Preparation of nitrogen heterocycles from aromatic amines using tris(isopropylthio)cyclopropenyl cation as a three-carbon building block

HIDEO KOJIMA, NOBORU MATSUMURA, AND HIROO INOUE[1]

Department of Applied Chemistry, College of Engineering, University of Osaka Prefecture, Sakai, Osaka 591, Japan

Received June 3, 1991

HIDEO KOJIMA, NOBORU MATSUMURA, and HIROO INOUE. Can. J. Chem. **70**, 1 (1992).

Quinolines (**2** and **3**) and naphthazepines (**8** and **9**) are prepared in high yields by the reaction of tris(isopropylthio)-cyclopropenylium perchlorate (**1**) with anilines and 1-naphthylamines, respectively, under nitrogen in *N*,*N*-dimethylformamide at 80–85°C. The reactions are proven to proceed through the intermediary formation of iminium salts (**5**, **10**, and **11**) derived from **1** and amines. The reaction of **1** with pyrrole and indole in dimethyl sulfoxide, containing sodium hydride, at 25°C gives 5,6,7-tris(isopropylthio)-1*H*-pyrrolizine (**12**) and 1,2,3-tris(isopropylthio)-9*H*-fluorazene (**14**), respectively, in high yields by intramolecular cyclization of a vinylcarbene intermediate. The possible pathway for the formation of these nitrogen heterocycles is proposed.

Key words: cyclopropenyl cation, aromatic amines, nitrogen heterocycles, three-carbon building block.

HIDEO KOJIMA, NOBORU MATSUMURA et HIROO INOUE. Can. J. Chem. **70**, 1 (1992).

En faisant réagir du perchlorate de tris(isopropylthio)cyclopropénylium (**1**) avec des anilines et des naphtyl-1-amines, sous azote, dans le *N*,*N*-diméthylformamide, à 80–85°C, on a préparé respectivement les quinoléines **2** et **3** et les naphtazépines **8** et **9**, avec d'excellents rendements. On a prouvé que les réactions se produisent par la formation des sels d'iminium **5**, **10** et **11**, dérivés du composé **1** et des amines, comme intermédiaires. Les réactions du composé **1** avec le pyrrole et l'indole, dans le diméthylsulfoxyde contenant de l'hydrure de sodium à 25°C, fournissent respectivement le 5,6,7-tris(isopropylthio)-1*H*-pyrrolizine (**12**) et le 1,2,3-tris(isopropylthio)-9*H*-fluorazène (**14**), avec d'excellents rendements, par la cyclisation intramoléculaire d'un vinylcarbène intermédiaire. On propose une voie éventuelle de formation de ces hétérocycles azotés.

Mots clés : cation cyclopropényle, amines aromatiques, hétérocycles azotés, possibilités d'ajouter trois carbones.

[Traduit par la rédaction]

Introduction

Cyclopropenyl cations have attracted special attention because of their high strain and aromatic character, and their reactions with various nucleophiles such as amines (1), enolates (2), and Grignard reagents (3) have been investigated extensively. Recent studies have shown that the reaction of tris(*tert*-butylthio)cyclopropenyl cation with aliphatic amines, such as 3-aminopropionitrile and 3-aminopropionates, in *N*,*N*-dimethylformamide (DMF) containing sodium hydride gives the corresponding substituted 1,2-dihydropyridines by C_3-ring opening followed by intramolecular cyclization (4). Despite this research, few have investigated the reaction of aromatic amines with this ring system to build nitrogen heterocycles by cyclization at the aromatic ring.

Due to our interest in using the cyclopropenyl cation as a three-carbon building block, we carried out the reaction of tris(isopropylthio)cyclopropenylium perchlorate (**1**) with aniline, *m*-aminophenol, 1-naphthylamine, 5-amino-1-naphthol, pyrrole, and indole. Herein we report experimental details on the preparation of quinolines, naphthazepines, and pyrrolizine and fluorazene derivatives from **1** and the corresponding aromatic amines. Part of the results have been reported in our preliminary papers (refs. 5 and 6).

Results and discussion

Preparation of quinolines from aniline and m-*aminophenol*

The reaction of the cyclopropenyl cation **1** with aniline (2 equiv.) under nitrogen in dry DMF at 80°C gave 2,3-bis(isopropylthio)quinoline (**2**) in a high yield. In this reaction, 3,4-bis(isopropylthio)quinoline was not obtained. The aniline/**1** molar ratio of 2:1 was necessary for raising the yield of **2**; in the molar ratio of 1:1, the yield of **2** after 50 h was 40% (recovery of **1**: 60%). 7-Hydroxy-2,3-bis(isopropylthio)quinoline (**3**) was also prepared under similar conditions from *m*-aminophenol and **1** (molar ratio of 2:1) in 96% yield after 24 h, accompanied by the formation of 5-hydroxy-2,3-bis(isopropylthio)quinoline (**4**) in 4% yield. Thus, the cyclopropenyl cation **1** served as a building block to form quinolines by ring opening followed by intramolecular cyclization.

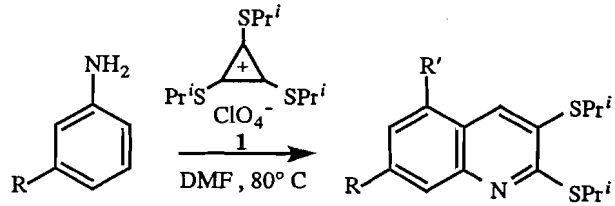

R = H, OH

2: R = R′ = H
3: R = OH; R′ = H
4: R = H; R′ = OH

Next the reactions were carried out in acetonitrile (MeCN) at 25°C. The reaction with aniline led to the formation of an iminium salt **5** in quantitative yield, although with *m*-aminophenol, quinolines **3** and **4** were isolated in 74 and 3% yields, respectively, after 73 h. The iminium salt **5** was isolated by the evaporation of MeCN after the reaction and its structure was established by measuring the ^1H and ^{13}C nmr spectra. The ^1H nmr spectrum showed a singlet (1H) for the CH=N$^+$ proton at δ 9.08, a broad singlet (2H) for the NH and NH$^+$ protons at δ 8.70–8.90, an unresolved multiplet (10H) for the aromatic ring protons at δ 7.38–7.43, and two doublets (12H, δ 1.18 and 1.26) and two septets (2H, δ 2.98 and 3.19) for the methyl and methine protons of two isopro-

[1]Author to whom correspondence may be addressed.

Printed in Canada / Imprimé au Canada

Can. J. Chem. Downloaded from www.nrcresearchpress.com by 123.30.183.119 on 09/08/12
For personal use only.

Can. J. Chem. Downloaded from www.nrcresearchpress.com by 123.30.183.119 on 09/08/12
For personal use only.

pylthio groups respectively. The ^{13}C nmr spectrum showed a signal due to the $C{=}N^+$ group at δ 175.2. Furthermore, the reaction of **1** with aniline at 25°C was carried out by using DMF instead of MeCN. The yield of **2** after 29 h increased to 14%, but the main product was the iminium salt **5** (84%). Next a solution of **5** in DMF was heated at 80°C for 25 h. It was found that **5** was converted quantitatively into the quinoline **2**. These facts indicate that **2** is produced through the intermediary formation of **5** which undergoes cyclization at 80°C.

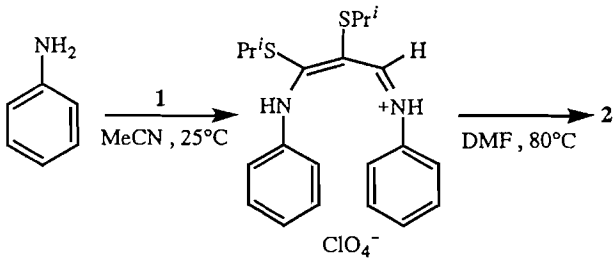

5

The possible pathway for the formation of **5** is proposed in Scheme 1. The nucleophilic attack of aniline on **1** is considered to form vinylcarbene (**6**), which is converted into an intermediate (**7**) by protonation. Formation and protonation of the vinylcarbene intermediate have been suggested in the reactions of 1-(diphenylamino)-2,3-diphenylcyclopropenyl cation with phenylmagnesium bromide (7) and of tris(*tert*-butylthio)cyclopropenyl cation with dimethylamine (8) and *o*-phenylenediamine (4), respectively. The reaction of intermediate **7** with aniline, accompanied by elimination of 2-propanethiol, leads to the formation of **5**. Cyclization of the iminium carbon of **5** at the *o*-position of the anilino group, followed by elimination of aniline, gives quinoline **2**. Quinolines **3** and **4** also are considered to be produced from *m*-aminophenol by this process, although the corresponding iminium salt was not detected.

Preparation of naphthazepines from 1-naphthylamine and 5-amino-1-naphthol

The cyclopropenyl cation **1** reacted under nitrogen with 1-naphthylamine and 5-amino-1-naphthol (2 equiv.) in MeCN under reflux or in DMF at 85°C to give 2,3-bis(isopropylthio)- (**8**) and 7-hydroxy-2,3-bis(isopropylthio)naphth[1,8-*bc*]azepine (**9**), respectively, in high yields. Thus, cyclopropenyl cation **1** undergoes cyclization at the 8-position of the naphthalene nucleus to form the azepine ring, but not at the 2-position to form the pyridine ring. When the reactions were carried out in DMF at 25°C, the yields of **8** and **9** decreased and iminium salts **10** and **11** were obtained as the main products. The iminium salts are considered to be produced by the pathway similar to that in Scheme 1. Furthermore, it was confirmed that iminium salts **10** and **11** were converted into naphthazepines **8** and **9**, respectively, in quantitative yields by heating at 85°C in DMF. From these results, the reaction pathway for the formation of naphthazepines **8** and **9** is considered to be similar to that in the reaction of **1** with anilines described above. Cyclization at the 8-position of the naphthalene ring implies that the carbon at the 8-position and the iminium carbon are favorably situated in positions that permit ring closure.

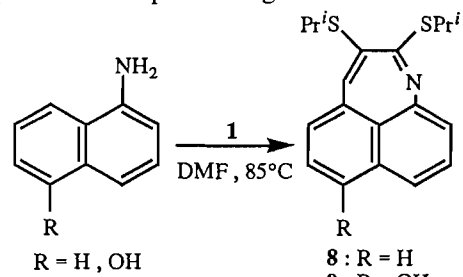

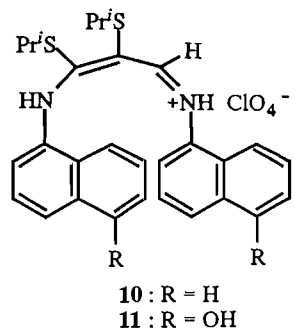

Preparation of pyrrolizine and fluorazene derivatives from pyrrole and indole

To prevent protonation of the vinylcarbene intermediate generated by ring opening, the reaction of cyclopropenyl cation **1** with *N*-anions of pyrrole and indole in dimethyl sulfoxide (DMSO) was conducted. Pyrrole was treated under nitrogen with sodium hydride (1 equiv.) in DMSO at 25°C and **1** (1 equiv.) was added. The reaction proceeded rapidly at 25°C to give 5,6,7-tris(isopropylthio)-1*H*(**12**) and -3*H* (**13**)-pyrrolizine in 53 and 11% yields, respectively, after 1 h. In this reaction, pyrrolizine **13** was found to be derived easily from **12** under irradiation with solar light. Therefore, reaction of **1** with the pyrrolyl *N*-anion was carried out in the dark, affording only **12** in 98% yield. Potassium *tert*-butoxide and potassium hydroxide also were useful, as a base, in this re-

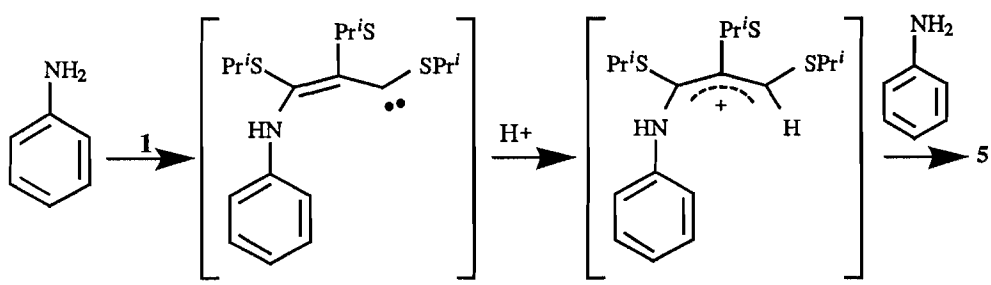

6 **7**

SCHEME 1

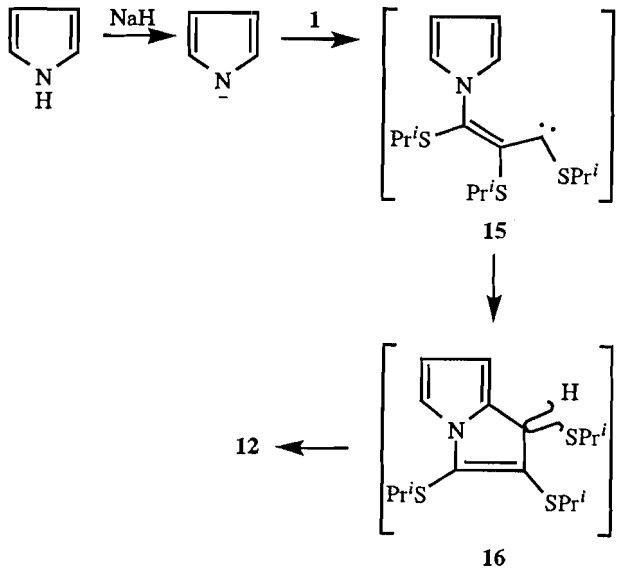

SCHEME 2

action. In the absence of a base, **12** and **13** were not produced, but a mixture of unidentified compounds was obtained.

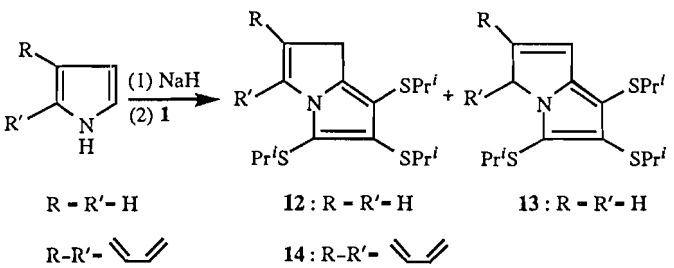

The reaction of **1** with the indole/NaH system (molar ratio of 1:1:1) was carried out under similar conditions. At 85°C, 1,2,3-tris(isopropylthio)-9*H*-fluorazene (**14**) was obtained in 84% yield after 1 h. Cyclization at the 7-position of indole did not occur. Thus, the cyclopropenyl cation **1** was proven to undergo cyclization at the 1,2 positions of pyrrole and indole to form pyrrolizine and fluorazene derivatives respectively.

Reaction with the pyrrolyl *N*-anion is rationalized to proceed through formation of the vinylcarbene intermediate **15** by nucleophilic attack of the pyrrolyl *N*-anion on the cyclopropenyl cation **1**, followed by intramolecular insertion of the carbene into the C—H bond in the 2-position of pyrrole to give **16**, as shown in Scheme 2. Intermediate **16** is converted into **12** by the migration of hydrogen. Fluorazene **14** also is considered to be produced from indole by this process.

Experimental

Melting points were determined on a Yanagimoto MP-S3 melting point apparatus and are uncorrected. The ir spectra of solids (KBr) and oil (neat) were recorded on a Hitachi 215 spectrometer. The ^{1}H nmr (270 MHz) and ^{13}C nmr (68 MHz) spectra were measured on a Jeol JNM-GX 270 FT nmr spectrometer with $CDCl_3$ as solvent and tetramethylsilane as an internal standard. Mass spectra were obtained at 70 eV with a Shimadzu LKB-9000 spectrometer. Elemental analyses of quinolines **2–4**, naphthazepines **8** and **9**, pyrrolizines **12** and **13**, and fluorazene **14** agreed within ±0.3% with the calculated values. Column chromatography was performed on silica gel (Wakogel C-300).

General procedure for the preparation of quinolines, iminium salts, and naphthazepines

Compound **1** (181 mg, 0.5 mmol) was added under nitrogen to a solution of amines (1.0 mmol) in dry DMF or MeCN (20 mL) in one portion and the mixture was stirred at the indicated reaction temperature for 24–73 h. Iminium salts **5**, **10**, and **11** were isolated by removal of the solvent *in vacuo*. The residue was subjected to the measurement of the ^{1}H and ^{13}C nmr spectra without further purification, because structural changes occurred on purification. For the isolation of quinolines **2–4** and naphthazepines **8** and **9**, the reaction mixture with DMF was poured into water (100 mL) and extracted with CH_2Cl_2 (2 × 50 mL). The organic layer was washed with water (3 × 50 mL), dried (Na_2SO_4), and concentrated *in vacuo*. The reaction mixture with MeCN was evaporated *in vacuo*. The residue was purified by silica gel chromatography using the eluent shown below.

2,3-Bis(isopropylthio)quinoline (2) (DMF, 80°C, 29 h): 80% yield; purified by column chromatography (hexane/CH_2Cl_2, 3:1); a colorless oil; ir (neat) ν: 3050, 2960, 2925, 2865, 1620, 1575, 1550, 1490, 1465, 1385, 1360, 1330, 1240, 1155, 1140, 1120, 1055, 990, 780, 750 cm^{-1}; ^{1}H nmr δ: 1.34 (d, J = 6.9 Hz, 6H, CH(CH_3)$_2$), 1.48 (d, J = 6.9 Hz, 6H, CH(CH_3)$_2$), 3.54 (sept, J = 6.9 Hz, 1H, CH(CH$_3$)$_2$), 4.23 (sept, J = 6.9 Hz, 1H, CH(CH$_3$)$_2$), 7.41 (m, 1H, arom), 7.61 (m, 1H, arom), 7.66 (m, 1H, arom), 7.91 (m, 1H, arom), 7.96 (s, 1H, H-4); ^{13}C nmr δ: 23.0 (2C), 35.6, 38.2, 125.3, 125.9, 127.0, 127.9, 128.3, 129.5, 138.5, 147.0, 162.2; ms m/z: 277 (M^+).

7-Hydroxy-2,3-bis(isopropylthio)quinoline (3) and 5-hydroxy-2,3-bis(isopropylthio)quinoline (4) (DMF, 80°C, 24 h): 96 and 4% yields; purified by column chromatography (hexane/CH_2Cl_2, 1:2); a colorless oil. **3**; ir (neat) ν: 3375, 1620, 1580, 1560, 1495, 1450, 1335, 1200, 1130, 1050, 995, 860, 810 cm^{-1}; ^{1}H nmr δ: 1.30 (d, J = 6.7 Hz, 6H, CH(CH_3)$_2$), 1.45 (d, J = 6.7 Hz, 6H, CH(CH_3)$_2$), 3.47 (sept, J = 6.7 Hz, 1H, CH(CH$_3$)$_2$), 4.17 (sept, J = 6.7 Hz, 1H, CH(CH$_3$)$_2$), 5.69 (br s, 1H, OH-7), 7.03 (dd, J = 8.6 and 2.7 Hz, 1H, arom), 7.25 (d, J = 2.7 Hz, 1H, arom), 7.56 (d, J = 8.6 Hz, 1H, arom), 7.93 (s, 1H, H-4); ^{13}C nmr δ: 22.9, 23.0, 35.6, 38.5, 110.0, 117.2, 120.9, 125.0, 128.8, 140.2, 148.4, 157.4, 163.5; ms m/z: 293 (M^+). **4**; ir (neat) ν: 3400, 1620, 1580, 1555, 1465, 1335, 1275, 1200, 1130, 1080, 1050, 805 cm^{-1}; ^{1}H nmr δ: 1.35 (d, J = 6.7 Hz, 6H, CH(CH_3)$_2$), 1.48 (d, J = 6.7 Hz, 6H, CH(CH_3)$_2$), 3.56 (sept, J = 6.7 Hz, 1H, CH(CH$_3$)$_2$), 4.21 (sept, J = 6.7 Hz, 1H, CH(CH$_3$)$_2$), 5.44 (br s, 1H, OH-5), 6.73 (m, 1H, arom), 7.39–7.51 (m, 2H, arom), 8.34 (s, 1H, H-4); ms m/z: 293 (M^+).

Iminium salt (5) (MeCN, 25°C, 25 h): 100% yield; a reddish oil; ^{1}H nmr δ: 1.18 (d, J = 6.7 Hz, 6H, CH(CH_3)$_2$), 1.26 (d, J = 6.7 Hz, 6H, CH(CH_3)$_2$), 2.98 (sept, J = 6.7 Hz, 1H, CH(CH$_3$)$_2$), 3.19 (sept, J = 6.7 Hz, 1H, CH(CH$_3$)$_2$), 7.38–7.43 (m, 10H, arom), 8.70–8.90 (br s, 2H, NH and N$^+$H), 9.08 (s, 1H, CH=N$^+$); ^{13}C nmr δ: 22.19, 22.49, 39.58, 40.15, 103.0, 115.2, 118.3, 118.7, 123.5, 126.8, 127.9, 128.8, 129.5, 129.6, 129.7, 137.3, 145.6, 154.5, 175.2 (CH=N$^+$).

2,3-Bis(isopropylthio)naphth[1,8-bc]azepine (8) (MeCN, reflux, 25 h and DMF, 85°C, 25 h): 91 and 92% yields; purified by column chromatography (hexane/CH_2Cl_2, 2:1); colorless solids, mp 86–87°C; ir (KBr) ν: 3040, 2950, 2915, 2850, 1620, 1600, 1570, 1550, 1495, 1470, 1435, 1385, 1360, 1240, 1150, 1130, 1050, 935, 810 cm^{-1}; ^{1}H nmr δ: 1.36 (d, J = 6.7 Hz, 6H, CH(CH_3)$_2$), 1.61 (d, J = 6.7 Hz, 6H, CH(CH_3)$_2$), 3.59 (sept, J = 6.7 Hz, 1H, CH(CH$_3$)$_2$), 4.41 (sept, J = 6.7 Hz, 1H, CH(CH$_3$)$_2$), 7.58 (m, 1H, arom), 7.65–7.72 (m, 3H, arom), 7.87 (m, 1H, arom), 8.02 (s, 1H, H-3), 9.19 (m, 1H, arom); ^{13}C nmr δ: 22.9, 23.1, 35.9, 38.2, 123.3, 124.4, 124.8, 126.4, 126.9, 127.8, 128.1, 128.3, 130.9, 133.9, 139.0, 144.8, 161.3; ms m/z: 327 (M^+).

7-Hydroxy-2,3-bis(isopropylthio)naphth[1,8-bc]azepine (9)

Can. J. Chem. Downloaded from www.nrcresearchpress.com by 123.30.183.119 on 09/08/12
For personal use only.

Can. J. Chem. Downloaded from www.nrcresearchpress.com by 123.30.183.119 on 09/08/12
For personal use only.

(MeCN, reflux, 30 h and DMF, 85°C, 25 h): 96 and 90% yields; purified by column chromatography (hexane/CH_2Cl_2, 1:2); colorless solids, mp 159–160°C; ir (KBr) ν: 3325, 1610, 1575, 1425, 1390, 1355, 1255, 1135, 910, 755 cm^{-1}; ^1H nmr δ: 1.37 (d, J = 6.7 Hz, 6H, $CH(CH_3)_2$), 1.59 (d, J = 6.7 Hz, 6H, $CH(CH_3)_2$), 3.59 (sept, J = 6.7 Hz, 1H, $CH(CH_3)_2$), 4.38 (sept, J = 6.7 Hz, 1H, $CH(CH_3)_2$), 5.76 (br s, 1H, OH-7), 7.03 (m, 1H, arom), 7.51 (m, 1H, arom), 7.57 (d, J = 9.2 Hz, 1H, arom), 8.01 (s, 1H, H-3), 8.09 (d, J = 9.2 Hz, 1H, arom), 8.77 (m, 1H, arom); ^{13}C nmr δ: 22.9, 23.1, 35.9, 38.1, 111.9, 117.1, 119.8, 123.5, 123.9, 124.0, 126.9, 128.6, 132.4, 138.8, 144.6, 151.5, 161.2; ms m/z: 343 (M^+).

*Iminium salt (**10**)* (DMF, 25°C, 26 h): 73% yield with **8** in 26% yield; a reddish oil; ^1H nmr δ: 1.12 (d, J = 6.7 Hz, 6H, $CH(CH_3)_2$), 1.35 (d, J = 6.7 Hz, 6H, $CH(CH_3)_2$), 3.11 (sept, J = 6.7 Hz, 1H, $CH(CH_3)_2$), 3.30 (sept, J = 6.7 Hz, 1H, $CH(CH_3)_2$), 7.45–8.02 (m, 14H, arom), 8.54–8.62 (br s, 2H, NH and N^+H), 9.15 (s, 1H, $CH=N^+$); ^{13}C nmr δ: 22.4, 23.0, 40.1, 40.9, 103.1, 117.8, 119.6 (2C), 121.3, 122.7, 125.3, 125.5, 125.6, 126.8, 126.9, 127.4, 127.6, 127.9, 128.0, 128.5, 128.6, 129.2, 133.1, 133.7, 133.9, 157.4, 178.3 ($CH=N^+$).

*Iminium salt (**11**) (DMF, 25°C, 25 h): 65% yield with **9*** in 35% yield; a reddish oil; ^1H nmr (CD_3CN) δ: 1.06 (d, J = 6.7 Hz, 6H, $CH(CH_3)_2$), 1.42 (d, J = 6.7 Hz, 6H, $CH(CH_3)_2$), 2.97 (sept, J = 6.7 Hz, 1H, $CH(CH_3)_2$), 3.44 (sept, J = 6.7 Hz, 1H, $CH(CH_3)_2$), 5.70–5.80 (br s, 2H, OH), 7.06 (m, 2H, arom), 7.46–7.60 (m, 8H, arom), 8.25–8.35 (m, 2H, NH and N^+H), 9.19 (s, 1H, $CH=N^+$).

General procedure for the preparation of pyrrolizine and fluorazene derivatives

Pyrrole (34 mg, 0.5 mmol) or indole (59 mg, 0.5 mmol) was added to a suspended solution of NaH (50% in mineral oil), Bu^{t}OK, and KOH (0.5 mmol) in dry DMSO (10 mL) and the mixture was stirred under nitrogen at 25°C for 1.5–2 h. To the resulting solution, a solution of cyclopropenyl cation **1** (181 mg, 0.5 mmol) in dry DMSO (10 mL) was added in one portion. After stirring at 25 or 85°C for 1–2 h, the mixture was poured into water (100 mL) and extracted with ether (3 × 50 mL). The organic layer was dried (Na_2SO_4) and evaporated *in vacuo*. The residue was purified by silica gel chromatography using the eluent shown below.

*5,6,7-Tris(isopropylthio)-1H-pyrrolizine (**12**) and 5,6,7-tris(isopropylthio)-3H-pyrrolizine (**13**):* Yield, %: 53 and 11 (NaH, 1 h), 49 and 9 (Bu^{t}OK, 1 h), and 41 and 8 (KOH, 2 h). Irradiation of **12** (0.5 mmol) in deuteriochloroform (1 mL) (nmr sample tube) with solar light for 6 h: 50% yield of **13** and 50% recovery of **12**. Purified by column chromatography (hexane/CH_2Cl_2, 3:1); a colorless oil. **12**; ir (neat) ν: 3100, 2950, 2920, 2860, 1590, 1465, 1450, 1410, 1360, 1295, 1270, 1240, 1155, 1145, 1050, 935, 890, 810, 700 cm^{-1}; ^1H nmr δ: 1.18 (d, J = 6.7 Hz, 6H, $CH(CH_3)_2$), 1.20 (d, J = 6.7 Hz, 6H, $CH(CH_3)_2$), 1.21 (d, J = 6.7 Hz, 6H, $CH(CH_3)_2$), 3.20 (sept, J = 6.7 Hz, 1H, $CH(CH_3)_2$), 3.33 (sept, J = 6.7 Hz, 1H, $CH(CH_3)_2$), 3.48 (m, 2H, H-1), 3.49 (sept, J = 6.7 Hz, 1H, $CH(CH_3)_2$), 5.89 (m, 1H), 7.17 (m, 1H); ms m/z: 327 (M^+). **13**; ir (neat) ν: 2950, 2920, 2860, 1465, 1450, 1395, 1370, 1250, 1240, 1155, 1050, 770, 735 cm^{-1}; ^1H nmr δ: 1.19 (d, J = 6.7 Hz, 6H, $CH(CH_3)_2$), 1.22 (d, J = 6.7 Hz, 12H, $CH(CH_3)_2$), 3.20 (sept, J = 6.7 Hz, 1H, $CH(CH_3)_2$), 3.37 (sept, J = 6.7 Hz, 1H, $CH(CH_3)_2$), 3.49 (sept, J = 6.7 Hz, 1H, $CH(CH_3)_2$), 4.52 (m, 2H, H-3), 6.37 (m, 1H), 6.71 (m, 1H); ms m/z: 327 (M^+).

*1,2,3-Tris(isopropylthio)-9H-fluorazene (**14**)* (NaH, 85°C, 1 h): 84% yield; purified by column chromatography (hexane/CH_2Cl_2, 2:1); a yellowish oil; ir (neat) ν: 3030, 2900, 2860, 1590, 1440, 1350, 1300, 1235, 1180, 1150, 1050, 735 cm^{-1}; ^1H nmr δ: 1.23 (d, J = 6.7 Hz, 6H, $CH(CH_3)_2$), 1.24 (d, J = 6.7 Hz, 6H, $CH(CH_3)_2$), 1.25 (d, J = 6.7 Hz, 6H, $CH(CH_3)_2$), 3.31 (sept, J = 6.7 Hz, 1H, $CH(CH_3)_2$), 3.38 (sept, J = 6.7 Hz, 6H, $CH(CH_3)_2$), 3.59 (sept, J = 6.7 Hz, 1H, $CH(CH_3)_2$), 3.89 (s, 2H, H-9), 7.12–7.17 (m, 1H, arom), 7.31–7.37 (m, 1H, arom), 7.42 (d, J = 6.7 Hz, 1H, arom), 8.26 (d, J = 6.7 Hz, 1H, arom); ms m/z: 377 (M^+).

Acknowledgements

This work was supported by the Grant-in-Aid for Scientific Research on Priority Areas No. 02230226 from the ministry of Education, Science, and Culture, Japanese Government.

1. Z. Yoshida. Top. Curr. Chem. **40**, 47 (1973).
2. H. Yoshida, T. Tamai, T. Ogata, and K. Matsumoto. Bull. Chem. Soc. Jpn. **61**, 2891 (1988).
3. A Padwa, S. I. Goldstein, and R. J. Rosenthal. J. Org. Chem. **52**, 3278 (1987); H. Yoshida, H. Sano, M. Kato, T. Ogata, and K. Matsumoto. Bull. Chem. Soc. Jpn. **59**, 2833 (1986).
4. Z. Yoshida, H. Hirai, S. Miki, and S. Yoneda. Tetrahedron, **45**, 3217 (1989).
5. H. Kojima, K. Ozaki, N. Matsumura, and H. Inoue. Chem. Lett. 1499 (1989).
6. H. Kojima, K. Ozaki, N. Matsumura, and H. Inoue. J. Heterocycl. Chem. **27**, 1845 (1990).
7. H. Yoshida, H. Sano, T. Ogata, and K. Matsumoto. Bull. Chem. Soc. Jpn. **61**, 4341 (1988).
8. S. Yoneda, H. Hirai, and Z. Yoshida. Heterocycles, **15**, 865 (1981).

Catalytic activity of vanadyl phosphate supported on TiO_2 (anatase) and SiO_2 (silica)

M. MARTINEZ-LARA, L. MORENO-REAL, R. POZAS-TORMO, A. JIMENEZ-LOPEZ,[1] AND S. BRUQUE
Universidad de Málaga, Facultad de Ciencias, Departamento de Química Inorgánica, Apartado 59, 29071 Málaga, Spain

AND

P. RUIZ AND G. PONCELET[1]
Groupe de physico-chimie minérale et de catalyse, Place Croix du Sud 1, B-1348 Louvain-la-Neuve, Belgium

Received December 11, 1990[2]

M. MARTINEZ-LARA, L. MORENO-REAL, R. POZAS-TORMO, A. JIMENEZ-LOPEZ, S. BRUQUE, P. RUIZ, and G. PONCELET. Can. J. Chem. **70**, 5 (1992).

Oxidation of *n*-butane was investigated on vanadyl phosphate (VP) prepared in the presence of titania (anatase) and silica as supports. In the case of silica, α-$VOPO_4$ was synthesized with no sign of interaction between the silica surface and vanadium phosphate. On the contrary, titania was coated with amorphous VP (P/V = 1), preventing the crystallization of $VOPO_4$ at least up to the VP content of 21%. *n*-Butane was completely converted into CO_2 for the VP/TiO_2 catalytic system. Upon impregnation with metal sulfates, maleic anhydride (MA) was produced with selectivities depending on the nature of the added metallic species, the best effect being observed with Fe^{2+} (V/Fe = 3). Selectivities to MA were influenced by the P/V ratio, with a maximum at P/V = 1.2.

Key words: vanadyl phosphate, maleic anhydride, butane oxidation, anatase, rutile.

M. MARTINEZ-LARA, L. MORENO-REAL, R. POZAS-TORMO, A. JIMENEZ-LOPEZ, S. BRUQUE, P. RUIZ et G. PONCELET. Can. J. Chem. **70**, 5 (1992).

On a étudié l'oxydation du butane sur de phosphate de vanadyle (PV) préparé en présence de titania (anatase) et de silica comme supports. Dans le cas de la silice, on a synthétisé du α-$VOPO_4$ sans signes d'interactions entre la surface de la silice et le phosphate de vanadium. Au contraire, le titania était couvert de PV (P/V = 1) et cette situation empêche la cristallisation du $VOPO_4$, au moins jusqu'à un contenu en PV de 21%. Avec le système catalytique PV/TiO_2, le butane est complètement transformé en CO_2. Après imprégnation sur des sulfates métalliques, il y a formation d'anhydride maléique (AM) avec des sélectivités qui dépendent de la nature des espèces métalliques ajoutées; les meilleurs résultats sont obtenus avec le Fe^{2+} (V/Fe = 3). Les sélectivités en AM sont influencées par le rapport P/V; le maximum se situe à P/V = 1, 2.

Mots clés : phosphate de vanadyle, anhydride maléique, oxydation du butane, anastase, rutile.

[Traduit par la rédaction]

Introduction

Two catalytic processes of industrial importance, namely, the production of maleic anhydride (MA) from C_4 hydrocarbons and phthalic anhydride from *o*-xylene, rely widely on vanadium-based catalysts. In the first process, C_4 hydrocarbons are oxidized into MA using vanadium phosphate catalytic systems (VPO catalysts), while in the second, titania-supported V_2O_5 catalysts are preferred. These two types of catalysts generally contain modifiers, promoters, etc. There has been significant evidence that TiO_2 imparts special properties to V_2O_5, which other more classical supports do not, or do so to a lesser extent. Several authors proposed that a solid solution forms between V^{4+} and TiO_2 (1, 2), though this question still remains debatable.

The VPO catalysts, in spite of the large number of studies on these compounds and the progress made in recent years, remain complex systems that are not yet understood. Three main aspects are still subject to some disagreement: the exact nature of the active phase (is it a crystalline phase and, if so, which one (3), or is it rather an amorphous phase (4)); the oxidation state of V and its control (5); the influence of the P/V ratio on the selectivity to MA (6, 7). These questions have been considered in reviews by Hodnett *et al.* (8) and Centi *et al.* (9).

One way to improve the performance of a catalyst is to increase the number of the active sites exposed to the reacting molecules. High surface area catalysts may be obtained from precursors prepared in nonaqueous solutions (10, 11) or, alternatively, by supporting the catalytic phase. This latter approach was preferred.

Up to now, very little work has been concerned with the study of supported VP catalytic systems. Chinchen *et al.* (12) mention patents to BASF wherein it is "suggested" that a titania/steatite is probably used to support VPO. The same authors also refer to patents to Mitsubishi quoting silica and alumina as supports for these catalysts. Cavani *et al.* (5) prepared a coprecipitated VPO–TiO_2 catalyst with 10% V_2O_5, but have not yet provided results showing how these systems compare with pure VPO catalysts. SiO_2 was taken as support for VPO by Varma and Saraf (13) for the oxidation of butenes, whereas Nakamura *et al.* (14) investigated VPO/α-Al_2O_3 systems.

In spite of the already complex nature of vanadium phosphate catalysts, it was challenging, due to the particular interaction between vanadium compounds and titania, to investigate the catalytic performance of supported VP in the oxidation of *n*-butane. TiO_2 (anatase) and a microfibrilous silica were chosen as supports, the VPO phase being prepared using a procedure that, in absence of support, yielded crystalline α-$VOPO_4 \cdot 2H_2O$ (15, 16). This paper summarizes the preliminary results obtained with these systems.

[1]Authors to whom correspondence may be addressed.
[2]Revision received August 1, 1991.

Can. J. Chem. Downloaded from www.nrcresearchpress.com by 123.30.183.119 on 09/08/12
For personal use only.

Can. J. Chem. Downloaded from www.nrcresearchpress.com by 123.30.183.119 on 09/08/12
For personal use only.

Experimental

Preparation of the catalysts

Crystalline α-$VOPO_4$ was synthesized according to the method described earlier (15). The supported "$VOPO_4$" (hereafter VP) systems were prepared using the standard method, the only difference being the addition of the support to the reaction mixture. Two supports were chosen: TiO_2 (Eurotitania from Tioxide, batch 1143; So = 61 m^2/g) and a microfibrous SiO_2 (from Redco; So = 550 m^2/g). After refluxing, the slurries were washed and freeze-dried. The amounts of the different reagents in the reaction mixture corresponded to $V_2O_5/(V_2O_5 + TiO_2)$ weight ratios of 5, 10, 15, and 22% (named T5, T10, T15, and T22 in Table 1) and $V_2O_5/(V_2O_5 + SiO_2)$ of 6.6, 12.6, 20, and 31%.

Metals (Me) supported on VP/TiO_2 were obtained by the wet impregnation (H_2O or MeOH) method, using the sulfates of Fe^{2+}, Co^{2+}, Cr^{3+}, and Mn^{2+}. Molybdenum-impregnated systems were prepared with ammonium heptamolybdate. In all cases the V/Me atomic ratio was 3. Impregnation and drying were carried out in a rotavapor.

Systems with different P/V ratios were obtained by impregnation of the (Me)VP/TiO_2 material with the amounts of H_3PO_4 necessary to achieve P/V ratios of 1.1, 1.2, 1.3, and 1.5.

All the solids prepared were pelleted, crushed, and sieved. The catalytic tests were performed on the 0.2–0.315 mm fraction.

Characterization methods

To determine the chemical composition of the solids, they were dissolved by melting with NaOH. Vanadium was determined by atomic absorption spectrometry and the content of phosphorus was obtained by colorimetric analysis as the blue molybdophosphate complex; previous precipitation of titanium and vanadium was with cupferron.

The catalytic systems were also characterized using various techniques: differential thermal and thermogravimetric analyses (Rigaku Thermoflex), infrared spectroscopy (IFS 88 Brucker), X-ray diffraction (Cu Kα radiation, Siemens D500 equipment with DACO-MP setup), scanning electron microscopy (Jeol Temscan 100CX), and electron microprobe analysis EDS (Kevex SC 100).

Catalytic measurements

The catalytic oxidation of *n*-butane (*n*-C_4) was carried out in a flow reactor operated at atmospheric pressure. A detailed description of the apparatus and measurement procedure has been given elsewhere (7). The tests were done on a constant catalyst volume basis (height of catalyst bed: 14 cm; internal diameter of the tubular reactor: 3.5 mm). In these conditions, the sample weight was between 1.2 and 1.8 g.

The reaction was performed in temperature-programmed mode with *n*-C_4 flowing at 0.5 mL/min and air at 35 mL/min. These conditions define a molar concentration of *n*-C_4 of 1.4%. The tubing and valves beyond the reactor were heated to prevent condensation of the reaction products. The analyses were performed by gas chromatography.

Results

Catalyst characterization

Chemical analyses

The chemical analysis data of solids before catalytic performances given in Table 1 indicate that, in the VP/TiO_2 systems, the molar ratio V/P is near 1. The total vanadium content of these catalysts represents 80% of the amount of V introduced in the synthesis mixture. For the VP/SiO_2 catalysts, only 60% of the starting vanadium is found in the final product.

X-ray diffraction and SE microscopy

The X-ray diagrams of the VP/TiO_2 series with different VP contents and of the pure α-$VOPO_4 \cdot 2H_2O$ phase are shown in Fig. 1. The 001 (7.4 Å), 002 (3.7 Å), 102 (3.16

TABLE 1. Chemical analysis data of the VP/TiO_2 catalysts (in wt.%)

Catalyst	V_2O_5 (%)	P_2O_5 (%)	H_2O (%)	TiO_2[a] (%)	P/V[b]	"$VOPO_4$"[c] (%)
T5	4.5	3.3	1.1	91.1	0.94	7.5
T10	8.1	6.1	2.9	82.9	0.96	13.9
T15	12.0	9.2	5.1	73.7	0.98	21.0
T22	18.4	14.0	7.9	59.7	0.97	31.9

[a]%TiO_2 = 100 − (%V_2O_5 + %P_2O_5 + %H_2O).
[b]Molar ratio.
[c]As inferred from P_2O_5 content.

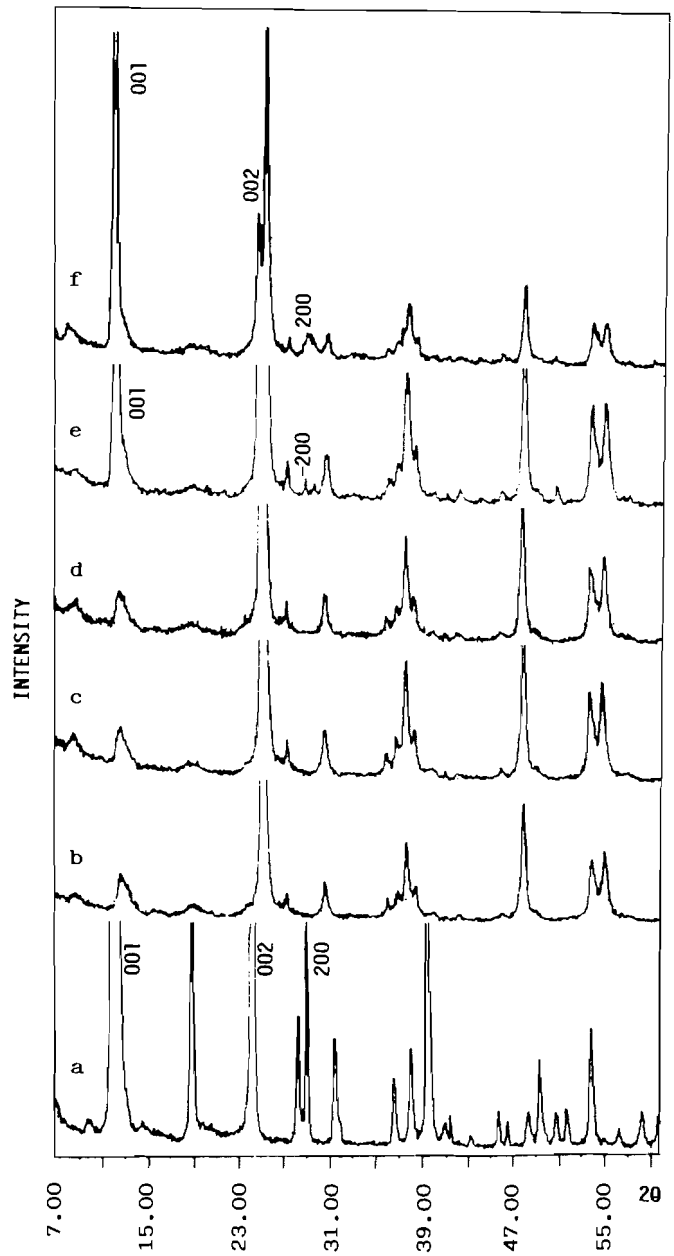

FIG. 1. X-ray powder diagrams of unsupported α-$VOPO_4$ (a), TiO_2 (b), and VP/TiO_2 containing 7.5%VP (c), 13.9%VP (d), 21%VP (c), and 31.9%VP (d).

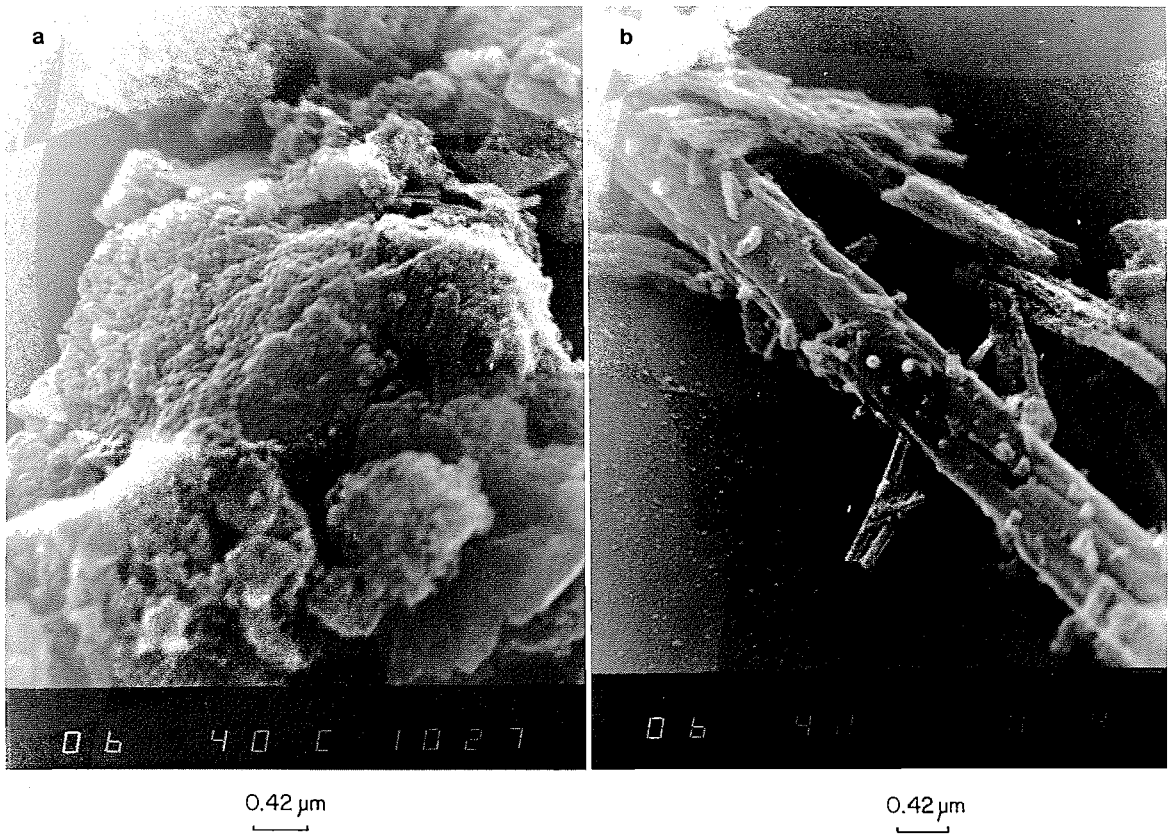

FIG 2. SEM photomicrograph of: (a) VP/TiO_2 and (b) VP/SiO_2. The bar in the lower right corresponds to 0.42 μm.

Å), and 200 (3.09 Å) reflections were taken to identify the crystalline α-$VOPO_4 \cdot 2H_2O$ phase. As can be seen, these diffraction lines are absent in the systems containing less than 21% VP. On the SE micrographs the anatase particles appear as homogeneously coated with VP (Fig. 2(a)). EDX studies verified this situation. Both analyses of aggregates and at various positions on individual particles show similar composition of Ti, V, and P. Only the samples with 31.9% VP contain, in addition, segregated particles of α-$VOPO_4$, thus in agreement with the X-ray diffraction analysis.

This situation was also observed by Fierro *et al.* (17) in the V_2O_5/TiO_2 system; X-ray diffraction data and Raman spectra showed that V_2O_5 was highly dispersed over TiO_2 in $V/(V + Ti) \leq 0.11$ catalyst; in more vanadium-rich systems the presence of tridimensional V_2O_5 crystallites was observed.

The picture is very different for the VP phases prepared in the presence of silica. Indeed, the X-ray diffraction spectra, given in Fig. 3, clearly show that crystalline α-$VOPO_4$ is present in all the samples, with peak intensities increasing with the VP content. Trace b in Fig. 3 indicates that the starting silica contains a small amount of residual quartz. The VP/SiO_2 with 4.1 and 14.6% VP contain, in addition to α-$VOPO_4$, small amounts of another phase characterized by reflections near 15°(2θ). This phase has not yet been identified. Examining these samples with SE microscopy confirms the existence of segregated α-$VOPO_4$, particles, the SiO_2 fibrils being uncoated. This fact is deduced from the microprobe analysis on the fibrous and lamellar materials in Fig. 2(b). Summarizing, the type of support plays an important role in the formation of the VPO phase. Anatase prevents the crystallization of α-$VOPO_4$, at least for VP contents up to 21.0%, and the TiO_2 particles are completely covered with VP. On the contrary, the silica used as support has no effect on the crystallization of the VPO phase, and there is no evidence of vanadium phosphate interacting with the surface of silica.

When V_2O_5 is supported on TiO_2 (anatase) a simultaneous reduction of V_2O_5 and transformation of TiO_2 (anatase) into TiO_2 (rutile) has been observed (1, 2). This polymorphic transformation is catalyzed by V^{5+} and is strongly dependent upon the calcination temperature, specially above 800 K. Taking into account that our VP/TiO_2 systems were air-dried and that the catalytic reactions were carried out up to 673 K, the catalysts will not undergo substantial phase transformation. The aforementioned authors (17) have not found any differences in the percentages of anatase and rutile in the supported catalysts after calcination at 773 K with respect to the unsupported anatase.

The addition of reducing metal ions (like Fe^{2+}, Mn^{2+}) provokes a gradual diminution of the 001 reflections of α-$VOPO_4 \cdot 2H_2O$, while a new peak appears at 13.4°(2θ) (6.6 Å) whose intensity increases with the amount of the reducing species. Such a change of the X-ray diagram had already been reported by Martinez *et al.* (15) in the case of redox intercalation in vanadyl phosphate for which the coexistence of a vanadium (4+) phosphate phase containing interlamellar cations and vanadium (5+) phosphate was proposed.

Can. J. Chem. Downloaded from www.nrcresearchpress.com by 123.30.183.119 on 09/08/12
For personal use only.

Can. J. Chem. Downloaded from www.nrcresearchpress.com by 123.30.183.119 on 09/08/12
For personal use only.

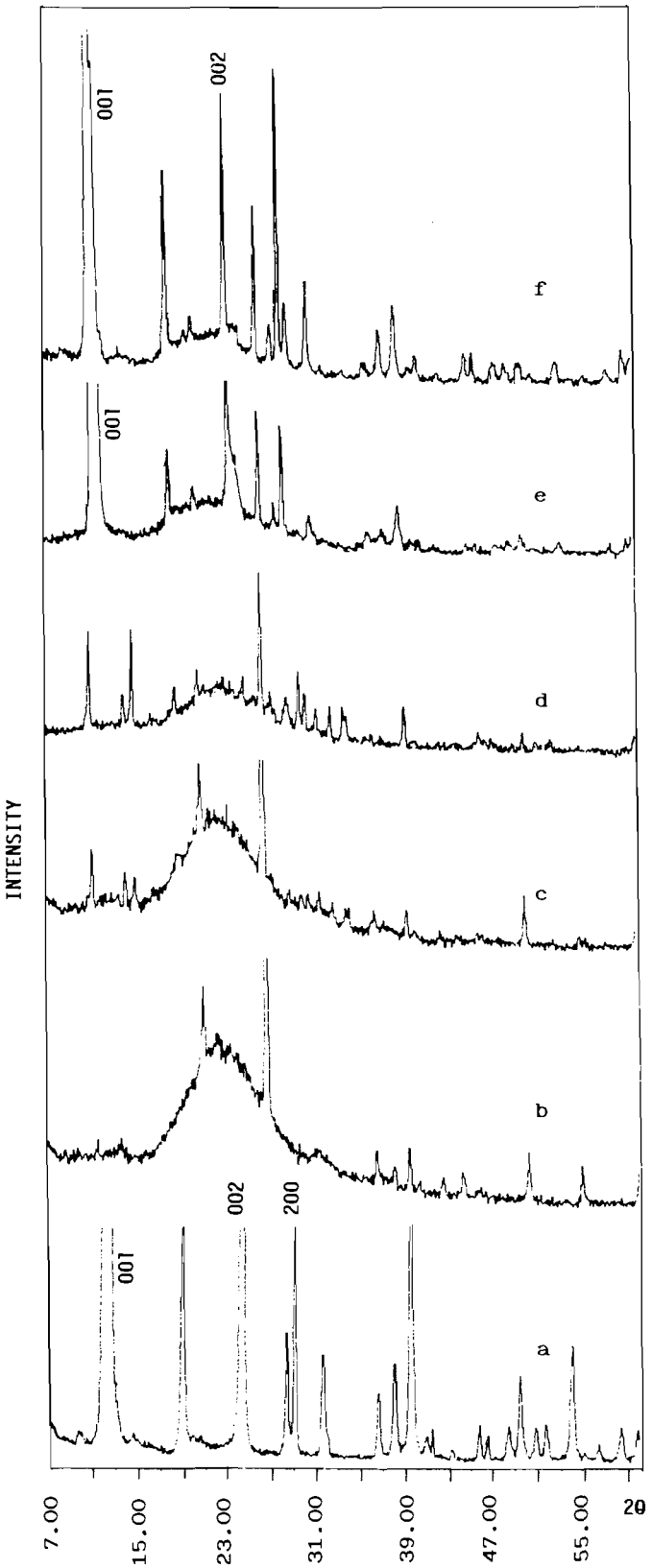

FIG 3. X-ray powder diagrams of unsupported α-$VOPO_4$ (a), SiO_2 showing the reflections of residual quartz (b), and with different amounts of VP: (c) 4.1%; (d) 14.6%; (e) 21.8%, and (f) 33.0%.

Infrared spectroscopy

The IR spectra of the VP/SiO_2 and VP/TiO_2 systems exhibit, without important modifications, the absorption band characteristic of the support and of the active phase. The spectral region between 900 and 1200 cm^{-1} is most sensitive to the modifications of the catalyst. Indeed, this is the frequency domain of the vibrations of PO_4^{3-} (1170, 1080, 1030 cm^{-1}) and V—O groups (1010, 990, 964 cm^{-1}) (15, 16). The spectrum of VP/TiO_2 impregnated with Fe^{2+} (Fig. 4B) clearly shows a band at 990 cm^{-1}, which is assigned to the V^{IV}—O vibration as a consequence of a partial reduction of V^V by Fe^{2+}. As compared to the spectrum of the iron-free sample (Fig. 4A), the intensity of the band at 964 cm^{-1} of the Fe^{2+}-containing catalyst is markedly diminished. This band may be attributed to the P—O stretching vibration of the PO_4^{3-} group within an asymmetrical environment, although Pulvin *et al.* (18) proposed to assign it to the pseudo-symmetrical vibration of O—V=O.

The IR spectrum of the Fe^{2+}-containing VP/TiO_2 sample impregnated with phosphoric acid (Fig. 4C) shows a broad absorption band centered at around 1050 cm^{-1}, which envelopes all the other bands due to the phosphate groups.

EPR measurements

The EPR spectra of the VP/TiO_2 samples (not shown here) are characteristic of vanadyl phosphate, with the signal of trace amounts of V(4+) centers diluted magnetically (19). The sample of VP/TiO_2 partially reduced with Fe^{2+} gives rise to EPR signals that denote the presence of V(4+) and Fe(3+) species, with a broad signal due to large amounts of paramagnetic centers.

Catalytic activity of the VP/TiO_2 systems

Influence of the "$VOPO_4$" content on the reaction of n-*butane*

The conversion of n-C_4 for the catalysts containing 7.5, 13.9, 21.0, and 31.9% VP depends upon the temperature. Thus, total conversion (C) of n-C_4 is achieved at around 380°C for the two catalysts containing the highest amounts of vanadium, and at temperatures above 400°C for those with lesser VP contents. For the four systems, there is a steep increase in activity between 250 and 350°C. In these runs, total oxidation of n-C_4 occurred, CO_2 being the sole reaction product. No maleic anhydride could be detected.

For the four catalysts, the relationship between ln C and $1/T$ does not yield a single straight line but, rather, two linear portions with different slopes. The corresponding activation energies calculated from Arrhenius' equation are 88 kJ/mol between 200 and 300°C, and 15 kJ/mol between 300 and 400°C, respectively. This last value is, of course, typical of a reaction limited by the diffusional process.

Influence of different metal species on the selectivity to maleic anhydride

The oxidizing power of VP/TiO_2 being too strong, it was necessary to temper it by adjoining another metal. This was done, as indicated above, by wet impregnations of VP/TiO_2 catalyst with the sulfates of different metals. The impregnations were carried out on the system containing 31.9% VP.

In a first series of preparations, the base catalyst was impregnated with $FeSO_4$ in order to deposit 2, 4, and 8 wt.% Fe^{2+}. The catalytic tests were performed under the same conditions as those in the preceding section.

Figure 5 compares the course of the conversion vs. reaction temperature obtained for the Fe^{2+}-loaded catalysts with

Can. J. Chem. Downloaded from www.nrcresearchpress.com by 123.30.183.119 on 09/08/12
For personal use only.

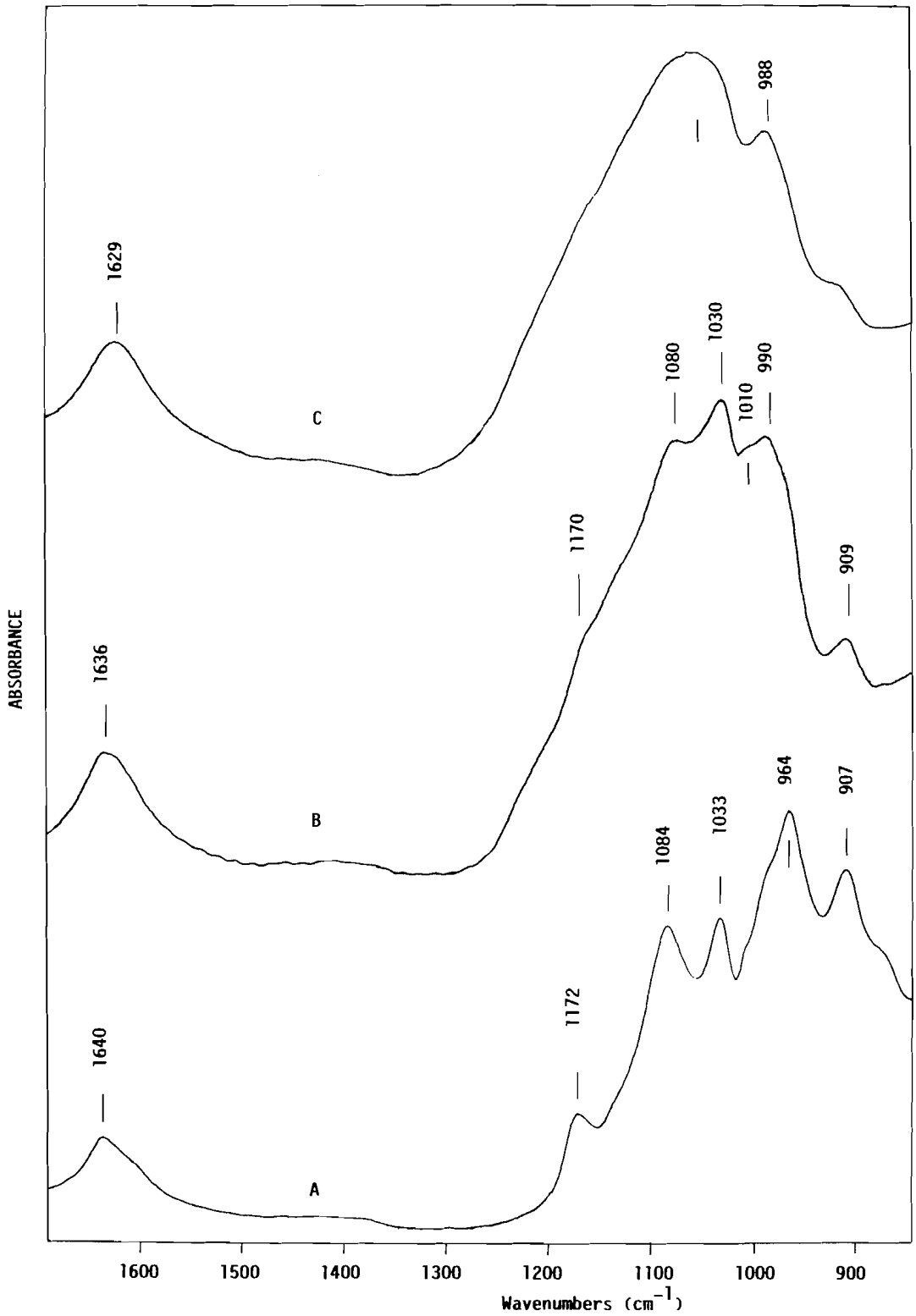

FIG 4. Infrared spectra of VP/TiO_2 (A); VP/TiO_2 impregnated with $FeSO_4$ (B), and the same as (B) with a P/V ratio of 1.2 (C).

that of the base VP/TiO_2 catalyst. Obviously, the addition of $FeSO_4$ lowers markedly the catalytic performance as compared with the reference catalyst. The catalysts containing 4 and 8% Fe^{2+} exhibit almost similar activities, slightly lower than that of the 2% Fe^{2+}-impregnated catalyst.

The effect of adding Fe^{2+} on the production of maleic anhydride is important. Whereas the base VP/TiO_2 produces only CO_2, upon addition of Fe^{2+} maleic anhydride is obtained, in addition to CO_2 as the main reaction product. In accordance with the IR and EPR results for the Fe^{2+}-impregnated catalysts, these systems have V(4+) and V(5+) centers. The selectivity to MA can be related to the pres-

Can. J. Chem. Downloaded from www.nrcresearchpress.com by 123.30.183.119 on 09/08/12
For personal use only.

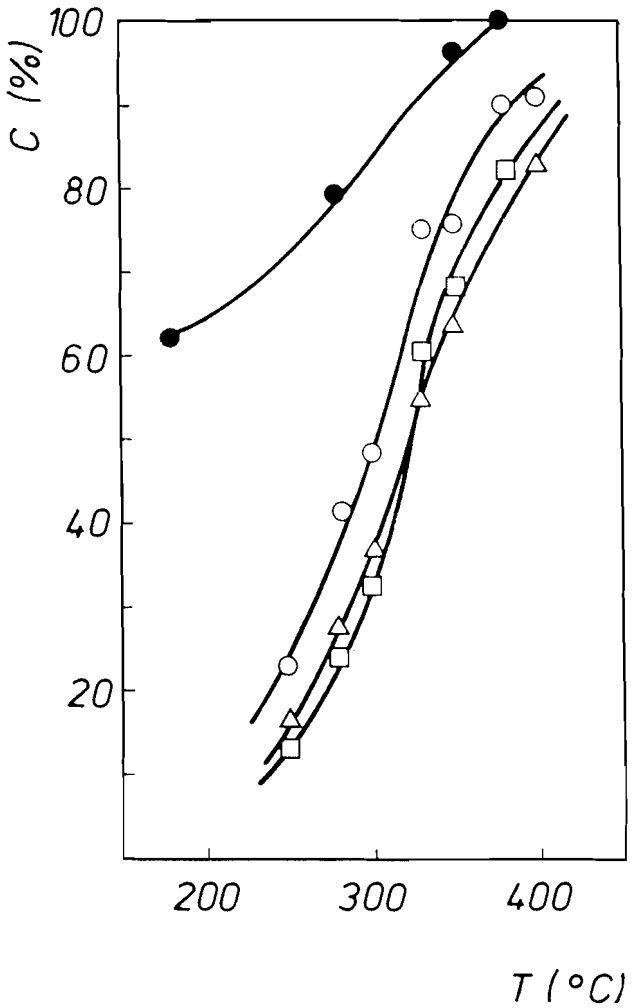

FIG. 5. Conversion of *n*-butane vs. temperature for: ● VP/TiO_2 (31.9% VP) and for the same catalyst impregnated with, respectively, 2% (○), 4% (△), and 8% (□) $FeSO_4$.

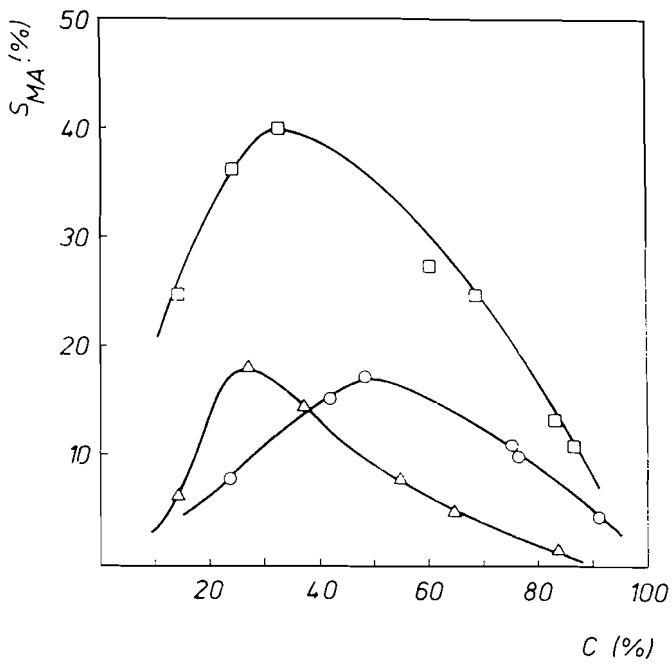

FIG. 6. Evolution of the selectivity to MA vs. conversion for the $FeSO_4$-impregnated VP/TiO_2: ○, □, △: 2, 4, and 8% Fe respectively.

ence of both oxidation states as has been established from EXAFS by other authors (20). A similar conclusion has been proposed by Batis *et al.* (21) with a catalyst based on $(VO)_2P_2O_7$ and V^{+5}, where high selectivity to MA was found when specific $VOPO_4$ phases (α_I, α_{II}, β, γ, etc) are simultaneously present with $(VO)_2P_2O_7$. Figure 6 compares, for the three iron-impregnated catalysts, the selectivities to MA as a function of the conversions obtained at the temperatures indicated in Fig. 5. At 50% conversion, the system containing 4% Fe^{2+} is twice as selective as the one with 2% Fe^{2+} and almost four times as selective as that for 8% Fe^{2+}. For the three catalysts, the maximum selectivity is attained at around 300°C.

In another series of preparations, VP/TiO_2 (31.9% VP) was impregnated with the sulfates of different metals in order to see the influence of the nature of the metal on the selectivity to MA. Except for Mo, which was introduced as ammonium molybdate, the sulfates were used in the amounts required to load the parent catalyst with 4% Me. This amount corresponds to a V/Me atomic ratio of 3.

Figure 7 compares the course of the conversion vs. temperature for the different systems investigated. Although the activity of these catalysts is lower than that of the metal-free catalyst, Co^{2+} and Mn^{2+} appear, among the different metals, to have the most effect on the activity, whereas the Mo^{6+}-impregnated system is the least active. The Co^{2+} and Mn^{2+}-modified catalysts transform approximately twice as much *n*-C_4 as the Mo^{+6}-loaded catalyst, at any temperature between 250 and 350°C. The Cr^{3+} system exhibits intermediate behaviour.

Considering the selectivities to maleic anhydride, for some of the conversion values obtained from Fig. 7 (Fig. 8), three systems are not very selective, namely those containing Mn^{2+}, Cr^{3+}, and Mo^{6+}. The other, the Co^{2+}-impregnated catalyst, appears with a higher selectivity to MA although slightly lower than those developed by the Fe^{2+}-impregnated catalyst. As observed for the system containing Fe^{2+}, the maximum selectivity is reached near 30% conversion, which occurs at around 280–300°C.

Influence of the P/V ratio on the selectivity to MA

The influence of the P/V ratio of unsupported VPO catalysts on the selectivity to MA is still debated. According to different authors (6, 7), the optimal ratio may vary significantly. It was interesting to consider this parameter in our systems, inasmuch as, as mentioned previously, TiO_2-supported VP catalysts are X-ray amorphous. VP/TiO_2 catalysts containing 4% Fe^{2+} were thus prepared with P/V ratios between 1 and 1.5, additional P being supplied by impregnation with the required amounts of phosphoric acid.

Figure 9 shows the evolution of the total conversion of *n*-C_4 as a function of reaction temperature. Obviously, P/V ratios higher than unity depress the catalytic activity as compared with the catalyst where P/V = 1. The catalyst with the highest P/V (1.5) is the least active.

Considering the selectivities to MA, on increasing the P/V ratio there is an influence on the production of MA at least for conversions that do not exceed 40%. This is in accordance with the suggestion of some authors (20) who report that an excess of phosphorus prevents the complete oxida-

Can. J. Chem. Downloaded from www.nrcresearchpress.com by 123.30.183.119 on 09/08/12
For personal use only.

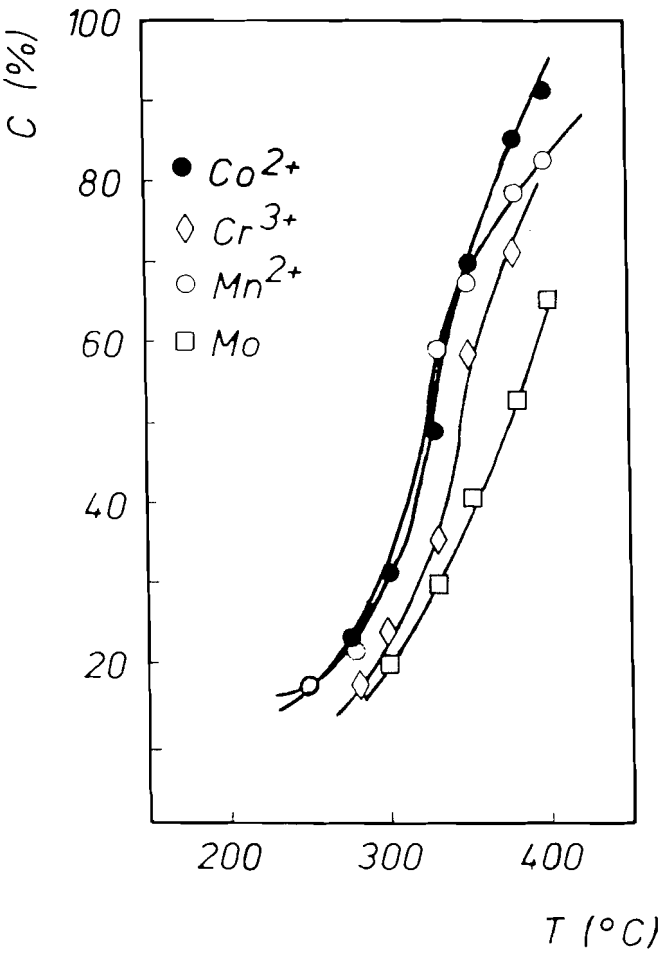

FIG. 7. Conversion of *n*-butane vs. temperature for the VP/TiO_2 (31.9% VP) impregnated with the sulfate (4%) of different metals (Mo from ammonium heptamolybdate).

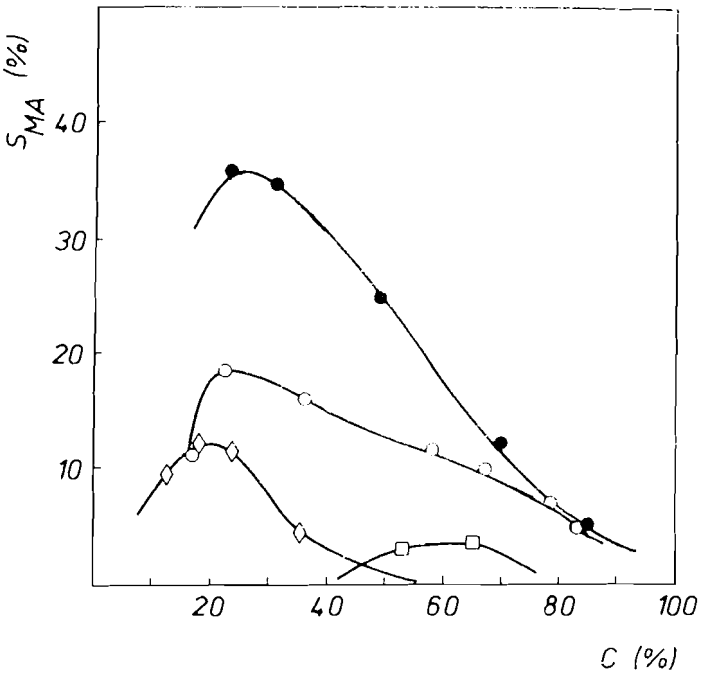

FIG. 8. Evolution of the selectivity to MA vs. conversion for the same catalysts as in Fig. 6: □ Mo^{6+}; ◇ Cr^{3+}; ○ Mn^{2+}; ● Co^{2+}.

tion of vanadium (V^{4+} to V^{5+}) by calcination in air. Beyond this value (40%), the effect is much less obvious (see Fig. 10). The system with P/V = 1.5 that is the least active is also the least selective and that with P/V = 1.2 is the most selective. At higher conversions, i.e., at higher temperatures, this effect vanishes. As for the other catalytic systems investigated, the maximum selectivity is obtained near 25% conversion.

Catalytic activity of unsupported crystalline α-$VOPO_4$

Oxidation tests of *n*-C_4 were performed, as well, under similar experimental conditions on bulk, well-crystallized α-$VOPO_4$ synthesized according to the method described in ref. 15.

These solids were found to be completely inactive in the temperature range investigated.

Catalytic activity of α-$VOPO_4/SiO_2$ systems

As shown previously, these systems always exhibit segregated crystalline α-$VOPO_4$ adjacent to silica whatever the VP content introduced in the preparation.

The catalytic runs carried out on these solids showed only partial conversion, which in no case was higher than 25% at 450°C. No maleic anhydride was produced.

VP/SiO_2 (21.8% VP) was then impregnated, first with $FeSO_4$ (4% Fe^{2+}) and subsequently with H_3PO_4, to realize a P/V ratio of 1.2, and tested. The conversion of *n*-C_4 increased slightly, to yield 30% at 450°C, 53% of the reaction product being maleic anhydride. The activity could be further improved when silica was precalcined at 700°C. Indeed, at 450°C, 55% of the hydrocarbon was converted, but lower selectivities to MA (11%) were obtained (with a maximum of 22% at 400°C).

These results agree with those found by Do *et al.* (22) for V_2O_5 supported on TiO_2 and Al_2O_3, where the TiO_2-supported catalyst was found to exhibit better selectivities for MA than the Al_2O_3-supported catalysts. Although the source of the support effect on the selectivity to MA of V_2O_5/P_2O_5 catalysts is not clear, Do *et al.* (23) related selectivity to MA to the presence of OH groups on the surface. Lopez Nieto *et al.* (24), in studies of the selective oxidation of propene on Al_2O_3, SiO_2, and TiO_2 (anatase)-supported V_2O_5 catalysts, found that V_2O_5/TiO_2 was the most active and selective phase because the V_2O_5 is highly dispersed on non-porous TiO_2, whereas for SiO_2 and Al_2O_3 part of the V_2O_5 species was deposited within the catalyst pores.

Discussion

The use of titania as support to VPO compounds makes difficult the comparison between the data in literature and the present results. Indeed, unsupported VPO catalysts used as starting materials are often, if not generally, well-defined crystalline phases. Nevertheless, as seen in this work, the presence of titania in the synthesis medium prevents the formation of a crystalline phase, up to VP contents near 21%. For this reason, this discussion will be restricted to the comparison of some of the main tendencies observed in this study with the results already published.

First of all, crystalline α-$VOPO_4$ is a much less active catalyst for the oxidation of *n*-butane (in the presence of SiO_2 as well as unsupported) than is its amorphous counterpart. This difference might possibly be only a surface effect, the fraction of the catalyst surface available to the reagents being

Can. J. Chem. Downloaded from www.nrcresearchpress.com by 123.30.183.119 on 09/08/12
For personal use only.

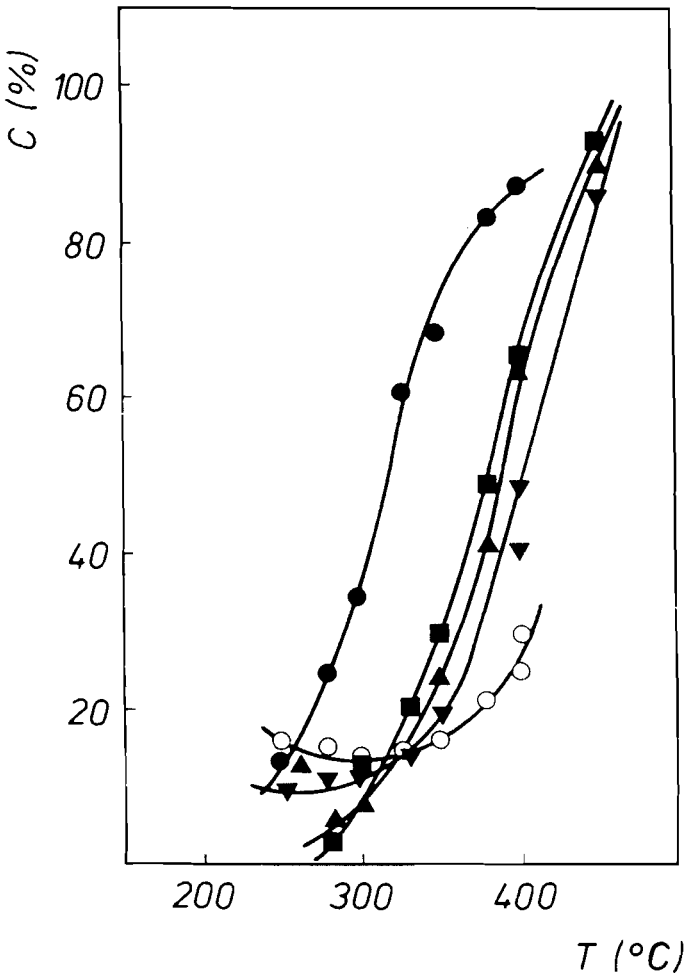

FIG. 9. Evolution of the conversion of *n*-butane vs. temperature for the Fe^{2+}-impregnated VP/TiO_2 with different P/V ratios: ●: 1.0; ■: 1.1; ▲: 1.2; ▼: 1.3; and ○: 1.5.

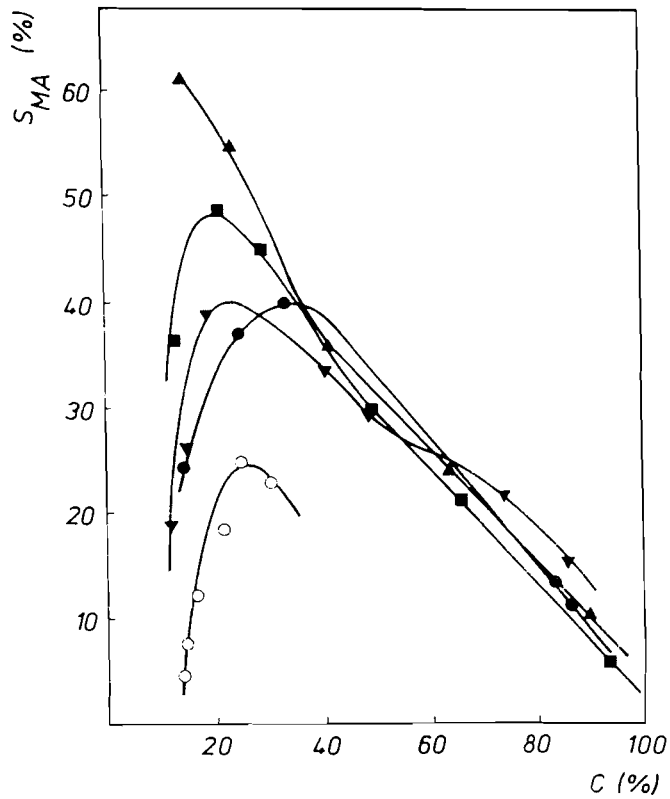

FIG. 10. Effect of the P/V ratio on the selectivity to MA (same symbols as in Fig. 9).

higher for the VP/TiO_2 systems. Nevertheless, independent of the crystalline or amorphous character of the VP phase, both systems yield only CO_2 as reaction product. These observations are consistent with the results reported by Bergeret *et al.* (4), Hodnett (8), and Védrine *et al.* (25), as well as the linear relationship between *n*-butane conversion and VP content (26). The results obtained with such catalytic systems are a clear illustration that it is not enough to reach high conversions if the oxidizing power of these catalysts is not under control in agreement with Cavani *et al.* (5).

In bulk VPO catalysts, the nature of the phase responsible for the formation of MA is not well identified. $(VO)_2P_2O_7$ has been advocated by Cavani *et al.* (27), Contractor *et al.* (3), and Védrine *et al.* (25), among other authors, as being the active phase, while no quantitative correlation between catalytic activity and selectivity and the content of vanadium pyrophosphate could be found by Van Geem *et al.* (6) and Hodnett *et al.* (7, 28). To other authors, it turns out rather that the best catalysts appear to be poorly crystallized or even amorphous VPO phases (25), while for Bordes and Courtine (29) and Morselli *et al.* (30) activity and selectivity are associated with the simultaneous presence of β-$VOPO_4$ and $(VO)_2P_2O_7$. Bergeret *et al.* (4) obtained the best results with a mixture of $(VO)_2P_2O_7$ and an amorphous phase produced upon activation. In this respect, our data show that completely amorphous supported VP with a P/V = 1 does not lead to MA. Maleic anhydride was formed only when the supported VP's were impregnated with a metal sulfate. The promotional effect of a series of elements on the selectivity to MA was investigated by Brutovsky and Gerej (31) and Brutovsky *et al.* (32) in the case of $(VO)_2P_2O_7$, the beneficial effect being in the following sequence: Mn > Co ≈ Sn > Fe > Cu > Li > Zn > Ce > Ni. Patent literature mentions catalysts containing promoters such as alkalis or alkaline earths (33) and Zn (34), which appear to prolong the life of the catalysts by diminishing the loss of phosphorus.

In our catalytic systems prepared by impregnation with metal sulfates, the improvement of the selectivity to MA was in the following order: $Fe^{2+} > Co^{2+} > Mn^{2+} > Cr^{3+} > Mo^{6+}$. It was established for the Fe^{2+}-impregnated VP/TiO_2 that the best selectivities to MA were obtained when the V/Fe atomic ratio was 3. If this sequence is different from the one previously reported, the catalysts are also not similar. These different elements do not simply improve the yield of MA, but in their absence no MA is formed. Their effect is merely to buffer the oxidizing power of VP. Since data on the oxidation state of V and on a possible change in that of the co-metal are not yet available, the way these catalytic systems act and favor the formation of MA cannot be discussed in more detail, although, as has been seen in the IR and EPR discussion of the Fe^{2+}-impregnated system, the higher value for selectivity may be related to the presence in the VP of V^{4+}/V^{5+} ions.

The influence of the P/V ratio on the reaction of *n*-butane has also been extensively investigated. If there seems to be a general consensus (from literature) that excess P with respect to a P/V ratio of 1 improves the selectivity to MA

with a parallel decrease in activity (35), the results reported by some authors are, at the very least, somewhat confusing. For instance, Van Geem and Nobel (6) observe a decrease in activity as the P/V ratio increases but with a maximum selectivity for P/V ratios between 0.58 and 1.06. These authors conclude, however, that selectivity to MA is only determined by the degree of conversion of the hydrocarbon. Nevertheless, it has been shown that low P/V ratios favor VPO phases (β-$VOPO_4$) with a vanadium oxidation number close to 5+, whereas higher P/V ratios stabilize vanadium as V^{4+}, in β or B phases (3), or $(VO)_2P_2O_7$ (5, 7, 14, 28, 29, 36, 37) yielding higher selectivities to MA. The influence of the P/V ratio on the selectivities to MA obtained for the $Fe/VP/TiO_2$ with a maximum at a value of 1.2 is hence consistent with the results of others. Further investigation is needed to characterize the oxidation state of vanadium in those systems, with particular attention to the effect of adding a co-metal on the oxidation state of vanadium, and to its distribution on the solid surface.

Acknowledgements

The authors gratefully acknowledge the financial support of the "Accords Culturels de la Communauté Française de Belgique," and PB 86-244 (CICYT) Spain.

1. P. J. Gellings. *In* Catalysis. Vol. 7. *Edited by* G. C. Bond and P. B. Webb. The Royal Society of Chemistry, London. 1985. p. 105.
2. F. Cavani, G. Centi, E. Foresti, and F. Trifiro. J. Chem. Soc. Faraday Trans. **84**, 237 (1988).
3. R. M. Contractor, H. E. Bergna, H. S. Horowitz *et al.* Catal. Today, **1**, 49 (1987).
4. G. Bergeret, M. David, J. P. Broyer *et al.* Catal. Today, **1**, 37 (1987).
5. F. Cavani, G. Centi, A. Riva, and F. Trifiro. Catal. Today, **1**, 17 (1987).
6. P. C. Van Geem and A. P. P. Nobel. Catal. Today, **1**, 15 (1987).
7. B. K. Hodnett, P. Permanne, and B. Delmon. Appl. Catal. **6**, 231 (1983).
8. B. K. Hodnett. Catal. Rev. Sci. Eng. **27**, 373 (1985).
9. G. Centi, F. Trifiro, J. R. Ebner, and V. M. Franchetti. Chem. Rev. **88**, 55 (1988).
10. R. A. Schneider. U.S. Patent No. 3,864,280 (1975).
11. K. Katsumoto and D. M. Marquis. U.S. Patent No. 4,132,670 (1979).
12. G. Chinchen, P. Davies, and R. J. S. Sampson. *In* Catalysis science and technology. Vol. 8. Edited by J. R. Anderson and M. Boudart. Springer-Verlag, Berlin, 1987. p. 1.
13. R. L. Varma and D. N. Saraf. J. Catal. **55**, 361 (1978).
14. M. Nakamura, K. Kawai, and Y. Fujiwara. J. Catal. **34,** 345 (1974).
15. M. Martinez-Lara, A. Jimenez-Lopez, L. Moreno-Real *et al.* Mat. Res. Bull. **20**, 549 (1985).
16. M. Martinez-Lara, L. Moreno-Real, A. Jimenez-Lopez *et al.* Mat. Res. Bull. **21**, 13 (1986).
17. J. L. G. Fierro, L. A. Arrua, J. M. Lopez Nieto, and G. Kremenic. Appl. Catal. **37**, 323 (1988).
18. S. Pulvin, E. Bordes, M. Romis, and P. Courtine. J. Chem. Res. **362**, 362 (1981).
19. J. W. Johnson, A. J. Jacobson, J. F. Brody, and S. M. Rich. Inorg. Chem. **21**, 3820 (1982).
20. G. Vlaic and F. Garbassi. J. Catal. **122**, 312 (1990).
21. N. Harrouch Batis, H. Batis, A. Ghorbel *et al.* J. Catal. **128**, 3248 (1991).
22. N. T. Do and M. Baerns. Appl. Catal. **45**, 1 (1988).
23. N. T. Do and M. Baerns. Appl. Catal. **45**, 9 (1988).
24. J. M. Lopez Nieto, G. Kremenic, and J. L. G. Fierro. Appl. Catal. **61**, 235 (1988).
25. J. C. Védrine, G. Coudurier, M. Forissier and J. C. Volta. Catal. Today, **1**, 261 (1987).
26. K. Mori, A. Miyamoto, and Y. Murakami. J. Phys. Chem. **89**, 4265 (1985).
27. F. Cavani, G. Centi, and F. Trifiro. J. Chem. Soc. Chem. Commun. 492 (1985).
28. B. K. Hodnett and B. Delmon. Appl. Catal. **15**, 841 (1985).
29. E. Bordes and P. Courtine. J. Catal. **57**, 236 (1979).
30. L. Morselli, F. Trifiro, and L. Urbain. J. Catal. **75**, 112 (1982).
31. M. Brutovsky and S. Gerej. Collect. Czech. Chem. Commun. **47**, 403 (1982).
32. M. Brutovsky, S. Gerej, F. Vasilco, and J. Gerejova. Collect. Czech Chem. Commun. **47**, 1290 (1982).
33. U.S. Patent No. 4.016.105. (1972).
34. Belg. Patent No. 791.294. (1973).
35. A. W. Sleight. Catal. Today, **1**, 347 (1987).
36. T. P. Moser, R. W. Wenig, and G. L. Schrader. Appl. Catal. **34**, 39 (1987).
37. G. Centi, G. Galassi, I. Manenti *et al. In* Preparation of catalysts III. *Edited by* G. Poncelet, P. Grange, and P. A. Jacobs. Elsevier Science, Amsterdam. 1983. pp. 543–551.

Can. J. Chem. Downloaded from www.nrcresearchpress.com by 123.30.183.119 on 09/08/12
For personal use only.

Réduction électrochimique de 4*H*-1,3-thiazines : obtention de 6*H*-1,3-thiazines et (ou) de pyrroles substitués

ABDESSELAM ABOUELFIDA ET JEAN PAUL PRADÈRE

Laboratoire de synthèse organique, Unité associée au Centre national de la recherche scientifique, n° 475, 2, Rue de la Houssinière, 44072 Nantes CEDEX 03, France

MICHEL JUBAULT[1]

Laboratoire de synthèse organique et d'électrochimie, Unité associée au Centre national de la recherche scientifique, n° 439, Faculté des sciences, 2, Boulevard Lavoisier, 49045 Angers CEDEX, France

ET

ANDRÉ TALLEC

Laboratoire d'électrochimie, Unité associée au Centre national de la recherche scientifique, n° 439, Université de Rennes I, 35042 Rennes CEDEX, France

Reçu le 18 avril 1991

ABDESSELAM ABOUELFIDA, JEAN PAUL PRADERE, MICHEL JUBAULT et ANDRÉ TALLEC. Can J. Chem. **70**, 14 (1992).

La réduction électrochimique à potentiel contrôlé, sur cathode de mercure et en milieu protique, des 2-éthoxy- et 2-phényl-4*H*-1,3-thiazines diversement substitutées en position 4 conduit aux 6*H*-1,3-thiazines et (ou) aux pyrroles substitués. La sélectivité observée dépend du pH du milieu et de la nature de la substitution : l'orientation de la réduction vers la formation de pyrroles est favorisée en milieu acide (H_2SO_4 à 0,5 mol L^{-1}) et par la présence d'un substituant phényle en position 2 et alkoxycarbonyle en position 4. L'orientation vers la formation de 6*H*-1,3-thiazines et leurs produits de réduction (thiobenzamides, carbamates et 2-thiazolines substitués) est favorisée par l'utilisation d'un milieu faiblement acide (tampon acétique) ou basique (tampon ammoniacal).

Mots clés : réductions electrochimiques, 4*H*- et 6*H*-1,3-thiazines, pyrroles, 2-thiazoline, régression cyclique.

ABDESSELAM ABOUELFIDA, JEAN PAUL PRADÈRE, MICHEL JUBAULT, and ANDRÉ TALLEC. Can. J. Chem. **70**, 14 (1992).

Controlled potential electroreduction (protic medium, mercury cathode) of substituted 2-ethoxy and 2-phenyl-4*H*-1,3-thiazines leads to 6*H*-1,3-thiazines and (or) pyrroles. The nature of the isolated products appears strongly dependent on pH of the medium and type of substitution: pyrrole formation takes place in acidic medium (0.5 mol L^{-1} H_2SO_4) and is favoured by phenyl and alkoxycarbonyl groups at positions 2 and 4, respectively; formation of 6*H*-1,3-thiazines and their reduction products (substituted thiobenzamides, carbamates and 2-thiazoline) occurs in weakly acidic (acetate buffer) or basic (ammoniacal buffer) medium.

Key words: electrochemical reductions, substituted 4*H*- and 6*H*-1,3-thiazines, pyrroles, 2-thiazoline, cyclic regression.

Introduction

L'intérêt d'utiliser les 6*H*-1,3-thiazines comme intermédiaires réactionnels ou comme précurseurs de céphèmes a été mentionné de nombreuses fois ces dernières années (1–6). Cependant, peu de méthodes permettent d'accéder directement aux dérivés 6*H*-1,3-thiaziniques polyfonctionnalisés **A**. En effet, l'introduction de groupements fonctionnels est généralement réalisée par cycloaddition 4+2 en utilisant des méthodes d'activation : catalyse acide (2, 3) ou hautes pressions (7). Nous avons envisagé d'accéder aux composés **A** par réduction de 4*H*-1,3-thiazines substituées **B** dont le mode de préparation a été précédemment décrit (8). La réduction chimique des 4,5,6-alkoxycarbonyl-4*H*-1,3-thiazines **B** (**1***c* et **2***c*) par l'aluminium amalgamé, utilisé dans le cas des dérivés 1,3-thiaziniques (9, 10), ne permet pas d'isoler les 6*H*-1,3-thiazines correspondantes **A**; l'hydrogénation conduit aux thiobenzamide ($R^2 = C_6H_5$) et carbamate ($R^2 = C_2H_5O$) substitués **C** résultant de l'hydrogénolyse du cycle thiazinique intermédiairement formé.[2] La diversité des composés obtenus par réduction chimique nous a conduit à mettre en oeuvre une méthode a priori plus sélective : la réduction électrochimique à potentiel contrôlé, appliquée précédemment au cas des 6*H*-1,3-thiazines (11, 12). Ce mémoire concerne l'extension de cette méthode aux 4*H*-1,3-thiazines substituées **B** (**1***a*–**1***c* et **2***a*–**2***c*), pour lesquelles une sélectivité satisfaisante a été observée lors des premiers essais d'électroréduction (8). Nous décrirons d'abord le comportement polarographique des composés étudiés puis nous exposerons successivement les résultats obtenus par réduction des 2-éthoxy-4*H*-1,3-thiazines **1***a*–**1***c* et des 2-phényl-4*H*-1,3-thiazines **2***a*–**2***c* substituées.

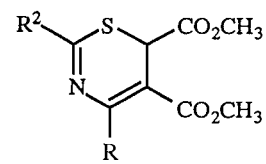

A

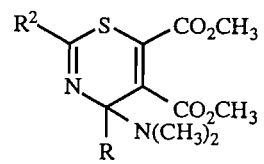

B

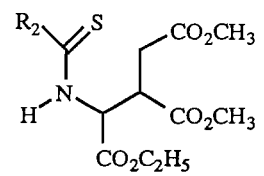

C

1*a*–**1***c* $R^2 = C_2H_5O$
2*a*–**2***c* $R^2 = C_6H_5$
a R = H
b R = CH_3
c R = $CO_2C_2H_5$

[1]Auteur à qui adresser toute correspondance.

[2]Abdesselam Abouelfida, thèse de doctorat de l'Université de Nantes, juillet 1990.

Printed in Canada / Imprimé au Canada

Can. J. Chem. Downloaded from www.nrcresearchpress.com by 123.30.183.119 on 09/08/12
For personal use only.

TABLEAU 1. Polarographie des 4*H*-1,3-thiazines **1***a*–**1***c* et **2***a*–**2***c*. Potentiel de demi-vague en V ECS et (nombre d'electrons échangés)

	Substituants		Milieu d'électrolyse		
Composés	R^2	R	H_2SO_4	Tampon acétique	Tampon ammoniacal
1*a*		H	−0,60 (4) −1,02(*)	−0,78 (2) −0,89 (2)	−0,95 (2) −1,25 (2)
1*b*	C_2H_5O	CH_3	Instable	Instable	−0,95 (2) −1,33 (2)
1*c*		$CO_2C_2H_5$	−0,59 (4)	−0,75 (2) −0,92 (2) −1,18 (2)	−0,95 (2) −1,06 (2) −1,17 (2)
2*a*		H	−0,45 (4)	−0,73 (4)	−0,92 (4)
2*b*	C_6H_5	CH_3	−0,68 (4)	−0,88 (4)	−1,02 (4)
2*c*		$CO_2C_2H_5$	−0,42 (4) −0,58 (2)	−0,68 (4) −1,06 (2)	−0,88 (4) −1,07 (2)

(*) Vague catalytique de dégagement d'hydrogène.

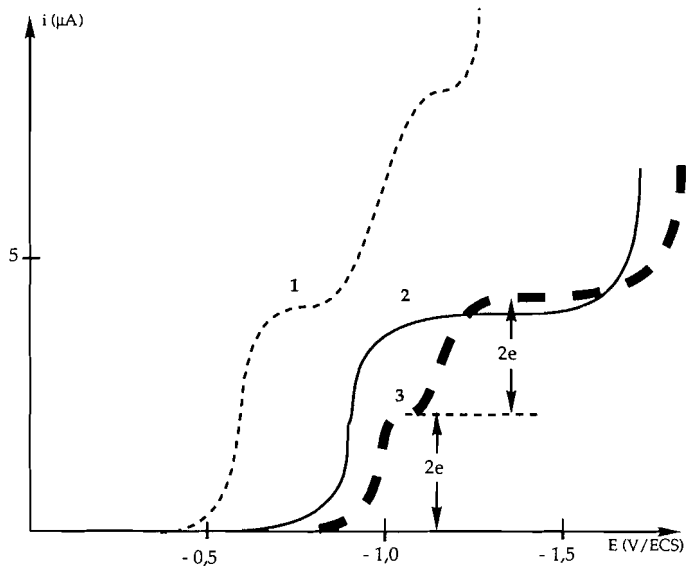

FIG. 1. Polarogrammes de **1***a* (solution à 10^{-3} mol L^{-1}); courbe **1** : H_2SO_4 à 0,5 mol L^{-1} + éthanol (1 : 1); la 2ème vague est une vague catalytique de dégagement d'hydrogène; courbe **2** : tampon acétique + éthanol (1 : 1); courbe **3** : tampon ammoniacal + éthanol (1 : 1).

Résultats

Les résultats des études polarographiques effectuées sur les 4*H*-1,3-thiazines substituées **1** et **2**, rassemblés dans le tableau 1, permettent d'effectuer les remarques suivantes :

Les 2-éthoxyl-4*H*-1,3-thiazines **1***a*–**1***c* présentent une première vague de réduction à 4 électrons en milieu très acide alors que cette vague correspond à un transfert biélectronique dans les autres milieux envisagés.

Les 2-phényl-4*H*-1,3-thiazines **2***a*–**2***c* présentent une première vague à 4 électrons, quelle que soit l'acidité du milieu.

La réduction globale des composés étudiés correspond généralement à 4 électrons; l'exception concerne les substrats **1***c* et **2***c* (R = $CO_2C_2H_5$) pour lesquels la réduction globale est à 6 électrons.

*Comportement électrochimique des 2-éthoxy-4*H*-1,3-thiazines substituées* ***1***

*(i) 2-Éthoxy-4*H*-1,3-thiazine* **1**a *(R = H)*

Les électrolyses préparatives ont été réalisées à la température de la glace fondante, compte-tenu de la stabilité limitée de ce composé en milieu protique. En milieu tampon ammoniacal, la réduction effectuée au palier de la première vague polarographique (potentiel de travail E_T = −1,1 V ECS, figure 1, courbe 3) fournit uniquement la 6*H*-1,3-thiazine **3***a* (Rdt = 90%). Dans cette réaction la réduction de la double liaison diactivée C5=C6 est suivie de l'élimination de diméthylamine (mécanisme EC). L'électrolyse, réalisée directement à potentiel très négatif (E_T = −1,6 V ECS) consomme 4 moles d'électron et permet d'isoler le thiocarbamate insaturé **7***a* (Rdt = 60%) (schéma 1). En milieu tampon acétique, les deux vagues successives sont trop peu séparées pour que l'on puisse obtenir une réduction sélective (cf. figure 1, courbe 2). L'électrolyse réalisée au palier de la seconde vague fournit comme précédemment le composé **7***a* (Rdt = 90%). Nous avons verifié que la réduction à −1,1 V ECS de la 6*H*-1,3-thiazine **3***a*, obtenue en tampon ammoniacal,conduit quantitativement au produit d'hydrogénolyse **7***a*. En milieu acide sulfurique, l'électrolyse effectuée à −0,75 V ECS, correspondant au palier de la vague de réduction à 4 électrons (figure 1, courbe 1), conduit à un mélange de carbamate **7***a* (Rdt = 20%) et de pyrrole **5***a* (Rdt = 40%) (schéma 1). Le composé **5***a* résulte d'une contraction du cycle thiazinique avec élimination de sulfure d'hydrogène. En effet, nous avons vérifié que ce pyrrole ne provient, ni de l'évolution du carbamate **7***a* retrouvé inchangé après un séjour de 24 h dans le milieu d'électrolyse, ni de la régression de la 4*H*-1,3-thiazine précurseur **1***a* en milieu acide (13). Par ailleurs, il ne semble pas que la 6*H*-1,3-thiazine **3***a* soit un intermédiaire de la transformation de **1***a* en **5***a* car nous avons constaté que le composé **3***a* est instable en milieu acide sulfurique dans les conditions de la réduction.

*(ii) 2-Éthoxy-4-méthyl-4*H*-1,3-thiazine* **1**b *(R = CH_3)*

Les électrolyses n'ont pu être réalisées qu'en milieu tampon ammoniacal compte-tenu de l'instabilité de ce substrat en milieu acide. À potentiel peu négatif (E_T = −1,1 V ECS), au palier de la première vague, la réduction de **1***b* fournit la 6*H*-1,3-thiazine **3***b* (Rdt = 83%); un polarogramme, enregistré en fin d'électrolyse, montre que la seconde vague de réduction du composé **1***b* est conservée. À potentiel directement très négatif (E_T = −1,4 V ECS), on isole le carbamate **7***b* (Rdt = 44%) (schéma 1).

*(iii) 2-Éthoxy-4-éthoxycarbonyl-4*H*-1,3-thiazine* **1**c *(R = $CO_2C_2H_5$)*

En milieu tampon ammoniacal, les trois vagues observées (figure 2, courbe 3) ne sont pas suffisamment séparées pour obtenir des réductions sélectives. L'électrolyse, réalisée directement à potentiel très négatif (E_T = −1,2 V ECS), consomme entre 5 et 6 moles d'électron et fournit un mélange de 2-éthoxypyrrole substitué **5***c* (Rdt = 50%) et de carbamates diastéréoisomères **9***c* et **9***c'* (Rdt = 38%).

En milieu tampon acétique, la séparation des vagues est encore insuffisante pour atteindre la sélectivité (figure 2, courbe 2) : À E_T = −0,75 V ECS (potentiel correspondant au potentiel de demi-vague), la réduction est très lente. Au bout de 48 h, le résultat coulométrique est de 2,2 moles

Can. J. Chem. Downloaded from www.nrcresearchpress.com by 123.30.183.119 on 09/08/12
For personal use only.

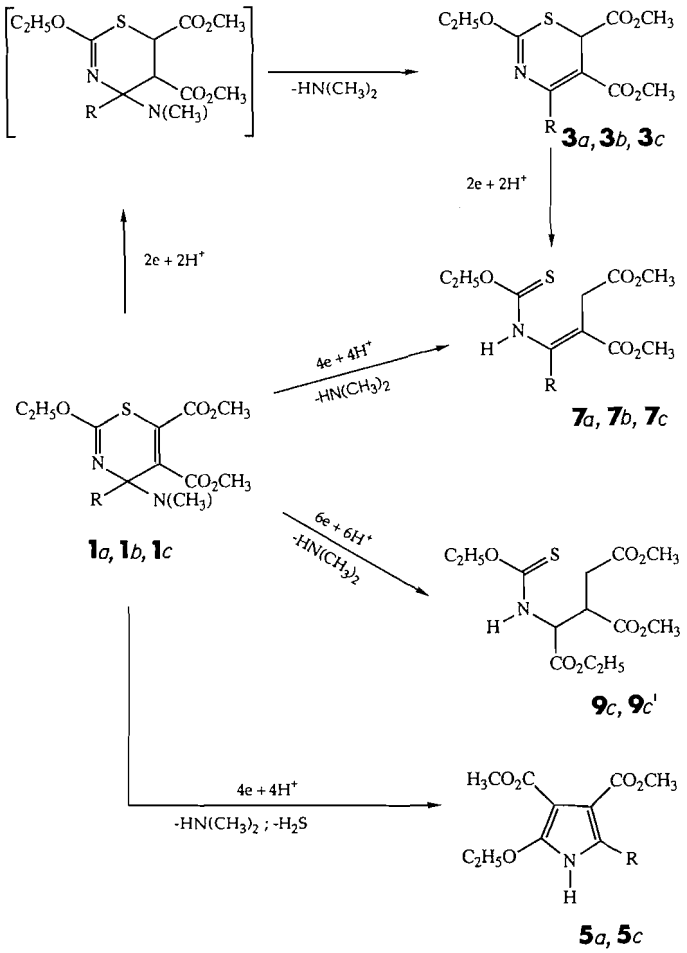

SCHÉMA 1. Réduction électrochimique des 2-éthoxy-4*H*-1,3-thiazines **1***a*–**1***c*.

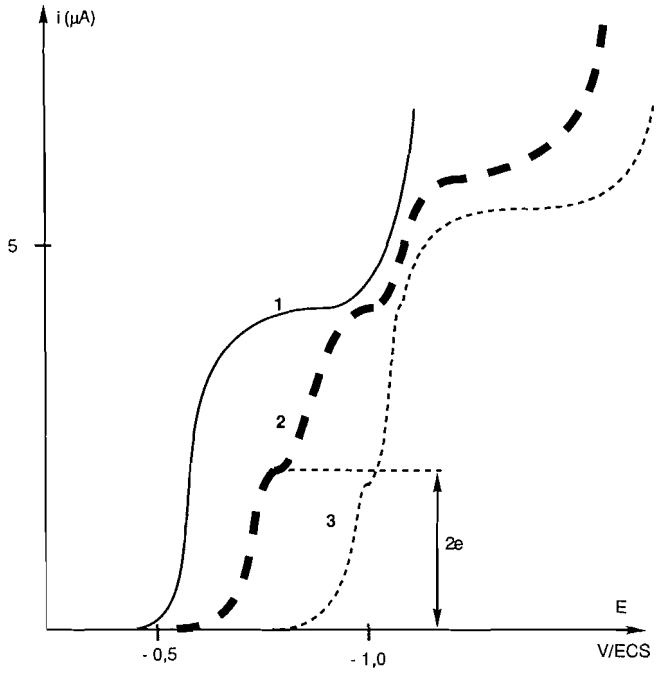

FIG. 2. Polarogrammes de **1***c* (solution à 10^{-3} mol L^{-1}); courbe **1** : H_2SO_4 à 0,5 mol L^{-1} + éthanol (1 : 1); courbe **2** : tampon acétique + éthanol (1 : 1); courbe **3** : tampon ammoniacal + éthanol (1 : 1).

d'électron alors qu'il reste 20% du substrat **1***c* non réduit; le traitement de la solution permet d'isoler la 6*H*-1,3-thiazine **3***c* (Rdt = 45%) et le pyrrole **5***c* (Rdt = 15%) (schéma 1). À E_T = −1,0 V ECS, les deux premières vagues de **1***c* ont disparu après passage de 3,8 moles d'électron; en outre, il apparaît une vague de réduction biélectronique dont le potentiel de demi-vague ($E_{1/2}$ = −1,22 V ECS) est différent de celui de la troisième vague de **1***c* ($E_{1/2}$ = −1,12 V ECS). Le traitement de la solution fournit un mélange de 6*H*-1,3-thiazine **3***c* (Rdt = 11%), de pyrrole **5***c* (Rdt = 18%) et de carbamate insaturé **7***c* (Rdt = 52%) auquel on peut attribuer la nouvelle vague de réduction.[3] Enfin, à E_T = −1,35 V ECS la réduction consomme 6 moles d'électron et conduit directement au mélange des carbamates diastéréoisomères **9***c* et **9***c'* (Rdt = 80%) (schéma 1).

En milieu acide sulfurique, la réduction effectuée au palier de la vague unique (E_T = −0,8 V ECS, figure 2, courbe 1) permet d'isoler un mélange de pyrrole **5***c* (Rdt = 46%) et de carbamates **9***c*, **9***c'* (Rdt = 40%); la formation de ces derniers apparaît surprenante puisque la vague polarographique correspond au transfert de 4 électrons. Par ailleurs, la réduction, dans ce milieu, de la 6*H*-1,3-thiazine **3***c* conduit uniquement au dérivé insaturé **7***c*; on peut en déduire que les composés **3***c* et **7***c* ne sont pas des intermédiaires formés lors de la réduction de la 6*H*-1,3-thiazine **1***c* en carbamates **9**. Cette observation permet de supposer que l'élimination de la diméthylamine à partir des composés de réduction est relativement lente en milieu acide sulfurique.

*Comportement électrochimique des 2-phényl-4*H*-1,3-thiazines substituées* **2**

*(i) 2-Phényl-4*H*-1,3-thiazine* **2**a *(R = H)*

Rappelons que le polarogramme présente, quel que soit le milieu, une vague de réduction unique à 4 électrons (figure 3). En tampon ammoniacal (E_T = −1,0 V ECS), la réduction fournit sélectivement le thiobenzamide insaturé **8***a* (Rdt = 89%) (schéma 2). En tampon acétique (E_T = −0,85 V ECS) on obtient un mélange de thiobenzamide **8***a* (Rdt = 55%) et de pyrrole **6***a* (Rdt = 35%). En milieu acide sulfurique (E_T = −0,7 V ECS) on isole le pyrrole **6***a* avec un excellent rendement (88%). La formation du composé **8***a* (Rdt = 7%) apparaît dans ce cas très minoritaire. On peut observer que dans ces réactions la 2-phényl-4*H*-1,3-thiazine **4***a*, vraisemblablement précurseur du composé **8***a*, n'est jamais isolée contrairement à ses homologues issus de la réduction des 2-éthoxy-4*H*-1,3-thiazines étudiées précédemment. Par ailleurs, le changement d'acidité du milieu d'électrolyse permet d'orienter la réduction, de façon quasi-sélective, soit vers la formation du thiobenzamide **8***a* (milieu basique) soit vers celle du pyrrole **6***a* (milieu très acide).

*(ii) 4-Méthyl-2-phényl-4*H*-1,3-thiazine* **2**b

Les électrolyses du composé **2***b* n'ont été réalisées que dans les deux milieux de pH extrême compte-tenu des résultats obtenus pour la 4*H*-1,3-thiazine précédente **2***a*. En tampon

[3]L'électroactivité du carbamate **7***c* est liée à l'activation de la double liaison par les deux groupements alcoxycarbonyles par comparaison aux carbamates **7***a* et **7***b*. L'obtention de diastéréoisomères dépendant de l'acidité du milieu a déja été observée lors de la réduction de diesters éthyléniques (14).

Can. J. Chem. Downloaded from www.nrcresearchpress.com by 123.30.183.119 on 09/08/12
For personal use only.

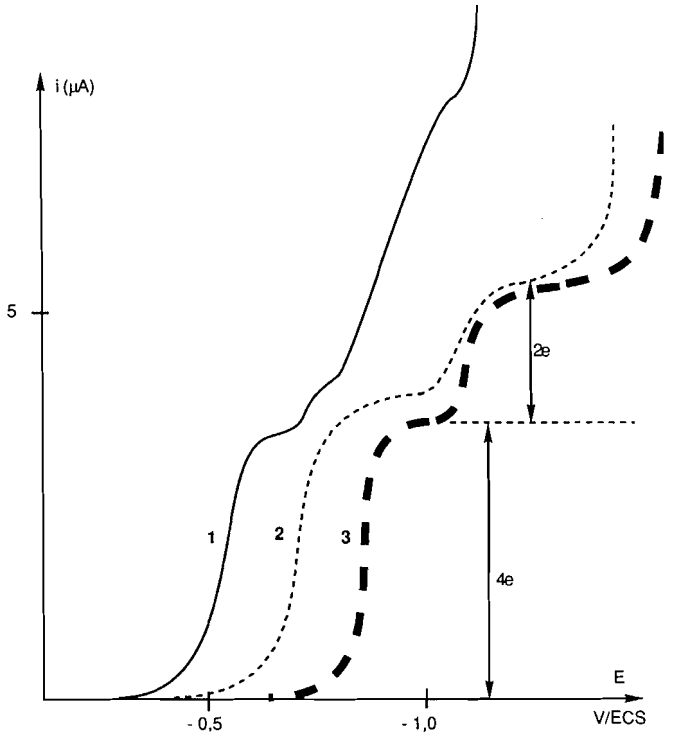

FIG. 3. Polarogrammes de **2***c* (solution à 10^{-3} mol L^{-1}); courbe **1** : H_2SO_4 à 0,5 mol L^{-1} + éthanol (1 : 1); courbe **2** : tampon acétique + éthanol (1 : 1); courbe **3** : tampon ammoniacal + éthanol (1 : 1).

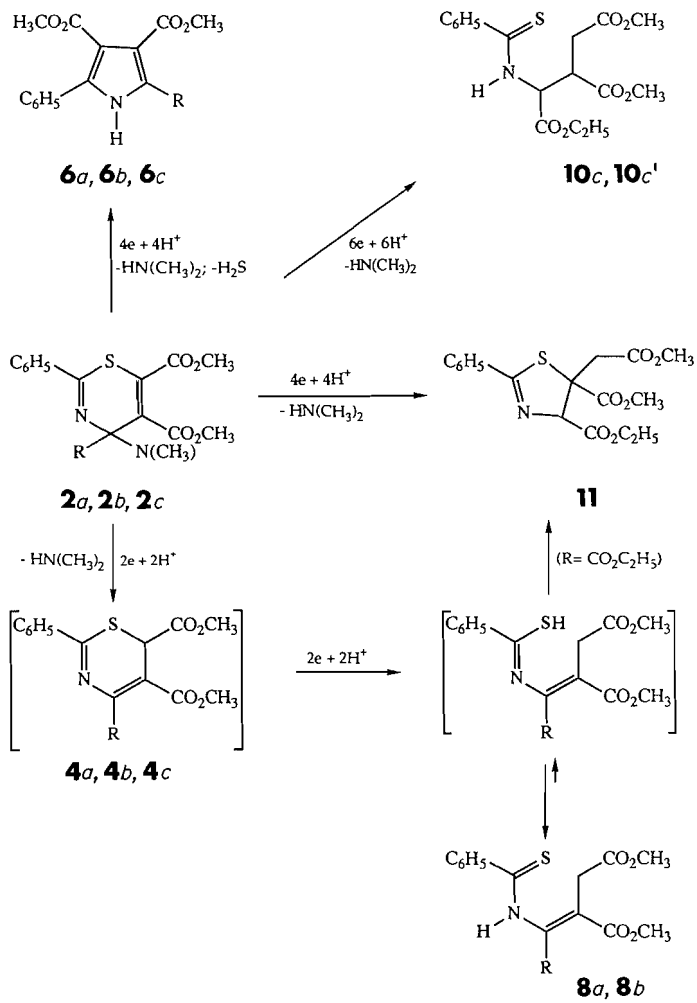

SCHÉMA 2. Réduction électrochimique des 2-phényl-4*H*-1,3-thiazines **2***a*–**2***c*.

ammoniacal (E_T = −1,1 V ECS), le résultat coulométrique est déficitaire par rapport aux 4 moles d'électron attendues. On isole, avec des rendements limités, le pyrrole **6***b* (Rdt = 18%) et le thiobenzamide *N*-substitué **8***b* (Rdt = 42%). En milieu acide sulfurique (E_T = −0,7 V ECS), la réduction n'est pas sélective, mais conduit majoritairement au pyrrole **6***b* (Rdt = 55%). La formation de celui-ci s'accompagne de celle du composé **8***b* (Rdt = 33%) (schéma 2).

*(iii) 4-Éthoxycarbonyl-2-phényl-4*H*-1,3-thiazine* **2***c*

Pour ce composé **2***c*, rappelons que la première vague à 4 électrons est suivie, à potentiel plus cathodique, d'une vague de réduction biélectronique (figure 3, courbes 2 et 3). En tampon ammoniacal, au potentiel de la première vague (E_T = −0,9 V ECS, figure 3, courbe 3) la réduction conduit à un mélange de pyrrole **6***c* (Rdt = 30%) et de 2-thiazoline **11** (Rdt = 52%). La formation de cette 2-thiazoline résulte probablement de la cyclisation intramoléculaire du thioamide insaturé **8***c*, issu lui-même de l'hydrogénolyse de la 6*H*-1,3-thiazine **4***c*, intermédiairement formée. En fin d'électrolyse, on observe, en polarographie, la présence d'une vague biélectronique ($E_{1/2}$ = −1,2 V ECS) que nous avons pu attribuer, par comparaison, à la réduction de l'hétérocycle **11**. Au potentiel de la seconde vague (E_T = −1,3 V ECS), l'électrolyse permet d'isoler minoritairement le pyrrole **6***c* (15%) et majoritairement les thiobenzamides diastéréoisomères **10***c* (Rdt = 32%) et **10***c'* (Rdt = 41%) (schéma 2). Ceux-ci peuvent résulter soit de la réduction du composé insaturé **8***c* dont la double liaison diactivée est électroactive au potentiel utilisé, soit de l'hydrogénolyse de la 2-thiazoline **11** intermédiairement formée.

En milieu tampon acétique, on obtient des résultats comparables. On isole soit le mélange de pyrrole **6***c* et de 2-thiazoline **11** à potentiel peu négatif (E_T = −1,0 V ECS, figure 3, courbe 2), soit le mélange de pyrrole **6***c* (Rdt = 30%) et de thiobenzamides diastéréoisomères **10***c* (Rdt = 30%) et **10***c'* (Rdt = 27%) au potentiel E_T = −1,3 V ECS). En milieu acide sulfurique la réduction de la 4*H*-1,3-thiazine **2***c* effectuée au potentiel E_T = −0,75 V ECS (figure 3, courbe 1) conduit à la formation du pyrrole **6***c* (Rdt = 76%) (schéma 2). Par comparaison au cas du substrat **2***a*, on remarquera que l'utilisation d'un milieu très acide oriente de la même façon la réduction vers la formation de dérivés pyrroliques.

Discussion

Les réductions, effectuées au potentiel de la première vague polarographique, conduisent soit à des 6*H*-1,3-thiazines ou à des produits issus de l'hydrogénolyse de ces dernières, soit à des pyrroles résultant d'une régression cyclique.

(*i*) La formation de 6*H*-1,3-thiazines implique une hydrogénation de la double liaison C5=C6, diactivée par les deux groupements alcoxycarbonyles, suivie d'une élimination de diméthylamine au niveau de la dihydrothiazine intermédiairement formée. La réduction peut s'arrêter à ce stade pour R^2 = C_2H_5O. Les 6*H*-1,3-thiazines obtenues (com-

Can. J. Chem. Downloaded from www.nrcresearchpress.com by 123.30.183.119 on 09/08/12
For personal use only.

Can. J. Chem. Downloaded from www.nrcresearchpress.com by 123.30.183.119 on 09/08/12
For personal use only.

posés **3**) sont réductibles avec hydrogénolyse de la liaison S—C6. L'affaiblissement de cette liaison serait lié à la présence d'un substituant électroattracteur en position 6. Ce comportement apparaît tout à fait différent de celui des 6*H*-1,3-thiazines monoactivées (R^5 attracteur : la réduction biélectronique porte sur la liaison imine) et diactivées (R^4 et R^5 attracteurs : la dihydrogénation concerne la double liaison C4=C5) précédemment étudiées (11). Il faut noter que toute modification de la substitution sur le cycle thiazinique entraîne un changement du site de réduction. Dans cette étude, les 6*H*-1,3-thiazines ne sont pas isolables pour R^2 = C_6H_5 (composés **4**). Leur réduction, qui s'accompagne de l'hydrogénolyse de la liaison S—C6, s'effectue au même potentiel que la réduction des 4*H*-1,3-thiazines précurseurs. Le groupement phényle, par rapport au groupement éthoxy en position 2, exerce probablement un effet attracteur qui rend plus fragile la liaison S—C6. La réduction s'arrête à la formation des carbamates **7** ou thiobenzamides **8** insaturés lorsque R = H ou CH_3. Par contre, pour R = $CO_2C_2H_5$, l'électroréduction conduit selon la nature du substituant en position 2, soit aux carbamates **9***c*, **9***c*′ ou thiobenzamides **10***c*, **10***c*′ saturés, soit à la 2-thiazoline **11** par une cyclisation intramoléculaire analogue à celle observée lors de la régression cyclique de la 4-éthoxycarbonyl-2-phényl-6*H*-1,3-thiazine-6-one (15).

(*ii*) L'obtention par électroréduction de pyrroles substitués (composés **5** et **6**) semble liée à l'existence d'une première vague de réduction à 4 électrons; par ailleurs, elle est favorisée par l'utilisation d'un milieu très acide, la présence d'un groupement phényle en position 2 et d'un substituant attracteur éthoxycarbonyle en position 4. Deux hypothèses ont été envisagées pour expliquer la formation de ces pyrroles. En effet, ces composés pourraient provenir de la réduction des 6*H*-1,3-thiazines (**3** ou **4**); cette hypothèse ne paraît pas devoir être retenue puisque, d'une part, ces hétérocycles n'ont pas été isolés lorsque R^2 = C_6H_5, d'autre part, ils apparaissent soit instables (composé **3***a*) soit réductibles en milieu acide (composé **3***c*), dans le cas de R^2 = C_2H_5O. Plus vraisemblablement, le cycle pyrrolique résulte de la réduction de la forme protonée de l'imine (schéma 3); un premier transfert biélectronique conduirait à un thiirane, lui-même réductible à 2 électrons avec élimination de sulfure d'hydrogène et de diméthylamine. Les effets de la substitution interviendraient d'une part sur la basicité de l'azote du cycle, d'autre part, sur le caractère électrophile du carbone en position 6. Ce mécanisme de régression cyclique est à rapprocher de celui mentionné pour expliquer la formation de pyrroles par réduction de 6*H*-1,3-thiazines-6-ones comportant un substituant électroattracteur en position 4 (16, 17).

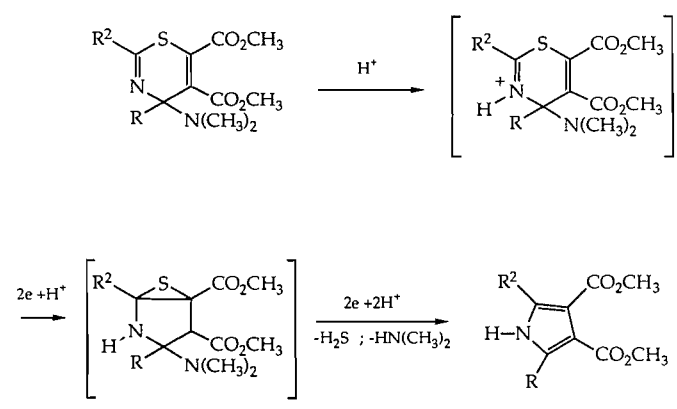

SCHÉMA 3. Mécanisme de formation de pyrroles en milieu acide.

(*iii*) L'obtention par voie chimique de pyrroles substitués peut être réalisée à partir des 6*H*-1,3-thiazines issues des électroréductions. Ainsi la transformation de **3***c* en **5***c* peut être effectuée avec 87% de rendement en traitant la 4-éthoxycarbonyl-6*H*-1,3-thiazine **3***c* par la triéthylamine (8). Le mécanisme de cette réaction est à rapprocher de ceux précédemment mentionnés pour la régression cyclique de 6*H*-1,3-thiazines en milieu fortement basique (18, 19). Dans notre cas, la présence d'un groupement alcoxycarbonylé en position 4 sur les dérivés thiaziniques permet d'effectuer la régression cyclique dans des conditions plus douces (20).

Conclusion

La réduction électrochimique à potentiel contrôlé, sur cathode de mercure et en milieu protique, des 4*H*-1,3-thiazines substituées permet d'accéder aux pyrroles et (ou) aux 6*H*-1,3-thiazines substituées ainsi qu'à leurs produits d'hydrogénolyse. La formation sélective de pyrroles peut être réalisée, soit directement par voie électrochimique, soit indirectement par traitement basique de 6*H*-1,3-thiazines préparées par électroréduction. La régression cyclique apparaît alors comme une méthode de choix pour accéder aux pyrroles substitués, si l'on se réfère à la diversité des dérivés thiaziniques fonctionnalisés mentionnés dans la littérature (2).

Partie expérimentale

Les spectres de RMN ^1H et ^{13}C ont été enregistrés au moyen d'un spectromètre Jeol JNM FX90 respectivement à 90 MHz et 20 115 MHz. Les déplacements chimiques δ sont exprimés en ppm/TMS et les constantes de couplage *J* en hertz. Les spectres ont été obtenus à partir de solutions dans $CDCl_3$. Un spectrophotomètre à transformée de Fourier Bruker IFS 85 est utilisé pour les déterminations infrarouges; les fréquences de vibration caractéristiques sont exprimées en cm^{-1}. Les spectres de masse sont enregistrés à l'aide d'un appareil Varian MAT 112 (énergie de faisceau électronique : 70 eV; intensité dans le filament : 1,5 mA). Les produits réactionnels ont été purifiés par chromatographie sur gel de silice (Merck Kieselgel 60, 70–230 ASTM). Les points de fusion ont été déterminés à l'aide d'un microscope RCH (C. Reichert) à platine chauffante Kofler. Les analyses centésimales ont été effectuées par les services de microanalyse du C.N.R.S. de Vernaison (France).

Réduction par l'aluminium amalgamé (Al/Hg)

L'aluminium amalgamé est préparé en traitant l'aluminium finement divisé (6–25 mmol) par une solution aqueuse contenant 5% de chlorure mercurique. Après quelques minutes, l'amalgame formé est lavé successivement par de l'eau (2 × 20 cm^3) et de l'éthanol (20 cm^3) puis recouvert par une solution éthanolique (20 cm^3) de 4*H*-1,3-thiazine (1 mmol). L'agitation magnétique est maintenue 1 h à température ambiante. L'hydroxyde d'aluminium formé est éliminé par filtration puis lavé par 20 cm^3 d'éthanol. Le filtrat est concentré et chromatographié sur gel de silice.

Polarographie

Les polarogrammes des composés **1***a*–**1***c* et **2***a*–**2***c* (tableau 1 et figures 1–3) ont été enregistrés à l'aide d'un polarographe Tacussel PRG3. Les solutions polarographiques sont constituées d'un mélange, volume à volume, d'une solution d'électrolyte-support et d'une solution à 2 × 10^{-3} mol L^{-1} du composé dans l'éthanol. Les trois solutions d'électrolyte-support utilisées ont la composition suivante : milieu acide, H_2SO_4 à 0,5 mol L^{-1}; milieu faiblement acide, tampon acétique (CH_3CO_2H à 0,5 mol L^{-1} + CH_3CO_2Na à 0,5 mol L^{-1}); milieu faiblement basique, tampon ammoniacal (NH_4Cl à 0,5 mol L^{-1} + NH_3 à 0,5 mol L^{-1}).

TABLEAU 2. Milieu d'électrolyse, pótentiel de travail (V ECS) et produits d'électroréduction (Rdt %) des 4*H*-1,3-thiazines **1***a*–**2***c*

Composés	Milieu sulfurique	Tampon acétique	Tampon ammoniacal
1*a*	$E_T = -0,75$ **5***a* (40%), **7***a* (20%)	$E_T = -1,35$ **7***a* (90%)	$E_T = -1,1$ **3***a* (90%)
			$E_T = -1,6$ **7***a* (60%)
1*b*	Instable	Instable	$E_T = -1,1$ **3***b* (83%)
			$E_T = -1,4$ **7***b* (44%)
1*c*	$E_T = -0,8$ **5***c* (46%), **9***c*/**9***c*′ (40%)	$E_T = 0,75$ **3***c* (45%), **5***c* (15%)	$E_T = -1,2$ **5***c* (50%), **9***c*/**9***c*′ (38%)
		$E_T = -1,0$ **5***c* (18%), **7***c* (52%)	
		$E_T = -1,35$ **9***c*/**9***c*′ (80%)	
2*a*	$E_T = -0,7$ **6***a* (88%)	$E_T = -0,85$ **6***a* (35%), **8***a* (55%)	$E_T = -1,0$ **8***a* (89%)
2*b*	$E_T = -0,7$ **6***b* (55%), **8***b* (33%)		$E_T = -1,1$ **6***b* (18%), **8***b* (42%)
2*c*	$E_T = -0,75$ **6***c* (76%)	$E_T = -1,0$ **6***c* et **11**	$E_T = -0,9$ **6***c* (30%), **11** (52%)
		$E_T = -1,3$ **6***c* (30%), **10***c*/**10***c*′ (57%)	$E_T = -1,3$ **6***c* (15%), **10***c*/**10***c*′ (73%)

Électroréductions préparatives

Elles ont toutes été réalisées, à potentiel controlé, sur cathode de mercure, dans la cellule d'électrolyse à épuisement précédemment décrite (21). Le potentiel de la cathode est maintenu constant à l'aide d'un potentiostat Tacussel PRT et la quantité d'électricité consommée est mesurée à l'aide d'un coulomètre IG5. Le déroulement d'une expérience-type d'électroréduction est le suivant : On introduit, dans la cellule d'électrolyse éventuellement refroidie à 2°C, 130 cm^3 d'un mélange électrolyte-support + éthanol (identique à celui utilisé en polarographie). Après désaération à l'aide d'azote et préélectrolyse de la solution, le composé électroactif ($(1–2) \times 10^{-3}$ mol), dissous dans 20 cm^3 d'éthanol, est ajouté dans la cellule. L'électrolyse est alors effectuée sous courant continu d'azote. Des polarogrammes, enregistés sur des prélèvements de la solution d'électrolyse effectués en cours de réduction, permettent de contrôler l'avancement de la réaction et de détecter la formation éventuelle d'intermédiaires ou de produits d'évolution électroactifs. Après électrolyse complète, le mercure est décanté puis l'éthanol est évaporé sous vide partiel et la solution aqueuse neutralisée par du bicarbonate de sodium. Après extraction au dichlorométhane, la solution organique est séchée sur sulfate de magnésium puis concentrée. Le mélange réactionnel est ensuite chromatographié sur gel de silice (éluant : hexane/éther diéthylique). Les résultats des électroréductions préparatives sont rassemblés dans le tableau 2.

4H-1,3-Thiazines substituées **1**a–c *et* **2**a–c

L'acétylène dicarboxylate de méthyle (5 mmol) est additionné, à température ambiante, à une solution de 3-aza-4-diméthylamino-1-thiabutadiène substitué (5 mmol) (22) dans 20 cm^3 de dichlorométhane. L'évolution de la réaction est suivie par chromatographie sur couche mince jusqu'à disparition de l'hétérodiène correspondant. Après évaporation du solvant, le mélange réactionnel est chromatographié sur gel de silice. (Elution : éther de pétrole/acétate d'éthyle 50 : 50.) Les 4*H*-1,3-thiazines purifiées sont cristallisées dans l'éther diéthylique. Les constantes physiques et les analyses spectroscopiques sont en accord avec les données de la littérature (8).

2-Éthoxy-5,6-bis(méthoxycarbonyl)-6H-1,3-thiazine **3**a : F = 36°C (éther de pétrole); IR ν_{max} (KBr) : 1740 et 1707 (CO_2CH_3) cm^{-1}; RMN ^1H δ : 1.35 (3H, t, CH_3), 3.73 et 3.79 (6H, 2s, $2CH_3O$), 4.44 (2H, q, CH_2), 4.75 (1H, s, H6), 7.82 (1H, s, H4); RMN ^{13}C δ : 14.0 (CH_3), 39.4 (C6 J_{C-H} = 143.6 Hz), 52.0 et 53.0 ($2CH_3O$), 65.8 (CH_2), 104.6 (C5), 146.9 (C4, J_{C-H} = 182.2 Hz), 164.2, 166.0 et 169.8 (C2 et CO). Anal. calc. pour $C_{10}H_{13}NO_5S$: C 46.32, H 5.05, S 12.36; tr. : C 46.32, H 5.26, S 11.95.

2-Éthoxy-5,6-bis(méthoxycarbonyl)-4-méthyl-6H-1,3-thiazine **3**b : huile; IR ν_{max} (CCl_4) : 1747 et 1721 (CO_2CH_3) cm^{-1}; RMN ^1H δ : 1.35 (3H, t, CH_3), 2.4 (3H, s, CH_3), 3.70 et 3.76 (6H, 2s, $2CH_3O$), 4.44 (2H, q, CH_2), 4.79 (1H, s, H6); RMN ^{13}C δ : 14.0 (CH_3), 23.9 (CH_3-C=); 41.4 (C6, J_{C-H} = 143.6 Hz), 51.6 et 52.7 ($2CH_3O$), 65.1 (CH_2), 101.4 (C5), 157.6, 160.7, 166.2 et 169.8 (C4, C2 et CO). Anal. calc. pour $C_{11}H_{15}NO_5S$: C 48.34, H 5.53, S 11.73; tr. : C 48.68, H 5.56, S 11.65.

2-Éthoxy-4-éthoxycarbonyl-5,6-bis(méthoxycarbonyl)-6H-1,3-thiazine **3**c : F = 81°C (éther diéthylique); IR ν_{max} (KBr) : 1740 et 1700 (CO_2CH_3 et $CO_2C_2H_5$) cm^{-1}; RMN ^1H δ : 1.36 (6H, 2t, $2CH_3$), 3.74 et 3.79 (6H, 2s, $2CH_3O$), 4.43 (4H, m, CH_2), 4.85 (1H, s, H6); RMN ^{13}C δ : 13.9 (CH_3), 40.3 (C6, J_{C-H} = 145.1 Hz), 52.4 et 53.3 ($2CH_3O$), 61.8 et 66.5 (CH_2), 101.9 (C5), 149.7 (C4), 164.6, 165.4, 165.9 et 169.1 (C2 et CO). Anal. calc. pour $C_{13}H_{17}NO_7S$: C 47.12, H 5.17, S 9.68; tr. : C 47.12, H 5.12, S 9.58.

2-Éthoxy-3,4-bis(méthoxycarbonyl)-pyrrole **5**a : F = 96°C (éther diéthylique); IR ν_{max} (KBr) : 3255 (NH), 1722 (CO_2CH_3) cm^{-1}; RMN ^1H δ : 1.30 (3H, t, CH_3), 3.77 et 3.81 (6H, 2s, $2CH_3O$), 4.16 (2H, q, CH_2), 6.92 (1H, d, H5, J_{H5-NH} = 3 Hz), 9.76 (1H, se, NH); RMN ^{13}C δ : 15.1 (CH_3), 51.6 ($2CH_3O$), 70.7 (CH_2), 97.9, 114.1, 117.9, 149.7 (C2–C5), 164.9 (CO). Anal. calc. pour $C_{10}H_{13}NO_5$: C 52.85, H 5.76, N 6.16; tr. : C 52.69, H 5.90, N 6.08.

2-Éthoxy-5-éthoxycarbonyl-3,4-bis(méthoxycarbonyl)-pyrrole **5**c : F = 128°C (éther diéthylique); IR ν_{max} (KBr) : 3276 (NH), 1744, 1700 et 1680 (CO_2CH_3 et $CO_2C_2H_5$) cm^{-1}; RMN ^1H δ : 1.31 et 1.42 (6H, 2t, $2CH_3$), 3.78 et 3.91 (6H, 2s, $2CH_3O$), 4.26 (4H, m, $2CH_2$), 9.64 (1H, se, NH); RMN ^{13}C δ : 14.0 et 14.9 ($2CH_3$), 51.4 et 52.5 ($2CH_3O$), 61.3 et 70.0 ($2CH_2$), 98.9, 111.5, 123.8 et 150.8 (C2–C5), 159.9, 162.9 et 165.9 (CO). Anal. calc. pour $C_{13}H_{17}NO_7$: C 52.16, H 5.72, N 4.68; tr. : C 51.93, H 5.56, N 4.66.

3,4-Bis(méthoxycarbonyl)-2-phényl-pyrrole **6**a : F = 96°C (éther diéthylique); IR ν_{max} (KBr) : 3306 (NH), 1733 et 1685 (CO_2CH_3) cm^{-1}; RMN ^1H δ : 3.66 et 3.68 (6H, 2s, $2CH_3O$), 7.11–7.30 (6H, m, C_6H_5 et H5), 10.4 (1H, se, NH); RMN ^{13}C δ : 51.0 et 51.8 ($2CH_3O$), 113.0, 115.3, 124.6, 127.0, 127.8, 128.2, 130.6 et 134.1 (C2–C5 et C_6H_5), 164.3 et 165.3 (CO). Anal. calc. pour $C_{14}H_{13}NO_4$: C 64.85, H 5.05, N 5.40; tr. : C 64.50, H 5.06, N 5.39.

3,4-Bis(méthoxycarbonyl)-5-méthyl-2-phényl-pyrrole **6**b : huile; IR ν_{max} (CCl_4) : 3302 (NH), 1712 (CO_2CH_3) cm^{-1}; RMN ^1H δ : 2.4 (3H, s, CH_3), 3.76 (6H, s, $2CH_3O$), 7.17–7.55 (5H, m, C_6H_5), 8.9 (1H, se, NH); RMN ^{13}C δ : 12.5 (CH_3) 51.0 et 51.9 ($2CH_3O$), 111.8, 114.0, 126.9, 127.6, 128.4, 130.9, 131.0 et 135.6 (C2–C5 et C_6H_5), 165.0 et 167.8 (CO).

5-Éthoxycarbonyl-3,4-bis(méthoxycarbonyl)-2-phényl-pyrrole **6**c : F = 106°C (éther diéthylique); IR ν_{max} (KBr) : 3310 (NH), 1739, 1727 et 1718 (CO_2CH_3 et $CO_2C_2H_5$) cm^{-1}; RMN ^1H δ : 1.3 (3H, t, CH_3), 3.70 et 3.90 (6H, 2s, $2CH_3O$), 4.14 (2H, q, CH_2), 7.35–8.20 (5H, m, C_6H_5) 9.99 (1H, se, NH); RMN ^{13} C δ : 14.1 (CH_3), 51.6 et 52.6 ($2CH_3O$), 61.5 (CH_2), 112.2, 119.9, 124.9, 128.2, 129.6, 130.3, 131.6 et 140.3 (C2–C5 et C_6H_5), 160.1, 163.4 et 166.1 (CO). Anal. calc. pour $C_{17}H_{17}NO_6$: C 61.62, H 5.17, N 4.23; tr. : C 61.27, H 5.14, N 4.20.

5-Aza-6-éthoxy-3-méthoxycarbonyl-6-thioxo-hex-3-ènoate de

Can. J. Chem. Downloaded from www.nrcresearchpress.com by 123.30.183.119 on 09/08/12
For personal use only.

méthyle **7**a : F = 81°C (éther diéthylique); IR ν_{max} (CCl_4) : 3280 (NH), 1714 (CO_2CH_3) cm^{-1}; RMN ^1H δ : 1.4 (3H, t, CH_3), 3.40 (2H, s, CH_2), 3.71 et 3.77 (6H, 2s, $2CH_3O$), 4.59 (2H, q, CH_2), 8.43 (1H, d, H4, J_{H4-NH} = 11.1 Hz), 9.17 (1H, d, NH); RMN ^{13}C δ : 13.9 (CH_3), 31.3 (C2), 52.2 et 52.6 ($2CH_3O$), 68.2 (CH_2O), 105.8 (C3), 139.1 (C4), 167.5 et 172.1 (2CO), 189.2 (CS). Anal. calc. pour $C_{10}H_{15}NO_5S$: C 45.98, H 5.79, S 12.27; tr. : C 46.03, H 5.73, S 12.36.

5-Aza-6-éthoxy-3-méthoxycarbonyl-4-méthyl-6-thioxo-hex-3-ènoate de méthyle **7**b : huile; IR ν_{max} (CCl_4) : 3254 (NH), 1742 et 1724 (CO_2CH_3) cm^{-1}; RMN ^1H δ : 1.37 (3H, t, CH_3), 2.42 (3H, s, CH_3), 3.39 (2H, s, CH_2), 3.71 et 3.89 (6H, 2s, $2CH_3O$), 4.51 (2H, q, CH_2), 8.93 (1H, se, NH); RMN ^{13}C δ : 13.9 et 20.2 ($2CH_3$), 34.3 (C2), 51.8 et 52.2 ($2CH_3O$), 67.7 (CH_2O), 116.8 (C3), 147.4 (C4), 166.9 et 172.1 (2CO), 188.7 (CS). Anal. calc. pour $C_{11}H_{17}NO_5S$: C 47.97, H 6.22, S 11.64; tr. : C 48.00, H 6.46, S 11.90.

5-Aza-6-éthoxy-4-éthoxycarbonyl-3-méthoxycarbonyl-6-thioxo-hex-3-ènoate de méthyle **7**c : huile; IR ν_{max} (CCl_4) : 3277 (NH), 1745 et 1731 (CO_2CH_3 et $CO_2C_2H_5$) cm^{-1}; RMN ^1H δ : 1.34 (6H, t, $2CH_3$), 3.38 (2H, s, CH_2), 3.68 et 3.79 (6H, 2s, $2CH_3O$), 4.33 et 4.52 (4H, m, $2CH_2$), 11.37 (1H, se, NH); RMN ^{13}C δ : 13.8 ($2CH_3$), 34.7 (C2), 52.6 et 52.9 ($2CH_3O$), 62.2 et 68.7 (CH_2O), 137.5, 162.9, 166.5 et 171 (C3, C4 et CO), 188.6 (CS).

5-Aza-3-méthoxycarbonyl-6-phényl-6-thioxo-hex-3-ènoate de méthyle **8**a : F = 97°C (éther diéthylique); IR ν_{max} (KBr) : 3348 (NH), 1700 (CO_2CH_3) cm^{-1}; RMN ^1H δ : 3.54 (2H, s, CH_2), 3.76 et 3.82 (6H, 2s, $2CH_3O$), 7.36–8.12 (5H, m, C_6H_5) 8.75 (1H, d, H4, J_{H4-NH} = 10.7 Hz), 10.91 (1H, d, NH); RMN ^{13}C δ : 32.1 (C2), 52.4 et 53.0 ($2CH_3O$), 109.5 (C3), 127.5, 128.8, 132.4, 139.0 et 140.6 (C_6H_5 et C4), 167.2 et 172.8 (CO), 198.7 (CS); SM m/z (I %) : 293 (M^+), 234(100). Anal. calc. pour $C_{14}H_{15}NO_4S$: C 57.32, H 5.15, S 10.93; tr. : C 57.26, H 5.02, S 11.07.

5-Aza-3-méthoxycarbonyl-4-méthyl-6-phényl-6-thioxo-hex-3-ènoate de méthyle **8**b : huile; IR ν_{max} (CCl_4) : 3340 (NH), 1742 et 1727 (CO_2CH_3) cm^{-1}; RMN ^1H δ : 2.65 (3H, s, CH_3), 3.43 (2H, s, CH_2), 3.72 et 3.74 (6H, 2s, $2CH_3O$), 7.38–7.96 (5H, m, C_6H_5), 13.01 (1H, se, NH); RMN ^{13}C δ : 30.9 (CH_3-C=), 32.2 (C2) 52.1 ($2CH_3O$), 116.9 (C3), 127.8, 128.8, 132.1 et 144.1 (C4 et C_6H_5), 168.0 et 169.8 (CO), 186.1 (CS).

5-Aza-6-éthoxy-4-éthoxycarbonyl-3-méthoxycarbonyl-6-thioxo-hexanoates de méthyle **9**c : huile; RMN ^1H δ : 1.28 et 1.34 (6H, 2t, CH_3), 2.5–2.9 (2H, m), 4.23 et 4.47 (2q, CH_2), 5.47 (dd, H4, J_{H4-H3} = 3.5 Hz, J_{H4-NH} = 9.2 Hz), 6.93 (d, NH, J_{NH-H4} = 9.2 Hz); RMN ^{13}C δ : 14.0 (CH_3CH_2), 32.5 (C2), 43.1 (C3), 51.1 et 52.5 ($2CH_3O$), 57.6 (C4), 62.2 et 67.2 (CH_2CH_3), 169.5 et 171.7 (CO), 191.9 (CS). Anal. calc. pour $C_{13}H_{21}NO_7S$: C 46.55, H 6.31, S 9.56; tr. : C 46.69, H 6.35, S 9.44.

5-Aza-4-éthoxycarbonyl-3-méthoxycarbonyl-6-phényl-6-thioxo-hexanoates de méthyle **10**c : F = 94°C (éther diéthylique); IR ν_{max} (KBr) : 3337 (NH), 1734 et 1720 (CO_2CH_3 et $CO_2C_2H_5$) cm^{-1}; RMN ^1H δ : 1.31 (3H, t, CH_3), 2.5–2.85 (2H, m, CH_2), 3.65 et 3.76 (6H, 2s, $2CH_3O$), 3.71 et 4.53 (3H, m, H3 et CH_2O), 5.9(1H, dd, H4, J_{H4-H3} = 3.4 Hz, J_{H4-NH} = 8.8 Hz), 7.17–7.93 (5H, m, C_6H_5), 8.36 (1H, d, NH); RMN ^{13}C δ : 14.1 (CH_3), 32.9 (C2), 43.1 (C3), 52.2 et 52.6 ($2CH_3O$), 58.1 (C4), 62.3 (CH_2O), 126.9, 128.6, 131.6 et 141.2 (C_6H_5), 169.3, 171.5 et 172.8 (CO), 200.8 (CS); SM m/z (I %) : 367 (M^+), 121(100). Anal. calc. pour $C_{17}H_{21}NO_6S$: C 55.57, H 5.76, S 8.72; tr. : C 56.0, H 5.86, S 8.46.

Composé **10**c′: huile; IR ν_{max} (CCL_4) : 3400 (NH), 1745 et 1718 (CO_2CH_3 et $CO_2C_2H_5$) cm^{-1}; RMN ^1H δ : 1.32 (3H, s, CH_3), 2.73 (1H, dd, H2a, $J_{H2a-H2b}$ = 17 Hz, J_{H2a-H3} = 5.9 Hz), 3.02 (1H, dd, H2b, $J_{H2b-H2a}$ = 17 Hz, J_{H2b-H3} = 8.5 Hz), 3.71 et 3.72 (6H, 2s, $2CH_3O$), 3.5–3.9 (1H, m, H3), 4.26 (2H, q, CH_2O), 5.56 (1H, dd, H4, J_{H4-H3} = 3.4 Hz, J_{H4-NH} = 7.8 Hz), 7.2–7.9 (5H, m, C_6H_5), 8.62 (1H, d, NH); RMN ^{13}C δ : 14.1 (CH_3), 33.4 (C2, J_{C-H} = 130.4 Hz), 43.0 (C3, J_{C-H} = 130.4 Hz), 51.9 et 52.5 ($2CH_3O$), 58.7 (C4, J_{C-H} = 140.6 Hz), 62.2 (CH_2O), 126.9, 128.5, 131.3 et 141.0 (C_6H_5), 169.1, 171.6 et 171.7 (CO), 198.9 (CS).

4-Éthoxycarbonyl-5-méthoxycarbonyl-5-méthoxycarbonylméthyl-2-phényl-2-thiazoline ***11*** : huile; IR ν_{max} (CCl_4) : 1744 (CO_2CH_3 et $CO_2C_2H_5$) cm^{-1}; RMN ^1H δ : 1.32 (3H, t, CH_3), 3.18 (2H, s, CH_2), 3.69 et 3.82 (6H, 2s, $2CH_3O$), 4.25 (2H, q, CH_2O), 5.65 (1H, s, H4), 7.17–7.9 (5H, m, C_6H_5); RMN ^{13}C δ : 13.9 (CH_3), 38.8 (CH_2, J_{C-H} = 132.9 Hz), 51.9 et 53.3 ($2CH_3O$), 61.5 (CH_2O), 63.2 (C5), 81.9 (C4, J_{C-H} = 148.7 Hz), 128.4 et 131.7 (C_6H_5), 167.9, 168.4, 170.3 et 170.9 (C2 et CO). SM m/z (I %) : 365 (M^+), 306(100). Anal. calc. pour $C_{17}H_{19}NO_6S$: C 55.87, H 5.24, S 8.77; tr. : C 55.69, H 5.34, S 8.60.

Régression cyclique en milieu basique de la 6H-1,3-thiazine **3**c : Une solution toluénique (20 cm^3) de *6H*-1,3-thiazine **3***c* (0,6 mmol) et de triéthylamine (0,1 cm^3) est chauffée à 80°C pendant 18 h. Après évaporation du solvant, le 2-éthoxy pyrrole substitué **5***c* obtenu est purifié par chromatographie sur gel de silice (élution : éther de pétrole/éther diéthylique 60 : 40).

1. G. C. Tea, J. P. Pradère, B. Bujoli, H. Quiniou et L. Toupet. Bull. Soc. Chim. Fr. 149 (1987).
2. H. Quiniou et O. Guilloton. *Dans* Adv. Heterocycl. Chem. **50**, 85 (1990).
3. J. P. Pradère, J. C. Rozé, R. Danion-Bougot, D. Danion, L. Toupet et H. Quiniou. Can. J. Chem. **64**, 597 (1986) et références citées.
4. A. Reliquet, J. C. Meslin, F. Reliquet et H. Quiniou. Tetrahedron, **44**, 1107 (1988).
5. M. Bakasse, A. Reliquet, F. Reliquet, G. Duguay et H. Quiniou. J. Org. Chem. **54**, 2889 (1989).
6. R. Tuloup, R. Danion-Bougot, D. Danion et J. P. Pradère. Can. J. Chem. **67**, 1125 (1989).
7. C. Cellerin, C. G. Tea, J. P. Pradère, A. Guingant et P. Guenot. Sulfur Lett. **8**, 205 (1988).
8. A. Abouelfida, M. Jubault, J. P. Pradère, J. C. Rozé et A. Tallec. Tetrahedron Lett. **32**, 2225 (1991).
9. J. C. Rozé, J. P. Pradère, G. Duguay, A. Guével, H. Quiniou et S. Poignant. Can. J. Chem. **61**, 1169 (1983).
10. S. H. Eggers, V. V. Kane et G. Lowe, J. Chem. Soc. 1262 (1965).
11. B. Bujoli, M. Jubault, J. C. Rozé et A. Tallec. Tetrahedron, **43**, 2709 (1987).
12. B. Bujoli, M. Jubault, C. Moinet et A. Tallec. Electrochim. Acta, **35**, 805 (1990).
13. R. R. Schmidt et M. Dimmler. Chem. Ber. **26**, 3971 (1975).
14. R. Hazard, J. Sarrazin et A. Tallec. Electrochem. Acta, **25**, 1071 (1980).
15. M. Chehna, J. P. Pradère, J. Vicens, L. Toupet et H. Quiniou. Bull. Soc. Chim. Fr. **5**, 897 (1988).
16. B. Bujoli, M. Chehna, M. Jubault et A. Tallec. J. Electroanal. Chem. Interfacial Electro. Chem. **2**, 461 (1986).
17. A. Tallec, M. Jubault et B. Bujoli. *Dans* Recent advances in electroorganic synthesis. *Editeur* : S. Torii. Elsevier, Amsterdam. 1987. pp. 203–210.
18. R. R. Schmidt et M. Dimmler. Chem. Ber. **108**, 6 (1975).
19. R. Spitzner et W. Schroth. Tetrahedron Lett. **26**, 3971 (1985).
20. C. G. Tea, J. P. Pradère, H. Quiniou et L. Toupet. J. Chem. Soc. Perkin Trans. **1**, 1875 (1985).
21. C. Moinet et D. Peltier. Bull. Soc. Chim. Fr. 690 (1969).
22. C. G. Quiniou, M. Chehna, J. P. Pradère, G. Duguay et L. Toupet. Phosphorus Sulfur **27**, 327 (1986).

Can. J. Chem. Downloaded from www.nrcresearchpress.com by 123.30.183.119 on 09/08/12
For personal use only.

On the role of the parent cation in the dynamics of formation of laser-induced hydrated electrons

ERNÖ KESZEI[1] AND JEAN-PAUL JAY-GERIN

Groupe du Conseil de recherches médicales du Canada en sciences des radiations, Département de médecine nucléaire et de radiobiologie, Faculté de médecine, Université de Sherbrooke, Sherbrooke (Québec), Canada J1H 5N4

Received June 5, 1991

ERNÖ KESZEI and JEAN-PAUL JAY-GERIN. Can. J. Chem. **70**, 21 (1992).

A short account is given of the continuum and molecular descriptions of the formation of hydrated electrons. Starting with a scheme of hydration dynamics of laser-induced electrons that accounts for the formation of hydrated electrons without invoking the "direct" ionization of water, a new model explaining the dynamics of electron hydration in terms of a molecular description is proposed. According to this model, the parent cation plays an active role in the trapping of electrons, deepening electron traps that preexist in the liquid before excitation. Consequences of this description to the transient absorption spectra are briefly discussed.

Key words: laser-induced electron – cation pairs, hydrated electron formation, liquid water.

ERNÖ KESZEI et JEAN-PAUL JAY-GERIN. Can J. Chem. **70**, 21 (1992).

On présente un court rapport sur les descriptions continue et moléculaire de la formation des électrons hydratés. Utilisant comme point de départ un schéma de la dynamique d'hydratation d'électrons induits par un laser qui tient compte de la formation d'électrons hydratés sans impliquer l'ionisation «directe» de l'eau, on propose un nouveau modèle qui explique la dynamique de l'hydratation des électrons en fonction d'une description moléculaire. D'après ce modèle, le cation parent joue un rôle actif dans le piégeage des électrons en abaissant les pièges d'électrons qui existent déjà dans le liquide avant l'excitation. On discute brièvement des conséquences de cette description sur les spectres d'absorption des espèces transitoires.

Mots clés : photolyse laser femtoseconde, piégeage et hydratation de l'électron, eau liquide.

[Traduit par la rédaction]

Since the discovery and identification of the hydrated electron (1–3), many models have been proposed for the structure of this species as well as for the mechanism and dynamics of its formation. Recent experimental results (4–11) using ultrafast laser spectroscopy techniques have revealed new evidence, which has given rise to new hypotheses for the dynamics of electron trapping and for the subsequent early events in water.[2]

Referring to a recent critical review summarizing current theories of the dynamics of solvation in dipolar liquids (13), continuum models are based on a frequency-dependent dielectric continuum picture of the solvent, where the solute is replaced by a cavity containing the charge. Molecular theories represent a different approach which is promising, but a consistent treatment of solvent structure should be included along with a nonlinear theory of polar solvent dynamics in order to get reliable theoretical results. In a recent paper, Long *et al.* (11) also conclude that the dielectric-relaxation picture of solvation is fundamentally inconsistent with their experimental results on electron hydration in pure water. The important role of molecular interactions in solvation dynamics is also supported from studies of femtosecond laser fluorescence spectroscopy of electronically excited molecules (14), and of femtosecond, laser-driven nonlinear optical responses of liquids (15).

Beside theoretical models, computer simulations (16–20) also provide an insight into the details of electron hydration dynamics, with the great advantage that they treat water as consisting of individual molecules. These simulations use a quantum-mechanical representation of the electron (through, for example, the Feynman path-integral technique), but a classical representation of water molecules and a pseudopotential approach for describing the electron–water interaction. The simulation results largely support an important role of molecular and structural effects of the solvent, but, while there is good qualitative agreement with experiment, quantitative discrepancies are still serious (17; for a review, see ref. 17*b*).

None of the current theories or simulations can explain the dynamical characteristics of electron hydration. Based on the most recent experimental and simulation results, we propose here a model of the dynamics of formation of laser-induced hydrated electrons that differs from the mechanism of hydrated electron formation via high-energy ionizing radiations. We think that a major shortcoming of current theories is that they do not take into account the active role of the positive parent ion in the early events during which localization of laser-induced electrons occurs.

Let us consider the following schematic representation of electron hydration:

$$H_2O \xrightarrow{2\,h\nu} H_2O^*$$

$$H_2O^* \rightarrow \begin{cases} H_2O^+ \xrightarrow{+\,H_2O} H_3O^+ + OH^\cdot \\ e^- \xrightarrow[\tau_1\ (\text{trapping})]{} e_{ir}^- \end{cases}$$

$$e_{ir}^- \xrightarrow[\tau_2]{} e_{aq}^- \text{ (“hydrated” electron)}$$

In this scheme, excitation of a water molecule can be regarded as instantaneous. Electron trapping is a complex

[1]Permanent address: Department of Physical Chemistry, L. Eötvös University, Budapest 112, P.O. Box 32, H-1088, Hungary.

[2]For a review of experimental and theoretical studies on the formation of laser-induced solvated electrons, see ref. 12.

Can. J. Chem. Downloaded from www.nrcresearchpress.com by 123.30.183.119 on 09/08/12
For personal use only.

Can. J. Chem. Downloaded from www.nrcresearchpress.com by 123.30.183.119 on 09/08/12
For personal use only.

event, where a transient absorption, attributed to the water cation H_2O^+, appears and disappears within 50 fs (i.e., within the time resolution of the femtosecond laser apparatus), during the formation of the e_{ir}^- species. The characteristic time τ_1 for the formation of the latter species has been found to vary from ~110 fs (5) to ~180 fs (11).

As indicated in the above scheme, we think that the precursor of the e_{ir}^- species is *not* a "dry" or quasi-free electron, but rather the excited water molecule itself. The energetics of photoionization of water, recently reviewed by Goulet *et al.* (21), suggests that the energy band gap of liquid water is 8.9 ± 0.2 eV. This is the minimum energy necessary to produce a "dry" electron, or, in other words, to promote an electron into the conduction band of liquid water, while the threshold energy to produce a fully relaxed hydrated electron (along with $H_3O^+_{aq}$ and $OH^{\cdot}_{aq}$) is found to be 6.5 ± 0.5 eV from both single (22–24) and two-photon (25) ionization experiments. Now, the usual excitation energy, supposing a two-photon ionization process, is about 8 eV in all published femtosecond electron hydration experiments (4–11). This energy is sufficient to allow a valence electron to be promoted into one of the localized states of the Urbach tail, which lies below the conduction-band edge of water (21, 26). This obviously means that the actual production of laser-induced hydrated electrons does not proceed via the initial formation of quasi-free (dry) electrons, but that electrons get trapped directly from excitonic states of the liquid. (An interesting and inspiring continuum-model treatment of this process was recently proposed by Schiller (27).)

According to our proposition, these (Mott–Wannier-type) excitonic states can be viewed as Rydberg states with a largely extended outer electron and a localized positively charged core at the center. As the region over which this outer electron extends comprises many water molecules, the electronic charge density at the site of the parent ion is likely to be very small. (It is hard to give an estimate of the spatial range of this exciton; as a reasonable approximation, its radius can be estimated from the initial separation of e_{aq}^- and its parent cation (H_3O^+) after the formation of the e_{aq}^- species, which is about 1 nm (8, 28). Thus, the exciton would extend over a distance of some six water molecules, that is, over a hundred water molecules within a spherical range.) Consequently, the water molecules surrounding the parent ion site experience mainly the Coulombic field of this central (localized) positive charge, and, immediately after excitation, they begin to orientate and be polarized according to this field. The development of such a first hydration shell around the cation has important consequences. In fact, the potential of the central positive core at distances where the charge density of the outer electron is concentrated will be weakened as a result of this "screening." At the same time, the preexisting trap states (of the Urbach tail) that are located in the outer regions of the exciton and are coupled to the excitonic state will be deepened, due to the orientation of the positive poles of the aligned water dipoles towards these outer regions. Now, the screening by the water molecules will tend to diminish the interactions between the outer electron and the parent ion, while the trapping probability of the electron increases with the deepening of the available electron traps. Thus, the presence of the localized positive core of the initial exciton largely facilitates electron trapping in its immediate neighborhood. Once localized in one of these traps, the electron also begins to form its own hydration shell, and the e_{ir}^- species is formed, with a more or less relaxed microenvironment, with a characteristic time τ_1. During this formation time, irrespective of the degree of polarization of the surrounding water molecules, the central H_2O^+ can react with H_2O, with a high proton transfer rate, to give rise to H_3O^+ and $OH^{\cdot}$ (28, 29). This very fast event correlates with the rise and decay of an ultrashort transient absorbance at 625 nm (11). Once the e_{ir}^- species has been formed, it then transforms, with a characteristic time τ_2, into the fully relaxed e_{aq}^- state. (τ_2 has been found to vary from ~240 fs (5) to ~540 fs (11).) The resulting charged species $H_3O^+_{aq}$ and e_{aq}^- can be considered as a kind of solvent-separated ion pair (30). Due to this close proximity, e_{aq}^- can recombine easily with H_3O^+ and $OH^{\cdot}$. Indeed, it has been found that about 50% of the initially formed hydrated electrons undergo recombination within the first 100 ps, and the remaining e_{aq}^- population stabilizes after this time (6, 8, 31). This is in contrast with pulse radiolysis results where the estimated total ionization yield in water, G_{tot}, is about 6 molecules/100 eV (32–34), which stabilizes at about 4.8 molecules/100 eV after 30–100 ps (35, 36), i.e., only some 25% of the initially formed e_{aq}^- recombine. To our opinion, this difference is the direct consequence of the formation of quasi-free (or dry) electrons with large excess kinetic energy in the case of pulse radiolysis.

Summing up the proposed model for laser-induced electron trapping in liquid water, we suggest that the localized central positive core of the Rydberg-like excitonic state, formed upon photoexcitation, polarizes its environment, thus "deepening" preexisting electron traps (of the Urbach conduction-band tail) in the range of the exciton, largely facilitating the trapping of the extended outer electron. Dipolar relaxation around the positive parent site and the trapped electron takes up the excess energy of the exciton, thus giving rise to the formation of the reactive species $H_3O^+_{aq}$, e_{aq}^-, and $OH^{\cdot}_{aq}$ within a 1-nm radius (8, 28), and the subsequent recombination products. It is clear from the proposed model that an ultrafast initial Stokes shift should precede the build-up of the characteristic infrared band of the e_{ir}^- species. However, this Stokes shift should be located in the far infrared region from wavelengths of a few microns down to about 1 μm, the location of the e_{ir}^- infrared band. The large wavelength and the short time scale (probably less than ~100 fs) make the detection of this blue shift very difficult.

The proposed localization dynamics supposes ultrafast solvent relaxation times. The detection of a ~30-fs early configurational relaxation in computer simulations (20) provides support for this interpretation. Moreover, we think that, in water, proton jumps play an important role even in the orientation of the water molecules via an exchange of protons shared in hydrogen bonds. In our opinion, satisfactory simulation results could be obtained only with water molecules whose protons are considered as quantum particles, taking properly into account the role of the (classical) parent cation in the trapping of an electron.

Acknowledgements

The authors are indebted to T. Goulet and J.-M. Lopez-Castillo for stimulating discussions. Financial support from the Medical Research Council of Canada is gratefully acknowledged.

1. C. W. Gilbert, J. P. Keene, P. F. Browne, and T. J. Davy. *In* British Empire Cancer Campaign, 38th Annual Report, Part II. 1960. p. 498; J. P. Keene. Nature, **188**, 843 (1960); **197**, 47 (1963).
2. M. S. Matheson. Annu. Rev. Phys. Chem. **13**, 77 (1962).
3. E. J. Hart and J. W. Boag. J. Am. Chem. Soc. **84**, 4090 (1962); J. W. Boag and E. J. Hart. Nature, **197**, 45 (1963).
4. J. M. Wiesenfeld and E. P. Ippen. Chem. Phys. Lett. **73**, 47 (1980).
5. Y. Gauduel, A. Migus, J. L. Martin, Y. Lecarpentier, and A. Antonetti. Ber. Bunsen-ges. Phys. Chem. **89**, 218 (1985); A. Migus, Y. Gauduel, J. L. Martin, and A. Antonetti. Phys. Rev. Lett. **58**, 1559 (1987).
6. Y. Gauduel, S. Pommeret, A. Migus, and A. Antonetti. Radiat. Phys. Chem. **34**, 5 (1989); J. Phys. Chem. **93**, 3880 (1989); Chem. Phys. **149**, 1 (1990); S. Pommeret. Thèse de Doctorat, Université de Paris-Sud, Orsay. 1991.
7. Y. Gauduel, S. Pommeret, A. Migus, N. Yamada, and A. Antonetti. J. Am. Chem. Soc. **112**, 2925 (1990).
8. H. Lu, F. H. Long, R. M. Bowman, and K. B. Eisenthal. J. Phys. Chem. **93**, 27 (1989).
9. F. H. Long, H. Lu, and K. B. Eisenthal. Chem. Phys. Lett. **160**, 464 (1989).
10. F. H. Long, H. Lu, and K. B. Eisenthal. J. Chem. Phys. **91**, 4413 (1989).
11. F. H. Long, H. Lu, and K. B. Eisenthal. Phys. Rev. Lett **64**, 1469 (1990).
12. J. C. Mialocq. J. Chim. Phys. **85**, 31 (1988).
13. B. Bagchi. Annu. Rev. Phys. Chem. **40**, 115 (1989).
14. W. Jarzęba, G. C. Walker, A. E. Johnson, M. A. Kahlow, and P. F. Barbara. J. Phys. Chem. **92**, 7039 (1988).
15. G. A. Kenney-Wallace, C. Kalpouzos, and W. Lotshaw. Radiat. Phys. Chem. **32**, 573 (1988).
16. C. D. Jonah, C. Romero, and A. Rahman. Chem. Phys. Lett. **123**, 209 (1986); C. Romero and C. D. Jonah. J. Chem. Phys. **90**, 1877 (1989).
17. (*a*) M. Sprik, R. W. Impey, and M. L. Klein. J. Stat. Phys. **43**, 967 (1986); (*b*) M. Sprik. J. Phys. Condens. Matter, **2**, SA161 (1990).
18. A. Wallqvist, D. Thirumalai, and B. J. Berne. J. Chem. Phys. **86**, 6404 (1987); A. Wallqvist, G. Martyna, and B. J. Berne. J. Phys. Chem. **92**, 1721 (1988). For a review, see D. F. Coker and B. J. Berne. *In* Excess electrons in dielectric media. *Edited by* C. Ferradini and J.-P. Jay-Gerin. CRC Press, Boca Raton, FL. 1991. p. 211.
19. J. Schnitker and P. J. Rossky. J. Chem. Phys. **86**, 3471 (1987); J. Phys. Chem. **93**, 6965 (1989); J. Schnitker, K. Motakabbir, P. J. Rossky, and R. A. Friesner. Phys. Rev. Lett. **60**, 456 (1988); P. J. Rossky and J. Schnitker. J. Phys. Chem. **92**, 4277 (1988); F. J. Webster, J. Schnitker, M. S. Friedrichs, R. A. Friesner, and P. J. Rossky. Phys. Rev. Lett. **66**, 3172 (1991).
20. R. B. Barnett, U. Landman, and A. Nitzan. J. Chem. Phys. **90**, 4413 (1989); **93**, 8187 (1990); E. Neria, A. Nitzan, R. N. Barnett, and U. Landman. Phys. Rev. Lett. **67**, 1011 (1991).
21. T. Goulet, A. Bernas, C. Ferradini, and J.-P. Jay-Gerin. Chem. Phys. Lett. **170**, 492 (1990), and references cited therein.
22. U. Sokolov and G. Stein. J. Chem. Phys. **44**, 3329 (1966).
23. J. W. Boyle, J. A. Ghormley, C. J. Hochanadel, and J. F. Riley. J. Phys. Chem. **73**, 2886 (1969).
24. M. Anbar, G. A. St. John, H. R. Gloria, and R. F. Reinisch. *In* Water structure at the water–polymer interface. *Edited by* H. H. G. Jellinek. Plenum, New York. 1972. p. 85.
25. D. N. Nikogosyan, A. A. Oraevsky, and V. I. Rupasov. Chem. Phys. **77**, 131 (1983).
26. C. Houée-Levin and J.-P. Jay-Gerin. J. Phys. Chem. **92**, 6454 (1988).
27. R. Schiller. Radiat. Phys. Chem. **34**, 61 (1989).
28. T. Goulet and J.-P. Jay-Gerin. J. Phys. Chem. **93**, 7532 (1989).
29. A. Mozumder and J. L. Magee. Int. J. Radiat. Phys. Chem. **7**, 83 (1975).
30. P. Chang, R. V. Slates, and M. Szwarc. J. Phys. Chem. **70**, 3180 (1966).
31. T. Goulet and J.-P. Jay-Gerin. J. Chem. Phys. In press.
32. J. E. Turner, J. L. Magee, H. A. Wright, A. Chatterjee, R. N. Hamm, and R. H. Ritchie. Radiat. Res. **96**, 437 (1983).
33. G. R. Freeman. *In* Kinetics of nonhomogeneous processes. *Edited by* G. R. Freeman. Wiley, New York. 1987. Chap. 6. p. 277.
34. C. Ferradini and J.-P. Jay-Gerin. J. Chem. Phys. **89**, 6719 (1988), and references cited therein.
35. C. D. Jonah, M. S. Matheson, J. R. Miller, and E. J. Hart. J. Phys. Chem. **80**, 1267 (1976).
36. T. Sumiyoshi and M. Katayama. Chem. Lett. 1887 (1982); T. Sumiyoshi, K. Tsugaru, T. Yamada, and M. Katayama. Bull. Chem. Soc. Jpn. **58**, 3073 (1985).

Can. J. Chem. Downloaded from www.nrcresearchpress.com by 123.30.183.119 on 09/08/12
For personal use only.

Étude thermodynamique de l'acridone et de la thioxanthone

RAPHAËL SABBAH ET LAHCEN EL WATIK

Centre de thermodynamique et de microcalorimétrie du Centre national de la recherche scientifique, 26, rue du 14 lème RIA, 13003 Marseille, France

Reçu le 2 août 1991

RAPHAËL SABBAH et LAHCEN EL WATIK. Can. J. Chem. **70**, 24 (1992).

Dans le présent travail, nous avons étudié l'acridone et la thioxanthone par calorimétrie de combustion de faibles quantités de substance, de sublimation, par analyse thermique différentielle et par mesures de capacités calorifiques. Les fonctions thermodynamiques obtenues sont les suivantes : Pour l'acridone : $\Delta_{sub}H^0_m(298{,}15\ K) = (136{,}15 \pm 0{,}45)$ kJ mol^{-1}, $\Delta_cH^0_m(s, 298{,}15\ K) = -(6300{,}3 \pm 2{,}5)$ kJ mol^{-1}, $\Delta_fH^0_m(s, 298{,}15\ K) = -(101{,}6 \pm 2{,}6)$ kJ mol^{-1}, $\Delta_fH^0_m(g, 298{,}15\ K) = (34{,}6 \pm 2{,}6)$ kJ mol^{-1}. Pour la thioxanthone : $\Delta_{sub}H^0_m(298{,}15\ K) = (114{,}81 \pm 0{,}41)$ kJ mol^{-1}, $\Delta_cH^0_m(s, 298{,}15\ K) = -(6840{,}5 \pm 3{,}5)$ kJ mol^{-1}, $\Delta_fH^0_m(s, 298{,}15\ K) = -(20{,}5 \pm 3{,}6)$ kJ mol^{-1}, $\Delta_fH^0_m(g, 298{,}15\ K) = (94{,}3 \pm 3{,}6)$ kJ mol^{-1}, $\Delta_{fus}H_m = (35{,}50 \pm 0{,}28)$ kJ mol^{-1}, $T_{pt} = (487{,}88 \pm 0{,}02)$ K. Elles nous ont permis de déterminer l'énergie de conjugaison expérimentale des deux molécules qui nous intéressent et de les comparer aux valeurs théoriques. La molécule d'acridone étant plane, cette comparaison est tout à fait satisfaisante. La différence observée entre la valeur théorique et expérimentale dans le cas de la thioxanthone confirme les résultats expérimentaux sur la structure non plane de cette molécule. À partir de l'enthalpie d'atomisation expérimentale de l'acridone, nous avons pu déterminer une valeur enthalpique pour la liaison C_b-N. Enfin, en utilisant les contributions enthalpiques précédemment déterminées au laboratoire, nous avons pu retrouver par le calcul l'enthalpie d'atomisation de la molécule de thioxanthone.

Mots clés : thermodynamique; calorimétrie; analyse thermique différentielle; acridone; thioxanthone; enthalpies de combustion, de sublimation, de fusion; énergie de conjugaison; enthalpies d'atomisation, de liaisons intramoléculaires; température du point triple.

RAPHAËL SABBAH and LAHCEN EL WATIK. Can. J. Chem. **70**, 24 (1992).

In the present work we studied acridone and thioxanthone by combustion calorimetry of small amounts of substance, by sublimation calorimetry, by differential thermal analysis, and by heat capacity measurements. The thermodynamic quantities derived are as follows: For acridone: $\Delta_{sub}H^0_m(298.15\ K) = (136.15 \pm 0.45)$ kJ mol^{-1}, $\Delta_cH^0_m(s, 298.15\ K) = -(6300.3 \pm 2.5)$ kJ mol^{-1}, $\Delta_fH^0_m(s, 298.15\ K) = -(101.6 \pm 2.6)$ kJ mol^{-1}, $\Delta_fH^0_m(g, 298.15\ K) = (34.6 \pm 2.6)$ kJ mol^{-1}. For thioxanthone: $\Delta_{sub}H^0_m(298.15\ K) = (114.81 \pm 0.41)$ kJ mol^{-1}, $\Delta_cH^0_m(s, 298.15\ K) = -(6840.5 \pm 3.5)$ kJ mol^{-1}, $\Delta_fH^0_m(s, 298.15\ K) = -(20.5 \pm 3.6)$ kJ mol^{-1}, $\Delta_fH^0_m(g, 298.15\ K) = (94.3 \pm 3.6)$ kJ mol^{-1}, $\Delta_{fus}H_m = (35.50 \pm 0.28)$ kJ mol^{-1}, $T_{tp} = (487.88 \pm 0.02)$ K. The experimental results permitted us to determine for each molecule its resonance energy and to compare it with the theoretical value. This comparison fits well for acridone, which is planar. The difference observed in the case of thioxanthone shows that this molecule is not planar, in accord with literature structural results. From the experimental enthalpy of atomization of acridone, we determined an enthalpy value for the C_b—N bond. Using the enthalpy contributions previously determined in our laboratory, we found a value for the enthalpy of atomization of thioxanthone in accord with the experimental result.

Key words: thermodynamics; calorimetry; differential thermal analysis; acridone; thioxanthone; enthalpies of combustion, of sublimation, of fusion; resonance energy; enthalpies of atomization, of intramolecular bonds; triple point temperature.

Introduction

Dans le cadre de l'étude thermodynamique des hétérocycles se trouvant dans les coupes lourdes du pétrole ou dans les produits issus de la pyrolyse du charbon, entreprise au laboratoire depuis quelques années, nous nous sommes intéressés aux deux molécules d'acridone et de thioxanthone.

Comme on le sait, diverses actions programmées depuis plus de dix ans ont eu pour but la valorisation de ces matériaux. Parmi elles, il faut citer les deux opérations d'hydrodésulfuration et de désazotation. Leur but est de convertir les molécules renfermant du soufre ou de l'azote en hydrocarbures afin d'obtenir des combustibles non polluants. La difficulté de pouvoir déterminer directement les enthalpies des différentes réactions liées à ces opérations nécessite le recours à des valeurs précises des enthalpies de formation des réactifs et produits. Malheureusement, pour ces deux substances, il n'existe aucune grandeur thermodynamique dans la littérature.

Possédant au laboratoire les moyens de déterminer avec une exactitude suffisamment bonne, tout en n'utilisant que peu de substance (une étude complète nécessite 200 mg environ de substance pure), certaines grandeurs thermodynamiques : enthalpie de formation aux états condensé et gazeux à partir des enthalpies de combustion et de sublimation, enthalpie de fusion, température du point triple . . . (1–3), nous les avons utilisés pour étudier les deux molécules d'acridone et de thioxanthone.

Partie expérimentale

1. Produits

L'acridone est un produit Fluka (purum, pureté initiale >99%) et la thioxanthone est un produit Aldrich, pureté initiale 98%. Nous les avons repurifiés par recristallisation, le premier dans l'éthanol absolu et le second dans le tétrachlorure de carbone, puis sublimés sous une pression résiduelle de 10^{-2} Torr à 180°C dans le cas de l'acridone et à 120°C dans celui de la thioxanthone (1 Torr = 133,322 Pa).

Il ne nous a pas été possible de déterminer par ATD le degré de pureté de l'acridone car cette substance se décompose à la fusion. Par contre, dans le cas de la thioxanthone, nos expériences d'ATD nous ont permis de déterminer le degré de pureté de l'échantillon repurifié; celui-ci est égal à (99,94 ± 0,01) mol%.

Printed in Canada / Imprimé au Canada

Can. J. Chem. Downloaded from www.nrcresearchpress.com by 123.30.183.119 on 09/08/12
For personal use only.

TABLEAU 1. Grandeurs physiques des molécules étudiées à 298,15 K

Substance	Formule	M/g mol^{-1} [a]	ρ/g cm^{-3}	$-(\delta U/\delta P)_T$/J g^{-1} atm^{-1} [b]
Acridone $C_{13}H_9ON$	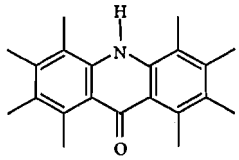	195,2206	1,201	(0,013)
Thioxanthone $C_{13}H_8OS$	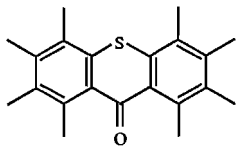	212,2719	1,422	(0,013)

[a] Calculée à partir du tableau des masses atomiques de 1987 (22).
[b] 1 atm = 101,325 kPa.
Les valeurs placées entre parenthèses ont été estimées.

2. Appareillage, techniques et mode opératoire

Pour mener à bien cette étude, nous avons utilisé la calorimétrie de combustion de faibles quantités de substance, la calorimétrie de sublimation, l'analyse thermique différentielle et la mesure des capacités calorifiques.

2.1. Calorimétrie de combustion

Pour réaliser les expériences par calorimétrie de combustion, nous avons utilisé l'appareillage décrit dans la référence 4*a*. Précisons ici que dans le cas de l'acridone, la microbombe qui lui est associée a été décrite dans un précédent mémoire (5). Avec la thioxanthone, nous avons utilisé une microbombe à revêtement de platine décrite dans la référence 4*a*. La sensibilité de la pile du calorimètre CRMT est de 62,4 μV mW^{-1} à 298,15 K; celle de l'amplificateur est de 30 mV. L'oxygène N45, utilisé dans nos expériences, provient de l'Air Liquide; son degré de pureté est égal à 99,995%.

2.2. Calorimétrie de sublimation

Pour mesurer diretement la quantité de chaleur mise en jeu par la sublimation des substances étudiées, nous avons utilisé un calorimètre Tian–Calvet, dont la sensibilité de la pile est de 16,87 μV mW^{-1} à 380 K et de 13,81 μV mW^{-1} à 432 K, associé à une cellule d'effusion de Knudsen. L'appareillage et le mode opératoire ont été décrits dans la référence 2. Toutefois, il y a lieu de préciser ici que le signal issu du calorimètre est amplifié par un nonovoltmètre Keithley modèle 147 (sensibilité utilisée : 30 μV (acridone) et 100 μV (thioxanthone)), puis digitalisé à l'aide d'un voltmètre numérique Keithley modèle 175. L'acquisition et le traitement des données ont été réalisés à l'aide d'un programme écrit par nos soins et traité par un ordinateur Zenith modèle 159.

La très faible pression de vapeur saturante des deux substances étudiées ne nous a pas permis de les sublimer à 298,15 K. En conséquence, la thioxanthone a été étudiée à 380 K et l'acridone à 432 K en utilisant un trou d'effusion respectivement de 1,5 et de 2 mm.

2.3. Analyse thermique différentielle

En utilisant l'appareillage et le mode opératoire décrits dans la référence 3, cette technique nous a permis de mesurer la température du point triple ainsi que l'enthalpie de fusion de la thioxanthone.

Résultats

Nous avons consigné dans le tableau 1 les grandeurs physiques à 298,15 K concernant les substances étudiées qui interviennent dans les calculs menant aux résultats expérimentaux.

1. Calorimétrie de combustion

L'équivalent énergétique du calorimètre (U_{calor}) a été obtenu à partir d'une série de combustions d'acide benzoïque, échantillon 39i du NBS, pour lequel $\Delta_c u^0$ (s, 298,15 K) = $-(26\ 414 \pm 3)$ J g^{-1}. Dans ces expériences, nous avons utilisé environ 5 mg d'acide et 0,2 mg de coton (dont l'énergie de combustion, préalablement déterminée au laboratoire, a pour valeur $\Delta_c u^0$(s, 298,15 K) = $-(16399 \pm 23)$ J g^{-1} (6)). Nous trouvons pour U_{calor}(298,15 K) la valeur (16,025 ± 0,007) J V^{-1} s^{-1} (acridone) et (15,957 ± 0,009) J V^{-1} s^{-1} (thioxanthone).

Les résultats expérimentaux obtenus par calorimétrie de combustion sont consignés dans les tableaux 2 et 3.

2. Calorimétrie de sublimation

L'étalonnage de notre système calorimétrique a été réalisé par effet Joule avant et après les expériences.

À cause de la très faible pression de vapeur saturante des substances étudiées, nous avons admis l'identité $\Delta_{sub}H_m(T) \equiv \Delta_{sub}H^0_m(T)$. Par ailleurs, pour calculer $\Delta_{sub}H^0_m$(298,15 K) à partir de $\Delta_{sub}H^0_m(T\ \text{K})$ (T = 432 K (acridone) et 380 K (thioxanthone)), nous avons utilisé la relation suivante :

$$\Delta_{sub}H^0_m(298{,}15\ \text{K}) = \Delta_{sub}H^0_m(T\ \text{K}) + \int_{T\text{K}}^{298{,}15\ \text{K}} [C^0_{p,m}(\text{g}) - C^0_{p,m}(\text{s})]\mathrm{d}T$$

après nous être assurés par ATD que la substance ne présente aucun changement de phase entre 298,15 et T K. En ce qui concerne l'intégrale $\int_{T\text{K}}^{298{,}15\ \text{K}}[C^0_{p,m}(\text{s})]\mathrm{d}T$, elle a été obtenue par la méthode de chute en utilisant un calorimètre Tian–Calvet et un four maintenus respectivement à 298,15 et T K. Quant à l'intégrale $\int_{T\text{K}}^{298{,}15\ \text{K}}[C^0_{p,m}(\text{g})]\mathrm{d}T$, elle a été déterminée à l'aide d'une méthode de contributions de groupes (7).

Nous avons consigné dans les tableaux 4 et 5 les résultats expérimentaux obtenus par calorimétrie de sublimation.

3. Enthalpie de formation de l'acridone et de la thioxanthone à l'état gazeux

Il est possible, à partir des résultats consignés dans les tableaux 2–5, de déterminer l'enthalpie de formation des substances étudiées à l'état gazeux et à 298,15 K. Celle-ci est égale à (34,6 ± 2,6) kJ mol^{-1} dans le cas de l'acridone et à (94,3 ± 3,6) kJ mol^{-1} dans celui de la thioxanthone.

Can. J. Chem. Downloaded from www.nrcresearchpress.com by 123.30.183.119 on 09/08/12
For personal use only.

TABLEAU 2. Combustion de l'acridone à 298,15 K

m(substance)/mg	m(coton)/mg	S/V s	$-\Delta U$/J	$-w_1$/J	w_2/J	$-\Delta_c U^0_m$(s, 298,15 K)/kJ mol^{-1}
4,1289	0,2055	8,541480	136,872	3,370	0,145	6305,31
6,0728	0,0755	12,313974	197,325	1,238	0,211	6296,75
4,8258	0,1652	9,883074	158,371	2,710	0,169	6290,21
6,7290	0,2054	13,772877	220,703	3,369	0,237	6298,38
6,1269	0,1312	12,473550	199,882	2,152	0,214	6293,42
4,7939	0,1880	9,864318	158,070	3,083	0,168	6304,63
5,1650	0,1991	10,624596	170,253	3,266	0,182	6304,75
6,5998	0,1618	13,435989	215,304	2,654	0,231	6283,31
5,5837	0,1841	11,441220	183,339	3,020	0,196	6297,59

$\Delta_c U^0_m$(s, 298,15 K) = $-$(6297,2 ± 2,5) kJ mol^{-1}
$\Delta_c H^0_m$(s, 298,15 K) = $-$(6300,3 ± 2,5) kJ mol^{-1}
$\Delta_f H^0_m$(s, 298,15 K) = $-$(101,6 ± 2,6) kJ mol^{-1}

Ces résultats corrspondent à la réaction suivante :
$C_{13}H_9ON$ (s) + $59/4O_2$ (g) → $13CO_2$ (g) + $9/2H_2O$ (l) + $1/2N_2$ (g)

S = aire des thermogrammes; ΔU = variation de l'énergie interne de la bombe et de son contenu; w_1 = énergie de combustion du coton; w_2 = corrections pour passer à l'état standard.

TABLEAU 3. Combustion de la thioxanthone à 298,15 K

m(substance)/mg	m(coton)/mg	S/V s	$-\Delta U$/J	$-w_1$/J	w_2/J	$-\Delta_c U^0_m$(s, 298,15 K)/kJ mol^{-1}
5,0149	0,1341	10,282158	164,073	2,199	0,311	6838,64
5,7210	0,1216	11,655741	185,991	1,994	0,345	6814,20
5,1760	0,1230	10,599366	169,134	2,017	0,319	6840,52
5,6892	0,1442	11,635941	185,675	2,365	0,344	6826,71
5,7484	0,1789	11,810700	188,464	2,934	0,348	6838,24
5,8164	0,1081	11,866640	189,356	1,773	0,349	6833,18
6,5254	0,1262	13,334600	212,781	2,070	0,383	6841,98
6,0561	0,1382	12,350709	197,081	2,267	0,361	6815,74
6,4263	0,1262	13,143486	209,731	2,070	0,378	6846,91
6,2312	0,1066	12,704631	202,728	1,748	0,369	6834,01

$\Delta_c U^0_m$(s, 298,15 K) = $-$(6833,0 ± 3,5) kJ mol^{-1}
$\Delta_c H^0_m$(s, 298,15 K) = $-$(6840,5 ± 3,5) kJ mol^{-1}
$\Delta_f H^0_m$(s, 298,15 K) = $-$(20,5 ± 3,6) kJ mol^{-1}

Ces résultats correspondent à la réaction suivante :
$C_{13}H_8OS$ (s) + $16O_2$ (g) + 112 H_2O (l) → $13CO_2$ (g) + $H_2SO_4.115H_2O$ (l)

S = aire des thermogrammes; ΔU = variation de l'énergie interne de la bombe et de son contenu; w_1 = énergie de combustion du coton; w_2 = corrections pour passer à l'état standard.

4. Pression de vapeur saturante de l'acridone et de la thioxanthone

Comme indiqué dans les références 8 et 9, il nous est possible, à partir de nos essais, d'évaluer la pression de vapeur saturante des substances étudiées en utilisant la relation suivante :

$$P(T) \approx \Delta P = \mathrm{d}m/\mathrm{d}t(2\pi RT/M)^{1/2}1/aF$$

dans laquelle ΔP est la pression de part et d'autre du trou d'effusion; $P(T)$, la pression mesurée par effusion à la température T; $\mathrm{d}m/\mathrm{d}t$, la masse effusée par unité de temps; R, la constante des gaz parfaits; M, la masse molaire de la substance; F, le facteur de Clausing et a, l'aire de l'orifice d'effusion.

Nous trouvons respectivement 4×10^{-4} et 2×10^{-3} Torr comme pression de vapeur saturante de l'acridone à 432 K et de la thioxanthone à 380 K.

5. Enthalpie de fusion et température du point triple

Comme précisé dans le paragraphe 2.3, il nous a été possible de déterminer par ATD l'enthalpie de fusion ainsi que la température du point triple de la thioxanthone. Nous avons trouvé $\Delta_{fus}H_m$ = (35,50 ± 0,28) kJ mol^{-1} et T_{pt} = (487,88 ± 0,02) K (définie par rapport à l'EIPT-68).

Le manque de valeurs thermodynamiques consignées dans la littérature pour les deux molécules qui nous intéressent ne nous a pas permis de les comparer à nos résultats expérimentaux.

L'incertitude qui accompagne nos résultats expérimentaux représente l'écart moyen, σ_m, et tient compte des erreurs sur les termes et facteurs de l'expression conduisant au calcul de ces résultats.

Discussion

L'ensemble des fonctions thermodynamiques obtenues et consignées dans la partie Résultats permet la détermination de plusieurs grandeurs énergétiques liées à la structure des molécules étudiées.

1. Energie de conjugaison

Comme on le sait, cette grandeur renseigne sur la stabilité d'une molécule et est étroitement liée à sa structure.

Can. J. Chem. Downloaded from www.nrcresearchpress.com by 123.30.183.119 on 09/08/12
For personal use only.

Can. J. Chem. Downloaded from www.nrcresearchpress.com by 123.30.183.119 on 09/08/12
For personal use only.

TABLEAU 4. Sublimation de l'acridone à 432 K

m(substance)/mg	S/V s	$\Delta_{sub}H_m$(432 K)/kJ mol^{-1}
10,3715	0,090508	123,34
11,5538	0,099214	121,37
14,2021	0,122214	121,67
15,8406	0,135795	121,21
21,9258	0,196770	122,16

$\Delta_{sub}H^0_m(432\ K) = (121,95 \pm 0,38)$ kJ mol^{-1}
$P_{sat}(432\ K) = 4 \times 10^{-4}$ Torr

$$\int_{298,15\,K}^{432\,K} C^0_{p,m}(s)dT = (38,1 \pm 0,2) \text{ kJ mol}^{-1}$$

$$\int_{298,15\,K}^{432\,K} C^0_{p,m}(g)dT = (23,9 \pm 0,2) \text{ kJ mol}^{-1}$$

$\Delta_{sub}H^0_m(298,15\ K) = (136,15 \pm 0,45)$ kJ mol^{-1}

S = aire des thermogrammes.

TABLEAU 5. Sublimation de la thioxanthone à 380 K

m(substance)/mg	S/V s	$\Delta_{sub}H_m$(380 K)/kJ mol^{-1}
17,1736	0,149275	109,39
30,0134	0,261159	109,51
28,2242	0,244874	110,19
25,2598	0,217132	108,18
22,3614	0,194219	109,31
21,4464	0,184249	108,12
30,9009	0,263116	107,16
29,2656	0,250964	107,93
33,4658	0,285185	107,25

$\Delta_{sub}H^0_m(380\ K) = (108,45 \pm 0,31)$ kJ mol^{-1}
$P_{sat}(380\ K) = 2 \times 10^{-3}$ Torr

$$\int_{298,15\,K}^{380\,K} C^0_{p,m}(s)dT = (20,3 \pm 0,3) \text{ kJ mol}^{-1}$$

$$\int_{298,15\,K}^{380\,K} C^0_{p,m}(g)dT = (13,91 \pm 0,09) \text{ kJ mol}^{-1}$$

$\Delta_{sub}H^0_m(298,15\ K) = (114,81 \pm 0,41)$ kJ mol^{-1}

S = aire des thermogrammes.

Construite à partir des modèles moléculaires, la molécule d'acridone est plane. Malheureusement nous n'avons trouvé dans la littérature aucune étude sur la structure cristalline ou (et) gazeuse de cette molécule permettant de confirmer cette observation. Il n'en est pas de même pour la thioxanthone qui présente un défaut de planéité confirmé par une étude structurale réalisée par diffraction électronique en phase gazeuse (10).

Dans l'une de nos précédentes publications (11), nous avions indiqué le procédé utilisé pour déterminer l'énergie de conjugaison expérimentale et théorique d'une molécule. Sur le plan pratique, on détermine la valeur expérimentale à partir des enthalpies de combustion à l'état gazeux de la molécule réelle et de la molécule fictive non conjuguée. La première de ces deux grandeurs s'obtient expérimentalement. Quant à la seconde, elle nécessite le recours aux systématiques. Pour notre part, nous avons utilisé celle de Klages qui est consignée par Wheland dans la référence 12.

En ce qui concerne la molécule d'acridone, compte tenu de sa structure plane, l'énergie de conjugaison expérimentale est égale à 390,1 kJ mol^{-1} et est tout à fait compatible avec la valeur théorique 386,7 kJ mol^{-1} obtenue en utilisant les paramètres suivants :

Pour la liaison C_b=0 :

$$\alpha(C) = \alpha + 0,250\beta_0$$
$$\alpha(O) = \alpha + 0,875\beta_0$$
$$\beta(C{=}O) = 1,375\beta_0$$

Pour la liaison C_b—N :

$$\alpha(C) = \alpha$$
$$\alpha(N) = \alpha + 1,750\beta_0$$
$$\beta(C{-}N) = 0,950\beta_0$$

La valeur de β(C—N) a été ajustée sur la molécule de pyrrole et a déjà été utilisée dans le calcul de l'énergie de conjugaison théorique de la molécule de carbazole (*4a*). β_0 représente, dans tous les calculs effectués dans la présente étude, l'intégrale de recouvrement dans la molécule de benzène et a pour valeur absolue 131,7 kJ mol^{-1}.

En ce qui concerne la molécule de thioxanthone, l'énergie de conjugaison expérimentale est égale à 353,2 kJ mol^{-1}. À partir des paramètres ci-dessus indiqués pour la liaison C_b=O et du même jeu de paramètres précédemment utilisés dans le cas du thiophène et de quelques-uns de ses dérivés (13) pour la liaison C_b—S ($\alpha(C) = \alpha$, $\alpha(S) = \alpha + 2,000\beta_0$ et $\beta(C{-}S) = 1,100\beta_0$), nous avons pu déterminer l'énergie de conjugaison théorique; celle-ci est égale à 409,5 kJ mol^{-1}. Étant supérieure à la valeur expérimentale, elle confirme bien le défaut de planéité de la molécule de thioxanthone.

Dans leur publication sur l'étude structurale de la molécule de thioxanthone en phase gazeuse, Iijima *et al.* (10) concluent à partir de leurs résultats et ceux de Gallaher et Bauer sur la molécule de thianthrène (14) que l'angle dièdre formé par les deux noyaux benzéniques est plus important dans le cas de la thioxanthone, ce qui voudrait dire que cette molécule serait plus plane que la molécule de thianthrène. Comme cette molécule a été précédemment étudiée au laboratoire (15), pour confirmer ce résultat, il suffisait de comparer la différence Δ entre les valeurs théorique et expérimentale de l'énergie de conjugaison pour chacune des deux molécules qui nous intéressent. Dans le cas présent, cette différence doit être plus grande dans le cas de la molécule de thianthrène. En utilisant le jeu de paramètres signalé ci-dessus, nous avons pu calculer la valeur théorique de l'énergie de conjugaison du thianthrène, ce qui nous a permis, connaissant $E_{conj,exp}$ = 364 kJ mol^{-1} (15), de déterminer Δ. Nous trouvons Δ = 72,7 kJ mol^{-1} dans le cas du thianthrène et 59,3 kJ mol^{-1} dans celui de la thioxanthone. Le même raisonnement peut être appliqué pour montrer que la molécule de xanthone, précédemment étudiée au laboratoire (1), est plus plane que celle de thioxanthone, confirmant ainsi les résultats expérimentaux d'études sur la structure de ces deux molécules (10, 16, 17) (Δ = 24,3 kJ mol^{-1} dans le cas de la molécule de xanthone).

Comme nous l'avons dit dans l'introduction, nous nous sommes intéressés à l'acridone et à la thioxanthone dans un cadre plus général visant l'étude de molécules polycycliques. De ce fait, il nous a paru intéressant de comparer entre elles les valeurs théoriques de l'énergie de conjugaison consignées dans le tableau 6. On constate que ces valeurs vont en ordre décroissant en passant de la molécule de

TABLEAU 6. Énergie de conjugaison expérimentale et théorique

Molécule	$E_{conj,exp.}$/kJ mol^{-1}	$E_{conj,théor.}$/kJ mol^{-1}
Thioxanthone	350,2	409,5
Xanthone	345,8 (l)	370,1 (l)
Acridone	390,1	386,7
Anthrone	325,6 (23)	336,7

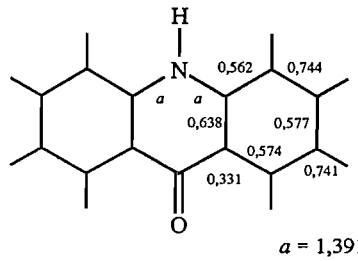

FIG. 1. Indices de liaison dans la molécule d'acridone.

thioxanthone, à celle d'acridone, à celle de xanthone. Ceci peut s'expliquer puisque la délocalisation, fonction de l'électronégativité, est plus grande dans le cas de la molécule de la thioxanthone qu'elle ne l'est dans les deux autres cas et dans l'ordre indiqué. Nous rejoignons ici la même conclusion tirée au moment de l'étude des molécules de dibenzothiophène, de carbazole et de dibenzofuranne (4). Quant à l'anthrone dont l'énergie de conjugaison théorique est égale à celle de la molécule de benzophénone (18), la valeur de celle-ci est inférieure aux trois autres car la conjugaison est incomplète (existence d'un chaînon -CH_2-). Par ailleurs, tout ce qui vient d'être dit trouve sa confirmation en comparant aussi entre elles les valeurs expérimentales de l'énergie de conjugaison. En effet, seule la molécule d'acridone est plane et sa conjugaison complète, ce qui explique la valeur élevée de l'énergie correspondante comparée à toutes les autres. L'énergie de conjugaison de la molécule de thioxanthone est plus élevée que celle de xanthone. Elle le serait encore plus si la molécule de thioxanthone était plane. Enfin, la faible valeur trouvée pour la molécule d'anthrone s'explique du fait que la conjugaison dans cette molécule est incomplète.

2. Enthalpie d'atomisation

L'enthalpie d'atomisation est liée à la transformation suivante : molécule (considérée comme gaz idéal, état fondamental, *T*) → atomes (chacun d'eux considéré comme gaz idéal, état fondamental, *T*).

À partir de l'enthalpie de formation d'une molécule à l'état gazeux et de celle des différents constituants C,H,O,N et S que l'on emprunte aux tables (19) et dont les valeurs sont respectivement égales à : (716,67 ± 0,44), (217,997 ± 0,006), (249,17 ± 0,10), (472,68 ± 0,40) et (276,98 ± 0,25) kJ mol^{-1}, il est possible de calculer son enthalpie d'atomisation expérimentale. Nous trouvons pour les molécules d'acridone et de la thioxanthone respectivement les valeurs : (11965,9 ± 3,9) et (11492,5 ± 4,6) kJ mol^{-1}.

Comme l'enthalpie d'atomisation est égale à la somme des enthalpies des liaisons intramoléculaires, compte tenu des facteurs de stabilisation et destabilisation, il nous a été possible de déterminer l'enthalpie de la liaison C_b—N dans le cas de la molécule d'acridone. Cela revient à retrancher de $\Delta_{a,exp}H(298,15\ K)$ la part enthalpique de toutes les autres liaisons intramoléculaires. Pour déterminer les contributions enthalpiques relatives aux différentes liaisons carbone–carbone, nous avons utilisé le procédé de calcul consigné dans la référence 4*a*. Celui-ci fait intervenir un paramètre lié à la géométrie de la molécule (l'indice de liaison l_{rs} entre deux atomes directement liés r et s), obtenu à partir du calcul théorique de l'énergie de conjugaison (cf. fig. 1). La relation reliant H_{rs} à l_{rs} s'écrit H_{rs}/kJ mol^{-1} = 246,0 l_{rs} + 342,6.

Quant aux enthalpies des liaisons C_b—H, C_b=O et N—H, nous avons respectivement utilisé les valeurs 415,88 758,19 (20) et 384,72 kJ mol^{-1} (21).

Nous trouvons $H(C_b—N)$ = 324,7 kJ mol^{-1} pour une distance interatomique de 1,391 Å. Ce résultat est tout à fait compatible avec le couple de valeurs $H(C_b—N)$ = 348,3 kJ mol^{-1} et $d(C_b—N)$ = 1,389 Å trouvée précédemment dans le cas de la molécule de carbazole (4*a*).

En ce qui concerne la molécule de thioxanthone, en utilisant les valeurs enthalpiques des différentes liaisons précédemment déterminées (15, 18), nous avons pu retrouver son enthalpie d'atomisation expérimentale à 2,4% près.

Remerciements

L'un de nous (L. El Watik) tient à remercier le gouvernement marocain pour l'octroi d'une bourse lui ayant permis de préparer une thèse de doctorat dont ce travail fait partie.

1. R. Sabbah et L. El Watik. Bull. Soc. Chim. Fr. 626 (1988).
2. R. Sabbah, I. Antipine, M. Coten et L. Davy. Thermochim. Acta, **115**, 153 (1987).
3. (*a*) R. Sabbah et I. Antipine. J. Therm. Anal. **32**, 1929 (1987); (*b*) R. Sabbah et L. El Watik. J. Therm. Anal. **36**, 2299 (1990).
4. (*a*) R. Sabbah et I. Antipine. Bull. Soc. Chim. Fr. 392 (1987); (*b*) R. Sabbah. Bull. Soc. Chim. Fr. **128**, 350 (1991).
5. R. Sabbah et L. El Watik. Thermochim. Acta, **176**, 163 (1991).
6. R. Sabbah et M. Coten. Thermochim. Acta, **49**, 307 (1981).
7. S. W. Benson. Thermochemical kinetics. 2 ed. Wiley–Interscience, New York. 1976. Chap. 2.
8. R. Sabbah, R. Chastel et M. Laffitte. Thermochim. Acta, **5**, 117 (1972).
9. R. Sabbah, R. Chastel et M. Laffitte. Can. J. Chem. **52**, 2201 (1974).
10. K. Iijima, I. Oonishi, S. Fujisawa et S. Shibata. Bull. Chem. Soc. Jpn. **60**, 3887 (1987).
11. R. Sabbah, M. Gilbert et A. Julg. Thermochim. Acta, **10**, 345 (1974).
12. G. W. Wheland. Resonance in organic chemistry. Wiley, New York. 1955.
13. A. Julg et R. Sabbah. C. R. Acad. Sci. Paris, Sér. C, **285**, 421 (1977).
14. K. L. Gallaher et S. H. Bauer. J. Chem. Soc. Faraday Trans. 2, **71**, 1173 (1975).
15. R. Sabbah et L. El Watik. Thermochim. Acta, **138**, 241 (1989).
16. K. Iijima, T. Misu, S. Ohnishi et S. Onuma. J. Mol. Struct. **213**, 263 (1989).
17. S. Onuma, K. Iijima et I. Oonishi. Acta Crystallogr. Sect. C: Cryst. Struct. Commun. **C46**, 1725 (1990).
18. R. Sabbah et M. Laffitte. Thermochim. Acta, **23**, 196 (1978).
19. Report of the Codata Task Group on Key Values for Thermodynamics 1977. J. Chem. Thermodyn. **10**, 903 (1978).
20. R. Sabbah et M. Laffitte. Thermochim. Acta, **25**, 376 (1978).
21. R. Sabbah et M. Laffitte. Bull. Soc. Chim. Fr. I-50 (1978).
22. Atomic weights of the elements 1987. Pure Appl. Chem. **60**, 841 (1988).
23. L. El Watik et R. Sabbah. Bull. Soc. Chim. Fr. **128**, 344 (1991).

Can. J. Chem. Downloaded from www.nrcresearchpress.com by 123.30.183.119 on 09/08/12
For personal use only.

Reactions of dimethyl polysulfides[1] with organomagnesium reagents

PETER D. CLARK,[2] RUSSELL S. MANN, AND KEVIN L. LESAGE
Department of Chemistry, The University of Calgary, 2500 University Drive N.W., Calgary, Alta., Canada T2N 1N4

Received April 11, 1991

PETER D. CLARK, RUSSELL S. MANN, and KEVIN L. LESAGE. Can. J. Chem. **70**, 29 (1992).

Reactions of a mixture of dimethyl polysulfides (DMPS, $CH_3S_xCH_3$, $x = 3 - 8$) with methyl- and phenylmagnesium halides are described. The type of product obtained was dependent on the molar ratio of DMPS to Grignard reagent. When a 6:1 methyl-Grignard to DMPS ratio was used, methanethiol and dimethyl sulfide were the major products obtained after acidification of the reaction mixture. Lesser quantities of methyl-Grignard favored the formation of dimethyl sulfide, dimethyl disulfide, and H_2S. Experiments with a 6:1 phenylmagnesium bromide to DMPS ratio produced benzenethiol and phenylmethyl sulfide as major products after acidification. No methanethiol was observed in these experiments. Mixtures of phenylmethyl mono-, di-, and trisulfides and H_2S were obtained with a 3:1 Grignard/DMPS molar ratio. From a mechanistic viewpoint, product distributions obtained from reaction of Grignard reagents with DMPS can be explained by the formation of magnesium thiolates that are most readily stabilized by adjacent structures. Experiments using phenyl Grignard reagent in limited supply suggested that the internal sulfur atoms of the polysulfide chains were most reactive.

Key words: organic polysulfides, Grignard reagents.

PETER D. CLARK, RUSSELL S. MANN et KEVIN L. LESAGE. Can. J. Chem. **70**, 29 (1992).

On décrit les réactions d'un mélange de polysulfures de diméthyle (PSDM, $CH_3S_xCH_3$, $x = 3 - 8$) avec les halogénures de méthyl- et de phénylmagnésium. Le type de produit obtenu dépend du rapport molaire entre le PSDM et le réactif de Grignard. Lorsqu'on a utilisé un rapport de 6 : 1 entre l'halogénure de méthyle magnésium et le PSDM, l'extraction du mélange réactionnel obtenu après acidification fournit du méthanethiol et du sulfure de diméthyle comme produits principaux. Lorsqu'on utilise des rapports plus faibles de ces réactifs, la formation de sulfure de diméthyle, de disulfure de diméthyle et de H_2S est favorisée. Des expériences avec un rapport de 6 : 1 entre le bromure de phénylmagnésium et le PSDM a conduit, après acidification, à la formation du benzènethiol et du sulfure de phényle et de méthyle comme produits principaux. On n'a pas observé la formation de méthanethiol dans ces expériences. On a obtenu des mélanges de mono-, di- et trisulfures de phényle et de méthyle et H_2S lorsqu'on a utilisé un rapport molaire de 3 : 1 de Grignard/PSDM. D'un point de vue mécanistique, les distributions de produits obtenus par réactions des réactifs de Grignard avec le PSDM peuvent être expliquées par la formation de thiolates de magnésium qui sont facilement stabilisées par des structures adjacentes. Des expériences réalisées avec des quantités limitées de réactif de Grignard suggèrent que les atomes internes de soufre des chaines polysulfurées sont les plus réactives.

Mots clés : polysulfures organiques, réactifs de Grignard.

[Traduit par la rédaction]

Introduction

Under the influence of basic catalysis, sulfur reacts with organic disulfides to form mixtures of organic polysulfides (for a review of polysulfide chemistry, see ref. 1). One industrial use of such chemistry is to inject suitably catalysed dimethyl disulfide into the tubulars of sour gas wells to remove deposited elemental sulfur (2–5):

$$CH_3SSCH_3 + S_8 \xrightarrow{\text{Base}} CH_3S_xCH_3 \qquad x = 3 - 17$$

The value of x depends on the amount of sulfur available and the temperature of reaction but, at 20°C, averages 5 when an amount of sulfur equal to the weight of disulfide is used (5). Organic polysulfides are unstable due to weak S—S bonds (6–12) but they can be shown to be present using NMR spectroscopy (13, 14) (for up to $x = 6$) and by reverse phase HPLC (see ref. 3 for general method) (for up to $x = 17$). In general, it is difficult to isolate organic polysulfides with $x > 3$ since they readily undergo equilibration to smaller polysulfides and sulfur.

Our interest stems from the industrial desire to convert organic polysulfides back to the disulfides and sulfur or to useful sulfur chemicals. This report describes the chemistry that occurs when methyl- and phenylmagnesium halides are contacted with dimethyl polysulfides (DMPS). To our knowledge, no studies on this type of chemistry have been reported. However, it is known that organic disulfides react with organomagnesium compounds to yield sulfides and magnesium thiolates (15–18):

$$R'MgX + RSSR \rightarrow RSR' + RSMgX$$

In similar chemistry, it was reported that organolithium and Grignard reagents cleave the S—S bond of μ-dithiobis-(tricarbonyl)iron (19). Consequently, it was expected that organomagnesium compounds would react readily with DMPS to yield mixtures of sulfides and disulfides and metal thiolates and that the amount of each product type should be dependent on relative reagent stoichiometries.

Experimental

Reagents

With the exception of sulfur, chemicals and solvents were obtained from the Aldrich Chemical Co. Sulfur was obtained from the Shell Canada Ltd. Jumping Pound, Alberta sour gas processing facility and had a purity >99.9%. Tetrahydrofuran (THF) was dried over $LiAlH_4$ and was distilled prior to use.

[1]According to IUPAC nomenclature rules, organic polysulfides are named as polysulfanes. Polysulfides are used throughout this article in keeping with common usage and to be consistent with the organic sulfides described herein.

[2]Author to whom correspondence may be addressed.

Can. J. Chem. Downloaded from www.nrcresearchpress.com by 123.30.183.119 on 09/08/12
For personal use only.

TABLE 1. Reaction of methylmagnesium iodide with dimethylpolysulfides

	$CH_3MgI/CH_3S_xCH_3$ molar ratio					
	3:1		4:1		6:1	
Products	Moles	Mol%[a]	Moles	Mol%[a]	Moles	Mol%[a]
H_2S	0.0495	28.5	0.0246	16.3	0.0139	11.6
CH_3SH	0.0222	12.8	0.0549	36.4	0.0664	55.1
CH_3SCH_3	0.0392	22.7	0.0360	23.9	0.0362	30.0
CH_3SSCH_3	0.0410	23.7	0.0290	19.2	0.00394	3.3
CH_3SSSCH_3	0.0213	12.3	0.0063	4.2	ND	ND
% Sulfur recovery	93.8		93.8		90.1	

[a]As percentage of total number of moles of products.
ND: not detected.

Dimethyl polysulfide preparation

Sulfur (100 g, 0.391 mol) was added to dimethyl disulfide (100 g, 1.042 mol) containing a trace of triethylamine and which had been saturated with H_2S. The mixture was stirred for 1 h or until all of the sulfur had dissolved. By calculation, this procedure gives a mixture of DMPS with an average value of approximately $x = 5$. HPLC analysis (see ref. 3) reveals a mixture of polysulfides with $x = 3 - 8$ as principal components and with $x = 5$ as the most abundant species.

Reactions with methylmagnesium iodide

All operations were conducted under a nitrogen atmosphere. A solution of DMPS (10.4 g, 0.0556 mol) in THF (50 mL) was added dropwise to a stirred solution of methylmagnesium iodide (prepared from iodomethane (24.1 g, 0.169 mol) and magnesium (4.0 g, 0.164 mol) in the usual way) in THF (200 mL) at 20°C. The mixture was stirred for 2 h and was acidified by dropwise addition of 6 M aqueous HCl. Evolved gases were collected in a calibrated gas syringe and were analysed for H_2S and methanethiol using standard gas chromatographic techniques (see below). Organic products were isolated by extraction with *m*-xylene (4 × 50 mL) and the organic extracts were dried ($MgSO_4$) and filtered. *m*-Xylene was chosen to simplify analysis of the volatile products formed in these reactions. Standard analytical transfer techniques were used to ensure that loss of solution was minimized and the final filtrate was diluted with *m*-xylene to a total volume of 250 mL. This solution was analysed for dimethyl sulfide and dimethyl di- and trisulfides (see below).

Gas analysis

Gases evolved during the acidification procedure were quantified using a HP 5890a gas chromatograph equipped with a 3.3 m Poropak N column linked in series to a 3 m Poropak QS column and a thermal conductivity detector. Analyses were carried out isothermally at 80°C.

Solution analyses

Xylene solutions were analysed using a HP 5890 gas chromatograph fitted with a Supelco SPB-5 fused silica capillary column and linked to an HP 5970 mass detector. The initial column temperature was 50°C; this was increased to 250°C at 10°C/min and was held at 250°C for 20 min. Compounds of interest elute before *m*-xylene. Analyses of solutions obtained from experiments with phenylmagnesium bromide (see below) required that the column temperature be raised to a final value of 300°C.

Compound response factors were obtained for both gas and solution analyses by calibration with pure compounds. Results of the analyses for the above experiment and experiments using 0.0417 and 0.0278 mol of DMPS (other reagent quantities were kept constant) are summarized in Table 1. These data are the average results of three experiments conducted for each of the initial quantities of DMPS; variations of ±5 mol% were observed for the data quoted in Tables 1 and 2.

Reactions with phenylmagnesium bromide

These experiments were conducted using procedures very similar to those described for methylmagnesium iodide. Four experiments (performed in triplicate each using 0.0556, 0.0417, 0.0278, and 0.0927 mol of DMPS) were carried out. Organic products were extracted into dichloromethane instead of *m*-xylene and were analysed for dimethyl di- and trisulfide, benzenethiol, methylphenyl sulfide, diphenyl sulfide, methylphenyl disulfide, diphenyl disulfide, and methylphenyl trisulfide. The average data of these experiments are compiled in Table 2. One series of experiments was performed in which the Grignard was added to the polysulfide (Table 2).

Results and discussion

Reactions of DMPS with methyl magnesium iodide

Planning and interpretation of experiments involving the reaction of DMPS with Grignard reagents is complicated by the fact that DMPS containing over three sulfur atoms can be used only as a mixture of compounds. The DMPS used in this study has the average formula $CH_3S_5CH_3$, although, as pointed out in the experimental section, it consists mostly of a range of compounds with three to eight sulfur atoms. It is probable that sulfur atoms other than those bonded to carbon will be the sites of reaction with Grignard reagents. Thus, a 3 mole excess of Grignard reagent should be sufficient to react with the three internal sulfur atoms in a DMPS mixture of average composition $CH_3S_5CH_3$, and produce dimethyl disulfide as the predominant product. Experiments with Grignard to DMPS ratios greater than 3:1 should promote further reaction with the disulfide to produce smaller compounds.

Data from the reaction of DMPS with methylmagnesium iodide at the 3:1 ratio (Table 1) show that after acidification of the reaction mixture H_2S, dimethyl sulfide, and dimethyl disulfide are the major products, along with lesser amounts of methanethiol and the trisulfide. When the relative amount of Grignard reagent was increased (the 4:1 and 6:1 data in Table 1), the quantities of H_2S and dimethyl disulfide formed decreased and methanethiol and dimethyl sulfide became the major products. No dimethyl trisulfide was observed in the 6:1 ratio experiments. These results can be explained by examination of the possible reactions outlined in Scheme 1.

Because DMPS exists as a mixture of compounds, the number of possible reactions is quite large. Scheme 1 only considers reactions up to and with the pentasulfide; reactions with larger polysulfides should follow similar pathways but need not be considered to explain the observations

Can. J. Chem. Downloaded from www.nrcresearchpress.com by 123.30.183.119 on 09/08/12
For personal use only.

TABLE 2. Reaction of phenylmagnesium bromide with dimethylpolysulfides

	$C_6H_5MgBr/CH_3S_xCH_3$ molar ratio							
	3:1		4:1		6:1		1:1[b]	
Products	Moles	Mol%[a]	Moles	Mol%[a]	Moles	Mol%[a]	Moles	Mol%[a]
H_2S	0.0225	11.9	0.0102	5.9	0.00588	4.7	0.00675	8.0
$CH_3S_2CH_3$	0.00579	3.1	0.0046	2.6	ND	ND	0.0136	16.1
$CH_3S_3CH_3$	0.00176	0.9	ND	ND	ND	ND	0.0266[c]	32.5
C_6H_5SH	0.0351	18.7	0.0837	48.0	0.064	50.7	0.00815	9.6
$C_6H_5SCH_3$	0.0740	39.5	0.0677	38.9	0.051	40.5	0.00620	7.3
$C_6H_5SC_6H_5$	0.0021	1.1	0.0029	1.7	0.0041	3.3	ND	ND
$C_6H_5SSCH_3$	0.0265	14.1	0.0039	2.2	ND	ND	0.0104	12.3
$C_6H_5SSC_6H_5$	0.0168	8.9	0.0013	0.7	0.00096	0.8	0.00195	2.3
$C_6H_5SSSCH_3$	0.00336	1.8	ND	ND	ND	ND	0.0101	11.9
% Sulfur recovery	90.5[d]		88[d]		93[d]		98[d]	

[a]As percentage of total number of moles of products.
[b]This experiment was conducted by adding the Grignard solution to the polysulfide.
[c]Includes $CH_3S_4CH_3$. This compound was not detected in the other experiments.
[d]Does not include S_8, which could not be measured accurately.
ND: not detected.

Primary reactions

[1] $CH_3S_5CH_3 + CH_3MgI \longrightarrow CH_3S_xCH_3 + CH_3S_{5-x}MgI$ ($x = 1 - 4$)

[2] $CH_3S_4CH_3 + CH_3MgI \longrightarrow CH_3S_xCH_3 + CH_3S_{4-x}MgI$ ($x = 1 - 3$)

[3] $CH_3S_3CH_3 + CH_3MgI \longrightarrow CH_3S_xCH_3 + CH_3S_{3-x}MgI$ ($x = 1 - 2$)

[4] $CH_3S_2CH_3 + CH_3MgI \longrightarrow CH_3SCH_3 + CH_3SMgI$

Secondary reactions

[5] $CH_3S_4MgI + CH_3MgI \longrightarrow CH_3S_{4-x}CH_3 + (MgI)_2S_x$ ($x = 1 - 3$)

[6] $CH_3S_3MgI + CH_3MgI \longrightarrow CH_3S_{3-x}CH_3 + (MgI)_2S_x$ ($x = 1 - 2$)

[7] $CH_3S_2MgI + CH_3MgI \longrightarrow CH_3SCH_3 + (MgI)_2S$

SCHEME 1. Possible reactions of methylmagnesium iodide with dimethylpolysulfides.

presented in Table 1. Three basic reactions with the pentasulfide are possible (eq. [1] in Scheme 1). Attack of the Grignard reagent at the sulfur adjacent to carbon would lead to dimethyl sulfide and a tetrathiolate. Attack at the next sulfur atom can lead to either a di- or a tetrasulfide and mono- or trithiolates depending on which S—S bond is cleaved. Attack at the central sulfur atom of the pentasulfide leads to the trisulfide and a dithiolate. Similar series of eqs. [2]–[4] can be written for reaction with the tetra-, tri-, and disulfides. Besides these primary reactions, secondary reactions between the produced thiolates and methylmagnesium iodide may occur (eq. [5]–[7] in Scheme 1). In writing these equations, the assumption was made that electron density in the Mg—S bond is polarized to the sulfur atom, thus promoting further reaction of the Grignard reagent with the other sulfur atoms of the thiolates.[3] As can be seen, reactions [5]–[7] produce magnesium sulfides, which on contact with acid would yield H_2S. In addition, these secondary reactions are likely to produce dimethyl sulfide as a final product when excess Grignard reagent is present.

In the initial phases of reaction of methylmagnesium iodide with DMPS, most reaction should be with larger polysulfides (e.g., the pentasulfide) simply because these species are present in the largest concentration. However, based on analysis of final products, it is difficult to decide which sulfur atom of the polysulfides is most susceptible to attack by the Grignard reagent. Regardless of this consideration, all reactions lead to smaller polysulfides, and, if enough Grignard reagent is present, continued reaction should lead to methanethiol (initially as a magnesium thiolate before acidification) and dimethyl sulfide as the major products. In general, this suggestion was confirmed by the observation of increased methanethiol production when high ratios of Grignard reagent to DMPS were used.

Overall, reactions detailed in Scheme 1 explain the type of products observed and the effect of varying the reactant molar ratios. It should be noted that only 90–94% of the sulfur in the reagents could be accounted for in the products (Table 1). Not all of this loss can be accounted for by experimental losses and errors since visual inspection of a typical experiment showed that some elemental sulfur was formed during the acidification stage. Although it was not possible to quantify this elemental sulfur (mostly because of difficulties in recovering it), its formation can be explained by acidification of $(MgI)_2S_x$ ($x > 1$) type species.

Reactions of DMPS with excess phenylmagnesium bromide

Table 2 summarizes the results of experiments in which DMPS was reacted with excess amounts of phenylmagnesium bromide. Other experiments using a deficit of the Grignard and reverse order of reagent addition are described in the following section. A 3:1 molar ratio of Grignard reagent to DMPS gave, after acidification of the

[3]It is assumed that the Mg—S bonds in these compounds are predominantly covalent as is the case for MgS and related compounds.

Can. J. Chem. Downloaded from www.nrcresearchpress.com by 123.30.183.119 on 09/08/12
For personal use only.

Can. J. Chem. Downloaded from www.nrcresearchpress.com by 123.30.183.119 on 09/08/12
For personal use only.

Primary reactions

[8] $CH_3S_5CH_3 + C_6H_5MgBr \longrightarrow CH_3S_xC_6H_5 + CH_3S_{5-x}MgBr$ ($x = 1 - 4$)

[9] $CH_3S_4CH_3 + C_6H_5MgBr \longrightarrow CH_3S_xC_6H_5 + CH_3S_{4-x}MgBr$ ($x = 1 - 3$)

[10] $CH_3S_3CH_3 + C_6H_5MgBr \longrightarrow CH_3S_xC_6H_5 + CH_3S_{3-x}MgBr$ ($x = 1 - 2$)

[11] $CH_3S_2CH_3 + C_6H_5MgBr \longrightarrow CH_3SC_6H_5 + CH_3SMgBr$

Secondary reactions

[12] $C_6H_5S_4CH_3 + C_6H_5MgBr \longrightarrow C_6H_5S_xC_6H_5 + CH_3S_{4-x}MgBr$ ($x = 1 - 3$)

[13] $C_6H_5S_4CH_3 + C_6H_5MgBr \longrightarrow C_6H_5S_xCH_3 + C_6H_5S_{4-x}MgBr$ ($x = 1 - 3$)

[14] $C_6H_5S_3CH_3 + C_6H_5MgBr \longrightarrow C_6H_5S_xC_6H_5 + CH_3S_{3-x}MgBr$ ($x = 1 - 2$)

[15] $C_6H_5S_3CH_3 + C_6H_5MgBr \longrightarrow C_6H_5S_xCH_3 + C_6H_5S_{3-x}MgBr$ ($x = 1 - 2$)

[16] $C_6H_5S_2CH_3 + C_6H_5MgBr \longrightarrow C_6H_5SC_6H_5 + CH_3SMgBr$

[17] $C_6H_5S_2CH_3 + C_6H_5MgBr \longrightarrow C_6H_5SCH_3 + C_6H_5SMgBr$

[18] $CH_3S_4MgBr + C_6H_5MgBr \longrightarrow C_6H_5S_{4-x}CH_3 + (MgBr)_2S_x$ ($x = 1 - 3$)

[19] $CH_3S_3MgBr + C_6H_5MgBr \longrightarrow C_6H_5S_{3-x}CH_3 + (MgBr)_2S_x$ ($x = 1 - 2$)

[20] $CH_3S_2MgBr + C_6H_5MgBr \longrightarrow C_6H_5SCH_3 + (MgBr)_2S$

[21] $CH_3S_xMgBr + C_6H_5S_yCH_3 \longrightarrow CH_3S_nCH_3 + C_6H_5S_mMgBr$ ($x + y = n + m$)

SCHEME 2. Possible reactions of phenylmagnesium bromide with dimethylpolysulfides.

reaction mixture, phenylmethyl sulfide as the major product along with phenylmethyl di- and trisulfides, benzenethiol, and H_2S in lesser quantities. Smaller amounts of diphenyl disulfide, phenylmethyl disulfide, and dimethyl di- and trisulfide were also detected. Higher ratios of Grignard reagent to DMPS (4:1 and 6:1) resulted in benzenethiol and phenylmethyl sulfide as the major products (50.7 and 40.5 mol% respectively). Other products such as H_2S were observed only in minor quantities when a 6:1 Grignard/DMPS ratio was used. As in reactions between DMPS and methylmagnesium iodide, small amounts of elemental sulfur were detected but we could not quantify this product accurately. However, since most of the sulfur added as DMPS was recovered in the organic products (88–93%, see Table 2), it is clear that elemental sulfur was a minor product. Interestingly, no methanethiol was produced in the reactions of DMPS with phenylmagnesium bromide.

Scheme 2 summarizes the possible reactions of phenylmagnesium bromide with polysulfides containing up to five sulfur atoms. Again, it should be remembered that the DMPS mixtures used in these experiments contained polysulfides with more than five sulfur atoms, but their reactions are not considered in detail because they should lead to the same products as the smaller polysulfides. As was the case in reactions with methylmagnesium iodide, it is conceivable that phenylmagnesium bromide may react with the pentasulfide at three different sulfur atoms (reaction [8] in Scheme 2) and that one of these reactions could yield phenylmethyl di- or tetrasulfide depending on which S—S bond is cleaved. However, since methanethiol was not observed in any of the reactions with phenylmagnesium bromide, it can be argued that reaction at the second sulfur atom always results in cleavage of the internal S—S bond to yield phenylmethyl disulfide and a methyl trithiolate species. It is not certain why internal S—S bond cleavage is favored although the disulfide formed in this reaction should be more stable than the tetrasulfide that would be formed from cleavage of the other S—S bond. One possibility is that methanethiolate product is formed but is consumed in subsequent reactions. Although this possibility cannot be discounted for reactions using a 3:1 Grignard to DMPS ratio, it seems probable that some methanethiol should have been formed in experiments using greater quantities of Grignard reagent. However, this was not the case.

Other primary reactions with smaller polysulfides, [9]–[11], should follow similar pathways (Scheme 2). However, once again it can be argued that reactions that would produce methanethiolate product did not occur because methanethiol was not observed on acidification of the reaction mixtures. In addition, reaction [11] is unlikely because only a trace of the disulfide was present in the initial DMPS mixture. Overall, reactions that produced phenylmethyl sulfide must have predominated as this was the major product observed at all Grignard to DMPS ratios (Table 2).

Because the primary reactions produce phenylmethyl polysulfides, more secondary processes (see Scheme 2) are possible with the phenyl-Grignard than was possible with the methyl-Grignard. Each of the sulfur atoms in these mixed polysulfides is chemically distinct. Thus, phenylmethyl tetrasulfide can react with phenylmagnesium bromide in six reactions, summarized by [12] and [13], which can yield different products depending on which S—S bond is broken. Similar reactions, [14]–[17], for the phenylmethyl tri- and disulfide can be written (Scheme 2), and explain the array of products noted in these reactions. As before, reactions leading to magnesium methylthiolate and hence methanethiol likely do not occur. Another series of secondary reactions with magnesium methyl polythiolates, CH_3S_xMgBr ($x = 2 - 4$), are also possible ([18]–[20] in Scheme 2). These reactions produce sulfides, which on acidification yield H_2S. Other reactions, not shown in Scheme 2, involving magnesium phenyl polythiolates formed in the secondary reactions of phenylmethyl polysulfides, are also possible.

Some of the secondary reactions can be used to explain why benzenethiol becomes a major product when excess phenylmagnesium bromide is present. In this regard, reactions [16] and [17] are of particular interest although related reactions occur in the series of reactions represented by [13] and [15]. Reaction [16] results in the formation of magnesium methylthiolate and reaction [17] produces magnesium phenylthiolate (which yields benzenethiol on acidification). The fact that benzenethiol was the predominant product suggests that the phenylthiolate species is more stable than the methyl counterpart. Presumably, this stabilization is based on the ability of the aromatic ring to delocalize electron density. The same arguments can be applied to the series

of reactions [13] and [15] and explain why phenylmethyl sulfide is formed in much greater amounts than diphenyl sulfide. In general, it is probable that attack of a phenyl Grignard reagent on a polysulfide will occur to produce the thiolates that can be stabilized by the aromatic ring.

Reactions of DMPS with a limited supply of phenylmagnesium bromide[4]

Experiments described above were designed to consume all of the polysulfide sulfur and so produce small organosulfur compounds. However, by using a limited amount of Grignard reagent, it should be possible to determine which sulfur atoms of the polysulfides are most reactive. Consequently, some experiments were conducted using a 1:1 molar ratio of DMPS to phenylmagnesium bromide (Table 2). Thus, remembering that the DMPS used in this study has the average molecular formula $CH_3S_5CH_3$ and that the three internal sulfur atoms are likely to be the most reactive, the actual ratio of "reactive sulfur" to Grignard is 3:1. In addition, the Grignard reagent was added dropwise to the polysulfide to ensure that it was present as the limiting reagent.

Data from these experiments show (Table 2) that methylphenyl di- and trisulfide were the major products (formed in almost equimolar amounts), along with lesser quantities of methylphenyl sulfide and benzenethiol. Unchanged DMPS was also detected in the reaction products. If we consider reaction of the phenyl Grignard with dimethyl pentasulfide (reaction [8] in Scheme 2) from a purely statistical viewpoint, twice as much phenylmethyl sulfide and disulfide should be produced in comparison to the trisulfide. Consequently, the data obtained infer that the central sulfur atom of the pentasulfide is the most reactive towards phenylmagnesium bromide and that the two sulfur atoms adjacent to the central one are the next most reactive. Clearly, attack of the sulfur atoms bonded to carbon is least favored. The observation of some benzenethiol and H_2S indicates that reactions were not limited entirely to primary reactions. In addition, reactions of type [21] could alter the distribution of the products observed. Overall, it is difficult to make a definitive statement on the relative reactivity of the polysulfide sulfur atoms, but the results obtained do suggest that the central and internal sulfur atoms are most reactive towards Grignard reagents.

Lastly, it should be noted that in the reaction of DMPS with either methyl- or phenyl-Grignard reagents, no evidence for attack of the Grignard at the carbon atoms of polysulfides or product organic sulfides was found. This in accord with other work that has shown that aliphatic sulfides are inert to Grignard reagents (20). The only exception to these findings appears to be the production of allylbenzene and phenylthiomagnesium bromide from the reaction of phenylallyl sulfide with phenylmagnesium bromide (21).

[4]We are indebted to a reviewer for suggesting these experiments.

Acknowledgments

The authors wish to thank the Natural Sciences and Engineering Research Council of Canada and Alberta Sulphur Research Ltd. for financial support of this project.

1. E. E. Reid. Organic chemistry of bivalent sulfur. Vol. III. Chemical Publishing Co., New York, NY. 1960. p. 387.
2. S. P. Sharp and L. F. Sudduth. U.S. Patent No. 3,846,311 (1974).
3. P. D. Clark, K. L. Lesage, and P. Sarkar. Energy Fuels, **3**, 315 (1990).
4. G. Henri and D. Yves. European Patent No. 269,517 A1 (1987).
5. P. D. Clark. Preprints of Sulphur 88, The British Sulphur Corporation, London. (1988). p. 257. (ISBN 0-902777-87-4).
6. D. Twiss. J. Am. Chem. Soc. **49**, 493 (1927).
7. S. O. Jones and E. E. Reid. J. Am. Chem. Soc. **60**, 2452 (1938).
8. G. F. Bloomfield. J. Chem. Soc. 1547 (1947).
9. R. C. Fuson, C. C. Price, D. M. Burness, R. E. Foster, W. R. Hatchard, and R. D. Lipscomb. J. Org. Chem. **11**, 487 (1946).
10. E. N. Guryanova, V. N. Vasilyeva, and L. S. Kuzina. Rubber Chem. Technol. **29**, 534 (1956).
11. I. Kende, T. L. Pickering, and A. V. Tobolsky. J. Am. Chem. Soc. **87**, 5582 (1965).
12. R. S. Laitenen, T. A. Pakkanen, and R. Steudel. J. Am. Chem. Soc. **109**, 710 (1987).
13. D. Grant and J. R. Van Wazer. J. Am. Chem. Soc. **86**, 1450 and 3012 (1964).
14. T. L. Pickering, K. J. Saunders, and A. V. Tobolsky. J. Am. Chem. Soc. **89**, 2364 (1967).
15. H. Wuyts. Bull. Soc. Chim. Fr. 166 (1906).
16. J. de Lattre. Bull. Soc. Chim. Belg. **26**, 323 (1912).
17. A. J. Parker and N. Kharasch. Chem. Rev. **59**, 583 (1959).
18. N. Kharasch and O. Reinmuth. *In* Grignard reactions of nonmetallic substances. Prentice-Hall, New York, NY. (1954). p. 1301.
19. D. Seyferth, R. S. Henderson, L.-C. Song, and G. B. Womack. J. Organomet. Chem. **9**, 292 (1985).
20. H. Gilman and J. B. Shumaker. J. Am. Chem. Soc. **47**, 514 (1925).
21. A. Luttringhaus, G. von Wagner-von Saaf, E. Sucker, and G. Borth. Justus Liebigs Ann. Chem. **557**, 46 (1945).

Can. J. Chem. Downloaded from www.nrcresearchpress.com by 123.30.183.119 on 09/08/12
For personal use only.

Molecular dynamics simulation of interhalogen compounds. 1. Liquid chlorine trifluoride (ClF_3): structure and thermodynamics

RAMESH K. WADI[1] AND VIVEK SAXENA
Department of Chemistry, University of Delhi, Delhi-110 007, India

Received June 5, 1991

RAMESH K. WADI and VIVEK SAXENA. Can. J. Chem. **70**, 34 (1992).

The results of a molecular dynamics (MD) simulation study of liquid chlorine trifluoride (ClF_3) at 217, 260, and 287 K are reported. The cubic simulation cell consists of 108 ClF_3 molecules assumed to be interacting via site–site Lennard–Jones 12–6 pair potential. The parameters for F–F and Cl–Cl interaction are the same as used for the simulation of F_2 and Cl_2, respectively, and those for the Cl–F cross interaction are calculated using Lorentz–Berthelot rules. These results are then used to calculate various radial distribution functions characteristic of the liquid structure. Thermodynamic properties, namely, configurational energy, constant volume specific heat, and internal pressure are also reported. The time-dependent properties, mean square force and torque, self diffusion coefficient, and the quantum corrections to the free energy, were also obtained. The dimer configuration drawn based on the observed contact distances was found to be in good agreement with the results of matrix isolation infrared and laser Raman spectroscopic studies.

Key words: MD simulation, interhalogens, liquid structure, thermodynamic properties.

RAMESH K. WADI et VIVEK SAXENA. Can. J. Chem. **70**, 34 (1992).

On a effectué une simulation par dynamique moléculaire du trifluorure de chlore liquide (ClF_3) à 217, 260 et 287 K. La cellule cubique de simulation comporte 108 molécules de ClF_3 qui interagiraient par potentiel de paires site–site 12–6 de Lennard–Jones. Les paramètres pour l'interaction F–F et Cl–Cl sont les mémes que ceux utilisés respectivement pour F_2 et Cl_2 alors que ceux pour l'interaction croisée Cl–F a été calculée à l'aide des règles de Lorentz–Berthelot. On utilise alors ces résultats pour calculer diverses fonctions de distributions radiales caractéristiques de la structure liquide. On rapporte aussi les propriétés thermodynamiques, soit l'énergie de configuration, la chaleur spécifique à volume constant et la pression interne. On a aussi déterminé les propriétés qui varient avec le temps, soit la force et le moment de torsion quadratique moyen, le coefficient d'autodiffusion et les corrections quantiques à l'énergie libre. On a trouvé que la configuration du dimère tracée en se basant sur les distances de contact observées est en bon accord avec les résultats des études par spectroscopie infrarouge et Raman réalisées avec des matrices isolées.

Mots clés : simulation par dynamique moléculaire, interhalogènes, structure liquide, propriétés thermodynamiques.
[Traduit par la rédaction]

Introduction

The list of molecular liquids studied by molecular dynamics (MD) computer simulation is fairly large (1). The major aim of such studies has been to test the adequacy of the proposed potentials and (or) the algorithms used and to obtain the thermodynamic and time-dependent properties, which may be experimentally determinable or even inaccessible. The studies have contributed significantly to the development of the theories of molecular interaction in the condensed state. MD simulations of the relatively simple liquid halogens have been reported by Singer *et al.* (2) using a "2-Lennard–Jones centers" pair potential and were found to reproduce their thermodynamic properties quite well. Further, Rodger, Stone, and Tildesley (3, 4) suggested an anisotropic atom–atom pair potential for molecular chlorine and studied its predictions for a wide range of properties of the crystalline and liquid states. Simulation of liquid hydrogen chloride, quite a complicated system due to H-bonding, required modifications of the usual Lennard–Jones 12–6 parameters. Interhalogens (viz., ClF, ClF_3, ClF_5, BrF_3, BrF_5, etc.) also form an interesting class of compounds as these are not as simple as halogens and not as complex as hydrogen chloride. The price to be paid to simulate with more sophisticated models is heavy computational cost. It is therefore natural that simple models should be fully exploited before they are abandoned in favour of more complicated ones. As most of these compounds are very reactive, hence difficult to purify and manipulate in the pure state, few experimental data are available for comparison purposes. We have started a systematic computer simulation study of the interhalogens with two aims: (*i*) to determine whether the potentials used for the simulation of halogens in the liquid state can also be used for the simulation of the interhalogens and (*ii*) to motivate experimentalists to further study this important class of liquids to determine their diffraction properties, equation of state, self-diffusion coefficients, etc.

In this paper we report the results of MD simulation of liquid ClF_3 at three average temperatures, 217 K, 260 K, and 287 K, so as to have an idea about the temperature variation of its properties in the liquid state. Gas phase microwave (5) and solid state X-ray diffraction studies (6) show that the ClF_3 molecule has a planar distorted "T" structure of C_{2v} symmetry, with the bond lengths and angles depicted in Fig. 1. On the basis of the results from the laser Raman spectroscopic study of ClF_3, Drifford *et al.* (7) suggested the presence of dimers in the liquid state. Evidence of dimers existing in the liquid state has also come from the IR spectra of ClF_3 in argon matrix (8). Though among the theoretical studies, quantum mechanical calculations have been reported for some of the interhalogens, the present work appears to be the first report of their computer simulation study.

Method

All calculations were carried out using the MDPOLY (9) program developed by Thompson, for a microcanonical ensemble of a system of 108 ClF_3 molecules in a cubic box satisfying the densities ρ given in Table 1 and using periodic boundary conditions to avoid surface effects. These

[1]Author to whom correspondence may be addressed.

Printed in Canada / Imprimé au Canada

Can. J. Chem. Downloaded from www.nrcresearchpress.com by 123.30.183.119 on 09/08/12
For personal use only.

TABLE 1. Average thermodynamic properties of liquid chlorine trifluoride

T (K)	ρ (g cm^{-3})	U (kJ mol^{-1})	v (kJ mol^{-1})	$P/\rho KT$	C_v (J mol^{-1} K^{-1})	γ (bar K^{-1})[a]
217.0	2.052	−21.28	−15.58	3.878	26.15	19.14
259.7	1.954	−19.77	−15.49	3.400	25.70	12.54
286.6	1.809	−18.08	−4.56	1.642	25.77	12.84

[a]1 bar = 100 kPa.;

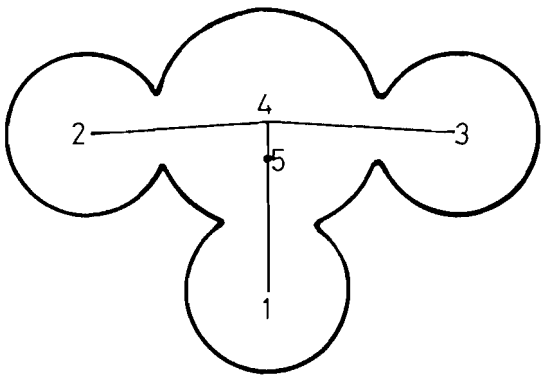

FIG. 1. Chlorine trifluoride molecule; sites 1, 2, and 3 represent fluorine; 4, chlorine, and 5, the centre of mass. Various distances and angles are $r_{24} = r_{34} = 1.698$ Å, $r_{14} = 1.598$ Å, $r_{45} = 0.36$ Å, and ∠ 142 = ∠ 143 = 87° 28′.

molecules were assumed to interact via a Lennard–Jones 12–6 site–site pair potential. The structure of the ClF_3 molecule as given in Fig. 1 was used and kept rigid during the simulation. The equations of motion were integrated by the predictor–corrector scheme of the second order; orientations of the molecules were expressed in terms of quaternions. At least 1000–1500 time steps, each corresponding to 7.5 fs, were required for the equilibration until the fluctuations in the total energy were reduced to about 0.001%. The statistics were then collected over 4000 steps of the production phase. The algorithm of the simulation has been well described by Allen and Tildesley (10).

The potential energy U of the system, assumed to be the sum of the pairwise interactions $u_{ab}(r_{ab})$ from the site a in molecule i at position r_{ia} and the site b in the molecule j at the position r_{jb}, can be represented as

$$[1a] \quad U = \sum_{i<j}\sum \sum_a \sum_b u_{ab}(r_{ab}) \qquad \text{for} \quad r_{ab} \le r_c$$

$$[1b] \quad = 0 \qquad \text{for} \quad r_{ab} > r_c$$

where r_c is the potential truncation distance and, in the present case, half of the box length,

$$r_{ab} = |r_{ia} - r_{jb}|$$

and

$$u_{ab}(r_{ab}) = 4\epsilon_{ab}\{(\sigma_{ab}/r_{ab})^{12} - (\sigma_{ab}/r_{ab})^{8}\}$$

σ_{ab} and ϵ_{ab} are obtained according to Lorentz–Berthelot rules: $\sigma_{ab} = (\sigma_{aa} + \sigma_{bb})/2$ and $\epsilon_{ab} = \sqrt{\epsilon_{aa}\epsilon_{bb}}$. The Lennard–Jones site–site potential parameters used in the simulation are $\sigma_{F-F} = 2.83$ Å, $\epsilon_{F-F} = 52.8$ K, $\sigma_{Cl-Cl} = 3.35$ Å, and $\epsilon_{Cl-Cl} = 173.5$ K (2).

The long-range corrections made to the virial sum v and the potential energy U assuming $g(r) = 1$ for $r_{ab} > r_c$ are

$$[2] \quad T_v = -(2/3)\pi N\, d \int_r^\infty r^2 v(r)\, dr$$

and

$$[3] \quad T_u = 2\pi N\, d \int_r^\infty r^2 u(r)\, dr$$

where d is the number density, N is the number of molecules in the system, and $v(r)$ is the virial function.

The schemes for the calculation of thermodynamic and other properties are described elsewhere (10). The self-diffusion coefficient D is calculated from the mean square displacement MSD(t), as it is linearly related to the diffusion coefficient by the corresponding Einstein equation

$$[4] \quad 2\,t\,D = (1/3)\,\mathrm{MSD}(t)$$

valid at sufficiently long times. D is then calculated as 1/6th of the slope of the MSD(t) line.

Results and discussion

The molecular trajectories obtained during the simulation run were simultaneously used to calculate the com–com (center of mass) and the various site–site radial distribution functions (rdf's) describing the gross structural features of liquid chlorine trifluoride at the three temperatures studied (Fig. 2). With rise in temperature the heights of these peaks can in general be seen to be reduced, and at longer r values the curves tend to flatten to $g(r) = 1$. The coordination number n_0 of the first shell around a moiety (a molecule or a site) was obtained by integration of the function $r^2g(r)$ up to the first minimum in the $g(r)$. The position r_{max} of the first maximum in the $g(r)$ was taken to be the most probable distance between the two moieties. These r_{max} and n_0 are collected in Table 2. Further examination of these rdf curves reveals the closest contact distances. The distance of closest approach of the sites is obtained as the intercept on the abcissa. These distances were 2.5 and 2.8 Å for F–F and Cl–F as compared to 2.8 and 3.06 Å, respectively, found in the crystals (6). Using these distances it is possible to visualize geometrically the positions in which a pair of molecules is likely to be found. Two such dimer configurations are shown in Fig. 3. The configuration of Fig. 3(a) matches well with the one derived from the IR spectral study of ClF_3 in argon matrix (6). In these dimers the molecules are assumed to lie in the molecular plane. As derived in the microwave study

Can. J. Chem. Downloaded from www.nrcresearchpress.com by 123.30.183.119 on 09/08/12
For personal use only.

Can. J. Chem. Downloaded from www.nrcresearchpress.com by 123.30.183.119 on 09/08/12
For personal use only.

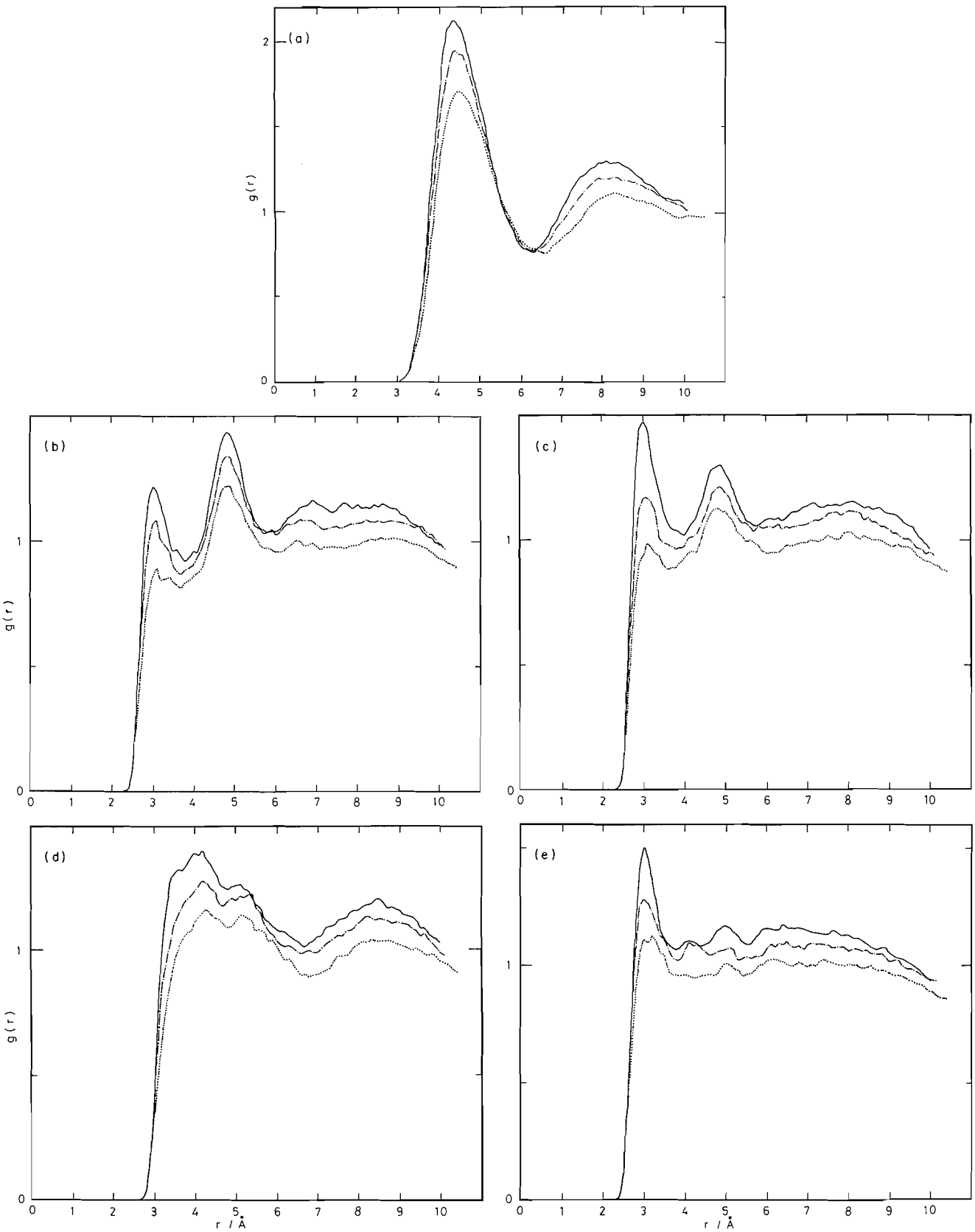

FIG. 2. Radial distribution function: (———) 217 K, (—·—·—) 260 K, (·····) 287 K. (a) 5–5; (b) 1–1; (c) 1–2; (d) 1–4; (e) 2–2; (f) 2–4; (g) 4–4. These numbers denote the sites as marked in Fig. 1.

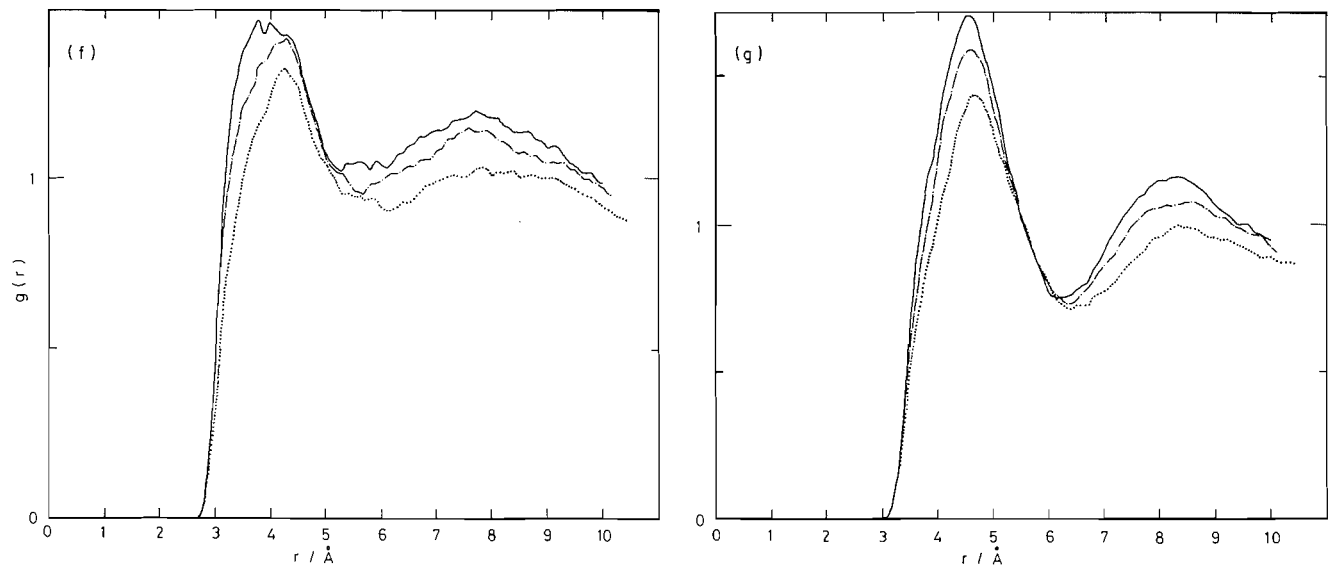

FIG. 2 (*concluded*)

TABLE 2. Position r_{max} of the first maximum in the $g(r)$ and the coordination number n_0 of the first shell around the moiety for liquid chlorine trifluoride at different temperatures

	217.0 K		259.7 K		286.6 K	
$g(r)^a$	r_{max} (Å)	n_0	r_{max} (Å)	n_0	r_{max} (Å)	n_0
5-5	4.3	13.19	4.4	12.68	4.5	13.31
1-1	3.0	1.92	3.1	1.56	3.1	1.36
1-2	3.0	2.46	3.1	1.93	3.1	1.49
1-4	4.2	5.83	4.2	4.48	4.2	4.76
2-2	3.0	2.22	3.0	2.12	3.1	2.80
2-4	3.8	7.56	4.3	9.02	4.3	10.27
4-4	4.5	12.74	4.6	12.70	4.7	11.86

[a]The numbers denote the sites as in Fig. 1.

TABLE 3. Time-dependent properties of liquid chlorine trifluoride

T (K)	$\langle F^2 \rangle$ (10^{-20} (J/m)^2)	$\langle \Gamma_i \rangle$ (10^{-40} J^2)	Q_c (K)	D (10^{-5} cm^2 s^{-1})
217.0	16.495	2.1396(*XX*)	0.0732	5.77
		8.9803(*YY*)		
		8.5983(*ZZ*)		
259.7	19.734	2.9946(*XX*)	0.0598	7.30
		10.2890(*YY*)		
		9.9870(*ZZ*)		
286.6	17.722	2.7728(*XX*)	0.0444	13.60
		9.3851(*YY*)		
		8.8276(*ZZ*)		

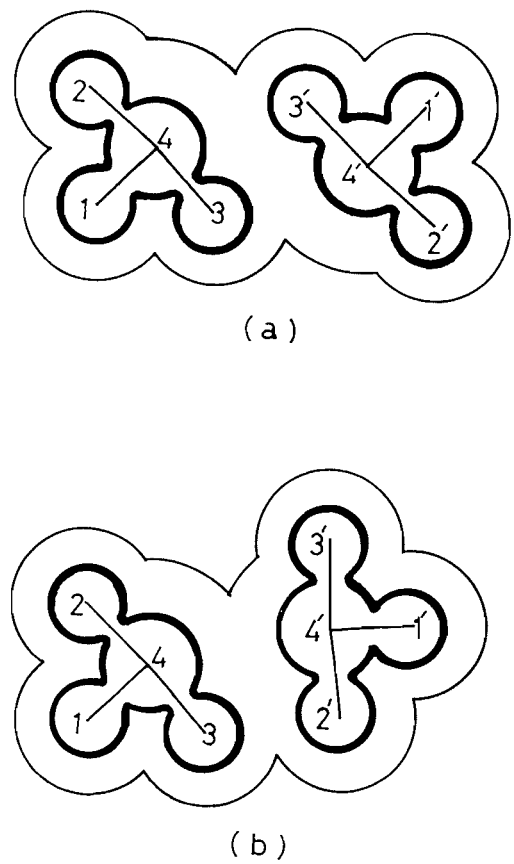

FIG. 3. Two possibilities of the closest approach of a pair of ClF_3 molecules derived from the rdf curves.

(3), the two lone pairs of electrons in the ClF_3 molecule lie above and below the plane of the molecule, thus reducing the chances of association from the two sides of the molecular plane in order to have the least interaction between the lone pairs.

Due to the fact that the nonbonded interactions among the halogens, except fluorine, show a characteristic feature of strong exchange interaction, anomalously shortened contact distances have been observed (11), indicating the existence of specific molecular interactions. The specific interaction described above results in shortened closest contact r_{ij} between the atoms of different molecules if $r_{ij} < (R_i + R_j - \delta)$ or $r_{ij} < 2\sqrt{R_i \cdot R_j} - \delta$, where R_i are the van der Waals radii and δ is the overlap of these spheres of atoms i and j. For a

Can. J. Chem. Downloaded from www.nrcresearchpress.com by 123.30.183.119 on 09/08/12
For personal use only.

normal contact δ is 0.15 Å for contacts between nonhydrogen atoms and 0.30 Å where one of the two atoms is hydrogen (11). Considering R_F = 1.35 Å and R_{Cl} = 1.8 Å, $R_i + r_j - \delta$ values are 2.55, 3.45, and 3.0 Å for F–F, Cl–Cl, and Cl–F, respectively. The corresponding r_{ij}(obs) values are 2.4, 3.2, and 2.8 Å, well in agreement with the above results.

The thermodynamic averages of the configurational energy U, the virial ν, the compressibilities $P/\rho KT$, constant volume specific heat C_v, and the thermal pressure coefficient γ, calculated over 4000 time steps for three average temperatures 217 K, 260 K, and 287 K, are listed in Table 1. Values for the mean squared force $\langle F^2 \rangle$ and torque $\langle \Gamma_i \rangle$ about the axis i, quantum corrections Q_c to the Helmholtz free energy, and the self-diffusion coefficients D are summarized in Table 3. The experimental data are unfortunately not available for comparison.

Acknowledgement

Liberal allocation of CPU time on the Zenith ENCORE mini-computer by the Delhi University Computer Centre and financial assistance from the CSIR, New Delhi, to V.S. are gratefully acknowledged.

1. Newsletters (1984–1989) of the CCP5 of SERC Daresbury Laboratory, Warrington WA4 4AD, U.K.
2. K. Singer, A. Taylor, and J. V. L. Singer. Mol. Phys. **33**, 1757 (1977).
3. P. M. Rodger, A. J. Stone, and D. J. Tildesley. J. Chem. Soc. Faraday Trans. 2, **83**, 1689 (1987).
4. P. M. Rodger, A. J. Stone, and D. J. Tildesley. Mol. Phys. **63**, 173 (1988).
5. D. F. Smith. J. Chem. Phys. **21**, 602 (1953).
6. R. D. Burbank and F. N. Bensey. J. Chem. Phys. **21**, 609 (1953).
7. M. Drifford, D. Martin, and R. Bongon. Rev. Chim. Miner. **7**, 1069 (1971).
8. R. A. Frey, R. L. Redington, and A. L. K. Aljibury. J. Chem. Phys. **54**, 344 (1971).
9. S. M. Thompson. MDPOLY. Daresbury Laboratory, Daresbury, Warrington WA4 4AD, England.
10. M. P. Allen and D. J. Tildesley. *In* Computer simulation of liquids. Clarenden Press, Oxford. 1987.
11. Yu. V. Zefirov and P. M. Zorkii. Russ. Chem. Rev. **58**, 421 (1989).

Can. J. Chem. Downloaded from www.nrcresearchpress.com by 123.30.183.119 on 09/08/12
For personal use only.

Kinetics of electron-transfer reactions of the $Co(bpyO_2)_3^{2+/3+}$ couple in acetonitrile

DONAL H. MACARTNEY[1] AND SAMUEL MAK
Department of Chemistry, Queen's University, Kingston, Ont., Canada K7L 3N6

Received June 25, 1991

DONAL H. MACARTNEY and SAMUEL MAK. Can. J. Chem. **70**, 39 (1992).

The kinetics of the outer-sphere electron transfer reactions of tris(1,1′-dioxo-2,2′-bipyridine)cobalt(II) and (III) with a series of nickel polyaza macrocycles, FeL_3^{n+} and OsL_3^{2+} complexes (L is 2,2′-bipyridine or 1,10-phenanthroline, and substituted derivatives), and $Rh_2(O_2CCH_3)_4(CH_3CN)_2^+$ have been investigated in acetonitrile at 25.0°C. An application of the Marcus theory relationship to the cross-reaction rate constants yielded apparent $Co(bpyO_2)_3^{2+/3+}$ self-exchange rate constants of 10^2 M^{-1} s^{-1} from the nickel macrocycle cross-reactions and 10^{-1} M^{-1} s^{-1} from the cross-reactions with the metal polypyridine complexes. The latter cross-reactions are considered to be non-adiabatic due to a mismatch in the donor/acceptor orbital symmetries. The electron exchange rate constant is compared with the exchange rate constants for other Co(II)/Co(III) complex couples and $M(bpyO_2)_3^{2+/3+}$ couples of other first-row transition metals, and discussed in terms of inner-sphere and solvent reorganization barriers.

Key words: electron transfer, Marcus theory relationship, cobalt(II)/(III) couples, 1,1′-dioxo-2,2′-bipyridine.

DONAL H. MACARTNEY et SAMUEL MAK. Can. J. Chem. **70**, 39 (1992).

Opérant en solution dans l'acétonitrile, à une température de 25°C, on a étudié la cinétique des réactions de transferts d'électrons de la sphère extérieure des tris(1,1′-dioxo-2,2′-biypridine)cobalt(II) ou (III) avec une série de macrocycles polyazotés de nickel, de complexes FeL_3^{n+} et OsL_3^{2+} (L = 2,2′-bipyridine ou 1,10-phénanthroline ainsi que leurs dérivés substitués) et du $Rh(O_2CCH_3)_4(CH_3CN)_2^+$. Une application de la relation de la théorie de Marcus aux sections efficaces des constantes de vitesse a permis d'évaluer les constantes de vitesse d'auto-échange apparentes du $Co(bpyO_2)_3^{2+/3+}$; en se basant sur les sections efficaces du nickel impliqué avec le macrocycle, cette valeur est égale à 10^2 M^{-1} s^{-1} alors qu'elle serait égale à 10^1 M^{-1} s^{-1} sur la base des sections efficaces des complexes métalliques de la polypyridine. On considère que ces dernières sections efficaces sont non-adiabatiques à cause du manque de similitude entre les symétries des orbitales donneur/accepteur. On a comparé la constante de vitesse de la réaction d'échange d'électrons avec celles d'autres couples de complexes Co(II)/Co(III) et d'autres couples $M(bpyO_2)_2^{2+/3+}$ d'autres métaux de transition de la première rangée et on en discute en fonction de la couche interne et des barrières à la réorganisation du solvant.

Mots clés : transfert d'électron, relation de la théorie de Marcus, couples cobalt (II)/cobalt (III), 1,1′-dioxo-2,2′-bipyridine.

[Traduit par la rédaction]

Introduction

The relationship between the bimolecular electron self-exchange rate constants (k_{11}) for transition metal complex couples and the nature of the donor–acceptor orbitals ($d\pi$ or $d\sigma^*$) has been demonstrated through both experimental and theoretical investigations (1, 2). Relatively slow electron exchange rate constants are found for couples in which the transferring electron resides in an antibonding $d\sigma^*$ (e_g in octahedral symmetry), and substantial reorganization of the metal–ligand bond distances is required prior to electron exchange. Electron exchange in the majority of Co(II)/Co(III) complex couples involves a transfer of an electron between a high-spin $t_{2g}^5 e_g^{*2}$ Co(II) state and a low-spin $t_{2g}^6 e_g^{*0}$ Co(III) state (3). The self-exchange rate constants for the couples $Co(NH_3)_6^{2+/3+}$, $Co(en)_3^{2+/3+}$ (en = 1,2-diaminoethane), $Co(sep)^{2+/3+}$ (sep = 1,3,6,8,10,13,16,19-octaazabicyclo[6.6.6]eicosane), $Co(phen)_3^{2+/3+}$ (phen = 1,10-phenanthroline) are $\geq 10^{-7}$ M^{-1} s^{-1} (25°C) (4), 7.7×10^{-5} (25°C, I = 0.98 M) (5), 5.0 (25.0°C, I = 0.2 M) (6), and 12 M^{-1} s^{-1} (25°C, I = 0.10 M) (7), respectively.

With strong-field cyclic polythiaether ligands the cobalt(II) center is found in a low-spin $t_{2g}^6 e_g^{*1}$ electronic configuration and the reduction in the inner-sphere reorganization barrier results in a more rapid electron exchange. The electron self-exchange rate constant for the $Co([9]aneS_3)_2^{2+/3+}$ couple ([9]aneS$_3$ = 1,4,7-trithiacyclononane), for example, is 9.5×10^4 M^{-1} s^{-1} (25.0°C, I = 0.1 M) (5), while for the analogous $Co([9]aneN_3)_2^{2+/3+}$ couple ([9]aneN$_3$ = 1,4,7-triazacyclononane), involving a high-spin $Co([9]aneN_3)_2^{2+}$ species, $k_{11} = 8 \times 10^{-2}$ M^{-1} s^{-1} (25.0°C, I = 1.0 M) (8). Self-exchange rate constants in the range of 45–640 M^{-1} s^{-1} have also been determined for a series of low-spin $Co\{(dioxime)_3(BF)_2\}^{0/+}$ couples in acetonitrile (9).

The ligand 1,1′-dioxo-2,2′-bipyridine ($bpyO_2$) complexes a variety of transition metal ions (10–14), including cobalt(II) and cobalt(III) (10, 11, 13). This bidentate oxygen donor ligand forms a puckered seven-membered ring when coordinated to metal ion.

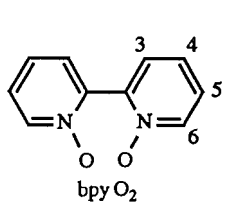

bpy O_2

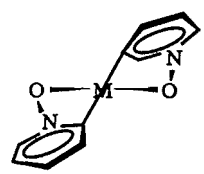

For the past several years, investigations concerning the kinetics of electron transfer reactions of $M(bpyO_2)_3^{2+/3+}$ complex couples of cobalt, nickel, manganese, and iron have been carried out in our laboratory (15, 16). One aim of this work has been to compare the electron transfer behaviour of these complexes with that the analogous tris(2,2′-bipyridine) couples of these first-row transition metals. The *N*-oxidation of the 2,2′-bipyridine ligand results in a change of the donor atom, a weakening of the ligand field, and changes in the ligand π^*-metal t_{2g} overlap interactions.

[1]Author to whom correspondence may be addressed.

Can. J. Chem. Downloaded from www.nrcresearchpress.com by 123.30.183.119 on 09/08/12
For personal use only.

Can. J. Chem. Downloaded from www.nrcresearchpress.com by 123.30.183.119 on 09/08/12
For personal use only.

In this paper we report the results of a kinetic study of the electron transfer reactions of $Co(bpyO_2)_3^{2+}$ and $Co(bpyO_2)_3^{3+}$ with a series of well-characterized nickel(III) polyaza macrocyclic complexes, FeL_3^{n+} and OsL_3^{2+} complexes (L is 2,2′-bipyridine or 1,10-phenanthroline, or substituted derivatives), and $Rh_2(O_2CCH_3)_4(CH_3CN)_2^+$, in acetonitrile containing 0.10 M tetraethylammonium perchlorate. The cross-reaction kinetic data are correlated in terms of the relationship from the Marcus theory (17), and the apparent self-exchange rate constant for the $Co(bpyO_2)_3^{2+/3+}$ couple in this medium has been estimated. The electron exchange rate constant for this couple is compared with those of other Co(II)/Co(III) complex couples and analogous $M(bpyO_2)_3^{2+/3+}$ couples, and discussed in terms of the inner- and outer-sphere barriers to electron exchange.

Experimental

Materials

Acetonitrile (BDH, OmniSolv) was used as received or dried with anhydrous sodium sulphate, filtered, and distilled from calcium hydride. The ligand 1,1′-dioxo-2,2′-bipyridine ($bpyO_2$) was prepared by a published method (11). ^1H NMR (CD_3CN) δ: 7.66 (d of d, 2H, H6), 7.02 (d of d, 2H, H3), 6.88 (t of d, 2H, H4), 6.85 (t of d, 2H, H5) with $J_{3,4}$ = 6.9 Hz, $J_{3,5}$ = 2.8 Hz, $J_{3,6}$ = 0.8 Hz, $J_{4,5}$ = 7.7 Hz, $J_{4,6}$ = 1.7 Hz, and $J_{5,6}$ = 5.9 Hz. Tris(1,1′-dioxo-2,2′-bipyridine)cobalt(II) perchlorate, $[Co(bpyO_2)_3](ClO_4)_2 \cdot 2H_2O$, was prepared from $Co(ClO_4)_2 \cdot 6H_2O$ (Alfa) and $bpyO_2$ in hot aqueous solution (11) and recrystallized from water. Anal. calcd. for $CoC_{30}H_{24}N_6O_{14}Cl_2 \cdot 2H_2O$: C 41.97, H 3.28, N 9.79; found: C 42.42, H 3.06, N 9.82.

The $[Co(bpyO_2)_3](ClO_4)_3$ complex was prepared by the electrochemical oxidation of $Co(bpyO_2)_3^{2+}$ in acetonitrile (containing 0.10 M tetraethylammonium perchlorate) at 0°C. The electrolysis was carried out in a H-shaped three-compartment cell containing platinum electrodes. A green solid, precipitated by concentration of acetonitrile solution, was washed with cold acetonitrile and dried under vacuum. Anal. calcd. for $CoC_{30}H_{24}N_6O_{18}Cl_3$: C 39.09, H 2.62, N 9.19; found: C 37.68, H 2.83, N 8.58. Elemental analyses were performed by Canadian Microanalytical Service, Delta, B.C. **Caution: Perchlorate salts of metal complexes with organic ligands are potentially explosive and should be prepared in small quantities and handled with care.**

The nickel(II) polyaza macrocycles: $Ni([14]aneN_4)^{2+}$ ([14]$aneN_4$ = 1,4,8,11-tetraazacyclotetradecane) (18), $Ni(rac\text{-}Me_6[14]aneN_4)^{2+}$ (*rac*-Me_6[14]$aneN_4$ = *rac*-5,7,7,12,12,14-hexamethyl-1,4,8,11-tetraazacyclotetradecane) (19), $Ni(Me_6[14]dieneN_4)^{2+}$ (Me_6[14]-$dieneN_4$ = 5,7,7,12,14,14-hexamethyl-1,4,8,11-tetraazacyclotetradeca-4,11-diene) (20), and $Ni([9]aneN_3)_2^{2+}$ ([9]$aneN_3$ = 1,4,7-triazacyclononane) (21) were prepared as perchlorate salts as described previously. The FeL_3^{2+} and OsL_3^{2+} (L is 2,2′-bipyridine or 1,10-phenanthroline, or substituted derivatives) complexes were prepared by reported synthetic procedures (22) and isolated as perchlorate salts. The analogous iron(III) complexes were prepared by an electrochemical oxidation of corresponding iron(II) species in acetonitrile as described above for $Co(bpyO_2)_3^{3+}$. Dirhodium(II) tetraacetate was prepared by a reported method (23).

Tetraethylammonium perchlorate (TEAP) was prepared by the metathesis of the tetraethylammonium bromide (BDH) with perchloric acid, recrystallized from water several times, and dried at 100°C for 24 h. Tetraethylammonium tetrafluoroborate was prepared and purified in a similar manner, using fluoroboric acid. Tetraethylammonium *p*-toluenesulphonate (Aldrich) was recrystallized twice from ethyl acetate and dried.

Kinetic experiments

The kinetic measurements were made using a TDI model IIA stopped-flow apparatus (Cantech Scientific) and data acquisition system interfaced to a Zenith ZF-151 microcomputer. Pseudo-first-order conditions of excess $Co(bpyO_2)_3^{n+}$ reductant or oxidant were employed and plots of $\ln(A_\infty - A_t)$ or $\ln(A_t - A_\infty)$ against time were linear for at least 3 half-lives. The first-order rate constants were determined from the average of four to six replicate experiments (Supplementary Material[2]). The reactions were conducted in acetonitrile, usually containing 0.10 M TEAP, at a temperature maintained at 25.0 ± 0.1°C by means of an external circulating water bath.

Physical and spectroscopic measurements

The cyclic voltammetric measurements were carried out in acetonitrile (0.10 M TEAP) with a BAS CV-1B cyclic voltammograph (Bioanalytical Systems) attached to a Houston Instruments 100 X–Y recorder. The working (Pt button) and auxilliary (Pt wire) electrodes in the sample solution were separated from the reference electrode (Ag/AgCl) by a glass frit. The ferricinium/ferrocene couple, $Fe(Cp)_2^{+/0}$, (+0.400 V vs. NHE 24)) was used as an internal reference. UV–visible spectra were measured on a Hewlett–Packard 8452A diode-array spectrophotometer. The ^1H NMR spectra were recorded on a Bruker AM-400 instrument operating at 400 MHz, and ^1H–^1H COSY spectra were obtained using Bruker software.

Results

^1H NMR and electronic spectra

The trischelate complex $Co(bpyO_2)_2^{3+}$ would theoretically exist in four diastereomers, each of which has a pair of enantiomers: Λ(δδδ) (= Δ(λλλ)), Λ(δδλ) (= Δ(λλδ)), Λ(δλλ) (= Δ(λδδ)), and Λ(λλλ) (= Δ(δδδ)). An examination of space-filling models of each of the diastereomers (considering only the Λ isomers) reveals that from a consideration of non-bonding interactions a stability order of Λ(δδδ) > Λ(δδλ) >> Λ(δλλ) >> Λ(λλλ) would be expected. The repulsive interactions that emerge upon conversions of δ to λ $bpyO_2$ ligand skew conformations take the form of a H6 proton on one $bpyO_2$ ligand interacting with the plane of a pyridine on another $bpyO_2$ ligand.

The ^1H NMR spectrum of the $Co(bpyO_2)_3^{3+}$ ion in CD_3CN revealed the presence of two of the four potential stereoisomers, which have been identified as Λ(δδδ) and Λ(δδλ) (along with the corresponding enantiomorphs) from one-dimensional ^1H and two-dimensional ^1H–^1H COSY NMR experiments (Fig. 1). The integration of the assigned peaks indicates that the Λ(δδλ) isomer is found in a slightly greater amount than the Λ(δδδ) isomer in acetonitrile at 25°C. A statistical entropy factor would favour the formation of Λ(δδλ) over Λ(δδδ) and this likely compensates for the greater steric instability of the Λ(δδλ) isomer (25).

In the Λ(δδδ) isomer the respective protons on the three $bpyO_2$ rings are equivalent, while on the Λ(δδλ) isomer there are three different pyridine ring types. The first set of protons (H′) are found on the unique λ $bpyO_2$ ligand. By converting a $bpyO_2$ ring from the δ to λ skew, the H6′ protons on the λ ligand are now placed over one of the pyridine rings on each of the other two δ $bpyO_2$ ligands, which form the second set (H″). The protons on the other pyridine ring on the δ $bpyO_2$ ligands form the third set (H‴). The H6′ and H5′ proton resonances are found at 6.48 and 7.67 ppm, respectively, shifted considerably upfield from H6 (9.40) and H5 (8.07) in the Λ(δδδ) isomer, due to the shielding of the aromatic ring (26). The shifts calculated by using the Johnson–

[2]Tables of kinetic data may be purchased from: The Depository of Unpublished Data, Document Delivery, CISTI, National Research Council Canada, Ottawa, Canada K1A 0S2.

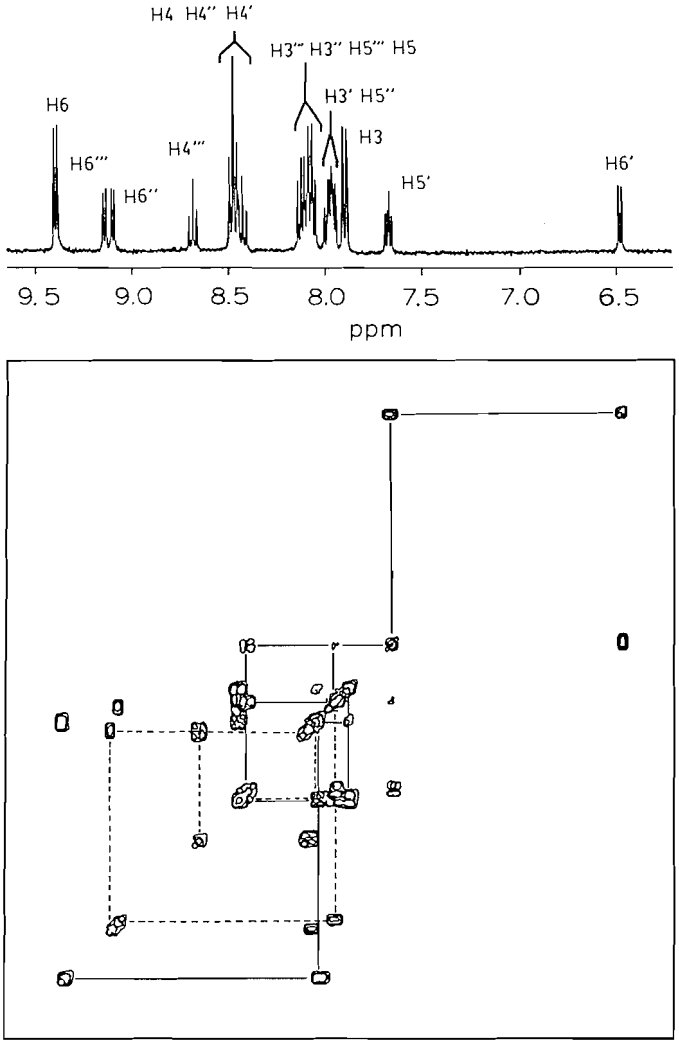

FIG. 1. ^1H–^1H COSY NMR spectrum of $Co(bpyO_2)_3^{3+}$ in CD_3CN. The connections between protons are indicated below the diagonal for the H (——) and H'' (– – –) protons and above the diagonal for the H' (——) and H''' (– – –) protons.

Bovey equation (26, 27) for the H5' (z = 3.50 and ρ = 0.8) and H6' (z = 1.75 and ρ = 0.0) protons on the basis of shielding contributions from the aromatic ring currents, by using the positions of the protons in the space-filling models, are in excellent agreement with the observed values.

The visible spectra of the $Co(bpyO_2)_3^{2+}$ and $Co(bpyO_2)_3^{3+}$ ions in acetonitrile are presented in Fig. 2. For the $Co(bpyO_2)_3^{2+}$ the maxima are found at 509 nm (ϵ = 140 M^{-1} cm^{-1}) and 552 nm (ϵ = 200 M^{-1} cm^{-1}), similar to the spectrum reported for the ion in nitromethane (12). The bands have been assigned to $^4T_{1g}(F) \rightarrow {}^4A_{2g}(F)$ and $^4T_{1g}(F) \rightarrow {}^4T_{1g}(P)$ transitions, respectively, and a D_q value of 1004 cm^{-1} has been reported (14). For the $Co(bpyO_2)_3^{3+}$ ion the visible maxima are found at 498 nm (ϵ = 225 M^{-1} cm^{-1}) and 676 nm (ϵ = 230 M^{-1} cm^{-1}, shoulder at 740 nm) and have been assigned to $^1A_{1g} \rightarrow {}^1T_{2g}$ and $^1A_{1g} \rightarrow {}^1T_{1g}$ transitions, respectively. From the asymmetric shapes of the peaks it is likely that the spectrum contains transitions for both the δδδ and δδλ isomers. A similar spectrum has been reported for the $Co(bpyO_2)_3^{3+}$ ion in aqueous media, with maxima at 466 and 671 nm, and D_q calculated to be 1560 cm^{-1} (13).

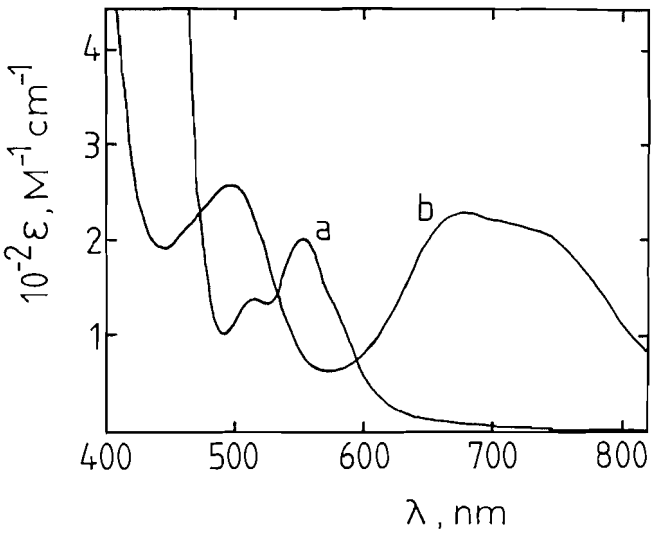

FIG. 2. Visible spectra of the (a) $Co(bpyO_2)_3^{2+}$ and (b) $Co(bpyO_2)_3^{3+}$ complexes in acetonitrile.

The reduction potential of the $Co(bpyO_2)_3^{3+}/Co(bpyO_2)_3^{2+}$ couple in acetonitrile containing 0.10 M TEAP was determined by cyclic voltammetry measurements. A quasi-reversible couple (ΔE_p = 80 mV) was observed with $E_{1/2}$ = 0.53 V vs. the $FeCp^+/FeCp$ internal reference. The reduction potentials of the cross-reactants used in this study were measured in the same medium and were found to be in good agreement with previously reported values in acetonitrile and (or) aqueous solution (28–31).

Kinetics studies

The electron transfer cross-reactions of $Co(bpyO_2)_3^{2+}$ and $Co(bpyO_2)_3^{3+}$ were carried out at 25.0°C in acetonitrile containing 0.10 M tetraethylammonium perchlorate (TEAP).

$$[1] \quad Co(bpyO_2)_3^{2+} + \text{oxidant} \overset{k_{12}}{\rightleftharpoons} Co(bpyO_2)_3^{3+} + \text{reductant}$$

The kinetics of the oxidations of the $Co(bpyO_2)_3^{2+}$ ion with a series of FeL_3^{3+} complexes (L = 2,2'-bipyridine or 1,10-phenanthroline or substituted derivatives) were monitored at the visible maximum of the FeL_3^{2+} species in the range of 510–530 nm. Using a pseudo-first-order excess of the reductant ((1–10) × 10^{-4} M) the kinetics followed the expression in eq. [2],

$$[2] \quad \frac{d[FeL_3^{2+}]}{dt} = k_{obs}[FeL_3^{3+}]$$

where $k_{obs} = k_{12}[Co(bpyO_2)_3^{2+}]$. Likewise for the reductions of $Co(bpyO_2)_3^{3+}$ by FeL_3^{2+} and OsL_3^{2+}, first-order dependences of k_{obs} on the pseudo-first-order excess concentrations of the $Co(bpyO_2)_3^{3+}$ were found. The reactions between $Co(bpyO_2)_3^{2+}$ and the nickel(III) polyaza macrocycles were followed by monitoring the disappearance of the oxidant at its maximum in the region of 300–400 nm, employing pseudo-first-order excess concentrations of the reductant. The kinetics of the oxidation of $Co(bpyO_2)_3^{2+}$ by $Rh_2(O_2CCH_3)_4(CH_3CN)_2^+$ were carried out under pseudo-first-order conditions of excess concentrations of the dirhodium cation, following the disappearance of the reductant at 410 nm. First-order plots for representatives of each group of cross-reaction are presented in Fig. 3. The second-order

Can. J. Chem. Downloaded from www.nrcresearchpress.com by 123.30.183.119 on 09/08/12
For personal use only.

Can. J. Chem. Downloaded from www.nrcresearchpress.com by 123.30.183.119 on 09/08/12
For personal use only.

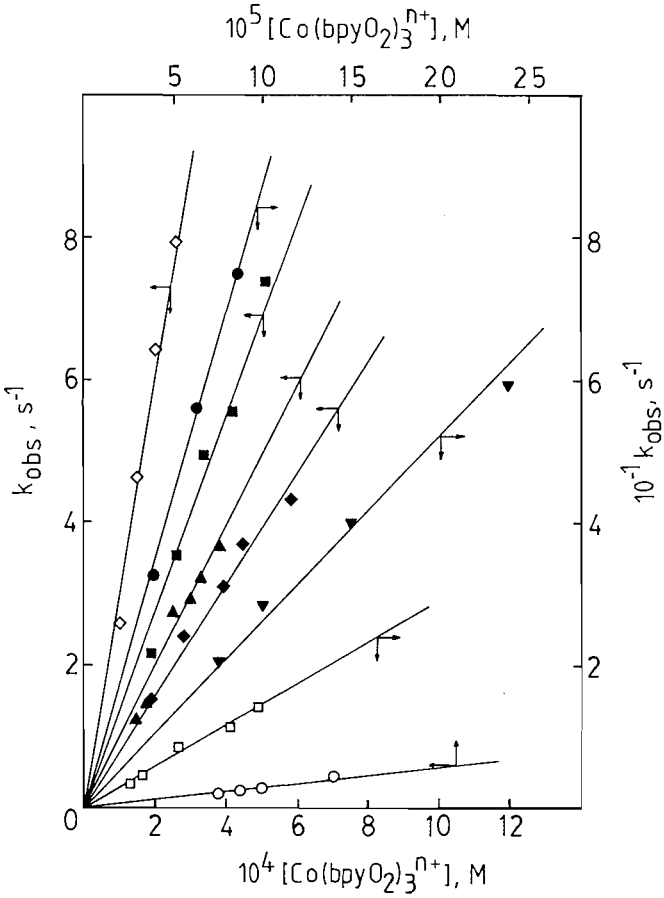

FIG. 3. Dependences of k_{obs} on $[Co(bpyO_2)_3^{n+}]$ for the oxidations of $Co(bpyO_2)_3^{2+}$ by $Fe(Cl\text{-}phen)_3^{3+}$ (●), $Fe(bpy)_3^{3+}$ (■), $Fe(5,6\text{-}Me_2phen)_3^{3+}$ (▲), $Ni(Me_6[14]dieneN_4)^{3+}$ (◆), and $Rh_2(O_2CCH_3)_4(CH_3CN)_2^{+}$ (▼, abscissa is $10^4[Rh_2^{+}]$), and the reductions of $Co(bpyO_2)_3^{3+}$ by $Os(5\text{-}Clphen)_3^{2+}$ (◇), $Os(phen)_3^{2+}$ (□), and $Fe(4,4'\text{-}Me_2bpy)_3^{2+}$ (○) in acetonitrile (0.10 M TEAP) at 25.0°C.

rate constants, k_{12}, for the cross-reactions in this study at 25.0°C are presented in Table 1.

For the $Co(bpyO_2)_3^{2+}/Fe(phen)_2^{3+}$ cross-reaction, determinations of the rate constant as a function of electrolyte concentration and the nature of the anion, using tetraethylammonium salts of ClO_4^-, BF_4^-, and *p*-tosylate (TEAX) as the electrolyte, were undertaken (Supplementary Material[2]). The rate constant increased with increasing concentration of electrolyte, with curvature towards a limiting value above 0.05 M TEAX. The rate constants at 0.01 and 0.10 M TEAX were 1.2×10^4 and 1.7×10^4 M^{-1} s^{-1} for $X^- = ClO_4^-$, 0.65×10^4 and 2.3×10^4 M^{-1} s^{-1} for $X^- = BF_4^-$, and 1.8×10^5 and 3.5×10^5 M^{-1} s^{-1} for X^- = *p*-tosylate, respectively.

An attempt was made to measure the electron self-exchange rate constant k_{11} for the $Co(bpyO_2)_3^{2+/3+}$ by using ^1H NMR line-broadening experiments.

[3] $Co(bpyO_2)_3^{2+} + Co(bpyO_2)_3^{3+} \overset{k_{11}}{\rightleftharpoons} Co(bpyO_2)_3^{3+} + Co(bpyO_2)_3^{2+}$

The addition of the paramagnetic $Co(bpyO_2)_3^{2+}$ ion ($\approx 1 \times 10^{-3}$ M, limited by its solubility) to a solution of the diamagnetic $Co(bpyO_2)_3^{3+}$ ion in CD_3CN at 25°C resulted in no discernible increase in the linewidths of the proton resonances. Using the equation for electron exchange in the slow-exchange domain (33): $k_{11}[Co(II)] = \pi(W_{DP} - W_D)$, where $W_{DP} - W_D$ is the difference in the linewidths of the diamagnetic resonances in the presence and the absence of the paramagnetic species, an upper limit of $k_{11} < 600$ M^{-1} s^{-1} is estimated, using $W_{DP} - W_D < 0.2$ Hz.

Discussion

The electron self-exchange rate constant for the $Co(bpyO_2)_3^{2+/3+}$ couple in acetonitrile is anticipated to be moderately small because the transfer involves changes in the population of the antibonding e_g^* orbitals and a change in the spin configuration from high-spin Co(II) (t_{2g}^5 e_g^{*2}) to low-spin Co(III) (t_{2g}^6 e_g^{*0}). The electron self-exchange rate constants for a number of transition metal complex couples have been predicted with reasonable success by using the semiclassical model for bimolecular electron exchange (1). The rate constant k_{11} may be expressed as the product of a preequilibrium constant K_A, an effective nuclear frequency ν_n, and electronic factor κ_{el}, and a nuclear factor that contains terms for both inner-sphere (ΔG_{in}^*) and solvent reorganizations (ΔG_{out}^*) as well as an inner-sphere nuclear tunneling factor Γ_n:

[4] $$k_{11} = K_A \nu_n \kappa_{el} \Gamma_n \exp[-(\Delta G_{in}^* + \Delta G_{out}^*)/RT]$$

The inner-sphere term, ΔG_{in}^*, corresponds to the reorganization of bond distances and angles required prior to electron transfer, and the outer-sphere term, ΔG_{out}^*, is the energy needed to change the orientations of the solvent molecules surrounding the reactants. The ΔG_{in}^* may be calculated with a knowledge of the bond distances and angles and vibrational frequencies and force constants for the two redox partners:

[5] $$\Delta G_{in}^* = \frac{1}{2} \sum f_i [\Delta d_0)_i/2]^2$$

While crystal structure determinations have not been reported for complexes containing either the $Co(bpyO_2)_3^{2+}$ or $Co(bpyO_2)_2^{3+}$ ion, the difference in the Co—O bond lengths between the two oxidation states is likely to fall in the range of 0.17–0.21 Å observed for other high-spin Co(II)/low-spin Co(III) complex couples, such as those mentioned in the Introduction. If it is assumed that f_i (34)[3] and Δd_0 for the $Co(bpyO_2)_3^{2+/3+}$ couple are similar to those for the $Co(bpy)_3^{2+/3+}$ couple ($\Delta d_0 = 0.19$ Å (2)), the difference in the electron exchange rate constants between the two couples would primarily reside in ΔG_{out}^* and K_A. With these two terms, it is calculated that the self-exchange rate constant for the $Co(bpyO_2)_3^{2+/3+}$ couple in acetonitrile would be about two or three times greater that the value for the $Co(bpy)_3^{2+/3+}$ exchange (20 M^{-1} s^{-1} (I = 0.1 M) (35)) in aqueous solution.

The cross-reaction kinetic data from this study may be correlated in terms of the Marcus equation (17), which relates the rate constant for a cross-reaction, k_{12}, to the rate constants for the component self-exchange reactions, k_{11} and

[3] A value of f_i = 169–176 N m^{-1} has been calculated for the $Co(bpy)_2^{2+/3+}$ couple (2, 34*a* (footnote 50)), and a value of 180 N m^{-1} is estimated for the $Co(bpyO_2)_3^{2+/3+}$ couple on the basis of Co—O stretching frequency for $Co(pyrO)_6^{2+}$ (34*b*).

TABLE 1. Rate constants for the cross-reactions of $Co(bpyO_2)_3^{2+}$ and $Co(bpyO_2)_3^{3+}$ in acetonitrile at 25.0°C, I = 0.10 M (TEAP)

No.	Reductant	Oxidant	ΔE^0 (V)	k_{12} ($M^{-1}s^{-1}$)	k_{22}[a] ($M^{-1}s^{-1}$)	k_{11}[b] ($M^{-1}s^{-1}$)
1	$Co(bpyO_2)_3^{2+}$	$Fe(phen)_3^{3+}$	0.15	1.65×10^4	1.2×10^7[c]	8×10^{-2}
2	$Co(bpyO_2)_3^{2+}$	$Fe(5\text{-Mephen})_3^{3+}$	0.10	1.13×10^4	2.0×10^7[c]	1×10^{-1}
3	$Co(bpyO_2)_3^{2+}$	$Fe(5,6\text{-Me}_2\text{phen})_3^{3+}$	0.09	9.81×10^3	2.0×10^7[c]	2×10^{-1}
4	$Co(bpyO_2)_3^{2+}$	$Fe(5\text{-Clphen})_3^{3+}$	0.26	1.74×10^5	1.5×10^7[c]	2×10^{-1}
5	$Co(bpyO_2)_3^{2+}$	$Fe(bpy)_3^{3+}$	0.13	1.35×10^4	3.5×10^6[c]	4×10^{-1}
6	$Co(bpyO_2)_3^{2+}$	$Fe(4,4'\text{-Ph}_2\text{bpy})_3^{3+}$	0.07	6.11×10^3	2.0×10^7[c]	1×10^{-1}
7	$Co(bpyO_2)_3^{2+}$	$Ni([14]aneN_4)^{3+}$	0.06	5.12×10^3	3.3×10^3[d]	6×10^2
8	$Co(bpyO_2)_3^{2+}$	$Ni([9]aneN_3)_2^{3+}$	0.03	3.0×10^3	6.0×10^3[d]	4×10^2
9	$Co(bpyO_2)_3^{2+}$	$Ni(rac\text{-}Me_6[14]aneN_4)^{3+}$	0.31	8.71×10^3	9.4[e]	9×10^1
10	$Co(bpyO_2)_3^{2+}$	$Ni(Me_6[14]dieneN_4)^{3+}$	0.40	1.02×10^4	1.1[e]	5×10^1
11	$Co(bpyO_2)_3^{2+}$	$Rh_2(O_2CCH_3)_4(CH_3CN)_2^+$	0.23	5.33×10^4	5.4×10^4[e]	4
12	$Fe(4,4'\text{-Me}_2\text{bpy})_3^{2+}$	$Co(bpyO_2)_3^{3+}$	−0.01	1.37×10^3	2.0×10^7[c]	1×10^{-1}
13	$Fe(4,7\text{-Me}_2\text{phen})_3^{2+}$	$Co(bpyO_2)_3^{3+}$	0.00	2.58×10^3	2.7×10^7[c]	3×10^{-1}
14	$Os(5\text{-Clphen})_3^{2+}$	$Co(bpyO_2)_3^{3+}$	0.00	8.78×10^3	3.8×10^7[c]	2
15	$Os(phen)_3^{2+}$	$Co(bpyO_2)_3^{3+}$	0.12	2.73×10^4	3.8×10^7[c]	2×10^{-1}

[a]The self-exchange rate constant for the cross-reactant.
[b]The self-exchange rate constant calculated for the $Co(bpyO_2)_3^{2+/3+}$ couple.
[c]Extrapolated from data in ref. 32.
[d]References 16 and 31.
[e]Reference 31.

k_{22}, and the equilibrium constant for the cross reaction K_{12} by eq. [6] (1*a*),

$$[6] \quad k_{12} = (k_{11}k_{22}K_{12}f_{12})^{1/2}W_{12}$$

where

$$[7] \quad \ln(f_{12}) = \frac{[\ln K_{12} + (w_{12} - w_{21})/RT]^2}{4\left[\ln\left(\frac{k_{11}k_{22}}{A_{11}A_{22}}\right) + \frac{w_{11} + w_{22}}{RT}\right]}$$

$$[8] \quad W_{12} = \exp[-(w_{12} + w_{21} - w_{11} - w_{22})/2RT]$$

$$[9] \quad w_{ij} = \frac{z_i z_j e^2}{D_s\sigma_{ij}(1 + \beta\sigma_{ij}I^{1/2})}$$

In the above expressions w_{ij} is the work required to bring ions i and j (charges z_i and z_j) to the separation distance σ_{ij} (taken equal to the sum of the radii of the ions), D_s is the static dielectric constant of the medium, $\beta = (8\pi Ne^2/1000D_skT)^{1/2}$, and $A_{ii} = (4\pi N\sigma_{ii}^2\nu_n(\delta r)/1000)_{ii}$, where δr is the thickness of the reaction shell ($\approx$ 0.8 Å). The values of D_s and β are 37.5 and 0.476 $M^{-1/2}$ $Å^{-1}$, respectively, for acetonitrile at 25°C. In the calculations of the work terms, radii of 8 Å for $Co(bpyO_2)_3^{n+}$, 7–8 Å for the iron and osmium complexes, 5.5 Å for $Rh_2(O_2CCH_3)_4(CH_3CN)_2^+$, and 5–7 Å for the nickel polyaza macrocycles, were employed.

The self-exchange rate constants of the nickel polyaaza macrocycle complexes used in the cross-reactions were determined by an application of the Marcus relationship to the kinetic data from reactions with other nickel complexes and iron or ruthenium tris(polypyridine) complexes in a previous study (16, 31). The self-exchange rate constants for the remainder of cross-reactants (in acetonitrile) were also determined previously from direct measurements or by the application of the Marcus relationship (31, 32).

From the results of several recent kinetic investigations of electron-exchange (9, 31, 36–40) and electron-transfer reactions of metal complexes in acetonitrile, it is becoming evident that ion pairing (and perhaps ion triplets) plays a major role in the rates of outer-sphere processes and their dependence on ionic strength in this medium. At an ionic strength of 0.10 M, ion pairing of the ClO_4^- ion with the cationic metal complexes used in this study is expected to be extensive. Conductivity measurements on the ion pairing between the ClO_4^- ion and ML_3^{2+}, ML_3^{3+} (L = polypyridine ligand) (40), and $Ni([14]aneN_4)^{2+}$ (41), in acetonitrile have yielded ion-pair association constants of <100, 170–900, and 190 M^{-1}, respectively. The observed dependence of k_{12} on the ionic strength and the nature of the anion in the reaction of $Co(bpyO_2)_3^{2+}$ with $Fe(phen)_3^{3+}$ is consistent with previous kinetic studies of electron transfer reactions between cationic complexes in acetonitrile (31, 32, 37). The analysis of these electrolyte dependences in terms of definitive ion-pair association constants and specific rate constants for free and ion-paired species is not simple (38, 40), and is beyond the scope of the present study. For the purposes of calculating the work-term parameters the trivalent metal oxidants are considered to be fully ion-paired (e.g., $\{ML_3,ClO_4\}^{2+}$). With the majority of the cross-reactions involving formally 2+/"2+" charge types, the terms w_{ij} in eq. [8] tend to cancel each other, such that W_{12} is not far from unity.

The electron transfer kinetic data in Table 1 have been correlated with the thermodynamic driving forces for the cross-reactions and presented in Fig. 4 as a plot of $\ln(k_{12}/k_{22}^{1/2}W_{12})$ against $\ln(K_{12}f_{12})^{1/2}$. From eq. [6], the slope and intercept of the plot are expected to be unity and $\frac{1}{2}\ln(k_{11})$, respectively. The points in Fig. 4 fall primarily on two lines, with the cross-reactions involving the nickel macrocycles forming one group and the remainder of the cross-reactants, primarily tris(polypyridine)metal complexes, the other group. The k_{11} values obtained from the cross-reactions involving the nickel macrocycles have a mean value of about 10^2 M^{-1} s^{-1}, while k_{11} calculated from the metal

Can. J. Chem. Downloaded from www.nrcresearchpress.com by 123.30.183.119 on 09/08/12
For personal use only.

Can. J. Chem. Downloaded from www.nrcresearchpress.com by 123.30.183.119 on 09/08/12
For personal use only.

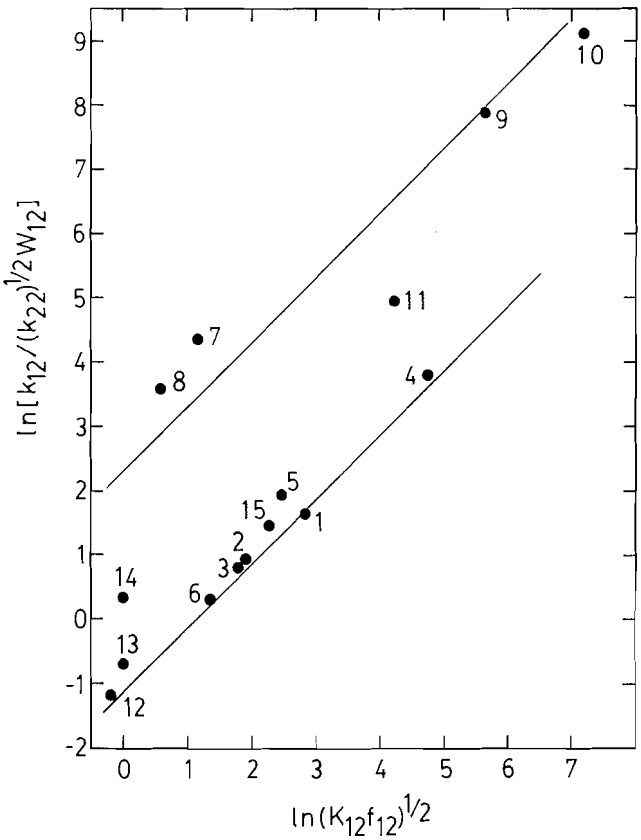

FIG. 4. Marcus correlation of $\ln[k_{12}/(k_{22})^{1/2}W_{12}]$ against $\ln(K_{12}f_{12})^{1/2}$ for the cross-reactions of the $Co(bpyO_2)_3^{2+/3+}$ couple in acetonitrile (I = 0.10 M). The reactions are numbered as in Table 1. The upper line corresponds to a value of k_{11} for the $Co(bpyO_2)_3^{2+/3+}$ couple of 10^2 M^{-1} s^{-1}, while the lower line corresponds to k_{11} = 10^{-1} M^{-1} s^{-1}.

tris(polypyridine) cross-reaction data are close to 10^{-1} M^{-1} s^{-1}. The k_{11} value obtained from the reaction with $Rh_2(O_2CCH_3)_4(CH_3CN)_2^+$, 4 M^{-1} s^{-1}, falls between these two groups. The ^1H NMR line-broadening experiment places k_{11} at less than 600 M^{-1} s^{-1}.

It has recently been suggested that cross-reactions of tris(polypyridine) complexes of Co(III) with Ru(II) amines are non-adiabatic (42), while those with tris(polypyridine)chromium(II) complexes are marginally non-adiabatic (43). From the present study it appears that the cross-reactions of the $Co(bpyO_2)_3^{2+/3+}$ couple with the tris(polypyridine) complexes of iron and osmium are non-adiabatic. We previously observed that significantly lower self-exchange rate constants are derived for high-spin Mn(II)/Mn(III) complex couples when metal tris(polypyridine) cross-reactants are employed, compared to the values obtained from reactions with the nickel macrocycles. These couples have included $Mn(H_2O)_6^{2+/3+}$ (44) and $Mn(edta)^{2-/-}$ ($edta^{4-}$ = ethylenediaminetetraacetate) (45) in aqueous solution and $Mn(urea)_6^{2+/3+}$ (46) in acetonitrile. The electron exchange pathway in the $M(bpy)_3^{2+/3+}$ complexes of Fe, Ru, and Os involves the t_{2g} orbitals and overlap with the π^* ligand orbitals. The exchange pathway of the Mn(II)/Mn(III), Co(II)/Co(III), and Ni(II)/Ni(III) couples involves the antibonding e_g^* orbitals. The incompatibility of the donor and acceptor orbital symmetries in the $Co(bpyO_2)_3/M(bpy)_3$ cross-reactions may account for the lower self-exchange rate constants derived for the $Co(bpyO_2)_3^{2+/3+}$ couple from these cross-reactions rather than from the reactions involving the nickel(II) macrocycles. Electron exchange and electron transfer reactions of the $Rh_2(O_2CCH_3)_4(CH_3CN)_2^{0/+}$ couple involve a weakly antibonding Rh—Rh π^* orbital and exhibit similar cross-reaction behaviour towards both nickel macrocycles and metal polypyridine complexes (31). It is perhaps not surprising, therefore, that the cross-reaction with $Co(bpyO_2)_3^{2+}$ yields a k_{11} value between those of the other two sets of reactants.

The self-exchange rate constant derived in this study for the $Co(bpyO_2)_3^{2+}/Co(bpyO_2)_3^{3+}$ couple may be compared with the value of 10^2 M^{-1} s^{-1} determined for the $Mn(bpyO_2)_3^{2+}/Mn(bpyO_2)_3^{3+}$ couple in acetonitrile (ref. 15, manuscript in preparation). The exchange process for this high-spin d^5/d^4 couple also involves the transfer of an antibonding e_g^* electron, as does exchange in the d^8/d^7 $Ni(bpyO_2)_3^{2+/3+}$ couple, for which an estimate of $k_{11} \approx 10^3$ M^{-1} s^{-1} (16) has been made from cross-reactions with tris(polypyridine)nickel(III) complexes in acetonitrile (16). Kinetic studies of the cross-reactions of the high-spin d^6/d^5 $Fe(bpyO_2)_3^{2+/3+}$ couple with tris(polypyridine)cobalt(II) and (III) complexes in acetonitrile are in progress and preliminary results (16) suggest an exchange rate constant of 10^6–10^7 M^{-1} s^{-1}, consistent with the lower inner-sphere reorganization barrier associated with the transfer of a nonbonding t_{2g} electron.

Acknowledgements

The financial support of this work by the Natural Sciences and Engineering Research Council of Canada in the form of operating and equipment grants is gratefully acknowledged. We thank Queen's University for a graduate scholarship (S.M.) and a grant (D.H.M.) from its Advisory Research Committee. We also thank S. Blake and D. Foucher for assistance in the NMR measurements and Dr. B. K. Hunter for helpful discussions.

1. (*a*) N. Sutin. Prog. Inorg. Chem. **30**, 441 (1983); (*b*) N. Sutin and M. D. Newton. Annu. Rev. Phys. Chem. **35**, 437 (1984).
2. B. S. Brunschwig, C. Creutz, D. H. Macartney, T.-K. Sham, and N. Sutin. Faraday Discuss. Chem. Soc. **74**, 113 (1982), and references therein.
3. J. F. Endicott, K. Kumar, T. Ramasami, and F. P. Rotzinger. Prog. Inorg. Chem. **30**, 141 (1983).
4. D. Geselowitz and H. Taube. Adv. Inorg. Bioinorg. Mech. **1**, 391 (1982).
5. F. P. Dwyer and A. M. Sargeson. J. Phys. Chem. **65**, 1892 (1961).
6. H. Doine and T. W. Swaddle. Inorg. Chem. **30**, 1858 (1991).
7. R. M. L. Warren, A. G. Lappin, B. D. Mehta, and H. M. Neumann. Inorg. Chem. **29**, 4185 (1990).
8. H.-J. Kuppers, A. Neves, C. Pomp, D. Ventur, K. Wieghardt, B. Nuber, and J. Weiss. Inorg. Chem. **25**, 2400 (1986).
9. D. Borchardt and S. Wherland. Inorg. Chem. **21**, 93 (1982); **23**, 2537 (1984); **25**, 901 (1986).
10. R. S. Nyholm and A. Turco. J. Chem. Soc. 1211 (1962).
11. P. G. Simpson, A. Vinciguerra, and J. V. Quagliano. Inorg. Chem. **2**, 282 (1963).
12. S. K. Madan and W. E. Bull. J. Inorg. Nucl. Chem. **26**, 2211 (1964).
12. A. R. Al-Karaghouli, R. O. Day, and J. S. Wood. Inorg. Chem. **17**, 3702 (1978).

13. L. C. Nathan, J. E. Armstrong, and R. O. Ragsdale. Inorg. Chim. Acta, **35**, 293 (1979).
14. S. Bhattacharya, R. Mukherjee, and A. Chakravorty. Inorg. Chem. **25**, 3448 (1986).
15. D. W. Thompson. M.Sc. Thesis, Queen's University, Kingston. 1987.
16. S. Mak. M.Sc. Thesis, Queen's University, Kingston. 1989.
17. R. A. Marcus. Annu. Rev. Phys. Chem. **15**, 155 (1966).
18. B. Bosnich, M. L. Tobe, and G. A. Webb. Inorg. Chem. **4**, 1102 (1965).
19. A. M. Tait and D. H. Busch. Inorg. Synth. **18**, 5 (1977).
20. N. F. Curtis, Y. M. Curtis, and H. J. K. Powell. J. Chem. Soc. A, 1015 (1966).
21. A. McAuley, P. R. Norman, and O. Olubuyide. J. Chem. Soc. Dalton Trans. 1501 (1984).
22. C. T. Lin, W. Bottcher, M. Chou, C. Creutz, and N. Sutin. J. Am. Chem. Soc. **98**, 6536 (1976).
23. G. A. Rempel, P. Legzdins, P. Smith, and G. Wilkinson. Inorg. Synth. **13**, 90 (1971).
24. R. R. Gagne, C. A. Koval, and G. C. Lisensky. Inorg. Chem. **19**, 2854 (1980).
25. F. A. Cotton and G. Wilkinson. Advanced inorganic chemistry. 5th ed. Wiley–Interscience, Toronto. 1988. pp. 53–56.
26. C. E. Johnson and F. A. Bovey. J. Chem. Phys. **29**, 1012 (1958).
27. J. W. Emsley, J. Feeney, and L. H. Sutcliffe. High resolution nuclear magnetic resonance spectroscopy. Vol. 1. Pergamon Press, Oxford. 1965. Appendix B.
28. R. Prasad and D. B. Scaife. J. Electroanal. Chem. **84**, 373 (1977).
29. C. R. Leidner and R. W. Murray. J. Am. Chem. Soc. **106**, 1606 (1984).
30. C. T. Lin, W. Bottcher, M. Chou, C. Creutz, and N. Sutin. J. Am. Chem. Soc. **98**, 6536 (1976).
31. M. A. S. Aquino, D. A. Foucher, and D. H. Macartney. Inorg. Chem. **28**, 3357 (1989).
32. M.-S. Chan and A. C. Wahl. J. Phys. Chem. **82**, 2542 (1978).
33. T. J. Swift and R. E. Connick. J. Chem. Phys. **37**, 307 (1962).
34. (*a*) D. J. Szalda, D. H. Macartney, and N. Sutin. Inorg. Chem. **23**, 3473 (1984); (*b*) A. D. Van Ingen Schenau, W. L. Groeneveld, and J. Reedijk. Spectrochim. Acta, **30A**, 213 (1974).
35. (*a*) B. R. Baker, F. Basolo, and H. M. Neumann. J. Phys. Chem. **63**, 371 (1959); (*b*) R. Farina and R. G. Wilkins. Inorg. Chem. **7**, 514 (1968).
36. (*a*) R. M. Nielson and S. Wherland. Inorg. Chem. **25**, 2437 (1986); (*b*) K. A. Anderson and S. Wherland. Inorg. Chem. **29**, 3822 (1990).
37. (*a*) R. Schmid, K. Kirchner, and F. L. Dickert. Inorg. Chem. **27**, 1530 (1988); (*b*) R. Schmid, K. Kirchner, and V. N. Sapunov. Inorg. Chem. **28**, 4167 (1989).
38. J. A. Goodwin, D. M. Stanbury, L. J. Wilson, C. W. Eigenbrot, and W. R. Scheidt. J. Am. Chem. Soc. **109**, 2979 (1987).
39. K. M. Davies, K. D. Whyte, and A. H. Gilbert. Inorg. Chim. Acta, **177**, 121 (1990).
40. T. G. Braga and A. C. Wahl. J. Phys. Chem. **89**, 5822 (1985).
41. E. Iwamoto, T. Yokoyama, S. Yamasaki, T. Yabe, T. Kumamaru, and Y. Yamamoto. J. Chem. Soc. Dalton Trans. 1935 (1988).
42. U. Furholz and A. Haim. J. Phys. Chem. **90**, 3686 (1986).
43. K. Zahir, J. H. Espenson, and A. Bakac. Inorg. Chem. **27**, 3144 (1988).
44. D. H. Macartney and N. Sutin. Inorg. Chem. **24**, 3403 (1985).
45. D. H. Macartney and D. W. Thompson. Inorg. Chem. **28**, 2195 (1989).
46. D. H. Macartney. Inorg. Chim. Acta, **127**, 9 (1987).

Can. J. Chem. Downloaded from www.nrcresearchpress.com by 123.30.183.119 on 09/08/12
For personal use only.

The ligand mediated pseudohypersensitivity of the $^3H_4 \rightarrow {}^3P_2$, $^3H_4 \rightarrow {}^3P_1$, $^3H_4 \rightarrow {}^3P_0$, and $^3H_4 \rightarrow {}^1D_2$ transitions of praseodymium(III) complexes in solution media

SUDHINDRA N. MISRA[1]

Chemical Laboratories, Bhavnagar University, Bhavnagar 364 002, India

AND

SHAUN O. SOMMERER

Penn State Erie, The Behrend College, Division of Science, Engineering and Technology, Erie, PA 16563-0203, U.S.A.

Received August 13, 1990[2]

SUDHINDRA N. MISRA and SHAUN O. SOMMERER, Can. J. Chem. **70**, 46 (1992).

The absorption difference, comparative absorption spectrophotometry, and quantitative analysis of 4*f*–4*f* spectra of praseodymium(III) complexes with ligands possessing varying structural features and binding capabilities have clearly indicated that the $^3H_4 \rightarrow {}^3P_2$, $^3H_4 \rightarrow {}^3P_1$, $^3H_4 \rightarrow {}^3P_0$, and $^3H_4 \rightarrow {}^1D_2$ transitions exhibit substantial intensification as well as a wide variation of oscillator strength. Since these transitions do not follow the selection rules they cannot be considered hypersensitive. Ligands such as β-diketones, Schiff bases, amino acids, diols, nucleic bases, nucleosides, nucleotides, alkoxides, and haloacetates with widely differing binding features in terms of coordinating ability, denticity, and normalized bite appear to induce, to varying degrees, high sensitivity in these non-hypersensitive transitions. The present article reports the high sensitivity of the $^3H_4 \rightarrow {}^3P_2$, $^3P_1$, $^3P_0$, and $^1D_2$ transitions of Pr(III) by considering the solution spectra of 173 species. This unique sensitivity is termed Ligand Mediated Pseudohypersensitivity.

Key words: praseodymium(III), 4*f*–4*f* transitions, hypersensitive transitions.

SUDHINDRA N. MISRA et SHAUN O. SOMMERER. Can. J. Chem. **70**, 46 (1992).

Les différences d'absorption, la spectrométrie d'absorption comparative et des analyses quantitatives des spectres 4*f*–4*f* de complexes du praséodyme(III) avec des ligands possédant diverses caractéristiques spectrales et diverses capacités de liaison indiquent clairement que les transitions $^3H_4 \rightarrow {}^3P_2$, $^3H_4 \rightarrow {}^3P_1$, $^3H_4 \rightarrow {}^3P_0$ et $^3H_4 \rightarrow {}^1D_2$ présentent une intensification importante ainsi que de grandes variations de la force de leur oscillateur. Puisque ces transitions ne suivent pas les règles de sélection, on ne peut les considérer comme hypersensibles. Des coordinats, comme des β-dicétones, des bases de Schiff, des acides aminés, des diols, des bases nucléiques, des nucléosides, des nucléotides, des alcoolates et des halogénoacétates qui possèdent des caractéristiques de liaison très différentes en termes de facilité de coordination, de «denticité» et de «prise» normalisée, semblent induire des sensibilités variables dans ces transitions non-hypertensives. Dans le présent travail, on a examiné la grande sensibilité des transitions $^3H_4 \rightarrow {}^3P_2$, $^3P_1$, $^3P_0$ et $^1D_2$ du Pr(III) en considérant les spectres en solution de 173 espèces. Cette sensibilité unique est appelée «pseudohypersensibilité obtenue par l'intermédiaire des coordinats».

Mots clés : praséodyme(III), transitions 4*f*–4*f*, transitions hypersensibles.

[Traduit par la rédaction]

Introduction

The intensity of hypersensitive transitions (1–3) has been used extensively to distinguish between outer and inner sphere coordination, in identifying the coordinating sites of ligands (4), in determining the immediate coordination environment, and in predicting the coordination number of lanthanides (5–10). Hypersensitivity has attracted much attention even though theories proposed to explain the phenomenon are far from quantitative. The majority of the quantitative work on these intensities has been done in the solid state (11–16) though a few of the studies have involved solution spectra (5–10). Due to phenomenon such as isomerization, dissociation, association, solvolysis, etc., the solution spectra can become quite complex, which in turn causes the data to become only approximate and the reproducibility of the experiment to become questionable. A new dimension to lanthanide coordination chemistry in solution has come of age with the increased use of lanthanides as probes in the exploration of the structural functions of biomolecular reactions (17–20). Moreover, the use of lanthanide hypersensitive bands as marker bands has increased the importance of solution spectra.

The quantitative analysis of the spectral data for Pr(III) complexes with a wide variety of ligands has clearly shown that hypersensitivity cannot be restricted to specific transitions only, but may under certain chemical conditions be extended to non-hypersensitive transitions as well. On the basis of 173 spectra of Pr(III) complexes, the high sensitivity of the $^3H_4 \rightarrow {}^3P_2$, $^3H_4 \rightarrow {}^3P_1$, $^3H_4 \rightarrow {}^3P_0$, and $^3H_4 \rightarrow {}^1D_2$ transitions (all pseudohypersensitive (21)) is reported and termed Ligand Mediated Pseudohypersensitivity.

Experimental

The spectral absorption studies were recorded on Shimadzu 260FS and Perkin Elmer Lambda-2 spectrophotometers. The regions of the pseudohypersensitive transitions were resolved and recorded in an expanded scale mode. All solutions were prepared from reagent grade materials.

The linear curve analysis of the absorption spectra followed by a Gaussian curve analysis of the individual bands led to the computation of the absorption spectral parameters: Slater–Condon F_k — Racah E^k — Coulombic interaction, Lande's ξ 4*f* spin-orbit interaction, nephelauxetic β bonding (*b*), and covalency parameters. The intensity parameter *P* (oscillator strength) and the Judd–

[1]Author to whom correspondence may be addressed.

[2]Revision received August 21, 1991.

Printed in Canada / Imprimé au Canada

Can. J. Chem. Downloaded from www.nrcresearchpress.com by 123.30.183.119 on 09/08/12
For personal use only.

Can. J. Chem. Downloaded from www.nrcresearchpress.com by 123.30.183.119 on 09/08/12
For personal use only.

Ofelt T_λ parameters were computed by partial and multiple regression methods on a HP-1000/45 computer (17, 21).

Results and discussion

Pr(III) (f^2) is the simplest tervalent lanthanide ion, yet it has not been extensively investigated when compared to Nd(III) (f^3) and Eu(III) (f^6). One possible reason may be that Judd–Ofelt (22, 23) theory does not work very well for Pr(III) nor does the calculation of oscillator strengths evidenced by the high RMS deviations. The $^3P_2 \leftarrow {}^3H_4$ transition of Pr(III) is hypersensitive, occurring at 5200 cm^{-1}, and is not generally studied in solution spectral investigations. Peacock (24) found that the $^3P_2 \leftarrow {}^3H_4$ and $^1D_2 \leftarrow {}^3H_2$ transitions of Pr(III) showed significant sensitivity and referred to them as pseudohypersensitive transitions. Siddall and Stewart (25) reported the hypersensitivity of the $^1I_6 \leftarrow {}^3H_4$ transition, which was contested by Peacock (24). To explain the anomalous behavior of Pr(III), Carnall *et al.* (26) together with Weber (27) put forward a theory in which certain assumptions made in Judd–Ofelt theory were considered to be invalid, in particular the assumption that the perturbation configurations are degenerate and lie at a higher energy level than $4f - 4f$ transitions. They also found that inclusion of the odd parts of the intensity expression improves the interpretation of Pr(III) absorption spectral intensities slightly. Using this method one finds that the $^3P_{2,1,0} \leftarrow {}^3H_4$ multiplets have $\lambda = 5$ reduced matrix values of 0.283, 0.502, and 0.0 respectively. If this is correct, the discrepancies in the oscillator strength would be more pronounced in the $^3P_1 \leftarrow {}^3H_4$ transition as the reduced matrix element has a higher value than that for $^3P_2 \leftarrow {}^3H_4$. Since this is not observed, the hypersensitivity of the $^3P_2 \leftarrow {}^3H_4$ transition observed by Peacock (24) cannot be explained by this argument.

The T_2 parameter, which is considered to be extremely sensitive towards even minor changes in the immediate coordination environment, is found generally to be negative in value (17, 21, 24). This is reasonable as only the $^3F_2 \leftarrow {}^3H_4$ transition has a significant **U** (2) matrix element but this has not been included in the data set of any of the compounds studied in solution (28, 29, 31). In Pr(III) the variation of the T_6 parameter appears to be related to changes in the immediate coordination sphere around Pr (Table 1).

There has been some difficulty in obtaining a good fit between the observed and calculated oscillator strength of the f–f transitions. Our method, however, of using partial and multiple regression has yielded quite satisfactory results for the $^3P_2 \leftarrow {}^3H_4$ and $^1D_2 \leftarrow {}^3H_4$ transitions while it marginally overestimates values for $^3P_1 \leftarrow {}^3H_4$ and underestimates the values for $^3P_0 \leftarrow {}^3H_4$ transitions (17, 21, 33). The RMS deviations in the oscillator strength values computed by our method were much smaller than those observed by Peacock (24).

An examination of Carnall's coefficients for **U** (2) shows that these are nearly the same for the $^3P_0$ and $^3P_1$ bands; consequently these bands should show the same strengths. One observes, however, that the intensity of the $^3P_1$ band is higher than that of $^3P_0$. There are two possible ways of making the oscillator strengths of $^3P_0$ and $^3P_1$ equal; the first is to use a positive correction factor by setting $T_7 = (^3P_1 - {}^3P_0)$ and the second is to use a negative correction factor $T_8 = (^3P_0 - {}^3P_1)$. At present it is not clear which one of these approaches is the correct one. As expected, however, the introduction of these correction factors does eliminate some of the discrepancy in the oscillator strengths of Pr(III). We are currently working on the detail and feasibility of these correction parameters (17, 21).

Values of the T_λ parameters consist of both vibronic and static components. The variation of T_λ with changes in the chemical environment can be determined by crystal field parameters A_{tP}, which depend upon the position (angular and radial) and the charges of the surrounding ligands. In lanthanide species other than Pr(III), T_2 varies significantly with minor changes in the immediate coordination sphere around the ion while T_4 and T_6 are relatively insensitive. This makes the intensities of non-hypersensitive transitions of little use in solving structural problems. In practice both the oscillator strengths of the transitions and the T_λ parameters have provided significant structural information about lanthanide coordination, especially in solution. In complexes of sufficiently low symmetry the oscillator strength of the hypersensitive transitions is of such magnitude that their description in terms of a forced electric dipole mechanism becomes meaningless.

The f–f transitions are weakly allowed if the energy of the excited state is lowered due to some mixing of the excited states with opposite parity into the ground state as a result of configuration interaction. Substantial intensification of the hypersensitive transitions may be gained by the mixing of metal $4f$ and ligand wave functions due to the increased probability of orbital overlap. With the introduction of covalency in the metal–ligand bond the possibility for a mixing of states with opposite parity improves and relaxes the rules for $4f$–$4f$ transitions leading to the intensification of the f–f bands. Iftikar *et al.* (31) have observed remarkably high intensification of the hypersensitive bands of Nd(III) and Er(III), which they ascribed to eigen perturbation.

During the course of our work with Pr(III) complexes (21) we noted that none of the observed transitions in the 350–1100 nm range (i.e., $^3P_2$, $^3P_1$, $^3P_0$, and $^1D_2 \leftarrow {}^3H_4$) can be considered hypersensitive in an orthodox sense. However, these transitions exhibit very high intensification and a wide variation of their oscillator strengths. The complexes investigated contain ligands with quite different binding features (e.g., haloacetate, amino acid derivatives, mixed ligand, diols (forming chelate rings of varying sizes 5–9-membered), β-diketonates, phenanthroline, nucleic bases, nucleosides, nucleotides, fluorinated nucleic bases, fluorinated nucleosides, Schiff bases, and alkoxides). These complexes have been well characterized by elemental analysis, IR spectroscopy, molecular weight determination, magnetic susceptibilities, conductivities, and thermal analysis.

Complexes with similar types of ligands have been tabulated together with the data on oscillator strengths and T_λ parameters and can be found in Table 1.

Pr(III) alkoxides

The alkoxides of Pr(III) of the general formula $Pr(OR)_3$ and $Pr[Al(OR)_4]_3$ where R = $C_3H_7^i$, $C_4H_9^n$, $C_4H_9^s$, $C_4H_9^t$, $C_5H_{11}^n$, $C_5H_{11}^{neo}$, $C_5H_{11}^t$ gave strong $4f$–$4f$ bands with very high oscillator strengths. These compounds also exhibit substantially high nephelauxetic, bonding, and covalency parameters, which is supported by their solubility in non-

TABLE 1. Observed oscillator strength (P) of $^3H_4 \rightarrow {}^3P_2$, $^3P_1$, $^3P_0$, and $^1D_2$ transitions and Judd–Ofelt (T_λ) parameters computed from the spectra of Pr(III) complexes with different ligands

Complexes 1	$P(^3H_4 \rightarrow {}^3P_2)$ 2	$P(^3H_4 \rightarrow {}^3P_1)$ 3	$P(^3H_4 \rightarrow {}^3P_0)$ 4	$P(^3H_4 \rightarrow {}^1D_2)$ 5	T_2 6	T_4 7	T_6 8
Complexes I: Alkoxides							
$Pr(OC_3H_7^i)_3$	28.53	10.88	3.40	10.18	−45.91	1.97	33.69
$Pr(OC_4H_9^n)_3$	16.44	4.74	2.84	5.37	−275.9	1.05	19.54
$Pr(OC_4H_9^s)_3$	20.19	5.30	3.46	10.37	−163.00	1.21	23.99
$Pr(OC_4H_9^i)_3$	34.45	18.23	5.23	15.39	468.6	3.24	39.65
$Pr(OC_5H_{11}^n)_3$	27.84	8.95	5.20	7.07	497.9	1.95	32.28
$Pr(OC_5H_{11}^{neo})_3$	34.04	20.36	4.90	10.63	558.2	4.15	38.42
$Pr(OC_5H_{11}^i)_3$	34.88	20.36	10.97	12.46	526.8	4.33	39.26
$Pr[Al(OC_3H_7)_4]_3$	40.68	25.40	14.87	10.69	−700.9	5.56	45.63
$Pr[Al(OC_4H_9^i)_4]_2$	50.45	30.30	17.53	12.53	−889.9	6.33	56.54
Complexes II: β-diketonates							
$Pr(acac)(H_2O)_6$, pH 2, EtOH	5.206	1.627	1.156	1.138	−110.13	0.187	6.447
$Pr(acac)(H_2O)_6$, pH 5, EtOH	6.647	2.400	1.753	1.717	−124.4	0.294	8.013
$Pr(acac)(H_2O)_6$, pH 2, DMF	8.432	3.607	1.839	2.694	−151.5	0.511	10.049
$Pr(acac)(H_2O)_6$, pH 5, DMF	9.502	4.199	3.1133	3.092	−158.6	0.571	11.341
Pr–butanediol(1:1), pH 2.0 (H_2O)	5.509	2.021	1.515	1.711	−93.20	0.425	6.464
Pr-butanediol (1:1), pH 2 (H_2O)	5.251	2.155	1.551	1.706	−86.83	0.432	6.135
Pr–butyne-1,4-diol (1:1), pH 2 (H_2O)	5.533	1.944	1.840	1.749	−95.41	0.407	6.513
Pr–butane-1,4-diol (1:1), pH 5.0 (H_2O)	5.951	2.542	1.840	1.749	−102.28	0.573	6.928
Pr-butene-1,4-diol (1:1), pH 5.0 (H_2O)	6.533	3.092	2.300	2.439	−99.43	0.641	7.524
Pr-butyne-1,4-diol (1:1), pH 5.0 (H_2O)	7.134	3.303	2.570	3.568	−87.84	0.716	8.202
Pr-butane-1,4-diol (1:1), pH 2, 80% DMF–20% H_2O	6.386	2.381	1.682	1.534	−118.65	0.469	7.517
Pr–butene-1,4-diol (1:1), pH 2, 80% DMF–20% H_2O	9.164	4.001	2.926	2.577	−160.05	0.817	10.675
Pr–butyne-1,4-diol (1:1), pH 2, 80% DMF–20% H_2O	9.180	3.694	2.845	2.487	−162.46	0.801	10.697
Pr–butane-1,4-diol (1:2), pH ~ 2	9.485	5.111	3.774	3.247	−168.69	1.055	10.838
Pr–butene-1,4-diol (1:2), pH ~ 2	10.140	4.682	3.536	3.247	−166.73	0.987	11.714
Pr–butyne-1,4-diol (1:2), pH ~ 2	12.088	6.516	4.363	2.526	−228.87	1.219	13.929
Class III: Complexes with nucleic bases, nucleosides, and nucleotides							
Solvent: water–DMSO 50:50							
Pr–adenine (1:2), pH ~ 2 (H_2O)	5.84	2.02	1.02	1.73	−101.24	0.42	6.89
Pr–adenine (1:4), pH ~ 2 (H_2O)	5.48	3.07	1.49	2.39	−76.04	0.30	6.35
Pr–adenine (1:6), pH ~ 2 (H_2O)	5.89	2.55	0.95	1.10	−115.84	0.48	6.89
Pr–adenine (1:2), pH ~ 4.5	9.76	3.63	2.86	3.36	−155.04	0.90	11.28
Pr–adenine (1:4), pH ~ 4.5	6.48	2.08	1.92	3.30	−86.20	0.55	7.54
Pr–adenine (1:6), pH ~ 4.5	7.92	3.66	2.61	3.35	−110.05	0.89	9.02
Pr–adenosine (1:1), pH ~ 2	6.62	2.77	2.21	2.18	109.67	0.61	7.67
Pr–adenosine (1:2), pH ~ 2	7.98	4.02	3.04	3.00	−120.54	0.84	9.13
Pr–adenosine (1:3), pH ~ 2	8.48	4.91	3.62	3.56	−124.34	0.99	9.60
Pr–adenosine (1:1), pH ~ 4.5	7.09	2.92	2.40	2.36	−114.47	0.67	8.18
Pr–adenosine (1:2), pH ~ 4.5	9.72	5.56	3.44	3.89	−141.85	0.96	11.20
Pr–adenoisine (1:3), pH ~ 4.5	9.95	5.97	4.70	5.29	−110.60	1.31	11.10
Pr–uracil (1:2), pH ~ 4.5	8.352	3.131	1.912	3.162	−143.80	0.698	10.570
Pr–uracil (1:4), pH ~ 4.5	9.180	3.694	2.868	2.487	−162.46	0.801	10.697
Pr–uracil (1:6), pH ~ 4.5	8.174	3.778	2.910	2.550	−149.27	0.813	10.106
Pr–bromouracil (1:2), pH ~ 4.5	5.592	1.442	1.074	0.817	−94.03	0.567	6.714
Pr–bromouracil (1:4), pH ~ 4.5	4.814	2.645	2.033	1.931	−93.985	0.567	6.714
Pr–bromouracil (1:6), pH ~ 4.5	5.928	2.658	1.957	1.952	−96.785	0.597	6.887
Pr–fluorouracil (1:2), pH ~ 4.5	5.594	2.168	1.656	1.320	−103.82	0.462	6.646
Pr–fluorouracil (1:4), pH ~ 4.5	6.084	1.925	1.572	0.892	−126.31	0.439	7.190
Pr–fluorouracil (1:6), pH ~ 4.5	6.138	2.165	1.728	1.067	−123.07	0.482	7.215
Pr–thymine (1:2), pH ~ 4.5	11.18	4.075	2.272	3.02	−197.87	0.877	13.050
Pr–thymine (1:4), pH ~ 4.5	14.412	4.727	2.927	2.790	−283.48	1.060	13.050
Pr–thymine (1:6), pH ~ 4.5	12.451	3.979	2.165	2.315	−198.566	0.821	13.625
Pr–thiouracil (1:2), pH ~ 4.5	5.653	2.376	1.760	0.618	−121.15	0.490	6.552
Pr–thiouracil (1:4), pH ~ 4.5	5.806	0.778	0.554	0.528	−131.62	0.152	7.132
Pr–thiouracil (1:6), pH ~ 4.5	5.592	1.442	1.074	0.817	−117.64	0.300	6.316
Pr–cytosine (1:2), pH ~ 4.5	4.383	1.946	0.930	1.280	−101.34	0.397	5.082

Can. J. Chem. Downloaded from www.nrcresearchpress.com by 123.30.183.119 on 09/08/12
For personal use only.

TABLE I (*continued*)

1	2	3	4	5	6	7	8
Pr–cytosine (1:4), pH ~ 4.5	5.615	2.222	1.057	1.823	−92.94	0.452	6.567
Pr–cytosine (1:6), pH ~ 4.5	5.837	2.082	1.117	1.358	−109.22	0.442	6.835
Pr–uridine (1:1), pH ~ 4.5	9.129	5.622	2.532	2.436	−157.9	1.128	10.306
Pr–uridine (1:2), pH ~ 4.5	11.033	4.566	2.582	1.453	−229.79	0.988	12.818
Pr–uridine (1:3), pH ~ 4.5	16.093	6.488	3.930	3.819	−296.91	1.442	18.736
Pr–thymidine (1:1), pH ~ 4.5	12.088	6.816	2.580	2.522	−228.99	1.219	13.929
Pr–thymidine (1:2), pH ~ 4.5	15.21	7.026	3.930	4.868	−250.10	1.48	17.570
Pr–thymidine (1:3), pH ~ 4.5	13.103	4.399	2.303	3.663	−250.04	0.740	17.57
Pr–cytidine (1:1), pH ~ 4.5	5.762	1.565	0.801	1.2281	−111.15	0.381	6.824
Pr–cytidine (1:2), pH ~ 4.5	6.172	2.089	1.038	1.531	−113.68	0.433	7.282
Pr–cytidine (1:3), pH ~ 4.5	6.370	2.428	1.148	1.767	−112.686	0.439	7.480
Pr–fluoroadenine (1:2), pH ~ 4.5	5.895	2.553	1.734	1.105	−115.82	0.483	6.888
Pr–fluoroadenine (1:4), pH ~ 4.5	5.847	2.021	1.508	1.773	−101.24	0.420	6.890
Pr–fluoroadenine (1:6), pH ~ 4.5	9.129	5.622	3.897	2.436	−157.90	1.128	10.306
Pr–fluorocytosine (1:2), pH ~ 4.5	5.594	3.363	2.380	2.075	−83.85	0.664	6.325
Pr–fluorocytosine (1:4), pH ~ 4.5	7.097	4.360	3.251	2.964	−97.85	0.906	7.960
Pr–fluorocytosine (1:6), pH ~ 4.5	9.600	4.514	3.180	3.44	−149.92	0.886	11.115
Pr–fluorothymine (1:2), pH ~ 4.5	4.89	2.198	1.792	1.482	−81.82	0.499	5.616
Pr–fluorothymine (1:4), pH ~ 4.5	5.408	1.904	1.573	1.485	−96.42	0.375	6.386
Pr–fluoroadenosine (1:1), pH ~ 4.5	5.361	2.135	1.636	1.303	−96.06	0.456	6.244
Pr–fluoroadenosine (1:2), pH ~ 4.5	7.928	3.667	2.619	3.558	−105.78	0.868	9.034
Pr–fluoroadenosine (1:3), pH ~ 4.5	9.763	3.635	2.865	3.364	−156.30	0.898	11.282
Pr–fluorouridine (1:1), pH ~ 4.5	5.176	2.393	1.746	1.740	−108.17	0.486	7.222
Pr–fluorouridine (1:2), pH ~ 4.5	6.083	1.829	1.356	1.546	−112.046	0.378	7.228
Pr–fluorouridine (1:3), pH ~ 4.5	10.792	5.393	4.272	2.772	−190.83	1.192	12.321
Pr–fluorocytidine (1:1), pH ~ 4.5	5.230	2.214	1.598	1.642	−87.50	0.445	6.093
Pr–fluorocytidine (1:2), pH ~ 4.5	5.442	1.901	2.347	1.482	−96.42	0.375	6.385
Pr–fluorocytidine (1:3), pH ~ 4.5	8.485	4.913	3.529	3.264	−66.521	0.983	5.908
Pr–fluorothymidine (1:1), pH ~ 4.5	6.620	2.765	2.161	2.108	−109.65	0.610	7.680
Pr–fluorothymidine (1:2), pH ~ 4.5	7.990	4.030	3.006	2.967	−120.50	0.836	9.136
Pr–fluorothymidine (1:3)	9.956	5.982	4.708	5.296	−110.51	1.316	11.108
(Solvent: water)							
Pr–AMP (1:1), pH ~ 3.0	5.87	1.83	1.53	1.47	−107.898	0.427	6.92
Pr–AMP (1:2), pH ~ 3.0	5.36	2.16	1.64	1.46	−96.060	0.456	6.245
Pr–AMP (1:3), pH ~ 3.0	5.34	2.07	1.58	1.41	−95.826	0.439	6.247
Pr–ADP (1:1), pH ~ 3.0	4.96	1.49	1.19	1.11	−94.34	0.334	5.873
Pr–ADP (1:2), pH ~ 3.0	4.27	1.46	1.11	1.04	−78.90	0.309	5.038
Pr–ADP (1:3), pH ~ 3.0	3.41	0.92	0.77	0.64	−67.85	0.215	4.058
Pr–ATP (1:1), pH ~ 3.0	5.40	1.90	1.35	1.48	−96.42	0.375	6.386
Pr–ATP (1:2), pH ~ 3.0	4.89	2.19	1.79	1.48	−81.82	0.498	5.616
Pr–ATP (1:3), pH ~ 3.0	5.64	2.03	1.57	1.75	−95.51	0.439	6.633
Pr–UMP (1:1), pH ~ 3.0	4.711	1.965	1.217	1.650	−74.34	0.439	5.447
Pr–UMP (1:2), pH ~ 3.0	5.306	1.808	1.142	1.487	−93.24	0.420	6.213
Pr–UMP (1:3), pH ~ 3.0	5.385	1.808	0.985	1.302	−99.70	0.397	6.334
Pr–CMP (1:1), pH ~ 3.0	5.508	2.077	1.173	1.661	−93.83	0.448	6.428
Pr–CMP (1:2), pH ~ 3.0	5.702	2.247	1.305	1.830	−94.25	0.490	6.627
Pr–CMP (1:3), pH ~ 3.0	6.673	2.43	1.445	2.072	−112.44	0.535	7.796
Solvent: DMSO–water 80:20, pH 3.0							
Pr–AMP (1:1)	5.97	2.32	1.647	1.459	−61.89	5.35	17.996
Pr–AMP (1:2)	7.597	2.295	1.501	1.259	−218.0	5.241	23.552
Pr–GMP (1:1)	6.854	3.468	1.715	3.187	264.02	7.15	20.548
Pr–GMP (1:2)	6.744	2.226	1.798	3.266	291.82	5.56	20.61
Pr–CMP (1:1)	5.704	2.884	1.472	3.532	419.71	6.009	17.089
Pr–CMP (1:2)	7.249	3.308	1.829	3.399	286.789	7.081	21.865
Pr–IMP (1:1)	11.434	4.220	2.410	2.631	−164.54	9.148	35.016
Pr–IMP (1:2)	12.944	4.713	2.780	3.178	−138.34	10.368	38.644
Pr–UMP (1:1)	7.833	2.829	1.752	3.344	236.79	6.32	23.98
Pr–UMP (1:2)	6.918	2.806	2.318	3.440	314.57	7.063	21.00
Pr–ATP (1:1)	6.667	2.455	1.269	1.286	−156.62	5.14	20.521
Pr–ATP (1:2)	6.286	2.306	1.487	1.638	−45.27	5.25	19.24
Haloacetates							
$Pr(MFA)_3$	13.8	5.0	2.6	2.8	3.03	1.05	4.21
$Pr(TFA)_3$	10.8	3.9	2.0	2.3	−2.14	0.81	3.29
$Pr(MC1A)_3$	11.6	4.8	2.9	2.7	−1.81	0.96	3.52

Can. J. Chem. Downloaded from www.nrcresearchpress.com by 123.30.183.119 on 09/08/12
For personal use only.

TABLE 1 (*concluded*)

1	2	3	4	5	6	7	8
$Pr(DC1A)_3$	11.6	4.7	3.4	3.3	−0.51	1.00	3.50
$Pr(TC1A)_3$	12.4	3.1	2.6	3.0	−1.65	0.73	3.84
$Pr(MBrA)_3$	15.8	7.1	2.7	2.2	−1.33	1.34	4.78
$Pr(DBrA)_3$	10.9	4.10	2.0	2.3	−2.20	0.84	3.32
$Pr(TBrA)_3$	10.7	3.5	1.8	2.5	−1.63	0.73	3.23
$Pr(HIA)_3$	11.6	4.2	2.0	2.0	−3.31	0.85	3.54
$Pr(MFA)_3$ in MeOH	17.187	3.317	0.880	2.807	−49.596	0.764	5.471
$Pr(MFA)_3$ in DMF	17.58	5.619	0.596	3.221	−42.87	0.852	5.519
$Pr(MFA)_3$ in DMSO	16.439	4.738	1.059	2.845	−14.238	0.7946	5.174
$Pr(MFA)_3$ in DMF + MeOH	16.837	4.530	2.810	3.622	55.44	1.012	5.2404
$Pr(MFA)_3$ in DMSO + MeOH	17.971	3.898	1.378	2.614	22.04	0.7266	5.6944
$Pr(MFA)_3$ in DMF + DMSO	18.507	3.663	2.079	2.814	2.103	0.7881	5.864
$Pr(MC1A)_3$ in MeOH	14.48	15.21	8.51	6.95	60.80	3.28	3.86
$Pr(MC1A)_3$ in DMF	28.53	10.88	3.06	10.12	43.11	1.99	8.81
$Pr(MC1A)_3$ in DMSO	27.38	8.95	5.14	6.95	23.00	1.94	8.40
$Pr(MC1A)_3$ in MeOH + DMF	16.59	2.68	3.53	7.40	57.85	8.62	5.20
$Pr(MC1A)_3$ in MeOH + DMSO	16.16	9.48	9.48	10.12	120.11	2.59	4.66
$Pr(MC1A)_3$ in DMF + DMSO	16.32	5.89	3.76	6.67	41.44	1.32	4.99
$Pr(MBrA)_3$ in MeOH	13.46	7.12	5.99	6.22	50.36	1.39	4.02
$Pr(MBrA)_3$ in DMF	30.72	11.57	3.48	5.36	−83.01	2.05	9.48
$Pr(MBrA)_3$ in DMSO	30.43	14.78	8.96	8.07	−21.97	3.25	9.09
$Pr(MBrA)_3$ in MeOH + DMF	16.81	5.62	2.70	2.88	−46.53	1.14	5.17
$Pr(MBrA)_3$ in MeOH + DMSO	16.88	8.99	3.24	4.69	−20.18	1.68	5.06
$Pr(MBrA)_3$ in DMF + DMSO	17.69	8.63	6.22	5.80	12.65	2.04	5.24
$Pr(MIA)_3$ in MeOH	34.45	20.26	9.18	10.59	9.34	4.04	10.21
$Pr(MIA)_3$ in DMF	52.48	30.40	8.61	12.58	−64.87	5.34	15.72
$Pr(MIA)_3$ in MeOH + DMF	27.89	22.90	22.71	15.34	−157.35	9.06	6.65
$Pr(MIA)_3$ in MeOH + DMSO	20.47	16.91	14.84	15.34	208.20	7.09	4.80
$Pr(MIA)_3$ DMF + DMSO	66.29	45.37	12.53	13.42	−97.51	7.92	17.46
Class V: Mixed ligand complexes: aminoacid and diol as ligand							
Solvent: water							
Pr(cysteine)(ethanediol) $(H_2O)_3$	13.3010	3.662	2.475	3.693	−4.906	0.845	4.152
Pr(cysteine)(propanediol) $(H_2O)_3$	14.7790	3.662	2.082	3.934	−35.06	1.412	3.832
Pr(cysteine)(butanediol) $(H_2O)_3$	16.634	5.0271	5.3538	0.5285	61.553	1.457	5.061
Pr(cysteine)(butenediol) $(H_2O)_3$	17.886	9.926	6.029	7.723	55.91	1.649	5.413
Pr(cysteine)(hexanediol) $(H_2O)_3$	17.747	5.280	2.2677	2.9373	56.612	0.632	5.6468
$Pr(cysteine)_2$(ethanediol) $(H_2O)_3$	14.4750	4.3517	4.5135	6.565	52.715	0.6325	5.6468
$Pr(cysteine)_2$(propanediol) $(H_2O)_3$	15.940	5.145	5.835	5.817	25.838	1.238	4.880
$Pr(cysteine)_2$(butenediol) $(H_2O)_3$	18.5070	5.668	5.998	5.498	2.870	0.789	5.846
Pr(cysteine)(hexanediol) $(H_2O)_3$	17.9710	3.898	4.289	4.289	13.390	0.7250	3.957
Pr(cysteine)(ethanediol) $(H_2O)_3$	12.920	2.880	1.197	2.587	−26.40	0.455	4.103
Pr(cysteine)(propanediol) $(H_2O)_3$	13.3620	2.472	2.051	3.591	−6.980	0.572	5.405
Pr(cysteine)(butenediol) $(H_2O)_3$	17.2920	3.487	3.326	5.716	15.326	0.927	5.405
Pr(cysteine)(hexanediol) $(H_2O)_3$	16.6130	3.662	3.107	5.420	13.005	0.867	5.199
Pr(histidine)(propanediol) $(H_2O)_3$	16.7140	3.9801	3.9228	5.7799	26.794	1.091	4.8503
Pr(histidine)(propanediol) $(H_2O)_3$	15.976	4.0956	3.9601	5.4150	16.643	1.1113	4.9380
Pr(histidine)(butanediol) $(H_2O)_3$	16.1790	4.4861	3.2748	5.6165	19.925	1.0681	5.016
Pr(histidine)(butenediol) $(H_2O)_3$	17.1940	3.9338	3.0348	3.4780	−34.710	0.8483	5.407
Pr(histidine)(pentanediol) $(H_2O)_3$	16.2920	6.3197	3.5288	5.7682	22.637	1.353	4.965
Pr(histidine)(hexanediol) $(H_2O)_3$	16.7020	7.4144	3.6338	4.9896	1.976	1.3848	5.0905
Pr(histidine)(ethanediol)$_2$ $(H_2O)_3$	14.309	4.5825	1.7172	4.6350	8.035	0.8671	4.446
Pr(histidine)(butenediol)$_2$ $(H_2O)_3$	16.6370	4.5301	3.6173	7.8667	68.223	1.009	5.1696
Pr(histidine)(pentanediol)$_2$ $(H_2O)_3$	15.7690	3.2629	1.9300	3.0154	−35.661	0.528	5.026
Pr(histidine)(hexanediol)$_2$ $(H_2O)_3$	16.4390	4.7382	1.5987	5.3678	13.163	0.7937	5.1624
Class VI: Schiff base derivatives							
Solvent: ethanol							
$Pr(VPDA)Cl(H_2O)_3$	10.98	4.51	3.12	3.71	−89.66	10.57	36.33
$Pr(VtZCZ)Cl(H_2O)_3$	11.57	4.72	3.60	4.02	−72.41	11.54	44.59
$Pr(V–PhDA)Cl(H_2O)_3$	11.96	4.89	3.51	4.09	−86.21	11.65	39.52
$Pr(V–NA)_2Cl(H_2O)_3$	12.46	4.96	3.90	4.41	−58.62	12.79	41.14
$Pr(V–DTA)Cl(H_2O)_3$	13.45	5.30	3.96	4.85	−48.28	12.87	44.29
$Pr(V–o\text{-phenet})Cl(H_2O)_3$	16.34	7.10	5.81	6.01	−34.48	17.95	53.57
$Pr(V–p\text{-phenet})Cl(H_2O)_3$	18.43	6.70	6.38	6.81	−31.03	18.48	60.95

Can. J. Chem. Downloaded from www.nrcresearchpress.com by 123.30.183.119 on 09/08/12
For personal use only.

Can. J. Chem. Downloaded from www.nrcresearchpress.com by 123.30.183.119 on 09/08/12
For personal use only.

polar organic solvents and the volatility of the *tert*-butoxide, neopentyl oxide, and *tert*-pentyl oxides. The bimetallic alkoxides are much more volatile as evidenced by the easy ability to either distil or sublime the compounds. These characteristics suggest that these compounds contain a substantial amount of covalency in hitherto predominantly ionic Pr–ligand bonds. The oscillator strengths (P) of the four pseudohypersensitive transitions are as follows:

$$^3P_2 \leftarrow {}^3H_4 \quad (16.44\text{–}50.45) \times 10^{-6}$$
$$^3P_1 \leftarrow {}^3H_4 \quad (4.74\text{–}30.30) \times 10^{-6}$$
$$^3P_0 \leftarrow {}^3H_4 \quad (2.84\text{–}17.53) \times 10^{-6}$$
$$^1D_2 \leftarrow {}^3H_4 \quad (5.37\text{–}15.39) \times 10^{-6}$$

The variation of oscillator strength is up to 600% though none of these transitions follow the selection rules for quadrapole transitions and thus cannot be considered to be hypersensitive. We regard these transitions as pseudohypersensitive in nature.

β-Diketonates and diol derivatives

Comprising bifunctional bidentate ligands such as acetylacetone, butane-1,4-, butene-1,4-, and butyne-1, 4-diols, these complexes were investigated at pH = 2.0 and 5.0 in water and DMF by following absorption difference and comparative absorption spectrophotometry. All show a significant variation of intensities for the pseudohypersensitive transitions. The diols are all related, differing only in the bond order (1–3) between the 2nd and 3rd carbon atoms of the diol function. Table 1 shows that the oscillator strength of the transition increases in the order: butane-1,4 < butene-1,4 < butyne-1,4. This ordering suggests that the π-electron density of the butene-1,4 and butyne-1,4 is having some effect of the Pr(III) diol binding.

$$^3P_2 \leftarrow {}^3H_4 \quad (5.206\text{–}12.088) \times 10^{-6}$$
$$^3P_1 \leftarrow {}^3H_4 \quad (1.627\text{–}6.516) \times 10^{-6}$$
$$^3P_0 \leftarrow {}^3H_4 \quad (1.158\text{–}4.363) \times 10^{-6}$$
$$^1D_2 \leftarrow {}^3H_4 \quad (1.138\text{–}3.568) \times 10^{-6}$$

The high sensitivity of these nonhypersensitive transitions is evidenced by the 350% variation in oscillator strengths.

Complexes of nucleic bases, nucleosides, and nucleotides including fluorinated nucleic bases and fluorinated nucleosides

The nucleic bases and nucleosides including their fluorinated analogues possess several potential donor sites yet these ligands form predominantly outer sphere complexes in aqueous medium. The complexes with nucleotides, on the contrary, are essentially ionic and show strong complexation in the solid state with an octa-coordinated environment around the Pr cation. These nucleic bases, nucleosides, and their fluorinated analogues behave differently in aqueous and semi-nonaqueous (equimolar mixture of DMSO and water) media. In water these biomolecules become highly hydrated by weakening the water structure while in semi-nonaqueous media they appear to strengthen the three-dimensional water structure and thus are less hydrated, behaving as better ligands. The presence of an electron-withdrawing fluorine on the biomolecules appears to make them a better ligand, as indicated by the higher oscillator strengths of the pseudohypersensitive transitions.

$$^3P_2 \leftarrow {}^3H_4 \quad (3.141\text{–}16.093) \times 10^{-6}$$
$$^3P_1 \leftarrow {}^3H_4 \quad (0.925\text{–}6.488) \times 10^{-6}$$
$$^3P_0 \leftarrow {}^3H_4 \quad (0.801\text{–}4.70) \times 10^{-6}$$
$$^1D_2 \leftarrow {}^3H_4 \quad (0.528\text{–}4.868) \times 10^{-6}$$

The variation in oscillator strengths observed here is up to 750%. Again all transitions are non-hypersensitive.

Haloacetates

These compounds are highly ionic in nature and soluble in water, ethanol, and polar organic solvents. They behave as 1:2 electrolytes and produce highly conducting aqueous solutions. In the solid state bidentate and dimeric haloacetate attachment is observed, which provides a noncoordinated Pr(III) with three additional water molecules of coordination. These compounds show small magnitudes for the nephelauxetic, covalency, and bonding parameters as well as weak $4f$–$4f$ bands

$$^3P_2 \leftarrow {}^3H_4 \quad (10.70\text{–}15.80) \times 10^{-6}$$
$$^3P_1 \leftarrow {}^3H_4 \quad (3.10\text{–}7.10) \times 10^{-6}$$
$$^3P_0 \leftarrow {}^3H_4 \quad (1.80\text{–}3.40) \times 10^{-6}$$
$$^1D_2 \leftarrow {}^3H_4 \quad (2.0\text{–}3.30) \times 10^{-6}$$

The variation of the observed oscillator strengths for the pseudohypersensitive transitions is of a much smaller magnitude, which is understandable in view of the highly ionic nature of these compounds. However, when the haloacetates are dissolved in methanol, DMF, DMSO, and equimolar binary mixtures the oscillator strengths of the pseudohypersensitive transitions show wide variations. This is most probably the result of a change in the immediate coordination environment around the Pr(III) cation when the coordinated solvent molecule changes from water (32) to polar nonaqueous (30).

$$^3P_2 \leftarrow {}^3H_4 \quad (13.46\text{–}87.01) \times 10^{-6}$$
$$^3P_1 \leftarrow {}^3H_4 \quad (2.68\text{–}45.37) \times 10^{-6}$$
$$^3P_0 \leftarrow {}^3H_4 \quad (0.596\text{–}22.71) \times 10^{-6}$$
$$^1D_2 \leftarrow {}^3H_4 \quad (2.614\text{–}18.07) \times 10^{-6}$$

The extremely wide range of oscillator strengths of the pseudohypersensitive transitions appears to be abnormally high. This evidence suggests that the immediate Pr(III)–haloacetate coordination environment normally consisting of three bidentate haloacetates and three water molecules changes to an environment consisting of eight DMF, DMSO, or MeOH molecules in some combination. This brings about a drastic change in the immediate coordination sphere of the Pr cation when contrasted to the other studies where only partial changes in the immediate coordination sphere were observed.

Mixed ligand complexes

These complexes comprise an aminoacid cysteine/histidine as the primary ligand (A) and various diols as secondary ligands (B) and are of the type MAB, MAB_2, and MA_2B. The size of the ring formed by the aminoacid is fixed but the diols form chelate rings numbering 5, 6, 7, and 8 members and in consequence have varying stability (as shown by the stability constants of the different complexes (33)).

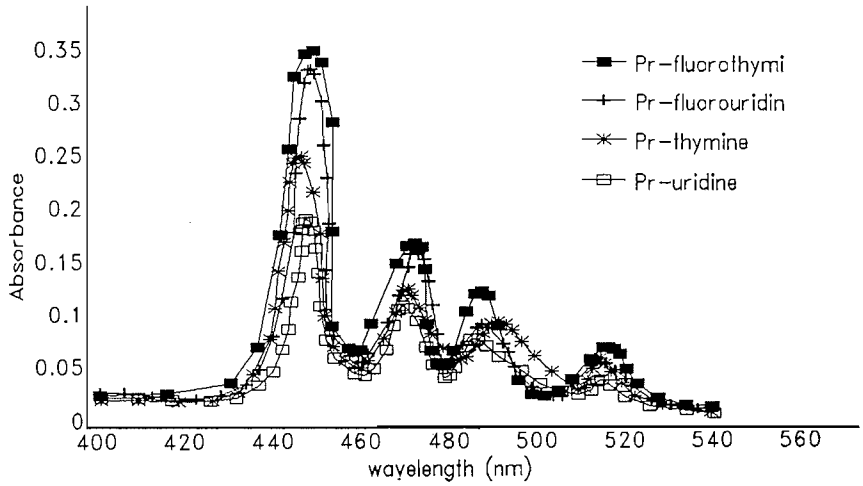

FIG. 1. Comparative absorption spectra of Pr(III)–uridine/thymidine/fluorouridine/fluorothymidine.

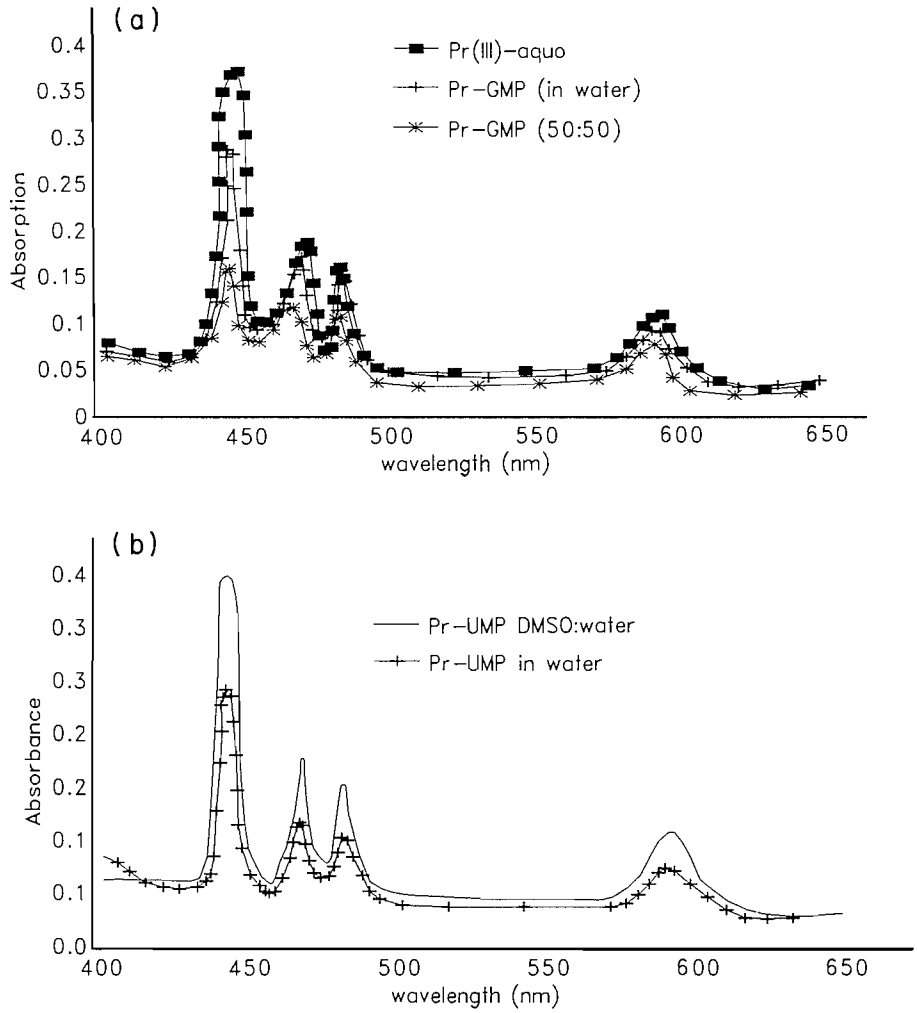

FIG. 2. (a) Comparative absorption spectra of $[Pr(aquo)_q]^{3+}$, $[Pr(GMP)H_2O)_x]^-$ in aqueous and DMSO–H_2O (50:50) media. (b) Comparative absorption spectra of Pr–UMP (1:1 molar ratio) in H_2O and DMSO–H_2O (50:50).

Can. J. Chem. Downloaded from www.nrcresearchpress.com by 123.30.183.119 on 09/08/12
For personal use only.

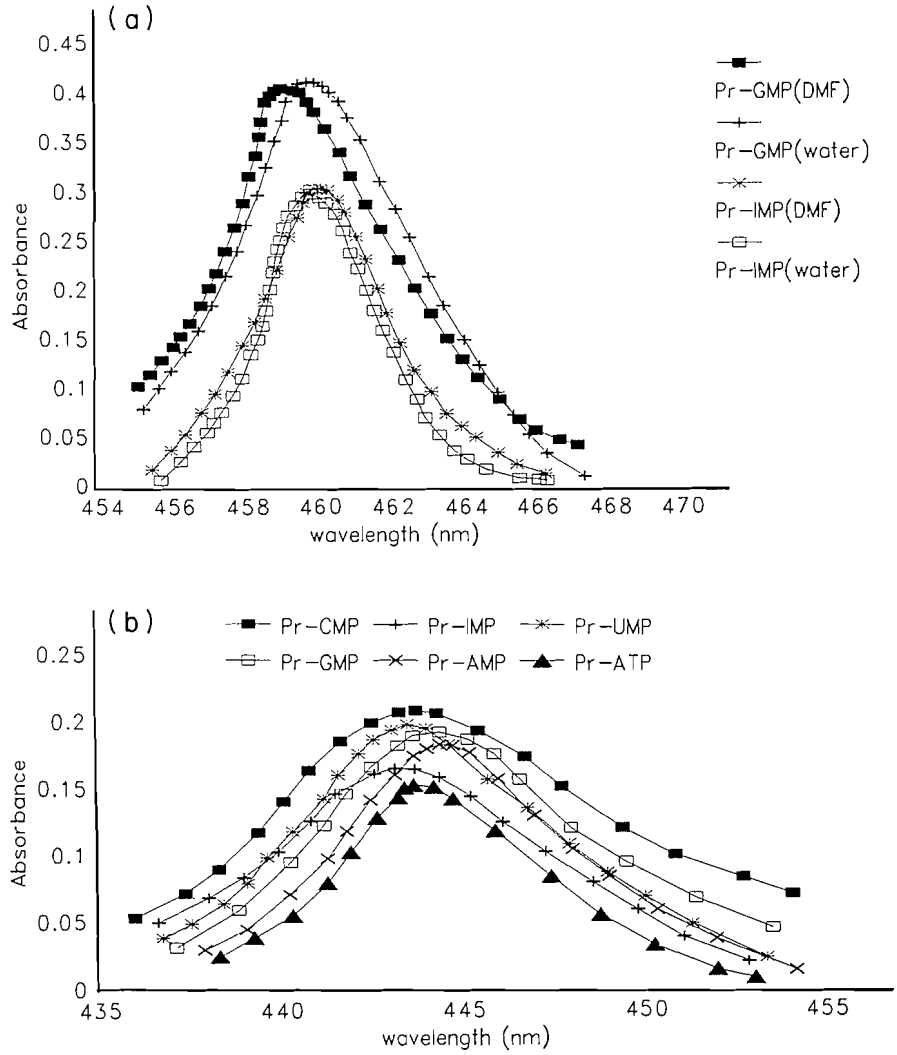

FIG. 3 (a) The pseudohypersensitive $^3H_4 \rightarrow {}^3P_2$ transition of Pr–GMP/IMP in H_2O and DMF. (b) The pseudohypersensitive $^3H_4 \rightarrow {}^3P_2$ transition of Pr(III) with various nucleotides.

$$^3P_2 \leftarrow {}^3H_4 \quad (13.301\text{–}18.5070) \times 10^{-6}$$
$$^3P_1 \leftarrow {}^3H_4 \quad (2.472\text{–}9.926) \times 10^{-6}$$
$$^3P_0 \leftarrow {}^3H_4 \quad (1.197\text{–}6.029) \times 10^{-6}$$
$$^1D_2 \leftarrow {}^3H_4 \quad (1.7172\text{–}8.5285) \times 10^{-6}$$

The values of the oscillator strengths are much lower than expected for such complexes with significant inner sphere complexation. The presence of the oxygen donor diol ligand enhances the overall stability of the complex and will naturally induce some intensification of the bands. The plots of the stability constants versus oscillator strengths of these pseudohypersensitive transitions, especially $^3P_2 \leftarrow {}^3H_4$ and $^1D_2 \leftarrow {}^3H_4$, give a linear correlation with a positive slope, which indicates that the stability of the species contributed towards the intensification of the $4f$–$4f$ bands (33). At the same time the nephelauxetic effect brings the metal closer to the ligand and thus enhances the probability of orbital overlap. The increased stability of the complexes appears to be due to the better participation of the metal $4f$ orbitals in bonding with the ligands (33).

Schiff base complexes

The Schiff bases derived from vanillin and propylene diamine, *o*-phenylene diamine, *oc*-naphthylamine, *o*-phenetidine, *p*-phenetidine, and thiosemicarbazide offer coordinating centers such as O, N, and S and can be either bidentate or tetradentate, which provides several different coordinating environments for Pr(III). These complexes are predominantly inner sphere complexes and have one chlorine and three water molecules in the inner sphere of coordination yielding an octacoordinated Pr(III) (34).

$$^3P_2 \leftarrow {}^3H_4 \quad (10.98\text{–}18.43) \times 10^{-6}$$
$$^3P_1 \leftarrow {}^3H_4 \quad (4.51\text{–}18.43) \times 10^{-6}$$
$$^3P_0 \leftarrow {}^3H_4 \quad (3.10\text{–}7.10) \times 10^{-6}$$
$$^1D_2 \leftarrow {}^3H_4 \quad (3.71\text{–}6.38) \times 10^{-6}$$

The comparatively low magnitude of the oscillator strengths for these pseudohypersensitive transitions in spite of the attached Schiff base is most probably due to the presence of a chloride anion in the inner sphere, which induces sufficient ionicity in these chelates to lower the observed intensities.

Can. J. Chem. Downloaded from www.nrcresearchpress.com by 123.30.183.119 on 09/08/12
For personal use only.

Can. J. Chem. Downloaded from www.nrcresearchpress.com by 123.30.183.119 on 09/08/12
For personal use only.

Comparative absorption spectral studies

The comparative absorption spectra of Pr–uridine, –thymine, –fluorouridine, and –fluorothymidine are shown in Fig. 1. The spectra show clearly that all four nonhypersensitive bands are varying in shape, energy, and oscillator strengths. These ligands coordinate to Pr(III) through the ribose hydroxyl group with weak participation of the carbonyl oxygen. Thus, nearly identical immediate coordination spheres are present around the Pr(III); however, the presence of fluorine in the fluorinated nucleosides induced substantial intensification of the pseudohypersensitive transitions.

Figures 2(a) and 2(b) show that even when Pr(III) is coordinated with the same ligand, changes in the solvent significantly influence the oscillator strengths of the $4f$–$4f$ bands.

Figure 3 shows the different affinities of various nucleotides towards Pr(III). Even though each of the nucleotides binds predominantly through the phosphate oxygen, clear differences in the band shape, energy, and oscillator strength are evident, which suggests that there is also involvement of the nucleic base.

These spectra taken together clearly show that minor changes in the immediate coordination environment of Pr(III) indeed cause significant intensification of these pseudohypersensitive bands.

Conclusion

Since the values of the T_2 parameters in most of the complexes are negative it becomes meaningless. The T_6 parameter, however, appears to show a definite trend with the changes in the coordination environment. The wide variation of oscillator strengths for the $4f$–$4f$ transitions in all the complexes described in the work are as follows:

$$^3P_2 \leftarrow {}^3H_4 \quad (3.410\text{–}87.01) \times 10^{-6}$$

$$^3P_1 \leftarrow {}^3H_4 \quad (0.925\text{–}45.37) \times 10^{-6}$$

$$^3P_0 \leftarrow {}^3H_4 \quad (0.596\text{–}22.71) \times 10^{-6}$$

$$^1D_2 \leftarrow {}^3H_4 \quad (0.528\text{–}18.07) \times 10^{-6}$$

In summary, one observes that the percentage variation in the oscillator strength of these pseudohypersensitive transitions is very high and they appear to behave much like hypersensitive transitions. The binding characteristics of the ligand, geometry of the complex formed, and the introduction of some covalency appear to relax the selection rules by lowering the energy of the excited state of these transitions. Other factors may also contribute to the enhancement and sensitivity of these transitions:

(*i*) The second-order interactions, which are two orders of magnitude less than the coulombic interactions (generally ignored), may become prominent by the ligating characteristics of the coordinating molecule. This may lower the excited state of these pseudohypersensitive transitions and in consequence their transition probability is enhanced.

(*ii*) The nephelauxetic effect may induce some broadening of the bands and hence may contribute to the intensification of the bands.

(*iii*) These transitions may be borrowing intensities from neighboring transitions.

1. D. E. Henrie, R. L. Fellows, and G. R. Choppin. Coord. Chem. Rev. **18**, 199 (1976).
2. K. B. Yatsimirskii and N. K. Davidenko. Coord. Chem. Rev. **27**, 223 (1979).
3. C. K. Jorgensen and B. R. Judd. Mol. Phys. **8**, 281 (1964).
4. D. G. Karraker. Inorg. Chem. **6**, 1863 (1967); **8**, 473 (1969); J. Inorg. Nucl. Chem. **33**, 3713 (1971).
5. C. K. Jorgensen. Oxidation number and oxidation states. Springer, New York. 1969.
6. C. K. Jorgensen. Struct. Bonding (Berlin), **13**, 199 (1973); Modern aspects of ligand field theory. North Holland Publishing Co., Amsterdam. 1971.
7. V. S. Khomenko, M. D. Lozinskii, Yu A. Fialkov, L. I. Krasovskaya, and I. Rasshinina. Koord. Khim. **12**, 740 (1986).
8. A. F. Borina. Zh. Neorg. Khim. **33**, 1696 (1988).
9. K. Bukeitynska and A. Mondry. Inorg. Chim. Acta, **130**, 145 (1987); **130**, 271 (1987).
10. (*a*) N. K. Davidenko and L. N. Lugina. J. Inorg. Chem. **13**, 980 (1968); J. Coord. Chem. **3**, 193 (1977); (*b*) A. G. Goryushko, N. K. Davidenko, and K. B. Yatsimirskin. J. Inorg. Chem. **18**, 1783 (1973); (*c*) A. G. Goryushko and N. K. Davidenko. J. Inorg. Chem. **19**, 1722 (1974).
11. K. Reisfeld. Struct. Bonding (Berlin), **13**, 53 (1973); **22**, 123 (1975).
12. (*a*) S. F. Mason, R. D. Peacock, and B. Stewart. Mol. Phys. **30**, 1829 (1975); (*b*) S. F. Mason and R. M. Seal. Mol. Phys. **31**, 755 (1976).
13. (*a*) S. F. Mason and B. Stewart. Mol. Phys. **35**, 611 (1986); (*b*) S. F. Mason. Inorg. Chim. Acta, **94**, 812 (1984); J. Indian Chem. Soc. **63**, 73 (1986).
14. J. C. Fuggle. NATO ASI Ser. Ser. B: **151**, 381 (1987).
15. W. C. Gorlla, P. Vandvelde, and Y. Hendrick. Inorg. Chim. Acta, **143**, 259 (1988).
16. (*a*) M. A. Tischenko, C. V. Malenleva, Z. A. Khafagi, M. P. Spirikhina, V. V. Tischenko, and U. A. Shaptun. Koord. Khim. **14**, 763 (1988); (*b*) M. T. Burry. Diss. Abstr. Int. B: **49**, 2204 (1988); Chem. Abstr. **110**, 124022 (1989).
17. (*a*) S. N. Misra. J. Sci. Ind. Res. **44**, 366 (1985); (*b*) S. N. Misra and A. Kothari. Can. J. Chem. **61**, 1778 (1983); (*c*) S. N. Misra and W. N. Cabalfin. Chem. Scr. **27**, 75 (1989); (*d*) S. N. Misra, G. Joseph, and K. Anjaiah. Chem. Scr. **28**, 333 (1990).
18. (*a*) K. Bukeitynska and P. Ngoethey. Inorg. Chim. Acta, **132**, 21 (1987); (*b*) K. Bukietynka and A. Mondry. Inorg. Chim. Acta, **130**, 145 (1987).
19. R. C. Holz and L. C. Thompson. Inorg. Chem. **27**, 4640 (1988).
20. M. T. Devlin, E. M. Stephens, and F. S. Richardson. Inorg. Chem. **27**, 1517 (1988).
21. S. N. Misra, K. J. Shah, G. Joseph, K. Anjaiah, and K. Venkatasubramanian. Indian J. Chem. **28A**, 267 (1990).
22. B. R. Judd. Phys. Rev. **A127**, 750 (1962).
23. G. S. Ofelt. J. Chem. Phys. **31**, 571 (1962).
24. R. D. Peacock. J. Chem. Soc. A, 2028 (1971); Chem. Phys. Lett. **7**, 187 (1970); Struct. Bonding (Berlin), **22**, 83 (1975).
25. T. H. Siddall and W. E. Stewart. J. Inorg. Nucl. Chem. **32**, 1147 (1970).
26. W. T. Carnall, P. R. Fields, and K. Rajnak. J. Chem. Phys. **49**, 4412 (1968).
27. M. J. Weber. J. Chem. Phys. **48**, 4774 (1968).
28. S. P. Tandon and P. C. Mehta. J. Chem. Phys. **52**, 4313 (1970).
29. K. Bukietynska and J. Choppin. J. Chem. Phys. **52**, 2875 (1970).
30. S. N. Misra, G. Joseph, K. Anjaiah, and K. Venkatasubramanian. Indian J. Chem. **26A**, 919 (1987); **28A**, 266 (1990).
31. K. Iftikar, S. Sayeed, and N. Ahmed. Inorg. Chem. **21**, 80 (1982).
32. S. S. L. Surana, M. Singh, and S. N. Misra. J. Inorg. Nucl. Chem. **42**, 61 (1980).
33. A. Kothari, S. N. Misra, A. Ahmed, and R. K. Jain. J. Inorg. Nucl. Chem. **43**, 2905 (1981).
34. S. N. Misra, G. K. Joshi, and M. Singh. Indian J. Chem. **23A**, 329 (1984).

Partial molar volumes of acidic gases in physical solvents and prediction of solubilities at high pressures

YUMING XU, LILI LI, AND LOREN G. HEPLER[1]

Department of Chemistry and Department of Chemical Engineering, University of Alberta, Edmonton, Alta., Canada T6G 2G2

Received March 22, 1991

YUMING XU, LILI LI, and LOREN G. HEPLER. Can. J. Chem. **70**, 55 (1992).

Partial molar volumes at infinite dilution for three acidic gases (carbon dioxide, hydrogen sulfide, and sulfur dioxide) in four physical solvents (propylene carbonate, methyl cyanoacetate, *N*-formyl morpholine, and Selexol) have been obtained using our new dilatometer. These partial molar volumes, in combination with the Henry's law constants obtained previously, have been used in the Krichevsky–Kasarnovsky equation for predicting the solubilities of acidic gases in physical solvents at high pressures.

Key words: partial molar volume, solubility, physical solvents.

YUMING XU, LILI LI et LOREN G. HEPLER. Can. J. Chem. **70**, 55 (1992).

Utilisant un nouveau dilatomètre, on a déterminé les volumes molaires partiels à dilution infinie de trois gaz acides (dioxyde de carbone, sulfure d'hydrogène et dioxyde de soufre) dans quatre solvants physiques (carbonate de propylène, cyanoacétate de méthyle, *N*-formyl morpholine et Séléxol). Dans le but de prédire les solubilités de ces gaz acides dans des solvants physiques à des pressions élevées, on a introduit ces volumes molaires partiels ainsi que les constantes de la loi de Henry obtenues antérieurement dans l'équation de Krichevsky–Kasarnovsky.

Mots clés : volume molaire partiel, solubilité, solvants physiques.

[Traduit par la rédaction]

Can. J. Chem. Downloaded from www.nrcresearchpress.com by 123.30.183.119 on 09/08/12
For personal use only.

Introduction

We have made measurements leading to the partial molar volumes of acidic gases (SO_2, H_2S, and CO_2) in "physical" solvents for two reasons. (1) One specific reason for making these measurements has been our interest in the use of physical solvents (called "physical" because there is no clear chemical reaction of acid–base type between solvent and solute) for the removal of acidic gases from industrial gas streams. (2) In addition to the specific reason mentioned above, we have a general interest in the use of results of low pressure measurements (partial molar volumes and Henry's law constants) for predicting the solubilities of gases at high pressures.

The simplest relationship between the pressure of a gas and its equilibrium solubility in a liquid solvent is Henry's law that we write as

$$[1] \quad f_2/X_2 = K_H \quad \text{or} \quad P_2/X_2 = K_H$$

in which f_2 and P_2 refer to the fugacity and pressure of the gas, and X_2 is the equilibrium mole fraction of the dissolved gas in the liquid phase. Because Henry's law is applicable only at low pressures, $f_2 \approx P_2$, it is proper to use either version of eq. [1].

Long ago Krichevsky and Kasarnovsky (1) considered the effects of high pressure on the solubilities of slightly soluble gases and derived the equation that is now known by their names:

$$[2] \quad \ln(f_2/X_2) = \ln K_H + [\bar{V}_2^0(P - P_1^0)]/RT$$

Symbols in this equation have the following meanings: f_2 is the fugacity of the gas at some specified total pressure P, X_2 is the equilibrium mole fraction of dissolved gas, K_H is the Henry's law constant, $\bar{V}_2^0$ is the low concentration partial molar volume of the dissolved gas, and P_1^0 is the equilibrium vapour pressure of the solvent at the specified temperature T. Prausnitz *et al.* (2) have provided a contemporary review of the thermodynamic basis of the Krichevsky–Kasarnovsky equation.

The Krichevsky–Kasarnovsky equation has been used most often as the basis of a method for convenient graphical presentation of gas solubility data and sometimes also as a method for screening such data for likely errors. Many of these applications refer to systems in which the vapour pressure of the pure solvent (P_1^0) is much smaller than the applied pressure so that eq. [2] can be simplified to

$$[3] \quad \ln(f_2/X_2) = \ln K_H + \bar{V}_2^0 P_2/RT$$

in which the total pressure and the partial pressure of gas are nearly identical as indicated by the use of P_2. In these common applications of the Krichevsky–Kasarnovsky equation [2] or [3], the fugacities are calculated for each pressure from the equation of state for the gas and then values of $\ln(f_2/X_2)$ are plotted against P_2, with the expectation of observing a (nearly) straight line. Points that fall far from an average smooth or straight line are often considered to be in error and are excluded from further consideration. One useful example of this kind of application has been provided recently by Lu *et al.* (3), who have screened reported solubilities of gases in bitumen.

Our principal interest has been in using the Krichevsky–Kasarnovsky equation in a different way; that is, we use values of K_H and $\bar{V}_2^0$ obtained from results of measurements at low pressures in eqs. [2] or [3] for prediction of the gas solubilities (X_2) at high pressures (P or P_2) and corresponding fugacities (f_2).

Because the Krichevsky–Kasarnovsky equation was derived specifically for gases that are very slightly soluble (such as H_2 in water), there has been considerable interest in modifying the original equation to allow for the kind of non-ideal solution effects that occur in less dilute solutions and that are represented by non-unity activity coefficients. The

[1]Author to whom correspondence may be addressed.

Can. J. Chem. Downloaded from www.nrcresearchpress.com by 123.30.183.119 on 09/08/12
For personal use only.

most commonly used equation of this type is the Krichevsky–Ilinskaya (4) equation that we write as

$$[4] \quad \ln (f_2/X_2) = \ln K_H + A(X_1^2 - 1)/RT + \bar{V}_2^0 P_2/RT$$

in which A is known as the Margules parameter and X_1 represents the equilibrium mole fraction of solvent in the solution that is saturated at pressure P_2. For slightly soluble gases (X_2 is very small and $X_1 \approx 1$), the middle term on the right side is negligible, and eq. [4] reduces to eq. [3].

There are several excellent reviews (5–8) of methods for measuring the partial molar volumes of gases in liquids. Most of these earlier methods are modifications of the method developed by Horiuti (9). Although these methods work well, we have chosen to use a simpler dilatometric and direct weighing method (10, 11) that is well suited to the present investigation of gases that are moderately soluble at ordinary atmospheric pressure.

Experimental

Our dilatometer consists of a Pyrex glass bulb (68 cm^3), fitted with a calibrated straight capillary tube (3 mm bore). To serve as a reference mark, a thin copper wire was attached halfway up the 100 mm long capillary. The open end of the capillary can be closed with a Nylon cap.

The solvent to be used is degassed with a vacuum pump and then loaded into the dilatometer with a hypodermic syringe until the solvent meniscus is about 10 mm up the capillary tube. The dilatometer is then closed with the Nylon cap and allowed to equilibrate in a constant temperature (±0.005 K) water bath. After thermal equilibrium has been achieved, the height (relative to the reference mark) of the meniscus is measured to ±0.2 mm with a cathetometer. The dilatometer is then removed from the water bath, dried, and weighed to ±0.0002 g.

The solute gas is introduced to the dilatometer under pressure slightly above atmospheric pressure, by way of Tygon tubing connecting the top of the capillary to a gas cylinder. The bulb is then placed in ice-water, causing the solvent to contract and a gas space of ≈1 cm^3 to be formed. This space is large enough to permit good mixing as a result of gentle shaking and rocking of the dilatometer. The intention is *not* necessarily to reach saturation as in most other methods, but merely to dissolve enough gas to permit determination of the amount of dissolved gas by accurate weighing.

The dilatometer is disconnected from the Tygon tubing, closed with the Nylon stopper, returned to the constant temperature bath, and left to equilibrate for 20–30 min. The final level of the meniscus (relative to the reference mark) and the final mass of the dilatometer plus contents are then measured.

The difference between the initial and final heights of the meniscus is combined with the cross-sectional area of the capillary to obtain the volume increase accompanying solution of the gas. Division of this volume by the number of moles of gas dissolved (calculated from masses) yields the apparent molar volume of the dissolved gas.

More information about construction and operation of the dilatometer is presented elsewhere (10, 11).

Propylene carbonate (99.0%) and methyl cyanoacetate (99.0%) were from Aldrich Chemicals. *N*-Formyl morpholine (99.0%) was from BASF. Selexol (a dimethyl ether of polyethylene glycol) from Harrisons and Crosfield Ltd. was examined in the Microanalytical Laboratory of the Department of Chemistry, University of Alberta, and found to contain 0.87% water and to have average molecular weight equal to 266 g/mol. High purity solute gases were from Matheson Gas Products Canada.

TABLE 1. Partial molar volumes ($cm^3\ mol^{-1}$)[a] of acidic gases in physical solvents at 25°C

Solvent	CO_2	H_2S	SO_2
Propylene carbonate	42.2	40.4	43.7
Methyl cyanoacetate	39.6	40.6	44.1
Selexol	42.2	38.5	39.8
N-Formyl morpholine	33.5	37.8[b]	33.1

[a]The standard deviations are all about 0.3 $cm^3\ mol^{-1}$ and total uncertainties are estimated to be ±0.5 $cm^3\ mol^{-1}$.

[b]The color of the solvent *N*-formyl morpholine changed from nearly colorless to light green to dark green as hydrogen sulfide dissolved.

Results

The apparent molar volumes ($V_{\phi,2}$) of solute gases that we have obtained directly from our measurements of volumes and masses are defined by

$$[5] \quad V_{\phi,2} = (V - n_1 v_1^0)/n_2$$

in which V is the total volume of solution, $n_1 v_1^0$ is the total volume of the pure solvent, and n_2 is the number of moles of dissolved gas. The partial molar volume ($\bar{V}_2$) of the dissolved gas is defined by

$$[6] \quad \bar{V}_2 = (\partial V/\partial n_2)_{T,P,n}$$

Combination of eqs. [5] and [6] leads to

$$[7] \quad \bar{V}_2 = V_{\phi,2} + n_2(\partial V_{\phi,2}/\partial n_2)_{T,P,n}$$

For sufficiently dilute solutions, the second term on the right of eq. [7] is negligible and we have the limiting equation

$$[8] \quad \bar{V}_2^0 = V_{\phi,2}^0$$

Typical mole fractions of dissolved gas in our experiments were in the range from 0.005 to 0.04. For these dilute solutions, as in previous investigations (10, 11), the second term on the right of eq. [7] is negligible so that eq. [8] permits evaluation of the desired limiting partial molar volumes from our experimental results, as summarized in Table 1. As discussed previously (10, 11), these partial molar volumes are accurate to about ±1% (≈ ±0.5 $cm^3\ mol^{-1}$).

We do not know of any volumetric measurements leading to partial molar volumes of CO_2, H_2S, or SO_2 in the solvents that we have investigated, so we are unable to make any direct comparisons of our results with those of prior investigations. We can, however, relate our present results to those from some other investigations as follows.

Previous investigations (7, 11) have shown that the partial molar volumes of SO_2 in "inert" solvents are all close to 55 $cm^3\ mol^{-1}$, while volumes of SO_2 in other solvents in which complexes are known or expected to form are distinctly smaller than 55 $cm^3\ mol^{-1}$. Although the "physical" solvents that we have investigated are not strongly basic (as are amines), it is still reasonable to expect that they are good solvents for acidic gases because of solvent–acidic gas interactions, which might be described as complex formation. Our partial molar volumes for SO_2 are all in the <55 $cm^3\ mol^{-1}$ range that has been identified (11) as characteristic of complex formation. Similar comparisons (7, 8) can be made for partial molar volumes of CO_2 in various solvents, again

with the conclusion that there are specific interactions between CO_2 and the solvents that we have investigated.

Jou *et al.* (12) have measured solubilities of CO_2 and H_2S in *N*-formyl morpholine and have analyzed their experimental results in terms of the Krichevsky–Ilinskaya equation [4] and thence calculated $\bar{V}_2^0 = 35.6$ cm^3 mol^{-1} for CO_2 and $\bar{V}_2^0 = 35.1$ cm^3 mol^{-1} for H_2S in this solvent. Considering the uncertainties in our experimental values (33.5 and 37.8 cm^3 mol^{-1}, respectively) for these same gases in the same solvent and the uncertainties that result from calculating (12) values of three parameters (K_H, A, and $\bar{V}_2^0$) from one set of experimental results, the agreement is satisfactory.

Because of our interest in using information (K_H and $\bar{V}_2^0$) obtained from results of measurements made conveniently at low pressures for calculations of solubilities at higher pressures, we now proceed to use the Krichevsky–Kasarnovsky equation [3] as follows. Fugacities of CO_2 at several pressures have been calculated from the virial coefficients (13). These fugacities and corresponding pressures have been combined with our previous values[2] for Henry's law constants (obtained by low-pressure GLC measurements) and the present partial molar volumes to calculate equilibrium solubilities of CO_2 in *N*-formyl morpholine and in propylene carbonate. Results can be summarized and compared with experimental solubilities as follows.

For CO_2 in *N*-formyl morpholine at $T = 298.15$ K, we calculate (as described above) that $X_2 = 0.37$ at $P_2 = 2950$ kPa, as compared to the directly measured (12) $X_2 = 0.34$. Agreement of calculated with experimental solubilities is better at lower pressures, worse at higher pressures. In similar fashion we have calculated that $X_2 = 0.23$ for CO_2 in propylene carbonate at $P_2 = 2104$ kPa, as compared to the directly measured (14) $X_2 = 0.21$ at this same pressure.

It is possible to obtain better agreement between calculated and experimental solubilities, especially at higher pressures, by using the Krichevsky–Ilinskaya equation [4]. Such improvement, however, is less likely to be useful for predictive purposes because the only reliable method at present for obtaining the needed values of the Margules parameter (A) is from additional solubility data.

Still another approach to solubilities of acidic gases in physical solvents where it is probable that moderately stable complexes are formed can involve explicit recognition of the complex by way of an appropriate equilibrium constant, as done previously for volumes of SO_2 in various solvents (11) and for solubilities of NH_3 in $HCCl_3$ (15).

[2]Y. Xu and L. G. Hepler. To be published.

Acknowledgements

We thank Dr. John F. Smith for helpful advice concerning measurements leading to our partial molar volumes and Professor Alan E. Mather for donating some solvents and for his helpful discussions about calculations with our results. We are also grateful to the Natural Sciences and Engineering Research Council of Canada and the Alberta Oil Sands Technology and Research Authority for financial support of this and related research on thermodynamic properties of gases in liquids.

1. I. R. Krichevsky and J. S. Kasarnovsky. J. Am. Chem. Soc. **57**, 2168 (1935).
2. J. M. Prausnitz, R. N. Lichtenthaler, and E. Gomes de Azevedo. Molecular thermodynamics of fluid phase equilibria. 2nd ed. Prentice–Hall, Inc., Englewood Cliffs, NJ. 1986.
3. B. C.-Y. Lu, W. K. Chung, Y. Adachi, and T. Boublik. AOSTRA J. Res. **2**, 139 (1986).
4. I. R. Kirchevsky and A. Ilinskaya. Acta Physicochim. URSS, **20**, 327 (1945).
5. R. Battino and H. L. Clever. Chem. Rev. **66**, 395 (1966).
6. H. L. Clever and R. Battino. *In* Solutions and solubilities. Part I. Techniques of chemistry. Vol. VIII. *Edited by* M. R. J. Dack. Wiley, New York. 1975. p. 379.
7. Y. P. Handa and G. C. Benson. Fluid Phase Equilib. **8**, 161 (1982).
8. Y. P. Handa, P. J. D'arcy, and G. C. Benson. Fluid Phase Equilib. **8**, 161 (1982).
9. J. Horiuti. Sci. Pap. Inst. Phys. Chem. Res. (Jpn.), **17**, 125 (1931).
10. G. A. Bottomley, J. F. Smith, R. P. Schutte, and L. G. Hepler. AOSTRA J. Res. **5**, 383 (1989).
11. J. F. Smith, G. A. Bottomley, L. Barta, and L. G. Hepler. J. Am. Chem. Soc. **112**, 153 (1990).
12. F.-Y. Jou, R. D. Deshmukh, F. D. Otto, and A. E. Mather. J. Chem. Soc. Faraday Trans. 1, **85**, 2675 (1989).
13. J. H. Dymond and E. B. Smith. The virial coefficients of pure gases and mixtures. Clarendon Press, Oxford. 1980.
14. F. Murrieta-Guevara, A. Romero-Martinez, and A. Trejo. Fluid Phase Equilib. **44**, 105 (1988).
15. J. F. Smith, C. Li, M. Roth, and L. G. Hepler. Can. J. Chem. **67**, 2213 (1989).

Can. J. Chem. Downloaded from www.nrcresearchpress.com by 123.30.183.119 on 09/08/12
For personal use only.

Étude de la conformation d'imines thiophéniques

BOUALEM OUSSAID, MOHAMED AYAD ET BERNARD GARRIGUES[1]

Unité de recherche associée au Centre national de la recherche scientifique, n° 454, Université Paul Sabatier, Laboratoire de synthèse, structure et réactivité de molécules phosphorées, 118 route de Narbonne, 31062 Toulouse CEDEX, France

JEAN-PIERRE FAYET

Université Paul Sabatier, Laboratoire de chimie des matériaux inorganiques, 118 route de Narbonne, 31062 Toulouse CEDEX, France

ET

LE TRANG TRAN

Université Paul Sabatier, Service commun de RMN, 118 route de Narbonne, 31062 Toulouse CEDEX, France

Reçu le 6 mai 1991

BOUALEM OUSSAID, MOHAMED AYAD, BERNARD GARRIGUES, JEAN-PIERRE FAYET et LE TRANG TRAN. Can. J. Chem. **70**, 58 (1992).

La conformation de 2-iminométhylthiophènes et du 2,5-bis(méthyliminométhyl)thiophène a été étudiée à partir de calculs théoriques, de mesures de moments dipolaires, de l'utilisation du couplage stéréospécifique à travers cinq liaisons et des expériences d'effets Overhauser. Une seule conformation a été mise en évidence : (2*c trans*) pour les 2-iminométhylthiophènes et (2*c* 5*c trans*) pour le 2,-5-bis(méthyliminométhyl)thiophène.

Mots clés : thiophène, imine, conformation.

BOUALEM OUSSAID, MOHAMED AYAD, BERNARD GARRIGUES, JEAN PIERRE FAYET, and LE TRANG TRAN. Can. J. Chem. **70**, 58 (1992).

Conformation of 2-iminomethylthiophenes and of the 2,5-bis(methyliminomethyl)thiophene has been elucidated from theoretical investigations, dipole moment measurements, use of stereospecific coupling through five bonds, as well as Overhauser effect experiments. Only one conformation has been found: (2*c trans*) for the 2-iminomethyl thiophenes and (2*c* 5*c trans*) for the 2,5-bis(methyliminomethyl)thiophene.

Key words: thiophene, imine, conformation.

Introduction

Dans la mesure où les répulsions d'origine stérique le permettent, l'effet de conjugaison des cycles thiophéniques avec le groupement carbonyle tend à imposer aux molécules une structure plane susceptible de présenter les conformations 2*c* ou 2*t*. Si la planéité des systèmes conjugués est admise, la nature de la conformation privilégiée fait l'objet d'une controverse entre différents auteurs (1–3). Des études spectrographiques par absorption dans l'infrarouge lointain et micro-ondes concluent à une prépondérance de la structure O—S *trans* (2*t*) pour les 2-formyl thiophènes (4).

Par contre, l'examen des moments dipolaires indique dans de nombreux systèmes thiényle-carbonyle une structure essentiellement O—S *cis* (2*c*), et il en est de même des mesures de l'intensité de la bande de vibration de valence du carbonyle (5–7). La stéréospécificité des couplages à longue distance est en faveur de la structure 2*c* (8, 9).

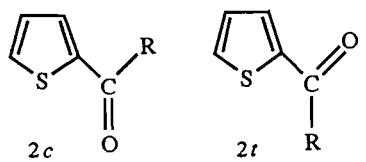

Le dédoublement des bandes d'absorption ν(C=O) et ν(CH) des 2,5-diformylthiophène est expliqué par l'existence de deux conformères 2*c* 5*c* et 2*c* 5*t* en équilibre à température ordinaire. On estime l'abondance relative de la forme 2*c* 5*t* à 40% (10). Des mesures de moments dipolaires concluent à l'existence d'un mélange de 74% de forme 2*c* 5*c* (7). Enfin, des études par RMN ^{1}H concluent à la présence des conformations 2*c* 5*c* et 2*c* 5*t* dans des pourcentages respectifs de 70–80% et 20–30% (11).

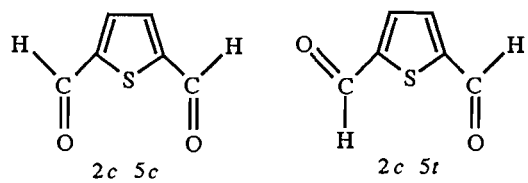

Nous nous proposons pour la première fois d'étudier la conformation de 2-iminomethylthiophène et du 2,5-bis-(methyliminométhyl)thiophène par calcul, mesure du moment dipolaire, utilisation du couplage stéréospécifique Zig-Zag (12) et effet Overhauser.

Partie expérimentale

Généralités

Points de fusion, non corrigés, en capillaires (appareil Tottoli, Büchi). Spectres IR : en suspension dans le Nujol ou sous forme de film, entre lames CaF_2, enregistrés sur un spectromètre Perkin–Elmer 257. Spectres de RMN ^{1}H : déplacements chimiques en ppm par rapport au TMS; constantes de couplage en Hz; appareil Bruker AC 250.

Les spectres ^{1}H ont été enregistrés avec une résolution digitale de 0,15 Hz/point. Celle des spectres ^{13}C est de 0,46 Hz/point.

Les expériences 2D-NOESY ont été réalisées dans des conditions tout à fait classiques, avec un temps de mélange $t_m \cong T_1$. Il est à remarquer que les molécules étudiées présentent un temps de relaxation assez important (jusqu'à 16 s pour H5 du produit **2***c*). D'autre part, pour permettre une relaxation optimum, nous avons

[1]Auteur à qui adresser toute correspondance.

Printed in Canada / Imprimé au Canada

Can. J. Chem. Downloaded from www.nrcresearchpress.com by 123.30.183.119 on 09/08/12
For personal use only.

Can. J. Chem. Downloaded from www.nrcresearchpress.com by 123.30.183.119 on 09/08/12
For personal use only.

choisi dans tous les cas un délai entre deux accumulations légèrement supérieur à $5 \times T_1$ (ex. : 90 s dans le cas du produit **2***c*).

Les analyses élémentaires ont été effectuées par le service de microanalyse de l'École Nationale Supérieure de Chimie de Toulouse. En outre, les chromatographies analytiques sont effectuées sur plaque de silice Merck réf. 5549.

Synthèse des dérivés **1**, **2**, **3**, **4**

Seuls les dérivés **1**, **2**, **3** sont signalés sans mode opératoire ni paramètres de RMN dans un travail précédent (13).

On mélange à la température ordinaire 0,01 mol de 2-formylthiophène ou de 2,5-diformylthiophène (14) et 0,05 mol d'amine en solution dans 30 mL de méthanol. Le milieu réactionnel est laissé sous agitation 48 h puis évaporé à sec. Après purification sur colonne de silice (éluant acétate d'éthyle) ou recristallisation dans le pentane on obtient le produit recherché analytiquement pur.

2-Méthyliminométhyl thiophène (**1**) : IR (Nujol) : 1637 (C=N) cm^{-1}. Rdt = 75%. RMN ^{13}C ($CDCl_3$) : 155,6 (s, CN), 142,5 (s, C2), 130,0 (s, C3), 128,5 (s, C5), 127,3 (s, C4), 47,7 (s, CH_3).

2-Isopropyliminométhyl thiophène (**2**) : IR (Nujol) : 1631 (C=N) cm^{-1}. Rdt = 83%. RMN ^{13}C ($CDCl_3$) : 151,5 (s, CN), 142,7 (s, C2), 129,9 (s, C3), 128,4 (s, C5), 127,2 (s, C4), 61,3 (s, CH), 24,1 (s, CH_3).

2-Tertiobutyliminométhyl thiophène (**3**) : IR (Nujol) : 1632 (C=N) cm^{-1}. Rdt = 71%. RMN ^{13}C ($CDCl_3$) : 148,7 (s, CN), 144,1 (s, C2), 129,6 (s, C3), 128,1 (s, C5), 127,2 (s, C4), 57,3 (s, C), 29,7 (s, CH_3).

2,5-Bis(methyliminomethyl)thiophène (**4**) : IR (KBr) : 1628 (C=N) cm^{-1}. Rdt = 90%. *F* = 78°C. RMN ^{13}C ($CDCl_3$) : 155,5 (s, CH), 144,6 (s, C2), 129,6 (s, C3), 48,0 (s, CH_3).

Les moments dipolaires des quatre imines thiophéniques (**1**, **2**, **3**, **4**) sont mesurés dans le dioxanne à 25°C (tableau 1). La formule de Debye est utilisée ainsi que la méthode d'extrapolation d'Halverstadt et Kumler (15) pour calculer la polarisation totale avec $\alpha = [d\epsilon/d\omega_2]\omega_2 \rightarrow 0$, $\beta = [dv/d\omega_2]\omega_2 \rightarrow 0$ et $0{,}001 < \omega_2 < 0{,}05$. ϵ est la constante diélectrique, ω_2 la fraction massique de l'échantillon et v le volume massique. Les polarisations électroniques sont assimilées aux refractions moléculaires R_{MD}.

Résultats et discussion

Nous avons pour notre part étudié la conformation des 2-iminométhylthiophènes **1–3** (**1** : R = Me, **2** : R = *i*Pr, **3** : R = *t*Bu) et du 2,5-bis(méthyliminométhyl)thiophène **4**.

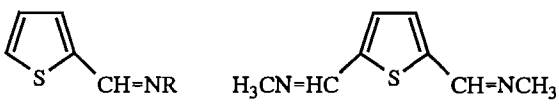

4

1 R = CH_3
2 R = *i* Pr
3 R = *t* Bu

Nous avons tout d'abord effectué un calcul théorique MNDO (16) pour les quatre conformations planes possibles 2*t cis*, 2*t trans*, 2*c trans* et 2*c cis*. Ce calcul montre, quelle que soit la nature du substituant R, que la structure la plus stable est la conformation 2*c trans* : −1309,713 eV (**1**), −1621,993 eV (**2**) et −1777,946 eV (**3**) (cf. tableau 2). Il est à noter que la conformation 2*c cis* n'a pas pu être calculée, à cause de l'encombrement stérique.

TABLEAU 1. Grandeurs intermédiaires pour la détermination des moments dipolaires expérimentaux

N°	α	β	R_{MD}	$P_{2\infty}$	$\mu_{(D)}$
1	5,09	−0,19	37,21	133,26	2,17
2	3,41	−0,18	42,35	121,03	1,96
3	3,34	−0,16	46,99	131,14	2,03
4	9,77	−0,25	48,87	302,41	3,52

TABLEAU 2. Valeur des énergies (eV) pour les conformations des composés **1–3** (la conformation 2*c cis* n'a pas pu être calculée)

R	N°	2*t cis*	2*t trans*	2*c trans*
Me	**1**	−1308,002	−1309,696	−1309,713
*i*Pr	**2**	−1613,519	−1621,976	−1621,993
*t*Bu	**3**	−1769,468	−1777,927	−1777,946

TABLEAU 3. Moments dipolaires calculés et mesurés (D) pour les composés **1–3**

R	N°	2*t cis*	2*t trans*	2*c trans*	μ_{exp}
Me	**1**	2,44	0,71	2,19	2,17
*i*Pr	**2**	2,55	0,66	2,14	1,96
*t*Bu	**3**	2,42	0,60	2,05	2,03

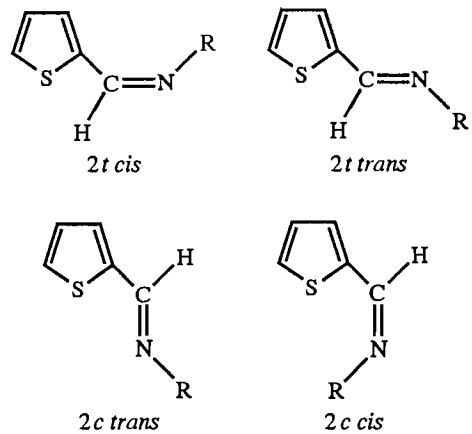

Le moment dipolaire théorique, calculé pour les trois conformations 2*t cis*, 2*t trans* et 2*c trans*, a été comparé à la mesure du moment dipolaire expérimental, effectué dans le dioxanne à 25°C. Les valeurs mesurées sont en faveur de la prépondérance de la conformation 2*c trans* dans le dioxanne : **1** : 2,17 (2,19); **2** : 1,96 (2,14); **3** : 2,03 (2,05) (tableau 3).

La stéréospécificité des couplages entre protons séparés par cinq liaisons dans une disposition Zig-Zag coplanaire ou *trans-trans* a été clairement établie dans de nombreux exemples et notamment en série thiophénique (12, 17, 18). Son existence a été démontrée par des expériences d'effets Overhauser (19), par rayons X dans des 4-bromo 2-formyl thiophènes (9) et enfin par des calculs théoriques de déplacements chimiques (9).

Nous avons pour notre part examiné les spectres des iminométhylthiophènes **1–3** (cf. tableau 4).

Un couplage spécifique Zig-Zag entre le proton imino et le proton H5 du cycle thiophénique a été observé. Sa valeur est comprise entre 0,7 et 0,9 Hz suivant la nature du substituant sur l'azote et confirme l'existence de la conformation 2*c trans*. Aucun dédoublement ni élargissement important n'apparaissent pour une solution refroidie dans le chloroforme à −60°C. La valeur nulle du couplage stéréospécifique $^5J(HCNH_4) = 0$ (**1–3**) qui résulterait des conformations 2*t trans* ou 2*t cis* permet d'éliminer ces deux dernières.

TABLEAU 4. Déplacements chimiques en ppm et constantes de couplages en Hz de 2-iminométhyl thiophène **1–3**

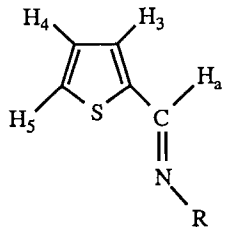

R	N°	H5	H4	H3	J_{45}	J_{35}	J_{34}	J(HaH5)	J(HaH4)
Me	**1**	7,22	6,88	7,15	4,3	1,2	3,7	0,7	0
*i*Pr	**2**	7,34	7,03	7,25	5,0	1,2	3,6	0,8	0
*t*Bu	**3**	7,32	7,02	7,27	4,8	1,2	3,7	0,9	0

Enfin, nous avons pu confirmer nos résultats par des expériences d'effets Overhauser. Dans le cas de **2**, nous avons observé une augmentation de l'intensité du signal du proton H3 de 8% lorsque l'on irradie le proton de la fonction imine; l'intensité des autres protons du cycle thiophénique n'est pas affecté par cette irradiation. Le spectre de RMN ^{2}D NOESY montre une très nette tache de corrélation entre le proton de la fonction imine et H3.

Nous avons étudié la conformation du 2,5-bis-(méthyliminométhyl)thiophène **4**. La simplicité du spectre de RMN ^{1}H dans un domaine de température de −60°C à +60°C ne peut s'expliquer que par la présence d'une conformation présentant un plan de symétrie qui rend équivalent les protons du cycle de la fonction imine et les groupements méthyle. Le composé **4** existe sous l'une des quatre conformations 2*t* 5*t cis*, 2*t* 5*t trans*, 2*c* 5*c trans* et 2*c* 5*c cis*.

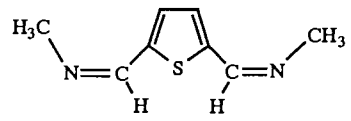

2*t* 5*t cis*

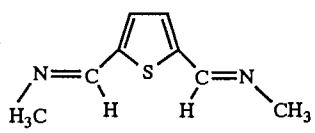

2*t* 5*t trans*

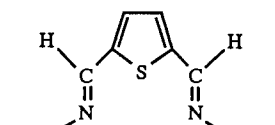

2*c* 5*c trans*

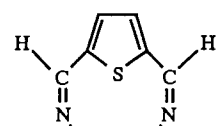

2*c* 5*c cis*

La conformation 2*c* 5*c cis*, trop encombrée stériquement, n'a pas pu être calculée. L'examen du calcul des énergies montre que la conformation 2*c* 5*c trans* est la plus basse en énergie (−1814,703 eV).

La mesure du moment dipolaire expérimental (3,52 D) est en accord avec cette conformation privilégiée (μ_{calc} = 3,39 D, cf. tableau 5). Enfin, dans cette conformation préférentielle, 2*c* 5*t trans*, aucun couplage stéréospécifique entre le proton de la fonction imine et le cycle ne doit exister : c'est ce qui est observé.

TABLEAU 5. Valeur des énergies (eV) et des moments dipolaires (D) pour les conformations de **4**

	2*t* 5*t cis*	2*t* 5*t trans*	2*c* 5*c trans*	μ_{exp}
E_T	−1811,276	−1814,665	−1814,703	
$\mu_{calc.}$	0,92	2,02	3,39	3,52

Conclusion

Alors que la conformation de formylthiophène a fait l'objet de controverses, les premières études que nous avons effectuées à partir de calculs théoriques, de mesures de moments dipolaires, de l'utilisation du couplage stéréospécifique à travers cinq liaisons et des expériences d'effets Overhauser montrent une convergence des résultats.

Dans le cas des iminométhyl thiophènes **1–3**, une seule conformation a été mise en évidence (2*c trans*). Le 2,5-bis(méthyliminométhyl)thiophène existe, lui, sous la conformation 2*c* 5*c trans*.

La conformation des imines hétérocycliques est sous la dépendance d'un certain nombre de facteurs : (*i*) l'attraction entre le soufre et l'azote; (*ii*) la différence de stabilité entre la conformation *cis* et *trans* dans l'enchaînement C=C—C=N, la forme *trans* étant thermodynamiquement la plus stable.

Nous remarquons que ces deux facteurs jouent dans le même sens pour conduire à une conformation *trans* de la fonction imine comme cela a déjà été observé pour les benzylidènes anilines (20).

Remerciements

Nous remerçions A. Colomer et G. Pelletier, respectivement, pour l'enregistrement des spectres IR et de RMN.

1. G. J. Karabastos et F. M. Vane. J. Am. Chem. Soc. **85**, 3886 (1963).
2. K. Dahlqvist et S. Forsen. J. Phys. Chem. **69**, 1760 (1965).
3. L. M. Jackman. Applications of NMR spectroscopy in organic chemistry. Pergamon Press, 1959. p. 124.
4. F. Monnig, H. Dreizler et H. D. Rudolf. Z. Naturforsch. A: Astrophys. Phys. Phys. Chem. **20A**, 1323 (1965); F. A. Miller. Spectrochim. Acta, Part A, **24A**, 891 (1967).
5. L. Felloni et F. Pulidori. Ann. Chim. (Rome), **51**, 1027 (1961).
6. K. V. Kovalenko, V. T. Minkin, Z. N. Nazarova et D. V. Kazachenko. Zh. Obshch. Khim. **32**, 549 (1962).
7. H. Lumbroso, D. M. Bertin, M. Robba et B. Roques. C. R. Seances Acad. Sci. Ser. C: **262**, 36 (1966).
8. S. Gronowitz et R. A. Hoffmann. Ark. Kemi, **13**, 279 (1958).
9. B. Roques, S. Combrisson, C. Riche et C. Pascard-Billy. Tetrahedron, **26**, 3555 (1970).
10. B. Antoine, J. J. Peron et P. Saumagne. C. R. Seances Acad. Sci. Ser. B: **272**, 1366 (1971).

Can. J. Chem. Downloaded from www.nrcresearchpress.com by 123.30.183.119 on 09/08/12
For personal use only.

11. L. Lunazzi, G. F. Pedulli, M. Tiecco et C. A. Veracini. J. Chem. Soc. Perkin Trans. 2, 755 (1972).
12. S. Sternhell. Q. Rev. Chem. Soc. **23**, 236 (1969).
13. Y. Hoshika. J. Chromatogr. **136**, 253 (1977).
14. B. L. Feringa, R. Hulst, R. Rikers et L. Brandsma. Synthesis, 316 (1988).
15. I. F. Halverstadt et Kumler. J. Am. Chem. Soc. **64**, 2888 (1942).
16. M. J. Dewar et W. Thiel. J. Am. Chem. Soc. **99**, 4899 (1977).
17. M. C. Fournie-Zaluski et B. Roques. Tetrahedron Lett. 4909 (1970).
18. B. Roques et M. C. Fournie-Zaluski. Tetrahedron Lett. 145 (1971).
19. S. Combrisson, B. Roques, P. Rigny et J. J. Basselier. Can. J. Chem. **49**, 904 (1971).
20. E. Fischer et Y. Frei. J. Chem. Phys. **27**, 808 (1957).

Can. J. Chem. Downloaded from www.nrcresearchpress.com by 123.30.183.119 on 09/08/12
For personal use only.

Intramolecular nucleophilic participation by the thiol group during amide hydrolysis. Part 2. The imidazole catalysis dilemma[1]

ROBERT S. MCDONALD,[2] PATRICIA PATTERSON, JUNE RODWELL, AND ANN WHALLEY
Department of Chemistry, Mount Saint Vincent University, 166 Bedford Highway, Halifax, N.S., Canada B3M 2J6

Received May 31, 1991

ROBERT S. MCDONALD, PATRICIA PATTERSON, JUNE RODWELL, and ANN WHALLEY. Can J. Chem. **70**, 62 (1992).

Catalysis by imidazole and *N*-methylimidazole buffers of the intramolecular thiolysis of *N*-*n*-propyl 2-mercaptomethylbenzamide (forming 2-thiophthalide) has been studied in aqueous solution at 40.0°C, μ = 1.0. Unlike other buffers previously studied, imidazole and *N*-methylimidazole are able to catalyze, by a general base route, formation of neutral tetrahedral intermediate; this pathway is rate limiting at pH $\leq$ 7.5. At higher pH, the previously reported general acid-catalyzed breakdown of this intermediate is rate limiting. The relevance of these observations to the currently accepted pathway for the acylation of papain by amide substrates is discussed.

Key words: amide hydrolysis, intramolecular, thiol participation, imidazole, papain model.

ROBERT S. MCDONALD, PATRICIA PATTERSON, JUNE RODWELL et ANN WHALLEY. Can. J. Chem. **70**, 62 (1992).

Opérant à 40.0°C, dans des solutions aqueuses à μ = 1,0, on a étudié l'effet de la catalyse par des tampons d'imidazole et de *N*-méthylimidazole sur la thiolyse intramoléculaire du *N*-propyl-2-mercaptométhylbenzamide (conduisant à la formation de 2-thiophtalides). Contrairement à ce qui a été observé antérieurement avec d'autres tampons, l'imidazole et le *N*-méthylimidazole peuvent catalyser, par le biais d'une catalyse générale basique, la formation d'un intermédiaire tétraédrique neutre; cette voie limite la vitesse à un pH $\leq$ 7,5. À des pH plus élevés, la décomposition de cet intermédiaire assistée par une catalyse générale acide est l'étape qui détermine la vitesse. On discute de l'importance de ces observations pour le mécanisme généralement accepté pour l'acylation de la papaïne par des substrats amides.

Mots clés : hydrolyse d'amides, intramoléculaire, participation d'un thiol, imidazole, modèle de la papaïne.

[Traduit par la rédaction]

A thiol group of a cysteine residue (Cys-25) has been been assigned a nucleophilic role in the acylation of papain by carboxylic ester and amide substrates (1). The acyl enzyme, a thiol ester, has been observed spectroscopically (2) and in certain cases can be isolated and its deacylation studied independently (3). Located within hydrogen bonding distance of the thiol group lies an imidazole residue (of His-159) (4), which has been assigned a general acid–base role on both acylation and deacylation pathways (1, 5, 6).

The key steps involving nucleophilic and general acid–base assistance on the catalytic pathways of several proteases have been modelled in simpler chemical systems that react by an intramolecular pathway (7). However, although the intramolecular thiolysis of an ester has been reported (8) and the corresponding intermolecular reaction is well known (9), there have been few previous reports of nucleophilic involvement by a thiol group during amide hydrolysis. A kinetic study of the reaction of 2-mercaptoethanol with the very reactive amide, acetylimidazole, allowed Jencks and Carriuolo (10) to conclude that the reaction proceeded by way of thiolate attack on the N-protonated substrate. Dafforn and Koshland (11) studied the intramolecular thiolactonization of one acyclic and two bicyclic thiol amides in anhydrous or slightly wet sulfolane solution. Although both an acid-catalyzed and a spontaneous pathway were observed, these authors proposed the intermediacy of both protonated and diprotonated intermediates, which may reflect the particular choice of solvent.

Thus our previous kinetic study (12) of the thiolactonization of amide **1** provided the first direct observation of nucleophilic thiol group participation in the hydrolysis of an unactivated amide in aqueous solution (Scheme 1).

The pH–rate profile and the influence of buffers on the reaction rate allowed the following conclusions to be made concerning the reaction pathway. At low pH ($\leq$2.5) or high buffer concentration, the rate-limiting step is the uncatalyzed formation of neutral tetrahedral intermediate, $\mathbf{I}_0$ (k_1 in Scheme 1 is 9.8×10^{-4} s^{-1} at 40.0°C, μ = 1.0). At higher pH, the (apparent) general acid-catalyzed breakdown of $\mathbf{I}_0$ becomes rate limiting. Actually, on the basis of the Brønsted catalysis plot, we proposed that the rate-limiting step involves the kinetically equivalent general base-catalyzed breakdown of N-protonated tetrahedral intermediate ($\mathbf{I}_+$) to form **2**.

Although imidazole was one of the buffers investigated in this previous study (12), kinetic results in this buffer were significantly different in several respects from those observed in the other buffers examined over the same pH range and were not reported there. Certainly it is most intriguing that it is catalysis by imidazole which is anomalous since it is catalysis by this buffer of the **1** → **2** transformation that provides the closest analogue to the acylation of papain by a substrate amide.

This paper then reports the kinetic results for the catalysis of the thiolactonization of **1** in a series of imidazole and *N*-methylimidazole buffers over the pH range 6–8 and provides a rationale for the "imidazole catalysis dilemma" that may be relevant to the mechanism of action of papain.

Experimental

General information, purification of materials, substrate preparation, product work, and a description of the kinetic methods have been previously described (12). Preparation of buffer solutions has also been described elsewhere (13).

Results and discussion

The identification of thiolactone **2** as the product of the reaction of **1** in imidazole buffers has been confirmed by uv

[1]For part 1, see ref. 12.
[2]Author to whom correspondence may be addressed.

Can. J. Chem. Downloaded from www.nrcresearchpress.com by 123.30.183.119 on 09/08/12
For personal use only.

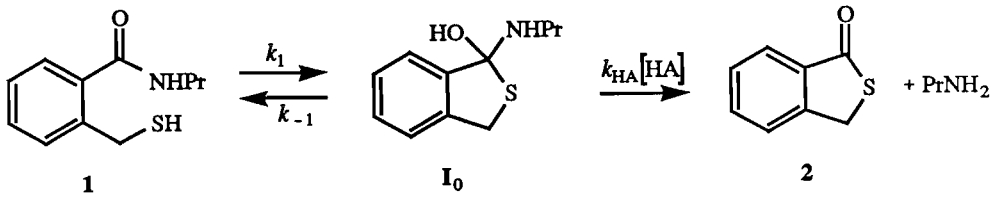

1 I_0 2

SCHEME 1

TABLE 1. Pseudo-first-order rate constants (k_{obs}) for the thiolactonization of **1** in (a) imidazole and (b) *N*-methylimidazole buffers in aqueous solution, t = 40.0°C, μ = 1.0

(a) Imidazole

	$10^4 \cdot k_{obs}(s^{-1})^a$				
[Bf] (M)	pH 5.99	pH 6.73	pH 7.11	pH 7.71	pH 8.17
0.10	6.79	—	6.41	—	—
0.20	9.38	10.5	11.9	8.87	—
0.40	10.9	16.0	18.0	14.7	8.03
0.50	—	—	22.1	—	—
0.60	13.5	20.4	26.6	21.3	12.0
0.80	14.5	25.0	30.6	27.0	15.5
1.00	16.3	29.5	37.6	32.6	19.2
1.50	—	—	55.7	—	—
2.00	—	—	66.8	—	—
$10^3 \cdot$ slope (M^{-1} s^{-1})	0.87 (±0.06)	2.35 (±0.06)	3.11 (±0.10)	2.99 (±0.05)	1.85 (±0.03)
$10^4 \cdot$ intercept (s^{-1})	7.7 (±0.4)	6.2 (±0.4)	6.4 (±1.0)	3.0 (±0.3)	0.7 (±0.2)
r	0.993	0.999	0.997	0.999	0.999

(b) *N*-Methylimidazole

	$10^4 \cdot k_{obs}$ (s^{-1})				
[Bf] (M)	pH 6.29	pH 6.82	pH 7.32	pH 7.87	pH 8.33
0.20	9.29	9.53	9.68	7.00	2.66
0.40	11.4	14.2	15.6	11.5	4.85
0.60	12.6	18.2	21.5	18.3	7.22
0.80	15.1	20.6	27.1	21.6	9.06
1.00	16.3	25.1	31.8	26.0	10.7
$10^3 \cdot$ slope (M^{-1} s^{-1})	0.89 (±0.06)	1.88 (±0.11)	2.79 (±0.07)	2.41 (±0.15)	1.01 (±0.04)
$10^4 \cdot$ intercept (s^{-1})	7.6 (±0.4)	6.3 (±0.7)	4.4 (±0.5)	2.5 (±1.0)	0.8 (±0.3)
r	0.994	0.995	0.999	0.994	0.997

[a]Quoted k_{obs} values are the average of at least duplicate runs; agreement between replicate runs was always within 10% and normally within 5–6%.

spectra of the reaction mixtures and by product isolation. In each case the final spectrum corresponded to an 80–95% yield of **2**. Although the oxidation of **1** to disulfide could be suppressed, it could not be completely eliminated (see experimental section of ref. 12). However, as long as disulfide formation was minimal and it remained in solution, this side reaction did not interfere appreciably with the thiolactonization kinetics.

Pseudo-first-order rate constants (k_{obs}) for the formation of **2** from **1** in a series of imidazole and *N*-methylimidazole buffers over the pH range 6–8.3 at 40.0°C, μ = 1.0 (with KCl), are collected in Table 1 and those in imidazole buffers are presented graphically in Figs. 1–3.

Several features of these data are strikingly different from those obtained in other buffers (phosphate, MES, Tris) previously reported over this pH range. Two of these are evident in Fig. 1 where the k_{obs} values in imidazole buffer at pH 7.11 are compared with those calculated assuming that imidazole conforms to the mechanistic pathway in Scheme 1 and obeys the Brønsted relationship in ref. 12 (i.e., $k_{HA}' = 2.51 \times 10^{-3}$ M^{-1} s^{-1} and $k_1 = 9.8 \times 10^{-4}$ s^{-1}). Clearly imidazole is a much more efficient catalyst than anticipated (in 2.0 M buffer, k_{obs} is 9-fold larger than predicted) and the buffer plot is essentially linear above 0.20 M, there being no apparent upper limit to k_{obs} at least up to 2.0 M. Previous buffer plots exhibited saturation-type behavior with an upper limit to k_{obs} in the range (0.9–1.6) $\times$ 10^{-3} s^{-1}. In this previous work, linear buffer plots were observed only where catalysis was very weak at high pH (see Table 1 and Fig. 2 of ref. 12). Similar behavior is observed for the other im-

Can. J. Chem. Downloaded from www.nrcresearchpress.com by 123.30.183.119 on 09/08/12
For personal use only.

Can. J. Chem. Downloaded from www.nrcresearchpress.com by 123.30.183.119 on 09/08/12
For personal use only.

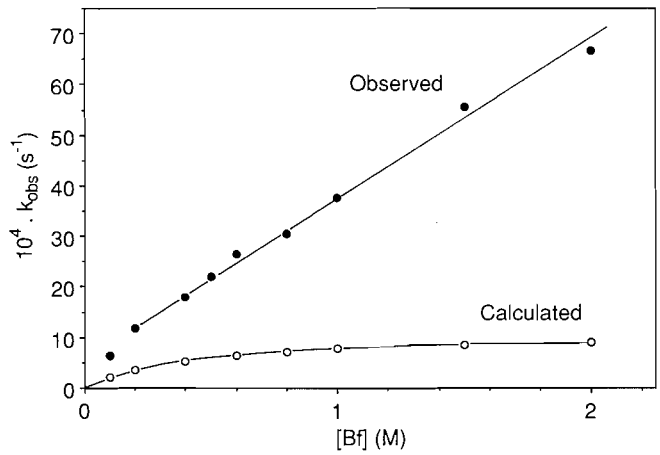

FIG. 1. Comparison of observed and calculated pseudo-first-order rate constants for the thiolactonization of **1** in imidazole buffer, pH 7.11, t = 40.0°C, μ = 1.0.

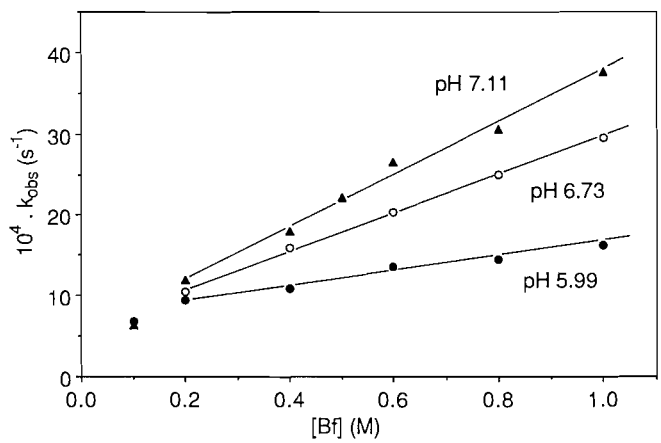

FIG. 2. Pseudo-first-order rate constants for the thiolactonization of **1** in imidazole buffers: pH 5.99, 6.73, and 7.11.

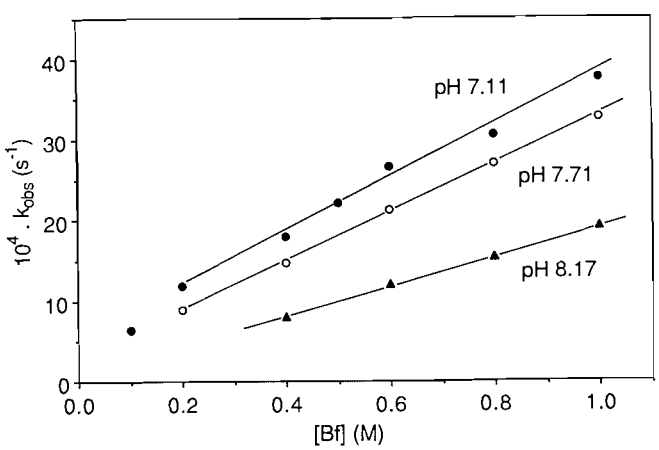

FIG. 3. Pseudo-first-order rate constants for the thiolactonization of **1** in imidazole buffers: pH 7.11, 7.71, and 8.17.

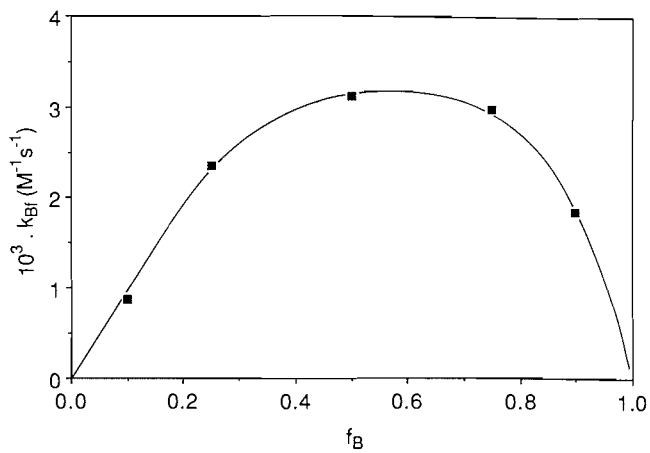

FIG. 4. Second-order buffer-catalyzed rate constants for the thiolactonization of **1** in imidazole buffers vs. f_B, the fraction of imidazole in its basic (neutral) form.

idazole buffers at higher and lower pH (although catalysis appears to be less efficient; see Figs. 2 and 3) and also for the series of *N*-methylimidazole buffers (not illustrated). The slopes, intercepts, and correlation coefficients for the linear portions of all these plots (at [Bf] $\geq$ 0.20 M) are also collected in Table 1.

The intercepts of these buffer catalysis plots are all larger than those that can be calculated from the known rate constants for the water- and hydronium ion-catalyzed terms (i.e., all k_0 values should be $\leq 1.3 \times 10^{-5}$ s^{-1}). Thus, there must be curvature in the buffer plots at *low* concentration, more pronounced at lower pH, which we take as evidence that the general acid-catalyzed (GAC) breakdown of $\mathbf{I}_0$ is still operative (*vide infra*).

Another noteworthy feature of these kinetic results is that catalysis is most efficient in the half-neutralized imidazole (or *N*-methylimidazole) buffer. This is illustrated in Fig. 4 where the apparent imidazole buffer-catalyzed rate constants (the slopes in Table 1) are plotted vs. the fraction of buffer in its basic form. This bell-shaped plot is certainly inconsistent with either GA or GBC (or both) on a single reaction step. Simultaneous cooperative GA–GBC can also be ruled out since this would require termolecular kinetics, which are not observed. Plots of k_{obs} vs. [Im][HIm^+] (not illustrated) are distinctly curved. Further, Breslow and Labelle (14) could detect no association between imidazole and its conjugate acid up to 1.0 M buffer concentration by nmr and cryoscopic measurements. The fact that *N*-methylimidazole buffers also show these characteristics allows us to eliminate the possibility of concerted bifunctional acid–base catalysis although this would be an unprecedented observation for this catalyst. It is also clear that our results are characteristic of the imidazole buffers and not simply due to a change in rate-limiting step of the reaction since other buffers over the same pH range exhibit GAC only.

A plot of the type illustrated in Fig. 4 has been obtained by Schmir and Cunningham (15) in the hydrolysis of an iminolactone catalyzed by acetate buffers. However, their substrate was undergoing significant changes in its state of protonation over the pH range examined. This cannot account for our results since we estimate the pK_a of the thiol

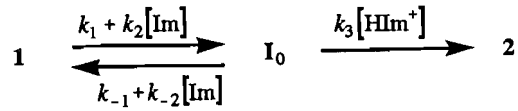

SCHEME 2

TABLE 2. Optimized rate constants and rate constant ratios for the thiolactonization of **1** in imidazole and *N*-methylimidazole buffers (40.0°C, μ = 1.0)

	Imidazole	*N*-Methylimidazole
$10^4 \cdot k_1$ (s^{-1})	11.0 ± 0.6	10.2 ± 0.9
$10^3 \cdot k_2$ (M^{-1} s^{-1})	7.74 ± 0.19	8.32 ± 0.51
k_{-2}/k_3	0.245 ± 0.021	0.516 ± 0.057
k_{-1}/k_3 (M)	0.040 ± 0.009	0.035 ± 0.017

group of **1** to be 9.0 ± 0.2 (12) and, again, other buffers over the same pH range do not show this effect.

One obvious conclusion that can be drawn from the lack of an upper limit to k_{obs} in imidazole buffers is that these buffers must also catalyze *formation* of I_0 (or provide an alternate route to **2**). Keeping in mind that the half-neutralized buffer provides the most efficient catalysis and assuming that breakdown of I_0 remains subject to GAC only, the minimum modification required to the pathway in Scheme 1 is the addition of a kinetic term involving imidazole for the formation of I_0 from **1** (and the reverse reaction). The revised pathway is represented in Scheme 2.

Making the steady-state assumption for I_0 leads to the following expression for k_{obs}:

$$[1] \quad k_{obs} = \frac{(k_1 + k_2[Im])[HIm^+]}{k_{-1}/k_3 + k_{-2}[Im]/k_3 + [HIm^+]}$$

Values of k_1, k_2, and the partitioning ratios k_{-1}/k_3 and k_{-2}/k_3 were adjusted iteratively using the Simplex algorithm (16) in order to minimize the least-squares difference between calculated and experimental k_{obs} values. The optimized values for these rate constants and rate constant ratios for imidazole and *N*-methylimidazole are given in Table 2. When these values are inserted into eq.[1], the k_{obs} values can be reproduced with an average deviation of 6–7%.

Worth noting here is the fact that Breslow and Labelle (14) also accounted for the observation of a bell-shaped buffer catalysis vs. pH profile in the imidazole-catalyzed hydrolysis of RNA by proposing sequential GA–GBC on successive steps of the reaction pathway.

It is reassuring that the optimized values for k_1 are in good agreement with one another and the value previously reported ($(9.8 \pm 1.1) \times 10^{-4}$ s^{-1}) (12). The fact that k_2 for *N*-methylimidazole is slightly larger than that for imidazole may reflect its slightly greater basicity.

The question remains as to how imidazole catalyzes the cyclization of **1** to I_0. We are unable to detect any specific interaction between a typical thiol (2-mercaptoethanol) and a 0.50 M imidazole buffer (pH 7.1) by uv measurements. Imidazole catalyzes the hydrolysis of activated esters and thiolesters (17); both nucleophilic and GBC pathways have been observed. As a general base, imidazole usually behaves normally, having a catalytic rate constant similar to that of hydrogen phosphate dianion, which has similar basicity. However, imidazole often exhibits enhanced nucleophilic reactivity as it does in the hydrolysis of *p*-nitrophenylacetate (18) and thiolesters (19). Intramolecular examples of both nucleophilic (20) and general base catalysis (21) by imidazole in thiolester hydrolysis have been found. There are, however, no reports of the catalysis of the hydrolysis of unactivated amides by imidazole buffers and we have been unable to detect any catalysis of the hydrolysis of *N*-*n*-propylbenzamide or the more reactive *p*-nitroacetanilide in 1.0 M imidazole (pH 7.1) over a period of 24 h.

It is interesting to note that the intramolecular thiolysis of both carboxylate (8) and carbamate (22) esters is not subject to GA–GBC. The sole kinetic pathway involves thiolate attack on the ester carbonyl.

Perhaps the closest analogue to our work is the kinetic study of acetyl group transfer from acetylimidazole to 2-mercaptoethanol catalyzed by imidazole carried out by Jencks and Carriuolo (10). The kinetic term involving [AcIm][RSH][Im] was proposed to correspond to true GBC of thiol attack at the amide carbonyl concerted with loss of imidazole. We also propose a general base role for imidazole in the ring closure of **1** to form I_0. Two kinetically equivalent pathways can be envisioned as outlined in Scheme 3.

Either imidazole provides true GB assistance to thiol attack on the amide carbonyl thus generating I_-, which rapidly becomes protonated (path a), or the thermodynamically unfavorable proton transfer between thiol group and imidazole to form the ion pair is followed by acid-assisted thiolate attack on the amide (path b). Analysis of the observed and estimated rate and equilibrium constants does not allow us to distinguish between these pathways.

This analysis implies that, in the presence of imidazole buffers, the reaction undergoes a change in rate-limiting step from the GBC formation of I_0 at pH $\leq$ 7.5 to its GAC breakdown at pH $\geq$ 7.5. The general base pathway becomes significant only for imidazole buffers for reasons which are as yet unclear.

What is most intriguing is that both pathways in Scheme 3 are analogous to those proposed for the acylation of papain by amide substrates. In his review, Lowe (23) proposed a mechanistic pathway for acylation analogous to path a, i.e., true GBC by imidazole. However, the position of the proton in the thiol–imidazole couple in the active enzyme has been debated for 20 years. The weight of recent evidence from uv (24), solvent isotope effects (25), potentiometric titration (26), and nmr (27) techniques reveals that this couple is from 50–100% in the form of the zwitterionic pair ($-S^-$ HIm^+-) such that imidazolinium might provide general acid assistance to thiolate attack. Unfortunately our results do not shine any light on the ambiguity but they do provide the first evidence that imidazole can catalyze acyl transfer from N to S in an unactivated amide.

There have been numerous previous attempts to observe cooperativity between proximate thiol and imidazole groups in a variety of 2- and 4-substituted imidazoles and appropriately functionalized peptides. Although the substrate chosen for this work was almost invariably the very reactive *p*-nitrophenyl acetate, only very modest rate enhancements (of 2–3 fold) have been observed. Brown and co-workers (21*b*, 30) have reasoned that the lack of success of these studies was due to the fact that the imidazole–thiol pair was not in the proper protonation state. Through a study of the

Can. J. Chem. Downloaded from www.nrcresearchpress.com by 123.30.183.119 on 09/08/12
For personal use only.

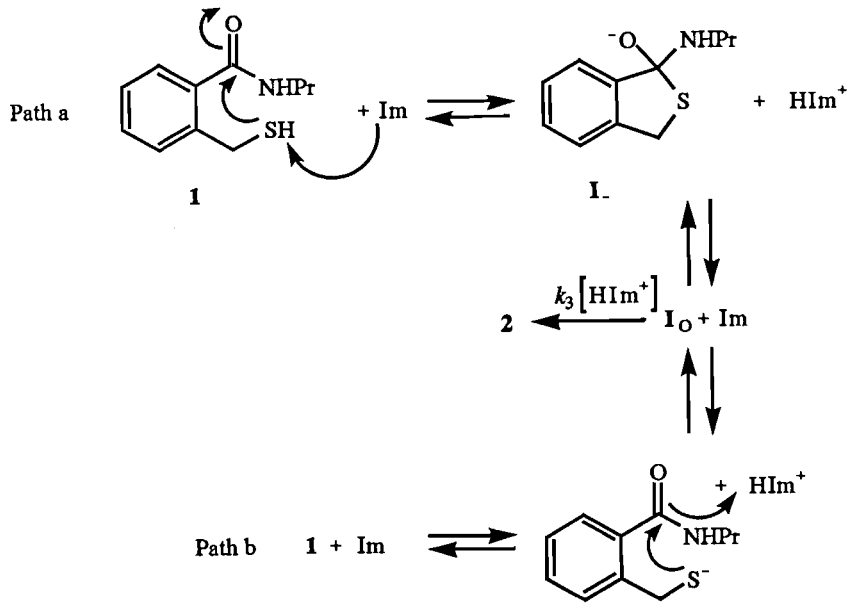

SCHEME 3

catalysis of PNPA hydrolysis by 2-mercaptomethylimidazole and its *N*-methyl derivative, in which the pK_a of the thiol group is lower than that of the imidazole group, they were able to observe significant attack on the ester carbonyl by the thiolate group of the zwitterionic form of the catalyst.

Turning back to our work, the question arises as to why imidazole can catalyze formation of $\mathbf{I}_0$ but other bases of similar or greater basicity cannot. In our previous work (12) we did notice that there was a systematic, if somewhat erratic, trend in k_1 from $(0.9–1.0) \times 10^{-3}$ s^{-1} (pH 0–6) up to 1.6×10^{-3} s^{-1} at pH 7.8. We ascribed this behavior to a modest medium or pH effect but, in retrospect, this may be due to a small general base contribution to the formation of $\mathbf{I}_0$. In any case, the contribution of this term by phosphate (pK 6.48) and Tris (pK 8.25) must be very small since in both of these cases the buffer-catalyzed rate constants decrease with increasing pH consistent with exclusive GAC. In an attempt to determine whether enhanced GBC by imidazole is a pK_a or a geometric effect, we are planning to study the catalytic effect of other substituted imidazoles, some of which have quite different pK_a and steric effects to those reported here.

Acknowledgements

The authors wish to thank the Natural Sciences and Engineering Research Council of Canada and Mount Saint Vincent University (Committee on Research and Publications) for financial support of this work. One of us (R.S.M.) is also pleased to acknowledge the hospitality of Professor Athel Beckwith and members of his research group at the Research School of Chemistry, The Australian National University, Canberra, during a recent sabbatical leave.

1. (*a*) A. N. Glazer and E. L. Smith. *In* The enzymes. Vol. 3. 3rd ed. *Edited by* P. D. Boyer. Academic Press, New York. 1971. Chap. 14; (*b*) G. Lowe. Tetrahedron, **32**, 291 (1976).
2. M. L. Bender and L. J. Brubacher. J. Am. Chem. Soc. **86**, 5333 (1964); G. Lowe and A. Williams. Proc. Chem. Soc. 104, (1964); Biochem. J. **96**, 189 (1965); A. C. Storer, W. F. Murphy, and P. R. Carey. J. Biol. Chem. **254**, 3163 (1979); J. P. G. Mallhouse, M. P. Gamcsik, A. S. F. Boyd, N. E. Mackenzie, and A. I. Scott. J. Am. Chem. Soc. **104**, 6811 (1982).
3. L. J. Brubacher and M. L. Bender. J. Am. Chem. Soc. **88**, 5871 (1966); P. M. Hinkle and J. F. Kirsch. Biochemistry, **9**, 4633 (1970); V. I. Zannis and J. F. Kirsch. Biochemistry, **17**, 2669 (1978).
4. J. Drenth, J. N. Jansonius, R. Koekoek, H. M. Swen, and B. G. Wolthers. Nature (London), **218**, 929 (1968); J. Drenth, J. N. Jonsonius, R. Koeboek, L. A. A. Sluyterman, and B. G. Wolthers. Philos. Trans. R. Soc. London B: **257**, 231 (1970); J. Drenth, J. N. Jansonius, R. Koeboek, and B. G. Wolthers. *In* The enzymes. Vol. 3. 3rd ed. *Edited by* P. D. Boyer. Academic Press, New York. 1971. Chap. 13.
5. S. S. Husain and G. Lowe. Biochem. J. **108**, 855 (1968); G. Lowe. Philos. Trans. R. Soc. London B: **257**, 237 (1970).
6. K. J. Angelides and A. L. Fink. Biochemistry, **17**, 2659 (1978); L. Polgar and P. Halasz. Biochem. J. **207**, 1 (1982), and references cited therein.
7. A. J. Kirby and A. R. Fersht. Prog. Bioorg. Chem. **1**, 1 (1971); T. H. Fife. *In* Bioorganic chemistry. Vol. 1. *Edited by* E. E. van Tamelen. Academic Press, New York. 1977. Chap. 5; A. J. Kirby. *In* Comprehensive organic chemistry. Vol. 5. *Edited by* E. Haslam. Pergamon Press, Oxford. 1979. pp. 401–409.
8. T. H. Fife and B. R. DeMark. J. Am. Chem. Soc. **98**, 6978 (1976).
9. J. R. Whitaker. J. Am. Chem. Soc. **84**, 1900 (1962); J. W. Ogilvie, J. T. Tildon, and B. S. Strauch. Biochemistry, **3**, 754 (1964); P. Lochon and J. Schoenleber. Tetrahedron, **32**, 3023 (1976).
10. W. P. Jencks and J. Carriuolo. J. Biol. Chem. **234**, 1280 (1958).
11. G. A. Dafforn and D. E. Koshland. J. Am. Chem. Soc. **99**, 7246 (1977).
12. R. S. McDonald, P. Patterson, and A. Stevens-Whalley. Can. J. Chem. **61**, 1846 (1983).
13. R. S. McDonald and E. V. Martin. Can. J. Chem. **57**, 506 (1979); R. S. McDonald and C. E. Sibley. Can. J. Chem. **59**, 1061 (1981).
14. R. Breslow and M. Labelle. J. Am. Chem. Soc. **108**, 2655 (1986).

Can. J. Chem. Downloaded from www.nrcresearchpress.com by 123.30.183.119 on 09/08/12
For personal use only.

15. G. L. Schmer and B. A. Cunningham. J. Am. Chem. Soc. **87**, 5692 (1965).
16. J. A. Nelder and R. Mead. Comput. J. **8**, 308 (1965).
17. T. C. Bruice and S. J. Benkovic. Bioorganic mechanism. Vol. 1. W. A. Benjamin, Inc., New York, NY. 1966. pp. 46–66, 279–285.
18. M. L. Bender and B. W. Turnquest. J. Am. Chem. Soc. **79**, 1656 (1957); T. C. Bruice and G. L. Schmir. J. Am. Chem. Soc. **79**, 1663 (1957); **80**, 148 (1958).
19. M. L. Bender and B. W. Turnquest. J. Am. Chem. Soc. **79**, 1652 (1957); L. R. Fedor and T. C. Bruice. J. Am. Chem. Soc. **86**, 4117 (1964).
20. T. C. Bruice. J. Am. Chem. Soc. **81**, 5444 (1959); T. H. Fife and B. R. DeMark. J. Am. Chem. Soc. **101**, 7379 (1979).
21. (*a*) J. P. Street and R. S. Brown. J. Am. Chem. Soc. **107**, 6084 (1985); (*b*) J. P. Street, K. I. Skorey, R. S. Brown, and R. G. Ball. J. Am. Chem. Soc. **107**, 7669 (1985).
22. T. H. Fife, J. E. C. Hutchins, and M. S. Wang. J. Am. Chem. Soc. **97**, 5878 (1975).
23. G. Lowe. Tetrahedron, **32**, 291 (1976).
24. L. Polgar. FEBS Lett. **32**, 187 (1974); **47**, 15 (1974); L. Polgar and P. Halasz. Biochem. J. **207**, 1 (1982).
25. D. G. Creighton, M. S. Gessousoun, and J. M. Heapes. FEBS Lett. **110**, 313 (1980); **110**, 319 (1980).
26. S. D. Lewis, F. A. Johnson, and J. A. Shafer. Biochemistry, **15**, 5009 (1976).
27. F. A. Johnson, S. D. Lewis, and J. A. Shafer. Biochemistry, **20**, 44 (1981); **20**, 48 (1981); **20**, 52 (1981).
28. F. Schneider. Z. Physiol. Chem. **348**, 1034 (1967); F. Schneider, E. Schaich, and H. Wenck. Z. Physiol. Chem. **349**, 1525 (1968); F. Schneider and H. Wenck. Z. Physiol. Chem. **350**, 1653 (1969); P. Lochon and J. Schoenleber. Tetrahedron, **32**, 3032 (1976).
29. K. Nakajima and K. Okawa. Bull. Chem. Soc. Jpn. **46**, 1811 (1973); D. Petz and F. Schneider. Z. Naturforsch. C: Biosci. **31C**, 534 (1976); M. J. Heller, J. A. Walder, and I. M. Klotz. J. Am. Chem. Soc. **99**, 2780 (1977).
30. K. I. Skorey and R. S. Brown. J. Am. Chem. Soc. **107**, 4070 (1985).

Can. J. Chem. Downloaded from www.nrcresearchpress.com by 123.30.183.119 on 09/08/12
For personal use only.

Charge distributions and chemical effects. XLVII. Density matrix contribution to the charge distribution in hydrocarbons, arising from singly excited configurations in CI calculations

CLAUDE MIJOULE,[1] JEAN-MARIE LECLERCQ,[1] MICHEL COMEAU, AND SÁNDOR FLISZÁR[2]
Département de chimie, Université de Montréal, C.P. 6128, Succ. A, Montréal (Quebec), Canada H3C 3J7

AND

MAUD PICARD
Laboratoire de dynamique des interactions moléculaires,
Unité propre de recherche du Centre national de la recherche scientifique A0271,
Université Pierre et Marie Curie, Campus Jussieu, tour 22, Paris, France

Received May 6, 1991

CLAUDE MIJOULE, JEAN-MARIE LECLERCQ, MICHEL COMEAU, SÁNDOR FLISZÁR, and MAUD PICARD. Can. J. Chem. **70**, 68 (1992).

The involvement of excited configurations in Mulliken charge analyses is examined for ethylene and acetylene, using an optimized 4-31G basis. The net charges of carbon, -346.4×10^{-3} (C_2H_4) and -335.3×10^{-3} e (C_2H_2) at the SCF level, are reduced to -269.9×10^{-3} and -271.2×10^{-3} e, respectively. Double excitations appear to contribute little to these corrections. In acetylene, three single $\sigma \rightarrow \sigma^*$ type excitations are responsible for ~83% of the charge correction whereas, as expected, the role of $\pi \rightarrow \pi^*$ type excitations is small. Similarly, four $\sigma \rightarrow \sigma^*$ configurations account for ~76% of the correction in ethylene. These effects are particularly important in comparisons with alkanes, whose charges are relatively little affected by CI corrections. Theoretical charges obtained from CI calculations appear to converge toward their empirical counterparts in a generalization of Mulliken's scheme, which allows for an uneven partitioning of CH overlap populations.

Key words: charge density, configuration interaction.

CLAUDE MIJOULE, JEAN-MARIE LECLERCQ, MICHEL COMEAU, SÁNDOR FLISZÁR et MAUD PICARD. Can. J. Chem. **70**, 68 (1992).

Utilisant une base 4-31G optimisée, on a étudié l'implication des configurations excitées dans les analyses de charge de Mulliken pour l'éthylène et l'acétylène. Les charges nettes du carbone calculées au niveau auto-cohérent, $-346{,}4 \times 10^{-3}$ (C_2H_4) et $-335{,}3 \times 10^{-3}$ e (C_2H_2), sont réduites respectivement à $-269{,}9 \times 10^{-3}$ (C_2H_4) et à $-271{,}2 \times 10^{-3}$ e (C_2H_2). Il semble que les doubles excitations n'apportent qu'une faible contribution à ces corrections. Dans l'acétylène, trois mono-excitations $\sigma \rightarrow \sigma^*$ sont responsables d'environ 83% de la correction de la charge alors que, comme on pouvait s'y attendre, le rôle des excitations du type $\pi \rightarrow \pi^*$ est faible. De la même manière, quatre configurations $\sigma \rightarrow \sigma^*$ sont la cause d'environ 76% de la correction dans l'éthylène. Ces effets sont particulièrement importants lorsqu'on les compare à ceux des alcanes pour lesquels les charges ne sont pratiquement pas affectées par des corrections d'IC. Les charges théoriques obtenues à l'aide de calculs d'IC semblent converger vers leurs contreparties empiriques, dans une généralisation du schéma de Mulliken.

Mots clés : densité électronique, interaction de configuration.

[Traduit par la rédaction]

Introduction

The theoretical energies of ground state molecules are only slightly improved by the inclusion of single excitations in configuration interaction (CI) calculations. In the case of H_2O, for example, single excitations improve the correlation energy associated with double excitations (DCI) by only 0.6%, in a situation where single and double excitations (SDCI) account for ~92% of the basis set correlation energy (full CI) (1). In contrast, the important role of single excitations is revealed (2) by the erroneous dipole moment predicted for CO when only multiple excitations are retained; inclusion of single excitations restores the correct sign and order of magnitude for μ_{CO}.

This study examines the role of single excitations in CI calculations, attention being focused on charge distributions. Our results thus differ from all the presently known population analyses that were obtained at the SCF level. Here we investigate in detail the atomic charges of ground state ethylene and acetylene and offer comparisons with methane and ethane. With the help of these results, we examine the validity of population analyses carried out with CI wave functions and learn that the charges obtained in this way do, indeed, converge toward those predicted earlier (3) from energy formulas featuring atomic charges in an explicit manner, in sharp contrast with what can be achieved at the SCF level.

Outline of Calculations

The SCF reference state

Using the double-zeta 4-31G basis, all scale factors and structural parameters were optimized following Davidson's optimally conditioned minimization technique (4) (Tables 1 and 2). This optimization, resulting in nearly theoretical virial ratios (as opposed to results deduced with standard exponents, giving $V/T \approx -1.98$), significantly improves the quality of the basis. The calculations of ethylene and acetylene were carried out under the appropriate D_{2h} and

[1]Visiting scientists, on temporary leave from the Laboratoire de dynamique des interactions moléculaires, Université Pierre et Marie Curie, Campus Jussieu, tour 22, 75252 Paris Cedex 05, France.

[2]Author to whom corespondence may be addressed.

Printed in Canada / Imprimé au Canada

Can. J. Chem. Downloaded from www.nrcresearchpress.com by 123.30.183.119 on 09/08/12
For personal use only.

Can. J. Chem. Downloaded from www.nrcresearchpress.com by 123.30.183.119 on 09/08/12
For personal use only.

TABLE 1 Optimized SCF geometries of ethylene and acetylene from 4-31G calculations

Molecule	Parameter	Calculated[a]	Experimental[a]
Ethylene	r_{CC}	1.3162	1.330 ± 0.005
	r_{CH}	1.0729	1.076 ± 0.005
	HCH	116.02	116.6 ± 0.8
Acetylene	r_{CC}	1.189603	1.203
	r_{CH}	1.051387	1.061

[a]Distances in Å, angles in degrees. Experimental geometries extracted from: (C_2H_4) K. Kuchitsu (13); (C_2H_2) M.D. Harmony *et al.* (14).

TABLE 2. Optimized scale factors for ethylene and acetylene in the 4-31G basis

Molecule	Scale factor	Standard[a]	Optimized
Ethylene	$C(s_K)$	1.0	0.99957
	$C(s'_L,p')$	1.0	0.99384
	$C(s''_L,p'')$	1.04	1.02030
	$H(s')$	1.20	1.18598
	$H(s'')$	1.15	1.14965
Acetylene	$C(s_K)$	1.0	0.999851
	$C(s'_L,p')$	1.0	1.004067
	$C(s''_L,p'')$	1.04	1.012648
	$H(s')$	1.20	1.18754
	$H(s'')$	1.15	1.128814

[a]Following the original recipe given by R. Ditchfield *et al.* (15).

$D_{\infty h}$ symmetry constraints, respectively. The corresponding ground state electron configurations are

$$1a_g^2\ 1b_{1u}^2\ 2a_g^2\ 2b_{1u}^2\ 1b_{2u}^2\ 3a_g^2\ 1b_{3g}^2\ 1b_{3u}^2$$

for the ^1A_g state of ethylene and

$$1\sigma_g^2\ 1\sigma_u^2\ 2\sigma_g^2\ 2\sigma_u^2\ 3\sigma_g^2\ 1\pi_u^4$$

for the $^1\Sigma_g^+$ state of acetylene.

Configuration interaction

Improvement of the wave functions was achieved by means of SDCI and DCI calculations, the many-electron wave functions being expanded as

$$[1]\qquad |\phi_0\rangle = c_0\,|\Psi_0\rangle + \sum_{k,v} c_k^v\,|\Psi_k^v\rangle + \sum_{k\geq l,v\geq t} c_{kl}^{vt}\,|\Psi_{kl}^{vt}\rangle$$

where $|\Psi_0\rangle$ stands for the appropriate SCF reference state; $|\Psi_k^v\rangle$ represents the single $k \rightarrow v$ and $|\Psi_{kl}^{vt}\rangle$ the double $k,l \rightarrow v,t$ type configurations. The summation indices in eq. [1] prevent double-counting of excited configurations. The $|\Psi_k^v\rangle$'s and $|\Psi_{kl}^{vt}\rangle$'s are space- and spin-adapted in a basis of eigenfunctions of S^2, as described earlier in detail (*5a*). Inclusion of the singly excited configurations is obviously needed for a proper description of one-electron properties such as charge densities and, hence, for properties that are sensitive to this quantity (dipole, quadrupole moments, . . .). The doubly excited configurations are required for two reasons. First, they allow us to indirectly introduce the single excitations by a coupling with the SCF reference state, the direct coupling being forbidden by the Brillouin theorem. Second, they can lead to non-negligible contributions to charge density corrections through a direct coupling with the reference state.

In the present CI developments, a core of two MO's was kept doubly occupied, i.e., the $1\sigma_g$, $1\sigma_u$ orbitals of C_2H_2 and the $1a_g$, $1b_{1u}$ orbitals of C_2H_4 corresponding to carbon *K* shells. The remaining 10 or 12 electrons of C_2H_2 or C_2H_4, respectively, were left available for fractional occupation of the corresponding 20 or 24 MO's.

Charge analysis

The following theoretical evaluation of atomic charges in an *N*-electron molecule involves the calculation of its charge density

$$[2]\qquad \rho(\boldsymbol{r}) = \langle\phi_0\,|\,\hat{\rho}(\boldsymbol{r})\,|\,\phi_0\rangle$$

i.e., the mean value of the density operator

$$\hat{\rho}(\boldsymbol{r}) = \sum_{i=1}^{N} \delta(\boldsymbol{r}_i - \boldsymbol{r})$$

where δ is the Dirac function.

Each molecular orbital $\varphi_a(\boldsymbol{r})$ is developed using the atomic basis set $\chi_\mu(\boldsymbol{r})$, giving

$$[3]\qquad \varphi_a(\boldsymbol{r}) = \sum_{\mu} d_{\mu a}\chi_\mu(\boldsymbol{r})$$

In this manner, inserting eqs. [1] and [3] into eq. [2], $\rho(\boldsymbol{r})$ can be expressed as follows:

$$[4]\qquad \rho(\boldsymbol{r}) = \rho_0(\boldsymbol{r}) + \rho_S(\boldsymbol{r}) + \rho_{SD}(\boldsymbol{r})$$

where $\rho_0(\boldsymbol{r})$ is the charge density involving the contribution of the SCF reference state to $\rho(\boldsymbol{r})$: $\rho_S(\boldsymbol{r})$ is the contribution to the density matrix including all non-diagonal elements of $\hat{\rho}(\boldsymbol{r})$ between the reference state and the singly excited configurations, and all diagonal and non-diagonal elements between the single excited configurations themselves; $\rho_{SD}(\boldsymbol{r})$ is the contribution to the charge density, which includes all the other terms (not contained in $\rho_0(\boldsymbol{r}) + \rho_S(\boldsymbol{r})$) coupling single with double excitations, and double excitations between themselves.

The appropriate expressions are (we assume real $\chi_\mu(\boldsymbol{r})$ and $d_{\mu a}$)

$$\rho_0(\boldsymbol{r}) = c_0^2 \sum_{\mu\nu} P_{d,\mu\nu}(0)\,\chi_\mu(\boldsymbol{r})\,\chi_\nu(\boldsymbol{r})$$

$$\rho_S(\boldsymbol{r}) = \sum_{K\equiv k\rightarrow v} \Bigg[c_k^{v2} \sum_{\mu\nu} P_{d,\mu\nu}(K)\chi_\mu(\boldsymbol{r})\chi_\nu(\boldsymbol{r}) + 2\,(-1)_K^0 c_0 c_k^v \sum_{\mu\nu} P_{n-d,\mu\nu}(0,K)\,\chi_\mu(\boldsymbol{r})\chi_\nu(\boldsymbol{r}) + 2 \sum_{K'\equiv k\rightarrow v'} (-1)_K^{K'} c_k^v c_k^{v'} \sum_{\mu\nu} P_{n-d,\mu\nu}(K,K')\,\chi_\mu(\boldsymbol{r})\chi_\nu(\boldsymbol{r}) + 2 \sum_{K''\equiv k'\rightarrow v} (-1)_K^{K''} c_k^v c_{k'}^v \sum_{\mu\nu} P_{n-d,\mu\nu}(K,K'')\,\chi_\mu(\boldsymbol{r})\chi_\nu(\boldsymbol{r}) \Bigg]$$

$$\rho_{SD}(\boldsymbol{r}) = \sum_{K\equiv k,l\rightarrow v,t} \Bigg[c_{kl}^{vt2} \sum_{\mu\nu} P_{d,\mu\nu}(K)\,\chi_\mu(\boldsymbol{r})\chi_\nu(\boldsymbol{r})$$

$$+ 2 \sum_{K' \in \{\{1/0\} \cap \{1/K\}\}} (-1)_K^{K'} c_{kl}^{vt} c_{k'}^{v'} \sum_{\mu\nu} P_{n-d,\mu\nu}(K,K') \times \chi_\mu(\boldsymbol{r})\chi_\nu(\boldsymbol{r})$$

$$+ 2 \sum_{K'' \in \{\{2/0\} \cap \{1/K\}\}} (-1)_K^{K''} c_{kl}^{vt} c_{k''l''}^{v''t''} \sum_{\mu\nu} P_{n-d,\mu\nu}(K,K'') \chi_\mu(\boldsymbol{r})\chi_\nu(\boldsymbol{r}) \Bigg]$$

with

$$P_{d,\mu\nu}(K) = \sum_a n_{Ka} d_{\mu,Ka} d_{\nu,Ka}$$

$$P_{n-d,\mu\nu}(K,L) = d_{\mu,Ki} d_{\nu,Lj}$$

The summations on k, l, and k', l', k'', l'', run over the MO's occupied in $|\Psi_0\rangle$, while the summations on v, t, and v', t', v'', t'', run over the MO's unfilled in $|\Psi_0\rangle$. The pair of indices K, L, with $L \equiv K'$ or K'', refer to the configurations $|\Psi_K\rangle$ and $|\Psi_L\rangle$, coupled through $\hat{\rho}(\boldsymbol{r})$, and which only differ by the φ_{Ki} and φ_{Lj} MO's. $(-1)_K^L = \pm 1$ following the parity of the permutation that locates at the same place the spin-orbitals present in K and L. n_{Ka} represents the occupancy (0, 1, or 2) of the ath molecular orbital in $|\Psi_K\rangle$. The subscript combination Ka stands for the absolute index of this molecular orbital (i.e., its index in the set defined by eq. [3]). The summation parameter $K' \in \{\{1/0\} \cap \{1/K\}\}$ ($K'' \in \{\{(2/0\} \cap \{1/K\}\}$ stands for the configurations K' (K''), which are, at once, a single-excited (double-excited) configuration with respect to the reference state $|\Psi_0\rangle$, and a single-excited configuration with respect to $|\Psi_K\rangle$.

Finally, using the **P** matrix, defined by

$$\rho(\boldsymbol{r}) = \rho_0(\boldsymbol{r}) + \rho_S(\boldsymbol{r}) + \rho_{SD}(\boldsymbol{r}) \equiv \sum_{\mu\nu} P_{\mu\nu}\chi_\mu(\boldsymbol{r})\chi_\nu(\boldsymbol{r})$$

Mulliken's net atomic charge q_A of atom A is deduced in the usual way (6),

$$[5] \qquad q_A^{\text{Mulliken}} = Z_A - \sum_{\mu \in A} (\mathbf{PS})_{\mu\mu}$$

where Z_A is the nuclear charge of atom A and **S** the effective overlap matrix of the atomic basis set. Charge normalization is ensured by $\Sigma_\mu (\mathbf{PS})_{\mu\mu} \equiv \text{tr}(\mathbf{PS}) = N$, i.e., $\Sigma_A q_A = 0$. In a more general partitioning scheme (3, 7), lifting the constraint of halving all overlap population terms, it is

$$N_A = \sum_{\mu \in A} \left(P_{\mu\mu} + \sum_{\nu \neq \mu} P_{\mu\nu} S_{\mu\nu} \lambda_{\mu\nu} \right)$$

$$q_A = Z_A - N_A$$

i.e.,

$$[6] \qquad q_A = q_A^{\text{Mulliken}} + \sum_{\mu \in A} \sum_{\nu \neq \mu} P_{\mu\nu} S_{\mu\nu} (1 - \lambda_{\mu\nu})$$

The inadequacy of Mulliken's charge analysis at the SCF level has been known for some time (8). Here, both Mulliken's scheme ($\lambda_{\mu\nu} = 1$), eq. [5], and its generalization, eq. [6], are instrumental in assessments regarding CI contributions in charge analyses and the physical validity of results deduced in this manner.

Selection of the relevant configurations

As we are interested in the mean value of a one-electron operator, the contribution of singly excited configurations in the full CI wave function requires attention. Using the Rayleigh–Schrödinger perturbation theory, with the partition of the Hamiltonian written as $\hat{H} = \hat{H}^{(0)} + \hat{V}$, expansion of the wave function up to the second order gives

$$[7] \qquad |\Psi_0\rangle = |\Psi_0^{(0)}\rangle + |\Psi_0^{(1)}\rangle + |\Psi_0^{(2)}\rangle$$

where the following expressions hold for $|\Psi_0^{(1)}\rangle$ and $|\Psi_0^{(2)}\rangle$:

$$[8] \qquad |\Psi_0^{(1)}\rangle = \sum_{K \neq 0} c_{0K}^{(1)} |\Psi_K^{(0)}\rangle \qquad \text{with } c_{0K}^{(1)} = \frac{V_{K0}}{E_0^{(0)} - E_K^{(0)}}$$

$$[8'] \qquad |\Psi_0^{(2)}\rangle = \left\{ -\frac{1}{2} \sum_{I \neq 0} \left\{ \frac{V_{I0}}{E_0^{(0)} - E_I^{(0)}} \right\}^2 \right\} |\Psi_0^{(0)}\rangle + \sum_{K \neq 0} c_{0K}^{(2)} |\Psi_K^{(0)}\rangle$$

with

$$c_{0K}^{(2)} = \left\{ \sum_{I \neq 0} \frac{V_{KI} V_{I0}}{(E_0^{(0)} - E_K^{(0)})(E_0^{(0)} - E_I^{(0)})} \right\} - \frac{V_{00} V_{K0}}{(E_0^{(0)} - E_K^{(0)})^2}$$

where $|\Psi_K^{(0)}\rangle$ is the Kth eigenfunction of $\hat{H}^{(0)}$, $E_K^{(0)} \equiv \langle \Psi_K^{(0)} | \hat{H}^{(0)} | \Psi_K^{(0)} \rangle$ is the associated eigenvalue, $V_{KI} \equiv \langle \Psi_K^{(0)} | \hat{V} | \Psi_I^{(0)} \rangle$ for $K = 0, 1, \ldots$ and $I = 0, 1, \ldots$ (the first term on the right-hand side of eq. [8′] has its origin in the normalization to second order of eq. [7]).

The first-order correction $|\Psi_0^{(1)}\rangle$ allows only the doubly excited configurations (hereafter, {2/0}) to mix with the SCF reference state $|\Psi_0\rangle$, all other excitations making a zero contribution at this stage because of the Brillouin theorem (as concerns single excitations) or the Slater rules otherwise. On the other hand, the second-order correction $|\Psi_0^{(2)}\rangle$ allows single excitations (hereafter, {1/0}) to mix indirectly with $|\Psi_0\rangle$ through the doubly excited configurations.

The first-order correction to $\rho_{SCF}(\boldsymbol{r})$ is

$$\rho^{(1)}(\boldsymbol{r}) = 2 \langle \Psi_0^{(0)}(\boldsymbol{r}) | \hat{\rho}(\boldsymbol{r}) | \Psi_0^{(1)}(\boldsymbol{r}) \rangle = 2 \sum_{K \neq 0} \frac{V_{K0}}{E_0^{(0)} - E_K^{(0)}} \langle \Psi_0^{(0)}(\boldsymbol{r}) | \hat{\rho}(\boldsymbol{r}) | \Psi_K^{(0)}(\boldsymbol{r}) \rangle = 0$$

($V_{K0} = 0$ if $K \notin \{2/0\}$, while $\langle \Psi_0^{(0)}(\boldsymbol{r}) | \hat{\rho}(\boldsymbol{r}) | \Psi_K^{(0)}(\boldsymbol{r}) \rangle = 0$ if $K \notin \{1/0\}$).

The second-order correction to $\rho_{SCF}(\boldsymbol{r})$ is

$$\rho^{(2)}(\boldsymbol{r}) = \langle \Psi_0^{(1)}(\boldsymbol{r}) | \hat{\rho}(\boldsymbol{r}) | \Psi_0^{(1)}(\boldsymbol{r}) \rangle + 2 \langle \Psi_0^{(0)}(\boldsymbol{r}) | \hat{\rho}(\boldsymbol{r}) | \Psi_0^{(2)}(\boldsymbol{r}) \rangle$$

$$= -\left\{ \sum_{I \in \{2/0\}} \left\{ \frac{V_{I0}}{E_0^{(0)} - E_I^{(0)}} \right\}^2 \right\} \langle \Psi_0^{(0)}(\boldsymbol{r}) | \hat{\rho}(\boldsymbol{r}) | \Psi_0^{(0)}(\boldsymbol{r}) \rangle$$

$$+ 2 \sum_{K \in \{1/0\}} \left\{ \sum_{I \in \{\{2/0\} \cap \{\{1/K\} \cup \{2/K\}\}} \frac{V_{KI} V_{I0}}{(E_0^{(0)} - E_I^{(0)})(E_0^{(0)} - E_K^{(0)})} \right\} \langle \Psi_0^{(0)}(\boldsymbol{r}) | \hat{\rho}(\boldsymbol{r}) | \Psi_K^{(0)}(\boldsymbol{r}) \rangle$$

$$+ \sum_{K \in \{2/0\}} \left\{ \frac{V_{K0}}{E_0^{(0)} - E_K^{(0)}} \right\}^2 \langle \Psi_K^{(0)}(\boldsymbol{r}) | \hat{\rho}(\boldsymbol{r}) | \Psi_K^{(0)}(\boldsymbol{r}) \rangle$$

$$+ \sum_{K \in \{2/0\}} \sum_{L \in \{\{2/0\} \cap \{1/K\}\}} \left\{ \frac{V_{K0}}{E_0^{(0)} - E_K^{(0)}} \right\} \left\{ \frac{V_{L0}}{E_0^{(0)} - E_L^{(0)}} \right\} \times \langle \Psi_K^{(0)}(\boldsymbol{r}) | \hat{\rho}(\boldsymbol{r}) | \Psi_L^{(0)}(\boldsymbol{r}) \rangle$$

Can. J. Chem. Downloaded from www.nrcresearchpress.com by 123.30.183.119 on 09/08/12
For personal use only.

TABLE 3. Contributions of excited configurations to the correlation energy, ΔE_{corr}, and the Mulliken net charge of carbon[a]

Molecule	Level of calculation	c_0^2	ΔE_{corr},au	Δq_C,me	q_C,me
Methane	SCF	1.0	0	0.0	−523.2
	SDCI	>0.99	−0.07303	7.5	−515.7
Ethane	SCF	1.0	0	0.0	−382.7
	SDCI	>0.99	−0.05717	4.5	−378.2
Ethylene	SCF	1.0	0	0.0	−346.4
	DCI	0.93443	−0.10505	6.7	−339.7
	SDCI	0.93053	−0.10677	76.5	−269.9
	Single contribution		−0.00172	69.8	
Acetylene	SCF	1.0	0	0.0	−335.3
	DCI	0.92472	−0.13468	2.0	−333.3
	SDCI	0.92084	−0.13678	64.1	−271.2
	Single contribution		−0.00209	62.1	

[a]The results for methane and ethane, deduced from optimized 4-31G calculations, are taken from ref. 8.

where the summation parameter $I \in \{\{2/0\} \cap \{\{1/K\} \cup \{2/K\}\}\}$ stands for the configurations I that are, at once, a double-excited configuration with respect to $|\Psi_0\rangle$, and a single- or a double-excited configuration with respect to $|\Psi_K\rangle$.

It follows immediately that the contribution of a single excitation $K \equiv k \rightarrow v$ to the second-order correction $P^{(2)}_{\mu\nu}$ of the element $P_{\mu\nu}$ of the density matrix is

$$[9] \quad 2\left\{\sum_{I\in\{\{2/0\}\cap\{\{1/K\}\cup\{2/K\}\}\}} \frac{V_{KI}V_{I0}}{(E_0^{(0)} - E_K^{(0)})(E_0^{(0)} - E_I^{(0)})}\right\} \times \{d_{\mu,k}d_{\nu,v}\}$$

To obtain the best possible wave function, eq. [1], while keeping the required computer space at an acceptable level, the configurations were selected (*i*) by retaining all singly excited symmetry- and spin-adapted configurations in the CI process and (*ii*) by picking in order of preference those double excitations that mix more efficiently with single excitations and the SCF reference state. The latter rule introduces a new constraint: one-electron properties are thus expected to converge more rapidly than the correlation energy, subject only to the constraint embodied in the construction of c_k. Hence, a selection of configurations that may be appropriate in charge calculations does not necessarily represent the best choice in problems of correlation energies. Briefly, we approach convergence of the charge results well before achieving that of the energy, as indicated by the results given below. Our calculations involve 20 single plus 283 double excitations for ethylene and 17 single plus 340 double excitations for acetylene, a selection that ensures convergence of the charge results.

Results

The 4-31G optimized geometries and scale factors of ethylene and acetylene are indicated in Tables 1 and 2. The structural parameters are in good agreement with their experimental counterparts though, as usual, the CC bond lengths appear to be somewhat underestimated. Slight uncertainties of this sort, however, do not result in significant errors in charge calculations. In both ethylene and acetylene, the s_L'' and p'' outer shells are those that are most perturbed by optimizations of the scale factors. As described elsewhere (3, 8), the use of well-adapted optimized basis sets is important in calculations of consistent charge distributions.

Table 3 reports the contributions of the excited configurations to the correlation energies and electronic charges of selected hydrocarbons. For ethylene and acetylene, inspection of the corrections contributed by the single and double excitations clearly indicates that the improvements of the energy, on the one hand, and charge distribution, on the other, follow distinct patterns. The modest contribution of the doubly excited configurations to the charges, in pure DCI calculations, suggests that the main correction to $\rho(r)$ primarily arises from interaction between single and double excitations and between single excitations themselves, which reflects in essence the one-electron nature of the operator $\hat{\rho}(r)$. Hence, the contribution of the single excitations can be understood by considering the second-order term $|\Psi_0^{(2)}\rangle$ of the Rayleigh–Schrödinger perturbation development eq. [7], as shown in eq. [9].

In addition, considering now the contribution, eq. [9], of each single excitation to the second-order correction $\rho_0^{(2)}(r)$ of the density matrix, it is clear that the singly excited configurations do not mix among themselves at this order of the perturbation expansion. It is thus straightforward to estimate the individual contributions of the various single excitations that are independently involved in the CI wave function. This results clearly from our numerical investigations (Tables 4 and 5). Indeed, the improvement of the CI wave function obtained by adding the single excitations one by one does not appreciably contaminate the weight of those already included in $|\phi_0\rangle$. The individual contributions of the $k \rightarrow v$ type configurations to the net charge corrections given in Tables 4 and 5 for ethylene and acetylene are vividly illustrated in Figs. 1 and 2. For acetylene, three singly excited configurations lead to ~83% of the net charge correction and are all of the $\sigma \rightarrow \sigma^*$ type, while the $\pi \rightarrow \pi^*$ excitation contributions are weak. The conclusions for ethylene are similar: four configurations are responsible for ~76% of the charge correction and the improvement due to $\pi \rightarrow \pi^*$ excitations is minor.

Convergence appears to be reached when all the single excitations are included in the configuration interaction and when the CI dimension reaches 400 determinants (i.e., nearly

Can. J. Chem. Downloaded from www.nrcresearchpress.com by 123.30.183.119 on 09/08/12
For personal use only.

TABLE 4. Individual contributions to Δq_C of the *s–s*-adapted configurations of ethylene

Configuration *i*	Coefficient[a]	Δq_C,me	%[b]
$1b_{3u} \rightarrow 2b_{3u}$	−0.031061	3.5	5.0
$1b_{3g} \rightarrow 2b_{3g}$	0.019898	23.4	33.5
$3a_g \rightarrow 4a_g$	0.014950	12.0	17.2
$1b_{2u} \rightarrow 2b_{2u}$	−0.008044	8.6	12.3
$2b_{1u} \rightarrow 3b_{1u}$	0.007144	9.3	13.3
$1b_{2u} \rightarrow 3b_{2u}$	0.006383	−4.2	−6.0
$1b_{2u} \rightarrow 4b_{2u}$	0.006038	2.4	3.4
$1b_{3g} \rightarrow 3b_{3g}$	−0.005472	4.2	6.0
$3a_g \rightarrow 5a_g$	−0.005326	−1.8	−2.6
$2b_{1u} \rightarrow 5b_{1u}$	−0.004166	−2.5	−3.6
$2a_g \rightarrow 4a_g$	0.004038	5.4	7.7
$2b_{1u} \rightarrow 6b_{1u}$	0.003810	2.3	3.3
$2b_{1u} \rightarrow 7b_{1u}$	0.003686	2.1	3.0
$3a_g \rightarrow 6a_g$	0.002973	−1.7	−2.4
$2a_g \rightarrow 5a_g$	0.002636	0.4	0.6
$3a_g \rightarrow 7a_g$	0.002371	0.6	0.9
$2b_{1u} \rightarrow 4b_{1u}$	−0.002097	1.8	2.6
$2a_g \rightarrow 7a_g$	0.002002	1.6	2.3
$1b_{3g} \rightarrow 4b_{3g}$	−0.001856	2.8	4.0
$2a_g \rightarrow 6a_g$	0.000604	−0.4	−0.6

[a]Expansion coefficient of configuration *i* in the complete CI wave function.
[b]Relative to the contribution of the singly excited configurations, 69.8 me.

TABLE 5. Individual contributions to Δq_C of the s–s-adapted configurations of acetylene

Configuration *i*	Coefficient[a]	Δq_C,me	%[b]
$2\pi_u \rightarrow 4\pi_u$	0.020745	1.2	1.9
$1\pi_u \rightarrow 3\pi_u$	0.020692	1.1	1.8
$3\sigma_g \rightarrow 4\sigma_g$	0.020323	21.8	35.1
$1\pi_u \rightarrow 4\pi_u$	0.016412	1.1	1.8
$2\pi_u \rightarrow 3\pi_u$	−0.016147	1.1	1.8
$2\sigma_u \rightarrow 3\sigma_u$	0.011482	20.3	32.7
$2\sigma_g \rightarrow 5\sigma_g$	0.008084	1.2	1.9
$2\sigma_u \rightarrow 4\sigma_u$	−0.007877	9.3	15.0
$2\sigma_u \rightarrow 6\sigma_u$	−0.004099	2.0	3.2
$2\sigma_g \rightarrow 4\sigma_g$	0.003160	−2.9	−4.7
$2\sigma_g \rightarrow 7\sigma_g$	−0.003084	−1.0	−1.6
$3\sigma_g \rightarrow 7\sigma_g$	−0.002882	2.4	3.9
$2\sigma_g \rightarrow 6\sigma_g$	0.002831	2.8	4.5
$3\sigma_g \rightarrow 5\sigma_g$	−0.001932	0.2	0.3
$2\sigma_u \rightarrow 5\sigma_u$	−0.001920	3.7	6.0
$2\sigma_u \rightarrow 7\sigma_u$	−0.001842	−4.4	−7.1
$3\sigma_g \rightarrow 6\sigma_g$	−0.001750	2.2	3.5

[a]Expansion coefficient of configuration *i* in the complete CI wave function.
[b]Relative to the contribution of the singly excited configurations, 62.1 me.

160 spin-adapted configurations). Indeed, a treatment of the excited states that effectively perturb the $k \rightarrow v$ type configurations (i.e., the single and the double excitations with respect to $k \rightarrow v$ that give non-zero CI matrix elements) may be regarded satisfactory with the inclusion of less than 300 spin-adapted configurations in the CI calculation. Present results suggest that a good description of charges in highly symmetric molecules does not necessarily involve very large CI calculations. It is also clear, however, that atomic charges would be plagued by serious errors if CI corrections were left out.

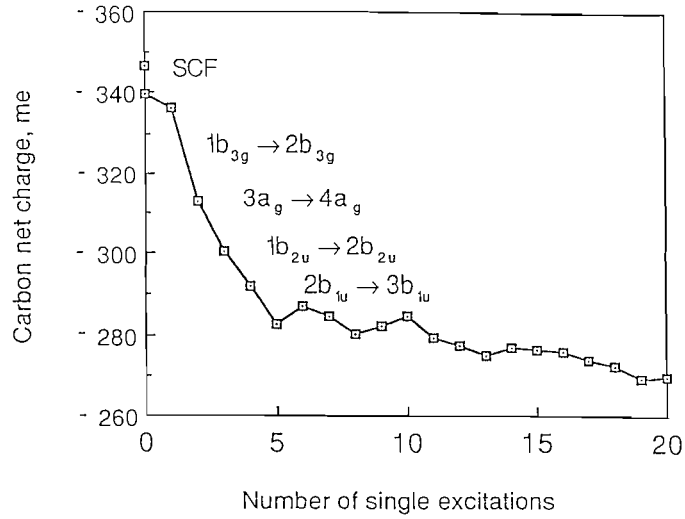

FIG. 1. Contribution of single excitations, in decreasing order of their weight in the CI wave function, to the carbon net charge of ethylene.

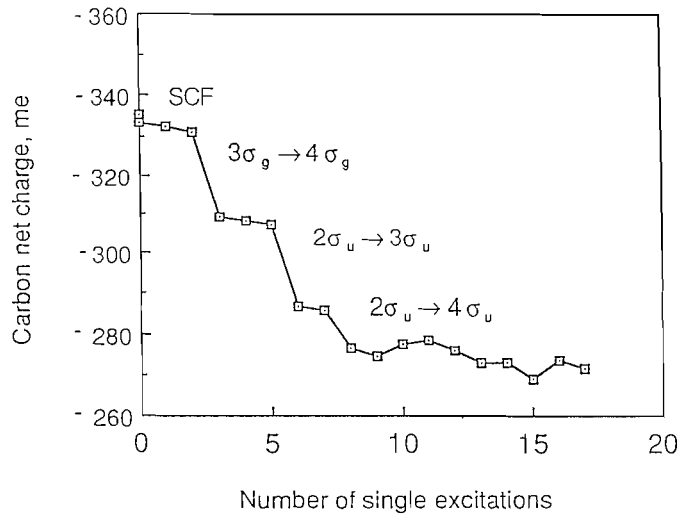

FIG. 2. Contribution of single excitations, in decreasing order of their weight in the CI wave function, to the carbon net charge of acetylene.

Charge analyses following eq. [6] have proven most appropriate in the study of physical properties, namely molecular energies (3), bond dissociation energies (9), and correlations with ^{13}C NMR shifts (10), explicitly involving atomic charges. For alkanes, eq. [6] gives (3, 7)

$$[10] \quad q_C = q_C^{\text{Mulliken}} + N_{CH}p$$

where p measures, for one CH bond, the departure from Mulliken's equipartitioning of overlap populations and N_{CH} counts the H atoms attached to C. The key is in the remarkable properties associated with a particular p value, that rendering all alkane carbons as similar to one another as possible, in a picture describing charge variations as events occurring most reluctantly. This p value is conveniently

Can. J. Chem. Downloaded from www.nrcresearchpress.com by 123.30.183.119 on 09/08/12
For personal use only.

deduced[3] from Mulliken net charges calculated for the ethane and methane carbons (3, 8), i.e.,

$$[11] \quad p = 3.412 q_C^{\text{Mulliken}}(C_2H_6)/3 - 4.412\, q_C^{\text{Mulliken}}(CH_4)/4$$

From our SDCI charges (Table 3) it follows that p = 138.68 me, a result which applies both to sp^3 and sp^2 carbons (3). The carbon net charges given by eq. [6] are thus 37.8 (C_2H_6) and 7.5 me (C_2H_4). These results compare favorably with their empirical counterparts (3) deduced from energy calculations, i.e., 35.1 (C_2H_6) (ref. 3, p. 107; ref. 11) and 7.7 me (C_2H_4) (ref. 3, p. 145; ref. 12). Clearly, realistic charge analyses require careful consideration of CI corrections. Configuration interaction removes the major inconsistencies plaguing the reference charges of ethane and ethylene at the SCF level and leads to the physically meaningful results that are suggested by energy calculations of alkanes and alkenes based on the electrostatic potentials at the nuclei.

Acknowledgements

The financial assistance given by the Natural Sciences and Engineering Research Council of Canada, and by the FCAR, Québec, are gratefully acknowledged. M. P. and J.M. L. are indebted to the Ministère de la Recherche et de la Technologie de France for the financial support offered by the Département de Chimie and the Département de Physique.

[3]Earlier studies (3, 7) indicated that the atomic charges of alkanes can be satisfactorily described in terms of a parameter, n, which determines their relative ordering. In particular, we have $q_C(CH_4)/q_C(C_2H_6) = 4(n + 1)/3n$. This parameter depends on the basis set (e.g., n = 1.3325 for optimized STO-3G Mulliken charges (7) or n = 39.454 for the SCF 4-31G Mulliken results of Table 3). The relative ordering of atomic charges, i.e., n, can be easily modified with the use of charges defined by eq. [10]. With the constraint that all alkane carbons should be as similar to one another as possible, a constraint whose validity is clearly revealed by the study of molecular energies (3, 11) and by correlations between ^{13}C nuclear magnetic resonance shifts and atomic charges (7, 10), it is $n = -4.412$. In this case, $q_C(CH_4)$ and $q_C(C_2H_6)$ represent corrected charges, suited for use in physical problems, namely $q_C(CH_4) = q_C^{\text{Mulliken}}(CH_4) + 4p$ and $q_C(C_2H_6) = q_C^{\text{Mulliken}}(C_2H_6) + 3p$ (from eq. [10]), i.e., $4(-3.412)/3(-4.412) = [q_C^{\text{Mulliken}}(CH_4) + 4p]/[q_C^{\text{Mulliken}}(C_2H_6) + 3p]$. The latter equation gives eq. [11] permitting the numerical evaluation of p for use in eq. [10]. The p correction for the sp^2 carbons of ethylenic hydrocarbons is the same as that determined for the sp^3 carbons, at least to a very good approximation (10*b*).

1. R. J. Bartlett and I. Shavitt. Chem. Phys. Lett. **50**, 190 (1977) (Erratum: Chem. Phys. Lett. **57**, 157 (1978); R. J. Bartlett and I. Shavitt. Int. J. Quantum Chem. Symp. **11**, 165 (1977) (Erratum: Int. J. Quantum Chem. Symp. **12**, 543 (1978)).
2. F. Grimaldi, A. Lecourt, and C. Moser. Int. J. Quantum Chem. **S1**, 153 (1967).
3. S. Fliszár. Charge distributions and chemical effects. Springer-Verlag, New York, N.Y. 1983.
4. W. C. Davidson. Math. Program. **9**, 1 (1975).
5. (*a*) J. Leclercq and J.-M. Leclercq. Chem. Phys. **22**, 221 (1977); (*b*) A. C. Hurley. Introduction to the electron theory of small molecules. Academic Press, London, New York. 1976. pp. 188–197.
6. R. S. Mulliken. J. Chem. Phys. **23**, 1833 (1955); **23**, 1841 (1955); **23**, 2338 (1955); **23**, 2343 (1955).
7. S. Fliszár, A. Goursot, and H. Dugas. J. Am. Chem. Soc. **96**, 4358 (1974); S. Fliszár. Can. J. Chem. **54**, 2839 (1976); V. H. Smith, Jr. Phys. Scr. **15**, 147 (1977).
8. C. Mijoule, J.-M. Leclercq, S. Odiot, and S. Fliszár, Can. J. Chem. **63**, 1741 (1985); S. Fliszár, J.-M. Leclercq, C. Mijoule, and S. Odiot. *In* Applied quantum chemistry. *Edited by* V. H. Smith, Jr., H. F. Schaefer III, and K. Morokuma. D. Reidel Publishing Company, Dordrecht, Holland. 1986. p. 395; J. Cioslowski, T. Hamilton, G. Scuseria, B. Andes Hess, Jr., Jiani Hu, L. J. Schaad, and M. Dupuis. J. Am. Chem. Soc. **112**, 4183 (1990), and references therein.
9. S. Fliszár and C. Minichino. Can. J. Chem. **65**, 2495 (1987).
10. (*a*) S. Fliszár, G. Cardinal, and M.-T. Béraldin. J. Am. Chem. Soc. **104**, 5287 (1982); (*b*) H. Henry and S. Fliszár. J. Am. Chem. Soc. **100**, 3312 (1978).
11. S. Fliszár. J. Am. Chem. Soc. **102**, 6946 (1980).
12. M.-T. Béraldin and S. Fliszár. Can. J. Chem. **61**, 197 (1983).
13. K. Kuchitsu. J. Chem. Phys. **44**, 906 (1966).
14. M. D. Harmony, V. W. Laurie, R. L. Kuczhowski *et al.* J. Phys. Chem. Ref. Data, **8**, 619 (1979).
15. R. Ditchfield, W. J. Hehre, and J. A. Pople. J. Chem. Phys. **54**, 724 (1971).

Can. J. Chem. Downloaded from www.nrcresearchpress.com by 123.30.183.119 on 09/08/12
For personal use only.

A comparative study of the liquid-phase reduction of acrylamide and methacrylamide with cyclohexene and with molecular hydrogen over sepiolite-supported catalysts

M. A. ARAMENDIA, V. BORAU, C. JIMENEZ, J. M. MARINAS,[1] M. E. SEMPERE, AND F. J. URBANO
Department of Organic Chemistry, University of Córdoba, E-14004 Córdoba, Spain

Received November 9, 1990[2]

M. A. ARAMENDIA, V. BORAU, C. JIMENEZ, J. M. MARINAS, M. E. SEMPERE, and F. J. URBANO. Can. J. Chem. **70**, 74 (1992).

This paper deals with the optimization of the variables involved in the synthesis of Pd/sepiolite catalysts used in the individual and competitive reduction of acrylamide and methacrylamide with molecular hydrogen and by hydrogen transfer with cyclohexene as donor. From the reaction profiles of the acrylamide/methacrylamide pair were determined the relative reactivities and relative coefficients of adsorption corresponding to the competitive liquid-phase reductions with molecular hydrogen obtained for different catalysts, solvents, and temperatures. A similar study on the competitive hydrogen transfer reduction of both amides was rendered unfeasible by the fact that acrylamide was strongly adsorbed on the same types of sites as cyclohexene. This completely hindered cyclohexene adsorption and, as a result, inhibited the reaction altogether.

Key words: reduction, acrylamide, methacrylamide, Pd/sepiolite, hydrogen transfer

M. A. ARAMENDIA, V. BORAU, C. JIMENEZ, J. M. MARINAS, M. E. SEMPERE et F. J. URBANO. Can. J. Chem. **70**, 74 (1992).

Dans ce travail on a optimisé les variables impliquées dans la synthèse de catalyseurs Pd/sépiolite utilisés dans la réduction individuelle et compétitive de l'acrylamide et du méthacrylamide à l'aide d'hydrogène et par transfert d'hydrogène à partir du cyclohexène agissant comme donneur. Sur la base des profils réactionnels de la paire acrylamide/méthacrylamide, on a déterminé les quantités relatives et les coefficients relatifs d'adsorption correspondants aux réductions compétitives en phase liquide avec de l'hydrogène moléculaire, obtenues avec divers catalyseurs ou solvants et à diverses températures. Une étude semblable sur les réductions compétitives par transfert d'hydrogène des deux amides n'est pas possible à cause du fait que l'acrylamide est fortement adsorbé sur les mêmes types de sites que le cyclohexène. Cette propriété a complètement empêché l'adsorption du cyclohexène et en conséquence a complètement inhibé la réaction.

Mots clés : réduction, acrylamide, méthacrylamide, Pd/sépiolite, transfert d'hydrogène.

[Traduit par la rédaction]

Introduction

Catalytic hydrogenations by transfer with a variety of hydrogen donors (1, 2) have been widely used in organic syntheses in the last few years, so much so that in many cases they have become viable alternatives to conventional catalytic hydrogenations with gaseous hydrogen.

For a few years now, our research team has investigated the application of aluminium orthophosphates and SiO_2–$AlPO_4$ and Al_2O_3–$AlPO_4$ systems as metals supports in the preparation of heterogeneous reduction catalysts. By supporting Pd on such systems we have prepared excellent catalysts (3–6) suitable for transfer reduction processes involving organic functions.

Sepiolites, namely hydrated magnesium silicates structurally consisting of internal channels capable of accommodating water and other molecules, are highly adsorptive to a number of gases and vapors (7–9) and have been used in chromatography and as catalysts or catalyst supports. Spain abounds with large deposits of this mineral, which is commercialized by TOLSA S.A., hence the great interest in the development of potential applications of this silicate. In this respect, our team has used sepiolites both as acid–base catalysts (10) and as supports for metals such as Pd, Pt, and Ni in order to obtain catalysts active in the reduction of aromatic nitro compounds (11) and in the deprotection of N-protected amino acids (12).

This work aims at comparing the catalytic selectivity of Pd/sepiolite systems in the competitive hydrogenation of acrylamide and methacrylamide, both with molecular hydrogen at a low pressure in a Parr system and by hydrogen transfer with cyclohexene as donor. It also studies the effect of the introduction of a methyl group into the double bond of acrylamide in both reduction processes. In the light of the theory of competitive hydrogenations (13–15), an explanation is provided for the hindered reduction of acrylamide, which, unlike methacrylamide, does not undergo hydrogen transfer with cyclohexene as donor.

Experimental

Supports

The Pd supports used were a sepiolite of the Pansil variety (PS) supplied by TOLSA S.A. and extracted from their ores in Vallecas (Spain), and a mixed SiO_2–$AlPO_4$ system named P2, gelled in propylene oxide, and prepared in our laboratory as described elsewhere (16).

The textural properties of both supports, determined by nitrogen adsorption at liquid-nitrogen temperature, were as follows: surface area (determined by the BET method), 410 and 280 $m^2\ g^{-1}$; pore volume, 0.54 and 0.48 mL g^{-1}; average pore diameter, 35 and 35 Å for support P2 and the sepiolite calcined at 673 K, respectively.

Supported palladium systems

Supported Pd catalysts were prepared by impregnation of the support with an aqueous solution of Na_2PdCl_4 (A), $(NH_3)_4PdCl_2$ (B), or $Pd(NO_3)_2 \cdot 2H_2O$ (C) by the incipient wetness technique.

The slurry was stirred for 24 h, after which the water was evaporated on a rotary vacuum evaporator and dried at 393 K for 24 h,

[1]Author to whom correspondence may be addressed.
[2]Revision received August 15, 1991.

Printed in Canada / Imprimé au Canada

Can. J. Chem. Downloaded from www.nrcresearchpress.com by 123.30.183.119 on 09/08/12
For personal use only.

followed by calcination (by increasing the temperature up to 493 K at a rate of 1 K min^{-1}) and subsequent reduction in a hydrogen stream (99.999% H_2, H_2O < 3 ppm) flowing at a rate of 60 mL min^{-1} and under the same thermal regime followed in the calcination.

One of the catalysts was doped with NaOH. It was labelled Pd_3-PS-A(4), the subscript denoting the Pd content (3%), PS the type of support, A the precursor salt used (Na_2PdCl_4), and (4) that the catalyst was doped with sodium hydroxide at a mole ratio of Na^+ to Pd of 4:1.

Chemicals

The Pd salts, hydrogen donor, acrylamide, methacrylamide, and solvents were commercially available reagents purchased from Merck and Fluka.

Product analysis

The reaction products were analysed by gas chromatography by using high-purity standards. Analyses were carried out on a Hewlett–Packard 5790A gas chromatograph fitted with an HP 18850GC terminal and furnished with a column packed with 10% diethyleneglycol succinate in Chromosorb PAW-60/80 mesh.

Experimental setup and conditions

Hydrogen transfer reductions

Hydrogen transfer reductions were carried out in a Berghof Heiz reactor by using 5×10^{-3} mol of the substrate to be reduced, 0.05 g of Pd catalyst (3% by weight), 5.9×10^{-3} mol of hydrogen donor (cyclohexene), and enough solvent to make up a volume of 6 mL. The reaction temperature varied from experiment to experiment as indicated below. The shaking rate was 1700 rpm, at which external diffusion was under control.

Reductions with gaseous hydrogen

According to a procedure described elsewhere (14), individual and competitive hydrogenation runs were carried out under vigorous shaking in a conventional low-pressure hydrogenator (Parr Instruments Co., model 3911) furnished with a manometer that continuously monitored the hydrogen pressure within the isolated reaction vessel (capacity, 500 mL). The reaction temperature was controlled by pumping water from a thermostatic bath through the vessel jacket, with an accuracy of ±0.5 K.

Individual reactions were carried out under essentially constant-volume conditions in 20 mL of a 0.5 M methanol solution of the substrate, under an initial hydrogen pressure of 0.276–0.414 MPa and at temperatures between 293 and 308 K. The apparent activation energies were calculated over the range 293–318 K. The amount of catalyst employed throughout was 0.045 g (3% Pd by weight).

The initial reaction rates for the individual hydrogenations were obtained from the variation of the hydrogen uptake (calculated from the decrease in the hydrogen pressure at the manometer) as a function of time. As the plots of the decrease in the hydrogen pressure with time were always linear up to 90% conversion, the determination of the initial slope was straightforward and reproducible to within about 6%.

As to the competitive hydrogenations, 20 mL of equimolar mixtures of acrylamide (AC) and methacrylamide (MAC), 0.25 M of each, in methanol were hydrogenated under experimental conditions identical to those used in the individual hydrogenations. The reactions were followed by GLC by analysing the reaction mixtures at appropriate intervals of hydrogen uptake.

Results and discussion

Individual hydrogenations

Hydrogen diffusion control in the reactions was examined. The effect of external diffusion was checked by decreasing the shaking rate from 300 to 100 strokes min^{-1}. The reaction rates were found to be independent of the shaking rate above 200 strokes min^{-1}. Internal diffusion was excluded by using catalysts with a grain diameter less than 0.149 mm.

TABLE 1. Application of the Koros–Nowak criterion

Catalyst	Surface[a] (m^2 g_{Pd}^{-1})	Turnover frequency (s^{-1}) 293 K	300 K	308 K	323 K
Pd_5-PS_{400}-A(4)	62	18.71	27.64	38.73	61.39
Pd_2-PS_{400}-A(4)	64	19.08	26.30	33.38	57.24

Reaction conditions: 20 mL of 0.5 M methacrylamide in 20 mL of MeOH. Initial H_2 pressure: 0.414 MPa. Reaction T: 300 K. Amount of catalyst: just as much as required to obtain 1.359 mg of Pd.

[a]The metal surface area was calculated from $S = 6/\rho d$, where ρ is the metal density and d is the average particle diameter, calculated by transmission electron microscopy (TEM) on a Phillips EM-300 instrument working at 100 kV and an IBAS II KONTRON image analyser, by counting between 600 and 900 particles per sample.

In addition, the hydrogen uptake, r, was found to vary linearly with the weight of catalyst, w. The plot of $1/r$ versus $1/w$ was also linear, and from the reciprocal of the intercept (17), a hydrogen transfer rate of 0.26×10^{-3} mol s^{-1} was obtained. As the hydrogen uptake rate of the fastest reaction was 9.13×10^{-5} mol s^{-1}, the kinetic data obtained must be free from any influence of transport phenomena throughout the variable operational ranges used. The absence of both internal and external heat and mass transfer constraints is apparent from the turnover frequencies listed in Table 1. Also, the absence of any significant changes in turnover between two catalysts that differed in their metal loading by a factor of 2.5 but had similar dispersion confirms that the reaction rates were correctly measured (18).

Table 2 reflects the influence of the type of precursor salt, doping with NaOH, type of support (sepiolite, PS, or mixed SiO_2–$AlPO_4$ system, P2), and calcination temperature of the support in the case of sepiolite, on the catalyst activity in the liquid-phase reduction of the double bond in acrylamide with molecular hydrogen. The reactivity per square meter of Pd of the catalysts supported on sepiolite is not significantly influenced by the calcination temperature. Yet, the doping with NaOH modifies the catalyst specific activity, which is maximum for an Na^+/Pd ratio of 4:1. The type of precursor salt and the solvent in which this is used significantly influence the catalyst specific activity of the resultant system, the best results being obtained with Na_2PdCl_4 in water.

The hydrogenation rate for all substrates, namely acrylamide (AC), methacrylamide (MAC), and cyclohexene (CHE), was zero order in the substrate concentration (0.25–2 M), while the order in the hydrogen pressure (0.414–0.551 MPa) was 0.5.

According to Horiuti–Polanyi (24), the addition of hydrogen to an olefin takes place via the following elementary process:

$$[1] \quad R + 2^* \underset{k_{-1}}{\overset{k_1}{=}} {}^*R^*$$

$$[2] \quad H_2 + 2^* \underset{k_{-2}}{\overset{k_2}{=}} 2H^*$$

$$[3] \quad {}^*R^* + H^* \underset{k_{-3}}{\overset{k_3}{=}} RH^* + 2^*$$

$$[4] \quad RH^* + H^* \overset{k_4}{\rightarrow} RH_2 + 2^*$$

Can. J. Chem. Downloaded from www.nrcresearchpress.com by 123.30.183.119 on 09/08/12
For personal use only.

TABLE 2. Influence of the calcination temperature of the support, precursor salt, and addition of NaOH on the catalyst activity

Catalyst	NaOH added (Na^+/Pd ratio)	$r_i \times 10^2$ (mmol s^{-1} m^{-2})	d (Å)[a]	S (m^2 g^{-1})
Pd_3-PS-B		19.4	36	139
Pd_3-PS_{300}-B		16.1	27	186
Pd_3-PS_{400}-B		17.2	26	193
Pd_3-PS_{500}-B		19.5	36	139
Pd_3-PS_{600}-B		20.0	41	122
Pd_3-PS_{400}-A (DMF)	2:1	13.8	34	147
Pd_3-PS_{400}-C (DMF)		24.5	34	147
Pd_3-PS_{400}-A (H_2O)	2:1	26.8	24	209
Pd_3-PS_{400}-A (H_2O)	3:1	27.0	23	218
Pd_3-PS_{400}-A (H_2O)	4:1	29.5	22	228
Pd_3-PS_{400}-A (H_2O)	5:1	28.1	23	218

Amount of catalyst: 0.0453 g. Total volume: 20 mL. T: 300 K. Initial pressure: 0.414 MPa. Substrate: AC in 0.5 M MeOH.
[a]Average metal particle diameter as calculated by TEM.

We shall now assume that the chemisorption of hydrogen (step [2]) is in equilibrium, with a constant k_2, and that the most abundant surface intermediate is the semihydrogenated state, RH*, covering almost entirely the available surface; both assumptions are compatible with a zero reaction order in the hydrocarbon. We shall also assume that chemisorbed hydrogen covers only a small fraction of the free sites. Thus:

$$[L] \simeq [RH^*]$$

$$[RH^*] >> [^*] >> [H^*]$$

where [L] is the number of active sites per unit metal area, and [RH*], [*], and [H*] are the concentrations of the semihydrogenated state, free active sites, and adsorbed atomic hydrogen, respectively.

Under these conditions, the overall reaction rate will be given by that of step [4], namely:

$$[5] \quad r = r_4 = [L]k_4k_2^{1/2}[H_2]^{1/2}$$

which is consistent with the kinetic results.

On the other hand, when the hydrogenation of AC or MAC was carried out to completion, the plot of the converted fraction of MAC or AC as a function of time deviated from linearity at a given conversion. This phenomenon cannot be attributed to catalyst poisoning and deactivation because a second introduction of reactant after the first sample had been completely converted gave the same reaction rate obtained for the first AC (or MAC) sample. This behavior is consistent with that found in the liquid-phase hydrogenation of 1-hexene, styrene, α-methylstyrene, acrolein, and methyl vinyl ketone on $Ni/AlPO_4$ catalysts (19–22) and in the liquid-phase hydrogenation of cyclohexene on Pt/Al_2O_3 and Pt/SiO_2 (23), where the reaction order in the olefin changes from zero to unity as a result of the catalyst "starvation" of olefin molecules at very low concentrations. Thus, our work was only concerned with the linear portion of the plot of the decrease in the hydrogen pressure as a function of the reaction time, where the reaction rate was zero order in AC, MAC, and CHE.

The hydrogenation rate is affected by the solvent. The best solvent was found to be methanol, which resulted in the highest reaction rates. We tried to correlate (Table 3) the logarithm of the hydrogenation rate of acrylamide in different solvents (log r) with typical parameters of some of their properties (25), according to the generic equation [6]

$$[6] \quad \log r = A_0 + A_1X$$

As can be seen, all the parameters for which the regression coefficient (r_{xy}) was equal to or greater than 0.94 were a function of the dielectric constant, so the solvent probably influences the bond energies of the activated complex through dielectric properties during the surface reaction.

On the other hand, we applied the multiple regression method to the Taft equation (26):

$$[7] \quad \log r = A_0 + A_1\Pi^* + A_2\beta + A_3\alpha$$

It is obviously correct to say that, with the inclusion of each new adjustable parameter (exploratory variable), the goodness of the fit, as judged by the multiple correlation constant, must either improve or at least remain the same. There are statistical procedures based either on the t test or on F statistics to demonstrate whether or not the inclusion of a new exploratory variable is statistically justified and, where appropriate, we applied such statistical tests. We found a correlation coefficient of 0.99 for a confidence limit of 98% by excluding the Π* term; such a limit dropped to 87% if this term was included. This seems to indicate that the acid–base character of the solvents, like their dielectric constant, plays a major role in the hydrogenation of AC.

The rates of reduction of MAC and AC at the same temperature and hydrogen pressure were rather different (7.5 and 32.7 mmol s^{-1} g_{Pd}^{-1}, respectively, at 308 K). This can be ascribed to steric hindrance in the adsorption of methacrylamide and (or) to the variation of the electron density of the double bond by the +I effect of the methyl group.

On the other hand, the apparent activation energies for AC and MAC were 29.8 ± 1.4 and 29.6 ± 0.8 kJ mol^{-1}, respectively, between 293 and 318 K.

Competitive hydrogenation

Figures 1*a*, *b*, and *c* show the distribution of reactants and products as a function of the extent of simultaneous hy-

Can. J. Chem. Downloaded from www.nrcresearchpress.com by 123.30.183.119 on 09/08/12
For personal use only.

TABLE 3. Influence of the solvent on the initial reduction rate of acrylamide. Regression coefficient (r_{XY}) and percent significance ($P(\%)$) of the fitting of each parameter to the dependent variable (log r)

	Methanol	Ethanol	Propanol	Butanol	Dioxane	r_{XY}	$P(\%)$
ϵ^a	32.63	24.30	20.10	17.10	2.20	0.94	98.2
$1/\epsilon^a$	0.031	0.041	0.049	0.057	0.453	0.98	99.7
μ^b	1.70	1.69	1.68	1.66	0.00	0.97	99.5
τ^c	0.000	0.194	−0.160	−0.162	−1.567	0.99	99.9
H^d	0.202	0.220	0.234	0.241	0.153	0.78	88.5
J^e	0.914	0.887	0.866	0.846	0.287	0.98	99.8
K^f	0.447	0.470	0.464	0.458	0.223	0.96	99.2
M^g	0.168	0.180	0.189	0.194	0.202	0.80	89.8
N^h	0.711	0.667	0.632	0.605	0.034	0.99	99.9
E_T^i	50.8	46.9	45.6	45.0	34.2	0.97	99.5
δ^j	14.45	12.90	12.00	10.70	9.73	0.81	90.8
α_H^k	0.087	0.073	0.069	0.063	0.051	0.85	93.6
π^l	0.60	0.54	0.52	0.47	0.55	0.04	6.0
β^m	0.62	0.77	0.81	0.88	0.37	0.76	86.0
α^n	0.93	0.83	0.78	0.79	0.00	0.98	99.85
$\log_r^o$	1.4928	1.4857	1.3729	1.3365	0.7993		Depend. variab.

Reaction conditions: 0.0453 g Pd_3PS_{400}-B, 20 mL of 0.5 M AC, 300 K, 0.414 MPa.
[a]Dielectric constant.
[b]Dipole moment.
[c]Parameter of the Drougard–Decroq equation.
[d]Onsager function, $H = (n^2 - 1)/(n^2 + 2)$ (n = refractive index).
[e]Davis and Hallam function, $J = (\epsilon - 1)/(\epsilon - 2)$.
[f]Kirkwood function, $K = (\epsilon - 1)/(2\epsilon + 1)$.
[g]McRae function, $M = (n^2 - 1)(2n^2 + 1)$.
[h]McRae function, $N = ((\epsilon - 1)/(\epsilon + 2)) - ((n^2 - 1)/(n^2 + 2))$.
[i]Dirmoth solvent polarity parameter.
[j]Hildebrand solubility parameter.
[k]Bunsen hydrogen adsorption coefficient.
[l]Taft polarity polarizability parameter.
[m]Taft solvent basicity parameter.
[n]Taft solvent acidity parameter.
[o]Logarithm of the hydrogenation rate of acrylamide.

drogenation for the couples MAC/AC, AC/CHE, and MAC/CHE, respectively.

The theory of competitive reactions on solid catalysts (13) states that the simultaneous reaction of two reducible molecules, 1 and 2, is a competitive process when the plot of log (C_A^0/C_A) vs. log (C_B^0/C_B) is linear. (C^0 is the initial concentration and C denotes the concentration at time t.) In our case, such a plot (Fig. 2) is linear for the couples AC/MAC (Fig. 2*a*) and MAC/CHE (Fig. 2*c*), so we can state that the simultaneous hydrogenation of A and B for these couples is a competitive process.

The slope of the plot provided the relative reactivity of A to B ($R_{A,B}$). We also calculated the relative equilibrium adsorption constant ($D_{A,B}$) from the expression

$$[8] \quad R_{A,B} = (r_A/r_B)D_{A,B}$$

where r_A and r_B are the individual reaction rates of A and B, respectively. This is only valid provided that the concentrations of A and B are high enough for r_A and r_B to be independent of the concentrations as previously confirmed.

On the other hand, as regards the couple AC/CHE (Fig. 2*b*), the double bond of cyclohexene is not reduced at AC concentrations above 0.025 M because both substrates are adsorbed on the same type of site and AC is retained much more strongly, which hinders cyclohexene adsorption and hence its reactivity. A comparison between the relative adsorption coefficients of the MAC/CHE and AC/CHE pairs (Table 4) reveals that the latter is about 15 times larger than the former, and that the incorporation of CH_3 (MAC) substantially modifies the adsorption.

We studied the variation of $R_{AC,MAC}$, $D_{AC,MAC}$, and the selectivities (S), defined as the ratio between reduced AC and reduced AC plus reduced MAC at half the hydrogen uptake required for the complete reduction of the double bond in both compounds, with the type of catalyst, solvent, and temperature used in the reaction (Table 5).

As can be seen for catalyst Pd_3-PS_{400}-A(4), the relative reactivity ($R_{A,B}$) is independent of the reaction temperature, which, according to Marinas and co-workers (27), by applying the equation

$$[9] \quad R\, \mathrm{d}(\ln R_{AC,MAC})/\mathrm{d}(1/T) = -(E_{a_{AC}} + W_{AC}) + (E_{a_{MAC}} + W_{MAC}) = -(\Delta E_{true})_{AC,MAC}$$

where E_a is the apparent activation energy, W the adsorption heat, and ΔE_{true} the real activation energy, reveals that the real activation energies of the two compounds are identical ($(\Delta E_{true})_{AC,MAC} = 0$). Since, as noted earlier, the apparent activation energies are also identical, the adsorption heats (W) will also be identical.

Since the rates of reduction of acrylamide and methacrylamide are different, there must be a difference in their activation entropies insofar as

$$[10] \quad k_v = (kT/h) \exp[n + \Delta S^{\neq}/R] \exp(E_a^{\neq}/RT)$$

where $\Delta S^{\neq}$ is the entropy increment and $E_a^{\neq}$ the activation

Can. J. Chem. Downloaded from www.nrcresearchpress.com by 123.30.183.119 on 09/08/12
For personal use only.

Can. J. Chem. Downloaded from www.nrcresearchpress.com by 123.30.183.119 on 09/08/12
For personal use only.

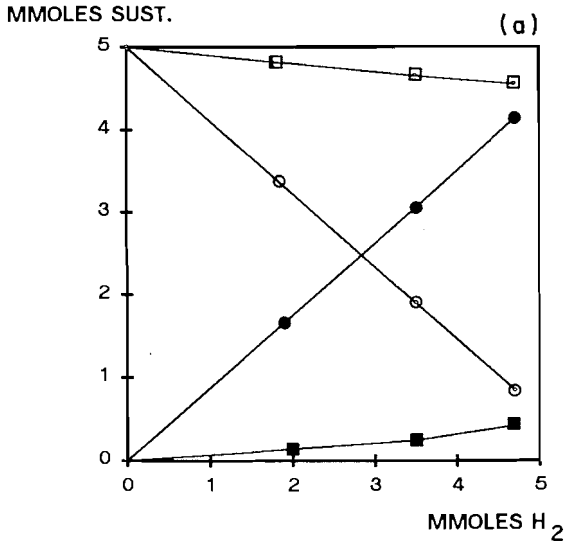

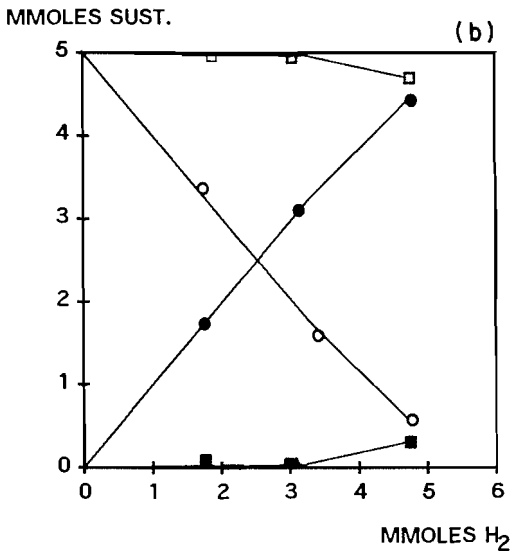

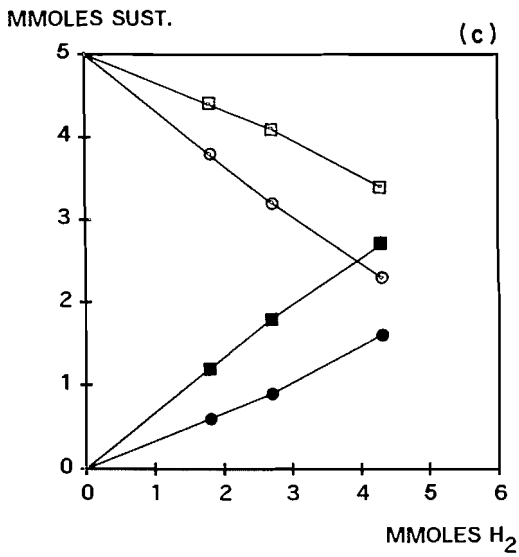

energy (equal for the two substrates), k Boltzman's constant, and h Planck's constant.

Insofar as the entropy factor can be ascribed to the steric hindrance of the adsorption, the decreased rate of reduction of methacrylamide must be attributed to a more negative value of the activation entropy of this process compared to the reduction of acrylamide. We can thus state that the steric effect of the methyl group plays a major role in the process.

On the other hand, Marinas and co-workers (27) derived the following equation:

[11] $$R \ln D_{AC,MAC} = \Delta S_{AC,MAC} - \Delta W_{AC,MAC}/T$$

As shown above, $\Delta W_{AC,MAC} = 0$. Therefore:

[12] $$\Delta S_{AC,MAC} = R \ln D_{AC,MAC}$$

In these cases, the relative adsorption coefficient can be exclusively determined by the entropy factor, which, as stated above, can be ascribed to steric effects on the adsorption.

The inductive effects of the substituents, reflected in changes in the strength of adsorption on the catalyst surface (by alteration of the electron density of the double bond), are directly related to the differential adsorption heat; as this last was virtually zero in our case, the inductive effects involved were clearly negligible.

On analysing the influence of the solvents used (tetrahydrofuran, ethyl acetate, dioxane, and methanol), methanol was found to yield the highest reaction rates and lowest selectivities and relative reactivities in the competitive hydrogenations. The selectivity order found was:

THF > dioxane > ethyl acetate > methanol

Regarding the influence of the catalyst, the order found for the relative reactivities was as follows: Pd_3-PS_{500}-B = Pd_3-PS_{600}-B > Pd_3-PS_{400}-C > Pd_3-PS_{400}-B = Pd/Al_2O_3 > Pd_3-P2-A > Pd/C > Pd_3-PS_{400}-A(4).

We should emphasize the major role played by the precursor Pd salt for a given support. In the case of sepiolite, the greatest selectivity is achieved by using $(NH_3)_4PdCl_2$ and calcining the support at 773 or 873 K prior to the impregnation. This catalyst is much more selective than the Pd/C (Merck) and Pd/Al_2O_3(Fluka) catalysts.

As can be seen, the selectivities are rather high: up to 93% under the optimum conditions, namely by using Na_2PdCl_4 doped with NaOH ($Na^+/Pd = 4$) as precursor, THF as solvent, and a temperature of 293 K.

In view of the above results (Table 4), those obtained in the hydrogen transfer reduction of acrylamide and methacrylamide with the same catalysts are quite logical. Only methacrylamide reduction is feasible under these conditions, as those of acrylamide reduction and cyclohexene disproportionation are inhibited. This shows the signifi-

FIG. 1. (*a*) Distribution of reactants and products as a function of the extent of simultaneous hydrogenation of AC/MAC: (○) acrylamide; (●) propanamide; (□) methacrylamide; (■) methylpropanamide. (*b*) Distribution of reactants and products as a function of the extent of simultaneous hydrogenation of AC/CHE: (○) acrylamide; (●) propanamide; (□) cyclohexene; (■) cyclohexane. (*c*) Distribution of reactants and products as a function of the extent of simultaneous hydrogenation of MAC/CHE: (○) methacrylamide; (●) methylpropanamide; (□) cyclohexene; (■) cyclohexane.

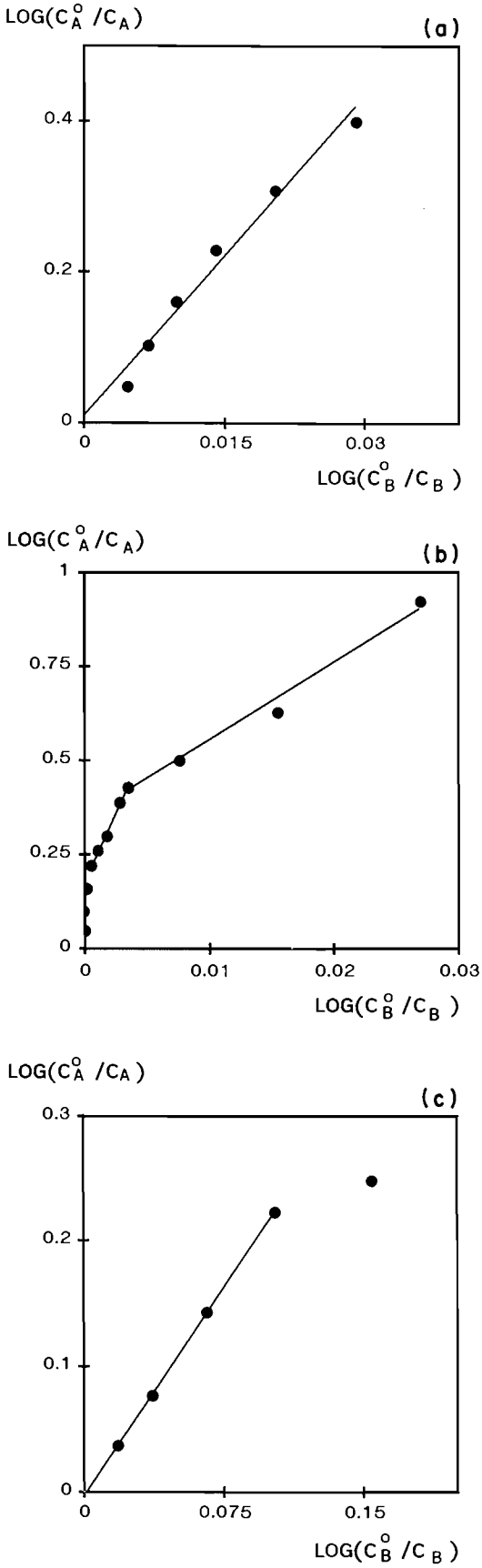

FIG. 2. (*a*) Logarithmic plot of the rate of disappearance of AC(A) vs. MAC(B). (*b*) Logarithmic plot of the rate of disappearance of AC(A) vs. CHE(B). (*c*) Logarithmic plot of the rate of disappearance of MAC(A) vs. CHE(B).

TABLE 4. Ratios between the rate constants (obtained individually), reactivities, and relative adsorption coefficients of the pairs AC/CHE, MAC/CHE, and MAC/AC

Pair	k_A/k_B	$R_{A,B}$	$D_{A,B}$
AC/CHE	3.92	117.6	30.0
MAC/CHE	0.96	2.2	2.3
MAC/AC	0.24	0.1	0.4

Reaction conditions: MeOH solution of the substrate; 0.5 M for the individual reactions and 0.25 M in each substrate in competitive reactions; total volume, 20 mL; 0.045 g of catalyst Pd_3-PS_{400}-A(4); 293 K; 0.414 MPa.

TABLE 5. Relative reactivities ($R_{AC,MAC}$) and relative coefficients of adsorption ($D_{AC,MAC}$) of acrylamide and methacrylamide for different temperatures, catalysts, and solvents

Catalyst	solvent	T(K)	$R_{AC,MAC}$	$D_{AC,MAC}$	S
Pd_3-PS_{400}-A(4)	MeOH	293	11.1	2.6	0.87
Pd_3-PS_{400}-A(4)	MeOH	298	11.9	2.5	0.88
Pd_3-PS_{400}-A(4)	MeOH	303	9.5	2.0	0.89
Pd_3-PS_{400}-A(4)	MeOH	308	9.8	2.2	0.83
Pd_3-PS_{400}-B	MeOH	293	17.9	3.9	0.88
Pd_3-PS_{500}-B	MeOH	293	25.6	5.7	0.87
Pd_3-PS_{600}-B	MeOH	293	25.6	5.1	0.87
Pd_3-PS_{400}-C	MeOH	293	21.7	3.7	0.86
Pd/C	MeOH	293	15.4	10.4	0.85
Pd/Al_2O_3	MeOH	293	17.9	6.9	0.85
Pd_3-P2-A	MeOH	293	16.1	6.5	0.75
Pd_3-PS_{400}-A	Dioxane	293	19.6	4.5	0.90
Pd_3-PS_{400}-A	EtAcO	293	17.2	4.2	0.89
Pd_3-PS_{400}-A	THF	293	25.3	7.1	0.93

cance of the adsorption coefficients of the substrate and the donor in hydrogen transfer reactions, as well as the influence of small structural modifications (presence of a methyl group or a proton) in the substrate to be adsorbed on such coefficients. On the other hand, the competitive reduction of AC and MAC by hydrogen transfer with cyclohexene as donor is also unfeasible as the latter cannot be adsorbed on the support to be converted to benzene and release the hydrogen required for the reduction of AC and (or) MAC. Both results confirm that cyclohexene, acrylamide, and methacrylamide are adsorbed on the same type of site, while hydrogen is adsorbed on different free sites, and that the type of donor used plays a significant role in hydrogen transfer processes.

Experiments under way are aimed at comparing the influence of the introduction of a methyl group in the double bond of acrolein, methyl acrylate, and styrene on both types of reduction process: with molecular hydrogen and by hydrogen transfer with cyclohexene as donor.

Acknowledgement

The authors wish to express their gratitude to the Consejería de Educación y Ciencia, of the Junta de Andalucía, and to the DGICyT for financial support received (Project PB89-0340).

Can. J. Chem. Downloaded from www.nrcresearchpress.com by 123.30.183.119 on 09/08/12
For personal use only.

1. G. Brieger and T. Nestrick. Chem Rev. **74**, 567 (1974).
2. R. A. W. Johnstone, A. H. Wilby, and I. Entwistle. Chem. Rev. **85**, 129 (1985).
3. M. A. Aramendía, V. Borau, A. García, C. Jiménez, J. M. Marinas, and J. A. Pajares. J. Catal. **78**, 188 (1982).
4. A. Alba, M. A. Aramendía, V. Borau, A. García-Raso, C. Jiménez, and J. M. Marinas. Can. J. Chem. **62**, 917 (1984).
5. A. Alba, M. A. Aramendía, V. Borau, C. Jiménez, and J. M. Marinas. Can. J. Chem. **63**, 3471 (1985).
6. A. Alba, M. A. Aramendía, V. Borau, C. Jiménez, and J. M. Marinas. J. Catal. **98**, 288 (1986).
7. R. M. Barrer, N. Mackenzie, and D. N. McLeod. J. Phys. Chem. **58**, 568 (1954).
8. A. J. Dandy. J. Phys. Chem. **72**, 334 (1968); J. Soil Sci. **20**, 278 (1969); J. Chem. Soc. *2383* (1971).
9. C. Serna and T. Fernández-Alvarez. An. Quim. **71**, 371 (1975).
10. J. M. Campelo, A. García, D. Luna, and J. M. Marinas. React. Solids, **3**, 263 (1987); Clay Minerals, **22**, 233 (1987).
11. M. A. Aramendía, V. Borau, C. Jiménez, and J. M. Marinas. Appl. Catal. **10**, 347 (1984).
12. M. A. Aramendía, V. Borau, C. Jiménez, J. M. Marinas, and M. E. Sempere. Can. J. Chem. **65**, 2791 (1987).
13. Ch. P. Rader and H. A. Smith. J. Am. Chem. Soc. **84**, 1443 (1962).
14. J. A. Cabello, J. M. Campelo, A. García, D. Luna, and J. M. Marinas. J. Catal. **94**, 1 (1985).
15. L. Cerveny and V. Ruzicka. Catal. Rev. Sci. Eng. **24**, 503 (1982).
16. C. Jiménez, J. M. Marinas, J. V. Sinisterra, and V. Borau. An. Quim. **73**, 1164 (1977).
17. (*a*) C. N. Satterfield. Mass transfer in heterogeneous catalysis. MIT Press, Cambridge, MA. 1970. p. 108; (*b*) J. M. Campelo, A. García, D. Luna, and J. M. Marinas. J. Catal. **97**, 108 (1986).
18. (*a*) M. E. Gonzo and M. Boudart. J. Catal. **52**, 462 (1978); (*b*) R. M. Koros and E. J. Novak. Chem. Eng. Sci. **22**, 470 (1967).
19. J. M. Campelo, A. García, D. Luna, and J. M. Marinas. Bull. Soc. Chim. Belg. **91**, 131 (1982).
20. J. M. Campelo, A. García, D. Luna, and J. M. Marinas. Bull. Soc. Chim. Belg. **92**, 851 (1983).
21. J. M. Campelo, A. García, D. Luna, and J. M. Marinas. J. Chem. Soc. Faraday Trans. 1, **80**, 659 (1984).
22. A. Alba, J. M. Gutiérrez, D. Luna, and J. M. Marinas. Appl. Catal. **7**, 397 (1983).
23. R. J. Madon, J. P. O'Connell, and M. Boudart. AIChE J. **24**, 904 (1978).
24. I. Horiuti and M. Polanyi. Trans. Faraday Soc. **30**, 1164 (1934).
25. L. Cerveny, B. Vostry, and V. Ruzicka. Collect. Czech. Chem. Commun. **46**, 2672 (1981).
26. M. S. Kamlet, J. L. M. Abboud, M. H. Abraham, and R. W. Taft. J. Org. Chem. **48**, 2877 (1983).
27. J. M. Campelo, A. García, D. Luna, and J. M. Marinas. J. Catal. **97**, 108 (1986).

Can. J. Chem. Downloaded from www.nrcresearchpress.com by 123.30.183.119 on 09/08/12
For personal use only.

Pressure dependences of the electrode potentials of some iron(III/II) and cobalt(III/II) couples in aqueous solution

HIDEO DOINE, TODD W. WHITCOMBE, AND THOMAS W. SWADDLE[1]

Department of Chemistry, The University of Calgary, Calgary, Alta., Canada T2N 1N4

Received May 10, 1991

HIDEO DOINE, TODD W. WHITCOMBE, and THOMAS W. SWADDLE. Can. J. Chem. **70**, 81 (1992).

The dependences of the electrode potentials E of aqueous $Fe(H_2O)_6^{3+/2+}$, $Fe(phen)_3^{3+/2+}$, $Fe(CN)_6^{3-/4-}$, and $Co(sep)^{3+/2+}$ upon pressure P (up to ca. 200 MPa) have been measured at 25.0°C relative to an AgCl/Ag(satd. KCl) electrode by cyclic voltammetry. For $Co(sep)^{3+/2+}$ at ionic strength I = 0.28 and 1.00 mol kg^{-1}, $(\partial E/\partial P)_T$ is independent of P as well as I, giving a volume of reaction $\Delta V = +13.7 \pm 0.4$ cm^3 mol^{-1} relative to AgCl/Ag; similarly, for $Fe(H_2O)_6^{3+/2+}$ at I = 0.28 mol kg^{-1} (CF_3SO_3H), $\Delta V = +5.0 \pm 0.3$ cm^3 mol^{-1}. For $Fe(CN)_6^{3-/4-}$ in KCl media, $(\partial E/\partial P)_T$ is independent of P and I at I = 0.28 and 0.51 mol kg^{-1}, giving $\Delta V = -36.1 \pm 1.0$ cm^3 mol^{-1}, but shows some slight dependence on P at I = 1.00 mol kg^{-1} (low-pressure limit $\Delta V_0 = -38 \pm 1$ cm^3 mol^{-1}; $(\partial \Delta V/\partial P)_T \approx +0.030$ cm^3 mol^{-1} MPa^{-1}). For $Fe(phen)_3^{3+/2+}$, $(\partial E/\partial P)_T$ is markedly pressure and medium dependent, with $\Delta V_0 = +14.2 \pm 0.5$ and $+6.2 \pm 0.5$ cm^3 mol^{-1} in KNO_3 media at I = 0.25 and 1.00 mol kg^{-1}, respectively. The peak-to-peak separation of the cyclic voltammograms increases with increasing P for $Fe(CN)_6^{3-/4-}$, but decreases slightly for the cationic couples; these trends can be accounted for in terms of the volumes of activation for the corresponding self-exchange reactions.

Key words: high pressures, electrode potentials, volume of reaction, iron complexes, cobalt complexes.

HIDEO DOINE, TODD W. WHITCOMBE et THOMAS W. SWADDLE. Can. J. Chem. **70**, 81 (1992).

Utilisant la voltampérométrie cyclique et opérant à 25°C, on a déterminé la relation entre la pression P (jusqu'à 200 MPa) et les potentiels à l'électrode E, mesurés par rapport à une électrode de AgCl/Ag (saturé en KCl), de solutions aqueuses de $Fe(H_2O)_6^{3+/2+}$, $Fe(phen)_3^{3+/2+}$, $Fe(CN)_6^{2-/4-}$ et de $Co(sep)^{3+/2+}$. Pour le $Co(sep)^{3+/2+}$, à des forces ioniques I = 0,28 et 1,00 mol kg^{-1}, $(\partial E/\partial P)_T$ est indépendant de la P ainsi que de I, conduisant à un volume de réaction $\Delta V = +13,7 \pm 0,4$ cm^3 mol^{-1} relatif à AgCl/Ag; de la même manière, pour le $Fe(H_2O)_6^{3+/2+}$ à I = 0,28 mol kg^{-1} (CF_3SO_3H), $\Delta V = +5,0 \pm 0,3$ cm^3 mol^{-1}. Pour le $Fe(CN)_6^{3-/4-}$ dans un milieu de KCl, alors que I = 0,28 et 0,51 mol kg^{-1}, $(\partial E/\partial P)_T$ est indépendant de la P et de I, donnant $\Delta V = -36,1 \pm 1,0$ cm^3 mol^{-1} qui est toutefois légèrement dépendant de P lorsque I = 1,00 mol kg^{-1} (la limite à basse pression est $\Delta V_0 = -38 \pm 1$ cm^3 mol^{-1}; $(\partial \Delta V/\partial P)_T \approx$ 0,30 cm^3 mol^{-1} MPa^{-1}). Pour le $Fe(phen)_3^{3+/2+}$, la valeur du $(\partial E/\partial P)_T$ varie beaucoup avec la pression et le milieu; ΔV_0 $= +1,42 \pm 0,5$ et $+6,2 \pm 0,5$ cm^3 mol^{-1} respectivement dans un milieu de KNO_3 avec I = 0,25 et 1,00 mol kg^{-1}. Avec le $Fe(CN)_6^{3-/4-}$, la séparation entre les pics des voltampérogrammes cycliques augmente avec un accroissement de la P, mais elle diminue légèrement pour les couples cationiques; on peut expliquer ces tendances en fonction des volumes d'activation des réactions correspondantes d'auto-échanges.

Mots clès : haute pression, potentiels à l'électrode, volume de réaction, complexes de fer, complexes de cobalt.

[Traduit par la rédaction]

Introduction

In connection with our continuing studies of the effects of pressure on the kinetics of electron transfer reactions in the context of Marcus-Hush theory (1–4), we have measured the pressure dependence of the electrode potentials of some typical metal complex couples in aqueous solution, viz., $Fe(H_2O)_6^{3+/2+}$, $Fe(phen)_3^{3+/2+}$, $Fe(CN)_6^{3-/4-}$, and $Co(sep)^{3+/2+}$ (phen = 1,10-phenanthroline; sep = sepulchrate (1,3,6,8,10,13,16,19-octaazabicyclo[6.6.6]eicosane)). The iron couples were chosen with the expectation that they would yield information on the influence of ionic size, charge, and spin state on the pressure response of the electrode potentials, while the cobalt(III/II) sepulchrate couple was included as an ideal example of an obligate outer-sphere low-spin/high-spin electrode transfer system, since neither the cobalt(III) nor the normally labile cobalt(II) ion can escape from the robust encapsulating ligand. For our present purposes, however, the most important consideration is that the pressure dependences of the *kinetics* of the self-exchange reactions of all four couples have been reported (1–6) and the use of those data together with the present results in testing the applicability of the Marcus "cross relation" (7) at high pressure will be described in a forthcoming article.

A variety of approaches to measurements of electrode phenomena at high pressures have been reported (5, 6, 8–15). We have found cyclic voltammetry to be well suited for the measurement of electrode potentials E_P as functions of the pressure P (12, 13); however, our attempts to obtain *kinetic* information from a combination of cyclic and AC voltammetry (16) gave inconsistent results under pressure, and are reported only in outline here.

Our potential measurements were made with reference to an AgCl/Ag electrode in saturated KCl solution. The standard free energy change ΔG^0 for a half-cell with a standard electrode potential E^0 is $-nFE^0$, where n is the number of (moles of) electrons transferred and F is the Faraday constant, and the associated standard volume change ΔV^0 is given by $(\partial \Delta G^0/\partial P)_T$. Thus, the pressure dependence of the potentials E of the single-electron redox half-cells relative to AgCl/Ag can be expressed as a reaction volume ΔV:

$$[1] \quad F(\partial E/\partial P)_T = -\Delta V$$

There is no reason to suppose, however, that ΔV is necessarily constant over pressure ranges of several hundred MPa. Theoretical analysis of the *kinetics* of electron transfer (1) suggests that volumes of activation for homogeneous

[1]To whom all correspondence should be addressed.

Can. J. Chem. Downloaded from www.nrcresearchpress.com by 123.30.183.119 on 09/08/12
For personal use only.

Can. J. Chem. Downloaded from www.nrcresearchpress.com by 123.30.183.119 on 09/08/12
For personal use only.

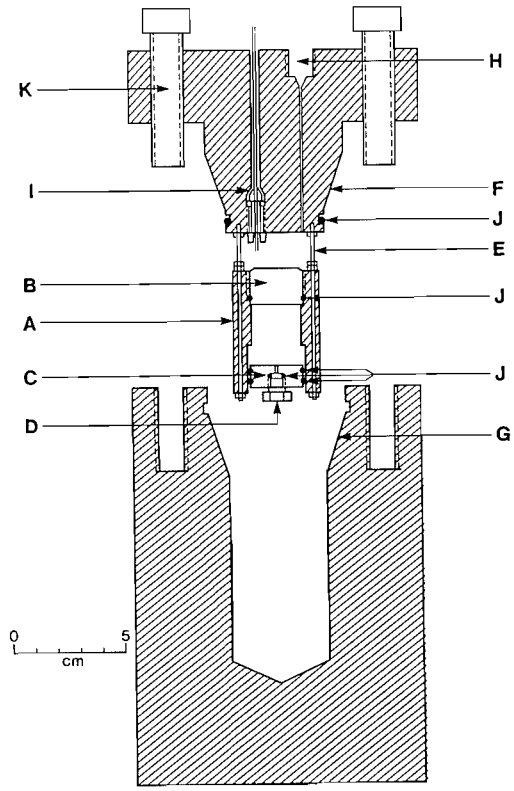

FIG. 1. Pressure vessel. A: Teflon cell containing sample and electrodes (see Fig. 3). B: Threaded Teflon plug through which electrode connections pass (see Fig. 3). C: Free piston (Teflon). D: Teflon plug sealing filling port. E: Threaded cell support (steel). F: Main sealing surface of pressure vessel cap (39° cone). G: Main sealing surface of pressure vessel body (40° cone). H: Standard quarter-inch high pressure connection (in plane in front of cell supports). I: High pressure electrical lead-through (in plane in front of cell supports E; two more are located in the corresponding plane behind cell supports; detailed structure shown in Fig. 2). J: Neoprene O-rings. K: Grade 8 hexhead bolts (0.625 in. NC, 2.25 in. long; eight of these, symmetrically placed around pressure vessel cap).

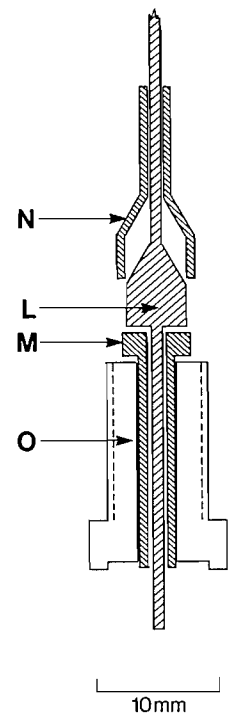

FIG. 2. High pressure electrical lead-through. L: Brass electrical connector. M: Vespel (Du Pont polyimide resin) insulating sleeve. N: Vespel pressure sealing sleeve. O: Thrust bolt, threading into bottom of pressure vessel cap.

self-exchange reactions might be markedly pressure dependent; thus, since the equilibrium electrode processes to which ΔV refers are dynamic, some pressure dependence of ΔV might also be anticipated. In any event, any significant differences between the partial molar compressibilities of the oxidized and reduced species would lead to a pressure-dependent ΔV. Accordingly, a further objective of this study was to assess the constancy of ΔV for some representative electrode reactions over a commonly used range of pressures (200 MPa). Finally, in view of the fact that substantial concentrations of inert electrolyte (at least 0.2 mol kg^{-1}) were necessary to obtain cyclic voltammograms of good quality, the effects of ionic strength I on ΔV were also investigated; however, most of the measurements were made at $I \simeq 0.28$ mol kg^{-1}, to correspond with kinetic studies to be reported later.

Experimental

Equipment

The pressure vessel (13.0 mm o.d., 4.4 mm i.d.) shown in Fig. 1 was machined from 17-4PH stainless steel, and heat-treated at 480°C for 1 h followed by air cooling (Rockwell hardness C44). The calculated ceiling pressure was 515 MPa (safety factor of 2), although the vessel was not tested or used beyond 300 MPa because the electrical lead-throughs (Fig. 2) may not be reliable beyond this pressure. The sample cell (Figs. 1 and 3; 3.85 mm o.d., 2.4 mm minimum i.d.) was machined from virgin Teflon. The electrode tips protruding from the sample cell cap were soldered to the electrical lead-through terminals as required. The helical counter electrode and straight working electrode were of Pt wire; trials with electrodes of other material (e.g., gold) or geometries gave results indistinguishable from those reported below. The reference electrode consisted of a silver rod, diameter 2 mm, enclosed in a 4 mm i.d. heat-shrink Teflon tube which was shrink-fitted at the top over a leak-tight adapter fitting into the cell gap and at the bottom over a 4 mm diameter Vycor porous plug (E. G. & G. Instruments Division, Markham, Ontario). The tube was filled with saturated KCl solution, and that part of the electrode that was exposed to this solution was coated beforehand with AgCl.

Materials

Potassium hexacyanoferrate(III) (BDH Analar reagent) was used as received. Iron(III) perchlorate hydrate (Aldrich, low chloride) was converted to the trifluoromethanesulfonate salt in aqueous CF_3SO_3H by addition of CF_3SO_3K to precipitate $KClO_4$; the iron concentration was determined spectrophotometrically with 1,10-phenanthroline after reduction to iron(II) with hydroxylamine, and the hydrogen ion concentration by titration with alkali. Cobalt(III) sepulchrate chloride monohydrate and tris(1,10-phenanthroline)-iron(II) sulfate 9-hydrate were made and checked for purity as described elsewhere (2, 4). All other reagents were of analytical reagent quality, and distilled water was passed through a Barnstead NANOpure purification train before use.

Measurements

Solutions were prepared by weight, deoxygenated with a nitrogen stream for at least 1 h, brought to 25°C, and injected with a syringe into the sample cell through the filling port in the free piston, leaving no air bubbles inside the cell. The filling port was then

Can. J. Chem. Downloaded from www.nrcresearchpress.com by 123.30.183.119 on 09/08/12
For personal use only.

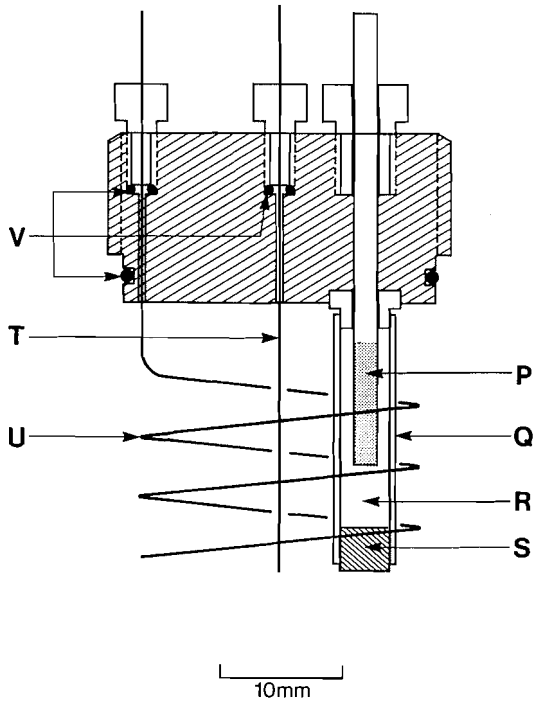

FIG. 3. Electrode assembly. P: Reference electrode (silver rod, 2.0 mm diameter, with AgCl coating over bottom 2 cm). Q: Heat-shrink Teflon tubing. R: Saturated KCl solution. S: Vycor porous disk. T: Working electrode (Pt wire). U: Helical counter-electrode (Pt wire). V: Neoprene O-rings.

sealed with a small O-ring and the threaded plug, and the assembly was lowered into the previously thermostated pressure vessel, which contained pure hexanes as the pressurizing fluid; excess fluid escaped through a weep hole in the pressure vessel at the level of the top of the conical surface (not shown in Fig. 1) or through the high pressure connection in the pressure vessel cap. The vessel was pressurized with a hand-pump and intensifier (capacity: 400 MPa); the hydraulic oil was prevented from mixing with the pressurizing hexanes by use of a large cylindrical separator with a free piston. The pressure was measured with a Heise Bourdon gauge, calibrated against a Pressurements T3800/4 deadweight pressure balance.

Since the assembly was to be operated close to room temperature, and because the number of high-pressure electrical leads had to be kept to a minimum, no provision was made to monitor the temperature of the sample cell *internally* during the electrochemical measurements. Rather, it was established, in a series of experiments in which the Pt electrodes were replaced with a Pt resistance sensor, that any temperature perturbation produced within the sample by (de)pressurization, 0–300 MPa, decayed to within 0.05°C of the temperature (25.0 ± 0.1°C) of the thermostat bath surrounding the pressure vessel within 50 min at worst, and that the temperature of the thermally equilibrated sample was within 0.05°C of that of the bath.

In the electrochemical experiments, measurements were made with a Princeton Applied Research Corporation model 173 potentiostat/galvanostat, model 178 electrometer, model 175 universal programmer, model 117 differential preamplifier, and model RE0074 X–Y recorder. The scan rate v was 50 mV s^{-1} except as noted below, and the scan ranges relative to the AgCl/Ag(satd. KCl) reference electrode were −750 to −200 mV for $Co(sep)^{3+/2+}$, 0 (or, in a few cases, −100) to 600 mV for $Fe(CN)_6^{3-/4-}$, 250 to 850 mV for $Fe(H_2O)_6^{3+/2+}$, and 500 to 1100 mV for $Fe(phen)_3^{3+/2+}$. Prior to making a measurement, a period of 90 min was allowed for complete thermal re-equilibration following set-up or pressure change.

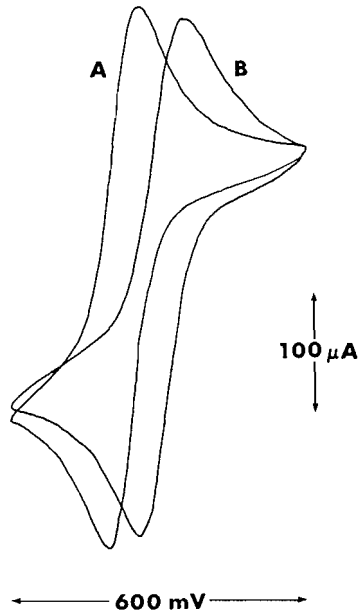

FIG. 4. Effect of pressure on the cyclic voltammogram of $Fe(CN)_6^{3-/4-}$ ([Fe] = 1.46 mmol kg^{-1}) in aqueous KCl (0.498 mol kg^{-1}) at 25.0°C. Cycle A: 4.6 MPa. Cycle B: 204.4 MPa.

Results

Figure 4 illustrates the typical effects of pressure on the cyclic voltammograms — in this case, two cycles for $Fe(CN)_6^{3-/4-}$ at ionic strength I = 0.5 mol kg^{-1}, taken 200 MPa apart. The average of the potentials E_{ox} and E_{red} corresponding to the peak oxidative and reductive currents, respectively, was identified with the reversible electrode potential E relative to that of the AgCl/Ag reference electrode at the prevailing pressure and ionic strength. The peak-to-peak potential separation $\delta E = (E_{ox} - E_{red})$ in this example varied monotonically with rising P from 80 mV at 4 MPa to 105 mV at 204 MPa; as explained below, this can be accounted for accurately in terms of the effect of pressure on the heterogeneous self-exchange rate constant k^{el} for $Fe(CN)_6^{3-/4-}$.

Complete listings of E and δE values as functions of P and I are given in the supplementary tables.[2] Here, values E_P of E for representative systems are presented as graphs (Figs. 5–11) which incorporate normalization of the results of replicate experiments to a common zero-pressure value E_0. This normalization was necessary because, although E values were reproducibly measurable to ±0.8 mV, drifts of some 5 mV in E typically developed from one day to the next for a given solution *in situ,* while still larger discrepancies could occur between experiments some days apart with different samples. Within a 6–8 h series of measurements on a given day, however, drift was negligible; this was demonstrated for each system by comparing series of measurements taken with rising pressure with ones taken with decreasing pres-

[2]Supplementary tables S1–S4 may be purchased from the Depository of Unpublished Data, Document Delivery, CISTI, National Research Council of Canada, Ottawa, Ont., Canada K1A 0S2.

Can. J. Chem. Downloaded from www.nrcresearchpress.com by 123.30.183.119 on 09/08/12
For personal use only.

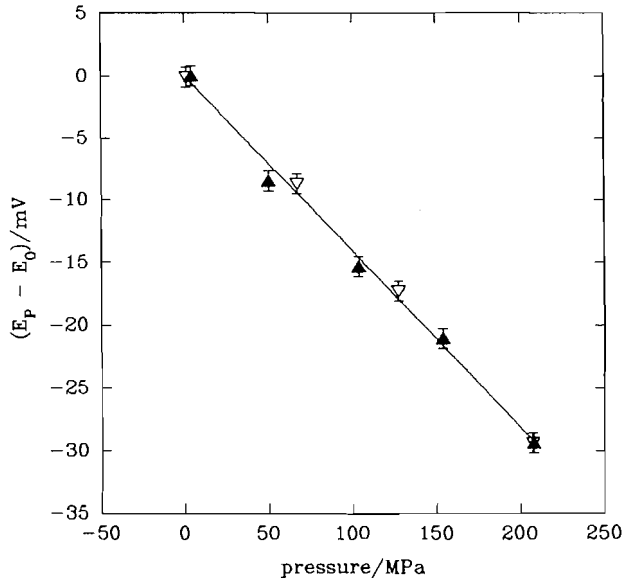

FIG. 5. Pressure dependence of E for $[Co(sep)]Cl_3$ (2.04 mmol kg^{-1}) in aqueous KCl solution (I = 1.02 mol kg^{-1}) at 25°C. Filled triangles: measurements with increasing pressure. Open triangles: measurements taken 1 day later with decreasing P and drift correction of 5.0 mV. Error bars are ±0.8 mV. Solid line: linear regression of all data.

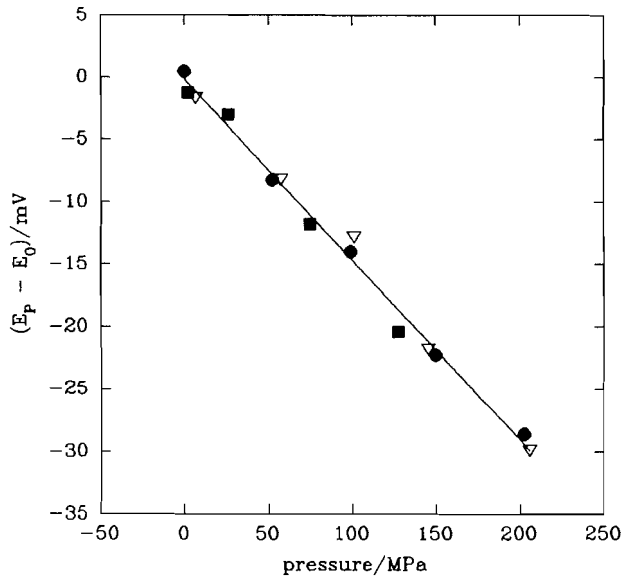

FIG. 6. Pressure dependence of E for $[Co(sep)]Cl_3$ (5.01 mmol kg^{-1}) in aqueous KCl (I = 0.26 mol kg^{-1}) at 25.0°C. Circles and triangles: pressure was first increased, then decreased. Squares: pressure decreasing from an initial 200 MPa.

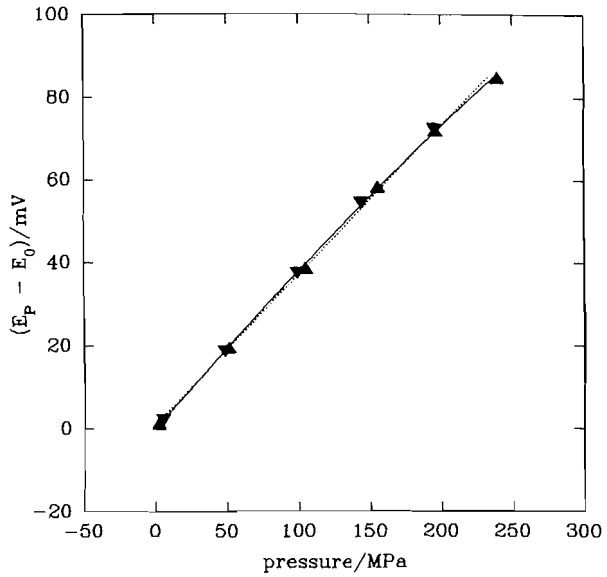

FIG. 7. Pressure dependence of E for $K_3[Fe(CN)_6]$ (4.78 mmol kg^{-1}) in aqueous KCl (I = 0.989 mol kg^{-1}) at 25.0°C. Up triangles: increasing pressure. Down triangles: decreasing pressure (separate experiment). Solid line: quadratic regression. Dotted line: linear regression.

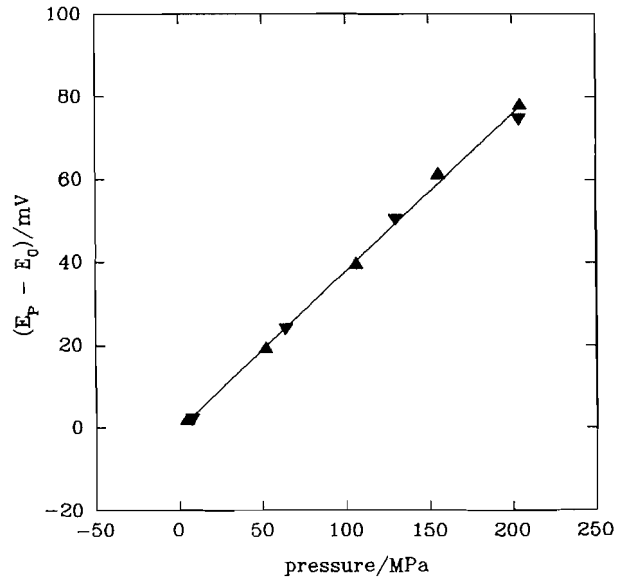

FIG. 8. Pressure dependence of E for $K_3[Fe(CN)_6]$ (1.46 mmol kg^{-1}) in aqueous KCl (I = 0.507 mol kg^{-1}) at 25.0°C. Up triangles: increasing pressure. Down triangles: decreasing pressure (separate experiment). Solid line: linear regression.

sure — in every case, the superposed plots of $(E_P - E_0)$ vs. P coincided within the experimental uncertainty. In other words, the absolute value of E at a given P could vary by several mV from one series of measurements to another, but the value of $(\partial E/\partial P)_T$ was typically reproducible to ±6 μV MPa^{-1}, corresponding to an uncertainty of ±0.6 cm^3 mol^{-1} in ΔV. For example, Fig. 5 shows that the slope of $(E_P - E_0)$ vs. P plots for a particular $Co(sep)^{3+}$ solution at I = 1.0 mol kg^{-1}, taken with ascending pressure on one day and with descending pressure the next, are indistinguishable within the natural scatter of the data, following application of a measured drift correction of −5.0 mV to the latter data set.

Drift in E seemed to be associated with the reference electrode. After several cycles, the Vycor porous plug tended to crack, leading to voltage changes of up to 30 mV, greater peak-to-peak separations, and the appearance of anomalous "spikes" in the CVs. The plug was therefore replaced periodically. No correction for the effect of pressure on junction potentials was applied; since the ultimate objective of this work was to evaluate the pressure effects on homoge-

Can. J. Chem. Downloaded from www.nrcresearchpress.com by 123.30.183.119 on 09/08/12
For personal use only.

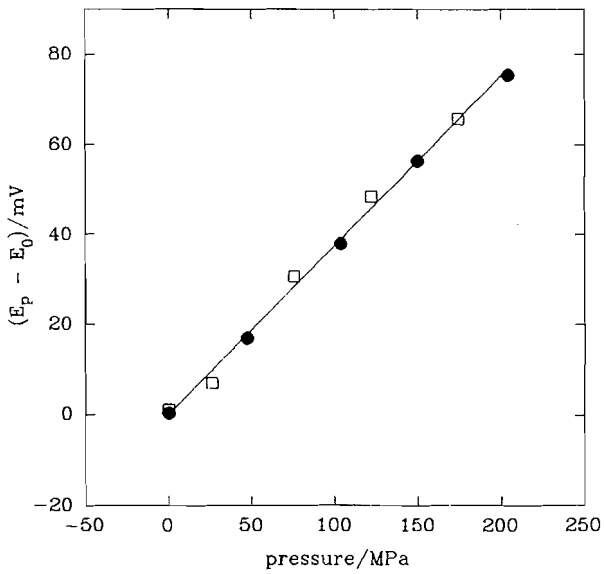

FIG. 9. Pressure dependence of E for $K_3[Fe(CN)_6]$ (4.80 mmol kg^{-1}) in aqueous KCl (I = 0.279 mol kg^{-1}) at 25.0°C. Circles and squares denote different experiments. Solid line: linear regression.

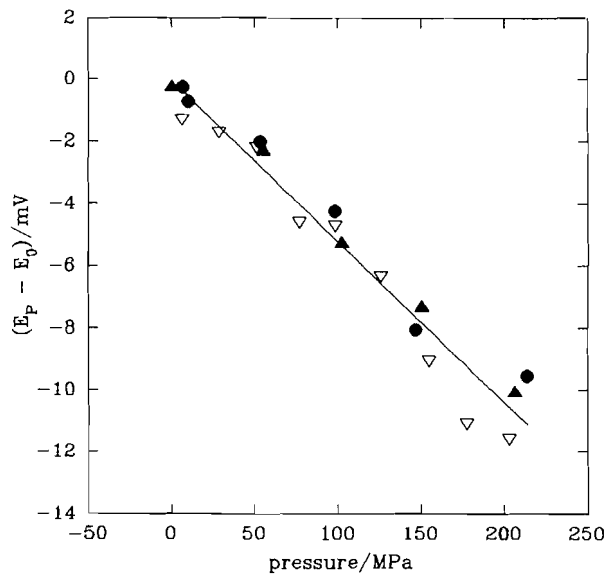

FIG. 10. Pressure dependence of E for $[Fe(H_2O)_6](CF_3SO_3)_3$ (5.00 mmol kg^{-1}) in aqueous CF_3SO_3H (0.250 mol kg^{-1}; I = 0.280 mol kg^{-1}) at 25°C. Different symbols indicate independent experiments. Solid line: linear regression.

neous redox equilibria from E values for the corresponding half-cells relative to the AgCl/Ag electrode, junction potential effects could be ignored.

Equation [1] implies that E will be a linear function of P if ΔV is constant, within the limits of detection, over the operational pressure range:

$$[2] \quad E_P = E_0 - P\Delta V/F$$

In certain of the cases described below, however, plots of E vs. P were distinctly curved. In the absence of a theoretical framework to account for this curvature, it was assumed that

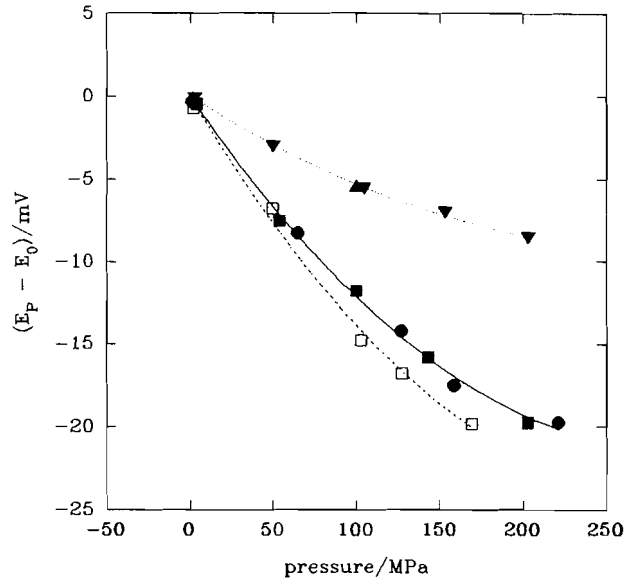

FIG. 11. Pressure dependence of E for $[Fe(phen)_3]SO_4$ in various aqueous media at 25°C. Curved lines are quadratic least-squares regressions; different symbols indicate independent experiments. Open squares and dashed curve: [Fe] = 2.53 mmol kg^{-1}, $[H_2SO_4]$ = 0.0506 mol kg^{-1}, $[Na_2SO_4]$ = 0.0739 mol kg^{-1}, $[phen]_{free}$ = 8.9 mmol kg^{-1}, I = 0.272 mol kg^{-1}. Filled circles: [Fe] = 0.946 mmol kg^{-1}, $[KNO_3]$ = 0.251 mol kg^{-1} $[phen]_{free}$ = 0.020 mol kg^{-1}, I = 0.254 mol kg^{-1}. Filled squares: [Fe] = 0.959 mmol kg^{-1}, $[KNO_3]$ = 0.249 mol kg^{-1}, no added phen, I = 0.253 mol kg^{-1}. Solid curve: I = 0.25 mol kg^{-1} (KNO_3). Triangles and dotted curve: [Fe] = 0.979 mmol kg^{-1}, $[KNO_3]$ = 1.001 mol kg^{-1}, no added phen, I = 1.005 mol kg^{-1}.

E was a quadratic function of pressure, i.e., that $(\partial\Delta V/\partial P)_T$ was sensibly constant over the experimental pressure range:

$$[3] \quad E_P = E_0 + AP + BP^2$$

where $A = -\Delta V_0/F$ and $B = -(\partial\Delta V/\partial P)_T/2F$. In practice, eq. [2] was adopted whenever nonlinear least-squares regression according to eq. [3] gave a standard error in B that was larger than B itself; interestingly, in all such cases, eq. [3] also gave a poorer fit of the data (larger mean square error) than did the simple linear eq. [2] despite the flexibility afforded by the additional parameter, since the quadratic regressions created outliers with relatively large residuals. Replicate data sets were normalized by calculating E_0 for each set according to the appropriate equation ([2] or [3]) and then combining values of $(E_P - E_0)$ to form a single data set for the particular couple and medium composition (Figs. 5–11, in each of which the various symbols indicate different data sets). The values of ΔV or ΔV_0 derived from the combined data sets, as explained below, are collected in Table 1. The sign of ΔV is correct for redox couples written in the standard IUPAC convention, i.e., as reduction potentials, but are relative to the AgCl/Ag(satd. KCl) electrode at ionic strength I rather than to the standard hydrogen electrode at infinite dilution.

For all but the $Fe(CN)_6^{3-/4-}$ couple, values of the peak-to-peak separation δE were typically 65–80 mV, and thus close to the "reversible" range (ref. 16, pp. 230, 231), but occasionally larger values were recorded. Increasing pressure appeared to cause a slight decrease in δE for the cat-

Can. J. Chem. Downloaded from www.nrcresearchpress.com by 123.30.183.119 on 09/08/12
For personal use only.

TABLE 1. Volumes of reaction ΔV for reduction half-cells at a Pt electrode relative to AgCl/Ag(satd. KCl), and volumes of activation ΔV_{ex}* for the corresponding self-exchange reactions in aqueous solution at 25.0°C.

Couple	I /mol kg^{-1}	ΔV or ΔV_0 /cm^3 mol^{-1}	ΔV_{ex}* /cm^3 mol^{-1}
$Co(sep)^{3+/2+}$	1.00 (KCl)	+13.5 ± 0.4	
	0.28 (KCl)	+13.9 ± 0.5	−6.4[a,b]
$Fe(CN)_6^{3-/4-}$	1.00 (KCl)	−38.3 ± 1.0[c]	+13.0[d]
	0.51 (KCl)	−36.6 ± 0.7	
	0.28 (KCl)	−36.2 ± 0.8	
	0.28 (LiCl)	−37.1 ± 1.3	
	0.28 (K_2SO_4)	−34.4 ± 0.6	
$Fe(H_2O)_6^{3+/2+}$	0.28 (CF_3SO_3H)	+5.0 ± 0.3	−11.1[b,e]
$Fe(phen)_3^{3+/2+}$	1.00 (KNO_3)	+6.2 ± 0.5[c]	
	0.25 (KNO_3)	+14.2 ± 0.5[c]	
	0.27 ($NaHSO_4$)	+16.3 ± 2.0[c]	−2.2[b,f]

[a]Reference 2.
[b]For homogeneous self-exchange.
[c]Zero-pressure limiting value, ΔV_0.
[d]For the electrode reaction; ref. 6.
[e]Reference 3.
[f]Reference 4.

ionic couples, but the δE values were insufficiently accurately reproducible from one run to the next to warrant detailed consideration (see supplementary tables).[2] For the $Fe(CN)_6^{3-/4-}$ couple, δE was relatively large (80 mV and more) and clearly *increased* with increasing pressure (cf. Fig. 4), but again reproducibility between runs was poor — generally, δE became large (up to 230 mV) after several repeated pressure cycles, possibly because of degradation of the Vycor porous plug in the reference electrode.

Cobalt(III/II) sepulchrate

The voltammograms exhibited good reversibility (δE typically 68–70 mV), with $E_0 \simeq -540$ mV vs. AgCl/Ag. The plots of E_P vs. P were accurately linear for $I = 1.0$ and 0.28 mol kg^{-1} (Figs. 5 and 6) and gave $\Delta V = +13.5 \pm 0.4$ cm^3 mol^{-1} and $+13.9 \pm 0.4$ cm^3 mol^{-1}, respectively.

Hexacyanoferrate(III/II)

The peak-to-peak separations δE in KCl media were typically 80–110 mV and *increased* with increasing pressure; thus, they departed further from the reversible range (18) than did δE for the other couples considered here. For $I = 1.0$ mol kg^{-1} (KCl), a slight curvature of the E vs. P plots was clearly discernable in two independent sets of data (Fig. 7) and was accurately represented by the quadratic eq. [3]. The combined data of Fig. 9 give $\Delta V_0 = -38.3 \pm 1.0$ cm^3 mol^{-1} and $(\partial\Delta V/\partial P)_T = 0.030 \pm 0.008$ cm^3 mol^{-1} MPa^{-1}; $E_0 \simeq +270$ mV. Linear regression gave $\Delta V = -34.8 \pm 0.4$ cm^3 mol^{-1}, but with a 2.4-fold increase in the mean standard error. For experiments in aqueous KCl with $I = 0.51$ (Fig. 8) and 0.28 mol kg^{-1} (Fig. 9), however, the data were statistically better represented by a linear regression (eq. [2]), giving $\Delta V = -36.6 \pm 0.7$ and -36.2 ± 0.8 cm^3 mol^{-1} with $E_0 \simeq 235$ and 243 mV, respectively. Cyclic voltammograms obtained at $I = 0.10$ mol kg^{-1} (KCl) were poorly reproducible, with anomalously large δE values, but gave an average ΔV of -34 ± 3 cm^3 mol^{-1}.

An experiment with LiCl rather than KCl as the supporting electrolyte ($I = 0.28$ mol kg^{-1}) gave a linear E_P vs. P plot with $\Delta V = -37.1 \pm 1.3$ cm^3 mol^{-1}, which is similar to the value obtained for the comparable KCl solutions, but the relatively large uncertainty in ΔV, a low E_0 (+214 mV), and a very large δE (194–227 mV) imply the need for caution in making this comparison. In another experiment, K_2SO_4 rather than KCl was used to bring the ionic strength to 0.28 mol kg^{-1}, so that the K^+ ion concentration was reduced from 0.264 to 0.181 mol kg^{-1} at constant I; E_0 (+233 mV), δE (83–141 mV) and ΔV (-34.4 ± 0.6 cm^3 mol^{-1}) were sufficiently close to the analogous data for the KCl medium to imply that changing the K^+ concentration or the nature of the supporting anion has no significant effect in this concentration regime.

Hexaaquairon(III/II)

It was necessary to maintain strongly acidic conditions ($[CF_3SO_3H] = 0.25$ mol kg^{-1}) to suppress hydrolysis of $Fe(H_2O)_6^{3+}$. Trifluoromethanesulfonate was chosen as the non-complexing anion because perchlorate, the logical choice, would have caused precipitation of $KClO_4$ in the reference electrode. The cyclic voltammograms came close to reversible behavior ($\delta E = 71$–79 mV) at a scan rate $v = 20$ mV s^{-1}. The results of three independent experiments are shown in Fig. 10; the vertical scale is expanded, relative to Figs. 6–9, because the pressure effect was small, so that the apparent scatter in the data is no worse than for the other couples. At $I = 0.28$ mol kg^{-1}, $E_0 \simeq +490$ mV, and linear regression of the combined E_P data gave $\Delta V = +5.0 \pm 0.3$ cm^3 mol^{-1}.

Tris(1,10-phenanthroline)iron(III/II)

Because of the insolubility of (for example) the perchlorate salt in perchlorate media, the sulfate salt of $Fe(phen)_3^{2+}$ was used in KNO_3 or $NaHSO_4$ media. Experience with $Fe(phen)_3^{3+}$ in solution (4) suggested a need to maintain high acidity and free phen (added as a 0.3% aqueous solution or as a 5% solution in ethanol), but, because the iron(III) complex is present only transiently in the course of a voltammetric cycle, these turned out to be unnecessary precautions (cf. filled squares and circles in Fig. 11). The salient features shown in Fig. 11 are (*i*) that E_P is clearly a nonlinear function of P, but is well represented by a quadratic regression (eq. [3]), and (*ii*) that E_P is very sensitive to medium effects.

In 1.0 mol kg^{-1} KNO_3, the voltammograms showed excellent reversibility ($\delta E = 61$–70 mV), with $E_0 \simeq +830$ mV, $\Delta V_0 = +6.2 \pm 0.5$ cm^3 mol^{-1}, and $(\partial\Delta V/\partial P)_T = -0.022 \pm 0.003$ cm^3 mol^{-1} MPa^{-1}. At $I = 0.254$ mol kg^{-1} (KNO_3), $\delta E \simeq 65$–76 mV, $E_0 \simeq +890$ mV, $\Delta V_0 = +14.2 \pm 0.5$ cm^3 mol^{-1}, and $(\partial\Delta V/\partial P)_T = -0.049 \pm 0.005$ cm^3 mol^{-1} MPa^{-1}. For the $NaHSO_4$ medium at $I = 0.272$ mol kg^{-1}, $\delta E = 73$–83 mV, $E_0 \simeq +910$ mV, $\Delta V_0 = +16.3 \pm 2.0$ cm^3 mol^{-1}, and $(\partial\Delta V/\partial P)_T = -0.057 \pm 0.024$ cm^3 mol^{-1} MPa^{-1}.

Discussion

The most obvious feature of Table 1 is that ΔV is a moderately positive number for the three cationic couples, but strongly negative for $Fe(CN)_6^{3-/4-}$, relative to AgCl/Ag. This phenomenon might be attributed, at least in part, to the *increase* in solvent electrostriction (17) expected for the effective net reaction [4]

[4] $Fe(CN)_6^{3-} + Ag(s) + Cl^- \rightarrow Fe(CN)_6^{4-} + AgCl(s)$

Can. J. Chem. Downloaded from www.nrcresearchpress.com by 123.30.183.119 on 09/08/12
For personal use only.

as compared with the *decrease* in electrostriction expected for the charge-dissipating reaction [5].

[5] $Fe(H_2O)_6^{3+} + Ag(s) + Cl^- \rightarrow Fe(H_2O)_6^{2+} + AgCl(s)$

This argument alone cannot, however, explain the fact that ΔV values for the corresponding electrode reactions of the larger (and so presumably less electrostrictive) $Fe(phen)_3^{3+}$ and $Co(sep)^{3+}$ ions are *more positive* than for reaction [5] at $I = 0.28$ mol kg^{-1}. The picture is further complicated by the marked pressure dependence of ΔV for the $Fe(phen)_3^{3+/2+}$ case; this is not due to some phenomenon involving ligand dissociation, since added phen had no effect, but the sensitivity of the pressure effect to the nature and concentration of the supporting electrolyte (Fig. 11) suggests the involvement of ion association or other medium effect.

Absolute molar volumes are available, or can be calculated, for all the reactants and products of reactions [4] and [5] (17–19),[3] so that the corresponding volumes of reaction ΔV^0 at infinite dilution, 25.0°C, and 0.1 MPa can be derived: $\Delta V^0 = -49.1$ cm^3 mol^{-1} for reaction [4] and $+12.8$ cm^3 mol^{-1} for reaction [5]. An approximate correction of these to ionic strength 0.28 mol kg^{-1} can be made as described elsewhere (19), but the results ($\Delta V = -47.1$ cm^3 mol^{-1} for $Fe(CN)_6^{3-/4-}$–Ag/AgCl, and $+10.1$ cm^3 mol^{-1} for $Fe(H_2O)_6^{3+/2+}$–Ag/AgCl) are in only slightly better agreement with the electrochemically measured values (-36.2 and $+5.0$ cm^3 mol^{-1}, respectively). It should be borne in mind that the values of ΔV measured electrochemically are in effect averages over the pressure range taken, so that, if an assumed linear dependence of E_P on P conceals a nonlinearity such as is observed for reaction [4] at $I = 1.0$ mol kg^{-1}, ΔV at 0.1 MPa could be numerically larger than the high pressure value, but no statistically significant nonlinearity could be detected for the cases in point, and besides the results for reaction [4] at $I = 1.0$ mol kg^{-1} indicate that no more than about 2–3 cm^3 mol^{-1} could be accounted for in this way.

As with the anomalous behavior of $Fe(phen)_3^{3+/2+}$ noted above, it is likely that a medium effect such as ion association is responsible (but in a different manner) for these discrepancies between calculation and experiment for reactions [4] and [5] — certainly, both the electrochemistry (20–23) and the high-pressure solution chemistry (6) of the highly charged cyanoferrates are well known to be sensitive to counterion effects, while $Fe(H_2O)_6^{3+}$ and $Co(sep)^{3+}$ can be expected to be more prone to association with anions than is the larger $Fe(phen)_3^{3+}$. One may surmise that 1:1 ion association may be largely complete in the cyanoferrate systems at $I = 0.2$–0.5 mol kg^{-1}, so that the electrochemical measurements refer to species such as $\{Fe(CN)_6^{n-}, K^+\}$ rather than the free ions to which the infinite-dilution molar volumes apply. Ion pairs are broken up by increasing pressure, which may explain the curved E_P vs. P plots for the $Fe(phen)_3^{3+/2+}$ case, but such breakup effects will be negligible if pairing is virtually complete at 0.1 MPa, so that the linearity of the E_P vs. P plots for the hexacyanoferrate system (except at the higher electrolyte concentrations, where ion triples could form) could be explained. Such speculation apart, it is reassuring that the signs and orders of magnitude of ΔV values calculated from molar volume data for reactions [4] and [5] are in qualitative agreement with the electrochemical observations. Molar volumes are not available for $Fe(phen)_3^{3+}$ or $Co(sep)^{2+}$, but the fact that ΔV is some 9 cm^3 mol^{-1} more positive for $Co(sep)^{3+/2+}$ than for $Fe(H_2O)_6^{3+/2+}$, despite expectations of similar contributions from electrostriction, may be qualitatively attributed to reorganization (expansion) associated with the spin change on going from Co^{III} to Co^{II}.

As noted above, AC and cyclic voltammetry gave insufficiently accurately reproducible kinetic information to warrant detailed discussion. It is worth noting, however, that the response of the peak-to-peak separation δE to increasing pressure (a marked increase for $Fe(CN)_6^{3-/4-}$, slight decreases for the other couples) is in accordance with the measured volumes of activation ΔV_{ex}^* for the corresponding self-exchange reactions (Table 1). The electrochemical kinetic parameter ψ (16) can be defined in terms of the standard heterogeneous electrochemical rate constant k^{el}, the diffusion coefficient D (assumed here to be the same for both the oxidized and the reduced species), and the scan rate v:

[6] $$\psi = k^{el}/(\pi D v n F/RT)^{1/2}$$

and ψ in turn can be correlated with δE (ref. 16, pp. 230, 231). Thus, the shift $\Delta\delta E_{200}$ in δE on going from atmospheric ("zero") pressure to 200 MPa can be estimated if we know the *relative* values of k^{el} and D at 0 and 200 MPa — it is not necessary to know their absolute values. Furthermore, application of Walden's rule allows use of the solvent viscosity η rather than D:

[7] $$\psi_{200}/\psi_0 = (k^{el}_{200}/k^{el}_0)(D_0/D_{200})^{1/2} = (k^{el}_{200}/k^{el}_0)(\eta_{200}/\eta_0)^{1/2}$$

For water at 25°C, η_{200}/η_0 is only 1.0406 (24), and for the $Fe(CN)_6^{3-/4-}$ electrode reaction ΔV_{ex}^* is $+13$ cm^3 mol^{-1} in 1.0 mol kg^{-1} KCl (6), so that $k^{el}_{200}/k^{el}_0 = 0.350$ and $\psi_{200}/\psi_0 = 0.357$. This means that, if $\delta E = 80$ mV at atmospheric pressure, δE at 200 MPa can be predicted to be about 105 mV — and this is exactly what was found in typical hexacyanoferrate experiments in aqueous KCl (see, for example, Fig. 4). Consideration of eq. [6] also explains the large (194 mV, rising to 227 mV at 194 MPa) δE values found for LiCl solutions, since k^{el} for $Fe(CN)_6^{3-/4-}$ in such solutions is only one-tenth that in aqueous KCl (20).

For the three cationic couples of Table 1, the ΔV_{ex}^* values refer to electron exchange in *homogeneous* solution (rate constants k^{ex}); adapting the theory of Marcus (25, 26), we can write

[8] $$k^{el}_{200}/k^{el}_0 = (k^{ex}_{200}/k^{ex}_0)^{1/2}$$

whence $\psi_{200}/\psi_0 = 1.38$, 1.67, and 1.16 for $Co(sep)^{3+/2+}$, $Fe(H_2O)_6^{3+/2+}$, and $Fe(phen)_3^{3+/2+}$, respectively. Taking typical observed atmospheric-pressure δE values,[4] these calculations predict that, on going to 200 MPa, δE will *decrease* from 70 to 67 mV for $Co(sep)^{3+/2+}$, from 79 to 72 mV for $Fe(H_2O)_6^{3+/2+}$, and from 65 to 64 mV for $Fe(phen)_3^{3+/2+}$. In short, negative activation volumes for the electrode reaction or for the corresponding homogeneous self-

[3]Following Millero (17), absolute molar volumes of aqueous ions may be calculated on the basis that the corresponding quantity for $H^+(aq)$ is -5.4 cm^3 mol^{-1}.

[4]The experimental δE values at 0.1 MPa for the cationic couples correlate with the square roots of the corresponding k_0^{ex} (2–4) in the manner predicted by eq. [6] and Marcus' theory of electrode kinetics (25, 26).

exchange mean that the cyclic voltammogram becomes "more nearly reversible" as the pressure is increased, but the limited accuracy of δE measurements at high pressures militates against extracting reliable volumes of activation from cyclic voltammograms.

Acknowledgements

We thank the Natural Sciences and Engineering Research Council of Canada for financial support, Drs. V. I. Birss and A. S. Hinman for technical advice, and Dr. P. A. Tregloan for discussions.

1. T. W. Swaddle. Inorg. Chem. **29**, 5017 (1990).
2. H. Doine and T. W. Swaddle. Inorg. Chem. **30**, 1858 (1991).
3. W. H. Jolley, D. R. Stranks and T. W. Swaddle. Inorg. Chem. **29**, 1948 (1990).
4. H. Doine and T. W. Swaddle. Can. J. Chem. **66**, 2763 (1988).
5. B. E. Conway and J. C. Currie. J. Electrochem. Soc. **125**, 252 (1978); **125**, 257 (1978).
6. M. Sato and T. Yamada. *In* High pressure science and technology. Vol. 2, *Edited by* B. Vodar and Ph. Marteau. Pergamon, Oxford. 1980. pp. 812–814.
7. R. A. Marcus. Annu. Rev. Phys. Chem. **15**, 155 (1964).
8. E. Cohen and K. Piepenbroek. Z. Phys. Chem. Abt. **A**: **167**, 365; **170**, 145 (1934).
9. A. H. Ewald and S. C. Lim. J. Phys. Chem. **61**, 1443 (1957).
10. G. J. Hills and P. J. Ovenden. Adv. Electrochem. Electrochem. Eng. **4**, 185 (1966).
11. G. J. Hills. Advances in high pressure research. Vol. 2, *Edited by* R. S. Bradley. Academic Press, New York. 1969. Chap. 4.
12. M. Fleischmann, W. B. Gara, and G. J. Hills. J. Electroanal. Interfac. Electrochem. **60**, 313 (1975).
13. A. C. McDonald, F.-R. F. Fan, and A. J. Bard. J. Phys. Chem. **90**, 196 (1986).
14. T. C. Franklin and S. A. Mathew. J. Electrochem. Soc. **134**, 760 (1987).
15. V. Jovancicevic and J. O'M. Bockris. Rev. Sci. Instrum. **58**, 1251 (1987).
16. A. J. Bard and L. R. Faulkner. Electrochemical methods. J Wiley and Sons, Toronto. 1980. Chaps. 6 and 9.
17. F. J. Millero. *In* Water and aqueous solutions. *Edited by* R. A. Horne. Wiley-Interscience, New York. 1972. Chapt. 13.
18. R. C. Weast. CRC Handbook of chemistry and physics. 61st. ed. Boca Raton, FL. 1980. B144.
19. T. W. Swaddle and M. K. S. Mak. Can. J. Chem. **61** 473 (1983).
20. R. C. McCreery. Electroanal. Chem. **17**, 221 (1991).
21. H. Bruhn, S. Nigam and J. F. Holzwarth. Faraday Disc. Chem. Soc. **74**, 129 (1982).
22. R. J. Campion, C. F. Deck, P. King, Jr., and A. C. Wahl. Inorg. Chem. **6**, 672 (1967).
23. M. Shporer, G. Ron, A. Loewenstein, and G. Navon. Inorg. Chem. **4**, 361 (1965).
24. J. V. Sengers and B. Kamgar-Parsi. J. Phys. Chem. Ref. Data, **13**, 185 (1984).
25. R. A. Marcus. Electrochim. Acta, **13**, 995 (1968).
26. R. D. Cannon. Electron transfer reactions. Butterworths, London, 1980. pp. 220–222.

Can. J. Chem. Downloaded from www.nrcresearchpress.com by 123.30.183.119 on 09/08/12
For personal use only.

Étude cinétique de la *N*-chloration de la succinimide en phase aqueuse

DENISE MATTE, BERNARD SOLASTIOUK, ANDRÉ MERLIN ET XAVIER DEGLISE[1]

Université de Nancy I, Laboratoire de photochimie appliquée,
Unité associée au Centre national de la recherche scientifique, n° 328, Boîte Postale n° 239,
54506 Vandoeuvre les Nancy CEDEX, France

Reçu le 28 novembre 1990[2]

DENISE MATTE, BERNARD SOLASTIOUK, ANDRÉ MERLIN et XAVIER DEGLISE. Can. J. Chem. **70**, 89 (1992).

Nous présentons une étude des mécanismes de la *N*-chloration de la succinimide en phase aqueuse en milieu acide (pH < 5) et en milieu basique (pH > 9). Nous avons déterminé les constantes de vitesse et les énergies d'activation des processus mis en cause. Les cinétiques rapides ont été étudiées par spectrophotométrie à écoulement bloqué. En absence d'ions chlorures et dans les domaines de pH étudiés, nos résultats sont en accord avec un modèle cinétique comprenant la contribution de deux processus indiscernables :

$$SH + ClO^- \xrightarrow{k_2} \text{produits}$$

ou

$$S^- + HOCl \xrightarrow{k_3} \text{produits}$$

Les valeurs limites des constantes de vitesse dans le cas où un seul des processus participe à la cinétique de chloration ont été évaluées : $k_2^0 = 1{,}6 \times 10^5\ M^{-1}\ s^{-1}$ à 293 K; $k_3^0 = 2{,}2 \times 10^7\ M^{-1}\ s^{-1}$ à 293 K.

En présence d'ions chlorures et en milieu acide, l'attaque nucléophile de S^- sur le chlore moléculaire Cl_2 s'ajoute à ces deux processus indiscernables.

Mots clés : cinétique, *N*-chloration, succinimide, phase aqueuse, spectrophotométrie à écoulement bloqué.

DENISE MATTE, BERNARD SOLASTIOUK, ANDRÉ MERLIN, and XAVIER DEGLISE. Can. J. Chem. **70**, 89 (1992).

A kinetic study of the *N*-chlorination, in aqueous medium, of succinimide (SH) at low pH (<5) and at high pH (>9) is presented. We have derived the rate constants and activation energies of the processes involved. A stopped-flow spectrophotometric technique was used to study the kinetics. Without chloride ions, our experimental results can be interpreted by two kinetically indistinguishable mechanisms:

$$SH + ClO^- \xrightarrow{k_2} \text{products}$$

$$S^- + HClO \xrightarrow{k_3} \text{products}$$

The limiting values of the rate constants for the case in which only one process is involved in the kinetics of chlorination were evaluated: $k_2^0 = 1.6 \times 10^5\ M\ s^{-1}$ at 293 K; $k_3^0 = 2.2 \times 10^7\ M^{-1}\ s^{-1}$ at 293 K.

In acid medium, in the presence of chloride ions, we observe a nucleophilic attack of the S^- ion on molecular chlorine Cl_2. This process is added to the two former processes.

Key words: kinetics, *N*-chlorination, succinimide, aqueous medium, stopped flow.

Introduction

En solution aqueuse, la succinimide réagit avec l'hypochlorite de sodium pour former la *N*-chlorosuccinimide. La succinimide est un acide faible; la forme acide notée SH et sa base conjuguée S^- peuvent exister sous différentes formes tautomères (figure 1).

La cinétique de cette réaction de *N*-chloration a été étudiée par Hussain et Higuchi (1) dans un domaine étroit de pH allant de 2 à 5 et en absence d'ions chlorures.

Dans ces conditions expérimentales, la réaction est assez lente pour être suivie par des techniques spectroscopiques classiques. Grâce à la spectroscopie à écoulement bloqué, nous avons pu étendre cette étude à toute la gamme de pH couverte par les solutions aqueuses et déterminer l'influence de la température et des ions chlorures sur la cinétique de cette réaction de chloration.

Techniques expérimentales

Les paramètres cinétiques de cette réaction de *N*-chloration ont été déterminés par spectrophotométrie à écoulement bloqué sur un appareil Applied Photophysics modèle 1705 couplé à un microordinateur. Cet appareillage est adapté à l'étude des cinétiques rapides en phase liquide à condition que l'on puisse détecter par absorption ultraviolette ou visible l'un des produits formés ou consommés durant la réaction (2).

En milieu basique (pH > 8), le chlore en solution existe principalement sous forme d'ions hypochlorites ClO^- (figure 2). Le maximum d'absorption de ClO^- se situant à 290 nm et la succinimide et son dérivé *N*-chloré absorbant à des longueurs d'onde plus faibles (figure 3), nous avons suivi la disparition de ClO^- à cette longueur d'onde. En opérant en large excès de succinimide par rapport au chlore, nous nous sommes placés dans les conditions d'une réaction du pseudo-premier ordre. Nous avons pu mesurer une constante de vitesse expérimentale du pseudo-premier ordre k_{obs}, pente de la droite $\ln(A - A_\infty)$ en fonction du temps, A étant la densité optique de la solution à 290 nm à un instant donné et A_∞ la densité optique à cette même longueur d'onde de la solution après réaction. La détermination expérimentale de cette constante de vitesse k_{obs} est détaillée dans l'annexe 1.

En milieu acide, le chlore est presque exclusivement sous forme d'acide hypochloreux HOCl (figure 2). Il n'est pas possible de suivre directement la disparition de ce composé à 235 nm, longueur d'onde de son maximum d'absorption, car la *N*-chlorosuccinimide absorbe également dans cette zone spectrale (figure 4). Toutefois, à cette longueur d'onde, le coefficient d'extinction molaire de la *N*-chlorosuccinimide étant beaucoup plus important que celui de la succinimide, nous pouvons étudier la cinétique de la *N*-chloration de la succinimide en suivant à 235 nm la formation de

[1]Auteur à qui adresser toute correspondance.
[2]Révision reçue le 18 septembre 1991.

Printed in Canada / Imprimé au Canada

Can. J. Chem. Downloaded from www.nrcresearchpress.com by 123.30.183.119 on 09/08/12
For personal use only.

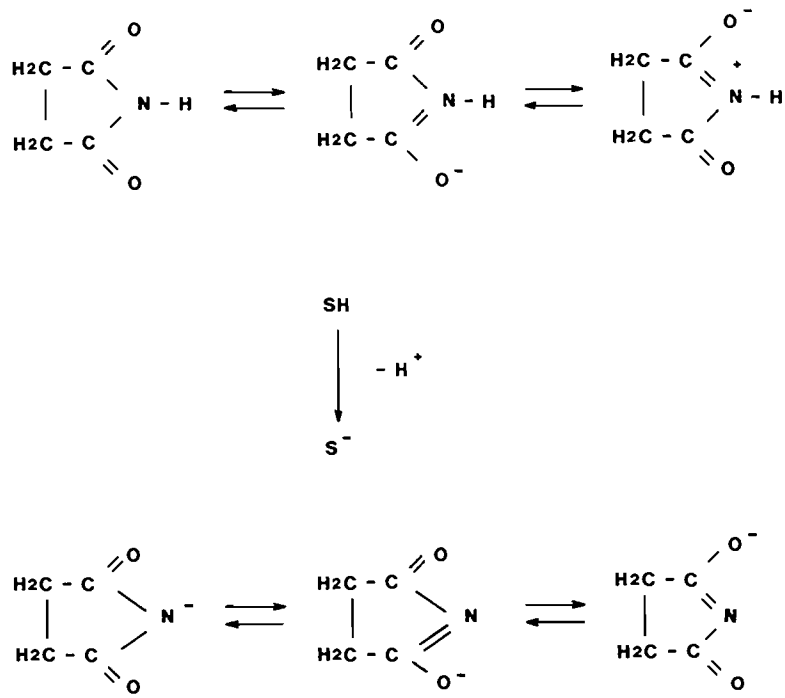

FIG. 1. Structures moléculaires de la succinimide SH et de sa base conjuguée S^-.

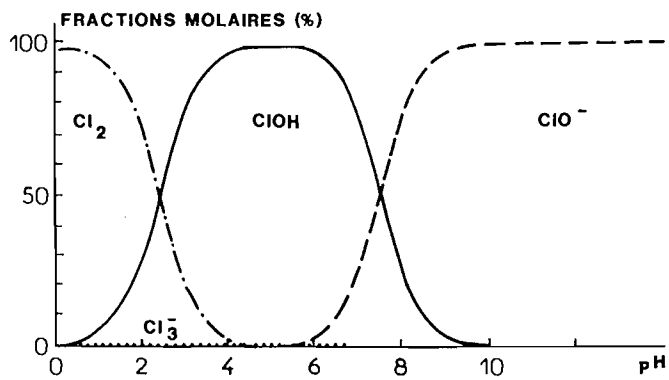

FIG. 2. Zone de prédominance des dérivés du chlore en solution aqueuse; $[Cl]_t = 10^{-3}$ M; $[Cl^-] = 0{,}1$ M.

la *N*-chlorosuccinimide au cours du temps. Dans le cas où la concentration initiale de succinimide est supérieure à la concentration initiale de chlore, la vitesse initiale de réaction v_0 est donnée par la relation :

$$[1] \qquad v_0 = \left(\frac{d}{dt}[SCl]_{t=0}\right) = \frac{(dA/dt)_{t=0}}{[A_\infty - A(0)]}[Cl]_T$$

$A(0)$ et A_∞ sont respectivement les densités optiques de la solution à 235 nm à l'instant initial et après réaction. $(dA/dt)_{t=0}$ est la pente à l'instant initial de la courbe donnant la variation de la densite optique de la solution avec le temps. $[Cl]_T$ représente la concentration totale de chlore. L'établissement de la relation [1] est donné en annexe 1.

La succinimide, de marque Fluka et de qualité Purum, contient moins de 2% d'impuretés. Les sels utilisés pour la fabrication des solutions tampon sont des produits Prolabo de qualité Normapur. Les solutions d'acide hypochloreux sont obtenues en faisant barboter du chlore gazeux dans de l'eau distillée. La solution et ensuite laissée pendant une journée en présence d'oxyde de mercure puis distillée sous pression réduite avant d'être titrée par du thiosulfate de sodium.

Résultats expérimentaux

Dans un premier temps, nous avons vérifié que les résultats expérimentaux, obtenus en milieu basique avec un excès de succinimide, étaient correctement représentés par un modèle d'une cinétique du pseudo-premier ordre. La réaction liant $\ln(A - A_\infty)$ avec le temps étant linéaire, la réaction est du premier ordre par rapport à la concentration en chlore «libre» total $[Cl]_t$ (on appelle chlore «libre» le chlore non lié à un atome d'azote).

La vitesse globale de réaction en milieu basique s'exprime donc par la relation :

$$[2] \qquad v = -\frac{d[Cl]_t}{dt} = k_{obs}[Cl]_t$$

À pH constant, nous avons observé que la constante k_{obs} en milieu basique et la vitesse initiale v_0 en milieu acide sont proportionnelles à la concentration totale de succinimide (figure 5). La réaction est donc globalement du second ordre et d'ordre 1 par rapport à chacun des deux réactifs :

$$[3] \qquad v = k_{exp}[S]_t[Cl]_t$$

avec k_{exp} : constante de vitesse globale du second ordre; $[Cl]_t$: concentration en chlore libre total; $[S]_t$: concentration totale de succinimide chlorée ou non (la succinimide étant en excès par rapport au chlore, sa concentration peut être considérée constante au cours de la réaction).

L'influence du pH sur la constante de vitesse k_{exp} a été étudiée à 293 K en milieu acide (pH < 5) et en milieu basique (pH > 9) (tableau 1 et figure 9). Nous avons aussi suivi l'influence de la température sur ce paramètre à pH fixé (pH = 9,25 dans le cas de la figure 6). La pente de la droite ln (k_{exp}) en fonction de $1/T$ permet de calculer l'énergie d'ac-

Can. J. Chem. Downloaded from www.nrcresearchpress.com by 123.30.183.119 on 09/08/12
For personal use only.

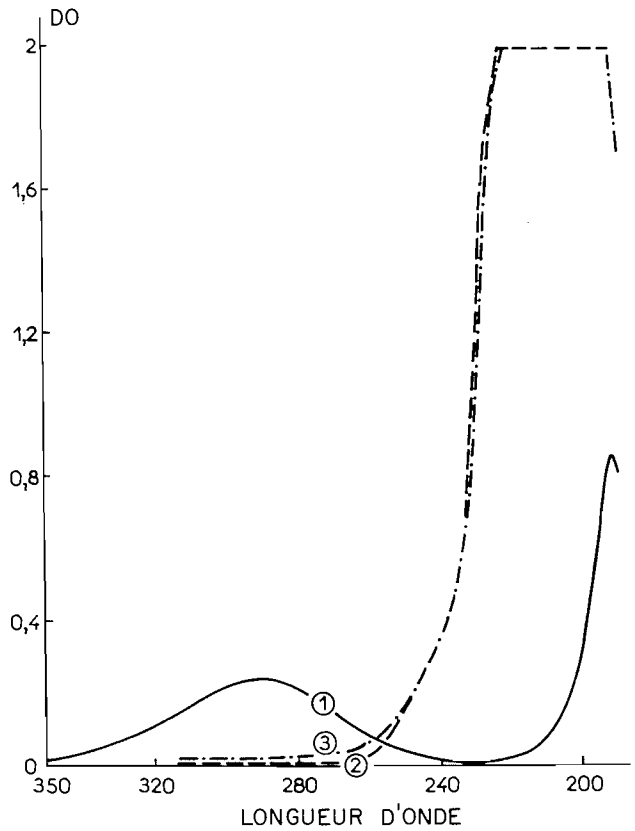

FIG. 3. Spectres d'absorption dans l'ultraviolet de la succinimide et de son dérivé *N*-chloré en milieu basique. DO : densité optique.
1 : NaOCl 8×10^{-4} M pH = 9,2;
2 : Succinimide 2×10^{-3} M pH = 9,2;
3 : NaOCl 8×10^{-4} M + succinimide 2×10^{-3} M pH = 9,2 après réaction

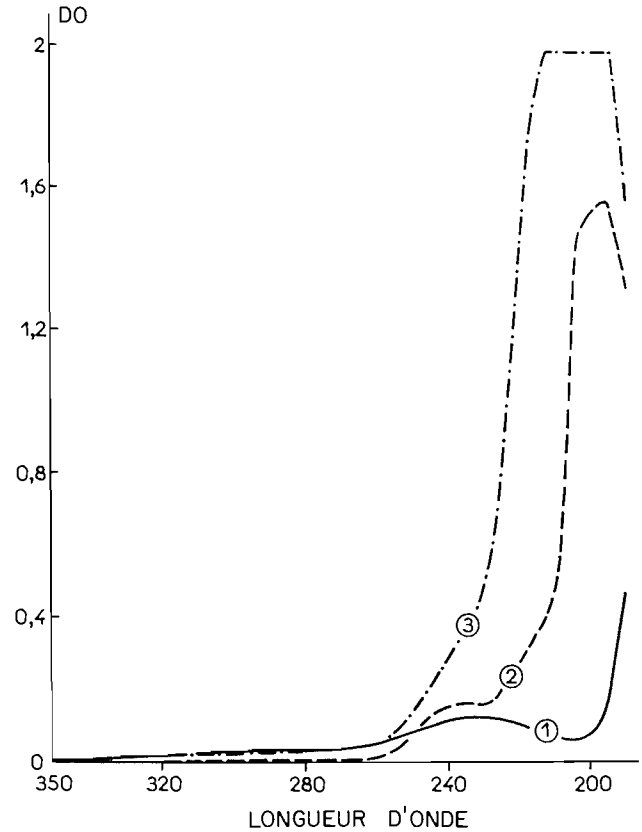

FIG. 4. Spectres d'absorption dans l'ultraviolet de la succinimide et de son dérivé N-chloré en milieu acide. DO : densité optique.
1 : HOCl $1,25 \times 10^{-3}$ M pH = 4,45
2 : Succinimide 2×10^{-3} M pH = 4,45
3 : HOCl $1,25 \times 10^{-3}$ M + succinimide 2×10^{-3} M pH = 4,45 } après réaction

tivation globale avec une précision de l'ordre de 20% : E = 48,8 kJ mol^{-1}.

En milieu acide (pH = 3), nous avons étudié l'augmentation de la vitesse de réaction avec la concentration en ions chlorures. On observe un accroissement linéaire de la constante de vitesse k_{exp} (figure 7) dans le domaine de concentration en ions chlorures étudié (10^{-2} M à 4×10^{-2} M).

Interprétation

Une solution aqueuse de succinimide contient les deux espèces SH et S^- en équilibre :

$$[I] \quad SH \leftrightarrows S^- + H^+ \qquad pK_I = 9,71 \text{ à } 293 \text{ K} \qquad (3)$$

En milieu acide ou neutre (pH < 8), la succinimide existe presque uniquement sous la forme SH. En milieu basique (pH > 11), l'ion S^- est prépondérant (figure 8). De même, le chlore en solution aqueuse peut exister sous quatre formes en équilibre dans des proportions qui dépendent du pH (figure 2).

$$[II] \quad HOCl \leftrightarrows ClO^- + H^+$$

$$pK_{II} = 7,58 \text{ à } 293 \text{ K} \qquad (4)$$

$$[III] \quad Cl_2 + H_2O \leftrightarrows HOCl + H^+ + Cl^-$$

$$pK_{III} = 3,48 \text{ à } 293 \text{ K} \qquad (5)$$

$$[IV] \quad Cl_2 + Cl^- \leftrightarrows Cl_3^-$$

$$pK_{IV} = 0,74 \text{ à } 298 \text{ K} \qquad (6)$$

Ces équilibres sont rapides devant la cinétique de la réaction de chloration et compte tenu de la mise en évidence expérimentale d'un ordre 1 par rapport à chacun des réactifs, nous pouvons envisager huit processus élémentaires différents de formation de SCl susceptibles de limiter la vitesse globale de réaction :

$$(P_1) \quad SH + HOCl \xrightarrow{k_1} SCl + H_2O$$

$$(P_2) \quad SH + ClO^- \xrightarrow{k_2} SCl + OH^-$$

$$(P_3) \quad S^- + HOCl \xrightarrow{k_3} SCl + OH^-$$

$$(P_4) \quad S^- + ClO^- + H_2O \xrightarrow{k_4} SCl + 2OH^-$$

$$(P_5) \quad SH + Cl_2 \xrightarrow{k_5} SCl + H^+ + Cl^-$$

$$(P_6) \quad SH + Cl_3^- \xrightarrow{k_6} SCl + H^+ + 2Cl^-$$

Can. J. Chem. Downloaded from www.nrcresearchpress.com by 123.30.183.119 on 09/08/12
For personal use only.

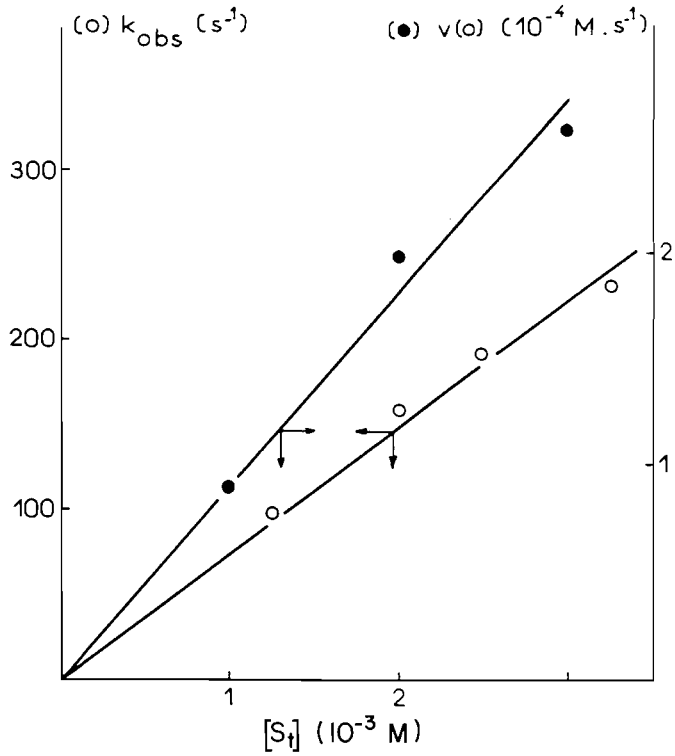

FIG. 5. Influence de la concentration de succinimide; (○) T = 293 K, pH = 9,25, $[Cl]_t = 3,35 \times 10^{-4}$ M; (●) T = 293 K, pH = 4,45, $[Cl]_t = 6 \times 10^{-4}$ M.

TABLEAU 1. Influence du pH sur les constantes de vitesse k_{exp}

pH	k_{exp} (10^3 M^{-1} s^{-1})	Conditions opératoires
10,90	8,59	T = 293 K
10,75	10,80	$[S]_t = 2,5 \times 10^{-3}$ M
10,70	13,00	$[Cl]_t = 3,35 \times 10^{-4}$ M
10,35	24,80	$\lambda_{analyse}$ = 290 nm
10,00	42,80	
9,75	60,70	
9,25	74,00	
4,45	153,00	T = 293 K
4,00	60,20	$[S]_t = 10^{-3}$ M
3,75	31,70	$[Cl]_t = 6 \times 10^{-4}$ M
3,35	18,10	$\lambda_{analyse}$ = 235 nm
3,00	15,10	

$$(P_7) \quad S^- + Cl_2 \xrightarrow{k_7} SCl + Cl^-$$

$$(P_8) \quad S^- + Cl_3^- \xrightarrow{k_8} SCl + 2Cl^-$$

Chloration en absence d'ions chlorures

Seuls les équilibres [I] et [II] et les processus (P_1), (P_2), (P_3), (P_4) qui ne font pas intervenir d'ions chlorures sont à considérer. Les concentrations courantes globales des réactifs sont donc données par les relations :

$$[4] \quad [Cl]_t = [ClO^-] + [HOCl]$$

et

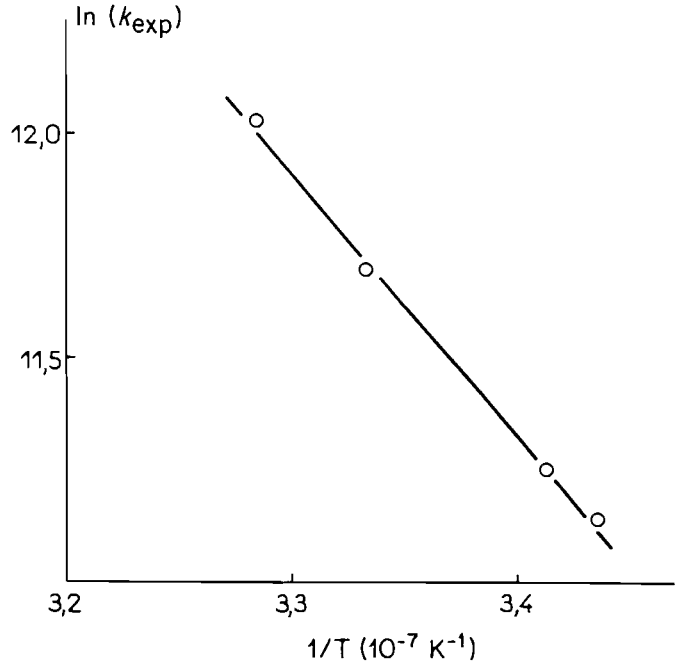

FIG. 6. Influence de la température : variation de $\ln(k_{exp})$ en fonction de $1/T$; pH = 9,25; $[S]_t = 2,5 \times 10^{-3}$ M; $[Cl]_t = 3,35 \times 10^{-4}$ M.

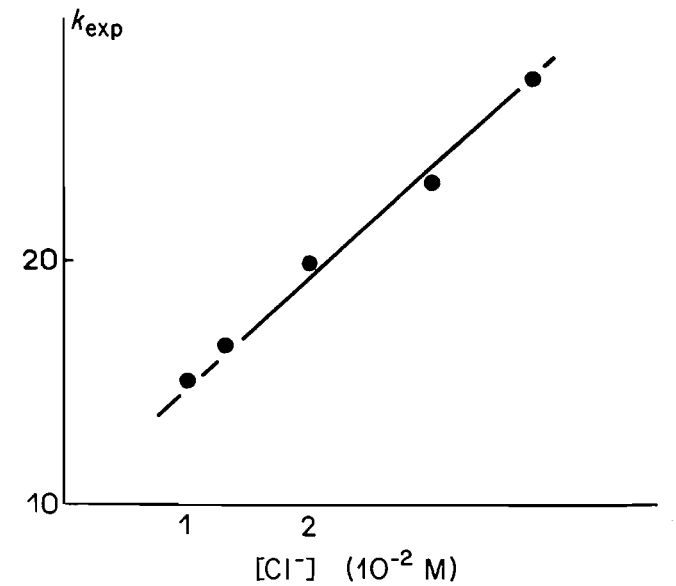

FIG. 7. Influence de la concentration en ions chlorures; T = 293 K; pH = 3,0; $[S]_t = 10^{-3}$ M; $[Cl]_t = 6 \times 10^{-4}$ M.

$$[S]_t = [SH] + [S^-] + [SCl]$$

Dans les conditions expérimentales du pseudo-premier ordre où nous nous sommes placés, la succinimide est en large excès par rapport au chlore et nous pouvons donc négliger la concentration en *N*-chlorosuccinimide [SCl] devant la concentration en succinimide totale :

$$[5] \quad [S]_t = [SH] + [S^-]$$

Les concentrations de ces différentes espèces peuvent être exprimées en fonction des constantes d'équilibre K_I et K_{II}, de leur coefficient d'activité γ_i, du pH, de $[Cl]_t$ et $[S]_t$.

Can. J. Chem. Downloaded from www.nrcresearchpress.com by 123.30.183.119 on 09/08/12
For personal use only.

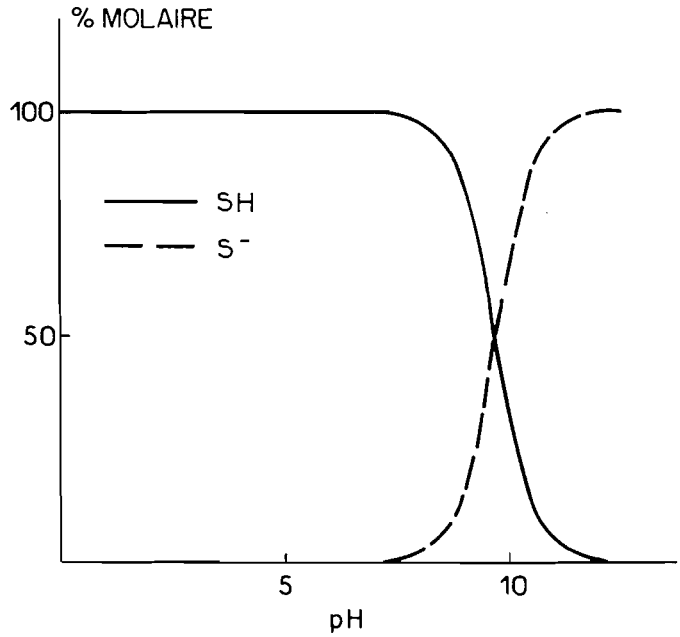

FIG. 8. Pourcentage molaire de succinimide sous forme de SH et S^- en fonction du pH à 293 K.

$$[6] \quad [SH] = \frac{\gamma_{S^-}(H^+)}{\mathcal{A}}[S]_t$$

$$[7] \quad [S^-] = \frac{\gamma_{SH}K_I}{\mathcal{A}}[S]_t$$

$$[8] \quad [HOCl] = \frac{\gamma_{ClO^-}(H^+)}{\mathcal{B}}[Cl]_t$$

$$[9] \quad [ClO^-] = \frac{\gamma_{HOCl}K_{II}}{\mathcal{B}}[Cl]_t$$

avec $\mathcal{A} = \gamma_{S^-}(H^+) + K_I\gamma_{SH}$ et $\mathcal{B} = \gamma_{ClO^-}(H^+) + K_{II}\gamma_{HOCl}$. Le détail du calcul qui conduit aux relations [6]–[9] est donné en annexe 2.

Si $v(P_i)$ est la participation de chacun des processus P_1–P_4 à la cinétique globale de la réaction de *N*-chloration, la vitesse peut s'exprimer par la relation :

$$[10] \quad v = \frac{d[SCl]}{dt} = \sum_{i=1}^{4} v(P_i)$$

Pour un processus bimoléculaire en solution réelle ($A + B \leftrightarrows C^{\neq} \rightarrow C$) où $C^{\neq}$ est le complexe activé du processus :

$$v(P_i) = k_i^0 \frac{\gamma_A\gamma_B}{\gamma_{C^{\neq}}}[A][B]$$

avec k_i^0 : constante de vitesse à dilution infinie.

Nous obtenons alors pour chacun des processus :

$$v(P_1) = k_1^0 \frac{\gamma_{SH}\gamma_{HOCl}}{\gamma_{1^{\neq}}}[SH][HOCl]$$

$$v(P_2) = k_2^0 \frac{\gamma_{SH}\gamma_{ClO^-}}{\gamma_{2^{\neq}}}[SH][ClO^-]$$

$$v(P_3) = k_3^0 \frac{\gamma_{S^-}\gamma_{HOCl}}{\gamma_{3^{\neq}}}[S^-][HOCl]$$

$$v(P_4) = k_4^0 \frac{\gamma_{S^-}\gamma_{ClO^-}}{\gamma_{4^{\neq}}}[S^-][ClO^-]$$

Soit en remplaçant les concentrations des espèces réagissantes par les expressions données par les relations [6]–[9] :

$$[11] \quad v(P_1) = \frac{k_1^0}{\gamma_{1^{\neq}}}(H^+)W[Cl]_t[S]_t$$

$$[12] \quad v(P_2) = \frac{k_2^0}{\gamma_{2^{\neq}}}K_{II}W[Cl]_t[S]_t$$

$$[13] \quad v(P_3) = \frac{k_3^0}{\gamma_{3^{\neq}}}K_IW[Cl]_t[S]_t$$

$$[14] \quad v(P_4) = \frac{k_4^0}{\gamma_{4^{\neq}}}\frac{K_IK_{II}}{(H^+)}W[Cl]_t[S]_t$$

avec

$$W = \frac{\gamma_{S^-}\gamma_{ClO^-}\gamma_{SH}\gamma_{HOCl}}{\mathcal{A}\mathcal{B}}(H^+)$$

En admettant une forme approchée par la loi de Debye–Hückel pour les coefficients des espèces ioniques, *W* prend la forme :

$$[15] \quad W = \gamma^2\frac{(H^+)}{[I_I + \gamma(H^+)][K_{II} + \gamma(H^+)]}$$

(avec $\gamma_{SH} = \gamma_{HOCl} = 1$ et $\gamma = \gamma_{S^-} = \gamma_{ClO^-} = 10^{-0,5\sqrt{I}}$), *I* étant la force ionique du milieu.

En milieu acide (pH < 5), K_I et K_{II} sont négligeables devant (H^+) et l'expression de *W* se simplifie : $W = 1/(H^+)$. La vitesse globale de la réaction s'exprime sous la forme :

$$v = \sum_{i=1}^{4} v(P_i) = \left[\frac{k_1^0}{\gamma_{1^{\neq}}} + \left(\frac{k_2^0K_{II}}{\gamma_{2^{\neq}}} + \frac{k_3^0K_I}{\gamma_{3^{\neq}}}\right)\frac{1}{(H^+)} + \frac{k_4^0K_IK_{II}}{\gamma_{4^{\neq}}}\frac{1}{(H^+)^2}\right][S]_t[Cl]_t$$

soit, d'après la relation [3] :

$$[16] \quad k_{exp} = \left[\frac{k_1^0}{\gamma_{1^{\neq}}} + \left(\frac{k_2^0K_{II}}{\gamma_{2^{\neq}}} + \frac{k_3^0K_I}{\gamma_{3^{\neq}}}\right)\frac{1}{(H^+)} + \frac{k_4^0K_IK_{II}}{\gamma_{4^{\neq}}}\frac{1}{(H^+)^2}\right]$$

Dans cette expression, nous avons regroupé les termes correspondants aux processus en fonction de leur dépendance vis-à-vis de l'activité du proton hydraté : P_1; (P_2,P_3); P_4. À l'intérieur du couple (P_2,P_3), les deux complexes activés ont même charge et même composition, leurs coefficients d'activité $\gamma_{2^{\neq}}$ et $\gamma_{3^{\neq}}$ varient donc de façon identique avec la force ionique. Comme le pH influence de la même manière leur contribution à la vitesse globale de réaction, ces deux processus sont indiscernables. Nous avons déjà rencontré ce phénomène d'indiscernabilité des processus pour la *N*-chloration d'amines secondaires (7) et de l'acide cyanurique (8).

En milieu basique (pH > 11), (H^+) devient négligeable devant les constantes K_{II} et K_I et *W* prend la forme :

Can. J. Chem. Downloaded from www.nrcresearchpress.com by 123.30.183.119 on 09/08/12
For personal use only.

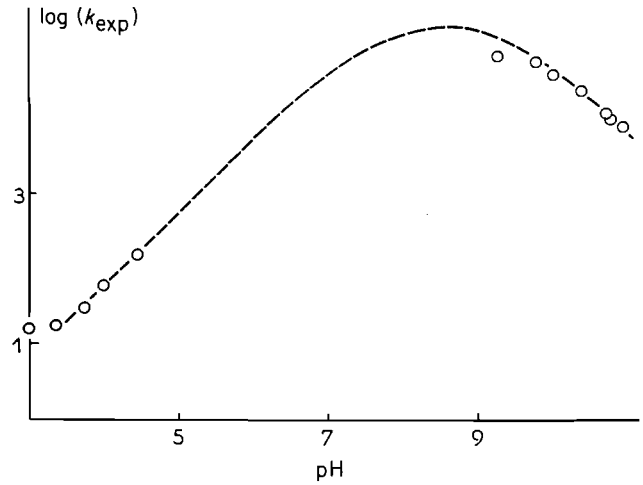

FIG. 9. Influence du pH sur k_{exp}; T = 293 K; pH < 5 : $[S]_t = 10^{-3}$ M, $[Cl]_t = 6 \times 10^{-4}$ M; pH > 8 : $[S]_t = 2{,}5 \times 10^{-3}$ M, $[Cl]_t = 3{,}35 \times 10^{-4}$ M.

$$W = \gamma^2 \frac{(H^+)}{K_I K_{II}}$$

soit :

$$[17] \quad k_{exp} = \left[\frac{k_1^0 \gamma^2}{\gamma_{1^\neq} K_I K_{II}} (H^+)^2 + \left(\frac{k_2^0 \gamma^2}{\gamma_{2^\neq} K_I} + \frac{k_3^0 \gamma^2}{\gamma_{3^\neq} K_{II}} \right)(H^+) + \frac{k_4^0 \gamma^2}{\gamma_{4^\neq}} \right]$$

Nous obtenons la même partition des processus P_1; (P_2,P_3); P_4 vis-à-vis de l'influence de l'activité du proton hydraté qu'en milieu acide et l'indiscernabilité des processus P_2, P_3 est conservée.

En étudiant la variation de la constante de vitesse k_{exp} déterminée à partir des points expérimentaux (tableau 1) en fonction du pH, nous observons, pour les pH inférieurs à 5 et supérieurs à 10, une variation linéaire de log(k_{exp}) avec le pH avec une pente voisine de +1 (±0,1) en milieu acide et de −1 (±0,1) en milieu basique (figure 9).

Ce résultat indique, d'après les relations [16] et [17], que seuls les processus P_2 ou P_3 interviennent dans la chloration de la succinimide en absence d'ions chlorures :

$$P_2 \quad SH + ClO^- \rightarrow SCl + OH^-$$

$$P_3 \quad S^- + HOCl \rightarrow SCl + OH^-$$

D'après les relations [12] et [13], la vitesse globale de la réaction est alors donnée par la relation :

$$v = v(P_2) + v(P_3) = \left[\frac{k_2^0 K_{II}}{\gamma_{2^\neq}} + \frac{k_3^0 K_I}{\gamma_{3^\neq}} \right] W [Cl]_t [S]_t$$

soit

$$k_{exp} = \left[\frac{k_2^0 K_{II}}{\gamma_{2^\neq}} + \frac{k_3^0 K_I}{\gamma_{3^\neq}} \right] W$$

Les deux complexes activés ayant une charge globale de −1, les coefficients d'activité $\gamma_{2^\neq}$ et $\gamma_{3^\neq}$ sont égaux à γ et l'expression de k_{exp} se simplifie :

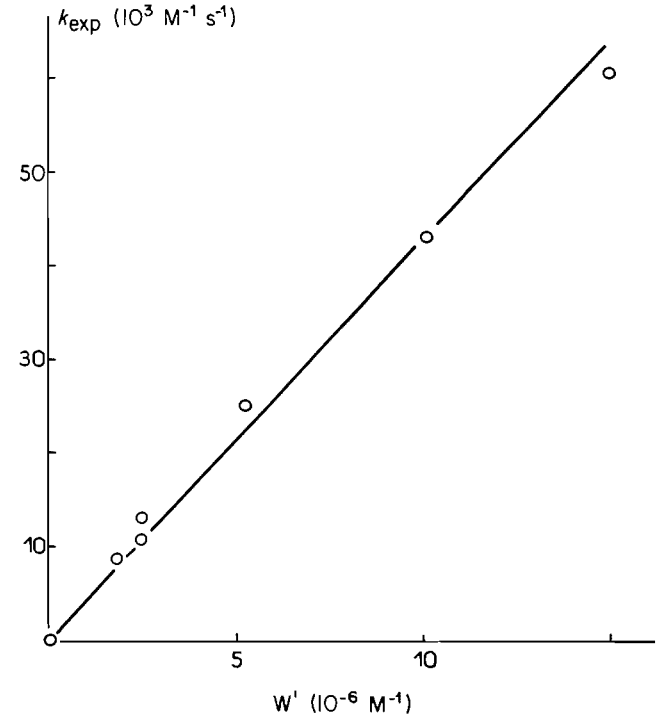

FIG. 10. k_{exp} en fonction de W'.

$$W' = \frac{\gamma(H^+)}{[K_I + \gamma(H^+)][K_{II} + \gamma(H^+)]}$$

$$[18] \quad k_{exp} = [k_2^0 K_{II} + k_3^0 K_I] W'$$

avec

$$W' = \frac{W}{\gamma} = \frac{\gamma(H^+)}{[K_I + \gamma(H^+)][K_{II} + \gamma(H^+)]}$$

La pente de la droite obtenue en portant les valeurs expérimentales des constantes de vitesse k_{exp} en fonction de W' (figure 10) nous permet de calculer, dans le cas limite où l'un des processus devient prépondérant, la valeur théorique maximale des constantes de vitesse k_2^0 et k_3^0 : si $k_2^0 K_{II} > k_3^0 K_I$, $k_2^0 = (1{,}6 \pm 0{,}3) \times 10^5$ M^{-1} s^{-1} à 293 K; si $k_2^0 K_{II} < k_3^0 K_I$, $k_3^0 = (2{,}2 \pm 0{,}4) \times 10^7$ M^{-1} s^{-1} à 293 K. Cette valeur de la constante de vitesse de la chloration de S^- par HOCl est en accord avec celle déterminée en milieu acide par Hussain et Higuchi : $k = 2{,}14 \times 10^7$ M^{-1} s^{-1} à 298 K (1).

La détermination des constantes de vitesse expérimentales obtenues à pH constant (pH = 9,25) à différentes températures (figure 6) a permis l'étude de l'influence de ce paramétre sur les constantes de vitesse k_2^0 et k_3^0 des deux processus P_2 et P_3. Le calcul du coefficient W dans la gamme de température étudiée a été fait en utilisant pour expression des constantes d'équilibre K_I et K_{II} les relations :

$$pK_I = \left(\frac{3000}{T} \right) - 10{,}0686 + 0{,}0253\, T \qquad (3)$$

$$pK_{II} = 36{,}92 - 0{,}167\, T + (2{,}53 \times 10^{-4}) T^2 \qquad (4)$$

Le logarithme des constantes de vitesse k_2^0 et k_3^0 en fonction de $1/T$ est porté par des droites (figure 11) dont les pentes

Can. J. Chem. Downloaded from www.nrcresearchpress.com by 123.30.183.119 on 09/08/12
For personal use only.

TABLEAU 2. Constante de vitesse, énergie d'activation, $\Delta H^{\neq}$ et $\Delta S^{\neq}$ des processus de chloration de la succinimide

	Processus	k^0_{293K} ($M^{-1}\,s^{-1}$)	$E^{\neq}$ (kJ mol^{-1})	$\Delta H^{\neq}$ (kJ mol^{-1})	$\Delta S^{\neq}$ (J K^{-1} mol^{-1})
P_2	$SH + ClO^- \rightarrow$	$1{,}6 \times 10^5$	62,7	60,2	61
P_3	$S^- + HOCl \rightarrow$	$2{,}2 \times 10^7$	48,0	45,5	51

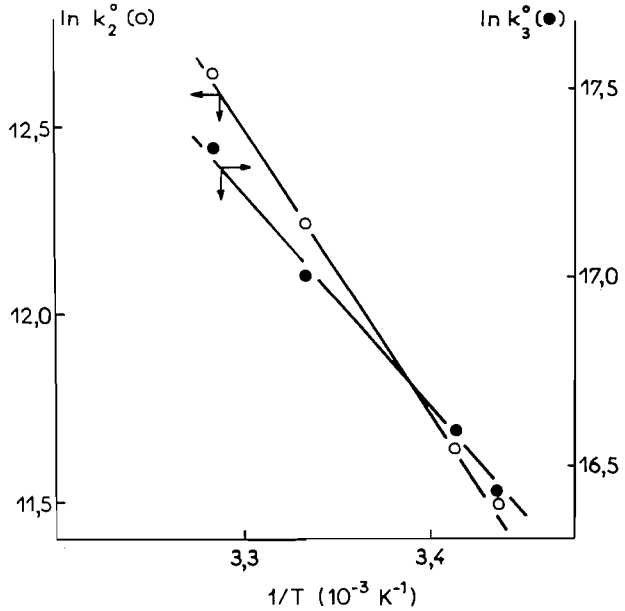

FIG. 11. Influence de la température; (○) ln k_2^0 en fonction de $1/T$; (●) ln k_3^0 en fonction de $1/T$.

donnent les énergies d'activation des processus P_2 et P_3 avec une précision de l'ordre de 20% :

$$\ln k_2^0 = -\frac{7528}{T} + 37{,}76 \qquad E_{2^{\neq}} = 62{,}7 \text{ kJ/mol}$$

$$\ln k_3^0 = -\frac{5770}{T} + 36{,}55 \qquad E_{3^{\neq}} = 48{,}0 \text{ kJ/mol}$$

Le tableau 2 résume les résultats obtenus pour les deux processus possibles de la *N*-chloration de la succinimide en absence d'ions chlorures. Les valeurs des enthalpies et des entropies d'activation des deux processus ont été calculées à partir des constantes de vitesse et des énergies d'activation déterminées précédemment.

Chloration en milieu acide en présence d'ions chlorures

En milieu acide et en présence d'ions chlorures, les concentrations en ions trichlorures Cl_3^- et surtout en chlore moléculaire Cl_2 ne sont plus négligeables (figure 2). En plus des processus P_2 et P_3 indiscernables qui limitent la vitesse de réaction globale en absence d'ions chlorures, nous devons considérer les quatre processus P_5–P_8 qui font intervenir les espèces Cl_3^- et Cl_2.

Les équilibres [I]–[IV] nous permettent d'exprimer la concentration de chaque espèce réagissante en fonction de la concentration en chlorure $[Cl^-]$, des concentrations totales en succinimide $[S]_t$ et en chlore libre $[Cl]_t$, du pH et du coefficient d'activité γ d'un ion de charge ± 1.

En tenant compte des approximations possibles en milieu acide (K_I et K_{II} négligeables devant $\gamma(H^+)$), nous obtenons :

$$[19] \quad [SH] = \frac{\gamma(H^+)}{K_I + \gamma(H^+)}[S]_t \approx [S]_t$$

$$[20] \quad [S^-] = \frac{K_I}{K_I + \gamma(H^+)}[S]_t \approx \frac{K_I}{\gamma(H^+)}[S]_t$$

$$[21] \quad [HOCl] \approx \frac{K_{III}}{\mathcal{D}}[Cl]_t$$

$$[22] \quad [ClO^-] \approx \frac{K_{II}K_{III}}{\mathcal{D}\gamma(H^+)}[Cl]_t$$

$$[23] \quad [Cl_2] \approx \frac{\gamma(H^+)[Cl^-]}{\mathcal{D}}[Cl]_t$$

$$[24] \quad [Cl_3^-] \approx \frac{K_{IV}\gamma(H^+)[Cl^-]^2}{\mathcal{D}}[Cl]_t$$

avec $\mathcal{D} = K_{III} + \gamma(H^+)[Cl^-]$. Le détail du calcul conduisant à ces expressions des concentrations est donné en annexe 3.

À partir des relations [19]–[24] et en utilisant la loi limite de Debye–Hückel pour expliciter les coefficients d'activité, nous pouvons exprimer la participation de chacun des processus P_1, P_2 et P_5–P_8 à la cinétique globale de la réaction :

$$v(P_2) = k_2^0 \frac{\gamma_{SH}\gamma_{ClO^-}}{\gamma_{2^{\neq}}}[SH][ClO^-] = k_2^0 \frac{K_{II}K_{III}}{\gamma(H^+)\mathcal{D}}[S]_t[Cl]_t$$

$$v(P_3) = k_3^0 \frac{\gamma_{S^-}\gamma_{HOCl}}{\gamma_{3^{\neq}}}[S^-][HOCl] = k_3^0 \frac{K_I K_{III}}{\gamma(H^+)\mathcal{D}}[S]_t[Cl]_t$$

$$v(P_5) = k_5^0 \frac{\gamma_{SH}\gamma_{Cl_2}}{\gamma_{5^{\neq}}}[SH][Cl_2] = k_5^0 \frac{\gamma(H^+)[Cl^-]}{\mathcal{D}}[S]_t[Cl]_t$$

$$v(P_6) = k_6^0 \frac{\gamma_{SH}\gamma_{Cl_3^-}}{\gamma_{6^{\neq}}}[SH][Cl_3^-] = k_6^0 \frac{K_{IV}\gamma(H^+)[Cl^-]^2}{\mathcal{D}}[S]_t[Cl]_t$$

Can. J. Chem. Downloaded from www.nrcresearchpress.com by 123.30.183.119 on 09/08/12
For personal use only.

$$v(P_7) = k_7^0 \frac{\gamma_S - \gamma_{Cl_3^-}}{\gamma_{7^\neq}} [S^-][Cl_2] = k_7^0 \frac{K_I[Cl^-]}{\mathcal{D}} [S]_t[Cl]_t$$

$$v(P_8) = k_8^0 \frac{\gamma_S - \gamma_{Cl_3^-}}{\gamma_{8^\neq}} [S^-][Cl_3^-] = k_8^0 \frac{1}{\gamma^2} \frac{K_I K_{IV}[Cl^-]^2}{\mathcal{D}} [S]_t[Cl]_t$$

L'expression de la vitesse globale en présence d'ions chlorures devient alors :

$$v = v(P_2) + v(P_3) + \sum_{i=5}^{8} v(P_i)$$

avec

$$v(P_2) + v(P_3) = \frac{k_2^0 K_{II} K_{III} + k_3^0 K_I K_{III}}{\gamma(H^+)\mathcal{D}} [S]_t[Cl]_t$$

Soit d'après la relation [3] :

$$[25] \quad k_{exp} = \frac{1}{\mathcal{D}\gamma(H^+)} \left[k_2^0 K_{II} K_{III} + k_3^0 K_I K_{III} + k_5^0 \gamma^2(H^+)^2[Cl^-] + k_6^0 K_{IV} \gamma^2(H^+)^2[Cl^-]^2 + k_7^0 K_I \gamma(H^+)[Cl^-] + k_8^0 K_I K_{IV} \frac{[Cl^-]^2(H^+)}{\gamma} \right]$$

Si nous nous plaçons dans le cas où le processus P_3 est prépondérant devant P_2 (ce choix arbitraire ne limite pas la généralité du résultat puisque nous n'avons pu évaluer que la valeur théorique maximale des constantes de vitesse k_2^0 et k_3^0 dans le cas où le processus P_2 ou P_3 est exclusif), nous aurons $k_3^0 K_I >> k_2^0 K_{II}$ et $k_3^0 K_I K_{III}$ vaut alors $1{,}44 \times 10^{-6}$ M^2 s^{-1}.

La réaction [25] peut s'écrire :

$$[26] \quad Y - 1{,}44 \times 10^{-6} = k_5^0 \gamma^2(H^+)^2[Cl^-] + k_7^0 K_I \gamma(H^+)[Cl^-] + k_6^0 K_{IV} \gamma^2(H^+)^2[Cl^-]^2 + k_8^0 K_I K_{IV} \frac{[Cl^-]^2(H^+)}{\gamma}$$

avec $Y = k_{exp}\mathcal{D}\gamma(H^+)$. Cette quantité Y peut être calculée à partir des points expérimentaux obtenus à pH constant (pH = 3) et pour des concentrations en chlorure variables. Nous constatons (figure 12) que c'est la proportionnalité qui rend le mieux compte des variations de $(Y - 1{,}44 \times 10^{-6})$ avec $\gamma[Cl^-]$ ou $\gamma^2[Cl^-]$ ce qui élimine les processus P_6 ou P_8. Ceci est d'autant plus vrai que $[Cl^-]$ est grand.

La variation linéaire de Y en fonction de $\gamma(H^+)[Cl^-]$ (figure 13) montre qu'en milieu acide et en présence d'ions chlorures, le processus P_7 semble prépondérant et intervient parallèlement au couple de processus (P_2, P_3) indiscernables. Le processus P_7 correspond à la chloration par le chlore moléculaire Cl_2 de l'ion S^- qui se trouve en très faible quantité dans ces conditions de pH. En admettant une variation linéaire de Y en fonction de $\gamma(H^+)[Cl^-]$, nous pouvons estimer la valeur de la constante de vitesse k_7^0 du processus P_7 : $k_7^0 = 1{,}1 \times 10^9$ M^{-1} s^{-1} à 293 K.

Nous notons également que l'ordonnée à l'origine de cette droite qui représente la quantité $k_3^0 K_{II} K_{III}$ conduit à une valeur expérimentale voisine de la valeur calculée à partir de la constante de vitesse k_3^0 déterminée par l'étude en absence d'ions chlorures et justifie l'interprétation de la courbe de la figure 13.

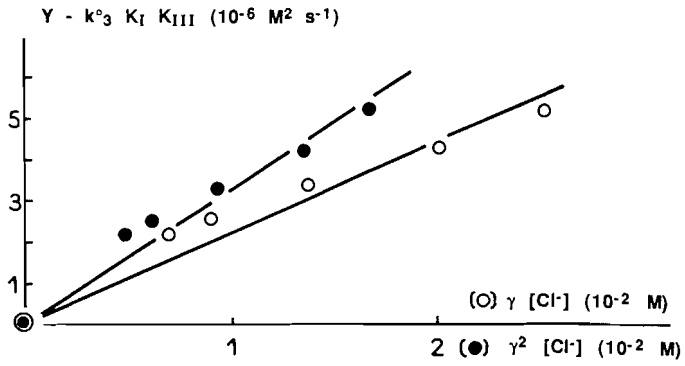

FIG. 12. Variation de $Y - k_3^0 K_I K_{III}$ en fonction de $\gamma[Cl^-]$ (○) et $\gamma^2[Cl^-]$ (●); pH = 3,0; T = 293 K.

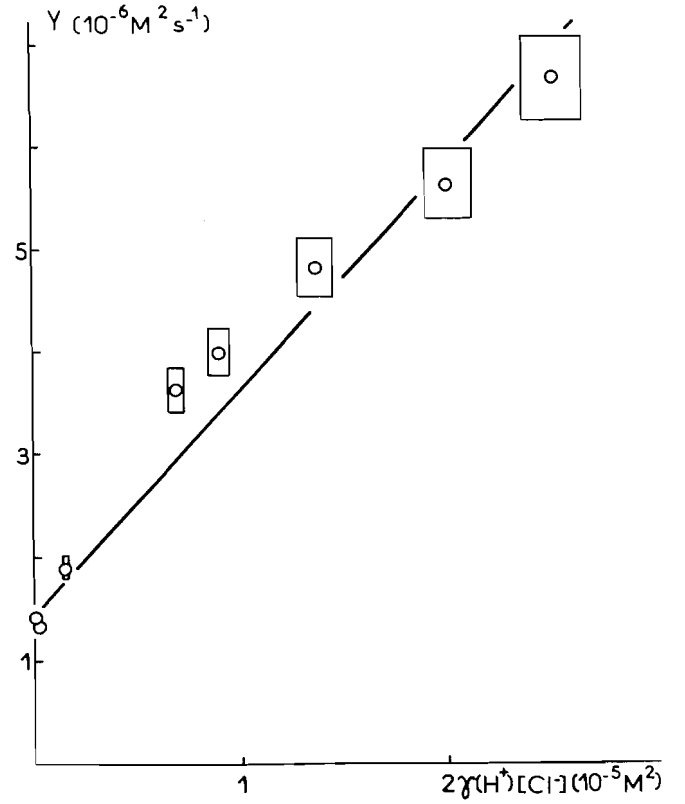

FIG. 13. Variation de Y en fonction de $\gamma(H^+)[Cl^-]$. Ces rectangles d'erreur sont calculés en ne tenant compte que de l'incertitude sur le pH (±0,025).

Conclusion

Cette étude par spectrophotométrie à écoulement bloqué nous a permis de mettre en évidence que, en milieu acide comme en milieu basique, la succinimide pouvait être chlorée soit sous sa forme acide SH par l'ion hypochlorite ClO^- soit sous sa forme basique S^- par l'acide hypochloreux HOCl.

Comme aucun paramètre cinétique ne permet de distin-

Can. J. Chem. Downloaded from www.nrcresearchpress.com by 123.30.183.119 on 09/08/12
For personal use only.

guer ces deux processus, la chloration de S^- par HOCl pourrait être la plus probable en supposant une attaque nucléophile de S^- sur HOCl en tout point semblable au mécanisme cinétiquement démontré en milieu acide : la chloration de S^- par Cl_2 :

$$S^- + HOCl \rightarrow SCl + OH^-$$

$$k_3^0 = 2{,}2 \times 10^7\ M^{-1}\ s^{-1} \text{ à } 293\ K$$

$$S^- + Cl\text{-}Cl \rightarrow SCl + Cl^-$$

$$k_7^0 = 1{,}1 \times 10^9\ M^{-1}\ s^{-1} \text{ à } 293\ K$$

Le facteur 50 entre les valeurs de k_3^0 et k_7^0 laisse penser que la cinétique de chloration par HOCl n'est pas totalement limitée par la diffusion. Les valeurs proches des coefficients de diffusion de HOCl et Cl_2 dans l'eau (D_{Cl_2} = 1,83 $m^2\ s^{-1}$ et D_{ClOH} = 1,28 $m^2\ s^{-1}$ à 298 K (8)) ne permettent pas d'expliquer l'écart entre les constantes de vitesse dans l'hypothèse de cinétiques limitées uniquement par la diffusion. La même observation a été faite pour la *N*-chloration des amines en phase aqueuse (9).

1. A. Hussain et T. Higuchi. J. Pharm. Sci. **61**, 371 (1972).
2. D. Matte. Thèse de Doctorat, Université de Nancy I. (1986).
3. H. F. Walton et A. A. Schilt. J. Am. Chem. Soc. **74**, 4995 (1952).
4. J. C. Morris. J. Phys. Chem. **70**, 3798 (1966).
5. R. E. Connick et Y. T. Chia. J. Am. Chem. Soc. **81**, 1280 (1959).
6. M. Eigen et K. Kustin. J. Am. Chem. Soc. **84**, 1355 (1962).
7. D. Matte, B. Solastiouk, A. Merlin et X. Deglise. Can. J. Chem. **67**, 786 (1989).
8. M. S. Chao. J. Electrochem. Soc. **115**, 1172 (1968).
9. D. Matte, B. Solastiouk, A. Merlin et X. Deglise. Can. J. Chem. **68**, 307 (1990).

Annexe 1 : Spectrophotométrie à écoulement bloqué. Exploitation des courbes cinétiques

La cinétique de la *N*-chloration de la succinimide en phase aqueuse peut être suivie en temps réel par spectrophotométrie à écoulement bloqué en mesurant, en fonction du temps, la tension V sortant du photomultiplicateur, qui est directement proportionnelle à l'intensité I de la lumière transmise par la solution. La densité optique A est obtenue en utilisant la loi de Beer–Lambert : $A = \log I_0/I$, soit $A = \log V_0/V$, I_0 et V_0 étant respectivement l'intensité de la lumière transmise et la tension à la sortie du photomultiplicateur.

1^er^ cas : Réaction du pseudo-premier ordre. On suit au cours du temps la concentration de l'ion ClO^-

Soit la réaction de chloration d'un substrat S par l'ion ClO^- d'ordre 1 par rapport à ClO^- et d'ordre α par rapport à S :

$$\alpha S + ClO^- \rightarrow P$$

L'ion hypochlorite est de plus en équilibre avec l'acide hypochloreux HOCl $\leftrightarrows$ $ClO^- + H^+$ avec la constante d'équilibre $K = [ClO^-](H^+)/[HClO]$. Cet équilibre est très rapide devant la réaction de chloration de telle sorte que les espèces HOCl et ClO^- restent toujours en équilibre entre elles. Si, à la longueur d'onde d'analyse, seules les espèces ClO^- et P absorbent la lumière, la densité optique est donnée par la relation : $A = \epsilon_1\,[ClO^-] + \epsilon_2\,[P]$, ϵ_1 et ϵ_2 étant respectivement les coefficients molaires d'extinction à cette longueur d'onde de ClO^- et de P.

En désignant par $[Cl]_t$ la concentration en chlore libre total (chlore non lié à un atome d'azote), $[Cl]_t = [HOCl] + [ClO^-] = [ClO^-](K + (H^+))/K$, la concentration totale de chlore $[Cl]_T$ devient :

$$[Cl]_T = [Cl]_t + P = [ClO^-]\frac{K + (H^+)}{K} + [P]$$

La densité optique de la solution prend alors la forme :

$$A = \epsilon[ClO^-] + \epsilon_2[Cl]_T$$

$\epsilon = \epsilon_1 - \epsilon_2 - \epsilon_2(H^+)/K$ reste constant au cours de la réaction, les solutions étant tamponnées.

La concentration du réactif S étant en large excès par rapport à l'hypochlorite, ce dernier sera entièrement consommé à la fin de la réaction et la densité optique à la longueur d'onde d'analyse de la solution après réaction devient :

$$A_\infty = \epsilon_2[Cl]_T$$

et

$$A = A_\infty + \epsilon[ClO^-] \text{ soit : } [ClO^-] = \frac{A - A_\infty}{\epsilon}$$

La réaction étant d'ordre 1 par rapport à $[ClO^-]$ et le réactif S étant en large excès par rapport à l'hypochlorite, on obtient $-\,d[ClO^-]/dt = k[ClO^-]$ avec k constante de vitesse du pseudo-premier ordre exprimée en s^{-1}. On en déduit donc :

$$-\frac{d(A - A_\infty)}{dt} = -\epsilon\frac{d[ClO^-]}{dt} = k(A - A_\infty)$$

soit, après intégration :

$$\ln\frac{A - A_\infty}{A(0) - A_\infty} = -kt$$

Ainsi, si la concentration de départ du réactif S est en large excès par rapport à la concentration d'hypochlorite et que les résultats expérimentaux vérifient la relation $\ln(A - A_\infty) = kt$ + constante, on peut en déduire que la réaction étudiée est du pseudo-premier ordre et déterminer la constante de vitesse apparente k.

2^e^ case : Réaction du deuxième ordre. On suit au cours du temps l'apparition du produit formé

Dans ce cas, on fixe la longueur d'onde de détection au maximum d'absorption de P. À cette longueur d'onde, les espèces HOCl, ClO^-, S ainsi que la solution tampon absorbent partiellement. La densité optique s'exprime alors par la relation :

$$A = \epsilon_1[P] + \epsilon_2[Cl]_t + \epsilon_3[S] + A_t$$

ϵ_1 et ϵ_3 sont respectivement les coefficients d'extinction molaire de P et S à la longueur d'onde d'analyse, ϵ_2 est un coefficient d'extinction molaire qui dépend du pH et A_t la densité optique due à la solution tampon. Ces deux derniers paramètres restent constants au cours de l'expérience. Comme

Can. J. Chem. Downloaded from www.nrcresearchpress.com by 123.30.183.119 on 09/08/12
For personal use only.

$[Cl]_T = [Cl]_t + [P]$ et $[S]_t = [S] + [P]$, $[S]_t$ étant la concentration totale du réactif chloré ou non, on en déduit :

$$[A] = (\epsilon_1 - \epsilon_2 - \epsilon_3)[P] + \epsilon_2[Cl]_T + \epsilon_3[S]_t + A_t$$

et

$$\frac{d[A]}{dt} = (\epsilon_1 - \epsilon_2 - \epsilon_3)\frac{d[P]}{dt}$$

La densité optique à l'instant initial est donnée par :

$$A(0) = \epsilon_2[Cl]_T + \epsilon_3[S]_t + A_t$$

Dans le cas où la concentration initiale de réactif $[S]_t$ est supérieure à la concentration initiale de chlore $[Cl]_T$, la densité optique de la solution à la fin de la réaction A_∞ est donnée par la relation :

$$A_\infty = (\epsilon_1 - \epsilon_3)[Cl]_T + \epsilon_3[S]_t + A_t$$

et

$$A_\infty - A(0) = (\epsilon_1 - \epsilon_2 - \epsilon_3)[Cl]_T$$

donc

$$\frac{dA}{dt} = \frac{[A_\infty - A(0)]}{[Cl]_T}\frac{dP}{dt}$$

soit

$$\left(\frac{dP}{dt}\right)_{t=0} = \frac{(dA/dt)_{t=0}}{[A_\infty - A(0)}[Cl]_T$$

Précision des résultats

Pour les réactions du pseudo-premier ordre, les constantes de vitesse sont déterminées en mesurant la pente de la droite $\ln(A - A_\infty)$ en fonction du temps par la méthode des moindres carrés. On peut estimer l'incertitude relative sur la constante de vitesse à environ 10%.

Pour les réactions du deuxième ordre, la constante de vitesse est calculée à partir de la pente dA/dt au début de la réaction et des densités optiques $A(0)$ et A_∞ au début et à la fin de la réaction. La précision sur les constantes de vitesse ainsi déterminée est d'environ 20%.

Annexe 2

Les expressions des concentrations des différentes espèces réagissantes sont établies à partir d'une part des bilans en succinimide et en chlore libre total :

[A1] $[Cl]_t = [ClO^-] + [HOCl]$

[A2] $[S]_t = [S^-] + [SH]$

et d'autre part des constantes des équilibres [I] et [II] :

[A3] $$K_I = \frac{(H^+)(S^-)}{(SH)} = \frac{(H^+)[S^-]}{[SH]}\frac{\gamma_{S^-}}{\gamma_{SH}}$$

[A4] $$K_{II} = \frac{(H^+)(ClO^-)}{(HOCl)} = \frac{(H^+)[ClO^-]}{[HOCl]}\frac{\gamma_{ClO^-}}{\gamma_{HOCl}}$$

Ces deux relations [A2] et [A3] forment un système de deux équations à deux inconnues [SH] et $[S^-]$ qui peut être résolu par exemple en exprimant $[S^-]$ en fonction de [SH] à partir de la relation [A3].

$$[S^-] = \frac{K_I[SH]\gamma_{SH}}{(H^+)\gamma_{S^-}}$$

En remplaçant $[S^-]$ par cette expression dans l'équation [A2], nous obtenons directement les relations [6] et [7]. De la même façon, les deux relations [8] et [9] sont déduites du système des deux équations [A1] et [A4] avec comme inconnues $[ClO^-]$ et [HOCl].

Annexe 3

En présence d'ions chlorures et dans les conditions d'une cinétique du pseudo-premier ordre (succinimide en large excès par rapport au chlore), les bilans en succinimide et en chlore libre total deviennent :

[A5] $[S]_t = [SH] + [S^-]$

[A6] $[Cl]_t = [ClO^-] + [HOCl] + [Cl_2] + [Cl_3^-]$

Ces concentrations sont liées entre elles par les lois d'action de masse des équilibres [I]–[IV] :

[A7] $$K_I = \frac{(H^+)[S^-]}{[SH]}\gamma \qquad \text{avec } pK_I = 9{,}71 \text{ à } 293 \text{ K}$$

[A8] $$K_{II} = \frac{(H^+)[ClO^-]}{[HOCl]}\gamma \qquad \text{avec } pK_{II} = 7{,}58 \text{ à } 293 \text{ K}$$

[A9] $$K_{III} = \frac{(H^+)[Cl^-][HOCl]}{[Cl_2]}\gamma$$

avec $pK_{III} = 3{,}48$ à 293 K

[A10] $$K_{IV} = \frac{[Cl_3^-]}{[Cl_2][Cl^-]}\gamma \qquad \text{avec } pK_{IV} = 0{,}74 \text{ à } 298 \text{ K}$$

Les deux équations [A5] et [A7] permettent facilement d'exprimer [SH] et $[S^-]$ en fonction de $[S]_t$. D'après [A5] : $[S^-] = [S]_t - [SH^-]$. En reportant cette expression dans [A7], nous obtenons :

$$[SH] = \frac{\gamma(H^+)}{K_I + \gamma(H^+)}[S]_t$$

et

$$[S^-] = [S]_t - \frac{\gamma(H^+)}{K_I + \gamma(H^+)}[S]_t = \frac{K_I}{K_I + \gamma(H^+)}[S]_t$$

En milieu acide (pH < 3), K_I devient négligeable devant $\gamma(H^+)$ et [SH] ≈ [S]t, $[S^-] \approx K_I/\gamma(H^+)[S]_t$.

À partir des trois lois d'action de masse [A8], [A9], [A10] correspondant aux équilibres [II]–[IV], nous pouvons obtenir par substitutions successives l'expression des concentrations des espèces chlorées en fonction de [HOCl] :

$$[ClO^-] = \frac{K_{II}[HOCl]}{\gamma(H^+)}$$

$$[Cl_2] = \frac{\gamma(H^+)[Cl^-][HOCl]}{K_{III}}$$

$$[Cl_3^-] = \frac{K_{IV}}{K_{III}}\gamma(H^+)[Cl^-]^2[HOCl]$$

Can. J. Chem. Downloaded from www.nrcresearchpress.com by 123.30.183.119 on 09/08/12
For personal use only.

Le bilan en chlore libre total [A6] s'écrit alors :

$$[Cl]_t = [HOCl]\left[1 + \frac{K_{II}}{\gamma(H^+)} + \frac{\gamma(H^+)[Cl^-]}{K_{III}} + \frac{K_{IV}}{K_{III}}\gamma(H^+)[Cl^-]^2\right]$$

En milieu acide pH < 3 et dans le domaine de concentration en ions chlorures étudié, $[K_{II}/\gamma(H^+)]$ et $(K_{IV}/K_{III})\gamma(H^+)[Cl^-]^2$ sont négligeables devant $1 + \gamma(H^+)[Cl^-]/K_{III}$.

$$[Cl]t \approx [HOCl]\left[\frac{K_{III} + \gamma(H^+)[Cl^-]}{K_{III}}\right]$$

En posant $\mathcal{D} = K_{III} + \gamma(H^+)[Cl^-]$, nous retrouvons l'équation [21] et par déductions successives, les relations [22]–[24].

Can. J. Chem. Downloaded from www.nrcresearchpress.com by 123.30.183.119 on 09/08/12
For personal use only.

The role of coupling in intramolecular proton transfer reactions. The hydrogen oxalate anion as an example

ENRIC BOSCH, MIQUEL MORENO, AND JOSÉ MARÍA LLUCH[1]

Departament de Química, Universitat Autònoma de Barcelona, 08193 Bellaterra, Barcelona, Spain

Received June 11, 1991

ENRIC BOSCH, MIQUEL MORENO, and JOSÉ MARÍA LLUCH. Can. J. Chem. **70,** 100 (1992).

Coupling between the proton motion and the internal degrees of freedom for intramolecular proton transfer in the hydrogen oxalate anion has been studied. A normal mode analysis at a sequence of points along the Intrinsic Reaction Coordinate (IRC) has been performed and the coupling functions $B_{k,F}$ have been obtained. It is shown that, although for the reactant the IRC direction essentially consists of the motion of oxygen atoms, the coupling changes this IRC direction towards the motion corresponding to proton transfer itself. From a quantum point of view, the curvature that appears as a consequence allows corner-cutting tunneling. Finally, the effect of isotope substitution is considered.

Key words: intramolecular proton transfer, coupling functions, IRC curvature, tunneling splitting, isotope substitution.

ENRIC BOSCH, MIQUEL MORENO et JOSÉ MARÍA LLUCH. Can. J. Chem. **70,** 100 (1992).

On a étudié le couplage entre le mouvement du proton et les degrés de liberté interne du transfert protonique intramoléculaire dans l'anion hydrogénoxalate. On a fait un analyse des modes propres de vibration sur une séquence de points de la coordonnée réactionnelle (CRI) et on a pu en tiré les fonctions de couplage $B_{k,F}$. On a démontré que, bien que la direction de la CRI dans le réactif peut être décrite principalement par le mouvement des atomes d'oxygène, le couplage change cette direction de la CRI vers le mouvement correspondant au transfert protonique lui-même. D'un point de vue quantique, la courbure qui apparait rend possible un effet tunnel qui coupe les coins. Enfin, on a considéré l'effet de la substitution isotopique.

Mots clés : transfert protonique intramoléculaire, fonctions de couplage, courbure de la CRI, dédoublement provoqué par l'effet tunnel, substitution isotopique.

[Traduit par la rédaction]

Introduction

It is generally accepted that proton transfer reactions are among the simplest and most common reactions in chemistry (1,2). Given that these processes primarily involve the motion of the transferring hydrogen, some calculations have frozen the other geometrical parameters (3, 4). In other studies this important restriction has been partially lifted so that the distance between H-donor and H-acceptor atoms is fixed, all other geometrical parameters being fully optimized at each stage of the proton transfer (5–7).

Over the past few years several authors have claimed that the proton motion is strongly coupled to intramolecular vibrational modes in the reaction system (8–18). In particular, we have shown that to have a reliable evaluation of the tunneling dynamics for intramolecular proton transfer in the hydrogen oxalate anion (HX), a bidimensional surface that takes into account the coupling between the proton transfer motion and the vibrations of the heavy atoms through a quadratic term must be considered. This quadratic term acts as a bath, which averages the effect of all the vibrational modes coupled to the system (proton transfer) motion (18).

The purpose of the present paper is to take the intramolecular proton transfer of HX as an example for discussing the importance and the nature of the coupling between the proton motion and the internal degrees of freedom. To this aim we will perform a quantitative analysis of the coupling that explicitly characterizes the interaction between the proton transfer motion and each of the vibrational modes. This study will be done in the full potential hypersurface by calculating the coupling functions $B_{k,F}$.

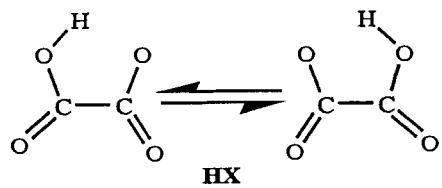

HX

SCHEME 1

Methodology

Ab initio self-consistent field (SCF) calculations were carried out with the Gaussian 86 series of programs (19), using the triply split valence basis set 3-21 + G (20, 21), which contains a diffuse *sp* shell on atoms other than hydrogen.

All geometrical parameters were completely optimized. Geometry optimization and direct location of minima and the transition state were carried out with the Schlegel gradient optimization algorithm (22).

We have constructed the Intrinsic Reaction Coordinate (IRC) (23–25). The IRC is a line in mass-weighted configuration space whose coordinates $\boldsymbol{x}$ are given parametrically in terms of the arc length s defined by

$$[1] \qquad ds = \left(\sum_{j=1}^{3N} dx_j^2 \right)^{1/2}$$

where $\boldsymbol{x}$ is a column vector whose components are the $3N$ mass-weighted Cartesian coordinates. The IRC is the solution of the differential equation:

$$[2] \qquad \frac{d\boldsymbol{x}}{ds} = -\frac{\nabla V}{|\nabla V|}$$

[1]Author to whom correspondence may be addressed.

Printed in Canada / Imprimé au Canada

Can. J. Chem. Downloaded from www.nrcresearchpress.com by 123.30.183.119 on 09/08/12
For personal use only.

Can. J. Chem. Downloaded from www.nrcresearchpress.com by 123.30.183.119 on 09/08/12
For personal use only.

where ∇ is the N-dimensional gradient operator in mass-weighted coordinates and V is the Born–Oppenheimer potential energy.

A normal mode analysis at a sequence of points along the IRC has been performed. Second energy derivatives with respect to the Cartesian coordinates were computed analytically (26). At a given point of the reaction coordinate we evaluate:

$$[3] \quad K^p = (1 - P) \cdot K \cdot (1 - P)$$

where K is the $3N \times 3N$ Hessian matrix and P is a projector, a $3N \times 3N$ matrix, whose elements are given by

$$[4] \quad P_{i,\gamma,i',\gamma'} = \sum_{k=3N-6}^{3N} L_{i,\gamma,k} \cdot L_{i',\gamma',k}$$

Here $i = 1, \ldots N$ labels the atoms and $\gamma = x, y, z$ the Cartesian coordinates. The quantities $\{L_{i,\gamma,k}\}$; $k = 3N - 6, \ldots, 3N - 1$ are the six $3N$-dimensional unit vectors that correspond to infinitesimal rotation and translations of the N-atom system, and $L_{i,\gamma,3N}$ is the unit vector along the reaction coordinate defined in eq. [2]. Thus, not only the direction of the reaction path but the direction corresponding to infinitesimal rotations and translations is projected out. An explicit expression of the $\boldsymbol{L}$ vectors has been given by Miller *et al.* (27).

Diagonalization of the projected Hessian matrix K^p was finally done in order to obtain the normal modes along the IRC. Note that for stationary points projections are not required.

In symmetrical double-well potentials the stationary states with energies less than the barrier height occur in nearly degenerate pairs consisting of a symmetric state and a higher energy antisymmetric state. The tunneling rate k is directly related to the energy splitting ΔE by (28)

$$[5] \quad k = \frac{2\Delta E}{h}$$

For a unidimensional path this tunneling splitting is given in the semiclassical WKB (29) approximation by

$$[6] \quad \Delta E = \frac{h\nu}{\pi} e^{-\theta}$$

where ν is the vibrational frequency in the well and θ is the classical action integral through the barrier defined by

$$[7] \quad \theta = \frac{1}{\hbar} \mathrm{Im} \int_{\text{barrier}} p(x)dx = \frac{1}{\hbar} \int_{s<}^{s>} (2m(V(x) - E))^{1/2} dx$$

where $s<$ and $s>$ are the initial and end points of the tunneling path. We note that since we use mass-weighted Cartesian coordinates, the mass m in eq. [1] must be a unit mass. To evaluate the tunneling feasibility the θ values at selected points along the IRC have been calculated using eq. [7].

Finally the isotope effect coming from the substitution of the transferring proton by a deuterium has been studied using a basis set method (30). In particular we have taken a basis set χ_i where the basis functions χ_i are localized Gaussian functions:

$$[8] \quad \chi_i(s) = \left(\frac{\alpha}{\pi}\right)^{1/4} \exp\left[\frac{-\alpha}{2}(s - s_i)^2\right]$$

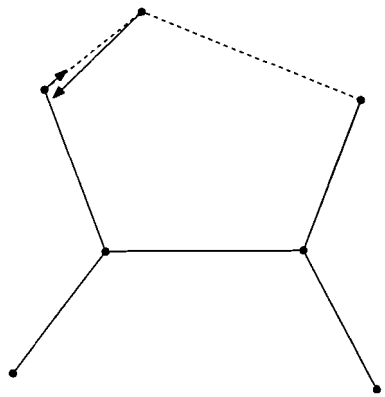

FIG. 1. Normal mode ν_1 of A' symmetry at the hydrogen oxalate minimum in mass-weighted Cartesian coordinates.

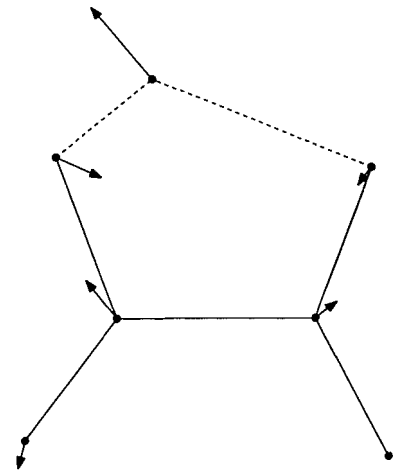

FIG. 2. Normal mode ν_4 of A' symmetry at the hydrogen oxalate minimum in mass-weighted Cartesian coordinates.

where α is an adjustable parameter and s_i values are equally spaced points along the s coordinate. A variational calculation using n localized Gaussian functions provides the lowest n eigenvalues and eigenfunctions of the one-dimensional system. The tunneling splitting ΔE can thereby be obtained. The adjustable parameter α is chosen to provide a balance of linear independence and completeness of the basis set. We have used 41 Gaussian functions for all the calculations.

Results and discussion

A chemical reaction involves a nuclear reorganization in going from reactants to products. In fact, only motions that strictly come from the geometric difference between reactant and product should be required. These motions would lead from reactants to products through the shortest path, a straight path known as the Linear Reaction Path (LRP) (11). For the proton transfer reaction in HX, the dominant component of this coordinate is the displacement of the transferring H.

A normal mode analysis of the reactant (HX) shows that the LRP arises mainly from the superposition of two modes displayed in Figs. 1 and 2. Note that the arrows indicate the direction of the atomic motion in mass-weighted Cartesian coordinates. Taking into account only the normal modes

corresponding to the C_s symmetry we can classify these modes in decreasing order of frequencies as the first and fourth.

Nevertheless the high values of the frequencies associated with these two modes $\nu_1 = 3639$ and $\nu_4 = 1418$ cm^{-1} suggest that motion along the LRP should require passage over a sizeable barrier. In fact an *ab initio* calculation provides a value of 21.24 kcal mol^{-1} for this barrier.

Therefore from a classical point of view it is clear that the reaction cannot proceed along the LRP. Instead, a structure of lower energy has to exist that fulfills the four conditions of a transition state as stated by McIver and Komornicki (31). In fact, when this transition state is located it is seen that an energy barrier of only 8.34 kcal mol^{-1} is imposed (17). From this transition state the IRC can be built as the steepest descent path that can go either way, to reactants or products. Its initial direction at the transition state is given by the normal mode of the imaginary frequency. Assuming the harmonic approximation, we choose the initial step size Δs that produces the appropriate energy lowering $k(\Delta s)^2/2$, where k is the negative force constant associated with the imaginary frequency. Then the IRC is followed, taking very small steps in the direction of the negative gradient, which is equivalent to the Euler method. An initial energy lowering of 0.0005 hartrees and successive steps of $\Delta s = 0.0265$ amu$^{1/2}$ Å have been used (17). The IRC ends up at the normal mode of the lower frequency (of the appropriate symmetry) (32).

Therefore, in contrast with the LRP, going from reactants to products through the transition state by following the IRC implies a distortion of the geometry of the reactant so that an approach to the geometry of the product is not initially provided, but a path with the lowest energy barrier is allowed.

Figure 3 shows the IRC direction for selected points along the IRC. In the reactant well ($s = -1.08$ amu$^{1/2}$ Å) the IRC follows the direction of the lowest normal mode at the geometry of the minimum whose frequency is $\nu_{10} = 320$ cm^{-1}. This low value clearly indicates a slow energy climbing. At this point the IRC essentially consists of the motion of oxygen atoms, the transferring hydrogen remaining attached to the donor oxygen.

In Fig. 4 we display the direction of the straight paths that depart from selected points along the IRC. Each straight path joins two points of the IRC with arc length values of $-s$ and $+s$ respectively. The path is defined by linear interpolation between both extremes in mass-weighted Cartesian coordinates. That is:

$$[9] \quad \mathbf{y}(v) = \frac{1}{2}(\mathbf{y}_s + \mathbf{y}_{-s}) + (\mathbf{y}_s - \mathbf{y}_{-s}) \cdot \frac{v}{\Delta v}$$

where:

$$[10] \quad \Delta v = |\mathbf{y}_s - \mathbf{y}_{-s}|$$

where $\mathbf{y}_{-s}$ and $\mathbf{y}_s$ are the $3N$ mass-weighted Cartesian coordinates of the atoms for the geometries corresponding to $-s$ and $+s$ values of the IRC respectively, v is the distance along the straight path, and $\mathbf{y}(v)$ the corresponding Cartesian coordinates along this path. Note that v varies from $-\Delta v/2$ to $+\Delta v/2$. When the straight path links reactant and product the LRP is obtained.

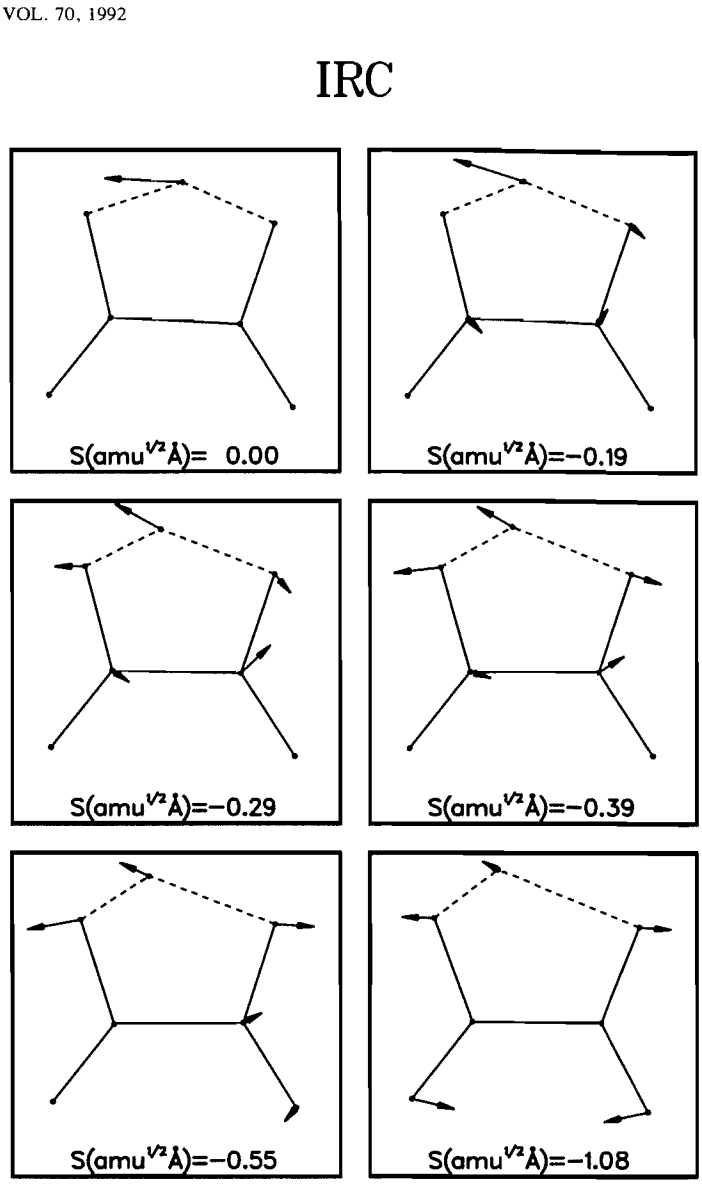

FIG. 3. Snapshots showing the direction in mass-weighted Cartesian coordinates of the IRC for hydrogen oxalate proton transfer at selected points.

To fulfill the requirement that any straight path have no linear nor angular momentum, the following conditions along this path $\boldsymbol{R}_i$ are imposed:

$$[11] \quad \sum_i m_i \cdot \boldsymbol{R}_i'(v) = 0$$

$$[12] \quad \sum_i m_i \cdot \boldsymbol{R}_i(v) \times \boldsymbol{R}_i'(v) = 0$$

where the prime denotes (d/dv). The first condition is satisfied by imposing the condition that the center of mass is always at the origin. The condition that angular momentum remain zero is satisfied by orienting the product axis system in precisely the correct way with respect to that of the reactant.

Can. J. Chem. Downloaded from www.nrcresearchpress.com by 123.30.183.119 on 09/08/12
For personal use only.

Can. J. Chem. Downloaded from www.nrcresearchpress.com by 123.30.183.119 on 09/08/12
For personal use only.

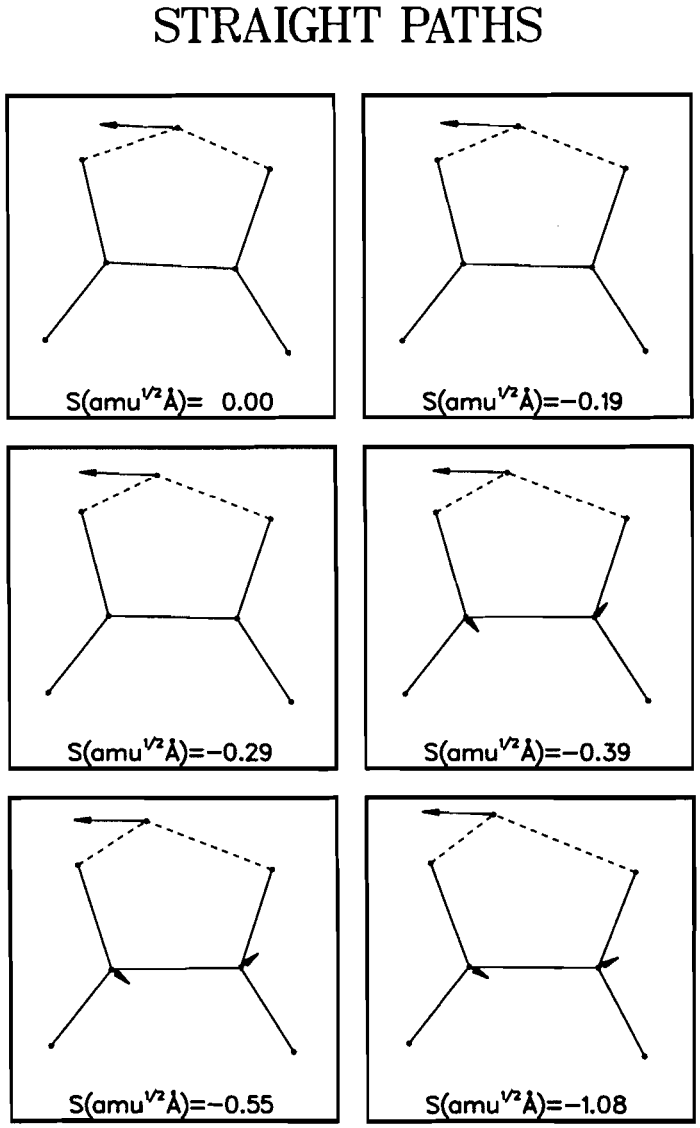

FIG. 4. Snapshots showing the direction in mass-weighted Cartesian coordinates of the straight paths that depart from selected points of the IRC.

In Fig. 4 it is shown that, as the reaction proceeds, the direction of the IRC changes, so that it progressively becomes the direction corresponding to the straight path. This point becomes clear when the snapshots depicted in Figs. 3 and 4 are compared. This way the transition vector entirely corresponds to the proton transfer, the other atoms remaining fixed.

The evolution of the IRC direction is the result of the coupling with the rest of the normal modes and, in particular, with modes 1 and 4. Quantitatively this coupling can be analyzed using the coupling functions $B_{k,F}$ that characterize the interaction between the kth vibrational generalized normal mode and the reaction coordinate F. The $B_{k,F}$ terms are given by

$$[13] \quad B_{k,F}(s) = \sum_{i=1}^{3N} (\delta L_{i,k}(s)/\delta s) \cdot L_{i,F}(s)$$

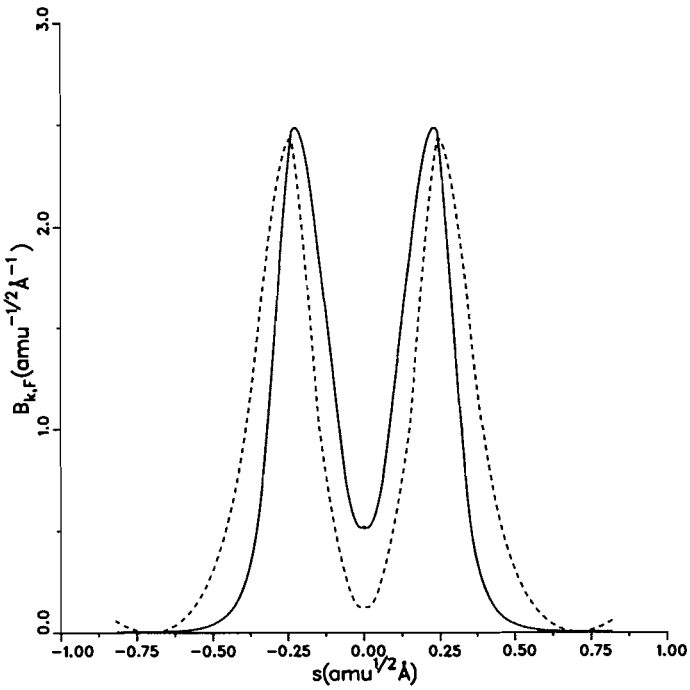

FIG. 5. Absolute value of coupling functions $B_{1,F}$ (solid line) and $B_{4,F}$ (dashed line) along the IRC.

where $L_{i,k}$ and $L_{i,F}$ are, respectively, the ith Cartesian component of the kth eigenvector of the projected force constant matrix and that of the reaction coordinate direction as a function of s. In practice the coupling elements are obtained via a finite difference approximation:

$$[14] \quad B_{k,F}\left(\frac{s_j + s_{j-1}}{2}\right) \approx \frac{\sum_{i=1}^{3N} [L_{i,k}(s_j) \cdot L_{i,F}(s_{j-1}) - L_{i,k}(s_{j-1}) \cdot L_{i,F}(s_j)]}{2(s_j - s_{j-1})}$$

The coupling functions $B_{1,F}$ and $B_{4,F}$ are shown in Fig. 5. Both display two significant peaks at about $s = \pm 0.25$ amu$^{1/2}$ Å. The variation of the adiabatic projected harmonic frequencies corresponding to the A' symmetry along the IRC is shown in Fig. 6. The important change of the 1 and 4 frequencies around $s = \pm 0.25$ amu$^{1/2}$ Å reflects the significant coupling of the corresponding modes with the reaction path.

This coupling is required to cause deviation of the IRC direction towards the motion corresponding to proton transfer itself. An important curvature appears as a consequence. This curvature of the reaction path is defined as

$$[15] \quad \kappa(s) = \left[\sum_{k=1}^{F-1} B_{k,F}(s)^2\right]^{1/2}$$

and has been represented by a solid line in Fig. 7.

It can be observed that two sharp peaks symmetrically appear, one before and one after the saddle point (s =

Can. J. Chem. Downloaded from www.nrcresearchpress.com by 123.30.183.119 on 09/08/12
For personal use only.

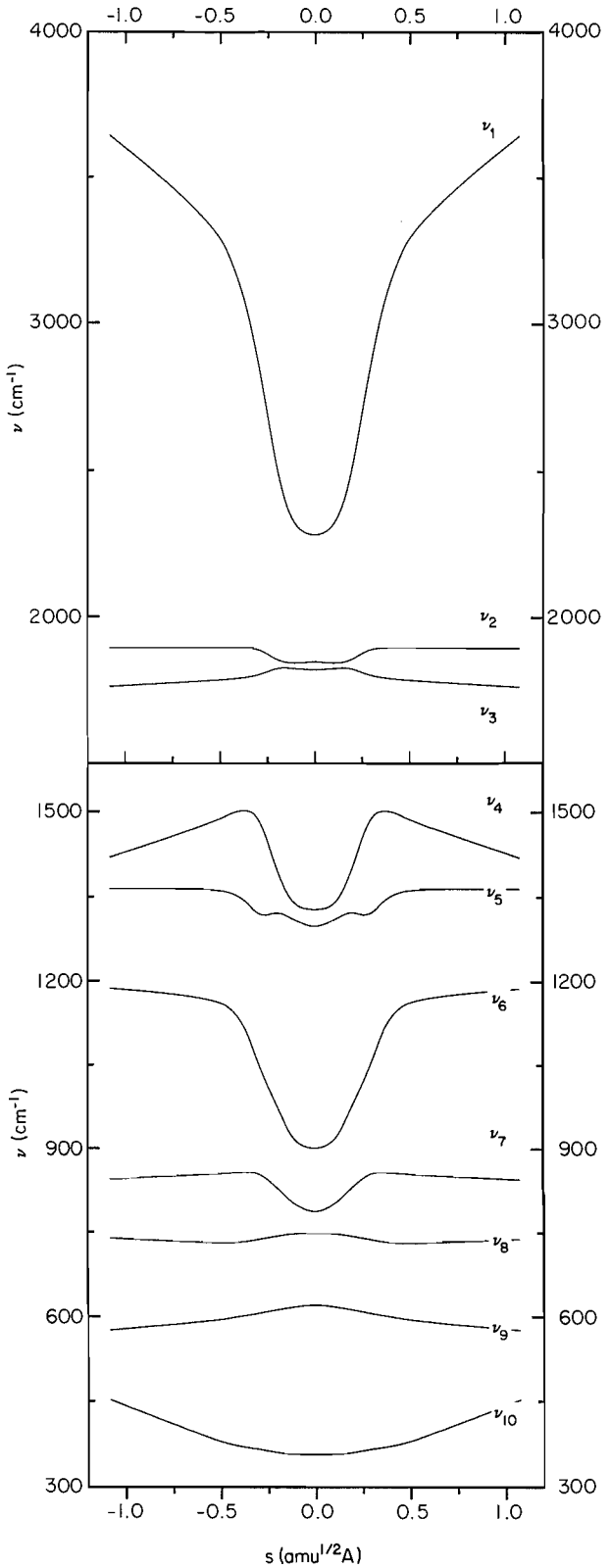

FIG. 6. Projected harmonic frequencies (in cm^{-1}) of the A' symmetry along the IRC.

0 $amu^{1/2}$ Å). These peaks are mostly due to the contribution of the coupling with modes 1 and 4.

From a quantum point of view the IRC curvature has the effect of allowing corner-cutting tunneling, thereby increasing the probability of tunneling. If only the height of the barrier is considered, the more appropriate tunneling path would be the IRC as this path implies the lowest value for such a barrier. However, when the curvature is large a straight line involves a shorter path that can compensate for the energy factor. To analyze this point, we have calculated several parameters at selected points along the IRC. We present these parameters in Table 1.

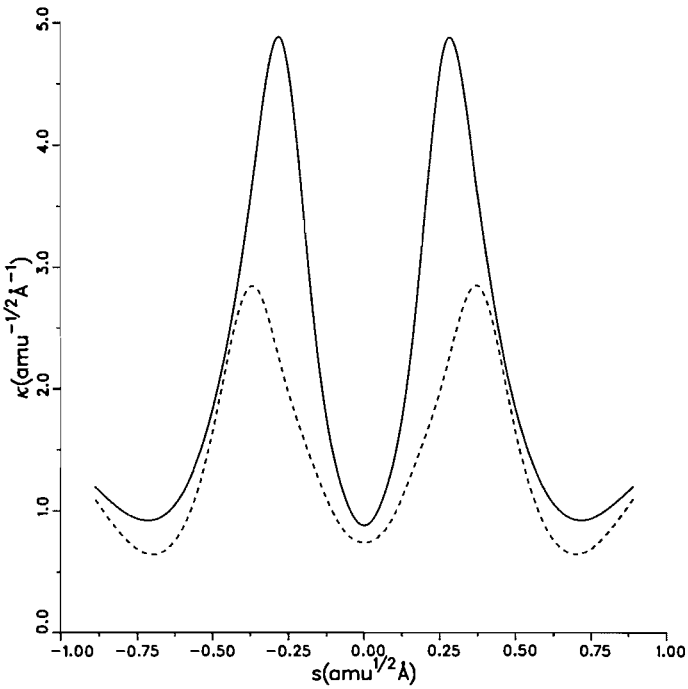

FIG. 7. Total curvature $\kappa(s)$ for hydrogen oxalate HX (solid line) and deuterated hydrogen oxalate DX (dashed line) anions along the IRC.

TABLE 1. Parameters that control the tunneling at selected points of the IRC (see text for details)

s^a	α^b	Δl^a	ΔB^c	$\Delta\theta$
−0.19	19.6	0.004	−0.05	0.004
−0.29	65.6	0.044	−0.43	0.103
−0.39	55.0	0.108	−1.39	0.198
−0.55	62.5	0.266	−3.40	0.643
−1.08	78.7	0.972	−12.91	2.416

[a] In $amu^{1/2}$ Å.
[b] In degrees.
[c] In kcal mol^{-1}.

In this table α stands for the angle obtained from the scalar product between the unitary vectors that define the IRC and the straight paths, respectively. As the IRC deviates more with respect to the straight paths, a higher value of α is obtained. Δl measures at each point the length difference between the IRC and its corresponding straight path. ΔB accounts for the difference of energy barriers between both paths. Finally, following eq. [7], these last two factors determine the value of $\Delta\theta$, the difference between the classical action integral through the barriers.

TABLE 2. Tunneling splittings[a] along the IRC and LRP for HX and DX

Path	ΔE^b
IRC	HX 2.72(−3)
	DX 2.75(−4)
LRP	HX 7.27(−3)
	DX 2.58(−4)

[a]Power of 10 in parentheses.
[b]In cm^{-1}.

In going from the transition state down to reactants the curvature tends to increase the value of the angle α. Then as the IRC deviates from the straight path, its length becomes progressively longer than the corresponding straight path. Table 1 shows that this last factor favors the tunneling through the straight path more and more, in spite of the fact that the barrier differences ΔB evolve unfavorably. Therefore, the LRP is a more feasible way to reach the product than the IRC when the quantum tunneling effect is accounted for.

The above-mentioned considerations can be useful in interpreting certain chemical phenomena. In particular it seems that in enzyme catalysis and protein chemistry the reduction of the distance between the proton-donor and the proton-acceptor atoms facilitates the proton transfer (33, 34). In fact, the effect of this "close packing" is equivalent to pushing the reactant system along the initial stage of the IRC, which, as mentioned above, essentially consists of the motion of the donor and acceptor atoms. Therefore from a classical point of view the energy barrier is lowered. In addition, from a quantum point of view the lengths of both the IRC and the straight paths are shortened in such a way that the proton tunneling is favored.

Another interesting problem is the isotope effect. When the transferring proton is substituted by a deuterium the IRC curvature is noticeably reduced as shown in the dashed curve in Fig. 7. This effect is reflected in Table 2 where the tunneling splittings for HX and DX (deuterated hydrogen oxalate anion) along the IRC and the LRP are shown.

A clear difference comes to light when looking at Table 2: whereas in the HX the splitting is clearly higher along the LRP (18), in the DX both paths lead to almost the same splitting values. On the other hand it is interesting to note that this unidimensional approach, although it underestimates the splitting, already shows that the tunneling frequency for HX is an order of magnitude greater than for DX.

Concluding remarks

From the results obtained in this work the following picture can be developed for intramolecular proton transfer in the hydrogen oxalate anion.

To achieve the minimum energy path the IRC is initiated with a direction in which the contribution of the hydrogen motion is very small. The coupling between the reaction path and the normal modes orthogonal to this path produces a progressive change in the direction of the IRC, the proton transfer itself taking place at the end of this path. This coupling leads to a curvature, so that from a quantum point of view the tunneling dynamics do not follow the IRC, allowing the tunneling path to cut the corner. When the transferring hydrogen is substituted by deuterium the curvature decreases so that this corner-cutting effect is diminished.

A final remark is that any feasible tunneling path not only involves the proton motion but other atom motions that come from the geometric difference of reactant and product. As a consequence the path in mass-weighted Cartesian coordinates becomes longer and the tunneling rate decreases.

We believe these features are general for a wide range of intramolecular proton transfers in chemical and biochemical systems.

1. E. F. Caldin and V. Gold (*Editors*). Proton-transfer reactions. Chapman & Hall, London. 1975.
2. M. T. Page. The chemistry of enzyme action. Elsevier, Amsterdam. 1974.
3. E. A. Hillenbrand and S. Scheiner. J. Am. Chem. Soc. **106**, 6266 (1984).
4. S. Scheiner, Paul Redfern, and M. M. Szczesniak. J. Am. Chem. Soc. **89**, 262 (1985).
5. S. M. Cybulski and S. Scheiner. J. Am. Chem. Soc. **109**, 4199 (1987).
6. S. M. Cybulski and S. Scheiner. J. Am. Chem. Soc. **111**, 23 (1989).
7. J. L. Esquivel and J. F. Mata-Segreda. Int. J. Quantum Chem. **38**, 521 (1990).
8. D. Borgis and J. T. Hynes. *In* The enzyme catalysis process. *Edited by* A. Cooper, J. Houben, and L. Chien. Plenum, New York. 1989.
9. D. Borgis, S. Lee, and J. T. Hynes. Chem. Phys. Lett. **162**, 19 (1989).
10. D. Borgis and J. T. Hynes. J. Chem. Phys. **94**, 3619 (1991).
11. W. H. Miller, B. A. Ruf, and Y. Chang. J. Chem. Phys. **89**, 6298 (1988).
12. N. Makri and W. H. Miller. J. Chem. Phys. **91**, 4026 (1989).
13. W. H. Miller. *In* New theoretical concepts for understanding organic reactions. *Edited by* J. Bertrán and I. G. Csizmadia. Kluwer, Dordrecht. 1989. p. 347.
14. N. Shida, P. F. Barbara, and J. E. Almlöf. J. Chem. Phys. **91**, 4061 (1989).
15. D. G. Truhlar, A. D. Isaacson, and B. C. Garrett. *In* Theory of chemical reaction dynamics. Vol. IV. *Edited by* M. Baer. CRC Press, Boca Raton, FL. 1985. p. 65.
16. K. K. Baldridge, M. S. Gordon, R. Steckler, and D. G. Truhlar. J. Phys. Chem. **93**, 5107 (1989).
17. E. Bosch, M. Moreno, J. M. Lluch, and J. Bertrán. Chem. Phys., **148**, 77 (1990).
18. E. Bosch, M. Moreno, J. M. Lluch, and J. Bertrán. J. Chem. Phys., **93**, 5685 (1990).
19. M. J. Frisch, J. S. Binkley, H. B. Schlegel *et al.* Gaussian 86. Carnegie–Mellon Quantum Chemistry Publishing Unit, Pittsburgh, PA, 1984.
20. G. W. Spitznagel, T. Clark, J. Chandrasekhar, and P. von R. Schleyer. J. Comput. Chem. **3**, 363 (1982).
21. T. Clark, J. Chandrasekhar, G. W. Spitznagel, and P. von R. Schleyer. J. Comput. Chem. **4**, 294 (1983).
22. H. B. Schlegel. J. Comput. Chem. **3**, 214 (1982).
23. D. G. Truhlar and A. Kupperman. J. Am. Chem. Soc. **93**, 1840 (1971).
24. K. Fukui. J. Phys. Chem. **74**, 4161 (1970).
25. K. Fukui. Pure Appl. Chem. **54**, 1825 (1982).
26. J. A. Pople, A. Krishnan, H. B. Schlegel, and J. S. Binkley. Int. J. Quantum Chem. Symp. **13**, 225 (1979).
27. W. H. Miller, N. C. Handy, and J. E. Adams. J. Chem. Phys. **72**, 99 (1980).

Can. J. Chem. Downloaded from www.nrcresearchpress.com by 123.30.183.119 on 09/08/12
For personal use only.

28. K. M. Christoffel and J. M. Bowman. J. Chem. Phys. **74**, 5057 (1981).
29. W. H. Miller. J. Phys. Chem. **83**, 960 (1979).
30. I. P. Hamilton and J. C. Light. J. Chem. Phys. **84**, 306 (1986).
31. J. W. McIver and A. Komornicki. J. Am. Chem. Soc. **94**, 2625 (1972).
32. B. A. Ruf and W. H. Miller. J. Chem. Soc. Faraday Trans. 2, **84**, 1523 (1988).
33. Y. Cha, C. J. Murray, and J. P. Klinman. Science, **243**, 1325 (1989).
34. L. Jaroszewski, B. Lesyng, J. T. Tanner, and J. A. McCammon. Chem. Phys. Lett. **175**, 282 (1990).

Can. J. Chem. Downloaded from www.nrcresearchpress.com by 123.30.183.119 on 09/08/12
For personal use only.

Copper(I)-catalyzed cross-dehydrocoupling reactions of silanes and amines

H. Q. Liu and J. F. Harrod
Chemistry Department, McGill University, Montreal, P.Q., Canada H3A 2K6

Received June 18, 1991

H. Q. Liu and J. F. Harrod. Can. J. Chem. **70**, 107 (1992).

In the presence of cuprous chloride, hydrosilanes and primary amines react to give silazanes. Methylphenylsilane reacts with (R)-(+)-α-methylbenzylamine to give the two diastereomeric monosilazanes as the only products. Aniline and benzylamine react with methylphenyl- and diphenylsilanes to give primarily the monosilazane, disilazane, or diazasilane as the main product, depending on the reactant ratios. Phenylsilane gives higher oligomers with aniline, mainly the trisilatriazane and trisiladiazanes, but no high molecular weight material.

Key words: silanes, amines, silazanes, cuprous chloride, dehydrocoupling, catalysis.

H. Q. Liu et J. F. Harrod. Can. J. Chem. **70**, 107 (1992).

En présence de chlorure cuivreux, les hydrosilanes et les amines primaires réagissent pour donner des silazanes. Le méthylphénylsilane réagit avec la (R)-(+)-α-méthylbenzylamine pour donner uniquement les deux monosilazanes diastéréoisomères. L'aniline et la benzylamine réagissent avec les méthylphényl- et diphénylsilanes et, suivant les rapport des réactifs, il se forme surtout des monosilazanes, des disilazanes ou des diazasilanes comme produits principaux. La réaction du phénylsilane avec l'aniline conduit à la formation d'oligomères, principalement le trisilatriazane et les trisiladiazanes; toutefois, il ne se forme pas de produits de poids moléculaires élevés.

Mots clés : silanes, amines, silazanes, chlorure cuivreux, couplage déshydrogénant, catalyse.

[Traduit par la rédaction]

Introduction

The potential use of polysilazanes as precursors to Si_3N_4 has stimulated the search for new methods for their synthesis (for general reviews, see ref. 1). Dehydrocoupling of silanes with amines is an attractive reaction, producing a relatively benign and light by-product, hydrogen. In general, the uncatalyzed reaction is too slow to be useful under any reasonable reaction conditions and hence requires catalysis. Strong bases are effective catalysts in certain cases (2, 3). In addition, a few transition metal catalysts have been found to work for the catalytic dehydrocoupling of silanes and primary or secondary amines. The most reactive catalysts are $Ru_3(CO)_{12}$, developed by Laine and co-workers (4–8), and $PdCl_2$, studied by Kinsley (9).

During our investigation of the dehydrocoupling reaction between silanes and acetylenic compounds, in the presence of an amine/copper(I) chloride catalyst (10), it was found that, besides the dehydrocoupling reaction of the silane with the acetylene, a dehydrocoupling reaction between silane and amine could also take place. This was particularly apparent when we tried to influence the stereochemical outcome of certain acetylene reactions through the use of a chiral secondary amine. We report here our ensuing investigation of copper(I) as a catalyst for the coupling of a variety of organosilanes and amines.

Results and discussion

In the presence of copper(I) chloride, the reaction of phenylmethylsilane and (R)-(+)-α-methylbenzylamine leads to the formation of the silazane in very good yield. In a typical reaction (mole ratio of silane:amine:CuCl = 1:1:0.067) after 21 h at 100°C an 84% conversion to a mixture of the two diastereoisomers, **1** and **2** was obtained (roughly 1:1 ratio by NMR integration of Si-H resonances at δ = 4.96 and 5.01). In the absence of catalyst, there was no detectable reaction under these conditions.

The reaction of phenylmethylsilane with benzylamine proceeds in essentially the same way as α-methylbenzylamine and leads to the formation of HPhMeSiNHBz, **3**, PhMeHSiN(Bz)SiHPhMe, **4**, and BzNHSi(PhMe)NHBz, **5**, in ratios depending on the initial molar ratio of silane to amine. With an equimolar ratio, the major product is **3**; with a molar ratio of 2:1, after extended reaction time, **4** is the only product, and with a molar ratio 1:2, and long reaction time, **5** is obtained in high yield (Table 1). The results from the reactions of equimolar amine and silane clearly show that the residual NH of **3** has a higher reactivity with methylphenylsilane than does the residual SiH of **3** with benzylamine. This effect allows the production of **4** in near quantitative yields if the reaction is run in the presence of a considerable excess of silane. On the other hand, the low reactivity of the residual SiH of **3** allows the clear demonstration of a stepwise passage from silazane to diazasilane when the reaction is run in the presence of excess amine. Again, there is essentially no reaction in the absence of catalyst.

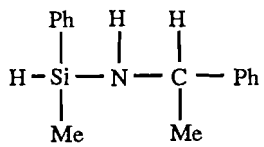

1, R,R; **2**, S,R

From Table 1, for the reactions with equimolar silane and amine, changes in reaction temperature or catalyst ratio do not have a significant effect on the formation of **5**. In addition, with a molar ratio of silane to amine of 1:2, the reaction took 3 days for complete conversion to **5**, while under otherwise similar conditions, the 2:1 molar ratio reaction, which yields mostly **4**, was complete in 21 h. It thus appears that the very low reactivity of the trisubstituted SiH intermediate with another NH bond is the major rate limiting factor, and the one which accounts for the failure of this combination of reactants to give polymers, or higher oligomers.

The reaction of diphenylsilane and benzylamine is similar to that of phenylmethylsilane and benzylamine. In toluene at reflux, the product is mainly $Ph_2HSiNHBz$, **6**, in the

Can. J. Chem. Downloaded from www.nrcresearchpress.com by 123.30.183.119 on 09/08/12
For personal use only.

TABLE 1. Dehydrocoupling reactions of phenylmethylsilane and benzylamine

$[PhMeSiH_2]/[BzNH_2]$	[Amine][a] M	[CuCl] M	T (°C)	t (h)	Main products[b] 3	4	5
3.8/4.3	—	0.26	110	8	53	34	0
3.8/3.8	0.26 (TMEDA)	0.26	145	9	49	28	4
1.5/1.5	1.75 (Bu_3N)	0.76	120	8	15	68	4
4.8/2.4	0.33 (Bu_3N)	0.33	107	6	6[c]	80	0
2.6/5.9	—	0.18	105	6	81	0	7
2.6/5.9	—	0.18	105	67	0	0	100

[a]Tertiary amine added as cocatalyst had little or no effect.
[b]The percentages are based on the conversion of phenylmethylsilane. The difference from 100% is due to unreacted silane.
[c]After 21 h, **4** is the only coupling product.

TABLE 2. Evolution of the coupling reaction between diphenylsilane and benzylamine[a]

t (h)	Conversion of Ph_2SiH_2(M%)	Composition of product (M%) 6	7	8
5	60	94	3	3
17	83	71	18	11
24	86	59	26	15

[a]$[Ph_2SiH_2]$ = $[PhCH_2NH_2]$ = 1.94 M; [CuCl] = [TMEDA] = 0.43 M; solvent: toluene; T: reflux.

first stage. Subsequently, the remaining monomers react with **6** to form $Ph_2HSiN(Bz)SiHPh_2$, **7**, and $BzHNSiPh_2NHBz$, **8**, (see Table 2). From the evolution of these reactions, it is again evident that the secondary silanes are much more reactive than the tertiary ones resulting from the coupling reaction, and the reactant primary amine is more reactive than the secondary one produced by the coupling reaction.

The above results indicate that high coupling reactivity requires a minimum of substitution on both the silane and the amine. This expectation is to some degree borne out by the results for reactions of phenylsilane with benzylamine and aniline. These reactions lead, in addition to the silazanes and disilazanes, to oligomers of somewhat higher molecular weight than are achievable with the secondary silanes. As is evident from the results listed in Table 3, the trisilatriazane, **9**, and trisiladiazane, **10**, can be the major products under appropriate reaction conditions. It should be noted, however, that very high CuCl concentrations are needed to produce higher oligomers. Using an equimolar mixture of reactants at 110°C, a near quantitative conversion of phenylsilane and aniline to 1,2-diphenylsilazane was achieved in 1 h, a rate that is not significantly different from the rates of silazane formation from the secondary silanes. One can therefore conclude that there is not a significant difference in reactivity between primary and secondary silanes, with respect to formation of the first SiN bond (see Table 4). However, the $RSiH_2$-N species retain sufficient reactivity to couple further with amine, while the R_2SiH-N species do not.

The reaction mechanism

The most probable mechanism for the CuCl-catalyzed cross-coupling of Si-H and N-H is a σ-bond metathesis involving a four center intermediate of the type:

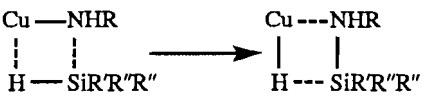

This type of intermediate is highly congested and analogous σ-bond metatheses also exhibit the kind of sensitivity to steric effects manifest in the present reactions (11). Although the above reaction is believed to be the productive step in dehydrocoupling, a number of other metatheses are probably occurring in the system as well, those shown in reactions [1]–[4] being of some possible importance.

[1] $R_1R_2R_3SiH + CuCl \rightarrow R_1R_2R_3SiCl + CuH$

[2] $RNH_2 + CuH \rightarrow RNHCu + H_2$

[3] $R_1R_2R_3SiH + CuH \rightarrow R_1R_2R_3SiCu + H_2$

[4] $R_1R_2R_3SiCu + RNH_2 \rightarrow CuH + R_1R_2R_3SiNHR$

Reaction [1] is known (12). We have established that preprepared CuH functions identically to CuCl as a catalyst and liberates hydrogen when heated with amines. We presently prefer [2] as the H_2-releasing step, although [3] cannot be excluded on the basis of presently available data. Silyl complexes of Cu(I) are known (13), but thermodynamics would appear to favour [2] over [4].

Conclusions

The CuCl-catalyzed coupling of silanes and amines provides a useful new route to the formation of Si-N bonds. Although this method works well for the synthesis of simple molecules, the activity is not high enough to permit the synthesis of high molecular weight polysilazanes. Given the reactivity patterns observed in the present study, it seems unlikely that copper-based catalysts will prove useful for polymer synthesis. However, the cost factor, relative to noble metal catalysts, certainly favours their use for the synthesis of simple silazanes.

Can. J. Chem. Downloaded from www.nrcresearchpress.com by 123.30.183.119 on 09/08/12
For personal use only.

TABLE 3. Dehydrocoupling polymerization of phenylsilane with aniline[a]

$[PhSiH_3]$ (M)	$[PhNH_2]$ (M)	$[Bu_3N]$ (M)	CuCl (M)	Solvent	T^b (°C)	t (h)	Product (mw[c])
4.6	4.6	—	0.29	—	110	1	Silazane
1.4	1.4	—	0.7	Bu_3N	110	5	
					150	15	Oligomer (395, 473)[d]
1.9	1.9	0.48	0.48	Xylene	100	18	
					145	7	Oligomer (248)
1.2	1.2	0.6	0.6	Xylene	145	17	Oligomer (393)[e]

[a]The conversions, based on silane consumption, for these polymerizations were in the range of 70–90%.
[b]Where two temperatures are cited, the reaction was run in two stages, for the times and temperatures indicated.
[c]Molecular weights determined by GPC against polystyrene standards.
[d]In this case, the reaction product separated into two liquid phases on cooling to room temperature. The denser, more viscous phase gave a molecular weight of 473 by GPC analysis and the second phase, after evaporating the volatiles, gave a molecular weight of 395.
[e]The oligomers obtained from this reaction were analyzed by MS and the results indicate the presence of the following ions: m/z (abundance): 592(28) for $[H(PhSiHNPh)_3]^+$, 577(100) for $[H(PhSiHNPh)_2SiPh_2]^+$, and 501(25) for $[H(PhSiHNPh)_2SiPhH]^+$.

TABLE 4. Comparison study of the coupling reaction of phenylsilane and phenylmethylsilane with benzylamine or aniline (t = 1 h)

Silane (M)	Amine (M)	CuCl (M)	T (°C)	Conversion[a] (%)
$PhSiH_3$(4.3)	$BzNH_2$(4.3)	0.27	110	68
$PhSiH_3$(4.6)	$PhNH_2$(4.6)	0.29	110	90
$PhMeSiH_2$(4.0)	$BzNH_2$(4.0)	0.26	105	100
$PhMeSiH_2$(4.4)	$PhNH_2$(4.4)	0.28	105	100
			80	55
			50	29

[a]Based on silanes.

Experimental

Materials and analytical methods

Phenylsilane, phenylmethylsilane, and diphenylsilane were prepared using a literature method (14). Benzylamine, aniline, butylamine, TMED, tributylamine, and (R)-(+)-α-methylbenzylamine (Aldrich Chemical Co.) were distilled from dry NaOH pellets immediately prior to use. CuCl (Anachemia) was used as received. CuH was prepared using a literature method (15). Tetrahydrofuran, toluene, and xylene were distilled from sodium.

^1H NMR spectra were recorded on a Varian XL-200FT spectrometer. Mass spectra were measured on a HP-5980A mass spectrometer using chemical ionization (NH_3). The molecular weights of polymers were measured on a Varian 5000 gel permeation chromatograph, equipped with a Waters Ultrastyragel 1000 Å column at 35°C. The carrier solvent was chloroform for the oligomers of phenylsilane with aniline, or benzylamine, and tetrahydrofuran for the products of the diphenyl- and phenylmethylsilane reactions. Polystyrene standards were used for calibration.

Reactions of diphenyl- and phenylmethylsilane with (R)-(+)-α-methylbenzylamine, aniline, and benzylamine

The reactions reported in Tables 1 and 2 were run by mixing reactants, catalyst, and (in the case of Table 2) solvent in a round bottomed flask and heating for the required length of time under an atmosphere of argon. On completion of the reactions, catalyst was removed by precipitation on cooling to room temperature, followed by filtration. Volatiles were removed by pumping and the residues were analyzed by a combination of GC/MS, ^1H NMR, and GPC. The products **4** and **5** were separated by vacuum distillation (135–140°C and 155–160°C at 0.01 Torr (133.3 Pa)). Some NMR and MS data for the products are listed in Table 5.

Copolymerization of phenylsilane and aniline

Phenylsilane (1 mL), aniline (0.73 mL), CuCl (400 mg), and xylene (4 mL) were introduced into an evacuated flask, equipped with a condenser and a gas inlet. The mixture was heated at reflux under nitrogen for 20 h. After cooling to room temperature to precipitate the catalyst, the liquid layer was decanted into a Schlenk tube and the volatiles were distilled off under vacuum at 100°C to give a very viscous yellow–orange gum (1.2 g, yield: 70%). The progress of the reaction was monitored by periodic sampling and

TABLE 5. ^1H NMR and MS data of selected coupling products[a]

Compounds	δSi-H	δSi-CH_3	δCH_2	δN-H	M^+(abundance)
PhMeSiHNHCHMePh (RR,RS)	4.96; 5.01(2xq)	0.4(2xd)	—	—	
$Ph_2HSiNHBz$	5.6(d)	—	4.2(d)	1.5(t)	
$(Ph_2HSi)_2NBz$	5.6(s)	—	4.5(s)	—	
$(BzHN)_2SiPh_2$	—	—	4.3(d)	1.8(t)	
$(BzHN)_2SiPhMe$	—	0.4(s)	4.1(s)	—	333(37)
					241(54)
					225(86)
$(PhMeHSi)_2NBz$	5.3(m)	0.62(d)	4.3(S)	—	348(19)
					269(30)
					195(100)

[a]s: singlet; d: doublet; t: triplet; q: quartet; m: multiplet.

Can. J. Chem. Downloaded from www.nrcresearchpress.com by 123.30.183.119 on 09/08/12
For personal use only.

following the disappearance of the Si-H resonance at 4.6 ppm by ^{1}H NMR.

1. (*a*) R. M. Laine, Y. D. Blum, D. Tse, and R. Glaser. *In* Inorganic and organometallic polymers. Am. Chem. Soc. Symp. Ser. No. 360, American Chemical Society, Washington, DC. 1988. p. 124; (*b*) R. M. Laine. Platinum Met. Rev. **32**, 64 (1988).
2. B. N. Dolgov, N. P. Kharatmov, and M. G. Voronkov. J. Gen. Chem. Moscow, **24**, 578 (1954).
3. W. Fink. Angew. Chem. Int. Ed. Engl. **5**, 760 (1966).
4. C. Biran, Y. D. Blum, R. Glaser, D. S. Tse, K. A. Youngdahl, and R. M. Laine. J. Mol. Catal. **48**, 183 (1988).
5. Y. D. Blum and R. M. Laine. Organometallics, **5**, 2081 (1986).
6. Y. D. Blum, R. M. Laine, K. B. Schartz, D. J. Rowcliffe, R. C. Bening and D. B. Colts. *In* Better ceramics through chemistry. II. *Edited by* C. J. Brinker, D. E. Clark, and D. R. Ulrich. Materials Research Society, Pittsburg. 1986. p. 389.
7. R. M. Laine, Y. D. Blum, R. Hamlin, and A. Chow. *In* Ultrastructure processing of ceramics, glass and composites. II. *Edited by* D. J. Mackenzie and D. R. Ulrich. J. Wiley, New York. 1988. p. 761.
8. A. W. Chow, R. D. Hamlin, Y. Blum, and R. M. Laine. J. Polym. Sci. Part C. Polym. Lett. **26**, 103 (1988).
9. N. Tillman and T. J. Barton. Main Group Metal Chem. **10**, 307 (1987).
10. H. Q. Liu and J. F. Harrod. Can. J. Chem. **68**, 1100 (1990).
11. T. D. Tilley. Comments Inorg. Chem. **10**, 37 (1990).
12. C. Eaborn. Organosilicon compounds. Butterworths, London. 1960. p. 208.
13. H. F. Klein, J. Montag, U. Zucha, U. Floerke, and H. J. Haupt. Inorg. Chim. Acta, **177**, 35 (1990).
14. R. A. Benkeser, H. Landesman, and D. Foster. J. Am. Chem. Soc. **74**, 648 (1952).
15. J. A. Dilts and D. F. Shriver. J. Am. Chem. Soc. **90**, 5769 (1968).

Can. J. Chem. Downloaded from www.nrcresearchpress.com by 123.30.183.119 on 09/08/12
For personal use only.

A MNDO study of planar thioacyl-substituted carbocations

JACK LEON GINSBURG
Department of Chemistry, Saint Mary's University, Halifax, N.S., Canada B3H 3C3

RICHARD FRANCIS LANGLER[1] AND RAJ KUMAR RAHEJA
Department of Chemistry, Mount Allison University, Sackville, N.B., Canada E0A 3C0

AND

LAURA PRECEDO
Department of Chemistry, Florida Institute of Technology, Melbourne, FL 32901, U.S.A.

Received July 19, 1990[2]

JACK LEON GINSBURG, RICHARD FRANCIS LANGLER, RAJ KUMAR RAHEJA, and LAURA PRECEDO. Can. J. Chem, **70**, 111 (1992).

Relative gas phase stabilities of pairs of planar regioisomeric thioacyl-substituted carbocations have been calculated using the MNDO method. These systems are stabilized by good π donors. The role of S π-electron population as a gauge of substituent effects is examined. Similar results were obtained using isodesmic reactions to gauge substituent effects. Results of this and earlier studies are consistent with the resonance saturation effect.

Key words: semiempirical calculations, carbonium ions.

JACK LEON GINSBURG, RICHARD FRANCIS LANGLER, RAJ KUMAR RAHEJA et LAURA PRECEDO. Can. J. Chem. **70**, 111 (1992).

Utilisant la méthode MNDO, on a calculé les stabilités relatives en phase gazeuse de paires de carbocations thioacyles substitués, régio-isomères et plans. Ces systèmes sont stabilisés par de bons donneurs d'électrons π. On a évalué le rôle de la population S d'électrons π comme mesure des effets de substituants. On a obtenu des résultats semblables lorsqu'on a utilisé des réactions isodesmiques comme mesure des effets de substituants. Ces résultats et ceux obtenus au cours d'études antérieures sont en accord avec un effet de saturation par résonance.

Mots clès : calculs semi-empiriques, carbocations.

[Traduit par la rédaction]

Introduction

The last decade has seen a burgeoning interest in the structures of carbocations which have strongly electron-withdrawing groups directly attached to the cationic center (**1***a–f*) (e.g., NO_2, CF_3, CN, and CO). Of course, stabilized carbocations have also been examined in detail (**1***g–o*).

We have undertaken a computational study of thioacyl-substituted carbonium ions **1** (Z = H) in order to (*i*) explore the relationship between the carbonyl and thiocarbonyl systems and (*ii*) to examine substituent effects in structures which are related to the thionium ions we have described previously (2).

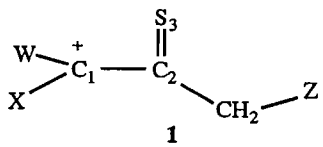

1

	W	X	Z
1*a*	NH_2	H	H
1*b*	H	H	NH_2
1*c*	H	OH	H
1*d*	H	H	OH
1*e*	$CH{=}CH_2$	H	H
1*f*	H	H	$CH{=}CH_2$
1*g*	SH	H	H
1*h*	H	H	SH
1*i*	H	BH_2	H
1*j*	H	H	BH_2
1*k*	H	F	H
1*l*	H	H	F
1*m*	CH_3	H	H
1*n*	H	H	CH_3
1*o*	H	Cl	H
1*p*	H	H	Cl
1*q*	CN	H	H
1*r*	H	H	CN
1*s*	H	CHO	H
1*t*	H	H	CHO
1*u*	CO_2CH_3	H	H
1*v*	H	H	CO_2CH_3
1*w*	CF_3	H	H
1*x*	H	H	CF_3
1*y*	H	H	H

While this study was in progress, Lien and Hopkinson (3) reported computational studies that included thioacyl-substituted carbonium ions **2** (W = H or NH_2).

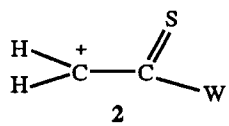

2

Their results permitted a convenient comparison of our MNDO results with high level *ab initio* calculations (6-31G*) and induced us to focus more on our second objective to avoid redundancy.

An examination of the isodesmic reaction [1] by MNDO furnished a $\Delta\Delta H_r$ of 21 kcal/mol, indicating more facile formation of the thioaldehyde cation.

[1]Author to whom correspondence may be addressed.
[2]Revision received August 23, 1991.

Printed in Canada / Imprimé au Canada

Can. J. Chem. Downloaded from www.nrcresearchpress.com by 123.30.183.119 on 09/08/12
For personal use only.

Can. J. Chem. Downloaded from www.nrcresearchpress.com by 123.30.183.119 on 09/08/12
For personal use only.

[1] $CH_2CHS^+ + CH_3CHO \longrightarrow CH_2CHO^+ + CH_3CHS$

Lien and Hopkinson (3) found a $\Delta\Delta H_f$ of 26 kcal/mol at the 6-31G* level.

Furthermore, the MNDO description of the oxycation **3** shows it to have a modest negative charge on oxygen, suggesting that **4** is not a significant resonance contributor.

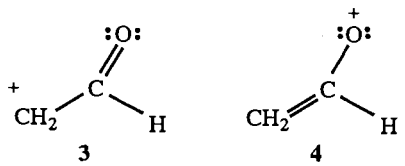

3 **4**

However, the MNDO picture of **2** (W = H) indicates substantial positive charge on sulfur, suggesting that **5** is an important contributor for **2** (W = H).

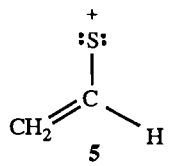

5

MNDO calculated CC bond lengths and π bond orders are in accord with these conclusions. Given the agreement between our MNDO results and the *ab initio* results on these acyl and thioacyl systems, we concluded that MNDO computations would be useful for a study of thioacyl-substituted carbocations **1**.

Lien and Hopkinson (3) have considered the question of open versus bridged cations, viz: **3** vs. **6** and **2** (W = H) vs. **7**.

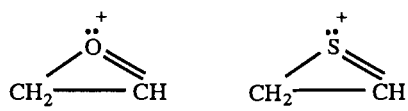

6 **7**

They conclude that sulfur bridges more readily than oxygen and that more heavily substituted structures tend to remain open. Examples of both structural types are known (3) for oxygen and sulfur systems. To confirm that planar thioacyl carbocations are local energy minima, we have examined the energy profile of the unsubstituted cation **2** (W = CH_3), for rotation of the thioacetyl group as depicted in reaction [2].

[2] 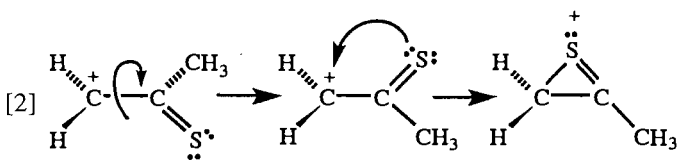

Results for the structure that has the geometry restricted to be planar at C^+ demonstrate that the eclipsed planar cation is at a minimum. Lifting the planarity restriction furnished the results presented in Table 1, which support the same conclusion. Consequently, we have examined acyclic thiocarbonyl-substituted carbocations using the MNDO method.

Method

MNDO computations were done on structures **1** using the improved set of *S* parameters (4). For each cation studied, the WXCCSC framework was constrained to be planar and all other geometric parameters were fully optimized. To permit a direct comparison with our earlier studies, calculations on **1** were also done using the original MNDO *S* parameters (5).

TABLE 1. Energy profile for change in XC_1C_2S (structure **1**) dihedral angle (ϕ)

ϕ (deg)	ΔH_f (kcal/mol)	$<C_1C_2S$ (deg)
180	245.1	120.1
160	245.7	119.8
140	247.4	118.9
120	249.9	117.3
110	251.4	114.9
106	232.9	70.6
100	233.3	71.3

TABLE 2. Calculated relative stabilities of regioisomeric thioacyl-substituted carbocations

Thioacyl carbocation		ΔH_f (kcal/mol)	$\Delta\Delta H_f$[a] (kcal/mol)
1*a*	NH_2	206.0	−41 (−46)
1*b*		247.2	
1*c*	OH	172.0	−29 (−32)
1*d*		200.7	
1*e*	$CH{=}CH_2$	238.6	−25 (−30)
1*f*		263.4	
1*g*	SH	230.1	−22 (−20)
1*h*		252.2	
1*i*	BH_2	241.2	−10 (−14)
1*j*		251.4	
1*k*	F	193.9	−12 (−14)
1*l*		205.8	
1*m*	CH_3	230.1	−9 (−10)
1*n*		239.4	
1*o*	Cl	239.4	−2 (−4)
1*p*		241.8	
1*q*	CN	283.6	−2 (−3)
1*r*		285.9	
1*s*	CHO	220.4	+2 (+2)
1*t*		218.2	
1*u*	CO_2CH_3	173.0	+3 (+4)
1*v*		169.7	
1*w*	CF_3	118.8	+12 (+13)
1*x*		106.9	
1*y*	H	245.1	—

[a]Numbers in parentheses are $\Delta\Delta H_f$ values obtained using the original set of *S* parameters (see Methods section).

As can be seen from Table 2, results obtained using the improved parameters are not significantly different from those obtained by using the original set. The same conclusion was reached for our recent study of S-substituted carbon radicals (6).

Results and Discussion

Relative regioisomeric stabilities

Table 2 presents relative gas phase stabilities, $\Delta\Delta H_f$, of regioisomeric pairs of thioacyl-substituted carbocations. $\Delta\Delta H_f$ is a measure of the stabilizing ability of a substituent relative to that of H. As is the case for thionium ions (2) and for

Can. J. Chem. Downloaded from www.nrcresearchpress.com by 123.30.183.119 on 09/08/12
For personal use only.

TABLE 3. Pertinent π-bond orders for thioacyl-substituted carbocations

Ion		π-Bond orders		
		C_1C_2	C_2S	C_1X/C_1W
1*a*	NH_2	0.31	0.93	0.84
1*b*		0.57	0.81	—
1*c*	OH	0.38	0.90	0.73
1*d*		0.57	0.81	—
1*e*	$CH{=}CH_2$	0.42	0.89	0.61
1*f*		0.59	0.79	—
1*g*	SH	0.43	0.88	0.79
1*h*		0.59	0.79	—
1*i*	BH_2	0.52	0.83	0.28
1*j*		0.59	0.79	—
1*k*	F	0.48	0.85	0.57
1*l*		0.58	0.80	—
1*m*	CH_3	0.53	0.83	0.29
1*n*		0.59	0.79	—
1*o*	Cl	0.54	0.81	0.50
1*p*		0.58	0.79	—
1*q*	CN	0.57	0.80	0.33
1*r*		0.59	0.79	—
1*s*	CHO	0.59	0.78	0.16
1*t*		0.58	0.80	—
1*u*	CO_2CH_3	0.62	0.76	0.19
1*v*		0.59	0.79	—
1*w*	CF_3	0.67	0.72	0.08
1*x*		0.59	0.79	—
1*y*	H	0.59	0.79	—

carbocations (7), there is no correlation between $\Delta\Delta H_f$ values and substituent electronegativities.

Examination of Table 3 indicates that stabilization is strongly related to the substituent's π-bonding ability as determined by substituent—C_1 π bond orders and by the differences between regioisomeric C_1—C_2 π bond orders. Thus, NH_2, the most strongly stabilizing substituent, has the largest substituent—C_1 π-bond order and the greatest weakening effect on the C_1—C_2 bond as measured by the difference between C_1—C_2 π-bond orders in the regioisomers. In general, the more strongly stabilizing substituents have relatively large substituent—C_1 π-bond orders while the destabilizing substituents have negligible substituent—C_1 π-bond orders. Also, stabilizing substituents weaken the C_1—C_2 π bond but destabilizing substituents have the opposite effect. There is a good inverse correlation between the stabilizing ability of the substituent and the weakening of the C_1—C_2 π bond. These results are consistent with those obtained for thionium ions (2) and carbocations (7).

Also consistent with thionium ion results is the fact that the π-electron population at S in the sp^2-substituted regioisomer is a much better indicator of the order and relative magnitudes of the $\Delta\Delta H_f$ values than is the π-electron population at C_1 (see Table 4).

Substituent stabilization of thioacyl carbocations

In order to verify our premise that $\Delta\Delta H_f$ is a measure of the stabilizing ability of a substituent, we have computed substituent stabilization effects directly by means of the following reaction.

[3] $XCH_2C(S)CH_3 + {}^+CH_2C(S)CH_3 \rightarrow {}^+CHXC(S)CH_3 + CH_3C(S)CH_3$

TABLE 4. Selected π-electron populations for thioacyl substituted carbocations **1**

Ion		π-Electron population	
		C_1	S
1*a*	NH_2	0.61	0.90
1*b*		0.32	0.65
1*c*	OH	0.51	0.81
1*d*		0.31	0.63
1*e*	$CH{=}CH_2$	0.53	0.83
1*f*		0.34	0.63
1*g*	SH	0.66	0.82
1*h*		0.34	0.61
1*i*	BH_2	0.37	0.70
1*j*		0.35	0.64
1*k*	F	0.46	0.70
1*l*		0.32	0.60
1*m*	CH_3	0.37	0.69
1*n*		0.34	0.62
1*o*	Cl	0.47	0.67
1*p*		0.32	0.60
1*q*	CN	0.43	0.64
1*r*		0.33	0.60
1*s*	CHO	0.38	0.62
1*t*		0.33	0.63
1*u*	CO_2CH_3	0.41	0.58
1*v*		0.33	0.62
1*w*	CF_3	0.45	0.52
1*x*		0.32	0.58
1*y*	H	0.34	0.62

TABLE 5. Substituent stabilization of thioacyl-substituted carbocations obtained using thioketone heats of formation

$\Delta H_f(X{-}H_2CCSCH_3)$ (kcal/mol)	*X*	ΔH_r[a] (kcal/mol)
9.2	H	—
15.5	NH_2	−45
−32.5	OH	−37
29.3	C_2H_3	−27
16.6	SH	−22
16.0	BH_2	−11
−33.7	F	−8
4.6	CH_3	−10
1.9	Cl	+2
44.9	CN	+3
−17.9	CHO	+2
−67.6	CO_2CH_3	+5
−13.4	CF_3	+18

[a] $XCH_2C(S)CH_3 + {}^+CH_2C(S)CH_3 \rightarrow {}^+XCHC(S)CH_3 + CH_3C(S)CH_3$

Results are given in Table 5. These results are in good agreement with the corresponding $\Delta\Delta H_f$'s, Table 2.

Sulfur π-electron population as a gauge of substituent stabilization effects

The planar thioacyl-substituted carbocation structures **1** may be described by a modest set of resonance contributors.

TABLE 6. Ionic bond orders for destabilizing substituents

Ion		C_1 ionic bond orders[a] C_1X	C_1H	C_1C_2	Sum of C_1 ionic bond orders (au)
1*s*	CHO	−0.024	−0.019	−0.042	−0.001
1*t*	CHO	−0.025	−0.023	+0.063	+0.015
1*u*	CO_2CH_3	−0.042	−0.020	+0.005	−0.007
1*v*	CO_2CH_3	−0.023	−0.024	+0.063	+0.016
1*w*	CF_3	−0.060	−0.022	+0.042	−0.040
1*x*	CF_3	−0.026	−0.024	+0.070	+0.020

[a]Ionic bond orders p^1 are defined (8, 9) as $P^1_{AB} = -q_Aq_B/R_{AB}$ where q_A = atomic charge on A, q_B = atomic charge on B, and R_{AB} = AB bond length.

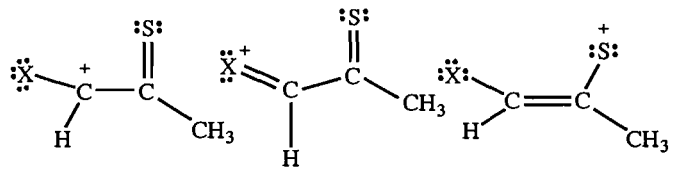

8 **9** **10**

As X becomes a better π donor, the relative importance of **10** is diminished leading to reduced charge on sulfur. For very poor π donors, X, contributor **10** becomes important and **9** is deemphasized. Thus the π-electron population at S is a useful measure of the stabilizing ability of X. It has the not inconsiderable advantage that it does not require a quantitative assessment of the significance of $2p$–$3p$ π bonding (e.g., Cl—C_1) versus $2p$–$2p$ π bonding (e.g., NH_2—C_1) in order to gauge substituent effects. Such an assessment would be required, for example, were one to attempt to use C_1—X π-bond orders to anticipate substituent stabilization effects (see Table 3).

Polarization destabilization

In accordance with our earlier carbocation study (7), we find that the destabilizing effects of CHO, CO_2CH_3, and CF_3 are not related to inductive effects. When positioned at C_1, CHO, CO_2CH_3, and CF_3 donate 0.18, 0.08, and 0.07 net electrons, respectively, to the CSC^+ moiety. Neither are their destabilizing effects related to the π-electron population at C_1. Each of the destabilizing substituents leads to π-electron populations at C_1 similar to those for CH_3 and BH_2 (see Table 4).

Our study of S-substituted radicals (6) led to the conclusion that the CF_3 group is a polarization stabilizer when attached to radical carbon but a polarization destabilizer when attached to positively charged carbon. CF_3 was also found to be a polarization destabilizer for carbocations (7).

Table 6 presents ionic bond orders (8, 9*a*), involving C_1 for the destabilizing substituents. A consideration of the differences in total ionic bond order at C_1 for pairs of regioisomers e.g., **1***w*, **1***x* indicates that polarization effects are dominant in the absence of strong π-bonding effects.

Hyperconjugation in **1**m *and* **1**i

As expected, hyperconjugation is an important stabilizing mechanism for the CH_3 group. The optimized geometry for **1***i* has the BH_2 unit perpendicular to the plane containing the BC_1C_2 unit. This geometry is calculated to be 15 kcal/mol more stable than the geometry having the BH_2 unit coplanar with the BC_1C_2 unit. We conclude that the BH_2 group stabilizes the thioacyl-substituted cations by a hyperconjugative effect. This is in accord with the *ab initio* results on simpler systems (9*b*). Comparison of $\Delta\Delta H_f$'s, π-bond orders, and π-electron populations at S leads to the conclusion that the hyperconjugative effects of BH_2 and CH_3 have the same order of magnitude.

Substituent effects in propyl carbocations (7), thionium ions (2), and thioacyl carbocations

Comparison of $\Delta\Delta H_f$ values and other relevant parameters for common sets of substituents shows that substituent effects are qualitatively similar for all three systems. For example, NH_2 is by far the best stabilizer of the thioacyl carbocations and of the propyl carbocation systems and is also the best π bonder in each system. CF_3 is the most destabilizing substituent in all three systems. The regioisomer in which CF_3 is positioned at the sp^2 carbon has the most negative π-bond order at that carbon. In general, the order of $\Delta\Delta H_f$ values and π-bonding parameters is similar for those substituents which are common to all three of our studies.

We can now present an overview of our MNDO studies on carbocations. For good π bonders there is a decrease in their stabilizing abilities as one goes from propyl carbocations **11** to thioacyl carbocations **8** to thionium ions **12**.

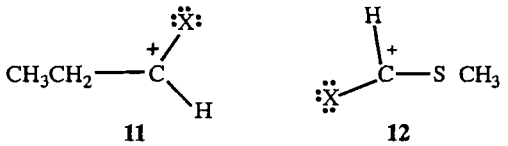

11 **12**

For example, $\Delta\Delta H_f$ for OH increases from −37 kcal/mol to −32 kcal/mol to −20 kcal/mol.[3] In terms of the isodesmic reaction shown in reaction [4] (R_i = C_2H_5 or $C(S)CH_3$ or SCH_3)

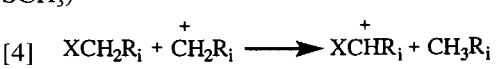

[4]

the stabilizing ability of X decreases as the stabilizing ability of R_i increases. This trend exemplifies the resonance saturation effect (10).

Frontier orbital analysis

The present study has created an opportunity to explore the possibility that some thioacyl carbocations might be expected to develop significant electrophilicity at sulfur. Such cations might serve as precursors in new preparations of vinyl sulfides. Both this novel potential behaviour and the "usual" expected outcome for thioacyl-substituted carbocations reacting with nucleophiles are shown below:

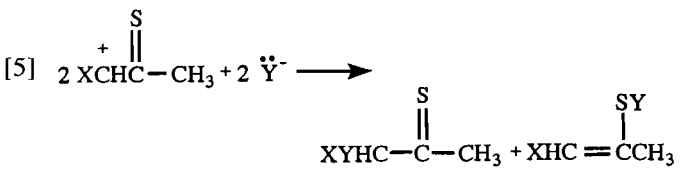

[5]

In order to explore the balance expected for these processes, we have calculated population numbers for the cation LUMO's, which are presented in Table 7. These population numbers indicate the preferred site for nucleophilic attack in accord with frontier orbital arguments (11).

The results in Table 7 permit two generalizations: (*i*) introduction of good electron donors (W or X in **1**), e.g., OH

[3]These numbers were obtained with the original *S* parameters.

Can. J. Chem. Downloaded from www.nrcresearchpress.com by 123.30.183.119 on 09/08/12
For personal use only.

TABLE 7. LUMO population numbers[a] for ions **1**

X	C_1	C_2	S_3	Additional atom
H	0.47	0.02	0.50	
Cl	0.49	0.01	0.43	Cl (0.06)
OH	0.47	0.05	0.34	O (0.13)
SH	0.47	0.02	0.30	S (0.21)
F	0.50	0.02	0.40	F (0.08)
NC	0.48	0.01	0.43	N (0.08)
CH_3CO_2	0.47	0.00	0.48	O[c] (0.03)
CHO	0.48	0.02	0.49	
C_2H_3	0.43	0.01	0.25	C[b] (0.30)
CF_3	0.45	0.01	0.54	
CH_3	0.50	0.02	0.43	
NH_2	0.38	0.09	0.34	N (0.18)
BH_2	0.50	0.02	0.43	

[a]Only the larger population numbers are included for each ion **1**.
[b]Terminal methylene of the vinyl group.
[c]O doubly bonded to C_1.

and NH_2, suppresses electrophilicity at sulfur and (*ii*) strong electron withdrawers (W or X in **1**), e.g., CO_2CH_3 and CF_3, maintain pronounced electrophilicity at sulfur.

Conclusions

1. Thioacyl-substituted carbocations are stabilized by good π donors.

2. Substituent stabilizing ability correlates well with electron population at S. Resonance contributor **10** is especially important for thioacyl systems in which the C^+ bears a poor π donor.

3. Inductive effects do not correlate with the destabilization of carbocationic species in which the C^+ bears -CHO or $-CO_2CH_3$ or CF_3. In these cases polarization effects dominate.

4. Both $-BH_2$ and $-CH_3$ stabilize carbocations through a hyperconjugative effect.

5. There is pronounced electrophilicity at thiocarbonyl sulfur in those cations in which the C^+ bears a strongly electron-withdrawing group.

1. (*a*) X. Creary. Acc. Chem. Res. **18**, 3 (1985); (*b*) P. G. Gassman and T. T. Tidwell. Acc. Chem. Res. **16**, 279 (1983); (*c*) T. T. Tidwell. Angew. Chem. Int. Ed. Engl. **23**, 20 (1984); (*d*) X. Creary and T. E. Aldridge. J. Org. Chem. **53**, 3888 (1988); (*e*) F. J. Ablenas, B. E. George, M. Maleki, R. Jain, A. C. Hopkinson, and E. Lee-Ruff. Can. J. Chem. **65**, 1800 (1987); (*f*) G. A. Olah, G. K. S. Prakash, M. Arvanaghi, V. V. Krishnamurthy, and S. C. Narang. J. Am. Chem. Soc. **106**, 1628 (1984); (*g*) A. Pross and L. Radom. Aust. J. Chem. **33**, 241 (1980); (*h*) X. Creary, M. E. Merhrsheikh-Mohammadi, and M. D. Eggers. J. Am. Chem. Soc. **109**, 2435 (1987); (*i*) J. A. Pople, Y. Apeloig, and P. v. R. Schleyer. Chem. Phys. Lett. **85**, 489 (1982); (*j*) A. C. Hopkinson and M. H. Lien. Can. J. Chem. **63**, 3582 (1985); (*k*) M. H. Lien and A. C. Hopkinson. J. Mol. Struct. (Theochem), **121**, 1 (1985); (*l*) M. Dorado, O. Mo, and M. Yanez. J. Am. Chem. Soc. **102**, 947 (1980); (*m*) C. F. Rodriquez and A. C. Hopkinson. J. Mol. Struct. (Theochem), **152**, 55 (1987); (*n*) C. F. Rodriquez and A. C. Hopkinson. J. Mol. Struct. (Theochem), **152**, 69 (1987); (*o*) J. C. White, R. J. Cave, and E. R. Davidson. J. Am. Chem. Soc. **110**, 6308 (1988).
2. J. L. Ginsburg and R. F. Langler. Can. J. Chem. **61**, 589 (1983).
3. M. H. Lien and A. C. Hopkinson. J. Am. Chem. Soc. **110**, 3788 (1988) and references therein.
4. (*a*) M. J. S. Dewar and C. S. Reynolds. J. Comput. Chem. **7**, 140 (1986); (*b*) Quantum Chemistry Program Exchange. Program No. 455.
5. M. J. S. Dewar, M. L. McKee, and H. S. Repza. J. Am. Chem. Soc. **100**, 3607 (1978).
6. J. L. Ginsburg, J. C. Baum, and R. F. Langler. J. Phys. Chem. **94**, 1750 (1990).
7. A. M. Aissani, J. C. Baum, R. F. Langler, and J. L. Ginsburg. Can. J. Chem. **64**, 532 (1986).
8. R. S. Mulliken. J. Chem. Phys. **23**, 1841 (1955).
9. (*a*) M. H. Whangbo, S. Wolfe, and F. Bernardi. Can. J. Chem. **53**, 3040 (1975); (*b*) Y. Apeloig, P. v. R. Schleyer, and J. H. Pople. J. Am. Chem. Soc. **99**, 1291 (1977).
10. F. G. Bordwell, J. E. Bares, J. E. Bartmess, G. J. McCollum, M. Van der Puy, N. R. Vanier, and W. S. Matthews. J. Org. Chem. **42**, 321 (1977).
11. I. Fleming. Frontier orbitals and organic chemical reactions. Wiley, London. 1976.

Can. J. Chem. Downloaded from www.nrcresearchpress.com by 123.30.183.119 on 09/08/12
For personal use only.

Electron paramagnetic resonance study of the reactions of the spin trap 2,4,6-tribromonitrosobenzene in benzene solutions

PETER SMITH,[1] KIRK RANDALL MAPLES, AND RAMONA LILLIAN LAU
Paul M. Gross Chemical Laboratory, Department of Chemistry, Duke University, Durham, NC 27706, U.S.A.

Received July 24, 1991

PETER SMITH, KIRK RANDALL MAPLES, and RAMONA LILLIAN LAU. Can. J. Chem. **70**, 116 (1992).

By means of static-sample studies involving the thermal decomposition of symmetric azo compounds and the oxidation of substrates with nickel peroxide, we have characterized by electron paramagnetic resonance 12 spin adducts of 2,4,6-tribromonitrosobenzene, **1**, in benzene at 25°C. In addition, we have used electron paramagnetic resonance spectroscopy to investigate benzene solutions of **1** both by itself and in the presence of olefins, and both in the presence and absence of light. Although **1** by itself did not give evidence for any free radical formation, when **1** was mixed with any one of the 11 olefins tested we could detect nitroxide formation. The presence of light did not affect our results. These observations support the "ene" reaction mechanism of nitroxide formation.

Key words: 2,4,6-tribromonitrosobenzene, spin trapping, nickel peroxide.

PETER SMITH, KIRK RANDALL MAPLES et RAMONA LILLIAN LAU. Can. J. Chem. **70**, 116 (1992).

Faisant appel à des études de résonance paramagnétique électronique (rpe) sur des échantillons statiques impliquant la décomposition thermique des composés azo symétriques et l'oxydation de substrats avec le peroxyde de nickel, on a caractérisé 12 adduits de spin du 2,4,6-tribromonitrobenzène, **1**, dans le benzène, à 25°C. De plus, on a utilisé la rpe pour étudier des solutions benzéniques du composé **1** soit seul ou en présence d'oléfines, tant en présence qu'en absence de lumière. Même si le composé **1** seul ne semble pas donner naissance à la formation de radicaux libres, on a pu détecter la présence de nitroxydes à chaque fois que le composé **1** a été mélangé avec l'une des 11 oléfines étudiées. La présence de lumière ne modifie pas nos résultats. Ces résultats sont en accord avec un mécanisme de réaction «ène» pour la formation du nitroxyde.

Mots clés : 2,4,6-tribromonitrobenzène, piégeage de radicaux, peroxyde de nickel.

[Traduit par la rédaction]

Introduction

The electron paramagnetic resonance, epr, technique of spin trapping has become a useful tool for studying a highly reactive radical, R•, in solution where the steady-state concentration is below the usual epr detection limit (1–6). This technique involves including in the reaction system a low concentration of a diamagnetic substance (the spin trap, ST) that reacts readily with R• to form R(ST)•, the spin adduct,

[1] $R^{\bullet} + ST \rightarrow R(ST)^{\bullet}$

The spin adduct must be an especially persistent (7) radical so that its concentration builds to a readily detectable value.

The most frequently used spin traps have been either nitrones or nitroso compounds, the latter generally providing more informative spin-adduct epr spectra than the former. Also, it is well known (1–5) to be advantageous to employ more than one spin trap to attempt to trap a radical of interest. This conclusion follows from the minimal variation of epr splitting constants for adducts of any one spin trap whereas there is greater variation of these constants for adducts of a particular radical with different spin traps. Thus, the introduction of new spin traps whose characteristics will aid in identifying which radical was indeed trapped provides a broader foundation for this technique. To that end, we have investigated the easily synthesized, inexpensive nitroso compound 2,4,6-tribromonitrosobenzene, $Br_3C_6H_2NO$ (which we denote as *Z*-N=O or **1**), in two reaction systems to discover its utility as a spin trap,

[2] $R^{\bullet} + Z\text{-}N{=}O \rightarrow Z\text{-}N(O^{\bullet})\text{-}R$

Employment of this compound as a spin trap has received relatively little attention in the literature (8–10), yet, based on its structure, **1** seems potentially useful. As **1** proved insufficiently soluble in aqueous solution for our use, we have generated radicals in the presence of **1** in benzene and characterized the resultant spin adducts by epr at 25°C. These studies involved using two radical sources, the oxidation of substrates by nickel peroxide (11, 12), and the thermal decomposition of symmetric aliphatic azo compounds (13–15). Also, we studied the reaction of **1** with several olefins. Our results show **1** forms very persistent (7) spin adducts and displays a quite useful variation of epr splitting constants with respect to the radicals trapped. However, **1**, like many nitroso compounds (16–26), reacts on contact with many olefins both in the light and in the dark to yield persistent radicals that could interfere with the analysis of spin adducts.

Experimental

The epr spectrometer, its accessories, and the general experimental arrangements and procedures were essentially as before (27, 28). However, in contrast to the earlier work (27, 28), we examined all solutions at 25.0 ± 1.0°C as static samples. If nonaqueous, these were contained in thin-walled 4 mm i.d. cylindrical Pyrex tubes, whereas, for aqueous solutions, we employed a Varian V-4548 aqueous-solution sample cell. All spectra were recorded as the first derivative with a field-modulation amplitude of 2.0×10^{-1} G. Unless specified otherwise, all water used was deionized tap water (27).

We synthesized 2,4,6-tribromonitrosobenzene, **1**, from 2,4,6-tribromoaniline (Aldrich, used as received) by a standard procedure (29), recrystallized the crystals so prepared from acetone (Reagent, ACS)/doubly distilled water (27) mixtures, mp 122–124°C (lit. (29*b*) mp 122–123°C), and stored the final product in the dark at room temperature until used. Benzene (Fisher, Certified ACS) was purified using H_2SO_4 (Reagent, ACS) by a standard method (30) and then distilled. Nickel peroxide, NiO_2, prepared by standard techniques (11, 12) from nickel sulfate (Mallinckrodt, ACS), contained $4.4_5 \times 10^{-3}$ g-atoms of available oxygen per gram of NiO_2.

[1]Author to whom correspondence may be addressed.

Printed in Canada / Imprimé au Canada

Can. J. Chem. Downloaded from www.nrcresearchpress.com by 123.30.183.119 on 09/08/12
For personal use only.

TABLE 1. Electron paramagnetic resonance data for Z-N(O•)-R spin-adduct radicals resulting from the trapping of R• radicals by **1**[a–c]

Substrate[d]	Spin adduct	Radical trapped, R•	Splitting constants (G) α-N	β-H(CH)	Δg[e]
2	**25**	$CH_3CH_2NHCH_2CH_2^{\bullet}$	12.43(1)	9.47(2)	70
3	**26**	$C_6H_5CH(NH_2)CH_2^{\bullet}$	12.35(2)	8.94(3)	81
4	**27**	$C_6H_5\dot{C}HCN$	12.72(2)	5.87(3)	94
5	**28**	$C_6H_5\dot{C}HCH_3$	12.82(1)	5.23(2)	64
			12.86	5.19	[f]
6	**29**	$C_6H_5\dot{C}HOC(O)CH_3$	12.44(1)	5.22(2)	56
7	**30**	$(CH_3)_2\dot{C}CN$	12.12(1)	—	73
			12.28	—	[g]
8	**31**	$CH_3CH_2(CH_3)\dot{C}CN$	12.21(4)	—	68
9	**32**	$CH(CH_3)_2CH_2(CH_3)\dot{C}CN$	12.32(1)	—	78
10	**33**	$(CH_3CH_2)_2\dot{C}CN$	12.40(1)	—	76
11	**34**	$HOC(O)CH_2CH_2(CH_3)\dot{C}CN$	12.17(1)	—	78
12	**35**	$(CH_3)_3C^{\bullet}$	12.38(1)	—	62
13	**36**	$(CH_3)_2\dot{C}C(O)OCH_3$	11.98(1)	—	71

[a]All protons of a given designation are magnetically equivalent.

[b]Unless stated otherwise, present work: at 25.0 ± 1.0°C; ΔH_{pp}, ca. 2.0 G; half-life, ca. 1.0–8.0 h.

[c]Each number in parentheses is the standard deviation of the mean, σ_{n-1}, times 10^2. The maximum error limits of the *a*-values are ca. ± $2\sigma_{n-1}$.

[d]See Experimental.

[e]Δg = (*g*-value − 2.00600) times 10^5. For each *g*-value, σ_{n-1} is ±0.00001 and the maximum error limit, ±0.00006, based on the reported error limits for the standard, potassium peroxylamine disulfonate in an aqueous solution saturated at room temperature with respect to potassium carbonate (27, 28, 31, 32).

[f]Spectrum observed during the photolysis at 25°C of anthraquinone in ethyl benzene in the presence of **1** and with oxygen excluded (8, 9).

[g]At room temperature; solvent, benzene; the method of generation of **30** was similar to that of the present work except that the reaction mixture was first freed of oxygen (10).

The substrates examined were diethylamine (**2**), (±)-α-methylbenzylamine (**3**), phenylacetonitrile (**4**), ethylbenzene (**5**), benzyl acetate (**6**), 2,2′-azobis-(2-methylpropanonitrile) (**7**), 2,2′-azobis-(2-methylbutanonitrile) (**8**), 2,2′-azobis-(2,4-dimethylpentanonitrile) (**9**), 2,2′-azobis-(2-ethylbutanonitrile) (**10**), 4,4′-azobis-(4-cyanopentanoic acid) (**11**), 2,2′-azobis-(2-methylpropane) (**12**), dimethyl 2,2′-azobis-(2-methylpropanoate) (**13**), methacrylic acid (**14**), methyl methacrylate (**15**), ethyl methacrylate (**16**), *n*-butyl methacrylate (**17**), isodecyl methacrylate (**18**), methacrylonitrile (**19**), methacrylamide (**20**), isopropenyl acetate (**21**), allyl chloride (**22**), allyl alcohol (**23**), and allyl benzoate (**24**). All substrates were either samples available in our laboratory (13), synthesized and purified by standard methods (**8–10**, **13**), or were used as received from Alfa (**12**), Aldrich (**3–5**, **11**, **21**), Fisher (**23**), Kodak (**2**, **7**, **19**, **20**, **22**, **24**), Pfaltz and Bauer (**6**), or Rohm and Haas (**14–18**).

NiO_2 redox studies

The reaction conditions were as follows: to a benzene solution 0.10 M in both **1** and the substrate at 25.0°C, we added 1.0 g of NiO_2 and mechanically stirred the mixture; mixtures reacted for ca. 2.0 min before supernatant samples were transferred into epr tubes for analysis. Control mixtures that did not include either **1** or the substrate were also examined in a like manner, these giving no evidence for adduct formation or any other epr radical signals. We examined each of **2–6** in this way.

Azo-compound thermal decomposition studies

The reaction conditions were as follows: we heated at 60°C for 3 min with stirring benzene solutions 0.025 M in both the azo compound and **1**, then cooled these solutions quickly (ca. 2.0 min) to 25.0°C in a constant temperature bath and analyzed samples by epr. Samples that did not contain either **1** or the azo compound were also examined, these not yielding evidence of adduct formation or any other epr radical signals. All azo compounds, **7–13**, received this treatment.

Direct reaction of **1** *with olefins*

The usual reaction conditions were as follows: we stirred benzene solutions 0.050–0.10 M in **1** and 0.050–0.20 M in olefin at 25.0°C, then removed samples for examination by epr at varying time intervals for each olefin/**1** mixture. These experiments were performed in the presence of normal laboratory light and again under photographic dark-room conditions. Finally, the experiments were initiated under photographic dark-room conditions and then the reaction mixtures were exposed to normal laboratory light. We followed this procedure for each of the olefins, **14–24**.

Photolysis studies

While keeping the temperature at 25.0 ± 1.0°C, we exposed 0.10 M solutions of **1** in benzene for 1–3 h to radiation from either normal laboratory lights, a tungsten filament lamp (Westinghouse, 60 W, 110–125 V) 12 cm from the sample, or by a sun lamp (Kenmore, 275 W, 110–125 V) positioned 10 cm from the sample, and then analyzed samples by epr.

Aqueous-system studies

Although **1** was not noticeably soluble in water, we made attempts to employ **1** as a spin trap in stirred aqueous slurries containing **7**. We heated these at 60°C for 3 min with stirring, cooled them quickly (ca. 2.0 min) to 25.0 ± 1.0°C in a constant temperature bath, and analyzed samples by epr. No evidence for **1** spin-adduct formation was obtained from such experiments.

Results

Table 1 summarizes the epr spectroscopic data obtained for all spin adducts of **1** successfully characterized and includes any comparable results in the literature (8–10).

NiO_2 redox studies

The reaction of NiO_2 with **2–6** yielded epr spectra consistent with the presence of only one spin adduct per sub-

Can. J. Chem. Downloaded from www.nrcresearchpress.com by 123.30.183.119 on 09/08/12
For personal use only.

TABLE 2. Electron paramagnetic resonance data for Z-N(Ȯ)-CH_2-C(R′)=CH(R″) radicals[a–c]

Substrate[d]	Radical	-R′	-R″	Splitting constants (G) α-N	Splitting constants (G) β-H(CH)	Δg[e]
14	**37**	-C(O)OH	-H	12.45(1)	8.74(2)	51
15	**38**	-C(O)OCH_3	-H	12.35(2)	8.51(4)	54
16	**39**	-C(O)OCH_2CH_3	-H	12.34(1)	8.26(2)	53
17	**40**	-C(O)O$(CH_2)_3CH_3$	-H	12.31(3)	8.14(2)	50
18	**41**	-C(O)O$(CH_2)_8CH(CH_3)_2$	-H	12.32(1)	8.14(3)	67
19	**42**	-CN	-H	12.38(1)	9.64(1)	73
20	**43**	-C(O)NH_2	-H	12.74(4)	8.45(4)	70
21	**44**	-$OC(O)CH_3$	-H	12.33(1)	9.16(2)	74
22	**45**	-H	-Cl	12.61(3)	9.83(2)	62
23	**46**	-H	-OH	12.79(2)	11.51(1)	50[f]
24	**47**	-H	-$OC(O)C_6H_5$	12.68(2)	10.29(4)	60

[a]See footnote *a*, Table 1.
[b]At 25.0 ± 1.0°C; ΔH_{pp}, ca. 2.0 G; half-life, ca. 1.0–8.0 h.
[c]See footnote *c*, Table 1.
[d]See footnote *d*, Table 1.
[e]See footnote *e*, Table 1.
[f]The more likely structure for this radical is that of the tautomer Z-N(Ȯ)-CH_2-CH_2-CH(O) (37).

strate. We reasonably attributed the spectra obtained to the **1** spin adducts of the radicals that might be produced from NiO_2 oxidation of **2–6** via hydrogen-atom abstraction (11, 12).

Of the **1** spin adducts characterized in our NiO_2-based work, **28** is the only one previously reported in the literature (8, 9). The earlier reported *a*-values, from studies of the photolysis of anthraquinone at 25°C in ethylbenzene in the presence of **1** (8, 9), and our present results are in good agreement.

Azo-compound thermal decomposition studies

The azo compounds decomposed in the presence of **1** to yield the expected radical spin adducts (14). The only corresponding literature report available for **1** spin adducts observed in this section of our studies is for **30** (10) at room temperature in benzene as solvent. The literature value for a_N, 12.28 G (10), is appreciably larger than our result, 12.12 G, and does not fit the trend in a_N with respect to the size of the alkyl groups of the trapped dialkylcyanomethyl radicals shown by our results; i.e., comparison of the epr data for **30–33** suggests that larger alkyl groups induce a larger a_N value for the **1** spin adduct and an a_N value of 12.28 G seems too large for **30**. We are unable to account for this discrepancy.

We obtained no evidence for the formation and trapping of >Ċ—C≡N radicals in the >C=C=N˙ form (33–35). A similar failure to trap 1-cyano radicals in the ketenimine form has been noted before (15, 26) and is perhaps not surprising as spin traps have not been routinely successful at trapping nitrogen-centered radicals (4).

Direct reaction of 1 with olefins

Previous work has shown that **1** reacted directly with unsubstituted long-chain alkenes in benzene at room temperature to produce persistent nitroxide radicals (36). In accordance with this report, we found that **1** reacted directly with all the substituted-ethylene substrates studied, **14–24**, to yield persistent radicals either in the presence or absence of light, their epr spectra consisting of a (1:1:1) triplet of (1:2:1) triplets, the characteristics of which were independent of room lighting conditions. For reactions of **1** with allyl compounds of structure CH_2=C(R′)CH_2R″, e.g., **14–24**, these radicals probably arise from the "ene" reaction sequence

[3] Z—N=O + CH_2=C(R′)—CH_2R″ → Z—N(OH)—CH_2—C(R′)=CHR″

[4] Z—N(OH)—CH_2—C(R′)=CHR″ $\xrightarrow{[O]}$ Z—N(Ȯ)—CH_2—C(R′)=CHR″

These reactions are analogous to those established (16–26) for the reaction of other nitroso spin traps with similar olefins. To detect a radical from a given allyl compound/**1** mixture, time delays varying from 1 to 30 min between mixing and epr examination were required. In addition, raising the concentration of both reactants above those usually employed produced a more intense epr signal in less time. All olefins examined gave evidence for reaction with **1**, and Table 2 lists the epr spectroscopic data for all radicals obtained.

Photolysis studies

We found no epr-detectable spin adducts in **1**/benzene solutions that were photolysed by either normal laboratory lights, a tungsten filament lamp, or a sun lamp.

Discussion

Although it has been stated that the reactivity of arylnitroso spin traps with olefins is probably not important for the hindered aliphatic and aromatic C-nitroso spin traps usually employed (3), our results show that **1** reacted with many alkenes to produce persistent radicals that could easily interfere with the detection and characterization of concurrently generated spin adducts. This radical formation, coupled with the relative insolubility of **1** in aqueous systems, tends to limit the usefulness of **1** as a spin trap.

However, for studies in nonaqueous solutions, **1**, like other arylnitroso spin traps (1–5, 12, 26), shows nice variation

Can. J. Chem. Downloaded from www.nrcresearchpress.com by 123.30.183.119 on 09/08/12
For personal use only.

Can. J. Chem. Downloaded from www.nrcresearchpress.com by 123.30.183.119 on 09/08/12
For personal use only.

in splitting constants with respect to the radical trapped. For instance, the results given in Table 1 show that the a_N values for the spin adducts from radicals of structure R′(R″)ĊCN, e.g., **27** and **30**, were consistently smaller than those for the analogous R′(R″)ĊCH$_3$ spin-adduct radicals, **28** and **35**, respectively. In addition, the a_N values for the spin adducts of R′(R″)ĊCN radicals where R′ and R″ are relatively small alkyl groups, **30–33**, showed noticeable increases upon extension of the alkyl chains, indicating that the epr spectroscopic data for **1** spin adducts appeared to be quite sensitive to the structure of the radical trapped. These phenomena are a reflection of how readily the nitroxide function responds to the substituents on the nitrogen (38), as illustrated by resonance structures

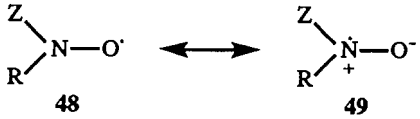

48 **49**

where structure **48** is favored when the R group is electron withdrawing, either −M or −I (39) and will have a lower a_N value than structure **49**, which is favored when the R group is electron donating, +M or +I. Thus, the differences between the a_N values in the spin adducts **27** and **30** and those in **28** and **35**, respectively, arise because the −CN group is electron withdrawing whereas the −CH$_3$ group is electron donating; and the a_N values for the spin adducts **30–33** vary as a consequence of the expected increase in the electron-donating power of the alkyl chains with increase in extension. In addition to the observed dependence of a_N values of Z-N(O·)-R radicals on the electrical properties of the R group, simple steric considerations predict that the $a_{\beta\text{-H}}$(CH) values tend to decrease as the bulkiness of the R group increases (40). All the $a_{\beta\text{-H}}$(CH) data in Table 1, i.e., for the addition radicals **25–29**, appear to follow this trend.

The radicals in Table 2 consist of two types, namely, **37–44**, for which -R′ varies with -R″ remaining the same, and **45–47**, for which the reverse holds. In the case of **37–44**, a_N is approximately constant except for **37** and **43**, in which the a_N values are noticeably larger than for the others. This fits in with the fact that, in all these radicals, -R′ is attached to the γ-C and so might not be expected to strongly affect a_N, in general. This follows because, although the -R′ groups are fairly strongly electron withdrawing (39, 41, 42), their electrical effects on the nitroxide group would be attenuated by the intervening β-CH$_2$ group. The two exceptions to this conclusion, **37** and **43**, have the only -R′ groups that might interact via intramolecular hydrogen bonding with the nitroxide group, thereby causing both a_N and $a_{\beta\text{-H}}$(CH) to increase (43). Inspection of the data shows that the $a_{\beta\text{-H}}$(CH) values for **37** and **43** are indeed relatively large. Simple steric considerations appear to be sufficient to account for the variation in the other $a_{\beta\text{-H}}$(CH) values, e.g., the fact that the $a_{\beta\text{-H}}$(CH) values for **42** and **44** are larger than those of **37** and **43**, and the variation of the $a_{\beta\text{-H}}$(CH) values in the series **37–41**. We would expect the results for **45–47** to be simply relatable to those for **37–44** as in each radical -R″ is attached to the δ-C and so should not have much influence on a_N. Accordingly, as -R′ in **45–47** is −H, which is much less electron withdrawing and bulky than the -R′ groups in **37–41**, it is not surprising that, in general, the a_N and $a_{\beta\text{-H}}$(CH) values in **45–47** are noticeably larger than those in **37–44**. It should be noted that **46** is not of the same structural type as the other radicals in Table 2, this doubtless being the reason its a values are somewhat out of line with those of **45** and **47**.

Chatgilialoglu and Ingold (44) have cautioned that reactions between nitroso compounds and olefins could appear to be spontaneous, when in fact they are photolytic in nature. In their reaction sequence, the aromatic nitroso spin trap, ArNO, is photolysed to yield aryl radicals, which then attack the solvent, benzene, to yield addition radicals, which finally react with the spin trap to give the detected spin adduct

[5] ArNO + visible light → Ar· + NO

[6] 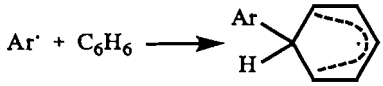

[7] 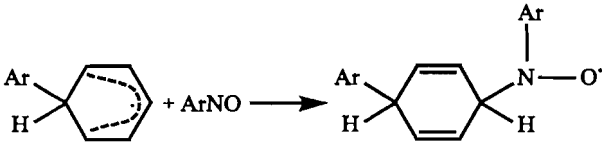

This spin-adduct epr spectrum would be characterized as a (1:1:1) triplet of (1:1) doublets. Our ability to detect nitroxide formation from mixtures of **1** with alkenes under darkroom conditions suggests that the reactions involved in this study are not photolytic, but are due to the "ene" addition reaction. This point is buttressed by our finding no spin adducts in **1**/benzene solutions that were directly photolysed. In addition, our **1** spin adducts generated using the alkenes all exhibited epr spectra characterized as a (1:1:1) triplet of (1:2:1) triplets, which is a different spin adduct epr pattern than that predicted via the photolytic reaction sequence.

In summary, **1** appears not to be light sensitive, can be synthesized easily and inexpensively, and demonstrates a quite useful variation in the spin-adduct splitting constants with respect to the radical trapped. However, in any reaction system that includes alkenes, **1** may react via the "ene" addition reaction to yield nitroxides that could interfere with the interpretation of the resultant epr spectra. Thus, **1** would seem to be an acceptable spin trap for selected systems.

Acknowledgements

We thank Rohm and Haas Company for gift samples of **14–18**, and the National Science Foundation and the North Carolina Board of Science and Technology for financial support. Also, we acknowledge with thanks useful discussions with Drs. Ann G. Motten, Ned A. Porter, Jeno Tomasz, and Pelham Wilder, Jr.

1. E. G. Janzen. Acc. Chem. Res. **4**, 31 (1971).
2. E. G. Janzen and D. L. Haire. Adv. Free Radical Chem. **1**, 253 (1990).
3. M. J. Perkins. Adv. Phys. Org. Chem. **17**, 1 (1980).
4. B. Kalyanaraman. Rev. Biochem. Toxicol. **4**, 73 (1982).
5. R. P. Mason, K. R. Maples, and K. T. Knecht. Electron Spin Reson. **11B**, 1 (1989).
6. C. Lagercrantz. J. Phys. Chem. **75**, 3466 (1971).
7. D. Griller and K. U. Ingold. Acc. Chem. Res. **9**, 13 (1976).
8. G. Móger and A. Rockenbauer. React. Kinet. Catal. Lett. **8**, 125 (1978).

9. G. Móger, A. Rockenbauer, and P. Simon. Radiochem. Radioanal. Lett. **42**, 407 (1980).
10. L. Sumegi, I. Mayer, I. Kende, and F. Tudos. Magy. Kem. Foly. **78**, 254 (1972).
11. K. Nakagawa, R. Konaka, and T. Nakata. J. Org. Chem. **27**, 1597 (1962).
12. S. Terabe and R. Konaka. J. Chem. Soc. Perkin Trans. 2, 2163 (1972).
13. L. B. Gilman. Ph.D. Dissertation, Duke University, Durham, NC. 1975.
14. C. H. Bamford and C. F. H. Tipper. *In* Comprehensive chemical kinetics. Free radical polymerization. Vol. 14A. Elsevier, Oxford. 1976.
15. J. C. Bevington, P. R. Fridd, and B. J. Tabner. J. Chem. Soc. Perkin Trans. 2, 1389 (1982).
16. D. Mulvey and W. A. Waters. J. Chem. Soc. Perkin Trans. 2, 1059 (1978); A. B. Sullivan. J. Org. Chem. **31**, 2811 (1966).
17. R. E. Banks, M. G. Barlow, and R. N. Haszeldine. J. Chem. Soc. 4714 (1965).
18. J. Hamer and A. Macaluso. Tetrahedron Lett. 381 (1963).
19. G. T. Knight. J. Chem. Soc. D, 1016 (1970).
20. R. E. Banks, R. N. Haszeldine, and P. J. Miller. Tetrahedron Lett. 4417 (1970).
21. R. W. Layer. Tetrahedron Lett. 4413 (1970).
22. R. K. Howe. J. Org. Chem. **33**, 2848 (1968).
23. W. B. Motherwell and J. S. Roberts. J. Chem. Soc. Chem. Commun. 329 (1972).
24. J. Lane and B. J. Tabner. J. Chem. Soc. Perkin Trans. 2, 1665 (1985).
25. W. A. Waters. J. Chem. Soc. Perkin Trans. 2, 1078 (1979).
26. P. Smith and J. S. Robertson. Can. J. Chem. **66**, 1153 (1988).
27. P. Smith and K. R. Maples. J. Magn. Reson. **65**, 491 (1985).
28. P. Smith, K. R. Maples, C. C. Devlin, and G. McCrohan. J. Magn. Reson. **67**, 539 (1986).
29. (*a*) A. I. Vogel. *In* Elementary organic chemistry. Longmans, Green, and Co., London. 1957. p. 245; (*b*) R. R. Holmes and R. P. Bayer. J. Am. Chem. Soc. **82**, 3454 (1960).
30. J. A. Riddick and W. B. Bunger. *In* Techniques of chemistry. Vol. II. *Edited by* A. Weissberger. Wiley–Interscience, New York. 1970. p. 606.
31. R. J. Faber and G. K. Fraenkel. J. Chem. Phys. **47**, 2462 (1967).
32. J. Q. Adams, S. W. Nicksic, and J. R. Thomas. J. Chem. Phys. **45**, 654 (1966).
33. M. Talât-Erben and S. Bywater. J. Am. Chem. Soc. **77**, 3710 (1955); **77**, 3712 (1955).
34. G. S. Hammond, C. S. Wu, O. D. Trapp, J. Warkentin, and R. T. Keys. J. Am. Chem. Soc. **82**, 5394 (1960).
35. P. Smith and S. Carbone. J. Am. Chem. Soc. **81**, 6174 (1959).
36. L. H. Sutcliffe and A. Zilnyk. J. Chem. Soc. Faraday Trans. 1, **81**, 1215 (1985).
37. J. March. *In* Advanced organic chemistry. 3rd ed. John Wiley, New York. 1985. Chap. 2.
38. E. G. Janzen. Acc. Chem. Res. **2**, 279 (1969).
39. J. March. *In* Advanced organic chemistry. 3rd ed. John Wiley, New York. 1985. Chaps. 1 and 9.
40. E. G. Janzen. Top. Stereochem. **6**, 177 (1971).
41. J. Hine. *In* Physical organic chemistry. 2nd ed. John Wiley, New York. 1962. Chap. 4.
42. O. Exner. *In* Correlation analysis in chemistry: Recent advances. *Edited by* N. B. Chapman and J. Shorter. Plenum Press, New York. 1978. Chap. 10.
43. E. G. Janzen and J. I-P. Liu. J. Magn. Reson. **9**, 510 (1973).
44. C. Chatgilialoglu and K. U. Ingold. J. Am. Chem. Soc. **103**, 4833 (1981).

Can. J. Chem. Downloaded from www.nrcresearchpress.com by 123.30.183.119 on 09/08/12
For personal use only.

Substituent and charge distribution effects on the redox potentials of radicals. Thermodynamics for homolytic versus heterolytic cleavage in the 1-naphthylmethyl system[1]

PAUL H. MILNE AND DANIAL D. M. WAYNER[2]
Steacie Institute for Molecular Sciences, National Research Council of Canada, Ottawa, Ont., Canada K1A 0R6

AND

DAYAL P. DECOSTA AND JAMES A. PINCOCK[2]
Department of Chemistry, Dalhousie University, Halifax, N.S., Canada B3H 4J3

Received May 22, 1991

PAUL H. MILNE, DANIAL D. M. WAYNER, DAYAL P. DECOSTA, and JAMES A. PINCOCK. Can. J. Chem. **70**, 121 (1992).

The electrochemical oxidation and reduction potentials of a number of substituted 1-methylnaphthalenes (**1***a-l*) and 1-naphthylmethyl radicals (**2***a-l*˙) as well as 2-methylnaphthalene (**3**) and the 2-naphthylmethyl radical (**4**˙) have been measured by cyclic voltammetry and photomodulation voltammetry. The oxidation potentials correlate with σ^+ ($\rho^+ = -7.1$ and -8.4 for **1** and **2**˙ respectively) while the reduction potentials correlate with σ^- ($\rho^- = 10.1$ and 13.0 for **1** and **2**˙ respectively). The relative magnitude of the ρ values can be rationalized when the charge density distribution in these systems is considered. This leads to the interesting conclusion that even though a full charge is placed in the π-system of **1** when it is oxidized or reduced, the fraction of the charge that accumulates at C_4 is actually less than in $\mathbf{2}^+$ or $\mathbf{2}^-$ where only 50–70% of the charge is delocalized into the ring. A correlation between ρ for the redox reactions of **1**, **2**˙, benzyl, diphenylmethyl, and cumyl and the calculated (AM1) charge density at C_4 is established, implying that the sensitivity of the corresponding ions to substituent effects increases as the fraction of charge at that site increases. The redox data have been used in thermochemical cycles in order to estimate the substituent effect on the homolytic, mesolytic, and heterolytic cleavage reactions of **1** and its corresponding radical ions. The implication of these results on the C—C cleavage versus deprotonation of radical cations and on the photochemical homolysis versus heterolysis of naphthylmethyl halides and acetates is discussed.

Key words: electrochemistry, homolysis, heterolysis, naphthylmethyl, substituent effect.

PAUL H. MILNE, DANIAL D. M. WAYNER, DAYAL P. DECOSTA et JAMES A. PINCOCK. Can. J. Chem. **70**, 121 (1992).

Faisant appel à la voltampérométrie cyclique et à la voltampérométrie de photomodulation, on a mesuré les potentiels d'oxydation et de réduction électrochimique d'un certain nombre de 1-méthylnaphtalènes substitués (**1***a-l*) et de radicaux 1-naphtylméthyles (**2***a-l*˙) ainsi que du 2-méthylnaphtalène (**3**) et du radical 2-naphtylméthyle (**4**˙). On peut établir une corrélation entre les potentiels d'oxydation et les α^+ ($\rho^+ = -7{,}1$ et $-8{,}4$ respectivement pour **1** et **2**˙). On peut rationaliser l'amplitude relative des valeurs de ρ en considérant la distribution de la densité de charge dans ces systèmes. Ceci conduit à la conclusion intéressante que, même si une charge complète est placée dans le système π du composé **1** (qu'il soit oxydé ou réduit), la fraction de la charge qui s'accumule en C_4 est en fait moindre que dans les entités $\mathbf{2}^+$ et **2**˙ dans lesquelles seulement 50–70% de la charge est délocalisée dans le cycle. On a établi une corrélation entre les valeurs de ρ des réactions rédox des entités **1**, **2**˙, benzyle, diphénylméthyle et cumyle et la densité de charge calculée (AM1) pour la position C_4; elle implique que la sensibilité des ions corespondants aux effets des substituants croit avec une augmentation de la fraction de la charge dans cette position. Les données rédox ont été utilisées dans des cycles thermodynamiques dans le but d'évaluer l'effet de substituant sur les réactions de clivage homolytique, mésolytique et hétérolytique du composé **1** et des ions radicaux correspondants. On discute de l'implication de ces résultats sur le clivage des liaisons C—C versus la déprotonation des cations radicaux et sur l'homolyse photochimique versus l'hétérolyse des halogénures et des acétates de naphtylméthyle.

Mots clés : électrochimie, homolyse, hétérolyse, naphtylméthyle, effet de substituant.

[Traduit par la rédaction]

Introduction

There has been continually growing interest in the use of electrochemical data in thermochemical cycles since Breslow and co-workers used this method to estimate the pK_a of a number of weak carbon acids (1–5). Recently, Arnold and co-workers (6–8) and Bordwell *et al.* (9–12) used this approach for the determination of pK_a's of radical cations and (or) the energies for the homolytic cleavage of C—H bonds. More recently, Arnett *et al.* (13–15) combined calorimetric and electrochemical measurements to obtain data for the heterolytic C—C cleavage reactions.

In essentially all of these cases the electrochemical measurements were made in solutions of very long-lived molecules or ions. We have shown that reliable electrochemical measurements can actually be made in solutions of transient radicals using the photomodulation voltammetry technique (16). We also have recently pointed out that all of the thermochemical cycles describing the homolytic and heterolytic cleavage reactions of molecules and their radical ions can be conveniently represented in a thermochemical mnemonic (Scheme 1, eqs. [1]–[7]) (17). In this mnemonic the vertical arrows represent the loss of R′ as a radical (i.e., the homolytic bond dissociation energy). The horizontal arrows represent the addition or removal of an electron while the diagonal arrows represent the loss of R'^+ (up to the right) or R'^- (up to the left). For the case where R′ = H, the reactions along the diagonals are representations of more familiar thermodynamic parameters; reactions [9] and [11] are

[1]NRCC No. 33271.
[2]Authors to whom correspondence may be addressed.

Can. J. Chem. Downloaded from www.nrcresearchpress.com by 123.30.183.119 on 09/08/12
For personal use only.

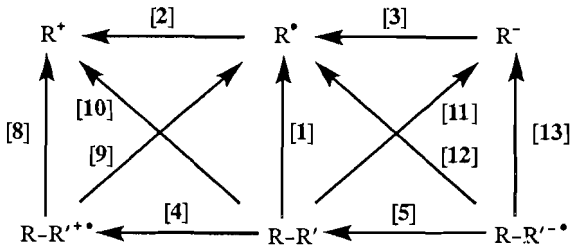

SCHEME 1

deprotonation reactions (pK_a's) while reactions [10] and [12] are hydride affinities. The latter two reactions are of particular importance to the chemistry of NADH/NAD^+ and its analogs (18–20).

[1] $R - R' \rightarrow R^{\bullet} + R'^{\bullet}$

[2] $R^{\bullet} \rightarrow R^+$

[3] $R^- \rightarrow R^{\bullet}$

[4] $R - R' \rightarrow R - R'^{+\bullet}$

[5] $R - R'^{-\bullet} \rightarrow R - R'$

[6] $R'^{\bullet} \rightarrow R'^+$

[7] $R'^- \rightarrow R'^{\bullet}$

The thermochemistry for all of the possible homolytic and heterolytic cleavage reactions can then be written simply as the sum of the homolytic bond dissociation energy (eq. [1]) with the difference between two potentials (eqs. [2]–[7]). It is important to keep in mind that an entropy correction must be applied to the bond dissociation enthalpies that are usually reported in the literature since the redox potentials are actually *free energy* differences. For R' = H, this correction is ca. −8 kcal mol^{-1} (16). These free energy relationships are given in eqs. [8]–[13].

[8] $R - R'^{+\bullet} \rightarrow R^+ + R'^{\bullet}$

$$\Delta G^0_8 = \Delta G^0_1 + F(E^0_2 - E^0_4)$$

[9] $R - R'^{+\bullet} \rightarrow R^{\bullet} + R'^+$

$$\Delta G^0_9 = \Delta G^0_1 + F(E^0_6 - E^0_4)$$

[10] $R - R' \rightarrow R^+ + R'^-$

$$\Delta G^0_{10} = \Delta G^0_1 + F(E^0_2 - E^0_7)$$

[11] $R - R' \rightarrow R^- + R'^+$

$$\Delta G^0_{11} = \Delta G^0_1 + F(E^0_6 - E^0_3)$$

[12] $R - R'^{-\bullet} \rightarrow R^{\bullet} + R'^-$

$$\Delta G^0_{12} = \Delta G^0_1 + F(E^0_5 - E^0_7)$$

[13] $R - R'^{-\bullet} \rightarrow R^- + R'^{\bullet}$

$$\Delta G^0_{13} = \Delta G^0_1 + F(E^0_5 - E^0_3)$$

We have now applied this thermochemical approach to the naphthylmethyl system. This system has an advantage over the benzyl system that has been reported (21), as the relative ease of oxidation and reduction makes the electrochemical characterization of the parent methylnaphthalenes more straightforward than it is for the toluenes. Recent results on the photochemical bond cleavage reactions of 1-naphthylmethyl derivatives (N-CH_2-X where N is a substituted naphthalene ring) (22–24) have indicated the importance of the 1-naphthylmethyl radical as an intermediate. Moreover, the rate of oxidation of this radical to the corresponding 1-naphthylmethyl cation seems to be critical in controlling the final product composition of these photoreactions (22). To understand these results in a quantitative sense, values for the oxidation potentials of the 1-naphthylmethyl radicals are needed. In this paper we report redox potential measurements for 12 substituted 1-methylnaphthalenes (**1***a-l*) and the corresponding 1-naphthylmethyl radicals (**2***a-l*') as well as similar values for 2-methylnaphthalene (**3**) and the 2-naphthylmethyl radical (**4**'). The implication of these results on the thermodynamic parameters in Scheme 1 and on the photochemistry of the 1-naphthylmethyl derivatives will be discussed.

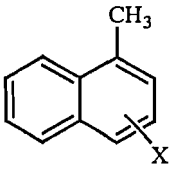

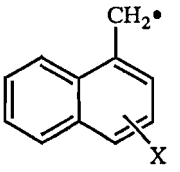

1*a*, X = 4-$CO_2CH_2CH_3$
1*b*, X = 3-CN
1*c*, X = 4-CN
1*d*, X = 3-OCH_3
1*e*, X = H
1*f*, X = 4-F
1*g*, X = 4-CH_3
1*h*, X = 2-OCH_3
1*i*, X = 4-OCH_3
1*j*, X = 4,8-di-OCH_3
1*k*, X = 4,5-di-OCH_3
1*l*, X = 4,7-di-OCH_3

2•

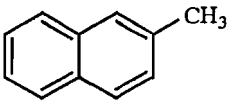

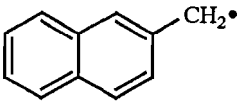

3 **4**•

Results and discussion

Substituent effects on redox properties

The oxidation and reduction potentials of the substituted **1** (measured by cyclic voltammetry) and the **2**• (measured by photomodulation voltammetry) are given in Table 1. Not surprisingly the series follow the trends expected; electron-donating groups make the oxidation of either **1** or **2**• easier and electron-withdrawing groups make the reduction of either easier. This can be put on a more quantitative basis by using Hammett correlations. Only data for the 4-substituted derivatives of **1** and the 3- and 4-substituted derivatives of **2** were included in this analysis to avoid the complication of adding σ values for the disubstituted cases. The usual benzene ring σ^+ and σ^- values were used since only a limited number of these parameters are available for naphthalene rings (25). The Hammett plots for oxidation of **1** ($\rho^+ = -8.4 \pm 0.9$) and **2**• ($\rho^+ = -7.1 \pm 0.7$) are shown in Fig. 1 and for the reduction of **1** ($\rho^- = 13.0 \pm 1.2$) and **2**• ($\rho^- = 10.1 \pm 0.9$) in Figure 2. Good fits ($r > 0.95$) were obtained in

Can. J. Chem. Downloaded from www.nrcresearchpress.com by 123.30.183.119 on 09/08/12
For personal use only.

Can. J. Chem. Downloaded from www.nrcresearchpress.com by 123.30.183.119 on 09/08/12
For personal use only.

TABLE 1. Oxidation and reduction potentials of compounds **1**–**4**

Compound	Substituent	$E_{1/2}^{ox}$ (V vs. SCE)		$E_{1/2}^{red}$ (V vs. SCE)	
		1[a]	**2**$^{\bullet}$[b]	**1**[c]	**2**$^{\bullet}$[b]
a	4-$CO_2CH_2CH_3$	1.81	0.81	−2.00	−0.71
b	3-CN	1.93	0.79	−2.04	−0.87
c	4-CN	1.99	0.72	−1.96	−0.55
d	3-OCH_3	1.30	0.52	−2.63	[d]
e	H	1.59	0.47	−2.55	−1.27
f	4-F	1.75	0.46	−2.50	−1.33
g	4-CH_3	1.57	0.35	−2.62	−1.35
h	2-OCH_3	1.30	0.13	−2.62	−1.36
i	4-OCH_3	1.34	0.04	−2.61	−1.55
j	4,8-Di-OCH_3	1.09[e]	−0.05	−2.80[e]	[d]
k	4,5-Di-OCH_3	1.09[e]	−0.05	−2.78[e]	[d]
l	4,7-Di-OCH_3	1.19[e]	−0.06	−2.68	−1.55
3[a]		1.64		−2.58[f]	
4$^{\bullet}$[b]		0.61		−1.25	

[a]Measured by cyclic voltammetry at a glassy carbon electrode in acetonitrile with 0.1 M TBAP as supporting electrolyte at a scan rate of 200 mV/s. All potentials are irreversible and potentials are reported as E_p − 30 mV.

[b]Measured by photomodulation voltammetry at a gold minigrid in acetonitrile/di-*tert*-butyl peroxide (9:1 v/v) with 0.1 M TBAP as supporting electrolyte.

[c]Measured by cyclic voltammetry at a glassy carbon electrode in acetonitrile with 0.1 M TBAP as supporting electrolyte at a scan rate of 200 mV/s. All potentials are reversible and potentials are reported as the mid-point between the cathodic and anodic peak.

[d]The reduction wave was not observed due to high background.

[e]Quasireversible wave.

[f]Reversible wave.

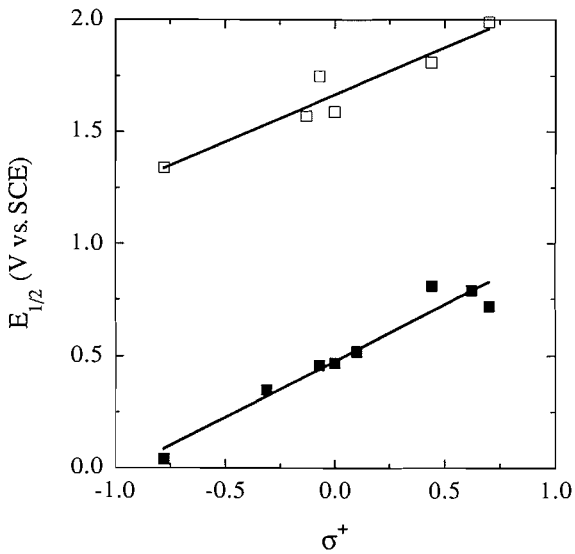

FIG. 1. Hammett plot for the oxidation of **1** (□, $\rho^+ = -7.1$, $r = 0.95$) and **2**$^{\bullet}$ (■, $\rho^+ = -8.4$, $r = 0.97$).

all cases. While most of these redox reactions are irreversible (Table 1), Bordwell *et al.* (9–12) have shown that for a series of structurally related species, the changes in redox properties closely approximate thermodynamic changes; i.e., ΔE_p from cyclic voltammetry $\approx \Delta E^0$, the thermodynamically significant potential. The oxidation and reduction potentials of the radicals (measured by photomodulation voltammetry) also have been shown to be close to E^0 (16, 17, 21).

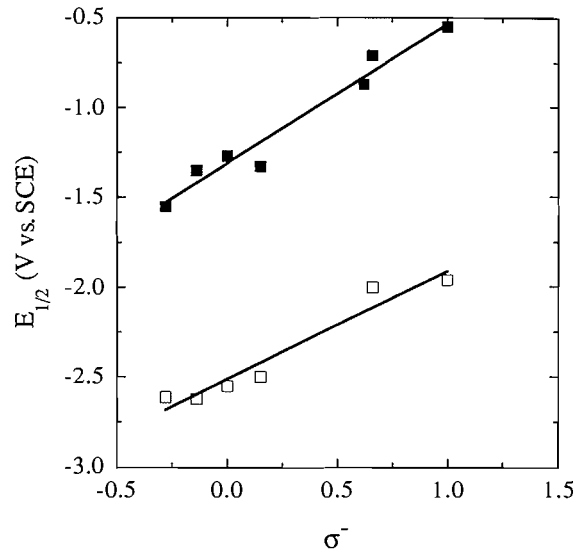

FIG. 2. Hammett plot for the reduction of **1** (□, $\rho^- = 10.1$, $r = 0.97$) and **2**$^{\bullet}$ (■, $\rho^- = 13.0$, $r = 0.98$).

It is interesting to note that for both the oxidations and the reductions, the Hammett ρ value was larger for the redox reaction of the radical than it was for the methylnaphthalene derivative (although the uncertainties in the ρ^+ are large enough that the difference between these values may not be significant). Intuitively one might expect this order to be reversed since a full charge is delocalized in the naphthalene ring in the radical ions ($\mathbf{1}^{+\bullet}$ and $\mathbf{1}^{-\bullet}$) whereas only a fraction (ca. 0.5) of the charge is expected to be delocalized into the ring for the naphthylmethyl ions ($\mathbf{2}^+$ and $\mathbf{2}^-$). It seemed reasonable to expect the sensitivity to substituent effects to be related to the extent of charge delocalization into the ring system.

To investigate this possibility, the charge distributions in these ions were calculated using the AM1 molecular orbital theory (26). The $2p_z$ charge densities for the parent ions $\mathbf{1}e^{+\bullet}$, $\mathbf{1}e^{-\bullet}$, $\mathbf{2}e^+$, and $\mathbf{2}e^{-\bullet}$ as well as the related benzyl ions are shown in Fig. 3 (the total atomic charges give an essentially identical distribution when the charge on the neighboring hydrogens is included). These data show some interesting parallels with the experimental results. Firstly, the charge distribution in the benzyl and the 1-naphthylmethyl systems is similar. This fits with the observation that the Hammett ρ values for the redox potentials of these systems also are the same within the experimental error (27). Secondly, the difference between the 1-naphthylmethyl and the 1-methylnaphthalene systems becomes clear. Because of the odd alternate nature of the arylmethyl ions ($\mathbf{2}^+$ or $\mathbf{2}^-$), more of the charge density accumulates at C_4 and C_2 while very little accumulates at C_3 or in the fused benzo ring. For the even alternate radical ions ($\mathbf{1}^{+\bullet}$ or $\mathbf{1}^{-\bullet}$) the charge is distributed more evenly since there are no nodes in the SOMO.

This result leads to the interesting conclusion that even though essentially a full charge is placed in the π-system of the naphthalene ring in the radical ions, the amount of that charge that ends up near the substituent is actually less than in those systems where only 50–70% of the charge in delocalized. This effect of charge distribution is clearly

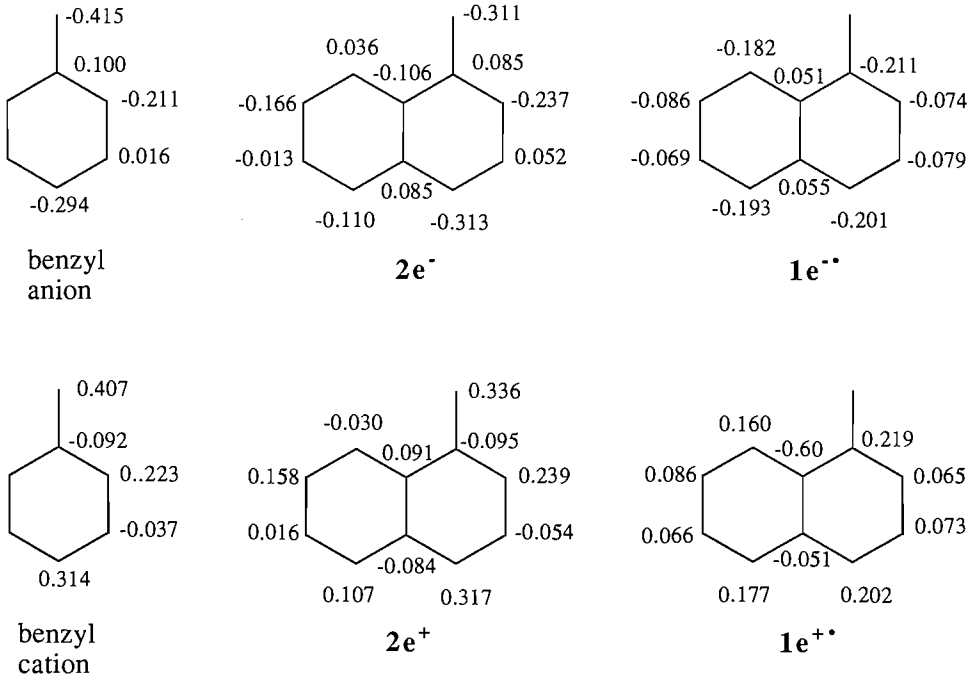

FIG. 3. Calculated (AM1) $2p_z$ charge densities for the cations and anions generated by the one-electron oxidation or reduction of the benzyl radical, **2**$^{\bullet}$ and **1***e*.

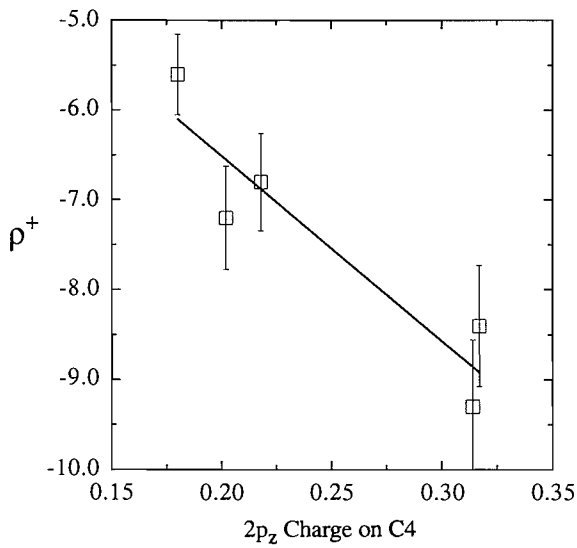

FIG. 4. Plot of ρ^+ for the oxidation of **1**, **2**$^{\bullet}$, benzyl, diphenylmethyl, and cumyl versus the calculated (AM1) $2p_z$ charge density at C_4 in the parent ion.

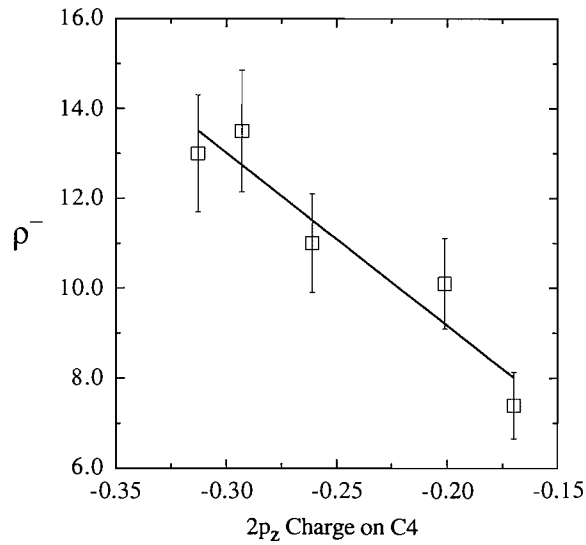

FIG. 5. Plot of ρ^- for the reduction of **1**, **2**$^{\bullet}$, benzyl, diphenylmethyl, and cumyl versus the calculated (AM1) $2p_z$ charge density at C_4 in the parent ion.

seen when the Hammett ρ values for the oxidation and reduction of substituted benzyl, diphenylmethyl, and cumyl (27) radicals along with those for **1** and **2**$^{\bullet}$ are plotted versus the calculated (AM1) $2p_z$ charge density at C_4 (Figs. 4, 5). Although there is some scatter in the plot (which contains electrochemical data for about 40 radicals), the trend is clear.

These observations are important inasmuch as they reinforce the idea that substituent effects in ionic species should not be additive. This issue has been addressed in detail by Dubois and co-workers (28, 29) and is supported by work on substituent effects on the redox properties of α,*p*-disubstituted benzyl radicals (30). In the latter work it was concluded that the effect of two "destabilizing" substituents on an ion is additive while the effect of two "stabilizing" substituents should be less than additive. The lack of additivity is usually rationalized as a saturation effect. However, it is equally well understood in terms of the effect that one substituent will have on the charge density at the site of the second. It is interesting to note that, in this case, the effect of two methoxy substituents on the redox potentials of **1** is essentially additive while the effect on **2** is less than addi-

Can. J. Chem. Downloaded from www.nrcresearchpress.com by 123.30.183.119 on 09/08/12
For personal use only.

TABLE 2. Heterolytic and mesolytic bond energies (kcal mol^{-1}) for some naphthylmethyl systems from thermochemical cycles[a]

Compound	Substituent	ΔG^0_8	ΔG^0_9	ΔG^0_{10}	ΔG^0_{11}	ΔG^0_{12}	ΔG^0_{13}
1*a*	4-CO_2Et	54.9	−6.9	104.9	51.2	107.7	40.1
b	3-CN	51.7	−9.7	104.5	54.9	104.9	39.2
c	4-CN	48.7	−11.1	102.8	47.5	110.5	41.0
d	3-OCH_3	60.0	4.8	98.2	[b]	[b]	25.6
e	H	52.1	−1.8	97.1	64.1	107.5	27.4
f	4-F	48.2	−5.5	98.9	65.5	104.9	28.6
g	4-CH_3	49.8	−1.4	94.3	66.0	107.2	25.8
h	2-OCH_3	51.0	4.8	89.2	66.2	107.0	25.8
i	4-OCH_3	48.0	3.9	87.2	70.6	102.4	26.1
j	4,8-Di-OCH_3	51.7	9.7	85.1	[b]	[b]	21.7
k	4,5-Di-OCH_3	51.7	9.7	85.1	[b]	[b]	22.1
l	4,7-Di-OCH_3	49.4	7.4	85.1	70.6	104.0	24.4
3		54.2	−3.0	100.3	65.6	108.6	26.8

[a]See text for equations.
[b]Insufficient data to complete the cycle.

Can. J. Chem. Downloaded from www.nrcresearchpress.com by 123.30.183.119 on 09/08/12
For personal use only.

tive. The configuration of the SOMO in the even alternate and odd alternate ions is consistent with this effect (Fig. 3).

Substituent effects on derived thermochemical parameters

The substituent effects on the C—H cleavage reactions of 1-methylnaphthalene and its radical ions (eqs. [8]–[13]) are given in Table 2. We have assumed that the bond energy for 1-methylnaphthalene derivatives is not dependent on ring substitution (ΔH^0_1 = 85 kcal mol^{-1}; ΔG^0_1 = 77 kcal mol^{-1} (31)). This assumption seems reasonable since there appears to be little effect of substitution on the C—H bond energy in toluenes (32, 33). The values of ΔG^0_6 and ΔG^0_7 have been estimated as −1.87 V and −0.36 V vs. SCE, respectively (17).

The substituent effect on ΔG^0_9 to ΔG^0_{12} depends only on the redox properties of one of the substituted species. For example, changes in ΔG^0_9 are determined only by changes in ΔG^0_4. Similarly ΔG^0_{10} is determined by ΔG^0_2, ΔG^0_{11} by ΔG^0_3, and ΔG^0_{12} by ΔG^0_5. On the other hand, ΔG^0_8 is determined by the difference between the oxidation potential of the naphthylmethyl radical (ΔG^0_2) and the oxidation potential of the methylnaphthalene (ΔG^0_4). In this case, since the Hammett slopes for these two processes are similar, the substituent effects partially cancel so the net effect is quite small. Although this cleavage reaction is not considered to be an important pathway for the substituted naphthalenes (**1**), the result has some important implications.

Arnold and co-workers (7, 8) and Maslak *et al.* (34, 35) have studied the C—C cleavage reactions of radical cations in solution. Maslak has suggested that the term "mesolytic" cleavage (34) be used to distinguish these reactions, which involve the cleavage of a formal one-electron bond, from those reactions that are truly homolytic or heterolytic. For reactions of symmetrical 1,2-diarylethanes the loss of proton (R′ = H, ΔG^0_9; eq. [14]) is expected to have a strong substituent effect while the competing pathway, C—C cleavage (R′ = R, ΔG^0_8; eq. [15]), will have a significantly smaller effect. Although Arnold *et al.* (36) and Tolbert *et al.* (37) have pointed out that kinetics of these competing pathways is strongly influenced by stereoelectronic factors, the relative thermochemistry for these pathways will have a significant impact on the interpretation of these data. Proton loss is usually more exoergonic than C—C cleavage. However, it may be possible to design a reaction, by using the appropriate substitution, in which the thermochemistry of these two pathways is reversed.

[14] $ArCH_2\text{-}CH_2Ar^{+\bullet} \rightarrow ArCHCH_2Ar + H^+$

[15] $ArCH_2\text{-}CH_2Ar^{+\bullet} \rightarrow ArCH_2^{\bullet} + ArCH_2^+$

Photoinduced homolytic and heterolytic cleavage reactions

The photocleavage of benzylic substrates with leaving groups (Ar-LG) is well known to give products that arise from both arylmethyl cations and radicals (38). However, the pathway for the formation of these critical intermediates is not well understood so that reliable predictions about product yields are still impossible. Early mechanisms proposed that the relative yield of cation and radical was controlled by the initial cleavage of the excited state and that the substituents on the aromatic ring could alter the ratio; i.e., the meta effect (39, 40). More recently, it has become obvious that electron transfer, converting the initially formed radical pair ($Ar^{\bullet}/LG^{\bullet}$) to an ion pair ($Ar^+/LG^-$), will be an important factor in determining these yields. Obviously, the data in Table 1 for the oxidation potentials of the substituted naphthylmethyl radicals as well as previous data for the substituted benzyl, cumyl, and diphenylmethyl radicals (16) are critical for understanding this electron transfer process. To this end, we have determined the free energy change (in acetonitrile) for the conversion of the radical pair $NpCH_2^{\bullet}/LG^{\bullet}$) to the ion pair ($NpCH_2^+/LG^-$) for LG = Cl (**5**), Br (**6**), I (**7**), and MeC(O)O (**8**) (Table 3).

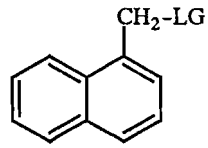

5, LG = Cl
6, LG = Br
7, LG = I
8, LG = $CH_3C(O)O$

TABLE 3. Homolytic and heterolytic bond energies for **1** and **5–8**[a]

$NpCH_2LG$	$(\Delta G^0_1)_g$	$(\Delta G^0_{10})_g$	$(\Delta G^0_{10})_{MeCN}$	$(\Delta G^0_{ET})_g$[b]	$(\Delta G^0_{ET})_{MeCN}$[c]
1*e* (H)	85.9	234.5	105.1	148.6	19.2
5 (Cl)	67.8	151.0	30.3	83.2	−37.5
6 (Br)	52.8	141.6	24.5	138.8	−28.3
7 (I)	40.0	136.1	23.2	96.1	−16.8
8 (OAc)	68.2	163.8	43.3	95.6	−24.9

[a]Subscript refers to the gas phase (g) or acetonitrile solution (MeCN). Values in kcal mol^{-1}.
[b]Free energy change for the conversion of a radical pair into an ion pair: $NpCH_2^{\bullet} + LG^{\bullet} \rightarrow NpCH_2^+ + LG^-$. $(\Delta G^0_{ET})_g = (\Delta G^0_{10})_g - (\Delta G^0_1)_g$.
[c]Free energy change for the conversion of a radical pair into an ion pair: $NpCH_2^{\bullet} + LG^{\bullet} \rightarrow NpCH_2^+ + LG^-$. $(\Delta G^0_{ET})_{MeCN} = (\Delta G^0_{10})_{MeCN} - (\Delta G^0_1)_g$

The redox data for $Cl^{\bullet}$ $Br^{\bullet}$, $I^{\bullet}$, and $MeC(O)O^{\bullet}$ in acetonitrile are easily derived from thermodynamic data in the literature (41). For acetate, a thermochemical cycle was used (based on eq. [11]) assuming a bond dissociation enthalpy (O—H) of 105 kcal mol^{-1} (30) and literature values for the free energy change associated with the transfer of the relevant ions from water into acetonitrile (42). The values in Table 3 are only for the unsubstituted naphthalene ring. Changes in these values for the substituted cases will parallel the oxidation potential of the 1-naphthylmethyl radicals (Scheme 1) so they have been omitted. Note also, that now LG refers to R′ in Scheme 1.

It is interesting to point out that (except for H, which is not photochemically labile) the ion pair is always more stable than the radical pair in solution. This is in contrast to the relative stability in the gas phase where the ions are not solvated (Table 3), clearly demonstrating that solvation of the product ions is the driving force for all of these reactions. The reasonable assumption that $(\Delta G^0_1)_g = (\Delta G^0_1)_{MeCN}$ is being used. The exoergonicity of these reactions spans a very wide range, from −9 kcal mol^{-1} for the reaction of 4-carboethoxy-1-naphthylmethyl iodide to −50 kcal mol^{-1} for 4-methoxy-1-naphthylmethyl chloride. Because of this fact, it is perhaps intitially surprising that products derived from the radical pair are ever observed. However, the Marcus theory of electron transfer (43) gives an explanation, since an activation barrier is provided by the reorganization energy that is necessary to convert the radical pair to an ion pair. These ideas have been confirmed (22) by results for the photolysis of 1-naphthylmethyl esters ($NpCH_2$-O_2CR). The product analysis leads to the conclusion that the excited state cleaves exclusively to the radical pair ($NpCH_2^{\bullet}/{}^{\bullet}O_2CR$) and the radical pair partitions between electron transfer (to form the ion pair) and decarboxylation of the acyloxy radical. The rates of the electron transfer process were shown to be rationalized by the Marcus equation even into the inverted region. A reorganization energy of ca. 9 kcal mol^{-1} was estimated. Obviously application of these ideas to other cleavage reactions must be considered.

Conclusions

The sensitivity of oxidation and reduction potentials of arylmethyl radicals to ring substitution is related not only to the extent of delocalization of the charge in the corresponding ions, but also to the charge distribution. Thus ρ^+ and ρ^- for the oxidation and reduction of 1-naphthylmethyl radicals are greater than those for the oxidation and reduction of the 1-methylnaphthalenes since the odd alternate nature of the former allows a greater fraction of the charge in the ions to accumulate at C_2 and C_4 even though only 50–70% of the charge is in the aryl ring (as calculated by AM1 molecular orbital theory).The SOMO of even alternate 1-methylnaphthalene radical ions leads to a more even distribution of the charge density at all of the sites. A correlation between the experimental ρ value and the fraction of charge in the $2p_z$ orbital at C_4 has been established.

The redox data lead to estimates of differences in bond energies for homolysis versus heterolysis of 1-naphthylmethyl halides and acetates. In all cases the heterolysis is the energetically favourable process. The electrochemical data complement observed photochemistry of these compounds in which electron transfer of an initially formed radical pair (to generate an ion pair) is found to compete with the intersystem crossing process.

Experimental

Methylnaphthalenes

1-Methyl, 2-methyl, and 1,4-dimethylnaphthalene were purchased from the Aldrich Chemical Company and purified by bulb-to-bulb distillation before use. 3-Cyano and 4-cyanomethyl naphthalene were prepared previously in our laboratory (23). All others were prepared as described below.

3-Methoxy-1-methylnaphthalene: prepared by the method of Bartoli and co-workers (44) and recrystallized from ethanol to give colourless crystals: mp 47–48°C (lit. (44) mp 48–49°C).

4.8-Dimethoxy-1-methylnaphthalene: prepared by the method of Buu-Hoi and Lavit (45). Recrystallization from ethanol gave colourless plates: mp 104–105°C (lit. (45) mp 105°C); ^1H nmr ($CDCl_3$) δ: 8.0 (d, 1H, J = 8.5 Hz), 7.4 (t, 1H, J = 7.8 Hz), 7.15 (d, 1H, J = 8.2 Hz), 6.8 (d, 1H, J = 8.0 Hz), 6.6 (d, 1H, J = 8.0 Hz), 3.9 (s, 3H), 3.8 (s, 3H), 2.8 (s, 3H).

4.7-Dimethoxy-1-methylnaphthalene: prepared by the method of Buu-Hoi and Lavit (46). Recrystallization from ethanol gave colourless plates: mp 54–55°C (lit. (46) mp 54°C); ^1H nmr ($CDCl_3$) δ: 8.2 (d, 1H, J = 8.5 Hz), 7.2–7.0 (m, 3H), 6.7 (d, 1H, J = 8.0 Hz), 3.95 (s, 3H), 3.9 (s, 3H), 3.9 (s, 3H), 2.7 (s, 3H).

4.5-Dimethoxy-1-methylnaphthalene: prepared by the method of Buu-Hoi and Lavit (47). Recrystallization from ethanol gave colourless plates: mp 64–65°C (lit (47) mp 65°C); ^1H nmr ($CDCl_3$) δ: 7.44–7.2 (m, 2H), 7.1 (d, 1H, J = 8.0 Hz), 6.8 (d, 1H, J = 8.0 Hz), 6.7 (d, 1H, J = 8.0 Hz), 3.9 (s, 3H), 3.85 (s, 3H), 2.6 (s, 3H).

4-fluoro-1-methylnaphthalene: prepared by the method of Sauer *et al.* (48): bp 64–66°C at 1 Torr (133.3 Pa) (lit. (48) bp 107.5–109.5°C at 12 Torr).

2-Methoxy-1-methylnaphthalene: prepared by the method of Buu-Hoi and Lavit (49). Recrystallization from ethanol gave colourless plates: mp 41–42°C (lit. (50) mp 39°C); ^1H nmr ($CDCl_3$)

Can. J. Chem. Downloaded from www.nrcresearchpress.com by 123.30.183.119 on 09/08/12
For personal use only.

δ: 8.1–7.5 (m, 3H), 7.4–7.2 (m, 2H), 7.1 (d, 1H, J = 8.0 Hz), 3.9 (s, 3H), 2.6 (s, 3H).

4-Carbomethoxy-1-methylnaphthalene: prepared by esterification of the acid with methanol: bp 80–82°C at 0.05 Torr. Crystallization from hexane gave colourless plates: mp 30–31°C (lit. (51) bp 192–194°C at 12 Torr); ^{1}H nmr ($CDCl_3$); δ: 9.1–8.9 (m, 1H), 8.0 (d, 1H, J = 8.0 Hz), 7.9–7.8 (m, 1H), 7.60 (t, 1H, J = 8.0 Hz), 7.50 (t, 1H, J = 8.0 Hz), 7.22 (d, 1H, J = 8.0 Hz), 3.91 (s, 3H), 2.60 (s, 3H).

The acid, 4-methylnaphthoic acid, was prepared by hydrolysis of 4-cyano-1-methylnaphthalene (23) with sodium hydroxide in ethanol/water. Recrystallization of the crude acid from ethanol–water gave colourless needles: mp 178–179°C (lit. (52) mp 180°C).

Electrochemical measurements

Solvents and electrolyte were purified as described previously (16). Radicals for photomodulation voltammetric measurements were generated by photolysis of a solution of acetonitrile/di-*tert*-butyl peroxide (9:1 v/v; 0.1 M tetrabutylammonium perchlorate as the supporting electrolyte) in the presence of the appropriate methylnaphthalene using a 1000-W Hg/Xe arc lamp (Oriel Corp). The output of the lamp was modulated as a sine wave with a mechanical light chopper that operated at frequencies between 20 and 250 Hz. The reference signal for the lock-in amplifier (PAR model 124A) was taken from the output of the light chopper. In electrochemical experiments the ac component of the electrolysis current was demodulated with the lock-in amplifier (Ithaco model 391A) interfaced to a microcomputer. The electrochemical cell was constructed from Teflon® and had a volume of 0.5 mL. The electrode, a gold minigrid (1000 wires/in.; Buckbee–Mears) was placed in the cell so that the exposed surface area was a circle with a radius of 2.5 mm. Currents in the range of 0–500 nA were measured with a PAR model 174A polarograph.

Cyclic voltammetric measurements were performed in acetonitrile/0.1 M tetrabutylammonium perchlorate at a glassy carbon electrode using an EG&G model 173 potentiostat and an EG&G model 175 universal cell programmer. All potentials are reported with respect to the saturated calomel electrode (SCE).

Can. J. Chem. Downloaded from www.nrcresearchpress.com by 123.30.183.119 on 09/08/12
For personal use only.

1. R. Breslow and K. Balasubramanian. J. Am. Chem. Soc. **91**, 5182 (1969).
2. R. Breslow and W. Chu. J. Am. Chem. Soc. **95**, 411 (1973).
3. M. R. Wasielewski and R. Breslow. J. Am. Chem. Soc. **98**, 4222 (1976).
4. R. Breslow and R. Goodin. J. Am. Chem. Soc. **98**, 6076 (1976).
5. B. Jaun, J. Schwarz, and R. Breslow. J. Am. Chem. Soc. **102**, 5741 (1980).
6. A. M. deP. Nicholas and D. R. Arnold. Can. J. Chem. **60**, 2165 (1982).
7. A. Okamoto, M. S. Snow, and D. R. Arnold. Tetrahedron, **22**, 6175 (1986).
8. R. Popielarz and D. R. Arnold. J. Am. Chem. Soc. **112**, 3068 (1990).
9. F. G. Bordwell and M. J. Bausch. J. Am. Chem. Soc. **108**, 2473 (1986).
10. F. G. Bordwell, J.-P. Cheng, and J. A. Harrelson, Jr. J. Am. Chem. Soc. **110**, 1229 (1988).
11. F. G. Bordwell and J.-P. Cheng. J. Am. Chem. Soc. **111**, 1792 (1989).
12. F. G. Bordwell and J. A. Harrelson, Jr. Can. J. Chem. **68**, 1714 (1990).
13. E. M. Arnett, K. Amarnath, N. G. Harvey, and J.-P. Cheng. J. Am. Chem. Soc. **112**, 344 (1990).
14. E. M. Arnett, K. Amarnath, N. G. Harvey, and S. Venimadhavan. J. Am. Chem. Soc. **112**, 7346 (1990).
15. E. M. Arnett, K. Amarnath, N. G. Harvey, and J.-P. Cheng. Science, **247**, 423 (1990).
16. D. D. M. Wayner, D. J. McPhee, and D. Griller. J. Am. Chem. Soc. **110**, 132 (1988).
17. D. Griller, J. A. Martinho-Simões, P. Mulder, B. A. Sim, and D. D. M. Wayner. J. Am. Chem. Soc. **111**, 7872 (1989).
18. D. Ostovic, I. H. Lee, R. M. G. Roberts, and M. M. Kreevoy. J. Org. Chem. **50**, 4206 (1985).
19. M. M. Kreevoy and I. H. Lee. J. Am. Chem. Soc. **106**, 2550 (1984).
20. D. Ostovic, R. M. G. Roberts, and M. M. Kreevoy. J. Am. Chem. Soc. **105**, 7629 (1983).
21. B. A. Sim, D. Griller, and D. D. M. Wayner. J. Am. Chem. Soc. **111**, 754 (1989).
22. D. P. DeCosta and J. A. Pincock. J. Am. Chem. Soc. **111**, 8948 (1989).
23. B. Foster, B. Gaillard, N. Mathur, A. L. Pincock, J. A. Pincock, and C. Sehmbey. Can. J. Chem. **65**, 1599 (1987).
24. B. Arnold, L. Donald, A. Jurgens, and J. A. Pincock. Can. J. Chem. **63**, 3140 (1985).
25. N. B. Chapman and J. B. Shorter. *In* Correlation analysis in chemistry. Plenum, New York. 1978.
26. M. J. S. Dewar, E. G. Zoebisch, E. F. Healy, and J. J. P. Stewart. J. Am. Chem. Soc. **107**, 3902 (1985).
27. B. A. Sim, P. H. Milne, D. Griller, and D. D. M. Wayner. J. Am. Chem. Soc. **112**, 6635 (1990).
28. J. E. Dubois, M. F. Ruasse, and A. Argile. J. Am. Chem. Soc. **106**, 4840 (1984).
29. M. F. Ruasse, A. Argile, and J. E. Dubois. J. Am. Chem. Soc. **106**, 4846 (1984).
30. D. D. M. Wayner, B. A. Sim, and J. J. Dannenberg. J. Org. Chem. **56**, 4853 (1991).
31. D. F. McMillen and D. M. Golden. Annu. Rev. Phys. Chem. **33**, 493 (1982).
32. W. A. Pryor, D. F. Church, F. Y. Tang, and R. H. Tang. *In* Frontiers of free radical chemistry. *Edited by* W. A. Pryor. Academic Press, New York. 1980. p. 355.
33. R. D. Gilliom. Theochem. **138**, 157 (1986).
34. P. Maslak and J. N. Narvaez. Angew. Chem. Int. Ed. Engl. **29**, 283 (1990).
35. P. Maslak and W. H. Chapman, Jr. Tetrahedron, **46**, 2715 (1990).
36. D. R. Arnold, L. J. Lamont, and A. L. Perrott. Can. J. Chem. **69**, 225 (1991).
37. L. M. Tolbert, R. K. Khanna, A. E. Popp, L. Gebaum, and L. A. Bottomley. J. Am. Chem. Soc. **112**, 2373 (1990).
38. S. J. Cristol and T. H. Bindel. *In* Organic photochemistry. Vol. 6. Marcel Dekker, New York. 1983. p. 327.
39. H. E. Zimmerman and V. R. Sandel. J. Am. Chem. Soc. **85**, 915 (1963).
40. H. E. Zimmerman and S. Somasekhara. J. Am. Chem. Soc. **85**, 922 (1963).
41. D. D. M. Wayner. *In* Handbook of photochemistry. Vol. II. *Edited by* J. C. Scaiano. CRC Press, Boca Raton, FL. p. 363.
42. Y. Marcus, M. J. Kamlet, and R. W. Taft. J. Phys. Chem. **92**, 3613 (1988).
43. L. Eberson. *In* Electron transfer reactions in organic chemistry. Springer-Verlag, New York. 1987. p. 32.
44. G. Baccolini, G. Bartoli, M. Bosco, and R. Dalpozzo. J. Chem. Soc. Perkin Trans. 2, 363 (1984).
45. N. P. Buu-Hoi and D. Lavit. J. Org. Chem. **20**, 1191 (1955).
46. N. P. Buu-Hoi and D. Lavit. Bull. Soc. Chem. Fr. 1419 (1955).
47. N. P. Buu-Hoi and D. Lavit. J. Chem. Soc. 2412 (1956).
48. J. Sauer, R. Huisgen, and A. Hauser. Ber. Dtsch. Chem. Ges. **91**, 1461 (1958).
49. N. P. Buu-Hoi and D. Lavit. J. Chem. Soc. 2776 (1955).
50. K. Fries and B. Huber. Ber. **39**, 442 (1906).
51. F. Mayer and A. Sieglitz. Chem. Ber. **55**, 1835 (1922).
52. J. M. Bonnier and J. Rinudo. Bull Soc. Chem. Fr. 3901 (1966).

Synthetic applications of glycidic thiolesters. Regioselective reduction to 1,3-diols and 2,3-epoxy alcohols

HSING-JANG LIU[1] AND WEIDE LUO

Department of Chemistry, University of Alberta, Edmonton, Alta., Canada T6G 2G2

Received July 10, 1991

HSING-JANG LIU and WEIDE LUO. Can. J. Chem. **70**, 128 (1992).

Glycidic thiolesters were shown to undergo regioselective reduction with Raney nickel to give 1,3-diols. With sodium borohydride at room temperature and lithium aluminum hydride at −78°C, the reduction of glycidic thiolesters was found to proceed chemoselectively to furnish 2,3-epoxy alcohols.

Key words: glycidic thiolesters, reduction, 1,3-diols, 2,3-epoxy alcohols.

HSING-JANG LIU et WEIDE LUO. Can. J. Chem. **70**, 128 (1992).

On montre que, en présence de nickel de Raney, les thiolesters glycidiques subissent une réduction régiosélective conduisant aux 1,3-diols. Avec le borohydrure de sodium à la température ambiante et avec l'hydrure double de lithium et d'aluminium à −78°C, la réduction de ces esters se produit d'une façon chimiosélective pour fournir des 2,3-époxy alcools.

Mots clés : thiolesters glycidiques, réduction, 1,3-diols, 2,3-époxy alcools.

[Traduit par la rédaction]

Can. J. Chem. Downloaded from www.nrcresearchpress.com by 123.30.183.119 on 09/08/12
For personal use only.

Introduction

It is well known that simple thiolesters are reduced to primary alcohols by Raney nickel (1–3). However, under the influence of other functionalities present in the molecule, the thiolester group may exert some unusual chemical properties. For example, β-keto thiolesters (4, 5) and derivatives of *S*,*S*′-diethyl dithiomalonate (6, 7) have been shown to undergo fragmentation reaction upon treatment with Raney nickel. In light of these previous findings in our laboratories, it became of interest to investigate the course of reduction of glycidic thiolesters with Raney nickel. Herein we wish to report the experimental results of this investigation as well as those obtained from the reduction of glycidic thiolesters with sodium borohydride and lithium aluminum hydride. Thiolesters have been shown to be more susceptible to reduction with metal hydride reducing agents than the corresponding oxygen analogues and could be reduced to the alcohol level under mild conditions with sodium borohydride in protic solvents (8) and tetrabutylammonium borohydride in aprotic solvents (9). It has also been shown that a clear differentiation of the thiolester group from other frequently encountered acid derivatives, namely ester, amide, and nitrile, could be achieved using sodium borohydride (8). The study on metal hydride reduction of glycidic thiolesters was undertaken in order to examine the viability of selectively reducing the thiolester group, with the intention of developing a new procedure for the preparation of 2,3-epoxy alcohols.

Results and Discussion

Synthesis of glycidic thiolesters

Glycidic thiolesters were first prepared by Wemple and co-workers from α-halo thiolesters and carbonyl compounds (10, 11) using a variant of Darzens condensation (12). In Darzens synthesis of glycidic esters, an alkoxide or sodium amide is generally used as a base. However, it is deemed necessary to use a non-nucleophilic base in the synthesis of glycidic thiolesters in order to avoid nucleophilic attack on the thiolester carbonyl group by the reagent. It has also been shown (11) that α-bromo thiolesters possessing a tertiary *S*-alkyl group are preferred over those with a primary or secondary *S*-alkyl group. One reason could be that the primary and secondary alkyl groups may undergo deprotonation under strongly basic conditions, as the hydrogen atom adjacent to the sulfur atom is quite acidic (13). Another possible reason is that a thiolester derived from a tertiary mercaptan is less prone to elimination reaction leading to ketene formation (14). In Wemple's synthesis (10, 11), lithium bis(trimethylsilyl)amide and sodium hydride were used as the base, and *S*-*tert*-butyl α-bromothiolesters were used as the main starting substrate. For our investigation, a number of glycidic thiolesters were prepared from *S*-*tert*-butyl 2-bromoethanethiolate (**1**) using lithium diisopropylamide as a base. This base was found to be more convenient to use and the results were more reproducible. In an early experiment, compound **1** was deprotonated with 1 equivalent of lithium diisopropylamide in tetrahydrofuran at −78°C. After addition of 1 equivalent of dihydrocinnamaldehyde, the reaction solution was stirred at −78°C for 2 h and then warmed up to room temperature. Under these conditions, a diastereomeric mixture of glycidic thiolesters **2** (1 : 1) was obtained in 25% yield.

To improve the yield, several runs of the reaction were carried out using increasing amounts of thiolester **1** and lithium diisopropylamide. With 2.5 equivalents each of **1** and the base, a 62% yield (based on the aldehyde) of glycidic thiolesters **2** was obtained. This yield could not be further improved by the use of an even greater amount of thiolester **1**.

It appears that the excess amount of thiolester **1** was required in order to cover its rapid consumption due to side reactions such as self-condensation. In a control experiment, thiolester **1** was treated with lithium diisopropylamide (1 equivalent) at −78°C in tetrahydrofuran for 2 h. The mixture was then allowed to warm up to room temperature (ca. 0.5 h). A substantial loss of material occurred and less than 60% of the starting thiolester **1** was recovered.

In the subsequent preparation of glycidic thiolesters, the

[1]Author to whom correspondence may be addressed.

TABLE 1. Preparation of glycidic thiolesters

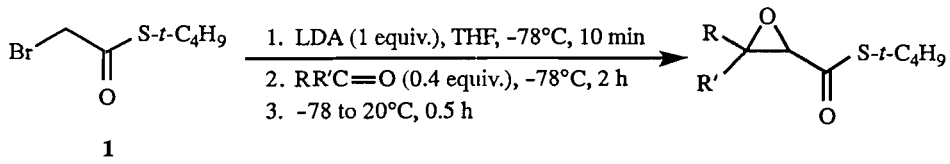

Glycidic thiolester(s)	% Yield	Glycidic thiolester(s)	% Yield
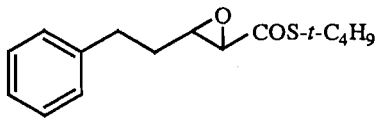 **2**	62 (*cis*:*trans* = 1:1)	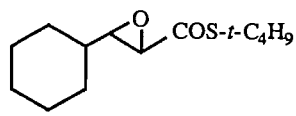 **3**	85 (*cis*:*trans* = 1:1)
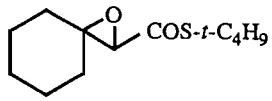 **4** (11)	83	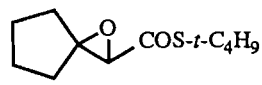 **5**	81
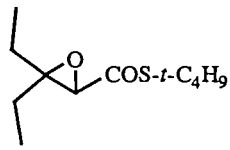 **6**	66	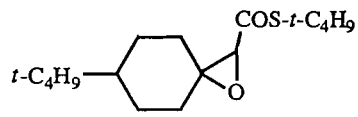 **7**	78 (*cis*:*trans* = 2:1)[a]
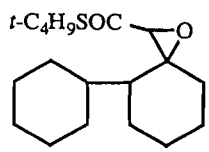 **8**[b]	70		

[a]The stereochemistry of these isomers follows from the subsequent reduction with Raney nickel (see Table 2). The terms *cis* and *trans* denote the relationship between the *tert*-butyl group and the oxygen atom of the epoxy ring.
[b]A single stereoisomer was obtained. Its stereochemistry remains to be determined.

following standard procedure was adopted. The enolate ion of thiolester **1** was preformed by treatment with lithium diisopropylamide (1 equivalent) in tetrahydrofuran at −78°C for 10 min. The carbonyl compound (0.4 equivalent) was then introduced. After 2 h at −78°C, the reaction mixture was warmed to room temperature (ca. 0.5 h). Under these conditions, several glycidic thiolesters were prepared in reproducible yields of 62–85%. The results are summarized in Table 1.

Similar to Darzens synthesis of glycidic esters, the formation of glycidic thiolesters is expected to proceed via the following three steps: deprotonation of an α-halo thiolester, nucleophilic addition of the enolate ion thus formed to a carbonyl compound, and cyclization to form the oxirane ring (Scheme 1). It was observed during the preparation of compound **2** that an intermediate was produced immediately following the addition of dihydrocinnamaldehyde at −78°C. This intermediate was slowly (ca. 5 h) converted to the desired product at low temperature (−78°C). This observation also indicated that the final cyclization was much slower than the addition of the enolate anion to the carbonyl compound.

We have also examined the condensation of *S*-*tert*-butyl 2-chloroethanethioate with carbonyl compounds. This reagent was found to be inferior to the corresponding bromo compound **1**. At −78°C over a period of 5 h, the reaction of its enolate ion with cyclohexanone gave rise to chloro alcohol **9** as the only product in 81% yield. When the reaction was carried out by slowly warming the reaction mixture to room temperature over a 2.5 h period, the desired product **4** was formed but only in poor yield (19%). Similarly, the condensation of *S*-*tert*-butyl 2-chloroethanethioate with dihydrocinnamaldehyde at −78°C gave chloro alcohol **10** as the only product (38% yield). In this case, the formation of the desired product **2** was not detected even after the reaction temperature was raised to 20°C.

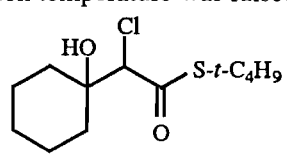

9

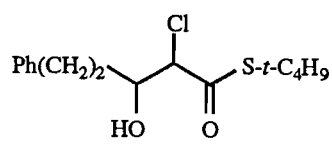

10

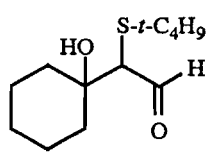

21

Can. J. Chem. Downloaded from www.nrcresearchpress.com by 123.30.183.119 on 09/08/12
For personal use only.

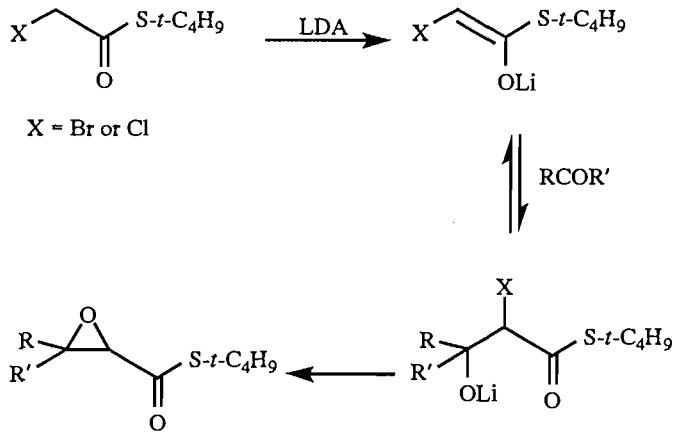

SCHEME 1

Treatment of compounds **9** or **10** with a base such as sodium hydride in tetrahydrofuran or 1,2-dimethoxyethane at room temperature did not yield any detectable amount of the desired glycidic thiolester. Instead, complete decomposition to give the original components, α-chloro thiolester and the carbonyl compound, occurred.

The above results clearly indicate that α-chloro thiolester is not an adequate reagent for the preparation of glycidic thiolesters via Darzens condensation. This is in agreement with the previous findings made by Wemple and co-workers (11). The isolation of intermediate chloro alcohols **9** and **10** and the observed reverse reaction of these intermediates lend support to the proposed mechanistic pathway depicted in Scheme 1.

Reduction of glycidic thiolesters with Raney nickel

Glycidic thiolester *cis*-**2** was treated with W-2 Raney nickel in 95% ethanol at room temperature for 1 h. After filtration and concentration of the filtrate, diol **11** (15) was obtained. The mass spectrum revealed its molecular formula of $C_{11}H_{16}O_2$. The ir spectrum indicated the presence of a hydroxy group showing a strong absorption at 3343 cm^{-1}. This was also confirmed by the signal at δ 2.3 for two D_2O exchangeable hydrogens in the ^1H nmr spectrum. However, at this stage the relationship (i.e., 1,2- or 1,3-) of the two hydroxy groups could not be determined by the ^1H nmr spectrum due to the complexity of the signals at δ 3.8–4.0 for the three hydrogens adjacent to the hydroxy groups.

To solve this problem, the diol was converted to the corresponding diacetate by treatment with excess acetic anhydride and pyridine in methylene chloride. The ^1H nmr spectrum clearly indicated that the product was a 1,3-diacetate derived from 1,3-diol **11**, displaying two low-field signals, a triplet at δ 4.10 (J = 6.5 Hz) for two hydrogen atoms, and a triplet of triplets at δ 5.04 (J = 7, 5.5 Hz) integrating to one hydrogen.

Similar treatment of glycidic thiolesters **3**, **4**, **7**, and **8** with Raney nickel gave rise to 1,3-diols **12** (16), **13** (17), **14** (18), and **15**, respectively. An examination of the results compiled in Table 2 reveals that the reduction in each case proceeded in a completely regioselective manner with preferential cleavage of the carbon–oxygen bond neighboring the thiolester group. As such, this bond is expected to be activated by the thiolester group. Furthermore, in compounds **4**, **7**, and **8**, this bond happens also to be sterically less congested than the other carbon–oxygen bond of the oxirane ring. Most likely, it is the combination of these electronic and steric effects that induced the observed high degree of regioselectivity.

Reduction of glycidic thiolesters with sodium borohydride and lithium aluminum hydride

In this part of the study, several glycidic thiolesters were subjected to sodium borohydride reduction in order to investigate the feasibility of reducing the thiolester group selectively without affecting the adjacent epoxy ring. Thus, compound **4** was treated with 4 molar equivalents of sodium borohydride in 98% ethanol at 20°C. The reduction was found to be completed within 5 h, giving rise to epoxy alcohol **16** (19) in 82% yield.

This procedure is apparently general for the selective reduction of glycidic thiolesters. Under similar conditions, compounds *cis*-**2**, *trans*-**2**, *cis*-**3**, and **8** were also smoothly reduced to their corresponding epoxy alcohols in good yields (80–95%). Results are compiled in Table 3.

It should be noted that up to 4 molar equivalents of the reducing agent were required for completion of the reaction, presumably because of partial consumption of the reagent by the solvent. The amount could be reduced to 2.5 molar equivalents by addition of the reagent in portions (0.5 molar equivalent over every 0.5 h period) during the reaction.

The formation of epoxy alcohols from glycidic thiolesters can also be achieved by the use of lithium aluminum hydride at low temperature. For example, when *trans*-**3** was treated with 3 molar equivalents of the reducing agent in ether at −78°C for 1 h, epoxy alcohol *trans*-**18** (16) was obtained in 89% yield.

The reduction was also attempted using 1 molar equivalent of lithium aluminum hydride. At −78°C, the reaction was found to be slow and incomplete after a long time of reaction (>5 h). When the reaction was carried out at room temperature, a complex mixture was produced, from which hydroxy aldehyde **21** was isolated in 5% yield. This compound was obviously produced as a result of the epoxy ring opening with *tert*-butyl mercaptide generated during the reduction.

Several other glycidic thiolesters were subjected to reduction with a large excess (3 molar equivalents) of lithium aluminum hydride at low temperature (−78°C). As indicated by the results outlined in Table 3, these conditions are generally effective for the selective reduction of the thiolester group.

Conclusion

Several new synthetic aspects of glycidic thiolesters, readily prepared by an α-bromo thiolester version of the Darzens condensation, were successfully explored. Reduction of glycidic thiolesters with Raney nickel was shown to give consistently the corresponding 1,3-diols as a result of the completely regioselective cleavage of the epoxy ring. On the other hand, with sodium borohydride at room temperature or lithium aluminum hydride at −78°C, glycidic thiolesters were readily reduced to give 2,3-epoxy alcohols resulting from the chemoselective reduction of the thiolester moiety. In conjunction with the Darzens glycidic thiolester condensation, these facile and apparently general reductions provide convenient access to 1,3-diols and 2,3-epoxy

Can. J. Chem. Downloaded from www.nrcresearchpress.com by 123.30.183.119 on 09/08/12
For personal use only.

TABLE 2. Reduction of glycidic thiolesters with Raney nickel

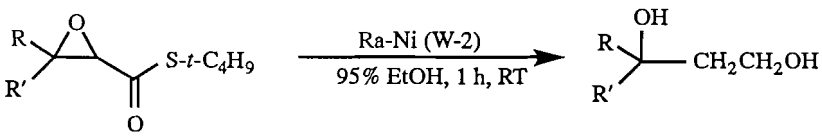

Thiolester(s)	Product(s)	% Yield
cis-**2**	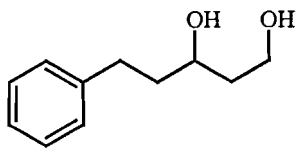 **11** (15)	80
3 (isomeric mixture)	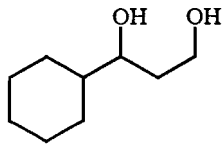 **12** (16)	88
4	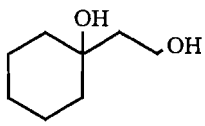 **13** (17)	87
7 (*cis*:*trans* = 1:2)	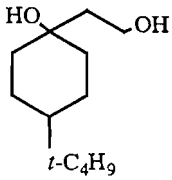 **14** (18) (*cis*:*trans* = 1:2)[a]	80
8	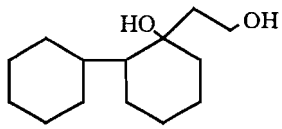 **15**[b]	96

[a]The stereochemistry of these isomers was tentatively assigned on the basis of the relative polarities (18) of the corresponding monoacetates (see Experimental). By inference the stereochemistry of the starting glycidic thiolesters 7 was deduced.
[b]The stereochemistry of this compound remains to be determined.

alcohols[2] that cannot be effectively prepared by similar transformations involving glycidic esters.

Experimental

General

Melting points (mp) were determined on a Köfler hot stage apparatus and are uncorrected. Elemental analyses were performed by the microanalytical laboratory of this department. Infrared (ir) spectra were recorded on a Perkin–Elmer model 457 or Nicolet 7-199 FT-IR spectrophotometer. Unless otherwise stated, ir samples were run as thin films. Proton nuclear magnetic resonance (^{1}H nmr) spectra were recorded on a Bruker WH-200 spectrometer and, except where otherwise stated, were obtained on solutions in deuterochloroform with tetramethylsilane as internal reference. The following abbreviations are used: s = singlet, d = doublet, t = triplet, q = quartet, m = multiplet, and br = broad. Carbon-13 nuclear magnetic resonance (^{13}C nmr) spectra were recorded on a Bruker WH-300 (75 MHz) spectrometer. The multiplicity of ^{13}C nmr signals was derived from off-resonance or Carr–Purcel–Meiboom–Gill spin echo *J*-modulated experiments (APT or Attached Proton Test). Peaks in antiphase (a) with deuteriochloroform were assigned as methyls or methines, while peaks in phase (p) correspond to methylenes or quarternary carbons. High resolution mass spectra (HRMS) were recorded using a Kratos A.E.I. model MS50 high-resolution mass spectrometer. Chemical ionization mass spectra (CIMS) were obtained using an A.E.I. MS12 mass spectrometer, with ammonia as the reagent gas. Concentrations of solvent systems used for column chromatography are given by volumes.

Materials

S-tert-Butyl 2-bromoethanethioate (**1**) was prepared by trapping, with *tert*-butyl mercaptan, of α-bromoacetyl bromide prepared by the Hell–Volhard–Zelinsky reaction (21). Methylene chloride was distilled from anhydrous magnesium sulfate. Ether, 1,2-dimethoxyethane, and tetrahydrofuran were distilled from so-

[2]For a review on the chemistry of 2,3-epoxy alcohols, see ref. 20.

Can. J. Chem. Downloaded from www.nrcresearchpress.com by 123.30.183.119 on 09/08/12
For personal use only.

TABLE 3. Reduction of glycidic thiolesters with sodium borohydride and lithium aluminum hydride

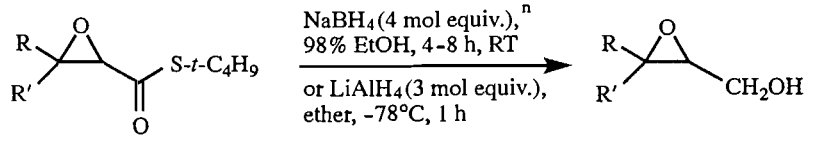

Thiolester(s)	Product(s)	% Yield with $NaBH_4$	% Yield with $LiAlH_4$
4	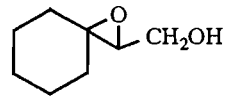 **16** (19)	82	
cis-**2**	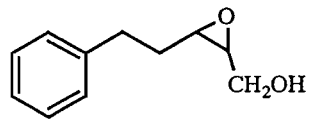 *cis*-**17**	94	94
trans-**2**	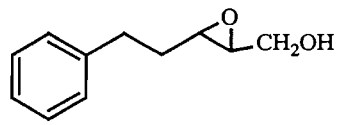 *trans*-**17**	80	
cis-**3**	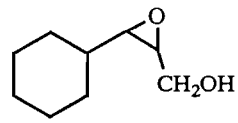 *cis*-**18** (16)	90	83
trans-**3**	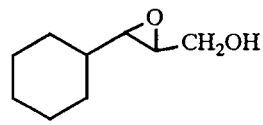 *trans*-**18** (16)		89
cis-**7**	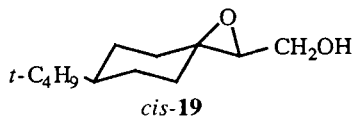 *cis*-**19**		92
8	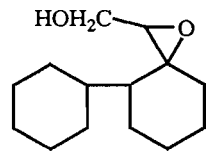 **20**[a]	95	86

[a]The stereochemistry of this compound remains to be determined.

dium metal and benzophenone under an argon atmosphere. Ethyl acetate, hexane, ether, and methylene chloride used for chromatography and extraction were purified by distillation. Argon was passed through a purification train of Fieser's solution, concentrated sulfuric acid, and potassium hydroxide pellets. Silica gel, 230–400 mesh ASTM, was used as absorbent for flash chromatography. Thin-layer chromatography was carried out using Merck TLC aluminum sheets silica gel 60 F_{254}. Unless otherwise stated, anhydrous magnesium sulfate was used for drying organic solutions.

Preparation of glycidic thiolesters

A number of glycidic thiolesters were synthesized from α-bromo thiolester **1** and the carbonyl compounds. A typical experimental procedure is given below with compounds **2**. Yields of products are shown in Table 1.

S-tert-*Butyl 3-(2-phenylethyl)oxirane-2-carbothioates* (**2**)

Under an argon atmosphere, diisopropylamine (1.11 g, 11.0 mmol) and tetrahydrofuran (30 mL) were placed in a flask and cooled to −78°C by a Dry Ice – acetone bath. A 2.0 M butyllithium solution in hexane (5.0 mL, 10.0 mmol) was slowly added with a syringe. After stirring for 10 min, a solution of compound **1** (2.11 g, 10.0 mmol) in tetrahydrofuran (5 mL) was added dropwise over a period of 10 min. Then a solution of dihydrocinnamaldehyde (0.536 g, 4.00 mmol) in tetrahydrofuran (5 mL) was added dropwise. The resulting mixture was stirred at −78°C for 2 h and the cooling bath was removed. After the mixture was warmed up to room temperature, it was poured into an aqueous

Can. J. Chem. Downloaded from www.nrcresearchpress.com by 123.30.183.119 on 09/08/12
For personal use only.

Can. J. Chem. Downloaded from www.nrcresearchpress.com by 123.30.183.119 on 09/08/12
For personal use only.

saturated ammonium chloride solution and extracted with ether (3 × 20 mL). The extracts were washed with aqueous saturated sodium chloride solution, combined, dried, filtered, and concentrated to give a brown oil. Flash chromatography (2–8% ether in hexane) gave *cis*-**2** (0.345 g, 1.31 mmol) and *trans*-**2** (0.310 g, 1.17 mmol). *cis*-**2**: ^{1}H nmr δ: 1.50 (s, 9H, -C(CH_3)$_3$), 2.00 (m, 2H, -$CH_2$$CH_2$Ph), 2.74 (dt, 1H, *J* = 13, 8 Hz, -C*H*HPh), 2.83 (dt, 1H, *J* = 13, 6 Hz, -CH*H*Ph), 3.21 (dt, 1H, *J* = 5, 6 Hz, -CH_2C*H*-), 3.58 (d, 1H, *J* = 5 Hz, -C*H*CO-), and 7.30 (complex, 5H, Ar*H*). *trans*-**2**: ir: 1670 (C=O) cm^{-1}; ^{1}H nmr δ: 1.50 (s, 9H, -C(CH_3)$_3$), 1.92 (m, 2H, -$CH_2$$CH_2$Ph), 2.77 (ddd, 1H, *J* = 13, 9, 4 Hz, -C*H*HPh), 2.80 (ddd, 1H, *J* = 13, 8.5, 4 Hz, -CH*H*Ph), 3.19 (ddd, 1H, *J* = 6.5, 6, 2 Hz, -CH_2C*H*-), 3.26 (d, 1H, *J* = 2 Hz, -C*H*CO-), and 7.23 (complex, 5H, Ar*H*); CIMS (M + NH_4)$^+$: 282 (calcd. for $C_{15}H_{24}NO_2S$: 282).

S-tert-*Butyl 3-cyclohexyloxirane-2-carbothioates (3) trans-3*: ^{1}H nmr δ: 1.48 (s, 9H, -C(CH_3)$_3$), 1.1–1.95 (complex, 11H), 2.98 (dd, 1H, *J* = 6.5, 2 Hz, -CHC*H*CO-), and 3.33 (d, 1H, *J* = 2 Hz, -C*H*CO-). *cis*-**3**: ^{1}H nmr δ: 1.51 (s, 9H, -C(CH_3)$_3$), 1.1–1.9 (complex, 11H), 2.95 (dd, 1H, *J* = 9, 4.5 Hz, -C*H*-), and 3.61 (d, 1H, *J* = 4.5 Hz, -C*H*CO-); HRMS M$^+$: 242.1327 (calcd. for $C_{13}H_{22}O_2S$: 242.1340).

S-tert-*Butyl 1-oxaspiro[2.5]octane-2-carbothioate (4)*: ir: 1695 and 1667 (C=O) cm^{-1}; ^{1}H nmr δ: 1.50 (s, 9H, -C(CH_3)$_3$), 1.5–1.8 (complex, 10H), and 3.36 (s, 1H, -C*H*CO-); HRMS M$^+$: 228.1183 (calcd. for $C_{12}H_{20}O_2S$: 228.1184).

S-tert-*Butyl 1-oxaspiro[2.4]heptane-2-carbothioate (5)*: ir: 1693 and 1668 (C=O) cm^{-1}; ^{1}H nmr δ: 1.50 (s, 9H, -C(CH_3)$_3$), 1.6–2.1 (complex, 8H), and 3.57 (s, 1H, -C*H*CO-); HRMS M$^+$: 214.1022 (calcd. for $C_{11}H_{18}O_2S$: 214.1027).

S-tert-*Butyl 3,3-diethyloxirane-2-carbothioate (6)*: ir: 1695 and 1668 (C=O) cm^{-1}; ^{1}H nmr δ: 0.95 (t, 3H, *J* = 8 Hz, -CH_2CH_3), 0.99 (t, 3H, *J* = 8 Hz, -CH_2CH_3), 1.52 (s, 9H, -C(CH_3)$_3$), 1.68 (q, 2H, *J* = 8 Hz, -$CH_2$$CH_3$), 1.70 (q, 2H, *J* = 8 Hz, -$CH_2$$CH_3$), and 3.42 (s, 1H, -C*H*-); HRMS M$^+$: 216.1178 (calcd. for $C_{11}H_{20}O_2S$: 216.1184).

S-tert-*Butyl* 6-tert-*butyl-1-oxaspiro[2.5]octane-2-carbothioates (7) trans-7*: ir: 1695 and 1669 (C=O) cm^{-1}; ^{1}H nmr δ: 0.87 (s, 9H, -C(CH_3)$_3$), 1.50 (s, 9H, -SC(CH_3)$_3$), 1.0–2.1 (complex, 9H), and 3.36 (s, 1H, -C*H*CO-). *cis*-**7**: ^{1}H nmr δ: 0.88 (s, 9H, -C(CH_3)$_3$), 1.40 (s, 9H, -SC(CH_3)$_3$), 1.0–2.1 (complex, 9H), and 3.38 (s, 1H, -C*H*CO-); HRMS M$^+$: 284.1810 (calcd. for $C_{16}H_{28}O_2S$: 284.1809).

S-tert-*Butyl 4-cyclohexyl-1-oxaspiro[2.5]octane-2-carbothioate (8)*: mp 91–93°C; ir: 1653 (C=O) cm^{-1}; ^{1}H nmr δ: 0.8–2.05 (complex, 20H), 1.49 (s, 9H, -C(CH_3)$_3$), and 3.23 (s, 1H, -C*H*-CO-); ^{13}C nmr ($CDCl_3$) δ: 196.7 (p), 69.3 (p), 64.1 (a), 48.5 (a), 35.9 (a), 31.4 (p), 30.7 (p), 29.8 (a), 27.6 (p), 26.5 (p), 26.4 (p), 25.7 (p), 25.3 (p), and 20.6 (p); HRMS M$^+$: 310.1969 (calcd. for $C_{18}H_{30}O_2S$: 310.1966). Anal. calcd. for $C_{18}H_{30}O_2S$: C 69.63, H 9.74, S 10.33; found: C 69.67, H 9.96, S 10.36.

Reduction of glycidic thiolesters with Raney nickel

The reactions were carried out using the general procedure described below. Yields of products are shown in Table 2.

To Raney nickel (W-2, ca. 4 g/mmol of substrate, 50% slurry in water), in a flask, was added water (5 mL). After stirring for 0.5 min, the liquid was carefully removed with a pipet. The residue was washed three times with 95% ethanol (5 mL each). Then a solution of glycidic thiolester (0.5–1.0 mmol) in 5 mL of 95% ethanol was added. After stirring at room temperature for 1 h, the reaction mixture was filtered through a layer of Celite 545. The residue was washed with 30 mL of ethanol. The filtrates were combined and concentrated to give the crude product, which was subjected to either flash chromatography (3% methanol and 30% ether in hexane) giving a pure diol, or direct acetylation as follows.

A pure or crude diol yielded from the reduction reaction was stirred with excess acetic anhydride and pyridine in methylene chloride at room temperature overnight. Then the mixture was poured into an ice-cold aqueous 1 N sodium hydroxide solution and extracted with methylene chloride. The extracts were washed with 1 N hydrochloric acid and aqueous saturated sodium chloride solution, combined, dried, filtered, and concentrated. The residue was chromatographed (10–40% ethyl acetate in hexane) to give mono- and (or) diacetate in good yield.

The diols and their corresponding mono- and (or) diacetates were shown to have the following spectral data.

5-Phenyl-1,3-pentanediol (11): ir: 3343 (br, -OH) cm^{-1}; ^{1}H nmr δ: 1.7–1.8 (complex, 4H), 2.3 (br s, 2H, D_2O exchangeable, -O*H*), 2.74 (ddd, 1H, *J* = 14, 7.5, 8.5 Hz, -C*H*HPh), 2.82 (ddd, 1H, *J* = 14, 7, 9 Hz, -CH*H*Ph), 3.8–4.0 (complex, 3H, -C*H*OH-$CH_2$$CH_2$OH), and 7.2–7.4 (complex, 5H, Ar*H*); CIMS (M + NH_4)$^+$: 198 (calcd. for $C_{11}H_{20}NO_2$: 198). Diacetate of **11**: ir: 1730 (C=O), 1500 and 1450 (Ph) cm^{-1}; ^{1}H nmr δ: 1.8–2.0 (complex, 4H), 2.05 (s, 6H, -COCH_3), 2.64 (td, 2H, *J* = 7, 2 Hz, -CH_2Ph), 4.10 (t, 2H, *J* = 6.5 Hz, -CH_2OAc), 5.04 (tt, 1H, *J* = 7, 5.5 Hz, -C*H*(OAc)-), and 7.15–7.40 (complex, 5H, Ar*H*); HRMS *m/z*: 204.1148 (M$^+$ − CH_3CO_2H, calcd. for $C_{13}H_{16}O_2$: 204.1150).

1-Cyclohexyl-1,3-propanediol (12): ir: 3342 (OH) cm^{-1}; ^{1}H nmr δ: 0.9–1.5 (complex, 6H), 1.5–2.0 (complex, 7H), 2.30 (br s, 1H, D_2O exchangeable, -O*H*), 2.46 (br s, 1H, D_2O exchangeable, -O*H*), 3.68 (dt, 1H, *J* = 7.5, 5.5 Hz, -C*H*(OH)-), 3.90 (dt, 1H, *J* = 11, 5.5 Hz, -C*H*HOH), and 3.95 (dt, 1H, *J* = 11, 5 Hz, -CH*H*OH); CIMS (M + NH_4)$^+$: 176 (calcd. for $C_9H_{22}NO_3$: 176). Diacetate of **12**: ^{1}H nmr δ: 0.9–1.9 (complex, 13H), 2.06 (s, 3H, -COCH_3), 2.08 (s, 3H, -COCH_3), 4.12 (t, 2H, *J* = 7 Hz, -CH_2-OAc), and 4.90 (ddd, 1H, *J* = 9, 6, 4 Hz, -C*H*(OAc)-).

1-(2-Hydroxyethyl)cyclohexanole (13): ^{1}H nmr δ: 1.3–1.8 (complex, 10H), 1.76 (dd, 2H, *J* = 6, 5 Hz, -$CH_2$$CH_2$OH), 2.35 (br s, 1H, D_2O exchangeable, -O*H*), 2.80 (br s, 1H, D_2O exchangeable, -O*H*), and 3.90 (ddd, 2H, *J* = 6, 5, 4.5 Hz, -$CH_2$$CH_2$OH; after addition of D_2O, dd 2H, *J* = 6, 5 Hz). Monoacetate of **13**: ir: 3450 (OH), 1716 (C=O) cm^{-1}; ^{1}H nmr δ: 1.2–1.8 (complex, 11H), 1.82 (t, 2H, *J* = 8 Hz, -$CH_2$$CH_2$ Ac), 2.06 (s, 3H, -COCH_3), and 4.27 (t, 2H, *J* = 8 Hz, -$CH_2$$CH_2$OAc); HRMS *m/z*: 169.1227 (M$^+$ − OH, calcd. for $C_{10}H_{17}O_2$: 169.1228). Diacetate of **13**: ir: 1725 (C=O) cm^{-1}; ^{1}H nmr δ: 1.2–1.6 (complex, 8H), 2.03 (s, 3H, -COCH_3), 2.06 (s, 3H, -COCH_3), 2.2 (complex, 2H), 2.25 (t, 2H, *J* = 8 Hz, -$CH_2$$CH_2$OAc), and 4.13 (t, 2H, *J* = 8 Hz, -$CH_2$$CH_2$-OAc); HRMS *m/z*: 169.1226 (M$^+$ − $OCOCH_3$, calcd. for $C_{10}H_{17}O_2$: 169.1228).

4-tert-Butyl-1-(2-hydroxyethyl)cyclohexanols (14): ir: 3356 (OH) cm^{-1}; HRMS M$^+$: 200.1776 (calcd. for $C_{12}H_{24}O_2$: 200.1776). *trans*-**14**: ^{1}H nmr δ: 0.86 (s, 9H, -C(CH_3)$_3$), 1.2–2.2 (complex, 9H), 1.84 (t, H, *J* = 5.5 Hz, -$CH_2$$CH_2$OH), 2.68 (br s, 1H, -O*H*), 2.23 (br s, 1H, -O*H*), and 3.92 (t, 2H, *J* = 5.5 Hz, -CH_2OH). *cis*-**14**: ^{1}H nmr δ: 0.88 (s, 9H, -C(CH_3)$_3$), 1.2–2.2 (complex, 9H), 1.73 (t, 2H, *J* = 5.5 Hz, -$CH_2$$CH_2$OH), 2.68 (br s, 1H, -O*H*), 2.23 (br s, 1H, -O*H*), and 3.95 (t, 2H, *J* = 5.5 Hz, -$CH_2$$CH_2$OH). Monoacetate of *trans*-**14**: ^{1}H nmr δ: 0.86 (s, 9H, -C(CH_3)$_3$), 1.0–2.0 (complex, 10H), 1.88 (t, 2H, *J* = 7 Hz, -$CH_2$$CH_2$OAc), 2.06 (s, 3H, -COC$H_3$), and 4.26 (t, 2H, *J* = 7 Hz, -CH_2OAc). Monoacetate of *cis*-**14**: ^{1}H nmr δ: 0.86 (s, 9H, -C(CH_3)$_3$), 1.2–1.8 (complex, 10H), 1.78 (t, 2H, *J* = 7 Hz, -$CH_2$$CH_2$OAc), 2.05 (s, 3H, -COC$H_3$), and 4.27 (t, 2H, *J* = 7 Hz, -CH_2OAc).

2-Cyclohexyl-1-(2-hydroxyethyl)cyclohexanol (15) mp 104–107°C; ir 3362 (OH) and 3357 (OH) cm^{-1}; ^{1}H nmr δ: 1.0–2.1 (complex, 22H), 2.28 (ddd, 1H, *J* = 14, 10, 6 Hz, -C*H*CH_2OH), 2.46 (br s, 1H, D_2O exchangeable, -O*H*), 3.80 (ddd, 1H, *J* = 10, 6, 4.5 Hz, -C*H*OH), and 4.01 (ddd, 1H, *J* = 10, 10, 4 Hz, -CH*H*OH); HRMS M$^+$: 226.1929 (calcd. for $C_{14}H_{26}O_2$: 226.1933). Monoacetate of **15**: ^{1}H nmr δ: 1.0–1.9 (complex, 21H), 1.97 (t, 2H, *J* = 7 Hz, -$CH_2$$CH_2$OAc), 2.10 (s, 3H, -COC$H_3$), and 4.23 (t, 2H, *J* = 7 Hz, -CH_2OAc).

Reduction of glycidic thiolesters with sodium borohydride

The reactions were carried out using the general procedure described below. Yields of products are shown in Table 3.

Can. J. Chem. Downloaded from www.nrcresearchpress.com by 123.30.183.119 on 09/08/12
For personal use only.

To a solution of a glycidic thiolester (0.5–1.0 mmol) in 98% ethanol (1–2 mL) cooled by an ice bath, was added sodium borohydride (4.0 molar equivalents) with stirring. After 10 min, the ice bath was removed and the reaction mixture was stirred at room temperature for 4–8 h. After the glycidic thiolester was completely consumed as shown by thin-layer chromatography, 1 N hydrochloric acid (5 mL) was carefully added to the mixture. The resulting mixture was poured into 1 N aqueous sodium hydroxide solution (50 mL) and extracted with methylene chloride (3 × 15 mL). The extracts were washed with aqueous saturated sodium chloride solution, combined, dried, filtered, and concentrated. The residue was chromatographed (30–60% ethyl acetate in hexane) to afford the epoxy alcohol.

Reduction of glycidic thiolesters with lithium aluminum hydride

The reactions were carried out using the general procedure described below. Yields of products are shown in Table 3.

At −78°C, to a solution of a glycidic thiolester (0.5–1.0 mmol) in ether (3–6 mL) under an atmosphere of argon was carefully added lithium aluminum hydride (3.0 molar equivalents). The reaction mixture was stirred at −78°C for 1 h, then quenched by addition of water (1 mL). The resulting mixture was acidified with 1 N hydrochloric acid and extracted with methylene chloride (3 × 10 mL). The extracts were washed with aqueous saturated sodium chloride solution, combined, dried, filtered, and concentrated. The residue was chromatographed (30–60% ethyl acetate in hexane) to give the corresponding epoxy alcohol.

The epoxy alcohols obtained from metal hydride reduction of glycidic thiolesters showed the following spectral data.

*2-Hydroxymethyl-1-oxaspiro[2.5]octane (**16**)*: ir: 3400 (OH) cm^{-1}; ^1H nmr δ: 1.4–1.9 (complex, 11H), 3.00 (dd, 1H, J = 7, 4.5 Hz, -C*H*CH_2OH), 3.70 (ddd, 1H, J = 12, 7, 4.5 Hz, -C*H*HOH), and 3.81 (ddd, 1H, J = 12, 8, 4.5 Hz, -CH*H*OH); CIMS $(M + NH_4)^+$: 160 (calcd. for $C_8H_{18}NO_2$: 160). Anal. calcd. for $C_8H_{14}O_2$: C 67.57, H 9.92, found: C 67.57, H 10.11.

*2-Hydroxymethyl-3-(2-phenylethyl)oxiranes (**17**)*:

cis-**17**: ir: 3417 and 3409 (OH) cm^{-1}; ^1H nmr δ: 1.57 (br s, 1H, D_2O exchangeable, -O*H*), 1.81 (dddd, 1H, J = 14, 8.5, 8, 6 Hz, -CH_2C*H*H-), 1.95 (dddd, 1H, J = 14, 9, 8, 6.5 Hz, -CH_2CH*H*-), 2.78 (dt, 1H, J = 13, 8 Hz, PhC*H*H-), 2.91 (ddd, 1H, J = 13, 9, 6. Hz, PhCH*H*-), 3.12 (ddd, 1H, J = 8.5, 6.5, 4 Hz, -CH_2C*H*-), 3.15 (dt, 1H, J = 4, 5 Hz, -C*H*CH_2OH), 3.62 (d, 2H, J = 5 Hz, -C*H*$_2$OH), and 7.25–7.45 (complex, 5H, Ar*H*); HRMS M^+: 178.0988 (calcd. for $C_{11}H_{14}O_2$: 178.0994). Acetate of *cis*-**17**: ^1H nmr δ: 1.94 (dt, 2H, J = 6, 8 Hz, -CH_2C*H*$_2$-), 2.12 (s, 3H, -COC*H*$_3$), 2.80 (dt, 1H, J = 14, 8 Hz, PhC*H*H-), 2.84 (dt, 1H, J = 14, 8 Hz, PhCH*H*-), 2.95 (ddd and dt, 2H, J = 6, 6, 3 and 6, 6 Hz, -CH_2C*H*OC*H*CH_2OAc), 3.90 (dd, 1H, J = 12, 6 Hz, -C*H*HOAc), 4.34 (dd, 1H, J = 12, 3 Hz, -CH*H*OAc), and 7.25–7.45 (complex, 5H, Ar*H*). *trans*-**17**: ir: 3417 and 3409 (OH) cm^{-1}; ^1H nmr δ: 1.58 (br s, 1H, D_2O exchangeable, -O*H*), 1.90 (ddd, 1H, J = 8.5, 8, 6 Hz, -CH_2C*H*H-), 1.94 (ddd, 1H, J = 8, 6.5, 6 Hz, -CH_2CH*H*-), 2.80 (ddd, 1H, J = 14, 8, 8 Hz, PhC*H*H-), 2.85 (ddd, 1H, J = 14, 8.5, 6.5 Hz, PhCH*H*-), 2.88 (ddd, 1H, J = 4.5, 2.5, 2 Hz, -CH_2C*H*-), 3.03 (dt, 1H, J = 2, 6 Hz, -C*H*CH_2OH), 3.62 (dd, 1H, J = 12, 4.5 Hz, -C*H*HOH), 3.88 (dd, 1H, J = 12.5, 2.5 Hz, -CH*H*OH), and 7.25–7.45 (complex, 5H, Ar*H*).

*2-Hydroxymethyl-3-cyclohexyloxiranes (**18**)*

cis-**18**: ir: 3418 (OH) cm^{-1}; ^1H nmr δ: 1.0–1.9 (complex, 11H), 2.02 (br s, 1H, -O*H*), 2.80 (dd, 1H, J = 8, 4 Hz, -CHC*H*-), 3.22 (ddd, 1H, J = 7, 4, 4 Hz, -C*H*CH_2-), 3.76 (dd, 1H, J = 12, 7 Hz, -C*H*HOH), and 3.93 (dd, 1H, J = 12, 4 Hz, -CH*H*OH); *trans*-**18**: ir: 3418 (OH) cm^{-1}; ^1H nmr δ: 1.0–2.0 (complex, 12H), 2.80 (dd, 1H, J = 7, 2.5 Hz, -CHC*H*-), 3.03 (ddd, 1H, J = 4, 2.5, 2.5 Hz, -C*H*CH_2-), 3.67 (ddd, 1H, J = 12, 7, 4 Hz, -C*H*HOH), and 3.95 (ddd, 1H, J = 12, 8, 2.5 Hz, -CH*H*OH); CIMS $(M + NH_4)^+$: 174 (calcd. for $C_9H_{20}NO_2$: 174).

cis- *6-tert-Butyl- 2-hydroxymethyl-1-oxaspiro[2.5]octane (**19**)*: ir: 3400 (OH) cm^{-1}; ^1H nmr δ: 0.90 (s, 9H, -C(CH_3)$_3$), 1.0–2.0 (complex, 10H), 3.05 (dd, 1H, J = 7, 4.5 Hz, -C*H*CH_2OH), 3.76 (ddd, 1H, J = 12, 7, 4 Hz, -C*H*HOH), and 3.87 (ddd, 1H, J = 12, 7, 4.5 Hz, -CH*H*OH); HRMS M^+: 198.1629 (calcd. for $C_{12}H_{22}O_2$: 198.1620).

*4-Cyclohexyl-2-hydroxymethyl-1-oxaspiro[2.5]octane (**20**)*: ir: 3420 (OH) cm^{-1}; ^1H nmr δ: 0.9–2.1 (complex, 21H), 2.85 (dd, 1H, J = 5, 7 Hz, -C*H*CH_2OH), 3.70 (ddd, 1H, J = 12, 7, 5 Hz, -CH*H*OH), and 3.90 (ddd, 1H, J = 12, 5, 7.5 Hz, -CH*H*OH); HRMS M^+: 224.1778 (calcd. for $C_{14}H_{24}O_2$: 224.1776). Anal. calcd. for $C_{14}H_{24}O_2$: C 74.95, H 10.78; found: C 74.82, H 10.45.

Acknowledgements

We are grateful to the Natural Sciences and Engineering Research Council of Canada and the University of Alberta for financial support.

1. O. Jeger, J. Norymberski, S. Szipilfogel, and V. Prelog. Helv. Chim. Acta, **29**, 684 (1946).
2. G. B. Spero, A. V. McIntosh, and R. H. Levin. J. Am. Chem. Soc. **70**, 1907 (1948).
3. M. L. Wolfrom and J. V. Karabinos. J. Am. Chem. Soc. **68**, 724 (1946); **68**, 1455 (1946).
4. H. J. Liu and H. K. Lai. Tetrahedron Lett. 1193 (1979).
5. H. J. Liu, H. K. Lai, and S. K. Attah-Poku. Tetrahedron Lett. 4121 (1979).
6. H. J. Liu and H. K. Lai. Can. J. Chem. **57**, 2522 (1979).
7. H. J. Liu and I. V. Oppong. Can. J. Chem. **60**, 94 (1982).
8. H. J. Liu, R. R. Bukownik, and P. R. Pednekar. Synth. Commun. **11**, 599 (1981).
9. H. J. Liu and W. Luo. Synth. Commun. **19**, 387 (1989).
10. D. J. Dagli and J. Wemple. J. Org. Chem. **39**, 2938 (1974).
11. D. J. Dagli, P.-S. Yu, and J. Wemple. J. Org. Chem. **40**, 3173 (1975).
12. H. O. House. Modern synthetic reactions. 2nd ed. W. A. Benjamin Inc., Menlo Park, CA. 1972. pp. 666–671.
13. A. I. Shatenshtein and H. A. Guozdeva. Tetrahedron, **25**, 2749 (1969).
14. H. Wynn. Ph.D. Dissertation, University of Alberta, 1985.
15. T. Harada, H. Karakawa, and A. Oku. Tetrahedron Lett. **28**, 4843 (1987).
16. S. M. Viti. Tetrahedron Lett. **23**, 4541 (1982).
17. P. Picard, D. Leclercq, J. P. Bats, and J. Moulines. Synthesis, 550 (1981).
18. J. Adams, L. Hoffman, Jr., and B. M. Trost. J. Org. Chem. **35**, 1600 (1970).
19. S. W. McCombie and W. A. Metz. Tetrahedron Lett. **28**, 383 (1987).
20. C. H. Behrens and K. B. Sharpless. Aldrichimica Acta, **16**, 67 (1983).
21. H. J. Liu and W. Luo. Synth. Commun. **21**, 2097 (1991).

Kinetics of the photochemical reactions of the croconate dianion in aqueous solution

B. ZHAO AND M. H. BACK
Ottawa–Carleton Chemical Institute, University of Ottawa, Ottawa, Ont., Canada K1N 6N5

Received July 5, 1991

B. ZHAO and M. H. BACK. Can. J. Chem. **70**, 135 (1992).

The kinetics of the photochemical reactions of the dianion of croconic acid (1,2-dihydroxycyclopentenetrione) have been studied in aqueous solution in the presence of electron acceptors. In neutral solutions the quantum yield for disappearance of croconate dianion was small ($<10^{-3}$) but was substantially increased in basic solution and in the presence of electron acceptors. At pH 12 in the presence of 4-nitrobenzylbromide and biacetyl a quantum yield of 1 was obtained. The kinetics of the rate of disappearance of croconate dianion as a function of pH and concentration of acceptor showed that the excited dianion is oxidized by acceptors and reacts with hydroxyl ion. A mechanism is proposed that, by assuming reasonable values for the rate constants involved, is shown to be consistent with the results.

Key words: photolysis, kinetics, croconate dianion, electron transfer.

B. ZHAO et M. H. BACK. Can J. Chem. **70**, 135 (1992).

Opérant en solution aqueuse, en présence d'accepteurs d'électrons, on a étudié la cinétique des réactions photochimiques du dianion de l'acide croconique (1,2-dihydroxycyclopentènetrione). Dans des solutions neutres, le rendement quantique pour la disparition du dianion croconate est faible ($<10^{-3}$); toutefois, il augmente considérablement en solution basique et en présence d'accepteurs d'électrons. À un pH de 12, en présence de bromure de 4-nitrobenzyle et de biacêtyl, on a obtenu un rendement quantique de 1. La cinétique de la vitesse de disparition du dianion croconate en fonction du pH et de la concentration d'accepteur montre que le dianion excité est oxydé par les accepteurs et qu'il réagit avec l'ion hydroxyle. On propose un mécanisme qui, en utilisant des valeurs raisonnables pour les constantes de vitesses impliquées, est en accord avec les résultats.

Mots clés : photolyse, cinétique, dianion croconate, transfert d'électrons.

[Traduit par la rédaction]

The cyclic dibasic acids, squaric, croconic, and rhodizonic, form symmetrical, resonance-stabilized structures when completely ionized.

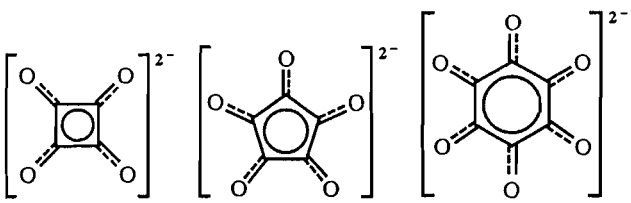

Squarate Croconate Rhodizonate

These dianions were named "oxocarbons" by West and Powell (1) and were recognized as members of an aromatic series containing only carbon and oxygen atoms (2, 3). These symmetrical structures have intrigued theoretical chemists who have discussed the structure and bonding, the properties of the molecular orbitals, and the excited electronic states (4–6). The dianions all show strong absorption in the first $\pi \rightarrow \pi^*$ electronic transition. The maximum in the absorption shifts from the visible, 483 nm (3.3×10^4 L mol^{-1} cm^{-1}), for rhodizonate to the near ultraviolet, 363 nm (3.9×10^4 L mol^{-1} cm^{-1}), for croconate, to the ultraviolet, 268 nm (2.4×10^4 L mol^{-1} cm^{-1}), for squarate. This property has led to several useful applications. Rhodizonic acid is an analytical reagent for metal ions, especially iron, lead, and barium (7–9). Squaric acid and croconic acid form condensation products with aminophenols and various types of pyrroles; these are intensely coloured and have found extensive use as photoreceptors in laser recording materials and other photoresponsive devices (10, 11). In spite of the importance of these anions and their derivatives, little is known about the chemical reactions occurring following absorption of light. Rhodizonic acid was known to be unstable when exposed to visible light but no study of the effect has been reported and no mechanism for the reaction proposed. We therefore began a systematic study of the kinetics of the photochemical reactions of these dianions, beginning with rhodizonate (12, 13).

The photochemical reaction of the rhodizonate dianion was shown to be inefficient, with quantum yields $<10^{-3}$ in neutral or weakly basic solutions (13). The rate of disappearance was significantly increased in the presence of electron acceptors, and quantum yields up to about 0.04 were obtained. The results were interpreted in terms of an initial electron transfer from the excited dianion to the acceptor, but a rapid reversal to ground state species prevented an efficient photodissociation. A similar mechanism was suggested to account for the slow thermal reaction.

In the present paper these studies have been extended to the croconate dianion in which the increased energy of the absorbed photon leads to a more efficient photodissociation process. Quantum yields of 1 have been observed in basic solution in the presence of certain additives. Two types of additives have been used to detect intermediates in the reaction: electron acceptors to oxidize the excited dianion of croconic acid, and diphenylpicrylhydrazyl (DPPH) and acrylamide to trap radicals that escaped from the solvent cage. A mechanism is proposed in which the excited dianion undergoes electron transfer to an acceptor molecule as well as direct reaction with hydroxyl ions.

Experimental

Disodium croconate, $Na_2C_5O_5$, was prepared by the thermal oxidation of sodium rhodizonate with hydrogen peroxide in basic solution, according to the procedure described by Schwartz, Gelb, and Yardley (14). The precipitate of sodium croconate was recrystallized from ethanol–water solution and dried at 120°C for 90 min. The ^{13}C NMR spectrum showed only one peak at 188 ppm and the extinction coefficient at the maximum of the strong $\pi \rightarrow \pi^*$ absorption, 363 nm, was 3.9×10^4 M^{-1} cm^{-1}, assuming the

Can. J. Chem. Downloaded from www.nrcresearchpress.com by 123.30.183.119 on 09/08/12
For personal use only.

Can. J. Chem. Downloaded from www.nrcresearchpress.com by 123.30.183.119 on 09/08/12
For personal use only.

salt was the monohydrate. Neutral solutions of sodium croconate were stable for several months when kept in the dark. Solutions for reaction were prepared daily from the stock solution using distilled and deionized water.

The light source was a medium-pressure mercury arc (Hanovia S-500) used with a Corning filter no. 7-37, which has a maximum transmission at 360 nm and a band pass of 35 nm. Thus the irradiating light was only the group of mercury emission lines in the range 365.0–366.3 nm (15). The intensity of light incident on the reaction cell was measured using a uranyl oxalate actinometer (16). During most of the experiments the incident intensity was in the neighbourhood of 1.1×10^{15} quanta cm^{-2} s^{-1}.

Solutions were irradiated in a spectrophotometer cell (1 cm × 1 cm) that was connected to a reservoir where solutions of croconate dianion and of additives were degassed, using five freeze–pump–thaw cycles, followed by mixing of the solutions in the spectrophotometer cell while under vacuum. The pH of the solutions ranged from 6 to 12, where the acid is fully ionized (pK_1 = 0.80; pK_2 = 2.25 (ref. 3, Chap 3)). The absorption spectra of the solutions were recorded using a Unicam SP-1800 spectrophotometer equipped with a thermostatted cell holder. The rate of disappearance of croconate was monitored at the maximum of its absorption, 363 nm. In all cases the initial rate was well defined and reproducible, with an uncertainty less than ±5%. Any effect of the presence of buffers was checked by irradiation at pH 12 using a trisodiumphosphate buffer or 0.01 M sodium hydroxide. Rates were the same in both solutions, showing that the ions associated with the buffer had no effect on the reaction. In the presence of acrylamide polymerization was measured by precipitating the polymer in methanol, followed by drying to constant weight at 60°C.

The additives used as electron acceptors were potassium ferricyanide, methyl viologen, 4-nitrobenzylbromide, and biacetyl. They were chosen to represent a range of compounds that easily accept electrons, subject to the restrictions imposed by solubility in water and little absorbance at 366 nm. Except for ferricyanide, where corrections for absorbance were made, the absorbance of the acceptors at 366 nm was <0.1% of that of croconate. The additive least soluble in water was 4-nitrobenzylbromide. Nevertheless at the highest concentration of this additive, 5×10^{-4} M, the absorbance was still linear with concentration. Hydrolysis of 4-nitrobenzylbromide is slow compared to the rate of disappearance of croconate even in strongly basic solutions. The absorption spectrum was unchanged in solutions of pH 12 for more than one-half hour.

All chemicals were reagent grade. Potassium ferricyanide was recrystallized from water–ethanol solutions and 4-nitrobenzyl bromide and acrylamide were recrystallized from methanol–water solution.

Results

Under all conditions croconic acid was more stable thermally than rhodizonic acid. The rhodizonate dianion was oxidized in the dark in aerated solutions, the rate increasing with increasing pH of the solution, and becoming too fast to allow photochemical measurements. Croconate dianion was stable in aerated neutral solutions for several months but the same trend of increasing instability in basic solution was observed. At pH 12, however, solutions of croconate were still stable for several hours. Photolysis in neutral or weakly basic aerated solutions was inefficient because of rapid quenching of the excited dianion by oxygen, but the rate of photolysis increased in basic solution. At pH 12 croconate dianion was converted to the squarate dianion, identified by the λ_{max} of its absorption spectrum, which showed the double maximum characteristic of all the oxocarbon dianions (Fig. 1). In degassed solutions about 30% of the croconate dianion was converted to squarate while in the presence of oxygen the conversion was 100%. Squarate dianion was the only product of the photolysis of croconate dianion identified by absorption over the wavelength range 200–700 nm, although minor absorption by other products at lower wavelength was observed in degassed solutions. Similar observations were made in the photolysis of rhodizonate dianion where croconate dianion was the only product that absorbed in the visible or the ultraviolet regions. Products that have lost the pseudo-aromatic structure of the oxocarbons would be too weakly absorbing to be detected at the concentrations used in the present experiments. The quantities produced were too small to be easily measured by other methods.

The conversion of croconate to squarate probably proceeds by an α-oxo alcohol rearrangement, by analogy with the mechanism discussed by West (3) for the conversion of rhodizonate to croconate, which occurs in the dark in basic solution in the presence of oxygen and some other oxidizing agents.

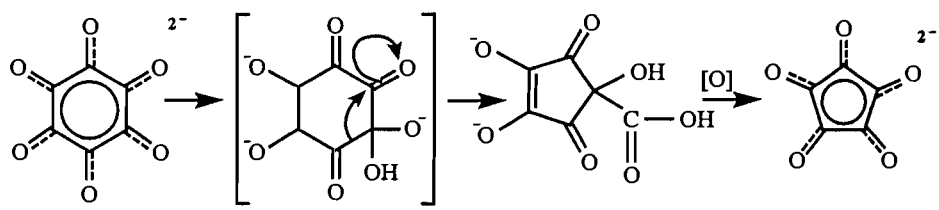

So efficient is this conversion that no other method has been developed for preparation of croconic acid. Formation of squarate from croconate has not previously been reported and it appears that photolysis under these conditions could provide a useful method for preparation of squaric acid.

In the presence of additives the characteristic spectrum of squarate was not as clear, since all of the additives themselves absorb in the neighbourhood of 270 nm. With ferricyanide a product was formed with λ_{max} 268 nm but the double maximum of squarate was obscured by the absorption due to ferrocyanide formed during the reaction. The product, if squarate, accounted for not more than 50% of the initial concentration of croconate and was observed both in the presence and absence of oxygen. The additive methyl viologen appeared not to be consumed in the reaction and when an equal concentration was used as reference the characteristic absorption spectrum of squarate was clearly seen. The amount corresponded to about 60% conversion of croconate. The absorption spectrum of 4-nitrobenzylbromide has a narrow band with a maximum at 280 nm. In

Can. J. Chem. Downloaded from www.nrcresearchpress.com by 123.30.183.119 on 09/08/12
For personal use only.

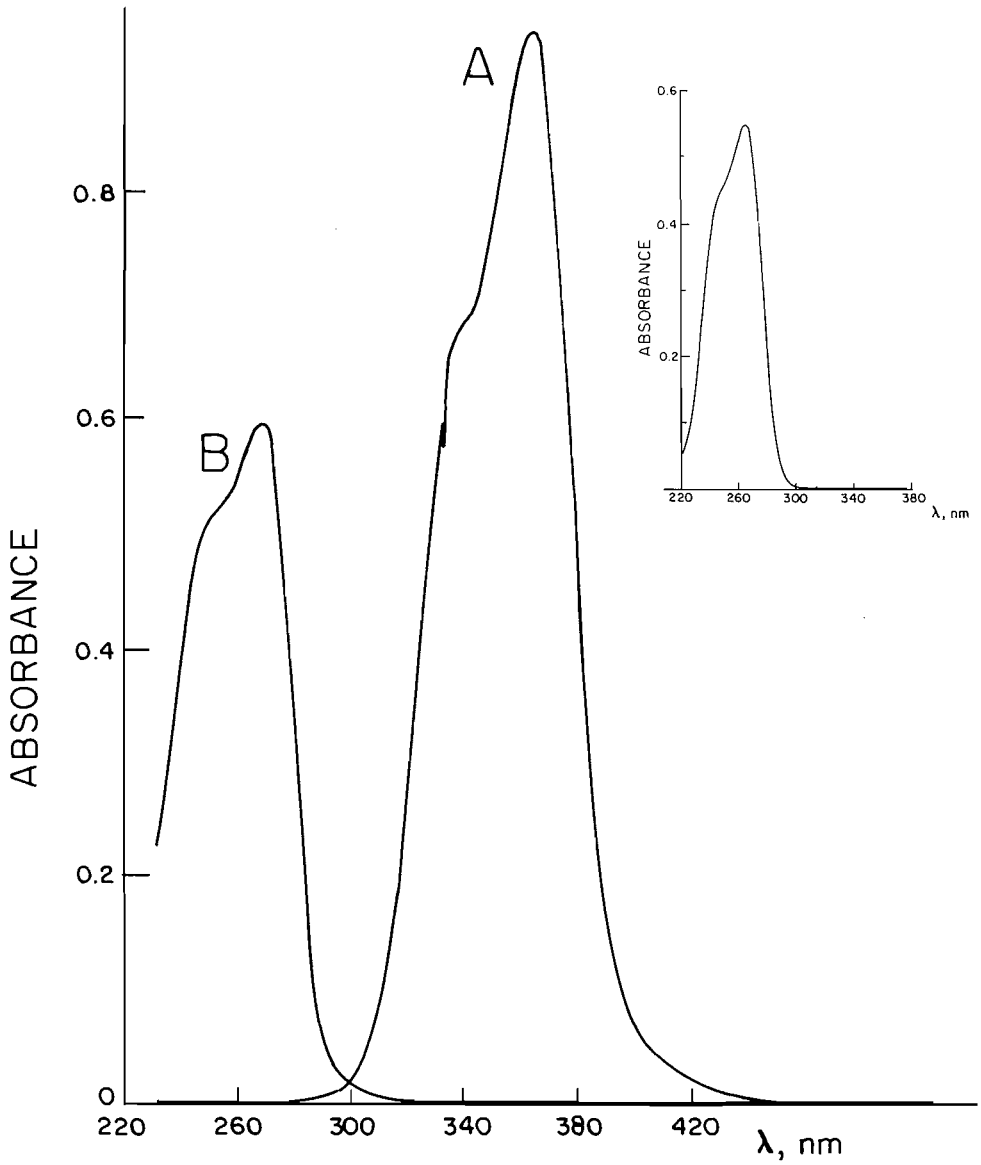

FIG. 1. Absorption spectra of a solution of croconate dianion before and after irradiation in the presence of oxygen, showing formation of squarate dianion. A. 2.4×10^{-5} M croconate dianion in 0.01 M sodium hydroxide before irradiation. B. Same solution after complete consumption of croconate dianion. The absorbance of the squarate dianion indicates quantitative conversion of croconate to squarate. Inset: absorption spectrum of 2.2×10^{-5} M squarate dianion in 0.01 M sodium hydroxide.

neutral solution, where formation of squarate from croconate alone was negligible, the absorbance at 280 nm decreased on photolysis, indicating that 4-nitrobenzylbromide was consumed in the reaction. In degassed basic solution the absorption maximum shifted to 268 nm and increased slightly. In the presence of oxygen the maximum also shifted to 268 nm and the absorbance increased substantially. Assuming that the molar loss of croconate is equal to the molar loss of 4-nitrobenzylbromide (unsubstantiated but reasonable) we estimate that conversion to squarate is 70% in the absence of oxygen and 100% in the presence of oxygen. With biacetyl, formation of squarate was not evident, possibly because of the strong absorption of biacetyl in this region. Hydration of biacetyl was observed at pH 12 and changes in the absorption spectrum were evident after about 10 min. The rate of photolysis of croconate was still much faster under these conditions and the rate was measured within 1 or 2 min of photolysis time. Further thermal reactions were observed after about 30 min.

Measurement of quantum yield

Deaerated solutions were photolyzed in the range of pH 6–12 in the presence and absence of the additives. In both the presence and absence of additives the quantum yield for disappearance of croconate dianion in acid solution was $<10^{-3}$ but increased in basic solution, approaching unity at pH 12 in the presence of biacetyl and 4-nitrobenzylbromide. These results are shown in Fig. 2 and summarized in Table 1.

The presence of an electron acceptor had a considerable effect on the quantum yield. As an illustration, the quantum yield for disappearance of croconate dianion is shown in Fig.

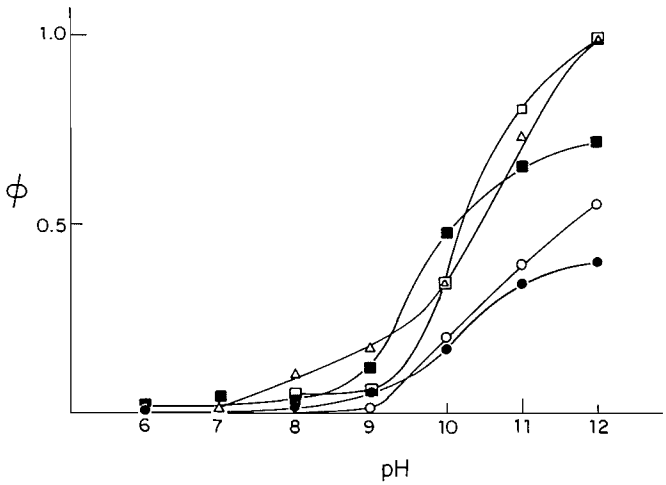

FIG. 2. The quantum yield for disappearance of croconate as a function of pH in the presence and absence of acceptors. The concentration of acceptor is given in Table 1. $[C_5O_5^{2-}] = 2.3 \times 10^5$ M. ●: no acceptor; ○: ferricyanide; ■: methylviologen; △: 4-nitrobenzylbromide; □: biacetyl.

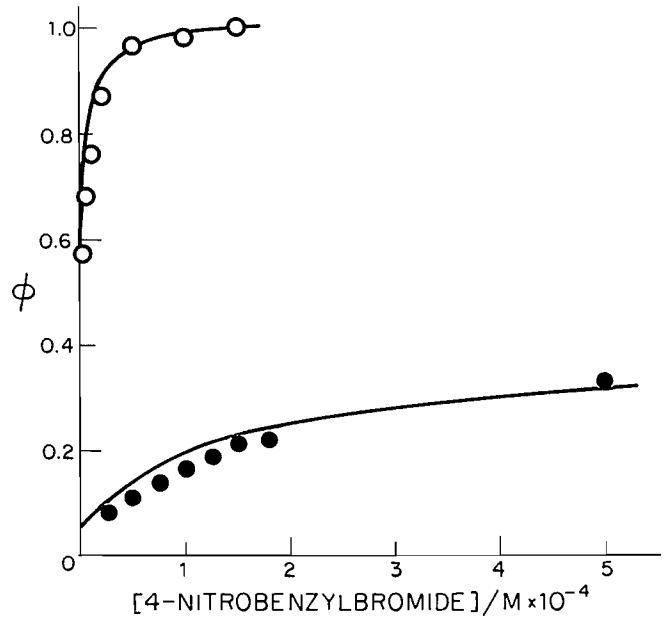

FIG. 3. The quantum yield for disappearance of croconate as a function of the concentration of 4-nitrobenzylbromide. The solid lines are calculated values (see text). $[C_5O_5^{2-}] = 2.3 \times 10^{-5}$ M. ●: pH 9; ○: pH 12.

3 as a function of the concentration of 4-nitrobenzylbromide at pH 9 and 12. The quantum yields as a function of concentration of each additive are given in Table 2. The dependence of the quantum yield on the concentration of croconate was measured with croconate alone at pH 12 and in the presence of 4-nitrobenzylbromide at pH 9. In both cases the quantum yield was independent of the concentration of croconate over the range $(1.3–3.3) \times 10^{-5}$ M.

Photolysis in the presence of radical traps

Photolyses in the presence of DPPH were performed in methanol solutions degassed under vacuum in the usual way. The spectrum and absorption maximum of croconate were not changed in methanol solution. Photolysis of mixtures of croconate and DPPH caused a loss of DPPH as measured by the absorbance of DPPH at 540 nm. Although DPPH has a strong absorbance at 366 nm, no measurable loss of DPPH occurred on photolysis in the absence of croconate. The rate of loss of DPPH was increased when biacetyl, 4-nitrobenzylbromide, and methyl viologen were added to the system but was not affected by the presence of potassium ferricyanide. The relative loss of DPPH as a function of time in the presence and absence of additives is shown in Fig. 4. The quantum yield for loss of DPPH, with respect to photons absorbed by croconate only at 366 nm, is given in Table 3.

Polymerization of acrylamide was observed on photolysis of croconate alone in aqueous solution and the rate was greatly increased in the presence of 4-nitrobenzylbromide and biacetyl. No increase in rate was observed with the additives ferricyanide or methyl viologen. The initial quantum yield for polymerization in aqueous solution at an initial pH of 4.1 is shown in Fig. 5 as a function of concentration of the additive 4-nitrobenzylbromide. Further measurements in buffered solutions showed that the quantum yield for polymerization increased to a maximum value of 2×10^3 at pH 8 and then declined in more basic solution. One experiment using an incident light intensity 14% of the original intensity showed that the rate was proportional to the square root of the light intensity. The results are summarized in Table 4.

The results of a more detailed study of the photopolymerization of acrylamide sensitized by croconate will be reported separately; the present limited results suggest that the photopolymerization follows the general mechanism involving mutual termination of radicals. The rate of polymerization may therefore be expressed by the general equation

$$[1] \quad R_p = k_p[M](\Phi_R I_{abs}/k_t)^{1/2}$$

where k_p and k_t are the rate constants for propagation and termination, respectively, for the acrylamide polymerization, [M] is the concentration of monomer, Φ_R is the quantum yield for production of radicals, and I_{abs} is the intensity of light absorbed by the initiator. Using the value for $k_p/k_t^{1/2}$ of 4.2 $M^{-1/2}$ $s^{-1/2}$ measured by Dainton and Tordoff (17), the quantum yield for production of radicals in the photolysis of croconate was obtained and is given in Table 4.

Discussion

The effect of all four additives on the quantum yield for reaction of croconate dianion is convincing evidence that an initial electron transfer occurs from the excited dianion. The fact that radical reactions (disappearance of DPPH and polymerization of acrylamide) are observed following photolysis indicates that the radical, or radicals, formed as a result of the electron transfer have sufficient lifetime to undergo reactions in the bulk solution. The increase in quantum yield observed in basic solutions (in the presence or absence of additive) suggests that the hydroxyl ion reacts directly with the excited croconate dianion. Excitation provides the energy required for this addition, which does not occur thermally at room temperature. By comparison, reaction of hydroxyl ion with rhodizonate dianion was observed in basic solution without photoexcitation.

A further interesting observation is an apparently synergistic effect of the additive and hydroxyl ions. For exam-

Can. J. Chem. Downloaded from www.nrcresearchpress.com by 123.30.183.119 on 09/08/12
For personal use only.

TABLE 1. Quantum yield for disappearance of $C_5O_5^{2-}$
$[C_5O_5^{2-}] = 2.3 \times 10^{-5}$ M

pH	No additive	$Fe(CN)_6^{3-}$ (5×10^{-4} M)	MV^{2+} (1×10^{-4} M)	$BrCH_2C_6H_4NO_2$ (1×10^{-4} M)	Biacetyl (1×10^{-4} M)
6	0.009		0.018	0.004	
7	0.012	0.0014	0.042	0.005	
8	0.012	0.0057	0.028	0.10	0.052
9	0.05	0.011	0.12	0.17	0.059
10	0.17	0.20	0.48	0.34	0.34
11	0.34	0.49	0.65	0.73	0.81
12	0.40	0.55	0.71	0.98	0.98

TABLE 2. Quantum yield for disappearance of $C_5O_5^{2-}$ at pH 9 and 12
$[C_5O_5^{2-}] = 2.3 \times 10^{-5}$ M

Additive concentration (M)	$Fe(CN)_6^{3-}$ pH = 12	MV^{2+} pH = 12	$BrCH_2C_6H_4NO_2$ pH = 12	$BrCH_2C_6H_4NO_2$ pH = 9	Biacetyl pH = 12
6.0×10^{-7}		0.62			
1.5×10^{-6}			0.57		
5.0×10^{-6}		0.71	0.68		
1.0×10^{-5}			0.76		0.5
2.0×10^{-5}	0.44	0.72	0.87	0.080	0.60
3.8×10^{-5}					0.73
5.0×10^{-5}	0.57	0.73	0.97	0.11	0.81
8.0×10^{-5}				0.14	0.95
1.0×10^{-4}	0.54	0.74	0.98	0.17	0.98
1.5×10^{-4}		0.71	1.0	0.21	1.0
2.0×10^{-4}	0.53			0.23	
3.0×10^{-4}		0.67			
5.0×10^{-4}	0.52			0.33	

ple, the increase in quantum yield observed on addition of 4-nitrobenzylbromide depends greatly on the pH of the solution. This is illustrated in Fig. 3 where the change in quantum yield is shown as a function of concentration of 4-nitrobenzylbromide at pH 9 and 12. If the effects of both reactants, hydroxyl ion and acceptor, were additive the rate of change of quantum yield with concentration of acceptor would not change with pH; only the quantum yield without additive would change. The limiting quantum yield at high concentration of additive is also quite different at pH 9 and pH 12. Such an effect requires an interaction of one of the reactants with an intermediate formed by the other reactant.

A mechanism for the reaction incorporating these features and allowing for deactivation of the excited state by both acceptor and hydroxyl ion is summarized below (Scheme 1), where A is an acceptor molecule and $(C_5O_5^{2-}...A^-)$ and $(C_5O_5^{2-}...OH^-)^*$ represent the transient intermediates formed between the excited state of the dianion and the reactant, which in each case may re-form the ground state reactants, proceed to products, or react with the other reactant.

Assuming a steady-state concentration of all intermediates the quantum yield may be expressed as

$$[2] \quad \Phi = \frac{k_1[A]}{k_D + k_1[A] + k_6[OH^-]}\left[\frac{k_3 + k_4[OH^-]}{k_2 + k_3 + k_4[OH^-]}\right] + \frac{k_6[OH^-]}{k_D + k_1[A] + k_6[OH^-]}\left[\frac{k_8 + k_9[A]}{k_7 + k_8 + k_9[A]}\right]$$

Photolysis in the absence of acceptors

In the absence of acceptor, eq. [2] may be simplified as follows:

$$[3] \quad \Phi = \frac{k_6[OH^-]}{k_D + k_6[OH^-]}\left[\frac{k_8}{k_7 + k_8}\right]$$

A plot of Φ^{-1} against $[OH^-]^{-1}$ is shown in Fig. 6. Values of $k_8/(k_7 + k_8)$ and k_D/k_6 obtained from the intercept and slope are given in Table 5*a*. Efficient reaction at these concentrations of reactant and hydroxyl ion requires a lifetime for the excited croconate in the microsecond range and preliminary measurements of the time constant for re-formation of the ground state croconate dianion following flash photolysis (18) indicated a value for k_D of 1.3×10^4 s^{-1}. The excited state of the dianion is undoubtedly the triplet. With this value for k_D, $k_6 = 10^8$ M^{-1} s^{-1}. The fact that the ratio $k_8/(k_7 + k_8)$ is smaller than 1 indicates that deactivation by the hydroxyl ion occurs concurrently with reaction.

Photolysis in the presence of acceptors

The addition of electron acceptors in every case increased the quantum yield of disappearance of croconate dianion. Thus energy transfer quenching of the excited croconate dianion by the additives appears of little importance, particularly in basic solution where the quantum yield was high and with biacetyl and 4-nitrobenzylbromide reached a value of 1. It follows that the quantum yield for intersystem crossing is unity and for these additives energy transfer

Can. J. Chem. Downloaded from www.nrcresearchpress.com by 123.30.183.119 on 09/08/12
For personal use only.

Can. J. Chem. Downloaded from www.nrcresearchpress.com by 123.30.183.119 on 09/08/12
For personal use only.

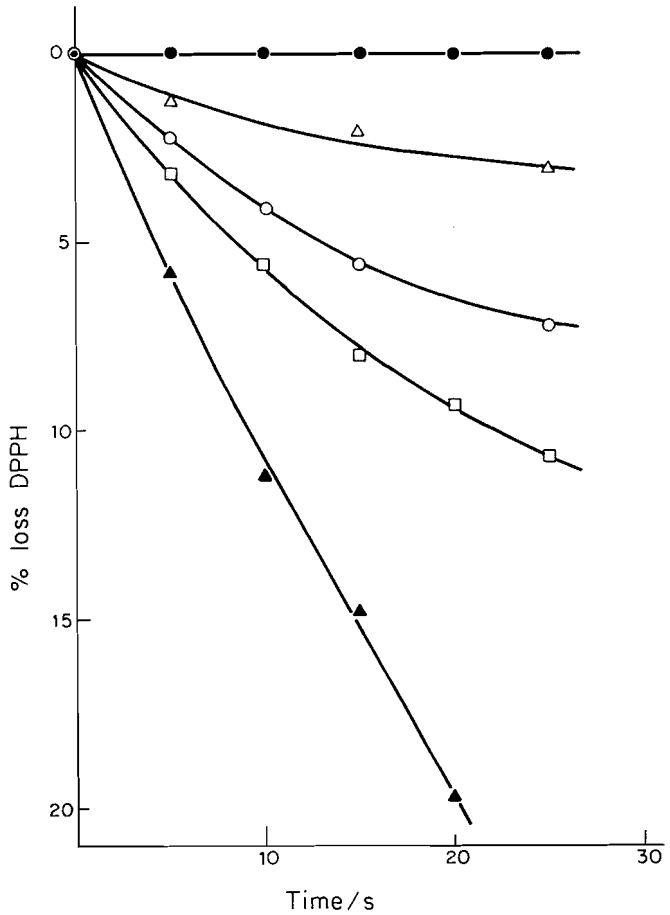

FIG. 4. The percentage loss of DPPH as a function of time. $[C_5O_5^{2-}] = 2.3 \times 10^{-5}$ M; [DPPH] = 3.1×10^{-5} M. ●: biacetyl + DPPH; △: DPPH + $C_5O_5^{2-}$; ○: DPPH + $C_5O_5^{2-}$ + methyl viologen, 6.4×10^{-5} M; □: DPPH + $C_5O_5^{2-}$ + 4-nitrobenzylbromide, 6.4×10^{-5} M; △: DPPH + $C_5O_5^{2-}$ + biacetyl, 3.2×10^{-5} M

TABLE 3. Quantum yield for disappearance of DPPH

Additive	[Additive] ($M/10^{-5}$)	[DPPH] ($M/10^{-5}$)	$[C_5O_5^{2-}]$ ($M/10^{-5}$)	Φ
No additive	0	3.1	2.3	0.055
Biacetyl	3.2	3.1	0	0
Biacetyl	3.2	1.5	2.3	0.52
Biacetyl	3.2	3.1	2.3	0.53
Biacetyl	3.2	4.7	2.3	0.52
Biacetyl	3.2	6.2	2.3	0.52
Biacetyl	6.4	3.1	2.3	0.52
$BrCH_2C_6H_4NO_2$	6.4	3.1	2.3	0.28
MV^{2+}	6.4	3.1	2.3	0.20

quenching must be negligible. For the additives where the quantum yield was less than unity, energy transfer quenching cannot be unequivocally ruled out, although the lower quantum yields can be accounted for by other reactions, as will be shown later.

At lower pH where the reaction with hydroxyl ion becomes negligible, eq. [2] may be written as

$$[4] \quad \Phi = \frac{k_1[A]}{k_D + k_1[A] + k_6[OH^-]} \left[\frac{k_3 + k_4[OH^-]}{k_2 + k_3 + k_4[OH^-]}\right]$$

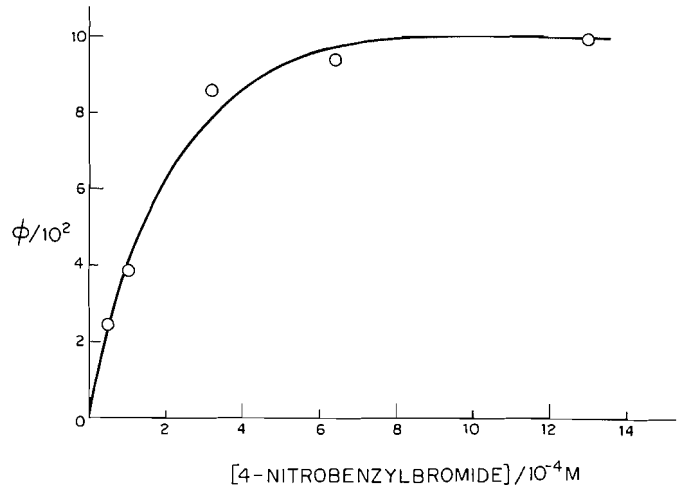

FIG. 5. The quantum yield for polymerization as a function of the concentration of 4-nitrobenzylbromide in aqueous solution. $[C_5O_5^{2-}] = 2.3 \times 10^{-5}$ M; [acrylamide] = 1.0 M.

TABLE 4. Rate and quantum yields of polymerization using 4-nitrobenzyl bromide
$[BrCH_2C_6H_4NO_2] = 6.4 \times 10^{-4}$ M, [Monomer] = 1.0 M

pH	Polymerisation (%)	Rate ($M\ s^{-1}/10^{-3}$)	Φ_p	Φ_R	Φ_3
4	15.4	0.86	1010	0.039	
5	21.1	1.17	1430	0.075	
6	25.7	1.43	1740	0.112	
7	27.3	1.52	1800	0.123	0.39
8	31.2	1.73	2110	0.162	0.38
9	26.2	1.46	1900	0.125	0.31
10	20.0	1.11	1610	0.08	0.10
11	18.4	1.02	1570	0.072	0.006
12	15.5	0.86	1480	0.037	1×10^{-4}

$[I_{abs}]$	$C_5O_5^{2-} + h\nu \rightarrow C_5O_5^{2-}*$
[D]	$C_5O_5^{2-}* \rightarrow C_5O_5^{2-}$
1.	$C_5O_5^{2-}* + A \rightarrow (C_5O_5^{\cdot-}\ldots A^-)$
2.	$(C_5O_5^{\cdot-}\ldots A^-) \rightarrow C_5O_5^{2-} + A$
3.	$(C_5O_5^{\cdot-}\ldots A^-) \rightarrow C_5O_5^{\cdot-} + A^-$
4.	$(C_5O_5^{\cdot-}\ldots A^-) + OH^- \rightarrow$ products
5.	$C_5O_5^{\cdot-} \rightarrow$ products
6.	$C_5O_5^{2-}* + OH^- \rightarrow (C_5O_5^{2-}\ldots OH^-)*$
7.	$(C_5O_5^{2-}\ldots OH^-)* \rightarrow C_5O_5^{2-} + OH^-$
8.	$(C_5O_5^{2-}\ldots OH^-)* \rightarrow$ products
9.	$(C_5O_5^{2-}\ldots OH^-)* + A \rightarrow$ products

SCHEME 1

Plots of Φ^{-1} as a function of $[A]^{-1}$ for the additive 4-nitrobenzylbromide at pH 8 and 9 are shown in Fig. 7 and the values of k_D/k_1 and the ratio $(k_3 + k_4[OH^-])/(k_2 + k_3 + k_4[OH^-])$ obtained from these results are given in Table 5*b*. If an upper limit of $10^9\ M^{-1}\ s^{-1}$ is assumed for k_4, then the corresponding upper limits for k_3 and $k_2 + k_3$ are 10^4 and $4 \times 10^4\ s^{-1}$, respectively.

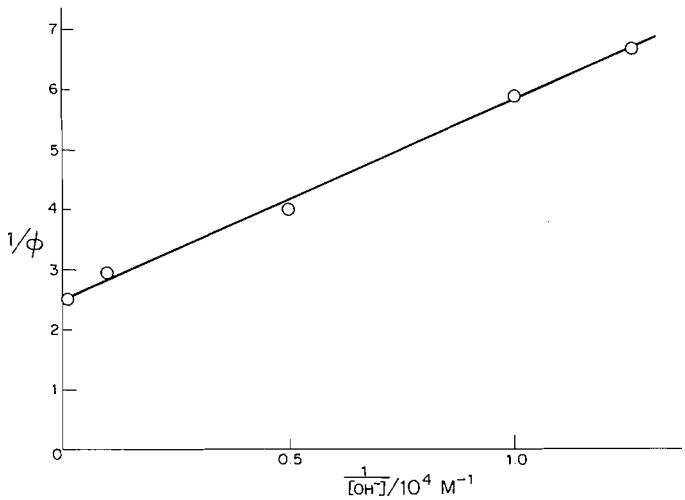

FIG. 6. Φ^{-1} for disappearance of croconate as a function of $[OH^-]^{-1}$ in the absence of acceptors. $[C_5O_5^{2-}] = 2.3 \times 10^{-5}$ M.

TABLE 5. Ratios of rate constants obtained from Figs. 5 and 6; $k_D = 1.3 \times 10^4$

(*a*)

$\frac{k_8}{k_7 + k_8}$	$\frac{k_D}{k_6}$
0.40	1.3×10^{-4}

(*b*)

pH	$\frac{k_3 + k_4[OH^-]}{k_2 + k_3 + k_4[OH^-]}$	$\frac{k_D}{k_1}$
8	0.25	1.5×10^{-4}
9	0.40	1.3×10^{-4}

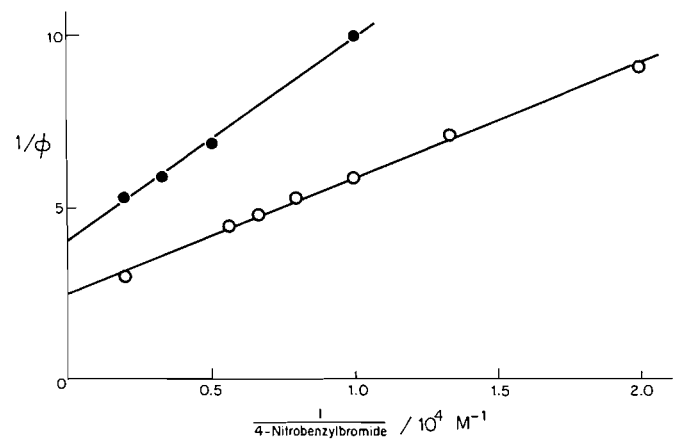

FIG. 7. Φ^{-1} for disappearance of croconate as a function of [4-nitrobenzylbromide]$^{-1}$. $[C_5O_5^{2-}] = 2.3 \times 10^{-5}$ M. ●: pH 8; ○: pH 9.

TABLE 6. Values for the rate constants in eq. [2]

k_1 (4-Nitrobenzylbromide)	8×10^7 M^{-1} s^{-1}
k_1 (Biacetyl)	8×10^8 M^{-1} s^{-1}
$k_2 + k_3$	4×10^4 s^{-1}
k_3	1×10^4 s^{-1}
k_4	1×10^9 M^{-1} s^{-1}
k_6	1×10^8 M^{-1} s^{-1}
$k_7 + k_8$	3.3×10^3 s^{-1}
k_8	1.3×10^3 s^{-1}
k_9 (4-Nitrobenzylbromide)	1×10^9 M^{-1} s^{-1}
k_9 (Biacetyl)	1×10^8 M^{-1} s^{-1}
k_D	1.3×10^4 s^{-1}

Evaluation of eq. [2]

With these guides to the values of the rate constants the quantum yield may be calculated from eq. [2] as a function of concentration of additive and of hydroxyl ion. If the rate constants for reactions 1 and 6 (Scheme 1) are similar, the fraction $k_6[OH^-]/(k_D + k_1[A] + k_6[OH^-])$ will be practically unity at pH 12 where $[OH^-] \gg [A]$, the fraction $k_1[A]/(k_D + k_1[A] + k_6[OH^-])$ will be negligible, and the increase in quantum yield as the concentration of additive increases to 10^{-4} M must be caused by the increasing contribution of reaction 9 through the fraction $(k_8 + k_9[A])/k_7 + k_8 + k_9[A])$. Both reactions 4 and 9 may also be diffusion controlled with rate constants close to 10^9 M^{-1} s^{-1}. At a concentration of 4-nitrobenzylbromide of 1×10^{-4} M, $k_9[A]$ must be much greater than $k_7 + k_8$ and therefore the maximum value for $k_7 + k_8$ will be approximately 1×10^3.

Minor modifications to these rate constants were made to maximize the agreement of the calculated quantum yields with the experimental measurements for the additive 4-nitrobenzylbromide at both pH 12 and pH 9. The final values for the rate constants are given in Table 6 and the calculated values for the quantum yield are shown as the solid lines in Fig. 3. At pH 12, as predicted, the first term in eq. [2] contributes a maximum of 1% to the quantum yield even at the highest concentration of 4-nitrobenzylbromide. At pH 9 both terms contribute to the reaction at lower concentrations of additive but at high concentrations the first term predominates. Examples of the values for the fractions in eq. [2] are given in Table 7.

With the additive biacetyl the approach of the quantum yield to the limiting value of 1 at pH 12 was slower over a comparable range of concentration, suggesting that reaction 9 was substantially slower than the corresponding reaction with 4-nitrobenzylbromide. The best agreement was obtained with $k_9 = 10^8$ M^{-1} s^{-1} and $k_1 = 10^{10}$ M^{-1} s^{-1}, the other constants remaining the same. The results for the measurements at pH 12 and pH 11 are shown in Fig. 8. Agreement is only qualitative, suggesting that additional reactions with this additive may be important, but the general pattern of the reaction and the change of quantum yield with pH are consistent with the mechanism.

The quantum yield in the presence of potassium ferricyanide and methyl viologen reached a limiting value less than 1 at pH 12, which suggests deactivation by the additive. To be effective at pH 12, deactivation must take place at the $(C_5O_5^{2-}...OH^-)^*$ complex rather than at the excited croconic dianion.

10. $(C_5O_5^{2-}...OH^-)^* + A \rightarrow C_5O_5^{2-} + OH^- + A$

Can. J. Chem. Downloaded from www.nrcresearchpress.com by 123.30.183.119 on 09/08/12
For personal use only.

TABLE 7. Values of the ratios in eq. [2] with 4-nitrobenzylbromide as additive

pH	[A] (M)	$\frac{k_1[A]}{k_D + k_1[A] + k_6[OH^-]}$	$\frac{k_3 + k_4[OH^-]}{k_2 + k_3 + k_4[OH^-]}$	$\frac{k_6[OH^-]}{k_D + k_1[A] + k_6[OH^-]}$	$\frac{k_8 + k_9[A]}{k_7 + k_8 + k_9[A]}$	Φ
9	1×10^{-5}	0.054	0.40	0.068	0.85	0.079
9	1×10^{-4}	0.364	0.40	0.045	0.98	0.19
12	1×10^{-5}	0.0007	1.00	1.00	0.85	0.85
12	1×10^{-4}	0.008	1.00	0.98	0.98	0.96

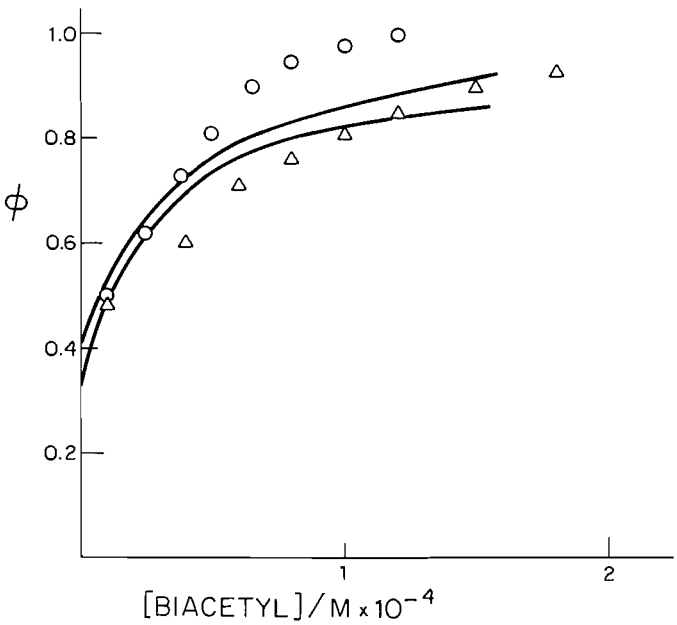

FIG. 8. The quantum yield for disappearance of croconate as a function of the concentration of biacetyl. $[C_5O_5^{2-}] = 2.3 \times 10^{-5}$ M. The solid lines are calculated values (see text). ○: pH 12; △: pH 11.

The fraction $(k_8 + k_9[A])/(k_7 + k_8 + k_9[A])$ in the second term in eq. [2] becomes $(k_8 + k_9[A])/(k_7 + k_8 + k_9[A] + k_{10}[A])$ and approaches the limit $k_9/(k_9 + k_{10})$ as the concentration of additive increases. The limit for potassium ferricyanide was 0.56 and was obtained at a concentration of 5×10^{-5} M^{-1} s^{-1}. For this additive the rate of reaction 9 is therefore slightly greater than for 4-nitrobenzylbromide. With methyl viologen the limiting quantum yield was observed at a concentration 10 times lower, 5×10^{-6} M, and the rate constant for reaction 9 would therefore be of the order of 5×10^{10} M^{-1} s^{-1}. Reaction 1 would likely be very fast as well but still would not make a significant contribution at pH 12. Such a large value for k_9 (or k_1) is reasonable considering the attraction of the positive ion towards the excited dianion and the excited hydroxyl ion complex.

The structure of the hydroxyl ion complex and the type of interaction involved in its formation are, of course, quite unknown. The spectrum of the dianion showed no change in basic solution, and interaction of the dianion and the hydroxyl ion in the ground state is probably unimportant. From studies of NMR spectra it was shown that the dianion was not hydrated in aqueous solution; only the undissociated acid gave evidence of hydration (19). The kinetic evidence clearly indicates reaction 6 is important but identification of the intermediate will require time-resolved experiments.

Further adjustment of rate constants or addition of new reactions to the mechanism was not attempted at this stage. The test of eq. [2] is sufficient to show that the mechanism, although oversimplified, gives a consistent picture of the type of reactions occurring on photolysis.

Polymerization of acrylamide

The rate of initiation of the polymerization of acrylamide is a measure of the rate of production of radicals in the solution. Polymerization occurred in slightly acid solutions and even in an aqueous solution of the monomer (pH 4.1) where the quantum yield for disappearance of croconate was not measurable, even in the presence of 4-nitrobenzylbromide. Polymerization is thus a very sensitive test for the presence of radicals. The rate of polymerization increased with increasing pH, achieved a maximum rate at pH 8, and then decreased in more basic solution. It may be concluded that reactions of the hydroxyl ion with the excited dianion or the intermediate complex do not lead to the formation of radicals. Reaction of the dianion with the additive, on the other hand, should produce radicals through electron transfer, reaction 3, and the quantum yield for this reaction is given by the following expression:

$$[5] \quad \Phi_3 = 2 \cdot \frac{k_1[A]}{(k_D + k_1[A] + k_6[OH^-])} \left[\frac{k_3}{(k_2 + k_3 + k_4[OH^-])}\right]$$

The product of these ratios, calculated using the rate constants in Table 6, is given in the last column in Table 4, where it may be compared with the quantum yield for initiation of radicals calculated from the quantum yield for polymerization and the rate constants for propagation and termination for the acrylamide polymerization. Taking into account the uncertainties in both calculation and measurement, the agreement between these two rates of initiation of radicals is reasonable and is convincing evidence that the electron transfer reaction produces radicals that have sufficient lifetime to diffuse into the solution. It is worth noting that one half of the value for the rate of formation of radicals by reaction 3 is very close to the initiation rate obtained for the rate of polymerization, particularly in the range of pH 7–10, suggesting that only one radical produced in reaction 3 may initiate polymerization. If only the radical formed by electron transfer to the acceptor, and not the croconate monoan-

Can. J. Chem. Downloaded from www.nrcresearchpress.com by 123.30.183.119 on 09/08/12
For personal use only.

ion, were effective in polymerization, the lack of initiation of polymerization in the presence of ferricyanide and methyl viologen would be more readily explained.

Comparison with the photochemical reaction of rhodizonate dianion

Several similarities and differences are evident in the photochemical behaviour of these two oxocarbon anions. Both excited dianions undergo oxidation by electron transfer to a suitable acceptor. The efficiency of the process appears much larger for croconate where a primary quantum yield of 1 for disappearance of the dianion was obtained for certain additives, whereas the quantum yield for disappearance of rhodizonate in the presence of additives did not exceed 4×10^{-2}. The large quantum yield for loss of croconate, however, was observed only in basic solution and was the result of the synergistic effect of the additive and the hydroxyl ion. The photochemical reaction of rhodizonate was measured only in neutral solution because the thermal reaction in basic solution was too fast to allow concurrent photochemical measurements. The similarity in these observations is the loss of the dianion through reactions with hydroxyl ion. In the case of rhodizonate the reaction occurs in the dark, whereas with croconate photochemical excitation of the dianion is required to induce reaction.

The product of the thermal reaction of rhodizonate dianion in basic solution in the presence of oxygen was croconate dianion. Conversion of croconate to squarate occurred photochemically in strongly basic solution in the presence of oxygen. This reaction is a possible easy route to the formation of squaric acid.

Summary and conclusions

The main conclusions from the results of this kinetic study of the photochemical reactions of croconate dianion are (1) both electron acceptors and hydroxyl ion react directly with the excited croconate dianion; (2) both electron acceptors and hydroxyl ion react further with the intermediates formed in the primary interaction of each reactant; (3) radicals are produced and diffuse into the solution following the electron transfer and not following the reactions with hydroxyl ion.

Acknowledgments

The authors thank Joanne Elliot, undergraduate student at the University of Ottawa, and Pamela Li, summer student in the Department of Chemistry, 1989, for valuable preliminary work on the photochemistry of the croconate dianion. The authors thank NSERC for continued financial support.

1. R. West and D. L. Powell. J. Am. Chem. Soc. **85**, 2577 (1963).
2. R. West and J. Niu. Non-benzenoid aromatics. Vol. 1. *Edited by* J. Snyder. Academic Press, New York. 1969. p. 311.
3. R. West (*Editor*). Oxocarbons. Academic Press, New York. 1980. Chap. 1.
4. M. Campos-Vallette, K. A. Figueroa, and C. Puebla. Spectrosc. Lett. **21**, 303 (1988).
5. J. Aikara. Bull. Chem. Soc. Jpn. **60**, 2268 (1987).
6. T-K. Ha and C. Puebla. J. Mol. Struct. **137**, 171 (1986); **137**, 183 (1986).
7. L. J. Silvestri, R. E. Hurst, L. Simpson, and J. M. Settine. Anal. Biochem. **123**, 303 (1982).
8. J. R. Preer and G. B. Murchison. Environ. Pollut. Ser. B, **12**, 1 (1986).
9. J. H. Gould, S. G. Capar, R. M. Jacobs, and R. Plunkett. Anal. Lett. **21**, 2145 (1988).
10. K-Y. Law and F. C. Bailey. Can. J. Chem. **64**, 2267 (1986).
11. K-Y. Law. J. Imaging Sci. **31**, 83 (1987).
12. G. Iraci and M. H. Back. Can. J. Chem. **66**, 1293 (1988).
13. B. Zhao and M. H. Back. Can. J. Chem. **69**, 528 (1991).
14. L. M. Schwartz, R. I. Gelb, and J. O. Yardley. J. Phys. Chem. **79**, 2246 (1975).
15. J. G. Calvert and J. N. Pitts. Photochemistry. John Wiley, New York. (1966). p. 696.
16. J. F. Rabek. Experimental methods in photochemistry and photophysics. Wiley–Interscience, New York. 1982.
17. F. S. Dainton and M. Tordoff. Trans. Faraday Soc. **53**, 499 (1957).
18. B. Zhao and M. H. Back. J. Polym. Sci. Part A: Polym. Chem. In press.
19. R. I. Gelb, L. M. Schwartz, D. A. Laufer, and J. O. Yardley. J. Phys. Chem. **81**, 1268 (1977).

Can. J. Chem. Downloaded from www.nrcresearchpress.com by 123.30.183.119 on 09/08/12
For personal use only.

Open-chain nitrogen compounds. Part XIV.[1] Synthesis of 1-aryl-3-aryloxymethyl-3-methyltriazenes and 1-aryl-3-(hydroxyaryl)methyl-3-methyltriazenes

M. P. MERRIN AND D. L. HOOPER
Dalhousie University, Halifax, N.S., Canada B3H 4J3

AND

R. J. LAFRANCE, R. SNOOKS, and K. VAUGHAN[2]
Saint Mary's University, Halifax, N.S., Canada B3H 3C3

Received May 13, 1991

M. P. MERRIN, D. L. HOOPER. R. J. LAFRANCE, R. SNOOKS, and K. VAUGHAN. Can. J. Chem. **70**, 144 (1992).

The synthesis of a new series of 1-aryl-3-aryloxymethyl-3-methyltriazenes (**2**) has been achieved by the reaction of the acetoxymethyltriazene (Ar-N=N-NMe-CH_2OAc) with the appropriate phenol in dry chloroform solution. Triazenes of type **2** are also formed by reaction of the acetoxymethyltriazene with the sodium phenolate, generated by reaction of the phenol with sodium hydride in dry chloroform, but under these conditions a second product is formed, which has been identified as an isomer of **2**. The structure of the second product has been elucidated by spectroscopic analysis to be the 1-aryl-3-(hydroxyaryl)methyl-3-methyltriazene (**3**). The formation of these two isomeric products is accounted for by the ambident nature of the nucleophilic phenolate ion in the displacement of the acetoxy leaving group. The mass spectra of all the triazenes of type **2** exhibit a fairly intense peak at M − 102, which is suggested to arise from a novel intramolecular rearrangement. Two examples of the triazenes of type **2** have been tested for antitumour activity on the NCI tumour panel and have shown statistically significant differential sensitivity in several cell lines. Preliminary investigation of the stability of these triazenes in physiological-pH buffer suggests that they may have the appropriate chemical stability for pro-drug application in therapy.

Key words: triazene, synthesis, antitumour, phenol, spectroscopy, aryloxymethyltriazene, prodrugs.

M. P. MERRIN, D. L. HOOPER, R. J. LAFRANCE, R. SNOOKS et K. VAUGHAN. Can. J. Chem. **70**, 144 (1992).

On a effectué la synthèse d'une nouvelle série de 1-aryl-3-aryloxyméthyl-3-méthyltriazènes (**2**) par la réaction, en solution dans du chloroforme sec, de l'acétoxyméthyltriazène (Ar-N=N-NMe-CH_2OAc) avec le phénol approprié. Le réaction de l'acétoxyméthyltriazène avec le phénolate de sodium, généré par une réaction du phénol avec l'hydrure de sodium dans du chloroforme sec, conduit aussi à la formation des triazènes du type **2**; toutefois, dans ces conditions, il y a formation concomitante d'un autre produit que l'on a identifié comme un isomère du produit **2**. Sur la base d'analyse spectroscopiques, on a établi que le second produit est le 1-aryl-3-(hydroxyaryl)méthyl-3-méthyltriazène (**3**). On explique la formation de ces deux produits isomèriques par la nature ambidente de l'ion phénolate nucléophile dans la réaction de substitution du groupement acétoxyle nucléofuge. Les spectres de masse des triazènes de type **2** présentent tous un pic assez intense à M − 102 qui proviendrait d'un nouvel exemple de réarrangement intramoléculaire. On a évalué deux des triazènes de type **2** pour leur activité antitumorale sur un ensemble de tumeurs NCI; ces produits présentent des sensibilités différentielles statistiquement significatives dans plusieurs lignées de cellules. Une étude préliminaire de la stabilité de ces triazènes dans des tampons à pH physiologique suggère qu'ils ont peut-être la stabilité chimique appropriée pour être utilisés comme pré-médicaments.

Mots clés : triazène, synthèse, antitumorale, phénol, spectroscopie, aryloxyméthyltriazène, pré-médicament.

[Traduit par la rédaction]

Introduction

1-Aryl-3,3-dimethyltriazenes (**1***a*) are an important class of antitumour agents (1), which have been shown to undergo metabolic activation to the short-lived 3-hydroxymethyltriazene (**1***b*) (2). Although the hydroxymethyltriazene (HMT) is inherently unstable under physiological conditions, it has been suggested (3) that a stable derivative of the HMT might be a suitable pro-drug for the active metabolite of the dimethyltriazene, the monomethyltriazene (Ar-N=N-NHMe), formed by loss of formaldehyde from **1***b*. Several derivatives of the HMT have been reported and some do indeed

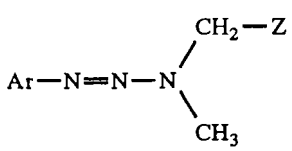

1*a*	Z = H
b	Z = OH
c	Z = OAc
d	Z = OMe
e	Z = N_3
f	Z = S—Ar

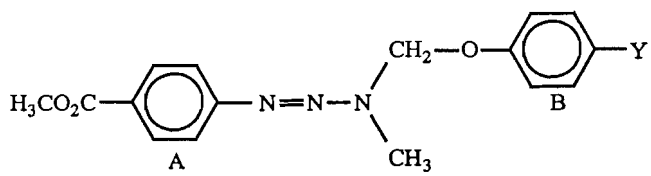

2*a*	Y = OCH_3
2*b*	CH_3
2*c*	H
2*d*	Cl
2*e*	Br
2*f*	CO_2CH_3
2*g*	CN
2*h*	NO_2

[1]For part XIII in this series see ref. 7.
[2]Author to whom correspondence may be addressed.

Can. J. Chem. Downloaded from www.nrcresearchpress.com by 123.30.183.119 on 09/08/12
For personal use only.

TABLE 1. Physical data for 1-aryl-3-aryloxymethyl-3-methyltriazenes (**2**)

Compound no.	Y	Method	Yield (%)	Melting point (°C)	Solvent	UV λ_{max} (nm)	Infrared (cm^{-1})	
2*a*	OCH_3	A	36	127–129	Ether	316	1705 (C=O)	1600 (R. st)
2*b*	CH_3	B	8.5	78–79	Hexane/ether	307	1705 (C=O)	1600 (R. st)
2*c*	H	A	57	46–47	Hexane/ether	320	1710 (C=O)	1590 (R. st)
		B	57					
2*d*	Cl	A	52	95–98	Ether	303	1710 (C=O)	1600 (R. st)
2*e*	Br	A	78	99–102	Hexane/ether	322	1710 (C=O)	1600 (R. st)
		B	39					
2*f*	MeO_2C	A	36	95–96	Ether/$CHCl_3$	303	1720 (C=O)	1600 (R. st)
2*g*	CN	A	34	136–139	Hexane/ether	314	1710 (C=O)	2225 (C≡N)
2*h*	NO_2	B	45	152–153	Ether/$CHCl_3$	312	1710 (C=O)	1605 (R. st)

R. st = Aromatic ring stretch.

TABLE 2. Physical data for 1-aryl-3-(hydroxyaryl)methyl-3-methyltriazenes (**3**)

Compound no.	Y	Method	Yield (%)	Melting point (°C)	Solvent	UV λ_{max} (nm)	Infrared (cm^{-1})	
3*a*	H	B	22	102–104	Hexane/Ether	—	1720 (C=O)	3400 (OH)
3*b*	CH_3	B	11	84–86	Ether	—	1710 (C=O)	3400 (OH)
3*c*	Br	B	5	118–119	Ether/Hexane	344	1705 (C=O)	3410 (OH)

TABLE 3. ^1H NMR data for 1-aryl-3-aryloxymethyl-3-methyltriazenes (**2**) in $CDCL_3$ at 20°C

Compound no.	CH_3O	Arom. A (AA'BB')	NCH_3 NCH_2	Arom. B	Y
2*a*	3.91	8.03–7.41	3.29 5.66	6.95–6.80	3.75 (OCH_3)
2*b*	3.91	8.04–7.43	3.29 5.69	7.07–6.83	2.28 (CH_3)
2*c*	3.91	8.04–7.45	3.30 5.72	7.31–6.82	
2*d*	3.91	8.05–7.45	3.29 5.70	7.26–6.93	
2*e*	3.92	8.04–7.46	3.29 5.70	7.40–6.89	
2*f*	3.92	8.06–7.41	3.31 5.79	7.98–7.03	3.88 (OCH_3)
2*g*	3.92	8.07–7.49	3.31 5.79	7.61–7.07	
2*h*	3.92	8.22–7.50	3.32 5.84	8.08–7.08	

TABLE 4. ^1H NMR data for 1-aryl-3-(hydroxyaryl)methyl-3-methyltriazenes (**3**) in $CDCl_3$ at 20°C

Compound no.	CH_3O	Arom. A AA'BB'	NCH_3	NCH_2	Arom. B.	Y	OH
3*a*	3.92	8.06–7.52	3.68	4.83	7.27–6.87		10.2 (br)
3*b*	3.91	8.05–7.50	3.67	4.78	7.23–6.63	2.28 (CH_3)	9.95 (br)
3*c*	3.91	8.05–7.50	3.68	4.75	7.36–6.82		10.3 (br)

have antitumour activity in animal models. Examples of such derivatives are the chemically reactive 3-acetoxymethyltriazenes (**1***c*; "acetates") and the relatively inert 3-methoxymethyltriazenes (**1***d*) (4).

The chemical reactivity of the acetates (**1***c*) has been employed in the synthesis of a variety of other derivatives. The acetates react smoothly with methanol to afford the methoxymethyltriazenes (**1***d*) (5) and with azide ion in aqueous acetone to afford the 3-azidomethyltriazenes (**1***e*) (6). Although the acetates do not react with neat thiols (5), we have recently shown that they react with a sodium thiophenolate in anhydrous dimethylformamide to afford a series of 1-aryl-3-arylthiomethyl-3-methyltriazenes (**1***f*) (7). In this paper we report an extension of this synthetic approach to the oxygen analogues, the 3-aryloxymethyltriazenes (**2**), which may represent a significant development in the search for a suitable pro-drug for the active metabolite of the anti-tumour dimethyltriazene.

Can. J. Chem. Downloaded from www.nrcresearchpress.com by 123.30.183.119 on 09/08/12
For personal use only.

TABLE 5. ^{13}C NMR data for 1-aryl-3-aryloxymethyl-3-methyltriazenes (**2**) in $CDCl_3$ at 20°C

Compound no.	CH_3O	C=O	Arom. A C_1	Arom. A $C_{2,6}$	Arom. A $C_{3,5}$	Arom. A C_4	NCH_3	NCH_2
2a	52.00	166.90	127.81	130.54	116.53	153.51	33.72	83.39
2b	51.92	166.89	127.90	131.80	116.72	153.67	33.67	83.78
2c	52.02	166.90	127.81	130.54	116.53	153.51	33.72	83.39
2d	52.05	166.83	127.96	130.57	117.79	153.29	33.76	83.50
2e	52.07	166.84	127.97	130.57	118.19	153.27	33.73	83.35
2f	51.96	166.82	128.11	131.59	120.95	153.20	33.77	82.84
2g	52.01	166.82	128.31	130.63	116.48	152.98	33.81	82.83
2h	52.01	166.72	128.35	130.78	115.68	152.88	33.85	83.00

Arom. B C_1	Arom. B $C_{2,6}$	Arom. B $C_{3,5}$	Arom. B C_4	Y
150.55	120.89	118.30	155.08	55.66 (OCH_3)
154.67	120.94	130.53	131.80	20.52 (CH_3)
156.70	120.91	129.59	122.28	
155.24	120.90	129.08	127.27	
155.75	120.90	132.43	114.61	
160.45	115.47	130.59	123.88	52.96 (OCH_3), 166.54 (C=O)
160.03	120.96	134.03	112.18	118.78 (C≡N)
161.69	120.96	125.85	142.24	

TABLE 6. ^{13}C NMR data for 1-aryl-3-arylmethyl-3-methyltriazenes (**3**) in $CDCL_3$ at 20°C

Compound no.	CH_3O	C=O	Arom. A C_1	Arom. A $C_{2,6}$	Arom. A $C_{3,5}$	Arom. A C_4	NCH_3	NCH_2
3a	52.01	166.81	130.62	130.78	119.78	152.10	42.22	50.02
3b	52.00	166.77	129.14	130.79	119.81	153.44	42.37	50.00
3c	52.05	166.74	127.60	130.82	119.80	151.76	42.34	49.52

Arom. B C_1	Arom. B C_2	Arom. B C_3	Arom. B C_4	Arom. B C_5	Arom. B C_6	Y
127.35	155.70	118.11	130.52	119.92	131.24	
130.79	145.65	120.34	117.92	131.55	131.08	20.42 (CH_3)
131.05	155.00	122.62	120.04	111.42	133.31	

Experimental

All solvents were purchased from BDH Chemicals Ltd. and were dried over molecular sieves type 4A except for acetone, which was dried over anhydrous sodium sulphate. In some instances the solvents were distilled prior to use. For some reactions chloroform was washed repeatedly with distilled water, dried overnight over anhydrous sodium sulphate, distilled, and stored in the dark.

Melting points were determined using a Reichert hot-stage microscope and are uncorrected.

Infrared spectra were obtained using a Perkin–Elmer 299 infrared spectrophotometer, calibrated against polystyrene film. Samples were prepared in $CHCl_3$ solution and the IR's run using matched KBr cells (Perkin–Elmer) with a $CHCl_3$ reference.

UV maxima were determined in a 2:1 mixture of 0.1 M phosphate buffer (pH 7.5) and isopropanol.

^{13}C (at 90 MHz) and ^1H NMR (at 361 MHz) spectra were acquired on the Nicolet 360 NB spectrometer of the Atlantic Region Magnetic Resonance Centre at Dalhousie University. Sweep widths for ^{13}C were 20 000 Hz and, for ^1H, 4000 Hz. The spectra were obtained at 20°C in deuterochloroform. Chemical shifts in ppm were measured relative to tetramethylsilane (1% internal standard).

Positive ion mass spectra were obtained from the MS service facility of Dalhousie University using a Consolidated Electrodynamics Corporation CEC 21-104 mass spectrometer. The operating parameters were as follows: source temperature 130–145°C; direct probe temperature 75–130°C; accelerating voltage 800 V; ionization voltage 70 eV; scan rate 6 dec s^{-1}.

1-Aryl-3-aryloxymethyl-3-methyltriazenes (2a–h)

Method A

The appropriate 1-aryl-3-acetoxymethyl-3-methyltriazene (**1***c*) (1.3 mmol) prepared by the method of Hemens *et al.* (4) was dissolved in dry chloroform (10 mL). A 50% excess of the phenol (1.9 mmol) was added and the mixture refluxed for 2–18 h depending on the desired product. With phenol itself, the mixture was not heated, but stirred for 24 h. The chloroform was removed under vacuum and the resulting oil washed with anhydrous ether. This usually resulted in the precipitation of the product, which was filtered off, dried, and recrystallized from a suitable solvent. Where

Can. J. Chem. Downloaded from www.nrcresearchpress.com by 123.30.183.119 on 09/08/12
For personal use only.

Can. J. Chem. Downloaded from www.nrcresearchpress.com by 123.30.183.119 on 09/08/12
For personal use only.

TABLE 7. Mass spectral intensities for the 1-aryl-3-aryloxymethyl-3-methyltriazenes (**2**)

Ion	Y					
	OCH_3	CH_3	Br	CO_2CH_3	CN	NO_2
$[M]^{\ddagger}$	1.28	1.45	0.13	2.51	0.40	1.46
$[M - CH_3O]^+$	2.44	3.11	1.60	3.80	2.98	3.01
$[M - CH_3O_2C]^+$	11.88	10.82	3.76	6.60	1.34	0.33
$[M - 102]^{+a}$	4.01	21.60	7.74	20.96	1.66	2.36
$[ArN_2]^+$	55.30	57.16	63.92	44.79	49.14	60.53
$[ArH]^+$	11.59	10.44	9.53	9.46	9.79	11.83
$[Ar]^+$	100.00	100.00	100.00	100.00	100.00	100.00
$[O_2CC_6H_4]^+$	10.26	10.60	9.76	17.52	13.95	38.61
$[Y - C_6H_4 - OCH_2]^+$	1.51	4.52	1.21	0.85	–	—[b]
$[Y - C_6H_4 - OH]^+$	24.26	14.63	6.05	3.80	15.38	10.97
$[Y - C_6H_4 - O]^+$	37.94	14.10	3.15	3.28	2.43	0.49
$[Y - C_6H_4]^+$	2.59	8.16	2.27	—[c]	4.63	4.29
$[Y - C_5H_4]^+$	9.39	7.43	4.58	9.53	6.86	0.73
$[C_7H_7]^+$	1.25	—[d]	1.00	2.09	4.18	4.65

[a]See Discussion.
[b]Coincident with $[ArH]^+$ (*m/e* 136).
[c]Coincident with $[Ar]^+$ (*m/e* 135).
[d]Coincident with $[Y - C_6H_4]$ (*m/e* 91).

TABLE 8. Mass spectral intensities for the 1-aryl-3-(hydroxyaryl)methyl-3-methyltriazenes (**3**)

Unit	**3***a* Y = H		**3***c* Y = Br	
	m/e	Rel. int. (%)	*m/e*	Rel. int. (%)
$[M]^{\ddagger}$	299	62	377/379	6
$[M - CH_3O]^+$	268	28	346/348	4
$[M - CH_3O_2C]^+$	239	5	317/319	1.5
$[M - 102]^+$	197	4	—	
$[M - ArN_2]^+$			214/216	60
			198/200	14
$[M - CH_2Ar']^+$	193	34	193	3
$[Ar'CH_2]^+$			185/187	69
$[ArN_3H]^+$	178	47	178	1.5
$[ArN_2]^+$	163	49	163	57
$[BrC_6H_5]^+$	—		156/158	4
$[ArNH]^+$	151	10	151	36
$[Ar]^+$	135	100	135	100
$[C_6H_4CO_2]^+$	120	34	120	79
	103	18	103	18
	92	10	92	27
	84	7		
	77	24	77	37

Ar = $MeOOC.C_6H_4$-; Ar′ = Y-C_6H_4 (OH)-.

TABLE 9. Elemental analyses for some 1-aryl-3-aryloxymethyl-3-methyltriazenes

Compound no.		C	H	N	O[a]	Br
2*a*	Calcd.	62.0	5.8	12.7	19.4	—
	Found	61.95	5.6	12.7	19.7	—
2*e*	Calcd.	50.8	4.3	11.1	12.7	21.1
	Found	51.0	4.4	11.2	12.3	21.05
2*h*	Calcd.	55.8	4.7	16.3	23.2	—
	Found	55.7	4.8	16.2	23.3	—

[a]Calculated by difference.

the product was an oil, it was chromatographed on silica gel with hexane/ether prior to recrystallization.

Method B

As in method A the 1-aryl-3-acetoxymethyl-3-methyltriazene was dissolved in chloroform. Sodium hydride 60% oily suspension (0.08 g) was placed in a round-bottomed flask fitted with a rubber septum and washed with dry petroleum ether (3 × 10 mL) to remove the oil, affording clean sodium hydride (2.0 mmol). The appropriate phenol (1.9 mmol) was dissolved in anhydrous chloroform and added carefully to the sodium hydride, provision being made for the safe egress of the hydrogen generated by the reaction. The resulting sodium phenolate solution was filtered to remove unreacted sodium hydride and added to the acetoxy methyltriazene solution and refluxed for 2–2½ h. Subsequent work-up was the same as for method A. Column chromatography of the reaction products of method B yielded a second product, identified as **3***a–c*, in addition to the main product (**2***c*, *b*, and *e*).

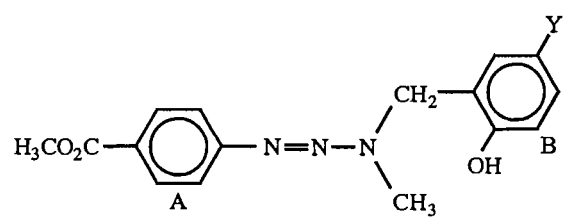

3*a* Y = H
3*b* CH_3
3*c* Br

In both methods the progress of the reaction was followed by TLC using 3:3:1 petroleum ether/ether/chloroform as solvent.

The physical data and yields for the compounds **2***a–h* are shown in Table 1, and those for compounds **3***a–c* in Table 2.[13]C and [1]H NMR shifts are presented in Tables 3–6. The relative intensities

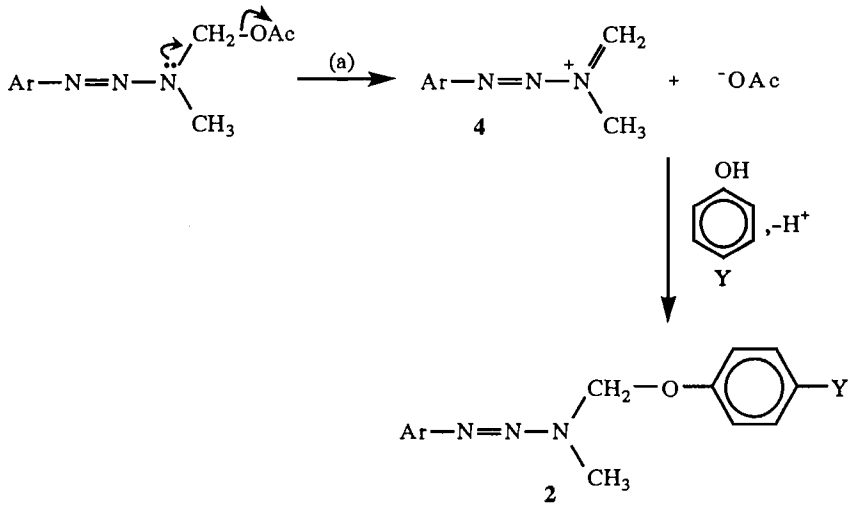

SCHEME 1

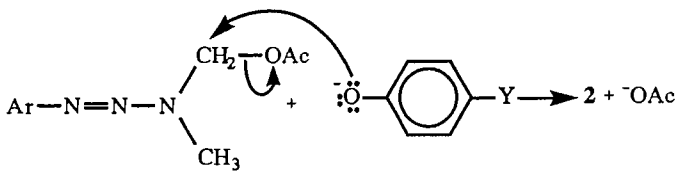

SCHEME 2

of the mass spectral peaks for compounds **2***a–h* are shown in Table 7, and for compounds **3***a* and **3***c* in Table 8.

Elemental analyses were performed on three of the aryloxymethyltriazenes by Canadian Microanalytical Service Ltd., Delta, British Columbia, and these assays are shown in Table 9.

Results and discussion

After the successful synthesis of the 3-arylthiomethyltriazenes (**1***f*) (7), it was regarded as important to prepare the *O*-aryl analogues (**2**), the objective being to develop a triazene pro-drug with the therapeutic advantages of the hydroxymethyltriazene but with a more useful half-life. The *S*-aryl derivatives (**1***f*) were found to be less reactive than the hydroxymethyltriazenes (**1***b*) under similar conditions. If the stability of these compounds depended to some extent on the leaving-group ability of -S-Ar, then comparison of the pK_a's of substituted phenols (pK_a = 7.15 for *p*-NO_2, 10.21 for *p*-OMe, and 9.98 for phenol itself) and thiophenol (7.8) suggests that an -O-Ar substituent should afford triazenes with hydrolysis profiles ranging from slightly faster to substantially slower than that of the *S*-aryl compounds. The appropriate substituted phenols are more readily available than the corresponding thiophenols, enabling us to examine a wider range of compounds to determine how leaving-group ability affects the hydrolysis rates. A further consideration was to eliminate the unpleasantness of the thiophenol, both as a reagent for synthesis and as a possible by-product of clinical treatment.

Simple replacement of a thiophenol with a phenol, using

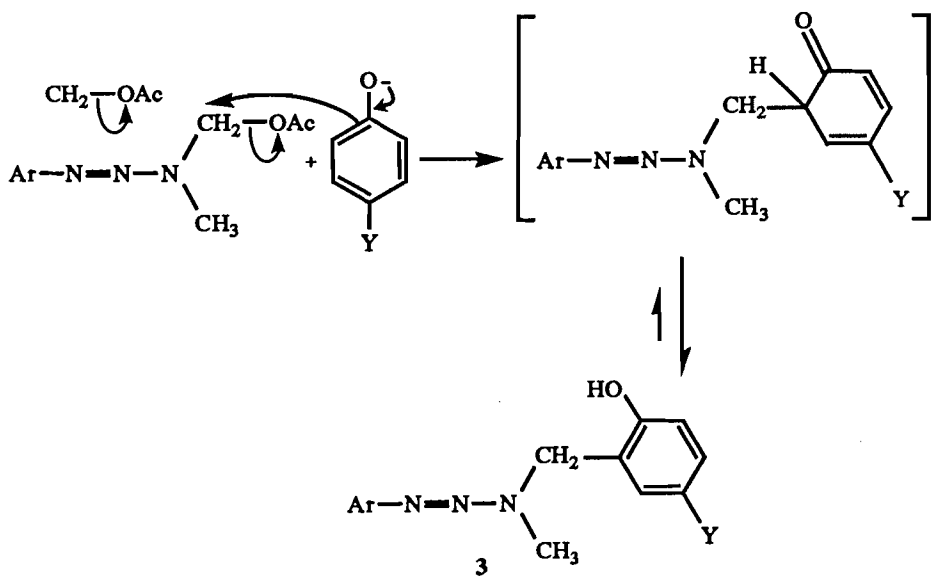

SCHEME 3

Can. J. Chem. Downloaded from www.nrcresearchpress.com by 123.30.183.119 on 09/08/12
For personal use only.

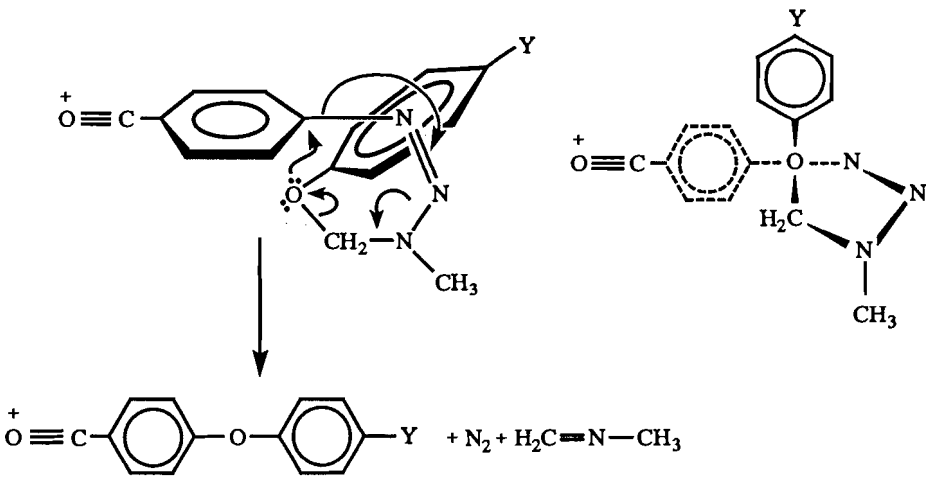

SCHEME 4

the methodology outlined in our previous report (7), was unsuccessful, the desired product being undetectable in the reaction mixtures. It turned out that a change of solvent was required to effect the desired substitution and, in some cases, the initial generation of a phenolate ion with sodium hydride was found to be unnecessary.

Using chloroform as solvent instead of dimethyl formamide enabled us to prepare the desired compounds in yields ranging from 8.5 to 78%. In two cases the generation of the phenolate ion with sodium hydride prior to reaction with the acetoxymethyltriazene (**1***c*) gave the best yields of the 1-aryl-3-aryloxymethyl-3-methyltriazenes (**2***b* and **2***h*).

It is noteworthy that in the reactions using sodium hydride, where the reaction time was extended from 2 to 18 h, a second product, the 1-aryl-3-(hydroxyaryl)methyl-3-methyltriazene (**3***a–c*), was formed. The low yields obtained by this method may be due to the formation of dichlorocarbene generated by refluxing chloroform in the presence of the base phenoxide ion, but there is no direct evidence to support this hypothesis.

The formation of **3** under these conditions could be due to a rearrangement of **2**, but so far we have been unable to produce **3** from pure **2** under the conditions of the reaction. A more likely explanation for the formation of the isomers **2** and **3** is as follows: The formation of the 3-aryloxymethyltriazenes (**2**) by method A is presumed to arise by an S_N1 mechanism as set out in Scheme 1. The initial step (a), in which the iminium ion (**4**) arises by dissociation of the acetate, is analogous to previously reported reactions (5, 6) and is more likely to occur in reaction with the neutral nucleophile, the phenol itself. Reaction of the phenol with the iminium ion and loss of a proton affords the product **2**.

However, in method B, the phenolate ion is generated prior to reaction with the acetate and it is possible that the alternative S_N2 pathway, Scheme 2, is preferred in this case. The formation of the 3-(hydroxyaryl)methyltriazenes (**3**), the isomers of **2**, lends support to this hypothesis and follows logically from the ambident nature of the nucleophilic phenolate ion. A suggested mechanism for the formation of **3** is shown in Scheme 3.

The identification of the 3-aryloxymethyltriazenes **2** and the isomeric 3-(hydroxyaryl)methyltriazenes **3** is based on elemental analyses, mass spectra, and IR and NMR spectroscopic data. The IR spectra of the ethers **2** show that the ester group attached to ring A is retained in the product; those of the isomers **3** also show the OH band at ca. 3400 cm^{-1} due to the phenolic substituent. In the NMR spectra, the triazene *N*-methyl resonance exhibits slightly different shifts for **2** (at ca. 3.30 ppm) than for **3** (at ca. 3.68 ppm). The N-CH_2 signals are distinctly different at ca. 4.80 ppm in **3** and in the range 5.66–5.84 ppm in **2**; the downfield shift is consistent with the deshielding effect of the O atom adjacent to the N-CH_2 group in **2**. Other features of the ^1H NMR spectra are entirely unpredictable.

The structures of **2** and **3** are also supported by the ^{13}C NMR data in Tables 5 and 6. The most significant difference is in the N-CH_2 signal at ca. 83 ppm in **2** and ca. 50 ppm in **3**. The ^{13}C aromatic peaks were assigned by consideration of their coupled multiplicities, peak heights, and additive substituent shift correlation calculations (8).

The mass spectra of all the 1-aryl-3-aryloxymethyl-3-methyltriazenes (**2**) exhibited a fairly intense peak at M − 102, which caused some puzzlement. Comparison with the mass spectra of the *S*-aryl analogues (**1***f*) indicated that the structural requirement for this feature was an ester function on the 1-aryl end of the molecule. Re-examination of the accurate-mass measurements for the *S*-aryl analogues showed that the mass lost in this reaction was 102.0668, corresponding to the empirical formula $C_3H_8N_3O$ for the methyl ester, and 116.0825 corresponding to $C_4H_{10}N_3O$ for the ethyl ester. These cannot be lost as single fragments, and the remaining charged species must arise from some kind of intramolecular rearrangement. One possibility is shown in Scheme 4.

Conclusions

Any further development of these new aryloxymethyltriazenes **2** as potential antitumour agents depends on two factors: (a) the antitumour activity; and (b) appropriate chemical stability. Two compounds of this series **2***e* and **2***h* have been subjected to screening on the investigational in vitro disease-oriented primary antitumour screen of the National Cancer Institute, Bethesda, Maryland. This screen consists of over 60 tumour cultures and each tumour type is tested with five tenfold dilutions of the drug candidate. Both com-

Can. J. Chem. Downloaded from www.nrcresearchpress.com by 123.30.183.119 on 09/08/12
For personal use only.

pounds tested have shown statistically significant differential sensitivity in the following cell lines: leukemia subpanel, renal subpanels, colon subpanels, and non-small lung panel. These results will be reported in more detail in an appropriate journal at a later date.

The 3-aryloxymethyltriazenes show a wide range of chemical stability depending on the nature of the substituent Y in the aryloxy moiety. The *p*-nitrophenyloxymethyltriazene (**2***h*) decomposed rapidly in phosphate buffer solution at pH 7.5. Measurement of the rate of this relatively fast reaction was made possible by following the growth of the absorbance at 400 nm in the UV spectrum arising from the *p*-nitrophenolate ion leaving group released into the buffer, to give a half-life of ca. 1 min for the initial decomposition to the hydroxymethyltriazene. In contrast, the *p*-bromophenyloxymethyltriazene (**2***e*) appeared not to decompose at all under identical conditions, but instead this triazene precipitated out of solution before any decomposition occurred. A more detailed study of the pH-dependent hydrolysis of these 3-aryloxymethyltriazenes (**2**) in various buffer media will be described in the next paper in this series.

1. T. A. Connors, P. M. Goddard, K. Merai, W. C. J. Ross, and D. E. V. Wilman. Biochem. Pharmacol. **25**, 241 (1976).
2. G. F. Kolar, M. Maurer, and M. Wildschutte. Cancer Lett. **10**, 287 (1980).
3. L. M. Cameron, R. J. LaFrance, C. M. Hemens, K. Vaughan, R. Rajaraman, D. C. Chubb, and P. M. Goddard. Anti-cancer Drug Des. **1**, 27 (1985).
4. C. M. Hemens, H. W. Manning, K. Vaughan, R. J. LaFrance, and Y. Tang. Can. J. Chem. **62**, 741 (1984).
5. C. M. Hemens and K. Vaughan. J. Chem. Soc. Perkin Trans. **2**, 11 (1986).
6. K. Vaughan, K. N. G. Nicholas, R. D. Singer, M. Roy, and N. W. Gibson. Anti-cancer Drug Des. **2**, 279 (1987).
7. M. P. Merrin, K. Vaughan, D. L. Hooper, and H. W. Manning. Can. J. Chem. **66**, 2487 (1988).
8. F. W. Wehrli and T. Wirthlin. Interpretation of ^{13}C NMR spectra. Heyden & Son Ltd., London. 1978.

Can. J. Chem. Downloaded from www.nrcresearchpress.com by 123.30.183.119 on 09/08/12
For personal use only.

Charge transfer and electron transfer processes in biologically significant systems. 1. Charge transfer complex formation between 1,3,5-trinitrobenzene and *N,N*-dimethyl-3,4-di-*O*-methyldopamine, a dopamine analogue

JULIAN M. DUST

Department of Chemistry, Sir Wilfred Grenfell College, Corner Brook, Nfld., Canada A2H 6P9

Received June 20, 1991

JULIAN M. DUST. Can. J. Chem. **70**, 151 (1992).

The interactions of *N,N*-dimethyl-3,4-di-*O*-methyldopamine, **1**, a structural analogue of the important neurochemical, dopamine, with 1,3,5-trinitrobenzene (TNB) were studied primarily by ^{1}H nuclear magnetic resonance (nmr). The dopamine analogue, a donor, forms a charge transfer complex with TNB, a model acceptor, in $CDCl_3$ and CD_3CN. Equilibrium constants were determined from the ^{1}H nmr charge transfer induced chemical shift changes. The results are discussed in terms of the probable type of donation from the amine, **1**, to TNB ($n \rightarrow \pi^*$ versus $\pi \rightarrow \pi^*$), comparison with dopamine, and with regard to possible charge transfer interactions in molecular receptors.

Key words: *N,N*-dimethyl-3,4-di-*O*-methyldopamine, charge transfer complex, equilibrium constant.

JULIAN M. DUST. Can. J. Chem. **70**, 151 (1992).

Utilisant principalement la RMN du ^{1}H, on a étudié les interactions entre le 1,3,5-trinitrobenzène (TNB) et la *N,N*-diméthyl-3,4-di-*O*-méthyldopamine (**1**), un analogue de la dopamine, un produit neurochimique important. En solution dans le $CDCl_3$ et dans le CD_3CN, l'analogue de la dopamine, un donneur, forme un complexe de transfert de charge avec le TNB, un accepteur modèle. On a déterminé les constantes d'équilibre à partir des changements dans les déplacements chimiques induits par le transfert de charge. On discute des résultats en termes du type probable de don d'électrons de l'amine **1** vers le TNB ($n \rightarrow \pi^*$ vs. $\pi \rightarrow \pi^*$), par comparaison avec la dopamine et en fonction des interactions possibles de transfert de charge dans les récepteurs moléculaires.

Mots clés : N,N-diméthyl-3,4-di-*O*-méthyldopamine, complexe de transfert de charge, constante d'équilibre.

[Traduit par la rédaction]

Introduction

A unifying concept in pharmacological studies is that of the receptor (1), a site on a muscle, nerve-ending, etc. at which specific bioactive agents can bind. If the bioactive agent or drug initiates a physiological response, such as the contraction of a muscle, either directly or via a transducer molecule (2), then the original bioactive agent is termed an agonist, whereas an antagonist binds with the receptor (or with an adjacent site that affects the conformation of the receptor) without producing the biological response.

Overall, the process can be visualized as an equilibrium (eq. [1]) between the agonist/antagonist (A) and the receptor site (R) to produce an equilibrium concentration of the bound bioactive agent (R–A):

[1] $\quad R + A \rightleftharpoons R\text{–}A$

The equilibrium may then be characterized by a binding constant, $K_{binding}$. Considerable progress has been made in quantifying the number, locations, and kinds of different receptors through binding constant measurements (3–5).

More importantly, the specific interactions involved in the binding of a given bioactive agent with a receptor have not always been fully elucidated. One approach to the problem has been that of "mapping" the receptor site, through the combination of computer modelling and series of binding studies using bioactive agents of similar structure, notably those that contain the functions associated with biological activity and, so, constitute the pharmacophore. These receptor mapping studies have emphasized the importance of the steric fit of the bioactive compound into the receptor site (6).

A somewhat different approach has come from the correlation of the bioactivity with the structure of series of structurally related drugs, using extended Hammett (Hansch) treatments (7, 8). Ariens (9), among others, has generalized such quantitative structure–activity relationships (QSAR's) as follows:

[2] $\quad \log(\text{biological response}) = a + b + c + d + \text{constant}$

where a is a lipophilic (hydrophobic) parameter, b is an electronic (substituent) parameter, c is a steric parameter, and d is a term that encompasses any other physically meaningful parameter, such as the ability to form hydrogen bonds (10). The most commonly used parameters for a, b, and c are $\log P_{oct}$, $\sigma(\sigma^+,\sigma^-)$, and E_s, respectively. P_{oct} is the partition constant between octanol and water for each member of the series of structurally related drugs (i.e., members of the pharmacophoric constellation). To give only a few examples of the efficacy of the approach, the binding of bioactive compounds with proteins (11) and cells (12) has been correlated and correlations between biological response and these parameters for antimalaria drugs (13) and anaesthetics (14) have been demonstrated.

Interestingly, among the interactions possible between the pharmacophore and the receptor, charge transfer (CT) complexation (15) has received relatively little attention (16). This is all the more striking in that CT complexation has been a well-known interaction since the early discoveries of Benesi and Hildebrand (15*a*), through the pioneering work of Briegleb (15*b*), and the valence-bond and molecular orbital descriptions of Mulliken (15*c*) and Dewar and Lepley (15*d*), respectively. For a pharmacophore that has begun the process of "docking" at the receptor site, CT complexation may represent an important binding interaction, a possible d-term interaction (eq. [2]).

The importance of CT interactions to biological systems has been reviewed recently (17). Among the recent literature, however, can be found examples that illustrate the

Can. J. Chem. Downloaded from www.nrcresearchpress.com by 123.30.183.119 on 09/08/12
For personal use only.

range and significance of CT complex (CTC) formation, including the correlation of carcinogenicity of 5-methylchrysene (as compared to isomeric methylchrysenes) with the disorder in the stacking of the 5-methylchrysene–1,3,5-trinitrobenzene (TNB) complexes, as shown by X-ray crystallography and molecular orbital (MO) calculations (18). CT complexation provides the basis for spectrophotometric assays for a variety of penicillins (19) and other drugs (20). CT complexation has also been found for amino acids and dimethoxybenzenes interacting with a highly electron-deficient synthetic molecular receptor (21). Evidence has recently been reported for the CT complexation of indoles with the acceptor 1-(2,4,6-trinitrophenyl)propan-2-one (22).

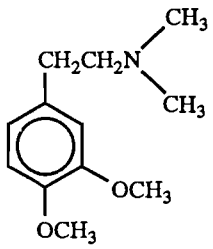

1

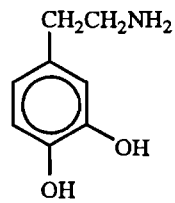

2

In the present article, we present evidence for the formation of CTC between *N*,*N*-dimethyl-3,4-di-*O*-methyldopamine (*N*,*N*-dimethyl-3,4-dimethoxyphenylethylamine, **1**), a dopamine analogue, and TNB, as a biophysical probe. Dopamine, **2**, is an important neurochemical, a precursor of noradrenaline; its absence in the neurosystem is implicated in Parkinson's disease (23) and cocaine addiction (23*c*). The information derived from the present in vitro study will be discussed in terms of the probable type of donation that occurs from donor, **1**, to acceptor, TNB ($n \rightarrow \pi^*$ versus $\pi \rightarrow \pi^*$), the possible bearing the results have on drug–receptor interactions, and, particularly, the extension of the conclusions to dopamine, itself.

Results

^{1}H nuclear magnetic resonance (nmr) studies

The three equivalent aromatic protons of TNB appear as a singlet at ca. 9 ppm in $CDCl_3$, CD_3CN, or $(CD_3)_2SO$. Addition of an excess of the amine, **1**, to a solution of TNB (in $CDCl_3$ or CD_3CN) causes the TNB singlet to shift to higher field. In $(CD_3)_2SO$ no detectable change in peak position or line shape could be seen. No new peaks are observed. The 8.6–5.0 ppm region of the spectra, where the protons of a trinitrocyclohexadienate moiety of anionic σ-adducts (Meisenheimer adducts) typically resonate (24), is clear of signals. Further, the TNB singlet is relatively sharp, as are the upfield peaks assignable to **1** (even in $(CD_3)_2SO$), indicating that electron transfer, to yield paramagnetic species like radical anions and cations, has not occurred (Fig. 1).

The change in chemical shift of the TNB singlet may be defined as Δ, that is, the difference in chemical shift between free TNB (δ_{TNB-f}) and the averaged shift of free and complexed TNB (δ_{TNB-av}). Hence,

$$[3] \quad \Delta = \delta_{TNB\text{-}f} - \delta_{TNB\text{-}av}$$

The chemical shift averaging is a result of a fast equilibrium

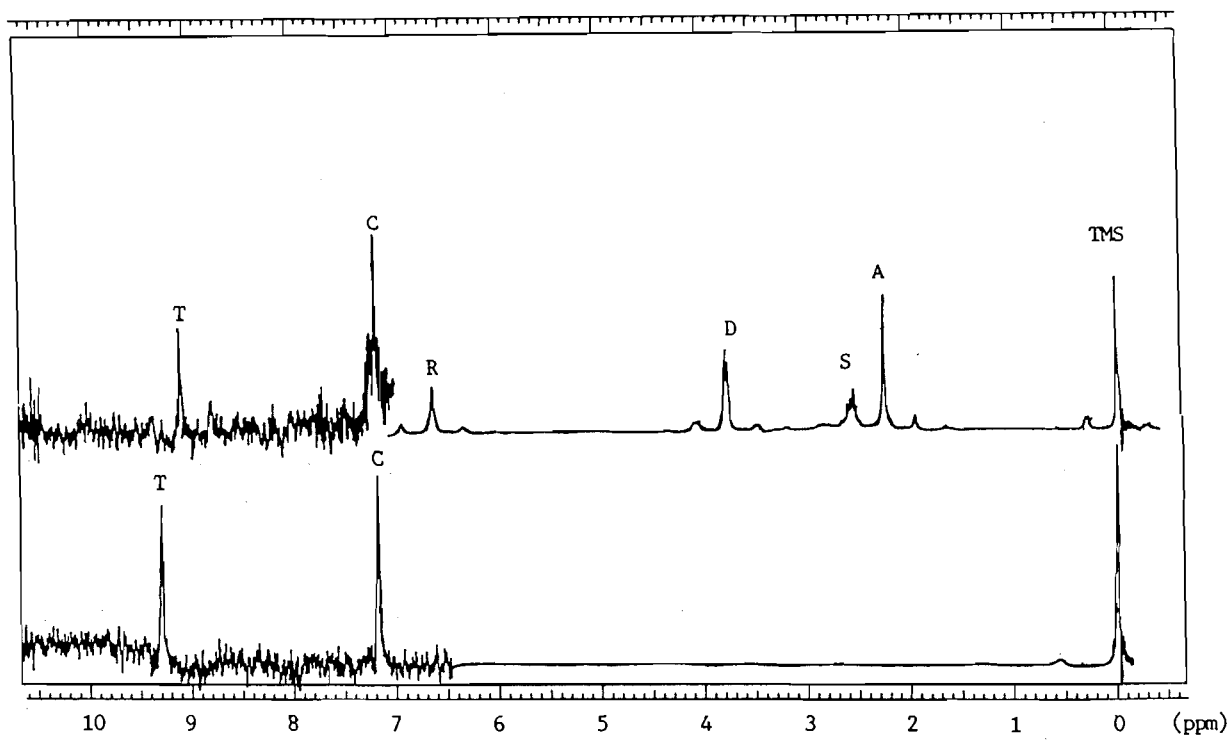

FIG. 1. Typical ^{1}H nmr spectra ($CDCl_3$ solvent). The region from 10.5 to ca. 7 ppm was scanned at a higher amplitude (factor of 100 greater) than that used for the upfield region. The lower spectrum shows the signals for TNB (T), $CHCl_3$(C), and tetramethylsilane (TMS). The top spectrum is that recorded after the addition of a 60-fold excess of **1**. The signals for **1** are labelled as follows: ring H's (R), 3,4-CH_3O's (D), -CH_2CH_2- (S), and -$N(CH_3)_2$ (A).

Can. J. Chem. Downloaded from www.nrcresearchpress.com by 123.30.183.119 on 09/08/12
For personal use only.

TABLE 1.[a] The ^{1}H nmr spectral data arranged for eq. [5] ($[TNB]_0 = 4.5 \times 10^{-3}$ M); $CDCl_3$ solvent

$[\mathbf{1}]_0/[TNB]_0$	$[\mathbf{1}]_0$ (mol L^{-1})	Δ (ppm)[b]	$\Delta/[\mathbf{1}]_0$ (ppm L mol^{-1})
200:1[c]	0.900	0.317	0.352
100:1	0.450	0.200	0.444
75:1	0.338	0.167	0.495
50:1	0.225	0.117	0.519
25:1	0.113	0.067	0.593

[a]The data from Table 1 are plotted on the graph, Fig. 1.
[b]Defined by eq. [3].
[c]The regression equation for the line is $\Delta/[\mathbf{1}]_0 = -0.937\,\Delta + 0.643$; $K_{CT} = 0.937$ L mol^{-1}, $\Delta_0 = 0.686$ ppm. $r = 0.991$.

TABLE 2. The ^{1}H nmr spectral data arranged for eq. [5] ($[TNB]_0 = 9.0 \times 10^{-3}$ M); $CDCl_3$ solvent

$[\mathbf{1}]_0/[TNB]_0$	$[\mathbf{1}]_0$ (mol L^{-1})	Δ (ppm)[a]	$\Delta/[\mathbf{1}]_0$ (ppm L mol^{-1})
120:1[b]	1.080	0.267	0.247
100:1	0.900	0.250	0.278
60:1	0.540	0.183	0.339
50:1	0.450	0.167	0.371
30:1	0.270	0.117	0.433
25:1	0.225	0.100	0.444

[a]Defined by eq. [3].
[b]The regression equation for the line is $\Delta/[\mathbf{1}]_0 = -1.18\,\Delta + 0.564$; $K_{CT} = 1.18$ L mol^{-1}, $\Delta_0 = 0.480$ ppm. $r = 0.996$.

(on the nmr time scale) between the free TNB and that bound in the CTC:

[4] $\mathbf{1} + TNB \rightleftharpoons \mathbf{1}$–TNB

Consequently, the upfield shift of the TNB singlet upon introduction of **1** into the system is diagnostic of formation of a CTC in which TNB accepts electron density from **1** (eq. [4]). In this context, the lack of detectable change in peak position with increasing concentration ratio of **1** to TNB in $(CD_3)_2SO$ (DMSO) as solvent suggests that the CTC, if formed, is formed in a concentration lower than the detection limit imposed by the nmr study. An alternative possibility is that either donor or acceptor or both interact more strongly with DMSO than with one another; this specific interaction (*vide infra*) may obscure any CTC formation between **1** and TNB in DMSO.

The change in chemical shift, as a function of the concentration of added **1** (Tables 1–6), was plotted according to the Scatchard equation for nmr data (25):

[5] $\Delta/[\mathbf{1}]_0 = -K_{CT}\Delta + K_{CT}\Delta_0$

where Δ refers to the change in chemical shift in the probe molecule, TNB, as defined above, $[\mathbf{1}]_0$ is the initial added concentration of *N*,*N*-dimethyl-3,4-di-*O*-methyldopamine, which is always present in excess, and K_{CT} is the equilibrium constant for CTC formation. Δ_0 represents the chemical shift change for the TNB probe at that point at which TNB is totally complexed.

A representative plot of the data for each solvent, $CDCl_3$ and CD_3CN, is shown in Fig. 2. All plots gave linear regression lines with satisfactory to good correlation coefficients (0.94–0.99). The regression equation for each separate experiment is given along with each table of data (Tables 1–6). The mean values for K_{CT} obtained from the K_{CT} values determined in the individual experiments are 1.06 ± 0.1 L mol^{-1} in $CDCl_3$ and 0.66 ± 0.24 L mol^{-1} in CD_3CN.

Solvents may interact preferentially with either the donor or the acceptor (26). No attempt has been made in the present study to correct for specific interactions between the

TABLE 3. The ^{1}H nmr spectral data arranged for eq. [5] ($[TNB]_0 = 9.0 \times 10^{-3}$ M); $CDCl_3$ solvent

$[\mathbf{1}]_0/[TNB]_0$	$[\mathbf{1}]_0$ (mol L^{-1})	Δ (ppm)[a]	$\Delta/[\mathbf{1}]_0$ (ppm L mol^{-1})
120:1[b]	1.080	0.250	0.231
60:1	0.540	0.190	0.352
50:1	0.450	0.167	0.371
30:1	0.270	0.107	0.396
25:1	0.225	0.093	0.415

[a]Defined by eq. [3].
[b]The regression equation for the line is $\Delta/[\mathbf{1}]_0 = -1.06\Delta + 0.524$; $K_{CT} = 1.06$ L mol^{-1}, $\Delta_0 = 0.494$ ppm. $r = 0.938$.

TABLE 4.[a] The ^{1}H nmr spectral data arranged for eq. [5] ($[TNB]_0 = 4.5 \times 10^{-3}$ M); CD_3CN solvent

$[\mathbf{1}]_0/[TNB]_0$	$[\mathbf{1}]_0$ (mol L^{-1})	Δ (ppm)[b]	$\Delta/[\mathbf{1}]_0$ (ppm L mol^{-1})
200:1[c]	0.900	0.150	0.167
140:1	0.630	0.125	0.198
100:1	0.450	0.100	0.222
50:1	0.225	0.058	0.259

[a]The data from Table 4 are plotted on the graph, Fig. 1.
[b]Defined by eq. [3].
[c]The regression equation for the line is $\Delta/[\mathbf{1}]_0 = -0.987\Delta + 0.318$; $K_{CT} = 0.987$ L mol^{-1}, $\Delta_0 = 0.322$ ppm. $r = 0.997$.

TABLE 5. The ^{1}H nmr spectral data arranged for eq. 5 $[TNB]_0 = 9.0 \times 10^{-3}$ M); CD_3CN solvent

$[\mathbf{1}]_0/[TNB]_0$	$[\mathbf{1}]_0$ (mol L^{-1})	Δ (ppm)[a]	$\Delta/[\mathbf{1}]_0$ (ppm L mol^{-1})
160:1[b]	1.440	0.142	0.098
100:1	0.900	0.100	0.111
80:1	0.720	0.083	0.116
50:1	0.450	0.060	0.133
40:1	0.360	0.050	0.139

[a]Defined by eq. [3].
[b]The regression equation for the line is $\Delta/[\mathbf{1}]_0 = -0.446\Delta + 0.158$; $K_{CT} = 0.446$ L mol^{-1}, $\Delta_0 = 0.355$ ppm. $r = 0.975$.

TABLE 6. The ^{1}H nmr spectral data arranged for eq. [5] ($[TNB]_0 = 9.0 \times 10^{-3}$M); CD_3CN solvent.

$[\mathbf{1}]_0/[TNB]_0$	$[\mathbf{1}]_0$ (mol L^{-1})	Δ (ppm)[a]	$\Delta/[\mathbf{1}]_0$ (ppm L mol^{-1})
160:1[b]	1.440	0.150	0.104
80:1	0.720	0.090	0.125
50:1	0.450	0.067	0.148
40:1	0.360	0.057	0.158

[a]Defined by eq. [3].
[b]The regression equation for the line is $\Delta/[\mathbf{1}]_0 = -0.553\Delta + 0.184$; $K_{CT} = 0.553$ L mol^{-1}, $\Delta_0 = 0.333$ ppm. $r = 0.965$.

Can. J. Chem. Downloaded from www.nrcresearchpress.com by 123.30.183.119 on 09/08/12
For personal use only.

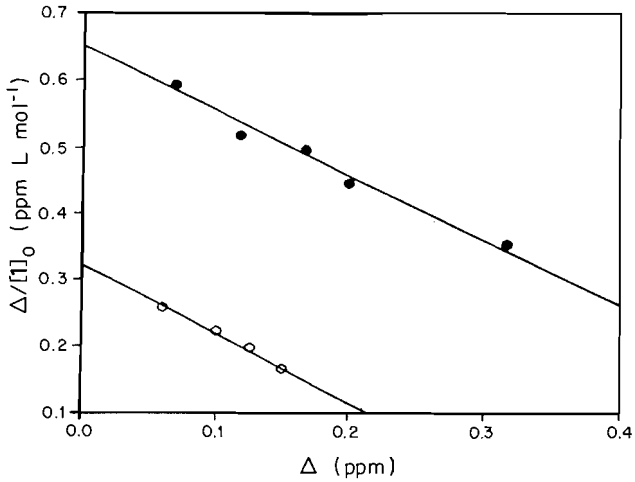

FIG. 2. Representative Scatchard plots (eq. 5), using the data from Table 1 (filled circles, $CDCl_3$ solvent) and from Table 4 (hollow circles, CD_3CN solvent). Regression analysis for the lines is given with the respective tables.

solvent and either of the interactants. It should be recognized, however, that such specific interactions have previously made comparison of gas-phase and solution data on CTC difficult (27). Consequently, the equilibrium constants measured in this study, K_{CT}, should be viewed as apparent equilibrium constants.

Ultraviolent–visible (uv–vis) spectroscopic study

When the ^{1}H nmr sample that contained the highest concentration ratio of **1** to TNB (200:1) was transferred, without dilution, to a semi-micro 0.1-cm-pathlength cuvette and the uv–vis spectrum was obtained (in either solvent) the orange-yellow solution did not contain the characteristic two-band spectrum found for anionic (1:1) Meisenheimer adducts of TNB (24). Instead the spectrum consisted of a single diffuse absorbance at 350–400 nm in $CDCl_3$ and 370–420 nm in CD_3CN. Such broad spectral bands, which are not attributable to either separate interactant, are consistent with CTC formation (eq. [4]) (15, 17).

Discussion

1. The nature of the interaction

(a) Nucleophilic versus CT behaviour

Charge transfer complexes occupy one extreme in a continuum of interactions that may occur between electron-rich species and electron-poor aromatic and heteroaromatic systems, exemplified by TNB. In charge transfer complexes, partial electron density is transferred from the HOMO of the donor to the LUMO of the acceptor. If a full electron is transferred, discrete species, namely the radical (D·) or the radical cation of the donor ($D^{+\cdot}$) and the radical anion of the acceptor ($TNB^{-\cdot}$), may form, giving rise to a radical ion pair. Transfer of a pair of electrons, however, with concomitant bonding of the donor to the acceptor produces an anionic Meisenheimer complex (24).

Interestingly, recent molecular orbital calculations (MNDO) have suggested that CT complexation precedes Meisenheimer adduct formation in nucleophilic aromatic substitution (S_NAr) reactions (28), in agreement with kinetic results involving nitrogen-centred nucleophiles in nonpolar solvents (29). Extensive work has also been done on polynitroaromatic systems with OH^- ion (30) in which CTC, radical anion – radical pairs, and Meisenheimer complexes have all been invoked as necessary intermediates. A previous study of the interactions of dopamine and 3,4-di-*O*-methyldopamine, **3**, with TNB in dimethyl sulfoxide (DMSO) demonstrated the presence of Meisenheimer complexes in these related reaction systems (*vide infra*) (31). Finally, Forlani and Cimarelli reported the observation and *isolation* of a zwitterionic adduct, **4**, formed in the reaction of the tertiary amine, 1,8-diazabicyclo[5.4.0]undec-7-ene (DBU), with TNB in toluene (32).

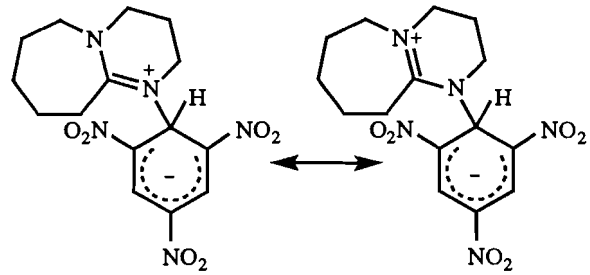

4

Clearly, in the present system only a CTC forms. There is no evidence from either the ^{1}H nmr or uv–vis spectroscopic studies for formation of radical ions or of a Meisenheimer adduct from **1** and TNB. The difference in reactivity between simple, tertiary amines like triethylamine (33) or **1** in contrast to DBU appears to lie, at least partially, in the ability of the DBU moiety of **4** to delocalize the positive charge of the ammonium ion centre, just as the trinitrocyclohexadienate portion of the complex delocalizes the negative charge. Steric hindrance to bond formation between **1** and TNB (as compared to DBU and TNB) may also account for the difference in reactivity between these two systems.

(b) Stoichiometry of the CTC

In the present study the Scatchard plots (eq. [5], Fig. 2) were found to be linear over the range of concentration ratios studied (200:1–25:1). Linearity of such plots has been taken as indicative of the presence of 1:1 CTC alone (34). Concave (upwards) plots have been found in some systems and these results were attributed either to the presence of CTC of higher stoichiometry (2:1, 3:1 etc.) (34) or to an Additional Unspecified Shielding (AUS) effect on the ^{1}H nmr spectra (35). The latter interpretation presumes that the chemical shift of free acceptor (TNB) and of totally complexed acceptor (**1**–TNB) could be different in the presence of donor, **1**, as compared to pure solvent, i.e., Δ would be incorrectly represented in the plot.

Further, in a recent article, Foster and co-workers demonstrated a Scatchard plot that increased to a maximum and then levelled off (22). This anomalous behaviour was attributed to self-association of the indoles used in that study.

It should be emphasized that for those plots that demonstrated only satisfactory correlation coefficients (r ca. 0.94), the points showed only scatter and no regular curvature could be seen. On these grounds, the CTC formed between **1** and TNB appears to have a 1:1 stoichiometry and the interaction is free from termolecular complexation or self-association of the donor, **1**.

Can. J. Chem. Downloaded from www.nrcresearchpress.com by 123.30.183.119 on 09/08/12
For personal use only.

Can. J. Chem. Downloaded from www.nrcresearchpress.com by 123.30.183.119 on 09/08/12
For personal use only.

(c) Classification of the type of partial electron donation

N,N-Dimethyl-3,4-di-*O*-methyldopamine can act as a partial electron donor in two ways: as an $n \rightarrow \pi^*$ donor via the amine function and as a $\pi \rightarrow \pi^*$ donor via the aromatic ring. This distinction between types of interaction in CT complexation was advanced previously (36), although assignment of one particular mode of donation from a given donor species has been problematic (37).

It should be noted that K_{CT} for *N,N*-dimethylaniline in chloroform (19.7°C) was ascribed a value of 1.3 L mol^{-1} (36), which is in reasonable agreement with the value found for the complex formed by **1** and TNB, i.e., **1**–TNB. There is a declining trend in the values of equilibrium constants for CT complexation between TNB and the following anilines: *N,N*-dimethyl-2,6-dimethylaniline, *N,N*-dimethylaniline, and *N,N*-dimethyl-2-methylaniline. The trend was explained on the basis of the varying ability of the aromatic ring to transfer electron density to TNB. Thus, the equilibrium constants decrease in magnitude in going from *N,N*-dimethylaniline to *N,N*-dimethyl-2-methylaniline, as would be anticipated if the introduction of the *ortho* methyl group leads to steric inhibition of delocalization of electron density from the amino nitrogen into the aniline ring and, thence, to the TNB ring in the complex. However, the steric inhibition of delocalization that would also be expected to apply to *N,N*-dimethyl-2,6-dimethylaniline is overwhelmed by the methyl inductive effect on the donor ability of the aromatic ring. Consequently, the equilibrium constant associated with CT complexation of *N,N*-dimethyl-2,6-dimethylaniline is larger than that found for *N,N*-dimethylaniline and larger still than that found for *N,N*-dimethyl-2-methylaniline (36). Consistent with the similarity in the magnitude of K_{CT} for *N,N*-dimethylaniline and **1** in complexation with TNB, the interaction of **1** with TNB may be $\pi \rightarrow \pi^*$, as found for *N,N*-dimethylaniline.

Some further support for this analysis can be found in the comparison of the magnitude of K_{CT} for **1**–TNB with the equilibrium constants for the complexation of TNB with a series of methyl-substituted benzenes, namely, mesitylene, durene, and pentamethylbenzene. In CCl_4 at 33.5°C the values of K_{CT} were determined to be 0.797 (mesitylene–TNB), 1.32 (durene—TNB), and 1.93 (pentamethylbenzene–TNB) L mol^{-1}. The values of K_{CT}, for these aromatic donors which are clearly unable to act in the $n \rightarrow \pi^*$ fashion, are again notably similar to that found for K_{CT} for CTC formation with **1** in $CDCl_3$ at 33.5°C (i.e., 1.06 L mol^{-1}) (25*c*). It should be noted that K_{CT} values are generally larger in CCl_4 than in $CDCl_3$ (15, 37).

Based upon these comparisons, the CT interaction between **1** and TNB is tentatively assigned as $\pi \rightarrow \pi^*$. However, we cannot rule out the possibility that both forms of interaction (i.e., $\pi \rightarrow \pi^*$ and $n \rightarrow \pi^*$) are operating in concert. Further evidence, including solid state nmr studies of the isolated complex and enthalpies and entropies of CTC formation, would be required for a more definitive assessment to be made.

A comment should be made concerning the trend found for the various solvents. The magnitude of K_{CT} declined from $CDCl_3$ to CD_3CN and, finally, to $(CD_3)_2SO$ where K_{CT} could not be measured, possibly due to specific interactions with the solvent. These results are in qualitative agreement with the generalization that CTC are essentially nonpolar in the ground state and are, therefore, stabilized in nonpolar solvents (15) or microenvironments.

2. Comparison with dopamine

The interactions of dopamine with TNB in DMSO solution were reported previously (31). Depending upon the degree of ionization of the hydroxyl groups (as a function of concentration and type of added base) a variety of Meisenheimer adducts were observed. In sequence, a nitrogen-bonded adduct was the first to be seen, followed by formation of a carbon-centred adduct, via attack of a ring carbon on TNB. Transient oxygen-centered adducts were postulated, but not observed.

Importantly, no CTC were found in the dopamine–TNB system in DMSO. This is in accord with the present study, where the CT interaction between the dopamine analogue, **1**, and TNB may be overwhelmed by specific interactions of the components with the $(CD_3)_3SO$ solvent.

However, the microenvironment of the receptor site may be relatively nonpolar. Hydrophobic interactions between a bioactive compound and the aqueous biological solution could force the bioactive compound into closer contact with a more nonpolar receptor site. In such a case, dopamine and other members of the series would be expected to bind to acceptor portions of the receptor much as **1** complexes with TNB.

We clearly recognize the importance of other interactions for dopamine, as compared to **1**, including hydrogen bonding of the phenolic OH groups of **2** with the receptor. In fact, 3,4-di-*O*-methyldopamine, **3**, which lacks these OH groups, is biologically active, although it does not affect the central nervous system as dopamine does (38). Nevertheless, CT complexation could be a general binding interaction for **2** and **3**, as well as **1**, and a suitable *d*-term in eq. [2].

In summary, *N,N*-dimethyl-3,4-di-*O*-methyldopamine, **1**, forms CTC with TNB, as a probe of biophysical interaction, in $CDCl_3$ and CD_3CN with K_{CT} values of 1.06 and 0.66 L mol^{-1}, respectively. Based upon comparison of the K_{CT} values with those found in related systems, the CT complexation is *probably* $\pi \rightarrow \pi^*$ in nature. Cooperative $\pi \rightarrow \pi^*$ and $n \rightarrow \pi^*$ interactions cannot be ruled out, however. The amine does not apparently form a CTC with TNB in $(CD_3)_2SO$. However, it is reasonable to conclude that dopamine, as well as **1**, could form CTC with suitable electron-deficient molecules (or moieties), particularly in low polarity solvents (or low polarity microenvironments, which may include receptor sites).

Experimental

General

3,4-Di-*O*-methyldopamine (3,4-dimethoxyphenylethylamine, Aldrich) was distilled; the fraction that boiled at 150–151°C at 9.0 Torr (1 Torr = 133.3 Pa) was collected and stored under N_2 at 10°C. *N,N*-Dimethyl-3,4-di-*O*-methyldopamine, **1**, was prepared by the Eschweiler–Clarke method (39). The purified yield was 46%; bp 120–130°C at 2.3–3.0 Torr (lit. (40)bp 85–90°C at 0.05 Torr). The colourless product, **1**, was stored under N_2 over 4Å molecular sieves at 10°C. In general, it was found necessary to redistill **1** immediately prior to use to obtain consistent results. 1,3,5-Trinitrobenzene (TNB, Eastman) was recrystallized thrice from benzene and once from ethanol, mp 124.5–125°C. $CDCl_3$, CD_3CN, and $(CD_3)_2SO$ (MSD) were allowed to stand over 4Å molecular sieves for 24 h and then used without further purification. The ^1H nmr

spectra were measured using a Varian EM-360 spectrometer operating at 60 MHz with a probe temperature of 33.5°C. Standard Wilmad PP-507 nmr tubes were used for all nmr experiments. The uv–vis spectra were recorded on a Beckman DU-8 spectrophotometer at ambient temperature (24 ± 3°C). Melting points were determined with a Fisher-Johns hotstage and the values reported are uncorrected.

The ^1H nmr experiments: preparation of solutions

Stock solutions of **1** in all solvents were prepared from weighed quantities of **1** in 1 mL volumetrics. Typically, **1** (376 mg, 1.80 mmol) was placed in a 1 mL volumetric flask and the flask then septum-capped, followed by flushing with dry N_2. Addition of $CDCl_3$ to the mark, via syringe, gave an initial stock solution (1.80 mol L^{-1}). A second stock solution was similarly prepared from **1** (451 mg, 2.16 mmol, 2.16 mol L^{-1}). Sequential dilution of the stock solution (0.5 mL in 1 mL volumetrics) gave concentration ratios of **1**:TNB ranging from 25:1 to 120:1. The same procedure was followed for CD_3CN and $(CD_3)_2SO$. The TNB stock solution (1.80×10^{-2} mol L^{-1}) consisted of TNB (19.2 mg, 4.50×10^{-5} mol) dissolved in N_2-purged solvent (5 mL).

A representative experiment

A sample tube contained 0.3 mL of the standard TNB solution in $CDCl_3$ and a drop of tetramethylsilane (TMS) as the internal shift standard. The initial spectrum of free TNB was recorded (0–10 ppm) and the chemical shift of the TNB singlet relative to TMS noted. A small quantity of the appropriate solution of **1** (0.3 mL) was injected into the septum-capped nmr tube via syringe and the spectrum rerecorded. The chemical shift of the averaged signal for free and complexed TNB were measured relative to TMS ($\delta_{TNB\text{-}av}$) (Fig. 1). The experimental data were plotted (Fig. 2) according to the Scatchard equation (25) (eq. [5]) to give the results reported above.

Acknowledgements

The author acknowledges the support and encouragement of the faculty at Sir Wilfred Grenfell College and helpful discussions with Prof. Erwin Buncel (Queen's University).

1. P. M. Dean. Molecular foundations of drug-receptor interaction. Cambridge University Press, Cambridge. 1987.
2. J. W. Black and P. Leff. Proc. R. Soc. London B, **220**, 141 (1983).
3. J. A. Apud. Pharmacol. Res. **23**, 217 (1991).
4. D. Colquhoun. Trends Pharmacol. Sci. **6**, 197 (1985).
5. (*a*) E. J. Ariens. Arch. Int. Pharmacodyn. **99**, 32 (1954); (*b*) E. J. Ariens and A. M. Simonis. Arch. Int. Pharmacodyn. **99**, 175 (1954).
6. Z. Simon, A. Chiriac, S. Holban, D. Ciubotaru, and G. I. Mihalas. Minimum steric difference. Wiley, New York. 1984.
7. (*a*) C. Hansch and A. Leo. Substituent constants for correlation analysis in chemistry and biology. Wiley–Interscience, New York. 1979; (*b*) C. Hansch, A. Leo, and R. W. Taft. Chem. Rev. **91**, 165 (1991).
8. J. G. Topliss (*Editor*). Quantitative structure–activity relationships of drugs. Academic Press, New York. 1983.
9. E. J. Ariens. *In* QSAR: Quantitative structure–activity relationships in drug design. Edited by J. L. Fauchere. A. R. Liss Inc., New York. 1989.
10. M. H. Abraham, P. L. Grellier, D. V. Prior, R. W. Taft, J. J. Morris, P. J. Taylor, C. Laurence, M. Berthelot, R. M. Doherty, M. J. Kamlet, J. L. M. Abboud, K. Sraidi, and G. Guiheneuf. J. Am. Chem. Soc. **110**, 8534 (1988).
11. F. Helmer, K. Kiehs, and C. Hansch. Biochemistry, **7**, 2858 (1968).
12. C. D. Selassie, C. D. Strong, C. Hansch, T. J. Delcamp, J. H. Freishein, and T. A. Khwaya. Cancer Res. **46**, 744 (1986).
13. K. H. Kim, C. Hansch, J. Y. Fukunaga, E. E. Steller, P. Y. C. Jow, P. N. Craig, and J. Page. J. Med. Chem. 366 (1979).
14. C. Hansch, A. Vittoria, C. Silipo, and P. Y. C. Jow. J. Med. Chem. **18**, 546 (1975).
15. (*a*) H. A. Benesi and J. H. Hildebrand. J. Am. Chem. Soc. **71**, 2703 (1949); (*b*) G. Briegleb. Electronen-donator–acceptor-komplexe. Springer-Verlag, Berlin. 1961; (*c*) R. S. Mulliken, J. Phys. Chem. **56**, 801 (1952); (*d*) M. J. S. Dewar and A. R. Lepley. J. Am. Chem. Soc. **83**, 4560 (1961); (*e*) R. Foster. Organic charge transfer complexes. Academic Press, London. 1969.
16. A. Chiriac, Z. Simon, R. Vilceanu, and V. Chiriac. An. Univ. Timisoara, Stiinte. Fiz.-Chim. 12, 59 (1978).
17. M. A. Slifkin. Mol. Interact. **2**, 271 (1981).
18. D. E. Zacharias, K. Prout, C. B. Myers and J. P. Glusker. Acta. Crystallogr. Sect. B: Struct. Sci. **B47**, 97 (1991).
19. H. F. Askal, G. A. Saleh, and N. M. Omar. Analyst (London), **116**, 387 (1991).
20. D. Kottke, T. Beyrich, and U. Meinkce. Pharmazie, **45**, 837 (1990).
21. (*a*) T. T. Goodnow, M. W. Reddington, J. F. Stoddart, and A. E. Kaifer. J. Am. Chem. Soc. **113**, 4335 (1991); (*b*) B. Odell, M. V. Reddington, A. M. Z. Slawin, N. Spencer, J. F. Stoddart, and D. J. Williams. Angew. Chem. Int. Ed. Engl. **27**, 1547 (1988).
22. J. A. Chudek, R. Foster, R. L. Mackay, F. M. Page, and D. R. Twiselton. J. Chem. Soc. Faraday Trans. 1, **84**, 1145 (1988).
23. (*a*) D. E. Metzler. Biochemistry. Academic Press, New York. 1977; (*b*) O. Walass (*Editor*). Molecular basis of some aspects of mental activity. Vol. 2. Academic Press, London. 1967; (*c*) E. K. Richfield. Brain Res. **540**, 1 (1991).
24. (*a*) E. Buncel, M. R. Crampton, M. J. Strauss, and F. Terrier. Electron deficient aromatic- and heteroaromatic-base interactions. The chemistry of anionic sigma complexes. Elsevier, Amsterdam. 1984; (*b*) E. Buncel, J. M. Dust, K. T. Park, R. A. Renfrow, and M. J. Strauss. *In* Nucleophilicity. *Edited by* J. M. Harris and S. P. McManus. Adv. Chem. Ser. Vol. 215. American Chemical Society, Washington, DC. 1987. p. 369; (*c*) J. M. Dust and J. M. Harris. J. Polym. Sci. Part A: Polym. Chem. **28**, 1875 (1990).
25. (*a*) G. Scatchard. Ann. NY Acad. Sci. **51**, 660 (1949); (*b*) P. H. Emslie and R. Foster. Tetrahedron, **20**, 1489 (1964); (*c*) R. Foster and C. A. Fyfe. Trans. Faraday Soc. **61**, 1626 (1965).
26. R. Foster. J. Phys. Chem. **84**, 2135 (1980).
27. J. Grudnes and S. D. Christian. J. Am. Chem. Soc. **90**, 2239 (1968).
28. S. K. Dotter and R. L. Harris. J. Org. Chem. **53**, 777 (1988).
29. (*a*) L. Forlani and V. Tortelli. J. Chem. Res. (S), 258 (1982); (*b*) J. Chem. Res. (S), 62 (1982); (*c*) L. Forlani, G. Guastadisegni, and L. Raffelini. J. Chem. Res. (S), 392 (1989).
30. (*a*) R. Bacaloglu, C. A. Bunton and G. Cerichelli. J. Am. Chem. Soc. **109**, 621 (1987); (*b*) R. Bacaloglu, C. A. Bunton and F. Ortega. J. Am. Chem. Soc. **110**, 3512 (1988); (*c*) J. Am. Chem. Soc. **111**, 1041 (1989).
31. E. Buncel, J. M. Dust, R. A. Manderville, K. T. Park, and I. Onyido. Bull. Soc. Chim. Fr. 371 (1988).
32. L. Forlani and C. Cimarelli. J. Phys. Org. Chem. **2**, 653 (1989).
33. M. R. Crampton and V. Gold. J. Chem. Soc. B, 23 (1967).
34. (*a*) B. Dodson, R. Foster, A. A. S. Bright, M. I. Foreman, and J. Gorton. J. Chem. Soc. B, 1283 (1971); (*b*) J. A. Chudek, R. Foster, and F. M. Jarrett. J. Chem. Soc. Faraday Trans. 1, **79**, 2729 (1983).

Can. J. Chem. Downloaded from www.nrcresearchpress.com by 123.30.183.119 on 09/08/12
For personal use only.

35. H. Stamm, W. Lamberty, and J. Shafe. J. Am. Chem. Soc. **102**, 1529 (1980).
36. R. Foster and J. W. Morris. J. Chem. Soc. B, 703 (1970).
37. (*a*) D. R. Kearns, P. Gardner, and J. Carmody. J. Phys. Chem. **71**, 931 (1967); (*b*) R. Foster and D. L. Hammick. J. Chem. Soc. 2685 (1954).
38. C. H. Jarboe, M. J. Bannon, and S. F. Lipson. J. Pharm. Pharmacol. **30**, 450 (1978).
39. R. Baltzly. J. Am. Chem. Soc. **75**, 6038 (1953).
40. P. A. Bather, J. R. Lindsay-Smith, and R. O. C. Norman, J. Chem. Soc. C, 3060 (1971).

Can. J. Chem. Downloaded from www.nrcresearchpress.com by 123.30.183.119 on 09/08/12
For personal use only.

Approaches towards the synthesis of a sulfur analog of ergosterol peroxide

YOULA S. TSANTRIZOS, PATRICIA L. FOLKINS, JAMES F. BRITTEN, AND DAVID N. HARPP[1]
Department of Chemistry, McGill University, Montréal (Qué.), Canada H3A 2K6

AND

KELVIN K. OGILVIE[1]
Vice President Academic, Acadia University, Wolfville, N.S., Canada B0P 1X0

Received February 18, 1991[2]

YOULA S. TSANTRIZOS, PATRICIA L. FOLKINS, JAMES F. BRITTEN, DAVID N. HARPP, and KELVIN K. OGILVIE. Can. J. Chem. **70**, 158 (1992).

In an analogous fashion to the preparation of ergosterol peroxide from singlet oxygen, the preparation of its sulfur analog was attempted via the Diels–Alder addition of diatomic sulfur to ergosterol. Two of the recently reported methods for generating and trapping diatomic sulfur were employed as well as "activated" sulfur. Although the desired target was not obtained, several interesting steroidal products were isolated including 3,5-cyclo-6,8(14),22-ergostatriene (**12**), ergosta-5,7,22-trien-3-thiol (**13**), and ergosta-4,6,8(14),22-tetraen-3-one (**16**). Mechanistic aspects are discussed.

Key words: diatomic sulfur, ergosterol, sulfur analog of ergosterol peroxide, ergosta-6,22-dien-5a,8a-epidisulfide-3-ol, ergosterol peroxide, 3,5-cyclo-6,8(14),22-ergostatriene, ergosta-5,7,22-trien-3-thiol, ergosta-4,6,8(14),22-tetraen-3-one.

YOULA S. TSANTRIZOS, PATRICIA L. FOLKINS, JAMES F. BRITTEN, DAVID N. HARPP et KELVIN K. OGILVIE. Can. J. Chem. **70**, 158 (1992).

Faisant appel à une méthode similaire à celle utilisée pour la préparation du peroxyde de l'ergostérol à partir de l'oxygène singulet, on a essayé de préparer l'analogue sulfuré via une addition de Diels–Alder du soufre diatomique sur l'ergostérol. On a utilisé du soufre «activé» ainsi que deux des méthodes décrites récemment pour générer et pour piéger le soufre diatomique. Même si l'on n'a pas obtenu la molécule désirée, on a pu isoler de nombreux produits stéroïdaux intéressants, dont du 3,5-cyclo-ergosta-6,8(14),24-triène (**12**), de l'ergosta-5,7,22-triène-3-thiol (**13**) et de l'ergosta-4,6,8(14),22-tétraèn-3-one (**16**). On discute des aspects mécanistiques.

Mots clés : soufre diatomique, ergostérol, analogue sulfuré du peroxyde de l'ergostérol, ergosta-6,22-diène-5a,8a-épidisulfure-3-ol, peroxyde de l'ergostérol, 3,5-cyclo-ergosta-6,8(14),22-triène, ergosta-5,7,22-tyriène-3-thiol, ergosta-4,6,8(14),22-tétraèn-3-one.

[Traduit par la rédaction]

Introduction

Ergosta-6,22-dien-5a,8a-epidioxy-3-ol (**1**), better known as ergosterol peroxide, was first isolated from the mycelium of *Aspergillus fumigatus* (1) and since then it has been found in several other fungi (2), lichens (3), and marine organisms (4). It exhibits a variety of biological effects including platelet aggregation (2*d*) and toxicity to plant tissues (5).

Recently, ergosterol peroxide was isolated from the liquid culture of *Phomopsis convolvulus* (6), a host-specific pathogen of the perennial plant *Convolvulus arvensis* (field bindweed) (7). This weed is classified as one of the most serious agricultural pests worldwide (8) that is hard to control at the present time. Ergosterol peroxide is a weakly phytotoxic compound that was found to be involved in the disease symptoms induced by *P. convolvulus* on field bindweed (6).

Sulfur analogs of biomolecules have been shown in the past to often mimic or even enhance the physiological effects of natural products. Most noteworthy are the examples of prostaglandin (9–11) and leukotriene (12) analogs, although several other sulfur derivatives of biologically important metabolites have been investigated (13). Hence, in hope of enhancing the herbicidal activity of ergosterol peroxide against field bindweed, studies towards the synthesis of ergosta-6,22-dien-5a,8a-epidisulfide-3-ol (**2**) were initiated.

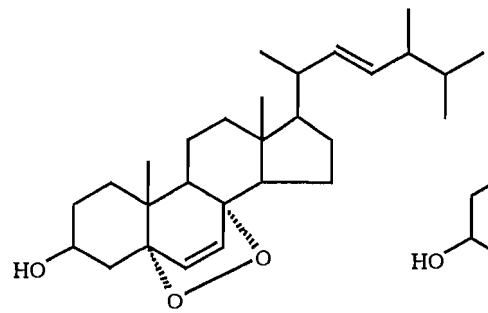

1 **2**

Ergosterol peroxide (**1**) has been synthesized from ergosterol (**3***a*) both enzymatically (2*c*, 14) and chemically (15). The Diels–Alder addition of singlet $O_2(^1\Delta_g)$ to the ergosterol diene is believed to be involved in the photochemical synthesis of the peroxide (15*a*, 16). Hence, it was considered appropriate to attempt the same reaction with diatomic sulfur precursors in an effort to synthesize its sulfur analog (**2**).

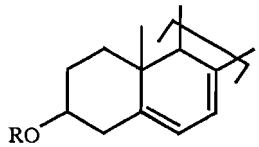

3*a* R = H

3*b* R = -Si(C_6H_5)$_2$ *tert*-butyl

[1]Authors to whom correspondence may be addressed.
[2]Revision received September 4, 1991.

Can. J. Chem. Downloaded from www.nrcresearchpress.com by 123.30.183.119 on 09/08/12
For personal use only.

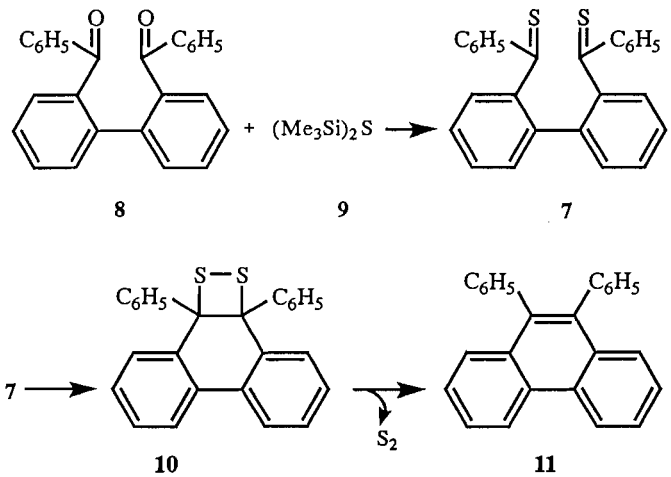

SCHEME 1

Results and discussion

A number of synthetically useful reagents for the generation of S_2 have been reported by Steliou *et al.* (17), Schmidt and Görl (18), and Harpp and MacDonald (19). In 1984, Steliou found that, in the presence of triphenyldibromophosphorane, organometallic trisulfides of general structure **4** deliver diatomic sulfur to a diene. The reaction mechanism could involve intermediate **5** or the formation of the four-membered ring intermediate **6**, analogous to that proposed in the phosphite-ozone generation of singlet oxygen (20). In 1987, the thermal rearrangement of the aromatic thioketone **7** was shown by Steliou *et al.* (17*b*) to generate S_2, which could be trapped by a number of dienes in high yield. Thioketone **7** is formed *in situ* from 2,2′-dibenzoylbiphenyl **8** (21), thiane **9**, and BCl_3. It has been proposed that a rearrangement takes place via intermediate **10**, which delivers S_2 to dienes (Scheme 1) (15*b*).[3]

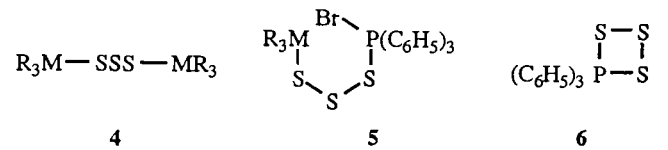

When the synthesis of the thioketone (**7**) was carried out in the presence of ergosterol (**3***a*) the main compounds isolated were 3,5-cyclo-6,8 (14),22-ergostatriene (**12**) and ergosta-5,7,22-trien-3-thiol (**13**) (in 41 and 19% yield respectively).

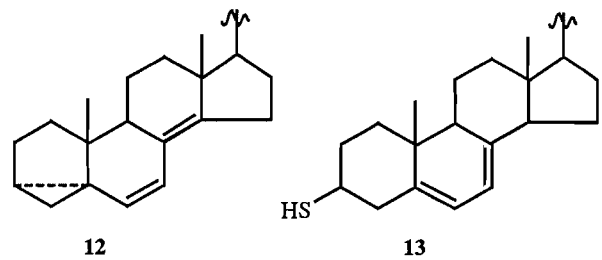

It was evident that these compounds were formed via OH elimination assisted by the Lewis acid even though the diene was not added until after the sulfurating agent was formed (as monitored by TLC) and conditions were kept such that the sulfurating reagent was the limiting reagent. When thiane **9** was added to ergosterol (**3***a*), a rapid silylation occurred to form the derivatives depicted in Scheme 2. In support of the proposed reactions, nearly 85% of unreacted 2,2′-dibenzoylbiphenyl was recovered. In addition, reaction of ergosterol with BCl_3 and **9** alone led to the isolation of the same two products (**12**, **13**) where omission of BCl_3 gave silylated ergosterol.

Structure determination for compound **12** was achieved by the combined NMR data from ^1H, ^{13}C, COSY, DEPT, APT, and HETCOR experiments. A literature search of the proposed structure revealed it to be a known compound (22); its UV and mp characteristics were in agreement with those previously reported (22). Compound **13** has nearly identical ^{13}C and ^1H NMR spectra to those of ergosterol (**3***a*) with appropriate deviations consistent with an -SH group at C-3. Further, an X-ray structure determination was carried out; the ORTEP diagram is shown in Fig. 1. The stereochemistry of the -SH group is identical to that of the -OH functionality in ergosterol (**3***a*), thus the mechanism of formation likely involves the attack of H_2S on the β face of the A ring of **12** (Scheme 2).

To inhibit the elimination reaction initiated by BCl_3 (Scheme 2), ergosterol (**3**) was protected with a *tert*-butyl diphenylsilyl group (**3***b*) and added to the reaction mixture long after it was estimated that thioketone **7** had formed in significant amounts while all of the BCl_3 had been consumed. However, even after refluxing in toluene for 72 h, there was no major product formed and most (70%) of the starting diene was recovered. Although 57% of starting dione **8** was also recovered, proof that some of the diatomic sulfur

[3]K. Steliou, Université de Montréal, Montréal, Québec. Personal communication.

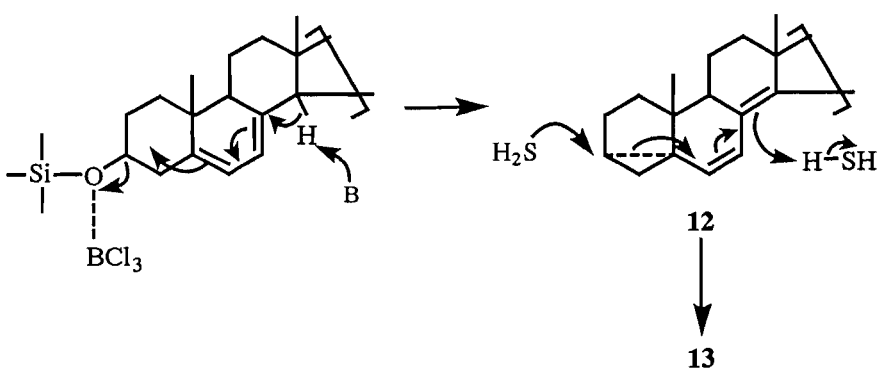

SCHEME 2

Can. J. Chem. Downloaded from www.nrcresearchpress.com by 123.30.183.119 on 09/08/12
For personal use only.

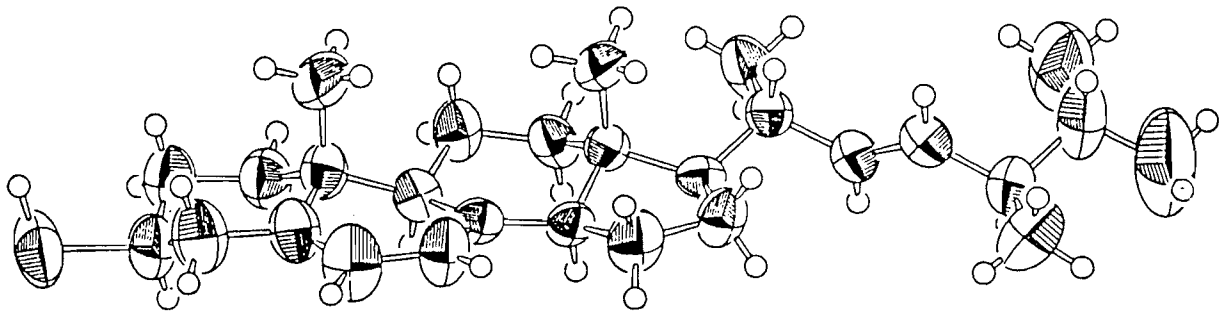

FIG. 1. ORTEP drawing of compound **13**.

precursor had actually been produced was evidenced by the formation of 21% of 9,10-diphenyl phenanthrene (**11**).

More recently, Harpp and MacDonald (19) reported the generation of diatomic sulfur from organometallic pentasulfides of titanium and zirconium complexes **14**. These reagents are analogous to the organometallic trisulfides **4** in that they undergo S_2 extrusion in the presence of triphenyldibromophosphorane.

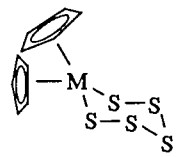

14*a* M = Ti
14*b* M = Zr

Several attempts to induce a Diels–Alder reaction between S_2 and ergosterol (**3***a*) using Ph_3PBr_2 and bis(*n*-cyclopentadienyl)titana(IV)cyclohexasulfane (**14***a*)[4] produced elemental sulfur (S_8); in addition, two minor products were isolated in low yield.[5]

[4]We are grateful to C. R. Williams for the preparation of this reagent. It was first prepared by McCall and Shaver (23).

[5]The ^1H NMR spectrum of the main steroidal product showed loss of the C-7 proton and a downfield shift of both the 18- and 19-CH_3 signals. The ^{13}C NMR spectrum showed a peak (170.74 ppm) at the characteristic shift of quaternary sp^2 carbons attached to sulfur, a downfield shift of the C-5 signal (139.78 to 150.85 ppm), and upfield shift of the C-8 signal (141.38 to 123.14 ppm). The ^1H NMR spectrum of the minor product showed a loss of the C-6 proton signal and a downfield shift of the C-3 proton signal to 3.90 ppm (from 3.63 ppm in ergosterol (**3***a*)) and the 19-CH_3 signal to 1.11 ppm (from 0.93 ppm in **3***a*). These data suggest that the major compound isolated was the C-7 mercapto ergosterol (ergosta-5,7,22-trien-7-mercapto-3-ol, **15***b*) and the minor, the C-6 mercaptan (ergosta-5,7,22-trien-6-mercapto-3-ol, **15***a*). These compounds do not give a parent ion in the ammonia CI mass spectrum and, due to their low yields, there was an insufficient amount of pure material available for elemental analysis. However, this class of compound is not unusual (24).

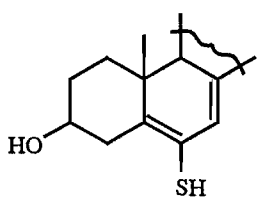

15*a*

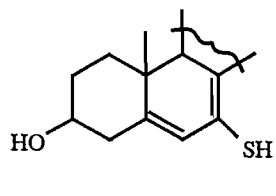

15*b*

In an attempt to understand the suggested addition of sulfur to ergosterol (compounds **15***a*, **15***b*) in the absence of any detectable Diels–Alder products, the behavior of ergosterol in the presence of elemental sulfur (S_8) (25)[6] was further investigated. S_8 alone failed to react with ergosterol in refluxing toluene over a period of several hours, thus an "activated" form of sulfur was employed. Triethylamine, which is widely used as an activating agent in reactions of elemental sulfur with organic compounds (25,26), was added to the reaction mixture. However, this combination of reagents gave several products, only one of which could be separated and identified. The unidentified products were the likely victims of aromatization as evidenced by the isolation of elemental sulfur (S_8) during flash column chromatography (27).[7]

The main product, isolated from the reaction of "activated" elemental sulfur with ergosterol, showed a downfield shift of the H6 and H7 olefinic protons and loss of the long-range coupling observed in the starting material and thus appeared consistent with anticipated structure **2** inasmuch as the spectrum closely resembled that of the ergosterol peroxide (**1**). However, the APT and DEPT NMR spectra and MS and IR data indicated that ergosta-4,6,8(14),22-tetraen-3-one (**16**) was in fact the correct structure. In addition, the mp and UV were consistent with earlier reports on this compound (28). The details of its structure were obtained by an X-ray structure analysis. The ORTEP diagram is displayed in Fig. 2. Compound **16** is an interesting fungal metabolite of *Penicillium rubrum* (29) and has been shown to be an important biosynthetic intermediate in the metabolism of ergosterol (29).

The mechanism (Scheme 3) that we believe led to the formation of **16** involves first the oxidation of the C-3 OH, by participation of the sulfur (26), followed by a temporary nucleophilic addition of the sulfur to the C-4 carbon and elimination of H-14 to give a conjugated carbonyl derivative.

Attempts to minimize side products of the above reaction by first converting the C-3 OH to its acetate were unsuccessful, leading to an even greater amount of unidentifiable products.

[6]It has been widely observed that sulfur reacts with olefinic carbons in ionic or radical type mechanisms (25).

[7]The formation of aromatic compounds produced by dehydration and dehydrogenation of six-membered ring secondary alcohols was observed previously in similar reactions of elemental sulfur under even milder experimental conditions (27).

Can. J. Chem. Downloaded from www.nrcresearchpress.com by 123.30.183.119 on 09/08/12
For personal use only.

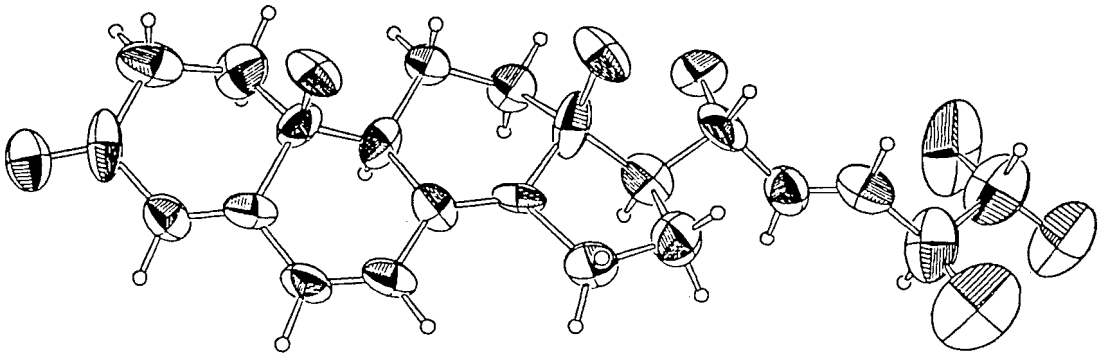

FIG. 2. ORTEP drawing of compound **16**.

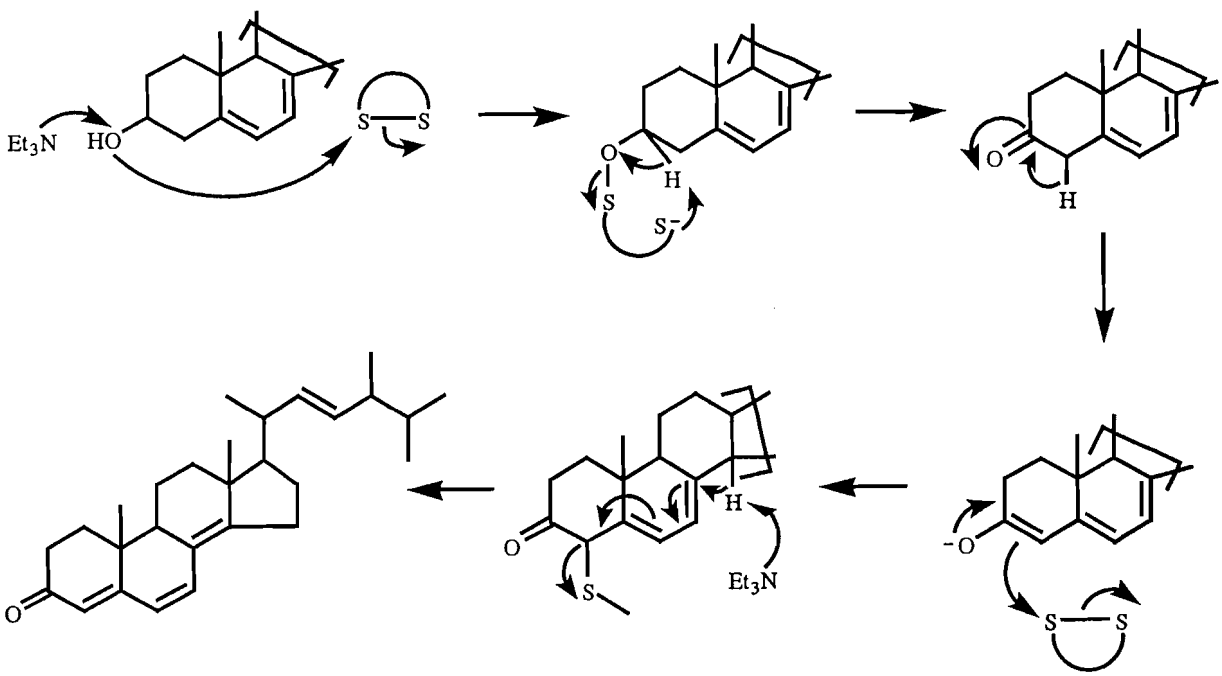

SCHEME 3

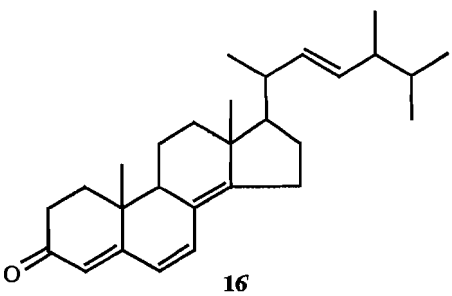

16

The fact that the main products isolated in the reaction of ergosterol and activated sulfur were not at all similar to those isolated in the reaction of ergosterol with bis(*n*-cyclopentadienyl)titana(IV)cyclohexasulfane (**14***a*) indicates that these two reactions must proceed by different routes. The products isolated from the reaction of ergosterol with **14***a* can be rationalized by insertion of diatomic sulfur into the double bonds of **3***a*; however, several closely related schemes can be envisaged which cannot be differentiated at this time.

Experimental

General methods

Nuclear Magnetic Resonance spectra were obtained at 20–22°C using Varian XL-200 and XL-300 MHz instruments. ^{1}H and ^{13}C NMR chemical shifts are quoted in ppm and are referenced to the internal deuterated solvent downfield from tetramethylsilane (TMS). Chemical shift assignments of all steroid products were based on the HETCOR and COSY NMR data of each compound and the literature chemical shifts of equivalent carbons in ergosterol and ergosterol peroxide (6). All mass spectra were measured at the Biomedical Mass Spectrometry Unit, McGill University, unless otherwise indicated. The low resolution chemical ionization (NH_3) spectra were obtained using a HP 5980A spectrometer. FAB and high resolution chemical ionization spectra (NH_3) were obtained using a ZAB 2F HS instrument. Ultraviolet spectra were recorded on a Hewlett Packard 8451A diode array spectrophotometer. Infrared spectra were recorded on an Analect ASQ-18 FTIR spectrophotometer calibrated to the 1602 cm^{-1} line of polystyrene. Sulfur analyses were performed on an Antek 771 pyroreactor and 714 sulfur detector system. Melting points were measured using a Gallenkamp capillary apparatus and are uncorrected.

Can. J. Chem. Downloaded from www.nrcresearchpress.com by 123.30.183.119 on 09/08/12
For personal use only.

Can. J. Chem. Downloaded from www.nrcresearchpress.com by 123.30.183.119 on 09/08/12
For personal use only.

Commercially available compounds were obtained from Aldrich Chemical Co. (Milwaukee, Wis.). Silica gel chromatography was performed on Merck Kieselgel 60 (230–400 mesh, no. 9385) using flash chromatography (30). Chromatographic solvents were fractionally distilled prior to use. All reactions were monitored by thin-layer chromatography carried out on 0.25 mm Merck silica gel plates (60F–254) using UV light and a 10% sulfuric acid ethanolic solution of ammonium molybdate-cerium sulfate developing dip.

*Preparation of 2,2′-dibenzoylbiphenyl (**8**)*

Prepared via oxidation of 2,2′-di(1-phenylmethanol)biphenyl. *o*-Dibromobenzene (4.00 g, 16.9 mmol) was dissolved in dry THF (100 mL) and cooled to −78°C under an atmosphere of nitrogen. *n*-Butyllithium (17 mL of a 2.5 M solution in hexanes, 42.4 mmol) was added (dropwise) and the mixture was allowed to stir at −78°C for 4 h and at room temperature for an additional 0.5 h. A solution of benzaldehyde (5.306 g, 50 mmol) in THF (25 mL) was added subsequently (dropwise) and the reaction was allowed to proceed for another 0.5 h before it was quenched with water (200 mL). The organic layer was then separated, washed with brine (2 × 200 mL), dried over $MgSO_4$, and evaporated under reduced pressure to a yellow oil. The excess benzaldehyde was removed by Kugelrohr distillation, and the remaining oil was allowed to crystallize from hexanes (in a freezer) to give 0.8785 g (28%) of 2,2′-di(1-phenylmethanol)biphenyl, mp 186–192°C. IR (KBr): 3500 (OH) cm^{-1}. ^1H NMR (200 MHz, $CDCl_3$) δ: 2.1 (s, 2H, 2 × CHOH), 2.6 (s, 2O*H*), and 7.1–7.6 (m, 18H, aromatic protons) ppm. ^{13}C NMR (300 MHz, $CDCl_3$) δ: 71.7 (2 × COH), 126.1, 126.9, 127.4, 128.1, 128.2, 128.3, 129.5, 140,0, 142.4 and 143.2 ppm.

Aqueous CrO_3 (0.25 g in 20 mL H_2O) was added dropwise to an acidic solution of 2,2′-di(1-phenylmethanol)biphenyl (0.217 g, 0.594 mmol, in 10 mL glacial acetic acid) at 65°C. The reaction was allowed to stir at 65°C for 0.5 h, then cooled to room temperature, neutralized with a saturated solution of Na_2CO_3, and extracted with ether (3 × 100 mL). The ether layer was dried over $MgSO_4$, evaporated to dryness, and recrystallized from ethanol to obtain 0.157 g (74% yield) of pure crystalline product (**8**). TLC: hexane/ethyl acetate (9:1), R_f 0.21; mp decomposes above 150°C. IR (KBr): 1654 (C=O) cm^{-1}. ^1H NMR (200 MHz, $CDCl_3$) δ: 7.20–7.40 (m, 14H) and 7.67–7.71 (m, 4H) ppm. ^{13}C NMR (300 MHz, $CDCl_3$) δ: 126.7 (C4 and C4′), 127.9 (C6 and C6′), 129.3 (C3″, C3‴), 130.1 (C3 and C3′), 130.3 (C1′, C1‴), 131.4 (C4″ and C4‴), 132.7 (C5 and C5′), 137.3 (C2 and C2′), 138.2 (C8 and C8′), 140.2 (C1 and C1′), and 197.5 (*C*=O) ppm.

*The formation of 3,5-cyclo-6,8(**14**),22-ergostatriene (**12**) and ergosta-5,7,22-trien-3-thiol (**13**)*[8]

To a solution of 2,2′-dibenzoylbiphenyl (0.169 g, 0.467 mmol) and ergosterol (0.185 g, 0.467 mmol) in dry toluene (30 mL), 1,1,1,3,3,3-hexamethyldisilylathiane (0.166 g, 0.933 mmol) was added via a syringe under an atmosphere of nitrogen. The resulting mixture was cooled to 0°C and boron trichloride (0.623 mL of a 1 M solution in CH_2Cl_2, 0.623 mmol) was added slowly via a syringe. The reaction was warmed to room temperature and then allowed to reflux for 9.5 h. Evaporation of the solvent, followed by flash column chromatography of the resulting crude with petroleum ether, led to the isolation of two compounds, 3,5-cyclo-6,8(14),22-ergostatriene (**12**) (fractions 3–6, 72.3 mg, 41% yield) and the ergosterol thiol **13** (fractions 8–13, 36.8 mg, 19% yield). Further elution with petroleum ether/ethyl acetate (3:1) led to the recovery of unreacted 2,2′dibenzoylbiphenyl (140 mg, 83%).

*3,5-Cyclo-6,8(14),22-ergostatriene (**12**):* TLC: Petroleum ether, R_f 0.57; mp 98.5–100°C (lit. (22) mp 102–102.5°C). IR ($CDCl_3$): 1458, 1600 (C=C), 2869 and 2961 (C—C) cm^{-1}. UV (EtOH): max 262 nm. ^1H NMR (200 MHz, $CDCl_3$) δ: 0.46 (dd, J = 5.0 and 8.2 Hz, 1H, H3), 0.76 (s, 3H, 18-CH_3), 0.79–0.84 (2d, J = 6.8 Hz, 6H, 26-CH_3 and 27-CH_3), 0.90 (s, 3H, 19-CH_3), 0.91 (d, J = 6.8 Hz, 3H, 28-CH_3), 1.02 (d, J = 6.7 Hz, 3H, 21-CH_3), 1.2–2.4 (m, 19H, steroid skeleton), 5.2 (m, 3H, H6, H22 and H23), and 6.19 (d, J = 9.5 Hz, 1H, H7) ppm. ^{13}C NMR (300 MHz, $CDCl_3$) δ: 15.56, 17.02, 17.65, 19.30, 19.65, 19.99, 20.39, 21.22, 25.18, 25.33, 26.52, 27.98, 30.79, 33.10, 37.37, 37.58, 39.44, 40.83, 42.86, 43.52, 43.86, 56.14, 124.06, 124.63, 130.57, 132.02, 135.49, and 147.04 ppm. APT (D2 = 4 ms) NMR (300 MHz, $CDCl_3$) δ: 37.58 (C10), 43.52 and 43.86 (C5 and C13), 124.63 (C14), and 147.04 (C8) ppm. DEPT NMR (300 MHz, $CDCl_3$) δ: $6CH_3$ (17.02 and 19.30 (C18 and C19), 17.66 (C28), 19.65 (C26), 19.99 (C27) and 21.22(C2) ppm); $7CH_2$ (15.56 (C4), 20.39 (C11), 25.18 and 25.33 (C2 and C15), 27.98 (C16), 30.79 (C1) and 37.37 (C12) ppm); 10CH (26.52 (C3), 33.10 (C25), 39.44 (C9), 40.83 (C20), 42.86 (C24), 56.14 (C17), 124.06 (C7), 130.57 (C6), 132.02 (C23) and 135.49 C22 ppm). MS (E.I., direct inlet, 65°C), m/z (% relative intensity, assignment): 378 (16, M^+).

*Ergosta-5,7,22-trien-3-thiol (**13**):* TLC: petroleum ether, R_f 0.42; mp 121.5–123°C. $[\alpha]_D^{20}$ −150 (*c* 0.02, CH_2Cl_2). IR ($CDCl_3$): 1458 (C=C), 2873 and 2960 (C—C) cm^{-1}. UV (EtOH): max 274, 284; min 296 nm. ^1H NMR (200 MHz, $CDCl_3$) δ: 0.61 (s, 3H, 18-CH_3), 0.79–0.83 (2d, J = 6.8 Hz, 6H, 26-CH_3 and 27-CH_3), 0.90 (d, J = 6.8 Hz, 3H, 28-CH_3), 0.94 (s, 3H, 19-CH_3), 1.02 (d, J = 6.6 Hz, 3H, 21-CH_3), 1.22–2.08 (m, 19H, steroid skeleton), 2.59–2.63 (m, 2H, 2 × H4), 3.80–3.86 (m, 1H, H3), 5.15–5.20 (m, 2H, H22 and H23), 5.37 (dd, 1H, H7), and 5.55 (bd, J = 5.62 Hz, 1H, H6) ppm. ^{13}C NMR (300 MHz, $CDCl_3$) δ: 12.06 (C18), 16.15 (C19), 17.60 (C28), 19.64 (C26), 19.95 (C27), 20.98 (C11), 21.10 (C21), 22.96 (C15), 28.26 (C16), 33.07 (C25), 33.63 (C2), 36.76 (C10), 38.98 (C12), 40.02 (C1), 40.41 (C20), 41.92 (C4), 42.82 (C13 and C24), 46.19 (C9), 54.55 (C14), 55.70 (C17), 59.09 (C3), 116.14 (C7), 119.84 (C6), 132.01 (C23), 135.50 (C22), 139.24 (C5), and 141.94 (C8) ppm. Chemical shift assignments were consistent with DEPT, APT, and COSY NMR experiments. MS (E.I., direct inlet, 95°C) m/z (% relative intensity, assignment): 378 ($M^+ - H_2S$). Sample analysis using the Antek analyzer confirmed the presence of sulfur in this compound. In addition, a nitroprusside (31) test for thiol was positive.

Protection of ergosterol with tert*-butylchlorodiphenylsilane (**3**b)*

Ergosterol (1.00 g, 2.50 mmol) and imidazole (0.85 g, 12.5 mmol) were dissolved in dry DMF (50 mL) under nitrogen and *tert*-butylchlorodiphenylsilane (1.39 g, 5.00 mmol) was added via syringe. The white precipitate formed was allowed to stir for 12 h at room temperature. The mixture was then extracted with ethyl acetate, the organic layer was washed with 1 M HCl (3 × 50 mL) and water (3 × 50 mL), dried over $MgSO_4$, and evaporated to dryness. The desired product (0.6824 g, 57% yield) and unreacted starting material were purified via flash column chromatography (24:1 hexanes:ethyl acetate). TLC: hexanes/ethyl acetate (4:1), R_f 0.55. ^1H NMR (200 MHz, $CDCl_3$) δ: 0.59 (s, 3H, Si-CH_3), 0.79–0.84 (2d, J = 6.7 Hz, 6H, 26-CH_3 and 27-CH_3), 0.88–0.91 (m, 6H), 1.02–1.05 (m, 12H), 1.2–1.9 (m, 18H, steroid skeleton), 2.31 (m, 2H, 2H4), 3.6 (m, 1H, H3), 5.15–5.20 (dd, 2H, H22 and H23), 5.29–5.34 (m, 1H, H7), and 5.36–5.43 (bd, J = 5.7 Hz, 1H, H6), 7.34–7.40 and 7.64–7.69 (2m, 6H and 4H respectively, phenyl) ppm. MS (C.I.(NH_3), direct inlet, 99°C) m/z (% relative intensity, assignment): 635 (5 M^+ +1), 379 (100, M^+ + 1 − $SiPh_2(C_4H_9)$).

*Reaction of ergosterol with bis(*n*-cyclopentadienyl)titana-(IV)cyclohexasulfane (**15**a,b)*

A solution of Br_2 (50 mL, 1.0 mmol) in dry CH_2Cl_2 (5.0 mL) was added dropwise to a solution of triphenylphosphine (275 mg, ~1.1 mmol in 5.0 mL dry CH_2Cl_2) at 0°C. The suspension of triphenyldibromophosphorane formed was allowed to warm up

[8]X-ray data for compounds **13** (22 pages) and **16** (10 pages), listing of structure factors for **13** (28 pages) and **16** (22 pages), and spectral data for compounds **3***b*, **13**, **15***a*, **15***b* have been deposited as supplementary material and may be purchased from: The Depository of Unpublished Data, Document Delivery, CISTI, National Research Council Canada, Ottawa, Canada K1A 0S2.

Can. J. Chem. Downloaded from www.nrcresearchpress.com by 123.30.183.119 on 09/08/12
For personal use only.

to room temperature and then it was added, dropwise, to a solution of ergosterol (800 mg, 1.0 mmol) and bis(*n*-cyclopentadienyl)titana(IV)cyclohexasulfane (340 mg, 1.0 mmol) in 15 mL dry CH_2Cl_2. The reaction mixture was stirred at room temperature for 4 h, evaporated to dryness, and purified by chromatography. Flash column chromatography of the crude mixture, using CH_2Cl_2 as the eluting solvent, led to separation of the isomeric mixture of thiols **15***a* and **15***b* from the remaining crude. Further thin-layer chromatography was carried out on preparative silica gel plates developed five times with petroleum ether/ethyl acetate (5:1) in order to achieve partial separation of the two compounds. The major product **15***b* was isolated in ~15% yield (~250 mg) and the minor product **15***a* in ~5% yield (~20 mg).

*Ergosta-5,7,22 trien-6-mercapto-3-ol (***15***a):* TLC: CH_2Cl_2/ethyl acetate (2:1), R_f 0.59. ^{1}H NMR (200 MHz, $CDCl_3$) δ: 0.80–0.85 (2d, J = 6.8 Hz, 6H, 26-CH_3 and 27-CH_3), 0.84 (s, 3H, 18-CH_3), 0.92 (d, J = 6.8 Hz, 3H, 28-CH_3), 1.03 (d, J = 6.6 Hz, 3H, 21-CH_3), 1.11 (s, 3H, 19-CH_3), 1.2–2.3 (m, 21H, steroid skeleton), 3.90 (m, 1H, H3), 5.20–5.25 (m, 2H, H22 and H23), and 5.36 (m, 1H, H7) ppm. There was a positive nitroprusside test indicating a thiol (31).

*Ergosta-5,7,22-trien-7-mercapto-3-ol (***15***b):* TLC: CH_2Cl_2/ethyl acetate (2:1), R_f 0.59; mp 133.5–135°C. ^{1}H NMR (200 MHz, $CDCl_3$) δ: 0.80–0.85 (2d, J = 6.8 Hz, 6H, 26-CH_3 and 27-CH_3), 0.82 (s, 3H, 18-CH_3), 0.92 (d, J = 6.8 Hz, 3H, 28-CH_3), 0.98 (s, 3H, 19-CH_3), 1.03 (d, J = 6.5 Hz), 1.2–2.4 (m, 21H, steroid skeleton), 3.63 (m, 1H, H3), 5.20–5.25 (m, 2H, H22 and H23), and 5.33 (m, 1H, H6) ppm. ^{13}C NMR (300 MHz, $CDCl_3$) δ: 15.83, 17.67, 18.39, 19.65, 19.98, 21.00, 21.87, 25.31, 26.60, 31.72, 33.10, 35.35, 36.57, 36.69, 36.95, 38.33, 38.91, 40.96, 42.83, 44.82, 57.10, 71.01, 117.79, 123.14, 132.07, 135.52, 140.74, and 150.85 ppm. MS (C.I. (NH_3), direct inlet, 250°C), m/z (% relative intensity, assignment): 397 (61, $M^+ + 1 - S$), 270 (17, $M^+ - S - 125$), 125 (100, side chain). Sample analysis using a "Sulfur analyzer" instrument confirmed the presence of sulfur in this compound; a nitroprusside (31) test was also positive.

*Reaction of ergosterol with elemental sulfur (***16***)*

Ergosterol (5.0 g, 12.6 mmol) and S_8 (3.00 g, 11.7 mmol = ~4 equiv. of S_2) were refluxed in dry toluene (~200 mL) in the presence of 1 equivalent of triethylamine (1.5 mL, ~12 mmol). After a period of 24 h the crude mixture was filtered, washed with water (3 × 100 mL), and evaporated to dryness. Flash column chromatography (2×) of the product mixture with petroleum ether/ethyl acetate (4:1) (2nd chromatography was performed on fractions 13–17 of the 1st column) led to the isolation of compound **16** (ergosta-4,6,8(14),22-tetraen-3-one) as an orange-yellow solid. Preparative thin-layer chromatography on silica gel plates, developed twice with hexane/ethyl acetate (9:1), followed by recrystallization from ethanol, gave crystalline compound **16** in approximately 5% yield (30 mg). TLC: pet. ether/ethyl acetate (3:1), R_f 0.45 (fluorescent spot under UV); mp 112.5–113°C (lit. (29) mp 114–115°C). IR ($CDCl_3$): 1646 (C=O), 1636, 1584 (C=C) cm^{-1}. UV (CH_3CH_2OH, nm): max 350. ^{1}H NMR (200 MHz, $CDCl_3$) δ: 0.78–0.83 (2d, J = 6.7 Hz, 6H, 26-CH_3 and 27-CH_3), 0.90 (d, J = 6.8 Hz, 3H, 28-CH_3), 0.93 and 0.96 (2s, 2 × 3H, 18-CH_3 and 19-CH_3), 1.03 (d, J = 6.7 Hz, 3H, 21-CH_3), 1.15–2.55 (m, 18H, steroid skeleton), 5.17–5.22 (m, 2H, H22 and H23), 5.70 (s, 1H, H2), 6.00 (d, J = 9.5 Hz, 1H, H6), and 6.57 (d, J = 9.5 Hz, 1H, H7) ppm. ^{13}C NMR (300 MHz, $CDCl_3$) δ: 16.62 (C18), 17.61 (C28), 2 × 18.95 (C19 and C2), 19.63 (C26), 19.96 (C27), 21.19 (C21), 25.33 (C11), 27.69 (C16), 33.05 (C25), 2× 34.09 (C1 and C12), 35.55 (C15), 36.71 (C10), 39.25 (C20), 42.83 (C24), 43.95 (C13), 44.28 (C9), 55.66 (C17), 122.95 (C4), 124.38 (C6), 124.42 (C8), 132.49 (C23), 133.97 (C7), 134.96 (C22), 156.04 (C14), 164.32 (C5), and 199.43 (C3) ppm. APT (D2 = 4 ms) NMR (300 MHz, $CDCl_3$) δ: 36.75 (C10), 43.96 (C13), 124.26 (C8), 155.89 (C9), 164.17 (C5), and 199.20 (C3) ppm. DEPT NMR (300 MHz, $CDCl_3$) δ: 6CH_3 (16.61, 17.61, 18.95, 19.63, 19.96, 21.19 ppm), 6CH_2 (18.95, 25.33, 27.69, 2 × 34.09, 35.55 ppm), 10CH (33.05, 39.25, 42.83, 44.28, 55.66, 122.95, 124.42, 132.49, 133.97, 134.96 ppm). MS (C.I. (NH_3), direct inlet, 150°C), m/z (% relative intensity, assignment): 394 (31, $M^+ + 1$), 393 (100, M^+).

Acknowledgements

We thank NSERC (Canada) and FCAR (Québec) for financial support of this work. The X-ray determination for **16** was carried out at the Molecular Structure Corporation, The Woodlands, TX 77381.

1. P. Wieland and V. Prelog. Helv. Chim. Acta, **30**, 1028 (1947).
2. (*a*) G. Bauslaugh, G. Just, and F. Blank. Nature, **202**, 1218 (1964); (*b*) E. P. Serebryakov, A. V. Simolin, V. F. Kucherov, and B. V. Rosynov. Tetrahedron, **26**, 5215 (1970); (*c*) J. Arditti, R. Ernst, M. H. Fisch, and B. H. Flick. J. Chem. Soc. Chem. Commun. 1217 (1972); (*d*) J. D. Weete. Phytochemistry, **12**, 1843 (1973); (*e*) L. C. Brown and J. J. Jacobs. Aust. J. Chem. **28**, 2317 (1975); (*f*) W. Lu, I. Adachi, K. Kano, A. Yasuta, K. Toriizuka, M. Ueno, and I. Horikoshi. Chem. Pharm. Bull. **33**, 5083 (1985); (*g*) G. Kusano, H. Ogawa, A. Takahashi, S. Nozoe, and K. Yokoyama. Chem. Pharm. Bull. **35**, 3482 (1987).
3. T. Hirayama, F.Fujikawa, I. Yosioka, and I. Kitagawa. Chem. Pharm. Bull. **23**, 693 (1975).
4. (*a*) A. A. L. Gunatilata, Y. Gopichand, F. J. Schmitz, and C. Djerassi. J. Org. Chem. **46**, 3860 (1981); (*b*) M. Guyot and M. Durgeat. Tetrahedron Lett. **22**, 1391 (1981).
5. N. Otomo, H. Sato, and S. Sakamura. Agric. Biol. Chem. **47**, 1115 (1983).
6. Y. S. Tsantrizos. Ph.D. Thesis, McGill University, Montreal, Quebec. 1990.
7. (*a*) J. Ormeno-Nunez, R. D. Reeleder, and A. K. Watson. Plant Dis. **72**, 338 (1988); (*b*) Can. J. Bot. **66**, 2228 (1988).
8. (*a*) J. F. Alex. *In* Biology and ecology of weeds. *Edited by* W. Holzner and M. Numata. W. Junk Publishers, The Hague. 1982. p. 309; (*b*) L. G. Holm, D. L. Plunknett, J. V. Pancho, and J. P. Herberger. *In* The world's worst weeds. University Press of Hawaii, Honolulu. 1977. Chap. 12; (*c*) S. S. Rosenthal. Calif. Agric. **37**, 16 (1983).
9. (*a*) K. C. Nicolaou, W. E. Barnette, G. P. Gasic, and R. L. Magolda. J. Am. Chem. Soc. **99**, 7736 (1977); (*b*) M. Shibasaki and S. Ikegami. Tetrahedron Lett. 559 (1978); (*c*) P. G. Baraldi, A. Barco, S. C. Benetti, A. Gandolfi, G. P. Pollini, E. Polo, and D. Simoni. Gazz. Chim. Ital. **114**, 177 (1984).
10. K. C. Nicolaou, W. E. Barnette, and R. L. Magolda. J. Am. Chem. Soc. **103**, 3486 (1981).
11. (*a*) H. Miyake, S. Iguchi, H. Itoh, and M. Hayashi. J. Am. Chem. Soc. **99**, 3536 (1977); (*b*) S. S. Ghosh, J. C. Martin, and J. Fried. J. Org. Chem. **52**, 862 (1987).
12. Y. Guindon and D. Delorme. Can. J. Chem. **65**, 1438 (1987).
13. (*a*) T. R. Bosin, R. P. Maickel, A. Dinner, A. Snell, and E. Campaigne. J. Heterocycl. Chem. **9**, 1265 (1972); (*b*) J. L. Douglas, A. Martel, G. Caron, M. Menard, L. Silveira, and J. Clardy. Can. J. Chem. **62**, 3382 (1984); (*c*) M. Iwata and H. Kuzuhara. Bull. Chem. Soc. Jpn. **58**, 2502 (1985); (*d*) K. Steliou, Y. Gareau, G. Milot, and P. Salama. Phosphorus, Sulfur Silica, **43**, 209 (1989).
14. M. L. Bates and W. W. Reid. J. Chem. Soc. Chem. Commun. 44 (1976).
15. (*a*) V. A. Windaus and J. Brunken. Justus Liebigs Ann. Chem. **465**, 225 (1928); (*b*) L. F. Fieser and M. Fieser *In* Steroids. Reinhold Publishing Corporation, New York; Chapman and Hall, London. 1959; (*c*) D. H. R. Barton, G. Leclerq, P. D. Magnus, and I. D. Menzies. J. Chem. Soc. Chem. Commun. 447 (1972); (*d*) D. H. R. Barton, R. K. Haynes, P. D.

Magnus, and I. D. Menzies. J. Chem. Soc. Chem. Commun. 511 (1972).
16. D. R. Kearns. J. Am. Chem. Soc. **91**, 6554 (1969).
17. (*a*) K. Steliou, Y. Gareau, and D. N. Harpp. J. Am. Chem. Soc. **106**, 799 (1984); (*b*) K. Steliou, P. Salama, D. Brodeur, and Y. Gareau. J. Am. Chem. Soc. **109**, 926 (1987).
18. M. Schmidt and U. Görl. Angew. Chem. Int. Ed. Engl. **26**, 887 (1987).
19. D. N. Harpp and J. G. MacDonald. J. Org. Chem. **53**, 3812 (1988).
20. (*a*) R. W. Murray,and M. L. Kaplan. J. Am. Chem. Soc. **90**, 537 (1968); (*b*) P. D. Bartlett and C. M. Lonzetta. J. Am. Chem. Soc. **105**, 1984 (1983).
21. D. Mullins. Ph.D. Thesis, McGill University, Montreal, Quebec. (1981).
22. M. Fieser, W. E. Rosen, and L. Fieser. J. Am. Chem. Soc. **74**, 5397 (1952).
23. J. M. McCall and A. Shaver. J. Organomet. Chem. **C37**, 193 (1980).
24. (*a*) G. Sauvé, N. Le Berre, and B. Zacharie. J. Org. Chem. **55**, 3002 (1990); (*b*) E. Campaigne and R. L. White, Jr. J. Heterocycl. Chem. **25**, 367 (1988); (*c*) T. Furuhata and W. Ando. Tetrahedron Lett. **42**, 5301 (1986).
25. M. G. Voronkov, N. S. Vyazankin, E. N. Deryagina, A. S. Nakhmanovich, and V. A. Usov. *In* Reactions of sulfur with organic compounds. *Edited by* J. S. Pizey. Plenum, New York. 1987.
26. R. Mayer. Z. Chem. **13**, 321 (1973).
27. L. Ruzicka. Angew. Chem. **51**, 5 (1938).
28. (*a*) D. H. R. Barton and T. Bruun. J. Chem. Soc. 2728 (1951); (*b*) H. Morimoto, I. Imada, T. Murata, and N. Matsumoto. Liebigs Ann. Chem. **708**, 230 (1967); (*c*) K. E. Schulte, G. Rucker, and H. Fachmann. Tetrahedron Lett. 4763 (1968).
29. J. D. White and S. I. Taylor. J. Am. Chem. Soc. **92**, 5811 (1970).
30. W. C. Still, M. Kahn, and A. Mitra. J. Org. Chem. **43**, 2923 (1978).
31. K. G. Krebs, D. Heusser, and H. Wimmer. *In* Thin layer chromatography. A laboratory handbook. *Edited by* E. Stahl. Springer Verlag, New York/Heidelberg. 1969. p. 890.

Can. J. Chem. Downloaded from www.nrcresearchpress.com by 123.30.183.119 on 09/08/12
For personal use only.

An investigation of the rotational isomers of *N*-acetyl-2,2-dimethyloxazolidine and related compounds by nuclear magnetic resonance spectroscopy and molecular mechanics[1]

WESLEY G. TAYLOR[2] AND TSE WAI HALL
Agriculture Canada Research Station, P.O. Box 3000, Main, Lethbridge, Alta., Canada T1J 4B1

AND

CARL E. SCHRECK
Medical and Veterinary Entomology Research Laboratory, Agricultural Research Service, Science and Education Administration, U.S. Department of Agriculture, Gainesville, FL 32604, U.S.A.

Received April 26, 1991

WESLEY G. TAYLOR, TSE WAI HALL, and CARL E. SCHRECK. Can. J. Chem. **70**, 165 (1992).

The 15 2,2-dimethyloxazolidines described here were found to exist in solution predominantly as a single rotational isomer, unlike *N*-acetyloxazolidine (**1**), *N*-acetyl-2-methyloxazolidine (**2**), *N*-acetyl-2-(*n*-octyl)oxazolidine (**3**), and other known 2-substituted *N*-acyloxazolidines. Using ^{13}C NMR spectroscopy, activation energies for interconversion of the *E* (minor) and *Z* (major) rotational isomers of **1–3** were determined from coalescence temperature measurements in pyridine-d_5. A sample of *N*-acetyl-2,2-dimethyloxazolidine (**4**) was isolated for comparison. The rotational isomer of **4** was found by two-dimensional nuclear Overhauser effect spectroscopy (NOESY) to possess the *Z* (or *trans*) stereochemistry. Molecular mechanics (MMX) calculations on the *E* and *Z* isomers of **1–4** helped to account for these findings. The conformation of the energy-minimized structures resembled a C-5 envelope. Samples of *N*-aroyl-2,2-dimethyloxazolidines (**5***a*–**5***n*) were isolated and the rotational isomers were assigned the *Z* stereochemistry by NOESY and ^{13}C NMR experiments. Most of these 2,2-dimethyloxazolidines were ineffective in a bioassay for mosquito repellent activity.

Key words: *N*-acyloxazolidines, *N*-aroyloxazolidines, NMR spectroscopy, rotational isomerism, molecular mechanics.

WESLEY G. TAYLOR, TSE WAI HALL et CARL E. SCHRECK. Can. J. Chem. **70**, 165 (1992).

On a trouvé que, en solution, les 15 2,2-diméthyloxazolidines décrites dans ce travail existent principalement sous la forme d'un seul isomère rotationnel; ce comportement diffère de celui des *N*-acétyl- (**1**), *N*-acétyl-2-méthyl- (**2**), *N*-acétyl-2-octyl- (**3**) oxazolidines et d'autres *N*-acétyloxazolidines substituées en position 2. Faisant appel à la RMN du ^{13}C et se basant sur des mesures des températures de coalescence dans la pyridine-d_5, on a déterminé les énergies d'activation d'interconversion des isomères rotationnels *E* (mineur) et *Z* (majeur) des composés **1–3**. Pour fins de comparison, on a isolé un échantillon de la *N*-acétyl-2,2-diméthyloxazolidine (**4**). En se basant sur l'effet Overhauser nucléaire bidimensionnel (NEOSY), on a démontré que l'isomère rotationnel du composé **4** possède la stéréochimie *Z* (ou *trans*). Des calculs de mécanique moléculaire (MMX) sur les isomères *E* et *Z* des composés **1-4** ont permis d'expliquer ces résultats. Les conformations des structures dont l'energie a été minimisée ressemblent à une enveloppe C-5. On a isolé des échantillons des *N*-aroyl-2,2-diméthyloxazolidines (**5***a*–**5***n*) et, sur la base d'expériences de RMN du ^{13}C et de NEOSY, on a attribué la stéréochimie *Z* à leurs isomères rotationnels. La plupart de ces 2,2-diméthyloxazolidines ne se sont pas avérées efficaces lors d'essais biologiques destinés à mesurer leur activité comme agent de répulsion des moustiques.

Mots clés : *N*-acetyloxazolidines, *N*-aroyloxazolidines, spectroscopie RMN, isomérie rotationnelle, mécanique moléculaire.

[Traduit par la rédaction]

Introduction

During studies on the insect repellent properties of oxazolidine heterocycles (1–3), various *N*-acetyl and *N*-alkylcarbonyl derivatives with alkyl or alkenyl groups at C-2 were found to exist in deuterochloroform solution as binary mixtures of rotational isomers (Fig. 1). The *Z* (or *trans*) rotational isomer was usually found in slight excess over the *E* (or *cis*) isomer. Rotational isomerism in five-membered cyclic nitrosamines, including *N*-nitrosooxazolidine and 2-methyl-*N*-nitrosooxazolidine, also has been studied by ^{13}C NMR spectroscopy (4).

The promising mosquito repellent activity of some of the *N*-acetyloxazolidines prompted us to investigate the rotational isomers of these and related compounds in detail, using high resolution NMR and computational chemistry techniques. We rationalized that comparative information on the conformational preferences of these highly mobile molecules might help in the design of better insect repellents. Thus, *N*-acetyloxazolidine (**1**), *N*-acetyl-2-methyloxazolidine (**2**), and *N*-acetyl-2-(*n*-octyl)oxazolidine (**3**) were selected as representative examples from our previous work (3)

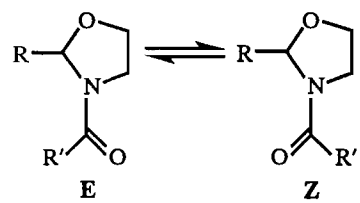

FIG. 1. Rotational isomers of 2-substituted *N*-acetyl- and *N*-alkylcarbonyloxazolidines. In refs. 1–3, these isomers were designated by *cis* and *trans* nomenclature, indicating relative orientation of the R and R′ groups. *E* and *Z* are used here, which means that the *cis* isomers of our earlier work are equivalent to *E* isomers and *trans* is equivalent to *Z*.

[1]LRS contribution No. 3879113.

[2]Author to whom correspondence may be addressed.

Can. J. Chem. Downloaded from www.nrcresearchpress.com by 123.30.183.119 on 09/08/12
For personal use only.

TABLE 1. Coalescence temperatures (K) and activation energies (kcal mol^{-1}) for the rotamers of **1–3** in pyridine-d_5

Oxazolidine	^{13}C site 2	4	5	6	7	9	$\Delta G^{\neq}_{ZE}$ (Mean ± SD)	$\Delta G^{\neq}_{EZ}$ (Mean ± SD)
1	320	360	355	357	[a]	—	17.4 ± 0.2	17.1 ± 0.2
2	330	351	338	338	338	346	17.4 ± 0.1	16.4 ± 0.1
3	325	353	348	339	[b]	[c]	17.6 ± 0.3	16.5 ± 0.3

[a]This carbon had the same chemical shift for both rotamers.
[b]A side-chain signal caused interference.
[c]Signals from the methylene carbons of the side chain were not assigned.

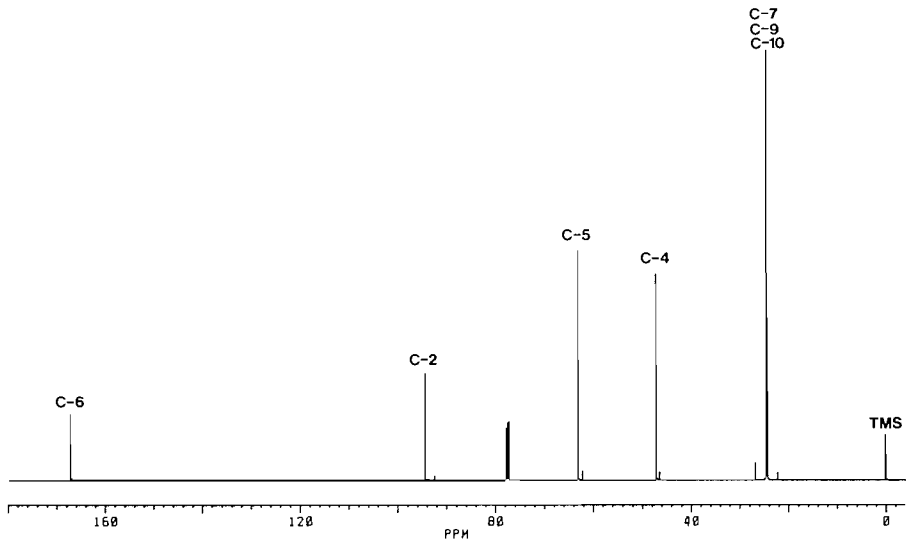

FIG. 2. Proton-decoupled ^{13}C NMR spectrum of a purified sample of **4** in 2.0 M $CDCl_3$ solution at 298 K.

for comparison here with *N*-acetyl-2,2-dimethyloxazolidine (**4**). The synthesis, ^{13}C NMR spectra, and mosquito repellent properties of 14 novel *N*-aroyl-2,2-dimethyloxazolidines (**5**), isolated as single rotational isomers, are also reported.

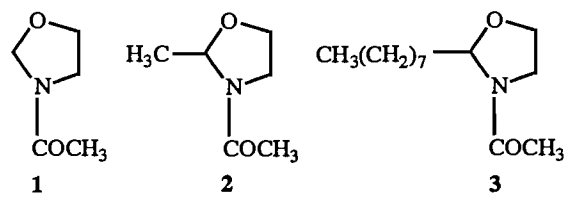

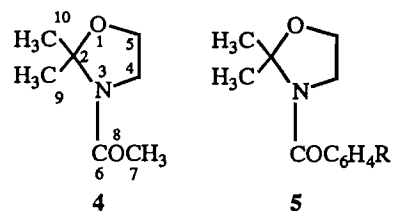

Results and discussion

N-*Acetyloxazolidines* ***1–4***

Rotational isomers of tertiary amides are capable of existing in solution as equilibrium mixtures because of the energy barrier to rotation about the N—CO bond. This barrier or free energy of activation is relatively high compared with other dynamic processes and has been estimated at 17.4 kcal mol^{-1} for **1** (5).

At room temperature, interconversion of the rotational isomers of *N*-acetyl and *N*-alkylcarbonyloxazolidines was sufficiently slow on the NMR time scale to allow the detection of the *E* and *Z* isomers by ^{13}C NMR spectroscopy (1–3). The major isomers were assigned the *Z* stereochemistry on the basis of ^{13}C chemical shift comparisons with the other isomer in the mixture.

The occurrence of unequal equilibrium isomer populations suggests that a higher free energy of activation is required for the *Z* to *E* conversion than that from *E* to *Z*. Activation energies were determined for **1–3** by measuring the coalescence temperatures of ^{13}C signals from isomeric mixtures of these representative *N*-acetyloxazolidines over a temperature range of 298–363 K in pyridine-d_5 (Table 1). Free energies of activation were calculated with the equations from Shanan-Atidi and Bar-Eli (6), which take into account the effect of unequal isomer populations and of course the frequency difference between the resolved signals. The same approach was used by Haky *et al.* (4) in their NMR study of rotational isomerism of *N*-nitrosooxazolidines in DMSO-d_6.

At 298 K, the *Z* isomer of **1** represented about 60% of the mixture, and the thermodynamic equations (6) confirmed that the activation energy for *Z* to *E* conversion (17.4 kcal mol^{-1}) was slightly greater than for the reverse process. This dif-

Can. J. Chem. Downloaded from www.nrcresearchpress.com by 123.30.183.119 on 09/08/12
For personal use only.

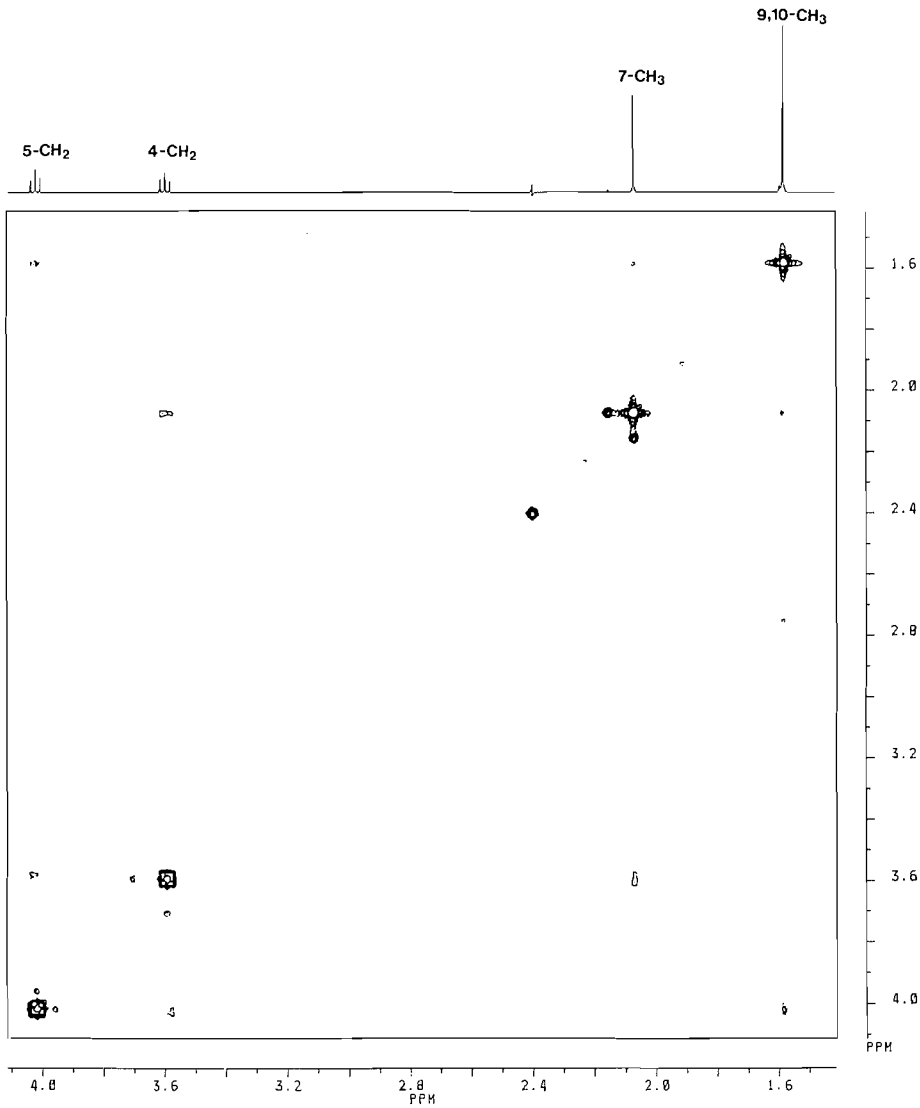

FIG. 3. Contour plot from a NOESY experiment on **4** recorded in $CDCl_3$ at 298 K. A conventional proton spectrum (1.47–4.12 ppm) is shown at the top. The signal at 2.42 ppm is due to folding of the TMS signal.

ference (0.3 kcal mol^{-1}) increased to about 1 kcal mol^{-1} for **2** and **3**, in accord with an increase to 80–85% in the *Z* isomer population. It seemed that unfavorable steric interactions between the C-2 alkyl and C-7 methyl groups in the *E* isomers of **2** and **3** were responsible for the shift in isomer populations. Equilibrium isomer populations of *N*-nitrosooxazolidines also were influenced by the steric crowding effect of a 2-methyl group.

The ^{13}C NMR spectra of **4** showed that one rotational isomer predominated in deuterochloroform and pyridine-d_5 solutions. In fact, the presence of any of the other rotational isomer could not be determined with certainty, implying that C-2 dimethyl substitution created an even greater difference in activation energies than was determined for **2** and **3**. In **4**, minor signals resonating upfield from the main signals for C-2, C-4, and C-5 were apparent (Fig. 2). Their chemical shifts were consistent with those expected from C-2, C-4, and C-5 of *E* **4** since, in the *E* isomers of **1**–**3**, the corresponding carbons resonated upfield compared to the signals of the *Z* isomers. Thus, ^{13}C chemical shift arguments as well as steric considerations suggested that *Z* **4** predominated but experimental evidence to confirm this assignment was sought.

To study the stereochemistry of the major component, proton–proton nuclear Overhauser enhancement (NOE) experiments were attempted on **4** using the two-dimensional NOESY pulse sequence (7). The recent literature illustrates several applications of these techniques to small organic molecules (8–11), sometimes in the phase-sensitive mode to distinguish NOE from intramolecular chemical exchange.

On the assumption that the main isomer of **4** had a favorable rotational correlation time, a potential dipolar interaction leading to an NOE cross-peak should occur between the protons at C-4 and C-7 in the *Z* isomer. Greater C-4 to C-7 interproton distances in the *E* isomer would result in a weaker cross-peak, or none at all, whereas the shorter distance between the methyl protons at C-7 and C-9,10 would be expected to give a stronger cross-peak. The contour plot (Fig. 3) showed a relatively intense cross-peak for the protons at C-4 and C-7 plus a relatively weak cross-peak for the methyl proton (C-7 and C-9,10) interactions. This indicated the *Z* stereochemistry. Although not of value for the stereochemical assignment, a relatively strong cross-peak also was ob-

Can. J. Chem. Downloaded from www.nrcresearchpress.com by 123.30.183.119 on 09/08/12
For personal use only.

TABLE 2. Relative steric energies from molecular mechanics calculations and equilibrium percentages (theoretical vs. experimental) of the rotamers of **1–4**

	Z Isomer			*E* Isomer		
		Population (%)			Population (%)	
Oxazolidine	Relative energy (kcal mol^{-1})	Theory[a]	^{13}C NMR[b]	Relative energy (kcal mol^{-1})	Theory[a]	^{13}C NMR[b]
1	0	65.1	61 (59)	0.37	34.9	39 (41)
2	0	88.5	82 (73)	1.21	11.5	18 (27)
3	0	92.9	84 (69)	1.52	7.1	16 (31)
4	0	98.6	>95 (>95)	2.53	1.4	<5 (<5)

[a]Calculated by ln (*E* isomer population/*Z* isomer population) = $-E/RT$ where the sum of the populations = 1 and T = 298 K.

[b]In pyridine-d_5 at 298 K. Values in parentheses are populations found in $CDCl_3$ at 298 K and, except for **4**, are taken from ref. 3.

TABLE 3. Selected torsional angles (degrees) from energy-minimized structures of the rotamers of **1–4**

	1		**2**[a]		**3**[a]		**4**	
Angle	*Z*	*E*	*Z*	*E*	*Z*	*E*	*Z*	*E*
O(1)—C(2)—N(3)—C(4)	−14.3	−15.1	−8.6	−6.9	−11.0	−4.8	−8.8	−14.6
C(2)—N(3)—C(4)—C(5)	−9.5	−8.6	−14.9	−16.5	−12.8	−18.4	−13.5	−7.8
N(3)—C(4)—C(5)—O(1)	30.1	29.4	33.4	34.2	32.3	35.2	31.2	27.6
C(4)—C(5)—O(1)—C(2)	−41.1	−40.9	−41.3	−41.1	−41.9	−41.1	−39.3	−39.2
C(5)—O(1)—C(2)—N(3)	34.2	34.5	31.0	29.9	32.8	28.7	29.9	33.4
C(6)—N(3)—C(2)—O(1)	166.8	165.7	173.8	175.0	171.6	177.2	171.8	165.7
C(6)—N(3)—C(4)—C(5)	169.4	170.7	162.7	161.8	164.6	159.7	165.9	172.0
C(7)—C(6)—N(3)—C(2)	−178.9	0.5	−175.7	6.1	−177.4	7.4	−176.7	0.3
C(7)—C(6)—N(3)—C(4)	2.4	−178.6	7.0	−171.8	5.6	−170.4	4.0	−179.3
O(8)—C(6)—N(3)—C(2)	1.0	−179.6	4.5	−174.9	2.6	−173.9	3.4	−179.7
O(8)—C(6)—N(3)—C(4)	−177.7	1.2	−172.8	7.1	−174.4	8.3	−175.9	0.6
C(9)—C(2)—N(3)—C(6)	—	—	55.5	57.3	52.6	59.7	56.3	51.1
C(9)—C(2)—O(1)—C(5)	—	—	155.1	154.2	157.9	152.2	151.0	155.8
C(9)—C(2)—N(3)—C(4)	—	—	−126.9	−124.6	−130.0	−122.3	−124.3	−129.2
C(10)—C(2)—N(3)—C(6)	—	—	—	—	—	—	−71.2	−78.6
C(10)—C(2)—O(1)—C(5)	—	—	—	—	—	—	−89.0	−85.4
C(10)—C(2)—N(3)—C(4)	—	—	—	—	—	—	108.1	101.1

[a]*R* enantiomer.

served for the C-5 methylene to C-9,10 methyl proton interactions. The cross-peak for the C-4,5 methylene proton interaction may be due to a combination of dipolar and scalar coupling effects.

It was of interest to attempt to account for the rotameric preferences of **1–4** by molecular mechanics, so the relative steric energies of the *E* and *Z* isomers of **1–4** were determined with the MMX force field of PCMODEL (see experimental section). During energy minimizations, the oxazolidine ring adopted a favorable conformation (*vide infra*) while retaining the essentially planar *E* or *Z* geometry of the acetamide group.

Equilibrium isomer populations derived from ^{13}C NMR spectroscopy showed that the *Z* isomer populations increased in a logical manner (**4** > **3** ≃ **2** > **1**), paralleling the steric bulk at C-2. Molecular mechanics calculations predicted that the *Z* isomers of these four oxazolidines also were preferred (Table 2). Differences in ground state steric energies of the minimized structures for the isomers of **1** were small (<0.5 kcal mol^{-1}) and may not be significant, but this increased to 2.5 kcal mol^{-1} on comparing the isomers of **4**. Quantitatively, the molecular mechanics calculations predicted more of the *Z* isomer than was found experimentally, especially for **3**.

It should be emphasized that the molecular mechanics calculations, furnishing total steric energies of isolated molecules in the gas phase, need not agree with the equilibrium populations found in solution. Indeed, solvent effects were evident as illustrated by the higher *Z* isomer populations in pyridine-d_5 than in deuterochloroform. Furthermore, some of the force field parameters for *N*-acetyloxazolidines have not been finalized. Despite these precautions, the agreement between experimental and theoretical results seen in this work was interesting. In a recent study on 2-ethynyl-*N*-acetylpyrrolidine (12), molecular mechanics calculations also predicted that the *Z* isomer would prevail, in agreement with the NMR data.

Minimum energy conformations from molecular me-

Can. J. Chem. Downloaded from www.nrcresearchpress.com by 123.30.183.119 on 09/08/12
For personal use only.

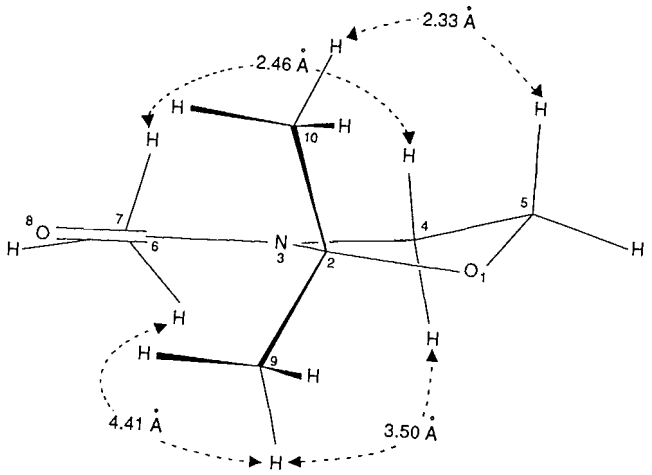

FIG. 4. The lowest energy conformation of the *Z* isomer of **4** found by molecular mechanics calculations and selected interproton distances.

chanics calculations gave ring-puckered structures resembling a C-5 envelope. This geometry has been reported before in molecular mechanics calculations on substituted oxazolidines (13) and was indicated here, for example, by the relatively large endocyclic torsional angles (−39 to −42°) for C(4) − C(5) − O(1) − C(2) and relatively small angles (−5 to −15°) for O(1) − C(2) − N(3) − C(4). Comparison of several torsional angles in *Z* **1–4** and in *E* **1–4** indicated only small differences in the conformations of the energy-minimized structures (Table 3).

The lowest energy conformation found for the *Z* isomer of **4** was of interest (Fig. 4). The interproton distances of 2.33 Å (C-5,10) and 2.46 Å (C-4,7) were consistent with the strong cross-peaks of the NOESY experiment. In fact, the weak NOE cross-peaks observed for C-4 methylene and C-7 methyl interactions to the C-9 methyl protons could be rationalized because the spatial proximity was less than 5 Å, which is approximately the maximum distance for which to expect a response in NOESY experiments (14).

N-*Aroyloxazolidines* **5**a–**5**n

These oxazolidines **5***a*–**5***n* (Table 4) were synthesized by reacting acetone with ethanolamine followed by acylation with various benzoyl chlorides.

The ^{13}C NMR spectra of **5***a*–**5***n* gave single resonances for each carbon of the oxazolidine ring. Chemical shift assignments to the unsubstituted **5***a* were made by reference to ^{13}C chemical shifts of **4** and of *N*,*N*-dimethylbenzamide. The ^{13}C signals for **5***b*–**5***n* could be assigned completely (Table 5) by spectral editing with DEPT and by use of substituent increments for monosubstituted benzenes (15) in conjunction with chemical shifts of the aromatic carbons from **5***a*. In the fluoro-substituted compounds **5***h*–**5***k*, ^{13}C–^{19}F couplings helped to confirm the assignments.

In the ^{13}C NMR spectrum of the *ortho*-trifluoromethyl compound **5***j*, the methyl carbons of the *gem*-dimethyl group were nonequivalent, appearing as two broad signals at 298 K. This observation might be related to slow rotation around the CO-aryl bond, as demonstrated with *ortho*-monosubstituted *N*,*N*-dialkylbenzamides (16). However, the *ortho*-methyl (**5***d*) and *ortho*-methoxy (**5***g*) compounds gave a sharp signal for the *gem*-dimethyl carbons.

The ^{13}C chemical shifts of C-2, C-4, and C-5 in **5***a*–**5***n* were very similar (Table 5), which indicated the same geometry about the amide bond. It was likely *Z* because the phenyl group would be expected to sterically favor that isomer, probably to even a greater extent than with the C-7 methyl group of **4**. To discount the possibility that the coalescence temperatures were less than ambient, the ^{13}C NMR spectrum of **5***b* was obtained at 218 K. That spectrum gave the same signals as those recorded at 298 K.

To assign the stereochemistry of **5***a*–**5***n*, it was anticipated that an NOE should be observed between a C-4 methylene proton and an *ortho* proton of the phenyl ring. This was demonstrated by a NOESY experiment on a sample of the 4′-methyl compound **5***b*. The ^{1}H NMR spectrum of **5***b* gave well-resolved doublets for the *ortho* (2′) and *meta* (3′) protons, and their chemical shifts were first assigned by a $^{1}H/^{13}C$ shift correlation experiment. The contour plot (Fig. 5) showed the anticipated cross-peak between the protons at C-2′ and C-4, which confirmed the *Z* stereochemistry. A strong NOE cross-peak was also observed for the *meta* protons and the protons of the 4′-methyl group.

Mosquito bioassays

Samples of **4** and **5***a*–**5***n* were applied to cloth and evaluated as potential insect repellents using two species of laboratory-reared mosquitoes and a published bioassay procedure (17). Against *Anopheles albimanus* Wiedeman, the compounds offered less than 1 day of protection from three or more mosquitoes biting through the cloth. With *Aedes aegypti* (Linn.), **5***a* and **5***c* showed repellency (6 days of protection) greater than that of the standard *N*,*N*-diethyl-*m*-toluamide (2–3 days) but less than that of other oxazolidine chemicals (2, 3).

Since marked differences in the bioactivity of rotational isomers of amides have recently been indicated, for example with antihypertensive dipeptides (18), it is possible that the relatively weak repellent activity of these 2,2-dimethyloxazolidines is related to an unfavorable *Z* stereochemistry. This hypothesis could be examined by studying conformationally restricted analogues that exist predominantly or exclusively as the *E* isomer. Further work in this direction is in progress.

Experimental

The acid chlorides were purchased from Aldrich Chemical Company (Milwaukee, Wis.) or from Pfaltz and Bauer (Stamford, Conn.), except for *m*-chlorobenzoyl chloride, which was prepared from *m*-chlorobenzoic acid using thionyl chloride. Ethanolamine and triethylamine were obtained from Aldrich. HPLC was performed with a Waters Prep LC/System 500 A instrument equipped with Prep PAK Silica cartridges (Waters Associates, Inc.) and a refractive index detector. GC was performed on a Hewlett–Packard 5838A instrument using a fused silica capillary column (30 m × 0.26 mm i.d.) of DB-1 (J and W Scientific) and splitless injections. A Hewlett–Packard 5985B mass spectrometer equipped with a capillary GC column of DB-1 or CP-Wax 57 CB (Chrompack) was used for GC–MS. Infrared spectra were recorded as liquid films on a Perkin–Elmer 137 instrument. Melting points, taken on a Fisher hot-stage or Büchi 530 apparatus, and boiling points, recorded during vacuum distillations, are uncorrected. Elemental analyses were obtained from C. Daessle, Montréal, Québec.

Synthesis

The preparation and characterization of **1–3** have been described (3). The sample of **4** was prepared from acetone (0.2 mol), ethanolamine (0.44 mol), and acetic anhydride (0.44 mol) by method B (19) and isolated in 21% yield as a colorless oil by HPLC with methylene chloride – ethyl acetate (3:1 v/v) followed by

Can. J. Chem. Downloaded from www.nrcresearchpress.com by 123.30.183.119 on 09/08/12
For personal use only.

TABLE 4. Analytical samples of *N*-aroyl-2,2-dimethyloxazolidines **5**

No.	Ar substituent	Formula (molecular weight)[a]	Boiling point °C (Torr)	Melting point (°C)	Yield (%)	Analyses (%) Found (calculated) C	H	N
a	H	$C_{12}H_{15}NO_2$ (205)	110–116(0.05)	32–35	48	70.04 (70.22)	7.58 (7.37)	6.96 (6.82)
b	4′-CH_3	$C_{13}H_{17}NO_2$ (219)	101–114(0.07)	53–54	58	70.95 (71.20)	7.87 (7.82)	6.50 (6.34)
c	3′-CH_3	$C_{13}H_{17}NO_2$ (219)	107–109(0.05)		22	71.41 (71.20)	8.06 (7.82)	6.30 (6.34)
d	2′-CH_3	$C_{13}H_{17}NO_2$ (219)	96–105(0.08)		53	70.94 (71.20)	7.83 (7.82)	6.26 (6.34)
e	4′-OCH_3	$C_{13}H_{17}NO_3$ (235)	130–138(0.08)	53–55	57	66.51 (66.36)	7.34 (7.28)	5.83 (5.95)
f	3′-OCH_3	$C_{13}H_{17}NO_3$ (235)	130–135(0.1)		68	66.34 (66.36)	7.00 (7.28)	6.10 (5.95)
g	2′-OCH_3	$C_{13}H_{17}NO_3$ (235)	120–126(0.1)	55–57	60	66.32 (66.36)	7.25 (7.28)	6.32 (5.95)
h	4′-CF_3	$C_{13}H_{14}F_3NO_2$ (273)	92–94(0.2)		36	57.41 (57.14)	5.32 (5.16)	5.26 (5.13)
i	3′-CF_3	$C_{13}H_{14}F_3NO_2$ (273)	105–111(0.2)	48–49	61	56.97 (57.14)	5.08 (5.16)	5.11 (5.13)
j	2′-CF_3	$C_{13}H_{14}F_3NO_2$ (273)	126(0.5)	74–76	44	57.29 (57.14)	5.22 (5.16)	5.08 (5.13)
k	3′-F	$C_{12}H_{14}FNO_2$ (223)	99–100(0.1)	40–42	66	64.36 (64.56)	6.51 (6.32)	6.39 (6.27)
l	3′-Cl	$C_{12}H_{14}ClNO_2$ (241)	114–117(0.1)	48–50	34	60.38 (60.13)	5.21 (5.05)	6.08 (5.84)
m	3′-Br	$C_{12}H_{14}BrNO_2$ (285)		54–56 (from hexane)	46	50.33 (50.72)	4.78 (4.97)	4.74 (4.93)
n	3′-NO_2	$C_{12}H_{14}N_2O_4$ (250)		59–60 (from hexane and methyl *t*-butyl ether)	66	57.74 (57.59)	5.85 (5.64)	10.94 (11.20)

[a]M + 1 ions (100% relative abundance) were observed for each compound during CI-MS analysis with isobutane as the reagent gas.

TABLE 5. ^{13}C NMR chemical shifts of *N*-aroyl-2,2-dimethyloxazolidines **5** in deuterochloroform solution[a]

No.	C=O	Ar 1′	2′	3′	4′	5′	6′	Substituents	Oxazolidine moiety 2	5	4	2-$(CH_3)_2$
a	167.67	137.84	126.47	128.37	129.76	128.37	126.47	—	94.92	63.44	48.76	24.51
b	167.80	135.00	126.61	128.94	139.91	128.94	126.61	21.39	94.90	63.44	48.79	24.57
c	167.89	138.24	127.10	137.87	130.43	128.22	123.37	21.35	94.86	63.44	48.77	24.53
d	167.83	138.18	133.23	128.83	130.52	124.98	126.05	18.62	94.59	63.33	47.91	24.50
e	167.41	130.14	128.60	113.53	160.77	113.53	128.60	55.34	94.98	63.47	48.87	24.58
f	167.42	139.09	111.92	159.58	115.69	129.50	118.57	55.39	94.92	63.45	48.76	24.50
g	165.86	128.05	154.96	111.21	130.35	120.99	127.30	55.74	94.66	63.37	47.12	24.49
h	166.25	141.14	126.89	125.58 (3.2 Hz)[b]	131.76 (33 Hz)	125.58 (3.2 Hz)	126.89	123.72 (272 Hz)	95.23	63.48	48.67	24.42
i	166.07	138.50	123.63 (3 Hz)	131.02 (33 Hz)	126.55 (3.2 Hz)	129.08	129.84	123.71 (272 Hz)	95.26	63.48	48.70	24.43
j	165.02	136.48	126.11 (32 Hz)	126.74 (4.4 Hz)	129.10	132.36	126.82	123.75 (274 Hz)	94.96	63.28	48.10	24.91 23.33
k	166.15	139.76 (6.4 Hz)	113.87 (22.7 Hz)	162.48 (248 Hz)	116.83 (21.1 Hz)	130.24 (7.9 Hz)	122.19	—	95.10	63.45	48.68	24.44
l	166.07	139.43	126.78	134.50	129.92[c]	129.85[c]	124.59	—	95.11	63.45	48.70	24.43
m	165.43	139.29	129.23[d]	122.11	132.42	129.75[d]	124.68	—	94.62	63.09	48.33	24.06
n	164.94	139.19	121.77	148.03	124.62	129.80	132.65	—	95.45	63.50	48.69	24.39

[a]In ppm from TMS. Precision ±0.02 ppm.
[b]The values in parentheses are ^{13}C–^{19}F coupling constants.
[c,d]These assignments may be reversed.

Can. J. Chem. Downloaded from www.nrcresearchpress.com by 123.30.183.119 on 09/08/12
For personal use only.

Can. J. Chem. Downloaded from www.nrcresearchpress.com by 123.30.183.119 on 09/08/12
For personal use only.

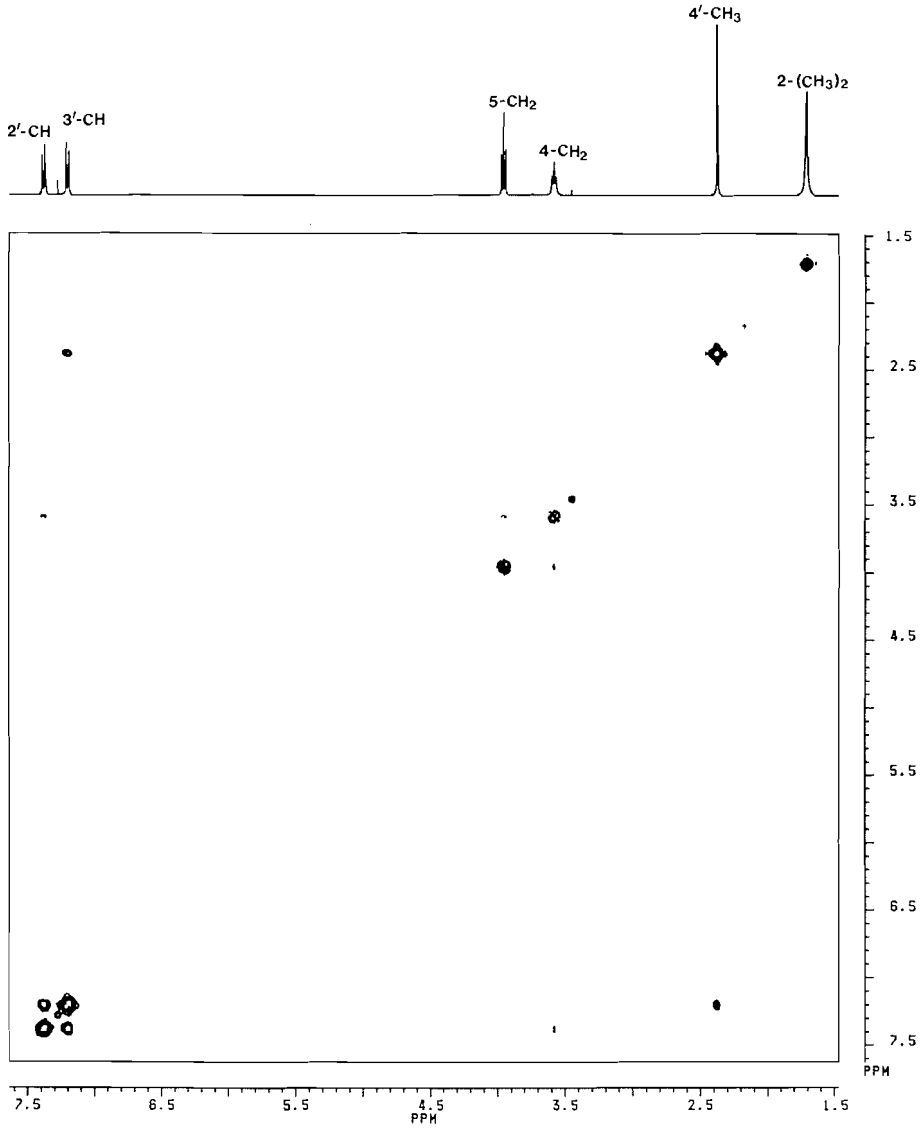

FIG. 5. Contour plot from a NOESY experiment on 2,2-dimethyl-*N*-(4'-methylbenzoyl)oxazolidine (**5***b*) recorded in $CDCl_3$ at 298 K. A conventional proton spectrum (1.47–7.63 ppm) is shown at the top.

distillation: bp 50–53°C (0.05 Torr; 1 Torr = 133.3 Pa) (lit. (20) bp 89–90°C (6 Torr)); IR: 1650 cm^{-1} (C=O); NMR (see Figs. 2 and 3); EI-MS (70 eV) *m/z* (% relative abundance): 143 (M^+, 0), 128 (40), 86 (100), 44 (31), 43 (27); CI-MS (isobutane): 144 (MH^+, 100). Anal. calcd. for $C_7H_{13}NO_2$: C 58.72, H 9.15, N 9.78; found: C 58.96, H 9.24, N 9.79.

Samples of **5***a*–**5***n* were prepared from acetone (0.1 mol), ethanolamine (0.22 mol), and a benzoyl chloride (0.1 mol) essentially following method B of ref. 19 except that triethylamine (0.11 mol) was added to the ice-cold reaction mixture prior to the dropwise addition of the acid chloride. The reaction solvent was dry benzene or toluene. After washing with brine (adjusted to pH 6), the organic layer was dried ($MgSO_4$) and concentrated on a rotary evaporator. Pure samples of **5***a*–**5***h* and **5***j*–**5***k* were obtained by distillation. Crude samples of **5***i* and **5***l* were purified by HPLC with methylene chloride – ethyl acetate – methanol (97: 2.5: 0.5 v/v/v) before distillation. The remaining samples were purified by silica gel (silicAR cc-7) column chromatography (**5***m*) and HPLC (**5***n*) before recrystallization. These samples were of high purity by capillary GC and silica gel TLC (methylene chloride – ethyl acetate, 1:1 v/v). IR spectra showed the amide carbonyl absorption at 1630–1650 cm^{-1}.

NMR spectroscopy

All NMR spectra were acquired in the Fourier transform mode with a Bruker AM-400 spectrometer and Bruker Aspect 3000 software. The ^1H (400.1 MHz) and ^{13}C (100.6 MHz) spectra and the $^1H/^{13}C$ chemical shift correlated two-dimensional spectra (XH-DEPT) were obtained in $CDCl_3$ (0.2 M sample concentrations unless otherwise specified) at 298 K essentially as described before (2).

Coalescence temperatures were determined on 2.0 M solutions of **1–3** in pyridine-d_5 (MSD Isotopes, Dorval, Québec) by variable temperature ^{13}C NMR spectroscopy with a Bruker BVT-1000 temperature control unit. Rotamer populations were derived from peak heights of the paired signals at 298 K.[3]

NOESY spectra were obtained in $CDCl_3$ at 298 K by the standard pulse sequence (recycle delay – 90° – t_1 – 90° – τ – 90° – acquisition) using a 5-mm selective probe with a ^1H 90° pulse length

[3]The following data (one table) may be purchased from: The Depository of Unpublished Data, Document Delivery, CISTI, National Research Council Canada, Ottawa, Canada K1A 0S2: ^{13}C chemical shifts recorded in pyridine-d_5 at 298 K for the rotational isomers of **1–4**.

of 4.9 μs. There were 256 values of t_1 with 16 scans per t_1 increment. These spectra were weighted with a standard sine bell function and zero-filled to 1K × 1K prior to transformation. The contour plots were displayed symmetrized with respect to the diagonal. Mixing times (τ) were chosen that corresponded to the longest spin-lattice relaxation time (T_1) for the protons of interest (8). This corresponded to 3.05 s for the C-7 methyl (acetyl) protons of **4** and to 4.29 s for the *ortho* protons at C-2′,6′ of **5***b*. The T_1 values were measured by the inversion–recovery method with standard Bruker software using NMR solutions previously bubbled with argon for 10 min. To suppress cross-peaks from scalar coupled protons in NOESY experiments (7), random variations to the mixing times were set at 10% of the mixing time.

Molecular mechanics

The molecular mechanics calculations were carried out using the MMX force field of the molecular modelling program PCMODEL (version 3.2), obtained from Serena Software (Bloomington, Ind.). This force field, purchased without the π routines, is similar to the Allinger force field of MM2 (QCPE-395). The program used generalized force field parameters for O-C-N-C (MM2 atom types 6-1-9-1), O-C-C-N (6-1-1-9), N-C-O-C (9-1-6-1), N-C-O-lone pair (9-3-7-20), and C-N-C-C (1-9-3-1). The starting geometry of the oxazolidine ring was flat and separate energy minimizations were performed with torsional angles of 0° and 180° for the C-C-N-C atoms of the acetamide group and C-2 or C-4. Use of the dihedral driver did not uncover more stable conformations than those reported. Calculations were performed using Coulombic (charge–charge) interactions and a value of 1.5 was chosen for the dielectric constant.

Acknowledgments

We thank J. Elder, A. Hewitt, and D. Vedres for technical assistance. We also thank K. Posey and D. Smith for their help in performing the mosquito bioassays. W.G.T. thanks the staff at the Queensland Medical Magnetic Resonance Research Center and Dr. D. J. Brecknell (Department of Chemistry, University of Queensland, Brisbane, Australia) for useful discussions during a transfer of work.

1. W. G. Taylor and T. T. Nakashima. Can. J. Chem. **62**, 96 (1984).
2. W. G. Taylor and C. E. Schreck. J. Pharm. Sci. **75**, 109 (1989).
3. W. G. Taylor and C. E. Schreck. Pesticide Sci. **33**, 1 (1991).
4. J. E. Haky, J. E. Saavedra, and B. D. Hilton. Org. Magn. Reson. **21**, 79 (1983).
5. J. B. Lambert and S. M. Wharry. J. Org. Chem. **47**, 3890 (1982).
6. H. Shanan-Atidi and K. H. Bar-Eli. J. Phys. Chem. **74**, 961 (1970).
7. D. Neuhaus and M. P. Williamson. The nuclear Overhauser effect in structural and conformational analysis. VCH Publishers, Inc., New York. 1989. Chap. 8.
8. D. J. Meyerhoff, R. Nunlist, and J. F. O'Connell. Magn. Reson. Chem. **25**, 843 (1987).
9. V. V. Krishnamurthy, J. E. Casida, and L. O. Ruzo. J. Agric. Food Chem. **35**, 504 (1987).
10. S. W. Fesik and E. T. Olejniczak. Magn. Reson. Chem. **25**, 1046 (1987).
11. N. H. Andersen, H. L. Eaton, and X. Lai. Magn. Reson. Chem. **27**, 515 (1989).
12. J. R. M. Lunkvist, H. M. Vargas, P. Caldirola, B. Ringdahl, and U. Hacksell. J. Med. Chem. **33**, 3182 (1990).
13. A. Bernardi, M. G. Beretta, V. Malatesta, and C. Tosi. Chem. Phys. Lett. **133**, 496 (1987).
14. B. A. Borgias and T. L. James. J. Magn. Reson. **79**, 493 (1988).
15. E. Breitmaier and W. Voelter. Carbon-13 NMR spectroscopy: high-resolution methods and applications in organic chemistry and biochemistry. 3rd ed. VCH Publishers, Inc., New York. 1987. pp. 319–320.
16. W. B. Jennings and M. S. Tolley. Tetrahedron Lett. 695 (1976).
17. W. G. Taylor and C. E. Schreck. J. Pharm. Sci. **74**, 534 (1985).
18. C. Bennion, R. C. Brown, A. R. Cook, C. N. Manners, D. W. Payling, and D. H. Robinson. J. Med. Chem. **34**, 439 (1991).
19. W. G. Taylor. J. Agric. Food. Chem. **30**, 409 (1982).
20. L. B. Dashkevich and F. G. Shepel. Khim. Geterotsikl. Soedin. Akad. Nauk Latv. SSR, 654 (1965); Chem. Abstr. **64**, 9700g (1966).

Can. J. Chem. Downloaded from www.nrcresearchpress.com by 123.30.183.119 on 09/08/12
For personal use only.

The reduction of α-bromocamphor by tertiary amines[1]

JIAN JEFFREY CHEN[2] AND DENNIS D. TANNER
Department of Chemistry, The University of Alberta, Edmonton, Alta., Canada T6G 2G2

Received May 30, 1991

JIAN JEFFREY CHEN and DENNIS D. TANNER. Can. J. Chem. **70**, 173 (1992).

The reduction of α-bromocamphor to camphor by *N,N*-dimethylaniline (DMA) at high temperatures (>200°C) proceeds via a free radical chain sequence. The reduction can be effected with DMA or triethylamine (TEA) in acetonitrile at much lower temperatures in the presence of di-*tert*-butylperoxide. The chain termination step is the dimerization of the camphor radical. These reductions presumably constitute an example of an electron transfer chain mechanism involving a tertiary amine as the chain propagating species.

Key words: reduction, tertiary amines, α-bromocamphor, chain reaction.

JIAN JEFFREY CHEN et DENNIS D. TANNER. Can. J. Chem. **70**, 173 (1992).

La réduction de l'α-bromocamphre en camphre par la *N,N*-diméthylaniline (DMA), à des températures élevées (>200°C), se produit par un mécanisme radicalaire en chaîne. En présence de peroxyde de di-*tert*-butyle, la réduction par de la DMA ou de la triéthylamine (TEA) dans de l'acétonitrile peut être réalisée à des températures beaucoup plus basses. L'étape de terminaison de la chaîne est la dimérisation du radical camphre. Ces réductions constituent probablement un autre exemple d'un mécanisme en chaîne de transfert d'électron impliquant une amine tertiaire comme espèce propageant la chaîne.

Mots clés : réduction, amines tertiaires, α-bromocamphre, réaction en chaîne.

[Traduit par la rédaction]

The reduction of α-bromocamphor (eq. [1]) has been reported to yield camphor (eq. [2]) in the presence of *N,N*-dimethylaniline (DMA) at 200°C (2). Scheme 1 was suggested as the mechanism for reductive debromination. The mechanism assumes that in a primary step the thermal cleavage of the carbon–bromine bond occurs readily at 200°C (eq. [1]). Since the bond dissociation energy (BDE) for the carbon–bromine bond in **1** is expected to be approximately 64 kcal/mol (the carbon–bromine bond dissociation energy for α-bromoacetone) (3), it does not appear to be reasonable,[3] even at these high temperatures, that a nonchain mechanism involving homolytic cleavage of the C—Br bond will lead to an efficient reductive debromination. In accord with this conclusion, the thermal decomposition of **1**, itself, at 200°C yields only a small amount of camphor and no other detectable products (2). The pathway leading to the oxidation product of DMA (eq. [4]) is likewise not clearly defined (2). Utilizing the thermolysis of **1** as an initiation step (eq. [1], Scheme 1) a chain sequence can be proposed that involves a halophilic abstraction of a bromine atom from **1** (eq. [6], Scheme 2). No direct evidence for this pathway is available, with the exception that the dehalogenation proceeds by a chain reaction.

Since the dehalogenation of a number of α-haloketones by 1,3-dimethyl-2-phenylbenzimidazoline (DMBI) (5) and *N*-benzyl-1,4-dihydronicotinamide (BNAH) (6) proceeds via an electron transfer hydrogen abstraction chain sequence (Scheme 3), a more likely mechanistic rationalization for the reported debromination of **1**, in the presence of an amine, is a similar chain sequence where ZH is *N,N*-dimethylaniline (DMA).

[1]Taken in part from ref. 1.

[2]Killam predoctoral fellow. University of Alberta. 1987–1990.

[3]If the preexponential constant reported for the homolysis of several alkyl bromides ($A = 2 \times 10^{13}$) (4) and a BDE of 64 kcal/mol is used for the calculation of the rate constant for the homolysis of α-bromocamphor (**1**) at 200°C (eq. [1]), a value of 1.3×10^{-16} s^{-1} was obtained for k_1. The half-life for **1** is 6×10^{10} days.

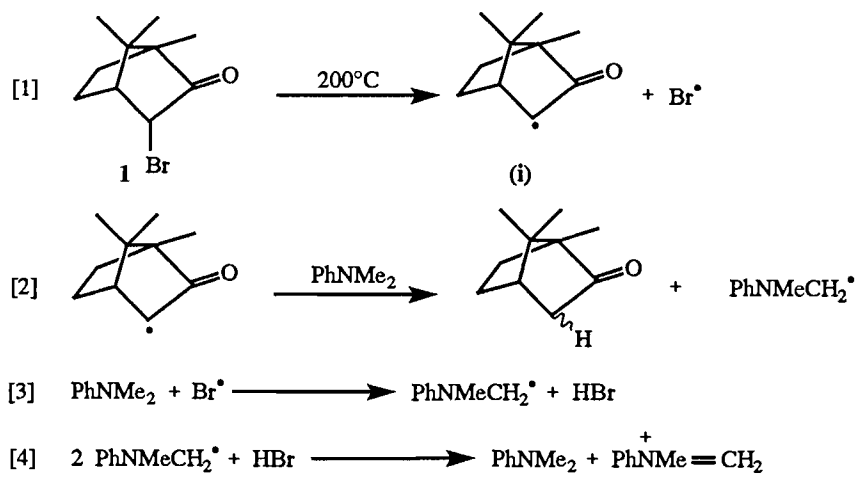

SCHEME 1

Can. J. Chem. Downloaded from www.nrcresearchpress.com by 123.30.183.119 on 09/08/12
For personal use only.

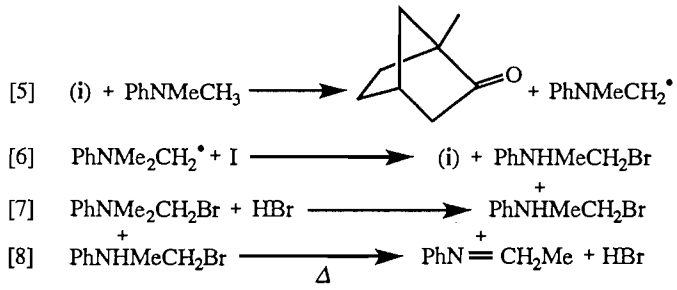

SCHEME 2

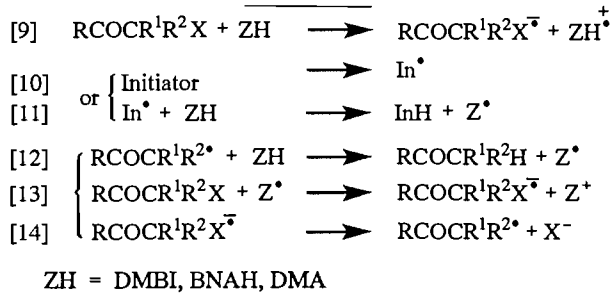

SCHEME 3

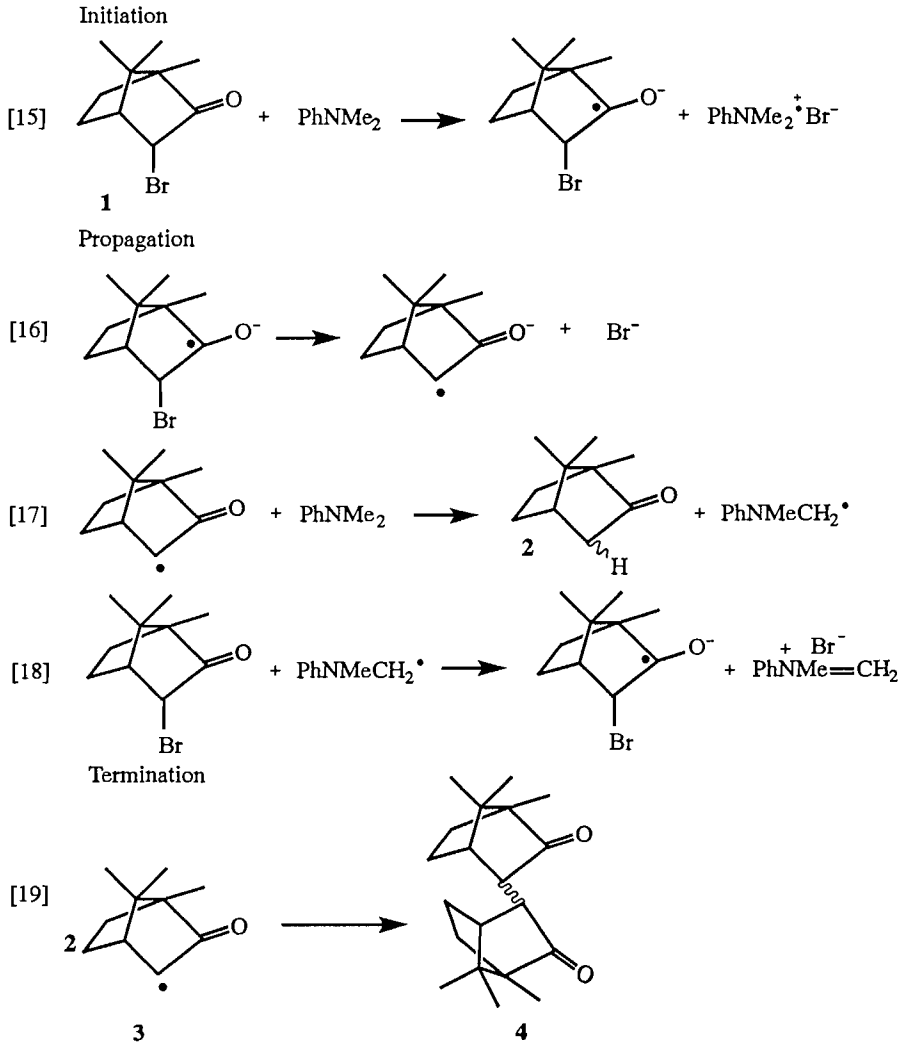

SCHEME 4

Amine radicals as chain carriers have previously been proposed (7).

By analogy to the mechanism established for the reduction of α-haloketones by DMBI (5) and BNAH (6), the reduction α-3-bromocamphor by DMA is likely to follow the radical chain process depicted in Scheme 4.

Initiation of the chain reaction is either thermal (200°C, reaction 1, Table 1), or peroxide initiated at a lower temperature (120°C, di-*tert*-butyl peroxide (BPO), reaction 4, Table 1). The chain was inhibited by the addition of *p*-dinitrobenzene (DMP), reaction 2, Table 1. When triethyl amine (TEA) was used as the reducing agent at the lower temperature (120°C) initiation by BPO is observed, see Table 1. The ability of amines to act as electron donors is well documented. The EPR spectra of quinone radical anions are observed in the reaction of amines with quinones at room temperature (8). EPR spectra were also recorded in the reaction of methylglyoxal with several amines (9). The observation

Can. J. Chem. Downloaded from www.nrcresearchpress.com by 123.30.183.119 on 09/08/12
For personal use only.

TABLE 1. The reduction of α-bromocamphor (**1**) to camphor (**2**) by *N*,*N*-dimethylaniline (DMA) and triethylamine (TEA)

Reaction	Amine	Conditions	Product Yield (%) **2**	**1**
1	DMA	Neat,[a] 200°C, 47 h	41.6 ± 0.6	63.4 ± 3.0
2		Neat,[a] 200°C, 47 h, 4% DNB	1.3 ± 0.4	103.5 ± 3.0
3		AN,[b] 120°C, 47 h	1.9 ± 0.2	98.0 ± 2.7
4		AN,[b] 120°C, 47 h, 9% BPO	10.4 ± 0.9	92.4 ± 2.0
5	TEA	AN,[b] 120°C, 47 h	2.2 ± 0.2	101.0 ± 2.2
6		AN,[b] 120°C, 47 h, 11% BPO	101.5 ± 5.5	4.0 ± 0.7
7		Neat,[a] 120°C, 49 h	1.8 ± 0.1	93.4 ± 2.0
8		Neat,[a] 120°C, 49 h, 9% BPO	33.6 ± 4.3	61.4 ± 6.5

[a][**1**] = 0.2 M.
[b][**1**] = 0.1 M, [amine] = 1.0 M.

of the EPR spectra is attributed to direct electron transfer from the amine to the carbonyl compound. In the BPO-initiated reaction the *tert*-butoxy radical reacts quite efficiently with an amine bearing an α-hydrogen to produce an α-aminoalkyl radical (eq. [20]) (10). The α-aminoalkyl radical has been proposed as an intermediate whose function is to act as an electron transfer agent in a radical chain reaction (7, 11).

[20] 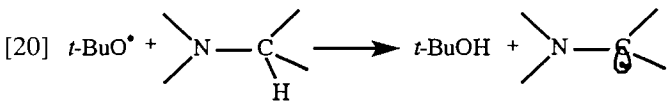

In further support of this proposal, the reduction of **1** by TEA proceeds more slowly in the less polar solvent, neat TEA (reactions 5–8, Table I) (dielectric constant, ε: TEA, 2.42; AN, 37.5) (12). Although this observation may be equivocal, it is consistent with a mechanism that involves an electron transfer process.

A termination step in the initiated free radical chain reduction of α-bromocamphor by amines is the dimerization of the camphor radical (eq. [19], Scheme 4). Three isomeric dimers of the camphor radical (**4**, approximately 0.02% of the starting **1**) were observed in the reaction of **1** with TEA. When the initiated reaction with TEA was carried out in CD_3CN, the product, camphor, was found to have a very low deuterium content (2.8%). The majority of the hydrogen transfer by the camphor radical takes place with TEA.

The reductive debromination of α-bromocamphor by tertiary amines proceeds via a free radical chain mechanism, Scheme 2 or 4. Although no definitive choice can be made between the two mechanisms, reduction by electron transfer – hydrogen atom abstraction appears to be the most attractive pathway, Scheme 4. This mechanistic scheme is also no doubt involved in the dehalogenation of other α-haloketones by DMA at high temperatures (13).

Experimental

Materials

The purification of (+)-α-bromocamphor, camphor, *p*-dinitrobenzene, *p*-di-*tert*-butylbenzene, and acetonitrile (AN) has been previously described (6). Di-*tert*-butylperoxide (BPO) (Aldrich, 98%) was used as supplied. Triethylamine (TEA) was distilled from calcium hydride before use. *N*,*N*-Dimethylaniline (DMA) (Fisher Scientific, reagent grade) was distilled from a small amount of acetic anhydride (14).

General procedure

An aliquot sample of a stock solution of α-bromocamphor (0.1 M or 0.2 M), *p*-di-*tert*-butylbenzene (0.05 M), and the additive in either neat amine or in AN containing the amine was placed in a reaction ampule. The ampule was degassed, sealed, and thermostated at the desired temperature (200°C or 120°C) for the time specified (see Table 1). After the reaction, the ampule was cooled, opened, and analyzed by GC (4,5) using a stainless steel column (20 ft × 1/8 in.) packed with 5% SE-30 on Chromo WAW DMCS 80/100 mesh. Products were identified by a comparison of their GC retention times, GC/IR spectra (using a 50 m Ultra-2 capillary column), and GC/MS spectra (using a 25-m DB-5 capillary column) with those of authentic samples. All reactions were carried out in duplicate.

The three dimers of camphor were detected by GC/MS in the reactions of **1** with TEA. The MS spectra of the three dimers were nearly identical; *m/e*: 302 (M^+), 287, 274, 259, 246, 203, 193, 177, 151, 121, 108, 95, 83, 81, 79, 55, and 41. Their GC/IR spectra were similar to that of camphor. The total yield of the dimers was estimated using their IR intensities relative to camphor. In the reaction of **1** with TEA the yield of the dimers accounted for 0.02% of the starting ketobromide, **1**.

Although no authentic samples of the dimers of camphor were available for comparison, the assignment of the dimers was supported by an indirect observation. A degassed hexane solution of **1** and hexaphenylditin ($Ph_3SnSnPh_3$) was irradiated with a 275-W sunlamp for 17 h. The product mixture was analyzed by GC/IR under the same conditions used for the analysis of the reduction mixture of **1**. Three compounds were detected that had the same GC retention times and GC/MS (*m/e*, 302, M^+) and GC/IR spectra as those observed in the reduction of **1**. These compounds were assigned the structures of the three dimers of camphor.

When the reactions were carried out in CD_3CN the same procedure was followed. The deuterium content of camphor (MW 152) was estimated from the GC/MS measurement of the reaction mixture. The ratio of the intensities of the camphor-d_1 molecular ion (*m/e*, 153, M^+) and camphor-d_0 molecular ion (*m/e*, 152, M^+) was used to determine the deuterium content of camphor.

1. J. J. Chen. Ph.D. thesis, University of Alberta. 1990.
2. A. G. Giumanini and M. M. Musiani. Z. Naturforsch. **32B**, 1314 (1977).
3. K. W. Egger and A. T. Cocks. The chemistry of the carbon–halogen bond. Part II. *Edited by* S. Patai. John Wiley & Sons, New York. 1973.
4. H. E. O'Neal and S. W. Benson. Free radicals. Vol. II. *Edited by* J. K. Kochi. John Wiley & Sons, New York. 1973. p. 295.
5. D. D. Tanner and J. J. Chen. J. Org. Chem. **54**, 3842 (1989).

Can. J. Chem. Downloaded from www.nrcresearchpress.com by 123.30.183.119 on 09/08/12
For personal use only.

6. D. D. Tanner, H. K. Singh, A. Kharrat, and A. R. Stein. J. Org. Chem. **52**, 2142 (1987).
7. G. A. Russell and K. Wang. J. Org. Chem. **56**, 3475 (1991).
8. K. Maruyama, S. Suzue, and J. Osugi. Bull. Chem. Soc. Jpn. **44**, 1161 (1971).
9. H. Kon and A. Szent-Gyorgyi. Proc. Natl. Acad. Sci. U.S.A. **70**, 1030 (1973).
10. D. Griller, J. A. Howard, P. R. Marriot, and J. C. Scaiano. J. Am. Chem. Soc. **103**, 619 (1981).
11. (*a*) G. A. Russell, S. V. Kulkarni, and R. K. Khanna. J. Org. Chem. **55**, 1080 (1990); (*b*) D. Cantacuzene, C. Wakselman, and R. Dorme. J. Chem. Soc. Perkin Trans. **1**, 1365 (1977); (*c*) I. Rico, D. Cantacuzene, and C. Wakselman. Tetrahedron Lett. **22**, 3405 (1981); J. Org. Chem. **48**, 1979 (1983); (*d*) G. A. Russell, R. K. Khanna, and D. Guo. J. Org. Chem. **50**, 3423 (1985). (*e*) K. Takagi, N. Miyake, E. Nakamura, Y. Sawaki, N. Koga, and H. Iwamura. J. Org. Chem. **53**, 1703 (1988).
12. A. A. Maryott and E. A. Smith. Table of dielectric constants of pure liquids. NBS Circular 514, Aug. 10, 1951.
13. A. G. Giumanini. Chimia, **21**, 464 (1967).
14. L. F. Fieser and M. Fieser. Reagents for organic synthesis. Vol. 1. 1967. p. 274.

Can. J. Chem. Downloaded from www.nrcresearchpress.com by 123.30.183.119 on 09/08/12
For personal use only.

Binding of water in aqua 18-crown-6 dichloropicric acid complexes in the solid state and its reversible thermal removal

IZAAK M. KOLTHOFF AND MIRAN K. CHANTOONI, JR.[1]
Department of Chemistry, University of Minnesota, Minneapolis, MN 55455-0431, U.S.A.

Received April 8, 1991

IZAAK M. KOLTHOFF and MIRAN K. CHANTOONI, JR. Can. J. Chem. **70**, 177 (1992).

Thermogravimetry, differential scanning calorimetry, and FT-IR vibrational spectral studies on the 1:1:1 18-crown-6:dichloropicric acid:water complex reveal that it remains unaltered when heated to melting. On the other hand, one molecule of water is expelled from the 1:2:2 complex by heating prior to melting. This results in an ionic microcrystalline product of undetermined crystal structure, in which the conformation of the crown is lower than D_{3d} in symmetry. The enthalpy accompanying this process, which involves rupturing of two water–crown hydrogen bonds, is −44 to −55 kJ mol^{-1}. The original 1:2:2 complex is regenerated by exposure of the heated adduct to water vapor. It was found that H_2O in the structure of the solid 1:2:2 adduct was partially replaced by D_2O at room temperature upon exposure to D_2O vapor. The crown–H_2O OH stretch in the IR exhibits a small or negligible positive isotope effect on deuteration.

Key words: crown ether, hydrogen bonding, water, dichloropicric acid.

IZAAK M. KOLTHOFF et MIRAN K. CHANTOONI, JR. Can. J. Chem. **70**, 177 (1992).

Des études de thermogravimétrie, de calorimétrie à balayage différentiel et de spectroscopie vibrationelle IR par TF, effectuées sur le complexe 1 : 1 : 1 18-couronne-6 : acide dichloropicrique : eau, révèlent que ce complexe n'est pas modifié lorsqu'on le chauffe jusqu'à son point de fusion. Par ailleurs, lorsque le complexe 1 : 2 : 2 est soumis à l'action de la chaleur, une molécule d'eau est expulsée avant la fusion. Cette expulsion conduit à la formation d'un produit ionique microcristallin de structure cristalline indéterminée, dans lequel la symétrie de la conformation de la couronne est inférieure à D_{3d}. L'enthalpie qui accompagne ce processus, qui implique le bris de deux liaisons hydrogènes reliant l'eau et l'éther couronne, se situe entre −44 et −55 kJ mol^{-1}. Lorsqu'on soumet le produit obtenu par chauffage à l'action de la vapeur d'eau, le complexe original 1 : 2 : 2 est régénéré. On a trouvé que le H_2O présent dans la structure de l'adduit 1 : 2 : 2 solide est partiellement remplacé par du D_2O lorsqu'on le laisse en présence de D_2O, à la température ambiante. Dans l'IR, la bande d'élongation OH de la couronne–H_2O présente un effet isotopique faiblement positif ou négligeable.

Mots clés : éther couronne, liaison hydrogène, eau, acide dichloropicrique.

[Traduit par la rédaction]

Introduction

The ability of the macrocyclic polyether $(-CH_2CH_2O-)_6$, denoted as 18-cr-6, to form crystalline binary 1:1 and 1:2 host:guest complexes with a large number of neutral organic guest molecules possessing -NH, $-NH_2$, or "acidic" -CH hydrogen bond donating groups has been well documented (1, 2). Water, acting in a dual role as hydrogen bond acceptor to the acidic functional group of the guest molecule, HX, and hydrogen bond donor to the crown heteroatoms, tends to bridge the crown (in its D_{3d} conformation) and monoprotic acid in the uncharged ternary complex 18-cr-6 $(HX \cdot H_2O)_2$ (2). The stereochemistry of the two inversion-related water molecules in this complex is *IA* in the classification scheme of Jeffrey and Maluszynska (3). An attempt to isolate the crystalline binary complex 18-cr-6 · 3,5-dichlorophenol in the absence of water has not been successful (4).

A number of crystalline 1:1:1, 1:1:2, and 1:2:2 18-cr-6:phenol:water adducts (2, 5–10) have been precipitated from organic solvents of intermediate or low polarity (e.g., ethyl acetate, toluene) and their crystal structures determined by X-ray diffraction. To our knowledge, the only neutral aqua 18-cr-6-phenol adduct crystallized from *water* is that of dichloropicric acid, 18-cr-6 $(HPiCl_2 \cdot H_2O)_2$ (**2** in Scheme 1). Crystal structures of both of the polymorphs have been determined (11). Dichloropicric acid, $HPiCl_2$, by far the most acidic of the phenols taken ($pK = -0.7$ in water (12)) participates in a very strong hydrogen bond to water in **2** (O . . . O distance = 2.462 Å).

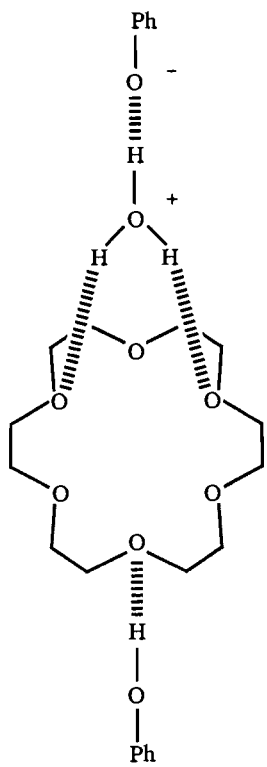

3A

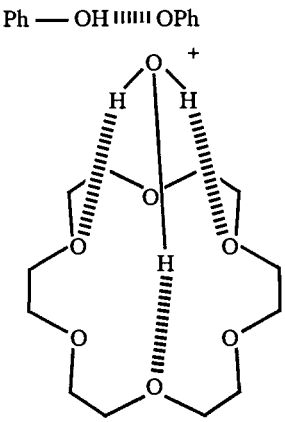

3B

[1]Author to whom correspondence may be addressed.

Printed in Canada / Imprimé au Canada

Can. J. Chem. Downloaded from www.nrcresearchpress.com by 123.30.183.119 on 09/08/12
For personal use only.

Thermal studies on the crown–acid–water adducts, which can yield information on the strength of binding of the water molecule(s), have not been reported in the literature, largely because of the low melting points of these adducts. In the present paper, results of a thermal analysis of **2** are presented. When heated, **2** is transformed without melting into **3**, which subsequently melts at 123°C (Scheme 1). The following techniques were employed: thermogravimetry (TGA), differential scanning calorimetry (DSC), FT-IR, and assay of the unheated and heated adduct. To establish that changes occur in the crystal structure of **2** upon heating, X-ray powder patterns were run. Using the above techniques, it has been demonstrated that **3** can be reversibly rehydrated on exposure to water vapor at 25°C (Results). Scheme 1 relates the various adducts composed of 18-cr-6, $HPiCl_2$, and water (or D_2O). At present, we are not able to

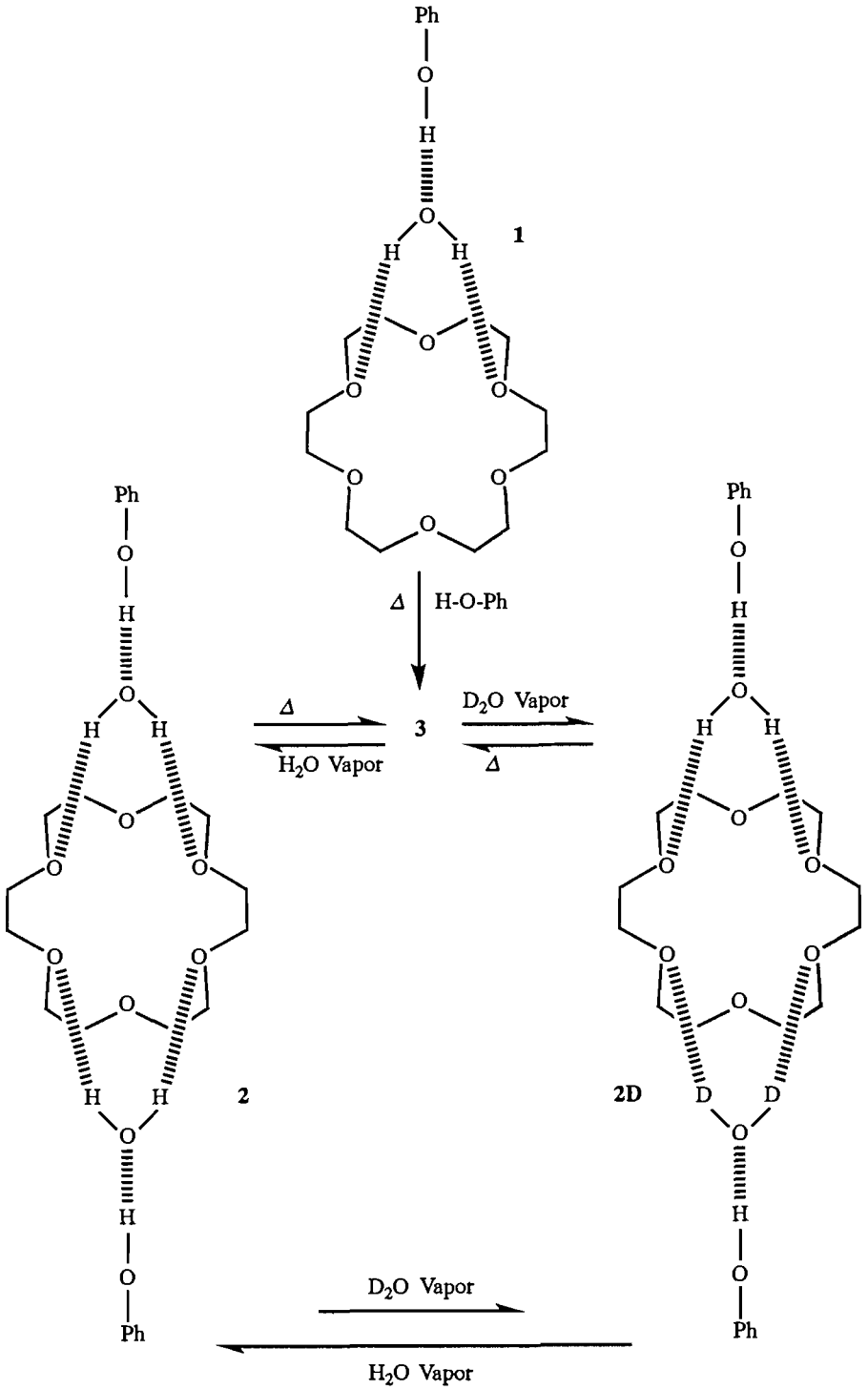

Ph = 2,4,6-trinitro-3,5-dichorophenyl

SCHEME 1

Can. J. Chem. Downloaded from www.nrcresearchpress.com by 123.30.183.119 on 09/08/12
For personal use only.

Can. J. Chem. Downloaded from www.nrcresearchpress.com by 123.30.183.119 on 09/08/12
For personal use only.

decide unambiguously whether **3** has a phenoxide-hydronium (**3***a*) or a phenol-phenoxide-hydronium structure (**3***b*). Although depicted in Scheme 1 as unionized, **1** may in fact be 18-cr-6 ($H_3O^+ \cdot PiCl_2^-$).

To gain insight into the nature of the potential well of the hydrogen bond of the crown oxygens to water, the OD and OH stretching frequencies were compared in the IR spectrum of **2D**. In addition, semiquantitative deuterium isotope exchange studies, which probe the labile character of H_2O in **2**, were

[1] **2** + $D_2O(g) \rightleftarrows$ **2D** + $H_2O(g)$

carried out at 25°C. Finally, the uptakes of D_2O and H_2O vapor by **3** have been compared (Scheme 1).

Experimental

Chemicals

Dichloropicric acid, 18-crown-6, and pentaethyleneglycol dimethylether, GLYME-6, were products used previously (13), while 4,4′-biphenol, 3,5-dichlorophenol, 3-nitrophenol, and 2,4-dinitrophenol (Aldrich Chemical Co.) were used as received. Preparation and purification of the 1:1:1, 1:1:2, and 1:2:2 adducts of the phenols, excepting that of $HPiCl_2$, were carried out by refluxing stoichiometric amounts in toluene and evaporating to crystallization (4). Adduct **1** was prepared by a phase transfer technique, in which 1.32 g (5.0 mmol) 18-cr-6 in 50 mL CH_2ClCH_2Cl (DCE) and 0.30 g (1.0 mmol) $HPiCl_2$ in 50 mL H_2O were stirred for 0.5 h. The organic phase was separated and slowly evaporated at atmospheric pressure (1.0×10^5 Pa) until crystallization. The crystals were washed with 1 mL DCE. Assay: 1:0.95:0.81 (18-cr-6:$HPiCl_2$:H_2O),[2] mp 97.6–99.3°C. The 1:2:1 adduct, **3**, prepared by reacting **1** with $HPiCl_2$ (Results, Scheme 1) softened at 116°C. Its mp, 121.0–122.0°C, was slightly lower than that of **2** when heated, 123–124°C (Table 1). Polymorph II of **2** was precipitated from H_2O at 25°C (11) by slowly adding 0.02 M 18-cr-6 to an equal volume of 0.04 M $HPiCl_2$ and stirring for 10 h. It was recrystallized at 25°C from H_2O by slow evaporation, without stirring, or from $CHCl_3$, DCE, DCE saturated with H_2O, or from DCE:cyclohexane 1:7 (also from the latter at 65°C and cooling). A layering technique between DCE and cyclohexane was also employed for crystallization. Assay: 1:1.96:1.71 from H_2O and 1:(1.975 ± 0.020):(2.035 ± 0.0125) from the organic solvents. Crystals of polymorph I of **2** were separated by hand under a microscope from a mixture of the two polymorphs (11).

The open-chain polyether adduct, GLYME-6 ($HPiCl_2 \cdot H_2O)_2$, was prepared in the same way as polymorph II of **2** and was recrystallized from H_2O at 25°C (mixture of polymorphs). Assay of mixture: 1:2.14:2.28, mp 66.0–67.0°C (square plates), 62.7–63.7°C (needles). All adducts were dried at 25°C over dry N_2 (or over P_2O_5 at 1.3×10^4 Pa pressure for 2 days in the case of GLYME-6 ($HPiCl_2 \cdot H_2O)_2$). Adducts **2** and GLYME-6 ($HPiCl_2 \cdot H_2O)_2$ were not hygroscopic, while **3**, **1**, and **2D** were. Almost completely deuterated 18-cr-6 ($DPiCl_2 \cdot D_2O)_2$ was prepared as described for **2** by precipitating and recrystallizing from D_2O.

Assay procedures

Dichloropicrate in the adducts was determined spectrophotometrically in aqueous 0.001 M NaOH at λ_{max} 380 nm (ε 4.18×10^3). This was checked by alkalimetric titration in H_2O using a glass electrode and was found to agree to within 0.91% of the spectrophotometric value.

[2]A detailed summary of the assays of the various adducts has been deposited as supplementary material and may be purchased from: The Depository of Unpublished Data, Document Delivery, CISTI, National Research Council Canada, Ottawa, Canada, K1A 052.

18-Crown-6 was determined by first neutralizing $HPiCl_2$ in the adduct in H_2O with KOH and then extracted exhaustively with 0.01 M $KPiCl_2$ (instead of picrate (14)) into CH_2Cl_2 as 18-cr-6 $KPiCl_2$. The latter was found spectrophotometrically at λ_{max} 398 nm (ε = (5.44–5.00) $\times 10^3$, the concentration range being (0–1.5) $\times 10^{-4}$ M). A calibration curve was run with known amounts of $KPiCl_2$ ((0–1) $\times 10^{-4}$ M) in presence of 0.005 M 18-cr-6. In the case of GLYME-6 ($HPiCl_2 \cdot H_2O)_2$, which is poorly extracted into CH_2Cl_2 by the above procedure, the ligand (0.05 M), was determined by ^1H NMR in $CDCl_3$, using 0.264 M *n*-decane as external proton concentration standard. The integrated signals per mol H of *n*-decane (δ 0.879, 1.264 ppm vs. TMS) were averaged and then compared with the integral per mol H of GLYME-6 from the following groups: terminal CH_3O- (6 3.374 ppm), -CH_2- adjacent to CH_3O- (4 3.553, 3.561, 3.571 ppm), and -CH_2-($CH_2CH_2O)_3OCH_2$- (16 3.653, 3.658 ppm). This yielded 1.037, 1.005, and 1.070 mmol GLYME-6/mg adduct, respectively.

The water content of all adducts was estimated from the integral of the ^1H NMR H^+, H_2O signal at δ 7.87–9.68 ppm for **1**, **2**, **3** and 6.597 ppm for GLYME-6 ($HPiCl_2 \cdot H_2O)_2$. The contribution of H^+ was taken equal to the dichloropicrate content. Assays of the partially or totally deuterated adducts were not performed in this study.

Instrumentation

Photomicrographs using either transmitted or reflected light were produced with a Nikon SMZ-10 stereomicroscope equipped with a photographic attachment. DSC scans were performed with a Mettler FP84TA microscopy cell in conjunction with a Mettler FD80 central processor. Aluminum sample cups were used. TGA consisted simply of keeping the sample in a stoppered weighing bottle at a given temperature for 20 min in a mineral oil bath (to constant weight), cooling in a desiccator, and weighing. **Caution**: *Although no detonation occurred in any of the experiments in which dichloropicric acid adducts were heated in 1 g quantities, care must be exercised.* X-ray powder patterns were scanned with a Siemens-D-500 automated diffractometer with CuKα radiation. The powder pattern of **3** exhibited peaks at 2θ = 21.35, 23.30, 19.70, 25.40, and 21.35°, in order of decreasing intensity, as compared to those of **2** at 8.50, 22.95, 21.40, 19.15, 11.40, and 29.40°. When **3** was exposed to H_2O vapor for 12 days at 25°C, peaks were found at 2θ = 23.00, 19.20, 29.50, 28.10, 8.60, 21.40, 23.75, 25.40, and 29.85°. Second harmonic generation capability of the adducts was probed using a homemade Kurtz and Dougherty device (15). Samples were dispersed with Flurolube on a glass slide. Melting points (corrected) were determined with a Thomas Hoover capillary device. UV–VIS absorbances at a single wavelength were taken on a GCA McPherson EU-700 spectrophotometer using 10 mm stoppered silica cells. ^1H NMR one-pulse sequence spectra were scanned by a Nicolet X-300 spectrometer. IR spectra were scanned by means of a Nicolet 5 DXB FT-IR spectrometer and were plotted by an HP 74470A plotter. NaCl discs were used for all samples. All experiments excepting those of DSC and TGA were performed at 20–25°C.

Results

Crystal morphology and X-ray powder pattern of adducts

Photomicrographs of the light yellow monoclinic crystals of polymorphs I and II of 18-cr-6 ($HPiCl_2 \cdot H_2O)_2$ are presented in Fig. 1.

These crystals become opaque, turn golden yellow, and soften when heated to ~75°C and ~87°C, respectively, presumably as a result of microcrystal formation (16). When cooled to 25°C in a dry atmosphere, they remain golden yellow, but again turn light yellow when exposed to water or D_2O vapor. It appears therefore, that **3** is ionic in character, as deduced from its IR spectrum (*vide infra*). Also in

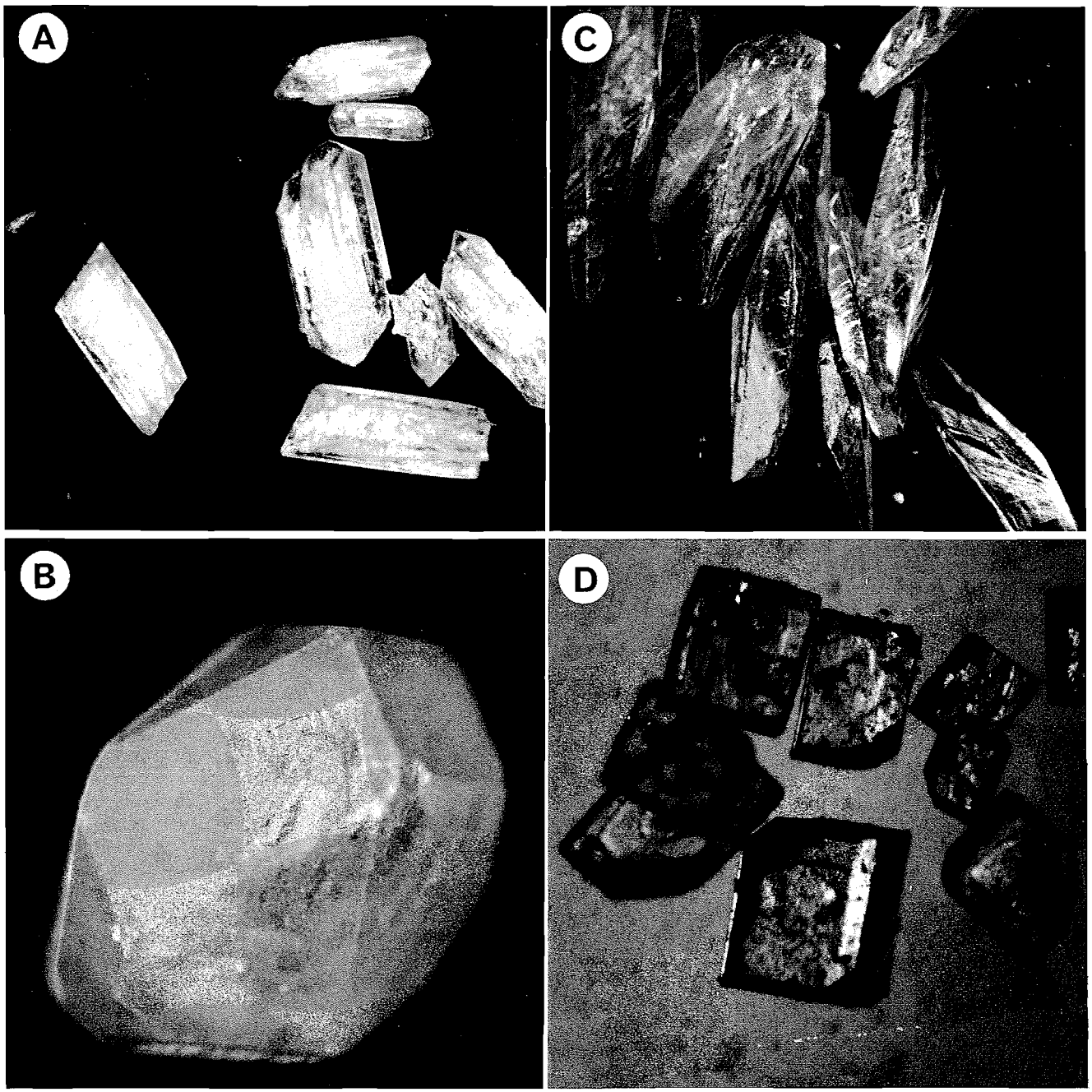

FIG. 1. Photomicrographs of unheated 18-crown-6 $(HPiCl_2 \cdot H_2O)_2$, **2**, and GLYME-6$(HPiCl_2 \cdot H_2O)_2$. A. Polymorph I of **2**. B. Polymorph II of **2** from layering of **2** dissolved in 1,2-dichloroethane with cyclohexane. C. Polymorph II of **2** from water by slow evaporation at 25°C. D. GLYME-6 $(HPiCl_2 \cdot H_2O)_2$ recrystallized in same way as C.

Can. J. Chem. Downloaded from www.nrcresearchpress.com by 123.30.183.119 on 09/08/12
For personal use only.

Fig. 1 is a photomicrograph of the very light yellow triclinic rectangular plates of a polymorph of GLYME-6 $(HPiCl_2 \cdot H_2O)_2$.[3] The other polymorph, as needles, is not shown.

The X-ray powder patterns of unheated **2** (polymorph II) and **3** (polymorph II of **2** heated to 113°C and cooled) are compared in Fig. 2. It is evident that **2** and **3** have different crystal structures. Not shown is that of **3** exposed to water vapor, which resembles that of **2** (Experimental).

Differential scanning calorimetry (DSC) and thermogravimetry (TGA) of dichloropicric acid adducts

A DSC scan of **1** (not shown) consists of only the baseline up to 80°C and a small endotherm (~4 kJ mol^{-1}) that merges into that of fusion at ~97°C. This indicates no significant phase change until fusion. A gradual loss in weight, ~2%, from 80 to 100°C is attributed to volatilization of **1** and

[3]D. Britton, J. M. Kolthoff, and M. K. Chantooni, Jr.; crystal structure determination to be published.

Can. J. Chem. Downloaded from www.nrcresearchpress.com by 123.30.183.119 on 09/08/12
For personal use only.

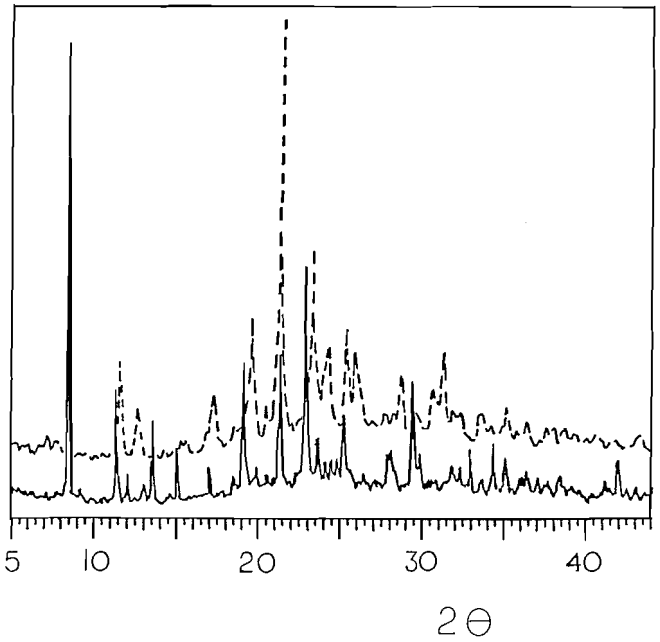

FIG. 2. X-ray powder patterns of unheated and heated **2**, polymorph II: (———) unheated; (— — —) heated to 113°C and cooled. Values of 2θ from 5.0 to 44.0°. λ = 1.541 Å.

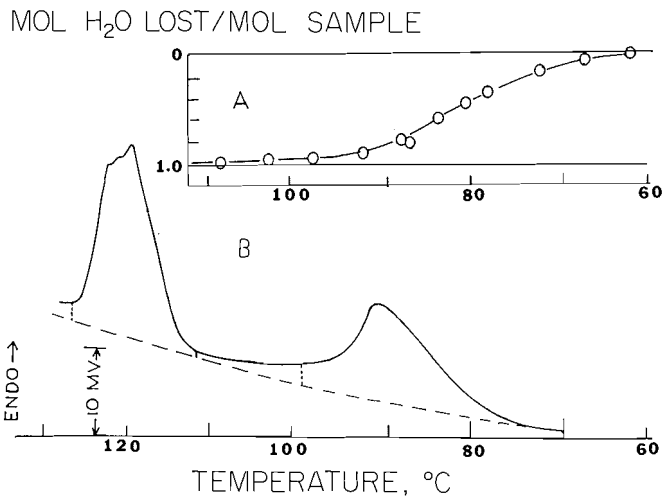

FIG. 3. Thermal studies on 18-crown-6 $(HPiCl_2 \cdot H_2O)_2$, polymorph II. A. TGA on 1618.3 mg 18-cr-6 · 1.96 $HPiCl_2$ · 1.71 H_2O, 10°/min; B. DSC on 5.4 mg 18-cr-6 · 2.00 $HPiCl_2$ · 2.23 H_2O, 3°/min. Vertical dashed lines indicates limits of endotherms.

(or) free $HPiCl_2$. A glass wool plug placed over the bottle containing the sample turned yellow. This does not occur when **2** is heated to 113°C. Both the TGA and DSC[4] of **2**, recrystallized from H_2O at 25°C, are presented in Fig. 3. The onset of loss of weight occurs at ~66°C, some 7°C lower than that of the beginning of the DSC endotherm. This currently is not explained. At higher temperatures a gradual increase in the endotherm is observed, followed by a maximum and subsequent steep decline. Uncertainty in ΔH due to uncertainty in locating the high-temperature limit of the endotherm is ~1.5 kJ mol^{-1}. Constant weight is attained at ~110°C. The loss in weight is linearly correlated with the DSC enthalpy change when the entire DSC is shifted to lower temperatures by 7°C.[5] DSC data of the various adducts are summarized in Table 1.

The loss in weight of **2** at 113°C corresponds to 0.96 mol H_2O/mol adduct, which is confirmed by assay of **3**, 1:2:00:1.16. When **3** is exposed to water vapor for 3 days at 25°C, constant weight is attained, to within 0.04% that of the original unheated sample, **2**. A DSC scan of the rehydrated adduct resembles that of **2** in Fig. 3. It consists of an endotherm at 95°C with $\Delta H = -51.8$ kJ mol^{-1} H_2O and a fusion endotherm of −60.1 kJ mol^{-1}. However, when **3** is rescanned without rehydration, only the baseline is obtained until fusion.

It may be added that exposure of **3** to MeOH vapor results in its superficial uptake, which is lost upon standing for 4 h at 25°C.

Nonlinear harmonic generation in adducts

Considering the dipolar nature of **3***a* or **3***b* and possible acentricity in the crystal structure, the second harmonic generation of **3** was probed, but not found. As expected GLYME-6 $(HPiCl_2 \cdot H_2O)_2$ (space group $P\bar{1}$)[3] and **2** (space group $C2/c$) lacked this capability.

IR spectra of adducts

In Table 2, frequencies of ν(OH) stretching vibrations of water to crown ether oxygens (3350–3550 cm^{-1}) and water to acid (1700–3200 cm^{-1}) in adducts (17–19) of 18-cr-6, water, and various phenols or aliphatic carboxylic acids are entered along with O . . . O distances, d(O . . . O), and O . . . H—O bond angles from X-ray diffraction data. In this study, FT-IR spectra of GLYME-6 $(HPiCl_2 \cdot H_2O)_2$ and aqua complexes of 18-cr-6 with 4,4′-biphenol, 3,5-dichlorophenol, 3-nitrophenol, 2,4-dintrophenol, and $HPiCl_2$ were run, since those of the first five are not available in the literature. FT-IR spectra of **2** and **2D** in the region 1700–3700 cm^{-1} are presented in Fig. 4. The spectrum of **1** (not shown) resembles that of **2**, with the exception of lack of absorption from 2100 to 2600 cm^{-1}. Fermi resonance (19) gives rise to a weak, but persistent, absorption at 1968, 1982, and 1982 cm^{-1} in spectra of unheated **1**, **2**, and **2D**, respectively (Fig. 4). When the crown possesses D_{3d}, or approximately D_{3d}, symmetry, as in unheated 1:1:1 and 1:2:2 aqua complexes of 18-cr-6 with phenols or carboxylic acids, the C-O-C, C-C stretching, and CH_2-CH_2 rocking mode bands occurring at ~1110, ~835, and ~960 cm^{-1} are not, or only slightly, split (19–21). This is found with adducts **1**, **2**, and **2D** in this study (Table 3). On the other hand, these bands are split extensively in the spectrum of unheated GLYME-6 $(HPiCl_2 \cdot H_2O)_2$ (not shown) as a result of the low symmetry of the polyether.[3]

The effects on their IR spectra of heating adducts **1** and **2** at 1.0×10^5 Pa pressure are described next. The entire spectrum of **1** from 400 to 4000 cm^{-1} is practically unchanged when heated to 103°C (Table 3), which is in ac-

[4]In some cases two distinct endotherms have been observed prior to fusion (Table 1). The sum of the ΔH values is the same as that when a single endotherm is encountered. The transition temperature of the first endotherm is not reproducible.

[5]A table of weight loss as ΔH has been deposited as supplementary material in the Depository of Unpublished Data, CISTI, National Research Council of Canada (see footnote 2). The slope of the linear plot is −53.0 kJ mol^{-1}.

TABLE 1. DSC results of 18-crown-6-dichloropicric acid–water adducts

Adduct composition[a]	$T_{transition}$[f] (°C)	$-\Delta H_{transition}$[g] (kJ/mol sample)	$-\Delta H_{fusion}$ (kJ/mol)	Melting point (°C)
1:1:1:0	—	—	80.3[h]	97.6–99.3
1:2:2:0[b]	86, 111.5	55.8	89.8	123.5–124.5
1:2:2:0[c]	88–98 or 80–92, 112	43.4 ± 3.8	66.2 ± 12.3	123–124
1:2:2:0[d]	109	42.4	79.8	123–124.5
1:2:1:1	102[e]	55.8[e]	78.0	120–121

[a]18-cr-6:$HPiCl_2$:H_2O:D_2O.
[b]Polymorph I from hot water.
[c]Polymorph II from water at 25°C.
[d]Polymorph II from DCE:cyclohexane 1:7 at 65°C.
[e]Accompanies release of D_2O (see text).
[f]Temperature at maximum of endotherm.
[g]Sum of ΔH of transitions excluding fusion.
[h]Includes endotherm from 80 to 94°C, associated with volatilization of adduct.

TABLE 2. X-ray crystallographic O ··· O distances, O—H ··· O angles (in brackets), and IR OH stretching frequencies of adducts[a]

		O ··· H — O distance (Å)			IR OH stretch (cm^{-1})		
No.	Adduct	Acid–H_2O	Crown–H_2O	Reference	Acid–H_2O	Crown–H_2O	Reference
1.	$L \cdot (—C_6H_5OH)_2 \cdot 2H_2O$	2.669	2.905 [179°] 2.945 [178°]	6	3142.2	3487 3529	This work
2.	$L(3—NO_2 \cdot C_6H_4OH \cdot H_2O)_2$	2.635 [168.1°]	2.876 [178.5°] 2.914 [175°]	10	3128	3458.6 3500.8	This work
3.	$L \cdot NCCH_2COOH \cdot H_2O$	2.595	2.917 [162.4°] 2.928 [168°]	21	2620	3490	19
4.	$L \cdot (2,4(NO_2)_2 \cdot C_6H_3OH \cdot H_2O)_2$	2.522 [173°]	2.847 [176°] 2.933 [159°]	9	~2550	3423.4 3529sh	This work
5.	$L(—COOH)_2 \cdot 2H_2O$	2.555 [166°] 2.650 [166°]	2.850 [169°] 2.877 [159°]	18	2500 2580	3425 3465	18
6.	$L(HPiCl_2 \cdot H_2O)_2$ (polymorph II)	2.462 [173°]	2.804 [167°] 2.904 [153°]	11	1771.1 1400	3378.5 3445 sh 3370 3500	This work 17
7.	$L \cdot HPiCl_2 \cdot H_2O$	2.47_4[b]	~2.72[c]		1700.8	3219.5	This work
7a.	$L \cdot HPiCl_2 \cdot H_2O$ (to 106°C)	2.47_4[b]	~2.75[c]		1700.8	3275.8	This work
8.	GLYME-6 $(HPiCl_2 \cdot H_2O)_2$	2.452 [173°] 2.473 [164°]	2.74_4 [176°] 2.86_7 [165°]		1722	3184sh 3336	This work
9.	$L \cdot 3,5—Cl_2C_6H_3OH \cdot H_2O$				3051	3508	This work

[a]L = 18-crown-6, GLYME-6 = pentaethyleneglycol dimethyl ether.
[b]O . . . H—O distance estimated from eq. [2]. using experimental value of ν(OH).
[c]O . . . H—O distance estimated from the solid curve in Fig. 4 using experimental value of ν(OH).

cord with DSC results. When **2** is heated to 113°C and cooled in a dry atmosphere, however, the water–crown and water–phenol stretching bands at 3379/3445 and 1771 cm^{-1} disappear, as well as the Fermi-resonance absorption at 1982 cm^{-1}, even though only one water molecule is expelled. These bands are replaced by a broad, moderately strong ν_1/ν_3 absorption of **3** in Fig. 4 (dashed line) from 2400 to 3100 cm^{-1} (centered at ~2650 cm^{-1}), which resembles that of H_3O^+ in 18-cr-6 $H_3O^+ \cdot BF_4^-$ (22) or in *cis-syn-cis*-dicyclohexano-18-cr-6 $H_3O^+ \cdot ClO_4^-$ (23). The pseudo hydronium ion in **3***a* is essentially that found in dicyclohexano-18-cr-6 $(H_3O^+ \cdot PiCl_2^-)_2$ by Peiju *et al.* (24) from X-ray diffraction.

In addition, the $2\nu_2$ symmetrical OH bending and ν_4(OH) asymmetrical bending modes characteristic of H_3O^+ (23) are observed at 2193 and ~1701 cm^{-1}, respectively, in the spectrum of **3**. Moreover, the symmetry of 18-cr-6 has been lowered from practically D_{3d} in **1** and **2** to possibly C_i in **3**, as extensive splitting is found in the C-O-C, C-C stretching, and CH_2CH_2 rocking modes.[6] Results are in Table 3. The presence of a strong absorption from <600 to 1000 cm^{-1} in the IR spectrum of **3** could be ascribed to either $PiCl_2^- \cdots H^+OH_2$ in **3***a* or to $H(PiCl_2)_2^-$ in **3***b*. A spectrum similar to that of **3** (produced when **2** is heated) is obtained when 1 mol $HPiCl_2$ is dissolved in 1 mol melted **1** at 98°C and the solidified mass, which forms after 3 min, remelted at 124°C and cooled (Fig. 4, open circles). This suggests that a mixed adduct, 18-cr-6 · $HPiCl_2$ · HA $(H_2O)_2$ (HA possibly being 2,4-dinitrophenol) could be prepared by reacting HA with melted **1** and hydrating over H_2O vapor.

[6]FT-IR spectra of **2** and **3** in the region 500–1700 cm^{-1} have also been deposited as supplementary material. See footnote 2.

Can. J. Chem. Downloaded from www.nrcresearchpress.com by 123.30.183.119 on 09/08/12
For personal use only.

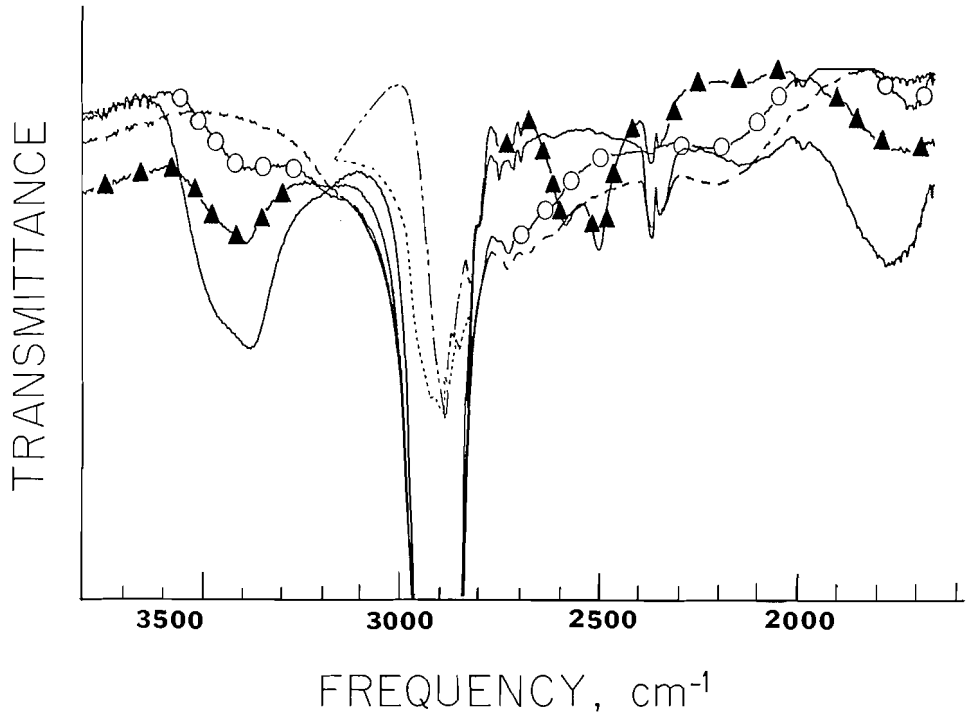

FIG. 4. FT-IR spectra of unheated and heated 18-crown-6 $(HPiCl_2 \cdot H_2O)_2$ in the region 1700–3700 cm^{-1}: (——) unheated **2**; (---▲---▲---) unheated **2D** (**3** over D_2O vapor); (---O---O---) reaction product between **1** and $HPiCl_2$ at 124°C; (-- -- --)**2** heated to 113°C; all with Nujol (— ·· — ··) and (· · · · ·) first and fourth entries, respectively, with Flurolube in the region 2850–3210 cm^{-1}.

TABLE 3. IR absorbance peaks of 18-cr-6 or GLYME-6 in dichloropicric acid adducts in the region 800–1200 cm^{-1} at 25°C

Adduct	Ligand IR frequency (cm^{-1})		
	C-O-C stretch	$-CH_2-CH_2-$ rocking	-C-C- stretch
1	1144.7 vw	954.3 s	844.4 w
	1112.0 s		830.9 s
1[a]	1143.4 vw	953.4 s	844.3 m
	1100.7 s		830.8 s
3[b]	1142.7 m	966.7 sh	843.3 m
	1093.3 s	948.7 m	826.1 m
3[c]	1142.9 w	950.1 m	842.9 m
	1096.7 s		829.5 m
2	1136.5 vw	960.9 m	840.1 vs
	1113.6 vs	950.0 w	
2D[d]	1136.4 vw	956.9 m	839.7 vs
	1113.4 vs	946.1 w	
3 · HDO	1138.5 vw	960.7 s	839.9 vs
	1113.9 vs	950.4 w	
GLYME-6	1140.1 m	950.1 s	860.5 m
$(HPiCl_2 \cdot H_2O)_2$	1104.2 s		835.9 m

[a]Heated to 103°C and cooled.
[b]**2** heated to 113°C and cooled.
[c]1:1 mixture of **1** and $HPiCl_2$ heated to 124°C and cooled (see text).
[d]Made by heating **2** to 117°C, cooling, and keeping over D_2O vapor.

Isotopic deuterium–hydrogen exchange study

In all experiments below the phenol in adducts **3**, **2**, **2D**, and 18-cr-6 $(HPiCl_2)_2$ $H_2O \cdot HDO$ (**3** · HDO) was in the OH form. These adducts were kept at ~25°C and 1.0×10^5 Pa pressure over nitrogen saturated with either H_2O or D_2O, or both, and their IR spectra recorded. When **3** (**2** heated to 117°C) was kept over D_2O for 11 days in a sealed container, **2D** was produced (Scheme 1, Table 3). The D_2O–crown and H_2O–crown doublets at 2502/2573 and 3395/3458 cm^{-1}, respectively, in Fig. 4 are about the same in intensity; the ratio of their integrated areas, $A(OD)/A(OH)$, being 0.92. Exposing **2D** or **3** to H_2O vapor for 4 days resulted in almost complete reversion to **2**. Incomplete exchange ($A(OD)/A(OH) = 0.42$) occurred when **2** was exposed to D_2O for 12 days (Scheme 1). Under these conditions equilibrium [1], the constant of which had not been determined, is displaced to the right. Incorporation of HDO into these adducts, is negligible, as the equilibrium

[2] $H_2O(g) + D_2O(g) \rightleftarrows 2\ HDO(g)$

must lie far to the left. From the above it is surmised that the O—H ··· O water–crown hydrogen bond is somewhat stronger than that of the deuterium analogue, even though a small positive isotope effect was deduced from the infrared (Discussion).

When **2D** was heated to 117°C, cooled, and exposed to D_2O vapor as above, and the procedure repeated three times, the IR spectrum of **2D** was observed ($A(OD)/A(OH) = 0.73$). From this it is inferred that one molecule of D_2O is lost when **2D** is heated and that H_3O^+ or possibly pseudohydronium ion (17) is favored in the structure of **3** over that of D_2OH^+ in the analogous D_2OH^+ compound. The high C_{3v} symmetry of H_3O^+ in **3***b* could be a factor. Replacing one H_2O molecule in **2** by HDO apparently is effected by keeping **3** over *both* H_2O and D_2O for 10 days. A single OD stretching band occurs at 2503 cm^{-1}. The ratio $A(OH)/A(OH)$ was found equal to 0.270, as compared to 0.306 expected for **3** · HDO.

Can. J. Chem. Downloaded from www.nrcresearchpress.com by 123.30.183.119 on 09/08/12
For personal use only.

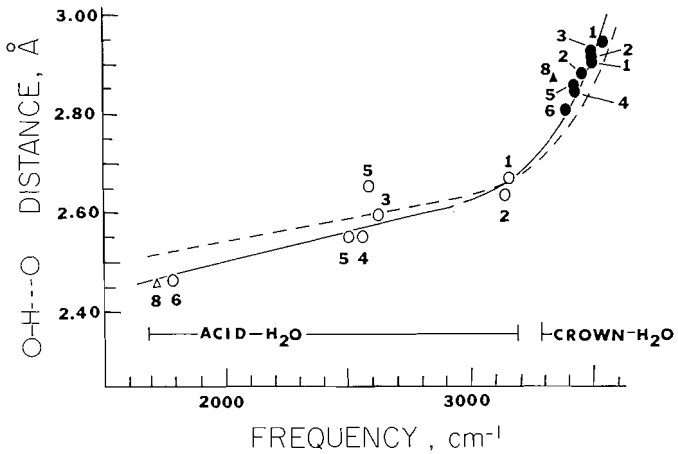

FIG. 5. Relation between O-H ··· O distance and OH stretching frequency of molecular adducts of 18-crown-6 (L) or GLYME-6, with carboxylic acids (or phenols) and water. 1. L·4,4′-biphenol·$2H_2O$. 2. L(3-nitrophenol·$H_2O)_2$. 5. L $(-COOH)_2(H_2O)_2$. 6. L (dichloropicric acid·$H_2O)_2$. 8. GLYME-6 (dichloropicric acid·$H_2O)_2$. Dashed curve is from ref. 25.

Discussion

Correlation between O ··· O distance and IR OH stretching frequency in adducts. Deuterium isotope effects

A plot of the O ··· O distances, d(O ··· O), in various 18-crown-6 aqua complexes vs. OH stretching frequency, ν(OH), in Fig. 5 has been constructed from the data in Table 2. Entries in which the O ··· H—O angle is ≤160° were excluded.

The water-to-crown points, which exhibit a weak dependence of ν(OH) on the acid in the adduct, lie slightly above a similar plot by Novack (25) (dashed line) of O—H ··· O hydrogen-bonded systems not containing crown ethers. Chênevert *et al.* (17) reported ν(OH) to be practically independent of d(O ··· O). It has been suggested (18) that poorly resolved ν(OH) doublets in this high-frequency range could be ascribed to the small difference in water–crown O ··· O distance, Δd(O ··· O). *Approximate* values of Δd(O ··· O) read off the d(O ··· O) vs. ν(OH) plot of Novak using experimental values of ν(OH) in Table 2 are ~0.041 and ~0.036 Å for the 4,4′-biphenol and 3-nitrophenol adducts, respectively, as compared to 0.045 and 0.038 Å from X-ray diffraction studies (Table 2). The presence of a D_2O–crown doublet in addition to a H_2O–crown doublet in the IR spectrum of **2D** in Fig. 4 stipulates that each water molecule in **2** has two different O—H ··· O (crown) distances as required by symmetry. Corresponding values of the ratio ν(OH)/ν(OD) equal to 1.344, 1.354 in the aqua dichloropicric acid 18-cr-6 complex and 1.35 reported in the aqua oxalic acid 18-cr-6 complex (18) characterize a small or negligible positive isotope effect. This is indicative of a single minimum potential well (25) with the proton situated near to the water oxygen.

For the phenolic or carboxylic acid-OH ··· OH_2 stretching band in the above adducts, the plot in Fig. 5 is linear from 1650 to 2700 cm^{-1}, conforming to the relation

$$[3] \quad d(\mathrm{O}\cdots\mathrm{O})(\text{Å}) = 2.21 + 1.40 \times 10^{-4}\nu(\mathrm{OH})(\mathrm{cm}^{-1})$$

The slope is somewhat greater than that of the linear portion of the plot by Novak, 0.8×10^{-4} (dashed line in Fig. 5). The phenolic ν(OD) band in the spectrum of the fully deuterated adduct, 18-cr-6 $(DPiCl_2 \cdot D_2O)_2$ (not shown) occurs at ≤1600 cm^{-1} (ν(OH)/ν(OD) ≥ 1.2), as expected for d(O ··· O) = 2.46 Å (25).

Thermal study on the 1:2:2 18-cr-6 aqua-dichloropicric acid adduct. Postulated mechanism of release of water

From comparison of the DSC and TGA plots of **2** in Fig. 3 it is evident that there is no enthalpy change prior to liberation of water. It is found from a single crystal X-ray diffraction study of **2** at 25°C (11) that there are large thermal vibrations of the proton in the (phenol) OH ··· OH_2 hydrogen bond (B_{eq} = 11 $Å^2$, isotropically refined) and in the H_2O to crown ether hydrogen bonds (B_{eq} 9, 16, $Å^2$). For comparison, the average value of B_{eq} of the methylene crown ring protons is 6.8 ± 1.3 $Å^2$. Apparently, the two hydrogen bonds of one H_2O molecule to the crown ether in **2** break upon heating, releasing $HPiCl_2 \cdot H_2O$, which is unstable ($HPiCl_2$ kept over H_2O vapor was found in this work to be $HPiCl_2 \cdot 0.071\ H_2O$). Picric acid is known not to form a hydrate (26). It is presumed that the remaining water molecule in structures **3***a* or **3***b* meanwhile becomes polarized, as a result of at least a partial proton transfer to it from the phenol. Polarizable hydrogen bonds are encountered in ionization and dissociation of strong acids in water (pK_a = 0–4) as described by Leuchs and Zundel (27). In solution, the critical O ··· O distance for proton transfer to occur is ~2.50 Å (28). This is slightly greater than d(O ··· O) of the 1:2:2 adduct. In this region the shallow double minimum potential well is very sensitive to the environment of the hydrogen-bonded system. The latter can readily be altered thermally.

$$[4] \quad \mathrm{AH}\cdots\mathrm{OH_2} \rightleftarrows \mathrm{A^-} + \mathrm{H^+OH_2}$$

Acknowledgements

I,M.K. thanks the National Science Foundation for Grants CHE-8401840 and CHE-8919860 for their generous support of this study. The authors are grateful to Professors D. Britton and M. C. Etter of the University of Minnesota for their timely suggestions. They also wish to thank M. C. Etter for the use of the microscope, and DSC and FT-IR facilities, in her laboratory.

1. R. D. Rogers and P. D. Richards. J. Inclusion Phenomen. **5**, 631 (1987), and references cited therein.
2. F. Vögtle, W. M. Müller, and W. H. Watson. Top. Curr. Chem. **125**, 148 (1985).
3. G. A. Jeffrey and H. Maluszynska. Acta Crystallogr. Sect. B: Struct. Sci. **B46**, 546 (1990).
4. C. Bavoux, B. Belamri, M. Perrin, R. Perrin, R. Lamertine, and J. Vicens. Mol. Cryst. Liq. Cryst. **156**, 49 (1988).
5. F. Vögtle and W. M. Müller. Chem. Ber. **114**, 3179 (1981).
6. D. A. Grossie, F. Vögtle, and W. M. Müller. Acta Crystallogr. Sect. B: Struct. Crystallogr. Cryst. Chem. **B38**, 3157 (1982).
7. B. Belamri and C. Bavoux, Acta Crystallogr. Sect. C: Cryst. Struct. Commun. **C44**, 2173 (1988).
8. B. Belamri, C. Bavoux, and M. Perrin. J. Crystallogr. Spectrosc. Res. **17**, 177 (1987).
9. M. R. Caira, W. H. Watson, F. Vögtle, and W. M. Müller.

Can. J. Chem. Downloaded from www.nrcresearchpress.com by 123.30.183.119 on 09/08/12
For personal use only.

Acta Crystallogr. Sect. C: Cryst. Struct. Commun. **C40**, 491 (1984).
10. W. H. Watson, J. Galloy, D. A. Grossie, F. Vögtle, and W. M. Müller. J. Org. Chem. **49**, 347 (1984).
11. D. Britton, M. K. Chantooni, Jr., and I. M. Kolthoff. Acta Crystallogr. Sect. C: Cryst. Struct. Commun. **C44**, 303 (1988).
12. P. J. Pearce and R. J. Simkins. Can. J. Chem. **46**, 241 (1968).
13. W. Ji-Wang, M. K. Chantooni, Jr., and I. M. Kolthoff. J. Coord. Chem. **22**, 43 (1990).
14. I. M. Kolthoff. Can. J. Chem. **59**, 1548 (1981).
15. J. R. Dougherty and S. K. Kurtz. J. Appl. Crystallogr. **9**, 145 (1976).
16. D. Curtin, I. Paul, E. Duesler, T. Lewis, B. Mann, and Wein-T Shiau. Mol. Cryst. Liq. Cryst. **50**, 25 (1979).
17. R. Chênevert, A. Rodigue, D. Chamberland, J. Ouellet, and R. Savoie. J. Mol. Struct. **131**, 187 (1985).
18. S. Deguire, F. Brisse, J. Ouellet, and R. Savoie. Can. J. Chem. **64**, 142 (1986).
19. R. Savoie, A. Rodigue, M. Pigeon-Gosselin, and R. Chênevert. Can. J. Chem. **63**, 1457 (1985).
20. M. Fouassier and J. Lassegues. J. Chim. Phys. **75**, 865 (1978).
21. A. Elbasyouny, H. J. Brügge, K. von Deuten, M. Dickel, A. Knöchel, K. U. Koch, J. Kopf, D. Melzer, and G. Rudolph. J. Am. Chem. Soc. **105**, 6568 (1983).
22. R. Chênevert, A. Rodigue, M. Pigeon-Gosselin, and R. Savoie. Can. J. Chem. **60**, 853 (1982).
23. R. M. Izatt, B. L. Haymore, and J. J. Christensen. J. Chem. Soc. Chem. Commun. 1308 (1972).
24. Z. Peiju, W. Ming, and W. Wenji. Acta Crystallogr. Sect. C: **C46**, 1522 (1990).
25. A. Novak. Structure Bonding (Berlin), **18**, 177 (1974).
26. E. Duesler, J. Engelmann, D. Curtin, and I. C. Paul. Cryst. Struct. Commun. **7**, 449 (1978).
27. M. Leuchs and G. Zundel. Can. J. Chem. **60**, 2118 (1982).
28. Th. Zeegers-Huyskens, and L. Sobczyk. J. Mol. Liq. **46**, 263 (1990).

Can. J. Chem. Downloaded from www.nrcresearchpress.com by 123.30.183.119 on 09/08/12
For personal use only.

Synthesis, C-13 NMR, and X-ray crystal structure of N6,N9-octamethylenepurinecyclophane

R. A. BELL,[1] R. FAGGIANI, H. N. HUNTER, AND C. J. L. LOCK[1]

Department of Chemistry, McMaster University, Hamilton, Ont., Canada L8S 4M1

Received June 14, 1990[2]

R. A. BELL, R. FAGGIANI, H. N. HUNTER, and C. J. L. LOCK. Can. J. Chem. **70**, 186 (1992).

The synthesis and structure determination of N6,N9-octamethylenepurine cyclophane by single crystal X-ray diffraction is reported. The cyclophane was prepared from 6-chloropurine and 8-aminooctanoic acid as starting materials. The aminooctyl fragment was first attached to N9 of 6-chloropurine by means of the Mitsunobu reaction and cyclization to the cyclophane effected by nucleophilic attack of the amino group at the C6 position and displacement of chloride ion. Reversing the reaction strategy did not result in formation of the cyclophane. Crystals of the cyclophane were monoclinic, $P2_1/n$, a = 9.620(3), b = 12.266(3), c = 11.994(2), Å, β = 111.25(2)°, Z = 4. Intensities were measured with a Nicolet P3 diffractometer and MoKα radiation at room temperature. The structure was solved by direct methods and refined to R = 0.0683, R_w = 0.0493 based on 1730 reflections. The molecule shows some strain, but bond lengths and angles are normal. Attempts to relieve the strain are made by a small distortion of the purine rings and bending of the N6 and C8′ atoms out of the planes to which they are attached (0.314(4), 0.459(5) Å). Further, the N6,H6,C1′ group is twisted by 30° from the pyrimidine plane and the torsion angles in the aliphatic chain are distorted from the idealized 60, 120, 180° (average, 13.6°; range 5.1–24.9°). These distortions result in some weakening of the π-bonding in the adenine moiety.

Key words: purinophane synthesis, nucleophilic aromatic substitution, conformational analysis, crystal structure.

R. A. BELL, R. FAGGIANI, H. N. HUNTER et C. J. L. LOCK. Can. J. Chem. **70**, 186 (1992).

On a réalisé la synthèse du cyclophane N6,N9-octaméthylène purine et on déterminé sa structure par diffraction des rayons-X par un cristal unique. On a préparé ce cyclophane en utilisant la 6-chloropurine et l'acide 8-amino-octanoïque comme produits de départ. On a d'abord relié la fragment amino-octyle à l'azote N9 de la 6-chloropurine à l'aide de la réaction de Mitsunobu et on a ensuite effectué la cyclisation en cyclophane en faisant appel à une attaque nucléophile du groupe aminé sur la position C6 qui provoque un déplacement de l'ion chlorure. Lorsque la stratégie des réactions est inversée, il n'y a pas de formation de cyclophane. Les cristaux du cyclophane sont monocliniques, $P2_1/n$, avec a = 9,620(3), b = 12,266(3) et c = 11.994(2) Å, β = 111,25(2)° et Z = 4. On a mesuré les intensité à l'aide d'un diffractomètre P3 de Nicolet et en utilisant la radiation MoKα, à la température ambiante. On a résolu la structure par des méthodes directes et on l'a affinée jusqu'à des valeurs de R = 0,683 et R_w = 0,0493 pour 1730 réflexions. La molécule présente des tensions, toutefois les longeurs des liaisons et les angles sont normaux. Une partie de la tension est éliminée par une faible distorsion des noyaux purines et un déplacement des atomes N6 et C8′ hors des plans auxquels ils sont attachés (0,314(4) et 0,459(5) Å respectivement). De plus, le groupe N6,H6,C1′ fait un angle de 30° avec le plan de la pyrimidine et les angles de torsions dans la chaîne aliphatique sont déformés par rapport aux valeurs idéales de 60, 120 et 180° (moyenne de 13,6° et écarts allant de 5,1, à 24,9°). Ces distorsions provoquent une diminution de la force de la liaison π dans la portion adénine.

Mots clés : synthèse du purinophane, substitution nucléophile aromatique, analyse conformationnelle, structure de cristaux.

[Traduit par la rédaction]

Introduction

Accounting for the chemical effects of the aromatic purine and pyrimidine rings found in ribo- and deoxyribonucleic acids has been the subject of intense study for some time (1).[3] The sequence-dependent arrangement of single (2) and double (3) stranded polynucleotides results in a variety of chemical shift values for neighbouring exchangeable and nonexchangeable heterobase protons. The ability to predetermine the diamagnetic shielding about these aromatic systems would be beneficial for the study of detailed conformational information for a specific sequence.

The two general methods of determining the anisotropy of the molecular diamagnetic susceptibility have involved the use of semi-empirical and quantum mechanics procedures. Originally, the semi-empirical investigations concentrated on calculating the contributions from ring currents (4), local atomic magnetic anisotropy (5), and polarization effects caused by protonation or hydrogen bonding (6). More recently, modifications have come by the comparison of ring current and ^{1}H shifts through correlation with crystal structure coordinates (7). A slightly different approach, which showed good agreement between theoretical and experimental results, was provided through a quantum mechanics study of the total shielding (8).

Despite the level of refinement obtained from the two theoretical approaches, a method of experimentally determining the diamagnetic shielding anisotropy is needed. A previous method of complementing and assessing the shielding anisotropy calculations for benzene involved the examination of the proton chemical shifts of a cyclophane molecule ([10]-paracyclophane) (9). The methylene proton chemical shifts furnished values for the spatial definition of the diamagnetic susceptibility anisotropy around the aromatic system and supplied a viable means of appraising the theoretical calculations.

In the work described here, the synthesis and crystal structure of a purine cyclophane (10) potentially suitable for

[1]Authors to whom correspondence may be addressed.

[2]Revision received September 18, 1991.

[3]For applications of heterobase anisotropy to N-H chemical shifts see ref. 1*b*.

Can. J. Chem. Downloaded from www.nrcresearchpress.com by 123.30.183.119 on 09/08/12
For personal use only.

Can. J. Chem. Downloaded from www.nrcresearchpress.com by 123.30.183.119 on 09/08/12
For personal use only.

the study of the diamagnetic shielding anisotropy about adenine is reported. Our approach to the shielding study necessitated the complete assignment of the ^{1}H NMR spectrum of the purine cyclophane **1** accompanied by the spatial location of the methylene protons relative to the purine system. Also described are the syntheses of two alkylated adenine derivatives used for comparison with the nuclear magnetic resonance (NMR) and ultraviolet (UV) spectroscopic properties of the cyclophane.

Considerations that must be taken into account when designing a cyclophane molecule derived from adenine are the location of the fusion sites on adenine and the length of the methylene chain. The methylene chain should be linked at opposite sides of adenine to enable the bridge to cross directly over the center of the aromatic plane. Purine reactivity and molecular models indicated that favourable fusion sites would be N6 and N9. The resulting methylene proton chemical shifts should provide a variety of shielding values representative of the different regions around the aromatic system. In considering the length of the methylene chain, the number of methylene units must be sufficient so that distortion of the aromatic plane resulting from strain imposed by the bridge is minimized. On the other hand, the chain should be relatively taut in order to restrict the movement of the methylene protons relative to the plane of the purine system. Again, inspection of molecular models revealed that an eight-carbon chain best satisfied these requirements.

Discussion and results

Synthesis

The route chosen for the synthesis of N6,N9-octamethylenepurine cyclophane, **1**, is shown in Scheme 1 and is the combination of two fragments, a purine ring system and a C8-methylene chain. The synthons were selected so that the purine ring was nucleophilic at N9 and electrophilic at C6 and the C8-methylene chain contained the nitrogen atom that was to become N6 in **1**. 6-Chloropurine, **10**, satisfied the first requirement and 8-aminooctanol, **5**, the second, with the hydroxyl group in the presence of the Mitsunobu reagent (11*a*) generating the electrophilic site.[4]

The initial synthetic work was directed towards developing a method of converting 8-aminooctanoic acid, **2**, into 8-aminooctanol. Although **2** is available commercially, it was convenient in the present instance to prepare the amino acid from cyclooctanone via the Beckmann rearrangement by standard procedures (12). Purification of **2** was achieved by adsorption on an ion exchange resin (13).

Initial attempts to reduce amino acid **2** to the amino alcohol with lithium aluminum hydride (LAH) proved fruitless because of the insolubility of the amino acid in suitable aprotic solvents. To overcome this problem, **2** was converted to the methyl ester, **3**, by use of thionyl chloride in methanol (14) and, although the ester could be isolated, it was prone to polyamide formation and difficult to handle. Reduction of freshly prepared samples of **3** with LAH, however, gave very poor yields (<10%) of 8-aminooctanol **5**, presumably because of the formation of insoluble poly(*N*-alkyliminoalane) complexes (15) that were immune to reduction by excess LAH. Reduction with the borane-methyl sulphide reagent (16) likewise led to poor yields of the amino alcohol, even where the potassium salt/18-crown-6 ether modification of Yoon and Cho (17) was used. During these trial reductions the remarkably stable borane-8-aminooctanol adduct was isolated and characterized (18). Fair yields (ca. 30%) of **5** could be obtained by reduction of the ethyl ester by use of the Bouvealt–Blanc procedure with excess sodium in ethanol (19). The ethyl ester **4** was synthesized in order to reduce the rate of polymerization and improve handling characteristics and, in the event, the ethyl group did prove to be of sufficient steric bulk to allow isolation of the amino ethyl ester **4** for brief periods at room temperature.

Since the synthetic scheme required a protected nitrogen atom for the Mitsunobu reaction (11), it was practical to improve the reduction procedure by first blocking the nitrogen atom of amino acid **2** (20). Two blocking groups were tried, the triphenylmethyl (trityl, Tr) group and the monomethoxytriphenylmethyl (methoxytrityl, MTr) group. Szammer (21) has reported the conversion of α-amino acids to the corresponding amino alcohol by reduction of the *N*-trityl ester. Thus, starting with the amino acid ethyl ester **4**, the trityl ester **6** was formed as shown in Scheme **1**. The reaction product was confirmed by the change in chemical shift of the methylene protons adjacent to the amine (from 1.53 to 2.15 ppm) together with the appearance of the expected aromatic protons at 7–7.4 ppm. Electron impact mass spectrometry failed to provide satisfactory molecular ion peaks for **6**, presumably because of thermal decomposition of the sample before ionization. Lithium aluminum hydride reduction of the *N*-trityl ester **6** then resulted in the formation of the *N*-trityl amino alcohol **8** in 87% yield. The ^{1}H NMR spectrum of this compound indicated the loss of ethoxy protons as well as the appearance of a triplet at 3.52 ppm for the methylene protons adjacent to the hydroxyl group. Preliminary trials were carried out on **8** to develop conditions for removal of the trityl group that would not affect the 6-chloropurine moiety. Reductive cleavage under mild conditions with Pd/C in ethyl acetate or ethanol proved unsatisfactory and, as more acidic conditions will remove the chlorine atom from 6-chloropurine, this avenue was not further explored. The trityl group could be successfully removed by acid hydrolysis (HCl–methanol), but these conditions again resulted in the solvolytic loss of the chlorine from 6-chloropurine, and it was concluded that the trityl group alone was not a useful protecting unit. Clearly a group with slightly greater acid lability, but similar steric bulk was required. Smith *et al.* (22) had suggested that the lability of the trityl group should increase as the number of *p*-methoxy substituents increased. With this in mind, the *N*-methoxytrityl ester **7** was prepared and reduced to the *N*-methoxytrityl amino alcohol **9** with LAH in greater than 97% yield from amino acid **2**. The C-13 NMR spectra for both the methoxytrityl ester and the methoxytrityl amino alcohol could be assigned by comparison with C-13 chemical shifts recorded for *n*-octanol, *n*-octylamine, ethyl octanoate, *p*-methoxybenzylamine, and triphenylcarbinol (23). Trial hydrolyses of compound **9** indicated that trifluoroacetic acid in methylene chloride followed by a methanol quench successfully cleaved the methoxytrityl group (24), and similar exposure of 6-chloropurine, **10**, to these mild reaction conditions showed that **10** was recovered completely unchanged.

Reaction of *N*-methoxytrityl amino alcohol **9** with 6-chloropurine, **10**, with use of the method of Mitsunobu (11*a*), afforded the N9-alkylated adduct **11** in 56% isolated yield.

[4]For an example of the use of this reaction using 6-chloropurine see ref. 11*b*.

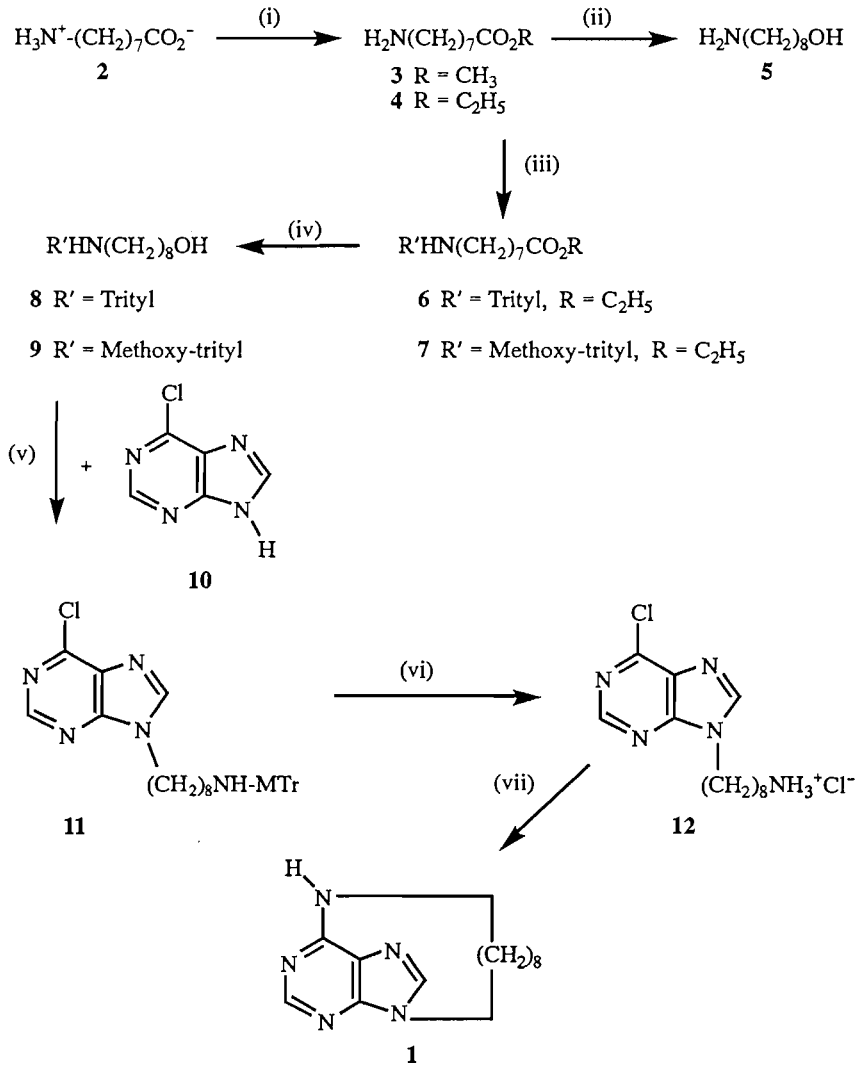

Reagents: (i) $SOCl_2$, MeOH or EtOH, 0°C. (ii) Sodium, ethanol, reflux. (iii) TrCl or MTrCl, Py, 0°C. (iv) $LiAlH_4$, ether, reflux. (v) DEAD, triphenylphosphine, THF, RT, 8 h. (vi) TFA, MeOH, 1 h. (vii) Acetonitrile, -20°C, 2 h; reflux, 24 h.

SCHEME 1

The proton NMR spectrum of **11** showed purine H-8 and H-2 absorptions at 8.74 and 8.08 ppm and the appearance of a triplet at 4.26 ppm arising from the methylene protons adjacent to N9 of the purine. The ^{13}C NMR spectrum was readily assigned by comparison with chemical shift data recorded for 6-chloropurine, *n*-octylamine, triphenylcarbinol, and *p*-methoxybenzyl-amine (23). Removal of the methoxytrityl group by the trifluoroacetic acid/methylene chloride/methanol procedure noted above yielded compound **12**, which was isolated as the hydrochloride salt and characterized by its proton NMR spectrum. Compound **12** appeared stable when stored as the hydrochloride salt.

The C8 methylene chain was chosen because, from the inspection of molecular models, it was expected to be reasonably taut across the purine ring, but not so strained as to cause extensive distortion of the purine. Intramolecular ring closure at the C6 site was expected to be less influenced by steric strain because of the geometry of nucleophilic attack at the C-6 site of a purine. Figure 1 shows the probable steps involved in the conversion of a substituted 6-chloropurine into an adenine cyclophane. The tetrahedral intermediate, **16**, arises from attack of the primary amine nitrogen of **12** on the *p* orbital at C6 (i.e., perpendicular to the plane of the purine). Thus, during the formation of **16**, there would be only a small constraint placed upon the conformation of the alkyl chain in order to allow the intermediate to be formed. The main imposition of the strain on the alkyl chain would be encountered in the subsequent collapse of the tetrahedral intermediate, when loss of chloride occurs causing the N6 nitrogen to move into the plane of the purine system and thus allows the C6 carbon to again become sp^2 hybridized.

The final ring closure was accomplished by taking into account observations from model experiments (see Scheme 2). These had indicated that primary amines reacted quickly with 6-chloropurine in polar, aprotic solvents such as dimethyl sulphoxide (DMSO), but it was undesirable to use DMSO in the large volumes required to ensure proper solute dilution for intramolecular reaction. Therefore, aceto-

Can. J. Chem. Downloaded from www.nrcresearchpress.com by 123.30.183.119 on 09/08/12
For personal use only.

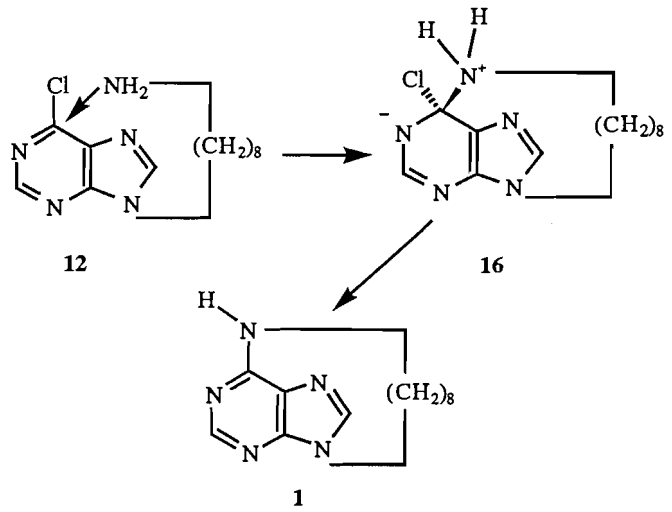

FIG. 1. Diagramatic view of the attack of the NH_2 nucleophile on the site of the 6-chlorine atom proceeding to the tetrahedral transition state **16**.

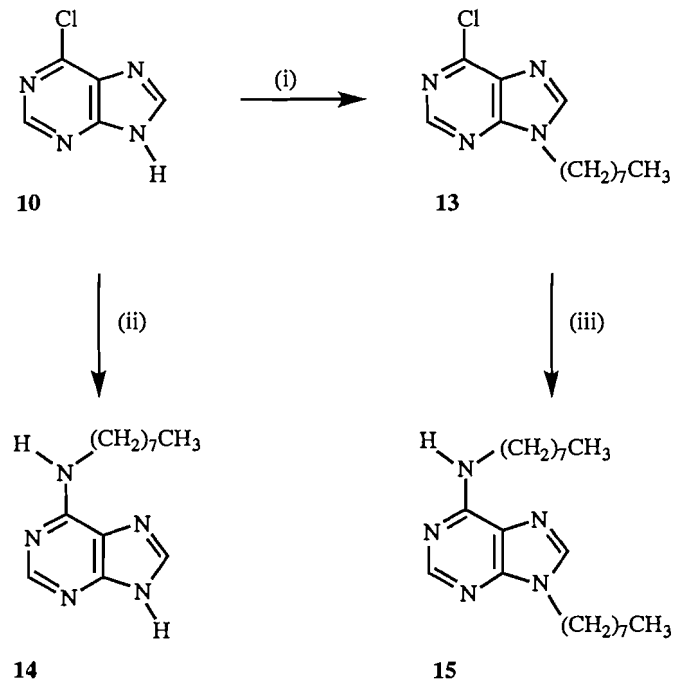

Reagents: (i) *n*-Octanol, triphenylphosphine, DEAD, THF, RT, 8 h; (ii) *n*-Octylamine, acetonitrile, 60°C, 24 h; (iii) *n*-Octylamine, acetonitrile, 60° C, 24 h.

SCHEME 2

nitrile was chosen as the solvent since it possessed similar solvent characteristics to DMSO (25) but was easier to remove upon completion of the reaction. The free amine was best generated from the hydrochloride salt **12** *in situ* and this was accomplished by combining the hindered non-nucleophilic base *N,N*-diisopropylethylamine with the **12** at low temperature (−23°C) and in relatively high concentration. The mixture was then diluted to 10^{-3} M with dry acetonitrile and heated. These reaction conditions gave the octamethylenepurine cyclophane **1** in 30% yield after chromatographic purification. The proton NMR spectrum of **1** was remarkable in showing all 16 methylene protons as diastereotopic and ranging in chemical shift from −0.6 to 4.8 ppm. Assignments were made initially from a two-dimensional COSY spectrum in conjunction with energy-minimized, computer-generated molecular models (26). Further confirmation came from two-dimensional $^{13}C-^{1}H$ heteronuclear shift correlated spectra together with the solid state conformation of the molecule demonstrated by the X-ray crystallographic study reported herein.

N6-Octylpurine, **14**, N9-octylpurine, **13**, and N6,N9-dioctylpurine, **15**, were prepared in model experiments (see Scheme **2**) to assist in refining experimental conditions for the preparation of **1** and also to act as models for the NMR and UV spectrum of **1**. The dialkyl compound **15** showed a UV maximum at λ 268 nm and **1** showed a maximum at λ 278 nm, indicating that some distortion of the purine ring has occurred (see discussion below).

It is of interest to note that during the synthetic work an attempt was made to prepare **1** by first forming the C6–N6 bond and then using the Mitsunobu reaction to carry out the intramolecular cyclization. 6-Chloropurine was readily *N*-alkylated at C6 with amino alcohol **5** by use of the method of Sutherland and Christensen (27), yielding 85% of **17**. The *N*-alkylation was confirmed by high resolution mass spectral data and comparison of the methylene CH_2NH chemical shift differences in the proton spectra of the product **17** (3.35 ppm) and amino alcohol **5** (1.53 ppm). In the final cyclization the electrostatic attraction within the intermediate **18** was expected to assist the ring closure (28). However, after prolonged reaction times and under a variety of reaction conditions, the cyclophane failed to form in detectable yields. This result could have arisen from two possible sources: (*i*) The Mitsunobu reaction proceeds by a number of bimolecular steps but, because intermolecular reaction must be minimized, the starting reactants are present at low concentration. Thus, the rate of these intermediate bimolecular steps would be extremely slow and other reaction pathways may occur before the Mitsunobu zwitterion could form. (*ii*) If the intermediate **18** was formed, reaction may not have taken place if the electron density in the highest occupied molecular orbital (HOMO) on N9 was not correctly oriented. If the HOMO at N9 is *perpendicular* to the ring then there will be minimal steric strain in the approach of the end $CH_2OP^+(Ph)_3$ unit, and an S_N2 transition state should be attainable with a normal activation barrier. If, however, the HOMO at N9 is *in the plane* of the purine ring, then to attain an S_N2 transition state would require severe stretching of the end methylene beyond N9 and **in the plane of the ring**. Molecular models suggest that such a transition state would be very difficult to attain without excessive strain on the alkyl chain and bending of the purine, and therefore make the intramolecular reaction inaccessible. Unfortunately our experiments did not distinguish between these two possibilities. It was noted that for prolonged reaction times there was incomplete recovery of **17**.

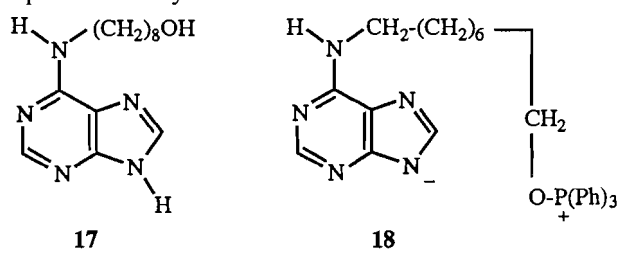

Can. J. Chem. Downloaded from www.nrcresearchpress.com by 123.30.183.119 on 09/08/12
For personal use only.

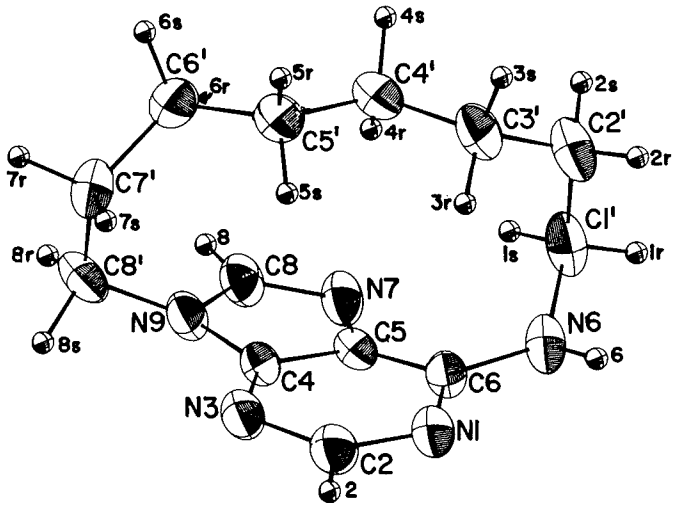

FIG. 2. The molecule of **1** showing the atom numbering. Hydrogen atoms are labelled by affix only in smaller print.

Diffraction studies and conformational analysis

The molecule is shown in Fig. 2 and bond lengths and angles are given in Table 3. One assumes that the structure has at least a small amount of strain present since there are a number of non-bonding distances that are shorter than the accepted van der Waals distances of 2.90–3.10 Å, C...H; 2.75–3.00 Å, N...H; 3.30 Å, C...C; 3.20–3.25 Å, C...N (29). These are C7′...C4, 3.154(4); C6′...N9, 2.941(4); H6r...C8, 2.72; H5s...C4, 1.94; H5s...N3, 2.66; H5s...C5, 2.44; H4s...N7, 2.52; H4s...C5, 2.80; H4s...C8, 2.84; C3′...C6, 3.134(4); H3r...C6, 2.57; H1s...C5, 2.64; H1s...C6, 2.63 (all in Å). Therefore, one looks for distortions in the structure that might indicate attempts to relieve the strain.

One can get an impression of the magnitude of the strain energies, which we pointed out above should be relatively small, from the nature of the distortions of the structure. Bond lengthening or shortening is energetically difficult and it is not surprising that the bond lengths within the adenine moiety agree very well with average values published previously (30). All values for the bond lengths lie within 0.51σ ($\sigma = (\sigma_1^2 + \sigma_2^2)^{1/2}$) of the average values, except C2—N3, which differs by 1.90σ. Similar agreement is obtained between the C—C and C—N distances in the aliphatic chain and published average values (31).

Angular distortions are energetically easier, but although variation is somewhat larger, all angles in the adenine moiety, except C8—N9—C8′ (2.86σ) lie within 2σ of the average values. Similarly C—C—C angles in the aliphatic chain (average value 115.1°, see Table 3) agree well with average values found in long-chain structures in which strain should be absent (114.9° (32), 114.3°, 114.6° (33), 114.9° (34)).

Twisting motions are energetically easiest and are observed. The adenine moiety shows small but significant distortions from planarity, whether one considers the molecule as a whole or the separate pyrimidine and imidazole rings. The dihedral angle between the pyrimidine and imidazole rings is 5.45(9)°, which is not excessive, but at the higher end of the normal range (30), and is not derived from bending about the C4—C5 bond like the pages of a book, but twisting of the imidazole ring relative to the pyrimidine ring about the C8-(centre of C4,C5) axis. The pyrimidine ring can be considered as a distorted boat with C2 and C5 forming the bow and stern. Both these distortions are to allow N6 and C8′ to move towards the aliphatic chain. This is reinforced by both N6 and C8′ being out of the planes of the rings to which they are attached (N6, 0.314(4) Å, C8′, 0.459(5) Å), again in the direction of the aliphatic chain. Further strain relief is achieved by the twist of the N6,H6,C1′ group from the pyrimidine plane by about 30° (C1′—N6—C6—C5, 30.6(3)°; C1′—N6—C6—N1, 147.4(3)°). All these distortions will tend to weaken the π-bonding within the adenine moiety, as can be seen in the bathochromic shift of the long wavelength UV absorption noted for **1** above. Further small distortions occur in the aliphatic chain. The chain is trying to lie as close as possible to the adenine ring system and this causes deviation of the N—C—C—C and C—C—C—C torsional angles from the idealized 60, 120, 180° values (average, 13.6°; range 5.1–24.9°). In particular the C2′—C3′—C4′—C5′, C3′—C4′—C5′—C6′, and C4′—C5′—C6′—C7′ angles (−158.0, 169.1, 139.0°) differ from the 180° found in unstrained aliphatic chains (32–34).

The packing is shown in Fig. 3. The molecules are arranged so that they lie in a layer centred on the 1 0 1 planes. The diagram shows the view normal to these planes. Surprisingly, the molecules are arranged so that there can be none of the expected π–π interaction between adenine moieties in adjacent molecules, perhaps also suggesting some weakening of the π-bonding. Thus both between layers and within layers only intermolecular van der Waals forces are present.

Experimental methods

Melting points were recorded on a Gallencamp capillary tube melting point apparatus and are uncorrected. Proton magnetic resonance (^{1}H NMR) spectra were recorded on a Varian EM-390 or Bruker WM-250 and AM-500 spectrometers with chloroform-*d* as the solvent unless otherwise noted. Unless specified, the usual internal references were tetramethylsilane (TMS) or chloroform. The abbreviations s = singlet, d = doublet, t = triplet, q = quartet, and m = multipet are used in the description of the spin–spin splitting pattern present in the spectra. The natural abundance carbon-13 magnetic resonances (^{13}C NMR) were recorded on Bruker WP-80 (at 20.115 MHz), WM-250 (at 62.896 MHz), and AM-500 (at 125.776 MHz) instruments using chloroform-*d* as the solvent and internal reference unless otherwise noted. All ^{13}C spectra were broad band decoupled. The ^{13}C NMR assignments based upon the literature were obtained from the following sources: *n*-octanol from the Bruker ^{13}C Data Bank (23); triphenylcarbinol from Olah *et al.* (35); 6-chloropurine from Szarek *et al.* (36); and *n*-octylamine and *p*-methoxybenzylamine from Sadtler Standard ^{13}C NMR spectra (23). Low resolution mass spectra (MS) and high resolution mass spectra (HRMS) were obtained at 70 eV on a VG Micromass 7070F double focussing mass spectrometer with the samples being introduced through a direct inlet system. Mass spectra obtained by the Fast Atom Bombardment (FAB) technique were recorded on a VG ZAB-E mass spectrometer. Infrared spectra (IR) were recorded on a Perkin Elmer 283 spectrometer. IR samples were run as neat liquids. The symbols s = strong, m = medium, w = weak, and sh = shoulder were used in the recording of the IR data to indicate the intensity of the recorded bands.

Dry ethanol was obtained by the method of Smith (37). *n*-Butanol, triethylamine, and pyridine were distilled over calcium hydride and stored over 4 Å molecular sieves until needed. Tetrahydrofuran (THF) was dried by refluxing and distilling from sodium and benzophenone under dry nitrogen. THF was collected from the distillation apparatus as required. Methanol was dried by

Can. J. Chem. Downloaded from www.nrcresearchpress.com by 123.30.183.119 on 09/08/12
For personal use only.

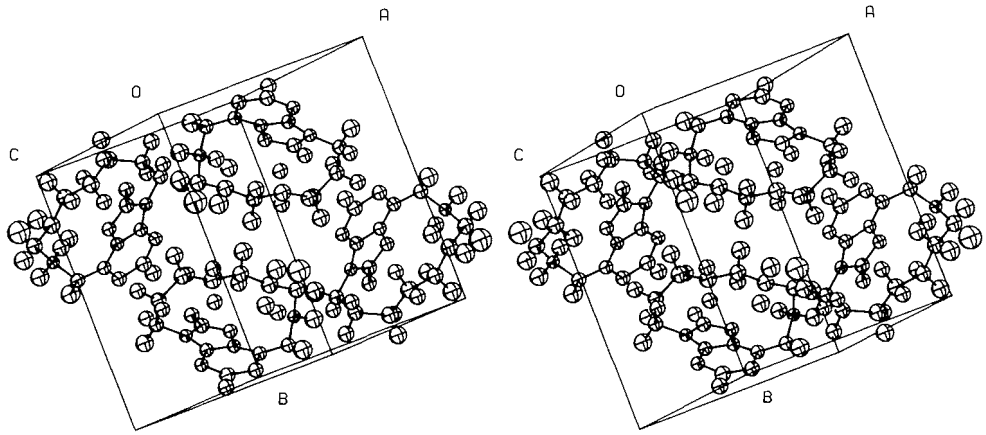

FIG. 3. The packing of the molecules within the unit cell. The view is roughly along [1 0 1].

Can. J. Chem. Downloaded from www.nrcresearchpress.com by 123.30.183.119 on 09/08/12
For personal use only.

refluxing over magnesium, distilled, and stored over molecular sieves. NMR solvents chloroform-*d*, methylene chloride-d_2, and dimethyl sulphoxide-d_6 were stored over molecular sieves before use.

Unless alternately specified, column chromatography was performed by the "flash" method of Still, Kahn, and Mitra (38). The silica gel used for column chromatography (5.0% of 100 mesh up, 47.6% of 100–200 mesh, and 47.4% of 200 mesh down) was purchased from Terochem. Silica gel 60 F254 (E. Merck Co.) plates of 0.2 mm thickness were used for analytical thin-layer chromatography. Reversed phase Sep-Pak C18 cartridges were obtained from Waters Associates. Reversed phase KC18F glass-backed thin-layer analytical plates (layer thickness 0.2 mm) were purchased from Whatman Co.

Cyclooctanone oxime

The procedure used was similar to the method of Coffman *et al.* (12). To a stirred solution of cyclooctanone (10 g, 0.079 mol) in dry absolute ethanol (50 mL), was added hydroxylamine hydrochloride (8.81 g, 0.127 mol). An aqueous solution of 50 mL of 1.3 M potassium carbonate was added dropwise and the solution was warmed to 50°C for 2 h. The ethanol solvent was evaporated under reduced pressure in a rotary evaporator and the remaining aqueous solution was extracted three times with 50-mL portions of chloroform. The chloroform extracts were combined, dried over anhydrous sodium sulphate, and the chloroform evaporated under reduced pressure in a rotary evaporator. This yielded 9.4 g (84%) cyclooctanone oxime (bp 87–88°C at 2.5 Torr (lit. (12) bp 123–124°C at 14 Torr; 1 Torr = 133.3 Pa). The oxime showed IR, ν_{max}: 1655 (m)(C=N) cm^{-1}. ^1H NMR (EM 390) δ: 1.47 (s, 6H, carbons 4,5,6 CH_2), 1.73 (s, 4H, carbons 3,7 CH_2), 2.40 (m, 4H, carbons 2.8 CH_2), 10.13 (s, 1H, OH). MS, *m/z* (RI%): 141 (21) [M^+], 124 (12) [M^+ − OH], 113 (100), 98 (32) [M^+ − CHNO], 73 (82), 55(50). HRMS, for $C_8H_{15}NO$, calcd.: 141.1154; found: 141.1130.

Cyclooctanone isooxime (2-azacyclononanone)

The procedure followed was similar to the method of Coffman *et al.* (12). To a stirred solution of sulphuric acid (4 mL of 96%) with distilled water (0.1 mL) at 110°C was added cyclooctanone oxime (951 mg, 6.74 mmol) dropwise. The solution was cooled to room temperature, poured onto ice (90 g), and neutralized with small portions of solid sodium hydroxide. The solution was extracted three times with 100-mL portions of chloroform. The combined extracts were dried over sodium sulphate (anhydrous) and evaporated under reduced pressure in a rotary evaporator, yielding 666.6 (70.0%) of a light brown solid, (mp 74.5–76.5°C (lit. (12) mp 77–79°C). The isooxime showed IR, ν_{max}: 3300 (s)[N-H], and 1650 (s)[CO] cm^{-1}. ^1H NMR (EM 390) δ: 1.6 (m, 10H, carbons 4,5,6,7,8 CH_2), 2.45 (*t*, *J* = 6 Hz, 2H, CH_2−CO), 3.35 (m, 2H, N-CH_2), 6.33 (br s, 1H, N-H). MS, *m/z* (RI%); 141 (35) [M^+], 124 (88) [M^+ − OH], 112 (24), 98 (62) [M^+ − CHNO], 56 (100). HRMS, for $C_8H_{16}NO$ [M + 1]$^+$, calcd.: 142.1232; found: 142.1243.

8-Aminooctanoic acid, 2

The method used was similar to that of Eck (39) or Takagi and Hayashi (13). To a stirred solution of 2-azacyclononanone (0.54 g, 3.8 mmol) dissolved in 5.2 mL of distilled water was added 1.5 mL of concentrated hydrochloric acid and the solution heated to reflux for 2 h. Amberlite IR-120 resin (40 mL) was washed three times with 20-mL portions of methanol and then washed five times with 20-mL portions of distilled water followed by 5 mL of 0.25 M hydrochloric acid. After cooling to room temperature, the hydrolysis solution was added to the resin and allowed to stir for 12 h. The solution was decanted and the resin was washed with distilled water until the washings were neutral. Distilled water (15 mL) and 1 M ammonium hydroxide were added to the resin until the solution was pH 9 and this mixture was stirred for 1 h. After decanting, more distilled water and ammonium hydride were added and the cycle repeated until four decantations were performed. These four solutions were combined and evaporated by use of a rotary evaporator under high vacuum. At the conclusion, benzene was used to form an azeotrope and remove remaining traces of water. Compound **2** was isolated as a cream-coloured solid (0.554 g, 98%) and it showed ^1H NMR (EM 390) D_2O solvent, δ:1.37 (m, 10H, carbons 3,4,5,6,7 CH_2), 2.17 (t, *J* = 6 Hz, 2H, CH_2COO), and 2.97 (t, *J* = 6 Hz, 2H, CH_2NH_2).

Ethyl 8-aminooctanoate, 4

The procedure described was similar to that of Huber and Brenner (14). To obtain the methyl ester, the same procedure was followed with methanol as the solvent. To 10 mL of ethanol stirred under nitrogen atmosphere at −5°C (ice/acetone bath) was added thionyl chloride (0.50 mL, 6.9 mmol) dropwise. After 5 min, 8-aminooctanoic acid, **2** (1.0 g, 6.3 mmol), was added and the solution stirred for 1 h at −5°C followed by 2 h at 40°C. The solvent was then evaporated under reduced pressure in a rotary evaporator and the residue was redissolved in 25 mL chloroform. Distilled water (25 mL) was added and the aqueous layer was adjusted to pH 8–9 with 1 M sodium hydroxide. The chloroform layer was removed and the aqueous layer was extracted twice with 25-mL portions of chloroform. The chloroform extracts were combined, dried over anhydrous sodium sulphate, and evaporated under reduced pressure in a rotary evaporator yielding 1.117 g (95%) ethyl 8-aminooctanoate which showed IR, ν_{max}: 3400 (m)[NH_2] and 1735 (s)[C=O] cm^{-1}. ^1H NMR (EM 390) δ: 1.23 (m, 15H, NH_2 and carbons 3,4,5,6,7 CH_2 and CH_3), 2.18 (t, *J* = 6 Hz, 2H, CH_2CO), 2.58 (t, *J* = 6 Hz, 2H, CH_2N), and 4.03 (q, *J* = 6 Hz, 2H, OCH_2). ^{13}C NMR (WP 80) δ: 173.6 (s, 1C, COO),

Can. J. Chem. Downloaded from www.nrcresearchpress.com by 123.30.183.119 on 09/08/12
For personal use only.

60 (s, 1C, OCH_2), 41.9 (s,1C,NCH_2), 34.2 (s,1C,CH_2CO), 33.2(s,1C,C7), 28.9 (s,2C,C4 and C5), 26.5 (s,1C,C6), 24.8 (s,1C,C3), and 14.1 (s,1C,CH_3). (Assignments based upon values for ethyl octanoate and *n*-octylamine (23).) HRMS, for $C_{10}H_{21}NO_2$ $(M + 1)^+$, calcd.: 187.1572; found: 187.1540. MS, *m/z* (RI%); 188 (33)$[M + 1]^+$, 158 (2)$[M^+ - CH_2CH_3]$, 142 (63)$[M^+ - OCH_2CH_3]$, 114 (4)$[M^+ - COOCH_2CH_3]$, and 100 (100)$[M^+ - CH_2COOCH_2CH_3]$.

8-Aminooctanol, 5

The procedure used was similar to that of Manske (19). Ethyl 8-aminooctanoate, **4** (97.5 mg, 0.518 mmol) was dissolved in anhydrous ethanol (5 mL). Without heating or stirring, sodium metal (145 mg, 6.3 mmol) was added as one piece. After the reaction was complete, distilled water (5 mL) was added dropwise. The ethanol was evaporated under reduced pressure in a rotary evaporator and the remaining aqueous solution was extracted three times with 10-ml portions of chloroform. The chloroform was evaporated under reduced pressure leaving the amino alcohol (22.5 mg, 30%) as a white solid. The aqueous extracts contained amino acid and were recovered for reuse. Amino alcohol **5** showed: ^1H NMR (EM 390) δ: 1.27 (s, 12H,carbons 2,3,4,5,6,7 CH_2), 1.53 (s,3H,OH and NH_2), 2.60 (t, J = 6 Hz,2H,CH_2N), and 3.53 (t, J = 6 Hz,2H,CH_2O). ^{13}C NMR (WP 80) δ: 62.22(s,1C,$HOCH_2$), 42.0 (s,1C,CH_2N), 33.5 (s,1C,C7), 32.7 (s,1C,C2), 29.2 (s,2C,C4 and C5), 26.6 (s,1C,C3), and 25.6 (s,1C,C6). (Assignments based upon values for *n*-octanol and *n*-octylamine (23).) MS, *m/z* (RI%): 144 (9)$[M^+ - 1]$, 128 (8)$[M^+ - NH_2]$, 115 (40)$[M^+ - CH_2NH_2]$, and 55 (100). HRMS, for $C_8H_{19}NO$ $(M^+ - 1)$, calcd.: 144.1388; found: 144.1343.

6-(8'-Hydroxy)octylaminopurine, 16

The procedure used was similar to that of Sutherland and Christensen (27). 9-Aminooctanol, **5** (45 mg, 0.3098 mmol) was dissolved in 2 mL of *n*-butanol. The solution was stirred at 80°C under nitrogen atmosphere and 6-chloropurine (43.2 mg, 0.28 mmol) was added. The solution was then heated to 110°C and stirred for 1.25 h. Potassium carbonate (23 mg, 0.166 mmol) was added and the solution stirred for 0.5 h. The solution was then evaporated under reduced pressure in a rotary evaporator. The crude product was recrystallized from hot water yielding 62.5 mg (85%). Compound **16** showed mp 164–166°C (dec.); ^1H NMR (WM-250) DMSO-d_6 solvent, δ: 1.256 (m, 10H, carbons 3',4',5',6',7' CH_2), 1.390 (m, 2H, CH_2), 3.355 (t, 2H, CH_2), 3.432 (t, 2H, CH_2), 7.495 (s, 1H, C2H), and 7.884 (s, 1H, C8H). MS, *m/z* (RI%): 263 (12)$[M^+]$, 246 (5)$[M^+ - OH]$, 232 (5)$[M^+ - CH_2OH]$, 218 (7)$[M^+ - (CH_2)_2OH]$, 204 (11)$[M^+ - (CH_2)_3OH]$, 190 (17)$[M^+ - (CH_2)_4OH]$, 176 (13)$[M^+ - (CH_2)_5OH]$, 162 (39)$[M^+ - (CH_2)_6OH]$, and 148 (100)$[M^+ - (CH_2)_7OH]$. HRMS, for $C_{13}H_{21}N_5O$, calcd.: 263.1745; found: 263.1741.

N-Trityl ethyl 8-aminooctanoate, 6

The method used was a modified version of the method described by Zervas and Theodoropoulos (40). To a stirred solution of ethyl 8-aminooctanoate (190.9 mg, 1.02 mmol) dissolved in 5 mL of chloroform were added triethylamine (103.7 mg, 1.02 mmol) and trityl chloride (1.05 equiv.). After 12 h, the solution was washed three times with 25-mL portions of distilled water. The organic phase was dried over anhydrous sodium sulphate and then evaporated under reduced pressure in a rotary evaporator. The yield of the trityl derivative **6** was 75%. The methoxy derivative was synthesized (by use of *p*-anisylchlorodiphenylmethane (4-methoxytrityl chloride)) under the same conditions yielding **7** in 95%. Compound **6** showed ^1H NMR (EM 390) δ: 1.39 (m, 13H, $(CH_2)_5$ and CH_3), 2.15 (m, 4H, CH_2N and CH_2CO), 4.02 (m, 2H, CH_2 ethyl), and 7.25 (m, 15H, aromatic). Compound **7** showed: ^1H NMR (AM 500) δ: 1253 (m, 9H, $(CH_2)_3$ and CH_3), 1.455 (m, 2H, CH_2-C-N), 1.584 (m, 2H, CH_2-C-COO), 2.107 (t, 2H, CH_2N), 2.258 (t, 2H, CH_2COO), 3.766 (s, 3H, OCH_3), 4.109 (m, 2H, OCH_2), and 7.448 (m, 14H, aromatic). ^{13}C NMR (AM500) δ: 14.25 (s, 1C, ethoxy CH_3), 24.92 (s, 1C, C3), 27.17 (s, 1C, C6), 29.07 (s, 1C, C4), 29.23 (s, 1C, C5), 30.81 (s, 1C, C7), 34.35 (s, 1C, C2), 43.73 (s, 1C, CC8), 55.15 (s, 1C, CH_3O), 60.12 (s, 1C, CH_2O), 70.26 (s, 1C, Tr-C-N), 113.00 (s, 2C, *meta*-anisyl), 126.04 (s, aromatic), 126.65 (s, aromatic), 127.84 (s, aromatic), 128.38 (s, aromatic), 128.56 (s, aromatic), 129.78 (s, aromatic), 130.52 (s, aromatic), 138.8 (s, 1C, *ipso*-anisyl), 146.74 (s, 2C, *ipso*-phenyl), 157.77 (s, 1C, *para*-anisyl) and 174.04 (s, 1C, COO). Assignments based upon values for ethyl octanoate, *n*-octylamine, triphenylcarbinol, and *p*-methoxybenzylamine (23).)

N-Tritylated ethyl 8-aminooctanols, 8, 9

The method used was similar to that used by Szammer (21). Lithium aluminum hydride (108 mg, 2.5 equiv.) was added to stirred anhydrous diethyl ether (8 mL) at 0°C under nitrogen atmosphere. To this solution was added an ethereal solution of *N*-trityl ethyl 8-aminooctanoate, **6** (1.09 mmol in 2 mL ether). The mixture was stirred at 0°C for 1 h and at reflux for 2 h. The reaction was quenched with 2 mL of methanol followed by 2 mL of distilled water. The mixture was filtered and the precipitate washed with 50 mL of ether and 25 mL of chloroform. The filtrate was concentrated (by rotary evaporation under reduced pressure) until only the water was remaining. This aqueous solution was extracted three times with 10-mL portions of chloroform. The combined chloroform extracts were dried over anhydrous sodium sulphate and evaporated under reduced pressure in a rotary evaporator. The yield of the trityl derivative **8** was 87%. The methoxytrityl compound was synthesized under the same conditions yielding 97% of the alcohol **9**. Compound **8** showed: ^1H NMR (EM 390) δ: 1.22 (m, 12H, $(CH_2)_6$), 2.10 (t, 2H, CH_2N), 3.52 (t, 2H, CH_2O), and 7.30 (m, 15H, aromatic). Compound **9** showed ^1H NMR (AM 500) δ: 1.274 (m, 8H, $(CH_2)_4$), 1.459 (m, 2H, CH_2-C-N), 1.529 (m, 2H, CH_2COH), 2.109 (m, 2H, CH_2N), 3.603 (t, 2H, CH_2O), 3.760 (s, 3H, CH_3O), and 7.230 (m, 15H, aromatic). ^{13}C NMR (WP 80) δ: 25.6 (s, 1C, C6), 27.2 (s, 1C, C3), 29.3 (s, 1C, C4), 29.4 (s, 1C, C5), 30.8 (s, 1C, C7), 32.7 (s, 1C, C2), 43.5 (s, 1C, C8), 55.0 (s, 1C, CH_3O), 62.8 (s, 1C, CH_2OH), 70.3 (s, 1C, Tr-C-N), 113.0 (s, 2C, *meta*-anisyl), 126.0 (s, aromatic), 127.6 (s, aromatic), 128.5 (s, aromatic), 129.8 (s, aromatic), 138.5 (s, 1C, *ipso*-anisyl), 146.6 (s, 2C, *ipso*-phenyl), and 157.8 (s, 1C, *para*-anisyl). (Assignments based upon values for *n*-octanol, *n*-octylamine, triphenylcarbinol and *p*-methoxybenzylamine (23).) MS, *m/z* (RI%): 340 (5)$[M^+ - C_6H_5]$, 318 (12), 288 (2)$[M^+ - (CH_2)_8OH]$, and 273 (100)$[M^+ - NH(CH_2)_8OH]$.

6-Chloro,9-(8'-N-methoxytritylaminooctyl)purine, 11

The procedure used was similar to that of Mitsunobu (11*a*), or Iwakawa *et al.* (11*b*). *N*-Methoxytrityl-8-aminooctanol (500 mg, 1.197 mmol) was dissolved in 5 mL of THF. To this stirred solution (under nitrogen atmosphere) was added a solution of triphenylphosphine (316 mg, 1.20 mmol) dissolved in 3 mL of THF. A solution of 6-chloropurine (185 mg, 1.197 mmol) together with diethyl azodicarboxylate (208.5 mg, 1.197 mmol) in 2 mL of THF was then added all at once. The mixture was stirred for 72 h at room temperature and the solvent then evaporated under reduced pressure in a rotary evaporator. The residue was washed three times with 10-mL portions of a solution consisting of 20% chloroform in hexanes. The combined washings were rotary evaporated under reduced pressure and redissolved in a volume of 40% acetonitrile in distilled water that was sufficient to effect dissolution (30–40 mL). A 2-mL portion of this solution was applied to a reversed phase Sep-Pak. The Sep-Pak was washed with 5 mL of fresh acetonitrile/water solution (40:60), followed by elution with 10 mL of acetonitrile. The Sep-Pak was then regenerated by washing with 5 mL of methanol followed by 5 mL of distilled water and the separation procedure was repeated with a fresh aliquot of the crude reaction product. The combined acetonitrile eluates were collected and evaporated under reduced pressure in a rotary evaporator. The yield of the partially purified product was 56% as indicated by ^1H NMR. TLC of **11** with acetonitrile on RP KC18F TLC

Can. J. Chem. Downloaded from www.nrcresearchpress.com by 123.30.183.119 on 09/08/12
For personal use only.

TABLE 1. Crystal data

Formula	$C_{13}H_{19}N_5$
Formula wt.	245.33
Crystal size (mm)	0.21 × 0.25 × 0.45
Systematic absences	$h0l$, $h + l = 2n + 1$, $0k0$, $k = 2n + 1$
Space group	$P2_1/n^a$
Unit cell parameters	a = 9.620(3)
(Å and °)	b = 12.266(3) β = 111.25(2)
	c = 11.944(2)
Volume (Å^3)	1313.7(5)
Z	4
μ, linear absorp. coeff. (cm^{-1})	0.86
absorp. coeff. factor. Å, range	1.016–1.028
σ_{calc}, σ_{obs} (g cm^{-3})	1.24, 1.22(2)
Max 2θ, reflections meas.	45°, $0 \leqslant h \leqslant 10$, $0 \leqslant k \leqslant 13$, $12 \leqslant l \leqslant 12$
Standard reflections (esd.%)	5 −2 −2 (1.66); 3 4 1 (1.13)
Temperature (°C)	22
Total number of reflections measured	1948
Number of independent reflections	1730
No. with $I > 0$ (used)	1730
R_{int}[b]	0.0113
Final R,[c] R_w[d]	0.0683, 0.0493
Final shift/error max. (ave.)	0.073, 0.009
Final difference map; max, min e Å^{-3}	0.233, −0.259
Weighting	$(\sigma_{F2} + 0.000335\ F_o^2)^{-1}$
Secondary extinction coefficient, x	0.00249
$F(000)$	528
Number of variables	240
Error in obs. of unit wt.	1.2448

[a]This cell can be converted to the conventional $P2_1/c$ cell; a = 9.620(3), b = 12.266(3), c = 12.325(2) Å, β = 114.52(2)° by the matrix (−1 0 1/0 −1 0/1 0 1).
[b]$R_{int} = (\Sigma(N\Sigma(w(\langle F\rangle - F)^2))/\Sigma(N-1)\Sigma wF^2)^{1/2}$.
[c]$R = \Sigma||F_o| - |F_c||/\Sigma|F_o|$.
[d]$R_w = (\Sigma w(|F_o| - |F_c|)^2/\Sigma wF_o^2)^{1/2}$.

plates gave R_f 0.51. Compound **11** showed ^{1}H NMR (WM 250) δ:1.283 (m, 8H, $(CH_2)_4$), 1.457 (m, 2H, $NCCH_2$), 1.921 (m, 2H, $N9CCH_2$), 2.102 (t, 2H, CH_2NH), 3.771 (s, 3H, OCH_3), 4.264 (t, 2H, $N9CH_2$), 6.810 (m, 4H, H_2OH2), 7.252 (m, 14H, Ph), 8.083 (s, 1H, C2H), 8.738 (s, 1H, C8H). ^{13}C NMR (WP 80) δ: 26.5 (s, 1C, C6′), 27.1 (s, 1C, C3′), 28.8 (s, 1C, C2′), 29.2 (s, 1C, C4′), 29.7 (s, 1C, C5′), 30.7 (s, 1C, C7′), 43.4 (s, 1C, C8′), 44.2 (s, 1C, C1′), 55.1 (s, 1C, CH_3O), 70.3 (s, 1C, Tr-C-N), 113.0 (s, 2C, *meta*-anisyl), 126.0 (s, aromatic), 127.6 (s, aromatic), 128.5 (s, aromatic), 129.8 (s, aromatic), 131.8 (s, 1C, C5), 138.5 (s, 1C, *ipso*-anisyl), 145.0 (s, 1C, C8), 146.6 (s, 2C, *ipso*-phenyl), 151.1 (s, 1C, C2), 151.9 (s, 2C, C4 and C6), and 157.8 (s, 1C, *para*-anisyl). (Assignments based upon values for *n*-octylamine, triphenylcarbinol, *p*-methoxybenzylamine, and 6-chloropurine (23).)

6-Chloro,9-(8′-aminooctyl)purine hydrochloride, 12

6-Chloro-9-(8′-*N*-methoxytritylaminooctyl)purine (46 mg, 0.083 mmol) was dissolved in 2 mL of methylene chloride. To this stirred solution was added 12 μL of trifluoroacetic acid and 20 μL of methanol. After 0.5 h more methanol (0.1 mL) and 8 mL of methylene chloride were added. The solution was extracted with twice with 10-mL portions of 0.01 M hydrochloric acid. The combined aqueous layers were evaporated under high vacuum in a rotary evaporator to dryness yielding 12 mg (50%) of **12** as a green solid. Compound **12** (HCl salt) showed ^{1}H NMR (EM 390) D_2O solvent, δ: 1.35 (m, 12H, $(CH_2)_6$), 3.07 (t, 2H, CH_2-N^+), 4.43 (m, 2H, CH_2-N9), and 8.86 (s, 1H, C2H). The free amine, isolated by methylene chloride extraction of a basic solution of the hydrochloride salt in water, was stable and showed ^{1}H NMR (EM 390) δ: 1.33 (br m, 12H, CH_2 on carbons 2′,3′,4′,5′,6′,7′), 3.63 (m, 2H, CH_2NH_2), 4.18 (t, J = 6 Hz, 2H, CH_2N9), 5.95 (s, 2H, NH_2), 7.77 (s, 1H, C2H), and 8.43 (s, 1H, C8H). MS, *m/z* (RI%): 281 (3)[M^+], 279 (14), 167 (32)[$M^+ - C_7NH_2$], 149 (84), and 92 (100).

N6,N9-Octamethylenepurine cyclophane, 1

6-Chloro-9-(8′-aminooctyl)purine hydrochloride (12 mg, 0.0378 mmol) was added to 1 mL of acetonitrile. The mixture was cooled to 0°C and *N*,*N*-diisopropylethylamine (10 mg, 0.080 mmol) was added dropwise. After 0.5 h, the mixture was added to 50 mL of acetonitrile. The solution was stirred at 60°C for 24 h followed by evaporation under reduced pressure in a rotary evaporator. The residue was redissolved in 10 mL of chloroform and extracted three times with 10-mL portions of 0.01 M hydrochloric acid. The organic layer was dried over anhydrous sodium sulphate and evaporated under reduced pressure in a rotary evaporator to dryness yielding 2.8 mg (0.0114 mmol, 30.2%) of crude **1**. The cyclophane was purified by medium pressure chromatography on silica gel using a Lobar column and elution with 1% methanol in chloroform. TLC with 5% methanol in chloroform gave R_f 0.198. The purified cyclophane showed: UV: λ_{max} 278 nm (ε = 10 557, ethanol). ^{1}H NMR (AM500) δ: −0.0636 (C5′*R*), 0.18 (C4′*S*), 0.18 (C3′*S*), 0.517 (C6′*S*), 0.606 (C4′*R*), 0.892 (C5′*S*), 1.030 (C3′*R*), 1.259 (C6′*R*), 1.377 (C2′*S*), 1.470 (C2′*R*), 1.644 (C7′*S*), 1.797 (C7′*R*), 3.350 (C1′*R*), 3.920 (C8′*S*), 4.546 (C8′*R*), 4.687 (C1′*S*). ^{13}C NMR (AM 500) δ: 23.146 (s, 1C, C6′), 25.213 (s, 1C, C3′), 26.128 (s, 1C, C4′), 28.722 (s, 1C, C7′), 30.924 (s, 1C, C2′), 31.322 (s, 1C, C5′), 43.030 (s, 1C, C1′), 45.032 (s, 1C, C8′), 121.313 (s, 1C, C5), 143.106 (s, 1C, C8), 152.417 (s, 1C, C4), 154.141 (s, 1C, C2), and 159.937 (s, 1C, C6). MS, *m/z* (RI%); 245 (79)[M^+], 216 (15)[$M^+ - NHCH_2$], 202 (19)[$M^+ - NH(CH_2)_2$], 188 (21)[$M^+ - NH(CH_2)_3$], 174 (21)[$M^+ - NH(CH_2)_4$], 160 (18)[$M^+ - NH(CH_2)_5$], 134

Can. J. Chem. Downloaded from www.nrcresearchpress.com by 123.30.183.119 on 09/08/12
For personal use only.

TABLE 2. Atomic positional parameters ($\times 10^4$) and temperature factors ($Å^2 \times 10^3$)

Atom	x	y	z	U_{eq}
N1	3392(2)	9609(2)	5456(2)	42
C2	1957(3)	9409(2)	5270(3)	43
N3	1358(2)	8714(2)	5825(2)	39
C4	2446(3)	8260(2)	6763(2)	32
C5	3953(3)	8462(2)	7146(2)	33
C6	4438(3)	9078(2)	6369(2)	37
N7	4719(2)	7887(2)	8193(2)	39
C8	3677(3)	7324(2)	8376(2)	40
N9	2271(2)	7492(2)	7539(2)	37
N6	5868(2)	9157(2)	6446(2)	47
C1′	6930(3)	8256(3)	6913(3)	50
C2′	6864(3)	7408(3)	5956(2)	58
C3′	5335(3)	6902(3)	5276(3)	51
C4′	4749(3)	6144(2)	6020(3)	46
C5′	3067(3)	6007(3)	5498(3)	45
C6′	2352(3)	5436(2)	6298(3)	46
C7′	887(3)	5955(2)	6262(3)	47
C8′	1012(3)	6735(4)	7285(2)	46

$U_{eq} = \frac{1}{3}(U_{11} + U_{22} + U_{33} + 2U_{13}\cos\beta)$.

(11)[$M^+ - (CH_2)_7CH$], 148 (51), 83 (90), and 55 (100). HRMS, for $C_{13}H_{19}N_5$, calcd.: 245.1640; found: 245.1669.

6-Chloro-9-octylpurine, ***13***

The same procedure was followed as for the synthesis of 6-chloro-9-(8′-*N*-methoxytritylaminooctyl)purine. The compound was purified by column chromatography with silica gel (5% methanol in chloroform) yielding 79% of **13**. Compound **13** showed ^{1}H NMR (EM 390) δ: 0.080 (m, 3H, CH_3), 1.23 (m, 10H, $(CH_2)_5$), 1.90 (m, 2H, CH_2-C-N), 4.27 (t, 2H, CH_2N), 8.10 (s, 1H, C2H) and 8.77 (s, 1H, C8H). ^{13}C NMR (AM 500) δ: 14.130 (s, 1C, CH_3), 22.466 (s, 1C, C7′), 26.520 (s, 1C, C3′), 28.833 (s, 1C, C5′), 28.919 (s, 1C, C4′), 29.774 (s, 1C, C6′), 31.574 (s, 1C, C2′), 44.477 (s, 1C, C1′), 131.550 (s, 1C, C5), 145.114 (s, 1C, C8), 150.934 (s, 1C, C2), and 151.815 (s, 2C, C4 and C6) (assigned by comparison with *n*-octylamine (23)). MS, *m/z* (RI%): 266 (10)[M^+], 237 (3)[$M^+ - CH_2CH_3$], 223 (4)[$M^+ - (CH_2)_2CH_3$], 209 (10)[$M^+ - (CH_2)_3CH_3$], 195 (7)[$M^+ - (CH_2)_4CH_3$], 181 (6)[$M^+ - (CH_2)_5CH_3$], 167 (11)[$M^+ - (CH_2)_6CH_3$], 104 (82), and 59 (100). HRMS, for $C_{13}H_{19}N_4Cl$, calcd.: 266.1298; found: 266.1285.

6-Aminooctylpurine and 6-aminooctyl-9-octylpurine, ***14, 15***

6-Chloropurine or 6-chloro-9-octylpurine was dissolved in 2.6 mL of acetonitrile. To this stirred solution were added octylamine (68 μL, 0.41 mmol) and *N,N*-diisopropylethylamine (71 μL, 0.41 mmol). After 24 h at 65°C, the solution was evaporated to dryness under reduced pressure in a rotary evaporator. The crude product was purified by column chromatography using 5% methanol in chloroform. The yield of the 6-amino compound **14** was 73%. The yield of the 6,9-dialkyl compound **15** was 50%. Compound **14** showed mp 169–170°C (lit.(41) mp 165–167°C). ^{1}H NMR (AM 500) δ: 0.855 (t, 3H, CH_3), 1.25 (m, 8H, $(CH_2)_4$), 1.416 (m, 2H, N-C-C-CH_2), 1.693 (m, 2H, N-C-CH_2), 3.600 (m, 2H, CH_2N), 6.068 (br s, 1H, NH), 7.240 (s, 1H, C2H), and 7.962 (s, 1H, C8H). ^{13}C NMR (AM 500) δ: 14.052 (s, 1C, CH_3), 22.614 (s, 1C, C7′), 26.937 (s, 1C, C3′), 29.208 (s, 1C, C5′), 29.321 (s, 1C, C4′), 29.723 (s, 1C, C6′), 31.779 (s, 1C, C2′), and 40.719 (s, 1C, C1′) (assigned by comparison with *n*-octylamine (23)). MS, *m/z* (RI%): 247 (10)[M^+], 204 (8)[$M^+ - (CH_2)_2CH_3$], 190 (14)[$M^+ - (CH_2)_3CH_3$], 176 (6)[$M^+ - (CH_2)_4CH_3$], 162 (25)[$M^+ - (CH_2)_5CH_3$], 148 (100)[$M^+ - (CH_2)_6CH_3$], and 119 (71)[$M^+ - NH(CH_2)_7CH_3$]. HRMS, for $C_{13}H_{21}N_5$, calcd.: 247.1797; found: 247.1784.

Compound **15** showed: UV: λ_{max} 268 (ε = 11 779, ethanol). ^{1}H NMR (EM 390) δ: 0.88 (m, 6H, $2CH_3$), 1.28 (m, 20H, $2(CH_2)_5$), 1.70 (m, 4H, $2CH_2$-C-N), 3.68 (m, 2H, CH_2N6), 4.17 (t, 2H, CH_2N9), 5.90 (br s, 1H, NH), 7.74 (s, 1H, C2H), and 8.45 (s, 1H, C8H). MS, *m/z* (RI%): 359 (41)[M^+], 343 (37), 330 (23)[$M^+ - CH_2CH_3$], 302 (57)[$M^+ - (CH_2)_3$], 288 (23)[$M^+ - (CH_2)_4CH_3$], 260 (92)[$M^+ - (CH_2)_6CH_3$], 247 (37)[$M^+ - CH(CH_2)_7CH_3$], 204 (23)[$M^+ - (CH_2)_8CH_3$], 176 (34)[$M^+ - (CH_2)_{10}CH_3$], 148 (100)[$M^+ - (CH_2)_{12}CH_3$], 104 (73), and 59(80). HRMS, for $C_{21}H_{37}N_5$, calcd.: 359.3049; found: 359.3036.

X-ray studies

A crystal of **1**, suitable for X-ray studies, was chosen after examination with a polarizing microscope. The acicular crystal was sealed in a Lindemann capillary and the space group determined with precession photographs. The cell parameters were determined by a least-squares refinement of the angular parameters of 15 automatically centred reflections in the range $19.1° < 2\theta < 26.5°$. Intensities were measured at 22° on a Nicolet P3 diffractometer with use of graphite-monochromated MoKα radiation (λ 0.71069 Å) and the θ(crystal)–2θ(counter) scan mode. Crystal data

TABLE 3. Selected interatomic distances (Å) and angles (°)

N1—C2	1.339(4)	C2–N3	1.332(4)	N3—C4	1.346(3)
C4—C5	1.375(3)	C5—C6	1.401(4)	C6—N1	1.353(3)
C5—N7	1.392(3)	N7—C8	1.299(4)	C8—N9	1.375(3)
N9—C4	1.374(3)	C6—N6	1.349(4)	N6—C1′	1.471(4)
C1′—C2′	1.530(5)	C2′—C3′	1.531(4)	C3′—C4′	1.528(5)
C4′—C5′	1.518(4)	C5′—C6′	1.534(5)	C6′—C7′	1.533(5)
C7′—C8′	1.522(4)	C8′—N9	1.468(4)		
C6—N1—C2	117.8(2)	N1—C2—N3	129.8(2)	C2—N3—C4	109.4(2)
N3—C4—C5	127.6(2)	C4—C5—C6	116.1(2)	C5—C6—N1	117.7(2)
N3—C4—N9	126.6(2)	C5—C4—N9	105.7(2)	C4—N9—C8	105.3(2)
N9—C8—N7	114.4(2)	C8—N7—C5	103.4(2)	N7—C5—C6	132.3(2)
N7–C5—C4	111.0(2)	C5—C6—N6	124.7(2)	N1—C6—N6	117.6(3)
C6—N6—C1′	121.5(3)	N6—C1′—C2′	113.1(2)	C1′—C2′—C3′	116.4(3)
C2′—C3′—C4′	115.1(3)	C3′—C4′—C5′	113.0(2)	C4′—C5′—C6′	116.5(2)
C5′—C6′—C7′	114.1(2)	C6′—C7′—C8′	115.7(2)	C7′—C8′—N9	112.5(3)
C8′—N9—C4	126.0(2)	C8′—N9—C8	125.2(2)		

and other numbers related to data collection are given in Table 1. Corrections were made for Lorentz polarization effects but not for absorption. This will introduce a maximum error in F_o of <0.3%. The structure was solved by direct methods. The phases were determined with the use of 321 reflections with $E > 1.2$ and 12 sets of starting phases. All non-hydrogen atoms were found in the subsequent E map. Hydrogen atoms were found from subsequent difference maps and the coordinates of all atoms (C and N with anisotropic temperature factors) were then refined, with minimization of the function $\Sigma w(|F_o| - |F_c|)^2$ until the final shift/error was less than 0.1. Reflections with $3\sigma_I > I > 3\sigma_I$ were treated by the method of French and Wilson (42). Scattering factors were those of Cromer and Waber (43). Secondary extinction was made by the method of SHELX (44).[5] Atomic positional parameters and U_{eq} for non-hydrogen atoms are given in Table 2.[6]

1. (*a*) P. Cruz, E. Bubienko, and P. N. Borer. Nature, **298**, 198 (1982); (*b*) D. R. Kearns. Prog. Nucleic Acids Res. Mol. Biol. **18**, 91 (1976); D. B. Arter and P. G. Schmidt. Nucleic Acids Res. **3**, 1437 (1976); H. A. M. Geerdes and C. W. Hilbers. Nucleic Acids Res. **4**, 207 (1977).
2. R. A. Bell, J. R. Everett, D. W. Hughes, J. M. Coddington, D. Alkema, P. A. Hader, and T. Neilson. J. Biomol. Struct. Dyn. **2**, 693–707 (1985).
3. P. N. Borer, L.-S. Kan, and P. O. P. Ts'o. Biochemistry, **14**, 4847 (1975).
4. C. Giessner-Prettre and B. Pullman. J. Theor. Biol. **27**, 87 (1976).
5. (*a*) C. Giessner-Prettre and B. Pullman. Biochem. Biophys. Res. Commun. **70**, 578 (1976). (*b*) F. Ribas Prado and C. Giessner-Prettre. J. Mol. Struct. (Theochem.) **76**, 81 (1981).
6. C. Giessner-Prettre, B. Pullman, and J. Caillet. Nucleic Acids Res. **4**, 99 (1977).
7. G. T. Robillard and B. R. Reid. *In* Biological applications of magnetic resonance. *Edited by* R. G. Shulman. Academic Press, New York. 1979. pp. 82–86.
8. C. Giessner-Prettre. J. Biomol. Struct. Dyn. **2**, 233 (1984).
9. A. Agarwal, J. A. Barnes, J. L. Fletcher, M. J. McGlinchey, and B. G. Sayer. Can. J. Chem. **55**, 2575 (1977).
10. R. A. Bell and H. N. Hunter. Tetrahedron Lett. **28**, 147 (1987).
11. (*a*) O. Mitsunobu. Synthesis, 1 (1981). (*b*) M. Iwakawa, B. M. Pinto, and W. A. Szarek. Can. J. Chem. **56**, 326 (1978).
12. D. D. Coffman, N. L. Cox, E. L. Martin, W. E. Mochel, and F. J. Van Natta. J. Polym. Sci. **3**, 85 (1948).
13. S. Tagaki and K. Hayashi. Chem. Pharm. Bull. **7**, 96 (1959).
14. W. Huber and M. Brenner. Helv. Chim. Acta, **36**, 1109 (1953).
15. S. Cucinella, T. Salvatori, C. Bussetto, G. Perego, and A. Mazzei. J. Organomet. Chem. **78**, 185 (1974). See also: S. Cucinella, G. Dozzi, A. Mazzei, and T. Salvatori. J. Organomet. Chem. **90**, 257 (1975).
16. A. Pelter and K. Smith. *In* Comprehensive organic chemistry. Vol. **3**. Edited by D. N. Jones. Pergamon, New York. 1979. pp. 687–940.
17. N. M. Yoon and B. T. Cho. Tetrahedron Lett. **23**, 2475 (1982).
18. T. Mancilla, F. Santiesban, R. Contreras, and A. Klaébe. Tetrahedron Lett. **23**, 1561 (1982); R. L. Letsinger and I. Skoog. J. Am. Chem. Soc. **77**, 2491 (1955).
19. R. H. Manske. Org. Synth. Coll. Vol. **2**. 154 (1943).
20. Z. Barneis, Y. Broeir, and S. Bittner. Chem. Ind. **19**, 526 (1976).
21. J. Szammer. Acta Chim. Acad. Scient. Hung. Tomus. **61**, 417 (1969).
22. M. Smith, D. H. Rammler, I. H. Goldberg, and H. G. Khorana. J. Am. Chem. Soc. **84**, 430 (1962).
23. Bruker ^{13}C Data Bank. Vol. **1**. Bruker Physik, Karlsruhe. 1976, Sadtler Standard ^{13}C NMR Spectra. VCH Verlagsgesellschaft, New York. 1987.
24. K. K. Ogilvie and K. Kroeker. Can J. Chem. **50**, 1211 (1972).
25. B. L. Karger, L. R. Snyder, and C. Horvath (*Editors*). *In* An introduction to separation science. Wiley, New York. 1973. pp. 272–274.
26. W. C. Still. Macromodel computer program. Version 1.5. Columbia University, New York. (1987).
27. M. Sutherland and B. E. Christensen. J. Am. Chem. Soc. **79**, 2251 (1957).
28. T. Kurihara, Y. Nakajima, and O. Mitsunobu. Tetrahedron Lett. 2455 (1976).
29. A. Bondi. J. Phys. Chem. **68**, 441 (1964); N. L. Allinger, J. A. Hirsch, M. A. Miller, I. J. Tyminski, and F. A. Van-Catledge. J. Am. Chem. Soc. **90**, 1199 (1968).
30. D. Voet and A. Rich. Prog. Nucl. Acid Res. Mol. Biol. **10**, 183 (1970).
31. L. E. Sutton, O. Kennard, H. M. Powell, and D. H. Whiffen (*Editors*). Tables of interatomic distances and configurations in molecules and ions. Supplement 1956–1959, Special Publication No. 18. The Chemical Society, London. 1965.
32. F. J. Zuniga and G. Chapuis. Cryst. Struct. Commun. **10**, 533 (1981).
33. I. Pascher, S. Sundell, and H. Hauser. J. Mol. Biol. **153**, 791 (1981).
34. M. Goto and E. Asada. Bull. Chem. Soc. Jpn. **53**, 2111 (1980).
35. G. A. Olah, P. W. Westerman, and J. Nishimura. J. Am. Chem. Soc. **96**, 3548 (1974).
36. W. A. Szarek, D. M. Vyas, A. Sepulchre, S. D. Gera, and G. Lukacs. Can. J. Chem. **52**, 2041 (1974).
37. E. L. Smith. J. Chem. Soc. 1288 (1927).
38. W. C. Still, M. Kahn, and A. Mitra. J. Org. Chem. **43**, 2923 (1978).
39. J. C. Eck. Org. Synth. **2**, 28 (1943).
40. L. Zervas and D. M. Theodoropoulos. J. Am. Chem. Soc. **78**, 1359 (1956).
41. M. Sutherland and B. E. Christensen. J. Am. Chem. Soc. **79**, 2251 (1957).
42. S. French and K. Wilson. Acta Crystallogr. **A34**, 517 (1978).
43. D. T. Cromer and J. T. Waber. International tables for X-ray crystallography. Vol. IV. *Edited by* J. A. Ibers and W. C. Hamilton. Kynoch Press, Birmingham, England. 1974. Table 2.2B, pp. 99–101.
44. G. M. Sheldrick. SHELX. Program for crystal structure determination. University of Cambridge, England. 1976.
45. J. M. Stewart and S. R. Hall. The XTAL system of crystallographic programs. Computer Sciences Technical Series, TR-1364. University of Maryland, College Park, MD. 1983.
46. G. Davenport. LSQPL. Calculation of least-squares planes.

[5]All calculations were carried out on a Vax 8600 computer. Calculations employed XTAL (45), SHELX (44), LSQPL (46), and CHEMX (47). Diagrams were made with SNOOPI (48).

[6]Tables of anisotropic temperature factors, atomic positional parameters, and temperature factors for hydrogen atoms, bond lengths and angles involving hydrogen atoms, best planes, dihedral and torsional angles and the moduli of F_o and F_c have been deposited. Complete sets of data may be purchased from: The Depository of Unpublished Data, Document Delivery, CISTI, National Research Council Canada, Ottawa, Canada K1A 0S2.

Tables of atomic positional parameters and bond lengths and angles involving hydrogen atoms have also been deposited with the Cambridge Crystallographic Data Centre and can be obtained on request from the Director, Cambridge Crystallographic Data Centre, University Chemical Laboratory, Lensfield Road, Cambridge CB2 1EW, U.K.

Can. J. Chem. Downloaded from www.nrcresearchpress.com by 123.30.183.119 on 09/08/12
For personal use only.

Crystallography Centre, University of West Australia, Nedlands, WA, Australia. 6009: Part of the XTAL system of crystallographic programs. *Edited by* J. M. Stewart and S. R. Hall. Computer Science Technical Series, TR-1364. University of Maryland, College Park, MD. 1983.

47. K. Davies. CHEM-X, developed and distributed by Chemical Design Ltd., Oxford, England. 1986.
48. K. Davies. CHEMGRAF Suite: Program SNOOPI, Chemical Design Ltd. Oxford, England. 1983.

Can. J. Chem. Downloaded from www.nrcresearchpress.com by 123.30.183.119 on 09/08/12
For personal use only.

The structure of 2,2-dibutyl-1,3,2-dioxastannane in the solid state and in solution

T. Bruce Grindley,[1] Rasiah Thangarasa, Pradip K. Bakshi, and T. Stanley Cameron[1]
Department of Chemistry, Dalhousie University, Halifax, N.S., Canada B3H 4J3

Received June 19, 1991

T. Bruce Grindley, Rasiah Thangarasa, Pradip K. Bakshi, and T. Stanley Cameron. Can. J. Chem. **70**, 197 (1992).

Crystals of 2,2-dibutyl-1,3,2-dioxastannane (**1**) are orthorhombic, of space group *Pnma*, with $a = 7.663(3)$, $b = 18.437(2)$, $c = 9.277(4)$ Å, $Z = 4$, $R = 0.0568$ ($R_w = 0.0551$) for 1183 independent reflections with $I > 3\sigma(I)$. Compound **1** is a polymer in which each monomer unit is joined to the next by a four-membered $(SnO)_2$ ring. The Sn—O bond lengths inside the monomer units average 2.04 Å while those between monomers average 2.57 Å. The mirror plane of the crystal contains the atoms in the four-membered rings and the other oxygen atoms. Two of the three remaining carbon atoms in the six-membered rings of the monomer units are close to the mirror plane. The other carbon atom is disordered above and below the plane. It was shown by ^{119}Sn NMR spectroscopy that solutions of **1** contain mixtures of oligomers that consist mainly of dimers, trimers, and tetramers in chloroform-*d*. ΔG^0 values for dimer–trimer equilibria and dimer–tetramer equilibria of -2.5 and -1.5 kcal mol^{-1} were obtained from integration of low temperature ^{119}Sn NMR spectra. These values favour the higher oligomers slightly less than those for 2,2-dibutyl-1,3,2-dioxastannolane.

Key words: 1,3,2-dioxastannanes, stannylene acetals, X-ray crystallography, ^{119}Sn NMR spectroscopy.

T. Bruce Grindley, Rasiah Thangarasa, Pradip K. Bakshi et T. Stanley Cameron. Can. J. Chem. **70**, 197 (1992).

Les cristaux de 2,2-dibutyl-1,3,2-dioxastannane (**1**) sont orthorhombiques, groupe d'espace *Pnma*, avec $a = 7,663(3)$, $b = 18,437(2)$, $c = 9,277(4)$ Å, $Z = 4$ et $R = 0,056$ ($R_w = 0,0551$) pour 1183 réflexions indépendantes avec $I \geq 3\sigma(I)$. Le composé **1** est un polymère dans lequel chaque unité de monomère est liée à la suivante par un cycle à quatre chaînons $(SnO)_2$. La longueur moyenne des liaisons Sn—O à l'intérieur des unités de monomère est égale à 2,04 Å alors que celle observée entre les monomères est de 2,57 Å. Le plan miroir du cristal contient les atomes des cycles à quatre chaînons ainsi que les autres atomes d'oxygène. Deux des trois autres atomes de carbone des cycles à six chaînons des unités de monomère se trouvent près du plan miroir. L'autre atome de carbone est désordonné au-dessus et au-dessous du plan. On a montré par RMN du ^{119}Sn que des solutions du composé **1** dans le chloroforme-*d* contiennent des mélanges d'oligomères formés principalement de dimères, de trimères et de tétramères. En se basant sur une intégration des spectres RMN du ^{119}Sn mesurés à basse température, on a pu déterminer que les valeurs de ΔG^0 des équilibres dimère/trimère et dimère/tétramère sont respectivement $-2,5$ et $-1,5$ kcal mol^{-1}. Ces valeurs sont un peu moins favorables aux oligomères plus élevés que celles mesurées pour le 2,2-dibutyl-1,3,2-dioxastannolane.

Mots clés : 1,3,2-dioxastannanes, acétals de stannylène, cristallographie par rayons-X, spectroscopie RMN du ^{119}Sn.
[Traduit par la rédaction]

Introduction

The reactions of 1,2-diols and 1,3-diols with dialkyltin oxides under conditions where water is removed azeotropically yield 1,3,2-dioxastannolanes and 1,3,2-dioxastannanes, respectively. These compounds, often termed stannylene acetals, have become widely used as intermediates for the regioselective monosubstitution of diols (1–3). Most of the reactions studied have involved 1,3,2-dioxastannolanes but those in which 1,3,2-dioxastannanes are intermediates also work efficiently (4, 5).

Structures of 1,3,2-dioxastannolanes in the solid state as determined by X-ray crystallography have ranged from dimers (6, 7), to a pentamer (8), to polymers (9). Derivatives with a few non-bulky substituents, e.g., 2,2-dibutyl-1,3,2-dioxastannolane (9, 10), or 2,2-dibutyl-4-methyl-1,3,2-dioxastannolane (10), are polymers in the solid. In solution, these compounds are less associated and the species present at concentrations observable by ^{119}Sn nmr spectroscopy range from dimers to mixtures of oligomers up to the pentamer (11). 1,3,2-Dioxastannolanes having large substituents on tin, e.g., *tert*-butyl groups (7), or many small substituents (11, 12) can exist solely as dimers both in solution and in the solid state. We have recently shown that highly substituted 1,3,2-dioxastannolanes, such as the 2,2-di-*tert*-butyl-4,4,5,5-tetramethyl derivative, exist as the monomer or as dimer–monomer mixtures (13).

The structure of 2,2-dibutyl-1,3,2-dioxastannane (**1**) has attracted considerable attention. A preliminary X-ray diffraction study published in 1973 suggested that solid **1** was a polymer but no details other than the Sn—O bond lengths were supplied (14). Recently, ^{119}Sn nmr spectra of **1** in the solid state have been measured and the results support the assignment of the structure of **1** as a polymer (10). Molecular weight measurements in pyridine by boiling point elevation gave values of 333 (14) and, for a higher concentration (4.2%), 550 (15). The molecular weight of the monomer is 307.

The most reliable technique for obtaining information about the structures of tin-containing compounds in solution is ^{119}Sn nmr spectroscopy (16). Smith *et al.* (17) and Kennedy (18) demonstrated that for dialkoxydialkyltin derivatives, tetracoordinate tin nuclei absorb between 0 and -40 ppm while pentacoordinate tin nuclei absorb between -150 and -170 ppm. Tetracoordinate tin atoms are present only in monomers. A dimer contains only pentacoordinate tin while higher oligomers contain both pentacoordinate and hexacoordinate tin atoms.

The ^{119}Sn nmr chemical shifts of cyclic derivatives are somewhat different. For 2,2-dibutyl-1,3,2-dioxastannolane (**2**) in solution, pentacoordinate tin nuclei in dimers and oligomers absorb between -126 and -132 ppm while hexacoordinate tin nuclei absorb between -260 and -285 ppm in trimers, tetramers, and pentamers (11). We have recently shown that tetracoordinate tin nuclei in mo-

[1]To whom correspondence should be addressed.

Can. J. Chem. Downloaded from www.nrcresearchpress.com by 123.30.183.119 on 09/08/12
For personal use only.

nomeric 2,2-dibutyl-1,3,2-dioxastannolanes absorb at about +80 ppm (13).

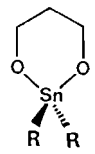

1

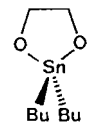

2

Smith *et al.* observed ^{119}Sn nmr chemical shifts for **1** of −228 and −288 ppm in saturated chloroform-*d* solution at room temperature and neat at 96°C, respectively. These workers concluded that **1** was probably present in solution as mixtures of oligomers based on their measurement of the chemical shift for a saturated solution of **2** in chloroform-*d* at room temperature of −189 ppm (17). Compound **2** was considered to be a dimer (17) although it has since been shown that a mixture of oligomers was present (11).

In this publication, we report an X-ray diffraction study of **1** at low temperature and variable temperature ^{119}Sn and ^{13}C nmr studies of **1** in solution in order to fully define the species present in both phases. These results will provide a basis for interpreting the spectra and reactions of substituted 1,3,2-dioxastannanes.

Experimental

Commercial 1,3-propanediol was dried over molecular sieves (4 Å) and converted to 2,2-dibutyl-1,3,2-dioxastannane (**1**) by refluxing with an equivalent amount of dibutyltin oxide in benzene in an apparatus for the azeotropic removal of water. Evaporation of the solvent on a vacuum line yielded a white powder. Distillation of dried hexane and toluene onto the sample, followed by heating and cooling cycles conducted in a vacuum, gave colourless crystals suitable for study by X-ray diffraction. The crystals were transferred into capillaries in a dry box and the capillaries were sealed. Crystal data and other experimental details are summarized in Table 1. The data were collected on an Enraf-Nonius CAD4 diffractometer using graphite monochromated MoK_α radiation (λ = 0.70926 Å) at 203 K. Cell dimensions were calculated from 25 reflections with 2θ angles in the range 26–30°. No correction was made for extinction but an absorption correction was applied (20). Atomic scattering factors and corrections for anomalous dispersion for Sn, C, O, and H were taken from the International tables for X-ray crystallography, Vol. IV (21).[2]

The structure was solved by the direct (SHELXS) method (19). All non-hydrogen atoms were refined with anisotropic thermal parameters. Hydrogen atoms were placed geometrically and refined riding on the attached carbon atoms with individual isotropic thermal parameters. C(5) and its attached hydrogens were found to be disordered above and below the mirror plane. C(4) and C(6) were also found to be slightly disordered (see Discussion).

Carbon-13 and tin-119 nmr spectra were measured on a Nicolet NT-360 NB spectrometer at 90.8 and 134.6 MHz, respectively. Chemical shifts are reported with respect to internal tetramethylsilane and external neat tetramethyltin at 20°C, respectively. The samples studied were prepared and sealed under vacuum as previously (11).

[2]Supplementary tables containing more experimental details, anisotropic thermal parameters, hydrogen atom positions, torsional angles, and observed and calculated structure factors may be purchased from the Depository of Unpublished Data, CISTI, National Research Council of Canada, Ottawa, Ont., Canada K2A 0S2.

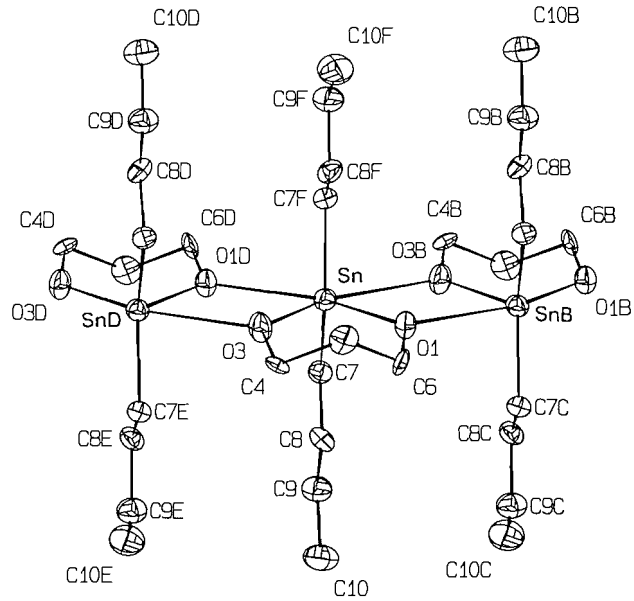

FIG. 1. A segment of the structure of polymeric 2,2-dibutyl-1,3,2-dioxastannane (**1**). The relationships between the labels here and the symmetry labels used in Table 3 and in the table of torsional angles (supplementary Table 4) are as follows: $B = iii = x + 0.5, -y + 0.5, -z + 0.5$; $C = iv = x + 0.5, y, -z + 0.5$; $D = ii = x - 0.5, -y + 0.5, -z + 0.5$; $E = v = x - 0.5, y, -z + 0.5$; $F = i = x, -y + 0.5, z$. Note that C(5), the atom between C(4) and C(6) in the figure, and also C(4) and C(6) have 1 : 1 disorders above and below the plane defined by O(3), Sn, O(1) and only one of the two locations for each are shown for each monomer unit.

Results and discussion

X-ray crystallography

The structure and numbering of the compound is shown in Fig. 1; the crystal data, atomic coordinates, bond lengths, and interbond angles are listed in Tables 1–3.

The individual 2,2-dibutyl-1,3,2-dioxastannane units are linked together through planar four-membered Sn—O—Sn—O rings to form an infinite ribbon polymer. The tin and oxygen atoms are all located on the mirror plane of space group *Pnma*. In initial refinements, the carbon atoms that are bonded to the oxygen atoms, C(4) and C(6), were also found to lie on the mirror plane but the third carbon atom, C(5), was disordered, occupying equally populated sites 0.52 Å above and below the plane. The thermal parameters for C(4) and C(6), particularly U_{22}, were found to be significantly larger than those of the other atoms. It appeared that C(4) and C(6) were slightly disordered as well, lying above the mirror plane when C(5) is below and vice versa. To define the extent of this disorder, several refinements were performed where C(4) and C(6) were fixed at varying distances away from the mirror plane. U_{22} was plotted against the distance away from the plane (see Fig. 2). The final distance away from the plane was that which minimized U_{22}. The two butyl groups are related by the mirror plane. Because the plane of the four-membered ring is the mirror plane of the crystal, all four-membered rings in a particular polymer lie in this plane. The conformation of each 1,3,2-dioxastannane ring is close to a half-chair with five atoms lying close to the plane defined by the two fused planar four-membered rings. All torsional angles involving O(1), Sn, O(3) and their symmetry-related atoms have values

Can. J. Chem. Downloaded from www.nrcresearchpress.com by 123.30.183.119 on 09/08/12
For personal use only.

Can. J. Chem. Downloaded from www.nrcresearchpress.com by 123.30.183.119 on 09/08/12
For personal use only.

TABLE 1. Crystal data for 2,2-dibutyl-1,3,2-dioxastannane (**1**)

Formula	$(C_{11}H_{24}O_2Sn)_n$
FW(monomer)	306.91
Crystal system	Orthorhombic
Space group	*Pnma*
a (Å)	7.663(3)
b (Å)	18.437(2)
c (Å)	9.277(4)
V (Å^3)	1311(2)
Z	4
D_{calcd} (g cm^{-3})	1.555
T	203 K
μ(MoKα) (cm^{-1})	19.3283
F(000)	624
Crystal dimensions (mm)	0.15 × 0.15 × 0.35
Scan type	ω/2θ
ω scan width (deg)	1.0 + 0.35 tan θ
θ range (deg)	3–25
Range of *h*, *k*, *l* (deg)	0–9, 0–11, 0–21
Measured reflections	1363
Unique reflections	1183
Observed reflections $\{I > 3\sigma(I)\}$	867
Parameters refined	104
Final *R*, R_w indices[a]	0.0568, 0.0551
Weighting scheme	$w = 1.000/[\sigma^2F + 0.000181F^2]$
S[b]	3.719
Highest peak (e Å^{-3})	3.38
Lowest peak (e Å^{-3})	−2.73

[a]$R = [\Sigma\|F_o| - |F_c|\|/\Sigma|F_o|$; $R_w = (\Sigma w(|F_o| - |F_c|)^2/\Sigma wF_o^2)^{1/2}$.
[b]$S = (\Sigma w(|F_o| - |F_c|)^2/(m - n)^{1/2}$; *m* = no. of reflections, *n* = no. of variables.

TABLE 2. Fractional atomic coordinates (× 10^4) with their estimated standard variations in parentheses

Atom	*x*/*a*	*y*/*b*	*z*/*c*	*U*(mod)
Sn	1282(2)	2500[a]	2270(1)	230(5)
C(7)	1299(13)	1415(4)	1451(8)	241(36)
C(8)	1266(23)	830(5)	2603(8)	267(37)
C(9)	1242(14)	75(5)	1961(10)	344(40)
C(10)	1268(17)	−533(6)	3060(12)	472(47)
O(1)	3233(12)	2500[a]	3770(10)	292(45)
C(6)	2966(18)	2365[b]	5278(16)	252(69)
C(5)	1374(20)	2778(9)	5826(16)	333(66)
C(4)	−301(19)	2365[b]	5346(15)	169(62)
O(3)	−594(13)	2500[a]	3812(10)	319(45)

[a]Fixed.
[b]Fixed by a procedure outlined in the text.

of 0 or 180° (supplementary Table 4). The torsional angles O—Sn—O—C have absolute values of 12.1(6)° with signs depending on the orientation of C(5).

The O—Sn—O bond angle inside the 1,3,2-dioxastannane ring is 93.2(2)° while the two O—Sn—O bond angles about a particular tin atom in its two attached four-membered rings are 65.7(2) and 67.3(2)°. The *trans*-O—Sn—O angles are 159.5(2) and 157.9(2)°. The exocyclic C—Sn—C bond angle is 138.4(3)°. Thus, the overall structure about tin is a severely distorted octahedron.

It is interesting to compare the structural features of **1** in the crystal with those of the 1,3,2-dioxastannolanes studied by X-ray crystallography (6–9). A comparison of bond angles and bond lengths is shown in Table 4. Because the *R* value for methyl 4,6-*O*-benzylidene-2,3-*O*-dibutylstannylene-α-D-glucopyranoside (**4**) was rather large (10.9%) and some carbon atoms in the butyl groups were not located (6*a*), we have recently reexamined this molecule by X-ray diffraction at low temperature and the data in Table 4 for **4** are from our study (6*b*).

TABLE 3. Selected bond lengths (Å) and bond angles (deg), with estimated standard deviations in parentheses[a]

Bond	Length	Bond	Length
Sn—C(7)	2.139(8)	Sn—C(7)^i	2.139(8)
Sn—O(1)	2.043(6)	Sn—O(1)^{ii}	2.527(6)
Sn—O(3)	2.028(6)	Sn—O(3)^{iii}	2.596(6)
C(7)—C(8)	1.519(14)	C(8)—C(9)	1.514(15)
C(9)—C(10)	1.516(15)	O(1)—C(6)	1.435(11)
O(1)—C(6)^i	1.435(11)	C(6)—C(5)	1.53(2)
C(6)—C(5)^i	1.35(2)	C(5)—C(4)	1.56(2)
C(5)—C(4)^i	1.38(2)	O(3)—C(4)	1.462(11)
O(3)—C(4)^i	1.462(11)		

Bonds	Angle	Bonds	Angle
C(7)—Sn—C(7)^i	138.4(3)	C(7)—Sn—O(1)	103.7(3)
C(7)—Sn—O(1)^{ii}	82.5(3)	C(7)—Sn—O(3)	104.8(3)
C(7)—Sn—O(3)^{iii}	81.8(3)	O(1)—Sn—O(1)^{ii}	159.5(2)
O(1)—Sn—O(3)	93.2(2)	O(1)—Sn—O(3)^{iii}	65.7(2)
O(1)^{ii}—Sn—O(3)	67.3(2)	O(1)^{ii}—Sn—O(3)^{iii}	134.8(2)
O(3)—Sn—O(3)^{iii}	157.9(2)	Sn—C(7)—C(8)	114.5(6)
C(7)—C(8)—C(9)	112.2(9)	C(8)—C(9)—C(10)	114.6(9)
Sn—O(1)—Sn^{iii}	114.6(3)	Sn—O(1)—C(6)	124.0(5)
Sn^{iii}—O(1)—C(6)	120.3(5)	O(1)—C(6)—C(5)	110.7(9)
O(1)—C(6)—C(5)^i	122.1(10)	C(6)—C(5)—C(4)	108.6(10)
C(6)—C(5)—C(4)^i	122.6(12)	C(6)^i—C(5)—C(4)	122.8(12)
C(6)^i—C(5)—C(4)^i	132.9(13)	Sn—O(3)—Sn^{ii}	112.4(3)
Sn—O(3)—C(4)	125.3(5)	Sn^{ii}—O(3)—O(1)^{ii}	46.7(2)
Sn^{ii}—O(3)—C(4)	121.2(5)	O(1)^{ii}—O(3)—C(4)	164.9(5)
C(5)—C(4)—O(3)	108.8(8)	C(5)^i—C(4)—O(3)	119.2(9)

[a]Atoms labelled with superscripts are related to the nonsuperscripted atoms by the following translational symmetry: *i*: *x* + 0.000, −*y* + 0.500, *z* + 0.000; *ii*: *x* − 0.500, −*y* + 0.500, −*z* + 0.500; *iii*: *x* + 0.500, −*y* + 0.500, −*z* + 0.500.

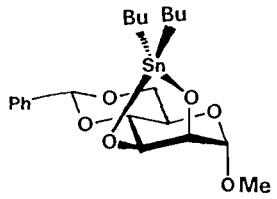

3

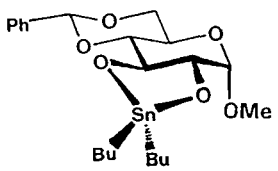

4

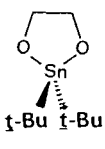

5

Polymeric molecules in which all tin atoms are hexacoordinate will be compared first. The bond angles and lengths for compound **1** do not differ significantly from those of its five-membered ring analogue, polymeric 2,2-dibutyl-1,3,2-dioxastannolane (**2**) (9), except that the intramonomer

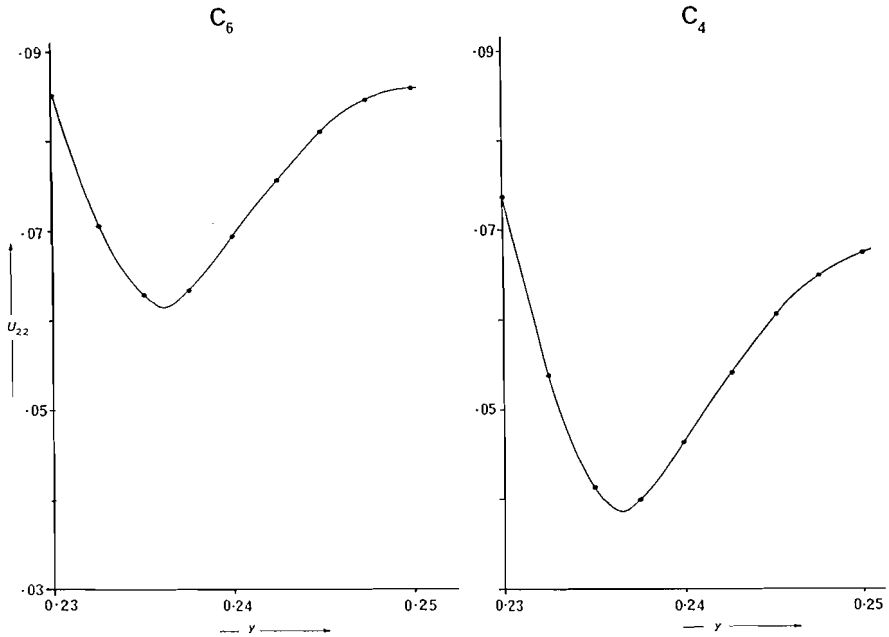

FIG 2. Plots of U_{22} versus the distance from the mirror plane (y, Å) for C(4) and C(6).

TABLE 4. Comparison of bond lengths and angles around tin in 1,3,2-dioxastannolanes and 1,3,2-dioxastannanes[a]

Parameter	Coordinate number of tin	Bond length (Å) on bond angle (deg)				
		Polymers		Pentamer	Dimers	
		1	**2**[b]	**3**[c]	**4**[d]	**5**[e]
Intramonomer	5			79.1(5), 80.7(7)	80.5(3)	79.7(3)
O—Sn—O	6	93.2(2)	79.0(5)	77.6(5)--78.3(5)		
Intermonomer	5–5				68.2(3)	67.4(4)
O—Sn—O	5–6			69.6, 70.6		
(inside 4-membered ring)	6–6	66.5(2)	66.0(6)	65.5--69.2		
Intercyclic	5			146.9, 149.0	148.6(3)	147.3(4)
O—Sn—O	6	158.7(2)	149.0(6)	143.9--145.2		
Exocyclic	5			127.4(13), 124.2(8)	128.5(5), 133.1(5)	125.0(5)
C—Sn—C	6	138.4(3)	138.6(6)	134.7(9)--142.7(8)		
Intramonomer	5			2.02(4)--2.07(4)	2.071(7)	2.063(7)
Sn—O	6	2.036(6)	2.04(1)	2.06(5)--2.13(5)		
Intermonomer	5			2.23--2.27	2.233(7)	2.249(7)
Sn—O	6	2.562(6)	2.51(2)	2.43--2.60		
Exocyclic	5			2.04(3)--2.25(8)	2.105(14)	2.186(7)
Sn—C	6	2.139(8)	2.14(2)	2.06(5)--2.13(5)		

[a]Where values reported are averages, the uncertainty reported is an average of the reported uncertainties.
[b]Reference 9.
[c]Reference 8.
[d]Reference 6*b*.
[e]Reference 21.

O—Sn—O bond angle in the six-membered ring is 14.2° larger and, as a result, the *trans*-O—Sn—O bond angle is also larger by 9.7°. These differences in the O—Sn—O bond angles in the two rings arise from the constraints imposed by closure of rings containing two long Sn—O bonds.

More extensive differences can be noted between the bond angles and lengths for five-coordinate tin centres when compared with those of six-coordinate centres. The magnitudes of exocyclic C—Sn—C bond angles at pentacoordinate tin centres in more highly substituted 1,3,2-dioxastannolanes, ranging from 124.2 to 133.1° (6, 8, 9), are about 10° smaller than those at hexacoordinate tin centres, which range from 134.7 to 142.7° (7, 8). This difference reflects the fact that the butyl groups are equatorial in the distorted trigonal bipyramid of five-coordinate tin and should be separated by 120° whereas the ideal separation for six-coordinate tin is 180°. The other major difference lies in the intermonomer Sn—O bond lengths, 2.23–2.27 Å for pentacoordinate tin (6, 8, 9) and 2.43–2.60 Å for hexacoordinate tin (7, 8). The larger bond lengths for hexacoordinate tin may be a response to the greater crowding about the more substituted centre.

Can. J. Chem. Downloaded from www.nrcresearchpress.com by 123.30.183.119 on 09/08/12
For personal use only.

TABLE 5. Chemical shifts for **1** (ppm)

Conditions		T	^{119}Sn			^{13}C					
								Butyl carbons			
Phase	Solvent	(°C)	Dimer	Trimer		C-4	C-5	C-α	C-β	C-γ	Me
Solution	$CDCl_3$	20	−193.5			66.7	36.9	21.9	27.0	27.5	13.7
Solution	$CDCl_3$	−65	−187.8	−195.1	−346.1	66.7, 66.3	36.5, 36.0, 35.4	26.7, 20.2	27.4	27.6	13.9
Solution	$CDCl_3$:CD_2Cl_2 2:1	20	−191.6			66.5	36.7	21.8[a]	26.9	27.4	13.5
Solution	$CDCl_3$:CD_2Cl_2 2:1	−85	−186.6	−194.2	−344.7[b]	66.5, 65.8	36.1, 34.7	27.0, 19.8[c]	27.3	27.5	13.8
Solution	Toluene-d_8	20	−234.1			66.7	37.0	21.8	27.0	27.5	13.6
Solid			−279.5, −281.8[d]								

[a] $^1J_{Sn,C}$ = 641 Hz.
[b] Also present in this spectrum were signals of the tetramer at −200.9 and −333.1 ppm.
[c] $^1J_{Sn,C}$ = 613 Hz.
[d] Polymer.

Solution nuclear magnetic resonance spectral results

The 134.6 MHz ^{119}Sn nmr spectra of **1** at 20°C consisted of one broad peak with a chemical shift of −193.5 ppm for a 0.41 M solution in chloroform-*d* and −234.1 ppm for a 0.38 M solution in toluene-d_8. The peak had a half-height linewidth of 1340 Hz in the chloroform-*d* solution at 20°C and it gradually narrowed to 810 Hz as the temperature was raised to 80°C but did not change position much (−199.4 ppm at 80°C). The peak in the spectrum from the toluene-d_8 solution shifted to −214.8 ppm on warming to 80°C and also narrowed (1200 to 375 Hz). When the temperature was lowered to about 10°C, the single peak in the chloroform-*d* spectrum divided into two, one with a shift close to the 20°C chemical shift and a second near −340 ppm that was smaller and broader. Further decrease in temperature caused the small peak to sharpen but the larger peak split again at about −45°C into two peaks having unequal intensities, with the less intense one being less shielded. The low temperature shifts are listed in Table 5. All three peaks sharpened as the temperature was lowered further but the smallest peak, at −187.8 ppm, remained broad, with a linewidth of 630 Hz and at a temperature of −65°C, at which the adjacent peak, at −195.1 ppm, had a linewidth of 72 Hz. Integrations of the two major peaks at −195 and −346 ppm at temperatures below −55°C where both were reasonably sharp showed that the intensity of the former was twice that of the latter (±10%). Of possible species, only a trimer contains two pentacoordinate tin atoms related by C_2 symmetry and one hexacoordinate tin atom. Therefore, it was concluded that the major species present at low temperature was a trimer.

The broad peak at −187.8 ppm lies in the region of the ^{119}Sn nmr spectrum where pentacoordinate tin atoms absorb and it can be assigned to a dimer. The dimer peak is broad at −65°C mainly because the dimer is still exchanging with a third species at this temperature as discussed below.

A 0.3 M sample of **1** in a 2:1 mixture of chloroform-*d* and dichloromethane-d_2 was prepared, to extend the study to lower temperatures. The ^{119}Sn spectra of this sample were very similar to those of the chloroform-*d* solutions at temperatures from 20 to −65°C (see Fig. 3). In spectra recorded at −75 to −95°C, the peak assigned to the dimer was sharper and two additional equal intensity peaks appeared at −200.9 and −333.1 ppm (chemical shifts at −85°C). A tetramer of **1** has C_2 symmetry and would give a ^{119}Sn nmr spectrum having this combination of two equal intensity peaks with the chemical shifts observed. Therefore, it is concluded that the tetramer is the species whose signals appear at temperatures lower than −65°C and exchange of a low concentration of the tetramer with the dimer causes the dimer signal to be broad at the lowest temperature accessible for chloroform-*d* solutions of **1** (see Fig. 4).

The ^{13}C nmr spectra of **1** are consistent with the conclusions drawn above. The spectra at room temperature and above are simple, having the number of signals expected for a monomer. Three signals show marked changes with variation in temperature which are similar in both chloroform-*d* and the mixed solvent system. The butyl C-α signal at 21.8 ppm in the mixed solvent spectra broadened as the temperature was lowered and split at about −20°C into two peaks, one at 19.8 ppm at −85°C, the other obscured by the butyl C-β and C-γ signals between 26.6 and 27.7 ppm. The average signal from the spectrum at 20°C had a $^1J_{Sn,C}$ value of 641 Hz and the signal at 19.8 ppm at −85°C had a $^1J_{Sn,C}$ value of 613 Hz. The magnitude of $^1J_{Sn,C}$ has been related to the size of the C—Sn—C bond angle, increasing with increasing angle size for both butyltin(IV) (23) and methyltin(IV) derivatives (24). C—Sn—C bond angles are larger about hexacoordinate tin than pentacoordinate tin in crystal structures containing dialkoxydialkyltin derivatives (6–9). Because the $^1J_{Sn,C}$ value for the room temperature peak, which is an average of values for pentacoordinate and hexacoordinate tin nuclei, was larger than the value for the peak at 19.8 ppm at −85°C, the peak at 19.8 ppm can be assigned to C-α for butyl groups on pentacoordinate tin.

The relationship obtained for butyltin(IV) derivatives, $^1J_{Sn,C} = 9.99\theta - 746$ Hz, was derived from a relatively small number of points (23). For a J value of 613 Hz, it gives a value of the C—Sn—C bond angle of 136.0°. The relationship obtained for methyltin(IV) derivatives, $^1J_{Sn,C} = 10.7\theta - 778$ Hz, was derived from an extensive set of data (24). It yields a value for the C—Sn—C bond angle of 130.4°. The

Can. J. Chem. Downloaded from www.nrcresearchpress.com by 123.30.183.119 on 09/08/12
For personal use only.

Can. J. Chem. Downloaded from www.nrcresearchpress.com by 123.30.183.119 on 09/08/12
For personal use only.

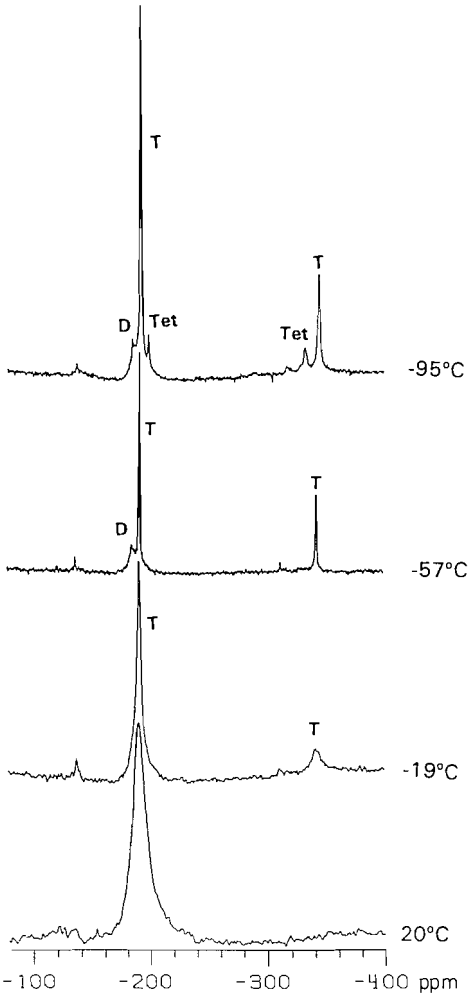

FIG 3. ^{119}Sn nmr spectra (134.6 MHz) of a 0.30 M solution of 2,2-dibutyl-1,3,2-dioxastannane (**1**) in a 2:1 mixture of chloroform-*d* and dichloromethane-d_2 at various temperatures. Labels: D, dimer peak; T, trimer peak; Tet, tetramer peak.

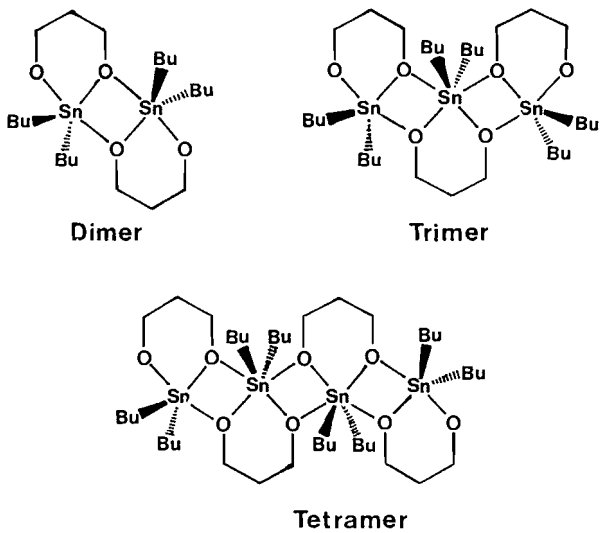

FIG. 4. Structures of those oligomeric species of 2,2-dibutyl-1,3,2-dioxastannane (**1**) observed in solution

X-ray C—Sn—C bond angle for **1** in which the tin atom is hexacoordinate in a polymer is 138.3(3)°, close to the average of C—Sn—C bond angles at hexacoordinate tin atoms in 1,3,2-dioxastannolanes (138.1 ± 3.0°) (7, 8). The average of C—Sn—C bond angles at pentacoordinate tin atoms in 1,3,2-dioxastannolanes is 127.8 ± 5.1° (6*b*, 8, 9). All structural features of analogous polymeric 1,3,2-dioxastannolanes and 1,3,2-dioxastannanes, i.e., **2** and **1**, are almost identical except for O—Sn—O bond angles in the five- and six-membered rings and directly related angles. Thus, the magnitude of the C—Sn—C bond angle for pentacoordinate tin atoms in the trimer of **1** is probably close to that of the same angle in the 1,3,2-dioxastannolanes, 127.8°. The relationship between $^1J_{Sn,C}$ and C—Sn—C bond angle derived for methyltin(IV) derivatives (24) appears to give an answer for **1** closer to this value than does the equation derived from a limited number of butyltin derivatives (23), suggesting that these relationships are independent of the nature of the alkyl group.

The peak at 36.7 ppm at 20°C in the mixed solvent splits at about −50°C into two major peaks at 36.1 and 34.7 ppm at −85°C with intensities in the ratio of about 2:1, respectively. Similarly, the peak at 66.5 ppm from the spectrum from the mixed solvent solution at 20°C splits at about −57°C into two peaks with chemical shifts of 66.5 and 65.8 ppm at −85°C having intensity ratios of about 2:1. It was concluded from the ^{119}Sn nmr spectra that the trimer was the major species present in solution at −85°C. The observation of two sets of signals present in 2:1 intensity ratios is consistent with a trimer, which consists of a central monomer unit containing hexacoordinate tin flanked by two equivalent monomer units containing pentacoordinate tin.

The coalescence temperatures for the signals at 36.7 ppm and 66.5 ppm at −50 ± 5°C and −57 ± 5°C and chemical shift differences of 56.1 and 126.9 Hz, respectively, were used to calculate rate constants at coalescence of 191.1 and 84.5 s^{-1}, respectively, by means of the method of Shanan-Atidi and Bar-Eli for unequally populated sites (25). Fractional populations for the two sites of 0.67 and 0.33 were used. Free energies of activation of 10.6 ± 0.2 and 10.6 ± 0.3 kcal mol^{-1} were obtained for coalescence at the two sites. The coalescence at 10 ± 5°C of the trimer hexacoordinate peak and its pentacoordinate peak, which have shifts of −344.0 and −194.6 ppm at −20°C, respectively, can be calculated in exactly the same way to have an activation energy of 10.8 ± 0.3 kcal mol^{-1}. These activation energies are slightly smaller than the comparable values of 12.1 ± 0.1 kcal mol^{-1} obtained for the dimer ⇄ trimer barrier for the 2,2-dibutyl-1,3,2-dioxastannolane derivative obtained from (*S*,*S*)-1,2-cyclohexanediol, (1*S*,6*S*)-8,8-dibutyl-7,9,8-dioxastannabicyclo[4.3.0]nonane (**6**) (11).

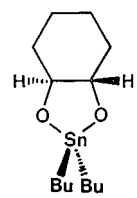

6

The activation barrier for the dimer ⇄ tetramer interchange appears to be considerably smaller for **1** than for the

Can. J. Chem. Downloaded from www.nrcresearchpress.com by 123.30.183.119 on 09/08/12
For personal use only.

1,3,2-dioxastannolanes, such as **2**, where coalescence for this process occurs simultaneously with that for the dimer ⇄ trimer process. The rate constant for a particular process is directly related to the chemical shift difference between the exchanging sites. Therefore, a rough estimate of the activation barrier for the dimer ⇄ tetramer interchange for **1** can be made from the ratio of the coalescence temperatures for the two processes occurring for **1** since the chemical shift differences are about the same for both. A value of 7.7 kcal mol^{-1} is obtained.

Integration of the trimer and dimer signals in the ^{119}Sn nmr spectra in chloroform-*d* allowed evaluation of the free energy difference for the dimer ⇄ trimer equilibrium. An equilibrium constant $K = [trimer]^2/[dimer]^3$ can be defined for the following equilibrium:

[1] 3Dimer ⇄ 2Trimer

Integrations of the spectra were performed at 208 and 213 K. The equilibrium constants, $K = [trimer]^2/[dimer]^3$, of 310 and 485, gave values of ΔG^0 of −2.4 and −2.6 kcal mol^{-1}, respectively, which yielded an average value of ΔG^0 of -2.5 ± 0.2 kcal mol^{-1} at 210 K. This value is somewhat smaller than that obtained for the same equilibrium for the dimers and trimers of **2**, -3.3 ± 0.1 kcal mol^{-1} at 200 K, obtained by the integration of spectra from a wide range of temperatures (11) for a 0.072 M solution in a 3:2 mixture of chloroform-*d* and dichlorofluoromethane. If the entropy term is the same as obtained earlier (11) for **2**, −27.6 cal mol^{-1} deg^{-1}, ΔH^0 for the equilibrium for **1** is −8.3 kcal mol^{-1}, very similar to the value of -8.8 ± 1.8 kcal mol^{-1} obtained for **2**.

The same procedure was performed on the mixed solvent spectra at 198 and 188 K, except that two equilibria could now be evaluated:

[1] 3Dimer ⇄ 2Trimer

[2] 2Dimer ⇄ Tetramer

For equilibria [1] and [2], ΔG^0 values at 193 K obtained by averaging the values at 198 and 188 K were −2.4 and −1.5 kcal mol^{-1}, respectively. For compounds **2** and **6**, the ΔG^0 values for equilibrium [2] at 200 K were 0.8 and 0.6 kcal mol^{-1}, respectively, algebraically greater than that measured for equilibrium [1] but similar to the difference in values for the two equilibria measured for **1** here.

The average chemical shifts observed by Smith *et al.* in a saturated chloroform-*d* solution at room temperature and neat at 96°C of −228 and −288 ppm, respectively, suggest that extensive oligomerization occurs under these conditions (17). If the chemical shifts from −65°C are used and it is assumed that only dimer and trimer are present, it can be calculated that the mole fraction of trimer is 0.70 for the chloroform-*d* solution. Probably the mixture present contained significant amounts of tetramer and perhaps higher oligomers. The chemical shift of −234 ppm observed for a 0.38 M solution of **1** at 20°C in toluene-d_8 here suggests more extensive oligomerization. The tendency of 1,3,2-dioxastannolanes to favour higher oligomers in less polar solvents had been noted previously (12). The shift to a less shielded position on heating is due to the expected (11) shift in the equilibria towards lower oligomers.

The mixture of species present in the neat liquid at 96°C (17) probably includes still higher oligomers. The average

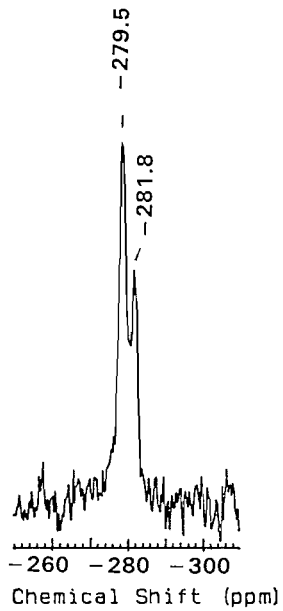

FIG. 5. Expansion of the isotropic peaks in the 74.6 MHz CP/MAS ^{119}Sn nmr spectrum of solid, 2,2-dibutyl-1,3,2-dioxastannane (**1**) spun at 4 kHz.

chemical shifts for the trimer and tetramer are −244.4 and −267.0 ppm from the mixed solvent data, both considerably less shielded than the signal from the neat liquid at −288 ppm. In the solid state, the average chemical shift for the polymer is −280 ppm and solution and solid-state ^{119}Sn chemical shifts are normally very similar (±5 ppm) (10, 26). Large variations in ^{119}Sn nmr chemical shifts with temperature preclude precise definition of the species present but average values more negative than −280 ppm would be expected for higher oligomers than the pentamer.

The ^{119}Sn nmr chemical shifts of **1** are 60–70 ppm more shielded than those for comparable species of its five-membered ring analogue, **2** (11) and 20–30 ppm more shielded than those for acyclic dibutyltin dialkoxide derivatives (17). Similar trends have been observed for tetraalkyltin and lead derivatives (16*d*).

Nuclear magnetic resonance spectral results for the solid

Static and CP/MAS ^{119}Sn nmr spectra of crystalline **1** were measured (10). An expansion of the region of the CP/MAS spectrum containing the isotropic peaks is shown in Fig. 5. Two isotropic peaks were observed close together at −279.5 and −281.8 ppm. These chemical shifts are in the region of the ^{119}Sn chemical shift range expected for hexacoordinate tin but are considerably less shielded than the hexacoordinate tin nuclei of **1** in trimers or tetramers in solution. Similar deshielding of hexacoordinate tin nuclei on moving from low oligomers to higher oligomers and polymers have been noted for tin atoms in 1,3,2-dioxastannolanes (10).

The observation of two peaks is probably due to the 1:1 disorder of C-5 in the crystal. Slightly different environments for tin atoms will arise depending on the orientations of the C-5 atoms in the neighbouring rings. If a particular tin nucleus in a 1,3,2-dioxastannane ring is considered, the C-5 atoms in adjacent rings can both be above the mirror plane of the molecule, both below, or one above and one below in a statistical ratio of 1:1:2, respectively. Three peaks are predicted with intensities in that ratio. The observation of only

two peaks indicates that the magnitude of the effect is small probably because the structural differences are five atoms away from the affected tin atom.

Conclusions

2,2-Dibutyl-1,3,2-dioxastannane (**1**) exists in the crystal as a polymer in which the individual monomer units are joined together by Sn—O bonds which are about 25% longer than those inside the monomer units. The tin atoms are present in highly distorted octahedral coordination. In liquid phases, compound **1** is present as mixtures of oligomers ranging from the dimer to high oligomers with compositions that vary widely depending on temperature and concentration. The tendency to form oligomers containing hexacoordinate tin for **1** is slightly less than that for 2,2-dibutyl-1,3,2-dioxastannolane (**2**) probably because the Sn—O—Sn bond angle inside the monomer ring for **1** is 93.2°, whereas that for **2** is 79.0°. The ^{119}Sn nmr chemical shifts of **1** are about 60–70 ppm more shielded than the five-membered ring analogue **2**, and 20–30 ppm more shielded than acyclic derivatives.

Acknowledgements

T.S.C. and T.B.G. are grateful to NSERC for financial support. We thank the Atlantic Region Magnetic Resonance Centre for nmr time and Dr. R. E. Wasylishen and W. P. Power for nmr spectra of solids.

1. D. Wagner, J. Verheyden, and J. G. Moffat. J. Org. Chem. **39**, 24 (1974); S. David. C. R. Acad. Sci. Ser. C, **278**, 1051 (1974).
2. S. David and S. Hanessian. Tetrahedron, **41**, 643 (1985); M. Pereyre, J.-P. Quintard, and A. Rahm. Tin in organic synthesis. Butterworths, London. 1987. Chapt. 11; S. J. Blunden, P. A. Cusak, and P. J. Smith. J. Organomet. Chem. **325**, 141 (1987).
3. G. Reginato, A. Ricci, S. Roelens, and S. Scapecchi. J. Org. Chem. **55**, 5132 (1990); A. Dureault, M. Portal, and J. C. Depezay. Synlett. **4**, 225 (1991).
4. S. David and A. Thieffry. J. Chem. Soc. Perkin Trans. 1, 1568 (1979); T. B. Grindley and R. Thangarasa. Carbohydr. Res. **172**, 311 (1988).
5. S. David, A. Thieffry, and A. Veyrières. J. Chem. Soc. Perkin Trans. 1, 1796 (1981).
6. (*a*) S. David, C. Pascard, and M. Cesario. Nouveau J. Chim. **3**, 63 (1979); (*b*) T. S. Cameron, P. K. Bakshi, R. Thangarasa, and T. B. Grindley. Can. J. Chem. To be published.
7. P. A. Bates, M. B. Hursthouse, A. G. Davies, and S. D. Slater. J. Organomet. Chem. **363**, 45 (1989).
8. C. W. Holzapfel, J. M. Koekemoer, C. F. Marais, G. J. Kruger, and J. A. Pretorius. S. Afr. J. Chem. **35**, 80 (1982).
9. A. G. Davies, A. J. Price, H. M. Dawes, and M. B. Hursthouse. J. Chem. Soc. Dalton Trans. 297 (1986).
10. T. B. Grindley, R. E. Wasylishen, R. Thangarasa, W. P. Power, and R. D. Curtis. Can. J. Chem. **70**, 205 (1992).
11. T. B. Grindley and R. Thangarasa. J. Am. Chem. Soc. **112**, 1364 (1990).
12. T. B. Grindley and R. Thangarasa. Can. J. Chem. **68**, 1007 (1990).
13. R. Thangarasa and T. B. Grindley. Organometallics. To be published.
14. J. C. Pommier, E. Mendes, J. Valade, and J. Housty. J. Organomet. Chem. **55**, C19 (1973).
15. R. C. Mehrotra and V. D. Gupta. J. Organomet. Chem. **4**, 145 (1965).
16. (*a*) B. Wrackmeyer. Annu. Rep. NMR Spectrosc. **16**, 73 (1985); (*b*) P. J. Smith and A. P. Tupciauskas. Annu. Rep. NMR Spectrosc. **8**, 291 (1978); (*c*) V. S. Petrosyan. Prog. NMR Spectrosc. **11**, 115 (1977); (*d*) J. D. Kennedy and W. McFarlane. *In* Multinuclear NMR spectroscopy. *Edited by* J. Mason. Pergamon Press, Oxford. 1988. p. 305; (*e*) R. K. Harris, P. Reams, and K. J. Packer. J. Mol. Struct. **141**, 13 (1986); (*f*) N. J. Clayden. Chem. Scr. **28**, 211 (1988).
17. P. J. Smith, R. F. M. White, and L. Smith. J. Organomet. Chem. **40**, 341 (1972).
18. J. D. Kennedy. J. Chem. Soc. Perkin Trans. 2, 242 (1977).
19. G. M. Sheldrick. SHELX. A system of computer programs for crystal structure determination. Cambridge University, Cambridge, U.K. 1976; G. M. Sheldrick. *In* Crystallographic Computing 3. *Edited by* G. M. Sheldrick, C. Kruger, and R. Goddard. Oxford University Press. Oxford, U.K. 1985. pp. 175–189.
20. N. Walker and D. N. Stuart. Acta Crystallogr. **A39**, 158 (1983).
21. International Tables for X-ray crystallography. Vol. IV. Kynoch Press, Birmingham, U.K. 1974.
22. J. R. Carruthers and D. L. Watkins. Crystals, Issue 8 (revised 1989), Chemical Crystallography Laboratory, Oxford, U.K. 1984.
23. J. Holeček and A. Lyčka. Inorg. Chim. Acta, **118**, L15 (1986); J. Holeček, M. Nádvorník, K. Handlíř, and A. Lyčka. J. Organomet. Chem. **315**, 299 (1986).
24. T. P. Lockhart and W. F. Manders. J. Am. Chem. Soc. **109**, 7015 (1987).
25. H. Shanan-Atidi and K. H. Bar-Eli. J. Phys. Chem. **74**, 961 (1970).
26. T. B. Grindley, R. D. Curtis, R. Thangarasa, and R. E. Wasylishen. Can. J. Chem. **68**, 2102 (1990).

Can. J. Chem. Downloaded from www.nrcresearchpress.com by 123.30.183.119 on 09/08/12
For personal use only.

Tin-119 NMR of 1,3,2-dioxastannolanes and a 1,3,2-dioxastannane in the solid state

T. Bruce Grindley,[1] Roderick E. Wasylishen,[1] Rasiah Thangarasa, William P. Power, and Ronald D. Curtis

Department of Chemistry, Dalhousie University, Halifax, N.S., Canada B3H 4J3

Received June 25, 1991

T. Bruce Grindley, Roderick E. Wasylishen, Rasiah Thangarasa, William P. Power, and Ronald D. Curtis. Can J. Chem. **70**, 205 (1992).

The cross-polarized static and high-resolution magic angle spinning ^{119}Sn NMR spectra of a number of 2,2-dialkyl-1,3,2-dioxastannolanes and one 1,3,2-dioxastannane have been measured in the solid state. For the four compounds on which X-ray studies had been performed, the numbers and positions of the isotropic peaks in the high-resolution spectra were related to the number of tin sites present and the state of oligomerization of the compounds. The chemical shifts of hexacoordinate Sn nuclei are 35–80 ppm larger in polymeric solids than for the same compounds in solution where the compounds exist as trimers and tetramers. States of oligomerization for solids that had not been previously studied by X-ray crystallography were determined using CP/MAS ^{119}Sn NMR spectroscopy. The principal components of the ^{119}Sn chemical shift tensors were obtained from the static spectra and used to calculate chemical shift anisotropies and asymmetry parameters. The values of the chemical shift anisotropies ranged from 600 to 800 ppm for 1,3,2-dioxastannolanes but the value for a 1,3,2-dioxastannane was larger, 919 ppm. The chemical shift anisotropies measured directly from the solid-state powder patterns are in excellent agreement with the values derived from previous variable temperature spin-lattice relaxation measurements in solution when the same oligomer was present in both states. Our results support our previous conclusion that the antisymmetric terms of the chemical shift tensor make a small or negligible contribution to the rate of ^{119}Sn spin-lattice relaxation in these compounds.

Key words: 1,3,2-dioxastannolanes, stannylene acetals, ^{119}Sn NMR, ^{119}Sn NMR of solids, ^{119}Sn chemical shift anisotropy.

T. Bruce Grindley, Roderick E. Wasylishen, Rasiah Thangarasa, William P. Power et Ronald D. Curtis. Can J. Chem. **70**, 205 (1992).

Opérant à l'état solide, on a mesuré les spectres RMN du ^{119}Sn, statiques avec polarisation croisée et tournant, à haute résolution, à l'angle magique, d'un certain nombre de 2,2-dialkyl-1,3,2-dioxastannolanes et d'un 1,3,2-dioxastannane. Pour les quatre composés pour lesquels on a déterminé des structures par diffraction des rayons-X, on a pu relié les nombres et les positions des pics isotropes dans les spectres à haute résolution avec le nombre des sites d'étain présents et l'état d'oligomérisation des composés. Les déplacements chimiques des noyaux de Sn hexacoordonnés sont de 35 à 80 ppm plus grands dans les polymères solides que dans les mêmes composés en solution alors que les composés existent sous la forme de trimères ou de tétramères. Faisant appel à la RMN du ^{119}Sn par CP/MAS, on a déterminé les états d'oligomérisation des solides que l'on n'avait pas étudiés antérieurement par diffraction des rayons-X. En se basant sur les spectres statiques, on a obtenu les principales composantes des tenseurs des déplacements chimiques du ^{119}Sn et on les a utilisées pour calculer les anisotropies des déplacements chimiques et les paramètres d'asymétrie. Pour les 1,3,2-dioxastannolanes, les valeurs des anisotropies des déplacements chimiques varient de 600 à 800 ppm; toutefois, pour un 1,3,2-dioxastannane, cette anisotropie est plus élevée, soit 919 ppm. Lorsque le même oligomère est présent dans les deux états, les anisotropies des déplacements chimiques mesurés directement à partir des patrons de poudres à l'état solide sont en très bon accord avec les valeurs obtenues à partir de mesures antérieures de relaxation spin-réseau à températures variables, en solution. Nos résultats supportent notre conclusion antérieure à l'effet que les contributions des termes antisymétriques du tenseur du déplacement chimique à la vitesse de relaxation spin-réseau du ^{119}Sn dans ces composés ne sont que faibles ou négligeables.

Mots clés : 1,3,2-dioxastannolanes, acétals de stannylène, RMN du ^{119}Sn, RMN du ^{119}Sn dans des solides, anisotropie du déplacement chimique du ^{119} Sn.

[Traduit par la rédaction]

Introduction

Tin-119 NMR spectroscopy has become established as a standard technique for evaluating the structures, reactions, and bonding of tin-containing compounds (1). There is now increasing interest in solid-state ^{119}Sn NMR spectroscopy to evaluate bonding at tin and also to provide a bridge between X-ray crystallographic results and solution NMR studies (2–10). A variety of compounds have been examined, including inorganic tin compounds (2), tetraalkyl or aryl tin compounds (3–5), organotin halides (3–6), organotin oxides, hydroxides, and sulfides (3, 4, 7), esters (3, 4, 8), and others (9, 10). Most investigators have only reported the isotropic chemical shift, δ_{iso}, obtained from CP/MAS measurements, even though it is possible to obtain the three principal components of the chemical shift tensor from solid-state NMR studies.

The compounds examined in this publication are 1,3,2-dioxastannolanes and 1,3,2-dioxastannanes, typical examples of the tin-containing intermediates employed in the widely used stannylene reaction (11). We have shown that these compounds are present in solution as dimers and (or) higher oligomers in which the tin atoms are pentacoordinate or hexacoordinate (12, 13). Tin-119 chemical shift ranges have been established for tin nuclei in 2,2-dibutyl-1,3,2-dioxastannolanes; pentacoordinate tin nuclei absorb in the region from −100 to −150 ppm with respect to tetramethyltin, while hexacoordinate tin nuclei absorb between −230 and −300 ppm in solution (12, 13).

We recently measured the ^{119}Sn NMR spin-lattice relax-

[1]Authors to whom correspondence may be addressed.

Can. J. Chem. Downloaded from www.nrcresearchpress.com by 123.30.183.119 on 09/08/12
For personal use only.

Can. J. Chem. Downloaded from www.nrcresearchpress.com by 123.30.183.119 on 09/08/12
For personal use only.

ation rates in solution for a number of 1,3,2-dioxastannolanes in which the tin atoms were in either pentacoordinate or hexacoordinate environments (14). The relaxation times in these compounds were short and the major mechanism of spin-lattice relaxation at 8.48 T was due to chemical shift anisotropy. The magnitudes of the chemical shift anisotropies were obtained from variable temperature solution spin-lattice relaxation data at 4.70 and 8.48 T. For one compound, methyl 4,6-*O*-benzylidene-2,3-*O*-dibutylstannylene-α-D-glucopyranoside (**1**), the principal components of the ^{119}Sn chemical shift tensor for the pentacoordinate site in its dimeric structure were determined directly from the static ^{119}Sn NMR spectrum of a powdered sample. The chemical shift anisotropy (CSA) determined from the solid-state experiments, 748 ± 20 ppm, was in good agreement with the value obtained from the solution T_1 data, 720 ± 50 ppm. This result is significant in that it suggests that the antisymmetric components of the ^{119}Sn chemical shielding tensor of **1** make a small or negligible contribution to the rate of spin-lattice relaxation. For compounds containing both pentacoordinate and hexacoordinate tin atoms, the solution ^{119}Sn spin-lattice relaxation data indicate that the tin chemical shift anisotropies for the hexacoordinate sites are approximately 1.5 times those of the pentacoordinate sites. This was a rather surprising result in view of the fact that the pseudo-octahedral environment of a hexacoordinate tin site has potentially high local symmetry. We decided to examine the solid-state ^{119}Sn NMR spectra of a number of other compounds containing five- or six-coordinate tin atoms in order to test the generality of the above conclusion. Furthermore, we were interested in comparing the ^{119}Sn chemical shift anisotropies measured directly in the solid state with those determined from earlier solution spin-lattice relaxation measurements. If these values are similar, the antisymmetric elements of the chemical shift tensors are probably insignificant.

Theory

The complete magnetic shielding tensor in the principal axis system (PAS) can be expressed as a sum of symmetric and antisymmetric tensors (15):

$$\sigma^{s}_{PAS} = \begin{pmatrix} \sigma_{11} & 0 & 0 \\ 0 & \sigma_{22} & 0 \\ 0 & 0 & \sigma_{33} \end{pmatrix} \text{ and}$$

$$\sigma^{a}_{PAS} = \begin{pmatrix} 0 & \sigma_{12} & \sigma_{13} \\ -\sigma_{12} & 0 & \sigma_{23} \\ -\sigma_{13} & -\sigma_{23} & 0 \end{pmatrix}$$

NMR measurements of a static powder sample in the solid state yield information concerning the principal components of the chemical shielding tensor (σ_{ii}, i = 1–3). To first order the antisymmetric tensor does not contribute to the NMR lineshape (16, 17). Any contribution that the antisymmetric terms make to the overall lineshape is expected to be small and would probably escape detection except possibly in careful single-crystal NMR studies of heavy nuclei that have enormous chemical shift ranges (17). The reader is referred to a recent paper by Ding and Ye for a complete discussion (18).

The contribution that the antisymmetric terms make to the rate of CSA relaxation in solution NMR studies is expected to be more profound. Blicharski (19) and other workers (17, 20) have shown that for relaxation by the CSA mechanism

$$[1] \quad \frac{1}{T_1} = \omega_0^2\left(\frac{2}{3}A^2\frac{\tau_1}{1+\omega_0^2\tau_1^2} + \frac{2}{15}S^2\frac{\tau_2}{1+\omega_0^2\tau_2^2}\right)$$

and

$$[2] \quad \frac{1}{T_2} = \omega_0^2\left(\frac{1}{3}A^2\frac{\tau_1}{1+\omega_0^2\tau_1^2} + \frac{1}{15}S^2\left(\frac{4}{3}\tau_2 + \frac{\tau_2}{1+\omega_0^2\tau_2^2}\right)\right)$$

where

$$A^2 = (\sigma^a_{12})^2 + (\sigma^a_{13})^2 + (\sigma^a_{23})^2 \text{ and}$$

$$S^2 = (\Delta\sigma)^2\left(1 + \frac{1}{3}\eta^2\right)$$

Here, $\Delta\sigma = (\sigma_{11} + \sigma_{22})/2 - \sigma_{33}$ and $\eta = (\sigma_{22} - \sigma_{11})/(\sigma_{33} - \sigma_{iso})$, where $\sigma_{iso} = (\sigma_{11} + \sigma_{22} + \sigma_{33})/3$.

For molecules that undergo small-step isotropic rotational diffusion, $\tau_1 = 3\,\tau_2$, and eqs. [1] and [2] become

$$[3] \quad \frac{1}{T_1} = \omega_0^2\left(2A^2\frac{\tau_2}{1+\omega_0^2(3\tau_2)^2} + \frac{2}{15}S^2\frac{\tau_2}{1+\omega_0^2\tau_2^2}\right)$$

$$[4] \quad \frac{1}{T_2} = \omega_0^2\left(A^2\frac{\tau_2}{1+\omega_0^2 9\tau_2^2} + \frac{1}{15}S^2\left(\frac{4}{3}\tau_2 + \frac{\tau_2}{1+\omega_0^2\tau_2^2}\right)\right)$$

The first point of interest is that eqs. [3] and [4] predict that T_2 can exceed T_1. In fact, in the limit where the antisymmetric terms dominate, $T_2 = 2T_1$. In contrast, if the antisymmetric terms do not contribute to CSA relaxation, then eqs. [3] and [4] indicate that $T_2 = (6/7)T_1$.

In ^{59}Co NMR studies of a series of pseudo-octahedral Co(III) complexes, Eaton and co-workers found that $T_2 > (6/7)T_1$ and implicated the antisymmetric terms as being responsible (21). More recently, Anet *et al.* (22) found that the ^{13}C T_2 value in tetrachlorocyclopropene is greater than T_1 and argued that the antisymmetric terms of σ must be responsible. The importance of the antisymmetric terms in this compound was predicted by *ab initio* IGLO calculations (23).

First, we would like to point out that compounds **1**, **2**, and **5** are excellent candidates to use to evaluate the importance of the antisymmetric terms. The mechanism for relaxation is the CSA mechanism (14) and the tin sites in these compounds lack any symmetry. Note that if a site has symmetry greater than C_{2v}, the antisymmetric terms disappear (24). Very similar chemical shifts in solution and from the solid state suggest that the structures of compounds **1**, **2**, and **5** are similar in both media.

The approach that we have taken here is to first assume that the antisymmetric terms do not contribute to T_1, i.e.,

$$[5] \quad \frac{1}{T_1} = \frac{2}{15}\omega_0^2 S^2\frac{\tau_2}{1+\omega_0^2\tau_2^2}$$

and evaluate S^2 from the T_1 minimum (14). We then compare this $\Delta\sigma$ (or S^2) with that measured directly in the solid state. If the two values are the same within experimental error, we suggest that the antisymmetric terms make a negligible contribution to the rate of relaxation. Note that on the basis of eq. [3], the antisymmetric term is much more heav-

Can. J. Chem. Downloaded from www.nrcresearchpress.com by 123.30.183.119 on 09/08/12
For personal use only.

ily weighted than the symmetric term (a factor of 15 under conditions of extreme narrowing).

Experimental

Solution ^{119}Sn and ^{13}C NMR spectra were recorded on a Nicolet NT-360 NB NMR spectrometer at 8.48 T (134.62 MHz). Solution data were referenced with respect to external tetramethyltin or tetramethylsilane, respectively. The 1,3,2-dioxastannolanes were prepared from the appropriate diols and a dialkyltin oxide as described previously (12, 13). The diols used for preparation of the 2,2-dibutyl-1,3,2-dioxastannolane derivatives were prepared as described elsewhere (diols for compounds **1–5**, refs. 12, 13, and 25) or were commercial compounds (diols for compounds **6–9**).

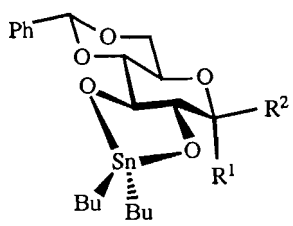

1 R^1 = OMe R^2 = H
2 R^1 = H R^2 = OCH_2Ph

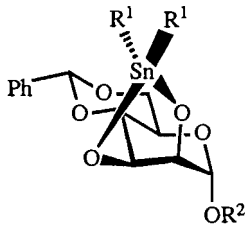

3 R^1 = Bu R^2 = Me
3*b* R^1 = Bu R^2 = CH_2Ph
4 R^1 = *t*-Bu R^2 = Me

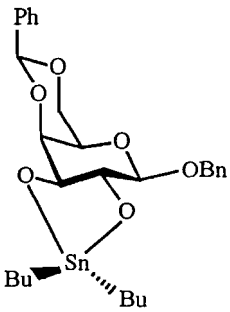

5

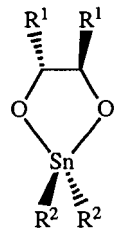

6 R^1 = H R^2 = Bu
7 R^1 = Me R^2 = Bu
8 R^1 = H R^2 = *t*-Bu

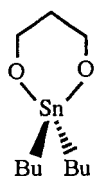

9

Crystalline samples of compounds **2–5** and **8** and **9** were obtained by recrystallization of samples prepared on a vacuum line as outlined elsewhere (12, 13). Sufficiently crystalline samples of **6** and **7** were obtained by evaporation of benzene solutions on the vacuum line. Recrystallization was also performed on the vacuum line so that the samples were never exposed to the atmosphere. The process started with the distillation of anhydrous solvents through the vacuum line onto the solid samples. Closed containers were taken off the vacuum line for cooling and heating during recrystallization and for transfer of crystals to a dry box where the samples were ground and packed in MAS rotors. The rotors were sealed with press-fitting caps, which limited exposure to atmospheric moisture sufficiently that these moisture-sensitive compounds showed no signs of hydrolysis after exposure of the spinners to the atmosphere for up to 2 weeks.

Solid-state MAS ^{119}Sn NMR spectra were recorded on a Bruker MSL-200 NMR spectrometer using a standard Bruker double air-bearing MAS probe. The rotors (7 mm o.d.) were spun at rates of 2.5–4.5 kHz. Conditions for the Hartmann–Hahn match were optimized using a sample of tetracyclohexyltin (26). All spectra were acquired with high-power proton decoupling and 90° pulse lengths of 3–4 μs. Contact times of 1.5–3 ms and recycle times of 5–10 s were used. Some of the static ^{119}Sn NMR spectra were acquired with the addition of a tin 180° pulse after the cross-polarization period in order to generate a Hahn echo before acquisition (27). This pulse sequence was found to be helpful in minimizing the spectral distortion present in experimental static spectra. Solid-state NMR spectra were referenced with respect to tetramethyltin at 0.0 ppm using as a secondary reference tetracyclohexyltin, which has a ^{119}Sn chemical shift of −97.35 ppm (26). The chemical shift of −97.35 ppm was erroneously identified as that of hexamethylditin in our previous paper (14). However, all chemical shifts in our previous study have correct values with respect to tetramethyltin.

Results and discussion

The molecules chosen for study were benzyl 4,6-*O*-benzylidene-2,3-*O*-dibutylstannylene-β-D-glucopyranoside (**2**), methyl 4,6-*O*-benzylidene-2,3-*O*-dibutylstannylene-α-D-mannopyranoside (**3**), methyl 4,6-*O*-benzylidene-2,3-*O*-di-*tert*-butylstannylene-α-D-mannopyranoside (**4**), benzyl 4,6-*O*-benzylidene-2,3-*O*-dibutylstannylene-β-D-galactopyranoside (**5**), 2,2-dibutyl-1,3,2-dioxastannolane (**6**), (4*R*, 5*R*)-2,2-dibutyl-4,5-dimethyl-1,3,2-dioxastannolane (**7**), 2,2-di-*tert*-butyl-1,3,2-dioxastannolane (**8**), and 2,2-dibutyl-1,3,2-dioxastannane (**9**). Compounds **3**, **6**, **8**, and **9** were chosen because information was available about their solid-state structures from X-ray crystallography. The other compounds provided complementary information about a range of environments for tin. Tin-119 CP/MAS NMR spectra of compounds **2–9** were obtained at various spinning rates and the static spectra of all compounds except **3** were also obtained. Typical CP NMR spectra are shown in Figs. 2–7.

Comparison of CP/MAS spectra at two or more spin rates yields values for the isotropic chemical shift, σ_{iso}. The isotropic chemical shift is $(\delta_{11} + \delta_{22} + \delta_{33})/3$, where δ_{ii} (i = 1–3) are the three principal components of the chemical shift tensor. We use the convention $\delta_{11} \geq \delta_{22} \geq \delta_{33}$, i.e., δ_{33} is the principal component of the chemical shift tensor with the smallest chemical shift (i.e., the most shielded component). Tin-119 cross-polarized NMR spectra of static samples allow direct and unambiguous measurement of the principal components of the chemical shift tensor when the signal-to-noise ratios are sufficient. Principal components were measured directly from the static spectra for all compounds except **3**. The magnitude of the chemical shift anisotropy, $\Delta\delta$, is defined according to the convention of Haeberlen (17):

$$[6] \quad \Delta\delta = (\delta_{11} + \delta_{22})/2 - \delta_{33}$$

The asymmetry parameter, η, is defined by eq. [7]:

$$[7] \quad \eta = (\delta_{11} - \delta_{22})/(\delta_{iso} - \delta_{33})$$

as, in all cases, $|\delta_{33} - \delta_{iso}| > |\delta_{11} - \delta_{iso}|$. The experimental chemical shift parameters are summarized in Table 1.

In the carbohydrate derivatives **1–5**, the oxygen atoms are diastereotopic; hence, three dimers are possible for each of these compounds. The different dimers will be designated using conventional carbohydrate nomenclature by means of

TABLE 1. Solid-state ^{119}Sn NMR data (all chemical shifts are in ppm)[a]

Compound	State of oligomer	δ_{11}	δ_{22}	δ_{33}	δ_{iso}	$\Delta\delta$	η	Reference
1	Dimer	246	−2	−627	−126.8, −128.6	748	0.49	14
2	Dimer	249	1	−618	−128	743	0.50	This work
3	Pentamer[b]	205	−11	−530	−119,	627	0.53	This work
		200	−16	−535	−127,	627	0.53	This work
		180	−89	−760	−223,	806	0.50	This work
		210	−102	−810	−234	864	0.54	This work
4	Dimer[c]	55	−68	−626	−213.0	620	0.30	This work
		77	−112	−642	−225.7	625	0.45	This work
5	Dimer	265	−13	−650	−141	776	0.54	This work
6	Polymer	160	−114	−739	−231	762	0.54	This work
7	Polymer	137	−66	−687	−205[d]	723	0.42	This work
8	Mixture of dimers	62	−105	−624	−222, −224, −225, −226	603	0.42	This work
9	Polymer	118	−67	−893	−278.5, −281.6	919	0.30	This work
SnO_2	Polymer	−560	−560	−685	−604.3	125	0	2

[a]Uncertainties unless otherwise indicated are ±20 ppm in δ_{ii}, ±28 ppm in $\Delta\delta$, and for η, range from 0.08 for **1**, **2**, and **5** to 0.12 for **7**.

[b]The δ_{11}, δ_{22}, and δ_{33} values for **3** were estimated from the spinning side-band patterns. Uncertainties are ±30 ppm for δ_{11} and δ_{22}, and ±50 ppm for δ_{33}. The uncertainty in $\Delta\delta$ is ±58 ppm. The uncertainties for η values are ±0.30 for the pentacoordinate sites and ±0.21 for the hexacoordinate sites.

[c]Uncertainties in δ_{ii} values from Herzfeld–Berger analysis, ±30 ppm; uncertainties in $\Delta\delta$ values, ±43 ppm.

[d]Calculated from static spectrum.

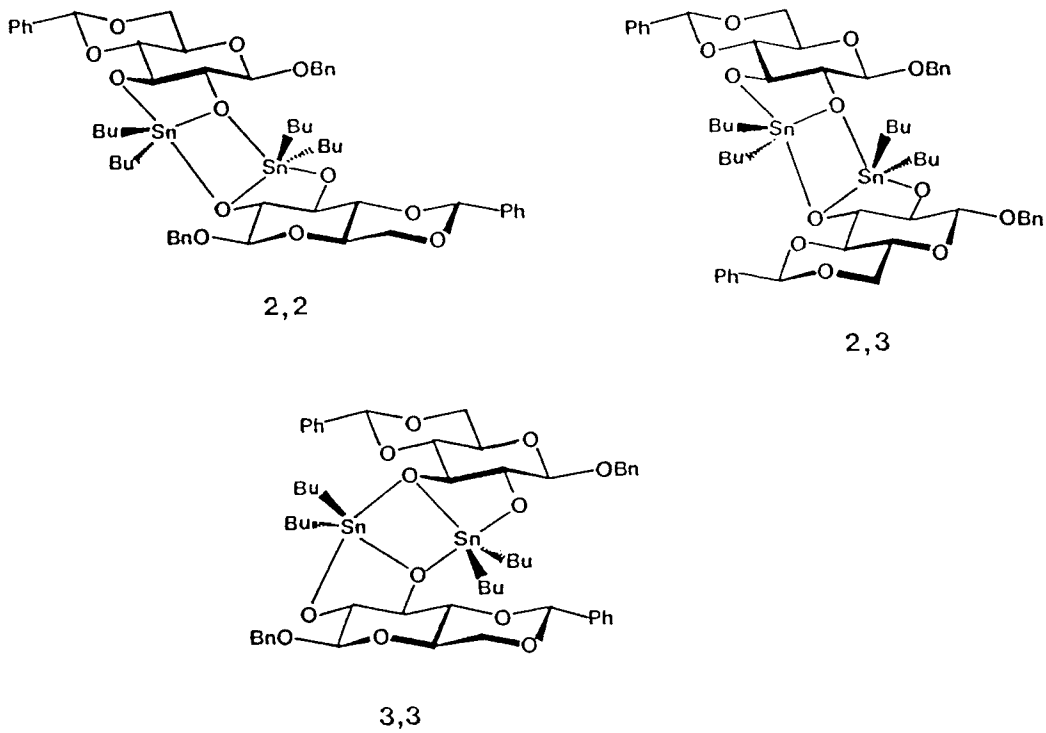

FIG. 1. Dimer structures possible for compound **2**.

the numbers of the two oxygen atoms that are tricoordinate (see Fig. 1). The formation of a dimer from two monomer molecules requires that one oxygen atom from each monomer becomes tricoordinate and that the two tin atoms become pentacoordinate.

A. Comparison of ^{119}Sn NMR spectra from the solid state and solution

In the discussion that follows, the ^{119}Sn NMR spectral data from solid-state (Table 1) and solution spectra (Table 2) will be compared and discussed in relation to what is known or

Can. J. Chem. Downloaded from www.nrcresearchpress.com by 123.30.183.119 on 09/08/12
For personal use only.

TABLE 2. ^{119}Sn NMR data from solution (all chemical shifts are in ppm)

Compound	Dimer	Trimer		Tetramer		Pentamer	
		Pentamer	Hexamer	Pentamer	Hexamer	Pentamer	Hexamer
1	−125[a]						
2	Major −132.6[a]						
	Minor −132.8,−133.0[a]						
3	−120.8[b]	−116.0,−119.4	−286.2[b]				
	−120.6[c]	−120.6	−280.8[c]				
		−120.6	−267.8[d]	−122.5	−245.9[d]	−125.5	−213.5,−236.6[d]
4	−217.7[e]						
5	−143.8[a]						
	−138.4[f]	−122.0,−133.6	−287.1[f]				
6	−126.8[g]	−126.8	−283.0[g]	−131.4	−266.1[g]	−134	−259,−261[g]
7	−132.0[g]	−132.0	−284.9[g]	−138.1	−266.0[g]		
8	−225[h]						
9	−188.2[i]	−195.1	−346.1[i]				

[a]Recorded for $CDCl_3$ solutions, ref. 13.
[b]For a 0.23 M solution in $CDCl_3$ at −60°C.
[c]For a 0.18 M solution in toluene-d_8 at −20°C.
[d]For the 0.18 M solution in toluene-d_8 at −60°C.
[e]For a 0.16 M solution in $CDCl_3$.
[f]For a toluene-d_8 solution at 25°C, ref. 13.
[g]For $CDCl_3$ solutions, ref. 12.
[h]For a $CDCl_3$ solution, ref. 25.
[i]For a 0.41 M solution in $CDCl_3$ at −65°C.

can be deduced about the structures of the compounds and the nature of the species present in the different phases.

The principal components of the chemical shift tensor for methyl 4,6-*O*-benzylidene-2,3-*O*-dibutylstannylene-α-D-glucopyranoside (**1**) are included for comparison purposes (14). Compound **1** has been studied by X-ray crystallography (28). Because of the large *R*-factor previously obtained (10.8%) and because some carbon atoms were not located, the solid-state structure was recently reevaluated from low temperature X-ray data (29). It is present as a 3,3-dimer in the solid state and in solution in chloroform-*d*, benzene-d_6, and toluene-d_8 (13, 28–30).

Compound **2** is a mixture of two dimers in solution (13); of the two dimers, the symmetrical 3,3-dimer constitutes the majority of the mixture in chloroform-*d*, benzene-d_6, and toluene-d_8. The sample studied here was recrystallized from a mixture of anhydrous toluene and anhydrous hexane. It gave a CP/MAS spectrum containing a single isotropic peak at −128 ppm, consistent with the symmetrical 3,3-dimer (Fig. 2). However, in solution, the chemical shifts of all three peaks, the major one from the 3,3-dimer and the two minor peaks from the unsymmetrical 2,3-dimer, were close together; the largest differences ranged from 0.4 ppm in chloroform-*d* to 4.2 ppm in toluene-d_8. Close inspection of peaks of **2** indicated that the major peak was accompanied by at least two other peaks present at low intensity and at slightly larger frequencies than that of the major peak, consistent with the presence of a small amount of the unsymmetrical dimer. Apparently, the crystalline material studied was a mixture in which the major 3,3-dimer was accompanied by a small proportion of the 2,3-dimer.

The principal components of the chemical shift tensor for tin in **2** are almost identical to those for **1**, suggesting that the bonding environment at tin is similar for these two compounds. In both, the tin atoms are in 1,3,2-dioxastannolane rings *trans*-fused to pyranose rings. It is therefore likely that the different regiochemistry observed in reactions of **1** and **2** (13) arises from factors other than the bonding of the tin atoms. The chemical shift anisotropy of the tin nuclei in the 3,3-dimer of **2**, obtained from spin-lattice relaxation measurements in a toluene-d_8 solution, was 810 ± 60 ppm (14), identical within experimental error to that measured here in the solid state.

Compound **3** is present as complicated mixtures in solution. The composition of the mixtures present depends on solvent and temperature. In chloroform-*d*, dimers and trimers are dominant; in toluene-d_8, the species observable by ^{119}Sn NMR includes tetramers and pentamers and their populations increase as the temperature is lowered. Below −50°C, the latter species are the major species present in toluene-d_8 (25). For the α-benzyl analog of **3** (**3***b*), oligomerization in toluene-d_8 only proceeds as far as the tetramer that becomes dominant below −40°C. Chemical shifts for a 0.22 M solution of **3***b* in toluene-d_8 at −40°C were as follows: trimer (~10%), −117.1, −124.1, and −291.2 ppm, and tetramer, −124.1 and −243.4 ppm.

Crystals of **3** obtained from hexane were found to be pentameric by X-ray crystallography (31). The solid-state ^{119}Sn NMR spectra were obtained on crystals also recrystallized from hexane. Tin-119 CP/MAS NMR spectra were obtained at three different spin rates, 2500, 3200, and 3730 Hz, to make the assignments of the isotropic peaks certain. Despite extensive overlap in the NMR spectra of **3**, it was possible to confirm the presence of two isotropic peaks in the hexacoordinate region and two in the pentacoordinate region. This observation is consistent with a pentameric structure in the solid state if one of the peaks assigned to hexacoordinate tin corresponds to two tin sites. As in the spectra of the solid sample, the spectra of the pentamer in toluene-d_8 solution also contained only four signals, two instead of the three expected in the hexacoordinate region of the spectra. There is no ambiguity in assignment of solution

Can. J. Chem. Downloaded from www.nrcresearchpress.com by 123.30.183.119 on 09/08/12
For personal use only.

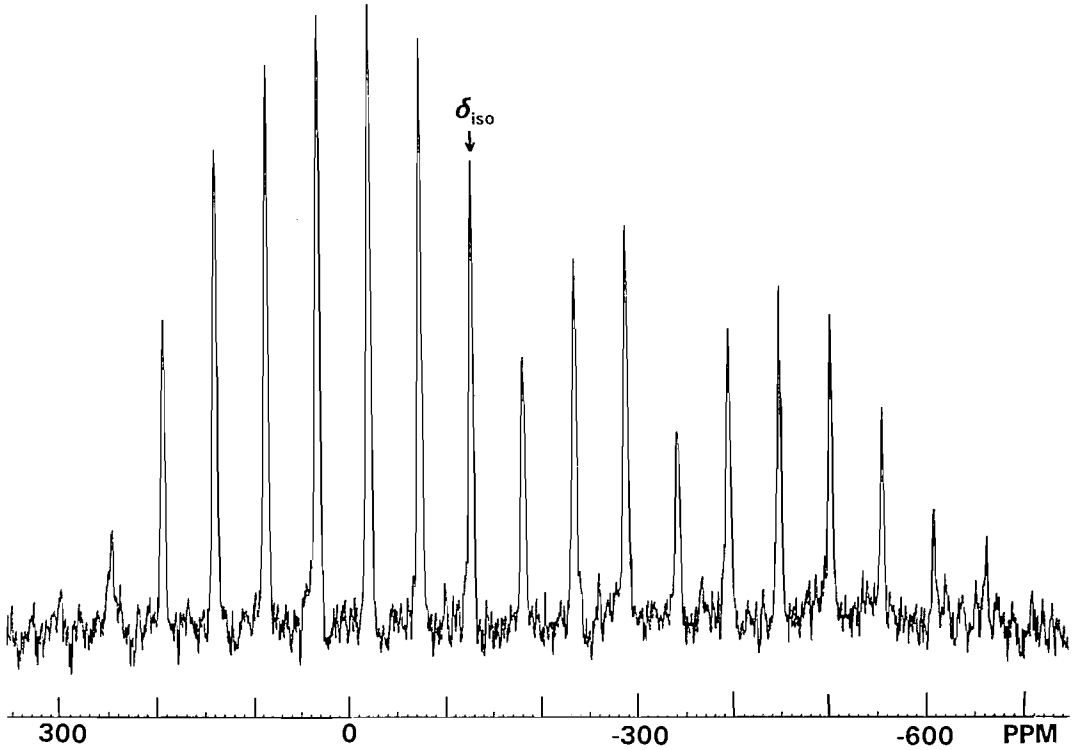

FIG. 2. Tin-119 solid-state CP/MAS NMR spectrum with magic angle spinning at 4.00 kHz for compound **2**.

Can. J. Chem. Downloaded from www.nrcresearchpress.com by 123.30.183.119 on 09/08/12
For personal use only.

spectra because the peaks due to trimers, tetramers, and pentamers are all present with relative intensities that vary in a predictable manner with temperature, concentration, and solvent. The relative intensities of the four peaks in the CP/MAS spectra were considerably different; also, there was some evidence for an additional small peak present at −270 ppm, perhaps due to the hexacoordinate site of a trimer contaminant in the sample studied. The relative intensity of the isotropic peak at −119 ppm was greater than those of the other peaks in all solid-state CP/MAS spectra of **3**.

The isotropic chemical shifts of hexacoordinate tin nuclei move to considerably higher frequencies as the size of the oligomer increases (12–14). For **3**, the isotropic ^{119}Sn chemical shifts obtained for hexacoordinate tin nuclei from solution spectra are −267.8 ppm for the trimer, −245.9 ppm for the tetramer, and −213.5 and −236.6 ppm for the pentamer. The corresponding solid-state shifts are −223 and −234 ppm for the pentamer. Differences between solution and solid-state chemical shifts for all compounds are given in Table 3.

The complex spectra of **3** precluded calculation of chemical shift tensor elements by graphical (32) or computer simulation methods (33). The δ_{11}, δ_{22}, and δ_{33} values for **3** given in Table 1 were estimated very approximately by examining the variation in intensity with frequency for the spinning side bands in the CP/MAS spectra and selecting shifts at positions in the spinning side-band patterns that matched those in other 1,3,2-dioxastannolane spectra that could be calibrated against static spectra. Although uncertainties in these δ_{ii} values may be as large as ±50 ppm, it is clear that the chemical shift anisotropies for the pentacoordinate sites are less than those in the hexacoordinate sites. The values of the chemical shift anisotropies measured here for the pentacoordinate sites in the solid-state pentamer are almost identical to those obtained for the two different pentacoordinate sites in the trimer of ***3b*** from T_1 minima in solution, 658 ± 33 ppm and 686 ± 34 ppm (14). The chemical shifts for these sites are also very similar and the total range in chemical shifts for pentacoordinate tin nuclei in **3** and ***3b*** is <10 ppm.

In marked contrast, the value of the chemical shift anisotropy for the hexacoordinate site in the trimer of ***3b*** in solution, 1080 ± 55 ppm (14), is significantly larger than the values obtained for the hexacoordinate sites in the solid-state pentamer of **3**, 806 ± 60 and 864 ± 60 ppm. As noted above, there are also significant chemical shift differences between the hexacoordinate sites of the trimer and tetramer in solution and those of the pentamer in the solid state or solution (see Table 3). These results suggest that both the chemical shifts and the chemical shift anisotropies reflect differences in bonding between the hexacoordinate tin nuclei in trimers and tetramers and those in pentamers and polymers. The principal components of the chemical shift tensor show much more variation with structure than do the isotropic averages. Unfortunately, no 1,3,2-dioxastannolane that has been studied by X-ray crystallography exists as either a trimer or tetramer.

Compound **4**, the first 2,2-di-*tert*-butyl-1,3,2-dioxastannolane derivative to be discussed here, is considered to be a single dimer in solution because the single peak observed in the ^{119}Sn NMR spectrum has a chemical shift of −217.7 ppm, similar to the chemical shifts observed for the parent di-*tert*-butyl derivative **8** from both solution and CP/MAS NMR spectra (34). Compound **8** was shown to be dimeric by X-ray crystallography (ref. 34 and discussion to follow). The CP/MAS ^{119}Sn NMR spectra of **4** contain two isotropic peaks at −213.0 and −225.7 ppm, chemical shifts consistent with pentacoordinate tin sites in dimeric structures (see Fig. 3).

TABLE 3. Comparison of ^{119}Sn NMR chemical shifts from solution and the solid state (all chemical shifts are in ppm)

	$\delta_{iso}^{solution} - \delta_{iso}^{solid}$				
	Pentacoordinate sites			Hexacoordinate sites	
Compound	Dimer–Dimer	Trimer–pentamer	Tetramer–pentamer	Trimer–pentamer or polymer	Tetramer–pentamer or polymer
1	3				
2	−5				
3		1, 4	5, −3	−58 to −34[a]	−23 to −12[a]
4	−5, 8				
5	−3				
6				−52[b]	−35[b]
7				−80[b]	−61[b]
8	−3 to +1				
9				−66[b]	

[a]With respect to pentamer.
[b]With respect to polymer.

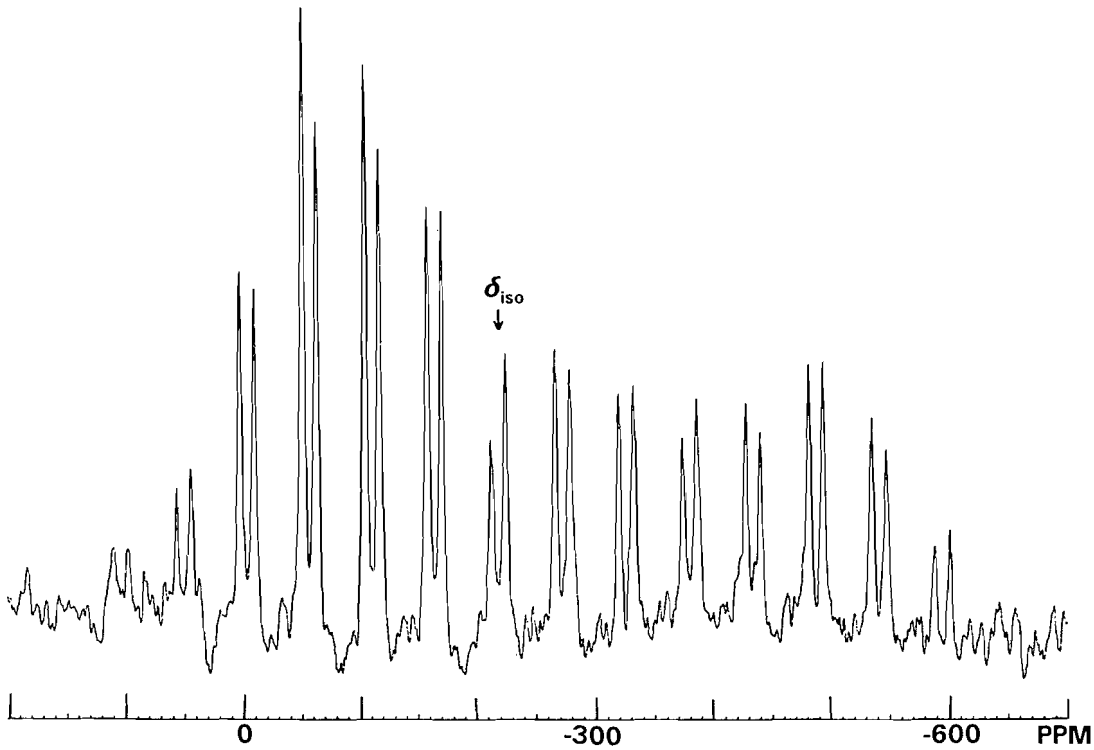

FIG. 3. Tin-119 solid-state CP/MAS NMR spectrum with magic angle spinning at 4.00 kHz for compound **4**.

The peak doubling observed in the solid-state spectra but not in those from solution could be caused by either one of two effects. The species present in the solid state could be one of the C_2-symmetric dimers whose intramolecular symmetry is lost due to crystal forces. Compound **1** was observed to deviate slightly from C_2 symmetry in the solid-state by X-ray diffraction (28, 29) and two peaks separated by 2.2 ppm were observed in its CP/MAS spectra (14). The two sites could also arise because symmetric dimers are present at two locations in the unit cell that are not related by symmetry as for **8** (ref. 34 and *vide infra*). Other possible explanations for the peak doubling could invoke dimers that are not populated in solution. However, there is no reason to expect that these species would form on crystallization.

The intensities and positions of the peaks in the spinning side-band pattern of the CP/MAS ^{119}Sn spectrum of **4** were analysed by an iterative version of the Herzfeld–Berger approach (32) to yield magnitudes of the principal components of the two chemical shift tensors. These values are listed in Table 1. The static spectrum of **4** gave averaged values of these components that, in each case, were intermediate between the values obtained by simulation of the CP/MAS NMR spectra.

The sample of compound **5** was obtained by recrystallization from a mixture of toluene and hexane. The isotropic chemical shift observed for **5** in the CP/MAS spectrum was −141 ppm, similar to the values obtained for the dimer of **5** in solutions in chloroform-*d* and toluene-d_8, −143.8 and

Can. J. Chem. Downloaded from www.nrcresearchpress.com by 123.30.183.119 on 09/08/12
For personal use only.

−138.4 ppm, respectively (Fig. 4). Thus, compound **5** was present as a dimer in the solid. The ^{119}Sn nuclei of **5** are about 13 ppm more shielded than those of the other two carbohydrate dibutylstannylene derivates that exist as dimers, compounds **1** and **2**. All three principal components of the chemical shift tensor contribute significantly to the difference, with δ_{33} showing the largest difference.

The chemical shift anisotropy calculated from solution T_1 data in chloroform-*d* at both 134.62 and 74.62 MHz for **5** was 773 ppm (14), almost identical to the value of 776 ppm obtained from the static spectrum. In calculating the solution value, it was necessary to assume a value for the asymmetry parameter, η. It was assumed that η had the same value as that for compound **1**, 0.49 (14). Substituting the value for η obtained from the static spectrum of the solid, 0.54, changes the solution chemical shift anisotropy slightly to 767 ppm, still very similar to the value from the solid.

Compound **6** has been shown by X-ray crystallography to exist as an infinite ribbon polymer in the crystalline state (35). The sample studied here was obtained by evaporation of a benzene solution. The observed δ_{iso} value, −231 ppm, is somewhat to higher frequency of those of the hexacoordinate tin nuclei of the trimers to pentamers present in solution (ref. 12, see Table 3). This result is consistent with a hexacoordinate tin atom in a highly oligomeric species, such as a polymer. The absence of isotropic peaks in the pentacoordinate region of the CP/MAS ^{119}Sn NMR spectrum confirms that the sample studied here was a polymer (see Fig. 5).

The individual principal components of the chemical shift tensor of **6** are all 100 ± 20 ppm more shielded than those of the pentacoordinate tin sites in the dimers of **1** and **2**. However, both the chemical shift anisotropies and asymmetry parameters for **6** are similar to those of **1** and **2**.

The crystalline sample of compound **7** was obtained by evaporation of a benzene solution. The only possible interpretation of its ^{119}Sn NMR spectra in the solid state is that **7** is an infinite ribbon polymer as observed for **6** although, as for **6**, it was present as a mixture of oligomers in solution (12). The isotropic chemical shifts in the solid-state spectrum were 80 and 61 ppm to higher frequency of those observed for hexacoordinate tin nuclei in spectra from solution, where **7** is present in the trimer and tetramer, respectively. These differences are of the same order of magnitude as noted above but are the largest observed. The actual chemical shift for **7** in the solid state, −205 ppm, is almost the same as that observed for the dimer of **9** in solution, −195 ppm. It is clear that caution must be used in deducing the coordination status of tin from ^{119}Sn NMR chemical shifts of this class of compound, particularly if shifts from compounds having different ring sizes are compared.

Compound **8** was considered to be a single dimer in the solid state based on X-ray crystallography and solid-state NMR spectroscopy (34). The solid powder sample examined here was prepared from large colourless cubically shaped crystals that were obtained by recrystallization from anhydrous toluene, the same solvent previously employed (34). Our high-resolution CP/MAS spectra indicate that the isotropic peak of **8**, earlier observed to be a singlet (34), actually contained four closely spaced peaks, three of which were intense and one that was small but reproducible (see Fig. 6). A single crystal of **8** was assigned to the space group *Pbam* and the unit cell contained two independent but chemically equivalent molecules. Although the structures of

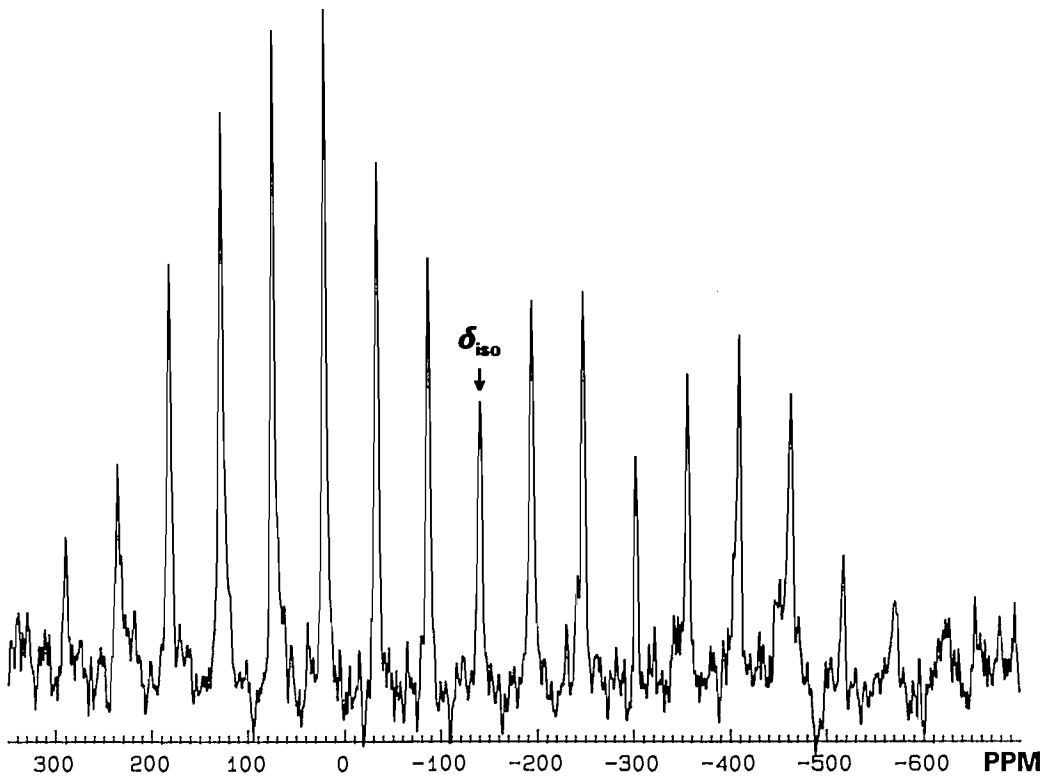

FIG. 4. Tin-119 solid-state CP/MAS NMR spectrum with magic angle spinning at 4.03 kHz for compound **5**.

Can. J. Chem. Downloaded from www.nrcresearchpress.com by 123.30.183.119 on 09/08/12
For personal use only.

Can. J. Chem. Downloaded from www.nrcresearchpress.com by 123.30.183.119 on 09/08/12
For personal use only.

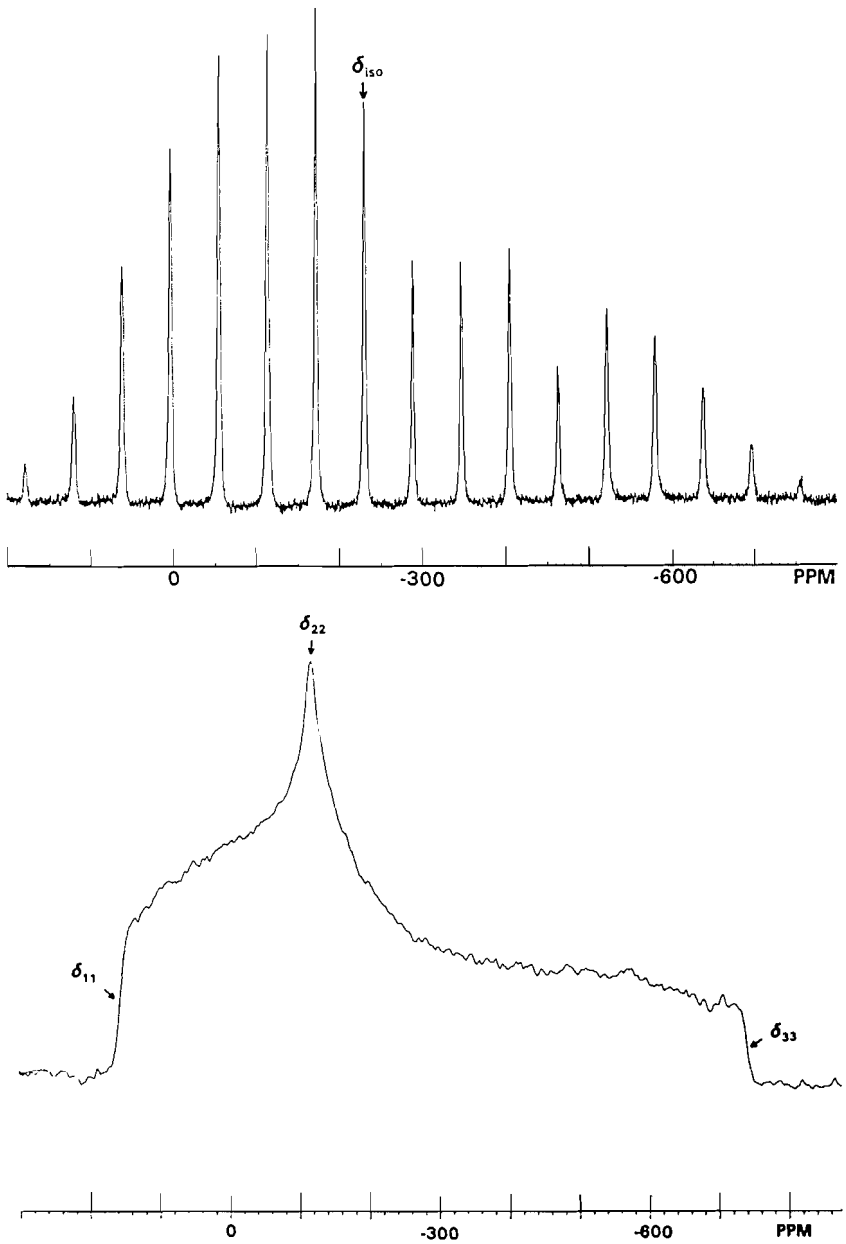

FIG. 5. Tin-119 solid-state NMR spectra for compound **6**; top, CP/MAS spectrum with magic angle spinning at 4.36 kHz; bottom, static spectrum.

the two independent molecules were nearly identical, small differences were observed; two of the 10 bond lengths involving heavy atoms and 8 of the 19 bond angles differed by more than the standard deviations in their respective values. The largest difference was 3.4 times the standard deviation. The X-ray crystallographic study (34) also indicated that the carbon atoms in the two 1,3,2-dioxastannolane rings in the dimeric structure were disordered. Each five-membered ring adopted twist conformations with the OSnO atoms in the mirror plane of the molecule. Each carbon atom in a 1,3,2-dioxastannolane ring was 50% disordered above and below the mirror plane containing the two oxygen atoms. In any one ring, one carbon atom is above the mirror plane and the other below. The crystal structure also had a C_2 axis through the centre of the four-membered SnOSnO ring (34).

If any motion in the 1,3,2-dioxastannolane rings occurs at a rate slower than the NMR chemical-shift time scale for this experiment (i.e., static disorder), two conformers that have C_2 and S_2 symmetry are possible, assuming that the four *tert*-butyl groups in each conformer assume static or averaged positions consistent with the symmetry. For discussion, the carbon atoms attached to the O atoms in the central SnOSnO ring will be designated α and α′ atoms. In the C_2 conformer, the α and α′ atoms are *syn* relative to the plane defined by the SnOSnO ring, while in the S_2 conformer they are *anti*. Each conformer should give rise to one ^{119}Sn NMR peak for a total of two peaks. Four peaks arise because each of the two independent molecules in the unit cell can be present as C_2 or S_2 conformers.

The principal components of the ^{119}Sn NMR chemical shift tensor reported earlier for **8** (34) are very different than those measured here directly from the static spectrum, presum-

Can. J. Chem. Downloaded from www.nrcresearchpress.com by 123.30.183.119 on 09/08/12
For personal use only.

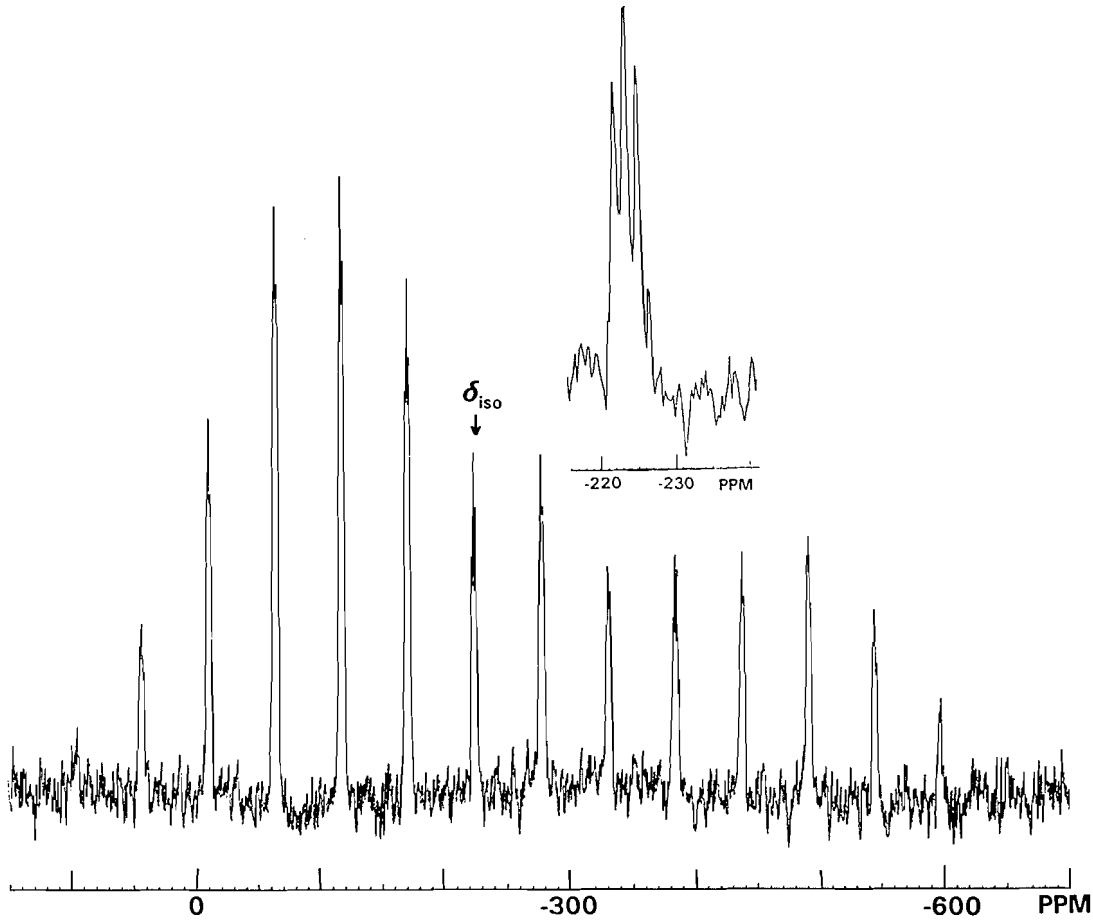

FIG. 6. Tin-119 solid-state NMR spectrum for compound **8** obtained with magic angle sample spinning at 3.99 kHz. The inset shows an expansion of the part of the spectrum containing the isotropic signals.

ably because of the difficulty of estimating these values from slow-spinning CP/MAS spectra.

A preliminary crystal structure of compound **9** has been published in which it was suggested that the structure contained monomer units linked together by long Sn—O bonds (36), which has been interpreted as **9** being a polymer (11). Since no details were published, it was not possible to compare conditions for recrystallization. The sample studied here consisted of needles that were obtained by recrystallization from hexane and toluene. A crystal from the same recrystallization has also been examined by X-ray crystallography (37). The CP/MAS ^{119}Sn NMR spectra of **9** contained two isotropic peaks at −278.5 and −281.6 ppm (Fig. 7). These peaks are on average 66 ppm less shielded than the peak assigned to the hexacoordinate tin atom in a trimer, consistent with the differences in shifts between polymers and trimers observed for **6** and **7** (see Table 3). Thus, these results support the earlier assignment of a polymeric structure to the crystals of **9** (11, 36). The new crystal structure confirmed the assignment of a polymeric structure to solid **9** (37).

Average bond angles at the six pentacoordinate (28–31, 34) and four hexacoordinate (31, 35) tin sites in 1,3,2-dioxastannolanes whose geometries are available from X-ray studies are shown in Fig. 8. An idealized octahedral environment at a dialkyltetraalkoxytin(IV) nucleus might be expected to be more symmetric than a pentacoordinate environment at a dialkyltrialkoxytin(IV) nucleus. However, it can be seen from Fig. 8 that the geometries are far from ideal and, thus, it is not surprising that large chemical shift anisotropies are observed for tin nuclei occupying six-coordinate sites. Where the distortions from octahedral geometry are much smaller, the chemical shift anisotropy is relatively small. For instance, SnO_2, cassiterite, crystallizes with the rutile structure in which each tin atom is surrounded by six oxygen atoms at equal distances, but with O—Sn—O angles of 78, 102, and 90° (38). The ^{119}Sn chemical shift anisotropy for SnO_2, calculated from the data in ref. 2, is 125 ppm, much less than the values observed in the 1,3,2-dioxastannolanes investigated here.

B. General observations

The total range in chemical shift anisotropy for the nine compounds studied here was 600–920 ppm, and some trends were observed within this range. The chemical shift anisotropy for 2,2-dibutyl-1,3,2-dioxastannolanes in pentacoordinate sites varied by over 120 ppm, much more than the range in isotropic chemical shifts (10 ppm).

Replacement of the *n*-butyl groups by *tert*-butyl groups, present in compounds **4** and **8**, results in marked decreases in the isotropic chemical shifts, −98 and −97 ppm for the changes from the dimer of **6** to that of **8** in solution and for the dimer of **3** to that of **4**, respectively. Direct comparisons of $\Delta\delta$ values of *n*-butyl and *tert*-butyl derivatives are not as readily made because values for comparable compounds in the same oligomeric form are not available. However, the $\Delta\delta$ values of **4**, which is dimeric, and those of the pentacoordinate sites of the pentamer **3** are almost identical. Each of the three δ_{ii} values of **4** are about 100 ppm smaller than

Can. J. Chem. Downloaded from www.nrcresearchpress.com by 123.30.183.119 on 09/08/12
For personal use only.

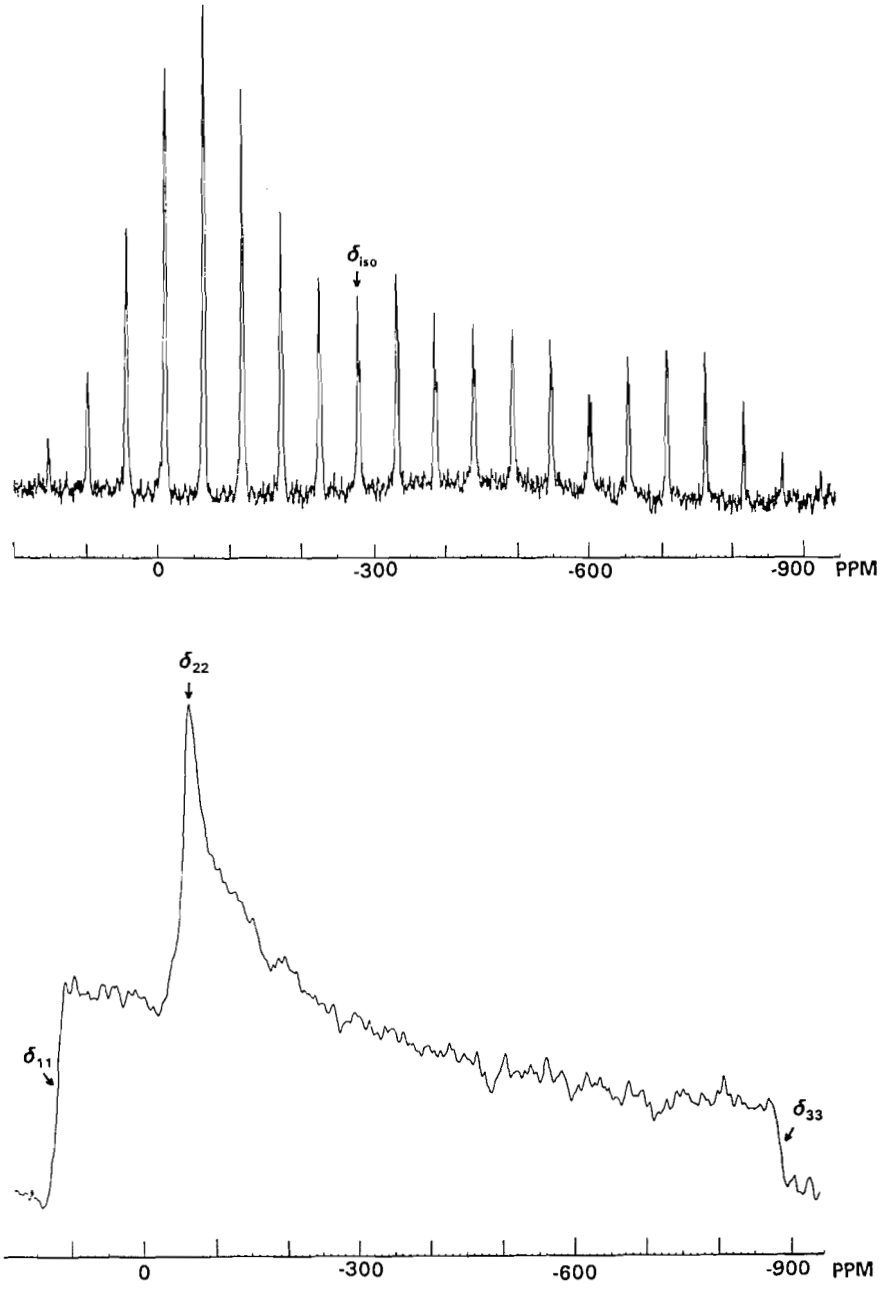

FIG. 7. Tin-119 solid state NMR spectra for compound **9**; top, CP/MAS spectrum with magic angle spinning at 4.00 kHz; bottom, static spectrum.

TABLE 4. Comparison of ^{119}Sn NMR chemical shift anisotropies and isotropic chemical shifts from solution and solid-state data

Compound	Oligomer present	Chemical shift anisotropies		Isotropic chemical shifts	
		Solution (14)	Solid state	Solution (13)	Solid state
1	Dimer	762 ± 50[a]	748 ± 30	−125,[a] −132[b]	−127, −128
2	Dimer	810 ± 60[b]	743 ± 30	−133,[a] −132[b]	−128
5	Dimer	767 ± 40[a,c]	776 ± 30	−144,[a] −138[b]	−141

[a]In chloroform-*d*.
[b]In toluene-d_8.
[c]The value from ref. 14 (773 ppm) was modified because the η value assumed (0.49) for its calculation was slightly different than that measured here (0.54) for solid **5**.

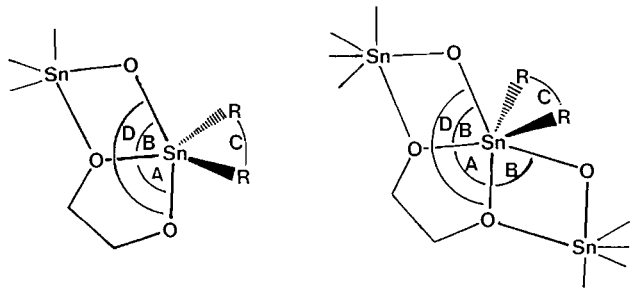

FIG. 8. Average bond angles around tin atoms in 1,3,2-dioxastannolanes obtained from X-ray crystallographic results where the tin atoms are in (a) pentacoordinate sites (28–31, 34) and (b) hexacoordinate sites (31, 35).

those of the pentacoordinate sites of **3**, resulting in the change in δ_{iso} observed.

The different bonding arrangements in the 1,3,2-dioxastannane **9** have a marked effect on the chemical shift anisotropy, which increases by 157 ppm with respect to that for 2,2-dibutyl-1,3,2-dioxastannolane **6**. The major cause of this marked increase in $\Delta\delta$ is the change in the δ_{33} value by −154 ppm. In view of the differences in δ_{33} between **9** and **6**, it is not surprising that the ^{119}Sn isotropic peaks of **9** are considerably more shielded (by about 50 ppm) than that of **6**. The asymmetry parameter is also considerably different for **9** compared to those of all sites in all 2,2-dibutyl-1,3,2-dioxastannolanes.

It was previously concluded from T_1 measurements in solution on compounds that were present as mixtures of oligomers, mainly trimers and tetramers, that $\Delta\delta$ values for hexacoordinate tin sites were approximately 1.5 times those from pentacoordinate sites (14). The $\Delta\delta$ values from ^{119}Sn NMR spectra of solids for hexacoordinate sites in polymers (compounds **6** and **7**) are about the same as those for pentacoordinate sites (compounds **1**, **2**, and **5**). Only one compound (**3**) is present in the solid in an oligomeric form that contains both hexacoordinate and pentacoordinate sites, a pentamer. For compound **3**, the ratios $\Delta\delta_{hexacoordinate}/\Delta\delta_{pentacoordinate}$ were 1.29 and 1.38 for the two hexacoordinate sites. Thus, the previous conclusion appears to apply to hexacoordinate sites in trimers and, perhaps, tetramers only. As the state of oligomerization increases, both the isotropic chemical shifts and the $\Delta\delta$ values for hexacoordinate sites decrease in absolute magnitude and, for the latter, the limiting value for the polymer appears to be of about the same size as those for pentacoordinate sites. Too few X-ray studies are available as yet to identify the factors causing these changes.

C. Do the antisymmetric terms of the shielding tensor contribute to the chemical shift anisotropy of tin in 1,3,2-dioxastannolanes?

Our results for the three compounds for which both solution (14) and solid-state data are available are summarized in Table 4. The similarity in the $\Delta\delta$ values derived from solution T_1 results and measured directly from the solid-state NMR powder spectra imply that the antisymmetric terms do not make a significant contribution to the rate of spin-lattice relaxation (eq. [3]). One could, of course, argue that there is no reason why the shielding tensors in solution and in the solid state should be identical. However, on the basis of the similar isotropic chemical shifts measured in solution and in the solid state, it is reasonable to assume similar values for the principal components in the two different phases. Also, given the extreme sensitivity of ^{119}Sn chemical shifts to subtle changes in molecular structure, this assumption is probably valid.

Conclusions

The ^{119}Sn isotropic chemical shifts of 1,3,2-dioxastannolanes from solid-state spectra and solution spectra are identical (±10 ppm) provided that the same oligomeric species is present in both media. Similarly, chemical shift anisotropies from solution T_1 measurements (14) are identical within experimental error to those from sites of the same species in the static solid-state spectra. This observation supports the previous conclusion (14) that the antisymmetric terms in the ^{119}Sn chemical shift tensor have negligible effects on spin-lattice relaxation rates in these compounds.

The marked and distinctive differences in isotropic chemical shifts of pentacoordinate and hexacoordinate tin sites are not mirrored by distinctive differences in the chemical shift anisotropies. It appears that other factors, such as bond angle variation, type of substituents, and local symmetry, have effects that are of a similar magnitude to that of coordination state on the chemical shift anisotropies and the latter factor is no longer dominant. One trend that is reflected in both the isotropic chemical shifts and the chemical shift anisotropies occurs for hexacoordinate tin sites for compounds for which data can be obtained for trimers, tetramers, pentamers, and polymers; as oligomerization proceeds to higher oligomers, the isotropic chemical shift is deshielded and the chemical shift anisotropy decreases. These changes probably are caused by subtle differences in geometry about the tin atoms.

Acknowledgements

T. B. G. and R. E. W. are grateful to NSERC for financial support. W. P. P. and R. D. C. thank NSERC for Postgraduate Scholarships and Dalhousie University for Killam Postgraduate Fellowships. We also want to thank Mr. B. Millier for his help in maintaining the NMR spectrometers and Dr. N. Burford for the use of his dry box. All NMR spectra were recorded at the Atlantic Region Magnetic Resonance Centre.

1. (*a*) B. Wrackmeyer. Annu. Rep. NMR Spectrosc. **16**, 73 (1985); (*b*) P. J. Smith and A. P. Tupciauskas. Annu. Rep. NMR Spectrosc. **8**, 291 (1978); (*c*) V. W. Petrosyan. Prog. NMR Spectrosc. **11**, 115 (1977); (*d*) J. D. Kennedy and W. McFarlane. *In* Multinuclear NMR spectroscopy. *Edited by* J. Mason. Pergamon Press, Oxford. 1988. p. 305; R. K. Harris, P. Reams, and K. J. Packer. J. Mol. Struct. **141**, 13 (1986); N. J. Clayden. Chem. Scr. **28**, 211 (1988).
2. N. J. Clayden, C. M. Dobson, and A. Fern. J. Chem. Soc. Dalton Trans. 843 (1989).
3. T. P. Lockhart and W. F. Manders. J. Am. Chem. Soc. **109**, 7015 (1987); R. K. Harris, T. N. Mitchell, and G. J. Nesbitt. Magn. Reson. Chem. **23**, 1080 (1985).

Can. J. Chem. Downloaded from www.nrcresearchpress.com by 123.30.183.119 on 09/08/12
For personal use only.

4. R. A. Komoroski, R. G. Parker, and A. M. Mazany. J. Magn. Reson. **73**, 389 (1988).
5. B. King, H. Eckert, D. Z. Denney, and R. H. Herber. Inorg. Chim. Acta, **122**, 45 (1986).
6. R. K. Harris, K. J. Packer, and P. Reams. Chem. Phys. Lett. **115**, 16 (1985); R. K. Harris, A. Sebald, D. Furlani, and G. Tagliavini. Organometallics, **7**, 388 (1988); D. C. Apperley, H. Bai, and R. K. Harris. Mol. Phys. **68**, 1277 (1989); H. Bai, R. K. Harris, and H. Reuter. J. Organomet. Chem. **408**, 167 (1991).
7. R. K. Harris and A. Sebald. J. Organomet. Chem. **331**, C9 (1987); R. K. Harris, K. J. Packer, P. Reams, and A. Sebald. J. Magn. Reson. **72**, 385 (1987); S. Kerschl, B. Wrackmeyer, D. Männig, H. Nöth, and R. Staudigl. Z. Naturforsch. B: Chem. Sci. **42**, 387 (1987).
8. T. P. Lockhart, J. C. Calabrese, and F. Davidson. Organometallics, **6**, 2479 (1987); K. C. Molloy. Inorg. Chim. Acta, **141**, 151 (1988).
9. F. Huber, A. Saxena, R. K. Harris, and A. Sebald. J. Organomet. Chem. **368**, 31 (1989); D. C. Apperley, N. A. Davies, R. K. Harris, A. K. Brimah, S. Eller and R. D. Fischer. Organometallics, **9**, 2672 (1990); C. Janiak, H. Schumann, C. Stader, B. Wrackmeyer, and J. J. Zuckerman. Chem. Ber. **121**, 1745 (1988).
10. A. Lyčka, J. Holeček, B. Schneider, and J. Straka. J. Organomet. Chem. **389**, 29 (1990).
11. S. David and S. Hanessian. Tetrahedon, **41**, 643 (1985); M. Pereyre, J.-P. Quintard, and A. Rahm. Tin in organic synthesis. Butterworths, London. 1987. Chap. 11.
12. T. B. Grindley and R. Thangarasa. J. Am. Chem. Soc. **112**, 1364 (1990).
13. T. B. Grindley and R. Thangarasa. Can. J. Chem. **68**, 1007 (1990).
14. T. B. Grindley, R. D. Curtis, R. Thangarasa, and R. E. Wasylishen. Can. J. Chem. **68**, 2102 (1990).
15. A. D. Buckingham and J. A. Pople. Trans. Faraday Soc. **59**, 2411 (1963); R. F. Schneider. J. Chem. Phys. **48**, 4905 (1968).
16. M. Mehring. Principles of high resolution NMR in solids. 2nd ed. Springer-Verlag, Berlin. 1983. p. 11.
17. U. Haeberlen. Phil. Trans. R. Soc. Lond. A: **299**, 497 (1981); U. Haeberlen. Adv. Magn. Reson. Suppl. 1. *Edited by* J. S. Waugh. Academic Press, New York, 1976.
18. S. Ding and C. Ye. Chem. Phys. Lett. **170**, 277 (1990).
19. J. S. Blicharski. Z. Naturforsch. A: Phys. Phys. Chem. Kosmophys. **27A**, 1456 (1972).
20. (*a*) R. M. Lynden-Bell. Mol. Phys. **29**, 301 (1975); (*b*) H. W. Spiess. NMR: Basic Princ. Prog. **15**, 55 (1978).
21. (*a*) S. C. F. Au-Yeung and D. R. Eaton. J. Magn. Reson. **52**, 351 (1983); (*b*) S. C. F. Au-Yeung, R. J. Buist, and D. R. Eaton. J. Magn. Reson. **55**, 24 (1983).
22. F. A. L. Anet, D. J. O'Leary, C. G. Wade, and R. D. Johnson. Chem. Phys. Lett. **170**, 401 (1990).
23. J. C. Facelli, A. M. Orendt, D. M. Grant, and J. Michl. Chem. Phys. Lett. **112**, 147 (1984).
24. A. D. Buckingham and S. M. Malm. Mol. Phys. **22**, 1127 (1971).
25. T. B. Grindley, R. Thangarasa, J. Allison, C. Keith, and M. D. Lumsden. Can. J. Chem. In preparation.
26. R. K. Harris and A. Sebald. Magn. Reson. Chem. **25**, 1058 (1987).
27. M. Rance and A. Byrd. J. Magn. Reson. **52**, 221 (1983).
28. S. David, C. Pascard, and M. Cesario. Nouv. J. Chim. **3**, 63 (1979).
29. T. S. Cameron, P. Bakshi, R. Thangarasa, and T. B. Grindley. Can. J. Chem. In press.
30. S. David, A. Thieffry, and A. Forchioni. Tetrahedron Lett. **22**, 2647 (1981).
31. C. W. Holzapfel, J. M. Koekemoer, C. F. Marais, G. J. Kruger, and J. A. Pretorius. S. Afr. J. Chem. **35**, 80 (1982).
32. J. Herzfeld and A. E. Berger. J. Chem. Phys. **73**, 6021 (1980).
33. N. J. Clayden, C. M. Dobson, L.-Y. Lian, and D. J. Smith. J. Magn. Reson. **69**, 476 (1986).
34. P. A. Bates, M. B. Hursthouse, A. G. Davies, and S. D. Slater. J. Organomet. Chem. **363**, 45 (1989).
35. A. G. Davies, A. J. Price, H. M. Dawes, and M. B. Hursthouse. J. Chem. Soc. Dalton Trans. **297**, (1986).
36. J. C. Pommier, E. Mendes, J. Valade, and J. Housty. J. Organomet. Chem. **55**, C19 (1973).
37. T. B. Grindley, R. Thangarasa, P. Bakshi, and T. S. Cameron. Can J. Chem. **70**, 197 (1992).
38. W. H. Baur. Acta Crystallogr. **9**, 515 (1956).

Can. J. Chem. Downloaded from www.nrcresearchpress.com by 123.30.183.119 on 09/08/12
For personal use only.

Antigenic and structural relationships within group 19 *Streptococcus pneumoniae:* chemical characterization of the specific capsular polysaccharides of types 19B and 19C[1]

LINDA M. BEYNON, JAMES C. RICHARDS,[2] AND MALCOLM B. PERRY
Institute for Biological Sciences, National Research Council of Canada, Ottawa, Ont., Canada K1A OR6

AND

PETER J. KNISKERN
Merck, Sharp and Dohme Research Laboratories, West Point, PA 19486, U.S.A.

Received April 23, 1991

LINDA M. BEYNON, JAMES C. RICHARDS, MALCOLM B. PERRY, and PETER J. KNISKERN. Can. J. Chem. **70**, 218 (1992).

The specific capsular polysaccharides of *Streptococcus pneumoniae* types 19B and 19C (American types 58 and 59) were investigated by a combination of ^{1}H, ^{13}C, and ^{31}P nuclear magnetic resonance spectroscopy and analytical methods based on mass spectrometry. The two polysaccharides were found to be high molecular weight polymers composed of L-rhamnose, 2-amino-2-deoxy-D-mannose, D-ribose, D-glucose, and phosphate. Homo- and heteronuclear chemical shift correlation techniques and nuclear Overhauser enhancement experiments led to the unambiguous assignment of the ^{1}H and ^{13}C resonances from the glycose residues and established their sequence within repeating oligosaccharide units. The oligosaccharide units are polymerized through phosphate diester linkages.

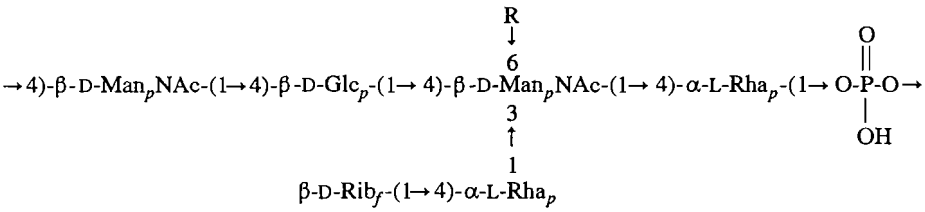

19B polysaccharide R = H
19C polysaccharide R = β-D-Glc$_p$-(1→

Both polysaccharides share a common hexasaccharide structural unit and they differ only in the degree of substitution at the branched 2-acetamido-2-deoxy-β-D-mannopyranosyl residue: the 19C polysaccharide is O-6 linked by β-D-glucopyranosyl end groups to form a heptasaccharide repeating unit, while the 19B polysaccharide is unsubstituted at that position. The serologic cross-reactivity between *S. pneumoniae* serotypes 19B and 19C can now be related to the structural similarity of the antigenic capsular polysaccharides.

Key words: *Streptococcus pneumoniae*, capsular polysaccharide, immuno chemistry.

LINDA M. BEYNON, JAMES C. RICHARDS, MALCOLM B. PERRY et PETER J. KNISKERN. Can. J. Chem. **70**, 218 (1992).

Faisant appel à une combinaison de spectroscopie en résonance magnétique nucléaire du ^{1}H, du ^{13}C et du ^{31}P et de méthodes analytiques basées sur la spectrométrie de masse, on a étudié les polysaccharides capsulaires spécifiques du *Streptococcus pneumoniae* des types 19B et 19C (types américains 58 et 59). On a trouvé que les deux polysaccharides sont des polymères de poids moléculaires élevés, composés de L-rhamnose, de 2-amino-2-désoxy-D-mannone, de D-ribose, de D-glucose et de phosphate. Les techniques de corrélations de déplacements chimiques homo- et hétéronucléaires et d'expériences d'effet Overhauser nucléaire ont permis de faire une attribution non-ambigüe des résonances ^{1}H et ^{13}C des résidus de sucre et d'établir leur séquence dans les unités d'oligosaccharides qui se répètent. Les unités d'oligosaccharides sont polymérisées par des liaisons diesters de l'acide phosphorique.

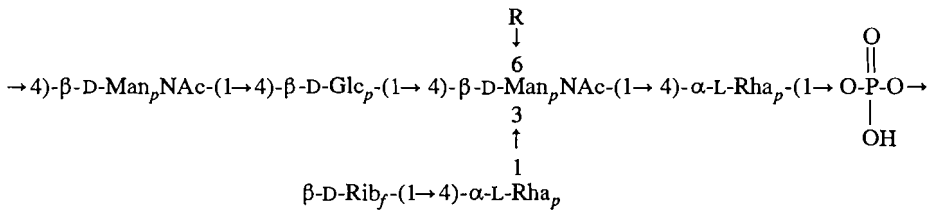

polysaccharide 19B R = H
polysaccharide 19C R = β-D-Glc$_p$-(1→

Les deux polysaccharides se partagent une unité structurale hexasaccharidique et ils ne diffèrent que par le degré de substitution au niveau de la ramification du résidu 2-acétamido-2-désoxy-β-D-mannopyranosyle : le polysaccharide 19C est lié par l'oxygène 6 aux groupes terminaux β-D-glucopyransoyle pour former une unité heptasaccharidique qui se répète

[1]NRCC No. 31992.
[2]Author to whom correspondence may be addressed.

Printed in Canada / Imprimé au Canada

Can. J. Chem. Downloaded from www.nrcresearchpress.com by 123.30.183.119 on 09/08/12
For personal use only.

alors que le polysaccharide 19B n'est pas substitué dans cette position. On peut maintenant établir une corrélation entre l'activité sérologique croisée des *S. pneumoniae* des sérotypes 19B et 19C et la similarité structurelle des polysaccharides capsulaires antigéniques.

Mots clés : *Streptococcus pneumoniae*, polysaccharide capsulaire, immunochimie.

[Traduit par la rédaction]

Introduction

Streptococcus pneumoniae are gram-positive bacteria that are associated with lower respiratory tract infections in adults and otitis media (middle ear infections) in children (1). In addition to a common group antigen (C-substance) (2), 85 type-specific capsular pneumococcal polysaccharide antigens are recognized that show serologic reactivity (3). The Danish serotyping system (4) places the cross-reactive types within groups designated by a number and a capital letter. The origin of serological cross-reactivity can be related to structural homologies among the pneumococcal polysaccharides within a group (3).

Group 19 *S. pneumoniae* is composed of four cross-reacting serotypes; 19A, 19F, 19B, and 19C. The chemical structures of the 19A and 19F specific capsular polysaccharides have been reported by Jennings and co-workers (5,6) and Ohno *et al.* (7). These polymers are composed of similar trisaccharide units,

$\rightarrow$4)-β-D-Man$_p$NAc-(1$\rightarrow$4)-α-D-Glc$_p$-(1$\rightarrow$3/2)-α-L-Rha$_p$-(1$\rightarrow$

polymerized through phosphate diester groups, and only differ in the position of the linkage to the α-L-Rha$_p$ residue. Both the 19A and 19F polysaccharides are included in the 23-valent pneumococcal vaccine currently in use in North America. To establish the molecular basis for the immunobiological activities and serological cross-reactivities among the group 19 pneumococci, we now report the results of the structural analysis of the serotypes 19B and 19C capsular polysaccharides.

Results

Type-specific capsular polysaccharide was obtained from the spent growth medium of *S. pneumoniae* serotype 19B and serotype 19C (8). The two polysaccharides eluted as the void volume fractions on a Sephadex G-50 gel filtration system, indicating each to be a high molecular weight polymer. These materials were further purified by DEAE–Sephacel ion exchange chromatography where the respective polysaccharides eluted as discrete homogeneous fractions in a sodium chloride salt gradient. The 19B and 19C polysaccharides so obtained had $[\alpha]_D$ −54.1 (*c* 1.7, water) and $[\alpha]$ −37.1 (*c* 1.4, water), respectively, and were homogeneous for neutral glycoses, aminodeoxy glycoses, and phosphate. Anal. found for 19B: C 37.7, H 5.4, N 3.1, and ash 15.5%, and for 19C: C 37.3, H 5.6, N 2.7, and ash 11.5%. The phosphate content of the 19B and 19C polymers was determined colorimetrically (9) to be 7.7 and 6.6% (PO_4), respectively.

Complete acid hydrolysis of 19B and 19C polysaccharides and GLC–MS of the derived alditol acetates showed both samples to contain L-Rha, D-Glc, D-ManN, and D-Rib. The relative increase in the amount of glucose released from the 19C polysaccharide after hydrolysis (Glc:Rha, 1.0:1.0), in comparison with that released from the 19B polysaccharide (Glc:Rha, 0.5:1.0), suggested that this polysaccharide contained an additional glucose residue. The absolute configurations of the residues were established by GLC of the

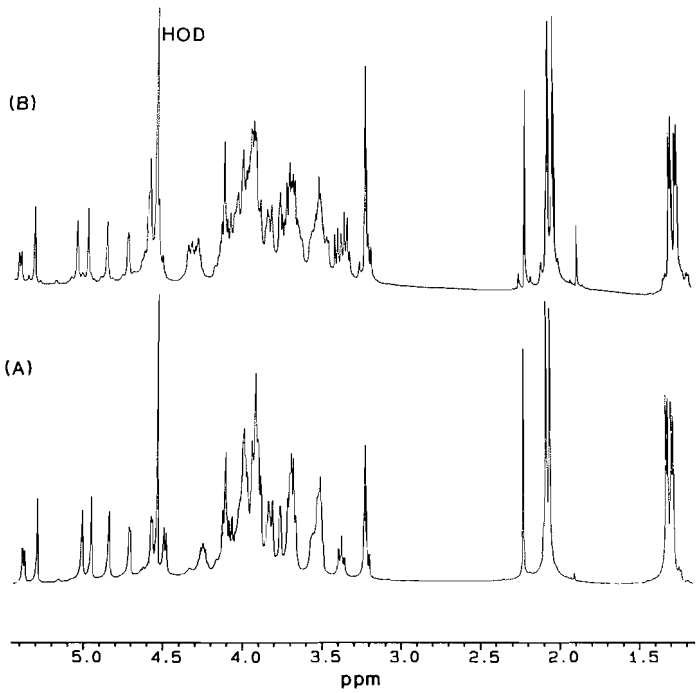

FIG. 1. Proton NMR spectra of the *S. pneumoniae* capsular polysaccharides recorded at 320 K; (A) serotype 19B, (B) serotype 19C.

corresponding (*R*)-2-octyl glycosides (10) and the identity of the D-ManN residues was confirmed by analysis of the nitrous acid-deaminated, reduced ($NaBH_4$), and acetylated products of hydrolysis (11).

The ^{1}H NMR spectra of the 19B and 19C polysaccharides were very similar (Fig. 1). Both spectra contained high-field doublets (J ~6 Hz) at 1.32 and 1.28 ppm for the methyl groups of two 6-deoxyhexoses and a pair of singlets of equal signal area at 2.10 and 2.07 ppm, which could be attributed to the methyl groups of two *N*-acetyl substituents. These findings, in conjunction with the analytical data, would suggest that the two polymers contain L-Rha and D-ManNAc in equal molar amounts. In the ^{13}C NMR spectra (Fig. 2), characteristic resonances at 18.2 and 17.9 ppm were indicative of the C-6 from two 6-deoxyhexoses, while the signals at 54.1 and 50.8 ppm were diagnostic of the C-2 from the 2-acetamido-2-deoxyhexopyranose residues. Resonances at 176.3, 176.0 ppm (C=O) and 23.6 and 22.9 ppm (CH_3) could be attributed to the two acetamido functions. A minor resonance at 55.2 ppm, together with the corresponding ^{1}H resonance at 3.22 ppm, could be attributed to the choline methyl groups from the pneumococcal group antigen, C-substance (2), which is often found as a contaminant of the specific capsular polysaccharide preparations. These resonances were absent from the spectra of the polysaccharides purified by ion exchange chromatography on DEAE–Sephacel.

The ^{13}C NMR spectrum of the 19B polysaccharide (Fig. 2A) exhibited six discrete anomeric carbon resonances at

Can. J. Chem. Downloaded from www.nrcresearchpress.com by 123.30.183.119 on 09/08/12
For personal use only.

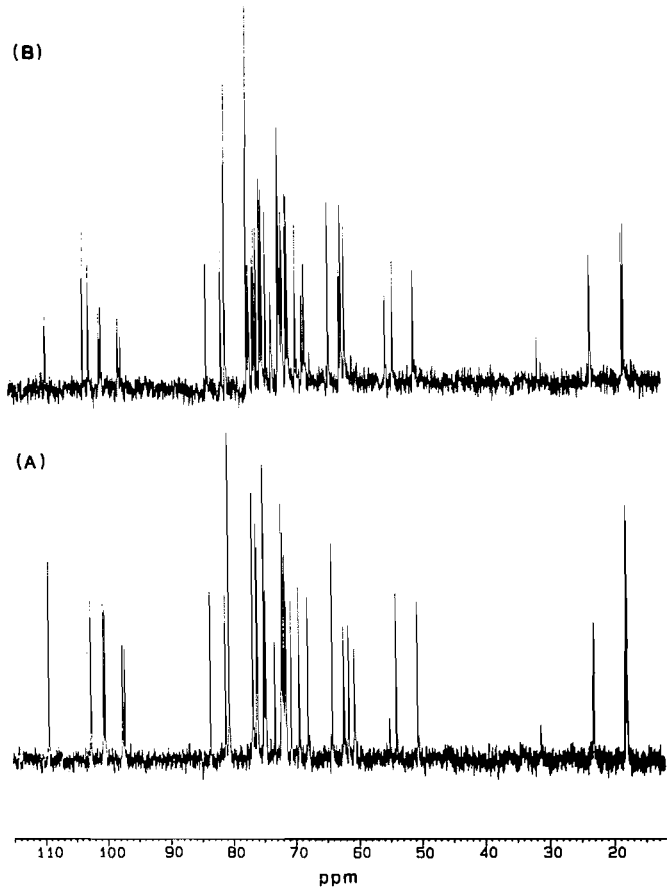

FIG 2. Partial ^{13}C NMR spectra of the *S. pneumoniae* capsular polysaccharides recorded at 310 K; (A) serotype 19B, (B) serotype 19C.

109.4, 102.5, 100.8, 100.5, 97.7, and 97.3 ppm, indicating the polymer to be composed of regular hexasaccharide repeating units. An additional resonance for an anomeric carbon was observed at 103.4 ppm in the ^{13}C NMR spectrum of the 19C polysaccharide (Fig. 2B) suggesting it to be composed of heptasaccharide units. The presence of an anomeric signal at 109.4 ppm in both spectra indicates that the polymers each contain residues having the β-furanosidic ring form (12).

Methylation analysis of the 19B and 19C polysaccharides gave the results recorded in Table 1. The data were consistent with the two polysaccharides being composed of branched repeating oligosaccharide units containing terminal D-Rib$_f$, 4-linked L-Rha$_p$, and 4-linked D-Glc$_p$ residues. The occurrence of the 6-*O*-methyl derivative of *N*-methyl-D-Man$_p$N in the acid hydrolysis products of the 19B polysaccharide indicated that one of the amino sugars was present as a di-*O*-substituted branch point linked through O-3 and O-4 (Table 1, column I). Although the corresponding partially methylated derivative was not detectable in the acid hydrolysate of the 19C polysaccharide, (Table 1, column VI), the presence of 2,3,4,6-tetra-*O*-methyl-D-glucose in addition to the 2,3,5-tri-*O*-methyl-D-ribose suggested that the repeating unit of this polymer contained two branch points. Aqueous hydrofluoric acid treatment of the 19C polysaccharide followed by methylation of the dephosphorylated product and hydrolysis gave approximately equal amounts of *N*-methyl-D-Man$_p$N and *N*-methyl-3,4,6-tri-*O*-methyl-D-ManN$_p$ (Table 1, column VII), indicating the presence of a tri-*O*-substituted 2-acetamido-2-deoxy-sugar residue in the repeating unit. The highly branched nature of the ManNAc residues may account for the low yield or absence of the corresponding derivatives obtained from the methylation analysis procedure.

The structures of the 19B and 19C polysaccharides were determined from an analysis of the fully assigned ^1H and ^{13}C NMR spectra by employing a combination of homo- and heteronuclear chemical shift correlation techniques and nuclear Overhauser enhancement experiments.

Examination of the *J*-connectivities observed in the 2D homonuclear chemical shift correlation (COSY) and relayed coherence transfer (relayed COSY) spectra led to the identification of the coupled spin networks that were representative of the individual glycose residues in the respective oligosaccharide repeating units. The ^1H chemical shift data and ^1H–^1H coupling constants, determined from the appropriate cross-peaks in these spectra, are recorded in Table 2. Assignments of the ^{13}C resonances were then made by direct correlation with the assigned ^1H resonances by heteronuclear ^{13}C–^1H chemical shift correlation (via $^1J_{C,H}$) and by comparison with ^{13}C data from the literature (13) (Table 3).

The COSY spectrum of the ring proton region of the 19C polysaccharide is shown in Fig. 3. In the low-field region of this spectrum (5.4–4.5 ppm), seven resonances for anomeric protons were readily identified from their single vicinal proton couplings. These resonances provided the starting point for spectral analysis and were labelled H-1**a** to H-1**g** according to their decreasing chemical shift values. Delineation of the connectivity pathways defined by the cross-peaks led to the identification of the subspectra associated with each of the component monosaccharide residues (**a**–**g**).

Subspectra corresponding to four of the component monosaccharide residues (**a**, **c**, **d**, and **e**) could readily be attributed to pyranosyl units having the *manno* configuration from the observed small magnitude (≤3 Hz) of the vicinal couplings $J_{1,2}$ and $J_{2,3}$ (14). Residues **a** and **d** were identified as the L-Rha$_p$ residues since the two high-field methyl doublets at 1.32 ($J_{5,6}$ 5.7 Hz) and 1.29 ppm ($J_{5,6}$ 5.6 Hz) could be mapped into the respective connectivity pathways via cross-peaks to H-5**a** (3.91 ppm) and H-5**d** (4.29 ppm) in the full-scale COSY, and to H-4**a** (3.70 ppm) and H-4**d** (3.51 ppm) in the relayed COSY. The resonances for H-2 of residues **c** and **e** occurred at relatively low field (4.5–4.7 ppm). Direct correlation of these resonances to the corresponding ^{13}C resonances for C-2 at 50.8 and 54.1 ppm, respectively, permitted the two residues to be identified as the D-Man$_p$NAc indicated by chemical analysis. The resonance for H-4**e** (4.07 ppm) showed additional heteronuclear coupling (*J* 9.8 Hz), which was apparent from the COSY cross-peak 3,4**e** indicating C-4 as the site of phosphate substitution. Phosphorus-31 coupling to the corresponding ^{13}C resonance, C-4**e** ($^2J_{C,P}$ 5.6 Hz), and the adjacent carbon, C-3**e** ($^3J_{C,P}$ 6.7 Hz), is consistent with phosphate substitution at C-4 of the D-Man$_p$NAc residue. The presence of phosphate at the O-4 position of one of the D-Man$_p$NAc residues may account for the low amount of the ManNAc derivatives detected by glycose and methylation analysis due to incomplete cleavage of the phosphate esters under the hydrolysis conditions employed. It is noteworthy that the COSY cross-peaks relating H-4 and H-5 of this D-

Can. J. Chem. Downloaded from www.nrcresearchpress.com by 123.30.183.119 on 09/08/12
For personal use only.

TABLE 1. Methylation analysis data from *S. pneumoniae* serotypes 19B and 19C capsular polysaccharides

Methylated sugar[a] (as alditol acetate)	T_{MG}[c]	Molar ratios[b] I	II	III	IV	V	VI	VII	VIII	IX
1,2,3,5-Rha	0.42		0.4	0.3	0.4	0.4		tr[d]	0.2	
2,3,5-Rib	0.62	0.8					1.0			
2,3,4-Rha	0.57		0.1	0.8	1.0			0.5		
2,3-Rha	0.89	1.7					1.0			
2,3,4,6-Glc	1.0				1.0	1.0	1.0	1.0	1.0	1.0
2,3,6-Glc	1.40	1.0	1.0	1.0			0.3	1.2		
1,2,3,5-ManNAc	2.12									0.2
2,3,4,6-ManNAc	2.51		0.3	0.3				0.4		
2,3,6-ManNAc	2.92	tr[d]	0.2			0.3				
2,6-ManNAc	3.32	0.5	tr[d]	0.4	0.1					
2,3-ManNAc	3.47								0.2	
2-ManNAc	3.73							0.3		

[a]2,3,4,6-Glc represents 1,5-di-*O*-acetyl-2,3,4,6-tetra-*O*-methyl-D-glucitol, etc.
[b]I, 19B polysaccharide; II, 19B HF product **1**; III, 19B HF product **2**; IV, 19B partial hydrolysis product **4**; V, 19B partial hydrolysis product **3**; VI, 19C polysaccharide; VII, 19C HF product **5**; VIII, 19C partial hydrolysis product **6**; IX, 19C partial hydrolysis product **7**. Values are not corrected for differences in detector response factors.
[c]Retention times relative to that of 1,5-di-*O*-acetyl-2,3,4,6-tetra-*O*-methyl-D-glucitol.
[d]Trace amounts present.

TABLE 2. Proton chemical shifts and coupling constants for the *S. pneumoniae* type 19C and 19B polysaccharides[a,b]

Glycose unit	H-1 ($J_{1,2}$)	H-2 ($J_{2,3}$)	H-3 ($J_{3,4}$)	H-4 ($J_{4,5}$)	H-5	H-6 ($J_{5,6}$)	H-6′ ($J_{5,6'}$,$J_{6,6'}$)
α-L-Rha$_p$	5.37	3.99	3.94	3.70	3.91	1.32	
a	(1.3)	(3.3)	(10.0)	(9.5)		(5.7)	
	(7.3)[c]						
β-D-Rib$_f$	5.29	4.10	4.12	4.02	3.83/3.69[d]		
b	(S)	(4.9)	(7.0)	(4.1)			
β-D-Man$_p$NAc[e]	5.03	4.71	3.99 [3.97]	3.93 [3.90]	3.63 [3.51]	4.33 [3.96]	4.04 [3.69]
c	(s)	(2.7)	(9.5)	(~10)		(~1)	(~4, 11.2)
α-L-Rha$_p$	4.97 [4.94]	3.76	3.92	3.51	4.29 [4.24]	1.29	
d	(s)	(3.7)	(9.1)	(10.0)		(5.6)	
β-D-Man$_p$NAc	4.83	4.57	3.98	4.07	3.56	3.94	3.83
e	(s)	(3.8)	(9.6)	(9.7)		(~2)	(4.8, 11.2)
				(9.8)[c]			
β-D-Glc$_p$	4.58 [4.48]	3.20	3.67	3.35	3.52	3.89	3.69
f	(7.5)	(9.8)	(101.0)	(9.8)		(~1)	(7.5, 11.3)
β-D-Glc$_p$[e]	4.52	3.34	3.53	3.39	3.47	3.93	3.73
g	(8.2)	(9.8)	(10.0)	(9.7)		(~2)	(6.2, 11.5)

[a]Observed first-order chemical shifts and coupling constants (±0.5 Hz).
[b]Data are for the native 19C polysaccharide in D_2O at 310 K. Chemical shift values in square brackets are for proton resonances shifted (>±0.01 ppm) in the spectrum of the 19B polysaccharide.
[c]$^3J_{H,P}$ value (Hz).
[d]H-5′ value; $J_{4,5'}$ = 7.2 Hz, $J_{5,5'}$ = 12.0 Hz.
[e]The β-D-Man$_p$NAc residues **c** are not substituted by β-D-Glc$_p$ end groups **g** at the O-6 position in the 19B polysaccharide.

Man$_p$NAc residue (4,5**e**) were of relatively low intensity (Fig. 3). A proton NOE experiment provided unambiguous assignment of the H-5**e** resonance.

Due to the axial disposition of the hydroxyl group at C-2 of the *manno*pyranosyl residues, the anomeric configurations were not evident from the $J_{1,2}$ values (≤3 Hz) (14). However, the configurations could be determined from the corresponding one-bond ^{13}C–^1H coupling constants (15). Values for $^1J_{C,H}$ of ca. 173 Hz indicated the α-configuration for the two L-Rha$_p$ residues (**a** and **d**), while $^1J_{C,H}$ values of 162–165 Hz were consistent with the β-configuration for the two D-Man$_p$NAc residues (**c** and **e**). The latter assignments were confirmed by intraresidue ^1H–^1H NOE experiments.

A ^1H–^{13}C connectivity between the H-1**b** resonance (5.29 ppm) and the anomeric carbon at lowest field (109.4 ppm) identified residue **b** as a β-furanoside moiety. The ^1H subspectrum corresponding to residue **b** comprised six ^1H resonances, for which the chemical shifts and ^3J-values (Table 2) were consistent with the residue being a β-D-Rib$_f$ (16). In addition, the residue **b** ^{13}C chemical shifts (Table

Can. J. Chem. Downloaded from www.nrcresearchpress.com by 123.30.183.119 on 09/08/12
For personal use only.

TABLE 3. Carbon-13 chemical shifts for the *S. pneumoniae* types 19C and 19B polysaccharides[a,b]

Glycose unit	C-1	C-2	C-3	C-4	C-5	C-6	C=O	CH_3
α-L-Rha_p	97.3[d]	72.1[d] [72.3]	70.7 [71.5]	80.6	69.4	18.2		
a	(173)[e]							
β-D-Rib_f	109.4	76.2	72.3	83.7	64.2			
b	(177)[e]							
β-D-Man_pNAc[c]	100.8	50.8	75.1	72.1 [71.9]	75.6 [76.1[h]]	68.4 [60.7]	176.3[i]	23.0[j]
c	(165)[e]							
α-L-Rha_p	97.7	71.5	71.6	80.6	68.1	17.9		
d	(172)[e]							
β-D-Man_pNAc	100.5	54.1	71.9	73.3	76.8[d]	61.6	176.0[i]	22.9[j]
e	(162)[e]		(6.7)[f]	(5.6)[g]				
β-D-Glc_p	102.5	74.7	75.0	81.3	75.9 [76.8[h]]	62.5		
f	(162)[e]							
β-D-Glc_p[c]	103.4	74.1	77.1	70.9	77.1	62.2		
g	(162)[e]							

[a]Data are for the native 19C polysaccharide at 310 K in D_2O. Chemical shift values in square brackets are for ^{13}C resonances shifted (>±0.01 ppm) in the spectrum of the 19B polysaccharide.
[b]Assignments were made by $^1H-^{13}C$ chemical shift correlation.
[c]The β-D-Man_pNAc residues **c** are not substituted by β-D-Glc_p end groups **g** at the O-6 position in the 19B polysaccharide.
[d]$J_{C,P}$ unresolved.
[e]$^1J_{C,H}$ (Hz).
[f]$^3J_{C,P}$ (Hz).
[g]$^2J_{C,P}$ (Hz).
[h–j]Assignments may be reversed.

Can. J. Chem. Downloaded from www.nrcresearchpress.com by 123.30.183.119 on 09/08/12
For personal use only.

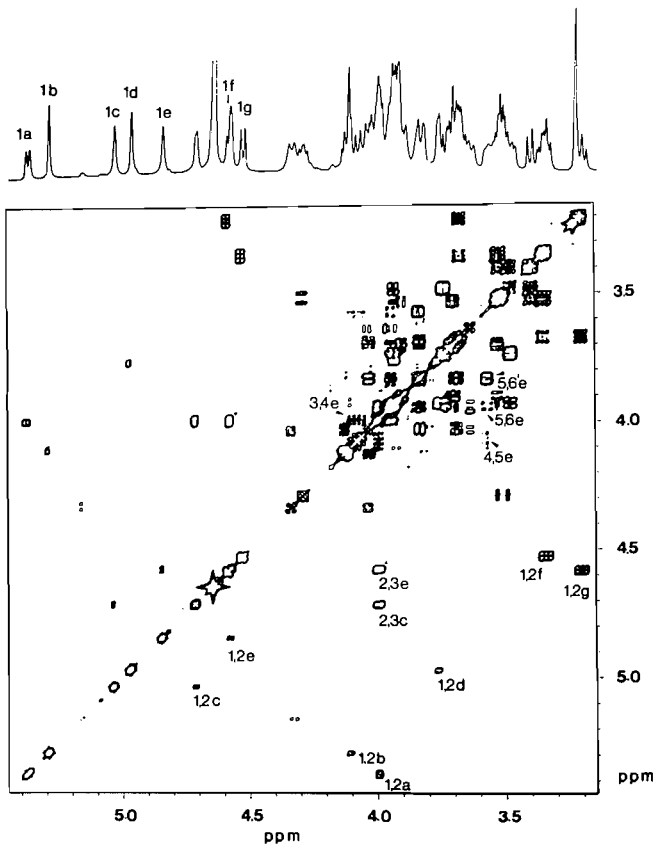

FIG. 3. The COSY contour plot of the ring proton region (5.45–3.15 ppm) of the *S. pneumoniae* serotype 19C capsular polysaccharide recorded at 310 K. Cross-peaks in the low-field region of the spectrum and from the residue **c** spin system are indicated.

3) were similar to those reported (17) for methyl β-D-ribofuranoside, indicating the residue to be present as a nonreducing end group.

Residues **f** and **g** each gave spin-systems comprising seven ^1H resonances. Based on the chemical shift data and the observed large values (8–10 Hz) for the ring proton coupling constants (Table 2), both residues could be identified as β-D-glucopyranose units (18).

The ^{13}C-decoupled ^1H-detected heteronuclear multiple quantum coherence spectrum (Fig. 4) of the 19C polysaccharide shows well-resolved cross-peaks for most of the $^{13}C-^1H$ single bond connectivities. Cross-peaks relating resonances at the 5-position of the β-pyranosyl residues **e**, **f**, and **g**, as well as the H-3**g**/C-3**g** contour, showed considerable overlapping, but a distinction between these residues could be made by comparison with data from the 19B polysaccharide in which the latter residue (**g**) is absent. The ^1H and ^{13}C NMR spectra of the 19B polysaccharide (Figs. 1B and 2B) were assigned similarly using COSY, relayed COSY, and $^{13}C-^1H$ correlation (CHORTLE) techniques (Tables 2 and 3).

For the 19C polysaccharide, the methylene carbon resonance at 68.4 ppm (identified by a DEPT experiment) was mapped into the residue **c** ^1H spin-system from connectivities to the proton resonances at 4.33 (H-6**c**) and 4.04 (H-6'**c**) ppm (Fig. 4), the downfield position of C-6**c** being indicative (19) of substitution at the corresponding position. This resonance is significantly upfield shifted in the spectrum of the 19B polysaccharide. The relatively deshielded values for C-3 (75.1 ppm) and C-4 (ca. 72.0 ppm) of this residue in the spectra of both the 19C and the 19B polysaccharides (Table 3) indicate **c** to be the branching D-Man_pNAc residue identified by methylation analysis. Indeed, from a comparison of the chemical shift data (Tables 2 and 3), it would appear that the only difference between the two serologically re-

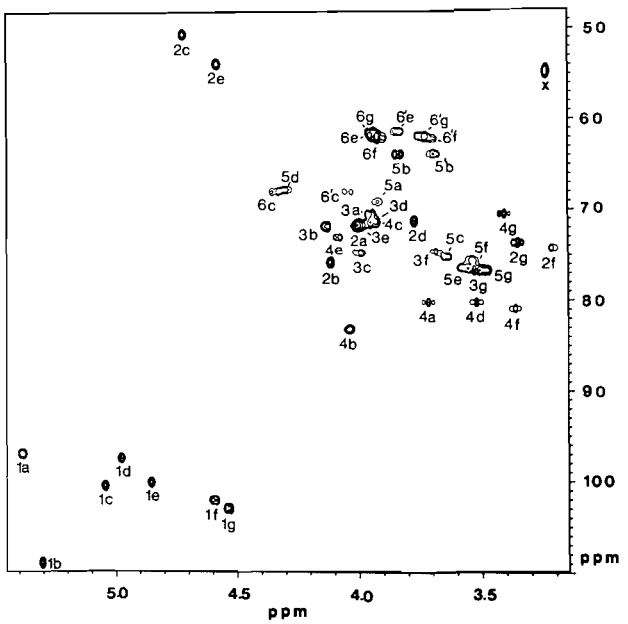

FIG. 4. The ^{13}C-decoupled ^{1}H-detected heteronuclear multiple quantum coherence spectrum of the ring proton region (5.45–3.15 ppm) of the *S. pneumoniae* serotype 19C capsular polysaccharide recorded at 310 K. The contour indicated by "X" is due to the choline methyl resonances from the pneumococcal C-substance.

TABLE 4. Proton NOE data for the *S. pneumoniae* types 19B and 19C polysaccharides[a]

Anomeric proton	Observed proton: Intraresidue NOE	Observed proton: Transglycosidic NOE	Partial sequence
1a	**2a**	—[b]	
1b	—[b]	**4d**	**b→d**
1c	**2c**, **3c**, **5c**	**4a**	**c→a**
1d	**2d**	**2c**, **3c**	**d→c**
1e	**2e**, **3e**, **5e**	**4f**	**e→f**
1f	**3f**, **5f**	**4c**	**f→c**
1g	**3g**, **5g**	**6′c**, **6c**[c]	**g→c**

[a]Measured from 2D NOESY spectra of the native polysaccharides at 310 K in D_2O.
[b]No detectable NOE.
[c]NOE of low intensity.

lated polysaccharides is the presence or absence of the β-D-Glc_p end groups **g** at the O-6 position of the β-D-Man_pNAc residues **c**.

The resonance for H-1**a** ($J_{1,2}$ ~1 Hz)) showed additional splitting (~7 Hz), which could be attributed to phosphorus-31 coupling, indicating that this α-L-Rha_p residue (residue **a**) is glycosidically linked to phosphate. This linkage was confirmed by $^{31}P-^{1}H$ chemical shift correlation, which established a connectivity (via $^{3}J_{H,P}$) between the phosphorus (δ_P −2.1 ppm) and proton (δ_H 5.37 ppm) resonances. In addition, the occurrence of a connectivity between the ^{31}P nucleus and H-4**e** (4.07 ppm) unequivocally established the position of the phosphate diester between residues **a** and **e**:

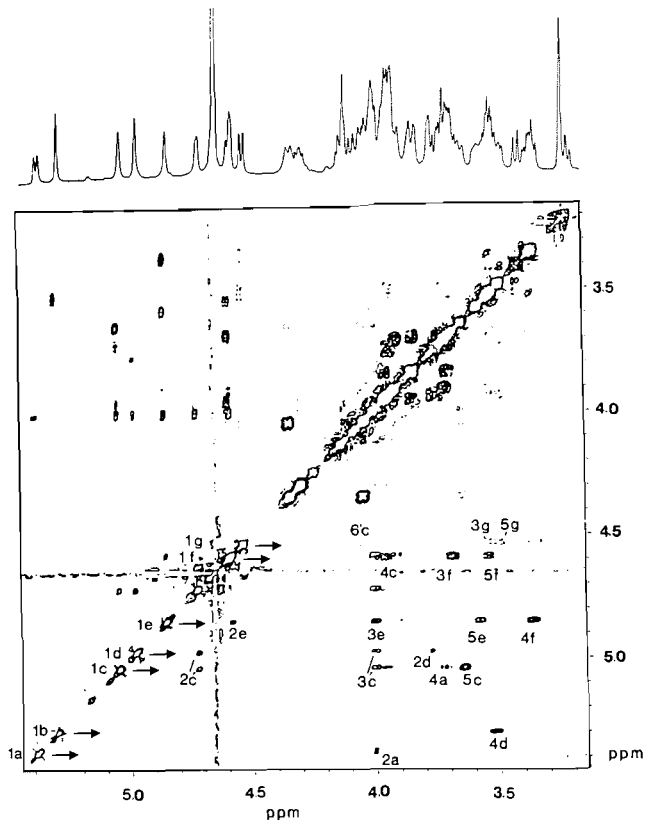

FIG. 5. Contour plot of the ^{1}H spectral region (5.45–3.15 ppm) of the NOESY spectrum for the *S. pneumoniae* serotype 19C capsular polysaccharide recorded at 310 K. Cross-peaks arising from NOE involving the anomeric protons are indicated.

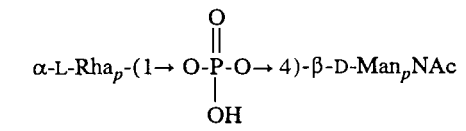

The sequences of the glycoses within the repeating units of the 19B and 19C polysaccharides were determined from NOE measurements that served to establish connectivities between the anomeric and aglyconic protons on adjacent glycosyl residues (Table 4). Two-dimensional experiments (NOESY) were employed and a contour plot of the spectrum obtained on the 19C polysaccharide is shown in Fig. 5.

Nuclear Overhauser effects relating the anomeric proton resonances with other protons within the same ring system provided confirmation of the configurations at the anomeric centres of the glycopyranosyl residues. The occurrence of intraresidue NOE between H-1 and H-3 and between H-1 and H-5 was diagnostic of the β-linked D-Man_pNAc (**c** and **e**) and D-Glc_p (**f** and **g**) residues, while intraresidue effects were observed between only H-1 and H-2 of the L-Rha_p residues (**a** and **d**) indicating the assigned α-configurations.

Transglycosidic NOE were observed between H-1**e**/H-4**f**, H-1**f**/H-4**c**, and H-1**c**/H-4**a**, which established the linear partial sequence, **e→f→c→a**. The anomeric proton reso-

Can. J. Chem. Downloaded from www.nrcresearchpress.com by 123.30.183.119 on 09/08/12
For personal use only.

nance of the α-L-Rha$_p$ residue **a** showed a strong NOE within the pyranosyl ring system to H-2**a** but none to adjacent glycosyl residues. The lack of any interresidue NOE is in accordance with the residue **a** being glycosidically linked to the phosphate moiety. It follows that the main chain of the polymer is composed of the repeating tetrasaccharide unit,

$$\rightarrow 4)\text{-}\beta\text{-D-Man}_p\text{NAc-}(1\rightarrow 4)\text{-}\beta\text{-D-Glc}_p\text{-}(1\rightarrow 4)\text{-}\beta\text{-D-Man}_p\text{NAc-}(1\rightarrow 4)\text{-}\alpha\text{-L-Rha}_p\text{-}(1\rightarrow$$
$$\quad\ \mathbf{e}\qquad\qquad\ \mathbf{f}\qquad\qquad\ \mathbf{c}\qquad\qquad\ \mathbf{a}$$

in which the β-D-Man$_p$NAc **c** provides the point for further substitution.

The occurrence of a transglycosidic NOE between H-1**b** and H-4**d** identifies the disaccharide side chain, **b**→**d**, which is in turn 1,3-linked to the branching β-D-Man$_p$NAc residue **c**, as evidenced from interresidue effects between H-1**d** and H-3**c**/H-2**c**. These effects were observed in the NOESY spectra of both the 19C and the 19B polysaccharides (Table 4), and thereby established the arrangement of the residues within the hexasaccharide unit of the 19B polymer (Fig. 6).

A transglycosidic connectivity between H-1**g** and the methylene proton pair (H-6**c** and H-6′**c**) in the NOESY of the 19C polysaccharide allows the terminal β-D-Glc$_p$ end group **g** to be positioned at O-6 of the trisubstituted β-D-Man$_p$NAc residue in the heptasaccharide unit. This is in accord with the conclusions arrived at from consideration of the ^{13}C chemical shift data. The accumulated evidence therefore establishes that the 19C *S. pneumoniae* capsular polysaccharide is composed of the heptasaccharide units,

$$\begin{array}{l}\qquad\qquad\qquad\qquad\qquad\qquad\beta\text{-D-Glc}_p\\ \qquad\qquad\qquad\qquad\qquad\qquad\ \ 1\\ \qquad\qquad\qquad\qquad\qquad\qquad\ \ \downarrow\\ \qquad\qquad\qquad\qquad\qquad\qquad\ \ 6\\ \rightarrow 4)\text{-}\beta\text{-D-Man}_p\text{NAc-}(1\rightarrow 4)\text{-}\beta\text{-D-Glc}_p\text{-}(1\rightarrow 4)\text{-}\beta\text{-D-Man}_p\text{NAc-}(1\rightarrow 4)\text{-}\alpha\text{-L-Rha}_p\text{-}(1\rightarrow\\ \qquad\qquad\qquad\qquad\qquad\qquad\ \ 3\\ \qquad\qquad\qquad\qquad\qquad\qquad\ \ \uparrow\\ \qquad\qquad\qquad\qquad\qquad\qquad\ \ 1\\ \qquad\qquad\qquad\qquad\qquad\qquad\beta\text{-D-Rib}_f\text{-}(1\rightarrow 4)\text{-}\alpha\text{-L-Rha}_p\end{array}$$

polymerized through phosphate diester groups. The repeating unit of the 19B polysaccharide has the same structure but lacks the β-D-Glc$_p$ end groups.

The positions of the glycosyl linkages and the sequence of the residues within the repeating units were confirmed by NMR and MS-based analyses of the oligosaccharide fragments obtained by partial acid hydrolysis of the 19B and 19C polysaccharides (Scheme 1).

Depolymerization of the 19B polysaccharide with 48% aqueous hydrofluoric acid, followed by fractionation of the products on Bio-gel P2, afforded two major phosphate-free products: a tetrasaccharide **1** (K_{av} 0.55,) and a pentasaccharide **2** (K_{av} 0.48).

The low-field region of the ^{1}H NMR spectrum of reduced **1** contained two singlets at 4.92 and 4.87 ppm for the anomeric protons of two β-D-Man$_p$NAc residues, two doublets (J ~4.6 Hz) at 4.62 and 4.55 ppm for their corresponding H-2 resonances, and a doublet ($J_{1,2}$ 8.4 Hz) at 4.52 ppm for

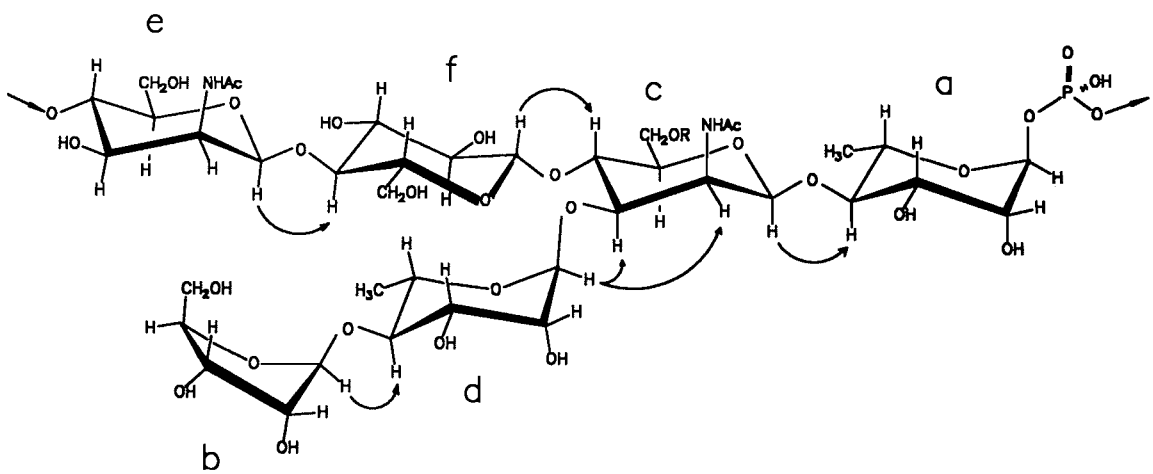

FIG. 6. Structure of the hexasaccharide repeating unit of *S. pneumoniae* serotype 19B capsular polysaccharide (R = H) showing through space connectivities identified by ^{1}H–^{1}H NOE analysis. For the heptasaccharide unit of the serotype 19C polysaccharide R = β-D-Glc$_p$.

Can. J. Chem. Downloaded from www.nrcresearchpress.com by 123.30.183.119 on 09/08/12
For personal use only.

SCHEME 1. Oligosaccharides obtained from the capsular polysaccharides of *S. pneumoniae* types 19B and 19C.

the anomeric proton of a β-D-Glc$_p$ residue (Table 5). Other characteristic signals were observed at 2.06 (s, 3H) and 2.08 (s, 3H) ppm and at 1.26 (d, 3H, $J_{5,6}$ 7.5 Hz) ppm for the methyl protons of two acetamido functions and a L-rhamnitol residue, respectively.

The ^{13}C NMR spectrum contained three signals in the anomeric region (Table 5), signals at 54.1 and 53.8 ppm for the C-2 resonances of the 2-amino-2-deoxyhexose residues, and one resonance at 19.2 ppm for the methyl carbon of a reduced rhamnose residue. A resonance at 63.7 ppm was assigned to C-1 of the reducing end residue of **1**.

The FAB mass spectrum of reduced, methylated **1** showed molecular ions at m/z 953 and 931, which correspond to $[M+Na]^+$ and $[M+H]^+$, respectively. The EI mass spectrum showed A-series fragment ions (20) at m/z 709, 464, and 260 produced by sequential cleavage of the glycosidic linkages from the reducing end of the tetrasaccharide, and a fragment ion at m/z 205 that was indicative of the terminal 6-deoxy-hexitol moiety (Fig. 7).

The downfield region of the ^{1}H NMR spectrum of reduced pentasaccharide **2** was similar to that of **1** (Table 5) except for the presence of an additional singlet at 4.96 ppm for the anomeric proton of an α-L-Rha$_p$ residue. Correspondingly, the ^{13}C NMR spectrum showed four signals in the anomeric carbon region (Table 5) and the presence of signals at 17.2 and 19.3 ppm indicated the presence of L-Rha$_p$ and reduced L-Rha residues, respectively.

The FAB mass spectrum of reduced, methylated **2** showed molecular ions at m/z 1105 $[M+H]^+$ and 1127 $[M+Na]^+$. Abundant fragment ions derived from the protonated molecular ion (m/z 1105) were observed at m/z 883, 677, and 196 in the collision-induced dissociation (CID) FAB mass spectrum obtained using linked scans at constant B/E (Fig. 8). The fragment ion at m/z 883 arises from a characteristic A-type cleavage (20), and subsequent loss of the terminal

Can. J. Chem. Downloaded from www.nrcresearchpress.com by 123.30.183.119 on 09/08/12
For personal use only.

TABLE 5. NMR data for the oligosaccharides derived from the *S. pneumoniae* 19B and 19C capsular polysaccharides[a]

	^{1}H NMR data			^{13}C NMR data	
Oligosaccharides	δ (ppm)	*J* (Hz)	Assignment[b]	δ (ppm)	Assignment[c]
1	4.92	s	β-D-ManNAc	103.3	β-D-Glc
	4.87	s	β-D-ManNAc	100.6	β-D-ManNAc
	4.62	4.6	H-2 of ManNAc	100.2	β-D-ManNAc
	4.55	4.6	H-2 of ManNAc	63.7	L-Rha-ol
	4.52	8.4	β-D-Glc		
2	4.96	s	α-L-Rha	102.8	β-D-Glc
	4.90	s	β-D-ManNAc	100.5	β-D-ManNAc
	4.84	s	β-D-ManNAc	100.3	β-D-ManNAc
	4.72	4.6	H-2 of ManNAc	97.6	α-L-Rha
	4.54	4.6	H-2 of ManNAc	63.7	L-Rha-ol
	4.50	8.4	β-D-Glc		
3	4.90	s	β-D-ManNAc	103.5	β-D-Glc
	4.60	1–2	H-2 of ManNAc	100.5	β-D-ManNAc
	4.51	8.4	β-D-Glc	63.8	L-Rha-ol
4	4.97	s	α-L-Rha	102.9	β-D-Glc
	4.92	s	β-D-ManNAc	100.5	β-D-ManNAc
	4.74	u	H-2 of ManNAc	97.8	α-L-Rha
	4.67	8.4	β-D-Glc	63.9	L-Rha-ol
5	4.95	s	β-D-ManNAc	103.0	β-D-Glc
	4.92	s	α-L-Rha	102.6	β-D-Glc
	4.86	s	β-D-ManNAc	100.7	β-D-ManNAc
	4.78	1–2	H-2 of ManNAc	100.3	β-D-ManNAc
	4.56	7.6	β-D-Glc	97.7	α-L-Rha
	4.54	1–2	H-2 of ManNAc	63.7	α-L-Rha-ol
	4.53	7.6	β-D-Glc		

[a]Measured in ppm from acetone as an internal standard (δ_H 2.225 ppm; δ_C 31.07 ppm)
[b]For example, β-D-Glc refers to the anomeric proton of a β-D-glucopyranosyl residue unless otherwise specified.
[c]As for *b*, but for the anomeric ^{13}C nuclei.

L-Rha$_p$ residue results in the formation of a fragment ion at *m/z* 677 having the possible structure

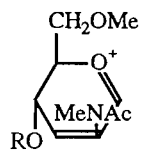

R = β-D-Man$_p$NAc-(1→4)-β-D-Glc$_p$-(1→

In conjunction with the data from methylation analysis (Table 1) of the two oligosaccharides, the foregoing results establish that the pentasaccharide **2** is representative of the 19B oligosaccharide repeating unit minus the terminal β-D-Rib$_f$ residue, and that the oligosaccharide **1** depicts the linear tetrasaccharide backbone (Scheme 1).

Partial hydrolysis of the 19B polysaccharide using 0.05 M trifluoroacetic acid (100°C, 3 h) afforded as the major products analogues of oligosaccharide **1** and **2** that were lacking the terminal nonreducing β-D-Man$_p$NAc residue. Gel filtration on Bio-gel P2 gave the trisaccharide **3** (K_{av} 0.57) and the tetrasaccharide **4** (K_{av} 0.47).

Reduced **3** showed ^{1}H NMR resonances at 4.90 (s) and 4.60 (d, $J_{1,2}$ 1–2 Hz) ppm for H-1 and H-2, respectively, of a β-D-Man$_p$NAc residue, and at 4.51 (d, $J_{1,2}$ 8.4 Hz) ppm for H-1 of a β-D-Glc$_p$ residue (Table 5). A singlet at 2.10 (3H) ppm and a doublet (3H, $J_{5,6}$ 7.5 Hz) at 1.27 ppm were indicative of the presence of a single acetamido function and an L-Rha residue, respectively. The ^{13}C NMR data (Table 5) showed two signals in the anomeric region, at 103.5 and 100.5 ppm, indicating **3** to be a trisaccharide. Resonances at 53.7 and 19.2 ppm confirmed the presence of a single amino sugar and a reduced L-Rha residue, respectively.

GLC–EI-MS analysis of reduced, methylated **3** gave a single peak (R_T 13.0 min, program *D*) that showed characteristic fragment ions at *m/z* 187, 205, 219, and 265. Identification of the partially methylated alditol acetates derived after hydrolysis of the reduced, methylated **3** allowed the trisaccharide to be characterized as β-D-Glc$_p$-(1→4)-β-D-Man$_p$NAc-(1→4)-L-Rha.

Examination of the ^{1}H and ^{13}C NMR data from **4** (Table 5) indicated it to be a tetrasaccharide (Scheme 1). Thus, the ^{13}C NMR spectrum of the reduced tetrasaccharide showed three signals in the anomeric region at 102.9, 100.5, and 97.8 ppm, while a single resonance at 50.5 ppm and two resonances at 19.2 and 17.1 ppm indicated the presence of one amino sugar, one reduced L-Rha, and one L-Rha$_p$, respectively.

The FAB mass spectrum of reduced, methylated **4** showed a molecular ion at *m/z* 860 $[M+H]^+$ and EI analysis gave fragment ions at *m/z* 189, 205, 219, 654, and 624 (Fig. 9). That the tetrasaccharide was branched at the D-Man$_p$NAc residue was verified by methylation analysis (Table 1, column IV).

Can. J. Chem. Downloaded from www.nrcresearchpress.com by 123.30.183.119 on 09/08/12
For personal use only.

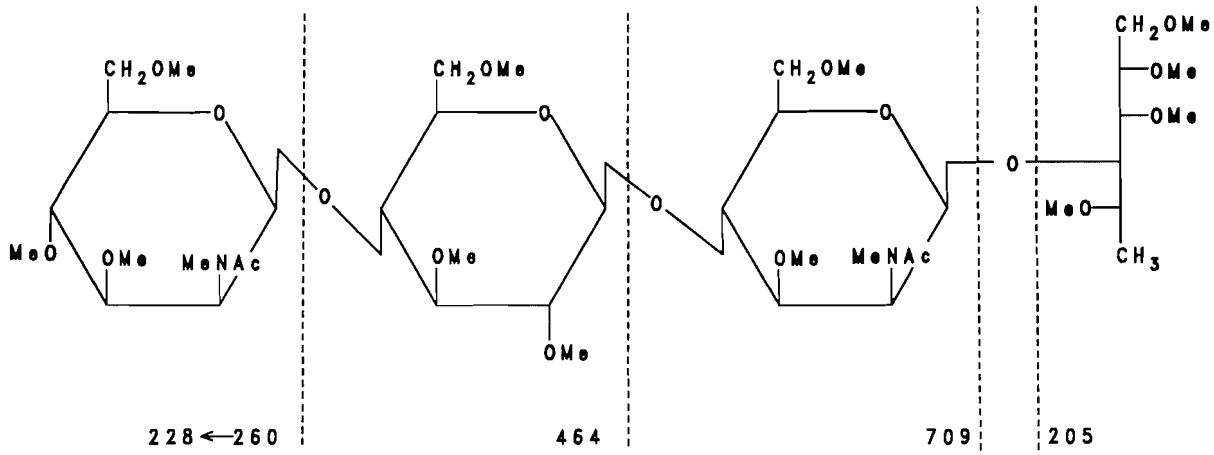

FIG. 7. EI-MS fragment ions of reduced, methylated oligosaccharide **1**.

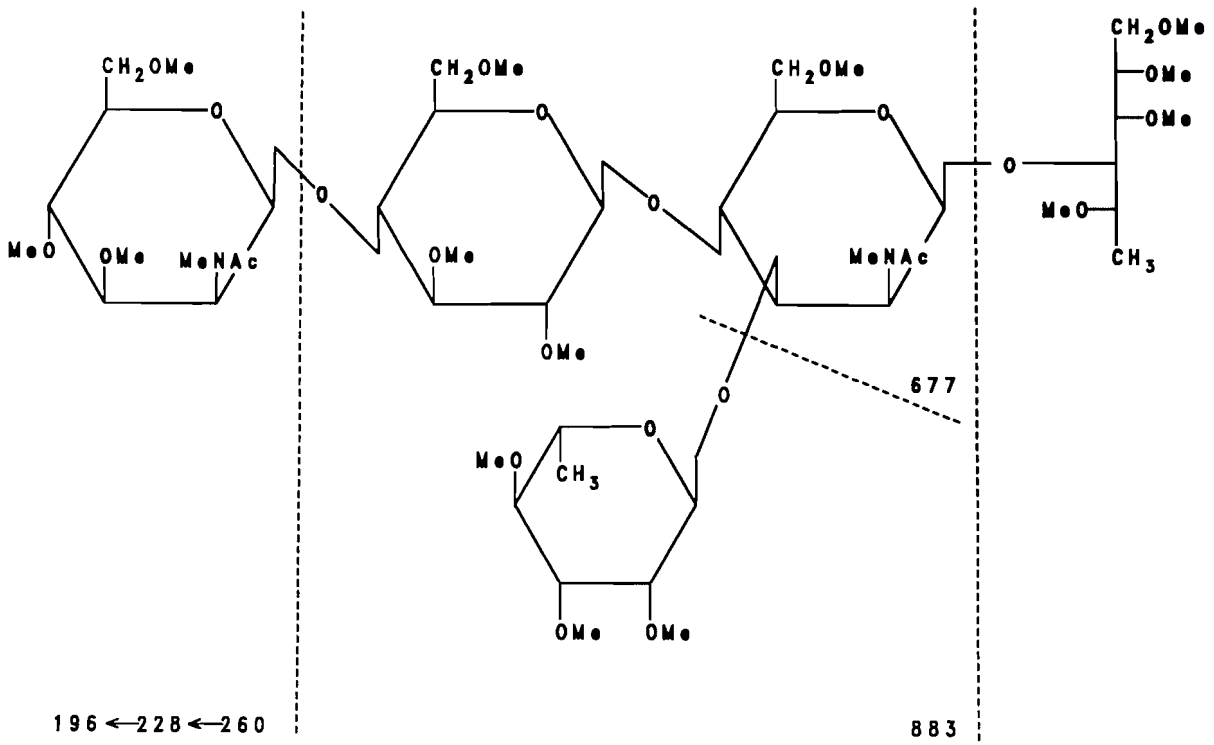

FIG. 8. FAB-MS fragment ions of reduced, methylated oligosaccharide **2**.

Depolymerization of 19C polysaccharide with 48% aqueous hydrofluoric acid, followed by fractionation of the products on Bio-gel P2, afforded a single major product, the phosphate-free hexasaccharide **5** (K_{av} 0.40).

The anomeric region of the ^{1}H NMR spectrum of reduced **5** showed two singlets (4.95 and 4.86 ppm) and two doublets (J ~1–2 Hz, 4.78 and 4.54 ppm) for the respective H-1 and H-2 resonances of two β-D-Man$_p$NAc residues, a singlet (4.92 ppm) from H-1 of an α-L-Rha$_p$ residue, and a pair of doublets ($J_{1,2}$ ~8 Hz, 4.56 and 4.53 ppm) from the H-1 resonances of two β-D-Glc$_p$ residues. The upfield region of the spectrum contained a singlet at 2.07 ppm (6H) and two doublets ($J_{5,6}$ 6.8 Hz) at 1.24 and 1.27 ppm from the methyl protons of two acetamido functions and two rhamnose residues, respectively.

The ^{13}C NMR spectrum of reduced **5** contained five signals in the anomeric region (Table 5), and several high-field resonances that confirmed the presence of the two 2-acetamido-2-deoxy sugars and L-Rha$_p$ residues.

The FAB mass spectrum of reduced, methylated **5** showed molecular ions at m/z 1347 $[M+K]^+$, 1331 $[M+Na]^+$, and 1309 $[M+H]^+$, and a major fragment ion at m/z 1087. The sequence of the glycoses was indicated from the FAB-MS by CID of the protonated molecular ion (m/z 1309) by linked scanning, and from the fragmentation pattern produced in the EI mass spectrum. In the EI mass spectrum characteristic A-

Can. J. Chem. Downloaded from www.nrcresearchpress.com by 123.30.183.119 on 09/08/12
For personal use only.

Can. J. Chem. Downloaded from www.nrcresearchpress.com by 123.30.183.119 on 09/08/12
For personal use only.

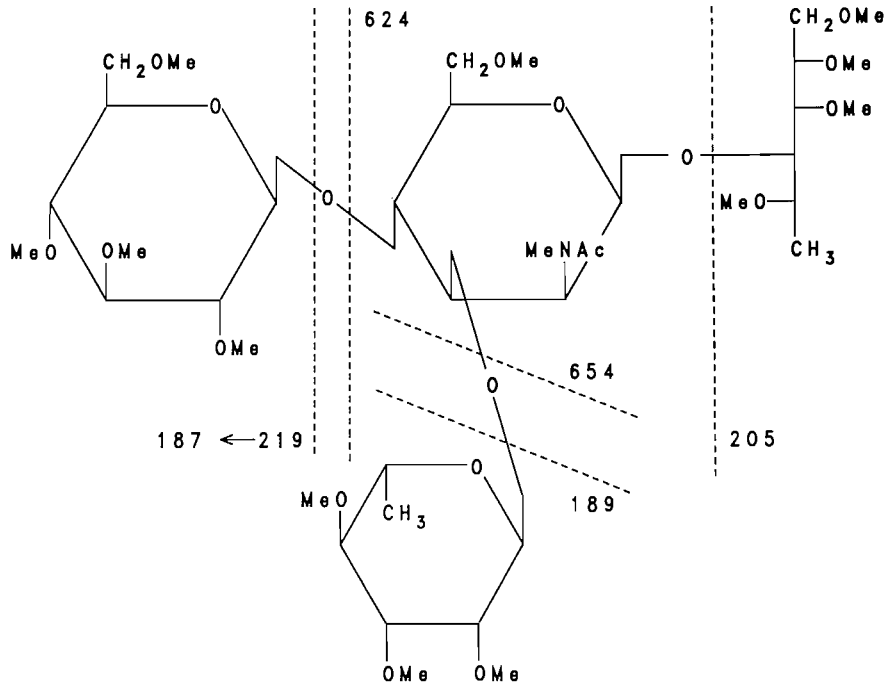

FIG. 9. EI-MS fragment ions of reduced, methylated oligosaccharide **4**.

type fragments at *m/e* 260, 219, 189, and 205 were indicative of ManNAc, Glc, and Rha nonreducing end groups and a terminal rhamnitol residue, respectively. A significant fragment ion at *m/z* 464 established the partial sequence ManNAc-O-Glc, while the ions at *m/z* 1087 and 828 in the CID-FAB-MS defined the position of the branching tri-*O*-substituted ManNAc residue (Fig. 10). Analysis by GLC–MS of hydrolysed, reduced, methylated **5**, after conversion of the partially methylated glycoses to their alditol acetates, identified the linkage positions (Table 1, column VII).

Treatment of the hexasaccharide **5** with trifluoracetic acid (0.5 M, 100°C, 1 h) and fractionation of the hydrolysis products on Bio-gel P2 afforded two oligosaccharides, **6** (K_{av} 0.34) and **7** (K_{av} 0.55).

The CI mass spectrum of methylated, reduced ($NaBH_4$) **6** showed a $[M+NH_4]^+$ ion at *m/z* 907, a $[M+H]^+$ ion at *m/z* 890, and fragment ions at *m/z* 654, 205, 187, and 155 (Fig. 11), which were indicative of a branched tetrasaccharide. On the other hand, the CI mass spectrum of the methylated derivative of reduced **7** contained molecular ions at *m/z* 733 $[M+NH_4]^+$ and 716 $[M+H]^+$, indicating it to be a related trisaccharide that was lacking the reducing L-Rha residue. The GLC–EI mass spectrum (R_T 13.6 min, program *D*) of **7** had fragment ions at *m/z* 219, 187, 174, 155, and 130. Hydrolysis of reduced, methylated **7** and analysis by GLC–MS of the partially methylated glycoses as their alditol acetates gave the results shown in Table 1, column VIII.

Thus the above results identify **5** as a β-D-Glc_p-containing analogue of **1**, which corresponds to the oligosaccharide repeating unit of the 19C polysaccharide minus the β-D-Rib_f end group (Scheme 1).

Comparison of the methylation analysis data for the 19B and 19C polysaccharides with those of the derived oligosaccharides (Table 1) confirmed the positions of the glycosyl linkages and the location of the side chains in the native polysaccharides.

Discussion

The structures of the *S. pneumoniae* group 19 capsular antigens are shown in Table 6. A number of common features can be identified that may be responsible for cross-serological activity within the group: (1) the trisaccharide units of the types 19A and 19F have almost identical structures, differing only in the substitution site of the α-L-Rha_p residues; (2) the 19C and 19B polysaccharides share a common hexasaccharide unit. However, the only common structural feature shared by all the four types is the region about the phosphate diester bridge, i.e., the trisaccharide fragment

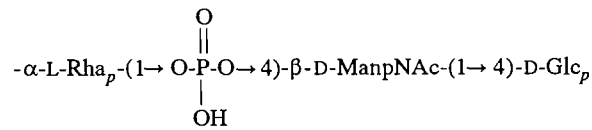

These structural aspects concur with serologically determined antigenic similarities.

Seven antigenic factors have been identified (21) within the group 19 of S. *pneumoniae* by the use of factor antisera (Table 6). The 19F and 19A pneumococcal types have two antigenic components in common (*19a* and *19d*). In addition, the type 19A expresses an antigenic determinant, *19c*, which, along with the *19a* determinant, is also a component of type 19B and 19C polysaccharides. The antigenic factor, *19b*, is unique to type 19F pneumococci and this factor may

Can. J. Chem. Downloaded from www.nrcresearchpress.com by 123.30.183.119 on 09/08/12
For personal use only.

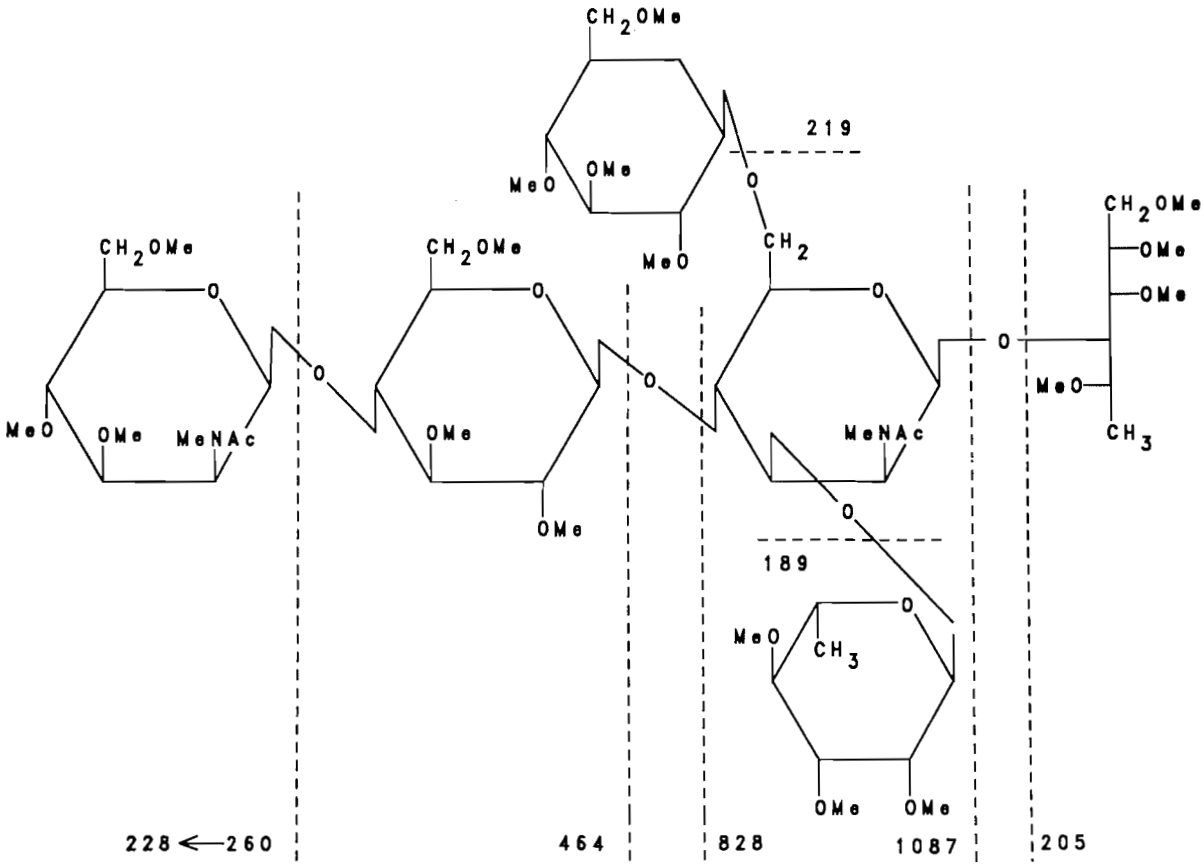

FIG. 10. EI-, CID-FAB-MS fragment ions of reduced, methylated oligosaccharide **5**.

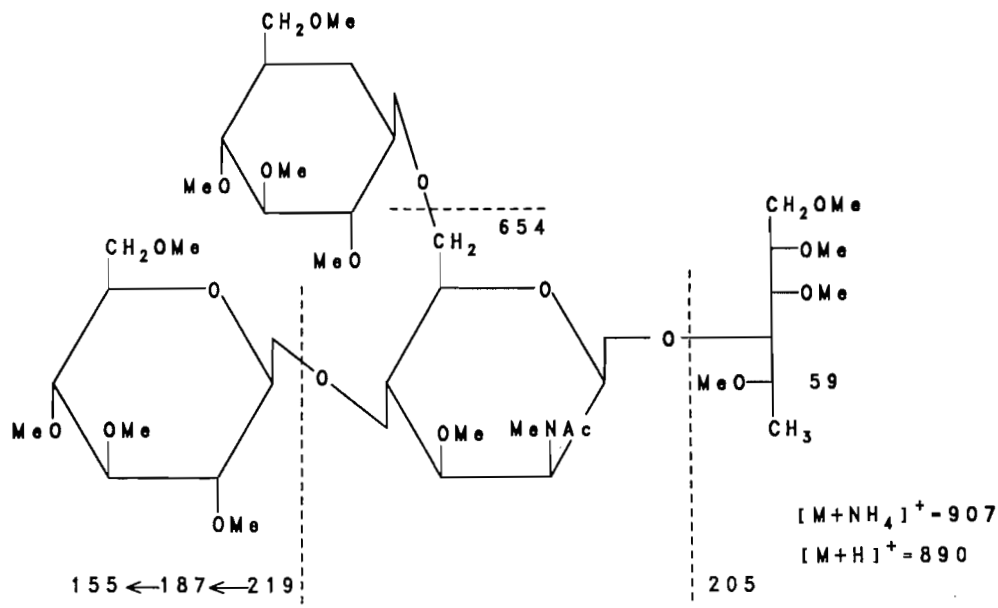

FIG. 11. CI-MS fragment ions of reduced, methylated oligosaccharide **6**.

TABLE 6. Structures[a] and antigenic formulae[b] of the group 19 *S. pneumoniae* specific capsular plolysaccharides

Serotype	Repeating unit	Antigenic factors
19F	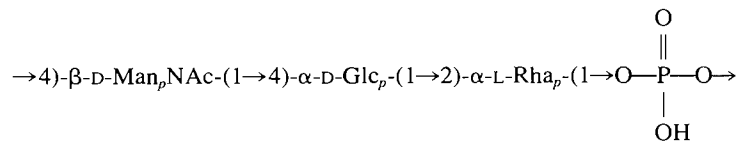	*19a*, *19b*, *19d*
19A	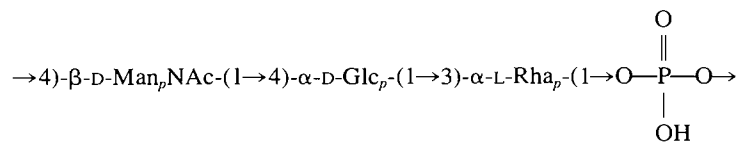	*19a*, *19c*, *19d*
19B	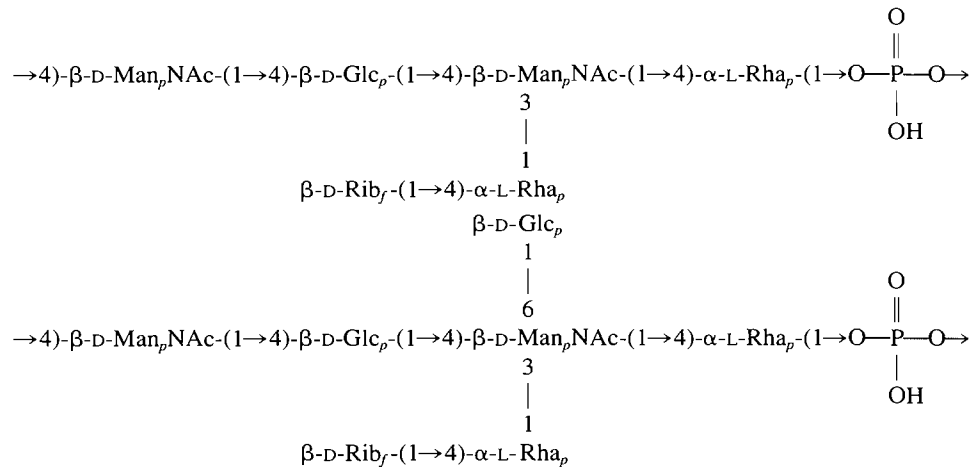	*19a*, *19c*, *19e*, **7h**
19C		*19a*, *19c*, *19f*, *7h*

[a]Structures of the 19F and 19A polysaccharides are from refs. 5–7.
[b]Antigenic factors are from ref. 21.

reflect the difference between the linkage to the α-L-Rha_p residues in the type 19F and 19A specific polysaccharides. *Streptococcus pneumoniae* types 19B and 19C have three antigenic factors in common, *19a*, *19c*, and *7h*; the latter determinant, which most probably resides in the β-D-Rib_f-(1→4)-α-L-Rha_p-(1→ disaccharide side chains, is also a component of the pneumococcal type 7B and 7C polysaccharides. Expression of the antigenic determinants *19f* and *19e* can be correlated to the presence or absence of the β-D-Glc_p end groups in the type 19C and 19B polysaccharides, respectively.

Rabbit antisera to either the 19F or 19A polysaccharide (22) react strongly with the heterologous polysaccharide, but only poorly with the 19B and 19C polysaccharides. On the other hand, the 19B and 19C polysaccharides and their antisera cross-react extensively with each other (22). It is noteworthy in this context that results in humans indicated much less cross-reactivity between types 19F and 19A and, as a consequence, both polysaccharide antigens are included in a 23-valent vaccine.

Experimental

Streptococcus pneumoniae *type 19B and 19C polysaccharides*

Types 19B and 19C polysaccharides were obtained from the respective bacterial growth media after digestion with trypsin, ribonuclease, and deoxyribonuclease by fractional precipitation with 2-propanol with serological probing (8). The polysaccharides were each eluted as single discrete peaks in a 0→1 M NaCl gradient on DEAE–Sephacel.

Analytical methods

Ion exchange chromatography on DEAE–Sephacel was carried out as described previously (23). Quantitative colorimetric methods used were (*i*) phenol – sulphuric acid for neutral glycoses (24), (*ii*) the method of Chen *et al.* for phosphate (9), and (*iii*) the modified Elson–Morgan for aminoglycoses (25).

Analytical GLC–MS was done with a Hewlett–Packard 5885B system and an OV-17 fused silica column (Quadrex Corp.) using an ionization potential of 70 eV (EI) or with ammonia as reagent gas (CI). The following programs were employed: *A* (for alditol acetates), 180°C for 2 min then 4°C/min to 240°C; *B* (for partially methylated alditol acetates), 180°C for 2 min then 2°C/min to 240°C; *C* (for acetylated (*R*)-2-octyl glycoside derivatives), 180°C for 2 min then 6°C/min to 240°C; *D* (for methylated oligosaccharide alditols), 180°C for 2 min then 10°C/min to 350°C.

For analysis of constituent sugars, samples (1 mg) of polysaccharide were hydrolysed with 4 M trifluoroacetic acid for 1 h at 125°C, and the excess acid was removed by evaporation under a stream of nitrogen gas. Glycoses were determined by GLC–MS of their derived alditol acetates (26).

Methylation of samples (1–2 mg) was carried out using a modification of the method of Hakomori (27,28) and the products isolated by partition between dichloromethane and water. Methylated oligosaccharides were analysed directly by FAB- and (or) CI- and EI-MS. The methylated products were subsequently hydrolysed as above and, after conversion of the partially methylated glycoses to their alditol acetates, analysed by GLC–EI-MS.

FAB-MS analyses were carried out in the positive ion mode using a JEOL AX505H or a VG 70-VS (VG Analytical Ltd., Manchester U.K.) mass spectrometer. An accelerating voltage of 3 kV and a mass resolution of 1500 was employed with the JEOL

Can. J. Chem. Downloaded from www.nrcresearchpress.com by 123.30.183.119 on 09/08/12
For personal use only.

Can. J. Chem. Downloaded from www.nrcresearchpress.com by 123.30.183.119 on 09/08/12
For personal use only.

AX505H instrument. Samples were dissolved in methylene chloride and dried onto the stainless steel probe tip. *m*-Nitrobenzyl alcohol was applied to the probe tip prior to FAB analysis, and a Xe atom beam of 6 kV was used to sputter and ionize the sample. Spectra were calibrated with Ultramark 1621. CID FAB-MS/MS experiments on M+H ions were performed using helium as the collision gas. Linked scans at constant B/E were generated by a JEOL DA-50,000 data system.

TLC was performed on silica gel (Merck) with 6:3:1 (v/v) *n*-propanol–conc. NH_3–water.

NMR spectroscopy

All measurements were made on solutions in D_2O using a Bruker AM-500 or AMX-500 spectrometer.

Proton spectra recorded at 500 MHz were obtained using a spectral width of 2.6 kHz, a 16-K data block, and a 90° pulse. Chemical shifts are expressed relative to internal acetone (δ_H, 2.225 ppm).

Broad-band proton decoupled ^{13}C NMR spectra were obtained at 125 MHz using a spectral width of 25 kHz, a 32-K data block, and a 90° pulse employing WALTZ decoupling (29). Heteronuclear $^1J_{C,H}$ values were measured using gated decoupling and DEPT spectra (30) were obtained with broad-band decoupling, a 135° proton pulse, and a 3.3-ms delay between pulses. Chemical shifts are referenced to internal acetone (δ_C, 31.07 ppm).

Two-dimensional homonuclear COSY, relayed COSY, and NOESY experiments were carried out as previously described (31) for sweep widths of 2600 or 1250 Hz, and the data were processed to give either magnitude (32) or phase-sensitive (33, 34) spectra.

Heteronuclear ^{13}C–^1H chemical shift correlations were measured using the CHORTLE pulse sequence (35), or in the ^1H-detected mode via multiple quantum coherence ($^1H\{^{13}C\}$HMQC) with a Bruker 5-mm inverse broad-band probe using reverse electronics. The HMQC experiment employed the pulse sequence described by Bax *et al.* (36, 37), and ^{13}C decoupling during ^1H acquisition was achieved using the GARP-1 composite pulse sequence (38). A data matrix of ($t_1 \times t_2$) 256 × 1024 complex points was employed over the full ^{13}C and ^1H spectral regions and 32 scans were acquired for each t_1 value. A squared sine-bell window function shifted over 60° was applied in both dimensions and the data are presented in the absorption mode in f_1 (^{13}C) and the absolute value mode in f_2 (^1H).

Phosphorus-31 spectra were recorded at 202 MHz by employing a spectral width of 10 kHz, a 16-K data set, and a 90° pulse. Chemical shifts are referenced to that of an external sample of aqueous 25% phosphoric acid (δ_P, 0.0 ppm). Two-dimensional ^{31}P–^1H chemical shift correlations were made by ^1H-detected multiple quantum coherence ($^1H\{^{31}P\}$HMQC) (36) for a 64 × 1024 data matrix, 64 scans per t_1 value and a 60-ms delay.

Dephosphorylation of the polysaccharides 19B and 19C

The 19B polysaccharide (42 mg) was dissolved in 48% aqueous hydrofluoric acid (2 mL) and kept at 4°C for 24 h. The reaction was quenched by pouring the mixture into a slurry of solid CO_2–calcium carbonate–dichloromethane (39) and the precipitate and dichloromethane were removed by centrifugation. The hydrolysis products were chromatographed on a column (1.5 × 95 cm) of Bio-Gel P2 with water as the eluant to give the phosphate-free products **1** (K_{av} 0.55, 9.7 mg) and **2** (K_{av} 0.48, 1.4 mg), which were pure by TLC (R_f 0.24 and 0.26, respectively). The oligosaccharides in water (0.5 mL) were each treated with $NaBH_4$ (~30 mg) at 20°C for 3 h, followed by decomposition of excess borohydride with acetic acid and repeated concentration of the solutions from methanol (5 × 1 mL). A sample of each reduced oligosaccharide was methylated, analysed by FAB- and EI-MS, hydrolysed, and the partially methylated glycoses analysed as their alditol acetates by GLC–EI-MS.

The 19C polysaccharide (20 mg) was dissolved in 48% aqueous hydrofluoric acid (1 mL) and kept at 4°C for 22 h. The reaction mixture was worked up as above to afford a single phosphate-free product **5** (K_{av} 0.40, R_f 0.11), which was reduced, methylated, and analysed as previously described for oligosaccharides **1** and **2**.

A sample of oligosaccharide **5** (10 mg) was treated with 0.5 M trifluoroacetic acid for 1 h at 100°C. The excess acid was removed by rotary evaporation and the remaining traces were neutralized with 5% NH_4OH. Separation of the products on Bio-gel P2 gave a tetrasaccharide **6** (K_{av} 0.34, R_f 0.12) and a trisaccharide **7** (K_{av} 0.55, R_f 0.08), which were reduced, methylated, analysed by CI- and EI-MS, and, following hydrolysis, the derived alditol acetates were analysed by GLC–MS.

Partial acid hydrolysis of 19B polysaccharide

The 19B polysaccharide (70 mg) dissolved in 0.05 M trifluoroacetic acid was heated on a boiling water bath for 3 h. The excess acid was removed by rotary evaporation and the remaining traces of acid neutralized with 5% NH_4OH. Separation of the products on Bio-gel P2 gave a trisaccharide **3** (K_{av} 0.57, R_f 0.30, yield 2.9 mg) and a tetrasaccharide **4** (K_{av} 0.47, R_f 0.27, yield 8.7 mg), which were reduced, methylated, and analysed by FAB- and EI-MS (**4**) or GLC–EI-MS (**3**). Each reduced, methylated oligosaccharide was then hydrolysed and analysed as described above.

General methods

Concentrations were made under reduced pressure at <40°C and optical rotations measure at 20°C in 10-cm microtubes, using a Perkin Elmer 243 polarimeter.

Acknowledgments

Fred Cooper provided expert FAB– and GLC–MS analyses and we thank VG Analytical Ltd., Manchester, UK, for mass spectra of oligosaccharides **1** and **2**.

1. J. O. Klein. Rev. Infect. Dis. **3**, 246 (1981).
2. H. J. Jennings, C. Lugowski, and N. M. Young. Biochemistry, **19**, 1011 (1980).
3. J. E. G. Van Dam, A. F. Snippe, and H. Snippe. Antonie van Leeuwenhoek, **58**, 1 (1990).
4. E. Lund and J. Henrichsen. Methods Microbiol. **12**, 241 (1978).
5. E. Katzenellenbogen and H. J. Jennings. Carbohydr. Res. **124**, 235 (1979).
6. H. J. Jennings, K.-G. Rosell, and D. J. Carlo. Can. J. Chem. **58**, 1069 (1980).
7. N. Ohno, T. Yadomae, and T. Miyazaki. Carbohydr. Res. **80**, 297 (1980).
8. V. Daoust, D. J. Carlo, J. Y. Zeltner, and M. B. Perry. Infect. Immun. **32**, 1028 (1981).
9. P. S. Chen, T. Y. Toribara, and H. Warner. Anal. Chem. **28**, 1756 (1956).
10. K. Leontein, B. Lindberg, and J. Lonngren. Carbohydr. Res. **62**, 359 (1978).
11. J. A. Cifonelli. Methods Carbohydr. Chem. **7**, 139 (1976).
12. P. A. J. Gorin and M. Mazurek. Carbohydr. Res. **48**, 171 (1976).
13. K. Bock, C. Pedersen, and H. Pedersen. Adv. Carbohydr. Chem. Biochem. **42**, 193 (1984).
14. C. Altona and C. A. G. Haasnoot. Org. Magn. Reson. **13**, 417 (1980).
15. K. Bock and C. Pedersen. J. Chem. Soc. Perkin Trans. **2**, 293 (1974).
16. S. J. Angyal. Carbohydr. Res. **77**, 37 (1979).
17. P. A. J. Gorin and M. Mazurek. Can. J. Chem. **53**, 1212 (1975).
18. M. L. Hayes, A. S. Serianni, and R. Barker. Carbohyr. Res. **100**, 87 (1982).
19. K. Bock and C. Pedersen. Adv. Carbohydr. Chem. Biochem. **41**, 27 (1983).

20. A. Dell. Adv. Carbohydr. Chem. Biochem. **45**, 19 (1987).
21. E. Lund and J. Henrichsen. Methods Microbiol. **12**, 241 (1978).
22. T. Krishnamurthy, C.-J. Lee, J. Henrichsen, D. J. Carlo, T. M. Stoudt, and J. B. Robbins. Infect. Immun. **22**, 727 (1978).
23. E. Altman, J.-R. Brisson, and M. B. Perry. Biochem. Cell Biol. **65**, 49 (1987).
24. M. Dubois, K. A. Gilles, J. K. Hamilton, P. A. Rebers, and F. Smith. Anal. Chem. **28**, 350 (1956).
25. R. Gatt and E. R. Berman. Anal. Chem. **15**, 167 (1965).
26. S. W. Gunner, J. K. N. Jones, and M. B. Perry. Can. J. Chem. **39**, 1892 (1961).
27. S. Hakomori. J. Biochem. (Tokyo), **55**, 205 (1964).
28. L. R. Phillips and B. A. Fraser. Carbohydr. Res. **90**, 149 (1981).
29. A. J. Shaka, J. Keeler, F. Frenkiel, and R. Freeman. J. Magn. Reson. **52**, 335 (1983).
30. D. M. Doddrell, D. T. Pegg, and M. R. Bendall. J. Magn. Reson. **48**, 323 (1982).
31. L. M. Beynon, M. Moreau, J. C. Richards, and M. B. Perry. Carbohydr. Res. **209**, 225 (1991).
32. A. Bax, R. Freeman, and G. Morris. J. Magn. Reson. **42**, 164 (1981).
33. A. Kumar, R. R. Ernst, and K. Wuthrich. Biochem. Biophys. Res. Commun. **95**, 1 (1980).
34. A. G. Wagner, R. R. Ernst, and K. Wuthrich. J. Am. Chem. Soc. **103**, 3654 (1981).
35. G. A. Pearson. J. Magn. Reson. **64**, 487 (1985).
36. A. Bax, R. H. Griffey, and B. L. Hawkins. J. Magn. Reson. **55**, 301 (1983).
37. A. Bax and S. Subramanian. J. Magn. Reson. **67**, 565 (1986).
38. A. J. Shaka and J. Keeler. Prog. NMR Spectrosc. **19**, 47 (1987).
39. A. J. Mort and W. D. Bauer. J. Biol. Chem. **257**, 1870 (1982).

Can. J. Chem. Downloaded from www.nrcresearchpress.com by 123.30.183.119 on 09/08/12
For personal use only.

Molecular recognition IX.[1] The synthesis of the H-type 2 human blood group determinant and congeners modified at the 6-position of the *N*-acetylglucosamine unit

EVA PETRAKOVA,[2] ULRIKE SPOHR,[3] AND RAYMOND U. LEMIEUX[4]
Department of Chemistry, University of Alberta, Edmonton, Alta., Canada T6G 2G2

Received July 26, 1991

EVA PETRAKOVA, ULRIKE SPOHR, and RAYMOND U. LEMIEUX. Can. J. Chem. **70**, 233 (1992).

The synthesis of the methyl glycosides of the H-type 2 human blood group determinant (α-L-Fuc-(1c → 2b)-β-D-Gal-(1b → 4a)-β-D-GlcNAc-OMe) and its 6a-deoxy, 6a-*O*-methyl, 6a-chloro-6a-deoxy, 6a-deoxy-6a-fluoro, 6a-amino-6a-deoxy, 6a-acetamido-6a-deoxy, and 6a-deoxy-6a-pivalamido congeners is reported. The compounds were prepared to test the hypothesis that the binding of the H-type 2 trisaccharide by the lectin I of *Ulex europaeus* requires OH-6a to become intramolecularly hydrogen bonded to the neighboring O-5a ring atom. The results obtained in the binding studies are reported in an accompanying publication (Spohr, Paszkiewicz-Hnatiw, Morishima, and Lemieux) where it is demonstrated that the formation of the intramolecular hydrogen bond is not required for effective binding. In view of the results reported in another accompanying paper (Nikrad, Beierbeck, and Lemieux), OH-6a most likely remains in contact with the aqueous phase near the periphery of the combining site.

Key words: *N*-acetylglucosamine derivatives, H-type 2 blood group determinant and congeners, oligosaccharide synthesis.

EVA PETRAKOVA, ULRIKE SPOHR et RAYMOND U. LEMIEUX. Can. J. Chem. **70**, 233 (1992).

On a réalisé les synthèses des glycosides de méthyle du déterminant du groupe sanguin humain H de type 2 (α-L-Fuc-(1c → 2b)-β-D-Gal-(1b → 4a)-β-D-GlcNAc-OMe) et de ses congénères 6a-désoxy, 6a-*O*-méthyl, 6a-chloro-6a-désoxy, 6a-désoxy-6a-fluoro, 6a-amino-6a-désoxy, 6a-acétamido-6a-désoxy et 6a-désoxy-6a-pivalamido. On a préparé ces composés pour vérifier que l'hypothèse selon laquelle il est nécessaire, pour que la liaison du trisaccharide du H de type 2 par la lectine I de l'*Ulex europaeus* puisse se produire, que le groupe OH en 6a soit impliqué dans une liaison hydrogène intramoléculaire avec l'atome d'oxygène en 5a du cycle voisin. Les résultats obtenus lors des études de liaisons font l'objet d'une publication parallèle (Spohr, Paszkiewicz-Hnatiw, Morishima et Lemieux) dans laquelle il est démontré que la formation d'une liaison hydrogène intramoléculaire n'est pas nécessaire pour conduire à une liaison efficace. À la lumière des résultats rapportés dans une autre publication parallèle (Nikrad, Beierbeck et Lemieux), il semble que le groupe OH en 6a demeure en contact avec la phase aqueuse près de la périphérie du site qui se combine.

Mots clés : dérivés du *N*-acétylglucosamine, déterminant du groupe sanguin H de type 2 et ses congénères, synthèse d'oligosaccharides.

[Traduit par la rédaction]

Introduction

The X-ray crystal structure of the complex formed between the lectin IV of *Griffonia simplicifolia* (GS-IV) and the Lewis b tetrasaccharide (α-L-Fuc-(1 → 2)-β-D-Gal-(1 → 3)-[α-L-Fuc-(1 → 4)]-β-D-GlcNAc-OMe) (Le^b-OMe) has revealed that 6 of the 10 hydroxyl groups of the tetrasaccharide reside near or at the periphery of the combining site (1, 2). Chemical modifications of the parent Lewis b-OMe compound have shown that 5 of these 6 hydroxyl groups may be replaced, one at a time, by hydrogen, halogen, or methoxy with only a small effect on the stability (ΔG^0) of the complex. Evidently, these interactions at the periphery of the combining site are weak and in competition with the solvation of the interacting groupings by water.

A similar situation appears to exist for the binding of the H-type 2 trisaccharide in the form of its β-methyl glycoside (H-type 2-OMe), namely, α-L-Fuc-(1c → 2b)-β-D-Gal-(1b → 4a)-β-D-GlcNAc-OMe (**23**), by the lectin I of *Ulex europaeus* in that the 2a-acetamido, OH-3a, OH-6a, and OH-6b proved not essential for productive binding (3–5). Therefore, these substituents appear to reside in the complex at the edge of the combining site and accessible for interaction with the bulk water. It was of particular interest to further examine the involvement of the OH-6a group since deoxygenation at this position increased the stability of the complex by near 0.5 kcal/mol. This paper reports the synthesis of compounds required for a study (5) of the effect on binding of substituting the OH-6a group by smaller, larger, more hydrophobic, and more hydrophilic groups.

Discussion

The synthesis of the 6a-deoxy-6a-fluoro H-type 2 trisaccharide **13** (Scheme 1) started from the *N*-acetylglucosamine derivative **1** (6), which was hydrolyzed in 80% acetic acid to give diol **2** (6). The primary position of **2** was selectively mesylated at −20°C to provide the mesylate **3** (77% yield). Replacement of the mesyloxy group of **3** by fluorine was achieved with tetraethylammonium fluoride in refluxing acetonitrile. Crystalline **4** was isolated in 62% yield. Galactosylation of **4** with bromide **5** (3) was promoted with silver trifluoromethanesulfonate and provided the β-linked disaccharide **8** in 65% yield. Compound **9** was obtained by Zemplen debenzoylation of **8** (98%) and was reacted with fucosyl bromide **10** (7) under halide-ion catalyzed conditions (8) to give trisaccharide **12** (82%). The benzyl groups of **12** were removed by hydrogenolysis to provide the trisaccharide **13** (93%). The ^{19}F nmr data supported the position of the F-atom. The ^1H and ^{13}C nmr data are reported in

[1]The previous publication in this series is ref. 14.
[2]University of Alberta Postdoctoral Fellow, 1984–1985.
[3]Research Associate, 1984–1988, 1991–present.
[4]Author to whom correspondence may be addressed.

Can. J. Chem. Downloaded from www.nrcresearchpress.com by 123.30.183.119 on 09/08/12
For personal use only.

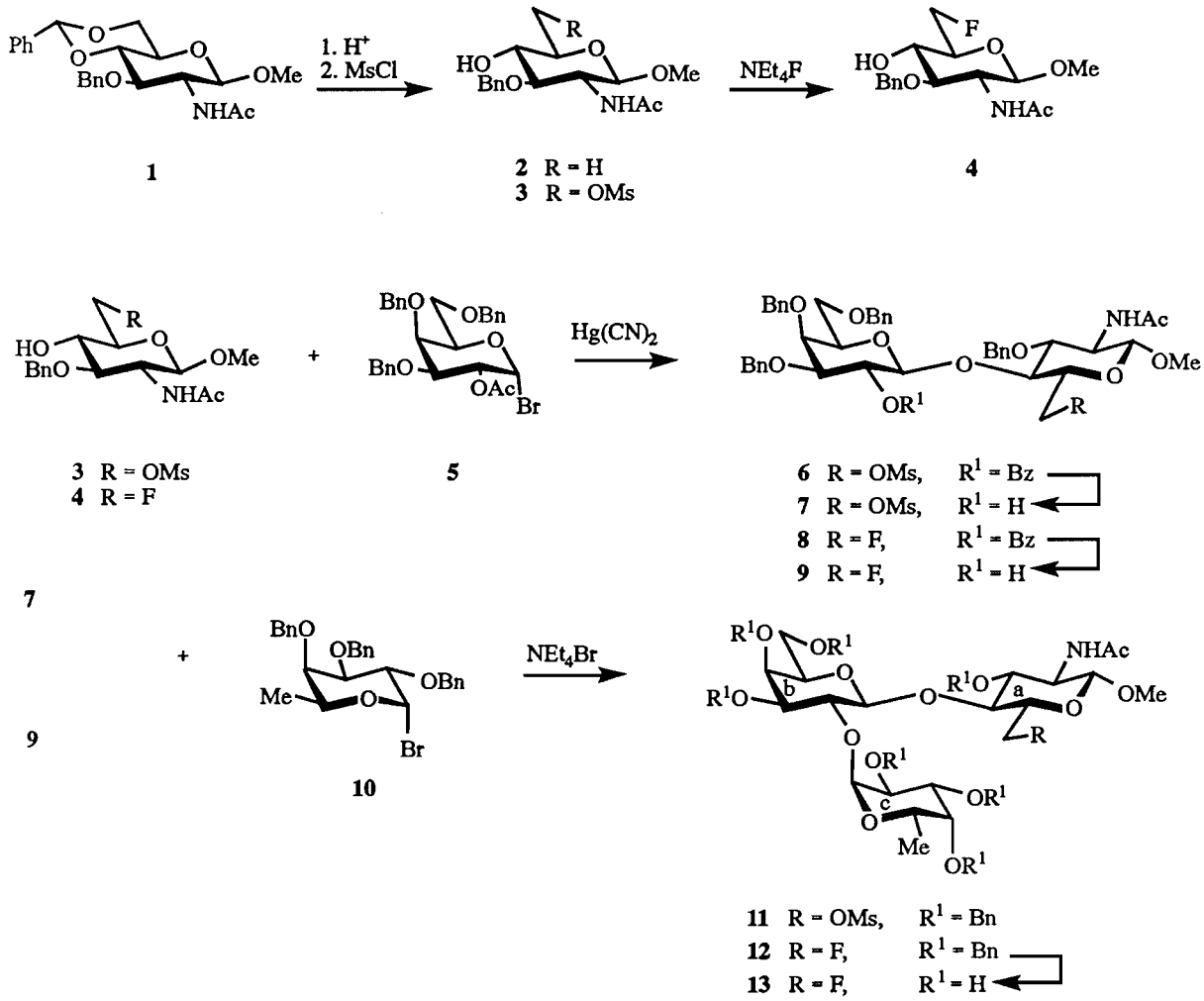

SCHEME 1

Tables 1 and 2 and confirmed the purity and structural assignment.

The blocked 6a-*O*-mesyl derivative **11** (Scheme 1) was prepared analogously. Coupling of galactosyl bromide **5** with alcohol **3** under Helferich conditions (9) furnished the β-linked disaccharide **6** (74%), which was debenzoylated with sodium methoxide to give **7** (75%). Reaction of **7** with the fucosyl bromide **10** in the presence of bromide ion then led to trisaccharide **11**, which was used as the intermediate for the preparation of the H-type 2 derivatives **23**–**29** (Scheme 2).

Mesylate **11** was converted into the benzoyl derivative **14** (84% yield) by replacement of the mesyloxy group by benzoate in *N*,*N*-dimethylformamide at 100°C. Debenzoylation then provided **15** in 98% yield. Hydrogenolysis of **15** in the presence of 5% palladium-on-carbon led to the H-type 2-OMe trisaccharide (**23**), which was to be used as the reference inhibitor.

Methylation of OH-6a of **15** (Scheme 2) using methyl iodide in the presence of barium oxide/barium hydroxide to avoid *N*-methylation of the acetamido group provided the methyl ether **16** in 79% yield. Debenzylation of **16** by catalytic hydrogenolysis then produced the desired 6a-*O*-methyl-H type 2-OMe (**24**).

Reduction of the 6a-mesylate (**11**) (Scheme 1) with sodium borohydride in dimethyl sulfoxide (10) provided the 6a-deoxy derivative **17** in 87% yield. Debenzylation then produced the desired 6a-deoxy H-type 2-OMe (**25**).

The blocked 6a-chloro-6a-deoxy compound **18** (Scheme 2) was prepared in 90% yield by treating the mesyl compound **11** with tetra-*n*-butylammonium chloride in benzene. Hydrogenolysis over palladium then provided **25** in 96% yield.

Reaction of the mesylate **11** with azide ion produced the 6a-azido-6a-deoxy compound (**19**), which was then reduced with zinc in acetic acid to form the amine **20** (Scheme 2) in 53% yield. Debenzylation by catalytic hydrogenolysis in acetic acid provided the desired 6a-amino-6a-deoxy H-type 2-OMe as its acetate salt (**27**). On the other hand, reduction of **19** in the presence of acetic anhydride produced the *N*-acetyl derivative **21** in 60% yield, which, in turn, was deblocked to produce the desired 6a-acetamido-6a-deoxy H-type 2-OMe (**28**). The amine (**20**) was treated with pivaloyl chloride in the presence of pyridine to form **22** in 84% yield. Hydrogenolysis then produced the desired 6a-deoxy-6a-pivalamido H-type 2-OMe (**29**) in 98% yield.

The ^{1}H and ^{13}C nmr data for H-type 2-OMe (**23**) and 6a-substituted derivatives reported in Tables 1 and 2 are seen to be in agreement with the structural assignments. The characteristic interunit deshielding of H-1c and H-5c of

Can. J. Chem. Downloaded from www.nrcresearchpress.com by 123.30.183.119 on 09/08/12
For personal use only.

TABLE 1. Comparison of ^{1}H nmr chemical shifts (ppm) and coupling constants (Hz) for the H-type 2 blood group determinant (**23**) and related structures[a]

		Derivatives of H-type 2-OMe (**23**)						
	H-type 2-OMe (**23**)	6a-OMe (**24**)[b]	6a-Deoxy (**25**)	6a-Chloro-6a-deoxy (**26**)	6a-Deoxy-6a-fluoro (**13**)	6a-Amino-6a-deoxy acetate (**27**)[d]	6a-Acetamido-6a-deoxy (**28**)[e]	6a-Deoxy-6a-pivalamido (**29**)[f]
βDGlcNAc a-unit								
H-1 ($J_{1,2}$)	4.44 (8.3)	4.43 (8.5)	4.43 (8.5)	4.52 (8.3)	4.50 (8.3)	4.48	4.45 (8.3)	4.45 (8.2)
H-2	3.73	3.73	3.73	3.75	3.74	3.75	3.75	3.74
H-3	*	*	3.74	*	*	*	*	*
H-4	3.76	3.75	3.56	*	3.87	*	3.73	*
H-5 ($J_{5,6}$)	3.47 (1.8)	3.53	3.53	3.68 (1.8)	3.63	3.75	3.55	*
H-6 ($J_{6,6'}$)	4.00 (11.5)	3.86	1.42 (5.7)	4.05 (12.5)	4.84 (10.5)[c]	3.48 (13.3)	3.66	*
H-6′ ($J_{5,6'}$)	3.79	3.66	—	3.89	4.76 (3.3)	3.26 (8.0)	3.49	*
CH_3O	3.51	3.49	3.48	3.51	3.51	3.51	3.50	3.50
CH_3CO	2.01	2.03	2.03	2.03	2.04	2.04	2.04	2.03
		$\Delta(\delta - \delta_{23})$ ppm						
βDGal b-unit								
H-1 ($J_{1,2}$)	4.54 (7.8)	−0.06	0.12	0.08	0.02	0.06	0.03	0.02
H-2 ($J_{2,3}$)	3.65 (10.0)	−0.01	0.0	0.01	0.02	0.0	−0.03	−0.03
H-3 ($J_{3,4}$)	3.88 (3.5)	0.0	−0.01	−0.01	−0.01	0.0	−0.01	0.0
H-4	3.89	0.0	0.0	*	0.0	0.0	0.01	0.0
H-5	3.65	−0.02[g]	*	*	*	*	*	*
H-6	3.76[g]	*	*	*	*	*	*	*
H-6′	3.75[g]	*	*	*	*	*	*	*
αLFuc c-unit								
H-1 ($J_{1,2}$)	5.31 (2.5)	−0.01	−0.02	0.03	0.01	0.0	−0.04	−0.03
H-2	3.78	0.01	0.02	0.02	0.0	0.01	−0.02	−0.02
H-3	3.80	0.0	0.01	*	*	*	*	*
H-4 ($J_{4,5}$)	3.79 (<1.0)	−0.01	0.01	0.03	−0.01	0.02	−0.03	0.01
H-5 ($J_{5,6}$)	4.23 (6.5)	0.0	0.04	−0.03	−0.03	0.02	−0.02	0.02
CH_3-6	1.23	0.0	−0.01	0.01	−0.01	0.0	−0.01	−0.01

[a]Measured at 360 MHz and 295 K using 0.04 M solutions in D_2O with acetone at 2.225 ppm as internal reference. The assignments were based on homonuclear shift-correlated 2-D experiments (COSY) and expected to be within ±0.01 ppm except for those marked with *g*, which are within ±0.03 ppm.
[b]CH_3O, δ = 3.43 ppm.
[c]$J_{F,6}$ = 47.5 Hz, $J_{F,6'}$ = 46.5 Hz.
[d]CH_3COOH, δ = 1.91 ppm.
[e]6a-CH_3CONH, δ = 2.04 ppm.
[f]$(CH_3)_3C$, δ = 1.20 ppm.
[g]Expected to be within ±0.03 ppm.
*Could not be assigned.

the fucose unit in the ^{1}H nmr spectrum of **23** by 0.54 and 0.19 ppm relative to α-L-Fuc-OMe (**11**) is similarly observed for the other derivatives. Since these deshieldings are interpreted as originating from the proximity of H-1c to O-3b of the β-D-Gal unit and H-5c to O-4a of the β-D-GlcNAc unit, the interglycosidic conformational preferences are not affected by changes in the 6a-substituent.

The immunochemical data are reported in an accompanying paper (5).

Experimental

General methods

The ^{1}H nmr spectra were measured at 360 and 400 MHz (Bruker WM 360 and WH 400) with tetramethylsilane as internal standard for $CDCl_3$ solutions. Reference standard for D_2O solutions was acetone (2.225 ppm). The ^{13}C nmr spectra were recorded at 100 and 75 MHz (Bruker WH 400 and AM 300) using D_2O as solvent and 1,4-dioxane (67.4 ppm) as internal standard. Optical rotations were measured at room temperature (23 ± 1°C) in a 1-dm cell on a Perkin–Elmer 241 polarimeter. Thin-layer chromatograms were performed on precoated plates of silica gel (60-F 254, E. Merck, Darmstadt) and visualized by spraying with 10% sulfuric acid in ethanol followed by heating. For column chromatography, silica gel 60 (230–400 mesh, E. Merck, Darmstadt) and distilled solvents were used. Solvents and reagents were purified and dried according to standard procedures. Melting points are uncorrected.

*Methyl 2-acetamido-3-O-benzyl-4,6-O-benzylidene-2-deoxy-β-D-glucopyranoside (**1**)*

Methyl 2-acetamido-4,6-*O*-benzylidene-2-deoxy-β-D-glucopyranoside (**12**) (30 g, 0.09 mol), barium oxide (42 g, 0.27 mol), barium hydroxide octahydrate (12 g, 0.04 mol), and benzyl bromide (15.3 mL, 0.13 mol) in *N*,*N*-dimethylformamide (360 mL) were stirred for 2 h. The reaction mixture was diluted with dichloromethane, filtered through a pad of Celite, and washed with cold aqueous 1 N hydrochloric acid, saturated aqueous sodium hydrogen carbonate, and water. The solution was concentrated, followed by the addition of diethyl ether. The precipitate was filtered to provide compound **1** (31.4 g, 82%). The analytical sample was recrystallized from ethanol, mp > 300°C, $[\alpha]_D$ −59.4 (*c* 0.8, di-

Can. J. Chem. Downloaded from www.nrcresearchpress.com by 123.30.183.119 on 09/08/12
For personal use only.

TABLE 2. Comparison of ^{13}C nmr chemical shifts (ppm) for the H-type 2 blood group determinant (**23**) and related structures[a]

		Derivatives of H-type 2-OMe (**23**)						
	H-type 2-OMe (**23**)	6a-OMe (**24**)[b]	6a-Deoxy (**25**)	6a-Chloro-6a-deoxy (**26**)	6a-Deoxy-6a-fluoro (**13**)	6a-Amino-6a-deoxy acetate (**27**)	6a-Acetamido-6a-deoxy (**28**)[c]	6a-Deoxy-6a-pivalamido (**29**)[d]
βDGlcNAc a-unit								
C-1	102.73	102.85	102.67	102.80	102.89	102.67	102.64	102.71
C-2	56.03	55.90	56.18	55.96	55.97	56.12	55.93	55.96
C-3	73.23	73.20	73.17	72.89	73.00	71.80[e]	73.05[e]	73.29[e]
C-4	77.26[e]	77.02	82.12	78.15	75.72	78.59[e]	78.01[e]	78.05[e]
C-5	76.14[f]	75.10	72.09	75.39	74.58	67.22[e]	73.51[e]	73.11[e]
C-6	61.10	71.56	17.60	44.36	82.40[g]	41.18	40.89	40.64
$CH_3(CO)$	23.05	23.01	23.03	23.02	23.01	23.02	23.02	23.01
CO	175.41	175.49	175.43	175.51	175.50	175.58	175.46	175.51
CH_3O	57.90	58.12	57.97	58.16	58.13	58.00	57.91	58.01
		$\Delta(\delta - \delta_{23})$ ppm						
βDGal b-unit								
C-1	101.19	−0.04	0.12	−0.06	−0.24	−1.17[e]	−0.18	−0.30
C-2	77.32[e]	−0.02	0.09	−0.22	−0.01	−0.08	0.56	0.39
C-3	74.43	−0.04	−0.02	−0.06	−0.18	−0.26	−0.11	−0.16
C-4	69.97	−0.02	0.02	0.0	−0.02	−0.14	−0.03	−0.05
C-5	76.09[f]	0.06	−0.06	0.10	0.02	0.02	0.17	0.28
C-6	61.87	0.06	0.07	0.0	0.05	0.01	0.04	0.09
αLFuc c-unit								
C-1	100.26	0.10	0.06	−0.10	0.02	−0.10[e]	0.29	0.22
C-2	69.13	−0.11	−0.04	−0.05	−0.03	−0.01	0.09	0.14
C-3	70.54	0.01	−0.02	−0.06	−0.07	0.04	−0.10	−0.14
C-4	72.56	−0.05	0.01	−0.04	0.09	−0.03	0.07	0.03
C-5	67.74	0.02	−0.04	0.08	0.12	0.12	−0.03	0.06
C-6	16.14	0.0	−0.05	0.0	−0.04	0.07	0.05	0.10

[a]0.05 M solutions in D_2O with dioxane as internal standard at 67.4 ppm were measured at 100 and 75 MHz at 295 K. The assignments were made by inspection.
[b]CH_3O, δ = 55.90 ppm.
[c]CH_3CO, δ = 22.52 ppm, CH_3CO, δ = 175.0 ppm.
[d]$NHCOC(CH_3)_3$, δ = 27.43 ppm, $NHCOC(CH_3)_3$, δ = 39.38 ppm, $NHCOC(CH_3)_3$, δ = 183.11 ppm.
[e,f]The corresponding assignments of the chemical shifts are tentative and may be reversed.
[g]$J_{6,F}$ = 168 Hz, $J_{5,F}$ = 18 Hz.

Can. J. Chem. Downloaded from www.nrcresearchpress.com by 123.30.183.119 on 09/08/12
For personal use only.

methyl sulfoxide) (lit. (6) $[\alpha]_D^{20}$ −58.2 (*c* 0.5, dimethyl sulfoxide)); ^1H nmr ($CDCl_3$) δ: 7.55–7.25 (m, 10H, 2Ph), 5.59 (s, 1H, C*H*Ph), 5.48 (d, 1H, $J_{NH,2}$ 7.5 Hz, NH), 4.89 (d, overlapped by CH_2Ph, $J_{1,2}$ 7.5 Hz, H-1), 4.90 and 4.64 (ABq, 2H, *J* 11.5 Hz, CH_2Ph), 4.36 (dd, 1H, $J_{6eq,6ax}$ 10.5 Hz, H-6eq), 4.27 (t, 1H, $J_{2,3} \sim J_{3,4} \sim$ 9.5 Hz, H-3), 3.80 (t, 1H, $J_{6ax,5}$ 10.0 Hz, H-6ax), 3.68 (t, 1H, $J_{4,5}$ 9.0 Hz, H-4), 3.53 (dt, 1H, H-5), 3.50 (s, 3H, CH_3O), 1.90 (s, 3H, CH_3CO). Anal. calcd. for $C_{23}H_{27}NO_6$: C 66.81, H 6.58, N 3.39; found: C 66.19, H 6.30, N 3.31.

*Methyl 2-acetamido-3-*O*-benzyl-2-deoxy-*β*-*D*-glucopyranoside (2)*

Compound **1** (2.0 g, 4.8 mmol) was heated in 80% acetic acid (60 mL) for 15 min at 80°C. The acid was removed by evaporation followed by co-distillation with water and ethanol to provide the title compound as a white solid (1.5 g, 96%). The analytical sample was recrystallized from ethanol, mp 214–215°C (lit. (6) mp 212–214°C (methanol–acetone–ether)), $[\alpha]_D$ −8.5 (*c* 1.0, dimethyl sulfoxide) (lit. (6) $[\alpha]_D^{20}$ −16, methanol)); ^1H nmr (D_2O) δ: 7.55–7.35 (m, 5H, Ph), 4.88 and 4.69 (ABq, 2H, *J* 12.0 Hz, CH_2Ph), 4.45 (d, 1H, $J_{1,2}$ 8.5 Hz, H-1), 3.97 (dd, 1H, $J_{6,6'}$ 12.0 Hz, $J_{5,6}$ 2.5 Hz, H-6), 3.78 (dd, 1H, $J_{5,6'}$ 6.0 Hz, H-6′), 3.75 (m, 1H, H-2), 3.59 (m, 2H, H-3, H-4), 3.51 (s, 3H, CH_3O), 3.49 (m, overlapped by CH_3O, H-5), 1.90 (s, 3H, CH_3CO). Anal. calcd. for $C_{16}H_{23}NO_6$: C 59.07, H 7.13, N 4.31; found: C 58.74, H 7.01, N 4.33.

*Methyl 2-acetamido-3-*O*-benzyl-2-deoxy-6-*O*-methanesulfonyl-*β*-*D*-glucopyranoside (3)*

Methanesulfonyl chloride (4 mL, 51.6 mmol) was added in three portions to a stirred solution of diol **2** (11 g, 33.8 mmol) in dry pyridine (240 mL) at −20°C. After 70 min, the reaction mixture was poured into aqueous sodium hydrogen carbonate and extracted with dichloromethane. The organic layer was washed twice with water, dried with sodium sulfate, and evaporated. The crude product was applied to a column of silica gel and eluted with dichloromethane–methanol (15:1) to give mesylate **3** (10.5 g, 77%). The analytical sample was obtained by recrystallization from ethanol, mp 164–165°C, $[\alpha]_D$ −14.2 (*c* 1.0, dichloromethane); ^1H nmr ($CDCl_3$) δ: 7.4–7.25 (m, 5H, Ph), 5.60 (d, 1H, $J_{2,NH}$ 8.0 Hz, NH), 4.83 (d, 1H, $J_{1,2}$ 8.0 Hz, H-1), 4.75 and 4.72 (ABq, 2H, *J* 12.0 Hz, CH_2Ph), 4.49 (d, 2H, $J_{5,6}$ 3.0 Hz, H_2-6), 4.07 (m, 1H, $J_{2,3}$ 10.5 Hz, $J_{3,4}$ 8.0 Hz, H-3), 3.58 (m, 2H, H-4, H-5), 3.48 (s, 3H, CH_3O), 3.25 (ddd, 1H, H-2), 3.06 (s, 3H, CH_3SO_2), 2.47 (d, 1H, $J_{OH,4}$ 3.0 Hz, OH), 1.95 (s, 3H, CH_3CO). Anal. calcd. for $C_{17}H_{25}NO_8S$: C 50.61, H 6.25, N 3.47, S 7.95; found: C 50.84, H 6.38, N 3.45, S 7.89.

*Methyl 2-acetamido-3-*O*-benzyl-2,6-dideoxy-6-fluoro-*β*-*D*-glucopyranoside (4)*

To a solution of mesylate **3** (2.5 g, 6.2 mmol) in acetonitrile (12 mL) was added a solution of tetraethylammonium fluoride

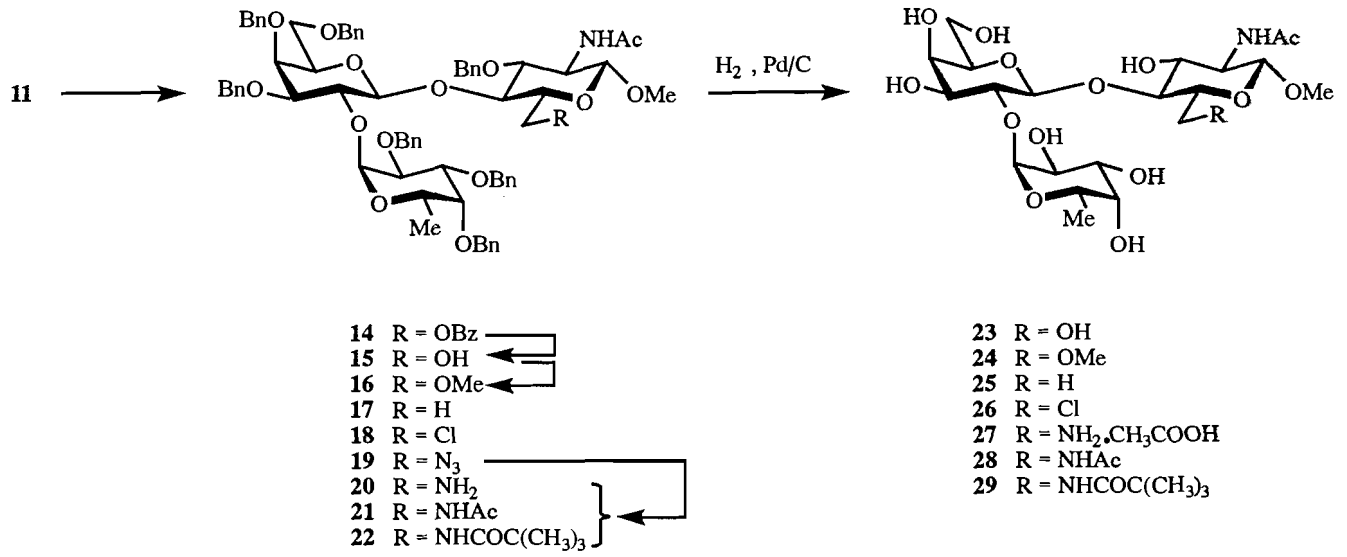

SCHEME 2

trihydrate (7 g, 34.4 mmol) in acetonitrile (12 mL) and the mixture was heated under reflux for 3 h. After evaporation of the solvent, the residue was applied to a column of silica gel (dichloromethane–methanol 30:1) and the resulting material crystallized from methanol–ether to provide **3** (1.25 g, 62%), mp 245–246°C, $[\alpha]_D$ −15.5 (*c* 0.6, methanol); ^{1}H nmr ($CDCl_3$) δ: 7.45–7.28 (m, 5H, Ph), 5.62 (d, 1H, $J_{NH,2}$ 7.5 Hz, NH), 4.87 (d, 1H, $J_{1,2}$ 8.5 Hz, H-1), 4.78 and 4.67 (ABq, 2H, *J* 11.5 Hz, CH_2Ph), 4.68 and 4.62 (m, 2H, $J_{6,6'}$ 10.5 Hz, $J_{5,6}$ 2.5 Hz, $J_{5,6'}$ 4.5 Hz, $J_{6,F} = J_{6',F}$ 47 Hz, H-6, H-6'), 4.13 (m, 1H, $J_{2,3}$ 10.0 Hz, $J_{3,4}$ 8.5 Hz, H-3), 3.58 (overlapped by H-5, 1H, H-4), 3.54 (m, overlapped by H-4 and CH_3O, H-5), 3.50 (s, 3H, CH_3O), 3.21 (dt, 1H, H-2), 1.98 (s, 3H, CH_3CO); ^{13}C nmr (CD_3CN, CD_3CN set at 118.9) δ: 171.35 (CH_3CO), 129.82, 129.47, 129.06 (Ph), 103.72 (C-1), 84.11 (C-3), 84.07 (d, $J_{C6,F}$ 169.8 Hz, C-6), 76.19 (d, $J_{C5,F}$ 17.4 Hz, C-5), 75.64 (CH_2Ph), 70.97 (d, $J_{C4,F}$ 7.6 Hz, C-4), 57.54, 56.02 (CH_3O, C-2), 24.03 (CH_3CO); ^{19}F nmr (376 MHz, $CDCl_3$, external standard C_6F_6 set at δ 0) δ: −72.31 (dt, $J_{F,H6} = J_{F,H6'}$ = 47 Hz, $J_{F,H5}$ 22.5 Hz, F-6). Anal. calcd. for $C_{16}H_{22}FNO_5$: C 58.71, H 6.77, N 4.28; found: C 58.62, H 6.75, N 4.10.

*Methyl 2-acetamido-4-*O*-(2-*O*-benzoyl-3,4,6-tri-*O*-benzyl-*β*-*D*-galactopyranosyl)-3-*O*-benzyl-2-deoxy-6-*O*-methanesulfonyl-*β*-*D*-glucopyranoside (6)*

A solution of 2-*O*-benzoyl-3,4,6-tri-*O*-benzyl-α-D-galactopyranosyl bromide (**5**, 15 mmol) (4) in toluene (25 mL) was added during a period of 1 h to a stirred solution of the alcohol **3** (4.0 g, 9.9 mmol) in nitromethane–toluene 1:1 (80 mL) containing mercuric cyanide (4.4 g, 17.4 mmol) at 40°C. After stirring for 1 h at 40°C, the solvent was evaporated, and the mixture was diluted with dichloromethane and washed successively with aqueous sodium hydrogen carbonate and water. The syrup obtained on evaporation was chromatographed on a column of silica gel (toluene – ethyl acetate 1:1, dichloromethane – ethyl acetate 2:1). The main component **6** was obtained as a foam in a yield of 74% (6.9 g), mp 68–69°C, $[\alpha]_D$ −4.5 (*c* 1.0, dichloromethane); ^{1}H nmr ($CDCl_3$) δ: 8.05–7.15 (m, 25H, 5Ph), 6.24 (d, 1H, $J_{NH,2a}$ 9.0 Hz, NH), 5.62 (dd, 1H, $J_{1b,2b}$ 7.5 Hz, $J_{2b,3b}$ 10.0 Hz, H-2b), 4.54 (d, 1H, H-1b), 4.43 (dd, overlapped by CH_2Ph, 1H, $J_{5a,6a}$ 4.5 Hz, H-6a), 4.33 (dd, 1H, $J_{6a,6a'}$ 11.0 Hz, $J_{5a,6a'}$ 5.5 Hz, H-6a'), 4.26 (d, 1H, $J_{1a,2a}$ 5.5 Hz, H-1a), 4.05 (m, 1H, $J_{2a,3a}$ 4.5 Hz, H-2a), 4.02 (d, 1H, $J_{3b,4b}$ 2.5 Hz, H-4b), 3.90 (t, 1H, $J_{3a,4a} \sim J_{4a,5a} \sim$ 4.5 Hz, H-4a), 3.80 (t, 1H, H-3a), 3.75 (m, H-5a), 3.71 (dd, 1H, H-3b), 3.66–3.50 (m, 3H, H-5b, H_2-6b), 3.14 (s, 3H, CH_3O), 2.75 (s, 3H, CH_3SO_2), 2.03 (s, 3H, CH_3CO). Anal. calcd. for $C_{51}H_{57}NO_{14}S$: C 65.16, H 6.11, N 1.49, S 3.41; found: C 65.36, H 6.12, N 1.45, S 3.53.

*Methyl 2-acetamido-3-*O*-benzyl-2-deoxy-6-*O*-methanesulfonyl-4-*O*-(3,4,6-tri-*O*-benzyl-*β*-*D*-galactopyranosyl)-*β*-*D*-glucopyranoside (7)*

Compound **6** (3.0 g, 3.2 mmol) was treated with methanolic 0.22 N sodium methoxide solution (35 mL) until *O*-debenzoylation was complete. The solution was made neutral with ion exchange resin Amberlite IR 120 H^+ and evaporated to a syrupy residue that was purified on a column of silica gel (carbon tetrachloride – methanol 15:1). Evaporation of the major fraction left a syrup that was crystallized from ethanol (2.0 g, 75%), mp 68–69°C, $[\alpha]_D$ +5.5 (*c* 1.0, dichloromethane); ^{1}H nmr ($CDCl_3$) δ: 7.5–7.2 (m, 20H, 4Ph), 5.71 (d, 1H, $J_{NH,2a}$ 8.3 Hz, NH), 4.86, 4.81, 4.72, 4.60, 4.55, 4.54 (3ABq, 6H, *J* 11.5 Hz, 3CH_2Ph), 4.71 (d, 1H, overlapped by CH_2Ph, $J_{1a,2a}$ 7.0 Hz, H-1a), 4.65 (dd, 1H, overlapped by CH_2Ph, $J_{5a,6a}$ 2.0 Hz, $J_{6a,6a'}$ 13.0 Hz, H-6a), 4.45 (d, 1H, $J_{1b,2b}$ 7.5 Hz, H-1b), 4.38 and 4.32 (ABq, 2H, *J* 11.5 Hz, CH_2Ph), 4.02 (m, 1H, H-3a), 3.96 (d, 1H, $J_{3b,4b}$ 2.5 Hz, H-4b), 3.91 (dd, 1H, $J_{2b,3b}$ 9.5 Hz, H-2b), ~3.81 (m, 2H, H-4a, H-5a), 3.57 (m, overlapped, H-2a), 3.46 (s, 3H, CH_3O), 3.40 (dd, overlapped, H-3b), 2.96 (s, 3H, CH_3SO_2), 1.85 (s, 3H, CH_3CO). Anal. calcd. for $C_{44}H_{53}NO_{13}S$: C 63.22, H 6.39, N 1.68, S 3.84; found: C 62.81, H 6.39, N 1.67, S 3.85.

*Methyl 2-acetamido-4-*O*-(2-*O*-benzoyl-3,4,6-tri-*O*-benzyl-*β*-*D*-galactopyranosyl)-3-*O*-benzyl-2,6-dideoxy-6-fluoro-*β*-*D*-glucopyranoside (8)*

A mixture of the alcohol **4** (0.5 g, 1.5 mmol), silver trifluoromethanesulfonate (1 g, 3.89 mmol), *sym*-collidine (0.2 mL, 1.5 mmol), and 4 Å molecular sieves (1 g) in dichloromethane (15 mL) was stirred at −30°C. A solution of bromide **5** (2 mmol) in dichloromethane (12 mL) was then added dropwise within 20 min. After 45 min at −30°C, tlc (ethyl acetate – methanol 10:1) indicated almost complete reaction. More *sym*-collidine (0.15 mL, 1.1 mmol) was added and after 15 min the reaction mixture was diluted with dichloromethane and filtered. The filtrate was washed with 3% hydrochloric acid, saturated sodium hydrogen carbonate, and water. The organic solution was dried and evaporated and the crude product purified on a column of silica gel (toluene – ethyl acetate 1:1, dichloromethane – ethyl acetate 2:1) to provide the title compound as a solid (0.85 g, 65%). The ana-

Can. J. Chem. Downloaded from www.nrcresearchpress.com by 123.30.183.119 on 09/08/12
For personal use only.

Can. J. Chem. Downloaded from www.nrcresearchpress.com by 123.30.183.119 on 09/08/12
For personal use only.

lytical sample was recrystallized from ethyl acetate – ether, mp 137–137.5°C, $[\alpha]_D$ −16.2 (*c* 0.6, chloroform); ^{1}H nmr ($CDCl_3$) δ: 8.05–7.1 (m, 25H, 5Ph), 6.07 (d, 1H, $J_{NH,2a}$ 8.5 Hz, NH), 5.64 (dd, 1H, $J_{1b,2b}$ 7.5 Hz, $J_{2b,3b}$ 10.0 Hz, H-2b), 4.53 (d, 1H, H-1b), 4.39 (d, overlapped by CH_2Ph, H-1a), 4.04 (d, 1H, $J_{3b,4b}$ 2.5 Hz, H-4b), 3.83 (m, H-2a), 3.65 (dd, 1H, H-3b), 3.21 (s, 3H, CH_3O), 1.97 (s, 3H, CH_3CO).

*Methyl 2-acetamido-3-*O*-benzyl-2,6-dideoxy-6-fluoro-4-*O*-(3,4,6-tri-*O*-benzyl-*β*-*D*-galactopyranosyl)-*β*-*D*-glucopyranoside (**9**)*

Compound **8** (0.3 g, 0.34 mmol) was debenzoylated in methanolic 0.5 N sodium methoxide solution (20 mL) at room temperature for 20 h. Deionization with Amberlite IR 120 H^+ followed by column chromatography on silica gel (dichloromethane–methanol 30:1) of the resulting material provided the title compound **9** (0.26 g, 98%). The analytical sample was obtained by recrystallization from ethyl acetate – ether, mp 157–158°C, $[\alpha]_D$ +7 (*c* 0.4 chloroform); ^{1}H nmr ($CDCl_3$) δ: 7.4–7.15 (m, 20H, 4Ph), 5.80 (d, 1H, $J_{NH,2a}$ 8.0 Hz, NH), 4.88, 4.84, 4.72, 4.59, 4.56 (3ABq, 6H, *J* 11.5 Hz, 3CH_2Ph), 4.87 (ddd, 1H, $J_{5a,6a}$ 3.5 Hz, $J_{6a,6a'}$ 10.5 Hz, $J_{6a,F}$ 46 Hz, H-6a), 4.75 (d, overlapped by CH_2Ph, H-1a), 4.71 (dd, overlapped by CH_2Ph, $J_{5a,6a'}$ 2.5 Hz, $J_{6a',F}$ 47 Hz, H-6a′), 4.43 (d, 1H, $J_{1b,2b}$ 7.5 Hz, H-1b), 4.38 and 4.31 (ABq, 2H, *J* 11.5 Hz, CH_2Ph), 4.08 (t, 1H, $J_{2a,3a} \sim J_{3a,4a} \sim$ 8.5 Hz, H-3a), 3.97 (d, 1H, $J_{3b,4b}$ 2.5 Hz, H-4b), 3.94 (dd, 1H, $J_{2b,3b}$ 9.5 Hz, H-2b), 3.88 (t, 1H, $J_{4a,5a}$ 7.5 Hz, H-4a), 3.68 (m, 1H, $J_{5a,F}$ 26.5 Hz, H-5a), ~3.51 (H-2a), 3.47 (s, CH_3O), 3.40 (dd, overlapped, H-3b), 1.85 (s, 3H, CH_3CO). Anal. calcd. for $C_{43}H_{50}FNO_{10}$: C 67.96, H 6.63, N 1.84; found: C 68.02, H 6.63, N 1.90.

*Methyl 2-acetamido-3-*O*-benzyl-2-deoxy-6-*O*-methanesulfonyl-4-*O*-[3,4,6-tri-*O*-benzyl-2-*O*-(2,3,4-tri-*O*-benzyl-α-*L*-fucopyranosyl)-β-*D*-galactopyranosyl]-β-*D*-glucopyranoside (**11**)*

A solution of 2,3,4-tri-*O*-benzyl-α-L-fucopyranosyl bromide (**10**, 2 mmol) (7) in dichloromethane (1 mL) was added to a mixture of compound **7** (0.6 g, 0.71 mmol), tetraethylammonium bromide (0.38 g, 1.8 mmol), and 4 Å molecular sieves (4.5 g) in *N*,*N*-dimethylformamide (0.5 mL) and dichloromethane (2 mL). After stirring for 20 h at room temperature, methanol (0.5 mL) was added and stirring continued for 2 h. The mixture was diluted with dichloromethane and filtered through Celite. The filtrate was extracted with saturated aqueous sodium hydrogen carbonate and water, followed by drying and evaporation. The residual solid was crystallized from hexane – ethyl acetate to give **11** (0.4 g, 45%). The mother liquor was evaporated and chromatographed on a column of silica gel with hexane – ethyl acetate 2:1 and then carbon tetrachloride – ethyl acetate 1:1 as eluent to provide an additional amount of compound **11** (0.40 g, total yield 90%), mp 68–69°C, $[\alpha]_D$ −60.8 (*c* 1.0, dichloromethane); ^{1}H nmr ($CDCl_3$) δ: 7.45–7.05 (m, 35H, 7Ph), 6.12 (d, 1H, $J_{2a,NH}$ 8.5 Hz, NH), 5.70 (d, 1H, $J_{1c,2c}$ 3.5 Hz, H-1c), 4.52 (d, 1H, $J_{1b,2b}$ 7.5 Hz, H-1b), 4.26 (q, 1H, $J_{5c,6c}$ 6.5 Hz, H_3-6c), 4.16 (dd, 1H, $J_{2b,3b}$ 9.5 Hz, H-2b), 4.03 (dd, 1H, $J_{2c,3c}$ 10.0 Hz, H-2c), 3.94 (d, 1H, $J_{3b,4b}$ 2.5 Hz, H-4b), 3.71 (dd, 1H, H-3b), 3.47 (s, 3H, CH_3O), 2.84 (s, 3H, CH_3SO_2), 1.78 (s, 3H, CH_3CO), 1.19 (d, 3H, H_3-6c). Anal. calcd. for $C_{71}H_{81}NO_{17}S$: C 68.09, H 6.52, N 1.12, S 2.56; found: C 68.01, H 6.42, N 1.10, S 2.58.

*Methyl 2-acetamido-3-*O*-benzyl-2,6-dideoxy-6-fluoro-4-*O*-[3,4,6-tri-*O*-benzyl-2-*O*-(2,3,4-tri-*O*-benzyl-α-*L*-fucopyranosyl)-β-*D*-galactopyranosyl]-β-*D*-glucopyranoside (**12**)*

A solution of fucosyl bromide **10** (0.40 mmol) in dichloromethane (2 mL) was added to a stirring mixture of the alcohol **9** (0.16 g, 0.21 mmol) and tetraethylammonium bromide (0.084 g, 0.4 mmol) in dry dichloromethane (2 mL) and *N*,*N*-dimethylformamide (0.5 mL) containing 4 Å molecular sieves (1.2 g). After 20 h at room temperature, methanol (2 mL) was added and the mixture was stirred for 2 h. The reaction mixture was worked up in the usual manner and purified on a column of silica gel (hexane – ethyl acetate 2:1, carbon tetrachloride – ethyl acetate 1:1) to provide compound **12** (0.204 g, 82%), $[\alpha]_D$ −46.4 (*c* 0.3, chloroform); ^{1}H nmr ($CDCl_3$) δ: 7.40–7.00 (m, 35H, 7Ph), 5.89 (d, 1H, $J_{NH,2a}$ 8.0 Hz, NH), 5.71 (d, 1H, $J_{1c,2c}$ 3.5 Hz, H-1c), 4.74 (d, overlapped by CH_2Ph, $J_{1a,2a}$ 7.5 Hz, H-1a), 4.47 (d, 1H, $J_{1b,2b}$ 7.5 Hz, H-1b), 4.28 (q, 1H, $J_{5c,6c}$ 6.5 Hz, H-5c), 4.21 (dd, 1H, $J_{2b,3b}$ 9.0 Hz, H-2b), 4.03 (dd, 1H, $J_{2c,3c}$ 10.0 Hz, H-2c), 4.02 (t, overlapped by H-3c, $J_{2a,3a} \sim J_{3a,4a} \sim$ 7.5 Hz, H-3a), 3.99 (d, 1H, $J_{3b,4b}$ 2.5 Hz, H-4b), 3.83 (dd, 1H, $J_{3c,4c}$ 3.0 Hz, H-3c), 3.78 (t, 1H, $J_{4a,5a}$ 7.0 Hz, H-4a), 3.71 (dd, 1H, H-3b), 3.69 (d, overlapped by H-3b, H-4c), 3.60–3.39 (m, 7H, H-5a, H-5b, H-6b, H-6b′ and CH_3O at 3.47), 1.83 (s, 3H, CH_3CO), 1.21 (d, 3H, H_3-6c). Anal. calcd. for $C_{70}H_{78}FNO_{14}$: C 71.47, H 6.68, N 1.19; found: C 71.23, H 6.43, N 1.30.

*Methyl 2-acetamido-2,6-dideoxy-6-fluoro-4-*O*-[2-*O*-(α-*L*-fucopyranosyl)-β-*D*-galactopyranosyl]-β-*D*-glucopyranoside (**13**)*

A mixture of compound **12** (0.058 g, 0.049 mmol) and 5% palladium-on-carbon (0.058 g) in 95% ethanol (2 mL) was hydrogenated at 100 psi (1 psi = 6.89 kPa) for 24 h. The catalyst was removed by filtration, the solvent evaporated, and the resulting material passed through a column of Sephadex LH 20 using ethanol–water 1:1 as eluant. Freeze-drying an aqueous solution provided compound **13** (0.025 g, 93%) as a light white powder; $[\alpha]_D$ −103.5 (*c* 0.5, water). The ^{1}H and ^{13}C nmr data are presented in Tables 1 and 2; ^{19}F nmr (376.5 MHz, D_2O, $CFCl_3$ as external standard set at 0) δ: −232.4 (dt, $J_{F,6a} = J_{F,6a'} = 47.0$ Hz, $J_{F,5a}$ 26.4 Hz, F-6a).

*Methyl 2-acetamido-6-*O*-benzoyl-3-*O*-benzyl-2-deoxy-4-*O*-[3,4,6-tri-*O*-benzyl-2-*O*-(2,3,4-tri-*O*-benzyl-α-*L*-fucopyranosyl)-β-*D*-galactopyranosyl]-β-*D*-glucopyranoside (**14**)*

A mixture of mesylate **11** (0.5 g, 0.4 mmol) and sodium benzoate (0.3 g, 2.1 mmol) in *N*,*N*-dimethylformamide (5 mL) was heated for 4.5 h at 100°C with stirring. The reaction mixture was diluted with dichloromethane and washed twice with water, dried with sodium sulfate, and evaporated. After purification of the crude product on a column of silica gel (ethyl acetate – carbon tetrachloride 2:1), the main fraction left, on evaporation, the benzoate **14** (0.43 g, 84%), $[\alpha]_D$ −38.7 (*c* 0.6, dichloromethane); ^{1}H nmr ($CDCl_3$) δ: 8.05–6.95 (m, 40H, 8Ph), 5.89 (d, 1H, $J_{2a,NH}$ 8.0 Hz, NH), 5.68 (d, 1H, $J_{1c,2c}$ 3.5 Hz, H-1c), 4.22 (dd, 1H, $J_{1b,2b}$ 8.0 Hz, $J_{2b,3b}$ 9.5 Hz, H-2b), 3.42 (s, 3H, CH_3O), 1.84 (s, 3H, CH_3CO), 1.24 (d, 3H, $J_{5c,6c}$ 6.0 Hz, H_3-6c). Anal. calcd. for $C_{77}H_{83}NO_{16}$: C 72.34, H 6.54, N 1.10; found: C 71.96, H 6.52, N 1.14.

*Methyl 2-acetamido-3-*O*-benzyl-2-deoxy-4-*O*-[3,4,6-tri-*O*-benzyl-2-*O*-(2,3,4-tri-*O*-benzyl-α-*L*-fucopyranosyl)-β-*D*-galactopyranosyl]-β-*D*-glucopyranoside (**15**)*

Compound **14** (0.15 g, 0.12 mmol) was debenzoylated in methanolic 0.5 M sodium methoxide (2 mL) for 20 h at room temperature. The product was isolated in the usual manner, purified on a column of silica gel (ethyl acetate – carbon tetrachloride 2:1), and obtained as a white foam (0.135 g, 98%), $[\alpha]_D$ −55 (*c* 0.5, dichloromethane); ^{1}H nmr ($CDCl_3$) δ: 7.4–7.0 (m, 35H, 7Ph), 5.69 (d, 1H, $J_{1c,2c}$ 3.5 Hz, H-1c), 5.59 (d, 1H, $J_{NH,2a}$ 8.0 Hz, NH), 4.79 (d, overlapped by CH_2Ph, $J_{1a,2a}$ 7.5 Hz, H-1a), 4.22 (dd, 1H, $J_{1b,2b}$ 7.5 Hz, $J_{2b,3b}$ 9.5 Hz, H-2b), 4.03 (dd, 1H, $J_{2c,3c}$ 10.0 Hz, H-2c), 3.48 (s, 3H, CH_3O), 1.90 (s, 3H, CH_3CO), 1.22 (d, 3H, $J_{5c,6c}$ 6.5 Hz, H_3-6c). Anal. calcd. for $C_{70}H_{79}NO_{15}$: C 71.59, H 6.78, N 1.19; found: C 71.87, H 6.79, N 1.14.

*Methyl 2-acetamido-3-*O*-benzyl-2-deoxy-6-*O*-methyl-4-*O*-[3,4,6-tri-*O*-benzyl-2-*O*-(2,3,4-tri-*O*-benzyl-α-*L*-fucopyranosyl)-β-*D*-galactopyranosyl]-β-*D*-glucopyranoside (**16**)*

A solution of methyl iodide (0.06 mL, 0.96 mmol) in *N*,*N*-dimethylformamide (3 mL) was added to a mixture of compound **15** (0.1 g, 0.085 mmol), barium oxide (0.08 g, 0.52 mmol), and barium hydroxide octahydrate (0.08 g, 0.25 mmol) in *N*,*N*-dimethylformamide (1.0 mL). After stirring for 20 h at room temperature,

Can. J. Chem. Downloaded from www.nrcresearchpress.com by 123.30.183.119 on 09/08/12
For personal use only.

the mixture was diluted with dichloromethane, filtered, and the filtrate washed with 3% hydrochloric acid, aqueous saturated sodium hydrogen carbonate, and water. Evaporation of the solvent, followed by column chromatography (ethyl acetate – dichloromethane 2:1) of the crude product provided **16** (0.08 g, 79%) as a white foam, $[\alpha]_D$ −59.3 (*c* 1.0, dichloromethane); ^{1}H nmr ($CDCl_3$) δ: 7.4–7.0 (m, 35H, 7Ph), 5.79 (d, 1H, $J_{NH,2a}$ 8.0 Hz, NH), 5.72 (d, 1H, $J_{1c,2c}$ 3.5 Hz, H-1c), 4.72 (d, 1H, $J_{1a,2a}$ 7.0 Hz, H-1a), 4.20 (t, 1H, $J_{1b,2b}$ 7.5 Hz, $J_{2b,3b}$ 9.5 Hz, H-2b), 3.45, 3.33 (2s, each 3H, $2CH_3O$), 1.84 (s, 3H, CH_3CO), 1.22 (s, 3H, $J_{5c,6c}$ 6.5 Hz, H_3-6c). Anal. calcd. for $C_{71}H_{81}NO_{15}$: C 71.76, H 6.87, N 1.18; found: C 71.66, H 6.79, N 1.19.

*Methyl 2-acetamido-3-*O*-benzyl-2,6-dideoxy-4-*O*-[3,4,6-tri-*O*-benzyl-2-*O*-(2,3,4-tri-*O*-benzyl-*α*-*L*-fucopyranosyl)-*β*-*D*-galactopyranosyl]-*β*-*D*-glucopyranoside (17)*

A mixture of **11** (0.5 g, 0.40 mmol), sodium borohydride (0.06 g, 1.6 mmol), and dimethyl sulfoxide (2 mL) was heated with stirring for 12 h at 85° C in an atmosphere of nitrogen. After cooling, the reaction mixture was poured into ice water, and the precipitate was filtered off and dissolved in dichloromethane. The solution was extracted twice with water, dried, and evaporated. After purification of the crude product by column chromatography on silica gel (carbon tetrachloride – ethyl acetate 1:1) pure **17** (0.4 g, 87%) was obtained as a syrup. Recrystallization from hexane – ethyl acetate 2:1 provided the analytical sample as white needles, mp 118–119°C, $[\alpha]_D$ −60.8 (*c* 1.0, dichloromethane); ^{1}H nmr ($CDCl_3$) δ: 7.40–7.00 (m, 35H, 7Ph), 5.69 (d, 1H, $J_{1c,2c}$ 3.5 Hz, H-1c), 5.54 (d, 1H, $J_{NH,2a}$ 7.5 Hz, NH), 4.75 (d, overlapped by CH_2Ph, 1H, $J_{1a,2a}$ 8.0 Hz, H-1a), 4.58 (d, overlapped by CH_2Ph, 1H, $J_{1b,2b}$ 7.5 Hz, H-1b), 4.35 (q, overlapped by CH_2Ph, H-5c), 4.24 (dd, 1H, $J_{2b,3b}$ 10.0 Hz, H-2b), 4.02 (dd, 1H, $J_{2c,3c}$ 10.0 Hz, H-2c), 4.00 (d, 1H, $J_{3b,4b}$ 2.5 Hz, H-4b), 3.92 (t, 1H, $J_{2a,3a} \sim J_{3a,4a} \sim$ 9.0 Hz, H-3a), 3.87 (dd, 1H, $J_{3c,4c}$ 2.5 Hz, H-3c), 3.71 (dd, 1H, H-3b), 3.66 (d, 1H, H-4c), ~3.5 (H-4a), 3.48 (s, 3H, CH_3O), 3.29 (m, H-5a), 3.20 (m, H-2a), 1.80 (s, 3H, CH_3CO), 1.32 (d, 3H, $J_{5a,6a}$ 6.5 Hz, H_3-6a), 1.22 (d, 3H, $J_{5c,6c}$ 6.5 Hz, H_3-6c). Anal. calcd. for $C_{70}H_{79}NO_{14}$: C 72.58, H 6.87, N 1.21; found: C 72.47, H 6.88, N 1.19.

*Methyl 2-acetamido-3-*O*-benzyl-6-chloro-2,6-dideoxy-4-*O*-[3,4,6-tri-*O*-benzyl-2-*O*-(2,3,4-tri-*O*-benzyl-*α*-*L*-fucopyranosyl)-*β*-*D*-galactopyranosyl]-*β*-*D*-glucopyranoside (18)*

A solution of **11** (0.5 g, 0.40 mmol) and tetra-*n*-butylammonium chloride (0.15 g, 0.54 mmol) in dry benzene (10 mL) was heated at 70°C for 20 h. After evaporation, the crude product was chromatographed on a column of silica gel (dichloromethane – ethyl acetate 2:1) to provide compound **18** (0.43 g, 90%) as a solid. Recrystallization from ethanol provided the analytical sample, mp 123–124°C, $[\alpha]_D$ − 56 (*c* 1.0, dichloromethane); ^{1}H nmr ($CDCl_3$) δ: 7.45–7.00 (m, 35H, 7Ph), 5.95 (d, 1H, $J_{NH,2a}$ 8.5 Hz, NH), 5.70 (d, 1H, $J_{1c,2c}$ 3.5 Hz, H-1c), 4.70 (d, overlapped by CH_2Ph, 1H, $J_{1a,2a}$ 7.5 Hz, H-1a), 4.50 (d, overlapped by CH_2Ph, 1H, $J_{1b,2b}$ 7.5 Hz, H-1b), 4.29 (q, overlapped by CH_2Ph, 1H, $J_{5c,6c}$ 6.5 Hz, H-5c), 4.18 (dd, 1H, $J_{2b,3b}$ 9.5 Hz, H-2b), 4.02 (dd, 1H, $J_{2c,3c}$ 10.0 Hz, H-2c), ~3.98 (H-4a), 3.96 (d, $J_{3b,4b}$ 2.5 Hz, H-4b), 3.89 (dd, 1H, $J_{3c,4c}$ 2.5 Hz, H-3c), 3.82 (t, 1H, $J_{2a,3a} \sim J_{3a,4a} \sim$ 6.5 Hz, H-3a), 3.73 (H-4c), 3.70 (dd, overlapped, H-3b), 3.60 (m, H-2a), 3.47 (s, 3H, CH_3O), 1.80 (s, 3H, CH_3CO), 1.20 (d, 3H, H_3-6c). Anal. calcd. for $C_{70}H_{78}ClNO_{14}$: C 70.49, H 6.59, Cl 2.97, N 1.17; found: C 70.34, H 6.51, Cl 3.24, N 1.20.

*Methyl 2-acetamido-6-azido-3-*O*-benzyl-2,6-dideoxy-4-*O*-[3,4,6-tri-*O*-benzyl-2-*O*-(2,3,4-tri-*O*-benzyl-*α*-*L*-fucopyranosyl)-*β*-*D*-galactopyranosyl]-*β*-*D*-glucopyranoside (19)*

A mixture of **11** (0.8 g, 0.64 mmol) and sodium azide (0.24 g, 3.7 mmol) in *N*,*N*-dimethylformamide (9 mL) was heated with stirring for 4 h at 70°C. It was diluted with dichloromethane, washed with water, and followed by drying and evaporation. The resulting product was purified on a column of silica gel (ethyl acetate – carbon tetrachloride 2:1) to give the title compound **19** (0.70 g, 91%) as a foam; $[\alpha]_D$ −62.7 (*c* 1.0, dichloromethane); IR ($CHCl_3$) *ν*: 3280 (NH), 2098 (N_3) cm^{-1}; ^{1}H nmr ($CDCl_3$) δ: 7.40–7.00 (m, 35H, 7Ph), 5.70 (d, 1H, overlapped by NH, $J_{1c,2c}$ 3.5 Hz, H-1c), 5.68 (d, overlapped by H-1c, NH), 4.79 (d, overlapped by CH_2Ph, $J_{1a,2a}$ 7.5 Hz, H-1a), 4.42 (d, overlapped by CH_2Ph, $J_{1b,2b}$ 8.0 Hz, H-1b), 4.22 (q, overlapped by H-2b, H-5c), 4.21 (dd, $J_{2b,3b}$ 9.5 Hz, H-2b), 4.03 (dd, overlapped, H-2c), 4.00 (overlapped, H-3a), 3.99 (overlapped, H-4b), 3.81 (dd, 1H, $J_{2c,3c}$ 10.0 Hz, $J_{3c,4c}$ 2.8 Hz, H-3c), 3.75 (d, H-4c), 3.71 (dd, 1H, $J_{3b,4b}$ 2.5 Hz, H-3b), 3.49 (overlapped, CH_3O), 3.36 (dt, H-2a), 1.85 (s, 3H, CH_3CO), 1.23 (d, 3H, $J_{5c,6c}$ 6.5 Hz, H_3-6c). Anal. calcd. for $C_{70}H_{78}N_4O_{14}$: C 70.10, H 6.56, N 4.67; found: C 70.26, H 6.54, N 4.67.

*Methyl 2-acetamido-6-amino-3-*O*-benzyl-2,6-dideoxy-4-*O*-[3,4,6-tri-*O*-benzyl-2-*O*-(2,3,4-tri-*O*-benzyl-*α*-*L*-fucopyranosyl)-*β*-*D*-galactopyranosyl]-*β*-*D*-glucopyranoside (20)*

Zinc dust (0.40 g) and activated zinc–copper couple (0.20 g) (13) were added to a solution of azido compound **19** (0.40 g, 0.33 mmol) in glacial acetic acid (2 mL) with stirring at 18°C. After 1 h, the mixture was filtered, and the filtrate evaporated and coevaporated three times with toluene. The resulting syrup was dissolved in dichloromethane and the solution washed with water, sodium hydrogen carbonate, and water. Purification of the crude product by column chromatography (silica gel, dichloromethane–methanol 30:1) provided **20** as a foam (0.206 g, 53%), $[\alpha]_D$ −31.5 (*c* 0.6, dichloromethane); IR ($CHCl_3$) *ν*: 3280 (NH_2) cm^{-1}; ^{1}H nmr ($CDCl_3$) δ: 7.40–7.00 (m, 35H, 7Ph), 5.69 (d, 1H, $J_{1c,2c}$ 3.5 Hz, H-1c), 5.55 (d, 1H, $J_{NH,2a}$ 7.5 Hz, NH), 4.75 (d, overlapped by CH_2Ph, H-1a), 4.54 (d, overlapped by CH_2Ph, $J_{1b,2b}$ 7.5 Hz, H-1b), 4.34 (q, overlapped by CH_2Ph, H-5c), 4.24 (dd, 1H, $J_{2b,3b}$ 9.5 Hz, H-2b), 4.03 (dd, 1H, $J_{2c,3c}$ 10.0 Hz, H-2c), 4.00 (d, 1H, $J_{3b,4b}$ 2.5 Hz, H-4b), 3.93 (t, 1H, $J_{3a,4a} \sim J_{4a,5a} \sim$ 9.0 Hz, H-3a), 3.87 (dd, 1H, $J_{3c,4c}$ 2.5 Hz, H-3c), 3.78 (d, 1H, H-4c), 3.76 (overlapped by H-4c and H-3b, H-4a), 3.72 (dd, 1H, H-3b), 3.60–3.43 (m, 6H, H-5b, H-6b, H-6b′, and CH_3O at 3.48), ~3.31 (m, 2H, H-2a, H-5a), 3.08 (dd, 1H, $J_{6a,6a'}$ 12.0 Hz, $J_{5a,6a}$ 2.5 Hz, H-6a), 2.91 (dd, 1H, $J_{5a,6a'}$ 6.5 Hz, H-6a′), 1.89 (s, 3H, CH_3CO), 1.25 (d, 3H, $J_{5c,6c}$ 6.5 Hz, H_3-6c). Anal. calcd. for $C_{70}H_{80}N_2O_{14}$: C 71.65, H 6.87, N 2.38; found: C 70.88, H 6.67, N 2.32.

*Methyl 2,6-diacetamido-3-*O*-benzyl-2,6-dideoxy-4-*O*-[3,4,6-tri-*O*-benzyl-2-*O*-(2,3,4-tri-*O*-benzyl-*α*-*L*-fucopyranosyl)-*β*-*D*-galactopyranosyl]-*β*-*D*-glucopyranoside (21)*

To a solution of azido compound **19** (0.20 g, 0.17 mmol) in glacial acetic acid (2 mL) and acetic anhydride (0.5 mL) were added zinc dust (200 mg) and activated zinc–copper (100 mg) couple. The mixture was stirred for 45 min at 18°C, filtered, evaporated, and coevaporated with toluene. The resulting syrup was dissolved in dichloromethane and the solution was washed with water, saturated sodium hydrogen carbonate, and water, followed by drying and evaporation. Column chromatography on silica gel (dichloromethane–methanol 30:1) provided in the main fraction compound **21** (0.124 g, 60%) as a foam, $[\alpha]_D$ −47 (*c* 0.5, dichloromethane); ^{1}H nmr ($CDCl_3$) δ: 7.40–7.00 (m, 35H, 7Ph), 5.83 (t, 1H, $J_{NH,6a} \sim J_{NH,6a'} \sim$ 5.0 Hz, NH-6a), 5.70 (d, 1H, $J_{NH,2a}$ 8.5 Hz, NH-2a), 5.62 (d, 1H, $J_{1c,2c}$ 3.0 Hz, H-1c), 4.59 (d, overlapped by CH_2Ph, $J_{1a,2a} \sim J_{1b,2b}$ 7.5 Hz, H-1a, H-1b), 4.34 (q, overlapped by CH_2Ph, H-5c), 4.16 (dd, 1H, $J_{2b,3b}$ 9.5 Hz, H-2b), 4.02 (s and d, 2H, H-2c, H-3c), 3.92 (d, overlapped by H-3a, $J_{3b,4b}$ 2.5 Hz, H-4b), 3.91 (t, 1H, overlapped by H-4b, H-3a), 3.85 (s, 1H, H-4c), 3.71 (2H, H-4a and H-3b), 3.62 (2H, H-2a and H-6a), 3.45 (s, overlapped, CH_3O), 1.82 (s, 3H, CH_3CO), 1.21 (s, 3H, H_3-6c). Anal. calcd. for $C_{72}H_{82}N_2O_{15}$: C 71.15, H 6.80, N 2.30; found: C 70.90, H 6.74, N 2.25

*Methyl 2-acetamido-3-*O*-benzyl-2,6-dideoxy-6-pivalamido-4-*O*-[3,4,6-tri-*O*-benzyl-2-*O*-(2,3,4-tri-*O*-benzyl-*α*-*L*-fucopyranosyl)-*β*-*D*-galactopyranosyl]-*β*-*D*-glucopyranoside (22)*

To a solution of **20** (0.15 g, 0.13 mmol) in dichloromethane (5 mL) were added dry pyridine (0.04 mL) and, dropwise, pival-

Can. J. Chem. Downloaded from www.nrcresearchpress.com by 123.30.183.119 on 09/08/12
For personal use only.

oyl chloride (0.03 mL, 0.24 mmol). After stirring at room temperature for 30 min, the reaction mixture was worked up conventionally and the product purified on a column of silica gel (dichloromethane–methanol 25:1). The main fraction gave **22** as a foam (0.143 g, 89%), $[\alpha]_D$ −39 (*c* 1.8, dichloromethane); ^{1}H nmr ($CDCl_3$) δ: 7.45–7.00 (m, 35H, 7Ph), 5.99 (6, 1H, $J_{NH,6a} \sim J_{NH,6a'} \sim 5$ Hz, NH-6a), 5.65 (d, 1H, $J_{1c,2c}$ 3.5 Hz, H-1c), 5.60 (d, 1H, $J_{NH,2a}$ 8.0 Hz, NH-2a), 4.65 (d, overlapped by CH_2Ph, $J_{1a,2a}$ 7.5 Hz, H-1a), 4.56 (d, overlapped by CH_2Ph, H-1b), 4.40 (q, overlapped by CH_2Ph, H-5c), 4.20 (dd, overlapped by H-2b, H-3c), 4.19 (dd, overlapped by H-3c, $J_{2b,3b}$ 9.5 Hz, H-2b), 4.02 (dd, overlapped by H-4c, H-2c), 4.00 (d, overlapped by H-2c, H-4c), 3.95 (d, overlapped by H-3a, H-4b), 3.93 (t, 1H, $J_{2a,3a} \sim J_{3a,4a} \sim 7.5$ Hz, H-3a), 3.85 (m, 1H, $J_{6a,6a'}$ 13.5 Hz, $J_{6a,5a}$ 2.5 Hz, H-6a), 3.74 (dd, 1H, $J_{3b,4b}$ 3.0 Hz, H-3b), 3.64 (t, 1H, $J_{4a,5a}$ 7.5 Hz, H-4a), 3.59–3.39 (m, 8H, H-5a, H-5b, H-6b, H-6b′, H-2a, and CH_3O at 3.46), 3.20 (m, 1H, H-6a′), 1.85 (s, 3H, CH_3CO), 1.22 (d, 3H, $J_{5c,6c}$ 6.5 Hz, H_3-6c), 1.14 (s, 9H, $(CH_3)_3C$). Anal. calcd. for $C_{75}H_{88}N_2O_{15}$: C 71.63, H 7.05, N 2.23; found: C 71.86, H 7.06, N 2.20

*Methyl 2-acetamido-2-deoxy-4-*O*-[2-*O*-(α-*L*-fucopyranosyl)-β-*D*-galactopyranosyl]-β-*D*-glucopyranoside (23)*

Compound **15** (0.05 g, 0.04 mmol) in 95% ethanol (2 mL) was hydrogenated over 5% palladium-on-carbon (0.1 g) for 24 h at 100 psi. Subsequent gel filtration of the hydrogenation product on a column of Bio-Gel P-2 (10% ethanol) followed by freeze-drying an aqueous solution provided compound **23** (0.022 g, 95%) as a light white powder, $[\alpha]_D$ −94.8 (*c* 0.4, water). The ^{1}H and ^{13}C nmr data are presented in Tables 1 and 2.

*Methyl 2-acetamido-2-deoxy-4-*O*-[2-*O*-(α-*L*-fucopyranosyl)-β-*D*-galactopyranosyl]-6-*O*-methyl-β-*D*-glucopyranoside (24)*

A solution of **16** (0.1 g, 0.084 mmol) in 95% ethanol (2 mL) containing 5% palladium-on-carbon (0.2 g) was hydrogenated for 24 h at 100 psi. Chromatography on a column of Bio-Gel P-2 (10% ethanol) provided **24** (45 mg, 96%) after lyophilization as a light white powder, $[\alpha]_D$ −62.5 (*c* 1.0, water). The ^{1}H and ^{13}C nmr data are reported in Tables 1 and 2.

*Methyl 2-acetamido-2,6-dideoxy-4-*O*-[2-*O*-(α-*L*-fucopyranosyl)-β-*D*-galactopyranosyl]-β-*D*-glucopyranoside (25)*

Compound **17** (0.1 g, 0.086 mmol) in 95% ethanol (2 mL) was hydrogenated over 5% palladium-on-carbon (0.1 g) for 20 h at 100 psi. After purification of the hydrogenation product on a column of Bio-Gel P-2 (10% ethanol) and lyophilization of an aqueous solution, **25** (0.044 g, 96%) was obtained as a light white powder, $[\alpha]_D$ −78.5 (*c* 1.0, water). The ^{1}H and ^{13}C nmr data are reported in Tables 1 and 2.

*Methyl 2-acetamido-6-chloro-2,6-dideoxy-4-*O*-[2-*O*-(α-*L*-fucopyranosyl)-β-*D*-galactopyranosyl]-β-*D*-glucopyranoside (26)*

Compound **18** (0.068 g, 0.057 mmol) was hydrogenated and the hydrogenation product purified as described for the preparation of **25** to provide trisaccharide **26** (0.03 g, 95%), $[\alpha]_D$ −57.5 (*c* 1.0, water). The ^{1}H and ^{13}C nmr data are reported in Tables 1 and 2.

*Methyl 2-acetamido-6-amino-2,6-dideoxy-4-*O*-[2-*O*-(α-*L*-fucopyranosyl)-β-*D*-galactopyranosyl]-β-*D*-gluocpyranoside acetate (27)*

Compound **20** (0.06 g, 0.051 mmol) and 5% palladium-on-carbon (0.06 g) were hydrogenated in glacial acetic acid (1 mL) at 20 psi. After 20 h, the mixture was filtered and evaporated at room temperature to provide, after freeze-drying an aqueous solution, compound **27** (0.027 g, 88%) as a white powder, $[\alpha]_D$ −56.5 (*c* 1.0, water). The ^{1}H and ^{13}C nmr data are reported in Tables 1 and 2.

*Methyl 2,6-diacetamido-2,6-dideoxy-4-*O*-[2-*O*-(α-*L*-fucopyranosyl)-β-*D*-galactopyranosyl]-β-*D*-glucopyranoside (28)*

Compound **21** (0.1 g, 0.082 mmol) was hydrogenated over 5% palladium-on-carbon as described for the preparation of **25** with subsequent gel filtration to provide **28** (0.047 g, 97%), $[\alpha]_D$ −77.5 (*c* 1.0, water). The ^{1}H and ^{13}C nmr data are reported in Tables 1 and 2.

*Methyl 2-acetamido-2,6-dideoxy-4-*O*-[2-*O*-(α-*L*-fucopyranosyl)-β-*D*-galactopyranosyl]-6-pivalamido-β-*D*-glucopyranoside (29)*

Compound **22** (0.130 g, 0.1 mmol) was hydrogenated in the presence of 5% palladium-on-carbon (0.13 g) as usual and the resulting product purified on a column of Bio-Gel P-2 (10% ethanol) to provide the title compound **29** (0.064 g, 98%), $[\alpha]_D$ −83.8 (*c* 1.0, water). The ^{1}H and ^{13}C nmr data are reported in Tables 1 and 2.

Acknowledgements

This research was supported by the Natural Sciences and Engineering Research Council of Canada (Grant A-172 to R.U.L.) and the Alberta Heritage Foundation for Medical Research.

1. L. T. J. Delbaere, M. Vandonselaar, L. Prasad, J. W. Quail, P. V. Nikrad, J. R. Pearlstone, M. R. Carpenter, L. B. Smillie, U. Spohr, and R. U. Lemieux. Can. J. Chem. **68**, 1116 (1990).
2. R. U. Lemieux, L. T. J. Delbaere, H. Beierbeck, and U. Spohr. Ciba Found. Symp. **158**, 231 (1990).
3. O. Hindsgaul, T. Norberg, J. LePendu, and R. U. Lemieux. Carbohydr. Res. **109**, 109 (1982).
4. O. Hindsgaul, D. P. Khare, M. Bach, and R. U. Lemieux. Can. J. Chem. **63**, 2653 (1982).
5. U. Spohr, E. Paszkiewicz-Hnatiw, N. Morishima, and R. U. Lemieux. Can. J. Chem. **70**, 254 (1992).
6. A. S. Shashkov, A. Y. Evstigneev, and V. A. Derevitskaya. Bioorg. Khim. **4**, 1495 (1978).
7. U. Spohr and R. U. Lemieux. Carbohydr. Res. **174**, 211 (1988).
8. R. U. Lemieux, K. B. Hendricks, R. V. Stick, and K. James. J. Am. Chem. Soc. **97**, 4056 (1975).
9. B. Helferich and K.-F. Wedemeyer. Justus Liebigs Ann. Chem. **563**, 139 (1949).
10. H. Weidmann, N. Wolf, and W. Timpe. Carbohydr. Res. **24**, 184 (1972).
11. H. Thøgersen, R. U. Lemieux, K. Bock, and B. Meyer. Can. J. Chem. **60**, 44 (1982).
12. W. Roth and W. Pigman. J. Am. Chem. Soc. **82**, 4608 (1960); J. Conchie and G. A. Levvy. Methods Carbohydr. Chem. **2**, 332 (1963).
13. L. F. Fieser and M. Fieser. Reagents for organic synthesis. J. Wiley and Sons, New York. 1967. p. 1292.
14. R. U. Lemieux, R. Cromer, and U. Spohr. Can. J. Chem. **66**, 3083 (1988).

Molecular recognition X. A novel procedure for the detection of the intermolecular hydrogen bonds present in a protein·oligosaccharide complex[1]

P. V. NIKRAD,[2] H. BEIERBECK,[3] AND R. U. LEMIEUX[4]

Department of Chemistry, University of Alberta, Edmonton, Alta., Canada T6G 2G2

Received July 26, 1991

P. V. NIKRAD, H. BEIERBECK, and R. U. LEMIEUX. Can. J. Chem. **70**, 241 (1992).

The relative potencies of both the monodeoxy and mono-*O*-methyl derivatives of the Le^b-OMe tetrasaccharide (α-L-Fuc-(1 → 2)-β-D-Gal-(1 → 3)-[α-L-Fuc-(1 → 4)]-β-D-GlcNAc-OMe) as inhibitors of the complexation of a Le^b artificial antigen by the lectin IV of *Griffonia simplicifolia* are interpreted in terms of the X-ray crystal structure at 2.5 Å resolution of the GS-IV · Le^b-OMe complex. Both kinds of derivatives maintain high potencies when the hydroxyl groups involved appear, in the crystal structure, to be in contact with the aqueous phase. Hydroxyl groups situated at the periphery of the combining site and hydrogen bonded to the protein can also be deoxygenated without important loss in potency. However, their methylation leads to a strong decrease in the stability of the complex, because the steric bulk of the introduced methyl group causes loss of complementarity. In contrast, the hydroxyl groups that form hydrogen bonds with the protein along the base of the shallow amphiphilic cleft of the combining site can neither be deoxygenated nor methylated without virtually complete loss of binding activity. Thus, the procedure can provide an appreciation of the various kinds of hydrogen bonds that are present in a protein · oligosaccharide complex. Hard-sphere calculations supported these contentions since an energetically favorable orientation was indicated for a methoxy group at any one of the five positions that were expected to remain in contact with the aqueous phase. However, the calculations, as expected, showed the introduction of strong destabilizing nonbonded interactions when the methylation involved hydroxyl groups that are hydrogen bonded to the protein in the complex. The results are in accord with the previously made rationalization of the near linear enthalpy–entropy compensation found for the active deoxy congeners.

Key words: molecular recognition, lectin IV of *Griffonia simplicifolia*, *O*-methyl derivatives of the Lewis b-OMe tetrasaccharide, detection of intermolecular hydrogen bonds, hard-sphere calculations.

P. V. NIKRAD, H. BEIERBECK et R. U. LEMIEUX. Can. J. Chem. **70**, 241 (1992).

On a déterminé les efficacités relatives des dérivés monodésoxy- et mono-*O*-méthyle du tétrasaccharide Le^b-OMe (α-L-Fuc-(1 → 2)-β-D-Gal-(1 → 3)-[α-L-Fuc-(1 → 4)]-β-D-GlcNAc-OMe) comme inhibiteurs de la complexation d'un antigène artificiel du Le^b par la lectine IV du *Griffonia simplicifolia;* on interprète les résultats en fonction de la structure cristalline d'un complexe GS-IV · Le^b-OMe, déterminée par diffraction des rayons-X, à une résolution de 2,5 Å. Les deux types de dérivés maintiennent des efficacités élevées lorsqu'il semble que, dans la structure cristalline, les groupes hydroxyles sont en contact avec la phase aqueuse. Lorsqu'on désoxygène les groupes hydroxyles qui sont situés à la périphérie du site qui se combine et qui sont liés à la protéine par des liaisons hydrogènes, il n'y a pas de perte importante de l'efficacité. Toutefois, leur méthylation conduit à une perte de complémentarité et à une baisse importante de la stabilité du complexe qui sont le résultat de l'encombrement stérique introduit par les groupes méthyles. Par ailleurs, pour ce qui est des groupes hydroxyles qui forment des liaisons hydrogènes avec la protéine le long de la base de l'interstice amphiphile peu profond du site de combinaison, on ne peut ni les déoxygéner ni les méthyler sans perdre presque complètement l'activité de liaison. Cette procédure permet donc d'apprécier les divers types de liaisons hydrogènes qui sont présents dans un complexe protéine · oligosaccharide. Des calculs de sphères dures corroborent ces conclusions; en effet, les calculs indiquent que les groupements méthoxyles présents dans les cinq positions qui devraient rester en contact avec la phase aqueuse seraient tous dans une orientation qui serait favorable d'un point de vue énergétique. Toutefois, les calculs ont démontré, comme on pouvait s'y attendre, qu'il y a introduction de fortes interactions déstabilisantes et non-liées lorsqu'on effectue la méthylation des groupes hydroxyles qui sont reliés à la protéine du complexe par des liaisons hydrogènes. Les résultats sont en accord avec la rationalisation faite antérieurement au sujet de la compensation pratiquement linéaire enthalpie–entropie détectée avec des congénères actifs déoxygénés.

Mots clés : reconnaissance moléculaire, lectins IV du *Griffonia simplicifolia*, dérivés *O*-méthyles du tétrasaccharide Le^b-OMe, détection des liaisons hydrogènes intermoléculaires, calculs de sphères dures.

[Traduit par la rédaction]

Introduction

The thermodynamic parameters for the association of the methyl glycoside (**1**) of the tetrasaccharide, known as the Lewis b human blood group determinant, with the lectin IV of *Griffonia simplicifolia* established the reaction to be enthalpy driven with an association constant of 4.4×10^4 [L/μmol] at 298 K (1). The thermodynamic studies were extended to include all 10 monodeoxy derivatives of **1** (2). The results, reported in Table 1, showed that three hydroxyl groups provide key polar interactions with the protein since their replacement by hydrogen provided virtually inactive structures. The seven other monodeoxy-Le^b-OMe were active inhibitors and, as previously commented upon (2), changes in the thermodynamic parameters showed virtual linear enthalpy–entropy compensation. Subsequently, the X-ray crystal structure at 2.5 Å resolution[5] indicated that,

[1]Presented at the 201st National Meeting of the American Chemical Society, Atlanta, Georgia, April 14–19, 1991.

[2]Research Associate, 1983–1990. Present address: Alberta Research Council, P.O. Box 8330, Station F, Edmonton, Alta., Canada T6H 5X2.

[3]Research Associate, 1985–present.

[4]Author to whom correspondence may be addressed.

[5]L. T. J. Delbaere, M. Vandonselaar, L. Prasad, and J. W. Quail. Private communication.

Can. J. Chem. Downloaded from www.nrcresearchpress.com by 123.30.183.119 on 09/08/12
For personal use only.

Can. J. Chem. Downloaded from www.nrcresearchpress.com by 123.30.183.119 on 09/08/12
For personal use only.

TABLE 1. Comparison of the effects of deoxygenation with those of *O*-methylation at the various hydroxyl positions of Le^b-OMe on the binding by the lectin GS-IV

Position substituted	Relative potencies as inhibitors		Thermodynamic parameters at 298 K for the binding of the monodeoxy derivatives, kcal/mol (2)		
	O-Me	Deoxy (2)	$\Delta\Delta G^0$	$\Delta\Delta H^0$	$\Delta(T\Delta S^0)$
None[a]	—	—	0	0	0
6a	110[b]	95	0	0.2	0.2
3b	[c]	Inactive	—	—	—
4b	[c]	Inactive	—	—	—
6b	250	91	0.1	4.6	4.5
2c	77	30	0.6	3.3	2.7
3c	<1[d]	26	0.8	6.7	5.9
4c	[c]	Inactive	—	—	—
2d	2.2	30	0.5	1.2	0.6
3d	~100[d]	38	0.7	4.7	3.9
4d	130	115	−0.1	5.9	6.0

[a]For Le^b-OMe, $\Delta G^0 = -6.3$, $\Delta H^0 = -13.3°$, $T\Delta S^0 = -7.0$ kcal/mol and setting its potency at 100.
[b]Inhibition provided by the 6a-*O*-mesyl derivative (1).
[c]Not determined since expected to be inactive.
[d]See Table 2.

except for the OH-6a group of the β-D-GlcNAc unit, which is remote from the combining site, the six other non-key hydroxyl groups all reside at or near the periphery of the combining site (see Fig. 1). Indeed, four of these hydroxyl groups, namely those at positions 6b, 2c, 3d, and 4d, appear to remain in contact with the aqueous phase. The three-dimensional geometry of the complex appeared acceptable for favorable hydrogen bonding of O-3c with proton donation from Arg 48 and of O-2d with proton donation from Asn 135, as projected in Fig. 1. The crystal structure at 2.5 Å resolution was not favorable for hydrogen bonding of OH-3d, either as a proton donor or acceptor, with His 114.

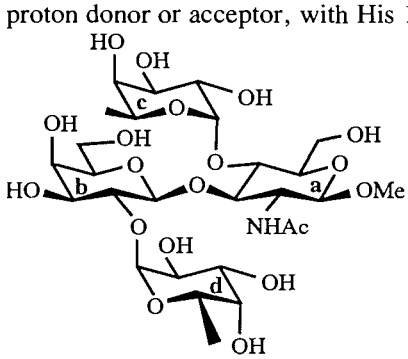

a-L-Fuc-(1→2b)-b-D-Gal-(1→3a)-[a-L-Fuc-(1→4a)]-β-D-GlcNAc-OMe (Le^b-OMe)

1

Discussion of results

Binding studies

In view of the above-mentioned indications for hydrogen bond formation, it became of interest to examine the effect on binding of introducing a methyl group at each of the hydroxyl positions of **1**. It was expected that the substitution of any one of the three key hydroxyl groups at positions 3b, 4b, and 4c would lead to loss of stereoelectronic complementarity. Consequently, the *O*-methyl derivatives at these positions were not prepared. Monomethyl derivatives of **1** were synthesized by substitutions at OH-6b, OH-2c, OH-3d, and OH-4d. In the case of OH-6a, it was to be expected that the substitution would not result in significant change in activity since the replacement of this hydroxyl group either by an iodine atom or *O*-mesylation, as previously reported (1), had no appreciable effect on the potency as an inhibitor of the binding of a Le^b-active artificial antigen in a competitive solid-phase radioimmunoassay. Consequently, the 6a-*O*-methyl derivative of **1** was not prepared. Instead, the thermodynamic parameters of the 6a-*O*-mesyl derivative of **1**, reported in Table 2, are accepted as representative of those for the 6a-*O*-methyl congener of **1**. Neither the 3c- nor the 3d-*O*-methyl derivatives of **1** were prepared since the potencies of these structures could be surmised from the potencies of the more readily synthesized 2c,3c- and 2d,3d-di-*O*-methyl derivatives. That is, since the 2c-*O*-

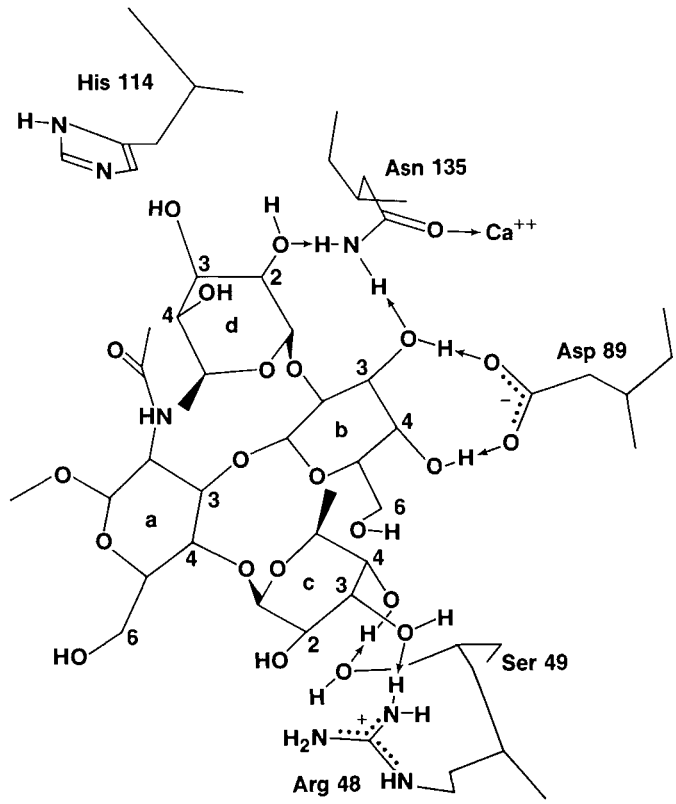

FIG. 1. Fragment of the X-ray crystal structure at 2.5 Å resolution of the complex formed by Le^b-OMe (**1**) and the lectin IV of *Griffonia simplicifolia* to show the intermolecular hydrogen bonds. The ϕ/φ torsion angles about the three intersugar glycosidic bonds are 46.3°/31.1° for α-L-Fuc-(1c → 4a), 55.7°/12.7° for β-D-Gal-(1b → 3a), and 45.6°/15.0° for α-L-Fuc-(1d → 2b), in good agreement with those estimated by HSEA calculation; namely, 55°/25°, 55°/10°, and 45°/15°, respectively. The OH-3b, OH-4b, and OH-4c groups provide the key polar interaction by donating protons to accepting groups located toward the bottom of the cleft that forms the combining site. The OH-3c and OH-2d groups act as proton acceptors from amino acids at the periphery of the combining site to form hydrogen bonds that are not essential to the stability of the complex. Although OH-6b, OH-2c, OH-3d, and OH-4d reside near the periphery of the combining site, these, together with OH-6a, remain in hydrogen bonding interactions with water molecules (see Fig. 3).

TABLE 2. The relative potencies of *O*-methyl derivatives of Le^b-OMe as inhibitors of the lectin IV of *Griffonia simplicifolia*

Compound	Positions substituted	Relative potency[a]
1	None	100
—	6a	110[b]
43	6b	250
37	2c	77
—	[3c	<1][c]
40	2d	2.2
—	[3d	~100][d]
—	4d	130[e]
38	2c,3c	<1
39	3c,4c	Inactive
42	2d,3d	2.3
41	3d,4d	110
44	6b,2c,3d,4d	230

[a]Calculated from the micromolar concentrations that provide 50% inhibition of the binding of an ^{125}I-labelled Le^b-BSA artificial antigen by the lectin GS-IV using a previously described (3) competitive, solid-phase radioimmunoassay.

[b]The value for the 6a-*O*-methanesulfonyl derivative.

[c]In view of the low potency of the 2c,3c-di-*O*-methyl derivative.

[d]In view of the high potencies of the 3d,4d-di-*O*-methyl and the 6b,2c,3d,4d-tetra-*O*-methyl derivatives.

[e]Unpublished.

methyl congener is highly potent but the 2c,3c-di-*O*-methyl derivative is not, evidently methylation at the 3c position strongly hinders complex formation. Also, since the 2d-mono-*O*-methyl and 2d,3d-di-*O*-methyl derivatives of **1** both had almost equally poor potencies, the indication was that methylation at the 3d position is compatible with complex formation. This conclusion was confirmed by preparation of the 6b,2c,3d,4d-tetra-*O*-methyl derivative, which proved to be, as expected, a highly active inhibitor (Table 2).

Semi-empirical energy calculations support the data presented in Table 2. These were accomplished by calculating the energy barriers to rotation about the C-OMe bond of the various GS-IV · mono-*O*-methyl-Le^b-OMe complexes in order to test whether or not there exists an orientation of the methyl group wherein no appreciable nonbonded interaction, either intra- or intermolecular, is present. These assessments were made using the same Kitaygorodsky expression for hard-sphere calculations that is employed in the HSEA method for estimating the conformational preferences about glycosidic linkages (4). In the present situation, coordinates were generated for the six mono-*O*-methyl derivatives of Le^b-OMe noncovalently bound to GS-IV that are presented in Table 1. The energy of interaction of the methyl group with the rest of the Le^b-OMe structure, as well as those with the amino acid residues of the combining site, were then calculated as a function of the Me/C_γ torsion angle defined by the CH_3-O bond and the vicinal C-C bond of the lowest numbered carbon atom of the pyranose ring and always proceeding clockwise for the rotation. These interaction energies were then added to provide the total energy changes with changes in torsion angle displayed in Fig. 2. Thus, with reference to the 6b-methoxy group, the energy of interaction over the range of torsion angles of near 180° to 270° is near zero or slightly negative and, therefore, the *O*-methylation was expected to have no adverse effect on complex formation, as was indeed observed. Similarly for the 2c, 3d, and 4d-*O*-methyl compounds, an orientation exists in which the methyl group has virtually no repulsive interaction, either intramolecularly or with the protein. Indeed, in accord with these observations, the inhibition data show that the addition of a methyl group at these positions does not interfere with com-

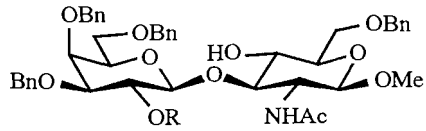

22, R = Ac

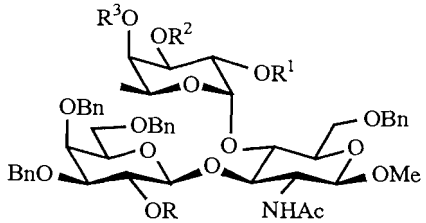

	R	R^1	R^2	R^3
23	Ac	Me	Bn	Bn
24	Ac	Bn	Me	Me
25	Ac	Me	Me	Bn
26	Ac	Bn	Bn	Bn
27	H	Me	Bn	Bn
28	H	Bn	Me	Me
29	H	Me	Me	Bn
30	H	Bn	Bn	Bn

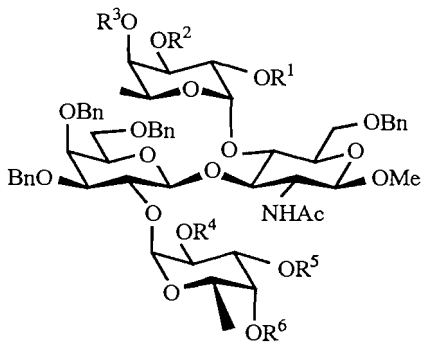

	R^1	R^2	R^3	R^4	R^5	R^6
31	Me	Bn	Bn	Bn	Bn	Bn
32	Me	Me	Bn	Bn	Bn	Bn
33	Bn	Me	Me	Bn	Bn	Bn
34	Bn	Bn	Bn	Me	Bn	Bn
35	Bn	Bn	Bn	Bn	Me	Me
36	Bn	Bn	Bn	Me	Me	Bn

Can. J. Chem. Downloaded from www.nrcresearchpress.com by 123.30.183.119 on 09/08/12
For personal use only.

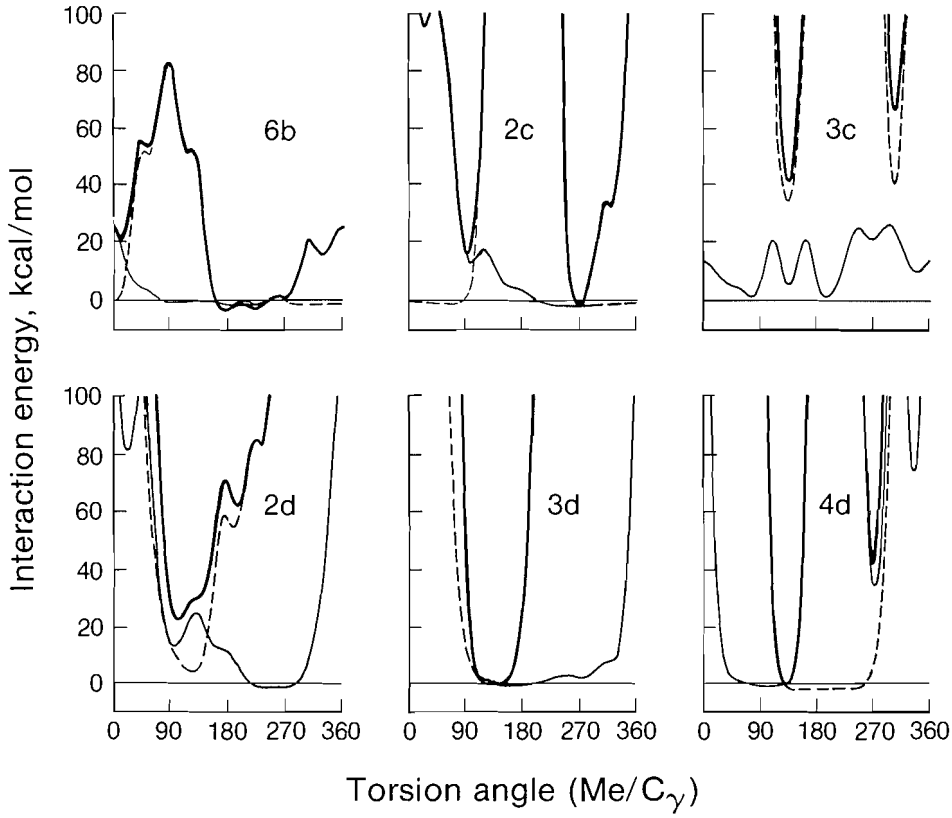

FIG. 2. Potential energy plots provided by hard-sphere calculation of the barriers to rotation about the C-OMe bond to assess whether or not *O*-methylation of hydroxyl groups of Le^b-OMe complexed with GS-IV is compatible with the structure of the complex. The heavy solid plot represents the total of the interaction of the methoxy group within the tetrasaccharide (light solid plot) and the interaction with the protein (dotted plot). Orientations that produce no repulsive interactions are possible only when a methyl group is introduced at either the 6b, 2c, 3d, or 4d positions since, as seen in Table 1, these congeners are highly active whereas the others are not.

plex formation. This is particularly interesting in the case of the 3d-*O*-methyl derivative since it requires that only a weak, if any, hydrogen bond exists between OH-3d and the imidazole group of His 114. It was to be expected, however, that *O*-methylation at either position 3c or 2d would lead to an inactive compound since the crystal structure, as displayed in Fig. 1, is in accord with hydrogen bond formation between the hydroxyl groups at these positions and the protein, and important loss in stereoelectronic complementarity would result. The calculations fully substantiated these expectations. However, the calculations did not anticipate the residual activities for compounds **38** and **42** (Table 2). It is apparent that these situations involve flexible peripheral groups that can offer some adjustment to steric demands for complexation, which our rigid hard-sphere model does not take into account.

It is of interest to note that the *O*-methylation at either position 6b or 4d causes an enhancement of the binding and that these results may be related to the fact that the methyl groups come into contact with hydrophobic residues at the periphery of the combining site: the indolyl group of Trp-133 in the case of CH_3O-6b and both Phe-108 and His 114 in the case of CH_3O-4d. In contrast, CH_3O-2c comes into contact with the strongly hydrophilic guanidine group of Arg 48 and the substitution causes a 23% loss in potency. These stereochemical relationships can be appreciated by examination of the partial CPK model for the complex formed between

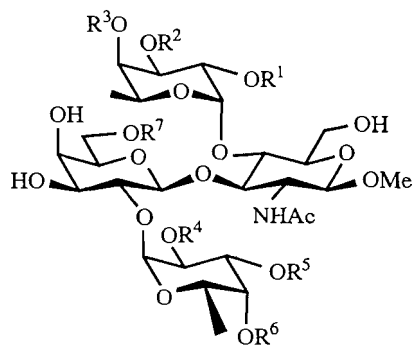

	R^1	R^2	R^3	R^4	R^5	R^6	R^7
37	Me	H	H	H	H	H	H
38	Me	Me	H	H	H	H	H
39	H	Me	Me	H	H	H	H
40	H	H	H	Me	H	H	H
41	H	H	H	H	Me	Me	H
42	H	H	H	Me	Me	H	H
43	H	H	H	H	H	H	Me
44	Me	H	H	H	Me	Me	Me

Can. J. Chem. Downloaded from www.nrcresearchpress.com by 123.30.183.119 on 09/08/12
For personal use only.

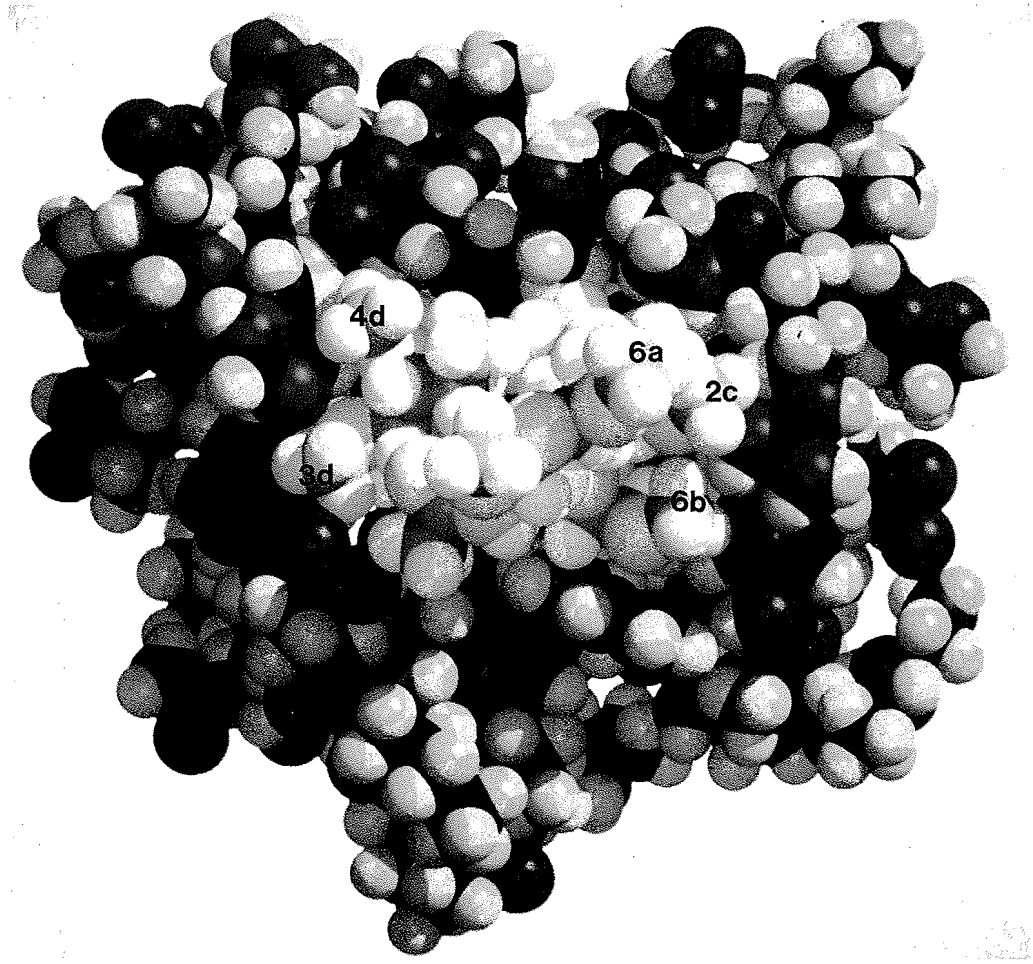

FIG. 3. CPK molecular model of the 6a,6b,2c,3d,4d-penta-*O*-methyl derivative of Le^b-OMe occupying the combining site of the lectin GS-IV, which is represented by the 62 amino acid residues that provide the combining site and the structure about its periphery. Note that both the methyl aglycon and the 6a-methyl groups are both well removed from the combining site. The methyl groups at positions 6b, 2c, 3d, and 4d are in favored orientations according to calculations reported in Fig. 2.

GS-IV and Le^b-OMe, which has positions 6a, 6b, 2c, 3d and 4d *O*-methylated with the methyl groups placed in the favorable orientations identified by the hard-sphere calculations and presented in Fig. 3.

The results achieved in this study thoroughly confirm the indications as to the disposition of the 10 hydroxyl groups present in Le^b-OMe after association with the lectin GS-IV. They also support our proposal (2) that the near-linear enthalpy–entropy compensation that is observed for the binding of Le^b-OMe congeners results from changes in water structure about both the position of structural change prior to complexation and about this position in close proximity to the periphery of the combining site in the complex. An important new insight gained from this research is the recognition that hydroxyl groups of an oligosaccharide that do not come into a hydrogen bonding interaction with the receptor site, but which come into close proximity to amino acid residues at the periphery of the site, may be substituted with little effect on the stability of the complex. In fact, substantial stability may be gained when the substitution leads to new energetically favorable interactions.

In conclusion, it is to be noted that a comparison of the activities of the monodeoxy derivatives of an oligosaccharide with those of the mono-*O*-methyl derivatives provides a powerful novel method for the probing of receptor sites that can yield information that, otherwise, can only be achieved in special cases by high-resolution X-ray crystallography. Thus, such findings may prove useful in efforts aimed at reducing the toxicities of medicinals where it is required to maintain strong recognition by the receptor sites of interest while depressing the interactions responsible for the undesirable side effects.

Chemical synthesis

The procedures used to synthesize the partially *O*-methylated derivatives of Le^b-OMe (**37–44**) followed closely those previously employed (U. Spohr and R. U. Lemieux, unpublished) to synthesize 4d-*O*-methyl-Le^b-OMe and to determine the potency reported in Tables 1 and 2.

The synthesis of the various *O*-alkylated derivatives of Le^b-OMe (**37–44**) required in the first instance the preparation of the substituted fucosyl bromides **15**, **17**, **19**, and **21** (Scheme 1) and the galactosyl bromide **47** (Scheme 2). In the case of the fucosyl bromides, the reactions used and outlined in Scheme 1 are all well-established procedures except for the opening of the stannylene ring (5) of compounds **8** and **9** using fluoride ion. David *et al.* (6) recommended iodide ion for this purpose. However, under the aprotic conditions, the much more strongly nucleophilic

Can. J. Chem. Downloaded from www.nrcresearchpress.com by 123.30.183.119 on 09/08/12
For personal use only.

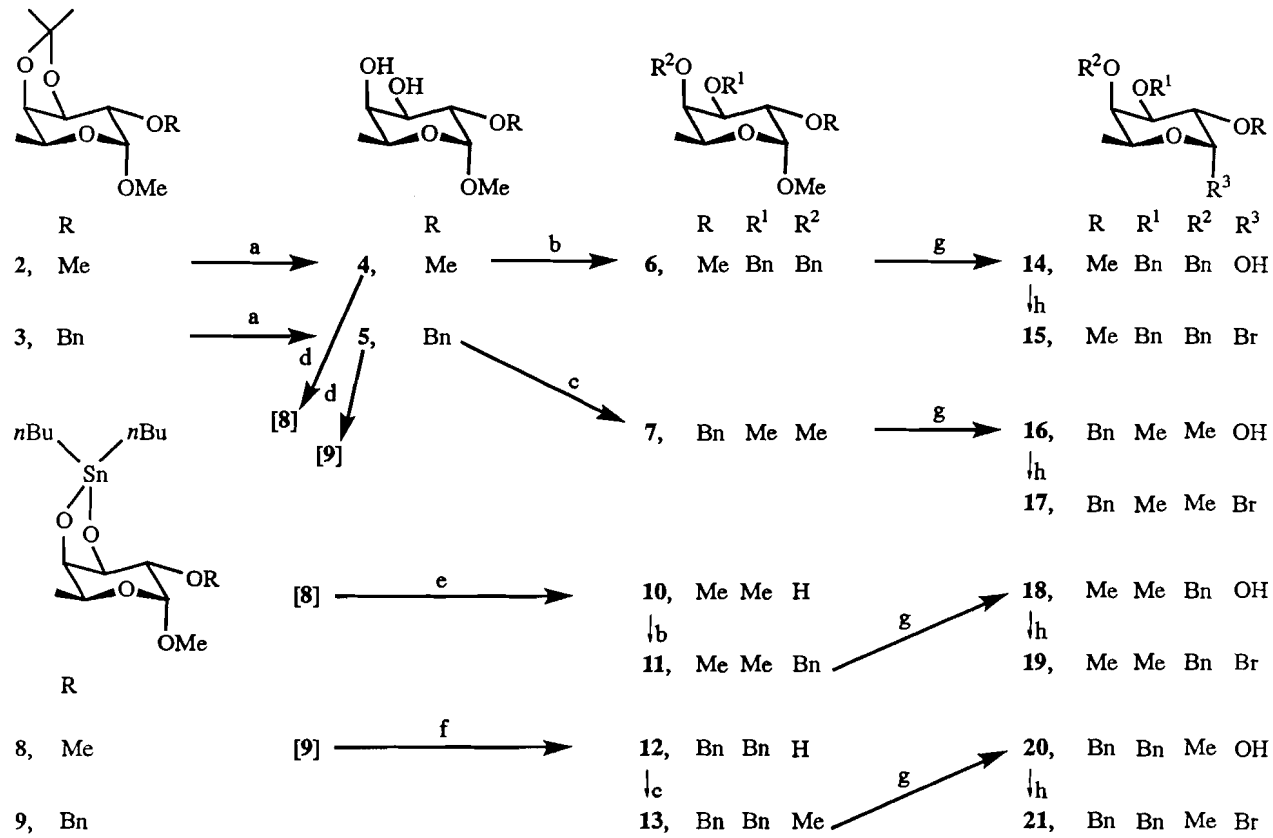

SCHEME 1. Preparation of *O*-alkylated fucosyl bromides. a: H_2O, AcOH; b: BnBr, NaH, DMF; c: MeI, NaH, DMF; d: C_6H_6, $(n\text{-Bu})_2SnO$; e: MeI, $(n\text{-Bu})_4N^+F^-$, C_6H_6; f: BnBr, $(n\text{-Bu})_4N^+F^-$, C_6H_6; g: HCl, AcOH, H_2O; h: $(BrCO)_2$, DMF, CH_2Cl_2.
2,3,4-Tri-*O*-benzyl-α-L-fucopyranosyl bromide (**55**) was prepared according to ref. 1.

fluoride ion could be expected to greatly accelerate the overall reaction. Indeed, a reaction that requires refluxing in benzene for up to 24 h using iodide was found to be finished within minutes with the yield of **12** increasing from 10 to 75% (R. U. Lemieux and N. Morishima, unpublished data).

The preparation of the appropriately protected core disaccharides **22** and **49** followed well-established procedures (7) and does not warrant comment further than reported in Scheme 2. The fucosylations of these compounds all resulted in good to excellent yield under the conditions for bromide-ion catalysis (8), which simply employ 4 Å molecular sieve (9) to absorb the liberated hydrogen bromide and *N,N*-dimethylformamide (DMF) in the dichloromethane solvent to accelerate, if need be, the reaction (10).

The various partially *O*-methylated derivatives of Le^b-OMe (**37–44**) are well characterized by the high resolution nmr spectral data reported in Tables 3 and 4. The ^1H nmr data presented in Table 3 confirm the structures and indicate that the introduction of the *O*-methyl groups causes little, if any, change in the conformational preference. These conclusions are further supported by the ^{13}C nmr data presented in Table 4. It is to be noted that the chemical shift assignments are based only on a comparison with those previously assigned to Le^b-OMe (1) and are strictly provisional.

Experimental

General methods

The ^1H nmr spectra were recorded at 300 MHz (Bruker AM 300 spectrometer) with tetramethylsilane as internal standard for $CDCl_3$ solutions. The reference standard for D_2O solutions was acetone (2.225 ppm). The ^{13}C nmr spectra were recorded at 75 MHz (Bruker AM 300 spectrometer), using D_2O as solvent and 1,4-dioxane (67.4 ppm) as internal standard. Optical rotations were measured at room temperature (23 ± 1°C) in a 1-dm cell with a Perkin–Elmer 241 polarimeter. Thin-layer chromatography was performed on a precoated plate of Silica Gel 60 F_{254} (Merck) with detection by spraying with 10% sulfuric acid in ethanol followed by heating. For column chromatography, Silica Gel 60 (230–400 mesh, Merck) and distilled solvents were used. Solvents and reagents were purified and dried according to standard procedures (11). Melting points are uncorrected.

The inhibition studies employed the previously reported competitive solid-phase radioimmunoassay (3) and the relative potencies were calculated from the relative molar amounts that provided 50% inhibition.

O-Benzylations

The benzylations of compounds **4** and **10** of Scheme 1 were performed essentially as follows. The alcohol (20 mmol) was dissolved in DMF (50 mL) and the solution cooled to 0°C. Sodium hydride (100 mmol) was added slowly and the mixture was stirred under nitrogen until the evolution of gas had stopped (about 1 h at 0°C). Benzyl bromide (85 mmol) was then added dropwise with efficient stirring. The mixture was allowed to reach room temperature while stirring for 16 h. The excess sodium hydride was decomposed with methanol (10 mL), and dichloromethane (200 mL) was added. The solids were removed by filtration and the filtrate was evaporated *in vacuo* to a syrup that was chromatographed on a silica gel column using toluene/ethyl acetate as eluent.

O-Methylations

These were conducted under essentially the same conditions as described above for the benzylations except that methyl iodide was substituted for the benzyl bromide.

Can. J. Chem. Downloaded from www.nrcresearchpress.com by 123.30.183.119 on 09/08/12
For personal use only.

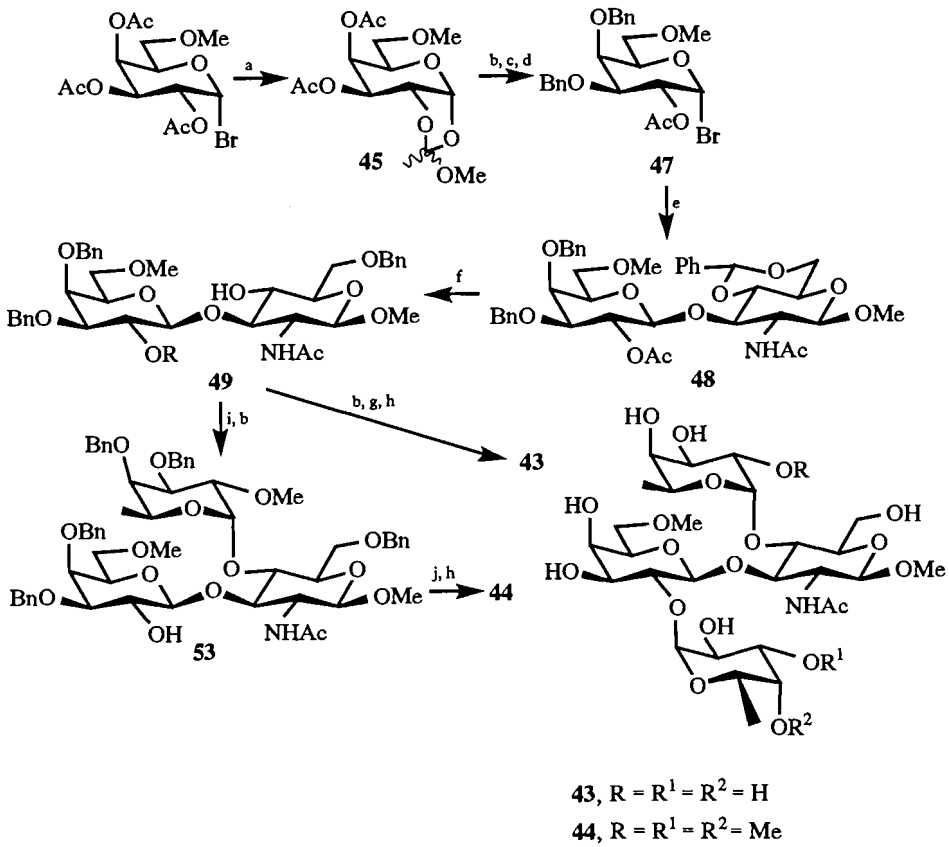

SCHEME 2. Preparation of *O*-methylated derivatives of Le^b-OMe. a: $Et_4N^+Br^-$, MeOH, *s*-collidine; b: NaOMe, MeOH; c: BnBr, NaH, DMF; d: AcBr, $Et_4N^+Br^-$; e: methyl 2-acetamido-4,6-*O*-benzylidene-2-deoxy-β-D-glucopyranoside, $Hg(CN)_2$; f: $NaBH_3CN$, HCl, THF; g: **55**, $Et_4N^+Br^-$, CH_2Cl_2, DMF; h: Pd, H_2, EtOH; i: **15**, $Et_4N^+Br^-$, CH_2Cl_2, DMF; j: **17**, $Et_4N^+Br^-$, CH_2Cl_2, DMF.

TABLE 3. The ^1H nmr chemical shifts,[a] ppm (coupling constant, Hz), of *O*-methyl derivatives of Le^b-OMe (**1**)

	Compound								
Hydrogen atom	**1**	**37**	**38**	**39**	**40**	**41**	**42**	**43**	**44**
β-D-GlcNAc a-unit									
H-1 ($J_{1,2}$)	4.32 (8.3)	4.32 (8.3)	4.33 (8.3)	4.32 (8.3)	4.30 (8.3)	4.32 (8.3)	4.32 (8.3)	4.31 (8.3)	4.29 (8.5)
H-3 ($J_{3,4}$)	4.12 (9.3)	4.09 (9.3)	4.12 (9.3)	4.14 (9.3)	4.11 (9.3)	4.12 (9.3)	4.11 (9.3)	4.11 (9.0)	4.05 (9.5)
CH_3O	3.48	3.47	3.45	3.47	3.46	3.45	3.47	3.47	3.40
CH_3CO	2.07	2.06	2.05	2.07	2.04	2.08	2.08	2.06	2.05
β-D-Gal b-unit									
H-1 ($J_{1,2}$)	4.64 (7.8)	4.64 (7.8)	4.65 (7.8)	4.66 (7.8)	4.62 (7.8)	4.66 (7.8)	4.64 (7.8)	4.64 (7.8)	4.61 (7.8)
CH_3O	—	—	—	—	—	—	—	3.44	3.46
α-L-Fuc c-unit									
H-1 ($J_{1,2}$)	5.01 (3.8)	5.14 (3.8)	5.14 (3.5)	4.99 (3.8)	5.00 (4.0)	5.23 (3.5)	5.01 (3.5)	5.00 (3.8)	5.08 (3.8)
H-5 ($J_{5,6}$)	4.84 (6.5)	4.82 (6.5)	4.80 (6.5)	4.82 (6.5)	4.83 (6.5)	4.85 (6.5)	4.84 (6.5)	4.87 (6.5)	4.81 (6.5)
CH_3-6	1.27	1.25	1.27	1.25	1.24	1.27	1.24	1.25	1.21
CH_3O	—	3.54	3.47, 3.51	3.53, 3.53	—	—	—	—	3.51
α-L-Fuc d-unit									
H-1 ($J_{1,2}$)	5.14 (3.8)	5.17 (3.5)	5.16 (4.0)	5.16 (3.0)	5.33 (3.5)	5.34 (3.5)	5.10 (4.0)	5.14 (3.8)	5.12 (3.5)
H-5 ($J_{5,6}$)	4.34 (6.5)	4.32 (6.5)	4.33 (6.5)	4.34 (6.5)	4.31 (6.5)	4.31 (6.5)	4.33 (6.5)	4.34 (6.5)	4.28 (6.5)
CH_3-6	1.27	1.25	1.25	1.33	1.24	1.27	1.32	1.27	1.29
CH_3O	—	—	—	—	3.48	3.48, 3.48	3.54, 3.56	—	3.51, 3.53

[a]See General methods.

Can. J. Chem. Downloaded from www.nrcresearchpress.com by 123.30.183.119 on 09/08/12
For personal use only.

TABLE 4. The ^{13}C nmr chemical shifts[a] of *O*-methyl derivatives of Le^b-OMe (**1**)

		Compound							
	1	**37**	**38**	**39**	**40**	**41**	**42**	**43**	**44**
Carbon atom	δ, ppm	Δδ, ppm[b]							
β-D-GlcNAc a-unit									
1	103.52	0.06	0.00	−0.02	0.07	0.12	0.17	0.02	0.14
2	56.35	0.02	0.05	0.03	−0.03	−0.17	−0.17	0.04	−0.06
3	75.63	0.06	0.10	0.02	−0.18	−0.07	−0.25	0.07	0.16
4	73.12	0.26	−0.06	0.17	1.32	0.81	1.22	0.04	0.48
5	76.33	−0.16	−0.17	−0.14	−0.10	−0.88	−0.15	−0.11	−0.16
6	60.60	−0.14	−0.22	−0.26	−0.20	−0.23	−0.26	−0.18	−0.19
CH_3CO	23.07	−0.05	−0.04	−0.03	0.21	0.19	0.22	−0.03	0.24
CH_3CO	147.45	0.11	0.08	−0.41	0.17	−0.12	−0.07	0.12	−0.12
CH_3O-1	58.02	0.05	0.05	0.04	0.07	−0.02	−0.01	0.04	0.03
β-D-Gal b-unit									
1	101.44	0.06	−0.02	−0.05	0.02	−0.06	0.00	−0.04	−0.03
2	77.39	0.04	0.15	0.03	−0.51	−0.03	−0.04	−0.19	−0.05
3	74.55	−0.07	−0.01	−0.02	−0.10	−0.21	−0.17	−0.20	−0.28
4	69.62	−0.10	−0.17	−0.05	0.02	0.25	−0.05	0.28	0.20
5	75.63	−0.05	−0.33	−0.35	−0.27	−0.15	−0.12	2.53	−2.63
6	62.38	−0.07	−0.08	−0.10	0.06	−0.02	0.00	6.45	−0.16
CH_3O[c]	—	—	—	—	—	—	—	1.46	1.49
α-L-Fuc c-unit									
1	98.67	−2.21	−2.16	−0.06	−1.09	−0.05	−1.29	0.03	−2.15
2	68.73	0.79	−0.06	−0.16	−0.07	−0.22	−0.14	1.17	−0.18
3	70.01	0.30	7.65	9.72	−0.06	−1.42	−0.13	0.24	−0.51
4	72.87	−0.10	5.84	6.45	−0.03	0.06	0.12	−0.07	−0.01
5	67.80	0.07	−0.14	0.11	0.10	0.03	0.05	−0.02	−0.02
6	16.21	−0.04	0.07	0.21	−0.03	0.11	−0.10	−0.01	0.17
CH_3O[c]	—	2.10	−1.62, 0.08	0.53, 0.53	—	—	—	—	2.12
α-L-Fuc d-unit									
1	100.42	0.04	0.01	−0.02	−1.71	−0.22	−1.72	0.02	−0.10
2	69.18	−0.06	−0.06	−0.07	9.21	0.36	8.94	−0.06	3.68
3	70.01	0.29	0.27	0.25	6.29	6.52	6.89	0.06	8.83
4	72.82	−0.05	−0.04	−0.05	−0.13	−0.04	−0.04	−0.02	6.42
5	67.06	0	0.01	0.03	−0.24	0.04	−0.44	0.03	0.10
6	16.09	0.04	0.01	−0.02	0.01	0	−0.02	0.00	0.00
CH_3O[c]	—	—	—	—	0.29	−0.42, −1.02	−0.01, 1.56	—	−0.34, 1.49

[a]See General methods. The chemical shifts for **1** are those previously reported (1, 7).
[b]Provisional assignments based on a comparison of the spectra with the spectrum of **1**, $\Delta\delta = \delta - \delta_1$.
[c]Relative to the chemical shift of CH_3O-1a of **1**.

*Methyl 3,4-di-O-benzyl-2-O-methyl-α-L-fucopyranoside (**6**)*

The syrupy product of the benzylation of **4** (Scheme 1) with $[\alpha]_D$ −90 (*c* 1.1, chloroform) was obtained in 79% yield; ^1H nmr data ($CDCl_3$) δ: 7.43–7.21 (m, 10H, 2Ph), 4.92 (d, 1H, *J* 12.0 Hz, CH_2Ph), 4.87 (d, 1H, $J_{1,2}$ 3.0 Hz, H-1, partly overlapped by CH_2Ph), 4.84 (d, 1H, *J* 12.0 Hz, CH_2Ph), 4.7 (d, 1H, *J* 12.0 Hz, CH_2Ph), 4.65 (d, 1H, *J* 12.0 Hz, CH_2Ph), 3.88–3.78 (m, 3H, H-5 overlapped by H-2 and H-3), 3.62 (dd, 1H, $J_{3,4}$ 2.5 Hz, $J_{5,6}$ 1.0 Hz, H-4), 3.57 (s, 3H, CH_3O), 3.39 (s, 3H, CH_3O), 1.15 (d, 3H, $J_{5,6}$ 6.5 Hz, 3H-6). Anal. calcd. for $C_{22}H_{28}O_5$: C 70.94, H 7.58; found: C 70.15, H 7.51.

*Methyl 2-O-benzyl-3,4-di-O-methyl-α-L-fucopyranoside (**7**)*

The syrupy product of the methylation of **5** (Scheme 1) with $[\alpha]_D$ −72 (*c* 0.34, chloroform) was obtained in 89% yield; ^1H nmr data ($CDCl_3$) δ: 7.22–7.45 (m, 5H, Ph), 4.55 (d, 1H, $J_{1,2}$ 3.5 Hz, H-1), 4.3 and 4.1 (2d, 2H, *J* 12.0 Hz, CH_2Ph), 3.86 (m, 1H, H-5), 3.82 (dd, 1H, $J_{2,3}$ 9.0 Hz, H-2), 3.62 (dd, 1H, $J_{3,4}$ 3.0 Hz, H-3), 3.59 and 3.55 (s, 3H, $2CH_3O$), 3.43 (dd, 1H, $J_{4,5}$ 1.0 Hz, H-4), 3.34 (s, 3H, CH_3O), 1.24 (d, 3H, $J_{5,6}$ 6.5 Hz, 3H-6). Anal. calcd. for $C_{16}H_{24}O_5$: C 64.84, H 8.16; found: C 64.22, H 7.94.

*Methyl 2,3-di-O-methyl-α-L-fucopyranoside (**10**)*

Compound **4** (5.16 g, 26.84 mmol) was dissolved in benzene (250 mL) and di-*n*-butyl tin oxide (7.1 g, 28.5 mmol) was added. The mixture was refluxed for 16 h with azeotropic removal of water formed during stannylation. After 16 h it was concentrated to 100 mL for addition of tetrabutylammonium fluoride (10 g, 38.24 mmol), molecular sieves 4 Å (25 g), and methyl iodide (10 mL, 160.5 mmol). The mixture was stirred at room temperature under nitrogen overnight. The progress of the reaction was monitored by tlc (methanol/dichloromethane 1:9). The solids were removed by filtration and the filtrate was concentrated to a syrup that was chromatographed on a silica gel column (methanol/dichloromethane, 1:19) to provide a highly volatile oily product (5.15 g, 79%) with $[\alpha]_D$ −110 (*c* 3.0, chloroform); ^1H nmr data ($CDCl_3$) δ: 4.75 (d, 1H, $J_{1,2}$ 3.0 Hz, H-1), 3.9 (m, 2H, H-5 overlapped by H-4), 3.55 (dd, 2H, H-2 overlapped by H-3 and CH_3O), 3.49 (s, 6H, $2CH_3O$), 3.4 (s, 3H, CH_3O), 2.38 (d, 1H, OH-4, D_2O exchanged), 1.32 (d, 3H, $J_{5,6}$ 6.5 Hz, 3H-6).

*Methyl 4-O-benzyl-2,3-di-O-methyl-α-L-fucopyranoside (**11**)*

The syrupy product of the benzylation of **10** (Scheme 1) with $[\alpha]_D$ −41 (*c* 1.1, chloroform) was obtained in 88% yield; ^1H nmr data

Can. J. Chem. Downloaded from www.nrcresearchpress.com by 123.30.183.119 on 09/08/12
For personal use only.

Can. J. Chem. Downloaded from www.nrcresearchpress.com by 123.30.183.119 on 09/08/12
For personal use only.

($CDCl_3$) δ: 7.42–7.25 (m, 5H, Ph), 4.95 (d, 1H, *J* 11.5 Hz, CH_2Ph), 4.87 (d, 1H, $J_{1,2}$ 3.5 Hz, H-1), 4.63 (d, 1H, *J* 11.5 Hz, CH_2Ph), 3.85 (m, 1H, H-5), 3.75 (dd, 1H, $J_{2,3}$ 10.0 Hz, H-2), 3.69 (dd, 1H, $J_{3,4}$ 2.5 Hz, $J_{4,5}$ 1.0 Hz, H-4), 3.57 (dd, 1H, H-3), 3.52, 3.51, 3.40 (3s, each 3H, $3CH_3O$), 1.19 (d, 3H, $J_{5,6}$ 6.5 Hz, 3H-6). Anal. calcd. for $C_{16}H_{24}O_5$: C 64.84, H 8.16; found: C 64.88, H 8.44.

Methyl 2,3-di-O-benzyl-α-L-fucopyranoside (12)

As already stated, this compound was prepared from **5** (Scheme 1) in a separate project under conditions similar to those described above for the synthesis of **10** except that benzyl bromide was used as the alkylating agent.

Methyl 2,3-di-O-benzyl-4-O-methyl-α-L-fucopyranoside (13)

As mentioned above, this compound was prepared in a separate project under conditions similar to those used for **4–10** by way of **8** (Scheme 1).

Hydrolysis of the substituted methyl fucosides

The compound, either **6**, **7**, or **11** (Scheme 1) (15 mmol), was dissolved in a mixture of acetic acid (100 mL) and 6 N hydrochloric acid (3 mL) and the solution heated at 65°C. The course of the reaction could be monitored by tlc (ethyl acetate–toluene) and found to be complete within 1 h. The mixture was concentrated *in vacuo* and coevaporated with toluene (200 mL × 5). The residue was chromatographed on silica gel with the solvent mixture used for the tlc. Compound **20** was prepared under similar conditions.

3,4-Di-O-benzyl-2-O-methyl-α/β-L-fucopyranose (14)

The syrupy product from the hydrolysis of **6** (Scheme 1) (86% yield) with $[\alpha]_D$ −100 (*c* 2.6, chloroform) was a 61:39 mixture of the α and β anomers; ^1H nmr data ($CDCl_3$), α isomer, δ: 7.5–7.15 (m, 10H, 2Ph), 5.4 (dd, $J_{1,2}$ 3.0 Hz, $J_{1,OH}$ 2.0 Hz, H-1), 4.57 (d, 1H, *J* 11.5 Hz, CH_2Ph), 4.71 (d, 1H, *J* 11.5 Hz, CH_2Ph), 4.1 (m, 1H, H-5), 3.81 (m, 2H, H-2α overlapped by H-3β), 3.65 (m, 1H, H-4), 3.55 (s, 3H, CH_3O), 3.46 (dd, 1H, $J_{2,3}$ 9.5 Hz, $J_{3,4}$ 3.0 Hz, H-3 overlapped by H-4β), 2.86 (d, 1H, $J_{1,OH}$ 2.0 Hz, OH-1, D_2O exchanged), 1.13 (d, 3H, $J_{5,6}$ 6.5 Hz, 3H-6). β-Isomer, δ: 7.5–7.15 (m, 10H, 2Ph), 4.79 (d, 1H, *J* 12.0 Hz, CH_2Ph), 4.67 (d, 1H, *J* 12.0 Hz, CH_2Ph), 4.67 (t, 1H, $J_{1,2}$ 7.5 Hz, $J_{1,OH}$ 7.0 Hz, H-1), 4.10 (m, 1H, H-5), 3.81 (m, 2H, H-3β overlapped by H-2α), 3.69 (s, 3H, CH_3O), 3.51 (dd, 1H, $J_{2,3}$ 9.0 Hz, H-2), 3.46 (dd, 1H, $J_{3,4}$ 3.0 Hz, $J_{4,5}$ 1.0 Hz, H-4), 3.1 (d, 1H, $J_{1,OH}$ 7.0 Hz, OH, D_2O exchanged), 1.18 (d, 1H, $J_{5,6}$ 6.0 Hz, 3H-6). Anal. calcd. for $C_{21}H_{26}O_5$: C 70.37, H 7.3; found: C 69.4, H 7.24.

2-O-Benzyl-3,4-di-O-methyl-α/β-L-fucofuranose (16)

The syrupy product from the hydrolysis of **7** (Scheme 1) (89% yield) with $[\alpha]_D$ −31 (*c* 0.51, chloroform) was a 64:36 mixture of the α and β anomers; ^1H nmr ($CDCl_3$), α-isomer, δ: 7.45–7.25 (m, 5H, Ph), 5.2 (dd, 1H, $J_{1,2}$ 3.5 Hz, $J_{1,OH}$ 2.0 Hz, H-1), 4.85 (d, 1H, *J* 11.5 Hz, CH_2Ph, overlapped by CH_2 β signal), 4.66 (d, 1H, *J* 11.5 Hz, CH_2Ph), 4.12 (m, 1H, H-5), 3.83 (dd, 1H, $J_{2,3}$ 9.5 Hz, H-2), 3.61 (2s, 6H, $2CH_3O$), 3.55 (s, 3H, CH_3O), 3.6 (dd, 1H, H-3 overlapped by CH_3O signal), 3.48 (dd, H-1, $J_{3,4}$ 3.0 Hz, $J_{4,5}$ 1.0 Hz, H-4), 2.885 (d, 1H, $J_{1,2}$ 2.0 Hz, OH-α, D_2O exchanged), 1.27 (d, 3H, $J_{5,6}$ 6.5 Hz, 3H-6). β-Isomer, δ: 7.45–7.25 (m, 5H, Ph), 4.89 (d, 1H, *J* 11.5 Hz, CH_2Ph), 4.6 (d, 1H, *J* 11.5 Hz, CH_2Ph), 4.60 (dd, 1H, $J_{1,2}$ 7.5 Hz, $J_{1,OH}$ 7.0 Hz, H-1), 4.12 (m, 1H, H-5), 3.61 (2s, 6H, $2CH_3O$), 3.55 (dd, 1H, H-2 overlapped by CH_3O signal), 3.415 (dd, 1H, $J_{3,4}$ 3.0 Hz, $J_{4,5}$ 1.0 Hz, H-4), 3.28 (dd, 1H, $J_{2,3}$ 9.5 Hz, H-3), 2.96 (d, 1H, $J_{1,OH}$ 7.0 Hz, OH-1, exchanged with D_2O), 1.34 (d, 3H, $J_{5,6}$ 6.0 Hz, 3H-6). Anal. calcd. for $C_{15}H_{22}O_5$: C 63.81, H 7.85; found: C 64.12, H 7.69.

4-O-Benzyl-2,3-di-O-methyl-α/β-L-fucopyranose (18)

The syrupy product from the hydrolysis of **11** (Scheme 1) (89% yield) with $[\alpha]_D$ −39 (*c* 0.63, chloroform) was a 59:41 mixture of the α and β anomers; ^1H nmr data ($CDCl_3$), α-isomer, δ: 7.4–7.15 (m, 5H, Ph), 5.4 (dd, 1H, $J_{1,2}$ 3.5 Hz, $J_{1,OH}$ 2.0 Hz, H-1α), 4.94 (d, 1H, *J* 11.5 Hz, CH_2Ph), 4.64 (d, 1H, *J* 11.5 Hz, CH_2Ph), 4.1 (m, 1H, H-5), 3.72 (dd, 2H, $J_{2,3}$ 10.0 Hz, H-3 partly overlapped by H-4α), 3.51, 3.53 (2s, each 3H, $2CH_3O$), 2.95 (d, 1H, $J_{1,OH}$ 2.0 Hz, OH-α, D_2O exchanged), 1.17 (d, 3H, $J_{5,6}$ 6.5 Hz, 3H-6). β-isomer, δ: 7.4–7.15 (m, 5H, Ph), 4.94 (d, 1H, *J* 11.5 Hz, CH_2Ph), 4.66 (d, 1H, *J* 11.5 Hz, CH_2Ph), 4.53 (t, 1H, $J_{1,2}$ 7.5 Hz, $J_{1,OH}$ 7.0 Hz, H-1), 4.1 (m, 1H, H-5), 3.62 (dd, 1H, $J_{3,4}$ 3.0 Hz, $J_{4,5}$ 1.5 Hz, H-4), 3.53, 3.51 (2s, each 3H, $2CH_3O$), 3.25 (d, 1H, $J_{1,OH}$ 7.0 Hz, OH-β, D_2O exchanged), 1.21 (d, 1H, $J_{5,6}$ 6.0 Hz, 3H-6). Anal. calcd. for $C_{15}H_{22}O_5$: C 63.81, H 7.85; found: C 63.91, H 7.70.

Substituted L-fucopyranosyl bromides

The compounds **15**, **17**, and **19** were prepared under the following conditions from compounds **14**, **16**, and **18** (Scheme 1). Compound **21** was prepared from **20** in a separate project under similar conditions. A solution of oxalyl bromide (8 mmol) in dichloromethane (5 mL) was added to the protected fucose (5 mmol) in a mixture of dichloromethane (5 mL) and DMF (0.5 mL). After stirring at room temperature for 30 min, the mixture was poured into ice-water. The organic layer was twice washed with cold water, and dried over sodium sulfate and 3 Å molecular sieves prior to concentration to a syrup that was used directly in the halide-ion catalyzed fucosylation reactions to be described below.

Bromide-ion catalyzed fucosylations

The protected fucopyranosyl bromide (**15**, **17**, **19**, or **55**) (5 mmol) in dichloromethane (4 mL) was added to a stirred solution of the alcohol (1 mmol), tetraethylammonium bromide (3 mmol), dichloromethane (8.5 mL), DMF (3.3 mL), and 4 Å molecular sieves under scrupulously anhydrous conditions. After stirring under nitrogen for 2 days, methanol (1.4 mL) was added and the stirring continued for a further 2 h. The mixture was freed of solids by filtration and washing with methylene chloride. After washing with aqueous sodium bicarbonate and water, the solution was dried over sodium sulfate and the solvent then removed *in vacuo*.

Methyl 2-acetamido-3-O-(2-O-acetyl-3,4,6-tri-O-benzyl-β-D-galactopyranosyl)-6-O-benzyl-2-deoxy-β-D-glucopyranoside (22)

This compound was prepared following the procedure previously described by Spohr and Lemieux (1).

Methyl 2-acetamido-3-O-(2-O-acetyl-3,4,6-tri-O-benzyl-β-D-galactopyranosyl)-6-O-benzyl-2-deoxy-4-O-(3,4-di-O-benzyl-2-O-methyl-α-L-fucopyranosyl)-β-D-glucopyranoside (23)

Alcohol **22** was reacted with bromide **15** under the conditions for bromide-ion catalyzed glycosylation. The product was chromatographed on a column of silica gel (ethyl acetate/toluene, 4:1) to provide a 79% yield of a white solid, $[\alpha]_D$ −66.3 (*c* 0.37, chloroform); ^1H nmr data ($CDCl_3$) δ: 7.4–7.2 (m, 30H, 6 Ph), 6.43 (d, 1H, $J_{NH,2a}$ 8.0 Hz, NH), 5.31 (dd, 1H, $J_{1b,2b}$ 8.0 Hz, $J_{2b,3b}$ 10.0 Hz, H-2b), 5.12 (d, 1H, $J_{1c,2c}$ 3.5 Hz, H-1c), 4.91 (d, 1H, $J_{A,B}$ 11.5 Hz, CH_2Ph), 4.38 (s, 2H, CH_2Ph), 4.31 (d, 1H, $J_{A,B}$ 11.5 Hz, CH_2Ph), 3.73 (dd, 1H, $J_{2c,3c}$ 10.0 Hz, H-2c), 3.50 (dd, 1H, $J_{3c,2c}$ 10.0 Hz, $J_{3c,4c}$ 3.0 Hz, H-3c), 3.43, 3.41 (2s, each 3H, $2CH_3O$), 2.05 (s, 3H, CH_3COO), 1.93 (s, 3H, $NHCOCH_3$), 1.09 (d, 3H, $J_{5c,6c}$ 6.5 Hz, 3H-6c). Anal. calcd. for $C_{66}H_{77}NO_{16}$: C 69.52, H 6.81, N 1.23; found: C 69.09, H 6.85, N 1.25.

Methyl 2-acetamido-3-O-(2-O-acetyl-3,4,6-tri-O-benzyl-β-D-galactopyranosyl)-6-O-benzyl-4-O-(2-O-benzyl-3,4-di-O-methyl-α-L-fucopyranosyl)-2-deoxy-β-D-glucopyranoside (24)

Alcohol **22** was reacted with bromide **17** under the conditions for bromide-ion catalyzed glycosylation. Chromatographic purification as described for the isolation of **23** provided a white foam (82% yield), $[\alpha]_D$ −61 (*c* 0.5, chloroform); ^1H nmr data ($CDCl_3$) δ: 7.4–7.15 (m, 25H, 5Ph), 6.48 (d, 1H, $J_{NH,2a}$ 8.0 Hz, NH), 5.31 (dd, 1H, $J_{1b,2b}$ 8.0 Hz, $J_{2b,3b}$ 10.0 Hz, H-2b), 5.15 (d, 1H, $J_{1c,2c}$ 3.5 Hz, H-1c), 4.95 (d, 1H, $J_{A,B}$ 11.5 Hz, CH_2Ph), 4.69 (t, 2H,

Can. J. Chem. Downloaded from www.nrcresearchpress.com by 123.30.183.119 on 09/08/12
For personal use only.

$J_{A,B}$ 11.5 Hz for both, CH_2Ph), 3.82 (dd, 1H, $J_{1c,2c}$ 3.5 Hz, $J_{2c,3c}$ 10.0 Hz, H-2c overlapped by H-5c), 3.52 (dd, 1H, $J_{3c,4c}$ 3.0 Hz, H-3c), 3.42, 3.41, and 3.37 (3s, each 3H, $3CH_3O$), 2.03 (s, 3H, CH_3COO), 1.17 (s, 3H, $NHCOCH_3$), 1.09 (d, 1H, $J_{5c,6c}$ 6.5 Hz, 3H-6c). Anal. calcd. for $C_{60}H_{73}NO_{16}$: C 67.71, H 6.91, N 1.32; found: C 67.36, H 6.94, N 1.29.

*Methyl 2-acetamido-3-*O*-(2-*O*-acetyl-3,4,6-tri-*O*-benzyl-β-D-galactopyranosyl)-6-*O*-benzyl-4-*O*-(4-*O*-benzyl-2,3-di-*O*-methyl-α-L-fucopyranosyl)-2-deoxy-β-D-glucopyranoside (25)*

Compound **22** was reacted with bromide **19** under the conditions for bromide-ion catalyzed glycosylation. Chromatographic purification as described for the isolation of **23** provided a white foam (78% yield), $[\alpha]_D$ −59 (*c* 0.3, chloroform); ^1H nmr data ($CDCl_3$) δ: 7.41–7.25 (m, 25H, 5Ph) 6.49 (d, 1H, $J_{NH,2a}$ 8.0 Hz, NH), 5.30 (dd, 1H, $J_{1b,2b}$ 8.0 Hz, $J_{2b,3b}$ 10.0 Hz, H-2b), 5.11 (d, 1H, $J_{1c,2c}$ 3.5 Hz, H-1c), 4.92 (d, 1H, $J_{A,B}$ 11.5 Hz, CH_2Ph), 4.69 (2d, 2H, $J_{A,B}$ 11.5 Hz, CH_2Ph), 4.44 (ABq, 2H, $J_{A,B}$ 11.5 Hz and $J_{A,B'}$ 11.5 Hz, CH_2Ph), 4.28 (d, 1H, $J_{A,B}$ 11.5 Hz, CH_2Ph), 3.91 (m, H-5c overlapped), 3.5 (dd, 1H, $J_{3c,2c}$ 10.0 Hz, $J_{3c,4c}$ 3.0 Hz, H-3c), 3.41 (2s, 6H, $2CH_3O$), 3.34 (s, 3H, CH_3O), 2.1 (s, 3H, CH_3COO), 1.9 (s, 3H, $NHCOCH_3$), 1.06 (d, 3H, $J_{5c,6c}$ 6.5 Hz, 3H-6c). Anal. calcd. for $C_{60}H_{73}NO_{16}$: C 67.71, H 6.91, N 1.32; found: C 67.07, H 6.94, N 1.33.

*Methyl 2-acetamido-3-*O*-(2-*O*-acetyl-3,4,6-tri-*O*-benzyl-β-D-galactopyranosyl)-6-*O*-benzyl-2-deoxy-4-*O*-(2,3,4-tri-*O*-benzyl-α-L-fucopyranosyl)-β-D-glucopyranoside (26)*

The previously described (1) tri-O-benzyl-α-L-fucopyranosyl bromide (**55**, Scheme 1) was reacted with **22** under the conditions for bromide-ion catalyzed focusylation and provided crystalline white needles from ethyl acetate (90% yield) with mp 148–149°C, $[\alpha]_D$ −66.4 (*c* 0.81, chloroform); ^1H nmr data ($CDCl_3$) δ: 7.4–7.10 (m, 35H, 7Ph), 6.57 (d, 1H, $J_{NH,2a}$ 8.0 Hz, NH), 5.2 (dd, 1H, $J_{1b,2b}$ 8.0 Hz, $J_{2b,3b}$ 10.0 Hz, H-2b), 5.18 (d, 1H, $J_{1c,2c}$ 4.0 Hz, H-1c), 4.92 (d, 1H, $J_{A,B}$ 11.5 Hz, CH_2Ph), 4.79 (d, 1H, $J_{A,B}$ 11.5 Hz, CH_2Ph), 4.05 (dd, overlapped, $J_{2c,3c}$ 10.0 Hz, H-2c), 3.72 (dd, 1H, $J_{3c,4c}$ 3.0 Hz, H-3c), 3.42 (s, 3H, CH_3O), 2.05 (s, 3H, CH_3CONH), 1.57 (s, 3H, CH_3COO), 1.07 (d, 3H, $J_{5c,6c}$ 6.5 Hz, 3H-6c). Anal. calcd. for $C_{72}H_{81}NO_{16}$: C 71.11, H 6.67, N 1.15; found: C 70.02, H 6.59, N 1.15.

*Methyl 2-acetamido-6-*O*-benzyl-2-deoxy-4-*O*-(3,4-di-*O*-benzyl-2-*O*-methyl-α-L-fucopyranosyl)-3-*O*-(3,4,6-tri-*O*-benzyl-β-D-galactopyranosyl)-β-D-gluocopyranoside (27)*

Compound **23** (500 mg, 0.44 mmol) was dissolved in methanolic 0.2 M sodium methoxide and kept overnight at room temperature. After neutralization with Amberlite IRC-50 (H^+) resin, the solution was evaporated to a white solid (405 mg, 85%), mp 90°C, $[\alpha]_D$ −64.4 (*c* 0.263, chloroform); ^1H nmr data ($CDCl_3$) δ: 7.45–7.2 (m, 30H, 6Ph), 7.03 (d, 1H, $J_{NH,2a}$ 8.0 Hz, NH), 5.14 (d, 1H, $J_{1c,2c}$ 3.5 Hz, H-1c), 4.9 (H-2b overlapped by CH_2Ph signals), 4.54 (s, 2H, CH_2Ph), 4.41 (s, 2H, CH_2Ph), 4.38 (d, 1H, $J_{1b,2b}$ 7.5 Hz, H-1b), 4.25 (bm, 1H, OH-2b), 4.18 (m, 1H, H-5c), 4.39, 3.45 (2s, each 3H, $2OCH_3$), 1.83 (s, 3H, $NHCOCH_3$), 1.10 (d, 3H, $J_{5c,6c}$ 6.5 Hz, 3H-6c). Anal. calcd. for $C_{64}H_{75}NO_{15}$: C 69.99, H 6.88, N 1.28; found: C 69.74, H 6.87, N 1.28.

*Methyl 2-acetamido-6-*O*-benzyl-4-*O*-(2-*O*-benzyl-3,4-di-*O*-methyl-α-L-fucopyranosyl)-2-deoxy-3-*O*-(3,4,6-tri-*O*-benzyl-β-D-galactopyranosyl)-β-D-glucopyranoside (28)*

Compound **24** was de-*O*-acetylated as described above for **23** to yield a white powder (91% yield), mp 87°C, $[\alpha]_D$ − 63.2 (*c* 0.43, chloroform); ^1H nmr data ($CDCl_3$) δ: 7.45–7.2 (m, 25H, 5Ph), 7.04 (d, 1H, $J_{2a,NH}$ 8.0 Hz, NH), 5.14 (d, 1H, $J_{1c,2c}$ 3.5 Hz, H-1c), 4.9 (dd, 3H, H-2b overlapped by CH_2Ph), 4.44 (s, 2H, CH_2Ph), 4.39 (d, 1H, $J_{1b,2b}$ 8.0 Hz, H-1b), 3.52, 3.5, 3.48 (3s, each 3H, $3CH_3O$ overlapped), 3.26 (dd, 1H, $J_{3c,4c}$ 2.5 Hz, $J_{4c,5c}$ 1.0 Hz, H-4c), 1.53 (s, 3H, $NHCOCH_3$), 1.16 (d, 3H, $J_{5c,6c}$ 6.5 Hz, 3H-6c). Anal. calcd. for $C_{58}H_{71}NO_{15}$: C 68.15, H 7.00, N 1.37; found: C 67.95, H 7.04, N 1.39.

*Methyl 2-acetamido-6-*O*-benzyl-4-*O*-(4-*O*-benzyl-2,3-di-*O*-methyl-α-L-fucopyranosyl)-2-deoxy-3-*O*-(3,4,6-tri-*O*-benzyl-β-D-galactopyranosyl)-β-D-glucopyranoside (29)*

Compound **25** was de-*O*-acetylated as described above for **23** to yield a white powder (93% yield), $[\alpha]_D$ −66.2 (*c* 0.22, chloroform); ^1H nmr data ($CDCl_3$) δ: 7.5–7.2 (m, 25H, 5Ph), 7.05 (d, 1H, $J_{2a,NH}$ 8.0 Hz, NH), 5.14 (d, 1H, $J_{1c,2c}$ 3.5 Hz, H-1c), 4.92 (d, 1H, $J_{A,B}$ 11.5 Hz, CH_2Ph), 4.62 (d, 1H, $J_{A,B}$ 11.5 Hz, CH_2Ph), 4.54 (s, 2H, CH_2Ph), 4.43 (s, 2H, CH_2Ph), 4.39 (d, 1H, $J_{1b,2b}$ 8.0 Hz, H-1b), 4.23 (bm, 1H, OH-2b), 4.17 (m, 1H, H-5c), 3.69 (dd, 1H, $J_{1c,2c}$ 3.5 Hz, $J_{2c,3c}$ 10.0 Hz, H-2c), 3.49 (s, 3H, CH_3O), 3.43 (s, 6H, $2CH_3O$), 1.88 (s, 3H, $NHCOCH_3$), 1.10 (d, 3H, $J_{5c,6c}$ 6.5 Hz, 3H-6c). Anal. calcd. for $C_{58}H_{71}NO_{15}$: C 68.15, H 7.00, N 1.37; found: C 67.97, H 7.00, N 1.39.

*Methyl 2-acetamido-6-*O*-benzyl-2-deoxy-4-*O*-(2,3,4-tri-*O*-benzyl-α-L-fucopyranosyl)-3-*O*-(3,4,6-tri-*O*-benzyl-β-D-galactopyranosyl)-β-D-glucopyranoside (30)*

Compound **26** was de-*O*-acetylated as described for the preparation of **27**. The yield was 92% of crystalline product, which was recrystallized from methanol and had mp 140–142°C, $[\alpha]_D$ −68.4 (*c* 0.6, chloroform); ^1H nmr data ($CDCl_3$) δ: 7.45–7.2 (m, 35H, 7Ph), 7.04 (d, 1H, $J_{2a,NH}$ 6.5 Hz, NH), 5.2 (d, 1H, $J_{1c,2c}$ 4.0 Hz, H-1c), 4.9 (dd, 3H, H-2b overlapped by CH_2Ph), 4.21 (bm, 1H, OH-2b exchanged with D_2O), 4.05 (dd, 2H, $J_{3c,2c}$ 10.0 Hz, H-2c overlapped by H-5c), 3.79 (dd, 1H, $J_{3c,4c}$ 3.0 Hz, H-3c overlapped by H-4c), 3.52 (s, 3H, CH_3O), 1.5 (s, 3H, CH_3CONH), 1.09 (d, 3H, $J_{5c,6c}$ 6.5 Hz, 3H-6c). Anal. calcd. for $C_{70}H_{79}NO_{15}$: C 71.6, H 6.75, N 1.19; found: C 71.40, H 6.59, N 1.33.

*Methyl 2-acetamido-6-*O*-benzyl-2-deoxy-4-*O*-(3,4-di-*O*-benzyl-2-*O*-methyl-α-L-fucopyranosyl)-3-*O*-[3,4,6-tri-*O*-benzyl-2-*O*-(2,3,4-tri-*O*-benzyl-α-L-fucopyranosyl)-β-D-galactopyranosyl]-β-D-glucopyranoside (31)*

Alcohol **27** was reacted with the bromide **55** (Scheme 1) under the conditions for bromide-ion catalyzed glycosylation. The product was purified by chromatography as described for **23** to provide a white foam (81% yield) with $[\alpha]_D$ −81 (*c* 0.43, chloroform); ^1H nmr data ($CDCl_3$) δ: 7.4–7.0 (m, 45H, 9Ph), 5.7 (d, 1H, $J_{1d,2d}$ 3.5 Hz, H-1d), 5.66 (d, 1H, $J_{2a,NH}$ 8.0 Hz, NH), 4.99 (d, 1H, $J_{1c,2c}$ 3.5 Hz, H-1c), 4.92 (d, 1H, $J_{A,B}$ 11.5 Hz, CH_2Ph), 4.11 (m, 1H, H-5d overlapped by H-2c), 3.41, 3.36 (2s, each 3H, $2CH_3O$), 3.2 (dd, 1H, $J_{3c,4c}$ 3.0 Hz, $J_{4c,5c}$ 1.0 Hz, H-4c), 1.78 (s, 3H, $NHCOCH_3$), 1.2, 1.117 (2s, each 3H, $J_{5c,6c}$ = $J_{5d,6d}$ = 6.5 Hz, 3H-6c, 3H-6d). Anal. calcd. for $C_{91}H_{103}NO_{19}$: C 72.15 H 6.85, N 0.93; found: C 71.66, H 6.99, N 1.01.

*Methyl 2-acetamido-6-*O*-benzyl-4-*O*-(4-*O*-benzyl-2,3-di-*O*-methyl-α-L-fucopyranosyl)-2-deoxy-3-*O*-[3,4,6-tri-*O*-benzyl-2-*O*-(2,3,4-tri-*O*-benzyl-α-L-fucopyranosyl)-β-D-galactopyranosyl]-β-D-glucopyranoside (32)*

Alcohol **29** was reacted with the bromide **55** (Scheme 1) under the conditions for bromide-ion catalyzed glycosylation. Purification of the product as described for **23** provided a white solid (70% yield) with $[\alpha]_D$ −67.3 (*c* 0.32, chloroform); ^1H nmr data ($CDCl_3$) δ: 7.4–7.0 (m, 40H, 8Ph), 5.69 (2d, 2H, $J_{2a,NH}$ 8.0 Hz, $J_{1d,2d}$ 3.5 Hz, NH partly overlapped by H-1d), 4.96 (d, 1H, $J_{1c,2c}$ 3.5 Hz, H-1c overlapped by CH_2Ph signal), 3.38, 3.34, 3.25 (3s, each 3H, $3CH_3O$), 3.11 (dd, 1H, $J_{3c,4c}$ 3.0 Hz, $J_{4c,5c}$ 1.0 Hz, H-4c), 1.90 (s, 3H, $NHCOCH_3$), 1.18, 1.07 (2d, each 3H, $J_{5c,6c}$ = $J_{5d,6d}$ = 6.5 Hz, 3H-6c, 3H-6d). Anal. calcd. for $C_{85}H_{99}NO_{19}$: C 70.96, H 6.94, N 0.97; found: C 70.70, H 6.93, N 0.97.

*Methyl 2-acetamido-6-*O*-benzyl-2-deoxy-4-*O*-(2-*O*-benzyl-3,4-di-*O*-methyl-α-L-fucopyranosyl)-3-*O*-[3,4,6-tri-*O*-benzyl-2-*O*-(2,3,4-tri-*O*-benzyl-α-L-fucopyranosyl)-β-D-galactopyranosyl]-β-D-glucopyranoside (33)*

Alcohol **28** was reacted with the bromide **55** (Scheme 1) under the conditions for bromide-ion catalyzed glycosylation. The product was purified by chromatography as described for **23** to provide a white powder (74.4% yield) with $[\alpha]_D$ −62 (*c* 0.3, chloroform); ^1H nmr data ($CDCl_3$) δ: 7.45–7.05 (m, 40H, 8Ph), 5.71 (d,

Can. J. Chem. Downloaded from www.nrcresearchpress.com by 123.30.183.119 on 09/08/12
For personal use only.

1H, $J_{2a,NH}$ 8.5 Hz, NH), 5.7 (d, 1H, $J_{1d,2d}$ 3.7 Hz, H-1d), 4.93 (d, 1H, $J_{1c,2c}$ 3.5 Hz, H-1c overlapped by CH_2Ph signal), 4.67 (d, 1H, $J_{1b,2b}$ 8.0 Hz, H-1b), 3.76 (dd, 1H, $J_{2c,3c}$ 10.0 Hz, H-2c), 3.44 (dd, 1H, $J_{3c,4c}$ 3.0 Hz, H-3c), 3.32, 3.29, and 3.15 (3s, each 3H, $3CH_3O$), 2.88 (dd, 1H, $J_{4c,5c}$ 1.0 Hz, H-4c), 1.85 (s, 3H, $NHCOCH_3$), 1.17, 1.04 (2d, each 3H, $J_{5c,6c} = J_{5d,6d} = 6.5$ Hz, 3H-6c, 3H-6d). Anal. calcd. for $C_{85}H_{99}NO_{19}$: C 70.96, H 6.94, N 0.97; found: C 70.49, H 7.01, N 1.01.

Methyl 2-acetamido-6-O-benzyl-2-deoxy-3-O-[3,4,6-tri-O-benzyl-2-O-(3,4-di-O-benzyl-2-O-methyl-α-L-fucopyranosyl)-β-D-galactopyranosyl]-4-O-(2,3,4-tri-O-benzyl-α-L-fucopyranosyl)-β-D-glucopyranoside (34)

Reaction of the bromide (**15**) (Scheme 1) with the alcohol **30** under the conditions for bromide-ion catalysis provided, after the chromatographic purification, a white foam (77.6% yield) with $[\alpha]_D$ −130.0 (*c* 0.32, chloroform); ^1H nmr data ($CDCl_3$) δ: 7.45–7.12 (m, 45H, 9Ph), 5.68 (d, 1H, $J_{NH,2a}$ 8.0 Hz, NH), 5.62 (d, 1H, $J_{1d,2d}$ 3.5 Hz, H-1d), 4.97 (d, 1H, $J_{1c,2c}$ 3.5 Hz, H-1c), 4.92 (d, 1H, $J_{A,B}$ 11.5 Hz, CH_2Ph), 4.67 (d, 1H, $J_{1b,2b}$ 7.5 Hz, H-1b), 3.56, 3.3 (2s, each 3H, $2CH_3O$), 1.88 (s, 3H, $NHCOCH_3$), 1.18, 1.12 (2d, each 3H, $J_{5c,6c} = J_{5d,6d} = 6.5$ Hz, 3H-6c, 3H-6d). Anal. calcd. for $C_{91}H_{103}NO_{19}$: C 72.15, H 6.85, N 0.93; found: C 71.64, H 6.83, N 0.91.

Methyl 2-acetamido-6-O-benzyl-2-deoxy-4-O-(2,3,4-tri-O-benzyl-α-L-fucopyranosyl)-3-O-[3,4,6-tri-O-benzyl-2-O-(2-O-benzyl-3,4-di-O-methyl-α-L-fucopyranosyl)-β-D-galactopyranosyl]-β-D-glucopyranoside (35)

Reaction of the alcohol **30** with the bromide **17** (Scheme 1) under the conditions for bromide-ion catalyzed glycosylation, followed by purification of the product by chromatography, provided a white solid (84% yield), $[\alpha]_D$ −78.6 (*c* 0.41, chloroform); ^1H nmr data ($CDCl_3$) δ: 7.4–7.05 (m, 40H, 8Ph), 5.81 (d, 1H, $J_{2a,NH}$ 8.5 Hz, NH), 5.65 (d, 1H, $J_{1d,2d}$ 3.5 Hz, H-1d), 5.03 (d, 1H, $J_{1c,2c}$ 3.5 Hz, H-1c), 3.57, 3.54 (2s, each 3H, $2CH_3O$ overlapped), 3.41 (s, 3H, CH_3O), 1.89 (s, 3H, $NHCOCH_3$), 1.28, 1.13 (2d, each 3H, $J_{5c,6c} = J_{5d,6d} = 6.5$ Hz, 3H-6c, 3H-6d). Anal. calcd. for $C_{85}H_{99}NO_{19}$: C 70.96, H 6.94, N 0.97; found: C 70.74, H 6.92, N 0.95.

Methyl 2-acetamido-6-O-benzyl-2-deoxy-3-O-[3,4,6-tri-O-benzyl-2-O-(4-O-benzyl-2,3-di-O-methyl-α-L-fucopyranosyl)-β-D-galactopyranosyl]-4-O-(2,3,4-tri-O-benzyl-α-L-fucopyranosyl)-β-D-glucopyranoside (36)

The alcohol **30** was reacted with the bromide **19** (Scheme 1) under the conditions for bromide-ion catalyzed glycosylation, followed by purification of the product by chromatography, and provided a white foam (79% yield) with $[\alpha]_D$ −145 (*c* 0.32, chloroform); ^1H nmr data ($CDCl_3$) δ: 7.45–7.25 (m, 40H, 8Ph), 5.83 (d, 1H, $J_{2a,NH}$ 8.0 Hz, NH), 5.60 (d, 1H, $J_{1d,2d}$ 3.5 Hz, H-1d), 5.01 (d, 1H, $J_{1c,2c}$ 3.5 Hz, H-1c), 3.5 (s, 3H, CH_3O), 3.343, 3.306 (2s, each 3H, $2CH_3O$), 1.91 (s, 3H, $NHCOCH_3$), 1.18, 1.12 (2d, each 3H, $J_{5c,6c} = J_{5d,6d} = 6.5$ Hz, 3H-6c, 3H-6d). Anal. calcd. for $C_{85}H_{99}NO_{19}$: C 70.96, H 6.94, N 0.97; found: C 70.33, H 6.96, N 0.96.

Deblocking by hydrogenolysis to remove the O-*benzyl groups*

Typical experiments involved dissolving the compound (**31**–**36**) (100 mg) in 95% ethanol (4.5 mL) and stirring the solution efficiently over the palladium-on-charcoal catalyst for 16 h under hydrogen at atmospheric pressure. After catalyst removal, the solution was taken to dryness and the resulting residue dissolved in 10% ethanol for passing through a column of Biogel-P2. The appropriate fraction was taken to dryness and then dissolved in water for freeze-drying.

Methyl 2-acetamido-2-deoxy-3-O-[2-O-(α-L-fucopyranosyl)-β-D-galactopyranosyl]-4-O-(2-O-methyl-α-L-fucopyranosyl)-β-D-glucopyranoside (37)

The hydrogenolysis of **31** produced a white powder, in 89% yield, $[\alpha]_D$ −102.2 (*c* 0.78, water). The ^1H and ^{13}C nmr data are reported in Tables 3 and 4.

Methyl 2-acetamido-2-deoxy-4-O-(2,3-di-O-methyl-α-L-fucopyranosyl)-3-O-[2-O-(α-L-fucopyranosyl)-β-D-galactopyranosyl]-β-D-glucopyranoside (38)

The hydrogenolysis of **32** provided a white powder in 74% yield, $[\alpha]_D$ −90 (*c* 0.72, water). The ^1H and ^{13}C nmr data are reported in Tables 3 and 4.

Methyl 2-acetamido-2-deoxy-4-O-(3,4-di-O-methyl-α-L-fucopyranosyl)-3-O-[2-O-(α-L-fucopyranosyl)-β-D-galactopyranosyl]-β-D-glucopyranoside (39)

The hydrogenolysis of **33** provided a white powder in 73% yield, $[\alpha]_D$ −69.4 (*c* 0.8, water). The ^1H and ^{13}C nmr data are reported in Tables 3 and 4..

Methyl 2-acetamido-2-deoxy-4-O-(α-L-fucopyranosyl)-3-O-[2-O-(2-O-methyl-α-L-fucopyranosyl)-β-D-galactopyranosyl]-β-D-glucopyranoside (40)

The hydrogenolysis of **34** led to a white powder in 83% yield, $[\alpha]_D$ −127 (*c* 0.7, water). The ^1H and ^{13}C nmr data are reported in Tables 3 and 4.

Methyl 2-acetamido-2-deoxy-4-O-(α-L-fucopyranosyl)-3-O-[2-O-(3,4-di-O-methyl-α-L-fucopyranosyl)-β-D-galactopyranosyl]-β-D-glucopyranoside (41)

The hydrogenolysis of **35** provided a white powder in 89% yield, $[\alpha]_D$ −134.5 (*c* 0.73, water). The ^1H and ^{13}C nmr data are reported in Tables 3 and 4.

Methyl 2-acetamido-2-deoxy-4-O-(α-L-fucopyranosyl)-3-O-[2-O-(2,3-di-O-methyl-α-L-fucopyranosyl)-β-D-galactopyranosyl]-β-D-glucopyranoside (42)

The hydrogenolysis of **36** provided a white powder in 76% yield, $[\alpha]_D$ −98.5 (*c* 0.63, water). The ^1H and ^{13}C nmr data are reported in Tables 3 and 4.

3,4-Di-O-acetyl-1,2-O-(1-methoxyethylidene)-6-O-methyl-α-D-galactopyranose (45)

The known 6-*O*-methyl-α/β-D-galactopyranose (12) (7.8 g, 21.5 mmol) was acetylated for conversion to the acetobromo derivative in the usual manner using hydrogen bromide in acetic acid. The syrupy product was dissolved in *sym*-collidine (40 mL) and tetraethylammonium bromide. Methanol (10 mL) was then added and the mixture was heated at 60°C for 24 h. The product was isolated in the usual manner (13) and purified by chromatography on a silica gel column (58% yield); ^1H nmr data ($CDCl_3$), *exo* and *endo* isomers δ: 5.82 (d, 1H, $J_{1,2}$ 5.0 Hz, H-1), 5.43 (m, 2H, H-4 overlapped by H-6a), 5.05 (dd, 1H, $J_{2,3}$ 7.0 Hz, $J_{3,4}$ 4.5 Hz, H-3), 4.36–4.1 (m, 3H, H-2, H-5, and H-6b), 3.38 and 3.35 (2s, each 3H, 2MeO), 2.12 (s, 6H, 2OAc), 1.68 (s, 3H, CH_3).

3,4-Di-O-benzyl-1,2-O-(1-methoxyethylidene)-6-O-methyl-α-D-galactopyranose (46)

The orthoester (**45**) (4.0 g, 12 mmol) was deacetylated in the usual manner using sodium methoxide in methanol and, without purification, was subjected to *O*-benzylation under the standard conditions described above. Chromatography on silica gel provided a syrupy product (3.3 g, 65% yield), $[\alpha]_D$ +111 (*c* 0.46, chloroform); ^1H nmr data ($CDCl_3$), *exo* and *endo* isomers, δ: 7.5–7.2 (m, 10H, 2Ph), 5.75 (d, 1H, $J_{1,2}$ 4.5 Hz, H-1), 4.93 and 4.64 (ABq, 2H, $J_{A,B}$ 11.5 Hz, CH_2Ph), 4.81 and 4.68 (ABq, 2H, $J_{A,B}$ 12 Hz, CH_2Ph), 4.49 (dd, 1H, $J_{1,2}$ 4.5 Hz, $J_{2,3}$ 7 Hz, H-2), 4.09–3.95 (m, 2H, H-6a and H-4), 3.65 (dd, 1H, $J_{3,4}$ 2.5 Hz, H-3), 3.57–3.48 (m, 2H, H-5 and H-6b), 3.31 and 3.28 (2s, each 3H, 2MeO), 1.58 (s, 3H, CH_3). Anal. calcd. for $C_{24}H_{30}O_7$: C 66.96, H 7.02; found: C 66.32, H 6.95.

2-O-Acetyl-3,4-di-O-benzyl-6-O-methyl-α-D-galactopyranosyl bromide (47)

Acetyl bromide (0.9 mL, 12.2 mmol) was added to a stirred mixture of **46** (2.5 g, 5.8 mmol), tetraethylammonium bromide (0.62 g, 3 mmol), 4 Å molecular sieves (1.0 g), and dichloromethane (23 mL). After 1 h, the solids were removed and the solution poured into a stirred mixture of aqueous sodium bicarbonate and ice. Work-up in the usual manner (1) provided a syrup (2.2 g, 79% yield).

Can. J. Chem. Downloaded from www.nrcresearchpress.com by 123.30.183.119 on 09/08/12
For personal use only.

*Methyl 2-acetamido-3-O-(2-O-acetyl-3,4-di-O-benzyl-6-O-methyl-β-D-galactopyranosyl)-4,6-O-benzylidene-2-deoxy-β-D-glucopyranoside (**48**)*

A mixture of methyl 2-acetamido-4,6-benzylidene-2-deoxy-β-D-glucopyranoside (7, 14) (1.16 g, 3.6 mmol), mercuric cyanide (1.86 g, 7.4 mmol), powdered calcium sulfate (1.16 g), and 4 Å molecular sieves (2 g) in toluene/nitromethane (1:1, 116 mL) was stirred under nitrogen and the bromide (**47**) (2.1 g, 4.4 mmol) in toluene/nitromethane (14 mL) was added over a 20 min period at room temperature. After 2 h, the solids were removed by filtration and the solution poured into a mixture of aqueous sodium bicarbonate and dichloromethane. The organic layer was washed with water, dried, and evaporated to leave a solid residue. The yield was 1.94 g (76%) of a crystalline solid, which was recrystallized from methanol, mp 145°C, $[\alpha]_D$ −44 (*c* 0.6, chloroform); ^{1}H nmr data ($CDCl_3$) δ: 7.5–7.2 (m, 15H, 3Ph), 5.76 (d, 1H, $J_{NH,2a}$ 6.5 Hz, NH), 5.50 (s, 1H, CHPh), 5.26 (dd, 1H, $J_{1b,2b}$ 8.0 Hz, $J_{2b,3b}$ 10.0 Hz, H-2b), 5.16 (d, 1H, $J_{1a,2a}$ 8.0 Hz, H-1a), 4.88 and 4.42 (ABq, 2H, $J_{A,B}$ 12.0 Hz, CH_2Ph), 4.61 (m, 3H, CH_2Ph overlapped by H-1b), 4.32 (dd, 1H, $J_{6Aa,6Ba}$ 10.0 Hz, $J_{6Aa,5a}$ 5.0 Hz, H-6Aa), 3.84 (d, 1H, $J_{3b,4b}$ 2.5 Hz, H-4b), 3.76 (t, 1H, $J_{5a,6Ba}$ 10.0 Hz, H-6Ba), 3.67 (t, 1H, $J_{4a,5a}$ 9.0 Hz, H-4a), 3.50 (s, 3H, MeO), 3.41 (dd, 1H, H-3b), 3.20 (bt, 1H, $J_{5b,6Ab}$ 5.5 Hz, $J_{5b,6Bb}$ 7.0 Hz, H-5b), 3.10 (s, 3H, OMe), 2.96 (m, 1H, H-2a), 1.96 and 1.98 (s, 3H each, NHAc and OAc). Anal. calcd. for $C_{39}H_{47}NO_{12}$: C 64.89, H 6.56, N 1.94; found: C 64.82, H 6.36, N 1.89.

*Methyl 2-acetamido-3-O-(2-O-acetyl-3,4-di-O-benzyl-6-O-methyl-β-D-galactopyranosyl)-6-O-benzyl-2-deoxy-β-D-glucopyranoside (**49**)*

Compound **48** (1.8 g, 2.5 mmol) was reduced with sodium cyanoborohydride (3.3 g) under the conditions described for the preparation of **22** (1). The yield was 1.3 g (72%) of a solid, which was recrystallized from methanol, mp 222°C, $[\alpha]_D$ +16.9 (*c* 0.64, chloroform); ^{1}H nmr data ($CDCl_3$) δ: 7.4–7.2 (m, 15H, 3Ph), 5.66 (d, 1H, $J_{NH,2a}$ 7.0 Hz, NH), 5.34 (dd, 1H, $J_{1b,2b}$ 8.0 Hz, $J_{2b,3b}$ 10.0 Hz, H-2b), 4.92 and 4.61 (ABq, 2H, J_{AB} 12 Hz, CH_2Ph), 4.90 (d, 1H, $J_{1a,2a}$ 8.0 Hz, H-1a), 4.69 and 4.5 (ABq, 2H, CH_2Ph), 4.60 (s, 2H, CH_2Ph), 4.41 (d, 1H, H-1b), 4.33 (dd, 1H, $J_{2a,3a}$ 10.0 Hz, $J_{3a,4a}$ 8.0 Hz, H-3a), 4.26 (bs, 1H, OH exchanged with D_2O), 3.86 (d, overlapped, 1H, $J_{3b,4b}$ 2.5 Hz, H-4b), 3.54 (dd, overlapped; H-3b), 3.49 (s, 3H, OMe) 3.46 (t, overlapped; $J_{4a,5a}$ 9.5 Hz, H-4a), 3.28 (s, 3H, OMe), 2.94 (m, 1H, H-2a), 2.05 and 1.98 (s, 3H each, NHAc and OAc). Anal. calcd. for $C_{39}H_{49}NO_{12}$: C 64.72, H 6.82, N 1.94; found: C 64.26, H 6.76, N 2.02.

*Methyl 2-acetamido-3-O-(3,4-di-O-benzyl-6-O-methyl-β-D-galactopyranosyl)-6-O-benzyl-2-deoxy-β-D-glucopyranoside (**50**)*

Compound **49** was de-*O*-acetylated under the standard conditions to provide a crystalline product, in 97% yield, which decomposed at >235°C; $[\alpha]_D$ −2.1 (*c* 0.7, chloroform); ^{1}H nmr data ($CDCL_3$) δ: 7.4–7.2 (m, 15H, 3Ph), 6.20 (d, 1H, NH), 4.87 and 4.55 (ABq, 2H, $J_{A,B}$ 12.0 Hz, CH_2Ph), 4.76 (d, 1H, $J_{1a,2a}$ 8.5 Hz, H-1a), 4.60 and 4.70 (ABq, 2H, $J_{A,B}$ 12.0 Hz, CH_2Ph), 4.59 (s, 2H, CH_2Ph), 4.26 (bs, 1H, OH), 4.23 (d, 1H, $J_{1b,2b}$ 8.0 Hz, H-1b), 4.16 (dd, 1H, $J_{2a,3a}$ 10.0 Hz, $J_{3a,4a}$ 8.0 Hz, H-3a), 3.96 (dd, 1H, $J_{2b,3b}$ 9.5 Hz, H-2b), 3.80 (d, 1H, $J_{3b,4b}$ 2.0 Hz, H-4b), 3.50 (s, 3H, MeO), 3.39 (dd, 1H, H-3b), 3.26 (s, 3H, MeO), 3.2 (bs, 1H, OH), 3.26 (m, 1H overlapped by MeO signal H-2a), 1.96 (s, 3H, NHAc). Anal. calcd. for $C_{32}H_{47}NO_{11}$: C 65.18, H 6.95, N 2.05; found: C 64.91, H 6.84, N 2.02.

*Methyl 2-acetamido-6-O-benzyl-2-deoxy-4-O-(2,3,4-tri-O-benzyl-α-L-fucopyranosyl-3-O-[3,4-di-O-benzyl-6-O-methyl-2-O-(2,3,4-tri-O-benzyl-α-L-fucopyranosyl)-β-D-galactopyranosyl]-β-D-glucopyranoside (**51**)*

Reaction of **50** (230 mg, 0.34 mmol) with the fucosyl bromide (**55**) (2.42 mmol) under the conditions for bromide-ion catalyzed glycosylation, followed by purification of the product by chromatography over silica gel, provided a white powder (325 mg, 65% yield), mp 84°C, $[\alpha]_D$ −67.0 (*c* 0.5, chloroform); ^{1}H nmr data ($CDCL_3$) δ: 7.4–7.0 (m, 45H, 9Ph), 5.72 (d, 1H, $J_{2a,NH}$ 8.5 Hz, NH), 5.7 (d, 1H, $J_{1d,2d}$ 3.8 Hz, H-1d), 4.98 (d, 1H, $J_{1c,2c}$ 4.0 Hz, H-1c), 3.31 and 3.26 (2s, each 3H, $2CH_3O$), 1.85 (s, 3H, $NHCOCH_3$), 1.19, 1.13 (2d, each 3H, $J_{5c,6c}$ = $J_{5d,6d}$ = 6.5 Hz, 3H-6c, 3H-6d). Anal. calcd. for $C_{91}H_{103}NO_{19}$: C 72.15, H 6.86, N 0.93; found: C 71.59, H 6.76, N 0.99.

*Methyl 2-acetamido-2-deoxy-4-O-(α-L-fucopyranosyl)-3-O-[6-O-methyl-2-O-(α-L-fucopyranosyl)-β-D-galactopyranosyl]-β-D-glucopyranoside (**43**)*

Hydrogenolysis of compound **51** and purification under the standard conditions described above provided a white amorphous solid (82 mg, 86% yield), $[\alpha]_D$ −104 (*c* 0.26, water). The ^{1}H and ^{13}C nmr data are reported in Tables 3 and 4.

*Methyl 2-acetamido-6-O-benzyl-2-deoxy-4-O-(3,4-di-O-benzyl-2-O-methyl-α-L-fucopyranosyl)-3-O-(2-O-acetyl-3,4-di-O-benzyl-6-O-methyl-β-D-galactopyranosyl)-β-D-glucopyranoside (**52**)*

Alcohol **49** (500 mg, 0.69 mmol) was reacted with the fucosyl bromide (**15**) (2 mmol) under the conditions for halide-ion catalyzed glycosylation. Purification of the product on a column of silica gel (ethyl acetate/methanol, 96:4) gave a white solid (529 mg, 72% yield), mp 177°C, $[\alpha]_D$ −64.0 (*c* 0.38, chloroform); ^{1}H nmr data ($CDCl_3$) δ: 7.4–7.2 (m, 25H, 5Ph), 6.38 (d, 1H, $J_{NH,2a}$ 8.0 Hz, NH), 5.3 (dd, 1H, $J_{1b,2b}$ 8.0 Hz, $J_{2b,3b}$ 10.0 Hz, H-2b), 5.14 (d, 1H, $J_{1c,2c}$ 3.8 Hz, H-1c), 4.91 and 4.34 (ABq, 2H, $J_{A,B}$ 11.5 Hz, CH_2Ph), 3.45, 3.41, and 3.23 (3s, each 3H, 3MeO), 2.05 and 1.91 (2s, each 3H, $NHCOCH_3$ and OAc), 1.14 (d, 3H, $J_{5c,6c}$ 6.5 Hz, 3H-6c). Anal. calcd. for $C_{60}H_{73}NO_{16}$: C 67.71, H 6.91, N 1.32; found: C 67.61, H 6.80, N 1.20.

*Methyl 2-acetamido-6-O-benzyl-2-deoxy-4-O-(3,4-di-O-benzyl-2-O-methyl-α-L-fucopyranosyl)-3-O-(3,4-di-O-benzyl-6-O-methyl-β-D-galactopyranosyl)-β-D-glucopyranoside (**53**)*

Compound **52** (450 mg, 0.45 mmol) was de-*O*-acetylated to produce a white solid (378 mg, 86% yield), mp 92°C, $[\alpha]_D$ −60.5 (*c* 0.4, chloroform); ^{1}H nmr data ($CDCl_3$) δ: 7.45–7.2 (m, 25H, 5Ph), 7.02 (d, 1H, $J_{NH,2a}$ 8.0 Hz, NH), 5.15 (d, 1H, $J_{1c,2c}$ 3.0 Hz, H-1c), 4.9 (H-2b overlapped by CH_2Ph signal), 4.55 (s, 2H, CH_2Ph), 4.37 (d, 1H, $J_{1b,2b}$ 7.5 Hz, H-1b), 4.2 (bs, 1H, OH-2b), 4.18 (m, 1H, H-5c), 3.48, 3.46 (2s, each 3H, 2MeO), 3.26 (s, 3H, MeO), 1.93 (s, 3H, NHAc), 1.12 (d, 3H, $J_{5c,6c}$ 6.5 Hz, 3H-6c). Anal. calcd. for $C_{58}H_{71}NO_{15}$: C 68.15, H 7.0, N 1.37; found: C 68.0, H 7.02, N 1.31.

*Methyl 2-acetamido-6-O-benzyl-2-deoxy-4-O-(3,4-di-O-benzyl-2-O-methyl-α-L-fucopyranosyl)-3-O-[3,4-di-O-benzyl-6-O-methyl-2-O-(2-O-benzyl-3,4-di-O-methyl-α-L-fucopyranosyl)-β-D-galactopyranosyl]-β-D-glucopyranoside (**54**)*

Compound **53** (300 mg, 0.3 mmol) was reacted with the fucosyl bromide (**17**) (2.10 mmol) under the conditions for halide-ion catalyzed glycosylation. Chromatographic purification of the product on a column of silica gel (ethyl acetate/methanol 96:4) gave **54** as a white foam (311 mg, 81%), mp 96°C, $[\alpha]_D$ −73.1 (*c* 0.35, chloroform); ^{1}H nmr data ($CDCl_3$) δ: 7.4–7.0 (m, 30H, 6Ph), 5.79 (d, 1H, $J_{2a,NH}$ 8.5 Hz, NH), 5.65 (d, 1H, $J_{1d,2d}$ 4.0 Hz, H-1d), 5.15 (d, 1H, $J_{1c,2c}$ 3.5 Hz, H-1c), 3.82 (dd, 1H, $J_{2c,3c}$ 10.0 Hz, H-2c), 3.58, 3.55, 3.45, 3.40, and 3.25 (5s, each 3H, 5MeO), 1.97 (s, 3H, NHAc), 1.31 and 1.17 (2d, each 3H, $J_{5c,6c}$ = $J_{5d,6d}$ = 6.5 Hz, 3H-6c, 3H-6d). Anal. calcd. for $C_{73}H_{91}NO_{19}$: C 68.15, H 7.13, N 1.1; found: C 68.44, H 6.94, N 1.08.

*Methyl 2-acetamido-2-deoxy-4-O-(2-O-methyl-α-L-fucopyranosyl)-3-O-[6-O-methyl-2-O-(3,4-di-O-methyl-α-L-fucopyranosyl)-β-D-galactopyranosyl]-β-D-glucopyranoside (**44**)*

Hydrogenolysis of **54** and purification of the product by passing it twice through a Biogel-P-2 column gave a white powder

TABLE 5. The r_0 values[a] used in the hard-sphere calculations

	H	C	N	O
H	2.66	3.22	3.06	3.00
C	—	3.78	3.61	3.56
N				3.37

[a] $r_0 = 1.11 \times$ (the sum of the van der Waals radii).

(32 mg, 65% yield), $[\alpha]_D$ −110 (*c* 0.14, water). The ^1H and ^{13}C nmr data are reported in Table 3 and 4.

Hard-sphere calculations

Using the X-ray diffraction-derived coordinates for the GS-IV · Le^b-OMe complex at 2.5 Å resolution,[5] methyl groups were substituted for the hydroxyl hydrogens at positions 6a, 6b, 2c, 2d, 3c, 3d, and 4d. In each case, a valency angle of 117° was adopted for CH_3-O-C_α with a CH_3-O_α bond length of 1.43 Å. The orientation of a methyl group (as CH_3, not as a pseudo atom), relative to the sugar unit to which it is attached, is described by the torsion angle defined by the CH_3 group and the lower-numbered vicinal carbon atom, Cγ, of a Me-O_α-C_β-C_γ fragment of the sugar unit. Thus, in Fig. 2, the zero torsion angles refer to the eclipsed conformations for Me/C-5b, Me/C-1c, Me/C-2c, Me/1d, Me/C-2d, and Me/C-3d, respectively.

The results reported in Fig. 2 were obtained using mono-*O*-methyl derivatives of Le^b-OMe only. Starting with the eclipsed conformation described above, the methoxy group was rotated through 360° in 5° steps. After each rotational step, the energy of the interaction of the methyl group with the rest of the Le^b-OMe molecule (except for the adjacent O_α and C_β atoms) was calculated and the results presented in Fig. 2 by the light solid line plot. At each step, the energy of interaction of the CH_3 group with all the amino acid atoms of the receptor GS-IV within 10 Å of the methoxy group oxygen (O_α) was calculated. The plots of these interaction energies versus torsion angles are presented as broken lines in Fig. 2. The heavy solid lines in Fig. 2 represent the sum of the two interaction energies. These nonbonded, hard-sphere interactions were calculated using the Kitaygorodsky expression that we have employed in HSEA calculations (4), namely, $E = 0.14z^{-6} + e^{10.31228-13z}$, when $z = r_{ij}/r_0$ and for which r_{ij} = internuclear distance and r_0, which is known as the equilibrium atomic radius, depends on the atoms involved in the interaction. The values used are reported in Table 5. The orientations displayed in Fig. 3 correspond to the methoxy group torsion angles at the midpoints of the energy minima in Fig. 2.

Acknowledgements

The research was supported by a Natural Sciences and Engineering Research Council of Canada operating grant (A-172) to R.U.L. The authors also wish to acknowledge and thank Dr. Ulrike Spohr for technical guidance and Chembiomed Ltd. for generous assistance. The chemical and immunochemical studies were performed by P.V.N. H.B. did the hard-sphere calculations and generated the computer graphics.

1. U. Spohr and R. U. Lemieux. Carbohydr. Res. **174**, 211 (1988).
2. R. U. Lemieux, L. T. J. Delbaere, H. Beierbeck, and U. Spohr. Ciba Foundation Symposium No. 158, Host–guest molecular interactions: from chemistry to biology. July 3–5, 1990. London, U.K. Wiley, Chichester. p. 231.
3. U. Spohr, O. Hindsgaul, and R. U. Lemieux. Can. J. Chem. **63**, 2644 (1985).
4. R. U. Lemieux, K. Bock, L. T. J. Delbaere, S. Koto, and V. S. Rao. Can. J. Chem. **58**, 631 (1980).
5. D. Wagner, J. P. H. Verheyden, and J. G. Moffat. J. Org. Chem. **39**, 24 (1974).
6. S. David, A. Thieffry, and A. Veyieres. J. Chem. Soc. Perkin Trans. 1, 1796 (1981).
7. R. U. Lemieux, R. Cromer, and U. Spohr. Can. J. Chem. **66**, 3083 (1988).
8. R. U. Lemieux, K. B. Hendricks, R. V. Stick, and K. James. J. Am. Chem. Soc. **97**, 4056 (1975).
9. O. Hindsgaul, T. Norberg, J. LePendu, and R. U. Lemieux. Carbohydr. Res. **109**, 109 (1982).
10. R. U. Lemieux and H. Driguez. J. Am. Chem. Soc. **97**, 4069 (1975).
11. D. D. Perrin, W. L. F. Armarego, and D. R. Perrin. Purification of laboratory chemicals. Pergamon Press, London. 1966.
12. E. B. Rathbone, A. M. Stephen, and K. G. R. Pachler. Carbohydr. Res. **20**, 357 (1971).
13. R. U. Lemieux and A. R. Morgan. Can. J. Chem. **43**, 2199 (1965).
14. W. Roth and W. Pigman. J. Am. Chem. Soc. **82**, 4608 (1960).

Can. J. Chem. Downloaded from www.nrcresearchpress.com by 123.30.183.119 on 09/08/12
For personal use only.

Molecular recognition XI. The synthesis of extensively deoxygenated derivatives of the H-type 2 human blood group determinant and their binding by an anti-H-type 2 monoclonal antibody and the lectin 1 of *Ulex europaeus*[1]

ULRIKE SPOHR,[2] EUGENIA PASZKIEWICZ-HNATIW,[3] NAOHIKO MORISHIMA,[4] AND RAYMOND U. LEMIEUX[5]
Department of Chemistry, University of Alberta, Edmonton, Alta., Canada T6G 2G2

Received July 26, 1991

ULRIKE SPOHR, EUGENIA PASZKIEWICZ-HNATIW, NAOHIKO MORISHIMA, and RAYMOND U. LEMIEUX. Can. J. Chem. **70**, 254 (1992).

The relative potencies of a wide variety of deoxygenated derivatives of the methyl glycoside of α-L-Fuc-(1 → 2)-β-D-Gal-(1 → 4)-β-D-GlcNAc (the H-type 2 human blood group related trisaccharide) for the inhibition of the binding of an artificial H-type 2 antigen by the lectin I of *Ulex europaeus* confirmed the previous evidence that the key and productive interaction involves only the three hydroxyl groups of the α-L-fucose unit, the hydroxyl at the 3-position of the β-D-galactose residue, and the nonpolar groups in their immediate environment. Except for the acetamido group and the hydroxymethyl of the β-D-Gal unit, which stay in the aqueous phase, on complex formation the remaining three hydroxyl groups appear to come to reside at or near the periphery of the combining site since their replacement by hydrogen causes relatively small changes ($<\pm 1$ kcal/mol) in the stability of the complex (ΔG^0). Relatively much larger but compensating changes occur for the enthalpy and entropy terms, and these may arise primarily from the differences in the water structure about the periphery of the combining site and the oligosaccharide both prior to and after complexation. It is proposed that steric constraints lead to an ordered state of the water molecules hydrogen-bonded to the polar groups within the cleft formed by the key region of the amphiphilic combining site. Their release to form less ordered clusters of more strongly hydrogen-bonded water molecules in bulk solution would contribute importantly to the driving force for complexation. It is demonstrated that the surface used for the binding of H-type 2-OMe by a monoclonal anti-H antibody is virtually identical to that used by the *Ulex* lectin.

Key words: molecular recognition, H-type 2 blood group determinant and deoxygenated derivatives, lectin I of *Ulex europaeus*, anti-H-type 2 monoclonal antibody, enthalpy–entropy compensation.

ULRIKE SPOHR, EUGENIA PASZKIEWICZ-HNATIW, NAOHIKO MORISHIMA et RAYMOND U. LEMIEUX. Can. J. Chem. **70**, 254 (1992).

Les efficacités relatives d'un grand nombre de dérivés désoxygénés du glycoside de méthyle de l'α-L-Fuc-(1 → 2)-β-D-Gal-(1 → 4)-β-D-GlcNAc (trisaccharide relié au groupe sanguin H de type 2 de l'homme) comme inhibiteurs de la fixation d'un antigène artificiel du H de type 2 par la lectine I de l'*Ulex europaeus* ont confirmé les données antérieures suggérant que cette interaction importante et productive n'implique que les trois groupes hydroxyles de l'unité α-L-fucose, le groupe hydroxyle en position 3 du résidu β-D-galactose et les groupes non-polaires qui se trouvent dans leur environnement immédiat. À l'exception du groupe acétamido et de l'hydroxyméthyle de l'unité β-D-Gal qui restent dans la phase aqueuse lors de la formation du complexe, il semble que les trois autres groupes hydroxyles se retrouvent à, ou près de, la périphérie du site qui effectue la combinaison; en effet, leur remplacement par de l'hydrogène ne provoque que de faibles changements ($<\pm 1$ kcal/mol) dans la stabilité du complexe (ΔG^0). Des changements relativement plus importants se font sentir dans les termes enthalpiques et entropiques; toutefois, ces derniers se compensent et il est possible qu'ils soient principalement le résultat de différences dans la structure de l'eau autour de la périphérie de l'oligosaccharide et du site qui se combine, tant avant qu'après la complexation. On suggère que des contraintes stériques conduisent à un état ordonné des molécules d'eau réunies par des liaisons hydrogènes aux groupes polaires contenues dans l'interstice formé par la région clé du site amphiphile qui se combine. Leur libération, conduisant à la formation d'agrégats moins ordonnés de molécules d'eau réunies par des liaisons hydrogènes plus fortes dans la masse de la solution, pourrait contribuer d'une façon importante à la force aidant à la complexation.

Mots clés : reconnaissance moléculaire, déterminant du groupe sanguin H de type 2 et dérivés désoxygénés, lectine I de l'*Ulex europaeus*, anticorps monoclonal d'anti-H de type 2, compensation enthalpie–entropie.

[Traduit par la rédaction]

Introduction

The specific, non-covalent binding of oligosaccharides by acceptor proteins has received much attention during the last decade. This laboratory has studied the combining sites of various monoclonal antibodies and lectins that specifically bind blood group determinants (1). The strategy was to slightly chemically alter the natural oligosaccharide substrate mainly by replacing hydroxyl, hydroxymethylene, methyl, and *N*-acetyl groups by hydrogen, one group at a time, and to study the effect on the binding. The relative potencies of the modified haptens, as inhibitors of artificial ^{125}I-labelled antigens, were determined using a solid-phase radioimmunoassay (2). Also, the changes in ultraviolet absorption accompanying complex formations were used to determine association constants at various temperatures in order to derive the changes in enthalpy and entropy (2). The striking finding of these binding studies was that only one to four, but mostly two to three, of the hydroxyl groups of a di-, tri-, or tetrasaccharide were indispensable for complex formation. Replacement of only one of these "essen-

[1]Presented at the Fuji '90 Post-Symposium, The Fuji Training Institute, Susono City, Shizuoka, Japan. August 18–21, 1990.
[2]Research Associate, 1984–1988; 1991–present.
[3]University of Alberta Postdoctoral Fellow, 1987–1989.
[4]Alberta Heritage Foundation for Medical Research Postdoctoral Fellow, 1983–1985.
[5]Author to whom correspondence may be addressed.

Can. J. Chem. Downloaded from www.nrcresearchpress.com by 123.30.183.119 on 09/08/12
For personal use only.

Can. J. Chem. Downloaded from www.nrcresearchpress.com by 123.30.183.119 on 09/08/12
For personal use only.

tial" hydroxyl groups virtually abolished complex formation. Usually, these hydroxyl groups, termed the "key polar grouping," occur as a tight cluster flanked by lipophilic surfaces of the oligosaccharide (3) and normally originate from different sugar units of the oligosaccharide. Less often observed, the key hydroxyl groups are provided by only one sugar unit.

The previous binding studies have shown that a particular oligosaccharide may be recognized differently by different acceptor proteins, though the general features recognized are similar in kind. For example, lectin IV of *Griffonia simplicifolia* recognizes a different topography of the Lewis b tetrasaccharide (2) than does a monoclonal anti-Lewis b antibody (4), and two monoclonal anti-Lewis a antibodies have different ways to accommodate the Lewis a trisaccharide (5). In contrast, two monoclonal anti-B antibodies appear to form very similar complexes with the B-trisaccharide (6). In this study, the binding of a monoclonal anti-H type 2 antibody is compared to that of the H-type 2-specific lectin I of *Ulex europaeus*.

That key polar groupings become involved in hydrogen-bond networks with polar groups of the acceptor protein, some of which may be negatively charged, was confirmed by the X-ray crystal structure of the complex formed by the lectin IV of *Griffonia simplicifolia* (GS-IV) and the Lewis b tetrasaccharide (α-L-Fuc-(1 → 2)-β-D-Gal-(1 → 3)-[α-L-Fuc-(1 → 4)]-β-D-GlcNAcOMe) (7, 8). The combining site proved to be a rather small shallow depression at the surface of the protein. The key polar interaction between protein and ligand occurs at the bottom of the cleft where conformational rigidity of the polypeptide chain is greatest. These polar groups are surrounded by aromatic amino acid side chains that may contribute to the stability of the complex by the exclusion of water molecules.

Whereas the hydroxyl groups of a key polar grouping are indispensable to complex formation, the replacement of other hydroxyl groups by hydrogen, halogen, amino, or methoxy groups has a relatively minor effect on the binding. The result may be either an increase or a decrease in the activity normally involving a differential change in free energy of less than 1 kcal/mol. In the case of the lectin GS-IV, these "nonessential" hydroxyl groups were found (8, 9) to be involved in interactions at or near the periphery of the combining site where the protein structure may be conformationally more flexible and interaction with water is more readily possible. Although the replacement of a "nonessential" peripheral hydroxyl group by hydrogen does not importantly affect the change in free energy, the structural change causes a substantial change in the thermodynamic parameters, which takes the form of a linear enthalpy–entropy compensation (9, 10).

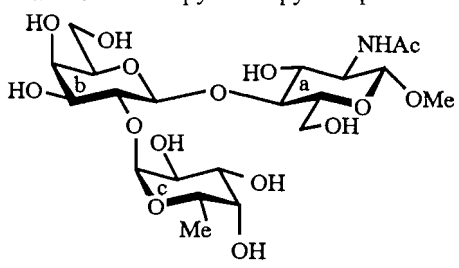

1

Probing of the combining site of the H-type 2 (α-L-Fuc-(1c → 2b)-β-D-Gal-(1b → 4a)-β-D-GlcNAc, **1**) specific lectin I of *Ulex europaeus* revealed the key polar grouping to comprise OH-2c, OH-3c, and OH-4c of the α-L-Fuc unit and OH-3b of the β-D-Gal unit (11, 12). Although all four hydroxyl groups provide important polar interactions, the effect on the stability of the complex of replacing either OH-2c or OH-3b by hydrogen was substantially less than for OH-3c and OH-4c. These four hydroxyl groups provide a cluster that is flanked by lipophilic regions of the β-side of the GlcNAc unit, and the α-sides of the Gal and Fuc units, thereby presenting the assortment of amphiphilic surfaces displayed in Fig. 1 (center). The inhibition data (12) indicated that the CH_3O-1a, NHAc-2a, OH-3a, and CH_2OH-6b groups remain in contact with the aqueous phase. As is indicated in the side projections of Fig. 1, OH-3a, OH-6a, and OH-4b are now considered to also interact with the lectin at or near the periphery of its combining site.

In view of the slightly higher activity of the 6a-deoxy H-type 2 congener (11, 12), the OH-6a group appeared to become involved in an interaction within a hydrophobic environment. For this reason, it was suggested that this hydroxyl group may be accepted into the complex by forming an intramolecular bond with O-5a (11, 12). However, this view must now be modified since the X-ray crystal structure of the complex formed by the Lewis b tetrasaccharide and the lectin GS-IV has shown (8), in a very similar situation, that, although the hydroxymethyl group of the β-D-Gal unit is near the indolyl group of a tryptophane unit, the hydroxyl group remains in the aqueous phase (9). In the case of the *Ulex* lectin, the steric complementarity provided for the CH_3-6c and H-5c atoms of the fucose unit contributes importantly to the stability of the complex (12) and infers an important hydrophobic component to the binding reaction.

We now wish to report that these conclusions, largely drawn from the immunochemical properties of monodeoxy derivatives of **1**, are supported by the inhibition data provided by polydeoxygenated congeners. The syntheses of several 6a-substituted derivatives of **1** are reported in a separate communication (13). It is demonstrated that major changes in the structural features that are not directly involved in the binding reaction may be made without causing substantial change in the thermodynamic stability of the complex although major but compensating changes occur for the changes in enthalpy and entropy.

Discussion

A. Synthesis

Scheme 1 outlines the synthesis leading to the H-type 2 derivative (**13**) that has the NHAc-2a, OH-3a, OH-6a, and CH_2OH-6b groups of the H-type 2 trisaccharide (**1**) replaced by hydrogen. To synthesize the starting alcohol (**6**), the enopyranoside (**2**) (14, 15) was hydrogenated in the presence of 5% palladium-on-carbon and triethylamine (16) to crystalline dideoxypyranoside (**3**) (17) in 94% yield. Oxidative cleavage of the benzylidene ring of **3** with *N*-bromosuccinimide (18) provided the 6-bromo compound **4** in 99% yield. Catalytic reduction of **4** to give **5** (98% yield) followed by debenzoylation with sodium methoxide provided the previously reported (19) trideoxy compound (**6**) as an oil in 86% yield. Glycosylation of **6** with acetobromoarabinose (**7**) (20, 21) in boiling toluene was promoted with mercuric cyanide under the conditions developed by Tanaka and co-workers (22) to provide, after deacetylation, the disaccharide (**9**) in 43% isolated yield. Protection of the 3b-

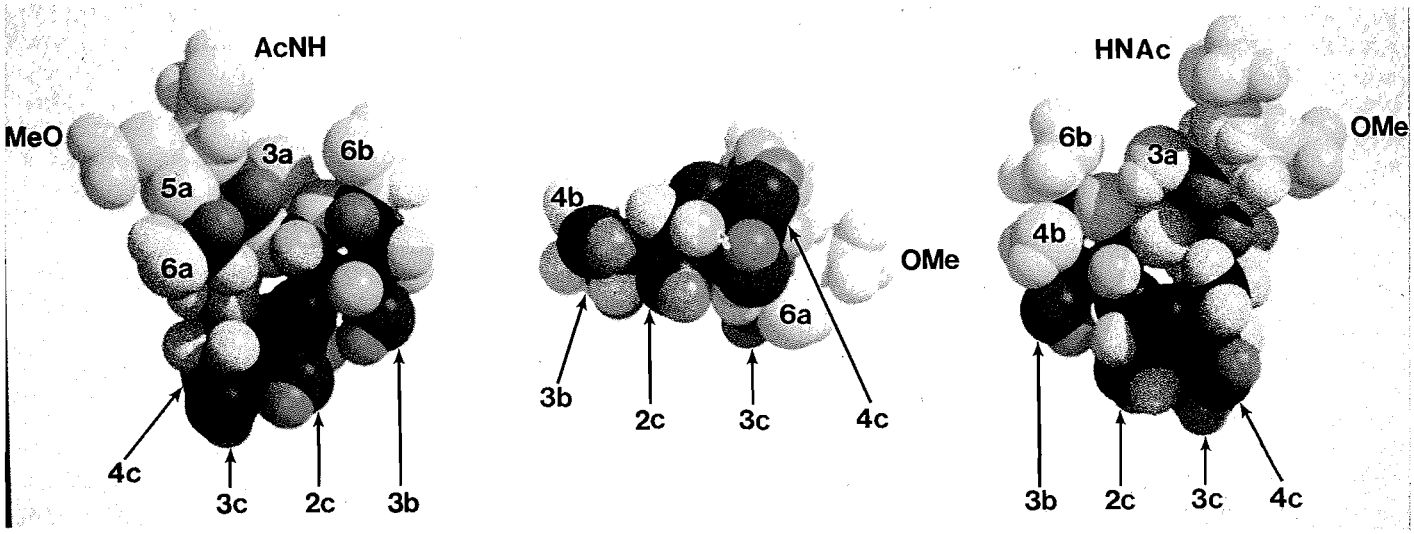

FIG. 1. CPK molecular model for H-type 2-OMe (α-L-Fuc(1c → 2b)-β-D-Gal(1b → 4a)-β-D-GlcNAc-OMe, **1**). Hydroxyl groups in the region for productive binding with the *Ulex* lectin are designated by dark red oxygen and green hydrogen atoms. The aliphatic hydrogen atoms are yellow. Oxygen atoms that come to reside in the complex at or near the periphery of the combining site are presented in light pink. Those groups which come into contact with the aqueous phase near the periphery of the combining site are presented in grey. The rest of the molecule, which is depicted in an off-white and which is derived from the GlcNAc residue, remains in the aqueous phase. The various projections allow an appreciation of the "polyamphiphilic" surface that becomes bound within the stereoelectronically complementary cleft that forms the combining site.

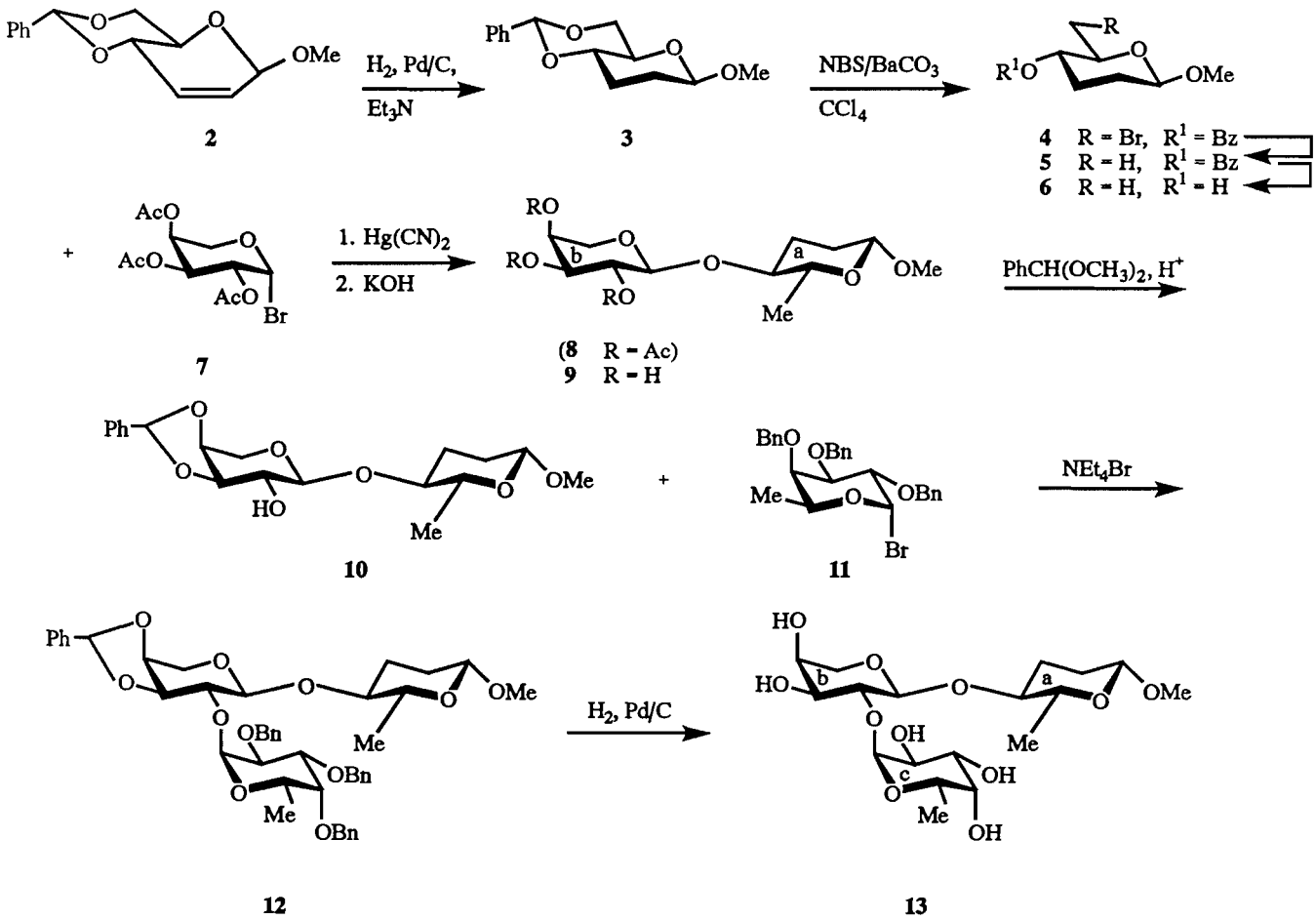

SCHEME 1

Can. J. Chem. Downloaded from www.nrcresearchpress.com by 123.30.183.119 on 09/08/12
For personal use only.

TABLE 1. ^{1}H nmr chemical shifts (ppm) and some coupling constants (Hz) for the H-type 2 blood group determinant (α-L-Fuc-(1 → 2)-β-D-Gal-(1 → 4)-β-D-GlcNAcOMe) (**1**) and related structures[a]

	H-type 2-OMe (**1**)	Derivatives of H-type 2-OMe					
		13	**20**	**30**	**31**	**50**	**51**
a-unit							
H-1 ($J_{1,2ax}$)	4.44 (8.3)	4.54 (9.2)	3.44 (8.9)[b]	4.58 (9.0)	4.56 (9.0)	3.40	3.35
H-2ax ($J_{2ax,3ax}$)	3.73	1.50		1.52 (12.0)	1.51 (13.0)	1.25	1.24
H-2eq ($J_{1,2eq}$)	—	1.94 (2.1)	1.80–1.51	1.94 (2.0)	1.93 (2.0)	2.10	2.09[c]
H-3ax ($J_{3ax,4}$)	*	1.64 (10.5)		1.69 (9.5)	1.62 (9.8)	1.47 (10.5)	1.41 (10.5)
H-3eq ($J_{3ax,3eq}$)	—	2.13 (13.0)	2.14	2.22 (13.0)	2.18 (13.0)	2.16	2.11[c]
H-4 ($J_{4,5}$)	3.76	3.43 (9.9)	3.39 (9.2)	3.69 (8.5)	3.52	3.68 (6.5)[c]	3.41 (10.5)
H-5 ($J_{5,6}$)	3.47 (1.8)	3.54 (6.2)	3.41 (5.7)	3.49 (2.5)	3.52 (5.5)	1.62	1.52
H-6 ($J_{6,6'}$)	4.00 (11.5)	1.33	1.31	3.93 (11.5)	1.35 H-7	3.81[c]	1.07
H-6′ ($J_{5,6'}$)	3.79	—	—	3.73 (8.5)	— H-7′	3.61[c]	—
					H-6ax	1.13	1.02
					H-6eq	2.20	2.06[c]
CH_3O	3.51	3.49	—	3.50	3.48	3.37	3.35
β-D-Gal or α-L-Ara b-unit							
H-1 ($J_{1,2}$)	4.54 (7.8)	4.60	4.62	4.51	4.62	4.51	4.62
H-2 ($J_{2,3}$)	3.65 (10.0)	3.64	3.68	3.61	3.62	3.62	3.62
H-3 ($J_{3,4}$)	3.88 (3.5)	3.90	3.91	3.85	3.85	3.85	3.85
H-4	3.89	3.94	3.95	3.89	3.89	3.89	3.89
H-5ax	3.65	3.63	3.65	3.66	3.67	3.65	3.65
H-5eq	—	3.88	3.90	—	—	—	—
H-6	3.76[c]	—	—	3.76	3.76	3.77	3.77
H-6′	3.75[c]	—	—	3.75	3.75	3.74	3.73
α-L-Fuc c-unit							
H-1 ($J_{1,2}$)	5.31 (2.5)	5.26	5.26	5.31	5.30	5.31	5.30
H-2	3.78	3.79	3.80	3.81	3.80	3.79	3.79
H-3	3.80	3.84	3.85	3.81	3.83	3.81	3.86
H-4 ($J_{4,5}$)	3.79 (<1)	3.81	3.82	3.81	3.82	3.81	3.79
H-5 ($J_{5,6}$)	4.23 (6.5)	4.26	4.28	4.26	4.30	4.31	4.41
H-6	1.23	1.21	1.22	1.23	1.22	1.22	1.21

[a]Measured at 400 or 300 MHz using 0.04 M solutions in D_2O with acetone at 2.225 ppm as internal reference. The assignments are expected to be within ±0.01 ppm except for those marked with [c] which are within ±0.03 ppm.
[b]H-1eq 3.88 ppm.
[c]Expected to be within ±0.03 ppm.
*Could not be assigned.

and 4b-positions of **9** was then achieved by benzylidenation with α,α-dimethoxytoluene in the presence of *p*-toluenesulfonic acid (23). The crystalline alcohol (**10**) was obtained in 63% yield and reacted, under halide-ion catalyzed conditions (24), with tri-*O*-benzyl-L-fucosyl bromide (**11**) prepared as previously reported (25). The trisaccharide derivative (**12**) was isolated in 81% yield and hydrogenolyzed over 5% palladium-on-carbon to provide crystalline **13** in 87% yield. The identities and high purities of the above products were all confirmed by appropriate nmr studies. The ^{1}H and ^{13}C nmr data for the H-type 2 related compounds are reported in Tables 1 and 2.

To examine the involvement of the aglyconic MeO-1a group in the binding of **13**, structure **20** was synthesized as described in Scheme 2. The starting alcohol (**14**) was prepared as previously reported (26). Glycosylation of **14** with acetobromoarabinose (**7**) under Helferich conditions produced **15**, which on deacetylation provided the β-linked disaccharide (**16**) in 54% yield. Reaction of **16** with 2,2-dimethoxypropane in the presence of *p*-toluenesulfonic acid led to the alcohol (**17**) (91% yield), which in turn was reacted with **11** under halide-ion catalyzed conditions. Chromatographic separation of the reaction products provided, besides the fully protected trisaccharide **18** (44% yield), the de-*O*-isopropylidinated derivative (**19**) (43% yield). Mild acid hydrolysis of **18** in aqueous acetic acid yielded **19**, which was hydrogenolyzed to the crystalline trisaccharide (**20**) in near quantitative yield.

The syntheses of the polydeoxygenated H-type 2 derivatives (**30** and **31**) (outlined in Scheme 3) started from the enopyranoside (**2**) (Scheme 1). Hydrogenation over 20% palladium hydroxide-on-carbon provided the known highly acid-labile product (**21**) (19), which had to be isolated in the presence of pyridine. The primary hydroxyl group of **21** was preferentially tosylated to form **22** (19) in 54% crystalline yield. The ditosylate **22***a* (19) (10%) was also isolated. Reaction of **22** with the galactosyl bromide (**23**) (27) under Helferich conditions provided the β-linked disaccharide (**24**) in 61% yield. Zemplen deacetylation of **24** furnished the alcohol (**25**) (90% yield) from which the trisaccharide (**26**) was prepared by using **11** under halide-ion catalysis (65% yield). Compound **26** was converted into the benzoate (**27**) by replacement of the tosylate group (68% yield). Debenzoylation with sodium methoxide then provided the alcohol (**28**) (89% yield). The tosylate (**26**) was also used to prepare the 6a-deoxy compound (**29**) (75% yield) by reduction with

Can. J. Chem. Downloaded from www.nrcresearchpress.com by 123.30.183.119 on 09/08/12
For personal use only.

TABLE 2. The ^{13}C nmr chemical shifts (ppm) for the H-type 2 blood group determinant (α-L-Fuc-(1→2)-β-D-Gal-(1→4)-β-D-GlcNAcOMe) (**1**) and related structures[a]

	H-type 2-OMe (**1**)	Derivatives of H-type 2-OMe					
		13	**20**	**30**	**31**	**50**	**51**
a-unit							
C-1	102.73	103.29	67.81	103.21	103.29	79.08	79.23
C-2	56.03	30.30[b]	25.48	29.91[b]	30.27[b]	30.03[b]	30.26[b]
C-3	73.23	29.27[b]	31.27	28.97[b]	29.23[b]	31.70[b]	31.94[b]
C-4	77.26	79.48	80.19	74.03	79.13	78.82	84.31
C-5	76.14	75.42	77.78	79.59	75.47	44.46	37.51
C-6	61.10	18.21	18.14	62.01	18.27	33.41	38.80
C-7	—	—	—	—	—	62.91	18.69
CH_3O	57.90	56.94	—	57.03	56.96	56.02	55.93
β-D-Gal or α-L-Ara b-unit							
C-1	101.19	102.49	102.49	102.19	102.36	102.58	102.88
C-2	77.32	77.13	77.11	76.87	77.03	77.27	77.31
C-3	74.43	73.23	73.25	74.57	74.60	74.62	74.71
C-4	69.97	68.80	68.82	69.85	69.88	69.91	69.96
C-5	76.09	65.76	65.76	75.86	75.81	75.74	75.65
C-6	61.87	—	—	61.65	61.66	61.64	61.66
α-L-Fuc c-unit							
C-1	100.26	100.15	100.14	100.03	100.09	100.12	100.12
C-2	69.13	69.07	69.06	69.04	69.07	69.08	69.09
C-3	70.54	70.43	70.42	70.42	70.43	70.43	70.42
C-4	72.56	72.62	72.62	72.59	72.62	72.50	72.61
C-5	67.74	67.70	67.71	67.66	67.62	67.69	67.58
C-6	16.14	16.10	16.10	16.15	16.11	16.14	16.12

[a]0.05 M solutions in D_2O with dioxane as internal reference at 67.4 ppm were measured at 100 or 75 MHz at 295 K. The assignments were made by inspection (11).

[b]The corresponding assignments of the chemical shifts are tentative and may be reversed.

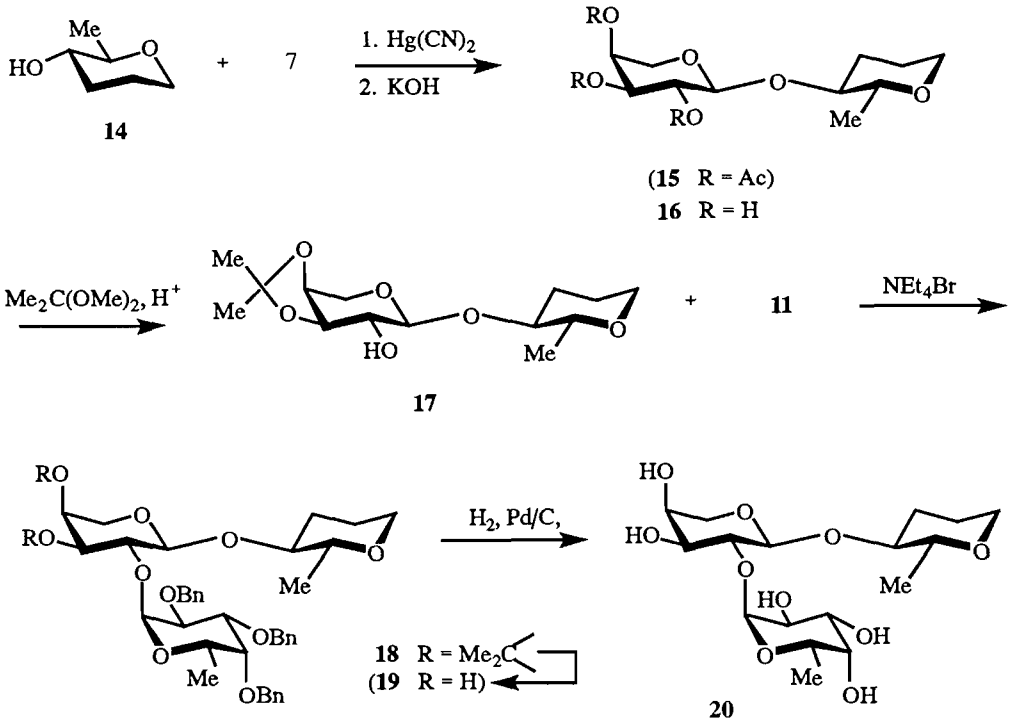

SCHEME 2

Can. J. Chem. Downloaded from www.nrcresearchpress.com by 123.30.183.119 on 09/08/12
For personal use only.

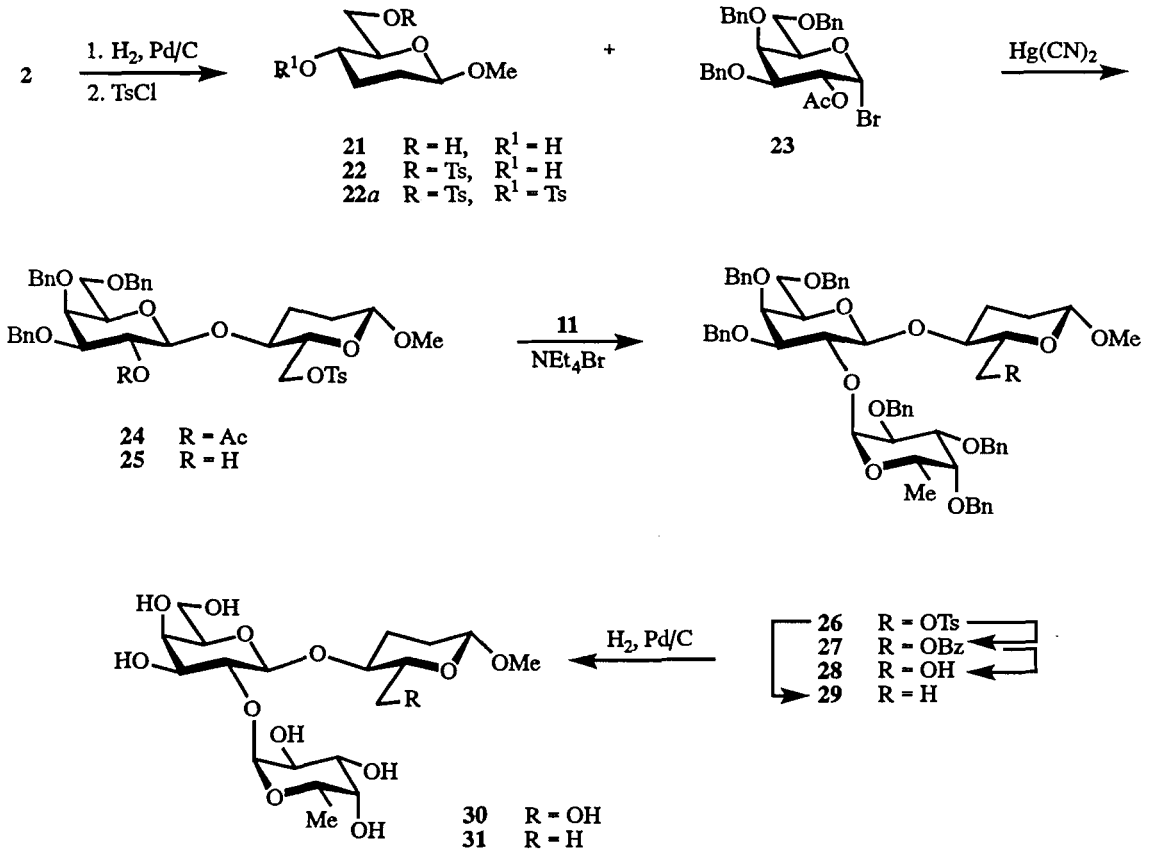

SCHEME 3

lithium aluminium hydride in refluxing tetrahydrofuran (28). Hydrogenolysis of **28** and **29** to remove the benzyl groups then furnished the trisaccharides **30** and **31**. The ^1H and ^{13}C nmr spectra are in complete agreement with the structural assignments (Tables 1 and 2).

The *pseudo*-trisaccharides **50** and **51** (Scheme 5) were prepared starting with racemic (1,5/4)-1-*O*-methyl-5-*C*-hydroxymethyl-1,4-cyclohexanediol (**37**) (Scheme 4), which was synthesized as follows. The known bicyclo carboxylic acid (**32**) (29) was obtained by catalytic hydrogenation of the Diels–Alder adduct of furan and acrylic acid (30). Acetolysis (31) of **32** occurred with about 80% regioselectivity at the 4-position to produce the all-equatorial cyclohexane derivative **33**. However, **33** was isolated by crystallization in only 35% yield. The structural assignment followed from the downfield shifts of the H-2 and H-5 signals and the large coupling constants for $J_{1,2}$, $J_{2,3ax}$, $J_{5,4ax}$, and $J_{5,6ax}$. Reduction with diborane–tetrahydrofuran complex (32) provided the triol (**34**), which was converted directly into the crystalline benzylidene derivative **35** (85%) with α,α-dimethoxytoluene in the presence of *p*-toluenesulfonic acid. The *O*-methyl derivative (**36**) (84% yield) was hydrogenolyzed to the diol

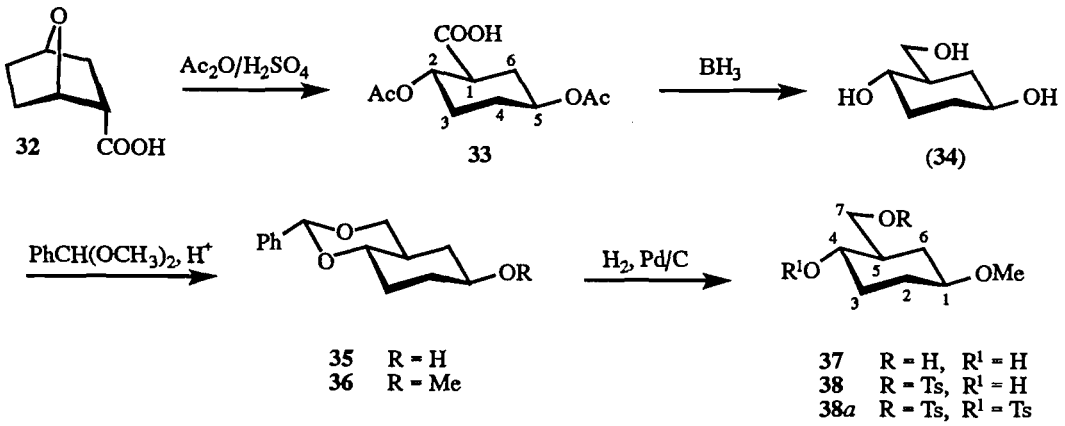

SCHEME 4 (Only one enantiomer of DL mixture displayed)

Can. J. Chem. Downloaded from www.nrcresearchpress.com by 123.30.183.119 on 09/08/12
For personal use only.

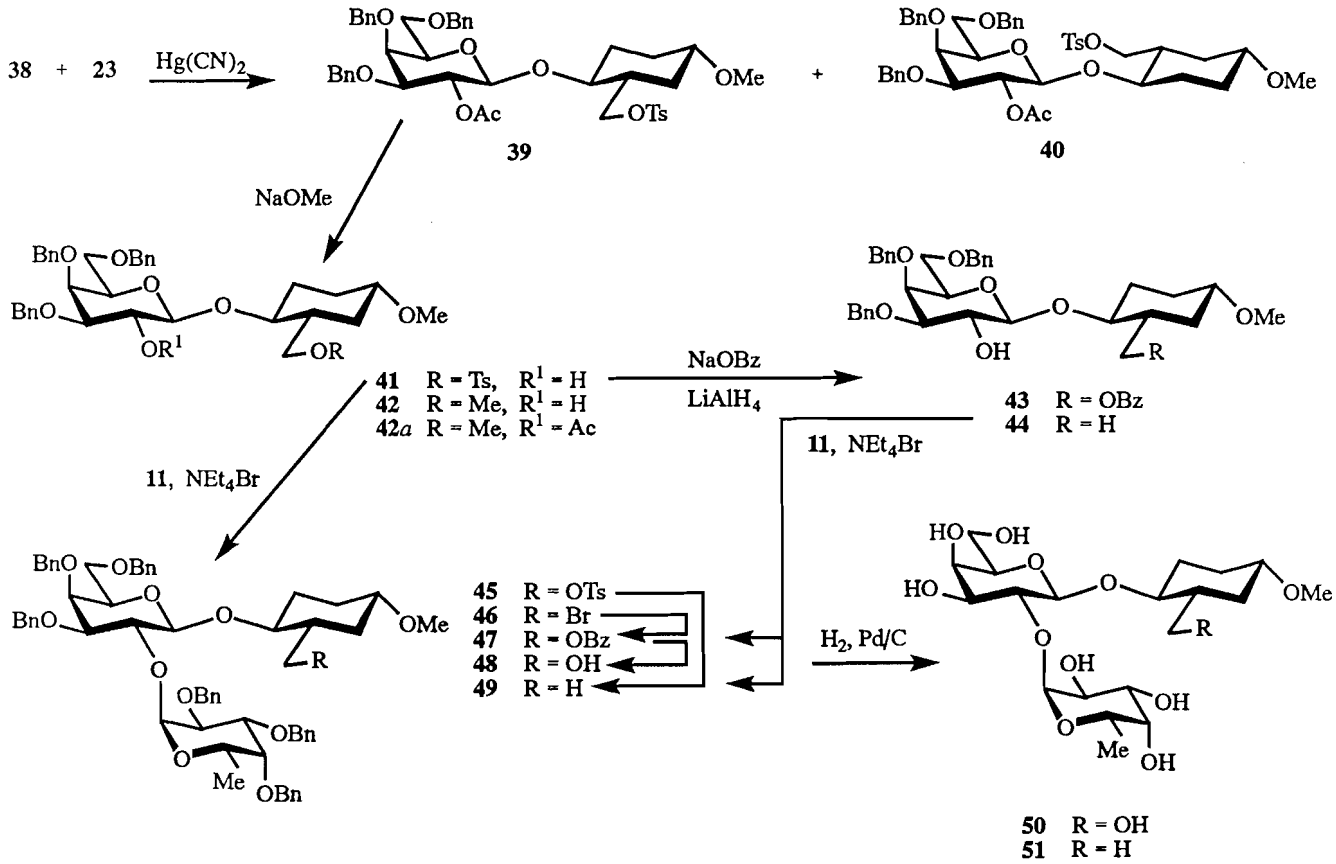

SCHEME 5

(**37**) (99% yield). Monotosylation of **37** provided both the mono- and ditosylates (**38** and **38***a*, respectively) in 72 and 16% yields, respectively.

As outlined in Scheme 5, the racemic tosylate (**38**) was coupled with galactosyl bromide (**23**) under Helferich conditions at room temperature. The two diastereoisomeric disaccharides (**39** and **40**) were separated by chromatography in yields of 22 and 18%, respectively. Their absolute configurations were anticipated from their optical rotations. The aglycon assigned to **39** is expected to reside largely in the conformation depicted by **39***a* wherein the tosyloxy group defines a positive screw pattern of asymmetry with CH_2-6 and, similarly, CH_2-7 with O-4. For the diastereoisomer **40**, these torsion angles are negative, as displayed in **40***a*. Therefore, following the notions introduced by Whiffen (33) and elaborated by Brewster (34) it could be expected that the aglycon of **39** would make a positive contribution to its molecular rotation ($[M]_D = +162°$) and that the molecular rotation would be more negative for **40**, that is, the isomer with $[M]_D = +63°$. Consequently, **39** was chosen for the preparation of the H-type 2 congeners **50** and **51**. Indeed, these products possessed activities for the inhibition of the binding of the H-type 2 trisaccharide compatible with expectation (Table 3).

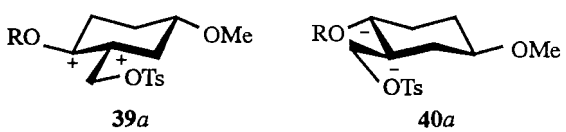

39*a* **40***a*

R = 2-*O*-acetyl-3,4,6-tri-*O*-benzyl-β-D-galactopyranosyl

Deacetylation of **39** with sodium methoxide provided the alcohol (**41**) in 62% yield. Some replacement of the tosyl group by methoxide occurred and gave rise to the 7a-O-methyl compound (**42**) (15%), which was also characterized as its 2-O-acetate (**42***a*). This replacement was not observed when the O-5a analog (**24**) (Scheme 3), which has a more electronegative neighboring group, was deacetylated under similar conditions.

Reaction of **41** with **11** in the presence of bromide ion provided the trisaccharide (**45**) in only 20% yield. The main reaction product (52% yield) was identified as the 7a-bromo-7a-deoxy substitution product (**46**). Its structural assignment followed from the upfield shift of C-7a in the ^{13}C nmr spectrum. In contrast, the similar fucosylation of the O-5a analog **25** produced only ~4% yield of the bromo substitution product. The tosylate (**45**) was reduced with lithium aluminium hydride to produce the 7a-deoxy derivative **49** in 53% yield. The 6-O-benzoate (**47**) was obtained in 66% yield by reaction of the bromide (**46**) with sodium benzoate. De-*O*-benzoylation then provided the alcohol **48**. An alternate route to **48** involved replacing the tosyloxy group of **41** by benzoate to form **43** in 65% yield. Compound **43** was used to prepare the trisaccharide (**47**) (64% yield) in the usual way. Reduction of **41** with lithium aluminium hydride provided the 7a-deoxy compound **44**, which was converted to the trisaccharide (**49**) (65% yield). Hydrogenolysis of **48** and **49** provided the target compounds **50** and **51**.

B. Structural and conformational assignments

The ^1H and ^{13}C nmr parameters for H-type 2-OMe (**1**) and the various modified structures are reported in Tables 1 and

Can. J. Chem. Downloaded from www.nrcresearchpress.com by 123.30.183.119 on 09/08/12
For personal use only.

TABLE 3. Inhibition data for the binding of the H-type 2-OMe trisaccharide (**1**) and congeners by the lectin I of *Ulex europaeus*

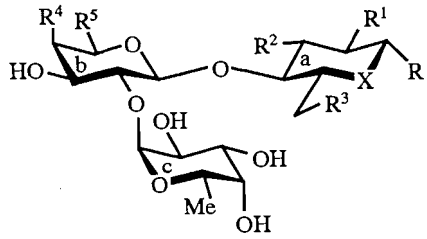

Compound (reference)	Structure R	R1	R2	R3	X	R4	R5	Relative potency	ΔΔG⁰ kcal/mole
1. Reference inhibitor									
1 (13)	OCH_3	NHAc	OH	OH	O	OH	CH_2OH	100[a]	0
2. Changes involving NHAc-2a, OH-3a and OH-6a									
52 (12)	OCH_3	NHAc	H	OH	O	OH	CH_2OH	46[b]	0.46[b]
53 (13)	OCH_3	NHAc	OH	H	O	OH	CH_2OH	250	−0.55
30	OCH_3	H	H	OH	O	OH	CH_2OH	25	0.83
31	OCH_3	H	H	H	O	OH	CH_2OH	67	0.24
3. Changes involving O-5a and OH-6a									
50	OCH_3	H	H	OH	CH_2	OH	CH_2OH	22	0.91
51	OCH_3	H	H	H	CH_2	OH	CH_2OH	55	0.36
4. Changes involving OH-6a									
54 (13)	OCH_3	NHAc	OH	F	O	OH	CH_2OH	450	−0.90
55 (13)	OCH_3	NHAc	OH	Cl	O	OH	CH_2OH	350	−0.75
56 (13)	OCH_3	NHAc	OH	OMe	O	OH	CH_2OH	150	−0.24
57 (13)	OCH_3	NHAc	OH	NH_2	O	OH	CH_2OH	17 (pH 9.1)	1.1
58 (13)	OCH_3	NHAc	OH	NH_2	O	OH	CH_2OH	1.7 (pH 5.3)	2.4
59 (13)	OCH_3	NHAc	OH	NHAc	O	OH	CH_2OH	40	0.55
60 (13)	OCH_3	NHAc	OH	NHPiv	O	OH	CH_2OH	5	1.8
5. Changes involving OH-4b and OH-6b									
61 ([c])	OCH_3	NHAc	OH	OH	O	H	CH_2OH	37	0.60
62 (12)	OCH_3	NHAc	OH	OH	O	OH	CH_3	60	0.31
6. Changes involving CH_3O-1a, NHAc-2a, OH-3a, and OH-6b									
63 (12)	$O(CH_2)_8CO_2Me$	NHAc	OH	OH	O	OH	CH_2OH	150	−0.24
13	OCH_3	H	H	H	O	OH	H	66	0.25
20	H	H	H	H	O	OH	H	28	0.76

[a]50% inhibition was provided by 150 μmol/L.
[b]Estimated from the potency of the 3a-deoxy derivative when R = $O(CH_2)_8CO_2Me$ (12).
[c]R. Cromer, U. Spohr, D. P. Khare, J. LePendu, and R. U. Lemieux. Can. J. Chem. Accepted.

2. These are considered to be in full agreement with the structural assignments.

The conformational preference with minimum energy at ϕ/ψ = 50°/15°, and 55°/0° about the glycosidic linkages α-L-Fuc(1 → 2) and β-D-Gal(1 → 4) of the H-type 2 trisaccharide, provided by HSEA calculations (35) is supported by ^1H and ^{13}C nmr data (11). The minimum energy conformer places H-1c of the α-L-Fuc c-unit in near van der Waals contact with O-3b of the β-D-Gal b-unit, and this conformational preference is supported by the interunit deshielding of H-1c by 0.54 ppm (Table 1) relative to α-L-Fuc-OMe (35). Examination of the chemical shifts reported in Table 1 for H-1c of the various derivatives of **1** shows that this interunit deshielding occurs for compounds **30**, **31**, **50**, and **51** and is only slightly less for the L-arabino derivatives **13** and **20**. Therefore, the orientation of the α-L-Fuc c-unit with respect to the β-D-Gal b-unit appears to be essentially the same for all these H-type 2 congeners. The H-5c of **1** is deshielded 0.19 ppm relative to H-5 of α-L-Fuc-OMe and this has been attributed to its proximity to O-4a (35). This interunit deshielding is slightly higher for derivatives **13**, **20**, **30**, **31**, and **50** and even higher (0.37 ppm) for pseudo oligosaccharide **51**. Therefore, it appears that the conformational preferences about the interglycosidic linkages of H-type 2-OMe (**1**) are essentially preserved and the immunochemical data will be interpreted accordingly.

C. Immunochemical studies

The inhibitions by the H-type 2-OMe compound and the various congeners of the binding of a ^{125}I-labelled H-type 2-bovine-serum-albumin artifical antigen by either the lectin or the antibody were determined using a solid phase, competitive radioimmunoassay, which has been reported in detail (2). Whenever possible, 50% inhibitions were determined in order to establish the relative potencies. Although the discussion of the results will be in terms of the effects of structural changes on relative potency, the differential changes in free energy, calculated from the relative potencies, are included in Table 3 to indicate the change in the strength of the driving force for the complexation relative to that of the reference inhibitor (**1**).

It is known that the binding of the H-type 2 structure by

Can. J. Chem. Downloaded from www.nrcresearchpress.com by 123.30.183.119 on 09/08/12
For personal use only.

Can. J. Chem. Downloaded from www.nrcresearchpress.com by 123.30.183.119 on 09/08/12
For personal use only.

the *Ulex* lectin is unaffected by replacement of the acetamido group (R^1 in Table 3) either by a hydroxyl or an amino group (11). As seen in Table 3, replacement of OH-3a of **1** by hydrogen to provide **52** leads to a 54% loss in potency. Therefore, the low potency of 25 found for compound **30** can be attributed, in large part, to the deoxygenation at position 3a.

The 6a-deoxy derivative of **1** (**53**) was found to be 2.5 times more potent than **1**. Therefore, it may have been expected that the 6a-deoxy derivative of **30** (**31**) would be about 2.5 times more potent an inhibitor than **30**. Indeed, **31** was found to be 2.7 times more potent than **30**. Remarkably, the 6a-deoxy derivative of **50** (**51**), wherein the a-unit is a *pseudo*-sugar, is also 2.5 times more potent than **50**. That changes at the 2a and 3a positions do not influence the effect of changes at the 6a position is not necessarily surprising since these reside on opposite sides of the pyranose ring.

It was suggested (11, 12) that the increase in the strength of the binding of about 0.5 kcal/mol, which results from the deoxygenation of position 6a of **1**, is related to a requirement for the CH_2OH-6a group to penetrate a hydrophobic region of the combining site for the complex to form. On this basis, it seemed reasonable to expect that OH-6a would become intramolecularly hydrogen-bonded to the vicinal O-5a. A very similar situation was discovered for the CH_2OH-6b group of the Le^b-OMe tetrasaccharide when bound by the lectin IV of *Griffonia simplicifolia* (GS-IV) (2). In this case, deoxygenation led to a slight (31%) decrease in potency. However, the 6b-chloro-6b-deoxy-Le^b-OMe was 1.9 times more potent (36), thereby suggesting that, on being bound, the CH_2OH-6b group penetrates a hydrophobic region. Indeed, the X-ray crystal structure has now shown the CH_2OH-6b to be in van der Waals contact with the indolyl group of the tryptophane-133 unit (9). An accompanying publication (37) provides unequivocal evidence that, in fact, OH-6b remains in contact with the aqueous phase on complex formation. Nevertheless, it is important to note that, as previously pointed out (36), improved binding resulting from the deoxygenation of a hydroxyl group is observed only when the hydroxyl group is sterically well disposed for intramolecular hydrogen bonding with a nearby proton-accepting atom. It seems likely, therefore, as was found for the GS-IV complex, that these hydroxyl groups occur near hydrophobic groups of the protein. Thus, under thermal agitation, the formation of the intramolecular bond may lead to as favorable a contribution to the stability of the complex as when the interaction is with a water molecule. Presumably, the intramolecular hydrogen bonding effect would be most extensively imposed when the hydroxyl group must become engulfed within the combining site.

The data presented in Table 3 show that, in fact, intramolecular hydrogen bonding is not required for the binding of the CH_2OH-6a group of **1** by the *Ulex* lectin. First of all, replacement of the ring oxygen (O-5a) of **30** by a methylene group to provide **50** has negligible effect on the potency. Therefore, O-5a of **1** does not participate directly in the binding reaction with the *Ulex* lectin and, certainly, the intramolecular hydrogen-bond hypothesis does not apply. That OH-6a remains in the aqueous phase is further indicated by the high potency of the 6a-*O*-methyl derivative **56** (37). On the other hand, the replacement of OH-6a by groups such as amino (**57**), ammonium (**58**), and acetamido (**59**), which strongly interact with water, importantly reduced the potency. These results indicate that, in the complex, although the OH-6a group remains hydrogen-bonded to water, it resides near protein structure. This latter conclusion is supported by the low potency of the pivalamide (**60**) as compared to the acetamide (**59**). In the case of Le^b-OMe, the CH_2-6b group interacts with the indolyl group of a tryptophane unit of the *Griffonia* lectin and proved essential to binding (36). Likely, therefore, the *Ulex* lectin comes into nonbonded nonpolar interaction with the CH_2-6a group of the β-D-GlcNAc unit. This conclusion is supported by the inhibition data observed for compounds **53**–**55** since, as seen in Table 3, the replacement of the OH-6a of **1** by either a fluorine or a chlorine atom importantly enhances the stability of the complex (0.90 and 0.75 kcal/mol, respectively).

It was previously established (12) that OH-3b provides part of the key polar interaction for the binding of **1** by the *Ulex* lectin. Therefore, in the complex, the neighboring *cis*-OH-4b must be in close proximity to the combining site if not actually in a direct interaction with the protein at the periphery of the combining site. Indeed, substitution of OH-4b by hydrogen to yield **61** reduced the potency to 37% of that of **1**. In the event that the involvement of OH-4b is at or near the periphery, CH_2OH-6b would not likely be importantly involved since it is even more remote from the combining site. The replacement of OH-6b by hydrogen to form **62** in fact caused only a weak loss in potency. Also, the replacement of the CH_2OH-6b group of **31** by hydrogen to form **13** had no significant effect on potency.

As mentioned above, the CH_2OH-6a group of **1** must be at the periphery of the combining site. Therefore, the protein structure on complex formation comes close to the aglyconic R group (Table 3). This is consistent with the observation that **63** is more potent than **1** and that **13** is more potent than **20**.

How structure **1** is bound by the *Ulex* lectin is depicted in Fig. 1. Since peripheral interactions are relatively weak, it was possible to establish the effects of some of the structural changes in this region on the thermodynamic parameters. These are presented in Fig. 2 where it is seen that, as found for the binding of Le^b-OMe by GS-IV (2, 9), structural changes near the periphery of the combining site have only a minor effect on the change in free energy as compared to the major but near-compensating changes in the enthalpy and entropy. This enthalpy–entropy compensation phenomenon appears related to changes in the structure of the water about the periphery of the combining site (9). It is especially remarkable that the compensation extended to include compound **13**.

The same conclusion was reached by Belleau and Lavoie (38, 39) over 20 years ago in a study of the thermodynamic parameters for the binding of acetylcholine by acetylcholinesterase. A wide range of congeners were prepared, varying only in the structure of the 2-acetoxyethyl group of acetylcholine. As presently found for congeners of H-type 2-OMe and previously reported for derivatives of Le^b-OMe (9), the various structural analogs of acetylcholine that remained *productive* as inhibitors were bound with little differential change in free energy but with a high degree of compensation for the relatively high changes in enthalpy and entropy. It was concluded (38) that in all cases the binding was essentially restricted to the recognition of the trimethylammonium group and that the driving force was derived from the disordering (melting) of water molecules *within* the

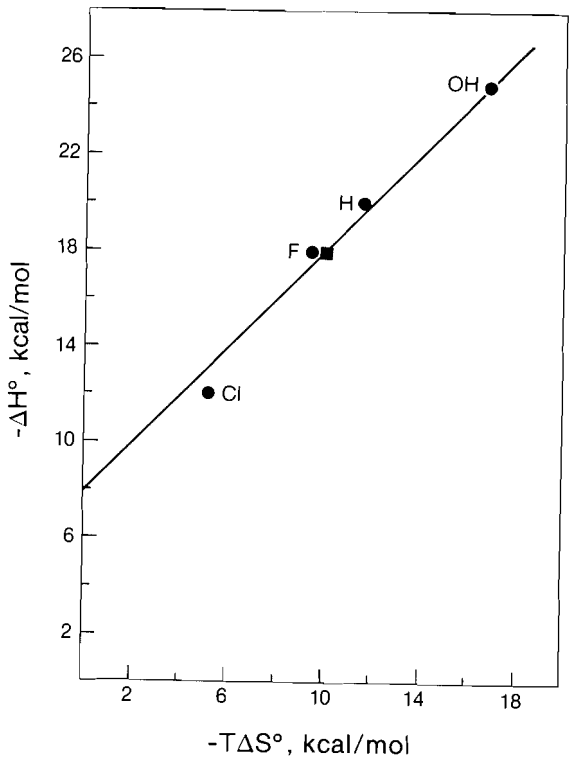

FIG. 2. The effect on the thermodynamic parameters at 298 K for the binding of H-type 2-OMe (**1**) by the lectin I of *Ulex europaeus* of changing the substituent at the 6a-position of the β-D-GlcNAc unit from OH (**1**) to H (**53**), to F (**54**), and to Cl (**55**). The data presented by a square are those for compound **13**, a structure that corresponds to **53** with the NHAc-2a, OH-3a, and CH_2OH-6b groups replaced by hydrogen atoms. The slope of 1 provided by the plot demonstrates the enthalpy–entropy compensation.

combining site. Since stereoelectronic complementarity was found to be the controlling parameter, it was further concluded that productive bindings depend uniquely on specific interactions within the combining site. On this basis, the enthalpy–entropy compensation phenomenon was attributed to changes in the peripheral involvements of water molecules.

The inhibition data presented in Table 3 show that wide variations in the structural features of H-type 2-OMe can be made without causing differential changes in free energy ($\Delta\Delta G^0$) that are greater than 1 kcal/mol. This has been found only when the changes do not involve the key polar grouping and its immediate surrounding. In view of data presented in Fig. 2, these small changes likely result from relatively large but compensating changes in enthalpy and entropy.

In contrast to the positively charged trimethylammonium ion of acetylcholine, the productive surface presented by H-type 2-OMe, as can be appreciated from Fig. 1 (center), is "polyamphiphilic" in the sense that it is made up of a variety of small amphiphilic parts. This surface, together with the stereoelectronically complementary combining site of the lectin, is hydrated prior to complex formation and these water molecules become replaced by the complementary ligand–protein structures, whereas the water molecules at the periphery achieve different states of organization (9). Thus, whereas the latter condition, being related to water only, can be expected to provide an enthalpy–entropy compensation, the productive binding within the combining site is expected to lead to a one-way release of water molecules to bulk.

In an attempt to assess the role of water in these binding reactions, Monte Carlo simulations were made of the hydration of the amphiphilic Le^b-OMe tetrasaccharide (40). It was concluded that the hydration of a polyamphiphilic surface leads to a host of water molecules that are less ordered and less strongly bound than in bulk water. In contrast, the steric constraints for binding water molecules to strongly polar groups within the potential combining site may immobilize water molecules to a greater extent than is present in the bulk condition. If so, the increase in entropy that would result from their release to bulk would contribute to the driving force for complexation. Indeed, Delbaere and Brayer (41) were able to locate water molecules within the active site of native *Streptomyces griseus* protease A. It was noted that this network of "immobilized" solvent molecules resembles the placement of the inhibitor in the complex with chymostatin. The proposed increase in entropy from the release to bulk of strongly bound water molecules from within the combining site would provide compensation for the demands in entropy required for specific organization and immobilization of the reacting species. Monte Carlo simulations of the hydration of the combining site of GS-IV and of its complex with Le^b-OMe may provide a useful test of this proposal and are being pursued.

In the course of this investigation, a monoclonal anti H-type 2 antibody became available and the relative potencies for its binding of H-type 2-OMe (**1**) and several of its congeners are reported in Table 4 where a comparison is made with those found for the *Ulex* lectin. It is readily appreciated that the two proteins recognize very similar regions of the trisaccharide and, therefore, regions about the key polar grouping presented in Fig. 1. It is seen that the 2c-deoxy derivative **66** (R^7 = H) is slightly more strongly bound by the lectin but that the reverse is strongly the case for the 4c-deoxy **68** (R^9 = H) compound. The high relative potency of this compound in inhibiting the antibody indicates that OH-4c is not part of the key polar grouping. The low potencies found for 3b-deoxy **65** (R^4 = H) are very similar and suggest involvement in both cases of OH-3b in a relatively strong polar interaction. The only other significant difference in the affinities is for the Y tetrasaccharide (**64**). In the case of the lectin, the introduction of the fucose unit at the 3a-position of **1** caused a slight decrease in potency relative to the 3a-deoxy compound (**52**, Table 3) (26 vs. 46). On the other hand, the introduction of the second fucose unit provided superior binding by the antibody. This result may arise from this fucose residue providing some additional attractive interactions at the periphery of the antibody combining site. The higher potencies displayed by **63** (R = $(CH_2)_8CO_2Me$) likely have a similar origin. The results presented in Table 4 indicate that the key polar grouping for the binding of the H-type 2 determinant by the *Ulex* lectin was the immunodominant surface of this antigenic determinant in the immune response that led to the production of the monoclonal antibody.

Experimental

Methods

The radioimmunoassays were performed following the procedure recently described (2) using an ^{125}I-labelled [α-L-Fuc-(1→

Can. J. Chem. Downloaded from www.nrcresearchpress.com by 123.30.183.119 on 09/08/12
For personal use only.

TABLE 4. Comparison of the inhibition of the binding of an H-type 2 artificial antigen by a monoclonal anti-H-type 2 antibody and the lectin I of *Ulex europaeus*

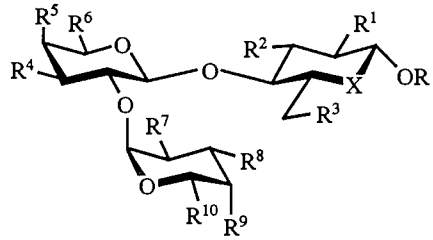

Compound	R	R^1	R^2	R^3	R^4	R^5	R^6	R^7	R^8	R^9	R^{10}	X	Relative potencies: Antibody	Relative potencies: Lectin
1	Me	NHAc	OH	OH	OH	OH	CH_2OH	OH	OH	OH	Me	O	100	100
63	$(CH_2)_8CO_2Me$	NHAc	OH	OH	OH	OH	CH_2OH	OH	OH	OH	Me	O	135	150[b]
64	Me	NHAc	α-L-FucO	OH	OH	OH	CH_2OH	OH	OH	OH	Me	O	130	26
53	Me	NHAc	OH	H	OH	OH	CH_2OH	OH	OH	OH	Me	O	142	250[c]
65	Me	NHAc	OH	OH	H	OH	CH_2OH	OH	OH	OH	Me	O	3	2.5[c]
61	Me	NHAc	OH	OH	OH	H	CH_2OH	OH	OH	OH	Me	O	43	37
62	Me	NHAc	OH	OH	OH	OH	Me	OH	OH	OH	Me	O	45	60[c]
66	Me	NHAc	OH	OH	OH	OH	CH_2OH	H	OH	OH	Me	O	Inactive	0.63[c]
67	Me	NHAc	OH	OH	OH	OH	CH_2OH	OH	H	OH	Me	O	Inactive	0.06[c]
68	Me	NHAc	OH	OH	OH	OH	CH_2OH	OH	OH	H	Me	O	45	Inactive[c]
69	$(CH_2)_8CO_2Me$	NHAc	OH	OH	OH	OH	CH_2OH	OH	OH	OH	H	O	8.5[a]	3.8[c]
31	Me	H	H	H	OH	OH	CH_2OH	OH	OH	OH	Me	O	60	67
13	Me	H	H	H	OH	OH	H	OH	OH	OH	Me	O	42	66
51	Me	H	H	H	OH	OH	CH_2OH	OH	OH	OH	Me	CH_2	48	55
50	Me	H	H	OH	OH	OH	CH_2OH	OH	OH	OH	Me	CH_2	33	22

[a]Estimated from the value when $(CH_2)_8CO_2Me$ was aglycon.
[b]Reference 11.
[c]Reference 12.

2)-β-D-Gal-(1→4)-β-D-GlcNAcO-$(CH_2)_8CONH]_{16}$-BSA antigen provided by Chembiomed Ltd., Edmonton, Alberta. The solution provided near 290 000 cpm/100 μL. In the absence of inhibitor, the coated tubes acquired about 40–50% of these counts in the case of the antibody and about 63–78% in the case of the lectin. The monoclonal anti-H-type 2 antibody (IgM, clone 92 FR A2) was available from Chembiomed Ltd. The lectin 1 of *Ulex europaeus* was purchased from Sigma Chemical Company.

The thermodynamic parameters presented in Fig. 2 were determined by difference ultraviolet absorption spectroscopy as previously described (2).

The ^1H nmr spectra were measured at 300, 360, and 400 MHz (Bruker AM300, WM360, and WH400) with tetramethylsilane as internal standard for $CDCl_3$ solutions. The reference standard for D_2O solutioins was acetone (2.225 ppm). The ^{13}C nmr spectra were recorded at 100 and 75 MHz using as a solvent either $CDCl_3$ (77.06 ppm) or D_2O with 1,4-dioxane (67.4 ppm) as internal standard. Optical rotations were measured at room temperature (23 ± 1°C) in a 1-dm cell on a Perkin–Elmer 241 polarimeter. Thin-layer chromatograms were performed on precoated plates of silica gel (60F254, E. Merck, Darmstadt) and visualized by spraying with 10% sulfuric acid in ethanol followed by heating. For column chromatography, silica gel 60 (230–400 mesh, E. Merck, Darmstadt) and distilled solvents were used. Solvents and reagents were purified and dried according to standard procedures. Melting points are uncorrected.

Methyl 4,6-O-benzylidene-2,3-dideoxy-β-D-erythro-*hexopyranoside (3)*

Methyl 4,6-*O*-benzylidene-β-D-*erythro*-hex-2-enopyranoside **2** (14) (1.68 g, 6.77 mmol) was hydrogenated in the presence of 5% palladium-on-carbon (0.85 g) in methanol (85 mL) containing 17 mL of triethylamine at 50 psi (1 psi = 6.89 kPa). Filtration and evaporation left a syrup, which was partitioned between benzene and water. The benzene layer was dried and evaporated to give crystalline **3** (1.59 g, 94%); mp 104–105°C, $[\alpha]_D$ −57 (*c* 0.6, chloroform) (lit. (14) mp 106–107°C; $[\alpha]_D$ −58.8 (*c* 2.55, chloroform)); ^1H nmr ($CDCl_3$) δ: 7.51–7.33 (m, 5H,Ph), 5.56 (s, 1H, PhC*H*), 4.51 (dd, 1H, $J_{1,2ax}$ 9.5 Hz, $J_{1,2eq}$ 2.4 Hz, H-1), 4.30 (dd, 1H, $J_{5,6eq}$ 5.0 Hz, $J_{6ax,6eq}$ 10.4 Hz, H-6eq), 3.80 (t, 1H, $J_{5,6ax}$ 10.0 Hz, H-6ax), 3.57 (ddd, 1H, $J_{3ax,4}$ 10.8 Hz, $J_{3eq,4}$ 4.5 Hz, $J_{4,5}$ 9.2 Hz, H-4), 3.53 (s, 3H, OCH_3), 3.45 (ddd, 1H, H-5), 2.15 (dt, 1H, $J_{2ax,3eq}$ 4.2 Hz, $J_{2eq,3eq}$ < 1.0 Hz, $J_{3ax,3eq}$ 12.0 Hz, H-3eq), 2.02 (ddd, 1H, $J_{2ax,2eq}$ 12.6 Hz, $J_{2eq,3ax}$ 3.5 Hz, H-2eq), 1.76 (dddd, 1H, $J_{2ax,3ax}$ 13.1 Hz, H-3ax), 1.68 (dddd, 1H, H-2ax). Anal. calcd. for $C_{14}H_{18}O_4$: C 67.18, H 7.25; found: C 66.71, H 6.99.

Methyl 4-O-benzoyl-6-bromo-2,3,6-trideoxy-β-D-erythro-*hexopyranoside (4)*

A mixture of compound **3** (1.59 g, 6.36 mmol), *N*-bromosuccinimide (1.38 g, 7.63 mmol), and barium carbonate (1.90 g, 9.54 mmol) in carbon tetrachloride (48 mL) (18) was boiled under reflux for 30 min. The solvent was evaporated and the remainder dissolved in dichloromethane (200 mL). The solution was washed with aqueous sodium bicarbonate and water, followed by drying and evaporation, to leave a crystalline residue (2.08 g, 99%) that was crystallized from a small quantity of methanol to yield pure **4**; mp 107–108°C, $[\alpha]_D$ +12 (*c* 0.8, chloroform); ^1H nmr ($CDCl_3$) δ: 8.05–7.44 (m, 5H, Ph), 4.92 (ddd, 1H, $J_{3ax,4}$ 9.7 Hz, $J_{3eq,4}$ 4.8 Hz, $J_{4,5}$ 8.7 Hz, H-4), 4.54 (dd, 1H, $J_{1,2ax}$ 8.4 Hz, $J_{1,2eq}$ 2.4 Hz, H-1), 3.87 (ddd, 1H, $J_{5,6A}$ 3.2 Hz, $J_{5,6B}$ 7.8 Hz, H-5), 3.63 (dd, 1H, $J_{6A,6B}$ 10.8, H-6A), 3.57 (s, 3H, OCH_3), 3.50 (dd, 1H, H-6B), 2.37 (dddd, 1H, $J_{2eq,3eq}$ 1.0 Hz, $J_{2ax,3eq}$ 3.4 Hz, $J_{3ax,3eq}$ 11.6 Hz, H-3eq), 2.01 (dddd, 1H, $J_{2ax,2eq}$ 12.0 Hz, $J_{2eq,3ax}$ 3.9 Hz, H-2eq), 1.76 (dddd,

Can. J. Chem. Downloaded from www.nrcresearchpress.com by 123.30.183.119 on 09/08/12
For personal use only.

Can. J. Chem. Downloaded from www.nrcresearchpress.com by 123.30.183.119 on 09/08/12
For personal use only.

$J_{2ax,3ax}$ 12.8 Hz, H-2ax), 1.70 (dddd, 1H, H-3ax). Anal. calcd. for $C_{14}H_{17}BrO_4$: C 51.08, H 5.21, Br 24.27; found: C 51.23, H 5.15, Br 24.62.

Methyl 4-O-benzoyl-2,3,6-trideoxy-β-D-erythro-*hexopyranoside (5)*

The bromo compound **4** (1.35 g, 4.10 mmol) was hydrogenated in the presence of 5% palladium-on-carbon (0.70 g) in methanol (100 mL) containing triethylamine (0.70 mL, 4.92 mmol) at 80 psi for 8 h. Filtration and evaporation left a syrup, which was dissolved in dichloromethane (50 mL). Washing with water and evaporation gave a syrupy product **5** (1.01 g, 98%); $[\alpha]_D$ +7 (*c* 0.8, chloroform); ^{1}H nmr ($CDCl_3$) δ: 8.04–7.44 (m, 5H, Ph), 4.72 (ddd, 1H, $J_{3ax,4}$ 10.3 Hz, $J_{3eq,4}$ 4.9 Hz, $J_{4,5}$ 9.0 Hz, H-4), 4.47 (dd, 1H, $J_{1,2a}$ 8.8 Hz, $J_{1,2eq}$ 2.2 Hz, H-1), 3.71 (dq, 1H, $J_{5,6}$ 6.3 Hz, H-5), 3.53 (s, 3H, OCH_3), 2.32 (dddd, 1H, $J_{2ax,3eq}$ 4.0 Hz, $J_{2eq,3eq}$ 1.5 Hz, $J_{3ax,3eq}$ 12.5 Hz, H-3eq), 1.98 (dddd, 1H, $J_{2eq,3ax}$ 3.9 Hz, $J_{2ax,2eq}$ 12.4 Hz, H-2eq), 1.74 (dddd, 1H, $J_{2ax,3ax}$ 13.1 Hz, H-2ax), 1.64 (dddd, 1H, H-3ax), 1.31 (d, 3H, 3H-6). Anal. calcd. for $C_{14}H_{18}O_4$: C 67.18, H 7.25; found: C 67.13, H 7.23.

Methyl 2,3,6-trideoxy-β-D-erythro-*hexopyranoside (6)*

Compound **6** (1.0 g, 4.0 mmol) was debenzoylated in the usual manner using methanolic sodium methoxide. After evaporation, the crude material was purified by chromatography on a column of silica gel (dichloromethane-10% methanol) to provide **6** (0.52 g, 89%) as an oil; $[\alpha]_D$ −50 (*c* 0.5, water) (lit. (19) $[\alpha]_D$ −21.9 (*c* 0.82, chloroform)); ^{1}H nmr ($CDCl_3$) δ: 4.38 (dd, 1H, $J_{1,2ax}$ 9.2 Hz, $J_{1,2eq}$ 2.2 Hz, H-1), 3.52 (s, 3H, OCH_3), 3.32 (dq, 1H, $J_{4,5}$ 8.5 Hz, $J_{5,6}$ 6.1 Hz, H-5), 3.29 (ddd, 1H, $J_{3ax,4}$ 10.6 Hz, $J_{3eq,4}$ 3.7 Hz, H-4), 2.08 (dddd, 1H, $J_{2ax,3eq}$ 4.1 Hz, $J_{2eq,3eq}$ 2.0 Hz, $J_{3ax,3eq}$ 12.3 Hz, H-3eq), 1.90 (dddd, 1H, $J_{2ax,2eq}$ 12.9 Hz, $J_{2eq,3ax}$ 4.0 Hz, H-2eq), ~1.60 (br, 1H, OH), 1.59 (dddd, 1H, $J_{2ax,3ax}$ 13.3 Hz, H-2ax), 1.49 (dddd, 1H, H-3ax), 1.36 (d, 3H, 3H-6).

*Methyl 4-O-(*α-L-*arabinopyranosyl)-2,3,6-trideoxy*-β-D-erythro-*hexopyranoside (9)*

A mixture of **6** (185 mg, 1.26 mmol), mercuric cyanide (446 mg, 1.76 mmol) and 2,3,4-tri-*O*-acetyl-β-L-arabinopyranosyl bromide (1.76 mmol) (20, 21) in dry toluene (18 mL) was kept under reflux for 2 h. Filtration and evaporation left a syrup, which was deacetylated with 5% potassium hydroxide in methanol (13 mL) for 30 min at room temperature. The precipitate was filtered off and the filtrate was treated with Amberlite MB-3, followed by filtration and evaporation of the solvent. Column chromatography on silica gel eluting with a gradient solvent system of dichloromethane and methanol gave syrupy **9** (151 mg, 43%); $[\alpha]_D$ +7 (*c* 1.0, water); ^{1}H nmr (D_2O) δ: 4.56 (dd, 1H, $J_{1a,2aax}$ 9.2 Hz, $J_{1a,2aeq}$ 2.2 Hz, H-1a), 4.44 (d, 1H, $J_{1b,2b}$ 7.5 Hz, H-1b), 3.94 (ddd, 1H, $J_{3b,4b}$ 3.7 Hz, $J_{4b,5bax}$ 1.2 Hz, $J_{4b,5beq}$ 2.1 Hz, H-4b), 3.89 (dd, 1H, $J_{5bax,5beq}$ 13.1 Hz, H-5beq), 3.65 (dd, 1H, H-5bax), 3.65 (dd, 1H, H-3b), 3.59 (dq, 1H, $J_{4a,5a}$ 9.0 Hz, $J_{5a,6a}$ 6.3 Hz, H-5a), 3.51 (dd, 1H, $J_{2b,3b}$ 9.6 Hz, H-2b), 3.48 (s, 3H, OCH_3), 3.40 (ddd, 1H, $J_{3aax,4a}$ 10.2 Hz, $J_{3aeq,4a}$ 3.8 Hz, H-4a), 2.20 (dddd, 1H, $J_{2aax,3aeq}$ 4.0 Hz, $J_{2aeq,3aeq}$ 3.3 Hz, $J_{3aax,3aeq}$ 12.6 Hz, H-3aeq), 1.93 (dddd, 1H, $J_{2aax,2aeq}$ 12.8 Hz, $J_{2aeq,3aax}$ 3.8 Hz, H-2aeq), 1.63 (dddd, 1H, $J_{2aax,3aax}$ 13.1 Hz, H-3aax), 1.50 (dddd, 1H, H-2aax), 1.33 (d, 3H, 3H-6a); ^{13}C nmr (D_2O) δ: 104.95 (C-1b), 103.29 (C-1a), 81.17 (C-4a), 75.22 (C-5a), 73.08 (C-3b), 71.76 (C-2b), 69.01 (C-4b), 66.84 (C-5b), 56.93 (CH_3O), 30.37, 29.47 (C-2a, C-3a), 18.02 (C-6a). Anal. calcd. for $C_{12}H_{22}O_7$: C 51.79, H 7.97; found: C 51.09, H 7.87.

*Methyl 4-O-(3,4-O-benzylidene-*α-L-*arabinopyranosyl)-2,3,6-trideoxy*-β-D-erythro-*hexopyranoside (10)*

A mixture of **9** (136 mg, 0.49 mmol), α,α-dimethoxytoluene (0.38 mL), *p*-toluenesulfonic acid monohydrate (5 mg), and *N,N*-dimethylformamide (1.1 mL) was heated at 50°C for 20 min. Neutralization with sodium methoxide, followed by evaporation, left a syrup, which was chromatographed on a column of silica gel (dichloromethane–ethyl acetate, 7:1) to give crystalline **10** (113 mg, 63%); mp 128–129°C, $[\alpha]_D$ −4 (*c* 0.5, chloroform); ^{1}H nmr ($CDCl_3$) δ: 7.56–7.38 (m, 5H, Ph), 5.97 (s, 1H, *CH*Ph), 4.39 (d, 1H, $J_{1b,2b}$ 7.5 Hz, H-1b), 4.38 (dd, 1H, $J_{1a,2aax}$ 8.9 Hz, $J_{1a,2aeq}$ 2.3 Hz, H-1a), 4.34 (dt, 1H, $J_{3b,4b}$ 6.3 Hz, $J_{4b,5bax} = J_{4b,5beq}$ 3.6 Hz, H-4b), 4.29 (dd, 1H, $J_{5bax,5beq}$ 13.2 Hz, H-5eq), 4.23 (dd, 1H, $J_{2b,3b}$ 7.5 Hz, H-3b), 3.90 (dd, 1H, H-5bax), 3.72 (dt, 1H, $J_{2b,OH}$ 2.2 Hz, H-2b), 3.51 (s, 3H, OCH_3), 3.46 (dq, 1H, $J_{4a,5a}$ 8.9 Hz, $J_{5a,6a}$ 6.2 Hz, H-5a), 3.26 (ddd, 1H, $J_{3aax,4a}$ 10.4 Hz, $J_{3aeq,4a}$ 4.5 Hz, H-4a), 2.36 (d, 1H, OH), 2.22 (m, 1H, H-3aeq), 1.91 (m, 1H, H-2aeq), 1.69–1.54 (m, 2H, H-2aax and H-3aax), 1.36 (d, 3H, 3H-6a). Anal. calcd. for $C_{19}H_{26}O_7$: C 62.28, H 7.15; found: C 61.52, H 7.11.

*Methyl 4-O-[3,4-O-benzylidene-2-O-(2,3,4-tri-O-benzyl-*α-L-*fucopyranosyl)-*α-L-*arabinopyranosyl]-2,3,6-trideoxy*-β-D-erythro-*hexopyranoside (12)*

A solution of bromide **11** (0.44 mmol) in dichloromethane (0.4 mL) was added to a mixture of **10** (64 mg, 0.17 mmol), tetraethylammonium bromide (55 mg, 0.26 mmol), diisopropylethylamine (76 μL, 0.44 mmol), powdered 4 Å molecular sieves (300 mg), *N,N*-dimethylformamide (0.15 mL), and dichloromethane (0.40 mL). After stirring for 20 h at room temperature, the mixture was diluted with dichloromethane and filtered through Celite. The filtrate was washed with aqueous sodium bicarbonate and water, followed by drying and evaporation. Column chromatography of the crude product on silica gel (toluene–ethyl acetate, 50:1 to 3:1, gradient) provided syrupy **12** (109 mg, 81%), $[\alpha]_D$ −53° (*c* 0.5, chloroform); ^{1}H nmr ($CDCl_3$) δ: 7.53–7.24 (m, 20H, 4Ph), 5.88 (s, 1H, *CH*Ph), 5.50 (d, 1H, $J_{1c,2c}$ 3.7 Hz, H-1c), 4.98 and 4.68 (AB, 2H, $J_{A,B}$ 11.2 Hz, CH_2Ph), 4.88 and 4.73 (AB, 2H, J_{AB} 11.7 Hz, CH_2Ph), 4.79 and 4.75 (AB, 2H, J_{AB} 13.0 Hz, CH_2Ph), 4.58 (d, 1H, $J_{1b,2b}$ 6.8 Hz, H-1b), 4.38 (t, 1H, $J_{2b,3b} = J_{3b,4b}$ 6.8 Hz, H-3b), 4.33 (ddd, 1H, $J_{4b,5bax}$ 4.6 Hz, $J_{4b,5beq}$ 4.2 Hz, H-4b), 4.30 (dd, 1H, $J_{1a,2aax}$ 8.9 Hz, $J_{1a,2aeq}$ 2.1 Hz, H-1), 4.11 (q, 1H, $J_{4c,5c}$ < 1.0 Hz, $J_{5c,6c}$ 6.3 Hz, H-5c), 4.09 (dd, 1H, $J_{5bax,5beq}$ 13.0 Hz, H-5beq), 4.05 (dd, 1H, $J_{2c,3c}$ 10.3 Hz, H-2c), 3.93 (t, 1H, H-2b), 3.91 (dd, $J_{3c,4c}$ 2.5 Hz, H-3c), 3.84 (dd, 1H, H-5bax), 3.62 (d, 1H, H-4c), 3.47 (s, 3H, OCH_3), 3.28 (dq, 1H, $J_{4a,5a}$ 8.9 Hz, $J_{5a,6a}$ 6.1 Hz, H-5a), 3.20 (ddd, 1H, $J_{3aax,4a}$ 10.0 Hz, $J_{3aeq,4a}$ 4.5 Hz, H-4), 2.12 (m, 1H, H-3aeq), 1.85 (m, 1H, H-2aeq), 1.58–1.45 (m, 2H, H-2aax, H-3aax), 1.22 (d, 3H, 3H-6a), 1.10 (d, 3H, 3H-6c). Anal. calcd. for $C_{46}H_{54}O_{11}$: C 70.57, H 6.95; found: C 71.03, H 7.04.

*Methyl 2,3,6-trideoxy-4-O-[2-O-(*α-L-*fucopyranosyl)-*α-L-*arabinopyranosyl]-*β-D-erythro-*hexopyranoside (13)*

Compound **12** (51 mg, 0.065 mmol) was hydrogenated in the presence of 5% palladium-on-carbon (25 mg) in 95% ethanol (2.5 mL) at 125 psi for 5 h. Filtration and evaporation left a crystalline residue that was purified by column chromatography on silica gel (dichloromethane–methanol, 5:1). Evaporation of chromatographically pure fractions gave **13** (24 mg, 87%), which was crystallized from methanol–ethyl acetate; mp 230–232°C, $[\alpha]_D$ −106 (*c* 0.5, water). The ^{1}H and ^{13}C nmr data are reported in Tables 1 and 2. Anal. calcd. for $C_{18}H_{32}O_{11}$: C 50.94, H 7.60; found: C 50.43, H 7.64.

*4-O-(*α-L-*Arabinopyranosyl)-1,2,3,6-tetradeoxy*-D-erythro-hexopyranose *(16)*

A mixture of 1,2,3,6-tetradeoxy-D-*erythro*-hexopyranose (**14**, 232 mg, 2.0 mmol) (26), 2,3,4-tri-*O*-acetyl-β-L-arabinopyranosyl bromide (**7**, 2.8 mmol), and mercuric cyanide (700 mg, 2.8 mmol) in dry toluene (23 mL) was boiled under reflux for 2 h. After filtration and evaporation, the residue was treated with methanolic 5% potassium hydroxide (21 mL) for 30 min. Filtration, neutralization with acetic acid, and evaporation followed by column chromatography on silica gel (dichloromethane–methanol, gradient) provided crystalline **16** (266 mg, 54%) as the main product; mp 145.5–146°C, $[\alpha]_D$ +63 (*c* 0.7, water); ^{1}H nmr (D_2O) δ: 4.43 (d, 1H, $J_{1b,2b}$ 7.6 Hz, H-1b), 3.93 (ddd, 1H, $J_{3b,4b}$ 3.7 Hz, $J_{4b,5bax}$ 1.3 Hz, $J_{4b,5beq}$ 2.2 Hz, H-4b), 3.90 (dd, 1H, $J_{5bax,5beq}$ 12.8 Hz, H-5beq), 3.86 (m, 1H, H-1aeq), 3.65 (dd, 1H, H-5bax),

Can. J. Chem. Downloaded from www.nrcresearchpress.com by 123.30.183.119 on 09/08/12
For personal use only.

3.65 (dd, 1H, $J_{2b,3b}$ 9.6 Hz, H-3b), 3.51 (dd, 1H, H-2b), 3.43 (ddd, 1H, $J_{1aax,1aeq}$ 11.4 Hz, $J_{1aax,2aax}$ 8.7 Hz, $J_{1aax,2aeq}$ 5.8 Hz, H-1aax), 3.43 (dq, 1H, $J_{4a,5a}$ 9.0 Hz, $J_{5a,6a}$ 6.1 Hz, H-5a), 3.48 (ddd, 1H, $J_{3aax,4a}$ 10.0 Hz, $J_{3aeq,4a}$ 4.1 Hz, H-4a), 2.21 (m, 1H, H-3aeq), 1.78–1.48 (m, 3H, H-2aax, H-2aeq, and H-3aax), 1.29 (d, 3H, 3H-6a); ^{13}C nmr (D_2O) δ: 104.91 (C-1b), 81.89 (C-4a), 77.57 (C-5a), 73.15 (C-3b), 71.86 (C-2b), 69.05 (C-4b), 67.96 (C-1a), 66.85 (C-5b), 31.44 (C-3a), 25.49 (C-2a), 18.15 (C-6a). Anal. calcd. for $C_{11}H_{20}O_6$: C 53.22, H 8.12; found: C 53.19, H 8.02.

*1,2,3,6-Tetradeoxy-4-*O*-(3,4-*O*-isopropylidene-α-L-arabinopyranosyl)-D-*erythro*-hexopyranose (17)*

To a solution of **16** (191 mg, 0.77 mmol) in 2,2-dimethoxypropane (0.4 mL, 3.0 mmol) and *N*,*N*-dimethylformamide (1.9 mL), 5% trifluoromethanesulfonic acid in *N*,*N*-dimethylformamide (50 μL) was added. After stirring for 20 min at room temperature, the solution was neutralized with sodium methoxide and evaporated to leave a syrup. Chromatography on a column of silica gel (dichloromethane–ethyl acetate, 3:1) afforded compound **17** (200 mg, 91%) as a syrup, $[\alpha]_D$ +53 (*c* 1.2, chloroform); ^{1}H nmr ($CDCl_3$) δ: 4.27 (d, 1H, $J_{1b,2b}$ 6.8 Hz, H-1b), 4.23 (ddd, 1H, $J_{3b,4b}$ 5.8 Hz, $J_{4b,5bax}$ 3.3 Hz, $J_{4b,5beq}$ 2.8 Hz, H-4b), 4.17 (dd, 1H, $J_{5bax,5beq}$ 13.2 Hz, H-5beq), 4.06 (dd, 1H, $J_{2b,3b}$ 7.6 Hz, H-3b), 3.86 (m, 1H, $J_{1aax,1aeq}$ 11.3 Hz, H-1aeq), 3.78 (dd, 1H, H-5bax), 3.60 (dt, 1H, $J_{2b,OH}$ 2.8 Hz, H-2b), 3.35 (m, 1H, $J_{1aax,2aax}$ 10.0 Hz, $J_{1aax,2aeq}$ 4.8 Hz, H-1aax), 3.28 (dq, 1H, $J_{4a,5a}$ 9.0 Hz, $J_{5a,6a}$ 6.1 Hz, H-5a), 3.20 (ddd, 1H, $J_{3aax,4a}$ 10.8 Hz, $J_{3aeq,4a}$ 4.7 Hz, H-4a), 2.37 (d, 1H, OH), 2.22 (m, 1H, H-3aeq), 1.75–1.64 (m, 2H, H-2aax and H-2aeq), 1.55 and 1.38 (2s, each 3H, Me_2C), 1.53 (m, 1H, H-3aax), 1.28 (d, 3H, 3H-6a). Anal. calcd. for $C_{14}H_{24}O_6$: C 58.32, H 8.39; found: C 58.23, H 8.38.

*1,2,3,6-Tetradeoxy-4-*O*-[3,4-*O*-isopropylidene-2-*O*-(2,3,4-tri-*O*-benzyl-α-L-fucopyranosyl)-α-L-arabinopyranosyl]-D-*erythro*-hexopyranose (18)*

A solution of freshly prepared 2,3,4-tri-*O*-benzyl-α-L-fucopyranosyl bromide **11** (1.73 mmol) in dichloromethane (1 mL) was added to a mixture of **17** (200 mg, 0.69 mmol), tetraethylammonium bromide (292 mg, 1.39 mmol), powdered 4 Å molecular sieves (2.4 g), dichloromethane (1.6 mL), and *N*,*N*-dimethylformamide (0.6 mL). After stirring for 6 h at room temperature, the mixture was diluted with dichloromethane, filtered through Celite, and washed with aqueous sodium bicarbonate and water successively, followed by drying and evaporation. Chromatography on a column of silica gel (benzene–ethyl acetate, 50:1 to 3:1, gradient) afforded two major fractions. Evaporation of the first fraction left a syrup (215 mg, 44%) that was identified as the fully protected trisaccharide **18**, $[\alpha]_D$ −34 (*c* 1, chloroform); ^{1}H nmr ($CDCl_3$) δ: 7.44–7.25 (m, 15H, 3Ph), 5.52 (d, 1H, $J_{1c,2c}$ 3.8 Hz, H-1c), 5.00 and 4.68 (AB, 2H, $J_{A,B}$ 11.5 Hz, CH_2Ph), 4.88 and 4.74 (AB, 2H, J_{AB} 12.0 Hz, CH_2Ph), 4.79 (s, 2H, CH_2Ph), 4.47 (d, 1H, $J_{1b,2b}$ 7.0 Hz, H-1b), 4.29 (dd, 1H, $J_{2b,3b}$ 7.0 Hz, $J_{3b,4b}$ 6.5 Hz, H-3b), 4.25 (ddd, 1H, $J_{4b,5bax}$ 3.8 Hz, $J_{4b,5beq}$ 3.3 Hz, H-4b), 4.13 (q, 1H, $J_{4c,5c}$ < 1 Hz, $J_{5c,6c}$ 6.8 Hz, H-5c), 4.07 (dd, 1H, $J_{2c,3c}$ 10.2 Hz, H-2c), 4.06 (dd, 1H, $J_{5bax,5beq}$ 12.8 Hz, H-5beq), 3.88 (dd, 1H, $J_{3c,4c}$ 2.8 Hz, H-3c), 3.85 (m, 1H, H-1aeq), 3.80 (t, 1H, H-2b), 3.75 (dd, 1H, H-5bax), 3.60 (d, 1H, H-4c), 3.29 (ddd, 1H, $J_{1aax,1aeq}$ 11.3 Hz, $J_{1aax,2aax}$ 10.0 Hz, $J_{1aax,2aeq}$ 4.8 Hz, H-1aax), 3.15 (ddd, 1H, $J_{3aax,4a}$ 10.5 Hz, $J_{3aeq,4a}$ 4.8 Hz, $J_{4a,5a}$ 9.0 Hz, H-4a), 3.07 (dq, 1H, $J_{5a,6a}$ 6.0 Hz, H-5a), 2.16 (m, 1H, H-3aeq), 1.70–1.60 (m, 2H, H-2aax, H-2aeq), 1.46 (m, 1H, H-3aax), 1.49 and 1.36 (2s, each 3H, Me_2C), 1.15 (d, 3H, 3H-6a), 1.08 (d, 3H, 3H-6c). Anal. calcd. for $C_{41}H_{52}O_{10}$: C 69.87, H 7.44; found: C 69.97, H 7.38.

The ^{1}H nmr spectrum of the product (199 mg, 43%) of the second fraction was superimposable with that of 1,2,3,6-tetradeoxy-4-*O*-[2-*O*-(2,3,4-tri-*O*-benzyl-α-L-fucopyranosyl)-α-L-arabinopyranosyl]-D-*erythro*-hexopyranose (**19**) formed by heating of **18** in aqueous acetic acid.

*1,2,3,6-Tetradeoxy-4-*O*-[2-*O*-(α-L-fucopyranosyl)-α-L-arabinopyranosyl]-D-*erythro*-hexopyranose (20)*

A solution of **18** (55 mg, 0.078 mmol) in 80% aqueous acetic acid (0.6 mL) was heated at 65°C for 2.5 h. Evaporation and coevaporation with toluene left a syrup, which was hydrogenated in 95% ethanol (2.5 mL) in the presence of 5% palladium-on-carbon (20 mg) at 128 psi for 7 h, when tlc (2-propanol/water, 9:1) indicated completion of the reaction. Filtration and evaporation left a clear syrup of **20** (31 mg, 100%), which was crystallized from ethyl acetate; mp 181–182°C, $[\alpha]_D$ −92 (*c* 0.7, water). The ^{1}H and ^{13}C nmr data are presented in Tables 1 and 2. Anal. calcd. for $C_{17}H_{30}O_{10}$: C 51.77, H 7.67; found: C 51.31, H 7.70.

*Methyl 2,3-dideoxy-*β*-D-*erythro*-hexopyranoside (21) (ref. 19)*

Compound **2** (35 mg, 0.14 mmol) (15) was hydrogenated over 20% palladium hydroxide-on-carbon (9 mg) in ethanol (3.5 mL) for 6 h at 20 psi. After removal of the catalyst and evaporation, pure diol **21** (18.5 mg, 81%) was obtained as a colourless syrup; ^{1}H nmr ($CDCl_3$) δ: 4.42 (dd, 1H, $J_{1,2eq}$ 2.0 Hz, $J_{1,2ax}$ 9.0 Hz, H-1), 3.87 (dd, 1H, $J_{5,6A}$ 4.0 Hz, $J_{6A,6B}$ 11.5 Hz, H-6A), 3.85 (dd, 1H, $J_{5,6B}$ 4.5 Hz, H-6B), 3.64 (m, 1H, H-4), 3.49 (s, 3H, OCH_3), 3.32 (m, 1H, $J_{4,5}$ 9.0 Hz, H-5), 2.32 (bs, 2H, 2OH), 2.10 (m, 1H, H-3eq), 1.90 (m, 1H, H-2eq), 1.62–1.47 (m, 2H, H-2ax, H-3ax); ^{13}C nmr ($CDCl_3$) δ: 102.93 (C-1), 78.99 (C-4), 66.35 (C-5), 63.25 (C-6), 56.54 (OCH_3), 30.68, 30.21 (C-2, C-3).

For larger scale preparations, after removal of the catalyst, the solution was treated with pyridine prior to evaporation to dryness.

*Methyl 2,3-dideoxy-6-*O*-p-toluenesulfonyl-*β*-D-*erythro*-hexopyranoside (22)*

Compound **21** (1.242 g, 5 mmol) was hydrogenated over 20% palladium hydroxide-on-carbon (311 mg) in ethanol (90 mL) at 20 psi for 3 h. The catalyst was removed by filtration and pyridine (10 mL) was added to the solution. It was evaporated to dryness. The residue was left overnight in an oil pump vacuum. The oily product (0.821 g) was dissolved in dry pyridine (12.5 mL), cooled to 0°C, and *p*-toluenesulfonyl chloride (1.012 g, 5.3 mmol) was added. The mixture was stirred at 0°C for 1 h, then more chloride (0.482 g, 2.5 mmol) was added. After 2.5 h, water (1 mL) was added and the mixture was kept stirring for 2 h at room temperature, then poured into ice-water. A precipitate was filtered off and the filtrate was extracted with chloroform. The combined extracts were washed with water, dried, and evaporated to provide compound **22** as a crystallizing syrup (0.72 g, 46%). The precipitate, which was a mixture of two compounds, was chromatographed on a column of silica gel (chloroform–ethyl acetate, 4:1) to provide crystalline methyl 2,3-dideoxy-4,6-di-*O*-*p*-toluenesulfonyl-β-D-*erythro*-hexopyranoside (**22***a*, 0.222 g, 10%) and compound **22** 0.6 g, 38%). Both samples of compound **22** were combined and recrystallized from ether–hexane (0.857 g, 54%); mp 87.5–88.5°C, $[\alpha]_D$ −53.5 (c 0.5, chloroform) (lit. (19) mp 95–96°C (chloroform–petroleum ether), $[\alpha]_D$ −43.8 (*c* 1.1, chloroform)); ^{1}H nmr ($CDCl_3$) δ: 7.82 and 7.35 (2d, 4H, C_6H_4), 4.38–4.32 (2dd overlapped, 2H, $J_{1,2eq}$ ~ 2.5 Hz, $J_{1,2ax}$ 8.5 Hz, H-1, $J_{5,6A}$ 4.5 Hz, $J_{6A,6B}$ 11.0 Hz, H-6A), 4.25 (dd, 1H, $J_{5,6B}$ 2.5 Hz, H-6B), 3.60 (m, 1H, H-4), 3.42 (s and m, 3H, OCH_3 and 1H, $J_{4,5}$ 9.5 Hz, H-5), 2.47 (s, 3H, CH_3 of Ts), 2.10 (m, 1H, H-3eq), 2.05 (d, 1H, $J_{4,OH}$ 5.5 Hz, OH), 1.88 (m, 1H, H-2eq), 1.62–1.44 (m, 2H, H-3ax, H-2ax); ^{13}C nmr ($CDCl_3$) δ: 144.98, 132.66, 129.68, 128.01 (C_6H_4), 102.67 (C-1), 77.48 (C-4), 69.60 (C-6), 65.48 (C-5), 56.36 (OCH_3), 30.36, 29.94 (C-2, C-3), 21.66 (CH_3 of Ts). Anal. calcd. for $C_{14}H_{20}O_6S$: C 53.15, H 6.37, S 10.13; found: C 53.32, H 6.41, S 10.12.

Ditosylate **22***a* melted at 124–125°C (ethyl acetate–hexane); $[\alpha]_D$ −9 (*c* 0.53, chloroform) (Lit. (19) mp 136–138°C (chloroform/petroleum ether)); ^{1}H nmr ($CDCl_3$) δ: 7.80–7.32 (m, 8H, $2C_6H_4$), 4.33 (dd, 1H, $J_{1,2eq}$ 2.0 Hz, $J_{1,2ax}$ 8.0 Hz, H-1), 4.25 (ddd, 1H, $J_{3eq,4}$ 4.5 Hz, $J_{4,5}$ 8.0 Hz, $J_{3ax,4}$ 9.5 Hz, H-4), 4.07 (dd, 1H, $J_{5,6A}$ 3.5 Hz, $J_{6A,6B}$ 11.0 Hz, H-6A), 3.83 (dd, 1H, $J_{5,6B}$ 6.0 Hz, H-6B),

Can. J. Chem. Downloaded from www.nrcresearchpress.com by 123.30.183.119 on 09/08/12
For personal use only.

3.60 (m, 1H, H-5), 3.34 (s, 3H, OCH_3), 2.48 and 2.45 (2s, each 3H, $2CH_3$ of Ts), 2.14 (m, 1H, H-3eq), 1.87 (m, 1H, H-2eq), 1.68 (m, 1H, H-3ax), 1.50 (m, 1H, H-2ax). Anal. calcd. for $C_{21}H_{26}O_8S_2$: C 53.60, H 5.57, S 13.63; found: C 53.65, H 5.61, S 13.41.

*Methyl 4-O-(2-O-acetyl-3,4,6-tri-O-benzyl-β-D-galactopyranosyl)-2,3-dideoxy-6-O-p-toluenesulfonyl-β-D-*erythro*-hexopyranoside (24)*

A mixture of compound **22** (0.19 g, 0.6 mmol), mercuric cyanide (0.304 g, 1.2 mmol), powdered calcium sulfate (0.1 g), and 4 Å molecular sieves (0.2 g) in toluene–nitromethane (1:1, 4 mL) was stirred under nitrogen for 1 h. Then a solution of bromide **23** (0.487 g, 0.887 mmol) in nitromethane–toluene (1:1, 2 mL) was added dropwise within 15 min. After stirring at room temperature for 1.5 h, the reaction mixture was filtered and poured into a mixture of aqueous sodium bicarbonate and dichloromethane. The organic solution was washed with water, dried, and evaporated. The crude product was chromatographed on a column of silica gel (toluene–ethyl acetate, 4:1) to provide pure disaccharide **24** as a white foam (0.289 g, 61%) and 20 mg (11%) of starting alcohol **22**. The analytical sample of compound **24** was recrystallized from ether–hexane and had mp 110–111°C, $[\alpha]_D$ +1.5 (*c* 0.6, chloroform); ^{1}H nmr ($CDCl_3$) δ: 7.80 (d, 2H) and 7.37–7.23 (m, 17H, 3Ph, C_6H_4), 5.31 (dd, 1H, $J_{1b,2b}$ 8.0 Hz, $J_{2b,3b}$ 10.0 Hz, H-2b), 4.91 and 4.59 (AB, 2H, $J_{A,B}$ 11.5 Hz, CH_2Ph), 4.66 and 4.51 (AB, 2H, $J_{A,B}$ 12.0 Hz, CH_2Ph), 4.41 (s, 2H, CH_2Ph), 4.36 (d, 1H, H-1b), 4.22 (dd, 1H, $J_{1a,2aeq}$ 2.0 Hz, $J_{1a,2aax}$ 9.0 Hz, H-1a), 4.17 (dd, 1H, $J_{6aA,6aB}$ 11.0 Hz, $J_{5a,6aA}$ 2.0 Hz, H-6aA), 4.15 (dd, 1H, $J_{5a,6aB}$ 3.5 Hz, H-6aB), 3.91 (d, 1H, $J_{3b,4b}$ 2.7 Hz, H-4b), 3.58–3.53 (m, 3H, H-5b, 2H-6b), 3.49 (dd, 1H, H-3b), 3.46–3.33 (m, 2H, H-4a, H-5a), 3.30 (s, 3H, OCH_3), 2.42 (s, 3H, CH_3 of Ts), 2.19 (m, 1H, H-3aeq), 2.08 (s, 3H, CH_3CO), 1.77 (m, 1H, H-2aeq), 1.57 (m, 1H, H-3aax), 1.40 (m, 1H, H-2aax). Anal. calcd. for $C_{43}H_{50}O_{12}S$: C 65.30, H 6.37, S 4.04; found: C 65.68, H 6.50, S 3.90.

*Methyl 2,3-dideoxy-6-O-p-toluenesulfonyl-4-O-(3,4,6-tri-O-benzyl-β-D-galactopyranosyl)-β-D-*erythro*-hexopyranoside (25)*

A solution of acetate **24** (82 mg, 0.104 mmol) in methanolic 0.1 M sodium methoxide (4.4 mL) and dichloromethane (0.7 mL) was kept overnight at room temperature. It was neutralized with Amberlite IRC-50 (H^+) and evaporated. The crude product was purified on a column of silica gel (toluene–ethyl acetate, 4:1) to provide pure alcohol **25** (70 mg, 90%) as a white foam; $[\alpha]_D$ −14 (*c* 0.5, chloroform); ^{1}H nmr ($CDCL_3$) δ: 7.80 (d, 2H) and 7.36–7.24 (m, 17H, 3Ph, C_6H_4), 4.87 and 4.62 (AB, 2H, $J_{A,B}$ 11.5 Hz, CH_2Ph), 4.72 and 4.69 (AB, 2H, $J_{A,B}$ 11.5 Hz, CH_2Ph), 4.43 (s, 2H, CH_2Ph), 4.37 (dd, $J_{5a,6aA}$ 4.0 Hz, $J_{6aA,6aB}$ 10.5 Hz, H-6aA), 4.31–4.26 (2dd, d, 3H, $J_{5a,6aB}$ 2.0 Hz, H-6aB, $J_{1a,2aeq}$ 2.0 Hz, $J_{1a,2aax}$ 7.0 Hz, H-1a, $J_{1b,2b}$ 7.5 Hz, H-1b), 3.88 (d overlapped by ddd, 2H, $J_{3b,4b}$ 2.5 Hz, H-4b, $J_{2b,3b}$ 10.0 Hz, $J_{2b,OH}$ 3.0 Hz, H-2b), 3.57 (bs, 3H, H-5b, 2H-6b), 3.52 (m, 1H, H-5a), 3.50 (m, 1H, H-4a), 3.40 (dd, 1H, H-3b), 3.39 (s, 3H, OCH_3), 2.67 (d, 1H, OH), 2.42 (s, 3H, CH_3 of Ts), 2.22 (m, 1H, H-3aeq), 1.81 (m, 1H, H-2aeq), 1.69–1.57 (m, 1H, H-3aax), 1.46 (m, 1H, H-2aax). Anal. calcd. for $C_{41}H_{48}O_{11}S$: C 65.76, H 6.46, S 4.28; found: C 65.55, H 6.59, S 4.33.

*Methyl 2,3-dideoxy-6-O-p-toluenesulfonyl-4-O-[3,4,6-tri-O-benzyl-2-O-(2,3,4-tri-O-benzyl-α-L-fucopyranosyl)-β-D-galactopyranosyl]-β-D-*erythro*-hexopyranoside (26)*

A solution of bromide **11** (0.981 mmol) in dichloromethane (1 mL) was added to a stirred mixture of alcohol **25** 0.245 g, 0.327 mmol), tetraethylammonium bromide (0.069 g, 0.327 mmol), dichloromethane (1 mL), *N*,*N*-dimethylformamide (0.4 mL), and 4Å molecular sieves (1 g, powdered). Stirring under nitrogen was continued for 27 h. Then methanol (1 mL) was added and the mixture was stirred for another 2 h. It was diluted with dichloromethane, filtered through Celite, washed with aqueous sodium bicarbonate, water, then dried and evaporated. The residue was chromatographed on a column of silica gel (hexane–ethyl acetate, 3:1, 3:2) to provide in the main fraction pure compound **26** (0.248 g, 65%) as a white foam; $[\alpha]_D$ −34.5 (*c* 0.5, chloroform); ^{1}H nmr ($CDCl_3$) δ: 7.78 (d, 2H) and 7.36–7.00 (m, 32H, 6Ph, C_6H_4), 5.69 (d, 1H, $J_{1c,2c}$ 3.5 Hz, H-1c), 4.95–4.42 (m, 12H, $6CH_2$Ph), 4.39 (d, 1H, $J_{1b,2b}$ 7.5 Hz, H-1b), 4.33 (dd, 1H, $J_{5a,6aA}$ 3.5 Hz, $J_{6aA,6aB}$ 10.0 Hz, H-6aA), 4.30 (q, 1H, $J_{5c,6c}$ 6.5 Hz, H-5c), 4.28 (dd, 1H, $J_{1a,2aeq}$ 2.0 Hz, $J_{1a,2aax}$ 7.0 Hz, H-1a), 4.17 (dd, 1H, $J_{2b,3b}$ 10.0 Hz, H-2b), 4.11 (dd, 1H, $J_{5a,6aB}$ 6.5 Hz, H-6aB), 4.01 (dd, 1H, $J_{2c,3c}$ 10.0 Hz, H-2c), 3.97 (dd, 1H, $J_{3c,4c}$ 2.0 Hz, H-3c), 3.88 (d, 1H, $J_{3b,4b}$ 2.5 Hz, H-4b), 3.81 (d, 1H, H-4c), 3.67 (dd, 1H, H-3b), 3.62–3.50 (m, 4H, H-5a, H-5b, 2H-6b), 3.42 (m, 1H, H-4a), 3.31 (s, 3H, OCH_3), 2.37 (s, 3H, CH_3 of Ts), 2.12 (m, 1H, H-3aeq), 1.84 (m, 1H, H-2aeq), 1.62 (m, 1H, H-3aax), 1.44 (m, 1H, H-2aax), 1.13 (d, 3H, 3H-6c). Anal. calcd. for $C_{68}H_{76}O_{15}S$: C 70.08, H 6.57, S 2.75; found: C 69.94, H 6.77, S 2.81.

From the minor fractions starting alcohol **25** (15 mg, 6%) was isolated, as well as methyl 6-bromo-2,3,6-trideoxy-4-*O*-[3,4,6-tri-*O*-benzyl-2-*O*-(2,3,4-tri-*O*-benzyl-α-L-fucopyranosyl)-β-D-galactopyranosyl]-β-D-*erythro*-hexopyranoside (15 mg, 4%); ^{1}H nmr ($CDCl_3$) δ: 7.35–6.95 (m, 30H, 6Ph), 5.17 (d, 1H, $J_{1c,2c}$ 3.5 Hz, H-1c), 4.96–4.42 (m, 13H, $6CH_2$Ph, at 4.45 d, 1H, $J_{1b,2b}$ 8.0 Hz, H-1b), 4.37 (dd, 1H, $J_{1a,2aeq}$ 2.0 Hz, $J_{1a,2aax}$ 8.0 Hz, H-1a), 4.26 (q, 1H, $J_{5c,6c}$ 6.5 Hz, H-5c), 4.21 (dd, 1H, $J_{2b,3b}$ 9.5 Hz, H-2b), 4.03 (dd, 1H, $J_{2c,3c}$ 10.0 Hz, H-2c), 3.95 (dd, 1H, $J_{3c,4c}$ 2.5 Hz, H-3c), 3.91 (d, 1H, $J_{3b,4b}$ 2.8 Hz, H-4b), 3.86 (d, 1H, H-4c), 3.73 (dd, 1H, $J_{6aA,6aB}$ 9.5 Hz, $J_{5a,6aA}$ 2.0 Hz, H-6aA), 3.70 (dd, 1H, H-3b), 3.60–3.52 (m, 3H, H-5b, 2H-6b), 3.50 (s, 3H, OCH_3), 3.47–3.36 (m, 3H, H-6aB, H-5a, H-4a), 2.21 (m, 1H, H-3aeq), 1.87 (m, 1H, H-2aeq), 1.69–1.49 (m, 2H, H-3aax, H-2aax), 1.16 (d, 3H, 3H-6c).

*Methyl 6-O-benzoyl-2,3-dideoxy-4-O-[3,4,6-tri-O-benzyl-2-O-(2,3,4-tri-O-benzyl-α-L-fucopyranosyl)-β-D-galactopyranosyl]-β-D-*erythro*-hexopyranoside (27)*

A mixture of tosylate **26** (0.175 g, 0.15 mmol), sodium benzoate (0.108 g, 0.75 mmol), and *N*,*N*-dimethylformamide (2 mL) was heated at 100°C with stirring for 4.5 h. After cooling, it was diluted with dichloromethane, the solution was washed twice with water, dried, and evaporated. The crude product was chromatographed on a column of silica gel (hexane–ethyl acetate, 3:1) to provide pure **27** (0.112 g, 68%) as a white foam; $[\alpha]_D$ −49 (*c* 0.5, chloroform); ^{1}H nmr ($CDCl_3$) δ: 8.02–6.96 (m, 35H, 7Ph), 5.70 (d, 1H, $J_{1c,2c}$ 2.5 Hz, H-1c), 4.85–4.43 (m, 12H, $6CH_2$Ph), 4.69 (dd, 1H, $J_{6aA,6aB}$ 11.0 Hz, $J_{6aA,5a}$ 3.0 Hz, H-6aA), 4.51 (d, 1H, $J_{1b,2b}$ 7.5 Hz, H-1b), 4.41 (q, 1H, overlapped, $J_{5c,6c}$ 6.0 Hz, H-5c), 4.36 (dd, 1H, overlapped, $J_{5a,6aB}$ 7.5 Hz, H-6aB), 4.40 (dd, 1H, overlapped, $J_{1a,2aax}$ ~ 7.0 Hz, $J_{1a,2aeq}$ ~ 2.5 Hz, H-1a), 4.22 (dd, $J_{2b,3b}$ 9.5 Hz, H-2b), 4.02–3.95 (m, 2H, H-2c, H-3c), 3.90 (d, 1H, $J_{3b,4b}$ 2.5 Hz, H-4b), 3.74 (dt, $J_{5a,6aA}$ ~ $J_{4a,5a}$ ~ 7.5 Hz, H-5a), 3.71 (d, 1H, $J_{3c,4c}$ 1.5 Hz, H-4c), 3.69 (dd, 1H, H-3b), 3.61–3.52 (m, 4H, H-4a, H-5b, 2H-6b), 3.43 (s, 3H, OCH_3), 2.28 (m, 1H, H-3aeq), 1.89 (m, 1H, H-2aeq), 1.69 (m, 1H, H-3aax), ~1.55 (m, 1H, H-2aax), 1.15 (d, 3H, 3H-6c). Anal. calcd. for $C_{68}H_{74}O_{14}$: C 73.23, H 6.69; found: 72.97, H 6.81.

*Methyl 2,3-dideoxy-4-O-[3,4,6-tri-O-benzyl-2-O-(2,3,4-tri-O-benzyl-α-L-fucopyranosyl)-β-D-galactopyranosyl]-β-D-*erythro*-hexopyranoside (28)*

Compound **27** (75 mg, 0.067 mmol) was debenzoylated in methanolic 0.5 M sodium methoxide (1.3 mL) at room temperature for 21 h. Then it was diluted with methanol, neutralized with Amberlite IRC-50 (H^+), filtered, and evaporated. Purification was achieved by column chromatography on silica gel (hexane–ethyl acetate, 3:2) to afford pure **28** (60 mg, 89%) as a colourless syrup; $[\alpha]_D$ −50 (*c* 0.5, chloroform); ^{1}H nmr ($CDCl_3$) δ: 7.38–6.99 (m, 30H, 6Ph), 5.70 (d, 1H, $J_{1c,2c}$ 3.5 Hz, H-1c), 4.97–4.43 (m, 12H, $6CH_2$Ph, 4.45 (d, 1H, $J_{1b,2b}$ 7.5 Hz, H-1b), 4.37 (dd, 1H, $J_{1a,2aax}$ 8.0 Hz, $J_{1a,2aeq}$ 2.0 Hz, H-1a), 4.29 (q, 1H, $J_{5c,6c}$ 6.5 Hz, H-5c),

Can. J. Chem. Downloaded from www.nrcresearchpress.com by 123.30.183.119 on 09/08/12
For personal use only.

4.19 (dd, 1H, $J_{2b,3b}$ 9.5 Hz, H-2b), 4.01 (dd, 1H, $J_{2c,3c}$ 10.0 Hz, H-2c), 3.92 (dd, 1H, $J_{3c,4c}$ 2.5 Hz, H-3c), 3.91 (d, 1H, $J_{3b,4b}$ 3.5 Hz, H-4b), 3.76 (m, 1H, $J_{6aA,6aB}$ 11.0 Hz, $J_{6aA,OH}$ 6.0 Hz, H-6aA), 3.72–3.64 (m, 3H, H-4c, H-6aB, H-3b), 3.59–3.49 (m, 4H, H-5b, 2H-6b, H-4a), 3.48 (s, 3H, OCH_3), 3.28 (ddd, 1H, $J_{4a,5a}$ 9.0 Hz, $J_{5a,6aA}$ 2.5 Hz, $J_{5a,6aB}$ 4.0 Hz, H-5a), 2.22 (m, 1H, H-3eq), 1.97 (dd, 1H, $J_{6aA,OH} \sim J_{6aB,OH}$ 6.0 Hz, OH), 1.85 (m, 1H, H-2aeq), 1.67–1.43 (m, 2H, H-3aax, H-2aax), 1.15 (d, 3H, 3H-6c).

*Methyl 2,3,6-trideoxy-4-*O*-[3,4,6-tri-*O*-benzyl-2-*O*-(2,3,4-tri-*O*-benzyl-α-L-fucopyranosyl)-β-D-galactopyranosyl]-β-D-*erythro*-hexopyranoside (29)*

A mixture of tosylate **26** (122 mg, 0.105 mmol), lithium aluminium hydride (10 mg, 0.26 mmol), and tetrahydrofuran (1.2 mL) was boiled under reflux for 2 h. After cooling, ethyl acetate (0.5 mL) was added and the mixture was poured into ice-water. The precipitate formed was filtered off and dissolved in dichloromethane. The organic solution was washed twice with water, dried, and evaporated. The crude product was purified on a column of silica gel (hexane–ethyl acetate, 3:1) to provide pure **29** (78 mg, 75%) as a white foam; $[\alpha]_D$ −60 (*c* 0.5, chloroform); ^{1}H nmr ($CDCl_3$) δ: 7.36–7.00 (m, 30H, 6Ph), 5.72 (d, 1H, $J_{1c,2c}$ 3.5 Hz, H-1c), 4.97–4.41 (m, 12H, 6CH_2Ph), 4.49 (d, 1H, $J_{1b,2b}$ 7.5 Hz, H-1b), 4.34 (q, 1H, $J_{5c,6c}$ 6.5 Hz, H-5c), 4.29 (dd, 1H, $J_{1a,2aeq}$ 2.0 Hz, $J_{1a,2aax}$ 8.0 Hz, H-1a), 4.20 (dd, 1H, $J_{2b,3b}$ 9.5 Hz, H-2b), 4.01 (dd, 1H, $J_{2c,3c}$ 10.0 Hz, H-2c), 3.73 (dd, d, 2H, $J_{3c,4c}$ 2.5 Hz, H-3c, overlapped by d, $J_{3b,4b}$ 2.5 Hz, H-4b), 3.70 (dd, 1H, H-3b), 3.62 (d, 1H, H-4c), 3.61–3.43 (m, 3H, H-5b, 2H-6b), 3.46 (s, 3H, OCH_3), 3.28–3.17 (m, 2H, H-4a, H-5a), 2.18 (m, 1H, H-3aeq), 1.83 (m, 1H, H-2aeq), 1.52 (m, 2H, H-3aax, H-2aax), 1.24 (d, 3H, $J_{5a,6a}$ 5.5 Hz, 3H-6a), 1.12 (d, 3H, 3H-6c). Anal. calcd. for $C_{61}H_{70}O_{12}$: C 73.62, H 7.09; found: C 73.43, H 7.31.

*Methyl 2,3-dideoxy-4-*O*-[2-*O*-(α-L-fucopyranosyl)-β-D-galactopyranosyl]-β-D-*erythro*-hexopyranoside (30)*

Compound **28** (102 mg, ~0.1 mmol) was hydrogenated in ethanol (6 mL) over 5% palladium-on-carbon (102 mg) at 20 psi for 3 h. The catalyst was removed by filtration. A drop of triethylamine was added to the filtrate and the solvent was evaporated. The product was applied to a column of Bio-Gel P-2 and eluted with 10% ethanol in water. Freeze-drying an aqueous solution provided pure **30** (42 mg, 88%) as a white powder; $[\alpha]_D$ −82.5 (c 0.6, water). The ^{1}H and ^{13}C nmr data are reported in Tables 1 and 2.

*Methyl 2,3,6-trideoxy-4-*O*-[2-*O*-(α-L-fucopyranosyl)-β-D-galactopyranosyl]-β-D-*erythro*-hexopyranoside (31)*

Compound **29** (97 mg, 0.097 mmol) was hydrogenated in ethanol (5.2 mL) over 5% palladium-on-carbon (97 mg) and then purified as described for the preparation of **30**. Pure **31** was obtained as a white powder (33 mg, 75%) after freeze-drying an aqueous solution; $[\alpha]_D$ −96.5 (*c* 0.5, water). The ^{1}H and ^{13}C nmr data are reported in Tables 1 and 2.

DL-(1,5/2)-2,5-Diacetoxycyclohexane carboxylic acid (33)

(±) *endo*-7-Oxabicyclo[2,2,1]-heptane-2-carboxylic acid (**32**, 13.6 g, 0.1 mol) (29) was heated in a mixture of 85% acetic acid (225 mL), acetic anhydride (113 mL), and sulfuric acid (9 mL) for 20 h at 80°C (28). Then sodium acetate trihydrate (18 g) was added and the slightly brown mixture was evaporated. The remainder was taken up in dichloromethane, the mixture washed with water, and the organic solution evaporated to leave a crystalline residue. The material was treated with charcoal in ethanol, followed by filtration, evaporation, and recrystallization from dichloromethane/ether to provide pure **33** (8.2 g, 35%), mp 154–155°C; ^{1}H nmr ($CDCl_3$) δ: 5.03 (dt, 1H, $J_{1,2}$ 10.0 Hz, $J_{2,3ax}$ 10.0 Hz, $J_{2,3eq}$ 4.5 Hz, H-2), 4.79 (m, 1H, H-5), 2.68 (ddd, 1H, $J_{1,6ax}$ 11.5 Hz, $J_{1,6eq}$ 4.5 Hz, H-1), 2.28 (m, 1H, $J_{6eq,6ax}$ 13.5 Hz, H-6eq), 2.18 (m, 1H, H-3eq), 2.04, 2.03 (2s, each 3H, 2CH_3CO), ~2.01 (overlapped, H-4eq), 1.81 (q, 1H, $J_{6ax,5}$ 11.0 Hz, H-6ax), 1.56 (m, 1H, $J_{4ax,5}$ ~11 Hz, H-4ax), 1.47 (m, 1H, H-3ax). Anal. calcd. for $C_{11}H_{16}O_6$: C 54.09, H 6.60; found: C 53.76, H 6.59.

*DL-(1,5/4)-4,7-*O*-Benzylidene-5-*C*-hydroxymethyl-1,4-cyclohexanediol (35)*

A 1 M borane solution in tetrahydrofuran (65 mL, 65 mmol) was added to a stirring solution of the diacetate **33** (4.9 g, 20.1 mmol) in tetrahydrofuran (15 mL) under argon at ice-bath temperature. After the gas evolution ceased, the mixture was kept at room temperature for 48 h. Then methanol (5 mL) was added, followed by evaporation and codistillation with methanol–acetic acid 1:1. The residue, diol **34**, was dried for 2 h at 70°C in an oil pump vacuum and was then taken up in acetonitrile (120 mL). *p*-Toluenesulfonic acid (700 mg) and α,α-dimethoxytoluene (3.8 mL, 25.3 mmol) were added to the turbid suspension. After 15 min, it was neutralized with triethylamine, evaporated, and the residue dissolved in dichloromethane. Washing with water, evaporation of the organic solution, and co-distillation with water and ethanol left a white solid, which was recrystallized from dichloromethane–ether–hexane to provide pure **35** (4.0 g, 85%), mp 126–126.5°C; ^{1}H nmr ($CDCl_3$) δ: 7.5–7.3 (m, 5H, Ph), 5.54 (s, 1H, C*H*Ph), 4.08 (dd, 1H, $J_{7eq,7ax}$ 11.0 Hz, $J_{7eq,5}$ 4.3 Hz, H-7eq), 3.77 (tt, 1H, $J_{1,2ax} \sim J_{1,6ax} \sim$ 11.5 Hz, $J_{1,2eq} \sim J_{1,6eq} \sim$ 4.5 Hz, H-1), 3.62 (t, 1H, $J_{7ax,5}$ 11.0 Hz, H-7ax), 3.47 (dt, 1H, $J_{4,3ax} \sim J_{4,5} \sim$ 11 Hz, $J_{4,3eq}$ 4.0 Hz, H-4), 2.09 (m, 1H, overlapped by H-3eq, H-2eq), 2.04 (m, 1H, H-3eq), 1.82 (m, 2H, H-5, H-6eq), 1.58 (m, 2H, H-3ax, OH), 1.41 (m, 1H, H-2ax), 1.04 (q, 1H, $J_{6ax,6eq} \sim J_{6ax,5} \sim J_{6ax,1} \sim$ 12 Hz, H-6ax). Anal. calcd. for $C_{14}H_{18}O_3$: C 71.77, H 7.74; found: C 71.39, H 7.78.

*DL-(1,5/4)-4,7-*O*-Benzylidene-1-*O*-methyl-5-*C*-hydroxymethyl-1,4-cyclohexanediol (36)*

Sodium hydride (1.5 g, ~50% oily suspension, 31.3 mmol) was added to a stirring solution of compound **35** (4.7 g, 20.1 mmol) in *N*,*N*-dimethylformamide (40 mL) at 0°C. After 30 min, methyliodide (2 mL, 32.1 mmol) was added and stirring continued for 1 h. After the addition of methanol (1 mL), the mixture was evaporated, the residue taken up in dichloromethane, and the solution washed with water and evaporated. The crystalline material was filtered through a column of silica gel (hexane–ethyl acetate, 3:1) to provide pure **36** (4.2 g, 84%). The analytical sample was recrystallized from ether–hexane, mp 63.5°C; ^{1}H nmr ($CDCl_3$) δ: 7.53–7.30 (m, 5H, Ph), 5.56 (s, 1H, C*H*Ph), 4.12 (dd, 1H, $J_{7eq,7ax}$ 11.3 Hz, $J_{5,7eq}$ 4.5 Hz, H-7eq), 3.63 (t, 1H, $J_{5,7ax}$ 11.3 Hz, H-7ax), 3.47 (dt, 1H, $J_{4,5} \sim J_{3ax,4} \sim$ 11 Hz, $J_{3eq,4}$ 4.3 Hz, H-4), 3.36 (s, 3H, OCH_3), 3.28 (tt, 1H, $J_{1,2ax} \sim J_{1,6ax} \sim$ 11 Hz, $J_{1,2eq} \sim J_{1,6eq} \sim$ 4.3 Hz, H-1), 2.19 (m, 1H, $J_{2eq,2ax}$ 13.0 Hz, H-2eq), 2.06 (ddd, 1H, $J_{3eq,3ax}$ 12.5 Hz, $J_{2ax,3eq}$ 7.5 Hz, H-3eq), 1.92 (m, $J_{6eq,6ax}$ 12.0 Hz, H-6eq), 1.77 (m, 1H, H-5), 1.56 (ddd, 1H, $J_{3ax,2ax} \sim$ 12 Hz, $J_{3ax,2eq}$ 3.8 Hz, H-3ax), 1.32 (ddd, 1H, H-2ax), 0.94 (q, 1H, $J_{6ax,5} \sim$ 11.5 Hz, H-6ax). Anal. calcd. for $C_{15}H_{20}O_3$: C 72.55, H 8.12; found: C 72.37, H 8.23.

*DL-(1,5/4)-1-*O*-Methyl-5-*C*-hydroxymethyl-1,4-cyclohexanediol (37)*

A mixture of compound **36** (3.83 g, 15.4 mmol) and 20% palladium-on-carbon (0.95 g) in 95% ethanol (100 mL) was hydrogenated in the hydrogen stream at 15 psi for 4 h. The catalyst was removed by filtration and the solvent evaporated to provide pure diol **37** (2.45 g, 99%) as a colourless syrup; ^{1}H nmr ($CDCl_3$) δ: 4.35 (bs, 1H, OH), 4.13 (bs, 1H, OH), 3.72 (dd, 1H, $J_{7eq,7ax}$ 11.0 Hz, $J_{5,7eq}$ 4.3 Hz, H-7eq), 3.67 (t, 1H, $J_{7ax,5}$ 10.0 Hz, H-7ax), 3.55 (dt, 1H, $J_{3ax,4}$ 11.0 Hz, $J_{4,5}$ 11.0 Hz, $J_{3eq,4}$ 4.5 Hz, H-4), 3.34 (s, 3H, OCH_3), 3.22 (tt, 1H, $J_{1,2ax} \sim J_{1,6ax} \sim$ 11 Hz, $J_{1,2eq} \sim J_{1,6eq} \sim$ 4.3 Hz, H-1), 2.08 (m, 1H, $J_{2eq,2ax}$ 12.5 Hz, H-2eq), 1.99 (m, 1H, overlapped by H-6eq, H-3eq), 1.92 (m, 1H, H-6eq), 1.38 (ddd, 1H, $J_{3ax,3eq} \sim$ 13 Hz, $J_{2ax,3ax} \sim$ 11.5 Hz, H-3ax), 1.20 (ddd, 1H, H-2ax), 0.92 (q, 1H, $J_{6ax,6eq} \sim J_{6ax,5} \sim$ 12 Hz, H-6ax). Anal. calcd. for $C_{18}H_{16}O_3$: C 59.98, H 10.07; found: C 59.98, H 10.11.

*DL-(1,5/4)-1-*O*-Methyl-5-*C*-(p-toluenesulfonyloxy)methyl-1,4-cyclohexanediol (38)*

p-Toluenesulfonyl chloride (1.221 g, 6.4 mmol) was added to a solution of diol **37** (0.933 g, 5.82 mmol) in dry pyridine (12 mL) at 0°C. The mixture was stirred at 0°C for 1.5 h. Then more chlo-

Can. J. Chem. Downloaded from www.nrcresearchpress.com by 123.30.183.119 on 09/08/12
For personal use only.

ride (0.6 g, 3.15 mmol) was added and stirring continued for 2 h. The reaction was quenched by the addition of water (1 mL). After 2.5 h at room temperature, it was poured into ice-water. The precipitate was filtered off and washed with water. The filtrate was extracted with chloroform and the combined extracts were washed with water, dried, and evaporated to leave pure **38** (1.29 g, 70%) as a colourless syrup. The precipitate was chromatographed on a column of silica gel (chloroform–ethyl acetate, 4:1) to provide 0.42 g (16%) of DL-(1,5/4)-1-*O*-methyl-4-*O*-*p*-toluenesulfonyl-5-*C*-(*p*-toluenesulfonyloxy)methyl-1,4-cyclohexanediol (**38***a*) and 25 mg of **38** (total yield 72%). The analytical sample of **38** was recrystallized from ether–hexane, mp 82–83°C; ^{1}H nmr ($CDCl_3$) δ: 7.79 and 7.36 (2d, 4H, C_6H_4), 4.23 (dd, 1H, $J_{7A,7B}$ 10.0 Hz, $J_{7A,5}$ 5.0 Hz, H-7A), 4.06 (dd, 1H, $J_{7B,5}$ 3.5 Hz, H-7B), 3.47 (dt, 1H, $J_{4,3eq}$ 4.0 Hz, $J_{4,3ax} \sim J_{4,5}$ 10.0 Hz, H-4), 3.32 (s, 3H, OCH_3), 3.16 (tt, 1H, $J_{1,2ax} \sim J_{1,6ax} \sim$ 11 Hz, $J_{1,2eq} \sim J_{1,6eq} \sim$ 4 Hz, H-1), 2.46 (s, 3H, CH_3 of Ts), 2.08–1.97 (m, 3H, H-2eq, H-3eq, H-6eq), 1.86 (s, 1H, OH), 1.62 (m, 1H, H-5), 1.41–1.10 (m, 3H, H-2ax, H-6ax, H-3ax); ^{13}C nmr ($CDCl_3$) δ: 144.91, 132.69, 129.61, 127.92 (C_6H_4), 77.81 (C-4), 71.49 (C-7), 69.56 (C-1), 56.03 (CH_3O), 42.75 (C-5), 32.62, 32.58, 29.79 (C-2, C-3, C-6), 21.66 (CH_3 of Ts). Anal. calcd. for $C_{15}H_{22}O_5S$: C 57.31, H 7.05, S 10.20; found: C 57.33, H 6.93, S 10.29.

The ditosyl derivative **38***a* was recrystallized from ether–ethyl acetate; mp 81–82°C; ^{1}H nmr ($CDCl_3$) δ: 7.76 and 7.34 (4d, 8H, $2C_6H_4$), 4.30 (dt, 1H, $J_{4,5} \sim J_{4,3ax} \sim$ 10 Hz, $J_{4,3eq}$ 4.5 Hz, H-4), 3.95 (dd, 1H, $J_{7A,5}$ 4.0 Hz, $J_{7A,7B}$ 10.0 Hz, H-7A), 3.74 (dd, 1H, $J_{7B,5}$ 6.5 Hz, H-7B), 3.27 (s, 3H, OCH_3), 3.12 (m, 1H, H-1), 2.47 and 2.46 (2s, 6H, $2CH_3$ of Ts), 2.11–1.82 (m, 4H, H-2eq, H-3eq, H-6eq, H-5), 1.49 (m, 1H, H-3ax), 1.26 (m, 1H, H-2ax), 1.12 (m, 1H, H-6ax). Anal. calcd. for $C_{22}H_{28}O_7S_2$: C 56.39, H 6.02, S 13.68; found: C 57.02, H 6.27, S 13.03.

*(1S,4S,5R)-1-Methoxy-5-*C*-(*p*-toluenesulfonyloxy)methylcyclohex-4-yl- and (1R,4R,5S)-1-methoxy-5-*C*-(*p*-toluenesulfonyloxy)methylcyclohex-4-yl 2-*O*-acetyl-3,4,6-tri-*O*-benzyl-β-D-galactopyranoside (39 and 40)*

A mixture of alcohol **38** (0.218 g, 0.69 mmol), mercuric cyanide (0.354 g, 1.4 mmol), powdered calcium sulfate (0.16 g), and 4 Å molecular sieves (0.32 g) in nitromethane–toluene (1:1, 4.5 mL) was stirred under nitrogen for 1 h. Then a solution of bromide **23** (0.719 g, 1.29 mmol) in nitromethane–toluene (1:1, 4 mL) was added dropwise within 20 min. After 2 h, the reaction mixture was filtered and poured into a stirred mixture of aqueous sodium bicarbonate and dichloromethane. The organic solution was washed with water, dried, and evaporated. The resulting material was chromatographed on a column of silica gel (toluene–ethyl acetate, 4:1) to provide two pure compounds: **39** (0.121 g, 22%; R_f 0.34, toluene–ethyl acetate, 4:1) and **40** (0.096 g, 18%; R_f 0.29) as white foams, and a mixture of both (0.039 g). The analytical sample of compound **39** was recrystallized from ether–hexane to provide white needles, mp 97–98°C, $[\alpha]_D$ +20.5 (*c* 0.6, chloroform); ^{1}H-nmr ($CDCl_3$) δ: 7.78–7.22 (m, 19H, 3Ph, C_6H_4), 5.31 (dd, 1H, $J_{1b,2b}$ 8.0 Hz, $J_{2b,3b}$ 10.0 Hz, H-2b), 4.91 and 4.59 (AB, 2H, $J_{A,B}$ 11.5 Hz, CH_2Ph), 4.66 and 4.51 (AB, 2H, $J_{A,B}$ 12.0 Hz, CH_2Ph), 4.42 (s, 2H, CH_2Ph), 4.35 (d, 1H, H-1b), 4.10 (dd, 1H, $J_{7aA,7aB}$ 9.5 Hz, $J_{5a,7aA}$ 5.5 Hz, H-7aA), 3.98 (dd, 1H, $J_{5a,7aB}$ 3.0 Hz, H-7aB), 3.91 (d, 1H, $J_{3b,4b}$ 2.7 Hz, H-4b), 3.60–3.51 (m, 3H, H-5b, 2H-6b), 3.48 (dd, 1H, H-3b), 3.31 (dt, 1H, overlapped, $J_{4a,5a} \sim J_{4a,3aax} \sim$ 9.5 Hz, $J_{4a,3aeq}$ 4.5 Hz, H-4a), 3.26 (s, 3H, overlapped, OCH_3), 3.03 (m, 1H, H-1a), 2.42 (s, 3H, CH_3 of Ts), 2.17 (m, 1H, H-3aeq), 2.08–1.83 (m, 2H, H-6aeq, H-2aeq overlapped by s, 3H at 2.05, CH_3CO), 1.70 (m, 1H, H-5a), 1.38 (m, 1H, H-3aax), 1.19–0.98 (m, 2H, H-2aax, H-6aax). Anal. calcd. for $C_{44}H_{52}O_{11}S$: C 66.99, H 6.64, S 4.06; found: C 67.23, H 6.50, S 4.21.

Compound **40** had $[\alpha]_D$ +8 (*c* 0.78, chloroform); ^{1}H nmr ($CDCl_3$) δ: 7.74–7.17 (m, 19H, 3Ph, C_6H_4), 5.18 (dd, 1H, $J_{1b,2b}$ 8.0 Hz, $J_{2b,3b}$ 10.0 Hz, H-2b), 4.92 and 4.60 (AB, 2H, $J_{A,B}$ 11.5 Hz, CH_2Ph), 4.65 and 4.48 (AB, 2H, $J_{A,B}$ 12.0 Hz, CH_2Ph), 4.51 and 4.45 (AB, 2H, $J_{A,B}$ 12.0 Hz, CH_2Ph), 4.29 (d, 1H, H-1b), 4.13 (dd, 1H, $J_{7aA,7aB}$ 9.5 Hz, $J_{5a,7aA}$ 3.5 Hz, H-7aA), 4.03 (dd, 1H, $J_{5a,7aB}$ 6.5 Hz, H-7aB), 3.97 (d, 1H, $J_{3b,4b}$ 2.7 Hz, H-4b), 3.70 (dd, 1H, $J_{6bA,6bB} \sim J_{6bA,5b}$ 8.5 Hz, H-6bA), 3.65 (dd, 1H, $J_{6bB,5b}$ 5.0 Hz, H-6bB), 3.53 (m, 1H, H-5b), 3.48 (dd, 1H, H-3b), 3.38 (dt, 1H, $J_{4a,3aeq} \sim$ 4.0 Hz, $J_{4a,5a} \sim J_{4a,3aax} \sim$ 10 Hz, H-4a), 3.28 (s, 3H, OCH_3), 3.08 (m, 1H, H-1a), 2.31 (s, 3H, CH_3 of Ts), 2.12–1.89 (m, 3H, H-3aeq, H-2aeq, H-6aeq, overlapped by s, 3H at 1.98, CH_3CO), 1.65 (m, 1H, H-5a), 1.20–1.02 (m, 3H, H-2aax, H-3aax, H-6aax).

*(1S,4S,5R)-1-Methoxy-5-*C*-(p-toluenesulfonyloxy)methylcyclohex-4-yl 3,4,6-tri-*O*-benzyl-β-D-galactopyranoside (41)*

Acetate **39** (137 mg, 0.174 mmol) was deacetylated in methanolic 0.11 M sodium methoxide (4.5 mL) at room temperature for 26 h. The solution was neutralized with Amberlite IRC-50 (H^+), filtered, and evaporated. The resulting material was chromatographed on a column of silica gel (toluene–ethyl acetate, 4:1) to provide pure **41** as a white foam (80 mg, 62%); $[\alpha]_D$ +1 (*c* 0,5 chloroform); ^{1}H nmr ($CDCl_3$) δ: 7.78 (d, 2H) and 7.39–7.22 (m, 17H, 3Ph and C_6H_4), 4.87 and 4.61 (AB,2H, $J_{A,B}$ 11.5 Hz, CH_2Ph), 4.73 and 4.69 (AB, 2H, $J_{A,B}$ 11.5 Hz, CH_2Ph), 4.43 (s, 2H, CH_2Ph), 4.41 (dd, 1H, $J_{7aA,5a}$ 5.0 Hz, $J_{7aA,7aB}$ 9.5 Hz, H-7aA), 4.27 (d, 1H, $J_{1b,2b}$ 8.0 Hz, H-1b), 3.97 (dd, 1H, $J_{7aB,5a}$ 3.0 Hz, H-7aB), 3.98 (ddd overlapped by d, 2H, $J_{2b,OH}$ 3.0 Hz, $J_{2b,3b}$ 9.5 Hz, H-2b, $J_{3b,4b}$ 3.0 Hz, H-4b), 3.57 (bs, 3H, H-5b, 2H-6b), 3.45 (dt, 1H, $J_{4a,5a} \sim J_{4a,3aax}$ 10.0 Hz, $J_{4a,3aeq}$ 4.0 Hz, H-4a), 3.40 (dd, 1H, H-3b), 3.29 (s, 3H, OCH_3), 3.10 (m, 1H, H-1a), 2.63 (d, 1H, OH), 2.42 (s, 3H, CH_3 of Ts), 2.19 (m, 1H, H-2aeq), 2.04–1.94 (m, 2H, H-2aeq, H-6aeq), 1.78 (m, 1H, H-5a), 1.41 (m, 1H, H-3aax), 1.27–1.08 (m, 2H, H-2aax, H-6aax). Anal. calcd. for $C_{42}H_{50}O_{10}S$: C 67.54, H 6.75, S 4.29; found: C 67.28, H 6.96, S 4.21.

A minor compound eluted from the column after **41** was found to be (1*S*,4*S*,5*R*)-1-methoxy-5-*C*-methoxymethylcyclohex-4-yl 3,4,6-tri-*O*-benzyl-β-D-galactopyranoside (**42**, 16 mg, 15%). It had $[\alpha]_D$ −7.5 (*c* 0.35, chloroform); ^{1}H nmr ($CDCl_3$) δ: 7.42–7.22 (m, 15H, 3Ph), 4.88 and 4.60 (AB, 2H, $J_{A,B}$ 12.0 Hz, CH_2Ph), 4.76 and 4.72 (AB, 2H, $J_{A,B}$ 12.0 Hz, CH_2Ph), 4.45 and 4.43 (AB, 2H, $J_{A,B}$ 12.0 Hz, CH_2Ph), 4.25 (d, 1H, $J_{1b,2b}$ 7.5 Hz, H-1b), 3.93 (ddd, 1H, $J_{2b,3b}$ 10.0 Hz, $J_{2b,OH}$ 1.0 Hz, H-2b), 3.88 (d, 1H, $J_{3b,4b}$ 3.0 Hz, H-4b), 3.63 (d, 1H, OH), 3.59 (bs, 3H, H-5b, 2H-6b), 3.52 (dd, 1H, $J_{7aA,7aB}$ 10.0 Hz, $J_{7aA,5a}$ 4.0 Hz, H-7aA), 3.44 (2dd, overlapped, $J_{7aB,5a}$ 5.0 Hz, H-7aB and H-3b), 3.40 (dt, overlapped, $J_{4a,5a} \sim J_{4a,3aax}$ 10.5 Hz, $J_{4a,3aeq}$ 4.0 Hz, H-4a), 3.34 and 3.33 (2s, each 3H, CH_3O and CH_2OCH_3), 3.61 (m, 1H, H-1a), 2.20 (m, 1H, H-3aeq), 2.19 (m, 2H, H-2aeq, H-6aeq), 1.80 (m, 1H, H-5a), 1.45 (m, 1H, H-3aax), 1.22–1.03 (m, 2H, H-2aax, H-6aax). The compound was acetylated (pyridine, acetic anhydride) and then recrystallized from ether–hexane. **42***a* had mp 91–92°C, $[\alpha]_D$ +22 (*c* 0.5, chloroform); ^{1}H nmr ($CDCl_3$) δ: 7.37–7.23 (m, 15H, 3Ph), 5.35 (dd, 1H, $J_{1b,2b}$ 7.8 Hz, $J_{2b,3b}$ 10.0 Hz, H-2b), 4.91 and 4.60 (AB, 2H, $J_{A,B}$ 11.5 Hz, CH_2Ph), 4.66 and 4.49 (AB, 2H, $J_{A,B}$ 12.0 Hz, CH_2Ph), 4.43 (s, 2H, CH_2Ph), 4.35 (d, 1H, H-1b), 3.92 (d, 1H, $J_{3b,4b}$ 2.5 Hz, H-4b), 3.61–3.52 (m, 3H, H-5b, 2H-6b), 3.48 (dd, 1H, H-3b), 3.39 (dd, 1H, $J_{5a,7aA}$ 6.0 Hz, $J_{7aA,7aB}$ 9.0 Hz, H-7aA), 3.31 and 3.29 (2s, each 3H, $2OCH_3$, overlapped by H-7aB and H-4a), 3.11 (m, 1H, H-1a), 2.20–1.93 (m, 6H, H-2aeq, H-3aeq, H-6aeq, and $COCH_3$ at 2.04), 1.64 (m, 1H, H-5a), 1.42 (m, 1H, H-3aax), 1.23–1.09 (m, 2H, H-2aax, H-6aax). Anal. calcd. for $C_{38}H_{48}O_9$: C 70.35, H 7.46; found: C 69.91, H 7.42.

*(1S,4S,5R)-5-*C*-Benzoyloxymethyl-1-methoxycyclohex-4-yl 3,4,6-tri-*O*-benzyl-β-D-galactopyranoside (43)*

A mixture of tosylate **41** (100 mg, 0.134 mmol) and sodium benzoate (100 mg, 0.694 mmol) in *N*,*N*-dimethylformamide (1.5 mL) was stirred at 80°C for 4 h. Then the mixture was diluted with dichloromethane, and the organic solution washed twice with water, dried, and evaporated. Chromatographic purification on a column of silica gel (hexane–ethyl acetate, 3:2) afforded pure **43**

Can. J. Chem. Downloaded from www.nrcresearchpress.com by 123.30.183.119 on 09/08/12
For personal use only.

(61 mg, 65%) as a white foam. It had $[\alpha]_D$ +8 (*c* 0.5, chloroform); ^{1}H nmr ($CDCl_3$) δ: 8.10–7.20 (m, 20H, 4Ph), 4.87 and 4.60 (AB, 2H, $J_{A,B}$ 11.5 Hz, CH_2Ph), 4.71 (s, overlapped by dd, 3H, $J_{A,B}$ 10.5 Hz, CH_2Ph, $J_{5a,7aA}$ 4.5 Hz, $J_{7aA,7aB}$ 11.0 Hz, H-7aA), 4.43 and 4.42 (AB, 2H, $J_{A,B}$ 12.0 Hz, CH_2Ph), 4.37 (dd, 1H, $J_{5a,7aB}$ 2.5 Hz, H-7aB), 4.28 (d, 1H, $J_{1b,2b}$ 7.5 Hz, H-1b), 3.97 (ddd, 1H, $J_{2b,3b}$ 10.0 Hz, $J_{2b,OH}$ 2.0 Hz, H-2b), 3.86 (d, 1H, $J_{3b,4b}$ 3.0 Hz, H-4b), 3.62–3.51 (m, 3H, H-5b, 2H-6b), 3.45 (dt, 1H, $J_{4a,3aeq}$ 4.0 Hz, $J_{4a,3aax} \sim J_{4a,5a}$ 10.0 Hz, H-4a), 3.40 (dd, 1H, H-3b), 3.35 (s, 3H, OCH_3), 3.20 (m, 1H, H-1a), 2.91 (d, 1H, OH), 2.29–2.17 (m, 2H, H-3aeq, H-6aeq), 2.06 (m, 1H, H-2aeq), 1.93 (m, 1H, H-5a), 1.49 (m, 1H, H-3aax), 1.39–1.15 (m, 2H, H-2aax, H-6aax).

*(1S,4S,5S)-1-Methoxy-5-*C*-methylcyclohex-4-yl 3,4,6-tri-*O*-benzyl-*β*-*D*-galactopyranoside (**44**)*

A mixture of tosylate **41** (67 mg, 0.09 mmol) and lithium aluminium hydride (10 mg, 0.27 mmol) in tetrahydrofuran (1.3 mL) was stirred under nitrogen at room temperature for 2 h. Then it was poured into ice-water and extracted with chloroform. The organic solution was washed twice with water, dried, and evaporated. Chromatography of the residue on a column of silica gel (hexane–ethyl acetate, 3:2) gave pure **44** (34 mg, 66%) as a colourless syrup; $[\alpha]_D$ +7 (*c* 0.5 chloroform); ^{1}H nmr ($CDCl_3$) δ: 7.38–7.24 (m, 15H, 3Ph), 4.88 and 4.61 (AB, 2H, $J_{A,B}$ 11.5 Hz, CH_2Ph), 4.72 and 4.67 (AB, 2H, $J_{A,B}$ 11.5 Hz, CH_2Ph), 4.45 (s, 2H, CH_2Ph), 4.29 (d, 1H, $J_{1b,2b}$ 7.5 Hz, H-1b), 3.95 (ddd, 1H, $J_{2b,3b}$ 10.0 Hz, $J_{2b,OH}$ 2.0 Hz, H-2b), 3.90 (d, 1H, $J_{3b,4b}$ 2.5 Hz, H-4b), 3.62–3.54 (m, 3H, H-5b, 2H-6b), 3.43 (dd, 1H, H-3b), 3.32 (s, 3H, OCH_3), 3.13 (m, 1H, overlapped, H-1a), 3.09 (dt, 1H, overlapped, $J_{4a,5a} \sim J_{4a,3aax} \sim$ 10.5 Hz, $J_{4a,3aeq}$ 4.5 Hz, H-4a), 2.34 (d, 1H, OH), 2.17 (m, 1H, H-3aeq), 2.07–1.97 (m, 2H, H-5aeq, H-6aeq), 1.59 (m, 1H, H-5a), 1.40 (m, 1H, H-3aax), 1.17 (m, 1H, H-2aax), 1.05 (d, 3H, $J_{5a,7a}$ 6.5 Hz, 3H-7), 0.98 (q, 1H, $J_{5a,6aax} \sim J_{6aax,6aeq} \sim J_{6aax,1a} \sim$ 12.0 Hz, H-6aax).

*(1S,4S-5R)-1-Methoxy-5-*C*-(p-toluenesulfonyloxy)methylcyclohex-4-yl- and (1S,4S,5S)-5-*C*-bromomethyl-1-methoxycyclohex-4-yl 3,4,6-tri-*O*-benzyl-2-*O*-(2,3,4-tri-*O*-benzyl-α-*L*-fucopyranosyl)-β-*D*-galactopyranoside (**45** and **46**)*

A solution of freshly prepared bromide **11** (0.38 mmol) in dichloromethane (0.5 mL) was added to a stirred mixture of alcohol **41** (79 mg, 0.106 mmol), tetraethylammonium bromide (23 mg, 0.109 mmol), dichloromethane (0.3 mL), *N*,*N*-dimethylformamide (0.12 mL), and powdered 4 Å molecular sieves. Stirring under nitrogen was continued for 21 h. Then methanol (0.5 mL) was added. After 2.5 h, the mixture was diluted with dichloromethane and filtered through a pad of Celite. The filtrate was washed with saturated aqueous sodium bicarbonate and water, dried, and evaporated. Subsequent chromatography on a column of silica gel (hexane–ethyl acetate, 3:1) afforded in the first main fraction compound **46** (59 mg, 52%) as a white foam; $[\alpha]_D$ −31.5 (*c* 0.6, chloroform); ^{1}H nmr ($CDCl_3$) δ: 7.37–6.94 (m, 30H, 6Ph), 5.71 (d, 1H, $J_{1c,2c}$ 3.5 Hz, H-1c), 4.96–4.41 (m, 13H, 6CH_2Ph, at 4.47 d, 1H, $J_{1b,2b}$ 7.5 Hz, H-1b), 4.30 (q, 1H, $J_{5c,6c}$ 6.5 Hz, H-5c), 4.22 (dd, 1H, $J_{2b,3b}$ 10.5 Hz, H-2b), 4.03 (dd, 1H, $J_{2c,3c}$ 10.5 Hz, H-2c), 3.95 (dd, 1H, $J_{3c,4c}$ 2.5 Hz, H-3c), 3.90 (d, 1H, $J_{3b,4b}$ 2.5 Hz, H-4b), 3.83 (d, 1H, H-4c), 3.70 (2dd, 2H, H-3b, $J_{5a,7aA}$ 3.0 Hz, $J_{7aA,7aB}$ 9.5 Hz, H-7aA), 3.60–3.51 (m, 3H, H-5b, 2H-6b), 3.35 (s, 3H, OCH_3), 3.29 (dt, 1H, $J_{4a,5a} \sim J_{4a,3aax}$ 10.0 Hz, $J_{4a,3aeq}$ 4.0 Hz, H-4a), 3.22 (dd, 1H, $J_{5a,7aB}$ 7.0 Hz, H-7aB), 3.15 (m, 1H, H-1a), 2.36 (m, 1H, H-3aeq), 2.20 (m, 1H, H-6aeq), 2.06 (m, 1H, H-2aeq), 1.62 (m, 1H, H-5a), 1.40 (m, 1H, H-3aax), 1.21 (m, 1H, H-2aax), 1.14 (d, 3H, 3H-6c), 1.04 (m, 1H, H-6aax); ^{13}C nmr ($CDCl_3$) δ: 102.92 (C-1b), 97.74 (C-1c), 69.13 (C-6b), 56.11 (CH_3O), 44.92 (C-5a), 36.67, 34.88, 31.59, 29.98 (C-2a, C-3a, C-6a, C-7a), 16.56 (CH_3-6c). Anal. calcd. for $C_{62}H_{71}BrO_{11}$: C 69.20, H 7.02; found: C 69.69, H 6.82.

Continued elution provided compound **45** (24 mg, 20%) as a colourless syrup; $[\alpha]_D$ −33 (*c* 0.45, chloroform); ^{1}H nmr ($CDCl_3$) δ: 7.77–7.03 (m, 34H, 6Ph and C_6H_4), 5.70 (d, 1H, $J_{1c,2c}$ 3.5 Hz, H-1c), 4.97–4.42 (m, 12H, 6CH_2Ph), 4.30 (d, 1H, $J_{1b,2b}$ 7.5 Hz, H-1b), 4.28 (q, 1H, $J_{5c,6c}$ 6.5 Hz, H-5c), 4.18 (dd, 1H, $J_{7aA,5a}$ 3.5 Hz, $J_{7aA,7aB}$ 9.5 Hz, H-7aA), 4.14 (dd, 1H, $J_{2b,3b}$ 10.0 Hz, H-2b), 4.08 (dd, 1H, $J_{5a,7aB}$ 6.5 Hz, H-7aB), 4.03 (dd, 1H, $J_{2c,3c}$ 10.0 Hz, H-2c), 3.96 (dd, 1H, $J_{3c,4c}$ 2.5 Hz, H-3c), 3.88 (d, 1H, $J_{3b,4b}$ 2.5 Hz, H-4b), 3.77 (d, 1H, H-4c), 3.60 (dd, 1H, H-3b), 3.56–3.44 (m, 3H, H-5b, 2H-6b), 3.38 (dt, 1H, $J_{4a,3aeq}$ 4.5 Hz, $J_{4a,5a} \sim J_{4a,3aax} \sim$ 9.0 Hz, H-4a), 3.25 (s, 3H, OCH_3), 3.06 (m, 1H, H-1a), 2.34 (s, 3H, CH_3 of Ts), 2.07 (m, 1H, H-3aeq), 1.99–1.86 (m, 2H, H-2aeq, H-6aeq), 1.68 (m, 1H, H-5a), 1.37 (m, 1H, H-3aax), 1.25–1.11 (m, 4H, H-2aax, overlapped by d at 1.12, 3H-6c), 1.01 (q, $J_{5a,6aax} \sim J_{6aeq,6aax} \sim J_{6aax,1a}$ 12.0 Hz, H-6aax); ^{13}C nmr ($CDCl_3$) δ: 102.13 (C-1b), 97.65 (C-1c), 71.37, 71.19 (*C*H_2Ph, C-7a), 69.02 (C-6b), 55.96 (CH_3O), 41.45 (C-5a), 32.24, 30.31, 29.06 (C-2a, C-3a, C-6a), 21.62 (CH_3 of Ts), 16.62 (CH_3-6c).

*(1S,4S,5R)-5-*C*-Benzoyloxymethyl-1-methoxycyclohex-4-yl 3,4,6-tri-*O*-benzyl-2-*O*-(2,3,4-tri-*O*-benzyl-α-*L*-fucopyranosyl)-β-*D*-galactopyranoside (**47**)*

*(a) By fucosylation of compound **43***

A solution of bromide **11** (0.297 mmol) in dichloromethane (0.4 mL) was added to a stirred mixture of alcohol **43** (62 mg, 0.089 mmol), tetraethylammonium bromide (19 mg, 0.09 mmol), dichloromethane (0.3 mL), *N*,*N*-dimethylformamide (0.1 mL), and powdered 4 Å molecular sieves (0.4 g). Stirring under nitrogen was continued for 24 h. Then methanol (0.1 mL) was added to the reaction mixture and after 2 h it was worked up as described for the preparation of **45**. Chromatographic purification on a column of silica gel (hexane–ethyl acetate, 3:1), provided **47** (63 mg, 64%) as a white foam, $[\alpha]_D$ −36.5 (*c* 0.5, chloroform); ^{1}H nmr ($CDCl_3$) δ: 8.01–6.94 (m, 35H, 7Ph), 5.70 (d, 1H, $J_{1c,2c}$ 3.5 Hz, H-1c), 4.86–4.42 (m, 15H, 6CH_2Ph, at 4.66, dd, 1H, $J_{7aA,7aB}$ 11.0 Hz, $J_{7aA,5a}$ 4.0 Hz, H-7A, at 4.53, d, 1H, $J_{1b,2b}$ 7.5 Hz, H-1b, ~4.44, m, H-5c, overlapped), 4.22 (dd, 1H, $J_{2b,3b}$ 10.5 Hz, H-2b), 4.19 (dd, 1H, $J_{5a,7aB}$ 8.0 Hz, H-7aB), 4.00 (dd, 1H, $J_{2c,3c}$ 10.5 Hz, H-2c), 3.98 (dd, 1H, $J_{3c,4c}$ 2.0 Hz, H-3c), 3.89 (d, 1H, $J_{3b,4b}$ 2.5 Hz, H-4b), 3.73 (d, 1H, H-4c), 3.69 (dd, 1H, H-3b), 3.63–3.52 (m, 3H, H-5b, 2H-6b), 3.47 (dt, 1H, $J_{4a,5a} \sim J_{4a,3aax}$ 9.5 Hz, $J_{4a,3aeq}$ 4.5 Hz, H-4a), 3.32 (s, 3H, OCH_3), 3.17 (m, 1H, H-1a), 2.26 (m, 1H, H-3aeq), 2.19 (m, 1H, H-6aeq), 2.05 (m, 1H, H-2aeq), 1.90 (m, 1H, H-5a), 1.46 (m, 1H, H-3aax), 1.28–1.10 (m, 5H, H-2aax, H-6aax, overlapped by d at 1.15, $J_{5c,6c}$ 6.5 Hz, 3H-6c).

*(b) By benzoate substitution of compound **46***

A mixture of compound **46** (35 mg, 0.033 mmol) and sodium benzoate (23 mg, 0.162 mmol) in *N*,*N*-dimethylformamide (0.5 mL) was heated at 120°C for 4.5 h with stirring. Then it was diluted with dichloromethane, washed twice with water, dried, and evaporated. Purification was achieved by column chromatography on silica gel (hexane–ethyl acetate, 3:1) to provide the pure title compound **47** (24 mg, 66%).

*(1S,4S,5R)-5-*C*-Hydroxymethyl-1-methoxycyclohex-4-yl 3,4,6-tri-*O*-benzyl-2-*O*-(2,3,4-tri-*O*-benzyl-α-*L*-fucopyranosyl)-β-*D*-galactopyranoside (**48**)*

Compound **47** (63 mg, 0.057 mmol) was debenzoylated in methanolic 0.5 M sodium methoxide (1.1 mL) at room temperature for 24 h. The reaction mixture was evaporated to dryness and the remainder was taken up in chloroform. The solution was washed twice with water, dried, and evaporated. The crude product was purified on a column of silica gel (hexane–ethyl acetate, 3:1) to provide the pure title compound **48** (43 mg, 76%) as a colourless syrup; $[\alpha]_D$ −43.5 (*c* 0.5, chloroform); ^{1}H nmr ($CDCl_3$) δ:7.38–7.01 (m, 30H, 6Ph), 5.68 (d, 1H, $J_{1c,2c}$ 3.5 Hz, H-1c), 4.97–4.44 (m, 13H, 6CH_2Ph, at 4.45 d, 1H, $J_{1b,2b}$ 7.5 Hz, H-1b), 4.32 (q, 1H, $J_{5c,6c}$ 6.5 Hz, H-5c), 4.20 (dd, 1H, $J_{2b,3b}$ 9.5 Hz, H-2b), 4.02 (dd, 1H, $J_{3c,2c}$ 10.5 Hz, H-2c), 3.94 (dd, 1H, $J_{3c,4c}$ 2.5 Hz, H-3c), 3.90 (d, 1H, $J_{3b,4b}$ 2.5 Hz, H-4b), 3.67 (dd, 1H, H-3b), 3.64 (d, 1H, H-4c), 3.64–3.47 (m, 5H, H-5b, 2H-6b, 2H-7a), 3.40 (ddd, 1H, $J_{4a,5a} \sim J_{4a,3aax}$ 10.0 Hz, $J_{4a,3aeq}$ 4.0 Hz, H-4a), 3.33 (s, 3H, CH_3O), 3.14 (m, 1H, H-1a), 2.19–1.95 (m, 3H, H-2aeq, H-3aeq, H-6aeq), 1.77 (t, 1H, OH), 1.53–1.33 (m, 2H, H-5a, H-3aax), 1.28–1.02

(m, 4H, H-2aax, overlapped by d at 1.13, 3H-6c), 1.08 (q, $J_{5a,6ax} \sim J_{6aax,6aeq} \sim J_{6aax,1a} \sim 12$ Hz, H-6aax).

*(1S,4S,5S)-1-Methoxy-5-*C*-methylcyclohex-4-yl 3,4,6-tri-*O*-benzyl-2-*O*-(2,3,4-tri-*O*-benzyl-α-L-fucopyranosyl)-β-D-galactopyranoside (**49**)*

*(a) By fucosylation of compound **44***

A solution of freshly prepared bromide **11** (0.266 mmol) in dichloromethane (0.2 mL) was added to a stirred mixture of alcohol **44** (43 mg, 0.075 mmol), tetraethylammonium bromide (16 mg, 0.076 mmol), dichloromethane (0.3 mL), *N*,*N*-dimethylformamide (0.1 mL), and powdered 4 Å molecular sieves (0.4 g). After stirring for 24 h, the mixture was processed conventionally and separated on a column of silica gel (hexane–ethyl acetate, 3:1) to provide pure **49** (48 mg, 65%) as a colourless syrup; $[\alpha]_D$ −50.5 (*c* 0.5, chloroform); ^{1}H nmr ($CDCl_3$) δ: 7.35–6.95 (m, 30H, 6Ph), 5.69 (d, 1H, $J_{1c,2c}$ 3.5 Hz, H-1c), 4.96–4.40 (m, 14H, 6CH_2Ph, at 4.50 d, 1H, $J_{1b,2b}$ 7.5 Hz, H-1b, at 4.46 q, 1H, $J_{5c,6c}$ 6.5 Hz, H-5c), 4.22 (dd, 1H, $J_{2b,3b}$ 9.5 Hz, H-2b), 4.02 (dd, 1H, $J_{2c,3c}$ 10.0 Hz, H-2c), 3.95 (dd, 1H, $J_{3c,4c}$ 2.0 Hz, H-3c), 3.92 (d, 1H, $J_{3b,4b}$ 2.5 Hz, H-4b), 3.70 (dd, 1H, H-3b), 3.61 (d, 1H, H-4c), 3.59–3.52 (m, 3H, H-5b, 2H-6b), 3.32 (s, 3H, OCH_3), 3.10 (m, 2H, H-1a, H-4a), 2.15 (m, 1H, H-3aeq), 2.00 (m, 2H, H-2aeq, H-6aeq), 1.39–1.24 (m, 2H, H-5a, H-3aax), 1.23–1.09 (m, 4H, H-2aax, overlapped by d at 1.12, 3H-6c), 0.98 (d, 3H, $J_{5a,7a}$ 6.5 Hz, 3H-7a), 0.95 (q, overlapped, 1H, $J_{5a,6aax} = J_{6aax,6aeq} = J_{6aax,1a}$ 12.0 Hz, H-6aax).

*(b) By reduction of tosylate **45***

Lithium aluminium hydride (5 mg, 0.13 mmol) was added to a solution of compound **45** (20 mg, 0.017 mmol) in tetrahydrofuran (0.3 mL). After stirring for 1 h at room temperature, the mixture was poured into ice-water and extracted with chloroform. The organic solution was washed with water, dried, and evaporated. The crude product was purified on a column of silica gel (hexane–ethyl acetate, 3:1) to provide pure **49** (9 mg, 53%).

*(1S,4S,5R)-5-*C*-Hydroxymethyl-1-methoxycyclohex-4-yl 2-*O*-(α-L-fucopyranosyl)-β-D-galactopyranoside (**50**)*

Compound **48** (58 mg, 0.058 mmol) was hydrogenated in ethanol (3.7 mL) over 5% palladium-on-carbon (58 mg) for 2.5 h at 20 psi. After removal of the catalyst, the solution was evaporated to dryness. The residue was applied to a column of Bio-Gel P-2 (10% ethanol-water) to provide pure **50** (22 mg, 82%) as a white powder after freeze-drying an aqueous solution; $[\alpha]_D$ −85 (*c* 0.55, water). The ^{1}H and ^{13}C nmr data are reported in Tables 1 and 2.

*(1S,4S,5S)-1-Methoxy-5-*C*-methylcyclohex-4-yl 2-O-(α-L-fucopyranosyl)-β-D-galactopyranoside (**51**)*

Compound **49** (52 mg, 0.052 mmol) in ethanol (3.3 mL) was hydrogenated and purified as described for the preparation of **50**. Freeze-drying an aqueous solution provided pure **51** (18 mg, 76%) as a white powder; $[\alpha]_D$ −90 (*c* 0.53, water). The ^{1}H and ^{13}C nmr data are reported in Tables 1 and 2.

Acknowledgements

This research was supported by the Natural Sciences and Engineering Research Council of Canada (Grant A-172 to R.U.L) and the Alberta Heritage Foundation for Medical Research. The authors thank Mrs. Mimi Bach for the determination of thermodynamic parameters and Mr. Roberto Mendez for his assistance in the preparation of compound **37**.

1. R. U. Lemieux. Chem. Soc. Rev. **18**, 347 (1989).
2. U. Spohr, O. Hindsgaul, and R. U. Lemieux. Can. J. Chem. **63**, 2644 (1985).
3. R. U. Lemieux. Med. Chem. Adv., Proc. 8th Int. Symp. Vol. 1. Swedish Pharmaceutical Press, Stockholm. (1985). p. 329.
4. U. Spohr, N. Morishima, O. Hindsgaul, and R. U. Lemieux. Can. J. Chem. **63**, 2659 (1985).
5. R. U. Lemieux, O. Hindsgaul, P. Bird, S. Narasimhan, and W. W. Young, Jr. Carbohydr. Res. **178**, 293 (1988).
6. R. U. Lemieux, A. P. Venot, U. Spohr, P. Bird, G. Mandal, N. Morishima, O. Hindsgaul, and D. R. Bundle. Can. J. Chem. **63**, 2664 (1985).
7. M. Vandonselaar, L. T. J. Delbaere, U. Spohr, and R. U. Lemieux. J. Biol. Chem. **262**, 10848 (1987).
8. L. T. J. Delbaere, M. Vandonselaar, L. Prasad, J. W. Quail, P. V. Nikrad, J. R. Pearlstone, M. R. Carpenter, L. B. Smillie, U. Spohr, and R. U. Lemieux. Can. J. Chem. **68**, 1116 (1990).
9. R. U. Lemieux, L. T. J. Delbaere, H. Beierbeck, and U. Spohr. Ciba Found. Symp. **158**, 231 (1990).
10. R. Lumry and S. Rajender. Biopolymers, **9**, 1125 (1970).
11. O. Hindsgaul, T. Norberg, J. LePendu, and R. U. Lemieux. Carbohydr. Res. **109**, 109 (1982).
12. O. Hindsgaul, D. P. Khare, M. Bach, and R. U. Lemieux. Can. J. Chem. **63**, 2653 (1985).
13. E. Petrakova, U. Spohr, and R. U. Lemieux. Can. J. Chem. **70**, 233 (1992).
14. R. U. Lemieux, E. Fraga, and K. A. Watanabe. Can. J. Chem. **46**, 61 (1968).
15. T. Yamazaki, H. Sugiyama, N. Yamaoka, K. Matsuda, and S. Seto. Carbohydr. Res. **50**, 279 (1976).
16. R. U. Lemieux, A. A. Pavia, J. C. Martin, and K. A. Watanabe. Can. J. Chem. **47**, 4427 (1969).
17. E. J. Hedgley, W. G. Overend, and R. A. C. Rennie. J. Chem. Soc. 4701 (1963).
18. S. Hanessian. Carbohydr. Res. **2**, 86 (1966).
19. E. H. Williams, W. A. Szarek, and J. K. N. Jones. Carbohydr. Res. **20**, 49 (1971).
20. J. Meisenheimer and H. Jung. Ber. Dtsch. Chem. Ges. **60**, 1462 (1927).
21. M. Gehrke and F. X. Aichner. Ber. Dtsch. Chem. Ges. **60**, 918 (1927).
22. K. Mizutani, A. Hayashi, R. Kasai, O. Tanaka, N. Yoshida, and T. Nakajima. Carbohydr. Res. **126**, 177 (1984).
23. M. E. Evans. Carbohydr. Res. **21**, 473 (1972).
24. R. U. Lemieux, K. B. Hendriks, R. V. Stick, and K. James. J. Am. Chem. Soc. **97**, 4056 (1975).
25. U. Spohr and R. U. Lemieux. Carbohydr. Res. **174**, 211 (1988).
26. R. U. Lemieux and J. C. Martin. Carbohydr. Res. **13**, 139 (1970).
27. S. Hanessian, T. J. Liak, and D. M. Dixit. Carbohydr. Res. **88**, C14 (1981).
28. H. Schmid and P. Karrer. Helv. Chim. Acta, **32**, 1371 (1949).
29. M. P. Kunstmann, D. S. Tarbell, and R. L. Autrey. J. Am. Chem. Soc. **84**, 4115 (1962).
30. T. Suami, S. Ogawa, K. Nakamoto, and I. Kasahara. Carbohydr. Res. **58**, 240 (1977).
31. S. Ogawa, M. Ara, T. Kondoh, M. Saitoh, R. Masuda, T. Toyokuni, and T. Suami. Bull. Chem. Soc. Jpn. **53**, 1121 (1980).
32. N. M. Yoon, G. S. Pak, H. C. Brown, S. Krishnamurthy, and T. P. Stocky. J. Org. Chem. **38**, 2786 (1973).
33. D. H. Whiffen. Chem. Ind. 964 (1956).
34. J. H. Brewster. J. Am. Chem. Soc. **81**, 5483 (1959).
35. H. Thøgersen, R. U. Lemieux, K. Bock, and B. Meyer. Can. J. Chem. **60**, 44 (1982).
36. R. U. Lemieux, R. Cromer, and U. Spohr. Can. J. Chem. **66**, 3083 (1988).
37. P. V. Nikrad, H. Beierbeck, and R. U. Lemieux. Can. J. Chem. **70**, 241 (1992).
38. B. Belleau. Ann. N.Y. Acad. Sci. **144**, 705 (1967).
39. B. Belleau and J. L. Lavoie. Can. J. Biochem. **46**, 1397 (1968).
40. H. Beierbeck and R. U. Lemieux. Can. J. Chem. **68**, 820 (1990).
41. L. T. J. Delbaere and G. D. Brayer. J. Mol. Biol. **183**, 89 (1985).

Can. J. Chem. Downloaded from www.nrcresearchpress.com by 123.30.183.119 on 09/08/12
For personal use only.

The importance of conformation in the reactivity of radical cations. Changing configuration at saturated carbon centres[1]

ALLYSON L. PERROTT AND DONALD R. ARNOLD[2]
Department of Chemistry, Dalhousie University, Halifax, N.S., Canada B3H 4J3

Received May 3, 1991

ALLYSON L. PERROTT and DONALD R. ARNOLD. Can. J. Chem. **70**, 272 (1992).

Irradiation of an acetonitrile solution of *cis* 1-methyl-2-phenylcyclopentane (**1***b cis*); 1,4-dicyanobenzene (**2**), an electron-accepting photosensitizer; and 2,4,6-collidine (**3**), a nonnucleophilic base, leads to configurational isomerization of the cyclopentane; the photostationary state lies >99% in favour of the *trans* isomer. The mechanism proposed for this reaction involves formation of the radical cation of **1***b cis* by photoinduced electron transfer to the singlet excited state of **2**, deprotonation of the radical cation assisted by the base **3**, reduction of the resulting benzylic radical by the radical anion $\mathbf{2}^{\cdot-}$, and reprotonation of the benzylic anion to give both the *cis* and the *trans* isomers of **1***b*. The photostationary state is controlled by the relative rates of deprotonation of the radical cations of **1***b cis* and *trans*; these rates are dependent upon the extent of overlap of the SOMO of the radical cation, which is largely associated with the phenyl ring, and the benzylic carbon–hydrogen bond. Molecular mechanics calculations (MM3 and MMP2) are used to calculate the preferred conformations of the isomers. The required orbital overlap is 31% effective with the global minimum conformation of the *cis* isomer and essentially ineffective for the low-lying conformations of the *trans* isomer. This proposed mechanism is supported by Stern–Volmer quenching studies, which indicate that both isomers quench the singlet excited state of **2** at the diffusion-controlled rate, and by deuterium incorporation studies. When irradiation of the *cis* isomer is carried out in acetonitrile–methanol-*O-d* as solvent, isomerization is accompanied by deuterium exchange at the benzylic position; the *trans* isomer is stable under these conditions.

Key words: photosensitized electron transfer, radical cation, deprotonation, configurational isomerization, conformation, molecular mechanics (MM3).

ALLYSON L. PERROTT et DONALD R. ARNOLD. Can. J. Chem. **70**, 272 (1992).

L'irradiation d'un mélange de *cis*-1-méthyl-2-phénylcyclopentane (**1***b cis*), de 1,4-dicyanobenzène (**2**, un sensibilisateur accepteur d'électrons) et de 2,4,6-collidine (**3**, une base qui n'est pas nucléophile) en solution dans l'acétonitrile conduit à une isomérisation configurationnelle du cyclopentane; l'état photostationnaire favorise l'isomère *trans* à plus de 99%. Le mécanisme proposé pour cette réaction implique la formation du cation radicalaire du produit **1***b cis* par le biais d'un transfert d'électron photo-induit vers l'état excité singulet du produit **2**, une déprotonation du cation radicalaire assistée par la base **3**, la réduction, par l'anion radicalaire $\mathbf{2}^{\cdot-}$; du radical benzylique qui en résulte et un reprotonation de l'anion benzylique qui fournit les isomères *cis* et *trans* du produit **1***b*. L'état photostationnaire est contrôlé par les vitesses relatives de déprotonation des cations radicalaires des produits **1***b cis* et *trans*; ces vitesses dépendent du degré de recouvrement de la liaison carbone–hydrogène benzylique et des orbitales moléculaires SO du cation radicalaire qui sont très associées au noyau phényle. On a fait appel à des calculs de mécanique moléculaire (MM3 et MMP2) pour calculer les conformations privilégiés des isomères. Le recouvrement orbitalaire requis est efficace à 31% dans la conformation globale minimale de l'isomère *cis* et est essentiellement inefficace pour les conformères les plus stables de l'isomère *trans*. Le mécanisme proposé est en accord avec les résultats d'études d'incorporation de deutérium et d'études de désactivation de Stern–Volmer qui indiquent que les deux isomères désactivent l'état excité singulet du produit **2** à une vitesse contrôlée par la diffusion. Lorsqu'on effectue l'irradiation de l'isomère *cis* dans un mélange d'acétonitrile et de méthanol-*O-d*, l'isomérisation s'accompagne d'un échange de deutérium dans la position benzylique; dans ces conditions, l'isomère *trans* est stable.

Mots clés : transfert d'électrons photosensibilité, cation radicalaire, déprotonation, isomérisation configurationnelle, conformation, mécanique moléculaire (MM3).

[Traduit par la rédaction]

Introduction

Removal of an electron from a neutral molecule weakens bonding interactions, making cleavage more likely. There are several recent reports of photosensitized (electron transfer) carbon–carbon bond cleavage and deprotonation from radical cations generated in this way, and progress has been made toward an understanding of the scope and mechanism of these reactions (1–4). Particularly relevant to this study is the report of contrasting behaviour of the radical cations of *trans* and *cis* methyl 2-phenylcyclopentyl ethers (**1***a*) (2). Irradiation of an acetonitrile–methanol (3:1) solution of *trans* methyl 2-phenylcyclopentyl ether (**1***a trans*) and 1,4-dicyanobenzene (**2**), an electron-accepting photosensitizer, leads to formation of the radical cation $\mathbf{1}a\ trans^{\cdot+}$, which undergoes carbon–carbon bond cleavage and ultimately forms acyclic products, mainly 5-phenylpentanal dimethyl acetal (**4**) (reaction [1]). In marked contrast, the radical cation of the *cis* isomer ($\mathbf{1}a\ cis^{\cdot+}$) does not undergo carbon–carbon bond cleavage; deprotonation resulting ultimately in formation of the *trans* isomer occurs instead (reaction [2]). Evidence for the deprotonation mechanism was provided by the observation that deuterium was incorporated at the benzylic position when the irradiation was carried out in acetonitrile–methanol-*O-d*. The mechanisms for the carbon–carbon bond cleavage and the deprotonation reactions are summarized in Scheme 1.

The key step in the mechanism leading to carbon–carbon bond cleavage (step 7) requires that the dissociation energy

[1]This is part 30 of the series Radical Ions in Photochemistry. The preceding publication in this series is ref. 1*a*.

[2]Author to whom correspondence may be addressed.

Can. J. Chem. Downloaded from www.nrcresearchpress.com by 123.30.183.119 on 09/08/12
For personal use only.

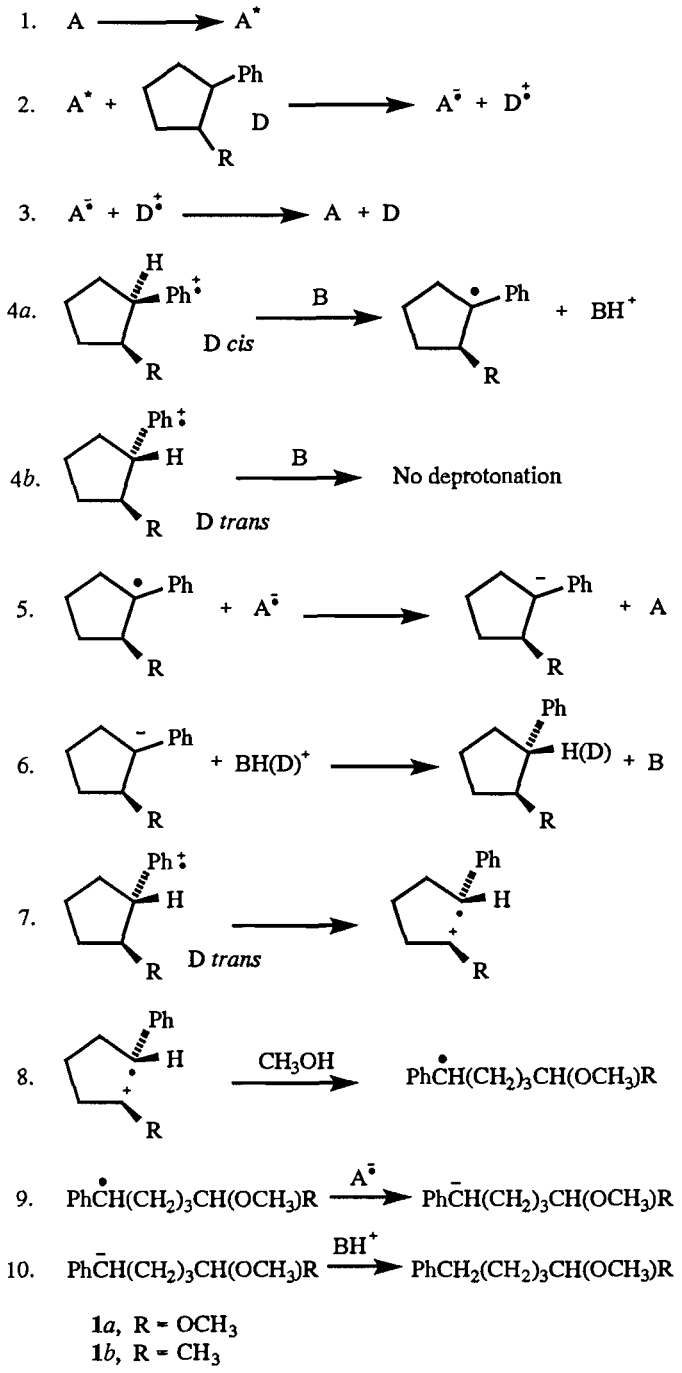

SCHEME 1

of the vulnerable bond of the radical cation be less than ca. 55 kJ mol^{-1}, that the conformation of the methoxy group allow interaction of a nonbonding electron pair on the oxygen with the σ* orbital of the vulnerable bond, and that the singly occupied molecular orbital (SOMO) of the radical cation overlap with this bond (2, 3*a*). These requirements are obviously met in the radical cation **1***a trans*$^{+\cdot}$; cleavage occurs. The lack of carbon–carbon bond cleavage of the radical cation **1***a cis*$^{+\cdot}$ was explained on the basis of an unfavourable conformation of the radical cation: insufficient overlap of a nonbonding pair of electrons on the oxygen with the σ* orbital of the vulnerable benzylic carbon–carbon bond. The preferred conformation of **1***a cis*$^{+\cdot}$ does, however, have the SOMO favourably orientated for overlap with the benzylic carbon–hydrogen bond and deprotonation occurs (step 4*a*) (2).

Reaction [1] (ref. 2)

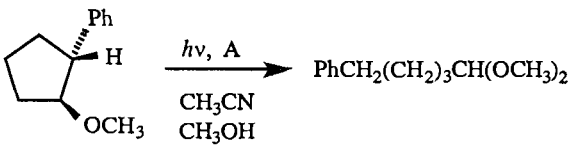

1*a trans*

A = 1,4-dicyanobenzene (2)

Reaction [2] (ref. 2)

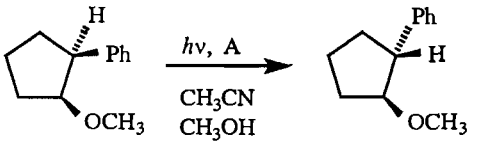

1*a cis* **1***a trans*

A = 1,4-dicyanobenzene (2)

It is well established that the thermodynamic acidity of radical cations is greatly increased relative to the neutral molecules (5). The pK_a of the benzylic hydrogen of the radical cation of toluene has been estimated to be in the range −11 to −13 (5*a*). This large increase in acidity is realized only when the SOMO and the benzylic carbon–hydrogen bond overlap. The interaction falls off in a $\cos^2$ relationship with this dihedral angle. Molecular mechanics calculations (MMP2) identify global minimum conformations of **1***a trans* and **1***a cis* that are consistent with this explanation for the difference in reactivity of these radical cations. Similar dependence of the rate of deprotonation on dihedral angle has been reported for other systems (4*b*, 6).

This study focuses on the configurational isomerization reaction exemplified by the conversion of **1***a cis* to **1***a trans*. The behaviour of the radical cations of the analogous 1-methyl-2-phenylcyclopentane isomers, **1***b cis* and **1***b trans*, has been studied. These compounds were chosen because the benzylic carbon–hydrogen bond of these radical cations should be acidic enough for the deprotonation reaction, but the carbon–carbon bond dissociation energy should be above the threshold for cleavage. Therefore, *cis–trans* isomerization should occur without competition from carbon–carbon bond cleavage.

This isomerization reaction involves changing the configuration at a saturated carbon. Such a procedure for the interconversion of diastereomers could prove to be of considerable synthetic utility.[3]

Results

Both *cis* and *trans* 1-methyl-2-phenylcyclopentane (**1***b cis*, *trans*) are known compounds (7). The stereospecific synthesis of the *cis* isomer began with a Grignard reaction, adding phenylmagnesium bromide to 2-methylcyclopentanone. The resulting alcohol was dehydrated with acid, and

[3]The diastereomeric relationship could also result from interaction of a racemic substrate (radical cation) with a chiral base. Differences in the rate of deprotonation of the diastereomeric pairs would then provide a new mechanism for chiral induction.

Can. J. Chem. Downloaded from www.nrcresearchpress.com by 123.30.183.119 on 09/08/12
For personal use only.

Can. J. Chem. Downloaded from www.nrcresearchpress.com by 123.30.183.119 on 09/08/12
For personal use only.

the conjugated alkene was reduced by catalytic hydrogenation. The *trans* isomer was synthesized via a two-step procedure. First, 6-phenyl-1-hexene was prepared by coupling 3-phenylpropylmagnesium bromide and allyl bromide. Then the 6-phenyl-1-hexene was cyclized to a mixture of the isomers, *trans* predominating (85%), by treatment with potassium. Pure *trans* isomer was isolated by preparative gas chromatography (gc).

The irradiation procedure was similar to that used in earlier studies (2). Solutions of the 1-methyl-2-phenylcyclopentane (**1***b*); 1,4-dicyanobenzene (**2**), an electron-accepting photosensitizer; and 2,4,6-collidine (**3**), a nonnucleophilic base, in acetonitrile or in a mixture of acetonitrile–methanol-*O*-*d* (3:1), were degassed by nitrogen ebullition and then irradiated through a Pyrex filter using a medium-pressure mercury vapour lamp. Progress of the reaction was followed by capillary column gas chromatography with a flame ionization detector (gc/fid). The results of the irradiations are illustrated in reactions [3]–[6].

Reaction [3]

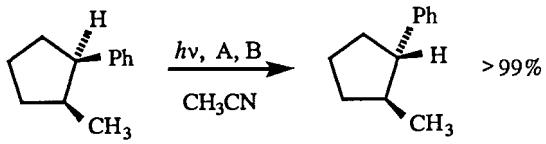

1*b cis* **1***b trans*

A = 1,4-dicyanobenzene (**2**)
B = 2,4,6-collidine (**3**)

Reaction [4]

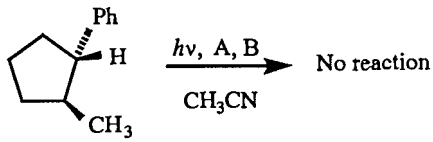

1*b trans*

A = 1,4-dicyanobenzene (**2**)
B = 2,4,6-collidine (**3**)

Reaction [5]

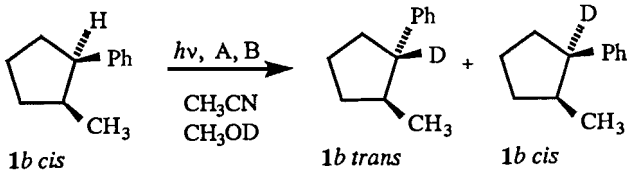

1*b cis* **1***b trans* **1***b cis*

Reaction [6]

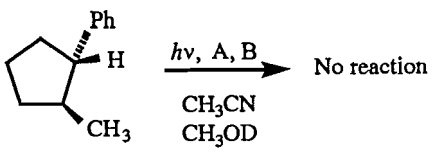

1*b trans*

Irradiation of the *cis* isomer resulted in isomerization to the *trans* isomer (reaction [3]). Starting with pure *cis* isomer, the ratio of *cis*:*trans* isomers was 79:21 after 4 days irradiation; continued progress of the reaction was impeded, presumably as a result of competitive light absorption by side products. When the irradiation was begun on a mixture of *cis* and *trans* isomers (14:86), the ratio of *cis* to *trans* isomers decreased further (3:97). When the irradiation was begun on the pure *trans* isomer (>99%), no *cis* isomer was detected (reaction [4]). A side product, formed after prolonged irradiation starting with the *cis* isomer, has been isolated and identified: 1-(4-cyanophenyl)-2-methyl-1-phenylcyclopentane (**4**). Only one of the diastereomers was detected (gc/fid, gc/ms). The stereochemical assignment (4-cyanophenyl- and methyl- *trans*) is based upon ^{1}H nmr evidence. This product was not detected when solutions of the *trans* isomer were similarly irradiated.

The deuterium incorporation studies involved similar irradiations of solutions of the cyclopentane (**1***b*), photosensitizer (**2**), and base (**3**) in acetonitrile–methanol-*O*-*d* (3:1). The extent of isomerization and deuterium incorporation was determined by capillary column gas chromatography coupled to a mass selective detector (gc/ms). Analysis of the photolysate following irradiation of the *cis* isomer indicated that all of the *trans* isomer formed had incorporated one atom of deuterium. Prolonged irradiation led to detectable amounts of deuterium incorporated in the *cis* isomer as well (reaction [5]). Analysis (^{1}H and ^{2}H nmr) of the resulting mixture of *cis* and *trans* isomers confirmed that deuterium was incorporated at the benzylic positions. Irradiation of the *trans* isomer in the acetonitrile–methanol-*O*-*d* solvent mixture did not produce the *cis* isomer and, furthermore, no deuterium was incorporated in the recovered *trans* isomer (reaction [6]).

Oxidation potentials of *cis* and *trans* 1-methyl-2-phenylcyclopentane (**1***b cis* and *trans*), required for the discussion of the initial electron transfer step, were determined by cyclic voltammetry. The voltammograms were typical of irreversible oxidation; the oxidation potentials were taken as 0.03 V preceding the anodic peak potentials (8). These values are summarized in Table 1.

Fluorescence quenching studies were carried out to confirm the initial electron transfer from the 1-methyl-2-phenylcyclopentanes (**1***b cis* and *trans*) to the singlet excited state of 1,4-dicyanobenzene (**2**). Stern–Volmer analysis of the fluorescence intensity from **2** as a function of concentration of **1***b cis* and *trans* confirms that both isomers quench the fluorescence of **2** with a rate constant 2.8×10^{10} M^{-1} s^{-1}: electron transfer takes place at the diffusion-controlled rate (Fig. 1).[4]

Molecular mechanics calculations can provide an accurate description of molecular structure (9). Since the introduction of the MMP2 program, additional experimental data have become available. Furthermore, some users have pointed out systematic errors in this program (9*d*): MMP2 underestimates the length of eclipsed single bonds. This is a particularly important deficiency in the case of cyclopentane derivatives. The development of the MM3 program (9*c*) has alleviated this problem by including a torsion-stretch interaction in the force field, and by giving cyclopentane rings distinct parameters, different from open-chain alkanes. Both MM3 and MMP2 molecular mechanics calculations were used to describe the conformers of *cis* and *trans* 1-methyl-2-phenylcyclopentane (**1***b cis* and **1***b trans*). The search for

[4]The slopes of the Stern–Volmer plots (Fig. 1) were $k_q\tau$ = 249.9 for **1***b trans* and 245.4 for **1***b cis*. The measured fluorescence lifetime of 1,4-dicyanobenzene (**2**) in acetonitrile is 8.8×10^{-9} s (10).

TABLE 1. Oxidation potentials of some of the compounds of interest

	E_p (V)[a]	$E_{p/2}$ (mV)
cis Methyl 2-phenylcyclopentyl ether (**1***a cis*)	2.05[b]	117
trans Methyl 2-phenylcyclopentyl ether (**1***a trans*)	2.05[b]	162
cis 1-Methyl-2-phenylcyclopentane (**1***b cis*)	2.30	197
trans 1-Methyl-2-phenylcyclopentane (**1***b trans*)	2.35	228

[a]Anodic peak potential taken from the cyclic voltammogram at a 100 mV/s sweep rate. The reference electrode was saturated calomel (sce). The oxidation potential can be estimated from the peak potential by subtraction 0.028 V (ref. 8).
[b]Reference 2.

conformers began with all permutations of structures having the phenyl or the methyl group on either side of the flap of the envelope cyclopentane structure. Four energy minima were identified for each isomer. These results are summarized in Table 2. The global minimum conformations of **1***b cis* and **1***b trans* are illustrated in Figs. 2 and 3.

Discussion

The first three steps in the proposed mechanism for both the carbon–carbon bond cleavage and the deprotonation reactions (Scheme 1) are the same. The first step involves excitation of the photosensitizer, 1,4-dicyanobenzene (**2**). The ultraviolet absorption spectrum of **2** extends out to 290 nm, beyond the short wavelength cutoff of the Pyrex filter. The other components of the irradiation mixture are transparent in this region.

The singlet excited state of **2** can accept an electron from either **1***b cis* or *trans*. The free-energy change (ΔG_{et}) associated with this electron transfer can be calculated from the oxidation potential of the donor, the reduction potential of the acceptor, and the singlet excited state energy by using the Weller equation (eq. [7]) (11). For both *cis* and *trans* **1***b*, electron transfer is exergonic by at least 30 kJ mol^{-1}. Under these conditions electron transfer is expected to occur at the diffusion-controlled rate and the observed fluorescence quenching rate constants, ca. 2.8×10^{10} M^{-1} s^{-1} for both isomers, are in agreement.

$$[7] \quad \Delta G_{et} = F[E^{ox}_{1/2}(D) - E^{red}_{1/2}(A) - e/\epsilon\alpha] - E_{0,0}(A)$$

$$[8] \quad \Delta G_{-et} = F(E^{red}_{1/2}(A) - E^{ox}_{1/2}(D))$$

The third step in the mechanism is back electron transfer, an energy-wasting step that regenerates the ground state starting materials. Back electron transfer, following photoinduced electron transfer, is always exergonic (eq. [8]). However, when the process is as favourable as it is in this case, $\Delta G_{-et} = -4$ eV, the rate falls within the Marcus inverted region and the process becomes relatively slow (12). Estimates based upon study of similar systems place the rate of back electron transfer within the radical ion pair in the range 10^6–10^8 s^{-1} (12*b*). That is, back electron transfer is slow enough to allow a rapid bimolecular reaction of the radical cation within the radical ion pair.

Rapid deprotonation (step 4) requires overlap of the SOMO with the benzylic carbon–hydrogen bond. Maximum interaction occurs when the SOMO and the benzylic bond are at an angle of 0°; there will be no increase in acidity when the benzylic hydrogen is in the same plane as the phenyl ring. The magnitude of the interaction follows a $\cos^2$ relationship with the angle between the SOMO and the benzylic bond (13).[5] Molecular mechanics calculations, both MM3 and MMP2, indicate that the angle (θ) between the plane of the phenyl ring and the benzylic carbon–hydrogen bond is ca. 1° in the global minimum conformation of **1***b trans* (Fig. 3). Furthermore, there is no reactive conformer readily accessible by thermal equilibration. The only potentially reactive conformer ($\theta = 32.5°$) is 15 kJ mol^{-1} above the global minimum (Table 2). It is therefore not surprising that the radical cation of this isomer is stable under these conditions. In marked contrast, this angle is 34° (31% effective overlap) according to the MM3 calculations (51°, or 60% maximum overlap according to the MMP2 calculations) in the global minimum of the *cis* isomer (Fig. 2). While this interaction

[5]Since the molecular mechanics calculations provide an angle (θ) between the plane of the phenyl ring and the benzylic bond, the orbital overlap is assessed with the 1-$\cos^2\theta$ relationship.

TABLE 2. Conformers of *cis* and *trans* 1-methyl-2-phenylcyclopentane (**1***b cis*, *trans*)

Initial conformation[a]	Angle[b]	Energy above the global minimum (kJ/mol)
1*b cis*		
Phenyl (flap-eq), methyl (ax)	34° (51°)	Global minimum (Global minimum)
Methyl (flap-eq), phenyl (ax)	c (8.6°)	c (1.6)
Phenyl (flap-ax), methyl (eq)	24.7° (26.8°)	0.5 (2.3)
Methyl (flap-ax), phenyl (eq)	d (28.3°)	d (6.5)
1*b trans*		
Phenyl (flap-eq), methyl (eq)	1° (1°)	Global minimum (Global minimum)
Methyl (flap-eq), phenyl (eq)	d (9.3°)	d (1.4)
Phenyl (flap-ax), methyl (ax)	32.5° (27.9°)	14.9 (10.0)
Methyl (flap-ax), phenyl (ax)	4.1° (d)	21.1 (d)

[a]The initial structure, all combinations of the phenyl and the methyl group on both sides of the flap.
[b]The dihedral angle between the plane of the phenyl ring and the benzylic hydrogen. The values in parentheses are from the MMP2 program.
[c]Calculation converged to the same conformer obtained with the initial structure phenyl (flap-ax), methyl (eq).
[d]Calculation converged to the global minimum.

Can. J. Chem. Downloaded from www.nrcresearchpress.com by 123.30.183.119 on 09/08/12
For personal use only.

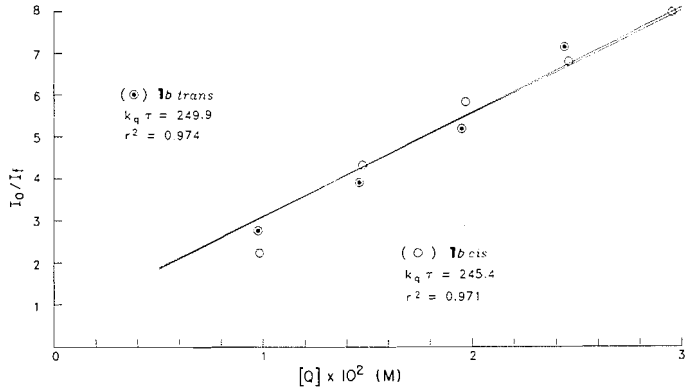

FIG. 1. Stern–Volmer plots of the fluorescence intensity from 1,4-dicyanobenzene (**2**) as a function of the concentration of *cis* and *trans* 1-methyl-2-phenylcyclopentane (**1***b cis* and **1***b trans*).

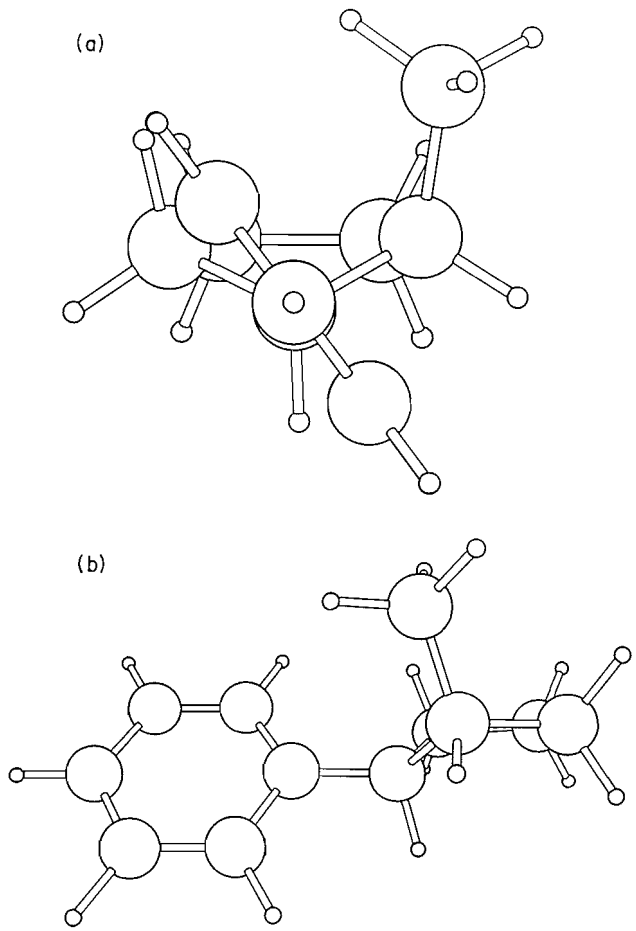

FIG. 2. The global minimum conformer (MM3) of *cis* 1-methyl-2-phenylcyclopentane (**1***b cis*): (a) looking down the plane of the phenyl ring, (b) with the plane of the phenyl ring nearly in the *x*,*y*-plane.

is less than optimal, the radical cation of **1***b cis* does deprotonate: exchange of deuterium for hydrogen at the benzylic position and isomerization to the *trans* isomer are observed.

Two obvious assumptions must be justified: the molecular mechanics calculations were performed on the neutral molecules while the reactive species are the radical cations,

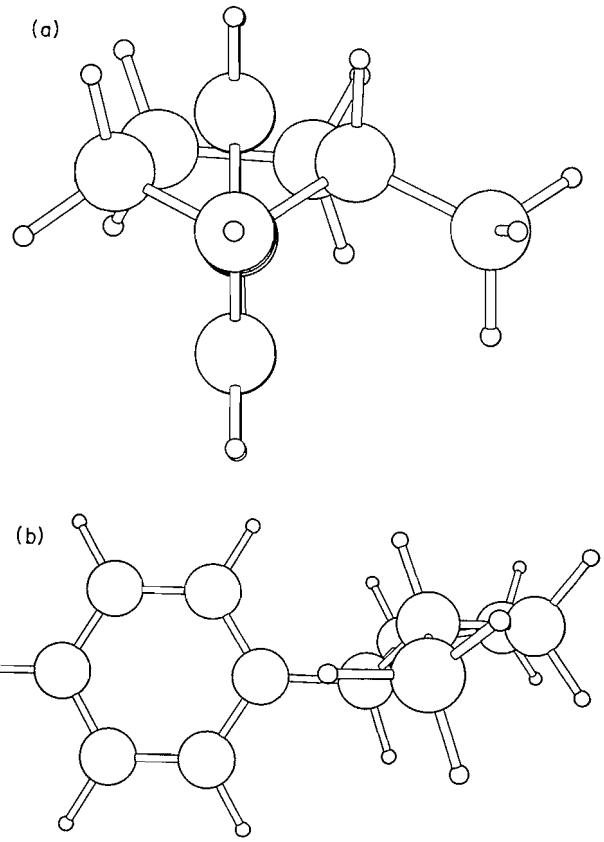

FIG. 3. The global minimum conformer (MM3) of *trans* 1-methyl-2-phenylcyclopentane (**1***b trans*): (a) looking down the plane of the phenyl ring, (b) with the plane of the phenyl ring nearly in the *x*,*y*-plane.

and even though the global minimum conformation does not have favourable orbital overlap, other conformers with the required overlap may be accessible by thermal equilibration. With these hydrocarbons, it is likely that the SOMO is largely associated with the phenyl ring, the preferred conformation of the neutral molecule and the radical cation will be similar, and the molecular mechanics calculations carried out on the neutral molecules can be extended to the radical cations. The lifetime of the radical cation is short, and competitive deactivation by back electron transfer is rapid; therefore, deprotonation will be inefficient if the global minimum conformer does not have favourable overlap.

The acidity of the benzylic hydrogen of the radical cations **1***b cis*$^{\ddagger\cdot}$ and **1***b trans*$^{\ddagger\cdot}$, estimated from a thermochemical cycle (eq. [9] (5*a*)), is pK_a = −15.[6] This high

[6]The acidity of the benzylic hydrogen of the radical cation **1***b trans*$^{\ddagger\cdot}$ can be estimated from the bond dissociation free-energy ($\Delta G^0_{BDE(RH)}$, using cumene as a model) and the standard oxidation potential (E^0_{RH}) using Method 1 (eq. [9]) described in ref. 5*a*. The required data are $\Delta H_{BDE(RH)}$ = 353 ± 6 kJ mol^{-1} (14*a*); $\Delta S_{BDE(RH)}$ = 110 ± 4 J mol^{-1} (14*b*); so, $\Delta G^0_{BDE(RH)}$ = 322 ± 25 kJ mol^{-1}; $E^{ox}_{1/2}$ (**1***b trans*$^{\ddagger\cdot}$) = 2.32 V (vs. sce) (Table 1), accepting this value as an estimate of the standard oxidation potential, E^0_{RH} = 2.56 V (vs. standard hydrogen electrode); $\Delta G^0_{tr(H^+)CH_3CN}$ = 46.0 kJ mol^{-1} (14*c*); $\Delta G^0_{f(H)g}$ = 203.2 kJ mol^{-1} (14*d*). The pK_a (**1***b trans*$^{\ddagger\cdot}$) = −15. The K_a (toluene$^{\ddagger\cdot}$) = −13 by this method.

Can. J. Chem. Downloaded from www.nrcresearchpress.com by 123.30.183.119 on 09/08/12
For personal use only.

Can. J. Chem. Downloaded from www.nrcresearchpress.com by 123.30.183.119 on 09/08/12
For personal use only.

thermodynamic acidity of the radical cation means that even the solvent, i.e., acetonitrile, might serve as the base.

$$[9]\quad pK_{a(RH^{+})sol} = \frac{1}{2.303\,RT}(-FE^{0}_{RH} + \Delta G^{0}_{tr(H^{+})sol} + \Delta G^{0}_{BDE(RH)g} - \Delta G^{0}_{f(H)g})$$

However, the reaction is significantly more efficient when the stronger base, 2,4,6-collidine (**3**), has been added. The effect of added base, assisting in the deprotonation of strongly acidic radical cations, has been observed before (15).

The final steps in the mechanism for isomerization (Scheme 1, steps 5 and 6), reduction of the radical by the radical anion of the photosensitizer followed by protonation (deuteration), are well understood. The reduction potential of the benzylic radical will be similar to that of the cumyl radical (−1.73 V vs. sce (16)), which is close to that of 1,4-dicyanobenzene (**2**) (−1.66 V). Equilibrium electron transfer is possible and protonation of the carbanion will be rapid. Competitive formation of the 1:1 adduct (1-(4-cyanophenyl)-2-methyl-1-phenylcyclopentane (**4**) results from coupling of the benzylic radical, on the least hindered side, and the radical anion of 1,4-dicyanobenzene, at the *ipso* position, followed by rearomatization of the resulting cyclohexadienyl anion by loss of cyanide ion.

We found no evidence, in any case, for carbon–carbon bond cleavage of either **1***b cis* or **1***b trans*. The global minimum conformer of **1***b trans* has the required overlap of the SOMO with the vulnerable bond; the angle between the plane of the phenyl ring and the benzylic carbon–carbon bond is 57° (70% effective overlap). Nevertheless, cleavage does not occur. This lack of reactivity is readily explained on energetic grounds. Thermochemical cycles used for estimating the bond dissociation energy of the vulnerable benzylic carbon–carbon bond of the radical cations (Scheme 1, step 7) are shown in Fig. 4.[7] Cleavage of the radical cation to the distonic radical cation is well below the threshold energy (ca. 55 kJ mol^{-1} (3*a*)) for the ethers (**1***a*) but is significantly above the maximum for the hydrocarbons (**1***b*). The major difference in the two systems is the lower oxidation potential of the α-oxy radical, relative to that of a secondary benzylic radical (16).

The photostationary state lies well in favour (>99%) of the *trans* isomer (reaction 3). This observation is consistent with the fact that no deuterium was incorporated in **1***b trans*, even after prolonged irradiation is acetonitrile–methanol-*O*-*d* (3:1) (reaction 6). The reported synthesis of **1***b* by the alkali metal catalyzed cyclization of 6-phenyl-1-hexene in refluxing butylcyclohexane gave a mixture of isomers, *trans*:*cis* = 5:1, which was presumed to be a thermodynamic equilibrium corresponding to a difference in energy ΔG = 6 kJ mol^{-1} at 185° (7). We repeated this synthesis, using decalin as solvent, and an 8:1 ratio of isomers (ΔG = 8 kJ mol^{-1} at 190°C) was obtained. The difference in the heat of formation of the isomers calculated with MM3 is 11 kJ mol^{-1} (5 kJ mol^{-1} by MMP2). Despite the lack of quantitative agreement among these estimates, it is evident that the photostationary state lies further in favour of the *trans* isomer than would be obtained at thermodynamic equilibrium.

In this case both the photostationary state and the thermodynamic equilibrium favour the *trans* isomer. In general, the conformational criterion controlling the photostationary state is unrelated to thermodynamic considerations. It will be possible to use this photosensitized (electron transfer) isomerization reaction to convert a more stable isomer to the less stable isomer. The ability to change configuration at a saturated carbon should prove to have signif-

[7]The data for Fig. 4 were taken from refs. 14*a*, *b*, 16, and 17.

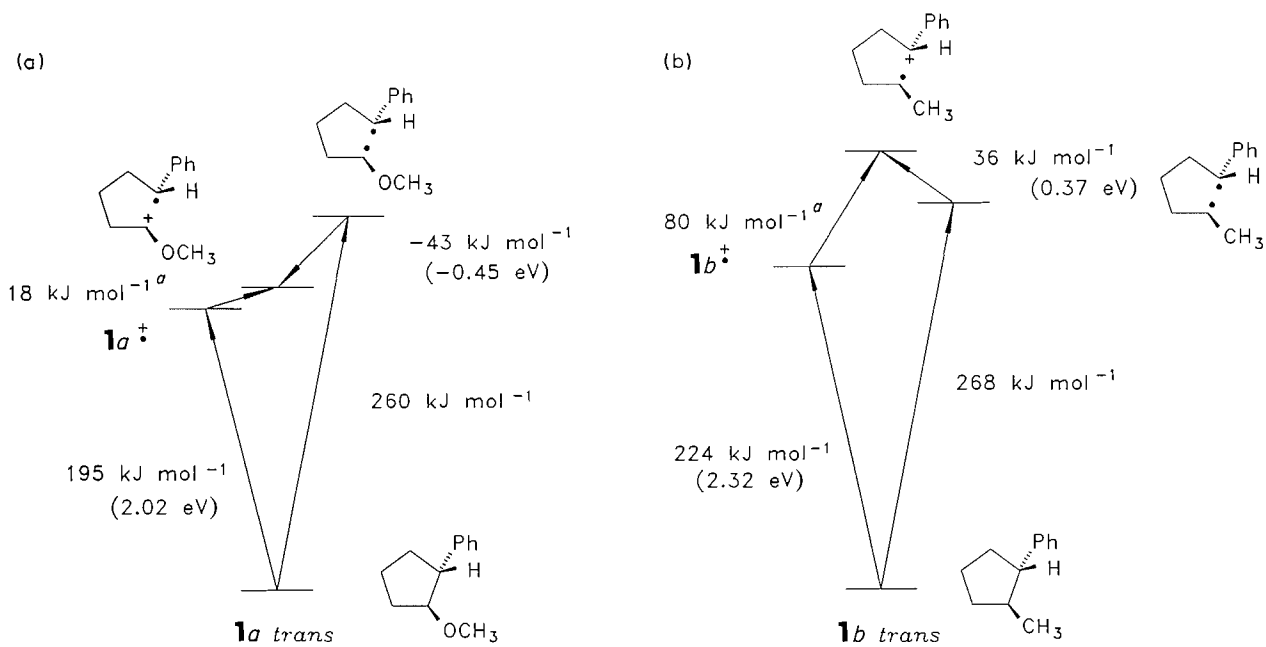

FIG. 4. Thermochemical cycles used for the estimation of the bond dissociation energy of the vulnerable benzylic carbon–carbon bond of the radical cations of the ether **1***a* and the hydrocarbon **1***b*.

[a]Value calculated by completing the cycle.

Can. J. Chem. Downloaded from www.nrcresearchpress.com by 123.30.183.119 on 09/08/12
For personal use only.

icant synthetic utility; our efforts to define the scope of the reaction and to improve the efficiency continue.

Experimental

General information

The ^1H and ^{13}C nmr spectra were recorded on a Nicolet Instruments Corp. narrow bore 360-MHz spectrometer and are reported in parts per million relative to tetramethylsilane. Infrared spectra were recorded on a Perkin–Elmer 180 spectrometer. Frequencies are reported in wavenumbers, relative to polystyrene film (1601.8 cm^{-1}). Gas chromatography with mass selective detection (gc/ms) was carried out on a Hewlett–Packard 5890 gc/5970 mass selective detector interfaced with a Hewlett–Packard 9816 microcomputer. The column used was 25 m × 0.2 mm 5% phenyl methyl silicone on fused silica with a film thickness of 0.25 μm. Gas chromatography with flame ionization detection (gc/fid) was carried out on a Hewlett–Packard 5890. The column used was 25 m × 0.25 mm OV-1701 fused silica. Preparative gas chromatography was carried out on an Aerograph A-700 gc fitted with a thermal conductivity detector, using a 6 ft × $\frac{1}{4}$ in. 20% SE-30 on Chromosorb 60/80 W column.

Electrochemical measurements

Oxidation potentials were obtained by cyclic voltammetry using a three-electrode cell, which has been described previously (18). The working electrode was a platinum sphere (1 mm diameter) and the counter electrode was a platinum wire. The reference electrode was saturated calomel (sce). The electrolyte was 0.1 M tetraethylammonium perchlorate (TEAP) in acetonitrile. Substrate concentrations were approximately 1 mM.

The peak potentials were measured with a 100 mV/s sweep rate. No cathodic wave was detected following the anodic sweep. The half-wave potentials were taken as 0.03 V before the anodic peak potentials (8).

Irradiations

Irradiations were carried out in Pyrex tubes using a Canadian General Electric Co. 1-kW medium-pressure mercury vapour lamp with a Pyrex cooling jacket immersed in a constant temperature bath held at 10°C. Samples were degassed by nitrogen ebullition for 5 min prior to irradiation.

Fluorescence quenching studies

Fluorescence quenching experiments were performed by using a Perkin–Elmer MPF-66 fluorescence spectrophotometer with a Perkin–Elmer MPF-66 xenon lamp power supply interfaced to a Perkin–Elmer 7500 computer. Solutions were 0.01 M in 1,4-dicyanobenzene (**2**). The quencher concentrations ranged from 0.01 to 0.03 M. Solutions were degassed on a vacuum line by three freeze–pump–thaw cycles. The excitation wavelength was 293 nm; the emission was monitored at 309.4 nm. From the previously measured singlet lifetime of **2**, 8.8 × 10^{-9} s (10), both isomers quench the fluorescence with a rate constant of 2.8 × 10^{10} s^{-1}.

Calculations

Molecular mechanics calculations were carried out on a VAX 8800 mainframe computer. The 1989 force field of MM3 and the 1987 force field of MMP2 were used. The dihedral driver option was used to rotate the phenyl group.

Materials

Solvents were distilled prior to use. Acetonitrile and 1,4-dicyanobenzene (**2**) (Aldrich Chem. Co.) were purified as previously described (19). Bromobenzene, 2-methylcyclopentanone, and 1-bromo-3-phenylpropane were obtained from the Aldrich Chemical Company. Decalin and 2,4,6-collidine were obtained from BDH, *o*-chlorotoluene was obtained from Matheson Coleman and Bell, allyl bromide was obtained from Fisher, and cyclododecane was obtained from K & K Laboratories.

Preparation of compounds

Preparation of cis *1-methyl-2-phenylcyclopentane (***1**b cis*)*

2-Methyl-1-phenylcyclopentanol was prepared by a Grignard reaction (7*a*). Bromobenzene (43 mL, 64 g, 0.41 mol) was added to magnesium turnings (10 g, 0.41 mol) in anhydrous diethyl ether. When reaction was complete, the flask was cooled in ice, and 2-methylcyclopentanone (15 mL, 14 g, 0.14 mol) was added dropwise. The reaction mixture was poured into a mixture of concentrated HCl and ice, and then extracted with ether. The combined organic layer was washed with 5% $NaHCO_3$ and with distilled water. Finally, the organic layer was dried over $MgSO_4$ and the solvent was evaporated.

The alcohol was refluxed with *p*-toluenesulfonic acid in benzene. Water was removed by using a Dean–Stark trap. The crude 1-methyl-2-phenylcyclopentene was chromatographed with hexanes on silica gel.

The cyclopentene was hydrogenated over 10% Pd on carbon in ethanol. Chromatography of the product on silica gel with hexanes gave 1-methyl-2-phenylcyclopentane in 88% purity, 30% yield. Preparative gas chromatography was used to prepare samples of 99% purity; ^1H nmr (360 MHz) in $CDCl_3$: 7.1–7.3 (m, 5H), 3.1 (m, 1H), 2.3 (m, 1H), 1.8–2.0 (m, 4H), 1.7 (m, 1H), 1.4 (m, 1H), 0.6 (d, 3H, J = 7.1 Hz).

Preparation of trans *1-methyl-2-phenylcyclopentane (***1**b trans*)*

The synthesis of the *trans* isomer followed the procedure of Pines and co-workers (7*b*, *c*). The first step involves the synthesis of 6-phenyl-1-hexene. 1-Bromo-3-phenylpropane (24 mL, 31 g, 0.16 mol) was added to magnesium turnings (3.8 g, 0.16 mol) in anhydrous diethyl ether. When reaction was complete, allyl bromide (14 mL, 20 g, 0.16 mol) was added dropwise. After the addition was complete, the reaction mixture was refluxed for 16 h. The mixture was cooled and poured into a slurry of concentrated HCl and ice. The aqueous layer was extracted with ether, and the combined organic extracts were washed with 5% $NaHCO_3$ and then with distilled water. The organic extract was dried over $MgSO_4$ and the solvent was evaporated. The crude product was chromatographed on silica gel with hexanes. 6-Phenyl-1-hexene was obtained in 68% yield.

Potassium (0.94 g, 0.024 mol) and *o*-chlorotoluene (0.40 mL, 0.43 g, 0.0034 mol) were refluxed in decalin (25 mL) for 15 min. 6-Phenyl-1-hexene (7.43 g, 0.046 mol) was added dropwise, and the mixture was refluxed for 25.5 h. The black, sludgy reaction mixture was chilled in ice, and isopropanol was added to decompose any remaining potassium. The mixture was diluted with hexanes (100 mL) and filtered to remove the sediment. The filtrate was washed with distilled water until neutral. The organic layer was dried over $CaCl_2$, and the hexanes were evaporated. The remaining solution was distilled under reduced pressure to remove most of the decalin. The residue was chromatographed on silica gel with hexanes as the eluent to give 85% pure *trans* in 34% yield from 6-phenyl-1-hexene. Small quantities of pure *trans* were obtained by preparative gas chromatography; ^1H nmr (360 MHz) in $CDCl_3$: 7.1–7.3 (m, 5H), 2.4 (m, 1H), 1.9–2.1 (m, 3H), 1.7–1.8 (m, 3H), 1.3 (m, 1H), 0.9 (d, 3H, J = 6.4 Hz).

Irradiations

Irradiations of cis *1-methyl-2-phenylcyclopentane (***1**b cis*)*

A solution of 99% pure *cis* isomer (14 mg, 8.7 × 10^{-5} mol), 1,4-dicyanobenzene (**2**) (7.2 mg, 5.6 × 10^{-5} mol), 2,4,6-collidine (**3**) (17 mg, 1.4 × 10^{-4} mol), and cyclododecane (5.2 mg, 3.1 × 10^{-5} mol) in acetonitrile (3 mL) was irradiated for 4 days. Progress of the reaction was followed by gc/fid, using the peak due to cyclododecane as an internal standard. The yield of *trans* isomer was 24% at 50% conversion.

A solution of 99% pure *cis* isomer (15 mg, 9.5 × 10^{-5} mol), (**2**) (8.8 mg, 6.9 × 10^{-5} mol), (**3**) (20 mg, 1.6 × 10^{-4} mol), and cyclododecane (6.3 mg, 3.7 × 10^{-5} mol) was irradiated in acetonitrile–methanol-*O*-*d* (3 mL, 3:1) for 4 days. The *trans* isomer was formed in 17% yield at 46% conversion (gc/fid). Some of the *cis*

isomer and all of the *trans* isomer had incorporated one atom deuterium (gc/ms). Analysis of the ^1H and ^2H nmr spectra indicate exchange occurred at the benzylic position.

A solution of 95% pure *cis* isomer (9.2 mg, 5.7×10^{-5} mol), (**2**) (6.4 mg, 5.0×10^{-5} mol), and cyclododecane (4.4 mg, 2.6×10^{-5} mol) in acetonitrile (2 mL) was irradiated for 1 day. At 74% conversion, the yield of the *trans* isomer was 7% (gc/fid).

A stirred solution of 99% pure *cis* isomer (0.18 g, 1.1×10^{-3} mol), (**2**) (0.56 g, 4.4×10^{-3} mol), and (**3**) (0.28 g, 2.3×10^{-3} mol) in acetonitrile (60 mL) was irradiated for 1 day. The photolysate was chromatographed on silica gel using 1:1 hexanes–CH_2Cl_2 as the eluent. 1-(4-Cyanophenyl)-2-methyl-1-phenylcyclopentane (**4**) was isolated in 36% yield (72% conversion); ir: 3065 (w), 3040 (w), 3010 (w), 2940 (s), 2860 (s), 2215 (s), 1730 (w), 1600 (s), 1500 (m), 1490 (s), 1455 (m), 1445 (m), 1400 (w), 1375 (w), 1015 (w), 885 (w), 815 (s), 740 (m), 715 (m), 685 (s). ^1H nmr (360 MHz) in $CDCl_3$: 7.0–7.5 (m, 9H), 2.8 (m, 1H), 2.6 (m, 1H), 1.8–2.1 (m, 3H), 1.6 (m, 1H), 1.4 (m, 1H), 0.8 (d, 3H); ^{13}C nmr (90 MHz) in $CDCl_3$: 155.4 (s), 145.0 (s), 131.8 (d), 128.8 (d), 128.0 (d), 127.8 (d), 126.0 (d), 119.1 (s), 109 (s), 58.8 (s), 39.3 (d), 38.8 (t), 32.1 (t), 21.4 (t), 17.6 (q). Exact Mass calcd. for $C_{19}H_{19}N$: 261.1517; found: 261.1517.

Irradiations of trans *1-methyl-2-phenylcyclopentane (***1**b trans*)*

A solution of a mixture of isomers, 86% *trans*:14% *cis* (12 mg, 7.8×10^{-5} mol), 1,4-dicyanobenzene (**2**) (11 mg, 8.7×10^{-5} mol), and 2,4,6-collidine (**3**) (15 mg, 1.2×10^{-4} mol) in acetonitrile (3 mL) was irradiated for 7 days. The ratio of isomers in the irradiated mixture was 97:3 *trans*:*cis*.

A solution of 99% pure *trans* isomer (10 mg, 6.2×10^{-5} mol), (**2**) (6.1 mg, 4.8×10^{-5} mol), (**3**) (14 mg, 1.2×10^{-4} mol), and cyclododecane (4.3 mg, 2.6×10^{-5} mol) in acetonitrile (3 mL) was irradiated for 6 days. No volatile products were detected by gc/fid.

A solution of 99% pure *trans* isomer (10 mg, 6.5×10^{-5} mol), (**2**) (5.4 mg, 4.2×10^{-5} mol), (**3**) (14 mg, 1.2×10^{-4} mol), and cyclododecane (4.2 mg, 2.5×10^{-5} mol) in acetonitrile-methanol-*O*-*d* (3 mL, 3:1) was irradiated for 6 days. No volatile products were detected by gc/fid. No deuterium incorporation was detected in the *trans* isomer (gc/ms).

Acknowledgements

This work was supported by the Natural Sciences and Engineering Research Council of Canada. We thank Dr. D. L. Hooper at the Atlantic Regional Magnetic Resonance Centre at Dalhousie University for the 360-MHz nmr spectra. We also thank Drs. T. B. Grindley and Y. R. Luo for helpful discussions.

1. (*a*) X. Du, D. R. Arnold, R. J. Boyd, and Z. Shi. Can. J. Chem. **69**, 1365 (1991); (*b*) D. R. Arnold, X. Du, K. M. Henseleit. Can. J. Chem. **69**, 839 (1991).
2. (*a*) D. R. Arnold, L. J. Lamont, and A. L. Perrott. Can. J. Chem. **69**, 225 (1991); (*b*) D. R. Arnold and L. J. Lamont. Can. J. Chem. **67**, 2119 (1989).
3. (*a*) R. Popielarz and D. R. Arnold. J. Am. Chem. Soc. **112**, 3068 (1990); (*b*) L. W. Reichel, G. W. Griffin, A. J. Muller, P. K. Das, and S. N. Ege. Can. J. Chem. **62**, 424 (1984); (*c*) D. F. Eaton. Pure Appl. Chem. **56**, 1191 (1984); (*d*) P. Maslak and W. H. Chapman, Jr. Tetrahedron, **46**, 2715 (1990); (*e*) X. Ci and D. G. Witten. J. Am. Chem. Soc. **111**, 3459 (1989).
4. (*a*) D. R. Arnold and S. A. Mines. Can. J. Chem. **67**, 689 (1989); (*b*) Can. J. Chem. **65**, 2312 (1987).
5. (*a*) A. M. de P. Nicholas and D. R. Arnold. Can. J. Chem. **60**, 2165 (1982); (*b*) F. G. Bordwell, J.-P. Cheng, and M. J. Bausch. J. Am. Chem. Soc. **110**, 2867 (1988); (*c*) M. M. Green, S. L. Mielke, and T. Mukhopadhyay. J. Org. Chem. **49**, 1276 (1984); (*d*) J. M. Masnovi, S. Sankararaman, and J. K. Kochi. J. Am. Chem. Soc. **111**, 2263 (1989); (*e*) V. D. Parker, Y. Chao, and B. Reitstoen. J. Am. Chem. Soc. **113**, 2336 (1991).
6. (*a*) L. M. Tolbert, R. K. Khanna, A. E. Popp, L. Gelbaum, and L. A. Bottomley. J. Am. Chem. Soc. **112**, 2373 (1990); (*b*) F. D. Lewis. Acc. Chem. Res. **19**, 401 (1986); (*c*) P. J. Wagner, R. J. Truman, A. E. Puchalski, and R. Wake. J. Am. Chem. Soc. **108**, 7727 (1986); (*d*) T. Shono and Y. Matsumura. J. Org. Chem. **35**, 4157 (1970).
7. (*a*) A. F. Platé, A. A. Mel'nikov, T. A. Italinskaya, and R. A. Zelenko. Zh. Obshchei Khim. **30**, 1250 (1960); (*b*) E. Lewicki, H. Pines, and N. C. Sih. Chem. Ind. 154 (1964); (*c*) H. Pines, N. C. Sih, and E. Lewicki. J. Org. Chem. **30**, 1457 (1965).
8. (*a*) R. S. Nicholson and I. Shain. Anal. Chem. **36**, 706 (1964); (*b*) **37**, 178 (1965).
9. (*a*) U. Burkert and N. L. Allinger. Molecular mechanics. American Chemical Society, Washington, DC. 1982; (*b*) N. L. Allinger. J. Am. Chem. Soc. **99**, 8127 (1977); (*c*) N. L. Allinger, Y. H. Yuh, and J.-H. Lii. J. Am. Chem. Soc. **111**, 8551 (1989); (*d*) K. B. Lipkowitz and N. L. Allinger. QCPE Bull. **7**, 19 (1987).
10. R. M. Borg, D. R. Arnold, and T. S. Cameron. Can. J. Chem. **62**, 1785 (1984).
11. D. Rehm and A. Weller. Isr. J. Chem. **8**, 259 (1970).
12. (*a*) R. A. Marcus. Discuss. Faraday Soc. **29**, 21 (1960); (*b*) I. R. Gould, D. Ege, S. L. Mattes, and S. Farid. J. Am. Chem. Soc. **109**, 3794 (1987); (*c*) I. R. Gould, D. Ege, J. E. Moser, and S. Farid. J. Am. Chem. Soc. **112**, 4290 (1990).
13. (*a*) M. Karplus. J. Chem. Phys. **30**, 11 (1959); (*b*) J. Am. Chem. Soc. **85**, 2870 (1963).
14. (*a*) D. A. Robaugh and S. E. Stein. Int. J. Chem. Kinet. **13**, 445 (1981); (*b*) S. W. Benson. Thermochemical kinetics. 2nd ed. Wiley–Interscience, New York. 1976; (*c*) B. G. Cox, G. R. Hedwig, A. J. Parker, and D. W. Watts. Aust. J. Chem. **27**, 477 (1974); (*d*) CODATA Bull. No. 28, ICSU CODATA, Paris 1978. J. Chem. Thermodyn. **10**, 903 (1978).
15. C. J. Schlesener, C. Amatore, and J. K. Kochi. J. Am. Chem. Soc. **106**, 7472 (1984).
16. D. D. M. Wayner, D. J. McPhee, and D. Griller. J. Am. Chem. Soc. **110**, 132 (1988).
17. J. B. Pedley and J. Rylance. Sussex N.P.L. Computer Analysed Thermochemical Data. Organic and Organometalic Compounds. University of Sussex, 1977.
18. D. D. M. Wayner and D. R. Arnold. Can. J. Chem. **63**, 871 (1985).
19. A. Okamoto, M. S. Snow, and D. R. Arnold. Tetrahedron, **42**, 6175 (1986).

Can. J. Chem. Downloaded from www.nrcresearchpress.com by 123.30.183.119 on 09/08/12
For personal use only.

Characterization of the triplet excited state of the phenylxanthenium carbocation[1]

L. J. JOHNSTON[2] AND D. F. WONG

Steacie Institute for Molecular Sciences, National Research Council Canada, Ottawa, Ont., Canada K1A 0R6

Received August 16, 1991

L. J. JOHNSTON and D. F. WONG. Can. J. Chem. **70**, 280 (1992).

The triplet excited state of the 9-phenylxanthenium cation has been observed directly by both luminescence and transient absorption techniques. The triplet–triplet absorption shows $\lambda_{max} \leq 300$ nm and decays over a period of several microseconds in the absence of easily oxidized donors. The triplet cation reacts with 9-phenylxanthydrol and biphenyl via electron transfer to give the corresponding radical and radical cation and also reacts rapidly with both oxygen and 1,3-cyclohexadiene.

Key words: carbocations, triplets, electron transfer, laser flash photolysis.

L. J. JOHNSTON et D. F. WONG. Can. J. Chem. **70**, 280 (1992).

Utilisant des techniques de luminescence et d'absorption d'espèces transitoires, on a observé l'état excité triplet du cation 9-phénylxanthénium directement. L'absorption triplet–triplet présente un λ_{max} à $\leq$300 nm et, en l'absence de donneurs facilement oxydables, elle décroit sur une période de plusieurs microsecondes. Le cation triplet réagit avec le 9-phénylxanthydrol et le biphényle par le biais d'un transfert d'électrons qui conduit au radical et au cation radical correspondant et il réagit aussi rapidement avec l'oxygène ainsi que le cyclohexa-1,3-diène.

Mots clés : carbocations, triplets, transfert d'électrons, photolyse éclair au laser.

[Traduit par la rédaction]

Despite the large volume of data on the reactivities of photogenerated ground state carbocations (1), there have been relatively few investigations of the excited state behavior of these intermediates (2–12). Most of the available information deals with intramolecular rearrangements such as the photo-cyclization of the triphenylmethyl cation (2) and valence isomerizations of protonated unsaturated carbonyl compounds (3, 5, 6) and a variety of aromatics (7). Until recently the excited states involved in these reactions were not characterized. We recently reported a detailed study of the fluorescent properties of a variety of arylmethyl carbocations and demonstrated that excited singlet xanthenyl and dibenzosuberenyl carbocations undergo efficient intermolecular reaction with aromatic donors via an electron transfer mechanism (8). Similar results have also been reported by Das and co-workers for the 9-phenylxanthenium system (9, 10). Further, reaction of triplet 1-methoxynaphthalene with bis(4-methoxyphenyl)methyl cation results in products derived from electron transfer (13). Herein we describe the first direct observation of the excited triplet state of the 9-phenylxanthenium carbocation using both transient absorption and luminescence techniques.

Stable solutions of the 9-phenylxanthenium carbocation (**1**) can be readily generated by protonation and subsequent dehydration of the parent alcohol (9-phenylxanthydrol, **2**) using moderate concentrations (1–10 mM) of trifluoroacetic acid in 2,2,2-trifluoroethanol (TFE). Laser excitation of **1** in TFE[3] using the third harmonic (355 nm) from a Nd:YAG laser results in a complex transient absorption spectrum (Fig. 1) that changes with both time and concentration of the precursor alcohol. Spectrum A in Fig. 1 shows both bleaching of the cation absorption in the 350–450 nm region and a transient (X) at shorter wavelengths ($\lambda_{max} < 300$ nm). This spectrum was recorded 0.5 μs after the laser pulse for a 10^{-4} M solution of **2**. At later times transient X has almost completely decayed, some of the initial cation bleaching has recovered, and an additional long-lived species is observed at 340 nm. These changes are more apparent at higher initial concentrations of alcohol **2**, as shown in Fig. 1, spectrum B; note that the same cation concentration was obtained for both alcohol concentrations by adjusting the amount of acid to give matched optical densities at 355 nm. The long-lived signal at 340 nm can be readily assigned to the 9-phenylxanthenyl radical (**3**) based on its similarity to the known spectrum for this species (9). Radical **3** has a lifetime in excess of 0.5 ms under our experimental conditions. Examination of kinetic traces at 300 and 340 nm on several different time scales demonstrates that X decays within 5–10 μs at low concentrations of alcohol **2** and that its lifetime decreases with increasing concentrations of **2**. The 340 nm signal assigned to the phenylxanthenyl radical shows a growth that is concomitant with the decay at 300 nm, as shown in Fig. 1, and its yield increases with increasing alcohol concentrations. At low alcohol concentrations very little radical is produced and most of the cation bleaching recovers, with kinetics that are identical to the decay of X at 300 nm. Under conditions where the lifetime of X has been shortened by the addition of **2** only a small amount of the cation bleaching recovers on the maximum time scale that we have examined (400 μs).

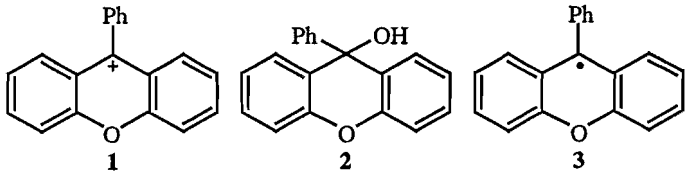

1 **2** **3**

The above observations are consistent with transient X

[1]Issued as NRCC No. 33253.

[2]Author to whom correspondence may be addressed.

[3]All experiments were done using flow samples to eliminate problems associated with sample depletion and product buildup. Samples were deaerated by nitrogen purging unless otherwise noted. The laser flash photolysis setup has been described elsewhere (14).

Can. J. Chem. Downloaded from www.nrcresearchpress.com by 123.30.183.119 on 09/08/12
For personal use only.

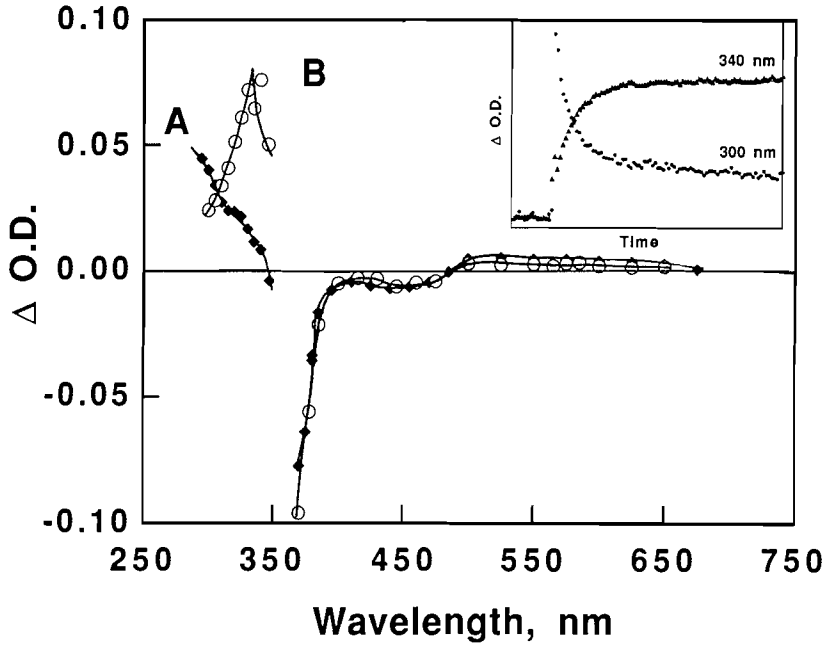

FIG. 1. Transient absorption spectra produced by 355 nm excitation of cation **1** in TFE/H^+: A, 0.13 mM **2**, 0.5 μs delay; B, 0.63 mM **2**, 5 μs delay. Insert: Decay and growth of the transient absorptions at 300 and 340 nm, respectively, following 355 nm excitation of cation **1** in TFE with 0.1 mM initial concentration of alcohol **2**.

reacting with alcohol **2** to generate radical **3**. The rate constants for decay of X at several alcohol concentrations (after correction for the amount of alcohol converted to cation) can be used to calculate an approximate rate constant of 5×10^9 M^{-1} s^{-1} for this reaction. Several additional experiments were carried out in an attempt to identify X. Firstly, the lifetime of X decreased in the presence of air or oxygen (k_q (O_2) ~ 8×10^9 M^{-1} s^{-1}); samples deaerated with oxygen showed no evidence for either X or radical **3**. This is not due to reaction of the singlet cation with oxygen since it was previously demonstrated that the fluorescence lifetime of **1** is the same within experimental error in either oxygen or nitrogen-purged TFE (8). However, addition of sufficient aromatic donor (e.g., anisole) to quench >90% of the excited singlet cations does prevent the formation of both species X and the radical. Secondly, the lifetime of X decreased in the presence of 1,3-cyclohexadiene, with $k_q = 3.5 \times 10^9$ M^{-1} s^{-1}. In this case radical **3** was still formed, again with kinetics that agreed with the decay of the 300 nm transient. Thirdly, excitation of cation **1** in TFE or in ethanol/H^+ glasses at 77 K in a fluorimeter gave weak phosphorescence at 600 nm; the excitation spectrum matched the ground state spectrum of the cation, indicating that the parent alcohol is not the emitting species.

These results suggest that transient X is the triplet excited state of cation **3**. In the absence of quenchers this species decays back to ground state cation with a rate constant that under our conditions is probably limited by traces of oxygen in the sample. The observed oxygen quenching and phosphorescence are consistent with the triplet assignment. The phosphorescence spectrum indicates a triplet energy of approximately 48 kcal, which is reasonable based on the singlet energy of 57 kcal. The triplet reacts with excess alcohol **2** to yield radical **3**, presumably via electron transfer as shown in reaction [1]. Based on the triplet energy and the redox potentials of 0.02 and 0.9 V for radical **3** (15) and alcohol **2** (9), respectively, calculation using the Rehm–Weller equation indicates that reaction [1] is exothermic by ~28 kcal (16). Radical cations in xanthenyl systems have strong absorptions at long wavelength (λ_{max} 900 nm) with a weaker band between 330 and 380 nm (17). The latter would not be readily detectable in our experiments due to overlap with the strong radical signal and cation bleaching. However, there are small differences between the spectrum of **1** and the bleaching observed in the transient experiment, which may indicate some additional absorption in the 350–450 nm region. Further, triplet **2** can be ruled out as a possible candidate for transient X since the latter is not formed by excitation of **2** alone and since the triplet–triplet absorption of **2** has been observed at 440 nm (9).

[1] $\mathbf{1}^* + \mathbf{2} \rightarrow \mathbf{3} + \mathbf{2}^{+\cdot}$

The triplet energy calculated from the phosphorescence spectrum suggests that energy transfer from triplet **1** to 1,3-cyclohexadiene is endothermic by 5–6 kcal/mol. This and the fact that radical **3** is formed efficiently when triplet **1** reacts with diene indicates that this reaction also occurs via electron transfer, which is exothermic by ~7 kcal in this case. The fact that triplet **1** undergoes an efficient electron transfer reaction is confirmed by its rapid reaction with electron donors such as biphenyl. In this case, triplet **1** is quenched with a rate constant of 4.0×10^9 M^{-1} s^{-1}, with the concomitant production of radical **3** and the biphenyl radical cation with its characteristic absorption at 650 nm (17). The efficient electron transfer quenching of triplet **1** is in good agreement with recent reports of efficient electron transfer reactions ($k_q \sim 5 \times 10^9$ M^{-1} s^{-1}) of singlet excited xanthenyl (8, 10) and dibenzosuberenyl (8) cations.

Can. J. Chem. Downloaded from www.nrcresearchpress.com by 123.30.183.119 on 09/08/12
For personal use only.

In conclusion, the present results provide direct luminescence and transient absorption evidence for the first excited triplet state of the phenylxanthenium carbocation. The triplet is formed by intersystem crossing from the first excited singlet state,[4] and has a lifetime on the order of 5–10 μs in TFE in the absence of easily oxidized additives. In accord with our earlier results on the behavior of singlet excited diarylmethyl cations, the triplet excited cation readily undergoes electron transfer reactions with various donors. To our knowledge, this represents the first direct observation and characterization of a triplet excited state arylmethyl carbocation, although protonated triplet benzophenones and xanthones have been reported (18) and triplet ground state aryl cations have been observed in glasses at 77 K (11, 12). In this regard it should also be noted that a triplet state has been postulated as an intermediate in some of the photochemistry of the triphenylmethyl cation, although this was not based on any direct spectroscopic evidence (2, 7). Work aimed at generating other diarylmethyl cations by either direct excitation or sensitization and examining their reactivity is currently in progress.

1. R. A. McClelland, V. M. Kanagasapathy, N. S. Banait, and S. Steenken. J. Am. Chem. Soc. **113**, 1009 (1991); J. Bartl, S. Steenken, H. Mayr, and R. A. McClelland. J. Am. Chem. Soc. **112**, 6918 (1990); S. L. Mecklenburg and E. F. Hilinski. J. Am. Chem. Soc. **111**, 5471 (1989); P. Wan and E. Krogh. J. Am. Chem. Soc. **111**, 4887 (1989).
2. E. E. van Tamelen and T. M. Cole. J. Am. Chem. Soc. **93**, 6158 (1971).
3. R. F. Childs. Rev. Chem. Intermed. **3**, 285 (1980).
4. H. Al-Ekabi and P. de Mayo. J. Org. Chem. **53**, 1471 (1988).
5. R. F. Childs, M. Mahendran, C. Blackburn, and G. Antoniadis. Can. J. Chem. **66**, 1355 (1988).
6. R. F. Childs and B. E. George. Can. J. Chem. **88**, 1343 (1988).
7. P. W. Cabell-Whiting and H. Hogeveen. Adv. Phys. Org. Chem. **10**, 129 (1973).
8. A. Azarani, A. B. Berinstain, L. J. Johnston, and S. Kazanis. J. Photochem. Photobiol. A: **57**, 175 (1991).
9. R. E. Minto and P. K. Das. J. Am. Chem. Soc. **111**, 8858 (1989).
10. A. Samanta, K. R. Gopidas, and P. K. Das. Chem. Phys. Lett. **167**, 165 (1990).
11. H. B. Ambroz and T. J. Kemp. J. Chem. Soc. Faraday Trans. 1, **78**, 1269 (1982).
12. H. B. Ambroz, G. K. Przybtniak, C. Stradowski, and M. Wolszczak. J. Photochem. Photobiol. A: **52**, 369 (1990).
13. L. J. Johnston and T. Kanigan. J. Am. Chem. Soc. **112**, 1271 (1990).
14. S. Kazanis, A. Azarani, and L. J. Johnston. J. Phys. Chem. **95**, 4430 (1991).
15. E. M. Arnett, K. Amarnath, N. G. Harvey, and J.-P. Cheng. J. Am. Chem. Soc. **112**, 344 (1990).
16. D. Rehm and A. Weller. Isr. J. Chem. **8**, 259 (1970).
17. T. Shida. Electronic absorption spectra of radical ions. Elsevier, Amsterdam. 1988.
18. J. F. Ireland and P. A. H. Wyatt. J. Chem. Soc. Faraday Trans. 1, **69**, 161 (1973).

[4]The strong fluorescence (τ = 36 ns) (8) from **1** makes it difficult to confirm that the absorption assigned to triplet **1** has a rise-time equal to the decay of excited singlet **1** or to detect transient absorptions due to the latter species.

Can. J. Chem. Downloaded from www.nrcresearchpress.com by 123.30.183.119 on 09/08/12
For personal use only.

Correlation of the effects of alkyl substituents on the basicities of indoles

PETER A. COHEN AND LOUIS A. COHEN[1]

Laboratory of Bioorganic Chemistry, National Institute of Diabetes and Digestive and Kidney Diseases, National Institutes of Health, Bethesda, MD 20892, U.S.A.

Received April 29, 1991

PETER A. COHEN and LOUIS A. COHEN. Can. J. Chem. **70**, 282 (1992).

Alkyl groups at C-2 of indole increase basicity at the site of protonation, C-3, while alkyl groups at C-3 decrease basicity. These opposing effects can be incorporated, for both the isomeric mono- and 2,3-dialkylindoles, into a single linear free energy correlation, $pK_a = -10.05\Sigma\sigma - 3.94$, in which $\Sigma\sigma = \sigma_p^+(\text{C-2}) + 0.60[\sigma_m^+(\text{C-3}) + 0.08D_s - 0.084]$ and D_s is the double bond stabilization parameter at C-3. An analogous correlation for *N*-methylindoles, $pK_a = -8.64\Sigma\sigma - 2.80$, reveals that the effect of *N*-alkylation on basicity is predictable but not additive.

Key words: alkylindoles, carbon basicity, free energy correlation, substituent effects, *N*-alkyl effect.

PETER A. COHEN et LOUIS A. COHEN. Can. J. Chem. **70**, 282 (1992).

Alors que la présence de groupes alkyles en C-2 des indoles augmente leur basicité, celle de groupes alkyles en C-3 provoque une diminution de cette basicité. Il est possible d'incorporer ces effets opposés, tant pour des dérivés mono- ou 2,3-dialkylindoles, dans une seule corrélation linéaire d'énergie libre, $pK_a = -10{,}05\Sigma\sigma - 3{,}94$, dans laquelle $\Sigma\sigma = \sigma_p^+(\text{C-2}) + 0{,}60[\sigma_m^+(\text{C-3}) + 0{,}08D_s - 0{,}084]$ et D_s est le paramètre de stabilisation de la liaison double en C-3. Une corrélation analogue pour les *N*-méthylindoles, $pK_a = -8{,}64\Sigma\sigma - 2{,}80$, révèle qu'il est possible de prédire l'effet de la *N*-alkylation sur la basicité, mais que cet effet n'est pas additif.

Mots clés : alkylindoles, la basicité de carbone, corrélation d'énergie libre, effets de substituant, effet de la *N*-alkylation.

[Traduit par la rédaction]

Our continuing studies on the chemistry of indoles and bioindoles (1) have sometimes required estimates of basicity at the normal site of protonation, C-3 (2). Since such estimates depend on extrapolation from linear free energy

[1]Author to whom correspondence may be addressed.

In conclusion, the present results provide direct luminescence and transient absorption evidence for the first excited triplet state of the phenylxanthenium carbocation. The triplet is formed by intersystem crossing from the first excited singlet state,[4] and has a lifetime on the order of 5–10 μs in TFE in the absence of easily oxidized additives. In accord with our earlier results on the behavior of singlet excited diarylmethyl cations, the triplet excited cation readily undergoes electron transfer reactions with various donors. To our knowledge, this represents the first direct observation and characterization of a triplet excited state arylmethyl carbocation, although protonated triplet benzophenones and xanthones have been reported (18) and triplet ground state aryl cations have been observed in glasses at 77 K (11, 12). In this regard it should also be noted that a triplet state has been postulated as an intermediate in some of the photochemistry of the triphenylmethyl cation, although this was not based on any direct spectroscopic evidence (2, 7). Work aimed at generating other diarylmethyl cations by either direct excitation or sensitization and examining their reactivity is currently in progress.

1. R. A. McClelland, V. M. Kanagasapathy, N. S. Banait, and S. Steenken. J. Am. Chem. Soc. **113**, 1009 (1991); J. Bartl, S. Steenken, H. Mayr, and R. A. McClelland. J. Am. Chem. Soc. **112**, 6918 (1990); S. L. Mecklenburg and E. F. Hilinski. J. Am. Chem. Soc. **111**, 5471 (1989); P. Wan and E. Krogh. J. Am. Chem. Soc. **111**, 4887 (1989).
2. E. E. van Tamelen and T. M. Cole. J. Am. Chem. Soc. **93**, 6158 (1971).
3. R. F. Childs. Rev. Chem. Intermed. **3**, 285 (1980).
4. H. Al-Ekabi and P. de Mayo. J. Org. Chem. **53**, 1471 (1988).
5. R. F. Childs, M. Mahendran, C. Blackburn, and G. Antoniadis. Can. J. Chem. **66**, 1355 (1988).
6. R. F. Childs and B. E. George. Can. J. Chem. **88**, 1343 (1988).
7. P. W. Cabell-Whiting and H. Hogeveen. Adv. Phys. Org. Chem. **10**, 129 (1973).
8. A. Azarani, A. B. Berinstain, L. J. Johnston, and S. Kazanis. J. Photochem. Photobiol. A: **57**, 175 (1991).
9. R. E. Minto and P. K. Das. J. Am. Chem. Soc. **111**, 8858 (1989).
10. A. Samanta, K. R. Gopidas, and P. K. Das. Chem. Phys. Lett. **167**, 165 (1990).
11. H. B. Ambroz and T. J. Kemp. J. Chem. Soc. Faraday Trans. 1, **78**, 1269 (1982).
12. H. B. Ambroz, G. K. Przybtniak, C. Stradowski, and M. Wolszczak. J. Photochem. Photobiol. A: **52**, 369 (1990).
13. L. J. Johnston and T. Kanigan. J. Am. Chem. Soc. **112**, 1271 (1990).
14. S. Kazanis, A. Azarani, and L. J. Johnston. J. Phys. Chem. **95**, 4430 (1991).
15. E. M. Arnett, K. Amarnath, N. G. Harvey, and J.-P. Cheng. J. Am. Chem. Soc. **112**, 344 (1990).
16. D. Rehm and A. Weller. Isr. J. Chem. **8**, 259 (1970).
17. T. Shida. Electronic absorption spectra of radical ions. Elsevier, Amsterdam. 1988.
18. J. F. Ireland and P. A. H. Wyatt. J. Chem. Soc. Faraday Trans. 1, **69**, 161 (1973).

[4]The strong fluorescence (τ = 36 ns) (8) from **1** makes it difficult to confirm that the absorption assigned to triplet **1** has a rise-time equal to the decay of excited singlet **1** or to detect transient absorptions due to the latter species.

Can. J. Chem. Downloaded from www.nrcresearchpress.com by 123.30.183.119 on 09/08/12
For personal use only.

Correlation of the effects of alkyl substituents on the basicities of indoles

PETER A. COHEN AND LOUIS A. COHEN[1]

Laboratory of Bioorganic Chemistry, National Institute of Diabetes and Digestive and Kidney Diseases, National Institutes of Health, Bethesda, MD 20892, U.S.A.

Received April 29, 1991

PETER A. COHEN and LOUIS A. COHEN. Can. J. Chem. **70**, 282 (1992).

Alkyl groups at C-2 of indole increase basicity at the site of protonation, C-3, while alkyl groups at C-3 decrease basicity. These opposing effects can be incorporated, for both the isomeric mono- and 2,3-dialkylindoles, into a single linear free energy correlation, $pK_a = -10.05\Sigma\sigma - 3.94$, in which $\Sigma\sigma = \sigma_p^+(\text{C-2}) + 0.60[\sigma_m^+(\text{C-3}) + 0.08D_s - 0.084]$ and D_s is the double bond stabilization parameter at C-3. An analogous correlation for *N*-methylindoles, $pK_a = -8.64\Sigma\sigma - 2.80$, reveals that the effect of *N*-alkylation on basicity is predictable but not additive.

Key words: alkylindoles, carbon basicity, free energy correlation, substituent effects, *N*-alkyl effect.

PETER A. COHEN et LOUIS A. COHEN. Can. J. Chem. **70**, 282 (1992).

Alors que la présence de groupes alkyles en C-2 des indoles augmente leur basicité, celle de groupes alkyles en C-3 provoque une diminution de cette basicité. Il est possible d'incorporer ces effets opposés, tant pour des dérivés mono- ou 2,3-dialkylindoles, dans une seule corrélation linéaire d'énergie libre, $pK_a = -10{,}05\Sigma\sigma - 3{,}94$, dans laquelle $\Sigma\sigma = \sigma_p^+(\text{C-2}) + 0{,}60[\sigma_m^+(\text{C-3}) + 0{,}08D_s - 0{,}084]$ et D_s est le paramètre de stabilisation de la liaison double en C-3. Une corrélation analogue pour les *N*-méthylindoles, $pK_a = -8{,}64\Sigma\sigma - 2{,}80$, révèle qu'il est possible de prédire l'effet de la *N*-alkylation sur la basicité, mais que cet effet n'est pas additif.

Mots clés : alkylindoles, la basicité de carbone, corrélation d'énergie libre, effets de substituant, effet de la *N*-alkylation.

[Traduit par la rédaction]

Our continuing studies on the chemistry of indoles and bioindoles (1) have sometimes required estimates of basicity at the normal site of protonation, C-3 (2). Since such estimates depend on extrapolation from linear free energy

[1]Author to whom correspondence may be addressed.

TABLE 1. Values of pK_a, σ^+, and $\Sigma\sigma$ for alkylindoles

Compound	C-2(α)	C-3(β)	a(NH) pK_a[a]	b(NMe) pK_a[a]	σ_p^+[b]	σ_m^+[b]	D_s[c]	$\Sigma\sigma$[d]
1	Me	H	−0.28	0.30	−0.31		3.18	−0.36
2	Et	H	−0.41		−0.30		3.18	−0.35
3	Me	*n*-Pr	−1.40		−0.31	−0.08	3.18	−0.26
4	Me	Me	−1.49	−0.66	−0.31	−0.07	3.18	−0.25
5	H	H	−3.50	−2.32	0	0	0	−0.05
6	H	*t*-Bu[e]	−3.84			−0.06	3.18	0.07
7	H	Et	−4.25			−0.08	3.18	0.05
8	H	*n*-Pr	−4.34			−0.08	3.18	0.06
9	H	Me	−4.55	−3.30		−0.07	3.18	0.06
10	H	CH_2COOH	−6.13	−4.60		0.17[f]	3.18	0.20
11	H	$CH_2CH_2NH_3^+$	−6.31			0.23[f]	3.00	0.23

[a]Data from ref. 3.
[b]Data from ref. 5.
[c]In the absence of D_s values for specific substituents (except methyl), the values used are estimates based on Table 2 in ref. 6.
[d]Calculated from eq. [1].
[e]Not included in statistical analysis.
[f]The value of σ_m^0 was taken as the approximate equivalent of σ_m^+.

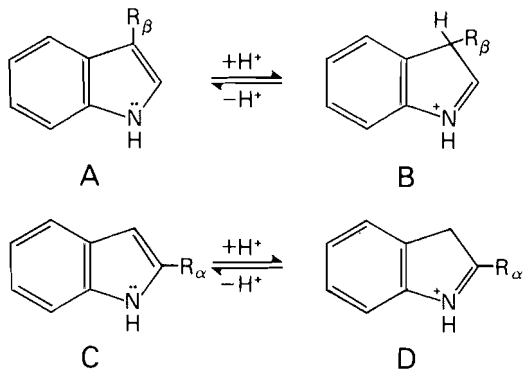

SCHEME 1

relationships, we have attempted to establish such relationships based on the series of pK_a values determined by Hinman and Lang (3) for alkylindoles. These investigators discovered an unexpected property of the pyrrole ring of indole: while an alkyl group at C-2 increases basicity at C-3, an alkyl group at C-3 *decreases* basicity. Quite appropriately, Hinman and Lang argued that an electron-releasing group at C-3 should stabilize the neutral indole (A in Scheme 1) at the expense of its protonated form (B); conversely, the same group at C-2 should stabilize D more effectively than C.

A useful but limited analogy is encountered in the acid-catalyzed hydration of substituted alkenes (4): while protonation of the alkene is consistently the rate-determining step in the hydration process (Scheme 2), we have found (1) that C-3 protonation of indoles is rate determining under conditions of intramolecular proton transfer, but is a rapid equilibrium process in the presence of stronger external acid. For the protonation of alkenes, Knittel and Tidwell (4) achieved a linear correlation of log *k* with a complex parameter, eq. [1], in which σ_p^+ is the electrophilic substituent constant (5)

$$[1]\quad \Sigma\sigma = \sigma_p^+(R_\alpha) + 0.60[\sigma_m^+(R_\beta) + 0.08D_s - 0.084]$$

for the group (R_α in Scheme 2) at the olefinic carbon which becomes the carbocation, σ_m^+ is the analogous constant for the substituent (R_β) on the adjacent carbon, and D_s is the double bond stabilization parameter (6) for the β substituent. Since there is a degree of parallelism between the electronic effects expected of substituents on the protonation of alkenes (Scheme 2) and of alkylindoles (Scheme 1), we applied Tidwell's analysis to the indole series (Table 1), taking C-2 as the α carbon and C-3 as β. We were indeed gratified to observe the correlations shown in Fig. 1 and summarized in eqs. [2] and [3]. The only deviant member

$$[2]\quad \text{NH Series(a)}\quad pK_a = -10.05\Sigma\sigma - 3.94 \quad (r = 0.9990)$$

$$[3]\quad \text{N-Me Series(b)}\quad pK_a = -8.64\Sigma\sigma - 2.80 \quad (r = 0.9997)$$

of the set is 3-*tert*-butylindole (**6***a*), which is almost one p*K* unit *more* basic than predicted. Indeed, space-filling models reveal that steric crowding between the *tert*-butyl group and H-4 in the neutral indole is markedly relieved by conversion of C-3 to a tetrahedral carbon, as would occur in protonation.

Of course, it would be desirable to test the validity of eqs.

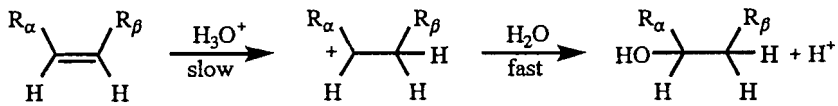

SCHEME 2

Can. J. Chem. Downloaded from www.nrcresearchpress.com by 123.30.183.119 on 09/08/12
For personal use only.

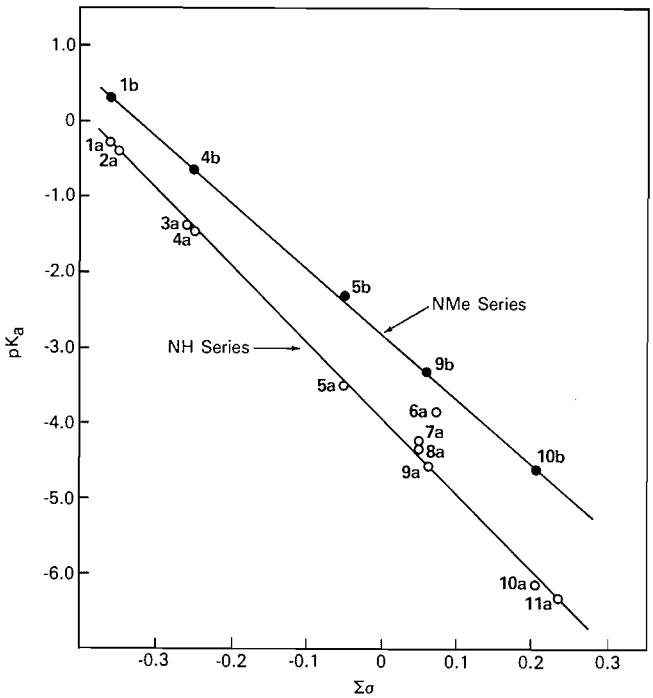

FIG. 1. Plots of the dependence of observed pK_a values for indoles (open circles) and for *N*-methylindoles (closed circles) on $\Sigma\sigma$ (see eq. [1] and Table 1); regression lines and correlation coefficients are given in eqs. [2] and [3], respectively.

[2] and [3] with other substituents. While 2- and 3-alkylindoles exist overwhelmingly as their indole tautomers (7), indoles with stronger electron-releasing groups at C-2 may have to be excluded from analysis because of their partial or total preference for the indolenine tautomer (8). Furthermore, strong electron-withdrawing groups should reduce indole basicity to a level at which measurement of protonation equilibria would become difficult. For example, pK_a values of -8.9 for 3-nitroindole and -12.8 for 2-nitroindole are predicted from eq. [2].

Figure 1 also reveals that the effect of *N*-methylation on pK_a is not constant, a phenomenon we have already observed in the imidazole series (9). While *N*-methylation generally increases basicity at C-3 (Table 1), extrapolation of the slopes of Fig. 1 beyond the point of intersection requires a reversal in order, in that *N*-methylation should result in a decrease in basicity for indoles containing stronger electron-releasing groups at C-2.

Even within the limited range of alkyl substituents, our method of correlation is probably not applicable to pyrroles, for which α-protonation is preferred but is often redirected by other substituents (10). On the other hand, there may be additional indole-like heterocyclic systems (e.g., carbolines) for which this treatment of substituent effects is applicable.

1. R. S. Phillips and L. A. Cohen. Tetrahedron Lett. **24**, 5555 (1983); J. Am. Chem. Soc. **108**, 2023 (1986).
2. R. L. Hinman and E. B. Whipple. J. Am. Chem. Soc. **84**, 2534 (1962).
3. R. L. Hinman and J. Lang. J. Am. Chem. Soc. **86**, 3796 (1964).
4. P. Knittel and T. T. Tidwell. J. Am. Chem. Soc. **99**, 3408 (1977).
5. O. Exner. *In* Correlation analysis in chemistry. *Edited by* N. B. Chapman and J. Shorter. Plenum Press, New York. 1978. p. 439.
6. J. Hine and N. W. Flachskam, J. Am. Chem. Soc. **95**, 1179 (1973).
7. L. A. Cohen, J. Daly, H. Kny, and B. Witkop. J. Am. Chem. Soc. **82**, 2184 (1960).
8. T. Hino, M. Nakagawa, T. Hashizume, N. Yamagi, and Y. Miwa. Tetrahedron, **27**, 775 (1971); J. Harley-Mason and T. J. Leeney. Proc. Chem. Soc. 369 (1964); J. Kebrle and K. Hoffmann. Helv. Chim. Acta, **39**, 116 (1956).
9. Y. Takeuchi, K. L. Kirk, and L. A. Cohen. J. Org. Chem. **43**, 3570 (1978).
10. Y. Chiang and E. B. Whipple. J. Am. Chem. Soc. **85**, 2763 (1963); J. Catalan and M. Yanez. J. Am. Chem. Soc. **106**, 421 (1984).

Can. J. Chem. Downloaded from www.nrcresearchpress.com by 123.30.183.119 on 09/08/12
For personal use only.

Molecular orbital calculation using spectral representation technique

SHINICHI KATSUKI

Department of Physics, College of General Education, Kyushu University, Fukuoka 810, Japan

Received June 25, 1991

This paper is dedicated to Professor Sigeru Huzinaga on the occasion of his 65th birthday

SHINICHI KATSUKI. Can. J. Chem. **70**, 285 (1992).

The spectral representation technique as a tool for molecular orbital calculation is introduced. The procedure for getting a potential in spectral representation is simple and straightforward. The technique is also shown to be versatile to apply to the so-called effective core-potential case, to the relativistic case, to the non-spherical frozen-area case, to the case of approximate estimation of the electronic structures of molecules without the self-consistent-field process, and to the case of incorporating external effect into the cluster by environment potential.

Key words: spectral representation, molecular orbital calculation, electronic structure, relativistic potential, environment potential.

SHINICHI KATSUKI. Can. J. Chem. **70**, 285 (1992).

On introduit la technique de la représentation spectrale comme outil pour calculer des orbitales moléculaires. La méthode permettant d'obtenir un potentiel dans la représentation spectrale est simple et directe. On a aussi démontré que la méthode est versatile et qu'on peut l'appliquer au soit-disant cas du potentiel efficace du noyau, au cas relativiste, au cas de la surface définie non-sphérique, au cas de l'évaluation approximative des structures électroniques de molécules sans processus de champ auto-cohérent et au cas de l'incorporation, grâce au potentiel de l'environnement, de l'effet externe dans l'agglomération.

Mots clés : représentation spectrale, calculs d'orbitales moléculaires, structure électronique, potentiel relativiste, potentiel de l'environnement.

[Traduit par la rédaction]

Can. J. Chem. Downloaded from www.nrcresearchpress.com by 92.62.229.171 on 09/08/12
For personal use only.

Introduction

Recently an *ab initio* effective Hamiltonian method was introduced for valence-electron molecular calculations (1, 2). In this method the mathematical technique of spectral representation was used to replace the core-valence interactions with a so-called effective core potential. The method has some characteristic features. First, once the reference all-electron Hartree–Fock–Roothaan calculations for constituent atoms are done, a practical effective Hamiltonian for active electrons of a molecule is obtained in a straightforward manner without any parameter fitting or adjustment procedure. Second, the relativistic effects can be included properly in the effective Hamiltonian (3, 4). Third, the method can handle cases in which the frozen area has a non-spherical shape.

The natural extension of the effective Hamiltonian formalism leads to the linear combination of atomic operator (LCAOP) method or the *ab initio* Hückel (abiHück) method (5), where the potential due not only to the core electrons but all electrons is expressed in the spectral representation.

The effective Hamiltonian method will be briefly reviewed with some newly obtained results in the next section and a description of the LCAOP method will follow. The last section summarizes our approach.

Effective Hamiltonian method and some applications

The molecular orbital theory within the Hartree–Fock approximation has been well established. According to the theory, the energy and many properties of a stationary state of a molecule can be obtained by solving the Schrödinger equation

$$[1] \quad H\Psi = E\Psi$$

where the eigenfunction Ψ is expressed in terms of molecular orbitals ψ_i that satisfy the Hartree–Fock equation

$$[2] \quad F\psi_i = \epsilon_i\psi_i$$

with the Fock operator F (in the case of closed-shell electron configuration)

$$[3] \quad F = -\frac{1}{2}\Delta - \sum_{\mathrm{A}} \frac{Z_{\mathrm{A}}}{r_{\mathrm{A}}} + \sum_{j}^{n} (2J_j - K_j)$$

where

$$[4] \quad J_j f(1) = \int d\upsilon_2 \psi_j^*(2)\psi_j(2) \frac{1}{r_{12}} f(1)$$

$$[5] \quad K_j f(1) = \int d\upsilon_2 \psi_j^*(2) f(2) \frac{1}{r_{12}} \psi_j(1)$$

We may rewrite the Fock operator, by introducing a *complete* set $\{\chi_a\}$ which is not necessarily an orthogonal set, as

$$[6] \quad F = -\frac{1}{2}\Delta + \left[-\sum_{\mathrm{A}} \frac{Z_{\mathrm{A}} - Z_{\mathrm{A}}^{\mathrm{C}}}{r_{\mathrm{A}}} + \sum_{j}^{n-m} (2J_j - K_j) \right] + \Omega \left[-\sum_{\mathrm{A}} \frac{Z_{\mathrm{A}}^{\mathrm{C}}}{r_{\mathrm{A}}} + \sum_{j}^{m} (2J_j - K_j) \right] \Omega$$

where

$$[7] \quad \Omega = \sum_{ab} |\chi_a\rangle (S^{-1})_{ab} \langle\chi_b|$$

$$[8] \quad S_{ab} = \langle\chi_a|\chi_b\rangle$$

$$[9] \quad \sum_{\mathrm{A}} Z_{\mathrm{A}}^{\mathrm{C}} = 2m$$

Printed in Canada

Can. J. Chem. Downloaded from www.nrcresearchpress.com by 92.62.229.171 on 09/08/12
For personal use only.

The operator

$$[10]\quad \Omega O \Omega = \sum_{abcd} |\chi_a\rangle (S^{-1})_{ab} \langle\chi_b| O |\chi_c\rangle (S^{-1})_{cd} \langle\chi_d|$$

is called a spectral representation of an operator O. The potential operator in the rewritten Fock operator (eq. [6]) is expressed partially in spectral representation. The division of $2n$ electrons into $2m$ and $2(n - m)$ electrons is optional as long as the self-consistent-field (SCF) is guaranteed. Z_A^C is a number of electrons which are assumed to belong to the nucleus A among $2m$ electrons. The total energy E_T is calculated as

$$[11]\quad E_T = \sum_i \left(\epsilon_i + \left\langle \psi_i \middle| -\frac{\Delta}{2} - \sum_A \frac{Z_A}{r_A} \middle| \psi_i \right\rangle\right) + \sum_{A>B} \frac{Z_A Z_B}{R_{AB}}$$

(a) Spectral representation of the potential due to core electrons

Core electrons of atoms remain nearly frozen in forming molecules. If a potential due to core electrons (V_{core}) is expressed in the spectral representation in eq. [6], it will change little in the SCF process of a molecular orbital calculation. We may consider only the active valence electrons on the stage, leaving the dormant core electrons behind the scenes. In this case V_{core} may be expressed as a linear combination of atomic core potentials

$$[12]\quad V_{core} = \sum_A V_{core}^A$$

$$[13]\quad V_{core}^A = \Omega_A \left[-\frac{Z_A^C}{r} + \sum_i (2J_i^A - K_i^A) \right] \Omega_A + P_A$$

$$[14]\quad P_A = \Omega_A \left[-\sum_i 2\epsilon_i^A |\psi_i^A\rangle\langle\psi_i^A| \right] \Omega_A$$

The operator P_A, which is called the energy shift operator, is included in eq. [13] for the sake of the lowest *valence* orbital energy (not the lowest *core* orbital energy) being obtained as the lowest eigenvalue of the Fock operator. In eq. [11], in this case, $-Z_A/r_A$ and Z_AZ_B/R_{AB} should be replaced by $-(Z_A - Z_A^C)/r_A + V_{core}^A$ and $(Z_A - Z_A^C)(Z_B - Z_B^C)/R_{AB}$, respectively, and Σ_i should run over just the valence orbitals. A practical choice of the representation basis function set $\{\chi_a\}$ is the atomic basis set used in the reference Hartree–Fock–Roothaan calculation, decontracted to the primitive form. The results of the preliminary applications to N_2, P_2, and As_2 show the usefulness of this method (2).

(b) Spectral representation of relativistic effects

The present approach based on the spectral representation of operator is very suitable to incorporate the relativistic effects in the Fock operator. The mass-velocity term V_{mv} and the Darwin term V_D in the Cowan–Griffin (6) – Wood–Boring (7) formalism are expressed in the spectral representation

$$[15]\quad V_{rel} = \sum_l \Omega^l [V_{mv}^l + V_D^l] \Omega^l$$

$$[16]\quad V_{mv}^l = -\frac{\alpha^2}{4} (\epsilon^l - V^l)^2$$

$$[17]\quad V_D = -\frac{\alpha^2}{4} \left\{ 1 + \frac{\alpha^2}{4} (\epsilon^l - V^l) \right\}^{-1} \frac{dV^l}{dr} \left(\frac{1}{G^l} \frac{dG^l}{dr} - \frac{1}{r} \right)$$

where ϵ^l and G^l are the eigenvalue and the large component radial function of l symmetry ($l = s, p, \ldots$), respectively. V^l is the potential acting on G^l and $\alpha = 1/137.037$. We note that no more than one valence orbital for each symmetry l should be included, because the relativistic effects are orbital index dependent. The method has been shown to work well at the level of one-component approximation (4); it may also work at the level of two- and four-component approximation (15).

(c) Spectral representation of non-spherical frozen area

The idea of active and dormant electrons in atoms can be extended to electrons in molecules. For instance, consider the $NH_3 + H^+$ interaction. Among the molecular orbitals of NH_3, $1a_1$, $1e_x$, and $1e_y$ will not interact with the $1s$ orbital of H^+ when H^+ approaches along the z axis. The effect of the six electrons occupying $1a_1$, $1e_x$, and $1e_y$ may be replaced with a static potential. Our approach is flexible to construct the static potential in spectral representation,

$$[18]\quad V_{eff} = \Omega \left[-\sum_A \frac{Z_A^{eff}}{r_A} + \sum_i (2J_i - K_i) - \sum_i 2\epsilon_i |\psi_i\rangle\langle\psi_i| \right] \Omega$$

where A = N, H_1, H_2, H_3; $i = 1a_1, 1e_x, 1e_y$. The expansion basis set for Ω are the primitive-Gaussian-type orbitals (PGTO) recovered by decontracting the atomic basis functions of N and H, and the spectral representation is a four-center representation. Z_A^{eff} may be calculated as

$$[19]\quad Z_A^{eff} = \sum_{ijk} 2c_{ij}^A c_{ik}^A \langle \phi_j^A \mid \phi_k^A \rangle$$

where c_{ij}^A is the renormalized coefficient for the jth atomic orbital ϕ_j^A of the ith molecular orbital ψ_i to satisfy $\Sigma_A \Sigma_{jk} c_{ij}^A c_{ik}^A \langle \phi_j^A \mid \phi_k^A \rangle = 1$ (8). Equation [19] is not unique to calculate Z_A^{eff}, because there is no definite way to calculate occupation numbers from the molecular orbitals that are not spherically symmetric. The molecular orbital $3a_1$ calculated by this method is listed in Table 1 along with those obtained by the ordinary Hartree–Fock SCF method and the effective Hamiltonian method with the N1s core potential. The results may be improved by using more sophisticated Z_A^{eff} values.

Linear combination of atomic operator method and some applications

If an intuitive "chemical building block" picture for a molecular structure is accepted, the potential field in the Fock operator for the molecule may be approximated by a linear

TABLE 1. Molecular orbital $3a_1$ and its orbital energy in NH_3H^+ (C_{3v}) ((721/61)CGTO basis set for N and (51)CGTO for H, R(N—H^+) = 2.0 au)

Orbital energy (au)	Effective Hamiltonian method ($1a_1$, $1e_x$, $1e_y$) −1.0745813	(N1s core) −1.0113908	Ordinary SCF −1.0113675
N s	−0.0015903	−0.0100632	−0.0099367
s	0.0056831	0.0184932	0.0184671
s	0.0357491	0.0484529	0.0485777
z	0.7111865	0.6769529	0.6769717
z	−0.0509031	−0.0218615	−0.0218490
H s	−0.1574238	−0.1622899	−0.1622976
s	0.0137643	0.0193287	0.0193291
H s	−0.1574238	−0.1622899	−0.1622976
s	0.0137643	0.0193287	0.0193291
H s	−0.1574238	−0.1622899	−0.1622976
s	0.0137643	0.0193287	0.0193291
H s	0.4542041	0.4747341	0.4747325
s	−0.0418995	−0.0564211	−0.0565674

combination of potential fields of the constituent atoms (in the spectral representation in our case).

$$[20] \quad F = -\frac{1}{2}\Delta + \sum_{A} G_A$$

$$[21] \quad G_A = \Omega_A\left[-\frac{Z_A}{r_A} + \sum_i n_i(J_i^A - \lambda K_i^A)\right]\Omega_A$$

The approach, thus, might be termed as the linear combination of atomic operator (LCAOP) method (5). We can shift up some of the orbitals ψ_i^A in energy, when we are not interested in these orbital states, by adding to eq. [21] the energy shift operator P_A (eq. [14]) which includes the corresponding orbitals ψ_i^A.

In this method molecular orbitals and orbital energies are obtained by non-iterative diagonalization of the one-electron operator (eq. [20]), just as is done in the Hückel method. This method might therefore be called the *ab initio* Hückel (abiHück) method (5, 9).

We introduced the parameter λ in eq. [21] to avoid a complication in the restricted Hartree–Fock formalism for the open-shell electron configuration (many atoms have the open-shell electron configuration) and to prepare a single Fock operator for all the orbitals (closed-shell and open-shell). A naive choice of the parameter is $\lambda = 1/2$ for each occupation number n_i. This choice was supported by calculations for Li_2 and F_2 molecules with several λ values.

Some of the results of test calculations by the abiHück method, such as those for H_2, Li_2, N_2, F_2, CH_4, were more or less acceptable but some other results, such as those for CO, LiF, H_2O, were not acceptable (5). A linear H_2O was obtained probably due to the neglect of multicenter energy integrals. An acceptable result for CO was obtained (Table 2) when one iteration was done, namely, the density matrix in the abiHück method was recalculated from the molecular orbitals that were the eigenfunctions of eq. [20].

Although the method is surely a crude approximation to the electronic structure calculation from the viewpoint of the sophisticated theory of modern quantum chemistry, the results obtained so far suggest several interesting applications.

TABLE 2. CO total energy and orbital energies at several R_{CO} distances ((721/61)CGTO for C and O)

R_{CO} (au)	LCAOP E_T (au)	Ordinary SCF E_T (au)
1.6	−109.82118	−112.21232
1.85	−110.35685	−112.56701
2.132	−110.37965	−112.67174
2.35	−110.05774	−112.65915
2.6	−109.37138	−112.60467
R_{CO} = 2.132	ε_i (au)	ε_i (au)
1σ	−20.2893	−20.6913
2σ	−11.5024	−11.4377
3σ	−1.5758	−1.5705
4σ	−0.7025	−0.8027
1π	−0.4391	−0.6572
5σ	−0.4378	−0.5547

TABLE 3. Electronic energy convergence for F_2 in SCF calculations

Cycle	abiHück+GAMESS (au)	Ordinary GAMESS (au) (H_{core} initial guess)
1	−227.630370019	−212.398206736
2	−0.004963762	9.648422837
3	−0.000439812	−23.214683732
4	−0.000027890	−1.421329814
5	−0.000000687	−0.245850602
6	−0.000000006	−0.004130185
7	−0.000000000	−0.000023413
8		−0.000000478
9		−0.000000007
10		−0.000000000

(a) Starting potential field for the standard SCF process

The results introduced above suggest that the linear combination of potential fields of the constituent atoms is a good starting potential field for a molecular orbital SCF calculation. As shown in Table 3, our approach stabilized the SCF process for F_2 with use of the (321111/21111) basis set. The exponents of the additional three diffuse functions for s and p orbitals are (0.18, 0.09, 0.045) and (0.24, 0.12.0.06), respectively, and the other CGTO are taken from the (33/3) basis set of Huzinaga *et al.* (10).

(b) Environment potential

The potential in the spectral representation generated from the electron distribution in an atom (or a molecule) may serve as an environment potential. The environment potential is necessary to get reliable results for the electronic structure of the cluster which simulates a part of crystal (11, 12). Ficticious surface atoms which appear as a result of cutting out the cluster from the crystal undergo a significantly different field from that in the bulk of the material. Even in the center region of the cluster the potential field may be different from that in the original crystal, owing to the limitation

Can. J. Chem. Downloaded from www.nrcresearchpress.com by 92.62.229.171 on 09/08/12
For personal use only.

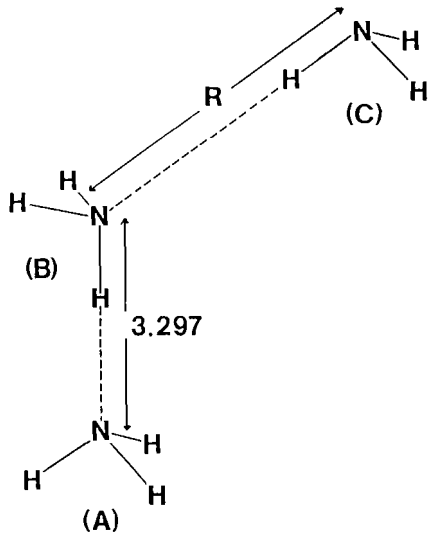

FIG. 1 Geometry of $(NH_3)_A$ + $(NH_3)_B$ + $(NH_3)_C$ (R(N—H) = 1.0124 Å and ∠ HNH = 106.67° are fixed for all ammonia molecules)

TABLE 4. Total energy and equilibrium distance $R(N_B—N_C)$ ((33/3)CGTO for N and (3)CGTO for H)

R (Å)	EP method E_T (au)	Full SCF E_T (au)
2.5	0.0198599	0.0191073
2.75	−0.0000493	−0.0005471
3.0	−0.0058696	−0.0062024
3.25	−0.0065412	−0.0067600
3.5	−0.0056075	−0.0057487
4.0	−0.0034063	−0.0034667
4.5	−0.0020958	−0.0021244
5.0	−0.0013876	−0.0014214
200.0	0.0	0.0
R (Å)	3.209	3.200
E_T (au)	−0.0068385	−0.0070744

of the size of the cluster. The environment potential could remedy the situation.

In the environment potential, the shift operator (eq. [14]) including all the occupied orbitals should be added to eq. [21] to prevent the molecular orbitals of the cluster from collapsing into the environment region.

We apply this approach to the interaction between three ammonia molecules $(NH_3)_A$ + $(NH_3)_B$ + $(NH_3)_C$ (cf. Fig. 1), replacing $(NH_3)_A$ with the environment potential. A similar arrangement was used by Ohta *et al.* (13). The environment potential embodying the effect of $(NH_3)_A$ is obtained by eq. [18], but this time Σ_i runs over all the occupied molecular orbitals, $1a_1$, $2a_1$, $1e_x$, $1e_y$, and $3a_1$. Z_A^{eff} is estimated by eq. [19]. We used this model because we can check the usefulness of the idea of the environment potential by comparing the result obtained by the environment potential (EP) method with that of the full SCF molecular orbital calculation. The agreement of the two results is quite good as shown in Table 4, indicating that the environment potential approach is very promising.

TABLE 5. Exponents ζ_i and coefficients c_i of the second CGTO for the s orbital and the CGTO for the p orbital of carbon

ζ_i	c_i for PAO	c_i for MAO
s orbital		
5.1547389	−0.0848630	−0.2014335
0.47514660	0.5718362	1.3573287
0.14935199	0.5114750	−0.3930986
p orbital		
33.635525	0.0056111	0.0059001
7.6995768	0.0375191	0.0394513
2.3051616	0.1467225	0.1542784
0.79317404	0.3461799	0.3640074
0.28343850	0.4599964	0.4836852
0.09961177	0.2440829	0.1810292

TABLE 6. Internuclear distance R(C—H) and total energy E_T for methane calculated using MAO, PAO, and SV basis sets

Basis set	R(C—H) (au)	E_T (au)
MAO	2.1164	−40.10876
PAO	2.2307	−40.07340
SV	2.0819	−40.14340

(c) Modified atomic orbital

Atomic orbitals used as basis functions for molecular orbital calculation are necessarily modified (or polarized) in a molecule. To cope with the modification, the split-valence (SV) basis set is usually used. If we prepare modified atomic orbitals in advance of the calculation, we can get results at the desired level of accuracy for a smaller size of the basis set (14). As a preliminary test of the idea, a carbon atom in CH_4 is chosen as a working example. The pure atomic orbital (PAO) basis set used for carbon is a (73/6) basis set of Huzinaga *et al.* (10), and a (721/51) SV basis set ψ_i is generated from the (73/6) basis set by decontracting the most diffuse PGTO. Wave functions ψ_i which are composed of the SV basis set and satisfy the following equation

$$[22] \quad \left(-\frac{\Delta}{2} + V(r) + \sum_k V_{env}^H(r - R_k^H)\right)\psi_i(r) = \epsilon_i\psi_i(r)$$

are modified by the environment potential of hydrogen atoms V_{env}^H placed at R_k^H = (1.2, 1.2, 1.2), (1.2, −1.2, −1.2), (−1.2, 1.2, −1.2), and (−1.2, −1.2, 1.2). Contracting the most diffuse PGTO again we get the modified atomic orbitals (MAO) for carbon. The contraction coefficients for MAO are given in Table 5 and the results are listed in Table 6. Better values are obtained by MAO than by PAO.

Summary

The spectral representation technique as a tool for the molecular orbital calculation is introduced. The process to get the potential operator in the spectral representation is simple and straightforward. *No special skill is needed.* One should only calculate one- and two-electron integrals, which

Can. J. Chem. Downloaded from www.nrcresearchpress.com by 92.62.229.171 on 09/08/12
For personal use only.

are at most two-center integrals and familiar to users of the Hartree–Fock–Roothaan method. Once the potentials in the spectral representation are calculated and stored in a file of a computer, one can incorporate them into calculations only by reading them from the file and evaluating them through overlap integrals. The spectral representation technique thus reduces computation cost by changing multicenter energy integral computations to the simple evaluation of one- and two-center overlap integrals.

This technique is versatile enough to apply to many interesting cases. Although the spectral representation technique as a tool for molecular orbital calculation is just underway and there is room for further improvement, such as a proper simulation of non-spherical distribution of frozen electrons, we hope it is established as one of the useful methods for the quantum mechanical calculations of electronic structures.

Acknowledgements

The approach introduced here originated with Professor Huzinaga's gifted idea. We are very grateful to Professor Huzinaga not only for his invaluable discussions, without which most of the results presented here would not have been obtained, but also for his hospitality while we were in Edmonton. We are also grateful to Professor Mariusz Klobukowski for his kind help in computer processing. The numerical calculations were done using the computer facilities at the University of Alberta and Kyushu University.

1. S. Huzinaga. J. Mol. Structure (Theochem), **234**, 51 (1991).
2. S. Katsuki and S. Huzinaga. Chem. Phys. Lett. **152**, 203 (1988).
3. S. Katsuki and S. Huzinaga. Chem. Phys. Lett. **147**, 597 (1988).
4. S. Katsuki. Chem. Phys. Lett. **165**, 535 (1990).
5. S. Huzinaga, S. Katsuki, and O. Matsuoka. J. Mol. Structure (Theochem). In press.
6. R. D. Cowan and D. C. Griffin. J. Opt. Soc. Am. **66**, 1010 (1976).
7. J. H. Wood and A. M. Boring. Phys. Rev. **B**, **18**, 2710 (1978).
8. S. Katsuki and H. Taketa. Int. J. Quantum Chem. **18**, 25 (1980).
9. G. Nicolas and Ph. Durand. J. Chem. Phys. **70**, 2020 (1979); **72**, 453 (1980).
10. S. Huzinaga (*Editor*). Gaussian basis sets for molecular calculations. Elsevier, Amsterdam. 1984.
11. Z. Barandiaran and L. Seijo. J. Chem. Phys. **89**, 5739 (1988).
12. S. Katsuki and H. Taketa. Solid State Commun. **54**, 669 (1985); **55**, 1069 (1985).
13. K. Ohta, Y. Yoshioka, K. Morokuma, and K. Kitaura. Chem. Phys. Lett. **101**, 12 (1983).
14. S. Katsuki. Chem. Phys. Lett. **127**, 231 (1986); **130**, 511 (1986).
15. Ph. Durand and J.-P. Malrieu. Adv. Chem. Phys. **67**, 321 (1987).

Can. J. Chem. Downloaded from www.nrcresearchpress.com by 92.62.229.171 on 09/08/12
For personal use only.

On the accuracy of the algebraic approximation in electronic structure calculations for the ground states of H_3^{2+} and H_4^{3+} using basis sets of atom-centred Gaussian-type functions

S. WILSON

Rutherford Appleton Laboratory, Chilton, Oxfordshire, OX11 0QX, England

Received July 25, 1991

This paper is dedicated to Professor Sigeru Huzinaga on the occasion of his 65th birthday

S. WILSON. Can. J. Chem. **70**, 290 (1992).

Sequences of even-tempered basis sets of atom-centered Gaussian-type functions are employed to explore the accuracy that can be achieved for the ground state energies of the H_3^{2+} and H_4^{3+} species in calculations using finite basis sets. These systems are considered as prototypes for the treatment of polyatomic molecules of arbitrary symmetry within the algebraic approximation.

Key words: algebraic approximation, basis sets, even-tempered, universal.

S. WILSON. Can. J. Chem. **70**, 290 (1992).

On utilise des séquences d'ensembles de base équilibrés de fonctions gaussiennes centrées sur les atomes pour examiner la précision que l'on peut atteindre lors du calcul des énergies de l'état fondamental des espèces H_3^{2+} et H_4^{3+}, en utilisant des ensembles de base finis. On considére ces systèmes comme des prototypes pour le traitement de molécules polyatomiques de symétrie arbitraire dans l'approximation algébrique.

Mots clés : approximation algébrique, ensembles de base, équilibrés, universal.

[Traduit par la rédaction]

1. Introduction

Huzinaga (1) has emphasized the "*quasi-empirical*" nature of the vast majority of contemporary *ab initio* electronic structure calculations associated with the error arising from basis set truncation. A similar point of view has been expressed in a review by Davidson and Feller (2) who comment that "the smaller the basis the more *ab initio* calculations assume an empirical flavor." Clementi and co-workers (3) observe that, because of the failure to address the problem of basis set construction in the 1970s, "the chemical literature . . . was flooded with computations which essentially compared experiments with basis set superposition error data." Even today, basis set truncation errors are a major and frequently dominant source of error in molecular electronic structure calculations. However, as long ago as 1963, Schwartz (4) emphasized the need to devise systematic schemes for extending basis sets employed in atomic and molecular electronic structure calculations and developing "an orderly plan of attack" which "is . . . essential for any mathematical analysis of the convergence rate. The old habit of picking the "best" (chosen by art) choice of a fixed number of terms is to be discarded if one wants to see how the problem converges." In more recent years, this point of view has been underlined by Ruedenberg and co-workers and by Wilson and co-workers. Following early work by Reeves (5), Ruedenberg and his colleagues (6–12) introduced the even-tempered basis sets that virtually eliminated at a stroke the tedious exponent optimization that had been the most time-consuming ingredient of many of the pioneering electronic structure calculations carried out in the 1960s. With the introduction of the algebraic approximation into powerful techniques based on many-body perturbation theory (13, 14) for handling the electron correlation problem in atoms and molecules, the basis set truncation error was seen to be the major source of error (15). (A similar conclusion has been reached from more recently reported full configuration interaction calculations (16).) The need to use a large flexible basis set in order to obtain high accuracy became apparent and the concept of the universal basis set was introduced (17–22). These large and flexible basis sets are not only capable of yielding high accuracy but are also transferable from system to system without regard to the nuclear charges or molecular environment involved. The investigation of the convergence of calculated properties of atoms and molecules with increasing size of basis set was realized in practice in the work of Feller and Ruedenberg (23) and Schmidt and Ruedenberg (24), and ultimately led to the concept of a universal systematic sequence of even-tempered basis sets (25, 26). Clementi *et al.* (27, 28) emphasized the simplifications that arise in evaluation of the two-electron integrals when universal even-tempered (or geometric) basis sets are employed. Wilson (29) presented a scheme based on the Cholesky decomposition of the two-electron integral matrix that allows the effective generation, storage, and processing of the integrals associated with a universal even-tempered basis set. The scheme becomes increasingly efficient as the size of the basis set is increased. Huzinaga (1) has stated that "these remarkable universal geometric basis sets . . . will certainly usher us to a new plateau of computational chemistry." More detailed reviews have been provided by the present author (30–32).

There appears to be a widely held belief (see, for example, Schaefer (33)) that finite difference approximations to atomic and molecular wave functions are superior to their finite basis set counterparts. Finite difference methods have, until recently, been the method of choice in atomic structure calculations (34, 35). Furthermore, the finite difference approach has been applied to a range of diatomic molecules containing light atoms (36–40). Numerical Hartree–Fock calculations for atoms and for diatomic molecules have been shown to afford a sub-μhartree level of accuracy for total electronic energies. Over the past decade, it has also been demonstrated that finite basis set expansions can provide equivalent or superior approximations for Hartree–Fock wave functions for atoms and diatomic molecules. By using systematic sequences of even-tempered basis

Printed in Canada

Can. J. Chem. Downloaded from www.nrcresearchpress.com by 123.30.183.119 on 09/08/12
For personal use only.

Can. J. Chem. Downloaded from www.nrcresearchpress.com by 123.30.183.119 on 09/08/12
For personal use only.

sets of either Gaussian-type functions (23, 24) or exponential-type functions (41–43), atomic self-consistent field energies, that are, in fact, often more accurate than those obtained by finite difference techniques can be obtained. For diatomic molecules, the accuracy achieved in fully numerical self-consistent field calculations can be matched by calculations performed within the algebraic approximation when elliptical basis functions are employed (44–46). Basis set expansions provide a compact representation of self-consistent field wave functions. Quiney *et al.* (47) point out that "The underlying reason for the success of the finite difference methods lies in the choice of coordinate system for the special cases in which they have found favour."

Systematically constructed sequences of basis sets can also be employed with advantage in studies of the effects of electron correlation in atomic and molecular systems. Use of basis sets yields a square-integrable representation of the complete spectrum and affords an effective quadrature over the continuum. Studies of a simple model problem (a hydrogenic atom perturbed by increasing the nuclear charge) using the techniques of many-body perturbation theory have established that integration over the continuum states can be carried out more accurately using systematically extended basis sets than by the numerical approach traditionally employed in atomic structure calculations (48). In relativistic electronic structure studies the use of the algebraic approximation has not only opened up the possibility of applications to molecules but has also provided representation of the negative energy branch of the spectrum, which is required if one is to go beyond the so-called "no virtual pair" approximation that has been employed even in atomic structure calculations carried out by employing finite differences (49). Finally, the computational advantages of the algebraic approximation should be emphasized since it leads to algorithms with basic linear algebra kernels, which can be executed with great efficiency on vector processing machines and parallel processing computers (50).

For molecular systems without special symmetry properties, the use of atomic basis functions transfers a local coordinate system to the region where the wave function is most rapidly changing, whereas the finite difference approach must, in practice, employ a Cartesian grid, which is a manifestly unsuitable coordinate system especially in the region of the nuclei. However, there appears to have been little systematic study of the accuracy that can be achieved in electronic structure studies of very simple polyatomic systems. In this work, we investigate the convergence of the total energies of the simplest polyatomic one-electron systems, H_3^{2+} and H_4^{3+}, obtained when a systematic sequence of even-tempered basis sets of Gaussian-type functions with *s* symmetry are employed. The convergence is compared with that observed for the H atom and the H_2 molecule. In Sect. 2, a brief description of systematic sequences of even-tempered basis sets, their completeness properties, and applications is given. The results of calculations on the H_3^{2+} and H_4^{3+} systems are presented in Sect. 3 and discussed in Sect. 4 where conclusions are also given.

2. Systematic sequences of even-tempered basis sets

The orbital exponents, $\zeta_k(N)$ in an even-tempered basis set are taken to form a geometric progression, thus

$$[1] \quad \ln \zeta_k(N) = \ln \alpha(N) + k \ln \beta(N) \qquad k = 1, 2, \ldots, N$$

where both $\alpha(N)$ and $\beta(N)$ depend on N, the number of functions in the basis set, as, therefore, do the orbital exponents. For the basis set to approach completeness as $N \rightarrow \infty$, α and β must be functions of N such that

$$[2] \quad \begin{aligned} &\alpha(N) \rightarrow 0 \\ &\beta(N) \rightarrow 1 \\ &\beta(N)^N \rightarrow \infty \end{aligned}$$

Ruedenberg and co-workers (23, 24) suggested empirical functional forms that ensure that these limits are satisfied. In particular, they suggested the forms

$$[3] \quad \ln \alpha(N) = a_0 \ln(\beta(N) - 1) + a_1$$

and

$$[4] \quad \ln \ln \beta(N) = b_0 \ln N + b_1$$

where a_0, a_1, b_0, and b_1 are constant for a given sequence. Basis sets generated according to eqs. [1], [3], and [4] are termed systematic sequences of even-tempered basis sets. Ruedenberg and co-workers take these constants to be different for different atomic species. If, however, they are taken to be independent of the particular system then this is termed a universal systematic sequence of even-tempered basis sets (26).

The set of Gaussian-type basis functions $\exp(-\zeta_k(N)r^2)$ generated in this fashion can be shown to be asymptotically total in $L^2(R^+)$ in the limit of large N since the generalized Muntz–Szasz theorem (51)

$$[5] \quad \lim_{N\rightarrow\infty} \sum_{k=1}^{N} \zeta_k(N)/(1 + (\zeta_k(N))^2) = \infty$$

holds. Note that for fixed α and β, the series of partial sums

$$[6] \quad \mathcal{S}(N) = \sum_{k=1}^{N} \zeta_k(N)/(1 + (\zeta_k(N))^2)$$

converge to a finite limit.

Schmidt and Ruedenberg (24) demonstrated that by employing a systematic sequence of even-tempered basis sets of Gaussian-type functions for the ground state of the hydrogen atom, the calculated energy is found to smoothly approach the exact energy as the basis set is extended. The convergence of the energies obtained by Schmidt and Ruedenberg, using a sequence containing 3, 4, 5, . . ., 10 Gaussian-type functions of *s* symmetry, is displayed in Fig. 1, where the change in the energies $\Delta E(N) = E(N) - E(N - 1)$ ($E(N)$ denoting the energy resulting from a calculation using N basis functions) is shown as a function of the size of the basis set. Results obtained by optimizing the orbital exponents for each basis set (designated "optimal") are compared with those obtained by using the relations [1], [3], and [4], which, following Schmidt and Ruedenberg, are designated "regular." It should be noted that although the variation principle ensures that $\Delta E(N)$ is negative for the "optimal" basis sets this is not necessarily the case for the "regular" basis sets. However, for the hydrogen atom ground state $\Delta E(N) < 0$ and $|\Delta E(N)|$ decreases monotonically as N is increased.

Wells and Wilson (52) demonstrated that sub-μhartree accuracy could be achieved in Hartree–Fock calculations for small diatomic molecules by using systematically constructed basis sets of atom-centered Gaussian-type func-

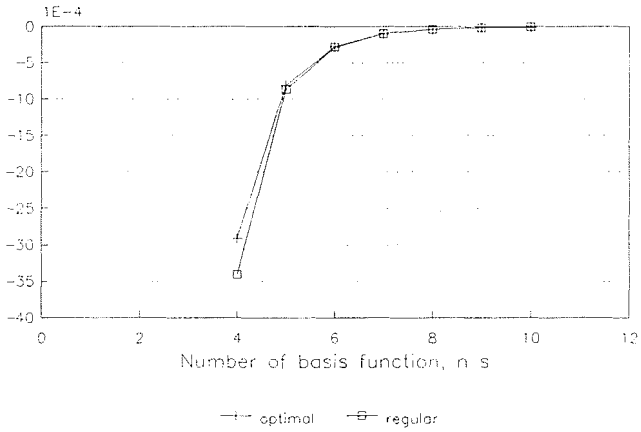

FIG. 1. Convergence of the ground state energy of the hydrogen atom using a sequence of optimized even-tempered basis sets of Gaussian-type functions and a systematic sequence of even-tempered basis sets of Gaussian-type functions (based on the work of Schmidt and Ruedenberg (24)).

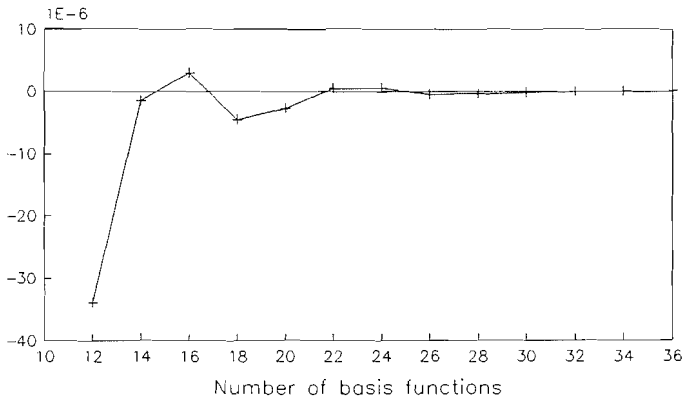

FIG. 2. Convergence of the ground state energy of the H_2 molecule using a systematic sequence of even-tempered basis sets of Gaussian-type functions of s symmetry (based on the work of Wells and Wilson (52)).

TABLE 1. Convergence of the ground state energy of the H_2 molecule with an internuclear separation of 1.4 bohr obtained by employing a systematic sequence of even-tempered basis sets of Gaussian-type functions of s symmetry centred on the two nuclei. See text for details. Energies are given in hartree units

Basis set	Energy
22s	−1.128 541 594
24s	−1.128 541 154
26s	−1.128 541 534
28s	−1.128 541 964
30s	−1.128 542 176
32s	−1.128 542 193
34s	−1.128 542 161
36s	−1.128 542 108

tions. Using a basis set consisting of 23s, 9p, 4d, 4f, 2g, and 1h Gaussian-type functions on each atom, these authors obtain a total ground state energy for the H_2 molecule with an internuclear separation of 1.400 bohr of −1133629.366 μhartree, which differs by only 0.21 μhartree from the energy obtained by employing basis sets of elliptical functions (44), −1133629.57 μhartree, and that obtained in fully numerical Hartree–Fock calculations (38), −1133629.57 μhartree.

The convergence of calculations of the ground state energy of H_2 obtained from a sequence of atom-centred even-tempered basis sets of Gaussian-type functions of s symmetry is displayed in Fig. 2, where the change in the calculated energy values on extending the basis set by two additional basis functions is displayed as a function of the number of basis functions. The internuclear distance is again 1.400 bohr. Satisfactory convergence of the calculated energy values with increasing size of basis set of functions with s symmetry is, of course, a necessary first step in any accurate calculation. The orbital exponents were generated from eqs. [1], [3], and [4] using the parameters given by Schmidt and Ruedenberg for the H atom. The energies obtained for basis sets containing 10, 12, 14, . . ., 20 are given in ref. 52. The energies resulting from calculations employing 22, 24, 26, . . . 36 basis functions are displayed in Table 1. It can be seen that the convergence pattern shows some oscillation but that sub-μhartree accuracy can be achieved by employing a sufficiently extended basis set. Obviously, these oscillations could be removed by optimizing the exponents for each of the basis sets in the sequence since this would ensure that the energy would decrease monotonically. However, such an optimization of the exponents is not usually practiced in molecular calculations. For the basis set of 26 s functions the smallest eigenvalue of the overlap matrix, a measure of computational linear dependence, was found to be 0.0000285 whilst for the largest basis set considered, the set of 36 s functions, this was found to decrease to 0.0000033.

3. Results of calculations for H_3^{2+} and H_4^{3+}

Calculations were carried out to investigate the convergence of the ground state electronic energy of the prototype triatomic system, the H_3^{2+} molecular ion, in an equilateral triangle configuration and internuclear separation R. Two internuclear separations were considered: R = 1.0 bohr and R = 2.0 bohr. A systematic sequence of even-tempered basis sets of Gaussian-type functions of s symmetry centred on each of the three nuclei was employed. The parameters given by Schmidt and Ruedenberg for the H atom and employed by Wells and Wilson (52) in their study of the H_2 ground state were again used.

The calculated electronic energies for the H_3^{2+} molecular ion are given in Table 2 for R = 1.0 and R = 2.0 bohr for a sequence of even-tempered basis sets containing 10, 11, 12, . . ., 32 functions. For each basis set, the smallest eigenvalue of the overlap matrix, ε_s, is given for the R = 1.0 bohr configuration. This provides a measure of computational linear dependence in the basis set. Values of ε_s for the R = 2.0 bohr configuration were found to be greater than or equal to those for R = 1.0 bohr.

For the H_3^{2+} ion the energy difference $\Delta E(N) = E(N) - E(N-1)$, where $E(N)$ denotes the energy obtained by using a basis set of N functions, is displayed in Figs. 3 and 4 for

Can. J. Chem. Downloaded from www.nrcresearchpress.com by 123.30.183.119 on 09/08/12
For personal use only.

TABLE 2. Convergence of the ground state electronic energy of the H_3^{2+} molecular ion with an equilateral triangle configuration and internuclear separation R in bohr obtained by employing a systematic sequence of even-tempered basis sets of Gaussian-type functions of s symmetry centred on the three nuclei. See text for details. Energies are given in hartree units. Distances are given in bohr. ε_s is the smallest eigenvalue of the overlap matrix and provides a measure of computational linear dependence

Basis set	Electronic energy $R = 1.0$	Electronic energy $R = 2.0$	ε_s $R = 1.0$
10s	−2.514 141 8	−1.689 499 3	0.002 544 1
11s	−2.513 999 0	−1.689 561 2	0.001 801 5
12s	−2.514 076 6	−1.689 343 6	0.001 278 6
13s	−2.514 248 0	−1.689 135 0	0.000 921 2
14s	−2.514 338 0	−1.689 084 2	0.000 675 5
15s	−2.514 316 0	−1.689 189 0	0.000 497 4
16s	−2.514 254 8	−1.689 371 6	0.000 367 6
17s	−2.514 229 4	−1.689 551 7	0.000 275 5
18s	−2.514 257 6	−1.689 678 7	0.000 208 9
19s	−2.514 313 0	−1.689 736 3	0.000 158 8
20s	−2.514 359 6	−1.689 735 3	0.000 121 0
21s	−2.514 377 6	−1.689 702 0	0.000 093 0
22s	−2.514 370 5	−1.689 662 0	0.000 072 3
23s	−2.514 353 0	−1.689 633 3	0.000 056 5
24s	−2.514 339 4	−1.689 624 0	0.000 044 2
25s	−2.514 337 4	−1.689 634 7	0.000 034 6
26s	−2.514 346 1	−1.689 659 5	0.000 027 4
27s	−2.514 360 5	−1.689 691 4	0.000 021 8
28s	−2.514 374 9	−1.689 723 7	0.000 017 5
29s	−2.514 384 9	−1.689 751 3	0.000 014 0
30s	−2.514 388 9	−1.689 772 0	0.000 011 2
31s	−2.514 387 9	−1.689 784 8	0.000 009 0
32s	−2.514 377 4	−1.689 790 3	0.000 000 4

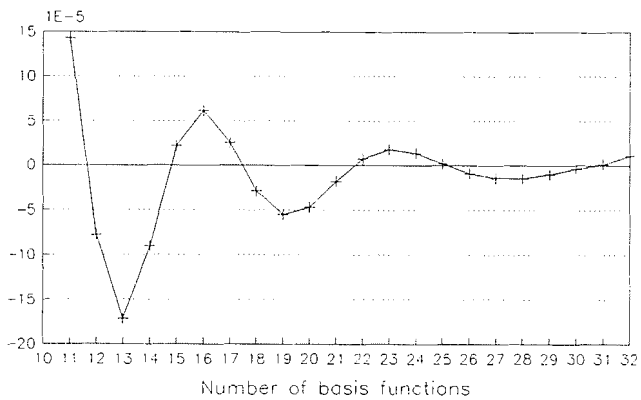

FIG. 3. Convergence of the ground state energy of the H_3^{2+} ion in an equilateral triangle configuration with an internuclear distance of 1.0 atomic units using a systematic sequence of even-tempered basis sets of Gaussian-type functions of s symmetry.

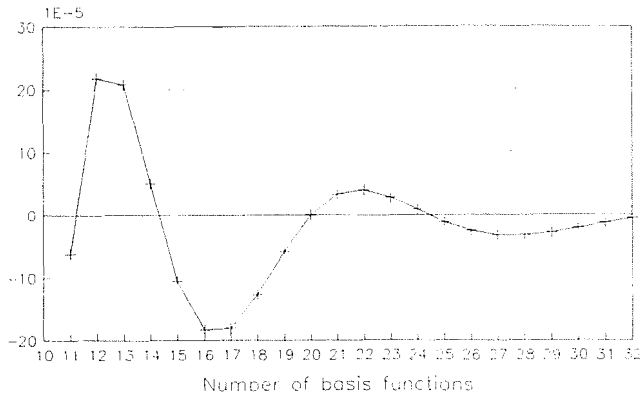

FIG. 4. Convergence of the ground state energy of the H_3^{2+} ion in an equilateral triangle configuration with an internuclear distance of 2.0 atomic units using a systematic sequence of even-tempered basis sets of Gaussian-type functions of s symmetry.

TABLE 3. Convergence of the ground state electronic energy of the H_4^{3+} molecular ion, in a square planar configuration with side 1.0 bohr, obtained by employing a systematic sequence of even-tempered basis sets of Gaussian-type functions of s symmetry centred on the three nuclei. See text for details. Energies are given in hartree units. ε_s is the smallest eigenvalue of the overlap matrix and provides a measure of computational linear dependence

Basis set	Electronic energy	ε_s
10s	−3.362 116 3	0.000 378 4
11s	−3.361 777 0	0.000 287 5
12s	−3.361 418 1	0.000 220 9
13s	−3.361 480 9	0.000 170 9
14s	−3.361 827 0	0.000 133 2
15s	−3.362 150 1	0.000 104 7
16s	−3.362 266 0	0.000 082 9
17s	−3.362 199 5	0.000 066 0
18s	−3.362 075 1	0.000 052 7
19s	−3.362 004 3	0.000 042 3
20s	−3.362 030 1	0.000 034 1
21s	−3.362 126 0	0.000 027 6
22s	−3.362 238 9	0.000 022 5
23s	−3.362 323 4	0.000 018 4
24s	−3.362 358 3	0.000 015 0
25s	−3.362 347 5	0.000 012 3
26s	−3.362 311 6	0.000 010 1
27s	−3.362 274 8	0.000 008 4
28s	−3.362 254 8	0.000 007 0
29s	−3.362 258 6	0.000 005 8
30s	−3.362 283 5	0.000 004 8
31s	−3.362 320 4	0.000 004 0
32s	−3.362 343 0	0.000 000 4

the $R = 1.0$ bohr and $R = 2.0$ bohr equilateral triangle configurations, respectively.

Calculations were also performed for the ground state electronic energy of the prototype tetra-atomic system, the H_4^{3+} ion, for a square planar arrangement of the nuclei with side 1.0 bohr. Again, a systematic sequence of even-tempered basis sets of Gaussian-type functions of s symmetry centred on each of the nuclei was employed together with the parameters given by Schmidt and Ruedenberg for the H atom. The results are displayed in Table 3. For each basis set in the sequence 10, 11, 12, . . ., 32 s functions we give the electronic energy together with the smallest eigenvalue of the overlap matrix, ε_s.

The energy difference $\Delta E(N)$ observed for the H_4^{3+} ion is plotted in Fig. 5 as a function of the number of basis functions.

Can. J. Chem. Downloaded from www.nrcresearchpress.com by 123.30.183.119 on 09/08/12
For personal use only.

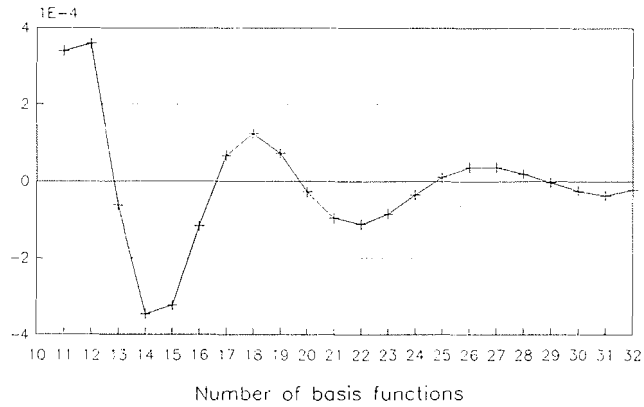

FIG. 5. Convergence of the ground state energy of the H_4^{3+} ion in a square planar configuration with side of 1.0 atomic units using a systematic sequence of even-tempered basis sets of Gaussian-type functions of *s* symmetry.

4. Discussion

The one-electron ions H_3^{2+} and H_4^{3+} afford the simplest prototypes for the study of the accuracy that can be achieved in electronic structure calculations for polyatomic molecules when systematically constructed sequences of even-tempered basis sets are employed. The results can be compared with previous studies of simple atomic and diatomic systems. In the present study, attention has been focused on the convergence patterns observed when Gaussian-type functions of *s* symmetry are centred on each of the nuclei in the system, which is, of course, a necessary first step in any accurate calculation.

Whilst smooth convergence of the calculated energies is observed for the hydrogen atom ground state shown in Fig. 1, there is some oscillation in the convergence pattern for the hydrogen molecule displayed in Fig. 2. For the hydrogen molecule the oscillations are of the order of 5 μhartrees. Convergence to sub-μhartree accuracy is ultimately achieved with a sufficiently large basis set.

For the prototype triatomic system, H_3^{2+}, the convergence with increasing size of basis set is also oscillatory. The oscillations are more pronounced than those observed for the H_2 ground state, being of the order of 200 μhartree in the $R = 1.0$ bohr case for the smaller basis sets considered diminishing, to about 5 μhartree for the larger sets employed. Somewhat improved convergence characteristics are observed for the $R = 2.0$ bohr geometry. It should be noted again that these oscillations could obviously be removed by optimization of the exponents for each of the basis sets in a sequence but in this work we have followed the usual practice of employing basis sets designed for atomic systems in a molecular environment. From the calculations reported in Table 2 it must be concluded that, as the basis set is systematically extended, sub-μhartree accuracy cannot be achieved before computational linear dependence renders the calculations unreliable. It would appear that an absolute accuracy of ~10 μhartree can be achieved for the ground state electronic energy of the H_3^{2+} ion at the nuclear geometries considered.

The convergence with increasing size of basis set is also oscillatory for the prototype tetra-atomic system, the H_4^{3+} ion. The oscillations are more pronounced than those observed for both the H_2 ground state and the H_3^{2+} ion, being of the order of 400 μhartree for the smaller basis sets considered, diminishing to about 40 μhartree for the larger sets. Again we have followed the usual practice of using atomic basis sets in a molecular system. From the calculations reported in Table 3 it must be concluded that, again, as the basis set is systematically extended, sub-μhartree accuracy cannot be achieved before computational linear dependence renders the calculations unreliable. An absolute accuracy of ~50 μhartree can be achieved for the ground state electronic energy of the H_4^{3+} ion at the nuclear geometry considered.

In the present study, we have restricted our attention to one-electron systems using basis functions of *s* symmetry. Certainly, functions of *p*, *d*, *f*, . . . and higher symmetries will be required to approach the exact electronic energies. It is also possible that for many-electron systems there could be some degree of cancellation of errors in the one- and two-electron components of the electronic energy. However, the accurate description of polyatomic, one-electron systems using basis sets of *s* symmetry must be regarded as a necessary first step in any high-precision treatment of polyatomic molecules.

In conclusion, it is useful to recall some empirical advice given by Schwartz (4) in 1963: "it seems quite general, working with computing machines of finite numerical accuracy, a poor choice of basis functions (implying a slow convergence rate) will be signaled by large and rapidly growing roundoff errors. The best cure for this disease will lie not in any improvement in the numerical capability of the machine, but requires the selection of a basis more appropriate to the problem in hand. Thus it appears that the two problems of getting an accurate (numerical) answer at each step, and having these successive answers converge rapidly, are strongly interwoven."

1. S. Huzinaga. Comput. Phys. Rep. **2**, 279 (1985).
2. E. R. Davidson and D. Feller. Chem. Rev. **86**, 681 (1986).
3. S. J. Chakravorty, G. Corongiu, J. R. Flores, V. Sonnad, E. Clementi, V. Carravetta, and I. Cacelli. *In* Modern techniques in computational chemistry. ESCOM, Leiden. 1989. p. 81.
4. C. Schwartz. Methods Comput. Phys. **2**, 241 (1963).
5. C. M. Reeves. J. Chem. Phys. **39**, 11 (1963).
6. K. Ruedenberg, R. C. Raffenetti, and R. Bardo. *In* Energy, structure and reactivity. Proc. 2nd Boulder Res. Conf. Theor. Chem., Wiley, New York. 1973.
7. R. C. Raffenetti. J. Chem. Phys. **58**, 4452 (1973).
8. R. C. Raffenetti. J. Chem. Phys. **59**, 5936 (1973).
9. R. C. Raffenetti and K. Ruedenberg. J. Chem. Phys. **59**, 5978 (1973).
10. R. Bardo and K. Ruedenberg. J. Chem. Phys. **59**, 5956 (1973).
11. R. Bardo and K. Ruedenberg. J. Chem. Phys. **59**, 5966 (1973).
12. R. Bardo and K. Ruedenberg. J. Chem. Phys. **60**, 918 (1974).
13. U. Kaldor. Phys. Rev. A, **7**, 427 (1973).
14. S. Wilson and D. M. Silver. Phys. Rev. A, **14**, 1949 (1976).
15. S. Wilson and D. M. Silver. J. Chem. Phys. **66**, 5400 (1977).
16. C. W. Bauschlicher and P. R. Taylor. J. Chem. Phys. **85**, 2779 (1986).
17. D. M. Silver, S. Wilson, and W. C. Nieuwpoort. Int. J. Quantum Chem. **14**, 635 (1978).
18. D. M. Silver and S. Wilson. J. Chem. Phys. **69**, 3787 (1978).
19. D. M. Silver and W. C. Nieuwpoort. Chem. Phys. Lett. **57**, 421 (1978).
20. S. Wilson and D. M. Silver. J. Chem. Phys. **72**, 2159 (1980).
21. S. Wilson and D. M. Silver. J. Chem. Phys. **77**, 3674 (1982).
22. S. Wilson. Mol. Phys. **49**, 1489 (1983).
23. D. F. Feller and K. Ruedenberg. Theor. Chim. Acta, **52**, 231 (1979).

Can. J. Chem. Downloaded from www.nrcresearchpress.com by 123.30.183.119 on 09/08/12
For personal use only.

24. M. W. Schmidt and K. Ruedenberg. J. Chem. Phys. **71**, 3951 (1979).
25. S. Wilson. Theor. Chim. Acta, **57**, 53 (1980).
26. S. Wilson. Theor. Chim. Acta, **58**, 31 (1980).
27. E. Clementi, G. Corongiu, M. Gratarola, P. Habitz, C. Lupo, P. Otto, and D. Vercauteren. Int. J. Quantum Chem. Symp. **16**, 409 (1982).
28. E. Clementi, G. Corongiu, and S. Chakravorty. *In* Modern techniques in computational chemistry. ESCOM, Leiden. 1990. p. 343.
29. S. Wilson. Comput. Phys. Commun. **58**, 71 (1990).
30. S. Wilson. Electron correlation in molecules. Clarendon Press, Oxford. 1984.
31. S. Wilson. *In* Methods in computational molecular physics. *Edited by* G. H. F. Diercksen and S. Wilson. Reidel, Dordrecht. 1983.
32. S. Wilson. Adv. Chem. Phys. **67**, 439 (1987).
33. H. F. Schaefer III. Quantum chemistry. The development of *ab initio* methods in molecular electronic structure theory. Clarendon Press, Oxford. 1984.
34. C. F. Fischer. The Hartree-Fock method for atoms. Wiley, New York. 1977.
35. I. P. Grant. Methods Comput. Chem. **2**, 1 (1988).
36. L. Laaksonen, P. Pyykkö, and D. Sundholm. Chem. Phys. Lett. **96**, 1 (1983).
37. L. Laaksonen, P. Pyykkö, and D. Sundholm. Int. J. Quantum Chem. **23**, 309 (1983).
38. L. Laaksonen, P. Pyykkö, and D. Sundholm. Int. J. Quantum Chem. **23**, 319 (1983).
39. L. Laaksonen, P. Pyykkö, and D. Sundholm. Comput. Phys. Rep. **4**, 313 (1986).
40. P. Pyykkö. *In* Numerical determination of the electronic structure of atoms, diatomic and polyatomic molecules. *Edited by* M. Defranceschi and J. Delhalle. Kluwer, Dordrecht. 1989.
41. D. L. Cooper and S. Wilson. J. Chem. Phys. **77**, 5053 (1982).
42. D. L. Cooper and S. Wilson. J. Chem. Phys. **77**, 4551 (1982).
43. D. L. Cooper and S. Wilson. J. Chem. Phys. **78**, 2456 (1983).
44. B. H. Wells and S. Wilson. J. Phys. B: At. Mol. Phys. **18**, L731 (1985).
45. B. H. Wells and S. Wilson. J. Phys. B: At. Mol. Phys. **19**, 17 (1986).
46. J. W. Thompson and S. Wilson. J. Phys. B: At. Mol. Phys. **23**, 2205 (1990).
47. H. M. Quiney, I. P. Grant, and S. Wilson. *In* Numerical determination of the electronic structure of atoms, diatomic and polyatomic molecules. *Edited by* M. Defranceschi and J. Delhalle. Kluwer, Dordrecht. 1989.
48. H. M. Quiney, I. P. Grant, and S. Wilson. J. Phys. B: At. Mol. Phys. **18**, 577 (1985).
49. H. M. Quiney, I. P. Grant, and S. Wilson. *In* Many-body methods in quantum chemistry. *Edited by* U. Kaldor. Lect. Notes Chem. **52**, 307 (1989); S. Wilson. *In* The effects of relativity in atoms, molecules and the solid state. *Edited by* S. Wilson, I. P. Grant, and B. L. Gyorffy. Plenum, New York. 1991; S. Wilson. *In* Methods in computational molecular physics. *Edited by* S. Wilson and G. H. F. Diercksen. Plenum, New York. 1992.
50. S. Wilson. Methods Comput. Chem. **3**, 1 (1989).
51. B. Klahn. J. Chem. Phys. **83**, 5748 (1985).
52. B. H. Wells and S. Wilson. J. Phys. B: At. Mol. Opt. Phys. **22**, 1285 (1989).

Can. J. Chem. Downloaded from www.nrcresearchpress.com by 123.30.183.119 on 09/08/12
For personal use only.

New scheme for large-scale eigenvalue problems of the RPA-type matrix equation

SUSUMU NARITA AND TAI-ICHI SHIBUYA

Department of Chemistry, Faculty of Textile Science and Technology, Shinshu University, Ueda, Nagano-ken 386, Japan

Received July 25, 1991

This paper is dedicated to Professor Sigeru Huzinaga on the occasion of his 65th birthday

SUSUMU NARITA and TAI-ICHI SHIBUYA. Can. J. Chem. **70**, 296 (1992).

A new method is proposed for obtaining a few eigenvalues and eigenvectors of a large-scale RPA-type equation. Some numerical tests are carried out to study the convergence behaviors of this method. It is found that the convergence rate is very fast and quite satisfactory. It depends strongly on the way of estimating the deviation vectors. Our proposed scheme gives a better estimation for the deviation vectors than Davidson's scheme. This scheme is applicable to the eigenvalue problems of nondiagonally dominant matrices as well.

Key words: large-scale eigenvalue problem, RPA-type equation, fast convergence.

SUSUMU NARITA et TAI-ICHI SHIBUYA. Can. J. Chem. **70**, 296 (1992).

On propose une nouvelle méthode d'obtention des valeurs propres et des vecteurs propres d'une équation importante de type RPA. On a effectué quelques évaluations numériques dans le but de déterminer les comportements de convergence de cette méthode. On a trouvé que la vitesse de convergence est très rapide et assez satisfaisante. La vitesse de convergence dépend beaucoup de la façon d'évaluer les vecteurs de déviation. Notre méthode donne une meilleure évaluation des vecteurs de déviation que celle de Davidson. On peut aussi appliquer cette méthode aux problèmes de valeurs propres de matrices principalement non-diagonales.

Mots clés : problème de valeurs propres, équation de type RPA, convergence rapide.

[Traduit par la rédaction]

1. Introduction

In computing quantities such as the transition energies and the transition properties related to electronic states of atoms and molecules, the equations-of-motion (EOM) method has various advantages over the traditional configuration interaction (CI) method. The EOM is set up directly for the electronic transition, taking into account the electron correlation at various levels of approximation, while the CI method deals with the ground and the excited states, separately. The first-level approximation to the EOM is known to be the random phase approximation (RPA), which is equivalent to the time-dependent Hartree–Fock method. At higher levels of approximation such as the higher RPA (1) and the second higher RPA (2), one often ends up with similar RPA-type equations.

The RPA-type equation is written

$$[1] \qquad \begin{bmatrix} \boldsymbol{A} & \boldsymbol{B} \\ -\boldsymbol{B} & -\boldsymbol{A} \end{bmatrix} \begin{bmatrix} \boldsymbol{Y}(k) \\ \boldsymbol{Z}(k) \end{bmatrix} = \omega_k \begin{bmatrix} \boldsymbol{Y}(k) \\ \boldsymbol{Z}(k) \end{bmatrix}$$

where $\boldsymbol{A}$ and $\boldsymbol{B}$ are symmetric $N \times N$ square matrices assumed to be real, $\boldsymbol{Y}(k)$ and $\boldsymbol{Z}(k)$ column vectors with N components, and ω_k the transition energy to the kth state. Because of the special structure of the RPA-type matrix, its eigenvectors show various interesting properties. Some of them were discussed in the monograph by Thouless (3). Mathematical solutions for negative ω are easily obtained from the solutions for positive ω (3). If

$$\begin{bmatrix} \boldsymbol{Y}(k) \\ \boldsymbol{Z}(k) \end{bmatrix}$$

is the eigenvector associated with the positive eigenvalue ω_k, then

$$\begin{bmatrix} \boldsymbol{Y}(-\boldsymbol{k}) \\ \boldsymbol{Z}(-\boldsymbol{k}) \end{bmatrix} \equiv \begin{bmatrix} \boldsymbol{Z}(k) \\ \boldsymbol{Y}(k) \end{bmatrix}$$

is the eigenvector associated with the negative eigenvalue $\omega_{-k} \equiv -\omega_k$.

Equation [1] may be solved by the direct diagonalization of the $2N \times 2N$ unsymmetric matrix unless N gets large. For large N, however, the direct diagonalization becomes formidable. Usually one is only interested in a few solutions of the lowest transition energies. Various iterative algorithms have been developed for this purpose (4–6). Although these methods are applicable to the RPA-type equations, they do not take advantage of the special paired structure of the RPA-type matrix. Recently, Olsen *et al.* (7) proposed iterative algorithms that utilize this structure. In their algorithms, however, computations with $2N$-component vectors are involved.

Alternatively, eq. [1] may be equivalently written as

$$[2a] \qquad \boldsymbol{A}\,\boldsymbol{Y}(k) + \boldsymbol{B}\,\boldsymbol{Z}(k) = \omega_k \boldsymbol{Y}(k)$$

$$[2b] \qquad -\boldsymbol{B}\,\boldsymbol{Y}(k) - \boldsymbol{A}\,\boldsymbol{Z}(k) = \omega_k \boldsymbol{Z}(k)$$

and the subtraction and addition of these equations give

$$[3a] \qquad (\boldsymbol{A} + \boldsymbol{B})\,\boldsymbol{P}(k) = \omega_k \boldsymbol{Q}(k)$$

$$[3b] \qquad (\boldsymbol{A} - \boldsymbol{B})\,\boldsymbol{Q}(k) = \omega_k \boldsymbol{P}(k)$$

where

$$[4] \qquad \boldsymbol{P}(k) = \boldsymbol{Y}(k) + \boldsymbol{Z}(k)$$
$$\boldsymbol{Q}(k) = \boldsymbol{Y}(k) - \boldsymbol{Z}(k)$$

The multiplication of eq. [3a] by $(\boldsymbol{A} - \boldsymbol{B})$ and eq. [3b] by $(\boldsymbol{A} + \boldsymbol{B})$, from the left on both sides, gives

$$[5a] \qquad \boldsymbol{G}\,\boldsymbol{P}(k) = W_k \boldsymbol{P}(k)$$

$$[5b] \qquad \boldsymbol{H}\,\boldsymbol{Q}(k) = W_k \boldsymbol{Q}(k)$$

where

$$[6] \qquad \boldsymbol{G} = (\boldsymbol{A} - \boldsymbol{B})(\boldsymbol{A} + \boldsymbol{B})$$
$$\boldsymbol{H} = (\boldsymbol{A} + \boldsymbol{B})(\boldsymbol{A} - \boldsymbol{B}) = \boldsymbol{G}^T$$

Can. J. Chem. Downloaded from www.nrcresearchpress.com by 92.62.229.171 on 09/08/12
For personal use only.

Can. J. Chem. Downloaded from www.nrcresearchpress.com by 92.62.229.171 on 09/08/12
For personal use only.

and

$$[7] \qquad W_k \equiv \omega_k^2$$

The associated eigenvectors $\boldsymbol{P}(k)$ and $\boldsymbol{Q}(m)$ must satisfy the orthonormality condition

$$[8] \qquad \boldsymbol{P}(k)^T \boldsymbol{Q}(m) = \delta_{km}$$

Many years ago, Tamura and Udagawa (8) proposed to solve eqs. [5*a*] or [5*b*] instead of solving eq. [1] directly. They proposed to obtain W_k and its associated eigenvector $\boldsymbol{P}(k)$ or $\boldsymbol{Q}(k)$ and then to obtain the other as a solution of the simultaneous equation. To obtain the properly normalized eigenvectors, however, one needs careful treatment of these equations.[1] In the following sections, we will propose a new scheme to solve the Tamura–Udagawa equations, eqs. [5*a*] and [5*b*] or eqs. [3*a*] and [3*b*], of large-N components, and will discuss its efficiency in actual applications.

2. Algorithms

2.1. The Newton–Raphson equation

First we define the Rayleigh quotient $f(\boldsymbol{P},\boldsymbol{Q})$ as

$$[9] \qquad f(\boldsymbol{P},\boldsymbol{Q}) = \frac{\boldsymbol{Q}^T\boldsymbol{G}\boldsymbol{P}}{\boldsymbol{Q}^T\boldsymbol{P}}$$

where $\boldsymbol{P}$ and $\boldsymbol{Q}$ are column vectors of N components and $\boldsymbol{G}$ is given by eq. [6]. The differentiation of eq. [9] with respect to the kth components P_k and Q_k gives

$$[10a] \qquad \left(\frac{\partial f}{\partial P_k}\right)(\boldsymbol{Q}^T\boldsymbol{P}) = \sum_j Q_j G_{jk} - fQ_k$$

and

$$[10b] \qquad \left(\frac{\partial f}{\partial Q_k}\right)(\boldsymbol{Q}^T\boldsymbol{P}) = \sum_j G_{kj} P_j - fP_k$$

It is then clear from eqs. [10*a*] and [10*b*] that the extremum conditions for f readily give eqs. [5*b*] and [5*a*], respectively.

The second derivatives of f are obtained by differentiating eqs. [10*a*] and [10*b*] with respect to the mth components P_m and Q_m:

$$[11a] \qquad \left(\frac{\partial^2 f}{\partial P_m\,\partial P_k}\right)(\boldsymbol{Q}^T\boldsymbol{P}) = -\left(\frac{\partial f}{\partial P_m}\right)Q_k - \left(\frac{\partial f}{\partial P_k}\right)Q_m$$

$$[11b] \qquad \left(\frac{\partial^2 f}{\partial Q_m\,\partial P_k}\right)(\boldsymbol{Q}^T\boldsymbol{P}) = G_{mk} - f\delta_{km} - \left(\frac{\partial f}{\partial P_k}\right)P_m$$

$$[11c] \qquad \left(\frac{\partial^2 f}{\partial P_m\,\partial Q_k}\right)(\boldsymbol{Q}^T\boldsymbol{P}) = G_{km} - f\delta_{km} - \left(\frac{\partial f}{\partial Q_k}\right)Q_m$$

$$[11d] \qquad \left(\frac{\partial^2 f}{\partial Q_m\,\partial Q_k}\right)(\boldsymbol{Q}^T\boldsymbol{P}) = -\left(\frac{\partial f}{\partial Q_m}\right)P_k - \left(\frac{\partial f}{\partial Q_k}\right)P_m$$

The higher order derivatives of f can be obtained similarly. Then, using eqs. [10*a*]–[11*d*], we obtain the Taylor expansion of eq. [9]:

$$[12] \qquad f = f^0 + \sum_j \left[\left(\frac{\partial f}{\partial P_j}\right)^0 \delta P_j + \left(\frac{\partial f}{\partial Q_j}\right)^0 \delta Q_j\right] + \frac{1}{2}\sum_{jk}\left[\left(\frac{\partial^2 f}{\partial P_j\,\partial P_k}\right)^0 \delta P_j\delta P_k + \left(\frac{\partial^2 f}{\partial P_j\,\partial Q_k}\right)^0 \delta P_j\delta Q_k\right] + \frac{1}{2}\sum_{jk}\left[\left(\frac{\partial^2 f}{\partial Q_j\,\partial P_k}\right)^0 \delta Q_j\delta P_k + \left(\frac{\partial^2 f}{\partial Q_j\,\partial Q_k}\right)^0 \delta Q_j\delta Q_k\right] + \ldots$$

where f^0 is equal to $f(\boldsymbol{P}_0,\boldsymbol{Q}_0)$. The derivative coefficients with superscript 0 are all evaluated at $\boldsymbol{P}_0$ and $\boldsymbol{Q}_0$.

The deviation vectors $\delta\boldsymbol{P}$ and $\delta\boldsymbol{Q}$ can be estimated from the Newton–Raphson equation

$$[13] \qquad \begin{bmatrix} f^0_{PP} & f^0_{PQ} \\ f^0_{QP} & f^0_{QQ} \end{bmatrix}\begin{bmatrix} \delta\boldsymbol{P} \\ \delta\boldsymbol{Q} \end{bmatrix} = -\begin{bmatrix} f^0_P \\ f^0_Q \end{bmatrix}$$

where subscripts P and Q denote the differentiation and, for instance,

$$(f^0_P)_k = \left(\frac{\partial f}{\partial P_k}\right)^0$$

and

$$(f^0_{PP})_{mk} = \left(\frac{\partial^2 f}{\partial P_m \partial P_k}\right)^0$$

The kth components of the first derivative coefficient vectors, f^0_P and f^0_Q can be evaluated from eqs. [10*a*] and [10*b*], respectively. Similarly, the (m,k) components of the Hessians, f^0_{PP}, f^0_{QP}, f^0_{PQ}, and f^0_{QQ}, can be evaluated from eqs. [11*a*]–[11*d*], respectively.

In the vicinity of the extremum, the first-order derivative coefficients $(f^0_P)_k$ and $(f^0_Q)_k$ in eqs. [11*a*]–[11*d*] become negligible, and eq. [13] becomes

$$[14a] \qquad (\boldsymbol{G} - f^0\boldsymbol{1})\delta\boldsymbol{P} = -f^0_Q$$

$$[14b] \qquad (\boldsymbol{H} - f^0\boldsymbol{1})\delta\boldsymbol{Q} = -f^0_P$$

Note that the matrix size here is reduced to $N \times N$ from $2N \times 2N$. When the f^0 value approaches the extremum, the Hessian matrices of eqs. [14*a*] and [14*b*] become nearly singular. However, the deviation vectors $\delta\boldsymbol{P}$ and $\delta\boldsymbol{Q}$ would then contain the dominant components of the eigenvectors whose eigenvalues are near to the f^0 value. This is the reason why the Newton–Raphson method shows fast convergence when the initial guess is close to the final solution.

Note that if all the off-diagonal elements of the Hessian matrices are ignored in eqs. [14*a*] and [14*b*], then we have

$$[15a] \qquad \delta P_k = \frac{-\left[\sum_j (G_{kj}P_j - f^0P_k)\right]}{(G_{kk} - f^0)}$$

$$[15b] \qquad \delta Q_k = \frac{-\left[\sum_j (H_{kj}Q_j - f^0Q_k)\right]}{(H_{kk} - f^0)}$$

which are the approximations employed in the Davidson algorithm (10). These approximations may be good when the matrix $\boldsymbol{G}$ is diagonally dominant (i.e., $\varepsilon' << 1$, where $\varepsilon' =$

[1] S. Narita, S. Kumei, and T. Shibuya. Unpublished results.

$|G_{ij}/(G_{ii} - G_{jj})|$) (11). If $\boldsymbol{G}$ is not diagonally dominant, however, they will give only poor deviation vectors.

2.2. The shifted inverse-power method

Now, let us consider the properties of $\boldsymbol{x}^{(1)}$ which is the solution of the equation

$$[16] \quad (\boldsymbol{G} - f\boldsymbol{1})\,\boldsymbol{x}^{(1)} = \boldsymbol{b}$$

f being a scalar and $\boldsymbol{b}$ an arbitrary column vector with a constant norm other than zero. This equation looks very much like eqs. [14]. If all the eigenvalues W_i's and associated eigenvectors $\boldsymbol{P}_i$'s and $\boldsymbol{Q}_i$'s of the matrix $\boldsymbol{G}$ are known, then the vector $\boldsymbol{x}^{(1)}$ of eq. [16] can be written as

$$[17] \quad \boldsymbol{x}^{(1)} = (\boldsymbol{G} - f\boldsymbol{1})^{-1}\boldsymbol{b} = \sum_i \boldsymbol{Q}_i^T\,\boldsymbol{b}(W_i - f)^{-1}\boldsymbol{P}_i$$

Note in this equation that $\boldsymbol{Q}_i^T\,\boldsymbol{b}(W_i - f)^{-1}$ is a coefficient of vector $\boldsymbol{P}_i$. When f is close to an eigenvalue, say W_i, the absolute value of the corresponding coefficient becomes very large compared with the rest, and then $\boldsymbol{x}^{(1)}$ becomes a very good approximation to the exact eigenvector $\boldsymbol{P}_i$ as all other terms in eq. [17] become negligible compared with this particular term of $\boldsymbol{P}_i$.

We obtain a more accurate vector $\boldsymbol{x}^{(2)}$ by replacing a vector $\boldsymbol{b}$ in eq. [17] by the vector $\boldsymbol{x}^{(1)}$:

$$[18] \quad \boldsymbol{x}^{(2)} = (\boldsymbol{G} - f\boldsymbol{1})^{-1}\boldsymbol{x}^{(1)} = \sum_i \boldsymbol{Q}_i^T\,\boldsymbol{b}(W_i - f)^{-2}\boldsymbol{P}_i$$

Note that the magnitude of the corresponding coefficient of $\boldsymbol{P}_i$ in eq. [18] becomes much larger than that in eq. [17]. In general, the result in the kth step of the iteration, $\boldsymbol{x}^{(k)}$, is related to that in the previous step, $\boldsymbol{x}^{(k-1)}$, as

$$[19] \quad \boldsymbol{x}^{(k)} = (\boldsymbol{G} - f\boldsymbol{1})^{-1}\boldsymbol{x}^{(k-1)}$$

The vector $\boldsymbol{x}^{(k)}$ approaches the exact eigenvector as k increases. We call this the inverse iteration effect. By repeating the above procedure we can improve an arbitrary vector $\boldsymbol{b}$ so as to give the exact eigenvalues around the value of f and their associated eigenvectors. This iterative method is well known as the shifted inverse-power method (9).

For small N, it is easy to solve eq. [16] and obtain the vector $\boldsymbol{x}^{(1)}$. For large N, however, it becomes formidable to handle the inverse matrix $(\boldsymbol{G} - f\boldsymbol{1})^{-1}$. This is the major drawback of the shifted inverse-power method. However it gives a more accurate estimation for the deviation vectors than the Davidson algorithm, and therefore is free from the problem of diagonal dominance. With this method, the convergence rate is also drastically improved.

2.3. A compromised method

The method we propose here is a compromise of the Newton–Raphson method, the shifted inverse-power method, and the variational method. Although $\boldsymbol{x}^{(n)}$ in the previous section may be a good approximation to the eigenvector, we can construct an even better vector by taking a linear combination of $\boldsymbol{x}^{(1)}, \boldsymbol{x}^{(2)}, \ldots, \boldsymbol{x}^{(n)}$. Let $\{\boldsymbol{x}^{(k)}\}$ be the set of the results obtained in sequence by eq. [19] and $\{\boldsymbol{y}^{(k)}\}$ be a set of vectors that satisfy the orthonormality conditions

$$[\boldsymbol{y}^{(i)T}\,\boldsymbol{x}^{(j)} = \delta_{ij}, \qquad i, j = 1 \ldots n]$$

n being the number of vectors in each set, and the dimension of vector $\boldsymbol{x}^{(j)}$ is N. The set $\{\boldsymbol{y}^{(k)}\}$ may form an $N \times n$ matrix

$$[20] \quad \boldsymbol{Y} = \boldsymbol{X}(\boldsymbol{X}^T\boldsymbol{X})^{-1}$$

where

$$\boldsymbol{X} = [\boldsymbol{x}^{(1)}, \boldsymbol{x}^{(2)}, \ldots, \boldsymbol{x}^{(n)}]$$

and

$$\boldsymbol{Y} = [\boldsymbol{y}^{(1)}, \boldsymbol{y}^{(2)}, \ldots, \boldsymbol{y}^{(n)}]$$

The coefficients of the linear combination of $\boldsymbol{x}^{(k)}$ may be determined so as to give the minimum value of f by the variational method. Given the basis sets $\boldsymbol{X}$ and $\boldsymbol{Y}$, approximate eigenvectors $\boldsymbol{P}'$ and $\boldsymbol{Q}'$ are represented as

$$[21a] \quad \boldsymbol{P}' = \boldsymbol{X}\,\boldsymbol{p}$$

$$[21b] \quad \boldsymbol{Q}' = \boldsymbol{Y}\,\boldsymbol{q}$$

where the coefficient vectors $\boldsymbol{p}$ and $\boldsymbol{q}$ consist of n elements. Then, eqs. [20] and [9] give

$$[22] \quad f(\boldsymbol{P}',\boldsymbol{Q}')\boldsymbol{q}^T\boldsymbol{p} = \boldsymbol{q}^T\boldsymbol{Y}^T\boldsymbol{G}\boldsymbol{X}\boldsymbol{p} = \boldsymbol{q}^T\boldsymbol{g}\boldsymbol{p}$$

where the matrix elements of the $n \times n$ matrix $\boldsymbol{g}$ are given by

$$[23] \quad g_{km} = \boldsymbol{y}^{(k)T}\,\boldsymbol{G}\,\boldsymbol{x}^{(m)}$$

The differentiation of eq. [22] with respect to the kth component q_k, together with the extremum conditions, give

$$[24] \quad \boldsymbol{g}\boldsymbol{p} = f\boldsymbol{p}$$

This equation can easily be solved by diagonalizing the matrix $\boldsymbol{g}$ giving n solutions. Using the ith eigenvectors $\boldsymbol{p}_i$ in eq. [24] and the basis-set $\boldsymbol{x}^{(j)}$'s, we can compute the corresponding approximate eigenvectors $\boldsymbol{P}_i'$ of $\boldsymbol{G}$ as

$$[25] \quad \boldsymbol{P}_i' = \sum_{j=1}^{n} (\boldsymbol{p}_i)_j\,\boldsymbol{x}^{(j)}$$

where $(\boldsymbol{p}_i)_j$ is the jth component of the eigenvector $\boldsymbol{p}_i$.

Suppose that we are looking for the lowest eigenvalue f_1 and its associated eigenvector $\boldsymbol{P}_1$. Let $\boldsymbol{x}^{(n)}$ be an approximate eigenvector obtained by the shifted inverse-power method, and $\boldsymbol{P}_1'$ be the approximate vector constructed by $\boldsymbol{x}^{(j)}$'s and coefficient vector $\boldsymbol{p}_1$, which belongs to the lowest eigenvalue in eq. [24]. As $\boldsymbol{P}_1'$ contains $\boldsymbol{x}^{(n)}$ as a basis, the f value corresponding to the vector $\boldsymbol{P}_1'$ becomes always less than or equal to that of $\boldsymbol{x}^{(n)}$ itself by virtue of the variational principle. Therefore $\boldsymbol{P}_1'$ becomes a more accurate eigenvector than $\boldsymbol{x}^{(n)}$ itself.

In calculating the basis set $\boldsymbol{X}$, we adopted $-\boldsymbol{f}_Q^0$ instead of $\boldsymbol{b}$ in eq. [16] as in eq. [14a]. The first result is then the same as $\delta\boldsymbol{P}$, the solution of the Newton–Raphson equation [14a]. After having obtained two sets $\{\boldsymbol{x}^{(k)}\}$ and $\{\boldsymbol{y}^{(k)}\}$, we solve the variational equation [24].

We now summarize our computational scheme. Here for simplicity, we look for the solution of the lowest excitation energy only. The extension to obtaining a few eigenvalues and eigenvectors is quite straightforward.

2.3.1. Initialization

Select a set of trial vectors $\boldsymbol{P}$ and $\boldsymbol{Q}$, which satisfy $\boldsymbol{P}^T\boldsymbol{Q} = 1$. As an initial guess, we choose $P_i = Q_i = 1$ and all the other elements of these vectors are set to be 0's, where i is the number corresponding to the smallest diagonal element in the matrix $\boldsymbol{G}$. Probably this choice of the initial guess is the simplest one.

2.3.2. Iteration

(*i*) Calculate f by eq. [9], the first derivative vector $\boldsymbol{f}_Q$ by

Can. J. Chem. Downloaded from www.nrcresearchpress.com by 92.62.229.171 on 09/08/12
For personal use only.

TABLE 1. Convergence rate in computing the transition energies to 1^1B_u state of decapentaene and dodecahexaene[a,b]

Iteration number	Decapentaene		Dodecahexaene	
	Transition energy (a.u.)	Residual[c] norm	Transition energy (a.u.)	Residual[c] norm
1	0.422 718 67D+00[d]	0.195 195 52D+00	0.316 762 78D+00	0.169 118 73D+00
2	0.388 150 64D+00	0.187 130 23D+00	0.259 144 97D+00	0.108 606 67D+00
3	0.314 586 94D+00	0.109 577 30D+00	0.206 902 30D+00	0.840 052 49D−01
4	0.275 961 33D+00	0.757 197 95D−01	0.177 476 22D+00	0.100 849 06D−01
5	0.175 994 64D+00	0.135 190 64D−01	0.176 793 97D+00	0.643 174 63D−04
6	0.156 830 60D+00	0.348 439 53D−02	0.176 793 95D+00	0.141 550 75D−13
7	0.156 784 95D+00	0.100 399 17D−05		

[a]The molecular geometries and parameters are given in ref. 12.
[b]The matrix sizes for decapentaene and dodecahexaene are 169 and 342, respectively.
[c]A tolerance value for convergence is $N \times 10^{-8}$.
[d]D−02, for instance, denotes $\times 10^{-2}$.

TABLE 2. Convergence rate in computing the transition energies to 2^1A_g state of decapentaene and dodecahexaene[a,b]

Iteration number	Decapentaene		Dodecahexaene	
	Transition energy (a.u.)	Residual[c] norm	Transition energy (a.u.)	Residual[c] norm
1	0.373 520 80D+00	0.179 012 10D+00	0.382 377 85D+00	0.189 892 28D+00
2	0.305 225 12D+00	0.111 158 62D+00	0.366 667 78D+00	0.158 804 94D+00
3	0.238 995 69D+00	0.630 000 85D−01	0.344 368 42D+00	0.175 851 91D+00
4	0.186 938 21D+00	0.100 980 48D+00	0.349 288 71D+00	0.200 779 01D+00
5	0.135 226 06D+00	0.208 384 19D−03	0.328 154 06D+00	0.154 125 06D+00
6	0.125 225 73D+00	0.955 922 68D−10	0.316 163 75D+00	0.155 694 06D+00
7			0.305 698 08D+00	0.160 158 62D+00
8			0.297 713 15D+00	0.157 414 23D+00
9			0.266 155 55D+00	0.108 526 83D+00
10			0.250 580 50D+00	0.883 587 93D−01
11			0.229 473 94D+00	0.376 795 00D−01
12			0.225 543 06D+00	0.597 362 09D−02
13			0.315 338 95D+00	0.285 768 40D+00
14			0.182 535 93D+00	0.635 268 30D−01
15			0.161 151 77D+00	0.451 062 50D−01
16			0.136 505 24D+00	0.370 732 06D−01
17			0.126 944 23D+00	0.159 311 37D−03
18			0.128 581 71D+00	0.170 543 14D−01
19			0.126 944 08D+00	0.819 043 11D−06

[a]The molecular geometries and parameters are given in ref. 12.
[b]The matrix sizes for decapentaene and dodecahexaene are 181 and 360, respectively.
[c]A tolerance value for convergence is $N \times 10^{-8}$.

eq. [10*b*], and the approximated Hessian matrix $(\boldsymbol{G} - f\mathbf{1})$ by eq. [14*a*].

(*ii*) Compute the residual norm of f_Q.

If it becomes smaller than ε(a tolerance value for convergence), stop the calculation. Then the computed value of f in step (*i*) is the eigenvalue to be obtained.

(*iii*) If the norm is greater than ε, then obtain a sequence of $\boldsymbol{x}^{(k)}$ in the shifted inverse iteration by eqs. [14*a*] and [19] to construct matrix $\boldsymbol{X}$, which consists of n column vectors. In our test calculations shown below, n will be 3. The larger n becomes, the faster is the convergence rate. There is no general rule for the determination of n and it should be chosen case by case.

If the Hessian matrix becomes singular, add a small number to all the diagonal elements and recalculate $\boldsymbol{X}$. Obtain $\boldsymbol{Y}$ from eq. [20]. After having obtained the basis sets $\boldsymbol{X}$ and $\boldsymbol{Y}$, calculate the matrix $\boldsymbol{g}$ in eq. [23].

(*iv*) Solve eq. [24] and choose the lowest eigenvalue f_1 and its associated eigenvector $\boldsymbol{p}_1$.

(*v*) Obtain a renewed trial vector $\boldsymbol{P}$ by eq. [25]. Compute the corresponding vector $\boldsymbol{Q}$ by eq. [3*a*] for the proper normalization, and normalize them by using eq. [8]. Note that ω_1 is equal to the square root of f_1. Jump back to step (*i*).

Needless to say, this scheme is also applicable to the eigenvalue problems of symmetric matrices.

3. Results and discussion

To illustrate the efficiency of the proposed algorithms we calculate the transition energies to 1^1B_u and 2^1A_g states of decapentaene and dodecahexaene by the parametrized EOM method at the $(1p–1h) + (2p–2h)$ level (12). These results are shown in Tables 1–3. In these test calculations, the $\sigma \rightarrow \sigma^*$ mixings are omitted for simplicity.

As is seen in these tables, the convergence rates are very

Can. J. Chem. Downloaded from www.nrcresearchpress.com by 92.62.229.171 on 09/08/12
For personal use only.

TABLE 3. Improvement of the convergence rate for the 2^1A_g state of dodecahexaene[a,b] by setting n to be 6

Iteration number	Dodecahexaene	
	Transition energy (a.u.)	Residual[c] norm
1	0.382 377 85D+00	0.189 892 28D+00
2	0.314 817 41D+00	0.118 202 24D+00
3	0.244 844 27D+00	0.655 926 70D−01
4	0.262 105 82D+00	0.198 492 55D+00
5	0.149 355 78D+00	0.449 902 01D−01
6	0.126 944 08D+00	0.119 220 30D−04
7	0.126 944 08D+00	0.619 471 40D−13

[a]The geometries and parameters are shown in ref. 12.
[b]The matrix sizes is 360.
[c]A tolerance value for convergence is $N \times 10^{-8}$.

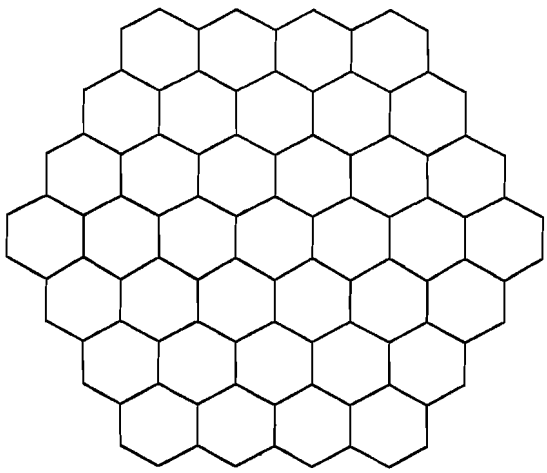

FIG. 1. The geometries of highly fused ring system $C_{96}H_{24}$. The bond angles (∠C—C—C) are all 120° and atomic distances between C—C are all 1.39 Å.

TABLE 4. The convergence rate for the lowest singlet excitation energy of the highly fused ring system[a,b] by setting n to be 3.

Iteration number	$C_{96}H_{24}$	
	Transition energy (a.u.)	Residual[c] norm
1	0.105 114 13D+00	0.139 340 42D−01
2	0.742 720 02D−01	0.152 197 97D−03
3	0.743 634 70D−01	0.811 655 87D−07

[a]The geometry is shown in Fig. 1.
[b]The matrix size is 2304.
[c]A tolerance value for convergence is $N \times 10^{-8}$.

fast and quite satisfactory except for the case of the 2^1A_g state of dodecahexaene in Table 2. It appears that the convergence rate does not depend on the matrix size. For the 2^1A_g state of dodecahexaene, a drastic improvement is attained when we set n to be 6, as is shown in Table 3.

The rapid convergence demonstrated in these examples is all due to the combined use of the shifted inverse power method and the variational method. The former extracts the dominant terms of the eigenvectors whose eigenvalues are close to f, and the latter determines the step length of the extracted vectors so as to give the optimum energy. To accelerate the convergence rate, the deviation vector must be properly evaluated. The numerical examples presented here indicate that the shifted inverse-power method is quite effective in evaluating these deviation vectors. It does not make any crude approximation in evaluating the deviation vectors as does the Davidson algorithm, so that it is applicable to the eigenvalue problems of nondiagonally dominant matrices.

It is well known that the Newton–Raphson method becomes very poor when the initial guess is far from the exact solution. However, the inverse sequence, $\boldsymbol{x}^{(k)}$ in eq. [19], obtained by the Newton–Raphson-type equation, provides a good approximation for the exact eigenvector. The reason is quite natural because of the inverse iteration effect discussed in Sect. 2.2. It is very interesting that the matrix in the shifted inverse-power method just corresponds to the Hessian matrix.

By virtue of the shifted inverse-power method, the set $\{\boldsymbol{P}_i\}$ obtained from eq. [25] contains not only the component of the wanted eigenvector but also those of the other eigenvectors whose eigenvalues are near to f. Therefore, once one solution is obtained, we have a good starting vector for the next solution.

Although the present method has good characteristics as mentioned above, the computation of the inverse matrix $(\mathbf{G} - f\mathbf{1})^{-1}$ is a time–memory consuming job particularly when N becomes large. As the matrices in our test calculations, which are shown in Tables 1–3, are not very large, we were able to calculate the inverse matrices of the Hessian and obtain the sequence $\{\boldsymbol{x}^{(k)}\}$ without any difficulty. If the sequence $\{\boldsymbol{x}^{(k)}\}$ is obtained directly without calculating the inverse matrix, then the eigenvalue problems for larger-scale matrices can be solved without consuming computer memory. To confirm this idea, we performed a "direct RPA" calculation on the highly fused ring system as shown in Fig. 1. In this calculation, we obtained the MO's by the PPP (Pariser–Parr–Pople) method and the sequence $\{\boldsymbol{x}^{(k)}\}$ by the Lanczos method (13). As we did not distinguish the symmetries, the RPA matrix size became 2304. The result is shown in Table 4. As expected from the previous results, the convergence rate is quite satisfactory. The fast convergence shows the efficiency of extracting the dominant terms of the eigenvectors whose eigenvalues are close to f.

1. (*a*) T. Shibuya and V. McKoy. Phys. Rev. A, **2**, 2208 (1970); (*b*) T. Shibuya, J. Rose, and V. McKoy. J. Chem. Phys. **58**, 500 (1970).
2. T. Shibuya, T. Funada, and H. Gotoh. Bull. Chem. Soc. Jpn. **61**, 1103 (1988).
3. D. T. Thouless. Nucl. Phys. **22**, 78 (1961).
4. J. P. Flament and H. P. Gervais. Int. J. Quantum Chem. **16**, 1347 (1979).
5. S. Rettrup. J. Comput. Phys. **45**, 100 (1982).
6. K. Hirao and H. Nakatsuji. J. Comput. Phys. **45**, 246 (1982).
7. J. Olsen, H. J. A. Jensen, and P. Jørgensen. J. Comput. Phys. **74**, 265 (1988).
8. T. Tamura and T. Udagawa. Nucl. Phys. **53**, 33 (1964).
9. G. Strang. Linear algebra and its applications. Academic Press Inc., New York. 1976.
10. E. Davidson. J. Comput. Phys. **17**, 87 (1975).
11. E. Davidson. J. Phys. A: Math. Gen. **13**, L170 (1980).
12. T. Shibuya, T. Funada, and S. Narita. Bull. Chem. Soc. Jpn. **62**, 701 (1988).
13. Y. Saad. SIAM J. Numer. Anal. **19**, 485 (1982).

Can. J. Chem. Downloaded from www.nrcresearchpress.com by 92.62.229.171 on 09/08/12
For personal use only.

Orbital reorganization and its energies in the interaction of CO with Sc, Fe, and Cu

KAZUO HIRAI AND NOBUHIRO KOSUGI[1]

Division of Molecular Engineering, Kyoto University, Yoshida, Kyoto 606, Japan

Received June 24, 1991

This paper is dedicated to Professor Sigeru Huzinaga on the occasion of his 65th birthday

KAZUO HIRAI and NOBUHIRO KOSUGI. Can. J. Chem. **70**, 301 (1992).

The interaction of CO with transition metals (M = Cu, Fe, and Sc) is analyzed using a newly developed method within the framework of the Hartree–Fock approximation. This method reveals reorganization of each orbital by the interaction and its energy contribution. To avoid the basis-set dependence in the energy partitioning, the orbital reorganization energy includes both polarization and charge-transfer effects; however, these effects are clearly distinguished by using orbital contours. The interaction in M–CO is discussed not only in terms of widely accepted components, such as metal $4s$–$4p\sigma$ polarization, CO 5σ – metal $3d\sigma$ donation, and metal $3d\pi$ – CO $2\pi^*$ backdonation, but also by using newly found components, metal $3d\sigma$–$4s$ and $4s$–$3d\sigma$ polarization, CO 5σ – metal $4p\sigma$ donation, metal $3d\sigma$ – CO $6\sigma^*$ backdonation, and CO 1π – $2\pi^*$ polarization.

Key words: metal carbonyl, interaction energy, orbital reorganization.

KAZUO HIRAI et NOBUHIRO KOSUGI. Can. J. Chem. **70**, 301 (1992).

On a analysé l'interaction du CO avec les métaux de transition (M = Cu, Fe et Sc) en utilisant une méthode développée récemment dans le cadre de l'approximation de Hartree–Fock. Cette méthode révèle la réorganisation de chaque orbitale sous l'influence de l'interaction ainsi que sa contribution à l'énergie. Afin d'éviter le problème d'une dépendance sur l'ensemble de base dans la répartition de l'énergie, l'énergie de réorganisation orbitalaire inclut les effets de polarisation ainsi que ceux du transfert de charge; toutefois, on fait une distinction claire entre ces effets en utilisant des contours orbitalaires. On ne discute pas de l'interaction M–CO seulement en fonction de composantes bien acceptées comme la polarisation métallique $4s$–$4p\sigma$, la donation CO 5σ – métal $3d\sigma$ et la rétrodonation métal $3d\pi$ – CO $2\pi^*$, mais aussi en utilisant les quatre nouvelles composantes suivantes : polarisation métal $3d\sigma$–$4s$ et $4s$–$3d\sigma$, la donation CO 5σ – métal $4p\sigma$, la rétrodonation métal $3d\sigma$ – CO $6\sigma^*$ et la polarisation CO 1π–$2\pi^*$.

Mots clés : métal carbonyle, énergie d'interaction, réorganisation orbitalaire.

[Traduit par la rédaction]

Introduction

In classical physics the molecular interaction is discussed in terms of the electrostatic forces among dipoles and induced dipoles. These correspond to the electrostatic (ES), polarization (PL), and dispersion terms. In quantum mechanics the exchange (EX) term is taken into account to satisfy the Pauli exclusion principle, and the charge-transfer (CT) term is very important. Several approaches to divide molecular interaction into the ES, EX, PL, and CT terms are proposed within the Hartree–Fock approximation and are applied to various interacting systems.

The interaction of CO with metals in adsorbed surfaces and in carbonyl compounds is an interesting issue for both experimental and theoretical chemists (1–9). It is widely accepted (1) that the interaction can be described as two major CT interactions: σ donation from CO 5σ to metal $3d\sigma$ and π backdonation from metal $3d\pi$ to CO $2\pi^*$, where the donation leads to a concentration of electron density on the metal and the backdonation reduces this charge. Some experiments indicated that the increase of $d\pi$ backdonation makes the M—C bond stronger and the C—O bond weaker (1). However, Bagus and co-workers (2, 4, 5) showed, in various systems involving CO and transition metals, that metal polarization (PL) and $d\pi$ backdonation are much more important than σ donation. In their theoretical work, they used the constrained space orbital variation (CSOV) method (6) to sequentially partition the interaction energy into contributions from intra-unit (PL) and inter-unit (CT) charge redistribution.

Recently, Frey and Davidson (3) investigated the SCF interaction energies for the $^2\Pi$, $^2\Delta$, $^2\Sigma^+$, $^4\Sigma^-$ states of ScCO by modifying the Kitaura–Morokuma (KM) analysis (10). They pointed out that the definition of polarization by Kitaura and Morokuma does not satisfy the Pauli exclusion principle. The concepts of PL and CT begin to lose their meanings as the distance between the fragments decreases or as the basis set becomes rather complete. Even if not complete, the distinction between PL and CT would depend on the basis set used. Furthermore, the concepts of ES and EX lose their meanings in strong interaction regions. To overcome these problems Frey and Davidson (3) redefined the polarization energy including the exchange repulsion, and showed that after the modification the results became reasonable even when the distance between the fragments was short or extended basis sets were used.

In the present work, based on a newly developed method, the features of σ donation, $d\pi$ backdonation, and metal polarization and other components are systematically clarified in the interaction of CO with different transition metals (M = Fe, Cu, and Sc). The total interaction energy is partitioned into the electrostatic plus exchange (ES + EX) term and the polarization plus charge transfer (PL + CT) term. The orbital reorganization through the PL + CT interaction is described as the change of the occupied orbital space from an isolated system to a combined system, and the PL + CT interaction energy is divided into each orbital reorganization. Orbital contours are used to see whether the interaction is PL, CT, or their mixture.

Method and computation

In the present work, the interaction is divided into two steps. In the first step, infinitely isolated fragments approach each other with no change in their wavefunctions. To

[1]Author to whom correspondence may be addressed.

Printed in Canada

Can. J. Chem. Downloaded from www.nrcresearchpress.com by 92.62.229.171 on 09/08/12
For personal use only.

satisfy the Pauli exclusion principle, the total wave function $\Phi(P)$ should be constructed by orthogonalization (or antisymmetrization, A) between the fragment wavefunctions, $\Phi(P_A)$ and $\Phi(P_B)$, as follows:

$$[1] \quad P = P_A \cup P_B \neq P_A + P_B$$

$$[2] \quad \Phi(P) = A\{\Phi(P_A) \cdot \Phi(P_B)\} \neq \Phi(P_A) \cdot \Phi(P_B)$$

where P, and P_A and P_B, are the occupied orbital spaces for the total and fragment systems, respectively. The first-step interaction arises from the interaction within the occupied orbital spaces of the fragments and includes only ES and EX terms. The ES + EX interaction energy E_{ES+EX} is obtained as the difference between the energy of the infinitely isolated system and the energy using the orbitals orthogonalized among all the occupied fragment orbitals. In the second step, the total wave function is reorganized from P to Q to satisfy the Hartree–Fock (HF) self-consistent field of the combined system, where Q denotes the HF occupied orbital space. The second-step interaction arises from stabilization through mixing with the vacant orbital space $(1 - P)$ and includes only PL and CT terms. The PL + CT interaction energy E_{PL+CT} is obtained by the difference between the energies for P and Q.

In addition to partitioning of the interaction energy, we have tried to see the change from P to Q by reorganization of each orbital. The first-step interaction is not to be divided into orbital components, but the second-step interaction within the HF approximation can be divided into orbital components as follows:

$$[3] \quad \Phi(P) = \|\phi_{o,1}\phi_{o,2} \cdots \phi_{o,N}\|$$

$$[4] \quad \Psi(Q) = \|\psi_{o,1}\psi_{o,2} \cdots \psi_{o,N}\|$$

where $P = \{\phi_{o,i} | i = 1, 2, \ldots, N\}$ and $Q = \{\psi_{o,i} | i = 1, 2, \ldots, N\}$ are the total occupied orbital spaces spanned by orthonormalized spin orbitals, $\phi_{o,i}$ and $\psi_{o,j}$, respectively, and Ψ denotes the HF wave function after the second-step interaction. The total vacant orbital space after the first-step interaction is $1 - P = \{\phi_{v,j} | j = 1, 2, \ldots, M\}$, where $\langle\phi_{o,i}|\phi_{v,j}\rangle = 0$. Then, $\psi_{o,i}$ can be uniquely described by mixing $\phi_{o,i}$ with $\phi_{v,i}$ as follows:

$$[5] \quad \psi_{o,i} = c_{o,i}\phi_{o,i} + c_{v,i}\phi_{v,i}$$

where

$$[6] \quad \langle\psi_{o,i}|\phi_{o,j}\rangle = c_{o,i}\delta_{ij}$$

$$[7] \quad \langle\psi_{o,i}|\phi_{v,j}\rangle = c_{v,i}\delta_{ij}$$

We can determine these spin orbitals by unitary transformation for the α-spin occupied orbitals and for the β-spin occupied orbitals of $\Phi(P)$ and $\Psi(Q)$ so that the overlap matrix between $\phi_{o,i}$ and $\psi_{o,j}$ is diagonalized as given by eq. [6] and the total energies remain unchanged. Such unitary transformation is achieved by the corresponding orbital transformation (11). Using the resulting relation [6], we obtain $\phi_{v,i}$ by normalizing the difference, $\psi_{o,i} - c_{o,i}\phi_{o,i}$. The orthogonal relation [7] $\langle\psi_{o,i}|\phi_{v,j}\rangle = 0$ $(i \neq j)$ is derived from the relations $\langle\psi_{o,i}|\psi_{o,j}\rangle = 0$ and $\langle\psi_{o,i}|\phi_{o,j}\rangle = 0$. When $M > N$, the orbitals $\phi_{v,i}$ $(i = 1, 2, \ldots, N)$ are uniquely defined to satisfy eqs. [5] and [7] but the remainder $(i = N + 1, \ldots, M)$ is not defined. When $M < N$, $\psi_{o,i} = \phi_{o,i}$ $(i = M + 1, \ldots, N)$. Thus, the change of $\phi_{o,i}(P)$ to $\psi_{o,i}(Q)$ by the inclusion of some part of $\phi_{v,i}(1 - P)$ is uniquely described by the mixture of the particular pair of orbitals.

TABLE 1. Interaction energies in Fe–CO and Cu–CO[a]

	FeCO $^5\Sigma^-(3d\sigma^1 3d\pi^4 3d\delta^2 4s^1)$			CuCO $^2\Sigma^+(3d\sigma^2 3d\pi^4 3d\delta^4 4s^1)$		
	α	β	Total	α	β	Total
E_{ES+EX}	–	–	−2.811	–	–	−1.755
E_{PL+CT}	1.363	1.006	2.369	0.800	0.369	1.169

[a]The values are given in eV, and positive value means stabilization. The SCF energies of CuCO and FeCO are −1751.1699 and −1374.6876 au, respectively.

Next, let us divide the second-step interaction energy E_{PL+CT} into each spin orbital component E_i as follows:

$$[8] \quad E_i = (Ea_i + Eb_i)/2$$

$$[9] \quad Ea_i = E\{\|\psi_{o,1}\psi_{o,2} \cdots \phi_{o,i} \cdots \psi_{o,N}\|\} - E\{\Psi(Q)\}$$

$$[10] \quad Eb_i = E\{\Phi(P)\} - E\{\|\phi_{o,1}\phi_{o,2} \cdots \psi_{o,i} \cdots \phi_{o,N}\|\}$$

$$[11] \quad E_{PL+CT} = \Sigma E_i = E\{\Phi(P)\} - E\{\Psi(Q)\}$$

where the first term in Ea_i is the energy when only the ith spin orbital $\psi_{o,i}$ of Q is substituted by the ith spin orbital $\phi_{o,i}$ of P, that is, $\psi_{o,i} \rightarrow \phi_{o,i}$ in Q; the second term in Eb_i is the energy when only the ith spin orbital of P is substituted by the ith spin orbital of Q, that is, $\phi_{o,i} \rightarrow \psi_{o,i}$ in P. Then, the total stabilization energy in the second-step interaction E_{PL+CT} is equal to a sum of contributions for each spin orbital. Let us call E_i the orbital reorganization energy.

The Cu, Fe, and Sc primitive functions used in the present work were taken from (5333/53/5) contracted Gaussian-type functions of Huzinaga *et al.* (12), and were augmented with three p functions: ζ_p(Cu) = 0.318, 0.142, 0.044, ζ_p(Fe) = 0.255, 0.118, 0.038, ζ_p(Sc) = 0.073, 0.042, 0.024, to describe the 4p orbital, and with a diffuse d function: ζ_d(Cu) = 0.15, ζ_d(Fe) = 0.11, and ζ_d(Sc) = 0.05, according to Hay's suggestion (13). The contraction scheme used was (532121/521111/3111). The C and O basis sets for CuCO and FeCO were of double ζ quality (621/311) from (63/5) of Huzinaga *et al.* (12). The C and O basis sets for ScCO were (73/7) augmented with polarization functions: ζ_d(C) = 0.600 and ζ_d(O) = 1.154, resulting in (721/511/1). The bond lengths R(M—C) and R(C—O) were 1.98 and 1.14 Å for CuCO (2), 1.84 and 1.15 Å for FeCO (2), and 2.12 and 1.183 Å for ScCO (3), respectively. The electronic states calculated were $^2\Sigma^+(3d\sigma^2 3d\pi^4 3d\delta^4 4s^1)$ for CuCO, $^5\Sigma^-(3d\sigma^1 3d\pi^4 3d\delta^2 4s^1)$ for FeCO, and $^2\Pi(3d\pi^1 4s^2)$ and $^4\Sigma^-(3d\pi^2 4s^1)$ for ScCO. The counterpoise method (14) was applied to the isolated systems. The correction energies were very small as follows: 0.0220 eV for Cu($d^{10}s^1$) and 0.0810 eV for CO; 0.0153 eV for Fe($d_{z^2}{}^1 d_{xz}{}^2 d_{yz}{}^2 d_{xy}{}^1 d_{x^2-y^2}{}^1 4s^1$) and 0.1023 eV for CO; 0.0075 eV for Sc($d_{xz}{}^1 4s^2$), 0.0063 eV for Sc($d_{xz}{}^1 d_{yz}{}^1 4s^1$), and 0.0432 eV for CO, where the single-configuration atomic SCF calculations were performed for Cu, Fe, and Sc($d_{xz}{}^1 d_{yz}{}^1 4s^1$) in the $C_{\infty v}$ symmetry and for Sc($d_{xz}{}^1 4s^2$) in the C_{2v} symmetry. The program GSCF3 (15, 16) was used for SCF calculations. All the computations were performed on the workstations DG AViiON 310 and SONY PWS 1550.

Can. J. Chem. Downloaded from www.nrcresearchpress.com by 92.62.229.171 on 09/08/12
For personal use only.

TABLE 2. The orbital reorganization energies (in eV) in the interaction between Fe and CO in FeCO $^5\Sigma^-(3d\sigma^1 3d\pi^4 3d\delta^2 4s^1)$

	E_i	Figure	Characterization
$\alpha 1(\sigma)$	0.824	Fig. 1a	Fe $4s$–$4p\sigma$ polarization
$\beta 1,2(\pi)$	0.764	Fig. 1b	Fe $3d\pi$ – CO $2\pi^*$ backdonation
$\alpha 2,3(\pi)$	0.409		
$\beta 3(\sigma)$	0.251	Fig. 1c	CO 5σ – Fe $3d\sigma$ donation
$\alpha 4(\sigma)$	0.086	Fig. 1d	CO 5σ – Fe $4p\sigma$ donation
$\alpha 5(\sigma)$	0.055	Fig. 1e	Fe $3d\sigma$ – CO $6\sigma^*$ backdonation
Others	−0.020		
Sum(E_{PL+CT})	2.369		

TABLE 3. The orbital reorganization energies (in eV) in the interaction between Cu and CO in CuCO $^2\Sigma^+(3d\sigma^2 3d\pi^4 3d\delta^4 4s^1)$

	E_i	Figure	Characterization
$\alpha 1(\sigma)$	0.581	(Fig. 1a)	Cu $4s$–$4p\sigma$ polarization
$\beta 1,2(\pi)$	0.135	(Fig. 1b)	Cu $3d\pi$ – CO $2\pi^*$ backdonation
$\alpha 2,3(\pi)$	0.123		
$\beta 3(\sigma)$	0.136	Fig. 2a	Cu $3d\sigma$–$4s$ polarization
$\alpha 4(\sigma)$	0.098	Fig. 2b	
$\beta 4(\sigma)$	0.097	(Fig. 2b)	CO 5σ – Cu $4p\sigma$ donation
Others	−0.001		
Sum(E_{PL+CT})	1.169		

Results and discussion

FeCO($^5\Sigma^-$) and CuCO ($^2\Sigma^+$)

Table 1 shows the first-step and second-step energies, E_{ES+EX} and E_{PL+CT}, in the interaction of CO with Fe and Cu in the $^5\Sigma^-(3d\sigma^1 3d\pi^4 3d\delta^2 4s^1)$ FeCO and $^2\Sigma^+(3d\sigma^2 3d\pi^4 3d\delta^4 4s^1)$ CuCO states, respectively. The positive value means stabilization. E_{ES+EX} for FeCO and CuCO are both negative, indicating repulsive interaction. The absolute values of E_{ES+EX} and E_{PL+CT} for FeCO are larger than for CuCO; the interaction between Fe and CO is stronger than between Cu and CO. This is because the metal–CO distance for FeCO (1.85 Å) is smaller than for CuCO (1.98 Å) and is partly because the $4s$ and $3d$ orbitals of Fe have larger radial extent than those of Cu (2).

Tables 2 and 3 show results of the orbital reorganization energies in the second-step interaction. Figures 1 and 2 show contour maps of the orbitals, $\phi_{o,i}$, $\phi_{v,i}$, and $\psi_{o,i}$ together with $c_{o,i}$ and $c_{v,i}$. Figure 1a shows the most contributive σ orbital reorganization in Fe–CO ($\alpha 1$, 35% of E_{PL+CT}, see Table 2). This reorganization demonstrates reduction of the repulsive ES + EX interaction between Fe and CO, which is achieved mainly by the Fe $4s$ orbital polarizing away from CO through $4s$–$4p\sigma$ hybridization and slightly by CO reorganization. The Cu $\alpha 1(\sigma)$ reorganization in Cu–CO shows very similar $4s$–$4p\sigma$ polarization away from CO, which is the most contributive of E_{PL+CT} (50%, see Table 3). Figure 2a shows the $\beta 3$ orbital reorganization in the $^2\Sigma^+(3d\sigma^2 3d\pi^4 3d\sigma^4 4s^1)$ CuCO state (0.136 eV, 12% of E_{PL+CT}), which corresponds to Cu σ polarization from $3d\sigma$ to $4s$ due to repulsive interaction between the doubly occupied CO 5σ and Cu $3d\sigma$ orbitals. This type of polarization is not found in the $^5\Sigma^-(3d\sigma^1 3d\pi^4 3d\delta^2 4s^1)$ FeCO state.

Figure 1b shows contour maps of π orbital reorganization in Fe–CO. The orbitals for α and β spins are exactly the same, because the restricted SCF wavefunctions are used and the α-spin and β-spin π electrons occupy the same orbitals. Figure 1b shows that the Fe $3d\pi$ electron moves towards the CO $2\pi^*$ orbital; that is, the $\beta 1,2$ and $\alpha 2,3$ reorganization of FeCO is typical $d\pi$ backdonation. The $\beta 1,2$ and $\alpha 2,3$ orbital contours of CuCO are nearly the same as those of FeCO. The sums of energy contributions from the π orbital reorganization $\beta 1,2$ and $\alpha 2,3$ are 50 and 22% of E_{PL+CT} in FeCO and CuCO, respectively.

Figures 1c and 1d show the $\beta 3$ and $\alpha 4$ orbital reorganization in the $^5\Sigma^-(3d\sigma^1 3d\pi^4 3d\delta^2 4s^1)$ FeCO state, respectively, both of which correspond to CO 5σ donation to Fe. The $\beta 3$ reorganization shown in Fig. 1c is typical σ donation from CO 5σ to Fe $3d\sigma$. On the other hand, the $\alpha 4$ reorganization shown in Fig. 1d corresponds to σ donation from CO 5σ to Fe $4p\sigma$ ($4sp\sigma$ hybrid directed to CO). Figure 2b shows the $\alpha 4$ orbital reorganization in CuCO, and the $\beta 4$ orbital reorganization in CuCO is almost the same as $\alpha 4$ in Fig. 2b. The $\alpha 4$ and $\beta 4$ reorganization is σ donation from CO 5σ to Cu $4p\sigma$ ($4sp\sigma$ hybrid directed to CO), which is similar to $\alpha 4$ of Fe–CO but is more contributive in energy (17% of E_{PL+CT}) than FeCO $\alpha 4$ (4% of E_{PL+CT}). In the $^2\Sigma^+(3d\sigma^2 3d\pi^4 3d\delta^4 4s^1)$ CuCO state, there is no σ donation from CO 5σ to Cu $3d\sigma$, because the $3d\sigma$ orbital is doubly occupied.

Figure 1e shows the $\alpha 5$ orbital reorganization in FeCO. Interestingly, this clearly indicates σ backdonation from Fe $3d\sigma$ to CO $6\sigma^*$. Other orbital reorganizations in FeCO and CuCO are complicated, but are energetically unimportant.

Bauschlicher *et al.* investigated the same systems based on the CSOV method (2). The FO interaction energies, which

Can. J. Chem. Downloaded from www.nrcresearchpress.com by 92.62.229.171 on 09/08/12
For personal use only.

Can. J. Chem. Downloaded from www.nrcresearchpress.com by 92.62.229.171 on 09/08/12
For personal use only.

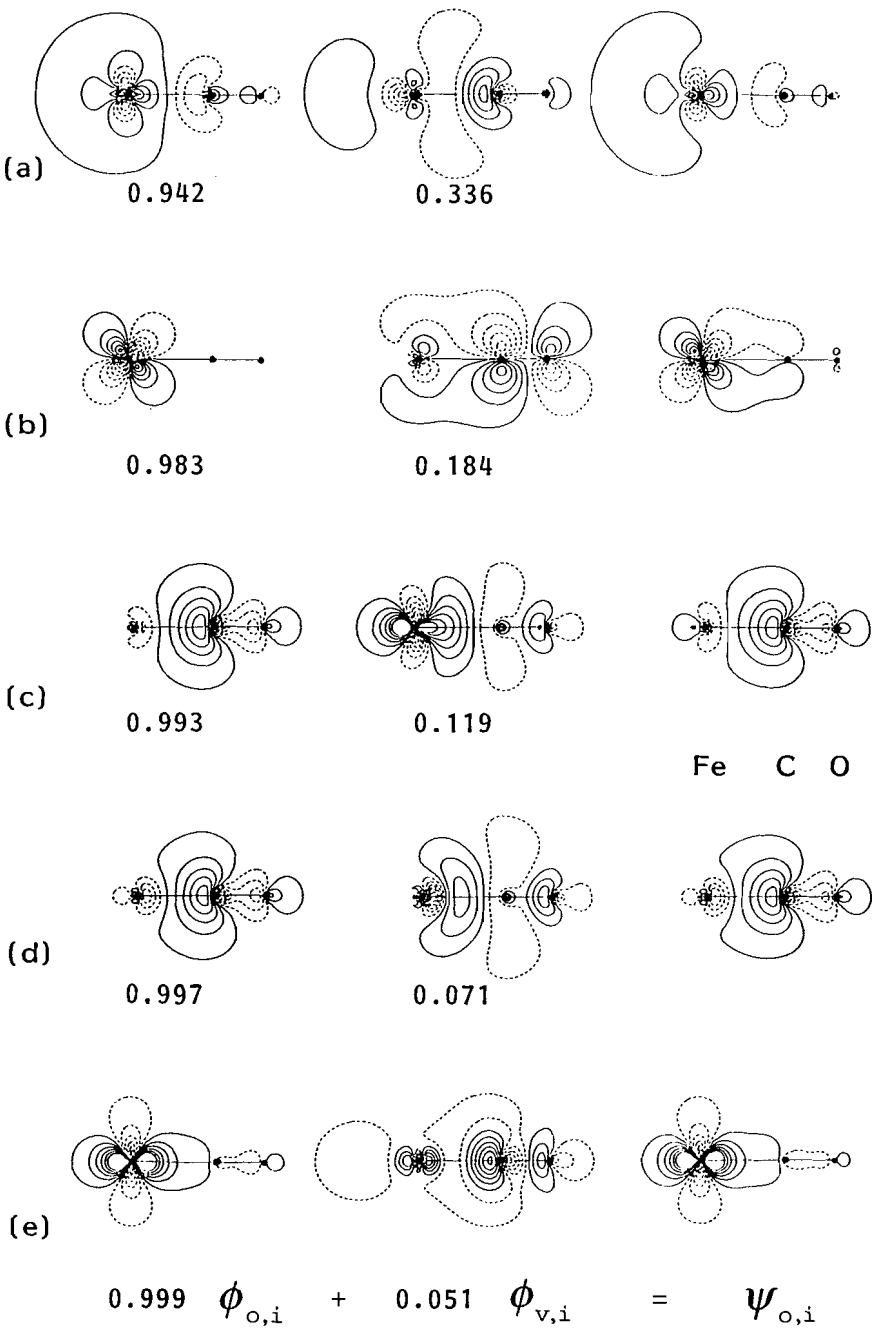

FIG. 1. Contour maps of the orbitals, $\phi_{o,i}$, $\phi_{v,i}$, and $\psi_{o,i}$ together with $c_{o,i}$ and $c_{v,i}$, where $c_{o,i}\phi_{o,i} + c_{v,i}\phi_{v,i} = \psi_{o,i}$, for the $^5\Sigma^-$ FeCO state. (a) $\alpha 1(\sigma)$, (b) $\beta 1,2(\pi)$ and $\alpha 2,3(\pi)$, (c) $\beta 3(\sigma)$, (d) $\alpha 4(\sigma)$, and (e) $\alpha 5(\sigma)$.

are defined with the frozen-orbital (FO) wavefunctions formed by superimposing (and antisymmetrizing) the wavefunctions of the isolated fragments, are -2.80 and -1.82 eV for FeCO and CuCO, respectively, and are nearly the same as the present results ($E_{ES+EX} = -2.811$ and -1.755 eV as shown in Table 1), though the basis functions used are different (but of the same quality) and in the present work the counterpoise method (14) is used. The PL + CT energies evaluated as the difference between their FO and SCF energies are 2.43 and 1.27 eV for FeCO and CuCO, respectively (2). Those are slightly larger than the present results ($E_{PL+CT} = 2.369$ and 1.169 eV). The CSOV stabilization energies within the π orbital space evaluated as [V(M;full basis) $-$ V(M;full σ basis)] + [V(CO;full basis) $-$ V(CO;full σ basis)] are 0.93 and 0.22 eV for FeCO and CuCO, respectively (2). Those are smaller than the present results for the sum of $\beta 1,2$ and $\alpha 2,3$ (1.173 and 0.258 eV). The present result shown in Fig. 1b demonstrates only $d\pi$ backdonation but no polarization at all; therefore, it is probable that the CSOV result underestimates the π orbital stabilization energies. The deficiency may be recovered by taking into account the unidentified (residual) interaction energies in the CSOV analysis, 0.21 and 0.05 eV for FeCO and CuCO, respectively (2). The sums of the metal and CO polarization energies of CSOV, V(M;M) and

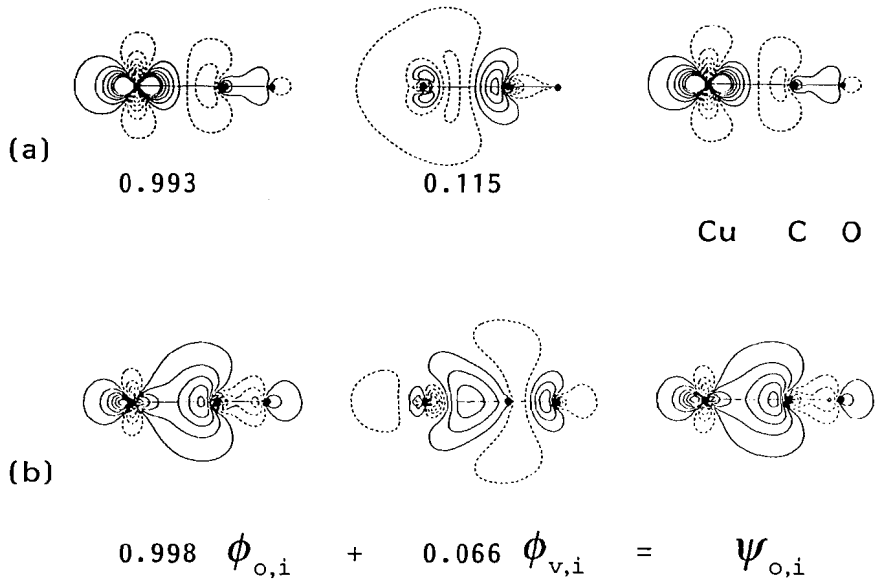

FIG. 2. Contour maps of the orbitals, $\phi_{o,i}$, $\phi_{v,i}$, and $\psi_{o,i}$ together with $c_{o,i}$ and $c_{v,i}$, where $c_{o,i}\phi_{o,i} + c_{v,i}\phi_{v,i} = \psi_{o,i}$, for the $^2\Sigma^+$ CuCO state. (a) β3(σ) and (b) α4(σ).

TABLE 4. Interaction energies in Sc–CO[a]

	ScCO $^2\Pi$ ($3d\pi^1 4s^2$)			ScCO $^4\Sigma^-$($3d\pi^2 4s^1$)		
	α	β	Total	α	β	Total
E_{ES+EX}	–	–	−3.096	–	–	−1.765
E_{PL+CT}	1.208	0.815	2.024	2.233	0.218	2.450

[a]The values are given in eV, and positive value means stabilization. The SCF energies of $^2\Pi$ and $^4\Sigma$ of ScCO are −872.2384 and −872.2570 au, respectively.

V(CO;CO), are 1.15 and 0.86 eV in FeCO and CuCO, respectively. The polarization energy coming from the α1 orbital reorganization in FeCO reaches 72% (0.824 eV) of the CSOV polarization energy, and the polarization energy from α1 and β3 in CuCO reaches 83% (0.717 eV).

ScCO($^2\Pi$, $^4\Sigma^-$)

Table 4 shows the first-step and second-step energies, E_{ES+EX} and E_{PL+CT}, of the interaction between Sc and CO in the $^2\Pi(3d\pi^1 4s^2)$ and $^4\Sigma^-(3d\pi^2 4s^1)$ states of ScCO. E_{ES+EX} for both the $^2\Pi$ and $^4\Sigma^-$ states are negative, indicating repulsive interaction. E_{ES+EX} for the $^2\Pi(3d\pi^1 4s^2)$ state is much larger than that of the $^4\Sigma^-(3d\pi^2 4s^1)$ state. This is consistent with the expectation that the repulsive interaction arises between the CO 5σ and Sc 4s electrons. The $^4\Sigma^-(3d\pi^2 4s^1)$ state is more favorable than the $^2\Pi(3d\pi^1 4s^2)$ state, and the E_{PL+CT} value for $^4\Sigma^-$ is larger than that for $^2\Pi$.

Tables 5 and 6 show results of the orbital reorganization energies in the second-step interaction. The orbital reorganization of the doubly occupied orbitals α1 and β1 for the $^2\Pi(3d\pi^1 4s^2)$ state (62% of E_{PL+CT}) seems to be large Sc polarization from 4s to 3$d\sigma$, or from d^1s^2 to d^2s^1, with small contribution of CO reorganization, resulting in reduction of the axial repulsive interaction, as is shown in Fig. 3a. This type of polarization is very unique. On the other hand, for the $^4\Sigma^-(3d\pi^2 4s^1)$ state, the singly occupied α3 orbital reorganization (19% of E_{PL+CT}) shown in Fig. 4b corresponds mainly to Sc σ polarization through 4s–4$p\sigma$ hybridization, which resembles the singly occupied α1 orbital reorganization of FeCO (Fig. 1a) and CuCO.

Figure 4a shows very large orbital reorganization of half-occupied α1,2 of the $^4\Sigma^-(3d\pi^2 4s^1)$ state (65% of E_{PL+CT}) which corresponds to $d\pi$ backdonation. This is similar to $d\pi$ backdonation of FeCO (Fig. 1b) and CuCO, but shows an increase of the density between Sc and C. This is consistent with the fact that the Sc 3$d\pi$ orbital has a relatively large radial extent. The orbital reorganization for quarterly occupied α2 in the $^2\Pi(3d\pi^1 4s^2)$ state (20% of E_{PL+CT}) corresponds to very similar $d\pi$ backdonation to α1,2 of the $^4\Sigma^-(3d\pi^2 4s^1)$ state.

The α4 and β1 orbital reorganization of the $^4\Sigma^-(3d\pi^2 4s^1)$ state corresponds to σ donation from CO 5σ to Sc 3$d\sigma$, which is very similar to the β3 orbital reorganization in the $^5\Sigma^-(3d\sigma^1 3d\pi^4 3d\delta^2 4s^1)$ FeCO state (Fig. 1c). Figure 3b shows β2 and α3 of the $^2\Pi(3d\pi^1 4s^2)$ state (14% of E_{PL+CT}) and is similar to Fig. 2b showing α4 and β4 of the $^2\Sigma^+(3d\sigma^2 3d\pi^4 3d\delta^4 4s^1)$ CuCO state; contribution of CO 5σ donation to Sc 4$p\sigma$ (not to 3$d\sigma$) is dominant. This is because the 4s orbital is doubly occupied in the $^2\Pi(3d\pi^1 4s^2)$ state and the Sc 4s–3$d\sigma$ polarization is very contributive, as is shown in Fig. 3a.

Figure 3c shows the α4 and β3 orbital reorganization of the $^2\Pi(3d\pi^1 4s^2)$ state. This reorganization contributes little in energy, but shows CO 1π–2π* polarization with very small π donation from CO 1π to Sc 3$d\pi$. It is interesting that this type of polarization is clearly found to be independent of the $d\pi$ backdonation α2.

Frey and Davidson (3) investigated the same states of ScCO based on the original and modified Kitaura–Morokuma (KM) methods. Their ES + EX energies (E_{el} + E_{ex}) based on the original KM method are 2.95 and 1.73 eV for the $^2\Pi$ and $^4\Sigma^-$ states, respectively. These are comparable with the present results (E_{ES+EX} = 3.096 and 1.765 eV). On the other hand, their total PL + CT energies evaluated as $E_{int} - E_{el} - E_{ex}$ with the original KM method, which they call the distortion term, are 1.74 and 2.30 eV for the $^2\Pi$ and $^4\Sigma^-$ states,

Can. J. Chem. Downloaded from www.nrcresearchpress.com by 92.62.229.171 on 09/08/12
For personal use only.

TABLE 5. The orbital reorganization energies (in eV) in the interaction between Sc and CO in ScCO $^2\Pi(3d\pi^1 4s^2)$

	E_i	Figure	Characterization
β1(σ)	0.630	Fig. 3a	Sc $4s-3d\sigma$ polarization
α1(σ)	0.616		
α2(π)	0.409	(Fig. 4a)	Sc $3d\pi$ – CO $2\pi^*$ backdonation
β2(σ)	0.145	Fig. 3b	CO 5σ – Sc $4p\sigma$ donation
α3(σ)	0.138		
α4(π)	0.036	Fig. 3c	CO $1\pi-2\pi^*$ polarization
β3(π)	0.033	(Fig. 3c)	
Others	0.017		
Sum(E_{PL+CT})	2.024		

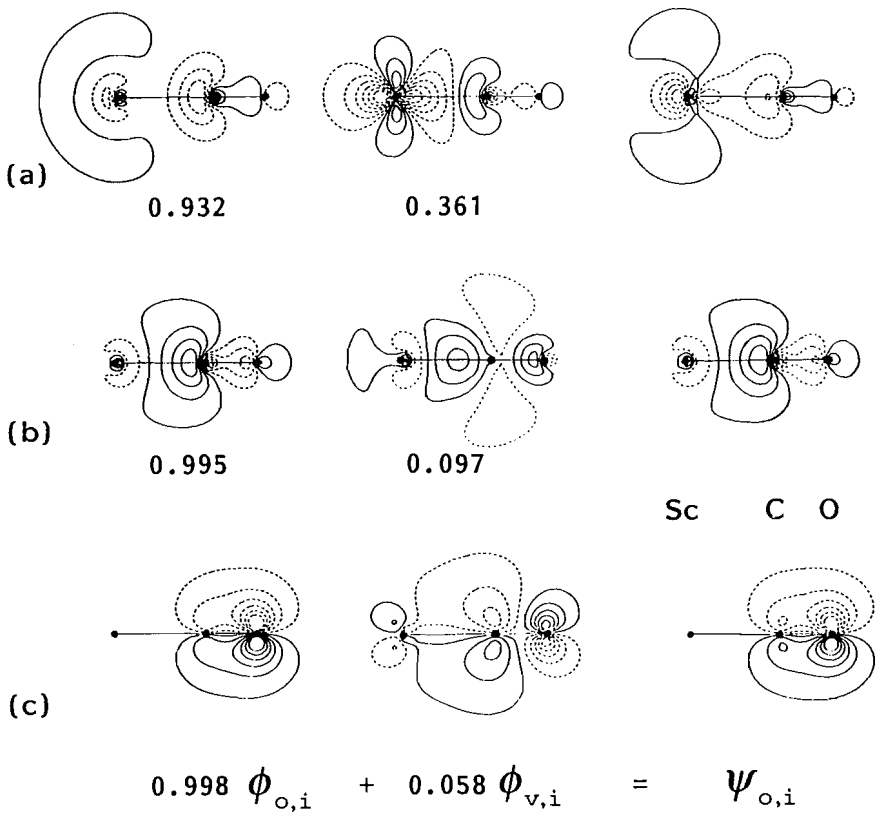

FIG. 3. Contour maps of the orbitals, $\phi_{o,i}$, $\phi_{v,i}$, and $\psi_{o,i}$ together with $c_{o,i}$ and $c_{v,i}$, where $c_{o,i}\phi_{o,i} + c_{v,i}\phi_{v,i} = \psi_{o,i}$, for the $^2\Pi$ ScCO state. (a) β1(σ) and α1(σ), (b) β2(σ) and α3(σ), and (c) α4(π).

respectively, and those evaluated as $E_{plctx}(Sc) + E_{plctx}(CO)$ with the modified KM method, which should be equal to the distortion term, are 1.73 and 2.09 eV, respectively. These discrepancies are attributed to coupling terms (3). The present results (E_{PL+CT} = 2.024 and 2.450 eV) are larger than their results. These discrepancies may arise from differences in the basis functions used; their basis functions for Sc seem to be better than the present ones, lowering the energies of the isolated systems. Furthermore, they divided the PL + CT energies E_{plctx} into the σ and π parts. The σ PL + CT energies $E_{plctx}(\sigma)$ are 1.28 and 0.76 eV and the π PL+CT energies $E_{plctx}(\pi)$ are 0.33 and 1.10 eV for the $^2\Pi$ and $^4\Sigma^-$ states, respectively. The present results ($E_{PL+CT}(\sigma)$ = 1.614 and 0.867 eV, $E_{PL+CT}(\pi)$ = 0.410 and 1.583 eV, respectively) are in qualitative agreement with those.

Conclusions

The present method is able to uniquely partition the interaction into the orbital reorganization. To avoid the basis-set dependence in the energy partitioning, the polarization and charge transfer are not separated within the algorithm; however, the orbital contours make it clear whether the reorganization is polarization or charge transfer in most cases. Centers of gravity of the reorganization orbitals may also be useful for the distinction. Even if polarization and charge transfer appear in the same orbital reorganization, it only

Can. J. Chem. Downloaded from www.nrcresearchpress.com by 92.62.229.171 on 09/08/12
For personal use only.

TABLE 6. The orbital reorganization energies (in eV) in the interaction between Sc and CO in ScCO $^4\Sigma^-(3d\pi^2 4s^1)$

	E_i	Figure	Characterization
$\alpha 1,2(\pi)$	1.583	Fig. 4a	Sc $3d\pi$ – CO $2\pi^*$ backdonation
$\alpha 3(\sigma)$	0.470	Fig. 4b	Sc $4s$–$4p\sigma$ polarization
$\alpha 4(\sigma)$	0.190	(Fig. 1c)	CO 5σ – Sc $3d\sigma$ donation
$\beta 1(\sigma)$	0.172		
Others	0.035		
Sum(E_{PL+CT})	2.450		

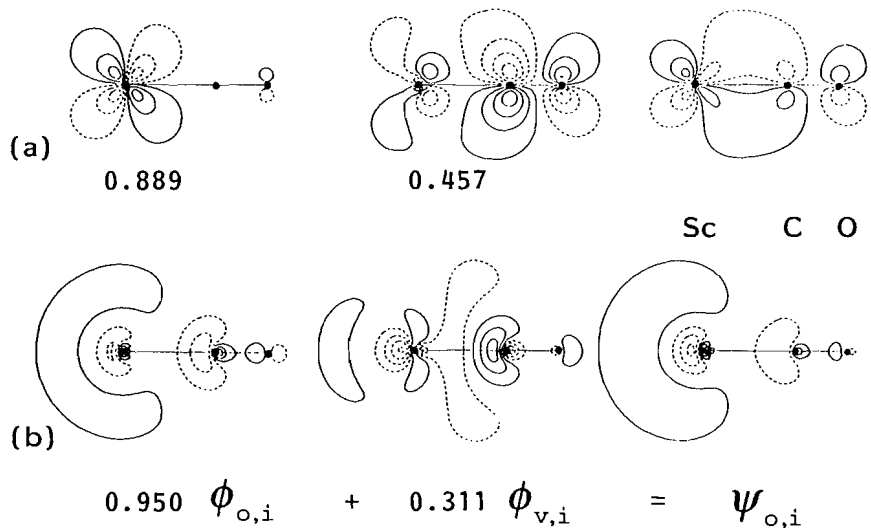

FIG. 4. Contour maps of the orbitals, $\phi_{o,i}$, $\phi_{v,i}$, and $\psi_{o,i}$ together with $c_{o,i}$ and $c_{v,i}$, where $c_{o,i}\phi_{o,i} + c_{v,i}\phi_{v,i} = \psi_{o,i}$, for the $^4\Sigma^-$ ScCO state. (a) $\alpha 1,2(\pi)$ and (b) $\alpha 3(\sigma)$.

suggests that the reorganization cannot be divided definitely into polarization and charge transfer. If we wish to develop a method to distinguish between polarization and charge transfer, it will fall into basis-set dependence. Although the present method is defined within the HF level, it may be extended beyond the HF level by using $\{\phi_{o,i}\}$ and $\{\phi_{v,i}\}$ defined within the HF level.

The interaction of CO with transition metals was analyzed in the high-spin states of the linear model carbonyls, FeCO, CuCO, and ScCO. The orbital reorganization contours were consistent with the conventional concepts of donation, backdonation, and polarization, though the polarization and charge transfer effects cannot be methodologically distinguished. For the $^5\Sigma^-(3d\sigma^1 3d\pi^4 3d\delta^2 4s^1)$ FeCO and $^2\Sigma^+(3d\sigma^2 3d\pi^4 3d\delta^4 4s^1)$ CuCO states, the metal $4s$–$4p\sigma$ polarization and the metal $3d\pi$ – CO $2\pi^*$ backdonation were dominant, where $E_{PL}(4s$–$4p\sigma) \sim 35$ and 50%, and $E_{CT}(3d\pi$–$2\pi^*) \sim 50$ and 22% of E_{PL+CT}, respectively. For the $^2\Pi(3d\pi^1 4s^2)$ and $^4\Sigma^-(3d\pi^2 4s^1)$ states of ScCO, the metal polarization and the metal $3d\pi$ – CO $2\pi^*$ backdonation were dominant, where E_{PL}(metal) ~ 62 and 19%, and $E_{CT}(3d\pi$–$2\pi^*) \sim 20$ and 65% of E_{PL+CT}, respectively. The reorganization orbital contours for the $d\pi$ backdonation (Figs. 1b and 4a) were almost independent of the metals and the electronic configurations, but the energy contributions were dependent on the number of $d\pi$ electrons and the radial extent of $d\pi$ orbitals. On the other hand, the orbital reorganization by the metal polarization was dependent on the electronic configurations. In the $^5\Sigma^-(3d\sigma^1 4s^1)$ FeCO, $^2\Sigma^+(3d\sigma^2 4s^1)$ CuCO, and $^4\Sigma^-(3d\sigma^0 4s^1)$ ScCO states, the dominant metal polarization corresponded to the $4s$–$4p\sigma$ rehybridization away from CO to reduce the repulsive interaction with CO (Figs. 1a and 4b). In the $^2\Pi(3d\sigma^0 4s^2)$ ScCO state, there was no $4s$–$4p\sigma$ polarization but the metal polarization corresponded to the de-excitation from $4s$ to $3d\sigma$, or from d^1s^2 to d^2s^1, to reduce the axially repulsive interaction with CO (Fig. 3a).

Other polarization and backdonation effects were found. In the $^2\Sigma^+(3d\sigma^2 4s^1)$ CuCO state the metal $3d\sigma$–$4s$ polarization was contributive (12% of E_{PL+CT}), indicating the rehybridization between $d\sigma^2 s^1$ and $d\sigma^1 s^2$ to reduce the axially repulsive interaction with CO 5σ (Fig. 2a). The CO 1π–$2\pi^*$ polarization (Fig. 3c) and Fe $3d\sigma$ – CO $6\sigma^*$ backdonation (Fig. 1e) were clearly found in the $^2\Pi(3d\sigma^0 4s^2)$ ScCO and $^5\Sigma^-(3d\sigma^1 4s^1)$ FeCO states, respectively, though less contributive (3.4 and 2.3% of E_{PL+CT}).

The CO 5σ donation to the metals was more complicated. There were two types of donation found in the $^5\Sigma^-(3d\sigma^1 4s^1)$ FeCO state: the donations to Fe $3d\sigma$ and to Fe $4p\sigma$ ($4sp$ hybrid directed to CO). The former corresponded to the well-accepted donation (Fig. 1c) and was more contributive (11% of E_{PL+CT}) than the latter (Fig. 1d, 3.6% of E_{PL+CT}). In the $^2\Sigma^+(3d\sigma^2 4s^1)$ CuCO and $^2\Pi(3d\sigma^0 4s^2)$ ScCO states with the $3d\sigma$ and $4s$ orbitals doubly occupied, respec-

Can. J. Chem. Downloaded from www.nrcresearchpress.com by 92.62.229.171 on 09/08/12
For personal use only.

tively, only the latter type of donation was contributive (17% of E_{PL+CT}, Fig. 2b; 14% of E_{PL+CT}, Fig. 3b). In the $^4\Sigma^-(3d\sigma^0 4s^1)$ ScCO state with the $3d\sigma$ orbital unoccupied, only the former type of donation was contributive (15% of E_{PL+CT}).

Acknowledgement

One of the authors (N.K.) is very grateful to Professor Sigeru Huzinaga for continuous encouragement and interest in his work.

1. F. A. Cotton and G. Wilkinson. Advanced inorganic chemistry, 5th ed. Wiley, New York. 1988.
2. C. W. Bauschlicher, Jr., P. S. Bagus, and B. O. Roos. J. Chem. Phys. **85**, 354 (1986).
3. R. F. Frey and E. R. Davidson. J. Chem. Phys. **90**, 5555 (1989).
4. P. S. Bagus, C. J. Nelin, and C. W. Bauschlicher, Jr. Phys. Rev. B, **28**, 5423 (1983).
5. P. S. Bagus, C. J. Nelin, and C. W. Bauschlicher, Jr. J. Vac. Sci. Technol. A: **2**, 905 (1984).
6. P. S. Bagus, K. Hermann, and Bauschlicher, Jr. J. Chem. Phys. **80**, 4378 (1984).
7. P. S. Bagus, K. Hermann and C. W. Bauschlicher, Jr. J. Chem. Phys. **81**, 1966 (1984).
8. C. W. Bauschlicher, Jr. and P. S. Bagus. J. Chem. Phys. **81**, 5889 (1984).
9. K. Hermann, P. S. Bagus, and C. J. Nelin. Phys. Rev. B, **35**, 9467 (1987).
10. K. Kitaura and K. Morokuma. Int. J. Quantum Chem. **10**, 325 (1976).
11. A. T. Amos and G. G. Hall. Proc. R. Soc. (London), **A263**, 483 (1961).
12. S. Huzinaga, J. Andzelm, M. Kłobukowski, E. Radzio-Andzelm, Y. Sakai, and H. Tatewaki. Gaussian basis sets for molecular calculations. Elsevier, Amsterdam. 1984.
13. P. J. Hay. J. Chem. Phys. **66**, 4377 (1977).
14. S. F. Boys and F. Bernardi. Mol. Phys. **19**, 533 (1970).
15. N. Kosugi and H. Kuroda. Chem. Phys. Lett. **74**, 490 (1980).
16. N. Kosugi. Theor. Chim. Acta, **72**, 149 (1987).

Can. J. Chem. Downloaded from www.nrcresearchpress.com by 92.62.229.171 on 09/08/12
For personal use only.

A configuration interaction study of the ground and first excited $^1\Sigma^+$ states of the NaI molecule

YOSHIKO SAKAI,[1] EISAKU MIYOSHI, AND TOSINOBU ANNO
College of General Education, Kyushu University, Ropponmatsu, Fukuoka, 810, Japan

Received June 13, 1991

This paper is dedicated to Professor Sigeru Huzinaga on the occasion of his 65th birthday

YOSHIKO SAKAI, EISAKU MIYOSHI, and TOSINOBU ANNO. Can. J. Chem. **70**, 309 (1992).

Multireference singly and doubly excited CI (MRSDCI) calculations are performed on the NaI molecule by using a model potential method. The potential energy curves of the ground and first excited $^1\Sigma^+$ states are generated over a wide range of internuclear distance R. The curves yield the avoided crossing, which is expected to arise by the mixing of the ionic and covalent configurations, and thus the curve of the first excited state shows a shallow minimum. The geometrical parameters, dipole moment, and dissociation energy are calculated. The agreement of those with the experimental results is satisfactory.

Key words: NaI, MRSDCI calculation, model potential method, potential curve, excited state.

YOSHIKO SAKAI, EISAKU MIYOSHI et TOSINOBU ANNO. Can. J. Chem. **70**, 309 (1992).

Utilisant une méthode avec potentiel modèle, on a effectué des calculs d'IC avec multi-références simplement ou doublement excitées (MRSDCI) sur la molécule de NaI. On a généré les courbes d'énergie potentielle de l'état fondamental et du premier état excité $^1\Sigma^+$ pour un grand ensemble de distances internucléaires R. Les courbes conduisent au croisement évité qui devrait augmenter par le mélange des configurations ionique et covalente; la courbe du premier état excité présente donc un minimum peu profond. On a calculé les paramètres géométriques, le moment dipolaire et l'énergie de dissociation. L'accord entre ces valeurs et les résultats expérimentaux est correct.

Mots clés : NaI, calculs MRSDCI, méthode du potentiel modèle, courbe de potentiel, état excité.

[Traduit par la rédaction]

Introduction

Over the last six decades, a number of spectroscopic studies have been done on diatomic alkali halides (1, 2). Although the ground state of these molecules has been well established, only a little knowledge has been gained for the excited states. The alkali halide dissociation reaction is influenced by the interaction between the ionic ground state and the lowest excited covalent state. The crossing (or avoided crossing) of the potential surfaces of these two states arises from the fact that the energy required to separate into ions ($M^+ + X^-$) is larger than the energy required to separate into neutral atoms (M + X), where M and X represent the alkali metal and halogen, respectively. This characteristic of alkali halides leads to interesting effects in the dynamics.

Schaefer *et al.* (3, 4) were the first to provide an analysis of the discrete ultraviolet (UV) spectrum obtained for NaI, and deduced the molecular parameters for the first excited state as well as for the ground state. Bluhm *et al.* (5) and Bower *et al.* (6) found a new bound state that leads to one of the Na(3*p*) asymptotes. Rose *et al.* (7, 8) performed femtosecond transition state spectra (FTS) measurements on the reaction of NaI, LiI, and NaBr. Their work focused particularly on NaI. The data showed that some NaI molecules were being trapped in a well formed by the avoided crossing of the covalent and ionic potential energy surfaces, indicating the presence of the excited bound state. Grice and Herschbach (9) calculated the splitting $\Delta V(R_x)$ between the pair of adiabatic potential energy curves that arise from pseudo-crossing of ionic and covalent states, where R_x is the crossing point of the diabatic potential curves. They pointed out that only when $R_x < 15$ au is $\Delta V(R_x)$ large enough to enable the adiabatic potential curves to govern the nuclear motion; otherwise the dissociation proceeds nonadiabatically, as if there were no mixing of the ionic and covalent configurations. The FTS measurements by Rose *et al.* (8) indicated that the fragments from the LiI dissociation were trapped similarly to the case of NaI, but then the dissociation of NaBr did not exhibit strong trapping. (R_x = 11.9 au for LiI, 13.3 au for NaI, and 15.4 au for NaBr (9).)

It is interesting to represent the potential energy curves of the alkali halides by theoretical calculations using the approach based on first principles. In the present work, we examine the potential energy curves of the ground state ($X^1\Sigma^+$) and the first excited state ($A^1\Sigma^+$) of the NaI molecule over a wide range of internuclear distance R. Careful configuration interaction (CI) calculations are required to describe properly the intermediate part of the potential curves, where the avoided crossing is expected to arise by the mixing of the ionic and covalent configurations. Multireference singly and doubly excited CI (MRSDCI) calculations are performed with extended Gaussian-type basis sets. The core electrons of the atoms are replaced by the model potentials (10–17). Our results include the potential energy curves, dipole moment curves, geometrical parameters, dissociation energy, and the values of R_x and $\Delta V(R_x)$.

Details of calculation

Basis sets and the scheme of calculation

Hartree–Fock–Roothaan (HFR) and MRSDCI calculations were performed on the ground and first excited $^1\Sigma^+$ states of the NaI molecule by using a model potential method (10–17). Nine electrons ($2s^22p^63s$) for the Na atom and seven electrons ($5s^25p^5$) for the I atom were treated explicitly and the remaining (core) electrons were replaced by the model potentials. Model potential parameters and basis sets were determined in the same way as in previous work (15). Major relativistic effects (mass–velocity and Darwin terms) were incorporated for the model potential of the I atom at the level

[1]Author to whom correspondence may be addressed.

Printed in Canada

Can. J. Chem. Downloaded from www.nrcresearchpress.com by 92.62.229.171 on 09/08/12
For personal use only.

TABLE 1. Gaussian-type basis sets for Na and I[a]

Type	Exponent	Coefficient	Type	Exponent	Coefficient
Na($2s^2 2p^6 3s^1$)			I($5s^2 5p^5$)		
s	184.432	0.066381	s	36.6348	0.125342
	24.7419	0.289568		9.69744	−0.481102
s	1.61226	1.0		2.42111	0.506331
s	0.489690	1.0	s	1.49193	1.0
s	0.0593791	1.0	s	0.284545	1.0
s	0.0233826	1.0	s	0.111568	1.0
p	34.5061	0.051633	s	0.030	1.0
	7.14634	0.286849	p	15.3022	0.144756
p	1.92832	1.0		2.25475	−0.348447
p	0.534480	1.0	p	0.308861	1.0
p	0.1432	1.0	p	0.120287	1.0
p	0.05235	1.0	p	0.0493516	1.0
d	0.582628	1.0	p	0.0150	1.0
d	0.117986	1.0	d	0.452	1.0
d	0.0378792	1.0	d	0.204	1.0
			d	0.0845	1.0

[a]The basis sets were contracted as (21111/21111/111) for Na and (31111/21111/111) for I.

Can. J. Chem. Downloaded from www.nrcresearchpress.com by 92.62.229.171 on 09/08/12
For personal use only.

of Cowan and Griffin's quasirelativistic HF method (13, 18). The valence basis set consists of six s- and four p-type Gaussian-type functions (GTF's) ($6s/4p$) for Na, and of ($6s/5p$) for I. In the molecular calculations, these basis sets were increased by one or two diffuse s- and p-type GTF's and three d-type GTF's, as shown in Table 1, in order to describe the Na^+ and I^- characters in the NaI molecule properly, and they were contracted as (21111/21111/111) for Na and (31111/21111/111) for I.

Following the SCF calculations, the MRSDCI calculations were performed to obtain the potential energy curves for the ground and first excited $^1\Sigma^+$ states. The calculations were done at 18 different distances of R = 4.0–20.0 au and at the dissociation limit ($R = 10^4$ au).

Computer programs JAMOL4 (19) and MICA3[2] were used for the SCF and MRSDCI calculations, respectively. A detailed description of the MRSDCI procedure will be given in the following section.

MRSDCI calculations

At the SCF-MO calculation, the configuration of the ionic state is $(4a_1^2)$, which is an abbreviation of $(1a_1^2 2a_1^2 3a_1^2 1b_1^2 2b_1^2 1b_2^2 2b_2^2 4a_1^2)$ in C_{2v} symmetry, and it turns into $(5a_1^2)$ at the dissociation limit. The highest occupied MO in the ionic state is of the I($6p$) character. The configuration of the covalent state is $(4a_1 5a_1)$, in which the $4a_1$ and $5a_1$ MO's are of the I($6p$) and Na($3s$) characters, respectively. We chose three configurations, $(4a_1^2)$, $(4a_1 5a_1)$, and $(5a_1^2)$, as the references in the MRSDCI calculations. All single and double excitations from these three reference configurations were considered without any orbital being kept frozen. To save configurational space, the configuration state functions (CSF's) were limited to first-order interaction space (20). The number of CSF's thus obtained is 89 252. Because the SCF-MO's of the ionic state are significantly different from those of the covalent state, the choice of the MO's in the CI is critical. We, therefore, adopted the procedure that consists of the following two steps.

1. The MRSDCI calculations with a small dimension were performed first, in which the SCF-MO's up to $10a_1$, $1a_2$, $5b_1$, and $5b_2$ in each representation were considered. Here, the SCF-MO's for the ionic state were used. The CI dimension was 3929.

2. Next, the MRSDCI calculations with full space were performed for the ionic and covalent states separately, using the natural orbitals for each of the states obtained by the above calculation. The dimension of CI was reduced to 3000–6000 (the smaller number of CSF's for the larger R values) by the second-order perturbation selection (21, 22) with an energy threshold of 5 μhartree. Weights of the reference space in the calculated ground and first excited states were 92–93% for all distances. The results of the CI calculations were modified by adding the energy lowering from the rejected CSF's, estimated by a second-order perturbation technique (21, 22), and also by a Davidson-like correction for multireference (23).

Results and discussion

The potential energy curves for the lowest two $^1\Sigma^+$ states obtained by the MRSDCI calculations are shown in Fig. 1. The ionic state produces an avoided crossing with the dissociation asymptote to the neutral atoms, and the curve of the excited state has a shallow minimum. Geometrical parameters (equilibrium Na—I distance R_e, vibrational constant ω_e, rotational constant B_e, and force constant k_e) were obtained by a third-degree polynomial fit to the total energies around the minimum shown in Table 2.

We shall discuss the properties of the ground state first. The results are given in Table 3 with the results of SCF calculation and the experimental data (24). The SCF values agree well with the experimental ones. The MRSDCI calculation improves the results further. The difference in R_e between the MRSDCI and experimental values is 0.02 Å (0.7%). Agreement of the calculated ω_e (256 cm^{-1}) and B_e

[2]A program package for CI calculations written by A. Murakami, H. Iwaki, H. Terashima, T. Kawaguchi, and T. Noro.

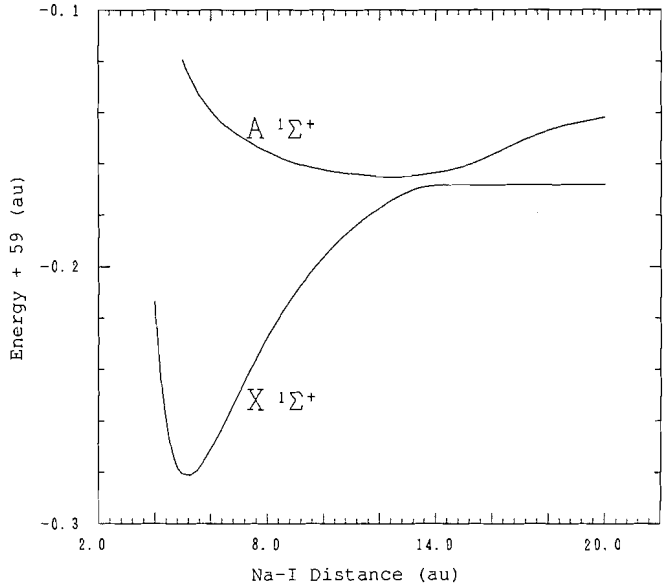

FIG. 1. Potential energy curves of the ground state ($X^1\Sigma^+$) and the first excited state ($A^1\Sigma^+$) obtained by the MRSDCI calculations as a function of the Na—I distance.

TABLE 2. Total energies around the energy minimum of the ground and excited states, and at the separation limit

	Total energy + 59 au	
R(au)	SCF	MRSDCI
Ground state		
5.0	−0.014707	−0.280825
5.1	−0.015435	−0.281434
5.15	−0.015590	−0.281532
5.165(R_e,MRSDCI)		−0.281539
5.188(R_e,SCF)	−0.015624	
5.2	−0.015621	−0.281511
5.4	−0.014699	−0.280371
10^4(Na + I)	+0.076300	−0.168531
First excited state		
7.5		−0.152285
10.0		−0.162164
11.5		−0.164371
12.5		−0.165029
13.5		−0.164037
15.0		−0.160745
10^4($Na^+ + I^-$)	+0.170616	−0.091756

(0.116 cm^{-1}) with the experimental values, 258 and 0.1178 cm^{-1}, respectively, is excellent.

To calculate the dissociation energy (D_e) of NaI, two methods were examined, the formulas of which are given as follows:

$$[1] \quad D_e = E(Na^+) + E(I^-) - E(NaI,R_e) - IP(Na) + EA(I)$$

and

$$[2] \quad D_e = E(Na) + E(I) - E(NaI,R_e)$$

TABLE 3. Results for the ground $^1\Sigma^+$ state of NaI

	SCF	MRSDCI	Exptl.
R_e(Å)	2.745	2.733	2.711145[a]
ω_e(cm^{-1})	252	256	258[a]
B_e(cm^{-1})	0.115	0.116	0.1178[a]
k_e(dyne/cm)	7.30×10^4	7.50×10^4	
μ_e(debye)		9.41	9.21[b]
D_0(eV)	2.98[c]	3.07[c]	3.00[d]
			3.13 ± 0.1[e]
			3.15 ± 0.05[f,g]
			3.18 ± 0.01[h]
			3.26 ± 0.03[i]

[a]See ref. 24.
[b]See ref. 38.
[c]A zero point correction of one-half ω_e was done on the calculated D_e.
[d]Photoionization, in ref. 29.
[e]Flame photometry, in ref. 33.
[f]Thermochemical, in ref. 32.
[g]Atomic fluorescence, in ref. 34.
[h]Photo-fragmentation, in ref. 30.
[i]Band convergence, in ref. 31.

where IP(Na) and EA(I) are the experimental ionization potential for Na and electron affinity for I, respectively. It has been confirmed that formula [1] gives more accurate D_e's than formula [2] for diatomic alkali halides (MX) (25), because the electronic structure of MX in the ionic ground $^1\Sigma^+$ state resembles that of the ion pair ($M^+ + X^-$) (25–28). When D_e is calculated by formula [1], most of the differential correlation and relativistic effects between MX and M + X are embedded in the experimental IP and EA (25–28). In the present work, the experimental values of IP(Na) = 5.138 eV and EA(I) = 3.063 eV (9) were used, and the total energy of the (Na^+I^-) system calculated at $R = 10^4$ au, given in Table 2, was used instead of the sum of the energy of the separated ions. By the use of formula [1], the MRSDCI and SCF calculations yielded D_e's of 3.09 and 3.00 eV, respectively. A number of experimental studies on the dissociation energy of the NaI molecule have been reported (29–34). As shown in Table 3, the experimental values of D_0 are in the range 3.00–3.26 eV. After a zero point correction of one-half ω_e on the calculated D_e's, we obtained D_0 = 3.07 and 2.98 eV for the MRSDCI and SCF calculations, respectively. The D_0's thus obtained are included in Table 3. Agreement of the MRSDCI D_0 value with the experimental values is satisfactory.

We also examined formula [2] to obtain D_e. D_e's of 3.08 and 2.50 eV were obtained for the MRSDCI and SCF calculations using the total energies given in Table 2. These D_e's, however, cannot be compared directly with the experimental values. The NaI molecule dissociates into the neutral Na($^2S_{1/2}$) and I($^2P_{3/2}$) atoms. Because of neglect of the spin-orbit interactions (13), our calculations yield the weighted average of the Na($^2S_{1/2}$) + I($^2P_{3/2}$) and Na($^2S_{1/2}$) + I($^2P_{1/2}$) asymptotes. The energy difference between the two atomic states, I($^2P_{3/2}$) and I($^2P_{1/2}$), is 0.94 eV, which is not negligible. Since the averaged energy of I(^2P,av) is higher by 0.31 eV than the energy of I($^2P_{3/2}$), the total energy of the supermolecule (Na + I) shown in Table 3 should be corrected by this amount. After this correction, formula [2] yielded D_e's of 2.77 and 2.19 eV for the MRSDCI and SCF calculations. These results are worse than those obtained by formula [1]. The difference in MRSDCI D_e's obtained by the

Can. J. Chem. Downloaded from www.nrcresearchpress.com by 92.62.229.171 on 09/08/12
For personal use only.

Can. J. Chem. Downloaded from www.nrcresearchpress.com by 92.62.229.171 on 09/08/12
For personal use only.

TABLE 4. Results for the first excited $^1\Sigma^+$ state of NaI

	MRSDCI
R_e(Å)	6.49
ω_e(cm^{-1})	39
B_e(cm^{-1})	0.0206
k_e(dyne/cm)	1.73×10^3

two methods is 0.32 eV. Bauschlicher *et al.* (28) have performed *ab initio* CI calculations on MgO (a^3II) and its component atoms and ions, and discussed which of the two methods gives a more accurate D_e value. They concluded that formula [1] gives a more accurate D_e than formula [2] and that the difference in the D_e's obtained by these two methods is very nearly the sum of errors in the calculated IP and EA. Their CI calculation has given an error of 0.21 eV for the IP(Mg) − EA(O) using large STO and GTO basis sets. The same is true of the present case. The experimental value for IP(Na) − EA(I) is 2.08 eV (9). After correcting the value of $\Delta E(\mathrm{I}(^2P,\mathrm{av}) - \mathrm{I}(^2P_{3/2}))$ by the amount 0.31 eV, the difference in the total energies of the systems, Na + I and $Na^+ + I^-$, calculated at $R = 10^4$ au is 2.40 eV, which corresponds to the calculated value of the IP(Na) − EA(I). Thus, the error of IP(Na) − EA(I) amounts to 0.32 eV. This is mainly caused by the difficulty in evaluating electron affinities of atoms (35, 36).

The true potential curves should provide their total energy difference at $R = \infty$, being equal to the experimental value of IP(Na) − EA(I). From this point of view, it is required that the $\mathrm{Na}(^2S_{1/2}) + \mathrm{I}(^2P_{3/2})$ asymptote lies lower, by 2.08 eV, than that of $Na^+(^1S_0) + I^-(^1S_0)$. Our potential curves shown in Fig. 1 yield an energy separation of 2.09 eV at $R = 10^4$ au. This agreement is a result of cancellation of the error caused by omitting the spin-orbit interaction and the above-mentioned error in IP(Na) − EA(I). The spin-orbit interaction will have little effect on the ionic system of $Na^+(^1S_0) + I^-(^2S_0)$ character over the whole range of R. The interaction affects significantly the covalent system of $\mathrm{Na}(^2S_{1/2}) + \mathrm{I}(^2P_{3/2})$ character, as discussed above. The effect will remain, however, nearly constant for a wide range of R, because the electronic structure of the covalent system changes little. Under these assumptions, we consider that the potential curves shown in Fig. 1 should be close to the true curves for the adiabatic ground ($X0^+$) and first excited ($A0^+$) states. We calculated the geometrical parameters for the first excited state by fitting a third-degree polynomial to the total energies around the minimum shown in Table 2. The results, which are given in Table 4, are R_e = 6.49 Å, ω_e = 39 cm^{-1}, and B_e = 0.0206 cm^{-1}. Schaefer *et al.* (3, 4) derived the potential curve of the first excited $^1\Sigma^+$ state ($A0^+$) of NaI, as well as the ground state, by analyzing the UV absorption spectrum. However, the intermediate part of the curve of the excited state is still unclear because of the assumption made to obtain the absolute v' numbering (4). They reported in their first paper (3) that vibrational spacing ω = 39.3 cm^{-1}, averaged rotational constant B = 744 MHz (=0.0248 cm^{-1}), and R = 5.90 Å for the adiabatic $A0^+$ state. These values agree qualitatively with our results. In the refined paper (4), however, they gave the values of Y_{10} ($\approx\omega$) = 27.3 cm^{-1} and Y_{01} ($\approx B$) = 0.0482 cm^{-1} for the adiabatic state ($A0^+$). This B value yields R = 4.24 Å, which is too

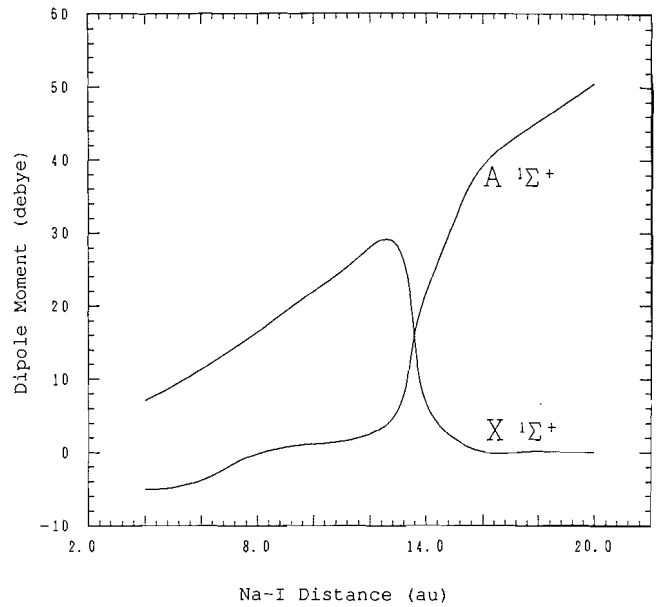

FIG. 2. Dipole moment curves of the ground state ($X^1\Sigma^+$) and the first excited state ($A^1\Sigma^+$) obtained by the MRSDCI calculations as a function of the Na—I distance.

short compared to our R_e of 6.49 Å. From the experimental potential curves of the excited state, we could not obtain quantitative geometrical parameters, because the intermediate part of the potential curve derived from an extrapolation is still questionable (4).

The crossing point of the diabatic potential curves, R_x, is estimated to be 13.3 au (7.04 Å) by a simple formula, IP(Na) − EA(I) = $1/R_x + \alpha/2R_x^4$ (9), where α is the sum of the polarizabilities of the positive and negative ions. From our adiabatic potential curves in Fig. 1, R_x is likely to be 13.5 au (7.14 Å), which is close to the estimated R_x value. The R_e given in Table 4 is shorter than the R_x, by 0.65 Å. We obtained a value of 0.13 eV for the energy splitting $\Delta V(R_x)$ between the adiabatic potential curves at the crossing point (R_x = 13.5 au), which is in good agreement with the result (0.10 ± 0.02 eV) derived from the chemical ionization process $Na + I \rightarrow Na^+ + I^-$ given by Los and coworkers (37). Grice and Herschbach have also obtained a splitting of 0.1 eV by semiempirical calculation (9). These facts give additional support to the reliability of the potential curve of the excited state in Fig. 1.

In Fig. 2 the dipole moment curves given by the MRSDCI calculation are plotted against R. The electronic structures of the two states change dramatically around R_x. The curve of the ground state goes down to zero at $R \simeq 15$ au. The gross populations on the atoms are 8.42 (Na) and 7.58 (I) at R_e, and 7.93 (Na) and 8.07 (I) at 12.5 au. They turn to 9.00 (Na) and 8.00 (I) for $R > 16$ au. On the contrary, the curve of the excited state goes up to the dissociation asymptote for the Na^+ and I^- ions at $R \simeq 16$ au. For $R < 8$ au, dipole moments are of $Na^{\delta-}I^{\delta+}$ character. For example, the gross populations are 9.16 (Na) and 6.83 (I) at 5.0 au. The polarity changes into $Na^{\delta+}I^{\delta-}$ at $R \simeq 8$ au. The gross populations are 8.00 for both atoms, (Na^+I^-), for $R > 16$ au. The dipole moment calculated at R_e is given in Table 3. The value of 9.41 debye agrees very well with the experimental value of 9.21 debye (38).

Acknowledgements

This paper is dedicated to Professor Sigeru Huzinaga on the occasion of his 65th birthday. The authors would like to thank Professor Huzinaga for his kind guidance in their research activities over many years. One of the authors (Y.S.) also would like to thank Professor Keiji Morokuma for his helpful suggestions for the present work. The calculations were done at the computer center of the Institute for Molecular Science.

1. R. S. Berry. *In* Alkali halide vapors. *Edited by* P. Davidovits and D. L. McFadden. Academic Press, New York, N.Y. 1979.
2. F. J. Lovas and E. Tiemann. J. Phys. Chem. Ref. Data, **3**, 609 (1974).
3. S. H. Schaefer, D. Bender, and E. Tiemann. Chem. Phys. Lett. **92**, 273 (1982).
4. S. H. Schaefer, D. Bender, and E. Tiemann. Chem. Phys. **89**, 65 (1984).
5. H. Bluhm, J. Lindner, and E. Tiemann. J. Chem. Phys. **93**, 4556 (1990).
6. R. D. Bower, P. Chevrier, P. Das, H. J. Foth, J. C. Polanyi, M. G. Prisant, and J. P. Viscot. J. Chem. Phys. **89**, 4478 (1988).
7. T. S. Rose, M. J. Rosker, and A. H. Zewail. J. Chem. Phys. **88**, 6672 (1988).
8. T. S. Rose, M. J. Rosker, and A. H. Zewail. J. Chem. Phys. **91**, 7415 (1989).
9. R. Grice and D. R. Herschbach. Mol. Phys. **27**, 159 (1974).
10. Y. Sakai. J. Chem. Phys. **75**, 1303 (1981).
11. Y. Sakai and S. Huzinaga. J. Chem. Phys. **76**, 2537 (1982).
12. Y. Sakai and S. Huzinaga. J. Chem. Phys. **76**, 2552 (1982).
13. M. Klobukowski. J. Comput. Chem. **4**, 350 (1983).
14. S. Huzinaga, M. Klobukowski, and Y. Sakai. J. Phys. Chem. **88**, 4880 (1984).
15. Y. Sakai, E. Miyoshi, M. Klobukowski, and S. Huzinaga. J. Comput. Chem. **8**, 226 (1987).
16. Y. Sakai, E. Miyoshi, M. Klobukowski, and S. Huzinaga. J. Comput. Chem. **8**, 256 (1987).
17. E. Miyoshi and Y. Sakai. J. Comput. Chem. **9**, 719 (1988).
18. R. D. Cowan and D. C. Griffin. J. Opt. Soc. Am. **66**, 1010 (1976).
19. H. Kashiwagi, S. Obara, T. Takada, F. Sasaki, and E. Miyoshi. Annu. Rev. Inst. Mol. Sci. (Japan), (1979). 121.
20. A. D. McLean and B. Liu. J. Chem. Phys. **63**, 980 (1975).
21. R. J. Buenker and S. D. Peyerimhoff. Theor. Chim. Acta, **35**, 33 (1974).
22. Z. Gershgorn and I. Shavitt. Int. J. Quantum Chem. **2**, 751 (1968).
23. E. R. Davidson. J. Comput. Phys. **17**, 87 (1975). P. E. M. Siegbahn. Chem. Phys. Lett. **55**, 386(1978).
24. K. P. Huber and G. Herzberg. *In* Constants of diatomic molecules, molecular spectra and molecular structure IV. Van Nostrand Reinhold Company, New York, N.Y. 1979.
25. S. R. Langhoff, C. W. Bauschlicher, Jr., and H. Partridge. J. Chem. Phys. **84**, 1687 (1986).
26. B. Liu, R. E. Olson, and R. P. Saxon. J. Chem. Phys. **74**, 4216 (1981).
27. P. Rosmus and W. Meyer. J. Chem. Phys. **74**, 4217 (1981).
28. C. W. Bauschlicher, Jr., B. H. Lengsfield III, and B. Liu. J. Chem. Phys. **77**, 4084 (1982).
29. J. Berkowitz and W. A. Chupka. J. Chem. Phys. **45**, 1287 (1966).
30. N. J. A. van Veen, M. S. de Vries, and A. E. de Vries. Chem. Phys. Lett. **64**, 213 (1979).
31. R. A. Berg and G. W. Skewes. J. Chem. Phys. **51**, 5430 (1969).
32. L. Brewer and E. Bracket. Phys. Rev. **61**, 425 (1961).
33. T. M. Sugden. Trans. Faraday Soc. **57**, 681 (1961).
34. H. Beutler and H. Levi. Z. Phys. Chem. Abt. B: **24**, 263 (1934).
35. F. Sasaki and M. Yoshimine. Phys. Rev. A, **9**, 17, 26 (1974).
36. D. Feller and E. R. Davidson. J. Chem. Phys. **90**, 1024 (1989).
37. A. P. M. Baede and J. Los. Physica, **52**, 422 (1971); A. M. C. Moutinho, J. A. Aten, and J. Los. Physica, **53**, 471 (1971); G. A. L. Delvigne and J. Los. Physica, **59**, 61 (1972).
38. A. J. Hebert, F. J. Lovas, C. A. Melenders, C. D. Hollowell, T. L. Story, Jr., and K. Street, Jr. J. Chem. Phys. **48**, 2824 (1968).

Can. J. Chem. Downloaded from www.nrcresearchpress.com by 92.62.229.171 on 09/08/12
For personal use only.

Ab initio study on radical anions of nitro compounds

FABIO RAMONDO

Dipartimento di Chimica, Università degli Studi di Roma, P.le A. Moro 5, 00185 Roma, Italy

Received June 10, 1991

This paper is dedicated to Professor Sigeru Huzinaga on the occasion of his 65th birthday

FABIO RAMONDO. Can. J. Chem. **70**, 314 (1992).

The results of *ab initio* molecular orbital calculations on some nitro compounds, RNO_2 (R = CH_3, CF_3, CH_2F, BH_2, BF_2, BHF, C_6H_5) and on the corresponding radical anions are reported. The geometries of the neutral and charged species were optimized at the SCF and MP2 levels of theory employing the 6-31G* and the 6-31+G* basis sets. The rotation about the CN and BN bonds reveals distinct conformations for each molecule and vibrational frequencies were determined for such structures. All the employed levels of theory predict structural differences between neutral and charged molecules. The major geometrical changes occurring by electron adding to RNO_2 consist in the lengthening of the NO bonds and in the shortening of the CN and BN bonds. The radical anions are calculated to be pyramidal at nitrogen in the stable conformers of $CH_3NO_2^-$, $CF_3NO_2^-$, $CH_2FNO_2^-$, while, for the π-electron-accepting substituents (BH_2, BHF, BF_2, C_6H_5), the anion is planar. Electron correlation energy corrections in the framework of Møller–Plesset perturbation theory were included to determine relative stabilities between different conformations. At the MP4/6-31G*//MP2/6-31G* level, an easy rotation of the NO_2 group is predicted for all the radical anions and neutral molecules with the exception of $BH_2NO_2^-$, $BF_2NO_2^-$, and $BHFNO_2^-$, which show high torsional barriers about the BN bond.

Key words: nitro compounds, radical anions, *ab initio* calculations, molecular structure.

FABIO RAMONDO. Can. J. Chem. **70**, 314 (1992).

On a effectué des calculs d'orbitales moléculaires *ab initio* sur quelques composés nitrés, RNO_2 (R = CH_3, CF_3, CH_2F, BH_2, BF_2, BHF et C_6H_5) et sur les anions radicaux correspondants. On a optimisé les géométries des espèces neutres et chargées aux niveaux auto-cohérent et MP2 de la théorie, en employant des ensembles de base 6-31G* et 6-31+G*. La rotation autour des liaisons CN et BN indique l'existence de conformations distinctes pour chaque molécule et on a déterminé les fréquences de vibration de chaque structure. Tous les niveaux de la théorie qui ont été utilisés permettent de prédire des différences structurales entre les molécules neutres et chargées. Les changements principaux de géométrie se produisent par l'addition d'un électron au RNO_2 et ils consistent en un allongement des liaisons NO et un raccourcissement des liaisons CN et BN. On a calculé que, dans les conformères stables du $CH_3NO_2^-$, $CF_3NO_2^-$ et $CH_2FNO_2^-$, les anions radicaux sont pyramidaux au niveau de l'azote alors que, avec des substituants qui acceptent les électrons π (BH_2, BHF, BF_2 et C_6H_5), l'anion est plan. Afin de déterminer les stabilités relatives des diverses conformations, on a introduit des corrections pour l'énergie de corrélation électronique dans le contexte de la théorie des perturbations de Møller–Plesset. Aux niveaux MP4/6-31G*//MP2/6-31G*, on prédit l'existence d'une rotation facile du groupe NO_2 pour tous les anions radicaux et les molécules neutres, à l'exception des anions $BH_2NO_2^-$, $BF_2NO_2^-$ et $BHFNO_2^-$ pour lesquels il existerait des barrières torsionnelles élevées autour de la liaison BN.

Mots clés : composés nitrés, anions radicaux, calculs *ab initio*, structure moléculaire.

[Traduit par la rédaction]

Introduction

Molecules containing the nitro group are involved in many electron-transfer processes both in the gas phase and in solution. Ion–molecule equilibria measurements in the gas phase were applied to determine electron affinities and ion thermochemical data (1, 2). Electron affinities were obtained for a wide variety of organic molecules and have been summarized in a recent review (3). Because of the high electron affinity of the NO_2 group, the formation of stable radical anions via electron attachment occurs easily. The lowest unoccupied molecular (π^*) orbital (LUMO) accepts an extra electron to become a singly occupied molecular orbital (SOMO) of the radical anion. The possibility of conjugation between NO_2 and other groups of the molecule and the presence of electronegative atoms or electron-withdrawing groups leads to the lowering of the LUMO energy and thus to higher electron affinities and to higher stability of the resulting radical anions. Accurate electron affinities were alternatively determined by photodetachment studies (4) but, when polyatomic molecules are investigated, knowledge of the geometry for both the neutral molecule and the anion is required to resolve the photoelectron spectrum. Geometrical changes and normal modes displacements are predicted as a consequence of electron attachment. However, any accurate experimental determination of the geometry and vibrational spectra of stable gas-phase radical anions represents a particularly difficult target. A general structural feature of nitro radical anions can be obtained from electron spin resonance investigations providing information about conformational preference of the nitro group in different organic radical anions (5). On the basis of ^{14}N anisotropic hyperfine splittings (5) and from experimental and theoretical studies of splitting constants (6), aliphatic anions show a tendency for pyramidal nitrogen, while nitroaromatic anions appear to be planar at nitrogen. Likewise, structural changes due to the negative charge are suggested by entropy variations derived from electron attachment measurements in the gas phase (1, 2). Negative entropy changes were determined for the nitrobenzene radical anion and substituted derivatives and this indicates a stiffening of the internal rotation of the NO_2 group moving from neutral to charged species (7, 8).

Detailed structures, relative energies between different isomers, and vibrational spectra of radical anions may be determined by *ab initio* molecular orbital calculations (9, 10). In general, it is desirable to employ extended basis sets including diffuse atomic orbitals for obtaining a correct de-

Can. J. Chem. Downloaded from www.nrcresearchpress.com by 92.62.229.171 on 09/08/12
For personal use only.

Can. J. Chem. Downloaded from www.nrcresearchpress.com by 92.62.229.171 on 09/08/12
For personal use only.

scription of diffuse charge densities. Self-consistent field (SCF) calculations frequently suffice for the determination of geometries and vibrational frequencies of anions and neutral precursors, and reproduce structural reorganization reliably upon electron attachment; this is valuable when molecular size renders post-SCF treatments non-feasible. The main aim of this work is to determine and compare structural features and stabilities of some radical anions containing the nitro group bonded to substituents with different electron properties, using uniform levels of *ab initio* theory. In particular, a comparative study of molecular parameters calculated for neutral and negatively charged species might provide indications about the change in molecular geometry upon adding an extra electron to the neutral compound and on the character of the molecular orbitals involved. The mutual influence between NO_2 and the substituent bonded to the nitro group can rationalize different conformational behaviours observed moving from a neutral molecule to an anion. The effect of the substituent on the geometry of nitro radical anions and the rotational barriers of the NO_2 framework are investigated with an aliphatic group, such as methyl, and with a π-electron-accepting group, such as BH_2. The influence of electronegative groups on such parameters is investigated by substitution of fluorine atoms in the CH_3 and BH_2 groups. An example of expansion of π conjugation, the radical anion of nitrobenzene, $C_6H_5NO_2^-$, is also included.

Method

Geometry optimizations of neutral and negatively charged molecules were accomplished at the SCF level of theory by analytical gradient-based techniques (11). Split-valence basis sets including polarization, 6-31G*(6D) (12), and (or) diffuse functions, 6-31+G* (12), were employed. The spin-unrestricted Hartree–Fock (UHF) formalism was used for the radical anions and calculated $\langle S^2 \rangle$ values are 0.75 for open-shell systems with the exception of the planar structure of $C_6H_5NO_2^-$, which gives $\langle S^2 \rangle$ values indicating contamination from higher spin states. Vibrational frequencies were calculated at the 6-31G* basis set level to characterize each stationary point on the corresponding potential energy surface and to determine the zero-point corrections (ZPE) to the total energies of the stable structures.

With the exceptions of CF_3NO_2 and $C_6H_5NO_2$, for which the sizes of the molecules render post-SCF calculations prohibitively expensive, geometries were optimized with the second-order Møller–Plesset theory (13) with all orbitals active, using the 6-31G* basis set. The geometries obtained in this way are indicated as MP2/6-31G*. Single-point calculations were carried out using the frozen core approximation (fc), with the Møller–Plesset perturbation theory up to the fourth order, by including single, double, triple, and quadruple excitations. The designation of these calculations is MP4(SDTQ)(fc)/6-31G*//MP2/6-31G* where // means "at the geometry of." Henceforth the term SDTQ(fc) will be omitted. All the energy differences between the different conformations are calculated as ΔHF, ΔMP2, and ΔMP4 for the neutral molecules or as ΔUHF, ΔPMP2, and ΔPMP4 for the radical anions where "P" indicates that the largest spin contamination has been projected out of the UHF correlation energies and will be generically represented by ΔMP2 and ΔMP4. All calculations were carried out using the IBM-VM/CMS version of the GAUSSIAN-88 (14) program on an IBM 3090-600J computer at the University of Rome.

Tables 1 and 2 show the total energies of the most stable molecules calculated at various levels of theory, the ZPE corrections, and the energy differences between conformers. Optimized geometries and vibrational frequencies of the less stable structures as well as the results of additional computations are available from the author upon request.

Results and discussion

Molecular structures

The geometry of the NO_2 group was determined by gas-phase electron diffraction and microwave spectroscopy starting from the simplest aliphatic compound, CH_3NO_2 (15, 16). Both techniques indicate that CH_3NO_2 has staggered conformation. Previous *ab initio* calculations on the staggered and eclipsed conformers of nitromethane were carried out at the SCF level (17, 18) and a slight preference (lower than 0.1 kJ/mol) was found for the staggered orientation at the MP2/6-31G*//HF/6-31G* level (18). To recalculate the equilibrium geometry of CH_3NO_2, the eclipsed and staggered conformations were optimized at the HF/6-31G** and MP2/6-31G* levels. The effect of electron correlation was estimated for both conformers with single point MP4/6-31G*//MP2/6-31G* calculations. The total energies indicate that the staggered conformer is more stable than the eclipsed one but the energy difference between them is extremely small, about 0.04 kJ/mol (MP4/6-31G*//MP2/6-31G*). HF/6-31G* frequency calculations indicate that the eclipsed conformation is a rotational transition state, as suggested by the imaginary frequency (53i cm^{-1}). The height of the rotational barrier is comparable to the small value, 0.025 kJ/mol, determined from microwave spectroscopy (19). Most of the geometrical parameters determined by HF/6-31G** calculations (Fig. 1) agree with the experimental ones, with the exception of the NO bond length, usually underestimated at this level of theory (20). The inclusion of electron correlation provides a better description of the molecular geometry. The bond angles are quite independent of the level of theory adopted but, as expected, the MP2 optimized bond lengths are longer than those obtained from the HF/6-31G** level and this effect is more considerable for the NO bond distances (see Fig. 1). The MP2 optimized geometry of the $-CNO_2$ moiety (r_{CN} = 1.485 Å; r_{NO} = 1.240 Å; $\angle$ONO = 125.7°) agrees with the experimental r_z geometry (16) (r_{CN} = 1.488 ± 0.005 Å; r_{NO} = 1.230 ± 0.004 Å; $\angle$ONO = 124.9 ± 0.5°). Based on these considerations and on previous calculations (18), a single electron configuration with inclusion of electron correlation by perturbation theory appears sufficient to predict satisfactorily the geometry of CH_3NO_2.

CF_3NO_2, as ascertained from gas-phase electron diffraction (21), has a staggered ethane-type conformation with one position missing and the $-CNO_2$ group is found to prefer a nonplanar arrangement. On the contrary, a planar conformation of the $-CNO_2$ moiety seems to be preferred at the HF/6-31G* level. In particular, the C_s eclipsed form of CF_3NO_2 with the O, C, N, and F atoms lying in the same plane and shown in Fig. 1 was calculated to be a minimum on the HF/6-31G* potential energy surface. Vibrational frequencies show that the C_s staggered conformation is a first-order saddle point with imaginary vibrational frequency of 31 cm^{-1}. The relative normal coordinate corresponds to the torsion mode about the CN bond. As a matter of fact, a small variation from planarity of the $-CNO_2$ group is observed in the staggered form of CF_3NO_2 but relaxation of the planarity constraint results in a very small stabilization (0.3 kJ/mol). The negligible energy change and the value of the dihedral angle between the CN bond and the NO_2 plane (177.3°) suggest that the $-CNO_2$ moiety is nearly planar at the HF/6-31G* level. By including these deviations from planarity, the

TABLE 1. Total energies (hartree) for stable conformations of CH_3NO_2, $CH_3NO_2^-$, CF_3NO_2, $CF_3NO_2^-$, CH_2FNO_2, and $CH_2FNO_2^-$; ZPE corrections (hartree); and rotational barriers (ΔE) (kJ/mol)[a]

	CH_3NO_2	$CH_3NO_2^-$	CF_3NO_2	$CF_3NO_2^-$	CH_2FNO_2	$CH_2FNO_2^-$
HF/6-31G*[b]	−243.66199[c]	−243.63654	−540.22117	−540.24579	−342.50363	−342.49574
ZPE//HF/6-31G*[b]	0.05457[c]	0.05119	0.03077	0.02734	0.04773	0.04427
ΔE HF/6-31G*[b]	0.04[c]	8.8	0.4	7.2	13.3	14.0
UHF/6-31+G*		−243.66806		−540.28271		−342.53281
ΔE UHF/6-31+G*		8.1		8.1		16.4
MP2/6-31G*[d]	−244.34533	−244.30078	−541.38815[e]	−541.39411[e]	−343.35700	−343.33075
ΔE MP2/6-31G*[d]	0.05	17.9	0.4[e]	9.5[e]	10.6	27.4
MP4/6-31G*[d,f]	−244.37427	−244.33063			−343.38697	−343.36030
ΔE MP4/6-31G*[d,f]	0.04	16.7			12.0	24.2

[a]1 hartree = 2625.5 kJ/mol.
[b]RHF for the neutral molecules and UHF for the radical anions.
[c]Reference 18.
[d]MP2 and MP4 for the neutral molecules and PMP2 and PMP4 for the radical anions.
[e]MP2(fc)/6-31G*//Hf/6-31G*.
[f]Short for MP4(SDTQ)(fc)/6-31G*//MP2/6-31G*.

TABLE 2. Total energies (hartree) for stable conformations of BH_2NO_2, $BH_2NO_2^-$, BF_2NO_2, $BF_2NO_2^-$, $BHFNO_2$, and $BHFNO_2^-$; ZPE corrections (hartree); and energy differences (ΔE) (kJ/mol)[a] between the planar and orthogonal structures.

	BH_2NO_2	$BH_2NO_2^-$	BF_2NO_2	$BF_2NO_2^-$	$BHFNO_2$	$BHFNO_2^-$
HF/6-31G*[b]	−229.88688	−229.90567	−427.74467	−427.76685	−328.81515	−328.83294
ZPE//HF/6-31G*[b]	0.03506	0.03299	0.02404	0.02168	0.02987	0.02799
ΔE HF/6-31G*[b]	25.0	92.5	5.1	40.9	8.6	56.7
UHF/6-31+G*		−229.92838		−427.80286		−328.86401
ΔE UHF/6-31+G*		71.7		36.2		46.5
MP2/6-31G*[c]	−230.51205	−230.53298	−428.71957	−428.72527	−329.61640	−329.62486
ΔE MP2/6-31G*[c]	21.9	128.6			6.2	73.9
MP4/6-31G*[c,d]	−230.53958	−230.55768	−428.73005	−428.74124	−329.64155	−329.64812
ΔE MP4/6-31G*[c,d]	26.8	118.6	6.0	50.4	8.8	67.8

[a]1 hartree = 2625.5 kJ/mol.
[b]RHF for the neutral molecules and UHF for the radical anions.
[c]MP2 and MP4 for the neutral molecules and PMP2 and PMP4 for the radical anions.
[d]Short for MP4(SDTQ)(fc)/6-31G*//MP2/6-31G* for BH_2NO_2, $BH_2NO_2^-$, $BHFNO_2$, and $BHFNO_2^-$ and MP4(SDTQ)(fc)/6-31G*//HF/6-31G* for BF_2NO_2 and $BF_2NO_2^-$.

barrier separating the staggered and eclipsed conformations of CF_3NO_2 is extremely small (0.4 kJ/mol) at the HF/6-31G* and MP2/6-31G*//HF/6-31G* levels. Based upon these results, the rotation about the CN bond in CF_3NO_2 as well as in CH_3NO_2 is virtually free. More accurate previsions of the torsional barrier of CF_3NO_2 might be provided by higher levels of theory but this would increase computational time prohibitively. The CH_2FNO_2 molecule is more suitable than the trifluorine derivative to investigate the effects of electron correlation at higher levels on the height of the rotational barrier of the nitro group. Geometry optimizations were carried out at the SCF and MP2 levels for two distinct orientations of the CH_2F group with respect to the NO_2 framework within the C_s symmetry constraint. The conformation where the CF bond is perpendicular to the NO_2 plane is designated as staggered and that where the fluorine atom is lying on the ONC plane and shown in Fig. 1 is indicated as eclipsed. Due to the asymmetry of the CH_2F group, intermediate orientations of the CF bond with respect to the NO_2 framework might correspond to other critical points. The SCF and MP2 results are consistent with those predicted for CF_3NO_2. In fact, the eclipsed conformer of CH_2FNO_2 is a minimum structure on the HF/6-31G* energy surface, while the staggered form corresponds to a first-order saddle point with CN torsional frequency of 82i cm^{-1}. Likewise, a slight nonplanarity of the -CNO_2 group is inferred from the HF/6-31G* (178.5°) and MP2/6-31G* (176.7°) optimized geometries of staggered CH_2FNO_2. The eclipsed structure is more stable than the staggered conformer at both MP2/6-31G* (10.6 kJ/mol) and MP4/6-31G*//MP2/6-31G* (12.0 kJ/mol) levels.

The most noticeable differences between the theoretical and experimental geometry of CF_3NO_2 (16, 21) are in the CN and NO bond lengths. The HF/6-31G* level predicts the CN bond distance (1.508 Å) shorter than the electron diffraction (1.56 ± 0.02 Å) (21) and microwave (1.534 ± 0.005 Å) (16) values. The r_z structure (16) shows the NO and CF bond distances equal to 1.217 ± 0.004 and 1.314 ± 0.003 Å, respectively, while the HF/6-31G* mean value for the NO bond length in both conformations of CF_3NO_2 is 1.184 Å and that for the CF bond is 1.295 Å. It is clear that the SCF method is not suitable to determine very accurately the molecular geometry of CF_3NO_2. However, as shown by the geometry optimizations of CH_2FNO_2 carried out at the MP2/6-31G* level (Fig. 1), the inclusion of electron correlation appreciably lengthens the CF and NO bonds with

Can. J. Chem. Downloaded from www.nrcresearchpress.com by 92.62.229.171 on 09/08/12
For personal use only.

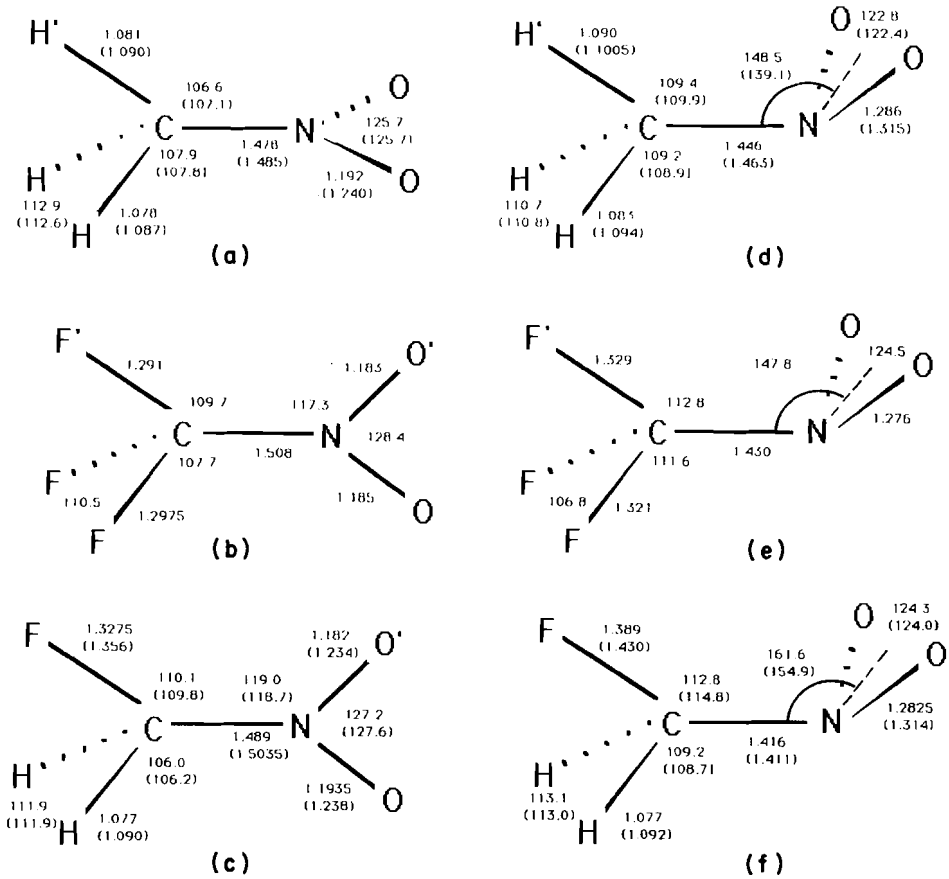

FIG. 1. HF geometries of the staggered CH_3NO_2 (a) (6-31G**) and eclipsed conformers of CF_3NO_2 (b) (6-31G*) and CH_2FNO_2 (c) (6-31G*). UHF/6-31+G* geometries of the staggered $CH_3NO_2^-$ (d), $CF_3NO_2^-$ (e), and $CH_2FNO_2^-$ (f). The MP2/6-31G* parameters are in parentheses (bond lengths in Å and bond angles in deg).

Can. J. Chem. Downloaded from www.nrcresearchpress.com by 92.62.229.171 on 09/08/12
For personal use only.

respect to the HF/6-31G* values but has a negligible effect on the CN bond. Indeed, it is known that for compounds containing the nitrosyl and nitro groups, such as CH_3NO and CH_3NO_2 (22, 23), the $\pi \rightarrow \pi^*$ configuration contributes significantly to the ground state wave function, but the molecular geometry is well described also by a single-determinant wave function. Instead, a previous MCSCF study on CF_3NO (24) showed that the largest contributions to the ground state wave function, other than the SCF and $\pi \rightarrow \pi^*$ configurations, come from the $\sigma_{CN} \rightarrow \sigma_{CN}^*$ and $\sigma_{NO} \rightarrow \sigma_{NO}^*$ configurations, and that the CN bond length can be satisfactorily reproduced by theoretical calculations by employing only a two-configuration (TCSCF) wave function by pairing the bonding and the antibonding CN orbitals ($\sigma_{CN} \rightarrow \sigma_{CN}^*$). Based on these results, a better description of the CN bond length in CF_3NO_2 would probably require a multideterminant wave function including the $\sigma_{CN} \rightarrow \sigma_{CN}^*$ configuration as a starting point. The radical anions $CH_3NO_2^-$, $CH_2FNO_2^-$, and $CF_3NO_2^-$ were studied at the UHF level employing the 6-31G* basis set. For a more reliable description of charge density, diffuse functions were added to the heavy atoms and the UHF/6-31+G* optimized geometries of staggered conformers are shown in Fig. 1. By analogy with the neutral molecule, $CH_2FNO_2^-$ was investigated assuming the C_s staggered and eclipsed conformers described above. Mulliken population analysis reveals that the π^* molecular orbital of the NO_2 fragment accepts the extra electron becoming the single occupied molecular orbital (SOMO) of the radical anion. It has a significant coefficient on nitrogen and, at the SCF level, this suggests that the unpaired electron is delocalized onto each atom of the NO_2 group but with a prevalent contribution at nitrogen. The highest values of atomic spin density were calculated on nitrogen for all the radical anions. The staggered conformations of the three anions are energy minima at the UHF/6-31G* level. Frequency calculations show that the eclipsed forms of $CH_3NO_2^-$, $CH_2FNO_2^-$, and $CF_3NO_2^-$ correspond to first-order saddle points. Geometry optimizations at the MP2/6-31G* level were performed for both conformers of $CH_3NO_2^-$ and $CH_2FNO_2^-$ and molecular parameters of the staggered conformation are reported in parentheses in Fig. 1. An MP2/6-31G*//UHF/6-31G* energy calculation predicts that staggered $CF_3NO_2^-$ is 9.5 kJ/mol lower than the eclipsed ion. Higher barriers are calculated at the MP4/6-31G*//MP2/6-31G* level for $CH_3NO_2^-$ (16.7 kJ/mol) and $CH_2FNO_2^-$ (24.2 kJ/mol).

Comparisons of the optimized geometries for the stable conformation of each neutral and negatively charged molecule reveal substantial structural differences at all levels employed. Addition of an electron into the π-antibonding orbital weakens and lengthens the NO bond. The lengthening is in fact 0.075 Å (MP2/6-31G*) for nitromethane, 0.078 Å (MP2/6-31G*) for $CH_2FNO_2^-$, and 0.092 Å (HF/6-31G*) for $CF_3NO_2^-$. Simultaneously, the CN bond short-

Can. J. Chem. Downloaded from www.nrcresearchpress.com by 92.62.229.171 on 09/08/12
For personal use only.

ens in these radical anions. The HF/6-31G* level predicts the CN bond length to be 1.478 Å for CH_2NO_2, 1.508 Å for CF_3NO_2, and 1.489 Å for CH_2FNO_2 while 1.446, 1.430, and 1.416 Å are the predicted values for the corresponding anions. The increment in overlap population between the carbon and nitrogen atoms occurring upon electron attachment rationalizes this observation. As a consequence of the weakening of the NO bond, the ONO angle narrows in the radical anions by 4.5° in $CH_3NO_2^-$ and 3.0° in $CF_3NO_2^-$. These remarkable differences in the NO and CN bond lengths are followed by appreciable changes in the geometry of the substituent bonded to NO_2. The CH and CF bond lengths of the charged molecules are longer than in the neutral systems and the lengthening is larger for the CF (0.03 Å) than for the CH bond distances (0.01 Å).

Different conformational aspects are found for the radical anions with respect to their neutral precursors. From the previous arguments it emerges that the calculations reproduce the experimental geometries of CH_3NO_2 and CF_3NO_2 with different accuracy. However, it is known that the differences in length between similar bonds in different conformations of the same molecule are reliable (25). For instance, the variation of geometry of the neutral molecules associated with a change in conformation might reveal conformationally dependent interactions between the substituent and the NO_2 group. A previous study on nitromethane (18) showed that geometric variations from the staggered to the eclipsed conformer could be rationalized by HOMO–LUMO interactions. In particular, the occupied orbital of the methyl group is expected to interact with the unoccupied orbital on the nitrogen of the NO_2 fragment. It was suggested that CH_3 donation into the vacant nitrogen orbital in the LUMO causes a methyl group tilt with respect to NO_2. Indicating H′ as the unique hydrogen and H as one of the two equivalent hydrogen atoms, the tilt angle of CH_3 with respect to the CN bond ($\Delta\alpha$), defined as the difference between the H′CN and HCN bond angles, is negative in the staggered conformer and positive in the eclipsed structure. In addition, the CH bonds involved in the donation into the LUMO are longer than those that cannot interact. These effects of hyperconjugation, previously shown at the HF/6-31G* level (18), are confirmed at the HF/6-31G** and MP2/6-31G* levels. A similar hyperconjugative interaction also can be predicted for the trifluorine derivative. Small geometric changes of the CF_3 group are observed in the rotation about the CN bond. The HF/6-31G* value of the CF′ bond distance perpendicular to NO_2 is 0.007 Å longer than that of the two equivalent CF bonds in the staggered conformer. The CF′ bond lying in the same plane of NO_2 in the eclipsed arrangement is 0.006_5 Å shorter than the out-of-plane CF bond. Moreover, a reversed tilt of the CF_3 group with respect to the CN bond in the two conformations appears. From the value of the difference ($\Delta\beta$) between the F′CN and FCN bond angles there emerges a trifluoromethyl tilt away from the nitro group ($\Delta\beta = 2.0°$) in the eclipsed conformer while CF_3 is tilted towards the NO_2 group ($\Delta\beta = -2.2°$) in the staggered arrangement. Except for these small geometric variations of the methyl and trifluoromethyl groups, the structural parameters of CH_3NO_2 and CF_3NO_2 do not change significantly during this internal motion.

On the contrary, more appreciable variations in the geometry of each charged molecule are observed upon torsion about the CN bond. The eclipsed conformations of $CH_3NO_2^-$, $CF_3NO_2^-$, and $CH_2FNO_2^-$ have a nearly planar configuration at nitrogen. UHF/6-31G* frequency calculations indicate that these structures are transition states with imaginary vibrational frequencies of 339i ($CH_3NO_2^-$), 216i ($CF_3NO_2^-$), and 381i ($CH_2FNO_2^-$) cm^{-1}. An analysis of the components of the eigenvector reveals that the rotation of the R group relative to NO_2 is accompanied by a simultaneous departure from planarity of the nitrogen. As evidence of this tendency, the minimum structure is calculated to be pyramidal at nitrogen and to prefer a conformation in which the NO bonds are placed on the same side of the orthogonal CH and CF bonds, as shown in Fig. 1.

Based on these results, the $-CNO_2$ group is markedly nonplanar in the staggered form of the radical anions and the dihedral angle between the CN bond and the NO_2 plane is 148.5° for $CH_3NO_2^-$, 147.8° for $CF_3NO_2^-$, and 161.6° for $CH_2FNO_2^-$ (UHF/6-31+G*). The tendency towards nonplanarity at nitrogen is also confirmed from the MP2 optimized structures of $CH_3NO_2^-$ and $CH_2FNO_2^-$ with dihedral angles equal to 139.1° and 154.9°, respectively. Additional information on the nonplanar character of the $-CNO_2$ moiety was obtained by forcing the radical anions into an artificially constrained geometry. UHF/6-31G* geometry optimizations were performed on $CH_3NO_2^-$ and $CF_3NO_2^-$ assuming the $-CNO_2$ group to be planar. Such calculations show that both these structures are about 9 kJ/mol above the respective stable isomer. The optimized molecular parameters are comparable with those calculated for the $-CNO_2$ nonplanar isomer with the exception of the CN bond lengths, which are close to the optimized values for the eclipsed conformer at the same computational level (1.437 Å for $CH_3NO_2^-$ and 1.417 Å for $CF_3NO_2^-$). Furthermore, inversion at nitrogen in the staggered $CH_3NO_2^-$ was studied at the UHF/6-31G* level. This stationary point was characterized as a second-order saddle point through its vibrational frequencies. The imaginary frequencies, 196i cm^{-1} and 188i cm^{-1}, can be assigned to the inversion motion of the NO_2 group through a plane containing the CN bond and to the rotation of CH_3 relative to the NO_2 framework. These observations suggest that the rotation about the CN bond is associated with the simultaneous flattening of nitrogen and this internal motion can be regarded as a rotation–inversion process.

Pyramidal nitrogen also is predicted for the simple radical species HNO_2^-. A nonplanar C_s structure and a C_{2v} planar arrangement were studied at different levels of theory. The optimized geometries of the two conformations are reported in Table 3. The C_{2v} structure lies about 11.1 kJ/mol (MP4/6-31G*//MP2/6-31G*) above the C_s structure. Frequency calculations indicate that the C_s structure is a minimum on the UHF/6-31G* and MP2/6-31G* potential energy surfaces while the C_{2v} isomer corresponds to a transition state connecting two equivalent C_s structures with pyramidal nitrogen. From the comparison between the energies of occupied molecular orbitals it emerges that the stabilization of the nonplanar form is substantially the result of the lowering of the SOMO energy on moving from a C_{2v} to a C_s structure. Additional *s*-character of nitrogen in the SOMO is observed in the C_s conformation with respect to the pure π character of this orbital in the planar molecule. As a consequence, increments of 1.9° (UHF/6-31+G**) and 3.3° (MP2/6-31+G**) are calculated for the ONO bond angle in going from the C_s to planar C_{2v} symmetry structure.

TABLE 3. Optimized geometries[a] and vibrational frequencies (cm^{-1}) of the C_s radical anion HNO_2^{-b}

Geometrical parameter	UHF/6-31G*	UHF/6-31+G**	MP2/6-31G*	MP2/6-31+G**
r_{NO}	1.284	1.284	1.314	1.317
	(1.284)	(1.284)	(1.310)	(1.312)
r_{NH}	1.014	1.008	1.042	1.027
	(1.007_5)	(1.003)	(1.026)	(1.015)
⟨O—N—O	125.05	124.6	123.8	123.0
	(127.4)	(126.5)	(127.8)	(126.3)
ΦH–NO_2[c]	147.1	148.4	139.0	138.6
	(180.0)	(180.0)	(180.0)	(180.0)
Vibrational frequencies				
A' NHstretching	3488		3064	
(A_1)	(3609)		(3354)	
A' NO_2 stretching	1309		1250	
(A_1)	(1302)		(1251)	
A'' NO_2 stretching	1316		1498	
(B_2)	(1322)		(1523)	
A' NO_2 bending	629		610	
(A_1)	(681)		(639)	
A'' HNO bending	1644		1451	
(B_2)	(1648)		(1453)	
A' HNO_2 deformation	847		898	
(A_2)	(616i)		(753i)	

[a]Bond distances in Å and bond angles in degrees.
[b]Geometry and vibrational frequencies of the C_{2v} planar isomer are reported in parentheses.
[c]Dihedral angle between the NH bond and the NO_2 plane.

HNO_2^- provides further evidence that R-NO_2^- is appreciably nonplanar at nitrogen if the R substituent is a weak π-electron donor.

An examination of the optimized geometries of the radical anions reveals that conformational changes cause appreciable variations in other geometrical parameters. As observed for the neutral molecules, the orthogonal CH and CF bond lengths of each staggered conformer are calculated to be 0.007 Å longer than the other two equivalent distances, also for the radical anions. Likewise, in the eclipsed conformation, the CH and CF bonds lying in the NO_2 plane are shorter than the nonplanar CH and CF bonds by 0.008 Å (CH) and by 0.014 Å (CF). Moreover, the changes are greater than those predicted for the neutral molecules. The structural features calculated for the radical anions containing the nitro group are similar to those obtained in a series of theoretical studies on $CH_3CH_2^-$, $CF_3CH_2^-$, and $CH_2FCH_2^-$ carbanions (26). These substituted ethyl anions provided the prototype systems for the theoretical investigation of the negative hyperconjugation. On the basis of computational results on $CH_2NO_2^-$, $CF_3NO_2^-$, and $CH_2FNO_2^-$ that predict appreciable electron density on the whole NO_2 fragment, it seems reasonable to attribute the conformational preference, as well as the lengthening of the CH and CF orthogonal distances, to negative hyperconjugation. In fact, a weak and stabilizing interaction between the π* SOMO on nitrogen and the orbitals of the CH_3, CF_3, and CH_2F groups might rationalize the small energetic preference for the staggered conformers of all radical anions studied. To investigate hyperconjugation, the CH_2F group represents a model system both for the neutral molecule and the radical anion. The CF bond of $CH_2FNO_2^-$ oriented for hyperconjugative interaction is calculated to be 0.024 Å (HF/6-31+G*) and 0.036 Å (MP2/6-31G*) longer than the eclipsed CF one. A less marked lengthening of the CF bond distance (0.010 Å) is observed at the HF/6-31G* and MP2/6-31G* levels on moving from the eclipsed to staggered conformation of the neutral molecule. Likewise, the MP2/6-31G* shortening of the CN bond length associated with the rotation of CH_2F from the eclipsed to the staggered conformer of $CH_2FNO_2^-$ (0.024 Å) and CH_2FNO_2 (0.010 Å) is in accord with computational results on $CH_2FCH_2^-$ (26). Moreover, the UHF/6-31+G* spin population shows a small increase of fluorine spin density on moving from the eclipsed to the orthogonal conformer. Thus CH_2F in the staggered orientation acts as a weak π-electron acceptor and the decrease in the pyramidalization angle with respect to $CH_3NO_2^-$ and $CF_3NO_2^-$ can be thought of as a structural consequence of hyperconjugation.

The influence of different substituents on the geometry and stability of the anions is indicated, for example, by the values of some molecular parameters. The HOMO/LUMO energy difference, calculated at the HF/6-31G* level, decreases on going from CH_3NO_2 (15.48 eV) to CF_3NO_2 (15.35 eV). Based on these values, the replacement of CH_3 with an electron-withdrawing group tends to lower the LUMO energy with a subsequent stabilization of the radical anion. Thus a small increase of electron affinity is expected going from nitromethane to trifluoronitromethane. Unfortunately, experimental values of electron affinity are available only for CH_3NO_2 from electron-transfer equilibria measurement (0.48 eV) (7) and from the electron-capture detector (0.45 ± 0.09 eV) (27). On the other hand, calculations of accurate electron affinities have proved to be a very delicate problem (9). Very recently, a general computational procedure to give accurate total energies was developed (28), but its application to moderately large molecules is a prohibitive task. The electron affinity of CH_3NO_2 was estimated by single point Møller–Plesset calculations up to

Can. J. Chem. Downloaded from www.nrcresearchpress.com by 92.62.229.171 on 09/08/12
For personal use only.

Can. J. Chem. Downloaded from www.nrcresearchpress.com by 92.62.229.171 on 09/08/12
For personal use only.

the fourth order employing the 6-31+G* basis set and including the zero-point contribution, but it was found that $CH_3NO_2^-$ lies energetically below the parent neutral molecule only at the UHF and MP3 levels. To observe a qualitative trend, electron affinities of CH_3NO_2, CH_2FNO_2, and CF_3NO_2 were calculated as the difference between the UHF/6-31+G*//UHF/6-31G* total energy of the radical anion and that of the neutral molecule including the zero-point contribution. These calculations indicate that the stability of the radical anion with respect to the neutral precursor increases in the series CH_3NO_2 (0.01 eV), CH_2FNO_2 (0.5 eV), and CF_3NO_2 (1.3 eV). Based on these qualitative results, the CH_2F and CF_3 groups should stabilize an adjacent NO_2^-, partly delocalizing the unpaired electron from the NO_2 framework. In both cases there is a hyperconjugative component to the stabilization. The smaller hyperconjugative effect of the CF_3 substituent is fully compensated for by a larger inductive effect. Such a stabilizing interaction should be more noticeable with strong π-electron acceptor substituents. As expected, their ability to accept *p*-electrons allows the unpaired electron of the anion to delocalize partially onto the R group, lowering the LUMO energy and changing the NO_2 geometry with respect to that of the unconjugated radical anions. To investigate in detail the effects of these substituents on the properties of the NO_2 group, theoretical calculations were carried out on some systems R-NO_2/R-NO_2^-. The nitroborane $BH_2NO_2/BH_2NO_2^-$ pair was chosen as a simple example where the BH_2 substituent has a very strong tendency to accept π-type electrons as a result of its low-lying empty orbital. The substitution of hydrogen with σ-inductive electron acceptor atoms such as fluorine should further stabilize the anion with respect to the neutral molecule, as predicted for the fluorine derivatives of nitromethane. On the other hand, the π-electron donor property of the fluorine atom should decrease the tendency to delocalize the unpaired electron from NO_2 to the boron atom. Therefore, substituents such as BH_2, BHF, and BF_2 show decreasing π-electron acceptor properties.

BH_2NO_2, $BHFNO_2$, and BF_2NO_2 and their respective radical anions were optimized at the HF and UHF levels employing the 6-31G* and the 6-31+G* basis sets. The optimized geometries of the stable conformations of each molecule are reproduced in Fig. 2. Electron correlation effects on the geometry were estimated at the MP2/6-31G* level. The neutral compounds were studied assuming a planar structure and an orthogonal arrangement with BH_2, BF_2, and BHF groups perpendicular to NO_2. Both the conformers are stationary points and all levels of calculation indicate the orthogonal structure (Fig. 2) as the most stable isomer. Vibrational frequencies were calculated at the HF/6-31G* level and show that this conformer is a minimum on the potential energy surface, while the planar one is a first-order saddle point. It corresponds to the rotational transition state connecting two equivalent orthogonal conformations. Small energy barriers separate the planar and orthogonal structures: the MP4/6-31G* values of the torsional barrier are 26.8 kJ/mol (BH_2NO_2), 8.8 kJ/mol ($BHFNO_2$), and 6.0 kJ/mol (BF_2NO_2). The geometry of the radical anions was optimized at the UHF and MP2 levels assuming a planar structure (Fig. 2). The predicted geometry changes upon electron attachment are consistent with those calculated for CH_3NO_2, CH_2FNO_2, and CF_3NO_2. The NO bond lengths are significantly increased while the ONO bond angles decrease and the BN bond lengths shorten. The NO_2 group was allowed to become nonplanar, but a preference for the planar arrangement was found. The positive values of the vibrational frequencies reveal that the planar isomers are minima and, in addition, the values of the A_2 torsional frequency indicate a greater rigidity of these systems with respect to the neutral precursors. The torsional barriers were investigated by geometry optimizations of structures with BH_2, BF_2, and BHF groups perpendicular to the NO_2 fragment, including the possibility of deviations from planarity at nitrogen within the C_s symmetry constraint.

According to frequency calculations, these stationary points were characterized as second-order saddle points. With regard to $BHFNO_2^-$, the asymmetry of the BHF group permits two C_s orthogonal conformations. The structure in which the NO bonds are placed on the side of hydrogen is found to be 4.0 kJ/mol (UHF/6-31G*) lower than the isomer with the opposite configuration at nitrogen. As a general trend, the UHF/6-31G* energy difference between the C_{2v} planar conformer and the C_s nonplanar structure is higher than the small rotational barriers of the neutral molecule; it decreases from BH_2NO_2 (92.5 kJ/mol), to $BHFNO_2$ (56.7 kJ/mol) and BF_2NO_2 (40.9 kJ/mol). The inclusion of electron correlation at the MP4/6-31G* level provides a similar order of stability: 118.6 kJ/mol for BH_2NO_2, 67.8 kJ/mol for $BHFNO_2$, and 50.4 kJ/mol for BF_2NO_2. By imposing the constraint of planarity of the -BNO_2 moiety in the orthogonal conformer of $BH_2NO_2^-$ and $BF_2NO_2^-$, another C_{2v} critical point was obtained; it was characterized by vibrational analysis as a third-order saddle point. The geometries of both the C_s and C_{2v} orthogonal conformers differ by a few thousandths of an Å and the UHF/6-31G* stability difference between them is about 2.0 kJ/mol for $BH_2NO_2^-$ and 0.5 kJ/mol for $BF_2NO_2^-$. These values are sufficiently small to allow free inversion of nitrogen when it is not involved in π-interaction with boron.

The electronic state of the planar structures of $BH_2NO_2^-$ and $BF_2NO_2^-$ is $^2B_1$ and that of $BHFNO_2^-$ is $^2A''$. An analysis of atomic spin density population predicts decreasing values on boron moving from $BH_2NO_2^-$ to $BF_2NO_2^-$ and, simultaneously, spin density increases on the nitrogen atom. On the contrary, negligible values on boron are calculated for the C_s orthogonal structures that show the nitrogen spin density as constant for all the substituents. Mulliken population analysis indicates that the negative charge on the oxygen atoms is nearly independent of the nature and orientation of the substituent while the distribution of atomic charge in the remaining portion of the molecule is strongly altered with the rotation of the NO_2 group. An appreciable charge transfer from boron to nitrogen is observed on moving from planar to orthogonal anions. Looking at the energy and population data, the torsional barrier is sensitive to the amount of π-delocalization of the unpaired electron from nitrogen to boron. Such a π-interaction is improved by the flattening of the NO_2 pyramid, which should increase the *p*-character of the SOMO, making nitrogen a better donor and allowing more complete spin delocalization onto the boron atom.

The calculation of HOMO/LUMO energy differences predicts noticeably smaller values than those reported for nitromethane and its fluorine derivatives. Moreover, an increase in the HF/6-31G* value is observed on moving from BH_2NO_2 (12.50 eV) to $BHFNO_2$ (13.34 eV) and to BF_2NO_2 (13.90 eV). These progressively increasing values are in

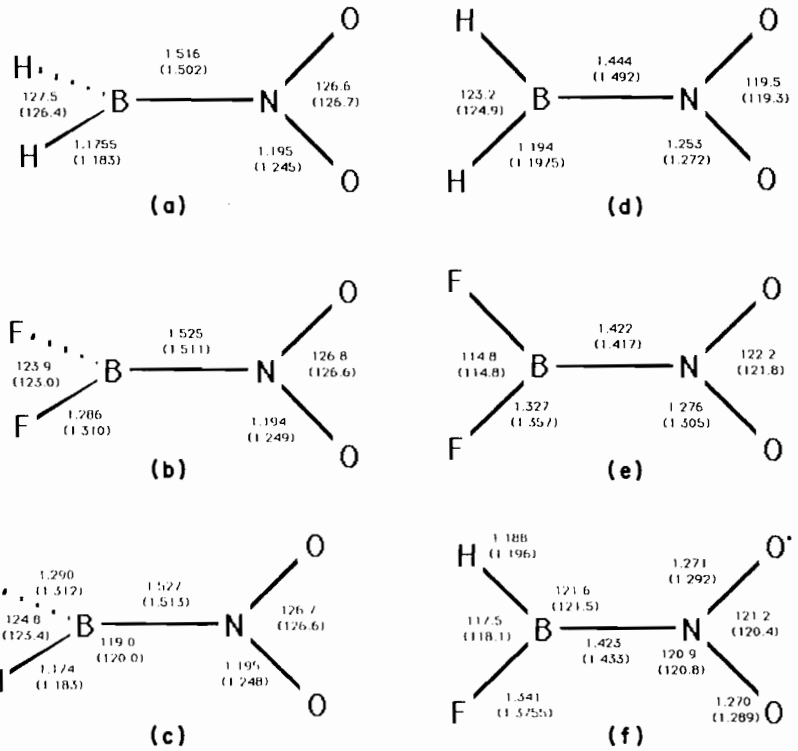

FIG. 2. HF/6-31G* geometries of orthogonal BH_2NO_2 (a), BF_2NO_2 (b), and $BHFNO_2$ (c) and UHF/6-31+G* geometries of planar $BH_2NO_2^-$ (d), $BF_2NO_2^-$ (e), and $BHFNO_2^-$ (f). The MP2/6-31G* parameters are in parentheses (bond lengths in Å and bond angles in deg).

reasonable agreement with the different π-electron acceptor properties of each R group. A higher HOMO/LUMO energy difference is calculated for the orthogonal structure of BH_2NO_2 (14.04 eV), $BHFNO_2$ (15.23 eV), and BF_2NO_2 (15.30 eV) where the π-stabilizing interaction is prevented. Such computational results suggest that the radical anions of nitro compounds with π-electron acceptor groups are appreciably stabilized in that the LUMO energy can be lowered by extension of the π conjugation. As a consequence of the electron-delocalizing property of the substituent, an appreciable lengthening of the NO bond is calculated upon torsion of the NO_2 group. The predicted value of the NO distance is about 1.290 Å for each orthogonal conformer while the UHF/6-31+G* value for the planar arrangement is significantly shorter for each radical anion (see Fig. 2), and this is consistent with the fact that the electron density in the π* orbital of the nitro group is increased when NO_2 is forced out-of-plane.

To extend the study of the structural consequences of electron attachment to molecules containing π-systems, the radical anion $C_6H_5NO_2^-$ was investigated. The molecular structure of nitrobenzene was determined by gas-phase electron diffraction and studied by *ab initio* calculation at the HF/6-31G* level (29). The internal rotation of the nitro group was investigated by including electron correlation effects at the MP2/6-311G**//MP2/6-31G* level (30). The low rotational barrier, 19.04 kJ/mol (30), and the small variations of bond lengths and angles calculated rotating NO_2 from the planar to the orthogonal conformation (29) indicate only a small degree of conjugation between the ring and the nitro group. Similarly, the distribution of net atomic charge remains essentially unaltered by changing conformation. The extent of π-electron transfer from the benzene ring to the nitro group can be investigated by a vibrational frequency study, bearing in mind that the addition of polarization functions is necessary to obtain a reliable description of nitrogen structural features (31). The planar structure was calculated to be at the minimum on the HF/6-31G* potential surface with NO stretchings equal to 1868 cm^{-1} (B_2) and 1640 cm^{-1} (A_1). However, the value of the A_2 torsional frequency about the CN bond (56 cm^{-1}) reveals an easy twist of the NO_2 group with respect to the benzene ring and this is consistent with the small torsional barrier determined for nitrobenzene (30). The previous *ab initio* calculations on the planar structure were repeated by employing a slightly more extended basis set (DZP) (12) or by adding polarization functions also to the hydrogen atoms (6-31G**). The optimized geometry at this latter level shows negligible variations with respect to those reported previously while the dependence of the geometry on the basis set is more appreciable at the DZP level. In particular, a systematic lengthening of NO and CC bond distances by about 0.004 Å is observed. The CN bond length is calculated equal to 1.465 Å while a smaller value (1.458 Å) is calculated at the 6-31G* level (29).

Except for these changes, the basis sets employed describe consistently the effect of the substituent on the ring geometry, predicting differences between CC bond distances and values of internal angles independent of the choice of the basis set. On the grounds of these results, employing only one basis set, 6-31G*, with addition of diffuse functions, 6-31+G*, is a reasonable compromise in investigating the radical anion of nitrobenzene. The planar structure was studied at the UHF level and the 6-31G* and 6-31+G* optimized geometries are reported in Fig. 3. The b_1 π* or-

Can. J. Chem. Downloaded from www.nrcresearchpress.com by 92.62.229.171 on 09/08/12
For personal use only.

Can. J. Chem. Downloaded from www.nrcresearchpress.com by 92.62.229.171 on 09/08/12
For personal use only.

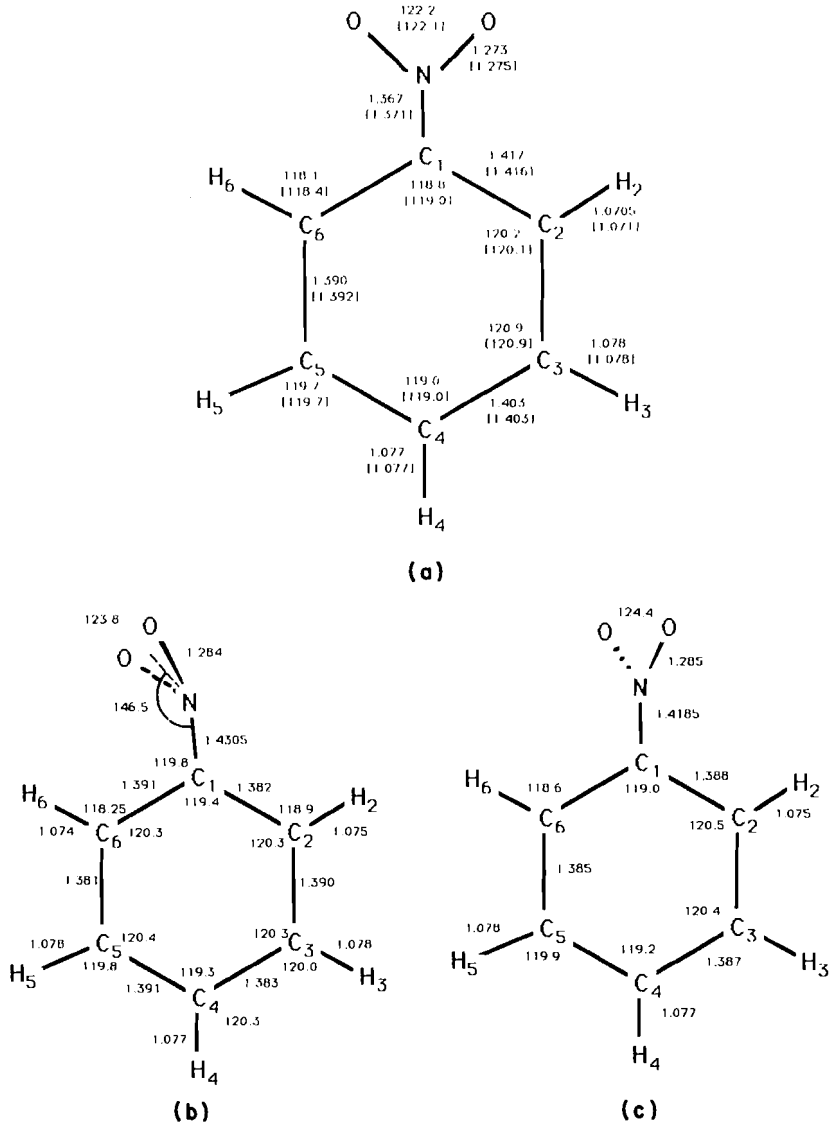

FIG. 3. UHF/6-31G* geometries of the C_{2v} planar (a), C_s (b), and C_{2v} orthogonal (c) structures of $C_6H_5NO_2^-$. The UHF/6-31+G* geometry is in square parentheses (bond lengths in Å and bond angles in deg).

bital is the singly occupied molecular orbital and the electronic state of the radical anion is $^2B_1$, but this conformer suffers spin contamination from higher energy quartet states ($\langle S^2 \rangle = 0.99$) and this is a frequent problem with UHF wave functions when low-lying states of higher spin multiplicity exist (32). However, the quartet state $^4B_1$ is estimated to be about 3.7 eV above the $^2B_1$ ground state by UHF/6-31G* single point calculation at the geometry of the doublet state. In addition, an analysis of atomic spin density for the $^2B_1$ state predicts a spin population on nitrogen and on the C_2, C_4, and C_6 atoms (Fig. 3) in agreement with the electron spin resonance results (33). Additional geometry optimizations carried out in the ROHF formalism provide an unreliable spin density population on the whole molecule, predicting a high value on nitrogen, but a negligible spin density on the benzene ring. Based on these considerations and notwithstanding the high spin contamination emerging from the UHF results, the optimized geometry at this computational level can be discussed.

The geometry of the NO_2 group of $C_6H_5NO_2^-$ reveals a remarkable increase in the value of the NO bond length (0.080 Å) and decrease in the ONO bond angle (2.5°) with respect to the calculated values for the neutral precursor (29). A more marked change is calculated for the CN bond length, which is 0.091 Å shorter in the molecular anion. With regard to the ring geometry, a general lengthening of the CC bond lengths is predicted but the amount is more relevant for the C_1C_2 (0.034Å) and C_3C_4 (0.016 Å) bonds than for the C_2C_3 (0.007 Å) bond. While the differences in the theoretical lengths of the ring CC bonds of the neutral molecule are equal to a few thousands of an angstrom, a noticeable alternation of long/short/long nonequivalent distances is predicted for the radical anion. By employing the 6-31+G* basis set, the C_1C_2 bond length is calculated to be 0.024 Å longer than the C_2C_3 distance while the latter is 0.011 Å shorter than C_3C_4. Concerning the bond angles of the ring, electron charging of nitrobenzene causes decreases of the $C_6C_1C_2$ (3.5°) and $C_3C_4C_5$ (1.4°) bond angles. The remaining ring angles, $C_1C_2C_3$ and $C_2C_3C_4$, increase by about 1.7° and 0.8°, respectively.

Can. J. Chem. Downloaded from www.nrcresearchpress.com by 92.62.229.171 on 09/08/12
For personal use only.

Such a comparison shows that the addition of an electron into the b_1 π^* molecular orbital of nitrobenzene simultaneously gives rise both to the expected geometry variations of the nitro group and to marked changes in the ring geometry. According to the Jahn–Teller theorem, the addition of an extra electron to benzene lowers the D_{6h} symmetry of the neutral molecule to D_{2h}. In fact, the $^2E_{2u}$ electronic state is split into ^2A_u and $^2B_{3u}$ components. The molecular geometries of each state were previously calculated at the UHF/STO-3G level (34). Both structures show comparable stability but their optimized geometries are very different. In addition, previous STO-3G calculations performed for a set of singly substituted benzene radical anions (35) reveal that the ^2A state is favoured by π-electron donor substituents while the ^2B state is preferred by π-electron acceptor groups. The expansion of π conjugation or the introduction of electron-withdrawing substituents stabilizes the radical anion, extending the π^*-type SOMO electron density over the aromatic ring and over the substituent. Based upon these arguments, the calculated differences for the ring geometry in going from neutral nitrobenzene to the radical anion should be strongly affected by the degree of conjugation between the aromatic ring and the substituent. In particular, indications of interactions between the nitro group and the ring in the radical anion are suggested by changes in the ring geometry calculated on going from the $C_6H_6^-$ to $C_6H_5NO_2^-$. Geometry optimizations have been carried out on the radical anion of benzene at the same level of theory employed for the nitro-substituted derivative. The ^2A_u and $^2B_{3u}$ electronic states were studied at the UHF level employing the 6-31G* basis set and each electronic state is predicted to have the optimized geometry reported in Fig. 4. The ring bonds and angles of the radical anion of nitrobenzene are close to those calculated for the $^2B_{3u}$ structure of $C_6H_6^-$. However, the shortening of the C_1C_2 and C_3C_4 distances and the increase of the C_2C_3 bond length observed in $C_6H_5NO_2^-$ suggest that the unpaired electron is partly shared between the ring and the substituent. Further evidence of this sharing is given by the values of the ring angles ranging between those of neutral $C_6H_5NO_2$ and those calculated for the $^2B_{3u}$ state of $C_6H_6^-$.

The degree of conjugation between the substituent and the aromatic ring can be alternatively investigated by rotating the nitro group out of the plane of the ring and observing the change in the molecular geometry. By forcing the NO_2 group into an orthogonal conformation, two stationary points are found at the UHF/6-31G* level, as shown in Fig. 3, and the relative $\langle S^2 \rangle$ values are 0.75. The C_s structure with pyramidal nitrogen ($^2A'$) is calculated to be more stable than the C_{2v} orthogonal isomer ($^2B_2$) by about 6.6 kJ/mol. The degree of nonplanarity at nitrogen is indicated by the value of the dihedral angle between the ONO plane and the CN bond (146.5°). In addition, a tilt of the CN bond away from the C_1C_4 axis is predicted for the C_s structure and the difference between the NC_1C_2 and NC_1C_6 angles is 1°. An electron spin resonance study of di-*ortho*-alkylnitrobenzene radical anions (36), in which the NO_2 group is forced out of the aromatic ring, shows a reduction in the spin delocalization from the nitro group into the ring, and a pyramidal nitrogen was proposed as the possible conformation of the NO_2 group. As a matter of fact, the differences in total atomic charges in going from the planar to the orthogonal structures reveal that the NO_2 group gains electronic charge, 0.026 on each oxygen and 0.041 on nitrogen. The largest variation in the ring atomic charge occurs for the C_1 atom, which loses 0.100, while the remaining carbon atoms undergo smaller changes. Simultaneously the atomic spin density on carbon ring atoms decreases down to negligible values in the orthogonal structures.

The reduction of spin density on the ring is reflected significantly in the values of certain parameters. The largest change in the geometry of the anion on going from planar to orthogonal arrangements occurs in the CN bond length, which increases by 0.052 Å in the C_{2v} structure and by 0.064 Å in the C_s conformer. This variation is accompanied by the simultaneous lengthening of the NO bond (0.012 Å) and increase in the ONO angle by 2.2° (C_{2v}) and 1.6° (C_s). The calculated value of the NO bond length (1.285 Å) is close to the value for NO_2 bonded to groups having weak π-electron-donating properties, such as CH_3 (1.286 Å). The considerable short/long/short alternation of the values of the CC ring distances calculated for the planar structure becomes less marked in the orthogonal structures. In particular, the C_{2v} isomer shows C_1C_2, C_2C_3, and C_3C_4 bond lengths equal to 1.388, 1.385, and 1.387 Å, respectively, indicating that the ring geometry is similar to that of the neutral molecule.

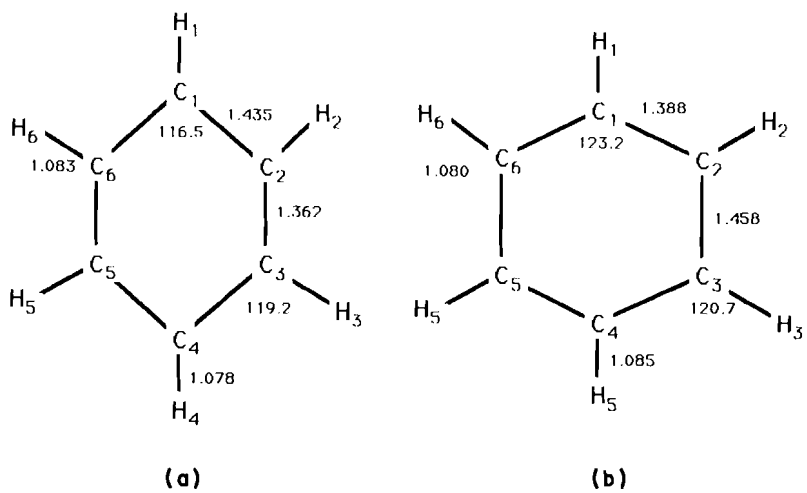

FIG. 4. UHF/6-31G* geometries of the ^2A_u (a) and $^2B_{3u}$ (b) electronic states of $C_6H_6^-$ (bond lengths in Å and bond angles in deg).

TABLE 4. HF/6-31G* vibrational frequencies[a] (cm^{-1}) of CH_3NO_2, CF_3NO_2, and CH_2FNO_2 and UHF/6-31G* values for $CH_3NO_2^-$, $CF_3NO_2^-$, and $CH_2FNO_2^-$ radical anions

CH_3NO_2[b] Staggered (C_s)		$CH_3NO_2^-$ Staggered (C_s)	CF_3NO_2 Eclipsed (C_s)		$CF_3NO_2^-$ Staggered (C_s)	CH_2FNO_2 Eclipsed (C_s)		$CH_2FNO_2^-$ Staggered (C_s)
A'' 3404	CH_3 stretch	3277 A''	A' 1927	NO_2 stretch	1533 A'	A'' 3397	CH_2 stretch	3333 A''
A' 3369	CH_3 stretch	3239 A'	A' 1693	NO_2 stretch	1372 A''	A' 3319	CH_2 stretch	3272 A'
A' 3272	CH_3 stretch	3161 A'	A' 1520	CF_3 stretch	1392 A''	A' 1908	NO_2 stretch	1505 A''
A'' 1880	NO_2 stretch	1440 A''	A'' 1479	CF_3 stretch	1337 A'	A' 1687	NO_2 stretch	1491 A'
A' 1688	NO_2 stretch	1428 A'	A' 1322	CF_3 stretch	1267 A'	A' 1652	CH_2 scissor	1657 A'
A' 1620	CH_3 deformation	1630 A'	A' 987	NO_2 scissor	898 A'	A' 1562	CH_2 rock	1587 A'
A'' 1607	CH_3 deformation	1638 A''	A'' 882	NO_2 wag	677 A'	A'' 1400	CH_2 twist	1352 A''
A' 1571	CH_3 deformation	1558 A'	A' 831	CN stretch	749 A'	A' 1307	CF stretch	1091 A'
A' 1271	CH_3 rock	1214 A'	A' 675	NO_2 rock	653 A''	A'' 1232	CH_2 rock	1131 A''
A'' 1233	CH_3 rock	1137 A''	A'' 578	CF_3 deformation	537 A'	A' 1051	CN stretch	989 A'
A' 1051	CN stretch	971 A'	A' 484	CF_3 deformation	470 A''	A' 784	NO_2 scissor	704 A'
A' 744	NO_2 scissor	637 A'	A' 460	CF_3 deformation	464 A'	A'' 667	NO_2 wag	520 A'
A' 690	NO_2 wag	443 A'	A' 319	CF_3 rock	314 A''	A' 563	NO_2 rock	483 A''
A'' 529	NO_2 rock	482 A''	A'' 317	CF_3 rock	262 A'	A' 335	CH_2F deformation	210 A'
A'' 21	CN torsion	217 A''	A'' 31	CN torsion	71 A''	A'' 86	CN torsion	108 A''

[a]The description of the modes is approximate and it has been done by analogy with CH_3NO_2.
[b]Assignments by ref. 18.

TABLE 5. HF/6-31G* vibrational frequencies[a] (cm^{-1}) of orthogonal BH_2NO_2, BF_2NO_2, and $BHFNO_2$ and UHF/6-31G* values for the planar $BH_2NO_2^-$, $BF_2NO_2^-$, and $BHFNO_2^-$ radical anions

BH_2NO_2 (C_{2v})		$BH_2NO_2^-$ (C_{2v})	BF_2NO_2 (C_{2v})		$BF_2NO_2^-$ (C_{2v})	$BHFNO_2$ (C_s)		$BHFNO_2^-$ (C_s)
B_2 2947	BH_2 stretch	2728 B_2	B_1 1833	NO_2 stretch	1310 B_2	A' 2916	BH stretch	2754 A'
A_1 2819	BH_2 stretch	2664 A_1	A_1 1746	NO_2 stretch	1686 A_1	A'' 1829	NO_2 stretch	1633 A'
B_1 1818	NO_2 stretch	1467 B_2	B_2 1648	BF_2 stretch	1444 B_2	A' 1737	NO_2 stretch	1358 A'
A_1 1721	NO_2 stretch	1366 A_1	A_1 1361	BF_2 stretch	1254 A_1	A' 1478	BF stretch	1317 A'
A_1 1309	BH_2 scissor	1293 A_1	A_1 959	NO_2 scissor	851 A_1	A' 1177	BHF scissor	1153 A'
B_1 1073	BH_2 wag	786 B_1	B_2 776	NO_2 + BF_2 rock	473 B_2	A' 1034	NO_2 scissor	997 A'
B_2 1049	BH_2 rock	973 B_2	B_1 712	BF_2 wag	675 B_1	A'' 949	BHF wag	870 A''
A_1 1033	NO_2 scissor	1035 A_1	A_1 673	BN stretch	635 A_1	A' 825	BHF rock	488 A'
A_1 680	BN stretch	679 A_1	A_1 387	BF_2 scissor	426 A_1	A' 621	BN stretch	695 A'
B_2 557	NO_2 wag	696 B_1	B_2 255	BF_2 + NO_2 rock	252 B_2	A' 300	NO_2 wag	556 A''
A_2 243	BN torsion	394 A_2	B_1 172	NO_2 wag	409 B_1	A'' 182	NO_2 rock	270 A'
B_1 139	NO_2 rock	399 B_2	A_2 30	BN torsion	102 A_2	A'' 64	BN torsion	197 A''

[a]The description of the modes is approximate.

Vibrational frequencies

The calculated vibrational frequencies of neutral and negatively charged species are reported in Tables 4 and 5. The comparison between assigned vibrational modes reveals variations that reflect the structural reorganization occurring upon electron attachment. The IR spectrum of the anion NO_2^- produced in low temperature matrix by electron transfer processes (37), shows that the ν_3 stretching mode (1240 cm^{-1}) is appreciably shifted with respect to the frequency of the neutral NO_2 (1617 cm^{-1}) (38). Likewise, the NO_2^- vibrational data gathered from condensed phase studies of nitrite ions (39, 40) (ν_1 = 1332, ν_2 = 821, and ν_3 = 1240 cm^{-1}) are different from the NO_2 vibrational modes (ν_1 = 1320, ν_2 = 750, and ν_3 = 1617 cm^{-1}) (38). A lowering of the NO stretchings as a consequence of the weakening of the NO bond upon electron charging is therefore expected. The values of the NO stretchings for CH_3NO_2 (A'' 1880 cm^{-1} and A' 1688 cm^{-1}) decrease to 1440 cm^{-1} (A'') and 1428 cm^{-1} (A') for $CH_3NO_2^-$; similar decreases are observed passing from CF_3NO_2 (A' 1927 and A' 1639 cm^{-1}) to $CF_3NO_2^-$ (A' 1533 and A'' 1372 cm^{-1}) and from CH_2FNO_2 (A' 1908 and A' 1687 cm^{-1}) to $CH_2FNO_2^-$ (A'' 1505 and A' 1491 cm^{-1}). Comparable lowerings of the NO stretching frequencies are predicted in the anions with NO_2 bonded to boron. The fundamental modes B_1 and A_1 of the orthogonal minimum structure of BH_2NO_2 are calculated to occur at 1818 and 1721 cm^{-1} and those of BF_2NO_2 are at 1833 and 1746 cm^{-1}. The planar structure of the respective radical anions shows the NO stretching modes equal to 1467 and 1366 cm^{-1} in $BH_2NO_2^-$ and 1686 and 1310 cm^{-1} in $BF_2NO_2^-$.

The change in conformation of the neutral molecules does not cause appreciable variations in the vibrational frequencies of the NO_2 group. On the contrary, small variations (ca. 50 cm^{-1}) of the NO stretching modes are calculated upon torsion about the CN bond for the radical anions: the eclipsed conformations have NO stretchings equal to 1478 and 1440 cm^{-1} ($CH_3NO_2^-$), 1577 and 1419 cm^{-1} ($CF_3NO_2^-$). Small changes are also calculated for $BH_2NO_2^-$ and

Can. J. Chem. Downloaded from www.nrcresearchpress.com by 92.62.229.171 on 09/08/12
For personal use only.

$BF_2NO_2^-$: the NO stretching frequencies of the C_s conformations are at 1536 (A') and 1308 (A'') cm^{-1} for $BH_2NO_2^-$ and at 1634 (A') and 1283 (A'') cm^{-1} for $BF_2NO_2^-$.

The minor geometry variations of the groups bonded to NO_2 calculated upon electron adding are reflected in small changes in the vibrational modes of these groups. In particular, the CF, CH, BH, and BF stretching modes for the radical anions are calculated as lowered by about 100 cm^{-1}, with the exception of the CF stretching of CH_2FNO_2, which moves from 1307 cm^{-1} for the neutral molecule to 1091 cm^{-1} for the radical anion. The shortening of the CN and BN bonds occurring by addition of an extra electron is not followed by displacements of the relative stretching modes, which show small lowerings.

As far as the torsional frequency about the CN and BN bonds is concerned, the highest value is calculated for $BH_2NO_2^-$ (394 cm^{-1}), and this is consistent with the high torsional barrier predicted for this anion. A general increase of rigidity of the NO_2 group upon electron attachment is suggested by the values of the NO_2 wagging and rocking modes, which increase for the boron-containing species. This is consistent with the results obtained from measurements of electron-attachment equilibria for the nitrobenzene radical anion and substituted derivatives (7, 8), which predict a stiffening of the NO_2 internal rotation on moving from neutral molecules to radical anions.

Conclusions

The equilibrium geometries and the vibrational frequencies of some radical anions and of the parent neutral molecules containing the nitro group have been studied by *ab initio* molecular orbital calculations at the SCF and MP2 levels. As a general trend, the $-CNO_2$ moiety is characterized by an appreciable structural reorganization upon electron attachment as a consequence of the π^* character of the SOMO. This work shows that both at the SCF and MP2 levels, the $-CNO_2$ framework undergoes major geometry variations in the NO bond, ONO bond angle, and in the CN bond. In fact, the NO and CN bond distances of the radical anions are found to lengthen and shorten, respectively, and the ONO bond angles to decrease. The conjugation between the nitro group and the substituent bonded to NO_2 can delocalize the unpaired electron from the NO_2 onto the remaining atoms of the molecules, influencing thus the structure and the geometry of the NO_2 group. The nonplanar character at nitrogen has been determined for the following substituents: H, CH_3, CH_2F, and CF_3. Planar structures at nitrogen have been predicted for radical anions with strong *p*-electron acceptors such as BH_2, BHF, and BF_2. Nonplanar geometries at nitrogen have been found for the latter substituents oriented perpendicularly with respect to the NO_2 plane. The orthogonal orientation prevents π interactions between the nitrogen and boron atoms of $BH_2NO_2^-$, $BHFNO_2^-$, and $BF_2NO_2^-$, increasing the electron density in the π^* orbital of the NO_2 fragment. The results accomplished from the UHF geometry optimizations of $C_6H_5NO_2^-$ are consistent with those predicted for the boron-containing radical anions.

Barriers to internal rotation of the NO_2 group have been calculated at various levels including Møller–Plesset perturbation theory up to the fourth order, and the barrier heights are consistent with the degree of π conjugation between the NO_2 and the substituent. The rotation about the CN bond is almost free, both for the neutral molecules and for the radical anions of the series CH_3NO_2 and CF_3NO_2; on the contrary, high torsional barriers about the BN bond are calculated for $BH_2NO_2^-$, $BHFNO_2^-$, and $BF_2NO_2^-$ radical anions, and the values of the related torsional frequencies reflect this trend.

Acknowledgments

The assistance of Dr. L. Bencivenni and Dr. F. Grandinetti, for their interest in this work, is acknowledged. The author gratefully acknowledges a generous grant of computer time by "Progetto NIC-Italia."

1. G. Caldwell and P. Kebarle. J. Chem. Phys. **80**, 577 (1984).
2. E. P. Grimsrud, G. Caldwell, S. Chowdhury, and P. Kebarle. J. Am. Chem. Soc. **107**, 4627 (1985).
3. P. Kebarle and S. Chowdhury. Chem. Rev. **87**, 513 (1987).
4. R. D. Mead, A. E. Stevens, and W. C. Lineberger. Gas Phase Ion Chem. **3**, 214 (1984).
5. D. H. Geske. Prog. Phys. Org. Chem. **4**, 125 (1967).
6. B. C. Gilbert and M. Trenwith. J. Chem. Soc. Perkin Trans. **2**, 2010 (1973).
7. S. Chowdhury, T. Heinid, E. P. Grimsurd, and P. Kebarle. J. Phys. Chem. **90**, 2747 (1986).
8. S. Chowdhury, H. Kishi, G. W. Dillow, and P. Kebarle. Can. J. Chem. **67**, 603 (1989).
9. J. Simons and K. D. Jordan. Chem. Rev. **87**, 535 (1987).
10. F. Ramondo, N. Sanna, L. Bencivenni, and F. Grandinetti. Chem. Phys. Lett. **180**, 369 (1991).
11. H. B. Schlegel. J. Comput. Chem. **3**, 214 (1982).
12. R. Poirer, R. Kari, and I. G. Csizmadia. Handbook of Gaussian basis sets. Elsevier, Amsterdam. 1985.
13. C. Møller and M. S. Plesset. Phys. Rev. **46**, 618 (1934).
14. M. J. Frisch, M. Head-Gordon, H. B. Schlegel *et al.*, GAUSSIAN 88. Gaussian Inc., Pittsburgh, PA. 1988.
15. L. O. Brockway, J. Y. Beach, and L. Pauling. J. Am. Chem. Soc. **57**, 2693 (1935).
16. A. P. Cox. J. Mol. Struct. **97**, 61 (1983).
17. C. W. Bock, S. V. Krasnoshchiokov, L. V. Khristenko, Yu. N. Panchenko, and Yu. A. Pentin. J. Mol. Struct. (Theochem), **149**, 201 (1987).
18. M. L. McKee. J. Am. Chem. Soc. **107**, 1900 (1985).
19. E. Tannenbaum, R. J. Myers, and W. D. Gwinn. J. Chem. Phys. **25**, 42 (1956).
20. W. J. Hehre, L. Radom, P. v. R. Schleyer, and J. A. Pople. *Ab initio* molecular orbital theory. Wiley, New York. 1986.
21. I. L. Karle and J. Karle. J. Chem. Phys. **36**, 1969 (1962).
22. D. S. Marynick, A. K. Ray, J. L. Fry, and D. A. Kleier. J. Mol. Struct. (Theochem), **108**, 45 (1984).
23. D. A. Kleier and M. A. Lipton. J. Mol. Struct. (Theochem), **109**, 39 (1984).
24. J. S. Tse and J. D. Goddard. J. Mol. Struct. (Theochem), **139**, 165 (1986).
25. I. Hargittai and M. Hargittai (*Editors*). Stereochemical applications of gas-phase electron diffraction. Part A. The electron diffraction technique. VCH Publishing, Weinheim. 1988.
26. P. v. R. Schleyer and A. J. Kos. Tetrahedron, **39**, 1141 (1983).
27. E. C. M. Chen and W. E. Wentworth. J. Phys. Chem. **87**, 45 (1983).
28. J. A. Pople, M. Head-Gordon, D. J. Fox, K. Raghavachari, and L. A. Curtiss. J. Chem. Phys. **90**, 5622 (1989).
29. A. Domenicano, G. Schultz, I. Hargittai, M. Colapietro, G. Portalone, P. George, and C. W. Bock. Struct. Chem. **1**, 107 (1990).
30. M. Head-Gordon and J. A. Pople. Chem. Phys. Lett. **173**, 585 (1990).
31. C. W. Bock, P. George, and M. Trachtman. Theor. Chim. Acta, **69**, 235 (1986).
32. H. B. Schlegel. J. Chem. Phys. **84**, 4530 (1986).

Can. J. Chem. Downloaded from www.nrcresearchpress.com by 92.62.229.171 on 09/08/12
For personal use only.

33. G. L. Swartz and W. M. Gulick, Jr. Mol. Phys. **30**, 869 (1975).
34. A. J. Birch, A. L. Hinde, and L. Radom. J. Am. Chem. Soc. **102**, 3370 (1980).
35. S. Chowdhury,. T. Heinis, and P. Kebarle. J. Am. Chem. Soc. **108**, 4662 (1986).
36. D. H. Geske, J. L. Ragle, M. A. Bambenek, and A. L. Balch. J. Am. Chem. Soc. **86**, 987 (1964).
37. D. E. Milligan and M. E. Jacox. J. Chem. Phys. **55**, 3404 (1971).
38. E. T. Arakawa and A. H. Nielsen. J. Mol. Spectrosc. **2**, 413 (1958).
39. R. E. Weston, Jr. and T. F. Brodasky. J. Chem. Phys. **27**, 683 (1957).
40. E. Herbst, I. A. Patterson, and W. C. Lineberger. J. Chem. Phys. **61**, 1300 (1974).

Can. J. Chem. Downloaded from www.nrcresearchpress.com by 92.62.229.171 on 09/08/12
For personal use only.

Electron thermalization distance distributions and thermal electron mobilities in dense liquid isobutane

TAKEHISA YOSHINARI,[1] NORMAN GEE, AND GORDON R. FREEMAN[2]

Chemistry Department and Radiation Research Centre, University of Alberta, Edmonton, Alta., Canada T6G 2G2

Received May 16, 1991

This paper is dedicated to Professor Sigeru Huzinaga on the occasion of his 65th birthday

TAKEHISA YOSHINARI, NORMAN GEE, and GORDON R. FREEMAN. Can. J. Chem. **70**, 327 (1992).

Free ion yields G_{fi}^{E} were measured at electric field strengths E up to 6.7 MV m^{-1} in liquid isobutane at $556 \leq d$/kg m$^{-3} \leq 739$ (294.4–114.6 K). The yields decreased with decreasing temperature and increasing density up to 677 kg m^{-3}; further increases in density led to little change in G_{fi}^{E}. The thermalization distance distribution $F(y)$ was estimated by fitting the field dependence of G_{fi}^{E} using the extended Onsager model. At lower densities $F(y)$ = YGP (three-dimensional Gaussian body with power tail) provided an adequate fit to the results, while at higher densities $F(y)$ = YE (one-dimensional exponential distribution) was better. Thus the electron-scattering properties of liquid isobutane change somewhat with density. The thermalizing ability of liquid isobutane increased with increasing density up to ~660 kg m^{-3}, then decreased at densities >690 kg m^{-3}. By comparison, the Arrhenius temperature coefficient of mobility of thermal electrons changed in the same density region: $E_{\mu} \approx 7$ kJ mol^{-1} at $d < 660$ kg m^{-3}, and ≈16 kJ mol^{-1} at $d > 690$ kg m^{-3}.

Key words: isobutane, electron thermalization distance, free ion yield, liquid, electron mobility, radiolysis.

TAKEHISA YOSHINARI, NORMAN GEE et GORDON R. FREEMAN. Can. J. Chem. **70**, 327 (1992).

Opérant dans de l'isobutane liquide à $556 \leq d$/kg m$^{-3} \leq 739$ (de 294.4 K à 114.6 K), on a mesuré les rendements en ions libres G_{fi}^{E} à des forces de champ électrique E allant jusqu'à 6.7 MV m^{-1}. Les rendements diminuent lorsque la température diminue et lorsque la densité augmente jusqu'à 677 kg m^{-3}; une augmentation plus poussée de la densité affecte très légèrement la valeur du G_{fi}^{E}. On a évalué la distribution de la distance de thermalisation $F(y)$ en ajustant l'influence du champ sur la valeur du G_{fi}^{E} en faisant appel au modèle étendu de Onsager. Pour des densités plus faibles, l'équation $F(y)$ = YGP (corps gaussien tridimensionnel et queue avec des puissances) permet d'obtenir une concordance adéquate avec les résultats; par ailleurs, pour des densités plus élevées, l'équation $F(y)$ = YE (distribution exponentielle unidimensionnelle) est meilleure. Les propriétés de dispersion des électrons par l'isobutane liquide varient donc un peu avec la densité. Lorsque la densité augmente jusqu'à environ 660 kg m^{-3}, la capacité de thermalisation de l'isobutane liquide augmente d'une façon parallèle; à des densités >690 kg m^{-3}, cette capacité commence à diminuer. Par comparaison, le coefficient de température d'Arrhénius pour la mobilité des électrons thermiques change aussi dans cette même région de densité : $E_{\mu} \approx 7$ kJ mol^{-1} à $d < 660$ kg m^{-3}, et $E_{\mu} \approx 16$ kJ mol^{-1} à $d > 690$ kg/m^{3}.

Mots clés : isobutane, distance de thermalisation de l'électron, rendement en ion libre, liquide, électron mobilité, radiolyse.

[Traduit par la rédaction]

Introduction

When ionizing radiation interacts with a fluid, electrons are ejected from molecules to form ion–electron pairs (1*b*). The ejected electron possesses excess kinetic energy, which it loses by inelastic collisions with molecules as it moves away from its sibling cation. The electron reaches thermal energy at some distance y, which is usually sufficiently small that there is Coulombic attraction between the sibling electron–ion pair that is significant in comparison with the random thermal energy k_BT. The creation of the electron ion pair is represented as

$$[1] \qquad M \rightsquigarrow [M^+ + e^-]$$

where the square brackets around the charged entities represent the significant electrostatic attraction between them. A competition (2) then takes place between recombination of the electron and ion (geminate neutralization),

$$[2] \qquad [M^+ + e^-] \rightarrow M$$

and diffusion apart of the ion and electron until their mutual Coulombic attraction becomes negligible compared to k_BT (free ion formation),

$$[3] \qquad [M^+ + e^-] \rightarrow M^+ + e^-$$

The free ions ultimately encounter other free ions at random and can neutralize each other (random neutralization),

$$[4] \qquad M^+ + e^- \rightarrow M$$

or they can be attracted to electrodes by a sufficiently large applied electric field E, collected, and measured,

$$[5] \qquad \begin{cases} e^- & \xrightarrow{E} \text{ anode} \\ M^+ & \xrightarrow{E} \text{ cathode} \end{cases}$$

The number of free ion pairs formed per 100 eV (16 aJ) of energy absorbed by the fluid, denoted G_{fi}^{E}, is determined by the magnitudes of the thermalization distance y, the dielectric relative permittivity ε of the fluid, the temperature T, and E.

The rate at which G_{fi}^{E} increases with E is strongly affected by the shape of the thermalization distance distribution function $F(y)$ (1*c*). In turn the shape of $F(y)$ and the mean value of y reflect the strength of the electron–molecule interactions in the liquid, mainly for electrons of energies be-

[1]Permanent address: Physics Department, Yamagata University, 4-12, 1-chome, Koshirakawa-Machi, Yamagata, Japan.

[2]Author to whom correspondence may be addressed.

Can. J. Chem. Downloaded from www.nrcresearchpress.com by 123.30.183.119 on 09/08/12
For personal use only.

Can. J. Chem. Downloaded from www.nrcresearchpress.com by 123.30.183.119 on 09/08/12
For personal use only.

tween about 1 eV (~200 zJ) and 1.5 k_BT (~5 zJ); z = zepto = 10^{-21}.[3]

For most liquids, as the temperature is decreased G_{fi}^E decreases (3, 4). The $F(y)$ distribution function that fits the (E, G_{fi}^E) data in the widest range of systems (1*d*) has a Gaussian body and a power tail, and is designated YGP (1*c*, 4). The Gaussian shape is attributed to randomness of the scattering (1*a*). The yields in liquid carbon disulfide behaved differently (5); as the temperature was decreased from 460 to 168 K (and density increased concomitantly from 1000 to 1444 kg m^{-3}) G_{fi}^E *increased*. Furthermore, the (E, G_{fi}^E) data could not be fitted by $F(y)$ = YGP. A distribution with an exponential body and a power tail, designated YEP, provided a better fit but was also inadequate at the lowest temperatures (densities >1350 kg m^{-3}). At these highest densities a simple power function designated YP (1*c*) gave satisfactory fits (5). These distribution functions indicate a lack of randomness in the scattering.

The behavior in dense liquid CS_2 brought to mind earlier studies of G_{fi}^E in isobutane (2-methylbutane) (6, 7). As the liquid was cooled from 296 to 169 K, with concomitant increase of density from 553 to 688 kg m^3, G_{fi}^E decreased and the variation of G_{fi}^E with E could be fitted by using YGP. However, on further cooling to 148 K (709 kg m^{-3}) the yields stayed about constant and their field dependence was consistent with YP (6).

In the present work G_{fi}^E was measured in isobutane from 294.4 to 114.6 K (556 to 739 kg m^{-3}). Particular attention was given to the behavior at T < 180 K, d > 677 kg m^{-3}. The effects of increasing density on $F(y)$ and on the mean thermalization distance $\langle y \rangle$ were examined by fitting the (E, G_{fi}^E) data.

The mobilities μ of thermal electrons were also measured to check the purity of the liquid and to extend the earlier range of measurements. The Arrhenius temperature dependence of μ changes in the same density region as does $F(y)$.

Experimental

Materials

Matheson research grade isobutane (>99.96 mol%) was further purified in a grease-free vacuum line, by the method used for *n*-butane described in ref. 4.

Apparatus

Low-pressure liquid conductance cells (8) with electrode separations l of 2.51 and 3.26 mm were used. The electron conductance amplifier, charge integrator, voltage supplies, and dosimetry are described or referenced in ref. 4. Temperature control and measurement are described in ref. 9.

The densities are dielectric permittivities were taken from ref. 10.

Results and discussion

Electron mobility

At all temperatures except the lowest (114.6 K, which is 0.9 K above the freezing point) the electron conductance signal decayed linearly, or nearly so (11), with time. This indicated that the liquid was sufficiently free of electron-attaching impurities. The applied field strengths were in the range 0.3–5 MV m^{-1}, and the measured electron drift times

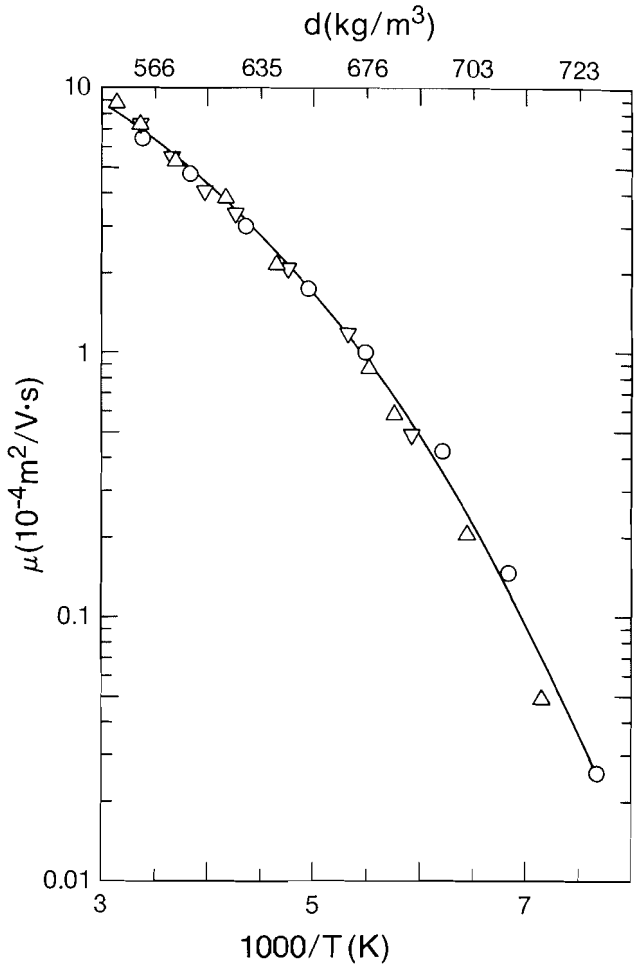

FIG. 1. Arrhenius plot of electron mobility μ in liquid isobutane. ○, present work; ▽, ref. 7; △, ref. 12. The full curve was calculated from eqs. [8]–[13], using the parameter values given in the text.

t_d were in the range 2–700 μs. The conductance signal at 114.6 K was convex toward the time axis and had a long tail, so was not used.

The electron mobilities were calculated from eq. [6],

$$[6] \qquad \mu = l^2/t_d \cdot V$$

where l is the distance between the parallel electrodes and V is the applied voltage. For the conditions of this work the diffusion correction (11) was negligible. At each temperature at least eight measurements, half obtained with positive and half with negative applied voltage, were averaged to give the results in Fig. 1 and Table 1. The present mobilities agree with earlier reports at the higher temperatures (7, 12), but are somewhat higher than those reported for the lower temperatures (12).

The variation of μ with liquid temperature T and density d is interpreted by a two-state model (12), which is summarized as follows. The electrons are in equilibrium between quasifree (qf) and localized (loc) states:

$$[7] \qquad e_{qf}^- + \text{medium} \rightleftharpoons e_{loc}^-$$

A fraction χ of the electrons is in the quasifree state:

$$[8] \qquad \chi = \int_{-\infty}^{\infty} N(E)[1 + \exp(E/k_BT)]^{-1} dE$$

[3]H. Preston-Thomas, private communication. The following prefixes were accepted by the Comité International des Poids et Mesures in Oct./90 to be put forward to the Conférence Générale des Poids et Mesures for adoption in Oct./91: 10^{-21}, zepto, z; 10^{21}, zetta, Z; 10^{-24}, yocto, y; 10^{24}, yotta, Y.

Can. J. Chem. Downloaded from www.nrcresearchpress.com by 123.30.183.119 on 09/08/12
For personal use only.

TABLE 1. Thermal electron mobilities in isobutane

T (K)	d (kg m^{-3})	μ (10^{-4} m^2 V^{-1} s^{-1})
130.5	725	0.026
146.6	710	0.143
161.1	696	0.424
182.2	676	1.00
201.5	656	1.72
229.4	627	3.00
261.5	594	4.76
294.5	555	6.51
294.8	555	6.37

where $N(E)dE$ is the fraction of localized states that lie at energies between E and $E + dE$ from the quasifree state, and k_B is Boltzmann's constant.

The distribution function $N(E)$ is taken to be a Gaussian about a mean value E_0 with a dispersion σ,

$$[9] \quad N(E) = \pi^{-1/2}\sigma^{-1} \exp[-(E - E_0)^2/\sigma^2]$$

The parameters E_0 and σ vary with temperature,

$$[10] \quad E_0 = E(0) - aT$$

$$[11] \quad \sigma = \sigma(0) + bT^{1.5}$$

In previous work the power of T in eq. [11] was taken as 1.0, but that value did not provide enough curvature for the data in Fig. 1.

The observed mobility is the sum of the contributions of e^-_{qf} of mobility μ_{qf} and e^-_{loc}:

$$[12] \quad \mu = \chi\mu_{qf} + (1 - \chi)\mu^0_{loc} \exp(-E_{loc}/k_BT)$$

where μ^0_{loc} and E_{loc} are respectively the preexponential factor and activation energy of e^-_{loc} mobility. The value of μ_{qf} is density and temperature dependent, taken as

$$[13] \quad \mu_{qf} = \mu_{ref}(d_{ref}/d)^2(T_{ref}/T)$$

where μ_{ref} is the mobility at the reference density d_{ref} and temperature T_{ref}.

Previously selected values of the parameters for isobutane (12) were used as far as possible: $E(0) = 32$ zJ entity^{-1} (0.20 eV ent^{-1}), $\sigma(0) = 0$, $\mu^0_{loc} = 1 \times 10^{-5}$ m^2 V^{-1} s^{-1}, $E_{loc} = 11$ zJ ent^{-1} (0.07 eV ent^{-1}), $\mu_{ref} = 3 \times 10^{-3}$ m^2 V^{-1} s^{-1} at $T_{ref} = 295$ K and $d_{ref} = 555$ kg m^{-3}. The new values $a = 43$ yJ ent^{-1} K^{-1} (0.27 meV ent^{-1} K^{-1}) and $b = 7.2$ yJ ent^{-1} K$^{-1.5}$ (0.0448 meV ent^{-1} K$^{-1.5}$) provided the full curve in Fig. 1. The contribution of e^-_{loc} is negligible (1% at the lowest T, and less at higher T's), so eq. [12] reduces to [12′] in this case:

$$[12'] \quad \mu = \chi\mu_{qf}$$

While we do not treat mobilities in low density liquids here, to fit data at $d/d_c < 2.5$ (13) using eq. [11], the variation of μ_{qf} with density in the low density liquid regime would have to change to $\mu_{qf} \propto d^{-4}$. Furthermore, near the critical region quasilocalization of the electrons lowers the measured μ (12).

Free-ion yields and thermalization distance distributions

The yields decreased relatively rapidly as the temperature was decreased from 294 to 180 K (density increased from 555 to 677 kg m^{-3}), then decreased more slowly as the temperature was decreased further to 130 K (density increased to 725 kg m^{-3}): see Figs. 2 and 3. At 114.6 K (740 kg m^3), which is 0.9 K above the freezing point, the G^E_{fi} curve lies below that for 130.9 K at low fields and above it at high fields (Fig. 3).

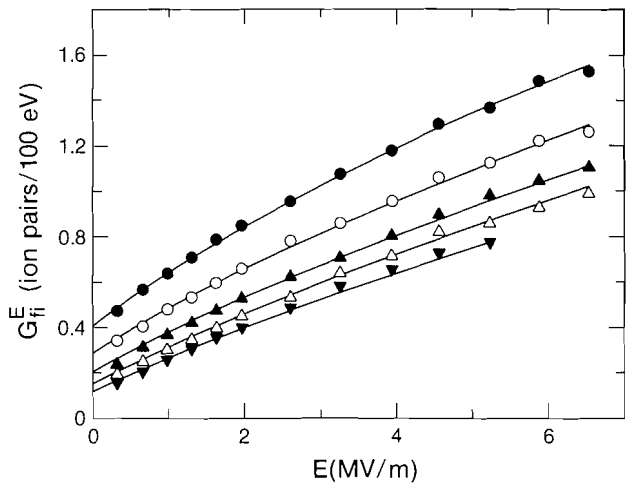

FIG. 2. Electric field strength dependence of free ion yields in liquid isobutane at $T = 294.4$ K (●), 261.9 K (○), 229.4 K (▲), 200.5 K (△), and 180.6 K (▼). The curves were calculated from eqs. [14]–[18] and $F(y) = YP$ (Table 3).

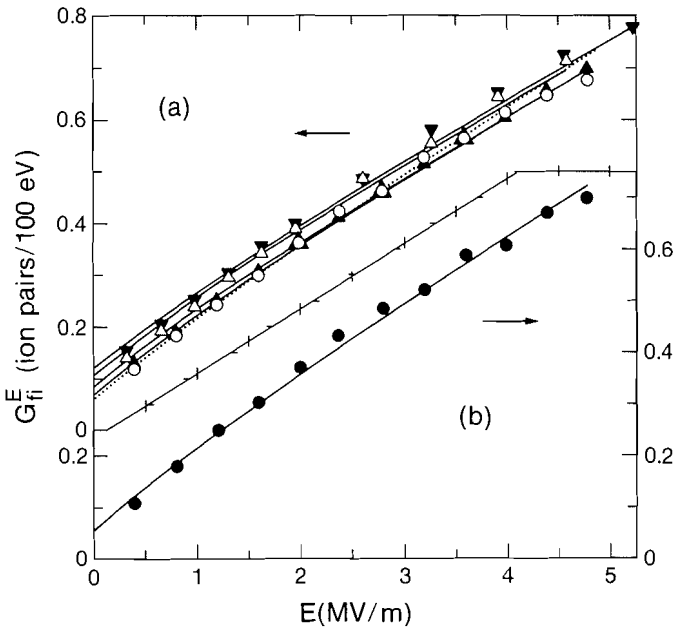

FIG. 3. Field strength dependence of free ion yields in liquid isobutane at (a) $T = 180.6$ K (▼), 169.7 K (△), 149.6 K (▲), 130.9 K (○), and (b) 114.6 K (●). Lines calculated as in Fig. 2. The · · · line in (a) is the line from (b), to show the cross-over.

The free ion yield at a given set of conditions can be calculated from (1*c*)

$$[14] \quad G^E_{fi} = \phi^E_{fi} G_{tot}$$

where G_{tot} is the total yield (ion pairs per 16 aJ) of reaction [1], which is measured chemically by electron capture in the liquid phase, or electrically in the gas phase. The probability ϕ^E_{fi} that an initial ion pair will become a free-ion pair is calculated from

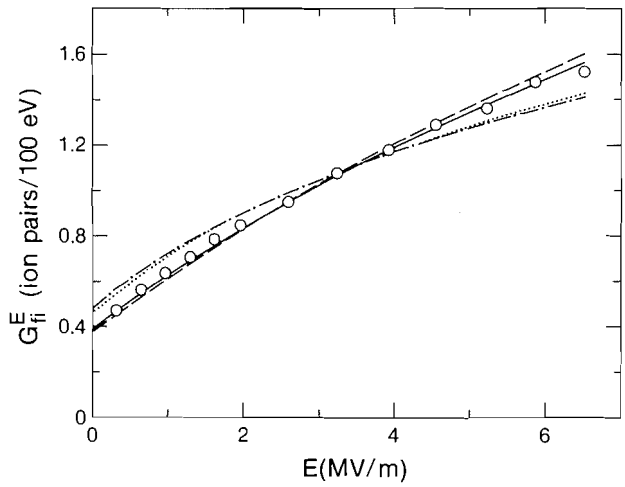

FIG. 4. Free ion yields at 294.4 K (○) compared to those calculated by eqs. [14]–[18] using G_{tot} = 4.2 and $F(y)$ = YGP (——), YG (– – –), YEP (—·—·), and YE (· · ·), with parameter values from Table 2.

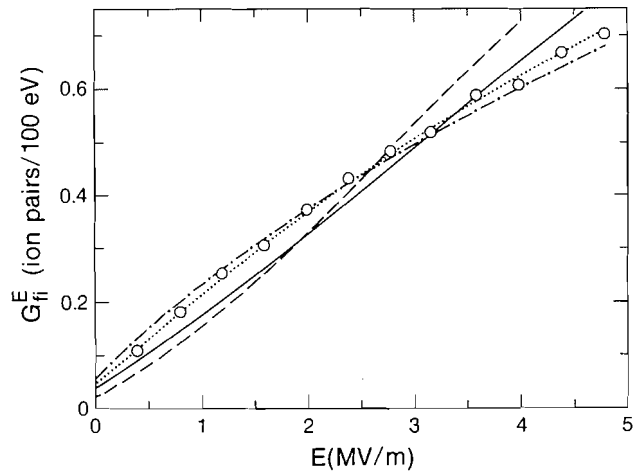

FIG. 5. Free ion yields at 114.6 K (○). Lines calculated as in Fig. 4.

TABLE 2. Parameter values for curves in Figs. 4 and 5[a]

	294.4 K		114.6 K	
Distribution	G_{fi}^{0}	b (nm)	G_{fi}^{0}	b (nm)
YG	0.373	11.4	0.025	9.7
YGP	0.392	10.7	0.040	8.7
YE[b]	0.459	12.7	0.046	8.3
YEP[b]	0.474	11.6	0.059	7.2

[a]Free ion yields in liquid isobutane. Assumed G_{tot} = 4.2. The equations for the distribution functions YG, YGP, YE, and YEP are given in refs. 1*c* and 13.
[b]y_0 = 1 nm.

$$[15] \quad \phi_{fi}^{E} = \int_0^\infty \phi_{fi}^{E}(y)F(y)dy$$

where y is the distance between the electron and ion at the time when the electron reaches thermal energy, $F(y)$ is the distribution function, and

$$[16] \quad \phi_{fi}^{E}(y) = \phi_{fi}^{0}(y)[1 + f(E,\varepsilon,T,y)]$$

The probability at zero field is (2)

$$[17] \quad \phi_{fi}^{0}(y) = \exp(-\xi^2/4\pi\varepsilon_0\varepsilon k_B T y) = \exp(-r_c/y)$$

where $-\xi$ is the electron charge, ε_0 is the permittivity of vacuum, ε is the relative permittivity of the medium between the electron and cation, and r_c is the distance at which the coulombic attraction energy between the electron and ion equals $k_B T$. The field enhancement term in eq. [16] is (1*c*)

$$[18] \quad f(E,\varepsilon,T,y) = e^{-2\beta y}\sum_{m=1}^{\infty}\frac{(2\beta y)^m}{(m+1)!}\sum_{j=0}^{m-1}(m-j)\frac{(r_c/y)^{j+1}}{(j+1)!}$$

where $\beta(m^{-1}) = \xi E/2k_B T = 5800\,E/T$, where E is in V m^{-1}.

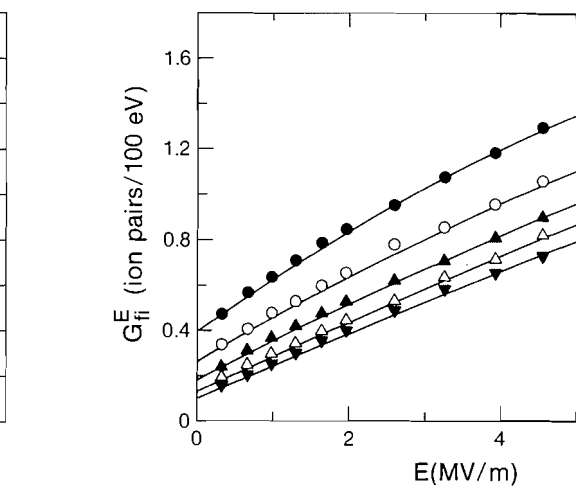

FIG. 6. Experimental free ion yields as in Fig. 2. Curves calculated using $F(y)$ = YGP and parameter values from Table 3.

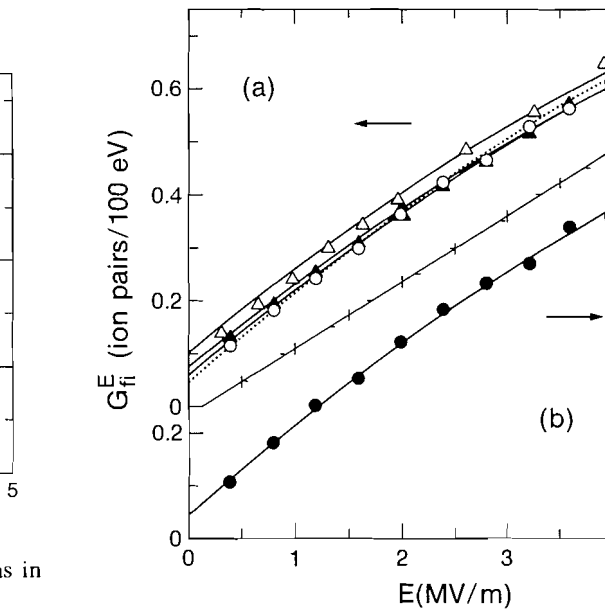

FIG. 7. Experimental free ion yields as in Fig. 3. Curves calculated using $F(y)$ = YE and parameter values from Table 3.

Can. J. Chem. Downloaded from www.nrcresearchpress.com by 123.30.183.119 on 09/08/12
For personal use only.

TABLE 3. Parameter values to fit field dependence of free ion yields[a]

T (K)	d (kg m^{-3})[b]	ε[c]	G_{fi}^0	b_{GP} or b_E (nm)[d]	$\langle y \rangle$ (nm)	$G_{fi}^{0\,d}$	y_{min} (nm)[d]	$\langle y \rangle$ (nm)[d]
294.4	555	1.752	0.39[e]	10.7[e]	13.8[e]	0.41	7.5	14.6
261.9	593	1.818	0.26[e]	9.5[e]	12.3[e]	0.29	6.7	13.1
229.4	627	1.880	0.18[e]	8.9[e]	11.5[e]	0.20	6.2	12.1
200.5	657	1.935	0.13[e]	8.5[e]	11.0[e]	0.15	5.9	11.5
180.6	677	1.973	0.096[e]	8.3[e]	10.7[e]	0.12	5.7	11.1
169.7	688	1.993	0.102[f]	8.1[f]	9.1[f]	0.11	5.7	11.1
165.1	692	2.003	0.093[f]	8.0[f]	9.0[f]	0.099	5.6	10.9
159.7	697	2.013	0.084[f]	7.9[f]	8.9[f]	0.092	5.6	10.9
149.6	707	2.033	0.076[f]	7.9[f]	8.9[f]	0.084	5.7	11.1
140.0	716	2.053	0.066[f]	8.0[f]	9.0[f]	0.076	5.7	11.1
135.3	721	2.063	0.063[f]	8.0[f]	9.0[f]	0.073	5.8	11.3
130.9	725	2.071	0.059[f]	8.1[f]	9.1[f]	0.068	5.8	11.3
114.6	740	2.107	0.047[f]	8.3[f]	9.3[f]	0.058	6.0	11.7

[a]Assumed $G_{tot} = 4.2$.
[b]Mass density, ref. 10. Freezing point 113.7 K. Critical point 408.1 K; $d_c = 221$ kg m^3.
[c]Relative dielectric permittivity, ref. 10.
[d]YP parameters with $x = 2.05$; Figs. 2 and 3.
[e]YGP parameters; $\langle y \rangle = 1.29\, b_{GP}$ (wrongly given as $1.34\, b_{GP}$ in ref. 5); Fig. 6.
[f]YE parameters; $\langle y \rangle = b_E + y_0$; Fig. 7.

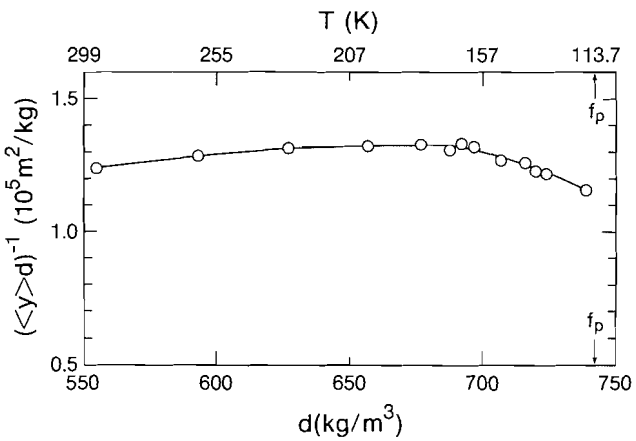

FIG. 8. Thermalizing ability plotted against density; $\langle y \rangle$ obtained using $F(y)$ = YP.

One may obtain information about $F(y)$ by fitting eqs. [14]–[18] to yields measured under a wide range of conditions. Many forms of $F(y)$ have been considered (1*c*, 13–17). The most common are based on Gaussian or exponential forms. A Gaussian-type distribution can arise from nearly random scattering of the thermalizing electrons by the fluid molecules, while an exponential-type might arise from a greater contribution of forward scattering in the more ordered, denser fluid (1*c*). Four example distributions (13) are a three-dimensional Gaussian designated YG, a one-dimensional exponential designated YE, and each with the addition of a y^{-3} power tail for a few percent of the pairs that have the largest y values, and therefore designated YGP and YEP, respectively. The power tail at large y values is an artifact of the model, in which it is assumed that there is only one ionization event per microzone, and is due to the rapid combination of the ions and electrons nearest the center of the few microzones that contain more than one ion–electron pair (1*c*). The explicit forms of these functions are given in refs. 1*c* and 13. In Figs. 4 and 5 yields calculated from these four distributions, with best-fit parameter values given in Table 2, are compared to the measured values at 294.4 K (555 kg m^{-3}) and 114.6 K (740 kg m^{-3}). In the former the best fit was obtained with YGP, while in the latter it was obtained with YE. This unusual change of the distribution function indicates that the scattering properties of the liquid are somewhat different at the lowest and highest densities.

Figure 6 shows that yields calculated with YGP are not unreasonable at densities up to 677 kg m^{-3} (temperatures down to 180.6 K). This is why measurements in isobutane at $d < 555$ kg m^{-3} could be fitted with YGP (18). Figure 7 shows that yields calculated with YE are not unreasonable at densities down to 725 kg m^{-3} (temperatures up to 130.9 K). The parameter values used to obtain the curves in Figs. 6 and 7 are listed in Table 3.

Less than 40% of the initial ionizations produce free ions at the highest field and temperature used in the present work. Therefore the low y value half of the $F(y)$ distribution makes a negligible contribution to the yields displayed in Figs. 6 and 7. We can therefore neglect the shape of the main body of the distribution and focus on the shape of the tail. For that purpose we use a simple power function, designated YP (1*c*, 7):

$$[19] \quad F(y) = \begin{cases} 0 & y < y_{min} \\ x y_{min}^{x} y^{-(x+1)} & y > y_{min} \end{cases}$$

where x and y_{min} are adjustable parameters. A reasonable fit to the yields at all temperatures and densities (Figs. 2 and 3) was obtained with $x = 2.05$, although the curvature of the lines is a bit too small. Parameter values for the curves in Figs. 2 and 3 are listed in Table 3. This compromise function varies as $y^{-3.05}$, compared to the y^{-3} tails in YGP and YEP. The mean values of y, $\langle y \rangle$, in YP are similar to those in YGP over the range of density and temperature where the latter is an adequate distribution (Table 3). However, the values of $\langle y \rangle$ in YE are significantly smaller than those in YP because the former has an unrealistically large number of pairs at the lowest y values.

The values of G_{fi}^0 obtained by extrapolation with YP are

Can. J. Chem. Downloaded from www.nrcresearchpress.com by 123.30.183.119 on 09/08/12
For personal use only.

slightly higher than those obtained with YGP or YE (Table 3). The preferred values would be the averages of those in the two columns of the table, but we do not list them because they do not have an associated distribution function.

Electron thermalizing ability of the liquid

The inverse of the average thermalization distance, normalized for the density of the liquid, $(\langle y \rangle d)^{-1}$, is a measure of the inherent ability of the liquid to remove excess kinetic energy from hot electrons. This quantity is plotted against isobutane density in Fig. 8. The plot has a slightly positive slope for densities up to about 660 kg m^{-3}, and a negative slope for densities above about 690 kg m^{-3}. In this same density region, 660–690 kg m^{-3}, the temperature dependence of the electron mobility undergoes a significant change (Fig. 1). In the lower density region, $d < 660$ kg m^{-3}, the Arrhenius temperature coefficient is $E_\mu \approx 7$ kJ mol^{-1}, whereas at $d > 690$ kg m^{-3} it is $E_\mu \approx 16$ kJ mol^{-1}. These changes in behavior are attributed to an undetermined change in liquid structure, or molecular packing. Values of the viscosity of the liquid in this low-temperature region are not available in the literature. A large program of studying liquids for their own sake is badly needed to assist programs in many other fields, such as the behavior of electrons in fluids.

Acknowledgements

We thank the staff of the Radiation Research Center for maintaining the equipment, and the Natural Sciences and Engineering Research Council for financial assistance.

1. G. R. Freeman. *In* Kinetics of nonhomogeneous processes. *Edited by* G. R. Freeman. Wiley–Interscience, New York. 1987; (*a*) pp. 35–36; (*b*) pp. 40–43; (*c*) pp. 51–57; (*d*) pp. 66–82.
2. L. Onsager. Phys. Rev. **54**, 554 (1938).
3. A. O. Allen. Natl. Stand. Ref. Data Ser. Natl. Bur. Stand. No. 57 (1976).
4. N. Gee, P. C. Senanayake, and G. R. Freeman. J. Chem. Phys. **89**, 3710 (1988).
5. N. Gee and G. R. Freeman. Can. J. Phys. **68**, 930 (1990).
6. J.-P. Dodelet, P. G. Fuochi, and G. R. Freeman. Can. J. Chem. **50**, 1617 (1972).
7. J.-P. Dodelet, K. Shinsaka, and G. R. Freeman. Can. J. Chem. **54**, 744 (1976).
8. J.-P. Dodelet, K. Shinsaka, U. Kortsch, and G. R. Freeman. J. Chem. Phys. **59**, 2376 (1973).
9. M. A. Floriano and G. R. Freeman. J. Chem. Phys. **85**, 1603 (1986).
10. W. M. Haynes and B. A. Younglove. Adv. Cryog. Eng. **27**, 883 (1982).
11. N. Gee and G. R. Freeman. Phys. Rev. A: Gen. Phys. **31**, 3496 (1985).
12. N. Gee and G. R. Freeman. J. Chem. Phys. **78**, 1951 (1983).
13. G. Ramanan, N. Gee, and G. R. Freeman. Can. J. Phys. **68**, 925 (1990).
14. W. F. Schmidt and A. O. Allen. J. Phys. Chem. **72**, 3730 (1968).
15. A. Mozumder and M. Tachiya. J. Chem. Phys. **62**, 979 (1975).
16. J. Casanovas, R. Grob, D. Blanc, G. Brunet, and J. Mathieu. J. Chem. Phys. **53**, 3673 (1975).
17. C. Ferradini and J.-P. Jay-Gerin. J. Chem. Phys. **89**, 6719 (1988).
18. N. Gee and G. R. Freeman. IEEE Trans. Electr. Insul. **23**, 505 (1988).

Can. J. Chem. Downloaded from www.nrcresearchpress.com by 123.30.183.119 on 09/08/12
For personal use only.

A theoretical study on the activation of hydrogen–hydrogen and hydrogen–alkyl bonds by electron-poor early transition metals

E. FOLGA AND T. ZIEGLER[1]

Department of Chemistry, University of Calgary, Calgary, Alta., Canada T2N 1N4

Received May 23, 1991

This paper is dedicated to Professor Sigeru Huzinaga on the occasion of his 65th birthday

E. FOLGA and T. ZIEGLER. Can. J. Chem. **70**, 333 (1992).

A theoretical study has been carried out on four σ-bond metathesis reactions mediated by the electron-poor lutetium metal centre. The four processes include hydrogen exchange, $X_2Lu\text{-}H + D_2 \rightarrow X_2Lu\text{-}D + HD$ (**1**), and hydrogenolysis $X_2Lu\text{-}CH_3 + H_2 \rightarrow Cl_2Lu\text{-}H + CH_4$ (**2**), in which a H—H bond is activated, as well as methane exchange, $X_2Lu\text{-}CH_3 + CH_4 \rightarrow X_2Lu\text{-}CH_3 + CH_4$ (**3**), and methylation, $Cl_2Lu\text{-}H + CH_4 \rightarrow X_2Lu\text{-}CH_3 + H_2$ (**4**), in which a C—H bond is activated. The Cp^*_2Lu fragment employed in a number of experimental studies was modelled by Cl_2Lu and all calculations were based on approximate Density Functional Theory (DFT). The study combined methods from quantum mechanics and statistical mechanics to obtain enthalpies and entropies of activation as well as transition state structures. All four processes were found to have an ordered four-centre transition state with negative entropies of activation given by $\Delta S^{\neq} = -109$ (**1**), -124 (**2**), -131 (**3**), and -134 (**4**) J mol^{-1} K^{-1} at $T = 298.15$ K. The Gibb's free energies of activation, $\Delta G^{\neq}(=\Delta H^{\neq} - T\Delta S^{\neq})$ were calculated as $\Delta G^{\neq} = 81.6$ (**1**), 126.0 (**2**), 136.7 (**3**), and 130.6 (**4**) kJ mol^{-1} at $T = 298.15$ K. The calculated trends in $\Delta G^{\neq}$ are consistent with the observed order of reactivity for σ-bond metathesis reactions between R—H and M—R′ bonds: R = R′ = H >> R = H, R′ = CH_3 > R = R′ = CH_3. The decrease in the reaction rate is related to the diffferent abilities of the 1*s* hydrogen orbital and the σ_{CH_3} methyl orbital to stabilize the four-centre transition state. Thus, the spherical 1*s* hydrogen orbital is better able to overlap fully with orbitals on adjacent centres than the directional σ_{CH_3} orbital. As a consequence, the electronic barrier is seen to increase from the hydrogen exchange reaction towards the hydrogenolysis and methane exchange processes as one or two hydrogens, respectively, are replaced by methyl groups in the four-centre transition state.

Key words: Density Functional Theory, C—H activation, metathesis, hydrogenolysis, H—H activation.

E. FOLGA et T. ZIEGLER. Can. J. Chem. **70**, 333 (1992).

On a effectué une étude théorique sur des réactions de métathèse impliquant quatre liaisons-σ et l'entremise du lutécium comme centre métallique pauvre en électrons. Les quatre processus comprennent : l'échange d'hydrogène, $X_2Lu\text{-}H + D_2 \rightarrow X_2Lu\text{-}D + HG$ (**1**), l'hydrogénolyse, $X_2Lu\text{-}CH, + H_2 \rightarrow Cl_2Lu\text{-}H + CH_4$ (**2**) dans laquelle une liaison H—H est activée, l'échange de méthane, $X_2Lu\text{-}CH_3 + CH_4 \rightarrow X_2Lu\text{-}CH_3 + CH_4$ (**3**) et la méthylation, $Cl_2Lu\text{-}H + CH_4 \rightarrow X_2Lu\text{-}CH_3 + H_2$ (**4**) dans laquelle il y a activation d'une liaison C—H. On a utilisé le Cl_2Lu comme modèle du fragment Cp^*_2Lu qui a été souvent employé dans un certain nombre d'études expérimentales et tous les calculs sont basés sur la théorie de la densité fonctionnelle (TDF) approximative. L'étude a combiné des méthodes de la mécanique quantique et de la mécanique statistique pour obtenir les enthalpies et les entropies d'activation ainsi que les structures des états de transition. On a trouvé que les quatre processus possèdent un état de transition ordonné à quatre centres avec des entropies d'activation calculées qui sont négatives : $\Delta S^{\neq} = -109$ (**1**), -124 (**2**), -131 (**3**) et -134 (**4**) J mol^{-1} K^{-1}, à 298,15 K. Les enthalpies libres d'activation, $\Delta G^{\neq}$ $(=\Delta H^{\neq} - T\Delta S^{\neq})$, calculées sont égales à 81,6 (**1**), 126,0 (**2**), 136,7 (**3**) et 130,4 (**4**) kJ mol^{-1}, à 298,15 K. Les tendances calculées pour les $\Delta G^{\neq}$ sont en accord avec l'ordre de réactivité observé pour les réactions de métathèses des liaisons-σ entre des liaisons R—H et M—R′ : R = R′ − H >> R = H, R′ − CH_3 > R − R′ = CH_3. L'abaissement de la vitesse de la réaction est relié aux pouvoirs différents de l'orbitale 1*s* de l'hydrogène et de l'orbitale σ_{CH_3} du méthyle de stabiliser l'état de transition à quatre centres. L'orbitale 1*s* sphérique de l'hydrogène donne donc lieu à un plus grand recouvrement des orbitales des centres adjacents que l'orbitale σ_{CH_3} orientée. En conséquence, alors qu'on remplace respectivement un ou deux hydrogènes par des groupes méthyles dans l'état de transition à quatre centres, on voit un accroissement de la barrière électronique lorsqu'on passe de la réaction d'échange d'hydrogène vers les processus d'hydrogénolyse et d'échange de méthane.

Mots clés : théorie de la densité fonctionelle, activation d'une liaison C—H, métathèse, hydrogénolyse, activation d'une liaison H—H.

[Traduit par la rédaction]

Introduction

The activation (breaking) of H—H and C—H bonds by transition metal centres has been studied extensively over the last decade by experimental (1–4) as well as theoretical (5, 6–9, 12) techniques. Electron-rich middle to late transition metal complexes are known (1, 5) to add H_2 oxidatively to form dihydride complexes.

[1] $ML_n + H_2 \rightarrow$ 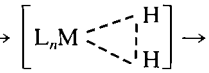 $\rightarrow L_nM(H)_2$

1

The process in eq. [1] is facile and proceeds through a three-centre transition state (1, 5) in a concerted manner. Electron-rich metal centres can also activate alkylic C—H bonds (2, 5*i–k*, 6*a–c*) by a concerted oxidative addition

[2] $ML_n + H\text{—}CH_3 \rightarrow$ 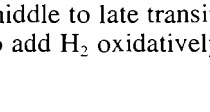 $\rightarrow L_nM(H)(CH_3)$

2

The reaction is not as facile as H—H addition and has only been realized (2) in a limited number of cases. The H—H and C—H bonds are of roughly the same strength. However, H—H activation is thermodynamically more favourable since M—H bonds of middle to late transition metals are stronger

[1]Author to whom correspondence may be addressed.

Can. J. Chem. Downloaded from www.nrcresearchpress.com by 92.62.229.171 on 09/08/12
For personal use only.

Can. J. Chem. Downloaded from www.nrcresearchpress.com by 92.62.229.171 on 09/08/12
For personal use only.

(2*g*, 6*d*–*e*, 12) than the corresponding M–alkyl bonds. Thus, oxidative addition of H_2 in eq. [1] is in general exothermic (5*i*–*l*, 6*c*) whereas the C—H addition of eq. [2], with some important exceptions (2), is endothermic (5*i*–1, 6*c*). The H—H addition is further kinetically more facile since the spherical $1s_H$ orbital (5*i*–*l*) is better able to stabilize the three-centre transition state, **1**, than the more directional σ_{CH_3} orbital in **2**.

Early transition metals are in general too electron poor to activate H—H and C—H bonds by oxidative addition. They are, nevertheless, able to activate H—H and C—H bonds in the recently discovered σ-bond metathesis reaction (3):

[3] $L_nM—R + H—R^* \rightarrow L_nM—R^* + H—R$

($M = d^0, f^{14}d^0$; R, R* = H, alkyl)

The general formulation of the σ-bond metathesis reaction in eq. [3] includes hydrogen exchange, eq. [4*a*], methane exchange, eq. [4*b*], and hydrogenolysis of metal alkyls, eq. [4*c*].

[4*a*] $L_nM—H + D_2 \leftrightarrow L_nM—D + HD$

[4*b*] $L_nM—CH_3 + {}^*CH_4 \leftrightarrow L_nM—{}^*CH_3 + CH_4$

[4*c*] $L_nM—R + H_2 \rightarrow L_nM—H + RH$

[4*d*] $L_nM—H + CH_4 \rightarrow L_nM—CH_3 + H_2$

(M = Lu, Sc; L = Cp*; *n* = 2)

The σ-bond metatheses by organo-lutetium and organo-scandium methyl complexes were studied experimentally by Watson (3*c*–*e*) and Bercaw and co-workers (3*a*–*b*) in connection with the Ziegler–Natta polymerization process. Both complexes were reported to readily undergo hydrogenolysis, eq. [4*c*], giving up metal hydrides that then rapidly underwent H/D exchange, eq. [4*a*]. Methane exchange, eq. [4*b*], was observed in several instances and kinetic studies were carried out for M = Sc (3*a*,*b*), Y, and Lu (3*c*–*e*). Hydrogenolysis of metal alkyls, eq. [4*c*], is postulated to take place during the chain-termination step in Ziegler–Natta polymerization (3). Electron-poor early *f*-block elements are also known (3*f*,*g*) to activate H—H and C—H bonds according to the reaction given in eq. [3].

The activation of the H—H bond by electron-poor metal centres in the σ-bond metathesis reactions of eqs. [4*a*] and [4*c*] has been postulated (3) to proceed via a four-centre transition state **3***a*.

[5] $L_nM—R + H—H \rightarrow \left[\begin{array}{cc} L_nM & R \\ H & H \end{array}\right]$ (**3***a*) $\rightarrow L_nM—H + R—H$

A similar four-centre transition state **3***b*

[6] $L_nM—R + H—CH_3 \rightarrow \left[\begin{array}{cc} L_nM & R \\ H_3C & H \end{array}\right]$ (**3***b*) $\rightarrow L_nM—CH_3 + R—H$

has been inferred for the activation of the C—H bond in the two reactions of eqs. [4*b*] and [4*d*]. Activation of H—H bonds via the four-centre transition state, **3***a*, might also occur in complexes of middle to late transition metals (9).

Up-to-date theoretical investigations on σ-bond metathesis include a GVB (Generalized Valence Bond) study of the reaction in eq. [4*a*] (M = Sc, Ti; L = Cl) by Steigerwald and Goddard (7*a*) and EHA (Extended Hückel Approximation) calculations of the reactions in eqs. [4*a*] and [4*b*] (M = Lu, L = Cp*) by Hoffmann and co-workers (7*c*). Recently, Rappé (7*b*) discussed σ-bond metathesis between C—H bonds of olefins or acetylenes and the Sc—R (R = H, CH_3) linkage. We (7*d*) have also reported preliminary calculations on the reaction in eq. [4*a*] with $ML_n = LuCl_2$.

The present investigation is concerned with a comparison between the activation of the H—H bond in eqs. [4*a*] and [4*c*], and the activation of the C—H bond in eqs. [4*b*] and [4*d*]. In particular, we shall contrast the degree to which the frontier orbitals on H and CH_3 are able to stabilize the four-centre transition states **3***a* and **3***b* and its implication (3*a*,*b*, 7*a*,*b*) for the activation energies of the processes in eqs. [4*a*]–[4*d*]. We have chosen Cl_2Lu to model the Cp^*_2Lu fragment employed by Watson (3*c*–*e*). The activation of H—H, eq. [1], and C—H bonds, eq. [2], by electron-rich metal centres has been studied previously in our group (6*c*).

Our calculations are based on Approximate Density Functional Theory (10), which over the past decade has emerged as a tangible and versatile computational method. It has been employed successfully to obtain thermochemical data (11, 12), molecular structures (13, 14), force fields and frequencies (15), assignments of NMR (16, 17), photoelectron (18), ESR (19), and UV spectra (15), and transition state structures as well as activation barriers (20), dipole moments (21), and other one-electron properties. Thus, approximate DFT is now applied to many problems previously covered exclusively by *ab initio* Hartree–Fock (HF) and post-HF methods. The recently acquired popularity of approximate DFT stems in large measure from its computational expedience, which makes it amenable even to large-size molecules at a fraction of the time required for HF or post-HF calculations. More important, perhaps, is the fact that expectation values derived from approximate DFT in most cases are better in line with experiment than results obtained from HF calculations. This is in particular the case for systems involving transition metals. An analysis of why approximate DFT affords more reliable results than HF has recently been published by Cook and Karplus (22) as well as by Tschinke and Ziegler (23).

Computational details

The reported calculations were all carried out by utilizing the HFS–LCAO program system developed by Baerends *et al.* (24, 25) and vectorized by Ravenek (25*b*). The numerical integration procedure applied for the calculations was developed by Becke (26). All molecular structures were optimized on the singlet energy surface within the C_s symmetry group. The geometry optimization procedure was based on the method developed by Versluis and Ziegler (13). Vibrational frequencies were evaluated from force constants calculated by numerical differentiation of the energy gradients (15). The transition states were optimized according to the method due to Simons *et al.* (27) in the implementation by Baker (28) that has been adopted to the HFS–LCAO program system by Fan *et al.* (15). The electronic configurations of the molecular systems were described by an uncontracted triple-ζ STO basis set (29) on lutetium for 5*d*, 6*s*, and 6*p* as well as a double-ζ STO basis set (22) on chlorine (3*s*,3*p*) and hydrogen (1*s*,2*p*). The $1s^22s^22p^63s^23p^63d^{10}4s^24p^64f^{14}5s^25p^6$ configuration on Lu and the $1s^22s^22p^2$ configuration on Cl were assigned to the core and treated by the frozen-core approximation (24). A set of auxiliary (30) *s*, *p*, *d*, *f*, and *g* STO functions, centred on all nuclei, was used to fit the molecular density and present Coulomb and exchange poten-

Can. J. Chem. Downloaded from www.nrcresearchpress.com by 92.62.229.171 on 09/08/12
For personal use only.

tials accurately in each SCF cycle. Relativistic effects were taken into account according to the approach by Snijders *et al.* (31) in its quasi-relativistic implementation (32).

Energy differences were calculated by including the local correlation potential by Stoll *et al.* (33*a*) and Becke's (33*b*) non-local exchange corrections. Calculations on metal carbonyls (34), binuclear metal complexes (35), alkyl and hydride complexes (6*c*–*f*, 36), as well as complexes containing M—L bonds for a number of different ligands (12, 37), have shown that the Approximate Density Functional method employed here affords metal–ligand and metal–metal bond energies of nearly chemical accuracy (±5 kcal mol^{-1}). More than 50 molecular structures optimized by Approximate Density Functional Theory have been compared with experiment (13). The agreement between experiment and theory is in most cases excellent. The application of Approximate Density Functional Theory to organometallic chemistry has recently been reviewed (36, 38).

H—H bond activation

Transition state structure for the hydrogen exchange reaction: $Cl_2Lu—H + H_2 \rightarrow Cl_2Lu—H + H_2$

A schematic energy profile for the hydrogen exchange reaction of eq. [4*a*] is given in Fig. 1. Our calculations indicate that a weak adduct, **4***a*, is formed in the early stages of the process. The formation energy for **4***a* was calculated to be only 4.9 kJ mol^{-1}. The equilibrium structure **4***a*, optimized under C_s symmetry constraints, reveals only a slight elongation of the H—H bond (by 0.002 Å) and a rather long distance of 3.724 Å from the midpoint of the H—H bond to the lutetium centre.

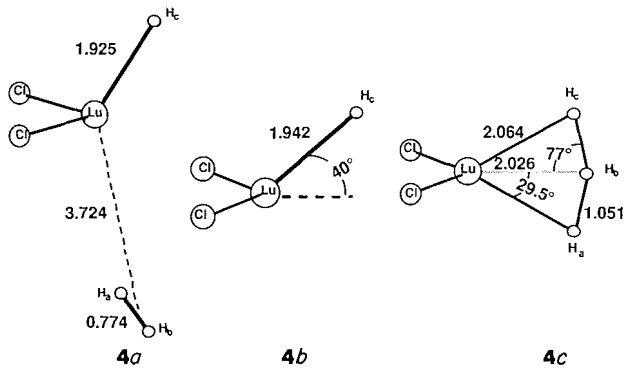

The Cl_2Lu—H framework in **4***a* resembles the optimized structure of free Cl_2LuH, **4***b*, which was found to have a nonplanar geometry with the hydride bent 40° out of the Cl_2Lu coordination plane. The barrier of inversion for free Cl_2LuH was calculated to be 8.7 kJ mol^{-1}.

There are two electron pairs involved in bond breaking and bond making during the exchange reaction in eq. [4*a*]. The two orbitals holding the electron pairs in the early stages of the reaction are shown to the left of the correlation diagram in Fig. 2. Of lowest energy is 2*a*′, which is made up of the σ_g orbital on the incoming H_2 molecule. This orbital describes the intact H—H bond. The 6*a*′ orbital of higher energy represents the Lu—H linkage. The bonding interaction in 6*a*′ is between a well-directed hybrid on lutetium (0.58 $6s - 0.43\ d_{x^2-y^2} + 0.43\ d_{z^2} + 0.50\ d_{yz}$) and $1s_{H_c}$.

The optimized transition state for the reaction in eq. [4*a*] was found to have a planar structure of C_{2v} symmetry, **4***c*. The two Lu—H distances of 2.064 and 2.026 Å are only slightly longer than the Lu—H hydride bond in **4***b* of 1.941 Å. The symmetrical H—H bond distances of 1.051 Å are substantially longer than the calculated H—H bond in free H_2 at 0.772 Å. The Lu—H_a—H_b—H_c ring structure in **4***c*

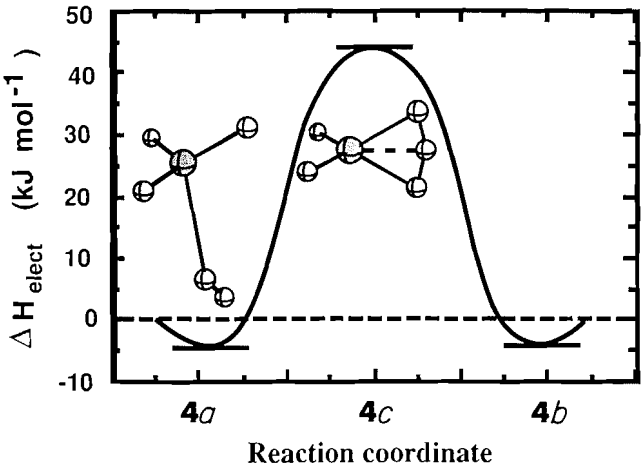

FIG. 1. Profile for the hydrogen exchange reaction $Cl_2LuH_c + H_a—H_b \rightarrow Cl_2LuH_a + H_b—H_c$. The energies are relative to the reactants (products).

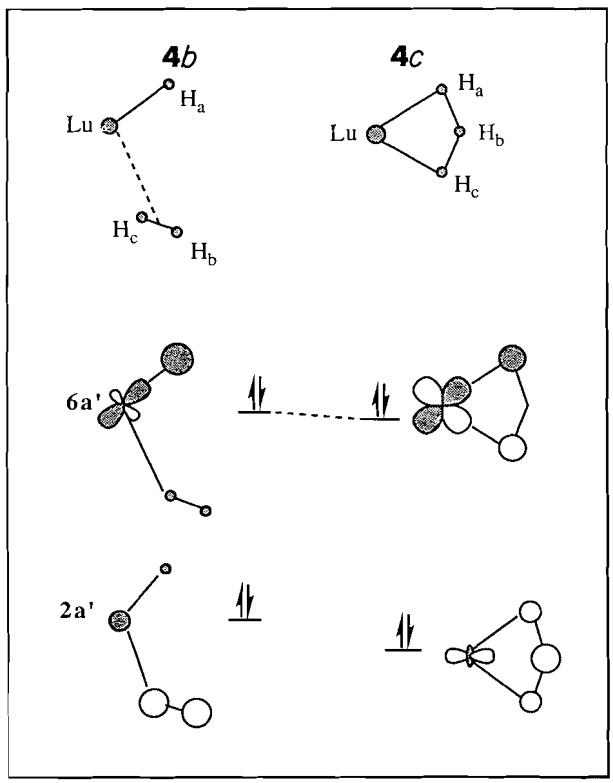

FIG. 2. Correlation diagram for the passage **4***a* → **4***c*.

clearly has the characteristics of a four-centre transition state with substantial bonding interaction between the adjacent atoms in the ring. In addition, there is some stabilizing interaction between Lu and H_b across the ring.

The two occupied orbitals responsible for the stabilizing interaction within the ring structure are shown to the right in Fig. 2. The 2*a*′ orbital represents a four-centre bonding interaction between the metal-based $d_{x^2-y^2}$ orbital on Cl_2Lu^+ and three in-phase 1*s* hydrogen orbitals on H_3^-. The 6*a*′ orbital of higher energy represents a three-centre bonding interaction involving the d_{yz} orbital on lutetium and an out-of-phase combination of 1*s* orbitals on the two equivalent hydrogen atoms.

Can. J. Chem. Downloaded from www.nrcresearchpress.com by 92.62.229.171 on 09/08/12
For personal use only.

The two electron pairs involved in the bond making and bond breaking through the passage from **4***a* to **4***c*, Fig. 2, remain in orbitals, 2*a*′ and 6*a*′, with strong stabilizing interactions. The electron pair of lowest energy is situated in an orbital 2*a*′, localized largely on the hydrogen atoms. This orbital will experience a loss in the bonding interaction between H_a and H_b as the H_a—H_b bond is stretched in the process **4***a* → **4***c*. The loss is, however, compensated for by an increase in the stabilizing interaction between H_b and H_c.

The electron pair of higher energy remains in a Lu—H bonding orbital, 6*a*′. The metal hybrid in 6*a*′ is able to change its nodal characteristics and directionality during the transit **4***a* → **4***c*, from a hybrid (0.58 6*s* − 0.43 $d_{x^2-y^2}$ + 0.43 d_{z^2} + 0.50 d_{yz}) pointing towards H_c in $\mathbf{4}_a$ to a pure d_{yz} orbital in $\mathbf{4}_c$. This is made possible by drawing on the pool of empty orbitals in the 5*d*, 6*s*, and 6*p* shells (7, 8). It should be noted that the stretch of the incoming H_a—H_b bond from 0.77 Å in $\mathbf{4}_a$ to 1.05 Å in $\mathbf{4}_c$ adds 85.7 kJ mol^{-1} to the calculated electronic barrier. This destabilization is only partially compensated for by the stabilizing interactions in 2*a*′ and 6*a*′ of **4***c*, Fig. 2.

The nodal flexibility distinguishes electron-poor early transition metals and *f*-block elements from hydrogen or alkylic carbon atoms. Thus in σ-bond metathesis involving H—H or C—H bonds neither the hydrogen nor the alkylic carbon have any empty orbitals of the same nodal characteristics as d_{yz} in $\mathbf{4}_c$. As a consequence, the electron pair of highest energy will reside in a two-centre nonbonding orbital rather than in the three-centre bonding orbital, 6*a*′, shown to the right in Fig. 2. The lack of stabilization for the upper electron pair in σ-bond metathesis involving H—H or alkylic C—H bonds will result in high barriers for this type of process. In fact, they are [2*s* + 2*s*] symmetry forbidden reactions. Our explanation for the reason that [2_s + 2_s] exchange reactions between H—H and Lu—H bonds are allowed is based on simple molecular orbital arguments. Similar explanations have been put forward by Steigerwald and Goddard (7*a*), Rappé (7*b*), as well as Jolly and Marynick (8).

The transition state structure **4***c* has a single negative force constant. The corresponding normal mode, **5**, represents the reaction coordinate that, as one might expect, primarily constitutes an asymmetric H–H–H stretch.

Using the GVB gradient program, Steigerwald and Goddard (7*a*) obtained a barrier of 17 kcal mol^{-1} (71.1 kJ mol^{-1}) for a similar isomerization process involving scandium rather than lutetium. The Sc—H_a bond distance in the transition state was optimized to be 1.887 Å, i.e., 0.213 Å shorter than the Lu—H_a bond distance calculated in this work. It is an acceptable difference if one takes into account the size of the ionic radii ($R_{Sc^{3+}}$ = 0.89 Å, $R_{Lu^{3+}}$ = 1.00 Å) (39). Goddard calculated the H_a—H_b distance as 1.014 Å and the

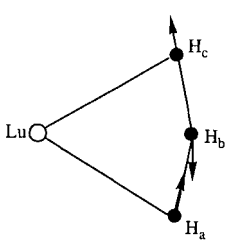

5

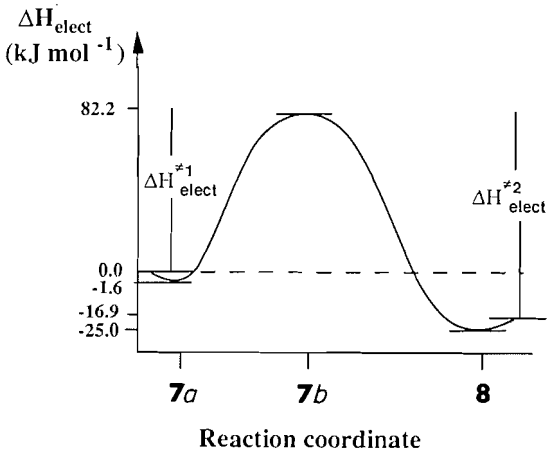

FIG. 3. Profile for the reaction $Cl_2LuCH_3 + H_2 \rightarrow Cl_2LuH + CH_4$. The energies are relative to the reactants.

H_a—Lu—H_c angle as 65°, compared to 1.057 Å and 59° reported here. As for the geometry of the scandium hydride, it was assumed to be planar and optimized as such with the Sc—H bond distance of 1.780 Å.

Transition state structure for the hydrogenolysis reaction:
Cl_2Lu—CH_3 + H_2 → Cl_2Lu—H + CH_4

We have discussed the hydrogen exchange reaction in the previous sections. In the following, we shall examine the related hydrogenolysis reaction of eq. [4*c*]. The results from our theoretical study are summarized in Fig. 3 where we present an energy profile for the process. It can be seen from Fig. 3 that the electronic energy of the products (Cl_2LuH and CH_4) is lower than the corresponding energy of the reactants (Cl_2LuCH_3 and H_2) by 16.9 kJ mol^{-1}. It is in fact observed experimentally (3*a*, 3*c*) that the equilibrium in eq. [4*c*] is shifted to the right. The reaction is further seen to have a substantial electronic barrier, $\Delta H^{\neq 1}_{elect}$, of 82.2 kJ mol^{-1}, Fig. 3.

We have optimized the geometry of the reactant Cl_2LuCH_3. The methyl complex has a structure, **6**, with the methyl group bent out of the Cl_2Lu coordination plane. Interestingly, the crystal structure of the related $Cp^*_2ScCH_3$ complex has a planar geometry (3*b*). We have calculated the barrier of inversion for the lutetium methyl to be 13.7 kJ mol^{-1}. In addition, we note that the methyl group can rotate freely about its C_3 axis.

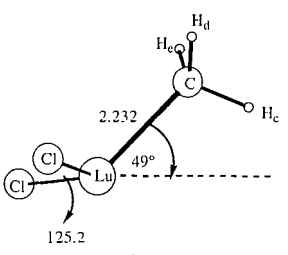

6

The incoming H_2 molecule forms a weak adduct, **7***a*, with Cl_2LuCH_3, **6**, in the early stages of the hydrogenolysis reaction. The adduct is similar to that, $\mathbf{4}_a$, found for the hydrogen exchange process. It has a moderately stretched H_a—H_b bond and the adduct stabilization energy is only 1.6 kJ mol^{-1}.

Can. J. Chem. Downloaded from www.nrcresearchpress.com by 92.62.229.171 on 09/08/12
For personal use only.

The transition state, **7***b*, was optimized without any symmetry constraints. The transition state comprises four centres: Lu, C, H_a, and H_b, arranged in a nearly planar geometry. The structure **7***b* represents an early, reactant-like transition state where the H_a—H_b bond of the dihydrogen is still intact, although stretched from 0.773 to 0.915 Å. On the other hand, the emerging C—H_b bond at 1.723 Å is still much longer than an ordinary aliphatic C—H bond of 1.10 Å. The methyl group in **7***b* can rotate almost freely around its C_3 axis with a relatively modest barrier of 18.2 kJ mol^{-1}.

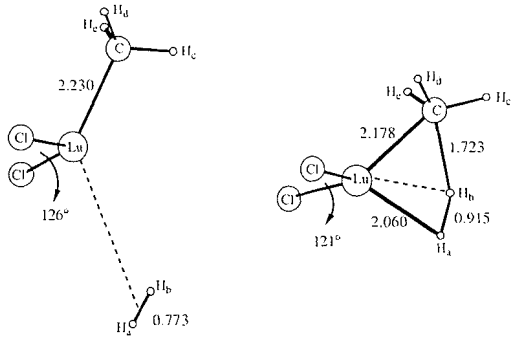

7*a* **7***b*

The product of the hydrogenolysis reaction is a weak methane adduct, **8**. The Lu—H_a bond distance in **8** is comparable to that of free Cl_2LuH and the methane fragment is only slightly distorted compared to that of free CH_4. The total adduct stabilization for **8** is calculated to be 8.2 kJ mol^{-1}.

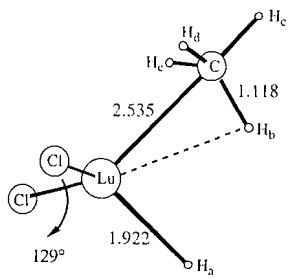

8

There are two substantial contributions to the calculated electronic activation barrier of $\Delta H^{\neq}_{elect}$ = 82.2 kJ mol^{-1}. They come from the energy required to deform the two fragments, H_a–H_b and Cl_2Lu–CH_3, to the shapes they take up in the transition state, **7***b*. The energy needed to stretch a hydrogen molecule to coincide with the H_a–H_b fragment of **7***b* is found to be 49.8 kJ mol^{-1}. Clearly, the H_2 molecule undergoes a smaller degree of stretching than in the case of the hydrogen exchange (85.2 kJ mol^{-1}). The energy required to deform the Cl_2LuCH_3 molecule, **6**, to the geometry taken up by the Cl_2Lu—CH_3 framework in **7***b* is calculated to be 35.6 kJ mol^{-1}. The deformation involves an increase in the angle, α, between the C_3 axis of the methyl group and the Lu—CH_3 bond vector by about 40°, Fig. 4. The deformation shown in Fig. 4 redirects the σ-orbital on CH_3 towards the incoming H_b atom at the expense of losing some of the bonding interaction with the d_{xy} orbital on lutetium.

A schematic correlation diagram for the process **7***a* → **7***b* → **8** is presented in Fig. 5. The diagram in Fig. 5 correlates

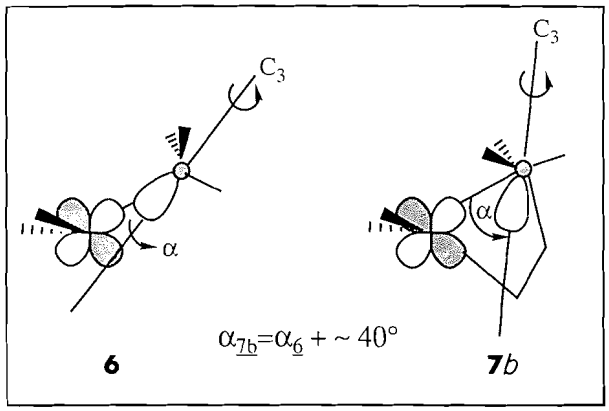

FIG. 4. Deformation of Cl_2LuCH_3 fragment in transition state **7***b*.

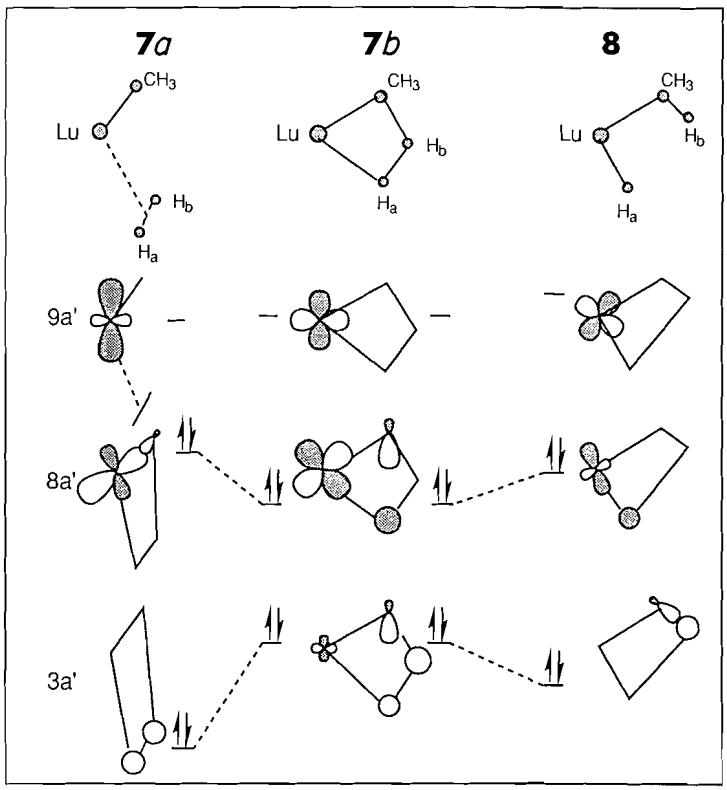

FIG. 5. Correlation diagram for the process $Cl_2LuCH_3(H_2)$ → $Cl_2LuH(CH_4)$. Chlorine and methyl hydrogen atoms are not included.

the two occupied orbitals 3*a*′ and 8*a*′ (HOMO) as well as the 9*a*′ (LUMO) from reactants, **7***a*, to products, **8**. The orbitals 3*a*′ and 8*a*′ hold the two electron pairs involved in bond breaking and bond making during the hydrogenolysis reaction.

The 3*a*′ orbital on the reactants' side represents the H_a—H_b σ-bond of the incoming hydrogen molecule. It correlates smoothly with the C—H_b bond at the product side, **8**, via the virtually ligand-only orbital of the transition state **7***b*. The 3*a*′ orbital is considerably destabilized in the transition state, as the H_a—H_b bond is stretched without any significant bonding interaction between H_b and the methyl carbon. This is in contrast to the previously discussed hydrogen exchange re-

TABLE 1. Contributions to the enthalpies of activation[a] for reactions in eq. [4]

	Hydrogen exchange Eq. [4a][b]	Hydrogenolysis Eq. [4c][c]	Methane exchange Eq. [4b][d]	Methylation Eq. [4d][e]
$\Delta H^{\neq}_{vib}$	2.08	1.57	5.05	5.69
$\Delta H^{\neq}_{rot}$	−2.25	−2.25	−2.48	−2.48
$\Delta H^{\neq}_{trans} + RT$	−6.19	−6.19	−6.19	−6.19
$\Delta H^{\neq}_{elect}$	44.54	82.20	108.60	99.07
$\Delta H^{\neq}_{0}$	10.87	13.69	−7.42	−5.54
$\Delta H^{\neq}_{tot}$	49.04	89.03	97.56	90.55
$\Delta G^{\neq}_{tot}$[f]	81.63	126.01	136.72	130.72

[a]All energies in kJ mol^{-1}, T = 298.15 K.
[b]$Cl_2Lu—H + H_2 \rightarrow Cl_2Lu—H + H_2$.
[c]$Cl_2Lu—CH_3 + H_2 \rightarrow Cl_2Lu—H + CH_4$.
[d]$Cl_2Lu—CH_3 + {}^*CH_4 \rightarrow Cl_2Lu—{}^*CH_3 + CH_4$.
[e]$Cl_2Lu—H + CH_4 \rightarrow Cl_2Lu—CH_3 + H_2$.
[f]$\Delta G^{\circ}_{tot} = \Delta H^{\circ} - T\Delta S^{\circ}$.

Can. J. Chem. Downloaded from www.nrcresearchpress.com by 92.62.229.171 on 09/08/12
For personal use only.

action of eq. [4*a*] where the corresponding 2*a*′ orbital in the transition state **4***c*, see Fig. 2, is characterized by a substantial interaction between H_b and H_c. In that case, the electron pair is residing in a truly three-centre orbital. As already mentioned, it is the lack of a strong three-centre stabilization in 3*a*′ of **7***b* that is primarily responsible for the larger electronic barrier in the hydrogenation reaction compared to the hydrogen exchange process.

The HOMO of the reactant **7***a*, representing the Lu—CH_3 bond, is made up of a $5d_{z^2}/5d_{x^2-y^2}/5d_{xy}/6s$ hybrid on the lutetium centre and σ_{CH_3}. The HOMO of the product **8**, which represents the Lu—H bond, on the other hand comprises another hybrid of different directionality on lutetium, and the 1*s* orbital on the lateral hydrogen atom, H_a. These two HOMOs correlate via the HOMO of the transition state, 8*a*′ (in the middle of Fig. 5).

The presence of several empty orbitals in the 5*d*, 6*s*, and 6*p* shells of lutetium is essential for the change in directionality of the hybrid on the metal. This change is required in order to maintain an optimal overlap with the adjacent ligand orbitals throughout the reaction. As one can easily see from Fig. 5, the $5d_{xy}$ orbital plays an appreciative role in the stabilization of 8*a*′ in the transition state.

Entropies and enthalpies of activation

We have calculated the enthalpies and entropies of activation for the reactions in eqs. [4*a*] and [4*c*]. The kinetic parameters were evaluated in the harmonic oscillator and rigid rotor approximation with the use of standard formulas of statistical mechanics (40). The calculated parameters for the reaction in eqs. [4*a*] and [4*c*] are presented in Tables 1 and 2.

It is clear that $\Delta H^{\neq}$ is dominated by the electronic energy barrier, ΔH_{elect}, of Figs. 1 and 3. The rotational and translational contributions to $\Delta H^{\neq}$ are negative, as one might expect from reactions with a highly ordered transition state, **4***c* and **7***b*. The negative contributions from $\Delta H^{\neq}_{rot}$ and $\Delta H^{\neq}_{trans}$ are simply a consequence of the fact that the reactants have six degrees of translational freedom and five degrees of rotational freedom, whereas the transition states have three of each. It is also consistent with an ordered transition state that the contribution to $\Delta H^{\neq}$ from $\Delta H^{\neq}_{vib}$ is positive. As the transition state is formed from the two reactants, three degrees of translational freedom and two degrees of rotational freedom are transformed into five degrees of vibrational freedom. The additional vibrational degrees of freedom will increase ΔH_{vib} in the transition state.

The vibrational zero-point energy has a positive contribution, $\Delta H^{\neq}_0$, to $\Delta H^{\neq}$. This contribution is given by

$$[7] \qquad \Delta H^{\neq}_0 = \frac{1}{2}\sum_{i=1}^{N(\text{transt.})} hc\omega_i - \frac{1}{2}\sum_{i=1}^{N(\text{reactant.})} hc\omega_i$$

In the two reactions of eqs. [4*a*] and [4*c*] $\Delta H^{\neq}_0$ is positive, Table 2, since

$$[8] \qquad \sum_{i=1}^{N(\text{transt.})} > \sum_{i=1}^{N(\text{reactant.})} \omega_i$$

There are two reasons for this. The first has to do with the fact that the vibrational degrees of freedom in the transition state, N(transt.), exceed the number of vibrational degrees of freedom among the reactants, N(reactant.), by five. The second factor stems from the fact that the weakening of the incoming H_a—H_b bond in the transition states **4***c* and **7***b* is counteracted by the formation of the Lu—H_b bond across the four-centre ring system. We have in addition for **4***c* the formation of an H_c—H_b bond. A transition state for which eq. [8] holds and $\Delta H^{\neq}_0$ is positive could appropriately be termed a bond-making transition state. The total enthalpy of activation at 298.15 K was calculated to be 49.0 kJ mol^{-1}, which is only 4.5 kJ mol^{-1} higher than the calculated electronic barrier, $\Delta H^{\neq}_{elect}$. Thus, the negative contributions from $\Delta H^{\neq}_{rot}$ and $\Delta H^{\neq}_{trans}$ are seen to nearly cancel $\Delta H^{\neq}_{vib}$ and $\Delta H^{\neq}_0$.

The entropies of activation at 298.15 K were calculated to be −109 and −124 J mol^{-1} for the hydrogen exchange and hydrogenolysis reaction respectively. It follows from Table 2 that the negative values for $\Delta S^{\neq}$ are primarily determined by the large negative translational contribution, $\Delta S^{\neq}_{trans}$, and to a lesser extent by the rotational component, $\Delta S^{\neq}_{rot}$. The vibrational term, $\Delta S^{\neq}_{vib}$, is on the other hand positive. The negative values of $\Delta S^{\neq}_{trans}$ and $\Delta S^{\neq}_{rot}$ stem from the decrease in the number of the translational (three) and rotational (two) degrees of freedom of the transition state whereas the posi-

TABLE 2. Contributions to the entropies of activation[a] for reactions in eq. [4]

	Hydrogen exchange Eq. [4a][a]	Hydrogenolysis Eq. [4c][c]	Methane exchange Eq. [4b][d]	Methylation Eq. [4d][e]
$S^{\neq}_{vib}$	20.37	6.21	41.20	35.93
$S^{\neq}_{rot}$	−12.14	−12.88	−29.87	−28.24
S_{trans}	−117.37	−117.27	−142.47	−142.42
$S^{\neq}_{tot}$	−109.04	−123.94	−131.14	−134.73

[a]All entropies in J mol^{-1} K^{-1}, T = 298.15 K.
[b]$Cl_2Lu—H + H_2 \rightarrow Cl_2Lu—H + H_2$.
[c]$Cl_2Lu—CH_3 + H_2 \rightarrow Cl_2Lu—H + CH_4$.
[d]$Cl_2Lu—CH_3 + {}^*CH_4 \rightarrow Cl_2Lu—{}^*CH_3 + CH_4$.
[e]$Cl_2Lu—H + CH_4 \rightarrow Cl_2Lu—CH_3 + H_2$.

tive value of $\Delta S^{\neq}_{vib}$ comes from the increase in the number of the vibrational degrees of freedom (five) in the transition state. The relatively large negative entropy of activation once again underlines the highly ordered nature of the transition state. It should be noted that the methyl group in the hydrogenolysis reaction of eq. [4*c*] maintains its free rotation around the C_3 axis from reactant, **7***a*, to the transition state, **7***b*. Thus this degree of freedom does not contribute to either $\Delta H^{\neq}$ or $\Delta S^{\neq}$.

H—C activation

Transition state structures for the methane exchange reaction: $Cl_2Lu—CH_3 + {}^*CH_4 \rightarrow Cl_2Lu—{}^*CH_3 + CH_4$

The methane exchange process in eq. [4*b*] has been studied experimentally for a number of metal centres, including lutetium (3*c–e*), yttrium (3*c–e*), and scandium (3*a,b*). The pioneering steps in this field were taken by Patricia Watson (3*c*), who discovered the methane exchange reaction of eq. [4*b*]. Her discovery was made during an investigation of the reaction between $Cp^*_2Lu—CH_3$ and benzene. Her studies demonstrated that the reaction in eq. [4*b*] has a rate of approximately 4.6 × 10^{-4} M^{-1} s^{-1} at 343 K in the case of Cp^*_2Lu. The reaction is enhanced by the more electrophilic yttrium (k = 2.6 × 10^{-3} M^{-1} s^{-1} at 343 K) and inhibited in the case of the more nucleophilic scandium (k = 1 × 10^{-5} M^{-1} s^{-1} at 353 K).

The results from our calculations are summarized in the reaction profile in Fig. 6. We have located a methane adduct, **9***a*, at the early stages of the methane reaction. The formation enthalpy for **9***a* was calculated to be 19.4 kJ mol^{-1}, which makes **9***a* less stable then the reactants Cl_2LuCH_3 and CH_4.

The methane exchange reaction has a substantial electronic barrier of 108.6 kJ mol^{-1}, Fig. 6. The associative transition state, **9***b*, is of C_{2v} symmetry. It follows from the optimized transition state structure that the $C_1—H_a$ bond of the incoming methane has been stretched almost to the breaking point with a $C_1—H_a$ bond distance of 1.56 Å. This stretch requires 150.3 kJ mol^{-1} and is thus a major contributor to the sizable electronic barrier of $\Delta H^{\neq}_{elect}$ = 108.6 kJ mol^{-1}. Each of the methyl groups in **9***b* has a tilting angle, α, of 38°, which is quite similar to that of 41° calculated for the methyl group in **7***b*. The tilting angle adopted in **9***b* is a compromise between a value of α ~ 5° for the optimal interaction between lutetium and the two methyl groups and a value of α ~ 55° for the optimal interaction between H_a and

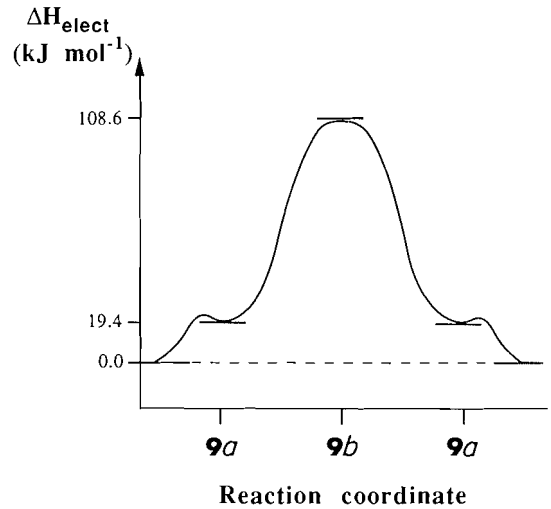

FIG. 6. Profile for the reaction $Cl_2LuCH_3 + {}^*CH_4 \rightarrow Cl_2Lu{}^*CH_3 + CH_4$. The energies are relative to the reactants (products).

the same two methyl groups. This compromise ensures the best simultaneous overlap between the highly directional σ_{CH_3} orbitals on the methyl groups and orbitals on the adjacent lutetium and H_a centres. The price paid for this compromise is a considerable elongation of the Lu—C and C—H_a links in the four-centre transition state, **9***b*. Thus, the Lu—C distance in **9***b* is 0.1 Å longer than the regular Lu—C bond in **6**, whereas the C—H_a distances in **9***b* are nearly 0.4 Å longer than a normal C—H bond. It should also be noted that the two CH_3 groups in **9***b* can rotate freely around their C_3 axis. The central H_a atom has a rather short distance to lutetium of 1.920 Å. The short distance, in conjunction with the spherical nature of the 1*s* orbital on H_a, facilitates a substantial Lu–H interaction in addition to the C—H_a bonds.

Both C—H_a distances are somewhat shorter than the corresponding C—H_b distance of **7***b* (1.723 Å). The $C_1—H_a—C_2$ angle is 167° in **9***b* and differs from the C—$H_b—H_a$ angle of 155° in **7***b* and from the $H_a—H_b—H_c$ angle of 154° in **4***c*. The across-the-ring Lu–H_a distance of 1.92 Å is slightly shorter than the calculated 1.96 Å in **7***b* and the corresponding Lu–H_b separation of 2.03 Å in **4***c*. These trends are facilitated by the wider $C_1—Lu—C_2$ angle of 84° in **9***b* compared to the C—Lu—H_a angle of 75° in **7***b* and the 59° $H_a—Lu—H_c$ angle in **4***c*. A Hückel calculation (5) performed on a comparable transition state with the Cp rings in

Can. J. Chem. Downloaded from www.nrcresearchpress.com by 92.62.229.171 on 09/08/12
For personal use only.

Can. J. Chem. Downloaded from www.nrcresearchpress.com by 92.62.229.171 on 09/08/12
For personal use only.

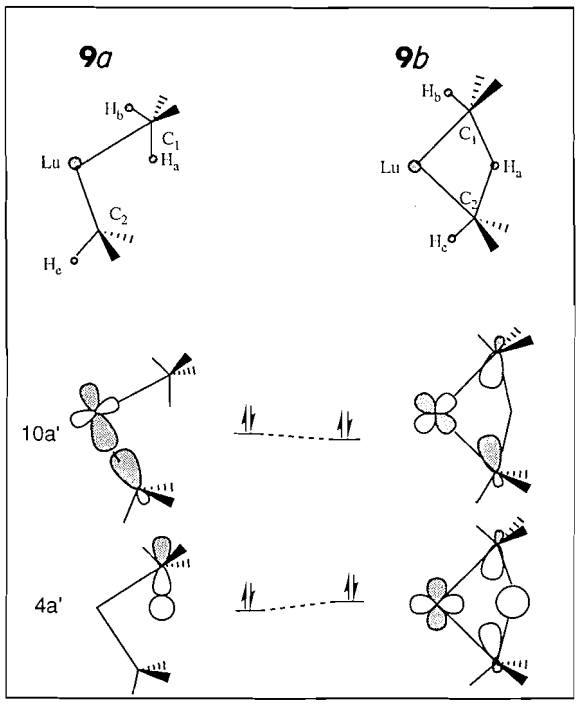

FIG. 7. Correlation diagram for the process $Cl_2Lu—CH_3 + {}^*CH_4 \rightarrow Cl_2LuCH_3({}^*CH_4)$. Chlorine atoms are not included.

place of chlorine atoms revealed a structure quite similar to **9***b*. The tilting angle α between the C_3 axis of each of the equivalent methyl groups and the corresponding Lu—C bond was calculated to be 43.0°. However, the Hückel calculation found a substantially higher electronic barrier, $\Delta H^{\neq}_{elect}$, of about 190 kJ mol^{-1}.

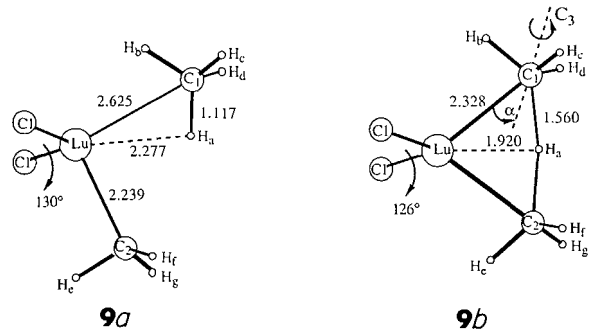

Figure 7 represents a correlation diagram for the passage from **9***a* to **9***b*. The occupied 4*a*′ and 10*a*′ (HOMO) orbitals are shown because of their role in bond breaking and bond formation during the methane exchange reaction. On the reactants' side, the 4*a*′ orbital represents the $C_1—H_a$ σ-bond of the methane molecule. It is composed of σ_{CH_3} on C_1 and the 1*s* orbital on H_a. In the transition state, the 4*a*′ orbital is a three-centre bonding orbital comprising the two σ_{CH_3} hybrids on the methyl groups and the 1*s* orbital on H_a. The orientation of the σ_{CH_3} hybrids is clearly not optimal for the $C_1—H_a—C_2$ interaction. An optimal interaction would have required a tilting angle of α = 55°.

The highest occupied molecular orbital on the reactants' side corresponds to the Lu—C σ-bond of the lutetium methyl molecule. It is made up of a $5d_{xy}/5d_{z^2}/5d_{x^2-y^2}/6s$ hybrid on the metal centre and a σ_{CH_3} orbital on the C_2 atom. It correlates with a three-centre HOMO in the transition state, representing a bonding interaction between the d_{xy} orbital on lutetium and an out-of-phase combination between the σ_{CH_3} orbitals on the two equivalent methyl groups. During the course of the reaction, the metal *d* component in 10*a*′ undergoes a rehybridization, analogous to that seen in the hydrogen exchange or the hydrogenolysis processes. The presence of the empty *d* orbitals, in particular d_{xy} and $d_{x^2-y^2}$, on the metal fragment, makes such a rehybridization possible. We note that the orientation of the σ_{CH_3} lobes is less than optimal for the interaction between σ_{CH_3} and d_{xy}. An optimal interaction would have required a tilting angle of α = 5°.

It follows from our analysis that two main factors contribute to the substantial electronic activation barrier of 108.6 kJ mol^{-1} for the methane exchange reaction. The first is related to the stretch of the $C_1—H_a$ bond in the incoming methane, which amounts to 152 kJ mol^{-1}. The second stems from the inability of the directional σ_{CH_3} orbital to attain at the same time optimal stability in the 4*a*′ and 10*a*′ orbitals of the transition state **9***b* for any orientation of the methyl groups.

Transition state structures for the methylation reaction:

$$Cl_2Lu—H + CH_4 \rightarrow Cl_2Lu—CH_3 + H_2$$

Entropies and enthalpies of activation

We have calculated the contributions to $\Delta H^{\neq}$ and $\Delta S^{\neq}$ for the two C—H activating processes in eqs. [4*b*] and [4*d*]. The results are compared in Tables 1 and 2 to similar calculations involving the two H—H activating processes of eqs. [4*a*] and [4*c*]. It is interesting to note that $\Delta H^{\neq}_0$, from the zero-point correction of eq. [7], is the only contribution to $\Delta H^{\neq}$ that differs qualitatively between the two types of reactions. Thus $\Delta H^{\neq}_0$ is positive for the H—H activating processes and negative for the C—H activating processes, Table 2. Both types of reactions have, as already discussed previously, four-centre transition states encompassing elements of bond making and bond breaking. However, the C—H activating processes involve a transition state in which a C—H bond has been stretched to the breaking point so that:

$$[9] \quad \sum_{i=1}^{N(transt.)} \omega_i < \sum_{i=1}^{N(reactant.)} \omega_i$$

As a consequence, the contribution to $\Delta H^{\neq}$ from the zero point energy, $\Delta H^{\neq}_0$, is negative. The H—H bonds of the incoming hydrogen molecules in the transition states of the H—H activating processes are not stretched to the same extent, with the result that eq. [8] applies and $\Delta H^{\neq}_0$ is positive. One might say, based on the different signs for $\Delta H^{\neq}_0$, that the C—H activating reactions approach the transition state in a process that is net bond breaking whereas the H—H activating reactions approach the transition state in a process that is net bond making.

The entropies of activation at 298.15 K were calculated to be −131.1 and −134.7 J mol^{-1} for the methane exchange and methylation reaction, respectively. Thus $\Delta S^{\neq}$ is somewhat more negative for the C—H activating processes compared to the reactions involving H—H activation, Table 2. The negative activation entropy is largely determined by the loss of three translational degrees of freedom as the incoming H_2 or CH_4 molecules are incorporated into the four-centre transition state. However, the decrease in entropy is

somewhat more pronounced for CH_4 due to its larger mass (40).

Concluding remarks

We have investigated four σ-bond metathesis reactions mediated by the electron-poor lutetium metal centre. The four processes include hydrogen exchange, eq. [4*a*], and hydrogenolysis, in which an H—H bond is activated, as well as methane exchange, eq. [4*b*], and methylation, eq. [4*d*], in which a C—H bond is activated. We find all processes to have a highly ordered transition state with a negative entropy of activation ($\sim$100 J mol^{-1} K^{-1}).

The calculated Gibb's free energy of activation, $\Delta G^{\neq}$ ($=\Delta H^{\neq} - T\Delta S^{\neq}$) increases from 81.6 kJ mol^{-1} for the hydrogen exchange reaction to 126.0 kJ mol^{-1} for the hydrogenolysis process and 136.7 kJ mol^{-1} for the methane exchange reaction, Table 2. This trend is a result of an increasing electronic barrier, which plays a dominating role in the determination of the activation enthalpy. Also, the entropy of activation contributes to this trend by adopting an increasingly negative value. The calculated trends in $\Delta G^{\neq}$ are consistent with the trend observed by Bercaw and coworkers (3) for the organo-scandium species and indicate the following decrease in the reactivity of the R—H bonds with various M—R′ linkages: R = R′ = H >> R = H, R′ = CH_3 > R = R′ = CH_3. The decrease in the reaction rate is related to the different abilities of the 1*s* hydrogen orbital and the σ_{CH_3} methyl orbital to stabilize the four-centre transition state. Thus, the spherical 1*s* hydrogen orbital is better able to overlap fully with orbitals on adjacent centres than the directional σ_{CH_3} orbital. As a consequence, the electronic barrier is seen to increase, Table 2, from the hydrogen exchange reaction towards the hydrogenolysis and methane exchange processes as one or two hydrogens, respectively, are replaced by methyl groups in the four-centre transition state.

The hydrogen exchange process as well as the hydrogenolysis reaction is characterized by a positive zero-point energy correction, $\Delta H_0^{\neq}$, to the total activation, see Table 2. This is understandable since the weakening of the H—H bond in the transition state for the two processes (**4***c* and **7***b*, respectively) is more than compensated for by the formation of strong Lu—H and H—H (**4***c*) bonding interactions. The result is a net bond formation. The methane exchange reaction has, on the other hand, a negative contribution from $\Delta H_0^{\neq}$, Table 2. This can be attributed to the "classical" character of the transition state, **9***b*, for this reaction. Thus, in **9***b* a C—H bond (C_1—H_a) of an incoming methane molecule has been broken, and this bond breaking has not yet been compensated for by the formation of a new C—H bond (C_2—H_a) or a full Lu–C (Lu–C_1) interaction.

Can. J. Chem. Downloaded from www.nrcresearchpress.com by 92.62.229.171 on 09/08/12
For personal use only.

1. G. Kubas. Acc. Chem. Res. **21**, 120 (1988).
2. (*a*) A. H. Janowicz and R. G. Bergman. J. Am. Chem. Soc. **104**, 352 (1982); (*b*) J. K. Hoyano and W. A. G. Graham. J. Am. Chem. Soc. **104**, 3727 (1982); (*c*) W. D. Jones and F. J. Feher. J. Am. Chem. Soc. **106**, 1650 (1984); (*d*) Acc. Chem. Res. **22**, 91 (1989); (*e*) I. P. Rothwell. Acc. Chem. Res. **21**, 153 (1988); (*f*) R. H. Crabtree. Chem. Rev. **85**, 245 (1985); (*g*) J. A. Marthino Simones and J. L. Beauchamp. Chem. Rev. **90**, 629 (1990).
3. (*a*) B. J. Burger, M. E. Thompson, W. D. Cotter, and J. E. Bercaw. J. Am. Chem. Soc. **112**, 1566 (1990); (*b*) M. E. Thompson, S. M. Buxter, A. R. Bulls, B. J. Burger, M. C. Nolan, B. D. Santarsiero, W. P. Schaefer, and J. E. Bercaw. J. Am. Chem. Soc. **109**, 203 (1987); (*c*) P. L. Watson. J. Chem. Soc. Chem. Commun. 276 (1983); (*d*) P. L. Watson and G. W. Parshall. Acc. Chem. Res. **18**, 51 (1985); (*e*) P. L. Watson. J. Am. Chem. Soc. **105**, 6491 (1983); (*f*) G. Jeske, H. Lauke, H. Mauermann, H. Schumann, and T. J. Marks. J. Am. Chem. Soc. **107**, 8111 (1985); (*g*) J. W. Bruno, G. M. Smith, T. J. Marks, C. K. Fair, A. T. Shultz, and J. M. Williams. J. Am. Chem. Soc. **108**, 40 (1986).
4. (*a*) C. S. Christ, Jr., J. R. Eyler, and D. E. Richardson. J. Am. Chem. Soc. **112**, 596 (1990); (*b*) J. Am. Chem. Soc. **110**, 4038 (1988).
5. (*a*) K. Kitaura, S. Obara, and K. Morokuma. J. Am. Chem. Soc. **103**, 2891 (1981); (*b*) S. Obara, K. Kitaura, and K. Morokuma. J. Am. Chem. Soc. **106**, 7482 (1984); (*c*) J. O. Noell and P. J. Hay. J. Am. Chem. Soc. **104**, 4578 (1982); (*d*) J. J. Low and W. A. Goddard III. J. Am. Chem. Soc. **106**, 6928 (1984); (*e*) M. R. A. Blomberg and P. E. M. Siegbahn. J. Chem. Phys. **78**, 986 (1983; (*f*) J. Chem. Phys. **78**, 5682 (1983); (*g*) U. B. Brandemark, M. R. A. Blomberg, L. G. M. Pettersson, and P. E. M. Siegbahn. J. Phys. Chem. **88**, 4617 (1984); (*h*) J. J. Low and W. A. Goddard III. J. Am. Chem. Soc. **106**, 8321 (1984); (*i*) Organometallics, **5**, 609 (1986); (*j*) J. Am. Chem. Soc. **108**, 6115 (1986); (*k*) J-Y. Saillard and R. Hoffmann. J. Am. Chem. Soc. **106**, 2006 (1984).
6. (*a*) P. Hofmann and M. Padmanabhan. Organometallics, **2**, 1273 (1983); (*b*) A. Dedieu. *In* Topics in physical organometallic chemistry. Vol. 1. *Edited by* M. F. Gielen. Freund Publishing House, London. 1989. p. 1; (*c*) T. Ziegler, L. Fan, V. Tschinke, and A. Becke. J. Am. Chem. Soc. **111**, 2018 (1989); (*d*) T. Ziegler, V. Tschinke, and A. Becke. J. Am. Chem. Soc. **109**, 1351 (1987); (*e*) T. Ziegler, C. Wendan, E. J. Baerends, and W. Rawenek. Inorg. Chem. **27**, 3458 (1988).
7. (*a*) M. L. Steigerwald and W. A. Goddard III. J. Am. Chem. Soc. **106**, 308 (1984); (*b*) A. K. Rappé. Organometallics, **9**, 466 (1990); (*c*) H. Rabaâ, J.-Y. Saillard, and R. Hoffmann. J. Am. Chem. Soc. **108**, 4327 (1986); (*d*) E. Folga, T. Ziegler, and L. Fan. Nouv. J. Chim. **15**, 741 (1991).
8. C. A. Jolly and D. S. Marynick. J. Am. Chem. Soc. **111**, 7968 (1989).
9. L. Versluis and T. Ziegler. Organometallics, **9**, 2985 (1990).
10. (*a*) R. G. Parr and W. Yang. *In* Density functional theory of atoms and molecules. Oxford University Press, New York. 1989; (*b*) E. S. Kryachko and E. V. Ludena. *In* Density functional theory of many electron systems. Kluwer Press, Dordrecht. In press; (*c*) T. Ziegler. Chem. Rev. **91**, 651 (1991).
11. A. D. Becke. Int. J. Quantum Chem. **S23**, 599 (1989).
12. T. Ziegler, V. Tschinke, E. J. Baerends, and W. Ravenek. Polyhedron, **7**, 1625 (1988).
13. L. Versluis and T. Ziegler. J. Chem. Phys. **88**, 322 (1988).
14. R. Fournier, J. Andzelm, and D. R. Salahub. J. Chem. Phys. **90**, 6371 (1989).
15. L. Fan, L. Versluis, T. Ziegler, E. J. Baerends, and W. Ravenek. Int. J. Quantum Chem. **S22**, 173 (1988).
16. (*a*) W. Bieger, G. Seifert, H. Eschrig, and G. Grossman. Chem. Phys. Lett. **115**, 275 (1985); (*b*) D. A. Freier, R. F. Fenske, and Y. Xiao-Zeng. J. Chem. Phys. **83**, 3526 (1985); (*c*) V. G. Malkin and Z. Zhidomirov. Zh. Strukt. Khim. **29**, 32 (1988).
17. A. J. Van der Est, P. B. Barker, E. E. Burnell, C. E. de Lange, and J. G. Snijders. Mol. Phys. **56**, 1 (1985).
18. D. A. Case. Annu. Rev. Phys. Chem. **33**, 151 (1982).
19. (*a*) L. Noodleman and J. G. Norman. J. Chem. Phys. **70**, 4903 (1979); (*b*) L. Noodleman. J. Chem. Phys. **74**, 5737 (1981); (*c*) L. Noodleman and E. J. Baerends. J. Am. Chem. Soc. **106**, 2316 (1984); (*d*) L. Noodleman, J. G. Norman, J. H. Osborne, A. Aizman, and D. A. Case. J. Am. Chem. Soc. **107**, 3418 (1985).

20. L. Fan and T. Ziegler. J. Chem. Phys. **92**, 3645 (1990).
21. M. Trsic, T. Ziegler, and W. G. Laidlaw. Chem. Phys. **15**, 383 (1976).
22. M. Cook and M. Karplus. J. Phys. Chem. **91**, 31 (1987).
23. V. Tschinke and T. Ziegler. J. Chem. Phys. **93**, 8051 (1990).
24. E. J. Baerends, D. E. Ellis, and P. Ros. Chem. Phys. **2**, 41 (1973).
25. (*a*) E. J. Baerends. Ph.D. Thesis, Vrije Universiteit, Amsterdam. 1975; (*b*) W. Ravenek. *In* Algorithms and applications on vector and parallel computers. *Edited by* H. J. J. te Riele, Th. J. Dekker, and H. A. van de Vorst. Elsevier, Amsterdam. 1987.
26. A. D. Becke. J. Chem. Phys. **88**, 2547 (1988).
27. J. Simons, P. Jorgensen, H. Taylor, and J. Ozment. J. Phys. Chem. **87**, 2745 (1983).
28. J. Baker. J. Comput. Chem. **7**, 385 (1986).
29. (*a*) J. G. Snijders, E. J. Baerends, and P. Vernooijs. *In* At. Data Nucl. Data Tables, **26**, 483 (1982); (*b*) P. Vernooijs, J. G. Snijders, and E. J. Baerends. *In* Slater type basis functions for the whole periodic system. Internal Report, Free University of Amsterdam, The Netherlands. 1981.
30. J. Krijn and E. J. Baerends. *In* Fit functions in the HFS-method. Internal Report (*in Dutch*), Free University of Amsterdam, The Netherlands. 1984.
31. J. G. Snijders, E. J. Baerends, and P. Ros. Mol. Phys. **38**, 1909 (1979).
32. T. Ziegler, V. Tschinke, E. J. Baerends, J. G. Snijders, and W. Ravenek. J. Phys. Chem. **93**, 3050 (1989).
33. (*a*) H. Stoll, E. Golka, and H. Preuss. Theor. Chim. Acta, **55**, 2 (1980); (*b*) A. D. Becke. Phys. Rev. A, **38**, 2398 (1988).
34. T. Ziegler, V. Tschinke, and C. Ursenbach. J. Am. Chem. Soc. **109**, 4825 (1987).
35. T. Ziegler, V. Tschinke, and A. Becke. Polyhedron, **6**, 685 (1987).
36. T. Ziegler and V. Tschinke. *In* Density functional methods in chemistry. *Edited by* J. K. Labanowski and J. W. Andzelm. Springer, Heidelberg. 1991. p. 139.
37. (*a*) L. Versluis and T. Ziegler. Inorg. Chem. **29**, 5340 (1990); (*b*) J. Harrod, T. Ziegler, and V. Tschinke. Organometallics, **9**, 89 (1990); (*c*) T. Ziegler, L. Fan, V. Tschinke, and A. Becke. J. Am. Chem. Soc. **111**, 2018 (1989); (*d*) J. Ball, M. Boormann, and T. Ziegler. J. Chem. Soc. Chem. Commun. 722 (1989); (*e*) T. Chivers, K. S. Dhathathreyan, and T. Ziegler. J. Chem. Soc. Chem. Commun. 86 (1989); (*f*) A. P. S. Masters, T. S. Sorensen, and T. Ziegler. Organometallics, **8**, 1088 (1989); (*g*) L. Versluis and T. Ziegler. J. Am. Chem. Soc. **112**, 6763 (1990).
38. (*a*) T. Ziegler. J. Pure Appl. Chem. **63**, 873 (1991); (*b*) T. Ziegler and L. Versluis. Adv. Chem. Res. In press; (*c*) T. Ziegler and V. Tschinke. ACS Symp. Ser. **428**, 277 (1990); (*d*) T. Ziegler, J. G. Snijders, and E. J. Baerends. ACS Symp. Ser. **383**, 322 (1989); (*e*) T. Ziegler, V. Tschinke, and L. Versluis. NATO ASI Ser. Ser. C: **176**, 189 (1986).
39. T. J. Marks and R. D. Ernst. *In* Comprehensive organometallic chemistry. *Edited by* G. Wilkinson, F. G. A. Stone, and E. W. Abel. Pergamon Press, Oxford. 1982. Chap. 21.2.1.
40. D. A. McQuarrie. *In* Statistical thermodynamics. Harper & Row, New York. 1973.

Can. J. Chem. Downloaded from www.nrcresearchpress.com by 92.62.229.171 on 09/08/12
For personal use only.

On the allowed symmetries of all distorted forms of conformers, molecules, and transition structures

PAUL G. MEZEY

Department of Chemistry and Department of Mathematics, University of Saskatchewan, Saskatoon, Sask., Canada S7N 0W0

Received June 17, 1991

This paper is dedicated to Professor Sigeru Huzinaga on the occasion of his 65th birthday

PAUL G. MEZEY. Can. J. Chem. **70**, 343 (1992).

Based on the catchment region point symmetry theorem, a general framework and some new results are presented on symmetry constraints of deformations preserving chemical identity. The point symmetries of the unique critical point (equilibrium) nuclear arrangement corresponding to a conformer, molecule, or a transition structure and those of a family of nuclear arrangements with an arbitrarily small limit on the allowed distortions provide a complete symmetry characterization of the entire potential surface catchment region of the chemical species. Consequently, the point symmetries of all distorted molecular forms that preserve chemical identity can be deduced by testing symmetry conditions only within an arbitrarily small domain of the potential surface, in the vicinity of the equilibrium arrangement. Additional constraints are deduced on the point symmetries of transition structures obtained directly from the given conformer.

Key words: molecular distortions, symmetry, catchment regions, new symmetry theorems, framework groups, point groups.

PAUL G. MEZEY. Can. J. Chem. **70**, 343 (1992).

En se basant sur le théorème de la symétrie du point dans la région de captation, on présente un cadre général et quelques nouveaux résultats relatifs à la symétrie des contraintes de déformation qui préservent l'identité chimique. Les symétries de point du point critique unique (équilibre) de l'arrangement nucléaire correspondant à un conformère, la molécule ou la structure de transition et celles d'une famille d'arrangements nucléaires, avec une faible tolérance arbitraire pour les distorsions permises, fournissent une caractérisation complète de la symétrie de toute la surface de potentiel de la région de captation des espèces chimiques. En vérifiant les conditions de symétrie uniquement à l'intérieur du faible domaine arbitraire de la surface de potentiel au voisinage de l'arrangement à l'équilibre, on peut alors déduire les symétries de point de toutes les formes moléculaires déformées qui préservent l'identité chimique. On déduit des contraintes additionnelles sur les symétries de point des structures de transition obtenues directement a` partir du conformère donné.

Mots clés : distorsions moléculaires, symétrie, régions de captation, nouveaux théorèmes de la symétrie, cadre général, groupes de point.

[Traduit par la rédaction]

Can. J. Chem. Downloaded from www.nrcresearchpress.com by 92.62.229.171 on 09/08/12
For personal use only.

Introduction

Point symmetries of equilibrium nuclear arrangements, of stable configurations and transition structures, have been recognized as important tools for the analysis of molecular properties and reaction processes (e.g., refs. 1–9). Whereas the early studies focussed on individual nuclear configurations or on specific reaction paths, in a recent study some new results have been derived using a global approach and a symmetry domain partitioning of the nuclear configuration space (10). In this note we shall extend this approach in order to derive some new results on the available symmetries of distorted nuclear configurations that preserve the chemical identity of the molecular species.

The range and type of distortions that preserve the chemical identity of molecular conformations, individual molecules, or transition structures are dependent on the potential energy hypersurface belonging to the given stoichiometry (and to the given electronic state, usually the electronic ground state). Even small distortions may lead to changes in conformational classification, and if the disortions are large enough then a molecule cannot preserve its identity; a chemical reaction occurs. Some of these distortions may preserve the point symmetry of nuclear configurations while some others do not, and, in fact, these distortions may lead to major symmetry changes. However, not all point symmetries are available for each chemical species of the given stoichiometry, even if the given stoichiometric family of nuclei does have possible arrangements with these symmetries. For example, any planar arrangement of an NH_3 system (of no coincident nuclei) belongs to the transition structure catchment region of the pyramidal inversion process of ammonia, or to the catchment region of another non-ammonia species, and no planar symmetry may occur within the family of distorted ammonia configurations that preserve chemical identity. Fortunately, the deformations leading to specified symmetry changes and those leading to chemical identity changes are interrelated. These interrelations can be studied by taking a global configuration space approach (11). A recent result on the global symmetry analysis of nuclear configuration spaces is the *catchment region point symmetry theorem* (10): *within each catchment region the critical point nuclear configuration has the highest point symmetry*. In addition, point symmetry groups occurring within a catchment region of a stable conformer or a molecule have an algebraic structure: they form an algebraic lattice (12). Although this result provides some constraints on the point symmetry groups, by itself it is insufficient to decide which actual point symmetry groups are available for distorted configurations. Based on these results, we shall provide here a general framework and a new rule for the study of symmetries of chemical identity preserving deformations.

We shall use the terminology and basic concepts re-

Can. J. Chem. Downloaded from www.nrcresearchpress.com by 92.62.229.171 on 09/08/12
For personal use only.

viewed recently in ref. 10; further background and more detail on the global properties of potential energy hypersurfaces may be found in ref. 11. Here only a brief summary of the background will be given.

A *stoichiometric family* of chemical species is defined by specifying N nuclei as well as an overall charge and electronic state. The stoichiometric family includes all conformers and isomers of all stable molecules, transition structures, reaction intermediates, decomposition products, as well as all their distorted conformations that have the given overall atomic composition. All possible internal (relative) nuclear arrangements (nuclear configurations) for $N \geq 3$ nuclei can be described by $3N - 6$ internal coordinates; the collection of all possible nuclear arrangements forms a $(3N - 6)$-dimensional *nuclear configuration space*. This space may be chosen as a *metric* space M with a global metric (11), that is, with a global distance function, where the distance between any two points K and K' of M is a measure of dissimilarity between the corresponding two nuclear configurations. For a given electronic state a potential energy value can be assigned to each configuration K; this assignment generates a *potential energy hypersurface* $E(K)$ over M. At each *critical point* of a potential energy surface the energy gradient vanishes. The second energy derivatives are the elements of the *Hessian matrix* of the critical point. For an ordinary (non-degenerate) energy minimum, all eigenvalues of the Hessian matrix are positive; for a simple saddle point of a transition structure, precisely one eigenvalue is negative. The *index* λ of the critical point $K(\lambda,i)$ is the number of negative eigenvalues of the Hessian matrix $H(K(\lambda,i))$ and i is a serial index. If the local internal coordinates are derived from the *mass-weighted Cartesian coordinates* of the nuclei, then a *steepest descent path* represents a formal, infinitely slow relaxation of nuclear configurations. A *catchment region* is a subset of M, representing the range of deformations that preserve chemical identity of a chemical species of a given electronic state. By an equivalent definition, a catchment region $C(\lambda,i)$ of a potential energy hypersurface is that subset of nuclear configurations from where the relaxation paths lead to a common critical point $K(\lambda,i)$ of the potential energy hypersurface. The catchment region $C(0,i)$ of the minimum point $K(0,i)$ represents the ith stable molecular species (conformer or molecule) of the given stoichiometry and the electronic state of the given potential energy hypersurface $E(K)$; the steepest descent paths from all points K of the catchment region $C(0,i)$ lead to the minimum point $K(0,i)$. The dimension of $C(0,i)$ is (almost always) $3N - 6$. A transition structure is (almost always) represented by a $(3N - 7)$-dimensional catchment region $C(1,j)$ of a saddle point $K(1,j)$ of critical point index $\lambda = 1$. For sake of simplicity in the terminology, the less important catchment regions of higher critical point indices are also referred to as formal chemical species.

We shall use the following terminology: an n-dimensional hypersurface C_n within a nuclear configuration space M is a *relaxed cross section* of M with respect to a given potential energy hypersurface $E(K)$ if at every point K of C_n the energy gradient is tangential to C_n (10). (Note that alternative definitions are also known; however, as it has been pointed out in ref. 10, these alternative definitions do not always satisfy some coordinate-invariance requirements.) Relaxed cross sections are of importance in potential surface analysis; for example, a typical catchment region of a transition structure is a $(3N - 7)$-dimensional subset of a relaxed cross section C_n of M, with $n = (3N - 7)$. Since neither steepest descent nor steepest ascent paths may leave such a hypersurface C_n, relaxed cross sections have many properties analogous to properties of the complete nuclear configuration space M, even if the dimension n is much lower than the dimension $3N - 6$ of M. In particular, the following catchment region point symmetry theorem is equally applicable within the configuration space M and within its relaxed cross sections C_n (10):

Within each catchment region $C(\lambda,i)$*, the nuclear configuration corresponding to the critical point* $K(\lambda,i)$ *has the highest point symmetry (a proof is given in ref. 10).*

The expression "highest point symmetry" refers to group–subgroup relations: within a catchment region $C(\lambda,i)$, the point symmetry group of the critical point $K(\lambda,i)$ contains as subgroups all other point symmetry groups occurring in $C(\lambda,i)$, where each point symmetry group is considered to be one of its own subgroups. The critical point $K(\lambda,i)$ is not necessarily the only point within the catchment region $C(\lambda,i)$ that has the highest point symmetry. For example, all points of the catchment region $C(\lambda,i)$ may have the same (and by default, the highest) point symmetry.

The simplest proof of this result is based on an earlier result of Pechukas (6): if mass-weighted coordinates are used, then all point symmetry (and all framework group) elements of nuclear configurations are preserved along segments of steepest descent paths between critical point. By limit arguments, the group element occurring along the path must also be present at the critical point at the end of the path, and additional elements may appear only at the critical points.

The catchment region point symmetry theorem provides a link between the point symmetry of the nuclear arrangement (a purely geometrical property) and molecular stability (an energy-dependent property). The theorem is applicable for the potential energy surfaces and catchment regions of all electronic states of all neutral and ionic species of the given stoichiometric family (10).

In what follows below, we shall apply a similar approach for deriving symmetry conditions on all chemical identity preserving deformations of molecules, testing only an arbitrarily small neighborhood of the critical points of catchment regions.

A symmetry theorem on neighborhoods of critical points

We shall consider a small limit r for distortions of an equilibrium nuclear configuration $K(\lambda,i)$. This limit r is given in terms of the configuration space distance function (metric) $d(K,K')$, expressing the dissimilarity of two nuclear configurations K and K'.

Take an n-dimensional catchment region $C(\lambda,i)$ of the nuclear configuration space M, where $n = 3N - 6 - \lambda$, the typical case. (Note that for a minimum point $K(\lambda,i)$ the index $\lambda = 0$ and the dimension of the corresponding catchment region $C(\lambda,i)$ is usually $n = 3N - 6$, whereas for saddle points of transition structures the typical case corresponds to $\lambda = 1$ and $n = 3N - 7$.) The catchment region $C(\lambda,i)$ is a subset of an n-dimensional relaxed cross section C_n of the nuclear configuration space M. Consider a radius $r > 0$, and the n-dimensional ball $B(C(\lambda,i), r)$ containing all those points K of the relaxed cross section C_n that are at distance r or less from the critical point $K(\lambda,i)$,

$$[1] \quad B(C(\lambda,i), r) = \{K : K \in C_n, d(K(\lambda,i), K) \leq r\}$$

The $(n - 1)$-dimensional boundary sphere of this ball $B(C(\lambda,i), r)$ is denoted by $S(C(\lambda,i), r)$,

[2] $S(C(\lambda,i), r) = \{K : K \in C_n, d(K(\lambda,i), K) = r\}$

If this radius r is a small enough positive value then the ball $B(C(\lambda,i), r)$ and, hence, its boundary sphere $S(C(\lambda,i), r)$ fall within the catchment region $C(\lambda,i)$:

[3] $B(C(\lambda,i), r) \subset C(\lambda,i)$

and

[4] $S(C(\lambda,i), r) \subset C(\lambda,i)$

Choose any configuration K from catchment region $C(\lambda,i)$, different from the critical point $K(\lambda,i)$,

[5] $K \in C(\lambda,i)$

[6] $K \neq K(\lambda,i)$

If K is not within $B(C(\lambda,i), r)$, that is, if

[7] $K \in C(\lambda,i) \backslash B(C(\lambda,i), r)$

then the steepest descent path from K must pass through $S(C(\lambda,i), r)$ at some point K' as it leads to $K(\lambda,i)$. Note that $C(\lambda,i)$ and $B(C(\lambda,i), r)$ are within the same relaxed cross section C_n of the nuclear configuration space M. Consequently, a path of steepest descent from K must stay within C_n, and hence it cannot avoid passing through the sphere $S(C(\lambda,i), r)$. Also note that, due to condition [4] and to the positivity of r, point K' of the boundary sphere $S(C(\lambda,i), r)$ cannot be a critical point. Consequently, by the preservation of point symmetry elements along steepest descent paths, sphere $S(C(\lambda,i), r)$ must have a point K' with precisely the same point symmetry elements as K.

Alternatively, if K is within $B(C(\lambda,i), r)$,

[8] $K \in B(C(\lambda,i), r)$

then the steepest ascent path from K must contain a point K' common with sphere $S(C(\lambda,i), r)$. Consequently, by the preservation of point symmetry elements along steepest ascent paths, sphere $S(C(\lambda,i), r)$ must have a point K' with precisely the same point symmetry elements as K. This proves the following theorem.

Theorem 1

Each point symmetry group $g(K)$ present for any distorted nuclear configuration K of a $(3N - 6 - \lambda)$-dimensional catchment region $C(\lambda,i)$ is also present at some configuration K' on a $(3N - 6 - \lambda - 1)$-dimensional sphere $S(C(\lambda,i), r)$ of center $K(\lambda,i)$ and of an arbitrarily small positive radius r, where r is small enough so that $S(C(\lambda,i), r)$ falls within the catchment region $C(\lambda,i)$.

Comment 1: Distortions are considered with reference to the equilibrium (critical point) nuclear configuration $K(\lambda,i)$, which is not regarded distorted. Of course, the point symmetry group $g(K(\lambda,i))$ (the group of highest symmetry within $C(\lambda,i)$) does not have to occur along the sphere $S(C(\lambda,i), r)$, but it does occur if for some other point K, $g(K) = g(K(\lambda,i))$ holds.

Comment 2: It is computationally much simpler to find a critical point on a potential surface than to find the boundaries of its catchment region. The above theorem allows one to obtain information on the extent of a catchment region by finding out all point symmetry groups that occur within the catchment region. This can be accomplished by testing the point symmetries only along a small sphere of distorted configurations around the critical point.

Comment 3: The above theorem provides more information than the catchment region point symmetry theorem. By knowing the point symmetry group $g(K(\lambda,i))$, and knowing that it is the largest point symmetry group within the catchment region $C(\lambda,i)$, there is often ambiguity concerning the actual point symmetry groups occurring within $C(\lambda,i)$. Note that it is not necessary for a catchment region to contain configurations having point symmetries corresponding to each subgroup of $g(K(\lambda,i))$. The same group $g(K(\lambda,i))$ may be obtained as a result of combining a different collection of its subgroups. A trivial example is the case where all configurations K of $C(\lambda,i)$ have the same point symmetry group $g(K(\lambda,i))$ and no configuration K of $C(\lambda,i)$ has any one of the nontrivial subgroups g of $g(K(\lambda,i))$ as its point symmetry group.

Spherical maps of point symmetries of catchment regions and their boundaries

We shall use the above theorem to compare point symmetry groups of a catchment region $C(\lambda,i)$ with those occurring on its boundary $B(\lambda,i)$. We have seen above that the point symmetry group $g(K)$ of any (non-critical) point K of a catchment region $C(\lambda,i)$ is present at some point K' of a small sphere $S(C(\lambda,i), r)$ around the critical point $K(\lambda,i)$. This generates a symmetry-preserving $K \rightarrow K'$ assignment of all points of $C(\lambda,i) \backslash K(\lambda,i)$ to points of the sphere $S(C(\lambda,i), r)$.

Let us denote by G_i the collection of all those points K' of the sphere $S(C(\lambda,i), r)$ where the three-dimensional point symmetry group of nuclear configurations is g_i:

[9] $G_i = \{K' : K' \in S(C(\lambda,i), r), g(K') = g_i\}$

Each set G_i may be disconnected and we shall consider their maximum connected components G_{ik}.

These sets G_{ik} provide a symmetry-domain partitioning of the sphere $S(C(\lambda,i), r)$ that reflects all possible point symmetries of distorted configurations of $C(\lambda,i)$. The pattern and neighbor relations of these symmetry domains G_{ik} on the sphere $S(C(\lambda,i), r)$ provide a detailed symmetry characterization of the catchment region.

Consider now another map on the sphere $S(C(\lambda,i), r)$ that describes the point symmetry groups occurring along the boundary $B(\lambda,i)$ of the catchment region $C(\lambda,i)$. If the catchment region $C(\lambda,i)$ is that of an energy minimum, $\lambda = 0$, then most of the nuclear configurations along the boundary $B(\lambda,i)$ are those of transition structure catchment regions. Hence, the results we shall describe below are of relevance to transition structures, which are the easiest to visualize in the two-dimensional case. However, we shall not rely on (often misleading) visualization and the derivation will be general for the multidimensional case of any catchment region $C(\lambda,i)$ of arbitrary index λ.

The $(3N - 6 - \lambda - 1)$-dimensional boundary $B(\lambda,i)$ divides the relaxed cross section C_n into two subsets: to the catchment region $C(\lambda,i)$ and the remainder $C_n \backslash C(\lambda,i)$ of the cross section C_n (we regard $B(\lambda,i)$ as a part of this second subset).

Each point K of the boundary $B(\lambda,i)$ has some point symmetry $g(K)$. In addition, to each point K of $B(\lambda,i)$ we assign a point symmetry $g'(K)$, which is one of point symmetries occurring within the catchment region $C(\lambda,i)$. To generate this assignment, we first note that the boundary surface $B(\lambda,i)$ is topologically equivalent to a $(3N - 6 - \lambda - 1)$-dimen-

Can. J. Chem. Downloaded from www.nrcresearchpress.com by 92.62.229.171 on 09/08/12
For personal use only.

sional smooth surface $S(\lambda,i,w)$ placed within $C(\lambda,i)$, where the homeomorphism

$$[10] \quad h(K) = K'', K \in B(\lambda,i), K'' \in S(\lambda,i,w)$$

establishing the topological equivalence between $B(\lambda,i)$ and $S(\lambda,i,w)$ is chosen so that

$$[11] \quad d(K,K'') < w$$

for some small positive value w. As $w \to 0$, $K'' \to K$ follows. By limit arguments, for an infinitesimal w, all the point symmetry elements of K'' must also be present for configuration K at the boundary $B(\lambda,i)$:

$$[12] \quad g(K'') \subset g(K)$$

However, K is not on any steepest descent path leading to the critical point $K(\lambda,i)$ of the catchment region $C(\lambda,i)$; consequently, the group $g(K)$ at point K may have some additional point symmetry elements besides those present in $g(K'')$. Hence the two groups, $g(K)$ and $g'(K) = g(K'')$ are not necessarily the same.

By the composition of the above $K \to K''$ assignment and the $K'' \to K'$ assignment generated by the paths of steepest descent from each point K'' of the $S(\lambda,i,w)$ surface to a point K' on the sphere $S(C(\lambda,i), r)$, one obtains a $K \to K'$ assignment of the boundary points K of $B(\lambda,i)$ to points K' on the sphere $S(C(\lambda,i), r)$. Take now the point symmetry $g(K)$ and assign it to the corresponding point K' on the sphere $S(C(\lambda,i), r)$. This assignment is denoted by

$$[13] \quad g_a(K') = g(K)$$

generating a new point symmetry map on sphere $S(C(\lambda,i), r)$.

The range of the $K \to K'$ assignment is denoted by $S'(C(\lambda,i), r)$. If the boundary surface $B(\lambda,i)$ is closed, then the $K \to K'$ assignment is onto $S'(C(\lambda,i), r) = S(C(\lambda,i), r)$, hence the new symmetry map of the $g_a(K')$ point symmetry groups covers the entire sphere $S(C(\lambda,i), r)$. Otherwise we obtain a new symmetry map only on a subset $S'(C(\lambda,i), r)$ of the sphere $S(C(\lambda,i), r)$, $S'(C(\lambda,i), r) \neq S(C(\lambda,i), r)$. This map represents the $g(K)$ point symmetry group distribution along the boundary $B(\lambda,i)$ of catchment region $C(\lambda,i)$.

Let us denote by G'_i the collection of all those points K' of the sphere $S(C(\lambda,i), r)$ where the assigned three-dimensional point symmetry group $g_a(K')$ is g'_i:

$$[14] \quad G'_i = \{K': K' \in S(C(\lambda,i), r), g_a(K') = g_i\}$$

As in the case of the previous partitioning, each set G'_i may be disconnected and we shall consider their maximum connected components G'_{ik}.

The symmetry domains G'_{ik} generate a partitioning of the sphere $S(C(\lambda,i), r)$ reflecting all the point symmetries of configurations along the boundary $B(\lambda,i)$ of catchment region $C(\lambda,i)$. *These are the configurations that are distorted to a critical extent, sufficient to change their chemical identity,* as compared to the chemical species represented by the catchment region $C(\lambda,i)$. The pattern and neighbor relations of the symmetry domains G'_{ik} on the sphere $S(C(\lambda,i), r)$ provide a detailed symmetry characterization of the boundary $B(\lambda,i)$ of the catchment region $C(\lambda,i)$.

The two maps on sphere $S(C(\lambda,i), r)$ are not independent. By taking into account the range of assignment $K \to K'$, a simple substitution of eq. [13] into relation [12] proves the following theorem.

Theorem 2

For any point $K' \in S'(C(\lambda,i), r)$, the actual point symmetry group $g(K')$ is a subgroup of the corresponding boundary point symmetry group $g_a(K')$:

$$[15] \quad g(K') \subset g_a(K'), \qquad K' \in S'(C(\lambda,i), r)$$

Comment 1: This result can be rephrased as follows. Consider the pattern of point symmetry group distribution along the boundary $B(\lambda,i)$ of a catchment region $C(\lambda,i)$, and the pattern of point symmetry groups along a sphere around the critical point $K(\lambda,i)$. These patterns can be interrelated so that the boundary pattern is "superior" to the pattern present along the sphere, where term "superior" indicates a pointwise group/subgroup relation.

Comment 2: Combining this result with the catchment region point symmetry theorem leads to an interesting observation. Ordinary points K' of a catchment region $C(\lambda,i)$ are "symmetry-dominated from both inside and outside" of the catchment region: both the critical point $K(\lambda,i)$ (dominance from the "inside") and the corresponding boundary point K (dominance from the "outside") have point symmetry groups that are never proper subgroups, but are possibly supergroups of the point symmetry group of K':

$$[16] \quad g(K(\lambda,i)) \supset g(K') \subset g(K)$$

Symmetry-wise, ordinary points K' of a catchment region are "squeezed" in between the critical point $K(\lambda,i)$ and the boundary $B(\lambda,i)$ of the catchment region $C(\lambda,i)$.

Two generalizations

For each symmetry operator R of a nuclear configuration K, one may assign a permutation operator P by the following rule: the rearrangement of identical nuclei caused by the symmetry operator R is undone by the permutation P of identical nuclei. For two different nuclear configurations, K_1 and K_2 of the same set of nuclei, both having a given symmetry operator R, the assigned permutation operators P_1 and P_2 may be different. That is, the point symmetry operator R does not determine the permutation operator P in general. For each configuration K the pairs (R,P) of associated operators form a group, often referred to as the framework group of configuration K. Framework groups provide more information than point symmetry groups.

As a consequence of framework group invariance along noncritical segments of steepest descent paths (6) and the catchment region framework group theorem (10), all results of this study remain valid if one replaces point symmetry groups and their elements with framework groups and their elements, respectively. This generalizes the two theorems of this study to framework groups and their maps.

Another generalization is provided by noting that point symmetry and framework group conservation are equally valid along steepest descent and steepest ascent paths. Hence the results derived in this study are also valid for the "upside down" energy hypersurface $-E(K)$. Note that the catchment regions of $E(K)$ and the formal catchment regions of $-E(K)$ are in general different, hence applying the theorems to $-E(K)$ does provide new information.

Can. J. Chem. Downloaded from www.nrcresearchpress.com by 92.62.229.171 on 09/08/12
For personal use only.

Conclusions

All the point symmetries available to the distorted nuclear configurations of a conformer, molecule, or transition structure can be accounted for by considering a small family of nuclear configurations along a sphere of arbitrarily small positive radius, centered on the equilibrium configuration of the species. The distortions are restricted to those preserving the chemical identity of the species, that is, to configurations within a catchment region. Distances (expressing dissimilarity of configurations), radii, and the corresponding spheres are taken within a metric configuration space M. By testing point symmetries within a small sphere around the equilibrium configuration, these results allow one to calculate and account for all possible symmetries actually present within the entire catchment region even if the extent and shape of the catchment region is not known. The pattern of point symmetry group distribution along the sphere shows an interesting relation with the pattern of point symmetry groups along the boundary of the catchment region, that is, along the hypersurface of configurations representing borderline distortions with respect to the preservation of chemical identity. An assignment between configurations of the sphere and those of the boundary surface implies a "symmetry dominance" of the ordinary interior configurations of the catchment region by the boundary configurations. Hence, ordinary configurations are symmetry-dominated both from the "inside," by the critical point, and from the "outside," by the boundary of the catchment region.

Analogous results are valid for framework groups and for the catchment regions of "upside down" energy hypersurfaces $-E(K)$.

Acknowledgements

This work was supported by both strategic and operating research grants from the Natural Sciences and Engineering Research Council of Canada.

1. H. Jahn and E. Teller. Proc. R. Soc. London, Ser. A, **161**, 220 (1937).
2. E. B. Wilson Jr., J. C. Decius, and P. C. Cross. Molecular vibrations. McGraw-Hill, New York. 1955.
3. (*a*) J. N. Murrell and K. Laidler. Trans. Faraday Soc., **64**, 371 (1968); (*b*) J. N. Murrell and G. L. Pratt. Trans. Faraday Soc. **66**, 1680 (1970).
4. R. E. Stanton and J. W. McIver. J. Am. Chem. Soc. **97**, 3632 (1975).
5. S. Kato and K. Fukui. J. Am. Chem. Soc. **98**, 6395 (1976).
6. P. Pechukas. J. Chem. Phys. **64**, 1516 (1976).
7. K. Ishida, K. Morokuma, and A. Komornicki. J. Chem. Phys. **66**, 2153 (1977).
8. T. D. Bouman, C. D. Duncan, and C. Trindle. Int. J. Quantum Chem. **11**, 399 (1977).
9. C. A. Mead and D. G. Truhlar. J. Chem. Phys. **70**, 2284 (1979).
10. P. G. Mezey. J. Am. Chem. Soc. **112**, 3791 (1990).
11. P. G. Mezey. Potential energy hypersurfaces. Elsevier, Amsterdam. 1987.
12. P. G. Mezey. J. Math. Chem. **4**, 377 (1990).

Can. J. Chem. Downloaded from www.nrcresearchpress.com by 92.62.229.171 on 09/08/12
For personal use only.

Structure and bonding in square-planar chalcogen rings

LEIF J. SAETHRE[1] AND ODD GROPEN[1]

Department of Chemistry, Institute of Mathematical and Physical Sciences, University of Tromsø, N-9000 Tromsø, Norway

Received August 19, 1991

This paper is dedicated to Professor Sigeru Huzinaga on the occasion of his 65th birthday

LEIF J. SAETHRE and ODD GROPEN. Can. J. Chem. **70**, 348 (1992).

The molecular structures of square-planar X_4^{2+}, X_4^{+}, and X_4 (X = S, Se, Te) have been calculated using the effective core potential model. For X_4^{2+} the agreement between experimental and calculated values is excellent provided that *d* orbitals are included in the basis set. For the hypothetical molecules X_4^{+} and X_4 the bond lengths are found to increase dramatically as one and, subsequently, two electrons are added to the systems. Extensive population analysis shows that this increase is almost exclusively due to loss of bonding in the π system, whereas the bonding in the σ system remains relatively unaltered. These results make it possible to predict covalent single bond radii for S, Se, and Te for which the influence of π repulsion is removed. From the calculated variation of bond lengths with atomic charge, bond lengths are predicted for a series of planar disulphide rings.

Key words: structure, bonding, chalcogen, theoretical, ECP.

LEIF J. SAETHRE et ODD GROPEN. Can. J. Chem. **70**, 348 (1992).

Utilisant le modèle du potentiel de coeur effectif, on a calculé les structures moléculaires des ions plans carrés X_4^{2+}, X_4^{+} et X_4 (X = S, Se et Te). Pour le X_4^{2+}, à la condition d'y inclure les orbitales *d* dans la base, l'accord est excellent entre les valeurs calculées et expérimentales. On a trouvé que, pour les molécules hypothétiques X_4^{+} et X_4, les longueurs des liaisons augmentent d'une façon dramatique lorsqu'on ajoute un, puis un deuxième, électron aux systèmes. Une analyse extensive de la population montre que cette augmentation est pratiquement complètement due à une perte de liaison dans le système π alors que la liaison par le système σ demeure pratiquement inchangée. Grâce à ces résultats, il est possible de prédire les rayons des liaisons covalentes simples du S, du Se et du Te desquelles on a éliminé la répulsion π. En se basant sur la variation des longueurs de liaisons avec les charges atomiques, on peut prédire les longueurs de liaison d'une série de cycles disulfurès plans.

Mots clés : structure, liaison, chalcogène, théorique, ECP.

[Traduit par la rédaction]

Introduction

The molecular structures of S_4^{2+}, Se_4^{2+}, and Te_4^{2+} have been determined by X-ray crystallography and found to possess square-planar symmetry (D_{4h}) or very nearly so (1–6). The slight variation in symmetry and bond lengths is attributed to the nature of the counterions and to differences in the crystallographic packing (5–7). The average S—S, Se—Se, and Te—Te bond lengths are found to be 2.00, 2.27, and 2.68 Å, respectively (5, 6). These bonds are all shorter than the corresponding single bonds (8), and the stability has been explained as due to an aromatic 6π-electron system.

Figure 1 shows a schematic drawing of the valence molecular orbitals of π symmetry. These orbitals represent the highest occupied and the lowest unoccupied orbitals for these systems. The six electrons occupy one bonding and two degenerate, essentially non-bonding, molecular orbitals. According to simple Hückel theory this results in a cyclic 2-electron 4-center bond with a π-bond order of 0.5, which accounts for the observed bond lengths. As can be seen from the figure, additional electrons are forced to enter into the antibonding b_{2u} orbital if the molecular symmetry is kept the same. This would remove the π stabilization and with two electrons in the b_{2u} orbital one would, to a first approximation, expect the bond lengths to be close to pure single bonds. The purpose of this investigation is to calculate the bond length increase and describe the bonding properties as one and, subsequently, two electrons are added to the molecular systems (Scheme 1).

The hypothetical neutral molecules may in fact serve as models for the study of structure and bonding in *cis*-planar

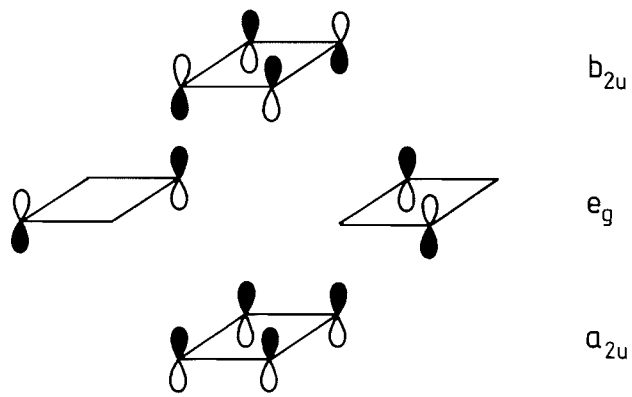

FIG. 1. Schematic representation of the valence molecular orbitals of π symmetry.

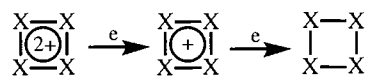

SCHEME 1

dichalcogen molecules. For example, from a survey of experimental S—S bond lengths between divalent sulphur atoms, Hordvik proposed that the bond length varies with the dihedral angle, being smallest (about 2.03 Å) at 90° and increasing to a maximum value (about 2.10 Å) for the *cis*-planar structure (9):

[1]Authors to whom correspondence may be addressed.

Printed in Canada

Can. J. Chem. Downloaded from www.nrcresearchpress.com by 123.30.183.119 on 09/08/12
For personal use only.

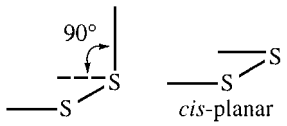

This relationship has been verified both experimentally and theoretically, and is believed to be due to the p_π lone-pair repulsion at 0° dihedral angle, and to π bonding, which is most pronounced at 90°(10).

In other classes of compounds the S—S bond is part of planar five-member rings of different π-electron population. For the dithiolium cation (Scheme 2) the ring is stabilized by a 6π-electron system (11). This results in a relatively short S—S bond of about 2.01 Å (12), which is close to the S—S bonds in S_4^{2+}. For the next two rings in Scheme 2 it is assumed that the positive charge is shared between two (13) and four (14) disulphide rings, respectively. The last compound represents a neutral *cis*-planar disulphide (9).

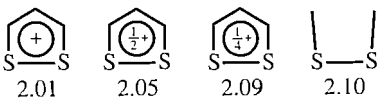

SCHEME 2

From the above it seems that the bonding in disulphides and related molecules is closely connected to the population of the π orbitals. In the present study we will therefore focus on the relationship between bond distances and the π-electron population of the bond. We believe that the square-planar chalcogens are ideally suited model compounds for this purpose, since the structures are homo-atomic, with bonding angles of 90°, and have no additional substituents or dihedral angles to complicate the analysis.

As expected for such an interesting class of compounds, several theoretical investigations have been performed. These include both *ab initio* (S_4^{2+}, S_4, S_4^{2-}) (15–17), effective core potential (Te_4^{2+}, Te_4) (18), and semiempirical methods (S_4^{2+}, Se_4^{2+}, and Te_4^{2+}) (19, 20). We earlier carried out preliminary calculations on X_4^{2+} and X_4 (X = S, Se, Te) using effective core potentials (21). In that paper "technical" details on basis sets, choice of parameters, as well as comparison with full *ab initio* calculations on S_4^{2+} and S_4 are discussed. In the present work we will emphasize the chemical bonding in these compounds and have for this reason also included results for the X_4^+ cations, which were not discussed earlier.

Method and computational details

The possibility of dividing the electrons into subshells and treating the valence electrons in the frozen sea of the core electrons was first proposed by Fock, Vesselow, and Petraschen (22). Today several groups have developed different schemes for simulating the valence-core interaction by Effective Core Potentials, ECP (23). Most of the schemes are the same, based on a projection operator and a local potential, but differing in the way the parameters are determined. There have been, basically, two different approaches. One was suggested by Goddard and Melius (24), who used an angular dependent projection operator. The other approach was suggested by Bonifacic and Huzinaga (25), who expressed the projection operator explicitly through the core orbitals. This latter approach has successfully been pursued by Huzinaga and co-workers (26). We have in our laboratory (27) developed an ECP scheme based on the ideas put forward by Huzinaga *et al.* This scheme, without the frozen orbitals, is applied in the present calculations. The one-electron operator then takes the following form:

$$F = h + \Sigma_i^c |f_i^c> B_i^c <f_i^c| + \Sigma_k A_k e^{-\alpha_k r^2}/r + \Sigma_j (J_j^v - K_j^v)$$

Here the first and the last terms are the well-known one-electron operator with reduced nuclear charge and the valence Coulomb and exchange operators. The second term is the projection operator where B_i^c's are taken equal to the core orbital energies with opposite sign. The third term is the local potential, which corrects for the incomplete screening, exchange interactions between core and valence, and effects of basis set reduction through the ECP operator. The parameters A_k and α_k are optimized so that the orbital energies of a selected atomic state are reproduced.

The *ab initio* reference calculations were carried out with double-ζ quality basis sets for S, Se, and Te, respectively (28). In the ECP calculations these were truncated to six *s* and five *p* functions and augmented with one *d* function with exponent values equal to 0.48, 0.33, and 0.22 respectively for S, Se, and Te. For further details see ref. 21.

Results and discussion

Bond lengths

The optimized bond lengths of square-planar X_4^{2+}, X_4^+, and X_4 are shown in Table 1. Also shown is the calculated bond length increase for X_4^+ and X_4 relative to those in X_4^{2+}. The calculations were performed both with and without valence *d*-orbitals. We will first focus on the results for X_4^{2+} where experimental results are available.

Table 1 shows that the agreement between experimental and calculated values is excellent when *d*-orbitals are included in the basis set. The calculations give bond lengths well within the range of the experimental values. Electron correlation was not included in these calculations. Such a correction would probably lead to an elongation of the bonds (17). On the other hand, a more complete basis set, such as inclusion of a second set of *d*-orbitals, would probably have decreased the bonds (17). It seems that in this study the effects of electron correlation and a somewhat limited basis set are mutually cancelling, and that the chosen basis set is able to reproduce the experimental values satisfactorily at the HF level. As mentioned in the introduction, the main object of the calculations is to calculate the relative increase in bond length as π electrons are added to the systems. The good agreement for the dications gives confidence that the predicted bond lengths for the monocations and neutral molecules are reasonably accurate.

When valence *d*-orbitals are excluded from the basis set, the calculated bond lengths are systematically overestimated. For S_4^{2+} they are about 11%, and for Se_4^{2+} and Te_4^{2+} about 7% too long. This *d*-orbital effect was noted earlier, and is well known for sulphur compounds (21, 29). The effect has generally been attributed to the ability of the *d* functions to act as polarization functions. In this study they are also active participants in the bonding by virtue of their symmetry, as will be shown below.

The calculated increase in bond lengths as additional electrons are added to the molecules is quite dramatic. When *d*-orbitals are included the increase is about 0.05 Å for one electron and about 0.12 Å when the b_{2u} orbital is com-

Can. J. Chem. Downloaded from www.nrcresearchpress.com by 123.30.183.119 on 09/08/12
For personal use only.

TABLE 1. Bond lengths in square-planar X_4^{2+}, X_4^{+}, and X_4

Basis[a]	X	X_4^{2+} Calcd.	X_4^{2+} Expt.[d]	X_4^{+} Calcd.	$(X_4^{+} - X_4^{2+})$[b] Calcd.	X_4 Calcd.	$(X_4 - X_4^{2+})$[c] Calcd.
WD	S	1.999	1.988–2.014	2.054	0.054	2.123	0.124
	Se	2.256	2.247–2.288	2.307	0.051	2.375	0.119
	Te	2.688	2.660–2.699	2.736	0.048	2.805	0.117
WOD	S	2.221	1.988–2.014	2.255	0.034	2.310	0.089
	Se	2.425	2.247–2.288	2.464	0.039	2.524	0.099
	Te	2.863	2.660–2.699	2.894	0.031	2.947	0.084

[a]Huzinaga basis (refs. 21, 28) with (WD) and without (WOD) inclusion of *d*-orbitals.
[b]Calculated bond length increase for X_4^{+} relative to X_4^{2+}.
[c]Calculated bond length increase for X_4 relative to X_4^{2+}.
[d]Range of experimental values.

TABLE 2. Calculated orbital and overlap populations without *d*-orbitals in X_4^{2+}, X_4^{+}, and X_4 (X = S, Se, Te). The populations are calculated at the minimum energy geometry

	Orbital populations			Overlap populations					
Molecule	*s*	p_x	p_z	*s*–*s*	*s*–p_x	p_x–p_x	σ	π	Total
S_4^{2+}	2.00	1.00	1.50	−0.07	−0.09	0.44	0.28	0.10	0.38
Se_4^{2+}	2.01	1.00	1.50	−0.07	−0.10	0.44	0.27	0.10	0.37
Te_4^{2+}	2.00	1.00	1.50	−0.06	−0.08	0.46	0.32	0.09	0.42
S_4^{+}	1.99	1.01	1.75	−0.07	−0.08	0.45	0.30	0.02	0.31
Se_4^{+}	2.00	1.00	1.75	−0.06	−0.10	0.45	0.29	0.01	0.30
Te_4^{+}	1.99	1.00	1.75	−0.05	−0.07	0.47	0.34	0.02	0.36
S_4	1.97	1.01	2.00	−0.05	−0.07	0.45	0.33	−0.07	0.26
Se_4	1.99	1.01	2.00	−0.05	−0.09	0.46	0.32	−0.08	0.24
Te_4	1.98	1.01	2.00	−0.05	−0.06	0.47	0.37	−0.06	0.30

TABLE 3. Calculated orbital populations with *d*-orbitals in X_4^{2+}, X_4^{+}, and X_4 (X = S, Se, Te). The populations are calculated at the minimum energy geometry[a]

Molecule	*s*	p_x	p_z	$d_{x^2-y^2}$	d_{xz}
S_4^{2+}	1.92	1.01	1.45	0.04	0.02
Se_4^{2+}	1.92	1.00	1.45	0.04	0.03
Te_4^{2+}	1.90	1.02	1.45	0.04	0.03
S_4^{+}	1.92	1.01	1.72	0.03	0.02
Se_4^{+}	1.93	1.00	1.71	0.03	0.02
Te_4^{+}	1.93	1.02	1.71	0.04	0.02
S_4	1.93	1.01	1.98	0.03	0.01
Se_4	1.95	1.00	1.97	0.03	0.01
Te_4	1.96	0.99	1.97	0.03	0.01

[a]Contributions from d_{z^2} and d_{xy} are small and are not included.

pletely filled. This lengthening is remarkably constant for all chalcogens, even though the atomic radii increase appreciably down the periodic table. The results when *d*-orbitals are omitted are essentially the same, although the increase is somewhat less. Both sets of results may be understood from an increase in the p_π repulsion, which is less dramatic as the atomic separation becomes larger.

Electron population

Extensive Mulliken population analyses have been performed for all molecules, both with and without valence *d*-orbitals. It is well known that this type of analysis is basis-set dependent, and should be used with caution (30). In this study, however, the analysis is simplified by the homogeneity of the rings, and the use of similar valence basis sets for all molecules. The populations are calculated for bond lengths corresponding to the optimized geometries in Table 1, and are shown in Tables 2, 3, and 4. In each case the X—X bond is along the Cartesian *x*-axis with the *z*-axis perpendicular to the molecular plane.

We will first discuss the results in the simple case when *d*-orbitals are omitted. Table 2 shows the orbital and overlap populations for the three sets of molecules, X_4^{2+}, X_4^{+}, and X_4. The table reveals a number of interesting features. We see first that the orbital *s* and p_x populations are remarkably constant both for all sets and for each chalcogen within the set. In all cases the molecules use p_x for bonding, leaving the *s* electrons essentially as *s* lone pairs. This is clearly seen from the overlap populations where the *s*–*s* and *s*–p_x interactions are antibonding and the p_x–p_x the strongest bonding. Second, the p_z (or π) populations and also the π bonding are essentially constant within each set of molecules, but as the π population increases to 1.75 the π bonding becomes very small. When the π system incorporates all 8 electrons, i.e., when p_π lone pairs are formed, the π interaction becomes antibonding. Thus, it is the π-population which is responsible for the variation in bonding properties; the σ-bonding remains constants.

Turning now to the results when *d*-orbitals are included in the basis set, Tables 3 and 4 show that the general features of the electron population are much the same as for the simple case without *d*-orbitals. Table 3 shows that the pop-

Can. J. Chem. Downloaded from www.nrcresearchpress.com by 123.30.183.119 on 09/08/12
For personal use only.

TABLE 4. Calculated overlap populations with d-orbitals in X_4^{2+}, X_4^{+}, and X_4 (X = S, Se, Te). The populations are calculated at the minimum energy geometry[a]

Molecule	s–s	s–p_x	p_x–p_x	s–d_σ	p_x–d_σ	p_z–p_z	p_π–d_π	σ	π	Total
S_4^{2+}	−0.12	−0.06	0.42	0.01	0.07	0.11	0.06	0.33	0.17	0.50
Se_4^{2+}	−0.08	−0.09	0.44	0.01	0.08	0.11	0.06	0.36	0.17	0.53
Te_4^{2+}	−0.04	−0.05	0.45	0.01	0.08	0.10	0.07	0.45	0.17	0.62
S_4^{+}	−0.10	−0.07	0.43	0.01	0.06	−0.02	0.04	0.33	0.02	0.35
Se_4^{+}	−0.08	−0.10	0.44	0.01	0.07	−0.02	0.05	0.34	0.03	0.38
Te_4^{+}	−0.04	−0.08	0.46	0.01	0.07	−0.00	0.05	0.42	0.05	0.47
S_4	−0.10	−0.08	0.44	0.01	0.05	−0.14	0.03	0.33	−0.11	0.22
Se_4	−0.07	−0.11	0.45	0.01	0.05	−0.14	0.04	0.33	−0.10	0.23
Te_4	−0.04	−0.11	0.46	0.01	0.06	−0.10	0.04	0.38	−0.06	0.32

[a]Overlap populations from d–d interactions are small and are not included.

Can. J. Chem. Downloaded from www.nrcresearchpress.com by 123.30.183.119 on 09/08/12
For personal use only.

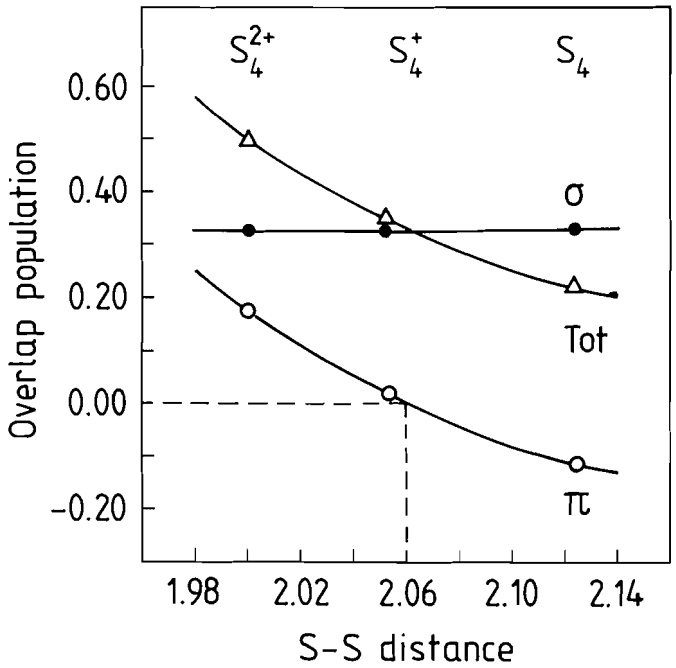

FIG. 2. Variation of σ, π, and total overlap population with S—S bond length in S_4^{2+}, S_4^{+}, and S_4.

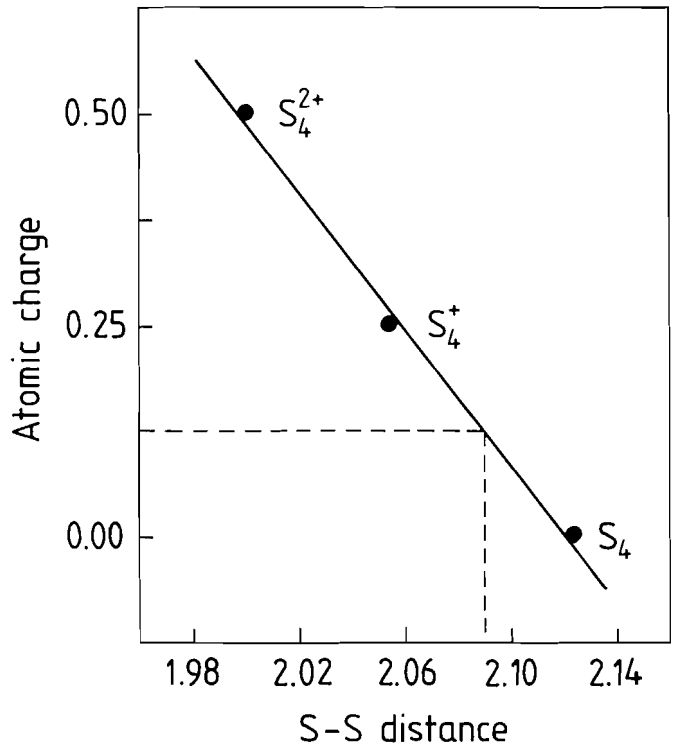

FIG. 3. Atomic charge on sulphur as a function of S—S bond length in S_4^{2+}, S_4^{+}, and S_4.

ulations of the most important d-orbitals are quite modest and that charge density is transferred from the s and p_z orbitals to the $d_{x^2-y^2}$ and d_{xz} orbitals, respectively. This polarization leads to a significant increase in both the σ(s–d_σ and p_x–d_σ) and the π (p_z–d_{xz}) bonding. The increase in π bonding is relatively large and may be explained from the fact that the d_{xz} (or d_π) orbital has the proper symmetry to bind to a neighbouring p_z orbital in the molecular orbital of e_g symmetry (see Fig. 1). For further discussion on the importance of adding d-orbitals to symmetry-deficient basis sets, see ref. 31. In the present case, the shorter bond lengths obtained with d-orbitals lead to stronger π bonds for X_4^{2+} and more antibonding π bonds for X_4.

Table 4 also shows the σ, π, and total overlap population. It is seen that for each chalcogen the total population decreases as more electrons are added to the molecular system. However, as found without d-orbitals, but even more pronounced here, the variation is almost exclusively due to the increase in π bonding. This remarkable result is illustrated for sulphur in Fig. 2, where the overlap population is plotted as a function of calculated bond lengths. Similar figures may be drawn for Se and Te.

Prediction of single bond radii for S, Se, and Te

The variation of X—X bond lengths with overlap population, such as depicted for S—S in Fig. 2, enables us to estimate the bond lengths for which the π population is zero. These distances should then correspond to pure covalent single bonds. Table 4 shows that this occurs for bond lengths slightly longer than those calculated for X_4^{+}. Simple interpolation on a smooth curve through the three points as shown in Fig. 2 gives the following bond distances: S—S = 2.06 Å, Se—Se = 2.32 Å, and Te—Te = 2.76 Å. These correspond to single bond radii of 1.03, 1.16, and 1.38 Å respectively for S, Se, and Te, which are very close to those proposed by Pauling, 1.04, 1.17, and 1.37 Å, respectively (8). As mentioned above, Hordvik arrived at 2.10 Å for S—S bonds in *cis*-planar disulphides, which corresponds to a sin-

gle bond radius of 1.05 Å (9). The two systems are of course not directly comparable, but it appears from this study that appreciable $\pi-\pi$ repulsion is present in both compounds.

Variation of bond lengths with atomic charge

Figure 3 shows how the calculated S—S bond lengths vary with the atom charge on sulphur. For simplicity the best straight line is drawn through the three points. This dependence is of course directly related to the overlap population in Fig. 2. As mentioned in the introduction, there seems to be a relationship between the S—S bond lengths and the ring charge (13). If we assume that the charge is mainly located on the sulphur atoms, we may use Fig. 3 to predict S—S bond lengths in these planar systems. We have already mentioned the resemblance between the S—S bonds in S_4^{2+} (2.00 Å) and those in the dithiolium cations (2.01 Å) for which a sulphur charge of 0.50 may be assumed. Similarly, S—S bond lengths of 2.05 and 2.09 Å are predicted for the charges 0.25 and 0.125. The latter value is obtained from interpolation, as shown in Fig. 3. Both of these S—S bonds correspond exactly to those found experimentally (13, 14). On the other hand, the predicted value of 2.12 Å for a neutral planar system is somewhat longer than the 2.10 Å value suggested by Hordvik.

1. J. Passmore, G. Sutherland, and P. S. White. J. Chem. Soc. Chem. Commun. 330 (1980).
2. I. D. Brown, D. B. Crump, and R. J. Gillespie. Inorg. Chem. **10**, 2319 (1971).
3. T. W. Couch, D. A. Lokken, and J. D. Corbett. Inorg. Chem. **11**, 357 (1972).
4. P. Boldrini, I. D. Brown, M. J. Collins, R. J. Gillespie, E. Maharajh, D. R. Slim, and J. F. Sawyer. Inorg. Chem. **24**, 4302 (1985).
5. R. C. Burns and R. J. Gillespie. Inorg. Chem. **21**, 3877 (1982).
6. G. Cardinal, R. J. Gillespie, J. F. Sawyer, and J. E. Vekris. J. Chem. Soc. Dalton Trans. 765 (1982).
7. M. J. Collins, R. J. Gillespie, J. F. Sawyer, and G. J. Schrobilgen. Inorg. Chem. **25**, 2053 (1986).
8. L. Pauling. The nature of the chemical bond. 3rd. ed. Cornell University Press, Ithaca, N.Y. 1960.
9. A. Hordvik. Acta Chem. Scand. **20**, 1885 (1966).
10. L. J. Saethre. Acta Chem. Scand. **A29**, 558 (1975).
11. A. Hordvik. Quart. Rep. Sulfur Chem. **5**, 21 (1970).
12. A. Hordvik, and H. Kjøge. Acta Chem. Scand. **23**, 1367 (1969); F. Grundtvik and A. Hordvik. Acta Chem. Scand. **25**, 1567 (1971).
13. A. Hordvik, K. Jynge, and L. K. Hansen. Acta Chem. Scand. **A42**, 79 (1988).
14. R. P. Shibaeva and V. F. Kaminskii. Kristallografiya, **23**, 499 (1978).
15. J. Kao. Inorg. Chem. **16**, 2085 (1977); J. Kao. J. Mol. Struct. **63**, 293 (1980); F. L. Skrezenek and R. D. Harcourt. Theor. Chim. Acta (Berlin), **67**, 271 (1985).
16. G. Van Zandwijk, R. A. J. Janssen, and H. M. Buck. J. Am. Chem. Soc. **112**, 4155 (1990).
17. G. E. Quelch, H. F. Schaefer III, and C. J. Marsden. J. Am. Chem. Soc. **112**, 8719 (1990).
18. M. J. Rothman, L. S. Bartell, C. S. Ewig, and J. R. Van Wazer. J. Comput. Chem. **1**, 64 (1980).
19. A. E. Foti, V. H. Smith, Jr., and D. R. Salahub. Chem. Phys. Lett. **57**, 33 (1978).
20. K. Tanaka, T. Yamabe, H. Terama-E, and K. Fukui. Inorg. Chem. **18**, 3591 (1979).
21. O. Gropen, L. J. Saethre, and E. Wisløff-Nilssen. Studies in physical and theoretical chemistry. Vol. 21. *Edited by* R. Carbo. Elsevier, Amsterdam. 1982. pp. 427–435.
22. V. Fock, M. Vesselow, and M. Petrashen. Zh. Eksp. Teor. Fiz. **10**, 723 (1940).
23. O. Gropen. *In* Methods in computational chemistry. Vol. 2. Relativistic effects in atoms and molecules. *Edited by* S. Wilson, Plenum Press, New York. 1988.
24. W. A. Goddard and C. F. Melius, Phys. Rev. A, **10**, 1528 (1974).
25. V. Bonifacis and S. Huzinaga, J. Chem. Phys. **60**, 2779 (1974).
26. S. Huzinaga, M. Klubokowski, and Y. Sakai, J. Chem. Phys. **88**, 4880 (1984); J. Andzelm, S. Huzinaga, M. Klubokowski, and E. Radzio. Mol. Phys. **52**, 1495 (1984).
27. O. Gropen, L. G. M. Petterson, and U. Wahlgren, Chem. Phys. **66**, 453 (1982); **66**, 459 (1982); L. G. M. Petterson, U. Wahlgren, and O. Gropen. Chem. Phys. **80**, 7 (1983); A. Strömberg, O. Gropen, and U. Wahlgren. J. Chem. Phys. **80**, 1593 (1984); L. G. M. Petterson, U. Wahlgren, and O. Gropen. J. Chem. Phys. **86**, 2174 (1987).
28. S. Huzinaga. Approximate atomic functions II. Technical Report, University of Alberta. 1971; J. Chem. Phys. **66**, 4245 (1977); **71**, 1980 (1979).
29. J. B. Collins, P. v. R. Schleyer, J. S. Binkley, and J. A. Pople. J. Chem. Phys. **64**, 5142 (1976); P. G. Mezey and A. Haas. J. Chem. Phys. **77**, 870 (1982); C. J. Marsden and B. J. Smith. J. Mol. Struct. **105**, 385 (1983).
30. W. J. Hehre, L. Radom, P. v. R. Schleyer, and J. A. Pople. Ab initio molecular orbital theory. John Wiley and Sons, New York. 1986. pp. 336–341.
31. E. E. Ball, M. A. Ratner, and J. R. Sabin. Chem. Scr. **12**, 128 (1977); R. A. J. Janssen, G. J. Visser, and H. M. Buck. J. Am. Chem. Soc. **106**, 3429 (1984).

Can. J. Chem. Downloaded from www.nrcresearchpress.com by 123.30.183.119 on 09/08/12
For personal use only.

AO integral evaluation using Cartesian exponential type orbitals (CETOs)[1]

RAMON CARBÓ[2] and EMILI BESALÚ
Laboratori de Química Computacional, Estudi de Ciències, Estudi General de Girona, 17071 Girona, Spain

Received July 15, 1991

This paper is dedicated to Professor Sigeru Huzinaga on the occasion of his 65th birthday

RAMON CARBÓ and EMILI BESALÚ. Can J. Chem. **70**, 353 (1992).

CETO functions and their properties are defined and described, to provide a means of obtaining general expressions for many-center many-electron integral formulae. Compact integral expressions are written by means of nested summation symbols, a new concept developed in this paper. Integrals over CETO functions are computed by means of a set of several auxiliary integral forms. No transformations other than frame rotations are needed to compute the usual integral terms. The formulae obtained are immediately programmable in any high level language and the parallelizable terms are obtained with a simple rule. Results can be considered an encouraging alternative way to solve the STO integral problem.

Key words: many-center AO integrals, molecular basis sets, ETO, STO, CETO.

RAMON CARBÓ et EMILI BESALÚ. Can. J. Chem. **70**, 353 (1992).

On définit et décrit des fonctions d'orbitales de type cartésien exponentiel (CETO) et leurs propriétés; ces fonctions pourraient ouvrir la voie pour obtenir des expressions générales pour des formules d'intégrales à plusieurs électrons et à plusieurs centres. On dérive des expressions intégrales compactes en utilisant des symboles de sommation emboîtés les uns dans les autres, un nouveau concept développé dans ce travail. Pour calculer les intégrales sur les CETO, on utilise un ensemble de quelques formes d'intégrales auxiliaires. Il n'est pas nécessaire de faire appel à d'autres transformations que des rotations du repère de référence pour calculer les termes des intégrales usuelles. Les formules qui sont obtenues peuvent immédiatement être programmées dans n'importe lequel language de haut niveau et on obtient des termes parallélisables avec une règle simple. On peut considérer que les résultats sont une alternative encourageante pour la solution du problème des intégrales du type de Slater.

Mots clés : intégrales d'orbitales atomiques à plusieurs centres, bases moléculaires, orbitales de type exponentiel, orbitales de type Slater, orbitales de type cartésien exponentiel.

[Traduit par la rédaction]

Introduction

Although defined in 1960 by Boys and Cook (1), Cartesian Exponential Type Orbital (CETO) functions did not attract notice until a GTO integral review made by Saunders (2), where they were cautiously manipulated as a subproduct.

As integrals over Exponential Type Orbitals (ETO) are raising interest among various research groups (3–8), we tried to open anew the CETO functions study as a way to approach the ETO integral problem from another point of view.

This paper approaches the computation of CETO integrals by using a notation where all the necessary elements, integrals plus coordinate transformations, are compactly expressed. We prove in this way how CETO integrals are expressible in terms of accessible concepts and auxiliary functions well known in the literature. Care has been taken to provide the simplest formulation possible, suited to easy translation to any high level programming language and well adapted to parallelization.

To fulfill this primary goal, the present paper will be roughly divided into four parts. The first one will introduce the concepts of CETO functions and their transformation properties. The second discusses one- and two-center one-electron integrals. The third is devoted to obtaining two-center Coulomb repulsion integrals and in the fourth part many-center integrals are analyzed.

1. CETO

1.1 Definition 1: CETO functions

Let us define a real normalized Cartesian Exponential Type Orbital (CETO) with the screening parameter α and centered at the point $\boldsymbol{A}$ as

$$[1.1] \quad \chi(\boldsymbol{A},\boldsymbol{a},n,\alpha) = N_n(\boldsymbol{a},\alpha)\, H_a(\boldsymbol{A},\boldsymbol{a})\, P_n(\mathbf{A},\alpha)$$

where the following conditions hold:

1 $\boldsymbol{a} = (a_1,a_2,a_3)$, a_i integer ≥ 0 $\forall i$
2 n integer ≥ 0
3 α real >0
4 $r_A = |\boldsymbol{r} - \boldsymbol{A}|$, $\boldsymbol{r} = (x_1,x_2,x_3)$, $\boldsymbol{A} = (A_1,A_2,A_3)$

and where one can distinguish the following terms:

(i) The normalization factor

$$[1.2] \quad N_n(\boldsymbol{a},\alpha) = \alpha(2\alpha)^{a+n+1/2} \cdot [(2a+1)!!\,(\pi\, p\,(2(a+n+1))!)^{-1}]^{1/2}$$

with $a = \Sigma_i a_i$ and $p = \Pi_i(2a_i - 1)!!$.

(ii) The angular part

$$[1.3] \quad H_a(\boldsymbol{A},\boldsymbol{a}) = \prod_i (x_i - A_i)^{a_i}$$

where a is defined in eq. [1.2].

(iii) The radial part

$$[1.4] \quad P_n(\boldsymbol{A},\alpha) = r_A^n \exp(-\alpha r_A)$$

In some cases condition 2 above can be relaxed, allowing negative values, and condition 3 may be extended with $\alpha =$

[1] A contribution of the Grup de Química Quàntica del Institut d'Estudis Catalans.

[2] Author to whom correspondence may be addressed.

Printed in Canada

Can. J. Chem. Downloaded from www.nrcresearchpress.com by 92.62.229.171 on 09/08/12
For personal use only.

Can. J. Chem. Downloaded from www.nrcresearchpress.com by 92.62.229.171 on 09/08/12
For personal use only.

1.2. Relationship of CETO with STO functions

Slater Type Orbital (STO) (2, 9*a*) functions have been well known since their description by Slater ca. 60 years ago (10). STO have been massively studied and used as atomic basis sets (11). In the convenient definition by Wahl *et al.* (12), normalized STO are constructed over spherical coordinates. After some elementary manipulations one can see that it is possible to write any STO in terms of CETO functions (9, 13*a*).

The interesting pattern here is the appearance of the structure of Cartesian STO functions, expressible as finite linear combinations of CETO functions. This property can be also used in similar contexts where spherical harmonic functions are present. Take also as an example the atomic spinor functions, see ref. 13. It will be easy to design relativistic one-electron orbitals as formed by four-dimensional vectors whose components are CETO linear combinations. CETO functions can be considered the building blocks of Cartesian STO. In this sense, solving the integral evaluation problem over CETO functions will be the same as solving the integral STO problem.

1.3. Practical details on CETO products

As is well known, basis functions when used in a LCAO framework appear in product pairs at the moment of computing molecular integrals. Analysis of the structure of these CETO products will permit easy definition of canonical integral forms.

1.3.1 Orientation of CETOs over the line joining a pair of centers

(*i*) To be useful for integral computation a product of two CETO functions must be *well-oriented,* in such a way that the x_3-axis (z-axis) coincides with the line joining the two centers involved.

(*ii*) Here we analyze how to perform an effective rotation over the coordinates $\boldsymbol{x}^0 = (x_1^0,x_2^0,x_3^0)$ using the Eulerian angles $\omega = (\varphi,\theta,\delta)$ and the rotation matrix $\boldsymbol{R}(\omega)$ (14). The rotation $\boldsymbol{R}(\omega)$ is chosen in order to express the coordinates $\boldsymbol{x}^0$ in terms of the coordinate system $\boldsymbol{x} = (x_1,x_2,x_3)$ having the same origin as $\boldsymbol{x}^0$, say $\boldsymbol{A}$, and which is well oriented with respect to another center, $\boldsymbol{B}$.

(*iii*) Thus, the rotations in the present paper will be used to orient well two CETO functions, centered at different sites. The rotation angles involved for this kind of manipulation will be constructed by the vector: $\omega_s = (\varphi,\theta,0)$. This is because of the cylindrical symmetry that the prolate spherical coordinates system (see Definition A1 in Appendix A) possesses with respect to a rotation around the axis line joining both centers.

(*iv*) Cartesian coordinate power products such as those forming the CETO angular part, $H_a^0(\boldsymbol{A},\boldsymbol{a})$, are of special interest when dealing with this kind of AO functions.

Using the result of the rotation matrix product over coordinate vectors, the following relationship can be found:

$$[1.5]\quad H_a^0(\boldsymbol{A},\boldsymbol{a}) = \Sigma\,(\boldsymbol{i} = \boldsymbol{0},\boldsymbol{a}) \cdot \Sigma(\boldsymbol{j} = \boldsymbol{0},\boldsymbol{i})\, \boldsymbol{M}(\boldsymbol{i},\boldsymbol{j},\boldsymbol{a}) f(\boldsymbol{i},\boldsymbol{j},\boldsymbol{a},\varphi,\theta)\, H_a(\boldsymbol{A},\boldsymbol{g})$$

where $a = \Sigma_i g_i = \Sigma_i a_i$. Certain definitions should be taken into account in order to interpet eq. [1.5]. They are written as follows:

1. We will call $\Sigma(\boldsymbol{i} = \boldsymbol{0},\boldsymbol{a})$, $\Sigma(\boldsymbol{j} = \boldsymbol{0},\boldsymbol{i})$ *nested summation symbols*. A general description of these is given in Appendix A, Definition A2.

2. The M coefficients correspond to the binomial coefficient product:

$$[1.6]\quad M(\boldsymbol{i},\boldsymbol{j},\boldsymbol{a}) = (-1)^{a_1-i_1+i_3}\binom{a_1}{i_1}\binom{a_2}{i_2}\binom{a_3}{i_3}\binom{i_1}{j_1}\binom{i_2}{j_2}$$

3. The f function is defined as

$$[1.7]\quad f(\boldsymbol{i},\boldsymbol{j},\boldsymbol{a},\varphi,\theta) = (\sin\theta)^{b_1}(\cos\theta)^{b_2}(\sin\varphi)^{b_3}(\cos\varphi)^{b_4}$$

where the four-dimensional vector $\boldsymbol{b}$ is built up in terms of vectors $\boldsymbol{a}$, $\boldsymbol{i}$, and $\boldsymbol{j}$ elements using the rules:

$$[1.8]\quad \boldsymbol{b} = \boldsymbol{b}(\boldsymbol{a},\boldsymbol{i},\boldsymbol{j}) = (i_1 + i_2 + i_3 - (j_1 + j_2), a_3 + j_1 + j_2 - i_3, a_1 + i_2 - i_1, a_2 + i_1 - i_2)$$

4. The three-dimensional vector $\boldsymbol{g}$ components are constructed by the rules:

$$[1.9]\quad \boldsymbol{g} = \boldsymbol{g}(\boldsymbol{a},\boldsymbol{i},\boldsymbol{j}) = (j_1 + j_2 + i_3, a_1 + a_2 - (i_1 + i_2), a_3 + i_1 + i_2 - g_1)$$

5. In the present framework the index j_3 must be considered constant and equal to zero.

1.3.2 General CETO products and their properties

(*i*) Using CETO Definition 1 one can easily find that if two CETO functions share the same center, that is, if $\boldsymbol{A} = \boldsymbol{B}$ and $R = 0$, their product is but a new CETO within the same center, or:

$$[1.10]\quad \Omega_{AA'} = \chi(\boldsymbol{A},\boldsymbol{a},n,\alpha)\,\chi(\boldsymbol{A},\boldsymbol{a}',n',\alpha') = \chi(\boldsymbol{A},\boldsymbol{a}+\boldsymbol{a}',n+n',\alpha+\alpha')$$

(*ii*) The product of two CETO functions placed at centers $\boldsymbol{A}$ and $\boldsymbol{B}$ respectively, separated by a distance R, giving a charge distribution Ω_{AB} when rotated, can be written as

$$\begin{aligned}[1.11]\quad \Omega_{AB} &= \chi(\boldsymbol{A},\boldsymbol{a},n,\alpha)\,\chi(\boldsymbol{B},\boldsymbol{b},m,\beta)\\ &= \Sigma(\boldsymbol{i} = \boldsymbol{0},\boldsymbol{a})\,\Sigma(\boldsymbol{j} = \boldsymbol{0},\boldsymbol{i})\,\Sigma(\boldsymbol{i}' = \boldsymbol{0},\boldsymbol{b})\\ &\quad\cdot \Sigma(\boldsymbol{j}' = \boldsymbol{0},\boldsymbol{i}')\,\boldsymbol{M}(\boldsymbol{i},\boldsymbol{j},\boldsymbol{a})\,\boldsymbol{M}(\boldsymbol{i}',\boldsymbol{j}',\boldsymbol{b})\\ &\quad\cdot f(\boldsymbol{i},\boldsymbol{j},\boldsymbol{a},\varphi_A,\theta_A)\,f(\boldsymbol{i}',\boldsymbol{j}',\boldsymbol{b},\varphi_B,\theta_B)\\ &\quad\cdot W(A,\boldsymbol{g},n,\alpha)\,W(B,\boldsymbol{g}',m,\beta)\end{aligned}$$

where the f and M coefficients and the $\boldsymbol{g}$ and $\boldsymbol{g}'$ vectors arise from the rotations that put each CETO in a well-oriented form with respect to the other. The W functions are a particular form of CETO functions, which are defined below in the next section.

1.3.3. Well-oriented CETO form

When observing eq. [1.5] it is easy to consider how the general CETO structure changes. The CETO functions, once transformed, become linear combinations of unnormalized Well-Oriented CETO (WO-CETO) functions, which can be defined as follows:

Definition 2: WO-CETO functions

Using the conventions:

1. $\boldsymbol{n} = (n_1,n_2,n_3)$
2. $m \in \{0,1\}$
3. $\alpha \geq 0$ and real
4. $R \geq 0$ and real
5. $s \in \{-1,0,+1\}$

6. $z(s) = sR/2$
7. $r(s) = (x_1^2 + x_2^2 + (x_3 - z(s))^2)^{1/2}$

an unnormalized WO-CETO function is written as

$$[1.12] \quad W(z(s),\boldsymbol{n},m,\alpha) = x_1^{n_1} x_2^{n_2} (x_3 - z(s))^{n_3} r(s)^m \exp\{-\alpha r(s)\}$$

One can represent unnormalized WO-CETO functions as a product of the following terms, when the convention $z(s) = (0,0,z(s))$ and the definitions [1.3] and [1.4] apply:

(*i*) An *angular part*:

$$[1.13] \quad H_n(z(s),\boldsymbol{n}) = x_1^{n_1} x_2^{n_2} (x_2 - z(s))^{n_3}$$

where $n = \Sigma_i n_i$.

(*ii*) A *radial part*:

$$[1.14] \quad P_m(z(s),\alpha) = r(s)^m \exp\{-\alpha r(s)\}$$

In this way $r_A = r(-1)$, so one can also use the symbol $W(A,\boldsymbol{n},m,\alpha)$ for $W(z(-1),\boldsymbol{n},m,\alpha)$; moreover, one can write $r_B = r(+1)$ and, consequently, $W(B,\boldsymbol{n},m,\alpha) = W(z(+1),\boldsymbol{n},m,\alpha)$.■

A still simpler expression, having the form of some sort of elementary CETO building block, can be also described:

Definition 3: E-CETO functions

Taking into account the same conventions as in Definition 2, an Elementary CETO (E-CETO) function is:

$$[1.15] \quad E(\boldsymbol{n},m,\alpha) = W(z(0),\boldsymbol{n},m,\alpha).■$$

1.3.4. WO-CETO products. Cartesian form in terms of E-CETOs

The product of two WO-CETO functions can be written in terms of the third axis components, so:

$$[1.16] \quad \Omega_{AB}^W = W(A,\boldsymbol{a},n,\alpha)\, W(B,\boldsymbol{b},m,\beta) = \Sigma(\boldsymbol{i} = \boldsymbol{0},\boldsymbol{p})\, \Gamma(\boldsymbol{i},\boldsymbol{a},\boldsymbol{b},R) \cdot x_1^{a_1+b_1} x_2^{a_2+b_2} x_3^{i_1+i_2} P_{nm}(\boldsymbol{A},\alpha,\boldsymbol{B},\beta)$$

with

$$\Gamma(\boldsymbol{i},\boldsymbol{a},\boldsymbol{b},R) = (-1)^{a_3-i_1}\binom{a_3}{i_1}\binom{b_2}{i_2}(R/2)^{a_3+b_3-(i_1+i_2)}$$

The two-dimensional vector $\boldsymbol{p}$ is defined as (a_3,b_3) and

$$[1.17] \quad P_{nm}(\boldsymbol{A},\alpha,\boldsymbol{B},\beta) = P_n(\boldsymbol{A},\alpha)\, P_m(\boldsymbol{B},\beta)$$

2. Integrals over one-electron operators

Although already described by Saunders (2), overlap and kinetic energy integrals over a CETO framework will be briefly discussed for the sake of completeness. One- and two-center nuclear attraction integrals will also be studied here.

The notation presented previously in the above discussion is used in all integral cases, leading in this way to a compact description of every integral form, usually needed in quantum chemical problems.

All one-electron integrals studied here can be written in terms of overlap integrals.

2.1. Overlap integrals

(*i*) *One center*

The one-center overlap integrals can be easily obtained considering the structure of eq. [1.10]:

$$[2.1] \quad S_{AA} = \langle\chi(\boldsymbol{A},\boldsymbol{a}',n',\alpha')|\chi(\boldsymbol{A},\boldsymbol{a}'',n'',\alpha'')\rangle = \langle\chi(\boldsymbol{A},\boldsymbol{a},n,\alpha)\rangle$$

where $\boldsymbol{a} = \boldsymbol{a}' + \boldsymbol{a}''$, $n = n' + n''$, $\alpha = \alpha' + \alpha''$, and

$$[2.2] \quad \langle\chi(\boldsymbol{A},\boldsymbol{a},n,\alpha)\rangle = \int \chi(\boldsymbol{A},\boldsymbol{a},n,\alpha)\, dV = \delta(\wedge_i(a_i = \dot{2}))\, F_t(a_1 + a_2 + 1, a_3) \cdot F_2(a_2,a_1)\, t!\, \alpha^{-(t+1)}$$

with $t = 2 + n + \Sigma_i a_i$.

The integral [2.2] vanishes unless $a_i = \dot{2}$, $\forall i$, as signaled by the logical Kronecker delta function, described in Appendix A, Definition A3, appearing as a first factor. The functions F_k, coming from the integration of the angular part of the CETO function, are defined in Appendix B, Definition B5.

(*ii*) *Two center*

Taking into account the rotations outlined in section 1.3.1, the two-center overlap integral can be expressed as

$$[2.3] \quad S_{AB} = \langle\chi(\boldsymbol{A},\boldsymbol{a},n,\alpha)|\chi(\boldsymbol{B},\boldsymbol{b},m,\beta)\rangle = \Sigma(\boldsymbol{i} = \boldsymbol{0},\boldsymbol{a})\, \Sigma(\boldsymbol{j} = \boldsymbol{0},\boldsymbol{i})\, \Sigma(\boldsymbol{i}' = \boldsymbol{0},\boldsymbol{b}) \cdot \Sigma(\boldsymbol{j}' = \boldsymbol{0},\boldsymbol{i}')\, M(\boldsymbol{i},\boldsymbol{j},\boldsymbol{a})\, M(\boldsymbol{i}',\boldsymbol{j}',\boldsymbol{b}) \cdot f(\boldsymbol{i},\boldsymbol{j},\boldsymbol{a},\varphi_A,\theta_A) f(\boldsymbol{i}',\boldsymbol{j}',\boldsymbol{b},\varphi_B,\theta_B) \cdot \langle W(A,\boldsymbol{g},n,\alpha)|W(B,\boldsymbol{g}',m,\beta)\rangle$$

where it is necessary to compute overlap integrals over WO-CETO functions, as

$$[2.4] \quad S_{AB}^W = \langle W(A,\boldsymbol{a},n,\alpha)|W(B,\boldsymbol{b},m,\beta)\rangle = \delta(a_1 + b_1 = \dot{2} \wedge a_2 + b_2 = \dot{2})\, (R/2)^{t+1} \cdot F_2(a_2 + b_2,\, a_1 + b_1) \cdot \Sigma(\boldsymbol{r} = \boldsymbol{0},\boldsymbol{t})\, \Gamma(\boldsymbol{r},\boldsymbol{c})\, A_{r_1}(\sigma)\, B_{r_2}(\tau)$$

with $\boldsymbol{t} = (t,t)$, $t = 2 + m + n + \Sigma_i(a_i + b_i)$, and having $\sigma = R(\alpha + \beta)/2$ and $\tau = R(\alpha - \beta)/2$. The coefficients $\Gamma(\boldsymbol{r},\boldsymbol{c})$ arise from the development of the prolate coordinates function $P(\boldsymbol{c},u,v)$, with the definition of the six-dimensional vector $\boldsymbol{c} = (n + 1, m + 1, a_3, b_3, k, k)$, as explained in Appendix A, Definition A4. The $A_k(x)$ and $B_k(x)$ integrals are defined in Appendix B, Definitions B1 and B2.

The sum $a_1 + b_1 + a_2 + b_2$ is even for nonvanishing integrals, due to the properties of the F_k functions, defined in Appendix B, Definition B5. Thus, the index $k = (a_1 + b_1 + a_2 + b_2)/2$, appearing in the expression of the vector $\boldsymbol{c}$, has always an integer value.

2.2. Kinetic energy integrals

Kinetic energy integrals may be computed using overlap integrals and the symmetric form of the associated kinetic energy operator derived from Green's first identity (15):

$$[2.5] \quad T_{AB} = \langle\chi_A|-1/2\, \nabla^2|\chi_B\rangle = 1/2\, \langle\nabla\chi_A|\nabla\chi_B\rangle$$

Furthermore, one obtains:

$$[2.6] \quad \partial W(A,\boldsymbol{a},n,\alpha)/\partial x_i = a_i\, W(A,\, \boldsymbol{a} - \boldsymbol{e}_i,\, n,\, \alpha) + n\, W(A,\, \boldsymbol{a} + \boldsymbol{e}_i,\, n - 2,\, \alpha) - \alpha\, W(A,\, \boldsymbol{a} + \boldsymbol{e}_i,\, n - 1,\, \alpha)$$

Can. J. Chem. Downloaded from www.nrcresearchpress.com by 92.62.229.171 on 09/08/12
For personal use only.

where $\{e_i\}$ are the rows of the (3×3) unit matrix.

The fact must be noted here that if a_i or n is zero in the original WO-CETO, the first or the second term on the right side of eq. [2.6] will vanish.

Once the rotations described in paragraph 1.3.1 are performed over the CETO functions appearing in eq. [2.5], this integral can be expressed as a sum involving overlap integrals of type [2.4] as

$$[2.7] \quad T_{AB} = 1/2 \sum_i T_{ABi}$$

employing the auxiliary definition:

$$\begin{aligned}[2.8] \quad K_i(s,p) = b_i \langle & W(A, \boldsymbol{a} + s\boldsymbol{e}_i, n - p, \alpha) \\ & \cdot |W(B, \boldsymbol{b} - \boldsymbol{e}_i, m, \beta)\rangle \\ & + m \langle W(A, \boldsymbol{a} + s\boldsymbol{e}_i, n - p, \alpha) \\ & \cdot |W(B, \boldsymbol{b} + \boldsymbol{e}_i, m - 2, \beta)\rangle \\ & - \beta \langle W(A, \boldsymbol{a} + s\boldsymbol{e}_i, n - p, \alpha) \\ & \cdot |W(B, \boldsymbol{b} + \mathbf{e}_i, m - 1, \beta)\rangle\end{aligned}$$

where $s \in \{-1,+1\}$ is a sign and $p \in \{0,1,2\}$ an integer, one obtains:

$$[2.9] \quad T_{ABi} = a_i K_i(-1,0) + n K_i(+1,2) - \alpha K_i(+1,1)$$

In one-center kinetic energy integrals, the term [2.9] can be written using the following combination:

$$\begin{aligned}[2.10] \quad U_{AAi} = & -a_i(a_i - 1) && \chi(\boldsymbol{A}, \boldsymbol{a} - 2\boldsymbol{e}_i, n, \alpha) \\ & -n(2a_i + 1) && \chi(\boldsymbol{A}, \boldsymbol{a}, n - 2, \alpha) \\ & +\alpha(2a_i + 1) && \chi(\boldsymbol{A}, \boldsymbol{a}, n - 1, \alpha) \\ & -\delta(n > 2)\, n(n - 2) && \chi(\boldsymbol{A}, \boldsymbol{a} + 2\boldsymbol{e}_i, n - 4, \alpha) \\ & +\alpha(n + (n - 1)\delta(n > 1)) && \chi(\boldsymbol{A}, \boldsymbol{a} + 2\boldsymbol{e}_i, n - 3, \alpha) \\ & -\alpha^2 && \chi(\boldsymbol{A}, \boldsymbol{a} + 2\boldsymbol{e}_i, n - 2, \alpha)\end{aligned}$$

then:

$$[2.11] \quad T_{AAi} = \langle U_{AAi} \rangle$$

where the symbol $\langle U_{AAi} \rangle$ stands for an integral like the one-center overlap including all the CETO functions present in eq. [2.10].

2.3. Nuclear attraction integrals

(i) One-center integrals of the form $\langle$AA:A$\rangle$

This type of integral can be computed by integrating within a spherical coordinates framework. They can be associated with a one-center overlap integral [2.2] as follows:

$$\begin{aligned}[2.12] \quad \langle AA':A \rangle &= \int \chi(\boldsymbol{A},\boldsymbol{a},n,\alpha)\, r_A^{-1}\, \chi(\boldsymbol{A},\boldsymbol{a}',n',\alpha')\, dV \\ &= \langle \chi(\boldsymbol{A}, \boldsymbol{a} + \boldsymbol{a}', n + n' - 1, \alpha + \alpha') \rangle\end{aligned}$$

(ii) Two-center integrals of the form $\langle$AA:B$\rangle$

This type of integral, and the following case, can be obtained by integrating in a prolate spherical coordinates framework.

One can see that the nuclear attraction integral is a linear combination of two-center overlap integrals:

$$\begin{aligned}[2.13] \quad \langle AA':B \rangle &= \int \chi(\boldsymbol{A},\boldsymbol{a}',n',\alpha')\, r_B^{-1}\, \chi(\boldsymbol{A},\boldsymbol{a}'',n'',\alpha'')\, dV \\ &= \int \chi(\boldsymbol{A},\boldsymbol{a},n,\alpha)\, r_B^{-1}\, dV \\ &= \Sigma(\boldsymbol{i} = \mathbf{0},\boldsymbol{a})\, \Sigma(\boldsymbol{j} = \mathbf{0},\boldsymbol{i})\, M(\boldsymbol{i},\boldsymbol{j},\boldsymbol{a}) \\ &\quad \cdot f(\boldsymbol{i},\boldsymbol{j},\boldsymbol{a},\varphi,\theta)\, \langle W(A,\boldsymbol{g},n,\alpha) | W(B,\mathbf{0},-1,0) \rangle\end{aligned}$$

where $\boldsymbol{a} = \boldsymbol{a}' + \boldsymbol{a}''$, $n = n' + n''$, and $\alpha = \alpha' + \alpha''$. The M and f coefficients and the vectors $\boldsymbol{g} = \boldsymbol{g}(\boldsymbol{a},\boldsymbol{i},\boldsymbol{j})$, constructed as in eq. [1.9], arise from the rotations transforming the CETO centered at $\boldsymbol{A}$ into a well-oriented form with respect to the CETO centered at $\boldsymbol{B}$.

Also the term $r_B^{-1} = \chi(\boldsymbol{B},\mathbf{O},-1,0) = W(B,\mathbf{O},-1,0)$ can be expressed either as a CETO or a WO-CETO, relaxing conditions 2 and 3 of CETO Definition 1.

The overlap-like integrals appearing in eq. [2.13], which involve the operator $W(B,\mathbf{0},-1,0)$, can be taken as a particular case of the two-center overlap integrals described in eq. [2.4].

(iii) Two-center integrals of the form $\langle$AB:A$\rangle$ *or* $\langle$AB:B$\rangle$

In this case, one has

$$\begin{aligned}[2.14] \quad \langle AB:A \rangle &= \int \chi(\boldsymbol{A},\boldsymbol{a},n,\alpha)\, r_A^{-1}\, \chi(\boldsymbol{B},\boldsymbol{b},m,\beta)\, dV \\ &= \langle \chi(\boldsymbol{A}, \boldsymbol{a}, n - 1, \alpha) | \chi(\boldsymbol{B},\boldsymbol{b},m,\beta) \rangle\end{aligned}$$

Thus, a finite linear combination of WO-CETO overlap integrals suffices to compute the two-center $\langle AB:A \rangle$ integrals.

3. Coulomb repulsion integrals

Coulomb repulsion integrals over CETO functions, conserving the important role already obtained in GTO and STO choices, are discussed here.

The one- and two-center Coulomb integral computation is set as was done in earlier classical work, see for example refs. 12 and 16. We use the structure of the nuclear attraction monoelectronic integrals to solve the integration over the coordinates of the first electron for the one-center problem, in the same way as Wahl *et al.* (12) proposed when dealing with STO functions in general. However, we reverse this integration scheme for the two-center case, as did O-ohata and Ruedenberg, also within the STO functions framework, in an interesting paper published in 1966 (16).

This twofold integration scheme was adopted after realizing that, when considering the two-center case, the potential first integration drives towards a second integration step with plenty of difficulties, if general analytical formulae are sought. In fact, Wahl *et al.* (12) proposed to perform the second integration numerically. The integral analytical evaluation over the coordinates of the second electron, in the two-center CETO function case, corresponds to a calculation of integrals, involving in the worst situation an infinite series if the O-ohata and Ruedenberg (16) scheme is used.

It must be said now, taking into account the property outlined in eq. [1.10], that all the Coulomb repulsion integrals will transform into integral forms, which we have called *reduced Coulomb integrals*. For example, a Coulomb integral written schematically in the form $\langle AA|r_{12}^{-1}|BB \rangle$ will be reduced to $\langle A|r_{12}^{-1}|B \rangle$. Only this kind of integral is discussed in the present paper, due to the fact that the coordinate rotations and the use of property [1.10] will transform

Can. J. Chem. Downloaded from www.nrcresearchpress.com by 92.62.229.171 on 09/08/12
For personal use only.

Coulomb integrals into this last form, $|A\rangle$ and $|B\rangle$ being WO-CETO functions. Moreover, as will be shown in Sect. 4, when following the approach outlined there, the many-center integrals require only reduced Coulomb integrals in order to be evaluated. Two kinds of reduced Coulomb integrals over WO-CETO functions will be studied here: one- and two-center.

3.1. Potential functions

The general integration structure adopted in order to obtain analytical formulae in the one-center case is based on the first integration, associated with a nuclear attraction integral like those appearing in eq. [2.14]. In fact, writing the following general reduced Coulomb integral:

$$[3.1]\quad R_{AB} = \langle A|r_{12}^{-1}|B\rangle = \iint [W(A,\boldsymbol{a},n,\alpha)\{1\}]\, r_{12}^{-1} \cdot [W(B,\boldsymbol{b},m,\beta)\{2\}]\, dV_1\, dV_2$$

integration with respect to the electron {2} is equivalent to computing a nuclear attraction integral such as:

$$[3.2]\quad \vartheta(1) = [\langle B|r_{12}^{-1}\rangle\{1\}] = [\langle W(B,\boldsymbol{b},m,\beta)|r_{12}^{-1}\rangle\{1\}]$$

which in turn is a function of electron {1} coordinates. Thus, in general, a reduced repulsion integral may be written:

$$[3.3]\quad R_{AB} = \int [W(A,\boldsymbol{a},n,\alpha)\{1\}]\, \vartheta(1)\, dV_1$$

The integration over the coordinates of the electron number {2} must be done over a prolate spherical coordinate system $\{r_{B2},r_{12},r_{B1}\}$ defined in Appendix A, Definition A1, and the obtained analytic expression of the nuclear attraction integral shown in eq. [3.2]. The intercenter distance, r_{B1}, will act here as a variable and it has to be integrated when considering the electron {1} coordinates. To have electron {2} in a well-oriented system with respect to electron {1}, it is necessary to perform a rotation, for each position of electron {1}, from the original system to the prolate spherical system.

Let the WO-CETO attached to electron {2} coordinates be symbolized by $W(B,\boldsymbol{b},m,\beta)$.

Electrons {1} and {2} are described by means of typical spherical coordinate systems $\{r_{A1},\theta_1,\varphi_1\}$ and $\{r_{B2},\theta_2,\varphi_2\}$, respectively.

After performing the needed rotations outlined in Sect. 1.3.1, one can express the $\vartheta(1)$ potential function [3.2] as

$$[3.4]\quad \vartheta(1) = \Sigma(\boldsymbol{i} = \boldsymbol{0},\boldsymbol{b})\, \Sigma(\boldsymbol{j} = \boldsymbol{0},\boldsymbol{i})\, M(\boldsymbol{i},\boldsymbol{j},\boldsymbol{b})\, f(\boldsymbol{i},\boldsymbol{j},\boldsymbol{b},\varphi_1,\theta_{B1})\langle W(B,\boldsymbol{g},m,\beta)|W(\{1\},\boldsymbol{0},-1,0)\rangle$$

where $\Sigma(\boldsymbol{i} = \boldsymbol{0},\boldsymbol{b})$ and $\Sigma(\boldsymbol{j} = \boldsymbol{0},\boldsymbol{i})$ are nested summation symbols and the coefficients $M(\boldsymbol{i},\boldsymbol{j},\boldsymbol{b})$ and $f(\boldsymbol{i},\boldsymbol{j},\boldsymbol{b},\varphi_1,\theta_{B1})$ are defined in Sect. 1.3.1. Note that the angle θ_{B1} is measured from the center $\boldsymbol{B}$. The $W(\{1\},\boldsymbol{0},-1,0)$ notation stands for a WO-CETO centered on the position of the electron {1}.

The vector $\boldsymbol{g}$, according to eq. [1.9], is defined here as $\boldsymbol{g}(\boldsymbol{b},\boldsymbol{i},\boldsymbol{j})$.

Using eq. [2.4], eq. [3.4] can be written:

$$[3.5]\quad \langle W(B,\boldsymbol{g},m,\beta)|W(\{1\},\boldsymbol{0},-1,0)\rangle = F_2(g_2,g_1)\, N(T_b,\beta)\Sigma(\boldsymbol{p} = \boldsymbol{0},\boldsymbol{q})\, A(\boldsymbol{p},\boldsymbol{h},\beta)\, r_{B1}^{T_b-s}\, \{(-1)^{p_4} - \exp(-\beta r_{B1})\}$$

where:

(*i*) $T_b = m + \Sigma_i b_i$

(*ii*) The function N is defined by

$$[3.6]\quad N(t,\beta) = 2^{-t}\, \beta^{-2}$$

(*iii*) The coefficients A are constructed by means of

$$[3.7]\quad A(\boldsymbol{p},\boldsymbol{h},\beta) = \Gamma(\boldsymbol{p},\boldsymbol{h})\, \Lambda(\boldsymbol{p})\, (2/\beta)^s$$

where Γ appears as in eq. [2.4] with $\boldsymbol{t} = (p_1,p_2)$. The Λ coefficient is defined as $\Lambda(\boldsymbol{p}) = (p_1!p_2!)/(p_3!p_4!)$ and $s = p_1 + p_2 - (p_3 + p_4)$.

(*iv*) The six components of the vector $\boldsymbol{h}$ are

$$[3.8]\quad \boldsymbol{h} = (m + 1,\, 0,\, g_3,\, 0,\, k,\, k)$$

with $k = (g_1 + g_2)/2$.

(*v*) Finally,

$$[3.9]\quad \boldsymbol{q} = (m + 1,\, m + 1,\, p_1,\, p_2)$$

Although the previous scheme seems very promising for both one- and two-center cases, we faced the same difficulties as Wahl *et al.* (12) have surely met, when integration over the second electron was to be performed. In consequence, we use this approach only for the one-center integrals, discussed next.

3.2. One-center reduced Coulomb integrals

Let be $W(1) = W(A,\boldsymbol{a},n,\alpha)$ and $W(2) = W(B,\boldsymbol{b},m,\beta)$ two WO-CETOs centered at the origin, that is, $\boldsymbol{A} = \boldsymbol{B} = \boldsymbol{0}$.

One can define the following quantities:

(*i*) $T_a = n + \Sigma_i a_i$ and $T_b = m + \Sigma_i b_i$ as the total order of each WO-CETO.

(*ii*) $T = T_a + T_b$ as the total order of the integral.

The integral to be calculated is

$$[3.10]\quad R_{AA} = \langle A|r_{12}^{-1}|A\rangle = \iint W(1)\, r_{12}^{-1}\, W(2)\, dV_1\, dV_2$$

which can be written using the potential integral described in eq. [3.2].

Can. J. Chem. Downloaded from www.nrcresearchpress.com by 92.62.229.171 on 09/08/12
For personal use only.

One can obtain the expression for $\vartheta(1)$ using eq. [3.5] where the prolate spherical system needed is configured by means of the parameters $\{r_2, r_{12}, r_1\}$.

Integration over the electron $\{1\}$ is carried out in a spherical coordinates framework $\{r_1, \theta_1, \varphi_1\}$ and leads to the final result:

$$[3.11] \quad R_{AA} = \delta(\wedge_i(a_i + b_i = \dot{2}))\, N(T_b - 1, \beta)\, \Sigma(\boldsymbol{i} = \boldsymbol{0}, \boldsymbol{b})\, \Sigma(\boldsymbol{j} = \boldsymbol{0}, \boldsymbol{i}) C(\boldsymbol{i}, \boldsymbol{a}, \boldsymbol{b})\, \Sigma(\boldsymbol{p} = \boldsymbol{0}, \boldsymbol{q})\, A(\boldsymbol{p}, \boldsymbol{h}, \beta)\, D(\boldsymbol{p}, n, \alpha, \beta)$$

where the following definitions hold.

(*i*) The C coefficients are defined as

$$[3.12] \quad C(\boldsymbol{i}, \boldsymbol{a}, \boldsymbol{b}) = B(\boldsymbol{i}, \boldsymbol{a}, \boldsymbol{b}) F_1(a_1 + a_2 + i_1 + i_2 + i_3 - (j_1 + j_2) + 1, a_3 + b_3 + j_1 + j_2 - i_3)$$

with the B coefficients being defined in turn by means of

$$[3.13] \quad B(\boldsymbol{i}, \boldsymbol{a}, \boldsymbol{b}) = M(\boldsymbol{i}, \boldsymbol{j}, \boldsymbol{b})\, F_2(b_1 + b_2 - (i_1 + i_2), j_1 + j_2 + i_3) F_2(a_2 + b_1 - i_1 + i_2, a_1 + b_2 + i_1 - i_2)$$

where $M(\boldsymbol{i}, \boldsymbol{j}, \boldsymbol{b})$ are the transformation coefficients constructed as in eq. [1.6].

(*ii*) N and A are the same as the coefficients defined in eqs. [3.6] and [3.7] respectively, and the functions F_k are described in Appendix B, Definition B5.

(*iii*) The six components of the vector $\boldsymbol{h}$ are the same as these defined in eq. [3.8], with the same definition of index g_3.

(*iv*) The vector $\boldsymbol{q}$ has its components constructed as: $(T_b + 1, T_b + 1, p_1, p_2)$.

(*v*) The coefficients D are defined as:

$$[3.14] \quad D(\boldsymbol{p}, n, \alpha, \beta) = (t - 1)!\, \{(-1)^{p_4} \alpha^{-t} - (\alpha + \beta)^{-t}\}$$

with $t = 3 + n - (p_1 + p_2) + p_3 + p_4$.

(*vi*) From the parity restrictions associated with the F_k functions, it is easy to determine that the following conditions necessarily hold: $\{\wedge_i(a_i + b_i = \dot{2})\}$, in order to have non-vanishing integrals. This generates the logical Kronecker delta appearing in eq. [3.11].

(*vii*) To avoid integration divergence when obtaining $\vartheta(1)$, before carrying out any calculation as described in this section, it is necessary to ensure that $T_a \geq T_b$.

3.3 Two-center reduced Coulomb integrals

Let W_A, W_B be two WO-CETO functions placed at the centers $\boldsymbol{A}$ and $\boldsymbol{B}$ respectively, with $\boldsymbol{A} \neq \boldsymbol{B}$ and R being the inter-center distance.

Due to the problems discussed at the end of Sect. 3.1, the integration in the two-center case has been done using the methodology outlined by O-ohata and Ruedenberg (16). The integral to be computed now is a reduced Coulomb integral written as

$$[3.15] \quad R_{AB} = \int\int W_A(\boldsymbol{r}_1 - \boldsymbol{r}_A)\, |\boldsymbol{r}_1 - \boldsymbol{r}_2|^{-1} W_B(\boldsymbol{r}_2 - \boldsymbol{r}_B)\, d\boldsymbol{r}_1\, d\boldsymbol{r}_2$$

Making a change of variable:

$$[3.16] \quad \boldsymbol{r}_2 - \boldsymbol{r}_B = \boldsymbol{r}_1 - \boldsymbol{r}_C$$

one must evaluate integral [3.15] in the form:

$$[3.17] \quad R_{AB} = \int\int W_A(\boldsymbol{r}_1 - \boldsymbol{r}_A)\, |\boldsymbol{r}_C - \boldsymbol{r}_B|^{-1} W_B(\boldsymbol{r}_1 - \boldsymbol{r}_C)\, d\boldsymbol{r}_1\, d\boldsymbol{r}_C = \int |\boldsymbol{r}_C - \boldsymbol{r}_B|^{-1}\, S(\boldsymbol{r}_C - \boldsymbol{r}_A)\, d\boldsymbol{r}_C$$

To obtain this final result an overlap integral has to be calculated between the CETO functions χ_A, χ_C, resulting from the translation of W_A, W_B to the new frame defined in eq. [3.16]:

$$[3.18] \quad S(\boldsymbol{r}_C - \boldsymbol{r}_A) = \int \chi_A(\boldsymbol{r}_1 - \boldsymbol{r}_A)\, \chi_C(\boldsymbol{r}_1 - \boldsymbol{r}_C)\, d\boldsymbol{r}_1 = \Sigma(\boldsymbol{i} = \boldsymbol{0}, \boldsymbol{a})\, \Sigma(\boldsymbol{j} = \boldsymbol{0}, \boldsymbol{i})\, \Sigma(\boldsymbol{i}' = \boldsymbol{0}, \boldsymbol{b})\, \Sigma(\boldsymbol{j}' = \boldsymbol{0}, \boldsymbol{i}')$$
$$\cdot M(\boldsymbol{i}, \boldsymbol{j}, \boldsymbol{a})\, M(\boldsymbol{i}', \boldsymbol{j}', \boldsymbol{b}) f(\boldsymbol{i}, \boldsymbol{j}, \boldsymbol{a}, \varphi_A, \theta_A)\, f(\boldsymbol{i}', \boldsymbol{j}', \boldsymbol{b}, \varphi_A, \theta_B) \langle W(A, \boldsymbol{g}, n, \alpha) | W(C, \boldsymbol{g}', m, \beta) \rangle$$

with $\boldsymbol{g} = \boldsymbol{g}(\boldsymbol{a}, \boldsymbol{i}, \boldsymbol{j})$ and $\boldsymbol{g}' = \boldsymbol{g}(\boldsymbol{b}, \boldsymbol{i}', \boldsymbol{j}')$ following the convention outlined in eq. [1.9].

Using the expression [3.18] in eq. [3.17] and the Laplace expansion of $|\boldsymbol{r}_C - \boldsymbol{r}_B|^{-1}$, one arrives at the final result:

$$[3.19] \quad R_{AB} = \delta(a_1 + b_1 = \dot{2} \wedge a_2 + b_2 = \dot{2}) R^2\, (R/2)^{t+1}\, \Sigma(\boldsymbol{i} = \boldsymbol{0}, \boldsymbol{a})\, \Sigma(\boldsymbol{j} = \boldsymbol{0}, \boldsymbol{i})\, \Sigma(\boldsymbol{i}' = \boldsymbol{0}, \boldsymbol{b})\, \Sigma(\boldsymbol{j}' = \boldsymbol{0}, \boldsymbol{i}')$$
$$\cdot M(\boldsymbol{i}, \boldsymbol{j}, \boldsymbol{a})\, M(\boldsymbol{i}', \boldsymbol{j}', \boldsymbol{b})\, F_2(g_2 + g_2', g_1 + g_1')\, F_2(c_1 + c_1', c_2 + c_2')$$
$$\cdot \sum(\boldsymbol{r} = \boldsymbol{0}, \boldsymbol{t})\, \Gamma(\boldsymbol{r}, \boldsymbol{d}) \sum_{s=0}^{\infty} P(s, c_3 + c_3', c_4 + c_4')\, J(\boldsymbol{u}, \sigma, \tau)$$

where:

(*i*) The $\boldsymbol{c}$ and $\boldsymbol{c}'$ vectors are defined by means of the general vector structure:

$$[3.20] \quad \boldsymbol{c} = \boldsymbol{c}(\boldsymbol{a}, \boldsymbol{i}, \boldsymbol{j}) = (a_1 - i_1 + i_2, a_2 + i_1 - i_2, i_1 + i_2 + i_3 - (j_1 + j_2), a_3 + j_1 + j_2 - i_3)$$

$\boldsymbol{c}' = \boldsymbol{c}(\boldsymbol{b}, \boldsymbol{i}', \boldsymbol{j}')$ being defined in a similar manner.

Can. J. Chem. Downloaded from www.nrcresearchpress.com by 92.62.229.171 on 09/08/12
For personal use only.

(*ii*) The function P is

$$[3.21]\quad P(k,m,n) = \int_0^{\pi} P_k(\cos\theta)(\sin\theta)^m(\cos\theta)^n\,d\theta = 2^{-k}\sum_{p=0}^{q}\frac{(-1)^p(2(k-p))!}{p!(k-p)!(k-2p)!}F_1(m,k+n-2p)$$

where $q = [k/2]$ is the largest integer in the quotient $k/2$, the function F_1 is defined in Appendix B, Definition B5, and $P_k(x)$ are Legendre polynomials of order k.

$$[3.22]\quad (iii)\ J(\boldsymbol{u},\sigma,\tau) = K(\boldsymbol{u},\sigma,\tau) + L(\boldsymbol{u},\sigma,\tau)$$

where $\boldsymbol{u} = (\boldsymbol{r},s,t)$, $\boldsymbol{r} = (r_1,r_2)$, and

$$[3.23]\quad K(\boldsymbol{u},\sigma,\tau) = \int_1^{\infty} x^{(t-s+2)}A_{r_1}(\sigma x)B_{r_2}(\tau x)\,dx$$

$$[3.24]\quad L(\boldsymbol{u},\sigma,\tau) = \int_0^{1} x^{(t+s+3)}A_{r_1}(\sigma x)B_{r_2}(\tau x)\,dx$$

One can use a product $A_k(x)B_l(y)$ expansion form avoiding negative powers of x in the expression of $L(\boldsymbol{u},\sigma,\tau)$. In this manner, the K and L integrals lead to computing the $C_k(x)$ and $D_k(x)$ auxiliary functions, defined in Appendix B, Definitions B3 and B4.

(*iv*) In this formulation $\boldsymbol{t} = (t,t)$, $t = 2 + m + n + \Sigma(a_i + b_i)$, the vector $\boldsymbol{d} = (n+1, m+1, g_3, g_3', h, h)$ with $h = (g_1 + g_1' + g_2 + g_2')/2$, as well as the parameters σ and τ, which are defined as in eq. [2.4].

(*vi*) The parity restrictions associated with the F_k functions have their origin in the logical Kronecker delta appearing in eq. [3.19].

4. Many-center integrals

To compute many-center integrals, two choices can be proposed in a first instance.

The first is based on optimally expressing a two-center CETO product in terms of a linear combination of CETOs, centered at each of the sites belonging to the product functions. This approach will be discussed here and then used to describe in the following sections how to compute three- and four-center integrals. More details will be given elsewhere.

The second option can be based on trivially expressing the 1*s* exponential part of the CETO functions in terms of a linear combination of primitive GTO, as did Fernández Rico (4*e*) when dealing with STO. This approach, which possesses an extreme simplicity and is well adapted to the same form as the Cartesian angular part of the CETO and GTO functions, seems very promising because the exponential part of the CETO functions only has to be expanded.

In fact, when using a Gaussian expansion, a unique fixed primitive GTO linear combination is needed, as a consequence of the scaling theorem demonstrated by O-ohata, Taketa, and Huzinaga (17) when dealing with a similar problem. In this easy numerical environment, integrals over CETO functions become transformations of primitive cartesian GTO integrals. This second approach will be studied in depth elsewhere.

4.1. Two-center expansion of a CETO function product

Let there be two CETO functions centered at points $\{\boldsymbol{A},\boldsymbol{B}\}$ at a distance R: $\{\chi_A,\chi_B\}$. In the present approach the product of both functions Ω_{AB} will be expanded, using a more general structure than the one proposed by Ruedenberg (18), consisting of the sum of two bilinear forms:

$$[4.1]\quad \Omega_{AB} \approx \sum_{\alpha\epsilon A}\sum_{\alpha'\epsilon A}\Gamma_\alpha\Gamma_{\alpha'}\Omega_{\alpha\alpha'} + \sum_{\beta\epsilon B}\sum_{\beta'\epsilon B}\Gamma_\beta\Gamma_{\beta'}\Omega_{\beta\beta'}$$

But, as has been shown before in eq. [1.10], the CETO products $\Omega_{\alpha\alpha'}$ and $\Omega_{\beta\beta'}$ can be substituted by unique CETO functions χ_a and χ_b, respectively. Thus the product Ω_{AB} can also be expressed in terms of WO-CETO functions $\{\Psi_\alpha^A,\Psi_\beta^B\}$ centered separately on $\boldsymbol{A}$ and $\boldsymbol{B}$. Connecting the present approach with earlier ideas of Harris and Rein (19*a*), Newton (19*b*), and Okninski (19*c*), one can also write eq. [4.1] as

$$[4.2]\quad \Omega_{AB} \approx \sum_{\alpha\epsilon A} c_\alpha^A\Psi_\alpha^A + \sum_{\beta\epsilon B} c_\beta^B\Psi_\beta^B$$

In fact, after obtaining this simplified result, it is crucial to prove the product Ω_{AB} can be expanded at the centers $\boldsymbol{A}$ and $\boldsymbol{B}$ with sufficient accuracy. A general theoretical discussion on the way these linear combinations can be calculated follows.

Optimal linear coefficients can be computed using the compact matrix form of eq. [4.2], supposing both sides equal:

$$[4.3]\quad \Omega_{AB} = \boldsymbol{\Psi}^A\boldsymbol{c}^A + \boldsymbol{\Psi}^B\boldsymbol{c}^B$$

then $\{\boldsymbol{c}^A,\boldsymbol{c}^B\}$, the column vectors of the expansion coefficients, can be obtained by multiplying equation [4.3] on the left by the WO-CETO basis set column vectors $(\boldsymbol{\Psi}^A)^+$ and $(\boldsymbol{\Psi}^B)^+$ where both basis sets are stored respectively, and integrating. The following linear system can be built up:

$$[4.4]\quad \boldsymbol{s}_A = \boldsymbol{S}_{AA}\,\boldsymbol{c}^A + \boldsymbol{S}_{AB}\,\boldsymbol{c}^B$$
$$\boldsymbol{s}_B = \boldsymbol{S}_{BA}\,\boldsymbol{c}^A + \boldsymbol{S}_{BB}\,\boldsymbol{c}^B$$

where $\boldsymbol{s}_A = \langle\boldsymbol{\Psi}^A|\Omega_{AB}\rangle$ and $\boldsymbol{S}_{AA} = \langle\boldsymbol{\Psi}^A|\boldsymbol{\Psi}^A\rangle$ is the metric matrix of the WO-CETO basis set centered on $\boldsymbol{A}$. The same definitions apply but with respect to center $\boldsymbol{B}$ for $\boldsymbol{s}_B$ and $\boldsymbol{S}_{BB}$.

Collecting $\{\boldsymbol{s}_A,\boldsymbol{s}_B\}$ and the other matrices in [4.4] in a hypermatrix system one can easily write:

$$[4.5]\quad \boldsymbol{s} = \boldsymbol{S}\,\boldsymbol{c}$$

with obvious definitions for the organization of the matrices in eq. [4.4] as hypermatrices in eq. [4.5]. As $\boldsymbol{S}$ is the metric matrix of the union of the basis sets $\{\boldsymbol{\Psi}^A,\boldsymbol{\Psi}^B\}$, and consequently $\boldsymbol{S} > 0$, then an inverse will always exist: $\boldsymbol{S}^{-1}$, which can be used to solve eq. [4.5].

After some tests, we recommend Cholesky's decomposition (20) in order to compute $\boldsymbol{S}^{-1}$, due to the numerical stability of the method and to the possibility of performing iterative computations when new functions are added to the linear combination [4.3]. When adding functions to the expansion [4.3] it is mandatory to choose them so as to achieve a good fitting between the expansion [4.3] and Ω_{AB}. The parameter taken as an indicator of the degree of fitting is the norm:

$$[4.6]\quad q^{(2)} = |\Omega_{AB} - (\boldsymbol{\Psi}^A\boldsymbol{c}^A + \boldsymbol{\Psi}^B\boldsymbol{c}^B)|^2$$

Supposing all the involved functions are normalized, then the measure:

$$[4.7]\quad \xi = \int \Omega_{AB}\,(\boldsymbol{\Psi}^A\boldsymbol{c}^A + \boldsymbol{\Psi}^B\boldsymbol{c}^B)\,dV$$

Can. J. Chem. Downloaded from www.nrcresearchpress.com by 92.62.229.171 on 09/08/12
For personal use only.

is nothing more than the degree of fitting of the linear combination [4.3] of the WO-CETO charge distribution Ω_{AB}: as $\xi \rightarrow 1$, Ω_{AB} is better covered by the two-center expansion and $q^{(2)} \rightarrow 0$. Numerical experience shows how the measure ξ tends to one with sufficient accuracy ($\approx 10^{-8}$) using a reasonable number of terms (≈ 20) in the combination [4.2].

4.2. Reduction of three- and four-center integrals to mono and bicentric terms

Using the CETO expansion method outlined in the preceding section, it can be seen that molecular integrals may be constructed as linear combinations of other integrals within a reduced number of centers. Three important cases can be considered:

(*i*) Three-center nuclear attraction integrals $\langle AB{:}C\rangle$ will reduce to an expression involving two-center integrals of the $\langle AA{:}C\rangle$ and $\langle BB{:}C\rangle$ type. Here, the expansion expressed in eq. [4.2] is used in order to compute the $\langle AB{:}C\rangle$ integral, and one can write:

$$[4.8]\quad \langle AB{:}C\rangle = \int \chi(\boldsymbol{A},\boldsymbol{a},n,\alpha)\, r_C^{-1}\, \chi(\boldsymbol{B},\boldsymbol{b},m,\beta)\, dV = \langle \Omega_{AB}|r_C^{-1}\rangle = \sum_{\alpha\epsilon A} c_\alpha^A \langle \Psi_\alpha^A|r_C^{-1}\rangle + \sum_{\beta\epsilon B} c_\beta^B \langle \Psi_\beta^B|r_C^{-1}\rangle$$

(*ii*) In general, it can be considered as the evaluation of a two-electron four-center integral of any kind: $\langle AB|\boldsymbol{T}|CD\rangle$. Expanding both charge distributions involved as described in expression [4.2], the integral will be a sum of four bilinear terms that will depend on the four kinds of integral $\{\langle A|\boldsymbol{T}|C\rangle, \langle A|\boldsymbol{T}|D\rangle, \langle B|\boldsymbol{T}|C\rangle, \langle B|\boldsymbol{T}|D\rangle\}$, reduced to bicentric forms:

$$[4.9]\quad \langle AB|\boldsymbol{T}|CD\rangle \approx \sum_a \sum_c C_a^{AC}\, C_c^{CA}\, \langle a|\boldsymbol{T}|c\rangle + \sum_a \sum_d C_a^{AD}\, C_d^{DA}\, \langle a|\boldsymbol{T}|d\rangle + \sum_b \sum_c C_b^{BC}\, C_c^{CB}\, \langle b|\boldsymbol{T}|c\rangle + \sum_b \sum_d C_b^{BC}\, C_d^{DB}\, \langle b|\boldsymbol{T}|d\rangle$$

Thus, three- and four-center Coulomb integrals will be expressed in terms of the reduced Coulomb integrals as defined in eq. [3.1].

(*iii*) An interesting situation, which can easily be solved within the present approach, corresponds to two-center integrals of the "exchange" type: $\langle AB|\boldsymbol{T}|AB\rangle$, which have not been previously discussed. It is well known that in the STO framework and with the Coulomb operator substituting the operator $\boldsymbol{T}$, they are not so trivially computed as the two-center "Coulomb" type integrals: $\langle AA|\boldsymbol{T}|BB\rangle$, as the papers by Ruedenberg (21) or Wahl *et al.* (12) prove. But, using eq. [4.9], they are simply expressed in terms of one-center $\langle A|\boldsymbol{T}|A'\rangle$, $\langle B|\boldsymbol{T}|B'\rangle$, and two-center $\langle A|\boldsymbol{T}|B\rangle$ integrals. The same can be said for the "hybrid" type integrals $\langle AA|\boldsymbol{T}|AB\rangle$.

Conclusions

A general but simple framework has been described in order to compute integrals over CETO functions. The proposed formulation has been written in such a way as to permit: (*a*) construction of a procedure to compute basic two-center and many-center integrals; (*b*) easy buildup of a program structure in any high level language for any integral; (*c*) parallelization of the terms lying inside nested summation symbols.

Acknowledgements

This work has been supported by the Spanish "Ministerio de Industria y Energía" under the "Programa Nacional de Investigatión y Desarrollo Farmacéuticos" through Grant No. FAR 88-0617. One of us (E. B.) benefits by a grant of the "Departament d'Ensenyament de la Generalitat de Catalunya." Comments made by the referees are gratefully acknowledged: they have generated considerable improvement in the paper.

1. S. F. Boys and G. B. Cook. Rev. Mod. Phys. **32**, 285 (1960).
2. V. R. Saunders. *In* Computational techniques in quantum chemistry and molecular physics. *Edited by* G. H. F. Diercksen *et al.* D. Reidel, Dordrecht. 1975. p. 347.
3. C. A. Weatherford and H. W. Jones (*editors*). ETO multicenter molecular integrals. D. Reidel, Dordrecht. 1982.
4. (*a*) R. López, G. Ramírez, J. M. García de la Vega, and J. Fernández Rico. J. Chim. Phys. **84**, 695 (1987); (*b*) J. Fernández Rico, R. López, and G. Ramírez. J. Comput. Chem. **9**, 790 (1988); (*c*) J. Comput. Chem. **10**, 869 (1989); (*d*) Int. J. Quantum Chem. **37**, 69 (1989); (*e*) J. Chem. Phys. **91**, 4204 (1989); **91**, 4213 (1989); (*f*) J. Chem. Phys. **94**, 5032 (1991).
5. (*a*) I. I. Guseinov. J. Chem. Phys. **72**, 2198 (1980); (*b*) Phys. Rev. **A**, **22** 369 (1980); (*c*) *In* ETO multicenter molecular integrals. *Edited by* C. A. Weatherford and H. W. Jones. D. Reidel, Dordrecht. 1982. p. 171; (*d*) J. Chem. Phys. **78**, 2801 (1983); (*e*) Phys. Rev. **A**, **31** 2851 (1985); (*f*) Int. J. Quantum Chem. (Q. C. Symp.), **19**, 149 (1986); (*g*) *In* Quantum chemistry: basic aspects, actual trends. *Edited by* R. Carbó. Stud. Phys. Theor. Chem. **62**, 37 (1989).
6. (*a*) H. W. Jones. Int. J. Quantum Chem. **20**, 1217 (1981); (*b*) Int. J. Quantum Chem. **21**, 1079 (1982); (*c*) Phys. Rev. **A**, **30** 1 (1984); (*d*) Int. J. Quantum Chem. **29**, 177 (1986); (*e*) H. W. Jones, B. Bussery, and C. A. Weatherford. Int. J. Quantum Chem. (Q. C. Symp.), **21**, 693 (1987); (*f*) H. W. Jones. Phys. Rev. **A**, **38** 1065 (1988); (*g*) H. W. Jones and B. Etemadi. Int. J. Quantum Chem. (Q. C. Symp.), **24**, 405 (1990).
7. (*a*) E. O. Steinborn. *In* ETO multicenter molecular integrals. *Edited by* C. A. Weatherford and H. W. Jones. D. Reidel, Dordrecht. 1975. p. 7, and references therein; (*b*) E. O. Steinborn. *In* Methods in computational molecular physics. *Edited by* G. H. F. Diercksen *et al.* D. Reidel, Dordrecht. 1983. p. 37; (*c*) E. O. Steinborn and H. H. H. Homeier. Int. J. Quantum Chem. (Q. C. Symp.), **24**, 349 (1990); (*d*) E. O. Steinborn and E. J. Weniger. J. Mol. Struc. (Theochem), **210**, 71 (1990); (*e*) H. H. H. Homeier and E. O. Steinborn. Int. J. Quantum Chem. **39**, 625 (1991).
8. (*a*) H. Tai. NASA Technical Memorandum 101545. Hampton, Va. (1989); (*b*) Phys. Rev. **A**, **40**, 6681 (1989); (*c*) Chin. J. Phys. **28**, 481 (1990).
9. (*a*) P. W. Atkins. Quanta. Oxford Chemistry Series. Clarendon Press, Oxford. 1974; (*b*) L. C. Biedenharn and J. D. Louck. Angular momentum in quantum physics. Addison-Wesley, Reading, Mass. 1981.
10. J. C. Slater. Phys. Rev. **36**, 51 (1930).
11. (*a*) S. Huzinaga. Approximate atomic functions. Technical reports I, II (1971), and III (1973). Division on Theoretical Chemistry. Department of Chemistry. University of Alberta; (*b*) E. Clementi and C. Roetti. At. Nucl. Data Tables, **14**, 177 (1974).
12. A. C. Wahl, P. E. Cade, and C. C. J. Roothaan. J. Chem. Phys. **41**, 2578 (1964).
13. (*a*) E. Clementi (*Editor*). Modern techniques in computa-

Can. J. Chem. Downloaded from www.nrcresearchpress.com by 92.62.229.171 on 09/08/12
For personal use only.

tional chemistry 1990. IBM Corporation, Kingston, 1990; (*b*) A. D. McLean and Y. S. Lee. *In* Current aspects of quantum chemistry 1981. *Edited by* R. Carbó. Stud. Phys. Theor. Chem. **21**, 219 (1982).
14. (*a*) C. G. Gray and K. E. Gubbins. Theory of molecular fluids. Vol. 1. Appendix A. Clarendon Press, Oxford. (1984); (*b*) R. N. Zare. Angular momentum. John Wiley & Sons, New York. 1988.
15. M. R. Spiegel. Mathematical handbook of formulas and tables. McGraw-Hill, New York. 1968.
16. K. O-ohata and K. Ruedenberg. J. Math. Phys. **7**, 547 (1966).
17. K. O-ohata, H. Tateka, and S. Huzinaga. J. Phys. Soc. Jpn. **21**, 2313 (1966).
18. K. Ruedenberg. J. Chem. Phys. **19**, 1433 (1951).
19. (*a*) E. Harris and R. Rein. Theort. Chim. Acta, **6**, 73 (1966); (*b*) M. D. Newton. J. Chem. Phys. **51**, 3917 (1969); (*c*) A. Okninski. J. Chem. Phys. **60**, 4098 (1974).
20. (*a*) J. H. Wilkinson. The algebraic eigenvalue problem. Clarendon Press. Oxford. 1965; (*b*) E. Durand. Solutions numériques des équations algebriques. Masson et Cie., Paris. 1961; (*c*) R. Carbó and Ll. Domingo. Algebra matricial y lineal. Serie Schaum. McGraw Hill, Madrid. 1987.
21. K. Ruedenberg. J. Chem. Phys. **19**, 1459 (1951).
22. E. Besalú and R. Carbó. Comput. Chem. Submitted.
23. R. Carbó and J. A. Hernández. Chem. Phys. Lett. **47**, 85 (1977).
24. M. Abramowitz and I. A. Stegun. Tables of mathematical functions. Dover, New York. 1972.
25. W. Gröbner and H. Hofreiter. Integraltafel. Springer-Verlag, Wien. 1966.

Appendix A: Definitions

Definition A1: Prolate spherical system

When we refer to the *prolate spherical parameter system* $\{r_A,r_B,R\}$ we mean to use the coordinates:

$$[A.1] \quad u = (r_A + r_B)/R, \qquad v = (r_A - r_B)/R, \qquad \varphi = \varphi_A = \varphi_B$$

the volume element being $dV = (R/2)^3(u^2 - v^2)\,du\,dv\,d\varphi$ and the integration limits: $u\epsilon\{1,\infty\}$, $v\epsilon\{-1,+1\}$, $\varphi\epsilon\{0,2\pi\}$.■

Definition A2: Nested summation symbols

Let us use a *nested summation symbol* as a general expression like $\Sigma(\boldsymbol{k} = \boldsymbol{r},\boldsymbol{s})$ describing a sequence of summation symbols.

The meaning of such a convention corresponds to performing all the sums involved in the generation of all possible forms of vector $\boldsymbol{k}$, whose elements are defined by the limits $k_i = r_i,s_i;\forall i$.

Nested summation symbolism is very convenient because successive generation of $\boldsymbol{k}$ vector elements can be programmed in a general way under any high level language, using a unique **do** or **for** loop irrespective of the number of sums involved. These symbols are well suited for programming in a parallel hardware environment. Inside a nested sum, all operations attached to each vector $\boldsymbol{k}$ can be run into a separate CPU. More details about nested summation symbology can be found in ref. 22.

Definition A3: Logical Kronecker delta

A logical Kronecker delta, $\delta(\{L\})$, is a symbolic factor that is unity when the logical expression $\{L\}$ is true and zero otherwise.■

An initial and crude form of this symbol was given some years ago by one of us within the context of the development of a MCSCF (23). More details concerning Logical Kronecker and related topics can be found in ref. 22.

Definition A4: $P(\boldsymbol{a},u,v)$ function and $\Gamma(\boldsymbol{r},\boldsymbol{a})$ coefficients

For some of the integrals appearing in this paper, it is helpful to obtain an expression for the expansion of the binomial products, which can be written as

$$[A.2] \quad P(\boldsymbol{a},u,v) = (u + v)^{a_1}(u - v)^{a_2}(1 + uv)^{a_3} \cdot (1 - uv)^{a_4}(u^2 - 1)^{a_5}(1 - v^2)^{a_6}$$

One can easily deduce the equivalent compact form:

$$[A.3] \quad P(\boldsymbol{a},u,v) = \Sigma(\boldsymbol{r} = \boldsymbol{0},\boldsymbol{p})\,\Gamma(\boldsymbol{r},\boldsymbol{a})\,u^{r_1}v^{r_2}$$

where $\boldsymbol{p} = (t + 2a_5, t + 2a_6)$ with $t = a_1 + a_2 + a_3 + a_4$.

The coefficients in eq. [A.3] are defined as

$$[A.4] \quad \Gamma(\boldsymbol{r},\boldsymbol{a}) = \Sigma(\boldsymbol{k} = \boldsymbol{0},\boldsymbol{a})\,\delta(k_1 + k_2 + k_3 + k_4 + 2k_5 = r_1)\delta(a_1 + a_2 - (k_1 + k_2) + k_3 + k_4 + 2k_6 = r_2)\,C(\boldsymbol{k},\boldsymbol{a})$$

where

$$[A.5] \quad C(\boldsymbol{k},\boldsymbol{a}) = (-1)^t \prod_{i=1}^{6} \binom{a_i}{k_i}$$

with the index definition: $t = a_2 + a_5 + k_2 + k_4 + k_5 + k_6$.

Appendix B: Auxiliary integrals

Definition B1: $A_k(x)$ integrals

$$[B.1] \quad A_k(x) = \int_1^\infty t^k\,e^{-xt}\,dt.■$$

Definition B2: $B_k(x)$ integrals

$$[B.2] \quad B_k(x) = \int_{-1}^{+1} t^k\,e^{-xt}\,dt.■$$

Definition B3: $C_k(x)$ integrals

$$[B.3] \quad C_k(x) = \int_1^\infty t^{-k}\,e^{-xt}\,dt.■$$

Definition B4: $D_k(x)$ integrals

$$[B.4] \quad D_k(x) = \int_0^1 t^k\,e^{-xt}\,dt.■$$

The evaluation and extensive computational properties of these integrals can be found in the handbook of Abramowitz and Stegun (24).

Definition B5: $F_k(m,n)$ functions

$$[B.5] \quad F_k(m,n) = \int_0^{k\pi} (\sin x)^m (\cos x)^n\,dx$$
$$= \delta(n = \dot{2})\{k\delta(m = \dot{2})(\Gamma(p)\Gamma(q)/\Gamma(p + q)) + \delta(k = 1 \wedge m \neq \dot{2})(2^{m+1}\,m! \prod_{r=0}^{m} [2(n + r) + 1])\}$$

with $k\epsilon\{1,2\}$, $p = (m + 1)/2$, $q = (n + 1)/2$, and $\Gamma(x)$ is the gamma function.■

Partial information on this definition can be found in ref. 25.

Can. J. Chem. Downloaded from www.nrcresearchpress.com by 92.62.229.171 on 09/08/12
For personal use only.

Improvement of the long-range behavior of Gaussian basis sets using asymptotic constraints

TOSHIKATSU KOGA
Department of Applied Chemistry, Muroran Institute of Technology, Muroran, Hokkaido 050, Japan

AND

AJIT J. THAKKAR[1]
Department of Chemistry, University of New Brunswick, Fredericton, N.B., Canada E3B 6E2

Received September 5, 1991

This paper is dedicated to Professor Sigeru Huzinaga on the occasion of his 65th birthday

TOSHIKATSU KOGA and AJIT J. THAKKAR. Can. J. Chem. **70**, 362 (1992).

It is suggested that atomic orbitals with improved long-range behavior can be obtained by using energy-optimized Gaussian basis sets to which Gaussians have been added to satisfy a subset of some recently derived constraints that must be satisfied by the exact Hartree–Fock orbitals. This procedure is demonstrated by illustrative calculations for helium. This method is found to be superior to the *ad hoc* method of adding diffuse Gaussians in an even-tempered fashion.

Key words: Gaussian basis sets, long-range behavior, asymptotic constraints.

TOSHIKATSU KOGA et AJIT J. THAKKAR. Can. J. Chem. **70**, 362 (1992).

On suggère que l'on peut obtenir des orbitales atomiques avec un meilleur comportement à longue distance en utilisant des bases gaussiennes optimisées pour l'énergie auxquelles on a ajouté des gaussiennes dans le but de satisfaire un sous-ensemble de contraintes dérivées récemment et qui doivent être satisfaites par des orbitales de Hartree–Fock exactes. On fait une démonstration de cette procédure par des calculs de l'hélium. On a trouvé que cette méthode est supérieure à la méthode *ad hoc* impliquant l'addition bien tempérée de gaussiennes diffuses.

Mots clés : bases gausiennes, comportement à longue distance, contraintes asymptotiques.

[Traduit par la rédaction]

Can. J. Chem. Downloaded from www.nrcresearchpress.com by 92.62.229.171 on 09/08/12
For personal use only.

Introduction

The long-range behavior of atomic orbitals is important in the calculation of many physically important properties. Examples of such properties include electric properties such as multipole moments, polarizabilities, and hyperpolarizabilities (1, 2), and momentum space properties such as the Compton profile peak height (3–5). Standard variationally optimized basis sets (for reviews, see refs. 6–10) are usually not sufficiently flexible at long range unless they are very large. Hence, it is common practice to augment standard basis sets with diffuse basis functions whenever properties such as those discussed above are to be computed.

There is no single standard method for choosing diffuse basis functions. If the basis set consists of Slater-type functions (STF), then the known asymptotic behavior of Hartree–Fock atomic orbitals (11–13) can be used to add diffuse STF whose exponents match the asymptotic behavior (4, 13). If the basis set consists of Gaussian-type functions (GTF), then one may add diffuse GTF with exponents chosen such that the augmented basis set produces a good fit to the asymptotic behavior in the physically important region (14). A common *ad hoc* prescription, followed in refs. 15–19 and in many other papers, is to choose diffuse GTF with exponents that form a geometric sequence with the exponents of the two most diffuse GTF in the variationally optimal basis set. We shall refer to the diffuse functions chosen by this *ad hoc* procedure as even-tempered diffuse functions.

The purpose of this paper is to demonstrate that self-consistent-field (SCF) orbitals with improved long-range behavior can be obtained by using energy-optimized GTF basis sets supplemented by GTF chosen to ensure that the SCF orbitals satisfy some of the linearly averaged position moment (LAPM) constraints that we recently derived (20).

The LAPM constraints

The LAPM relationships (20) that must be satisfied by the exact solutions of the closed shell Hartree–Fock equations are given by

$$[1] \quad e_i(K,L,M) = \epsilon_i$$

in which ϵ_i is the orbital energy corresponding to the ith orbital ψ_i and

$$[2] \quad e_i(K,L,M) = e_{1,i}(K,L,M) + e_{2,i}(K,L,M)$$

The one-electron component in eq. [2] is given by

$$[3] \quad e_{1,i}(K,L,M) = \{-K(2K+2L+1)[r^{2K+L-2}Y^*_{LM}(\Omega)]_i + [r^{2K+L}v(\boldsymbol{r})Y^*_{LM}(\Omega)]_i\}/[r^{2K+L}Y^*_{LM}(\Omega)]_i$$

and the two-electron component by

$$[4] \quad e_{2,i}(K,L,M) = \sum_{j=1}^{N} \{2[r^{2K+L}w_{jj}(\boldsymbol{r})Y^*_{LM}(\Omega)]_i - [r^{2K+L}w_{ji}(\boldsymbol{r})Y^*_{LM}(\Omega)]_j\}/[r^{2K+L}Y^*_{LM}(\Omega)]_i$$

In the above equations, $v(\boldsymbol{r})$ is the one-electron potential,

$$[5] \quad w_{ij}(\boldsymbol{r}) = \int [\psi_i^*(\boldsymbol{r}')\psi_j(\boldsymbol{r}')]\,|\boldsymbol{r}-\boldsymbol{r}'|^{-1}\,d\boldsymbol{r}'$$

Y_{LM} are spherical harmonics, and square brackets are used to denote *linear* averages as follows:

$$[6] \quad [f(\boldsymbol{r})]_i = \int f(\boldsymbol{r})\psi_i(\boldsymbol{r})\,d\boldsymbol{r}$$

in which ψ_i is a Hartree–Fock orbital. Equation [1] is valid for all $K \geqq 0$, but, in atoms, only for some L and M deter-

[1]Author to whom correspondence may be addressed.

Printed in Canada

Can. J. Chem. Downloaded from www.nrcresearchpress.com by 92.62.229.171 on 09/08/12
For personal use only.

mined by the angular momentum symmetry of ψ_i. The acronym LAPM for the set of relationships embodied in eq. [1] arises from the occurrence of *l*inear *a*verages over *p*osition *m*oments (20–23). The special case $K = L = M = 0$ is the Hartree–Fock counterpart of the original zero-momentum energy expression (24–26), and the full set of LAPM equations is a Hartree–Fock analog of the modified zero-momentum expression (27).

Since the LAPM relationships place emphasis on the outer reaches of the electron density (20), it is plausible that they can somehow be used to determine diffuse basis functions. We found that attempting to satisfy a subset of the LAPM equations by modifying exponents of basis functions that are present in variationally optimized basis sets does not work well. A more suitable procedure is to begin with a variationally optimized basis set, add m basis functions to it, and vary the exponents of the added functions until the augmented basis set satisfies m constraints given by the LAPM eq. [1]. Note that this requires an additional layer of iterations to ensure that the orbital energies used in the constraints coincide with those obtained from the SCF procedure in that basis set.

Results for atomic helium

A large number of calculations based on the above procedure were performed for the helium atom. In this case, symmetry dictates that $L = M = 0$ in eq. [1]. To construct GTF basis sets of dimension N, we began with variationally optimal basis sets containing $(N - m)$ GTF, added m GTF, and varied the exponents of the m added functions to ensure that self-consistent-field (SCF) solutions of the Hartree–Fock (HF) equations in the full N-GTF basis set satisfied the LAPM eq. [1] with $L = M = 0$ and $0 \leqq K \leqq m - 1$. This was done with $N = 4, 6, 8, 10, 12, 14$ and with $m = 0, 1, 2$. In some cases no satisfactory solutions were obtained for $m = 2$. The variationally optimal basis sets with 6 GTF or less were refined versions of the basis sets of van Duijneveldt (28), and those with 7 or more GTF were taken from the work of Partridge (29). For the sake of comparison, N-GTF basis sets constructed by the *ad hoc* addition of an even-tempered diffuse GTF to a variationally optimal basis set with $N - 1$ GTF were also considered.

A summary of the results is presented in Table 1, which lists the total and orbital energies, and the average percent error Δ in the moments $\langle r^k \rangle$ ($-2 \leqq k \leqq 10$ excluding $k = 0$) with respect to the numerically determined Hartree–Fock values (13, 30). The standard energy-optimal basis sets appear as the $m = 0$ cases, the basis sets constructed by the *ad hoc* procedure are denoted by a d after the number of constraints, and those constructed via the LAPM constraints are denoted by an L after the number of constraints.

We found that it is not always possible to apply two or more LAPM constraints. No solutions were found for $N = 10, 12, 14$ with $m = 2$L. Moreover, in the $N = 4$ and 6 cases, the $m = 2$L solutions are not satisfactory because the exponent of one of the two added GTF is larger than an exponent in the underlying $(N - 2)$ GTF energy-optimal basis set. We think the constraint procedure must be considered unsuccessful for atomic helium if it does not produce diffuse functions. Furthermore, in the $N = 8$, $m = 2$L case, even though the two added GTF are more diffuse than any functions in the substrate, their exponents (0.11 and 0.16) are rather close to each other and this leads to near-linear dependence. In view of the above results, we believe that the LAPM procedure should be restricted to one constraint per orbital.

TABLE 1. Overall performance of Gaussian basis sets for helium. N is the number of basis functions. m is the number of constraints; d indicates that the geometric sequence method is used for the diffuse functions whereas L indicates that LAPM constraints (see text) have been used. E and ϵ are the total and orbital energies respectively. Δ is the mean percent error for the moments $\langle r^k \rangle$ with $k = -2, -1, 1, \ldots, 10$

N	m	E	ϵ	Δ
4	0	−2.855160	−0.914151	25.18
4	1d	−2.838713	−0.913247	46.51
4	1L	−2.838603	−0.913421	9.67
4	2L	−2.776531	−0.893048	15.64
6	0	−2.861153	−0.917625	10.79
6	1d	−2.860011	−0.917680	4.78
6	1L	−2.860024	−0.917699	2.84
6	2L	−2.856377	−0.916450	1.34
8	0	−2.861625	−0.917919	4.22
8	1d	−2.861520	−0.917922	3.44
8	1L	−2.861523	−0.917933	0.67
8	2L	−2.861225	−0.917842	0.21
10	0	−2.861673	−0.917951	1.59
10	1d	−2.861661	−0.917950	1.49
10	1L	−2.861662	−0.917953	0.16
12	0	−2.861679	−0.917955	0.59
12	1d	−2.861677	−0.917955	0.58
12	1L	−2.861677	−0.917955	0.06
14	0	−2.861680	−0.917955	0.22
14	1d	−2.861680	−0.917955	0.22
14	1L	−2.861680	−0.917955	0.02
Hartree–Fock limit		−2.861680	−0.917956	0

Next, we turn to a comparison of standard basis sets ($m = 0$), one-LAPM constraint basis sets ($m = 1$L), and basis sets containing one diffuse function added in an even-tempered fashion ($m = 1$d). Table 1 shows clearly that, for a fixed basis set size N, the $m = 1$L sets yield a substantially lower Δ than either the $m = 0$ or $m = 1$d sets. It is rather surprising that the *ad hoc* $m = 1$d sets do *not* have a smaller Δ than the $m = 0$ sets except for $N = 6, 8$. Table 2 contains a detailed comparison of the moments for $N = 8$. Evidently, the $m = 1$L set has a much smaller Δ because it produces high moments $\langle r^k \rangle$ ($k \geqq 5$) that are in much better agreement with the HF limit values than the $m = 0$ and $m = 1$d sets. Since the high moments weight the outer reaches of the electron density, we can conclude that the SCF orbital in the $m = 1$L basis set has much more accurate long-range behavior than the SCF orbitals in the $m = 0$ and $m = 1$d basis sets.

Moreover, Table 1 shows that the $m = 1$L sets lead to better orbital energies than the $m = 1$d and $m = 0$ sets, except for $N = 4$. The relatively poor behavior of the $N = 4$, $m = 1$L basis set leads us to suggest that the LAPM constraints are not suitable for very small basis sets. Table 2 shows that the price for the better long-range behavior and orbital energies of the $m = 1$L set is a slightly worse disagreement with the HF limit values of the lower moments. Not unexpectedly, the $m = 1$L sets predict a somewhat worse energy than the energy-optimized $m = 0$ basis sets. However, the $m = 1$L energies are generally better than the $m =$

TABLE 2. Comparison of moments $\langle r^k \rangle$ for some basis sets. N and m are defined in Table 1. Quantities in parentheses are percent errors relative to the Hartree–Fock (HF) limit[a]

k	$N = 8, m = 0$	$N = 8, m = 1d$	$N = 8, m = 1L$	HF limit [a]
−2	5.99112 (−0.07)	5.98552 (−0.17)	5.98546 (−0.17)	5.99550
−1	1.68726 (−0.00)	1.68710 (−0.01)	1.68708 (−0.01)	1.68728
1	0.927204 (−0.01)	0.927451 (0.02)	0.927493 (0.02)	0.927273
2	1.18435 (−0.04)	1.18557 (0.06)	1.18582 (0.08)	1.18483
3	1.93773 (−0.15)	1.94274 (0.11)	1.94410 (0.18)	1.94064
4	3.87067 (−0.44)	3.88971 (0.05)	3.89759 (0.25)	3.88795
5	9.11806 (−1.12)	9.18792 (−0.36)	9.23591 (0.16)	9.22120
6	24.6589 (−2.45)	24.9139 (−1.44)	25.2229 (−0.22)	25.2784
7	74.9061 (−4.76)	75.8696 (−3.54)	77.9817 (−0.85)	78.6525
8	250.983 (−8.35)	255.005 (−6.88)	270.345 (−1.28)	273.845
9	913.67 (−13.4)	933.63 (−11.5)	1051.84 (−0.28)	1054.83
10	3568.98 (−19.9)	3689.83 (−17.2)	4652.95 (4.48)	4453.56

[a] $\langle r^{-2} \rangle$ is from ref. 30 and the remaining moments are the results of C. Froese-Fischer as tabulated in ref. 13.

TABLE 3. GTF basis sets for He with $N = 4, 6, 8, 10, 12, 14$ and $m = 1L$

α	c	α	c
0.089246	0.056376	0.057034	0.012639
0.382943	0.618518	0.244599	0.387370
1.998933	0.413430	0.874139	0.490814
13.62310	0.079350	3.318584	0.219889
		14.76441	0.054946
		98.07836	0.007568
0.041188	0.003361	0.032075	0.001026
0.183374	0.235818	0.149063	0.145034
0.536663	0.454918	0.384431	0.384592
1.610484	0.307754	1.000152	0.344250
5.091302	0.127803	2.672134	0.191598
18.07366	0.035887	7.497970	0.076632
79.42142	0.007206	23.03610	0.023555
529.1919	0.000938	81.36230	0.005787
		357.4945	0.001113
		2385.290	0.000143
0.026204	0.000348	0.022122	0.000128
0.126976	0.090840	0.111469	0.057981
0.299700	0.311309	0.246205	0.246330
0.706113	0.347170	0.538883	0.330400
1.693235	0.236324	1.194470	0.262872
4.163660	0.119118	2.689537	0.156402
10.73075	0.047365	6.218651	0.074795
29.75039	0.015593	15.01941	0.029945
91.21340	0.004393	38.51539	0.010466
322.0648	0.001048	106.6876	0.003258
1415.193	0.000200	327.0232	0.000899
9448.327	0.000026	1154.558	0.000213
		5073.383	0.000041
		33881.84	0.000005

1d ones. In fact, the $m = 1L$ sets are better than the $m = 1d$ sets on almost all counts. The exponents α and the linear coefficients c for the $m = 1L$ basis sets for helium are listed in Table 3.

Conclusions

We have demonstrated that, for atomic helium, basis sets with improved asymptotic behavior can be obtained from standard energy-optimized GTF basis sets by adding one GTF with an exponent chosen such that the augmented basis set satisfies one LAPM constraint. The resulting basis sets are superior to those produced by the commonly used *ad hoc* procedure of adding a diffuse GTF in an even-tempered fashion. We are performing tests to see whether the LAPM basis sets in Table 3 lead to less basis set superposition error in interatomic potential energy calculations, and whether they offer any advantages in polarizability calculations.

It remains to be seen whether this procedure can be successfully used for heavier atoms, and whether it can be extended to open-shell atoms. Such extensions are being explored in our laboratories. If both of these objectives can be met, then the LAPM procedure will become a generally useful method for adding a diffuse function to a GTF basis set.

Acknowledgement

This work has been supported in part by the Natural Sciences and Engineering Research Council of Canada.

1. M. Urban, I. Cernusak, V. Kello, and J. Noga. Method. Comput. Chem. **1**, 117 (1987).
2. C. E. Dykstra. Ab initio calculation of the structures and properties of molecules. Elsevier, Amsterdam. 1988.
3. B. G. Williams. (*Editor*). Compton scattering: the investigation of electron momentum distributions. McGraw–Hill, New York. 1977.
4. P. E. Regier, J. Fisher, B. S. Sharma, and A. J. Thakkar. Int. J. Quantum Chem. **28**, 429 (1985).
5. A. J. Thakkar. J. Chem. Phys. **86**, 5060 (1987).
6. T. H. Dunning, Jr. and P. J. Hay. *In* Methods of electronic structure theory. *Edited by* H. F. Schaefer, III. Plenum, New York. 1977. pp. 1–27.
7. R. Ahlrichs and P. R. Taylor. J. Chim. Phys. **78**, 315 (1981).
8. S. Huzinaga. Comput. Phys. Rep. **2**, 279 (1985).
9. E. R. Davidson and D. Feller. Chem. Rev. **86**, 681 (1986).
10. S. Wilson. Adv. Chem. Phys. **67**, 439 (1987).
11. N. C. Handy, M. T. Marron, and H. J. Silverstone. Phys. Rev. **180**, 45 (1969).
12. G. S. Handler, D. W. Smith, and H. J. Silverstone. J. Chem. Phys. **73**, 3936 (1980).
13. C. L. Davis, H. J. A. Jensen, and H. J. Monkhorst. J. Chem. Phys. **80**, 840 (1984).
14. M. E. Casida and D. P. Chong. Chem. Phys. **132**, 391 (1989).

Can. J. Chem. Downloaded from www.nrcresearchpress.com by 92.62.229.171 on 09/08/12
For personal use only.

15. H. J. Werner and W. Meyer. Mol. Phys. **31**, 855 (1976).
16. A. J. Sadlej. Collect. Czech. Chem. Commun. **53**, 1995 (1988).
17. A. J. Sadlej. Theor. Chim. Acta, **79**, 123 (1991).
18. G. Maroulis and A. J. Thakkar. J. Chem. Phys. **88**, 7623 (1988).
19. G. Maroulis and A. J. Thakkar. J. Chem. Phys. **93**, 4164 (1990).
20. T. Koga, H. Matsuyama, and A. J. Thakkar. Phys. Rev. A, **43**, 3299 (1991).
21. T. Koga. J. Chem. Phys. **89**, 5961 (1988).
22. T. Koga. J. Chem. Phys. **90**, 5887 (1989).
23. T. Koga. J. Chem. Phys. **91**, 4774 (1989).
24. B. H. Armstrong. Bull. Am. Phys. Soc. **9**, 401 (1964).
25. B. H. Armstrong. Lockheed Missiles and Space Company technical report, Physics No. 6-74-64-26 (1964).
26. A. J. Thakkar and V. H. Smith, Jr. Phys. Rev. A, **18**, 841 (1978).
27. T. Koga, K. Ohta, and A. J. Thakkar. Phys. Rev. A, **37**, 1411 (1988).
28. F. B. van Duijneveldt. Gaussian basis sets for the atoms H-Ne for use in molecular calculations. IBM research report RJ945, San Jose, Calif. 1971.
29. H. Partridge. Near Hartree–Fock quality GTO basis sets for the second-row atoms. NASA technical memorandum 89449, Ames Research Center, Moffet Field, Calif. 1987.
30. A. M. Simas, A. J. Thakkar, and V. H. Smith, Jr. Int. J. Quantum. Chem. **24**, 527 (1983).

Can. J. Chem. Downloaded from www.nrcresearchpress.com by 92.62.229.171 on 09/08/12
For personal use only.

Optimization of quantum Monte Carlo wavefunctions using analytical derivatives[1]

HARTMUT BUECKERT AND STUART M. ROTHSTEIN
Department of Chemistry, Brock University, St. Catharines, Ont., Canada L2S 3A1

AND

JAN VRBIK
Departments of Chemistry and Mathematics, Brock University, St. Catharines, Ont., Canada L2S 3A1

Received May 29, 1991

This paper is dedicated to Professor Sigeru Huzinaga on the occasion of his 65th birthday

HARTMUT BUECKERT, STUART M. ROTHSTEIN, and JAN VRBIK. Can. J. Chem. **70**, 366 (1992).

We show how to optimize many-parameter wavefunctions for use in quantum Monte Carlo by deriving and utilizing formulas for analytical rather than numerical evaluation of the required derivatives. We present these in a form which is easily vectorizable for use on a supercomputer. We also discuss several technical issues of variational Monte Carlo to ensure both an unbiased and efficient optimization. Finally, we illustrate our optimization scheme's numerical performance by optimizing ground-state wavefunctions for LiH and H_2O, each with more than 100 variational parameters.

Key words: quantum Monte Carlo, optimization, electron correlation, LiH, H_2O.

HARTMUT BUECKERT, STUART M. ROTHSTEIN et JAN VRBIK. Can J. Chem. **70**, 366 (1992).

On démontre comment optimiser des fonctions d'onde à plusieurs paramètres, utilisables en mécanique quantique selon Monte Carlo; pour réaliser cette optimisation, on met au point et on utilise des formules permettant de faire une évaluation analytique plutôt que numérique des dérivées requises. On les présente sous une forme que l'on peut facilement vectoriser en vue d'une utilisation à l'aide d'un super-ordinateur. On discute aussi de plusieurs points techniques de la méthode de Monte Carlo variationnelle qui permettent d'effectuer une optimisation à la fois impartiale et efficace. Enfin, on donne une démonstration de la performance de notre schéma d'optimisation à l'aide des fonctions d'onde de l'état fondamental du LiH et du H_2O qui contiennent chacun plus de 100 paramètres variationnels.

Mots clés : mécanique quantique de Monte Carlo, optimisation, corrélation électronique, LiH, H_2O.

[Traduit par la rédaction]

Introduction

Our objective is to optimize wavefunctions for use in quantum Monte Carlo which involve a large number of variational parameters. Our optimization scheme shares features of that reported by Umrigar, Wilson, and Wilkins (1) (U.W.W.), who propose minimizing the *variance* of the local energy, and that of Huang, Sun, and Lester, Jr. (2) (H.S.L.), who update the parameters stochastically to avoid ensemble dependency (unlike U.W.W. who use a fixed Monte Carlo sample). Another related paper is Schmidt and Moskowitz (3). They did optimization using analytical derivatives only for the electron correlation parameters. Our emphasis will be on optimizing all the remaining, yet primary parameters (basis set orbital exponents and the molecular orbital coefficients). (Others may also have used analytical derivatives, but even in that event, the relevant formulas are lacking.)

It is absolutely essential for efficient optimization of a large number of parameters to use analytical (as opposed to numerical) evaluation of the required derivatives. The improvement in efficiency (over numerical differentiation) is proportional to the number of parameters to be optimized, and can thus easily reach a factor of 100 or more. (Numerical differentiation takes two extra evaluations of the local energy for each variational parameter, whereas our technique does all these derivatives as a byproduct of a single evaluation, with only a small extra cost.)

We will present the relevant formulas, which are in a form readily vectorizable for use on supercomputers. We also discuss several technical issues to ensure both an unbiased and efficient optimization. We then illustrate our optimization scheme's numerical performance with applications to the ground states of LiH and H_2O molecules, using wavefunctions having more than 100 variational parameters.

Quantum Monte Carlo has virtually unlimited flexibility in its choice of atomic orbitals and correlation functions; the optimization technique represented here provides a useful tool for an in-depth study of the efficiency (in terms of speed of convergence to a complete set) of these. Work in this direction is reported here with the ultimate objective to design a procedure capable of reducing (almost arbitrarily, we hope) the trial function's error for any given molecule.

Analytical derivatives

In this section we report the formulas for the first and second derivatives of the wavefunction (ψ) and the corresponding local energy (E_L), with respect to the parameters of ψ. We assume a trial function of the form $\psi^\uparrow\psi^\downarrow\psi^c$, where $\psi^\uparrow$ is a Slater determinant of molecular orbitals (LCAO in our case) for the spin up electrons, $\psi^\downarrow$ the analog for spin down electrons, and ψ^c is the correlation function. Extension to linear combinations of such functions, as in multiconfiguration Hartree–Fock, is straightforward.

The local energy is conveniently computed as follows:

$$[1] \quad E_L = -\frac{1}{2}(g^\uparrow + g^\downarrow + 2(\mathbf{F}_\alpha^\uparrow \cdot \mathbf{F}_\alpha^{c\uparrow} + \mathbf{F}_\beta^\downarrow \cdot \mathbf{F}_\beta^{c\downarrow}) + g^c) + U$$

where $E_L = H\psi/\psi$, $g^\uparrow = \nabla_N^2\psi^\uparrow/\psi^\uparrow$, $\mathbf{F}_i^\uparrow = \nabla_i\psi^\uparrow/\psi^\uparrow$, etc, and U is the potential energy function. Also, ∇_i is the 3-di-

[1]This work is suported in part by grants from the Natural Sciences and Engineering Research Council of Canada.

Can. J. Chem. Downloaded from www.nrcresearchpress.com by 123.30.183.119 on 09/08/12
For personal use only.

Can. J. Chem. Downloaded from www.nrcresearchpress.com by 123.30.183.119 on 09/08/12
For personal use only.

mensional gradient operator corresponding to the ith electron, and ∇_N is its $3N$-dimensional analog, where N is the number of spin up ($\uparrow$) or down ($\downarrow$) electrons. (In general $N^\uparrow \neq N^\downarrow$, but we omit the superscript on N.) Here, and throughout this paper, two *or more* repeated Greek indices α, β, ... imply summation over all the N electrons. Repeated Roman do *not* imply summation.

It is now necessary to introduce some additional notation. Let $\mathbf{A}^\uparrow$ be the $J \times N$ matrix of values of J atomic orbitals, each evaluated N times, corresponding to the location of the individual electrons. Each atomic orbital is a function of an electron's location $\boldsymbol{r}$, and a single orbital exponent ζ. Extension to two or more non-linear parameters is possible.

Let $\mathbf{B}^\uparrow$ and $\mathbf{D}^\uparrow$ be the matrix of the corresponding gradients and ∇_i^2 values of the atomic orbitals, respectively. ($\mathbf{B}$ has three components for each entry; *i.e.*, it is a $J \times N \times 3$ matrix.) Let $\mathbf{A}^{\uparrow\zeta}$ be the matrix of elements of $\mathbf{A}^\uparrow$, differentiated with respect to the individual (*one for each row*) orbital exponents ζ. We stress this non-standard definition of a matrix of derivatives by using a matrix with superscript ζ rather than with a simple prime. Similarly for $\mathbf{B}^{\uparrow\zeta}$ and $\mathbf{D}^{\uparrow\zeta}$. Finally, let $\mathbf{C}$ be the $N \times J$ matrix of MO coefficients. Thus $\mathbf{CA}^\uparrow$ is the Slater matrix of N molecular orbitals evaluated at each electron's position, and $\psi^\uparrow = \det(\mathbf{CA}^\uparrow)$. The parameters of $\psi^\uparrow$ are the ζ's and the elements of $\mathbf{C}$.

One can easily compute the quantities appearing in eq. [1] by calculating the inverse of the Slater matrix $(\mathbf{CA}^\uparrow)^{-1}$, and some simple matrix algebra (4). In particular,

$$[2] \qquad g^\uparrow = (\mathbf{CD}^\uparrow)_{\alpha\beta}(\mathbf{CA}^\uparrow)^{-1}_{\beta\alpha}$$

and

$$[3] \qquad \mathbf{F}_i^\uparrow = (\mathbf{CB}^\uparrow)_{\alpha i}(\mathbf{CA}^\uparrow)^{-1}_{i\alpha}$$

Here we again stress that $\mathbf{B}$ has the extra dimension of 3, corresponding to the x, y, z components of the gradient. Thus, in effect we are taking the ith diagonal component (3 dimensional) from each of three $N \times N$ matrices.

We can also show that

$$[4] \qquad \frac{\partial \psi^\uparrow}{\partial c_{ij}} = \psi^\uparrow \mathbf{A}^\uparrow_{j\alpha}(\mathbf{CA}^\uparrow)^{-1}_{\alpha i}$$

and

$$[5] \qquad \frac{\partial g^\uparrow}{\partial c_{ij}} = \mathbf{D}^\uparrow_{j\alpha}(\mathbf{CA}^\uparrow)^{-1}_{\alpha i} - \mathbf{A}^\uparrow_{j\alpha}(\mathbf{CA}^\uparrow)^{-1}_{\alpha\beta}(\mathbf{CD}^\uparrow)_{\beta\gamma}(\mathbf{CA}^\uparrow)^{-1}_{\gamma i}$$

where $i = 1, \ldots, N$, and $j = 1, \ldots, J$.

Similarly, for the drift contribution to E_L:

$$[6] \qquad \mathbf{F}^\uparrow_\alpha \cdot \mathbf{F}^{c\uparrow}_\alpha = (\mathbf{CA}^\uparrow)^{-1}_{\beta\alpha}(\mathbf{CB}^\uparrow)_{\alpha\beta} \cdot \mathbf{F}^{c\uparrow}_\beta$$

we obtain

$$[7] \qquad \frac{\partial \mathbf{F}^\uparrow_\alpha \cdot \mathbf{F}^{c\uparrow}_\alpha}{\partial c_{ij}} = (\mathbf{B}^\uparrow_{j\gamma} - \mathbf{A}^\uparrow_{j\alpha}(\mathbf{CA}^\uparrow)^{-1}_{\alpha\beta}(\mathbf{CB}^\uparrow)_{\beta\gamma}) \cdot \mathbf{F}^{c\uparrow}_\gamma(\mathbf{CA}^\uparrow)^{-1}_{\gamma i}$$

where the scalar product (the standard 3-component operation) is between $\mathbf{F}_\gamma^{c\uparrow}$ and the extra third dimension of $\mathbf{B}^\uparrow$.

Now let us turn to the derivatives with respect to ζ_i, the orbital exponents:

$$[8] \qquad \frac{\partial \psi^\uparrow}{\partial \zeta_i} = \psi^\uparrow \mathbf{A}^{\uparrow\zeta}_{i\alpha}(\mathbf{CA}^\uparrow)^{-1}_{\alpha\beta}\mathbf{C}_{\beta i}$$

$$[9] \qquad \frac{\partial g^\uparrow}{\partial \zeta_i} = (\mathbf{D}^{\uparrow\zeta}_{i\alpha} - \mathbf{A}^{\uparrow\zeta}_{i\gamma}(\mathbf{CA}^\uparrow)^{-1}_{\gamma\delta}(\mathbf{CD}^\uparrow)_{\delta\alpha})(\mathbf{CA}^\uparrow)^{-1}_{\alpha\beta}\mathbf{C}_{\beta i}$$

and

$$[10] \qquad \frac{\partial \mathbf{F}^\uparrow_\alpha \cdot \mathbf{F}^{c\uparrow}_\alpha}{\partial \zeta_i} = (\mathbf{B}^{\uparrow\zeta}_{i\gamma} - \mathbf{A}^{\uparrow\zeta}_{i\alpha}(\mathbf{CA}^\uparrow)^{-1}_{\alpha\beta}(\mathbf{CB}^\uparrow)_{\beta\gamma}) \cdot \mathbf{F}^{c\uparrow}_\gamma(\mathbf{CA}^\uparrow)^{-1}_{\gamma\delta}\mathbf{C}_{\delta i}$$

Derivatives of g^c and of $\mathbf{F}^\uparrow_\alpha \cdot \mathbf{F}^{c\uparrow}_\alpha$ with respect to the parameters appearing in ψ^c are also required. For our applications we chose the usual Jastrow factor which contains two parameters. (The same function for all electron pairs was used in our trial functions.) In this case the derivative formulas are too straightforward to be presented here.

Design of the computer program

Following the approach of U.W.W., we seek the parameters of ψ which minimize the variance of the local energy:

$$[11] \qquad V = \frac{\sum_i (E_L(i) - E_g)^2 w(i)}{\sum_i w(i)}$$

Here $w(i) = (\psi(i)/\psi^0(i))^2$, where ψ_0 is the trial function computed with the "current" values of the optimized parameters, and ψ reflects any possible change of these. Now E_g is an estimate of the energy of the state of interest; our optimization proved fairly robust to the actual choice of E_g, and will perform well given just about any reasonable estimate. The sum is taken over a large number (a "block") of configurations drawn from ψ_0^2. (To use weights in this manner is the only proper way to estimate the variance, and to ignore them may (in our experience) adversely affect the performance of the algorithm.)

When attempting to optimize V with a fixed collection of configurations one immediately encounters a very serious obstacle: as the nodes of ψ change, it is very common for only a few (often just one) configurations to acquire an enormous weight $w(i)$, effectively disabling the other configurations and rendering the results of any further optimization of V virtually useless. We follow H.S.L.'s recommendations for dealing with this: ψ_0^2 is reset and a new block of configurations generated correspondingly after each update of the parameters, where the previous block averages of the analytical derivatives of V with respect to the individual variational parameters are used for this update. (A block is typically 20 Metropolis-sampling type of iterations (5) of a few hundred configurations (an ensemble).) However, we do not necessarily accept each such parameter update, as some moves may lead to variance deoptimization (backtracking being a standard feature of almost all optimizations). Our criteria for accepting/rejecting an update are described below.

We now discuss some important features of the procedure in detail:

Can. J. Chem. Downloaded from www.nrcresearchpress.com by 123.30.183.119 on 09/08/12
For personal use only.

Equilibration

The parameters in ψ are modified at the end of each block of Monte Carlo iterations. At that point the ensemble is distributed according to the previous ψ_0. Then we want to simulate a new block according to the updated ψ (to be called ψ_0 now), but we know that it will take several iterations just to re-equilibrate the ensemble. To do so, special care must be taken to remove the "locked-in" configurations which, under Metropolis sampling, would effectively never move (or only after extremely many attempts). They arise because the probability of moving a configuration goes to zero when a node of the new (updated) ψ gets into its immediate vicinity (6). Each such configuration is a remnant of ψ_0 and not at all representative of the current ψ. Keeping it and its likes would significantly bias the averaging process. (This problem, even though not well publicized, applies to any quantum Monte Carlo algorithm which employs an acceptance/rejection step.)

We deal with this problem by monitoring the "staleness" of each configuration — the number of times its move has been consecutively rejected. (A configuration which moves is assigned a staleness of zero.) When the staleness reaches a fixed value (such as 8), the corresponding configuration is replaced by another one, randomly selected from those whose staleness is zero. With this feature near-equilibration is achieved relatively quickly; we usually discard the first 2–8 iterations of each block to allow the ensemble to adjust to the new values of the parameters. Thereafter we start averaging: the local energies, their derivatives with respect to individual variational parameters, the derivatives of ψ, and the values of $(E_L - E_g)^2$ (whose average defines the block variance).

The variance

Since the block variance is subject to statistical fluctuation (unlike in standard optimization), it is important not to reject all changes which result in its increase. For this purpose we use the following scheme:

The average block variance is computed as follows:

$$[12] \quad M^{-1} \sum_{i=1}^{M} (E_L(i) - E_g)^2 \equiv \overline{(E_L(i) - E_g)^2}$$

(This is effectively a double summation, where the implied sum is over all configurations of the contributing part of the block. Thus, M equals the number of configurations times the number of contributing iterations.)

If the current block variance is higher than 1.5 times the "best" variance, the move is rejected — the procedure backtracks to the "best" results (wavefunction and ensemble) so far. At the same time the value of the "best" variance is increased by a factor of 1.5 to prevent the procedure from being "cornered" by statistical fluctuations. (These factors were determined empirically.) Also, the value of the optimization parameter λ (to be described shortly) is doubled, which results in a more conservative parameter "move" for the next block. Otherwise, the parameter update is accepted. But should the current variance actually be smaller than the "best" variance, this too is updated, and the value of λ modified to $\sqrt{(5\lambda)}$ (so that the next move can be more "daring").

To estimate the derivatives of the variance [11], it is important to realize that both ψ and E_L will vary with the parameters, but ψ_0 is fixed (defining the distribution of configurations in the current block). Then the first derivative of the variance with respect to a variational parameter (say, p_j) is obtained from the first derivatives of E_L and ψ as follows:

$$[13] \quad \frac{1}{2}\frac{\partial V}{\partial p_j} = \overline{(E_L - E_g)\frac{\partial E_L}{\partial p_j}} + \overline{(E_L - E_g)^2\left(\frac{1}{\psi}\frac{\partial \psi}{\partial p_j}\right)} - \overline{(E_L - E_g)^2} \cdot \overline{\frac{1}{\psi}\frac{\partial \psi}{\partial p_j}}$$

For the second derivative, to a good approximation:

$$[14] \quad \frac{1}{2}\frac{\partial^2 V}{\partial p_j^2} \approx \sum_{i=1}^{M} \left\{ \frac{\partial}{\partial p_j} \left[\frac{(E_L(i) - E_g)w(i)}{\left(\sum_{i=1}^{N} w(i)^2\right)^{1/2}} \right] \right\}^2$$

$$= \overline{\left(\frac{\partial E_L}{\partial p_j}\right)^2} + \overline{2(E_L - E_g)\left(\frac{\partial E_L}{\partial p_j}\right)\left(\frac{1}{\psi}\frac{\partial \psi}{\partial p_j}\right)} + \overline{(E_L - E_g)^2\left(\frac{1}{\psi}\frac{\partial \psi}{\partial p_j}\right)^2} - 2\left[\overline{(E_L - E_g)\frac{\partial E_L}{\partial p_j}} + \overline{(E_L - E_g)^2\left(\frac{\partial \psi}{\psi \partial p_j}\right)}\right] \cdot \overline{\left(\frac{1}{\psi}\frac{\partial \psi}{\partial p_j}\right)} + \overline{((E_L - E_g)^2)} \cdot \left[\overline{\left(\frac{1}{\psi}\frac{\partial \psi}{\partial p_j}\right)}\right]^2$$

This approximation is standard with least-squares fits used by statisticians and applies equally well here (7).

Updating quantities

Using the variance derivatives eq. [13] the variational parameters are updated by the steepest-descent technique:

$$[15] \quad p_j \rightarrow p_j - \frac{\overline{\frac{\partial V}{\partial p_j}}}{\overline{\frac{\partial^2 V}{\partial p_j^2}}} \cdot \lambda^{-1}$$

Typically λ assumes values between 5 and 10, starting with an initial value of 10.

Estimating the variational parameters

This procedure will optimize ψ even from very rough initial estimates of the variational parameters and a randomly generated ensemble. However, scores of blocks are required to reach a good variance minimum (to achieve "stabilization"), so for increased efficiency this is done in two stages:

First we perform a coarse optimization with a very small block size (we used 5 iterations) with only one or two iterations discarded to allow for equilibration within a block. The parameters very quickly assume quite reasonable values, and these are then used as improved initial values to perform one or more fine optimizations. This consists of several much larger blocks (we used 20 iterations) and more allowance made for equilibration (8 iterations were discarded). Upon stabilization one can still observe small changes in the variational parameters (essentially random fluctuations), and we

TABLE 1. Optimized variance and corresponding ground-state energy for various LiH and H_2O wavefunctions at the experimental geometry[a]

Wavefunction	Verification		Optimization	
	Variance	Energy	Variance	Energy
LiH				
Single configuration[b,c]				
Li: $1s^*2s2p3s3p3d$; H: $1s^*2s2p$	0.092 1(7)	−8.051 5(4)	0.087	−8.054
Many configurations[d,e]				
Li: $1s^*1s'1s''2s2p2p'$; H: $1s^*1s'2s2p$	0.092 7(3)	−8.045 7(4)	0.089	−8.048
Li: $1s^*2s^*2p3s3p3d$; H: $1s2s2p$	0.062 8(2)	−8.048 4(5)	0.063	−8.049
Li: $1s^*2s2p3s3p3d$; H: $1s2s2p^*$	0.067(2)	−8.050 2(6)	0.060	−8.051
Li: $1s^*2s2p^*3s3p3d$; H: $1s2s2p$	0.056 3(8)	−8.055 8(5)	0.054	−8.058
H_2O[b,f]				
O: $1s2s2p3s3p3d4s4p4d4f$; H: $1s2s2p$	2.08(2)	−76.227(6)	2.07	−76.233

[a]The "dominant" orbitals are marked with asterisks.
[b]Cartesian-like STO basis set, eq. [17].
[c]"Exact" non-relativistic energy is −8.0700 au (ref. 10).
[d]"Exact" hydrogen-like orbital basis set, eq. [19].
[e]The first line corresponds to a single configuration. The second line corresponds to a linear combination of the first two configurations, etc.
[f]Estimated "exact" non-relativistic energy is −76.438(2) au (ref. 11); full CI calculation yields −76.257 805 au (ref. 12).

TABLE 2. Variance optimized single configuration wavefunction for LiH ground state at R = 3.015 bohr[a]

Orbital	$[a,d]^b$	ζ (au)	MO Coefficients	
			ϕ_1	ϕ_2
1s(Li)	[0,0]	3.015 8	1	0
2s(Li)	[1,0]	1.203 9	2.762 2E−2	9.768 2E−2
2p(Li)	[0,1]	3.133 0	−1.888 0E−2	−7.272 1E−3
3s(Li)	[2,0]	3.101 8	1.878 4E−2	−2.937 4E−3
3p(Li)	[1,1]	1.791 1	−7.351 1E−4	−4.257 1E−2
3d(Li)	[0,2]	1.970 4	6.917 0E−3	1.012 8E−2
1s(H)	[0,0]	1.131 3	0	1
2s(H)	[1,0]	0.783 3	−2.510 8E−2	0.407 3
2p(H)	[0,1]	1.155 3	−1.649 4E−3	0.122 0

[a]Jastrow parameters (eq. [16]): a = 0.487 45; b = 0.710 50.
[b]Equation [17] with $b = c = 0$.

choose to simply average these over several dozen extra blocks.

It is important to stress that some components of our sampling technique will bias the variance estimate: random replacement of stale configurations; use of a relatively small number of iterations to near-equilibrate within each block; rejection of blocks with large variances; etc. All this will usually slightly exaggerate the quality of the achieved results, both in terms of the variance and ground-state energy. (See Table 1.) This will be more pronounced in the coarse optimizations, but still visible in fine-tuning runs as well. Thus it is necessary to subsequently perform a standard Metropolis-sampling verification to get proper estimates of these quantities. For this purpose we significantly increase the ensemble size as well.

Applications

We apply our scheme to optimize wavefunctions for the ground state of the LiH and H_2O molecules, taken at the experimental geometry. Initially we consider wavefunctions as expressed as a single product of two determinants (one for each spin possibility) multiplied by a Jastrow-type electron correlation function:

$$[16] \quad \psi^c = \exp\left(\sum_{i>j} \frac{ar_{ij}}{1 + br_{ij}}\right)$$

For the sake of programming convenience the basis set was created from Cartesian-like STO's:

$$[17] \quad [a,b,c,d] \equiv \zeta^m r^a x^b y^c z^d \exp(-\zeta r)$$

where $m = a + \ldots + d + 3$. (The non-standard "normalization" constant was intentional.)

For the c_{ij} matrix we start with an $N \times N$ unit matrix for the anticipated "dominant" N basis functions, and zero otherwise. (Without any loss of generality, for our choice of wavefunction the unit matrix can and should be kept fixed throughout the optimization.) For LiH the initial ζ's for all orbitals were equal to the corresponding atomic number. The initial (200) configurations were distributed randomly. The Metropolis iterations were done using a time-step value of 0.05 au. For the "fine" optimizations we used 500 blocks, discarding 300 to allow for stabilization. For the verification of our results, we used 1000 configurations; after equilibration we averaged the energy and variance over 10 blocks of 500 iterations each.

For H_2O the oxygen 1s orbital exponent was initially set at 8; for the second shell orbitals we used the value of 3. The initial random ensemble was distributed randomly as well. The Metropolis time-step was 0.005 au. The optimization was done in stages: first using only a few orbitals (10), then reoptimizing with more oxygen orbitals (initial orbital exponent equal to 6.)

The verified energy and variance, and the corresponding optimized parameters for both molecules appear in Tables 1–3, respectively.

It is obvious that our trial function is not general enough to give us the exact answer even in the limit of using infinitely many atomic orbitals. In fact, we reach this limit with

Can. J. Chem. Downloaded from www.nrcresearchpress.com by 123.30.183.119 on 09/08/12
For personal use only.

Can. J. Chem. Downloaded from www.nrcresearchpress.com by 123.30.183.119 on 09/08/12
For personal use only.

TABLE 3. Variance optimized single configuration wavefunction for H_2O ground state[a,b]

Orbital	[a,b,c,d][c]	ζ (au)	MO coefficients ϕ_1	ϕ_2	ϕ_3	ϕ_4	ϕ_5
1s(O)	[0,0,0,0]	7.98	1.	0	0	0	0
2s(O)	[1,0,0,0]	4.61	0	1	0	0	0
$2p_x$(O)	[0,1,0,0]	5.50	0	0	1	0	0
$2p_y$(O)	[0,0,1,0]	5.65	0	0	0	1	0
$2p_z$(O)	[0,0,0,1]	5.62	0	0	0	0	1
$3p_x$(O)	[1,1,0,0]	3.65	0	0	1.19	0	0
$3p_y$(O)	[1,0,1,0]	3.21	0	0	0	2.36	0
$3p_z$(O)	[1,0,0,1]	4.06	1.42E−2	−0.140	0	0	1.40
$3d_{yz}$(O)	[0,0,1,1]	4.45	0	0	0	−9.46E−2	0
$3d_{xz}$(O)	[0,1,0,1]	3.51	0	0	−0.143	0	0
3s(O)	[2,0,0,0]	4.62	−2.99E−2	1.49	0	0	6.85E−2
$3d_{x^2}$(O)	[0,2,0,0]	2.56	−2.52E−2	2.37	0	0	8.91E−2
$3d_{y^2}$(O)	[0,0,2,0]	2.17	−1.84E−2	1.94	0	0	0.809
$3d_{z^2}$(O)	[0,0,0,2]	2.19	−3.67E−2	3.15	0	0	−4.66E−2
4s(O)	[3,0,0,0]	4.07	−9.83E−3	0.851	0	0	−4.20E−2
$4f_{x^3}$(O)	[0,3,0,0]	7.52	0	0	1.66E−2	0	0
$4f_{y^3}$(O)	[0,0,3,0]	7.30	0	0	0	2.64E−2	0
$4f_{z^3}$(O)	[0,0,0,3]	2.20	−3.62E−3	0.207	0	0	0.168
$4p_x$(O)	[2,1,0,0]	3.29	0	0	0.219	0	0
$4p_y$(O)	[2,0,1,0]	1.91	0	0	0	0.630	0
$4p_z$(O)	[2,0,0,1]	2.66	4.29E−3	4.69E−2	0	0	0.484
$4d_{x^2}$(O)	[1,2,0,0]	8.77	1.05E−3	6.42E−2	0	0	−3.11E−3
$4d_{y^2}$(O)	[1,0,2,0]	8.58	9.78E−4	7.33E−2	0	0	−3.15E−3
$4d_{z^2}$(O)	[1,0,0,2]	8.68	1.00E−3	6.97E−2	0	0	−3.52E−3
$4d_{xz}$(O)	[1,1,0,1]	3.85	0	0	−4.05E−2	0	0
$4d_{yz}$(O)	[1,0,1,1]	7.78	0	0	0	4.82E−3	0
$4f_{x^2y}$(O)	[0,2,1,0]	7.07	0	0	0	2.92E−2	0
$4f_{x^2z}$(O)	[0,2,0,1]	2.25	9.96E−4	−0.226	0	0	0.405
$4f_{y^2z}$(O)	[0,0,2,1]	0.84	−7.84E−3	1.66	0	0	2.01
$4f_{xy^2}$(O)	[0,1,2,0]	7.93	0	0	1.30E−2	0	0
$4f_{xz^2}$(O)	[0,1,0,2]	7.27	0	0	1.93E−2	0	0
$4f_{yz^2}$(O)	[0,0,1,2]	7.22	0	0	0	2.84E−2	0
$1s(H_a)$	[0,0,0,0]	2.25	−8.40E−2	4.65	2.87	0	−2.38
$2p_x(H_a)$	[0,1,0,0]	2.01	1.54E−2	−1.38	−0.483	0	0.371
$2p_z(H_a)$	[0,0,0,1]	1.37	−2.08E−2	3.39	2.58	0	1.11
$2s(H_a)$	[1,0,0,0]	1.71	−6.33E−2	3.79	3.99	0	−2.30
$2p_y(H_a)$	[0,0,1,0]	1.28	0	0	0	2.49	0
$1s(H_b)$	[0,0,0,0]	2.25	−8.40E−2	4.65	−2.87	0	−2.38
$2p_x(H_b)$	[0,1,0,0]	2.01	−1.54E−2	1.38	−0.483	0	−0.371
$2p_z(H_b)$	[0,0,0,1]	1.37	−2.08E−2	3.39	−2.58	0	1.11
$2s(H_b)$	[1,0,0,0]	1.71	−6.33E−2	3.79	−3.99	0	−2.30
$2p_y(H_b)$	[0,0,1,0]	1.28	0	0	0	2.49	0

[a]Geometry (bohr); O(0,0,0); H_a(1.4315,0,−1.1094); H_b(−1.4315,0,−1.1094).
[b]Jastrow parameters (eq. [16]): $a = 0.487$; $b = 1.971$.
[c]Cartesian-like STO basis set (eq. [17]).

9 orbitals for LiH and 42 for H_2O. For LiH the single configuration wavefunction recovers roughly 77% of the correlation energy, for H_2O it is 46%.

Our initial choices of ζ (described above) were purposely made rather arbitrarily. In practice one may elect to use known well-studied basis sets originally designed for Hartree–Fock calculations to speed up the optimization.

The derivatives of the wavefunction and of the local energy of a single-product trial function can be easily extended to a multiconfiguration wavefunction augmented by the electron-correlation Jastrow (8):

$$[18] \quad \psi = (\psi_0^{\uparrow}\psi_0^{\downarrow} + C_1\psi_1^{\uparrow}\psi_1^{\downarrow} + \ldots)\psi^c$$

where the ψ_i's are several different Slater determinants, and the C's are additional optimization parameters. Here the leading term corresponds to the already optimized single-configuration wavefunction, so only the c_{ij}'s, ζ's, and the C's of the additional components need be optimized. We suggest doing this in stages: first optimize C_1 and $\psi_1^{\uparrow(\downarrow)}$, then C_2 and $\psi_2^{\uparrow(\downarrow)}$ (with fixed $\psi_0^{\uparrow(\downarrow)}$, C_1 and $\psi_1^{\uparrow(\downarrow)}$), etc.

To illustrate that this is indeed easily done, we optimized trial function [18] with up to four configurations for the case of LiH. Also, primarily for the sake of curiosity, we changed the basis set to one of "exact" hydrogen-like orbitals:

$$[19] \quad \chi = \rho^l L_n^l(\rho) P_l(\cos(\theta)) \exp(-\rho/2)$$

TABLE 4. Variance optimized multiconfiguration wavefunction for LiH ground state at R = 3.015 bohr[a]

Orbital[b]	ζ (au)	MO coefficients ϕ_1	MO coefficients ϕ_2
ψ_0 (C_0 = 1)			
1s(Li)	7.384 3	1	0
1s′(Li)	4.605 5	5.286 9E−2	−1.033 8
1s″(Li)	3.170 0	5.196 5E−2	0.467 4
2s(Li)	6.337 0	−0.163 4	0.154 9
2p(Li)	6.613 7	−8.767 5E−3	−4.085 6E−3
2p′(Li)	2.584 2	−8.509 8E−3	−0.232 6
1s(H)	2.454 1	0	1
1s′(H)	1.257 5	3.556 3E−2	0.579 8
2s(H)	1.723 6	1.611 2E−2	1.127 1E−2
2p(H)	1.984 2	3.241 8E−3	0.119 8
ψ_1 (C_1 = −4.223 5E−2)			
1s(Li)	7.198 5	1	0
2s(Li)	6.721 8	0	1
2p(Li)	5.643 6	0.256 3	−0.236 3
3s(Li)	7.869 2	−0.251 3	−0.331 5
3p(Li)	4.428 0	−0.263 4	0.226 5
3d(Li)	10.021 9	−4.963 2E−3	5.068 6E−3
1s(H)	1.579 2	−0.735 5	0.682 9
2s(H)	20.093 5	0.225 0	−0.159 0
2p(H)	2.012 5	−7.843 0E−2	7.238 0E−2
ψ_2 (C_2 = −1.228 6E−2)			
1s(Li)	4.898 1	1	0
2s(Li)	7.603 8	9.663 6E−2	0.176 2
2p(Li)	1.067 5	−1.018 5E−2	7.309 1E−2
3s(Li)	3.130 8	6.603 5E−2	−9.938 6E−2
3p(Li)	4.404 8	−1.256 9E−2	0.291 6
3d(Li)	1.159 1	1.382 1E−3	2.056 8E−2
1s(H)	1.856 1	−0.1064	1.168 3
2s(H)	1.661 3	−9.180 7E−3	1.848 9
2p(H)	2.397 3	0	1
ψ_3 (C_3 = −0.130 0)			
1s(Li)	5.337 2	1	0
2s(Li)	7.077 1	6.864 5E−2	0.986 1
2p(Li)	4.512 4	0	1
3s(Li)	4.210 7	1.395 1E−2	−0.864 5
3p(Li)	3.035 6	−6.511 1E−3	−1.000 3
3d(Li)	3.696 7	3.213 0E−5	−1.872 3E−2
1s(H)	1.769 6	−4.972 8E−3	1.172 7
2s(H)	1.545 3	3.384 1E−3	0.603 9
2p(H)	1.441 3	−3.086 2E−4	−0.100 9

[a]Jastrow parameters (eq. [16]): a = 0.495; b = 0.743 7.
[b]"Exact" orbitals, eq. [19].

where $\rho = \zeta r$, P is the standard Legendre polynomial, and L is a Laguerre polynomial, scaled such that the constant term is equal to one:

$$[20]\quad L_\alpha^\beta = 1 - \frac{\alpha-\beta}{\beta+1}\rho + \frac{(\alpha-\beta)(\alpha-\beta-1)}{(\beta+1)(\beta+2)2!}\rho^2 - \frac{(\alpha-\beta)(\alpha-\beta-1)(\alpha-\beta-2)}{(\beta+1)(\beta+2)(\beta+3)3!}\rho^3 + \ldots$$

The energy and variance results for each of four stages of optimization are shown in Table 1. (Note that the single-configuration result was not an improvement over the previous one using the Cartesian Slater orbital basis.) As we continued the optimization, the variance improved at each stage, with the net improvement of about 40%. The energy improved in tandem with the variance. Our optimized four-component wavefunction (Table 4) recovered roughly 85% of the correlation energy. (In our final optimization stage we kept fixed only the parameters for dominant (first) configuration.)

In our applications to LiH and H_2O we used the common choice of both the electron correlation function and the molecular orbitals. Our derivative formulas will also apply (with only minor changes) to other choices, such as the one made by Sun *et al.* (9), who allow the basis function orbital exponents to be different for each molecular orbital. For the sake of curiosity, we extended their wavefunction to 42 orbitals, but this resulted in no significant improvement over the 42 orbital wavefunction we reported above.

Our paper has focused on the technicalities of wavefunction optimization by the Monte Carlo technique. Having concentrated on the technical aspects, we tried to identify the basic ingredients needed for any successful future development, the use of analytical derivatives in particular. We hope to have provided a valuable tool for further research into the electron correlation problem.

Acknowledgements

Our research was supported by grants from the Natural Sciences and Engineering Research Council (NSERC) of Canada. We also acknowledge generous technical support from the Centre for Large Scale Computation at the University of Toronto. Work on this project done by Mr. Allan L. L. East and Mr. Hong Tao Chen was valuable to us and is gratefully acknowledged. And finally, we thank the Mathematics Department at the University of Queensland for supplying computer resources for this project while one of us (J.V.) was on sabbatical leave.

1. C. J. Umrigar, K. G. Wilson, and J. W. Wilkins. Phys. Rev. Lett. **60**, 1719 (1988); *In* Computer simulation studies in condensed matter physics: recent developments. *Edited by* D. P. Landau, K. K. Mon, and H. B. Schutter. Springer-Verlag, New York. 1988. pp. 185–194; C. J. Umrigar. Int. J. Quantum Chem. Symp. **18**, 217 (1989).
2. S. Huang, Z. Sun, and W. A. Lester, Jr. J. Chem. Phys. **92**, 597 (1990).
3. K. E. Schmidt and J. W. Moskowitz. J. Chem. Phys. **93**, 4172 (1990).
4. D. M. Ceperley, G. V. Chester, and M. H. Kalos. Phys. Rev. B**16**, 3081 (1977); B. H. Wells. *In* Methods in computational physics. Vol. 1. *Edited by* S. Wilson. Plenum Press, New York. 1987. pp. 311–350.
5. P. J. Reynolds, D. M. Ceperley, B. J. Alder, and W. A. Lester, Jr. J. Chem. Phys. **77**, 5593 (1982).
6. A. L. L. East. Unpublished results.
7. W. H. Press, B. P. Flannery, S. A. Teukolsky, and W. T. Vetterling. Numerical recipes. Cambridge University Press, Cambridge. 1986. pp. 522–523.
8. R. J. Harrison and N. C. Handy. Chem. Phys. Lett. **113**, 257 (1985).
9. Z. Sun, S.-y. Huang, R. N. Barnett, and W. A. Lester, Jr. J. Chem. Phys. **93**, 3326 (1990).
10. M. F. DePasquale, S. M. Rothstein, and J. Vrbik. J. Chem. Phys. **89**, 3629 (1988).
11. B. J. Rosenberg and I. Shavitt. J. Chem. Phys. **63**, 2162 (1975).
12. C. W. Bauschlicher, Jr. and P. R. Taylor. J. Chem. Phys. **85**, 2779 (1986).

Can. J. Chem. Downloaded from www.nrcresearchpress.com by 123.30.183.119 on 09/08/12
For personal use only.

Polarizabilities of *trans* and *cis* polyacetylene and interactions among chains in crystalline polyacetylene

ZHONGHAO HUANG[1]
Department of Chemistry, Northeast Normal University, Changchun 130024, People's Republic of China

DANIEL A. JELSKI[2]
Department of Chemistry, State University of New York, College at Fredonia, Fredonia, NY 14063, U.S.A.

RONGSHUN WANG, DEMIN XIE, AND CHENDA ZHAO
Department of Chemistry, Northeast Normal University, Changchun 130024, People's Republic of China

XINFU XIA
Department of Chemistry and Physics, 239 Fronczak Hall, State University of New York at Buffalo, Buffalo, NY 14260, U.S.A.

AND

THOMAS F. GEORGE
Departments of Chemistry and Physics, Washington State University, Pullman, WA 99164, U.S.A.

Received April 4, 1991

This paper is dedicated to Professor Sigeru Huzinaga on the occasion of his 65th birthday

ZHONGHAO HUANG, DANIEL A. JELSKI, RONGSHUN WANG, DEMIN XIE, CHENDA ZHAO, XINFU XIA, and THOMAS F. GEORGE. Can. J. Chem. **70**, 372 (1992).

In this paper, we use the semi-empirical Hartree–Fock method introduced within the finite electric field perturbation approach, to calculate the molecular and π-system polarizabilities of *trans* and *cis* polyene H(-CH=CH-)$_n$H (n = 3, 4, 5, ..., 18). The result is that for a given n, the order of both molecular and π-system polarizabilities of polyene is *trans* > *cis*. This result is consistent with the order of experimental values of *trans* and *cis* hexatriene. When the n increases from 3 to 18, the contribution of π-system polarizability to the molecular polarizability increases from 45 to 70%. Using these results, we have extrapolated the polarizabilities of both *trans* and *cis* polyacetylene. The order is *trans* > *cis*. These results and crystal parameters lead to an estimate of the dispersion energies among polyacetylene chains. The result is also $E_{disp}(trans) > E_{disp}(cis)$.

Key words: polarizability, polyacetylene, *cis*/*trans*, CNDO, dispersion energy.

ZHONGHAO HUANG, DANIEL A. JELSKI, RONGSHUN WANG, DEMIN XIE, CHENDA ZHAO, XINFU XIA et THOMAS F. GEORGE. Can. J. Chem. **70**, 372 (1992).

Dans ce travail, on utilise la méthode semi-empirique de Hartree–Fock introduite dans une approche de perturbation d'un champ électrique défini pour calculer les polarisabilités moléculaires et des systèmes-π des polyènes *cis* et *trans* H(-CH=CH-)$_n$H (n = 3, 4, 5, ..., 18). Le résultat est que, pour une valeur donnée de n, l'ordre des polarisabilités moléculaires et des systèmes-π du polyène est *trans* > *cis*. Ce résultat est en accord avec les valeurs expérimentales de l'ordre des *trans*- et *cis*-hexatriènes. Lorsque la valeur de n augmente de 3 à 18, la contribution de la polarisabilité du système-π à la polarisabilité moléculaire augmente de 45 à 70%. Utilisant ces résultats, on a extrapolé les polarisabilités des *cis*- et *trans*-polyacétylènes. L'ordre est *trans* > *cis*. Ces résultats et les paramètres cristallins conduisent à une évaluation des énergies de dispersion entre les chaînes de polyacétylène. On en déduit que $E_{disp}(trans) > E_{disp}(cis)$.

Mots clés : polarisabilité, polyacétylène, *cis*/*trans*, CNDO, énergie de dispersion.

[Traduit par la rédaction]

Introduction

Polyacetylene (PA) is an important conductive polymer that has two isomers, *trans* and *cis* (see Fig. 1). Since PA was synthesized (1,2) and it was found that the conductivity of doped PA rapidly increases from 10^{-6} $(\Omega\ cm)^{-1}$ to as high as 10^3 $(\Omega\ cm)^{-1}$ with increasing dopant concentration (3), much experimental and theoretical research (4,5) has been reported, including differences between *trans* and *cis* PA (6–8). Polarizability is an important property of a material and closely related to interactions among molecules and the dielectric coefficient of the material. Because PA is relatively insoluble and decomposes before melting (9), these experimental difficulties have so far precluded the measurement of the polarizability of either *trans* or *cis* PA.

Davies (10) studied the π-system polarizabilities of the *trans* polyene series, using the perturbed HMO method. He found that the α^{π}_{xx}, which is the component of π-system polarizability along the carbon chain, is proportional to L^3, where L is the length of carbon chain. Recently, Hurst *et al.* (11) calculated the polarizabilities of *trans* polyene series, H(-CH=CH-)$_n$H (n = 2, 3, ..., 11), using the *ab initio* coupled–perturbed Hartree–Fock method, and the extrapolated polarizability of *trans* PA is 60.3 au/C_2H_2. To our knowledge, no study of the polarizability of *cis* PA and the contribution of the π-system polarizability to molecular polarizability has yet been reported. It is therefore interesting to calculate and compare the π system and the molecular polarizabilities of both *cis* and *trans* PA, and to discuss their differences, which is the purpose of this article.

[1]Part of this research was performed while visiting at SUNY-Fredonia.

[2]Author to whom correspondence may be addressed.

Printed in Canada

Can. J. Chem. Downloaded from www.nrcresearchpress.com by 92.62.229.171 on 09/08/12
For personal use only.

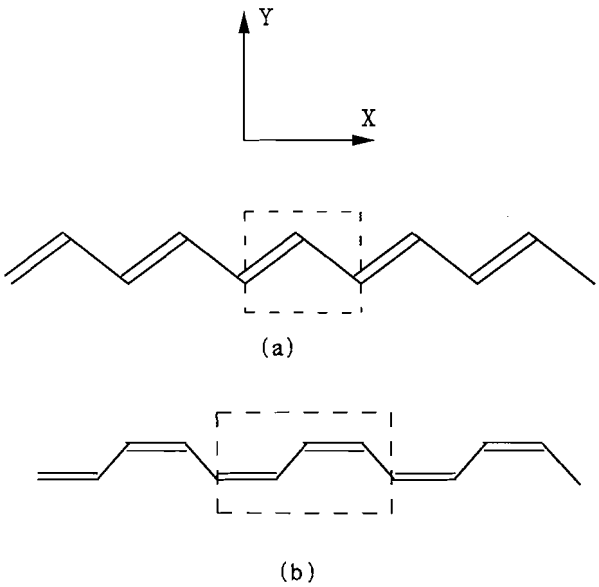

FIG. 1. Diagram of the geometry of *trans* (*a*) and *cis* (*b*) polyacetylene. The polyacetylene unit cell is indicated by the dashed lines. The coordinates used in this calculation are illustrated, with the *z*-axis taken as perpendicular to the page. The origin is chosen as the center of mass for each member of the polyene series.

Method

Because PA can be considered an infinite polyene, and given the difficulty of directly calculating the polarizability of an infinite polymer, the best method available is to calculate the polarizabilities of a series of polyenes with finite chain length, and then extrapolate to the infinite limit, i.e., PA. Hence the longer the polyene chain, the more reliable the extrapolated result for PA may be expected to be. We therefore choose a method for which chain length is not a severe limitation.

Zyss *et al.* (12,13) calculated the polarizabilities of many conjugated molecules using the semi-empirical Hartree–Fock method introducing a finite electric field perturbation, and obtaining good results. This method can be briefly described as follows. If $\hat{H}_0$ is the single-electron Hamiltonian operator of an unperturbed system and **F** is a finite external electric field, the single-electron Hamiltonian of the perturbed system is

$$[1] \quad \hat{H} = \hat{H}_0 + \mathbf{r} \cdot \mathbf{F}$$

where **r** is the coordinate vector of the electron, and where we have used $F = 10^{-4}$ au (13). Substituting eq. [1] into the Hamiltonian operator in the Roothaan equations (14), one obtains the molecular polarizability as

$$[2] \quad \alpha_{ii} = [\mu_i(F = F_i) - \mu_i(F = 0)]/F_i$$

$$[3] \quad \alpha = \frac{1}{3}\sum_i \alpha_{ii} \qquad (i = x, y, z)$$

where μ_i is the component of the molecular dipole moment along the *i*-axis.

Given the desirability of performing the calculation on as large a polyene molecule as possible, we choose a semi-empirical method (CNDO/2) (15) instead of an *ab initio* technique. Considering the importance of the π system in polyene and PA, we are especially interested in the contributions of the $2p_z$ (π) electron to the molecular polarizability, and these are reported separately as α^π.

TABLE 1. Polarizabilities (au) of *trans* and *cis* hexatriene

	Present work α	Experimental data (ref. 16)		
		Refractivity	Density (g/cm^3)	α
trans	73.1920	1.5135	0.7369	87.4565
cis	71.1604	1.4577	0.7175	81.4466

In Table 1, we list the relative experimental values (16) and our calculated results for the polarizabilities of *trans* and *cis* hexatriene. The structure parameters of hexatriene come from experimental values (17,18). Our results are consistent with experiment and demonstrate the reliability of this method.

Only a few structure parameters of polyene molecules have been determined, and these all approach the standard values: L(C=C) = 1.35 Å, L(C—C) = 1.45 Å, $\measuredangle$CCC = 120°, the same as the case for the determined and optimized PA parameters (19,20). Therefore we take the standard parameters as the structure parameters of both *trans* and *cis* polyene. The coordinate system is as shown in Fig. 1. It is possible to distinguish between *trans* and *cis* forms only for $n \geq 3$, and hence our calculation starts with $n = 3$.

Results

In Table 2 we list π-system and molecular polarizabilities and the contributions of the π system to molecular polarizability. Some of these data are illustrated in Fig. 2. From these results, we derive the following conclusions:

1. When *n* is the same, the order of both molecular and π-system polarizabilities of *trans* and *cis* polyene is *trans* > *cis*, also shown in Fig. 2. This order is consistent with the order of experimental polarizabilities of *trans* and *cis* hexatriene.

2. The molecular polarizability of polyene mainly comes from the contribution of the π system. The longer the carbon chain, the larger the contribution of the π system. When *n* increases from 3 to 18, the contribution of the π system increases from 45 to 70%.

3. A value for $\alpha^\sigma/n = \alpha/n - \alpha^\pi/n$ is easily calculated. This difference is nearly constant over the entire range of *n*, as shown in Fig. 2. This means that the polarizability of the σ system in a -CH=CH- unit for various polyenes is the same, which obviously differs from the π system. The σ polarizability is essentially independent of chain length. This differs from the π polarizability because of the delocalized nature of the π system.

To generalize the polyene results to PA, we require a function that accounts for the fact that $d(\alpha/n)/dn \rightarrow 0$ for large *n*. The proposed function (11) is

$$[4] \quad \log(\alpha/n) = a + b/n + c/n^2$$

This implies that $\lim_{n\rightarrow\infty} \alpha/n = 10^a$ for PA. Our values and Hurst's are compared in Table 3. The relative polarizabilities of the *cis* and *trans* PA are in the same order as for the polyene series. However, the π-electron contribution for PA is larger than for polyene, as shown in Table 3.

Can. J. Chem. Downloaded from www.nrcresearchpress.com by 92.62.229.171 on 09/08/12
For personal use only.

Can. J. Chem. Downloaded from www.nrcresearchpress.com by 92.62.229.171 on 09/08/12
For personal use only.

TABLE 2. Polarizabilities (au) of *trans* and *cis* polyene H(-CH=CH-)$_n$H

	trans			*cis*		
n	α^{π}	α	$\alpha^{\pi}/\alpha(\%)$	α^{π}	α	$\alpha^{\pi}/\alpha(\%)$
3	33.03	73.20	45.13	31.62	71.62	44.16
4	55.37	109.01	50.80	51.45	104.71	49.14
5	82.24	149.22	55.11	74.59	141.05	52.88
6	112.84	193.06	58.45	100.40	180.02	55.77
7	146.54	239.94	61.07	128.37	221.10	58.06
8	182.39	289.13	63.17	157.94	263.76	59.88
9	221.13	340.31	64.98	188.91	307.78	61.37
10	260.65	393.11	66.30	220.64	352.54	62.59
11	302.33	447.67	67.53	253.61	398.50	63.64
12	344.77	502.97	68.55	287.06	444.98	64.51
13	388.20	559.97	69.40	321.05	491.95	65.26
14	432.54	616.34	70.18	355.52	539.39	65.91
15	477.17	673.86	70.81	390.16	586.98	66.47
16	522.56	731.85	71.40	425.08	634.87	66.95
17	568.11	790.25	71.89	460.35	683.11	67.39
18	614.15	848.86	72.35	495.77	731.47	67.78

TABLE 3. Polarizabilities (au) per -C_2H_2- of *trans* and *cis* PA

	a	α^{π}	*a*	*b*	*c*	α	$\alpha^{\pi}/\alpha(\%)$
Present work							
trans PA	1.6903	49.012	1.7782	−2.0830	2.7304	60.007	81.67
cis PA	1.5710	37.239	1.6918	−1.6389	2.0907	49.181	75.72
Ab initio (6-31G) (ref. 11)							
trans PA			1.7803	−1.8398	1.8920	60.298	

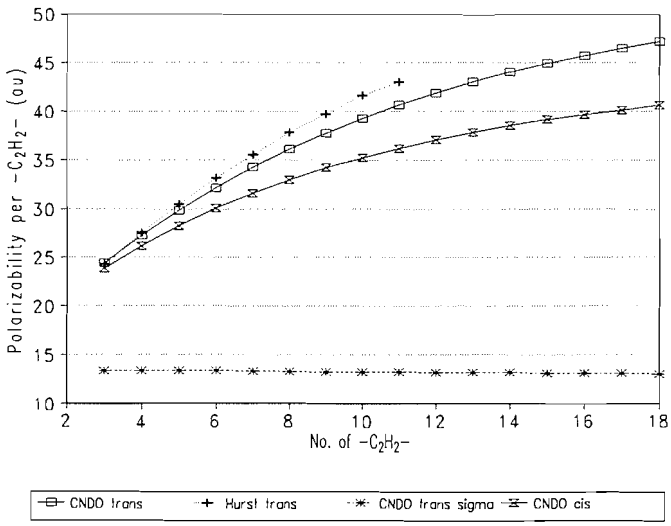

FIG. 2. Polarizability of polyene as a function of chain length, comparing the *trans* and *cis* isomers. Also shown are the *ab initio* (11) results and the σ-electron polarizability for the *trans* species. The σ-electron polarizability for the *cis* isomer is almost identical.

Discussion

We begin by considering the reasons why the *trans* isomer polarizability is larger than the *cis*. First are geometric considerations. If L is the length of the carbon chain, $L = n \times l$, then l is the length of the projection of a unit cell (-CH=CH-) (including both a C=C and a C—C bond) on the x-axis. In our calculation, l is equal to 2.425 Å and 2.125 Å for *trans* and *cis* polyene, respectively. The projection of *trans* is larger than *cis* by 0.3 Å. This makes the conjugation length of the *trans* polyene π system longer than that of *cis* polyene by $n \times 0.3$ Å, when n is the same. This is the main reason that both π-system and molecular polarizabilities of *trans* polyene are larger than those of *cis* polyene.

Besides the difference in x-axis projection length between the *trans* and *cis* unit structures, we consider another factor affecting polarizability magnitude. The unit cell of *trans* PA consists only of one -CH=CH- segment, whereas a unit cell of *cis* PA consists of two -CH=CH- segments, as shown in Fig. 1. This demonstrates that the translational symmetry of *trans* PA is higher than that of *cis* PA. Clearly, the higher the translational symmetry, the larger the delocalizability, and the larger the polarizability. Thus one would expect the *trans* and *cis* isomers to differ in subtle chemical respects in addition to geometrical effects. We expect similar effects for finite polyenes as well.

Two functional forms to describe the polarizability of *trans* polyene have been given in the literature. Hurst *et al.* (11) suggest that $\alpha \approx N^{\gamma}$, where they find $\gamma \approx 1.6$ for small polymers. However, if the delocalization length is finite, then γ must also be a function of n and must eventually tend toward 1, i.e., the polarizability is proportional to n. We specify the proportionality constant as

$$[5] \quad \alpha = Cn^{\gamma}$$

where two parameters, C and γ, are to be fitted to the data.

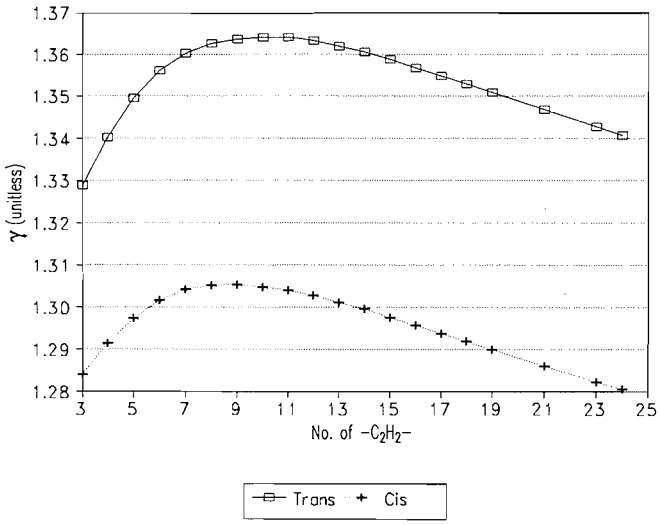

FIG. 3. Parameter γ versus polyene length.

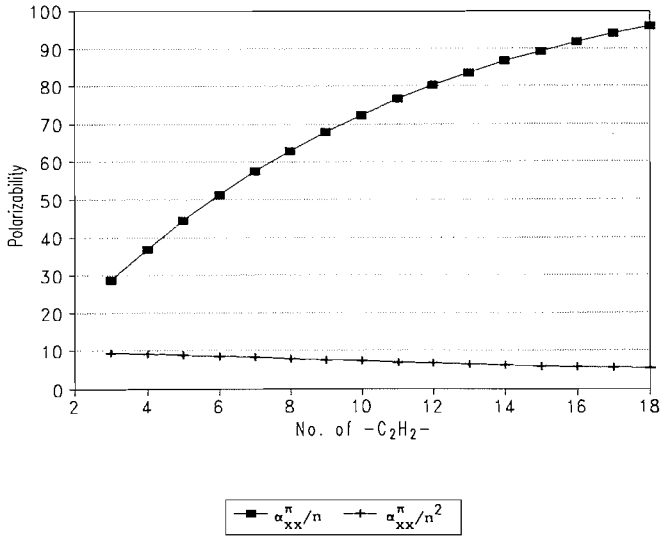

FIG. 4. α^{π}_{xx}/n and α^{π}_{xx}/n^2 for *trans*-polyene.

Equation [5] will provide some significant physical insight in what follows.

Hurst *et al.* (11) have proposed yet another function, given by eq. [4]. Parameter a has clear physical significance, already mentioned. Parameters b and c only influence the behavior at small n, and from physical arguments (i.e., a less conjugated system), we know that $b < 0$. We have fitted our data to the Hurst function for *trans* PA, with the results shown in Table 3. It is seen that our value for a corresponds very closely with that of Hurst, and thus our value for the PA polarizability is close to that obtained by Hurst. This implies that as the chain becomes longer, the values obtained for the polarizability will more closely match the *ab initio* results. Since Hurst used polyenes with $n = 2, 3, \ldots, 11$, and we use $n = 3, 4, \ldots, 18$ from which to extrapolate the polarizability of PA, this implies that the semi-empirical method with minimal Slater type basis can closely match the *ab initio* result. However, parameters b and c, which affect short-chain behavior, are less reliable.

The physical significance of the power law (eq. [5]) depends on how C is defined. If C is defined as C_∞, the limiting value of α/n as $n \rightarrow \infty$, then $C_\infty = 10^a$, identical to the limiting value in eq. [4], and eq. [5] is valid for large n when $\gamma = 1$. On the other hand, if C is defined as C_0, the polarizability of the $-C_2H_2-$, i.e., α for $n = 1$, the form can be fitted to small n but will be incorrect in the large n limit if γ is assumed to be constant. Further, in this case it is apparent that γ cannot converge to unity since then the polarizability of the infinite chain would equal that for $n = 1$. Finally, C_0 must be equal for both *cis* and *trans* polymers, and therefore has a very definite physical meaning. It is clear that γ has a different physical interpretation depending on how C is chosen.

A least-squares fit to determine C_0 in the *trans* and *cis* cases reveals 17 au ± 1 au. Given $C_0 = 17$, it is then possible to plot the necessary value of γ from the CNDO and Hurst data. This is shown in Fig. 3, and several points can be made. First, we note that values for γ are larger in the *trans* case than in the *cis*. This is consistent with the value of a, and with the notion that the *trans* form has a larger polarizability. Secondly, it is apparent that γ goes through a maximum at approximately $n = 9$ for the *cis* isomer, and $n = 10$–11 for the *trans* isomer. This probably reflects a distance related to the delocalization effect in polyene, indicating that electrons are delocalized over a larger region in the *trans* isomer than in the *cis*.

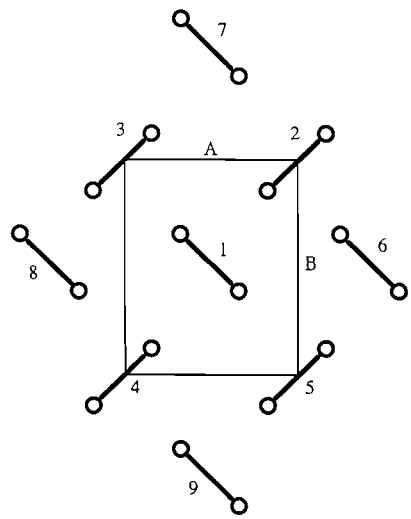

FIG. 5. The (001)-plane for the crystal unit cell of *trans* and *cis* polyacetylene.

Figure 4 illustrates the α^{π}_{xx}/n and the α^{π}_{xx}/n^2 for *trans* polyene. Using HMO theory (infinite delocalization length), Davies (10) showed that this ratio should increase proportionally to n^2 for *trans* PA. If the delocalization length were infinite, then one would expect the HMO theory to be accurate, but Fig. 4 indicates that it is not valid. Therefore, the existence of a typical delocalization length is further indicated.

The dispersion energy of crystalline PA

The crystal structure parameters of both *trans* and *cis* PA have been determined (20,21) and are similar to each other (see Fig. 5 and Table 4). Because PA is a nonpolar mate-

Can. J. Chem. Downloaded from www.nrcresearchpress.com by 92.62.229.171 on 09/08/12
For personal use only.

TABLE 4. The E_{disp} among chains and relevant parameters of *trans* and *cis* PA

	trans PA	*cis* PA
Cell parameter (refs. 20, 21)		
A (Å)	4.24	7.61
B (Å)	7.32	4.39
C^a (Å)	2.46	4.47
α (deg)	90.	90.
β (deg)	91.5	90.
γ (deg)	90.	90.
Ionization energy (au)	0.243	0.246 (ref. 22)
E_{disp}(kcal/mol)	9.873	5.194

[a]The C-axis is along the carbon chain, and the repeat unit along the C-axis is $-C_2H_2-$ for *trans* PA and $-C_4H_4-$ for *cis* PA.

rial, we can estimate the dispersion energy among PA chains in crystals as

$$[6] \quad E_{disp} = -\frac{3}{4} \times \frac{\alpha^2 I}{R^6}$$

where I is the ionization energy of PA (22), and R is the distance between centers of two chains. The calculated results and relevant parameters are listed in Table 4, and E_{disp} is the sum of the dispersion energies between chain 1 and chains 2, 3, 4, 5, 6, 7, 8, and 9, respectively. We use the extrapolated α/n for PA, as calculated above, and all the centers of nine PA units are on the same plane. Consistent with our previous results, E_{disp} for the *trans* PA is larger than for the *cis*. These are shown in Table 4.

Conclusion

We have calculated the polarizability of a series of *trans* and *cis* polyene molecules. Our results compare favorably with those of Hurst (10). The data have been fitted to an appropriate function, and it is found that our data and Hurst's have the same limiting behavior. We therefore conclude that the polyene data may be extrapolated to provide information about polyacetylene.

Further, we have considered the relative polarizability of *trans* and *cis* polyene, and we show that *trans* has a larger polarizability than *cis*. An inquiry into the reasons for this phenomenon indicates that it is a function of geometry and of symmetry.

Finally, we have presented data on the crystal dispersion energy. We find dramatic differences between the *trans* and *cis* forms, which should in principle be measurable, thereby allowing experimental confirmation of our results.

Acknowledgments

The Changchun authors acknowledge that this research was supported by the National Science Foundation of the People's Republic of China. Acknowledgment is made by D.A.J. to the Donors of the Petroleum Research Fund, administered by the American Chemical Society, for partial support of this research. D.A.J. also acknowledges that this research was partially supported by a grant from the Research Corporation, and he thanks the SUNY Research Foundation for an Equipment Matching Grant. T.F.G. acknowledges support by the Office of Naval Research and the National Science Foundation under Grant No. CHE-9016789.

1. H. Shirakawa and S. Ikeda. Polym. J. **2**, 231 (1971).
2. G. L. Baker and F. S. Bates. Mol. Cryst. Liq. Cryst. **117**, 15 (1985).
3. A. J. Heeger and A. G. MacDiarmid, *In* The physics and chemistry of low dimensional solids. *Edited by* L. Alcacer. Reidel, Dordrecht. 1980. p. 394 ff.
4. W. P. Su, J. R. Shrieffer, and A. J. Heeger. Phys. Rev. Lett. **42**, 1698 (1979).
5. Z. Huang, C. Zhao, and Q. Fu. Synth. Met. **36**, 229 (1990).
6. Y. Sun, C. Zhao, and R. Wang. Acta Chim. Sin. (Chin.), **44**, 380 (1986).
7. H. Teramae, T. Yamabe, and A. Imamura. J. Chem. Phys. **81**, 3564 (1984).
8. H. W. Gibson, S. Karplan, R. A. Mosher, W. M. Prest, Jr., and R. J. Weagley. J. Am. Chem. Soc. **108**, 6843 (1986).
9. T. Ito, H. Shirakawa, and S. Ikeda. J. Polym. Sci. Polym. Chem. Ed. **13**, 1943 (1975).
10. P. L. Davies. Trans. Faraday Soc. **48**, 789 (1952).
11. G. J. B. Hurst, M. Dupuis, and E. Clementi. J. Chem. Phys. **89**, 385 (1988).
12. J. Zyss. J. Chem. Phys. **70**, 3333 (1979).
13. R. Mathies and R. C. Albrecht. J. Chem. Phys. **60**, 2500 (1974).
14. C. C. J. Roothaan. Rev. Mod. Phys. **23**, 69 (1951).
15. J. A. Pople and G. A. Segal. J. Chem. Phys. **44**, 3289 (1966).
16. C. R. Weast (*Editor*). CRC handbook of chemistry and physics. 66th ed. CRC Press, Boca Raton, Fla. 1985–86. p. C308.
17. M. Traetteberg. Acta Chem. Scand. **22**, 628 (1968).
18. M. Traetteberg. Acta Chem. Scand. **22**, 2294 (1968).
19. A. Karpfen. Solid State Commun. **37**, 179 (1981).
20. C. R. Fincher, Jr. C.-E. Chen, A. J. Heeger, A. G. MacDiarmid, and J. B. Hastings. Phys. Rev. Lett. **48**, 100 (1982).
21. R. H. Baugh, S. L. Hsu, G. P. Pez, and A. J. Signorell. J. Chem. Phys. **68**, 5405 (1978).
22. J. L. Bredas, R. R. Chance, R. Silbey, G. Nicolas, and Ph. Durand. J. Chem. Phys. **75**, 255 (1981).

Can. J. Chem. Downloaded from www.nrcresearchpress.com by 92.62.229.171 on 09/08/12
For personal use only.

Ab initio calculations and the chemical reaction molecular dynamics simulation

MASATAKA NAGAOKA,[1] YOSHISHIGE OKUNO,[2,3] TOKIO YAMABE,[2] AND KENICHI FUKUI
Institute for Fundamental Chemistry, 34-4, Takano-Nishihiraki-cho, Sakyo-ku, Kyoto 606 Japan

Received July 5, 1991

This paper is dedicated to Professor Sigeru Huzinaga on the occasion of his 65th birthday

MASATAKA NAGAOKA, YOSHISHIGE OKUNO, TOKIO YAMABE, and KENICHI FUKUI. Can. J. Chem. **70**, 377 (1992).

To clarify the mechanism of chemical reactions in solution, each solvent molecule was classified as either a reactive-solvent molecule or a medium-solvent molecule in accordance with its role in the reaction. The proton transfer reaction of formamidine in water was treated as a model reaction. *Ab initio* molecular orbital calculations were performed for the complex made up of a formamidine, a reactive-water molecule, and a medium-water molecule. The optimized geometries and the solvation energies were obtained and the orbital interaction analysis carried out along the intrinsic reaction coordinate (IRC). It was found that the medium-water molecule influences the reaction dynamically rather than energetically. There was no energy change in the potential barrier under the influence of the medium-water molecule, in contrast to the remarkable barrier-reducing effect of the reactive-water molecule. The situation is different from that in chemical reactions involving ionic states. Chemical reaction molecular dynamics (CRMD) simulation for this system was performed in order to investigate the energy relaxation mechanism. It was found that just after the reaction finishes, a relative translational motion is first induced between the supermolecule, which consists of a formamidine and a reactive-water molecule, and the medium-water molecule, and is then followed by a rotational motion of the medium-water molecule.

Key words: formamidine, chemical reaction molecular dynamics method, reactive-solvent molecule, medium-solvent molecule, energy relaxation mechanism.

MASATAKA NAGAOKA, YOSHISHIGE OKUNO, TOKIO YAMABE et KENICHI FUKUI. Can. J. Chem. **70**, 377 (1992).

Dans le but de clarifier les mécanismes de réactions chimiques en solution, on a classifié chaque molécule de solvant, suivant son rôle dans la réaction, soit comme une molécule de solvant réactive soit comme une molécule de solvant agissant comme milieu réactionnel. On a utilisé la réaction de transfert de proton de la formamidine dans l'eau comme modèle. On a effectué des calculs d'orbitales moléculaires *ab initio* sur le complexe formé d'une formamidine, d'une molécule d'eau réactive et d'une molécule d'eau agissant comme milieu réactionnel. On a obtenu les géométries optimisées et les énergies de solvatation et on a réalisé une analyse des interactions orbitalaires le long des coordonnées intrinsèques de la réactions (CIR). On a trouvé que l'eau agissant comme milieu réactionnel n'a pas d'influence sur l'énergie de la réaction; elle agit toutefois sur la dynamique de la réaction. Sous l'influence de la molécule d'eau agissant comme milieu réactionnel, il n'y a pas de changement d'énergie dans la barrière de potentiel; ce comportement diffère d'une façon notable avec l'effet remarquable de réduction de la barrière de la molécule d'eau réactive. La situation est différente de celle qui prévaut dans les réactions chimiques impliquant des états ioniques. Afin d'évaluer le mécanisme de relaxation moléculaire, on a effectué une simulation de la dynamique moléculaire de la réaction chimique (DMRC). On a trouvé que, immédiatement après la fin de la réaction, il se produit d'abord un mouvement relatif de translation entre la supermolécule, qui consist d'une formamidine et d'une molécule d'eau réactive, et la molécule d'eau agissant comme milieu réactionnel qui est suivi d'un mouvement de rotation de la molécule d'eau agissant comme milieu réactionnel.

Mots clés : formamidine, méthode de la dynamique moléculaire de la réaction chimique, molécule de solvant réactive, molécule de solvant agissant comme milieu réactionnel, mécanisme de relaxation d'énergie.

[Traduit par la rédaction]

Introduction

Based on extensive gas phase research using molecular orbital (MO) theories, theoretical chemists have recently been challenged to resolve problems in solution chemistry in terms of molecular language (1–4). It is true that most treatments were developed in combination with techniques that were originally invented in the field of condensed phase physics. Hence the chemical and physical quantities of their concern are closely related to equilibrium properties of solution and ensemble-averaged properties. However, as far as solvent effects are concerned, not only *long-range interactions* but also *short-range interactions* should be taken into consideration. In particular, a chemical reaction in solution, with accompanying recombination and reorientation of constituent atoms, is essentially a nonequilibrium process, with both energy concentration and dissipation. Thus, we must inevitably deal with such short-range interactions as *exchange-exclusion* and *electron transfer interactions* between a solute molecule and certain solvent molecules, in addition to long-range interactions, i.e., *electrostatic*, *polarization*, and *dispersion interactions*.

Under the circumstances, one can be led naturally to the notion that solvent molecules in solution should be classified in two categories; the *reactive-solvent* molecule and the *medium-solvent* molecule. The former is defined as a solvent molecule that interacts with a solute molecule through short-range interaction, while the latter interacts through long-range interaction. A reactive-solvent molecule might be included in a reactant in addition to the solute molecules themselves, if the short-range interaction were regarded as part of the chemical bonding interaction. Although the simulation that deals with both a solute and a number of medium-solvent molecules at the same time must represent a good approach to the study of the medium-solvent effect, it

[1]Author to whom correspondence may be addressed.
[2]Also associated with the Department of Hydrocarbon Chemistry, Faculty of Engineering, Kyoto University, Kyoto 606, Japan.
[3]Permanent address: Daicel Chemical Industries, Ltd., 1239, Shinzaike, Aboshi-ku, Himeji, Hyogo 671-12, Japan.

Printed in Canada

Can. J. Chem. Downloaded from www.nrcresearchpress.com by 92.62.229.171 on 09/08/12
For personal use only.

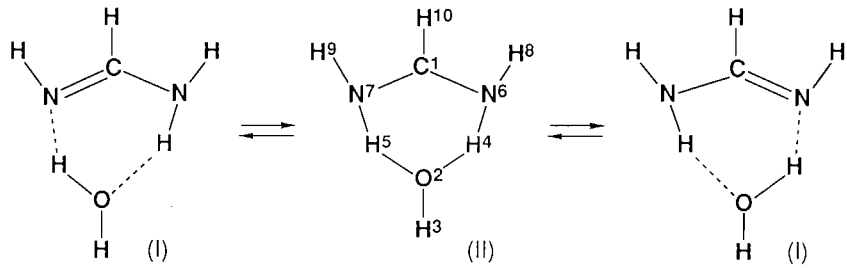

FIG. 1. Intrasupermolecular proton transfer scheme of the formamidine–water system.

Can. J. Chem. Downloaded from www.nrcresearchpress.com by 92.62.229.171 on 09/08/12
For personal use only.

cannot be denied that the reactive-solvent effect might play a dominant role in solving the mechanism of chemical reaction dynamics in solution.

We have therefore investigated the proton transfer reaction of formamidine in water as one model of chemical reactions in solution (5, 6). The proton transfer reaction is worthwhile investigating because its study contributes in general to a deeper understanding of chemical reactivity, and is of special importance to biochemical systems. In fact, extensive theoretical studies for solvation in biological systems have been examined by several researchers (7). Moreover, much attention has been paid to studies of formamidine on the relation between molecular conformation and biological activity (8–11).

Previously, we determined that the potential energy barrier, 59.11 kcal/mol, of the intramolecular proton transfer process of formamidine is reduced to 21.56 kcal/mol, with the assistance of only a water molecule, which corresponds to the energy difference between the stable state (I) and the transition state (II) for the intrasupermolecular proton transfer reaction process of the formamidine–water (FW) system (Fig. 1) (5, 6). On the other hand, the potential energy barrier calculated recently by MP4/6-311G(*d*,*p*) wave functions was reported by Truhlar and co-workers (12) to be 24.6 kcal/mol for the FW system. Although it was also reported that the potential energy barrier is 6.8 kcal/mol and is significantly lower than the value 21.56 kcal/mol, Truhlar and co-workers must have misunderstood the definition of the "potential energy barrier" adopted in ref. 6. Therefore, the value that should have been compared with 21.56 kcal/mol is 24.6 kcal/mol for the reaction E → F in their Table II(B). The difference between their value (24.6 kcal/mol) and ours is just 3.0 kcal/mol and, moreover, no striking difference in the geometries can be recognized. Hence, it is expected that the energetics for the proton transfer reaction process of the FW system can be described sufficiently by the basis set used in our study.

On the basis of these static studies for the proton transfer reaction of formamidine in water, the dynamic investigation for the FW system was performed by chemical reaction molecular dynamics (CRMD) simulation and the existence of the dynamic transition state (DTS) was postulated (13, 14). The water molecule in the FW system can be recognized as a reactive-water molecule because it plays a central role in proton rearrangement. However, after taking the *reactive solvent* effect into consideration, the next step for understanding solution chemistry is to clarify the role of the medium-solvent molecule in the chemical reaction mechanism.

The aim in the present article, therefore, is to show the *medium-solvent* effect not only from the static, but also from the dynamic, viewpoint. For the purpose, another water molecule (i.e., a medium-solvent molecule) is added to the original FW system and the static medium-solvent effect is investigated first by an *ab initio* MO method. On the basis of the supermolecular treatment of the formamidine–water–water (FWW) complex, *ab initio* MO calculations are performed and then the transition state (TS) obtained as a saddle point on the potential energy surface is compared with that of the FW system. The interaction between the FW system and the medium-water molecule is certified to be the long-range interaction, by analysis of optimized geometries, solvation energies, and orbital interactions. The intrinsic reaction coordinate (IRC) is carefully traced and then the potential energy barrier is estimated. It is clear that the medium-water molecule does not influence both the original FW geometry and then the potential energy barrier and, as a result, the solvation energy is small, as well as the orbital interaction between the FW system and the medium-water molecule.

After constructing the intermolecular potential function between the FW system and a medium-water molecule, the CRMD simulation for the FWW complex is performed in the constant-temperature scheme (CTS) (13) and hence the energy relaxation mechanism can be investigated precisely. (The CRMD studies in the constant-energy scheme (CES) will be discussed in another publication (15).) It is understood that the medium-solvent effect in the energy relaxation/supply is observed after/before the reaction finishes/starts. The relative translational kinetic energy between the FW system and the medium-water molecule first increases. Then it transfers to the rotational kinetic energy of the medium-water molecule.

In the following section, the method utilized in the present article is precisely explained and, in the Results and discussion, the calculational results are presented, with discussion in terms of *ab initio* MO theory and CRMD treatment. Finally, a concise summary is drawn in the Conclusions.

Method

Ab initio *MO calculations and IRC analysis*

Ab initio MO calculations (16) were carried out by using the GAUSSIAN86 program (17) with the minimal STO-3G basis set (18) at the Hartree–Fock level of theory (19). All the geometries of the complexes were optimized with the analytical energy gradient method (20). All optimizations were accomplished under the tight convergence criterion.

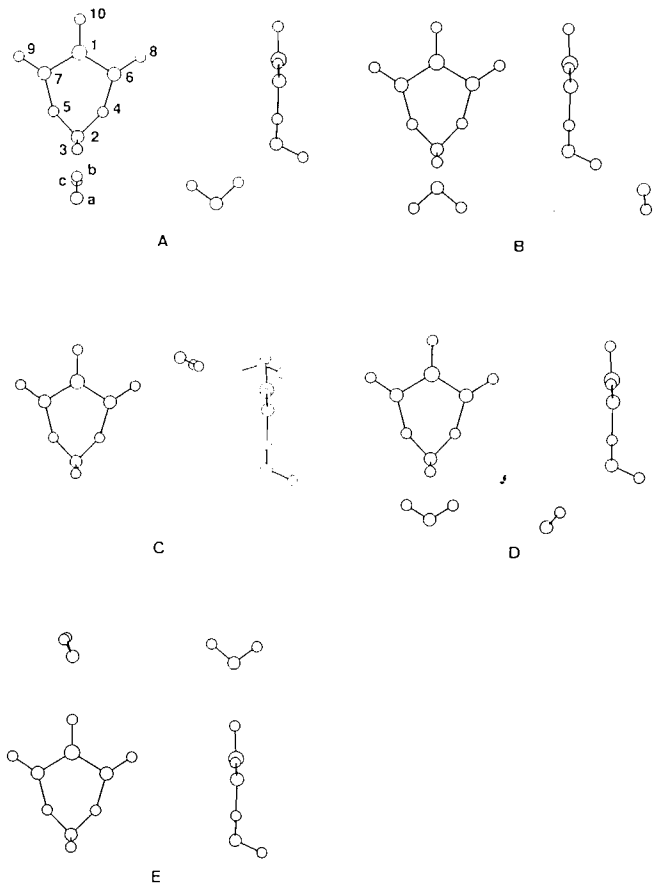

FIG. 2. Optimized geometries of the FW(TS)–W(SS) complex.

In the supermolecular treatment where another water molecule (i.e., a medium-solvent molecule) is added to the FW system, the geometry optimization of TS should be performed straightforwardly for the total FWW complex and may then be denoted as FWW(TS). It is, however, easily understood that the direct optimization of FWW(TS) should be difficult because of its high dimensionality. Therefore, the TS-optimization was first executed for the complex that consists of the TS structure of the FW system (i.e., FW(TS)) and the stable state (SS) structure of a water molecule (i.e., W(SS)), namely, for the FW(TS)–W(SS) complex. From the viewpoint of chemical reaction dynamics, it is expected that, for the reaction to occur, the medium-water molecule should take the favorable position and orientation to the TS geometry of FW, and the optimized geometry of the FW(TS)–W(SS) complex cannot be very different from the optimized geometry of the FWW(TS) complex.

As a matter of fact, such a large complex as the FW(TS)–W(SS) system can possess several stable structures. Thus, before the optimization calculation, we examine some possibilities by carrying out orbital interaction analysis for MOs of each isolated molecule and can select certain orientations as candidates for stable structures. After obtaining optimized stable geometries, for the sake of completeness we execute the random search procedure for other possible stable geometries that might exist, by choosing 2000 orientations between the FW(TS) and W(SS) systems within the cubic box (22 Å each side). The total energies for these orientations can be used later for the fitting of the intermolecular potential function between them, which is employed for the CRMD studies of the FWW complex together with the previous intrasupermolecular potential function of the FW supermolecule (13, 21).

TABLE 1. Total potential energy of the optimized geometries

	Total energy (hartree)
W(SS)	−74.96590
F(SS)	−147.15328
FW(TS)	−222.10898
FW(SS)	−222.13399
FW(TS)–W(SS)	
A	−297.08422
B	−297.08415
C	−297.08121
D	−297.07966
E	−297.07826
FWW(TS)	−297.08503
FWW(SS)	−297.10995

To obtain the FWW(TS) structures and information about their electronic states, full optimization is also performed on the basis of those optimized geometries obtained above for the FW(TS)–W(SS) complex. The solvation energy of a medium-water molecule is estimated from the difference between an optimized total energy of FWW(TS) and the sum of the energies of two isolated systems, FW(TS) and W(SS). The IRC of the FWW complex is analyzed by using the GAUSSIAN86 program equipped with the IRC algorithm (22) and comparing with that of the FW system (6, 13, 14). To explain the medium-solvent effect in terms of MO language, Mulliken population analysis (23) is utilized as a supplement for the FW(TS) system, the SS of the FW system (i.e., FW(SS)), W(SS), and the SS of formamidine (i.e., F(SS)). Hence, the energetics for a chemical reaction in solution can be analyzed, and how many varieties of approach a medium-solvent takes can also be understood.

Potential function

Intramolecular motions, i.e., vibrations and librations, are usually related to much higher frequencies than intermolecular motions. This fact allows us to utilize the rigid-body approximation of the medium-water molecule. Thus, during the CRMD simulation for the FWW complex, three internal degrees of freedom of a medium-water molecule are restricted to correspond to the SS structure. Other degrees of freedom, which correspond to the translation and the rotation at a distance, are included in order to express the intermolecular potential energy surface.

The intrasupermolecular potential function for the FW system:

$$[1] \quad V_{FW} = \sum \left\{ \frac{a_{1ij}}{r_{ij}} + \frac{a_{2ij}}{r_{ij}^2} + \frac{a_{3ij}}{r_{ij}^3} + \frac{a_{4ij}}{r_{ij}^4} + \frac{a_{6ij}}{r_{ij}^6} \right\}$$

was fitted to reproduce the potential energy surface along the IRC by our newly developed heuristic potential function (HPF) method (21, 24). On the contrary, the intermolecular potential energy function between the FW system and a medium-water molecule was constructed similarly by the least-

Can. J. Chem. Downloaded from www.nrcresearchpress.com by 92.62.229.171 on 09/08/12
For personal use only.

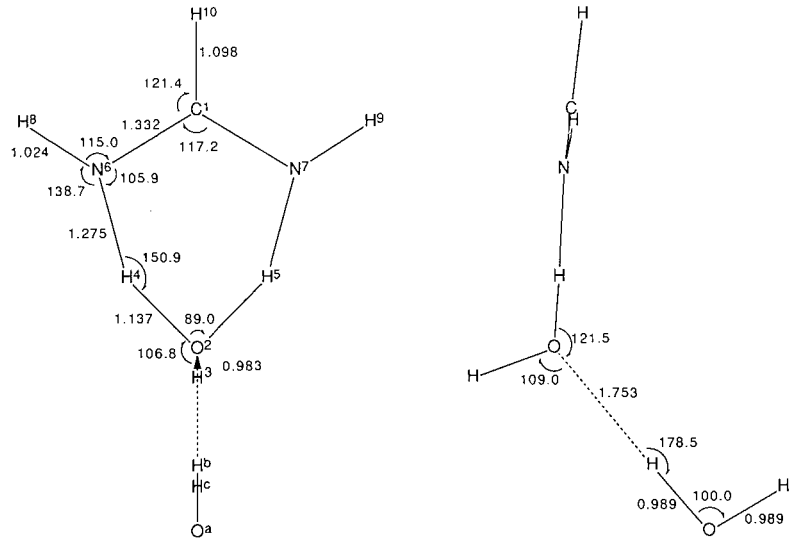

FIG. 3. Bond distances and bond angles in the optimized structure A of the FW(TS)–W(SS) complex (shown in Fig. 2). Numerical values are given in angstrom for bond length and in degrees for bond angle.

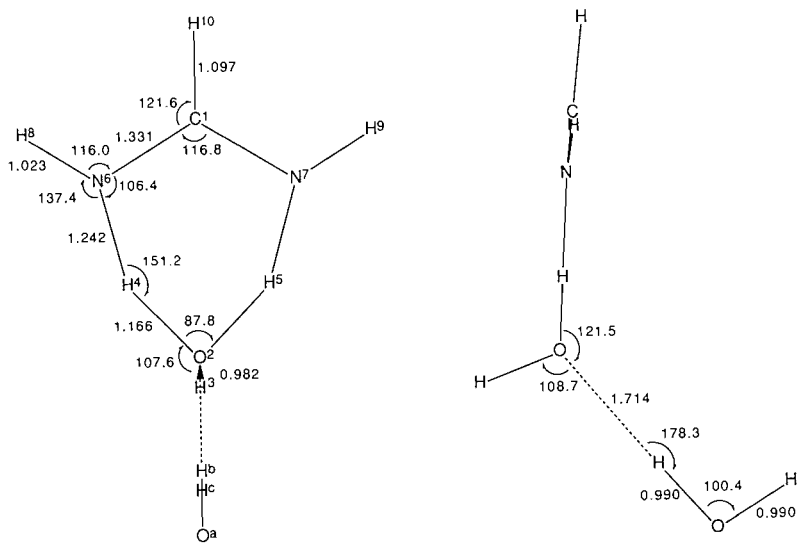

FIG. 4. Bond distances and bond angles in the optimized structure of the FWW(TS) complex. Numerical values are given in angstrom for bond length and in degrees for bond angle.

mean-squares method (25). Although the intermolecular potential function for the CRMD simulation should be fitted in the neighborhood of the true IRC of the FWW complex, the present potential energy function was prepared to reproduce relative energies of various orientations between the FW(TS) system and the W(SS) molecule. The functional form is assumed to be as follows:

$$[2] \quad V_{\text{FW-W}} = \sum \left\{ \frac{b_{3ij}}{r_{ij}^{3}} + \frac{b_{6ij}}{r_{ij}^{6}} + \frac{b_{12ij}}{r_{ij}^{12}} \right\}$$

where

$$[3] \quad b_{12ij} > 0$$

Although 2000 randomly selected configurations within the cubic box explained previously were used for the electronic energy calculation and were stored as the data base for fitting to the above potential functional form, those configurations with energies higher than the energy threshold of the sum of the isolated FW(TS) and W(SS) energies plus 2 kcal/mol were excluded from the first because the preferential sampling by the bath mode partition function (21) gives them small weightings. Finally, including 5 optimized stable geometries, 1912 configurations between the FW(TS) system and the W(SS) as a whole form the data base. The parameter optimization of eq. [2] was performed by the modified Levenberg–Marquardt method (26–28). Optimized parameters were checked by another test data base than the above initial data base and were found to represent the potential energy surface.

CRMD simulation

The Hamiltonian equations of motion for the atoms in the FWW complex were solved numerically by using the Verlet algorithm (29). For the sake of comparing the dynamical difference between the FW system and the FWW complex, the constant-temperature scheme (CTS) simulation was re-

Can. J. Chem. Downloaded from www.nrcresearchpress.com by 92.62.229.171 on 09/08/12
For personal use only.

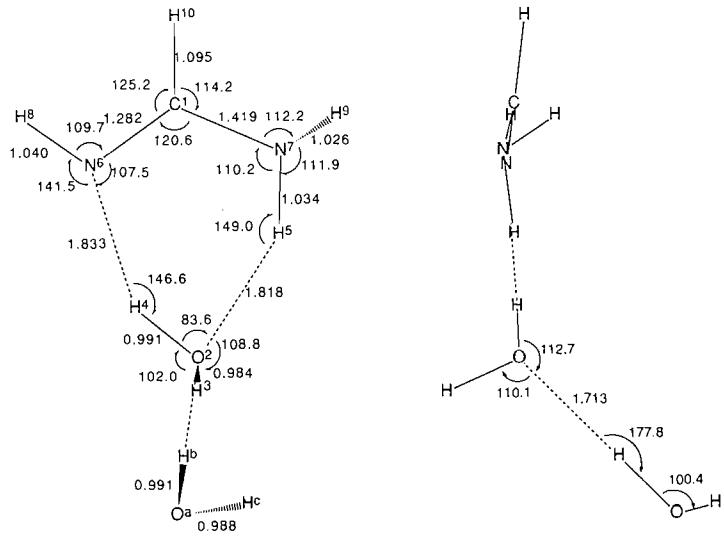

FIG. 5. Bond distances and bond angles in the optimized structure of the FWW(SS) complex. Numerical values are given in angstrom for bond length and in degrees for bond angle.

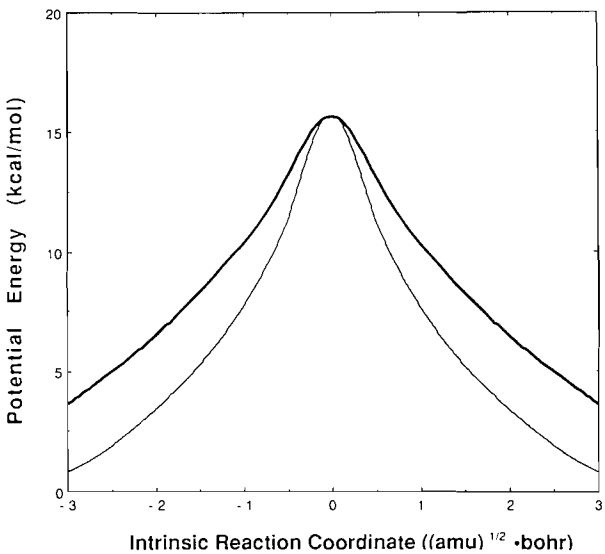

FIG. 6. Potential energy profiles along the intrinsic reaction coordinate (IRC) of the FW system (thin solid line) and the FW–W system (thick solid line).

alized for the FW part of the FWW complex in the CRMD simulation (13), where each atom in the FW part of the FWW complex was assigned the same initial configuration and velocity as those in the CRMD simulation for the isolated FW system. In other words, those trajectories were initiated at the saddle-point (i.e., TS) geometry of the isolated FW system with initial internal temperature $T_0 = 1$ K;

$$[4] \quad T_0 = \sum \frac{m_i v_i^2}{3Nk_B}$$

where m_i and v_i denote the mass and the velocity of the ith atom in the FW system, respectively, and N is the total number of atoms.

Two initial conditions were employed: the randomly directed initial velocity (R-D IV) condition and the IRC-directed initial velocity (IRC-D IV) condition. So that the velocity distribution can reproduce the Maxwell–Boltzmann distribution at a given initial internal temperature T_0, a random number generator was used for determining a set of R-D IVs. Using an optimized conformation for the total of the FW(TS) and W(SS) systems, after 10 ps equilibration with the FW(TS) geometry fixed (i.e., the dynamic equilibration), the CRMD simulation was started for the FWW complex as a whole. As explained before, the two O—H bond lengths and the angle between them of the medium-water molecule are constrained to hold the SS geometry during the whole simulation. This constrained dynamics was realized by using a set of Lagrangian multipliers, which adjust the magnitudes of the forces of constraint involving two hydrogen and one oxygen atoms (29, 30). This treatment is called the SHAKE algorithm.

Results and discussion

TS-optimization of the FW(TS)–W(SS) complex

Five optimized geometries (A–E in Fig. 2) were found by geometry optimization of the complex that consists of the FW(TS) supermolecule and the W(SS) molecule. Those potential energies calculated for them can be compared with the sum of energies for the isolated FW(TS) and W(SS) (Table 1). As explained in the Introduction, since our present attention is being paid to chemical reaction dynamics in solution, it is necessary to select the most influential medium-water molecule for the reaction, and to investigate the effect of the medium-water molecule on the original FW reaction system. The optimized geometry A is, for that reason, chosen because it is the most energetically stable among these optimized geometries (Table 1), and the distance between the transferring proton, the H4 atom or the H5 atom, and the medium-water molecule, is the shortest among them (Fig. 2). Still more important is that the medium-water molecule of geometry A is supposed to play an effective role for energy relaxation because its orientation is the most favorable for energy transfer from the vibrational energy between the transferring proton and the O2 atom to the ro-

Can. J. Chem. Downloaded from www.nrcresearchpress.com by 92.62.229.171 on 09/08/12
For personal use only.

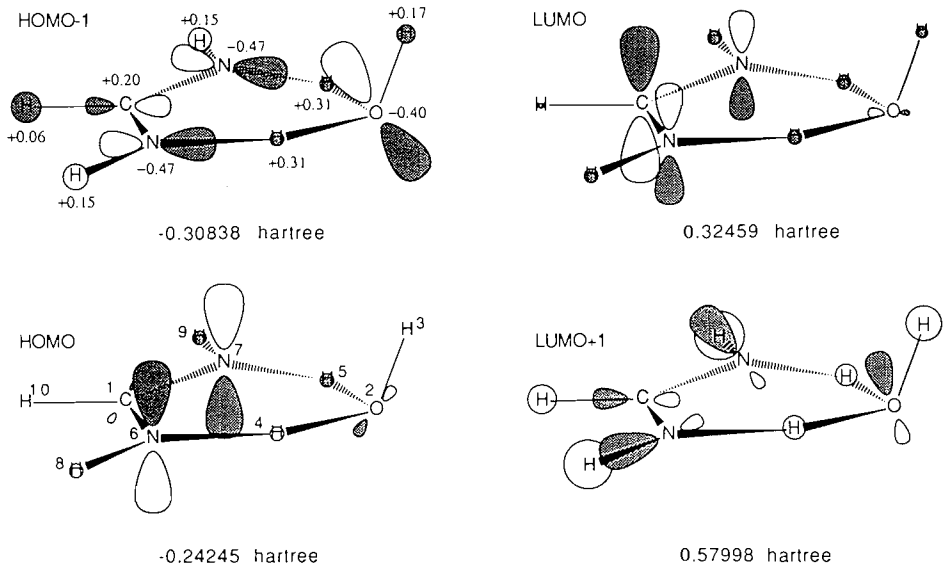

FIG. 7. Molecular orbitals and total atomic charges of the FW(TS) system. Orbital energies are also given in hartree.

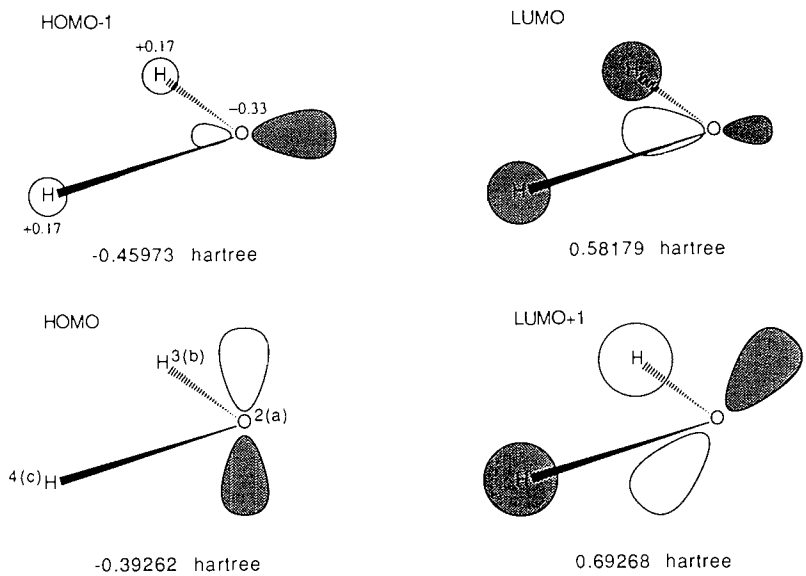

FIG. 8. Molecular orbitals and total atomic charges of the W(SS). Orbital energies are also given in hartree.

tational kinetic energy of the medium-water molecule (31). This conjecture is also supported by the remarkable H3 motion in the CRMD simulation in the previous studies (13). Thus, we recognize the character of the optimized geometry A and, hereafter, denote it solely as that of the FW(TS)–W(SS) system. The bond distances and bond angles of the optimized FW(TS)–W(SS) geometry are shown in Fig. 3. This optimized geometry is also classified as the C_s symmetry group.

Full TS-optimization of the FWW complex

Full TS-optimization of the FWW(TS) complex was carried out on the basis of the optimized FW(TS)–W(SS) geometry and the vibrational analysis confirmed that the geometry obtained corresponds to the TS structure of FWW. It can be recognized that there is no striking geometric difference between the FWW(TS) complex and the FW(TS)–W(SS) one, although the distance of the hydrogen bond r_{2b} and the r_{46} and r_{57} of the FWW(TS) system is a little shorter and the bond length of r_{24} and r_{25} is a little longer (Fig. 4). Thus it is concluded that the geometric effect of the medium-water molecule on the original FW(TS) supermolecule is almost negligible. The energy of the FWW(TS) complex is −297.08503 hartree and the energy difference from the FW(TS)–W(SS) complex is just 0.5 kcal/mol (Table 1). Consequently, the fully optimized geometry, i.e., the FWW(TS) complex, can be approximated sufficiently by the optimized geometry between the original FW(TS) system and the W(SS).

Can. J. Chem. Downloaded from www.nrcresearchpress.com by 92.62.229.171 on 09/08/12
For personal use only.

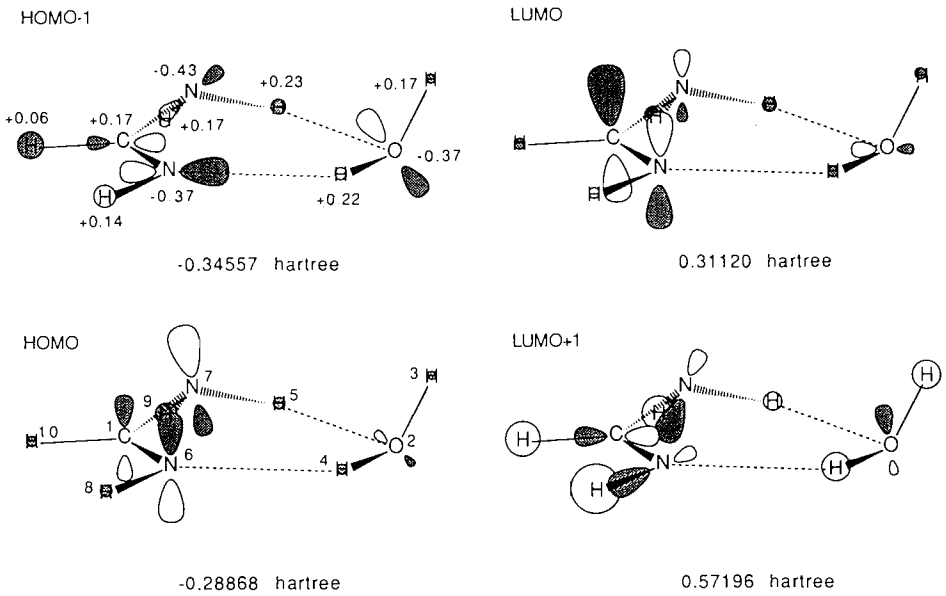

FIG. 9. Molecular orbitals and total atomic charges of the FW(SS) system. Orbital energies are also given in hartree.

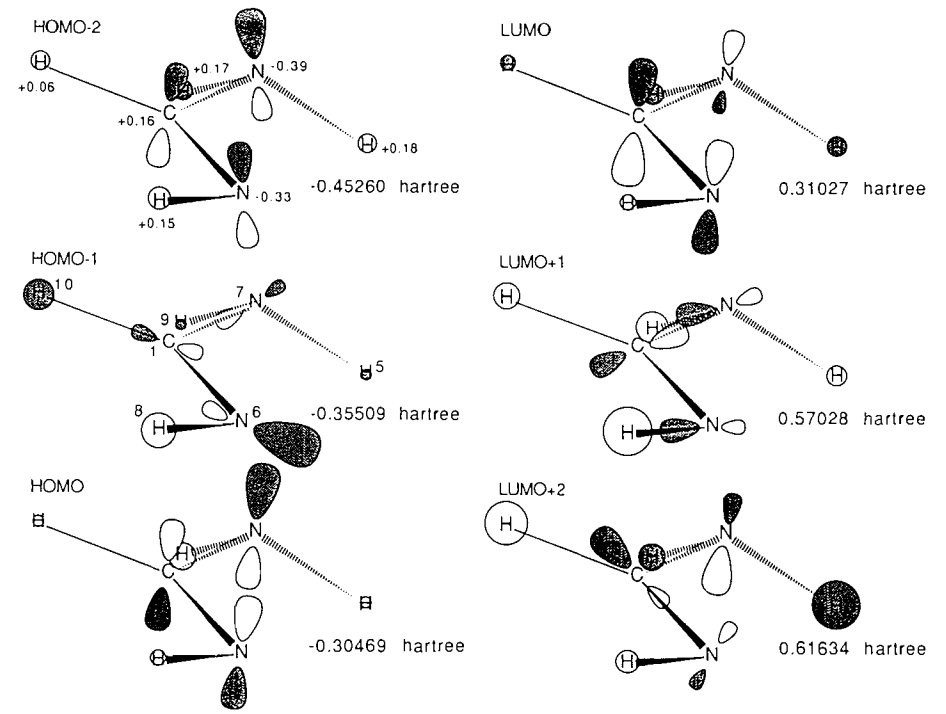

FIG. 10. Molecular orbitals and total atomic charges of the formamidine. Orbital energies are also given in hartree.

The solvation energies of the medium-water and the reactive-water molecule are 6.95 and 58.23 kcal/mol, respectively. The solvation energy of the medium-water molecule is almost one eighth that of the reactive-water molecule and it confirms that the medium-water molecule should be distinguished from the reactive-water one.

IRC analysis of the FWW complex and the stable states

The IRC analysis was performed for the supermolecular model of the total FWW complex and compared with that of the FW system. The SS of the FWW complex (i.e., FWW(SS)) can be found by IRC analysis (Fig. 5) and it was observed that the optimized SS geometry is not influenced by a water molecule so much as the previously optimized geometry of the FW(SS) system (6). The medium-water solvation energy, 6.91 kcal/mol, was almost the same as that in the FW(TS) system. This is clearly in contrast to the fact that the reactive-water solvation energy of the SS, 9.32 kcal/mol, was much less than that of the TS, 58.23 kcal/mol,

Can. J. Chem. Downloaded from www.nrcresearchpress.com by 92.62.229.171 on 09/08/12
For personal use only.

TABLE 2. Optimized values for the disposable parameters in the intermolecular potential function between the FW(TS) system and the W(SS)

Atom pair		Optimized parameters		
i	j	b_{3ij} (Å^3 · hartree)	b_{6ij} (Å^6 · hartree)	b_{12ij} (Å^{12} · hartree)
1	*a*	−0.478	4.243	1309.466
1	*b*	0.264	−2.599	215.310
1	*c*	0.264	−2.599	215.310
2	*a*	0.433	−1.635	461.669
2	*b*	−0.197	0.232	0.002
2	*c*	−0.197	0.232	0.002
3	*a*	−0.211	0.233	0.027
3	*b*	0.094	−0.062	1.252
3	*c*	0.094	−0.062	1.252
4	*a*	−0.094	−0.885	122.962
4	*b*	0.058	0.280	0.002
4	*c*	0.058	0.280	0.002
5	*a*	−0.094	−0.885	122.962
5	*b*	0.058	0.280	0.002
5	*c*	0.058	0.280	0.002
6	*a*	0.358	−0.098	524.092
6	*b*	−0.200	0.260	3.001
6	*c*	−0.200	0.260	3.001
7	*a*	0.358	−0.098	524.092
7	*b*	−0.200	0.260	3.001
7	*c*	−0.200	0.260	3.001
8	*a*	−0.115	−0.042	0.161
8	*b*	0.054	0.068	0.003
8	*c*	0.054	0.068	0.003
9	*a*	−0.115	−0.042	0.161
9	*b*	0.054	0.068	0.003
9	*c*	0.054	0.068	0.003
10	*a*	−0.026	−0.334	12.573
10	*b*	0.014	0.078	0.020
10	*c*	0.014	0.078	0.020

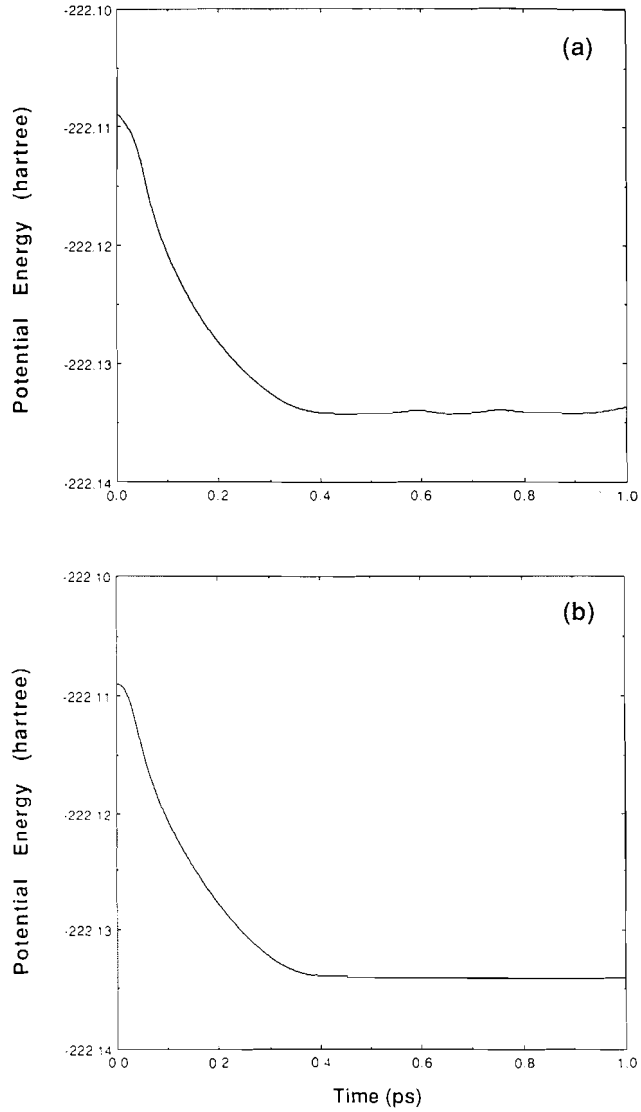

FIG. 11. Potential energy curve of the CRMD simulation in the case of IRC-directed initial velocity for (*a*) the FW system and (*b*) the FW–W system.

which was attributed to the potential energy reducing effect through the short-range interactions.

The potential energy profile along the IRC shows that the potential energy barrier of the FWW complex, 15.65 kcal/mol (Fig. 6), is almost the same as that of the FW system, 15.69 kcal/mol (13). This is also because a medium-water molecule solvates energetically both the FW(SS) and the FW(TS) system to the same extent.

Molecular orbital analysis

The schematic picture of the frontier orbitals and the total atomic charges for the FW(TS) system and the W(SS) molecule are shown in Figs. 7 and 8, respectively. There exist two kinds of electron lone pair, one in the FW system and the other in the W molecule. As explained later, the orbital interaction between FW and W is found less charge-transfer-interactive. However, if we use a term, *the donor and acceptor interaction*, the HOMO–LUMO interaction may be explained by the interaction between a lone pair orbital of W/FW and an unoccupied orbital of FW/W. Taking the second-order perturbation theory into consideration, the larger the magnitude of overlapping and the smaller the energy difference between the orbitals involved, the larger is the stabilization energy associated with the interaction between them. Accordingly, it can be found that the following orbital combinations are important for the effective orbital interaction for each structure of the FW(TS)–W(SS) complex.

	FW(TS)	W(SS)
A	HOMO−1	← LUMO
B	LUMO+1	→ HOMO
C	LUMO+1	→ HOMO
D	HOMO−1	← LUMO
E	LUMO+1	→ HOMO

As is easily understood from Table 1, the solvation energy for each orientation is equal to ~6.0 kcal/mol and is known as the stabilization energy of hydrogen bonding. According to the energy decomposition analysis developed by Yamabe and Morokuma (32, 33), it is concluded that the stabilization energy of a hydrogen bond originates mainly from the electrostatic energy. Although it was reported also that the contribution of the charge transfer energy turns out to be equally large by using the minimal STO-3G basis set,

Can. J. Chem. Downloaded from www.nrcresearchpress.com by 92.62.229.171 on 09/08/12
For personal use only.

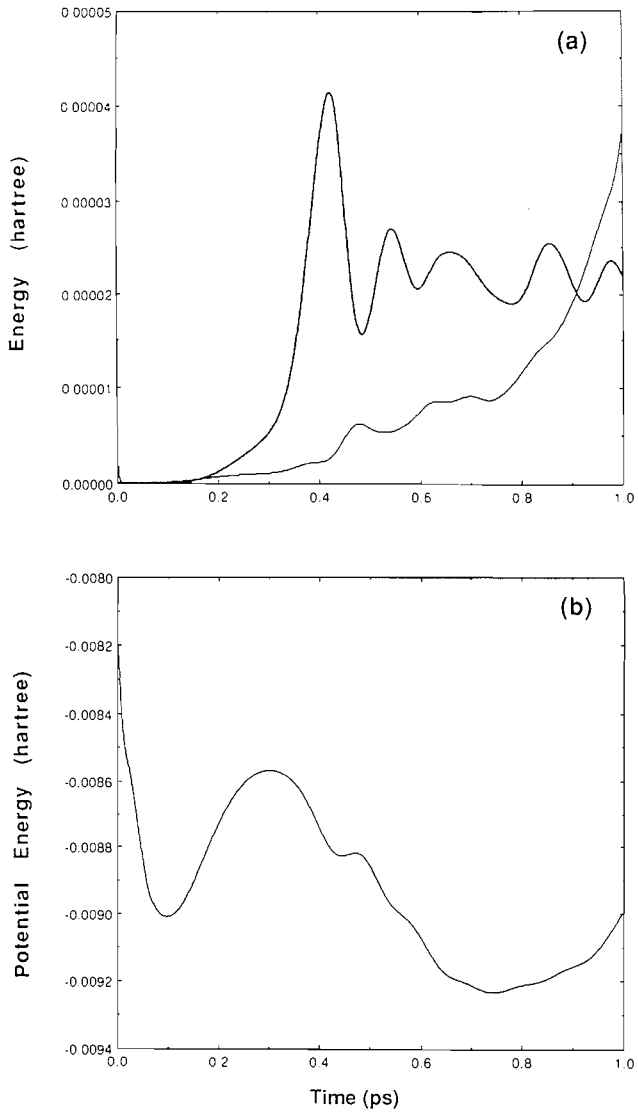

FIG. 12. Energy flows for the FW–W system in the case of IRC-directed initial velocity: (*a*) the rotational kinetic energy of W (thin solid line) and the relative translational one between FW and W (thick solid line), and (*b*) the potential energy between FW and W.

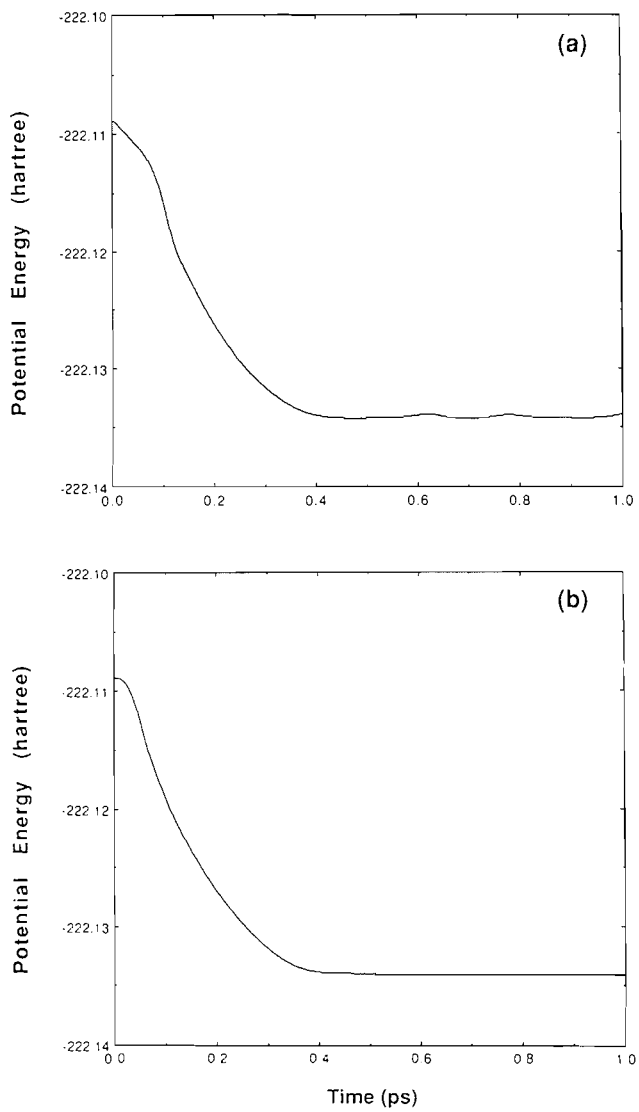

FIG. 13. Potential energy curve of the CRMD simulation in the case of randomly directed initial velocity for (*a*) the FW system and (*b*) the FW–W system.

it is due to the superposition error of the basis set. The present calculation has been executed by the minimal STO-3G basis set and, therefore, the present stabilization energy, i.e., the solvation energy by hydrogen bond creation, arises mainly by the electrostatic interaction between the FW system and the W molecule.

The energetic order and phases of the orbitals for the FW(SS) system (Fig. 9) are similar to those of the FW(TS) system (Fig. 7). Furthermore, no striking differences are observed with respect to the charge distribution between the FW(TS) and FW(SS) systems. These facts suggest that not only the orbital symmetry but also electrostatic interaction does not change along the IRC in the present reaction system. The barrier-reducing effect of a medium-water molecule does not appear because nearly the same stabilization is accomplished for TS and SS, respectively. Thus the circumstances contrast with chemical reactions involving ionic states. For example, Bohme and Mackay reported that the hydration in S_N2 reactions in solution gives rise to smaller rate constants than those in the gas phase (34). Several theoretical studies have concluded that the energy barrier increases with the assistance of water (2, 35–37). On the other hand, Warshel reported that in a heterolytic bond cleavage reaction, the specific orientation of surrounding solvent molecules or a protein cage reduces the energy barrier on the free energy surface (38). These results are attributed to the fact that the electrostatic coupling between the solute charge distribution and that of the solvent determines the energetics of chemical reaction systems (36, 39, 40). It is true that the entropy factor also depends on the long-range interaction between the solute and solvent. However, it is expected that its contribution to the factor is equivalent for both FW(TS) and FW(SS) and, therefore, the dynamic effect caused by the medium-water should become more important for understanding the proton transfer reaction in the FW system.

On the contrary, the situation is in clear contrast to that of a formamidine and a water molecule (i.e., a reactive-solvent molecule), where "stabilization" of a few hundred kcal/mol is observed and the orbital symmetry between the SS and TS structures is quite different. This is why the water mol-

Can. J. Chem. Downloaded from www.nrcresearchpress.com by 92.62.229.171 on 09/08/12
For personal use only.

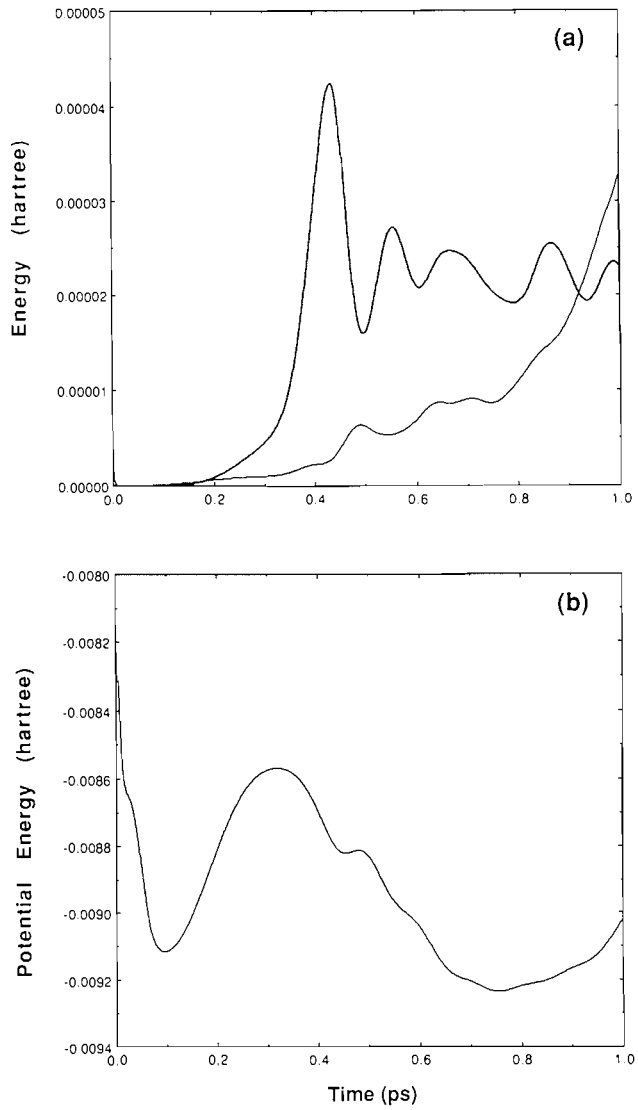

FIG. 14. Energy flows for the FW–W system in the case of randomly directed initial velocity: (*a*) the rotational kinetic energy of W (thin solid line) and the relative translational one between FW and W (thick solid line), and (b) the potential energy between FW and W.

ecule should be treated as a reactive-solvent molecule in this article. While electrostatic interaction can be also expected between the N6 and the H4 and between the H5 and the O2 (see, Figs. 8 and 10), the charge transfer interaction, which may be considered as one of the donor–acceptor interactions between the HOMO − 1 of the formamidine and the LUMO of the W(SS) and that between the LUMO + 2 of the formamidine and the HOMO of the W(SS), should play the more dominant role in this system.

Intermolecular potential function

The intermolecular potential function between the FW system and the W molecule was fitted by using the configurations and their total energies between the FW(TS) and the W(SS) structures. Although the fitted potential function was approximated for the FW(TS)–W(SS) intermolecular potential energies in the neighborhood of the IRC on the potential energy surface, this approximation can be allowed because interaction energies between FW(TS) and W(SS) are found to be small. The fitting of parameters, shown in Table 2, was accomplished with a standard deviation of 1.40×10^{-4} hartrees. Further, the standard deviation, 2.03×10^{-4} hartrees, for the test data base suggests that the present fitting is satisfactory enough to be in good agreement with *ab initio* MO energies.

CRMD simulation and the energy relaxation mechanism

In simulations with IRC-D IV, except for the slight oscillation in the SS region for the FW system in the time-dependent potential energy profile, there is little difference between the FW system and the FW part of the FWW system (Fig. 11). As shown in Fig. 12, the change in internal vibrational kinetic energy shows that the medium-water molecule has little movement with respect to the FW supermolecule around the saddle-point region. The relative translational kinetic energy between the FW system and the W molecule increases at the entrance of the SS region, followed by the increase of the rotational kinetic energy of the W molecule.

In simulations with R-D IV, the slow decrease of the potential energy over the starting 0.2 ps for the FW system disappears for the case of the FWW system as shown in Fig. 13. This fact can be observed for each of the 10 trajectories calculated and is considered the most important result brought about by the participation of the medium-water molecule. It is explained by the IRC stabilization effect, which can result in the rate constant increase (14). On the other hand, the kinetic energy flow is similar to that in the IRC-D IV case (Fig. 14); that is, the internal vibrational kinetic energy of FW transfers, by way of relative translational kinetic energy, to the rotational kinetic energy of W. Since the 10 trajectories show also the same characteristic, it can be concluded that there is a temporal order in the energy relaxation mechanism for the FWW(TS) complex.

Conclusion

The solvent effect for chemical reactions in solution was investigated by classifying solvent molecules as reactive-solvent or medium-solvent. The proton transfer reaction of formamidine in the solvent water was treated in this study as a model for the biological system. The FW(TS) system can be largely stabilized in comparison to the TS structure of isolated formamidine and the corresponding stabilization between the SS structures is not found. This phenomenon explains the remarkable potential energy barrier-reducing effect of the reactive-water molecule. On the other hand, the solvation energy of a medium-water molecule for the FW supermolecule is quite small. Therefore, the potential energy barrier does not change in the presence of a medium-water molecule in comparison with reactions involving ionic states. The solvation energy of the medium-water molecule in the FWW complex consists mainly of the electrostatic interaction and was discussed by *ab initio* MO analysis according to frontier orbital theory based on second-order perturbation theory.

The energy relaxation mechanism was clarified by the CRMD simulation. The averaged position of the center of mass of the medium-water molecule does not change during the reaction process. After the decrease of the internal vibrational kinetic energy occurs, the relative translational kinetic energy between the FW system and the medium-water molecule first increases and is then followed by the increase

Can. J. Chem. Downloaded from www.nrcresearchpress.com by 92.62.229.171 on 09/08/12
For personal use only.

of the rotational kinetic energy of the medium-water molecule. The IRC stabilization effect was found by comparing the CRMD simulations for the FW and the FWW systems. This effect is important and will be discussed in detail in a future publication (15).

Acknowledgments

We would like to thank the referee for some helpful comments and suggested references. The numerical calculations were performed by CONVEX C201 and C210 at the IFC computer room and by FACOM VP400E at the Data Processing Center of Kyoto University. This work was supported by a Grant-in-Aid for Scientific Research from the Ministry of Education, Science and Culture in Japan.

1. I. H. Williams. J. Am. Chem. Soc. **109**, 6299 (1987).
2. K. Morokuma. J. Am. Chem. Soc. **104**, 3732 (1982).
3. M. T. Nguyen and A. F. Hegarty. J. Mol. Struct. (Theochem), **93**, 329 (1983).
4. J. D. Madura and W. L. Jorgensen. J. Am. Chem. Soc. **108**, 2517 (1986).
5. K. Yamashita, M. Kaminoyama, T. Yamabe, and K. Fukui. Theoret. Chim. Acta (Berlin), **60**, 303 (1981).
6. T. Yamabe, K. Yamashita, M. Kaminoyama, M. Koizumi, A. Tachibana, and K. Fukui. J. Phys. Chem. **88**, 1459 (1984).
7. B. Chance *et al* (*Editor*). Tunneling in biological systems. Academic Press, New York. 1979.
8. T. J. Zielinski, M. R. Peterson, I. G. Csizmadia, and R. Rein. J. Comput. Chem. **3**, 62 (1982).
9. W. Kinasiewicz, A. Les', and I. Wawer. J. Mol. Struc. (Theochem), **168**, 1 (1988).
10. L. Radom, W. J. Hehre, and J. A. Pople. J. Am. Chem. Soc. **93**, 289 (1971).
11. J. Andres, J. Krechl, M. Carda, and E. Silla. Int. J. Quantum Chem. **40**, 127 (1991).
12. K. A. Nguyen, M. S. Gordon, and D. G. Truhlar. J. Am. Chem. Soc. **113**, 1596 (1991).
13. M. Nagaoka, Y. Okuno, and T. Yamabe. J. Am. Chem. Soc. **113**, 769 (1991); D. Heidrich, W. Kliesch, and W. Quapp. Properties of chemically interesting potential energy surfaces. Lect. Notes Chem. **56**, 176 (1991).
14. M. Nagaoka, Y. Okuno, and T. Yamabe. To be submitted.
15. M. Nagaoka, Y. Okuno, and T. Yamabe. To be published.
16. R. Daudel, G. Leroy, D. Peeters, and M. Sana. Quantum chemistry. Willey, New York. 1983.
17. M. J. Frisch, J. S. Binkley, H. B. Schlegel *et al.* GAUSSIAN86. Carnegie–Mellon Quantum Chemistry Publishing Unit, Pittsburgh, PA. 1984.
18. W. J. Hehre, R. F. Stewart, and J. A. Pople. J. Chem. Phys. **51**, 2657 (1969).
19. C. C. J. Roothaan. Rev. Mod. Phys. **23**, 69 (1951).
20. P. Pulay and H. F. Schaefer III (*Editors*). Modern theoretical chemistry. Vol. 4. Plenum, New York. 1977.
21. M. Nagaoka, Y. Okuno, T. Yamabe, and K. Fukui. Int. J. Quantum Chem. In press.
22. J. Baker and P. M. W. Gill. J. Comput. Chem. **9**, 465 (1988).
23. R. S. Mulliken. J. Chem. Phys. **23**, 1841 (1955).
24. S. Swaminathan, R. J. Whitehead, E. Guth, and D. L. Beveridge. J. Am. Chem. Soc. **99**, 7817 (1977).
25. A. F. Carley and P. H. Morgan. Computational methods in the chemical sciences. Ellis Horwood, Chichester. 1989.
26. K. Levenberg. Q. Appl. Math. **2**, 164 (1944).
27. D. W. Marquardt. J. Soc. Ind. Appl. Maths. **11**, 431 (1963).
28. J. J. More, B. S. Garbow, and K. E. Hillstrom. User guide for MINPACK-1. Argonne National Labs Report ANL-80-74, Argonne, IL. 1980.
29. M. P. Allen and D. J. Tildesley. Computer simulation of liquids. Oxford University Press, New York. 1987.
30. J. P. Ryckaert, G. Ciccotti, and H. J. C. Berendsen. J. Comput. Phys. **23**, 327 (1977).
31. I. Ohmine. J. Chem. Phys. **85**, 3342 (1986).
32. K. Morokuma. J. Chem. Phys. **55**, 1236 (1971).
33. S. Yamabe and K. Morokuma. J. Am. Chem. Soc. **97**, 4458 (1975).
34. D. K. Bohme and G. I. MacKay. J. Am. Chem. Soc. **103**, 978 (1981).
35. J. Chandrasekhar, S. F. Smith, and W. L. Jorgensen. J. Am. Chem. Soc. **106**, 3049 (1984).
36. S. E. Huston, P. J. Rossky, and D. A. Zichi. J. Am. Chem. Soc. **111**, 5680 (1989).
37. J. K. Hwang, G. King, S. Creighton, and A. Warshel. J. Am. Chem. Soc. **110**, 5297 (1988).
38. A. Warshel. Proc. Natl. Acad. Sci. U.S.A. **81**, 444 (1984).
39. O. Tapia, R. Cardenas, J. Andres, J. Krechl, M. Campillo, and F. Colonna-Cesari. Int. J. Quantum Chem. **39**, 767 (1991).
40. H. J. Kim and J. T. Hynes. J. Chem. Phys. **93**, 5194 (1990).

Can. J. Chem. Downloaded from www.nrcresearchpress.com by 92.62.229.171 on 09/08/12
For personal use only.

Molecular integrals over Laguerre Gaussian-type functions of real spherical harmonics

OSAMU MATSUOKA

Department of Physics, The University of Electro-Communications, Chofu, Tokyo 182, Japan

Received May 9, 1991

This paper is dedicated to Professor Sigeru Huzinaga on the occasion of his 65th birthday

OSAMU MATSUOKA. Can. J. Chem. **70**, 388 (1992).

Molecular integrals are formulated over the Laguerre Gaussian-type functions (LGTF) of *real* spherical harmonics. They include the overlap integrals and the energy integrals of kinetic, nuclear attraction, and electron repulsion. For the nuclear-attraction integrals the formulations based on the point as well as the Gaussian nuclear charge distribution models are presented. Integral formulas over the LGTFs of *real* spherical harmonics are found a little more complicated than those of the LGTFs of *complex* spherical harmonics due to the summations over magnetic quantum numbers.

Key words: molecular integral, Gaussian-type function, spherical harmonic, solid harmonic, Sonine polynomial.

OSAMU MATSUOKA. Can. J. Chem. **70**, 388 (1992).

On formule des intégrales moléculaires pour les fonctions de Laguerre de type gaussien (FLTG) des harmoniques sphériques *réelles*. Elles comprennent les intégrales de recouvrement et les intégrales d'énergie cinétique, d'attraction nucléaire et de répulsion électronique. Pour les intégrales d'attraction nucléaire on présente les formulations basées sur des modèles de distributions de charges ponctuelles ainsi que gaussiennes. On a trouvé que, à cause des sommations sur les nombres quantiques magnétiques, les formules intégrales pour les FLTG des harmoniques sphériques *réelles* sont un peu plus compliquées que les FLTG des harmoniques sphériques *complexes*.

Mots clés : intégrale moléculaire, fonction de type gaussien, harmonique sphérique, harmonique solide, polynôme de Sonine.

[Traduit par la rédaction]

Can. J. Chem. Downloaded from www.nrcresearchpress.com by 92.62.229.171 on 09/08/12
For personal use only.

1. Introduction

The Laguerre Gaussian-type function (LGTF) is a spherical harmonic Gaussian and is defined as

$$L_n^{(l+1/2)}(\alpha r^2)\exp(-\alpha r^2)r^l Y_{lm}(\theta,\phi)$$

where $L_n^{(l+1/2)}$ is the generalized Laguerre (or Sonine) polynomial, Y_{lm} is the spherical harmonic, α is the exponent parameter, n, l, and m are quantum numbers, and (r,θ,ϕ) denotes the spherical coordinates. The LGTF shares with other spherical harmonic Gaussians a common desirable feature that all members with the same angular quantum number l but with different magnetic quantum numbers $m = -l, \ldots, +l$ are independent of each other in contrast to those of the Cartesian Gaussians of higher angular quantum numbers than of d types. Furthermore, the molecular integral of electron repulsion over the LGTFs is of particularly simple form to facilitate fast computation.

In a previous paper (1) (which will be referred to as I hereafter) by the present author, Fieck's (2) analysis of molecular integrals over the LGTFs was reformulated so that it is suitable for computation and his analysis was generalized to include such various kinds of molecular properties as the multipole moments and transitions, the electric field and gradient, the quasi-relativistic interactions, etc. Recently, it was further generalized (3) to include the molecular integrals of Breit interaction for relativistic calculation.

In previous works (1–3), the formulations were done over the LGTFs of *complex* spherical harmonics (CSH) (or the complex LGTFs). The complex LGTFs could be appropriately adopted for *linear* molecules. However, for general *polyatomic* molecules the LGTFs of *real* spherical harmonics (RSH) (or the real LGTFs) are more suitable. Thus, in the present paper the real LGTFs have been employed for the analysis. The formulas of molecular integrals over the real LGTFs have been found a little more complicated than those over the complex LGTFs but their analysis has been done almost parallel to the one on the complex LGTFs. In I, the analysis was done on various molecular properties and the formulas of the energy integrals (i.e., the overlap, the kinetic energy, the nuclear attraction, and the electron-repulsion integrals) were derived indirectly as special cases of integral formulas of more general properties. In the present paper, analysis has been limited to the one on the energy integrals but their formulas have been derived directly through the definitions and properties of the real LGTFs so that their derivations might be more transparent. For nuclear-attraction integrals the formulas based on the point as well as the Gaussian nuclear charge distribution models are presented.

In Sect. 2 the real LGTFs are defined and the Talmi transformation among them is described. In Sect. 3 the formulas of the energy integrals are derived directly using the definitions and the properties of the real LGTFs. Section 4 gives some concluding remarks. In the appendices some of the formulas and properties used in Sects. 2 and 3 are derived and discussed.

2. Laguerre Gaussian-type functions and Talmi transformation

2.1. Laguerre Gaussian-type functions

The unnormalized LGTF of *real* spherical harmonic is defined by

$$[2.1]\qquad \chi_{\alpha N}(\boldsymbol{r}) = (-1)^l \hat{Y}_N(\nabla)\exp(-\alpha r^2),$$

where N is a set of integers (quantum numbers):

$$[2.2]\qquad N = (n, l, m)$$

n and l being nonnegative and $|m| \leq l$. The operator $\hat{Y}_N(\nabla)$ is obtained by substituting the differential operators $\partial/\partial x$, $\partial/\partial y$, and $\partial/\partial z$ into the Cartesian coordinates x, y, and z in the homogeneous solid harmonic $Y_{nlm}(\boldsymbol{r}) = r^{2n+l}Y_{lm}(\theta,\phi)$. In

Printed in Canada

Can. J. Chem. Downloaded from www.nrcresearchpress.com by 92.62.229.171 on 09/08/12
For personal use only.

the present paper the RSHs $Y_{nl}(\theta,\phi)$ are defined through the CSHs $\bar{Y}_{lm}(\theta,\phi)$ of Condon–Shortley as:

[2.3]
$$Y_{l,0}(\theta,\phi) = \bar{Y}_{l,0}(\theta,\phi)$$
$$Y_{l,|m|}(\theta,\phi) = (1/\sqrt{2})[\bar{Y}_{l,-|m|}(\theta,\phi) + (-1)^m \bar{Y}_{l,|m|}(\theta,\phi)]$$
$$Y_{l,-|m|}(\theta,\phi) = (i/\sqrt{2})[\bar{Y}_{l,-|m|}(\theta,\phi) - (-1)^m \bar{Y}_{l,|m|}(\theta,\phi)]$$

where i is the imaginary unit. The real LGTF defined by [2.1] is written explicitly as

[2.4]
$$\chi_{\alpha N}(\boldsymbol{r}) = N_{\alpha nl} L_n^{(l+1/2)}(\alpha r^2) \exp(-\alpha r^2) Y_{0lm}(\boldsymbol{r})$$

where

[2.5]
$$N_{\alpha nl} = (-1)^n 2^{2n+l} n! \alpha^{n+l}$$

and the generalized Laguerre (or Sonine) polynomial is defined by

[2.6]
$$L_n^{(s)}(x) = \sum_{m=0}^{n} \frac{\Gamma(n+s+1)}{m!(n-m)!\Gamma(m+s+1)} (-x)^m$$

$\Gamma(x)$ being the Gamma function. A derivation of [2.4] is given in Appendix 1.

The real LGTF located at position $\boldsymbol{A}$ is thus written as

[2.7]
$$\chi_{\alpha_A N_A}(\boldsymbol{r}_{\mu A}) = \hat{Y}_{N_A}(\nabla_A) \exp(-\alpha_A r_{\mu A}^2)$$

where $\boldsymbol{r}_{\mu A} = \boldsymbol{r}_\mu - \boldsymbol{A}$, $\boldsymbol{r}_\mu$ being position of the electron μ and ∇_A is the differential operator with respect to the position vector $\boldsymbol{A}$. Here we have used the fact that $\hat{Y}_{N_A}(\nabla_{\mu A}) = (-1)^{l_A} \hat{Y}_{N_A}(\nabla_A)$ when operating on a function of argument $r_{\mu A}$.

For analysis of nuclear-attraction and electron-repulsion integrals, it is convenient to generalize the definition of the real LGTF, [2.1], to include the case when $n = -1$:

[2.8]
$$\chi_{\alpha(-1)lm}(\boldsymbol{r}) = -(2\alpha)^{l-1} F_l(\alpha r^2) Y_{0lm}(\boldsymbol{r})$$

where the incomplete Gamma function is defined by

[2.9]
$$F_l(t) = \int_0^1 du u^{2l} \exp(-tu^2)$$

2.2. *Talmi transformation*

A product of two real LGTFs $\chi_{\alpha_1 N_1}(\boldsymbol{r}_1)$ and $\chi_{\alpha_2 N_2}(\boldsymbol{r}_2)$ can be written as a finite sum over the products of two real LGTFs $\chi_{\alpha_3 N_3}(\boldsymbol{r}_3)$ and $\chi_{\alpha_4 N_4}(\boldsymbol{r}_4)$ of coordinates $\boldsymbol{r}_3 = \boldsymbol{r}_1 - \boldsymbol{r}_2$ and $\boldsymbol{r}_4 = (\alpha_1 \boldsymbol{r}_1 + \alpha_2 \boldsymbol{r}_2)/(\alpha_1 + \alpha_2)$ with $\alpha_3 = \alpha_1\alpha_2/(\alpha_1 + \alpha_2)$ and $\alpha_4 = \alpha_1 + \alpha_2$:

[2.10]
$$\chi_{\alpha_1 N_1}(\boldsymbol{r}_1)\chi_{\alpha_2 N_2}(\boldsymbol{r}_2) = \sum_{N_3 N_4} \chi_{\alpha_3 N_3}(\boldsymbol{r}_3)\chi_{\alpha_4 N_4}(\boldsymbol{r}_4) T(\alpha_3 N_3, \alpha_4 N_4 \mid \alpha_1 N_1, \alpha_2 N_2)$$

The indices N_1, N_2, N_3, and N_4 have to satisfy the relation

[2.11]
$$2n_1 + l_1 + 2n_2 + l_2 = 2n_3 + l_3 + 2n_4 + l_4$$

Relation among magnetic quantum numbers m_1, m_2, m_3, and m_4 is a little more complicated than the one for the complex LGTFs ([2.14] of I) and is discussed in Appendix 2. The relation [2.10] is known as Talmi transformation (4) and the coefficients T are called Talmi coefficients which are expressed in terms of the Moshinsky–Smirnov coefficients (5, 6) and Niukkanen coefficients (7) (see also [2.16] and [2.24] of I).

Using [2.10] a product of two real LGTFs located at $\boldsymbol{A}$ and $\boldsymbol{B}$ with exponent parameters α_A and α_B respectively, can be expressed again in terms of real LGTFs located at $\boldsymbol{P} = (\alpha_A \boldsymbol{A} + \alpha_B \boldsymbol{B})/(\alpha_A + \alpha_B)$:

[2.12]
$$\chi_{\alpha_A N_A}(\boldsymbol{r}_{\mu A})\chi_{\alpha_B N_B}(\boldsymbol{r}_{\mu B}) = \sum_{N_P} \chi_{\alpha_P N_P}(\boldsymbol{r}_{\mu P}) W(N_P; \alpha_A N_A, \alpha_B N_B \mid \boldsymbol{BA})$$

where

[2.13]
$$W = \sum_{N_R} \chi_{\alpha_R N_R}(\boldsymbol{BA}) T(\alpha_R N_R, \alpha_P N_P \mid \alpha_A N_A, \alpha_B N_B)$$

In [2.12] and [2.13] $\alpha_P = \alpha_A + \alpha_B$, $\alpha_R = \alpha_A\alpha_B/(\alpha_A + \alpha_B)$, and $\boldsymbol{BA} = \boldsymbol{B} - \boldsymbol{A}$ and the indices N_P and N_R have to satisfy the relation

[2.14]
$$2n_A + l_A + 2n_B + l_B = 2n_P + l_P + 2n_R + l_R.$$

3. Molecular integrals

In this section the formulas of the energy integrals are derived. For the analysis an operator identity will be used:

[3.1]
$$\hat{Y}_{N_1}(\nabla)\hat{Y}_{N_2}(\nabla) = \sum_N \hat{Y}_N(\nabla)\, \Xi(lm \mid l_1 m_1, l_2 m_2)$$

Here the summations over n and l are done under the restriction

[3.2]
$$2n + l = 2n_1 + l_1 + 2n_2 + l_2$$

and m takes two values m_+ and m_- given by (8, 9)

[3.3]
$$m_\pm = \text{sign}(m_1)\,\text{sign}(m_2)\,|\,(|m_1| \pm |m_2|)\,|$$

where

[3.4]
$$\text{sign}(x) = +1 \text{ for } x \geq 0 \quad \text{and sign}(x) = -1 \text{ for } x < 0$$

In Appendix 2 the Gaunt coefficients Ξ of RSHs are related to those of CSHs.

3.1. *Overlap integral*

Using [2.12] the overlap integral is reduced to

[3.5]
$$\langle \alpha_A N_A \mid \alpha_B N_B \rangle = \int d^3 \boldsymbol{r}_1 \chi_{\alpha_A N_A}(\boldsymbol{r}_{1A})\chi_{\alpha_B N_B}(\boldsymbol{r}_{1B}) = \sum_{N_P} W(N_P; \alpha_A N_A, \alpha_B N_B \mid \boldsymbol{BA})[\alpha_P N_P \mid 1]$$

Using the orthogonality properties of the Sonine polynomials and the RSHs the basic integral in [3.5] reads

[3.6]
$$[\alpha_P N_P \mid 1] = \int d^3 \boldsymbol{r}_1 \chi_{\alpha_P N_P}(\boldsymbol{r}_{1P}) = \delta_{n_P 0}\delta_{l_P 0}\delta_{m_P 0}\sigma(\alpha_P)$$

where

[3.7]
$$\sigma(\alpha) = \pi/2\alpha^{2/3}$$

Hence the overlap integral, [3.5], is further reduced to

[3.8]
$$\langle \alpha_A N_A \mid \alpha_B N_B \rangle = \sigma(\alpha_P) W(000; \alpha_A N_A, \alpha_B N_B \mid \boldsymbol{BA})$$

The formula [3.8] can be adopted in practice for the computation. However, using a formula of the Talmi coeffi-

Can. J. Chem. Downloaded from www.nrcresearchpress.com by 92.62.229.171 on 09/08/12
For personal use only.

cient in [2.10] when $N_3 = (0, 0, 0)$, the W function of [3.8] is further reduced to

$$[3.9] \quad W = (-1)^{l_B}(4\pi)^{1/2} \times \sum_{N_R} \chi_{\alpha_R N_R}(\boldsymbol{BA})\Xi(l_R m_R) \mid l_A m_A, l_B m_B)$$

where, due to the properties of the Gaunt coefficients Ξ (eqs. [3.2] and [3.3]), the summations over n_R and l_R are done under the restriction

$$[3.10] \quad 2n_R + l_R = 2n_A + l_A + 2n_B + l_B$$

and m_R takes two values

$$[3.11] \quad m_R = \text{sign } (m_A) \text{ sign } (m_B) \mid (|m_A| \pm |m_B|) \mid$$

The derivation of the expression [3.9] is very much analogous to the one for the complex LGTFs (eq. [3.15] of I). The formulas [3.8] and [3.9] can also be adopted in the computation.

3.2 Kinetic-energy integral

Using the definition of the LGTFs, [2.1], the kinetic-energy integral in nonrelativistic calculations is reduced to an overlap integral:

$$[3.12] \quad \langle \alpha_A N_A \mid \nabla^2 \mid \alpha_B N_B \rangle = \int \mathrm{d}^3 \boldsymbol{r}_1 \chi_{\alpha_A N_A}(\boldsymbol{r}_{1A}) \nabla_1^2 \chi_{\alpha_B N_B}(\boldsymbol{r}_{1B}) = \langle \alpha_A N_A \mid \alpha_B, (n_B + 1), l_B, m_B \rangle$$

In relativistic (Dirac–Fock) calculations the kinetic-energy operator is $\boldsymbol{\sigma}\cdot\boldsymbol{p}$, where $\boldsymbol{\sigma} = (\sigma_x, \sigma_y, \sigma_z)$ are Pauli 2×2 matrices and $\boldsymbol{p} = -i\nabla$ is the momentum operator. Thus the integral appearing in the calculation is

$$[3.13] \quad \langle \alpha_A N_A \mid \hat{Y}_{01m}(\nabla) \mid \alpha_B N_B \rangle = \int \mathrm{d}^3 \boldsymbol{r}_1 \chi_{\alpha_A N_A}(\boldsymbol{r}_{1A}) \hat{Y}_{01m}(\nabla_1) \chi_{\alpha_B N_B}(\boldsymbol{r}_{1B})$$

where $m = 0, \pm 1$. Using [2.7] and [3.1] it can be shown that

$$[3.14] \quad \hat{Y}_{01m}(\nabla_1)\chi_{\alpha_B N_B}(\boldsymbol{r}_{1B}) = -\sum_{l'm'} \Xi\,(l'm' \mid 1m, l_B m_B)\chi_{\alpha_B n_B l'm'}(\boldsymbol{r}_{1B})$$

Here, due to the Gaunt coefficient Ξ, $l' = l_B \pm 1$ and $m' = m_B$, $m_B \pm 1$ and it has been used that $\hat{Y}_{01m}(\nabla_1) = -\hat{Y}_{01m}(\nabla_B)$ when operating on a function of argument $\boldsymbol{r}_{1B}$. Then integral [3.13] is also reduced to the overlap integrals:

$$[3.15] \quad \langle \alpha_A N_A \mid \hat{Y}_{01m}(\nabla) \mid \alpha_B N_B \rangle = -\sum_{l'm'} \Xi(l'm' \mid 1m, l_B m_B) < \alpha_A N_A \mid \alpha_B n_B l'm' \rangle$$

3.3. Nuclear-attraction integral

Using [2.12] the nuclear-attraction integral is reduced to

$$[3.16] \quad \langle \alpha_A N_A \mid V(r_C) \mid \alpha_B N_B \rangle = \int \mathrm{d}^3 \boldsymbol{r}_1 \chi_{\alpha_A N_A}(\boldsymbol{r}_{1A}) V(r_{1C}) \chi_{\alpha_B N_B}(\boldsymbol{r}_{1B}) = \sum_{N_P} W(N_P; \alpha_A N_A, \alpha_B N_B \mid \boldsymbol{BA})[\alpha_P N_P \mid V(r_C)]$$

where the attractive center of nuclear potential $V(r_C)$ is assumed on location (atom) $\boldsymbol{C}$ and the basic integral is defined as

$$[3.17] \quad [\alpha_P N_P \mid V(r_C)] = \int \mathrm{d}^3 \boldsymbol{r}_1 \chi_{\alpha_P N_P}(\boldsymbol{r}_{1P}) V(r_{1C})$$

If the *point-charge* model for the atomic nucleus is adopted, $V(r_{1C}) = 1/r_{1C}$. Then using the definition of the LGTFs, [2.7], we obtain

$$[3.18] \quad [\alpha_P N_P \mid 1/r_{1C}] = \hat{Y}_{N_P}(\nabla_P) \int \mathrm{d}^3 \boldsymbol{r}_1 \exp(-\alpha_P r_{1P}^2)(1/r_{1C})$$

For the integral in [3.18] Boys (10) gives a formula

$$[3.19] \quad \int \mathrm{d}^3 \boldsymbol{r}_1 \exp(-\alpha_P r_{1P}^2)(1/r_{1C}) = (2\pi/\alpha_P) F_0(\alpha_P \overline{CP}^2)$$

After differentiation of [3.19] by $\hat{Y}_{N_P}(\nabla_P)$, we get

$$[3.20] \quad [\alpha_P N_P \mid 1/r_{1C}] = -4\pi \chi_{\alpha_P (n_P - 1) l_P m_P}(\boldsymbol{CP})$$

where $\boldsymbol{CP} = \boldsymbol{C} - \boldsymbol{P}$. Fieck (2) gives a proof of [3.20] using the Poisson equation. A more direct and straightforward derivation is given in Appendix 1.

If the *Gaussian nuclear charge distribution* model (11) for the atomic nucleus is adopted,

$$[3.21] \quad V(r_{1C}) = \int \mathrm{d}^3 \boldsymbol{r}_2 \exp(-\alpha_C r_{2C}^2)(1/r_{12})$$

where α_C is a nuclear parameter. Then noting that $\exp(-\alpha r^2) = \chi_{\alpha 000}(\boldsymbol{r})$, the basic integral [3.19] is shown to be written as

$$[3.22] \quad [\alpha_P N_P \mid V(r_C)] = \int \mathrm{d}^3 \boldsymbol{r}_1 \int \mathrm{d}^3 \boldsymbol{r}_2 \chi_{\alpha_P N_P}(\boldsymbol{r}_{1P}) \chi_{\alpha_C 000}(\boldsymbol{r}_{2C})(1/r_{12})$$

This is a basic integral for the electron-repulsion integral and is written (see [3.28] of next subsection)

$$[3.23] \quad [\alpha_P N_P \mid V(r_C)] = -4\pi\sigma(\alpha_P + \alpha_C)\chi_{\alpha_T (n_P - 1) l_P m_P}(\boldsymbol{CP})$$

where σ is defined by [3.7] and $\alpha_T = \alpha_P \alpha_C/(\alpha_P + \alpha_C)$.

Both of the basic integrals, [3.20] and [3.23], are expressed in terms of the generalized LGTFs, [2.1] and [2.8].

3.4 Electron-repulsion integral

Using [2.12] separately for the two charge distributions of electrons 1 and 2, the electron-repulsion integral is reduced to

$$[3.24] \quad \langle \alpha_A N_A, \alpha_B N_B \mid 1/r_{12} \mid \alpha_C N_C, \alpha_D N_D \rangle = \int \mathrm{d}^3 \boldsymbol{r}_1 \int \mathrm{d}^3 \boldsymbol{r}_2 \chi_{\alpha_A N_A}(\boldsymbol{r}_{1A}) \chi_{\alpha_B N_B}(\boldsymbol{r}_{1B}) \chi_{\alpha_C N_C}(\boldsymbol{r}_{2C}) \times \chi_{\alpha_D N_D}(\boldsymbol{r}_{2D})(1/r_{12}) = \sum_{N_P N_Q} W(N_P; \alpha_A N_A, \alpha_B N_B \mid \boldsymbol{BA}) \times W(N_Q; \alpha_C N_C, \alpha_D N_D \mid \boldsymbol{DC})[\alpha_P N_P \mid 1/r_{12} \mid \alpha_Q N_Q]$$

where $\alpha_Q = \alpha_C + \alpha_D$. Using the definition of LGTFs, [2.7], for $\chi_{\alpha_P N_P}(\boldsymbol{r}_{1P})$ and $\chi_{\alpha_Q N_Q}(\boldsymbol{r}_{2Q})$, where $\boldsymbol{Q} = (\alpha_C \boldsymbol{C} + \alpha_C \boldsymbol{D})/(\alpha_C + \alpha_D)$, the basic integral in [3.24] is written as

$$[3.25] \quad [\alpha_P N_P \mid \alpha_Q N_Q] = \int \mathrm{d}^3 \boldsymbol{r}_1 \int \mathrm{d}^3 \boldsymbol{r}_2 \times \chi_{\alpha_P N_P}(\boldsymbol{r}_{1P}) \chi_{\alpha_Q N_Q}(\boldsymbol{r}_{2Q})(1/r_{12}) = \hat{Y}_{N_P}(\nabla_P) \hat{Y}_{N_Q}(\nabla_Q) \int \mathrm{d}^3 \boldsymbol{r}_1 \int \mathrm{d}^3 \boldsymbol{r}_2 \times \exp(-\alpha_P r_{1P}^2 - \alpha_Q r_{2Q}^2)(1/r_{12})$$

For the integral in [3.25] Boys (10) gives a formula

$$[3.26] \quad \int \mathrm{d}^3 \boldsymbol{r}_1 \int \mathrm{d}^3 \boldsymbol{r}_2 \exp(-\alpha_P r_{1P}^2 - \alpha_Q r_{2Q}^2)(1/r_{12}) = [2\pi^{5/2}/\alpha_P \alpha_Q (\alpha_P + \alpha_Q)^{1/2}] F_0(\alpha_T \overline{QP}^2)$$

where $\alpha_T = \alpha_P\alpha_Q/(\alpha_P + \alpha_Q)$. As [3.26] shows the integral in [3.25] depends on $\boldsymbol{QP} = \boldsymbol{Q} - \boldsymbol{P}$ so that $\hat{Y}_{N_Q}(\nabla_Q)$ in [3.25] can be replaced by $(-1)^{l_Q}\hat{Y}_{N_Q}(\nabla_P)$. Then using [3.1] for the product $\hat{Y}_{N_P}(\nabla_P)\hat{Y}_{N_Q}(\nabla_Q)$ and noting

$$[3.27] \quad \hat{Y}_N(\nabla_P)F_0(\alpha_T\overline{QP}^2) = -2\alpha_T\chi_{\alpha_T(n-1)lm}(\boldsymbol{QP})$$

we obtain for the basic integral of [3.25]

$$[3.28] \quad [\alpha_P N_P|1/r_{12}|\alpha_Q N_Q] = (-1)^{l_Q+1}(4\pi)^{3/2}\sigma(\alpha_P + \alpha_Q) \times \sum_{N_T} \Xi(l_T m_T \mid l_p m_p, l_Q m_Q)\chi_{\alpha_T(n_T-1)l_T m_T}(\boldsymbol{QP})$$

where σ is defined by [3.7] and the summations over $N_T = (n_T, l_T, m_T)$ are done under the restrictions

$$[3.29] \quad 2n_T + l_T = 2n_P + l_P + 2n_Q + l_Q$$

and

$$[3.30] \quad m_T = \text{sign}\,(m_P)\,\text{sign}\,(m_Q)\,|\,(|m_P| \pm |m_Q|)\,|$$

A derivation of [3.27] is given in Appendix 1.

4. Concluding remarks

In previous works (1–3), the formulations of molecular integrals were done over the *complex* LGTFs so that they are suitable for the calculations of *linear* molecules. In the present work the formulation has been done over the *real* LGTFs so that it is expected to be useful for general *polyatomic* molecules.

The formulas of molecular integrals over the real LGTFs are a little more complicated than those over the complex LGTFs. The complications in the case of real LGTFs are due to two reasons: (*1*) The total magnetic quantum number m in the Gaunt coefficient Ξ defined for the RSHs takes two values, [3.3], while the corresponding quantum number for the CSHs takes only one value such that $m = m_1 + m_2$ ([3.3] of I). (*2*) In the Talmi coefficients $\tilde{T}$ defined for the complex LGTFs there is a simple relation [A2.6], while in the T for the real LGTFs the relation among the magnetic quantum numbers is a little more complicated. Thus except for these complications the formulas over the real LGTFs are almost the same as those over the complex LGTFs.

In nonrelativistic calculations the LGTFs, [2.1], with quantum number $n = 0$ are usually employed and in relativistic calculations the LGTFs with quantum number $n = 0$ and 1 are needed. Thus if we restrict ourselves to adopt only the LGTFs with quantum number $n = 0$ (and 1), we should get some simplifications for the integral formulas.

1. Matsuoka. J. Chem. Phys. **92**, 4364 (1990).
2. G. Fieck. Theoret. Chim. Acta, **54**, 323 (1980).
3. N. Fujimura and O. Matsuoka. Int. J. Quantum Chem. In press.
4. I. Talmi. Helv. Phys. Acta, **25**, 185 (1952).
5. M. Moshinsky. Nucl. Phys. **13**, 104 (1959).
6. Yu. F. Smirnov. Nucl. Phys. **27**, 177 (1961); **39**, 346 (1962).
7. A. W. Niukkanen. Chem. Phys. Lett. **69**, 174 (1980).
8. K. O-ohata and K. Ruedenberg. J. Math. Phys. **7**, 547 (1966).
9. K. O-ohata. Mem. Fac. Sci. Kyushu Univ. **5**B, 7 (1974).
10. S. F. Boys. Proc. R. Soc. London Ser. A. **200**, 542 (1950).
11. O. Visser, P. J. C. Aerts, D. Hegarty, and W. C. Nieupoort. Chem. Phys. Lett. **134**, 34 (1987).
12. B. F. Bayman. J. Math. Phys. **19**, 2558 (1978).

Appendix 1. Explicit expressions of Laguerre Gaussian-type function and of basic integrals for nuclear-attraction and electron-repulsion integrals.

Fieck (2) suggested a derivation of the expression [2.4] via recursion formula and sketched the proof of the expression [3.20] and [3.27] via Poisson equation. In this appendix other direct derivations of these expressions will be presented using a generalized gradient formula (3).

Fujimura and Matsuoka (3) generalized Bayman's gradient formula (12) of solid harmonic to include the *homogeneous* solid harmonic. For an arbitrary radial function $f(r)$ the generalized gradient formula (3) reads

$$[A1.1] \quad \hat{Y}_{n_1l_1m_1}(\nabla)[f(r)Y_{l_2m_2}(\theta,\phi)] = \sum_{lm} \Xi(lm \mid l_1m_1, l_2m_2)g_{2n_1+l_1,l_2,l}(r)Y_{lm}(\theta,\phi)$$

where the summation over l extends from $|l_1 - l_2|$ to $l_1 + l_2$ in step of 2, Ξ is the Gaunt coefficient defined by [3.1], and

$$[A1.2] \quad g = \sum_k \frac{(2n_1 + l_1 + l_2 + l + 1)!!}{(2l + 2k + 1)!!} \times \binom{(2n_1 + l_1 + l_2 - l)/2}{k} \times r^{l+2k}\left(\frac{1}{r}\frac{d}{dr}\right)^{(l+2n_1+l_1-l_2)/2+k} [f(r)/r^{l_2}]$$

the summation over k being done in the range $[0, (2n_1 + l_1 + l_2 - l)/2]$.

Using [A1.1] for $\exp(-\alpha r^2)$ and noting the definition of Sonine polynomial, [2.6], it is straightforward to get an explicit expression of the real LGTF:

$$[A1.3] \quad \hat{Y}_{nlm}(\nabla)\exp(-\alpha r^2) = (-1)^l\chi_{\alpha nlm}(\boldsymbol{r}).$$

If one notes that

$$[A1.4] \quad (r^{-1}d/dr)^lF_0(\alpha r^2) = (-2\alpha)^lF_l(\alpha r^2)$$

and using [A1.1] for $F_0(\alpha r^2)$ it is also straightforward to derive

$$[A1.5] \quad \hat{Y}_{0lm}(\nabla)F_0(\alpha r^2) = (-2\alpha)^lF_l(\alpha r^2)Y_{0lm}(\boldsymbol{r}) = -2\alpha(-1)^l\chi_{\alpha(-1)lm}(\boldsymbol{r})$$

where on the second line the generalized definition of the LGTF, [2.8], has been used.

In order to prove [3.20] and [3.27] for $n = 1, 2, 3, \ldots$, we use [A1.1] for $F_0(\alpha r^2)$ and also use the recursion relation:

$$[A1.6] \quad (2m + 1)F_m(t) - 2tF_{m+1}(t) = \exp(-t)$$

Then we get

$$[A1.7] \quad \hat{Y}_{100}(\nabla)F_0(\alpha r^2) = -2\alpha\exp(-\alpha r^2)/(4\pi)^{1/2}$$

If we note that

$$[A1.8] \quad \hat{Y}_{nlm}(\nabla) = \hat{Y}_{n-1,lm}(\nabla)\hat{Y}_{100}(\nabla)/Y_{00}(\theta,\phi)$$

and use [A.13] in this equality, then we get

$$[A1.9] \quad \hat{Y}_{nlm}(\nabla)F_0(\alpha r^2) = -2\alpha(-1)^l\chi_{\alpha(n-1)lm}(\boldsymbol{r}) \quad (n = 1, 2, 3, \ldots)$$

Equations [A1.5] and [A1.9] prove [3.20] and [3.27].

Can. J. Chem. Downloaded from www.nrcresearchpress.com by 92.62.229.171 on 09/08/12
For personal use only.

Appendix 2. Talmi and Gaunt coefficients of real spherical harmonics

The RSHs $Y_{lm}(\theta, \phi)$ are obtained from the CSHs $\tilde{Y}_{lm}(\theta, \phi)$ by a unitary transformation:

$$[A2.1] \quad Y_{lm} = \sum_{m'=-l}^{l} U_{mm'} \tilde{Y}_{lm'}$$

From [2.3] it is seen that only the following elements of the unitary matrix **U** are nonvanishing:

$$[A2.2] \quad U_{00} = 1$$

$$U_{|m|,-|m|} = 1/\sqrt{2}, \qquad U_{|m|,|m|} = (-1)^m/\sqrt{2}$$

$$U_{-|m|,-|m|} = i/\sqrt{2}, \qquad U_{-|m|,|m|} = i(-1)^{m+1}/\sqrt{2}$$

Thus the inverse transformation is written as

$$[A2.3] \quad \tilde{Y}_{lm} = \sum_{m'=-l}^{l} Y_{lm'} U^*_{m'm}$$

Hence, using [A2.1]–[A2.3], all the quantities defined for the CSHs in I can be transformed to those for the RSHs.

The Talmi transformation for the complex LGTFs $\tilde{\chi}_{\alpha N}(\boldsymbol{r})$ is defined as (eqs. [2.12]–[2.14] of I)

$$[A2.4] \quad \tilde{\chi}_{\alpha_1 N_1}(\boldsymbol{r}_1)\tilde{\chi}_{\alpha_2 N_2}(\boldsymbol{r}_2) = \sum_{N_3 N_4} \tilde{\chi}_{\alpha_3 N_3}(\boldsymbol{r}_3)\tilde{\chi}_{\alpha_4 N_4}(\boldsymbol{r}_4)\tilde{T}(\alpha_3 N_3, \alpha_4 N_4 \mid \alpha_1 N_1, \alpha_2 N_2)$$

Using [A2.1] and [A2.3] in [A2.4] the Talmi coefficients T of real LGTFs, eq. [2.10], are written by those of the CSHs, $\tilde{T}$, as

$$[A2.5] \quad T(\alpha_3 n_3 l_3 m_3, \alpha_4 n_4 l_4 m_4 \mid \alpha_1 n_1 l_1 m_1, \alpha_2 n_2 l_2 m_2) = \sum_{\mu_1\mu_2\mu_3\mu_4} \tilde{T}(\alpha_3 n_3 l_3 \mu_3, \alpha_4 n_4 l_4 \mu_4 \mid \alpha_1 n_1 l_1 \mu_1, \alpha_2 n_2 l_2 \mu_2) \times U^*_{m_3\mu_3} U^*_{m_4\mu_4} U_{m_1\mu_1} U_{m_2\mu_2}$$

Among the indices the relations [2.11] and

$$[A2.6] \quad \mu_1 + \mu_2 = \mu_3 + \mu_4$$

hold. Among the indices m_1, m_2, m_3, and m_4, relations like [A2.6] hold but their explicit expressions would not be necessary for writing the computer program for the coefficients. It should be noted that the coefficients T as well as $\tilde{T}$ are real.

The Gaunt coefficients $\tilde{\Xi}$ for complex homogeneous solid harmonics $\tilde{Y}_{nlm}(\boldsymbol{r})$ are defined by (eq. [3.1] of I)

$$[A2.7] \quad \tilde{Y}_{N_1}(\boldsymbol{r})\tilde{Y}_{N_2}(\boldsymbol{r}) = \sum_{N} \tilde{Y}_N(\boldsymbol{r})\tilde{\Xi}(lm \mid l_1 m_1, l_2 m_2)$$

where relations [3.2] and

$$[A2.8] \quad m_1 + m_2 = m$$

hold. Thus, using [A2.1] and [A2.3] in [A2.7], the Gaunt coefficients Ξ for real homogeneous solid harmonics are written as

$$[A2.9] \quad \Xi(lm \mid l_1 m_1, l_2 m_2) = \sum_{\mu_1\mu_2} \Xi(l\mu \mid l_1\mu_1, l_2\mu_2) U^*_{m\mu} U_{m_1\mu_1} U_{m_2\mu_2},$$

where $\mu = \mu_1 + \mu_2$ and index m takes two values given by [3.3]. O-ohata and Ruedenberg (8, 9) give more explicit expressions for [A2.9]. It should be noted that the coefficients Ξ as well as $\tilde{\Xi}$ are real.

Can. J. Chem. Downloaded from www.nrcresearchpress.com by 92.62.229.171 on 09/08/12
For personal use only.

Electronic structure of lower singlet states of binuclear copper acetate monohydrate

KATSUYUKI OGASAWARA,[1] YUJI MOCHIZUKI,[2] TAKESHI NORO, AND KIYOSHI TANAKA[3]
Department of Chemistry, Faculty of Science, Hokkaido University, Sapporo, 060, Japan

Received June 10, 1991

This paper is dedicated to Professor Sigeru Huzinaga on the occasion of his 65th birthday

KATSUYUKI OGASAWARA, YUJI MOCHIZUKI, TAKESHI NORO, and KIYOSHI TANAKA. Can. J. Chem. **70**, 393 (1992).

The electronic structures of the ground state and the excited states due to the $3d$–$3d$ transition of copper acetate monohydrate are investigated by *ab initio* calculations. No direct bond is obtained between the two Cu ions, but they are bonded by bridges of the four acetates. The excited states represented by the one-electron excitation of an occupied $3d$ electron to an unoccupied $3d$ orbital in either of the two Cu's are located around 1.6–1.8 eV, which corresponds to the energy region of band I. Those of the simultaneous one-electron $3d$–$3d$ excitation in both Cu's (i.e., two-electron excitation) are located around 3.2–3.4 eV. They correspond to the energy region of band II.

Key words: copper acetate monohydrate, binuclear compound, bridged bond, $3d \rightarrow 3d$ excited states.

KATSUYUKI OGASAWARA, YUJI MOCHIZUKI, TAKESHI NORO et KIYOSHI TANAKA. Can. J. Chem. **70**, 393 (1992).

Faisant appel à des calculs *ab initio*, on a étudié la structure électronique de l'état fondamental et des états excités résultant de la transition $3d$–$3d$ du monohydrate de l'acétate de cuivre. On n'a pas observé de liaison directe entre les deux ions de Cu; ils sont toutefois reliés aux quatre acétates par des ponts. Les états excités, représentés par l'excitation d'un électron de l'orbitale $3d$ occupée vers l'orbitale $3d$ inoccupée de l'un ou l'autre des deux Cu, sont situés autour de 1,6–1,8 eV et ceci correspond à la région d'énergie de la bande I. Ceux de l'excitation simultanée d'un électron $3d$–$3d$ des deux Cu (c'est-à-dire une excitation à deux électrons) sont situés autour de 3,2–3,4 eV. Ils correspondent à la région d'énergie de la bande II.

Mots clés : monohydrate de l'acétate de cuivre, composé binucléaire, liaison pontée, états excités $3d \rightarrow 3d$.
[Traduit par la rédaction]

1. Introduction

Many dimeric copper(II) compounds exhibit subnormal magnetic moments and have long been studied extensively (1). Binuclear copper acetate monohydrate is a typical example of this type and has been investigated by experiments on its geometrical structure, magnetic properties, and electronic spectra (2). The two copper ions are bridged symmetrically by four acetates, and two waters coordinate along the Cu–Cu axis (3, 4). The Cu–Cu distance is about 2.62 Å, which is a little larger than that in the Cu metal (2.56 Å). There is some controversy on the bonding character (δ-bond (5) or σ-bond (6)) between the Cu unpaired $3d$ electrons, and no direct bond between two Cu's (1, 2).

Measurements of the magnetic succeptibility of the system indicated that the ground state of the complex is singlet (1, 2); the magnetic moment of this system is lower than the values usually found for copper(II) compounds and the magnetic susceptibility decreases as the temperature declines.

Copper acetate monohydrate is known to have three broad-band systems in its electronic transition spectra: band I (1.6–1.8 eV), band II (3.2–3.4 eV), and band III (3.7–6.2 eV). Since the experimental work by Tsuchida *et al.* (7), the origin of these bands has been a topic of great discussion (2*b*). The bands that correspond energetically to bands I and III have been observed in mononuclear Cu complexes such as $CuSO_4(OH_2)_5$ (1). The assignment of band I has been established to be $3d$–$3d$ single-electron excitation in a Cu ion (8) and band III has been assigned as a ligands-to-metal charge transfer (CT) band (9). Band II is a weak shoulder on band III, which is much broader and stronger. The origin of band II has not yet been established. It has been tentatively assigned by various researchers: single $3d$ electron excitation (9, 10), double excitation of $3d$ electrons (11), and CT transition from ligands to copper (12, 13). Recently, Ross *et al.* (14) performed a detailed investigation of band I by the use of magnetic circular dichroism (MCD) and considered the spin–spin coupling between the two coppers in the excited states making up band I. They also discussed the assignment of band II (they called it the dimer band) and tentatively concluded that the band is due to CT from the ligands to the copper ion.

Several simple theoretical studies (9–11, 13, 15, 16) were carried out on the spin coupling between the coppers and the electronic structure of the ground and excited states. Otherwise, only one *ab initio* calculation has been carried out, by de Loth *et al.* (17). They used a split valence basis set and calculated the energy separation between the lowest singlet and triplet states. They discussed the exchange mechanism of the two Cu's in the ground state.

In this work, we carry out *ab initio* calculations on this system and discuss the electronic structure of the ground state and the lower singlet excited states. We focus our attention especially on the character of bonding between the two Cu's and the classification of the excited states corresponding to bands I and II.

2. Method of calculation

The geometrical structure of a copper acetate monohydrate is shown in Fig. 1. The molecular plane of the two waters (axial ligands) is assumed to bisect the two bridging acetate planes. The CH_3 group in each acetate ion is replaced by a hydrogen. This may help to reduce computing

[1]Present address: Software Development Department, Personal System Division, Fujitsu Limited, 1015, Kamikodanaka, Nakahara-ku, Kawasaki 211, Japan.
[2]Present address: Department of Exploratory Research, NEC Tsukuba Research Laboratory, Miyukigaoka 34, Tsukuba 305, Japan.
[3]Author to whom correspondence may be addressed.

Printed in Canada

Can. J. Chem. Downloaded from www.nrcresearchpress.com by 92.62.229.171 on 09/08/12
For personal use only.

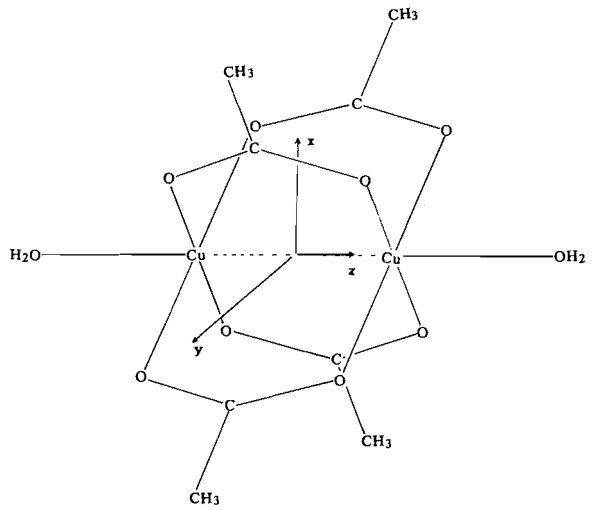

FIG. 1. Schematic geometrical structure of copper acetate monohydrate.

effort without sacrificing the reliability of the calculated results. The structure belongs to the D_{2h} symmetry point group. The geometrical parameters are taken from the neutron diffraction data obtained by Brown and Chidambaram (3) and they are shown as follows:

R(Cu—Cu)	= 2.614 Å	R(Cu—OH_2)	= 2.162 Å
R(Cu—O)	= 1.967 Å	R(Cu—Cu)	= 1.260 Å
∠Cu—O—C	= 122.8°	∠O—C—O	= 124.9°

The basis set used is composed of the MIDI4, split valence type, given by Huzinaga and Tatewaki (18), (3,3,3,2, 1/3,3/4,1) for Cu, (4,2,1/3,1) for O and C, and (3,1) for H. A diffuse p-type primitive Gaussian function (exponent = 0.117) is augmented to the Cu basis set. The total number of basic orbitals is 190. In calculating molecular integrals, we employ the integral approximation based on the semi-orthogonalized orbitals by Osanai and Kashiwagi (19).

We carry out a self-consistent field (SCF) calculation on the lowest $^3B_{1u}$ state. The wave function may be represented by the use of a component of $3d_8$ ($3d_{xy}$) as follows

[1] (Closed shell structure)$[3d_{xy}(8b_{1g})^1 3d_{xy}(6a_u)^1]$

where $3d_{xy}$ is directed toward the four oxygens of the equilateral ligands around each copper and the MO's $3d_{xy}(8b_{1g})$ and $3d_{xy}(6a_u)$ are primarily represented by bonding and antibonding of the two $3d_{xy}$'s, respectively. The closed-shell part of the wave function is expressed by the following electronic configuration

$$[2]\quad (1\text{-}17a_g)^{34}\cdot(1\text{-}7b_{1g})^{14}\cdot(1\text{-}9b_{2g})^{18}\cdot(1\text{-}9b_{3g})^{18}\cdot(1\text{-}5a_u)^{10}\cdot(1\text{-}15b_{1u})^{30}\cdot(1\text{-}11b_{2u})^{22}\cdot(1\text{-}11b_{3u})^{22}$$

This wave function ensures possible diradical form where two parallel spins are localized primarily on the $3d_{xy}$ atomic orbitals (AO's) of the two coppers. Starting from the molecular orbitals (MO's) thus obtained, we carry out a two-configuration self-consistent field (TCSCF) calculation where the two configurations are as follows:

[3] (Closed shell structure)$[3d_{xy}(8b_{1g})^2]$

[4] (Closed shell structure)$[3d_{xy}(6a_u)^2]$

The mixing of these two configurations is also possible, to describe the diradical form of the singlet coupling of the two unpaired electrons localized on $3d_{xy}$ AO's of the two coppers.

FVCI (full valence configuration interaction) calculations for the singlet ground state and excited states are carried out by the use of the resultant TCSCF MO's. As the predominant configurations are not well known for the lower excited states, especially for the doubly excited states, the FVCI scheme may help to avoid generating an inappropriate set of configuration state functions (CSF). In the FVCI calculation, the following orbitals are taken as frozen core orbitals:

$$1\text{-}14a_g,\ 1\text{-}6b_{1g},\ 1\text{-}7b_{2g},\ 1\text{-}7b_{3g},$$
$$1\text{-}4a_u,\ 1\text{-}12b_{1u},\ 1\text{-}9b_{2u},\ 1\text{-}9b_{3u}.$$

They are mainly composed of the core orbitals of Cu($1s$, $2s$, $3s$, $2p$, and $3p$), the occupied orbitals of C and H, and the occupied orbitals of O except for the $2p_\sigma$ orbitals, which belong to the equilateral oxygen ligands. In generating CSF's, we take all possible distributions of the 34 valence electrons on the 20 valence orbitals, which are mainly represented by $3d$, $4s$ orbitals of the coppers and oxygen $2p_\sigma$ orbitals of acetic acids. These $2p_\sigma$ orbitals are directed toward the copper. Those orbitals are shown in Table 1 in connection with the irreducible representations. As the resulting occupied MO's of the TCSCF wave function are not eigenfunctions of a Fock-like operator, it is easy to partition those MO's of the closed-shell part into core orbitals and valence orbitals. This is because any unitary transformation among the closed-shell MO's does not change the total wave function. The valence MO's, mostly representing $3d$ and $2p_\sigma$, are projected out from the TCSCF wave function by the corresponding orbital technique (20). In projecting out the valence MO's, we prepare the MO's of the SCF wave functions on the fragments, $(Cu^{2+})_2$ and $(HCOO^-)_4(H_2O)_2$, separately. By the use of the $3d$ dominant MO's of the $(Cu^{2+})_2$ triplet wavefunction of the configuration

[5] (Closed shell structure)$[3d_{xyg}{}^1 3d_{xyu}{}^1]$

the $3d$ type valence MO's are projected out from the occupied orbitals of the TCSCF wave function of the complex. The $2p_\sigma$(O) MO's of the ground state SCF wavefunction of $(HCOO^-)_4(H_2O)_2$ are used to project out those $2p_\sigma$-type valence MO's of the compound system. The unoccupied $4s$-type MO's are projected out from the unoccupied orbital space so as to maximize the overlap with the $4s$ dominant MO's of $(Cu^{2+})_2$ obtained from the SCF MO's of the septed wavefunction of

[6] (Closed shell structure)$[3d_{z^2g}{}^1 3d_{z^2u}{}^1 3d_{xyg}{}^1 3d_{xyu}{}^1 4s_g{}^1 4s_u{}^1]$

The number of CSF's of the FVCI are of the order of 47 300–47 900 for the states under consideration (^1A_g, $^1B_{1g}$, $^1B_{2g}$, $^1B_{3g}$, ^1A_u, $^1B_{1u}$, $^1B_{2u}$, and $^1B_{3u}$).

Can. J. Chem. Downloaded from www.nrcresearchpress.com by 92.62.229.171 on 09/08/12
For personal use only.

TABLE 1. The valence MO's in the FVCI

Symmetry	Orbital number	Assignment			
A_g	$15a_g$–$18a_g$	O $2p\sigma$	Cu $3d_{z^2}$	Cu $3d_{x^2-y^2}$	Cu $4s$
B_{1g}	$7b_{1g}$–$8b_{1g}$	O $2p\sigma$	Cu $3d_{xy}$		
B_{2g}	$8b_{2g}$–$9b_{2g}$	O $2p\sigma$	Cu $3d_{zx}$		
B_{3g}	$8b_{3g}$–$9b_{3g}$	O $2p\sigma$	Cu $3d_{yz}$		
A_u	$5a_u$–$6a_u$	O $2p\sigma$	Cu $3d_{xy}$		
B_{1u}	$13b_{1u}$–$16b_{1u}$	O $2p\sigma$	Cu $3d_{z^2}$	Cu $3d_{x^2-y^2}$	Cu $4s$
B_{2u}	$10b_{2u}$–$11b_{2u}$	O $2p\sigma$	Cu $3d_{yz}$		
B_{3u}	$10b_{3u}$–$11b_{3u}$	O $2p\sigma$	Cu $3d_{zx}$		

TABLE 2. Mulliken population analysis of the ^1A_g, $^3B_{1u}$ states by the use of the (TC)SCF wave function[a]

		p		d			
Atom	s	σ	π	σ	π	δ	Total
Cu	6.351	4.120	8.341 (12.461)	1.974	3.992 (9.050)	3.084	27.862
O[b]	3.868	1.445	3.369 (4.814)				8.682
C[b]	3.066	0.772	1.566 (2.338)				5.404
H[b]	0.844						0.844
O[c]	3.787	1.607	3.254 (4.845)				8.648
H[c]	0.631						0.631

[a]The numbers for population are the same within the given digits for the two states: TCSCF for ^1A_g, and SCF for $^3B_{1u}$.
[b]Belonging to the acetic acid.
[c]Belonging to water.

3. Results and discussion

3.1. (TC)SCF results: character of the lowest ^1A_g and $^2B_{1u}$ states

The TCSCF energy of the lowest ^1A_g state is −4169.11130 hartree. This is slightly lower than the SCF energy of the lowest $^3B_{1u}$ state by about 0.0005 eV. By experiment, the ground state of the system is singlet and its energy is lower than the lowest triplet state by about 0.035 eV (2). The energetical order of the two states is in accord with experiment, but this energy separation is very small. As was pointed out by de Loth *et al.* (17), we should employ a much more extensive computational method than the TCSCF or SCF scheme to obtain energy separation comparable to experiment.

The Mulliken-type population analysis is performed for the ^1A_g and $^3B_{1u}$ states by the use of the (TC)SCF wave functions. The results are summarized in Table 2. In both states, each Cu is populated by about 28 electrons, i.e., Cu^+ rather than Cu^{2+}. If one sees the results in more detail, one notes that the $3d$ shell is occupied by about 9 electrons and the electron population of the $4s$ and $4p$ shell is about 0.8. The population of the $3d_\delta$ orbitals in the two states is about 3 for each copper. The two unpaired electrons are localized on the $3d_{xy}$ of the coppers. All oxygens are occupied by about 8.6–8.7 electrons, which means that oxygens are nearly O^-. The overlap population between the two coppers is about −0.02, whereas that of Cu—O (acetic acid) is about 0.29.[4]

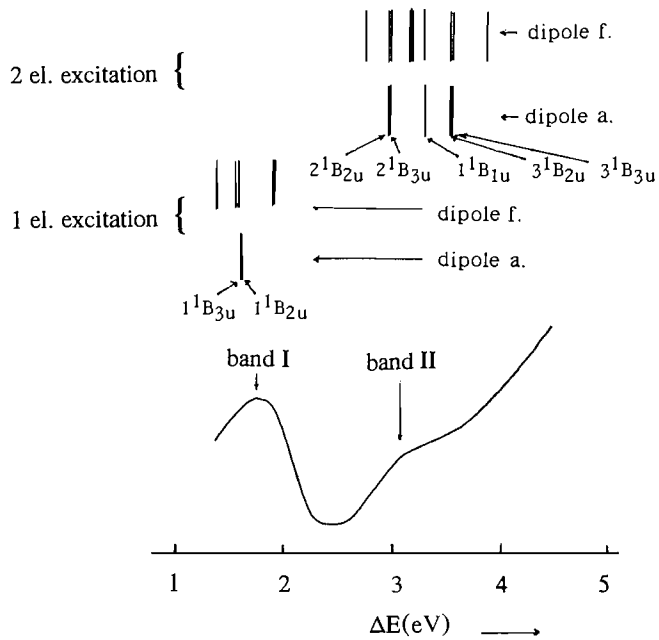

FIG. 2. Calculated vertical excitation energies in comparison with bands I and II. Note: The term "dipole f." means dipole-forbidden transition and "dipole a." represents dipole-allowed transition.

[4]The overlap population of Cu—O(water) is 0.17.

Can. J. Chem. Downloaded from www.nrcresearchpress.com by 92.62.229.171 on 09/08/12
For personal use only.

This indicates that the two coppers are not bonded directly but bridged by the four acetic acids.

3.2 The FVCI results: the d–d *singlet excited states*

Using the results of the FVCI, we are going to discuss the lower excited states. The total energy of the ground state (^1A_g) is −4169.46775 hartree. The calculated excitation energies are also compared with the observed excitation spectra in Fig. 2. Table 3 shows excitation energies, leading configurations, and their coefficients for the excited states below 4 eV relative to the ground state. The configurations A and B that are shown in the table correspond to those given by eqs. [3] and [4], respectively. They contribute primarily to the ground state wave functions. The lower 3*d* to 3*d* excited states are described by excitation to the $3d_{xy}(a_u)$ MO, which is empty in configuration A, or by excitation to an empty MO of $3d_{xy}(b_{1g})$ in configuration B.

The wave function of the ground state is expressed by the out-of-phase combination of the two configurations with almost the same weight. This may be schematically expressed by

$$[7]\quad \{3d_{xy}(1) + 3d_{xy}(2)\}^2 - \{3d_{xy}(1) - 3d_{xy}(2)\}^2 \propto [3d_{xy}(1)^1 3d_{xy}(2)^1]^{[1]}$$

where $3d_{xy}(1)$ is an AO of a copper and $3d_{xy}(2)$ is that of another copper and $[3d_{xy}(1)^1 3d_{xy}(2)^1]^{[1]}$ represents the singlet coupling of two electrons occupying the two AO's.

Every excited state given in the table is also expressed by two primary configurations and they mix with almost equal weight. The excited states are described as essentially intra-3*d* excitations. All the excited states that lie below 2.0 eV are represented mainly by single electron excitations from A or B. They are primarily described as 3*d* to 3*d* single electron excitation in either of the two coppers. As an example, we show a schematic form of the wave function of the 1^1B_{2u} state in terms of AO's in a form similar to eq. [6]:

$$[8]\quad [\{3d_{zx}(1) + 3d_{zx}(2)\}^1\{3d_{zx}(1) - 3d_{zx}(2)\}^2\{3d_{xy}(1) + 3d_{xy}(2)\}^2\{3d_{xy}(1) - 3d_{xy}(2)\}^1]^{[1]} - [\{3d_{zx}(1) + 3d_{zx}(2)\}^2 \times \{3d_{zx}(1) - 3d_{zx}(2)\}^1\{3d_{xy}(1) + 3d_{xy}(2)\}^1\{3d_{xy}(1) - 3d_{xy}(2)\}^2]^{[1]} \propto [3d_{zx}(1)^2 3d_{zx}(2)^1 3d_{xy}(1)^1 3d_{xy}(2)^2]^{[1]} - [3d_{zx}(1)^1 3d_{zx}(2)^2 3d_{xy}(1)^2 3d_{xy}(2)^1]^{[1]}$$

This wave function represents the single electron excitation ($3d_{zx} \rightarrow 3d_{xy}$) in either of the Cu's.

Our interest has been drawn to the ordering of the 3*d* levels. By the present calculation, the first two excited states are $3d_{x^2-y^2}(d_\delta')$ to $3d_{xy}(d_\delta)$ excitation and the excitation energy is about 1.4 eV. The lobe of $3d_{x^2-y^2}$ bisects the O—Cu—O angle where the O's are equilateral ligands. The next four levels are d_π ($3d_{yz}$ and $3d_{zx}$) to $3d_{xy}$ excited levels. They are located around 1.6 eV. The $3d_{z^2}$ (d_σ) level is the most stable and $3d_{z^2}$ to $3d_{xy}$ excitation is found at about 1.9 eV. It is interesting to compare the excitation energies of these excited states with band I. Dipole-allowed transitions of the 1^1B_{3u} and 1^1B_{2u} states (1.58 and 1.61 eV) are in especially good agreement with the center of the peak of band I (1.8 eV). The present results indicate that band I is composed of 3*d* to 3*d* single electron excitation in either of the two coppers. All 3*d* to 3*d* singly excited states lie below 2 eV and the assignment of 3*d* to 3*d* single electron excitation (9, 10) to band II is not supported.

The excited states higher than 2.7 eV are led by doubly excited configurations, double electron excitation to the empty $3d_{xy}(a_u)$ MO in configuration A or, in other words, excitation to the empty $3d_{xy}(b_{1g})$ MO in configuration B. They are essentially described as simultaneous single electron 3*d*–3*d* excitation in both coppers. As an example, the wave function of the 1^1B_{1u} state is given in terms of AO's as follows:

$$[9]\quad [\{3d_{x^2-y^2}(1) + 3d_{x^2-y^2}(2)\}^1\{3d_{x^2-y^2}(1) - 3d_{x^2-y^2}(2)\}^2\{3d_{z^2}(1) + 3d_{z^2}(2)\}^2\{3d_{z^2}(1) - 3d_{z^2}(2)\}^1\{3d_{xy}(1) + 3d_{xy}(2)\}^2 \times \{3d_{xy}(1) - 3d_{xy}(2)\}^2]^{[1]} - [\{3d_{x^2-y^2}(1) + 3d_{x^2-y^2}(2)\}^2\{3d_{x^2-y^2}(1) - 3d_{x^2-y^2}(2)\}^1\{3d_{z^2}(1) + 3d_{z^2}(2)\}^1\{3d_{z^2}(1) - 3d_{z^2}(2)\}^2 \times \{3d_{xy}(1) + 3d_{xy}(2)\}^2\{3d_{xy}(1) - 3d_{xy}(2)\}^2]^{[1]} \propto [3d_{x^2-y^2}(1)^2 3d_{x^2-y^2}(2)^1 3d_{z^2}(1)^1 3d_{z^2}(2)^2 3d_{xy}(1)^2 3d_{xy}(2)^2]^{[1]} - [3d_{x^2-y^2}(1)^1 3d_{x^2-y^2}(2)^2 3d_{z^2}(1)^2 3d_{z^2}(2)^1 3d_{xy}(1)^2 3d_{xy}(2)^2]^{[1]}$$

This wave function represents two-electron excitation ($3d_{x^2-y^2} \rightarrow 3d_{xy}$ in one Cu and $3d_{z^2} \rightarrow 3d_{xy}$ in another Cu).

Although the transition probability to these doubly excited states should be small even in the dipole-allowed $^1B_{1u}$, $^1B_{2u}$, and $^1B_{3u}$ states, it is interesting to note that the five dipole-allowed excited states, $^1B_{2u}$ (2.96 eV, 3.52 eV), $^1B_{3u}$ (2.99 eV, 3.55 eV), and $^1B_{1u}$ (3.30 eV), are located at comparable transition energies of band II, which is centered around 3.3 eV. As band II is a very weak shoulder of band III, it is highly possible that band II originated from one-electron 3*d* to 3*d* transitions in both coppers simultaneously. Hansen and Ballhausen (11) assigned band II as doubly excited ($(d_\sigma)^2$ to $(d_\delta)^2$) transition. This excited state is the 6^1A_g state by the present calculation. This state is represented by singlet coupling of the unpaired d_σ electrons in both Cu's and is unstable relative to the ground state by about 3.9 eV.

Apart from these states, we also calculated the energies of the CT states. The excitation energies for the CT states are about 10 eV or more. They are much higher than those for the broad peak of band III, which are supposed to have originated from CT excitation. The variational space selected in this calculation is limited to the one that is appropriate to describe only *d*–*d* transitions, and CT states would not be predicted well by the present calculation. In this context, possible contribution of CT to band II (12–14) is not denied by the present calculation. More extensive calculation is desired for this purpose.

Can. J. Chem. Downloaded from www.nrcresearchpress.com by 92.62.229.171 on 09/08/12
For personal use only.

TABLE 3. Excitation energies (eV) and a rough description of the wave functions of the ground state and the lower singly excited states

Symmetry representation	Excitation energy (eV)	Type of configuration	Transition[a]	Coefficient
1^1A_g	0.0	A	$3d_{xy}(b_{1g})^2 3d_{xy}(a_u)^0$	−0.694
		B	$3d_{xy}(b_{1g})^0 3d_{xy}(a_u)^2$	0.715
1^1A_u	1.38	A	$3d_{x^2-y^2}(a_g) \rightarrow 3d_{xy}(a_u)$	0.698
		B	$3d_{x^2-y^2}(b_{1u}) \rightarrow 3d_{xy}(b_{1g})$	−0.711
1^1B_{1g}	1.38	A	$3d_{x^2-y^2}(b_{1u}) \rightarrow 3d_{xy}(a_u)$	0.701
		B	$3d_{x^2-y^2}(a_g) \rightarrow 3d_{xy}(b_{1g})$	−0.708
1^1B_{2g}	1.57	A	$3d_{yz}(b_{2u}) \rightarrow 3d_{xy}(a_u)$	0.689
		B	$3d_{yz}(b_{3g}) \rightarrow 3d_{xy}(b_{1g})$	0.713
1^1B_{3u}[b]	1.58	A	$3d_{yz}(b_{3g}) \rightarrow 3d_{xy}(a_u)$	0.702
		B	$3d_{yz}(b_{2u}) \rightarrow 3d_{xy}(b_{1g})$	0.700
1^1B_{3g}	1.60	A	$3d_{zx}(b_{3u}) \rightarrow 3d_{xy}(a_u)$	0.688
		B	$3d_{zx}(b_{2g}) \rightarrow 3d_{xy}(b_{1g})$	−0.713
1^1B_{2u}[b]	1.61	A	$3d_{zx}(b_{2g}) \rightarrow 3d_{xy}(a_u)$	−0.702
		B	$3d_{zx}(b_{3u}) \rightarrow 3d_{xy}(b_{1g})$	0.700
2^1A_u	1.90	A	$3d_{z^2}(a_g) \rightarrow 3d_{xy}(a_u)$	−0.673
		B	$3d_{z^2}(b_{1u}) \rightarrow 3d_{xy}(b_{1g})$	0.728
2^1B_{1g}	1.93	A	$3d_{z^2}(b_{1u}) \rightarrow 3d_{xy}(a_u)$	0.718
		B	$3d_{z^2}(a_g) \rightarrow 3d_{xy}(b_{1g})$	−0.686
2^1A_g	2.75	A	$(3d_{x^2-y^2}(a_g))^2 \rightarrow (3d_{xy}(a_u))^2$	0.702
		A	$(3d_{x^2-y^2}(b_{1u}))^2 \rightarrow (3d_{xy}(a_u))^2$	−0.707
2^1B_{3g}	2.96	A	$3d_{x^2-y^2}(a_g), 3d_{yz}(b_{3g}) \rightarrow (3d_{xy}(a_u))^2$	−0.706
		A	$3d_{x^2-y^2}(b_{1u}), 3d_{yz}(b_{2u}) \rightarrow (3d_{xy}(a_u))^2$	0.696
2^1B_{2u}[b]	2.96	A	$3d_{x^2-y^2}(b_{1u}), 3d_{yz}(b_{3g}) \rightarrow (3d_{xy}(a_u))^2$	−0.709
		A	$3d_{x^2-y^2}(a_g), 3d_{yz}(b_{2u}) \rightarrow (3d_{xy}(a_u))^2$	0.693
2^1B_{2g}	2.99	A	$3d_{x^2-y^2}(a_g), 3d_{zx}(b_{2g}) \rightarrow (3d_{xy}(a_u))^2$	0.705
		A	$3d_{x^2-y^2}(b_{1u}), 3d_{zx}(b_{3u}) \rightarrow (3d_{xy}(a_u))^2$	0.696
2^1B_{3u}[b]	2.99	A	$3d_{x^2-y^2}(b_{1u}), 3d_{zx}(b_{2g}) \rightarrow (3d_{xy}(a_u))^2$	0.709
		A	$3d_{x^2-y^2}(a_g), 3d_{zx}(b_{3u}) \rightarrow (3d_{xy}(a_u))^2$	0.693
3^1A_g	3.17	A	$(3d_{yz}(b_{3g}))^2 \rightarrow (3d_{xy}(a_u))^2$	0.709
		A	$(3d_{yz}(b_{2u}))^2 \rightarrow (3d_{xy}(a_u))^2$	−0.685
3^1B_{1g}	3.20	A	$3d_{yz}(b_{3g}), 3d_{zx}(b_{2g}) \rightarrow (3d_{xy}(a_u))^2$	0.710
		A	$3d_{yz}(b_{2u}), 3d_{zx}(b_{3u}) \rightarrow (3d_{xy}(a_u))^2$	0.684
3^1A_u	3.20	A	$3d_{yz}(b_{2u}), 3d_{zx}(b_{2g}) \rightarrow (3d_{xy}(a_u))^2$	0.697
		A	$3d_{yz}(b_{3g}), 3d_{zx}(b_{3u}) \rightarrow (3d_{xy}(a_u))^2$	0.697
4^1A_g	3.23	A	$(3d_{zx}(b_{2g}))^2 \rightarrow (3d_{xy}(a_u))^2$	0.707
		A	$(3d_{zx}(b_{3u}))^2 \rightarrow (3d_{xy}(a_u))^2$	−0.683
5^1A_g	3.30	A	$3d_{x^2-y^2}(a_g), 3d_{z^2}(a_g) \rightarrow (3d_{xy}(a_u))^2$	0.677
		A	$3d_{x^2-y^2}(b_{1u}), 3d_{z^2}(b_{1u}) \rightarrow (3d_{xy}(a_u))^2$	−0.719
1^1B_{1u}[b]	3.30	A	$3d_{x^2-y^2}(a_g), 3d_{z^2}(b_{1u}) \rightarrow (3d_{xy}(a_u))^2$	0.721
		A	$3d_{x^2-y^2}(b_{1u}), 3d_{z^2}(a_g) \rightarrow (3d_{xy}(a_u))^2$	−0.685
3^1B_{2u}[b]	3.52	A	$3d_{yz}(b_{3g}), 3d_{z^2}(b_{1u}) \rightarrow (3d_{xy}(a_u))^2$	0.723
		A	$3d_{yz}(b_{2u}), 3d_{z^2}(a_g) \rightarrow (3d_{xy}(a_u))^2$	0.672
3^1B_{3g}	3.53	A	$3d_{yz}(b_{2u}), 3d_{z^2}(b_{1u}) \rightarrow (3d_{xy}(a_u))^2$	0.711
		A	$3d_{yz}(b_{3g}), 3d_{z^2}(a_g) \rightarrow (3d_{xy}(a_u))^2$	0.686
3^1B_{3u}[b]	3.55	A	$3d_{xz}(b_{2g}), 3d_{z^2}(b_{1u}) \rightarrow (3d_{xy}(a_u))^2$	0.723
		A	$3d_{xz}(b_{3u}), 3d_{z^2}(a_g) \rightarrow (3d_{xy}(a_u))^2$	−0.672
3^1B_{2g}	3.56	A	$3d_{xz}(b_{2g}), 3d_{z^2}(a_g) \rightarrow (3d_{xy}(a_u))^2$	0.685
		A	$3d_{xz}(b_{3u}), 3d_{z^2}(b_{1u}) \rightarrow (3d_{xy}(a_u))^2$	−0.710
6^1A_g	3.88	A	$(3d_{z^2}(a_g))^2 \rightarrow (3d_{xy}(a_u))^2$	0.659
		A	$3d_{z^2}(b_{1u}))^2 \rightarrow (3d_{xy}(a_u))^2$	−0.735

[a]Transition relative to the type of configuration (A or B) described by the primary character of the MO's.
[b]Dipole allowed relative to the ground state.

Can. J. Chem. Downloaded from www.nrcresearchpress.com by 92.62.229.171 on 09/08/12
For personal use only.

4. Summary

By using a split valence basis set and employing the limited FVCI scheme, we have investigated the electronic structure of the ground and lower Cu $3d$–$3d$ excited states of the binuclear copper acetate monohydrate. Each copper has almost nine $3d$ electrons, but it is formally not Cu^{2+} but Cu^{+}. About 0.8 electron is back-donated to $4s$ and $4p$ shells.

The excited states due to $3d$ to $3d$ single electron transition in either Cu contributes to band I, as is well established. The excited states distributed between 3.0 and 3.6 eV are primarily led by $3d$ to $3d$ single electron excitation in both coppers simultaneously. The present result suggests that these states contribute to band II, which is a weak shoulder of the strong absorption band III.

5. Acknowledgements

The authors are grateful to Professors K. Ohno and F. Sasaki for their discussions on this problem. This work has been supported by a grant-in-aid of the Japanese Ministry of Education. All calculations were carried out using the computer codes JAMOL4 (21) and JASON2 (22), on systems HITAC M-680H, M-682H, and S-820/20 at the Institute for Molecular Science and the Computing Center of Hokkaido University.

The authors feel it a great honor to contribute this paper to the special issue of the Canadian Journal of Chemistry dedicated to Professor Huzinaga. They are indebted to Professor Huzinaga for his leadership, over a long period, in the field of theoretical molecular physics and quantum chemistry. They express their deep gratitude for his enlightening them through his papers and books.

1. M. Kato, H. B. Jonassen, and J. C. Fanning. Chem. Rev. **64**, 99 (1964).
2. (*a*) R. J. Doedens. Prog. Inorg. Chem. **21**, 209 (1976) and references therein; (*b*) J. Catterick and P. Thornton. Adv. Inorg. Chem. and Radiochem. **20**, 291 (1977), and references therein.
3. G. M. Brown and R. Chidambaram. Acta Crystallogr. Sect. B: Struct. Crystallogr. Cryst. Chem. **B29**, 2393 (1973).
4. P. de Meester, S. R. Fletcher, and A. C. Skapski. J. Chem. Soc. Dalton Trans. 2575 (1973).
5. B. N. Figgis and R. L. Martin. J. Chem. Soc. 3837 (1956).
6. L. S. Forster and C. J. Ballhausen. Acta Chem. Scand. **16**, 1385 (1962).
7. R. Tsuchida and S. Yamada. Nature (London), **176**, 1192 (1956); **182**, 1230 (1955); R. Tsuchida, S. Yamada, and H. Nakamura. Nature (London), **178**, 1171 (1955); **181**, 479 (1958).
8. G. W. Reimann, G. F. Kokoszka, and G. Gordon. Inorg. Chem. **4**, 1082 (1965).
9. D. P. Graddon. J. Inorg. Nucl. Chem. **17**, 222 (1961).
10. G. F. Kokoszka, H. C. Allen, Jr., and G. Gordon. J. Chem. Phys. **42**, 3693 (1965).
11. A. E. Hansen and C. J. Ballhausen. Trans. Faraday Soc. **61**, 631 (1965).
12. L. Dubicki and R. L. Martin. Inorg. Chem. **5**, 2203 (1966).
13. L. Dubicki. Aust. J. Chem. **25**, 1141 (1972).
14. P. K. Ross, M. D. Allendorf, and E. I. Solomon. J. Am. Chem. Soc. **111**, 4009 (1989).
15. M. L. Tonnet, S. Yamada, and I. G. Ross. Trans. Faraday Soc. **60**, 840 (1964).
16. P. J. Hay, J. C. Thibeault, and R. Hoffmann. J. Am. Chem. Soc. **97**, 4884 (1975).
17. P. de Loth, P. Cassoux, J. P. Daudey, and J. P. Malrieu. J. Am. Chem. Soc. **103**, 4007 (1981).
18. S. Huzinaga, J. Andzelm, M. Klobukowski, E. Radzio-Andzelm, Y. Sakai, and H. Tatewaki. Gaussian basis sets for molecular calculations, physical science data. Vol. 16. Elsevier, Amsterdam. 1984.
19. Y. Osanai and H. Kashiwagi. Int. J. Quantum Chem. **17**, 1031 (1980).
20. A. T. Amos and G. G. Hall. Proc. R. Soc. London, A: **263**, 483 (1961).
21. H. Kashiwagi, T. Takada, E. Miyoshi, S. Obara, and F. Sasaki. RHF program JAMOL4. 1989.
22. S. Yamamoto, U. Nagashima, T. Aoyama, and H. Kashiwagi. CASSCF program JASON2. 1987.

Can. J. Chem. Downloaded from www.nrcresearchpress.com by 92.62.229.171 on 09/08/12
For personal use only.

Relativistic many-body perturbation theory using discrete basis expansion method: accurate representation of second-order energy of Xe atom with contracted well-tempered Gaussian basis set

YASUYUKI ISHIKAWA

Department of Chemistry and The Chemical Physics Program, University of Puerto Rico, Rio Piedras, PR 00931 U.S.A.

Received June 26, 1991

This paper is dedicated to Professor Sigeru Huzinaga on the occasion of his 65th birthday

YASUYUKI ISHIKAWA. Can. J. Chem. **70**, 399 (1992).

Relativistic many-body perturbation theory calculations on Xe have been performed with basis sets of well-tempered Gaussian-type functions of Huzinaga and Klobukowski. The well-tempered Gaussian-type functions were used in both contracted and uncontracted form. The contracted Gaussian basis sets used in the relativistic many-body study are designed to retain flexibility for correlated calculations both in the core and the valence region. They reproduce second-order energy corrections computed with uncontracted Gaussian basis sets to an accuracy of greater than 99%. A compact representation of the relativistic wave functions in terms of contracted well-tempered Gaussian functions used in the present study provides a useful means of curtailing integral storage requirements and the time needed for correlated calculations, while still retaining high accuracy in relativistic electron correlation effects.

Key words: Dirac–Fock, relativistic many-body perturbation theory, well-tempered Gaussian basis, xenon.

YASUYUKI ISHIKAWA. Can. J. Chem. **70**, 399 (1992).

Utilisant des ensembles de base de fonctions gaussiennes de Huzinaga et Klobukowski bien aplanies, on a effectué des calculs relativistes de la théorie perturbationnelle à plusieurs centres sur le Xe. On a utilisé les formes tant contractée que non-contractée de ces fonctions de type gaussien. Les ensembles gaussiens de type contracté sont utilisés dans l'étude relativiste à plusieurs centres afin de conserver une certaine flexibilité dans les calculs comportant une corrélation dans les régions tant du coeur que de valence. Ils permettent de reproduire, avec une précision de plus de 99%, les corrections d'énergie du deuxième ordre calculées avec des ensembles de base gaussiens non-contractés. Une représentation compacte des fonctions d'onde relativistes en termes de fonctions gaussiennes bien aplanies contractées utilisées dans la présente étude fournit un moyen utile de réduire les besoins d'emmagasinage intégral et le temps nécessaire pour effectuer des calculs corrélés, tout en maintenant une grande précision dans les effets relativistes de corrélation électronique.

Mots clés : Dirac–Fock, théorie perturbationnelle relativiste à plusieurs centres, ensemble de base gaussien bien aplani, xénon.

[Traduit par la rédaction]

Introduction

Many-body perturbation theory (MBPT) has been recognized as a powerful approach to the non-relativistic correlation problem for atoms and molecules (1). In the last few years, a relativistic version of the many-body theory, which accounts for both relativistic and electron correlation effects, was developed by a number of groups by using analytic basis functions (2–11). The relativistic MBPT algorithm, based on an expansion in analytic basis functions (2–11), has the advantage that it provides the compact representation of the complete Dirac spectrum, and greatly facilitates the evaluation of the many-body diagrams using finite summations (2, 6).

The technique of basis set contraction has not been widely employed in atomic calculations. In view of the computational difficulties in many-body calculations on heavy-atom systems, a basis set contraction that does not affect the accuracy in electron correlation energy would be especially useful in applications to heavier atoms. The approach to contraction in molecular calculations has been articulated by Dunning (12), Huzinaga (13), Pople and co-workers (14), and Wilson (15). In this approach, Gaussian-type functions (GTF) that represent the core region are extensively contracted, while valence functions are left uncontracted to provide flexibility in describing bond formation. The contracted basis sets reproduce the relativistic corrections well at the Dirac–Fock (DF) SCF level (16). However, they give relatively poor values for second- and third-order MBPT energy corrections (16). These basis sets have been derived to reproduce valence, but not core or core–valence interactions.

Atomic calculations, which aim at much higher accuracy, must employ the largest practical basis sets. Provided that the error introduced by basis set contraction is a fraction of the absolute error in an atomic calculation, contracted basis sets should provide a useful means of curtailing computation time as well as integral storage in relativistic MBPT calculations on heavier atoms. In a previous study (17), we explored a way to reduce the computational burden in relativistic MBPT calculations on Kr by using contracted and uncontracted GTF basis sets. In the present study, the feasibility of a practical relativistic MBPT on heavy atoms is examined by electronic structure calculations of the ground state Xe atom by using contracted well-tempered GTF. The Xe atom possesses 54 electrons, and is one of the heaviest atoms to which non-relativistic and relativistic MBPT employing analytic basis functions have ever been applied.

Methods

In c-number theory, the approximate N-electron Hamiltonian for our development of relativistic MBPT calculations is the so-called relativistic "no-pair" Dirac–Coulomb (DC) Hamiltonian (18, 19),

$$[1] \qquad H_+ = \sum_i h_D(i) + \mathcal{L}_+\left(\frac{1}{2}\sum_{i,j} 1/r_{ij}\right)\mathcal{L}_+$$

Printed in Canada

Can. J. Chem. Downloaded from www.nrcresearchpress.com by 92.62.229.171 on 09/08/12
For personal use only.

Can. J. Chem. Downloaded from www.nrcresearchpress.com by 92.62.229.171 on 09/08/12
For personal use only.

where $\mathcal{L}_+ = L_+(1) \cdot L_+(2) \cdots L_+(N)$, and $L_+(i)$ is the projection operator onto the space spanned by the positive-energy eigenfunctions, $\{\phi^+_{n\kappa}\}$ of the radial Dirac–Fock operator, F_κ (19, 20).

$$[2] \quad F_\kappa \phi^+_{n\kappa}(r) = \epsilon_{n\kappa} \phi^+_{n\kappa}(r)$$

where

$$[3] \quad F_\kappa = \begin{bmatrix} V^{LL} & c\Pi_\kappa + V^{LS} \\ c\Pi_\kappa + V^{SL} & V^{SS} - 2c^2 \end{bmatrix}$$

and

$$[4] \quad \phi^+_{n\kappa}(r) = \begin{bmatrix} P_{n\kappa}(r) \\ Q_{n\kappa}(r) \end{bmatrix}$$

The radial functions $P_{n\kappa}(r)$ and $Q_{n\kappa}(r)$ are referred to as the large and small components, respectively. $P_{n\kappa}(r)$ and $Q_{n\kappa}(r)$ may be expanded in sets of basis functions.

In the second-quantized, particle-hole formalism, the "no-pair" DC Hamiltonian may be expressed in terms of normally ordered products of the spinor operators, $[r^+s]$ and $[r^+s^+ut]$,

$$[5] \quad H_N = \sum_{r,s} f_{rs}[r^+s] + \frac{1}{4} \sum_{r,s,t,u} \langle rs \| tu \rangle [r^+s^+ut]$$

Here f_{rs} and $\langle rs \| tu \rangle$ are, respectively, one-electron DF and antisymmetrized two-electron Coulomb interaction matrices over the DF four-component spinors, r, s, t, and u. Normal ordering implies that, in the vacuum state, annihilation operators are moved to the right of creation operators as if all anticommutators vanish. The Fermi level is shifted to the highest occupied positive energy state. The creation operator then appears to the right of a normally ordered set when it refers to an occupied positive energy state, while the annihilation operator remains on the right for a positive energy virtual state. In this form, the no-pair Hamiltonian is restricted to contributions from the positive energy branch of the spectrum.

In a series of studies (9, 21), we have performed DF Gaussian basis expansion calculations on one- and many-electron systems with a finite nucleus model. In these studies, we have emphasized alteration of the boundary conditions such that GTF become the best form for basis functions. Representing the nucleus as a finite body of uniform proton charge accomplishes that feat. With this representation of the potential, for example, the exact $s_{1/2}$ solutions of the Dirac equation near the origin are

$$[6] \quad P(r)/r = 1 + g_2 r^2 + g_4 r^4 + \ldots$$

$$[7] \quad Q(r)/r = f_1 r + f_3 r^3 + \ldots$$

so that, for α arbitrary parameters

$$[8] \quad P(r) = r + g_2 r^3 + \ldots \approx r \exp(-\alpha r^2)$$

$$[9] \quad Q(r) = f_1 r^2 + f_3 r^4 + \ldots \approx r^2 \exp(-\alpha r^2)$$

Thus, in the finite nuclear model, the GTF of an integer power of r are appropriate basis functions because imposition of the finite nuclear boundary results in a solution that is Gaussian at the origin. In a previous study, we have shown that the failure to satisfy the proper boundary conditions near the origin may lead to a spurious solution (21).

The GTF basis functions that satisfy the boundary conditions associated with the finite nucleus automatically satisfy the condition of the so-called "kinetic balance" for a finite value of c. The kinetically balanced GTF basis functions are precisely the form given in eqs. [8] and [9]. This is a consequence of the fact that the exponent of r in the GTF basis functions does not depend on the speed of light. In this sense, the GTF are chosen to satisfy the condition of kinetic balance and relativistic boundary conditions associated with a finite nucleus.

The expansion scheme is applied to basis sets of contracted functions in a direct extension of its application to uncontracted functions. Large-component radial functions, $P_{n\kappa}(r)$, are expanded in a basis of contracted functions, $\{X_{\kappa i}{}^L(r)\}$ with expansion coefficients $\{C_{n\kappa i}{}^L\}$ as (16)

$$[10] \quad P_{n\kappa}(r) = \sum_i C_{n\kappa i}{}^L X_{\kappa i}{}^L(r)$$

where

$$[11] \quad X_{\kappa i}{}^L(r) = \sum_p d_{\kappa ip} f_{\kappa p}{}^L(r)$$

Here the $\{d_{\kappa ip}\}$ are the contraction coefficients. The $\{f_{\kappa p}{}^L(r)\}$ are the primitive GTFs. The small-component radial function, $Q_{n\kappa}(r)$ are expanded in a basis of $\{X_{\kappa i}{}^S(r)\}$,

$$[12] \quad Q_{n\kappa}(r) = \sum_i C_{n\kappa i}{}^S X_{\kappa i}{}^S(r)$$

To insure proper balance, $X_{\kappa i}{}^S(r)$ is related to $X_{\kappa i}{}^L(r)$ as

$$[13] \quad X_{\kappa i}{}^S(r) = (d/dr + \kappa/r) X_{\kappa i}{}^L(r)$$

We performed DF and MBPT calculations on ground state xenon with the well-tempered GTF basis sets of Huzinaga and Klobukowski (22) in a contracted and an uncontracted form. The well-tempered GTF basis sets have proven very useful in accurate DF SCF (23) and relativistic MBPT calculations (9). The Xe nucleus was represented as a sphere of uniform proton charge distribution. The atomic mass used in the calculations was 131.30 amu. The speed of light used was 137.0370 au. To simulate the non-relativistic limit, a value of c of 10^4 was used.

The virtual orbitals used in the study were calculated in the field of the nucleus and of all the electrons (V_N potential). Goldstone diagrams have been summed to compute Dirac–Coulomb correlation corrections to second order. Diagrammatic summation was done within the subspace of the positive energy branch, i.e., in the no-pair approximation (18, 19).

The DC Hamiltonian used in the present study is approximate. In the DC Hamiltonian, one-electron interactions are treated relativistically as a sum of Dirac one-electron Hamiltonians, whereas the two-electron interaction is treated non-relativistically as the instantaneous Coulomb repulsion. However, the energy shift induced by the low-frequency Breit interaction in the SCF and correlated calculations is known to be significant for inner-shell orbitals of heavy systems (24). In the present study, we have neglected the Breit interaction along with the radiative corrections, mass polarization, and reduced mass effects.

TABLE 1. Basis-set composition of the $21s17p12d7f6g5h$ primitive set for relativistic DF and MBPT calculations on the Xe atom

Exponent	Symmetry					
	$s_{1/2}$	$p_{1/2,3/2}$	$d_{3/2,5/2}$	$f_{5/2,7/2}$	$g_{7/2,9/2}$	$h_{9/2,11/2}$
0.049856		X				
0.124201	X	X				
0.267022	X	X				
0.525944	X	X	X			
1.235243	X	X	X	X		
2.634090	X	X	X	X	X	X
5.546456	X	X	X	X	X	X
11.720477	X	X	X	X	X	X
24.524048	X	X	X	X	X	X
52.022218	X	X	X	X	X	X
110.24499	X	X	X	X	X	
237.19332	X	X	X			
522.83644	X	X	X			
1201.3225	X	X	X			
2951.2282	X	X	X			
7854.5129	X	X	(X)[a]			
22818.101	X	X				
71055.064	X	(X)[a]				
230587.85	X	(X)[a]				
792091.87	X					
3011538.7	X					
17406192.0	X					

[a]Included in the DF calculations using a $21s19p13d$ basis.

Results and discussion

We performed DF and MBPT calculations on the Xe atom by systematically enlarging the order of partial wave expansion, i.e., L_{max}. Throughout this work, the non-relativistically optimized well-tempered basis set of Huzinaga and Klobukowski (22) was used in a contracted and an uncontracted form. Table 1 contains the uncontracted well-tempered GTF exponents for Xe. Exponents of higher angular momentum functions used to generate the virtual orbitals are also tabulated in the table for the $21s17p12d7f6g5h$ primitive GTF basis set. Basis functions in the $21s$, $17p$, and $12d$ primitive sets in Table 1 were contracted to generate the $[14s13p10d]$ contracted set. The contracted basis set was derived by grouping the functions of highest exponents. Table 2 displays the contraction coefficients for the contracted $[14s13p10d]$ set. The contraction coefficients were taken from the results of the Hartree–Fock calculations obtained by Huzinaga and Klobukowski (22).

Table 3 displays the total DF energies, E_{DF} computed by using contracted and uncontracted GTF basis sets. In the table, the $21s17p12d$ primitive functions are those of non-relativistically optimized well-tempered Gaussians. The $21s19p13d$ primitive set was constructed by augmenting the $21s17p12d$ basis with two $2p$ and one $3d$ Gaussian functions whose exponents are the next highest in Table 1. The results reveal that contracting basis functions of high exponents raises the total DF energy markedly. The DF energy is sensitive to the type of contraction used in the present study. This is understandable because relativistic dynamics near the origin are described by the GTF of high exponents, and contracting these functions affects the accuracy of the relativistic energies.

Table 4 displays the second-order (E_2) correlation energy corrections computed with a partial-wave expansion up to $L_{max} = 5$. The reductions in the second-order energies, ΔE_2, caused by basis set contraction, are given in the third column of the table. The results show that such a contraction scarcely affects the computed correlation energy corrections. Comparison of the second-order energy obtained by using an uncontracted $21s17p12d$ basis with that obtained by using a contracted $14s13p10d$ basis set shows that the reduction of the second-order correlation energy due to the basis set contraction is only 0.0168 au. The overall reduction amounts to 1.7% of the second-order energies obtained by using a $21s17p12d$ primitive GTF basis set. This is in contrast to the DF SCF calculations in which contracting basis functions of high exponents noticeably affects the total DF SCF energy. The error in E_2 is primarily due to the reduction of the virtual space in size caused by the basis set contraction in $s_{1/2}$ and $p_{1/2,3/2}$ symmetries. Consequently, this error in the second-order energy remains constant even when the virtual space is enlarged by including the partial wave expansion up to $L_{max} = 3$: Use of a $14s13p10d7f$ contracted basis gives the error of 0.01695 au, which accounts for 0.76% of the second-order energy, −2.2297 au, obtained by using the $14s14p10d7f$ contracted basis set.

The basis set with the highest L_{max} used in the present study is the contracted $14s13p10d7f6g5h$ set. The second-order many-body energy obtained by using this basis is −2.74029 au. The experimental estimate of the correlation energy in Xe is not known. Using a density functional approximation for the correlation energy of the inhomogeneous electron gas, Perdew estimated theoretically the non-relativistic correlation energy of Xe to be −3.31 au (25).

For neutral atoms, the error in the computed correlation correction, caused by the truncation of the partial wave expansion for $L_{max} \geq 6$, varies between 1 and 3% depending

Can. J. Chem. Downloaded from www.nrcresearchpress.com by 92.62.229.171 on 09/08/12
For personal use only.

TABLE 2. Contraction coefficients of the [14s13p10d] contracted GTF basis sets

Exponent	Contraction coefficient		
	$s_{1/2}$	$p_{1/2,3/2}$	$d_{3/2,5/2}$
0.049856		1.0	
0.124201	1.0	1.0	
0.267022	1.0	1.0	
0.525944	1.0	1.0	1.0
1.235243	1.0	1.0	1.0
2.634090	1.0	1.0	1.0
5.546456	1.0	1.0	1.0
11.720477	1.0	1.0	1.0
24.524048	1.0	1.0	1.0
52.022218	1.0	1.0	1.0
110.24499	1.0	1.0	1.0
237.19332	1.0	1.0	1.0
522.83644	1.0	9.40556(−2)	4.94760(−3)
1201.3225	1.0	2.87601(−2)	8.86000(−4)
2951.2282	1.58650(−1)	7.32970(−3)	1.64300(−4)
7854.5129	5.96087(−2)	1.41760(−3)	
22818.101	1.81052(−2)	3.14400(−4)	
71055.064	4.68230(−3)		
230587.85	1.12190(−3)		
792091.87	2.54000(−4)		
3011538.7	5.51000(−5)		
17406192.0	9.10000(−6)		

TABLE 3. Dirac–Fock energies of Xe computed in contracted and uncontracted basis sets (in au)

Basis set	E_{DF}
21s19p13d	−7446.88356
21s17p12d	−7446.80485
14s13p10d	−7443.27479
Numerical limit[a]	−7446.9010

[a]Computed by using finite difference DF program (ref. 26).

TABLE 4. Second-order many-body energies of Xe computed in contracted and uncontracted basis sets (in au)

Basis set	E_2	ΔE_2
21s17p12d	−1.03044	
14s13p10d	−1.01356	0.01688
21s17p12d7f	−2.24665	
14s13p10d7f	−2.22970	0.01695
14s13p10d7f6g	−2.59315	
14s13p10d7f6g5h	−2.74029	

on the system (9). Thus, the error caused by the basis set contraction is less than the error in the correlation correction caused by the truncation of the partial wave expansion.

We have computed the non-relativistic limit of E_2 by taking $c = 10^4$ in our relativistic DF and MBPT calculations. This gave −2.7077 au. The results give an estimate of the nonadditive contribution due to the interference between relativity and Coulomb correlation to be 0.0326 au, which is twice as large as that of the Kr atom (17).

Conclusion

The present study reveals that the DF energy is sensitive to the contraction of GTF of high exponents because of the importance of the relativistic dynamics near the origin, while electron correlation is insensitive to such a contraction. This fact makes it possible to contract the GTF of high exponents without sacrificing the accuracy in correlated calculations. Relativistic atomic structure calculations, which aim at high accuracy, must employ uncontracted Gaussian basis sets at the SCF level, while contraction can be employed at the correlated level.

The contraction scheme discussed in the present study works well for heavy systems because there are a number of primitive GTF of high exponents used to represent the core region of high Z nucleus, and they may be contracted without significantly affecting the accuracy of the computed correlation energy. The contracted basis sets are kept flexible both in the core and the valence region to enable us to recover accurate correlation energies both in the core and the valence region. The results obtained in the present study indicate that it is possible to contract the Xe primitive basis to a size comparable to those used in MBPT calculations on the neon atom (9), while maintaining the accuracy in the correlation energy. Contracting the 21s17p12d primitive set into 14s13p10d reduces both the storage of integrals and the computation time by more than 30%. We believe that this type of contraction would be very useful for accurate relativistic many-body calculations on heavy systems because the contraction considerably curtails integral storage requirements and the time needed for correlated calculations.

Acknowledgements

This research has been supported by the National Science Foundation under Grant PHY-9008627. All the calculations reported in this work were performed on an Alliant FX-8

Can. J. Chem. Downloaded from www.nrcresearchpress.com by 92.62.229.171 on 09/08/12
For personal use only.

superminicomputer, which was acquired by the University of Puerto Rico with a grant from the National Science Foundation.

1. H. P. Kelly. Adv. Chem. Phys. **14**, 129 (1969).
2. W. R. Johnson and J. Sapirstein. Phys. Rev. Lett. **57**, 1126 (1986).
3. W. R. Johnson, S. A. Blundell, and J. Sapirstein. Phys. Rev. A, **37**, 307 (1988); **41**, 1689 (1990).
4. S. Salomonson and P. Oster. Phys. Rev. A, **40**, 5548 (1989).
5. H. M. Quiney, I. P. Grant, and S. Wilson. Phys. Scr. **36**, 460 (1987).
6. H. M. Quiney, I. P. Grant, and S. Wilson. *In* Many-body methods in quantum chemistry (Lecture Notes in Chemistry 52). *Edited by* U. Kaldor. Springer, Berlin. 1989.
7. H. M. Quiney, I. P. Grant, and S. Wilson. J. Phys. B: At. Mol. Opt. Phys. **23**, L271 (1990).
8. Y. Ishikawa, H. Sekino, and R. C. Binning, Jr. Chem. Phys. Lett. **160**, 206 (1989).
9. Y. Ishikawa. Phys. Rev. A, **42**, 1142 (1990).
10. A. Rutkowski. J. Phys. B: At. Mol. Phys. **19**, 3443 (1986).
11. A. Rutkowski and W. H. E. Schwarz. Theor. Chim. Acta, **76**, 391 (1990).
12. T. H. Dunning. J. Chem. Phys. **55**, 716 (1971).
13. S. Huzinaga (*Editor*). Gaussian basis sets for molecular calculations. Elsevier, Amsterdam. 1984.
14. R. Krishnan, J. S. Brinkley, R. Seeger, and J. A. Pople. J. Chem. Phys. **72**, 650 (1980).
15. S. Wilson. Adv. Chem. Phys. **67**, 439 (1987).
16. Y. Ishikawa, H. Sekino, and R. C. Binning, Jr. Chem. Phys. Lett. **165**, 237 (1990).
17. Y. Ishikawa. Chem. Phys. Lett. **179**, 291 (1991).
18. J. Sucher. *In* Relativistic effects in atoms, molecules, and solids. Proc. of NATO Advanced Study Institute. *Edited by* G. L. Malli. Plenum Press, New York. 1983.
19. M. H. Mittleman. Phys. Rev. A, **24**, 1167 (1981).
20. Y.-K. Kim. Phys. Rev. **154**, 17 (1967).
21. Y. Ishikawa and H. M. Quiney. Int. J. Quantum Chem. Quantum Chem. Symp. **21**, 523 (1987); Y. Ishikawa, R. Baretty, and R. C. Binning, Jr. Chem. Phys. Lett. **121**, 130 (1985).
22. S. Huzinaga and M. Klobukowski. J. Mol. Struct. Theochem. **167**, 1 (1988); S. Huzinaga, M. Klobukowski, and H. Tatewaki. Can. J. Chem. **63**, 1812 (1985).
23. O. Matsuoka and S. Huzinaga. Chem. Phys. Lett. **140**, 567 (1987); S. Okada and O. Matsuoka. J. Chem. Phys. **91**, 4193 (1989).
24. Y. Ishikawa, H. M. Quiney, and G. L. Malli. Phys. Rev. A, **43**, 3270 (1991).
25. J. P. Perdew. Phys. Rev. B, **33**, 8822 (1986).
26. I. P. Grant, B. J. McKenzie, P. H. Norrington, D. F. Mayers, and N. C. Pyper. Comput. Phys. Commun. **21**, 207 (1980).

Can. J. Chem. Downloaded from www.nrcresearchpress.com by 92.62.229.171 on 09/08/12
For personal use only.

Dipped adcluster model study for the end-on chemisorption of O_2 on an Ag surface

HIROSHI NAKATSUJI[1] AND HIROMI NAKAI

Department of Synthetic Chemistry, Faculty of Engineering, Kyoto University, Kyoto 606, Japan

Received June 10, 1991

This paper is dedicated to Professor Sigeru Huzinaga on the occasion of his 65th birthday

HIROSHI NAKATSUJI and HIROMI NAKAI. Can. J. Chem. **70**, 404 (1992).

Theoretical study for the end-on adsorption of an O_2 molecule on an Ag surface is carried out with the use of the dipped adcluster model (DAM). The adcluster of AgO_2 is taken and the highest spin coupling model is employed. Electron transfer from the bulk metal to the adcluster considered by DAM is important for the occurrence of the chemisorption, and this cannot be described by the small-size cluster model. Electron correlations are also quite important and are described by the SD-CI method based on the corresponding parent configurations. In the end-on geometry, the superoxide species is the ground state, and there are no peroxide species in the lower energy region. The calculated adsorption energy compares reasonably with the experimental value. The O—O axis of the superoxide is inclined by 70°–80° from the surface normal. The outside oxygen atom of the adsorbed species seems to be more reactive than the inside one, while the net charge on the former is smaller than that on the latter.

Key words: DAM (dipped adcluster model), silver, superoxide, chemisorption.

HIROSHI NAKATSUJI et HIROMI NAKAI. Can. J. Chem. **70**, 404 (1992).

Utilisant le modèle de l'«adagrégat» plongé (DAM), on a effectué une étude théorique de l'adsorption par le bout de la molécule d'oxygène sur une surface. On a pris l'«adagrégat» du AgO_2 et on a utilisé le modèle du couplage des spin les plus élevés. Sur la base du DAM, le transfert d'électron de l'ensemble du métal vers l'«adagrégat» semble une condition importante pour que la chemisorption puisse se produire; cette importance ne peut pas être décrite par le modèle des petits agrégats. Les corrélations d'électrons sont aussi très importantes et elles peuvent être décrites par la méthode SD-CI basée sur les configurations des parents correspondants. Dans le géométrie d'addition par le bout, l'espèce superoxyde est dans l'état fondamental et il n'y a pas d'espèce peroxyde dans la région d'énergies plus faibles. L'énergie d'adsorption calculée se compare raisonnablement bien avec la valeur expérimentale. L'axe O—O du superoxyde est incliné de 70° à 80° par rapport à la surface normale. L'atome d'oxygène qui se trouve à l'extérieur de l'espèce adsorbée semble plus réactif que celui qui se trouve à l'intérieur alors que la charge nette du premier est plus faible que celle du dernier.

Mots clés : DAM (modèle de l'«adagrégat» plongé), argent, superoxyde, chemisorption.

[Traduit par la rédaction]

Introduction

An oxygen molecule adsorbed on a silver surface can undergo several important catalytic reactions. In particular, the partial oxidation of ethylene (1) is a very useful reaction in chemical industry. Several studies for clarifying the nature of the adsorbed oxygen have been performed in order to understand the mechanism of this reaction (2–4). However, there still remain many questions about the structure and electronic states of the adsorbed oxygen species involved in the epoxidation.

Two different observations have been made about the structure of the adsorbed oxygen. The NEXAFS study of O_2/Ag(110) shows that the O—O axis is parallel to the surface along the [1$\bar{1}$0] azimuthal axis with the O—O distance of 1.47 ± 0.05 Å (5). The ESDIAD experiment of O_2/Ag(110) indicates that O_2 is bonded end-on to a single Ag atom, slightly inclined away from the surface normal along the [001] azimuth (6).

In our previous study (7), we examined a side-on adsorption of O_2 onto an Ag surface by using the dipped adcluster model (DAM) (8, 9) combined with the SAC (symmetry adapted cluster)/SAC-CI method (10, 11). It has been shown that two superoxide (O_2^-) and one peroxide (O_2^{2-}) species exist in that geometry, while the latter is 13 kcal/mol more stable than the former. The peroxide species leads to dissociative adsorption with further stabilization. It was concluded that electron correlations in low-lying surface states and electron transfer from bulk metal to the adcluster are important for the oxygen chemisorption. The heats of molecular and dissociative chemisorptions and the O—O vibrational frequencies agreed well with the experimental values. In addition to other theoretical studies (12–16) on the side-on adsorptions of O_2 onto the silver surface, which use the cluster model, the structures and electronic states of the side-on oxygen species are considerably clarified.

In this study, we investigate the end-on adsorption of an O_2 molecule on an Ag surface with the use of DAM. Electron correlation is described by the SD-CI method based on the respective parent configurations. On the other hand, cluster-model SCF calculations for AgO_2 were carried out by Broomfield and Lambert (17). They showed the existence of two superoxide species in the end-on geometry with inclined O—O axis, but no stabilization energies were presented.

Dipped adcluster model

The dipped adcluster model was proposed as a theoretical model for studying chemisorptions and surface reactions involving electron transfers between admolecules and surfaces (8, 9). The "adcluster," a combined system of an admolecule and a cluster, is dipped onto the electron "bath" of a solid metal and an equilibrium is established for electron and (or) spin transfers between them. The equilibrium condition is described by using the chemical potentials of the

[1]Author to whom correspondence may be addressed.

Printed in Canada

Can. J. Chem. Downloaded from www.nrcresearchpress.com by 92.62.229.171 on 09/08/12
For personal use only.

Can. J. Chem. Downloaded from www.nrcresearchpress.com by 92.62.229.171 on 09/08/12
For personal use only.

adcluster and the solid surface. Namely, at equilibrium, the adcluster is at the min[$E(n)$] in the range,

$$[1] \quad -\frac{\partial E(n)}{\partial n} \geq \mu$$

where $E(n)$ is the energy of the adcluster, with n being the number of electrons transferred from the bulk metal to the adcluster and μ the chemical potential of the electrons of the metal surface. While all the electrons transferred into the admolecule must be supplied by the cluster alone in the conventional cluster model, some of the electrons are supplied from the electron bath of the bulk metal in DAM. The admolecule charged by this electron transfer induces an electrostatic polarization on the metal surface and receives an electrostatic attractive force. In DAM, the energy of the adcluster is given by

$$[2] \quad E = E^{(0)} + E^{(1)}$$

where $E^{(0)}$ is the electronic energy of the adcluster alone and $E^{(1)}$ the energy of the electrostatic interaction between the adcluster and the bulk metal. For $E^{(0)}$, the molecular orbital model of the dipped adcluster was proposed (8) and, for $E^{(1)}$, estimation by the method of image force was suggested (9). The energy E of the system is calculated as a function of n.

In the present study, a linear Ag—O_a—O_b system is taken as an adcluster. At infinite separation, the O_2 molecule is in the $^3\Sigma_g^-$ state and the Ag atom in the ^2S ($d^{10}s^1$) state. The highest (or parallel) spin coupling model is adopted, since it gives a continuous picture leading to the correct separation limit. In the linear AgO_2 system, the frontier MOs are mainly composed of the degenerate π^* MOs of O_2. Since the π^* orbitals of O_2 are already singly occupied by two α-spin electrons, an $n/2$ β-spin electron is added to each of the degenerate π^* orbitals.

The DAM calculations have been performed with the *ab initio* RHF SCF MO program. The Gaussian basis set for the silver atom is (3*s*3*p*4*d*)/[3*s*2*p*2*d*] and the Kr core is replaced by the relativistic effective core potential (18). For oxygen, we use the (9*s*5*p*)/[4*s*2*p*] set of Huzinaga–Dunning (19) augmented by the diffuse *s*,*p* functions of $\alpha = 0.059$ as anion bases (20) and the polarization *d* function of $\alpha = 0.30$.

Figure 1 is a display of the $E(n)$ curves, energy as a function of n. This figure is for the Ag—O_a distance at 2.20 Å, which is almost the most stable distance. The O—O distance is changed from 1.20741 Å, which is an equilibrium length of O_2 (21), to 1.35 Å, which is an equilibrium length for O_2^- (22). The curves are upper convex and the curvature is discontinuous at $n = 0.0$ and $n = 1.0$. At $n = 0.0$, $R_{O—O} = 1.20741$ Å is more stable, but at $n = 1.0$, $R_{O—O} = 1.35$ Å is more stable. The tangents of the curves coincide with the experimental chemical potential $-\mu$ of the solid silver metal (4.52 eV) (23) at $n = 0.7$. Therefore, as judged from the equilibrium condition of eq. [1], one electron flows from the bulk metal into the adcluster after a certain barrier.

O_2 approaching process

We next investigate the end-on approach of the O_2 molecule to the silver surface. Electron correlations in the low-lying states of the adcluster are calculated by including all the single and double (SD) excitation configurations relative to the corresponding parent configurations. Zero- and

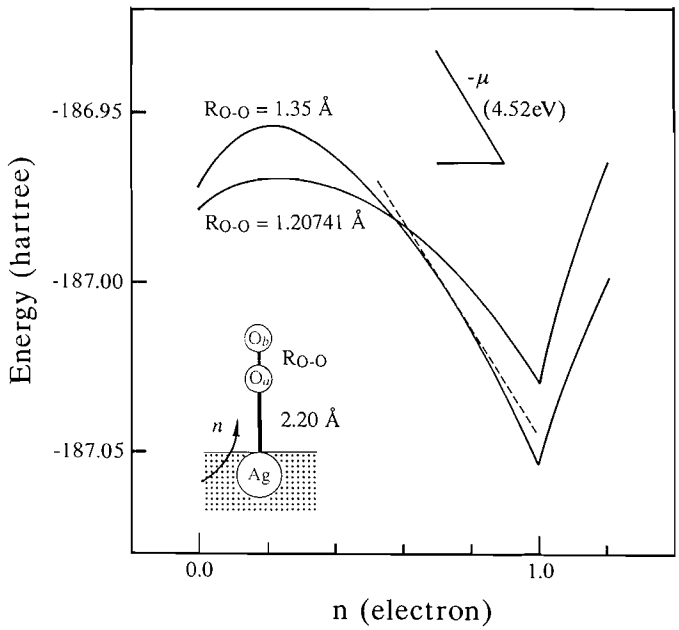

FIG. 1. $E(n)$ curve for the Ag—O_a—O_b system in the highest spin coupling model with the O_a—O_b distance of 1.20741 and 1.35 Å, and the Ag—O_a distance of 2.20 Å.

one-electron transferred states are calculated in relation to the results of Fig. 1. The active space in the SD-CI calculations consists of 11 higher occupied orbitals and 16 lower unoccupied orbitals calculated by the HF method. The 11 occupied orbitals are mainly made up from the 4*d* and 5*s* atomic orbitals of Ag and the 2*p* atomic orbitals of O. The CI calculations are carried out with the use of the program GAMESS (24).

Figure 2 shows the potential energy curves for the approaching process. The ground state of the separated system, Ag plus O_2, corresponds to the $^4\Sigma^+$ state. The energy of the separated system is estimated to be −187.089988 hartree by SD-CI calculation of the supermolecule. On the other hand, it is estimated to be −187.108991 hartree by SD-CI calculation of the free Ag plus O_2 system, of which the active spaces are [6 × 7] and [5 × 9], respectively. The energy scale on the right-hand side in Fig. 2 is in kcal/mol relative to the free system. The energy difference between the two estimations is due to the truncated nature of the CI method, which causes an unsatisfactory size consistency, as is well known. Therefore, the adsorption energy calculated from the CI of the separated free system is always smaller than that obtained from the CI for the supermolecule.

The $^4\Sigma^+$ state does not involve electron transfer between the bulk metal and the adcluster. The potential energy curve of the $^4\Sigma^+$ state rises monotonously as O_2 approaches and shows that O_2 is not adsorbed on the silver surface along this state. While the curve of the $^4\Sigma^+$ state is calculated for $R_{O—O}$ fixed at 1.20741 Å, a similar repulsive curve is also obtained for $R_{O—O}$ fixed at 1.35 Å and lies at higher energy than the curve shown in Fig. 2.

On the other hand, the ground state of the adsorbed system is the $^3\Pi$ state and involves one-electron transfer from the bulk metal. The potential energy curve of the $^3\Pi$ state is attractive and has a minimum at the Ag—O distance of

Can. J. Chem. Downloaded from www.nrcresearchpress.com by 92.62.229.171 on 09/08/12
For personal use only.

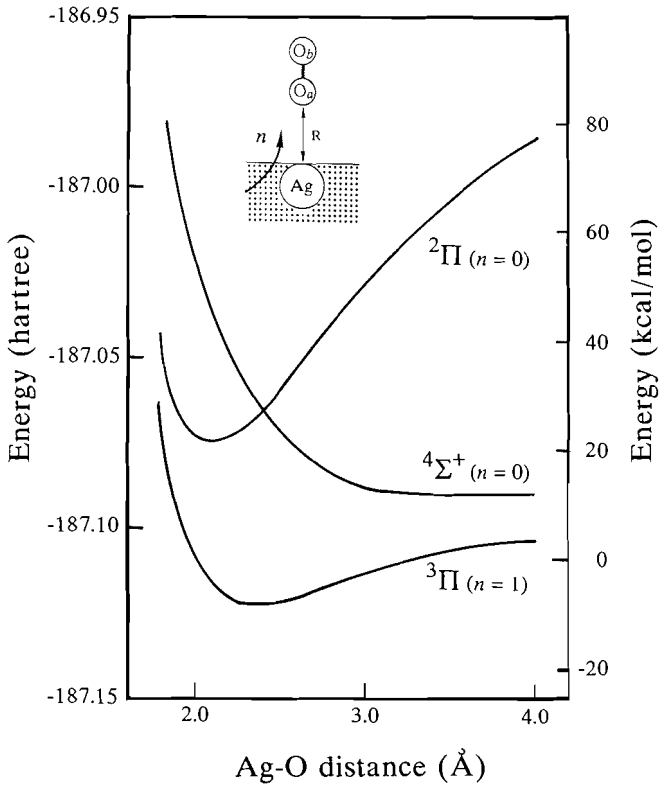

FIG. 2. Potential energy curves for the end-on approach of the O_2 molecule onto silver, calculated by the SD-CI method. The O—O length is fixed at 1.20741 Å for the $^4\Sigma^+$ state and at 1.35 Å for the $^2\Pi$ and $^3\Pi$ states. n denotes the number of electrons transferred into the adcluster from the bulk metal. The energy scale on the right-hand side is in kcal/mol relative to the free Ag plus O_2 system.

2.2 Å. The $^3\Pi$ state corresponds to the superoxide species O_2^-, since the degenerate π^* orbitals of O_2 are formally occupied by three electrons. The adsorption energy of the superoxide is calculated to be 19.4 kcal/mol relative to the energy of the supermolecule, and to be 7.5 kcal/mol relative to the energy of the free system. These calculated adsorption energies are positive in both cases and comparable with the experimental value of 9.2 kcal/mol (25).

The $^2\Pi$ state is an electron-transferred state from Ag to O_2, but no electron is supplied from the bulk metal. The potential energy curve of the $^2\Pi$ state has a minimum at the Ag—O distance of 2.0 Å, but the energy is always higher than that of the separated system (negative adsorption energy). This state corresponds to the superoxide species obtained by the conventional cluster model, though the present potential energy contains the electrostatic energy correction $E^{(1)}$. This result shows that the electron transfer from the bulk metal to the adcluster considered by DAM is important, though this cannot be dealt with by the conventional cluster model.

Table 1 shows Mulliken's atomic charges of the AgO_2 adcluster with R_{Ag-O} = 2.20 Å and R_{O-O} = 1.35 Å. In the $^4\Sigma^+$ state, which does not involve electron transfer from the bulk metal, as mentioned above, the charge of O_2 is small. The large negative charge −0.75 of O_2 in the $^2\Pi$ state is transferred from the Ag atom alone, since no electron is supplied from the bulk metal. This electron transfer is unfavorable in energy as seen in Fig. 2. On the other hand, in the $^3\Pi$ state all the electrons transferred to O_2 are supplied from the bulk metal. Note that the charge distribution of O_2 in the $^3\Pi$ state, the superoxide described by the DAM, is similar to that in the $^2\Pi$ state, the superoxide in the cluster model. The negative charge on the Ag atom seems to reflect the smallness of the size of the adcluster. It also seems to be due to the use of the highest spin coupling model, which is an extreme model. Actually, in the calculation of the PdO_2 adcluster based on the paired spin coupling model, the Pd atom has positive charge (9).

TABLE 1. Mulliken's atomic charges for the Ag—O_a—O_b adcluster[a]

State	n	Mulliken's atomic charge			
		Ag	O_a	O_b	O_a + O_b
$^4\Sigma^{+b}$	0.0	−0.103	−0.017	+0.120	+0.103
$2\Pi^b$	0.0	+0.751	−0.637	−0.114	−0.751
$^3\Pi^b$	1.0	−0.328	−0.507	−0.165	−0.672
$^3A''^c$	1.0	−0.184	−0.501	−0.315	−0.816

[a]Ag—O and O—O lengths are at 2.20 and 1.35 Å, respectively.
[b]Linear Ag—O—O adcluster.
[c]Declining angle θ of 70°.

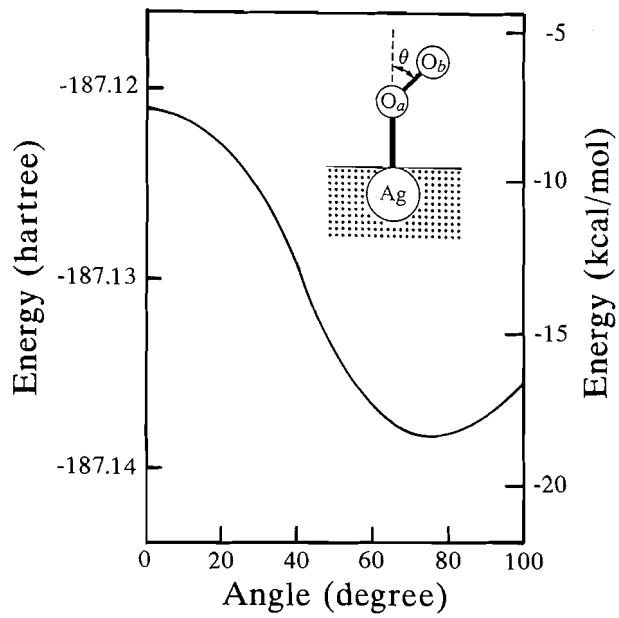

FIG. 3. Potential energy curve for the ground state of the AgO_2 adcluster calculated by the SD-CI method for the O_2 declining process. The declining angle θ is defined in the figure. The Ag—O_a and O_a—O_b lengths are fixed at 2.20 and 1.35 Å, respectively. The energy scale on the right-hand side is in kcal/mol relative to the free Ag plus O_2 system.

O_2 declining process

We examine the O—O axis declining on the silver surface. While the π^* MOs of O_2, which have three electrons for the superoxide species, are degenerate in the linear system, they are separated into a' MO (in-plane) and a'' MO (out-of-plane) in the declining process. The $^3A''$ state, in

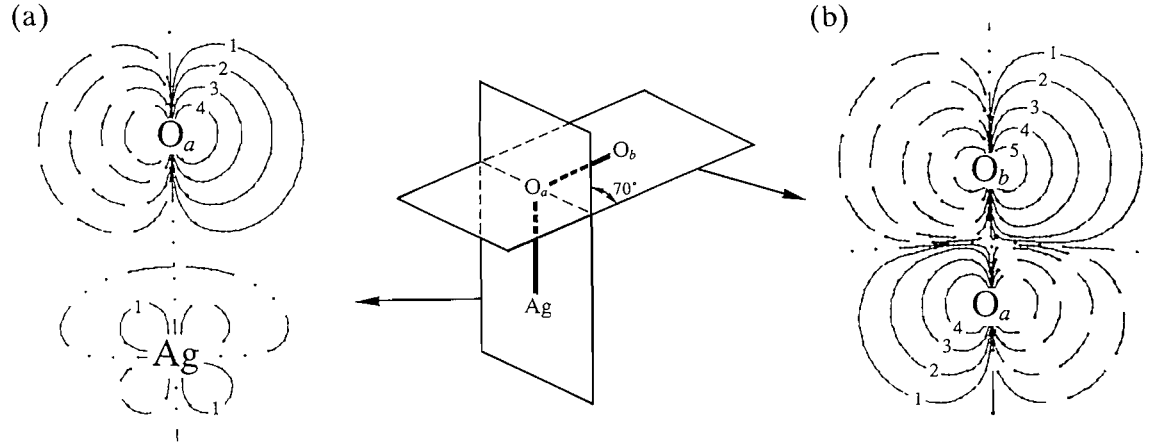

FIG. 4. Contour maps of the frontier orbital of the superoxide on silver calculated from the AgO_2 adcluster with Ag—O_a and O_a—O_b distances of 2.20 and 1.35 Å, respectively, and the declining angle θ of 70°; (*a*) and (*b*) are the maps on the planes including the Ag—O_a and O_a—O_b bonds, respectively. Solid and broken lines correspond to plus and minus signs in the MO. Double dotted line shows the node of the MO. The numbers 1–5 on the contours correspond to the values 0.01, 0.03, 0.10, 0.30, 1.00, respectively.

Can. J. Chem. Downloaded from www.nrcresearchpress.com by 92.62.229.171 on 09/08/12
For personal use only.

which the π* MOs are splitting into doubly occupied *a'* and singly occupied *a"* MOs, is more stable than the $^3A'$ state, in which the occupations in the π* MOs are reversed. Figure 3 shows the potential energy curve of the $^3A''$ state for the declining angle from the linear system. It is calculated by the SD-CI method with the Ag—O and O—O distances fixed at 2.20 and 1.35 Å, respectively. We find a minimum at the declining angle of 70–80°, which is similar to the result of Broomfield and Lambert (17). The energy at the minimum is more stable by 10.4 kcal/mol than that of the linear system. The adsorption energy is calculated to be 18.0 and 29.8 kcal/mol, relative to the energies of the separated system calculated for free molecules and supermolecule, respectively. The experimental value is 9.2 kcal/mol (25). The calculated state corresponds to the superoxide species, and no peroxide species is found in the lower energy region.

At the potential minimum, the net charges on O_a and O_b are calculated to be −0.50 and −0.32, respectively, as shown in Table 1. Namely, the negative charge on the inside O_a atom is larger than that on the outside O_b atom, which seems to be opposite to the charge distribution expected from the covalent Ag—O—O^- system.

Reactivity of superoxide

The frontier orbital of the superoxide species is the out-of-plane π* MO, which is the singly occupied (SO) MO, while the in-plane π* MO is doubly occupied as mentioned above. Figure 4 illustrates the frontier orbital map, which is related to the reactivity of the adsorbed oxygen species. Figures 4(*a*) and (*b*) correspond to the maps on the planes including the Ag—O_a and O_a—O_b bonds, respectively. These figures show much contribution of the π* orbital of O_2, but little of the $4d_{yz}$ orbital of Ag. Furthermore, in contrast to the charge distribution, the frontier orbital is larger at O_b than at O_a, which indicates that the former is more reactive than the latter.

Finally, we summarize the properties of the superoxide in the end-on form in contrast to the side-on dioxygen species studied in the previous work (7).

1. The O—O bond of the superoxide is moderately relaxed: Since the π* orbitals of the species are formally occupied by three electrons, the O—O bond is weaker than the neutral species, but stronger than the peroxide species. As shown in the previous paper (7), the peroxide species leads to the dissociative oxygen on an Ag surface.

2. In the end-on geometry, the superoxide is not liable to become the peroxide: The present study shows that in the end-on geometry the superoxide is the ground state and no peroxide state exists in the lower energy region. On the contrary, the superoxide in the side-on form seems to be easily transformed into the peroxide, since the peroxide is more stable than the superoxide (7).

3. The outside oxygen of the superoxide is more reactive than the inside oxygen: The amplitude of the frontier orbital is larger at the outside oxygen than at the inside one, in contrast to the charge distribution. Furthermore, since the frontier orbital, which is SOMO, is mainly composed of the π* MO of O_2, one-electron flow into this orbital causes a breaking of the O—O bond.

4. The charge distribution of the end-on superoxide is favorable for the approach of electron-rich molecules: By the above reasoning, the electron-rich molecule may attack the outside oxygen of the end-on superoxide. The electrostatic repulsion in this attacking process is reduced, since the negative charge on the outside oxygen atom is smaller than that on the inside one. On the other hand, in the side-on form there is no charge polarization between the two oxygen atoms.

Acknowledgements

One of the authors (H. Nakatsuji) would like to thank Mr. N. Kishimoto of Nippon Shokubai Co., Ltd. for valuable discussions at the beginning of this study. The calculations were carried out with the FACOM M780 computer at the Data Processing Center of Kyoto University and the HITAC M-680H at the Institute for Molecular Science. The author thanks the IMS computer center for the grants of computing time. Part of this study was supported by the Grant-in-Aid for Scientific Research from the Japanese Ministry of Education, Science, and Culture, and by the Kurata Foundation.

1. A. Ayame and H. Kanoh. Shokubai, **20**, 381 (1978), in Japanese.
2. G. H. Twigg. Proc. R. Soc. London, A: **188**, 92 (1946).
3. E. L. Force and A. T. Bell, J. Catal. **40**, 356 (1975).
4. N. W. Cant and W. K. Hall. J. Catal. **52**, 81 (1978).
5. D. A. Outka, J. Stöhr, W. Jark, P. Stevens, J. Solomon, and R. J. Madix. Phys. Rev. B, **35**, 4119 (1987); J. Stöhr and D. A. Outka. Phys. Rev. B, **36**, 7891 (1987).
6. K. Bange, T. E. Madey, and J. K. Sass. Chem. Phys. Lett. **113**, 56 (1985).
7. H. Nakatsuji and H. Nakai. Chem. Phys. Lett. **174**, 283 (1990).
8. H. Nakatsuji. J. Chem. Phys. **87**, 4995 (1987).
9. H. Nakatsuji, H. Nakai, and Y. Fukunishi. J. Chem. Phys. **95**, 640 (1991).
10. H. Nakatsuji and K. Hirao. J. Chem. Phys. **68**, 2035 (1978); H. Nakatsuji. Chem. Phys. Lett. **59**, 362 (1978); **67**, 329 (1979); **67**, 334 (1979).
11. H. Nakatsuji. Reports in molecular theory. CRC Press, Boca Raton, FL. In press.
12. A. Selmani, J. M. Sichel, and D. R. Salahub. Surf. Sci. **157**, 208 (1985); A. Selmani, J. Andzelm, and D. R. Salahub. Int. J. Quantum Chem. **29**, 829 (1986).
13. M. L. McKee. J. Chem. Phys. **87**, 3143 (1987).
14. T. H. Upton, P. Stevens, and R. J. Madix. J. Chem. Phys. **88**, 3988 (1988).
15. E. A. Carter and W. A. Goddard III. Surf. Sci. **209**, 243 (1989).
16. P. J. van den Hoek and E. J. Baerends. Surf. Sci. **221**, L791 (1989); P. J. van den Hoek, E. J. Baerends, and R. A. van Santen. J. Phys. Chem. **93**, 646 (1989).
17. K. Broomfield and R. M. Lambert, Mol. Phys. **66**, 421 (1989).
18. P. J. Hay and W. R. Wadt. J. Chem. Phys. **82**, 270 (1985).
19. S. Huzinaga. J. Chem. Phys. **42**, 1293 (1965); T. H. Dunning, Jr. J. Chem. Phys. **53**, 2823 (1970).
20. T. H. Dunning, Jr. and P. J. Hay. *In* Modern theoretical chemistry. Vol. 3. *Edited by* H. F. Schaeffer III. Plenum, New York. 1977.
21. E. Sutton. Tables of interatomic distances and configuration in molecules and ions. The Chemical Society, London. 1965.
22. K. P. Huber and G. Herzberg. Molecular spectra and molecular structure. IV. Constants of diatomic molecules. Van Nostrand Reinhold, New York. 1979.
23. A. W. Dweydari and C. H. B. Mee. Phys. Status Solidi A: **27**, 223 (1975).
24. B. R. Brooks, P. Saxe, W. D. Laidig, and M. Dupuis. Program System GAMESS; Program Library No. 481, Computer Center of the Institute for Molecular Science, Okazaki. 1981.
25. C. T. Campbell. Surf. Sci. **157**, 43 (1985).

Can. J. Chem. Downloaded from www.nrcresearchpress.com by 92.62.229.171 on 09/08/12
For personal use only.

The *ab initio* model potential method. Cowan–Griffin relativistic core potentials and valence basis sets from Li ($Z = 3$) to La ($Z = 57$)

ZOILA BARANDIARÁN AND LUIS SEIJO

Departamento de Química Física Aplicada, C-14, Universidad Autónoma de Madrid, 28049 Madrid, Spain

Received June 25, 1991

This paper is dedicated to Professor Sigeru Huzinaga on the occasion of his 65th birthday

ZOILA BARANDIARÁN and LUIS SEIJO. Can. J. Chem. **70**, 409 (1992).

A comprehensive tabulation of Cowan–Griffin relativistic *ab initio* core model potentials and valence basis sets corresponding to the Cowan–Griffin *ab initio* model potential method is presented. It includes those for the elements from Li ($Z = 3$) to La ($Z = 57$), the alkaline M^+ and alkaline earth M^{2+} cations, and for the halogen X^- anions. Molecular results are presented in order to test the potentials and basis sets and to estimate the extent of the mass–velocity and Darwin relativistic effects considered within the method, which lie within the expected margins.

Key words: relativistic, model potential, effective core potential, basis sets, *ab initio*.

ZOILA BARANDIARÁN et LUIS SEIJO. Can. J. Chem. **70**, 409 (1992).

On présente un tableau exhaustif des bases de valence et des potentiels de polarisation interne du modéle relativiste *ab initio* interne de Cowan–Griffin correspondant à la méthode CG-AIMP. Il comporte les données relatives aux éléments allant du Li ($Z = 3$) au La ($Z = 57$), aux cations alcalins M^+, aux cations des métaux alcalino-terreux M^{2+} et aux anions des halogènes X^-. Afin de vérifier les potentiels et les bases ainsi que pour évaluer l'importance des effets de masse–vélocité et les effets relativistes de Darwin considérés dans cette méthode, on présente des résultats moléculaires qui tombent à l'intérieur des marges attendues.

Mots clés : relativiste, potentiel modèle, potentiel interne, bases, *ab initio*.

[Traduit par la rédaction]

1. Introduction

The *ab initio* model potential method (AIMP) for valence-electron molecular calculations has been presented in previous papers (1–3). It shows the following characteristics.

(*i*) It makes use of valence orbitals with the correct nodal structure.

(*ii*) The atomic core model potentials are obtained directly from the operators they represent, without resorting to any parametrization procedure making use of valence reference orbitals. This characteristic is peculiar to the method. As a consequence of it, the AIMP can also be used to obtain complete-ion potentials (both cations and *anions*), becoming a useful tool to represent crystal lattices in solid state calculations (4).

(*iii*) The model potentials result from the addition of *explicit* representations of the core Coulomb exchange and projection operators, as well as the mass–velocity and Darwin operators that appear if the relativistic effects are handled within the Cowan–Griffin (CG) approximation (3, 5, 6). This gives the opportunity to analyze the physical effects associated with each operator.

(*iv*) The atomic valence basis sets are optimized according to the variational principle; their design and optimization is a replica of the procedure followed for all-electron basis sets.

Systematic studies on atomic and molecular calculations have been conducted, with the objective of reproducing, within an acceptable margin of error, the corresponding all-electron results if the same kind of wave function and valence basis set is used. As a consequence of them, nonrelativistic core model potentials and valence basis sets from Li to Xe have already been proposed (1–3), as well as Cowan–Griffin relativistic ones for the second series transition metal elements (3).

Numerical experimentation at the Hartree–Fock level has shown that nonrelativistic all-electron (AE) results are acceptably reproduced at a fraction of the cost. Furthermore, the effects of changes in the valence part of molecular basis sets run parallel in the AE and AIMP calculations. This is particularly important, since it means that the experience already gathered in the design of AE molecular basis sets from atomic basis sets (splitting of outermost contracted GTF's, addition of polarization functions, . . .) can safely be used for model potential calculations. Also, the high quality of the core operators used and, hence, the close reproduction of the AE basis set dependencies point out subtle effects on the molecular results, leading to the conclusion that, if there are symmetry blocks having core orbitals but lacking inner components in the molecular basis set, they must be supplied with *orthogonalization* functions in order to provide the ability to reach sufficient orthogonality between the core orbitals and the *molecular* valence orbitals. Finally, the Cowan–Griffin relativistic version of the AIMP method reproduces fairly well not only the absolute value of the equilibrium distance of AgH calculated by Lee and McLean (7) at the AE Dirac–Fock level, but also its relativistic contraction (3). The result of this test may be taken only as an additional support for the use and expected quality of the CG-AIMP method in molecules where relativistic effects other than mass–velocity and Darwin (such as spin-orbit) are not very significant, since a systematic comparison of results with AE Dirac–Fock (DF) calculations is not possible for molecules containing atoms up to La: All-electron DF calculations are available for molecules containing heavier atoms (8), where the inclusion of spin-orbit effects is compulsory.

In addition to the Cowan–Griffin relativistic core model potentials and valence basis sets already published for the second series transition metal elements, those for Sr, Ba, Br, and I have been obtained prior to conducting theoretical

Can. J. Chem. Downloaded from www.nrcresearchpress.com by 92.62.229.171 on 09/08/12
For personal use only.

TABLE 1. Sizes of the core orbitals, local core Coulomb model potentials, and valence basis sets

	Orbitals		Core orbital size			Coulomb MP size	Valence basis set	
	Core	Valence	*s*	*p*	*d*		Pattern	Structure
Li,Be	|He|	2*s*	6	—	—	8	(5)	(32
B–Ne,Na^+,Mg^{2+},F^-	|He|	2*s*2*p*	6	—	—	7	(5/5)	(32/5)
Na,Mg	|Ne|	3*s*	8	7	—	10	(7)	(322)
	|Be|	2*p*3*s*	8	—	—	10	(7/5)	(322/5)
Al–Ar,K^+,Ca^{2+},Cl^-	|Ne|	3*s*3*p*	8	7	—	9	(7/6)	(322/33)
K,Ca	|Ar|	4*s*	10	8	—	11	(9)	(3222)
	|Mg|	3*p*4*s*	10	8	—	11	(9/6)	(3222/33)
Sc–Zn	|Mg|	3*p*4*s*3*d*	10	6	—	10	(9/5/5)	(3222/32/5)
Ga–Kr,Rb^+,Sr^{2+},Br^-	|Ar|3*d*	4*s*4*p*	10	8	6	11	(9/8)	(3222/323)
Rb,Sr	|Kr|	5*s*	12	10	6	12	(11)	(32222)
	|Zn|	4*p*5*s*	12	10	6	12	(11/8)	(32222/323)
Y–Cd[a]	|Zn|	4*p*5*s*4*d*	12	10	6	11	(11/7/6)	(32222/322/33)
In–Xe,Cs^+,Ba^{2+},I^-	|Kr|4*d*	5*s*5*p*	12	9	7	12	(11/10)	(32222/3223)
Cs,Ba	|Xe|	6*s*	15	12	8	13	(13)	(322222)
	|Cd|	5*p*6*s*	15	12	8	13	(13/10)	(322222/3223)
La	|Xe|	6*s*5*d*	15	12	8	13	(13//7)	(322222//322)
	|Cd|	5*p*6*s*5*d*	15	12	8	13	(13/10/7)	(322222/3223/322)

[a]From ref. 3.

studies of the equilibrium geometry of alkaline earth dihalides (9). The latter are presented in this paper together with those of their respective periods, in order to facilitate the systematic performance of CG-AIMP molecular calculations. We have also obtained relativistic potentials and basis sets for the lighter elements, for completeness, even though the relativistic effects are known to be almost negligible for them (10). Finally, we include here the relativistic model potentials and basis sets for La($6s^25d^1$—^2D) as well as for the alkaline and alkaline earth cations and halogen anions. The results of molecular calculations performed in order to test the potentials and basis sets and to assess the extent of the mass–velocity and Darwin relativistic effects are presented.

2. Method

The nonrelativistic and Cowan–Griffin relativistic versions of the AIMP method, as applied to the valence electrons of a molecule, have already been described in refs. 1–3 and are simply summarized here. The one-electron contribution to the AIMP Hamiltonian for the valence electrons of a molecule is

$$[1]\quad h(i) = -\frac{1}{2}\Delta_i - \sum_I \frac{Z^I - Z^I_{\text{core}}}{r_{Ii}} + \sum_I \{V^{I,\text{MP}}_{\text{Coul}}(i) + V^{I,\text{MP}}_{\text{exch}}(i) + V^{I,\text{MP}}_{\text{MV}}(i) + V^{I,\text{MP}}_{\text{DW}} + P^I(i)\}$$

where I runs over the nuclei. The atomic core model potential components are as follows.

(*i*) The Coulomb core model potential,

$$[2]\quad V^{I,\text{MP}}_{\text{Coul}}(r_{Ii}) = \sum_k \frac{A^I_k \exp(-\alpha^I_k r^2_{Ii})}{r_{Ii}}$$

where the parameters $\{A^I_k, \alpha^I_k\}$ are determined through least-squares fitting to the genuine core Coulomb operator (including $-Z^I_{\text{core}}/r_{Ii}$).

(*ii*) The core exchange potential plus the relativistic mass–velocity and Darwin model potentials, which are the spectral representations of the genuine operators on the subset of the molecular primitive basis set that is centered on each nuclei:

$$[3]\quad V^{I,\text{MP}}_{\text{exch}}(i) + V^{I,\text{MP}}_{\text{MV}}(i) + V^{I,\text{MP}}_{\text{DW}}(i) = \sum_I \sum_{m=-l}^{+l} \sum_{a,b} |alm;I\rangle\, A^{I,\text{MP}}_{l;ab}\, \langle blm;I|$$

the $\{|alm;I\rangle\}$ are the spherical primitive Gaussian-type functions in the molecular basis set centered on I, and the coefficients $A^{I,\text{MP}}_{l;ab}$ are the elements of the matrix

$$[4]\quad A^{I,\text{MP}} = (S^I)^{-1} V^I_{\text{EMD}} (S^I)^{-1}$$

where S^I and V^I_{EMD} are, respectively, the overlap matrix and

Can. J. Chem. Downloaded from www.nrcresearchpress.com by 92.62.229.171 on 09/08/12
For personal use only.

TABLE 2. Valence energy, orbital energies, and radial expectation values for the IA–IIA main group elements, corresponding to the Cowan–Griffin relativistic *ns*-valence and $(n-1)p$,*ns*-valence calculations. The all-electron results (last entry) correspond to numerical Cowan–Griffin–Hartree–Fock calculations. All numbers in atomic units

					ns			$(n-1)p$		
		E(val)	$-\varepsilon(s)$	$-\varepsilon(p)$	$\langle 1/r\rangle$	$\langle r\rangle$	$\langle r^2\rangle$	$\langle 1/r\rangle$	$\langle r\rangle$	$\langle r^2\rangle$
Li	$2s^1-{}^2S$	−0.195 515	0.1955		0.342	3.889	17.875			
			0.1963		0.345	3.874	17.738			
Be	$2s^2-{}^1S$	−0.958 888	0.3083		0.518	2.656	8.460			
			0.3093		0.523	2.649	8.424			
Na	$3s^1-{}^2S$	−0.181 767	0.1818	—	0.300	4.216	20.759	—	—	—
	$2p^6\ 3s^1-{}^2S$	−27.782 634	0.1814	1.5141	0.299	4.222	20.826	1.698	0.796	0.814
			0.1823	1.5174	0.302	4.204	20.656	1.698	0.798	0.822
Mg	$3s^2-{}^1S$	−0.784 231	0.2528	—	0.397	3.254	12.412	—	—	—
	$2p^6\ 3s^2-{}^1S$	−38.395 385	0.2524	2.2794	0.397	3.258	12.439	1.953	0.683	0.593
			0.2534	2.2812	0.400	3.248	12.384	1.953	0.685	0.597
K	$4s^1-{}^2S$	−0.147 539	0.1475	—	0.236	5.240	31.486	—	—	—
	$3p^6\ 4s^1-{}^2S$	−16.260 555	0.1478	0.9522	0.237	5.232	31.393	0.937	1.437	2.442
			0.1480	0.9534	0.237	5.225	31.324	0.940	1.436	2.437
Ca	$4s^2-{}^1S$	−0.606 406	0.1958	—	0.299	4.211	20.375	—	—	—
	$3p^6\ 4s^2-{}^1S$	−22.138 283	0.1960	1.3381	0.300	4.208	20.345	1.057	1.275	1.909
			0.1963	1.3392	0.301	4.202	20.303	1.060	1.273	1.905
Rb	$5s^1-{}^2S$	−0.139 325	0.1393	—	0.220	5.571	35.411	—	—	—
	$4p^6\ 5s^1-{}^2S$	−13.736 977	0.1396	0.8079	0.220	5.562	35.294	0.755	1.728	3.451
			0.1400	0.8083	0.222	5.546	35.123	0.756	1.727	3.449
Sr	$5s^2-{}^1S$	−0.558 514	0.1806	—	0.271	4.580	23.939	—	—	—
	$4p^6\ 5s^2-{}^1S$	−18.369 409	0.1808	1.0958	0.272	4.576	23.896	0.833	1.571	2.834
			0.1812	1.0955	0.274	4.564	23.801	0.834	1.570	2.832
Cs	$6s^1-{}^2S$	−0.127 463	0.1275	—	0.198	6.122	42.462	—	—	—
	$5p^6\ 6s^1-{}^2S$	−11.520 385	0.1274	0.6811	0.198	6.121	42.451	0.614	2.089	4.966
			0.1282	0.6811	0.200	6.087	42.015	0.614	2.089	4.967
Ba	$6s^2-{}^1S$	−0.500 503	0.1620	—	0.240	5.119	29.676	—	—	—
	$5p^6\ 6s^2-{}^1S$	−15.262 623	0.1624	0.9015	0.240	5.119	29.675	0.670	1.924	4.191
			0.1631	0.8998	0.243	5.084	29.312	0.669	1.924	4.191

the matrix of the genuine core exchange, mass–velocity, and Darwin operators on the basis set $\{|alm;I\rangle\}$.

(*iii*) The core projection operator,

$$[5]\quad P^l(i) = -\sum_{c}^{\text{core}-l} 2\varepsilon_c^l |\phi_c^l\rangle\langle\phi_c^l|$$

where ε_c^l and ϕ_c^l are the core orbital energies and functions of atom I.

The necessary atomic core orbitals, as well as the genuine (numerical) mass–velocity and Darwin relativistic operators, are obtained in an atomic AE numerical Cowan–Griffin–Hartree–Fock calculation. The numerical core orbitals are represented by linear combinations of primitive GTF's (using a maximum overlap criterium (11)) to facilitate integral calculations. Once the atomic core operators are well defined, none of them needs to be parametrized in an atomic valence-electron calculation. The atomic valence basis set is obtained by minimization of the valence energy following standard all-electron methods (12).

The Cowan–Griffin relativistic AIMP method, as it has been summarized, does not take into account spin-orbit interactions. A procedure to also include these effects in molecular calculations has already been proposed (5, 13).

3. Model potentials, basis sets, and atomic results

We present in this section Cowan–Griffin relativistic core model potentials and valence basis sets for the elements from Li (Z = 3) to La (Z = 57), except those for the second series transition metal elements, which have already been presented in ref. 3. We also include model potentials and basis sets for alkaline cations M^+, alkaline earth cations M^{2+}, and halogen anions X^-.

We use the experience already gathered with the nonrelativistic atoms in order to establish the size of the model potentials and the basis set patterns as those which led to optimum results for the nonrelativistic elements. They are described in Table 1, where, together with the size of the expansions of the core orbitals in terms of primitive GTF's and of the Coulomb model potentials, eq. [2], the pattern and structure of the valence basis sets are also shown. The notation of ref. 12 is followed for the basis set pattern, which is accompanied by the *structure* of the basis set, that is, the number of primitive GTF's used to represent the inner parts of the valence orbitals and, thus, to provide a high degree of core-valence orthogonality. Let us take In–Xe as an example: The actual minimal basis set is (11/10), meaning that an 11-GTF expansion is used for the 5*s* orbital and a 10-GTF expansion for the 5*p* orbital; its structure is (32222/3223),

Can. J. Chem. Downloaded from www.nrcresearchpress.com by 92.62.229.171 on 09/08/12
For personal use only.

TABLE 3. Valence energy, orbital energies, and radial expectation values for the IIIA–VIIIA main group elements, corresponding to the Cowan–Griffin relativistic *ns*,*np*-valence calculations. The all-electron results (second entry) correspond to numerical Cowan–Griffin–Hartree–Fock calculations. All numbers in atomic units

					ns			*np*		
		E(val)	$-\varepsilon(s)$	$-\varepsilon(p)$	$\langle 1/r\rangle$	$\langle r\rangle$	$\langle r^2\rangle$	$\langle 1/r\rangle$	$\langle r\rangle$	$\langle r^2\rangle$
B	$2s^2\,2p^1-{}^2P$	−2.537 816	0.4924	0.3107	0.707	1.982	4.727	0.606	2.196	6.075
			0.4949	0.3098	0.713	1.976	4.706	0.605	2.205	6.147
C	$2s^2\,2p^2-{}^3P$	−5.320 301	0.7020	0.4338	0.889	1.593	3.062	0.784	1.709	3.706
			0.7061	0.4332	0.897	1.589	3.049	0.784	1.715	3.747
N	$2s^2\,2p^3-{}^4S$	−9.655 884	0.9401	0.5675	1.070	1.335	2.155	0.959	1.405	2.520
			0.9463	0.5674	1.079	1.331	2.146	0.958	1.410	2.548
O	$2s^2\,2p^4-{}^3P$	−15.687 946	1.2372	0.6307	1.256	1.144	1.584	1.112	1.228	1.948
			1.2463	0.6316	1.267	1.141	1.584	1.112	1.228	1.948
F	$2s^2\,2p^5-{}^2P$	−23.912 868	1.5635	0.7275	1.440	1.003	1.218	1.273	1.080	1.520
			1.5759	0.7297	1.452	1.000	1.213	1.272	1.085	1.543
Ne	$2s^2\,2p^6-{}^1S$	−34.678 133	1.9195	0.8464	1.622	0.893	0.967	1.437	0.961	1.208
			1.9357	0.8500	1.636	0.891	0.964	1.436	0.965	1.228
Al	$3s^2\,3p^1-{}^2P$	−1.876 640	0.3935	0.2091	0.504	2.600	7.885	0.377	3.444	14.079
			0.3944	0.2096	0.508	2.594	7.861	0.379	3.436	14.026
Si	$3s^2\,3p^2-{}^3P$	−3.674 534	0.5404	0.2962	0.601	2.206	5.666	0.476	2.758	9.016
			0.5417	0.2967	0.605	2.202	5.650	0.477	2.753	8.987
P	$3s^2\,3p^3-{}^4S$	−6.352 763	0.6977	0.3907	0.692	1.931	4.335	0.568	2.326	6.407
			0.6994	0.3912	0.697	1.927	4.324	0.570	2.323	6.391
S	$3s^2\,3p^4-{}^3P$	−9.949 044	0.8817	0.4364	0.783	1.719	3.431	0.648	2.063	5.074
			0.8841	0.4369	0.789	1.715	3.422	0.650	2.061	5.065
Cl	$3s^2\,3p^5-{}^2P$	−14.734 551	1.0764	0.5053	0.873	1.553	2.801	0.730	1.844	4.063
			1.0795	0.5058	0.879	1.550	2.793	0.732	1.842	4.058
Ar	$3s^2\,3p^6-{}^1S$	−20.878 788	1.2826	0.5900	0.960	1.419	2.339	0.813	1.664	3.312
			1.2865	0.5904	0.967	1.416	2.331	0.815	1.662	3.308
Ga	$4s^2\,4p^1-{}^2P$	−1.985 966	0.4318	0.2068	0.522	2.456	7.017	0.372	3.425	13.902
			0.4342	0.2071	0.526	2.449	6.982	0.373	3.423	13.904
Ge	$4s^2\,4p^2-{}^3P$	−3.664 030	0.5636	0.2859	0.586	2.197	5.582	0.446	2.863	9.629
			0.5666	0.2861	0.590	2.190	5.554	0.447	2.861	9.626
As	$4s^2\,4p^3-{}^4S$	−6.060 665	0.6998	0.3682	0.645	2.003	4.622	0.511	2.506	7.337
			0.7033	0.3684	0.650	1.997	4.599	0.512	2.505	7.336
Se	$4s^2\,4p^4-{}^3P$	−9.158 774	0.8556	0.4017	0.704	1.844	3.907	0.564	2.293	6.161
			0.8598	0.4018	0.709	1.839	3.887	0.565	2.292	6.162
Br	$4s^2\,4p^5-{}^2P$	−13.165 957	1.0158	0.4561	0.760	1.715	3.371	0.618	2.105	5.190
			1.0209	0.4561	0.766	1.709	3.354	0.619	2.104	5.191
Kr	$4s^2\,4p^6-{}^1S$	−18.186 149	1.1818	0.5235	0.816	1.606	2.952	0.672	1.944	4.422
			1.1877	0.5233	0.821	1.601	2.937	0.673	1.944	4.423
In	$5s^2\,5p^1-{}^2P$	−1.803 117	0.3927	0.1945	0.463	2.740	8.636	0.338	3.764	16.550
			0.3964	0.1947	0.468	2.725	8.553	0.334	3.761	16.548
Sn	$5s^2\,5p^2-{}^3P$	−3.264 385	0.5027	0.2631	0.509	2.496	7.121	0.390	3.225	12.037
			0.5070	0.2630	0.515	2.483	7.058	0.391	3.224	12.041
Sb	$5s^2\,5p^3-{}^4S$	−5.314 755	0.6146	0.3336	0.552	2.309	6.072	0.439	2.876	9.510
			0.6197	0.3331	0.558	2.297	6.019	0.439	2.876	9.518
Te	$5s^2\,5p^4-{}^3P$	−7.919 223	0.7409	0.3591	0.593	2.154	5.267	0.477	2.667	8.194
			0.7471	0.3585	0.600	2.142	5.220	0.477	2.667	8.203
I	$5s^2\,5p^5-{}^2P$	−11.244 930	0.8694	0.4028	0.633	2.025	4.646	0.516	2.478	7.070
			0.8769	0.4021	0.640	2.014	4.604	0.516	2.478	7.076
Xe	$5s^2\,5p^6-{}^1S$	−15.364 053	1.0014	0.4574	0.671	1.915	4.149	0.555	2.314	6.156
			1.0103	0.4566	0.679	1.905	4.110	0.554	2.314	6.159

Can. J. Chem. Downloaded from www.nrcresearchpress.com by 92.62.229.171 on 09/08/12
For personal use only.

TABLE 4. Valence energy, orbital energies, and radial expectation values for the first-series transition metal elements, corresponding to the Cowan–Griffin relativistic $3p,4s,3d$-valence calculations, and for lanthanum. The all-electron results (second entry) correspond to numerical Cowan–Griffin–Hartree–Fock calculations. All numbers in atomic units

						$3p$			$4s$			$3d$		
		E(val)	$-\varepsilon(3p)$	$-\varepsilon(4s)$	$-\varepsilon(3d)$	$\langle 1/r\rangle$	$\langle r\rangle$	$\langle r^2\rangle$	$\langle 1/r\rangle$	$\langle r\rangle$	$\langle r^2\rangle$	$\langle 1/r\rangle$	$\langle r\rangle$	$\langle r^2\rangle$
Sc	$4s^2\,3d^1-{}^2D$	−29.229 124	1.5694	0.2097	0.3351	1.152	1.171	1.604	0.319	3.958	18.053	0.796	1.670	3.561
			1.5753	0.2114	0.3358	1.154	1.173	1.615	0.322	3.938	17.882	0.793	1.691	3.709
Ti	$4s^2\,3d^2-{}^3F$	−37.817 714	1.7902	0.2204	0.4299	1.241	1.090	1.391	0.335	3.776	16.467	0.905	1.456	2.691
			1.7978	0.2224	0.4316	1.243	1.092	1.400	0.339	3.754	16.294	0.902	1.471	2.782
V	$4s^2\,3d^3-{}^4F$	−48.102 530	2.0204	0.2303	0.4972	1.332	1.019	1.217	0.351	3.619	15.172	0.997	1.318	2.204
			2.0242	0.2326	0.4995	1.330	1.023	1.230	0.354	3.599	15.010	0.993	1.332	2.281
Cr	$4s^1\,3d^5-{}^7S$	−60.032 374	2.0459	0.2204	0.3568	1.398	0.973	1.112	0.346	3.669	15.671	1.001	1.360	2.422
			2.0537	0.2460	0.3625	1.400	0.975	1.122	0.364	3.499	14.197	0.998	1.377	2.539
Mn	$4s^2\,3d^5-{}^6S$	−73.802 894	2.4771	0.2475	0.6202	1.496	0.909	0.970	0.376	3.374	13.245	1.164	1.128	1.614
			2.4905	0.2507	0.6259	1.498	0.911	0.976	0.381	3.349	13.058	1.162	1.137	1.662
Fe	$4s^2\,3d^6-{}^5D$	−89.468 379	2.7412	0.2578	0.6248	1.582	0.861	0.870	0.392	3.249	12.310	1.234	1.070	1.462
			2.7573	0.2616	0.6329	1.584	0.862	0.876	0.397	3.222	12.115	1.232	1.079	1.510
Co	$4s^2\,3d^7-{}^4F$	−107.326 921	3.0071	0.2670	0.6496	1.667	0.819	0.787	0.405	3.143	11.541	1.307	1.013	1.315
			3.0261	0.2714	0.6600	1.668	0.820	0.792	0.411	3.114	11.341	1.305	1.022	1.361
Ni	$4s^2\,3d^8-{}^3F$	−127.468 191	3.2810	0.2758	0.6771	1.751	0.781	0.715	0.418	3.047	10.869	1.380	0.961	1.189
			3.3031	0.2809	0.6899	1.752	0.782	0.720	0.425	3.017	10.663	1.378	0.970	1.232
Cu	$4s^2\,3d^9-{}^2D$	−150.030 683	3.5632	0.2843	0.7059	1.835	0.746	0.653	0.431	2.960	10.277	1.453	0.915	1.079
			3.5886	0.2901	0.7215	1.835	0.747	0.658	0.438	2.928	10.063	1.451	0.924	1.120
Zn	$4s^2\,3d^{10}-{}^1S$	−175.213 392	3.8496	0.2922	0.7437	1.918	0.714	0.600	0.443	2.883	9.767	1.527	0.872	0.981
			3.8783	0.2986	0.7618	1.918	0.715	0.604	0.451	2.849	9.548	1.525	0.880	1.019
						$5p$			$6s$			$5d$		
		E(val)	$-\varepsilon(5p)$	$-\varepsilon(6s)$	$-\varepsilon(5d)$	$\langle 1/r\rangle$	$\langle r\rangle$	$\langle r^2\rangle$	$\langle 1/r\rangle$	$\langle r\rangle$	$\langle r^2\rangle$	$\langle 1/r\rangle$	$\langle r\rangle$	$\langle r^2\rangle$
La	^2D core-$5p$	−1.216 537		0.1773	0.2350				0.259	4.762	25.718	0.452	2.821	9.211
	^2D core-$4d$	−19.662 512	1.0521	0.1770	0.2349	0.714	1.810	3.698	0.259	4.763	25.734	0.452	2.819	9.195
			1.0538	0.1796	0.2355	0.714	1.810	3.703	0.263	4.723	25.324	0.447	2.891	9.890

that is, the three innermost GTF s provide the ability to reach $1s$–$5s$ orthogonality, the following two GTF s are used for $2s$–$5s$ orthogonality, etc.

The core orbitals, Coulomb model potentials, and valence basis sets are all tabulated and deposited as supplementary material.[1] A list of libraries containing these tables as well as the numerical mass–velocity and Darwin potentials are available from the authors upon request. These are all the data necessary to perform molecular CG-AIMP calculations. The fact that the coefficients of the nonlocal spectral representation, eq. [3], depend on the actual molecular basis set (they vary with the addition of diffuse functions, etc.) makes a tabulation of them impractical: alternatively, they can be actually computed, eq. [4], along the input processing part of the molecular calculation, since their evaluation is not time consuming.

The molecular basis set for an AIMP calculation can be built up from the atomic valence basis sets in the very same manner as the AE molecular basis sets are obtained from the atomic AE minimal segmented basis sets of ref. 12: the *splitting* of the contracted functions (note that here we only have one per symmetry) is used to increase the flexibility of the basis set, and the *addition* of extra functions available in the literature provides specific abilities to the molecular basis set. For instance, *polarization functions* are available in ref. 12. *Diffuse functions* for Rydberg states and for anions can be taken from ref. 14, and, for those not available, the same obtention procedure can be followed, i.e., p-type GTF with exponents 0.043 and 0.039 for Br and I provide an excellent agreement with the numerical HF atomic electron affinities and they can be used as diffuse functions for anions (9). *Diffuse* d-*functions* able to provide a balanced description of s^2d^n, s^1d^{n+1}, and s^0d^{n+2} configurations of first-row and second-row transition metal elements are available in refs. 15 and 16, respectively. *Extra d-functions* for alkaline earth elements that allow for the participation on the bonding of the unoccupied (in the atom) $(n-1)d$ orbitals, are available in ref. 17 for Ca. We tabulated[1] these d functions for Sr and Ba, which correspond to the valence $(n-1)d$ orbital optimized along atomic calculations on $Sr^+(4d^1-{}^2D)$ and $Ba^+(5d^1-{}^2D)$, and used them in molecular calculations in ref. 9. We include the functions for Rb and Cs optimized in the corresponding $Rb(4d^1-{}^2D)$ and $Cs(5d^1-{}^2D)$ atomic calculations. As we comment in the Introduction, in cases where atomic symmetry blocks having core orbitals lack inner components in the basis set, *orthogonalization functions* have

[1]The set of Tables 7–24 may be purchased from: The Depository of Unpublished Data, Document Delivery, CISTI, National Research Council Canada, Ottawa, Canada K1A 0S2.

Can. J. Chem. Downloaded from www.nrcresearchpress.com by 92.62.229.171 on 09/08/12
For personal use only.

TABLE 5. Valence energy, orbital energies, and radial expectation values for the alkaline and alkaline-earth cations and for the halogen anions corresponding to the Cowan–Griffin relativistic *ns*,*np*-valence calculations. The all-electron results (second entry) correspond to numerical Cowan–Griffin–Hartree–Fock calculations. All numbers in atomic units

				ns			*np*		
	E(val)	$-\varepsilon(s)$	$-\varepsilon(p)$	$\langle 1/r\rangle$	$\langle r\rangle$	$\langle r^2\rangle$	$\langle 1/r\rangle$	$\langle r\rangle$	$\langle r^2\rangle$
Na(+)	−47.443 978	3.0637	1.7946	1.857	0.780	0.732	1.701	0.794	0.808
		3.0823	1.7968	1.872	0.778	0.729	1.770	0.796	0.815
K(+)	−27.890 054	1.9717	1.1695	1.073	1.274	1.873	0.940	1.432	2.417
		1.9770	1.1703	1.081	1.271	1.866	0.943	1.430	2.413
Rb(+)	−23.732 243	1.7599	1.0099	0.889	1.478	2.483	0.759	1.720	3.410
		1.7672	1.0097	0.895	1.473	2.469	0.759	1.719	3.408
Cs(+)	−19.829 772	1.4791	0.8632	0.724	1.780	3.562	0.618	2.078	4.902
		1.4902	0.8621	0.732	1.770	3.527	0.617	2.078	4.902
Mg(++)	−62.239 007	4.4741	3.0047	2.098	0.691	0.571	1.961	0.679	0.584
		4.4964	3.0062	2.114	0.689	0.568	1.960	0.681	0.588
Ca(++)	−35.841 085	2.7896	1.8760	1.188	1.156	1.536	1.064	1.264	1.870
		2.7967	1.8773	1.196	1.154	1.530	1.067	1.262	1.867
Sr(++)	−29.868 920	2.4256	1.5827	0.963	1.371	2.126	0.840	1.555	2.767
		2.4346	1.5826	0.969	1.366	2.114	0.840	1.555	2.765
Ba(++)	−24.710 066	2.0205	1.3315	0.776	1.666	3.108	0.677	1.903	4.083
		2.0344	1.3305	0.785	1.657	3.078	0.675	1.903	4.083
F(−)	−23.957 230	1.0603	0.1730	1.401	1.037	1.317	1.164	1.242	2.112
		1.0779	0.1807	1.414	1.034	1.315	1.162	1.256	2.211
Cl(−)	−14.828 473	0.7360	0.1488	0.850	1.599	2.995	0.678	2.028	5.087
		0.7397	0.1498	0.857	1.596	2.990	0.680	2.029	5.116
Br(−)	−13.260 020	0.7070	0.1371	0.744	1.760	3.579	0.577	2.295	6.368
		0.7125	0.1376	0.749	1.754	3.563	0.578	2.298	6.407
I(−)	−11.339 425	0.6004	0.1264	0.619	2.077	4.925	0.484	2.678	8.480
		0.6080	0.1261	0.626	2.065	4.880	0.484	2.680	8.516

Can. J. Chem. Downloaded from www.nrcresearchpress.com by 92.62.229.171 on 09/08/12
For personal use only.

been found necessary in molecular model potenial calculations, to provide sufficient core-valence orthogonality (1–3). The following cases appear in the set of atoms covered here.

(*i*) Alkaline and alkaline earth elements. In *ns*-valence calculations, a *p* orthogonalization function is needed, starting on Na, to provide orthogonality between the atomic core *p* orbitals and the *molecular* valence orbitals: a contracted function corresponding to the outermost lobe of the $(n-1)p$ orbital in the tabulated $(n-1)p$,*ns*-valence basis set may be used as orthogonalization function. In addition, starting on Rb, a *d* orthogonalization function is needed as well to provide high orthogonality with the *d* core orbitals. In these cases, if the *extra* $(n-1)d$ functions are used, their inner lobes provide the desired ability and no additional function is needed. If, on the contrary, they are not used, their inner lobes may be taken as orthogonality functions.

(*ii*) IIIA to VIIA main group elements from Ga to Kr and In to Xe. Analogously, these elements demand a *d* orthogonalization function. We have tabulated (see footnote 2) 3-GTF contracted *d* functions for Ga–Kr, which maximize the overlap with the Cowan–Griffin relativistic numerical orbitals; for In–Xe, the 3-GTF contracted functions corresponding to the three outermost components of the tabulated GTF expansion of the relativistic 4*d* core orbitals are valid orthogonalization functions.

In Tables 2–5 the orbital energies and radial expectation values of the CG-AIMP atomic valence orbitals can be compared with those corresponding to the numerical Cowan–Griffin calculation. The discrepancies are comparable with the ones obtained for nonrelativistic AIMP versus numerical HF calculations. It should be noted that, for the nonrelativistic atomic tests, the deviations of the AIMP results from the AE numerical HF results are very similar to those of the AE calculations with limited basis sets having a valence part of the same size, the AIMP results being slightly better (1–3).

4. Molecular calculations

The ability of the method to reproduce the results of AE molecular calculations if the same kind of wave function and valence basis set is used has already been shown (1–3), as well as its ability to represent genuine mass–velocity and Darwin relativistic effects in molecules containing second-row transition metal elements (3), where the spin-orbit effects are not expected to be very significant. The size of the relativistic effects on equilibrium distances and angles, vibrational frequencies, and bending barriers of alkaline earth dihalides, as calculated by means of the potentials and basis sets for Sr, Ba, Br, and I presented here, have been analyzed in ref. 9. We present here results of CG-AIMP restricted HF calculations on molecules of main group elements and first series transition metal elements. The results are

TABLE 6. Nonrelativistic (refs. 1–3) and Cowan–Griffin relativistic (this work) RHF results of the equilibrium distances and vibrational frequencies for the ground states of some molecules

Cores and basis sets	Core	Valence basis set
N	|He|	(41/311/1*)
P	|Ne|	(61/411/1*)
As	|Ar|3*d*	(711/5111/3°1*)
Sb	|Kr|4*d*	(911/7111/3°1*)
Sc,Mn,Cu	|Mg|	(81/321*1*/311)
O	|He|	(41/41)
S	|Ne|	(61/51/1*)

Results	R_e(Å)		$\bar{\nu}_e$(cm^{-1})	
	NR-AIMP	CG-AIMP	NR-AIMP	CG-AIMP
N_2	1.079	1.079	2746	2760
P_2	1.877	1.876	906	908
As_2	2.067	2.064	511	505
Sb_2	2.492	2.460	314	313
$ScO(\sigma^1-{}^2\Sigma)$	1.658	1.659	1088	1087
$ScS(\sigma^1-{}^2\Sigma)$	2.136	2.136	622	621
$MnO(\delta^2\pi^2\sigma^1-{}^6\Sigma)$	1.789	1.787	649	641
$CuO(\sigma^2\delta^4\pi^3-{}^2\Pi)$	1.873	1.854	589	530

summarized in Table 6. The relativistic effects on the equilibrium distance and vibrational frequency of N_2, P_2, and As_2 are negligible, becoming significant only on Sb_2, where a bond-length contraction of 0.03 Å is found, the vibrational frequency being unaffected. The effects on the first-row transition metal molecules increase towards the end of the series: they are insignificant for ScO, ScS, and MnO, whereas for CuO a contraction of 0.02 Å in r_e is found (in agreement with the results of previous calculations (10)) as well as a reduction of 10% in $\bar{\nu}_e$. This tendency along the series has also been observed in the second-row transition metal elements (3), where the effects are, however, larger.

5. Conclusions

In this paper we complete the tabulation of Cowan–Griffin relativistic *ab initio* core model potentials and valence basis sets for the elements from Li ($Z = 3$) to La ($Z = 57$); we also include those for alkaline and alkaline earth cations, as well as for halogen anions. Even though the relativistic effects are only expected to be important starting from the fifth period of the periodic table, the tabulation for the lighter elements is also presented for the sake of completeness and in order to facilitate systematic studies on mass–velocity and Darwin relativistic effects. Tests of the potentials and basis sets on restricted Hartree–Fock molecular calculations are presented, which complete those previously performed with second-row transition metal elements (3), and alkaline earth dihalides (9). The relativistic effects along the periodic table, as estimated by the CG-AIMP method, lie within the expected margins (10).

Acknowledgements

In 1984 we had the fortune to meet Professor Sigeru Huzinaga at the University of Alberta, where he received us as post-doctoral fellows. Since then, we have enjoyed working with him. As a consequence of his sharing with us both his scientific knowledge and experience, and his friendship, we have learned from him many important things of both scientific and human nature. As a scientist, he is the person who has most influenced our present scientific attitudes. As a person, his behaviour has left an indelible impression on us. We have developed deep and intimate feelings of gratitude and respect towards Professor Huzinaga. This work was partly supported by a grant from MEC (DGICYT PS89-0021), Spain.

1. S. Huzinaga, L. Seijo, Z. Barandiarán, and M. Klobukowski. J. Chem. Phys. **86**, 2132 (1987).
2. L. Seijo, Z. Barandiarán, and S. Huzinaga. J. Chem. Phys. **91**, 7011 (1989).
3. Z. Barandiarán, L. Seijo, and S. Huzinaga. J. Chem. Phys. **93**, 5843 (1990).
4. Z. Barandiarán and L. Seijo. J. Chem. Phys. **89**, 5739 (1988).
5. S. Katsuki and S. Huzinaga. Chem. Phys. Lett. **147**, 597 (1988).
6. R. D. Cowan and D. C. Griffin. J. Opt. Soc. Am. **66**, 1010 (1976).
7. Y. S. Lee and A. D. McLean. J. Chem. Phys. **76**, 735 (1982).
8. G. L. Malli. *In* The challenge of d and f electrons: Theory and computation. *Edited by* D. R. Salahub and M. C. Zerner. ACS Symp. Ser. **394**, ACS, Washington, D.C. 1989. pp. 291–308, and references therein.
9. L. Seijo, Z. Barandiarán, and S. Huzinaga. J. Chem. Phys. **94**, 3762 (1991).
10. P. Pyykko. Chem. Rev. **88**, 563 (1988).
11. E. Francisco, L. Seijo, and L. Pueyo. J. Solid State Chem. **63**, 391 (1986); Comput. Phys. Commun. **43**, 269 (1987).
12. J. Andzelm, M. Klobukowski, E. Radzio-Andzelm, Y. Sakai, and H. Tatewaki. Gaussian basis sets for molecular calculations. *Edited by* S. Huzinaga. Elsevier, Amsterdam. 1984.
13. S. Huzinaga. J. Mol. Struct. (Theochem), **80**, 51 (1991).
14. T. H. Dunning and P. J. Hay. *In* Modern theoretical chemistry. *Edited by* H. F. Schaefer III. Plenum Publishing Corp., New York. 1977. p. 1.
15. P. J. Hay. J. Chem. Phys. **66**, 4377 (1977).
16. S. P. Walch, Ch. W. Bauschlicher, Jr., and C. J. Nelin. J. Chem. Phys. **79**, 3600 (1983).
17. L. G. M. Petterson, P. E. M. Siegbahn, and S. Ismail. Chem. Phys. **82**, 355 (1983).

Can. J. Chem. Downloaded from www.nrcresearchpress.com by 92.62.229.171 on 09/08/12
For personal use only.

The use of special coordinate axes in direct and semi-direct implementations of second-order perturbation theory, including the derivation of a horizontal recurrence relation

TRACY P. HAMILTON AND HENRY F. SCHAEFER III[1]

Center for Computational Quantum Chemistry, University of Georgia, Athens, GA 30602, U.S.A.

Received June 25, 1991

This paper is dedicated to Professor Sigeru Huzinaga on the occasion of his 65th birthday

TRACY P. HAMILTON and HENRY F. SCHAEFER III. Can. J. Chem. **70**, 416 (1992).

A horizontal recurrence relation (HRR) is derived which may be used in the generation of two-electron repulsion integrals (ERIs). Also, special Cartesian coordinate axes may be used to reduce the number of intermediate terms. Heretofore, the use of local axis systems entailed rotations every time a shell quadruple of ERIs was computed. Recently, we pointed out the possibility of postponing the transformation using choices of Cartesian reference frames based on nuclear positions. In our pilot implementation of direct and semi-direct Møller–Plesset second-order perturbation theory (MP2) we construct the integrals in local coordinate systems and perform the back-transformation in the middle of the AO to MO integral transformation, rather than rotating the ERIs after the computation of each shell quadruple. The efficacy of this approach depends on whether the gains in ERI computation are greater than the losses incurred in transformation. Preliminary CPU profiles indicate that the increased time spent in rotating axes is quite small.

Key words: horizontal recurrence relation, second-order perturbation theory.

TRACY P. HAMILTON et HENRY F. SCHAEFER III. Can. J. Chem. **70**, 416 (1992).

On a développé une relation de récurrence horizontale (RRH) qui peut être utilisée dans la génération d'intégrales de répulsion de deux électrons (IRE). On peut aussi utiliser des axes de coordonnées cartésiennes pour réduire le nombre des termes intermédiaires. Jusqu'à maintenant, l'utilisation de systèmes d'axes locaux impliquait des rotations chaque fois que l'on calculait une couche quadruple d'IRE. Récemment, on a démontré la possibilitié de retarder la transformation en utilisant des ensembles de références cartésiens basés sur les positions nucléaires. Dans nos essais pilotes de la théorie de perturbation du deuxième ordre de Møller–Plesset directe ou semi-directe (MP2), on a construit des orbitales dans des systèmes de coordonnées locales et, au lieu de faire subir une rotation aux IRE après la calcul de chaque couche quadruple, on a effectué la rétro-transformation au milieu de la transformation de l'intégrale d'OA à OM. L'efficacité de cette approche suppose que le gains dans le calcul de l'IRE sont plus grands que les pertes encourues dans la transformation. Des profils préliminaires de CPU indiquent que le temps supplémentaire nécessaire pour la rotation des axes est très petit.

Mots clés : relation de récurrence horizontale, théorie de perturbation du deuxième ordre.

[Traduit par la rédaction]

Can. J. Chem. Downloaded from www.nrcresearchpress.com by 92.62.229.171 on 09/08/12
For personal use only.

Introduction

With the development of direct SCF (1) and direct Møller–Plesset second-order perturbation theory (MP2) (2, 3), in which ERIs are recomputed many times rather than stored because of disk access limitations, interest in efficient ERI evaluation has increased. The 1986 paper of Obara and Saika (4) (OS) derived a recursion relation that has prompted recent, intense activity in this field. This relation was implicit in earlier work on integral derivatives by Schlegel (5). A 1988 Head-Gordon and Pople paper (6) (HGP) presented another recursion relation, which they used in conjunction with that of OS to compute ERIs. Again, the recurrence formula given by HGP was previously used as the "transfer" equations in the Rys polynomial procedure (7). Recently, another recurrence relation was derived for ERIs over Cartesian Gaussians that moved powers of coordinates from electron one to electron two (8, 9). An alternative derivation to the one given in ref. 8 is reported in this paper. Considering the intertwined relationships between the use of these recurrence equations in ERI and ERI derivatives, new formulas using the rotational invariance conditions may be possible. Using recursion relations involving Hermite Gaussians as well, Gill, Head-Gordon, and Pople (10–12) (GHP) are investigating various integral and integral derivative algorithms.

Many of the intermediate terms involved in ERI computation become zero in special Cartesian coordinate systems; this is a main feature of the original Pople–Hehre (13) (PH) algorithm. We recently pointed out the possibility of moving the back-transformation (rotation) from the level of the ERIs to the level where the quantities to be transformed are smaller in number, enabling the rotation of axes to be done less frequently. To achieve this, the special axis systems cannot depend on orbital exponents. In the present paper, we use this idea in a preliminary implementation of direct and semi-direct second-order perturbation theory (MP2) to gauge the CPU requirements for the transformations needed.

Recurrence relations among Cartesian Gaussian ERIs

We shall only consider Cartesian Gaussian functions in this paper, and will use the notation of HGP (6):

$$[1] \qquad \phi_{ak}(\boldsymbol{r}) = (x - A_x)^{a_x}(y - A_y)^{a_y} \times (z - A_z)^{a_z} \exp(-\alpha_k(\boldsymbol{r} - \boldsymbol{A})^2)$$

The centers of the basis functions are denoted by $\boldsymbol{A}$, $\boldsymbol{B}$, $\boldsymbol{C}$, $\boldsymbol{D}$ where $\boldsymbol{A} = (A_x, A_y, A_z)$, etc. The angular momentum of the Gaussian on center $\boldsymbol{A}$ is $\boldsymbol{a} = (a_x, a_y, a_z)$ where $a_x + a_y + a_z$ is the total angular momentum. The exponents are given by the Greek letters α, β, γ, and δ. The product of the Gaussian centered on $\boldsymbol{A}$ and the Gaussian on $\boldsymbol{B}$ is a charge

[1]Author to whom correspondence may be addressed.

Printed in Canada

	FLOP	Core
Loop over i batches		
Loop over atoms A,B		
Choose local coordinate system		
Make transformation matrices		
Transform $\boldsymbol{C}$	$a^*n_i^*(\mathrm{NAT})^{2*}N^2$	N^2
Transform $\boldsymbol{P}$	$n_i^*(\mathrm{NPRIM})^{2*}(\mathrm{NAT})^{2*}11/4$	$(\mathrm{NPRIM})^2$
Loop over shells on A,B		
Loop over atoms $\boldsymbol{C}$,$\boldsymbol{D}$		
Loop over shells on C,D		
Make $(\rho\sigma\|\mu\nu)$	$n_i^*k^*N^4$	m^2N^2
End shells on C,D		
End atoms C,D		
Accumulate $(\rho\sigma\|\mu\nu)$ for μ in one shell, ν in one shell, and $\rho\sigma$ for all $\rho > \sigma$		
Make $(\rho i\|\mu\nu)$ and $(\sigma i\|\mu\nu)$	ON^4	$m^2\mathrm{IN}$
Make $(ia\|\mu\nu)$	OVN^3	$m^2\mathrm{IV}$
Transform $(ai\|\mu\nu)$ to original axes, making μ, ν run fast	$2^*a^*OVN^2$	
Make $(j\mu\|ia)$ and $(j\nu\|ia)$	O^2VN^2	$m\mathrm{IOV}$
Transform μ and ν to symmetry orbitals, to reduce storage	O^2VN^2	IOVN
End shells on A,B		
End atoms A,B		
Make $(jb\|ia)$	O^2V^2N	V^2
Compute pair energy	O^2V^2	
End i batch		

FIG. 1. Loop structure for direct MP2 energy evaluation. The maximum number of basis functions in a shell is m.

Can. J. Chem. Downloaded from www.nrcresearchpress.com by 92.62.229.171 on 09/08/12
For personal use only.

distribution on point $\boldsymbol{P}$ with exponent $\zeta = \alpha + \beta$ where $\boldsymbol{P}$ is given by

$$[2] \qquad \boldsymbol{P} = \frac{\alpha\boldsymbol{A} + \beta\boldsymbol{B}}{\alpha + \beta}$$

Similarly, a function with exponent $\eta = \gamma + \delta$ centered at $\boldsymbol{Q}$ results from the product of the functions centered at $\boldsymbol{C}$ and $\boldsymbol{D}$. Repeating this process for the product of the charge distributions centered at $\boldsymbol{P}$ and $\boldsymbol{Q}$, we obtain a Gaussian of exponent $\zeta + \eta$ with a center

$$[3] \qquad \boldsymbol{W} = \frac{\zeta\boldsymbol{P} + \eta\boldsymbol{Q}}{\zeta + \eta}$$

The OS approach (4) for ERI calculation was based on their recurrence relation for incrementing angular momentum, which HGP (6) call the vertical recurrence relation (VRR):

$$[4] \qquad [(a + \boldsymbol{l}_i)\boldsymbol{b}|\boldsymbol{cd}]^{(m)} = (P_i - A_i)[\boldsymbol{ab}|\boldsymbol{cd}]^{(m)} + (W_i - P_i)[\boldsymbol{ab}|\boldsymbol{cd}]^{(m+1)} + \frac{a_i}{2\zeta}\left\{[(\boldsymbol{a} - \boldsymbol{l}_i)\boldsymbol{b}|\boldsymbol{cd}]^{(m)} - \frac{\eta}{\zeta + \eta}[(\boldsymbol{a} - \boldsymbol{l}_i)\boldsymbol{b}|\boldsymbol{cd}]^{(m+1)}\right\}$$
$$+ \frac{b_i}{2\zeta}\left\{[\boldsymbol{a}(\boldsymbol{b} - \boldsymbol{l}_i)|\boldsymbol{cd}]^{(m)} - \frac{\eta}{\zeta + \eta}[\boldsymbol{a}(\boldsymbol{b} - \boldsymbol{l}_i)|\boldsymbol{cd}]^{(m+1)}\right\} + \frac{c_i}{2(\zeta + \eta)}[\boldsymbol{ab}|(\boldsymbol{c} - \boldsymbol{l}_i)\boldsymbol{d}]^{(m+1)}$$
$$+ \frac{d_i}{2(\zeta + \eta)}[\boldsymbol{ab}|\boldsymbol{c}(\boldsymbol{d} - \boldsymbol{l}_i)]^{(m+1)}$$

where $\boldsymbol{l}_i = (\delta_{ix}, \delta_{iy}, \delta_{iz})$. Square brackets represent primitive integrals, whereas rounded ones (parentheses) denote ERIs over contracted Gaussians. They recursively generate ERIs using eq. [4], starting from the $[\boldsymbol{00}|\boldsymbol{00}]^{(0)}$ to $[\boldsymbol{00}|\boldsymbol{00}]^{(m)}$ auxiliary integrals generated by a $F_m(T)$ subroutine, where

$$[5] \qquad m = \sum_{i=1}^{3}(a_i + b_i + c_i + d_i)$$

For integrals of low total angular momentum, $F_m(T)$ can be one of the more computation-intensive steps. The superscript m denotes whether the integral is a true ERI ($m = 0$) or an intermediate ($m \neq 0$) that can be used in the assembly of true ERIs. Similar equations may be written to increment the angular momenta of $\boldsymbol{b}$, $\boldsymbol{c}$, and $\boldsymbol{d}$.

HGP noted that subtracting the VRR for $[\boldsymbol{a}(\boldsymbol{b} + \boldsymbol{l}_i)|\boldsymbol{cd}]^{(m)}$ from $[(\boldsymbol{a} + \boldsymbol{l}_i)\boldsymbol{b}|\boldsymbol{cd}]^{(m)}$ yields

$$[6] \qquad [\boldsymbol{a}(\boldsymbol{b} + \boldsymbol{l}_i|\boldsymbol{cd}]^{(m)} = [(\boldsymbol{a} + \boldsymbol{l}_i)\boldsymbol{b}|\boldsymbol{cd}]^{(m)} + (A_i - B_i)[\boldsymbol{ab}|\boldsymbol{cd}]^{(m)}$$

Since eq. [6] does not involve exponents or different values of m, it may be applied to true *contracted* ERIs:

$$[7] \qquad (\boldsymbol{a}(\boldsymbol{b} + \boldsymbol{l}_i)|\boldsymbol{cd}) = ((\boldsymbol{a} + \boldsymbol{l}_i)\boldsymbol{b}|\boldsymbol{cd}) + (A_i - B_i)(\boldsymbol{ab}|\boldsymbol{cd})$$

HGP (6) construct integrals of the form $(\boldsymbol{e}\,\mathbf{0}|\boldsymbol{f}\,\mathbf{0})$ using the VRR, with $\boldsymbol{e}$ ranging from $\boldsymbol{a}$ to $\boldsymbol{a} + \boldsymbol{b}$ and $\boldsymbol{f}$ ranging from $\boldsymbol{c}$ to $\boldsymbol{c} + \boldsymbol{d}$. They then use eq. [7], which they called the horizontal recurrence relation (HRR). The advantages are threefold: there are fewer $(\boldsymbol{e}\mathbf{0}|\boldsymbol{f}\mathbf{0})$ integrals to construct inside loops over contractions, there are a maximum of five non-zero terms in the VRR instead of eight, and eq. [9] is used after all contractions have been done.

Recently, a new horizontal recurrence relation was derived (8) by considering ERI derivatives. However, an alternative is to consider the OS relation for $[\boldsymbol{ab}|(\boldsymbol{c} + \boldsymbol{l}_i)\boldsymbol{d}]^{(m)}$:

$$[8]\quad [\boldsymbol{ab}|(\boldsymbol{c}+\boldsymbol{l}_i)\boldsymbol{d}]^{(m)} = (Q_i - C_i)[\boldsymbol{ab}|\boldsymbol{cd}]^{(m)} + (W_i - Q_i)[\boldsymbol{ab}|\boldsymbol{cd}]^{(m+1)} + \frac{c_i}{2\eta}\left\{[\boldsymbol{ab}|(\boldsymbol{c}-\boldsymbol{l}_i)\boldsymbol{d}]^{(m)} - \frac{\zeta}{\zeta+\eta}[\boldsymbol{ab}|(\boldsymbol{c}-\boldsymbol{l}_i)\boldsymbol{d}]^{(m+1)}\right\}$$
$$+ \frac{d_i}{2\eta}\left\{[\boldsymbol{ab}|\boldsymbol{c}(\boldsymbol{d}-\boldsymbol{l}_i)]^{(m)} - \frac{\zeta}{\zeta+\eta}[\boldsymbol{ab}|\boldsymbol{c}(\boldsymbol{d}-\boldsymbol{l}_i)]^{(m+1)}\right\} + \frac{a_i}{2(\zeta+\eta)}[(\boldsymbol{a}-\boldsymbol{l}_i)\boldsymbol{b}|\boldsymbol{cd}]^{(m+1)}$$
$$+ \frac{b_i}{2(\zeta+\eta)}[\boldsymbol{a}(\boldsymbol{b}-\boldsymbol{l}_i)|\boldsymbol{cd}]^{(m+1)}$$

The $(m + 1)$ terms can be eliminated by adding $\zeta/\eta\,[(\boldsymbol{a} + \boldsymbol{l}_i)\boldsymbol{b}|\boldsymbol{cd}]^{(m)}$ to $[\boldsymbol{ab}|(\boldsymbol{c} + \boldsymbol{l}_i)\boldsymbol{d}]^{(m)}$ to get

$$[9]\quad \frac{\zeta}{\eta}[(\boldsymbol{a}+\boldsymbol{l}_i)\boldsymbol{b}|\boldsymbol{cd}]^{(m)} + [\boldsymbol{ab}|(\boldsymbol{c}+\boldsymbol{l}_i)\boldsymbol{d}]^{(m)} = \left\{\frac{\zeta}{\eta}(P_i - A_i) + (Q_i - C_i)\right\}[\boldsymbol{ab}|\boldsymbol{cd}]^{(m)} + \left\{\frac{\zeta}{\eta}(W_i - P_i) + (W_i - Q_i)\right\}[\boldsymbol{ab}|\boldsymbol{cd}]^{(m+1)}$$
$$+ \frac{a_i}{2\eta}[(\boldsymbol{a}-\boldsymbol{l}_i)\boldsymbol{b}|\boldsymbol{cd}]^{(m)} + \frac{b_i}{2\eta}[\boldsymbol{a}(\boldsymbol{b}-\boldsymbol{l}_i)|\boldsymbol{cd}]^{(m)} + \frac{c_i}{2\eta}[\boldsymbol{ab}|(\boldsymbol{c}-\boldsymbol{l}_i)\boldsymbol{d}]^{(m)} + \frac{d_i}{2\eta}[\boldsymbol{ab}|\boldsymbol{c}(\boldsymbol{d}-\boldsymbol{l}_i)]^{(m)}$$

The prefactor of the remaining $(m + 1)$ term is identically zero. Solving for $[\boldsymbol{ab}|(\boldsymbol{c} + \boldsymbol{l}_i)\boldsymbol{d}]^{(m)}$ and dropping the superscript (m) gives

$$[10]\quad [\boldsymbol{ab}|(\boldsymbol{c}+\boldsymbol{l}_i)\boldsymbol{d}] = \frac{1}{(2\gamma+2\delta)}\{-2(\alpha+\beta)[\boldsymbol{a}+\boldsymbol{l}_i)\boldsymbol{b}|\boldsymbol{cd}] - [2\beta(A_i - B_i) + 2\delta(C_i - D_i)][\boldsymbol{ab}|\boldsymbol{cd}]$$
$$+ a_i[(\boldsymbol{a}-\boldsymbol{l}_i)\boldsymbol{b}|\boldsymbol{cd}] + b_i[\boldsymbol{a}(\boldsymbol{b}-\boldsymbol{l}_i)|\boldsymbol{cd}] + c_i[\boldsymbol{ab}|(\boldsymbol{c}-\boldsymbol{l}_i)\boldsymbol{d}] + d_i[\boldsymbol{ab}|\boldsymbol{c}(\boldsymbol{d}-\boldsymbol{l}_i)]\}$$

TABLE 1. Theoretical FLOP counts and number of ERIs for C_6H_6 with DZP and TZ2P basis sets (no symmetry)

	DZP	TZ2P
N	126	234
O	16	16
V	98	206
NPRIM	120	150
a	5.3	5.9
n_i	1	1
$N^4/8$	31 500 000	374 800 000
n_i*NPRIM^2*NAT^2*11/4	5 700 000	8 900 000
a*n_i*NAT^2*N^2/2	12 100 000	46 500 000
a*OVN^2	66 000 000	532 400 000

Inspection of eq. [10] shows that it can be used to move powers of coordinates from center $\boldsymbol{A}$ to center $\boldsymbol{C}$, and so can be used as a second type of HRR in ERI algorithms. Equation [10] can be used to modify the HGP method (6) in a straightforward way. Instead of creating $[\boldsymbol{e}\mathbf{0}|\boldsymbol{f}\mathbf{0}]$ using the VRR, we can make $[(\boldsymbol{e} + \boldsymbol{f})\mathbf{0}|\mathbf{00}]$ using the VRR, and then use eq. [10] to shift coordinate dependence from $\boldsymbol{A}$ to $\boldsymbol{C}$ to form $[\boldsymbol{e}\mathbf{0}|\boldsymbol{f}\mathbf{0}]$. The remaining part of the HGP scheme is unaltered. Equation [10] has an exponent dependence that includes α, β, γ, and δ, so that in this form it must be applied inside all of the loops over contractions. Included in our implementation of this algorithm will be the computation of the ERIs in coordinate axes specified by prescriptions based on atom positions. In local coordinate axes, some of the terms in the recurrence equations discussed above become zero. Research on the optimal computational implementation of this algorithm is in progress in our group. Therefore, the MP2 programs discussed in the next section used integrals computed by our Rys polynomial code to gauge the extra effort induced by the transformations to and from local Cartesian reference frames. Other improvements to the HGP method may be possible using different techniques to generate the $[\boldsymbol{e}\mathbf{0}|\boldsymbol{f}\mathbf{0}]$ integrals that are required (9, 10).

Direct and semi-direct MP2 energy evaluation

Figure 1 shows a scheme for the direct MP2 energy method that uses local Cartesian coordinate axes. The axes are chosen such that $\boldsymbol{A}$ is at the origin, $\boldsymbol{B}$ is on the z-axis, and the other two axes are arbitrary. This is essentially a modification of the program structure outlined in ref. 2. A check is made at the level of loops over atoms using

$$[11]\quad Q_{AB} = \max_{\substack{\mu\in A\\ \nu\in B}} Q_{\mu\nu}$$

with

$$[12]\quad Q_{\mu\nu} = (\mu\nu|\mu\nu)^{1/2}$$

and the upper bound of (14, 15):

$$[13]\quad (\mu\nu|\rho\sigma) \le (\mu\nu|\mu\nu)^{1/2}(\rho\sigma|\rho\sigma)^{1/2}$$

If Q_{AB}*Q_{CD} is lower than a certain threshold, then all of the integrals on the center combinations $ABCD$ are neglected.

The local axis transformation steps scale as 2*a*n_i*(NAT)^2*N^2/4 and a*OVN^2, where n_i is the number of passes through the integral list, NAT is the number of atoms, N is

Can. J. Chem. Downloaded from www.nrcresearchpress.com by 92.62.229.171 on 09/08/12
For personal use only.

	FLOP	Core
Loop over i batches		
Loop over atoms A,B		
Choose local coordinate system		
Make transformation matrices		
Transform $\boldsymbol{C}$	$a*n_i*(\mathrm{NAT})^2*N^2$	N^2
Transform $\boldsymbol{P}$	$n_i*(\mathrm{NPRIM})^2*(\mathrm{NAT})^2*11/4$	$(\mathrm{NPRIM})^2$
Loop over shells on A,B		
Loop over atoms C,D		
Loop over shells on C,D		
Make $(\rho\sigma\|\mu\nu)$	n_i*k*N^4	m^2N^2
End shells on C,D		
End atoms C,D		
Accumulate $(\mu\nu\|\rho\sigma)$ for μ in one shell, ν in one shell, and $\rho\sigma$ for all $\rho > \sigma$		
Make $(\rho i\|\mu\nu)$ and $(\sigma i\|\mu\nu)$	ON^4	$m^2\mathrm{IN}$
Make $(ai\|\mu\nu)$	OVN^3	$m^2\mathrm{IV}$
Transform $(ai\|\mu\nu)$ to original axes	$2*a*OVN^2$	
Write $(ai\|\mu\nu)$ to disk		
End shells on A,B		
End atoms A,B		
Sort to $(\mu\nu\|ai)$ with μ, ν running fast		
Read $(\mu\nu\|ai)$ for all μ, ν, a		$N^2V/2$
Make $(\mu j\|ai)$ and $(\nu j\|ai)$	O^2VN^2	OVN
Make $(bj\|ai)$	O^2V^2N	V^2
Compute pair energy	O^2V^2	
End i batch		

FIG. 2. Loop structure for semi-direct MP2 energy evaluation. The maximum number of basis functions in a shell is m.

the number of basis functions, O is the number of occupied orbitals, V is the number of virtual orbitals, and a is the average number of FLOPs needed to rotate a basis function ($2l - 1$ FLOPs for a basis function with angular momentum l). P and Q cannot be precomputed any longer, so they need to be reconstructed at an ultimate cost of $n_i*(\mathrm{NPRIM})^2(\mathrm{NAT})^2*11/4$. NPRIM is the number of primitive exponents, not the number of primitive basis functions. Table 1 contains some of these quantities for C_6H_6 with DZP and TZ2P basis sets (six frozen cores and virtuals, no symmetry). The number of FLOPs for ERI evaluation is $kN^4/8$, where k is usually a large number ($\sim$100). The Δk needed for breakeven with respect to an algorithm that does not use special Cartesian axes is obtained by dividing the number of integrals ($N^4/8$) by the sum of the last three terms. Δk is 2.6 for the DZP basis set and 1.5 for the TZ2P basis set in this example. For larger values of n_i, Δk is even smaller, with limiting values of 0.57 and 0.15.

In a somewhat more formal manner, we may consider the number of FLOPs required for the computation of important blocks of integrals. For the 81 electron repulsion integrals in a $(pp|pp)$ block the FLOP count is

$$836K^4 + 30K^2 + 324$$

for the HS algorithm (8), where K is the contraction length, i.e., the number of primitive Gaussians in the contracted function. In the present local axes scheme ($C_y - D_y \neq 0$) the FLOP count is

$$738K^4 + 30K^2 + 216$$

For the case $K = 4$ (found in the standard double zeta $9s5p/4s2p$ basis sets for C, N, and O), the number of FLOPs is 215 000 for the earlier scheme (8) and 190 000 for the present local axes algorithm.

For the 1296 integrals in the larger $(dd|dd)$ block, the FLOP count expressions are

$$13\,900K^4 + 30K^2 + 11\,300$$

for our earlier method (8) and

$$13\,200K^4 + 30K^2 + 6\,300$$

with the present scheme. For the common, uncontracted $K = 1$ case the FLOP counts are 25 200 and 19 500 for the two methods. One concludes from this analysis that there should be an advantage to the new algorithm.

Profiling of our pilot direct MP2 program for DZ, C_{10} showed that the time spent in axis transformation was only 0.29%. Given that the transformation time is less than 0.5%, a well-designed integral algorithm should recover the miniscule effort involved. Figure 2 shows a modification of Fig. 1 in ref. 16 that gives our current algorithm for semi-direct MP2 energy computation using local axes. The largest MP2 energy evaluation done with the semi-direct program to date is C_8H_6 with a DZ + d basis set (C_{2v} symmetry with 132 basis functions). The integrals evaluation for SCF took 2048 s on the IBM 3090-400E computer, and the semi-direct MP2 energy required 2201 s. The program that computes the ERIs only in symmetry orbitals has a more stringent threshold for computation, thus accounting for some of the "speedup" in the MP2 program.

Concluding remarks

We have introduced a new recursion relation that may be useful in reducing the CPU time required to evaluate ERIs. Because eq. [10] is exponent dependent, the reduction in work is inside the loops over primitives. Direct MP2 may benefit from calculating ERIs in a special Cartesian axis system that depends only on nuclear positions, because the

Can. J. Chem. Downloaded from www.nrcresearchpress.com by 92.62.229.171 on 09/08/12
For personal use only.

extra work introduced appears to be insignificant. The semi-direct algorithm modifications are the same as in the direct MP2 program, since the $(\mu\nu|ia)$ integrals are already rotated to the original coordinate system specified by the user. The IBM Almaden group (9) has derived eq. [10] independently and has written a computer program using an algorithm like the one outlined here, without the use of local axis systems, however.

Acknowledgements

This research was supported by the U.S. National Science Foundation, Grant CHE-8718469. This paper is based on material presented in the workshop "Methodology of the Evaluation of Integrals in LCAO Calculations" at Argonne National Laboratory, August 22–25, 1990.

1. J. Almlöf, K. Faegri, and K. Korsell. J. Comput. Chem. **3**, 385 (1982).
2. J. Head-Gordon, J. A. Pople, and M. J. Frisch. Chem. Phys. Lett. **153**, 503 (1988).
3. S. Saebø and J. Almlöf. Chem. Phys. Lett. **154**, 83 (1989).
4. S. Obara and A. Saika. J. Chem. Phys. **84**, 3963 (1986).
5. H. B. Schlegel. J. Chem. Phys. **77**, 3676 (1982).
6. M. Head-Gordon and J. A. Pople. J. Chem. Phys. **89**, 5777 (1988).
7. J. Rys, M. Dupuis, and H. F. King. J. Comput. Chem. **4**, 154 (1983).
8. T. P. Hamilton and H. F. Schaefer. Chem. Phys. **150**, 163 (1991).
9. R. Lindh, U. Ryu, and B. Liu. J. Chem. Phys. **95**, 5889 (1991).
10. P. M. W. Gill, M. Head-Gordon, and J. A. Pople. Int. J. Quantum. Chem. **S23**, 269 (1989).
11. P. M. W. Gill, M. Head-Gordon, and J. A. Pople. J. Phys. Chem. **94**, 5564 (1990).
12. P. M. W. Gill and J. A. Pople. To be published.
13. J. A. Pople and W. J. Hehre. J. Comput. Phys. **27**, 161 (1978).
14. J. D. Power and R. M. Pitzer. Chem. Phys. Lett. **24**, 478 (1974).
15. M. Häser and R. Ahlrichs. J. Comput. Chem. **10**, 104 (1989).
16. M. J. Frisch, M. Head-Gordon, and J. A. Pople. Chem. Phys. Lett. **166**, 281 (1990).

Can. J. Chem. Downloaded from www.nrcresearchpress.com by 92.62.229.171 on 09/08/12
For personal use only.

Ab initio relativistic molecular orbital self-consistent field calculations for the thorium–platinum diatomic

G. L. MALLI

Department of Chemistry, Simon Fraser University, Burnaby, B.C., Canada V5A 1S6

Received September 12, 1991

This paper is dedicated to Professor S. Huzinaga on the occasion of his 65th birthday

G. L. MALLI. Can. J. Chem. **70**, 421 (1992).

Ab initio relativistic as well as the corresponding non-relativistic limit (NRL) MO calculations are reported for the ground state ($\Omega = 0$) of the closed-shell diatomic ThPt. It is found that relativistic effects lead to a very *pronounced* bond shortening of ca 1.68 bohr. The predicted bond length of 2.7398 Å with the relativistic molecular orbital (RMO) wavefunction (WF) for the diatomic ThPt is ca. 0.25 Å *shorter* than the Th—Pt distance reported in a recently synthesized complex with a thorium–platinum bond as well as the shortest Th—Pt bond distance reported for the Th–Pt alloy. The calculated relativistic total molecular energy and the force constant at the predicted bond distance of 5.1774 bohr are −44 963.5050 hartree and 0.34650 hartree/(Å)^2, whereas the corresponding predicted non-relativistic values are 6.824 bohr, −41 690.6970 hartree, and 0.08388 hartree/(Å)^2, respectively. The vibrational frequencies predicted by the RMO and the non-relativistic limit MO SCF wavefunctions are 155.4 cm^{-1} and 76.46 cm^{-1}, respectively. The relativistic effects are very pronounced for ThPt and lead to a very *significant* bond contraction, an almost *fourfold* increase in the force constant, and *doubling* of the vibrational frequency.

Key words: relativistic effects, ThPt, RMO, bond contraction, DF SCF.

G. L. MALLI. Can. J. Chem. **70**, 421 (1992).

On a effectué des calculs d'OM *ab initio* relativistes ainsi que les calculs correspondants de limites non-relativistes (LNR) pour l'état fondamental ($\Omega = 0$) de la couche fermée diatomique ThPt. On a observé que les effets relativistes conduisent à un raccourcissement important de la liaison d'environ 1,68 bohr. La longueur de 2,7398 Å prédite pour la liaison ThPt diatomique à l'aide d'une fonction d'onde (FO) de l'orbitale moléculaire relativiste (OMR) est environ 0,25 Å plus courte que la distance rapportée pour une liaison thorium–platine d'un complexe synthétisé récemment ainsi que la plus courte liaison Th—Pt observée dans un alliage de Th—Pt. L'énergie moléculaire totale et la constante de force calculées d'une façon relativiste à le longueur de liaison prédite de 5,1774 bohr sont respectivement −44963,5050 hartree et 0,34650 hartree/(Å)^2 alors que les valeurs correspondantes calculées par des méthodes non-relativistes sont respectivement 6,8624 bohr, −41690,6970 hartree et 0,08388 hartree/(Å)^2. Les fréquences de vibration prédites par les orbitales moléculaires relativistes et les fonctions d'onde d'orbitales moéculaires auto-cohérentes limites non-relativistes sont respectivement 155,4 cm^{-1} et 76,46 cm^{-1}. Les effets relativistes sont très prononcés pour le ThPt et ils conduisent à un important raccourcissement de liaison alors que la constante de force est pratiquement quadruplée et que la fréquence vibrationnelle est doublée.

Mots clés : effets relativistes, ThPt, OMR, raccourcissement de liaison, DF SCF.

[Traduit par la rédaction]

Introduction

The theoretical aspects of the chemistry of heavy elements with 5*d*, 5*f*, 6*d*, and 7*s* valence electrons present a formidable challenge to computational quantum chemists because both the relativistic and the electron correlation effects are expected to be very significant for systems involving atoms of these heavy elements.

We recently discussed in detail the methodology for performing *ab initio* all-electron Dirac–Fock (DF) self-consistent-field (SCF) and relativistic configuration interaction (RCI) calculations with all single and pair-type double excitations (RCISPD) taking the DF SCF wavefunction as the reference (1, 2).

We have reported *ab initio* DF SCF and the RCISPD calculations for AuH and have discussed in detail the effects of relativity and electron correlation in bonding, spectroscopic properties, dipole moment, etc., for diatomics of heavy elements (1, 3, 4). In addition, we have reported *ab initio* fully relativistic RMO SCF calculations for the diatomics UO and ThO and have shown that the relativistic (and the correlation) effects are very pronounced for the systems involving atoms of heavy third-row transition elements and actinides (1–5). Recently Dyall *et al.* (6) reported Dirac–Hartree–Fock calculations for the tetrahydrides of the group IV elements and discussed the relativistic effects for the ground states of these systems.

In this paper, we report the RMO SCF calculations for the closed-shell ground state of the diatomic ThPt, a hetero bimetallic species involving atoms of an actinide and a third-row transition element. Our objective in this study is twofold, viz., firstly to assess the relativistic effects in this species and secondly to understand the nature of the metal–metal bond involving an actinide and a third-row transition element; we will ignore the electron correlation effects at present, however. It is well established (7) that all metallic elements participate in metal–metal bonding and that bonds between elements with *d* orbitals (valence) are especially strong. Examples of the metal–metal bonds are also well known for the lightest metal Li in $[LiCH_3]_4$ and the heaviest metal U in $U_6O_4(OH)_4(SO_4)_6$.

Gingerich (8) used an empirical valence bond approach for calculating bond energies of diatomic intermetallic compounds of platinum and compared these with the experimental bond energies obtained using Knudsen-cell mass spectroscopy. Recently, Hay *et al.* (9) used their effective-core-potential (ECP) scheme for calculations on $C_{12}Th(\mu\text{-}PH_2)_2Pt(PH_3)$, using the Th—Pt distance reported in the recently synthesized $Cp^*_2Th(\mu\text{-}PPh_2)_2(Pt(PMe_3)$ complex.

Can. J. Chem. Downloaded from www.nrcresearchpress.com by 123.30.183.119 on 09/08/12
For personal use only.

Can. J. Chem. Downloaded from www.nrcresearchpress.com by 123.30.183.119 on 09/08/12
For personal use only.

However, *ab initio* all-electron RMO SCF calculations for the diatomic ThPt have not been reported and we present such calculations and discuss the relativistic effects in this species, since such a hetero bimetallic system is of great interest to both experimental and theoretical chemists.

Methodology

Our DF SCF methodology has been delineated in detail elsewhere (1–5) and only a brief summary of the salient features relevant to relativistic diatomic calculations is presented here.

The basic idea behind the Relativistic Integral Program (RIP) (10, 11) used in our calculations is to express the wavefunction for the diatomic molecule in terms of the Dirac–Fock atomic orbitals (DFAO) of the constituent atoms. The DFAOs for the atoms can be easily calculated using the Dirac–Fock programmes (12). In addition, since the innermost electrons of the heavy atoms (with $Z \geq 75$) are hardly expected to be affected by the formation of the molecule, a frozen core approximation is used in which the wavefunction $\Psi(\boldsymbol{r}_1, \ldots, \boldsymbol{r}_N)$ for the closed-shell N-electron diatomic molecule system is written as:

$$[1] \quad |\Psi(\boldsymbol{r}_1, \ldots, \boldsymbol{r}_N)\rangle = S\hat{A}'[|\Phi_{ca}(\boldsymbol{r}_1, \ldots, \boldsymbol{r}_{n_{ca}})\rangle \times |\Phi_{cb}(\boldsymbol{r}_{n_{ca}+1}, \ldots, \boldsymbol{r}_{n_{ca}+n_{cb}})\rangle \times |\Phi_V(\boldsymbol{r}_{n_{ca}+n_{cb}+1}, \ldots, \boldsymbol{r}_N)\rangle]$$

where in eq. [1] S is a normalization constant. The $|\Phi_{ca}\rangle$ and $|\Phi_{cb}\rangle$ in eq. [1] are wavefunctions for the cores containing n_{ca} and n_{cb} electrons of the atoms "a" and "b" of the diatomic and these core wavefunctions are taken to be single determinants (SD) of the DFAOs of the isolated atoms, viz.,

$$[2] \quad |\Phi_{ca}(\boldsymbol{r}_1, \ldots, \boldsymbol{r}_{n_{ca}})\rangle = \hat{A}\left(\prod_{i=1}^{n_{ca}} |\boldsymbol{u}_{a,i}(\boldsymbol{r}_{a,i})\rangle\right)$$

$$[3] \quad |\Phi_{cb}(\boldsymbol{r}_{n_{ca}+1}, \ldots, \boldsymbol{r}_{n_{ca}+n_{cb}})\rangle = \hat{A}\left(\prod_{i=1}^{n_{cb}} |\boldsymbol{u}_{b,i}(\boldsymbol{r}_{b,i} + \boldsymbol{n}_{ca})\rangle\right)$$

In eqs. [2] and [3] $|u_{b,i}\rangle$ is the ith core orbital for atom b, $r_{b,i}$ is the position vector of the ith electron with respect to the nucleus b, and $\hat{A}$ is the antisymmetrizer, while in eq. [1] $\hat{A}'$ is the partial antisymmetrizer, which contains, besides the identity, only permutations interchanging coordinates belonging to one of the set $(r_1, \ldots, r_{n_{ca}})$, $(r_{n_{ca}+1}, \ldots, r_{n_{ca}+n_{cb}})$, and $(r_{n_{ca}+n_{cb}+1}, \ldots, r_N)$ with those belonging to a different set. The $|\Phi_V\ (r_{n_{ca}+n_{cb}+1}, \ldots, r_N)\rangle$ appearing in eq. [1] is an antisymmetric wavefunction for the $(N - n_{ca} - n_{cb})$ valence electrons, which is built from those DFAOs of the isolated atoms not appearing in the core wavefunctions Φ_{ca} and Φ_{cb} defined in eqs. [2] and [3].

Each of the DFAO in eqs. [2] and [3] is taken to be of the standard central field form with respect to the nucleus on which it is centred and therefore carries the additional labels κ and m (13), so that

$$[4] \quad |\boldsymbol{u}_{\mu,b}\kappa\boldsymbol{m}\rangle = \boldsymbol{r}_\mu^{-1}\begin{pmatrix} \boldsymbol{P}_B(\boldsymbol{r}_\mu) & \boldsymbol{\chi}_{\kappa,m}(\boldsymbol{\theta}_\mu, \boldsymbol{\phi}_\mu) \\ i\boldsymbol{Q}_B(\boldsymbol{r}_\mu) & \boldsymbol{\chi}_{-\kappa,m}(\boldsymbol{\theta}_\mu, \boldsymbol{\phi}_\mu) \end{pmatrix}$$

where $P_B(r_\mu)$ and $Q_B(r_\mu)$ are the large and small radial functions, respectively centered on nucleus μ. The $(2j + 1)$ orbitals differing only in the m_j quantum number are said to constitute a subshell (14) denoted by B, and are taken to have the same radial functions. The label b in eq. [4] defines the orbital uniquely after specification of the centre μ, thus defining the κ and m quantum numbers, which may both carry the additional subscript b. The $\boldsymbol{\chi}_{\kappa,m}$ is a vector-coupled two-component spinor eigenfunction of the operators j^2 and j_z corresponding to the total and z-component of the angular momentum ($\boldsymbol{j} = \boldsymbol{l} + \boldsymbol{s}$) of an electron with eigenvalues $j(j + 1)$ and m respectively, so that m is the m_j quantum number. These functions can be written as

$$[5] \quad \boldsymbol{\chi}_{\kappa,m}(\boldsymbol{\theta}_\mu, \boldsymbol{\phi}_\mu) = \sum_{m_s=-1/2}^{1/2} \left\langle \ell\, \frac{1}{2}\, (m - m_s)\, \frac{1}{2}\, m_s \middle| jm \right\rangle \times Y_{\ell,m-m_s}(\theta_\mu, \phi_\mu) \left| \frac{1}{2}\, m_s \right\rangle$$

where in eq. [5] the $Y_{\ell,m-m_s}$ are the normalised spherical harmonics and $|\frac{1}{2}\, m_s\rangle$ is a two-component spin function:

$$|1/2\ 1/2\rangle = \begin{pmatrix} 1 \\ 0 \end{pmatrix} \equiv |\alpha\rangle, \quad |1/2\ -1/2\rangle = \begin{pmatrix} 0 \\ 1 \end{pmatrix} \equiv |\beta\rangle$$

The quantum number κ defines both the total angular momentum (j) and the orbital angular momentum (ℓ) as follows:

$$[6] \quad \kappa = -\left(j + \frac{1}{2}\right) a, \qquad \begin{aligned} a &= +1 \text{ for } j = \ell + \frac{1}{2} \\ a &= -1 \text{ for } j = \ell - \frac{1}{2} \end{aligned}$$

It should be borne in mind that only completely filled subshells (B), namely those in which each of the $(2j_B + 1)$ orbitals contains one electron, can be included in the core wavefunction in order to ensure both that the core has no net angular momentum, and that it is symmetric under the symmetry operators of the (double) symmetry group of the diatomic molecule (15, 16).

The valence wavefunction $|\Phi_V(r_{n_{ca}+n_{cb}+1,\ldots}\, r_N)\rangle$ is constructed from a set of relativistic orbitals, each member of which is orthogonal to all the orbitals entering the core functions of the two atoms given by eqs. [2] and [3]. The number of electrons to be included in the valence wavefunction depends upon the accuracy required; however, the electrons in the open shells of the isolated atoms of the diatomic *must* be included in Φ_V, which can be enlarged to include those outermost orbitals of the isolated atoms that are expected to be significantly affected by the formation of the molecule, e.g., 5*d** and 5*d* DFAO in the gold atom in AuH.

The valence wavefunction $|\Phi_V\rangle$ for most diatomic calculations is taken to be a single Slater determinant (SD) or antisymmetrized product (AP) of valence relativistic molecular orbitals (RMO), which are taken as eigenfunctions of the operator $\hat{j}_z$ with eigenvalue m. In this case the N-electron wavefunction becomes a molecular relativistic self-consistent-field (SCF) wavefunction and the SCF valence wavefunction Φ_V^{SCF} can be written as:

$$[7] \quad |\Phi_V^{SCF}\rangle = \hat{A}\left(\prod_{m>0}\prod_{a=1}^{N_{V_m}} |\psi_a m\rangle|\psi_a - m\rangle\right)$$

where N_{V_m} is the number of valence RMO's occurring in eq. [7] that have $m_j = m$.

Can. J. Chem. Downloaded from www.nrcresearchpress.com by 123.30.183.119 on 09/08/12
For personal use only.

The wavefunction $|\Phi_V^{SCF}\rangle$ is an eigenfunction of the z-component of the total angular momentum J_{zT} with zero eigenvalue and furthermore it is symmetric under both the N-electron relativistic operators $\boldsymbol{H}_{XT}$ and $\boldsymbol{H}_{YT}$, i.e., for reflections in the YZ and XZ planes (15, 16). Moreover, it can be shown either by double group arguments (15) or by using the properties of the $\boldsymbol{H}_{YT}$ operator (16) that the pair of orbitals $|\Psi_a \pm m\rangle$ occurring in Φ_V^{SCF} of eq. [7] is degenerate and constitutes a closed shell.

The Dirac–Fock atomic orbitals used to construct the core wavefunctions given in eqs. [2] and [3] describe automatically the behaviour of *electrons* and not positrons. Furthermore, all the orbitals used in the construction of the valence wavefunction $|\Phi_V\rangle$ have the form given in eq. [4] and are constructed to maintain the appropriate relation between the large and small components (17), and therefore lie within the subspace of the electron-like solutions of some single particle Dirac–Fock hamiltonian. The energy $E(R)$ of the wavefunction given in eq. [1], which depends on the internuclear separation (R), can therefore be calculated as

$$[8] \quad \boldsymbol{E(R)} = \langle \boldsymbol{\Psi}(\boldsymbol{r}_1, \ldots, \boldsymbol{r}_N)|\boldsymbol{H}|\boldsymbol{\Psi}(\boldsymbol{r}_1, \ldots, \boldsymbol{r}_N)\rangle$$

i.e., as the expectation value of the N-electron relativistic hamiltonian $\boldsymbol{H}$, *without* the need to introduce any projection operators (18) where

$$[9] \quad \boldsymbol{H} = \sum_{\mu=1}^{N} H_D(\mu) + \sum_{\mu<\nu} \boldsymbol{r}_{\mu\nu}^{-1}$$

$$[10] \quad H_D(\mu) = \boldsymbol{c}\boldsymbol{\alpha}_\mu \cdot \boldsymbol{p}_\mu + \boldsymbol{c}^2(\boldsymbol{\beta}_\mu - \boldsymbol{I}_4) - \sum_{a=1}^{n} \frac{\boldsymbol{Z}_a}{\boldsymbol{r}_{a\mu}}$$

In eq. [9] $r_{\mu\nu}^{-1}$ is the Coulomb repulsion between electrons μ and ν and $H_D(\mu)$ is the Dirac Hamiltonian for the μth electron in the potential of all the nuclei of the molecular system. In eq. [10], c is the velocity of light (c = 137.037 in a.u.), Z_a is the nuclear charge on the ath nucleus, $r_{a\mu}$ is the distance between the ath nucleus and the μth electron, and the sum over "a" runs over all the "n" nuclei. The α and β are well-known 4 × 4 matrices defined below, and I_4 is the 4 × 4 unit matrix:

$$\alpha = \begin{pmatrix} 0 & \sigma \\ \sigma & 0 \end{pmatrix}, \qquad \beta = \begin{pmatrix} I & 0 \\ 0 & -I \end{pmatrix}$$

In eq. [10], the rest mass energy of an electron has been subtracted in order to obtain its binding energy, and H of eq. [9] is the so-called Dirac–Coulomb Hamiltonian for molecules. The I in the definition of β is the 2 × 2 unit matrix.

Moreover, the strong orthogonality between the core and valence wavefunctions ensured by the orthogonality between the core and valence orbitals enables eq. [8] to be decomposed into core and valence contributions (19) as follows,

$$[11] \quad E(R) = E_{ca}^{(M)} + E_{cb}^{(M)} + \Delta E_{core}^{int}(R) + E_V(R)$$

where in eqs. [11] $E_{ca}^{(M)}$ and $E_{cb}^{(M)}$ are the energies of the core functions given in eqs. [2] and [3], respectively, and $\Delta E_{core}^{int}(R)$, which includes the nuclear–nuclear repulsion, is the difference between the energy of this core in the molecule and that of the same core in the isolated atoms. The $E_V(R)$ is the energy of the valence electrons and it contains both the direct and exchange interactions between the core and the valence electrons.

The dissociation energy (D_e) defined as positive (1) for a bound molecule, equals the negative of the interaction energy $\Delta E_{int}(R)$ at the predicted equilibrium internuclear separation (R_e) and $\Delta E_{int}(R)$ is given by the expression:

$$[12] \quad \Delta E_{int}(R) = E(R) - E_a - E_b$$

where E_μ, the total energy of the isolated atom μ, is given by

$$[13] \quad E_\mu = E_{\mu c} + E_{\mu v}$$

where in eq. [13] $E_{\mu c}$ and $E_{\mu v}$ are energies of the core and valence electrons, respectively, in the isolated atom μ. It should be borne in mind that the $E_{\mu c}$ only equals the energy $E_{\mu c}^{(M)}$ in the molecule if the same set of core orbitals is used both in the free μth atom wavefunction and in the molecular core function given in eqs. [1] and [2], and in this case $\Delta E_{int}(R)$ simplifies to

$$[14] \quad \Delta E_{int}(R) = \Delta E_{core}^{int}(R) + E_V(R) - E_{aV} - E_{bV}$$

Calculations and results

Ab initio RMO SCF calculations were performed for the ground state (Ω = 0) of the closed-shell ThPt molecule, assuming point nucleii at four internuclear distances, viz., 4.50, 5.50, 6.00, and 6.50 bohr.

The Oxford MCDF program of Grant *et al.* (12) was used to generate a nine-configuration state function (CSF) WF and the corresponding NRL WF for the neutral Th atom with the ground state electronic configuration [Rn] $6d^27s^2$, where [Rn] stands for the ground state electronic configuration of the radon atom (Z = 86). Similarly, wavefunctions were generated for the ground J = 3 state of the Pt atom with the configuration $1s^2 \ldots 5d^{*4}\ 5d^5\ 6s$, where the $5d^*$ stands for the ($5d$) AO with j = 3/2. In these calculations, the inner 86 electrons of the Th atom and the 68 electrons of the Pt atom were treated as "core" and the $6d$, $7s$ Dirac–Fock atomic orbitals (DFAO) of Th and the $5d$, $6s$ DFAOs of Pt were included in the valence RMO SCF WF of ThPt. It should be pointed out that although the core orbitals are taken to be unchanged from the isolated atoms, the following three important effects of the core on the valence wavefunctions are *exactly* calculated and therefore taken explicitly into account (1): (*i*) A direct Coulombic potential is generated by the core and is easily calculated by the Relativistic Integral Program (RIP) (10, 11). (*ii*) Core-valence exchange, whose exact computation by RIP or any other program requires explicitly the presence of the core orbitals in the total wavefunction, which is written as an antisymmetrized product of the core and valence wavefunctions (see ref. 1 for details). (*iii*) The strong orthogonality between the core and valence wavefunctions, which is ensured in the RIP program by construction of the valence wavefunction from the orbital set, which is orthogonal to the core orbitals.

Our approach, therefore, is to be clearly distinguished from the effective-core-potential (ECP) and the so-called relativistic pseudo-potential schemes, which *do not* explicitly incorporate the core orbitals and thus introduce approximations to the effects (*ii*) and (*iii*) of the core.

Moreover, the inclusion of inner-shell orbitals in the core wavefunction is for the sake of computational cost considerations, since it is not mandatory to do so, and we have re-

TABLE 1. Calculated total molecular relativistic MO (RMO) SCF energies (E_{Rel}) for ThPt in hartree (1 hartree = 27.211 eV) at various internuclear distances R in bohr (1 bohr = 0.529177 Å)

R (bohr)	$-E_{Rel}$ (hartree)	$R_{min,Rel}$(bohr)[a]	k_{Rel}[a]	$\bar{\nu}_{Rel}$(cm^{-1})[a]
4.50	44 963.475 51	5.1774	0.346 50	155.4
5.50	44 963.500 63			
6.00	44 963.484 85			
6.50	44 963.473 12			

[a]The values of $R_{min,Rel}$, the force constant k_{Rel}, and $\bar{\nu}_{Rel}$ (cm^{-1}), the vibrational frequency, are obtained by fitting the results of RMO SCF calculations for ThPt at four points to a cubic polynomial.

TABLE 2. Calculated total molecular non-relativistic limit MO SCF energies (E_{NR}) for ThPt in hartree (1 hartree = 27.211 eV) at various internuclear distances R in bohr (1 bohr = 0.529177 Å)

R (bohr)	$-E_{NR}$ (hartree)	$R_{min,NR}$(bohr)[a]	k_{NR}[a]	$\bar{\nu}_{NR}$(cm^{-1})[a]
4.50	41 690.665 72	6.8624	0.083 88	76.46
5.50	41 690.681 76			
6.50	41 690.695 57			
7.50	41 690.691 55			

[a]The values of $R_{min,NR}$, the force constant k_{NR}, and $\bar{\nu}_{NR}$ (cm^{-1}), the vibrational frequency, are obtained by fitting the non-relativistic limit MO SCF calculations for ThPt at four points to a cubic polynomial.

Can. J. Chem. Downloaded from www.nrcresearchpress.com by 123.30.183.119 on 09/08/12
For personal use only.

cently performed all-electron calculations for CdH^+, in which all the 24 RMOs were expressed as linear combination of DFAOs of Cd^+ and H; however, such calculations even for this 48-electron system are prohibitively expensive at present, even using supercomputers.[1] Moreover, it was found[1] that the first 23 RMOs consist of pure atomic DFAOs for this species. In the near future, we plan to perform similar calculations for non-hydride diatomics but, until then, we will content ourselves with calculations on ThPt with the core and valence wavefunctions described above, since even such calculations are very expensive for ThPt at our IBM 3081G mainframe computer.

We are aware of the limitations of our calculations; however, even such calculations are nonexistent for the diatomic ThPt, with 168 electrons. A full DF SCF calculation using about 100 DFAOs as valence basis set would require hundreds of CPU hours for RMO SCF calculations even with the CRAY XMP28 supercomputer. We believe that we can obtain fairly reliable understanding of the effects of relativity in bonding of the diatomics involving atoms of actinide and third-row transition elements even using the type of WF's we are reporting here for ThPt.

The seven doubly occupied valence relativistic molecular orbitals or molecular spinors (MS) were constructed as linear combinations of the (numerical) relativistic atomic orbitals or atomic spinors (AS), whereas the core wavefunction for ThPt was taken as the appropriate antisymmetrized products (AP) of the "cores" of the Th and Pt atoms as detailed elsewhere (1–5).

A cubic polynomial fit of the calculated total RMO SCF molecular energies at various internuclear separations was employed to predict R_{min}, total molecular energy energy at R_{min}, force constant k_{Rel}, and vibrational frequency ($\bar{\nu}_{Rel}$) and the results are collected in Table 1.

It should be pointed out, however, that the RMO SCF calculations predict the ThPt diatomic to be unbound only by 0.05075 hartree (1.38 eV) at R_{min}. Therefore, an RCI treatment taking the DF SCF WF with a very extended basis as the reference will be mandatory to obtain the dissociation energy of 109 kcal mol^{-1}, predicted (8) from the empirical valence-bond approach, and the experimental dissociation energy of 130.7 kcal mol^{-1} for ThPt reported by Gingerich (20) from a mass spectrometric study. However, such calculations will entail very enormous computational costs and can only be performed using dedicated state-of-the-art supercomputer technology, and are not feasible at present.

An RMO SCF calculation was also performed at the predicted R_{min} for ThPt and the calculated seven RMO energy eigenvalues are −0.3459, −0.3297, −0.2872, −0.2829, −0.2713, −0.2121, and −0.1817 hartree.

The non-relativistic limit (NRL) MO SCF calculations were performed for ThPt at four internuclear separations of 4.5, 5.5, 6.5, and 7.5 bohr. The NRL wavefunctions for the atoms Th and Pt were also generated using the Oxford MCDF program (12), and the calculations were performed in a similar manner to those of the RMO SCF calculations as discussed above. A cubic polynomial fit of the calculated total molecular energies using the NRL MO SCF wavefunctions for ThPt at various internuclear separations was performed to predict R_{min}, total molecular energy (at R_{min}), force constant (k_{NR}), and vibrational frequency ($\bar{\nu}_{NR}$) and the results are given in Table 2.

It should be pointed out that the NRL MO SCF wavefunction predicts the ThPt molecule to be almost bound at R_{min} (predicted binding energy of 0.000453 hartree, i.e., 0.0123 eV). However, this should not be construed to conclude that the NRL MO SCF WF is better for ThPt than the RMO SCF WF, since the calculated relativistic total molecular energy at the relativistically predicted R_{min} (5.1774 bohr) is *lower* by about 3273 hartree, i.e., 89 062 eV, than the NRL total molecular energy at the NRL predicted R_{min} (6.8624 bohr).

An NRL MO SCF calculation was also performed at the internuclear separation of 6.8624 bohr and the calculated seven orbital eigenvalues are found to be −0.2401, −0.2389, −0.2339, −0.2338, −0.2332, −0.2006, and −0.1534 hartree.

The RMO and the NRL MO SCF wavefunctions (at the respective predicted R_{min}) using Koopman's theorem predict ionization potentials (IP) of 4.944 and 4.174 eV, respectively; however, both predicted values of IP differ significantly from the value reported by Gingerich (20) for the appearance potential of 8 ± 2 eV for ThPt. It should also be mentioned that Gingerich (20) estimated molecular parameters for ThPt by means of standard statistical thermodynamic relations, and his estimates for bond distance and vibrational frequency are 2.54 Å and 221 cm^{-1}, respectively, which are in better agreement with the R_{min} and vibrational frequency ($\bar{\nu}$) predicted with our RMO SCF wavefunctions, viz., 2.7398 Å and 155.4 cm^{-1}, than the values predicted by the NRL MO SCF wavefunctions, viz., 3.6314 Å and 74.46 cm^{-1}, respectively.

To discuss bonding in ThPt, it is instructive to use the four-component functions defined through equations (3.5a)–(3.5d) of Malli and Pyper (1), to express the calculated valence

[1]G. L. Malli, A. J. Stacey, and N. C. Pyper. Unpublished.

Can. J. Chem. Downloaded from www.nrcresearchpress.com by 123.30.183.119 on 09/08/12
For personal use only.

RMOs in terms of the large components of the $|\ell_m m_s\rangle$ functions, where $|s_m m_s\rangle$, $|p_m m_s\rangle$, $|d_m m_s\rangle$ functions have s, p, d-like angular functions with m_ℓ quantum number m and $m_s = \pm 1/2$ (the z-component of the spin angular momentum corresponds to the two-component spin functions $|\alpha\rangle$ and $|\beta\rangle$). Therefore, the valence RMOs (and the NRL MOs) can be expressed in terms of $|p\sigma\alpha\rangle$, $|p\pi\beta\rangle$, $|d\sigma\alpha\rangle$, $|d\pi\beta\rangle$, $|f\sigma\alpha\rangle$, $|f\sigma\beta\rangle$ functions, etc., which can give insight into the bonding characteristics of the valence RMOs and the NRL MOs of the molecular species under study. The valence relativistic HOMO (RHOMO) of ThPt designated as $|7e3/2\rangle$ using the double group theoretical notation for the extra or additional irreducible representations of heteronuclear diatomics (at R = 5.1744 bohr) has the following form:

$$|7e3/2\rangle = -0.971|6d\delta\beta\rangle_{Th} + 0.171|6d\pi\alpha\rangle_{Th} - 0.159|5d\delta\beta\rangle_{Pt} - 0.156|5d\pi\alpha\rangle_{Pt}$$

It consists of almost pure $|6d\delta\beta\rangle$ on the Th atom (plus a small contribution of $|6d\pi\alpha\rangle$ on Th) with very small contributions from the $|5d\delta\beta\rangle$ and $|5d\pi\alpha\rangle$ orbitals on Pt.

The valence RMO $|6e1/2\rangle$, lying just below the RHOMO, however, is found to consist of a bonding combination of a $7s\sigma$–$6d\sigma$ hybrid on Th with a $6s\sigma$–$5d\sigma$ hybrid on Pt, but the dominating contributions are from the bonding arising from the interaction of the $7s$ DFAO on Th with the $6s$ DFAO of Pt:

$$|6e1/2\rangle = 0.661|7s\sigma\alpha\rangle_{Th} - 0.426|6s\sigma\alpha\rangle_{Pt} - 0.271|5d\sigma\rangle_{Pt} - 0.137|6d\sigma\alpha\rangle_{Th}$$

The next five calculated valence RMOs (lying below the $|6e1/2\rangle$ RMO) are of the following form:

$$|5e5/2\rangle = 0.995|5d\delta\alpha\rangle_{Pt}$$

$$|4e3/2\rangle = 0.792|5d\pi\alpha\rangle_{Pt} + 0.498|5d\delta\beta\rangle_{Pt} + 0.220|6d\pi\alpha\rangle_{Th} - 0.131|6d\delta\beta\rangle_{Th}$$

$$|3e1/2\rangle = 0.670|5d\pi\beta\rangle_{Pt} + 0.584|5d\sigma\alpha\rangle_{Pt} - 0.240|6d\sigma\alpha\rangle_{Th} + 0.196|6d\pi\beta\rangle_{Th} - 0.166|7s\sigma\alpha\rangle_{Th}$$

$$|2e3/2\rangle = -0.853|5d\delta\beta\rangle_{Pt} + 0.497|5d\pi\alpha\rangle_{Pt} + 0.0853|6d\pi\alpha\rangle_{Th}$$

$$|1e1/2\rangle = -0.698|5d\sigma\alpha\rangle_{Pt} + 0.653|5d\pi\beta\rangle_{Pt} + 0.164|6d\sigma\alpha\rangle_{Th} + 0.105|6d\pi\beta\rangle_{Th} - 0.0971|7s\sigma\alpha\rangle_{Th}$$

It can be seen that except for the $|5e5/2\rangle$ valence RMO (VRMO), the VRMOs lying below the RHOMO involve bonding mostly due to the interaction of the $5d$ DFAOs of Pt with the $6d$ DFAOs of Th or a hybrid of the $6d$ DFAO with small amounts of the $7s$ DFAO on Th. This is easily understood, since whereas the $7s$ DFAO is *stabilized* (i.e., lowered in energy) due to the *direct* relativistic effect, the $6d$ DFAOs of Th are *destabilized* due to the *indirect* relativistic effect, i.e., pushed up in energy, and thus the $7s$ DFAO of Th is involved in bonding (as can be seen from the VRMO $|6e1/2\rangle$) due to its interaction with the $6s$ DFAO of Pt, which is also lowered in energy due to the direct relativistic effect. The contribution of the $6d$ DFAOs of Th in lower lying VRMOs is fairly small; however, the destabilized $6d$ DFAOs of Th contribute significantly to the RHOMO.

The calculated NRL valence HOMO (at $R_{min,NR}$ = 6.8624 bohr) of ThPt has the following form:

$$7|e1/2\rangle_{NR} = 0.66|7s\sigma\alpha\rangle_{Th} - 0.510|6d\pi\beta\rangle_{Th} - 0.400|6d\sigma\alpha\rangle_{Th} - 0.221|5d\sigma\alpha\rangle_{Pt} - 0.146|6s\sigma\alpha\rangle_{Pt}$$

It consists of a $7s$–$6d$ hybrid on Th in a bonding interaction with a $5d$–$6s$ hybrid containing very small amounts of the $5d$ and $6s$ DFAOs of Pt. This is in contrast to the calculated RHOMO for ThPt, which, as discussed above, contains very substantial contributions from the $6d$ DFAOs of the Th atom, but very small contributions from the $5d$ DFAO of Pt, again due to the indirect relativistic effect on the $6d$ DFAO of Th. However, the next six lower lying valence nonrelativistic limit (NRL) MOs, with the exception of the $6|e3/2\rangle$ NRL MO, are calculated to consist almost of the pure $5d$ NRL AOs of Pt with very small contributions from the $6d$ NRL AOs of Th and almost negligible amounts of the $7s$ NRL AO of Th. The calculated NRL MO, $|6e3/2\rangle_{NR}$, has the following form:

$$|6e3/2\rangle_{NR} = -0.896|6d\delta\beta\rangle_{Th} - 0.394|6d\pi\alpha\rangle_{Th} + 0.208|5d\pi\alpha\rangle_{Pt} - 0.0860|5d\delta\beta\rangle_{Pt}$$

Thus the RHOMO is $|7e3/2\rangle$ and the VRMO lying below it is $|6e1/2\rangle$; however, the NRL calculations predict reversal of the symmetries, since the NR HOMO is $|7e1/2\rangle$ and the NR VMO lying below is $|6e3/2\rangle$.

We conclude, therefore, that the main features of bonding characteristics, the calculated valence RMOs and the NRL MOs of ThPt, can be understood due to the interplay of both the direct and indirect effects of relativity, as discussed here, and that the relativistic effects are very pronounced in bonding, bond length contraction, force constant, and vibrational frequency for ThPt.

Acknowledgements

I sincerely thank Professor Russell J. Boyd and Dr. Mariusz Klobukowski for inviting me to contribute to this issue on the occasion of the 65th birthday of Professor Sigeru Huzinaga, a pioneering theoretical chemist, whom I have known as an esteemed colleague and a very valuable personal friend for over 30 years. This work was supported in part by Grant No. A3598 from the Natural Sciences and Engineering Research Council (NSERC) of Canada, which is gratefully acknowledged. I wish to express my sincerest thanks to Ms. Vanessa Mah who has word-processed the manuscript very diligently and carefully.

1. G. L. Malli and N. C. Pyper. Proc. R. Soc. London, A: **407**, 377 (1986).
2. G. L. Malli. *In* Molecules in physics, chemistry, and biology. Vol. II. *Edited by* Jean Maruani. Kluwer Academic Publishers, Dordrecht. 1988. pp. 85–144.
3. A. F. Ramos, N. C. Pyper, and G. L. Malli. Phys. Rev. A, **38**, 2729 (1988).
4. G. L. Malli. *In* Self-consistent field: theory and applications. *Edited by* R. Carbo and M. Klobukowski. Elsevier, Amsterdam. 1990. pp. 447–530.
5. G. L. Malli. *In* The challenge of *d* and *f* electrons: theory and

computation. *Edited by* D. R. Salahub and M. C. Zerner. ACS Symp. Ser. **394**, 291 (1989).
6. K. G. Dyall, P. R. Taylor, K. Faegri, Jr., and H. Partridge. J. Chem. Phys. **95**, 2583 (1991).
7. (*a*) F. A. Cotton and G. Wilkinson. Advanced inorganic chemistry. 5th ed. John Wiley & Sons, New York, 1988; (*b*) F. A. Cotton and R. A. Walton. Multipole bonds between metal atoms. John Wiley, New York. 1982.
8. K. A. Gingerich. Int. J. Quantum Chem. Symp. **12**, 489 (1978).
9. P. J. Hay, R. R. Ryan, K. V. Salazar, D. A. Wrobleski, and A. P. Sattleberger. J. Am. Chem. Soc. **108**, 313 (1986).
10. (*a*) C. P. Wood and N. C. Pyper. Chem. Phys. Lett. **84**, 614 (1981); (*b*) C. P. Wood. Ph.D. Thesis, Cambridge University, England. 1984.
11. C. P. Wood and N. C. Pyper. Philos. Trans. R. Soc. London, A:**320**, 71 (1986).
12. (*a*) I. P. Grant, B. J. Mckenzie, P. H. Norrington, D. F. Mayers, and N. C. Pyper. Comput. Phys. Commun. **21**, 207 (1980); (*b*) I. P. Grant. Comput. Phys. Commun. **11**, 397 (1976); (*c*) J. P. Desclaux. At. Data Nuclear Data Tables, **12**, 311 (1973); Comput. Phys. Commun. **9**, 31 (1975).
13. I. P. Grant. Adv. Phys. **19**, 747 (1970).
14. I. P. Grant, D. F. Mayers, and N. C. Pyper. J. Phys. B: At. Mol. Phys. **9**, 2777 (1976).
15. J. Oreg and G. Malli. J. Chem. Phys. **61**, 4349 (1974).
16. N. C. Pyper. Philos. Trans. R. Soc. London, A: **304**, 567 (1982).
17. (*a*) Y. Ishikawa. Int. J. Quantum Chem: Quantum Chem. Symp. **18**, 375 (1984); (*b*) R. E. Stanton and S. Havriliak. J. Chem. Phys. **81**, 1910 (1984); (*c*) K. G. Dyall, I. P. Grant, and S. Wilson. J. Phys. B: At. Mol. Phys. **17**, L45 (1984); **17**, 1201 (1984).
18. J. Sucher. Phys. Rev. A, **22**, 348 (1980).
19. R. McWeeny. Methods of molecular quantum mechanics. Academic Press, New York. 1989.
20. K. A. Gingerich. Chem. Phys. Lett. **23**, 270 (1973).

Can. J. Chem. Downloaded from www.nrcresearchpress.com by 123.30.183.119 on 09/08/12
For personal use only.

Atomic orbital-wise characterization of the vibronic attractive interaction in a model of an oxygen-containing organic polymer

AKITOMO TACHIBANA[1]

Department of Hydrocarbon Chemistry, Faculty of Engineering and Division of Molecular Engineering, Graduate School of Engineering, Kyoto University, Kyoto 606, Japan

SHIGERU ISHIKAWA AND WATARU SAHARA

Division of Molecular Engineering, Graduate School of Engineering, Kyoto University, Kyoto 606, Japan

AND

TOKIO YAMABE[2]

Department of Hydrocarbon Chemistry, Faculty of Engineering and Division of Molecular Engineering, Graduate School of Engineering, Kyoto University, Kyoto 606, Japan

Received June 27, 1991

This paper is dedicated to Professor Sigeru Huzinaga on the occasion of his 65th birthday

AKITOMO TACHIBANA, SHIGERU ISHIKAWA, WATARU SAHARA, and TOKIO YAMABE. Can. J. Chem. **70**, 427 (1992).

The extended local vibronic constant (ELVC) is introduced for the study of the strength of local electron pairing for superconductivity based on vibronic interaction using a model of an oxygen-containing organic polymer. The ELVC consists of the electrostatic part and the two-electron part, which originates in the response of the electron density to the nuclear vibration. It is found that the two-electron part has opposite sign to, and almost the same magnitude as, that of the electrostatic part. The difference between the ELVC and the Fock matrix derivative, which is related to the derivative of the Hückel parameters used as the electron–phonon coupling constant, is discussed. The vibronic interaction in the in-plane orbitals, which is characteristic of the interaction in a two-dimensional conductor, is also discussed.

Key words: vibronic interaction, superconductivity, local electron pairing, extended local vibronic constant, *ab initio* calculation.

AKITOMO TACHIBANA, SHIGERU ISHIKAWA, WATARU SAHARA et TOKIO YAMABE. Can. J. Chem. **70**, 427 (1992).

Utilisant comme modèle un polymère organique contenant de l'oxygène, on fait appel à la constante vibronique locale étendue (CVLE) pour étudier la force du couplage électronique local dans la supraconductivité causée par l'interaction vibronique. La CVLE est formée de la partie électrostatique et de la partie à deux électrons qui trouve son origine dans la réponse à la densité électronique par rapport à la vibration nucléaire. On a trouvé que la partie à deux électrons est d'une amplitude égale, mais de signe opposé, à la partie électrostatique. On discute de la différence entre la CVLE et la dérivée de la matrice de Fock qui est reliée à la dérivée des paramètres de Hückel utilisés comme constante de couplage électron–phonon. On discute aussi de l'interaction vibronique dans les orbitales dans le plan qui est caractéristique de l'interaction dans un conducteur bidimensionnel.

Mots clés : interaction vibronique, supraconductivité, couplage électronique local, constante vibronique locale étendue, calculs *ab initio*.

[Traduit par la rédaction]

Introduction

The discovery of high-T_c copper-oxide superconductors (1) has renewed interest in the search for the origin of the attractive interaction between a Cooper pair of superconducting electrons. In this connection, various mechanisms of superconductivity, such as bipolaron (2, 3), exciton (4), plasmon (5), spin-polaron (6), and resonating valence bond (RVB) (7), have been proposed in addition to the conventional electron–phonon coupling mechanism (8–10). We have proposed a vibronic electron pairing mechanism (11), which is based on a specific vibronic interaction in molecules.

Vibronic interaction in molecules has been one of the primary subjects in molecular spectroscopy. Various theories for determining the vibronic coupling constants have been proposed (12–14). However, these theories are not specific to the attractive interaction for superconductivity.

Our vibronic attractive interaction originates from nonadiabatic coupling, and is obtained in closed form using normal coordinates Q_n of molecular vibration as parameters, in contrast with the use of the diabatic perturbation series for the attractive interaction in the conventional electron–phonon coupling mechanism (8–10). The vibronic attractive interaction is instantaneous with respect to the electronic interaction because it is caused by nuclear vibrational momentum $-i\partial/\partial Q_n$ acting on the electronic wavefunction, while the conventional electron–phonon coupling is delayed because it is caused by small but finite displacement of Q_n. The vibronic attractive interaction is negative definite, while conventional electron–phonon coupling contains repulsive interaction. Calculation of the attractive interaction of arbitrary chemical species can be done using *ab initio* molecular orbital methods, which enables us to design novel vibronic processes for superconductivity. Orbital and vibrational mode-specific characterization of the vibronic attractive interaction can be done using the extended orbital vibronic constant (EOVC) (15), which is related to the orbital vibronic constant (OVC) in Bersuker's study of the Jahn–Teller effect (14).

The EOVC is a measure of the vibronic interaction for the electronic stationary state. We may now ask the following

[1]Author to whom correspondence may be addressed.

[2]Also associated with the Institute for Fundamental Chemistry, 34-4 Nishihiraki-cho, Takano, Sakyo-ku, Kyoto 606, Japan.

Printed in Canada

Can. J. Chem. Downloaded from www.nrcresearchpress.com by 92.62.229.171 on 09/08/12
For personal use only.

Can. J. Chem. Downloaded from www.nrcresearchpress.com by 92.62.229.171 on 09/08/12
For personal use only.

question: how does the molecular vibration give rise to the local polarization of the electrostatic field and of the electron density? This will be represented by the extended local vibronic constant (ELVC) defined by eq. [3] in this paper. The ELVC gives a measure of the favorable atomic site and the interaction range for vibronic electron pairing.

We have calculated the vibronic interaction for superconductivity in heteroatom-substituted polyacetylene such as $(CHO)_n$, and found that the polar bond between oxygen and carbon is interesting for local electron pairing (16–19). Hence we shall examine in this paper the ELVC of $(CHO)_n$ using a structural model molecule $(CH_2)_2O$. The difference between the ELVC and the Fock matrix derivative, which is often used as the electron–phonon coupling constant, will be discussed. Another interesting aspect of this molecule is the vibronic interaction for the in-plane orbitals, which is characteristic of the interaction in a two-dimensional conductor. We have found that large vibronic attractive interaction is obtained in the in-plane orbitals centered at the oxygen atom (17). Hence, we shall examine the ELVC for the in-plane atomic orbitals.

Theory

The vibronic interaction for superconductivity

The effective interaction energy V^{ij}_{eff} of a Cooper pair or a time-reversal pair of electrons associated with the vibronic scattering process in between the ith molecular orbital ψ_i and the jth one ψ_j is given as (11, 15–19)

$$[1a] \quad V^{ij}_{\text{eff}} = V^{ij}_{\text{Coul}} - \Delta_{ij}$$

$$[1b] \quad V^{ij}_{\text{Coul}} = \langle\psi_j(1)\psi_j(2)|1/r_{12}|\psi_i(1)\psi_i(2)\rangle$$

$$[1c] \quad \Delta_{ij} = \sum_n |\langle\psi_i|\partial\psi_j/\partial Q_n\rangle|^2$$

where V^{ij}_{Coul}, Δ_{ij}, and Q_n denote the Coulombic repulsion energy, the vibronic attraction energy, and the nth normal vibrational coordinate, respectively. Δ_{ij} represents the nonadiabatic coupling between a pair of different electronic states ψ_i and ψ_j. V^{ij}_{Coul} is positive and is normally larger than Δ_{ij}. Δ_{ij} is positive definite and reduces the magnitude of V^{ij}_{Coul}, acting as the *attractive force*. The alternative form of Δ_{ij} is written as

$$[2a] \quad \Delta_{ij} = \sum_n |f^{ij}_n|^2/(\varepsilon_i - \varepsilon_j)^2$$

$$[2b] \quad f^{ij}_n = \langle\psi_i|\partial f/\partial Q_n|\psi_j\rangle$$

where f^{ij}_n, ε_i, and f denote the extended orbital vibronic constant (EOVC), the ith orbital energy, and the dynamic Fock operator that determines $\{\psi_i\}$ and $\{\varepsilon_i\}$ incorporating the vibronic interaction. The EOVC characterizes the selection rule and the strength of the vibronic interaction (15). If the EOVC is nonzero, a small orbital energy difference brings about a large vibronic attraction energy.

As the size of the system becomes large, V^{ij}_{Coul} decreases to zero in proportion to the volume of the system, whereas Δ_{ij} grows to infinity for a one-dimensional system, converges to a finite value for a two-dimensional system, and decreases to zero for a three-dimensional system if only the longitudinal vibrational modes are used for simple Hückel molecular orbitals (19). Even for a three-dimensional system, Δ_{ij} decreases much more slowly than does V^{ij}_{Coul} (19). This shows that a net attractive interaction responsible for superconductivity emerges if the system becomes large enough.

Definition of the ELVC

To elucidate the attractive interaction for local electron pairing, atomic orbital-wise characterization of the EOVC is required. Adopting the linear combination of the atomic orbital (LCAO) approximation for ψ_i, we get the expression for the EOVC in the atomic orbital basis $\{\chi_r\}$

$$[3a] \quad f^{rs}_n = \langle\chi_r|\partial f/\partial Q_n|\chi_s\rangle$$

Moreover, since Q_n is given by a linear combination of atomic cartesian coordinates, we have more basic representation of the EOVC as follows:

$$[3b] \quad f^{rs}_{\xi_a} = \langle\chi_r|\partial f/\partial\xi_a|\chi_s\rangle$$

where ξ_a denotes the Cartesian coordinates x_a, y_a, or z_a of atom a. We call f^{rs}_n and $f^{rs}_{\xi_a}$ the extended local vibronic constant (ELVC) with respect to Q_n and ξ_a, respectively. Differentiating f with respect to ξ_a, we get

$$[4] \quad \partial f/\partial\xi_a = \partial V_{eN}/\partial\xi_a + \partial G/\partial\xi_a + \partial\hat{\Delta}/\partial\xi_a$$

where V_{eN}, G, and $\hat{\Delta}$ denote the nuclear attraction potential, the two-electron operator, which consists of the Coulombic repulsion and the exchange interaction operators, and the vibronic interaction operator, respectively. The first and second terms in eq. [4], respectively, represent the instantaneous polarization of the electrostatic field and of the electron density brought about by the nuclear momentum. In Hartree–Fock theory, we may write $\partial G/\partial\xi_a$ in the functional form

$$[5] \quad \partial G(\rho)/\partial\xi_a = \int\delta G(\rho)/\delta\rho(r)\cdot\partial\rho(r)/\partial\xi_a\cdot d^3r$$

where r and ρ denote the electron coordinate and the electron density, respectively. The third term in eq. [4] is neglected in this paper, because the $\hat{\Delta}$ itself is negligible for small molecules like the one treated here.

The ELVC is different from the Fock matrix derivative simply because the ELVC does not have the atomic orbital derivative. The Fock matrix derivative is related to the derivative of the atomic α and resonance β integrals in the Hückel treatment, which are often used to study the electron–phonon coupling in the frame of a tight-binding approximation such as the Su–Schrieffer–Heeger (SSH) model (20).

Method of calculation

Ab initio calculations were performed with a 3-21G basis set by the GAUSSIAN80 and GAUSSIAN82 programs (21), incorporating new subroutines to calculate the vibronic interaction. Because we neglected the vibronic coupling term in eq. [4], the adiabatic Fock operator was used for the dynamic Fock operator. The EOVC was obtained using the relation

$$[6] \quad \langle\psi_i|\partial f/\partial Q_n|\psi_j\rangle = (\varepsilon_i - \varepsilon_j)\langle\partial\psi_i/\partial Q_n|\psi_j\rangle + \partial\varepsilon_j/\partial Q_n\delta_{ij}$$

The ELVC was calculated by transforming the EOVC from the molecular orbital basis to the atomic orbital basis:

$$[7] \quad \langle\psi_i|\partial f/\partial Q_n|\psi_j\rangle \rightarrow \langle\chi_r|\partial f/\partial Q_n|\chi_s\rangle$$

Results and discussion

The out-of-plane ELVC

A possible structure of the model polymer is shown in Fig. 1(*a*). The polymer is formally metallic; however, it may be

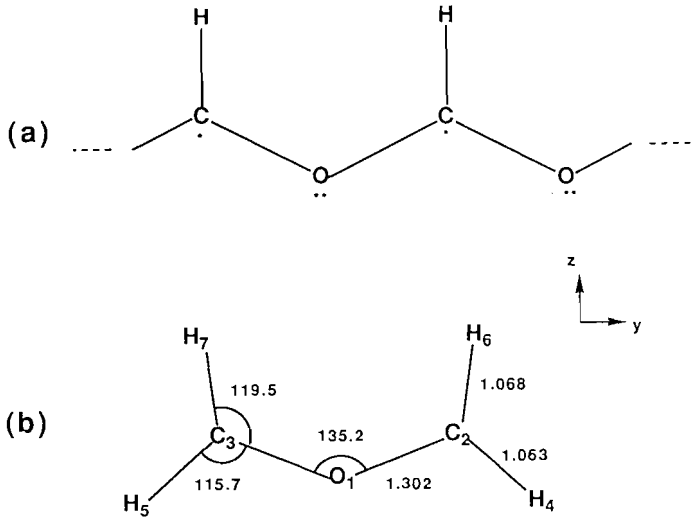

FIG. 1. (*a*) A possible structure of the oxygen-containing model organic polymer $(CHO)_n$. (*b*) Optimized C_{2v} geometry of the structural unit molecule $(CH_2)_2O$. The molecule is lying in the y–z plane. Units of bond lengths and angles are Å and degrees, respectively. The Cartesian coordinate of atom α is denoted as $(x_\alpha, y_\alpha, z_\alpha)$.

TABLE 1. The Fock matrix for the out-of-plane p orbitals of $(CH_2)_2O$. Only outer orbitals are shown. Units are au

		O_1 p_x(o)	C_2 p_x(o)	C_3 p_x(o)
O_1	p_x(o)	−0.1394		
C_2	p_x(o)	−0.2172	−0.0695	
C_3	p_x(o)	−0.2172	−0.0434	−0.0695

unstable with respect to generation of the spin density wave (SDW) or the charge density wave (CDW), which are characteristic of low-dimensional conductors. To suppress the generation of the insulating phase, two- or three-dimensional contact between polymer chains and doping of conducting carriers should be necessary as in the case of known organic superconductors. In Fig. 1(*b*), the optimized geometry of the structural unit molecule $(CH_2)_2O$ is shown. The molecule has C_{2v} symmetry, and is lying in the y–z plane. The diradical character of this molecule has been reported (22).

In Table 1, the Fock matrix elements for the out-of-plane p orbitals are shown. Since we are interested in the attractive interaction for the Cooper pair, we consider only outer atomic orbitals of the split-valence basis set because the outer atomic orbitals are thought to play a major role in electron conduction. The diagonal elements correspond to the Hückel α parameters and the nearest-neighbor elements to the Hückel β parameters. In Table 2, the Fock matrix derivatives with respect to the in-plane vibration of the oxygen and carbon atoms are shown. The nearest-neighbor vibrations, such as $\xi_a = y_1$ for the O_1—$C_{2,3}$ elements and $\xi_a = y_2$ and z_2 for the O_1—C_2 element, have large values. The sign is positive (negative) if the bond length increases (decreases). As distinct from the derivative of the Hückel parameters, the Fock

TABLE 2. The Fock matrix derivative for the out-of-plane p orbitals of $(CH_2)_2O$ with respect to the in-plane motions of oxygen and carbon atoms. Units are au. The Cartesian coordinates of atom a are denoted as (x_a, y_a, z_a)

			O_2 p_x(o)	C_2 p_x(o)	C_3 p_x(o)
$\xi_a = y_1$	O_1	p_x(o)	0.0		
	C_2	p_x(o)	−0.1410	−0.0529	
	C_3	p_x(o)	0.1410	0.0	0.0529
$\xi_a = z_1$	O_1	p_x(o)	−0.1023		
	C_2	p_x(o)	−0.0392	−0.0256	
	C_3	p_x(o)	−0.0392	−0.0236	−0.0256
$\xi_a = y_2$	O_1	p_x(o)	0.1493		
	C_2	p_x(o)	0.1348	0.0529	
	C_3	p_x(o)	−0.0067	0.0481	0.0081
$\xi_a = z_2$	O_1	p_x(o)	0.0563		
	C_2	p_x(o)	0.0487	0.0224	
	C_3	p_x(o)	−0.0098	0.0107	0.0005

matrix derivative originates not only from the nearest-neighbor vibration, but also the non-nearest-neighbor one. Moreover, the diagonal Fock matrix element derivative exists, which is conventionally set equal to zero in the Hückel framework. A large diagonal element is found in the O_1 site for $\xi_a = z_1$, y_2, and z_2. The diagonal elements of O_1 for $\xi_a = y_2$ and z_2 are larger than the O_1—C_2 element. The nearest-neighbor elements with respect to remote atom vibration, such as the O_1—C_3 elements for $\xi_a = y_2$ and z_2, are found to be small. The non-nearest-neighbor elements, such as the C_2—C_3 element for $\xi_a = z_1$, y_2, and z_2, are not negligible.

Various modes of the Fock matrix element derivatives appear according to the motion of the nuclei. The magnitude of the Fock matrix element derivative does not necessarily reflect that of the corresponding Fock matrix element shown in Table 1.

In Table 3, the ELVC's for the out-of-plane p orbitals are shown (bold-face type) with separation into the electrostatic contribution (upper parentheses) and the two-electron contribution (lower parentheses). The ELVC can be classified into three types: the on-site type, the nearest-neighbor type, and the non-nearest-neighbor or long-range type. This is the same as the Fock matrix element derivative. Indeed, *the ELVC originating from remote atom vibration coincides with the corresponding Fock matrix element derivative.* On the other hand, *the ELVC originating from the local atom vibration shows different sign and magnitude from the Fock matrix element derivative.* This is simply because the Fock matrix element derivative includes the derivative of the atomic orbital that is attached to the local atom vibration. For instance, the diagonal element of O_1 for $\xi_a = z_1$ is positive although the corresponding Fock matrix element is negative. As the interaction energy for the Cooper pair is related to the product of the ELVC, the sign and magnitiude of the ELVC are important in determining favourable site and interaction range for the electron pairing.

As shown in Table 3, *the two-electron contribution has opposite sign to, and almost the same magnitude as, that of the electrostatic contribution.* Therefore, *the two-electron contribution cancels the electrostatic contribution and makes the ELVC small.*

Can. J. Chem. Downloaded from www.nrcresearchpress.com by 92.62.229.171 on 09/08/12
For personal use only.

TABLE 3. The ELVC for the out-of-plane p orbitals of $(CH_2)_2O$. Units are au. The electrostatic and two-electron contributions are shown in the upper and lower parentheses, respectively

			O_1 p_x(o)	C_2 p_x(o)	C_3 p_x(o)
$\xi_a = y_1$	O_1	p_x(o)	**0.0**		
			(0.0)		
			(0.0)		
	C_2	p_x(o)	**−0.1040**	**−0.0529**	
			(−0.2759)	(−0.5612)	
			(0.1719)	(0.5083)	
	C_3	p_x(o)	**0.1040**	**0.0**	**0.0529**
			(0.2759)	(0.0)	(0.5612)
			(−0.1719)	(0.0)	(−0.5083)
$\xi_a = z_1$	O_1	p_x(o)	**0.0513**		
			(0.0)		
			(0.0513)		
	C_2	p_x(o)	**−0.0253**	**−0.0256**	
			(−0.1136)	(−0.2311)	
			(0.0884)	(0.2055)	
	C_3	p_x(o)	**−0.0253**	**−0.0236**	**−0.0256**
			(−0.1136)	(−0.0630)	(−0.2311)
			(0.0884)	(0.0395)	(0.2055)
$\xi_a = y_2$	O_1	p_x(o)	**0.1493**		
			(0.6190)		
			(−0.4697)		
	C_2	p_x(o)	**0.1714**	**−0.0397**	
			(0.2626)	(0.0)	
			(−0.0912)	(−0.0397)	
	C_3	p_x(o)	**−0.0066**	**0.0192**	**0.0081**
			(0.1788)	(0.0619)	(0.2363)
			(−0.1854)	(−0.0427)	(−0.2281)
$\xi_a = z_2$	O_1	p_x(o)	**0.0563**		
			(0.2549)		
			(−0.1986)		
	C_2	p_x(o)	**0.0775**	**−0.0152**	
			(0.1081)	(0.0)	
			(−0.0306)	(−0.0152)	
	C_3	p_x(o)	**−0.0098**	**−0.0081**	**0.0005**
			(0.0359)	(0.0)	(0.0)
			(−0.0457)	(−0.0081)	(0.0005)

For $\xi_a = y_1$, the diagonal element of O_1 and the non-nearest-neighbor elements of C_2—C_3 vanish because of the symmetry. The nearest-neighbor elements of O_1—$C_{2,3}$ are the largest in magnitude. The electrostatic contribution to the O_1—C_2 element is negative, −0.2759, because the bond length between O_1 and C_2 decreases as O_1 moves in the $+y_1$ direction. On the contrary, the two-electron contribution is positive, 0.1719, so that it cancels the electrostatic contribution. The magnitude of the electrostatic contribution is 1.6 times that of the two-electron contribution. The magnitude of the diagonal element of C_2 is smaller than that of the O_1—C_2 element although the magnitude of the electrostatic and two-electron contributions to it are larger than those of the O_1—C_2 element. Since the magnitude of the electrostatic contribution is 1.1 times that of the two-electron contribution, they cancel each other and make the ELVC small.

For $\xi_a = z_1$, the diagonal element of O_1 is the largest in magnitude. This element may bring about the on-site pairing of electrons on the oxygen site. As the electrostatic contribution vanishes because of the symmetry, only the two-electron contribution remains. This element is positive although the corresponding element of the Fock matrix derivative is negative. The magnitude of the non-nearest-neighbor element for C_2—C_3 is comparable to the other elements.

For $\xi_a = y_2$, the O_1—C_2 element is the largest in magnitude. The magnitude of the electrostatic contribution to it is 2.9 times that of the two-electron contribution. The diagonal element of O_1 is smaller than the O_1—C_2 element due to the cancellation between electrostatic and two-electron contributions, although their magnitude is large. On the contrary, for the Fock matrix element derivative, the O_1 element is larger than the O_1—C_2 element. The non-nearest-neighbor C_2—C_3 element is comparable to the on-site C_2 element.

For $\xi_a = z_2$, the O_1—C_2 element is the largest in magnitude. The magnitude of the electrostatic contribution to it is 3.5 times that of the two-electron contribution. The diagonal element of O_1 is smaller than the O_1—C_2 element due to the cancellation between two contributions.

The ELVC's originating from the vibration of hydrogen atoms are smaller than those for heavy atoms. However, if we substitute a polarizable side chain for a hydrogen atom, a large ELVC is brought about by the vibration of the side chain. The vibronic interaction produced by a polarizable side chain is interesting in connection with Little's model of an organic superconductor (23).

The out-of-plane ELVC with respect to the normal vibrational coordinate

We have shown that the ELVC with respect to the Cartesian coordinate can be characterized by three types: the on-site type, the nearest-neighbor type, and the non-nearest-neighbor type. We shall examine now the ELVC with respect to the normal vibrational coordinate. The normal coordinates adopted in this paper are depicted in Fig. 2. In Table 4, the ELVC with respect to these normal coordinates are shown.

For $n = 1$, the magnitude of the diagonal element of O_1 is the largest. The magnitude of the nearest-neighbor elements and the diagonal element of C_2 are about 0.3 times that of the O_1 element. Hence this mode, $n = 1$, is characterized by the on-site type of the ELVC.

For $n = 9$, the elements largest in magnitude are the nearest-neighbor elements of O_1—$C_{2,3}$. The diagonal element of C_2 is smaller by about one order of magnitude than the nearest-neighbor element. Hence this mode, $n = 9$, is characterized by the nearest-neighbor type of the ELVC.

For $n = 9$, the diagonal element of O_1 and the non-nearest-neighbor element of C_2—C_3 vanish because of the symmetry. In an actual organic polymer, these elements do not necessarily vanish because the dispersion of the lattice vibration gives different motions to C_2 and C_3.

For comparison, we also calculated the Fock matrix derivatives. The Fock matrix derivative with respect to the normal coordinate $n = 1$ was not the on-site type, while the other was the nearest-neighbor type.

The in-plane ELVC

The vibronic interactions among the in-plane orbitals are thought to be characteristic of two-dimensional conductors. In our previous study, a large vibronic attractive interaction is found in the in-plane orbitals in $(CH_2)_2O$ with respect to the transverse vibration of the spine (17). In this connection, we calculated the ELVC for the in-plane atomic orbit-

Can. J. Chem. Downloaded from www.nrcresearchpress.com by 92.62.229.171 on 09/08/12
For personal use only.

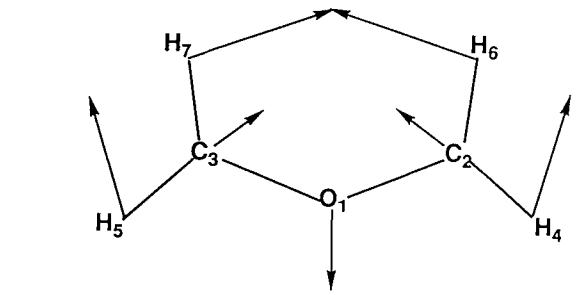

n=1 419 cm^{-1}

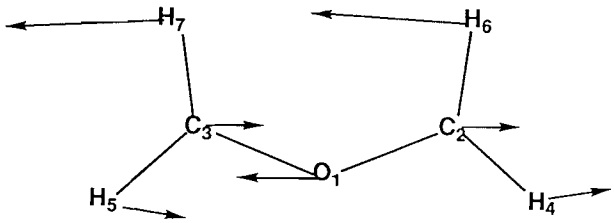

n=9 1383 cm^{-1}

FIG. 2. Normal vibrational coordinates of $n = 1$ and 9.

TABLE 4. The ELVC for the out-of-plane p orbitals of $(CH_2)_2O$ with respect to normal vibrational coordinates. Units are 10^{-4} au

			O_1 p_x(o)	C_2 p_x(o)	C_3 p_x(o)
$n = 1$	O_1	p_x(o)	−5.1107		
	C_2	p_x(o)	−1.1694	1.1264	
	C_3	p_x(o)	−1.1694	−0.3073	1.1264
$n = 9$	O_1	p_x(o)	0.0		
	C_2	p_x(o)	8.9995	0.4948	
	C_3	p_x(o)	−8.9995	0.0	−0.4948

TABLE 5. The ELVC for the in-plane orbitals of the C_{2v} form of $(CH_2)_2O$. Units are au

		O_1		
$\xi_a = z_1$		s(o)	p_y(o)	p_z(o)
O_1	s(o)	**0.0732**		
		(0.0)		
		(0.0732)		
	p_y(o)	**0.0**	**0.1936**	
		(0.0)	(0.0)	
		(0.0)	(0.1936)	
	p_z(o)	−1.9175	**0.0**	**0.1801**
		(−3.1803)	(0.0)	(0.0)
		(1.2629)	(0.0)	(0.1801)
C_2	s(o)	**−0.1138**	**−0.0046**	**−0.4970**
		(−0.2792)	(−0.1144)	(−0.9722)
		(0.1654)	(0.1098)	(0.4802)
	p_y(o)	**0.2186**	**−0.0064**	**0.9263**
		(0.4793)	(0.0697)	(1.6724)
		(−0.2607)	(−0.0761)	(−0.7461)
	p_z(o)	**−0.2518**	**−0.0944**	**0.3245**
		(−0.4760)	(−0.2004)	(0.4615)
		(0.2242)	(0.1060)	(−0.1369)
		C_2		
		s(o)	p_y(o)	p_z(o)
C_2	s(o)	**−0.0765**		
		(−0.4068)		
		(0.3303)		
	p_y(o)	**0.1418**	**−0.2448**	
		(0.3538)	(−0.6511)	
		(−0.2120)	(0.4063)	
	p_z(o)	**−0.0588**	**0.0968**	**0.1050**
		(−0.3449)	(0.2537)	(0.0491)
		(0.2861)	(−0.1570)	(0.0559)
C_3	s(o)	**−0.0611**	**0.1225**	**−0.0380**
		(−0.1487)	(0.2995)	(−0.1083)
		(0.0876)	(−0.1770)	(0.7027)
	p_y(o)	**−0.1225**	**0.2376**	**−0.0768**
		(−0.2995)	(0.5399)	(−0.2181)
		(0.1770)	(−0.3023)	(0.1413)
	p_z(o)	**−0.0380**	**0.0768**	**0.0647**
		(−0.1083)	(0.2181)	(0.0672)
		(0.0703)	(−0.1413)	(−0.0025)

als as shown in Table 5. In some elements, the magnitude of the electrostatic and two-electron contributions is larger than that for the out-of-plane atomic orbitals. However, as is similar to the ELVC for the out-of-plane p orbitals, the two-electron contribution is of opposite sign to the electrostatic contribution, and they cancel each other.

As O_1 moves in the z direction, the change of hybridization between s and p_z orbitals of O_1 gives a large on-site ELVC between them. The magnitude of this ELVC is larger by about one order of magnitude than that ELVC for the out-of-plane atomic orbitals. The sign of the electrostatic contribution is opposite that of the two-electron contribution. The magnitude of the electrostatic contribution is 2.5 times that of the two-electron contribution.

A large element is also found in between the p_z orbital of O_1 and the p_y orbital of C_2. This coupling is interesting from the point of view of two-dimensional coupling (17, 18). The sign of the electrostatic contribution is opposite to that of the two-electron contribution. The magnitude of the electrostatic contribution is 2.2 times that of the two-electron contribution.

There is no extremely large value for the on-site elements in C_2 and for the non-nearest-neighbor elements in C_2—C_3.

To see the two-dimensional character of the vibronic interaction in the in-plane atomic orbitals, we calculated the ELVC for the D_{2h} form of $(CH_2)_2O$. The optimized structure of the D_{2h} form is shown in Fig. 3, where the molecular axis is set to the y axis. The ELVC for the D_{2h} form is shown in Table 6. As O_1 moves in the z direction, a large element also appears in between the s and p_z orbital of O_1 due to the instantaneous hybridization between them. The sign of the electrostatic contribution is opposite that of the two-electron contribution. The magnitude of the electrostatic contribution is 2.5 times that of the two-electron contribution.

Can. J. Chem. Downloaded from www.nrcresearchpress.com by 92.62.229.171 on 09/08/12
For personal use only.

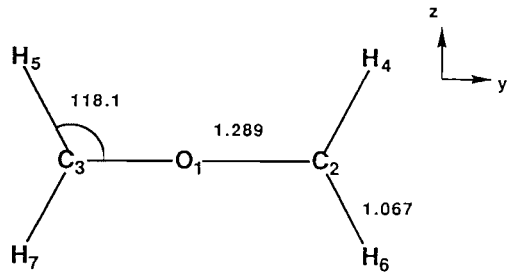

FIG. 3. Optimized D_{2h} structure of $(CH_2)_2O$. Units of bond lengths and angles are Å and degrees, respectively.

TABLE 6. The ELVC for the in-plane orbitals of the D_{2h} form of $(CH_2)_2O$. Units are au

		O_1		
$\xi_a = z_1$		$s(o)$	$p_y(o)$	$p_z(o)$
O_1	$s(o)$	**0.0**		
		(0.0)		
		(0.0)		
	$p_y(o)$	**0.0**	**0.0**	
		(0.0)	(0.0)	
		(0.0)	(0.0)	
	$p_z(o)$	**−1.9088**	**0.0**	**0.0**
		(−3.1803)	(0.0)	(0.0)
		(1.2716)	(0.0)	(0.0)
C_2	$s(o)$	**0.0**	**0.0**	**−0.4950**
		(0.0)	(0.0)	(−0.9494)
		(0.0)	(0.0)	(0.4545)
	$p_y(o)$	**0.0**	**0.0**	**1.0042**
		(0.0)	(0.0)	(1.7453)
		(0.0)	(0.0)	(−0.7411)
	$p_z(o)$	**−0.3473**	**−0.0929**	**0.0**
		(−0.6873)	(−0.3011)	(0.0)
		(0.3401)	(0.2081)	(0.0)
		C_2		
		$s(o)$	$p_y(o)$	$p_z(o)$
C_2	$s(o)$	**0.0**		
		(0.0)		
		(0.0)		
	$p_y(o)$	**0.0**	**0.0**	
		(0.0)	(0.0)	
		(0.0)	(0.0)	
	$p_z(o)$	**−0.1131**	**0.2083**	**0.0**
		(−0.5010)	(0.4699)	(0.0)
		(0.3878)	(−0.2616)	(0.0)
C_3	$s(o)$	**0.0**	**0.0**	**−0.0786**
		(0.0)	(0.0)	(−0.1634)
		(0.0)	(0.0)	(0.0848)
	$p_y(o)$	**0.0**	**0.0**	**−0.1706**
		(0.0)	(0.0)	(−0.3521)
		(0.0)	(0.0)	(0.1815)
	$p_z(o)$	**−0.0786**	**0.1706**	**0.0**
		(−0.1634)	(0.3521)	(0.0)
		(0.0848)	(−0.1815)	(0.0)

The ELVC between the p_z orbital of O_1 and the p_y orbital of C_2 is also large. This coupling has two-dimensional character since these orbitals have no overlaps between them. The sign of the electrostatic contribution is opposite to that of the two-electron contribution. The magnitude of the electrostatic contribution is 2.3 times that of the two-electron contribution. This large ELVC represents the instantaneous electronic polarization due to the sudden overlap of the nonoverlapping atomic orbitals.

We also calculated the Fock matrix element derivatives for the in-plane atomic orbitals. It is found that the Fock matrix element derivatives between the s and p_z orbitals of O_1, and between the p_z orbital of O_1 and the p_y orbital of C_2 are not the largest for both C_{2v} and D_{2h} forms. For the D_{2h} form, the values of the Fock matrix element derivatives between the s and p_z orbitals of O_1, and between the p_z orbital of O_1 and the p_y orbital of C_2, are 0.2290 and −0.1926, respectively. These values are smaller in magnitude than those of the corresponding ELVC's.

Conclusion

We have applied the ELVC using a model molecule to evaluate the strength of the vibronic attractive interaction for the local electron pairing of superconducting electrons. The ELVC is brought about by the Fock operator derivative, which represents the instantaneous electronic polarization due to the presence of the nuclear momentum as well as the polarization of the electrostatic field. However, the Fock matrix derivative cannot represent the instantaneous electronic polarization correctly because it is concomitant with the atomic orbital derivative, which represents the motion of the atomic orbital following local nuclear motion. The ELVC consists of electrostatic and two-electron contributions. The two-electron contribution originates in the response of the electron density to the nuclear vibration. This has an opposite sign to that of the electrostatic contribution and often cancels the electrostatic contribution. The vibronic interaction can be characterized by three types of the ELVC: the on-site type, the nearest-neighbor type, and the long-range type. This sheds new light on the electron–phonon coupling constant of the tight-binding approximation, where the on-site and the long-range interactions are neglected and only the nearest-neighbor interaction remains. Indeed, we have found that a large ELVC out-of-plane element with respect to a certain normal coordinate appears locally on the oxygen site. The long-range type may play an important role if the nuclear vibrational mode has a large dispersion as the system becomes large.

The ELVC's with respect to the vibration of the hydrogen atoms are found to be small. However, if we substitute a polarizable side chain for a hydrogen atom, a large ELVC is expected with respect to the vibration of the side chain.

A large in-plane ELVC appears locally on the oxygen site because of the change of hybridization between s and p_z orbitals as O_1 moves transversally. A large ELVC also appears in between the p_z orbital of O_1 and the p_y of C_2, which represents the two-dimensional vibronic coupling. The magnitude of these in-plane ELVC's is larger than that of the largest out-of-plane ELVC.

The vibronic interactions that we calculated may be too small to create a Cooper pair in the model molecule; however, if the system becomes large enough, a large vibronic attraction would be expected, because the energy gap between a pair of the electronic states becomes small and then the vibronic attraction becomes large. To generate a superconducting phase in the $(CHO)_n$ polymer, the instability characteristic of low-dimensional conductors such as SDW or CDW should be suppressed. This would be done by two- or three-dimensional contact between polymer chains,

Can. J. Chem. Downloaded from www.nrcresearchpress.com by 92.62.229.171 on 09/08/12
For personal use only.

which would also serve to generate long-range order in the superconducting phase. Vibronic coupling between in-plane orbitals is considered to be important in designing two-dimensional superconductors.

Acknowledgment

This work was supported by a Grant-in-Aid for Scientific Research from the Ministry of Education, Science and Culture of Japan. We are grateful to the Data Processing Center of Kyoto University and the Computer Center of the Institute for Molecular Science, for their generous permission to use FACOM M780, VP2600 and HITAC M680-H, S-820 computers, respectively.

1. W. E. Pickett. Rev. Mod. Phys. **61**, 433 (1989).
2. R. Micnas, J. Ranninger, and S. Robaszkiewicz. Rev. Mod. Phys. **62**, 113 (1990).
3. A. S. Alexandrov and D. K. Ray. Philos. Mag. Lett. **63**, 295 (1991).
4. C. M. Varma, S. Schmitt-Rink, and E. Abrahams. Solid State Commun. **62**, 681 (1987).
5. T. M. Rice. Z. Phys. B: Condens. Matter, **67**, 141 (1987).
6. H. Kamimura. Jpn. J. Appl. Phys. **26**, L627 (1987).
7. P. W. Anderson. Science, **235**, 1196 (1987).
8. J. Bardeen, L. N. Cooper, and J. R. Schrieffer. Phys. Rev. **108**, 1175 (1957).
9. J. R. Schrieffer. Theory of superconductivity. Benjamin–Cummings, Reading, Mass. 1964.
10. D. Adler. *In* Handbook on semiconductors. Vol. 1. *Edited by* W. Paul. North-Holland, Amsterdam. 1980. p. 806.
11. A. Tachibana. Phys. Rev. A, **35**, 18 (1987); Synth. Met. **19**, 105 (1987).
12. L. S. Cederbaum, W. Domcke, J. Schirmer, and H. Köppel. J. Chem. Phys. **72**, 1348 (1980).
13. N. O. Lipari, C. B. Duke, and L. Pietronero. J. Chem. Phys. **65**, 1348 (1976).
14. I. B. Bersuker. The Jahn–Teller effect and vibronic interactions in modern chemistry. Plenum Press, New York. 1984.
15. A. Tachibana, S. Ishikawa, T. Inoue, and T. Yamabe. Chem. Phys. Lett. **154**, 403 (1989).
16. A. Tachibana, K. Hori, and T. Yamabe. Chem. Phys. Lett. **112**, 279 (1984); A. Tachibana, T. Inoue, T. Yamabe, and K. Hori. Int. J. Quantum Chem. **30**, 575 (1986); A. Tachibana, T. Inoue, H. Fueno, T. Yamabe, and K. Hori. Synth. Met. **19**, 99 (1987); A. Tachibana, T-X. Lü, and T. Yamabe. Mol. Eng. **1**, 89 (1991); A. Tachibana, S. Ishikawa, and T. Yamabe. Mol. Eng. **1**, 101 (1991).
17. A. Tachibana, S. Ishikawa, T. Tada, and T. Yamabe. *In* The physics and chemistry of organic superconductors. *Edited by* G. Saito and S. Kagoshima. Springer-Verlag, Berlin, Heidelberg. 1990.
18. A. Tachiabana, H. Fueno, S. Ishikawa, and T. Yamabe. Chem. Phys. Lett. **160**, 353 (1989).
19. A. Tachibana. Int. J. Quantum Chem. In press.
20. W. P. Su, J. R. Schrieffer, and A. J. Heeger. Phys. Rev. Lett. **42**, 1698 (1979).
21. J. S. Binkley, R. A. Whiteside, R. Krishnan *et al.* GAUSSIAN 80. Carnegie–Mellon University, Pittsburgh, PA. 1981; J. S. Binkley, M. J. Frisch, D. J. Defrees *et al.* GAUSSIAN 82. Carnegie–Mellon University, Pittsburgh, PA. 1983.
22. K. Yamaguchi. J. Mol. Struct. (Theochem), **103**, 101 (1983).
23. W. A. Little. Phys. Rev. **134**, 1416 (1964).

Can. J. Chem. Downloaded from www.nrcresearchpress.com by 92.62.229.171 on 09/08/12
For personal use only.

Analytic derivative theory based on the Hellmann–Feynman theorem

K. HIRAO

Department of Chemistry, College of General Education, Nagoya University, Nagoya, Japan

Received August 2, 1991

This paper is dedicated to Professor Sigeru Huzinaga on the occasion of his 65th birthday

K. HIRAO. Can. J. Chem. **70**, 434 (1992).

General formulae for the second, third, and fourth derivatives of the energy with respect to the nuclear coordinates of a molecule are derived from the Hellmann–Feynman theorem. Hurley's condition is used to obtain approximations to the first-order wavefunction, from which the second, third, and fourth energies can be obtained, leading to quadratic, cubic, and quartic force constants. The procedure is equivalent to minimizing the derivative energy by perturbed variation techniques. The expressions for these higher energy derivatives are much simpler than those of the direct analytic derivative method. The electrostatic calculation involves only one-electron integrals. The coupled Hartree–Fock equations to obtain the wavefunction derivatives become much simpler. The present theory provides a great conceptual simplification. However, the theory is correct only if the basis set is complete or basis functions are independent of the perturbation.

Key words: analytic derivative theory, Hellmann–Feynman theorem, force constants, the curvature theorem.

K. HIRAO. Can. J. Chem. **70**, 434 (1992).

En utilisant le théorème de Hellmann–Feynman, on a dérivé des formules générales pour les deuxième, troisième et quatrième dérivées de l'énergie par rapport aux coordonnées nucléaires d'une molécule. On a utilisé la condition de Hurley pour obtenir des approximations de la fonction d'onde du premier ordre, à partir de laquelle on a obtenu les deuxième, troisième et quatrième énergies, qui ont conduit aux constantes de force quadratique, cubique et quartique. La procédure équivaut à minimiser l'énergie dérivée à l'aide des techniques de la variation perturbée. Les expressions de ces dérivées élevées de l'énergie sont beaucoup plus simples que celles obtenues grâce à la méthode de la dérivée analytique directe. Le calcul électrostatique n'implique que les intégrales d'un seul électron. Les équations couplées de Hartree–Fock nécessaires pour obtenir les dérivées de la fonction d'onde deviennent beaucoup plus simples. La présente théorie présente une grande simplification conceptuelle. Toutefois, la théorie n'est correcte que si la base est complète ou si les fonctions de base sont indépendantes de la perturbation.

Mots clés : théorie de la dérivée analytique, théorème de Hellmann–Feynman, constantes de force, théorème de courbure.

[Traduit par la rédaction]

1. Introduction

Many important molecular properties are directly defined as the derivatives of an electronic energy. Electric moments and polarizabilities are property defined as the derivatives of the energy with respect to the applied electric fields. Magnetic properties such as diamagnetic susceptibilities and nuclear magnetic resonance chemical shifts are related to energy derivatives with respect to external and nuclear magnetic fields. Differentiation of the energy with respect to nuclear coordinates corresponds to the calculation of forces and force constants. These nuclear displacement energy derivatives are very important in the exploration of potential surfaces.

The first derivatives of the energy with respect to nuclear coordinates give the force acting on the nucleus and are used to find the stationary points such as equilibrium structures and transition structures. The second derivatives are related to the harmonic force constants as well as to the nature of the stationary point. The third and fourth derivatives are related to the cubic and quartic force constants, respectively. The knowledge of these derivatives yields anharmonic spectroscopic constants.

There are two general approaches to the calculation of analytic energy derivatives. The first method is the direct analytic differentiation of the expectation value of the Hamiltonian. The procedure has been the most commonly used and has been the focus of many investigations in recent years. The idea underlying the direct analytical derivative method is to rigorously differentiate the true quantum mechanical energy. Generally this involves solving a type of eigenfunction equation or a simultaneous system of linear equations. Consequently n differentiations are necessary to reach nth energy derivatives.

Direct analytic first derivatives of the SCF energy were first derived by Pulay (1). It is now relatively straightforward to calculate the first derivatives with respect to nuclear coordinates for any method. Pople *et al.* (2) presented the analytical method for the evaluation of SCF second derivatives. To obtain second derivatives it is necessary to solve the coupled perturbed Hartree–Fock equations of Gerratt and Mills (3). The most severe bottleneck in this approach is the drastic increase in the number of basis molecular integrals to be computed. In spite of this, such a second derivative approach is used rather routinely for SCF and some MC-SCF schemes. The formulations of SCF third derivatives were first given by Gaw, Yamaguchi, and Schaefer (4). Some simplifications in the formula were given by Gaw and Handy (5). The fourth derivatives have been presented by Handy and coworkers.[1] This requires the solution of the second-order coupled perturbed Hartree–Fock equations. However, the scheme becomes more time consuming and complicated as the order of the energy derivatives increases. This is mainly due to the error terms, which vanish when the wavefunctions obeying the Hellmann–Feynman theorem are used. Nothing will be gained if we evaluate the unphysical error terms.

An alternative method is possible, based on the use of the

[1] S. M. Colwell, D. Jayatilaka, P. E. Maslen, R. D. Amos, and N. Handy, private communication.

Printed in Canada

Can. J. Chem. Downloaded from www.nrcresearchpress.com by 92.62.229.171 on 09/08/12
For personal use only.

Can. J. Chem. Downloaded from www.nrcresearchpress.com by 92.62.229.171 on 09/08/12
For personal use only.

Hellmann–Feynman theorem (6, 7). The Hellmann–Feynman theorem gives the first derivatives of the energy with respect to the nuclear coordinates as a simple expectation value. Consequently, $n - 1$ differentiations are required to reach the nth derivatives of the energy. In addition we have the so-called Hurley's condition (8) for the optimal variational wavefunction, which serves as an auxiliary condition. Thus, the Hellmann–Feynman approach seems to be much superior to the direct differentiation method. However, although there have been isolated successes of the Hellmann–Feynman approach (9),[2] thus far there is no general theoretical understanding of the situation. This is mainly due to the unreliability of the Hellmann–Feynman method for evaluating forces on nuclei. Although the Hellmann–Feynman theorem is valid for true Hartree–Fock wavefunctions, it is found to be of little value for the finite basis sets typically used in molecular calculations. Thus, the error in the Hellmann–Feynman theorem arises essentially from basis set inadequacies in the underlying calculations.

The Hellmann–Feynman theorem provides a great conceptual simplification and may lead to practical advantages. We will develop here the analytic derivative theory based on the Hellmann–Feynman theorem. In Sect. 2, the second, third, and fourth energy derivatives for a diatomic molecule will be derived from the Hellmann–Feynman theorem. In Sect. 3, general analytic expressions for these higher energy derivatives will be given. Results will be discussed in the final section.

2. Analytic derivative theory for diatomic molecules

Let Ψ be a normalized optimal variational wavefunction and E the corresponding energy

$$[1] \qquad \langle\Psi|H - E|\Psi\rangle = 0$$

By differentiating eq. [1] with respect to a nuclear coordinate λ we obtain

$$[2] \qquad E^1 = \langle\Psi|H^1|\Psi\rangle + \langle\Psi^1|H - E|\Psi\rangle + \langle\Psi|H - E|\Psi^1\rangle$$

Here we used the notation

$$H^n = \frac{\partial^n H}{\partial\lambda^n}$$

and analogous notation for Ψ^n and E^n. The variational condition ensures that

$$[3] \qquad \langle\Psi^1|H - E|\Psi\rangle + \langle\Psi|H - E|\Psi^1\rangle = 0$$

whence we have the Hellmann–Feynman theorem

$$[4] \qquad E^1 = \langle\Psi|H^1|\Psi\rangle$$

The negative energy gradient is called the Hellmann–Feynman force. Such a condition as eq. [3] was first given by Hurley (8) and is known as Hurley's condition. True Hartree–Fock approximations (as distinct from the SCF approximations), be they restricted, unrestricted, open-shell, closed-shell, multi-configurational, or whatever, satisfy the Hellmann–Feynman theorem.

For simplicity, in this paper we will consider $2n$ electron closed-shell systems. The wavefunction is expressed as a Slater determinant

$$[5] \qquad \Psi = \|\varphi_1\alpha\varphi_1\beta \ldots \varphi_i\alpha\varphi_i\beta \ldots\|$$

The Hartree–Fock orbitals $\varphi_1 \ldots \varphi_n$ are eigenfunctions of the Fock operator, the corresponding eigenvalues being $\varepsilon_1 \ldots \varepsilon_n$

$$[6] \qquad F\varphi_i = \varepsilon_i\varphi_i$$

Orbital labels $i, j, k \ldots$ denote occupied orbitals, $a, b, c \ldots$ denote virtual orbitals, and $p, q, r \ldots$ denote general orbitals. The Hellmann–Feynman theorem is satisfied if Hurley's condition, eq. [3], is fulfilled. The wavefunction derivative is given by

$$[7] \qquad \Psi^1 = \sum_i^{\text{occ}} \|\varphi_1\alpha\varphi_1\beta \ldots \varphi_i^1\varphi_i\,(\alpha\beta - \beta\alpha) \ldots\|$$

Taking account of the one-electron property of H^1, we assume that the derivative of the orbital is expressed as a linear combination of the other orbitals

$$[8] \qquad \varphi_i^1 = \varphi_p U_{pi}/\sqrt{2}$$

where $p = i$ is excluded from the orthogonality condition of orbitals. We used Einstein summation notation for repeated indices. Substituting eq. [8] into eq. [7], we have

$$[9] \qquad \Psi^1 = U_{ai}\Psi_{ai}$$

with

$$\Psi_{ai} = \|\varphi_1\alpha\varphi_1\beta \ldots \varphi_a\varphi_i(\alpha\beta - \beta\alpha)/\sqrt{2} \ldots\|$$

The Ψ_{ai} are singly excited configurations. Thus Hurley's condition of eq. [3] is equivalent to the Brillouin theorem

$$[10] \qquad \langle\Psi_{ai}|H - E|\Psi\rangle + \langle\Psi|H - E|\Psi_{ai}\rangle = 0$$

As well known, the Hellmann–Feynman theorem is satisfied for the optimal wavefunction as a consequence of the variational principle.

The differentiation of the Fock equations $\langle\varphi_j|F - \varepsilon_i|\varphi_i\rangle = 0$ leads to

$$[11] \qquad \langle\varphi_j|F^1 - \varepsilon_i^1|\varphi_i\rangle + (\varepsilon_j - \varepsilon_i)\langle\varphi_j|\varphi_i^1\rangle = 0$$

In the case of $i = j$ we have the Hellmann–Feynman theorem with respect to the orbital energy

$$[12] \qquad \varepsilon_i^1 = \langle\varphi_i|F^1|\varphi_i\rangle$$

Now let us derive the second, third, and fourth energy derivatives based on the Hellmann–Feynman theorem. For the sake of formal simplicity, we will consider the $2n$-electron closed-shell SCF wavefunction for a diatomic molecule. The electron energy is given by eq. [1]. The nuclear coordinates are understood to have been written in terms of the internuclear distance R. Thus only R appears as a parameter. Differentiation of eq. [1] results in the Hellmann–Feynman theorem if Hurley's condition is fulfilled. We observe that R is real so that the derivative wavefunctions are

[2]Other formulations are possible based on the use of the virial theorem to define $\partial E/\partial\lambda$, see for example, ref. 10.

Can. J. Chem. Downloaded from www.nrcresearchpress.com by 92.62.229.171 on 09/08/12
For personal use only.

assumed to be real. This is not a serious restriction. The normalization condition of the wavefunction requires

$$[13] \quad \langle\Psi^1|\Psi\rangle = 0$$

(i) Second derivative

Differentiation of the Hellmann–Feynman theorem with respect to R yields

$$[14] \quad E^2 = \langle\Psi|H^2|\Psi\rangle + 2\langle\Psi^1|H^1|\Psi\rangle$$

The second derivative of the energy requires knowledge of the first derivative of the wavefunction. The essential difficulty in calculating higher energy derivatives lies in finding a good approximation to the first derivative of the wavefunction. By differentiating Hurley's condition we have the first-order Hurley's condition

$$[15] \quad \langle\Psi^1|H^1|\Psi\rangle + \langle\Psi^1|H - E|\Psi^1\rangle + \langle\Psi^2|H - E|\Psi\rangle = 0$$

Equation [15] is the equation to determine the first derivative of the wavefunction. As shown later, finding Ψ^1 based on the use of eq. [15] is equivalent to finding the optimal Ψ^1 by the perturbation variation method (11). We assume that Ψ^1 can be expanded in terms of the singly excited configurations

$$[16] \quad \Psi^1 = U^{(1)}_{ai} S^+_{ai}\Psi$$

Here $U^{(1)}_{ai}$ are expansion coefficients, namely the first-order variational parameters, and S^+_{ai} are the single excitation operators defined by

$$[17] \quad S^+_{pq} = (a^+_{p\alpha}a_{q\alpha} + a^+_{p\beta}a_{q\beta})/\sqrt{2}$$

The a^+_p and a_q are the creation and destruction operators that satisfy the Fermion anticommutation relation. From the orthogonality relations of orbitals, we have

$$[18] \quad U^{(1)}_{pq} + U^{(1)}_{qp} = 0$$

The S^+_{ai} generates a singlet, singly excited, configuration when operating on Ψ

$$[19] \quad S^+_{ai}\Psi \equiv S^+_{ai}|\rangle = \| \ldots \varphi_a\varphi_i(\alpha\beta - \beta\alpha)\sqrt{2} \ldots \|$$

Equation [15] involves the second derivative of the wavefunction Ψ^2. So we must eliminate Ψ^2. Ψ^2 can be written in general in terms of the excitation operators as

$$[20] \quad \Psi^2 = U^{(1)}_{pq}U^{(1)}_{rs}S^+_{pq}S^+_{rs}|\rangle$$

The orbital pairs pq, rs run over all orbitals. Thus Ψ^2 consists of the ground, singly, and doubly excited configurations

$$[21] \quad \Psi^2 = [U^{(2)} + U^{(2)}_{ai}S^+_{ai} + U^{(2)}_{ai,bj}S^+_{ai}S^+_{bj}]|\rangle$$

The ground state component comes from the excitations $S^+_{ia}S^+_{ai}|\rangle$ and singly excited configurations arise from $S^+_{ab}S^+_{bi}|\rangle$ and $S^+_{ji}S^+_{aj}|\rangle$. Ψ^2 can be expressed in terms of the first-order parameters as

$$[22] \quad \Psi^2 = [U^{(1)}_{ia}U^{(1)}_{ai}S^+_{ia}S^+_{ai} + U^{(1)}_{ab}U^{(1)}_{bi}S^+_{ab}S^+_{bj} + U^{(1)}_{ji}U^{(1)}_{aj}S^+_{ji}S^+_{aj} + U^{(1)}_{ai}U^{(1)}_{bj}S^+_{ai}S^+_{bj}]|\rangle$$

Comparing eqs. [21] and [22] we have

$$[23a] \quad U^{(2)} = -|U^{(1)}_{ai}|^2$$

$$[23b] \quad U^{(2)}_{ai} = U^{(1)}_{ab}U^{(1)}_{bi} + U^{(1)}_{ji}U^{(1)}_{aj}$$

$$[23c] \quad U^{(2)}_{ai,bj} = U^{(1)}_{ai}U^{(1)}_{bj}$$

The $U^{(2)}$ can also be obtained from the second-order normalization condition

$$[24] \quad \langle\Psi^2|\Psi\rangle + \langle\Psi^1|\Psi^1\rangle = 0$$

Returning to eq. [15], we observe that the last term requires only the knowledge of the doubly excited configurations of Ψ^2. Using the relation given by eq. [23*c*], we can rewrite eq. [15] as

$$[25] \quad \langle|S_{ai}H^1|\rangle + [\langle|S_{ai}(H - E)S^+_{bj}|\rangle + \langle|S_{ai}S_{bj}H|\rangle]U^{(1)}_{bj} = 0$$

These are a set of linear equations, which are sufficient for finding $U^{(1)}_{ai}$. We only need solutions of eq. [25] to obtain Ψ^1. There is no iteration involved. From a practical point of view, the iterative scheme is preferred simply because it is less expensive. Equations [25] are known as the coupled perturbed Hartree–Fock equations, as discussed by Stevens *et al.* (12). Note here that once the first-order wavefunction has been determined, the second-order wavefunction Ψ^2 can be obtained, except for $U^{(2)}_{ai}$. $U^{(2)}_{ai}$ requires knowledge of $U^{(1)}_{ab}$ and $U^{(1)}_{ji}$, which cannot be fixed from the first-order wavefunction.

Finally, the second energy derivative can be written in terms of the excitation operators as

$$[26] \quad E^2 = \langle|H^2|\rangle + 2U^{(1)}_{ai}\langle|S_{ai}H^1|\rangle$$

Equation [26] can be formulated in another way. Let us consider the general expression of E^2 obtained by double differentiation of eq. [1]

$$[27] \quad E^2 = \langle\Psi|H^2|\Psi\rangle + 4\langle\Psi^1|H^1|\Psi\rangle + 2\langle\Psi^1|H - E|\Psi^1\rangle + 2\langle\Psi^2|H - E|\Psi\rangle$$

It can be shown (13) for any approximate Ψ^1, say $\tilde{\Psi}^1$, that

$$[28] \quad \langle\Psi|H^2|\Psi\rangle + 4\langle\tilde{\Psi}^1|H^1|\Psi\rangle + 2\langle\tilde{\Psi}^1|H - E|\tilde{\Psi}^1\rangle + 2\langle\tilde{\Psi}^2|H - E|\Psi\rangle \equiv \tilde{E}^2 \geq E^2$$

Thus we may choose an arbitrary trial function with variable parameters and optimize it by minimizing $\tilde{E}^2$. If $\tilde{\Psi}^1$ contains only linear parameters and $\tilde{\Psi}^2$ can be written as in eq. [21], it is easy to show that the optimized trial function Ψ^1_{opt} satisfies

$$[29] \quad \langle\Psi^1_{opt}|H|\Psi\rangle + \langle\Psi^1_{opt}|H - E|\Psi^1_{opt}\rangle + \langle\Psi^2_{opt}|H - E|\Psi\rangle = 0$$

This implies that Ψ^1_{opt} satisfies eq. [15] derived from Hurley's condition. Also we have the expression of E^2 for the optimal Ψ^1_{opt}

$$[30] \quad E^2 = \langle\Psi|H^2|\Psi\rangle + 2\langle\Psi^1_{opt}|H^1|\Psi\rangle$$

which takes the same form as given in eq. [14]. Thus, finding approximate Ψ^1 from the Hurley's condition of eq. [15] is equivalent to optimizing Ψ^1 using the perturbation variation technique (11).

That is, the analytic energy derivative derived from the Hellmann–Feynman theorem is the optimal function determined by the variation perturbation method. It must be emphasized that the variational perturbation method will lead to successful results only for the wavefunction obeying the Hellmann–Feynman theorem.

Equation [25] can be expressed in a simple matrix form

$$[31] \quad \mathbf{b} + (\boldsymbol{A} + \boldsymbol{B})\mathbf{U} = 0$$

The **b** and **U** are column vectors of $\langle|S_{ai}H^1|\rangle$ and first-order variational parameters $U^{(1)}_{ai}$, respectively. The $\boldsymbol{A}$ and $\boldsymbol{B}$ matrices are defined by

$$[32a] \quad (\boldsymbol{A})_{ai,bj} = \langle|S_{ai}(H - E)S^+_{bj}|\rangle$$

$$[32b] \quad (\boldsymbol{B})_{ai,bj} = \langle|S_{ai}S_{bj}H|\rangle$$

Since we are dealing with closed-shell systems, all the integrals can be chosen as real. So the $\boldsymbol{A}$ and $\boldsymbol{B}$ matrices are symmetric. Now let us consider the unitary transformation among singly excited configurations, which diagonalizes the $(\boldsymbol{A} + \boldsymbol{B})$ matrix

$$[33] \quad \boldsymbol{O}^\dagger(\boldsymbol{A} + \boldsymbol{B})\boldsymbol{O} = \boldsymbol{d}$$

Here $\boldsymbol{O}$ is the unitary matrix and $\boldsymbol{d}$ is a diagonal matrix. If we further define the unitary transformed excitation operators by

$$[34a] \quad R^+_{ai} = S^+_{bj}O_{bj,ai}$$

together with

$$[34b] \quad T^{(1)}_{ai} = U^{(1)}_{bj}O_{bj,ai}$$

then we have

$$[35] \quad \Psi^1 = T^{(1)}_{ai}R^+_{ai}|\rangle$$

and

$$[36] \quad T^{(1)}_{ai} = -\langle|R_{ai}H^1|\rangle/\Delta E_{ai}$$

with

$$[37] \quad \Delta E_{ai} = \langle|R_{ai}(H - E)R^+_{ai}|\rangle + \langle|R_{ai}R_{ai}H|\rangle$$

Finally, the second energy derivative can be written as

$$[38] \quad E^2 = \langle|H^2|\rangle - 2|\langle|R_{ai}H^1|\rangle|^2/\Delta E_{ai}$$

Equation [38] is derived without any approximation in spite of its simplicity. Namely, by choosing $\boldsymbol{O}$ as diagonalizing the matrix $(\boldsymbol{A} + \boldsymbol{B})$, the second energy derivative can be expressed in a form similar to a simple sum-over-state perturbation method (14). A similar procedure has been used to analyze the second-order perturbation energy of the coupled Hartree–Fock theory and the unlinked terms of the SCF effect of orbitals (15). Note here that ΔE_{ai} is not really the excitation energy; it includes the additional term originated from the $\boldsymbol{B}$ matrix. It is called the generalized exchange integral (15) since $\langle|S_{ai}S_{ai}H|\rangle$ equals the usual exchange integral $(\varphi_a\varphi_i|\varphi_a\varphi_i)$. The generalized exchange integral represents the higher order effect of the change in the orbitals due to the displacement of the internuclear distance.

The first term of the right-hand side of eq. [38] is the classical formula for the force constant and corresponds to moving the nuclei while holding the electrons fixed. It is positive. The second terms are often referred to as relaxation terms since they represent the effect of the changes in charge distribution due to the movement of the nuclei. From eq. [38], we have

$$[39] \quad E^2 - \langle|H^2|\rangle = -2|\langle|R_{ai}H^1|\rangle|^2/\Delta E_{ai} < 0$$

if

$$[40] \quad \Delta E_{ai} = \langle|R_{ai}(H - E)R^+_{ai}|\rangle + \langle|R_{ai}R_{ai}H|\rangle > 0$$

This is an alternative proof of the upper bound relation of second derivatives of the energy (the curvature theorem) (16). Equation [40] is the stability condition for the optimized variational wavefunction (17). The stability condition ensures that the wavefunction represents a true minimum of the energy. Thus, the upper bound condition is equivalent to the stability condition and provides an additional criterion to that of the variational principle for judging the quality and stability of an approximate wavefunction.

(ii) Third derivative

The third energy derivative is obtained by further differentiating eq. [14] with respect to R:

$$[41] \quad E^3 = \langle\Psi|H^3|\Psi\rangle + 4\langle\Psi^1|H^2 - E^2|\Psi\rangle + 2\langle\Psi^1|H^1 - E^1|\Psi^1\rangle + 2\langle\Psi^2|H^1 - E^1|\Psi\rangle$$

This expression of the third energy derivative contains the second derivative of the wavefunction Ψ^2. The unknown quantities of Ψ^2 are the parameters $U^{(2)}_{ai}$ for the singly excited configurations. So it is necessary to look at the second-order Hurley's condition obtained by differentiating eq. [15]

$$[42] \quad \langle\Psi^3|H - E|\Psi\rangle + 2\langle\Psi^2|H^1 - E^1|\Psi\rangle + 3\langle\Psi^2|H - E|\Psi^1\rangle + \langle\Psi^1|H^2|\Psi\rangle + 2\langle\Psi^1|H^1 - E^1|\Psi^1\rangle = 0$$

However, eq. [42] includes the third derivative of the wavefunction, Ψ^3. Therefore, we shall try to eliminate the third-order wavefunction. This is possible. The general form of Ψ^3 is

$$[43] \quad \Psi^3 = [U^{(3)} + U^{(3)}_{ai}S^+_{ai} + U^{(3)}_{ai,bj}S^+_{ai}S^+_{bj} + U^{(3)}_{ai,bj,ck}S^+_{ai}S^+_{bj}S^+_{ck}]|\rangle$$

However, we can express $U^{(3)}_{ai}$, $U^{(3)}_{ai,bj}$, and $U^{(3)}_{ai,bj,ck}$ in terms of the lower order parameters by analyzing the excitations,

$$[44a] \quad U^{(3)} = -3U^{(2)}_{ai}U^{(1)}_{ai}$$

$$[44b] \quad U^{(3)}_{ai,bj} = 3U^{(2)}_{ai}U^{(1)}_{bj}$$

$$[44c] \quad U^{(3)}_{ai,bj,ck} = U^{(1)}_{ai}U^{(1)}_{bj}U^{(1)}_{ck}$$

The relation of eq. [44*a*] can be derived directly from the third-order normalization condition of the wavefunction

$$[45] \quad \langle\Psi^3|\Psi\rangle + 3\langle\Psi^2|\Psi^1\rangle = 0$$

Note here that only the doubly excited configurations of Ψ^3 can contribute to the first term of eq. [42]. Thus, eq. [42] contains only unknown parameters $U^{(2)}_{ai}$ if $U^{(1)}_{ai}$ are known. Expressing eq. [42] in terms of $U^{(2)}_{ai}$ and $U^{(1)}_{ai}$, we have the following relations

$$[46] \quad U^{(2)}_{ai}\langle|S_{ai}H^1|\rangle = U^{(1)}_{ai}[\langle|S_{ai}H^2|\rangle + 2\langle|S_{ai}(H^1 - E^1)S^+_{bj}|\rangle U^{(1)}_{bj} + \{2\langle|S_{ai}S_{bj}HS^+_{ck}|\rangle + \langle|S_{bj}S_{ck}HS^+_{ai}|\rangle\}U^{(1)}_{bj}U^{(1)}_{ck}]$$

Thus, the $U^{(2)}_{ai}$ can be expressed explicitly in terms of the first-order parameters. The third energy derivative is now rewritten as

$$[47] \quad E^3 = \langle|H^3|\rangle + 6U^{(1)}_{ai}\langle|S_{ai}H^2|\rangle + 6U^{(1)}_{ai}U^{(1)}_{bj}\langle|S_{ai}(H^1 - E^1)S^+_{bj}|\rangle + 6U^{(1)}_{ai}U^{(1)}_{bj}U^{(1)}_{ck}\langle|S_{ai}S_{bj}HS^+_{ck}|\rangle$$

The formula is much simpler than that of the direct analytic derivative method. Note here that the final expression of E^3

Can. J. Chem. Downloaded from www.nrcresearchpress.com by 92.62.229.171 on 09/08/12
For personal use only.

contains only the first-order variational parameters. Explicit knowledge of Ψ^2 is not necessary. This point will be discussed later.

If we use the unitary transformed excitation operators, the above expression can be expressed in the form of the sum-over-state perturbation method

$$[48]\quad E^3 = \langle|H^3|\rangle - 6\langle|H^1R_{ai}^+|\rangle\langle|R_{ai}H^2|\rangle/\Delta E_{ai} + 6\langle|H^1R_{ai}^+|\rangle\langle|R_{ai}(H^1 - E^1)R_{bj}^+|\rangle\langle|R_{bj}H^1|\rangle/(\Delta E_{ai}\Delta E_{bj}) - 6\langle|H^1R_{ai}^+|\rangle\langle|H^1R_{bj}^+|\rangle\langle|R_{ai}R_{bj}HR_{ck}^+|\rangle\langle|R_{ck}H^1|\rangle/(\Delta E_{ai}\Delta E_{bj}\Delta E_{ck})$$

This equation is also exact. There is no approximation employed.

Now let us consider the general analytic expression of E^3 derived by successive differentiation of eq. [1]

$$[49]\quad E^3 = \langle\Psi|H^3|\Psi\rangle + 6\langle\Psi^1|H^2 - E^2|\Psi\rangle + 6\langle\Psi^1|H^1 - E^1|\Psi^1\rangle + 6\langle\Psi^2|H^1 - E^1|\Psi\rangle + 6\langle\Psi^2|H - E|\Psi^1\rangle + 2\langle\Psi^3|H - E|\Psi\rangle$$

Expanding the wavefunction derivatives in terms of the excitation operators as before and minimizing E^3 with respect to the unknown parameter $U_{ai}^{(2)}$, we have

$$[50]\quad \frac{\partial E^3}{\partial U_{ai}^{(2)}} = \langle|S_{ai}H^1|\rangle + [\langle|S_{ai}(H - E)S_{bj}^+|\rangle + \langle|S_{ai}S_{bj}H|\rangle]U_{bj}^{(1)} = 0$$

Equation [50] holds automatically if Ψ^1 is chosen optimal, that is, if $U_{ai}^{(1)}$ satisfies eq. [25]. The E^3 expression for the optimal Ψ^2 takes the same form as given by eq. [41]. Thus, the first-order wavefunction suffices to determine the third energy derivatives. This property is also utilized to derive the third energy derivatives of the direct analytic method (4).

(iii) Fourth derivative

The fourth derivative is obtained by differentiating eq. [41] again with respect to R:

$$[51]\quad E^4 = \langle\Psi|H^4|\Psi\rangle + 6\langle\Psi^1|H^3|\Psi\rangle + 6\langle\Psi^2|H^2 - E^2|\Psi\rangle + 6\langle\Psi^1|H^2 - E^2|\Psi^1\rangle + 6\langle\Psi^2|H^1 - E^1|\Psi^1\rangle + 2\langle\Psi^3|H^1 - E^1|\Psi\rangle$$

The last term on the right-hand side of eq. [51] involves the third derivative of the wavefunction. We need the singly excited components of Ψ^3 to evaluate this term due to the one-electron property of H^1. To determine the unknown quantities, we start with the third-order Hurley's condition

$$[52]\quad \langle\Psi^4|H - E|\Psi\rangle + 3\langle\Psi^3|H^1 - E^1|\Psi\rangle + 4\langle\Psi^3|H - E|\Psi^1\rangle + 3\langle\Psi^2|H^2 - E^2|\Psi\rangle + 9\langle\Psi^2|H^1 - E^1|\Psi^1\rangle + 3\langle\Psi^2|H - E|\Psi^2\rangle + \langle\Psi^1|H^3|\Psi\rangle + 3\langle\Psi^1|H^2 - E^2|\Psi^1\rangle = 0$$

Again, the above condition contains the fourth derivative of the wavefunction. However, the quantities required to evaluate the first term of eq. [52] are the doubly excited configurations of Ψ^4. From analysis of the excitation operators, we observe that

$$[53]\quad U_{ai,bj}^{(4)}S_{ai}^+S_{bj}^+ = (4U_{ai}^{(3)}U_{bj}^{(1)} + 3U_{ai}^{(2)}U_{bj}^{(2)})S_{ai}^+S_{bj}^+$$

Thus we can find the unknown parameters $U_{ai}^{(3)}$ from eq. [52]. The final expression of $U_{ai}^{(3)}$ becomes

$$[54]\quad U_{ai}^{(3)}\langle|S_{ai}H^1|\rangle = U_{ai}^{(1)}[\langle|S_{ai}H^3|\rangle + 3\langle|S_{ai}(H^2 - E^2)S_{bj}^+|\rangle U_{bj}^{(1)} + 9\langle|S_{ai}S_{bj}H^1S_{kc}^+|\rangle U_{bj}^{(1)}U_{kc}^{(1)} + \{3\langle|S_{ai}S_{bj}(H - E)S_{ck}^+S_{dl}^+|\rangle + 4\langle|S_{ai}S_{bj}S_{ck}HS_{dl}^+|\rangle\}U_{bj}^{(1)}U_{ck}^{(1)}U_{dl}^{(1)}] + 3U^{(2)}U_{ai}^{(1)}\langle|S_{ai}H^1|\rangle + 3U_{ai}^{(2)}[\langle|S_{ai}H^2|\rangle + 3\langle|S_{ai}(H^1 - E^1)S_{bj}^+|\rangle U_{bj}^{(1)} + \{\langle|S_{ai}(H - E)S_{bj}^+|\rangle + \langle|S_{ai}S_{bj}H|\rangle\}U_{bj}^{(2)} + 2\{2\langle|S_{ai}S_{bj}HS_{ck}^+|\rangle + \langle|S_{bj}S_{ck}HS_{ai}^+|\rangle\}U_{bj}^{(1)}U_{ck}^{(1)}]$$

Note here that it is not necessary to solve the second-order coupled perturbed Hartree–Fock equations for the calculation of the third-order parameters. It is also possible to represent $U_{ai}^{(3)}$ in terms of the first-order parameters $U_{ai}^{(1)}$ if we utilize the relations given by eq. [46].

The fourth energy derivative can be expressed in terms of the excitation operators:

$$[55]\quad E^4 = \langle|H^4|\rangle + 6U_{ai}^{(1)}\langle|S_{ai}H^3|\rangle + 6U_{ai}^{(2)}\langle|S_{ai}H^2|\rangle + 6U^{(2)}\langle|H^2 - E^2|\rangle + 6U_{ai}^{(1)}U_{bj}^{(1)}\langle|S_{ai}(H^2 - E^2)S_{bj}^+|\rangle + 6U^{(2)}U_{ai}^{(1)}\langle|S_{ai}^+H^1|\rangle + 6U_{ai}^{(2)}U_{bj}^{(1)}\langle|S_{ai}(H^1 - E^1)S_{bj}^+|\rangle + 6U_{ai}^{(1)}U_{bj}^{(1)}U_{ck}^{(1)}\langle|S_{ai}S_{bj}H^1S_{ck}^+|\rangle + 2U_{ai}^{(3)}\langle|S_{ai}H^1|\rangle$$

Utilizing the relations given in eq. [54] we can eliminate $U_{ai}^{(3)}$ and have

$$[56]\quad E^4 = \langle|H^4|\rangle + 8U_{ai}^{(1)}\langle|S_{ai}H^3|\rangle + 12U_{ai}^{(1)}U_{bj}^{(1)}\langle|S_{ai}(H^2 - E^2)S_{bj}^+|\rangle + 24U_{ai}^{(1)}U_{bj}^{(1)}U_{ck}^{(1)}\langle|S_{ai}S_{bj}H^1S_{ck}^+|\rangle + 6U_{ai}^{(1)}U_{bj}^{(1)}U_{ck}^{(1)}U_{dl}^{(1)}\langle|S_{ai}S_{bj}(H - E)S_{ck}^+S_{dl}^+|\rangle + 8U_{ai}^{(1)}U_{bj}^{(1)}U_{ck}^{(1)}U_{dl}^{(1)}\langle|S_{ai}S_{bj}S_{ck}HS_{dl}^+|\rangle + 6U_{ai}^{(2)}U_{bj}^{(2)}\{\langle|S_{ai}(H - E)S_{bj}^+|\rangle + \langle|S_{ai}S_{bj}H|\rangle\}12U_{ai}^{(2)}[\langle|S_{ai}H^2|\rangle + 2U_{bj}^{(1)}\langle|S_{ai}(H^1 - E^1)S_{bj}^+|\rangle + \{2\langle|S_{ai}S_{bj}HS_{ck}^+|\rangle + \langle|S_{ai}HS_{bj}^+S_{ck}^+|\rangle\}U_{bj}^{(1)}U_{ck}^{(1)}]$$

since, according to the relations of eq. [46], the last four terms on the right-hand side of the above equation are

$$[57]\quad 12U_{ai}^{(2)}[\langle|S_{ai}H^2|\rangle + 2U_{bj}^{(1)}\langle|S_{ai}(H^1 - E^1)S_{bj}^+|\rangle + \{2\langle|S_{ai}S_{bj}HS_{ck}^+|\rangle + \langle|S_{ai}HS_{bj}^+S_{ck}^+|\rangle\}U_{bj}^{(1)}U_{ck}^{(1)}] = 12|U_{ai}^{(2)}|^2\langle|S_{ai}H^1|\rangle/U_{ai}^{(1)}$$

provided that $U_{ai}^{(1)} \neq 0$. If we further use the relations given by eq. [46] we can express E^4 only in terms of the first-order parameters $U_{ai}^{(1)}$. Although the formula looks complicated, it consists only of straightforward combinations of known quantities. There are no algebraic problems.

The fourth energy derivatives can be expressed in terms of the unitary transformed excitation operators as

Can. J. Chem. Downloaded from www.nrcresearchpress.com by 92.62.229.171 on 09/08/12
For personal use only.

[58] $$E^4 = \langle|H^4|\rangle - 8\langle|H^1R_{ai}^+|\rangle\langle R_{ai}H^3|\rangle/\Delta E_{ai} + 12\langle|H^1R_{ai}^+|\rangle\langle|R_{ai}(H^2 - E^2)R_{bj}^+|\rangle\langle|R_{bj}H^1|\rangle/(\Delta E_{ai}\Delta E_{bj})$$
$$- 24\langle|H^1R_{ai}^+|\rangle\langle|H^1R_{bj}^+|\rangle\langle|R_{ai}R_{bj}H^1R_{ck}^+|\rangle\langle|R_{ck}H^1|\rangle/(\Delta E_{ai}\Delta E_{bj}\Delta E_{ck})$$
$$+ 6\langle|H^1R_{ai}^+|\rangle\langle|H^1R_{bj}^+|\rangle\langle|R_{ai}R_{bj}(H - E)R_{ck}^+R_{dl}^+|\rangle\langle|R_{ck}H^1|\rangle\langle|R_{dl}H^1|\rangle/(\Delta E_{ai}\Delta E_{bj}\Delta E_{ck}\Delta E_{dl})$$
$$+ 8\langle|H^1R_{ai}^+|\rangle\langle|H^1R_{bj}^+|\rangle\langle|H^1R_{ck}|\rangle\langle|R_{ai}R_{bj}R_{ck}HR_{dl}^+|\rangle\langle|R_{dl}H^1|\rangle/(\Delta E_{ai}\Delta E_{bj}\Delta E_{ck}\Delta E_{dl}) - 6|T_{ai}^{(2)}|\Delta E_{ai}$$

Here, $T_{ai}^{(2)}$ are the transformed second-order parameters

[59] $$T_{ai}^{(2)} = (\Delta E_{ai})^{-1}[\langle|R_{ai}H^2|\rangle - 2\langle|R_{ai}(H^1 - E^1)R_{bj}^+|\rangle\langle|R_{bj}H^1|\rangle/\Delta E_{bj}$$
$$+ \{2\langle|R_{ai}R_{bj}HR_{ck}^+|\rangle + \langle|R_{ai}HR_{bj}^+R_{ck}^+|\rangle\}\langle|R_{bj}H^1|\rangle\langle|R_{ck}H^1|\rangle/(\Delta E_{bj}\Delta E_{ck})]$$

Equation [59] is also an exact equation.

Let us again consider the general formula for E^4 obtained by successive differentiations of eq. [1]:

[60] $$E^4 = \langle\Psi|H^4|\Psi\rangle + 8\langle\Psi^1|H^3|\Psi\rangle + 12\langle\Psi^2|H^2 - E^2|\Psi\rangle + 12\langle\Psi^1|H^2 - E^2|\Psi^1\rangle + 24\langle\Psi^2|H^1 - E^1|\Psi^1\rangle$$
$$+ 8\langle\Psi^3|H^1 - E^1|\Psi\rangle + 6\langle\Psi^2|H - E|\Psi^2\rangle + 8\langle\Psi^3|H - E|\Psi^1\rangle + 2\langle\Psi^4|H - E|\Psi\rangle$$

Taking account of eq. [53], we minimize E^4 with respect to $U_{ai}^{(3)}$. This yields

[61] $$\frac{\partial E^3}{\partial U_{ai}^{(3)}} = \langle|S_{ai}H^1|\rangle + [\langle|S_{ai}(H - E)S_{bj}^+|\rangle + \langle|S_{ai}S_{bj}H|\rangle]U_{bj}^{(1)} = 0$$

This is also satisfied if Ψ^1 is chosen optimal and the E^4 for the optimal Ψ^3 becomes identical to that in eq. [51]. Thus, the optimal Ψ^1 is sufficient to evaluate the derivatives of the energy up to fourth order. Analogous results for E^5, E^6, ... may be derived. The only difficulty is that these lower-order wavefunctions must be known exactly.

3. General formulae for the second, third, and fourth energy derivatives

In this section we shall give the general formulae for the second, third, and fourth energy derivatives based on the Hellmann–Feynman theorem. We will start with the energy expression given by eq. [1]. By differentiating eq. [1] with respect to a nuclear coordinate λ, we obtain the Hellmann–Feynman theorem

[62] $$E^\lambda = \langle\Psi|H^\lambda|\Psi\rangle$$

and the Hurley's condition

[63] $$\langle\Psi^\lambda|H - E|\Psi\rangle + \langle\Psi|H - E|\Psi^\lambda\rangle = 0$$

We assume the wavefunction is normalized to unity and have

[64] $$\langle\Psi^\lambda|\Psi\rangle + \langle\Psi|\Psi^\lambda\rangle = 0$$

Second energy derivatives can be obtained by differentiating eq. [62] with respect to μ

[65] $$E^{\lambda\mu} = \langle\Psi|H^{\lambda\mu}|\Psi\rangle + 2\langle\Psi^\lambda|H^\mu|\Psi\rangle$$

Here, assuming that all the functions are real, we used the relations

[66] $$\langle\Psi^\lambda|H^\mu|\Psi\rangle = \langle\Psi^\mu|H^\lambda|\Psi\rangle$$

The second derivatives require the first derivative wavefunctions Ψ^λ. By differentiating eq. [63] with respect to μ we have the first-order Hurley's condition

[67] $$\langle\Psi^\lambda|H^\mu|\Psi\rangle + \langle\Psi^\lambda|H - E|\Psi^\mu\rangle + \langle\Psi^{\lambda\mu}|H - E|\Psi\rangle = 0$$

As shown in the previous section, Ψ^λ may be expanded in terms of the singly excited configurations

[68] $$\Psi^\lambda = U_{ai}^\lambda S_{ai}^+|\rangle$$

Then $\Psi^{\lambda\mu}$ can be expressed as

[69] $$\Psi^{\lambda\mu} = [-|U_{ai}^\lambda|^2 + U_{ai}^{\lambda\mu}S_{ai}^+ + U_{ai}^\lambda U_{bj}^\mu S_{ai}^+S_{bj}^+]|\rangle$$

Equation [67] with $\lambda = \mu$ gives

[70] $$\langle|S_{ai}H^\lambda|\rangle + [\langle|S_{ai}(H - E)S_{bj}^+|\rangle + \langle|S_{ai}S_{bj}H|\rangle]U_{bj}^\lambda = 0$$

By solving a set of linear equations we can obtain Ψ^λ and then $E^{\lambda\mu}$,

[71] $$E^{\lambda\mu} = \langle|H^{\lambda\mu}|\rangle + 2U_{ai}^\lambda\langle|S_{ai}H^\mu|\rangle$$

The third energy derivatives are derived by further differentiating eq. [65] with respect to ν. It is not symmetrized with respect to λ, μ, ν. It can be recast in a symmetrical form. The third energy derivatives are given by

[72] $$E^{\lambda\mu\nu} = \langle\Psi|H^{\lambda\mu\nu}|\Psi\rangle + \frac{4}{3}P_1^{(3)}\langle\Psi^\lambda|H^{\mu\nu} - E^{\mu\nu}|\Psi\rangle$$
$$+ \frac{2}{3}P_2^{(3)}\langle\Psi^{\lambda\mu}|H^\nu - E^\nu|\Psi\rangle$$
$$+ \frac{2}{3}P_3^{(3)}\langle\Psi^\lambda|H^\mu - E^\mu|\Psi^\nu\rangle$$

The notation $P_1^{(3)}$, $P_2^{(3)}$, $P_3^{(3)}$ means the permutation of the superscripts

$$P_1^{(3)} = (\lambda)(\mu\nu) + (\mu)(\nu\lambda) + (\nu)(\lambda\mu)$$
$$P_2^{(3)} = (\lambda\mu)(\nu) + (\mu\nu)(\lambda) + (\nu\lambda)(\mu)$$
$$P_3^{(3)} = (\lambda)(\mu)(\nu) + (\mu)(\nu)(\lambda) + (\nu)(\lambda)(\mu)$$

This implies there are three forms from each $P^{(3)}$. The third energy derivatives require the second-order parameters, $U_{ai}^{\lambda\mu}$. The second-order Hurley's condition is given by

[73] $$\langle\Psi^{\lambda\mu\nu}|H - E|\Psi\rangle + \frac{2}{3}P_2^{(3)}\langle\Psi^{\lambda\mu}|H^\nu - E^\nu|\Psi\rangle$$
$$+ P_2^{(3)}\langle\Psi^{\lambda\mu}|H - E|\Psi^\nu\rangle + \frac{1}{3}P_1^{(3)}\langle\Psi^\lambda|H^{\mu\nu} - E^{\mu\nu}|\Psi\rangle$$
$$+ \frac{2}{3}P_3^{(3)}\langle\Psi^\lambda|H^\mu - E^\mu|\Psi^\nu\rangle = 0$$

Can. J. Chem. Downloaded from www.nrcresearchpress.com by 92.62.229.171 on 09/08/12
For personal use only.

Using the relations

[74] $$U^{\lambda\mu\nu}_{ai,bj} = P^{(3)}_2 U^{\lambda\mu}_{ai} U^{\nu}_{bj}$$

we can express $U^{\lambda\mu}_{ai}$ in terms of U^{λ}_{ai} from eq. [73] as

[75] $$\frac{1}{3} P^{(3)}_2 U^{\lambda\mu}_{ai} \langle|S_{ai}H^{\nu}|\rangle = \frac{1}{3} P^{(3)}_1 U^{\lambda}_{ai}\langle|S_{ai}H^{\mu\nu}|\rangle + \frac{2}{3} P^{(3)}_3 U^{\lambda}_{ai}\langle|S_{ai}(H^{\mu} - E^{\mu})S^{+}_{bj}|\rangle U^{\nu}_{bj} + P^{(3)}_2 U^{\lambda}_{ai}\langle|S_{ai}S_{bj}HS^{+}_{ck}|\rangle U^{\mu}_{bj}U^{\nu}_{ck}$$

In the case of $\lambda = \mu = \nu$, eqs. [75] are reduced to

[76] $$U^{\lambda\lambda}_{ai}\langle|S^{+}_{ai}H^{\lambda}|\rangle = U^{\lambda}_{ai}[\langle|S_{ai}H^{\lambda\lambda}|\rangle + 2\langle|S_{ai}(H^{\lambda} - E^{\lambda})S^{+}_{bj}|\rangle U^{\lambda}_{bj} + \{2\langle|S_{ai}S_{bj}HS^{+}_{ck}|\rangle + \langle|S_{ai}HS^{+}_{bj}S^{+}_{ck}|\rangle\}U^{\lambda}_{bj}U^{\lambda}_{ck}]$$

Also we have the following relations by putting $\lambda = \nu$ in eq. [75]

[77] $$2U^{\lambda\mu}_{ai}\langle|S_{ai}H^{\lambda}|\rangle + U^{\lambda\lambda}_{ai}\langle|S_{ai}H^{\mu}|\rangle = 2U^{\lambda}_{ai}\langle|S_{ai}H^{\lambda\mu}|\rangle + U^{\mu}_{ai}\langle|S_{ai}H^{\lambda\lambda}|\rangle + 4U^{\lambda}_{ai}\langle|S_{ai}(H^{\lambda} - E^{\lambda})S^{+}_{bj}|\rangle U^{\mu}_{bj}$$
$$+ 2U^{\lambda}_{ai}\langle|S_{ai}(H^{\mu} - E^{\mu})S^{+}_{bj}|\rangle U^{\lambda}_{bj} + 3U^{\lambda}_{ai}\langle|S_{ai}S_{bj}HS^{+}_{ck}|\rangle U^{\lambda}_{bj}U^{\mu}_{ck} + 6U^{\lambda}_{ai}\langle|S_{ai}S_{bj}HS^{+}_{ck}|\rangle U^{\mu}_{bj}U^{\lambda}_{ck}$$

So once $U^{\lambda\lambda}_{ai}$ have been determined from eq. [75], the remaining $U^{\lambda\mu}_{ai}$ can be obtained from eq. [77]. Now the third energy derivatives given in eq. [72] can be rewritten in terms of the excitation operators as

[78] $$E^{\lambda\mu\nu} = \langle|H^{\lambda\mu\nu}|\rangle + 2P^{(3)}_1 U^{\lambda}_{ai}\langle|S_{ai}H^{\mu\nu}|\rangle + 2P^{(3)}_3 U^{\lambda}_{ai}U^{\mu}_{bj}\langle|S_{ai}(H^{\nu} - E^{\nu})S^{+}_{bj}|\rangle + 2P^{(3)}_2 U^{\lambda}_{ai}U^{\mu}_{bj}U^{\nu}_{ck}\langle|S_{ai}S_{bj}HS^{+}_{ck}|\rangle$$

Thus, we only need solutions of linear equations of eq. [70] to evaluate the third energy derivatives.

The fourth energy derivatives are given in a symmetrical expression by

[79] $$E^{\lambda\mu\nu\kappa} = \langle\Psi|H^{\lambda\mu\nu\kappa}|\Psi\rangle + \frac{3}{2} P^{(4)}_1\langle\Psi^{\lambda}|H^{\mu\nu\kappa}|\Psi\rangle + P^{(4)}_2[\langle\Psi^{\lambda\mu}|H^{\nu\kappa} - E^{\nu\kappa}|\Psi\rangle + \langle\Psi^{\lambda}|H^{\mu\nu} - E^{\mu\nu}|\Psi^{\kappa}\rangle$$
$$+ \frac{1}{2}\{\langle\Psi^{\lambda\mu}|H^{\nu} - E^{\nu}|\Psi^{\kappa}\rangle + \langle\Psi^{\lambda\mu}|H^{\kappa} - E^{\kappa}|\Psi^{\nu}\rangle\}] + \frac{1}{2} P^{(4)}_1\langle\Psi^{\lambda\mu\nu}|H^{\kappa} - E^{\kappa}|\Psi\rangle$$

with

$$P^{(4)}_1 = (\lambda)(\mu\nu\kappa) + (\mu)(\nu\kappa\lambda) + (\nu)(\kappa\lambda\mu) + (\kappa)(\lambda\mu\nu)$$
$$P^{(4)}_2 = (\lambda\mu)(\nu\kappa) + (\mu\nu)(\kappa\lambda) + (\nu\kappa)(\lambda\mu) + (\kappa\lambda)(\mu\nu) + (\mu\kappa)(\lambda\nu) + (\lambda\nu)(\mu\kappa)$$

The above expression includes third derivatives of the wavefunction, which requires knowledge of the singly excited configurations of $\Psi^{\lambda\mu\nu}$. The variational parameters $U^{\lambda\mu\nu}_{ai}$ of $\Psi^{\lambda\mu\nu}$ can be determined by the third-order Hurley's conditions obtained by differentiating eq. [73] and the relations

[80] $$U^{\lambda\mu\nu\kappa}_{ai,bj} S^{+}_{ai}S^{+}_{bj} = \left(P^{(4)}_3 U^{\lambda\mu\nu}_{ai}U^{\kappa}_{bj} + \frac{1}{2} P^{(4)}_2 U^{\lambda\mu}_{ai}U^{\nu\kappa}_{bj}\right)S^{+}_{ai}S^{+}_{bj}$$

with

$$P^{(4)}_3 = (\lambda\mu\nu)(\kappa) + (\mu\nu\kappa)(\lambda) + (\nu\kappa\lambda)(\mu) + (\kappa\lambda\mu)(\nu)$$

Then we have the following relations

[81] $$\frac{1}{4} P^{(4)}_3 U^{\lambda\mu\nu}_{ai}\langle|S_{ai}H^{\kappa}|\rangle = \frac{1}{4} P^{(4)}_1 U^{\lambda}_{ai}\langle|S_{ai}H^{\mu\nu\kappa}|\rangle + \frac{1}{4} P^{(4)}_2 U^{\lambda}_{ai}U^{\mu}_{bj}\langle|S_{ai}(H^{\nu\kappa} - E^{\nu\kappa})S^{+}_{bj}|\rangle + P^{(4)}_3 U^{\lambda}_{ai}U^{\mu}_{bj}U^{\nu}_{ck}U^{\kappa}_{dl}$$
$$\times\left[\frac{9}{4}\langle|S_{ai}S_{bj}(H - E)S^{+}_{ck}S^{+}_{dl}|\rangle + 2\langle|S_{ai}S_{bj}S_{ck}HS^{+}_{dl}|\rangle\right] + \frac{1}{4} P^{(4)}_2[U^{\lambda}_{ai}\langle|S_{ai}H^{\mu}|\rangle U^{\nu\kappa} + U^{\mu}_{ai}\langle|S_{ai}H^{\lambda}|\rangle U^{\nu\kappa}]$$
$$+ \frac{1}{2} P^{(4)}_2 U^{\lambda\mu}_{ai}\Bigg[\langle|S_{ai}H^{\nu\kappa}|\rangle + \frac{3}{2}\{\langle|S_{ai}(H^{\nu} - E^{\nu})S^{+}_{bj}|\rangle U^{\kappa}_{bj} + \langle|S_{ai}(H^{\kappa} - E^{\kappa})S^{+}_{bj}|\rangle U^{\nu}_{bj}\} + \{\langle|S_{ai}(H - E)S^{+}_{bj}|\rangle$$
$$+ \langle|S_{ai}S_{bj}H|\rangle\}U^{\nu\kappa}_{bj} + 2\{2\langle|S_{ai}S_{bj}HS^{+}_{ck}|\rangle + \langle|S_{ai}HS^{+}_{bj}S^{+}_{ck}|\rangle\}U^{\nu}_{bj}U^{\kappa}_{ck}\Bigg]$$

In the case of $\lambda = \mu = \nu = \kappa$, the above equations are reduced to eq. [54]. Once $U^{\lambda\lambda\lambda}_{ai}$ have been determined, $U^{\lambda\lambda\mu}_{ai}$ can be obtained by putting $\lambda = \nu = \kappa$ in eq. [81]. Finally we can determine the remaining $U^{\lambda\mu\nu}_{ai}$ using the known $U^{\lambda\lambda\lambda}_{ai}$ and $U^{\lambda\lambda\mu}_{ai}$. Now the fourth derivatives can be evaluated in terms of known quantities. Although the equations are rather complicated, there are no algebraic problems. Finally, the fourth energy derivatives can be written as

Can. J. Chem. Downloaded from www.nrcresearchpress.com by 92.62.229.171 on 09/08/12
For personal use only.

$$[82]\quad E^{\lambda\mu\nu\kappa} = \langle|H^{\lambda\mu\nu\kappa}|\rangle + 2P_1^{(4)}U_{ai}^{\lambda}\langle|S_{ai}H^{\mu\nu\kappa}|\rangle + 2P_2^{(4)}U_{ai}^{\lambda}U_{bj}^{\mu}\langle|S_{ai}(H^{\nu\kappa} - E^{\nu\kappa})S_{bj}^{+}|\rangle + 6\,P_3^{(4)}U_{ai}^{\lambda}U_{bj}^{\mu}U_{ck}^{\nu}\langle|S_{ai}S_{bj}H^{\kappa}S_{ck}^{+}|\rangle$$
$$+ 8\,U_{ai}^{\lambda}U_{bj}^{\mu}U_{ck}^{\nu}U_{dl}^{\kappa}\langle|S_{ai}S_{bj}S_{ck}HS_{dl}^{+}|\rangle + 6\,U_{ai}^{\lambda}U_{bj}^{\mu}U_{ck}^{\nu}U_{dl}^{\kappa}\langle|S_{ai}S_{bj}(H - E)S_{ck}^{+}S_{dl}^{+}|\rangle$$
$$+ P_2^{(4)}U_{ai}^{\lambda\mu}U_{bj}^{\nu\kappa}\{\langle|S_{ai}(H - E)S_{bj}^{+}|\rangle + \langle|S_{ai}S_{bj}H|\rangle\} + 2\,P_2^{(4)}U_{ai}^{\lambda\mu}[\{\langle|S_{ai}H|\rangle + \langle|S_{ai}(H^{\nu} - E^{\nu})S_{bj}^{+}|\rangle U_{bj}^{\kappa}$$
$$+ \langle|S_{ai}(H^{\kappa} - E^{\kappa})S_{bj}^{+}|\rangle U_{bj}^{\nu} + \{2\langle|S_{ai}S_{bj}HS_{ck}^{+}|\rangle + \langle|S_{ai}HS_{bj}^{+}S_{ck}^{+}|\rangle\}U_{bj}^{\nu}U_{ck}^{\kappa}]$$

Of course we can express $E^{\lambda\mu\nu\kappa}$ in terms of the first-order parameters by eliminating $U_{ai}^{\lambda\mu}$ with the help of eq. [77].

4. Discussion

We have derived equations that provide the second, third, and fourth derivatives of the energy of a molecule based on the Hellmann–Feynman theorem. Hurley's condition can be used to obtain approximations to the first-order wavefunction, from which the second, third, and fourth energies can be obtained.

The present theory is correct if the basis set is complete or basis functions are independent of the perturbation. Thus the derived formulae can be applicable to any real one-electron perturbation such as electric properties if the basis functions are independent of the perturbation. It is easy to modify the formulae for the purely imaginary perturbed wavefunctions in the case of magnetic properties. If the spin-dependent perturbations are considered, the singlet excitation operators defined in eq. [16] should be replaced by the triplet excitation operators

$$[83]\quad S_{pq}^{+} = (a_{p\alpha}^{+}a_{q\alpha} - a_{p\beta}^{+}a_{q\beta})/\sqrt{2}$$

We have also derived these higher derivatives in a form similar to the sum-over-state perturbation method. These expressions will help us to understand the physical meaning associated with each energy derivative.

Let us now consider the derivatives of the energy with respect to nuclear coordinates in the SCF approximation. The molecular orbitals are defined in terms of the finite basis functions $\chi_1 \cdots \chi_m$

$$[84]\quad \varphi_i = \chi_\alpha C_{\alpha i} = \mathbf{X}\mathbf{C}_i$$

The $\mathbf{X}$ and $\mathbf{C}_i$ are the row and column vectors of χ_α and $C_{\alpha i}$, respectively. The derivative of φ_i with respect to λ is given by

$$[85]\quad \varphi_i^1 = \mathbf{X}^1\mathbf{C}_i + \mathbf{X}\mathbf{C}_i^1$$

in a matrix representation. The first term on the right-hand side of eq. [85] arises from the fact that the basis functions will generally be defined in such a way that they move with the nucleus. The second term arises from the fact that the coefficients may also depend on λ. Hurley's condition is satisfied if

$$[86a]\quad \mathbf{F}\mathbf{C}_i = \varepsilon_i\mathbf{S}\mathbf{C}_i$$

and

$$[86b]\quad \sum_i \mathbf{C}_i^{\ddagger}(\mathbf{F}_i^{(1)} - \varepsilon_i\mathbf{S}^{(1)})\mathbf{C}_i = \sum_i \Delta_i = 0$$

where

$$(\mathbf{F}^{(1)})_{\alpha\beta} = \langle\chi_\alpha^1|F|\chi_\beta\rangle, \qquad (\mathbf{S}^{(1)})_{\alpha\beta} = \langle\chi_\alpha^1|\chi_\beta\rangle$$

Equations [86*a*] are the Fock equations and hold for any SCF orbitals. However, eqs. [86*b*] are not fulfilled in general. Thus the Hellmann–Feynman theorem is not necessarily satisfied for SCF wavefunctions with finite basis set.

There are two approaches to obtaining the wavefunction obeying the Hellmann–Feynman theorem. One way is to employ floating functions (8). In floating functions the individual orbitals are not fixed a priori on the nuclei. Rather, the centers are allowed to float, the variational method then determining the optimal centering. Floating functions obey the Hellmann–Feynman theorem and therefore both eqs. [86*a*] and [86*b*] are satisfied. However, it does not mean that the basis functions are independent of the perturbation in the first order. The fact that a wavefunction constructed from floating functions satisfies the Hellmann–Feynman theorem is only due to the fact that the energy is stationary with respect to variation of the centers of the floating functions. If each Δ_i in eq. [86*b*] is forced to be zero, then the enlarged basis functions composed of $\boldsymbol{X}$ and $\boldsymbol{X}^1$ become independent of the nuclear coordinates.

Alternatively, one may leave the basis set fixed at the nuclei but basis sets $\boldsymbol{X} = \{\chi, \chi^1, \chi^2, \ldots\}$ are employed, where χ^n denotes the nth derivative of χ. It is necessary to include the derivative basis functions for every basis function. Then eq. [86*b*] is fulfilled and the SCF wavefunction obeys the Hellmann–Feynman theorem (18). If these basis sets are used, the space spanned by derivatives of the basis functions is included in the original basis function space. Thus we can expand the derivatives of the basis functions $\boldsymbol{X}^1$ in terms of the original basis functions. However, from a practical point of view, we must truncate χ^n at some low order.

In both cases we should introduce the approximation to apply the present theory. Practical applications are now being investigated in order to check a theoretical and numerical justification.

Acknowledgement

This work was partly supported by a Grant-in-Aid for Scientific Research from the Japanese Ministry of Education, Science and Culture.

1. P. Pulay. Mol. Phys. **17**, 197 (1969); **18**, 473 (1970); Adv. Chem. Phys. **69**, 241 (1987).
2. J. A. Pople, K. Raghavachari, H. B. Schlegel, and J. S. Binkley. Int. J. Quantum Chem. **S13**, 225 (1979).
3. J. Gerratt and I. M. Mills. J. Chem. Phys. **49**, 1719 (1968); **49**, 1730 (1968).
4. J. F. Gaw, Y. Yamaguchi, and H. F. Schaefer. J. Chem. Phys. **81**, 6395 (1984).
5. J. F. Gaw and N. Handy. Chem. Phys. Lett. **121**, 321 (1985).
6. H. Hellmann. Einfuhrung in die Quantenchemie. Deuticke, Leipzig. 1937. p. 285; R. P. Feynman. Phys. Rev. **56**, 340 (1939).
7. S. T. Epstein. The variational methods in quantum chemistry. Academic Press, New York. 1974; *In* The force concept in chemistry. *Edited by* B. M. Deb. Van Nostrand Reinhold Company, New York. 1981. p. 1.

Can. J. Chem. Downloaded from www.nrcresearchpress.com by 92.62.229.171 on 09/08/12
For personal use only.

8. A. C. Hurley. Proc. R. Soc. London, A: **226**, 179, 193 (1954); *In* Molecular orbitals in chemistry, physics, and biology. *Edited by* P. O. Lowdin and B. Pullman. Academic Press, New York. 1964. p. 161.
9. T. Berlin. J. Chem. Phys. **19**, 208 (1951); L. Salem. J. Chem. Phys. **38**, 1227 (1963); R. H. Schwendeman. J. Chem. Phys. **44**, 556 (1966); H. Kim. J. Chem. Phys. **48**, 301 (1968); H. Nakatsuji, K. Kanda, and T. Yonezawa. J. Chem. Phys. **77**, 1961 (1982); Int. J. Quantum Chem. **23**, 387 (1983); J. Goodisman. *In* The force concept in chemistry. *Edited by* B. M. Deb. Van Nostrand Reinhold Company, New York. 1981. p. 246.
10. W. L. Clinton. J. Chem. Phys. **33**, 1603 (1960); P. Phillipson. J. Chem. Phys. **39**, 3010 (1963); **44**, 633 (1966).
11. I. M. Mills. Mol. Phys. **1**, 107 (1957); M. L. Benson and B. Kirtman. J. Chem. Phys. **44**, 126 (1966).
12. A. Dalgarno. Adv. Phys. **11**, 281 (1962); R. M. Stevens, R. M. Pitzer, and W. N. Lipscomb. J. Chem. Phys. **38**, 550 (1963); R. M. Stevens and W. N. Lipscomb. J. Chem. Phys. **40**, 2238 (1964); K. Thomsen and P. Swanstrom. Mol. Phys. **26**, 735 (1973).
13. J. O. Hirschfelder, W. B. Brown, and S. T. Epstein. Adv. Quantum Chem. **1**, 255 (1964); J. H. Epstein and S. T. Epstein. J. Chem. Phys. **42**, 3630 (1965).
14. A. Unsold. Z. Phys. **43**, 569 (1927).
15. H. Nakatsuji. J. Chem. Phys. **61**, 3728 (1974); K. Hirao and H. Nakatsuji. J. Chem. Phys. **69**, 4535 (1978); **69**, 4548 (1978).
16. J. N. Silverman and J. C. van Leuven. Chem. Phys. Lett. **7**, 37 (1979); B. M. Deb. Chem. Phys. Lett. **17**, 78 (1972).
17. J. Cizek and J. Paldus. J. Chem. Phys. **47**, 3976 (1967); H. Fukutome. Prog. Theor. Phys. **40**, 1227 (1969); K. Hirao and H. Nakatsuji. J. Chem. Phys. **69**, 4535 (1978).
18. H. Nakatsuji, K. Kanda, and T. Yonezawa. Chem. Phys. Lett. **75**, 340 (1980); H. Nakatsuji, T. Hayakawa, and M. Hada. Chem. Phys. Lett. **80**, 94 (1981).

Can. J. Chem. Downloaded from www.nrcresearchpress.com by 92.62.229.171 on 09/08/12
For personal use only.

Universality among topological properties of electron density associated with the hydrogen–hydrogen nonbonding interactions

JERZY CIOSLOWSKI[1] AND STACEY T. MIXON

Department of Chemistry and Supercomputer Computations Research Institute, Florida State University, Tallahassee, FL 32306-3006, U.S.A.

Received July 29, 1991

This paper is dedicated to Professor Sigeru Huzinaga on the occasion of his 65th birthday

JERZY CIOSLOWSKI and STACEY T. MIXON. Can. J. Chem. **70**, 443 (1992).

Nonbonding repulsive interactions between hydrogen atoms, separated by less than ca. 2.18 Å and connected to two carbon atoms in the 1,4-positions, are associated with additional pairs of bond and ring critical points in the electron density, $\rho(\boldsymbol{r})$, and the corresponding attractor interaction lines. Such topological features of $\rho(\boldsymbol{r})$ are present in some planar benzenoid hydrocarbons, including chrysene, benzanthracene, and phenanthrene. They also appear in conformations of the biphenyl molecule with the torsional angles between the benzene rings lying within the range of 0°–27°. Properties such as the bond point – ring point distance, the difference in $\rho(\boldsymbol{r})$ at the bond point and the ring point, and the bond ellipticity are found to follow *universal* functional dependencies with the hydrogen–hydrogen distance as the controlling variable. The same is true about the corresponding difference in the second derivatives of $\rho(\boldsymbol{r})$ in the direction of the vector connecting the bond and ring points.

Key words: atoms in molecules, electron density, attractor interaction lines, steric repulsions.

JERZY CIOSLOWSKI et STACEY T. MIXON. Can. J. Chem. **70**, 443 (1992).

Les interactions répulsives non-liées entre des atomes d'hydrogène séparés par moins de 2.18 Å et liés à deux atomes de carbone situés dans les positions 1 et 4 sont associées aux paires de liaisons additionnelles, aux points critiques de cycles dans la densité électronique, $\rho(\boldsymbol{r})$, et aux lignes d'interactions attractives correspondantes. Des telles caractéristiques topologiques du $\rho(\boldsymbol{r})$ sont aussi présentes dans les hydrocarbures benzénoïdes plans, y compris dans le chrysène, le benzanthracène et le phénanthrène. Elles apparaissent aussi dans les conformations de la molécule du biphényle alors que les angles de torsion entre les noyaux benzéniques se situent entre 0° et 27°. On a trouvé que les propriétés telles que la distance entre le point de la liaison et le point du cycle, la différence dans les $\rho(\boldsymbol{r})$ au point de liaison et au point du cycle et l'ellipticité suivent des relations fonctionnelles *universelles* dans lesquelles la distance hydrogène–hydrogène est la variable qui agit comme contrôle. Ceci est aussi vrai pour la différence correspondante dans les deuxièmes dérivées de $\rho(\boldsymbol{r})$ dans la direction du vecteur qui relie les points de la liaison et du cycle.

Mots clés : atomes dans les molécules, densité électronique, lignes d'interactions attractives, répulsions stériques.

[Traduit par la rédaction]

Can. J. Chem. Downloaded from www.nrcresearchpress.com by 92.62.229.171 on 09/08/12
For personal use only.

Introduction

It is well known that analysis of the topological properties of the electron density, $\rho(\boldsymbol{r})$, provides a comprehensive description of electronic structures of chemical systems (1). Identification of the critical (extremal or stationary) points in Cartesian space, at which the gradient of electron density disappears

$$[1] \qquad \nabla\rho(\boldsymbol{r}_{crit}) = 0$$

constitutes the first step in such an analysis. Depending on the number of negative eigenvalues of the corresponding Hessian matrix,

$$[2] \qquad h_{pq} = \frac{\partial}{\partial p}\frac{\partial}{\partial q}\rho(\boldsymbol{r})\bigg|_{\boldsymbol{r}=\boldsymbol{r}_{crit}}, \quad p, q = x, y, z$$

the critical points are classified as belonging to one of the four categories: attractors, bond points, ring points, or cage points. The unions of two gradient paths (the lines of steepest ascent in $\rho(\boldsymbol{r})$) originating at the bond points and terminating at the corresponding attractors are known as the attractor interaction lines.

The second step of the topological analysis is based upon the *empirical* observation that, in most chemical systems, the only attractors are nuclei. The existence of a bond point between a pair of attractors was originally thought to be the necessary and sufficient condition for the existence of a chemical bond between the nuclei [2], justifying the name bond paths for the attractor interaction lines in chemical systems at equilibrium geometries. Indeed, in his comprehensive monograph on the topological theory of atoms in molecules [1], Bader states that "the presence of a bond path linking a pair of nuclei implies that the corresponding atoms are bonded to one another" (ref. 1, p. 33). Although such an identification is supported by the "strong" bonds, which are characterized by large values of the corresponding $\rho(\boldsymbol{r}_{crit})$, the recent findings about "weak" bonds (3) cast doubts about its validity.

The unexpected bond points, found in several chemical systems, fall into two categories (3). In charge-transfer complexes, ionic pairs, and other systems with weak interactions, the Hopf–Poincaré theorem (4) dictates the presence of at least one bond point corresponding to the bond path linking the interacting moieties. The resulting paths can usually be interpreted as those describing delocalized bonding interactions, although the coordination numbers of some atoms involved in such bonding turn out to be unexpectedly high (such as 30 for the Ne atom in the $C_{60} \cdot Ne$ complex (3, 5). The additional bond atoms are characterized by low values of the electron density and large ellipticities with the major axes pointing in a direction (almost) *parallel* to the respective ring surfaces, if any ring points are present. One should note that these bond points are persistent in the sense

[1]Author to whom correspondence may be addressed.

Printed in Canada

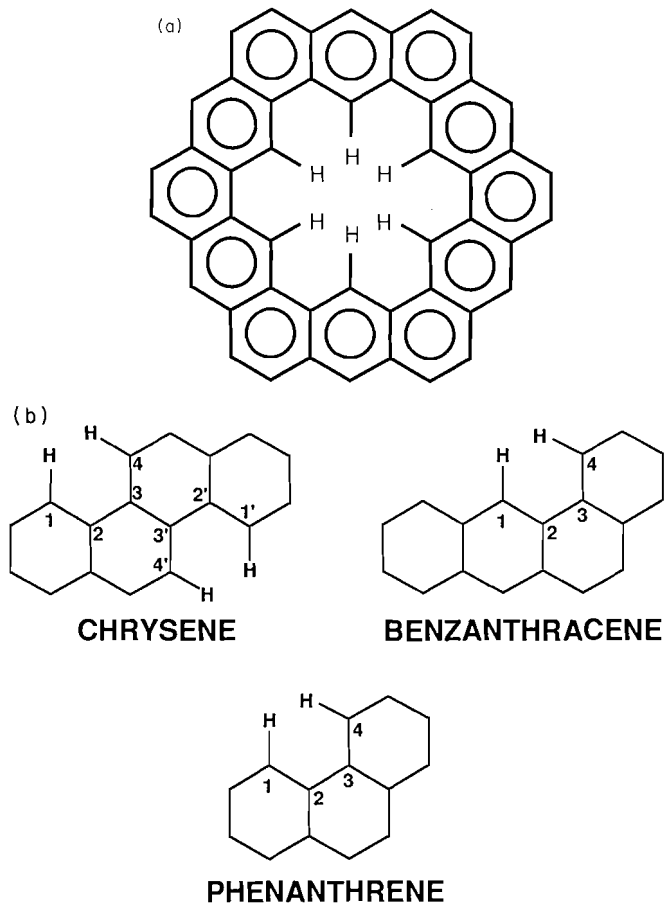

FIG. 1. (*a*) Molecular skeleton of the kekulene molecule. The sterically interacting hydrogen atoms are displayed. (*b*) Molecular skeletons of the chrysene, benzanthracene, and phenanthrene molecules. The sterically interacting hydrogen atoms, as well as the corresponding tetrads of carbon atoms are displayed.

that they do not vanish even at very large separations between the moieties. Typical examples of systems exhibiting such topological features of $\rho(\boldsymbol{r})$ are (3), to name a few, the benzene–tetracyanoethylene complex, the $C(NH_2)_3^+$ $C(CN)_3^-$ ionic pair, and the $C_{60} \cdot Ne$ endohedral complex (5).

The second category encompasses molecules and ions in which the presence of additional bond points indicates significant *nonbonding repulsive* interactions. The case of the kekulene molecule (Fig. 1*a*) is a typical example of such a situation (6). In this molecule, the six inner hydrogen atoms, which are separated by ca. 1.85 Å, are linked by highly curved interaction lines forming an inner hexagonal ring. Another example is provided by the $C(NO_2)_3^-$ ion, in which the steric interactions between the oxygen atoms give rise to three unexpected pairs of bond and ring points (7). These bond points again correspond to low electron densities; however, their ellipticities are much smaller than those of the bond points belonging to the aforementioned first category. More importantly, the major axes of their ellipticities lie in the directions *perpendicular* to the ring surfaces (3).

The existence of the second class of weak bonds hints that one should abandon the current interpretation of interaction lines in favor of a new one stating that interaction lines delineate major (not necessarily bonding!) interactions present within a given chemical system. Such a change would make it consistent with the notion that the molecular graph "isolates the pairwise interactions present in an assembly of atoms which dominate and characterize the properties of the system" (ref. 1, p. 33). The term bond path should be reserved for the interaction lines describing ordinary strong bonds.

Thus far, the major emphasis of research on the properties of $\rho(\boldsymbol{r})$ reported in the chemical literature has been directed toward bond paths (1, 2, 8). Therefore, in this paper we attempt to elaborate on the properties of interaction lines describing steric repulsive interactions. The particular example of the interaction lines linking the hydrogens connected to 1,4-carbon atoms is used for this purpose.

Topological features of electron density associated with interactions between hydrogens connected to 1,4-carbon atoms

In the following discussion, the characteristics of electron densities obtained from the HF/6-31G** calculations, pertinent to molecular geometries optimized at the same level, are used. Taking into account the results of numerical experiments with different theoretical levels, we do not expect the described topological properties of $\rho(\boldsymbol{r})$ to change qualitatively upon replacing the present wave functions by more accurate ones. We also believe that the corresponding quantitative changes should be rather small.

As mentioned in the introduction, in the kekulene molecule, the unique arrangement of six hydrogen atoms inside the inner molecular cavity leads to a quite unusual pattern of six highly curved H–H interaction lines forming a hexagonal ring. However, isolated H–H interaction lines indicating significant steric repulsions between pairs of hydrogen atoms occur in many other systems. In particular, spatial arrangements of two hydrogen atoms that result in short H–H distances are present in molecules in which the two hydrogens in question are bonded to a pair of 1,4-carbon atoms in the *Z*(*cis*) configuration. Such a bonding situation exists, for example, in all benzenoid hydrocarbons possessing the phenanthrene fragment.

Analysis of the topological properties of $\rho(\boldsymbol{r})$ in three such hydrocarbons with planar geometries, namely chrysene, benzanthracene, and phenanthrene (Fig. 1*b*), confirms these expectations. In benzanthracene and phenanthrene, one finds, in addition to "ordinary" critical points, a single bond point – ring point pair originating from the H–H repulsive interactions. In chrysene, two such pairs exist owing to molecular symmetry. In all three cases, the respective electron densities at the bond and ring points (ρ_B and ρ_R, respectively, Table 1) assume low values. The same is true about the corresponding Laplacians, $\nabla^2\rho_B$ and $\nabla^2\rho_R$. In accordance with our previous observations (3), the bond ellipticities (ε) are quite small, with the major axes directed perpendicularly to the vector connecting the corresponding bond and ring points. The H–H interaction lines are highly curved, as reflected in the large differences (Δl) between their lengths and the H–H internuclear separations (R_{HH}). The curvatures generally increase with increasing R_{HH}, whereas the bond point – ring point distances (z_{BR}) follow the opposite trend.

To gain a deeper insight into the properties of these critical points and the corresponding interaction lines, one needs a simple molecular system in which the H–H distance can be continuously varied and the accompanying variations in

Can. J. Chem. Downloaded from www.nrcresearchpress.com by 92.62.229.171 on 09/08/12
For personal use only.

TABLE 1. Topological properties of the electron density associated with the H—H bond points in benzenoid hydrocarbons

Molecule	R_{HH} (au)	z_{BR} (au)	Δl (au)	ρ_B (au)	ρ_R (au)	$\nabla^2\rho_B$ (au)	$\nabla^2\rho_R$ (au)	ϵ (au)
Chrysene	3.736	0.914	0.309	0.0127	0.0111	0.0548	0.0662	0.401
Benzanthracene	3.830	0.816	0.330	0.0116	0.0105	0.0505	0.0617	0.460
Phenanthrene	3.834	0.826	0.331	0.0115	0.0104	0.0503	0.0608	0.465

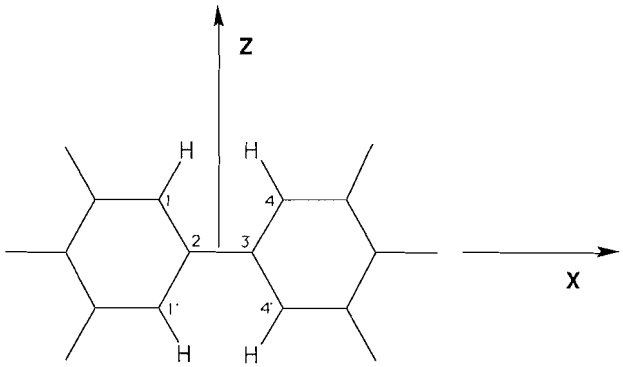

FIG. 2. The molecular skeleton of the biphenyl molecule with the sterically interacting hydrogen atoms displayed. The torsional angle (φ) is defined as the dihedral angle between the atoms 1–2–3–4 (or equivalently 1–2–3–4'). Note the coordinate axes.

the topological properties of the electron density can be monitored and, even more importantly, analyzed. The biphenyl molecule, with a variable torsional angle between the benzene rings and all other geometrical parameters fully optimized, affords such a system.

The fold catastrophe in the electron density of the biphenyl molecule

Optimization of the molecular geometry of biphenyl (Fig. 2) at the HF/6-31G** level yields the value of 45.5° for the torsional angle (φ). This is in excellent agreement with both the experimental data (φ = 44.4° ± 1.2°) (9) and previous *ab initio* calculations (HF/6-31G: φ = 44.7°) (10). Although the biphenyl molecule possesses two pairs of hydrogen atoms linked to (*Z*)-1,4-carbon atoms, at the equilibrium geometry the H–H distances are large enough to prevent the appearance of the H–H interaction lines. On the other hand, in the planar structure (φ = 0°), which is a transition state separating two identical minima, two H–H interaction lines with the corresponding four (two bond and two ring) critical points located along the *z* axis (Fig. 2) are present. These interaction lines persist up to the critical torsional angle φ_0 = 27.2°. At that geometry, in which the H–H distance equals R_0 = 2.178 Å (4.118 au, Fig. 3), the bond and ring critical points merge, annihilating each other through a fold catastrophe (4, 11).

The above observations are nicely illustrated by Figs. 4–6, in which the dependencies of the positions of the critical points, the corresponding electron densities, and the Laplacians on the torsional angle displayed. As φ_0 is approached, the properties of the bond and ring points become indistinguishable. The data displayed in these and other figures are based upon the HF/6-31G** calculations car-

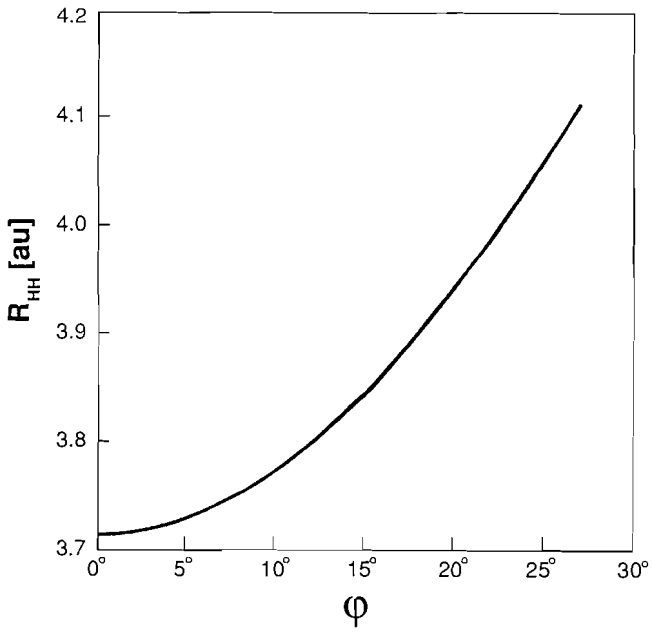

FIG. 3. The H—H separation vs. the torsional angle.

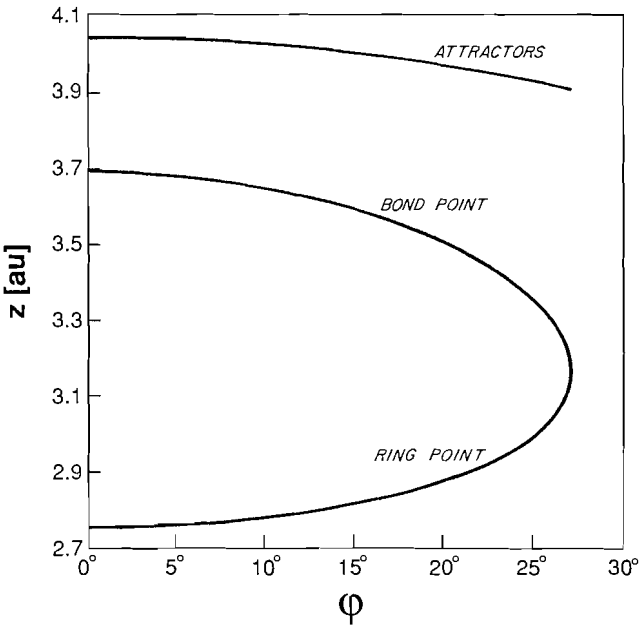

FIG. 4. The *z* coordinates of the critical points relevant to the H—H steric interactions vs. the torsional angle.

Can. J. Chem. Downloaded from www.nrcresearchpress.com by 92.62.229.171 on 09/08/12
For personal use only.

Can. J. Chem. Downloaded from www.nrcresearchpress.com by 92.62.229.171 on 09/08/12
For personal use only.

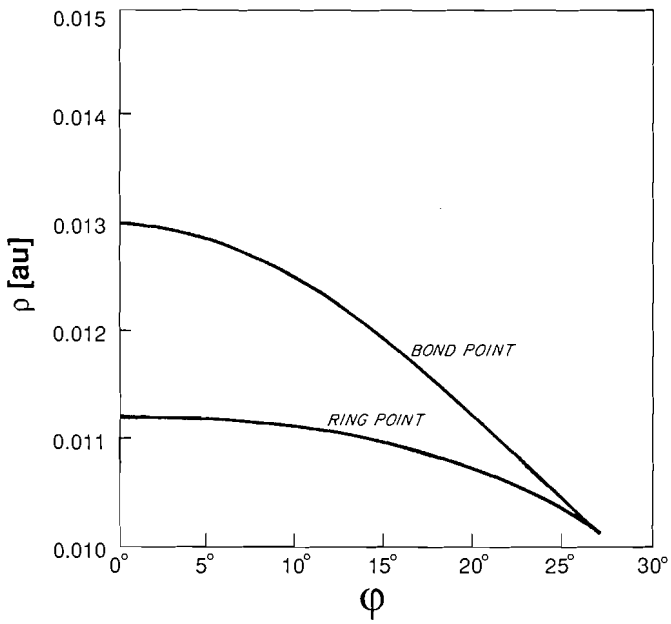

FIG. 5. The electron densities at the bond and ring critical points vs. the torsional angle.

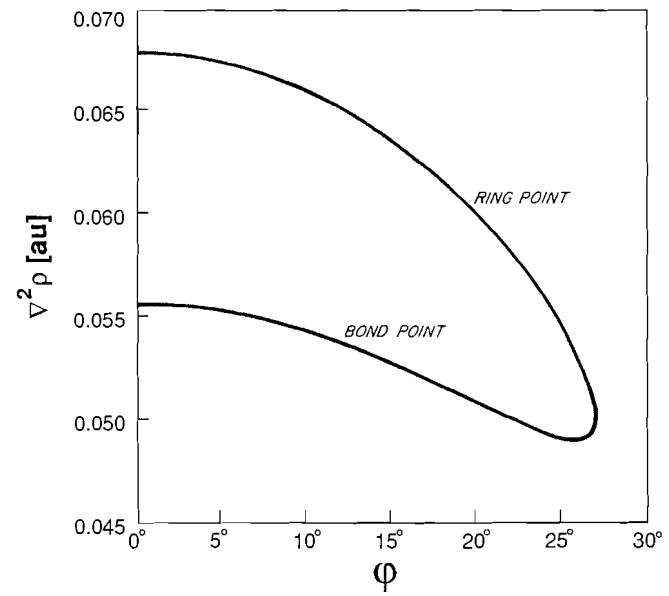

FIG. 6. The electron density Laplacians at the bond and ring critical points vs. the torsional angle.

ried out for the following values of φ: 0.0°, 5.0°, 10.0°, 15.0°, 20.0°, 21.0°, 22.0°, 23.0°, 24.0°, 25.0°, 26.0°, 26.8°, 26.9°, 27.0°, 27.1°, and 27.2°.

The calculated properties of $\rho(r)$ can be accounted for with the help of catastrophe theory (1, 4, 11, 12). In the particular case of the biphenyl molecule, the one-dimensional control and behavior spaces (11, 12) consist of the H–H distance (R_{HH}) and the distance along the z axis (z, Fig. 2), respectively. In the vicinity of the catastrophe point, the electron density is described by the unfolding (11)

$$[3] \quad \rho(R_{HH},z) = A\,(z - z_0)^3 + B(R_{HH})\,(z - z_0) + C$$

where $A < 0$, and $B(R_{HH})$ is positive for R_{HH} smaller than the critical H–H distance (R_0), while $B(R_{HH}) < 0$ for $R_{HH} > R_0$. For $R_{HH} < R_0$, the first derivative

$$[4] \quad \frac{\partial}{\partial z}\rho(R_{HH},z) = 3A\,(z - z_0)^2 + B(R_{HH})$$

has two zeros corresponding to one bond and one ring point, yielding

$$[5] \quad z_{BR}(R_{HH}) = z_B(R_{HH}) - z_R(R_{HH}) = 2\left[\frac{-B(R_{HH})}{3A}\right]^{1/2}$$

for the bond point – ring point distance. The corresponding difference in the electron densities equals

$$[6] \quad \begin{aligned}\Delta\rho(R_{HH}) &= \rho_B(R_{HH}) - \rho_R(R_{HH}) \\ &= \rho(R_{HH},z_B) - \rho(R_{HH},z_R) \\ &= \left(\frac{4}{3}\right) B(R_{HH}) \left[\frac{-B(R_{HH})}{3A}\right]^{1/2}\end{aligned}$$

Finally, for the difference between the second derivatives of $\rho(r)$ *along the direction of the vector connecting the corresponding bond and ring points*, one obtains

$$[7] \quad \begin{aligned}\Delta h(R_{HH}) &= h_B(R_{HH}) - h_R(R_{HH}) \\ &= \frac{\partial^2}{\partial z^2}\rho(R_{HH},z_B) - \frac{\partial^2}{\partial z^2}\rho(R_{HH},z_R) \\ &= 6A\left[\frac{-B(R_{HH})}{3A}\right]^{1/2}\end{aligned}$$

Since, in the vicinity of R_0, $B(R_{HH})$ changes linearly with R_{HH}, one expects the following critical behavior:

$$[8a] \quad z_{BR}(R_{HH}) = k_z\,(R_0 - R_{HH})^{1/2}$$

$$[8b] \quad \Delta\rho(R_{HH}) = k_\rho\,(R_0 - R_{HH})^{3/2}$$

$$[8c] \quad \Delta h(R_{HH}) = k_h\,(R_0 - R_{HH})^{1/2}$$

as R_{HH} approaches R_0 from below. An asymptotic analogous to [8*c*] is also expected for the difference between the electron density Laplacians,

$$[8d] \quad \Delta(\nabla^2\rho) = \nabla^2\rho_B - \nabla^2\rho_R$$

Plots of the appropriate powers of z_{BR}, $\Delta\rho$, Δh, and $\bar{\Delta}(\nabla^2\rho)$ vs. R_{HH} (Fig. 7–10) indeed reveal such behavior. However, the domains of validity of eqs. [8*a*] and [8*b*] are much broader than expected. Thus, the plot of z_{BR}^2 vs. R_{HH} (Fig. 7) shows a very small deviation from linearity throughout the entire range of R_{HH}. The same is true, although to a lesser extent, about the plot of $\Delta\rho^{2/3}$ vs. R_{HH} (Fig. 8). On the other hand, the relationships between Δh^2 and R_{HH} (Fig. 9) and between $\Delta(\nabla^2\rho)$ and R_{HH} (Fig. 10) are markedly nonlinear for larger differences between R_0 and R_{HH}.

An equation relating the values of z_{BR}, $\Delta\rho$, and Δh can be derived by combining eqs. [8*a*]–[8*c*]. The characteristic ratio is given by

$$[9] \quad \kappa = -\Delta h\,\frac{z_{BR}^2}{\Delta\rho} = 12.$$

This relationship is satisfied to a high degree of accuracy for the entire range of R_{HH}, as the plot of $-\Delta h\ z_{BR}^2$ vs. $\Delta\rho$

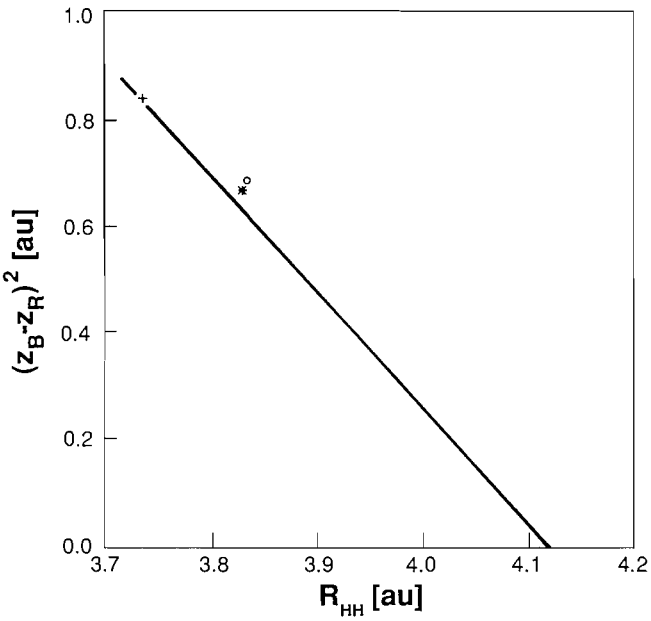

FIG. 7. The critical behavior of z_{BR}. +, chrysene; *, benzanthracene; o, phenanthrene.

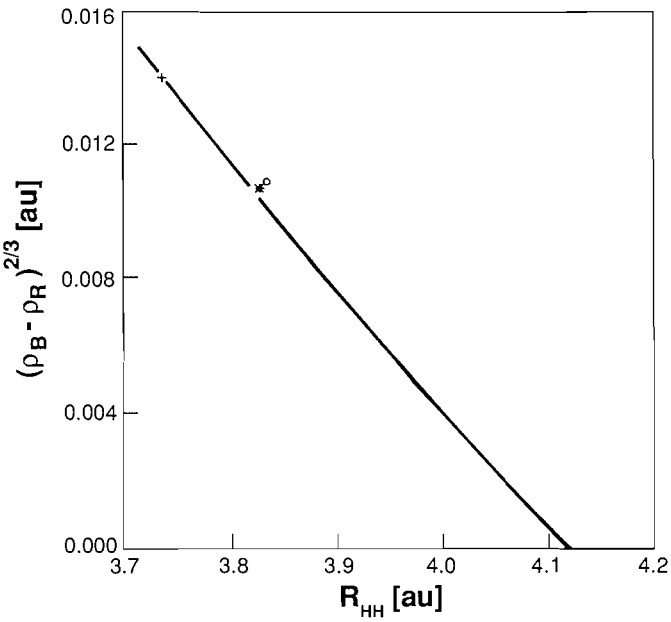

FIG. 8. The critical behavior of $\Delta\rho$. +, chrysene; *, benzanthracene; o, phenanthrene.

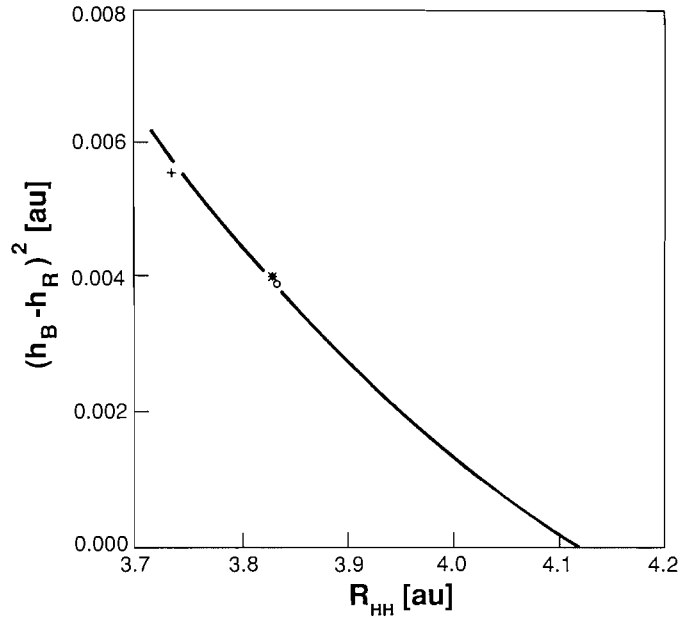

FIG. 9. The critical behavior of Δh. +, chrysene; *, benzanthracene; o, phenanthrene.

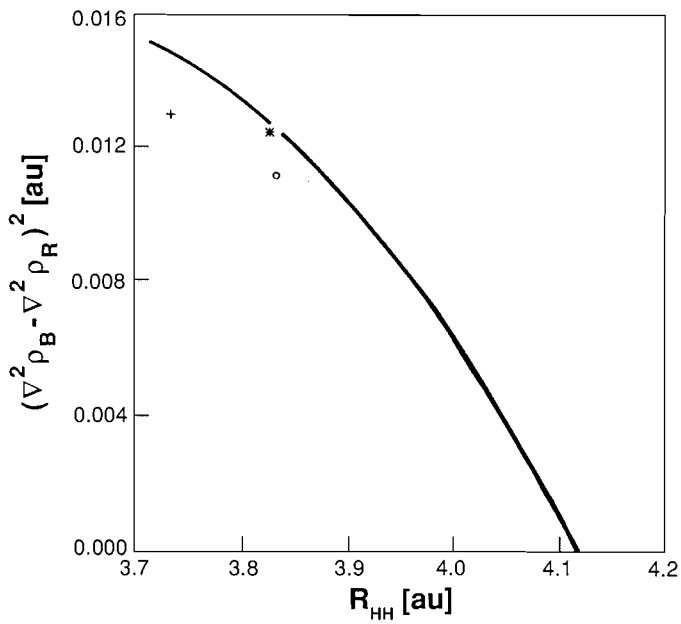

FIG. 10. The critical behavior of $\Delta(\nabla^2\rho)$. +, chrysene; *, benzanthracene; o, phenanthrene.

(Fig. 11) is indistinguishable from a straight line with a slope of 12. The singularity of the bond ellipticity (ϵ) (1, 2, 8) at $R_{HH} = R_0$ (Fig. 12) is also easily understood from eq. [8*c*]: As the critical value of R_{HH} is approached, one of the eigenvalues of the Hessian matrix becomes vanishingly small resulting in the singularity of ϵ. On the other hand, we are unable to explain the observed dependence of Δl on R_{HH} (Fig. 13).

Universality among the topological properties of electron density associated with the hydrogen–hydrogen nonbonding interactions

Inspection of Figs. 7–13 reveals that some of the aforementioned properties follow *universal* functional dependencies on the distance between the hydrogen atoms involved in the repulsive interactions. Such universality, which is exhibited by the values of z_{BR} (Fig. 7), $\Delta\rho$ (Fig. 8), Δh (Fig. 9), κ (Fig. 11), and ϵ (Fig. 12) is quite unexpected. One should note that, in planar benezoid hydrocarbons, the four carbon atoms and the two hydrogen atoms linked by a six-membered ring of interaction lines are coplanar. On the other hand, in the twisted biphenyl molecule, this coplanarity is nonexistent. This difference in the arrangement of the relevant nuclei is the probable cause of deviations present in the plots of $\Delta(\nabla^2\rho)$ vs. R_{HH} (Fig. 10) and Δl vs. R_{HH} (Fig. 13). Indeed, inspection of the eigenvalues of the Hessian matrix

Can. J. Chem. Downloaded from www.nrcresearchpress.com by 92.62.229.171 on 09/08/12
For personal use only.

Can. J. Chem. Downloaded from www.nrcresearchpress.com by 92.62.229.171 on 09/08/12
For personal use only.

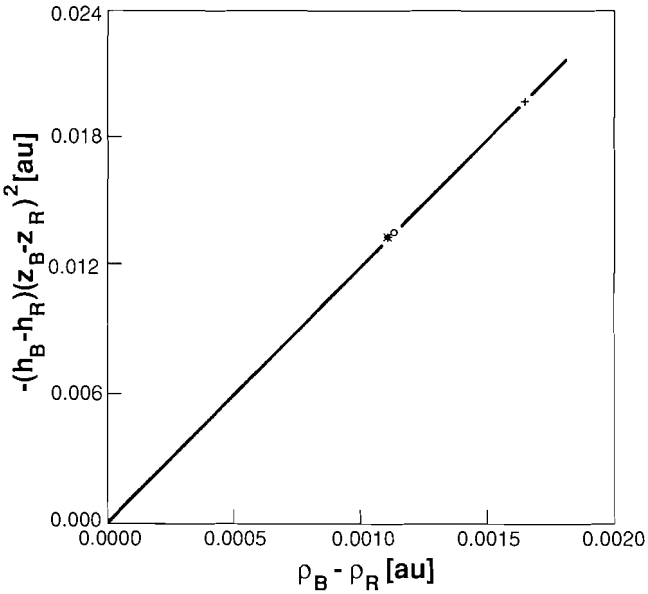

FIG. 11. Constancy of the characteristic ratio. +, chrysene; *, benzanthracene; o, phenanthrene.

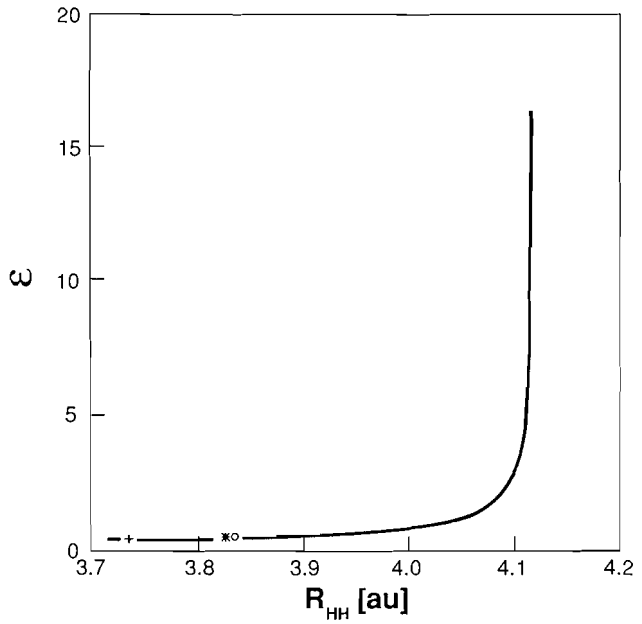

FIG. 12. The bond ellipticity vs. the torsional angle. +, chrysene; *, benzanthracene; o, phenanthrene.

makes it possible to conclude that most of the observed deviations in $\Delta(\nabla^2\rho)$ come from the component of $\nabla^2\rho_B$ perpendicular to the interaction line.

The remarkable accuracy to which the universal relationships are satisfied is particularly apparent from the values of the characteristic ratio (κ), eq. [9], computed for the benzenoid hydrocarbons. The values listed in Table 2 deviate from 12 by less than 0.5%! The projected Hessians, used in eq. [9] and in Fig. 9, are calculated by contracting the Hessian matrices, eq. [2], with the components of the vector (r_{BR}) connecting the respective bond and ring points and applying the appropriate normalization; z_{BR} is the length of r_{BR}.

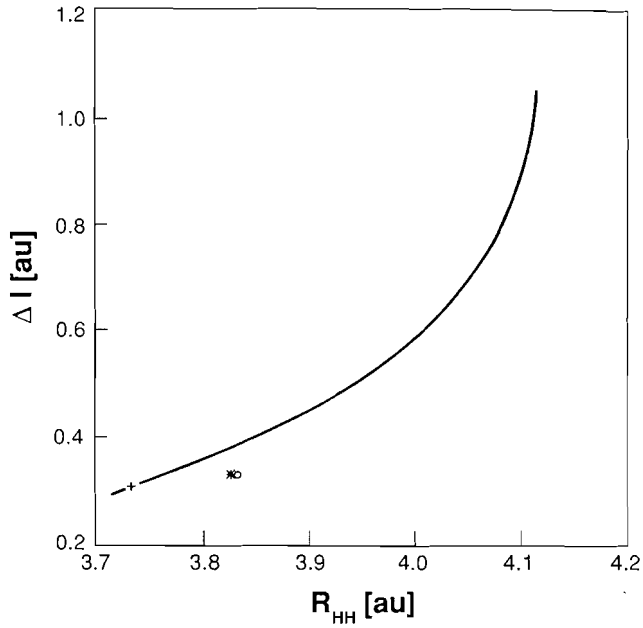

FIG. 13. The difference between the interaction line length and the H—H distance vs. the torsional angle. +, chrysene, *, benzanthracene; o, phenanthrene.

TABLE 2. Differences in the electron densities and the corresponding projected Hessians at the H—H bond and ring points in benzenoid hydrocarbons

Molecule	$\Delta\rho$ (au)	Δh (au)	κ (au)
Chrysene	0.001 654	−0.023 63	11.94
Benzanthracene	0.001 111	−0.020 02	12.00
Phenanthrene	0.001 127	−0.019 79	11.98

Finally, one should note that the low values of bond ellipticities found in the aforementioned benzenoid hydrocarbons (including kekulene, see Table 1 and ref. 6) are a consequence of the universality of ϵ, as displayed in Fig. 12, and the fact that the relevant H–H distances are quite small in these molecules.

Conclusions

The calculated properties of $\rho(r)$ in some benzenoid systems lead us to the following conclusions:

1. The existence of an attractor interaction line between a pair of nuclei does not necessarily imply the presence of bonding between those nuclei. Instead, the attractor interaction lines should be interpreted as those delineating major (either bonding or nonbonding, attractive or repulsive) interactions in a given molecular system.

2. In organic molecules in which two hydrogen atoms attached to carbon atoms separated by three carbon—carbon bonds (1,4-carbon atoms) are present, there is a possibility of the existence of H–H interaction lines. If present, such interaction lines result in an additional pair of bond and ring critical points.

3. The hydrogen–hydrogen distance (R_{HH}) appears to be the controlling variable that not only determines whether the

H–H interaction lines are present, but also controls the values of several properties of $\rho(r)$ pertinent to the critical points associated with such interaction lines.

4. One should expect the H–H interaction lines to be present if R_{HH} is less than ca. 2.18 Å. Therefore, the H–H interaction lines are present in the kekulene, chrysene, benzanthracene, and phenanthrene molecules, but are absent in the biphenyl molecule at its equilibrium geometry. For the same reason, the molecular graph of the planar transition state of (*Z*)-butadiene is devoid of the H–H interaction lines, because the relevant H–H distance equals 2.335 Å (at the HF/6-31G** level). The value of 2.18 Å can be therefore regarded as the contact interatomic separation (CIS) (13) for the H–H pair. This should be compared with double the van der Waals radius of the hydrogen atom, which equals ca. 2.4 Å (14). The values of CIS for other pairs of atoms or functional groups can be defined in a similar fashion (13).

5. The CIS values are expected to depend not only on the pair of atoms involved, but also on the manner in which they are bonded. For this reason, the H–H interaction lines are absent in $C_{60}H_{60}$, although the H–H separation (2.0 Å at the HF/6-31G** level (15) in this molecule is less than CIS for the pair of hydrogens bonded to 1,4-carbon atoms. However, in the $C_{60}H_{60}$ molecule, the two hydrogen atoms in question are bonded in a highly unusual manner to two adjacent carbon atoms through two almost parallel bonds.

We believe that the present work will contribute to a better understanding of the attractor interaction lines. The interaction lines associated with nonbonding steric repulsions certainly deserve no less attention than the more common bond paths.

Acknowledgement

This work was partially supported by the National Science Foundation under contract CHE-9015566, the Camille and Henry Dreyfus Foundation New Faculty Award Program, and Florida State University through time granted on its Cray Y-MP digital computer.

1. R. F. W. Bader. Atoms in molecules: a quantum theory. Clarendon Press, Oxford. 1990.
2. R. F. W. Bader. Acc. Chem. Res. **18**, 9 (1985).
3. J. Cioslowski, S. T. Mixon, and W. D. Edwards. J. Am. Chem. Soc. **113**, 1083 (1991).
4. K. Collard and G. G. Hall. Int. J. Quantum Chem. **12**, 623 (1977).
5. J. Cioslowski and E. D. Fleischmann. J. Chem. Phys. **94**, 3730 (1991).
6. J. Cioslowski, P. B. O'Connor, and E. D. Fleischmann. J. Am. Chem. Soc. **113**, 1086 (1991).
7. J. Cioslowski, S. T. Mixon, and E. D. Fleischmann. J. Am. Chem. Soc. **113**, 4751 (1991).
8. R. F. W. Bader, T. S. Slee, D. Cremer, and E. Kraka. J. Am. Chem. Soc. **105**, 5061 (1983); D. Cremer and E. Kraka. Croat. Chem. Acta, **57**, 1265 (1984).
9. A. Almenningen, O. Bastiansen, L. Fernholt, B. N. Cyvin, S. J. Cyvin, and S. Samdal. J. Mol. Struct. **128**, 59 (1985).
10. G. Häfelinger and C. Regelmann. J. Comput. Chem. **9**, 1057 (1987).
11. J. Cioslowski. J. Phys. Chem. **94**, 5496 (1990).
12. R. Thom. Stabilité structurelle et morphogènése. Benjamin-Addison-Wesley, New York. 1973.
13. J. Cioslowski and S. T. Mixon. J. Am. Chem. Soc. In press.
14. L. Pauling. The nature of the chemical bond. Cornell University Press, Ithaca, N.Y. 1960.
15. J. Cioslowski. Chem. Phys. Lett. **181**, 68 (1991).

Can. J. Chem. Downloaded from www.nrcresearchpress.com by 92.62.229.171 on 09/08/12
For personal use only.

The relationship between the rate–equilibrium coefficient α and transition state properties: a second-order Møller–Plesset perturbation study of S_N2 reactions

ZHENG SHI AND RUSSELL J. BOYD
Department of Chemistry, Dalhousie University, Halifax, N.S., Canada B3H 4J3

Received January 25, 1991

This paper is dedicated to Professor Sigeru Huzinaga on the occasion of his 65th birthday

ZHENG SHI and RUSSELL J. BOYD. Can. J. Chem. **70**, 450 (1992).

Ab initio calculations including electron correlation are used to study rate–equilibrium relationships in gas-phase S_N2 reactions. The difference between the "intrinsic" α and "group" α is emphasized. In general, the "group" α cannot be used as a measure of the transition state structure. The relationships between the "intrinsic" α and other properties, such as reaction endothermicity, geometry change, and the charge transfer, are discussed. A geometry change parameter R_α, defined by analogy with the definition of the "intrinsic" α, is shown to be linearly related to the "intrinsic" α. The charge transfer at the transition state is related not only to energy changes but also to the electronegativities of the entering nucleophile and leaving group in the product and reactant, respectively, and to the electronic structures at the transition state. Thus, the charge transfer parameter Q_α, unlike the "intrinsic" α and R_α, is affected by the electronegativities of the groups involved in the reaction. The systems studied are S_N2 reactions of the type $N^- + CH_3X \rightarrow CH_3N + X^-$, where X = H, NH_2, OH, OOH, F, CCH, *C*N, *N*C, PH_2, SH, and Cl when N = H, and where X = H, NH_2, OH, F, *C*N, *N*C, PH_2, SH, and Cl when N = F.

Key words: S_N2 reactions, rate–equilibrium relationships, transition state properties.

ZHENG SHI et RUSSELL J. BOYD. Can. J. Chem. **70**, 450 (1992).

On a utilisé les calculs *ab initio* incluant la corrélation d'électrons pour étudier la relation existant entre la vitesse et l'équilibre des réactions S_N2. On a mis l'accent sur la relation entre le α «intrinsèque» et le groupe α. En général on ne peut pas utiliser le groupe α comme mesure de la structure de l'état de transition. On discute de la relation entre le α «intrinsèque» et les autres propriétés tels le caractère endothermique de la réaction, le changement de géométrie et le transfert de charge. On démontre que le paramètre de changement de géométrie R_α, défini par analogie avec la définition de α «intrinsèque», est relié de façon linéaire au α «intrinsèque». Le transfert de charge au niveau de l'état de transition est relié non seulement aux changements d'énergie mais également à l'électronégativité du nucléophile attaquant et du groupe labile dans le produit et dans le réactif respectivement et à la structure électronique de l'état de transition. Ainsi, le paramètre de transfert de charge Q_α, contrairement au α «intrinsèque» et au R_α, est affecté par l'électronégativité des groupes impliqués dans la réaction. Les systèmes étudiés sont des réactions S_N2 du type $N^- + CH_3X \rightarrow CH_3N + X^-$ où X = H, NH_2, OH, OOH, F, CCH, *C*N, *N*C, PH_2. SH et Cl lorsque N = H, et où X = H, NH_2, OH, F, *C*N, *N*C, PH_2, SH et Cl lorsque N = F.

Mots clés : réactions S_N2, relations vitesse–équilibre, propriétés de l'état de transition.

[Traduit par la rédaction]

Introduction

Rate–equilibrium relationships have enjoyed widespread usage and success for many years. They have been used not only to predict reaction rates and equilibrium constants but also to discover under what conditions a change in mechanism occurs (1). Furthermore, the α coefficient of rate–equilibrium relationships is used to measure the position of the transition state (TS) along the reaction coordinate. This is based on the Leffler–Hammond postulate (2), according to which the transition state properties are intermediate between reactant and product. A more exothermic reaction has a small α and the TS resembles the reactant more than the product. Moreover, α should have a value between zero and one. However, anomalous values ($\alpha < 0$ and $\alpha > 1$) have been observed (3) and questions about the validity of using α as an indicator of TS structure have been raised (4). Thus, further studies on the subject are needed, especially with respect to geometry changes and charge transfer at the transition state. Such properties cannot be obtained directly from experiments and much remains to be done (5).

In this paper, we present an *ab initio* study of gas-phase S_N2 reactions at the second-order Møller–Plesset perturbation level. The study is done within the framework of the Marcus equation. The intention is to provide a better understanding of rate–equilibrium relationships and to see whether or not there is a relationship between α and transition state properties, especially the geometry change and charge transfer.

The Marcus equation (6) has been applied to a wide range of reactions including electron transfer, proton transfer, and methyl transfer reactions (5*b*, 7). According to the Marcus equation, the free energy of activation ($\Delta G^{\ddagger}$) is related (eq. [1]) not only to the free energy of a reaction (ΔG^0) but also to the intrinsic barrier ($\Delta G_0^{\ddagger}$)

$$[1] \qquad \Delta G^{\ddagger} = \Delta G_0^{\ddagger} + 0.5\Delta G^0 + \frac{(\Delta G^0)^2}{16\Delta G_0^{\ddagger}}$$

or in the potential energy form (6*b*)

$$[2] \qquad \Delta E^{\ddagger} = \Delta E_0^{\ddagger} + 0.5\Delta E^0 + \frac{(\Delta E^0)^2}{16\Delta E_0^{\ddagger}}$$

Thus, when $\Delta E_0^{\ddagger}$ is a constant,

$$[3] \qquad \alpha = \frac{\partial \Delta E^{\ddagger}}{\partial \Delta E^0} = 0.5\,(1 + x)$$

Can. J. Chem. Downloaded from www.nrcresearchpress.com by 92.62.229.171 on 09/08/12
For personal use only.

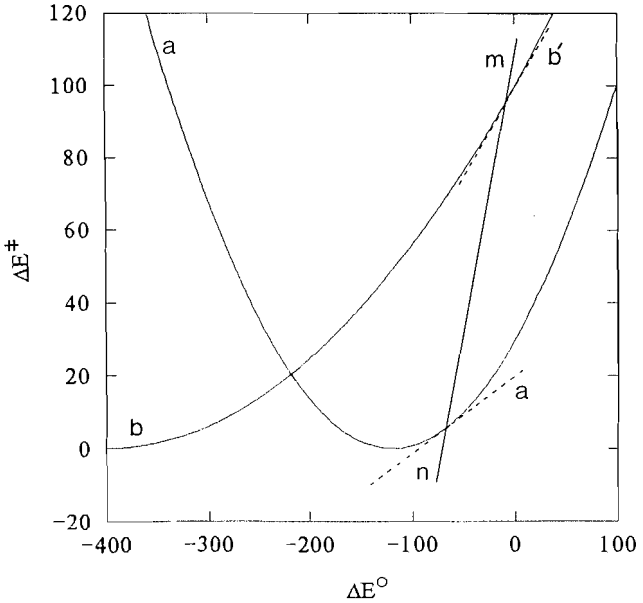

FIG. 1. Illustration of $\Delta E^{\ddagger}$ versus ΔE^0 (eq. [2]). In curve *a*, $\Delta E_0^{\ddagger} = 30$ kJ/mol and in curve *b*, $\Delta E_0^{\ddagger} = 100$ kJ/mol.

whereas if $\Delta E_0^{\ddagger}$ is not a constant

$$[4] \qquad \alpha = \frac{\partial \Delta E^{\ddagger}}{\partial \Delta E^0} = 0.5\,(1 + x) + (1 - x^2)\,\frac{\partial \Delta E_0^{\ddagger}}{\partial \Delta E^0}$$

where $x = \Delta E^0/4\Delta E_0^{\ddagger}$. Equations [3] and [4] were originally given by Marcus (6*c*).

For any reaction, α can be calculated from eq. [3] provided the ΔE^0 and $\Delta E_0^{\ddagger}$ values are known, and also α can be calculated according to eq. [4] if $\partial \Delta E_0^{\ddagger}/\partial \Delta E^0$ is known. Thus, at least two possible α values can be calculated for each reaction (by putting different reactions into one group, i.e., by changing $\partial \Delta E_0^{\ddagger}/\partial \Delta E^0$, different α values can be obtained from eq. [4]). The mathematical and physical differences between α's obtained from eqs. [3] and [4] should be understood and stressed as they often cause misinterpretations and confusion. The α obtained from eq. [3] is the derivative of the energy barrier with respect to the reaction energy in the absence of any variation in the intrinsic barrier. This α, which we call the "intrinsic" α, is characteristic of each reaction. On the other hand, the α obtained from eq. [4] includes the variation of intrinsic barriers; it involves information about other reactions ($\partial \Delta E_0^{\ddagger}/\partial \Delta E^0$). Thus, the α obtained from eq. [4] is characteristic of each group and is referred to as the "group" α. Figure 1 illustrates the difference between the "intrinsic" α and the "group" α. In this simplified example, we have two reactions; one (reaction [I]) has an intrinsic barrier $\Delta E_0^{\ddagger} = 30$ kJ/mol and $\Delta E^0 = -70$ kJ/mol and the other reaction (reaction [II]) has an intrinsic barrier $\Delta E_0^{\ddagger} = 100$ kJ/mol and $\Delta E^0 = -10$ kJ/mol. Using the Marcus equation (eq. [2]), when $\Delta E_0^{\ddagger} = 30$ kJ/mol, we obtain curve *a* and when $\Delta E_0^{\ddagger} = 100$ kJ/mol, we obtain curve *b* (see Fig. 1). The tangent of curve *a* at $\Delta E^0 = -70$ kJ/mol (*a'*) corresponds to the intrinsic α for reaction [I]. Similarly, the tangent of curve *b* at $\Delta E^0 = -10$ kJ/mol (*b'*) corresponds to the intrinsic barrier for reaction [II], whereas the slope of line mn corresponds to the group α of the two reactions.

Marcus indicated that only the intrinsic α, which has a normal range between zero and one (6*c*), can be used as a TS index. Lewis noted that the group α does not reflect product-like character as it is related to $\partial \Delta E_0^{\ddagger}/\partial \Delta E^0$ (5*d*). Other people (4*d*, *e*) also pointed out that the group α is not a reliable measure of the TS structure. At best, if the last term in eq. [4] is small, the group α is close to the average of the intrinsic α's.

In this paper, we present studies of the gas-phase S_N2 reactions $N^- + CH_3X \rightarrow CH_3N + X^-$, where X = H, NH_2, OH, OOH, F, CCH, *C*N, *N*C, PH_2, SH, and Cl when N = H, and where X = H, NH_2, OH, F, *C*N, *N*C, PH_2, SH, and Cl when N = F. The emphasis is on energy changes, geometry changes, and charge transfer at the TS and their relationship with α.

Computational methods

In earlier papers of our series on gas-phase S_N2 reactions (8*a–d*) we described the computational methods and results obtained at three levels of sophistication (8*b*, *c*). In this paper, the method denoted by MP2′ in previous papers is used (8*a–d*), unless stated otherwise. That is, the geometries were optimized at the Hartree–Fock level using the analytic gradient method and energies were calculated by use of second-order Møller–Plesset perturbation theory. Details about optimized geometries and energies can be found elsewhere (8*b*, *c*). The 6-31G basis set supplemented with diffuse and polarization functions (standard notation 6-31++G**) was used for all atoms except the three methyl hydrogens for which the 6-31G basis set was used. The justification for using single point Møller–Plesset calculations carried out at the geometries optimized at the Hartree–Fock level has been discussed in previous papers (8*b–d*). It has been shown that for those properties which involve at least two states, for example, energy differences and configuration contribution analysis of the TS, the MP2′ method gives results which are consistent with the full MP2 treatment (second-order Møller–Plesset perturbation calculations carried out at the geometries optimized at the same level).

The calculations were done by using the GAUSSIAN 80 and GAUSSIAN 86 programs (9) and the topological properties were calculated using the PROAIM and modified PROAIM packages (10).

Results and discussion

To repeat our earlier discussion, the intrinsic α is characteristic of each reaction, whereas the group α is a group property. In the following discussion, the intrinsic α's are used and the elementary step of converting the reactant ion–molecule complex ($N^- \cdots RX$) to the product ion–molecule complex ($NR \cdots X^-$) is considered unless stated otherwise.

Values of the α coefficients calculated from eqs. [3] and [4] and from linear plots of $\Delta E^{\ddagger}$ versus ΔE^0 (8*b*, *e*) are listed in Table 1. For exothermic reactions, the intrinsic α's are <0.5 (the second column), whereas the group α's (the third column) are usually >0.5. This is a direct result of the large gradient $\partial \Delta E_0^{\ddagger}/\partial \Delta E^0$ for these groups of reactions (8*b*, *e*). For the group of reactions in which X = CCH, *C*N, and *N*C the gradients ($\partial \Delta E_0^{\ddagger}/\partial \Delta E^0$) are 0.27 and 0.18 when N = H and F, respectively; for the group of reactions in which X = PH_2, SH, and Cl the gradients are 0.30 and 0.23 when N =

Can. J. Chem. Downloaded from www.nrcresearchpress.com by 92.62.229.171 on 09/08/12
For personal use only.

TABLE 1. Comparison of α coefficients calculated by different means[a]

N	X	α^b	α^c	α^d	ΔE^0
H	CCH	0.43	0.70	0.62	−127.13
H	*C*N	0.38	0.64	0.62	−206.61
H	*N*C	0.29	0.51	0.62	−308.41
H	PH_2	0.38	0.66	0.52	−187.31
H	SH	0.30	0.55	0.52	−275.74
H	Cl	0.17	0.33	0.52	−364.49
H	NH_2	0.44	0.80	0.69	−87.92
H	OH	0.37	0.70	0.69	−176.57
H	OOH	0.33	0.65	0.69	−203.77
H	F	0.25	0.52	0.69	−257.47
F	CCH	0.64	0.81	0.73	137.26
F	*C*N	0.57	0.75	0.73	67.92
F	*N*C	0.46	0.63	0.73	−32.97
F	PH_2	0.60	0.82	0.68	80.23
F	SH	0.49	0.72	0.68	−7.70
F	Cl	0.32	0.51	0.68	−93.71
F	NH_2	0.71	0.92	0.84	158.58
F	OH	0.62	0.86	0.84	74.09

[a]The reactant ion–molecule complex is taken as the reactant and the product ion–molecule complex is taken as the product. Thus, $\Delta E^0 = E(CH_3N\cdots X^-) - E(N^-\cdots CH_3X)$ and $\Delta E^+ = E([N\cdots CH_3\cdots X]^-) - E(N^-\cdots CH_3X)$.
[b]From eq. [3].
[c]From eq. [4].
[d]From the ΔE^+ versus ΔE^0 linear plot of ref. 8*e*.

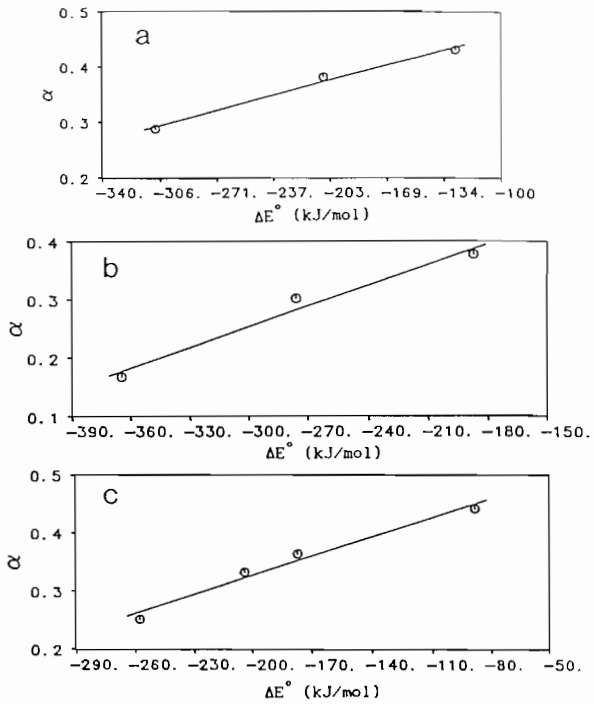

FIG. 2. Plot of α values versus ΔE^0 for the reactions $H^- + CH_3X \rightarrow CH_4 + X^-$. (*a*) X = CCH, *C*N, and *N*C; (*b*) X = PH_2, SH, and Cl; (*c*) X = NH_2, OH, OOH, and F.

H and F, respectively; for the group of reactions X = NH_2, OH, OOH, and F the gradients are 0.36 and 0.25 when N = H and F, respectively (8*b*, *e*). The α values obtained from ΔE^+ versus ΔE^0 linear plots (the fourth column) are averages of the values obtained from eq. [4] for each group and therefore they are larger than 0.5 as well.

Plots of intrinsic α versus ΔE^0 are shown in Fig. 2. Linear plots between α and ΔE^0 are observed within groups X = CCH, *C*N, *N*C, or X = PH_2, SH, Cl or X = NH_2, OH, OOH, and F. The observed linear relationship is due to the linear relationship between $\Delta E_0^{\ddagger}$ and ΔE^0 within these groups (8*b*, *e*). Detailed rationalization of the establishment of the reaction groups is provided elsewhere (8*b*, *e*). A brief explanation about the relationship between the intrinsic barrier and the reaction energy is provided by the following.

There are six important valence bond configurations in S_N2 reactions (11)

$N^{\cdot}\,R\cdot\cdot X$ $\quad$ $N\cdot\cdot R:X^-$ $\quad$ $N^{\cdot}R^+:X^-$ $\quad$ $N\cdot\,R^{\cdot}\cdot X$

1 $\quad$ **2** $\quad$ **3** $\quad$ **4**

$N^{\cdot}\,R^{\cdot}X^+$ $\quad$ $N^+:R^-:X^-$

5 $\quad$ **6**

The reactant and product wavefunction can be approximated as (12)

[5] $\quad \Psi_R = a_1\psi_1 + a_2\psi_3 + a_3\psi_5$

[6] $\quad \Psi_P = b_1\psi_2 + b_2\psi_3 + b_3\psi_6$

and the TS wavefunction can be approximated as (8*ab*, *d*)

[7] $\quad \Psi_{TS} = a\Psi_R + b\Psi_P + c\psi_3 + d\psi_4$

It has been shown that the intrinsic barrier is affected by the TS electronic structure, the hybridization factor of X and the electronegativity of X (8*b*, *e*). A considerable contribution of $N^{\cdot}R^+:X^-$ to the transition state (in addition to its contribution to the reactant and product) indicates a large difference in progress of the two reaction events (the main reaction and disparity reaction (8*e*, 13)) and a low intrinsic barrier. An *sp*-hybridized leaving group leads to a rapid ascent of the energy barrier and it increases the intrinsic barrier. Thus variation of TS electronic structures and the hybridization of the leaving group results in different relationships between $\Delta E_0^{\ddagger}$ and ΔE^0. For those reactions which have similar TS structures (similar values of *c* or *d* in eq. [7]) and the same hybridization of the leaving group, a linear relationship between $\Delta E_0^{\ddagger}$ and ΔE^0 is observed.

α *and geometry changes*

From the definition of α, it is clear that α is related to energy. In fact, it can be shown that α is related to the forward ($\Delta E_f^{\ddagger}$) and reverse energy barriers ($\Delta E_r^{\ddagger}$). By using eq. [2], and since $\Delta E_r^0 = -\Delta E_f^0$ ($\Delta E_f^0 = \Delta E^0$), we obtain

$$[8] \quad \frac{\Delta E_f^{\ddagger}}{\Delta E_f^{\ddagger} + \Delta E_r^{\ddagger}} = 0.5 + 0.25\,\frac{\Delta E^0}{\Delta E_0^{\ddagger} + \dfrac{(\Delta E^0)^2}{16\Delta E_0^{\ddagger}}}$$

and by omitting the quadratic term, we obtain

$$[9] \quad \frac{\Delta E_f^{\ddagger}}{\Delta E_f^{\ddagger} + \Delta E_r^{\ddagger}} \approx 0.5 + 0.25\,\frac{\Delta E^0}{\Delta E_0^{\ddagger}}$$

Thus, combining eq. [3] with eq. [9] yields

$$[10] \quad \alpha \approx 0.5\,\frac{\Delta E_f^{\ddagger}}{\Delta E_f^{\ddagger} + \Delta E_r^{\ddagger}} + 0.25$$

However, it is not obvious that a relationship between α and

Can. J. Chem. Downloaded from www.nrcresearchpress.com by 92.62.229.171 on 09/08/12
For personal use only.

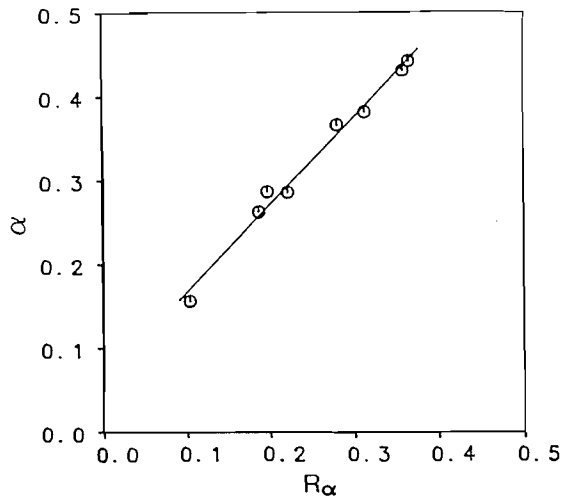

FIG. 3. A plot of α versus R_α for the reactions $H^- + CH_3X \rightarrow CH_4 + X^-$ at the MP2 level, where X = CCH, *C*N, *N*C, SH, Cl, NH_2, OH, and F.

transition state structure changes exists, although it is often assumed to exist. Furthermore, there is a lack of an unambiguous definition of geometry changes. For the latter problem, we may follow the example of the intrinsic α. According to eq. [10] the index for the energy change is related to the ratio of the forward and the sum of the forward and reverse activation energies. Similarly, an index for the geometry change (R_α) can be defined as the ratio of the forward and the sum of the forward and reverse geometry changes at the TS. Thus, we define

$$[11] \quad R_\alpha = \frac{f_f}{f_f + f_r}$$

In principle, f_f and f_r should be defined such that they measure the major geometry change of the reaction (for example, the breaking and forming of bonds). For the S_N2 reactions we have studied, f_f and f_r are defined as

$$[12] \quad f_f = \frac{R_{C-X}(TS) - R_{C-X}(R)}{R_{C-X}(R)}$$

and

$$[13] \quad f_r = \frac{R_{C-N}(TS) - R_{C-N}(P)}{R_{C-N}(P)}$$

where $R_{C-A}(TS)$ is the bond length between C and A in the transition state and $R_{C-A}(R)$ and $R_{C-A}(P)$ are the bond lengths between C and A in the reactant and product, respectively. Hence, if the TS resembles the reactant more than the product, $f_f < f_r$ and $R_\alpha < 0.5$. Otherwise, $R_\alpha > 0.5$. A plot of R_α versus intrinsic α is shown in Fig. 3 in which the ground state is taken to be the ion–molecule complex and the reactions have the same nucleophile, N = H. The results are obtained at the MP2 level (i.e., the geometries are optimized at the MP2 level).

It is interesting to note that even though a simple relationship between intrinsic α and ΔE^0 (see Fig. 2) only exits within each group, a simple relationship between intrinsic α and R_α can exist between members of more than one group. The rationalization is that the intrinsic α is related to the forward and reverse activation energies (eq. [10]) while the geometry change measured by f_f is related to the forward activation energy and that of f_r is related to the reverse activation energy. Therefore, R_α (eq. [11]) which is related to f_f and f_r is related to the forward and reverse activation energies as well. Thus, the relationship between α and R_α is not surprising. Furthermore, we can expect to observe a similar relationship between R_α and ΔE^0 as between α and ΔE^0, that is the linear relationship between R_α and ΔE^0 only exists within each reaction group.

TABLE 2. Calculated Q_α and ΔE^0 (kJ/mol) at the MP2 level[a]

	N = H		N = F	
X	Q_α	ΔE^0	Q_α	ΔE^0
CCH	0.38	−145.90		
*C*N	0.34	−251.55	0.74	33.31
*N*C	0.07	−361.34		
SH	0.41	−296.02	0.80	−11.20
Cl	0.27	−399.08	0.65	−114.22
NH_2	0.29	−91.44	0.80	193.42
OH	0.15	−186.42	0.66	98.44
F	0.09	−284.86	0.50	0.00

[a] $N^- + CH_3X$ and $CH_3N + X^-$ are taken as the reactant and product, respectively, for convenience. $\Delta E^0 = E(CH_3N + X^-) - E(N^- + CH_3X)$.

α and charge transfer at the transition state

The extent of charge transfer at the transition state is difficult to measure. Thus, in experiments, substituent or solvent effects are used as a means to measure the relative charge transfer at the TS (5). The study of charge transfer at the TS is also not trivial for theoretical calculations. It involves a proper definition of atoms in molecules and a proper partition of the charge distribution among atoms.

In this work, we used the charge partition scheme due to Bader and co-workers, according to which an atom in a molecule is defined as a real space surrounded by a zero-flux surface (a closed surface which is not traversed by any trajectories of ∇ρ) (14). The charge on an atom is obtained by subtracting the total number of electrons over the atomic basin from its nuclear charge.

By analogy with α and R_α, we can define a charge transfer index Q_α by

$$[14] \quad Q_\alpha = \frac{q_f}{q_f + q_r}$$

where

$$[15] \quad q_f = |Q_X(TS) - Q_X(R)|$$

and

$$[16] \quad q_r = |Q_N(TS) - Q_N(P)|$$

$Q_A(B)$ is the integrated charge on A in wavefunction B. For example, $Q_X(TS)$ is the integrated charge on X in the TS. Calculated Q_α values for reactions with N = H and N = F are listed in Table 2. Unlike intrinsic α and R_α, which have values <0.5 when $\Delta E^0 < 0$ and > 0.5 when $\Delta E^0 > 0$, Q_α can be >0.5 even when $\Delta E^0 < 0$ (for example, see Table 2 when N = F and X = Cl). The special behaviour of Q_α can be rationalized in terms of the factors discussed elsewhere

Can. J. Chem. Downloaded from www.nrcresearchpress.com by 92.62.229.171 on 09/08/12
For personal use only.

(8*b*, *d*). In previous papers, we have shown that the charge on atom A at the TS can be approximated as (8*b*, *d*)

$$[17] \quad Q_A(TS) = a^2Q_A(\Psi_R) + b^2Q_A(\Psi_P) + c^2Q_A(\psi_3) + d^2Q_A(\psi_4)$$

where a^2, b^2, c^2, and d^2 are the contributions of the reactant, product, and valence bond configurations ψ_3 and ψ_4 to the TS, respectively (see eq. [7]). $Q_A(\Psi_R)$, $Q_A(\Psi_P)$, $Q_A(\psi_3)$, and $Q_A(\psi_4)$ are the charges on A in the reactant, product, and valence bond configurations ψ_3 and ψ_4, respectively.

From eq. [17], the charge at the TS is related to the charges of A in various states ($Q_A(\Psi_R)$, $Q_A(\Psi_P)$, etc.). The charge on A in the reactant ($Q_A(\Psi_R)$ is A = X) and the charge on A in the product ($Q_A(\Psi_P)$ if A = N) are related to the electronegativity of A in the reactant and product, respectively. For example, a more electronegative A will attract more electrons, and hence a large negative value of $Q_A(\Psi_R)$ (when A = X). Therefore, the charge development at the TS is related to the electronegativity of A in the reactant and product. Furthermore, it is related to the contribution of various configurations to the TS (i.e., a^2, b^2, c^2, and d^2). All other things being equal, a large c^2 (i.e., large contribution of configuration $N^-{:}R^+{:}X^-$, in addition to its contribution to reactant and product, to the TS) tends to make the charge on A (A = N or X) at the transition state more negative. Moreover, as shown in previous papers (8*b*, *d*), if the reactions have similar electronic structures at the TS (i.e., similar values of *c* or *d* in eq. [7]), the ratio b^2/a^2 (product to reactant contribution to the TS) is related to the reaction energies. The smaller b^2/a^2 is, the more exothermic the reaction (8*a*, *b*, *d*). To sum up, the factors which affect charge transfer on A at the TS are the electronegativity of A, the electronic structure at the TS (i.e., whether there is a significant contribution of $N^-{:}R^+{:}X^-$, in addition to its contribution to the reactant and product, to the TS) and the reaction energy.

As we discussed above, only when the other two factors (electronic structure at the TS and electronegativities of N and X) are similar or at least change linearly with ΔE^0 will the simple relationship between q_f (and q_r) and ΔE^0 exist (see Figs. 1 to 4 in ref. 8*d*). Similarly, for a series of reactions, the simple relationship between Q_α and ΔE^0 will exist only when the reactions have similar TS electronic structures and the electronegativities of the X's are similar (or change linearly with ΔE^0).

It should be noted that the requirement for a simple relationship between Q_α and ΔE^0 discussed above is not sufficient to guarantee that $Q_\alpha < 0.5$ when $\Delta E^0 < 0$ or $Q_\alpha > 0.5$ when $\Delta E^0 > 0$. For that to be true, the electronegativity of the entering nucleophile N must be similar to that of the leaving group X. The relative charge transfer q_f and q_r is related to the relative electronegativities of N and X (8*b*, *d*). If N has a smaller electronegativity than X (for example N = H), $q_f < q_r$ and Q_α will tend to be smaller than when the electronegativities of N and X are similar. On the other hand, if N has a larger electronegativity than X (for example, N = F), q_f will be larger than q_r and Q_α would tend to be larger than when the electronegativities of N and X are similar.

The relationship between Q_α and ΔE^0 is illustrated in Fig. 4. For those X's which have similar electronic structures at the TS and electronegativities (for example, X = H and SH; X = CCH, CN, and Cl; X = OH, F, and NC; see refs. 8*b*, *d*), a simple relationship between Q_α and ΔE^0 is observed.

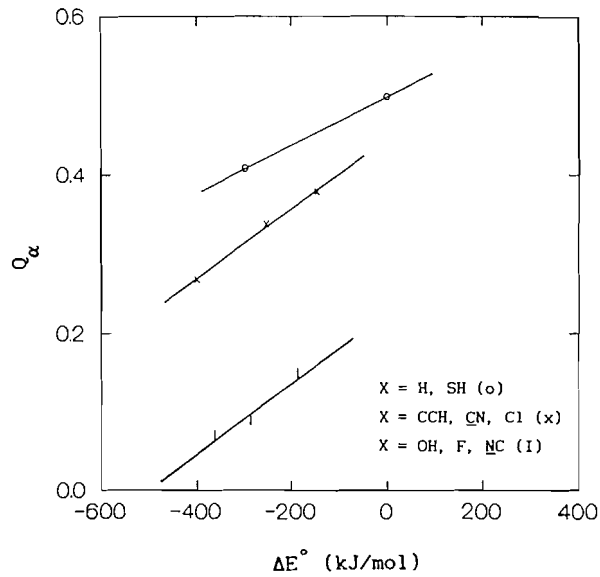

FIG. 4. Plot of Q_α versus ΔE^0 for the reactions $H^- + CH_3X \rightarrow CH_4 + X^-$ at the MP2 level.

Summary

The group α and the intrinsic α are different concepts. The α obtained experimentally is usually the group α. As noted by other workers (4*d*, *e*, 5*d*, 6*c*) and confirmed herein, the group α cannot be used as a measure of the TS structure in general. The intrinsic α is characteristic of each reaction. In this paper, we have discussed the relationships between the intrinsic α and other properties.

For gas-phase S_N2 reactions, the rate–equilibrium relationship is governed by the TS electronic structure and hybridization of the leaving group. Those reactions which have the same TS electronic structure and hybridization of the leaving group have a linear relationship between the intrinsic α and ΔE^0. In this case, a smaller intrinsic α indicates a more exothermic reaction.

An appropriate definition of the geometry change parameter is required in order to relate changes in geometry to the intrinsic α. R_α is proposed as the normalized TS geometry change. It measures the major geometry change of the forward reaction at the TS as compared to that of the sum of the forward and reverse reactions. A linear relationship between α and R_α is observed and explained by the fact that both α and R_α measure the forward activation energy as compared to the sum of the forward and reverse activation energies. Based on the relationships between R_α and α, and between α and ΔE^0, a linear relationship between R_α and ΔE^0 within each reaction group is expected.

The extent of charge transfer at the TS is related not only to energy changes but also to the electronegativities of the reactant and product and to the electronic structures at the TS. The explicit dependence of Q_α on electronegativity makes Q_α different from α and R_α. In order to observe a linear relationship between Q_α and ΔE^0, the electronegativities of X within the group must be similar.

Acknowledgements

A Killam Postgraduate Scholarship (to Z.S.) from Dalhousie University and the financial assistance of the Natural Sciences and Engineering Research Council of

Can. J. Chem. Downloaded from www.nrcresearchpress.com by 92.62.229.171 on 09/08/12
For personal use only.

Canada in the form of an Operating Grant (to R.J.B.) are gratefully acknowledged. We thank Dalhousie University Computing and Information Services for a generous allocation of computer time.

1. T. H. Lowry and K. S. Richardson. Mechanism and theory in organic chemistry. 3rd ed. Harper and Row, New York. 1987. p. 143 and references therein.
2. (*a*) J. E. Leffler. Science, **117**, 340 (1953); (*b*) G. S. Hammond. J. Am. Chem. Soc. **77**, 334 (1955); (*c*) J. E. Leffler and E. Grunwald. Rates and equilibria of organic chemistry. John Wiley and Sons Inc., New York, N.Y. 1963.
3. (*a*) F. G. Bordwell, W. J. Boyle, Jr., J. A. Hautala, and K. C. Yee. J. Am. Chem. Soc. **91**, 4002 (1969); (*b*) F. G. Bordwell, W. J. Boyle, Jr., and K. C. Yee. J. Am. Chem. Soc. **92**, 5926 (1970); (*c*) F. G. Bordwell and W. J. Boyle, Jr. J. Am. Chem. Soc. **94**, 3907 (1972); (*d*) F. G. Bordwell and W. J. Boyle, Jr. J. Am. Chem. Soc. **97**, 3447 (1975).
4. (*a*) J. R. Murdoch. J. Am. Chem. Soc. **94**, 4410 (1972); (*b*) F. G. Bordwell and D. L. Hughes. J. Am. Chem. Soc. **107**, 4737 (1985); (*c*) F. G. Bordwell and D. L. Hughes. J. Am. Chem. Soc. **108**, 7300 (1986); (*d*) H. Yamataka and S. J. Nagase. J. Org. Chem. **53**, 3232 (1988); (*e*) A. Pross and S. S. Shaik. New. J. Chem. **13**, 427 (1989).
5. (*a*) J. M. Sayer and W. P. Jencks. J. Am. Chem. Soc. **99**, 464 (1977); (*b*) W. J. Albery and M. M. Kreevoy. Adv. Phys. Org. Chem. **16**, 87 (1978); (*c*) W. P. Jencks. Chem. Rev. **85**, 511 (1985); (*d*) E. S. Lewis. J. Phys. Org. Chem. **3**, 1 (1990).
6. (*a*) R. A. Marcus. J. Phys. Chem. **72**, 891 (1968); (*b*) A. O. Cohen and R. A. Marcus. J. Phys. Chem. **72**, 4249 (1968); (*c*) R. A. Marcus. J. Am. Chem. Soc. **91**, 7224 (1969); (*d*) L. Eberson. *In* Electron transfer reactions in organic reaction. *Edited by* K. Hafmer. Springer-Verlag, Berlin, Heidelberg. 1987.
7. (*a*) R. P. Bell. The proton in chemistry. 2nd ed. Chapman and Hall, London. 1973; (*b*) E. Caldin and V. Gold (*Editors*). Proton transfer reaction. Chapman and Hall, London. 1973; (*c*) M. M. Kreevoy and S.-W. Oh. J. Am. Chem. Soc. **95**, 4805 (1973); (*d*) A. Kresge. Chem. Soc. Rev. **2**, 475 (1973); (*e*) W. J. Albery. Annu. Rev. Phys. Chem. **31**, 227 (1980); (*f*) E. S. Lewis, S. Kukes and C. D. Slater. J. Am. Chem. Soc. **102**, 1619 (1980). (*g*) M. J. Pellerite and J. I. Brauman. J. Am. Chem. Soc. **102**, 5993 (1980); (*h*) S. Wolfe, D. J. Mitchell, and H. B. Schlegel. J. Am. Chem. Soc. **103**, 7692 (1981); (*i*) S. Wolfe, D. J. Mitchell, and H. B. Schlegel. J. Am. Chem. Soc. **103**, 7694 (1981); (*j*) M. J. Pellerite and J. I. Brauman. J. Am. Chem. Soc. **105**, 2672 (1983); (*k*) M. M. Kreevoy and I.-S. H. Lee. J. Am. Chem. Soc. **106**, 2550 (1984); (*l*) E. S. Lewis and D. D. Hu. J. Am. Chem. Soc. **106**, 3292 (1984); (*m*) E. S. Lewis. J. Phys. Chem. **90**, 3756 (1986); (*n*) M. M. Kreevoy, D. Ostovic, I.-S. H. Lee, D. A. Binder, and G. W. King. J. Am. Chem. Soc. **110**, 524 (1988); (*o*) J. W. Bunting and D. Stefanidis. J. Am. Chem. Soc. **110**, 4008 (1988).
8. (*a*) Z. Shi and R. J. Boyd. J. Am. Chem. Soc. **111**, 1575 (1989); (*b*) Z. Shi. Ph.D. Thesis. Dalhousie University, Halifax, N.S. 1989; (*c*) Z. Shi and R. J. Boyd. J. Am. Chem. Soc. **112**, 6789 (1990); (*d*) Z. Shi and R. J. Boyd. J. Am. Chem. Soc. **113**, 1072 (1991); (*e*) Z. Shi and R. J. Boyd. J. Am. Chem. Soc. **113**, 2434 (1991).
9. (*a*) J. S. Binkley, R. A. Whiteside, R. Krishnan, R. Seeger, D. J. DeFrees, H. B. Schlegel, S. Topiol, L. R. Kahn, and J. A. Pople. GAUSSIAN 80, Carnegie–Mellon Quantum Chemistry Publishing Unit. Pittsburgh, Pa. 1980; (*b*) M. J. Frisch, J. S. Binkley, H. B. Schlegel, K. Raghavachari, C. F. Melius, R. L. Martin, J. J. P. Stewart, F. W. Bobrowicz, C. M. Rohlfing, L. R. Kahn, D. J. DeFrees, R. Seeger, R. A. Whiteside, D. J. Fox, E. M. Fleuder, and J. A. Pople. GAUSSIAN 86, Carnegie–Mellon Quantum Chemistry Publishing Unit, Pittsburgh, Pa. 1984.
10. (*a*) F. W. Biegler-König, R. F. W. Bader, and T. Tang. J. Comput. Chem. **3**, 317 (1982); (*b*) R. J. Boyd and L. C. Wang. J. Comput. Chem. **10**, 367 (1989).
11. (*a*) S. S. Shaik. J. Am. Chem. Soc. **103**, 3692 (1981); (*b*) A. Pross and S. S. Shaik. J. Am. Chem. Soc. **103**, 3702 (1981); (*c*) S. S. Shaik and A. Pross. J. Am. Chem. Soc. **104**, 2708 (1982); (*d*) A. Pross and S. S. Shaik. Acc. Chem. Res. **16**, 363 (1983); (*e*) S. S. Shaik. Prog. Phys. Org. Chem. **15**, 197 (1985); (*f*) A. Pross. Adv. Phys. Org. Chem. **21**, 99 (1985).
12. R. D. Harcourt. Theochem, **165**, 329 (1988).
13. E. Grunwald. J. Am. Chem. Soc. **107**, 125 (1985).
14. (*a*) R. F. W. Bader, Y. Tal, S. G. Anderson, and T. T. Nguyen-Dang. Isr. J. Chem. **8**, 19 (1980); (*b*) R. F. W. Bader and T. T. Nguyen-Dang. Adv. Quantum Chem. **14**, 63 (1981); (*c*) R. F. W. Bader, T. T. Nguyen-Dang, and Y. Tal. Rep. Prog. Phys. **44**. 893 (1981).

Can. J. Chem. Downloaded from www.nrcresearchpress.com by 92.62.229.171 on 09/08/12
For personal use only.

The calculation of atomic oscillator strengths: the lithium atom revisited

A. W. WEISS

National Institute of Standards and Technology, Gaithersburg, MD 20899, U.S.A.

Received May 30, 1991

This paper is dedicated to Professor Sigeru Huzinaga on the occasion of his 65th birthday

A. W. WEISS. Can. J. Chem. **70**, 456 (1992).

Extensive configuration interaction calculations have been done for the ground and first excited states of neutral lithium and singly ionized beryllium. While the calculations reproduce the ionization and excitation energies to within 3 cm^{-1} for Li and 10 cm^{-1} for Be^+, the main purpose of this work is the accurate evaluation of the $2s$–$2p$ resonance line oscillator strength. The calculated value of 0.7478 agrees to within less than 1% with the very accurate laser excitation lifetime measurement of 0.7416 ± 0.0012. However, internal consistency checks of the accuracy of these calculations suggest that more precise calculations are unlikely to reduce this discrepancy significantly. Furthermore, when placed together with other independent calculations that should be of comparable, if not better, accuracy, all theoretical predictions strongly indicate an f-value of 0.7475 ± 0.0010, which differs from the experiment by 4 experimental standard deviations.

Key words: configuration interaction, correlation, oscillator strength.

A. W. WEISS. Can. J. Chem. **70**, 456 (1992).

On a effectué des calculs étendus d'interactions de configuration de l'état fondamental et du premier état excité du lithium neutre et du béryllium mono-ionisé. Alors que les calculs permettent de reproduire les énergies d'ionisation et d'excitation à moins de 3 cm^{-1} pour le Li et à moins de 10 cm^{-1} pour le Be^+, le but principal de ce travail est d'évaluer d'une façon précise la force de l'oscillateur de la raie de résonance $2s$–$2p$. La valeur calculée, 0,7478, est à moins de 1% de la valeur très précise, 0,7416 ± 0,0012, obtenue par des mesures de temps de vie d'excitation au laser. Toutefois, des évaluations d'auto-cohérence de la précision de ces calculs laissent croire que des calculs plus précis ne réduiraient pas cette différence d'une façon significative. De plus, lorsqu'on utilise cette valeur avec celles obtenues par d'autres calculs indépendants d'une précision au moins semblable, si non meilleure, on en déduit que toutes les prédictions théoriques indiquent fortement que la valeur de f est égale à 0,7475 ± 0,0010 qui diffère de la valeur expérimentale par 4 écarts types expérimentaux.

Mots clés : interaction de configuration, corrélation, force de l'oscillateur.

[Traduit par la rédaction]

Introduction

The accurate calculation of atomic structures over the past 30 years has been driven primarily by the steady development of greater and greater computing power. The most accurate calculations have been, and continue to be, those on the bound states of the helium atom and its isoelectronic ions (1–4). For the two-electron atom, it is possible to carry out exhaustive variational calculations using trial functions that explicitly incorporate the interelectronic coordinate, r_{12}.

The next atom in complexity after helium is lithium, which, with a single electron outside a closed shell $1s$ core, remains a very simple system. Nevertheless, calculations of the energy of the atom comparable in precision to those on helium have not generally been possible, and the best calculations that have been done, although quite precise for a greater-than-two electron atom, have been of substantially lower accuracy (5). It is only recently that variational r_{ij} calculations have been reported which approach the precision of the two-electron calculations (6). Lithium has therefore been the beginning proving ground of truly many-electron methodologies, such as many-body perturbation theory (7) (MBPT) and the various versions of configuration interaction (8, 9).

For the most part these calculations, as well as many of those on more complex atoms and molecules, have concentrated on accurate determinations of the total energy of the system. This paper too reports variational configuration interaction (CI) or superposition of configurations (SOC) calculations of total energies and wave functions for lithium and singly ionized beryllium. However, the main emphasis here is on the *ab initio* determination of the spectroscopic properties of the atom, in particular energy differences, i.e., ionization and transition energies, and especially the transition oscillator strength, or f-value. Special attention will therefore be given to the contribution to the f-value and transition energies of the various classes of correlation configurations, as well as the convergence of these properties with respect to the CI partial wave expansion. All calculations begin with the Hartree–Fock approximation and are based on expansions in a basis set of Slater type orbital functions (STO). As it happens, the initial round of these wave function calculations had already been done in connection with a model study of transition moment bounding theorems (10).

Lithium is also of special interest in that the $2s$–$2p$ resonance line f-value is among the most accurately yet measured experimentally. Laser excitation lifetime measurements on Li and other alkali atoms have been reported (11) with an uncertainty of ±0.15%, a truly remarkable achievement, considering the longstanding extreme difficulty of measuring this property with a precision better than ≈5%. Unfortunately, the present calculations are unable to predict an f-value within these error limits, irrespective of the expansion lengths, the class of pair correlations, and the extent of the partial wave expansion included in the CI wave function. A comparison with all the other theoretical calculations that account for correlation at a comparable level of sophistication supports a predicted value that differs from the experimental one by more than 3 times the experimental uncertainty.

The next section will describe the details of the wave

Printed in Canada

Can. J. Chem. Downloaded from www.nrcresearchpress.com by 123.30.183.119 on 09/08/12
For personal use only.

function calculations, the systematics of incorporating the various aspects of correlation into the trial functions, and the method of choosing the basis sets. This section will also include a summary of the results on correlation energies and an analysis of the various correlation contributions to the ionization and excitation energies, as well as the total energy. The following section will present the results for the resonance transition oscillator strengths, with a parallel analysis of the various correlation components of the calculations. Comparisons with other comparable calculations and with the experimental results will also be given and discussed.

Description of calculations and energy results

For an atom of this simplicity, one should expect pair correlation corrections to the Hartree–Fock to provide the overwhelmingly dominant correlation effect. The trial wave function, therefore, was initially taken to be a single/double (SD) substitution CI function. For the ground state this has the form

$$[1]\quad \Psi = a_0 1s^2 2s + \sum_i a^i_{2s} 1s^2 n_i s + \sum_i a^i_{1s}[1s2s\ ^{1,3}S]n_i s + \sum_{i,j,l} a^{ijl}_{1s2s} 1s[n_i l n_j l\ ^{1,3}S] + \sum_{i,j,l} a^{ijl}_{1s^2} 2s[n_i l n_j l\ ^1S]$$

and for the $2p$ excited state,

$$[2]\quad \Psi = b_0 1s^2 2p + \sum_i b^i_{2p} 1s^2 n_i p + \sum_i b^i_{1s}[1s2p\ ^{1,3}P]n_i s + \sum_{i,j,l} b^{ijl}_{1s2p} 1s[n_i l n_j (l+1)\ ^{1,3}P] + \sum_{i,j,l} b^{ijl}_{1s^2} 2p[n_i l n_j l\ ^1S]$$

where all summations are assumed to run over some set of correlation orbitals, which will be described later on.

The first double sum in both cases represents the *KL* intershell correlation, since one valence and one core orbital are replaced by a correlation orbital. The single sum terms belong naturally to this class of correlation, since one of the $1s$ functions is left undisturbed. These single replacement terms also include the semi-internal (12) configurations such as

$$1s2s^2,\ 1s2sns\ ^2S \quad \text{and} \quad 1s2s2p,\ 1s2pns\ ^2P$$

The second double sum, of course, represents the *K*-shell core correlation corrections, and it too includes semi-internal, or configuration interference (8), terms that contribute differently to the correlation energies of the two states, as well as the ion limit. These are terms like

$$2s^2ns,\ 2p^22s, \quad \text{and} \quad (2pnp\ ^1S)\ 2s$$

for the ground state, and

$$2s^22p,\ (2sns\ ^1S)\ 2p,\ 2p^3, \quad \text{and} \quad 2p^2(^3P,^1D,^1S)\ np$$

for the $2p$ state. As will be discussed shortly, the CI wave function expansions [1] and [2] were also augmented beyond the SD scheme in a very selective way so as to include the largest of the triple substitution configurations, i.e., configurations where all three H–F orbitals have been replaced by correlation functions.

The starting point for these calculations, for each state, was the expansion method Hartree–Fock approximation, based on the usual normalized Slater type orbitals (STO),

$$[3]\quad \chi^\zeta_{plm} = \sqrt{\frac{(2\zeta)^{2p+1}}{(2p+1)!}}\, r^p e^{-\zeta r} Y_{lm}(\vartheta,\varphi)$$

The Hartree–Fock basis was augmented by a set of functions designed to represent the intershell correlation and an additional set to represent the *K*-shell core correlation. The set of correlation orbitals of eqs. [1] and [2] was then generated by sequential Schmidt orthogonalization of this full STO basis.

Since the core correlation is expected to be very similar for the atom and the helium-like ion limit, the additional *K*-shell correlation basis set was determined by independent configuration interaction calculations on the ground states of the helium-like ions, Li^+ and Be^{2+}. The partial wave expansion here was carried through *i*-orbitals, i.e., $l = 6$, and all exponential parameters were determined by minimizing the ground state energy for these ions. After some numerical experimentation, a double ζ set was decided on for each symmetry, with principal quantum numbers for each ζ running up to some maximum, much like the bases recently used for helium r_{12} calculations (2, 3) and those used in some of the earliest of the CI calculations (13). These calculations recover better than 99% of the correlation energy of the ground state of the helium-like ions, which should be adequate to represent core correlation contributions to the three-electron atom ionization and excitation energies. This Slater basis is included in the basis set tabulation given in the appendix.

Even tempered basis sets, defined as a set of STO's all with the same principal quantum number, but with the zetas defined by the geometric sequence (14)

$$[4]\quad \zeta_k = \alpha_0\beta^k, \qquad k = 0, 1, 2, \ldots,$$

were also examined and, upon optimizing α_0 and β, were found to give approximately the same improvement in energy as the double ζ set of the same number of basis functions. The double ζ set was chosen here, however, since the comparable, variationally optimized even-tempered set appeared to show a somewhat greater degree of linear dependence, as measured by the magnitude of the expansion coefficients in a Schmidt orthogonalized set of functions.

With the *K*-shell STO correlation basis established, a natural orbital transformation (15) was carried out for the helium-like ion wave functions in order to provide an orthonormal basis in which the correlation information was condensed, as much as possible, in the first few orbitals. This made it possible to slough off, without degrading the correlation calculations, the last natural orbital of some of the lower *l*-value symmetries where there was a suggestion of linear dependency. The total number of correlation orbitals was therefore smaller than the number of basis functions. This set of *K*-shell correlation functions was added to the Hartree–Fock function for each state, and then augmented further by a set of functions designed specifically to account for the intershell correlation.

The approach followed for the intershell correlation set was more direct, adding to the core correlation set a sequentially Schmidt orthogonalized group of STO's variationally opti-

Can. J. Chem. Downloaded from www.nrcresearchpress.com by 123.30.183.119 on 09/08/12
For personal use only.

TABLE 1. Energies for Li and Li^+ with basis set A {9-*s*,10-*p*,8-*d*,6-*f*,6-*g*,5-*h*,3-*i*}. The highest orbital angular symmetry included is indicated in parentheses

Level of approximation	Total energy (au)			Ionization energy (cm^{-1})		Excitation energy (cm^{-1})
	$1s^2 2s\ ^2S$	$2s^2 2p\ ^2P$	$1s^+\ ^1S$	$1s^2 2s\ ^2S$	$1s^2 2p\ ^2P$	$2s-2p$
H–F	−7.43273	−7.36507	−7.23641	−43082	−28234	14848
$KL(d)$	−7.43520	−7.36666		−43625	−28583	15042
$KL(f)$	−7.43522	−7.36672		−43630	−28597	15033
$KL(g)$	−7.43523	−7.36674		−43632	−28600	15032
$KL(h)$	−7.43523	−7.36674		−43632	−28601	15031
$KL(i)$	−7.43524	−7.36674		−43633	−28601	15032
$KL(i) + K(p)$	−7.47393	−7.40603	−7.27585	−43470	−28570	14900
$KL(i) + K(d)$	−7.47668	−7.40879	−7.27861	−43468	−28568	14900
$KL(i) + K(f)$	−7.47738	−7.40948	−7.27930	−43468	−28568	14900
$KL(i) + K(g)$	−7.47762	−7.40973	−7.27955	−43468	−28568	14900
$KL(i) + K(h)$	−7.47772	−7.40983	−7.27965	−43468	−28568	14900
$KL(i) + K(i)$	−7.47777	−7.40987	−7.27970	−43468	−28568	14900
$KL + K$ + trip(d)	−7.47781	−7.40990		−43477	−28574	14903
$KL + K$ + trip(g)	−7.47781	−7.40990		−43477	−28574	14903
Pauli ΔE (HF)	−7.47849	−7.41057	−7.28036	−43480	−28574	14906
Experiment[a]				−43487.15	−28583.27	14903.88

[a]Johansson, ref. 16.

mized on the intershell correlation only. That is, for purposes of variationally determining the STO exponential parameters, the core correlation configurations, i.e., the last double summations of eqs. [1] and [2], were omitted from the calculations. The *K*-shell basis set was included in these intershell calculations, but *K*-shell correlation configurations were not. The point of this exercise was to circumvent the distortion imposed on the variational problem by the much larger core correlation energy, which would otherwise dominate the ζ optimization procedure.

Here too, orbitals with angular symmetry through $l = 6$ were included in the calculations, with basis functions added within each symmetry until the energy appeared stable to $\approx 10^{-5}$ au. These basis sets for both the $2s$ and $2p$ states are included in the tabulation in the Appendix. It soon became clear that, except for *s*-functions, the same basis set could be used for both the ground and excited state. Repeated attempts to optimize parameters independently led to so small an energy improvement as to make it not worthwhile to pursue this approach.

The calculations included all possible configurations in [1] and [2] that could be constructed from this set of correlation orbitals. The total energies (in atomic units) calculated with this basis set, and labeled set A, are given in Table 1 for neutral lithium and in Table 2 for Be^+ and compared with experiment (16, 17). The number of basis functions for each symmetry is also shown in each case. The tables display the sequence of total energies (in au) obtained with the addition of successively higher angular momentum configurations representing the intershell correlation, followed by a similar sequence for core correlation. The corresponding computed energy differences, ionization and excitation energies (in cm^{-1}), are also given. In every case, the binding energies are computed relative to the energy of the helium-like ion at exactly the same level of approximation. All the KL intershell correlation calculations are, of course, referred to the $1s^2$ Hartree–Fock approximation of the ion limit.

An additional set of calculations including selected triple excitation configurations was also performed, based on the dominant double replacement core configurations,

$$s_1^2 2s + p_1^2 2s\ ^2S \quad \text{and} \quad s_1^2 2p + p_1^2 2p\ ^2P$$

Here s_1 and p_1 are the first natural correlation orbitals of *s*- and *p*-symmetry for the He-like core. For these calculations all possible single and double and substitution configurations referred to these configurations, but distinct from those already used, were added to the SD configuration interaction wave function. The improvements so obtained are indicated by the entries labeled "triples." This procedure generated a total of 1044 symmetry-adapted configuration state functions (CSF) for the ground state and 1773 for the $2p$ excited state. Relativistic energy shifts were estimated from Hartree–Fock calculations of the lowest order, single-particle Pauli approximation, and these corrections were added to the final calculated total energies.

Finally, for the case of neutral lithium, the entire set of calculations was repeated utilizing a larger set of STO's for the core and intershell correlation, here labeled basis set B. An enhanced basis set was optimized for the Li^+ ground state, the helium-like natural orbitals were obtained, and this set was added to the neutral atom H–F and an augmented intershell basis, generating 1695 CSF's for the ground state and 2895 for the $2p$ state. This basis is also given in the Appendix, and the energy results so obtained are shown in Table 3 in exactly the same way as Table 1.

Several conclusions stand out from these numerical results. Firstly, convergence of the total intershell correlation energy with respect to the partial wave expansion has been achieved to within $\approx 10^{-5}$ au. Results obtained with the larger basis, set B, are similar. The additional SD calculations of the core correlation also show that, for purposes of computing total energies, convergence with respect to this *l*-series has reached the regime of maddeningly slow convergence so common for helium and its isoelectronic ions. Furthermore, the absolute total energy corrections are quite large. No attempt has been made here to extrapolate the *l*-series; all

Can. J. Chem. Downloaded from www.nrcresearchpress.com by 123.30.183.119 on 09/08/12
For personal use only.

TABLE 2. Energies for Be^+ and Be^{2+} with basis set A {9-*s*,10-*p*,8-*d*,6-*f*,6-*g*,5-*h*,3-*i*}. The highest orbital angular symmetry included is indicated in parentheses

Level of approximation	Total energy (au)			Ionization energy (cm^{-1})		Excitation energy (cm^{-1})
	$1s^2 2s\ ^2S$	$1s^2 2p\ ^2P$	$1s^+\ ^1S$	$1s^2 2s\ ^2S$	$1s^2 2p\ ^2P$	$2s-2p$
H–F	−14.27739	−14.13085	−13.61128	−146186	−114027	32159
$KL(d)$	−14.28159	−14.13508		−147108	−114955	32153
$KL(f)$	−14.28164	−14.13530		−147119	−115002	32116
$KL(g)$	−14.28166	−14.13535		−147122	−115013	32109
$KL(h)$	−14.28166	−14.13536		−147123	−115016	32107
$KL(i)$	−14.28166	−14.13536		−147124	−115017	32107
$KL(i) + K(p)$	−14.32020	−14.17475	−13.65106	−146851	−114930	31921
$KL(i) + K(d)$	−14.32323	−14.17778	−13.65409	−146850	−114929	31921
$KL(i) + K(f)$	−14.32401	−14.17855	−13.65487	−146850	−114929	31921
$KL(i) + K(g)$	−14.32429	−14.17883	−13.65515	−146850	−114929	31921
$KL(i) + K(h)$	−14.32440	−14.17895	−13.65526	−146851	−114929	31921
$KL(i) + K(i)$	−14.32445	−14.17900	−13.65531	−146851	−114930	31921
$KL + K$ + trip(d)	−14.32448	−14.17903		−146858	−114936	31922
$KL + K$ + trip(g)	−14.32448	−14.17903		−146858	−114936	31922
Pauli ΔE (HF)	−14.32697	−14.18142	−13.65769	−146881	−114939	31942
Experiment[a]				−146882.9	−114949.7	31933.1

[a]Johansson, ref. 17.

TABLE 3. Energies for Li and Li^+ with basis set B {12-*s*,12-*p*,11-*d*,8-*f*,7-*g*,5-*h*,3-*i*}. The highest orbital angular symmetry included is indicated in parentheses

Level of approximation	Total energy (au)			Ionization energy (cm^{-1})		Excitation energy (cm^{-1})
	$1s^2 2s\ ^2S$	$1s^2 2p\ ^2P$	$1s^+\ ^1S$	$1s^2 2s\ ^2S$	$1s^2 2p\ ^2P$	$2s-2p$
H–F	−7.43273	−7.36507	−7.23641	−43082	−28234	14848
$KL(d)$	−7.43521	−7.36666		−43627	−28584	15043
$KL(f)$	−7.43524	−7.36673		−43633	−28599	15034
$KL(g)$	−7.43525	−7.36675		−43635	−28602	15033
$KL(h)$	−7.43525	−7.36675		−43636	−28603	15033
$KL(i)$	−7.43525	−7.36675		−43636	−28604	15032
$KL(i) + K(p)$	−7.47397	−7.40608	−7.27588	−43473	−28573	14900
$KL(i) + K(d)$	−7.47674	−7.40885	−7.27865	−43474	−28573	14901
$KL(i) + K(f)$	−7.47745	−7.40955	−7.27935	−43474	−28573	14901
$KL(i) + K(g)$	−7.47770	−7.40980	−7.27960	−43474	−28574	14900
$KL(i) + K(h)$	−7.47780	−7.40990	−7.27970	−43475	−28574	14901
$KL(i) + K(i)$	−7.47784	−7.40994	−7.27974	−43475	−28574	14901
$KL + K$ + trip(d)	−7.47788	−7.40997		−43483	−28580	14903
$KL + K$ + trip(g)	−7.47788	−7.40997		−43484	−28580	14904
Pauli ΔE (HF)	−7.47856	−7.41064	−7.28040	−43487	−28580	14907
Experiment[a]				−43487.15	−28583.27	14903.88

[a]Johansson, ref. 16.

numbers are exactly as calculated. Comparison of results for basis sets A and B also indicate slow convergence with respect to radial basis functions.

However, it is also clear that, for purposes of predicting energy differences for valence shell spectroscopy, all correlations of the core involving *d*-orbitals or higher are very nearly irrelevant, at least to within 1–2 cm^{-1}. The total energies, of course, show much larger changes with these core correlations. However, the shifts are all virtually the same for both the ground and $2p$ states as well as the $1s^2$ of the helium-like ion. This is not so for the correlations $1s^2 \rightarrow s^2$ and $1s^2 \rightarrow p^2$, where differential correlation shifts are produced because of the occupancy status of *s*- and *p*-symmetries in the reference state wave functions. Higher symmetry triple substitution terms are likewise of little consequence, once the occupied symmetries have been included. Even the intershell contributions to ionization and excitation energies stabilize with respect to the *l*-series after the addition of *f*- or *g*-type orbitals. It is now of interest to pursue the effects of these various correlation contributions on the transition oscillator strengths.

Oscillator strength results

The oscillator strength, or *f*-value, for an electric dipole transition is given, in the length gauge, by

Can. J. Chem. Downloaded from www.nrcresearchpress.com by 123.30.183.119 on 09/08/12
For personal use only.

$$[5] \quad f_{\text{len}} = \frac{2\Delta E}{3g_i} |\langle \Psi_i | \mathbf{r} | \Psi_f \rangle|^2$$

where ΔE is the transition energy in au, g_i is the statistical weight of the initial state, and the squared transition moment, the multiplet strength, is presumed summed over all degeneracies in both initial and final states, i and f. One can also compute f-values using the formally equivalent velocity form of the transition moment,

$$[6] \quad f_{\text{vel}} = \frac{2}{3g_i} \frac{1}{\Delta E} |\langle \Psi_i | \nabla | \Psi_f \rangle|^2$$

If the exact bound state wave functions are used to calculate the f-value, the length and velocity forms must agree exactly. With approximate wave functions, they need not, and frequently do not, agree, and it is common practice to compute both forms, taking the agreement as some measure of the accuracy of the calculation. Unfortunately, it is not at all clear how well this agreement or disagreement measures the accuracy. Length–velocity agreement is a necessary, not sufficient, condition of the correctness of the prediction. It can easily happen that both values agree quite well and both are wrong. Nevertheless, it is frequently a useful extra handle on one's calculations, albeit a potentially embarassing one. While the question of which form is to be preferred has been discussed at some length throughout the literature (18, 19), there is no hard and fast rule. It has been the author's experience that the length form seems to be preferable more often than not, but this is little better than a rough rule of thumb.

All CI contributions to the lithium transition moment were computed exactly, with no numerical approximations such as assuming orbital orthogonality for the two states. In principle, there is no reason for the orbitals used in the ground state to be orthogonal to those used in the $2p$ state calculations, and all requisite determinants of overlap integrals were dutifully computed here. In this case, because of the choice of a uniform correlation basis for $l > 0$, this is a minor point. Furthermore, since the K-shell electrons are so tightly bound, moving a single outer electron around among different valence orbitals, or removing it entirely, should cause negligible core relaxation. It is important to note, however, that this unimportance of the non-orthogonality problem is almost certainly peculiar to this particular application. In larger atoms, with larger and more polarizable cores, relaxation effects may well be substantially more important. Also, in atoms with more than one valence electron, term-dependent orbital relaxation can be, and often is, very significant. In such cases, orbital non-orthogonality must be incorporated into the calculations, either by direct calculation or indirectly, simulating this orbital relaxation by the appropriate configuration interaction. In the latter case, of course, care must be taken to include all the pertinent simulation configurations in the calculation.

The results of the oscillator strength calculations, using the sequences of wave functions indicated in Tables 1–3, are summarized in Table 4 and compared with the relevant experimental measurements (11, 20). In each case, the wave functions of both states of the transition have been truncated in exactly the same way. Thus, for example, $KL(i)$ means the CI wave function using all intershell correlation configurations through i-orbitals, and was used for both the $2s$ and $2p$ states. Several selected intermediate calculations in the sequences shown in Tables 1–3 have been omitted, since it is clear that they would add little to any conclusions one might derive from the results. In every case, the experimental transition energies were used to compute the oscillator strengths, since this throws the burden of any discrepancies or trends unambiguously onto the transition moment calculation itself.

Within each class of correlation configurations — intershell, core, and triple substitutions — we see that the higher angular momentum terms, as with the transition energy calculations, have virtually no effect on the oscillator strength. Adding intershell correlations through d-orbitals makes a significant change in the f-value compared with the Hartree–Fock and brings the length and velocity forms into much better agreement. However, adding f- and g-orbitals to the intershell correlation terms has only a marginal effect on the results, and adding h- and i-orbitals has none at all. Similar comments apply for the core correlation and triple substitution configurations, even though the former have a large effect on the total energy. The net effect for lithium of adding core and triple replacement terms to the wave function is to change the length and velocity f-values by 0.8% and 0.3% respectively from the intershell calculation.

It should be noted, of course, that these effects are all quite small. The Hartree–Fock values differ by only 3–4% from the final calculated numbers, a result that is already as good as, or better than, most current experimental measurements, and which is probably as accurate as needed for most applications. This, of course, is the point of the strategy followed in most current correlated calculations of f-values. By correlating only the valence electrons sufficiently, one hopes to bring the f-value calculations to the level of accuracy of the Hartree–Fock approximation for the corresponding alkali atom. For example, for carbon the procedure is to correlate the outer electrons only, which would then be expected to produce f-values of the precision of the Li Hartree–Fock. To go beyond this requires the inclusion of intershell and selected core correlation corrections, as has been done here.

The lithium results are somewhat disappointing in not being any more stable with respect to expansion lengths or categories of correlation configurations. It would also be nice to have seen better agreement of the length and velocity forms. The trends in the calculated values, however, strongly suggest that the f-value is unlikely to come down much closer to the experimental value than it already has. It is conceivable that a still more exhaustive correlation basis set would do the trick, but the very near equality of the two sets of calculated values produced by basis sets A and B suggests otherwise. It is possible that the addition of still more triple substitution configurations will depress the f-value still further. However, the set of triples that have been included already brings the ionization energy to within 3 cm^{-1} of the experiment, and it is difficult to see how the omitted remainder could make a change in the f-value three times larger than that due to the triple replacement terms already present. The calculations for Be^+ appear to be in much better shape than lithium, which is not surprising since isoelectronic ions generally tend to become rapidly less sensitive to correlation than the neutral atom. Also, the Be^+ experimental data are not claimed to be nearly as accurate as for lith-

Can. J. Chem. Downloaded from www.nrcresearchpress.com by 123.30.183.119 on 09/08/12
For personal use only.

TABLE 4. Summary of oscillator strength calculations for the $2s$-$2p$ resonance transition in Li and Be^+ (λ = 6709 Å, 3131 Å respectively)

Level of approximation	Li, basis set A		Li, basis set B		Be^+, basis set A	
	len	vel	len	vel	len	vel
H–F	0.7671	0.7909	0.7671	0.7909	0.5109	0.5505
$KL(d)$	0.7422	0.7531	0.7420	0.7530	0.4973	0.5009
$KL(g)$	0.7418	0.7521	0.7415	0.7519	0.4969	0.4997
$KL(i)$	0.7417	0.7520	0.7415	0.7519	0.4969	0.4996
$KL(i) + K(p)$	0.7496	0.7486	0.7495	0.7485	0.4990	0.4990
$KL(i) + K(f)$	0.7498	0.7490	0.7497	0.7489	0.4991	0.4994
$KL(i) + K(h)$	0.7498	0.7491	0.7497	0.7489	0.4991	0.4994
$KL(i) + K(i)$	0.7498	0.7491	0.7497	0.7489	0.4991	0.4994
$KL + K$ + trip(d)	0.7480	0.7500	0.7478	0.7498	0.4987	0.4998
$KL + K$ + trip(g)	0.7479	0.7500	0.7478	0.7498	0.4987	0.4997
Experiment	0.7416 ± 0.0012[a]				0.47 ± 0.01[b]	

[a]Gaupp *et al.*, ref. 11.
[b]Bromander, ref. 20.

TABLE 5. Comparison of theoretical and experimental resonance transition oscillator strengths and ionization potentials

	Var.[a] (r_{12})	Opacity[b] project	MCHF[c] + CI	MBPT[d]	Present	Expt.[e]
f_{len}	0.7476	0.7475	0.7480	0.7467	0.7478	0.7416 ± 0.0012
f_{vel}			0.7487	0.7471	0.7498	
$IP_{2s}(cm^{-1})$	43480	43377	43450	43487	43487	43487.15
$IP_{2p}(cm^{-1})$	28558	28539	28590	28581	28580	28583.27

[a]Sims *et al.* (1976), ref. 21.
[b]Peach *et al.* (1988), ref. 22.
[c]Froese-Fischer (1988), ref. 23.
[d]Blundell *et al.* (1989), ref. 7.
[e]Gaupp *et al.* (1982), ref. 11.

ium, although here too there appears to be reason to question the precision of the measurement.

One caveat would seem to be in order with regard to truncating a sequence of calculated f-values as given for lithium in Table 4. Had the calculations been stopped at only the level of intershell correlation, the length form would have been in virtually exact agreement with the cited experimental value. While this would have given the appearance of an extremely accurate calculation, it would clearly have been quite misleading. On the other hand if one had stopped the calculations at the intershell correlation but used the theoretical transition energy, which is 100 cm^{-1} too large, the length and velocity values would have been 0.7465 and 0.7469 respectively. As it happens, this beautiful, but fortuitous, agreement is not even far from the length value finally obtained with the fully correlated wave functions.

The bothersome situation for neutral lithium becomes yet more puzzling when placed in the context of all the other published calculations designed to fully account for correlation (7, 21–23). This is illustrated in Table 5, which compares all these values with the experiment and with each other. The table also includes the ionization energies predicted for both states by each calculation. Except for the MBPT calculation, which is relativistic, these ionization energies have been adjusted by adding the Hartree–Fock relativistic shifts computed here.

The opacity calculation (22) is part of a recent large-scale project to generate atomic data needed for modelling stellar opacities. The wave function calculations are all done within a uniform framework for treating both radiative and collisional processes in both the discrete and continuous spectrum. For bound state calculations this methodology is equivalent to a configuration interaction calculation. The MC + CI calculation (23) is a calculation using numerical multiconfiguration Hartree–Fock orbitals in a follow-on full-scale CI. Both of these calculations are therefore similar to the present ones. The calculation labeled r_{12} is a variational calculation that selectively includes the interelectronic coordinate in the wave function, by allowing only one r_{ij} factor per term (21). Although this represents a real restriction, for this kind of system it can be argued that it should not be a severe one. The MBPT result (7) has been obtained by a relativistic many-body perturbation calculation applied directly to the ionization energy. The calculation therefore assumes no orbital relaxation in going from Li to Li^+, simulating this effect by higher order perturbative corrections, which as discussed above should be easily done for this system. For neutral lithium, the fact that the calculations are relativistic is of little importance.

The consistently close agreement of the f-values, particularly for the dipole length form, is striking. An oscillator strength of 0.7474 ± 0.0007 encompasses all of the length

Can. J. Chem. Downloaded from www.nrcresearchpress.com by 123.30.183.119 on 09/08/12
For personal use only.

values, and 0.7482 ± 0.0016 would include all the calculated f-values, both length and velocity. The fact that these are all entirely independent calculations, each one designed to fully account for correlation, makes this consistency still more persuasive. Since the smallest of these theoretical predictions differs from the experimental value by more than 4 standard deviations, it would appear that either a new measurement or a careful reevaluation of the old one would be called for.

Conclusions

This paper has reported extensive configuration interaction calculations of correlated wave functions at the level of single and double substitution configurations plus selected triples for the ground and first excited states of lithium and singly ionized beryllium. The calculations were based entirely on a Slater function basis, with the K-shell correlation basis determined by variational calculations on the helium-like ions, followed by a natural orbital transformation to compress the correlation information into a rapidly converging set of core correlation orbitals. These calculations generated a sequence of CI wave functions, which were then used to calculate a sequence of putatively more accurate oscillator strengths for the resonance transition.

The results clearly show that core correlation configurations are necessary in addition to intershell ones. While core correlation energies are large, only the s- and p-wave contributions make a significant contribution to the ionization and excitation energies. Similarly, only the lowest orbital angular momentum triple replacement terms are needed for the final 10 cm^{-1} accuracy for energy differences. Similar conclusions hold for the oscillator strength calculations. Here, however, only the lowest angular terms (through d-orbitals) in the intershell correlation as well are important.

Although the computed f-value for lithium agrees to within 1% with the most accurate measurement, which in turn carries a stated uncertainty of ±0.15%, analysis of the calculations suggests that the agreement should be better. When juxtaposed with a broad variety of other independent *ab initio* calculations, all of which agree closely with one another, there is a strong indication that this discrepancy is real, and that the experiment should be reevaluated. Another more recent laser excitation experiment, using delayed coincidence, has produced (24) an f-value of 0.7435, but with an uncertainty of ±0.0055. While this would tend to support the measurement of Gaupp *et al.* (11), the error bars are large enough to encompass all the values quoted here.

On the other hand, very accurate variational wave function calculations on lithium, involving extensive use of the interelectronic coordinates, are currently being reported in the literature (6,25). It would be of considerable interest therefore to apply them to the calculation of the resonance line oscillator strength to attempt to resolve this discrepancy.

1. C. L. Pekeris. Phys. Rev. **126**, 1470 (1962); B. Schiff, C. L. Pekeris, and Y. Accad. Phys. Rev. A, **4**, 885 (1971).
2. A. Kono and S. Hattori. Phys. Rev. A, **29**, 2981 (1984).
3. G. W. F. Drake. Nucl. Instrum. Methods Phys. Res. Sect. B: **B31**, 7 (1988).
4. D. E. Freund, B. D. Huxtable, and J. D. Morgan III. Phys. Rev. A, **29**, 980 (1984).
5. J. S. Sims and S. A. Hagstrom. Phys. Rev. A, **11**, 418 (1975).
6. F. W. King. Phys. Rev. A, **40**, 1735 (1989).
7. S. A. Blundell, W. R. Johnson, Z. W. Liu, and J. Sapirstein. Phys. Rev. A, **40**, 2233 (1989).
8. C. Froese-Fischer. Phys. Rev. A, **41**, 3481 (1990).
9. D. Sundholm and J. Olsen. Phys. Rev. A, **42**, 2614 (1990).
10. D. Roginsky and A. W. Weiss. Phys. Rev. A, **38**, 1760 (1988).
11. A. Gaupp, P. Kuske, and H. J. Andrä. Phys. Rev. A, **26**, 3351 (1982).
12. O. Sinanoğlu. Advances in chemical physics. Vol. 14. Interscience, New York. 1969. p. 237.
13. A. W. Weiss. Phys. Rev. **122**, 1826 (1961).
14. R. D. Bardo and K. Ruedenberg. J. Chem. Phys. **60**, 918 (1974).
15. P. O. Löwdin and H. Shull. Phys. Rev. **101**, 1730 (1956).
16. I. Johansson. Ark. Fys. **15**, 169 (1959).
17. I. Johansson. Ark. Fys. **20**, 489 (1961).
18. R. Crossley. Phys. Scr. T, **T8**, 117 (1984).
19. M. T. Andersen and F. Weinhold. Phys. Rev. A, **10**, 1457 (1974).
20. J. Bromander. Phys. Scr. **4**, 61 (1971).
21. J. S. Sims, S. A. Hagstrom, and J. R. Rumble. Phys. Rev. A, **13**, 242 (1976).
22. G. Peach, H. E. Saraph, and M. J. Seaton. J. Phys. B: At. Mol. Opt. Phys. **21**, 3669 (1988).
23. C. Froese-Fischer. Nucl. Instrum. Methods Phys. Res. Sect. B: **B31**, 265 (1988).
24. J. Carlsson and L. Sturesson. Z. Phys. D: At. Mol. Clusters, **14**, 281 (1989).
25. D. K. McKenzie and G. W. F. Drake. Bull. Am. Phys. Soc. **35**, 1176 (1990).

Appendix

Tables A1 and A2 display the STO parameters for the two Slater basis sets labeled A and B respectively. The parameters are the principal quantum number, p, and the value of ζ, defined by eq. [3] in the main text. The basis sets are divided into two groups, the first referring to the Hartree–Fock and intershell bases, and the second the pure K-shell basis. In the latter case, e.g., the notation such as $2p$–$6p$ denotes a set of five p-type STOs all with the same value of ζ, but with principal quantum numbers, p, ranging from 2 through 6.

TABLE A1. Slater type orbitals for basis set A

	Li		Be^+	
	$1s^2 2s$	$1s^2 2p$	$1s^2 2s$	$1s^2 2p$
H–F + *KL* basis				
1*s*	2.468	2.478	3.399	3.421
1*s*	4.680	4.700	6.070	6.030
2*s*	1.760	1.680	2.420	1.980
2*s*	1.130	1.130	1.710	1.550
2*s*	0.665	0.665	1.174	1.160
3*s*	0.600	0.600	1.000	1.000
2*p*	0.512		1.025	
2*p*	0.920		1.420	
2*p*	1.380		2.450	
2*p*	2.850		4.500	
3*p*	2.800		4.450	
3*d*	0.720		1.420	
3*d*	1.050		1.850	
3*d*	1.950		3.400	
4*f*	1.100		1.950	
4*f*	2.000		3.600	

Can. J. Chem. Downloaded from www.nrcresearchpress.com by 123.30.183.119 on 09/08/12
For personal use only.

TABLE A1. (*concluded*)

	Li		Be^+	
	$1s^2 2s$	$1s^2 2p$	$1s^2 2s$	$1s^2 2p$
$5g$	1.350		2.450	
$5g$	2.500		4.000	
$6h$	1.550		2.750	
$6h$	4.000		6.500	
$7i$	2.000		3.800	
K-shell basis				
$2s$	5.600		7.700	
$2s$–$3s$	8.450		10.900	
$2p$	3.700		5.150	
$2p$–$5p$	9.000		12.300	
$3d$	4.890		6.720	
$3d$–$6d$	11.100		15.100	
$4f$	6.500		8.900	
$4f$–$6f$	12.000		16.300	
$5g$	8.000		10.900	
$5g$–$7g$	13.900		18.900	
$6h$	9.950		13.600	
$6h$–$7h$	14.800		20.000	
$7i$–$8i$	14.000		19.000	

TABLE A2. Slater type orbitals for basis set B

	Li	
	$1s^2 2s$	$1s^2 2p$
H–F + *KL* basis		
$1s$	2.468	2.478
$1s$	4.680	4.700
$2s$	1.760	1.680
$2s$	1.130	1.130
$2s$	0.665	0.665
$3s$	0.600	0.600
$3s$	1.720	1.720
$2p$	0.512	
$2p$	0.920	
$2p$	1.380	
$2p$	2.850	
$3p$	2.800	
$3d$	0.720	
$3d$	1.050	
$3d$	1.950	
$3d$	3.200	
$4f$	1.100	
$4f$	2.000	
$4f$	3.800	
$5g$	1.350	
$5g$	2.500	
$5g$	4.800	
$6h$	1.550	
$6h$	4.000	
$7i$	2.000	
K-shell basis		
$2s$	4.800	
$2s$–$5s$	11.250	
$2p$–$3p$	4.060	
$2p$–$6p$	12.000	
$3d$–$4d$	5.670	
$3d$–$6d$	13.200	
$4f$	6.180	
$4f$–$7f$	13.200	
$5g$	8.000	
$5g$–$7g$	13.900	
$6h$	9.950	
$6h$–$7h$	14.800	
$7i$–$8i$	14.000	

Can. J. Chem. Downloaded from www.nrcresearchpress.com by 123.30.183.119 on 09/08/12
For personal use only.

The infrared spectrum of 2-methylaziridine from scaled *ab initio* force fields

ARVI RAUK,[1] T. EGGIMANN, H. WIESER, AND DANYA YANG
Department of Chemistry, The University of Calgary, Calgary, Alta., Canada T2N 1N4

Received July 29, 1991

This paper is dedicated to Professor Sigeru Huzinaga on the occasion of his 65th birthday

ARVI RAUK, T. EGGIMANN, H. WIESER, and DANYA YANG. Can. J. Chem. **70**, 464 (1992).

The structures of the *cis* and *trans* invertomers of 2-methylazirdine were optimized at the RHF/6-31G*$^{(0.3)}$ level of theory and the composition of the equilibrium mixture was determined to be *trans*/*cis* = 0.71:0.29, in good agreement with the experimental value, 0.66:0.35. The *ab initio* force field was scaled and a complete assignment of the vibrational spectra of the two conformers is presented. The IR spectrum of 2-methylazirdine was recorded in the vapor phase and in solution (cyclohexane and CCl_4). The predicted IR spectrum of the equilibrium mixture agrees very well with the experimental spectrum. The 6-31G*$^{(0.3)}$ basis set is found to provide better geometries and more uniformly scalable force fields than the conventional 6-31G* basis set.

Key words: *ab initio* force fields, 2-methylaziridine.

ARVI RAUK, T. EGGIMANN, H. WIESER et DANYA YANG. Can. J. Chem. **70**, 464 (1992).

On a optimisé les structures des invertomères *cis* et *trans* de la 2-méthylaziridine au niveau RHF/6-31G*$^{(0.3)}$ de la théorie et on a évalué que l'équilibre de mélange devrait se situer à *trans*/*cis* = 0,71 : 0,29, en bon accord avec la valeur expérimentale de 0,66 : 0.34. On a attribué une échelle au champ de force *ab initio* et on présente une attribution complète du spectre de vibration des deux conformères. On a enregistré le spectre IR de la 2-méthylaziridine tant en phase vapeur qu'en solution (cyclohexane et CCl_4). Le spectre IR prédit pour le mélange à l'équilibre est en bon accord avec le spectre expérimental. On a trouvé que, comparé à l'ensemble de base conventionnel 6-31G*, l'ensemble de base 6-31G*$^{(0.3)}$ fournit de meilleures géométries et des champs de force que l'on peut fixer d'une façon plus uniforme sur une échelle.

Mots clés : champs de force *ab initio*, 2-méthylaziridine.

[Traduit par la rédaction]

Introduction

The explicit connection between the infrared (IR) spectrum of a substance and its molecular structure began to be elucidated in the last decade with the increasing availability of reliable *ab initio* force fields and atomic polar tensors (APT) for intensity calculations. The coincident introduction of chiroptical techniques in the form of vibrational circular dichroism (VCD) spectroscopy and the Raman equivalent has promised further insights. Extraction of the inherent information from the latter techniques (and to some extent the former) has been hampered by theoretical difficulties that have largely been overcome with the introduction of practical nonempirical formalisms by Nafie and Freedman (1), Stephens (2), and Buckingham, Fowler, and Galwas (3) and their computer implementations by Stephens and co-workers (4), Morokuma and Sugeta (5), and Dutler and Rauk (6). The structural rigidity and relatively small size of three-membered ring compounds makes them ideal platforms for the assessment of both experimental and theoretical procedures. The parent achiral compounds can be rendered optically active by isotopic substitution. Investigations have been reported on 1,2-dideuterio- (4) and 1,2-dicyanocyclopropane (7), the deuterated oxiranes (6, 8, 9) and their methyl (10–12) and dimethyl (12) derivatives, and on methyl- (13, 14) and dimethylthiirane (14). The analogous nitrogen heterocycle has escaped attention, perhaps since it lacks the conformational rigidity of the carbon, oxygen and sulfur analogues. 2-Methylaziridine exists as an equilibrium mixture of *trans* and *cis* diastereoisomeric forms whose composition has been determined by nuclear magnetic resonance (15) and IR (16) measurements. The present compound as well as numerous other amines have been the subject of exhaustive IR and Raman spectroscopic studies by Lattes and co-workers (16, 17). A partial assignment of the observed IR and Raman frequencies in the frequency range 100–4000 cm^{-1} was carried out by Durig *et al.* (18) and repeated in the region above 400 cm^{-1} by Razumova and Kostyanovsky (19). Both groups concentrated on the dominant *trans* isomer. The two sets of assignments were in agreement except in the position of the lower frequency N—H bending mode. A number of absorptions due to the *cis* invertomer could clearly be assigned (for a discussion, see ref. 20). In the present work, the gas phase and solution IR spectra are remea-

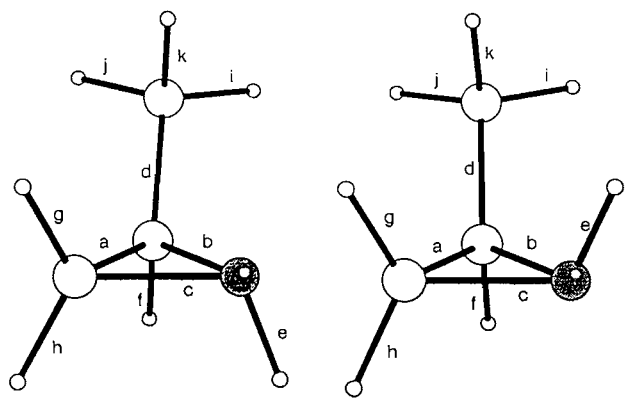

FIG. 1. The RHF//6-31G*$^{(0.3)}$ geometries of (1*R*,2*R*)-2-methylaziridine (*trans*) and (1*S*,2*R*)-2-methylaziridine (*cis*). See Table 1 for numerical details.

[1]Author to whom correspondence may be addressed.

Can. J. Chem. Downloaded from www.nrcresearchpress.com by 92.62.229.171 on 09/08/12
For personal use only.

TABLE 1. 6-31G*$^{(0.3)}$ and 6-31G*$^{(0.8)}$ geometries of *trans*-2-methylaziridine, and *cis*-2-methylaziridine

	trans-2-Methylaziridine			*cis*-2-Methylaziridine	
Parameter[a]	6-31G*$^{(0.3)}$	6-31G*$^{(0.8)}$	Expt.[b]	6-31G*$^{(0.3)}$	6-31G*$^{(0.8)}$
a	1.483	1.472	1.480[c]	1.482	1.471
b	1.475	1.449	1.488[c]	1.475	1.449
c	1.477	1.452	1.488[c]	1.479	1.453
d	1.512	1.508	1.517	1.513	1.510
e	1.007	1.001	1.010	1.008	1.002
f	1.083	1.080		1.082	1.078
g	1.080	1.076		1.081	1.078
h	1.081	1.077		1.079	1.076
i	1.091	1.086		1.091	1.086
j	1.092	1.086		1.091	1.086
k	1.089	1.084		1.091	1.087
ab	59.9	59.6		60.0	59.7
ac	59.8	59.4		59.8	59.4
ad	122.6	122.5	120.5	121.3	120.8
af	115.4	115.7		116.9	117.7
ag	119.8	120.1		117.9	117.8
ah	118.4	118.5		120.5	120.8
bc	60.3	61.0		60.2	60.9
bd	116.7	116.7		120.6	120.5
be	111.4	112.1		110.9	111.6
bf	115.6	116.5		112.0	112.9
ce	111.0	111.7		110.6	111.5
cg	114.4	115.0		117.7	118.4
ch	117.9	118.6		114.7	115.1
df	115.2	114.7		114.8	114.4
di	110.7	110.7		111.0	110.9
dj	110.8	110.9		110.7	110.8
dk	110.4	110.4		111.0	111.1
gh	115.1	114.3	116.7[c]	115.0	114.4
adi	−150.7	−150.6		−149.2	−149.2
adj	89.2	89.3		90.0	90.9
adk	−31.2	−31.1		−29.0	−29.0

[a]See Fig. 1 for a definition of the parameters: the letters denote bonds, e.g., a is the length in Å, ab is the bond angle (°), and abc is the dihedral angle (°).
[b]Reference 31.
[c]Assumed from aziridine.

TABLE 2. Energies of *trans*-2-methylaziridine, and *cis*-2-methylaziridine

Method[a]	*trans*-2-Methylaziridine energy (hartrees)	*cis*-2-Methylaziridine energy (hartrees)	$E_{cis} - E_{trans}$ (kJ/mol)
RHF/6-31G*$^{(0.8)}$//6-31G*$^{(0.8)}$	−172.078952	−172.077982	2.55
RHF/6-31G*$^{(0.3)}$//6-31G*$^{(0.3)}$	−172.036213	−172.035814	1.05
RHF/6-31G**//6-31G*$^{(0.3)}$	−172.091571	−172.090546	2.69
MP2/6-31G**//6-31G*$^{(0.3)}$	−172.690241	−172.689510	1.92
ZPVE(RHF/6-31G*$^{(0.3)}$//6-31G*$^{(0.3)}$)	273.170[b]	273.442[b]	0.25[c]

[a]The notation XXX/YYY//ZZZ means that the theoretical method XXX was used with the basis set YYY at a geometry optimized at the RHF level of theory with basis set ZZZ.
[b]In kJ/mol.
[c]× 0.912.

sured in the range 400–4000 cm^{-1} and the relative frequencies and intensities are determined. On the basis of the present study, many of the previous assignments must be revised.

Use of scaled *ab initio* force fields is fraught with several difficulties, not the least of which is the unfortunate fact that the conventional 6-31G* basis set does not yield as satisfactory a geometry for a heteroatom containing three-membered rings as for less strained systems. Typically, the C—X bond is too short by about 0.04 Å. While it is possible to transfer the *ab initio* field from the equilibrium geometry to the experimental geometry, there remains the

Can. J. Chem. Downloaded from www.nrcresearchpress.com by 92.62.229.171 on 09/08/12
For personal use only.

Can. J. Chem. Downloaded from www.nrcresearchpress.com by 92.62.229.171 on 09/08/12
For personal use only.

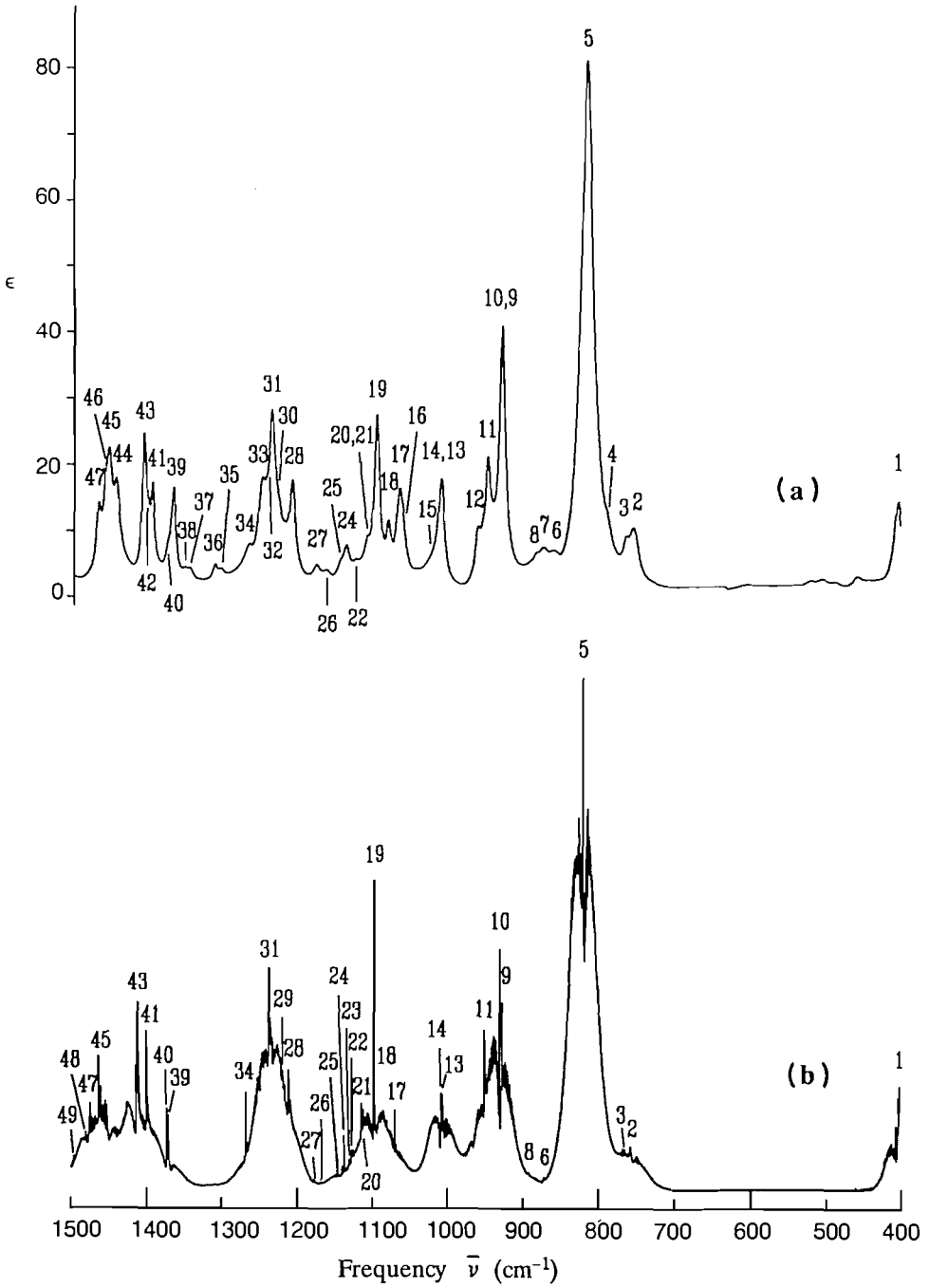

FIG. 2. Experimental IR spectrum of 2-methylaziridine (for experimental conditions, see text), 400–1500 cm^{-1}: (*a*) CCl_4 solution; (*b*) gas phase, 50 Torr.

suspicion that deficiencies in the structure are due to underlying deficiencies in the force field itself. It is well known that Hartree–Fock force fields are subject to a systematic, nearly constant, error (21), a theoretical rationalization of which has recently been presented (22). They are also subject to structure-related nonsystematic errors, which arise in part from deficiencies in the theoretical model (e.g., lack of electron correlation) but primarily from deficiencies in the basis set. Scaling of the force field attempts to correct for these deficiencies. *Uniform* scaling by a factor of 0.8 (21) largely compensates for systematic overestimation of force constants at the HF level and does not modify the normal mode descriptions from which intensity data may be derived. *Non*uniform scaling to match specific assigned frequencies is necessary to correct for basis set deficiencies. The success of nonuniform scaling procedures is contingent upon correct assignments being made in the first instance. Use of multiple scale factors also alters the normal mode descriptions and therefore the derived intensities. Ideally, the scaling should be as uniform as possible to avoid the latter difficulties. The recently introduced 6-31G*$^{(0.3)}$ basis set (12) yields geometries and "raw" *ab initio* force fields that appear to be superior to those derived using the standard 6-31G* (hereafter re-

Can. J. Chem. Downloaded from www.nrcresearchpress.com by 92.62.229.171 on 09/08/12
For personal use only.

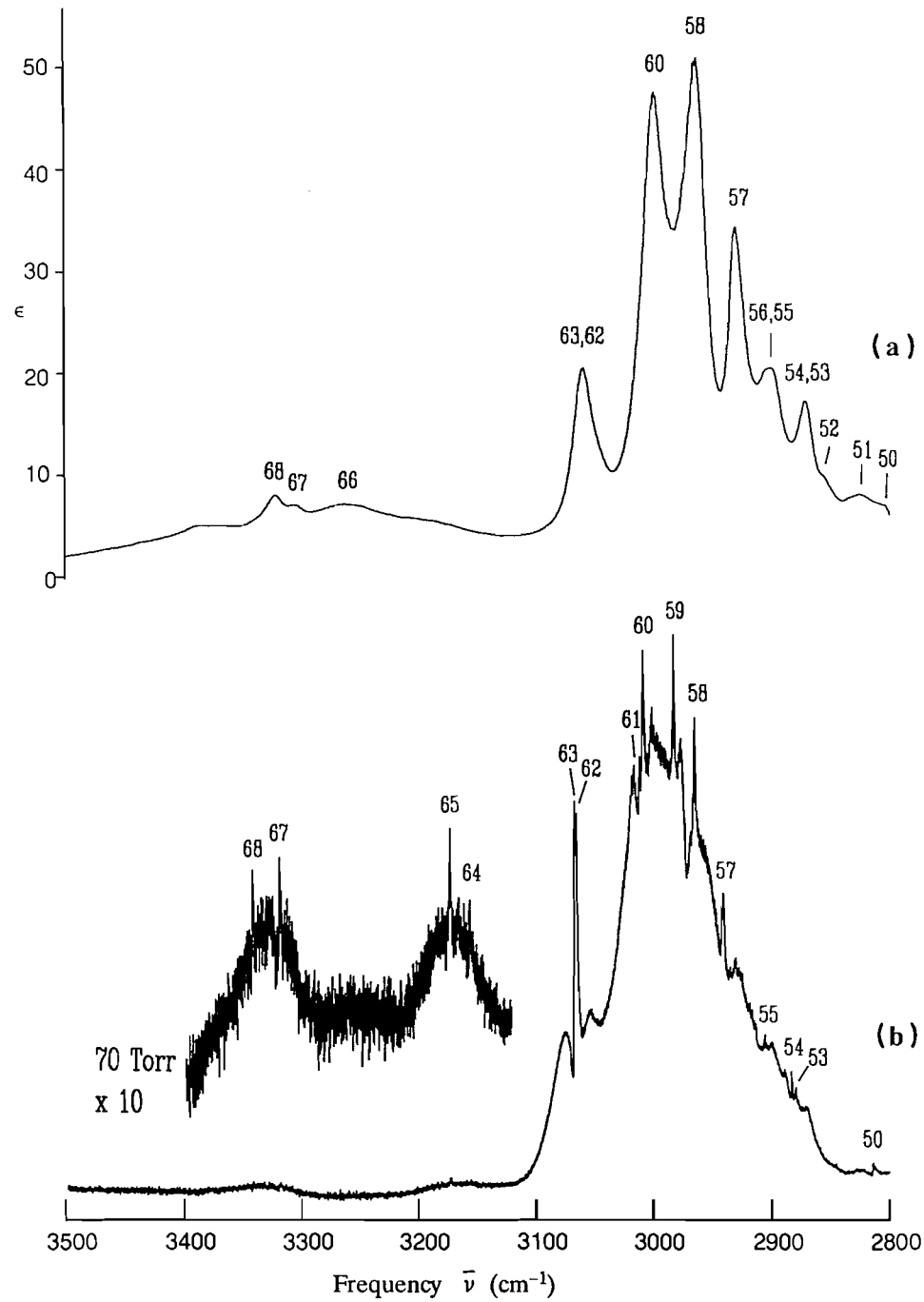

FIG. 3. Experimental IR spectrum of 2-methylaziridine (for experimental conditions, see text) 2800–3500 cm^{-1}: (*a*) CCl_4 solution; (*b*) gas phase, 50 Torr.

ferred to as 6-31G*$^{(0.8)}$) basis set for first row atoms. We report herein scaled *ab initio* 6-31G*$^{(0.3)}$ force fields for the two invertomers of 2-methylaziridine, and compare the calculated IR spectra with the spectrum simulated for the equilibrium mixture. In a following paper we report on a theoretical investigation of the vibrational circular dichroism spectra of the individual invertomers and of the equilibrium mixture (23).

Computational details

The geometries of *trans*- and *cis*-2-methylaziridine were determined by complete optimization at the restricted Hartree–Fock level of theory using the analytical procedures of the GAUSSIAN 82 (24) or GAUSSIAN 86 (25) systems of programs and the internal 6-31G*$^{(0.8)}$ (12, 26) basis set and the modified 6-31G*$^{(0.3)}$ (12) basis set. We distinguish the original and modified 6-31G* basis sets by indicating explicitly the value of the *d* exponent. Thus 6-31G*$^{(0.8)}$ is equivalent to the original 6-31G* basis set for C, N, and O (26). Since bond lengths are calculated to be a little longer by the 6-31G*$^{(0.3)}$ basis set, an effect also observed with optimization at the MP2 level of theory, an improved estimate of the relative energies of the two isomers was obtained by single point recalculation of the energies at the MP2 level of

TABLE 3. Observed vibrational frequencies and absorption intensities for 2-methylaziridine

No.[a]	Positions vapor (cm^{-1})	Positions solution[b] (cm^{-1})		Dipole strength[c] ($esu^2\ cm^2$)	No.[a]	Positions vapor (cm^{-1})	Positions solution[b] (cm^{-1})		Dipole strength[c] ($esu^2\ cm^2$)
1	400.9	402.7	m	49.6	35		1304.7	w,dcn	0.6
2	756.1	753.1	(CY) w,dcn	13.0	36		1312.3	w,dcn	3.2
3	763.8	763.7	(CY) w,dcn	7.3	37		1346.5	w,dcn	0.9
4		789.7	(CY) w,sh,dcn	2.0	38		1352.8	w,dcn	0.3
5	818.4	814.6	(CY) s	268	39	1371.0	1368.0	m	9.3
6	870.5	860.4	w	2.0	40	1373.1	1375.4	m,sh,dcn	2.8
7		873.5	w	3.0	41	1400.4	1396.2	m,dcn	7.3
8	891.1	884.2	w,dcn	1.1	42		1401.9	m,sh,dcn	4.4
9	926.2	929.2	s	52.5	32	1412.2	1407.6	s,dcn	11.2
10	929.4				44	Series of bands	1444.4	m,dcn	15.1
11	949.4	948.2	m	27.4	45	1463.6	1453.5	m,dcn	8.7
12		961.3	m,dcn	5.7	46	Series of bands	1457.4	m,sh,dcn	8.7
13	1004.9	1009.5	m	18.8	47	1474.8	1468.0	m,dcn	5.3
14	1007.0				48	1480.8			
15		1020.	w,sh,broad,dcn	10.9	49	1496.3			
16		1062.	m,sh,dcn	3.9	50	2812.0	2802.5	w,dcn	1.4
17	1068.6	1065.7	m	14.0	51		2823.7	w,broad,dcn	4.2
18	1079.5	1080.4	m	5.2	52		2854.1	w,sh,dcn	1.8
19	1095.8	1095.9	s	25.0	53	2878.3	2869.5	m	7.3
20	1110.8	1108.8	m,dcn	6.5	54	2881.6			
21	1113.8				55	2904.0	2896.5	m,dcn	3.0
22	1127.1	1124.7	w,dcn	1.7	56		2903.	m,sh,dcn	18.6
23	1130.2				57	2939.1	2928.4	s	14.9
24	1137.1	1137.5	w	4.8	58	2962.8	2961.6	s	43.9
25	1146.3	1145.0	w,sh,dcn	2.1	59	2981.1			
26	1167.7	1164.6	w	3.4	60	3007.1	2997.1	s	51.1
27	1176.7	1177.4	w	3.1	61	3014.8			
28	1210.5	1210.0	m	12.3	62	3064.8	3058.5	m	13.7
29	1218.4				63	3066.3			
30		1229.	m,sh,dcn	11.1	64	3155.1			
31	1236.9	1236.5	s	24.3	65	3172.6			
32		1243.	m,sh,dcn	3.1	66		3259.	very broad	
33		1250.1	m,dcn	13.7	67	3319.6	3305.3	w	0.3
34	1267.6	1267.0	w,dcn	5.0	68	3342.9	3321.2	w	1.7

[a]The numbers correspond to peak positions numerically identified in Figs. 2 and 3.
[b]Measured in CCl_4 except marked CY (cyclohexane), w = weak, m = medium, s = strong, sh = shoulder, dcn = position measured after Fourier self-deconvolution.
[c]$\times 10^{40}$.

theory using the internal 6-31G** basis set at the 6-31G*$^{(0.3)}$ geometry, i.e., MP2/6-31G**//6-31G*$^{(0.3)}$ in the accepted notation. Normal coordinate analysis at the 6-31G*$^{(0.3)}$ equilibrium geometry was carried out by analytical second differentiation of the Born–Oppenheimer RHF energy (27). IR intensities were accomplished by the program system Freq85 (6), which implements the vibronic coupling theory (VCT) of Nafie and Freedman (1) at the *ab initio* level, and permits recalculation for arbitrary isotopic substitutions. For IR intensities, VCT is identical to the atomic polar tensor (APT) theory that is implemented in GAUSSIAN 86 and subsequent versions of the GAUSSIAN system of quantum chemistry codes. For improved agreement with experiment, frequencies were either uniformly scaled (28), or selectively scaled according to the procedure of Pulay *et al.* (29, 30). The VCT intensity evaluations were computed using the 6-31G*$^{(0.3)}$ basis set (VCT/6-31G*$^{(0.3)}$). Simulated IR spectra were obtained assuming a Lorentzian lineshape of width at half height 10 cm^{-1}.

Geometries

Neither complete experimental nor theoretical structures of the 2-methylaziridines have previously been reported. The RHF/6-31G*$^{(0.3)}$//6-31G*$^{(0.3)}$ geometries of *trans*- and *cis*-2-methylaziridine are shown in Fig. 1. Complete details of the structures in terms of parameters defined in Fig. 1 are shown in Table 1. The RHF/6-31G*$^{(0.8)}$//6-31G*$^{(0.8)}$ structural parameters are also listed in Table 1. Partial experimental data deduced from MW studies (31) are compared to the calculated values. With the 6-31G*$^{(0.3)}$ basis set, the C—C and C—N bonds of the ring are very similar in length, the C—N bonds being calculated to be about 0.025 Å longer than with the 6-31G*$^{(0.8)}$ basis set. Examination of the structures of Fig. 1 reveals a tipping of the external H—C*—Me plane (the plane of the bonds d and f) away from the N—H bond (or toward the N lone pair) in each isomer. Although not apparent from the figure, examination of the data of Table 1 reveals a similar effect of the N configuration on the tilt of the CH_2 plane. The influence of the N lone pair, n_N, is

Can. J. Chem. Downloaded from www.nrcresearchpress.com by 92.62.229.171 on 09/08/12
For personal use only.

TABLE 4. Definitions of local symmetry coordinates (LSC) for *cis*- and *trans*-2-methylaziridine

	LSC type[a]	Definition[b]
1	C—N stretch	c
2	C—N stretch	b
3	C—C stretch	a
4	C—C stretch	d
5	N—H stretch	e
6	C—H stretch	g
7	C—H stretch	h
8	C—H stretch	f
9	C—H stretch	k
10	C—H stretch	j
11	C—H stretch	i
12	N—H ⊥bend	α(be) − α(ce)
13	N—H ∥ bend	α(be) + α(ce)
14	C—H ⊥bend	α(af) − α(bf)
15	C—H ∥ bend	2α(df) − α(af) − α(bf)
16	CH_2 scissor	α(gh)
17	CH_2 rock	α(ag) + α(cg) − α(ah) − α(ch)
18	CH_2 wag	α(ag) − α(cg) + α(ah) − α(ch)
19	CH_2 twist	α(ag) − α(cg) − α(ah) + α(ch)
20	CH_3 ⊥bend	α(ad) − α(bd)
21	CH_3 ∥ bend	α(ad) + α(bd)
22	CH_3 sym. deform.	α(di) + α(dj) + α(dk) − α(ij) − α(ik) − α(jk)
23	CH_3 asym. deform.	2α(ij) − α(ik) − α(jk)
24	CH_3 asym. deform.	α(ik) − α(jk)
25	CH_3 ⊥rock	α(di) − α(dj)
26	CH_3 ∥ rock	2α(dk) − α(di) − α(dj)
27	CH_3 torsion	τ(idb) + τ(jdf) + τ(kda)

[a] ⊥ = perpendicular to df or gh plane or equivalent at N (Fig. 1), ∥ = parallel to df or gh.
[b] Letters refer to bonds as defined in Fig. 1, α are angles, τ are dihedral angles.

TABLE 5. Force field scale factors

Mode	Uniform scaling	Azetidine[a]	2-methylaziridine refinements[b] 3sf	4sf	6sf	6sf
α C—H stretch		0.809	0.844	0.844	0.844	0.844
N—H stretch		0.792	0.817	0.817	0.817	0.817
C—C stretch		0.883			0.839	0.843
C—N stretch		0.784			0.828	0.827
CH_3 ∥ , ⊥ defs.				0.958	0.959	0.959
Rest[c]	0.832	0.785	0.833	0.825	0.820	0.818
No. of assigned bands	25		25	25	30	33
Average error (cm^{-1})	12.6		7.9	4.6	4.3	4.2

[a] 6-31G*$^{(0.8)}$ force field, see ref. 34.
[b] 6-31G*$^{(0.3)}$ force field, see text.
[c] Includes all CH_2, CH, and NH deformations, all CH_3 deformations, rocks, and torsion, and the other tabulated modes for which a scale factor is not explicitly listed.

probably electronic rather than simply steric, and may be rationalized in terms of perturbative MO theory as causing a distortion so as to improve the energetically favorable n_N–σ* interaction, where σ* is the out-of-phase combination of the antibonding orbitals of the d, f, and (or) g, h bonds.

Relative energies

2-Methylaziridine exists as an equilibrium mixture of the *trans*- and *cis*- isomeric forms. Both ^{1}H NMR (15) and IR (16) data indicate that the *trans* form is favored by about (ΔG^0 =) 1.6–1.7 kJ/mol in dilute solution, corresponding to a *trans*/*cis* ratio of 0.66:0.35 at ambient temperature. Total energies and relative energies of the two isomers computed by several methods are shown in Table 2. As discussed in the Computational Details section, the most accurate practical estimate of the relative energies of the Born–Oppenheimer minima should be obtained by single point MP2 calculation using the 6-31G** basis set at the 6-31G*$^{(0.3)}$ geometry (MP2/6-31G**//6-31G*$^{(0.3)}$ in Table 2). The zero point vibrational energy (ZPVE) is found to be slightly higher for the *cis* form. Correction for the change in ZPVE yields

Can. J. Chem. Downloaded from www.nrcresearchpress.com by 92.62.229.171 on 09/08/12
For personal use only.

TABLE 6. 6-31G*$^{(0.3)}$ frequencies and electric dipole strengths of (1*R*,2*R*)-2-methylaziridine (*trans*)

No. ν	Frequencies (cm^{-1}) Calcd.	Calcd.[b]	Calcd.[c]	Obsd.[e]	$D^{a,b}$	$D^{a,c}$	Assignments[d]
27	218	199	198	200[f,g]	4.0	4.4	CH_3 torsion
26	378	345	371	387[f,g]	52.7	53.8	$\perp CH_3$
25	415	378	408	401	86.8	82.5	$\parallel$ CH_3
24	830	757	757	764	33.9	28.9	asym ring def
23	903	824	823	818	283.9	288.1	asym ring def
22	950	867	861	871	7.6	8.8	CH_2 rock + $\perp$CH
21	1025	935	928	929	62.0	61.4	CH_2 rock + $\perp$NH
20	1062	969	966	961[h]	44.6	50.3	C—CH_3 str + ring def
19	1097	1001	996	1005	36.0	32.2	$\parallel$ NH + $\perp$CH
18	1188	1084	1084	1069	42.6	32.5	CH_3 rock + $\perp h^h$ + $\perp$CH
17	1213	1107	1100	1096	12.4	25.0	CH_2 wag
16	1256	1146	1142	1137	8.7	10.5	$\perp$CH + CH_2 twist
15	1327	1211	1209	(1210)	6.6	4.3	$\parallel$ CH + $\perp$NH
14	1373	1252	1253	(1243)[i]	38.0	17.6	$\perp$NH + CH_2 rock
13	1388	1266	1258	(1250)[i]	66.2	82.1	$\parallel$ NH + CH_2 rock
12	1512	1379	1369	1371	7.0	7.1	CH_3 umb
11	1565	1428	1420	1412	21.8	20.5	CH_2 scis + CH_3 umb
10	1614	1473	1460	(1444)	9.2	9.2	asym CH_3 def
9	1623	1481	1469	(1457)[i]	14.0	14.1	asym CH_3 def
8	1642	1498	1489	(1496)[i]	14.9	16.8	CH_2 scis
7	3135	2860	2880	2882	40.1	39.8	CH_3 sym str
6	3211	2929	2950	(2939)	42.9	42.7	CH_3 asym str
5	3226	2943	2964	j	2.3	2.2	CH_3 asym str + CH str
4	3235	2951	2972	j	49.2	48.8	CH_2 sym str
3	3254	2968	2989	2981	52.8	52.7	CH str
2	3336	3043	3065	3065	26.9	26.7	CH_2 asym str
1	3693	3369	3338	3343	3.9	3.9	NH str

[a]In $esu^2\ cm^2$ ($\times 10^{-40}$).
[b]Uniformly scaled force field, ×0.832.
[c]Optimally scaled force field (see text); average error 4.6 cm^{-1} (0.41%).
[d]Symbols and abbreviations: $\perp$ = perpendicular to df or gh plane or equivalent at N (Fig. 1), $\parallel$ = parallel to df or gh, str = stretch, def = deformation, umb = umbrella motion, scis = scissor.
[e]Numbers in parentheses are tentative assignments and were not included in the refinement.
[f]Below instrument cutoff.
[g]Reference 18.
[h]Bond h (see Fig. 1).
[i]Position measured from solution spectrum.
[j]Unassigned peaks, see Table 3.

an estimate of $\Delta H^0 = 2.17$ kJ/mol for the gas phase difference. Assuming that $\Delta S \approx 0$, a *trans/cis* mixture of 0.706:0.294 at 298 K is predicted. Since it is quite close to the experimental estimates and the effects of differential solvation are unknown, the theoretical ratio is used in the simulation of the IR spectra shown in Figs. 4 and 5, and discussed below.

Experimental methods

The racemic 2-methylaziridine was purchased from Aldrich (90%) and purified by distillation in a vacuum line before use. The solution absorption spectra (Figs. 2 and 3) were recorded at various concentrations in the solvents cyclohexane (700–850 cm^{-1}) and CCl_4 (rest of the spectral range) using a Nicolet 8000 FT-IR interferometer running at 1 cm^{-1} resolution (1000 scans). For the vapor phase absorption spectra (400–4000 cm^{-1}, see Figs. 2 and 3), 300 scans were collected with a resolution of 0.12 cm^{-1} in a 10 cm cell with KBr windows, at pressures of 50 and 70 Torr (1 Torr = 133.3 Pa).

In spite of the initial daunting appearance, the IR spectrum of the 2-methylaziridine yielded to modern techniques. Fourier self-deconvolution (32) provided exact frequency measurements for many of the overlapping bands that dominate the condensed phase spectrum. These band positions were then used for the determination of the intensities, some of which could not be measured precisely due to severe overlapping. A list of the observed frequencies and intensities may be found in Table 3. The intensities of bands 66 and 35–38 are concentration dependent, likely caused by hydrogen bonding. The intensities were measured with a sample concentration of 0.8 mol/L.

A number of vapor phase bands exhibit two distinct *Q*-branches clearly arising from the two conformers (e.g., nos. 9/10, 13/14, and 39/40). Some regions of the spectrum are so complex as to prevent firm identification of the fundamental transitions on the basis of the vapor phase spectrum alone.

Force field refinements and assignments

The *ab initio* Cartesian force constants for both conformers were transferred to a nonredundant set of local symmetry coordinates (Table 4), chosen in accordance to the recommendations of Pulay *et al.* (29). The scaling of the local symmetry force constants, K_{ij}, was achieved by the method, $F_{ij} = (c_i c_j)^{1/2} K_{ij}$, where F_{ij} are the scaled force constants and c_i and c_j are the scale factors associated with the local modes i and j, respectively (30). Our scaling and refining proce-

Can. J. Chem. Downloaded from www.nrcresearchpress.com by 92.62.229.171 on 09/08/12
For personal use only.

TABLE 7. 6-31G*$^{(0.3)}$ frequencies and electric dipole strengths of (1*S*,2*R*)-2-methylaziridine (*cis*)

No. ν	Frequencies (cm^{-1}) Calcd.	Calcd.[b]	Calcd.[c]	Obsd.[e]	$D^{a,b}$	$D^{a,c}$	Assignments[d]
27	232	212	210	213[f,g]	4.8	4.9	CH_3 torsion
26	381	347	374	f	17.9	15.8	$\perp CH_3$
25	416	379	408	401	26.5	23.8	$\parallel CH_3$
24	826	754	754	756	44.2	42.8	asym ring def
23	899	821	818	818	281.5	286.6	asym ring def
22	973	888	882	891	2.4	3.9	CH_2 rock + $\perp CH$
21	1024	934	927	926	43.7	44.2	CH_2 rock + $\perp NH$
20	1043	951	950	949	94.3	92.8	C—CH_3 str + ring def
19	1104	1007	1002	1007	95.1	101.5	$\parallel NH + \perp CH$
18	1199	1094	1090	1080	7.0	7.1	CH_2 wag + h^h wag
17	1231	1123	1121	1114	9.4	13.4	$\perp h^h$ wag
16	1268	1157	1151	1146	12.1	13.8	$\perp CH$
15	1336	1219	1218	(1218)	39.7	27.3	$\parallel CH + \perp NH$
14	1364	1245	1240	(1237)	33.5	34.5	$\perp NH + CH_2$ rock
13	1398	1275	1276	1268	24.1	22.7	$\parallel NH + CH_2$ rock
12	1514	1381	1370	1373	20.0	19.0	CH_3 umb + $\parallel CH$
11	1555	1419	1412	1400	30.9	31.4	CH_2 scis + CH_3 umb
10	1615	1473	1461	(1464)	8.8	8.9	asym CH_3 def
9	1625	1483	1471	(1475)	20.9	21.0	asym CH_3 def
8	1640	1496	1487	(1481)	4.4	5.7	CH_2 scis
7	3130	2855	2875	2878	35.5	35.3	CH_3 sym str
6	3208	2926	2947	i	26.9	26.7	CH_3 asym str
5	3212	2930	2951	i	36.6	36.3	CH_3 asym str + CH str
4	3236	2952	2973	i	42.5	42.1	CH_2 sym str
3	3269	2982	3003	3007	40.9	40.8	CH str
2	3337	3044	3066	3066	28.7	28.6	CH_2 asym str
1	3679	3356	3324	3320	3.1	3.1	NH str

[a] In $esu^2\ cm^2$ ($\times 10^{-40}$).
[b] Uniformly scaled force field, ×0.832.
[c] Optimally scaled force field (see text); average error 3.8 cm^{-1} (0.32%).
[d] Symbols and abbreviations: $\perp$ = perpendicular to df or gh plane or equivalent at N (Fig. 1), $\parallel$ = parallel to df or gh, str = stretch, def = deformation, umb = umbrella motion, scis = scissor.
[e] Numbers in parentheses are tentative assignments and were not included in the refinement.
[f] Below instrument cutoff.
[g] Reference 18.
[h] Bond h (see Fig. 1).
[i] Unassigned peaks, see Table 3.

dures have been described in more detail in earlier publications (33).

Great caution was mandatory for the refinements of the 6-31G*$^{(0.3)}$ force fields since no scale factors have been developed to date for this basis set. The favorable reference point for the refinement of the 2-methylaziridine force fields appears to be the 6-31G*$^{(0.8)}$ scale factors for azetidine (34). However, a direct transfer of the parameters is not advisable because the differences between the force fields of the two basis sets are not known. Therefore, the force fields were initially scaled uniformly with a factor ($f = 0.813$) that is the average of the six optimized azetidine 6-31G*$^{(0.8)}$ parameters. With the resulting frequency predictions, 25 of the 54 fundamental transitions for both conformers including the N—H stretches (ν_1) and C—H stretches (ν_2) were assigned unambiguously. The uniform scale factor was then divided up into three separate factors, one each for N—H stretching, C—H stretching, and the remaining modes, respectively. The optimized values after the first refinement run are given in Table 5 (column 3sf). Most frequencies below 1500 cm^{-1} were calculated high while the vibration, ν_{25}, which is an almost pure methyl out-of-plane bend, was predicted 22 cm^{-1} low for both conformers. This coordinate has been shown to require an unusually high scale factor for the 3-21G force field of methyloxetane (33*c*). It seemed justified and appropriate therefore to allow a separate scale factor just for this mode. With this modification, the previous refinement was repeated with a much improved frequency fit (column 4sf, Table 5).

It was now possible to assign with confidence another five fundamentals and to define two separate scale factors for the C—C stretch and C—N stretch. Starting with the preoptimized factors, all six parameters were allowed to vary independently in another refinement (6sf-1, Table 5). Column 6sf-2 in Table 5 contains the results from the final optimization including a total of 33 firmly assigned transitions, showing that all parameters remain constant and are well defined within this refinement. The average deviation experiment of the calculated frequencies is 4.2 cm^{-1} (0.37%). The absolute numbers of these new 6-31G*$^{(0.3)}$ force field scale factors are similar to previously optimized factors for other basis sets. The parameter for the CH_3 out-of-plane deformation is again found to be much larger than the others. All the factors except for the C—C stretch are higher than

Can. J. Chem. Downloaded from www.nrcresearchpress.com by 92.62.229.171 on 09/08/12
For personal use only.

Can. J. Chem. Downloaded from www.nrcresearchpress.com by 92.62.229.171 on 09/08/12
For personal use only.

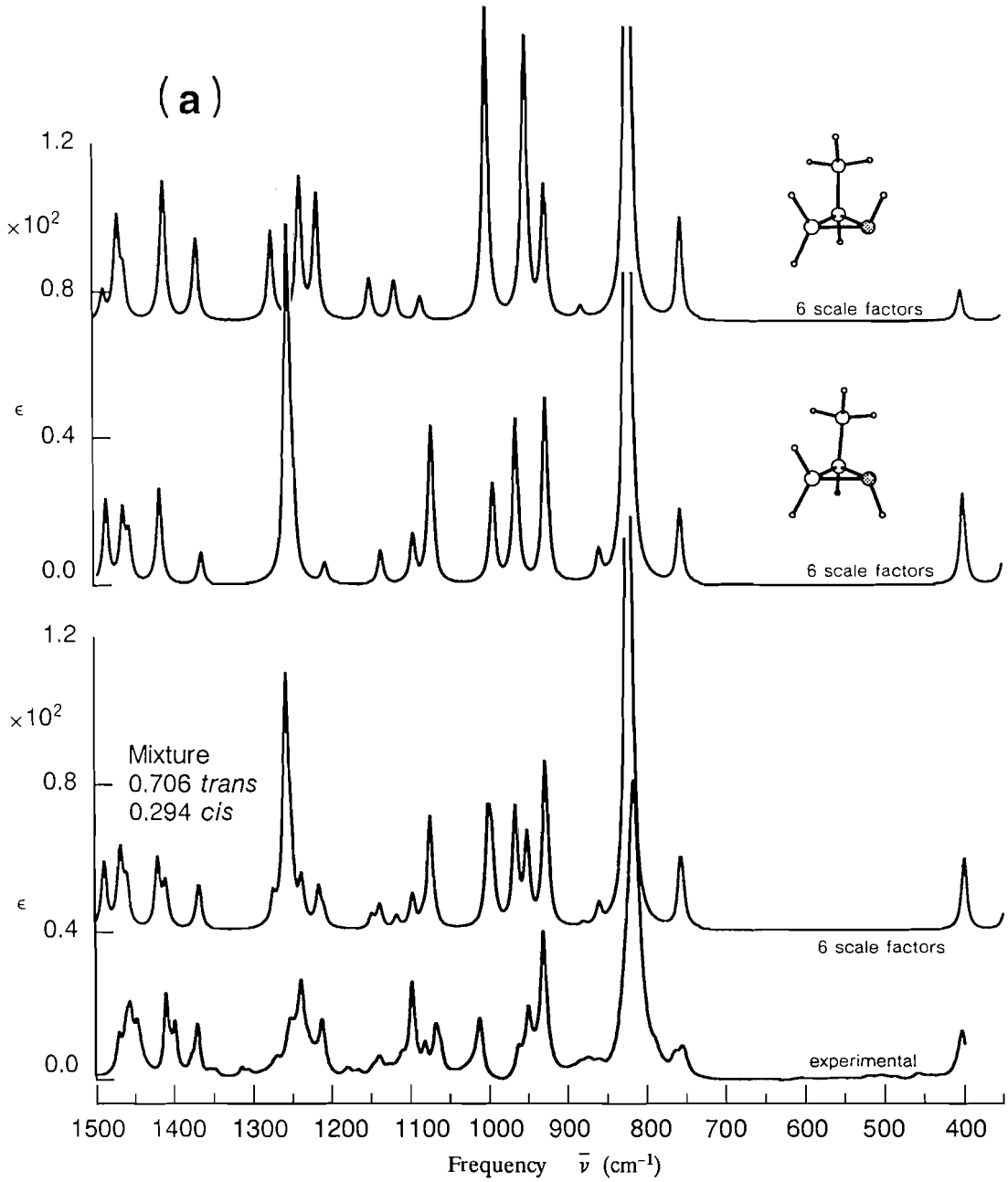

FIG. 4. Simulated IR spectra by VCT/6-31G*$^{(0.3)}$ theory in the region 350–1500 cm^{-1} for the individual invertomers of 2-methylaziridine, and of the theoretical equilibrium mixture at 298 K compared with the experimental spectrum in CCl_4 (bottom spectrum); the linewidth for simulations is 8 cm^{-1}: (*a*) scaled with six scale factors; (*b*) uniformly scaled.

the corresponding 6-31G*$^{(0.8)}$ values for azetidine. The parameters for C—C and C—H stretching remarkably resemble the corresponding 6-31G** scale factors of oxirane (9). Finally, the 6-31G*$^{(0.3)}$ factors are considerably more uniform than for the 6-31G*$^{(0.8)}$ or any smaller basis sets, indicating a more balanced treatment of the various intramolecular motions by the original *ab initio* 6-31G*$^{(0.3)}$ force field.

The refinements were also carried out with the 6-31G*$^{(0.8)}$ force constants for 2-methylaziridine. Although it was possible here to transfer directly the scale factors from azetidine, the spectral assignments were more tedious because of inferior frequency predictions compared to the 6-31G*$^{(0.3)}$ basis set. The final spectral assignment was essentially the same as above, included 33 bands as well, but required eight scale factors to reproduce the frequencies with an average error of 6.2 cm^{-1} (0.56%). The additional parameters had to be employed for the C—CH_3 stretch and for the methyl C—H stretches in order to achieve a reasonable fit. The optimized values are similar to the azetidine factors but generally lower.

Thus the present experience indicates that the errors of the 6-31G*$^{(0.3)}$ force constants for 2-methylaziridine are smaller and more uniform than for the conventional 6-31G*$^{(0.8)}$ basis set. The 6-31G*$^{(0.3)}$ force constants therefore lie closer to the Hartree–Fock limit values. It would be

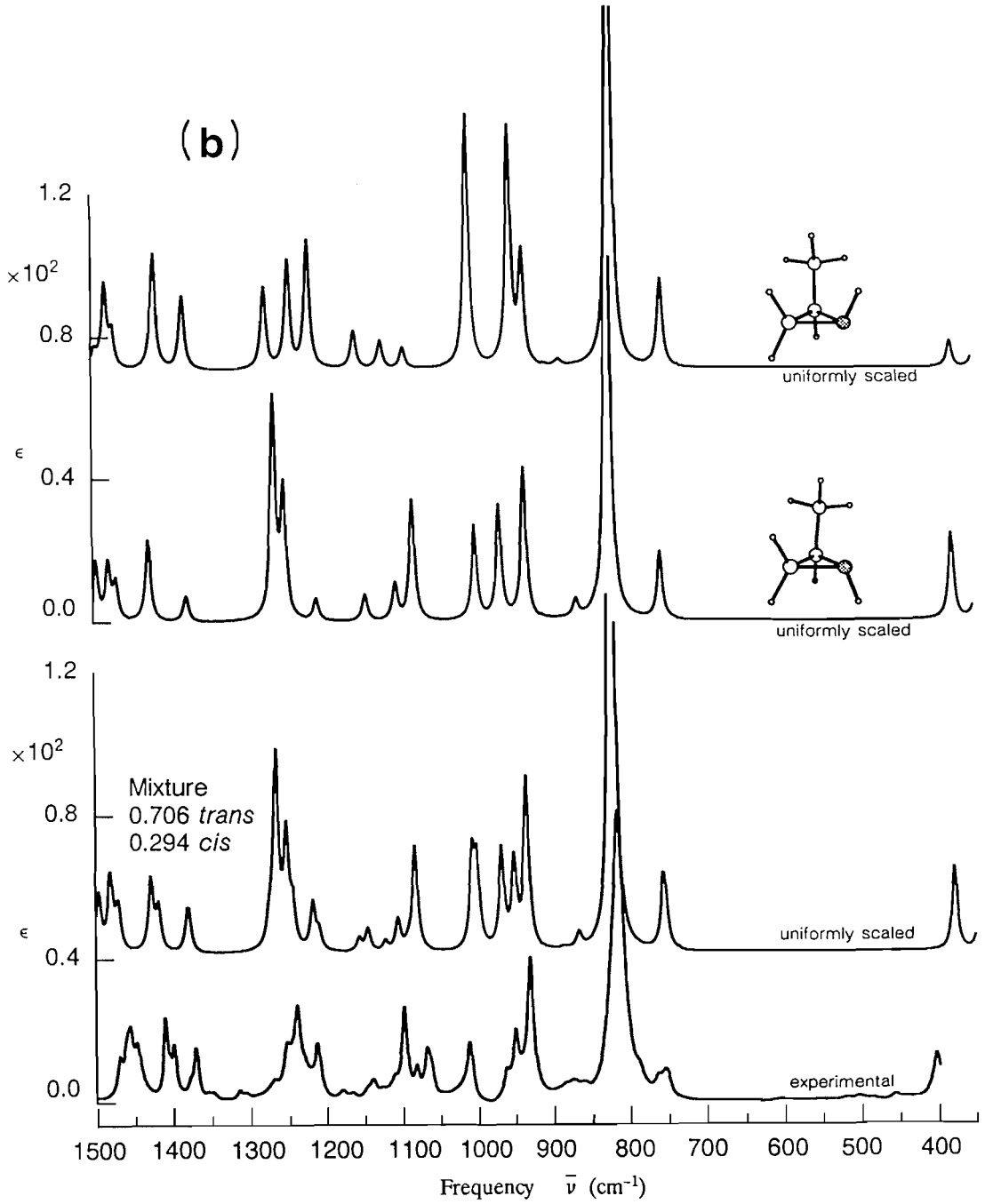

FIG. 4 (*concluded*)

necessary now to test the performance of this basis set with other molecules.

Results and discussion

The experimental solution and vapor phase spectra of 2-methylaziridine are shown in Fig. 2 (400–1500 cm^{-1}) and Fig. 3 (2800–3500 cm^{-1}). The numbering on the bands corresponds to the listing of observed bands in Table 3. A number of the bands cannot be assigned to fundamental transitions. Most of them are probably overtone or combination bands. However, there are relatively strong bands in the solution spectra (in both CCl_4 and cyclohexane) that are not observed in the gas phase. Examples are the signals between 420 and 520 cm^{-1} and the four bands, nos. 35–38, that we believe arise from N—H bending modes (ν_{13}, ν_{14}) of hydrogen-bonded molecules. The corresponding modes for ν_{19} and ν_{21}, which also involve the N—H deformations, should then be shifted up into the region 980–1050 cm^{-1}. Indeed, two unassigned bands are observed in or nearby this region (nos. 15, 16). The broad feature in the solution spectrum around 3260 cm^{-1} (no. 66) clearly corresponds to the N—H stretch involved in hydrogen bonding. One of the two vapor phase bands near 3180 cm^{-1}, no. 65 (3172.6 cm^{-1}), has been observed by Durig *et al.* (18) and assigned to a combination band due to the methyl torsion and an asymmetric stretch of the methyl group of the *trans* isomer, $\nu_5 + \nu_{27} = 3161$ cm^{-1}

Can. J. Chem. Downloaded from www.nrcresearchpress.com by 92.62.229.171 on 09/08/12
For personal use only.

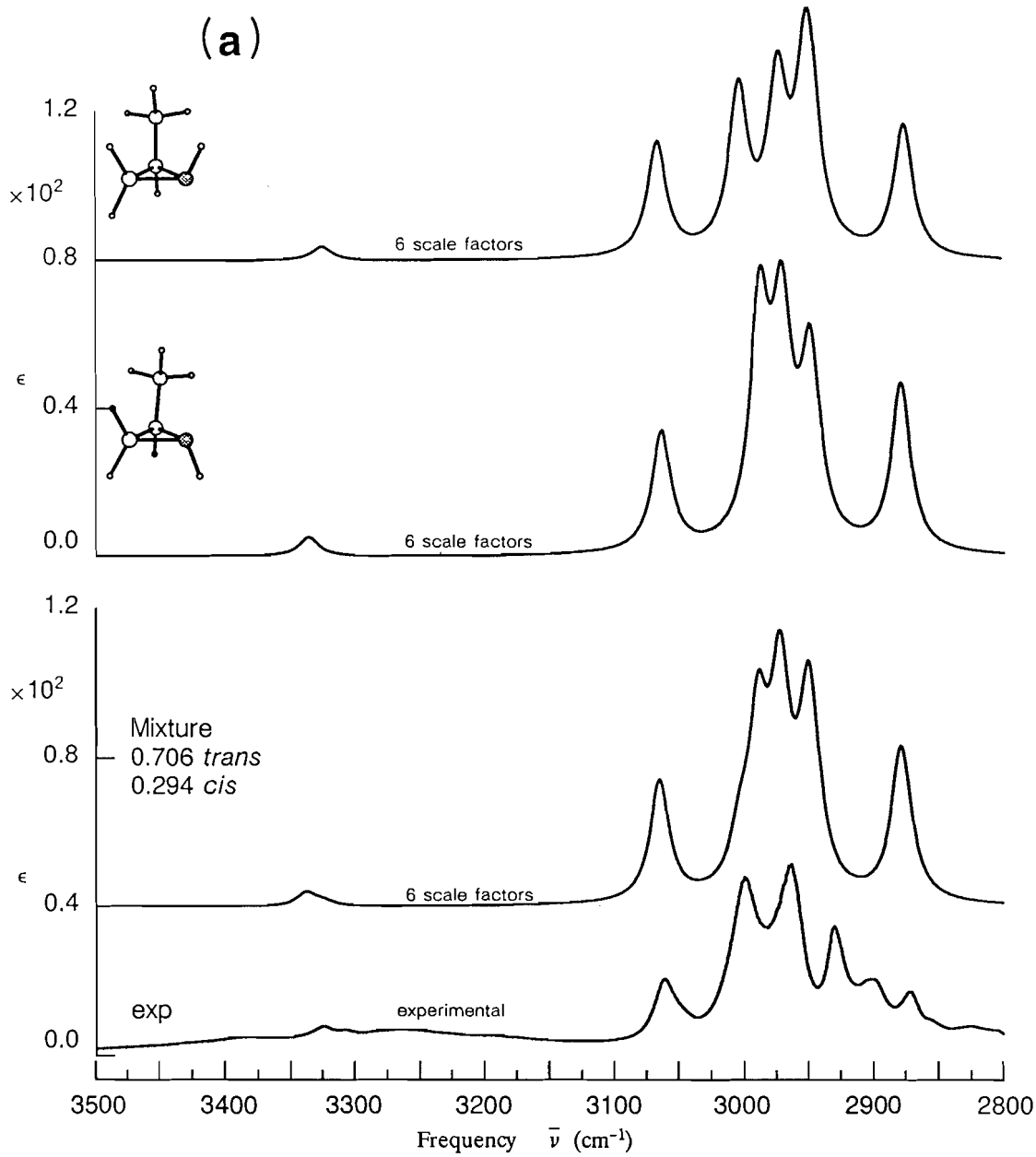

FIG. 5. Simulated IR spectra by VCT/6-31G*$^{(0.3)}$ theory in the region 2800–3500 cm^{-1} for the individual invertomers of 2-methylaziridine, and of the theoretical equilibrium mixture at 298 K compared with the experimental spectrum in CCl_4 (bottom spectrum); the linewidth for simulations is 18 cm^{-1}: (*a*) scaled with six scale factors; (*b*) uniformly scaled.

(calcd.). Band 65 (3155.1 cm^{-1}) may originate from a second combination of the same kind, namely $\nu_6 + \nu_{27} = 3147$ cm^{-1} (calcd.) since the calculated separation of the two asymmetric stretches (assumed to be degenerate by Durig *et al.*) is similar to the observed separation of bands 64 and 65.

Frequencies calculated by RHF/6-31G*$^{(0.3)}$//6-31G*$^{(0.3)}$ for the *trans* and *cis* isomer of 2-methylaziridine are listed in Tables 6 and 7, respectively. Also listed are the uniformly scaled frequencies, the optimally scaled values (six scale factors), and the corresponding observed bands. Dipole strengths were calculated from the uniformly and optimally scaled force fields by VCT/6-31G*$^{(0.3)}$ (= APT), and descriptions of the normal modes. The descriptions of the bands are assigned on the basis of visualizations of the animated normal modes and inspection of the normal modes in displacement vector representation (see Fig. 6, discussed below). The subsequent discussion is based on the optimally scaled results, which are very similar to the uniformly scaled values.

Vibrational frequencies and assignments

Some substantial differences are predicted in the frequencies of equivalent vibrational modes of the two isomers. Normal modes, ν_{22} and ν_{17}, primarily rocking and wagging motions of the CH_2 group, are predicted to occur 20 and 19 cm^{-1} to lower frequency in *trans*-2-methylaziridine than in the *cis* diastereomer. On the other hand, ν_{20}, a mixed mode consisting of C—CH_3 stretch and ring distortion, is predicted to be at higher frequency by 15 cm^{-1}. Lesser pertur-

Can. J. Chem. Downloaded from www.nrcresearchpress.com by 92.62.229.171 on 09/08/12
For personal use only.

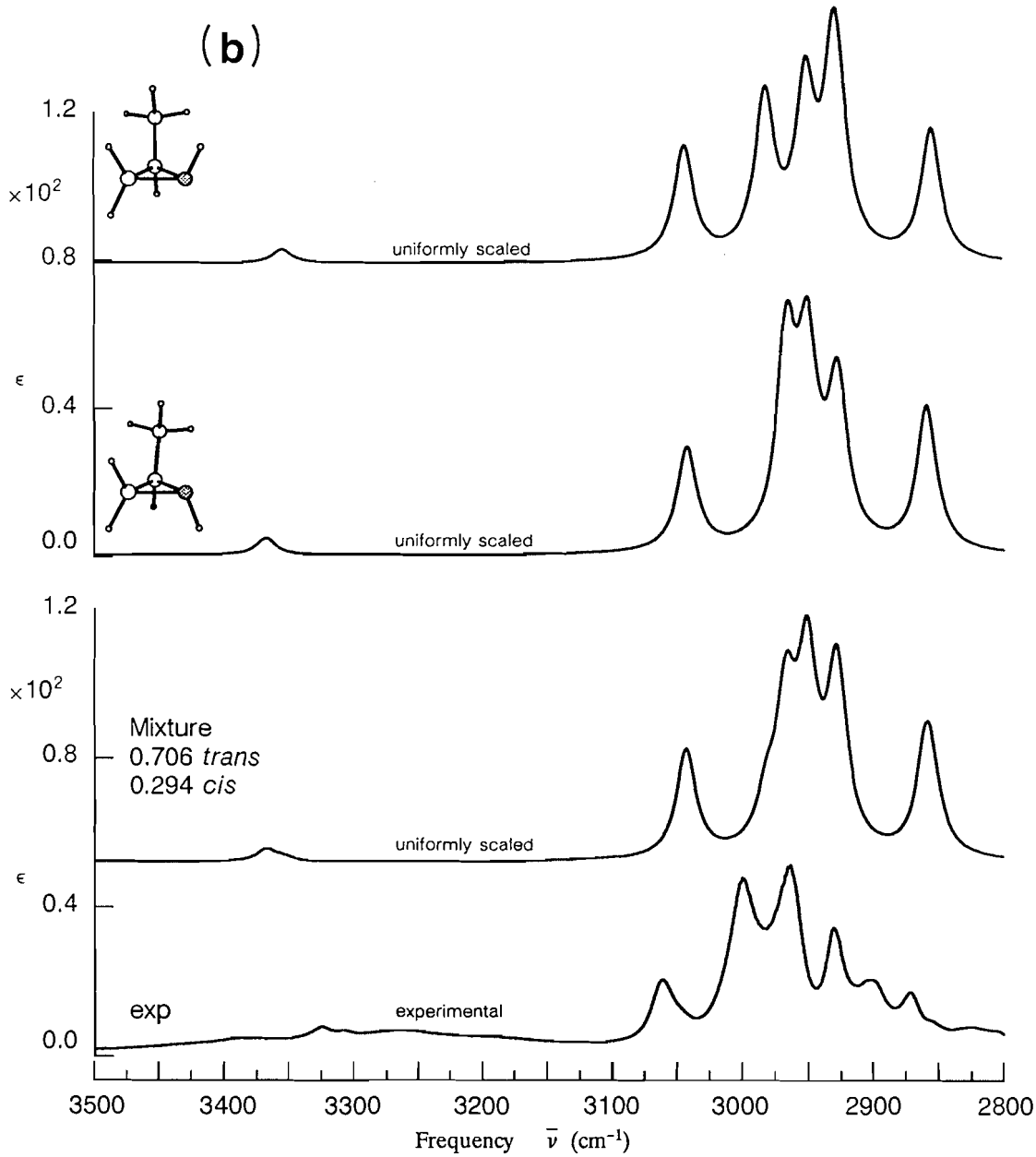

FIG. 5 (*concluded*)

bations to lower (ν_{27}, ν_{18}, ν_{16}, ν_{15}, ν_{13}, and ν_3) and higher (ν_{14}, ν_{11}, ν_5, and ν_1) frequencies in the *trans* compared to the *cis* conformer are easily resolved experimentally and therefore are significant for the scaling of the force fields and the interpretation of the IR spectra of the equilibrium mixture. The nature of the vibrations is particularly complex in the range 800–1400 cm^{-1}. In the assignments listed in Tables 6 and 7, only the major group motions are identified, in decreasing order of their apparent involvement. The modes are discussed further in their connection to the predicted IR intensities.

Comparison of the uniformly scaled and optimally scaled frequencies (columns 3 and 4 in Tables 6 and 7) reveals that the two sets are very similar, the greatest deviations occurring in the N—H and C—H stretching regions where the uniformly scaled values differ by +31 cm^{-1} (N—H) and −21 cm^{-1} (C—H) from the optimally scaled values. In the mid-IR region, most of the uniformly scaled values are too high, the maximum difference being 13 cm^{-1}.

The IR spectrum of 2-methylaziridine

The calculated electric dipole strengths are listed in Tables 6 and 7. Very little difference is found between the values obtained from the nonuniformly scaled force field and the uniformly scaled values.

On the basis of previous studies with the 6-31G*$^{(0.3)}$ basis set (12, 14), most of the calculated dipole strengths are expected to be within a factor of two of the most accurate results achievable with the present level of theory and with experiment. The most prominent feature, near 820 cm^{-1} in both isomers, is due to ν_{23} (a deformation of the three-membered ring). The observed intensity of this mode (268×10^{-40} esu^2 cm^2) is very close to the calculated values. For the majority of the modes, it is difficult to compare observed intensities with the predicted values. The simulated IR spectra

Can. J. Chem. Downloaded from www.nrcresearchpress.com by 92.62.229.171 on 09/08/12
For personal use only.

Can. J. Chem. Downloaded from www.nrcresearchpress.com by 92.62.229.171 on 09/08/12
For personal use only.

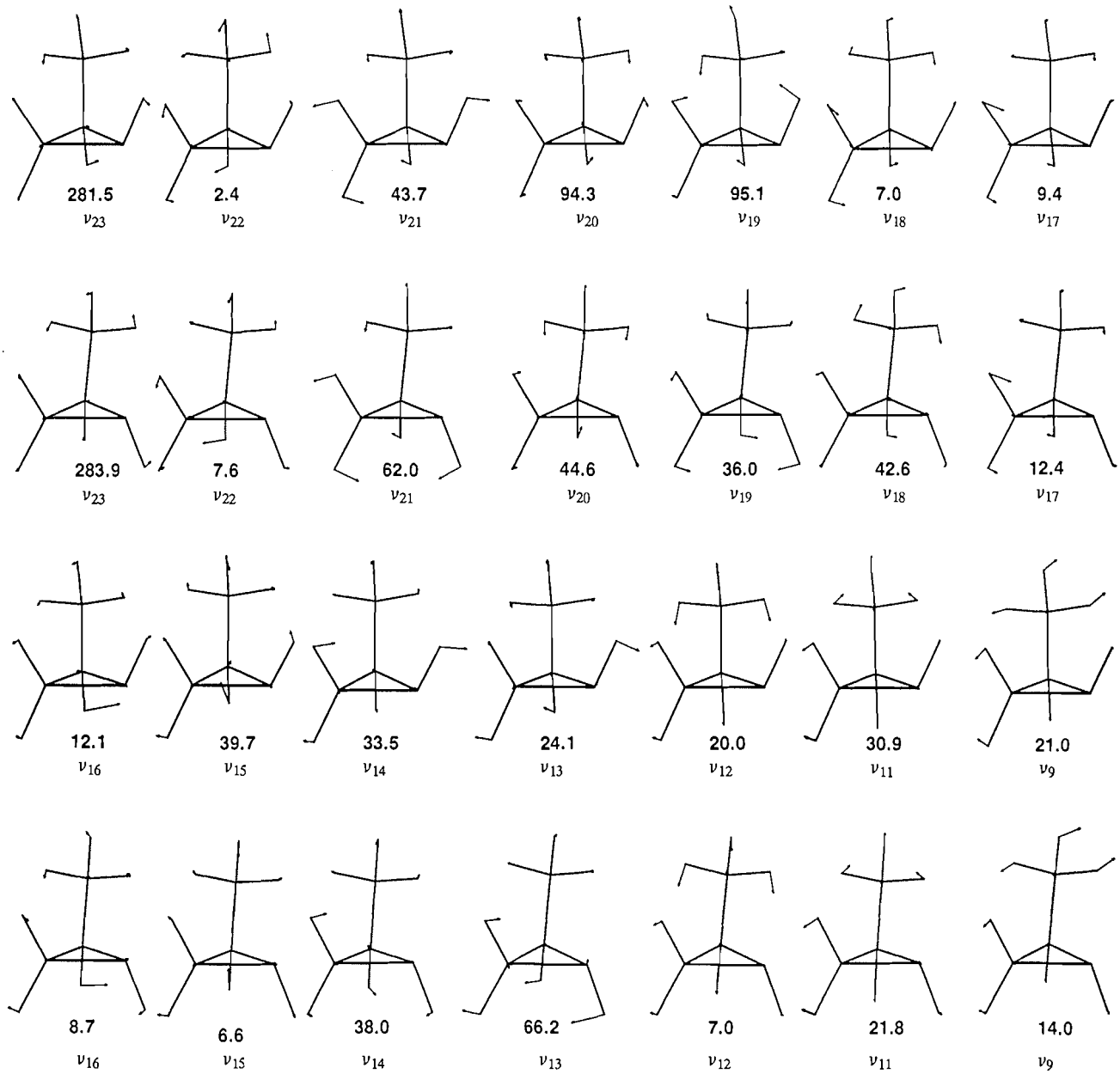

FIG. 6. Cartesian displacement vector representation of some of the normal modes between 800 and 1100 cm^{-1} of *cis*- and *trans*-2-methylaziridine. The bold-face numbers are the calculated dipole strengths in units of $esu^2\ cm^2$ ($\times 10^{40}$). The numbering is consistent with Tables 6 and 7.

of *trans*- and *cis*-2-methylaziridine, and of the calculated equilibrium mixture at room temperature (298 K), are compared to the experimental spectra in Figs. 4 and 5. In the region 400–1500 cm^{-1}, the majority of the line widths are in the range 5–12 cm^{-1}. The single major exception is the strong band at 820 cm^{-1}, which has a measured width of 19 cm^{-1}. In the simulations (Fig. 4), a constant linewidth of 8 cm^{-1} has been employed. As a consequence, the appearance of the 820 cm^{-1} feature is misleading. The remaining bands have about the correct overall intensity. The most obvious error occurs for the band at 1250 cm^{-1} in the spectrum of the *trans* isomer. This band is predicted to be much too intense, a situation exacerbated somewhat by the nonuniform scaling procedure. The associated normal mode, ν_{13}, involves motion of the N—H bond along the coordinate for pyramidal inversion (Fig. 6). Two other bands of the *trans* isomer are calculated to be anomalously intense, namely ν_{20} and ν_{18}, and one, ν_{17}, appears to be too weak, although the predicted intensity is only about a factor of two too low. The first of these, ν_{20} (and also ν_{19}) is predicted to be even more intense in the *cis* invertomer, while the second, ν_{18}, is a factor of six weaker.

Initial experience with the 6-31G*$^{(0.3)}$ basis set, based on comparison with calculations employing a much larger basis set, has suggested that the performance of this basis set with respect to the prediction of intensities in the C—H stretching region would be inferior to its performance in the mid-IR (12). The simulated spectra of the two isomers, the predicted equilibrium spectrum, and the experimental solution spectrum in the C—H and N—H stretching region are com-

pared in Fig. 5. The observed lines in this region are substantially broader than in the mid-IR. A width of 18 cm^{-1} (approximately the average of the observed values) has been used in the simulation. It is apparent that the predicted intensities are in the correct range and the simulated spectrum is, in fact, in reasonable agreement with the observed spectrum. It appears that with a few notable exceptions, the 6-31G*$^{(0.3)}$ basis set, originally developed to facilitate calculation of vibrational circular dichroism intensities, provides an economical means to obtain reasonable predictions of molecular geometries, force fields, and IR intensities.

Acknowledgements

The financial support of the Natural Sciences and Engineering Research Council of Canada is gratefully acknowledged. We also thank Supercomputer Services of the University of Calgary for generous allocations of CPU time on the CDC Cyber 205.

1. L. A. Nafie and T. B. Freedman. J. Chem. Phys. **78**, 7108 (1983).
2. P. J. Stephens. J. Phys. Chem. **89**, 748 (1985).
3. A. D. Buckingham, P. W. Fowler, and P. A. Galwas. Chem. Phys. **112**, 1 (1987).
4. M. A. Lowe, G. A. Segal, and P. J. Stephens. J. Am. Chem. Soc. **108**, 248 (1986).
5. K. Morokuma and H. Sugeta. Chem. Phys. Lett. **134**, 23 (1987).
6. R. Dutler. Ph.D. Dissertation, The University of Calgary. (1988).
7. K. J. Jalkanen, P. J. Stephens, R. D. Amos, and N. C. Handy. J. Am. Chem. Soc. **109**, 7193 (1987).
8. (*a*) K. J. Jalkanen, P. J. Stephens, R. D. Amos, and N. C. Handy. J. Am. Chem. Soc. **110**, 2012 (1988); (*b*) J. Am. Chem. Soc. **110**, 5598 (1988).
9. R. Dutler and A. Rauk. J. Chem. Soc. **111**, 6957 (1989).
10. M. A. Lowe, P. J. Stephens, and G. A. Segal. Chem. Phys. Lett. **123**, 108 (1986).
11. R. W. Kawiecki, F. Devlin, P. J. Stephens, R. D. Amos, and N. C. Handy. Chem. Phys. Lett. **145**, 411 (1988).
12. A. Rauk and D. Yang. J. Phys. Chem. **96**, 437 (1992).
13. H. Dothe, M. A. Lowe, and J. S. Alper. J. Phys. Chem. **92**, 6246 (1988).
14. P. L. Polavarapu, S. T. Pickard, H. E. Smith, T. M. Black, A. Rauk, and D. Yang. J. Am. Chem. Soc. **113**, 9747 (1991).
15. A. Lopez, M. M. Gauthier, R. Martino, and A. Lattes. Org. Magn. Reson. **12**, 418 (1979).
16. R. Martino, A. Lattes, F. Imberlin, and R. Mathis. C. R. Acad. Sci. Ser. C: **274**, 156 (1972).
17. (*a*) R. Martino, A. Lopez, R. Mathis, and A. Lattes. Bull. Soc. Chim. Fr. 1849 (1976); (*b*) R. Martino, R. Mathis, F. Imberlin, and A. Lattes. Spectrochim. Acta, Part A, **30A**, 741 (1974); (*c*) R. Mathis, R. Martino, and A. Lattes. Spectrochim. Acta, Part A, **30A**, 713 (1974); (*d*) R. Mathis-Noel, R. Martino, A. Secches, and A. Lattes. C. R. Acad. Sci. Ser. A: **266**, 926 (1968).
18. J. R. Durig, S. F. Bush, and W. C. Harris. J. Chem. Phys. **50**, 2851 (1969).
19. E. R. Razumova and R. G. Kostyanovskii. Izv. Akad. Nauk SSSR Ser. Khim. **9**, 2003 (1974).
20. W. C. Wurrey and A. B. Nease. *In* Vibrational spectra and structure. *Edited by* J. R. Durig. Elsevier Scientific Publishing Co., Amsterdam. 1978. pp. 181–185.
21. W. J. Hehre, L. Radom, P. v. R. Schleyer, and J. A. Pople. *Ab initio* molecular orbital theory. John Wiley and Sons, New York. 1987. pp. 226–251.
22. V. I. Pupyshev, Y. N. Panchencko, C. W. Bock, and G. Pangor. J. Chem. Phys. **94**, 1247 (1991).
23. A. Rauk, T. Eggimann, H. Wieser, and D. Yang. To be published.
24. (*a*) J. S. Binkley, M. J. Frisch, D. J. Defrees *et al.* Department of Chemistry, Carnegie–Mellon University, Pittsburgh, Pa; (*b*) A. Rauk and R. Dutler. J. Comput. Chem. **8**, 324 (1987).
25. M. J. Frisch, J. S. Binkley, H. B. Schlegel *et al.* Carnegie–Mellon Publishing Unit, Pittsburgh, Pa. 1984.
26. (*a*) W. J. Hehre, R. Ditchfield, and J. A. Pople. J. Chem. Phys. **56**, 2257 (1972); (*b*) M. M. Francl, W. J. Pietro, W. J. Hehre, J. S. Binkley *et al.* J. Chem. Phys. **77**, 3654 (1982).
27. P. Pulay. *In* Modern theoretical chemistry. Vol. 3. Methods of electronic structure theory. *Edited by* H. F. Schaefer III. Plenum, New York. 1977.
28. J. A. Pople, H. B. Schlegel, R. Krishnan *et al.* Int. J. Quantum Chem. Symp. **15**, 269 (1981).
29. P. Pulay, G. Fogarasi, F. Pang, and J. E. Boggs. J. Am. Chem. Soc. **101**, 2550 (1979).
30. P. Pulay. *In* Modern theoretical chemistry. Vol. 4. *Edited by* H. F. Schaefer III. Plenum, New York. (1977); pp. 153–185.
31. Y. S. Li, M. D. Harmony, D. Hayes, and E. L. Beeson, Jr. J. Chem. Phys. **47**, 4514 (1967).
32. J. K. Kauppinen, D. J. Moffatt, H. H. Mantsch, and D. G. Cameron. Appl. Spectrosc. **35**, 271 (1981).
33. (*a*) R. A. Shaw, C. Ursenbach, A. Rauk, and H. Wieser. Can. J. Chem. **66**, 1318 (1988); (*b*) R. A. Shaw, C. Castro, R. Dutler, A. Rauk and H. Wieser. J. Chem. Phys. **89**, 716 (1988); (*c*) R. A. Shaw, N. Ibrahim, and H. Wieser. J. Phys. Chem. **93**, 3920 (1989); (*d*) R. A. Shaw, N. Ibrahim, and H. Wieser. Can. J. Chem. **68**, 90 (1990).
34. R. Dutler, A. Rauk, and R. A. Shaw. J. Phys. Chem. **94**, 118 (1990).

Can. J. Chem. Downloaded from www.nrcresearchpress.com by 92.62.229.171 on 09/08/12
For personal use only.

Statistical theory of electron densities at nonzero temperatures

GARY G. HOFFMAN
Department of Chemistry, Florida International University, Miami, FL 33199, U.S.A.
ROBERT A. HARRIS
Department of Chemistry, University of California, Berkeley, CA 94720, U.S.A.
AND
LAWRENCE R. PRATT[1]
Chemical and Laser Sciences Division, Los Alamos National Laboratory, Los Alamos, NM 87545, U.S.A.

Received August 13, 1991

This paper is dedicated to Professor Sigeru Huzinaga on the occasion of his 65th birthday

GARY G. HOFFMAN, ROBERT A. HARRIS, and LAWRENCE R. PRATT. Can. J. Chem. **70**, 478 (1992).

This paper derives the finite temperature *optimized* Thomas–Fermi theory applicable to the electronic structure of atoms, molecules, and ions under conditions where both the bulk electron density and the electron temperature are substantial. The derivation provides a simple rule for transcribing the finite temperature case from the previous ground-state statistical electron-density functional theories.

Key words: plasma simulation, plasma chemistry, statistical theory of electron densities, Thomas–Fermi theory, optimized Thomas–Fermi theory.

GARY G. HOFFMAN, ROBERT A. HARRIS et LAWRENCE R. PRATT. Can. J. Chem. **70**, 478 (1992).

Dans ce travail, on a dérivé la théorie de Thomas–Fermi *optimisée* pour une température finie qui pourrait s'appliquer à la structure atomique d'atomes, de molécules et d'ions dans des conditions sous lesquelles la densité électronique globale ainsi que la température électronique sont importantes. Cette dérivation fournit une règle simple pour transcrire le cas de la température finie à partir des théories fonctionnelles de densité électronique statistique de l'état fondamental.

Mots clés : simulation de plasmas, chimie des plasmas, théorie statistique des densités électroniques, théorie de Thomas–Fermi, théorie optimisée de Thomas–Fermi.

Can. J. Chem. Downloaded from www.nrcresearchpress.com by 92.62.229.171 on 09/08/12
For personal use only.

Introduction

Interesting current research has focused on the ability to carry out numerical simulations of plasmas while explicitly treating electronic degrees of freedom (1). Such an ability is expected to further the understanding of a wide spectrum of problems (2, 3) including advanced methods for synthesis, processing, and characterization of exotic materials. The chemistry that takes place in laboratory plasmas is clearly important in plasma polymerization or plasma-assisted chemical vapor deposition (4–7), and in many analytical chemical methods (8), including methods involving laser ablation of surfaces.

Theoretical descriptions of plasmas of chemical interest typically focus first on identification of chemical species and of elementary chemical processes. These data are then often used as building blocks in modelling the dynamics of the plasma. The identification of chemical species usually begins with the Saha equation and the description of the ionic composition under equilibrium conditions at a temperature T (9). The primitive Saha treatment is physically sound for plasmas in the limit of low densities. But it will incur errors for higher densities because the electronic structures of the chemical constituents are not treated self-consistently with the electronic milieu. Going beyond the conditions of the primitive Saha treatment (10), there is special interest in circumstances where the electronic degrees of freedom equilibrate at a temperature $T = T_{\text{electron}}$ on a time scale that is short compared with the time required for equilibration of the nuclear translations. If the nuclear translations separately achieve thermal equilibrium, at least approximately, at a different temperature, the system would be regarded as a "two-temperature plasma." But if the nuclei are considered motionless on the electronic time scale this is just the familiar Born–Oppenheimer approximation (11).

The determination of the electron density as a function of nuclear coordinates is a first step towards a broader theory. In addition, it is just the information required by recent simulation calculations (1). The electron-density theory derived below starts from the assumption of the Born–Oppenheimer approximation and determines the electron densities self-consistently. No assumption of the equilibrium of the nuclear degrees of freedom is required. It will be clear that the present treatment is most natural when the electron density in the plasma is not too low. The present treatment is, therefore, complementary to the more traditional theoretical approaches that are correct at low density (9).

These developments build from recent work on statistical theories of electron densities in extended systems (12–17). The principal objective here is to work out the finite temperature version of the *optimized* Thomas–Fermi theory (14–17). The new result is indeed presented below. However, the finite temperature results can be *directly* transcribed from the previous ground state electron-density theory. This can be established by a simple, general, and physically transparent argument that is also given below. Some formal aspects of the finite temperature extension of our ground state approach have been derived previously (18). However, the present general derivation is important because of its simplicity in comparison with the previous derivation.

The corresponding spin density functional theory is formally a straightforward extension of these statistical meth-

[1]Author to whom correspondence may be addressed.

Printed in Canada

Can. J. Chem. Downloaded from www.nrcresearchpress.com by 92.62.229.171 on 09/08/12
For personal use only.

ods (18, 19). Such an extension should be important in practical applications. However, since the consideration of spin densities is entirely independent of the issue of finite temperature, we ignore that extension here.

Statistical formulation of finite temperature electron density theory

Our previous developments studied the *ground state* electron density given by filling all levels below the Fermi energy μ:

$$[1] \quad \rho(\boldsymbol{r};\mu) = 2\sum_{\zeta} |\phi_\zeta(\boldsymbol{r})|^2 \eta(\mu - \varepsilon_\zeta)$$

where $\eta(z)$ is the Heaviside function and $\phi_\zeta(\boldsymbol{r})$ and ε_ζ are, respectively, eigenfunctions and eigenvalues of the density-dependent, single-particle Hamiltonian

$$[2a] \quad \boldsymbol{H} = -\frac{\hbar^2}{2m}\nabla^2 + v(\boldsymbol{r};\rho)$$

It is known as a matter of principle that a $v(\boldsymbol{r};\rho)$ exists, which produces the exact density (20–22). Furthermore, approximate $v(\boldsymbol{r};\rho)$ are available, which produce reasonable densities (23). Double occupancy has been assumed in [1] and this accounts for the factor of 2.

The density theories we will construct here are based upon the fact that, at a nonzero temperature $T \equiv \beta^{-1}$, the density can be obtained from thermal population of the self-consistent eigenstates of a thermal $\boldsymbol{H}(\beta)$:

$$[3] \quad \rho(\boldsymbol{r};\mu,\beta) = 2\sum_{\zeta} \frac{|\psi_\zeta(\boldsymbol{r},\beta)|^2}{1 + \exp\{\beta(\varepsilon_\zeta(\beta) - \mu)\}}$$

Here $\psi_\zeta(\boldsymbol{r},\beta)$ and $\varepsilon_\zeta(\beta)$ are eigenfunctions and eigenvalues of the Hamiltonian $\boldsymbol{H}(\beta)$:

$$[2b] \quad \boldsymbol{H}(\beta) = -\frac{\hbar^2}{2m}\nabla^2 + v(\boldsymbol{r};\beta,\rho)$$

The structure of this theory is analogous to the thermal Hartree or Hartree–Fock theories (24). However, it is clear that a functional $v(\boldsymbol{r};\beta,\rho)$ exists that would produce the exact thermal density (25). The dependence of the $v(\boldsymbol{r};\beta,\rho)$ on β has been made explicit in [2*b*]. Although the β dependence, beyond the functional dependence on the density, should be assumed throughout, we subsequently drop this explicit notation.

The density matrix associated with this theory is just

$$[4] \quad \rho(\boldsymbol{r},\boldsymbol{r}') = 2\sum_{\zeta} \frac{\psi_\zeta(\boldsymbol{r})\psi_\zeta^*(\boldsymbol{r}')}{1 + \exp\{\beta(\varepsilon_\zeta - \mu)\}}$$

We next focus on expressing [4] so that it provides a natural description of the electron densities in disordered, extended materials where the manipulation of the orbitals $\psi_\zeta(\boldsymbol{r})$ is likely to be awkward. To this end, the density matrix [4] is written as

$$[5] \quad \rho(\boldsymbol{r},\boldsymbol{r}') = 2\int_{-\infty}^{\infty} \sum_{\zeta} \frac{\psi_\zeta(\boldsymbol{r})\psi_\zeta^*(\boldsymbol{r}')\delta(\varepsilon - \varepsilon_\zeta)}{1 + \exp\{\beta(\varepsilon - \mu)\}} d\varepsilon$$

An integration-by-parts yields

$$[6] \quad \rho(\boldsymbol{r},\boldsymbol{r}') = 2\int_{-\infty}^{\infty} \left\{\sum_{\zeta} \psi_\zeta(\boldsymbol{r})\psi_\zeta^*(\boldsymbol{r}')\eta\left(\mu + \frac{4\alpha}{\beta} - \varepsilon_\zeta\right)\right\} \times \operatorname{sech}^2(2\alpha)\, d\alpha$$

This extremely simple formula allows us to transcribe corresponding finite-β theories from all the previous ground state results. Note that $\operatorname{sech}^2(2\alpha)$ is a simple probability density on the interval $(-\infty,\infty)$. Therefore, [6] shows that the finite β result corresponds to an averaging of ground state densities according to a distribution of Fermi energies. Because of this, the Monte-Carlo methods devised elsewhere (13, 15, 16) to implement the ground state theory are directly applicable to the finite temperature theory as well. In particular, the thermal result can be implemented by considering cyclic paths $\{\boldsymbol{r},\boldsymbol{r}_1,\ldots,\boldsymbol{r}_{p-1},\boldsymbol{r}\}$ and evaluating the integrals

$$[7a] \quad \rho(\boldsymbol{r}) = \frac{4}{2^{3p/2}\,\Gamma\left[\frac{3(p-1)}{2}\right]\pi^{3/2}} \lim_{z^*\to\infty} \int_0^{\infty} \langle (k_p z)^{3p/2} J_{3p/2}(k_p z)\eta(k_p^2)\rangle_{z,\beta} \frac{e^{-z/z^*}\,dz}{z^4}$$

with the definitions:

$$[7b] \quad \langle f(k_p^2)\rangle_{z,\beta} = \frac{\int d^3a_1 \ldots \int d^3a_{p-1}\,\delta\left(z^2 - \sum_{m=1}^{p-1} a_m^2\right)\int_{-\infty}^{\infty} d\alpha\, f(k_p^2)\operatorname{sech}^2(2\alpha)}{\int d^3a_1 \ldots \int d^3a_{p-1}\,\delta\left(z^2 - \sum_{m=1}^{p-1} a_m^2\right)}$$

$$[7c] \quad \frac{\mathbf{a}_m}{\sqrt{2p\left\{1 - \cos\left(\frac{m\pi}{p}\right)\right\}}} = \sqrt{\frac{2}{p}}\sum_{j=1}^{p-1} (\boldsymbol{r}_j - \boldsymbol{r})\sin\left(\frac{mj\pi}{p}\right)$$

$$[7d] \quad \frac{\hbar^2 k_p^2}{2m} = \mu + \frac{4\alpha}{\beta} - \frac{1}{p}v(\boldsymbol{r};\rho) - \frac{1}{p}\sum_{j=1}^{p-1} v(\boldsymbol{r}_j;\rho)$$

The $p \to \infty$ limit identifies the exact density. Reference 15 can be consulted for further discussion of these formulae.

Finite temperature optimized Thomas–Fermi theory

If the potential was weakly varying over lengths compa-

rable with the Fermi wavelength $(8\pi/3\rho)^{1/3}$ then the Thomas–Fermi approximation for the ground state density,

$$[8] \quad \rho(\boldsymbol{r};\mu,\beta=\infty) = \frac{1}{3\pi^2}\left\{\frac{2m}{\hbar^2}[\mu - v(\boldsymbol{r};\rho)]\right\}^{3/2} \times \eta[\mu - v(\boldsymbol{r};\rho)]$$

would be appropriate (14–17, 26). When β is finite the familiar thermal Thomas–Fermi approximation obtains

$$[9] \quad \rho(\boldsymbol{r};\mu,\beta) = \left(\frac{1}{\pi}\right)^2 \int_0^\infty \frac{k^2\,dk}{1 + \exp\left\{\beta\left[\frac{\hbar^2k^2}{2m} + v(\boldsymbol{r};\rho) - \mu\right]\right\}}$$

The functional relation between the density and the potential depends on β.

The *optimized* Thomas–Fermi approximation is motivated by the view that it is rather draconian to evaluate the potential $v(\boldsymbol{r};\rho)$ only at the point where the density is sought. More physically, the density depends on the potential in the neighborhood of the point in question. In the interest of simplicity, we can agree to retain the simple form, [9], but we can make it more accurate by replacing $v(\boldsymbol{r};\rho)$ with a parameter v_r chosen so as to make the first-order corrections to [9] vanish (14–17). Using [6] together with the results of ref. 14 or 17, we can express the finite temperature *optimized* Thomas–Fermi theory as the two equations:

$$[10] \quad \rho(\boldsymbol{r};\mu,\beta) = \left(\frac{1}{\pi}\right)^2 \int_0^\infty \frac{k^2\,dk}{1 + \exp\left\{\beta\left(\frac{\hbar^2k^2}{2m} + v_r - \mu\right)\right\}}$$

and

$$[11] \quad 0 = \int d^3r'\left[\frac{v(\boldsymbol{r}';\rho) - v_r}{|\boldsymbol{r} - \boldsymbol{r}'|^2}\right]\int_0^\infty dk\, k^3 j_1(2k|\boldsymbol{r} - \boldsymbol{r}'|) \times \operatorname{sech}^2\left[\frac{\beta}{2}\left(\frac{\hbar^2k^2}{2m} + v_r - \mu\right)\right]$$

$j_1(z)$ is the spherical Bessel function of order $\nu = 1$. Equation [11], although implicit and nonlinear, operationally determines the v_r that is required in [10]. The functional relation between density and v_r depends on β in just the same way as the thermal Thomas–Fermi theory. But the effective potential v_r acquires additional temperature dependence.

Discussion

Several aspects of this theory deserve further discussion. Firstly, the electron density provided by the Thomas–Fermi theory becomes infinitely large near an atomic nucleus. There is a long history of concern with just this behavior. The *optimized* Thomas–Fermi theory removes this divergence and this advantage is inherited by the finite temperature *optimized* Thomas–Fermi theory. Alternatively, the use of effective core potentials can lead to improvements in the theory. This procedure accurately reflects the finite temperature quantum behavior of electrons near an atomic nucleus (1, 27). Incorporation of such an effective potential in the present theory could lead to a concomitant, self-consistent improvement of the theoretical description.

Secondly, these methods can be further extended to establish the equilibrium concentrations of ions of various types, as the Saha equation does in its regime of validity. The spectroscopy of the plasma (3) can also be treated by similar methods. The connection is that all these quantities intrinsically depend, as does the electronic correlation energy (28), upon the density of states defined by

$$[12] \quad g(\boldsymbol{r},\boldsymbol{r}';\varepsilon) = \sum_\zeta \psi_\zeta(\boldsymbol{r})\psi_\zeta^*(\boldsymbol{r}')\delta(\varepsilon - \varepsilon_\zeta)$$

Since this density of states can be expressed by the statistical methods utilized here, the physical quantities mentioned above also can be worked-out within the present approach.

Finally, it deserves to be emphasized that statistical methods are especially natural for extended systems without explicit simplifying symmetries associated with nuclear positions. The computational study of irregular many atom systems is no more difficult than that of a single atom. Therefore, we expect that these results should help in understanding chemistry that can occur in laboratory plasmas. We hope to return to those problems with more applied results in the future.

Acknowledgements

We wish to thank J. P. Hansen for fruitful discussions of his research. Discussions with D. Chandler have been helpful also. This research is supported by the National Science Foundation and the PRF/ACS.

1. J. Clerouin, G. Zerah, D. Benisti, and J. P. Hansen. Europhys. Lett. **13**, 685 (1991), and references therein.
2. R. B. Laughlin. Phys. Rev. A: Gen. Phys. **33**, 510 (1986).
3. J. A. Ball, J. A. Wheeler, and E. L. Fireman. Rev. Mod. Phys. **45**, 333 (1973).
4. H. Yasuda. Plasma polymerization. Academic Press Inc., New York. 1985.
5. Mater. Res. Soc. Symp. Proc. **86**, (1986).
6. P. K. Bachmann, G. Gartner, and H. Lydtin. MRS Bull. December, 52 (1988).
7. Pure Appl. Chem. **57**, (1985).
8. A. Montaser and D. W. Golightly (*Editors*). Inductively coupled plasmas in analytical atomic spectrometry. VCH Publishers Inc., New York. 1987.
9. L. D. Landau and E. M. Lifshitz. Statistical physics. 3rd. ed. Vol. 5. Pergamon Press, Elmsford, N.Y. 1980. Sect. 104.
10. I. Prigogine. Bull. Cl. Sci. Acad. R. Belg. **26**, 53 (1940); D. Kannappan and T. K. Bose. Phys. Fluids, **20**, 1668 (1977); A. Morro and M. Romeo. J. Plasma Phys. **39**, 41 (1988); M. C. M. van den Sanden, P. P. J. M. Schram, A. G. Peeters, J. A. M. van der Mullen, and G. M. W. Kroesen. Phys. Rev. A: Gen. Phys. **40**, 5273 (1989).
11. M. Born and R. Oppenheimer. Ann. Phys. (N.Y.), **84**, 457 (1927).
12. R. A. Harris and L. R. Pratt. J. Chem. Phys. **82**, 856 (1985).
13. G. G. Hoffman, L. R. Pratt, and R. A. Harris. Chem. Phys. Lett. **148**, 313 (1988).
14. L. R. Pratt, G. G. Hoffman, and R. A. Harris. J. Chem. Phys. **88**, 1818 (1988).
15. L. R. Pratt, G. G. Hoffman, and R. A. Harris. J. Chem. Phys. **92**, 6687 (1990).
16. G. G. Hoffman and L. R. Pratt. Proceedings of the International Workshop on Quantum Simulation of Condensed Matter Phenomena. *Edited by* J. D. Doll and J. E. Gubernatis. World Scientific Publishing Co. Pte. Ltd., Teaneck, N.J. 1990. pp. 105–115.

Can. J. Chem. Downloaded from www.nrcresearchpress.com by 92.62.229.171 on 09/08/12
For personal use only.

17. G. G. Hoffman and L. R. Pratt. Proc. R. Soc. London A: **435**, 245 (1991).
18. W. Yang. Phys. Rev. A: Gen. Phys. **38**, 5504 (1988).
19. W. Yang. Phys. Rev. A: Gen. Phys. **38**, 5494 (1988).
20. W. Kohn and L. J. Sham. Phys. Rev. **140**, A1133 (1965).
21. N. Hadjisavvas and A. Theophilou. Phys. Rev. A: Gen. Phys. **30**, 2183 (1984).
22. M. Levy and J. P. Perdew. *In* Density functional methods in physics. *Edited by* R. M. Dreizler and J. da Providencia. Plenum Press Inc., New York. 1985.
23. J. K. Labanowski and J. W. Andzelm (*Editors*). Density functional methods in chemistry. Springer-Verlag New York, Inc., New York. 1991.
24. A. L. Fetter and J. D. Walecka. Quantum theory of many-particle systems. McGraw-Hill Book Co., New York. 1971. Chap. 8; L. P. Kadanoff and G. Baym. Quantum statistical mechanics. Benjamin, Reading MA. 1976. Chap. 3; N. D. Mermin. Ann. Phys. (N.Y.), **21**, 99 (1963).
25. N. D. Mermin. Phys. Rev. **137**, A1441 (1965).
26. L. D. Landau and E. M. Lifshitz. Quantum mechanics (non-relativistic theory). 3rd ed. Vol. 3. Pergamon Press Inc., New York. 1980. Sections 46 and 70.
27. D. Chandler. *In* Liquids, freezing and glass transitions. *Edited by* J. P. Hansen et al., Les Houches L1, (1989) Elsevier Science Publishers, Amsterdam. 1991. p. 193.
28. R. A. Harris and L. R. Pratt. J. Chem. Phys. **83**, 4024 (1985).

Can. J. Chem. Downloaded from www.nrcresearchpress.com by 92.62.229.171 on 09/08/12
For personal use only.

A lattice of foam flow in porous media: a random walker approach

W. G. LAIDLAW[1] AND W. G. WILSON
Chemistry Department, University of Calgary, Calgary, Alta., Canada T2N 1N4

AND

DENNIS A. COOMBE
Computer Modelling Group, 3512-33rd Street N.W., Calgary, Alta., Canada T2L 2A6

Received August 7, 1991

This paper is dedicated to Professor Sigeru Huzinaga on the occasion of his 65th birthday

W. G. LAIDLAW, W. G. WILSON, and DENNIS A. COOMBE. Can. J. Chem. **70**, 482 (1992).

We introduce two simple foam blockage rules and examine their effect on sweep efficiency through a porous medium. Applying a random walk simulation method, it is found that an efficient sweep can be performed by a blockage mechanism where every invaded throat is blocked upon invasion. The blocking foam lamella must also have a large, but not necessarily infinite, decay time. This result is interpreted as a reduction in the interface speed.

Key words: porous media, viscous fingering, foam flow.

W. G. LAIDLAW, W. G. WILSON et DENNIS A. COOMBE. Can. J. Chem. **70**, 482 (1992).

On présente plusieurs régles relatives au blocage de mousses simples et on examine leur effet sur l'efficacité de déplacement à travers un milieu poreux. Lorsqu'on applique une méthode de simulation aléatoire, on trouve qu'un déplacement efficace nécessite un mécanisme de blocage par lequel chaque gorge doit être bloquée lorsqu'elle est envahie. Le temps de dégradation de la lamelle de mousse qui assure le blocage doit être assez grand, sans être nécessairement égal à l'infini. On interprète ce résultat en fonction d'une suppression des longueurs d'onde instables d'un point de vue de la diffusion; normalement cette suppression conduirait à la croissance de doigts du liquide qui envahit et un encerclement du fluide qui assure la défense.

Mots clés : milieux poreux, doigts du liquide visqueux, écoulement de mousses.

[Traduit par la rédaction]

Introduction

Foam has been introduced into the invading phase of a flood of an oil-saturated porous medium in an attempt to reduce the residual oil saturation (1). The expectation is that local regions of high permeability (invader-saturated regions) will become blocked, forcing the invader fluid into regions of lower permeability (oil-saturated regions). Network simulations of the effect of foam on the mobility of two-phase displacements in porous media have been suggested by a number of authors (2). Of particular interest is the pore-scale percolation-like treatment of Rossen, who suggested that the presence of blocking "foam lamella" could be accommodated by a rescaling of percolation results (2*a*). We have extended this idea to a number of foam-blockage scenarios (3). Unfortunately percolation treatments do not provide any dynamic information and so preclude an investigation of the effect of foam on phenomena such as viscous fingering. Methods of generating structures dynamically using systems of "random walkers" have been developed and applied to a variety of problems from simple invasion (4*a*) to local representations of rate processes (4*b*). In previous work we applied these concepts to pore-scale simulation of an immiscible displacement process in porous media and discussed in some detail a computer simulation based on the use of two armies of random walkers, the invaders and the defenders (5). Since a random walker method is essentially a diffusion process we were able to assess dynamic effects such as viscous fingering in two-phase flow.

In this report we apply our random walk pore-scale simulations in an attempt to understand foam effects on flow through porous media. The "foam rules" that we have implemented in the following work have sufficient complexity to produce the qualitative features expected with blockage by foam lamella under a variety of viscosity ratio values.

Incorporating the effects of foam at the microscopic scale involves knowledge of the precise mechanisms operating at that scale. However, most of the known results come from either the core scale or the field scale (1). In our simulations we would ideally utilize qualitative results, if not quantitative results, from pore-scale micromodels as the input to our simulations. The input would be framed as a rule or set of rules governing lamella creation, motion, and destruction while in the network. Although there is some information available to stipulate microscopic rules (6) we will consider a variety of plausible mechanisms. Simple rules can be incorporated within the two-species simulation, implicitly assuming that the foam has some statistical behavior that can be "integrated" out of the problem. More complex rules may require the introduction of a third "species" of random walker in the simulation.

Simple foam rules

Although we have examined only two of the potential simple rules, let us discuss several. The first, and trivial, case is to consider simple entrainment of lamella. As long as no other properties of foam are added, such as hanging up in small throats, this amounts to a simple change in the viscosity of the invading phase. The effects of viscosity on the invaded network are known (7) and range from the viscous fingering situation (low viscosity invader phase) to the stable displacement situation (highly viscous invader). In the

[1]Author to whom correspondence may be addressed.

Can. J. Chem. Downloaded from www.nrcresearchpress.com by 123.30.183.119 on 09/08/12
For personal use only.

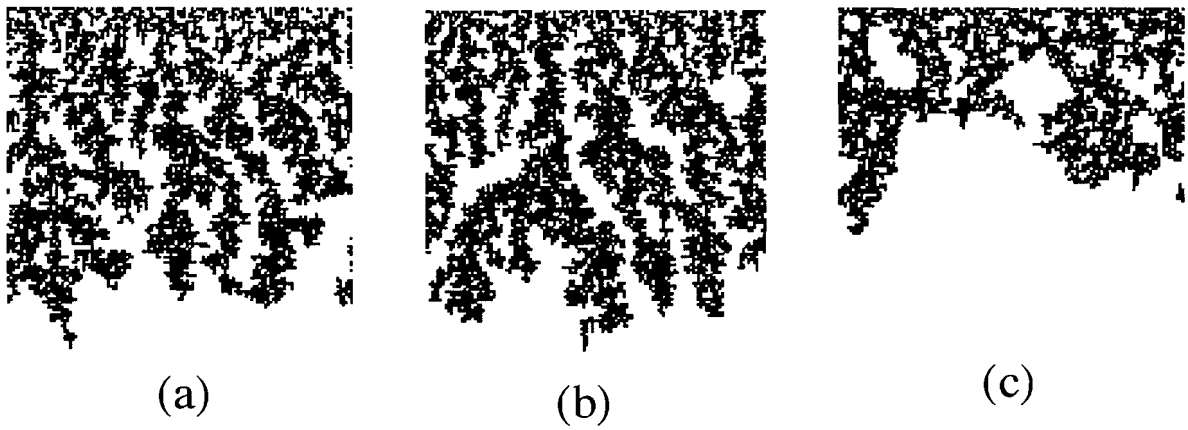

FIG. 1. The effect of static foam blockage on a viscous fingering displacement process with a viscosity ratio $\mu_r = 0.1$ and blockage probabilities (*a*) $\rho_b = 0.05$, (*b*) $\rho_b = 0.25$, and (*c*) $\rho_b = 0.5$. Very little effect on the invader saturation is observed.

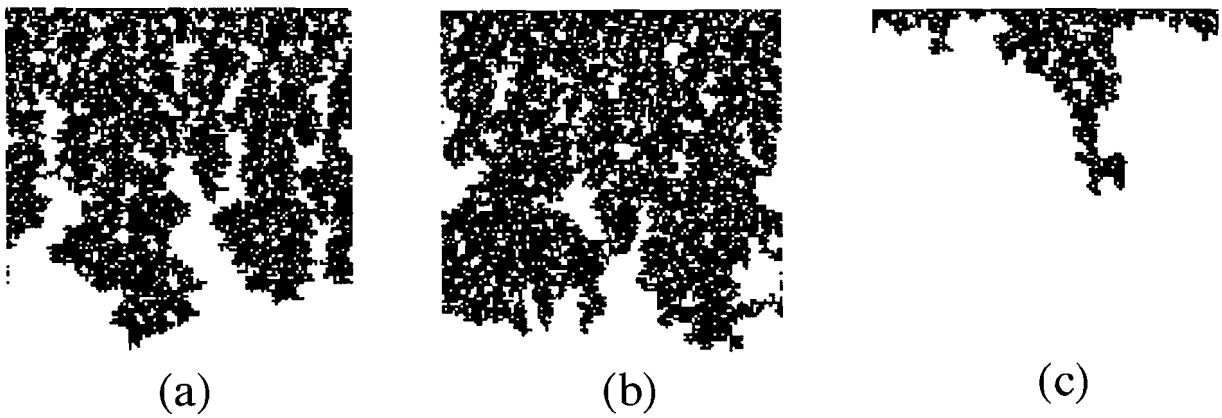

FIG. 2. The effect of static foam blockage on a displacement process with a viscosity ratio $\mu_r = 1.0$ and blockage probabilities (*a*) $\rho_b = 0.05$, (*b*) $\rho_b = 0.25$, and (*c*) $\rho_b = 0.5$. As in Fig. 1, very little effect on the invader saturation is observed. In (*c*), the invasion process has been halted by complete front blockage.

Can. J. Chem. Downloaded from www.nrcresearchpress.com by 123.30.183.119 on 09/08/12
For personal use only.

"entrained lamella interpretation," the viscous fingering would give way to stable displacement, to some extent, when lamella are included. In this case, the question becomes how lamella density changes the invader viscosity (1*a*, 8). But this viscosity change also depends on how easily the lamella are pushed through the network, which must depend on local conditions such as throat size. However, this is more of a hydrodynamic problem than a network problem and will not be treated in our simulations at this time.[2]

Static foam blockage

A nontrivial incorporation of lamella (at the macroscopic scale) is to allow lamella to block throats through the network. Two levels of complexity can be included. The most difficult scenario is to follow the lamella's movement throughout the network; then, via some microscopic rules, let it stop and permanently block a throat. These rules could be arbitrarily complex, depending on such things as throat size, local pressure gradients, and so on. However, this complexity adds to the simulation time. We instead make an appeal to statistical arguments.

As shown in our earlier work (9), no significant qualitative change is observed in the invaded structure when details such as individual throat sizes are included in the simulation. The exact configuration of randomly positioned throats is of no consequence to the global displacement process. Hence, to increase speed, we have chosen to perform simulations on networks with throats of a single size. Given this consideration, we can assume that a single simulation represents a possible outcome from an ensemble of different specific configurations of throat sizes. From some presumed understanding of lamella blocking behavior with respect to throat size, we could calculate the probability that a randomly chosen throat is blocked. It is this probability that we incorporate in our algorithm. Consider blocking at the invader front: all that is needed is to block a newly invaded throat with the chosen probability. Once blocked, no more of the invader phase is allowed to pass through that particular throat. This process is simple to add to the algorithm. A set of bits (one per throat) is distributed with one's and zero's according to the blockage probability. A second set of bits representing throat states (0 = flowing, 1 = blocked)

[2]The effect of throat and pore size on the conductivity of a network was investigated extensively in earlier work; see ref. 9, especially sections 4B and 4C using the method of Kirkpatrick to calculate the conductivity of small networks.

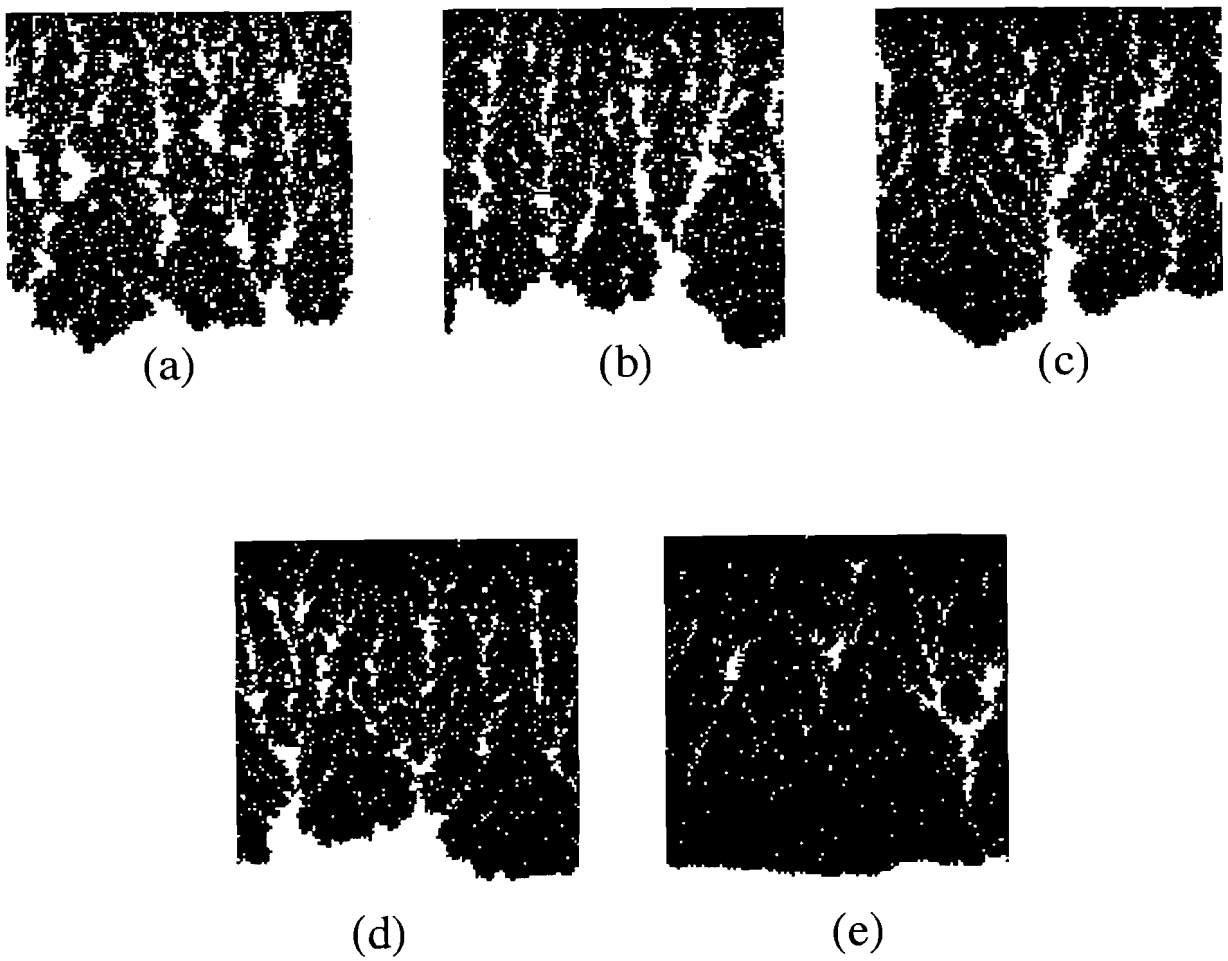

FIG. 3. The effect of dynamic foam blockage on a displacement process with a viscosity ratio $\mu_r = 1.0$, blockage probability $\rho_b = 1.0$, and unblockage probabilities (*a*) $\rho_u = 0.1$, (*b*) $\rho_u = 0.01$, (*c*) $\rho_u = 0.005$, (*d*) $\rho_u = 0.0025$, and (*e*) $\rho_u = 0.001$. A large effect on the invader saturation is observed.

is also included. At every simulation step the probability bits are randomly shuffled, and if the invasion of a throat takes place when its "blockage probability bit " is one, the throat is not invaded, but rather blocked by setting its state to one.

Figures 1 and 2 show results for such a blocking mechanism under a variety of conditions. In each pattern the dark regions represent invader fluid and the light parts the defender fluid. These simulations have been performed on a square lattice with a width of 128 and length of 200 sites. The runs in Fig. 1 represent a viscous fingering situation with an invader-to-defender viscosity ratio, denoted by $\mu_r = 0.1$, and with throat blockage probabilities, denoted by ρ_b, of (*a*) 0.05, (*b*) 0.25, and (*c*) 0.5. Figure 1(*a*) is essentially identical to a no-blockage scenario. It is obvious that this specific form of the foam mechanism is of no help in enhancing the removal of the defender phase. In fact, for any blockage probabilities greater than one-half, the two-dimensional bond-percolation threshold fraction, the invasion process must stop due to blockage of all throats along the invader front. The runs in Fig. 2 have identical blockage probabilities, but represent the case when the two phases have identical viscosities. It may appear that a blockage probability of 0.25 increased the invader saturation, but this is a statistically unsound conclusion from comparing just this one run. However, at 0.5, the front has completely stopped due to complete blockage at the front. Clearly, more structure must be included in the foam model.

The runs in Figs. 1 and 2 represent only one of three possible blocking mechanisms, blockage that occurs in throats as the invading phase sweeps through the throat for the first time. Another scenario would permit blockage to occur at any time and at any place within the invader-saturated region. This latter mechanism is called "behind-the-front" blockage, while what we have treated is "at-the-front" blockage. Behind-the-front blockage likewise suffers from the percolation threshold problem. A final scenario is the "leave-behind" blockage, which is the blockage of throats whose attached pores have been invaded, but the throat itself has not been invaded. This mechanism may result in an anisotropic percolation problem, meaning the percolation threshold problem may not have a significant effect.

Dynamic foam blockage

The treatment discussed in the previous section assumed that the lifetime of a blocking lamella is infinite. Thus, once a throat is blocked, it is forever blocked, leading to the front stoppage shown in Fig. 2(*c*). It is well known that lamella are not infinitely long-lived; thin film drainage is a major

Can. J. Chem. Downloaded from www.nrcresearchpress.com by 123.30.183.119 on 09/08/12
For personal use only.

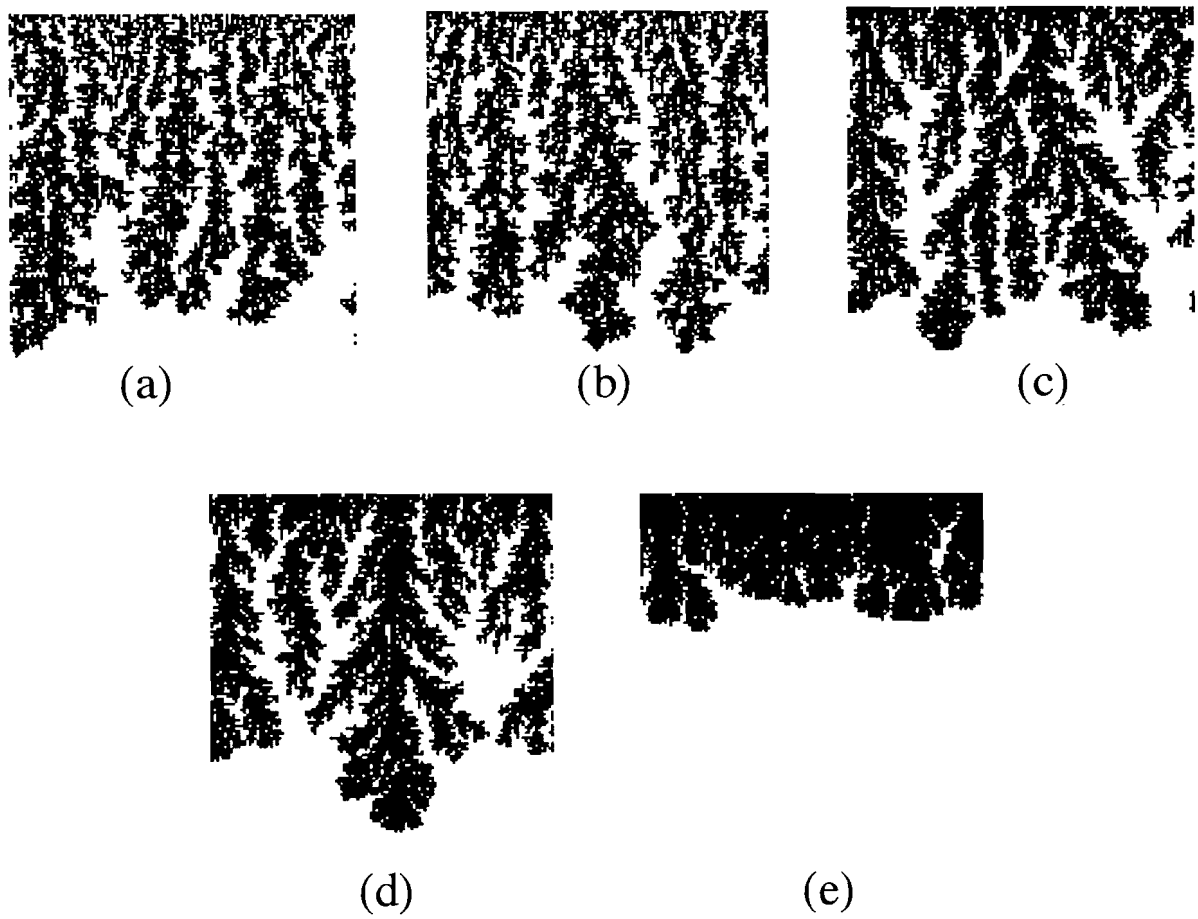

FIG. 4. The effect of dynamic foam blockage on a displacement process with a viscosity ratio $\mu_r = 0.1$, blockage probability $\rho_b = 1.0$, and unblockage probabilities (*a*) $\rho_u = 0.1$, (*b*) $\rho_u = 0.01$, (*c*) $\rho_u = 0.001$, (*d*) $\rho_u = 0.0005$, and (*e*) $\rho_u = 0.0001$. As in Fig. 3, a large effect on the invader saturation is observed, but at smaller unblockage probabilities.

problem in stability of foams (6, 8, 10). We have made an attempt to incorporate this feature by adding a half-life to the lamella. This is accomplished by giving each "living" lamella blockage some probability to "die" every simulation step and subsequently unblock the throat. Again, this is included within simple foam constructs since no additional walker species are needed in order to perform the simulation. What is required, however, is an additional set of bits distributed according to the "unblockage probability per simulation step."

Figure 3 displays the results for a viscosity ratio of $\mu_r = 1.0$ for the two phases, with various lamella half-lives $\tau_{1/2}$. In all of the following simulations, blockage occurs in every invaded throat, i.e., $\rho_b = 1.0$. This could not be allowed in the static blockage scenario, as discussed above, since a blockage probability greater than one half results in a fully plugged network. We anticipate that lower blockage probabilities would show the same relative shifts with sweeps of lower efficiency. Figures 3(*a*)–(*e*) show the final configurations for the unblocking probabilities, denoted ρ_u, of 0.1, 0.01, 0.005, 0.0025, and 0.0010, respectively. These probabilities correspond to lamella half-lives of roughly 7, 69, 140, 280, and 690 timesteps, respectively. As can be seen, the effect is to increase the invader saturation to nearly 100% for the large half-life case. This is the same effect as is seen by changing the viscosity ratio to ever increasing values: the invader phase becomes effectively more viscous, resulting in a much more stable displacement.

Figure 4 presents the corresponding pictures for a viscosity ratio of 0.1, where the defender phase is an order of magnitude more viscous than the invader phase. Given in Figs. 4(*a*)–(*e*) are the final configurations for lamella unblockage probabilities of 0.1, 0.01, 0.001, 0.0005, and 0.0001, respectively. The smallest unblockage probability corresponds to a lamella half-life of approximately 6 900 simulation steps. Again, one can see the increasing invader saturation for increasing lamella half-life.

The effect of keeping the lamella half-life constant at $\rho_u = 0.001$ while changing the viscosity ratio is shown in Figs. 5(*a*)–(*d*) for the viscosity ratios 1.0, 0.5, 0.25, and 0.1. It is apparent that the stability of the foam need not be as great for the higher viscosity ratios in order to obtain a complete sweep of the network, but the same foam has little effect on viscous fingering situations.

These pictorial representations of dynamic foam blockage are given a more quantitative representation in Fig. 6. Each simulation for a given viscosity ratio and chosen decay rate was repeated five times to obtain an average value of the invader saturation in a central portion of the lattice. For an adverse viscosity ratio ($\mu_r = 0.125$) and a very unstable foam ($\rho_u = 0.01$) the invader saturation is quite low, typical of a viscous fingering displacement process. However, for this

Can. J. Chem. Downloaded from www.nrcresearchpress.com by 123.30.183.119 on 09/08/12
For personal use only.

Can. J. Chem. Downloaded from www.nrcresearchpress.com by 123.30.183.119 on 09/08/12
For personal use only.

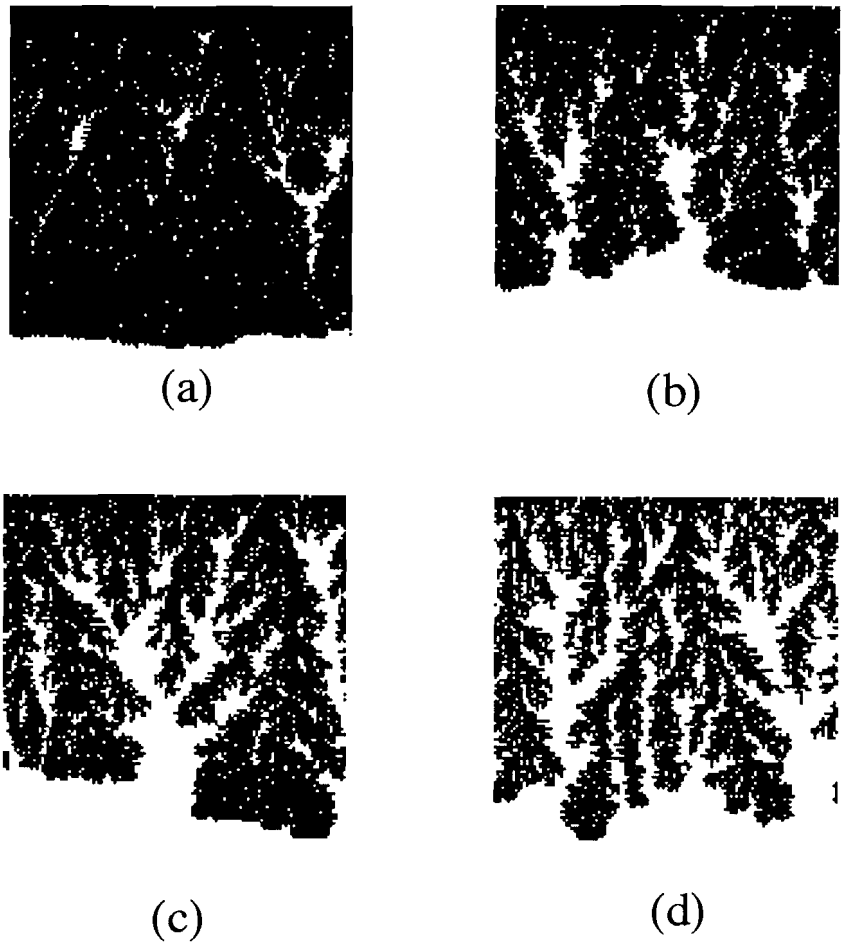

FIG. 5. The effect of dynamic foam blockage on a displacement process with a blockage probability $\rho_b = 1.0$, unblockage probability $\rho_u = 0.001$, and viscosity ratios (*a*) $\mu_r = 1.0$, (*b*) $\mu_r = 0.5$, (*c*) $\mu_r = 0.25$, and (*d*) $\mu_r = 0.125$.

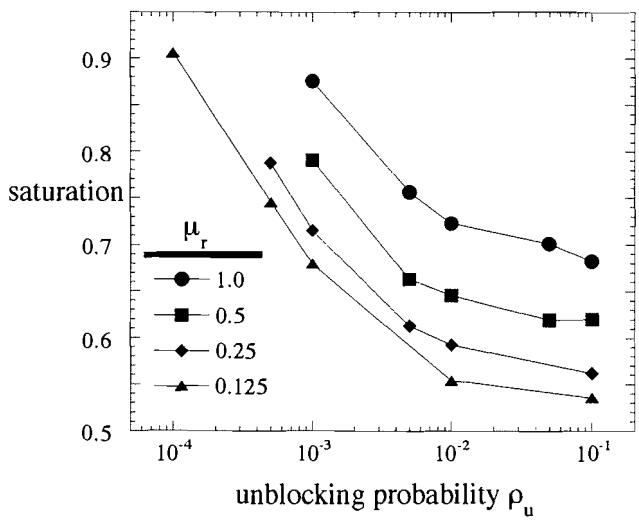

FIG. 6. The effect of dynamic foam blockage on the invader phase saturation as a function of the unblockage probability for various viscosity ratios. The lower right region represents viscous fingering while the upper left region represents stable displacements.

same viscosity ratio but a more stable foam ($\rho_u = 0.0001$) the invader saturation rises dramatically to about 90%.

Discussion

Inefficient sweeps occur, in part, because of an instability present in the coupled equations governing fluid flow through porous media, as discussed by Saffman and Taylor (*7a*). For a viscosity ratio $\mu_r < 1$, the growth of these instabilities is proportional to the speed of the interface between the two fluids. Without the dynamic foam blockage presented here, advance occurs randomly in throats all along the surface of the front, the front velocity is high, and viscous fingering erupts. There are two approaches to remove the instability, one involving a bulk mechanism, and the other involving a surface mechanism. For the bulk mechanism the approach would be to reduce the viscosity of the invader fluid phase. We have not considered this mechanism in this paper. The other approach is to reduce the velocity of the interface. This is exactly what is accomplished by the foam blockage we have presented. While a throat is blocked, advance of the front at that location cannot occur and, for a long lamella half-life, this is the case for most of the throats. Thus advance is occurring, on average, only in widely separated throats, and the interface speed is very low. As shown in our

results, this lowered interface speed is sufficient to supress the fingering instabilities.

In summary, we have examined two foam blockage scenarios for their effect on enhanced sweeps of porous media. Limited foam blockage by infinitely stable lamella does not result in greater sweep efficiency. Very high blockage is required, and even then one must have lamella that decay with a half-life appropriate for the invasion-to-defender viscosity ratio.

Clearly, there are practical difficulties with such a blocking process. The lamella that are introduced to the medium at the source must be completely stable against decay while moving to the front. Once a lamella has reached the front, it must then decay with the appropriate half-life.

Acknowledgements

It is a pleasure to acknowledge the support of AOSTRA grant no. 795, the award of a University of Calgary Fellowship to W.G.W., and the NSERC operating grant of W.G.L.

1. (*a*) G. Kular, K. Lowe, and D. A. Coombe. Foam application in an oil sands steam flood process. Paper SPE 19690 Annu. Tech. Meet. SPE. San Antonio, Tex. Oct. 8, 1989; (*b*) S. S. Mohammadi, D. C. van Slyke, and B. Ganong. Steam-foam pilot project in Dome-Tumbador, Midway Sunset Field. Paper SPE 16736. 1987 Annu. Tech. Conf. SPE. Dallas, Tex. Sept., 1987; (*c*) J. Chad, P. Matsalla, and J. J. Novosad. Foam forming surfactants in Pembina/Ostracod G. Pool. Paper 88-39-40. 39th Annu. Tech. Meet. CIM. Calgary, Alta. June 12, 1988; (*d*) D. G. Huh and L. L. Handy. SPE Reservoir Eng. **4**, 77 (1989); (*e*) F. Friedmann, W. M. Chen, and P. A. Gauglitz. Experimental and simulation study of high-temperature foam displacement in porous media. Paper SPE/DOE 17357. SPE/DOE Enhanced Oil Recovery Symp. Tulsa, Okla. April 12, 1988.
2. (*a*) W. R. Rossen, and P. A. Gauglitz. AIChE. J. **36**, 1176 (1990); W. R. Rossen. Theories of foam mobilization pressure gradient. Paper SPE/DOE 17358. SPE/DOE Enhanced Oil Recovery Symp. Tulsa, Okla. April 12, 1988; (*b*) S. I. Chou. Percolation theory of foam in porous media. SPE/DOE 20239. 7th Symp. Enhanced Oil Recovery. Tulsa, Okla. April 1990; (*c*) F. Friedmann, W. M. Chen, and P. A. Gauglitz. Experimental and simulation study of high-temperature foam displacement in porous media. Paper SPE/DOE 17357. SPE/DOE Enhanced Oil Recovery Symp. Tulsa, Okla. April 12, 1988.
3. W. G. Laidlaw, W. G. Wilson, and D. A. Coombe. Transp. Porous Media. In press.
4. (*a*) L. P. Kadanoff. J. Stat. Phys. **39**, 267 (1985); (*b*) J. Hoshen and R. Kopelman. J. Chem. Phys. **65**, 2817 (1976).
5. W. G. Wilson and W. G. Laidlaw. J. Stat. Phys. **66**, 1129 (1991).
6. (*a*) O. S. Owete and W. E. Brigham. SPE Reservoir Eng. **2**, 315 (1987); (*b*) F. Friedmann and J. A. Jensen. Some parameters influencing the formation and propagation of foams in porous media. Paper SPE 15087. 56th California Regional Meeting SPE. Oakland, Calif. April 1986; (*c*) G. J. Hirasaki and J. B. Lawson. SPEJ, Soc. Pet. Eng. J. **26**, 176 (1985).
7. (*a*) P. G. Saffman and G. Taylor. Proc. R. Soc. London, A: **245**, 213 (1958); (*b*) L. Patterson. Phys. Rev. Lett. **52**, 1621 (1984).
8. A. H. Falls, J. J. Musters, and J. Ratulowski. SPE Reservoir Eng. **4**, 155 (1989).
9. W. G. Laidlaw, W. G. Wilson, and D. A. Coombe. AOSTRA Contract no. 795 Report.
10. A. J. DeVries. Rubber Chem. Technol. Vol. 1. 36th ed. 1958. p. 1142.

Can. J. Chem. Downloaded from www.nrcresearchpress.com by 123.30.183.119 on 09/08/12
For personal use only.

Dynamical barriers to transport in pulsed spin systems: quantum–classical correspondence in the kicked top

J. L. BOORSTEIN[1] AND T. UZER[2]

School of Physics, Georgia Institute of Technology, Atlanta, GA 30332-0430, U.S.A.

Received August 13, 1991

This paper is dedicated to Professor Sigeru Huzinaga on the occasion of his 65th birthday

J. L. BOORSTEIN and T. UZER. Can. J. Chem. **70**, 488 (1992).

Classical phase space is not homogeneous, but contains barriers (such as KAM tori) that, whether intact or broken, affect the temporal evolution of dynamical systems. In this article, we study the quantal manifestations of these classical-mechanical structures. Here, the particular system is the kicked top, which consists of an angular momentum vector precessing about one direction and experiencing periodic sudden kicks around another direction. We find that a suitably defined probability distribution function (constructed from the time-dependent state vector) shows transitions from classically allowed regions to inaccessible regions at the locations where the classical dynamics places the KAM tori.

Key words: bottlenecks, phase space, transport, spin systems, Correspondence Principle.

J. L. BOORSTEIN et T. UZER. Can. J. Chem. **70**, 488 (1992).

L'espace d'une phase classique n'est pas homogène, mais comporte des barrières (telles que des tores de KAM) qui, intactes ou brisées, affectent l'évolution temporale des systèmes dynamiques. Dans cet article, on étudie les manifestations en termes quantiques de ces structures de la mécanique classique. Ici, le système particulier est le «kicked top» qui consiste en un vecteur de moment angulaire effectuant une précession dans une direction et éprouvant d'une façon périodique des sauts soudains dans une autre direction. On a observé qu'une fonction de distribution de probabilités définie adéquatement (construite à partir d'un vecteur d'état dépendant du temps) montre que les transitions entre les régions permises d'une façon classique et les régions inaccessibles sont situées là où la dynamique classique place les tores de KAM.

Mots clés : goulots, espace d'une phase, transport, systèmes de spin, principe de correspondance.

[Traduit par la rédaction]

Introduction

The two key assumptions of the Rice–Ramsperger–Kassel–Marcus (RRKM) theory of unimolecular reactions are that intramolecular energy redistribution is complete and fast compared with the time scale for unimolecular dissociation (1, 2). Notwithstanding the widespread success of this theory, even early on it was recognized that its hypotheses did not seem to apply to some chemical reactions (such as chemical activation experiments (1)). Another particularly severe breakdown was seen in the predissociation of excited van der Waals molecules like HeI_2, where the molecule has more than enough energy to dissociate, but lives for a very long time because the dissociation energy has great difficulty reaching the reactive mode (3).

With the application of classical mechanics to molecular systems through classical trajectories (4) it became possible to gain insight into the microscopic dynamical processes that are subsumed by statistical theories. These and related applications of nonlinear dynamics (5) have demonstrated that phase space is not homogeneous, but contains barriers that can steer the dynamics away from some energetically allowed regions. For example, when the mode energies of the molecule OCS were explored by classical trajectories (6), it was found that they did not decay or increase monotonically to their statistical limits. Instead, trajectories were sometimes trapped behind intramolecular bottlenecks for many vibrational periods, resulting in nonstatistical relaxation (7). Clearly, the dissociation behavior of such molecular systems can also be expected to be nonstatistical and nonrandom.

These chemical observations are among the many manifestations of how dynamical phase-space barriers affect transport phenomena. Their identification in widely differing physical systems attests to their universality (for a review, see ref. 8). According to the Kolmogorov–Arnol'd–Moser (KAM) theorem (9), these barriers must exist in generic nearly integrable systems, and are therefore referred to as KAM tori. As some nonlinearity parameter is varied, however, these impenetrable barriers gradually break up, giving rise to partially penetrable barriers called "cantori" (10). The latter structures may still act as obstacles to phase-space flow, and determine the transport properties of mechanical systems.

Based on earlier work on the transition to global stochasticity (5), MacKay *et al.* (11) and Bensimon and Kadanoff (12) developed a quantitative approach to transport that predicts relaxation rates even when nonstatistical correlations persist (13). Davis (7) undertook the application of these ideas to intramolecular energy transfer (for a recent review, see ref. 14), and coined the term "intramolecular bottleneck" to describe cantori. This terminology emphasizes the connection of this recent work with earlier statistical theories.

Since molecular systems are subject to the laws of quantum rather than classical mechanics, it is necessary to question whether or not these phase-space barriers are relevant for the quantum mechanical regime. The answer turns out to be affirmative and, perhaps surprisingly, these barriers assert their existence and significance even away from the Correspondence Principle limit (8, 15). Furthermore, while one usually associates confinement (of particles) with clas-

[1]Present address: Department of Physics, University of Chicago, Chicago, Ill. 60637, U.S.A.

[2]Author to whom correspondence may be addressed.

Printed in Canada

Can. J. Chem. Downloaded from www.nrcresearchpress.com by 92.62.229.171 on 09/08/12
For personal use only.

Can. J. Chem. Downloaded from www.nrcresearchpress.com by 92.62.229.171 on 09/08/12
For personal use only.

sical mechanics and spreading (of wavepackets) with quantum mechanics, many times these barriers are found (8, 15) to be more confining in quantum mechanics than in classical mechanics!

A thorough investigation of these barriers in realistic quantum mechanical systems is a difficult task. The difficulties are both technical (a large parameter space, complicated classical behavior, corresponding quantum mechanics being further complicated by the very large number of states involved) as well as conceptual (the need to use subtle forms of the quantum–classical correspondence to mimic classical phase space). These barriers have now been seen in the quantal multiphoton dissociation calculations of HF (16), in the comparison of quantal and classical dynamics for OCS (17, 18), and in the microwave ionization of hydrogen atoms (for reviews, see ref. 19).

While such efforts are continuing, most salient features of the quantum–classical correspondence at these barriers can be readily researched on relatively simple systems. Since these structures are generic and universal, understanding them in a particular model can (and does) provide understanding for a very broad class of related problems. This approach is very much in keeping with the great success and decisive impact that simple, generic models such as the Standard Map (5) and kicked rotator (5, 20, 21) have had in chaos research. The Standard Map has been the proving ground for chaos in classical mechanics (thus the name), while much of our understanding of the quantal manifestations of chaos is derived from research on the kicked rotor (or pendulum). In fact, a most illuminating study on the effects of KAM barriers on quantum dynamics was recently performed on the kicked rotor (8, 15).

Because of our interest in the classical–quantal correspondence for rotating systems (22), we investigated the effect of KAM barriers on quantum–mechanical probability flow when rotations (rather than only translations, as in the kicked rotor) are involved. As our model, we have chosen the paradigm for chaotic rotations, namely the kicked top (23–26). The kicked top is a spin system in which an angular momentum vector $\boldsymbol{J}$ (of fixed magnitude $j(j + 1)$) undergoes a linear precessional motion about one direction, and receives impulsive nonlinear kicks about an orthogonal direction. The classical dynamics of this system shows both regular and chaotic motion. Quantum mechanically, the system can be described in terms of a finite dimensional Hilbert space of dimension $2j + 1$, and therefore no artificial truncation in the number of states needs to be imposed. This, in addition to the generic nature, is one of the most desirable aspects of the model. In this article, we show that the KAM barriers and cantori can hinder probability flow in rotational systems, and that tunneling allows probability to penetrate into classically forbidden regions, as was observed in the kicked rotor.

The model

Consider a compass needle in a oscillating magnetic field (27). The quantum-mechanical generalization of that classical system is governed by the Hamiltonian

$$[1] \qquad H = AS_z^2 - \mu \boldsymbol{B}(t) \cdot \boldsymbol{S}$$

where μ is the magnetic moment of the quantum-mechanical particle with spin $\boldsymbol{S}$, A is the anisotropy in an easy plane of magnetization (28), and $\boldsymbol{B}(t)$ is the external time-varying magnetic field. When $\boldsymbol{B}$ has the form $\boldsymbol{B} = B_0 \cos \omega t \, \hat{x}$, chaotic trajectories are observed (27) for any B_0, and the system becomes completely stochastic at a critical field strength. The semiclassical dynamics of Hamiltonian [1] was studied by Frahm and Mikeska (29).

The kicked top is obtained from eq. [1] by replacing the continuous action of the magnetic field by a periodic train of impulsive kicks, i.e.,

$$[2] \qquad H = \frac{\hbar k}{2j\tau} J_z^2 + \hbar p J_y \sum_{n=-\infty}^{\infty} \delta(t - n\tau)$$

where j is the angular momentum quantum number, τ is the duration between kicks, and k and p are related respectively to A and μB in eq. [1]. Here, the system is characterized by an angular momentum vector $\hbar \boldsymbol{J} = \hbar(J_x, J_y, J_z)$, where the components of the angular momentum satisfy the usual commutation relation $[J_k, J_l] = i\hbar\epsilon_{\mathrm{klm}}\mathrm{J_m}$.

One of the technical advantages of this system is the resulting "stroboscopic" view of the dynamics, which then can be easily converted to a map. Quantum mechanically this is achieved by constructing a relatively simple time evolution operator U which takes the system from kick to kick. This way, Nakamura *et al.* (23) studied the changes in the wave function structure of the system as a function of external parameters. They showed how KAM tori, dominant in the weak-field regime, gradually collapse with increasing field. A number of experimental realizations of kicked systems have been suggested (30). Haake *et al.* (24, 31) have proposed two such scenarios for the kicked top. For example, in magnetized solids, crystal anisotropies allowing for an easy plane of magnetization can be represented as in the first term in the Hamiltonian, and a temporally periodic sequence of very short pulses could be imposed to generate the dynamics of the kicked top (24). They have also shown (31) how the dynamics of two laser modes in a medium with quartic nonlinearities corresponds to the kicked top.

Our Hamiltonian H, defined by

$$[3] \qquad H = \frac{\hbar p}{\tau} J_y + \frac{\hbar k}{2j} J_z^2 \sum_{n=-\infty}^{\infty} \delta(t - n\tau)$$

has been shown (25) to be equivalent to the Hamiltonian in eq. [2], and was originally used by Haake *et al.* (24). This Hamiltonian represents the dynamics of the system as a function of time with the first term representing the precession around the y axis with the angular frequency p/τ and the second term accounting for the train of periodic nonlinear kicks experienced by the system. These kicks can be thought of as an impulsive rotation around the z axis by an angle proportional to J_z.

In a classical-mechanical treatment, symmetries (such as invariance of the classical map under rotation around the precession axis by π and invariance of the composition of the classical map with itself around the x axis by π) may be introduced into this model by the appropriate selection of the strength of the magnetic field (which is related to p) and the kick strength. These special cases aid greatly in the study of critical points and periodic orbits. Under these symmetries Haake *et al.* (24) have studied the expectation value of the y component of the angular momentum of an initial state

Can. J. Chem. Downloaded from www.nrcresearchpress.com by 92.62.229.171 on 09/08/12
For personal use only.

chosen to be localized in the vicinity of a fixed point. They showed that the expectation value of this state initially exhibits damped oscillations and that for short time the quantum and classical distributions are indistinguishable. However, for long times the quantal expectation value exhibits periodic recurrences of the initial value while the classical mean has died off. Initial states in the chaotic region exhibit recurrence in the expectation value of the y component of the angular momentum; however, these recurrences occur irregularly.

Our aim is to study the quantum mechanical effects of KAM barriers (which characterize the dynamics for the kicked rotator) in the kicked top model. Since the introduction of symmetries used by other authors constrains the dynamics of the kicked top, it is found to be expedient to move away from these symmetries in order to find dynamics that is more suitable for comparison to the kicked rotator.

The Standard Map (5, 21)

$$[4]\qquad P_{n+1} = P_n + K \sin \theta_{n+1}$$
$$\theta_{n+1} = [\theta_n + P_n] \text{ modulo } 2\pi$$

describes how a kicked rotor with the Hamiltonian

$$[5]\qquad H = \frac{1}{2}p^2 + \epsilon_0 \cos\theta \sum_{n=-\infty}^{\infty} \delta(t - nT)$$

evolves from the nth to the $(n + 1)$st kick. Here, $K = \epsilon_0 T$.

In the Standard Map there exist barriers (KAM-tori) (20) that wrap around the map parallel to the angle coordinate and that act to separate the dynamics into bounded regions. As the strength of the nonlinearity, K, is varied, these barriers begin to break down, with the last one being a torus that is formed when the ratio of the relevant local frequencies, α, is related to the Golden Mean γ (5), viz.

$$[6]\qquad \alpha = 1 + \gamma, \qquad \gamma = (\sqrt{5} - 1)/2$$

The break-up of the "Golden Torus" has attracted the attention of researchers searching for a transition to global stochasticity (5). Simply put, the Golden Mean is the irrational number that is the hardest to approximate by rationals (5). Intuitively, the Golden Torus as the last obstacle to unrestricted transport in phase space is appealing, because it is found in phase-space regions where the coupled oscillators have the greatest difficulty driving each other resonantly (7). When propagated, the quantum-mechanical system exhibits only limited expansion into classically prohibited areas in the form of an exponential drop-off at these barriers.

The symmetric cases studied earlier (e.g., ref. 24) do not readily exhibit this bounding of the probability distribution for initial states that are eigenstates of the z component of the angular momentum. To produce barriers that limit the spreading of such an initial state it is convenient to break these symmetries. Allowing p to vary as well as k gives a doubly rich system of dynamics from which to study the correspondence between the classical and quantum models of the kicked top. For appropriate levels of precession rate and kick strength we encounter dynamics that qualitatively resembles the Standard Map. These regimes are shown to be more suitable for the investigation of structures in the phase space and the correspondence between the classical chaos and its quantal manifestations.

For the kicked top, both Hamiltonians (eqs. [2], [3]) can be studied with the help of a unitary operator that acts to propagate the state vector from kick to kick in time steps of length τ. This time evolution operator can be written in the form[3]

$$[7]\qquad U = \exp\left[-i\left(\frac{k}{2j}\right)J_z^2\right]\exp(-ipJ_y)$$

We will choose to interpret U in terms of the second Hamiltonian (eq. [3]) with the precession around the y axis and the nonlinear kick around the z axis. The unitary operator develops the initial state $|t = 0\rangle$ with n applications of U over a period of time $n\tau$ into the state $|t = n\tau\rangle = U^n|t = 0\rangle$.

Since the commutation relations

$$[8]\qquad [J^2,H] = 0; \qquad [J^2,U] = 0$$

hold for the kicked top, it is apparent that the magnitude of the angular momentum is a conserved quantity. We will therefore define our system on a $(2j + 1)$-dimensional Hilbert space spanned by the usual eigenvectors of J_z and J^2 with

$$[9]\qquad J_z|jm\rangle = m|jm\rangle$$
$$J^2|jm\rangle = j(j + 1)|jm\rangle \qquad (\hbar = 1)$$

We will see later that this is also an appropriate selection of eigenfunctions because the horizontal barriers that characterize the system limit the spreading of state vectors formed by composition of these eigenvectors. Furthermore, whereas the kicked rotator calls for a truncation scheme because the dynamics takes place in an infinite dimensional space, we are able to represent the dynamics from kick to kick in an exact matrix representation of the unitary operator expanded in this finite basis. Actual computational problems occur only for very large j. For our dynamical studies, we have chosen j's that do not exceed 60.

In the classical limit, the dynamics can also be represented by a recursive map (24). From the Heisenberg picture one can generate the discrete time evolution sequence of operators

$$[10]\qquad J_{in} = U^{+n}J_iU^n$$

The corresponding Heisenberg equations take the form of nonlinear recursion relations, which in the classical limit as $j \to \infty$ reduce to the following map:

$$[11]\qquad \begin{aligned} X' &= \text{Re} \\ Y' &= \text{Im} \\ Z' &= -X \sin p + Z \cos p \end{aligned} \Big\{(X \cos p + Z \sin p + iY)e^{ik(Z\cos p - X\sin p)}\Big\}$$

where the rescaled quantities $\boldsymbol{X} = \boldsymbol{J}/j$ have been introduced. As one immediately notices, this map reduces considerably with the selection of $p = \pi/2$ to

$$[12]\qquad \boldsymbol{X}' = F(\boldsymbol{X}) = \begin{bmatrix} Z \cos kX + Y \sin kX \\ -Z \sin kX + Y \cos kX \\ -X \end{bmatrix}$$

This map possesses various symmetries (24) that allow for

[3]This particularly simple form of the time evolution operator results from the presence of a δ-function, which simplifies the time-ordered expression. The derivation follows the argument outlined in eqs. [7.1]–[7.3]. of ref. 32.

a systematic study of the fixed points and periodic orbits of the system. In particular Haake *et al.* (24) have shown that

$$[13] \quad FR_x = R_x F R_y; \qquad FR_y = R_y F$$

where R_x and R_y define rotations of π radians around the x and y axes, respectively. Similarly the unitary operator U with $p = \pi/2$ exhibits these symmetries with R_x and R_y replaced by unitary operators defining rotations of π around the x and y axes.

To better understand the map [11] we define a coordinate system on the unit sphere given by

$$[14] \quad \begin{aligned} x &= \sin\theta\cos\phi \\ y &= \sin\theta\sin\phi \\ z &= \cos\theta \end{aligned}$$

which are the natural coordinates for the model because the magnitude of the angular momentum is conserved. This coordinate system is in turn projected onto the x–z plane with both hemispheres visible. Other useful coordinate systems are the flat local coordinates of Zhang *et al.* (33), which were used to study the effect of quantum fluctuations in the system.

In Fig. 1 we show a series of classical maps with p ranging from $\pi/2$ to 0.1, which exhibit a wide range of dynamics as k is varied. Though Figs. 1*a*–*d* exhibit periodic orbits and regions of bound motion, we notice that the dynamics on the sphere are not localized vertically, i.e., orbits are allowed to range widely in the z component as they are propagated in time. Immediately noticeable, however, is the breakdown of symmetry between the hemispheres as p is varied away from $\pi/2$. Figure 1*d* shows a mostly chaotic scenario. As p is decreased further away from $\pi/2$, trajectories begin to align themselves with the equator as expected; however, eventually all chaotic motion is suppressed with p close to zero. In Fig. 1*e* we notice the dynamics has resolved into periodic orbits parallel to the x–y plane, which suggests that in the limit, as p becomes small compared to k, the dynamics should separate into periodic orbits perpendicular to the z axis. These orbits correspond to barriers that limit the spreading in the z component of the angular momentum in the classical as well as the quantum regime.

Selection of parameters

For the kicked rotator, where only the kick strength may be varied, there is a critical value $K = K_c$ which corresponds to the destruction of the last invariant nonresonant curve. This critical value has been found (34) to be $K_c \approx 0.9716$. Similarly for the kicked top there exists a family of critical k's each corresponding to a specific set value of p. For $p = 0.1$ we find $k_c \approx 9.716$ (see Fig. 1*f*), and for $p = 0.2$ we obtain $k_c \approx 4.858$. We also note that there exists a critical value for k only in the range that p is small, hence confirming the idea that the kicked top system can be studied as a kicked rotator for p far from $\pi/2$. Indeed, the kicked rotor is a limiting case of the kicked top (35). This connection can be readily explained by taking a closer look at the classical dynamics of the Hamiltonian [3] when the initial z component of the angular momentum is approximately zero. In terms of the conjugate variables (36, 37)

$$[15] \quad \begin{aligned} J_y &= (J^2 - J_z^2)^{1/2}\cos\psi \\ J_x &= (J^2 - J_z^2)^{1/2}\sin\psi \end{aligned}$$

where ψ is the angle conjugate to J_z. If p is small, the second term in the Hamiltonian of eq. [3] will not change J_z much, so that J_z is approximately constant. The Hamiltonian can then be approximated by

$$[16] \quad H = \frac{\hbar k}{2j\tau} J_z^2 + \hbar p j \cos\psi \sum_{n=-\infty}^{\infty} \delta(t - n\tau)$$

This classical dynamics obeys the following Hamilton's equations:

$$[17] \quad \begin{aligned} \dot{\psi} &= \frac{\partial H}{\partial J_z} = \frac{\hbar k}{j\tau} J_z \\ \dot{J}_z &= -\frac{\partial H}{\partial \psi} = \hbar p j \sin\psi \sum_{n=-\infty}^{\infty} \delta(t - n\tau) \end{aligned}$$

Integrating these equations over one kick gives the recursion relations:

$$[18] \quad \begin{aligned} \psi_{n+1} &= \psi_n + \frac{\hbar k}{j}(J_z)_n \\ (J_n)_{n+1} &= (J_z)_n + \hbar p j \sin\psi_{n+1} \end{aligned}$$

which may be normalized by setting $(\hbar k/j)\, J_z \rightarrow J_z$. The result is the map

$$[19] \quad \begin{aligned} \psi_{n+1} &= \psi_n + (J_z)_n \\ (J_z)_{n+1} &= (J_z)_n + \hbar^2 p k \sin\psi_{n+1} \end{aligned}$$

which is equivalent to the Standard Map for the kicked rotator where the kick strength of the kicked rotator is $K = \hbar^2 p k$.

Measurements on the quantum system

Having determined appropriate combinations of the rate of precession and the nonlinear kick strength that give rise to vertical separation of the dynamics on the spherical projection of the classical map, we expect to be able to determine similar structures in the quantum phase space that also act to isolate the dynamics. If the state vector is described as an ensemble of eigenvectors of the z component of the angular momentum, then the propagation from kick to kick can readily be determined in the matrix representation of the unitary operator U. Furthermore, in the quantum regime, the dynamics is represented in the development of the coefficients of the expansion of the state vector.

For this reason we choose to study the asymptotic average of the projection of the angular momentum, which has been studied by Geisel *et al.* (15) for the kicked rotator. This value $P(m|m_0)$ is simply the time-averaged probability of finding the system in the state $|jm\rangle$ if the system is initially prepared in the state $|jm_0\rangle$. For the most readily evaluated distribution we choose the initial state to consist of a single eigenvector of J_z, namely $|jm_0\rangle = |j0\rangle$. The choice of /this state as the initial state also makes sense in light of the fact that for m approximately zero the system behaves locally as the kicked rotator. This quantity is defined for each eigenvector of the z component of the angular momentum as

$$[20] \quad P(m|m_0) = \lim_{N\to\infty} \frac{1}{N} \sum_{n=1}^{N} |\langle jm|U^n|jm_0\rangle|^2$$

Can. J. Chem. Downloaded from www.nrcresearchpress.com by 92.62.229.171 on 09/08/12
For personal use only.

Can. J. Chem. Downloaded from www.nrcresearchpress.com by 92.62.229.171 on 09/08/12
For personal use only.

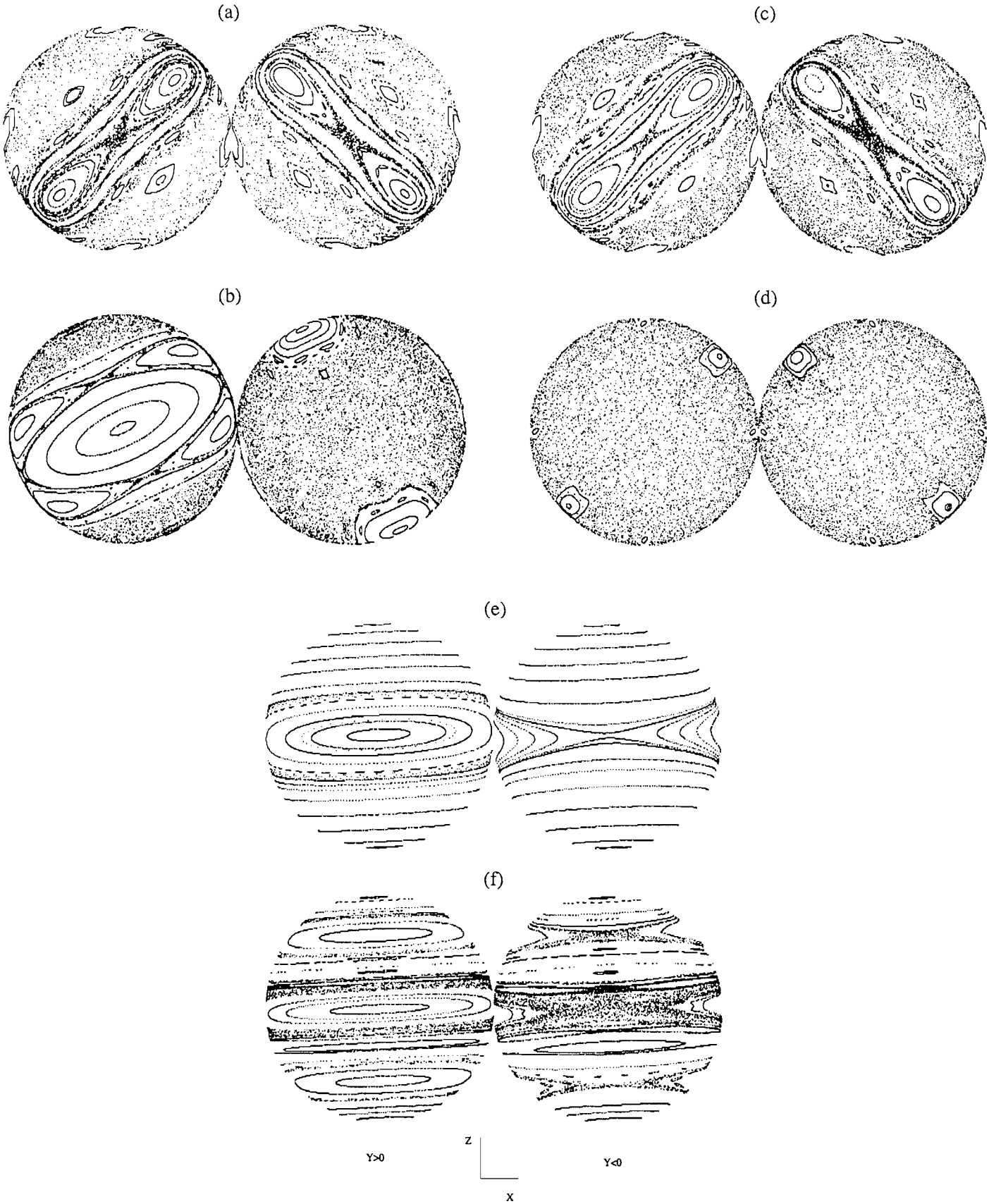

FIG. 1. (*a*)–(*f*) Classical maps on the unit sphere showing trajectories of selected points for up to 5000 iterations. (*a*) $p = \pi/2$, $k = 2.5$; (*b*) $p = 0.9$, $k = 2.5$; (*c*) $p = 1.54$, $k = 2.5$; (*d*) $p = \pi/2$, $k = 3.3$; (*e*) $p = 0.1$, $k = 2.5$; (*f*) $p = 0.1$, $k = 9.716$.

which can be expressed analytically for the kicked top in terms of the Wigner function (38) for rotation around the y axis as

$$[21] \quad \langle jm|U|jm'\rangle = \exp\left[-i\left(\frac{k}{2j}\right)m^2\right] d^{(j)}_{mm'}(p)$$

A linear plot of this distribution reveals that the system remains within the region bounded by the KAM torus (mostly within the band on the equator of Fig. 1*f*). However, there exist slight populations in the states outside the barriers, which in classical mechanics would prevent any diffusion. To see the effects of barriers in the quantum regime the natural logarithm of the asymptotic distribution among the eigenvectors of J_z is displayed. Figure 2 shows the convergence of this distribution as a function of the number of iterations. In this case we exhibit the critical case for $p = 0.1$, which shows a large amount of variation even over J_z even for $j = 20$. In principle an infinite number of iterations would be necessary to define this distribution; however, in practice after 50 iterations the distribution is approximately stable. Hence we are able to derive information of a particular system without lengthy computations (on the order of an hour) even on an Apple MacIntosh using the symbolic manipulation software Mathematica.

In Fig. 3 we take $j = 20$ and $k = 2.5$ while p is varied from $\pi/2$ to 0.25. Initially with $p = \pi/2$ the distribution shows approximately equal population of the even states while there is virtually no population in the odd states. This can be explained by the high level of symmetry in this case along with the absence of horizontal barriers, which allows the state to spread freely in the z direction. As p is varied we see the immediate breakdown of the even-odd state populations corresponding to the break in symmetry. As p moves into a system showing horizontal barriers in the classical map the distribution conforms in such a way as to follow these barriers as they narrow. In other words, as p moves away from $\pi/2$ the nonlinear kick around the z axis begins to dominate the dynamics, causing flattened trajectories on the sphere. This corresponds to confining the wave packet in phase space and a localization of the probability flow. In Fig. 3 as p approaches 0.5 the confinement is more precisely defined and

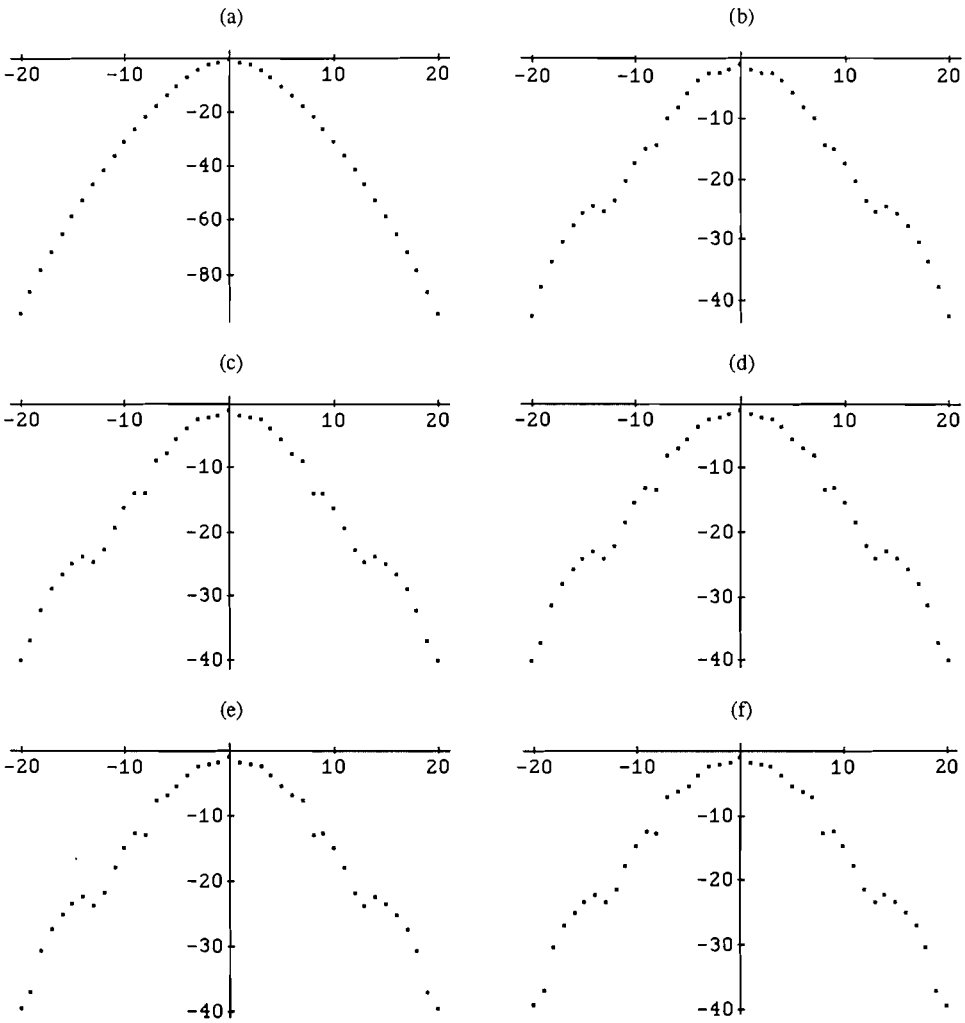

FIG. 2. The asymptotic distributions for the kicked top with $k = 9.716$ and $p = 0.1$ is shown to reach an approximately stable value after only 50 iterations. Each figure is shown at 10 iterations after the preceding figure with (*a*) shown after only one iteration of the initial state. The vertical axis denotes ln P (see eq. [20]), the horizontal axis is m.

Can. J. Chem. Downloaded from www.nrcresearchpress.com by 92.62.229.171 on 09/08/12
For personal use only.

Can. J. Chem. Downloaded from www.nrcresearchpress.com by 92.62.229.171 on 09/08/12
For personal use only.

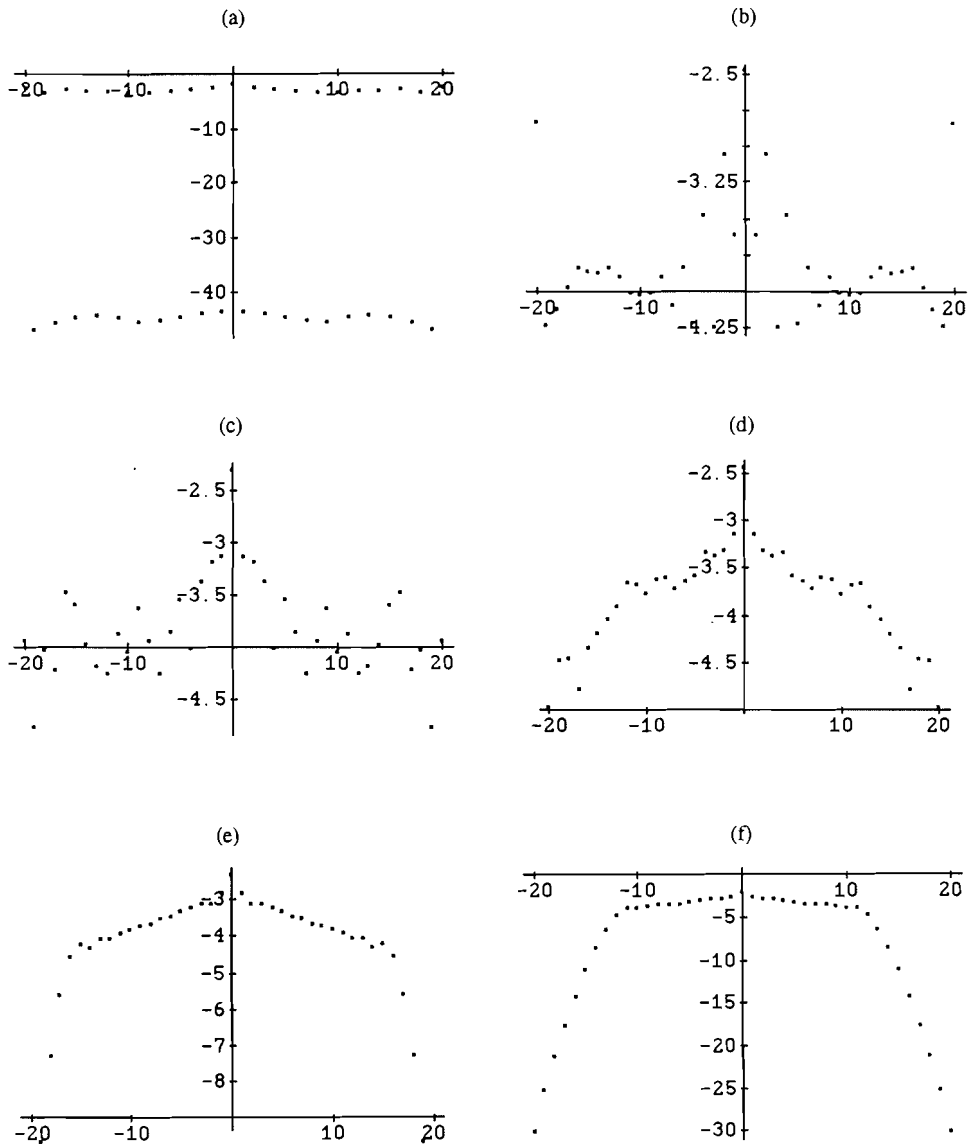

FIG. 3. Asymptotic distributions plotted on a logarithmic scale for a fixed $k = 2.5$. The precession angle p is varied from $\pi/2$ to 0.25 showing the effect of the cantori on confinement of the distribution. (*a*) $p = \pi/2$; (*b*) $p = 1.5$; (*c*) $p = 1.0$; (*d*) $p = 0.75$; (*e*) $p = 0.5$; (*f*) $p = 0.25$. The axes are the same as in Fig. 2.

the distribution outside the barriers decays exponentially away from the classically allowed regions.

In the kicked rotator model the critical value of the kick strength corresponds to a boundary between regular and chaotic motion in the dynamics. Hence any $K > K_c$ will allow trajectories to move more readily into classically forbidden regions. Similarly, for $K < K_c$ trajectories will be more strongly bound, providing less information to the structure of the phase space outside the barriers. The dynamics of the kicked top also exhibits this loss of information for kick strengths above and below k_c. In Fig. 4 we set $p = 0.1$ and $j = 20$, allowing k to vary around the critical nonlinear value $k_c = 9.716$ (for which we obtain KAM-tori in the classical map, see Fig. 1*f*). As expected, the distribution has difficulty sampling structures outside the barriers as k is decreased below k_c, whereas when k is increased above k_c the distribution reveals the breaking down of the tori, which allows the probability to flow more easily into classically inaccessible regions. However, as with the kicked rotator, the quantum phase-space structures work to greatly inhibit this probability flow as the asymptotic distributions still show exponential decay.

We also investigated the effect of increasing the size of j in order to study the distribution with more resolution. Figure 5 shows a series of distributions with $p = 0.1$ and $k = k_c = 9.716$. The actual shape of the distribution appears to be suppressed for very low values of j. However, the distribution takes on a distinctive shape with increasing j by revealing plateaus that mark other barriers on the sphere outside the initial bounded region.

Concluding remarks

In this article, we studied the quantum mechanics of the kicked top by constructing its time-dependent state and interrogating it for manifestations of KAM tori. The effect of these tori was revealed through the examination of a suita-

Can. J. Chem. Downloaded from www.nrcresearchpress.com by 92.62.229.171 on 09/08/12
For personal use only.

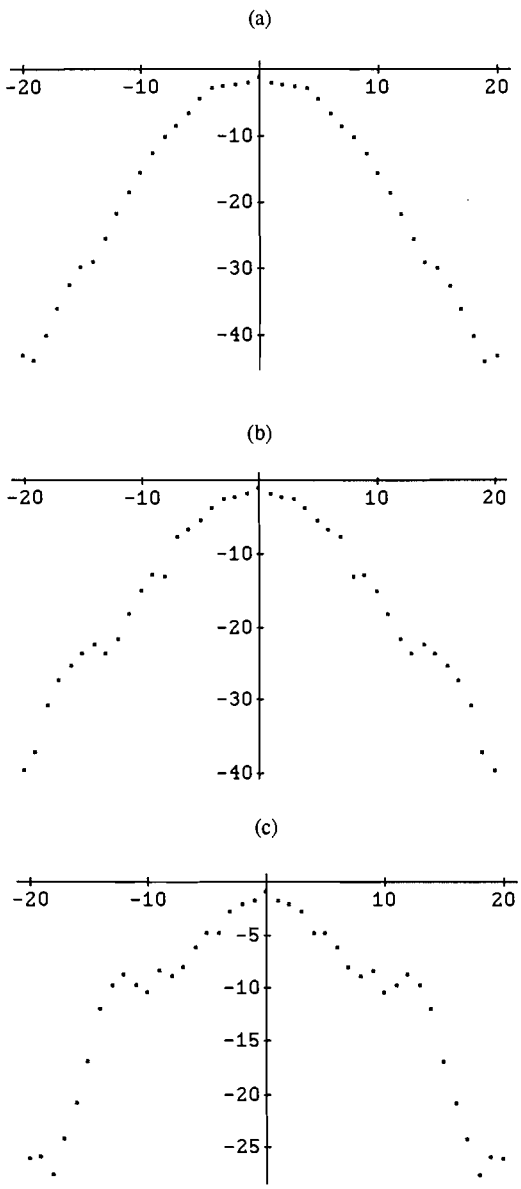

FIG. 4. The asymptotic distribution for $p = 0.1$ and (*a*) $k = 8.216$; (*b*) $k = 9.716$; and (*c*) $k = 11.216$. Below the critical value of k the cantori overly constrain the system, while above the critical value the distribution spreads more freely into classically inaccessible regions. The axes are the same as in Fig. 2.

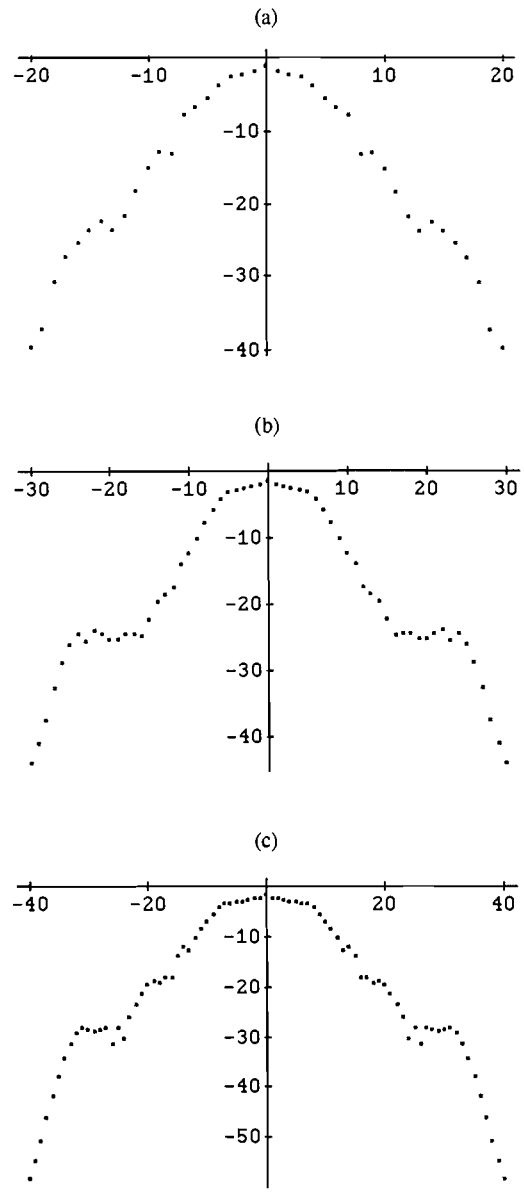

FIG. 5. The asymptotic distributions for the critical case $k = 9.716$ and $p = 0.1$. Here the magnitude of J is increased showing greater detail in the distribution outside the KAM-tori. All figures were obtained after 50 iterations, and j increases according to the sequence $j = 20$, 30, and 40. The axes are the same as in Fig. 2.

bly defined distribution function, and by moving away from special sets of parameters used by previous researchers. The connection between the kicked rotator and the kicked top was very useful to our investigation. We found a close correspondence between the locations of KAM tori as revealed by classical maps and by shoulders or kinks in the distribution functions, showing that for appropriate combinations of system parameters, probability flow in rotational systems is strongly affected by these phase-space structures.

In some recent research, the kicked rotator has been used as a testing ground for a number of interrelated speculations concerning the effect of measurements (39, 40), the dynamics of pure-state density matrices (39), localization (34), coherent quantum tunneling (25), as well as the effect of small variations in the parameters on the quantum dynamics (26). However, all these studies were restricted to the highly symmetric case $p = \pi/2$, which, as we have shown in this article, eliminates some very interesting dynamics. An analogous series of investigations, but performed in parameter ranges where the KAM barriers restrict probability flow, are expected to contribute to our understanding of the phenomenon of quantum state localization in rotational systems. Such work is currently in progress.

Acknowledgements

This research was supported by the U.S. National Science Foundation through grant CHE89-22420 and the REU program.

1. W. Forst. Theory of unimolecular reactions. Academic Press, New York. 1973.
2. D. M. Wardlaw and R. A. Marcus. Adv. Chem. Phys. **70**, 231 (1987); D. L. Truhlar, W. L. Hase, and J. T. Hynes. J. Phys. Chem. **87**, 2664 (1983); W. L. Hase. Acc. Chem. Res. **16**, 258 (1983).
3. C. E. Wozny and S. K. Gray. Ber. Bunsen-ges. Phys. Chem. **92**, 236 (1988).
4. L. M. Raff and D. L. Thompson. *In* Theory of chemical reaction dynamics. Vol. III. *Edited by* M. Baer. CRC Press, Boca Raton, Fla. 1985.
5. A. J. Lichtenberg and M. A. Lieberman. Regular and stochastic motion. Springer, New York. 1983.
6. M. J. Davis. Chem. Phys. Lett. **110**, 491 (1984); M. J. Davis and A. J. Wagner. *In* Resonance in electron-molecule scattering, van der Waals complexes and reactive chemical dynamics. ACS. Symp. Ser. **236**. *Edited by* D. G. Truhlar. American Chemical Society, Washington, D.C. 1984.
7. M. J. Davis. J. Chem. Phys. **83**, 1016 (1985).
8. G. Radons, T. Geisel, and J. Rubner. Adv. Chem. Phys. **73**, 891 (1989).
9. M. V. Berry. *In* Topics in nonlinear dynamics. AIP Conf. Proc. No. 46, *Edited by* S. Jorna. American Institute of Physics, New York. 1978.
10. I. C. Percival. *In* Nonlinear dynamics and beam–beam interactions. AIP Conf. Proc. No. 57. *Edited by* M. Month and J. C. Herrera. American Institute of Physics, New York. 1979.
11. R. S. McKay, J. D. Meiss, and I. C. Percival. Physica D: **13**, 55 (1984).
12. D. Bensimon and L. P. Kadanoff. Physica D: **13**, 82 (1984).
13. J. D. Meiss and E. Ott. Physica D: **20**, 387 (1986).
14. T. Uzer. Phys. Rep. **199**, 73 (1991).
15. T. Geisel, G. Radons, and J. Rubner. Phys. Rev. Lett. **57**, 2883 (1986).
16. R. C. Brown and R. E. Wyatt. Phys. Rev. Lett. **57**, 1 (1986); J. Phys. Chem. **90**, 3590 (1986).
17. M. J. Davis. J. Phys. Chem. **92**, 3124 (1988).
18. L. L. Gibson, G. C. Schatz, and M. A. Ratner. J. Chem. Phys. **86**, 3263 (1987).
19. G. Casati, B. V. Chirikov, D. L. Shepelyansky, and I. Guarneri. Phys. Rep. **154**, 77 (1987); R. V. Jensen, S. M. Suskind, and M. M. Sanders. Phys. Rep. **201**, 1 (1991); R. S. MacKay and J. D. Meiss. Phys. Rev. A, **37**, 4702 (1988).
20. G. Casati, B. V. Chirikov, F. M. Izrailev, and J. Ford. Lect. Notes Phys. **93**, 334, (1979).
21. F. M. Izrailev. Phys. Rep. **196**, 299 (1990).
22. V. Postell and T. Uzer. Phys. Rev. A, **41**, 4035 (1990).
23. K. Nakamura, Y. Okazaki, and A. R. Bishop. Phys. Rev. Lett. **57**, 5 (1986).
24. F. Haake, M. Kus, and R. Scharf. Z. Phys. B: Condens. Matter, **65**, 381 (1987).
25. B. C. Sanders and G. J. Milburn. Z. Phys. B: Condens. Matter, **77**, 497 (1989).
26. A. Peres. *In* Quantum chaos. *Edited by* H. A. Cerdeira, R. Ramaswamy, M. C. Gutzwiller, and G. Casati. World Scientific, Singapore. 1991. p. 73.
27. V. Croquette and C. Poitou. J. Phys. (Paris), **42**, L537 (1981).
28. R. M. White. Quantum theory of magnetism. 2nd (corrected and updated) ed. Springer Ser. Solid-State Sci. Vol. **32**, Springer-Verlag, New York. 1983.
29. H. Frahm and H. J. Mikeska. Z. Phys. B: Condens. Matter, **60**, 117 (1985).
30. R. E. Prange and S. Fishman. Phys. Rev. Lett. **63**, 704 (1989).
31. F. Haake, G. Lenz, and R. Puri. J. Mod. Optics **37**, 155 (1990).
32. G. M. Zaslavsky. Phys. Rep. **80**, 157 (1981).
33. W.-M. Zhang, J.-M. Yuan, D. H. Feng, Q. Pan, and J. Tjon. Phys. Rev. A, **42**, 3646 (1990).
34. J. M. Greene. J. Math. Phys. **20**, 1183 (1979).
35. F. Haake and D. L. Shepelyansky. Europhys. Lett. **5**, 671 (1988).
36. A. Deprit. Am. J. Phys. **35**, 424 (1967).
37. S. D. Augustin and W. H. Miller. J. Chem. Phys. **61**, 3155 (1974).
38. D. A. Varshalovich, A. N. Moshalev, and V. K. Khersoniskii. Quantum theory of angular momentum. World Scientific, Singapore. 1988.
39. E. R. Pike, S. Sarkar, and J. S. Satchell. *In* Quantum measurement and chaos. *Edited by* E. R. Pike and S. Sarkar. NATO ASI Ser. Ser. B: Physics Volume 161. Plenum Press, New York, 1987. pp. 119–146.
40. S. Sarkar and J. S. Satchell. Europhys. Lett. **4**, 133 (1987); Physica D: **29**, 343 (1988).

Can. J. Chem. Downloaded from www.nrcresearchpress.com by 92.62.229.171 on 09/08/12
For personal use only.

Stationary phase Monte Carlo methods: interference effects in quantum Monte Carlo dynamics

J. D. DOLL[1] AND STEVEN W. RICK
Department of Chemistry, Brown University, Providence, RI 02912, U.S.A.

AND

DAVID L. FREEMAN
Department of Chemistry, University of Rhode Island, Kingston, RI 02881, U.S.A.

Received May 23, 1991

This paper is dedicated to Professor Sigeru Huzinaga on the occasion of his 65th birthday

J. D. DOLL, STEVEN W. RICK, and DAVID L. FREEMAN. Can. J. Chem. **70**, 497 (1992).

As summarized by Hamming's motto, "the purpose of computing is insight, not numbers." In the spirit of this dictum, we describe here recent algorithmic developments in the theory of quantum dynamics. Through the use of the somewhat unlikely combination of modern numerical simulations and a visualization device borrowed from 19th century optics, the present efforts suggest the existence of an important, underlying structure in the general problem. This structure, verified for a relatively simple class of model problems, provides broad guidelines for the formulation and treatment of the general quantum dynamical problem.

Key words: Monte Carlo, stationary phase, quantum dynamics.

J. D. DOLL, STEVEN W. RICK et DAVID L. FREEMAN. Can. J. Chem. **70**, 497 (1992).

Comme l'a résumé la devise de Hamming, «le but des calculs par ordinateur n'est pas les valeurs numériques obtenues, mais l'aperçu général qu'on peut en dégager». Dans l'esprit de ce dicton, on décrit des développements récents d'algorithmes dans la théorie de la dynamique quantique. Par le biais de l'usage d'une combinaison saugrenue de simulations numériques modernes et d'un appareil de visualisation emprunté à l'optique du 19^{e} siècle, nos efforts suggèrent l'existence d'une structure sous-jacente importante dans le problème général. Cette structure, vérifiée par une classe relativement simple de problèmes modèles, fournit des lignes directrices importantes pour la formulation et le traitement du problème général de la dynamique quantique.

Mots clés : Monte Carlo, phase stationnaire, dynamique quantique.

[Traduit par la rédaction]

1. Introduction

In his autobiography Stan Ulam (1), one of the pioneers of modern computational science, made a series of surprisingly accurate observations concerning the likely future impact of numerical simulation methods in science. He correctly anticipated that the greatest significance of such methods was their ability to liberate one's thinking concerning the proper formulation and treatment of physical phenomena from the limitations imposed by purely analytic methods of analysis. These general numerical methods allow one to examine broad problem areas, to identify particular topics whose phenomenology warrants further investigation, and, most importantly, to produce the insight necessary to produce a unified, conceptual theory from the particular results so obtained. In this process, computational machines become significantly more than merely devices for producing answers to particular problems of the moment. Rather, they become the central enabling technology, the very engines that drive the analysis of complex physical phenomena.

The extent to which Ulam's program can be implemented is, of course, governed by the power of the computational machines that are available. Starting with postwar machines of relatively limited capabilities, these devices have undergone a dramatic evolution. In this relatively brief period, they have reached the stage where it is now possible to probe important classes of physically significant questions concerning the behavior of systems of realistic complexity. It is likely, moreover, that this rapid expansion of computational capability will accelerate, thus significantly extending the class and scale of problems that can be considered.

Broadly speaking, computational problems in finite temperature condensed matter theory can be broken into categories depending on whether they are essentially classical (e.g., Newtonian) or quantum mechanical in character and depending on whether they involve the study of equilibrium or time-dependent properties. This division is summarized by the simple "computational matrix," depicted in Fig. 1. This matrix serves to highlight the comments made by Ulam discussed above and to set the stage for the present discussion.

The computational machines available in the two decades following WWII, although primitive by current standards, were adequate to begin the study of equilibrium and dynamical properties of classical systems. A number of particular results from these calculations, such as the hard sphere freezing transition (2, 3) and the discovery of the long-time tails for the velocity autocorrelation functions for dense fluids (4), were of special interest. The lasting importance of these studies, however, did not reside in the particulars of these problems. Rather, the greater significance of these investigations was that they led to the development of general purpose tools for the analysis of many-body classical systems. As envisioned by Ulam, the resulting Monte Carlo (see, for example, ref. 5) and molecular dynamics methods (ref. 6 for a general review) freed investigators from the limitations imposed by uncontrolled numerical approximations typical of prior work and ultimately provided them with insight necessary to develop intelligent, physically well-founded theories of classical many-body systems.

[1]Author to whom correspondence may be addressed.

Can. J. Chem. Downloaded from www.nrcresearchpress.com by 92.62.229.171 on 09/08/12
For personal use only.

	Classical	Quantum-mechanical
Equilibrium	Monte Carlo	Quantum Monte Carlo
Dynamical	Molecular dynamics	Present work

FIG. 1. The computational "matrix" indicating the broad categories of current physical computations and the principal algorithms utilized within each.

Can. J. Chem. Downloaded from www.nrcresearchpress.com by 92.62.229.171 on 09/08/12
For personal use only.

Over the past decade, the statistically based, Monte Carlo methods designed for the classical equilibrium studies described above have been extended to treat corresponding quantum mechanical problems (7). The basic conceptual development involved was the realization that the quantum mechanical problem could be recast as a related classical problem in a higher-dimensional space. Since Monte Carlo methods are relatively insensitive to dimensionality, this formulation of the equilibrium problem proves a practical one. Current applications of the resulting "Quantum Monte Carlo" methods encompass a diverse range of problems in physics, chemistry, and biology and represent many of the largest computational problems yet undertaken (see ref. 8 for a cross section of recent activity.)

Anticipating the continued rapid expansion in computational capabilities, attention has now turned to the remaining entry in the computational matrix of Fig. 1, the study of general, time-dependent quantum mechanical methods. While lying at the outer edges of current algorithmic and computational capabilities, such problems are at the center of broad areas of chemistry and physics. Our particular interest in such developments will be their application to the areas of spectroscopy (the response of physical systems to time-dependent perturbations) and kinetics (the rates of chemical and physical processes). The time-dependent problem is formally similar in nature to its equilibrium counterpart. However, the time-dependent problem is substantially more "complex," both technically and in practical terms, than the equilibrium situation. Mathematically, these technical difficulties are related to the appearance of highly oscillatory quantities in the result. The treatment of these difficulties has prompted the search for new classes of more suitable Monte Carlo methods (9, 10) and the present efforts are a part of that search.

We describe here an observation concerning the composition of the general quantum dynamics problem. Exploiting a combination of numerical and graphical methods, we find indications that the principal quantum mechanical object of interest has an appreciably simpler theoretical structure than has heretofore been appreciated. This insight, gained through a series of particular model investigations, offers a number of general, and hopefully significant, suggestions for the formulation of the quantum dynamical problem.

Much of the present work is directed at extracting information concerning general theoretical structure that underlies objects obtained from numerical procedures. Section 2 describes and illustrates a visual device that we have found to be particularly useful in this regard. Section 3 presents a brief summary of the physical context of the present discussion and identifies the primary computational objects under consideration. The central result required for subsequent discussion is contained in eq. [12] and the associated discussion. The physical applications and associated conclusions are contained in Sects. 4 and 5, respectively.

2. Cornu analysis

In the theory of optics, a convenient visual device was developed for the analysis of certain classes of problems relating to diffraction (11). This device utilizes an elegant geometrical representation introduced by Cornu (12). Besides being rather pleasing aesthetically, we have found this instrument to be quite useful in the present work. This technique proves particularly valuable for revealing structure otherwise hidden within purely numerical procedures.

To appreciate the character of the Cornu analysis, consider a complex integral of the form

$$[1] \qquad I(t) = \int_{-\infty}^{\infty} dx\, \rho(x) e^{itf(x)}$$

As indicated above, integrals of this type arise naturally in the theory of optics. We will see in the following section that similar integrals also arise in the treatment of the dynamics of quantum mechanical systems. In the present illustrations, the functions $\rho(x)$ and $f(x)$ are specified. This generic integral is an example of what is typically termed the "stationary phase" problem (13). That is, if the parameter t is large, then the integral $I(t)$ will generally be dominated by those regions of x for which the phase of the complex exponential is "stationary" (i.e., locally constant). Within nonstationary phase regions, the complex exponential will oscillate rapidly for a small variation in the position x, thus effectively cancelling the region's contribution to the final integral. If $f(x)$ is known, then such stationary phase behavior can be readily anticipated. If, however, the integrand of eq. [1] is produced numerically, then such behavior is typically far from obvious.

In numerical applications, integrals of the type in eq. [1] are often approximated by quadrature. If these are written as an ordinary Reimann sum, the result becomes

$$[2] \qquad I(t) \approx \sum_{n=1}^{N} \Delta x_n \rho(x_n) e^{itf(x_n)}$$

where the summation is over the numerical grid points, $\{x_n\}$,

Can. J. Chem. Downloaded from www.nrcresearchpress.com by 92.62.229.171 on 09/08/12
For personal use only.

$n = 1, 2, \ldots N$, that cover the integration interval and Δx_n is the spacing between successive quadrature points.

We now consider the sequence of partial sums that make up eq. [2],

$$[3] \qquad I_M(t) = \sum_{n=1}^{M} \Delta x_n \rho(x_n) e^{itf(x_n)}$$

The partial sums defined by eq. [3] are the accumulation of M successive vectors, whose individual lengths and orientations are governed by the magnitudes and phases of the corresponding complex numbers in the original sum. The Cornu construction consists of following the real and imaginary parts of the sequence of partial sums defined in eq. [3] parametrically as a function of the index M. For $M = 1$, the partial sum consists of a single vector pointing from the origin to the first complex number in the summation of eq. [2]. With increasing values of M, successive complex vectors corresponding to the terms in eq. [2] are added sequentially to the preceding partial sum. The sequence of partial sums so produced thus begins at the origin in the complex plane and traces out a contour that provides a graphical representation of the original integral. So written, the integral is analogous to a many jointed, folding "carpenter's rule." In this representation, the integral's numerical value is given by the single, complex vector that corresponds to the ruler's end-to-end distance. What makes this construction convenient is that it provides a ready visual indication of those integration regions that contribute strongly to the overall result. Specifically, in regions where the phase function varies rapidly, the contributions from successive terms in the summation are tightly "knotted" and thus contribute little to the integral. Conversely, regions where the phase function is relatively constant tend to add coherently and thus to dominate. The geometry of the resulting construction is thus a convenient way of revealing the underlying structure of the original integral.

To illustrate these ideas, we examine the integral

$$[4] \qquad I(t) = \frac{1}{\sqrt{2\pi}} \int_{-\infty}^{\infty} \exp(-x^2/2 + itx^2)\, dx$$

Easily evaluated by analytic means, this integral is equal to $1/\sqrt{(1 - 2it)}$. The corresponding Cornu analysis is shown in Fig. 2 for the particular case of $t = 10$. In this case the integral was approximated by a simple trapezoidal quadrature with a numerical mesh of a sufficiently fine scale that the resulting Cornu plot in Fig. 2 appears continuous. This analysis vividly reveals the stationary phase character that underlies this integral, a character not immediately apparent if one considers merely the integral's exact numerical value. As anticipated, the bulk of the integration region from minus infinity up to zero forms a tightly knotted spiral centered at the origin of the complex plane (the lower left hand corner) in Fig. 2. As the integration variable nears the stationary phase point at zero, however, the Cornu spiral begins to open. Once past this region, the phase oscillations again become severe and the spiral collapses to a new accumulation point. The numerical value of the integral is given by the complex vector connecting the ends of the Cornu spiral. Changing the value of the parameter t in eq. [4] changes the orientation and absolute scale of the associated spiral, but the characteristic sigmoidal structure is a reflection of the stationary phase structure of the original integral and remains qualitatively undisturbed.

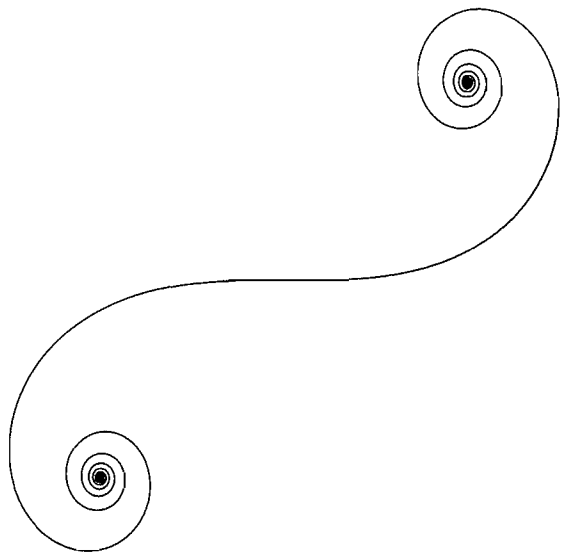

FIG. 2. Cornu analysis of the integral

$$I(t) = \frac{1}{\sqrt{2\pi}} \int_{-\infty}^{\infty} dx\, e^{-x^2/2}\, e^{itf(x)}$$

where $f(x) = x^2$ and $t = 10$. The plot displays the real and imaginary parts of the integral from $-\infty$ up to a point y parametrically as a function of the variable y over the range $-\infty < y < \infty$. The plot begins at the origin (the lower left-hand spiral) and proceeds to the upper right. The value of the integral is thus the vector connecting the ends of the curve. In this case the integral has the value $1/\sqrt{(1 - 20i)}$. Note the characteristic spiral corresponding to the single stationary phase point (the region near $y = 0$).

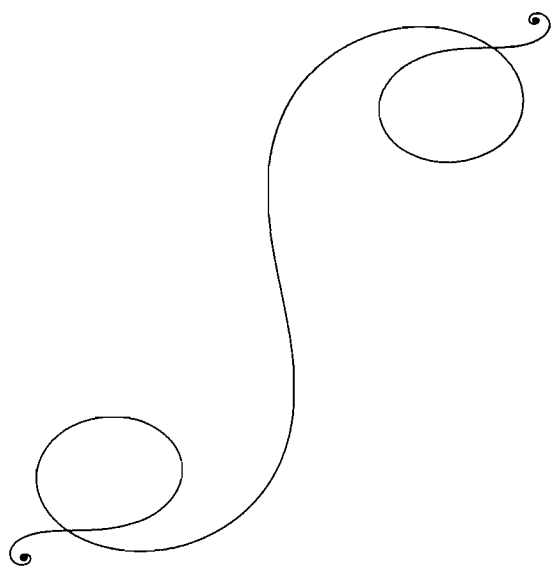

FIG. 3. As in Fig. 2, except that $f(x) = (x^2 - 2)^2$ and $t = 2$. Here the Cornu spiral reflects three stationary phase regions (corresponding to $y = 0$ and $y = \pm\sqrt{2}$). The value of the integral is 0.231 + 0.300 i.

Shown in Figs. 3–5 are examples of the Cornu analysis of more elaborate integrals. In Fig. 3 and 4 we display the results for the integral

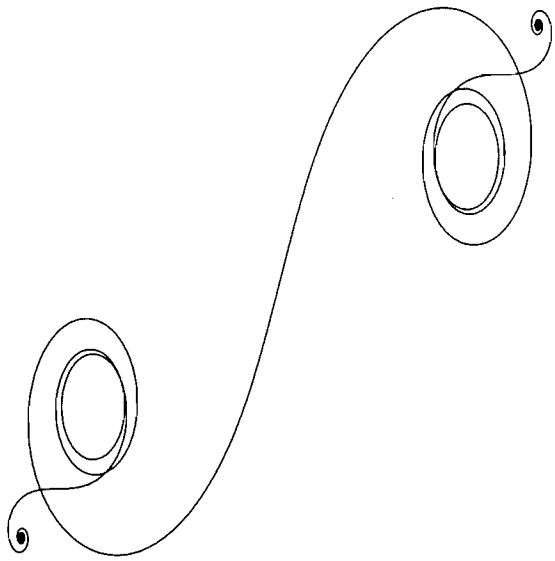

FIG. 4. As in Fig. 3 with $t = 5$. With the larger t value, the stationary phase structure in the Cornu spirals is more highly developed. The value of the integral for this value of t is 0.203 + 0.117 i.

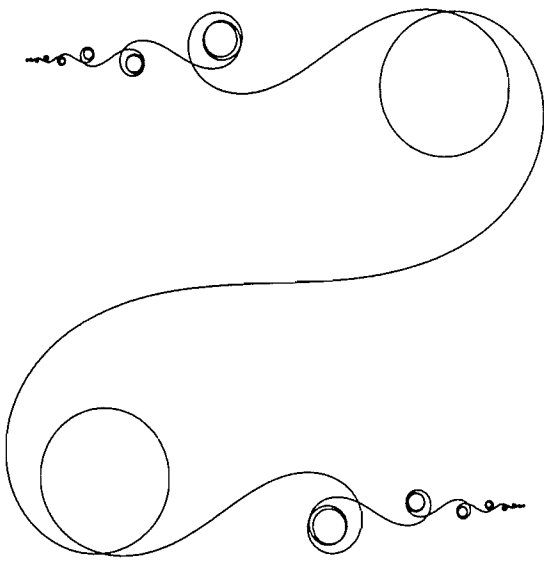

FIG. 5. Cornu analysis of the integral

$$I(t) = \frac{1}{\sqrt{8\pi}} \int_{-\infty}^{\infty} dx\, e^{-x^2/8}\, e^{itf(x)}$$

where $f(x) = \sin(x^2)$ and $t = 10$. The intricate structure arises from the multiple stationary phase regions ($f'(x) = 0$). The value of the integral is $-0.1085 + 0.0969$ i. This corresponds to the complex vector that connects the lower right to upper left ends of the figure.

$$[5] \qquad I(t) = \frac{1}{\sqrt{2\pi}} \int_{-\infty}^{\infty} \exp(-x^2/2 + it(x^2 - 2)^2)\, dx$$

We see that the Cornu spirals in this case are effectively a composite of three separate spirals of the type shown in Fig. 2. This composite nature reflects the contributions from the three stationary phase points of the original integrand, located at $x = 0$ and $x = \pm\sqrt{2}$, respectively. The existence and relative magnitudes of these stationary phase regions are easily visible in Figs. 3 and 4. Examination of the sequence of partial sums in the Cornu analysis reveals that the central portion of the figures corresponds to the contributions from the stationary phase region near $x = 0$. As the parameter t increases, the various portions of the Cornu construction pivot about in the complex plane, a "dynamics" that introduces additional "windings" into its spiral structure. Consequently, the central portion of Fig. 4 where $t = 5$ is more strongly developed than that of Fig. 3 where $t = 2$. We note in passing that the asymmetry in the outer spirals in Figs. 3 and 4 reflects the symmetry of the Gaussian term about the outer ($\pm\sqrt{2}$) stationary phase regions.

Shown in Fig. 5 is our final example. We hope that the reader will agree that Fig. 5 is one of the more lovely ways to write the integral

$$[6] \qquad I(t) = \frac{1}{\sqrt{8\pi}} \int_{-\infty}^{\infty} \exp(-x^2/8 + it \sin(x^2))\, dx$$

This majestic beast, resplendent in its myriad of stationary phase accoutrements, has a "dynamics" that is equally flamboyant!

The Cornu analysis described above represents an algorithm for the construction of an analog device that corresponds to our original mathematical problem. This device, is, in effect, a "clock" whose ornate hands pinwheel about in the complex plane chronicling not the passage of time but rather the "temporal" evolution of the particular object under study. The significance of this result for the present discussion is that it is possible to design such "timepieces" so that they follow the quantum dynamics of physical systems. The following section briefly summarizes the tools necessary for such developments.

3. Time-dependent quantum mechanics

Classically, physical systems and their time evolution are characterized by the positions and momenta of their constituents and their associated equations of motion. Once the interactions between the various constituents are specified, these well-known classical (Newtonian) equations of motion provide a complete description of the time development of the physical systems.

Quantum mechanically, this simple picture is valid only as an asymptotic, limiting case of a more general theory. Rather than simple, sharply defined classical variables, the objects of interest become various complex valued amplitudes whose functional form and time dependence are governed by the equations of wave mechanics.

To be concrete, let us consider a simple one-dimensional system characterized by a position variable, x, a mass m, a momentum p, and a potential energy function, $V(x)$. Classically, we proceed by constructing the Hamiltonian of the system, $H(p,x)$, given by

$$[7] \qquad H(p,x) = \frac{p^2}{2m} + V(x)$$

Can. J. Chem. Downloaded from www.nrcresearchpress.com by 92.62.229.171 on 09/08/12
For personal use only.

Can. J. Chem. Downloaded from www.nrcresearchpress.com by 92.62.229.171 on 09/08/12
For personal use only.

The time dependence of the system is governed by the classical equations of motion,

$$[8] \quad \frac{\partial x}{\partial t} = \frac{\partial H(p,x)}{\partial p} \qquad \frac{\partial p}{\partial t} = -\frac{\partial H(p,x)}{\partial x}$$

where t is the physical time. Once the initial positions and momenta are specified, eq. [8] permits us to determine the classical trajectory (the subsequent positions and momenta as functions of time) for all time.

Quantum mechanically, the problem is formulated rather differently. For example, the quantum mechanical generalization of the classical Hamiltonian turns out to be an "operator," $\hat{H}$. The explicit forms for such operators, the rules for their manipulation, and their mathematical properties are well known (14) and need not concern us further. We simply summarize here the basic results necessary for the present discussion. In terms of the quantum mechanical Hamiltonian, the time dependence of the physical system is governed by the related "time development operator," $\exp(-it\hat{H}/\hbar)$, where $\hbar$ is Planck's constant, a fundamental constant of nature. Here the exponential operator is understood in terms of the actions of its formal power series expansion. The second basic result that we will require is that the motion of a system from a position x at $t = 0$ to a position x' at a subsequent time t is governed by the quantum mechanical "matrix element," $\langle x'|\exp(-it\hat{H}/\hbar)|x\rangle$, a quantity that depends on the time development operator and on the coordinate labels, x and x'. Finally, we utilize the fact that the thermodynamic properties of a quantum mechanical system maintained at a finite temperature, T, are determined by matrix elements of the type $\langle x'|\exp(-\beta\hat{H})|x\rangle$, where $\beta = 1/(k_B T)$ and where k_B is another fundamental natural constant, Boltzmann's constant.

We note in passing that Newtonian physics is recovered from the above results in the limit that Planck's constant tends to zero. As will be discussed below, we can anticipate that this limit will be rather subtle since it is the *reciprocal* of Planck's constant that appears in the exponential of the time development operator. A large body of previous work (15) indicates that this "semiclassical" regime is an important and interesting one for chemistry and physics.

The above discussion reveals that the temperature and time dependence of a quantum mechanical system are intimately related. The reader will thus perhaps not be too surprised when we state the basic result we require for the present developments, that the complete *time dependence* of a *finite temperature* quantum mechanical system can be deduced from the knowledge of matrix elements of the type $\langle x'|\exp(-\beta_c\hat{H})|x\rangle$. Here the complex temperature has a real (imaginary) part related to the physical temperature (time) in the problem. For completeness, the parameter β_c is defined by

$$[9] \quad \beta_c = \beta/2 + it/\hbar$$

where the factor of two is included in the definition as a matter of convention.

Except for a relatively restricted set of model systems, the requisite quantum mechanical objects described above are not available analytically. Consequently, general equilibrium and dynamical quantum mechanical studies must ultimately make use of numerical methods of some type to produce the required results. The numerical approach adopted depends intimately on the scale of the problem under study. For problems where there are relatively few quantum mechanical variables (e.g., three or less), a number of efficient numerical methods are available. These include direct numerical solutions of the basic partial differential equations of wave mechanics, fast Fourier transform based methods, and approaches based on the exact diagonalization of a suitable matrix representation of the quantum mechanical Hamiltonian. Unfortunately, these more direct methods are of intrinsically limited utility in the treatment of larger scale quantum mechanical problems.

For larger scale applications, we must adopt methods whose inherent difficulty is only weakly related to the dimensionality of the problem. Much recent progress in the formulation of such methods (7, 9, 10) for larger systems is based on the use of Feynman's path integral formulation of quantum mechanics (14). In this approach the necessary quantum mechanical density matrix elements are written in the form of a formal sum over alternative ways for the quantum mechanical system to travel from one point to another. Numerical applications proceed by introducing a labeling procedure to enumerate the various alternatives in this sum, thereby recasting the formal path integral results in a form amenable to practical numerical calculation.

For the case of quantum dynamics, the path integral representation of the relevant matrix element is given symbolically as

$$[10] \quad \langle x'|\exp(-it\hat{H}/\hbar)|x\rangle = \sum_{\text{paths}} \exp\left(\frac{i}{\hbar} S([\text{path}])\right)$$

where the sum is over all possible paths, $x(t)$, that connect the position x at time zero with position x' at the time t. The amplitude for the contribution of each path depends on that particular path through a known function, S. As exploited by Feynman and Hibbs (14), eq. [10] constitutes the gateway between the classical and quantum mechanical worlds. The particular result that makes this connection possible is that the function S that appears in eq. [10] is a *classical mechanical* object. In particular, $S([x(t)])$ turns out to be the classical "action," the time integral along the path $x(t)$ of a known and relatively simple classical mechanical function. In the limit that Planck's constant tends to zero, only those paths in eq. [10] for which the variation in this action vanishes will contribute to the final result. That is, unless the variation in the action vanishes, the contributions of a particular path will be obliterated by neighboring paths, a cancellation induced by the rapid phase oscillations of the complex exponential in eq. [10]. As is well known from classical physics, the requirement that the variation of the action vanish is precisely the condition that the path be a classical trajectory, that is, a solution of eq. [8]. Thus, in the limit that Planck's constant tends to zero, the "stationary phase" character of eq. [10] reduces the summation over *all* paths to a summation over *classical* paths. Moreover, past experience indicates (15) that the contributions from these classical path regions frequently prove dominant in the actual quantum mechanical

problem. In general, for fixed values of x and x', the number of such paths is an increasing function of time.

The path integral formulation of the equilibrium problem is constructed similarly. For this problem, the corresponding matrix element is

$$[11] \quad \langle x'|\exp(-\beta\hat{H})|x\rangle = \sum_{\text{paths}} \exp\left(-\frac{1}{\hbar}\bar{S}([\text{path}])\right)$$

where $\bar{S}$ is also a related and known function of the path. The positive, exponential weight associated with each path from x to x' makes it a relatively simple matter to accumulate the various contributions. As Planck's constant tends to zero, the paths that minimize $\bar{S}$ tend to dominate the result.

Statistical methods have proved of use in equilibrium problems and numerous examples of the application of such formulations have appeared in the literature. The essential result behind such applications is that the importance of a particular path in the equilibrium problem can be considered in isolation, independently from the contribution of its neighbors. The significance of a particular path can be judged by an examination of the exponential weight associated with the path in question. By contrast, however, in the dynamics problem the significance of a particular path tends to be judged only retroactively, through an analysis of its interaction and possible phase cancellation with neighboring paths. This difference prevents the trivial extension of equilibrium statistical methods to the dynamical problem.

With the above discussion as background, we now consider the principal quantum mechanical objects in the present study, the matrix elements $\langle x'|\exp(-\beta_c\hat{H}|x\rangle$. Using a primary result of matrix mechanics (the matrix element of a product of operators is the matrix product of the corresponding elements of the individual operators), we can write an integral representation of our matrix elements as

$$[12] \quad \langle x'|\exp(-\beta_c\hat{H})|x\rangle = \int_{-\infty}^{\infty} dy\, \langle x'|\exp(-it\hat{H}/\hbar)|y\rangle\, \langle y|\exp(-\beta\hat{H}/2)|x\rangle$$

The familiar matrix multiplication formula appears here with a continuous integration rather than the usual discrete summation since the relevant coordinate labels are themselves continuous. This integral is generically similar in form to those considered in Sect. 2 (cf. eq. [1]) and proves useful in the discussion of the properties of the quantum mechanical matrix elements.

Equation [12] is not for the faint of heart! Taken superficially, it suggests that the matrix elements we desire are a continuous superposition of what are individually quite complicated objects. Even in the classical limit, where the matrix elements on the right-hand side are in some sense relatively simple, the outlook is not promising. In particular, it would appear at minimum that the calculation of a particular complex temperature density matrix element for specified value of x' in the classical limit will require us to include the contributions from *all* classical paths of temporal duration t that connect a continuously varying position, y, and our desired position, x'. Since the number of such paths grows with time in a generally unlimited fashion, finding and including the contributions arising from this multiply infinite set of trajectories would appear to be a rather hopeless endeavor.

The principal result of the present work is the suggestion that this rather bleak conclusion may be premature. To see how this may be the case, let us consider the case where the dynamical term in eq. [12] is given by its classical limiting expression (eq. [10] with only classical paths contributing). In this limit, the same stationary phase argument that was used to suggest the classical limit of eq. [10] implies that not all integration regions will contribute to the final result. In particular, the only regions that will contribute strongly to eq. [12] will be those for which the variation in the classical object S with respect to y vanishes. However, from classical physics, the y-variation of S corresponds to the initial momentum of the classical trajectory that begins at the point y and travels to the point x' in a time t. The requirement that the variation of S vanish implies that a particular region will contribute to the final result only if there exists a classical trajectory that begins with zero momentum at that point and travels to the point x' in a time t. The number of such classical trajectories for given values of y, x', and t is typically zero and *rigorously* never more than one. We thus obtain the rather startling suggestion that the matrix elements we require are not hopelessly complicated, but instead have a rather simple structure.

To investigate this suggestion further, we analyze the integral in eq. [12] for suitable model systems by means of a Cornu analysis. The objective will be to see if such an analysis confirms the existence of the underlying structure suggested above. If the presence of such a structure is demonstrated, it may provide a valuable focal point for the organization of the general quantum dynamical problem.

4. Results

As a model system, we consider a specific one-dimensional problem, that of a simple harmonic oscillator perturbed by an interaction term that varies as the fourth power of the oscillator displacement. The quantum mechanical Hamiltonian for the perturbed system can be written as

$$[13] \quad \hat{H} = \frac{p^2}{2} + \frac{x^2}{2} + \lambda x^4$$

where λ is a dimensionless constant. The conventional harmonic oscillator is recovered in the limit that λ is set to zero. We are using units in which the natural unit of energy is the spacing between successive energy levels of the conventional oscillator and the natural unit of distance is the square root of the ratio of Planck's constant to the product of the oscillator mass and unperturbed frequency.

We solve this quantum mechanical problem numerically by means of established matrix techniques. Specifically, we construct a matrix representation of the Hamiltonian operator in eq. [13] using information contained in the problem's unperturbed ($\lambda = 0$) solutions. As the number of such unperturbed solutions included in the treatment tends to infinity, the resulting matrix eigenvalues and vectors yield the exact energy levels and quantum mechanical wavefunctions of the problem. After they were so obtained, the energy levels and wavefunctions for the problem were utilized to construct the various matrix elements appearing in eq. [12] and to perform the associated Cornu decomposition of the final results.

We begin with a simple problem, the case of the simple harmonic oscillator (i.e., $\lambda = 0$). For this situation, all the

Can. J. Chem. Downloaded from www.nrcresearchpress.com by 92.62.229.171 on 09/08/12
For personal use only.

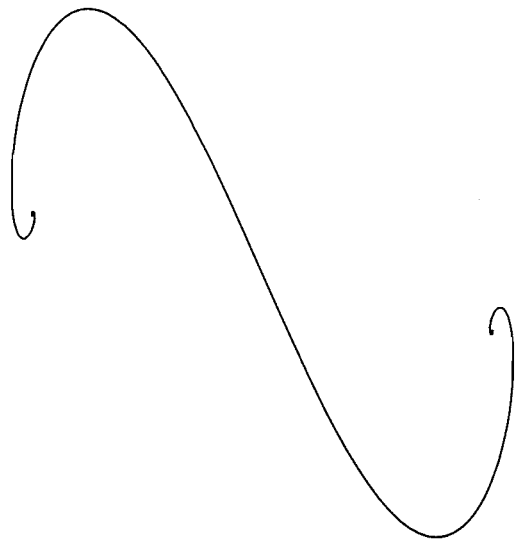

FIG. 6. Cornu analysis (eq. [12]) of the quantum mechanical amplitude $\langle x'|\exp(-\beta_e H)|x\rangle$ for the harmonic oscillator. The result shown corresponds to $x' = x = 0$ and reduced values of β and t of 1 and 0.1, respectively. As expected, the analysis reveals that a single stationary phase point is present. For scale, the numerical value of the matrix element (the complex vector from the left to right-hand ends of the figure) is equal to $0.545 - 0.058$ i.

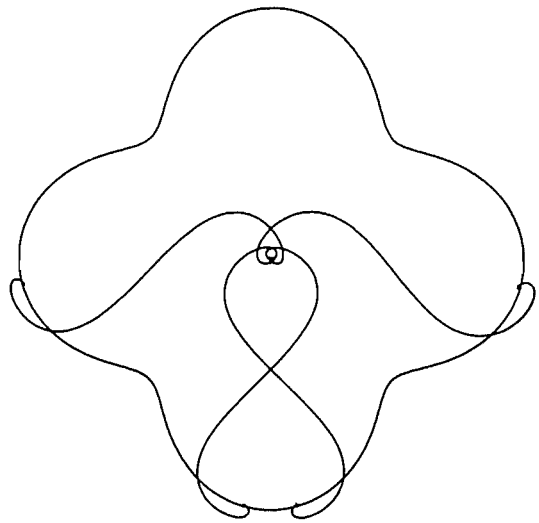

FIG. 7. The quantum mechanical oscillator matrix element of Fig. 6 is plotted in the complex plane parametrically as a function of time over the range $0 < t < 4\pi$. The resulting clover-leaf pattern represents the time-dependent locus of points that is swept out by the moving tip of the Cornu spiral in Fig. 6 as t advances over this interval. Superimposed on the figure are the Cornu spirals (cf. Fig. 6 and eq. [12]) for $t = .01$, $\pi - 0.1$, $\pi + 0.1$, and $2\pi - 0.1$. These results proceed from the $t = 0.1$ result (roughly in the three o'clock position) around the figure in a clockwise order. As expected, behavior corresponding to a single stationary phase point is seen for all times.

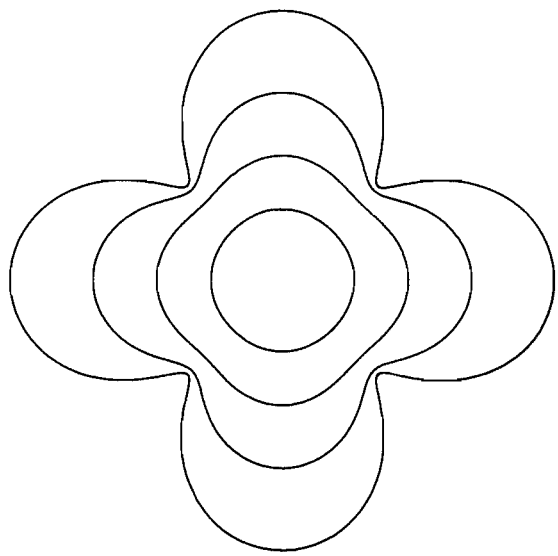

FIG. 8. Parametric time (cf. Fig. 7) plots of the complex temperature matrix elements for the harmonic oscillator described in Fig. 7 for temperatures corresponding to $\beta = 4.0$, 2.0, 1.0, and 0.5. The temperature dependence is monotonic with the outer (inner) curve corresponding to $\beta = 0.5$ (4.0).

necessary quantities are known exactly, and the various numerical pieces can thus be checked against their analytic counterparts. Furthermore, the various matrix elements involved for the oscillator contain a very simple coordinate dependence that leads to a simple, single stationary phase point behavior. Displayed in Fig. 6 is the Cornu analysis of a particular complex temperature density matrix element for the oscillator. As anticipated, the results indicate the presence of a single stationary phase point (cf. Fig. 2). Moreover, the particular results displayed in Fig. 6 agree with the corresponding analytic values.

As the parameter t advances, the spiral in Fig. 6 pivots about, coiling and uncoiling as illustrated in Fig. 7. For the oscillator, the locus of points traced out by the tip of the spiral forms a closed figure (Fig. 7), a figure whose overall physical extension varies with temperature (Fig. 8). The quantum dynamics of the physical system are thus monitored by the dynamics of its associated Cornu clock, which, perhaps cognizant of its role, even runs in a "clockwise" fashion! Although not explicitly of concern here, the precession of this clock reflects the details of the energy levels of the quantum mechanical system.

For a nonzero perturbation, the simple results of Figs. 6–8 are modified. As illustrated in Fig. 9, small perturbations introduce a slight dephasing into the dynamics and the locus of points traced out by the Cornu spiral no longer forms a simple closed curve. Although significant remnants of the original harmonic structure are evident for this case of $\lambda = 0.001$, we also see evidence of a modest precession in the dynamics.

The modifications of the harmonic results become more pronounced as the strength of the perturbation is increased. Relatively little of the original harmonic structure remains as λ is increased to a value of 0.05 (Fig. 10). In addition to the time development of the overall locus of points for the Cornu decompositions of the system, we also display in Fig. 10 specific constructions for various intermediate times. At the relatively short time of 0.1, the result is virtually identical to that of the corresponding harmonic system displayed in Fig. 7, indicating that the results are dominated by single stationary point phase behavior (cf. Figs. 2 and 6). This is consistent with the fact that with a zero initial momen-

Can. J. Chem. Downloaded from www.nrcresearchpress.com by 92.62.229.171 on 09/08/12
For personal use only.

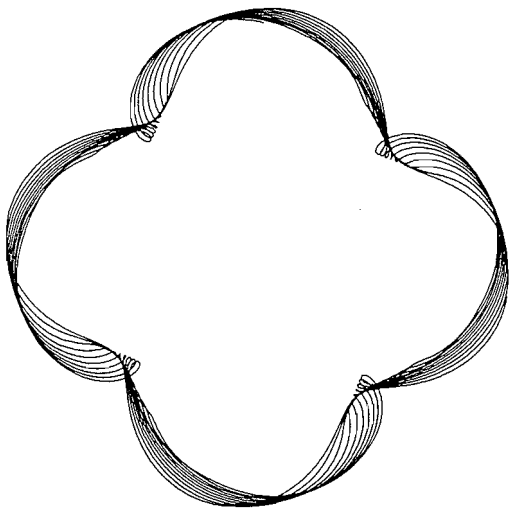

FIG. 9. The efect of a small anharmonic perturbation on the time dependence of the complex temperature density matrix element displayed in Fig. 7. The perturbation ($0.001\ x^4$) introduces a modest dephasing into the problem, as is evidenced by the slight precession evident in the figure. The time here ranges up to $t = 40\pi$.

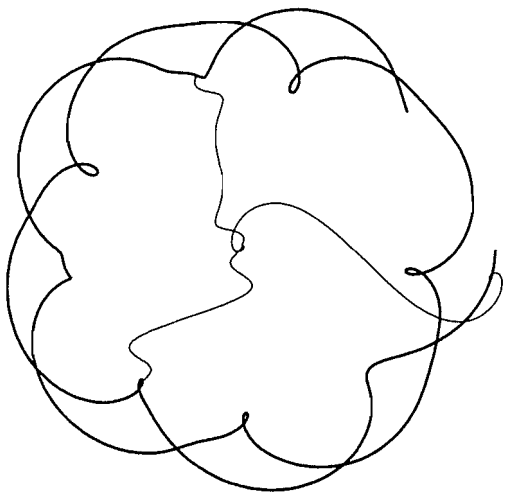

FIG. 10. The effect of a large anharmonic perturbation on the time dependence of the complex temperature density matrix element described in Fig. 7. The outer spiral follows the time dependence of the anharmonic ($\lambda = 0.05$) density matrix element parametrically in the complex plane as a function of t over the range $0 < t < 22$. The outer spiral begins at the three o'clock position at $t = 0$ at the value of $0.544 - 0.059$ i, a value only slightly different from the analogous harmonic result shown in Fig. 6. Superimposed on this figure clockwise from the three o'clock position are three Cornu constructions (eq. [12]) of the matrix element for three values of t (0.1, 4.0, and 20.0). At short times, the Cornu analysis reveals single stationary phase point behavior. At longer times, however, multiple stationary phase points are indicated. As confirmed in Figs. 11 and 12, the location and nature of these stationary phase points are correctly predicted by the analysis of Sect. 4.

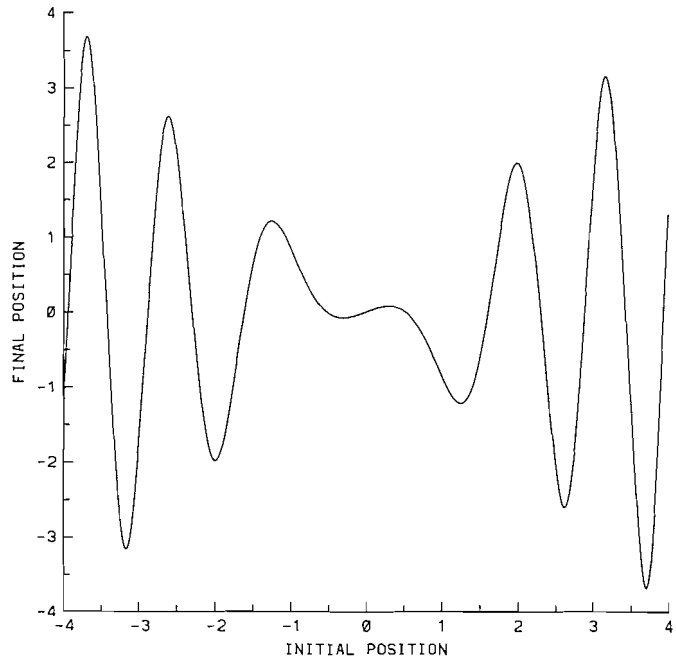

FIG. 11. Shown are the final positions of a classical particle that begins at various initial positions and proceeds forward 20 units of time on the anharmonic potential, $V(x) = x^2/2 + \lambda x^4$, where $\lambda = 0.05$. The initial positions that would lead to a final position of $x' = 0$ are thus the intersections of the curve plotted with a horizontal line at $x' = 0$. For example, the region $-0.3 < x < 0.3$ contains one such solution, the region $-1.2 < x < 1.2$ contains three and so on.

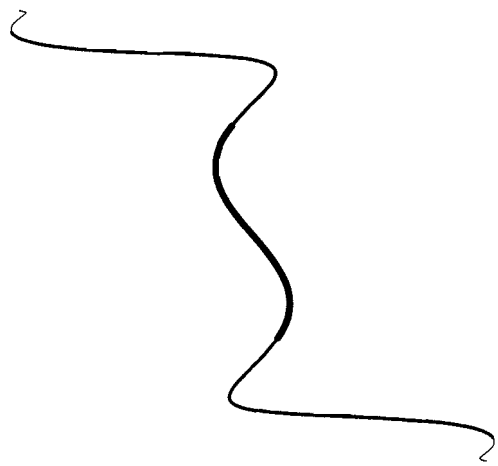

FIG. 12. A decomposition of the Cornu construction of the $t = 20$ result of Fig. 10 (cf. eq. [12]). The darkest portion corresponds to contributions that arise from the region $(-0.3,0.3)$, the next darkest portion from the region $(-1.2,1.2)$, and so on. This result combined with Fig. 11 confirms that the matrix element in question is dominated by the zero momentum stationary phase regions described in Sect. 4.

tum, the only particles that can reach the desired final position ($x' = 0$) in such a brief period are those that start at the origin. At longer times zero momentum trajectories can reach the origin from a variety of other positions, as illustrated in Fig. 11. However, from eq. [12] we see that each of the contributions from the various starting positions will be weighted by its associated equilibrium factor. Thus positions that are thermally inaccessible will effectively be eliminated from the problem. This important fact means that

Can. J. Chem. Downloaded from www.nrcresearchpress.com by 92.62.229.171 on 09/08/12
For personal use only.

the number of stationary phase regions contributing to the final result will ultimately saturate with time. The Cornu decomposition at $t = 20$ displayed in Fig. 12 exhibits multiple stationary phase character. As indicated in the figure, a careful analysis of the various contributions to the result reveals that the stationary phase regions involved are precisely the ones that would be predicted by the zero momentum classical analysis shown in Fig. 11. Although not explicitly shown here, a similar conclusion also holds for the $t = 4.0$ result shown in Fig. 10. Figure 12 is this a visual confirmation of the underlying structure in the quantum mechanical objects of interest.

5. Summary/Conclusions

The present work has considered a variety of topics of relevance in the development of quantum dynamical algorithms. Using a combination of numerical and graphical techniques, we have examined the principal computational objects of interest for a series of model problems. This analysis has revealed the presence of a significant underlying structure in the dynamical problem, a structure that we feel is rather general and that likely extends well beyond the particular model problems considered here. The significance of this structure is twofold. First, it demonstrates that the general quantum dynamical problem may be appreciably simpler than has previously been feared. Second, it provides a specific identification of the dominant contributions in the dynamical problem. In the spirit of Hamming's maximum (16) cited at the outset, we are hopeful that the insight gained in the present study will prove valuable in the ongoing efforts directed at the development of general, statistically based dynamical algorithms.

Acknowledgements

J.D.D. and S.W.R. would like to thank Brown University and the Department of Chemistry for its generous support of the present work. D.L.F. acknowledges the donors of the Petroleum Research Fund of the American Chemical Society for partial support of this work. The author would like to thank Dr. D. Lynch for valuable discussions concerning the present work. The present work is related to material submitted to the 1990 IBM Supercomputing Competition.

1. S. Ulam. Adventures of a mathematician. Scribners, New York. 1976.
2. W. W. Wood and J. D. Jacobson. J. Chem. Phys. **27**, 1207 (1957).
3. B. J. Alder and T. E. Wainwright. J. Chem. Phys. **27**, 1208 (1957).
4. B. J. Alder and T. E. Wainwright. Phys. Rev. Lett. **18**, 988 (1967); J. Phys. Soc. Jpn. Suppl. **26**, 267 (1968); Phys. Rev. A, **1**, 18 (1970).
5. M. Kalos and P. A. Whitlock. Monte Carlo methods. Wiley, New York. 1986.
6. B. J. Berne, (*Editor*). Statistical mechanics. Vol. 6. Plenum Press, New York. 1977.
7. B. J. Berne and D. Thirumalai. Annu. Rev. Phys. Chem. **37**, 401 (1986).
8. J. D. Doll and J. E. Gubernatis (*Editors*). Quantum simulations of condensed matter phenomena. World Scientific, New York, 1990.
9. J. D. Doll, D. L. Freeman, and T. L. Beck. Adv. Chem. Phys. **78**, 61 (1990).
10. N. Makri. Chem. Phys. Lett. **159**, 489 (1989), and refs. therein.
11. M. Born and E. Wolf. Principles of optics. 5th ed. Pergamon Press, New York. 1975. pp. 431–435.
12. A. Cornu. Phys. **3**, 5 (1874); **3**, 44 (1874).
13. G. F. Carrier, M. Krook, and C. E. Pearson. Functions of a complex variable. McGraw–Hill, New York. pp. 272–275.
14. R. P. Feynman and A. R. Hibbs. Quantum mechanics and path integrals. McGraw–Hill, New York. 1965.
15. W. M. Miller. Science, **233**, 171 (1986).
16. R. W. Hamming. Numerical methods for scientists and engineers. Dover, New York. 1986.

Can. J. Chem. Downloaded from www.nrcresearchpress.com by 92.62.229.171 on 09/08/12
For personal use only.

An investigation of atomic structure in position and momentum space by means of "ideal shells"

HARTMUT SCHMIDER, ROBIN P. SAGAR, AND VEDENE H. SMITH, JR.[1]
Department of Chemistry, Queen's University, Kingston, Ont., Canada K7L 3N6

Received September 3, 1991

This paper is dedicated to Professor Sigeru Huzinaga on the occasion of his 65th birthday

HARTMUT SCHMIDER, ROBIN P. SAGAR, and VEDENE H. SMITH, JR. Can. J. Chem. **70**, 506 (1992).

For atomic systems, the boundaries in position and momentum space that enclose the exact electron number given by the aufbau principle have been numerically calculated. Their relatively irregular behavior as a function of the atomic number Z is demonstrated and explained in terms of corresponding irregularities of the aufbau principle. Direct comparisons of these radii with those derived from density functionals that are known to exhibit atomic shell structure are shown to be useful in judging the ability of the latter to define "physical" shells compatible with the aufbau principle.

Key words: atomic radii, shell structure, aufbau principle, charge density, momentum density.

HARTMUT SCHMIDER, ROBIN P. SAGAR et VEDENE H. SMITH, JR. Can. J. Chem. **70**, 506 (1992).

Pour des systèmes atomiques, on a calculé les limites de la position et du moment spatial qui délimitent le nombre électronique exact données par le principe d'aufbau. On démontre que leur comportement en fonction du nombre atomique Z est relativement irrégulier et on l'explique en fonction des irrégularités correspondantes du principe d'aufbau. On montre qu'une comparaison directe de ces rayons avec ceux que l'on peut obtenir à partir de densités fonctionnelles connues pour présenter une structure de la couche atomique est utile pour juger de l'habilité de cette dernière à définir les couches «physiques» compatibles avec le principe d'aufbau.

Mots clés : rayons atomiques, structure de la couche, principe d'aufbau, densité de charge, densité de vitesse acquise.

[Traduit par la rédaction]

Can. J. Chem. Downloaded from www.nrcresearchpress.com by 92.62.229.171 on 09/08/12
For personal use only.

Introduction

In recent years, there have been several investigations into the ability of various functionals of the position density (1–9) $\rho(r)$ and the momentum (10–12) density $\Pi(p)$ of atomic systems to represent the atomic shell structure as suggested by the aufbau principle of the periodic table. That this structural feature could be exhibited by the charge or momentum densities themselves is excluded by the finding that the former is a monotonically decaying function (2, 13–15) of r, whereas the latter shows a maximum at $p > 0$ (10, 16–18) for some atomic systems. It has been shown that some of the above-mentioned functionals show a relatively large number of critical radii (roots and extrema) that can be meaningfully assigned to particular shell contributions.

On the other hand, the ability of these radii to define physical regions corresponding to an atomic shell with the "correct" number of electrons is much less pronounced. Partitioning schemes analogous to the so-called Politzer–Parr partitioning (19) show somewhat limited success for some (19, 20) and practically none for other (21) functionals.

Though most of these critical-point analyses fail to exhibit all shells for all atoms, the behavior of the resulting radii as a function of the atomic number Z shows remarkable regularities in many cases. For $D(r) = 4\pi r^2\rho(r)$ and $\nabla^2\rho(r)$ as quantities defined in position space, the inverse of the critical radii is proportional to Z (2, 4, 5) according to Bohr theory, whereas the corresponding radii p (or k) in the momentum (or reciprocal) space quantities $I(p) = 4\pi p^2\Pi(p)$, $\nabla^2\Pi(p)$, and $\nabla^2F(k)$ show direct linear behavior as a function of the atomic number (9, 11, 12).

One of the goals of this paper is to investigate if this kind of simple regular behavior is compatible with the notion of a given number of electrons in fixed shells as suggested by the aufbau principle of the periodic table. For this, "ideal-shell" radii have to be calculated.

[1]Author to whom correspondence may be addressed.

"Ideal-shell" radii for the neutral atoms

To judge if a given partitioning scheme, based for example on the critical radii of a density functional, is suitable for the definition of shell boundaries that comply with the aufbau principle, one has to check if the integral

$$[1a] \quad N_n = 4\pi \int_{r_{n-1}}^{r_n} \rho(r) r^2 dr$$

yields approximately the number of electrons, N_n^{HF}, that occupy orbitals with the corresponding principal quantum number n in the Hartree–Fock description of the atom. In eq. [1*a*] r_n denotes the radius that has been assigned to the boundary between the nth and the $(n + 1)$st shell, with $r_0 = 0$ by definition. The analogous expression in a momentum space description of the system is

$$[1b] \quad N_n = 4\pi \int_{p_n}^{p_{n-1}} \Pi(p) p^2 dp$$

Note that in position space $r_n > r_{n-1}$, whereas in momentum space $p_n < p_{n-1}$, since the K shell (i.e., $n = 1$) is the innermost shell in position, but the most diffuse one in momentum space. Analogously, high principal quantum numbers correspond to electrons that are far from the nucleus but relatively slow. Note that $p_0 = \infty$ by definition.

The extent to which these "shell occupations" agree with the expected values gives a measure of how strongly the corresponding region of space is dominated by a particular shell. To construct radii that fulfill the above condition *perfectly*, one has to solve the integral equations

$$[2] \quad N_n^{HF} = N_n$$

in position and momentum space for r_n and p_{n-1}, respectively. Note that in this labeling scheme $r_{n_{max}}$ and p_0 lie at infinity in the corresponding space, n_{max} denoting the maximum principal quantum number of the atom. The equations have to be solved recursively by starting at $r_0 = 0$ in position and at $p_{n_{max}} = 0$ in momentum space, respectively.

This can be done with small computational expense by a Newton algorithm, noting that the first derivatives of the integrals on the right-hand side of eq. [2] with respect to r and p are just the integrands, i.e., the radial position and momentum densities $D(r)$ and $I(p)$. The resulting iterative equations are

$$[3a] \quad r_n^{(i+1)} = r_n^{(i)} - \frac{\int_{r_{n-1}}^{r_n^{(i)}} D(r)\mathrm{d}r - N_n^{HF}}{D(r_n^{(i)})}$$

and

$$[3b] \quad p_{n-1}^{(i+1)} = p_{n-1}^{(i)} - \frac{\int_{p_n}^{p_{n-1}^{(i)}} I(p)\mathrm{d}r - N_n^{HF}}{I(p_{n-1}^{(i)})}$$

Here the superscript (i) denotes the result of the ith iteration. With a reasonable initial guess (e.g., from a binary search), these equations show quadratic convergence.

It is interesting to note that constraints similar to the ones in eq. [2] have been employed in density functional schemes where the density was represented by piecewise-exponentially decaying functions (22). The resulting values of r_n naturally deviate from the ones obtained here, since the underlying functions are of entirely different origin. As we will see later, the differences are not extreme.

Values of ideal-shell radii obtained from eqs. [3*a*] and [3*b*] can be used as a reference to judge how closely a given set of radii produces shells corresponding to the aufbau principle, from which they were derived. They have, however, no direct counterpart in any of the above-mentioned density functionals, but are a quite arbitrary partitioning scheme based on the (uncorrelated) orbital description in the framework of the independent-particle model. The assumption is made that the electrons of an atomic shell are confined exclusively to a well-defined region of space, whereas in reality each shell extends over all space. Note that it is only in the independent-particle model that the notion of atomic shells has any clear-cut meaning. As we will see in the following, it is also the aufbau principle that is responsible for the relatively spiky behavior of the "ideal" shells of the ground state atoms in the Hartree–Fock picture.

Results and discussion

Since most of the calculations on atomic shell structure and its expression in topographical features of density functionals have been based on the nonrelativistic Hartree–Fock calculations of Clementi and Roetti (23) and McLean and McLean (24), we have computed the ideal-shell radii for the neutral atoms ($3 \leq Z \leq 92$) in their ground states from the corresponding densities. Note that the Hartree–Fock ground state configurations were used, which do not in all cases coincide with the experimental ones. The necessary numerical integrations have been performed using a 50-point Fejér-quadrature and were checked with a 100-point quadrature of the same kind. The above algorithm was employed until a given accuracy of the resulting electron numbers was reached (10^{-10}). The starting values were chosen by a binary search with a small step size (0.02). Since the wave functions are given with an accuracy of five significant figures, and the algorithm works from the origin outwards, the number of electrons in the outermost shell (in the respective space) deviates somewhat from the expected integer value, i.e., the limited accuracy of normalization is entirely concentrated on these shells.

Tables 1 and 2 give the radii for the atoms with $3 \leq Z \leq 92$ in position and momentum space, respectively. The general trend of an inverse behavior in position space and a linear behavior in momentum space with respect to the atomic number Z is already visible from these values.

This trend can also be seen in Figs. 1 and 2, where the inverse radii r_n^{-1} (position space) and the radii p_n (momentum space) are plotted against the atomic number. The points have been connected to avoid confusion. As can be seen from Figs. 1*b* and 2*b* this general trend is frequently interrupted by spikes and jumps. For the boundaries between higher shells (M/N upwards), this becomes so prevalent that it is difficult to speak of a linear behavior at all. The linearity holds obviously only "piecewise." Note also that the figures for position and momentum space bear an amazing similarity.

This kind of behavior is rooted in the nature of the aufbau principle itself. As an example, consider the sudden jump in the radius r_5 corresponding to the O/P boundary after $Z = 79$ (gold). Up to $Z = 78$ (platinum), the 5*d* subshell has been gradually filled, whereas the P shell consists of a doubly occupied 6*s*. For Pt, however, the configuration $(Xe)5d^{10}6s^0$ becomes energetically favorable, and the corresponding ideal-shell boundary vanishes altogether. This phenomena occurs also for element 46 (palladium). With the following elements the P shell ($n = 6$) gets gradually filled and the shell boundary returns, but moves inward much faster. The reason for this is clear: the contractive effect of the growing nuclear charge is no longer counterbalanced by the increasing electron numbers in the O shell, since all "new" electrons are now filled into the outer, the P shell. The stronger movement of the radii inward results in a larger slope of the corresponding r^{-1}–Z plot.

As for the spikes, they may be explained on a similar basis of the filling of subshells. We take the example of $Z = 43$ (technetium). The (smaller) slope before this element corresponds to the filling of the 4*d* subshell. With Mo, this is half filled and the 43rd electron goes rather into the 5*s* orbital, which was only half occupied in the few preceding elements. Ru, however, shows again a singly occupied 5*s* and goes on with the population of 4*d* orbitals. The filling of the higher, rather than the lower, shell of a given boundary always has the effect of moving the shell boundary inward faster, which leads to higher slopes in the graphs or, in case only one element is affected, to spikes. The opposite scheme of filling inner shells may counterbalance the contractive increase in Z so strongly that the shell boundary moves outward, rather than inward. This leads to negative slopes in the graphs. Analogous, although less pictorial, arguments can be made in momentum space.

With the exception of the K/L and the L/M boundaries, which are naturally not much affected by irregularities in the

Can. J. Chem. Downloaded from www.nrcresearchpress.com by 92.62.229.171 on 09/08/12
For personal use only.

TABLE 1. Radii r_i in position space of boundaries between atomic shells that contain the exact number of electrons as given by the aufbau principle. The numbering of r corresponds to $r_0 = 0$ and the last shell extends to infinity.

	r_1	r_2	r_3	r_4	r_5	r_6
3	1.53206					
4	0.98522					
5	0.70192					
6	0.53714					
7	0.43189					
8	0.36027					
9	0.30775					
10	0.26781					
11	0.23684	2.12677				
12	0.21221	1.62852				
13	0.19214	1.35391				
14	0.17545	1.15658				
15	0.16134	1.00710				
16	0.14927	0.89100				
17	0.13882	0.79758				
18	0.12969	0.72084				
19	0.12166	0.65779	3.05934			
20	0.11456	0.60499	2.44774			
21	0.10832	0.55804	2.46515			
22	0.10275	0.51650	2.40024			
23	0.09773	0.47992	2.32838			
24	0.09323	0.44757	2.80248			
25	0.08904	0.41903	2.18359			
26	0.08525	0.39379	2.13231			
27	0.08177	0.37113	2.07772			
28	0.07857	0.35077	2.02427			
29	0.07564	0.33246	2.45480			
30	0.07287	0.31571	1.92317			
31	0.07028	0.30051	1.65946			
32	0.06786	0.28668	1.47114			
33	0.06559	0.27408	1.32687			
34	0.06347	0.26255	1.21201			
35	0.06147	0.25189	1.11791			
36	0.05958	0.24206	1.03806			
37	0.05781	0.23289	0.96961	3.45588		
38	0.05613	0.22444	0.91105	2.83290		
39	0.05456	0.21656	0.86045	2.94347		
40	0.05307	0.20916	0.81589	3.58384		
41	0.05166	0.20225	0.77487	3.41137		
42	0.05032	0.19575	0.73746	3.25372		
43	0.04905	0.18966	0.70307	2.64587		
44	0.04785	0.18390	0.67210	3.07804		
45	0.04670	0.17845	0.64321	2.98812		
46	0.04560	0.17331	0.61672			
47	0.04455	0.16845	0.59177	2.83635		
48	0.04355	0.16376	0.56929	2.32541		
49	0.04259	0.15949	0.54746	2.06212		
50	0.04167	0.15533	0.52765	1.86656		
51	0.04078	0.15139	0.50924	1.71291		
52	0.03994	0.14763	0.49205	1.58821		
53	0.03912	0.14406	0.47594	1.48311		
54	0.03834	0.14064	0.46088	1.39322		
55	0.03758	0.13739	0.44670	1.31501	4.01264	
56	0.03686	0.13427	0.43338	1.24671	3.34168	
57	0.03616	0.13129	0.42082	1.18772	3.42410	
58	0.03550	0.12859	0.40801	1.24720	3.22125	
59	0.03486	0.12594	0.39614	1.24023	3.16942	
60	0.03424	0.12340	0.38486	1.23185	3.12115	
61	0.03364	0.12096	0.37409	1.22244	3.07520	
62	0.03307	0.11862	0.36381	1.21177	3.03267	
63	0.03251	0.11637	0.35403	1.20020	2.99296	
64	0.03197	0.11415	0.34486	1.13794	3.10648	
65	0.03145	0.11211	0.33585	1.18105	2.91307	
66	0.03095	0.11010	0.32736	1.17050	2.87670	
67	0.03046	0.10816	0.31923	1.15981	2.84270	

Can. J. Chem. Downloaded from www.nrcresearchpress.com by 92.62.229.171 on 09/08/12
For personal use only.

TABLE 1. (*concluded*)

	r_1	r_2	r_3	r_4	r_5	r_6
68	0.02998	0.10629	0.31149	1.14941	2.80889	
69	0.02952	0.10448	0.30408	1.13888	2.77652	
70	0.02908	0.10274	0.29699	1.12804	2.74613	
71	0.02865	0.10102	0.29021	1.07131	2.93372	
72	0.02822	0.09935	0.28374	1.02188	2.93337	
73	0.02781	0.09773	0.27755	0.97781	2.89039	
74	0.02742	0.09615	0.27162	0.93812	2.83311	
75	0.02703	0.09462	0.26593	0.90203	2.76766	
76	0.02665	0.09314	0.26047	0.86890	2.72003	
77	0.02629	0.09169	0.25523	0.83841	2.66536	
78	0.02593	0.09029	0.25020	0.81126		
79	0.02559	0.08893	0.24534	0.78430	3.00065	
80	0.02525	0.08760	0.24068	0.75923	2.50363	
81	0.02492	0.08632	0.23618	0.73593	2.25089	
82	0.02460	0.08507	0.23184	0.71414	2.06006	
83	0.02428	0.08385	0.22767	0.69374	1.90912	
84	0.02398	0.08266	0.22363	0.67448	1.78606	
85	0.02368	0.08151	0.21974	0.65643	1.68238	
86	0.02339	0.08039	0.21597	0.63932	1.59236	
87	0.02310	0.07929	0.21233	0.62320	1.51468	4.30108
88	0.02282	0.07823	0.20881	0.60793	1.44606	3.61777
89	0.02255	0.07719	0.20540	0.59347	1.38657	3.71918
90	0.02229	0.07619	0.20205	0.57972	1.39934	3.62782
91	0.02203	0.07522	0.19880	0.56675	1.46628	3.42743
92	0.02178	0.07427	0.19567	0.55421	1.46057	3.37407

TABLE 2. Radii p_i in momentum space of boundaries between atomic shells that contain the exact number of electrons as given by the aufbau principle. The numbering of p corresponds to the innermost shell (K) extending to infinity, i.e., p_1 is the K/L boundary and the highest occupied shell starts at $p_{n_{max}} = 0$

	p_1	p_2	p_3	p_4	p_5	p_6
3	0.61095					
4	1.02737					
5	1.68164					
6	2.32060					
7	2.96399					
8	3.60474					
9	4.26459					
10	4.93938					
11	5.63725	0.53456				
12	6.34274	0.76708				
13	7.05210	1.03697				
14	7.76704	1.30349				
15	8.48786	1.56650				
16	9.21428	1.82130				
17	9.94737	2.08146				
18	10.68527	2.34431				
19	11.42690	2.61786	0.40178			
20	12.17348	2.89374	0.55840			
21	12.90562	3.22069	0.59055			
22	13.63487	3.56679	0.62090			
23	14.36330	3.91961	0.64952			
24	15.08126	4.27848	0.55834			
25	15.81710	4.63805	0.70363			
26	16.54551	4.99601	0.72973			
27	17.27321	5.35838	0.75517			
28	18.00164	5.72379	0.78007			
29	18.71720	6.08561	0.64642			
30	19.45722	6.46329	0.82668			
31	20.19560	6.83939	1.02609			
32	20.94134	7.21382	1.21696			
33	21.69273	7.58894	1.39716			
34	22.44540	7.96361	1.56409			

Can. J. Chem. Downloaded from www.nrcresearchpress.com by 92.62.229.171 on 09/08/12
For personal use only.

TABLE 2. (*concluded*)

	p_1	p_2	p_3	p_4	p_5	p_6
35	23.20383	8.33958	1.73282			
36	23.96271	8.71582	1.90084			
37	24.72149	9.08871	2.07155	0.36575		
38	25.48668	9.46804	2.24239	0.49732		
39	26.24951	9.84975	2.41680	0.52617		
40	27.00545	0.23418	2.59666	0.46523		
41	27.76832	0.62023	2.78052	0.48902		
42	28.53125	11.00825	2.96711	0.59061		
43	29.29566	11.39918	3.15946	0.62047		
44	30.03763	11.79191	3.34373	0.53562		
45	30.82164	12.18581	3.53373	0.54572		
46	31.58103	12.58357	3.71855			
47	32.34884	12.98343	3.91509	0.56528		
48	33.12596	13.36491	2.12217	0.71425		
49	33.89311	13.78472	4.31308	0.86920		
50	34.65986	14.18576	4.51022	1.01281		
51	35.43727	14.58865	4.70785	1.14637		
52	36.21298	14.99186	4.90552	1.26845		
53	36.99206	15.39593	5.10321	1.38994		
54	37.76937	15.80036	5.30222	1.51152		
55	38.55158	16.20838	5.50231	1.63547	0.32166	
56	39.33242	16.61470	5.70206	1.75563	0.43316	
57	40.11180	17.02261	5.90240	1.87839	0.45733	
58	40.87866	17.39958	6.17691	1.81570	0.44698	
59	41.64915	17.78960	6.42251	1.84759	0.45294	
60	42.42080	18.18070	6.67129	1.87934	0.45876	
61	43.19287	18.57063	6.92135	1.91025	0.46417	
62	43.96418	18.95966	7.17363	1.94101	0.46954	
63	44.73526	19.34879	7.42832	1.97157	0.47440	
64	45.51264	19.75217	7.67135	2.10048	0.49629	
65	46.27770	20.12889	7.93343	2.02947	0.48529	
66	47.04959	20.51875	8.18842	2.05847	0.49046	
67	47.81461	20.90855	8.44396	2.08776	0.49601	
68	48.58583	21.29818	8.70040	2.11585	0.50099	
69	49.35665	21.68767	8.95797	2.14375	0.50576	
70	50.12739	22.07713	9.21692	2.17180	0.51038	
71	50.90513	22.47823	9.47551	2.30102	0.53159	
72	51.68300	22.88210	9.73297	2.43331	0.55320	
73	52.46120	23.28722	9.98930	2.56532	0.57139	
74	53.24019	23.69484	10.24467	2.69913	0.58961	
75	54.01976	24.10425	10.49938	2.83367	0.60655	
76	54.80039	24.51491	10.75389	2.96556	0.62258	
77	55.58076	24.92709	11.00785	3.09824	0.63799	
78	56.35721	25.34219	11.25996	3.22345		
79	57.14044	25.75764	11.51388	3.36019	0.54597	
80	57.92451	26.17358	11.76819	3.49777	0.68170	
81	58.70920	26.59049	12.02261	3.63408	0.81709	
82	59.49519	27.00822	12.27787	2.76994	0.94155	
83	60.28155	27.42701	12.53411	3.90566	1.05637	
84	61.06845	27.84610	12.78814	4.03984	1.15940	
85	61.85615	28.26591	13.04457	4.17513	1.26103	
86	62.64567	28.68727	13.30083	4.31046	1.36229	
87	63.43689	29.10845	13.55648	4.44550	1.46276	0.30344
88	64.22673	29.53066	13.81237	4.58112	1.56106	0.40554
89	65.01615	29.95400	14.06877	4.71759	1.65991	0.42695
90	65.80301	30.37344	14.32525	4.85680	1.68129	0.43370
91	66.58605	30.78738	14.59040	5.00444	1.62971	0.42690
92	67.37215	31.20570	14.85300	5.15046	1.65567	0.43236

aufbau principle, these effects lead to a relatively poor description of the r_n^{-1}/Z (p_i/Z) relation by a linear least-squares fit. Resulting slopes and y intercepts, together with R^2 coefficients, are collected in Tables 3 and 4 to underline this point. The comparison of the correlation coefficients with those in the corresponding fits for radii derived from density functionals (2, 4, 6, 9) makes it quite clear that one side effect of the general deviation of the latter from the "correct" shell-occupation numbers is a much smoother behavior as a function of Z. The ideal (inverse) linearity of the radii in Z would not be compatible with the aufbau principle.

It is finally interesting to compare our results with the ones obtained for the r_n by Wang (22) in his density functional calculations that employ eq. [2] as a constraint for the first-row atoms. Table 5 contains a compilation of his results and ours. Taking into account the entirely different premises, the

Can. J. Chem. Downloaded from www.nrcresearchpress.com by 92.62.229.171 on 09/08/12
For personal use only.

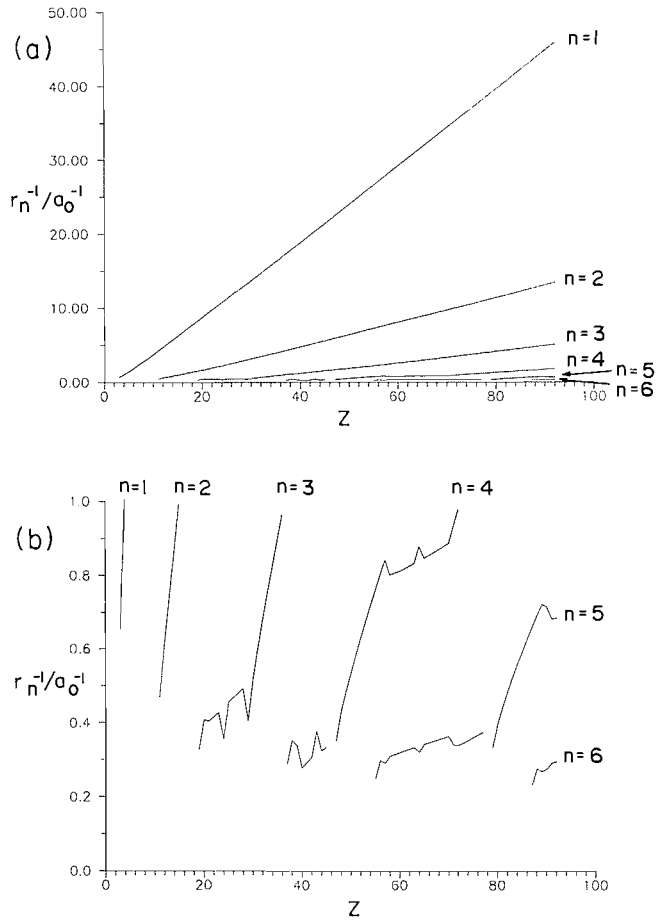

FIG. 1. (*a*) Inverse of the radii r_n in position space of boundaries between atomic shells that contain the exact number of electrons as given by the aufbau principle as a function of the atomic number Z. The numbering is the same as in Table 1. The r^{-1} range is chosen to depict the values for all elements with $3 \leq Z \leq 92$. (*b*) Inverse of the radii r_n in position space as in Fig. 1*a*. A subrange of r^{-1} was chosen to make details in the valence shells visible.

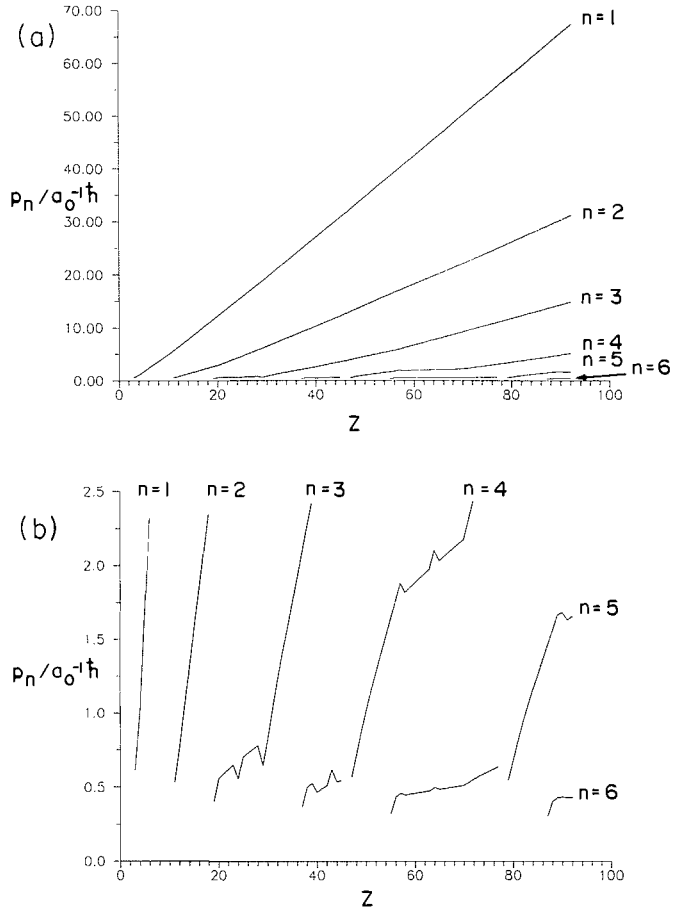

FIG. 2. (*a*) Radii p_n in momentum space of boundaries between atomic shells that contain the exact number of electrons as given by the aufbau principle as a function of the atomic number Z. The numbering is the same as in Table 2. The p range is chosen to depict the values for all elements with $3 \leq Z \leq 92$. (*b*) Radii p_n in momentum space as in Fig. 2*a*. A subrange of p was chosen to make details in the valence shells visible.

values are surprisingly similar. Calculations analogous to Wang's with radii fixed to the HF values would perhaps yield reasonable results. How far the values of r enclosing fixed electron numbers coincide with areas of approximately piecewise-exponential decay would have to be investigated by studying the logarithm of ρ or connected density functionals.

Conclusions

Since any atomic partitioning scheme based on functionals of the position or momentum density has to be judged on its ability to reproduce the aufbau principle in terms of the number of electrons enclosed by its shell regions, we have in this study computed the radii, for which this criterion is met exactly. We have done this for the neutral atoms in their ground states with $3 \leq Z \leq 92$, employing HF–SCF wavefunctions (23, 24).

These values should serve as a quick reference as to the extent with which a certain partitioning scheme is compatible with the underlying aufbau principle. They may as well be used to define radii of "inner parts" of atoms, e.g., core regions, if one wishes to represent these by "hard spheres" based solely on the density normalization. Their "spiky" behavior as a function of the atomic number Z shows their sensitivity towards irregularities in the filling of shells in the periodic table. They provide a quite pictorial map of these "ups and downs." This is not surprising, since the radii have been calculated with the *ad hoc* knowledge of the electron configuration.

From these relatively strong deviations from an (inverse) linear behavior of the resulting radii in Z, it can be inferred

TABLE 3. Radii $r_n(a_0)$ in position space of boundaries between atomic shells that contain the exact number of electrons as given by the aufbau principle. Slopes, y intercepts, and squares of correlation coefficients for a linear least-squares fit of r_n^{-1} as a function of Z (see Fig. 1)

n	Slope (a_0^{-1})	y-intercept (a_0^{-1})	R^2	Number of points
1	0.51313	−1.5233	0.99987	90
2	0.16270	−1.3075	0.99944	82
3	0.06925	−1.1705	0.99071	74
4	0.02676	−0.6477	0.96043	55
5	0.01139	−0.3169	0.79048	37
6	0.01064	−0.5719	0.76945	6

Can. J. Chem. Downloaded from www.nrcresearchpress.com by 92.62.229.171 on 09/08/12
For personal use only.

TABLE 4. Radii $p_n(\hbar a_0^{-1})$ in momentum space of boundaries between atomic shells that contain the exact number of electrons as given by the aufbau principle. Slopes, y intercepts, and squares of correlation coefficients for a linear least-squares fit of p_n as a function of Z (see Fig. 2)

n	Slope ($\hbar a_0^{-1}$)	y-intercept ($\hbar a_0^{-1}$)	R^2	Number of points
1	0.75890	−2.9751	0.99970	90
2	0.38692	−4.1330	0.99869	82
3	0.20996	−4.5049	0.98103	74
4	0.08352	−2.6239	0.95750	55
5	0.03449	−1.4696	0.78372	37
6	0.02044	−1.2202	0.56911	6

TABLE 5. Radii $r_n(a_0)$ in position space of boundaries between atomic shells that contain the exact number of electrons as given by the aufbau principle. Comparison of the Hartree–Fock values (23, 24) with values obtained from a density functional calculation by Wang[a]

	This work		Wang	
	$r_1(a_0)$	$r_2(a_0)$	$r_1(a_0)$	$r_2(a_0)$
Li	1.532		1.341	
Be	0.985		0.844	
C	0.537		0.489	
O	0.360		0.346	
Ne	0.268		0.268	
Na	0.237	2.127	0.236	2.376
Mg	0.212	1.629	0.212	1.717
Si	0.176	1.157	0.175	1.146
S	0.149	0.891	0.149	0.871
Ar	0.130	0.721	0.128	0.686

[a]See ref. 22; the values are the ones obtained using the Thomas–Fermi–Dirac–$\frac{1}{9}$–Singular–Weizsäcker model (FTFD$\frac{1}{9}$SW).

that such a behavior is of quite limited compatibility with the aufbau principle, which is inherently somewhat irregular. The fact that this behavior is nevertheless followed by many partitioning radii based on density functionals, can be assigned to a tendency of these functionals to "wash out details" of the latter.

Earlier results of Wang (22), employing fixed-electron number constraints in a piecewise exponential description of the atomic charge density, seem not too different from the ones in the paper, given the different nature of the underlying densities.

Acknowledgments

This research was supported by NSERCC (Natural Sciences and Engineering Research Council of Canada). H.S. thanks the School of Graduate Studies and Research of Queen's University for an R.S. McLaughlin Fellowship.

1. R. J. Boyd. J. Phys. B: At. Mol. Phys. **9**, L69 (1976).
2. A. M. Simas, R. P. Sagar, A. C. T. Ku, and V. H. Smith, Jr. Can J. Chem. **66**, 1923 (1988).
3. R. F. W. Bader. Atoms and molecules: a quantum theory. Oxford University, Oxford. 1990, and references therein.
4. R. P. Sagar, A. C. T. Ku, V. H. Smith, Jr., and A. M. Simas. J. Chem. Phys. **88**, 4367 (1988).
5. Z. Shi and R. J. Boyd. J. Chem. Phys. **88**, 4375 (1988).
6. R. P. Sagar, A. C. T. Ku, V. H. Smith, Jr., and A. M. Simas. Can. J. Chem. **66**, 1005 (1988).
7. A. D. Becke and K. E. Edgecombe. J. Chem. Phys. **92**, 5397 (1990).
8. M. Kohout, A. Savin, and H. Preuss. J. Chem. Phys. **95**, 1928 (1991).
9. H. Schmider, R. P. Sagar, and V. H. Smith, Jr. J. Chem. Phys. **94**, 4346 (1991).
10. S. R. Gadre, S. Chakravorty, and R. K. Pathak. J. Chem. Phys. **78**, 4581 (1983).
11. A. M. Simas, W. M. Westgate, and V. H. Smith, Jr. J. Chem. Phys. **80**, 2636 (1984).
12. R. P. Sagar, A. C. T. Ku, V. H. Smith, Jr., and A. M. Simas. J. Chem. Phys. **90**, 6520 (1989).
13. H. Weinstein, P. Politzer, and S. Srebenik. Theor. Chim. Acta, **38**, 159 (1975).
14. G. Sperber. Int. J. Quantum Chem. **5**, 189 (1971).
15. M. Hoffman-Ostenhoff and T. Hoffman-Ostenhoff. Phys. Rev.. A, **16**, 1782 (1977).
16. W. Weyrich, P. Pattison, and B. G. Williams. Chem. Phys. **41**, 271 (1979).
17. A. Harmalkar, A. M. Simas, V. H. Smith, Jr., and W. M. Westgate. Int. J. Quantum Chem. **23**, 811 (1983).
18. W. M. Westgate, A. M. Simas, and V. H. Smith, Jr. J. Chem. Phys. **83**, 4045 (1985).
19. P. Politzer and R. G. Parr. J. Chem. Phys. **64**, 4634 (1976).
20. R. J. Boyd. J. Chem. Phys. **66**, 356 (1977).
21. H. Schmider, R. P. Sagar, and V. H. Smith, Jr. J. Chem. Phys. **94**, 8627 (1991).
22. W. Wang. Phys. Rev. A, **25**, 2901 (1982).
23. E. Clementi and C. Roetti. At. Data Nucl. Data Tables, **14**, 177 (1974).
24. A. D. McLean and R. S. McLean. At. Data Nucl. Data Tables, **26**, 197 (1981).

Can. J. Chem. Downloaded from www.nrcresearchpress.com by 92.62.229.171 on 09/08/12
For personal use only.

A GTO basis set calculation of properties of the continuum. Photoionization and resonances of He

ROBERTO MOCCIA[1]

Dipartimento di Chimica e Chimica Industriale, Universita' di Pisa, Via Risorgimento 35, I-56126 Pisa, Italy

AND

PIETRO SPIZZO

Istituto di Chimica Quantistica ed Energetica Molecolare del CNR, Via Risorgimento 35, I-56126 Pisa, Italy

Received June 11, 1991

This paper is dedicated to Professor Sigeru Huzinaga on the occasion of his 65th birthday

ROBERTO MOCCIA and PIETRO SPIZZO. Can. J. Chem. **70**, 513 (1992).

By using the K-matrix technique for the continuum states that was previously employed with particularly diffuse L^2 basis sets, it is shown that GTO bases are also capable of yielding accurate values for the properties belonging to the electronic continuum. The method has been tested for helium and proved of satisfactory accuracy also for the analysis of the autoionizing states. The results include the phase shifts of the continuum states of the $^1S^e$ and $^1P^o$ manifolds, the properties of the lowest resonances of these symmetries, the ground state photoionization cross section, and the S contribution to the $1s2p\ ^1P^o$ photoionization cross section. The results obtained suggest that the proposed technique should be useful for computing molecular differential photoionization cross sections by exploiting the widely used codes that employ GTO bases.

Key words: photoionization, Gaussian basis sets, helium, autoionizing states.

ROBERTO MOCCIA et PIETRO SPIZZO. *Can. J. Chem.* **70**, 513 (1992).

Utilisant la technique de la matrice K pour le continuum des états qui a été employée antérieurement avec des ensembles de base L^2 particulièrement diffus, on a montré que les bases GTO peuvent aussi fournir des valeurs précises pour les propriétés appartenant au continuum électronique. On a vérifié la méthode avec l'hélium et on a prouvé que sa précision est aussi satisfaisante pour l'analyse d'états auto-ionisants. Les résultats incluent les déplacements de phase du continuum des états de multiplicités $^1S^e$ et $^1P^o$, les propriétés des résonances les plus basses de ces symétries, la section efficace de la photo-ionisation de l'état fondamental et la contribution S à la section efficace de la photo-ionisation de l'état $^1P^o$ $1s2p$. Les résultats obtenus suggèrent que, en exploitant des codes fréquemment utilisés qui utilisent des bases GTO, la technique proposée pourrait étre utile pour calculer les sections efficaces de la photo-ionisation différentielle moléculaire.

Mots clés : photo-ionisation, ensembles de base gaussiens, hélium, états auto-ionisants.

[Traduit par la rédaction]

Introduction

Electron emission is one of the most efficient decay mechanisms for atoms and molecules excited above the first ionization threshold. This makes a knowledge of reliable photoionization cross sections very valuable in a variety of fields. Their importance has also grown due to the development of laser sources and of synchrotron radiation, which have greatly extended both the range of photon energies and the number of photons involved in the experiments. In the numerical evaluation of photoionization cross sections, a pivotal role is played by the transition matrix elements involving states of the electronic continuum. It should be stressed that the differential cross section, in contrast to the integral, requires a more detailed knowledge of the states lying in the continuum, such as the individual phase shifts of their degenerate partial wave components.

The calculation of the matrix elements involving the continuum may be accomplished by several techniques characterized either by the use of purely L^2 basis sets or by the utilization of truly continuum orbitals. These latter techniques, derived from the calculations of scattering cross sections and known as scattering methods, should afford, in principle, a more accurate evaluation of the properties pertaining to the continuum; on the other hand, the former methods appear to have some decisive computational advantages. In fact, the L^2 algorithms may be reduced to a sequence of matrix operations that can be efficiently implemented on modern computers. In addition, the L^2 methods may exploit the well-established computer codes available to compute the electronic bound states of molecules employing L^2 bases, generally of the GTO type.

The lack of spherical symmetry in molecules curtails the possibility of directly applying the methods developed and extensively used to study the photoionization of atoms, such as the Close-Coupling (1) or many-body methods (2, 3). Specific approaches were thus developed for the molecular cases. Among those which truly determine continuum orbitals by solving differential or integral equations, the most extensively used are the Iterative Schwinger Variational method (4), the Multiple Scattering Xα method (5), and the Linear Algebraic method (6). The most widely applied L^2 methods are the Complex Basis method (7), the Reaction K-matrix method (8, 9), and the Stieltjes Moment Theory method (10). This last one may be employed usefully only to calculate integral cross sections.

To use L^2 methods for computing the differential cross sections, particular basis functions and numerical techniques were employed to obtain the partial wave phase shifts (11). These techniques rely upon a correct behavior of the more extended part of the wavefunction in order to interpolate it by an adequately phase-shifted Coulomb wave. These methods cannot be applied with the GTO bases since,

[1]Author to whom correspondence may be addressed.

Printed in Canada

Can. J. Chem. Downloaded from www.nrcresearchpress.com by 92.62.229.171 on 09/08/12
For personal use only.

Can. J. Chem. Downloaded from www.nrcresearchpress.com by 92.62.229.171 on 09/08/12
For personal use only.

at large distance from their origin, the GTO cannot give a reliable description of a Coulomb wave.

In this paper it is shown how, exploiting the reaction K-matrix technique, this shortcoming may be overcome. Thus the possibility of obtaining useful knowledge about the electronic continuum may be added to the many services already supplied by the GTO. Section 2 describes the method, while Sect. 3 reports some preliminary calculations, which, although made for the simple atomic system He, represent a stringent test of the methods due to the accuracy required by the quantities evaluated.

2. Method of calculation

The theory of the K-matrix technique and its implementation upon L^2 bases to represent the properties belonging to the continuum have been thoroughly described elsewhere. Here only a brief outline is given and the reader is referred to a previous paper (9) for details. This work will therefore focus on the differences needed to employ short-range basis orbitals like the Gaussian instead of the more suitable STOCOS functions (11) employed in our previous K-matrix calculations (8, 9, 12).

The present approach is an extension of the K-matrix method, in which all orthogonality constraints have been removed to achieve the fastest convergence of the variational expansion with the basis size. The method, as pioneered by Fano (13), is essentially a configuration interaction (CI) in the continuum, carried out for a fixed energy, and allows us (at a formal level) to expand the variational solution upon continuous basis sets. It turns the Schrödinger equation into a system of integral equations for the K-matrix elements, which is then transformed into a linear system by a quadrature upon a finite L^2 basis set. The formal basis employed to expand the continuum states includes a discrete subset of localized functions, which more efficiently represent the autoionizing states and the correlation effects, in addition to the relevant partial wave channel (pwc) subspaces. In the atomic case, these are defined by the ion level I and the l value of the electron partial wave. In the following the subspaces will be indexed with greek letters; a subspace index α will designate explicitly an open pwc subspace, while an index β designates an arbitrary subspace; $\hat{Q}_\beta$ will denote the projector inside the subspace.

In the present calculation, the formal basis functions $|\Phi_{\beta E}\rangle = |\Phi_I^+ \chi_{\epsilon l}\rangle$ of the pwc subsets are the eigenfunctions of the channel Hamiltonian $\hat{H}_\beta = \hat{Q}_\beta \hat{H} \hat{Q}_\beta$. They are therefore (antisymmetrized spin- and symmetry-adapted) products of the ion states $|\Phi^+_{IM_LM_S}\rangle$ and of the partial l-waves $|\chi_{\epsilon lmm_s}\rangle$ that diagonalize the effective channel Hamiltonian for the outer electron. These waves behave asymptotically as standing shifted Coulomb waves and the pwc basis functions may be indexed by the corresponding energy $E = E_I^+ + \epsilon$. To allow a safe representation upon a discrete basis, it is required that these states possess properties (phase shifts, off-diagonal overlap, and Hamiltonian matrix elements) weakly dependent upon the energy indexes.

In the case of helium, the effective channel Hamiltonians $\hat{H}_\beta$ do not support shape resonances, so these conditions are satisfied. If narrow shape resonances occur, as is often the case in molecular systems, $\hat{H}_\beta$ may be properly redefined to avoid this occurrence, while localized representations of these states must be included in the localized correlating subspace.

The calculation of the differential cross sections requires the phase shifts of the pwc basis functions $|\Phi_{\beta E}\rangle$, which in the present approach are obtained via K-matrix calculations performed inside the separate channels. In fact, according to the formula given in the next subsection, these phase shifts are immediately obtained when the K-matrix technique is employed to diagonalize the channel Hamiltonians in bases of zero phase shift; i.e., those obtained by coupling hydrogenic eigenfunctions $|\chi^{(0)}_{\epsilon l}\rangle$ to the ion levels. In the present L^2 approach, the $|\chi^{(0)}_{\epsilon l}\rangle$ are conveniently represented by diagonalizing the Coulomb Hamiltonian upon the same bases employed for the $|\chi_{\epsilon l}\rangle$; we stress that this procedure yields the phase shifts of the pwc basis functions even if the L^2 representations actually employed do not have a correct long-range behavior. It is also worth noting that the basis functions $|\Phi^{(0)}_{\beta E}\rangle = |\Phi_I^+ \chi^{(0)}_{\epsilon l}\rangle$ are not necessarily orthonormal nor do they diagonalize any model Hamiltonian. This preliminary step, hereafter referred to as the SC-KM (Separate Channel K-Matrix) step, yields the phase shifts of the basis functions $|\Phi_{\alpha E}\rangle$ employed to calculate the correlated eigenfunctions in the subsequent step, referred to as the IC-KM (Interacting Channel KM) step.

The present approach may be considered equivalent to a Close-Coupling calculation with the same open and closed channels plus a large number of pseudostates for the correlation effects. It should be clear, however, that the K-matrix method is much more suitable for a molecular calculation: it may be directly linked to the L^2 methods employed in molecular structure and may more easily handle the large number of channels that are needed in a molecular calculation.

The K-matrix method

The method will be outlined employing the notation proper of the IC-KM step, but the equations for the SC-KM step may be immediately derived from them. In this last case, of course, $\hat{H}$ stands for the channel Hamiltonian. For ease of writing, the same notation $|\Phi_{\beta E}\rangle$ will be employed for discrete and continuous eigenfunctions, normalized to unity and $\delta(E - E')$ respectively.

Corresponding to the n channels that are open at energy E (at the energies investigated in the present work the only open channel is that corresponding to the ion ground level), one may define n linearly independent trial functions $|\Psi_E\rangle = (|\Psi_{1E}\rangle \ldots |\Psi_{nE}\rangle)$ of the form

$$[1] \quad |\Psi_{\alpha E}\rangle = |\Phi_{\alpha E}\rangle + \sum_{\beta'} \oint\!\!\!\!\!\!\int dE' |\Phi_{\beta' E'}\rangle P \frac{1}{E - E'} K_{\beta' E', \alpha E}$$

where P denotes the principal part of the integral and for each subset β' denotes the summation over its discrete part and the integration over the continuous one. The expansion coefficients are determined by imposing $\langle \Phi_{\beta' E'} | \hat{H} - E | \Psi_{\alpha E}\rangle = 0$ and this leads to the system of coupled integral equations

$$[2] \quad K_{\beta' E', \alpha E} - \sum_{\beta''} \oint\!\!\!\!\!\!\int dE'' V_{\beta' E', \beta'' E''}(E) P \frac{1}{E - E''} K_{\beta'' E'', \alpha E} = V_{\beta' E', \alpha E}(E)$$

$$V_{\beta' E', \beta'' E''}(E) = \langle \Phi_{\beta' E'} | \hat{H} - E | \Phi_{\beta'' E''}\rangle - (E' - E)\delta_{\beta' \beta''}\delta(E' - E'')$$

In the present calculations, in the IC-KM step the matrix

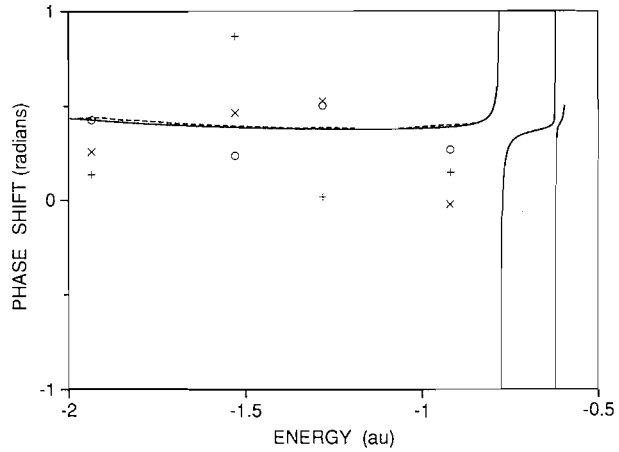

FIG. 1. Phase shifts of the $^1S^e$ states. Full line: K-matrix calculation with extended bases. Broken line: K-matrix calculation with GTO bases. +: wave analysis in the range 5–20 au, GTO basis. ×: wave analysis in the range 10–20 au, GTO basis. ○: wave analysis in the range 20–30 au, GTO basis.

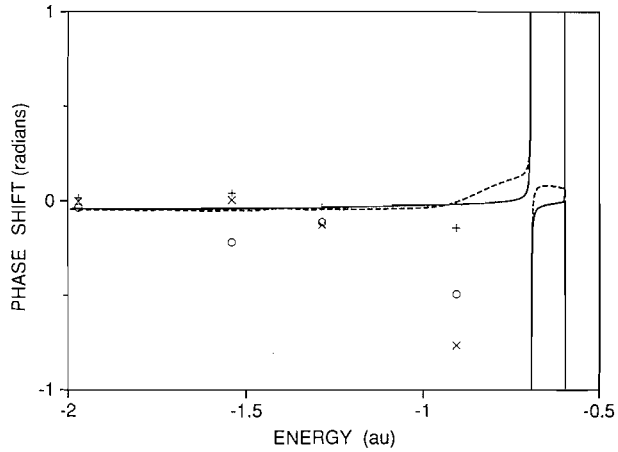

FIG. 2. Phase shifts of the $^1P^o$ states. Full line: K-matrix calculation with extended bases. Broken line: K-matrix calculation with GTO bases. +: wave analysis in the range 5–20 au, GTO basis. ×: wave analysis in the range 10–20 au, GTO basis. ○: wave analysis in the range 20–30 au, GTO basis.

TABLE 1. Parameters of the autoionizing states: position E (au), width Γ (au), Fano parameter q, absorption maximum σ_{max} (Megabarn). $a(b)$ means $a \times 10^b$

		GTO basis	Extended basis	A[c]	B[c]
$2s^2 + 2p^2\ ^1S^e$	E	−0.77769	−0.77783	−0.7778	−0.7778
	Γ	4.53(−3)	4.57(−3)	4.57(−3)	4.58(−3)
	q (LG)[a]	−53.2	−49.7	−30.7[d]	
	q (VG)[a]	−53.5	−49.7		
	σ_{max} (LG)[a]	7.65	7.68	8.2[d]	
	σ_{max} (VG)[a]	7.63	7.66		
$2s^2 - 2p^2\ ^1S^e$	E	−0.62049	−0.62055	−0.6195	−0.62052
	Γ	2.22(−4)	2.22(−4)	2.36(−4)	2.31(−4)
	q[a]	≈100	≈100	237[d]	
	σ_{max} (LG)[a]	419	409	404[d]	
	σ_{max} (VG)[a]	423	408		

		GTO basis	Extended basis	C[c]	B
$2s2p\ ^1P^o$	E	−0.69167	−0.69260	−0.69172	−0.69280
	Γ	1.43(−3)	1.36(−3)	1.48(−3)	1.33(−3)
	q (LG)[b]	−2.54	−2.772	−2.63	
	q (VG)[b]	−2.51	−2.770	−2.70	
$2s3p - 2p3s\ ^1P^o$	E	−0.59624	−0.59700	−0.59708	−0.59707
	Γ	3.54(−6)	3.71(−6)	4.15(−6)	3.89(−6)
	q (LG)[b]	−4.59	−4.29	−4.00	
	q (VG)[b]	−4.74	−4.32	−4.07	

[a]From $1s2p\ ^1P^o$.
[b]From $1s^2\ ^1S^e$.
[c]A: ref. 17, scattering variational calculation; B: ref. 16, 14 states close-coupling; C: ref. 3, nine-channel K-matrix calculation.
[d]Computed from the data in Tables III and V of A.

elements $V_{\beta E',\beta E''}(E)$ inside a channel are identically zero, since the pwc bases are the eigenfunctions of the projected Hamiltonian $\hat{Q}_\beta \hat{H} \hat{Q}_\beta$.

For real energies the K-matrix on the energy shell $\mathbf{K}(E)$, defined by $K_{\alpha'\alpha}(E) = K_{\alpha' E,\alpha_E}$, is a real symmetric matrix. As discussed in ref. 9, it is related to the scattering matrix and contains the quantities needed to analyze the resonances. Moreover, when only one open channel is present (e.g., in the SC-KM step), the solution $|\Psi_{\alpha E}\rangle$ is a standing wave with phase shift

$$\delta_\alpha(E) = \delta_{\alpha 0}(E) - \tan^{-1}[\pi K_{\alpha\alpha}(E)]$$

where $\delta_{\alpha 0}(E)$ is the phase shift of the pwc basis function. In the SC-KM step, this basis satisfies $\delta_{\alpha 0}(E) = 0$ and this makes

Can. J. Chem. Downloaded from www.nrcresearchpress.com by 92.62.229.171 on 09/08/12
For personal use only.

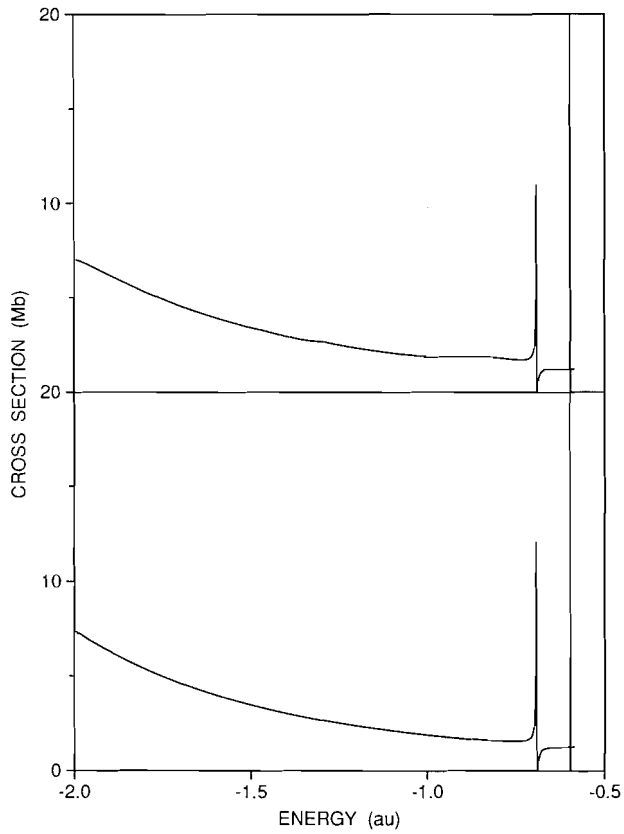

FIG. 3. Ground state photoionization cross section. Upper figure: GTO basis; lower figure: extended basis. LG and VG results are indistinguishable on this scale.

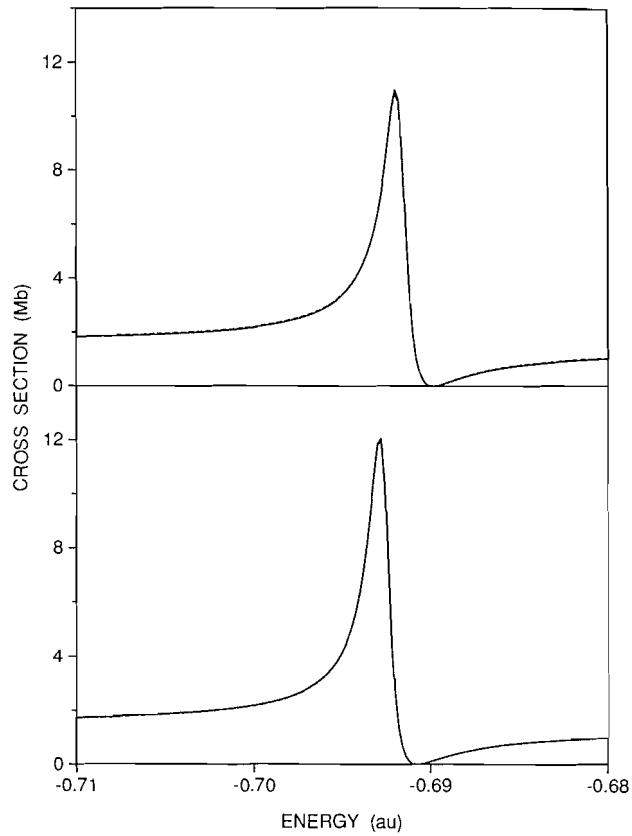

FIG. 4. Ground state photoionization cross section across the $2s2p\ ^1P^o$ resonance. Upper figure: GTO basis; lower figure: extended basis. Full line: LG results; broken line: VG results.

it possible to obtain the phase shifts of the pwc basis for the IC-KM step.

The variational wavefunctions so obtained satisfy

$$\langle \Psi_{E'} | \hat{H} - E'' | \Psi_E \rangle = (E - E'')[1 + \pi^2 \mathbf{K}(E)^2]\delta(E - E')$$

and two sets of complex orthonormal eigenfunctions may be obtained by:

$$|\Psi_E^{(\pm)}\rangle = (|\Psi_{1E}^{(\pm)}\rangle \ldots |\Psi_{nE}^{(\pm)}\rangle)$$
$$= (|\Psi_{1E}\rangle \ldots |\Psi_{nE}\rangle)[1 \pm i\pi \mathbf{K}(E)]^{-1} \mathbf{\Delta}^{(\pm)}(\mathrm{E})$$

where $\Delta_{\alpha'\alpha}^{(\pm)}(E) = \delta_{\alpha\alpha'} e^{\pm i\xi_{\alpha E}}$ and $\xi_{\alpha E}$ is the total phase shift of $|\Phi_{\alpha E}\rangle$, inclusive of $-\pi l_\alpha/2$ (i.e., the i^l factor). The states $|\Psi_{\alpha E}^{(-)}\rangle$ contain an outgoing Coulomb wave (with zero phase shift) only in the channel α and are therefore suitable for photoionization calculations.

The L^2 *representation of the partial wave channels*

The present work is concerned with the $^1S^e$ and $^1P^o$ continua from the ionization threshold at -2 au up to about -0.59 au; beyond this energy the GTO bases employed in the present work are unable to represent the higher resonances. All the calculations performed upon Gaussian bases have been checked, employing also extended bases that include, beside Slater and Hydrogenic orbitals, a large number of STOCOS functions

$$\chi_{\xi lm}(\mathbf{r}) = N_{\xi kl}\, r^l e^{-\xi r} \cos(kr) Y_{lm}(\theta,\phi)$$

These are probably the most efficient L^2 bases for calculations in the electronic continua; previous work has discussed in great detail their capabilities (11) and applications (9, 12, 14, 15).

The L^2 sets employed to represent the pwc subspaces in the IC-KM step were obtained by diagonalizing the Hamiltonian upon (spin- and symmetry-adapted) configurations of the form $1s\ nl$, where $1s$ is the exact (extended basis case) or an approximate (GTO case) ground state of He^+, while nl are diffuse orbitals for representing the electron wave. With both bases, the variational states $|\phi_{\beta j}\rangle$ obtained in this way include accurate representations for the lowest bound states of the channel Hamiltonian, a few wavepackets in the higher Rydberg region, a number of narrow wavepackets in the lowest continuum, and broad wavepackets at higher energy. The narrow wavepackets are those variational states whose waves resemble closely (apart from an energy-normalization constant $C_{\beta j}$) the true waves of the same energy inside a sufficiently large portion of space. The advantage of the present method is that this portion must include only the rather limited region where the potential deviates from $-1/r$, i.e., the "molecular region." The L^2 basis for the discretized K-matrix calculations is formed by the states $|\varphi_{\beta j}\rangle$, defined by $|\varphi_{\beta j}\rangle = C_{\beta j}|\phi_{\beta j}\rangle$ for the narrow wavepackets and by $|\varphi_{\beta j}\rangle = |\phi_{\beta j}\rangle$ for all the other states.

The K-matrix calculations may obviously be performed only at energies inside the range covered by the narrow wavepackets, which should allow interpolation of the matrix elements and the phase shifts of the channel basis functions. The contributions to the integrals in eqs. [1] and [2] from the high-energy regions, which should be small and

Can. J. Chem. Downloaded from www.nrcresearchpress.com by 92.62.229.171 on 09/08/12
For personal use only.

Can. J. Chem. Downloaded from www.nrcresearchpress.com by 92.62.229.171 on 09/08/12
For personal use only.

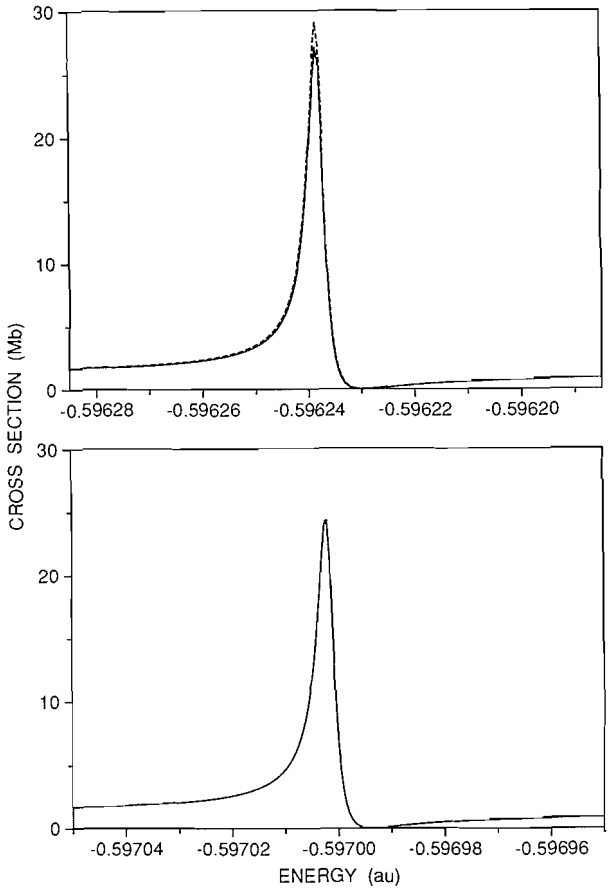

FIG. 5. Ground state photoionization cross section across the $2s3p-2p3s\ ^1P^o$ resonance. Upper figure: GTO basis; lower figure: extended basis. Full line: LG results, broken line: VG results.

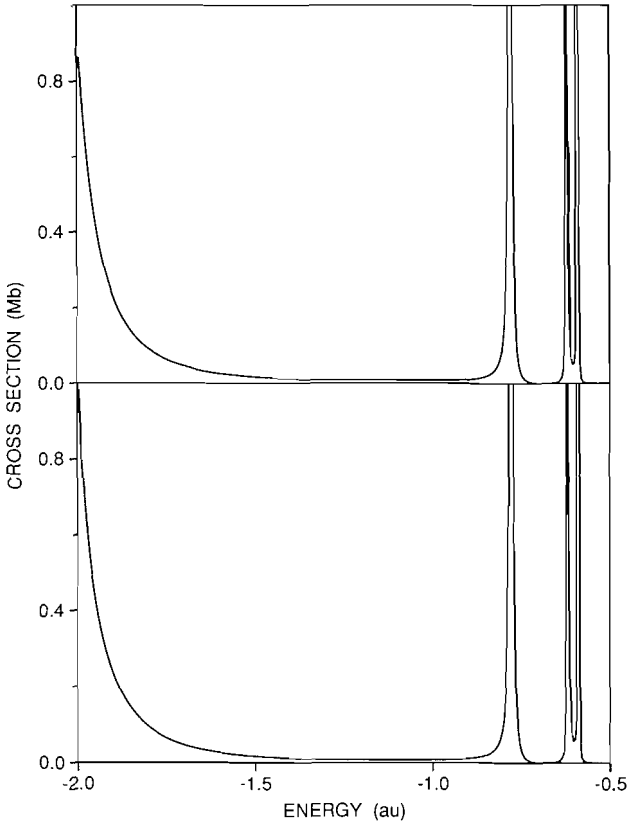

FIG. 6. $1s2p\ ^1P^o$ photoionization cross section. Upper figure: GTO basis; lower figure: extended basis. LG and VG results are indistinguishable on this scale. $^1S^e$ contribution.

weakly energy dependent, are instead approximated by summing the contributions of the broad wavepackets.

The GTO are poorly suited to represent the short-period oscillatory behavior of the high-energy continuum states; instead it appears that they are able to describe the long oscillations of the higher Rydberg and of the lower continuum. In this energy region, GTO and extended bases yield about the same number of states, while at higher energies the GTO variational states are much more spaced. With the GTO bases described in the next subsection, the variational waves propagate up to about 70 au, but they are reasonably close to the true waves of the same energy only in a more limited region, whose radius is about 20 au for the lowest states and shrinks for the higher ones. In the present case, the ion is very compact and the potential may be considered Coulombic already at 5 au from the nucleus, so the analysis of the waves in the range 5–20 au yields the normalization and the phase shift of the lowest variational states with good accuracy. However, this procedure is clearly inapplicable to larger atoms or molecular systems, and therefore a method independent of the wave analysis in a Coulombic region, like that proposed here, is in general required. The energy-normalization constants may be fairly well approximated from the energy spacings, $C^2_{\beta j} \approx 2/(E_{\beta,j+1} - E_{\beta,j-1})$, while the phase shifts may be obtained by the SC-KM step described above.

The discretized (on the first energy index) representation $K^{\text{disc}}_{\beta j,\alpha E}$ of the K-matrix on the variational basis is solution of

$$\sum_{\beta' j'} [1 - V(E)\mathbf{P}(E)]_{\beta j,\beta' j'} K^{\text{disc}}_{\beta' j',\alpha E} = V^{\text{int}}_{\beta j,\alpha E}$$

$$V_{\beta j,\beta' j'}(E) = \langle \varphi_{\beta j}|\hat{H} - E|\varphi_{\beta' j'}\rangle - (E_{\beta j} - E)\delta_{\beta,\beta'}\delta_{j,j'}$$

$$V^{\text{int}}_{\beta j,\alpha E} = \langle \varphi_{\beta j}|\hat{H} - E|\Phi_{\alpha E}\rangle^{\text{int}}$$

where the superscript "int" denotes interpolated matrix elements and $\mathbf{P}(E)$ is an almost diagonal matrix that represents the principal part of the integration and whose structure has been discussed elsewhere (9).

The GTO basis set

The $1s$ orbital of He^+ has been approximated by a linear combination of 6 GTO with $n = 1$ and orbital exponents 205, 31.5, 7.41, 2.241, 0.799, 0.306, and 0.1933. The ground state He^+ energy with this orbital is -1.999701 au.

The GTO basis for the localized $^1S^e$ configurations included all the configurations arising from the following orbitals: 14 s (with $n = 1$ and orbital exponents Z ranging from 87.36 to 0.01), 11 p (with $n = 2$ and Z from 8 to 0.005), 11 d (with $n = 3$ and Z from 8 to 0.01), and 8 f (with $n = 4$ and Z from 8 to 0.08).

The s-wave basis set includes the $1s$ ion orbital plus 63 GTO with $n = 3$ and orbital exponents in geometric progression of ratio 0.81 and first term 250. This basis yields 13 narrow wavepackets with energies between -2 and 0 au.

The GTO bases for the localized $^1P^o$ configurations included all the configurations arising from the following orbitals: 13 s (with $n = 1$ and orbital exponents Z ranging from

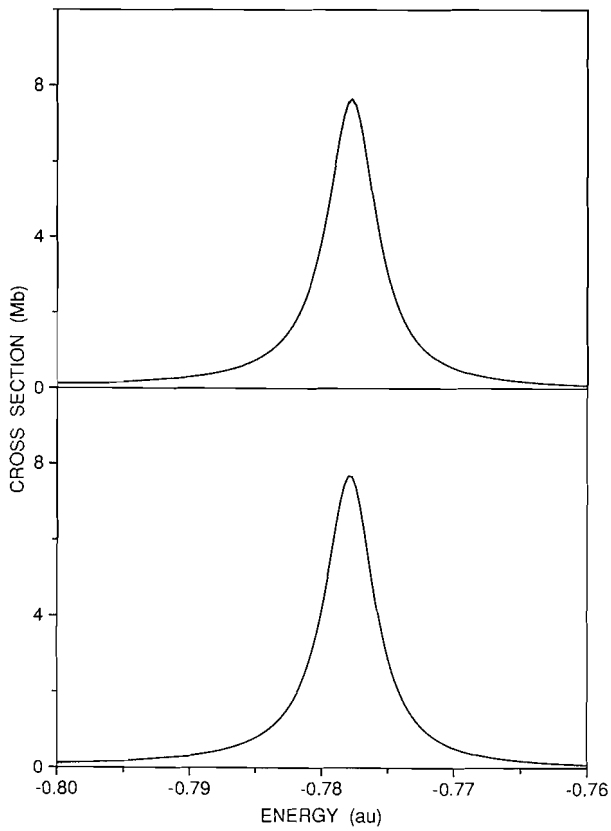

FIG. 7. $1s2p\ ^1P^o$ photoionization cross section across the $2s^2 + 2p^2\ ^1S^e$ resonance. Upper figure: GTO basis; lower figure: extended basis. LG and VG results are indistinguishable on this scale. $'S^e$ contribution.

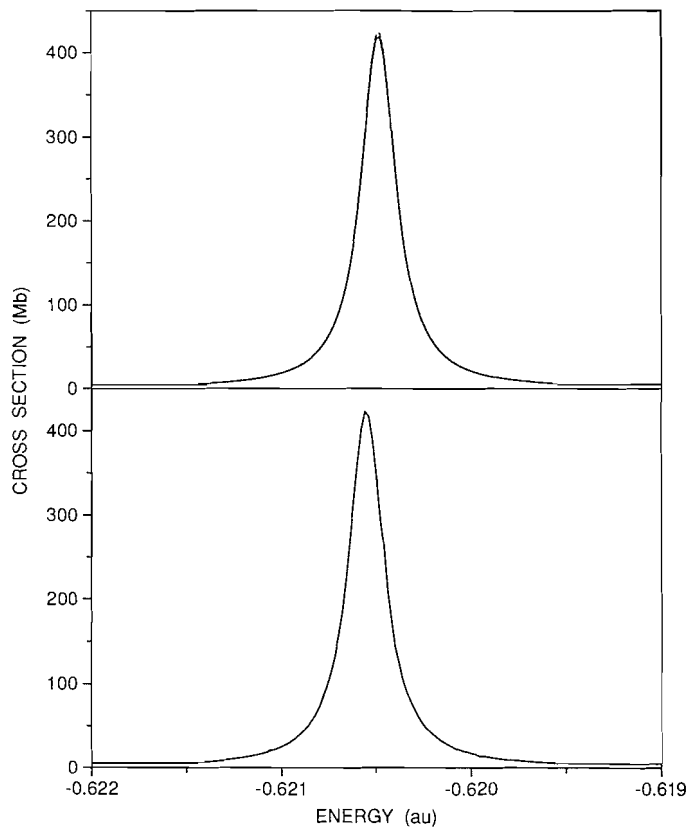

FIG. 8. $1s2p\ ^1P^o$ photoionization cross section across the $2s^2-2p^2\ ^1S^e$ resonance. Upper figure: GTO basis; lower figure: extended basis. Full line: LG results; broken line: VG results. $'S^e$ contribution.

87.36 to 0.01), 10 p (with $n = 2$ and Z from 8 to 0.01), 10 d (with $n = 3$ and Z from 8 to 0.02), and 9 f (with $n = 4$ and Z from 8 to 0.08). The p-wave basis set includes 44 GTO with $n = 2$; the first three of them have orbital exponents 8, 4, and 2; the other 41 of them have exponents in geometrical progression of ratio 0.77 and first term 1. This basis yields 12 narrow wavepackets with energies between -2 and 0 au.

3. Results

The calculated helium ground state energy was -2.903592 au in the STO basis and -2.900315 au in the GTO basis. For the $1s2p\ ^1P^o$ state, the calculated energies were respectively -2.123812 and -1.121688 au.

The $^1S^e$ and $^1P^o$ phase shifts calculated with the GTO and the extended bases are plotted in Figs. 1 and 2. Since in this case there is only one open channel, a variational representation of the continuum may also be obtained by diagonalizing the whole variational space (i.e., the localized correlating and the pwc subsets $1swl$). The phase shifts and the normalization constants may then be extracted by interpolating their long-range behavior with shifted Coulomb waves. With the extended basis, this calculation yields results practically coincident with the K-matrix ones. On the contrary, this procedure proved quite unreliable with the GTO basis, since these waves do not extend sufficiently outside the region where the correlation effects are important, i.e., where the localized states of the correlating subset have significant amplitudes. For the GTO basis, a few phase shifts computed in this way in various ranges of r are also shown in these figures.

The lowest resonances of the two mainfolds were analyzed by the methods described in ref. 9 and the S-matrix results are listed in Table 1 together with a few data reported in the literature (3, 16, 17). Many classification schemes are currently in use for these resonances. Here they are labelled in the Fano notation (18), which employs the dominant configurations. The correspondence between the various notations may be found in ref. 16. Our present extended-basis results update those reported in our previous work (14). The analysis of Table 1 shows that the GTO bases reproduce quite well the widths of the autoionizing states, while the positions are slightly too high.

The ground state photoionization cross section is reported in Fig. 3 and its details around the two lowest $^1P^o$ resonances are expanded in Figs. 4 and 5. The $^1S^e$ contribution to the cross section of the $1s2p\ ^1P^o$ level is plotted in Fig. 6 and its details around the two lowest resonances are expanded in Figs. 7 and 8. In all cases the calculations were performed in both the Length Gauge (LG) and in the Velocity Gauge (VG); the gauge agreement is very satisfactory with the extended basis and only slightly inferior with the GTO basis. The greatest differences are found for the second $^1P^o$ resonance, which projects mainly on the $2s3p$ and $2p3s$ configurations, since the GTO localized basis set does not reproduce the $3s$ and $3p$ orbitals very accurately.

The cross sections at these resonances were fitted to a Fano profile; the positions and the widths so obtained were practically coincident with the S-matrix results. The q values for

Can. J. Chem. Downloaded from www.nrcresearchpress.com by 92.62.229.171 on 09/08/12
For personal use only.

shapes like those of the $^1S^e$ resonances have hardly a definite meaning; indeed our values differ greatly from those which may be computed from the data of Cordes and Altick (17), although our absorption maxima are in good agreement with theirs.

4. Conclusions

The present results strongly suggest that, if properly handled, the GTO basis sets may yield accurate values for several properties of the states lying in the continuum. This increases still more the importance of the GTO's, whose usefulness was recognized long ago by Huzinaga, who in several papers has shown how to use them effectively. In our opinion, several of the rather sophisticated codes available to compute the lower-lying electronic states of molecular systems should be amenable for adaptation to the method proposed here. This should extend their capabilities to the calculation of accurate differential photoionization cross sections.

To test this contention, work is in progress here to calculate the differential ionization cross section of some simple polyatomic molecules using GTO bases and different levels of approximation.

Acknowledgement

One of the authors (R.M.) gratefully acknowledges the financial help of the Progetto Finalizzato Chimica Fine of C.N.R. and wishes to express his pleasure in dedicating this work to Prof. S. Huzinaga, with whom he has had the privilege of enjoying a long and lasting friendship.

1. R. J. W. Henry and L. Lipsky. Phys. Rev. **153**, 51 (1967).
2. M. S. Pindzola and H. P. Kelly. Phys. Rev. A, **11**, 1543 (1975).
3. S. Salomonson, S. L. Carter, and H. P. Kelly. Phys. Rev. A, **39**, 5111 (1989).
4. R. R. Lucchese and V. McKoy. Phys. Rev. A, **21**, 112 (1980); M. Braunstein, V. McKoy, L. E. Machado, L. M. Brescansin, and M. A. P. Lima. J. Chem. Phys. **89**, 2998 (1988); L. E. Machado, L. M. Brescansin, M. A. P. Lima, M. Braunstein, and V. McKoy. J. Chem. Phys. **92**, 2362 (1990); M. Braunstein and V. McKoy. J. Chem. Phys. **92**, 4887 (1990).
5. J. Siegel, D. Dill, and J. L. Dehmer. J. Chem. Phys. **64**, 3204 (1976); A. Görling and N. Rösch. J. Chem. Phys. **93**, 5563 (1990); W. Thiel. Chem. Phys. **57**, 227 (1981); J. D. Bozek, G. M. Bancroft, J. N. Cutler, K. H. Tan, B. W. Yates, and J. S. Tse. Chem. Phys. **132**, 257 (1989); J. S. Tse. Chem. Phys. Lett. **163**, 392 (1989).
6. B. I. Schneider and L. A. Collins. Comput. Phys. Rep. **10**, 49 (1989); B. I. Schneider and R. B. Walker. J. Chem. Phys. **70**, 2466 (1979); D. L. Lynch, B. I. Schneider, and L. A. Collins. Phys. Rev. A, **38**, 4927 (1988).
7. T. N. Rescigno and C. W. McCurdy. Phys. Rev. A, **31**, 624 (1985); S. Yabushita, C. W. McCurdy, and T. N. Rescigno. Phys. Rev. A, **36**, 3146 (1987); T. N. Rescigno. Phys. Rev. A, **31**, 607 (1985); C. W. McCurdy and T. N. Rescigno. Phys. Rev. A, **35**, 657 (1987).
8. I. Cacelli, V. Carravetta, and R. Moccia. J. Chem. Phys. **85**, 7038 (1986).
9. R. Moccia and P. Spizzo. Phys. Rev. A, **39**, 3855 (1991).
10. P. W. Langhoff and C. T. Corcoran. J. Chem. Phys. **61**, 146 (1974); P. W. Langhoff. *In* Electron–molecule and photon–molecule collisions. *Edited by* T. N. Rescigno, B. V. McKoy, and B. I. Schneider. Plenum, New York. 1979. pp. 183–224, and references therein; F. Müller-Plathe and G. Diercksen. Phys. Rev. A, **40**, 696 (1989); I. Cacelli, V. Carravetta, and R. Moccia. J. Phys. Chem. **92**, 979 (1988); I. Cacelli, V. Carravetta, R. Moccia, and A. Rizzo. J. Chem. Phys. **89**, 7301 (1988).
11. I. Cacelli, R. Moccia, and V. Carravetta. *In* Collisions and half collisions with lasers. *Edited by* N. K. Rahman and C. Guidotti. Harwood, Chur. 1982. pp. 229–248; Chem. Phys. **90**, 313 (1984); I. Cacelli, V. Carravetta, A. Rizzo, and R. Moccia. *In* MOTECC-90: modern techniques in computational chemistry. *Edited by* E. Clementi. ESCOM, Leiden. 1990. pp. 639–691; Phys. Rep. **205**, 284 (1992).
12. R. Moccia and P. Spizzo. J. Phys. B: At. Mol. Opt. Phys. **23**, 3557 (1990); Nuovo Cimento Soc. Ital. Fis. D: **13D**, 757 (1991).
13. U. Fano. Phys. Rev. **124**, 1866 (1961).
14. R. Moccia and P. Spizzo. J. Phys. B: At. Mol. Phys. **20**, 1423 (1987).
15. R. Moccia and P. Spizzo. J. Phys. B: At. Mol. Opt. Phys. **21**, 1121 (1988); Phys. Rev. A, **39**, 3855 (1989).
16. D. H. Oza. Phys. Rev. A, **33**, 824 (1986).
17. D. Cordes and P. L. Altick. Phys. Rev. A, **40**, 20 (1989).
18. J. W. Cooper, U. Fano, and F. Prats. Phys. Rev. Lett. **10**, 518 (1963).

Can. J. Chem. Downloaded from www.nrcresearchpress.com by 92.62.229.171 on 09/08/12
For personal use only.

Infrared intensities of liquids. IX. The Kramers–Kronig transform, and its approximation by the finite Hilbert transform via fast Fourier transforms

JOHN E. BERTIE AND SHULIANG L. ZHANG
Department of Chemistry, University of Alberta, Edmonton, Alta., Canada T6G 2G2

Received September 16, 1991

This paper is dedicated to Professor Sigeru Huzinaga on the occasion of his 65th birthday

JOHN E. BERTIE and SHULIANG L. ZHANG. Can. J. Chem. **70**, 520 (1992).

It is well known that the infinite Kramers–Kronig transform is equivalent to the infinite Hilbert transform, which is equivalent to the allied Fourier integrals. The Hilbert transform can thus be implemented using fast Fourier transform routines. Such implementation is usually some 60 times faster than the Kramers–Kronig transform for a data file containing about 7 points. This paper reports that, for transformations between the real and imaginary refractive indices, $n(\tilde{\nu})$ and $k(\tilde{\nu})$ in $\hat{n} = n(\tilde{\nu}) + ik(\tilde{\nu})$, the FFT-based Hilbert transform can be much less accurate than, or as accurate as, the Kramers–Kronig transform, depending on the algorithm used. The Kramers–Kronig transform, incorporating Mclaurin's formula for finding the principal value of the integral, transforms $k(\tilde{\nu})$ spectra into $n(\tilde{\nu})$ spectra that are accurate to about 0.05%. Some Hilbert transform algorithms in the literature yield only about 4% accuracy. The BZ algorithm for the Hilbert transform is presented, for use on a laboratory computer running under DOS, that yields $n(\tilde{\nu})$ spectra accurate to 0.05%. For the transform from $n(\tilde{\nu})$ to $k(\tilde{\nu})$, the BZ algorithm gives $k(\tilde{\nu})$ accurate to about −0.2% of the largest k value in the spectrum. This compares with an accuracy of 0.5% for the Kramers–Kronig transform. In cases where the $k(\tilde{\nu})$ spectrum is truncated at low wavenumbers, a simple method is presented that improves by a factor of ~10 the accuracy at low wavenumber of the $n(\tilde{\nu})$ spectrum obtained by Hilbert or Kramers–Kronig transforms of the k($\tilde{\nu}$) spectrum.

Key words: infrared intensities, complex refractive indices, Kramers–Kronig transform, Hilbert transform, optical constants.

JOHN E. BERTIE et SHULIANG L. ZHANG. Can. J. Chem. **70**, (1992).

Il est bien connu que la transformation infinie de Kramers–Kronig est l'équivalent d'une transformation infinie de Hilbert qui est elle-même l'équivalent des intégrales allied Fourier. On peut donc réaliser une transformation de Hilbert en utilisant des routines rapides de transformation de Fourier. Pour une base de données contenant 7000 points, une telle réalisation est généralement 60 fois plus rapide qu'une transformation de Kramers–Kronig. Dans ce travail, on montre que, pour des transformations entre des indices de réfraction réels et imaginaires, $n(\tilde{\nu})$ et $k(\tilde{\nu})$ dans $\hat{n} = n(\tilde{\nu}) + ik(\tilde{\nu})$, la transformation de Hilbert basée sur FFT est beaucoup moins ou aussi précise que la transformation de Kramers–Kronig suivant l'algorithme utilisé. La transformation de Kramers–Kronig, incorporant les formules de McLaurin pour trouver la valeur principale de l'intégrale, transforme des spectres $k(\tilde{\nu})$ en spectres $n(\tilde{\nu})$ qui sont précis à environ 0,05%. Quelques algorithmes rapportés dans la littérature pour la transformation de Hilbert ne conduisent qu'à une précision de 4%. On présente l'algorithme BZ qui peut être utilisé sur un ordinateur de laboratoire, opérant sous DOS, qui permet d'effectuer la transformation de Hilbert et qui donne des spectres $n(\tilde{\nu})$ précis à 0,05%. Pour la transformation $n(\tilde{\nu})$ en $k(\tilde{\nu})$, l'algorithme BZ conduit à une précision d'environ −0,2% pour la valeur la plus importante du spectre. Cette valeur se compare à une précision de 0,5% pour la transformation de Kramers–Kronig. Pour les cas où le spectre $k(\tilde{\nu})$ est tronqué aux faibles valeurs des nombres d'onde, on présente une méthode simple qui améliore la précision par un facteur d'environ 10 aux faibles valeurs des nombres d'onde de spectres $n(\tilde{\nu})$ obtenus par des transformations de Hilbert ou Kramers–Kronig de spectres $k(\tilde{\nu})$.

Mots clés : intensités infrarouges, indices de réfraction complexes, transformation de Kramers–Kronig, transformation de Hilbert, constantes optiques.

[Traduit par la rédaction]

Can. J. Chem. Downloaded from www.nrcresearchpress.com by 92.62.229.171 on 09/08/12
For personal use only.

Introduction

Equations [1*a*] and [1*b*] give the Kramers–Kronig transform (1, 2) between the optical constants (3–5), which are the real and imaginary components of the complex refractive index, $\hat{n}(\tilde{\nu}) = n(\tilde{\nu}) + ik(\tilde{\nu})$.

$$[1a] \quad n(\tilde{\nu}_i) - n(\infty) = \frac{2}{\pi} P \int_0^\infty \frac{\tilde{\nu}\, k(\tilde{\nu})}{\tilde{\nu}^2 - \tilde{\nu}_i^2} \, d\tilde{\nu}$$

$$[1b] \quad k(\tilde{\nu}_i) = -\frac{2\tilde{\nu}_i}{\pi} P \int_0^\infty \frac{n(\tilde{\nu}) - n(\infty)}{\tilde{\nu}^2 - \tilde{\nu}_i^2} \, d\tilde{\nu}$$

The real and imaginary components of the complex dielectric constant (6), $\hat{\epsilon}(\tilde{\nu}) = \epsilon'(\tilde{\nu}) + i\epsilon''(\tilde{\nu})$, are usually called the dielectric constant and the dielectric loss, respectively. The Kramers–Kronig transform between them (6) is obtained by replacing n and k by ϵ' and ϵ'' in eqs. [1]. Similarly, the Kramers–Kronig transform between the reflectance, $R(\tilde{\nu})$, and the phase, $\phi(\tilde{\nu})$, of reflection (4, 7, 8) can be written by substitution. The complex reflection is $\hat{r}(\tilde{\nu}) = r(\tilde{\nu}) \times e^{i\phi(\tilde{\nu})}$, and the reflectance, $R(\tilde{\nu})$, is $\hat{r}(\tilde{\nu}) \times \hat{r}^*(\tilde{\nu}) = |\hat{r}(\tilde{\nu})|^2$. Since $\ln \hat{r}(\tilde{\nu}) = \ln r(\tilde{\nu}) + i\phi(\tilde{\nu})$ and $\ln r(\tilde{\nu}) = 1/2 \ln R(\tilde{\nu})$, the Kramers–Kronig transform is obtained by substituting $(1/2 \ln R)$ for n and ϕ for k in eqs. [1].

The Kramers–Kronig transform has been used by several authors in recent years to aid the determination of the optical constants or dielectric constants from infrared transmission (9, 10), reflection (7, 11), or multiple attenuated total reflection (12, 13) spectra.

It is well known (6, 14–18) that the infinite Kramers–Kronig transform is equivalent to two successive Fourier

transforms, usually called the allied Fourier integrals. Stated more fully, the Kramers–Kronig transform is equivalent to the infinite Hilbert transform, provided that the real variable is an even function of wavenumber and the imaginary variable is an odd function of wavenumber, i.e., $n(\tilde{\nu}) = +n(-\tilde{\nu})$ and $k(\tilde{\nu}) = -k(-\tilde{\nu})$. Further, the Hilbert transform is equivalent to the allied Fourier integrals (6, 14–18). The Hilbert transform between the optical constants is shown in eqs. [2*a*] and [2*b*], and in eqs. [3*a*] and [3*b*] in its Fourier transform representation.

$$[2a] \quad n(\tilde{\nu}_i) - n(\infty) = \frac{1}{\pi} P \int_{-\infty}^{\infty} \frac{k(\tilde{\nu})}{\tilde{\nu} - \tilde{\nu}_i} \, d\tilde{\nu}$$

$$[2b] \quad k(\tilde{\nu}_i) = -\frac{1}{\pi} P \int_{-\infty}^{\infty} \frac{n(\tilde{\nu}) - n(\infty)}{\tilde{\nu} - \tilde{\nu}_i} \, d\tilde{\nu}$$

$$[3a] \quad n(\tilde{\nu}) - n(\infty) = -2 \int_0^{\infty} dt \cos(2\pi c\tilde{\nu}t) \int_{-\infty}^{\infty} k(\tilde{\nu}) \sin(2\pi c\tilde{\nu}t) \, d\tilde{\nu}$$

$$[3b] \quad k(\tilde{\nu}) = -2 \int_0^{\infty} dt \sin(2\pi c\tilde{\nu}t) \int_{-\infty}^{\infty} [n(\tilde{\nu}_i) - n(\infty)] \cos(2\pi c\tilde{\nu}t) \, d\tilde{\nu}$$

For the remainder of this paper we will use the term Hilbert transform to mean the use of eqs. [3] to perform a Hilbert transform via fast Fourier transform routines. We have not used eqs. [2] at all.

The Kramers–Kronig transform is slow on most laboratory computers. For example, a fairly efficient program written in Microsoft Fortran version 5.0 and running under Microsoft DOS on a 16 MHz laboratory computer with an Intel 28386 cpu chip requires 13 min for the Kramers–Kronig transform of a spectrum containing 8192 data points. In contrast, fast Fourier transform (FFT) routines are available, which transform a data file of this length in seconds. The routines used by most FT-IR spectrometer systems to transform the interferogram into the spectrum are fast and can sometimes be used in application programs written by the user. Thus authors have described the use of FFT routines supplied by the instrument manufacturers to accomplish the Hilbert transform (19, 20). Other authors have described the use of FFT routines to Hilbert transform largely specular reflection data (16–18).

We have recently developed computer programs that run under Microsoft DOS to permit more efficient computation of our spectral data than on the Aspect 2000 computer of our (1982) Bruker IFS 113V FT-IR spectrometer. To check our programs, we have used the classical damped harmonic oscillator model (21–23) to synthesize real and imaginary refractive index spectra. This model calculates, for dielectric loss bands that are essentially Lorentzian in shape, the correct real refractive index spectrum to accompany the calculated imaginary refractive index spectrum.

This work began when we compared these correct real refractive index spectra with those obtained by Hilbert transformation of the imaginary refractive index spectra using our original algorithm (20). Unless all of the bands are very sharp, which is frequently not the case for liquids, the Hilbert $n(\tilde{\nu})$, i.e., the $n(\tilde{\nu})$ spectrum obtained by Hilbert transform, deviates by several percent from the correct result.

We have also obtained the $n(\tilde{\nu})$ spectra by Kramers–Kronig (KK) transformation of the imaginary refractive index spectra. The KK $n(\tilde{\nu})$ spectra differ significantly from the Hilbert $n(\tilde{\nu})$ spectra, but are, however, in excellent agreement with the correct ones. Exceptions occur if the imaginary refractive index is not near zero at the low-wavenumber limit of the spectrum.

At about the time that we discovered the discrepancies between the Hilbert and KK transforms empirically, Bracewell (24) reported that discrepancies are to be expected, but he gave no details of their magnitude. Thus, the appealing very fast method of Hilbert transform gave results that are in considerable error, while the slow Kramers–Kronig transform gave correct answers. It was clearly worthwhile to explore whether the accuracy of the fast Hilbert transform method could be improved. Most previous authors considered the accuracy of the transform qualitatively. Only Ohta and Ishida (25) have addressed the accuracy of the Hilbert transform at this level.

In this paper we present the results of our exploration of the magnitude of the discrepancies between the correct $n(\tilde{\nu})$ spectra, the KK $n(\tilde{\nu})$ spectra, and the Hilbert $n(\tilde{\nu})$ spectra. We explore different literature algorithms for the Hilbert transform to determine the important parameters for accuracy. We present an algorithm that yields 0.05% agreement with the correct $n(\tilde{\nu})$ spectrum. In 1988 Ohta and Ishida (25) reported in less detail a similar study, which we have found very helpful. The algorithm we recommend from this work is similar to theirs, but uses symmetry to reduce the size of the transforms by a factor of two, and real variables rather than complex ones to speed computation.

The Hilbert transform also converts $n(\tilde{\nu})$ spectra to $k(\tilde{\nu})$ spectra, although we use this less frequently. For this Hilbert transform, we give an algorithm that yields very good agreement with the correct $k(\tilde{\nu})$ spectrum.

We also discuss procedures to follow when the experimental data are available over most of the fingerprint region, but do not extend to the very low wavenumbers where the imaginary refractive index often returns to near zero. This situation is common due to experimental limitations and difficulties. When the $k(\tilde{\nu})$ spectrum terminates at low wavenumber on a peak, rather than at $k(\tilde{\nu})$ values near zero, the real refractive index spectrum calculated by either the Kramers–Kronig transform or the Hilbert transform is seriously in error over the last several hundred wavenumbers. A method is presented that allows very good results to be obtained in those cases in which the entire $k(\tilde{\nu})$ spectrum is known. In such cases the $n(\tilde{\nu})$ spectrum can be calculated from the full $k(\tilde{\nu})$ as well as from the truncated version of it, so the accuracy of our method of treating the truncated spectrum can be evaluated. We believe this method also gives the best result available when the full $k(\tilde{\nu})$ spectrum is not known. But we cannot be sure of its accuracy in such cases until the influence of the missing part of the $k(\tilde{\nu})$ spectrum is known.

General methods

The Classical Damped Harmonic Oscillator model (21–23) gives eqs. [4*a*] and [4*b*] for the real and imaginary parts of the dielectric constant in terms of the wavenumbers, $\tilde{\nu}_j$, the

Can. J. Chem. Downloaded from www.nrcresearchpress.com by 92.62.229.171 on 09/08/12
For personal use only.

intensities, S_j, and the damping constants γ_j, of the oscillators.

$$[4a] \quad \epsilon'(\tilde{\nu}) = \epsilon'(\infty) + \sum_j \frac{S_j(\tilde{\nu}_j^2 - \tilde{\nu}^2)}{(\tilde{\nu}_j^2 - \tilde{\nu}^2)^2 + \gamma_j^2\tilde{\nu}^2}$$

$$[4b] \quad \epsilon''(\tilde{\nu}) = \sum_j \frac{S_j\gamma_j\tilde{\nu}}{(\tilde{\nu}_j^2 - \tilde{\nu}^2)^2 + \gamma_j^2\tilde{\nu}^2}$$

The optical constants $n(\tilde{\nu})$ and $k(\tilde{\nu})$ are calculated from these dielectric constants by eqs. [5]

$$[5a] \quad n(\tilde{\nu}) = \sqrt{(\sqrt{(\epsilon'(\tilde{\nu}))^2 + (\epsilon''(\tilde{\nu}))^2} + \epsilon'(\tilde{\nu}))/2}$$

$$[5b] \quad k(\tilde{\nu}) = \sqrt{(\sqrt{(\epsilon'(\tilde{\nu}))^2 + (\epsilon''(\tilde{\nu}))^2} - \epsilon'(\tilde{\nu}))/2}$$

In these equations, the intensity parameter S_j is related to the molecular dipole moment derivative, $\partial\mu/\partial Q_j$, in the approximation of mechanical and electrical harmonicity by $S_j = \{N/3\pi c^2\}(\partial\mu/\partial Q_j)^2 F_j^2$. Here N is the number of molecules in unit volume, c is the velocity of light in vacuum, and F_j^2 is the local field correction for a molecule in a liquid. In general theory, S_j is related to the sum of the squares of the molecular transition moments that contribute to the band, $|R_{v_j''v_j'}|^2$ by

$$S_j = \frac{8\pi^3}{3\,h\,c} \sum [\tilde{\nu}_j |R_{v_j''v_j'}|^2 (N_{v_j''} - N_{v_j'})]$$

where one must sum over all v_j'' states that are significantly populated.

Equations [4] and [5] were used to calculate corresponding pairs of $k(\tilde{\nu})$ and $n(\tilde{\nu})$ spectra through the Fortran program FHARM. The program reads ASCII input and produces spectral files in the **.SPC** format of Galactic Industries Spectracalc program.

In the first half of this work, the $k(\tilde{\nu})$ spectrum so calculated was entered into the Hilbert transform program under consideration, with the appropriate value for $n(\infty)$, and the $n_H(\tilde{\nu})$ spectrum was calculated. The $k(\tilde{\nu})$ spectrum was also entered into the Kramers–Kronig transform program, and the $n_K(\tilde{\nu})$ spectrum was calculated.

We are interested in obtaining values of $n(\tilde{\nu})$ to suitable accuracy, approximately 0.1% being all that our experimental absorption data can justify. Accordingly, we have chosen to show in most of our figures the percentage deviation of the Hilbert $n(\tilde{\nu})$ spectrum from the correct $n(\tilde{\nu})$ spectrum at each wavenumber, $100\{n_H(\tilde{\nu}) - n(\tilde{\nu})\}/n(\tilde{\nu})$. For the $n(\tilde{\nu})$ spectrum calculated via the Kramers–Kronig transform, we show $100\{n_K(\tilde{\nu}) - n(\tilde{\nu})\}/n(\tilde{\nu})$ to illustrate the accuracy.

For the purpose of demonstrating the actual error in the Hilbert transform routines it would be better to subtract the value of $n(\infty)$, and to compare $\Delta n_H(\tilde{\nu}) = n_H(\tilde{\nu}) - n(\infty)$ or $\Delta n_K(\tilde{\nu}) = n_K(\tilde{\nu}) - n(\infty)$ with $\Delta n = n(\tilde{\nu}) - n(\infty)$, because the transforms calculate these differences, which are converted to the $n_H(\tilde{\nu})$ and $n_K(\tilde{\nu})$ spectra simply by adding $n(\infty)$. We give this comparison for our initial and final Hilbert transform algorithms.

In the second half of this work, the $n(\tilde{\nu})$ spectra are entered into the Kramers–Kronig or Hilbert transform after subtracting $n(\infty)$ from each value, and the $k_K(\tilde{\nu})$ or $k_H(\tilde{\nu})$ spectra are calculated. In these cases the deviation of the calculated k from the correct one is calculated as a percentage of the largest k value in the spectrum to illustrate the accuracy of the transform.

TABLE 1. Parameters used for spectra[a] calculated from the classical damped harmonic oscillator model

j	$\tilde{\nu}_j$ (cm^{-1})	γ_j (cm^{-1})	S_j (cm^{-2})
Single band spectrum[b]			
1	1600	4	14 400
"Methanol" spectrum			
1	3346	250	280 000
2	2945	100	58 000
3	2833	50	25 000
4	1450	100	30 000
5	1115	30	2 500
6	1030	22	35 000
7	657	200	40 000
8	370	300	3 000
"Acetic acid" spectrum			
1	3543	100	50 000
2	3487	50	6 000
3	3416	200	150 000
4	3326	50	5 000
5	3248	140	50 000
6	3171	50	5 000
7	3139	200	25 000
8	3037	180	90 000
9	2937	50	3 000
10	2870	100	10 000
11	2794	100	5 000
12	2759	100	8 000
13	2622	150	40 000
14	1719	55	100 000
15	1634	100	40 000
16	1396	60	30 000
17	1280	80	70 000
18	1054	20	2 000
19	1014	30	7 500
20	925	250	38 000
21	887	30	2 000
22	723	250	50 000

[a]The spectra were calculated between 7800 and 50 cm^{-1}, data points are 0.964 cm^{-1} apart, and $n(\infty) = 1.325$.

[b]$\gamma_j = 50$ cm^{-1} was also used with $S_j = 180\,000$ and $\tilde{\nu}_j = 1600$ cm^{-1}.

The correct spectra

Three different types of spectra have been calculated via the classical damped harmonic oscillator model for this work. The first consists of a single band at 1600 cm^{-1} with a full width at half height (FWHH) ranging from 4 cm^{-1} up to 50 cm^{-1}. The second is a complex spectrum based on that of pure liquid methanol, and the third is a complex spectrum based on liquid acetic acid. The classical damped harmonic oscillator parameters used for these spectra are tabulated in Table 1. The $k(\tilde{\nu})$ and $n(\tilde{\nu})$ spectra are shown in Figs. 1–3. It should be noted that each $k(\tilde{\nu})$ spectrum is complete, i.e., contains completed bands. Thus, the k values at the highest and lowest wavenum-

Can. J. Chem. Downloaded from www.nrcresearchpress.com by 92.62.229.171 on 09/08/12
For personal use only.

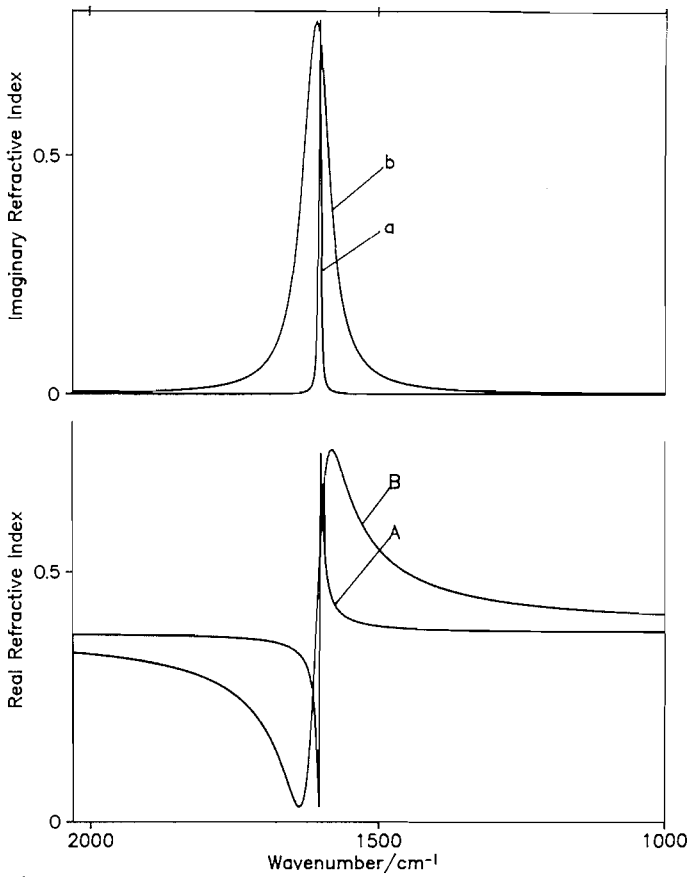

FIG. 1. Refractive index spectra calculated with the classical damped harmonic oscillator model. Single band spectra with FWHH 4 cm^{-1} and 50 cm^{-1} (Table 1).

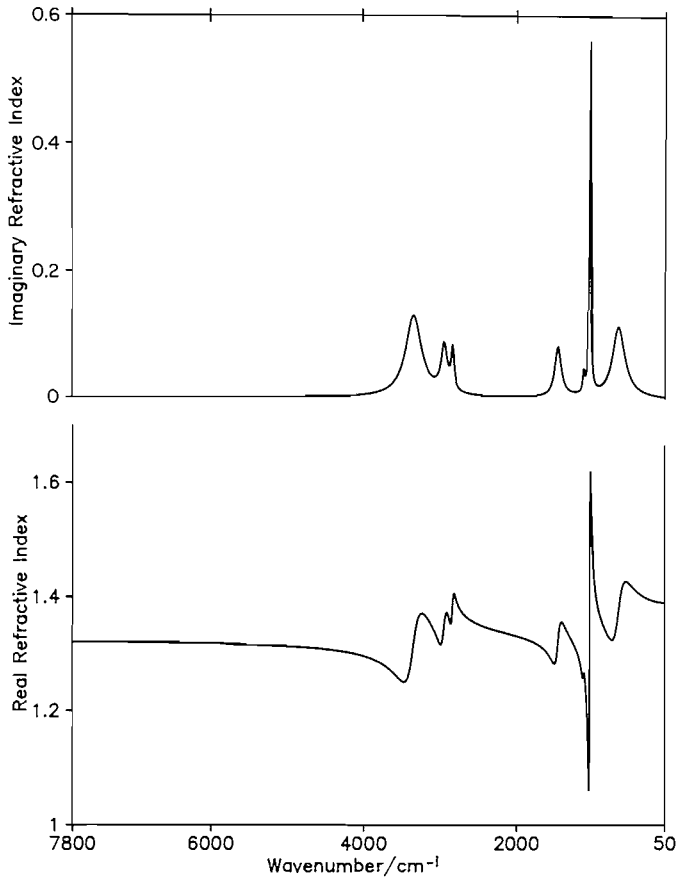

FIG. 2. Refractive index spectra calculated with the classical damped harmonic oscillator model. Simulated spectra of liquid methanol (Table 1).

ber points were about 10^{-5} of the peak value for the single band spectra and about one thousandth of the maximum peak height for the methanol and acetic acid simulations.

The Kramers–Kronig transform

A Fortran program, KKTRANS, for this transform was based on that included in program 46 of the National Research Council of Canada's Bulletins of Computer Programs for Infrared Spectroscopy (26). Several changes were made to improve the speed of the program on the laboratory computer by a factor of about eight, and a further factor of two was obtained by incorporating Ohta and Ishida's (25) Maclaurin formula method of calculating the principal value of the integral. This latter feature also considerably improved the accuracy of the transform near the intense peaks. Program KKTRANS takes 13 min to transform a file containing 8192 REAL (4 byte) data points on our 16 MHz 386SX computer with a 387 math coprocessor. It reads and writes files in the **.SPC** format of Spectracalc.

Hilbert transforms

The Hilbert transform via two successive fast Fourier transforms (FFTs), following eqs. [3], consists of the following five steps.

Step 1. Arranging the input spectral data into the appropriate form

Step 2. The first FFT

Step 3. Arranging the output of the first FFT into the appropriate form

Step 4. The second FFT

Step 5. Obtaining the desired spectrum from the output of the second FFT.

The details of the first, third, and fifth step depend on the algorithm used for the Hilbert transform, and depend on whether the transform is from $k(\tilde{\nu})$ to $n(\tilde{\nu})$ or vice versa. These features will be discussed in the Results sections.

The FFT is common to all algorithms, but may be used to transform real data or complex data. The output is complex in both cases, but is written into two arrays of real variables. To improve execution speed, complex variables are not used.

We tested four FFT subroutines by ensuring that they give the transform of a Gaussian peak of unit height correct (15, 27) to six decimal places. All subroutines gave correct transforms, and we chose to use the fastest subroutine, the Fortran subroutine described by Ng and Horlick (28). This subroutine is based on the algorithm first suggested by Gentleman and Sande (in ref. 29), and its listing is in the Ph.D. thesis of Ng (30). It is also given in the appendix to this paper, because there is a version of it in circulation that contains incorrect signs.

The subroutine is written with real variables to find the

Can. J. Chem. Downloaded from www.nrcresearchpress.com by 92.62.229.171 on 09/08/12
For personal use only.

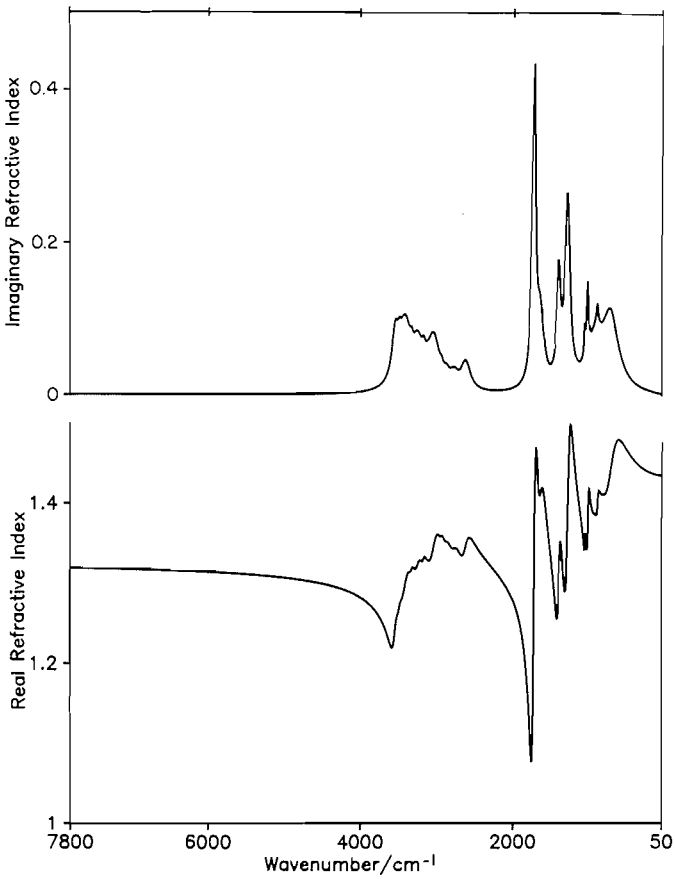

FIG. 3. Refractive index spectra calculated with the classical damped harmonic oscillator model. Simulated spectra of liquid acetic acid (Table 1).

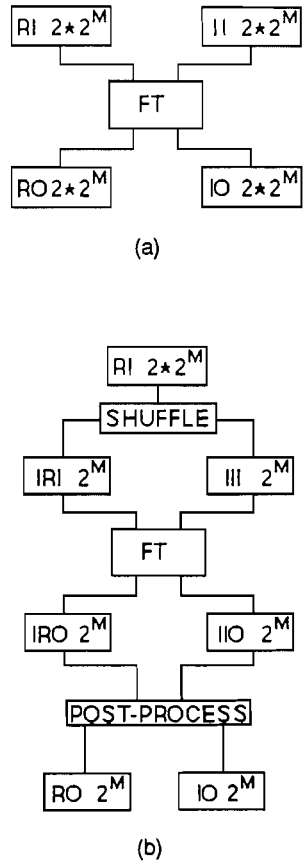

FIG. 4. Schematic representation of the fast Fourier transform subroutine used in this work. (a) The COMPLEX data mode; (b) The REAL data mode.

complex Fourier transform of a real function. It consists of three phases. (*a*) The "shuffle" of the real input array into half-sized real and imaginary input arrays to a complex FFT. (*b*) The complex FFT of real and imaginary input arrays to real and imaginary output arrays. (*c*) The "post-processing" phase to reconstruct the complex FFT of the original real input array. The shuffle consists of placing the odd- and even-indexed points of the real input array into the real and imaginary, respectively, arrays input to the complex FFT. The post-processing phase is that described by Zachor in an advertisement (31).

As noted above, this subroutine can be used in its REAL mode to obtain the complex transform of real data, or in its COMPLEX mode to obtain the transform of complex data. The REAL mode uses all three phases of the subroutine, while the COMPLEX mode uses only the middle phase. We have found the diagrams shown in Fig. 4 to be helpful illustrations of these two modes. In Fig. 4, RI, IO, etc. stand for Real Input, Imaginary Output, etc., and IRI, IIO, etc. stand for Intermediate Real Input, Intermediate Imaginary Output, etc. Figure 4 also notes that a Real Input array of size 2×2^M in REAL mode yields all other arrays of size 2^M. In COMPLEX mode all arrays have the same size.

The details of the use of this subroutine in the different Hilbert transform algorithms is given in the Results sections. All of our programs that use this subroutine read and write spectral files in the **.SPC** format of Spectracalc.

Results: transforms from $k(\tilde{\nu})$ to $n(\tilde{\nu})$ for complete $k(\tilde{\nu})$ spectra

We present first the results for those cases in which the $k(\tilde{\nu})$ spectrum is complete. Results for cases in which the $k(\tilde{\nu})$ spectrum contains incompleted bands at the lowest wavenumbers will be discussed later. It should be noted that all of our spectral files start at high wavenumber and run to low wavenumber.

Kramers–Kronig transforms

Figure 5 shows the percent deviation of the $n_K(\tilde{\nu})$ values calculated via KKTRANS from the $k(\tilde{\nu})$ spectra of Figs. 1–3. The greatest deviation of the n_K values from the correct ones is 0.07% for the single band of 4 cm^{-1} FWHH, 0.004% for the single band of 50 cm^{-1} FWHH, and 0.05% for the complex spectra. Thus, to the accuracy of our experimental data, program KKTRANS gives the correct $n(\tilde{\nu})$ spectrum, provided the $k(\tilde{\nu})$ spectrum is complete.

Hilbert transforms

Our original Hilbert transform algorithm

This has been described only in general terms (20). It uses the FFT subroutine in REAL mode (Fig. 4).

Consider a $k(\tilde{\nu})$ spectrum that contains NP data points. Step 1 of the Hilbert transform consists of three actions. First, adding zeros to the (low-wavenumber) end of the spectral data to make the number of points a power of 2, 2^M, as required by the FFT subroutine. Second, adding a zero point. Third, folding the file about that zero point to create a symmetrical

Can. J. Chem. Downloaded from www.nrcresearchpress.com by 92.62.229.171 on 09/08/12
For personal use only.

Can. J. Chem. Downloaded from www.nrcresearchpress.com by 92.62.229.171 on 09/08/12
For personal use only.

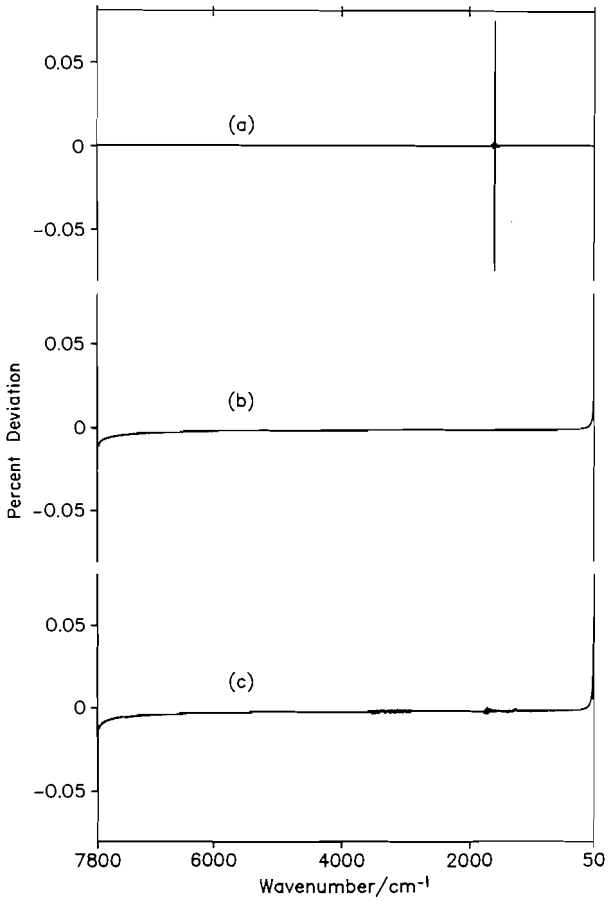

FIG. 5. Percent deviations from the correct spectra of $n(\tilde{\nu})$ spectra calculated by Kramers–Kronig transformation of $k(\tilde{\nu})$. Curve (a), Single band $k(\tilde{\nu})$, FWHH = 4 cm^{-1}; curve (b), simulated methanol spectrum; curve (c), simulated acetic acid spectrum.

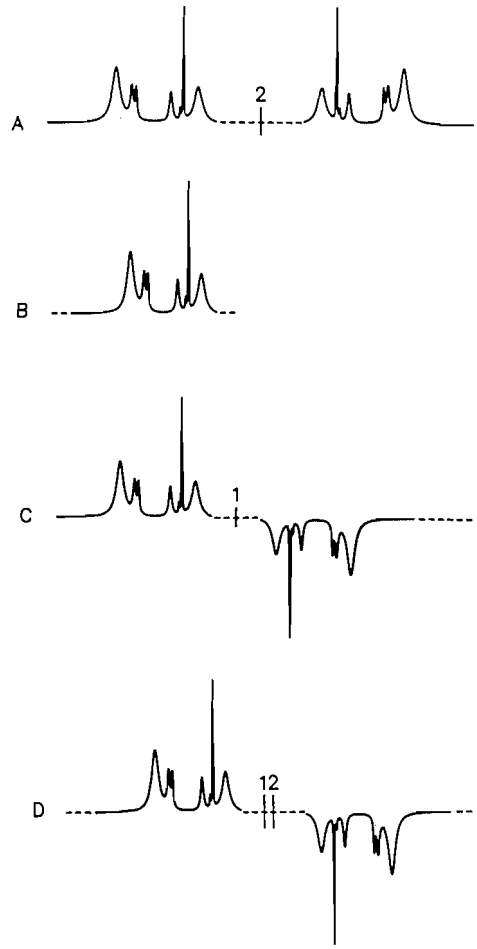

FIG. 6. Schematic representation of the input arrays to step 2 of the Hilbert transform algorithms. Curve A, Our original algorithm; curve B, Marshall's algorithm; curve C, Ohta and Ishida's algorithm; curve D, the BZ algorithm, our preferred algorithm. 1 indicates a zero value at 0 cm^{-1}; 2 indicates an additional zero value added as a folding or inverting centre.

array centered on the added zero. In fact the array is not quite symmetrical, because the first data point in the file must be omitted from its folded position at the end of the file to keep the number of points equal to a power of 2 (2×2^M). Figure 6, curve A, shows the resulting real input array schematically. This array is then input to step 2, the FFT in REAL mode.

The FFT of this real array consists of a zero imaginary transform array and a nonzero real transform array, both of size 2^M. Step 3 of this algorithm consists of 2 actions, replacing the second half of the real transform array by zeros and adding an additional 2^M zeros to restore the file to the full length of the real input to step 2. The resulting file is put into step 4, the FFT in REAL mode.

Step 5 of this algorithm is to obtain the NP values of $-\Delta n_H(\tilde{\nu}) = n(\infty) - n(\tilde{\nu})$ from the first NP points in the imaginary transform array, with wavenumber decreasing with increasing point index, and to subtract them from $n(\infty)$ to obtain the desired $n(\tilde{\nu})$ in the same wavenumber sequence as in the original $k(\tilde{\nu})$ array with NP points.

This algorithm programmed in Fortran takes 14 s to Hilbert transform an 8192-point $k(\tilde{\nu})$ spectrum.

This Hilbert transform program was checked in 1983 before it was used. However, the check was made using the single-band $k(\tilde{\nu})$ spectrum shown in Fig. 1, with a 4 cm^{-1} FWHH, by comparing the correct and Hilbert $n(\tilde{\nu})$ spectra (curves (a) and (b) of Fig. 7, lower box). The agreement appears very good. If the percent deviation is compared (curve (B) of Fig. 7, upper box) the agreement appears less good. As the FWHH of the single band is increased, problems become evident, as curve (C) of Fig. 7 upper shows for a single band of FWHH 50 cm^{-1}. If a more complex spectrum is used, the magnitude of the problem that initiated this work is seen. Curves (a) and (b) of Fig. 8 lower show the correct $n(\tilde{\nu})$ spectrum for the simulated methanol $k(\tilde{\nu})$ spectrum of Fig. 2 and that calculated from this Hilbert transform program. Curve (B) of Fig. 8 upper shows the percent deviation. Recall that the KK transform gave exact results for this spectrum (Curve (C) of Fig. 8). Clearly this Hilbert transform program yields an error in $n(\tilde{\nu})$ that increases in magnitude with decreasing wavenumber, from +0.3% to −4%. The error in the quantity actually calculated by the Hilbert transform, $\Delta n_H(\tilde{\nu}) = n(\tilde{\nu}) - n(\infty)$, reaches 80% at the lowest wavenumber.

Marshall's Hilbert transform algorithm

We turned next to an algorithm presented by Marshall and co-workers (32, 33). This was presented for the transformation of electron spin resonance absorption spectra to dis-

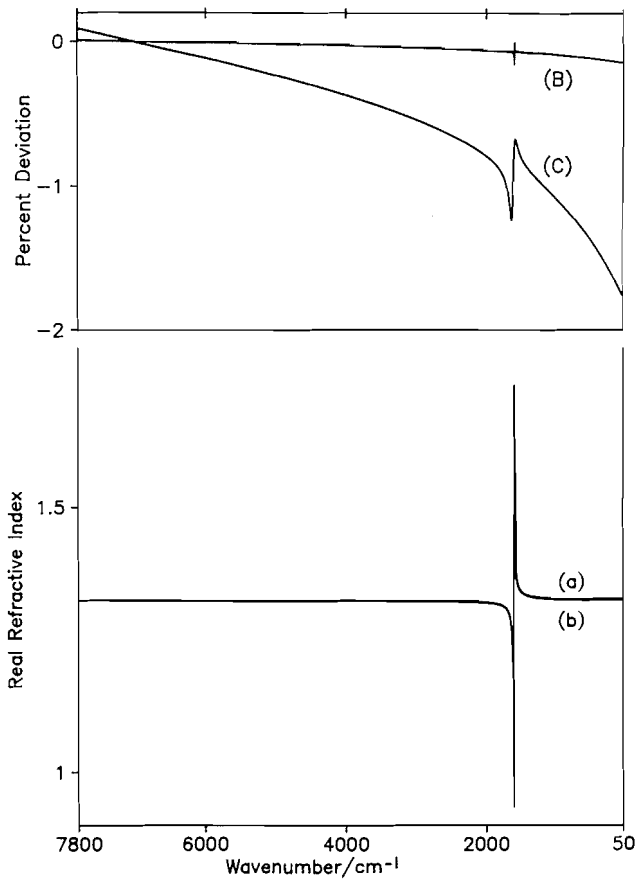

FIG. 7. Results for our original Hilbert transform algorithm. Lower box: curve (a), correct $n(\tilde{\nu})$ spectrum, single band, FWHH = 4 cm^{-1} (Fig. 1, Table 1); curve (b), $n_H(\tilde{\nu})$ calculated by Hilbert transformation of the corresponding $k(\tilde{\nu})$ spectrum. Curves (a) and (b) are indistinguishable on this scale. Upper box: percent deviation of the Hilbert transformed $n_H(\tilde{\nu})$ from the correct $n(\tilde{\nu})$ for: curve (B), single band spectrum, FWHH = 4 cm^{-1}; curve (C), single band spectrum, FWHH = 50 cm^{-1}.

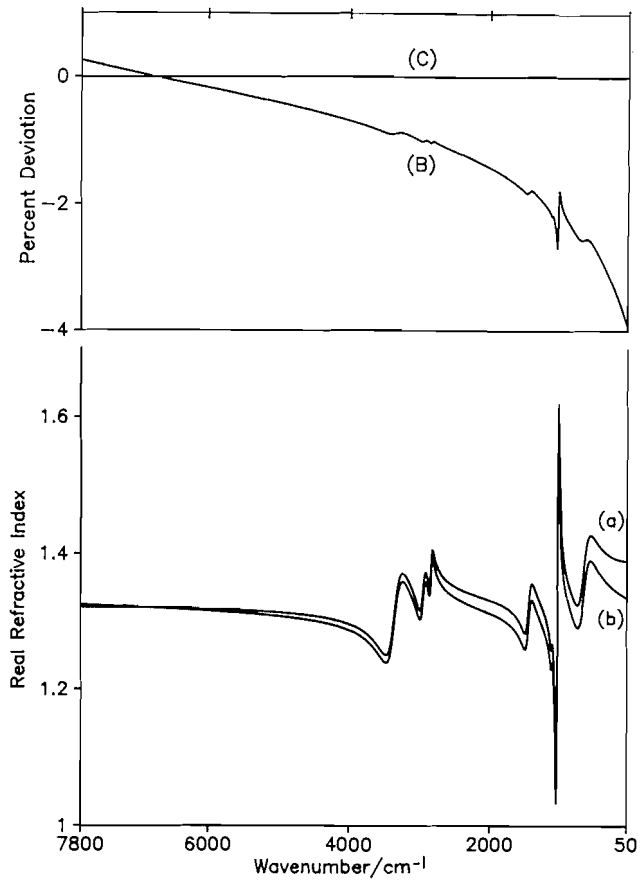

FIG. 8. Results for the simulated methanol spectrum (Fig. 2). Lower box: (a) correct $n(\tilde{\nu})$ and (b) our original Hilbert transformed $n_H(\tilde{\nu})$ spectra. Upper box: percent deviations from the correct $n(\tilde{\nu})$ spectrum of Kramers–Kronig transformed $n_K(\tilde{\nu})$ spectrum (curve (C)) and our original Hilbert transformed $n_H(\tilde{\nu})$ spectrum (curve (B)).

persion spectra, but the theoretical considerations are identical (33) to those for optical absorption and dispersion.

This algorithm uses the FFT in its COMPLEX mode. Step 1 is to add zeros to increase the number of data points to 2^M from the NP $k(\tilde{\nu})$ values. These zeros are added symmetrically, i.e., half at the beginning of the array and half at the end. The resulting array is shown schematically in Fig. 6 curve B. This array is input as the real array to step 2, the FFT in COMPLEX mode, and an array of zeros is input as the imaginary array. The FFT of this complex input is complex, with nonzero real and imaginary transform arrays. Step 3 of this algorithm is to negate the second half of the real and imaginary transform arrays. These arrays are then input to the complex FFT in step 4. The $\Delta n(\tilde{\nu})$ values are found in the imaginary transform array output from step 4. The $\Delta n(\tilde{\nu})$ value for the highest wavenumber is at point index $\{2^{M+Z} - 0.5\,(2^{M+Z} - 2^M) + 1\}$, where Z is the level of zero-filling used (see below), and they run to lower point indices with decreasing wavenumber.

This algorithm takes about the same time as the previous one. The result for the simulated methanol spectrum (Fig. 2) is shown as curve (a) in Fig. 9. The percent deviations cover a 4% range, as for the previous algorithm, but range

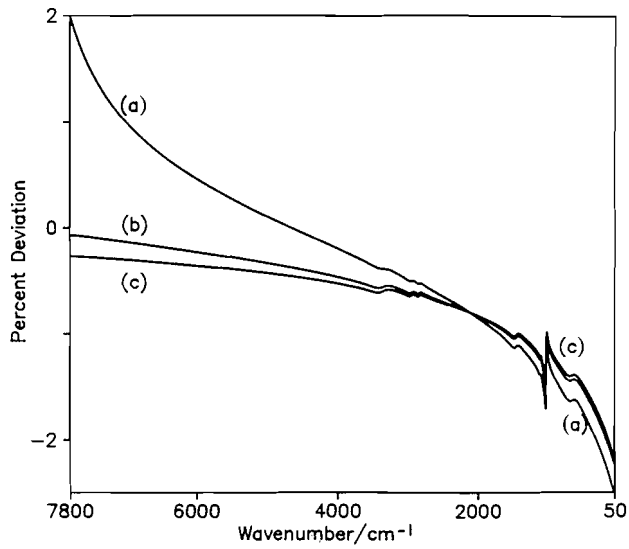

FIG. 9. Results for Marshall's Hilbert transform algorithm applied to the simulated methanol spectrum (Fig. 2). Percent deviations from the correct $n(\tilde{\nu})$ spectrum of the Hilbert $n_H(\tilde{\nu})$ spectrum transformed with no zero-filling (curve (a)), one level of zero-filling (curve (b)), and two levels of zero-filling (curve (c)).

Can. J. Chem. Downloaded from www.nrcresearchpress.com by 92.62.229.171 on 09/08/12
For personal use only.

Can. J. Chem. Downloaded from www.nrcresearchpress.com by 92.62.229.171 on 09/08/12
For personal use only.

from +2% to −2%. The agreement can be improved to some extent by additional zero-filling. To use one level of zero-filling you add, in step 1 of the algorithm, 2^M zero points to the 2^M points described above. These points are added symmetrically, half at the beginning and half at the end of the array, leaving the rest of the algorithm as described. The result for one level of zero-filling is shown as curve (b) of Fig. 9. One level of zero-filling considerably improves the accuracy at the high-wavenumber end of the spectrum, reducing the percent deviation to about −0.1%, but does little to improve the low-wavenumber end of the $n(\tilde{\nu})$ spectrum. A second level of zero-filling[1] (curve (c) of Fig. 9) makes little improvement. The errors involved in both of these algorithms are too large to allow them to be used with current experimental data.

Ohta and Ishida's Hilbert transform algorithm

At this stage of our study we became aware of the recent paper by Ohta and Ishida (25) who carried out a similar study. We programmed the algorithm they concluded was the most accurate. They emphasized the importance of continuing the data set to 0 cm^{-1}, and of folding the data to simulate $k(-\tilde{\nu}) = -k(\tilde{\nu})$. The latter is in keeping with the condition under which the Hilbert transform is equivalent to the Kramers–Kronig transform, while the former ensures that the correct phase relationship is maintained between the data for $\tilde{\nu}$ and that for $-\tilde{\nu}$.

Ohta and Ishida's algorithm uses the FFT in its COMPLEX mode. In step 1 of the algorithm, the $k(\tilde{\nu})$ spectrum, which consists of NP data points extending from XSP to XEP cm^{-1}, is extended to 0 cm^{-1} by adding N_1 zeros, and is then inverted in the zero wavenumber point to yield an array of 2(NP + N_1) −1 points, which is antisymmetric about the 0 cm^{-1} point. $2N_2 + 1$ zero points are then added to the end of the array to make the array contain 2×2^M points. The resulting array is shown schematically as curve C in Fig. 6. This array forms the real input array to the FFT of step 2, with an array of zeros as the imaginary input array.

The FFT of this complex input consists of nonzero real and imaginary transform arrays, each containing 2×2^M points. In step 3 of this algorithm, the second half of each transform array is replaced with zeros. The resulting real and imaginary arrays form the real and imaginary, respectively, inputs to step 4. In step 5, the values of $\Delta n_H(\tilde{\nu}) = n_H(\tilde{\nu}) - n(\infty)$ are obtained from the imaginary array. However, we found that they are not in the first 2^M points of the imaginary output as stated in Ohta and Ishida's paper, but they start at point $2N_2 + 3$ for the highest wavenumber and proceed to increasing index for decreasing wavenumber.

This algorithm uses arrays that are twice as long as those of previous algorithms, so it takes twice as long to execute. The result for the simulated methanol spectrum is shown in Fig. 10, curve (a). The percent deviations are now −0.4% at the high-wavenumber end and reduce to −0.2% at the low-wavenumber end of the spectrum. If one level of zero-filling is used, by simply adding a further 2×2^M zero points to the end of the array in step 1, the agreement is improved to about 0.07% (curve (b) of Fig. 10), but the program then takes twice as long to execute, about 70 s for a spectrum containing between 4096 and 8192 data points. The same result was found for the simulated acetic acid spectrum (Fig. 3).

[1]The second level of zero-filling consists of adding 2^M zero points to each end of the data set used for one level of zero-filling.

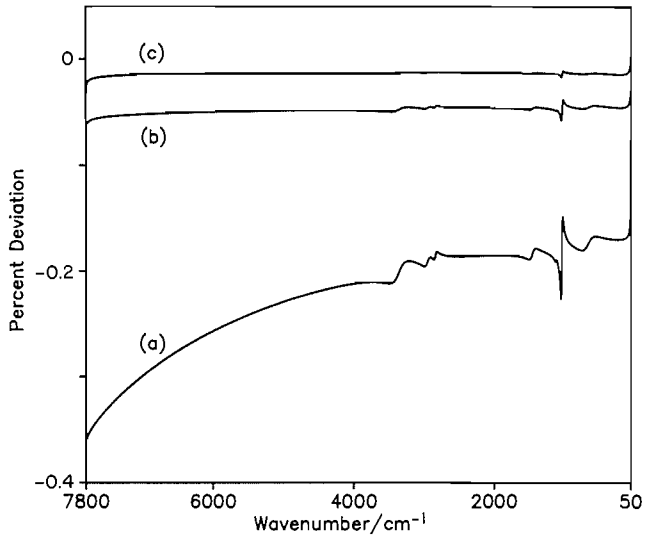

FIG. 10. Results for the simulated methanol spectrum (Fig. 2). Curves (a) and (b): percent deviations from the correct $n(\tilde{\nu})$ of Ohta and Ishida's Hilbert transformed $n_H(\tilde{\nu})$, calculated with no zero-filling (curve (a)) and one level of zero-filling (curve (b)). Identical results were obtained from the BZ algorithm, our preferred algorithm. Curve (c), percent deviation from the correct $n(\tilde{\nu})$ of $n_H(\tilde{\nu})$ calculated by the BZ algorithm with two levels of zero-filling.

The BZ algorithm: our preferred algorithm

We have built on the indication from Ohta and Ishida's work that it is important to extend the data to 0 cm^{-1}, thus maintaining the correct phase difference between $k(-\tilde{\nu})$ and $k(\tilde{\nu})$, and to ensure that $k(-\tilde{\nu}) = -k(\tilde{\nu})$. In fact eqs. [2] and [3] suggest that the equivalence of the Hilbert and Kramers–Kronig transforms hinges on these two points, in spite of their omission from some current algorithms.

Accordingly, step 1 of this algorithm consists of extending the $k(\tilde{\nu})$ spectrum, which contains NP points between XSP and XEP cm^{-1}, to 0 cm^{-1} by adding zeros, adding an extra zero, inverting the array in this added zero point to generate an antisymmetric array, then adding N_2 zero points to the beginning of the file and $N_2 - 1$ zero points to the end of the file, to generate an antisymmetric array of length 2×2^M. This array is shown schematically in Fig. 6 as curve D.

This algorithm uses the FFT in its REAL mode, and the array is input as the real input to the FFT in step 2. The transform consists of a zero real transform array and a nonzero imaginary transform array, each of length 2^M. In step 3 of the algorithm, the second half of the imaginary transform array is zeroed, and a further 2^M zeros are added to the end of the array. The resulting array is the real input to the FFT in step 4. Step 5 of the algorithm is to obtain the $\Delta n_H(\tilde{\nu}) = n_H(\tilde{\nu}) - n(\infty)$ values from the real transform array from step 4, starting at the $N_2 + 1$ point for the highest wavenumber and running to increasing index for decreasing wavenumber. This algorithm uses arrays half as large as those of Ohta and Ishida's method, but gives identical results to those shown in Fig. 10. We show as curve (c) of Fig. 10 the result with this, our preferred, algorithm, which was obtained with two levels of zero-filling. This level of zero-filling is not possible with Ohta and Ishida's algorithm under the memory limitations of Microsoft DOS, because of their

Can. J. Chem. Downloaded from www.nrcresearchpress.com by 92.62.229.171 on 09/08/12
For personal use only.

double length arrays. The percent deviation with two levels of zero-filing is up to 0.05%, which is the same as the percent deviation from the Kramers–Kronig transform. The same result was found for the simulated acetic acid spectrum. For single band spectra, the maximum percent deviation using two levels of zero-filling was 0.15% for 4 cm^{-1} FWHH and 0.007% for 50 cm^{-1} FWHH.

It is not immediately obvious why the BZ algorithm and that of Ohta and Ishida give identical results. In fact the identity stems from the FFT routines. To the FFT, Ohta's input array is identical to ours except that it is phase-shifted by a constant amount for each point. Thus neither the real nor the imaginary transform arrays from step 2 of Ohta and Ishida's algorithm is zero while the real one is zero in our algorithm. Provided both of the transform arrays are used in step 4, Ohta and Ishida's method allows correctly for their asymmetrical input, but at the expense of using larger arrays.

Summary

The FFT-based Hilbert transform of $k(\tilde{\nu})$ to $n(\tilde{\nu})$ can be as accurate as the Kramers–Kronig transform, provided the $k(\tilde{\nu})$ spectrum is extended with zeros to 0 cm^{-1}, and provided it is then inverted to yield an antisymmetric array to input to the FFT. The percent deviation of the calculated $n(\tilde{\nu})$ from the correct values is up to 0.05% for complex spectra.

It has been noted that this percent deviation is $100\{n_H(\tilde{\nu}) - n(\tilde{\nu})\}/n(\tilde{\nu})$, which overestimates the accuracy of the computation of the Hilbert transform that actually calculates $\Delta n_H(\tilde{\nu}) = n_H(\tilde{\nu}) - n(\infty)$. A percent deviation of 0.05% in n_H corresponds to a percent deviation of about 1% in $\Delta n_H(\tilde{\nu})$. The accuracy appears to be limited by the resolution with which the first Fourier transforms are defined. Zero-filling increases this resolution, and leads to a more accurate result for $\Delta n_H(\tilde{\nu})$ from the second transform.

In passing it should be noted that the addition of an extra zero point after the 0 cm^{-1} point in some of the algorithms is not essential. For the BZ algorithm, omission of this extra zero causes the $\Delta n_H(\tilde{\nu})$ output to start at point $N_2 + 2$ instead of at $N_2 + 1$, and for Ohta's algorithm its inclusion causes the $\Delta n_H(\tilde{\nu})$ output to start at point $2N_2 + 1$ instead of $2N_2 + 3$.

We have tested the effect of relaxing the requirements of extending the data to zero and making the $k(\tilde{\nu})$ spectrum antisymmetric. We have used the BZ algorithm, but (*a*) without extending the $k(\tilde{\nu})$ spectrum to 0 cm^{-1}, and (*b*) extending it to 0 cm^{-1} but folding the array to make a symmetrical array instead of inverting it to make an antisymmetrical array. In case (*b*) the accuracy of the results was as poor as that in our original method and Marshall's method. In case (*a*), the accuracy at high wavenumber was essentially the same as for the BZ algorithm, but deteriorated at low wavenumbers. The deterioration was to 0.4% and 1% when the lowest wavenumbers in the $k(\tilde{\nu})$ spectrum were 50 and 250 cm^{-1}, respectively. Thus both requirements are necessary for results accurate to 0.05 to 0.1%.

Results: transform from $n(\tilde{\nu})$ to $k(\tilde{\nu})$

We have based an algorithm for Hilbert transformation from $n(\tilde{\nu})$ to $k(\tilde{\nu})$ on the BZ algorithm for $k(\tilde{\nu})$ to $n(\tilde{\nu})$, with the necessary logical changes. First $n(\tilde{\nu}_{MAX})$ is subtracted from the $n(\tilde{\nu})$ to give $\Delta n(\tilde{\nu})$. The $\Delta n(\tilde{\nu})$ spectrum is then extended to 0 cm^{-1} by adding the value of $\Delta n(\tilde{\nu})$ at the lowest wavenumber instead of by adding zeros. The extra point below 0 cm^{-1} is added, not as a zero but as the value of $\Delta n(\tilde{\nu})$ at the lowest wavenumber, and the array is then folded about this point to create an array that is symmetrical. N_2 zero points are then added to the beginning of the array and $N_2 - 1$ are added to the end, to create a symmetric array of length 2×2^M.

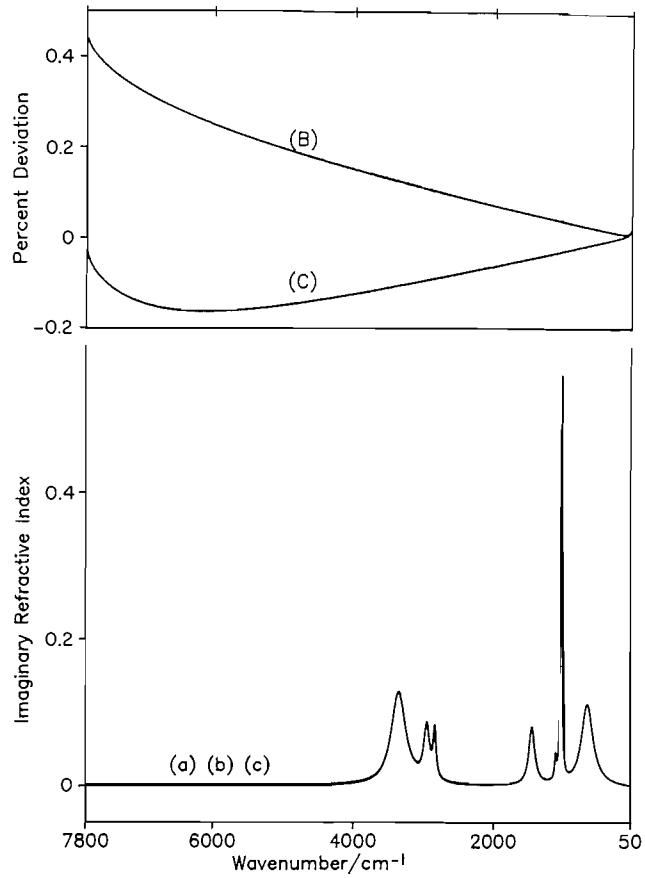

FIG. 11. Results of Kramers–Kronig and Hilbert transforms from $n(\tilde{\nu})$ to $k(\tilde{\nu})$. Lower box, the correct $k(\tilde{\nu})$ (curve (a)) and those calculated by KK (curve (b)) and Hilbert (curve (c)) transformation of the simulated $n(\tilde{\nu})$ spectrum of methanol. The three are indistinguishable on this scale. Upper box, deviations of the transformed $k(\tilde{\nu})$ from the correct $k(\tilde{\nu})$ as a percentage of the largest k value in the spectrum (Fig. 2) for the KK transform (curve (b)) and the BZ Hilbert transform (curve (c)).

If the $\Delta n(\tilde{\nu})$ spectrum is extended to 0 cm^{-1} with zeros, the calculated $k(\tilde{\nu})$ decreases steadily with decreasing wavenumber to a value −10% of the highest peak. If the extra point is zero instead of the constant value, the discontinuity on the input to the FFT causes ripples on the transform.

This array is the real input to the FFT in REAL mode in step 2 of the Hilbert transform algorithm. The Fourier transform consists of a zero imaginary array and a nonzero real array, both of size 2^M. In step 3 of the algorithm, the second half of the real transform is zeroed, and a further 2^M zero points are added to the end of the array. The resulting array is input to the FFT in step 4 and in step 5 the $k(\tilde{\nu})$ spectrum is obtained from the imaginary transform array from step 4, starting at the $N_2 + 1$ point for the highest wavenumber and running to increasing index with decreasing wavenumber.

Figure 11 shows the results obtained for the simulated methanol spectrum of Fig. 2. The lower box contains the correct $k(\tilde{\nu})$ spectrum (curve (a)), that calculated by Kramers–

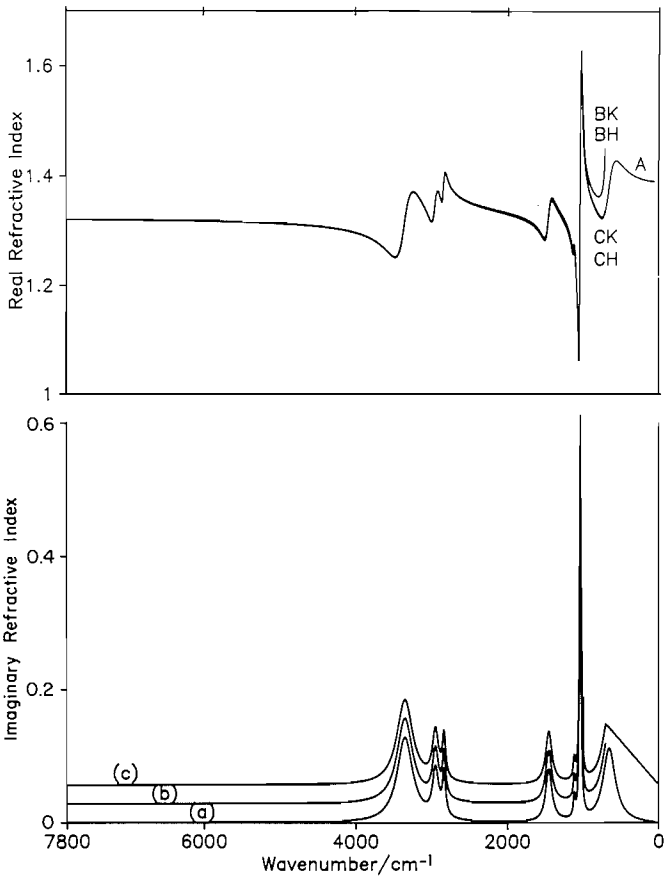

FIG. 12. $k(\tilde{\nu})$ to $n(\tilde{\nu})$ transform of truncated $k(\tilde{\nu})$ files. Lower box: curve (a), the complete $k(\tilde{\nu})$ spectrum; curve (b), the $k(\tilde{\nu})$ spectrum truncated at 700 cm^{-1}; curve (c), curve (b) extended linearly to 0 at 0 cm^{-1}; curves (b) and (c) are offset for clarity. Upper box: curve A, the correct $n(\tilde{\nu})$ spectrum; curves BK and CK, $n_K(\tilde{\nu})$ obtained by KK transformation of curves (b) and (c) of the lower box; curves BH and CH, $n_H(\tilde{\nu})$ obtained by BZ Hilbert transformation of curves (b) and (c) of the lower box.

Kronig transform (curve (b)), and that calculated by this BZ Hilbert transform (curve (c)). The KK transform is slightly higher than the other two at high wavenumbers. The upper box shows the deviation of the calculated and correct k values as a percentage of the largest k value in the spectrum for the Kramers–Kronig transform (curve B) and for the BZ Hilbert transform (curve C). The maximum deviation is about -0.2% of the largest k value for the Hilbert transform and about $+0.5\%$ for the Kramers–Kronig transform. The same result was obtained for acetic acid. For single band spectra (Fig. 1) deviations were smaller; the greatest deviation for the BZ Hilbert transform was 0.06% for FWHH = 4 cm^{-1} and -0.04% for FWHH = 50 cm^{-1}, and for the KK transform 0.07% for 4 cm^{-1} FWHH and +0.1% for 50 cm^{-1}. For 4 cm^{-1} FWHH the deviations were on the sides of the peak while for 50 cm^{-1} FWHH and the complex spectra they were as shown in Fig. 11, upper. Zero-filling does not improve the accuracy of our $n(\tilde{\nu})$ to $k(\tilde{\nu})$ Hilbert transforms.

Results: transforms from $k(\tilde{\nu})$ to $n(\tilde{\nu})$ for truncated $k(\tilde{\nu})$ spectra

It frequently happens that experimental $k(\tilde{\nu})$ spectra are incomplete and end halfway up an absorption band rather than in the baseline. In such cases neither Kramers–Kronig nor Hilbert transforms can be expected to give correct results, indeed the correct results are unknown. Sometimes, however, the complete spectrum is known, but it is necessary to refine a partial spectrum on its own before merging it with previously recorded spectra to cover a broader wavenumber range. Thus it is of interest to explore whether modifications can be made to a $k(\tilde{\nu})$ spectrum that terminates above the baseline, in order to improve the $n(\tilde{\nu})$ spectrum calculated from it.

We have found that a simple procedure similar to triangular apodisation usually improves the transformed result. Figure 12 shows in the lower box the full $k(\tilde{\nu})$ spectrum simulated for methanol (curve (a)), offset from the $k(\tilde{\nu})$ spectrum truncated at 700 cm^{-1} (curve (b)), which in turn is offset from the $k(\tilde{\nu})$ spectrum truncated at 700 cm^{-1} and linearly extended from the last point to $k = 0$ at 0 cm^{-1} (curve (c)). The upper box shows the correct $n(\tilde{\nu})$ spectrum (curve A) and those obtained by KK transformation (curves BK and CK) and by BZ Hilbert transformation (curves BH and CH). The $n(\tilde{\nu})$ spectra obtained by KK transformation are indistinguishable from those obtained by BZ Hilbert transformation in the figure. Comparison of curves BK and CK (or BH and CH) shows that the linear extension to low wavenumber improves the transform of the truncated file. Quantitatively, the percent deviations from the correct $n(\tilde{\nu})$ are reduced from about 10% to about 1%.

This method of extending the $k(\tilde{\nu})$ spectrum to zero at 0 cm^{-1} has been applied to acetic acid, and to many other test systems with and without peaks below the truncation point. It leads to an improvement in the deviations at low wavenumbers by a factor of about 10 in all cases.

Acknowledgements

J. E. B. thanks the Natural Sciences and Engineering Research Council of Canada for their support of this work. J. E. B. and S. L. Z. thank Dr. K. Ohta, Professor R. Wallace, and Professor W. R. Thorson for helpful discussions.

1. R. de L. Kronig. J. Opt. Soc. Am. **12**, 547 (1926); Physica, **3**, 1009 (1936).
2. H. A. Kramers. Atti Congr. Int. Fis. Como, **2**, 545 (1927).
3. S. Maeda and P. N. Schatz. J. Chem. Phys. **36**, 571 (1962).
4. F. Stern. Solid State Phys. **15**, 331 (1963).
5. E. E. Bell. Handbuch der Physik. *Edited by* S. Flugge. Vol. xxv/12a. Light and Matter 1a. *Edited by* L. Genzel. Springer-Verlag, Berlin, Heidelberg. 1967. pp. 28–31.
6. H. Frohlich. Theory of dielectrics. 2nd ed. Oxford University Press, London. 1958. p. 8.
7. F. C. Jahoda. Phys. Rev. **107**, 1261 (1957).
8. F. W. King. J. Chem. Phys. **71**, 4726 (1979).
9. T. G. Goplen, D. G. Cameron, and R. N. Jones. Appl. Spectrosc. **34**, 657 (1980).
10. J. E. Bertie, V. Behnam, and R. N. Jones. Appl. Spectrosc. **39**, 401 (1985); **40**, 427 (1986).
11. G. M. Hale, M. R. Querry, A. N. Rusk, and D. Williams. J. Opt. Soc. Am. **62**, 1103 (1972).
12. A. E. Tshmel and V. I. Vettegren. Spectrochim. Acta, **29A**, 1681 (1973).
13. V. M. Zolotarev, B. A. Mikhailov, L. I. Alperovich, and S. I. Popov. Opt. Spectrosc. **27**, 430 (1969).
14. B. Gross. Phys. Rev. **59**, 748 (1941).
15. E. C. Titchmarsh, Introduction to the theory of Fourier integrals. 2nd ed. Clarendon Press, Oxford. 1948. Chap. 5; 3rd ed. Oxford University Press, London. 1962. pp. 119–120.
16. M. G. Sceats and G. C. Morris. Phys. Status Solidi A: **14**, 643 (1972).

Can. J. Chem. Downloaded from www.nrcresearchpress.com by 92.62.229.171 on 09/08/12
For personal use only.

17. C. W. Peterson and B. W. Knight. J. Opt. Soc. Am. **63**, 1238 (1973).
18. B. Harbecke. Appl. Phys. A: **40**, 151 (1986).
19. J. A. Bardwell and M. L. Dignam. Anal. Chim. Acta, **172**, 101 (1985).
20. J. E. Bertie and H. H. Eysel. Appl. Spectrosc. **39**, 392 (1985).
21. G. R. Fowles. Introduction to modern optics. Holt Rinehart & Winston, New York. 1975.
22. J. A. Fahrenfort. *In* Infrared spectroscopy and molecular structure. *Edited by* M. Davies. Elsevier, New York. 1963. Chap. XI.
23. J. C. Decius and R. M. Hexter. Molecular vibrations in crystals. McGraw–Hill, New York. 1977.
24. R. N. Bracewell. Science, **248**, 697 (1990).
25. K. Ohta and H. Ishida. Appl. Spectrosc. **42**, 952 (1988).
26. D. G. Cameron, J. P. Hawranek, P. Neelakantan, R. P. Young, and R. N. Jones. National Research Council of Canada Bulletin **16**. Computer programs for infrared spectrophotometry. Program 46.
27. D. C. Champeney. Fourier transforms and their physical applications. Academic Press, London. 1973. p. 22.
28. R. C. L. Ng and G. Horlick. Spectrochim. Acta, **36B**, 529 (1981).
29. Bede Liu (*Editor*). Digital filters and the fast Fourier transform. Halsted Press, New York. 1975.
30. R. C. L. Ng. Ph.D. Thesis, University of Alberta. 1981.
31. A. Zachor. J. Opt. Soc. Am. **56**, VI (1966).
32. A. G. Marshall. *In* Fourier, Hadamard, and Hilbert transforms in chemistry. *Edited by* A. G. Marshall. Plenum, New York. 1982. p. 108.
33. F. G. Herring, A. G. Marshall, P. S. Phillips, and D. C. Roe. J. Magn. Reson. **37**, 292 (1980).

Appendix

```
C     SUBROUTINE FFT(HLBT,N,N2POW,X,Y)
C     X — REAL ARRAY, Y — IMAGINARY ARRAY
C     2N — NUMBER OF POINTS IN ARRAY X ON
C     ENTERING SUBROUTINE FOR FFT OF REAL
C     DATA.
C     N — NUMBER OF POINTS TO BE TRANS-
      FORMED IN EACH ARRAY, X,Y; N=2^N2POW
C     HLBT=0 — COMPLEX FFT, OTHERWISE, REAL
C     FFT

      SUBROUTINE FFT(HLBT, N, N2POW, X, Y)
      REAL I, I1, I2, I3, I4
      INTEGER HLBT, PASS, SEQLOC, L(15)
      DIMENSION X(1), Y(1)
      EQUIVALENCE (L13,L(1)), (L12,L(2)), (L11,L(3)),
      (L10,L(4)), (L9,L(5)), (L8,L(6)), (L7,L(7)),
     +   (L6,L(8)), (L5,L(9)), (L4,L(10)), (L3,L(11)),
     +   (L2,L(12)), (L1,L(13)), (L0,L(14)), (LA,L(15))

C     SHUFFLING DATA FOR REAL FFT
      IF(HLBT.EQ.0) GOTO 102
      DO 101 K=1,N
      K2=K*2
      X(K)=X(K2-1)
101   Y(K)=X(K2)

C     FFT; COOLEY–TUKEY ALGORITHM
102   NTHPOW=2**N2POW
      N4POW=N2POW/2
      IF(N4POW.EQ.0) GOTO 3
      DO 2 PASS=1,N4POW
      NXTLTH=2**(N2POW-2*PASS)
      LENGTH=4*NXTLTH
      SCALE=6.283185307/LENGTH
      DO 2 J=1,NXTLTH
      ARG=(J-1)*SCALE
      C1=COS(ARG)
      S1=SIN(ARG)
      C2=C1*C1-S1*S1
      S2=C1*S1*2
      C3=C1*C2-S1*S2
      S3=C2*S1+S2*C1
      DO 2 SEQLOC=LENGTH,NTHPOW,LENGTH
      J1=SEQLOC-LENGTH+J
      J2=J1+NXTLTH
      J3=J2+NXTLTH
      J4=J3+NXTLTH
      R1=X(J1)+X(J3)
      R2=X(J1)-X(J3)
      R3=X(J2)+X(J4)
      R4=X(J2)-X(J4)
      I1=Y(J1)+Y(J3)
      I2=Y(J1)-Y(J3)
      I3=Y(J2)+Y(J4)
      I4=Y(J2)-Y(J4)
      X(J1)=R1+R3
      Y(J1)=I1+I3
      IF(J.EQ.1) GOTO 1
      X(J3)=C1*(R2+I4)+S1*(I2-R4)
      Y(J3)=-S1*(R2+I4)+C1*(I2-R4)
      X(J2)=C2*(R1-R3)+S2*(I1-I3)
      Y(J2)=-S2*(R1-R3)+C2*(I1-I3)
      X(J4)=C3*(R2-I4)+S3*(I2+R4)
      Y(J4)=-S3*(R2-I4)+C3*(I2+R4)
      GOTO 2
1     X(J3)=R2+I4
      Y(J3)=I2-R4
      X(J2)=R1-R3
      Y(J2)=I1-I3
      X(J4)=R2-I4
      Y(J4)=I2+R4
2     CONTINUE
3     IF(N2POW.EQ.2*N4POW) GOTO 5
      DO 4 J=1,NTHPOW,2
      R=X(J)+X(J+1)
      X(J+1)=X(J)-X(J+1)
      X(J)=R
      I=Y(J)+Y(J+1)
      Y(J+1)=Y(J)-Y(J+1)
4     Y(J)=I
5     DO 6 J=1,15
      L(J)=1
6     IF(J.LE.N2POW) L(J)=2**(N2POW+1-J)
      IJ=1
      DO 7 JA=1,LA
      DO 7 J0=JA,L0,LA
      DO 7 J1=J0,L1,L0
      DO 7 J2=J1,L2,L1
      DO 7 J3=J2,L3,L2
      DO 7 J4=J3,L4,L3
      DO 7 J5=J4,L5,L4
      DO 7 J6=J5,L6,L5
      DO 7 J7=J6,L7,L6
      DO 7 J8=J7,L8,L7
      DO 7 J9=J8,L9,L8
      DO 7 J10=J9,L10,L9
```

Can. J. Chem. Downloaded from www.nrcresearchpress.com by 92.62.229.171 on 09/08/12
For personal use only.

```
      D0 7 J11=J10,L11,L10
      DO 7 J12=J11,L12,L11
      DO 7 JI=J12,L13,L12
      IF(IJ.GE.JI) GOTO 7
      R=X(IJ)
      X(IJ)=X(JI)
      X(JI)=R
      I=Y(IJ)
      Y(IJ)=Y(JI)
      Y(JI)=I
7     IJ=IJ+1

C     POST-PROCESSING FOR REAL FFT
      IF (HLBT.EQ.0) RETURN
      ARG=3.1415927/FLOAT(N)
      C1=COS(ARG)
      S1=-SIN(ARG)
      C1JX=1.
      S1JX=0.
      N2=N/2
      N2P1=N2+1
      DO 20 J=2,N2P1
      NP2MJ=N+2-J
      SORR1=X(J)+X(NP2MJ)
      SORI1=Y(J)-Y(NP2MJ)
      R=C1JX
      C1JX=C1JX*C1-S1JX*S1
      S1JX=R*S1+S1JX*C1
      SORR2=X(J)-X(NP2MJ)
      SORI2=Y(J)+Y(NP2MJ)
      SORR3=C1JX*SORR2-S1JX*SORI2
      SORI3=C1JX*SORI2+S1JX*SORR2
      Y(J)=0.5*(SORI1-SORR3)
      X(J)=0.5*(SORR1+SORI3)
      IF(J.EQ.N2P1) GOTO 20
      Y(NP2MJ)=-0.5*(SORI1+SORR3)
      X(NP2MJ)=0.5*(SORR1-SORI3)
20    CONTINUE
      X(1)=X(1)+Y(1)
      Y(1)=0.
      RETURN
      END
```

Can. J. Chem. Downloaded from www.nrcresearchpress.com by 92.62.229.171 on 09/08/12
For personal use only.

A test of composite natural orbitals for benzene

YUICHI YAMAMOTO,[1] TAKESHI NORO, AND KIMIO OHNO[2]
Department of Chemistry, Faculty of Science, Hokkaido University, Sapporo 060, Japan

Received June 10, 1991

This paper is dedicated to Professor Sigeru Huzinaga on the occasion of his 65th birthday

YUICHI YAMAMOTO, TAKESHI NORO, and KIMIO OHNO. Can. J. Chem. **70**, 532 (1992).

Approximate natural orbitals (NO's) of a larger system can be constructed from the NO's of smaller fragment systems. These orbitals, called composite NO's (CNO's) are expected to be useful in configuration interaction (CI) calculations. The effectiveness of these NO's is shown for the benzene molecule. This molecule is considered a combination of three ethylenes. The CI calculations were carried out for the $S_1 - S_3$ and $T_1 - T_3$ states. We take into account single and double excitations from σ and π electrons in the CI calculations. The calculated excitation energies are in good agreement with the experimental values.

Key words: benzene, π–π^* excited state, composite natural orbital, ionic and covalent, SDCI.

YUICHI YAMAMOTO, TAKESHI NORO et KIMIO OHNO. Can. J. Chem. **70**, 532 (1992).

On peut construire des orbitales naturelles (ON) approximatives de systèmes plus grands à partir d'ON de systèmes formés de fragments plus petits. On s'attend à ce que ces orbitales, que l'on appelle orbitales naturelles composites (ONC), soient utiles dans les calculs d'interactions de configuration (IC). On a démontré l'efficacité de ces ON avec la molécule de benzène. On considère la molécule comme une combinaison de trois molécules d'éthylène. On a effectué des calculs d'IC sur les états $S_1 - S_3$ et $T_1 - T_3$. Dans les calculs d'IC, on tient compte des excitations simples et doubles à partir des électrons σ et π. Les énergies d'excitation calculées sont en bon accord avec les valeurs expérimentales.

Mots clés : benzène, état excité π–π^*, orbitale naturelle composite, ionique et covalent, ICSD.

[Traduit par la rédaction]

1. Introduction

In quantum-chemical calculations beyond the Hartree–Fock level, CI is widely used for obtaining electronic states of molecules because of its simple concept and highly developed codes available for many types of computers. But CI has a serious defect in that the number of configuration state functions (CSF's) increases rapidly as the used orbital basis set becomes larger. For most molecules, therefore, a full CI calculation is almost impossible to carry out without the truncation of its expansion. It is well known that the convergence of CI expansion depends on the choice of the orbital set. Self-consistent field molecular orbitals (SCFMO's) commonly used in CI are not adequate for describing electron correlation. The canonical SCF virtual MO's are determined under the influence of $N + 1$ electron potential, so that they have only small amplitudes in the region of space covered by the occupied orbitals and thus are not suitable in describing electronic correlation. It was proved that NO's give the fastest convergence in two-electron systems. It is generally believed that NO's give the fastest convergence in CI expansion. A drawback about NO's is that they cannot be obtained before a CI calculation.

There are several attempts (1–4) to obtain approximate NO's without actually carrying out the CI calculation of a target system. These approximate NO's show definitely better convergence than the ordinary canonical SCFMO's. We have proposed another way of preparing approximate NO's. A molecule can usually be regarded as consisting of fragments. Composite natural orbitals (CNO's) are constructed from NO's of fragments. These orbitals gave excellent convergence in the calculation of excitation energies of C_4H_6 (5) and bipyrrole (6). Its effectiveness has also been shown in a CI calculation of free base porphine (7). The aim of this work is to investigate convergence of the CNO that is constructed from C_2H_4 as a fragment of benzene.

The benzene molecule is a typical aromatic molecule. The π-electron theory of Hückel (8) and the resonance theory of Pauling and Wheland (9) were formulated using benzene as an example. The first *ab-initio* SCF calculation was carried out by Schulman and Moskowitz (10). A large SCF calculation for the ground state by Almlöf and Faegri yielded SCF energy within 0.03 hartree of the estimated Hartree–Fock limit (11). The first CI calculation was carried out by Buenker, Whitten, and Petke (12). An extensive CI study of the excited states was carried out by Hay and Shavitt using a double zeta basis set and included single, double, and triple excitations of π electrons (13). The excitation energies of S_1, T_1, and T_2 were in agreement with experiment. However, for S_2, S_3, and T_3 the excitation energies were still higher than the experimental result by 1.0 eV. Matos, Roos, and Malmqvist performed CASSCF (14–18) contracted CI (CCI) (17) calculations using a double zeta basis set augmented with a $3d$-type polarization function and diffuse p-type functions on carbon (18). They included correlation effects of σ electrons that reduced the errors in the S_2, S_3, and T_3 states to less than 0.6 eV. Kitao and Nakatsuji carried out the SAC-CI (19, 20) calculation on valence and Rydberg excited states and ionized states of benzene using a double zeta basis set plus a $3d_\pi$-type polarization function and diffuse functions on carbon (21). They also considered the σ correlation effects and some higher excitations. The calculated excitation energies agreed with the experimental values to within 0.5 eV except T_1.

The second purpose of this work is to find out how close the present calculations using CNO's compare with the previous CI calculations of benzene (18, 21).

[1]Present address: Center for Information Processing Education, Hokkaido University, Sapporo 060, Japan.

[2]Present address: National Center for Science Information Systems, Otsuka 3-29-1, Bunkyo-ku, Tokyo 112, Japan.

Printed in Canada

Can. J. Chem. Downloaded from www.nrcresearchpress.com by 92.62.229.171 on 09/08/12
For personal use only.

Can. J. Chem. Downloaded from www.nrcresearchpress.com by 92.62.229.171 on 09/08/12
For personal use only.

The method of calculation is described in Sect. 2, results and discussion in Sect. 3, followed by concluding remarks.

2. Method

2.1 Basis set and molecular structure

Split-valence basis sets of Tatewaki and Huzinaga (22) were employed. Two diffuse p functions were added on the carbon atoms. The exponents are 0.03477 and 0.01074 as recommended by Hay and Shavitt (13). The total number of contracted Gaussian-type orbitals (CGTO's) is 102. However, the set has near linear dependence. To remove numerical difficulty, the basis set was reduced by projecting out the lowest two eigenvectors of the overlap matrix. The eliminated orbitals were both σ type.

For benzene, we took the bond lengths of C—C and C—H to be 1.397 and 1.084 Å as determined by Raman spectroscopy (23).

2.2 Computational procedures

The procedure of the calculation was as follows: (*1*) A SCF calculation was carried out on the ground state. (*2*) Preliminary CI calculations were performed to identify the main configurations of $S_1 - S_3$, $T_1 - T_3$ states by using the canonical ground state SCF orbital. These CI's included all single excitations from the ground state configuration except the 1*s* orbitals of carbon. A few main configurations were selected as a reference function (cf. Table 3). (*3*) SCF or single excitation CI(SCI) calculation from the reference functions mentioned above was performed for each state to prepare the occupied MO's. (*4*) A SDCI calculation was carried out on the ground state of ethylene to obtain the natural orbitals (NO's). (*5*) By merging the occupied MO's with the approximate NO's constructed from the fragment systems, a CNO set was prepared for each state (5). (*6*) The following three different levels of CI calculations were carried out using the CNO sets. (*a*) In the first level of CI, referred to πCI, single and double excitations of π electrons from the reference configurations were taken into account. (*b*) In the second level of CI, referred to σπCI1, we included single and double excitations of σ and π electrons from the reference configurations except simultaneous double excitations of σ electrons. By this CI, electronic correlations between σ and π electrons are considered but those among σ electrons are not. (*c*) In the third and most extensive CI in our treatment, referred to σπCI2, all single and double excitations of σ and π electrons from the reference configurations were taken into account.

Since the number of configuration state functions (CSF's) was too large, we used the second order perturbation theory to select the more important CSF's from the set of produced CSF's. The selection threshold of −50 μHartree was used. The effect of the rejected configurations on the energy, ΔE, was estimated by

$$[1] \quad \Delta E = \sum_{i}^{c\text{-space}} \left| \sum_{k}^{a\text{-space}} H_{ik} C_k \right|^2 \Big/ (E_{CI} - H_{ii})$$

where a and c spaces were spanned by the reference functions and the rejected CSF's, respectively, and C_k and E_{CI} are the eigenvector and eigenvalue of the Hamiltonian within the selected space (24). When all virtual orbitals are used as correlating orbitals, the eigenvalue should not depend on the orbital set by which excitations are represented. However, when we select more important CSF's, the resultant energy $E_{CI} + \Delta E$ depends on the choice of orbital set. The CNO set is expected to give a more accurate estimated energy than the SCFMO set.

TABLE 1. SCF results for the ground state

Orbital	Orbital energy (au)
$1a_{1g}$	−11.2337
$1e_{1u}$	−11.2331
$1e_{2g}$	−11.2319
$1b_{1u}$	−11.2313
$2a_{1g}$	−1.1627
$2e_{1u}$	−1.0240
$2e_{2g}$	−0.8303
$3a_{1g}$	−0.7174
$2b_{1u}$	−0.6447
$1b_{2u}$	−0.6276
$3e_{1u}$	−0.5960
$1a_{2u}$	−0.5069
$3e_{2g}$	−0.4970
$1e_{1g}$	−0.3417
$2a_{2u}$	0.0278
$2e_{1g}$	0.0417
$1e_{2u}$	0.0457

TABLE 2. Total energies[a] (au)

	KN[b]	MRM[c]	This work
SCF	−230.660466	−230.7282	−230.35476
πCI	−230.74818 (2.39eV)		−230.43452 (2.17eV)
σπCI1			−230.60321 (6.76eV)
σπCI2	−230.85811 (5.38eV)	−231.1131 (10.47eV)	−230.84359 (13.30eV)

[a]Correlation energies in parentheses.
[b]Reference 21.
[c]Reference 18.

3. Results and discussion

3.1 Total energies resulting from SCF and CI calculations

The SCF orbital energy is shown in Table 1. Table 2 gives the total energies and the correlation energies of the ground state obtained by the SCF and CI calculations compared with the previous calculations.

The correlation energy of σπCI2 is −13.30 eV, which is more than twice that of σπSACCI (21). Kitao and Nakatsuji truncated 35% of σ orbitals and selected the important operators by a perturbation selection technique to decrease the size of calculations. The SCFMO's of the ground state were used to represent the reference configurations and the excitation operator. As shown in the following section, truncation of orbitals causes serious loss of correlation energies when the SCFMO's are employed. This is probably the reason they obtained only 40% of the correlation energy in the present calculation in spite of the inclusion of a polarization function and higher excitations. Thus, their good agreement on excitation energies might be a result of fortuitous cancellation of errors. Although Matos *et al.* obtained the lowest total energy published so far, their correlation energy of 10.47 eV is still smaller than ours. They employed a larger

TABLE 3. Reference configurations and weights in σπCI2

State		Configuration	No. of CSF	Weight
	$^1A_{1g}$	$(1a_{2u})^2(1e_{1g})^4$	95611	88.3%
S_1	$^1B_{2u}$	$(1a_{2u})^2(1e_{1g})^3(1e_{2u})^1$ $(1a_{2u})^2(1e_{1g})^2(1e_{2u})^1(2e_{1g})^1$	437495	87.1%
S_2	$^1B_{1u}$	$(1a_{2u})^2(1e_{1g})^3(1e_{2u})^1$ $(1a_{2u})^2(1e_{1g})^1(1e_{2u})^3$	414453	87.7%
S_3	$^1E_{1u}$	$(1a_{2u})^2(1e_{1g})^3(1e_{2u})^1$ $(1a_{2u})^2(1e_{1g})^2(1e_{2u})^1(2e_{1g})^1$ $(1a_{2u})^2(1e_{1g})^1(1e_{2u})^3$	519813	87.2%
T_1	$^3B_{1u}$	$(1a_{2u})^2(1e_{1g})^3(1e_{2u})^1$	211290	86.4%
T_2	$^3E_{1u}$	$(1a_{2u})^2(1e_{1g})^3(1e_{2u})^1$	211290	87.0%
T_3	$^3B_{2u}$	$(1a_{2u})^2(1e_{1g})^3(1e_{2u})^1$	211330	88.3%

TABLE 4. Excitation energies

State		MRM[a]	KN[b]	πCI	σπCI1	σπCI2	Expt.
S_1	$^1B_{2u}$	5.6	5.25	4.95	5.19	5.15	4.90[c]
S_2	$^1B_{1u}$	6.8	6.60	7.60	6.93	6.50	6.20[c]
S_3	$^1E_{1u}$	7.4	7.47	8.41	7.76	7.35	6.95[c]
T_1	$^3B_{1u}$	4.3	4.06	3.84	4.27	3.89	3.95[d]
T_2	$^3E_{1u}$	4.3	5.02	4.96	5.12	4.68	4.45[d]
T_3	$^3B_{2u}$	5.1	6.02	6.93	6.20	5.70	5.60[d]

[a]Reference 18.
[b]Reference 21.
[c]Reference 26.
[d]Reference 27.

basis set than ours and they also took into account the double excitations of σ electrons with the CCI approach. In the CCI, doubly excited configurations are contracted into pair functions whose coefficients are obtained through second order perturbation theory. This contraction might explain some of the loss of the correlation energy.

Table 3 gives the reference configurations and the weight of reference functions $\Sigma_{i=1}^{\text{ref}}|C_i|^2$, which is expected to be a good index to measure the accuracy of a CI wavefunction (25). Since the weight of the each level was the same for all states of interest, our CI calculations seem to be impartial for all states.

3.2 Excited states

In Table 4 and Fig. 1, we show the calculated excitation energies of CI calculations with the experimental results for $S_1 - S_3$, $T_1 - T_3$. The πCI calculation yielded good results for S_1, T_1, and T_2. But the excitation energies for S_2, S_3, and T_3 are 1 eV higher than experiments.

Inclusion of correlation effects of π and σ electrons (σπCI1) caused the lowering of 0.7 eV for S_2, S_3 and T_3; however, it raised the excitation energies thus increasing discrepancies with experiment for S_1, T_2, and T_3. Inclusion of σ–σ correlation effects (σπCI2) gave considerable lowering in all excitation energies. For S_1 and triplet states, we obtained excellent agreement with experiment. For S_2 and S_3, we still had a small discrepancy of 0.25–0.30 eV that would be reduced by using the larger basis sets.

From the valence bond theory, these valence excited states can be classified in ionic and covalent states. The covalent states include S_2, T_1, and T_2. The ionic states are S_2, S_3, and T_3. The importance of σ–π and σ–σ correlation effects has been stressed for the ionic states (28–32). The results of

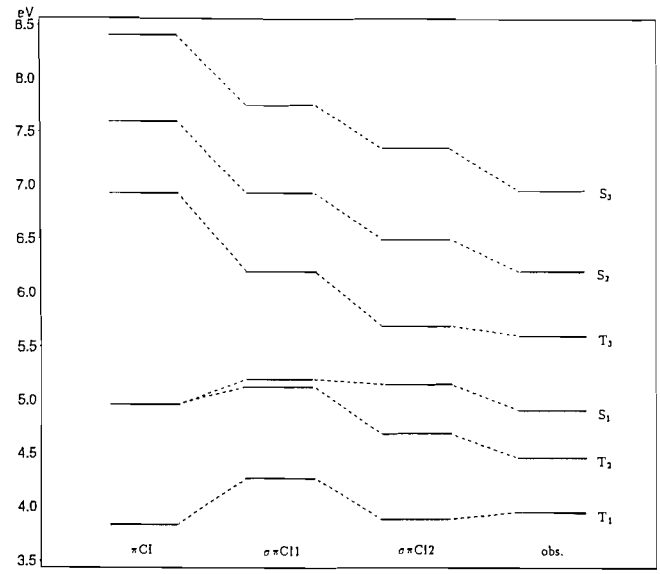

FIG. 1. Comparison of the theoretical and observed excitation energy of $S_1 - S_3$, $T_1 - T_3$ states.

σπCI1 and σπCI2 show that they also exert a significant effect to the covalent states.

Matos *et al.* (18) included σ–σ correlation effects; however, they could not obtain good excitation energies. They selected the reference configurations having the largest weight in the CASSCF wavefunction. The weight of reference space varied from 80% to 95% for different excited states. They mentioned that this imbalance might explain some of the remaining errors even if this part of the error is rather small. However, the present result shows that a well-balanced treatment for all states is extremely important to obtain more reliable results.

3.3 Convergence of CNO

To demonstrate the effectiveness of CNO, a series of truncated CI calculations were performed for σπCI2. First, we tested the convergence for the truncation of σ correlating orbitals. The number of σ correlating orbitals was reduced from 58 to 52, 44, 36, 32, 28, 24, 20, 16, and 12 and all π correlating orbitals was kept. To show the kind of calculations, we used (N_σ/N_π) as symbols, where N_σ and N_π mean the number of correlating orbitals used for σs and π orbitals, respectively. The calculation (58/21) corresponds to the untruncated CI.

The result is shown in Fig. 2. The CI calculations using CNO's give a rapid convergence in comparison with SCFMO's. In (24/21), the correlation energy of about 90% is obtained with CNO but only about 20% with SCFMO. In the calculation of Kitao and Nakatsuji, 35% of the σ SCFMO's (15 MO'S) were truncated to reduce the size of calculation. From Fig. 2, the truncation of 35% of σ SCFMO's would cause a loss of 55% of the total correlation energy.

Second, we tested the convergence for the truncation of π correlating orbitals. The number of π correlating orbitals was reduced from 21 to 17, 13 and 9 while keeping the number of σ correlating orbitals to be 36.

The results are shown in Figs. 3 and 4. For the ground state, S states and T states, the total energies for (36/9) went up only about 0.5 eV in comparison with (58/21). In

Can. J. Chem. Downloaded from www.nrcresearchpress.com by 92.62.229.171 on 09/08/12
For personal use only.

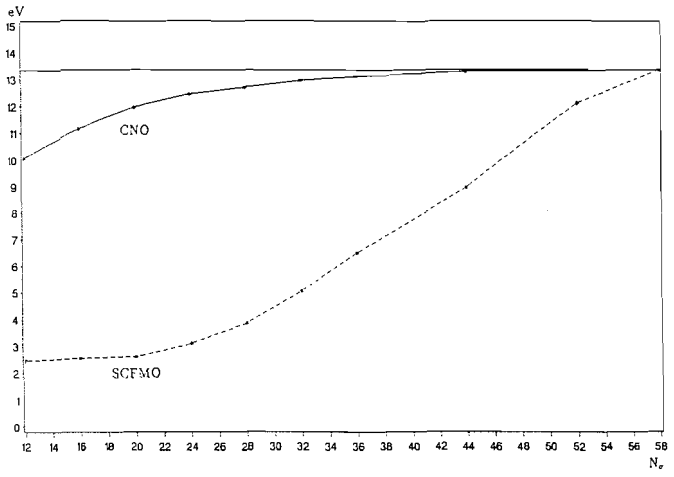

FIG. 2. Convergence of total energies of the ^1A_g state for the truncation of σ correlating orbitals. The lines show the correlation energies.

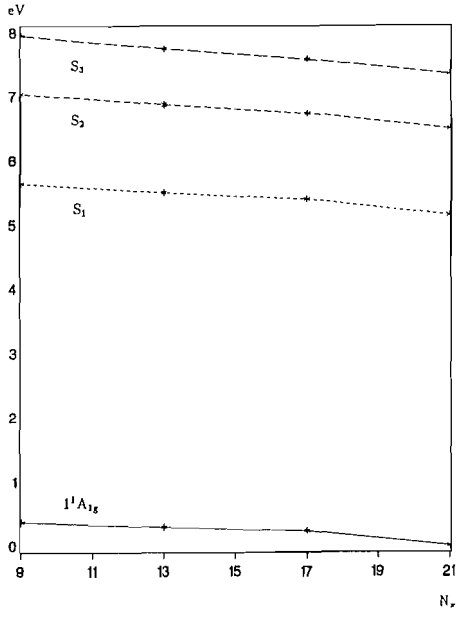

FIG. 3. Convergence of total energies of $S_1 - S_3$ states for the truncation of π correlating orbitals. N_σ is kept at 36. The lines show the energy differences, $(36/N_\pi) - (36/21)$ (^1A_g).

Table 5, we show the calculated excitation energies of truncated CI calculations for $S_1 - S_3$, $T_1 - T_3$. The excitation energies have changed only about 0.2 eV between (58/21) and (36/9). This means that the truncated CI for the ground state and excited states using CNO produces the results close to the untruncated CI values.

4. Concluding remarks

The present CI calculations used CNO, which yields excellent convergence of the CI expansion for the ground state and excited states. For the ground state, the correlation energy of 90% can be obtained when we truncate the σ correlation orbitals from 50 to 24. The error in excitation energies caused by the truncation of π orbitals from 21 to 9 is only 0.2 eV. Thus, the CNO's are expected to be quite useful for

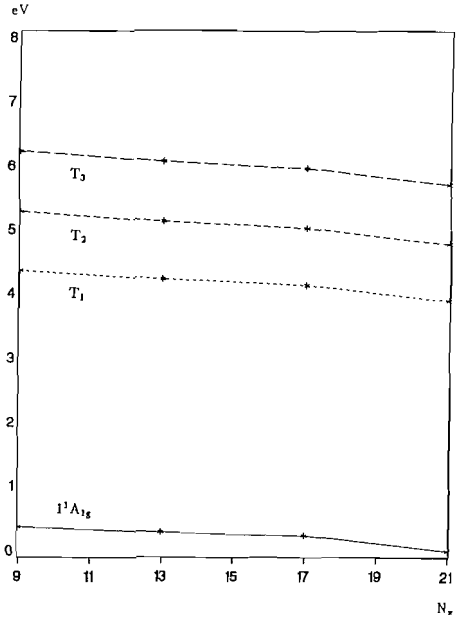

FIG. 4. Convergence of total energies of $T_1 - T_3$ states for the truncation of π correlating orbitals. N_σ is kept at 36. The lines show the energy differences, $(36/N_\pi) - (36/21)$ (^1A_g).

TABLE 5. Excitation energies by truncated CI

State		(58/21)	(36/17)	(36/13)	(36/9)	Expt.
S_1	$^1B_{2u}$	5.15	5.15	5.20	5.26	4.90[a]
S_2	$^1B_{1u}$	6.50	6.50	6.57	6.66	6.20[a]
S_3	$^1E_{1u}$	7.35	7.36	7.46	7.58	6.95[a]
T_1	$^3B_{1u}$	3.89	3.89	3.93	3.98	3.95[b]
T_2	$^3E_{1u}$	4.68	4.69	4.73	4.79	4.45[b]
T_3	$^3B_{2u}$	5.70	5.73	5.77	5.85	5.60[b]

[a]Reference 26.
[b]Reference 27.

CI calculations of a larger system including a cyclic system, where orbital truncation is necessary.

The CI calculation gave better results for excitation energies compared with the previous calculations. For S_1 and triple states, we obtained excellent agreement with experiment. For S_2 and S_3, we still have a small discrepancy of 0.25–0.30 eV that will be reduced by using a much larger basis set. Inclusion of correlation effect of σ electrons is important in both the so-called covalent and ionic states.

Acknowledgements

The authors thank Professors F. Sasaki and K. Tanaka for many helpful discussions. We are also grateful to Mr. A. Murakami for his helpful suggestions. All calculations were performed on the computers at the Hokkaido University Center for Information Processing Education and the Institute of Molecular Science using JAMOL3 (SCF) (33) and MICA3 (SDCI) (34) programs.

It is our great pleasure to dedicate this paper to Professor Sigeru Huzinaga. Having known Professor Sigeru Huzinaga for almost 40 years, one of the authors (K.O.) would like to offer his tribute of admiration to a man of conscience and

Can. J. Chem. Downloaded from www.nrcresearchpress.com by 92.62.229.171 on 09/08/12
For personal use only.

kindness. Professor Huzinaga has always been sincere, gentle, nice, and good to his friends all these years.

1. E. R. Davidson. J. Chem. Phys. **57**, 1999 (1972); L. Stenkamp and E. R. Davidson. Theor. Chim. Acta, **30**, 283 (1973).
2. I. L. Cooper and C. N. M. Pounder. J. Chem. Phys. **71**, 957 (1979).
3. C. W. Bauschlicher, Jr. ICASE Report No. 79-3, NASA Langley Research Center, Hampton, VA. 1979; C. W. Bauschlicher, Jr. J. Chem. Phys. **72**, 880 (1980).
4. D. Feller and E. R. Davidson. J. Chem. Phys. **74**, 3977 (1981).
5. Y. Yamamoto, T. Noro, and K. Ohno. Collect. Czech. Chem. Commun. **53**, 2266 (1988).
6. Y. Yamamoto, T. Noro, and K. Ohno. Chinese J. At. Mol. Phys. **7**, 1580 (1990).
7. Y. Yamamoto, T. Noro, and K. Ohno. Int. J. Quant. Chem. To be published.
8. E. Hückel. Z. Phys. **70**, 206 (1931); **72**, 310 (1931); **76**, 628 (1932).
9. L. Pauling and G. W. Wheland. J. Chem. Phys. **1**, 362 (1933); **2**, 484 (1934).
10. J. H. Shulman and J. W. Moskowitz. J. Chem. Phys. **43**, 3491 (1967).
11. J. Almlöf and K. Faegri, Jr. J. Chem. Phys. **79**, 2284 (1983).
12. R. J. Buenker, J. L. Whitten, and J. D. Petke. J. Chem. Phys. **49**, 2261 (1968).
13. R. J. Hay and I. Shavitt. J. Chem. Phys. **60**, 2865 (1974).
14. B. O. Roos, P. R. Taylor, and P. E. Siegbahn. J. Chem. Phys. **48**, 157 (1980).
15. P. E. Siegbahn, A. Heiberg, B. O. Roos, and B. Levy. Phys. Sci. **21**, 323 (1980).
16. P. E. Siegbahn, A. Heiberg, B. O. Roos, and B. Levy. J. Chem. Phys. **74**, 2384 (1981).
17. P. E. Siegbahn. *In* Current Aspects of Quantum Chemistry: Proceedings of the International Congress, Barcelona, Spain, 1981. *Edited by* R. Carbo. (Elsevier, Amsterdam, 1981); W. Meyer. Phys. Sci. **58**, 1017 (1973).
18. J. M. O. Matos, B. O. Roos, and P-Å. Malmqvist. J. Chem. Phys. **86**, 1458 (1987).
19. H. Nakatsuji and K. Hirao. J. Chem. Phys. **68**, 2035 (1978).
20. H. Nakatsuji. (*a*) Chem. Phys. Lett. **59**, 362 (1978); (*b*) **67**, 329 (1979); **67**, 334 (1979).
21. O. Kitao and H. Nakatsuji. J. Chem. Phys. **87**, 1169 (1987).
22. H. Tatewaki and S. Huzinaga. J. Comput. Chem. **1**, 205 (1980).
23. A. Langeth and B. P. Stoicheff. Can. J. Phys. **34**, 350 (1956).
24. T. Nomura, K. Tanaka, and F. Sasaki. Private communication.
25. T. Noro and M. Yoshimine. J. Chem. Phys. **91**, 3012 (1989).
26. E. N. Lassettre, A. Skerbele, M. A. Dillon, and K. J. Ross. J. Chem. Phys. **48**, 5066 (1968).
27. J. P. Doering. J. Chem. Phys. **51**, 2866 (1969).
28. S. Iwata and K. F. Freed. J. Chem. Phys. **61**, 1500 (1974).
29. T. Shibuya, Y. J. I' Haya, and V. McKoy. Int. J. Quant. Chem. **9**, 5059 (1975).
30. L. E. McMurchie and E. R. Davidson. J. Chem. Phys. **66**, 2959 (1977).
31. K. Tanaka. Int. J. Quantum. Chem. **6**, 1087 (1972).
32. J. A. Ryan and J. L. Whitten. Chem. Phys. Lett. **15**, 119 (1972).
33. H. Kashiwagi, T. Takada, E. Miyoshi, and S. Obara. User's manual of Center Library No. 1. 1977. Hokkaido University Computing Center (in Japanese).
34. A. Murakami, H. Iwaki, H. Terashima, T. Shoda, T. Kawaguchi, and T. Noro. User's manual Center Library No. 16. 1986. Hokkaido University Computer Center (in Japanese).

Can. J. Chem. Downloaded from www.nrcresearchpress.com by 92.62.229.171 on 09/08/12
For personal use only.

Valence and core region energies of atoms in Hartree–Fock theory

S. FLISZÁR, N. DESMARAIS, AND G. DANCAUSSE
Département de chimie, Université de Montréal, C.P. 6128, Succ. A, Montréal (Québec), Canada H3C 3J7

Received August 19, 1991

This paper is dedicated to Professor Sigeru Huzinaga on the occasion of his 65th birthday

S. FLISZÁR, N. DESMARAIS, and G. DANCAUSSE. Can. J. Chem. **70**, 537 (1992).

The subdivision of an atom into an inner core and an outer valence region reveals an interesting statistical aspect about the Hartree–Fock (HF) eigenvalues, ε_i, and the electron populations in the valence region, N_i^v, namely $\Sigma_i N_i^v \varepsilon_i = T^v + V_{ne}^v + V_{ee}^{cv} + 2V_{ee}^{vv}$, where T^v and V_{ne}^v are, respectively, the kinetic energy and the nuclear-electronic potential energy of the $\Sigma_i N_i^v$ valence electrons, V_{ee}^{vv} the interelectronic repulsion confined within the valence region, while V_{ee}^{cv} is the repulsion between the core electrons and those of the valence region. This relationship (and a similar one for the core region) holds for any number of electrons arbitrarily assigned to the core, but is accurate only for HF (or near-HF) wave functions. This leads to a definition of the valence region energy, $\Sigma_i N_i^v \varepsilon_i - V_{ee}^{vv} = T^v + V_{ne}^v + V_{ee}^{cv} + V_{ee}^{vv}$, which, however, cannot be compared to the energy actually required for the removal of the outer electrons, because relaxation is not accounted for. An accurate energy expression has also been derived, $E^v = \frac{1}{3}(V_{ne}^v + V_{ee}^{cv} + \Sigma_i N_i^v \varepsilon_i)$, which measures the actual withdrawal of the valence electrons. The latter expression requires the use of discrete values of N^c, the number of electrons assigned to the core, namely $N^c = 2$ for the first-row and $N^c = 10$ e for the second-row elements.

Key words: atoms, core–valence separation.

S. FLISZÁR, N. DESMARAIS et G. DANCAUSSE. Can. J. Chem. **70**, 537 (1992).

Le découpage d'un atome en une région interne et une région de valence externe conduit à une relation exacte impliquant les populations électroniques de valence, N_i^v, et les valeurs propres de Hartree–Fock, ε_i, soit $\Sigma_i N_i^v \varepsilon_i = T^v + V_{ne}^v + V_{ee}^{cv} + 2V_{ee}^{vv}$, où T^v and V_{ne}^v sont, respectivement, l'énergie cinétique et l'énergie potentielle noyau-électron des électrons de valence, V_{ee}^{vv} est la répulsion interélectronique dans cette région et V_{ee}^{cv} est la répulsion entre les électrons internes et ceux de valence. Cette relation (ainsi qu'une expression similaire pour la région interne) s'applique quelque soit le nombre d'électrons, N^c, associés à la région interne. Elle conduit à une énergie de la couche de valence, $\Sigma_i N_i^v \varepsilon_i - V_{ee}^{vv} = T^v + V_{ne}^v + V_{ee}^{cv} + V_{ee}^{vv}$, qui traduit un état de fait mais ne correspond pas à une ionisation physique. Cette dernière est bien décrite par l'énergie de valence $E^v = \frac{1}{3}(V_{ne}^v + V_{ee}^{cv} + \Sigma_i N_i^v \varepsilon_i)$, qui n'est valable que pour des valeurs discrètes de N^c, soit $N^c = 2$ pour les éléments de la première rangée et $N^c = 10$ e pour ceux de la deuxième.

Mots clés : atomes, énergie de valence.

Can. J. Chem. Downloaded from www.nrcresearchpress.com by 92.62.229.171 on 09/08/12
For personal use only.

1. Introduction

The idea of subdividing an atom into an inner core and an outer valence region is not a new one. Though intuitively appealing — "much of the chemistry resides in the valence region" — such a core–valence separation is by no means obvious. Indeed, no electron can be assigned to any region in particular, because each individual electron occupies the entire atom. In turn, we can construct arguments rooted in the notion of electron density, $\rho(\boldsymbol{r})$, building on the fact that the exact nonrelativistic ground-state energy of an atom, E, can be expressed in terms of the electrostatic potential at its nucleus (1) or, more generally (2), because E is a functional of $\rho(\boldsymbol{r})$.

Along these lines, Politzer and Parr (3) offered an approximation for the valence region energy, E^v,

$$[1] \qquad E^v = -\frac{3}{7}(Z - N^c)\int_{r_b}^{\infty} 4\pi r\rho(r)\mathrm{d}r$$

in which N^c is the number of electrons in the core region of an atom with nuclear charge Z and r_b defines the boundary separating the core from the valence region. The factor 3/7 is brought in by the Thomas–Fermi theory (4) involved in the derivation of eq. [1]. A number of studies (5) have exploited this Thomas–Fermi-like approach and have ultimately led to an approximate but accurate description of molecules (6).

The Politzer–Parr partitioning defines the boundary surface separating the core and valence regions at the minimum of the radial distribution function, $R(r) = R(r) = 4\pi r^2\rho(r)$. It is certainly reassuring to find a recognizable feature suggesting a justification for the selection of a boundary surface. But it remains that, in the last resort, any selection is largely arbitrary. Here we reformulate the question by asking about the energy of the outer electrons, which could be measured by the energy required to remove them. This implies the notion of integral numbers of electrons in the core and valence regions. Specifically, we consider here first-row elements with two core electrons, and second-row elements with 10 core electrons. Inroads will also be discussed, however, taking r_b at the minimum of the radial distribution function, as well as other possible definitions of the core region.

Sharply contrasting with approaches rooted in the Thomas–Fermi model, we tackle the problem within the framework of Hartree–Fock theory. The familiar Hartree–Fock orbital energies are part of our description and we take full advantage of these eigenvalues. A core–valence separation is described, new energy formulas are given, but, at the end, all this will bring us back to an expression resembling eq. [1], assessing its true merits.

2. Methodology

Consider a sphere of radius r, centered at the nucleus. The electron populations N_{1s}, N_{2s}, . . ., contained in this sphere are

$$[2] \qquad N_i(r) = \nu_i \int_0^r 4\pi r^2 |\phi_i(r)|^2 \mathrm{d}r$$

Can. J. Chem. Downloaded from www.nrcresearchpress.com by 92.62.229.171 on 09/08/12
For personal use only.

where the ϕ_i's are normalized Hartree–Fock orbitals occupied by ν_i electrons. The total core population, N^c, is then

$$N^c = \sum_i N_i(r_b)$$

where $r = r_b$ defines the boundary surface separating the core and valence regions. Similarly, the valence populations are

$$[3] \qquad N_i^v = \nu_i \int_{r_b}^{\infty} 4\pi r^2 |\phi_i(r)|^2 dr$$

The $1s$, $2s$, ..., electrons are well entangled in the inner region and, of course, also in the outer valence region. Briefly, in examining the energy associated with the "valence electrons" we must deal with a mix-up of electrons assigned to different Hartree–Fock orbitals ϕ_i, each one with its own eigenvalue ε_i.

These Hartree–Fock energies are reasonably good approximations to the orbital energies of an atom, as determined by X-ray and optical spectroscopy term values. We take them at their face value, in their integrality, as the energies of the individual electrons, knowing, of course, that each of these orbital energies is computed over the entire atom and that no localization of the individual electrons in certain regions of space should be attempted. Under these circumstances, all we can do is to evaluate the amount of energy statistically accumulated in a given region, using the densities of the electrons assigned to the various orbitals ϕ_{1s}, ϕ_{2s}, ..., with orbital energies ε_{1s}, ε_{2s}, ..., respectively. Hence we associate the electronic energies

$$[4] \qquad \sum_i N_i^c \varepsilon_i = \sum_i \varepsilon_i \nu_i \int_0^{r_b} 4\pi r^2 |\phi_i(r)|^2 dr$$

and

$$[5] \qquad \sum_i N_i^v \varepsilon_i = \sum_i \varepsilon_i \nu_i \int_{r_b}^{\infty} 4\pi r^2 |\phi_i(r)|^2 dr$$

with the core and valence regions, respectively. Our objective is to find the relationship between $\Sigma_i N_i^v \varepsilon_i$ and the energy of the valence region. The precise definition of the latter is momentarily postponed.

Now we switch to something else and pay attention to the individual kinetic and potential energy components of interest, namely

$V_{nc}^c = -Z \int_0^{r_b} \frac{\rho(r)}{r} dr$ = nuclear-electronic potential energy involving only the core electrons (inside the boundary r_b),

$V_{nc}^v = -Z \int_{r_b}^{\infty} \frac{\rho(r)}{r} dr$ = nuclear-electronic potential energy of the valence electrons (outside the boundary r_b),

T^c = kinetic energy of the core electrons,

T^v = kinetic energy of the valence electrons,

V_{ee}^{cv} = repulsion between the $(Z - N^c)$ valence and the N^c core electrons,

V_{cc}^{vv} = electron–electron repulsion involving only the electrons of the valence region,

V_{cc}^{cc} = electron–electron repulsion between core electrons.

The nuclear-electronic potential energies are readily obtained from

$$-Z \sum_i \nu_i \int 4\pi r |\phi_i(r)|^2 dr$$

and the use of the appropriate limits of integration. Similarly, it is easy to separate the kinetic energy, $T = \Sigma_i \nu_i \int \phi_i^* \hat{T} \phi_i d\boldsymbol{r}$, into a core contribution and a part associated with the valence region by using the appropriate limits of integration.

The separation of the V_{ee}^{cv}, V_{cc}^{vv}, and V_{cc}^{cc} parts of the total interelectronic repulsion V_{ee} also follows from appropriate selections of the integration limits. The Coulomb integrals

$$J_{ij} = \int^{\tau_1} \int^{\tau_2} \phi_i(1)\phi_j(2) \frac{1}{r_{12}} \phi_i(1)\phi_j(2) d\tau_1 d\tau_2$$

and the exchange integrals

$$K_{ij} = \int^{\tau_1} \int^{\tau_2} \phi_i(1)\phi_j(2) \frac{1}{r_{12}} \phi_j(1)\phi_i(2) d\tau_1 d\tau_2$$

were deduced with the help of the standard expansion of $1/r_{12}$ in terms of spherical harmonics (7). The integration goes over the spatial coordinates of electrons 1 and 2, with $d\tau_1 = r_1^2 \sin\theta_1 d\theta_1 d\varphi_1 dr_1$ and a similar expression for $d\tau_2$. Let us write these integrals in shorthand notation:

$$I = \int^{\tau_1} \int^{\tau_2} \ldots d\tau_1 d\tau_2 = \int_0^{2\pi} \int_0^{2\pi} \int_0^{\pi} \int_0^{\pi} \int_0^{\infty} \int_0^{\infty} \ldots dr_1 dr_2 d\theta_1 d\theta_2 d\varphi_1 d\varphi_2$$

Representing the angular part by A,

$$A = \int_0^{2\pi} \int_0^{2\pi} \int_0^{\pi} \int_0^{\pi} \ldots d\theta_1 d\theta_2 d\varphi_1 d\varphi_2$$

we rewrite I as follows:

$$I = A\int_0^\infty\int_0^\infty \ldots \mathrm{d}r_1\mathrm{d}r_2 = A\int_0^{r_b}\int_0^{r_b} \ldots \mathrm{d}r_1\mathrm{d}r_2 + A\int_0^\infty\int_{r_b}^\infty \ldots \mathrm{d}r_1\mathrm{d}r_2$$

$$= A\int_0^{r_b}\int_0^{r_b} \ldots + A\int_{r_b}^\infty\int_0^{r_b} \ldots + A\int_0^{r_b}\int_{r_b}^\infty \ldots + A\int_{r_b}^\infty\int_{r_b}^\infty \ldots$$

i.e.,

$$I = \int^{\tau_1^c}\int^{\tau_2^c} \ldots \mathrm{d}\tau_1\mathrm{d}\tau_2 + \int^{\tau_1^v}\int^{\tau_2^c} \ldots \mathrm{d}\tau_1\mathrm{d}\tau_2 + \int^{\tau_1^c}\int^{\tau_2^v} \ldots \mathrm{d}\tau_1\mathrm{d}\tau_2 + \int^{\tau_1^v}\int^{\tau_2^v} \ldots \mathrm{d}\tau_1\mathrm{d}\tau_2$$

The Coulomb and exchange integrals are thus conveniently separated into three contributions, namely

$$I^{cc} = \int^{\tau_1^c}\int^{\tau_2^c} \ldots \mathrm{d}\tau_1\mathrm{d}\tau_2$$

$$I^{vv} = \int^{\tau_1^v}\int^{\tau_2^v} \ldots \mathrm{d}\tau_1\mathrm{d}\tau_2$$

$$I^{cv} = \int^{\tau_1^v}\int^{\tau_2^c} \ldots \mathrm{d}\tau_1\mathrm{d}\tau_2 + \int^{\tau_1^c}\int^{\tau_2^v} \ldots \mathrm{d}\tau_1\mathrm{d}\tau_2$$

for the calculation of the V_{ee}^{cc}, V_{ee}^{vv}, and V_{ee}^{cv} repulsion energies, respectively.

This completes the breakdown of the kinetic and potential energies into core and valence contributions, for future use. We now proceed with the theory.

3. Theory. The "unperturbed" atom

Let us begin with a simple energy balance involving orbital energies. The potential energy part of ε_i includes, in an average way, the repulsion energy between electron i and all the other electrons of the atom. The sum of orbital energies, $\Sigma_i \nu_i\varepsilon_i = \Sigma_i N_i^v\varepsilon_i + \Sigma_i N_i^c\varepsilon_i$, thus counts each interelectronic repulsion twice. And the Hartree–Fock energy of an atom is

$$[6] \qquad E = \sum_i \nu_i\varepsilon_i - V_{ee}$$

where V_{ee} is the interelectronic repulsion energy including exchange. This means that $\Sigma_i N_i^v\varepsilon_i$ includes some double-counting of interelectronic repulsions, say V_{ee}(valence). So does $\Sigma_i N_i^c\varepsilon_i$, with V_{ee}(core). On these grounds we define

$$[7] \qquad E(\text{valence}) = \sum_i N_i^v\varepsilon_i - V_{ee}(\text{valence})$$

$$[8] \qquad E(\text{core}) = \sum_i N_i^c\varepsilon_i - V_{ee}(\text{core})$$

So far, we are deliberately vague as regards the energies, but this is just a temporary situation. Let us proceed with our energy balance. $\Sigma_i N_i^v\varepsilon_i$ also includes V_{ee}^{cv}, the repulsion between the valence and the core electrons. So does $\Sigma_i N_i^c\varepsilon_i$. But the double-counting of V_{ee}^{cv} only occurs when we form the sum $\Sigma_i N_i^v\varepsilon_i + \Sigma N_i^c\varepsilon_i$, which includes twice

$$[9] \qquad V_{ee} = V_{ee}^{cv} + V_{ee}(\text{valence}) + V_{ee}(\text{core})$$

Finally, we obtain from eqs. [6]–[9] that

$$[10] \qquad E(\text{valence}) + E(\text{core}) = E + V_{ee}^{cv}$$

We now use eq. [7] for the description of $E_{\text{unp.}}^v$, the valence energy of an unperturbed ground-state atom, meaning that there is no intent on our side of stripping it of its electrons. We observe this atom "as it is," after our mental subdivision into a core and a valence region. The interelectronic repulsion energy involving only the electrons associated with the valence region is V_{ee}^{vv}, which is unambiguously given by applications of standard formulas for Coulomb and exchange integrals. This V_{ee}^{vv} is used in eq. [7], which becomes

$$[11] \qquad E_{\text{unp.}}^v = \sum_i N_i^v\varepsilon_i - V_{ee}^{vv}$$

The validity of this equation rests entirely with the validity of our description, $\Sigma_i N_i^v\varepsilon_i$, of the electronic energy statistically accumulated in the valence region.

On the other hand, we can also express the total energy found in the valence region in a more conventional way, namely as the sum of the kinetic and potential energies associated with the valence electrons, i.e.,

$$[12] \qquad E_{\text{unp.}}^v = T^v + V_{ne}^v + V_{ee}^{cv} + V_{ee}^{vv}$$

Thus we obtain that

$$[13] \qquad \sum_i N_i^v\varepsilon_i = T^v + V_{ne}^v + V_{ee}^{cv} + 2V_{ee}^{vv}$$

and its companion

$$[14] \qquad \sum_i N_i^c\varepsilon_i = T^c + V_{ne}^c + V_{ee}^{cv} + 2V_{ee}^{cc}$$

(The latter follows immediately because the individual core and valence terms add up correctly to give the corresponding totals for the entire atom, e.g., $T^{\text{total}} = T^v + T^c$.) This result is exact and holds for any arbitrarily selected value of N^c, as illustrated by the numerical examples presented and discussed in Sect. 5. The statistical concept embodied in $\Sigma_i N_i^v\varepsilon_i$ is now clearly identified, eq. [13], in terms of the familiar kinetic and potential energies that can be associated with the valence region. It follows from the definition of these energy components and integration of the Hartree–Fock equations, $\hat{F}\phi_i = \varepsilon_i\phi_i$, i.e., after multiplication by ϕ_i^*, integration from r_b to ∞, and sum over i.

Up to this point we have described an atom left alone. Its valence energy corresponds to a hypothetical ionization in which the valence electrons would be simply skimmed off as they are in the unperturbed atom, with no relaxation of the core. This does not occur, of course. But this atom offers a convenient term of reference.

Can. J. Chem. Downloaded from www.nrcresearchpress.com by 92.62.229.171 on 09/08/12
For personal use only.

Can. J. Chem. Downloaded from www.nrcresearchpress.com by 92.62.229.171 on 09/08/12
For personal use only.

4. Theory. Valence energy including relaxation

Now we look for a valence-region energy, E^v, which is not any longer subject to the constraints having led to $E^v_{unp.}$. We hope to achieve this by examining the general properties of an atom in which the core and valence electrons are interdependent. This amounts to considering implicitly a relaxation energy term from which one region would benefit at the expense of the other in the event of an actual ionization. But this E^v and its core counterpart E^c are still tied by the general energy balance given in eq. [10]. Thus we write

$$[15] \quad E = E^v + E^c - V^{cv}_{ee}$$

Consider first the electronic energy of a ground-state atom with nuclear charge Z, $E = \langle\psi|\hat{H}|\psi\rangle$, and apply the Hellmann–Feynman theorem taking Z as parameter. This gives, in conventional notation,

$$\left(\frac{\partial E}{\partial Z}\right)_\rho = \left\langle\psi\left|\frac{\partial \hat{H}}{\partial Z}\right|\psi\right\rangle = \left\langle\psi\left|-\sum_i r_i^{-1}\right|\psi\right\rangle$$

where the sum over i runs over all electrons. The well-known result is

$$[16] \quad \left(\frac{\partial E}{\partial Z}\right)_\rho = \frac{V_{ne}}{Z}$$

On the other hand, the virial theorem, $2E = V_{ne} + V_{ee}$, and the Hartree–Fock formula, eq. [6], combine to give

$$[17] \quad 3E = V_{ne} + \sum_i \nu_i\varepsilon_i$$

This result and eq. [16] lead to

$$[18] \quad 3E - Z\left(\frac{\partial E}{\partial Z}\right)_\rho = \sum_i \nu_i\varepsilon_i$$

Now we define

$$[19] \quad \gamma = \frac{Z}{E}\left(\frac{\partial E}{\partial Z}\right)_\rho$$

and rewrite eq. [18] as follows

$$[20] \quad (3 - \gamma)E = \sum_i \nu_i\varepsilon_i$$

Moreover, it follows from eqs. [16] and [19] that

$$[21] \quad E = \frac{1}{\gamma}V_{ne}$$

Equations [20] and [21] represent an identity in Hartree–Fock theory. The particular interest offered by eq. [21] lies in the fact that $\gamma = 7/3$ appears to be the characteristic homogeneity of both Thomas–Fermi (8) and local density functional theory (9), in which case eq. [20] gives the Ruedenberg approximation (10), $E = (3/2)\,\Sigma_i\nu_i\varepsilon_i$, while eq. [21] gives the Politzer formula (11), $E = (3/7)\,V_{ne}$, contained in eq. [1]. Equations [15], [20], and [21] are our working formulas.

We pick up things where we left them with eq. [15] and write

$$[22] \quad \gamma E = \gamma^v E^v + \gamma^c(E^c - V^{cv}_{ee})$$

This expression is more general than what would follow from a simple multiplication by γ. It is noncommittal as to whether the atomic γ suits the individual core and valence parts: in writing eq. [22], γ is taken as the average of γ^v (with a weight of E^v) and γ^c (weighted by $E^c - V^{cv}_{ee}$), i.e.,

$$\gamma = \frac{\gamma^v E^v + \gamma^c(E^c - V^{cv}_{ee})}{E^v + E^c - V^{cv}_{ee}}$$

Next we consider $V_{ne} = V^v_{ne} + V^c_{ne}$, which we write

$$V_{ne} = (V^v_{ne} + V^{cv}_{ee}) + (V^c_{ne} - V^{cv}_{ee})$$

The reason for this association of terms is physical: in a central force problem, V^v_{ne} and V^{cv}_{ee} play roles that are similar in nature. V^v_{ne} measures the attraction of the valence electrons by the nucleus and V^{cv}_{ee} the accompanying repulsion by the core electrons. With eq. [21] in mind we now write

$$[23] \quad \frac{1}{\gamma}V_{ne} = \frac{1}{\gamma^v}(V^v_{ne} + V^{cv}_{ee}) + \frac{1}{\gamma^c}(V^c_{ne} - V^{cv}_{ee})$$

In this case $1/\gamma$ is the weighted average of $1/\gamma^v$ (with a weight of $V^v_{ne} + V^{cv}_{ee}$) and of $1/\gamma^c$ (with a weight of $V^c_{ne} - V^{cv}_{ee}$).

At this point we use eqs. [22] and [23] and solve for γ^v. After some algebra one obtains $(\gamma^v)^2 + b\gamma^v + c = 0$ with $b = -[(V^v_{ne} + V^{cv}_{ee})/E^v + \gamma]$ and $b^2 - 4c = [(V^v_{ne} + V^{cv}_{ee})/E^v - \gamma]^2$. The trivial root is $\gamma^v = \gamma$. The other root gives

$$[24] \quad E^v = \frac{1}{\gamma^v}(V^v_{ne} + V^{cv}_{ee})$$

So far we have exploited eq. [21]. We have one more step to go. Using eqs. [15] and [22] we write

$$(3 - \gamma)E = (3 - \gamma^v)E^v + (3 - \gamma^c)(E^c - V^{cv}_{ee})$$

and compare this expression with $\Sigma_i\nu_i\varepsilon_i = \Sigma_i N^v_i\varepsilon_i + \Sigma_i N^c_i\varepsilon_i$. Equation [20] tells us that

$$\left[(3 - \gamma^v)E^v - \sum_i N^v_i\varepsilon_i\right] + \left[(3 - \gamma^c)(E^c - V^{cv}_{ee}) - \sum_i N^c_i\varepsilon_i\right] = 0$$

This equation achieves a core–valence separation. The terms in brackets are certainly individually zero at the limits $N^c = 0$ and $N^v = 0$, but this does not warrant that these terms are individually zero for any value of N^c, i.e., that any N^c satisfies a meaningful core–valence separation. We shall tentatively proceed with

$$[25] \quad (3 - \gamma^v)E^v = \sum_i N^v_i\varepsilon_i$$

and examine which, if any, N^c values are acceptable. Equation [25] defines E^v. It is the "valence counterpart" of eq.

TABLE 1. Electron populations, nuclear-electronic and core-valence interelectronic potential energies of first-row atoms and ions, calculated for $N^c = 2$ e (au)

Atom/ion	r_b	N^c_{1s}	N^c_{2s}	N^c_{2p}	V^c_{ne}	V^v_{ne}	V^{cv}_{ee}
Li	1.5321	1.96689	0.03311		−16.24236	−0.90429	0.57772
Be^+	1.0249	1.95081	0.04919		−29.89775	−1.99171	0.94155
Be	0.9852	1.93972	0.06028		−30.06061	−3.57420	1.72566
B^+	0.7323	1.92322	0.07678		−48.16989	−6.42345	2.46890
B	0.7019	1.90507	0.05567	0.03926	−48.01617	−8.88107	3.41673
B^-	0.7019	1.90489	0.04975	0.04535	−47.91952	−10.25207	3.96644
C^+	0.5476	1.88114	0.06328	0.05558	−70.39599	−14.47298	4.60912
C	0.5371	1.87008	0.05249	0.07743	−70.20604	−17.93001	5.73185
C^-	0.5370	1.86967	0.04743	0.08290	−70.06753	−20.17176	6.47990
N^+	0.4365	1.84512	0.05825	0.09663	−96.88562	−27.06171	7.37360
N	0.4319	1.83795	0.05111	0.11094	−96.66557	−31.68660	8.66583
N^-	0.4331	1.83963	0.04817	0.11220	−96.52614	−34.42102	9.46578
O^+	0.3617	1.81390	0.05605	0.13005	−127.67476	−45.16864	10.76570
O	0.3603	1.81070	0.05135	0.13795	−127.44282	−50.63349	12.12703
O^-	0.3608	1.81172	0.04867	0.13961	−127.27411	−54.42949	13.08823
F^+	0.3086	1.78802	0.05552	0.15646	−162.79666	−69.25112	14.69211
F	0.3078	1.78543	0.05163	0.16294	−162.53664	−76.13084	16.21466
F^-	0.3081	1.78611	0.04914	0.16475	−162.33695	−81.14789	17.33979
Ne^+	0.2683	1.76416	0.05531	0.18053	−202.25916	−100.69703	19.24879
Ne	0.2678	1.76216	0.05197	0.18587	−201.97398	−109.15783	20.93433

[20]. Comparison with eq. [24] yields the new energy formula

$$[26] \quad E^v = \frac{1}{3}\left(V^v_{ne} + V^{cv}_{ee} + \sum_i N^v_i \varepsilon_i\right)$$

which is visibly the "valence counterpart" of eq. [17]. Extensive numerical verifications are presented in Sect. 5 in order to assess the range of validity of eq. [25]. E^v expresses a valence region energy that takes the relaxation of the core into proper account. It corresponds to the appropriate sum of ionization potentials.

In closing, let us compare this physically observable E^v with $E^v_{unp.}$, which reflects the description of the electrons as they are found in the valence region of an unperturbed atom. We eliminate V^{vv}_{ee} from eq. [12] with the help of eq. [11] and compare the result with eq. [26]. This gives

$$[27] \quad E^v_{unp.} = \frac{1}{2}(3E^v + T^v)$$

Surely, $E^v \neq E^v_{unp.}$. Equation [27] indicates that the virial theorem, $-T^v = E^v$, and thus $-T^v = E^v_{unp.}$, is not obeyed in the valence region.

5. Numerical verifications

All our calculations are based on normalized wave functions

$$\phi_i = \sum_k c_k \chi^{lm}_k \qquad (e.g., \phi_{1s}, \phi_{2s}, \ldots)$$

constructed from normalized Slater basis functions

$$\chi^{lm}_k = A_k r^{n_k - 1} e^{-\varsigma_k r} Y^m_l(\theta,\varphi)$$

$$A_k = (2\varsigma_k)^{n_k + 1/2}/[(2n_k)!]^{1/2}$$

Unless stated otherwise, we have used the near-Hartree–Fock wave functions of Clementi and Roetti (12) as well as the corresponding orbital energies ε_{1s}, ε_{2s}, ... Correlation and relativistic effects are not included in these calculations. The core and valence electron populations were calculated from eqs. [2] and [3], respectively. The boundary surfaces (i.e., r_b) are those that collect exactly $N^c = 2$ or $N^c = 10$ e in the core regions of the first- and second-row atoms and ions, respectively. The core results are given in Tables 1 and 2. The corresponding valence populations are readily deduced by difference. These populations are instrumental in the evaluation of $\Sigma_i N^v_i \varepsilon_i$. Table 3 reports the breakdown of V_{ee} and T for the atoms Li–Ar. This concludes the presentation of the input data required for our intended verifications of the new energy formulas.

Let us begin with eq. [26], using the data collected in Tables 1 and 2. The orbital energies were taken from the literature (12) and the ionization potentials used for comparisons are those given by Moore (13). The results presented in Table 4 for the first-row atoms and ions are self-explanatory. Those given for the second-row elements (Table 5) reveal discrepancies between calculated and observed quantities, particularly for the larger atoms. Now, the present results were entirely obtained from Hartree–Fock wave functions, which, of course, do not reproduce the experimental energies of the atoms. So it is only natural that non-inclusion of correlation and relativistic effects will show up in our comparisons. Taking these limitations into account, it seems fair to conclude that our verification of eq. [26] is acceptable both for the neutral atoms and their ions.

The following verification is instructive. When we subtract the calculated E^v's from the total Hartree–Fock energies of the corresponding atoms or ions, we obtain, eq. [15],

$$E - E^v = E^c - V^{cv}_{ee} = E^{ion}$$

This is what we did in Table 6, using the Hartree–Fock energies of ref. 12. Our results for $E^c - V^{cv}_{ee}$ are compared with independent calculations (12) of the helium isoelectronic series (for the first-row elements) and with the neon

Can. J. Chem. Downloaded from www.nrcresearchpress.com by 92.62.229.171 on 09/08/12
For personal use only.

TABLE 2. Electron populations and nuclear-electronic potential energies of second-row atoms and ions, calculated for N^c = 10 e (au)

Atom/ion	r_b	N^c_{1s}	N^c_{2s}	N^c_{3s}	N^c_{2p}	N^c_{3p}	V^c_{ne}	V^v_{ne}	V^{cv}_{ee}
Na	2.1268	2.00000	1.99323	0.07495	5.93182		−386.79497	−2.93877	2.61764
Na^-	2.1358	1.99997	1.99356	0.07317	5.93330		−386.78396	−4.56345	4.09925
Mg^+	1.6810	2.00000	1.98504	0.10942	5.90554		−470.52808	−4.54023	3.68083
Mg	1.6285	2.00000	1.98111	0.13737	5.88151		−470.74134	−8.30334	6.79125
Al^+	1.3584	2.00000	1.97024	0.17369	5.85607		−562.88200	−11.64124	8.75941
Al	1.3539	2.00000	1.96945	0.14655	5.85278	0.03123	−562.95265	−15.54499	11.76158
Al^-	1.3592	2.00000	1.96980	0.13622	5.85647	0.03750	−562.88449	−18.05726	13.70187
Si^+	1.1611	2.00000	1.95697	0.16494	5.82695	0.05114	−663.50017	−20.91780	14.66551
Si	1.1566	1.99999	1.95576	0.14346	5.82315	0.07763	−663.60709	−25.80117	18.15187
Si^-	1.1587	2.00000	1.95595	0.13185	5.82566	0.08651	−633.57878	−29.41788	20.74307
P^+	1.0107	1.99999	1.94221	0.15404	5.79664	0.10713	−772.66885	−33.45493	21.79709
P	1.0071	1.99997	1.94044	0.13712	5.79302	0.12945	−772.81824	−39.39692	25.89257
P^-	1.0088	2.00000	1.94113	0.12933	5.79450	0.13502	−772.75135	−43.57413	28.68900
S^+	0.8932	1.99998	1.92594	0.14446	5.76606	0.16357	−890.48672	−49.61457	30.53261
S	0.8796	2.00000	1.91849	0.16263	5.74580	0.17308	−891.57503	−56.94850	35.09536
S^-	0.8918	2.00000	1.92468	0.12511	5.76332	0.18687	−890.55774	−61.53634	37.99853
Cl^+	0.7994	2.00000	1.90931	0.13795	5.73555	0.21716	−1016.94014	−69.40726	40.24284
Cl	0.7976	2.00000	1.90775	0.12776	5.73178	0.23270	−1017.08080	−77.25045	44.86058
Cl^-	0.7978	2.00000	1.90764	0.12094	5.73388	0.23752	−1017.07811	−83.65198	48.63602
Ar^+	0.7224	2.00000	1.89211	0.13241	5.70457	0.27089	−1152.18440	−93.55104	51.27149
Ar	0.7208	1.99997	1.89041	0.12371	5.70366	0.28224	−1152.38159	−102.66604	56.33979

TABLE 3. Breakdown of V_{ee} and T for first-row atoms, with N^c = 2, and second-row atoms, with N^c = 10 e (au)

Atom	V^{cc}_{ee}	V^{vv}_{ee}	V^{cv}_{ee}	T^v
Li	1.69504	0.00825	0.57772	0.03838
Be	2.40265	0.36076	1.72566	0.24186
B	3.14506	1.27739	3.41673	0.91948
C	3.92512	3.10261	5.73185	2.31472
N	4.73588	6.14383	8.66583	4.71403
O	5.56818	10.76072	12.12703	8.20375
F	6.42460	17.20917	16.21466	13.23734
Ne	7.30271	25.80118	20.93433	20.11724
Na	63.38257	0.01726	2.61764	−0.00460
Mg	72.71274	0.31442	6.79125	0.06959
Al	82.05247	0.93367	11.76158	0.35877
Si	91.48340	2.07175	18.15187	0.90781
P	101.02263	3.86961	25.89257	1.77654
S	111.14501	6.64012	35.09536	2.94699
Cl	120.39047	10.13171	44.86058	4.56885
Ar	130.25206	14.82953	56.33979	6.70032

TABLE 4. The calculation of valence region energies of first-row atoms and ions (au)

Atom/ion	$V^v_{ne} + V^{cv}_{ee}$	$\Sigma_i N^v_i \varepsilon_i$	E^v	$-\Sigma$ IP
Li	−0.3266	−0.2719	−0.199	−0.198
Be^+	−1.0502	−0.8861	−0.645	−0.669
Be	−1.8485	−0.8852	−0.911	−1.012
B^+	−3.9546	−2.3090	−2.088	−2.318
B	−5.4643	−1.9901	−2.485	−2.623
B^-	−6.2856	−1.2302	−2.505	−2.634
C^+	−9.8639	−4.5032	−4.789	−5.026
C	−12.1982	−3.6788	−5.292	−5.440
C^-	−13.6919	−2.3800	−5.357	−5.486
N^+	−19.6881	−7.4748	−9.054	−9.276
N	−23.0208	−6.0148	−9.679	−9.810
N^-	−24.9552	−3.9412	−9.632	−9.805
O^+	−34.4029	−11.2814	−15.228	−15.416
O	−38.5065	−8.7778	−15.761	−15.916
O^-	−41.3413	−6.0181	−15.786	−15.970
F^+	−54.5590	−15.5717	−23.377	−23.572
F	−59.9162	−12.2559	−24.057	−24.212
F^-	−63.8081	−8.6761	−24.161	−24.339
Ne^+	−81.4482	−20.7634	−34.071	−34.252
Ne	−88.2235	−16.4997	−34.908	−35.045

For boron we used the electron affinity (0.3 eV) calculated by Clementi and McLean (14).

isoelectronic series (for the second row). Moreover, a comparison is offered with the corresponding sums of ionization potentials. The overall agreement is generally satisfactory. Finally, we show the deviations between our results and their experimental counterparts. The sum of these "core" and "valence" deviations equals, of course, the true error introduced by the neglect of correlation and relativistic effects. This analysis permits an estimate regarding the distribution of errors in the core and valence regions.

Additional tests were performed in order to learn about the selection of N^c. Calculations made for the series Na–Ar, assuming now a core N^c = 2, gave valence region energies that, on the whole, are of the same quality as those deduced for N^c = 10. Interestingly, this also holds true for the results obtained with N^c = 12. It should not be inferred, however, that the appropriate selection of N^c is not important. Calculations made for the series B–Ne with N^c = 4, for example, reveal major discrepancies, up to ~3.4 au for Ne. This N^c is definitely a bad choice. Core populations between 1.8 and 2.2 e were also examined for the first-row atoms, using experimental estimates along the lines given in ref. 3 for comparisons with eq. [26]. For carbon, the deviations are 1.607 (N^c = 1.8), 0.928 (N^c = 1.9), 0.148 (N^c = 2), 0.450 (N^c = 2.1), and 0.639 au (N^c = 2.2 e). N^c = 2 is the obvious choice for the first-row elements. Our results concur with the general idea (3) that the minima of the radial distribution function represent physically meaningful

Can. J. Chem. Downloaded from www.nrcresearchpress.com by 92.62.229.171 on 09/08/12
For personal use only.

TABLE 5. Valence region energies of second-row atoms and ions, for $N^c = 10$ e (au)

Atom/ion	$V^v_{ne} + V^{cv}_{ee}$	$\Sigma_i N^v_i \varepsilon_i$	E^v	$-\Sigma$ IP[a]
Na	−0.3211	−0.2909	−0.204	−0.189
Na^-	−0.4642	−0.1336	−0.199	−0.218
Mg^+	−0.8594	−0.7891	−0.550	−0.553
Mg	−1.5121	−0.8128	−0.775	−0.834
Al^+	−2.8818	−1.8535	−1.578	−1.737
Al	−3.7834	−1.5565	−1.780	−1.957
Al^-	−4.3554	−1.0048	−1.788	−1.976
Si^+	−6.2523	−3.1726	−3.142	−3.490
Si	−7.6493	−2.5985	−3.416	−3.790
Si^-	−8.6748	−1.6993	−3.458	−3.841
P^+	−11.6578	−4.9103	−5.523	−6.112
P	−13.5044	−3.9887	−5.831	−6.497
P^-	−14.8851	−2.5922	−5.826	−6.526
S^+	−19.0820	−7.1071	−8.730	−9.783
S	−21.8531	−5.7216	−9.192	−10.163
S^-	−23.5378	−3.7605	−9.099	−10.239
Cl^+	−29.1644	−9.5514	−12.905	−14.550
Cl	−32.3899	−7.5676	−13.319	−15.026
Cl^-	−35.0160	−5.2338	−13.417	−15.159
Ar^+	−42.2796	−12.5041	−18.261	−20.653
Ar	−46.3263	−9.9664	−18.764	−21.232

[a]For Na, Al, Si, and P we used the electron affinities computed by Clementi, McLean, Raimondi, and Yoshimine (15), using correlation plus relativistic corrections obtained from ionization processes.

core–valence boundary surfaces, but also suggest that this should not be taken too literally with Hartree–Fock wave functions. The latter reproduce quite accurately the electronic shell structure, as revealed by electron diffraction data (16), but small differences evidently persist. A final assessment on this matter is left to future studies, at a post Hartree–Fock level.

We now examine eq. [13], using the data collected in Tables 1–3 and the ε_i's of Clementi and Roetti (12). The example presented for argon (Table 7) illustrates that eq. [13] holds for any arbitrarily selected N^c. This result is not automatic, however: it reflects a property of Hartree–Fock (or near Hartree–Fock) spin orbitals. This point is revealed by an analysis of the numerical differences between $\Sigma_i N^v_i \varepsilon_i$ and $(T^v + V^v_{ne} + V^{cv}_{ee} + 2V^{vv}_{ee})$. They were calculated using $N^c = 1, 2, \ldots, N - 1$ for each individual atom, from Li through Ar, by means of the single-ζ, double-ζ, and near-HF basis sets of ref. 12. The selection of results offered in Table 8 vividly illustrates that $\Sigma_i N^v_i \varepsilon_i$ and $(T^v + V^v_{ne} + V^{cv}_{ee} + 2V^{vv}_{ee})$ converge as we approach the Hartree–Fock limit.

Finally, we examine the valence energy $E^v_{unp.}$ using eqs. [11] and [12] (Table 9) and consider, in an approximate way, the correlation and relativistic corrections suggested by the deviations reported in Table 6. We also indicate the results deduced from eq. [27], using "experimental" E^v's (as given by the appropriate sums of ionization potentials) and the calculated values of T^v (Table 3). The latter are only a minor part of the corresponding total kinetic energies. Hence, we can reasonably anticipate that no serious bias is introduced by their use. As a consequence, the results thus obtained for $E^v_{unp.}$ should represent the closest possible approximation to their "true" values. Surely, these valence energies are for valence regions containing fractional electron populations, those given by eq. [3]. For comparison, we offer the sum of ionization potentials accounting for the fractional populations by linear interpolation. This, of course, represents only a rough estimate, to be taken with a grain of salt, but gives a physical feeling for the energy accumulated in the valence region of an unperturbed atom. The last three entries of Table 9 reveal the general agreement between these different estimates of $E^v_{unp.}$ and support the basic tenets underlying their derivation.

Turning now to the Thomas–Fermi-like description of valence energy, eq. [1], we inquire whether it resembles E^v or $E^v_{unp.}$.

6. Alternate energy formulas. Approximations

Consider first eq. [24] and examine the physical nature of its V^{cv}_{ee} part. This potential energy describes the repulsion between an outer electron cloud (the valence electrons) and the N^c core electrons. Gauss' theorem tells us that the V^{cv}_{ee}

TABLE 6. Core region energies and distribution of errors, au

Atom	Isolated core energy[a]	$E^c - V^{cv}_{ee}$	$-\Sigma^{core}$IP	Deviation	
				Core	Valence
Li	−7.236	−7.237	−7.280	0.043	−0.001
Be	−13.611	−13.665	−13.657	−0.008	0.101
B	−21.986	−22.059	−22.035	−0.024	0.138
C	−32.361	−32.429	−32.416	−0.013	0.148
N	−44.736	−44.780	−44.802	0.022	0.131
O	−59.111	−59.127	−59.194	0.067	0.155
F	−75.486	−75.456	−75.595	0.139	0.155
Ne	−93.861	−93.772	−94.006	0.234	0.137
Na	−161.677	−161.660	−162.240	0.580	−0.015
Mg	−198.831	−198.617	−199.477	0.860	0.059
Al	−240.000	−240.121	−240.756	0.635	0.177
Si	−285.181	−285.460	−286.079	0.619	0.374
P	−334.370	−334.906	−335.451	0.545	0.666
S	−387.565	−388.303	−388.874	0.571	0.971
Cl	−444.764	−446.157	−446.356	0.199	1.707
Ar	−505.968	−508.031	−507.882	−0.149	2.468

[a]Computed energy (12) of the He isoelectronic series for Li–Ne, and of the Ne isoelectronic series for Na–Ar.

Can. J. Chem. Downloaded from www.nrcresearchpress.com by 92.62.229.171 on 09/08/12
For personal use only.

Can. J. Chem. Downloaded from www.nrcresearchpress.com by 92.62.229.171 on 09/08/12
For personal use only.

TABLE 7. Argon. Calculation of $\Sigma_i N_i^v \varepsilon_i$

	$\Sigma_i N_i^v \varepsilon_i$	
N^c	Calcd.[a]	Calcd.[b]
1	−216.7425	−216.7542
2	−125.7992	−125.7990
5	−60.2659	−60.2684
10	−9.9664	−9.9669
12	−4.6437	−4.6353
16	−1.3967	−1.3995

[a]Using valence populations, N_i^v, deduced from eq. [3] and the orbital energies of Clementi and Roetti.
[b]Using $T^v + V_{ne}^v + V_{ee}^{cv} + 2V_{ee}^{vv}$, for arbitrary selections of N^c (au).

TABLE 8. Basis set effects: the differences between $\Sigma_i N_i^v \varepsilon_i$ and $(T^v + V_{ne}^v + V_{ee}^{cv} + 2V_{ee}^{vv})$, expressed as root-mean-square (RMS) deviations of the results obtained with $N^c = 1, 2, \ldots, N - 1$ electron

	RMS deviation, au		
Atom	Single-ζ	Double-ζ	Near HF
B	0.0353	0.0136	0.0012
O	0.2409	0.0319	0.0025
F	0.4302	0.0429	0.0046
Ne	0.6891	0.0715	0.0051
Al	0.7140	0.0577	0.0042
Ar	0.8171	0.0624	0.0075

potential is just as though all the core electron charge were lumped at the nuclear position. Hence, the $\int_{r_b}^{\infty} [\rho(r)/r]dr$ integrals being the same in the evaluation of V_{ee}^{cv} and V_{ne}^v, and taking into account that the nuclear charge Z has been replaced by N^c, it follows that $V_{ee}^{cv} = -(N^c/Z)V_{ne}^v$. It is readily seen that, in this approximation,

$$[28] \quad V_{ne}^v + V_{ee}^{cv} = -(Z - N^c)\int_{r_b}^{\infty} \frac{\rho(r)}{r}\,dr$$

is the nuclear-electronic potential energy of the outer electrons in the field of an expanded "effective nucleus" $(Z - N^c)$.

This is an approximation, of course, because it does not consider the spin of the core electrons. We evaluated V_{ee}^{cv} energies by means of Gauss' theorem (using the V_{ne}^v results of Tables 1 and 2) and subtracted the appropriate exchange integrals, ΣK_{ij}^{cv}, involving the core and valence electrons. In this approximation we considered that for $N^c = 2$ the core consisted only of 1*s* electrons and computed all the 1*s*2*s* and 1*s*2*p* exchange integrals occurring in first-row atoms. For the second row we proceeded similarly, assuming a $N^c = 10$ core consisting only of 1*s*, 2*s*, and 2*p* electrons, and calculated all the relevant integrals with 3*s* and 3*p* electrons. The results obtained in this approximation are compared in Table 10 with their genuine counterparts, i.e., those that correspond to SCF calculations. The spin part is relatively small (e.g., ~0.499 au for Ne and ~0.765 au for Ar) but not negligible. These results are in general agreement with those of Politzer and Daiker (17). In short, eq. [28] is not bad, but is approximate.

On the other hand, this approximation is valuable for the physical picture it conveys, that of a valence electron cloud in the field of a nucleus partially screened by its core electrons. Using it in eq. [24] we get

$$[29] \quad E^v \simeq -\frac{1}{\gamma^v}(Z - N^c)\int_{r_b}^{\infty} \frac{\rho(r)}{r}\,dr$$

which is visibly the counterpart of eq. [1]. The $V_{ne}^v + V_{ee}^{cv}$ and E^v results (Tables 4 and 5) and eq. [24] reveal that, except for Li, Be, Na, and Mg, γ^v is of the order of 7/3. For the neutral atoms Be–Ne it appears that, in this approximation, $\gamma^v = 7/3$ works best under the conditions explored by Politzer and Parr (3). The point is that the straightforward use of Gauss' theorem for the evaluation of V_{ee}^{cv}, i.e., the simple approximation $V_{ne}^v + V_{ee}^{cv} = (Z - N^c)V_{ne}^v/Z$, introduces no major bias in applications of eq. [26]: the root-mean-square deviation between the calculated and experimental results has risen to 0.31 au for the first-row atoms and ions, from 0.16 au in calculations not involving this approximation.

Finally, there is one additional relevant point deserving attention. **Equation [29] represents a valence energy in which relaxation effects are included.** It was derived from eq. [24]. It cannot be mistaken for $E_{unp.}^v$. This particular aspect was not recognizable in earlier derivations (3, 18) of energy formulas like eq. [29]. It holds true for eq. [1].

In the light of these results we can now substantiate two important aspects regarding the appropriateness of the Politzer–Parr-like core–valence separation that was described earlier (6, 18) for molecules. This separation postulated, in a generalization including internuclear repulsions, the approximate validity of eq. [29]. This generalization and the energy formulas that were thus derived for the molecules involved the systematic use of Gauss' theorem: this approximation is now clearly justified. More importantly, it also appears that this generalization, which was entirely derived from a consideration of the valence electrons on the basis of eq. [29], does, indeed, include core relaxation effects as well, although originally the latter had not been contemplated in an explicit manner in the description of molecular systems. We thus retrace a posteriori at least part of the possible reasons explaining the accuracy of molecular energy formulas rooted in the core–valence separation approximated by eq. [29], as revealed by extensive numerical applications (6, 18) pertaining to the calculation of atomization energies and bond dissociation energies.

7. Conclusions

The mental subdivision of a Hartree–Fock atom into an inner core and an outer valence region leads to an amazingly simple statistics involving the eigenvalues, ε_i, of the spin orbitals. The electronic energies statistically accumulated in the core and valence regions are adequately described by $\Sigma_i N_i^c \varepsilon_i$ and $\Sigma_i N_i^v \varepsilon_i$, respectively, where N_i^c and N_i^v are the corresponding electron populations. The result $\Sigma_i N_i^v \varepsilon_i = T^v + V_{ne}^v + V_{ee}^{cv} + 2V_{ee}^{vv}$ for the valence region (with a similar equation for the core) does not depend on the number of electrons assigned to the core. This result is exact.

TABLE 9. Valence region energies of "unperturbed" atoms, with $N^c = 2$ for Li–Ne, and $N^c = 10$ for Na–Ar (au)

Atom	$E^v_{unp.}$ Eq. [11]	Eq. [12]	Eq. [12] + corr	Eq. [27]	$-\Sigma N_i^v(\mathrm{IP})_i$
Li	−0.280	−0.280	−0.280	−0.278	−0.284
Be	−1.246	−1.246	−1.347	−1.397	−1.312
B	−3.267	−3.267	−3.405	−3.475	−3.439
C	−6.781	−6.781	−6.929	−7.003	−7.118
N	−12.159	−12.163	−12.294	−12.358	−12.721
O	−19.539	−19.542	−19.697	−19.772	−20.406
F	−29.465	−29.470	−29.625	−29.699	−30.698
Ne	−42.301	−42.306	−42.443	−42.509	−43.961
Na	−0.308	−0.308	−0.293	−0.286	−0.359
Mg	−1.127	−1.128	−1.187	−1.216	−1.334
Al	−2.490	−2.491	−2.668	−2.756	−2.894
Si	−4.670	−4.670	−5.044	−5.231	−5.364
P	−7.858	−7.858	−8.524	−8.857	−8.932
S	−12.362	−12.266	−13.237	−13.771	−13.913
Cl	−17.699	−17.689	−19.401	−20.255	−19.885
Ar	−24.796	−24.796	−27.264	−28.498	−27.679

The ionization potentials were taken from ref. 13. For the interpolations using fractional electron populations, we included the second-last IP with the 1*s* population in the valence region. Similarly, we subtracted the 2*s* and 2*p* contributions from the valence region by including the corresponding fractions of the larger IP's in the core. The same approximation was used for 3*s* and 3*p* electrons.

TABLE 10. V^{cv}_{ee} results obtained from an application of Gauss' theorem and from SCF calculations

Atom	V^{cv}_{ee}, au Gauss' theorem[a]	SCF
Li	0.58856	0.57772
Be	1.73640	1.72566
B	3.46083	3.41674
C	5.83067	5.73185
N	8.83861	8.66583
O	12.36297	12.12703
F	16.52766	16.21466
Ne	21.33217	20.93433
Na	2.65201	2.61764
Mg	6.85205	6.79125
Al	11.82958	11.76158
Si	18.21751	18.15187
P	25.94621	25.89257
S	35.06381	35.09536
Cl	44.84264	44.86058
Ar	56.27189	56.33979

[a]Results deduced from $-(N^c/Z)V^v_{ne}$, using the results of Tables 1 and 2, and corrected for the core-valence exchange terms, ΣK^{cv}_{ij}.

It reflects a property of Hartree–Fock (or near Hartree–Fock) atomic orbitals. As a corollary of this property of $\Sigma_i N_i^v \varepsilon_i$, we can define the energy of the valence region as $E^v_{unp.} = \Sigma_i N_i^v \varepsilon_i - V^{vv}_{ee}$, where this valence region consists of an entangled mix-up of electrons belonging to different spin orbitals, with fractional populations defined by their densities. This description is in harmony with the fact that each electron occupies the entire atom, that its energy is represented by that of its spin orbital in its integrality, and, finally, with the usual concepts embodied in that of electron density.

This novel assignation of orbital energies to the core and valence regions of an atom and the notion of repulsion between these regions, V^{cv}_{ee}, are instrumental in the derivation of E^v, the energy that mirrors the actual removal of electrons from the valence shell. The key is in the use of Hartree–Fock identities describing the relationships between the total energy of the atom and the sum of occupied orbital energies, on one hand, and the nuclear-electronic potential energy, on the other. A combination of these relationships leads to a simple formula for E^v and establishes a clear relationship between E^v and $E^v_{unp.}$. But, unlike the latter energy, which is meaningful for any arbitrary choice of N^c, E^v is meaningful only for discrete values of N^c, namely integer core populations confined within boundaries lying in the vicinity of the minima of the radial distribution function. This result casts light on the physical involvement of the electronic shell structure in a meaningful separation of an atom into core and valence regions.

Acknowledgment

We wish to thank the referees for very helpful suggestions. The financial support given by the Natural Sciences and Engineering Research Council of Canada is gratefully acknowledged.

1. L. L. Foldy. Phys. Rev. **83**, 397 (1951); A. Froman. Phys. Rev. **112**, 870 (1958); P.-O. Löwdin. J. Mol. Spectrosc. **3**, 46 (1959); E. B. Wilson, Jr. J. Chem. Phys. **36**, 2232 (1962); P. Politzer and R. G. Parr. J. Chem. Phys. **61**, 4258 (1974).
2. P. Hohenberg and W. Kohn. Phys. Rev. B, **136**, 864 (1964); W. Kohn and L. J. Sham. Phys. Rev. A, **140**, 1133 (1965).
3. P. Politzer and R. G. Parr. J. Chem. Phys. **64**, 4634 (1976).
4. L. H. Thomas. Proc. Cambridge Philos. Soc. **23**, 542 (1926); E. Fermi. Z. Phys. **48**, 73 (1928); P. Gombás. Die Statis-

Can. J. Chem. Downloaded from www.nrcresearchpress.com by 92.62.229.171 on 09/08/12
For personal use only.

tische Theorie des Atoms und ihre Anwendungen. Springer-Verlag, Vienna. 1949.
5. R. J. Boyd. J. Chem. Phys. **66**, 356 (1977); S. Fliszár and H. Henry. J. Chem. Phys. **67**, 2345 (1977); S. Fliszár. J. Chem. Phys. **69**, 237 (1978); S. Fliszár and D. Salahub. J. Chem. Phys. **69**, 3321 (1978); S. Fliszár. J. Chem. Phys. **79**, 3874 (1983).
6. S. Fliszár. Charge distributions and chemical effects. Springer-Verlag, Heidelberg, New York. 1983.
7. H. Eyring, J. Walter, and G. E. Kimball. Quantum chemistry. Wiley, New York. 1944.
8. N. H. March. Adv. Phys. **6**, 1 (1957).
9. R. G. Parr, S. R. Gadre, and L. J. Bartolotti. Proc. Natl. Acad. Sci. USA, **76**, 2522 (1979).
10. K. Ruedenberg. J. Chem. Phys. **66**, 375 (1977).
11. P. Politzer. J. Chem. Phys. **64**, 4239 (1976); **69**, 491 (1978).
12. E. Clementi and C. Roetti. At. Data Nucl. Data Tables, **14**, 179 (1974).
13. C. E. Moore. Natl. Stand. Ref. Data Ser. (U.S. Natl. Bur. Stand.), **34** (1970).
14. E. Clementi and A. D. McLean. Phys. Rev. A, **133**, 419 (1964).
15. E. Clementi, A. D. McLean, D. L. Raimondi, and M. Yoshimine. Phys. Rev. A, **133**, 1274 (1964).
16. L. S. Bartell and L. O. Brockway. Phys. Rev. **90**, 833 (1953).
17. P. Politzer and K. C. Daiker. Chem. Phys. Lett. **20**, 309 (1973).
18. S. Fliszár. J. Am. Chem. Soc. **102**, 6946 (1980); *In* Chemistry and physics of energetic materials. *Edited by* S. N. Bulusu. NATO ASI Ser. C: **309**, 143 (1990).

Can. J. Chem. Downloaded from www.nrcresearchpress.com by 92.62.229.171 on 09/08/12
For personal use only.

Orbital exponent optimization for molecular self-consistent-field wave functions including the polarization function

KENRO HASHIMOTO[1]

Molecular Photochemistry Laboratory, The Institute of Physical and Chemical Research (RIKEN), Wako, Saitama 351-01, Japan

AND

YOSHIHIRO OSAMURA

Department of Chemistry, Faculty of Science and Technology, Keio University, 3-14-1 Hiyoshi, Kohoku-ku, Yokohama 223, Japan

Received July 18, 1991

This paper is dedicated to Professor Sigeru Huzinaga on the occasion of his 65th birthday

KENRO HASHIMOTO and YOSHIHIRO OSAMURA. Can. J. Chem. **70**, 547 (1992).

We have applied the analytical energy gradient method with respect to the orbital exponents for molecular self-consistent-field wave functions including the polarization functions. The gradients for Gaussian-type functions in Huzinaga–Dunning's double zeta basis set with and without polarization functions were compared for some hydrides of the first-row elements. The changes in the gradients caused by the polarization functions were observed. It was found that the polarization functions on hydrogen play a role in reducing the gradients produced in the absence of these functions. Although optimization of the exponents gives results depending on the molecules, the total energies as well as the dipole moments are insensitive to the exponent values. We could confirm that the exponents for Gaussian functions in the standard double zeta plus polarization basis set work adequately by coupling with the variational parameters for the simple hydrides even if they have gradients in the molecules.

Key words: orbital exponent, Gaussian-type functions, analytical energy gradient, molecular SCF wave function, polarization function.

KENRO HASHIMOTO et YOSHIHIRO OSAMURA. Can. J. Chem. **70**, 547 (1992).

On a appliqué la méthode du gradient de l'énergie analytique aux exposants orbitalaires des fonctions d'onde moléculaires en champ auto-cohérent, y compris aux fonctions de polarisation. Pour quelques hydrures des éléments de la première rangée, on a comparé les gradients des fonctions de type gaussien de bases double zêta de Huzinaga–Dunning avec et sans fonctions de polarisation. On a observé les changements dans les gradients, causés par les fonctions de polarisation. On a trouvé que les fonctions de polarisation affectent l'hydrogène en réduisant les gradients produits en l'absence de ces fonctions. Même l'optimisation des exposants donne des résultats qui dépendant des molécules; les énergies totales ainsi que les moments dipolaires ne sont pas sensibles aux valeurs des exposants. On a pu confirmer que les exposants des fonctions gaussiennes, dans la base standard de polarisation double zêta plus, donne des résultats adéquats en se couplant à des paramètres variationnels pour les hydrures simples, même s'ils possèdent des gradients dans les molécules.

Mots clés : exposant orbitalaire, fonctions de type gaussian, gradient de l'énergie analytique, fonction d'onde moléculaire en SCF, fonction de polarisation.

[Traduit par la rédaction]

Introduction

Since Gaussian-type functions (GTF's) were introduced as basis sets for *ab initio* molecular orbital (MO) methods, many were made to obtain adequate GTF exponents in the basis functions for the precise description of the electronic wave function. The energy gradient method as well as variational and numerical optimization has often been utilized in determining the orbital exponent of the GTF's. Kari *et al.* first introduced the gradient method to develop a basis set that has uniform quality for various atoms (1). Partridge reported many basis functions using this gradient method (2). He carefully assessed the quality of the basis set by varying the number of GTF's. Faegri and Almlof continued the research by examining the efficiency of the analytical Hessian in optimization (3).

Orbital exponents for GTF's in currently available basis sets were determined to be optimum for atoms (4–6), based on the concept and methodology of the Linear Combination of Atomic Orbitals (LCAO–MO) scheme. Thus, the computation for molecules could sometimes be biased, depending on the molecules and on how the basis set was constructed (7).

It would be desirable to optimize all parameters to describe the electronic wave function in each particular system. Some attempts have been made for variational parameters, e.g., orbital exponents, not only in atoms but also in molecules (8, 9). Such an approach to obtaining the molecular basis set would be feasible if an analytical gradient were available. However, the difficulty in evaluating multicenter integrals for the products of GTF's with high angular quantum numbers has obstructed the extension of the gradient method from atoms to molecules.

The recent development of the energy gradient technique for molecular wave functions enables us to examine the extent to which gradients for atomic exponents emerge in molecular wave functions. Tonachini and Schlegel (10) first overcame the difficulty in computing the integrals by using Rys polynomials (11). In this pioneering work (10), the au-

[1]Special Researcher, Basic Science Program, RIKEN. Present address: Institute for Molecular Science, Myodaiji, Okazaki 444, Japan.

Printed in Canada

Can. J. Chem. Downloaded from www.nrcresearchpress.com by 92.62.229.171 on 09/08/12
For personal use only.

TABLE 1. Energy gradients for the standard exponents of GTF's in the DZ+P basis set together with optimized exponents and scale factors in the BH_3 molecule[a]

Standard GTF exponents[b]	$\partial E/\partial \ln \alpha$ in atom[c]		$\partial E/\partial \ln \alpha$ in BH_3[c]		Optimized exponents[d]	Scale factor[e]
B 9*s* GTF's						
2788.41	0.0000	(−0.0000)	0.0000	(0.0000)	3851.21	1.175
419.039	−0.0000	(0.0000)	−0.0000	(−0.0000)	596.303	1.193
96.4683	−0.0008	(−0.0010)	−0.0003	(−0.0003)	140.211	1.206
28.0694	−0.0000	(0.0003)	−0.0009	(−0.0010)	40.8440	1.206
9.37597	0.0002	(0.0004)	0.0010	(0.0011)	13.5181	1.200
3.40623	0.0001	(−0.0009)	−0.0010	(−0.0002)	4.82277	1.190
1.30566	−0.0006	(0.0003)	−0.0002	(−0.0002)	1.73719	1.153
0.32448	−0.0009	(−0.0002)	−0.0002	(0.0016)	0.308691	0.975
0.102190	0.0009	(0.0002)	−0.0006	(0.0004)	0.0903640	0.940
B 5*p* GTF's						
11.3413	−0.0000	(−0.0000)	0.0004	(0.0010)	13.3940	1.087
2.43599	0.0000	(0.0001)	0.0021	(−0.0054)	2.93246	1.097
0.683580	0.0004	(0.0003)	0.0064	(.0170)	0.824396	1.098
0.213360	−0.0007	(−0.0007)	−0.0076	(−0.0118)	0.280425	1.146
0.070114	0.0000	(0.0000)	0.0020	(0.0024)	0.0729070	1.020
B 1*d* GTF						
0.7	0.0001		0.0008		0.579858	0.910
H 4*s* GTF's						
19.2406		(−0.0000)	0.0001	(0.0002)	22.4897	1.081
2.89915		(0.0000)	−0.0003	(−0.0009)	3.44874	1.091
0.653410		(0.0001)	0.0003	(0.0013)	0.772133	1.087
0.177576		(−0.0001)	−0.0006	(−0.0001)	0.203685	1.071
H 1*p* GTF						
1.0			0.0004		1.01933	1.010
		$E = -26.397147$ hartree			$E = -26.398731$ hartree ($\Delta E = 0.99$ kcal/mol)	

[a]Bond distance of BH_3 is 1.1098 Å, which is optimized by the SCF method with the DZ basis set.
[b]Exponents of Huzinaga's 9*s*5*p* GTF's for the B atom and 4*s* GTF's with a scale factor of 1.2 for the H atom. Exponents of polarization functions are taken from the values by Dunning and Hay (ref. 21).
[c]Values in parentheses are obtained without polarization functions (ref. 15).
[d]Optimization criterion is max $|\partial E/\partial \ln \alpha| \leq 0.0001$ in atomic units.
[e]Square root of {(optimized exponent for molecule)/(standard exponent)}.

thors showed the variation in energy gradients with respect to the orbital exponents of GTF's on sulfur by comparing the S atom and HS^-, H_2S, and H_3S^+ molecules. They also demonstrated that the exponents of *d* functions vary, depending on the molecular geometries during the course of the reaction pathway (12). In their approach, however, they limit the optimization to polarization exponents only.

In our own approach (13), we use the McMurchie–Davidson formulas (14) for derivative integral evaluation. By optimizing all of the orbital exponents using this technique, we can investigate whether or not the atomic exponents work adequately in the molecular calculations. We can also study the deviation of the orbital exponents for molecules from those for atoms, caused by chemical bond formation. In the present study, we focus on the effect of the polarization function, whose exponent can only be determined by molecular calculations. We also discuss the effect of optimization of the exponents upon the value of the dipole moment, which is one of the important one-electron properties of a molecule.

Method

The analytical energy gradient method with respect to the orbital exponent is applied to GTF sets including a single polarization function for each atom. Details of the method for calculating the gradients were described in our previous paper (15).

The molecules investigated are BH_3, CH_4, NH_3, H_2O, and HF. The molecular structures of BH_3 were optimized with the double zeta (DZ) basis set (16) and those for the other molecules were taken from the literature (16–19). For comparison, these structures are the same as those used in the case without polarization functions (15).

The size of the GTF sets is (9*s*5*p*1*d*) for the first-row elements and (4*s*1*p*) for hydrogen. We did not contract the GTF's but employed the primitive functions. The initial exponents of (9*s*5*p*) functions for the first-row elements are taken from Huzinaga (20). Huzinaga's exponents of (4*s*) functions for the hydrogen atom (20) with a molecular scale factor (1.2) are also used as initial exponents. The initial exponent of the *d*-type polarization function on heavy at-

Can. J. Chem. Downloaded from www.nrcresearchpress.com by 92.62.229.171 on 09/08/12
For personal use only.

TABLE 2. Energy gradients for the standard exponents of GTF's in the DZ+P basis set together with optimized exponents and scale factors in the CH_4 molecule[a]

Standard GTF exponents[b]	$\partial E/\partial \ln \alpha$ in atom[c]		$\partial E/\partial \ln \alpha$ in CH_4[c]		Optimized exponents[d]	Scale factor[e]
C 9*s* GTF's						
4232.61	0.0000	(0.0000)	0.0000	(0.0000)	5930.37	1.171
634.882	0.0001	(0.0000)	−0.0001	(−0.0001)	912.050	1.199
146.097	−0.0007	(−0.0011)	−0.0002	(−0.0002)	212.408	1.206
42.4974	−0.0009	(0.0001)	−0.0020	(−0.0018)	61.1714	1.200
14.1982	0.0020	(0.0001)	0.0030	(0.0026)	20.1278	1.191
5.14773	0.0010	(0.0001)	−0.0034	(−0.0031)	7.15225	1.179
1.96655	−0.0034	(−0.0005)	0.0004	(−0.0003)	2.57371	1.144
0.496240	0.0047	(−0.0000)	0.0024	(0.0031)	0.471162	0.974
0.153310	0.0023	(−0.0002)	−0.0021	(−0.0012)	0.151445	0.994
C 5*p* GTF's						
18.1557	0.0000	(0.0000)	0.0006	(0.0001)	17.2714	0.975
3.98640	0.0000	(0.0000)	−0.0035	(−0.0061)	3.78794	0.975
1.14293	0.0007	(0.0007)	0.0092	(0.0203)	1.06883	0.967
0.359450	−0.0013	(−0.0007)	−0.0082	(−0.0118)	0.346278	0.982
0.114600	−0.0000	(−0.0000)	0.0024	(0.0071)	0.0947105	0.909
C 1*d* GTF						
0.75	−0.0001		−0.0019		0.843533	1.061
H 4*s* GTF's						
19.2406		(−0.0000)	−0.0000	(−0.0000)	23.0078	1.094
2.89915		(0.0000)	0.0001	(0.0003)	3.64673	1.122
0.653410		(0.0001)	−0.0005	(−0.0022)	0.848556	1.140
0.177576		(−0.0001)	−0.0002	(0.0015)	0.229526	1.137
H 1*p* GTF						
1.0			−0.0004		1.22238	1.106
		$E = -40.208591$ hartree			$E = -40.210371$ hartree ($\Delta E = 1.12$ kcal/mol)	

[a]CH bond distance is 1.094 Å (ref. 17).
[b]Exponents of Huzinaga's 9*s*5*p* GTF's for the C atom and 4*s* GTF's with a scale factor of 1.2 for the H atom. Exponents of polarization functions are taken from the values by Dunning and Hay (ref. 21).
[c]Values in parentheses are obtained without polarization functions (ref. 15).
[d]Optimized criterion is max $|\partial E/\partial \ln \alpha| \leq 0.0001$ in atomic units.
[e]Square root of {(optimized exponent for molecule)/(standard exponent)}.

oms and that of the *p*-type polarization function on hydrogen are values reported by Dunning and Hay (21). Six *d* functions (d_{xx}, d_{yy}, d_{zz}, d_{xy}, d_{yz}, and d_{zx}) are included in a set of *d*-type polarization functions. This initial set of GTF's is one of the most frequently used basis-function sets in the double zeta plus polarization basis (DZ+P) with a contraction.

Energy gradients are calculated with respect to the natural logarithm of the orbital exponents, instead of the genuine exponents, as shown in our previous papers (13, 15). The modified quasi Newton–Raphson method proposed by Schlegel (22) is employed in optimization of the exponents.

Numerical computations were carried out with a Fujitsu FACOM M-780 computer at the computation center in the Institute of Physical and Chemical Research (RIKEN).

Results and discussion

Tables 1–5 summarize the results of the exponent optimization for BH_3, CH_4, NH_3, H_2O, and HF molecules, respectively. Each of the tables contains the gradients for atoms and molecule, optimized exponents, and their molecular scale factors relative to the standard exponents. We tabulated the results for each molecule because the correspondence between the standard exponents and the molecular exponents is important. However, we had better look at the items in the tables comparing the molecules to make the discussion clear and to understand the molecular characteristics. We will first pay attention to the gradients in the atoms.

Atomic gradients for GTF's on heavy atoms

The gradients for the standard exponents in the atoms are given in the second left column of the tables. Since we used six *d* functions as a set of polarization functions on heavy atoms, the gradients in the atom are affected by the additional *s*-type function due to the contribution from the sum of d_{xx}, d_{yy}, and d_{zz} functions. As pointed out in the previous paper (15), the standard exponents without the *d*-type polarization function are shown to be well optimized for B and C atoms, while not so much for N, O, and F atoms. Addition of the *d*-type function generally allows the gradients for the *s*-type functions to increase in all of the first-row atoms we examined. This increment in the gradients for *s*-type functions in atoms can be seen not only in the exponents of

Can. J. Chem. Downloaded from www.nrcresearchpress.com by 92.62.229.171 on 09/08/12
For personal use only.

TABLE 3. Energy gradients for the standard exponents of GTF's in the DZ+P basis set together with optimized exponents and scale factors in the NH_3 molecule[a]

Standard GTF exponents[b]	$\partial E/\partial \ln \alpha$ in atom[c]		$\partial E/\partial \ln \alpha$ in NH_3[c]		Optimized exponents[d]	Scale factor[e]
N 9*s* GTF's						
5909.44	0.0000	(0.0000)	0.0000	(0.0000)	10103.4	1.308
887.451	−0.0001	(0.0000)	−0.0001	(−0.0001)	1553.72	1.323
204.749	−0.0007	(−0.0015)	−0.0006	(−0.0007)	361.881	1.329
59.8376	−0.0019	(−0.0003)	−0.0022	(−0.0020)	104.458	1.321
19.9981	0.0033	(0.0010)	0.0040	(0.0035)	34.4499	1.313
7.19274	−0.0019	(0.0008)	−0.0033	(−0.0031)	12.3638	1.311
2.68598	−0.0004	(−0.0014)	−0.0002	(−0.0003)	4.62808	1.313
0.700040	0.0021	(−0.0001)	0.0013	(0.0080)	0.532921	0.873
0.213290	−0.0021	(−0.0006)	−0.0020	(−0.0043)	0.191697	0.948
N 5*p* GTF's						
26.7860	−0.0001	(−0.0002)	0.0003	(0.0001)	23.1917	0.930
5.95635	0.0008	(0.0008)	−0.0017	(−0.0010)	5.14422	0.929
1.70740	0.0019	(0.0018)	0.0106	(0.0106)	1.48886	0.934
0.531360	−0.0035	(−0.0035)	−0.0166	(−0.0253)	0.474264	0.945
0.165370	−0.0000	(0.0000)	0.0143	(0.0187)	0.137144	0.911
N 1*d* GTF						
0.8	−0.0002		−0.0004		0.799150	0.999
H 4*s* GTF's						
19.2406		(−0.0000)	−0.0001	(−0.0003)	24.3301	1.125
2.89915		(0.0000)	0.0005	(0.0022)	3.81164	1.147
0.653410		(0.0001)	−0.0011	(−0.0061)	0.880043	1.161
0.177576		(−0.0001)	−0.0003	(0.0024)	0.242972	1.170
H 1*p* GTF						
1.0			−0.0000		1.09164	1.045
		$E = -56.210611$ hartree			$E = -56.213509$ hartree ($\Delta E = 1.82$ kcal/mol)	

[a]NH bond distance is 1.0123 Å and ∠HNH angle is 106.7° (ref. 18).
[b]Exponents of Huzinaga's 9*s*5*p* GTF's for the N atom and 4*s* GTF's with a scale factor of 1.2 for the H atom. Exponents of polarization functions are taken from the values by Dunning and Hay (ref. 21).
[c]Values in parentheses are obtained without polarization functions (ref. 15).
[d]Optimized criterion is max $|\partial E/\partial \ln \alpha| \leq 0.0001$ in atomic units.
[e]Square root of {(optimized exponent for molecule)/(standard exponent)}.

diffuse *s*-type functions but also in those of some *s*-type functions with a middle range of exponent values for C, N, O, and F atoms. On the other hand, the gradients for *p*-type functions in the atom do not change much in the presence of the *d*-type polarization function, irrespective of the kind of atom. The atomic gradient of the *d*-type function itself is generally small in all these atoms.

Gradients in hydride molecules

Gradients for the standard exponent in the hydride molecules are shown in the third column of Tables 1–5. The gradients in the molecule depend not only on the molecule itself but also on each exponent value of the GTF's. It is convenient for our discussion to divide the *s*-type GTF's into three groups according to their exponent values. One is the *inner* group of three GTF's with large exponents, another is the *middle* group of three GTF's with middle values of exponents, and the rest belong to the *outer* group of three GTF's whose exponents are small. Almost all of the gradients for the outer group functions are found to be reduced or kept small by adding the *d*-type polarization function in all molecules. Because adding the *d*-type polarization function does not reduce the gradients for the middle group functions so much as for the outer group functions, we observe a large gradient for the middle group GTF's instead of for the outer ones, in the presence of the polarization function. The molecular gradients for the inner group functions with large exponents are small with and without the *d*-type function.

The gradient values of *p*-type functions are calculated to be fairly large in a molecule without a polarization function. We found that the large gradients of the *p*-type functions decreased by adding the *d*-type function in BH_3 and CH_4 molecules. In NH_3, the molecular gradients for only two diffuse *p*-type functions become small with the *d*-type function. In H_2O and HF molecules, the absolute value of the gradients for *p*-type functions becomes greater with the *d*-type function than for those without the polarization function. The gradients for the *d*-type function increase from atomic gradients in CH_4, H_2O, and HF molecules. They are, however, still small compared to other large gradients in *s* and *p* functions.

The gradients for four *s*-type functions on hydrogen are larger in NH_3, H_2O, and HF molecules than in BH_3 and CH_4 when the *p*-type polarization function is not included on the H atom. The *p*-type polarization function plays a role in conspicuously reducing the gradients for *s*-type functions on

Can. J. Chem. Downloaded from www.nrcresearchpress.com by 92.62.229.171 on 09/08/12
For personal use only.

TABLE 4. Energy gradients for the standard exponents of GTF's in the DZ+P basis set together with the optimized exponents and scale factors in the H_2O molecule[a]

Standard GTF exponents[b]	$\partial E/\partial \ln \alpha$ in atom[c]		$\partial E/\partial \ln \alpha$ in H_2O[c]		Optimized exponents[d]	Scale factor[e]
O 9*s* GTF's						
7816.54	0.0000	(0.0000)	0.0000	(0.0000)	13517.9	1.315
1175.82	−0.0001	(0.0000)	−0.0001	(−0.0000)	2066.75	1.326
273.188	−0.0016	(−0.0020)	−0.0013	(−0.0014)	478.659	1.324
81.1696	−0.0037	(−0.0027)	−0.0045	(−0.0041)	137.456	1.301
27.1836	0.0108	(0.0090)	0.0120	(0.0109)	45.1293	1.288
9.53223	−0.0058	(−0.0035)	−0.0075	(−0.0064)	16.1455	1.301
3.41364	−0.0006	(−0.0016)	−0.0004	(−0.0010)	6.03438	1.330
0.939780	−0.0017	(−0.0005)	−0.0012	(0.0074)	1.59410	1.303
0.284610	0.0003	(−0.0008)	0.0008	(−0.0038)	0.258176	0.952
O 5*p* GTF's						
35.1832	−0.0002	(−0.0002)	0.0002	(−0.0001)	34.0217	0.983
7.90403	0.0009	(0.0009)	−0.0015	(0.0008)	7.65230	0.984
2.30512	0.0009	(0.0009)	0.0099	(0.0034)	2.25255	0.989
0.717060	−0.0016	(−0.0016)	−0.0216	(−0.0172)	0.699557	0.988
0.213730	0.0000	(0.0000)	0.0228	(0.0227)	0.187741	0.937
O 1*d* GTF						
0.85	0.0000		−0.0011		1.04770	1.110
H 4*s* GTF's						
19.2406		(−0.0000)	−0.0001	(−0.0003)	22.5221	1.082
2.89915		(0.0000)	0.0008	(0.0022)	3.61070	1.116
0.653410		(0.0001)	−0.0018	(−0.0063)	0.875131	1.157
0.177576		(−0.0001)	−0.0001	(0.0016)	0.265759	1.223
H 1*p* GTF						
1.0			0.0007		0.667290	0.817
		$E = -76.048160$ hartree			$E = -76.052462$ hartree ($\Delta E = 2.70$ kcal/mol)	

[a]OH bond distance is 0.9584 Å and ∠HOH angle is 104.5° (ref. 16).
[b]Exponents of Huzinaga's 9*s*5*p* GTF's for the O atom and 4*s* GTF's with a scale factor of 1.2 for the H atom. Exponents of polarization functions are taken from the values by Dunning and Hay (ref. 21).
[c]Values in parentheses are obtained without polarization functions (ref. 15).
[d]Optimized criterion is max $|\partial E/\partial \ln \alpha| \leq 0.0001$ in atomic units.
[e]Square root of {(optimized exponent for molecule)/(standard exponent)}.

hydrogen in all of the molecules we studied, although the gradient for the *p*-type polarization function itself is small throughout these hydrides.

Optimized exponents in molecules and their scale factors

The optimized exponents in hydrides and their scale factors relative to the standard exponents are presented in the two right columns of Tables 1–5. The scale factor is defined as the square root of the ratio of the molecular exponent over the standard exponent. It is convenient for us to use scale factors rather than the molecular exponents themselves in order to see the change in the exponent values from atom to molecule. A scale factor greater than 1.0 means that the GTF shrinks compared to the standard function, while the GTF with a scale factor less than 1.0 diffuses as a result of the optimization in the molecule.

Throughout Tables 1–5, we note a general trend for the scale factors of *s*-type functions on heavy atoms. The scale factor of *s*-type functions whose exponents are smaller than that of the added *d*-type function becomes less than 1.0. When the exponent values of the *s*-type functions are larger than that of the *d*-type function, the scale factors for *s*-type functions turn out to be greater than 1.0 by the optimization. This result clearly indicates that the interaction between the normal *s*-type function and the extra *s*-type function involved in the six *d*-function sets is important in determining optimum values of the orbital exponents.

The scale factors of the *p*-type functions depend on the molecules much more than those of the *s*-type functions on heavy atoms. All *p*-type functions on the B atom tend to shrink in the BH_3 molecule. The deviation of orbital exponents of the *p*-type functions from the standard values is not so large after optimization in the BH_3 molecule.

The *p*-type functions on C, N, O, and F tend to diffuse in the order CH_4, NH_3, H_2O, and HF molecules. The largest change in orbital exponents of the *p*-type function is observed in the case of NH_3. The most diffuse function tends to diffuse more than the other four *p*-type functions except in the BH_3 molecule.

The optimized values of the orbital exponents of the *d*-type polarization functions on heavy atoms are 0.5799, 0.8435, 0.7992, 1.0477, and 1.1710 for BH_3, CH_4, NH_3, H_2O, and HF, respectively.

The scale factors obtained for the *s*-type functions on hydrogen are greater than 1.0 by optimization in all the hydrides. The shrinkage is larger in NH_3, H_2O, and HF

Can. J. Chem. Downloaded from www.nrcresearchpress.com by 92.62.229.171 on 09/08/12
For personal use only.

TABLE 5. Energy gradients for the standard exponents of GTF's in the DZ+P basis set together with optimized exponents and scale factors in the HF molecule[a]

Standard GTF exponents[b]	$\partial E/\partial \ln \alpha$ in atom[c]		$\partial E/\partial \ln \alpha$ in HF[c]		Optimized exponents[d]	Scale factor[e]
F 9*s* GTF's						
9994.79	0.0000	(−0.0000)	0.0000	(−0.0000)	17804.2	1.335
1506.03	−0.0001	(−0.0000)	−0.0001	(−0.0001)	2684.47	1.335
350.269	−0.0016	(−0.0021)	−0.0013	(−0.0018)	613.757	1.324
104.053	−0.0037	(−0.0042)	−0.0045	(−0.0048)	174.277	1.294
34.8432	0.0108	(0.0122)	0.0120	(0.0129)	56.6789	1.275
12.2164	−0.0058	(−0.0041)	−0.0075	(−0.0054)	20.1294	1.284
4.36885	−0.0006	(−0.0022)	−0.0004	(−0.0017)	7.47042	1.308
1.20775	−0.0017	(−0.0008)	−0.0012	(0.0033)	1.81819	1.227
0.363400	0.0003	(−0.0014)	0.0008	(−0.0008)	0.302617	0.913
F 5*p* GTF's						
44.3555	−0.0002	(−0.0002)	0.0002	(−0.0002)	43.1541	0.986
10.0820	0.0009	(−0.0007)	−0.0015	(−0.0004)	9.75513	0.983
2.99586	0.0009	(0.0000)	0.0099	(0.0005)	2.87365	0.979
0.938260	−0.0016	(0.0025)	−0.0216	(−0.0072)	0.884109	0.971
0.273290	0.0000	(−0.0001)	0.0228	(0.0207)	0.246935	0.951
F 1*d* GTF						
0.90	0.0000		−0.0011		1.17103	1.141
H 4*s* GTF's						
19.2406		(−0.0000)	−0.0001	(−0.0004)	23.8433	1.113
2.89915		(0.0000)	0.0008	(0.0030)	3.92119	1.163
0.653410		(0.0001)	−0.0018	(−0.0071)	0.950393	1.206
0.177576		(−0.0001)	−0.0001	(0.0004)	0.284874	1.267
H 1*p* GTF						
1.0			0.0007		0.766081	0.875
		E = 100.050209 hartree			E = −100.055069 hartree (ΔE = 3.05 kcal/mol)	

[a]FH bond distance is 0.9171 Å (ref. 19).
[b]Exponents of Huzinaga's 9*s*5*p* GTF's for the F atom and 4*s* GTF's with a scale factor of 1.2 for the H atom. Exponents of polarization functions are taken from the values by Dunning and Hay (ref. 21).
[c]Values in parentheses are obtained without polarization functions (ref. 15).
[d]Optimization criterion for is max $|\partial E/\partial \ln \alpha| \leq 0.0001$ in atomic units.
[e]Square root of {(optimized exponent for molecule)/(standard exponent)}.

molecules than in BH_3 and CH_4 molecules. The optimized exponents of *p*-type polarization functions on hydrogen atoms are 1.0193, 1.2224, 1.0916, 0.6673, and 0.7661 for BH_3, CH_4, NH_3, H_2O, and HF, respectively. These results clearly indicate that the orbital shape of the hydrogen atom strongly depends on each molecular environment.

General discussion on exponent optimization

Here, we will discuss some other features commonly seen in the molecules examined.

Firstly, the total energy is not very sensitive to the exponent optimization. Energy lowering by exponent optimization without the polarization function is calculated to be 1.00, 1.28, 1.78, 1.38, and 1.25 kcal/mol for the BH_3, CH_4, NH_3, H_2O, and HF molecules, respectively (15). When the polarization function is included in the optimization, the largest improvement in energy (3.05 kcal/mol) is obtained in the case of the HF molecule. The small improvement in the energy might be because the GTF's used are uncontracted.

Secondly, the shrinking and diffusing of the GTF's by molecular optimization cannot be predicted by the sign of their initial gradients, as is also true for the case without polarization function (15). Moreover, the largest deviation from 1.0 in the scale factors shown in Tables 1–5 is not always found for the exponent whose initial gradient is largest. This means that the exponents are strongly coupled in the optimization procedure.

Effect of exponent optimization on dipole moment

To see how much the electron distribution or density is improved by exponent optimization, we calculated the dipole moments for NH_3, H_2O, and HF molecules with standard and molecular optimized basis functions. The dipole moments are evaluated both with the optimized geometries and with the experimental structures. The results are summarized in Tables 6–8. The values obtained with the DZ and DZ+P contracted basis functions are also presented.

The dipole moments at the experimental geometries calculated without polarization functions deviate greatly from

Can. J. Chem. Downloaded from www.nrcresearchpress.com by 92.62.229.171 on 09/08/12
For personal use only.

TABLE 6. Effect of exponent optimization and geometry optimization on the dipole moment[a] of the NH_3 molecule calculated by using [9*s*5*p*(N) and 4*s*(H)] and [9*s*5*p*1*d*(N) and 4*s*1*p*(H)] GTF's

Basis set	Experimental geometry[b] Energy (hartree)	Experimental geometry[b] Dipole moment (debye)	Optimized geometry Energy (hartree)	Optimized geometry Dipole moment (debye)	r_{NH} (Å)	∠HNH (degree)
[9*s*5*p*(N) and 4*s*(H)]						
Contracted as DZ	−56.175954	2.3466	−56.180541	1.3618	0.9944	116.28
Standard exponent	−56.179356	2.2868	−56.182810	1.5242	0.9961	114.95
Optimized exponent	−56.181746	2.2882	−56.185308	1.5257	0.9954	114.93
[9*s*5*p*1*d*(N) and 4*s*1*p*(H)]						
Contracted as DZ+P	−56.209297	1.8974	−56.209685	1.8054	1.0010	108.19
Standard exponent	−56.210611	1.8907	−56.211030	1.8017	1.0003	108.15
Optimized exponent	−56.213509	1.9350	−56.214084	1.8044	0.9989	108.64

[a]Experimental dipole moment of NH_3 is 1.472 debye (ref. 26).
[b]r_{NH} = 1.0123 Å, ∠HNH = 106.7° (ref. 18).

TABLE 7. Effect of exponent optimization and geometry optimization on the dipole moment[a] of the H_2O molecule calculated by using [9*s*5*p*(O) and 4*s*(H)] and [9*s*5*p*1*d*(O) and 4*s*1*p*(H)] GTF's

Basis set	Experimental geometry[b] Energy (hartree)	Experimental geometry[b] Dipole moment (debye)	Optimized geometry Energy (hartree)	Optimized geometry Dipole moment (debye)	r_{OH} (Å)	∠HOH (degree)
[9*s*5*p*(O) and 4*s*(H)]						
Contracted as DZ	−76.009253	2.6837	−76.011000	2.5295	0.9513	112.52
Standard exponent	−76.013438	2.6498	−76.014897	2.5116	0.9524	111.79
Optimized exponent	−76.015634	2.6808	−76.017265	2.5315	0.9513	112.13
[9*s*5*p*1*d*(O) and 4*s*1*p*(H)]						
Contracted as DZ+P	−76.046436	2.2308	−76.046948	2.1799	0.9441	106.60
Standard exponent	−76.048160	2.2258	−76.048683	2.1771	0.9437	106.57
Optimized exponent	−76.052462	2.1863	−76.052950	2.1436	0.9437	105.97

[a]Experimental dipole moment of H_2O is 1.855 debye (ref. 27).
[b]r_{OH} = 0.9584 Å, ∠HOH = 104.5° (ref. 16).

TABLE 8. Effect of exponent optimization and geometry optimization on the dipole moment[a] of the HF molecule calculated by using [9*s*5*p*(F) and 4*s*(H)] and [9*s*5*p*1*d*(F) and 4*s*1*p*(H)] GTF's

Basis set	Experimental geometry[b] Energy (hartree)	Experimental geometry[b] Dipole moment (debye)	Optimized geometry Energy (hartree)	Optimized geometry Dipole moment (debye)	r_{FH} (Å)
[9*s*5*p*(F) and 4*s*(H)]					
Contracted as DZ	−100.021972	2.3791	−100.021980	2.3828	0.9196
Standard exponent	−100.026148	2.3520	−100.026150	2.3537	0.9184
Optimized exponent	−100.028143	2.3804	−100.028143	2.3806	0.9173
[9*s*5*p*1*d*(F) and 4*s*1*p*(H)]					
Contracted as DZ+P	−100.047686	2.0465	−100.047932	2.0196	0.9033
Standard exponent	−100.050209	2.0407	−100.050471	2.0141	0.9027
Optimized exponent	−100.055069	2.0392	−100.055376	2.0067	0.9015

[a]Experimental dipole moment of HF is 1.797 debye (ref. 28).
[b]r_{FH} = 0.9171 Å (ref. 19).

the experimental values (23–25) for all three molecules. They moved closer to the experimental values, by about 0.31–0.45 debye, by adding the polarization functions. It is very interesting that the change in dipole moments by exponent optimization is one order smaller than that obtained by adding the polarization functions without optimizing the exponents. We can also see that the polarization function is indispensable for geometry optimization, while the structures are rather insensitive to the exponent optimization when a high enough number of atomic optimized GTF's are uti-

Can. J. Chem. Downloaded from www.nrcresearchpress.com by 92.62.229.171 on 09/08/12
For personal use only.

lized. This result indicates that the wave function is greatly improved by the augmentation of polarization functions rather than the electron redistribution being optimized by the orbital exponents. Furthermore, it is important that our results show the standard exponents in the DZ+P basis set work adequately, without exponent optimization in molecules, to obtain the property as well as the electronic energy within this size of the basis functions.

Concluding remarks

We have applied the analytic energy gradient method with respect to the orbital exponent of GTF's for molecular SCF wavefunctions. In the present study, we have focused on the effect of polarization functions in order to see how the energy gradients change from those without polarization functions. We have observed that the gradients vary not only for small exponents but also for medium and large exponents when the polarization functions are included. The change in gradient values by adding the polarization function depends on the molecules. The coupling between the six *d*-type functions and the *s*-type functions plays a role in changing the gradients for both *s*-type and *p*-type functions. On the other hand, the *p*-type polarization function on the hydrogen atom tends to reduce the gradients for the original *s*-type GTF's.

The interaction between the six *d*-type functions and the *s*-type functions is found to be important in determining the optimum orbital exponents for molecules. Scale factors indicate how the exponents change from the atomic exponents. The scale factors for *s*-type functions on hydrogen indicate that the optimum orbital exponents depend on the molecular environment of the hydrogen atom. However, it is very interesting that the molecular energies as well as the dipole moments are confirmed to be quite insensitive to exponent optimization. The effect of the polarization functions is very important in describing the optimum electron distribution in the molecule so that the expectation values of the wave functions are much improved. Consequently, our present results support the suitability of the exponents in the Huzinaga–Dunning double zeta plus polarization basis set for simple hydride molecules with stable structures.

It is also important to know whether the basis functions work properly for any molecular structure. Sola *et al.* demonstrated recently, by optimizing only the exponents of the polarization functions (12), how the exponents of the polarization functions change at the transition state of the isomerization reaction of H_2SO and CH_3SH. Although it may be costly to optimize all the exponents, it is effective to use the gradient method to investigate how they couple with each other depending on structural changes in the molecules and whether their deficiency is acceptable even for unusual structures.

The effect of multiple-polarization functions for various molecules is more interesting and its importance will grow, since multiple polarization functions have been increasingly utilized for simple molecules in recent *ab initio* MO calculations. A study designed to give the optimum exponents of double polarization functions is now in progress and the results will be presented in a separate paper.

Acknowledgements

We thank Professor S. Iwata of Keio University for many helpful comments. This work was carried out as a subject of the Special Researchers' Basic Science Program by K. H. at the Institute of Physical and Chemical Research (RIKEN). K. H. expresses his sincere gratitude to the program. K. H. is also grateful to Professor H. Hayashi (RIKEN) for his encouragement. The present research was, in part, financially supported by a Scientific Research Grant from the Ministry of Education, Science and Culture of Japan.

1. R. E. Kari, P. G. Mezey, and I. G. Csizmadia. J. Chem. Phys. **63**, 581 (1975); **64**, 632 (1976); **66**, 964 (1977).
2. H. Partridge. J. Chem. Phys. **90**, 1043 (1989); NASA Technical Memorandum, 89449 (1987); 101044 (1989).
3. K. Faegri and J. Almlof. J. Comput. Chem. **7**, 396 (1986).
4. J. Andzelm, S. Huzinaga, M. Klobukowski, E. Radzio-Andzelm, Y. Sakai, and H. Tatewaki. Gaussian basis sets for molecular calculations. Elsevier, Amsterdam. 1984.
5. R. Piorier, R. Kari, and I. G. Csizmadia. Handbook of Gaussian basis sets. Elsevier, Amsterdam. 1984.
6. E. R. Davidson and D. Feller. Chem. Rev. **86**, 681 (1986).
7. W. J. Hehre, L. Radom, P. v. R. Schleyer, and J. A. Pople. Ab initio molecular orbital theory. Wiley–Interscience, New York. 1986.
8. R. Moccia. Theor. Chim. Acta, **8**, 8 (1967).
9. R. A. Poirier, R. Daudel, and I. G. Csizmadia. Int. J. Quantum. Chem. **19**, 711 (1981).
10. G. Tonachini and H. B. Schegel. J. Chem. Phys. **87**, 514 (1987).
11. M. Dupuis, J. Rys, and H. F. King. J. Chem. Phys. **65**, 111 (1976).
12. M. Sola, C. Gonzales, G. Tonachini, and H. B. Schlegel. Theor. Chim. Acta, **77**, 281 (1991).
13. K. Hashimoto and Y. Osamura. Chem. Phys. Lett. **164**, 353 (1989).
14. L. E. McMurchie and E. R. Davidson. J. Comput. Phys. **26**, 218 (1978).
15. K. Hashimoto and Y. Osamura. J. Chem. Phys. **95**, 1121 (1991).
16. T. H. Dunning. J. Chem. Phys. **53**, 2823 (1970).
17. J. H. Callomon, E. Hirota, T. Iijima, K. Kuchitsu, and W. J. Lafferty. *In* Landolt-Børnstein, New Series II-15. Structure data of free polyatomic molecules. *Edited by* K. H. Hellwege and A. M. Hellwege. Springer, Berlin. 1987.
18. R. E. Kari and I. G. Csizmadia. Theor. Chim. Acta, **22**, 1 (1971).
19. A. D. Mclean and M. Yoshimine. J. Chem. Phys. **47**, 3256 (1967).
20. S. Huzinaga. J. Chem. Phys. **42**, 1293 (1965).
21. T. H. Dunning and P. J. Hay. *In* Method of electronic structure theory. *Edited by* H. F. Schaefer. Plenum Press, New York. 1977. pp. 1–27.
22. H. B. Schlegel. J. Comput. Chem. **3**, 214 (1982).
23. W. S. Benedict and E. K. Plyer. Can J. Phys. **35**, 1235 (1957).
24. A. R. Hoy, I. M. Mills, and G. Strey. Mol. Phys. **24**, 1265 (1972).
25. K. P. Huber and G. Hertzberg. Constants of diatomic molecules. Van Nostrand Reinhold, New York. 1979.
26. J. L. Duncan and I. M. Mills. Spectrochim. Acta, **20**, 523 (1964).
27. S. A. Clough, Y. Beers, G. P. Kein, and L. S. Rothman. J. Chem. Phys. **59**, 2254 (1973).
28. J. S. Muenter and W. Klemperer. J. Chem. Phys. **52**, 6033 (1970).

Can. J. Chem. Downloaded from www.nrcresearchpress.com by 92.62.229.171 on 09/08/12
For personal use only.

Higher order exponential split operator method for solving time-dependent Schrödinger equations

ANDRÉ D. BANDRAUK[1]

Département de chimie, Faculté des sciences, Université de Sherbrooke, Sherbrooke (Québec), Canada J1K 2R1

AND

HAI SHEN

Département de mathématique-informatique, Faculté des sciences, Université de Sherbrooke, Sherbrooke (Québec), Canada J1K 2R1

Received July 2, 1991

This paper is dedicated to Professor Sigeru Huzinaga on the occasion of his 65th birthday

ANDRÉ D. BANDRAUK and HAI SHEN. Can J. Chem. **70**, 555 (1992).

A new method of splitting exponential operators is proposed for the exponential form of the operator solution to the time-dependent Schrödinger equation. The method is shown to hold for any desired accuracy in the time increment. A comparison of different algorithms is made as a function of accuracy and computation time.

Key words: splitting operator, Fast Fourier Transform (FFT), Schrödinger equations.

ANDRÉ D. BANDRAUK et HAI SHEN. Can. J. Chem. **70**, 555 (1992).

On propose une nouvelle méthode pour diviser les opérateurs exponentiels de la forme exponentielle de la solution basée sur l'opérateur de l'équation de Schrödinger. On démontre que la méthode possède la précision désirée lors de l'augmentation du temps. On présente une comparaison des divers algorithmes en fonction de leur précision et de leur temps de calcul.

Mots clés : méthode pour diviser les opérateurs, FFT, équations de Schrödinger.

[Traduit par la rédaction]

Can. J. Chem. Downloaded from www.nrcresearchpress.com by 92.62.229.171 on 09/08/12
For personal use only.

1. Introduction

Recent developments in laser physics and laser chemistry have pointed out the need for efficient algorithms to solve the time-dependent Schrödinger equation (1–4). In general, in describing molecular multiphoton transition, we have recourse to a linear parabolic partial differential equation, which can be written as

$$[1]\quad i\hbar\frac{\partial\varphi_n(\boldsymbol{R},t)}{\partial t} = -\frac{\hbar^2}{2m}\frac{\partial^2\varphi_n(\boldsymbol{R},t)}{\partial\boldsymbol{R}^2} + V_{nn}(\boldsymbol{R})\varphi_n(\boldsymbol{R},t) + \sum_{n'} V_{nn'}(\boldsymbol{R},t)\varphi_{n'}(\boldsymbol{R},t)$$

In the above, $V_{nn}(\boldsymbol{R})$ is the time-independent field free molecular (electronic) potential and $V_{nn'}(\boldsymbol{R},t)$ is the time-dependent electromagnetic–molecule interaction,

$$[2]\quad V_{nn'}(\boldsymbol{R},t) = \boldsymbol{\mu}_{nn'}(\boldsymbol{R})\boldsymbol{E}(\boldsymbol{r},t)$$

$\boldsymbol{R}$ is a molecular coordinate whereas $\boldsymbol{r}$ is the electromagnetic pulse coordinate, and $\mu_{nn'}(\boldsymbol{R})$ is a transition moment representing transitions between different electronic states of quantum number n.

In refs. 5 and 6, we developed a fourth order accurate formula for splitting the exponential operator $\exp[\lambda(A + B)]$ and used it to solve the time-dependent Schrödinger equation. The comparison of this new method and the standard second order accurate method (7–9) showed the new method to be more accurate and more efficient.

In the present note we wish to present an improved scheme for solving numerically the linear parabolic equation [1] to high order by the splitting exponential operator method. We extend here our previous work in refs. 5 and 6. The new improved method can give any desired order of accuracy. A comparison will be made of the order of the accuracy versus computation time (CPU).

[1]Author to whom correspondence may be addressed.

2. Symmetric formulas for splitting exponential operators $\exp[\lambda(A + B)]$

The most general method of splitting exponential operators is based on the Trotter product form for the operator $\exp[\lambda(A + B)]$ (10–15),

$$[3]\quad e^{\lambda(A+B)} = \lim_{m\to\infty}(e^{\lambda A/m}\, e^{\lambda B/m})^m$$

From this follows the most currently used standard *second order* accurate formula (7–9),

$$[4]\quad e^{\lambda(A+B)} = S_2(\lambda) + C_3\lambda^3 + O(\lambda^4)$$

where

$$[5]\quad S_2(\lambda) = e^{\lambda A/2}\, e^{\lambda B}\, e^{\lambda A/2}$$

and C_3 is some remnant combination of commutators of A and B (5, 6).

We showed previously that eq. [4] can be expressed as

$$[6]\quad e^{\lambda(A+B)} = e^{\lambda s(A+B)}\, e^{\lambda(1-2s)(A+B)}\, e^{\lambda s(A+B)}$$

so that higher order accuracy is obtained, i.e., by substituting eq. [5] in eq. [6],

$$[7]\quad e^{\lambda(A+B)} = S_2(s\lambda)S_2((1-2s)\lambda)S_2(s\lambda) + C_3\lambda^3(2s^3 + (1-2s)^3) + O(\lambda^4)$$

To get third order accuracy, the leading error term $O(\lambda^3)$ must vanish, i.e.,

[8] $2s^3 + (1 - 2s)^3 = 0$

Thus, if s is a root of eq. [8], we can obtain

[9] $e^{\lambda(A+B)} = S_3(\lambda) + C_4\lambda^4 + O(\lambda^5)$

where we have now defined

[10] $S_3(\lambda) = S_2(s\lambda)S_2((1 - 2s)\lambda)S_2(s\lambda)$

Equation [10] gives therefore a third order accurate formula for the exponential operator [3]. By iterating [7] further, we can obtain the general iteration:

[11] $e^{\lambda(A+B)} = S_{n-1}(s\lambda) + C_n\lambda^n + O(\lambda^{n+1})$

from which follows, by one more iteration, that

[12] $e^{\lambda(A+B)} = S_n(s\lambda) + O(\lambda^{n+2})$

where now

[13] $S_n(\lambda) = S_{n-1}(s\lambda)S_{n-1}((1 - 2s)\lambda)S_{n-1}(s\lambda)$

and s is a root of the more general equation

[14] $2s^n + (1 - 2s)^n = 0$

In ref. 5, we pointed out that if eq. [14] does not have real roots, the formula $S_n(\lambda)$ will not preserve unity since $\lambda = i\Delta t$, a complex number. This will create divergent exponentials in any iteration with concomitant loss of accuracy. One can shown that eq. [14] always has a real root when n is *odd*, i.e., for such cases, the symmetric expansion [13] for S_n is always unitary.

In summary, we have developed the iterations,

[15] $e^{\lambda(A+B)} = S_{2n-1}(\lambda) + O(\lambda^{2n+1}), \qquad n = 2,3, \ldots$

where

$$S_2(\lambda) = e^{\lambda A/2}\, e^{\lambda B}\, e^{\lambda A/2}$$

$$S_n(\lambda) = S_{n-1}(s\lambda)S_{n-1}((1 - 2s)\lambda)S_{n-1}(s\lambda)$$

and s is the real root of equation

$$2s^{2n-1} + (1 - 2s)^{2n-1} = 0$$

The symmetric decomposition of the general exponential operator [13] by the above algorithm furnishes, by construct, unitary approximations to propagator $e^{-iH\Delta t}$ to any order of accuracy, $O(\lambda^{2n+1})$, in the time increment Δt when we choose $\lambda = i\Delta t$, as shown in the next section.

3. Formal solution of TDSE and higher order propagation

We consider the Schrödinger equation

[16] $i\hbar \dfrac{\partial\varphi(x,t)}{\partial t} = H\varphi(x,t)$

If we choose a *time-independent* Hamiltonian,

[17] $H = -\dfrac{\hbar^2}{2m}\dfrac{\partial^2}{\partial x^2} + V(x)$

then the formal solution of eq. [16] is

[18] $\varphi(x,t + \Delta t) = e^{-i\Delta tH/\hbar}\varphi(x,t)$

We can therefore apply eq. [15] to solve [16] with [17] numerically with any desired accuracy in the time increment Δt.

On the other hand if one is dealing with a *time-dependent problem*,

[19] $H = -\dfrac{\hbar^2}{2m}\dfrac{\partial^2}{\partial x^2} + V(x,t)$

the formal solution of eq. [16] become more complicated. The general time-dependent solution can now be written (16),

[20] $\varphi(x,t + \Delta t) = U(t + \Delta t,t)\varphi(x,t)$

where

[21] $U(t + \Delta t,t) = T\exp\left[-\dfrac{i}{\hbar}\int_t^{t+\Delta t} H\, dt\right]$

and T is the time ordering operator. One can truncate eq. [20] and obtain

[22] $U(t + \Delta t,t) = \exp\left[-\dfrac{i}{\hbar}\int_t^{t+\Delta t} H\, dt\right] + D_3(t)(i\Delta t)^3 + D_4(t)(i\Delta t)^4 + \ldots$

Since $U(t + \Delta t,t)$ is unitary, we have at all time

[23] $U(t + \Delta t,t)U^\dagger(t + \Delta t,t) = 1$

Since the operator $\exp[-i/\hbar \int_t^{t+\Delta t} H\, dt]$ is also unitary, then by comparing the two unitarity conditions, one finds that any approximation to $U(t + \Delta t,t)$ has always odd order in the leading error, i.e.,

[24] $U(t + \Delta t,t) = \exp\left[-\dfrac{i}{\hbar}\int_t^{t+\Delta t} H\, dt\right] + D_3(t)(i\Delta t)^3 + D_5(t)(i\Delta t)^5 + \ldots$

Clearly, by using S_2, eq. [4], to approximate $U(t + \Delta t,t)$, we will obtain only a second order accurate propagation scheme.

We will now develop a propagation technique based on the group property of the operator $U(t + \Delta t,t)$ and eq. [15] to solve the Schrödinger equation for time-dependent potentials, in order to obtain high order accurate algorithms.

We divide $[t,t + \Delta t]$ into three subintervals $[t,t + s\Delta t]$, $[t + s\Delta t, t + (1 - s)\Delta t]$, and $[t + (1 - s)\Delta t, t + \Delta t]$. On each subinterval, we use eqs. [22] and [4]. Thus for the first interval we obtain

---

[25] $U(t + s\Delta t,t) = \exp\left[-\dfrac{i}{\hbar}\int_t^{t+s\Delta t} H\, dt\right] + D_3(t)(s\Delta t)^3 + O(\Delta t)^5$

$$= S_2(s\Delta t,t) + (C_3(t) + D_3(t))(s\Delta Dt)^3 + O(\lambda^5)$$

where

Can. J. Chem. Downloaded from www.nrcresearchpress.com by 92.62.229.171 on 09/08/12
For personal use only.

$$[26]\quad S_2(s\Delta t,t) = e^{-is\Delta tA/2\hbar}\, e^{-iB(t)/\hbar}\, e^{-is\Delta tA/2\hbar}, \qquad A = -\frac{\hbar^2}{2m}\frac{\partial^2}{\partial x^2}, \qquad B(t) = \int_t^{t+s\Delta t} V(x,t)\, dt$$

For the second interval, one has

$$[27]\quad U(t + (1-s)\Delta t, t + s\Delta t) = \exp\left[-\frac{i}{\hbar}\int_{t+s\Delta t}^{t+(1-s)\Delta t} H\, dt\right] + D_3(t)((1-2s)\Delta t)^3 + O(\Delta t)^5$$
$$= S_2((1-2s)\Delta t, t + s\Delta t) + (C_3(t) + D_3(t))((1-2s)s\Delta t)^3 + O(\Delta t)^5$$

where

$$S_2((1-2s)\Delta t, t + s\Delta t) = e^{-i\Delta t(1-2s)A/2\hbar}\, e^{-iB(t+s\Delta t)}\, e^{-i(1-2s)\Delta tA/2\hbar}$$

Finally for the last interval one obtains the equation,

$$[28]\quad U(t + (1-s)\Delta t, t + \Delta t) = \exp\left[-\frac{i}{\hbar}\int_{t+(1-s)\Delta t}^{t+\Delta t} H\, dt\right] + D_3(t)(s\Delta t)^3 + O(\Delta t)^5$$
$$= S_2(s\Delta t, t + (1-s)\Delta t) + (C_3(t) + D_3(t))(s\Delta Dt)^3 + O(\Delta t^5)$$

where

$$S_2(s\Delta t, t + (1-s)\Delta t) = e^{-is\Delta tA/2\hbar}\, e^{-iB(t+(1-s)\Delta t)/\hbar}\, e^{-is\Delta tA/2\hbar}$$

By the group property of $U(t + \Delta t,t)$ we have

$$[29]\quad U(t + \Delta t,t) = U(t + s\Delta t,t)U(t + (1-s)\Delta t, t + s\Delta t)U(t + \Delta t, t + (1-s)\Delta t)$$

and substituting eqs. [25], [27], and [28] into eq. [29], we obtain

$$[30]\quad U_3(t + \Delta t,t) = S_2(s\Delta t,t)S_2((1-2s)\Delta t, t + s\Delta t)S_2(s\Delta t, t + (1-s)\Delta t) + O(\Delta t^5)$$

where s is the real root of eq. [8].

The above procedure gives a fourth order accurate algorithm to calculate the evolution operator U for the time-dependent Schrödinger equation, using products of these second order accurate propagators. The results holds for both time-dependent and time-independent Hamiltonians. Iterating eq. [30] according to the scheme explicited in eq. [15] will generate schemes of any desired accuracy in the time increment Δt.

4. Numerical comparison

We previously compared the second and fourth order accurate splitting operators [26] and [30]. The latter is always more accurate (5, 6). In the preceding two sections we obtained higher order accurate formulas. Now we try to find the optimum algorithm with respect to maximum accuracy and minimum computation time (CPU). First, we note that the second order formula, S_2 in eq. [5], has three exponential operators; the fourth order one, S_3 in eq. [10], has seven exponential operators; the sixth order one, S_5, has 19 exponential operators, and the eighth order one, S_7, has 55 exponential operators. Thus from the eighth order formula, one does not seem to have practical algorithms due to the growing number of exponential operators.

We consider eq. [18] (we set $m = \hbar = 1$) with $V(x) = x^2$ as a test. This *time-independent* harmonic oscillator model has an exact ground state solution,

$$[31]\quad \varphi(x,t) = \left[\frac{\sqrt{2}}{\pi}\right]^{1/4} \exp\left[\frac{-(x^2 + it)}{\sqrt{2}}\right]$$

We solved this problem numerically using the various exponential splitting schemes presented in Sect. 2, using Fast Fourier Transform techniques (FFT) for the exponential of the Laplacian. All reported calculations were performed in an IBM RISC 6000/530 workstation (10 megaflop performance). In Fig. 1 a detailed comparison is presented of the L^2 errors (defined as: L^2 error = $(\Delta x \Sigma e_i^2)^{1/2}$, $e_i = |s^n - s^r|$ where s^n is a numerical solution and s^r is an exact solution) of the amplitudes of wavefunctions as a function of CPU computation time (seconds).

We see directly that the second order accurate formula S_2 (3rd order error) takes much CPU time for high accuracy. The eighth order accurate expansion S_7 is also not efficient because of too many exponential operators. So we focus on the fourth (S_3) and sixth (S_5) order accurate formulas. In the high accurate range (about 10^{-3}), the sixth order formula S_5 is better than the fourth one S_3. In view of the numerical results of Fig. 1, in general, the sixth order formula S_5 seems to be the optimum method, i.e., with minimum CPU seconds one obtains the highest accuracy. In practice, if a problem does not require high accuracy, the fourth order accuracy formula S_3 seems to be preferred to the sixth order one (seventh order error), S_5.

We next solve eq. [20] ($m = \hbar = 1$) with $V(x,t) = x^2 + x * \sin(t)$, i.e., the forced harmonic oscillator, using 2nd, 4th, 6th order accurate formulas S_2, S_3, S_5. We compare with these numerical results, the exact solution to eqs. [16] and [19] for an initial vibrational ground state (17),

$$[32]\quad \varphi(x,t) = \left[\frac{\sqrt{2}}{\pi}\right]^{1/4} \exp\left[-\frac{(x - \xi(t))^2}{\sqrt{2}}\right] * \exp\left[\frac{i\dot{\xi}(t)}{\sqrt{2}} + \dot{\xi}(x - \xi) + \int_0^t L\, dt\right]$$

where

$$\xi(t) = \sqrt{2}\,[\sin(\sqrt{2}t) - \sqrt{2}\sin(t)]/2$$

and

Can. J. Chem. Downloaded from www.nrcresearchpress.com by 92.62.229.171 on 09/08/12
For personal use only.

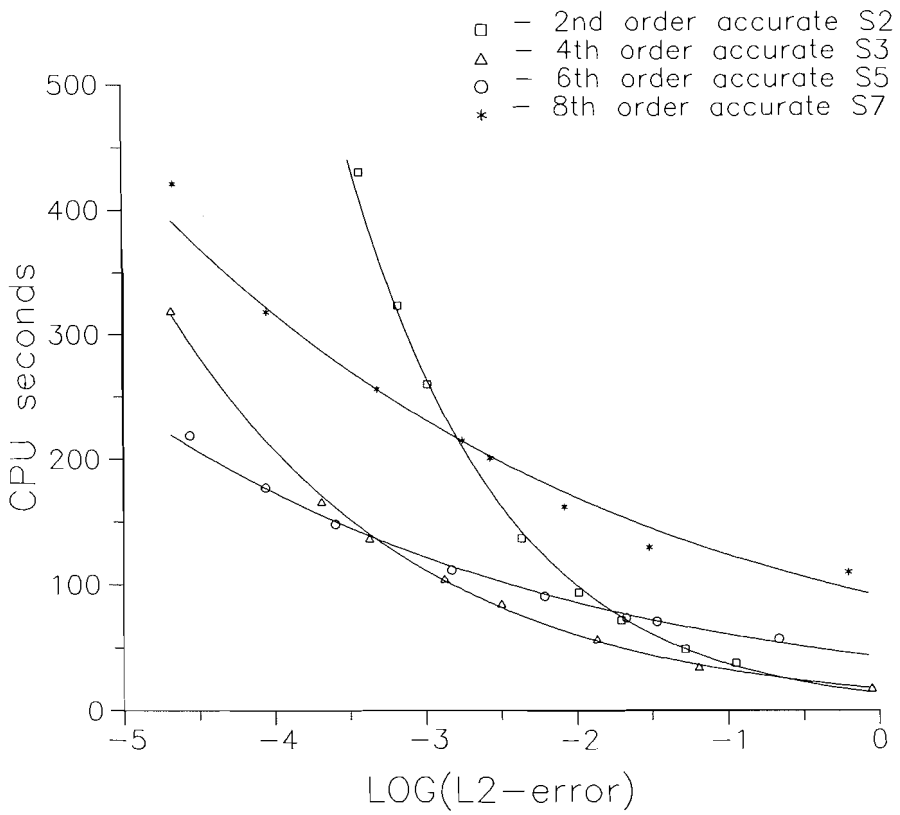

FIG. 1. Log of L^2 error of the amplitude of the time-dependent wavefunction (eq. [31]) as a function of CPU computation time on an IBM RISC 6000-530 workstation for different splitting operators, S_2, S_3, S_5, and S_7.

TABLE 1. The second order accurate splitting operator S_2 for time-dependent potential $V(x,t) = x^2 + x \sin(t)$. $-3.5\pi \leq x \leq 3.5\pi$, $\Delta x = 7\pi/128$, $t = 600$ ($\simeq$100 cycles)

Time	Amplitude error	Phase error	CPU(s)
0.06	0.14	0.95	53
0.03	0.36E−01	0.26	102
0.015	0.90E−02	0.65E−01	194
0.0075	0.23E−02	0.17E−01	376
0.00375	0.56E−03	0.42E−02	739

TABLE 2. The fourth order accurate splitting operator S_3 for time-dependent potential $V(x,t) = x^2 + x \sin(t)$. $-3.5\pi \leq x \leq 3.5\pi$, $\Delta x = 7\pi/128$, $t = 600$ ($\simeq$100 cycles)

Time	Amplitude error	Phase error	CPU(s)
0.2	0.21	0.86	45
0.1	0.13E−01	0.64E−01	86
0.05	0.80E−03	0.40E−02	169
0.025	0.50E−04	0.25E−03	322
0.0125	0.31E−05	0.16E−04	625

$$L = \frac{1}{2}\dot{\xi}^2 - \xi^2 + \xi \sin(t)$$

L is the Lagrangian of the classical forced harmonic oscillator. This time-dependent problem was solved numerically in Sect. 3 using the exponential splitting scheme for the propagator U.

In Tables 1–3 we present, for various orders of accuracy in the time increments, the L^2 errors for the amplitude and the phase of the numerical time-dependent wavefunctions as a function of the computation time in CPU seconds. These tables show that the sixth order accurate formula S_5 requires fewer CPU seconds and gives the best results. For instance, when the errors of the amplitude and phase are about 10^{-3} and 10^{-2} respectively, the second order formula S_2 requires 739 CPU seconds (Table 1), the fourth order one S_3 re-

TABLE 3. The sixth order accurate splitting operator S_5 for time-dependent potential $V(x,t) = x^2 + x \sin(t)$. $-3.5\pi \leq x \leq 3.5\pi$, $\Delta x = 7\pi/128$, $t = 600$ ($\simeq$100 cycles)

Time	Amplitude error	Phase error	CPU(s)
0.3	0.67E−01	0.39	81
0.2	0.56E−02	0.33E−01	120
0.1	0.85E−04	0.50E−03	235
0.05	0.13E−05	0.76E−05	456
0.03	0.61E−07	0.36E−06	745

Can. J. Chem. Downloaded from www.nrcresearchpress.com by 92.62.229.171 on 09/08/12
For personal use only.

TABLE 4. The second order accurate splitting operator S_2 for time-dependent potential $V(x,t) = x^2 + x \sin(t)$. $-3.5\pi \leq x \leq 3.5\pi$, $\Delta x = 7\pi/128$, $t = 1200$ ($\simeq$200 cycles)

Time	Amplitude error	Phase error	CPU(s)
0.06	0.20	1.14	106
0.03	0.60E−01	0.56	204
0.015	0.16E−01	0.14	388
0.0075	0.39E−02	0.35E−01	755
0.00375	0.98E−03	0.86E−02	1480

TABLE 5. The fourth order accurate splitting operator S_3 for time-dependent potential $V(x,t) = x^2 + x \sin(t)$. $-3.5\pi \leq x \leq 3.5\pi$, $\Delta x = 7\pi/128$, $t = 1200$ ($\simeq$200 cycles)

Time	Amplitude error	Phase error	CPU(s)
0.2	0.40	1.18	88
0.1	0.23E−01	0.15	171
0.05	0.14E−02	0.92E−02	332
0.025	0.86E−04	0.53E−03	644
0.0125	0.54E−05	0.36E−04	1260

TABLE 6. The sixth order accurate splitting operator S_5 for time-dependent potential $V(x,t) = x^2 + x \sin(t)$. $-3.5\pi \leq x \leq 3.5\pi$, $\Delta x = 7\pi/128$, $t = 1200$ ($\simeq$200 cycles)

Time	Amplitude error	Phase error	CPU(s)
0.3	0.11	0.81	161
0.2	0.98E−02	0.72E−01	238
0.1	0.15E−03	0.10E−02	470
0.05	0.23E−05	0.17E−04	914
0.03	0.11E−06	0.78E−06	1492

quires 322 s (Table 2), and the sixth, S_5, gives $0.85*10^{-4}$ in amplitude and $0.5*10^{-3}$ in phase using only 235 s (Table 3).

When we double the time interval from [0,600] to [0,1200], the results for 2nd, 4th, and 6th order accurate formulas in Tables 4–6 show that accumulations of the error in the sixth order formula are fewer than those of the other two lower order schemes. Therefore in long time propagation the sixth order formula offers the best possible algorithm in terms of maximum accuracy in amplitude and phase for the least CPU time.

In conclusion, we have shown that the sixth order accurate formula S_5 as given by eq. [14] allows explicit exponential numerical integration of parabolic partial differential equations, such as the time-dependent Schrödinger equation, with sixth order accuracy, i.e., errors depend on $(\Delta t)^7$. This method is shown to be superior in accuracy over the second and fourth order accurate methods. The second order scheme is the most frequently used method in current time-dependent problems (7–9). For high order accuracy ($\simeq 10^{-3}$), the sixth order operator, S_5, is optimum. For low order accuracy ($\simeq 10^{-2}$), the fourth order accurate operator S_3, previously proposed by us (5, 6), seems to be a more useful algorithm (see Fig. 1). Both methods are always superior to the standard second order accurate methods based on S_2 (7–9). We are currently examining the efficiency of these algorithms for coupled equations, as occur in multiphoton electronic transitions (1). Of note is that the present algorithms are always unitary as compared to other efficient propagation schemes that are not unitary, such as Chebyshev polynomial expansions (18).

Acknowledgment

We thank the Natural Sciences and Engineering Research Council of Canada for grants supporting this research. We also thank IBM Canada for partial support of a RISC machine.

1. A. D. Bandrauk. Atomic and molecular processes with intense laser pulses. Vol. 171B. NATO Advanced Studies Institute. Plenum Press, New York. 1988.
2. A. D. Bandrauk. *In* Advances in multiphoton spectroscopy. Vol. 6. *Edited by* S. H. Lin. Academic Press, New York. 1990.
3. S. Chelkowski and A. D. Bandrauk. J. Chem. Phys. **98**, 3618 (1988).
4. S. Chelkowski, A. D. Bandrauk, and P. B. Corkum. Phys. Rev. Lett. **65**, 2355 (1990).
5. A. B. Bandrauk and H. Shen. Chem. Phys. Lett. **176**, 428 (1991).
6. H. Shen. M. Sc. Thesis, Université de Sherbrooke. 1991.
7. M. D. Feit and J. A. Fleck. J. Chem. Phys. **78**, 2578 (1984).
8. H. Kono and S. H. Lin. J. Chem. Phys. **84**, 1071 (1986).
9. J. N. Barddey, A. Szöke, and J. M. Comella. J. Phys. B: At. Mol. Opt. Phys. **21**, 3899 (1989).
10. H. F. Trotter. Proc. Am. Math. Soc. **10**, 545 (1959).
11. R. M. Willcot. J. Math. Phys. **8**, 962 (1967).
12. S. I. Berstein and A. A. Mirin. J. Comput. Phys. **5**, 547 (1970).
13. H. D. Raedt and B. D. Readt. Phys. Rev. A, **26**, 3575 (1983).
14. M. Suzuki. J. Math. Phys. **26**, 601 (1985).
15. Q. Sheng. IMA J. Numer. Anal. **9**, 199 (1988).
16. P. Pechukas and J. C. Light. J. Chem. Phys. **44**, 3897 (1966).
17. H. Husimi. Prog. Theor. Phys. **9**, 381 (1953).
18. C. Leforestier *et al.* J. Comput. Phys. **94**, 59 (1991).

Can. J. Chem. Downloaded from www.nrcresearchpress.com by 92.62.229.171 on 09/08/12
For personal use only.

Optimization of Gaussian-type basis sets for local spin density functional calculations. Part I. Boron through neon, optimization technique and validation

NATHALIE GODBOUT AND DENNIS R. SALAHUB[1]
Département de chimie, Université de Montréal, C.P. 6128 Succursale A, Montréal (Québec), Canada H3C 3J7

AND

JAN ANDZELM[2] AND ERICH WIMMER
Cray Research Inc., 655E Lone Oak Drive, Eagan, MN 55121, U.S.A.

Received September 19, 1991

This paper is dedicated to Professor Sigeru Huzinaga on the occasion of his 65th birthday

NATHALIE GODBOUT, DENNIS R. SALAHUB, JAN ANDZELM, and ERICH WIMMER. Can J. Chem. **70**, 560 (1992).

Gaussian-type orbital and auxiliary basis sets have been optimized for local spin density functional calculations. This first paper deals with the atoms boron through neon. Subsequent papers will provide a list through xenon. The basis sets have been tested for their ability to give equilibrium geometries, bond dissociation energies, hydrogenation energies, and dipole moments. These results indicate that the present optimization technique yields reliable basis sets for molecular calculations.

Key words: Gaussian basis sets, density functional theory, boron–neon, geometries, energies of reactions.

NATHALIE GODBOUT, DENNIS R. SALAHUB, JAN ANDZELM et ERICH WIMMER. Can. J. Chem. **70**, 560 (1992).

Des bases orbitalaires et auxiliaires de type gaussienne ont été optimisées pour des calculs de la fonctionelle de la densité de spin locale. Ce premier article étudie les atomes de bore jusqu'au néon. Des articles subséquents fourniront des bases pour tous les atomes jusqu'au xénon. Les bases ont été vérifiées pour leurs capacités à reproduire des géométries d'équilibre, énergies de dissociation de liaison, énergies d'hydrogénation et moments dipolaires. Ces résultats indiquent que la présente technique d'optimisation produit des bases fiables pour les calculs moléculaires.

Mots clés : Bases orbitalaires gaussienne, théorie de la fonctionnelle de la densité, bore–néon, géométries, énergies de réactions.

1. Introduction

1.1 General considerations

Ever since their introduction, orbital basis sets have been the subject of extensive efforts and discussions. Because of their critical role in determining the accuracy and because of computational cost, the subject of basis sets in molecular calculations continues to be of great interest. All computational approaches that solve the Schrodinger equation with the expansion method express the molecular wave functions in terms of a basis set that contains a finite number of basis functions. As mentioned in a review by Huzinaga (1), "it is this finiteness that is the cause of all the frustrations and fascinations about the basis set."

A number of reviews about basis sets have been published (2–7). The fact that there has been many a review article about the subject serves to show that the field is important and very much alive. There exists no one finite basis set for each element that is small enough to be used in molecular calculations with today's computers, yet is flexible enough to universally describe all properties. In fact, results of various degrees of accuracy are obtained depending on the choice of the basis set. The choice of the basis set is critical.

1.2 Basis set functions

Several types of functions have been proposed. The two more commonly used are the Slater-type functions (STF), introduced by Slater (8) in 1930, and the Gaussian-type functions (GTF) proposed by Boys (9) in 1950. The STO's are functions that represent the main features of the radial part of an atomic orbital. The problem in using these functions comes from the difficulty in calculating the integrals.

Boys showed that by taking GTF, complete systems of functions can be constructed appropriate to any molecule, and that the necessary integrals can be evaluated explicitly. Although they do not describe the atom as well as does the STF (a linear combination has to be used in order to represent an STO), they retain the advantage that the molecular integral formulas are straightforward to derive and to code.

The usefulness of GTF as basis functions for large-scale molecular calculations was put forward by Huzinaga (10) in 1965. He concluded that even if the number of GTF needed in the analytical Hartree–Fock expansion calculation would be larger than if STF were used, the number of GTF would not be prohibitively large. Currently, most molecular calculations are done using CGTF (Contracted Gaussian-Type Functions).

1.3 Basis sets of GTF

Various methods to obtain expansions of STO in terms of GTO have already been proposed. A variational method (11) was developed but it suffered from the difficulty of achieving true minimization because of the multiple minima problem which grew rapidly with the number of variational parameters. A least-squares method had also been proposed, Boys and Shavitt (12), but it also had the problem of multiple minima. Huzinaga (10, 13) proposed a method based on a least-squares-fit procedure that could avoid such a problem. In parallel, Pople and co-workers proposed the STO-nG method (14–18).

A method based on least-squares fitting and atomic optimisation was proposed by Tavouktsoglou and Huzinaga (19). The emphasis was put on bonding valence orbitals in order to achieve accurate molecular results. In this method,

[1]Author to whom correspondence may be addressed.
[2]Present address: Biosym Technologies, 10065 Barnes Canyon Road, San Diego Calif. 92121, U.S.A.

Can. J. Chem. Downloaded from www.nrcresearchpress.com by 92.62.229.171 on 09/08/12
For personal use only.

Can. J. Chem. Downloaded from www.nrcresearchpress.com by 92.62.229.171 on 09/08/12
For personal use only.

the orbital exponents are optimized together with the contraction coefficients. While they remain at the 3G level (3 Gaussians to represent 1 STF), this was a new approach to their formation. This technique yielded very good molecular results for main group elements and succeeded with third row elements where the STO-3G basis sets had failed. This was mainly due to the fact that no least-squares fit to the STO was done and therefore the basis set did not inherit the defects of the STO. A similar contraction scheme had been proposed by Clementi and co-workers (20) but was limited to the contraction coefficients.

This method was further improved by Tatewaki and Huzinaga (21) and applied to third row transition metals. The main problem with the Tavouktsoglou and Huzinaga method (19) was that, with the limited number of Gaussian functions used, primitive Gaussians were overspent in the inner core region of the atom. Pople's method was a success in that sense since it considered the electronic distribution throughout the atom. Huzinaga's new scheme was able to achieve a proper electron distribution. Valence shell orbital energies that were quite close to those of double-zeta quality were obtained using a minimal basis set with a modest representation of the core orbitals. The authors concluded that basis sets constructed in that manner should provide good molecular results.

These minimal basis sets could be improved further for molecular calculations by splitting the valence shell orbitals into two parts in order to better describe a molecular environment, as suggested by the work of Pople and co-workers (22) and Hehre and Latham (23) with the 4-31G basis sets. The success of the method intitiated a series of articles by Huzinaga and co-workers in which basis sets were systematically prepared for the atoms helium through cadmium (24–29). A monograph by Huzinaga *et al.* (30) contains various basis sets developed in this method for all atoms of the periodic table.

1.4 Basis sets in density functional theory

The major drawback of the Hartree–Fock theory (HFT) is that it neglects electron correlation, which is known to be important for many systems including transition metal complexes, organometallic compounds, and even relatively small highly correlated molecules like FOOF (31, 32), C_2F_2 (34), and CH_3NO_2 and CH_3NH_2 (33). The HFT formally scales as N^4, N being the number of primitive basis functions, although some programs can perform as N^3 or N^2 due to the Gaussian-type decay of the localized basis sets and (or) the use of pseudospectral techniques (35, 36). When electron correlation is included, the scaling factor grows rapidly, making calculations on large molecular systems impossible unless some approximations are made to the integrals. There is growing evidence (33, 37–40) that density functional theory (DFT) (41–44) is a promising alternative to the Hartree–Fock approach (33). The DFT includes electron correlation and it scales formally as N^3. With increasing system size, the computational effort scales between N_2 and N_3, while correlated Hartree–Fock based methods giving results of similar quality scale at least with the fifth power of N. It is believed (33) that these features of molecular DTF open opportunities for the study of large and complex molecular systems that are out of reach for other *ab initio* molecular orbital methods.

Various techniques are used to solve the Kohn–Sham equations. Those techniques can use various types of functions. There have been implementations using Slater-type functions (45, 46), numerical functions (47–49), numerical functions generated from a muffin-tin potential (50, 51) plane-waves (52, 53), augmented plane-waves (54, 56), and Gaussian-type functions (57, 58). Basis set free solutions have also been introduced (59). The reason for using GTF in DFT, apart from the straight-forwardness of the integral evaluations, is that one can benefit from extensive Hartree–Fock experience.

The Gaussian-based implementation of the DFT equations relies on a variational, analytical approximation to the density. To achieve a variational fit to the density, the Coulomb energy term arising from the difference between the exact and the fitted density is minimized. This procedure was proposed by Dunlap *et al.* (58). It leads to an analytical expression for the fitting coefficients involving Coulomb-type three-index two-electron integrals. It may be noted that, with Gaussians, the Coulomb terms may be evaluated exactly, if desired, by the usual methods involving N^4 integrals.

The first implementation of DFT that used Gaussian functions (LCGTO–LSD, Linear Combination of Gaussian-Type Orbitals–Local Spin Density) employed extended uncontracted Hartree–Fock Gaussian basis sets, which inevitably limited the size of the systems that could be studied. Contracted basis sets were optimized in the LSD approximation for a series of transition metal atoms by Andzelm, Radzio, and Salahub (60) using Huzinaga's method (19, 21). It was actually found (60) that using contracted HF optimized basis sets in LSD calculations might not be appropriate since there are quite pronounced differences in the valence region between LSD and HF atoms that could influence the molecular results. Furthermore, it was shown that Hartree–Fock optimized basis sets used in DFT calculations would likely create basis set superposition errors (BSSE). Hartree–Fock optimized basis sets such as 6-31G* (61, 62) can be used in DFT calculations to give good geometries, but accurate, and economical, predictions of reaction energies require the use of DFT optimized Gaussian-type basis sets (33).

1.5 Overview of the present paper

In this first paper of a series, LSD optimized Cartesian Gaussian basis sets for boron to neon are reported and their performance in molecular calculations is discussed. For that purpose, we have used a recent implementation of the density functional Gaussian-type orbital approach, DGauss (for Density-Gaussian) (33, 34). Subsequent papers will include basis sets for atoms through xenon. Equilibrium geometries, bond dissociation and hydrogenation energies, and electric dipole moment results obtained with the proposed basis sets will be presented and compared with experimental and *ab initio* results. It seems that the present technique of optimizing LSD basis sets yields high quality double-zeta-split-valence + polarization (DZVP) basis sets.

2. Theory

2.1 Atomic numerical calculation

The optimization scheme of the contracted LSD-VWN (Vosko, Wilk, and Nusair (63)) basis sets, based on the Huzinaga method (21) as implemented by Andzelm, has been described elsewhere (60). Only an abbreviated version will be given here. The atomic numerical calculations were done as a first iteration because they provide an exact solution to

Can. J. Chem. Downloaded from www.nrcresearchpress.com by 92.62.229.171 on 09/08/12
For personal use only.

the LSD equations and therefore a reference for the atomic calculation with an orbital basis set. The radial Schrödinger equation can be written in the following way:

$$[1] \quad (-1/2\nabla_i^2 + V_i(r))R_{nl}(r) = \epsilon_i R_{nl}(r)$$

where ϵ_i is the orbital energy, $R_{nl}(r)$ is the radial function, and $V_i(r)$ is the total potential. There is one radial function attributed for each sub-shell. For example, for carbon, there are three radial functions: $R_{1s}(r)$, $R_{2s}(r)$, and $R_{2p}(r)$ and they are obtained by solving [1].

2.2 Atomic calculation with an orbital basis set

In the analytical SCF (Self-Consistent Field) method, the radial functions are approximated by a linear combination of basis functions denoted by $s_1(r),s_2(r),\ldots,s_{Ms}(r);p_1(r),p_2(r),\ldots,p_{Mp}(r);d_1(r),d_2(r),\ldots,d_{Md}(r)$ for s, p, and d symmetry respectively.

The radial functions can then be written in the following way:

$$[2] \quad R_{ns}(r) \simeq \sum_{i=1}^{M_s} c_{ns,i}s_i(r)$$

$$[3] \quad R_{np}(r) \simeq \sum_{i=1}^{M_p} c_{np,i}p_i(r)$$

$$[4] \quad R_{nd}(r) \simeq \sum_{i=1}^{M_d} c_{nd,i}d_i(r)$$

These radial functions can approach those obtained numerically if the basis functions and the length of the expansions M_s, M_p, and M_d are well chosen. Theoretically there is an optimal form for these basis functions. It can be obtained by expressing it as a linear combination of simple functions, the primitives. The primitives chosen for this work, as mentioned in the introduction, are GTF,

$$[5] \quad g_s(\alpha;r) \sim e^{-\alpha r^2}$$

$$[6] \quad g_p(\alpha;r) \sim re^{-\alpha r^2}$$

$$[7] \quad g_d(\alpha;r) \sim r^2e^{-\alpha r^2}$$

The CGTF are then defined as

$$[8] \quad s_i(r) = \sum_{k=1}^{K_{si}} d_{si,k}g_s(\alpha_{si,k};r)$$

$$[9] \quad p_i(r) = \sum_{k=1}^{K_{pi}} d_{pi,k}g_p(\alpha_{pi,k};r)$$

$$[10] \quad d_i(r) = \sum_{k=1}^{K_{di}} d_{di,k}g_d(\alpha_{di,k};r)$$

where K_{si}, $d_{si,k}$, and $\alpha_{si,k}$ are the parameters to be varied. For example, substituting the s basis function in eq. [8], the radial s function in eq. [2] becomes

$$[11] \quad R_{ns}(r) \simeq \sum_{l=1} a_{ns,l}g_s(\alpha_l;r)$$

where $R_{ns}(r)$ are the approximate functions. Once the size of the K_{si} expansions has been chosen, the optimization of the atomic orbital basis set is done by optimization of the exponents and linear coefficients so as to minimize the total atomic energy.

For example, the procedure to optimize an orbital basis set for carbon can be described as follows. If the $K2s(2)2p(2)$ electronic configuration is approximated using a (63/3) basis set, there are 6, 3, and 3 GTO used to represent the s_1, s_2, and p_1 CGTO (Contracted Gaussian-Type Orbital) of carbon respectively. First, the $s_1(r)$ basis function is varied so as to minimize the energy while keeping the $s_2(r)$ and $p_1(r)$ frozen, that is, the exponents and coefficients are not varied. The $s_2(r)$ function is then varied while the others are kept frozen. This process is repeated until consecutive calculations do not produce any improvement in the total energy within 10^{-5} a.u. Most of the computing time was spent on the core orbitals as this is where most of the energy resides. The Hartree–Fock optimized basis sets (30) were used as the starting basis sets.

TABLE 1. Coefficients and exponents for (41/1*) orbital basis sets of hydrogen

Hydrogen	
50.9991800	0.00966048
7.4832180	0.07372886
1.7774680	0.29585810
0.5193295	0.71590530
0.1541100	1.00000000
0.7500000	1.00000000

In ref. 60, a (4333/43/41+) expansion pattern was chosen for all the first row transition metal atoms. This choice was based on the orbital energies and molecular calculations as it fulfilled reasonable requirements of accuracy and economy. In the present work, three expansion patterns, which differ in the number of primitives used for the core orbitals, were optimized: (63/5) for boron through neon, (73/6) for boron through fluorine, and (83/7) for carbon and fluorine. The augmented number of primitive functions for the core orbitals is expected to reduce the BSSE. The orbital basis for hydrogen (Table 1) was derived from a least-squares fit to numerical LSD results followed by scaling by the usual factor (1.44, which corresponds to 1.2 for a hydrogenic orbital (64)).

The basis sets are optimized as minimal basis sets but they are decontracted for molecular calculations. For example, the (63/5) set was split to a (621/41) set. To further improve the molecular results, a d polarization function was added and the basis set would become a (621/41/1*) set. The polarization functions were chosen from the previous experience in LCGTO-LSD calculations and from Pople's 6-31G* basis sets. This brings the basis sets to the quality of DZVP for the valence electrons.

3. Results and discussion

3.1 Basis sets and orbital energies

The LSD-VWN optimized orbital basis sets are shown in Tables 1–4. The basis sets found in these tables are as they were optimized, except for the d polarization functions, which was not optimized, and the hydrogen basis set that was decontracted as it was used. The electronic configurations of the atoms are $K2s^22p^n$ where n takes the value 1–6 when going from boron to neon.

The orbital energies as a function of the expansion pattern are shown in Table 5. The orbital energies calculated with the (63/5) basis sets are in very good agreement with

TABLE 2. Coefficients and exponents for (63/5/1*) orbital basis sets for boron through neon

Boron		Carbon		Nitrogen	
1915.1670000	−0.00203952	2808.0640000	0.00201783	3845.4150000	0.00201861
287.1831000	−0.01559658	421.1383000	0.01543320	577.5332000	0.01540776
65.1571700	−0.07624424	95.5866200	0.07558155	131.3198000	0.07537140
18.1958300	−0.24792440	26.7390000	0.24782820	36.8237800	0.24821220
5.7015380	−0.47908230	8.4328270	0.47937250	11.6701200	0.47982740
1.8438370	−0.33529530	2.7605820	0.33383440	3.8542600	0.33180120
3.4914300	0.07742237	5.4470040	−0.07784077	7.8295610	−0.07766687
0.3050560	−0.57412390	0.4792422	0.56895600	0.6877351	0.5654980
0.0964865	−0.50571170	0.1461565	0.51437071	0.2040388	0.52030018
11.6874200	0.01508612	18.1308500	0.01585473	26.8098400	0.01546631
2.6307750	0.08881570	4.0998830	0.09568277	6.0681540	0.09643968
0.7442269	0.29036820	1.1858370	0.30491190	1.7676260	0.30836100
0.2304761	0.49944330	0.3685974	0.49350170	0.5466728	0.49115970
0.0699380	0.35425713	0.1097200	0.34415952	0.1587289	0.34703886
0.4000000	1.00000000	0.6000000	1.00000000	0.7000000	1.00000000
Oxygen		**Fluorine**		**Neon**	
5222.9020000	−0.00193637	6384.7140000	−0.00203016	7883.8260000	0.00203748
782.5399000	−0.01485067	958.8865000	−0.01549810	1184.4060000	0.01554681
177.2674000	−0.07331870	218.1901000	−0.07577869	269.6731000	0.07596377
49.5166900	−0.24511620	61.3647300	−0.25027240	75.9416500	0.25110270
15.6664400	−0.48028470	19.6029000	−0.48010860	24.3210900	0.48047650
5.1793600	−0.33594270	6.5648830	−0.32716140	8.1832560	0.32511420
10.6014400	0.07880582	13.8106900	0.07907066	17.4495200	−0.07900997
0.9423171	−0.56769520	1.2298670	−0.56812160	1.5516320	0.56762740
0.2774746	−0.51927687	0.3584713	−0.51990419	0.4476986	0.52130115
33.4241300	0.01756033	42.4699100	0.01831704	52.9038100	0.01879106
7.6221710	0.10763000	9.7138810	0.11245130	12.1233600	0.11576050
2.2382090	0.32352550	2.8640390	0.32977710	3.5859220	0.33426270
0.6867300	0.48322290	0.8746054	0.47997720	1.0921630	0.47780380
0.1938135	0.33844880	0.2425071	0.33547361	0.2994419	0.33280000
0.8000000	1.00000000	1.0000000	1.00000000	1.2000000	1.00000000

the ones calculated numerically and the ones with the (73/6) are in even better agreement. They are all calculated higher in energy than the numerical ones. This is also the case for the (73/6) set with the exception of the $1s\downarrow$ orbitals for boron, carbon, nitrogen, and fluorine, which are lower in energy. The average difference between the orbital energies calculated with an expansion and numerically ($\bar{x}$) along with the standard deviations are shown in Table 5. The errors in the orbital energies for the (63/5) set are in the tenth of an eV range for both valence and core levels. We would therefore expect a good valence representation for most purposes, and also a small BSSE. The errors are even smaller for the (73/6) set. The (83/7) set, for fluorine, leads to some further improvement but probably not enough to justify the additional expense. Finally, the total energy of the system decreases with the size of the expansion as a better description of the atoms is provided. With these results in mind, we expect that these basis sets will perform well in molecular calculations.

3.2 *Auxiliary sets*

Besides the orbital basis sets, fitting basis sets have to be introduced to approximate the electron density and the exchange-correlation potential and energy. Sambe and Felton (57) first proposed fitting the electron density and the exchange-correlation potential, thereby obtaining a method that scaled as N^3 rather than N^4. The fit to the electron density was later made variational by the work of Dunlap *et al.* (58). The electron density and exchange-correlation potential are expanded in auxiliary sets of Gaussian-type basis functions. The expansion of the *s*-, *p*-, and *d*-type uncontracted Gaussians provides a flexible enough representation of the atomic density provided the variational method of fitting is chosen. As for the exchange-correlation terms, the determination of the expansion coefficients has to be carried out numerically using a grid. The fit to the electron density is done analytically.

These auxiliary sets are derived from the orbital basis sets, according to a procedure similar to that developed by Dunlap. The smallest exponent of the orbital set is used to start the expansion for the electron density set. Since the charge density is the sum of the squares of the molecular orbitals, this small exponent is multiplied by two. It was found that an economical expansion could be built, to represent the density well, by using an even-tempered expansion for the lowest $n - 1$ exponents, and then breaking the even-tempered sequence for the tightest exponent. The auxiliary set is built using *s*-type functions and blocks of *s*-type, *p*-type, and *d*-type functions with shared exponents. This facilitates the calculation of molecular integrals. For carbon-like atoms,

Can. J. Chem. Downloaded from www.nrcresearchpress.com by 92.62.229.171 on 09/08/12
For personal use only.

Can. J. Chem. Downloaded from www.nrcresearchpress.com by 92.62.229.171 on 09/08/12
For personal use only.

TABLE 3. Coefficients and exponents for (73/6/1*) orbital basis sets for boron through fluorine

Boron		Carbon		Nitrogen		Oxygen		Fluorine	
3862.5990000	0.0008493277	5784.1570000	0.0008189950	8104.1760000	0.0007969164	10814.4000000	0.0007809405	13652.1000000	0.0007873155
581.4507000	0.0065080950	869.3035000	0.0062934710	1217.3140000	0.0061288990	1623.7530000	0.0060102170	2050.2870000	0.0060549950
133.1696000	0.0326348400	198.5116000	0.0317811800	277.7399000	0.0310470800	370.1827000	0.0305221800	467.6871000	0.0307289000
37.9878700	0.1191406000	56.4299000	0.1172734000	78.8476000	0.1153682000	104.9747000	0.1140089000	132.7635000	0.1146453000
12.3278500	0.3030930000	18.2854600	0.3034763000	25.5371600	0.3025738000	33.9844200	0.3019574000	43.0763800	0.3037706000
4.3449640	0.4512283000	6.4487150	0.4535214000	9.0045710	0.4557913000	11.9843100	0.4571107000	15.2288300	0.4573067000
1.5637310	0.2449106000	2.3418600	0.2430591000	3.2835280	0.2430208000	4.3859710	0.2432478000	5.6051180	0.2395779000
3.4966260	−0.0774017500	5.4595330	−0.0778043800	7.8493570	−0.0776364200	10.6300300	−0.0787653500	13.8479400	−0.0790344700
0.3045523	0.5763720000	0.4781968	0.5714946000	0.6862239	0.5679815000	0.9398525	0.5706303000	1.2266890	0.5708482000
0.0962327	0.5034960900	0.1457301	0.5118248000	0.2035026	0.5177469200	0.2766213	0.5162995800	0.3574564	0.5171159700
22.2584600	0.0055288170	34.2585600	0.0058042900	49.0146100	−0.0059006540	61.5442200	0.0066238050	78.9617500	0.0067826750
5.0508640	0.0385616100	7.8638950	0.0406403400	11.3166700	−0.0416444200	14.2761900	0.0464641700	18.3478800	0.0478976000
1.4846510	0.1440193000	2.3445190	0.1550219000	3.4034050	−0.1610249000	4.3317680	0.1744229000	5.5871890	0.1793841000
0.4979771	0.3428421000	0.7961715	0.3531444000	1.1611110	−0.3583538000	1.4766040	0.3666115000	1.9018470	0.3692988000
0.1710900	0.4662248000	0.2726804	0.4550062000	0.3953358	−0.4488415000	0.4959857	0.4369361000	0.6333652	0.4332780000
0.0570744	0.2565595300	0.0892605	0.2503745700	0.1268981	−0.2492758300	0.1544836	0.2463995200	0.1933455	0.2465505300
0.4000000	1.0000000000	0.6000000	1.0000000000	0.7000000	1.0000000000	0.8000000	1.0000000000	1.0000000	1.0000000000

the use of three *s*-type and three *p*-type functions having the same exponents in addition to four *s*-type functions was found to work well. In our notation, this corresponds to a (4,3;4,3) auxiliary set where the semi-colon separates the charge density from the exchange correlation. The resulting set is shown in Table 6. The same pattern is used for the exchange-correlation set. It is built from the electron density set by dividing the exponents by 3 since the exchange correlation goes essentially as $\rho^{1/3}$ (58).

The auxiliary sets shown in Tables 6 and 7 were made to be used with the (63/5) and the (73/6) orbital sets respectively. Each of the sets in Table 7 have one more *p*- and *d*-type function. Typically, the calculations were performed with triple-zeta *p*- and *d*-type fitting sets, i.e., (4,3;4,3). It was found (Dixon in ref. 33) that quadruple-zeta sets do not change molecular results significantly.

3.3 *Equilibrium geometries*

The LSD optimized basis sets presented in this paper have already been successfully used in LSD (and NLSD, Non-LSD) calculations by several authors to study fluorinated methanes (Dixon *et al.* in ref. 33), a methylamine complex (Hill *et al.* in ref. 33), nitro compounds (Redington and Andzelm in ref. 33), organic molecules (Andzelm in ref. 33), and many small organic compounds (34) as a part of the validation of the DGauss code to study various properties such as equilibrium geometries, vibrational frequencies, energetics of different types of reactions, and electric dipole moments. For completeness, some of these results will also be shown in the present paper.

The (63/5) basis set pattern was chosen for the present calculations as we initially hoped it would become the default pattern for DGauss. From other studies, this basis set seemed, at least on paper, to be a good compromise between economy and quality. In ref. 33, Dixon *et al.* tested these LSD basis sets as a function of the number of primitive functions for the core orbitals and the expansion pattern (DG-1 to DG-9 in their notation) for the study of isodesmic reactions for fluoromethanes. Hartree–Fock optimized 6-31G** and 6-311G** basis sets were also included in the study. Their finding was that all the levels predict about the same bond distances but that the LSD bonds calculated with the Hartree–Fock basis sets come out shorter, but still they are respectable. This is in agreement with the statement by Andzelm (in ref. 33) that Hartree–Fock basis sets used in DFT calculations lead to accurate molecular geometries for this class of molecules (see Redington in ref. 33).

Andzelm and Wimmer (34) used the CH_3NH_2 molecule to study the sensitivity of calculated geometric, vibrational, and energetic properties on the computational level. They found that the calculated bond lengths differ by 0.004 Å or less when the different levels are compared. The largest variation in bond angles is 1.4° (for HCN). Overall they concluded that there is relatively little sensitivity of the geometric variables on the choice of the computational levels. For small molecules and fragments containing C, N, O, and F atoms with the (621/41/1*) orbital basis sets and (41/1*) set for hydrogen, they found that the C—C single bond lengths are typically 0.01–0.02 Å too short whereas the C—C double bond and C—C aromatic bond are within a few thousandths of an Å of experiment. As for the C—H bond length, it is usually too long by about 0.01–0.02 Å and this trend is even more pronounced for the O—H, N—H, and

TABLE 4. Coefficients and exponents for (83/7/1*) orbital basis sets for carbon and fluorine

Carbon		Fluorine	
10798.8798828	0.0003827	28040.8398438	−0.0003205
1593.5169678	0.0030609	4189.2768555	−0.0025069
350.5501099	0.0167198	946.5355835	−0.0130835
94.0320969	0.0716948	265.9798889	−0.0529400
28.4737091	0.2266096	86.2899933	−0.1615474
9.3243723	0.4610515	30.9276409	−0.3524703
3.1331151	0.3815948	11.7157898	−0.4170229
0.1947443	−0.0585223	4.6249661	−0.1545233
5.4464412	−0.0779336	13.8498898	0.0790351
0.4792618	0.5694732	1.2243130	−0.5727925
0.1465912	0.5136164	0.3566824	−0.5151669
10.8737497	−0.0252670	142.6250000	0.0025472
46.9549713	−0.0034754	33.3321495	0.0197242
3.3925080	−0.0974677	10.4582195	0.0848059
1.2213171	−0.2483324	3.7320230	0.2323348
0.4671699	−0.3844518	1.3840370	0.3783796
0.1789529	−0.3666219	0.4925209	0.3840546
0.0658785	−0.1382337	0.1618818	0.1847055
0.6000000	1.0000000	1.0000000	1.0000000

TABLE 5. Total energy (hartree) and orbital energies (eV) for atoms boron through xenon as a function of the number of primitives in the expansion pattern

Atom	Basis	−TE	$-\epsilon 1s\uparrow$	$-\epsilon 1s\downarrow$	$-\epsilon 2s\uparrow$	$-\epsilon 2s\downarrow$	$-\epsilon 2p\uparrow$	$-\epsilon 2p\downarrow$
Boron	(63/5)	24.349	178.481	178.149	9.770	8.658	4.078	3.047
	(73/6)	24.351	178.513	178.181	9.776	8.664	4.091	3.061
	Num.[a]	—	178.518	178.178	9.804	8.667	4.103	3.079
Carbon	(63/5)	37.462	270.323	269.398	14.385	11.817	6.141	3.682
	(73/6)	37.466	270.371	269.444	14.398	11.832	6.165	3.709
	Num.	—	270.373	269.428	14.451	11.834	6.189	3.789
Nitrogen	(63/5)	54.124	380.585	378.845	19.491	15.223	8.316	4.133
	(73/6)	54.131	380.662	378.918	19.520	15.254	8.361	4.184
	Num.	—	380.669	378.898	19.604	15.268	8.400	4.371
Oxygen	(63/5)	74.509	510.193	508.877	24.672	21.740	10.153	7.302
	(73/6)	74.518	510.293	508.973	24.720	21.790	10.223	7.376
	Num.	—	510.444	508.994	24.902	21.804	10.367	7.408
Fluorine	(63/5)	99.091	657.992	657.250	30.075	28.546	11.811	10.319
	(73/6)	99.104	658.118	657.373	30.144	28.616	11.910	10.420
	(83/7)	99.108	658.162	657.417	30.169	28.641	11.940	10.451
	Num.	—	658.239	657.403	30.301	28.670	12.026	10.443
Neon	(63/5)	128.202	824.053	824.053	35.757	35.757	13.336	13.336
	Num.	—	824.289	824.289	35.979	35.979	13.546	13.546
$\bar{x} \pm \sigma$	(63/5)	—	0.151 ± 0.104	0.103 ± 0.082	0.148 ± 0.089	0.080 ± 0.081	0.133 ± 0.090	0.136 ± 0.756
	(73/6)	—	0.0572 ± 0.0727	0.018 ± 0.0098	0.101 ± 0.066	0.0174 ± 0.0212	0.067 ± 0.073	0.068 ± 0.071

[a]Num. refers to the numerical calculation.

H—F distances. For C—O, C—N, C—F, N—O, and N—F bonds, they find agreement within 0.02 Å or less. The bond angles deviate from experiment by less than 1°. The homonuclear diatomics are fairly well described.

The orbital basis set effect, i.e., the effect of the number of primitive basis functions and decontraction pattern, on the geometrical parameters can be seen in Tables 8 and 11. The basis set notation is given at the end of Table 8. The orbital basis sets are given on the left side of the semi-colon and the auxiliary sets on the right side. The notation used in ref. 34 is also indicated. From Table 8, we conclude that the C—H bond distance in CH_4 and in the CH_3 radical does not vary significantly with the basis sets. The standard deviation is 0.002 Å for both systems. In the case of the C—C, C—N, and C—O bonds, the addition of a *d* polarization function affects the bond lengths more than in the case of the C—H bond. The average bond lengths and the standard deviations when considering the results from the five basis sets studied for the C—C, C—N, and C—O bond lengths respectively are 1.518 ± 0.005, 1.450 ± 0.003, and 1.418 ± 0.016 Å.

Can. J. Chem. Downloaded from www.nrcresearchpress.com by 92.62.229.171 on 09/08/12
For personal use only.

Can. J. Chem. Downloaded from www.nrcresearchpress.com by 92.62.229.171 on 09/08/12
For personal use only.

TABLE 6. Exponents for the (4,3;4,3) auxiliary sets for boron through neon, for use with the (63/5) orbital set

Boron	Carbon	Nitrogen	Oxygen	Fluorine	Neon
716.800	1114.000	1640.000	2000.000	2458.000	3072.000
143.400	223.000	328.000	400.000	492.000	614.000
35.840	55.720	82.000	100.000	123.000	153.600
8.960	13.900	20.500	25.000	30.700	38.400
2.800	4.400	6.400	7.800	9.600	12.000
0.560	0.870	1.280	1.560	1.920	2.400
0.140	0.220	0.320	0.390	0.480	0.600
238.900	371.000	550.000	667.000	819.000	1024.000
47.790	74.200	110.000	133.000	164.000	204.800
11.950	18.600	27.000	33.300	41.000	51.200
2.990	4.640	6.830	8.300	10.200	12.800
0.930	1.470	2.100	2.600	3.200	4.000
0.190	0.290	0.430	0.520	0.640	0.800
0.047	0.073	0.110	0.130	0.160	0.200

TABLE 7. Exponents for the (4,4;4,4) auxiliary sets for boron through neon, for use with the (73/6) orbital set

Boron	Carbon	Nitrogen	Oxygen	Fluorine	Neon
992.000	1500.000	2066.000	2566.000	3100.000	4150.000
220.000	330.000	459.000	570.000	690.000	923.000
63.000	94.300	131.000	163.000	197.000	264.000
18.000	27.000	37.500	46.500	56.300	75.000
6.620	9.920	13.800	17.000	21.000	27.500
1.470	2.200	3.060	3.800	4.600	6.150
0.420	0.630	0.880	1.080	1.330	1.750
0.120	0.180	0.250	0.310	0.380	0.500
331.000	500.000	688.000	855.000	1035.000	1380.000
73.000	110.000	153.000	190.000	230.000	308.000
21.000	31.400	43.700	54.000	65.700	88.000
6.000	9.000	12.500	15.500	18.800	25.000
2.210	3.300	4.600	5.660	7.000	9.200
0.500	0.730	1.020	1.270	1.530	2.050
0.140	0.210	0.290	0.360	0.440	0.600
0.040	0.060	0.083	0.100	0.130	0.170

If we exclude the results obtained with the basis set without the polarization function, on the ground that polarization functions are necessary, these results become 1.517 ± 0.005, 1.451 ± 0.002, and 1.411 ± 0.002 Å and all the standard deviations are in the thousandths of an Å. These results reinforce the previous conclusion that the geometrical parameters are not significantly affected by the orbital and auxiliary basis sets chosen for this study.

The equilibrium geometries for a series of compounds containing first-row atoms are shown in Tables 9 and 10. These geometries were obtained using the LSD (621/41/1*) orbital basis sets for carbon-like atoms and (41) orbital basis set for hydrogen. The triple-zeta auxiliary sets were built as previously described. The equilibrium geometries for ethane, ethene, and ethyne are shown in Table 9. The results show that this bond is very well described using our basis sets. The differences with the experimental values are of 0.014, 0.003, and 0.014 Å for the triple, double, and single bonds respectively. The carbon–hydrogen bond is well reproduced, being too long by 0.01–0.02 Å.

Table 10 shows the calculated equilibrium geometries for first-row heteroatom compounds. Again, we find our results to be in excellent agreement with the experimental data. With the somewhat limited number of compounds studied, we have derived some statistics using the average difference between the calculated and experimental bond lengths and angles ($\overline{\Delta r}$). For the C—F(1), C—N(2), C—O(3), C—H(8), N—H(2), and O—H(1) bond types we find the values of ($\overline{\Delta r}$) of 0.005, 0.010, 0.009, 0.011, 0.013, and 0.011 Å respectively, the numbers in parentheses being the number of values from which the values of ($\overline{\Delta r}$) were tabulated. On average, all the bond lengths are calculated within 0.02 Å and in many cases within 0.01 Å of experiment, which is respectable. The highest deviation for the bond angles is 2.3° but most (six out of ten) are predicted within 1° of experiment. The average deviation regardless of the types of angles is 1°. These values are in agreement with the previous statement that LSD can predict bond angles within 2.0° of experiment and bond lengths within 0.02 Å. Out of the 11 angles calculated, four are calculated higher than the ex-

Can. J. Chem. Downloaded from www.nrcresearchpress.com by 92.62.229.171 on 09/08/12
For personal use only.

TABLE 8. C—X(X = C,N,O) bond lengths as a function of the basis set

Basis	CH_3-CH_3	CH_3-NH_2	CH_3-OH
A	1.524	1.446	1.446
B	1.519	1.453	1.410
C	1.519	1.451	1.410
D	1.520	1.453	1.414
E	1.510	1.448	1.409

The following notation reads as: orbital set for C-like atoms, orbital set for H; auxiliary set for C-like atoms, auxiliary set for H

A: (621/41),(41);(4,3;4,3),(4;4) or DZV[a]

B: (621/41/1*),(41); (4,3;4,3),(4;4) or DZVP[a]

C: (621/41/1*),(41/1); (4,3;4,3),(3,1;3,1) or DZVPP[a]

D: (721/51/1*),(41/1); (4,4;4,4),(3,1;3,1) or DZVP2[a]

E: (7111/411/1*),(41/1); (4,4;4,4),(3,1;3,1) or TZVP[a]

[a]Notation of ref. 34.

TABLE 9. Calculated and experimental equilibrium geometries for a series of organic molecules using the (621/41/1*) orbital basis set for carbon and (41/1*) for hydrogen

Molecule	Point group	Geometrical parameter		Explt.
C_2H_2	$D_{\infty h}$	r(CC)	1.217	1.203
		r(CH)	1.080	1.061
C_2H_4	D_{2h}	r(CC)	1.336	1.339
		r(CH)	1.098	1.085
		∠(HCH)	116.8	—
C_2H_6	D_{3d}	r(CC)	1.517	1.531
		r(CH)	1.105	1.096

perimental value, six are smaller, and one is exact. As for the calculated bond distances, most overestimate the corresponding experimental value. In conclusion, the equilibrium geometries that we showed, calculated using the proposed LSD basis sets, provide structures that compare favorably with MP2 results, obtained with 6-31G* basis sets, and experiment.

3.4 Bond dissociation energies

The bond dissociation energies, and the hydrogenation energies, are calculated by subtracting the sum of the energies of the reactants from those of the products. Fully optimized geometries were used. The non-local corrections to the energy are calculated as a perturbation at the end of the LSD calculation using the functional forms proposed by Becke for exchange (65) and Perdew for correlation (66) and using the LSD equilibrium geometries.

The results from the study of the $CH_4 \rightarrow CH_3^{\cdot} + H^{\cdot}$ reaction are in Table 11. At the MP4(6-31G**//6-31G*) level, a 6-31G** MP4 single-point calculation using a Hartree–Fock 6-31G* equilibrium geometry, a 3 kcal/mol difference with experiment still remains. Increasing the size of the basis set (6-311G**) at the same level of theory does not change the accuracy. The LSD(VWN) results overestimated the dissociation energy by an average of 11.9 kcal/mol. This result is not suprising since it is known that the binding energy is overestimated in the LSD approximation. The use of non-local corrections, Becke–Perdew potential, greatly improves the D_e, which is then only overestimated by 0.9 kcal/mol. This conclusion has been drawn by other authors (33). The D_e is basis set independent as is the geometry and the zero point energy. For the D_e, this can be seen by the small value of 0.2 kcal/mol of the standard devia-

TABLE 10. Equilibrium geometries for a series of organic molecules using the (621/41/1*) orbital basis set for carbon-like atoms and the (41/1*) set for hydrogen

Molecule	Geometrical parameter	LSD	MP2 (6-31G*)	Exptl
CO_2	r(CO)	1.175	—	1.162
CH_3F	r(CF)	1.378	1.392	1.383
	r(CH)	1.106	1.092	1.100
	∠(HCH)	109.5	109.8	110.6
CH_2NH	r(CN)	1.274	1.282	1.273
	r(NH)	1.035	1.027	1.023
	$r(CH_s)$	1.110	1.096	1.103
	$r(CH_a)$	1.106	1.090	1.081
	$\angle(H_sCN)$	125.4	125.4	123.4
	$\angle(H_sCN)$	118.2	116.1	119.7
	∠(HCN)	111.0	109.7	110.5
H_2CO	r(CO)	1.212	1.221	1.208
	r(CH)	1.123	1.104	1.116
	∠(HCN)	115.9	115.6	116.5
CH_3NH_2	r(CN)	1.451	1.465	1.471
	$r(CH_t)$	1.114	1.100	1.099
	$r(CH_g)$	1.105	1.092	1.099
	r(NH)	1.025	1.018	1.010
	∠(HNH)	107.1	105.9	107.1
	$\angle(NCH_t)$	116.2	115.4	113.9
	$\angle(H_gCH_{g'})$	106.2	107.5	108.0
CH_3OH	r(CO)	1.410	1.424	1.421
	r(OH)	0.974	0.970	0.963
	$r(CH_t)$	1.103	1.090	1.094
	$r(CH_g)$	1.110	1.097	1.094
	$\angle(OCH_t)$	106.8	106.4	107.2
	$\angle(H_gCH_{g'})$	108.4	108.7	108.5
	∠(HOC)	108.6	107.4	108.0

TABLE 11. Calculated and experimental[a] CH bond length (Å) and dissociation energy, D_e (kcal/mol), of methane

Basis sets/ method	D_e		RC-H		ZPE	
	VWN	BP	CH_3	CH_4	CH_3	CH_4
A	124.5	113.4	1.094	1.100	18.4	27.6
B	124.7	113.7	1.095	1.103	18.1	27.3
C	124.2	113.4	1.093	1.101	18.2	27.3
D	124.6	113.6	1.095	1.101	18.1	27.3
E	124.3	113.2	1.091	1.099	18.1	27.2
HF[b]	87					
MP2[b]	109					
MP3[b]	110					
MP4[b]	110					
MP4[c]	109.4					
GVB	98					
CCCI	111					
Exptl.	112.6					27

[a]Hartree–Fock, non-DFT, and experimental values from ref. 61.
[b]6-31G**//6-31G*.
[c]6-311G**.

TABLE 12. Bond dissociation energies (kcal/mol) for the dissociation of a series of molecules

Basis sets/ method	CH_3-CH_3		CH_3-NH_2		CH_3-OH	
	LSD	NLSD	LSD	NLSD	LSD	NLSD
A	115.1	94.0	112.4	90.0	114.8	90.5
B	117.2	96.3	115.6	91.4	124.0	99.0
C	115.1	94.9	114.3	90.5	122.3	98.0
D	115.9	94.9	114.2	90.3	122.6	97.5
E	115.8	94.1	114.3	89.9	122.6	97.3
HF[a]		69		58		58
MP2[b]		99		93		98
MP4[b]		97		88		92
Expt.		97		93		98

[a]Orbital basis set: 6-31G**//6-31G*.
[b]Orbital basis set: 6-31G**//6-31G*.

tion at the LSD and NLSD level. Since the decontraction pattern and the number of core primitive functions does not affect the D_e significantly, it is not certain that larger or more decontracted basis sets may improve the results.

Andzelm and Wimmer (34) computed the bond energies for the successive removal of H atoms from methane with a (621/21/1*) orbital basis set for carbon and (41/1*) set for hydrogen. They found that the CH—H bond is overestimated at the LSD level by as much as 15 kcal/mol. The NLSD calculations bring results to within 2 kcal/mol of experiment. The C—C bond dissociation energies were also studied and the same conclusions as for the C—H bond were obtained in terms of the need to include non-local corrections to the energy. None of the correlated Hartree–Fock based methods came as close to experiment as the NLSD approach.

The bond dissociation energies involving the atoms C, N, O, and F in a reaction of the type A—B → A + B represent a difficult problem for the *ab initio* approach. The Hartree–Fock approach gives poor agreement with experiment whereas MP2 often brings agreement within a few kilocalories per mole. Table 12 shows the dissociation energies for the C—C, C—N, and C—O bonds for the CH_3-CH_3, CH_3-NH_2, and CH_3-OH molecules as a function of the basis sets at the LSD and NLSD levels. The average D_e and the standard deviations for these bonds in the order given above are 115.8 ± 0.8, 114.2 ± 1.1, and 121.3 ± 3.7 kcal/mol. At the NLSD level, these values are 94.8 ± 0.9, 90.4 ± 0.6, and 96.5 ± 3.4 kcal/mol. The deviations are larger than in the case of the C—H bonds, the highest being for the dissociation of the C—O bond. The NLSD level is necessary to bring agreement to within 3 kcal/mol of experiment.

These results are preliminary and it would be dangerous to draw too general conclusions from them, but they are very encouraging since reasonable D_e, within 1–2 kcal/mol of the experimental results, could be obtained and this at a lesser cost than that of perturbation theory. Certainly, more results are needed to complement the present ones but one conclusion that seems unavoidable is that non-local corrections are needed if a close agreement with experiment is to be expected.

3.5 *Hydrogenation reactions*

The LSD and NLSD hydrogenation energies for a series of reactions are found in Table 13 along with the Hartree–Fock and Moller–Plesset results as compiled by Hehre *et al.* (61). In ref. 61 it is said that, at the Hartree–Fock level, the 6-31G* and 6-31G** sets are needed to bring the agreement to within 3–5 kcal/mol of experiment.

The calculation of energies of hydrogenation is quite new in DFT. When looking at the LSD and NLSD results in Table 13, what is first surprising is that the inclusion of a *d* polarization function to the DZV (double-zeta-split-valence) basis set slightly deteriorates the agreement with experiment. In general, a polarization function improves the results. The average energies of hydrogenation and the standard deviations for the CH_3-CH_3, CH_3-NH_2, and CH_3-OH molecules at the LSD level are respectively 17.8 ± 0.7, 24.7 ± 1.4, and 27.5 ± 1.7. At the NLSD level, these values are 18.9 ± 0.6, 25.7 ± 1.2, and 27.7 ± 1.8. The standard deviations indicate a basis set sensitivity of 1–2 kcal/mol. Even if the basis sets cause fluctuations in the energies, the extent of this behavior is restrained to within 2 kcal/mol, which is reasonable. Further, no large discrepancies with experiment are found. At the LSD level, the agreement with experiments is on average within 1–3 kcal/mol. The non-local corrections to the density bring the agreement to within 2 kcal/mol or less. The correction is not as large as was the case with dissociation energies. With a few exceptions, the energies are underestimated.

Again, the present LSD optimized basis sets provide quality results. In their study Andzelm and Wimmer (34) found that there were some serious deficiencies for reactions involving triple bonds while the hydrogenation of the single bonds is fairly well described at the LSD level. The NLSD level performs as well as the MP2 with 6-31G**//6-31G* orbital basis sets and is closer to the MP4 approach with the same basis sets. They also found that the agreement between NLSD and the experimental values corrected for zero-point energies is quite reasonable for many of the reactions but significant discrepancies of up to about 10% do exist.

3.6 *Electric dipole moments*

The calculation of the electric dipole moments provides an insight into the overall distribution of charge, which may be important to know when structures and reactivities of molecules are to be evaluated. This one-electron property can be measured experimentally so that comparisons with theory can be made. Generally, this comparison is limited to the

Can. J. Chem. Downloaded from www.nrcresearchpress.com by 92.62.229.171 on 09/08/12
For personal use only.

TABLE 13. Calculated and experimental energies of hydrogenation reactions (kcal/mol)[a]

Method	Basis set	$CH_3CH_3 + H_2 \rightarrow 2CH_4$	$CH_3NH_2 + H_2 \rightarrow CH_4 + NH_3$	$CH_3OH + H_2 \rightarrow CH_4 + H_2O$
HF	STO-3G//STO-3G	19	20	16
	3-21G//3-21G	25	30	28
	3-21G*//3-21G*	25	30	28
	6-31G*//6-31G*	22	27	27
	6-31G**//6-31G*	21	28	30
MP2	6-31G**//6-31G*	18	25	28
MP3	6-31G**//6-31G*	19	26	29
MP4SDQ	6-31G**//6-31G*	19	26	30
MP4	6-31G**//6-31G*	18	25	29
LDS	A	18.7	26.2	28.1
	B	16.9	22.5	24.4
	C	17.9	24.3	27.9
	D	17.9	25.3	28.6
	E	17.4	25.0	28.4
NLSD	A	19.8	26.9	27.9
	B	18.1	23.7	24.7
	C	18.7	25.5	28.0
	D	19.1	26.3	29.0
	E	18.9	26.3	28.9
Expt.		19	26	30

[a]All expt., Hartree–Fock, and Moller–Plesset results as compiled by W. Hehre in ref. 61.

Can. J. Chem. Downloaded from www.nrcresearchpress.com by 92.62.229.171 on 09/08/12
For personal use only.

magnitude of the vector as a lot of uncertainties often exist in the experimental directions. The dipole moments were calculated by computing the expectation value of the dipole moment operator, μ.

Again we turn to the Hartree–Fock experience to give us an idea of the basis set effect (61) on the electric dipole moments. For diatomic and small polyatomic molecules, the 6-31G* model is the most successful of the theoretical models as it provides a reasonable description of the magnitude of the dipoles for a variety of different compounds. In going from STO-3G to 6-31G*, the mean absolute deviation difference is 0.35 D and from 3-21G* to 6-31G* it is 0.04 D. From this we may conclude that once a somewhat high quality of basis set is reached, the calculated dipole moment is not affected as much by the choice of the basis set. This conclusion can also be applied to compounds containing heteroatoms. Still, significant errors remain if we consider that the typical range of values for dipole moments is 0 to about 5 D. Near the Hartree–Fock limit, the magnitudes of the electric dipole moments are frequently in error by a few tenths of a debye. From this comparative study, we expect that our basis sets will provide at least as good dipole moments as does the 6-31G* level.

The LSD dipole moments of two compounds as a function of the basis sets are shown in Table 14 along with the Hartree–Fock values. They were calculated with the equilibrium geometry as calculated by each of the basis sets. We do not feel that this will prevent us from having a discussion in terms of the basis set pattern as no major differences are found between the geometries. Looking at the LSD results as a function of the basis set, it is apparent that it is necessary to include a *d* polarization function to get agreement with experiment within 0.2 D or less. Disregarding the results without the *d* function, the highest deviation from experiment is of 0.193 D (CH_3NH_2) and the lowest one is of 0.046 D (CH_3OH). The best agreement is found with the basis set C. In all cases the dipole moments are overestimated. On average, the dipole moments for CH_3NH_2 and CH_3OH, when considering all the basis sets studied, are 1.34 ± 0.26 and 1.89 ± 0.2 D respectively. If we neglect the results obtained with basis set A from our statistics, these values become 1.46 ± 0.04 and 1.80 ± 0.04 D. The important conclusion is that the deviations become smaller.

TABLE 14. Dipole moments (debye) for heteratom-containing compounds

Method	Basis set	CH_3-NH_2	CH_3-OH
HF	STO-3G//STO-3G	1.62	1.51
	3-21G//STO-3G	1.92	2.21
	3-21G*//STO-3G	1.92	2.21
	6-31G*//STO-3G	1.74	2.04
LSD	A	0.877	2.237
	B	1.503	1.816
	C	1.410	1.746
	D	1.471	1.838
	E	1.436	1.810
Expt.		1.31	1.70

The effect of electron correlation can be tentatively accounted for as our basis sets are of similar size as the 6-31G* Hartree–Fock set. If that comparison can be made, the correlation has lowered the dipole moment by 0.2 D. The NLSD dipole moments are not shown here but other preliminary results tend to show that the correction should not be large (0.1–0.2 D) (67). In conclusion, for the two systems studied, the basis sets provide reasonable results but a more lengthy study is needed to determine trends and account for the 0.2 D (or less) difference with experiment that remains.

3.7 Final conclusions

We have proposed all-electron LSD optimized Gaussian basis sets for the atoms boron through neon. The optimization procedure used, based on the Tatewaki and Huzinaga method, provides high quality valence orbitals as judged by comparison with the energies and orbitals obtained by the numerical solution of the Kohn–Sham equations. We be-

Can. J. Chem. Downloaded from www.nrcresearchpress.com by 92.62.229.171 on 09/08/12
For personal use only.

lieve that these sets will cause only small BSSE since they have a good representation of the core orbitals.

The equilibrium geometries, bond dissociation and hydrogenation energies, and electric dipole moments have been calculated with the newly optimized basis sets. The results that we have shown make us believe that we have basis sets that can provide information with a reliable accuracy. The equilibrium geometry parameters are predicted at least within 0.02 Å and 1° of experiment.

The bond dissociation energies for one homolytic dissociation process could be predicted within 1 kcal/mol of experiment and other results obtained using the proposed basis sets are quite encouraging. They are as good as the MP2 and MP4 results, with the 6-31G**//6-31G* orbital basis sets, in reproducing the experimental values. Such an agreement is obtained, though, only if non-local corrections to the energies are included. The hydrogenation energies can be calculated within 1–3 kcal/mol and 2 kcal/mol of experiment at the LSD and NLSD levels respectively using the proposed basis sets. The electric dipole moments were calculated within 0.2 D of the experimental values. These conclusions are based on very preliminary studies. At first glance, the basis sets that we have proposed give results that are as good as those of calculations with other correlated methods and this can be an indication that they are adequate.

These basis sets were also used in other studies to calculate harmonic vibrational frequencies and energies of isodesmic reactions. Dixon (in ref. 33) found a much better agreement with experiment when using LSD optimized basis sets in LSD calculations than when using Hartree–Fock optimized basis sets for isodesmic reactions. He studied several patterns and sizes and concluded that the results are sensitive to the number of contracted functions in the core orbitals. The basis set with six primitives for the 1*s* orbital gives an error of about 4 kcal/mol whereas an improved treatment of the core by just one additional function decreases this error by more than 1 kcal/mol.

The vibrational frequencies in DFT are currently calculated with the second derivatives being obtained by numerical differentiation of the gradient at the equilibrium geometries, since the analytical second derivatives are not available yet. Andzelm (in ref. 33) calculated the vibrational frequencies, using the basis sets proposed in this paper, for a series of simple organic molecules containing C, N, O, H, and F using the basis sets found in this paper. He found a good agreement between the LSD and experimental data. Typically, the high energy frequencies are overestimated while the low frequencies are smaller than the corresponding experimental frequencies. The average percentage deviations in the calculated frequencies from the measured harmonic values are 4.5% at the DZVPP/LSD level. Andzelm and Wimmer (34), again using the present basis sets, calculated vibrational frequencies consistently closer to experiment than those obtained with the Hartree–Fock theory. The LSD results were at least as close to experiment as those obtained from the MP2 theory with similar size and quality of orbital basis sets.

Acknowledgments

We would like to thank Cray Research Inc. for their summer intern program which has rendered this work possible. We also acknowledge the contribution of D. Dixon for helpful discussions. Financial support from the Natural Sciences and Engineering Research Council of Canada and la Fondation pour la Formation des Chercheurs et l'Aide à la Recherche is also acknowledged.

1. S. Huzinaga. Comput. Phys. Rep. **2**, 6 (1985).
2. T. H. Dunning, Jr. and P. J. Hay. *In* Methods of electronic structure theory. *Edited by* H. F. Schaefer III. Plenum Press, New York. 1977. p. 1.
3. P. Čársky and M. Urban. Ab initio calculations. Springer-Verlag, Heidelberg. 1980.
4. E. R. Davidson and D. Feller. Chem. Rev. **86**, 681 (1986).
5. S. Wilson. Ab initio methods in quantum chemistry-I. Vol. 67. *Edited by* K. P. Lawley. John Wiley and Sons, New York. 1987. 439–500.
6. J. Almlöf and P. R. Taylor. Modern basis sets for quantum chemical calculations. University of Minnesota Supercomputer Institute Research Report, UMSI 90/190 (1990).
7. K. Lipkowitz and D. Boyd (*Editors*). Reviews in computational chemistry. VCH Publishers, Inc., New York. 1990. pp. 1–37.
8. J. C. Slater. Phys. Rev. **36**, 57 (1930).
9. S. F. Boys. Proc. R. Soc. (london), A: **200**, 542 (1950).
10. S. Huzinaga. J. Chem. Phys. **42**, 1293 (1965).
11. R. McWeeny. Acta Crystallogr. **6**, 631 (1953).
12. S. F. Boys and I. Shavitt. Proc. R. Soc. (London), A: **254**, 487 (1960).
13. O-ohata, H. Taketa, and S. Huzinaga. J. Phys. Soc. Jpn. **21**, 2306 (1966).
14. W. J. Hehre, R. F. Stewart, and J. A. Pople. J. Chem. Phys. **51**, 2657 (1969).
15. W. J. Hehre, R. Ditchfield, R. F. Stewart, and J. A. Pople. J. Chem. Phys. **52**, 2769 (1969).
16. M. D. Newton, W. A. Lathan, W. J. Hehre, and J. A. Pople. J. Chem. Phys. **52**, 4064 (1970).
17. W. J. Hehre, R. Ditchfield, and J. A. Pople. J. Chem. Phys. **53**, 932 (1970).
18. J. A. Pople. Applications of electronic structure theory. *In* Modern Theoretical Chemistry. Vol. 4. *Edited by* H. F. Schaefer III. Plenum Press, New York. 1977. p. 1.
19. A. N. Tavouktsoglou and S. Huzinaga. J. Chem. Phys. **72**, 1385 (1980).
20. L. Gianolio, R. Pavani, and E. Clementi. Gazz. Chim. Ital. **108**, 181 (1978).
21. H. Tatewaki and S. Huzinaga. J. Chem. Phys. **71**, 4339 (1979).
22. R. Ditchfield, W. J. Hehre, and J. A. Pople. J. Chem. Phys. **54**, 724 (1971).
23. W. J. Hehre and W. A. Lathan. J. Chem. Phys. **56**, 5255 (1972).
24. H. Tatewaki and S. Huzinaga. J. Comput. Chem. **1**, 205 (1980).
25. H. Tatewaki, Y. Sakai, and S. Huzinaga. J. Comput. Chem. **2**, 96 (1981).
26. Y. Sakai, H. Tatewaki, and S. Huzinaga. J. Comput. Chem. **2**, 100 (1981).
27. Y. Sakai, H. Tatewaki, and S. Huzinaga. J. Comput. Chem. **2**, 108 (1981).
28. H. Tatewaki, Y. Sakai, and S. Huzinaga. J. Comput. Chem. **2**, 278 (1981).
29. Y. Sakai, H. Tatewaki, and S. Huzinaga. J. Comput. Chem. **3**, 6 (1982).
30. S. Huzinaga, J. Andzelm, H. Klobukowski, E. Radzio-Andzelm, E. Sakai, and H. Tatewaki. Gaussian basis sets for molecular calculations. Elsevier, Amsterdam. 1984.
31. D. A. Dixon, J. Andzelm, G. Fitzgerald, and E. Wimmer. J. Phys. Chem. **95**, 9197 (1991).
32. T. J. Lee, J. E. Rice, G. E. Scuseria, and H. F. Schaefer III. Theor. Chim. Acta, **75**, 81 (1989), and references therein.

33. J. K. Labanowski and J. K. Andzelm (*Editors*). Density functional methods in chemistry. Springer-Verlag, New York. 1991.
34. J. Andzelm and E. Wimmer. J. Chem. Phys. **96**, 1280 (1992).
35. R. A. Friesner. J. Chem. Phys. **85**, 1462 (1986).
36. M. N. Ringnalda, Y. Won, and R. A. Friesner. J. Chem. Phys. **92**, 1163 (1990).
37. E. Wimmer, A. J. Freeman, C.-L. Fu, P.-L. Cao, S.-H. Chou, and B. Delley. *In* Supercomputer research in chemistry and chemical engineering. *Edited by* K. F. Jensen and D. G. Truhlar. ACS Symp. Ser. **353**, 49 (1987).
38. R. O. Jones and O. Gunnarsson. Rev. Mod. Phys. **61**, 689 (1990).
39. T. Ziegler. Chem. Rev. **91**, 651 (1991).
40. D. R. Salahub and M. C. Zerner (*Editors*). The challenge of *d* and *f* electrons. Theory and computation. ACS Symp. Ser. **394** (1989).
41. P. Hohenberg and W. Kohn. Phys. Rev. B, **136**, 864 (1964).
42. W. Kohn and L. J. Sham. Phys. Rev. A, **140**, 1133 (1965).
43. M. Levy. Proc. Natl. Acad. Sci. (U.S.A.) **76**, 6062 (1979).
44. R. G. Parr and W. Yang. Density-functional theory of atoms and molecules. Oxford University Press, New York. 1989.
45. E. J. Baerends, D. E. Ellis, and P. Ros. Chem. Phys. **2**, 41 (1973).
46. A. Rosén and D. E. Ellis. J. Chem. Phys. **65**, 3629 (1976).
47. F. W. Averill and D. E. Ellis. J. Chem. Phys. **59**, 6412 (1973).
48. B. Delley and D. E. Ellis. J. Chem. Phys. **76**, 1949 (1982).
49. B. Delley. J. Chem. Phys. **92**, 508 (1990).
50. O. K. Anderson and R. G. Woolley. Mol. Phys. **26**, 905 (1973).
51. (*a*) O. Gunnarsson, J. Harris, and R. O. Jones. Phys. Rev. B, **15**, 3027 (1977); (*b*) J. Chem. Phys. **67**, 3970 (1977).
52. R. Car and M. Parrinello. Phys. Rev. Lett. **55**, 2471 (1985).
53. M. P. Teter, M. C. Payne, and D. C. Allan. Phys. Rev. B, **40**, 12255 (1989).
54. J. C. Slater. Phys. Rev. **51**, 846 (1937).
55. O. K. Anderson. Phys. Rev. B, **12**, 3060 (1975).
56. E. Wimmer, H. Krakauer, M. Weinert, and A. J. Freeman. Phys. Rev. B, **24**, 864 (1981).
57. (*a*) H. Sambe and R. H. Felton. J. Chem. Phys. **61**, 3862 (1974); (*b*) J. Chem. Phys. **62**, 1122 (1975).
58. B. I. Dunlap, J. W. D. Connolly, and J. R. Sabin. J. Chem. Phys. **71**, 3396 (1979); **71**, 4993 (1979).
59. A. D. Becke. Int. J. Quantum Chem. Symp. **23**, 599 (1989).
60. J. Andzelm, E. Radzio, and D. R. Salahub. J. Comput. Chem. **6**, 520 (1985).
61. W. J. Hehre, L. Radom, P. v. R. Schleyer, and J. A. Pople. Ab initio molecular orbital theory. John Wiley and Sons, New York. 1986.
62. P. C. Hariharan and J. A. Pople. Chem. Phys. Lett. **66**, 217 (1972).
63. S. H. Vosko, L. Wilk, and M. Nusair. Can. J. Phys. **58**, 1200 (1980).
64. H. Tatewaki and S. Huzinaga. J. Comput. Chem. **3**, 205 (1980).
65. A. D. Becke. Phys. Rev. A, **38**, 3098 (1988).
66. J. P. Perdew. Phys. Rev. B, **33**, 8822 (1986).
67. A. St-Amant. Ph.D. Thesis, Université de Montréal. 1992.

Can. J. Chem. Downloaded from www.nrcresearchpress.com by 92.62.229.171 on 09/08/12
For personal use only.

Theoretical study of nitro–nitrite rearrangement of CH_3NO_2

ROBERTA P. SAXON
Molecular Physics Laboratory, SRI International, Menlo Park, CA 94025, U.S.A.

AND

MEGUMU YOSHIMINE
IBM Research Division, Almaden Research Center, San Jose, CA 95120-6099, U.S.A.

Received July 18, 1991

This paper is dedicated to Professor Sigeru Huzinaga on the occasion of his 65th birthday

ROBERTA P. SAXON and MEGUMU YOSHIMINE. Can. J. Chem. **70**, 572 (1992).

Calculations designed to characterize the transition state and determine the barrier height for rearrangement of nitromethane to methyl nitrite are reported. Structures of CH_3NO_2, CH_3ONO, dissociation products, CH_3 + NO_2 and CH_3O + NO, and the transition state for nitro–nitrite rearrangement have been optimized at the MCSCF/4-31G level. The geometry of the transition state may be approximately described as separated CH_3 and NO_2 species with extremely long C—N and C—O bond lengths, 3.396 and 3.654 Å, respectively. Energies have been obtained by large-scale multireference single- and double-excitation CI calculations (6-31G* basis). The transition state is calculated to lie 56.7 kcal/mol above nitromethane (with zero-point energy). A C—N bond dissociation energy of 51.7 kcal/mol is obtained. Results are compared with the infrared multiphoton dissociation experiment of Wodtke, Hintsa, and Lee.

Key words: nitromethane, *ab initio* calculations, transition state, rearrangement, dissociation.

ROBERTA P. SAXON et MEGUMU YOSHIMINE. Can. J. Chem. **70**, 572 (1992).

On rapporte les résultats de calculs effectués dans le but de caractériser l'état de transition et de déterminer la hauteur de la barrière au réarrangement du nitrométhane en nitrite de méthyle. Opérant au niveau MCSCF/4-31G, on a optimisé les structures du CH_3NO_2, du CH_3ONO, des produits de dissociation, CH_3 + NO_2 et CH_3O + NO, et de l'état de transition du réarrangement nitro–nitrite. La géométrie de l'état de transition ressemble approximativement aux espèces CH_3 et NO_2 séparées dans lesquelles les liaisons C—N et C—O sont extrémement allongées, à des distances respectives de 3,396 et 3,654 Å. On a obtenu les énergies à l'aide de calculs d'IC (base 6-31G*) avec multi-références simplement ou doublement excitées. On a calculé que l'état de transition se trouve à 56,7 kcal/mol au-dessus du nitrométhane (avec énergie du point zéro). On obtient une énergie de dissociation de la liaison C—N de 57,1 kcal/mol. On a comparé les résultats avec ceux d'expériences de dissociation par infrarouge multiphotonique de Wodtke, Hintsa et Lee.

Mots clés : nitrométhane, calculs *ab initio*, état de transition, réarrangement, dissociation.

[Traduit par la rédaction]

Introduction

The decomposition kinetics of nitro compounds is complicated by the competition between different mechanisms, e.g., simple bond cleavage, concerted molecular dissociation, and rearrangement or elimination through cyclic transition states. The high energy content of such molecules both provides alternative decomposition pathways and makes them attractive as prototype energetic materials.

Experimental evidence for unimolecular nitro–nitrite rearrangement, R—NO_2 → R—ONO, as an initial step in thermal decomposition has been reported in several systems. Wodtke, Hintsa, and Lee (1), using a molecular beam, infrared multiphoton dissociation technique, and an analysis based on RRKM theory to relate their results to pyrolysis experiments, observed isomerization of nitromethane, CH_3NO_2, to methyl nitrite, CH_3ONO, by detecting the CH_3O and NO products from dissociation of the nitrite.

In a study (2) of the kinetics of thermal decomposition of dimethylnitramine, $(CH_3)_2NNO_2$, numerical modeling satisfactorily reproduces the observed temperature and product formation only when rearrangement to the nitrite is included as a competitive process. Another experiment (3) on the same compound, which mass spectrometrically sampled the initial products, reported observation of NO and fragment ions of the nitroxyl radical $(CH_3)_2NO$, presumably formed from the nitrite. However, a recent IRMPD study (4) of dimethylnitramine reported no evidence of the isomerization channel. Finally, evidence of the rearrangement in nitrobenzene, detection of C_6H_5OH in the presence of radical scavenger, has also been reported (5).

Because of the great interest in the chemistry of nitro compounds, theoretical studies have been carried out over many years (6–8), although the multiconfigurational methods needed to describe open shell transition states and even the ground states of the stable isomers have only recently been applied to mechanistic studies (9–11).

In an effort to understand the mechanism of nitro–nitrite rearrangement in N—NO_2 compounds, we recently reported (9) MCSCF/CI calculations of stable isomers and the rearrangement transition state of NH_2NO_2, the unsubstituted analog of dimethylnitramine. Optimized at the MCSCF/4-31G level, the geometry of the transition state may be approximately described as separated NH_2 and NO_2 species with an N—N bond length of 2.8 Å. The wavefunction of the transition state is characterized by two singly occupied orbitals. At the CI level, the energy of the transition state is within 1 kcal/mol of the NH_2 + NO_2 asymptote. From these results, isomerization is expected to be competitive with N—NO_2 bond scission, as observed experimentally.

A similar computational approach was used in a careful study (10) by Mowrey *et al.* to determine the 5-membered ring transition state for elimination of HONO from CH_2NNO_2, which was predicted to have an activation energy below the N—NO_2 bond dissociation energy, consistent with indirect evidence from molecular beam experiments.

Printed in Canada

Can. J. Chem. Downloaded from www.nrcresearchpress.com by 92.62.229.171 on 09/08/12
For personal use only.

Can. J. Chem. Downloaded from www.nrcresearchpress.com by 92.62.229.171 on 09/08/12
For personal use only.

The nitromethane system has been studied theoretically by various techniques. However, a consistent mechanism for nitro–nitrite rearrangement in CH_3NO_2 has yet to emerge. The possibility of decomposition of nitro compounds by isomerization to nitrites was suggested by Dewar *et al.* (6). Rice and Thompson (12) recently reported a classical trajectory study of the rearrangement process, using three different model potential energy surfaces. They found best agreement with the reported branching ratio of isomerization vs. C—NO_2 dissociation for the model surface with a barrier 7.5 kcal/mol below the dissociation energy. This surface goes through what may be termed a tight transition state, C—N and C—O bond lengths on the order of 2 Å. A tight transition state with similar bond lengths, optimized at the SCF level, with an energy significantly above the C—N bond energy was reported by McKee (8). He indicated, however, that the result was likely to be an artifact of the SCF computational model. In a subsequent paper (11), McKee found a loose transition state, bond lengths > 3.6 Å, in a small active space MCSCF optimization. However, at the highest level CI calculation reported, the energy remained 10 kcal/mol above the C—N bond energy. The N—O bond lengths at the transition state geometry were quite uneven, indicative of an NO_2 radical in an energetically unfavorable conformation, in contrast to the situation found (9) for NH_2NO_2.

In this paper, we apply the MCSCF/CI computational model used to determine the nitro–nitrite rearrangement transition state in NH_2NO_2 to isomerization of nitromethane. Structures of the stable isomers as well as that of the transition state have been optimized as the MCSCF level by the gradient technique. Large-scale configuration interaction (CI) calculations were performed at the optimized geometries for determinations of energy differences. In the next section, the design of appropriate MCSCF and subsequent CI calculation is described. Results and discussion, including comparison with previous determinations and with the nitramine transition state, are presented in the following section.

Calculations

Geometries of the stable isomers, the rearrangement transition state, and the dissociation products were optimized at the MCSCF level with a standard 4-31G Gaussian basis set using analytic second derivatives at each step to facilitate the optimization. Calculations for the asymptotes were carried out on the supermolecule. The choice of the active space of the MCSCF calculation is crucial. Following the procedure described for NH_2NO_2, the active space should consist of seven orbitals: a complete valence space of 19 orbitals less the two O 2*s* orbitals, two N—O bonds, two N—O antibonds, three C—H bonds, and three C—H antibonds. This would provide, in principle, one orbital of C character and six orbitals of N—O character. In practice, at the equilibrium geometry, all seven orbitals in the active space describe the NO_2 (using σ and π to describe the NO_2 plane): two N—O σ bonds, one O σ lone pair, one O π lone pair, one N—O π bond, and N—O π^* and σ^* correlating orbitals. At the transition state, one N—O σ bonding orbital and the N—O σ^* orbital become the singly occupied orbitals on carbon and nitrogen.

Energies were determined by multireference single- and double-excitation CI calculations with the standard 6-31G* basis set using MCSCF molecular orbitals. In constructing the CI expansions, the orbitals were divided into four spaces: frozen; inactive, composed of 10 orbitals; active, composed of four orbitals; and external, composed of the remaining 48 orbitals. The four lowest occupied orbitals, corresponding to the C, N, and O 1*s* were kept doubly occupied. The configuration list included all single and double excitations from the inactive and active spaces with at most one electron in the external space and all double excitations from the inactive and active spaces to the external space, which differed by no more than two electrons from a set of reference configurations. Interacting space restrictions on the coupling were imposed for double excitations from the inactive space.

A four-orbital active space was used to construct the CI expansions, in contrast to the seven-orbital active space used in the MCSCF optimization calculations, in order to provide a more compact CI expansion. MCSCF orbitals determined with the four-orbital active space were used in these CI calculations. CI calculations were also performed for the isomers and the CH_3O + NO asymptote with the seven-orbital active space. The weight of the reference configurations in the CI wavefunctions was approximately 0.87 for all calculations. This resulted in CI expansions of up to 400 000 configurations with the four-orbital active space in C_s symmetry (900 000 with the seven-orbital active space) and 700 000 (four-orbital active space) in C_1 symmetry. Preliminary geometry optimizations were carried out with the GAMESS program (13); final geometry determinations (14) and all other calculations used the ALCHEMY II program system (15).

Results and discussion

Structures of stable isomers

Geometrical parameters for CH_3NO_2, CH_3ONO, and the dissociation products optimized at the MCSCF level are given in Tables 1–3. Experimentally obtained geometries and results of previous calculations, with which reasonable agreement is noted, are also given. The numbering of the atoms is illustrated in Fig. 1. In nitromethane, the four heavy atoms are predicted to be nearly coplanar. The angle between the CN bond and the NO_2 plane is 1.8°. Results are presented for the *cis* staggered isomer of methyl nitrite, which has been shown by experiment (16) and calculations (8) to be the lowest energy form. In this form, the four heavy atoms and the hydrogen labeled H1 are strictly coplanar. The *cis* eclipsed form with the in-plane H on the opposite side of the C—O bond was found to be a transition state for methyl group rotation.

Comparison with structural parameters obtained from microwave spectra shows excellent agreement for most bond lengths and all bond angles. For methyl nitrite, the analysis has been done with and without a small tilt of the methyl group off the C—O axis. Other parameters are insensitive to this assumption. The greatest discrepancy between the calculated and experimental geometries is found for the N—O bond length in CH_3NO_2 and the terminal N—O2 bond length in CH_3ONO, which are calculated to be longer by 0.02 and 0.06 Å, respectively, than the experimental determinations. In both cases, the dominant correlation in the MCSCF wavefunction is excitation to N—O antibonding orbitals. As discussed previously for NH_2NO_2, it is possible that the length of these bonds is overestimated by the 4-31G basis set as well as by the present MCSCF model, which does not correlate

TABLE 1. Optimized geometrical parameters for CH_3NO_2 (in angstroms and degrees)

	MC7/[a] 4-31G	SCF/[b] 6-31G*	MC2/[c] 6-31G*	Experiment[d]
C—N	1.474	1.478	1.474	1.489
N—O[e]	1.259	1.192	1.205	1.224
C—H1	1.078	1.080	1.081	(1.088)[f]
C—H2[g]	1.074	1.076	1.077	(1.088
∠O—N—O	125.6	125.8	124.9	125.3
∠C—N—O	117.2	117.1	117.6	117.4
∠H1—C—N	108.2			107.2
∠H2—C—N	108.0			107.2
$(NO_2)(CH)$[h]	1.8			
∠H2—C—N—O1[i]	30.5			

[a]Present work, MC*n* denotes MCSCF with *n* orbital active space.
[b]McKee, ref.8
[c]McKee, ref. 11.
[d]Cox and Waring, ref. 16. Isomer with one H in plane of NO_2.
[e]O atoms are equivalent.
[f]C—H distance assumed.
[g]H2 and H3 are equivalent.
[h]Angle between NO_2 plane and CN bond.
[i]Torsion angle.

TABLE 2. Optimized geometrical parameters for CH_3ONO *cis* staggered (in angstroms and degrees)

	MC7/[a] 4-31G	SCF/[b] 6-31G*	MC2/[c] 6-31G*	Experiment	
				Ref. 17[d]	Ref. 18[e]
C—O1	1.451	1.421	1.417	1.437	1.437	1.436
O1—N	1.373	1.326	1.339	1.398	1.420	1.418
N—O2	1.246	1.162	1.179	1.182	1.179	1.181
C—H1	1.073	1.078	1.078	(1.09)[f]	1.090	1.089
C—H2[g]	1.077	1.080	1.081	1.102	1.090	1.094
∠N—O—C	119.5	117.6	117.8	114.7	114.2	114.5
∠O—N—O	113.7	115.2	114.5	114.8	114.5	114.3
∠H1—C—O	103.8	104.4		101.8	102.4	102.6
∠H2—C—O	110.5	110.8		109.9	112.7	110.4
∠H2—C—O1—N[h]	61.0					

[a]Present work, MC*n* denotes MCSCF with *n* orbital active space.
[b]McKee, ref. 8.
[c]McKee, ref. 11.
[d]Turner, Corkill, and Cox, ref. 17.
[e]van der Veken *et al.*, ref. 18.
[f]C—H distance assumed.
[g]H2 and H3 are equivalent.
[h]Torsion angle.

all bonds to the same extent. These bond lengths appear to be underestimated, however, by the RHF model. The correlation included in the two electron in two orbital MCSCF calculations reported previously (11) had a modest effect on optimized geometries.

Vibrational frequencies for CH_3NO_2, CH_3ONO, and the dissociation products are reported in Table 4. Those modes that were identified as corresponding to pure motions of portions of the molecules in the experimental analysis are indicated in the table. They also correspond to pure motions in the calculated normal modes except for the *a"* NO_2 stretch in CH_3NO_2 for which some mixing was found. For the methyl stretches and bends noted, the calculated frequencies are larger than the observed values by an average of 12%. The calculated NO_2 or NO frequencies are smaller than experimental values by 2–19% (26–260 cm^{-1}). Similar comparisons are noted for the CH_3 modes of the dissociation products except for the low-frequency mode of the methyl radical, which is calculated to be anomalously low. The calculated NO and NO_2 frequencies in the isolated molecules are in excellent agreement with experiment. Summing the frequencies, the calculated zero point energies are in good agreement with experimental values. For CH_3NO_2 a value of 32.2 kcal/mol is predicted vs. 30.2 kcal/mol from the experimental frequencies. For CH_3ONO, the calculated zero point energy is 32.0 kcal/mol, vs. 29.0 from experiment.

Can. J. Chem. Downloaded from www.nrcresearchpress.com by 92.62.229.171 on 09/08/12
For personal use only.

TABLE 3. Optimized geometrical parameters for dissociation products (in angstroms and degrees)

CH_3:			NO_2:		
	MC7/ 4-31G	Experiment[a]		MC7/ 4-31G	Experiment[a]
C—H	1.069	1.079	N—O	1.211	1.193
∠HCH	120.		∠O—N—O	133.0	134.1
CH_3O:			NO:		
	MC7/ 4-31G	SCF/[b] DZ		MC7/ 4-31G	Experiment[c]
C—O	1.426	1.434	N—O	1.166	1.151
C—H5	1.082	1.084			
C—H6	1.080	1.081			
∠H5—C—O	106.1	106.3			
∠H6—C—O	110.7	110.6			

[a]Herzberg, ref. 19.
[b]Colwell, Amos, and Handy, ref. 20.
[c]Huber and Herzberg, ref. 21.

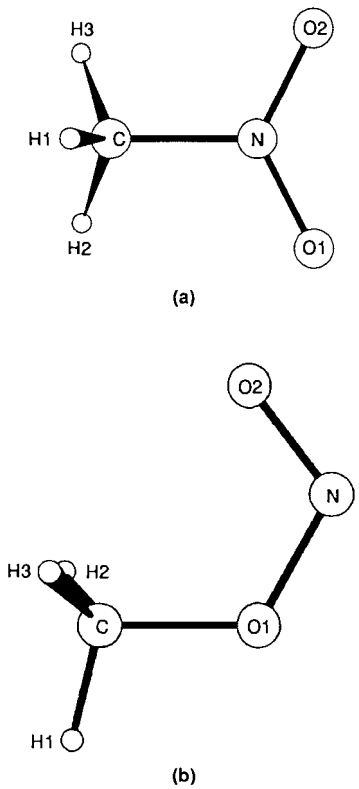

FIG. 1. MCSCF/4-31G optimized equilibrium geometry of (*a*) CH_3NO_2 and (*b*) CH_3ONO, *cis* staggered isomer. In (*b*), H1 and the heavy atoms are strictly coplanar and H2 and H3 are equivalent.

Transition state

The geometry of the transition state for rearrangement of CH_3NO_2 to CH_3ONO is illustrated in Fig. 2. Optimized geometrical parameters and calculated harmonic frequencies are given in Table 5. The transition state has one small imaginary frequency. The geometry may be approximately described as separated CH_3 and NO_2 species. The C—N bond is extremely long, 3.396 Å. The distance between C and O1, the atom with which the carbon will become bonded in CH_2ONO, is, however, slightly shorter at the transition state, 3.654 Å, than the C—O2 distance, 3.668 Å. All of the C—H and N—O parameters have very nearly the same values given for the isolated species at the same level of calculation in Table 3. The C—N bond makes an angle of 83° with the plane of the NO_2. The average plane of the nearly planar methyl radical fragment is virtually parallel to the NO_2 plane. Looking along the N—C bond, the oxygens and hydrogens are staggered, as shown in Fig. 2*b*. The MCSCF wavefunction at the transition state is characterized by two singly occupied orbitals, singlet coupled, as expected for this loose combination of radical species.

All of the significant frequencies for the transition state in Table 5 readily can be identified with frequencies of the fragments. They differ by less than 10 cm^{-1} from the frequencies of the separated species, calculated at the same level, except for the low methyl bend. The frequencies below 100 cm^{-1} correspond to motions connecting the two fragments.

The energy profile along an approximate reaction path shown in Fig. 3 demonstrates that the transition state that has been located does in fact smoothly connect nitromethane and methyl nitrite, as claimed. In constructing this plot, the C—N bond distance was taken as the reaction coordinate for the path between CH_3NO_2 and the transition state. Fixing the C—N distance at the plotted values, the remaining coordinates were optimized at the MCSCF/4-31G level. Relative energies obtained by MCSCF calculations with the 6-31G* basis are plotted in Fig. 3. The C—O1 bond distance was used as the reaction coordinate for the path between the transition state and CH_2ONO. For the first two points to the right of the transition state, C—O1 = 3.0 and 2.5 Å, it was necessary to fix the C—O1—N internal angle at interpolated values of 95 and 105.9°, respectively. The reaction path shown leads to the *cis*, staggered methyl nitrite, the lowest isomer.

Can. J. Chem. Downloaded from www.nrcresearchpress.com by 92.62.229.171 on 09/08/12
For personal use only.

TABLE 4. Calculated frequencies (cm^{-1}) (MC7/4-31G) for CH_3NO_2, CH_3ONO, and dissociation products

	CH_3NO_2		CH_3ONO	
	Calcd.	Experiment[a]	Calcd.	Experiment[a]
a'	598	607	355	346
	665	655	775	624
	918	917	888	838
	1275	1103	1111	995
	1376 NO_2 stretch	1402	1299	1239
	1603	1379	1359 N=O	1620
	1642 CH_3	1426	1615	1409
	3254 CH_3 stretch	2967	1659 CH_3	1458
	3351 CH_3 stretch	3065	3240 CH_3 stretch	2891[c]
			3367 CH_3 stretch	3032
a''	19		216	150
	507	480	289	256
	1007	1103	1275	988
	1360[d] NO_2 stretch	1561	1652 CH_3	1441
	1646 CH_3	1426	3327 CH_3 stretch	3015
	3381 CH_3 stretch	3045		

	CH_3		NO_2	
	Calcd.	Experiment[e]	Calcd.	Experiment[f]
	285	a_2'' 606	747	750 bend
	1554	e' 1396	1314	1320 sym
	3281	a_1' 3005	1714	1618 asym
	3467	e' 3161		

	CH_3O		NO	
	Calcd.[g]	Experiment[h]	Calcd.	Experiment[i]
	735	e 653	1890	1904
	1043			
	1166	a_1 1047		
	1599	a_1 1362		
	1619			
	1674	e 1487		
	3196	a_1 2840		
	3278	e 2774		
	3283			

[a]Trinquecoste, M. Rey-Lafon, and Forel, ref. 22.
[b]Rook and Jacox, ref. 23.
[c]From fit to spectrum.
[d]Some mixing with CH_3 motion.
[e]Jacox, ref. 24.
[f]Herzberg, ref. 19.
[g]C_s symmetry.
[h]C_{3v} symmetry, Jacox, ref. 24.
[i]Huber and Herzberg, ref. 21.

Energies

Total energies for all calculations carried out in this study, as well as relative energies with respect to CH_3NO_2 and calculated zero point energies, are given in Table 6. As mentioned above, CI calculations based on the same seven-orbital active space used for the MCSCF optimizations were performed for CH_3NO_2, CH_3ONO, and the CH_3O + NO asymptote, taking advantage of C_s symmetry, in order to test the four active orbital CI model. Relative energies for the nitrite and the asymptote from the two CI calculations are in good agreement, within 1.0 kcal/mol. Including the multireference Davidson correction for quadruple excitations, i.e., comparing the calculations labeled CI7D and CI4D in Table 6, the relative energies agree to within 0.1 kcal/mol. Note that the energy predictions with the small active space MCSCF calculations are not reliable. However, the structure of the MCSCF wavefunction and the molecular orbitals from the two MCSCF calculations are very similar.

Final results of this study are given by the quadruple corrected CI calculations, CI4D, with calculated zero point

Can. J. Chem. Downloaded from www.nrcresearchpress.com by 92.62.229.171 on 09/08/12
For personal use only.

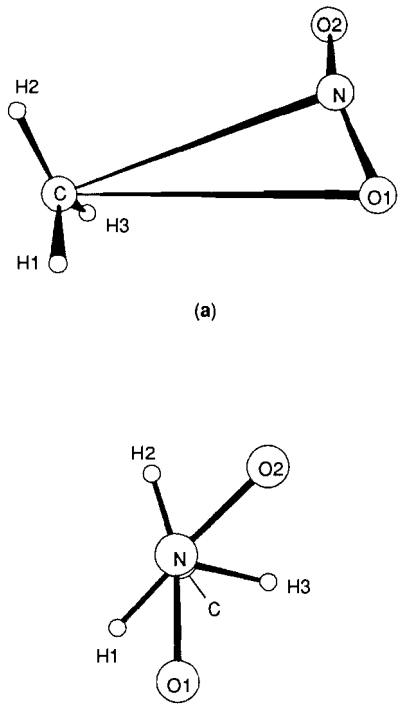

FIG. 2. MCSCF/4-31G optimized structure of the transition state for rearrangement of CH_3NO_2 to CH_3ONO: (*a*) viewed from above the C—N—O1 plane, (*b*) viewed along the N—C bond.

energies. These numbers correspond to energies at temperatures of 0°C. Nitromethane and methyl nitrite are calculated to be essentially isoenergetic. The transition state is predicted to lie 56.7 kcal/mol above nitromethane and 0.4 kcal/mol below the $CH_3 + NO_2$ asymptote. The energy to break the CH_3O—NO bond from these calculations is 34.5 kcal/mol.

Experimental energies given for comparison in Table 6 have been obtained from room temperature heats of formation extrapolated to 0°C assuming a rigid rotator, harmonic oscillator approximation.[1] The nitromethane, methyl nitrite energy difference, and C—NO_2 bond dissociation energy are in excellent agreement with experimental energies. The calculated energy of the $CH_3O + NO$ asymptote lies almost 6 kcal/mol below the value from experimental heats of formation.

Discussion

The goal of this work was to theoretically determine the mechanism for the rearrangement of nitromethane to methyl nitrite. These calculations predict an energy barrier to rearrangement of 56.7 kcal/mol, via a loose transition state. This barrier is very close in magnitude to the calculated energy to break the C—NO_2 bond, 57.1 kcal/mol. Furthermore, the preexponential Arrhenius A factors calculated from the vibrational frequencies in an RRKM treatment should be similar for isomerization and bond dissociation, leading to the prediction of comparable rates for isomerization and dissociation. This prediction should be compared with the results of the IRMPD experiment of Wodtke, Hinsta, and Lee (1) (WHL). Comparable reaction rates are consistent with the

[1]Heats of formation at 298 K of −17.76 kcal/mol for CH_3NO_2 and of −15.85 kcal/mol for CH_3ONO were taken from ref. 25*a*. For CH_3O, the value 3.99 kcal/mol from ref. 25*b* was used. Reference 25*c* was used for NO_2 and NO. Experimental structures and frequencies were used in the rigid rotator, harmonic oscillator extrapolation to 0°C except for CH_3O for which the calculated structure was adopted.

TABLE 5. Optimized geometrical parameters (in angstroms and degrees) and frequencies (cm^{-1}) for the $CH_3NO_2 \rightarrow CH_3ONO$ transition state

	Geometry				
	MC7/[a] 4-31G	SCF/[b] 6-31G*	MC4/[c] 66-31G*	Frequencies	
C—O	3.654	2.010	3.700	(63i)	
C—N	3.396	1.926	3.617	34	
N—O1	1.210	1.251	1.371	41	
N—O2	1.210	1.881	1.155	55	
C—H[d]	1.069	1.070	1.070	110	
∠O—N—O	133.1	119.9	113.0	111	
∠H1—C—H2	119.8	116.0	119.0	430	CH_3
∠H1—C—H3	119.7	116.0	119.0	749	NO_2
∠H2—C—H3	119.7	116.0	119.0	1316	NO_2
∠H1—C—O1	76.8			1556	CH_3
∠H2—C—O1	110.7			1556	CH_3
∠H3—C—O1	90.9			1719	NO_2
∠O2—N—O1—C[e]	96.7			3276	CH_3
				3459	CH_3
				3461	CH_3

[a]Present work, MC*n* denotes MCSCF with *n* orbital active space.
[b]McKee, ref. 8.
[c]McKee, ref. 11.
[d]All C—H bond lengths equal.
[e]Torsion angle.

Can. J. Chem. Downloaded from www.nrcresearchpress.com by 92.62.229.171 on 09/08/12
For personal use only.

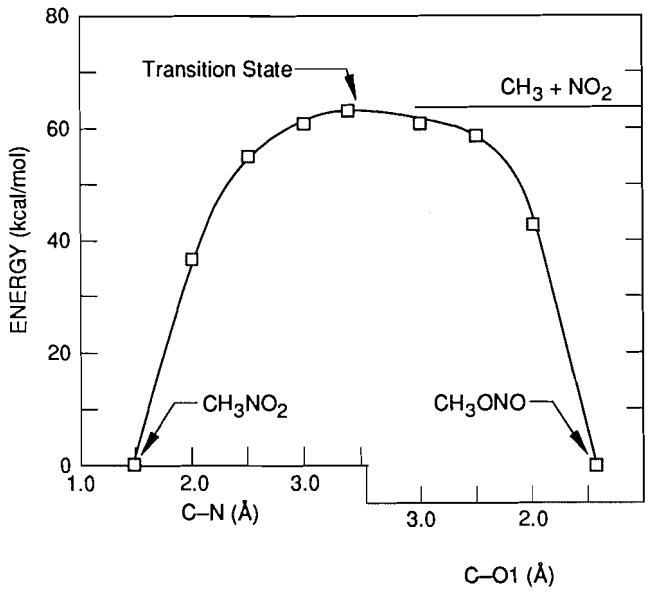

FIG. 3. Energy (kcal/mol) with respect to CH_3NO_2 (MC7/6-31G*) for the path connecting CH_3NO_2, the transition state, and CH_3ONO. Left side: reaction coordinate is C—N bond length. Right side: reaction coordinate is C—O1 bond length. See text.

branching ratio of isomerization to dissociation (0.6) inferred from the experimental observations.

The calculated barrier height is compared in Table 6 with the barrier height reported by WHL. This value is not observed directly in these experiments but emerges from an RRKM analysis with stated assumptions. The most critical of these, as discussed previously by McKee (11), may be the assumed A factor for the isomerization channel. WHL adopted the value reported by Dewar *et al.* (6) from the tight transition state indicated by semiempirical MINDO/3 calculations. This A factor is two orders of magnitude smaller than that taken for bond dissociation, which should be similar to the A factor from the loose transition state reported here. WHL estimated the uncertainty in the barrier height from a factor of three variation in the assumed A factor.

We may also note that while none of the model potential surfaces used by Rice and Thompson (12) in their classical trajectory study corresponds to a loose transition state, their results raise the possibility that trajectories that sample the rearrangement transition state may dissociate to $CH_3 + NO_2$, presumably via another transition state, rather than rearrange to the methyl nitrite. This introduces a subtlety that needs to be considered in rigorous calculations of reaction rates.

The structure of the transition state is compared in Table 5 with previously reported determinations. The C—N and C—O bond distances from the four electron in four orbital MCSCF optimization of McKee (11) are similar to the present results. The main differences in geometry are that the transition state has equal N—O bond lengths in the present work, while the previous MCSCF study reported one long and one short N—O bond, i.e., the present results correspond to the NO_2 radical portion of the loose transition state at its ground state equilibrium geometry while the previous work (11) describes the NO_2 fragment at the transition state as promoted to the O-N=O electronic configuration. In an attempt to explain these results, we investigated whether there are metastable states of the NO_2 radical at asymmetric geometries similar to that reported at the transition state. Using a nine electron in six orbital MCSCF with a 6-31G* basis, a minimum of $^2A''$ symmetry with bond lengths of 1.318 and 1.212 Å and an ONO bond angle of 109° was obtained. We may speculate that the transition state reported in ref. 11 corresponds to reaction on an excited electronic surface.

The transition state geometry obtained from SCF optimi-

TABLE 6. Calculated total energies (hartrees), zero-point-energies (kcal-mol), and relative energies (kcal/mol) with respect to CH_3NO_2 (6-31G* basis, MC7/4-31G geometries)

	Total energies[a]						Zero pt. energy
	MC7[b]	CI7[c]	CI7D[a]	MC4[b]	CI4[c]	CI4D[d]	
CH_3NO_2	−0.752935	−1.272106	−1.343826	−0.707666	−1.263188	−1.337278	32.3
CH_3ONO	−0.753136	−1.271839	−1.343300	−0.725977	−1.264320	−1.336653	32.0
Transition state	−0.652370			−0.602348	−1.159629	−1.236039	25.5
$CH_3 + NO_2$	−0.651532			−0.601387	−1.158259	−1.234397	24.8
$CH_3O + NO$	−0.719342	−1.218253	−1.281653	−0.691812	−1.208345	−1.275050	27.8

	Relative energies							
	MC7	CI7	CI7D	MC4	CI4	CI4D	CI4D/ZP	Expt.
CH_3ONO	−0.1	0.2	0.3	−11.5	−0.7	0.4	0.1	1.5[e]
Transition state	63.1			66.1	65.0	63.5	56.7	55.5[f]
$CH_3 + NO_2$	63.7			66.7	565.9	64.6	57.1	58.6[e]
$CH_3O + NO$	21.1	33.8	39.0	10.0	34.4	39.1	34.6	40.2[e]

[a] With respect to −243.0 hartrees.
[b] Defined in Table 1.
[c] CI*n* denotes CI with *n* orbital active space.
[d] CI*n*D denotes CI*n* with Davidson correction for quadruple excitations.
[e] Extrapolated to 0°C, see footnote 1.
[f] Deduced from IRMPD experiment, Wodtke, Hintsa, Lee, ref. 1.

Can. J. Chem. Downloaded from www.nrcresearchpress.com by 92.62.229.171 on 09/08/12
For personal use only.

zation (8) is also listed in Table 5. The determination of much longer C—N and C—O bond distances by MCSCF optimization than those predicted by the closed shell SCF model is expected. The SCF transition state is reported (8) to be significantly higher in energy than the C—N bond dissociation energy. While the energetics from semiempirical calculations should be interpreted with caution, the tight transition state, C—N = 1.516 Å, C—O1 = 1.584 Å, and N—O1 = 1.299 Å, from the MINDO/3 study of nitro–nitrite rearrangement (6) have been widely quoted (1, 12). We therefore investigated both of the tight transition states reported previously (6, 8) using the current MCSCF model to make sure that they do not correspond to another stationary point on the potential energy surface. In both cases, the structure of the MCSCF wavefunction is indeed closed shell. The gradients of the energy were far from zero; in particular, the gradients with respect to the C—N bond distance were quite large. At the MCSCF level, the energies were very high, >40 kcal/mol above the $CH_3 + NO_2$ asymptote. While it is not possible to prove that a tight transition state does not exist, our results suggest the tight transition states reported previously (6, 8) are artifacts of the approximate computational methods employed and do not represent stationary points on the potential energy surface of nitromethane.

In summary, the results reported here for nitro–nitrite rearrangement of nitromethane are very similar to those obtained previously (9) for rearrangement of NH_2NO_2 with a comparable MCSCF/CI computational model. The transition state in both cases can be characterized as a loose combination of radical species, CH_3 and NO_2 for nitromethane, and the energy of the transition state is within 1 kcal/mol of that of the separated fragments. The rate of unimolecular dissociation of CH_3NO_2 to $CH_3 + NO_2$ can be estimated using the hindered rotational Gorin model (26) while RRKM theory can be used to estimate the rate of the unimolecular isomerization reaction to CH_3ONO. The predicted loose transition state configuration will give an entropy contribution in the RRKM calculation very similar to the entropy contribution of the Gorin transition state and the activation energies are also calculated to be quite similar, leading to the prediction that the rate of isomerization to the nitrite is comparable to the rate of bond dissociation, consistent with experiment. The MCSCF approach is essential to determining the open shell transition state for nitro–nitrite rearrangement. Application of this model to other reactions should lead to improved understanding of detailed reaction mechanisms.

Can. J. Chem. Downloaded from www.nrcresearchpress.com by 92.62.229.171 on 09/08/12
For personal use only.

Acknowledgments

We are grateful to Dr. Jeff Manion for extrapolating thermochemical data and Drs. Alan Rodgers and Greg Smith for helpful conversations. This work was performed under a joint studies agreement between SRI International and IBM. R.P.S. was supported by SRI internal research and development funds.

1. A. M. Wodtke, E. J. Hintsa, and Y. T. Lee. J. Phys. Chem. **90**, 3549 (1986).
2. S. E. Nigenda, D. F. McMillen, and D. M. Golden. J. Phys. Chem. **93**, 1124 (1989).
3. P. H. Stewart, J. B. Jeffries, J.-M. Zellweger, D. M. Golden, and D. F. McMillen. J. Phys. Chem. **93**, 3557 (1989).
4. Y. G. Lazarou and P. Papagiannakopoulos. J. Phys. Chem. **94**, 7114 (1990).
5. A. C. Gonzalez, C. W. Larson, D. F. McMillen, and D. M. Golden. J. Phys. Chem. **89**, 4809 (1985); W. Tsang, D. Robaugh, and W. G. Mallard. J. Phys. Chem. **90**, 5968 (1986).
6. M. J. S. Dewar, J. P. Ritchie, and J. Alster. J. Org. Chem. **50**, 1031 (1985).
7. D. A. Kleier and M. A. Lipton. J. Mol. Struct. **109**, 39 (1984); D. S. Marynick, A. K. Ray, J. L. Fry, and D. A. Kleirer. J. Mol. Struct. **108**, 45 (1984); D. S. Marynick, A. K. Ray, and J. L. Fry. Chem. Phys. Lett. **116**, 429 (1985); C. Chabalowski, P. C. Hariharan, J. J. Kaufman, and R. Buenker. Int. J. Quantum Chem. Symp. **17**, 643 (1983); J. J. Kaufman, P. C. Hariharan, C. Chabalowski, and M. Hotokka. Int. J. Quantum Chem. Symp. **19**, 221 (1986); S. Roszak and J. J. Kaufman. J. Chem. Phys. **94**, 6030 (1991); M. L. McKee. Chem. Phys. Lett. **164**, 520 (1989); M. L. McKee. J. Am. Chem. Soc. **107**, 1900 (1985).
8. M. L. McKee. J. Am. Chem. Soc. **108**, 5784 (1986).
9. R. P. Saxon and M. Yoshimine. J. Phys. Chem. **93**, 3130 (1989).
10. R. C. Mowrey, M. Page, G. F. Adams, and B. H. Lengsfield. J. Chem. Phys. *93*, 1857 (1990).
11. M. L. McKee. J. Phys. Chem. **93**, 7365 (1989).
12. B. M. Rice and D. L. Thompson. J. Chem. Phys. **93**, 7986 (1990).
13. M. Dupuis, J. J. Wendoloski, and D. Spangler. Natl. Res. Comput. Chem. Software Cat. **1**, QG01 (1980).
14. M. Page, P. Saxe, G. E. Adams, and B. H. Lengsfield III. J. Chem. Phys. **81**, 434 (1984).
15. B. H. Lengsfield III. J. Chem. Phys. **73**, 382 (1980); B. H. Lengsfield III and B. Liu. J. Chem. Phys. **75**, 478 (1981); B. Liu and M. Yoshimine. J. Chem. Phys. **74**, 612 (1981).
16. A. P. Cox and S. Waring. J. Chem. Soc. Faraday Trans. **2**, 1060 (1972).
17. P. H. Turner, M. J. Corkill and A. P. Cox. J. Phys. Chem. **83**, 1473 (1979).
18. B. J. van der Veken, R. Maas, G. A. Guirgis, H. D. Stidham, T. G. Sheehan, and J. R. During. J. Phys. Chem. **94**, 4029 (1990).
19. G. Herzberg. Molecular spectra and molecular structure. *In* Electronic spectra of polyatomic molecules. Vol. III. Van Nostrand, New York. 1966.
20. S. M. Colwell, R. D. Amos, and N. C. Handy. Chem. Phys. Lett. **109**, 525 (1984).
21. K. P. Huber and G. Herzberg. Molecular spectra and molecular structure. *In* Constants of diatomic molecules. Vol. IV. Van Nostrand, New York. 1979.
22. C. Trinquecoste, M. Rey-Lafon, and M.-T. Forel. Spectrochim. Acta, **30A**, 813 (1974).
23. F. L. Rook and M. E. Jacox. J. Mol. Spectrosc. **93**, 101 (1982).
24. M. E. Jacox. J. Phys. Chem. Ref. Data, **19**, 1387 (1990).
25. (*a*) J. B. Pedley, R. D. Naylor, and S. P. Kirby. Thermochemical data of organic compounds. Chapman and Hall, London. 1986; (*b*) L. Batt, J. P. Burrows, and G. N. Robinson. Chem. Phys. Lett. **78**, 467 (1981); (*c*) The JANAF thermochemical tables. 3rd ed. J. Phys. Chem. Ref. Data, Supplement No. 1. **14**, (1985).
26. G. P. Smith and D. M. Golden. Int. J. Chem. Kinet. **10**, 489 (1978); A. C. Baldwin and D. M. Golden. J. Phys. Chem. **82**, 644 (1978).

The application of an optimization technique to the development of universal basis sets

R. CUSTODIO[1] AND J. D. GODDARD[2]

Guelph–Waterloo Centre for Graduate Work in Chemistry, Department of Chemistry and Biochemistry, University of Guelph, Guelph, Ont., Canada N1G 2W1

AND

M. GIORDAN AND N. H. MORGON

Instituto de Química, Departamento de Físico-Química, Universidade Estadual de Campinas, Barão-Geraldo, 13081-Campinas, São Paulo, Brazil

Received August 19, 1991

This paper is dedicated to Professor Sigeru Huzinaga on the occasion of his 65th birthday

Can. J. Chem. Downloaded from www.nrcresearchpress.com by 92.62.229.171 on 09/08/12
For personal use only.

R. CUSTODIO, J. D. GODDARD, M. GIORDAN, and N. H. MORGON. Can. J. Chem. **70**, 580 (1992).

The Simplex method was used to define atomic and universal meshes using the integral discretization technique for the Griffin–Hill–Wheeler–Hartree–Fock equations. This technique represents a basis set as an exponential set of the form:

$$\alpha_i(k) = \exp[\Delta\Omega_o(k) + (i-1)\Delta\Omega(k)], \qquad i = 1, \ldots, N$$

For atoms, the minimum total energy criterion was employed. For the universal basis, three different procedures were tested: (*a*) defining the universal basis using information on the isolated atoms, (*b*) determining the universal $\Omega_0(k)$ through atomic calculations and reoptimizing the $\Delta\Omega(k)$ for different symmetries employing simultaneously a single atomic calculation as a reference point, and (*c*) optimizing the universal mesh using a statistical criterion such as the squares of the deviations of the total energy. The meshes obtained by the minimum total energy criterion or the squares of deviations of the total energy for the universal basis are accurate for the total energy but the weight functions are deficient in the valence region. Shifting the optimized $\Omega_0(k)$ to $\Omega_0'(k) = \Omega_0(k) - \Delta\Omega(k)$, fixing $\Omega_0'(k)$, and reoptimizing $\Delta\Omega(k)$ for each symmetry species produces a better description of weight functions at the expense of a less accurate total energy. In general, no significant statistical difference was observed for the various universal bases generated by procedures (*a*) and (*b*) or by (*c*) provided the shift correction was made to the latter. Application of these bases to diatomic molecules (N_2, CO, P_2, CS) showed that the universal bases are as accurate as those optimized for atomic systems. If the bases are transferred from atoms to molecules, the shift corrections to the weight functions of the atoms are not useful in molecular calculations. The almost equivalent molecular properties and the good total energies show that the best basis for molecular calculations is that optimized by procedure (*c*).

Key words: universal basis sets, integral discretization technique.

R. CUSTODIO, J. D. GODDARD, M. GIORDAN et N. H. MORGON. Can. J. Chem. **70**, 580 (1992).

On a fait appel à la méthode Simplex utilisant la technique de la discrétisation intégrale des équations de Griffin–Hill–Wheeler–Hartree–Fock pour définir des mailles atomiques et universelles. Cette technique représente un ensemble de base sous la forme d'un ensemble exponentiel de la forme :

$$\alpha_i(k) = \exp[\Delta\Omega(k) + (i-1)\Delta\Omega(k)], \qquad i = 1, \ldots, N$$

Pour les atomes, on a employé le critère de l'énergie totale minimale. Pour les bases universelles, on a vérifié trois méthodes différentes : (*a*) en définissant la base universelle à l'aide d'information sur des atomes isolés; (*b*) en déterminant un $\Omega_0(k)$ universel à l'aide de calculs atomiques et en réoptimisant le $\Delta\Omega(k)$ pour diverses symétries en employant simultanément un calcul atomique unique comme point de référence et (*c*) en optimisant la maille universelle à l'aide d'un critère statistique comme les carrés des déviations de l'énergie totale. Les mailles obtenues par le critère de l'énergie totale minimale ou par les carrés des déviations de l'énergie totale pour les bases universelles sont précises pour l'énergie totale; les fonctions pondérales présentent toutefois des déficiences dans la région de valence. En remplaçant $\Omega_0(k)$ par $\Omega_0'(k) = \Omega_0(k) - \Delta\Omega(k)$, puis en fixant $\Omega_0'(k)$ et en réoptimisant $\Delta\Omega(k)$ pour chaque espèce de symétrie, on obtient une meilleure description des fonctions pondérales au dépens d'une énergie totale moins précise. En général, on n'a observé aucune différence statistique importante pour les diverses bases universelles générées par les méthodes (*a*) et (*b*); c'est aussi le cas avec la méthode (*c*) à condition de faire une correction pour le déplacement. L'application de ces bases à des molécules diatomiques (N_2, CO, P_2 et CS) a permis de montrer que les bases universelles sont aussi précises que celles qui sont optimisées pour des systèmes atomiques. Lorsqu'on transfère des bases d'atomes à des molécules, les corrections de déplacement aux fonctions pondérales des atomes ne sont pas utiles dans les calculs moléculaires. Les propriétés moléculaires pratiquement équivalentes et les bonnes énergies totales montrent que le meilleur ensemble pour des calculs moléculaires est optimisé par la méthode (*c*).

Mots clés : bases universelles, technique de la discrétisation intégrale.

[Traduit par la rédaction]

1. Introduction

The possibility of creating universal bases for atomic systems (1–3) is an interesting development in basis set design. In addition, the universal basis for different atoms has

---

[1]Permanent address: Instituto de Química, Departamento de Físico-Química, Universidade Estadual de Campinas, Barão-Geraldo, 13081-Campinas, São Paulo, Brazil.

[2]Author to whom correspondence may be addressed.

Can. J. Chem. Downloaded from www.nrcresearchpress.com by 92.62.229.171 on 09/08/12
For personal use only.

some practical advantages with respect to conventional basis sets (4). The most important advantage is the transferability with little loss of accuracy of one- and two-electron integrals among different molecules with the same internuclear distances.

Two methods have been employed to create the universal basis: the even-tempered (ET) technique (1–5), and integral discretization (ID) of the Griffin–Hill–Wheeler–Hartree–Fock (GHWHF) equations (6, 7). These methods employ three parameters to define the universal basis for each symmetry function. The general form is

$$[1] \quad \alpha_i = x.y^{(i-1).z}, \qquad i = 1, \ldots, N$$

where N is the number of primitives in the mesh. For the ET method $z = 1$. For the ID technique $x = \exp(\Omega_0.A)$ and $y^{(i-1).z} = e^{[(i-1).\Delta\Omega.A]}$. N, Ω_0, $\Delta\Omega$, and A are referred to as the discretization parameters. The parameter "x" defines the first element of the mesh and "y" or "z" the distances among exponents. Both methods require that the parameter "x" must be small to ensure a wide range of exponents, while the parameter "y" (ET bases) or "z" (ID technique) must be sufficiently large to avoid linear dependencies. N must represent an almost complete set. The choice of these parameters in the ET method has been somewhat arbitrary (1–3). The ID technique employs an additional criterion through the GHWHF equations. These are a set of integral equations of the form:

$$[2] \quad \int[F(\alpha,\beta) - \varepsilon_i.S(\alpha,\beta)]f_i(\beta)d\beta = 0, \qquad i = 1, \ldots, n$$

where $F(\alpha,\beta)$ and $S(\alpha,\beta)$ are the Fock and overlap kernels, respectively. They are obtained by use of the one-electron functions as an integral transform:

$$[3] \quad \psi_i(1) = \int\phi_i(1,\alpha)f_i(\alpha)d\alpha$$

where ϕ_i and f_i are the generator and weight functions, respectively, and α the generator coordinate. The ID technique solves eq. [2] numerically employing the mesh defined by eq. [1]. This procedure searches for universal parameters through analysis of the weight functions by probe calculations (8–11). With N constant, the Hartree–Fock method is applied to different atoms to find the extreme cut-off points of the basis set. N and the value of $\Delta\Omega$ are then varied with these extreme exponents held constant to obtain a desired precision in the energy. $\Delta\Omega$ and N are considered interdependent.

In a recent paper (12), we adjusted the ID parameters for an s generator function for atomic systems containing two or four electrons and the H_2 molecule employing an optimization technique. The application of an optimization procedure systematizes the search for the discretization parameters. Our earlier application of the optimization procedure led us to test this technique for obtaining universal bases (12). The objective of this work is to test the applicability of an optimization technique to define the meshes with s and p generator functions for neutral, ground state atoms from He to Ar using the ID method. Analysis of the optimized meshes should establish systematic ways to search for atomic universal bases for the elements of the first and second period. An analysis of the transferability of the optimized meshes as well as the universal ones from atomic to diatomic calculations also is evaluated.

2. Computational methods

Optimization of the meshes was performed both for single atoms and for the universal basis for the neutral, ground state atoms He to Ar. s and p Gaussian generator functions were employed in these calculations. The ID definition of the mesh (eq. [1]) was applied in this work (6, 7). As discussed above, the original ID technique relabels the generator coordinate space α according to:

$$[4] \quad \Omega_i = \frac{\ln \alpha_i}{A}, \qquad A \geq 1$$

A previously was set to 6 (8–11). This parameter contracts the relabelled space and facilitates the detection of the cut-off points of the weight functions. Optimization eliminates the necessity of defining the A parameter. In this work, $A = 1$ was employed.

The individual bases or the universal ones were evaluated maintaining the number of s and p type functions constant at $(16s10p)$. The choice of $(16s10p)$ is based on the existence of a universal basis with this same number of Gaussians (9). The values of $\Omega_0(s)$, $\Delta\Omega(s)$, $\Omega_0(p)$, and $\Delta\Omega(p)$ were optimized simultaneously. For individual atoms, the minimum total energy criterion was adopted to define the best meshes. The optimum universal parameters were chosen to minimize the squares of the deviations of the calculated total energies with respect to the optimized $(16s10p)$ basis sets of this work.

The SIMPLEX method of Nelder and Mead (13) was chosen as the optimization procedure. The algorithm in ref. 14 was used to optimize $\Omega_0(k)$ and $\Delta\Omega(k)$. As in our previous work (12), different values of the starting simplex were tested. The initial values of $\Omega_0(k)$ and $\Delta\Omega(k)$ multiplied by 0.05 were adequate simplex parameters. Truncation of the overlap matrix ($\boldsymbol{S}$) was employed to eliminate problems with linear dependence (15, 16). A cut-off value of the eigenvalues of $\boldsymbol{S}$ was kept at 10^{-6}.

The SIMPLEX program requires that the decrease in the function value being minimized in the terminating step be fractionally smaller than a certain tolerance. Optimizing the basis sets for the individual atoms, the tolerance was set at 10^{-8}–10^{-9} to achieve accurate results. The definition of this parameter for the universal bases is more difficult to establish since the mimimum in the squares of the deviations of the total energies depends on the limiting energy values. One way to define the tolerance is to set it at a relatively high value (10^{-3}–10^{-4}), and then restart the calculation with the optimized simplex employing a smaller tolerance (0.1 or 0.01 of the previous parameter). The Hartree–Fock convergence criterion was maintained at 10^{-8} au.

3. Optimization for the atoms

The development of universal bases depends on the regularity of basis sets and presupposes a good knowledge of the meshes employed for the atoms. To obtain additional information on the individual atoms, this work initially analyses the applicability of the SIMPLEX method to define meshes using the ID technique. The characteristics of the optimized $(16s10p)$ basis set and their influence on atomic properties also are examined.

Table 1 shows the optimized data for the $(16s10p)$ meshes. The use of the optimized integral discretization technique (OID) provides very good energies when compared with the

Can. J. Chem. Downloaded from www.nrcresearchpress.com by 92.62.229.171 on 09/08/12
For personal use only.

TABLE 1. Optimized total energies and discretization parameters obtained employing the integral discretization (OID) technique for a (16s10p) Gaussian basis set. Energies are in atomic units

Atom	E	Ω_0	$\Delta\Omega$	ΔE^a	ΔE^b
He(^1S)	−2.8616795	−2.2111(s)	0.8175(s)	0.0000004	0.0000010
Li(^2S)	−7.4327169	−3.7066(s)	0.8875(s)	0.0000089	0.0000208
Be(^1S)	−14.573002	−3.1704(s)	0.8852(s)	0.000019	0.000045
B(^2P)	−24.529024	−2.7043(s)	0.8799(s)	0.000033	0.000082
		−2.9989(p)	0.8798(p)		
C(^3P)	−37.688558	−2.4227(s)	0.8810(s)	0.000054	0.000144
		−2.6691(p)	0.8856(p)		
N(^4S)	−54.400844	−2.1277(s)	0.8832(s)	0.000080	0.000228
		−2.3681(p)	0.8724(p)		
O(^3P)	−74.809272	−1.7781(s)	0.8786(s)	0.000098	0.000383
		−2.2682(p)	0.8667(p)		
F(^2P)	−99.409177	−1.4827(s)	0.8815(s)	0.000123	0.000437
		−2.0593(p)	0.8931(p)		
Ne(^1S)	−128.54687	−1.2673(s)	0.8892(s)	0.00018	0.00069
		−1.8392(p)	0.8787(p)		
Na(^2S)	−161.85776	−3.5342(s)	0.9653(s)	0.00114	0.00303
		−1.4105(p)	0.8740(p)		
Mg(^1S)	−199.61330	−3.1715(s)	0.9573(s)	0.00131	0.00332
		−1.5041(p)	0.8593(p)		
Al(^2P)	−241.87363	−2.7113(s)	0.9513(s)	0.00305	0.01079
		−2.9449(s)	0.9820(p)		
Si(^3P)	−288.85094	−2.4125(s)	0.9444(s)	0.00337	0.01225
		−2.6499(p)	0.9696(p)		
P(^4S)	−340.71488	−2.1816(s)	0.9376(s)	0.00381	0.01423
		−2.3937(p)	0.9588(p)		
S(^3P)	−397.50017	−1.9608(s)	0.9317(s)	0.00468	0.01832
		−2.2892(p)	0.9580(p)		
Cl(^2P)	−459.47651	−1.7644(s)	0.9265(s)	0.00536	0.02134
		−2.1133(p)	0.9528(p)		
Ar(^1S)	−526.81105	−1.5904(s)	0.9220(s)	0.00634	0.02477
		−1.9392(p)	0.9472(p)		

[a]The calculated total energies minus the total energies from ref. 17.
[b]Same as (a) substituting $\Omega_0(k)$ by $\Omega_0'(k) = \Omega_0(k) - \Delta\Omega(k)$.

accurate results of Clementi and Roetti (17). The fifth column in Table 1 shows that the error in the total energy for the first row elements is between 4×10^{-7} and 1.8×10^{-4} au and for the second row between 1.14×10^{-3} and 6.34×10^{-3} au. This is the greatest accuracy that can be obtained with a (16s10p) universal basis using the OID method. Obviously, to increase the precision of this universal basis a larger number of primitives as well as polarization functions are required. The possibility of the optimized bases being trapped in local minima has been examined. Independent of reasonable initial values of the discretization parameters, trapping in local minima can occur and some care is required to find the absolute minima.

The optimized discretization parameters depend strongly on the atomic species (see the third and fourth columns in Table 1). The plots of $\Omega_0(s)$ and $\Delta\Omega(s)$ vs. atomic number in Figs. 1(a) and 1(b) show that the discretization parameters depend on the occupation of the s and p sub-shells. In Fig. 1(a) the presence of one electron in the 2s orbital of Li drastically changes the value of $\Omega_0(s)$ with respect to the He parameter. The necessity of more diffuse primitives to describe adequately the 2s orbitals shifts the $\Omega_0(s)$ of Li to more negative values relative to He. On the other hand, Fig 1(b) shows $\Delta\Omega(s)$ increasing in magnitude to maintain a reasonable description of the inner shell of Li. Further changes in the nuclear charge and in the occupation of the p orbitals provide constant increments to $\Omega_0(s)$ up to Ne (Fig. 1(a)). The almost constant values of $\Delta\Omega(s)$ for these elements (Fig. 1(b)) show that the meshes are being shifted in the direction of the nucleus. Adding one electron to the 3s orbital diminishes $\Omega_0(s)$ (Fig. 1(a)) and the magnitude of $\Delta\Omega(s)$ increases (Fig. 1(b)). These two effects maintain an "equilibrium" between an adequate description of the 3s orbital and the inner shells.

Nevertheless, Fig. 1(a) shows nearly equivalent values of $\Omega_0(s)$ for different elements with the same valence electronic combination. Thus the same $\Omega_0(s)$ may be used for elements with the same electronic configuration. However, the $\Delta\Omega$ for the second row elements are very different from those for the first period. This difference in the $\Delta\Omega$ parameter governs the spacing between the exponents. Due to the number of inner orbitals and the greater nuclear charge for the second row elements, the meshes are more widely spaced than for the first row elements (Fig. 1(a)). Thus reasonable descriptions of the inner shells of the second row elements are retained. The differences between the calculated energies and Clementi and Roetti's values (17) in the fifth column of Table 1 indicate the need for larger bases for the

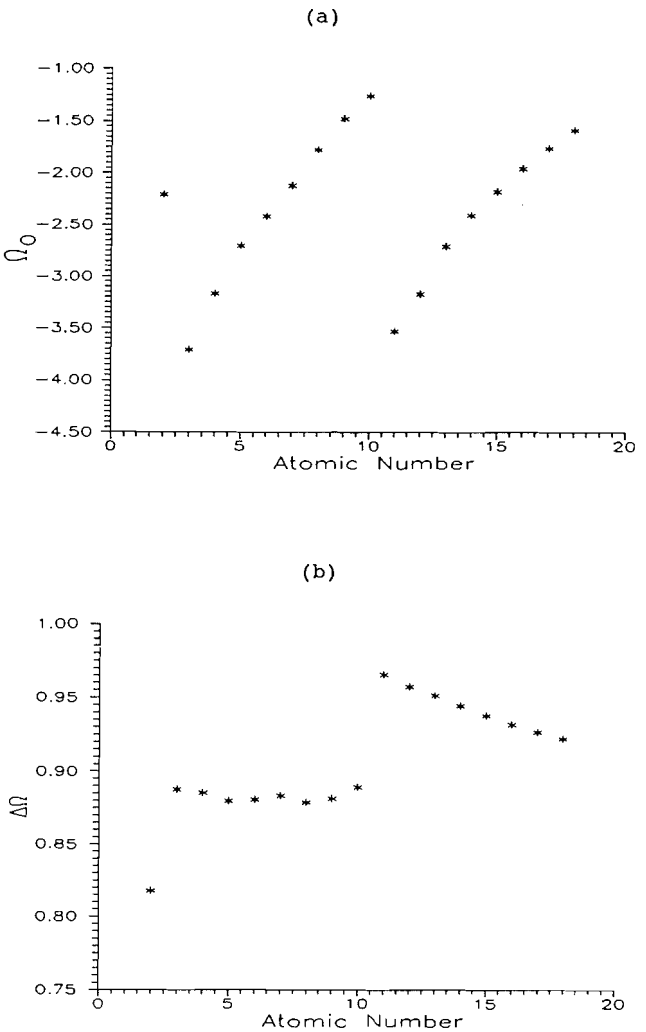

FIG. 1. Dependence of (*a*) $\Omega_0(s)$ and (*b*) $\Delta\Omega(s)$ with atomic number for the optimized (16*s*10*p*) basis sets.

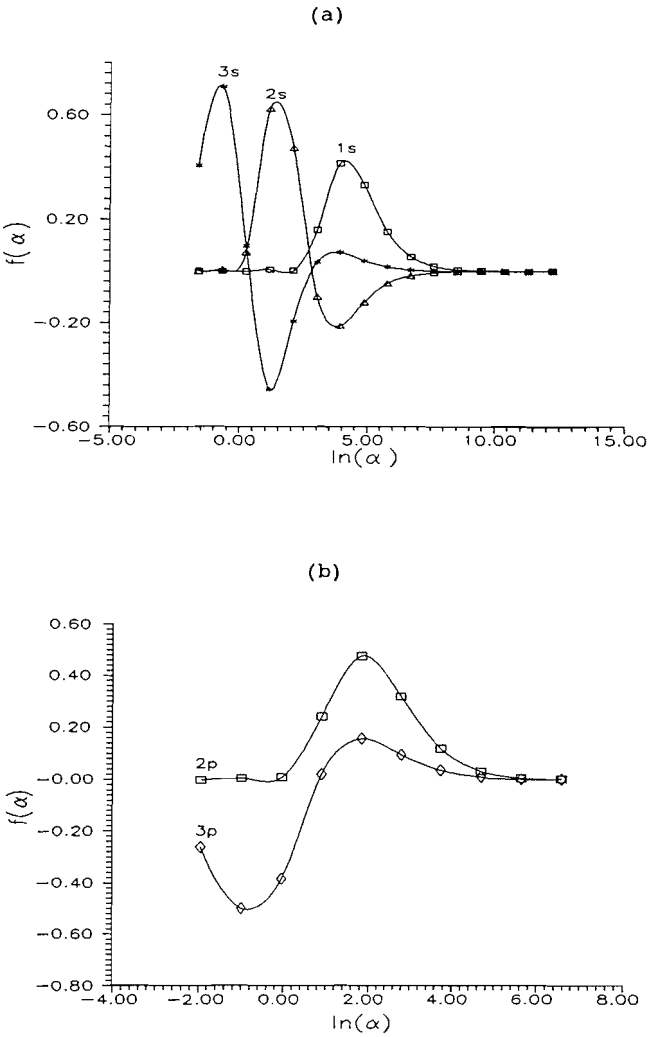

FIG. 2. The (*a*) *s* and (*b*) *p* weight functions for Ar obtained with the optimized (16*s*10*p*) basis set.

second row elements to reach a better precision in the total energy using OID. All these observations also hold for the *p* type functions.

The necessity of a good description of the weight function was stressed previously (6–11). Figures 2(*a*) and 2(*b*) show examples of the weight functions for the *s* and *p* atomic orbitals of Ar. The minimum energy criterion emphasizes the innermost region (more positive ln(α)). The primitives with small weight functions are more important in the minimization of the total energy than the outer Gaussians. All the inner orbitals in Ar have well-described weight functions in the sense that their coefficients are almost zero in that region. The outer functions require improvement for the 3*s* and 2*p* functions (Figs. 2(*a*) and 2(*b*)) since these outer orbitals do not have weight functions close to zero for the most negative value of ln(α). All the optimized meshes for the other atoms present the same behaviour. Figures 2(*a*) and 2(*b*) show that the description of the outer region can be improved after optimization if $\Omega_0(k)$ is changed by $\Omega_0'(k) = \Omega_0(k) - \Delta\Omega(k)$. Thus a better representation of the outer *s* and *p* type functions is obtained. However, the total energies increase, as shown in the sixth column in Table 1. The ΔE are a factor of 3.91 to 2.5 times larger. An improvement is possible if, after shifting $\Omega_0'(k)$, this parameter is maintained constant and $\Delta\Omega(k)$ is reoptimized. In this way, a more reasonable balance between the cutoff of the weight functions and the minimum energy criterion is obtained. Table 2 shows the improvement in the total energies after shifting the mesh and the reoptimized $\Delta\Omega(k)$. The ratios of the ΔE values of Table 2 to those of Table 1 on an atom by atom basis are now between 2.54 and 1.76.

Are the meshes adjusted by the last procedure improving other atomic properties? For Table 3, the orbital energies ε_i, $\langle p^n \rangle$, and $\langle r^n \rangle$, where $n = -2, -1, 1, 2, 3$, and 4, for the Ar atom were calculated. In the second column (SLT) are the results obtained with Clementi's accurate Slater basis functions (17), in the third column (AT1) the optimized (16*s*10*p*) Gaussian mesh data, and in the last column the results fixing $\Omega_0'(k)$ and reoptimizing $\Delta\Omega(k)$(AT2). The orbital energies and the $\langle r^n \rangle$ properties of the last column show a better correlation with Clementi's results (17) than those obtained with the optimized meshes. The opposite is concluded for $\langle p^n \rangle$. The sensitivity of $\langle p^n \rangle$ to small changes near the nuclei and the fixing of $\Omega_0'(k)$ far from the nucleus explains this trend. More detailed analysis shows that even the $\langle p^n \rangle$ properties calculated by the translated meshes and reoptimiza-

Can. J. Chem. Downloaded from www.nrcresearchpress.com by 92.62.229.171 on 09/08/12
For personal use only.

TABLE 2. Total energies and discretization parameters obtained by the substitution of $\Omega_0(k)$ by $\Omega_0'(k) = \Omega_0(k) - \Delta\Omega(k)$, fixing $\Omega_0'(k)$ and reoptimizing $\Delta\Omega'(k)$ for a $(16s10p)$ Gaussian basis set. Energies are in atomic units

Atom	E	$\Omega_0'^{a}$	$\Delta\Omega'$	ΔE^{b}
He(^1S)	−2.8616791	−3.0286(s)	0.8436(s)	0.0000008
Li(^2S)	−7.4327081	−4.5941(s)	0.9169(s)	0.0000176
Be(^1S)	−14.572986	−4.0556(s)	0.9196(s)	0.000035
B(^2P)	−24.528995	−3.5842(s)	0.9192(s)	0.000062
		−3.8787(p)	0.9029(p)	
C(^3P)	−37.688501	−3.3037(s)	0.9212(s)	0.000111
		−3.5547(p)	0.9139(p)	
N(^4S)	−54.400752	−3.0109(s)	0.9173(s)	0.000172
		−3.2405(p)	0.9192(p)	
O(^3P)	−74.809139	−2.6567(s)	0.9158(s)	0.000231
		−3.1349(p)	0.9351(p)	
F(^2P)	−99.408988	−2.3642(s)	0.9142(s)	0.000312
		−2.9524(p)	0.9404(p)	
Ne(^1S)	−128.54661	−2.1565(s)	0.9129(s)	0.00044
		−2.7179(p)	0.9409(p)	
Na(^2S)	−161.85666	−4.4995(s)	1.0107(s)	0.00224
		−2.2844(p)	0.9228(p)	
Mg(^1S)	−199.61223	−4.1289(s)	1.0067(s)	0.00238
		−1.9135(p)	0.9097(p)	
Al(^2P)	−241.87036	−3.6626(s)	0.9885(s)	0.00632
		−3.9269(p)	1.0497(p)	
Si(^3P)	−288.84704	−3.3569(s)	0.9782(s)	0.00727
		−3.6195(p)	1.0354(p)	
P(^4S)	−340.71023	−3.1192(s)	0.9711(s)	0.00846
		−3.3525(p)	1.0243(p)	
S(^3P)	−397.49396	−2.8925(s)	0.9640(s)	0.01089
		−3.2472(p)	1.0211(p)	
Cl(^2P)	−459.46916	−2.6909(s)	0.9602(s)	0.01271
		−3.0661(p)	1.0152(p)	
Ar(^1S)	−526.81105	−2.5124(s)	0.9550(s)	0.01486
		−2.8864(p)	1.0088(p)	

[a]$\Omega_0'(k) = \Omega_0(k) - \Delta\Omega(k)$, where $\Omega_0(k)$ and $\Delta\Omega(k)$ are the optimized parameters of Table 1.

[b]The calculated total energies minus the total energies from ref. 17.

tion of $\Delta\Omega(k)$ are in general closer to Clementi's results than those obtained with the optimized meshes.

Since atomic properties have significant differences in magnitude, some preprocessing of the data is needed before any general analysis. The atomic properties are renormalized with respect to Clementi's results (17). The sum of the squares of the deviations of the renormalized properties with respect to Clementi's data are taken as measures of the correlation between the models. Table 4 shows a generally better description of the electronic structure when the meshes are shifted to $\Omega_0'(k)$ and the $\Delta\Omega(k)$ are reoptimized. The $\langle p'' \rangle$ also show an improvement employing this method. The loss in accuracy in the total energy due to the shift of $\Omega_0'(k)$ and reoptimization of $\Delta\Omega(k)$ is compensated for by this improvement in other properties.

4. The universal bases

Three procedures were studied to obtain the universal bases (UBn): (*i*) the use of the optimized atomic meshes, (*ii*) the choice of selected parameters from these meshes (1) with reoptimization of the universal mesh employing a single atom as reference, or (*iii*) determining a mesh for a set of atoms simultaneously. With procedures (*i*) and (*ii*), the discussion above shows that there are two adequate meshes. The first is optimized based on the minimum energy criterion (Table 1) and the second involves substitution of the previously optimized $\Omega_0(k)$ for the s and p symmetry functions by $\Omega_0'(k) = \Omega_0(k) - \Delta\Omega(k)$, then fixing $\Omega_0'(k)$ and reoptimizing the $\Delta\Omega(k)$ parameter for each symmetry species simultaneously (Table 2).

The universal $\Omega_0(k)$ and $\Delta\Omega(k)$ must adequately cover the space of the generator functions for all atoms. In this sense, $\Omega_0(k)$ can easily be chosen as the most negative parameter in either Table 1 or Table 2. For the atoms studied the best choices for $\Omega_0(s)$ and $\Omega_0(p)$ are the values for Li and B that possess the most diffuse basis functions. The choice of $\Delta\Omega(k)$ for the s and p meshes requires knowledge of the magnitude of the largest exponent among all the atoms. Employing the equation, $\Omega_f(k) = \Omega_0(k) + (N_k - 1) \cdot \Delta\Omega(k)$, the largest s and p exponents of the atoms can be evaluated. In either Table 1 or Table 2 the Ar atom can be used for the s and p type functions. The most negative $\Omega_0(k)$ and the greatest $\Omega_f(k)$ provide an adequate representation of the weight functions for the atoms covered by this universal basis. The universal $\Delta\Omega$ for each symmetry species can be obtained through: $\Delta\Omega(k) = (\Omega_f^{\max.}(k) - \Omega_0^{\min.}(k))/(N_k - 1)$.

The second (UB1) and third (UB2) columns of Table 5 show the universal parameters using the data from Tables 1

Can. J. Chem. Downloaded from www.nrcresearchpress.com by 92.62.229.171 on 09/08/12
For personal use only.

Can. J. Chem. Downloaded from www.nrcresearchpress.com by 92.62.229.171 on 09/08/12
For personal use only.

TABLE 3. Ar (^1S) atomic properties calculated using accurate Slater basis functions (SLT), the optimized ($16s10p$) Gaussian mesh (AT1), and the ($16s10p$) Gaussian mesh using $\Omega_0'(k)$ and reoptimizing $\Delta\Omega(k)$ (AT2). Data are in atomic units

	SLT[a]	AT1	AT2
		Orbital energies	
$1s$	−118.610390	−118.608369	−118.614973
$2s$	−12.322187	−12.320150	−12.323909
$3s$	−1.277346	−1.275814	−1.277601
$2p$	−9.571502	−9.569238	−9.570398
$3p$	−0.591022	−0.589503	−0.590975
		$\langle p^n \rangle$	
$\langle p^{-2} \rangle$	$1.31065.10^1$	$1.28537.10^1$	$1.31091.10^1$
$\langle p^{-1} \rangle$	$1.01277.10^1$	$1.00788.10^1$	$1.01280.10^1$
$\langle p^1 \rangle$	$8.86994.10^1$	$8.87101.10^1$	$8.86874.10^1$
$\langle p^2 \rangle$	$1.05363.10^3$	$1.05362.10^3$	$1.05339.10^3$
$\langle p^3 \rangle$	$2.43507.10^4$	$2.43440.10^4$	$2.43324.10^4$
$\langle p^4 \rangle$	$1.13929.10^6$	$1.11715.10^6$	$1.11124.10^6$
		$\langle r^n \rangle$	
$\langle r^{-2} \rangle$	$1.46502.10^3$	$1.64520.10^3$	$1.46404.10^3$
$\langle r^{-1} \rangle$	$6.97252.10^1$	$6.97262.10^1$	$6.97153.10^1$
$\langle r^1 \rangle$	$1.60709.10^1$	$1.60512.10^1$	$1.60730.10^1$
$\langle r^2 \rangle$	$2.60352.10^1$	$2.58888.10^1$	$2.60408.10^1$
$\langle r^3 \rangle$	$5.60095.10^1$	$5.51153.10^1$	$5.60032.10^1$
$\langle r^4 \rangle$	$1.45106.10^2$	$1.39778.10^2$	$1.44771.10^2$

[a]Calculated with the Slater basis set of ref. 17.

and 2, respectively, and the statistical data for the atomic properties. The universal basis obtained using the data from Table 2 (UB2) produces a reasonable improvement in $\langle r^n \rangle$ at the expense of all other properties. The mesh that represents correctly the initial and final cutoffs of the weight functions for all the atoms is basis UB2. Table 5 shows that the UB1 mesh with a smaller $\Delta\Omega(k)$ produces a more reasonable description of the orbital energies ε_i, $\langle p^n \rangle$, and total energies. However, the inadequate representation of the weight functions for some atoms causes the inferior statistics for $\langle r^n \rangle$ with UB1.

TABLE 4. Averages of the squares of the deviations of the normalized atomic properties with the results of Clementi and Roetti (17) for He to Ar using the ($16s10p$) optimized Gaussian meshes (AT1), and fixing $\Omega_0'(k)$ and reoptimizing $\Delta\Omega(k)$ (AT2). Data are in atomic units

	AT1	AT2
ε_i^a	5.661×10^{-7}	9.680×10^{-9}
$\langle p^n \rangle^b$	5.425×10^{-5}	4.609×10^{-5}
$\langle r^n \rangle^b$	1.385×10^{-4}	1.781×10^{-6}
E^c	3.969×10^{-6}	1.013×10^{-5}

[a]Orbital energy.
[b]$n = -2, -1, 1, 2, 3, 4$.
[c]Total energy.

Further attempts to improve these universal meshes through optimization were made. The simplest possibility is to fix the $\Omega_0(k)$ parameters of UB1 and UB2 and to reoptimize $\Delta\Omega(k)$ to look for the most contracted Gaussians. For these most contracted primitives it is possible to use one atom that provides a good description of these Gaussians. Thus, it is possible to define the universal basis applying the optimization procedure to a single atom. That possibility was tested using the $\Omega_0(k)$ from UB1 and UB2 with Ar as the reference. The fourth (UB3) and fifth (UB4) columns in Table 5 present the meshes obtained and the statistical results for the properties for all the atoms with these meshes. The use of the minimum energy criterion has improved the total energy as well as the $\langle r^n \rangle$ properties for UB3 and UB4 by decreasing the range of the meshes (Table 5) when compared with UB1 and UB2, respectively. Because this decrease in the range of the meshes was at the expense of the large exponents, the quality of the $\langle p^n \rangle$ properties diminished. Thus, the optimization procedure with reference to only one atom can yield bases similar in quality to those determined using all atoms as UB1 and UB2 universal basis set.

A more general procedure to optimize universal bases involves minimization of a statistical property for a set of the atoms as suggested by Mezey (5). This possibility was verified by minimizing the sum of the squares of the deviations of the total energy. The optimized energies for the atoms from

TABLE 5. ($16s10p$) universal bases (UBn) and the averages of the squares of the deviations of the normalized atomic properties with the results of Clementi and Roetti (17) for He to Ar. Data are in atomic units

	UB1[a]	UB2[b]	UB3[c]	UB4[d]
$\Omega_0(s)$	−3.7066	−4.5941	−3.7066	−4.5941
$\Omega_0(p)$	−2.9989	−3.9269	−2.9989	−3.9269
$\Delta\Omega(s)$	1.0630	1.0939	1.0022	1.0467
$\Delta\Omega(p)$	1.0649	1.1108	1.0153	1.0904
ε_i^e	4.038×10^{-8}	4.172×10^{-8}	4.049×10^{-8}	2.420×10^{-8}
$\langle p^n \rangle^f$	1.847×10^{-5}	2.234×10^{-5}	3.587×10^{-5}	4.309×10^{-5}
$\langle r^n \rangle^f$	3.672×10^{-5}	4.850×10^{-6}	2.609×10^{-5}	3.111×10^{-6}
E^g	2.000×10^{-5}	3.428×10^{-5}	1.083×10^{-5}	2.373×10^{-5}

[a]Obtained using the optimized meshes in Table 1.
[b]Obtained using the meshes of Table 2.
[c]Same as (a), fixing $\Omega_0(k)$ and reoptimizing $\Delta\Omega(k)$ using Ar as a reference.
[d]Same as (b), fixing $\Omega_0(k)$ and reoptimizing $\Delta\Omega(k)$ using Ar as a reference.
[e]Orbital energy.
[f]$n = -2, -1, 1, 2, 3, 4$.
[g]Total energy.

TABLE 6. (16s10p) universal bases (UBn) and the average of the squares of the deviations of the normalized atomic properties with respect to the results of Clementi and Roetti (17) for He to Ar. Data are in atomic units

	UB5[a]	CTMUB[b]	UB6[c]	UB7[d]
$\Omega_0(s)$	−3.3195	−3.30	−4.2941	−4.2731
$\Omega_0(p)$	−2.4956	−2.40	−3.4863	−3.4934
$\Delta\Omega(s)$	0.9746	0.96	1.0156	1.0162
$\Delta\Omega(p)$	0.9908	0.96	1.0499	1.0562
ε_i^e	5.182×10^{-6}	1.033×10^{-5}	1.224×10^{-8}	1.386×10^{-8}
$\langle p^n \rangle^f$	1.289×10^{-4}	1.555×10^{-4}	5.052×10^{-5}	4.915×10^{-5}
$\langle r^n \rangle^f$	8.675×10^{-4}	1.210×10^{-3}	4.435×10^{-6}	4.761×10^{-6}
E^g	8.806×10^{-6}	9.053×10^{-6}	1.592×10^{-5}	1.619×10^{-5}

[a]Optimized minimizing the sum of the squares of the deviations of the total energy of all the atoms.
[b]Universal basis from ref. 9.
[c]Same as (*a*), fixing $\Omega_0(k)$ and reoptimizing $\Delta\Omega(k)$.
[d]Same as (*c*) using the {Li,B,Ne,Na,Al,Ar} reference set.
[e]Orbital energy.
[f]$n = -2, -1, 1, 2, 3, 4$.
[g]Total energy.

this work (Table 1) were taken as references. The second column in Table 6 represents the (16s10p) optimized universal basis (UB5) as well as the statistical information. There is a considerable difference in these discretization parameters from those presented in Table 5. The statistical information for UB5 in Table 6 shows a considerable improvement in the total energy. The total energy of Ar is the poorest and is 0.00721 au higher than the optimized value in Table 1. However, using the minimum of the squares of the deviations of the total energy as a criterion, the range for the meshes decreases, thus producing a poorer description of other atomic properties. The discretization parameters of this UB5 are very similar to those of the (16s10p) universal basis of da Costa, Trsic, and Mohallem (9) (CTMUB). Results with this basis are given in the third column of Table 6. Although the discretization parameters are almost identical for both methods, the optimized universal parameters of this work produce slightly better statistical results. The differences between the normalized total energies employing UB5 from this work and CTMUB of da Costa *et al.* are on the order of 10^{-5} hartree.

UB5 in Table 6 was obtained looking for the best total energies by minimizing the squares of the deviations of the total energy with respect to the optimized energy (Table 1). The small values of $\Omega_0(k)$ when compared with those of Table 5 suggest that this mesh can be improved for other properties using the technique discussed previously: change $\Omega_0(k)$ by $\Omega_0'(k) = \Omega_0(k) - \Delta\Omega(k)$, then fix $\Omega_0'(k)$ and reoptimize $\Delta\Omega(k)$. This universal basis (UB6) and the statistical results are given in the fourth column of Table 6. Comparing with the results of UB5, a significant improvement in the atomic properties was obtained without a great loss in total energy. UB6 in Table 6 provides the smallest sum of the squares of the deviations of the orbital energies and $\langle r^n \rangle$ of all the bases studied. The magnitude of the $\Omega_0(k)$ parameters for UB6 is close to reasonable cutoffs of the weight functions, as can be seen by comparing Table 6 with Tables 2 or 5. The accuracy of the total energies for this universal basis is poorer only in comparison with UB3 (Table 5) and UB5 and CTMUB (Table 6).

Although all atoms were used to define the sum of the squares of the deviations, a smaller set could be employed. A reasonable choice uses the atoms that have the most diffuse Gaussians as well as the most contracted ones for each period. For the set of atoms studied, the family {Li,B,Ne,Na,Al,Ar} yields the following mesh:

$$\Omega_0(s) = -3.2995 \qquad \Omega_0(p) = -2.4991$$

$$\Delta\Omega(s) = 0.9736 \qquad \Delta\Omega(p) = 0.9943$$

which is close to the values of the optimized universal basis (UB5 in Table 6). This mesh does not provide good atomic properties overall, and, thus, the $\Omega_0(k)$ were shifted by $\Omega_0'(k) = \Omega_0(k) - \Delta\Omega(k)$, $\Omega_0'(k)$ fixed, and the $\Delta\Omega(k)$ reoptimized. The fifth column (UB7) in Table 6 shows that this mesh is almost equivalent to that obtained including all atoms.

Three different procedures were applied to generate universal bases in atomic systems. Eight universal bases were generated for the atoms He to Ar. The choice of the best method can be done statistically, for example, using the Manhattan (city block) distance (18, 19) with respect to the Clementi–Roetti results (17). Taking all the properties calculated for all the atoms with all the bases in Tables 5 and 6, employing an autoscaling to remove the weighting that arises due to different units, and measuring the Manhattan distance from the Clementi–Roetti results indicates that the best bases are UB3, UB1, and UB6. However, the information in Tables 5 and 6 shows that there are no large statistical differences, except for UB5 and CTMUB, which were optimized considering exclusively the minimum energy criterion. The UB5 energy-optimized set could be modified by the inclusion of other atomic properties in the least-squares procedure, thus increasing the similarity of this basis to the others.

5. Applications to molecular systems

The bases discussed above attempt to improve the wavefunction such that good total energies and other atomic properties can be obtained simultaneously. A natural extension of this work is to evaluate the effect of these corrections in molecular systems. Calculations for N_2, CO, P_2, and CS were performed with two atom-optimized bases (AT1 and

Can. J. Chem. Downloaded from www.nrcresearchpress.com by 92.62.229.171 on 09/08/12
For personal use only.

TABLE 7. Molecular properties calculated with different (16s10p) bases for N_2, P_2, CO, and CS at the equilibrium geometry. Data in atomic units

	AT1	AT2	UB5	UB6	Hartree–Fock accurate
			Total energy		
N_2	−108.9101	−108.9095	−108.9083	−108.9082	−108.9939[a]
P_2	−681.4080	−681.4003	−681.4047	−681.3914	−681.5004[b]
CO	−112.7169	−112.7167	−112.7155	−112.7154	−112.7910[a]
CS	−435.2844	−435.2778	−435.2806	−435.2689	−435.7949[c]
			Bond length		
N_2	2.0458	2.0477	2.0492	2.0509	2.068[a]
P_2	3.6663	3.6653	3.6697	3.6706	3.497[b]
CO	2.1197	2.1208	2.1237	2.1239	2.132[a]
CS	2.9523	2.9570	2.9478	2.9548	2.906[c]
			Dipole moment		
CO	−0.1982	−0.1992	−0.2013	−0.2020	−0.104[a]
CS	0.3621	0.3515	0.3624	0.3547	0.902[c]
			Second moment		
N_2: $\langle x^2 \rangle$	−10.27804	−10.29750	−10.29964	−10.30894	
N_2: $\langle z^2 \rangle$	−12.66858	−12.67186	−12.67123	−12.66625	
P_2: $\langle x^2 \rangle$	−26.71693	−27.03795	−26.97925	−27.04992	
P_2: $\langle z^2 \rangle$	−29.38439	−29.66829	−29.51028	−29.66180	
CO: $\langle x^2 \rangle$	−10.16617	−10.17710	−10.18096	−10.18705	
CO: $\langle z^2 \rangle$	−13.16742	−13.16330	−13.16538	−13.15905	
CS: $\langle x^2 \rangle$	−18.67595	−18.75038	−18.71621	−18.74954	−18.25879[c]
CS: $\langle z^2 \rangle$	−22.09739	−22.14284	−22.13654	−22.15637	−21.02941[c]
			Electric field		
N_2: $\boldsymbol{E}_N$	0.14872	0.14884	0.14904	0.14711	
P_2: $\boldsymbol{E}_P$	0.05944	0.05861	0.05856	0.05850	
CO: $\boldsymbol{E}_C$	−0.09357	−0.09284	−0.09308	−0.09188	
CO: $\boldsymbol{E}_O$	0.17687	0.17733	0.17677	0.17559	
CS: $\boldsymbol{E}_C$	−0.07649	−0.07632	−0.07722	−0.07783	
CS: $\boldsymbol{E}_S$	0.07649	0.06617	0.06630	0.06805	
			Potential		
N_2: $\langle 1/r \rangle_N$	−18.24958	−18.24864	−18.24796	−18.24738	
P_2: $\langle 1/r \rangle_P$	−54.11066	−54.10501	−54.10662	−54.10352	
CO: $\langle 1/r \rangle_C$	−14.61680	−14.61631	−14.61520	−14.61527	
CO: $\langle 1/r \rangle_O$	−22.22985	−22.22958	−22.22924	−22.22899	
CS: $\langle 1/r \rangle_C$	−14.61063	−14.60908	−14.61047	−14.60882	−14.70994[c]
CS: $\langle 1/r \rangle_S$	−59.16101	−59.15745	−59.15949	−59.15570	−59.17182[c]

[a]Reference 20. Experimental equilibrium geometry.
[b]Reference 21. Theoretical equilibrium geometry.
[c]Calculated at the 6-311G (2df) MP2 level with Gaussian 90 (22). Theoretical equilibrium geometry.

AT2 of Tables 1 and 2) and with two universal ones (UB5 and UB6 of Table 6). The choice of these two universal bases was made considering that UB5 presents the worst results for atomic properties and good total energies, while UB6 was corrected to improve the atomic properties and to provide reasonable total energies. No contraction of the bases was employed to preserve the character of the numerical integration of eq. [2]. Table 7 presents the results of some molecular properties.

There is great similarity among the results obtained with the four bases. The universal bases provide results that are as accurate as the optimized ones independent of the property being analyzed. The correction of the weight functions for atomic systems does not produce significant changes in the molecular systems using either the optimized bases or the universal ones. Figure 3 shows that, in a molecule, bases optimized with respect to the total energy are deficient in their description of the weight function in the diffuse region. However, the nearly equivalent molecular properties calculated with different bases show that the best set for molecular calculations is UB5, which also gives the best energy.

The relatively large size of the bases may be responsible for the nearly equivalent results in Table 7. The incorrect magnitudes of the electric fields at the nuclei suggest that the deficiencies in the bases probably are due to the absence of polarization functions.

6. Conclusions

The SIMPLEX method defined the meshes of the s and p generator functions for the discretized version of the Griffin–Hill–Wheeler–Hartree–Fock equations. Analysis of the optimized basis sets showed that the meshes obtained through the minimum total energy criterion are accurate with respect to the total energy but deficient in the valence region. This deficiency leads to a poor description of other atomic properties such as orbital energies, $\langle r^n \rangle$ and $\langle p^n \rangle$. Changing

Can. J. Chem. Downloaded from www.nrcresearchpress.com by 92.62.229.171 on 09/08/12
For personal use only.

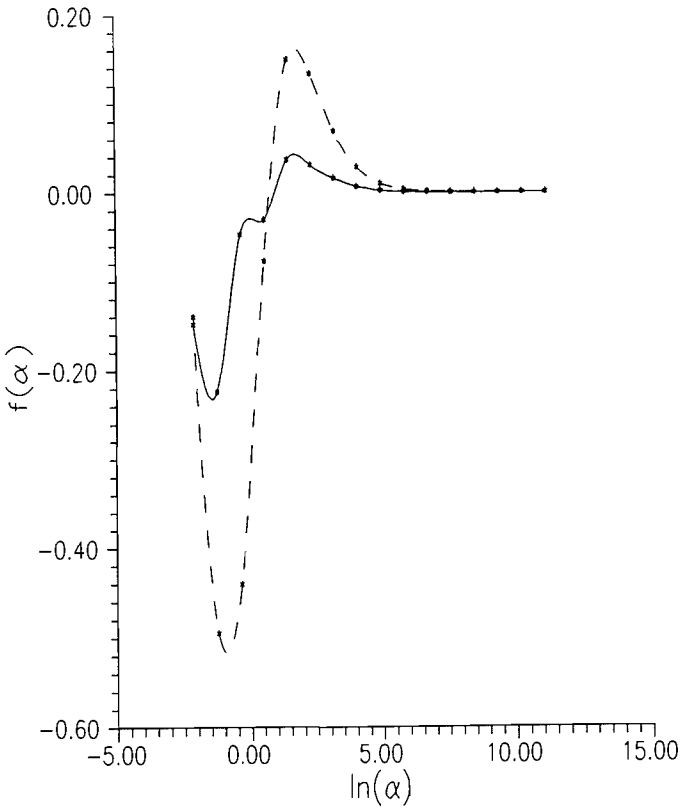

FIG. 3. The *s* weight function (dashed line) and the *p* weight function of the $3\sigma_g$ orbital for one nitrogen atom in the N_2 molecule obtained with the AT1 basis at the theoretical equilibrium bond length (continuous line).

the parameters $\Omega_0(k)$ to $\Omega_0'(k) = \Omega_0(k) - \Delta\Omega(k)$, fixing $\Omega_0'(k)$, and reoptimizing $\Delta\Omega(k)$ for each symmetry species simultaneously produces a better general description of the atomic properties at the expense of a somewhat poorer energy. Methods that maintain a good description of the weight function in both the outer and inner regions are needed.

Three different procedures were explored to obtain universal bases: (*a*) defining the universal basis using information from the isolated atoms, (*b*) defining the universal $\Omega_0(k)$ through atomic calculations and reoptimizing the $\Delta\Omega(k)$ for the different symmetries simultaneously with a single atom calculation as a reference, and (*c*) optimizing the universal mesh using statistical criteria such as the sum of the squares of the deviations of the total energy.

The universal bases generated by these procedures are almost equivalent statistically except for the basis obtained employing method (*c*). If the universal mesh is optimized with respect to the minimum deviation in the total energies, the mesh will yield a poor description of the weight function for a set of atoms. Changing $\Omega_0(k)$ to $\Omega_0'(k) = \Omega_0(k) - \Delta\Omega(k)$ and further reoptimization of $\Delta\Omega(k)$ improves the mesh and produces results statistically close to the other bases.

Applications of the atom-optimized and universal bases to diatomic molecules (N_2, CO, P_2, CS) show that the universal bases are as accurate as the atom-optimized ones. Bases AT1 and UB5 are deficient in the descriptions of the weight functions in the valence region. However, the shift corrections in the weight functions that improve the atomic properties are not useful in the molecular calculations when the bases are transferred from the atoms to a molecule. The bases yield nearly equivalent molecular properties. The important requirement of good total energies shows that the best basis for molecular calculations is that optimized by procedure (*c*), that is UB5.

7. Acknowledgements

We acknowledge financial support from NSERC (Canadian Agency), and from FAPESP and CNPq (Brazilian Agencies). We are grateful to J. R. Mohallem, H. F. M. da Costa, and M. Trsic for useful conservations on the discretized version of the GHWHF equations.

1. D. M. Silver, S. Wilson, and W. C. Nieuwport. Int. J. Quantum Chem. **14**, 635 (1978).
2. D. M. Silver and W. C. Nieuwport. Chem. Phys. Lett. **57**, 421 (1978).
3. D. M. Silver and S. Wilson. J. Chem. Phys. **69**, 3787 (1978).
4. S. Wilson. Adv. Chem. Phys. **67**, 440 (1987).
5. P. G. Mezey. Theor. Chim. Acta (Berlin) **53**, 183 (1979).
6. J. R. Mohallem. Z. Phys. D: At. Mol. Clusters, **3**, 339 (1986).
7. J. R. Mohallem, R. M. Dreizler, and M. Trsic. Int. J. Quantum Chem. **20**, 45 (1986).
8. J. R. Mohallem and M. Trsic. J. Chem. Phys. **86**, 5043 (1987).
9. H. F. M. da Costa, M. Trsic, and J. R. Mohallem. Mol. Phys. **62**, 91 (1987).
10. A. B. F. da Silva, H. F. M. da Costa, M. Trsic, and J. R. Mohallem. Mol. Phys. **68**, 433 (1989).
11. H. F. M. da Costa, A. B. F. da Silva, M. Trsic, A. M. Simas, and A. J. A. Aquino. J. Mol. Struct. (THEOCHEM), **210**, 63 (1990).
12. R. Custodio, M. Giordan, N. H. Morgan, and J. D. Goddard. Int. J. Quantum Chem. In press.
13. J. A. Nelder and R. Mead. Comput. J. **7**, 308 (1965).
14. W. T. Vetterling, S. A. Teukolsky, W. H. Press, and B. P. Flannery. Numerical recipes: The art of scientific computing. Cambridge University Press, London. 1985.
15. J. G. R. Tostes and T. Pizza. Phys. Rev. A, **28**, 538 (1983).
16. P. Chattopadyay, R. M. Dreizler, M. Trsic, and M. Fink. Z. Phys. A: At. Nucl. **285**, 7 (1978).
17. E. Clementi and C. Roetti. At. Data Nucl. Data Tables, **14**, 177 (1974).
18. M. A. Sharaf, D. L. Illman, and B. Kowalski. Chemometrics. John Wiley & Sons, New York. 1986. p. 179.
19. B. R. Kowalski and C. F. Bender. J. Am. Chem. Soc. **94**, 5632 (1972).
20. P. A. Christiansen and E. A. McCullough, Jr. J. Chem. Phys. **67**, 1877 (1977).
21. R. S. Mulliken and B. Liu. J. Am. Chem. Soc. **93**, 6738 (1971).
22. GAUSSIAN90. Revision F. M. J. Frisch, M. Head-Gordon, G. W. Trucks *et al.*, GAUSSIAN, Inc., Pittsburgh, PA. 1990.

Can. J. Chem. Downloaded from www.nrcresearchpress.com by 92.62.229.171 on 09/08/12
For personal use only.

Computational studies on hydrates of alkaline-earth dications

MARIUSZ KLOBUKOWSKI
Department of Chemistry, University of Alberta, Edmonton, Alta., Canada T6G 2G2

Received August 9, 1991

This paper is dedicated to Professor Sigeru Huzinaga on the occasion of his 65th birthday

MARIUSZ KLOBUKOWSKI. Can. J. Chem. **70**, 589 (1992).

SCF and Møller–Plesset calculations were done for the hydrated alkaline-earth ions in the gas phase. The systems studied were $M^{2+}(H_2O)_n$, where M = Mg, Ca, and Sr, and n = 1, 2, 3, 4, and 6. The successive ion–water bond energies were in the range anticipated on the basis of extrapolation of results from experimental studies on larger hydrates.

Key words: hydrates, alkaline-earth cations, quantum-chemical calculations.

MARIUSZ KLOBUKOWSKI. Can. J. Chem. **70**, 589 (1992).

On a effectué des calculs SCF et des calculs de Møller–Plesset sur les ions hydratés de métaux alcalino-terreux en phase gazeuse. On a étudié les systèmes $M^{2+}(H_2O)_n$, dans lesquels M = Mg, Ca et Sr et n = 1, 2, 3, 4 et 6. Les valeurs des énergies de liaison ion–eau successives sont dans l'ordre des valeurs attendues sur la base de l'extrapolation de résultats obtenus avec des hydrates plus importants.

Mots clés : hydrates, cations de métaux alcaline-terreux, calculs de la chimie quantique.

[Traduit par la rédaction]

Can. J. Chem. Downloaded from www.nrcresearchpress.com by 92.62.229.171 on 09/08/12
For personal use only.

Introduction

Recently, an experimental breakthrough achieved by Kebarle and co-workers (1) allowed for experimental studies *in the gas phase* of the equilibria involving water molecules and bivalent ions of the alkaline-earth elements:

$$M^{2+}(H_2O)_{n-1} + H_2O \rightleftharpoons M^{2+}(H_2O)_n$$

The electrospray technique used in the experiments provides accurate data on the ion–ligand bond energies for larger coordination numbers; in the case of divalent alkaline-earth ions the smallest clusters for which reliable data were reported contained as many as seven to eight water molecules. However, the interactions in the inner hydration shell involving a doubly charged metal ion and one to six water molecules and leading to binding energies in the 40–80 kcal/mol range, while interesting from a chemical viewpoint, are beyond the range of the present experimental apparatus (1).

Fortunately, the small-cluster range is amenable to computational studies, especially when the interacting systems possess high charges and closed electronic shells. The present work was conceived as a preliminary study in the computational continuation of the experimental investigation of the metal-ion–water clusters. To gain insight into the importance of basis set composition and the role played by the electron correlation, various large basis sets were used in SCF and post-SCF calculations. Furthermore, the accuracy of valence-electron representation in such studies, important for studies involving heavier atoms, was also investigated. Full geometry optimization of all species involved was done, thus furnishing not only the required energy data (which could be easily obtained from a refined experiment) but also the structural information (which is more difficult to acquire by experimental techniques).

In experiment, the successive ligands adapt the geometric arrangement corresponding to the lowest total energy. In computations, the imposed symmetry of the ligand arrangement can be utilized to reduce the computational effort. To establish the ligand conformation that is most favorable energetically, in the present work various possible symmetries were considered.

Calculations, results, and discussion

Basis sets

Basis sets of triple-zeta quality in the valence region were used in the present study. For hydrogen, Huzinaga's (5*s*) basis (2) was contracted to (3*s*). For oxygen, Huzinaga's (10*s*6*p*) basis (2) was used, contracted to (5*s*3*p*) following Dunning (3) and augmented with a diffuse *p*-type function (ζ_p = 0.059) (4). For magnesium, the McLean–Chandler (12*s*9*p*) basis, contracted to (6*s*5*p*), was used (5). Calcium was represented in the all-electron calculations by the (8*s*4*p*) basis obtained from the uncontracted (14*s*9*p*) set of Wachters (6). In the valence-electron calculations, the (5*s*5*p*) basis set, corresponding to the effective core potential including outer core electrons as developed by Hay and Wadt (7), was used in the contraction (5*s*4*p*) (with the two innermost *p*-type primitives contracted). In the valence-electron calculations on $Sr^{2+}(H_2O)_n$, the strontium (5*s*5*p*) basis of Hay and Wadt (7) was contracted as for calcium.

The exponents of the polarization functions were developed for all systems by optimization in the Møller–Plesset calculations (8) on the monohydrates (at geometries close to the optimum, with both the core orbitals and their counterparts among the virtual space removed from the active space). The polarization functions for hydrogen and oxygen were determined in the calculations on $Mg^{2+}(H_2O)$ and used for all the complexes.

The values of the exponents in the basis sets with single polarization functions (denoted here TZ1P) were: ζ_d^O = 1.2976, ζ_p^H = 0.9399, ζ_d^{Mg} = 0.2218, ζ_d^{Ca} = 1.1419, and ζ_d^{Sr} = 0.699. The exponents of the polarization functions in the TZ2P basis were: ζ_d^O = {2.3803,0.6844}, ζ_p^H = {1.4647,0.4261}, ζ_d^{Mg} = {0.4131,0.1580}, and ζ_d^{Ca} = {1.7336,0.5576}.

The optimization of exponents was done with the HONDO 7.0 program (9); the code was modified in this laboratory to allow for the geometry optimization in the Møller–Plesset

TABLE 1. Energy and structure of isolated water[a]

Method	Basis[b]	E_T	OH	HOH
SCF	AE1P	−76.05685	0.941	106.9
SCF	VE1P	−16.86446	0.946	106.4
SCF	AE2P	−76.06177	0.940	106.3
MP2	AE1P	−76.27615	0.960	104.2
MP2	AE2P	−76.30201	0.960	103.9

[a]Energies in atomic units, bond lengths in angstrøms, angles in degrees.
[b]AEnP = all-electron calculations with TZnP basis, VEnP = valence-electron calculations with TZnP basis.

calculations via the conjugate gradient method of Powell (10). For all systems studied, the complete optimization of geometry using gradient techniques was done using the GAMESS program (11). For the evaluation of electric moments and polarizabilities HONDO 8.1 code was used (12).

All calculations were done on a SUN SPARCstation 4/370.

Monohydrates

The data on energy and structure of the isolated water are collected in Table 1. The calculated geometries, both on the SCF and MP level, are almost independent of the polarization space. The valence-electron results are satisfactorily close to the corresponding all-electron values. On the SCF level, the geometric parameters of water are quite close to the near Hartree–Fock results (13) (especially when two polarization exponents are employed). Corrections for the electron correlation bring the computed geometry close to the experimental structure with OH = 0.957 Å and HOH = 104.5° (14).

To gain insight into the quality of the various basis sets used, dipole and quadrupole moments are tabulated in Table 2 together with the values of static dipole polarizabilities. The results are compared with recent accurate values of Szczęsniak and Scheiner (15), who used very large basis sets (for oxygen, (15*s*10*p*3*d*) was contracted to (7*s*6*p*3*d*); for hydrogen, (10*s*3*p*) basis was contracted to (5*s*3*p*); the exponents of the polarization functions were optimized in molecular Møller–Plesset and polarizability calculations). Expansion of the polarization space brings about reduced dipole and quadrupole moments and increased polarizabilities. The best SCF values differ by 3, 15, 29, and 21% for μ_z, α_{xx}, α_{yy}, and α_{zz}, respectively (the corresponding errors in the MP2 values are 11, 15, 33, and 21%).

The results for the complexes of Mg^{2+}, Ca^{2+}, and Sr^{2+} are presented in Table 3. Coordination of water by metal ions results in the lengthening of the OH bond (by 0.02 Å for the magnesium complex and 0.01 Å for calcium and strontium); the bond angle in the coordinated water becomes smaller, by 1°–2°, than that in free water (the only exception is found in the magnesium complex treated at the MP level). The metal–oxygen bond length increases with the size of the metal ion while the total hydration energy ΔE decreases. For the magnesium and calcium hydrates, the MOH bond angle changes only slightly with the change in the composition of the polarization space; small changes (less than 1°) are induced by the use of the MP method. The length of the metal–oxygen bond responds in expected fashion when the polarization set is expanded or correction for the electron correlation is added.

The total hydration energies are relatively stable with respect to both the size of the polarization space and the treatment of electron correlation. The largest absolute changes are seen in the magnesium complex, where they are about 1–2 kcal/mol. The valence-electron results (for the calcium hydrate) are very close to the corresponding all-electron values; it may be expected that the results for the strontium hydrate are equally accurate.

Ågren and co-workers (16) studied the $Mg^{2+}(H_2O)$ complex using fairly large basis sets in SCF and CASSCF calculations aiming at the evaluation of infrared intensities. However, only the geometry of water was optimized, while the Mg—O distance was kept fixed at 2.05 and 2.10 Å (these distances bracket the interval of ion–water distances found in various Mg^{2+} crystalline compounds (17)). Their computed OH bond lengths were 0.959 and 0.979 Å at the SCF and CASSCF levels, respectively; these values are very close to the ones obtained in the present work.

Calcium dication hydrates were recently studied by Castro and co-workers (18), who used a variety of basis sets for the monohydrate. However, only one basis set used in that work gives the total energy comparable to the ones shown in Table 3; the remaining six lead to total energies differing by 1–3 E_h from the present values. Davy and Hall (19) also used a rather small basis set (of about STO-3G quality for the core orbitals and DZ1P for the valence ones) in SCF calcula-

TABLE 2. Components of dipole moment (μ), quadrupole moment (Θ), and static dipole polarizability (α) of water[a]

		Property						
Method	Basis[b]	μ_z	Θ_{xx}	Θ_{yy}	Θ_{zz}	α_{xx}	α_{yy}	α_{zz}
SCF	AE1P	0.8874	1.985	−1.774	−0.211	7.209	4.488	5.611
SCF	VE1P	0.8979	1.960	−1.766	−0.193	7.407	4.274	5.654
SCF	AE2P	0.8026	1.940	−1.770	−0.169	7.807	5.592	6.712
SCF	AESS[c]	0.7800				9.163	7.898	8.478
MP2	AE1P	0.8867				7.721	5.273	6.404
MP2	AE2P	0.7900				8.470	6.402	7.618
MP2	AESS[c]	0.7077				9.998	9.559	9.689

[a]All values (in atomic units) were calculated at the center of mass for the equilibrium geometry (cf. Table 1). The molecule was located in the *OXZ* plane, with the oxygen atom below the hydrogens.
[b]AEnP = all-electron calculations with TZnP basis, VEnP = valence-electron calculations with TZnP basis.
[c]See ref. 15.

Can. J. Chem. Downloaded from www.nrcresearchpress.com by 92.62.229.171 on 09/08/12
For personal use only.

TABLE 3. Energy and structure of monohydrates in C_{2v} symmetry[a]

Metal	Model	Basis[b]	E[c]	$-\Delta E$[d]	MO	MOH	OH	HOH
Mg	SCF	AE1P	−0.01017	81.7	1.920	127.0	0.959	105.9
		AE2P	−0.01364	80.6	1.907	127.0	0.956	106.0
	MP2	AE1P	−0.33827	81.3	1.939	127.4	0.975	105.2
		AE2P	−0.36516	79.5	1.924	127.4	0.975	105.2
Ca	SCF	AE1P	−0.27013	51.7	2.324	127.9	0.953	104.1
		VE1P	−0.55964	52.5	2.328	128.1	0.958	103.9
		AE2P	−0.27610	51.5	2.280	127.6	0.952	104.7
	MP2	AE1P	−0.64409	51.5	2.330	128.9	0.970	102.3
		AE2P	−0.69424	51.9	2.269	128.3	0.971	103.4
Sr	SCF	VE1P	−0.47985	45.5	2.487	128.0	0.956	103.9

[a]Energies (E) in atomic units, stabilization energies (ΔE) in kcal/mol, bond lengths (MO and OH) in angstrøms, and bond angles (MOH and HOH) in degrees.
[b]AEnP = all-electron calculations with TZnP basis, VEnP = valence-electron calculations with TZnP basis.
[c]The total energies shifted by 275, 752, 52, and 46 atomic units for the Mg, Ca(AE), Ca(VE), and Sr(VE) complexes, respectively.
[d]$\Delta E = E[M^{2+}(H_2O)] - \{E[M^{2+}] + E[H_2O]\}$.

tions, obtaining the geometry of the monohydrate similar to the ones reported in the present work, despite a rather large difference in the total energy (about 6 E_h).

All three monohydrates were the subject of a computational study by Zahradník and co-workers (20) who used very small MINI-1 basis sets of Huzinaga and co-workers (21) without polarization functions (to minimize the basis set superposition errors). The metal–oxygen distances, affected by BSSE, were significantly shorter than the present ones; the interaction energies computed with the MINI-1 basis sets and corrected for BSSE were fairly close to the present values for the three systems studied. However, the (BSSE corrected) energies obtained with the more flexible MIDI basis sets were about 10 kcal/mol larger than the ones obtained with the large basis sets in the present work.

Dihydrates

Table 4 shows the results of calculations for the ions coordinated by two water molecules. The calculations were done for two symmetries of the complex, D_{2h} and D_{2d}.

As seen in the previous section, coordination lengthens the OH bond and decreases the bond angle in water (again, the exception is found in the magnesium complex treated on the MP level). Extension of the polarization space reduces the total hydration energies by about 2–3 kcal/mol; the changes brought about by the electron correlation effects are smaller. Again, the valence-electron description of the calcium dihydrate is adequately close to the all-electron picture, reinforcing confidence in the quality of the results for the strontium complex.

The two structures, D_{2h} and D_{2d}, lead to almost equal hy-

TABLE 4. Energy and structure of dihydrates[a]

Metal	Symmetry	Model	Basis	E[b]	$-\Delta E$[c]	MO	MOH	OH	HOH
Mg	D_{2h}	SCF	AE1P	−0.18487	155.7	1.938	127.0	0.957	106.0
			AE2P	−0.18963	152.3	1.928	127.0	0.955	106.0
		MP2	AE1P	−0.73205	155.1	1.955	127.5	0.974	105.1
			AE2P	−0.77969	150.1	1.946	127.3	0.972	105.4
	D_{2d}	SCF	AE1P	−0.18517	155.9	1.937	126.9	0.957	106.1
			AE2P	−0.18995	152.5	1.928	127.0	0.955	106.1
		MP2	AE1P	−0.73244	155.4	1.954	127.4	0.974	105.2
			AE2P	−0.78003	150.3	1.945	127.4	0.973	105.1
Ca	D_{2h}	SCF	AE1P	−0.40255	99.1	2.351	127.9	0.952	104.3
			VE1P	−0.50032	100.0	2.358	128.0	0.956	104.1
			AE2P	−0.41066	97.2	2.324	127.6	0.951	104.7
		MP2	AE1P	−0.99560	98.8	2.353	128.7	0.970	102.5
			AE2P	−1.06936	97.8	2.320	128.4	0.970	103.2
	D_{2d}	SCF	AE1P	−0.40263	99.1	2.351	127.9	0.952	104.3
			VE1P	−0.50049	100.1	2.357	127.9	0.956	104.1
			AE2P	−0.41076	97.2	2.324	127.6	0.951	104.8
		MP2	AE1P	−0.99572	98.9	2.353	128.7	0.970	102.6
			AE2P	−1.06952	97.9	2.319	128.4	0.970	103.2
Sr	D_{2h}	SCF	VE1P	−0.40991	86.7	2.531	127.9	0.955	104.1
	D_{2d}	SCF	VE1P	−0.41004	86.8	2.530	127.9	0.955	104.1

[a]See footnotes to Table 3.
[b]The total energies were shifted by 351, 828, 69, and 63 atomic units for Mg, Ca(AE), Ca(VE), and Sr(VE), respectively.
[c]$\Delta E = E[M^{2+}(H_2O)_2] - \{E[M^{2+}] + 2E[H_2O]\}$.

Can. J. Chem. Downloaded from www.nrcresearchpress.com by 92.62.229.171 on 09/08/12
For personal use only.

TABLE 5. Energy and structure of trihydrates from SCF calculations[a]

Metal	Symmetry[b]	Basis	E^c	$-\Delta E^d$	MO	MOH	OH	HOH
Mg	$D_{3h}^{\perp}$	AE1P	−0.33407	213.6	1.972	127.0	0.953	106.0
		AE2P	−0.34166	208.9	1.964	127.0	0.952	106.0
	$D_{3h}^{\parallel}$	AE1P	−0.33625	215.0	1.967	127.0	0.953	105.9
		AE2P	−0.34349	210.1	1.959	127.0	0.952	105.9
	C_3	AE1P	−0.33754	215.8	1.965	126.9	0.954	106.3
		AE2P	−0.34494	211.0	1.957	126.9	0.952	106.3
Ca	$D_{3h}^{\perp}$	AE1P	−0.52719	141.6	2.373	127.7	0.951	104.6
		AE2P	−0.53806	138.3	2.346	127.3	0.949	105.3
	$D_{3h}^{\parallel}$	AE1P	−0.52777	142.0	2.371	127.7	0.951	104.5
		AE2P	−0.53868	138.7	2.343	127.5	0.950	104.9
	C_3	AE1P	−0.52843	142.4	2.369	127.6	0.951	104.7
		VE1P	−0.43456	143.8	2.372	127.8	0.955	104.5
		AE2P	−0.53939	139.2	2.341	127.3	0.950	105.5
Sr	C_3	VE1P	−0.33593	125.3	2.542	127.8	0.954	104.4

[a]See footnotes to Table 3.

[b]In $D_{3h}^{\perp}$ symmetry the hydrogen atoms are perpendicular to the plane of heavy atoms; in $D_{3h}^{\parallel}$ symmetry they are located in the plane.

[c]The total energies were shifted by 427, 904, 86, and 80 atomic units for Mg, Ca(AE), Ca(VE), and Sr(VE), respectively.

[d]$\Delta E = E[M^{2+}(H_2O)_3] - \{E[M^{2+}] + 3E[H_2O]\}$.

dration energies, with the D_{2d} structure being infinitesimally more stable.

Castro and co-workers (18) in the studies on Ca^{2+} dihydrate with small basis sets obtained poorer energies (by about 2 E_h) and shorter metal–oxygen distance.

Trihydrates

In view of the great similarity in the interaction energies obtained with and without the corrections due to the electron correlation, only the SCF calculations were performed for trihydrates (and all larger complexes). The results, for the three geometric configurations of the complex, are shown in Table 5.

The water molecules respond to coordination in the manner seen in the smaller complexes, by increasing the bond length and reducing the bond angle. The angle between metal, oxygen, and hydrogen is quite similar to those found in the mono- and dihydrates (about 127°). The larger size of the central ion correlates with the longer metal–oxygen bond distance and smaller interaction energies. The larger polarization set reduces the hydration energies by 2–5 kcal/mol.

The interaction energies increase slightly in the series $D_{3h}^{\perp}$, $D_{3h}^{\parallel}$, and C_3 corresponding to a decreased repulsive contact between the lone electron pairs in water molecules. This change is accompanied by a diminutive lengthening of the metal–oxygen bond.

The total energies by Castro and co-workers (18) are again more than 2 E_h above the present values and their Ca—O bond lengths shorter.

Tetrahydrates

The larger size of these complexes, and the correspondingly larger basis sets, allowed for the use of the extended polarization space only for the tetrahydrates of magnesium in the highest symmetry D_{2h}.

The complexes with the "tetrahedral" S_2 symmetry have the largest binding energies (see Table 6). It is interesting to note, though, that as the size of the central ion increases, the difference between the hydration energies in C_4 and S_2 conformations becomes smaller. This is consistent with the recent experimental study on the structure of the Sr^{2+} ion in aqueous solution, which demonstrated lack of orientational order in the hydration shell (22). The reaction of water to coordination is similar to that seen in the smaller hydrates. The distances between the oxygen atoms in S_2 symmetry are fairly large, hence the metal–oxygen bond length is only slightly larger than in trihydrates.

The Ca—O bond lengths from the study by Castro and co-workers (18) are smaller (by about 0.7 Å for their best basis used).

Hexahydrates

For reasons of computational economy only the smallest, TZ1P, basis sets were used in T_h symmetry (see Table 7). The deviation of the geometric structure of the coordinated water from that of the free water is smaller in hexahydrates than in all other hydrates. The water molecules are found at relatively large distances from the metal ion. For the alkaline earth ions studied here, six water molecules are usually found in the first hydration shell. The Sr—O distance was found to be about 2.65 Å in solution (22), 2.61 Å in crystal (23).

In a recent theoretical study of hydrated Be^{2+} ions (24) it was found that two of the water molecules in the hexacoordinated ion form the second hydration shell, connecting with the first hydration shell via hydrogen bonds. The ions studied here are much larger than Be^{2+} and the first hydration shell could easily accommodate six water molecules. To check the relative stabilities of the two possible distributions of the six water molecules around the central ion, full geometry optimization was done for the magnesium ion hexahydrate in T_h and C_1 symmetries (the latter structure could be best written as $[Mg^{2+}(H_2O)_4](H_2O)_2$); following Iwata and co-workers (24), the 3–21G* basis set was used. The Mg—O distance in the T_h structure was found to be 2.075 Å, shorter than the value obtained with the TZ1P basis set, and the total hydration energy was 408 kcal/mol. The geometry of the C_1 structure is defined in Fig. 1 and in Table 8, and the corresponding interaction energy is only 385 kcal/mol, more than 20 kcal/mol smaller than in the T_h

Can. J. Chem. Downloaded from www.nrcresearchpress.com by 92.62.229.171 on 09/08/12
For personal use only.

TABLE 6. SCF energy and structure of tetrahydrates[a]

Metal	Symmetry[b]	Basis	E[c]	$-\Delta E$[d]	MO	MOH	OH	HOH
Mg	$D_{4h}^{\perp}$	AE1P	−0.44367	246.7	2.055	127.0	0.950	106.0
		AE2P	−0.45201	239.4	2.049	127.0	0.949	105.9
	$D_{4h}^{\parallel}$	AE1P	−0.45209	252.0	2.034	127.4	0.950	105.2
		AE2P	−0.46021	244.6	2.027	127.4	0.948	105.1
	C_4	AE1P	−0.45831	255.9	2.027	126.7	0.950	106.6
	S_2	AE1P	−0.47212	264.6	2.000	126.2	0.951	106.5
Ca	C_4	AE1P	−0.64240	178.2	2.398	127.4	0.949	105.2
	S_2	AE1P	−0.64653	180.8	2.391	127.5	0.950	105.1
		VE1P	−0.36077	182.6	2.392	127.6	0.952	104.8
Sr	S_2	Ve1P	−0.25530	159.8	2.563	127.6	0.953	104.7

[a]See footnotes to Table 3.
[b]In $D_{3h}^{\perp}$ symmetry the hydrogen atoms are perpendicular to the plane of heavy atoms; in $D_{3h}^{\parallel}$ symmetry they are located in the plane.
[c]The total energies were shifted by 503, 980, 103, and 97 atomic units for Mg, Ca(AE), Ca(VE), and Sr(VE), respectively.
[d]$\Delta E = E[M^{2+}(H_2O)_4] - \{E[M^{2+}] + 4E[H_2O]\}$.

TABLE 7. SCF energy and structure of hexahydrates[a]

Metal	Symmetry	Basis	E[b]	$-\Delta E$[c]	MO	MOH	OH	HOH
Mg	T_h	AE1P	−0.68501	326.8	2.102	126.3	0.947	107.3
Ca	T_h	AE1P	−0.85722	241.7	2.443	127.0	0.947	106.0
		VE1P	−0.18729	243.8	2.445	127.1	0.951	105.8
Sr	T_h	VE1P	−0.07307	215.5	2.616	127.2	0.951	105.5

[a]See footnotes to Table 3.
[b]The total energies were shifted by 655, 1132, 137, and 131 atomic units for Mg, Ca(AE), Ca(VE), and Sr(VE), respectively.
[c]$\Delta E = E[M^{2+}(H_2O)_6] - \{E[M^{2+}] + 6E[H_2O]\}$.

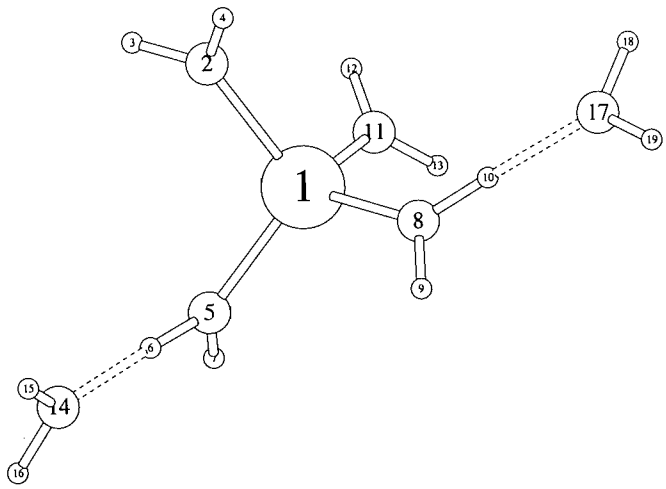

FIG. 1. Geometry of the $[Mg^{2+}(H_2O)_4](H_2O)_2$ ion in C_1 symmetry.

TABLE 8. Selected geometrical parameters of $[Mg^{2+}(H_2O)_4](H_2O)_2$[a]

Distance[b]		Angle[b]	
Label	Value	Label	Value
Mg1—O2	1.991	H3—O2—H4	106.1
Mg1—O5	1.928	H6—O5—H7	106.4
Mg1—O8	1.992	H15—O14—H16	105.5
Mg1—O11	1.927	O2—Mg1—O8	109.2
O2—H3	0.970	O2—Mg1—O11	107.1
O5—H7	0.968	O2—Mg1—O5	108.9
O5—H6	1.007	O5—Mg1—O8	113.0
H6—O14	1.579	O5—Mg1—O11	109.3
O14—H15	0.965		
O14—H16	0.966		

[a]Distances in angstrøms, angles in degrees.
[b]See Fig. 1 for notation.

complex. Even though both the geometries and the interaction energies are affected by the basis set superposition errors, unavoidable with the small 3–21G* basis set, the energy difference is probably large enough to allow for concluding that the first hydration shell of the divalent alkaline earth atoms consists of six molecules. For the Sr^{2+} hexahydrate, Castro and co-workers (18) used only the MINI-3 basis of Huzinaga and co-workers (21). The resulting geometry in T_h symmetry, with the Sr—O bond length 0.3 Å shorter than the present value, indicates considerable effects of the BSSE.

Conclusions

The energy changes obtained in the present study can be recast in the format that gives more information about the hydration process. The total energy change, $\Delta E(n)$, for the reaction:

$$M^{2+} + n\,H_2O \rightleftharpoons M^{2+}(H_2O)_n$$

Can. J. Chem. Downloaded from www.nrcresearchpress.com by 92.62.229.171 on 09/08/12
For personal use only.

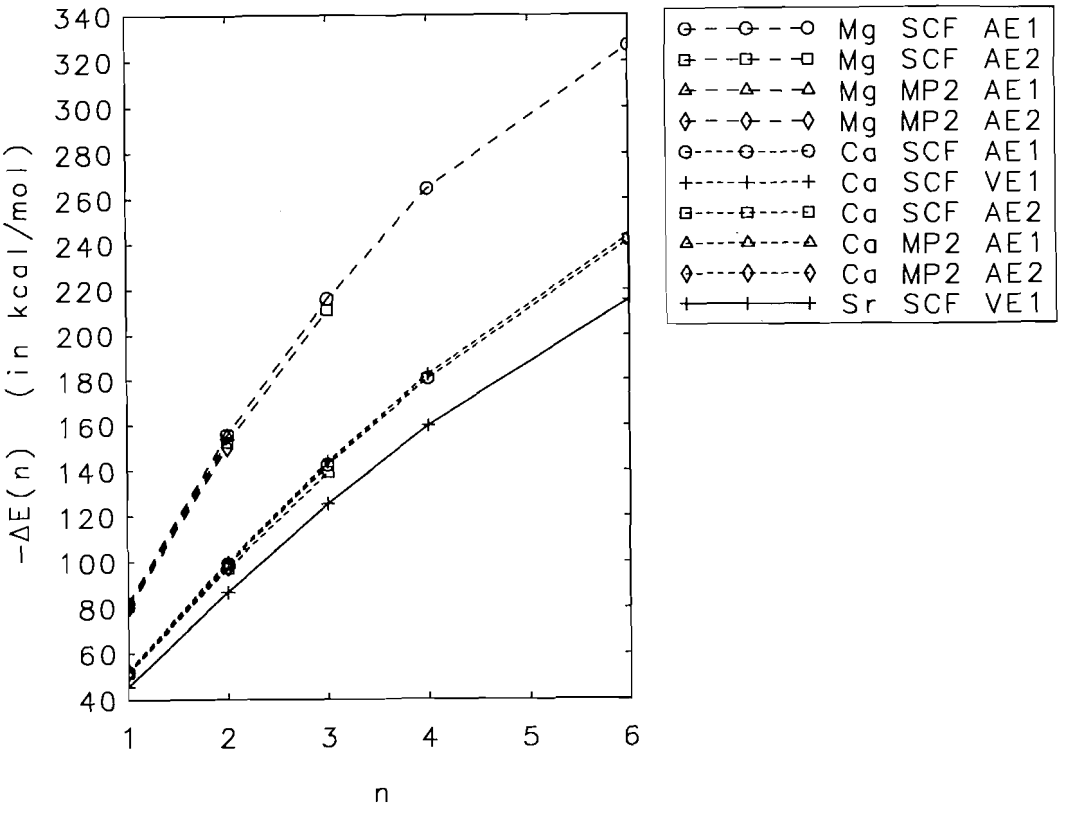

FIG 2. The total hydration energy.

is shown in Fig. 2. The average metal–water bond energies,

$$\Delta E(n)_{av} = \Delta E(n)/n$$

are depicted in Fig. 3. Finally, the successive metal–water bond energies that are closest to the quantities measured experimentally (1) in the reaction

$$M^{2+}(H_2O)_{n-1} + H_2O \rightleftharpoons M^{2+}(H_2O)_n$$

and which are defined as

$$\Delta E_{n-1,n} = E[M^{2+}(H_2O)_n] - \{E[M^{2+}(H_2O)_{n-1}] + E[H_2O]\}, \quad \text{for } n = 1, \ldots, 4$$

and

$$\Delta E_{n-1,n} = (E[M^{2+}(H_2O)_n] - \{E[M^{2+}(H_2O)_{n-2}] + 2E[H_2O]\})/2, \quad \text{for } n = 6$$

are presented in Fig. 4. Only the data for the symmetries with the lowest total energies are shown in the figures.)

It is interesting to note the behavior of $\Delta E_{n-1,n}$ for the magnesium hydrates: considering that the $\Delta H^0_{8,9}$ values for the three ions are in the 14.9–15.1 kcal/mol range (1), the rapid decrease of the calculated values may indicate that the structure of the hydration shell for $n > 6$ (and possibly even for $n = 6$) in the magnesium complex differs from the structure of the corresponding complexes with calcium and strontium ions. Clearly, the extension of the computational studies to the higher hydrates is needed.

The binding energies of all the hydrates studied decrease

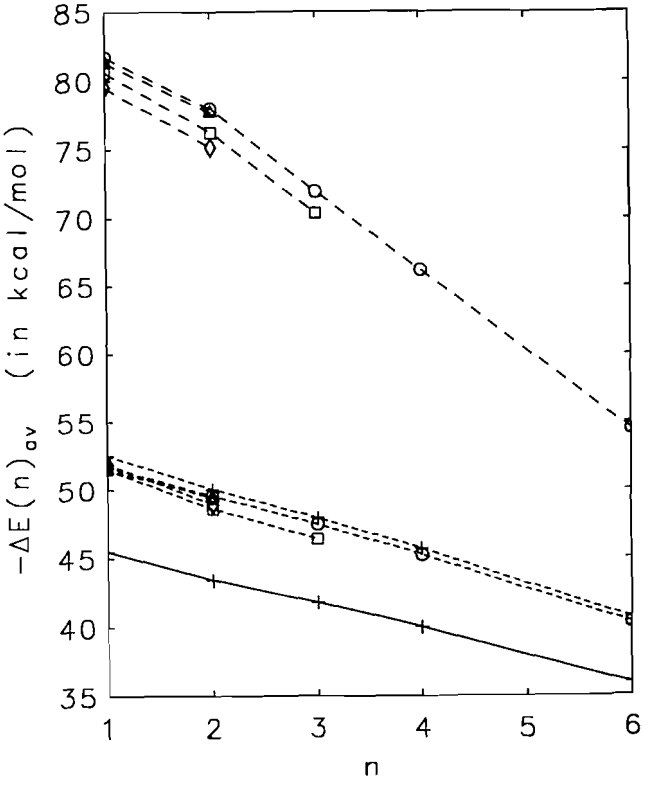

FIG. 3. The average metal–water bond energy (see the legend in Fig. 2 for explanation of symbols).

Can. J. Chem. Downloaded from www.nrcresearchpress.com by 92.62.229.171 on 09/08/12
For personal use only.

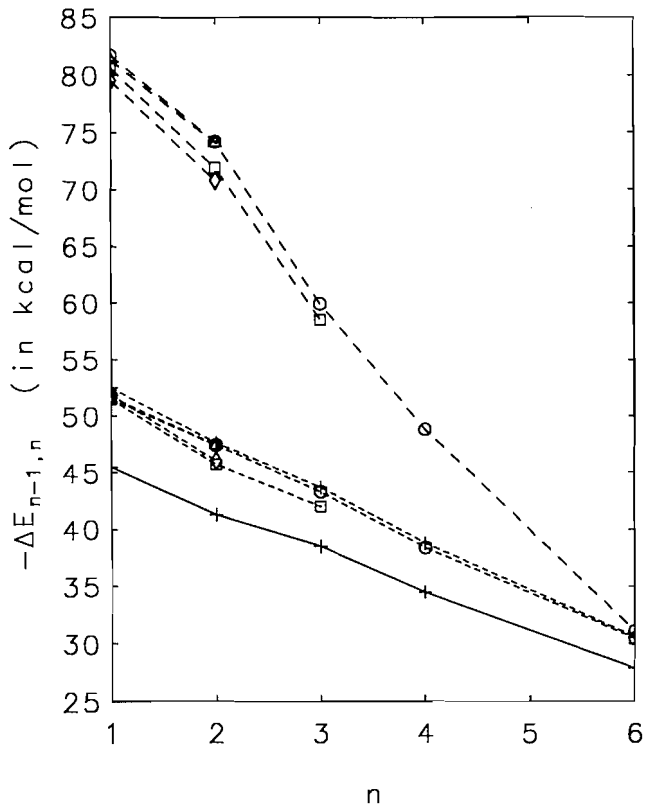

FIG. 4. The successive metal–water bond energy (see the legend in Fig. 2 for explanation of symbols).

when the basis set is increased. Considering that the bonding in the complexes is mainly electrostatic, the possible cause of the decreased interaction energies is the decrease of the dipole and quadrupole moments and increase of the dipole polarizability of the water molecule (cf. Table 2) upon extension of the basis set.

The present results indicate that neither extended (and expensive) polarization space nor electron correlation effects have to be necessarily considered in the studies on the hydrates involving the divalent alkaline earth atoms. Furthermore, the effective core potential method used with the basis set equipped with a small polarization space was found to be an adequate, and economical, computational approach to such calculations. The computational savings will be substantial especially in the studies on the harmonic vibrational frequencies.

The successive metal–water bond energies fall within the range of values predicted by Kebarle in the experimental studies (40–80 kcal/mol) (1). The agreement may be even better if the zero-point-energy corrections are added to the present values.

Can. J. Chem. Downloaded from www.nrcresearchpress.com by 92.62.229.171 on 09/08/12
For personal use only.

Acknowledgments

I am very grateful to Professor Kebarle for sharing the results of his work prior to publication and for the many discussions that followed. The comments by an anonymous referee, which resulted in an improved version of the manuscript, are greatly appreciated. This work was partly supported by the Natural Sciences and Engineering Research Council of Canada (under Operating Grant No. OGP0046770) and by the Central Research Fund of the University of Alberta (Grant No. 55-48938).

1. A. T. Blades, P. Jayaweera, M. G. Ikonomou, and P. Kebarle. J. Chem. Phys. **92**, 5900 (1990); Int. J. Mass Spectrom. Ion Processes, **102**, 251 (1990).
2. S. Huzinaga. J. Chem. Phys. **42**, 1293 (1965).
3. T. H. Dunning, Jr. J. Chem. Phys. **55**, 716 (1971).
4. T. H. Dunning, Jr. and P. J. Hay. *In* Modern theoretical chemistry. Vol. 3. Methods of electronic structure theory. *Edited by* H. F. Schaefer III. Plenum, New York. 1977. p. 1.
5. A. D. McLean and G. S. Chandler. J. Chem. Phys. **72**, 5639 (1980).
6. A. J. H. Wachters. J. Chem. Phys. **52**, 1033 (1970).
7. P. J. Hay and W. R. Wadt. J. Chem. Phys. **82**, 299 (1984).
8. C. Møller and M. S. Plesset. Phys. Rev. **46**, 618 (1934).
9. M. Dupuis, J. D. Watts, H. O. Villar, and G. J. B. Hurst. HONDO 7.0, QCPE Program No. 544, QCPE Bull. **8**, 79 (1988).
10. M. J. D. Powell. Comput. J. **7**, 155 (1964).
11. M. W. Schmidt, K. K. Baldridge, J. A. Boatz *et al.* QCPE Bull. **10**, 52 (1990).
12. M. Dupuis, P. Mougenot, J. D. Watts, G. J. B. Hurst, and H. O. Villar. *In* MOTECC: Modern techniques in computational chemistry. *Edited by* E. Clementi. ESCOM Science Publishers, Leiden. 1989. p. 307.
13. B. J. Rosenberg, W. C. Ermler, and I. Shavitt. J. Chem. Phys. **65**, 4072 (1976).
14. D. Feller, C. M. Boyle, and E. R. Davidson. J. Chem. Phys. **86**, 3424 (1987).
15. M. Szczęsniak and S. Scheiner. Collect. Czech. Chem. Commun. **53**, 2214 (1988).
16. K. Hermansson, J. Lindgren, and H. Ågren. Mol. Phys. **57**, 857 (1986).
17. G. Ferraris and M. Franchini-Angela. Acta Crystallogr. Sect. B: Struct. Crystallogr. Cryst. Chem. **B28**, 3572 (1972).
18. R. E. Cachau, H. O. Villar, and E. A. Castro. Theor. Chim. Acta, **75**, 299 (1989).
19. R. D. Davy and M. B. Hall. Inorg. Chem. **27**, 1417 (1988).
20. H.-J. Hoffmann, P. Hobza, R. Cammi, J. Tomasi, and R. Zahradník. J. Mol. Struct. (Theochem), **201**, 339 (1989).
21. H. Tatewaki and S. Huzinaga. J. Comput. Chem. **1**, 205 (1980); Y. Sakai, H. Tatewaki, and S. Huzinaga. J. Comput. Chem. **2**, 101 (1981), 108 (1981); J. Andzelm, S. Huzinaga (*Editor*), M. Klobukowski, E. Radzio-Andzelm, H. Tatewaki, and Y. Sakai. Gaussian basis sets for molecular calculations. Elsevier, Amsterdam. 1984.
22. G. W. Neilson and R. D. Broadbent. Chem. Phys. Lett. **167**, 429 (1990).
23. R. Camaniti, A. Musimu, G. Paschina, and G. Pinna. J. Appl. Crystallogr. **15**, 482 (1982).
24. K. Hashimoto, N. Yoda, and S. Iwata. Chem. Phys. Lett. **116**, 193 (1987).

Low-energy conformational domains of polypeptides, characterized by a random-search and minimization procedure

ANDRÉ G. MICHEL,[1] CHAKIB AMEZIANE-HASSANI, AND NATHALIE BREDIN
Laboratoire de chimie structurale, Département de chimie, Université de Sherbrooke, Sherbrooke (Québec), Canada J1K 2R1

Received September 2, 1991

This paper is dedicated to Professor Sigeru Huzinaga on the occasion of his 65th birthday

ANDRÉ G. MICHEL, CHAKIB AMEZIANE-HASSANI, and NATHALIE BREDIN. Can. J. Chem. **70,** 596 (1992).

In the framework of molecular mechanics conformational energy calculations, a random-search and minimization procedure is presented to characterize low-energy domains of polypeptidic structures. Rather than striving for global minima, populations of conformers are randomly generated, and their energy is minimized in order to study their intrinsic properties. The application to the opioid peptide Met-Enkephalin allowed the identification of low-energy domains that are compared with previous results of conformational studies on this molecule. Our method gives a complete overview of the conformational behaviour of the polypeptide under study, including previously reported structures as determined from experimental and theoretical studies. To illustrate the usefulness of this method to determine bioactive peptidic structures and their active conformers, the application to geometrically constrained chemotactic tripeptides is presented.

Key words: peptides, conformation, theoretical prediction.

ANDRÉ G. MICHEL, CHAKIB AMEZIANE-HASSANI et NATHALIE BREDIN. Can. J. Chem. **70,** 596 (1992).

Une méthode théorique de caractérisation des domaines conformationnels des molécules polypeptidiques est présentée. Les calculs d'énergie conformationnelle sont effectués dans le cadre empirique de la mécanique moléculaire. Plutôt que chercher à localiser le minimum global d'une hypersurface énergétique, des populations de conformères sont générées en vue d'en étudier les propriétés intrinsèques. L'application au peptide opiacé Met-Enképhaline a permis d'identifier des domaines dans la population générée et de comparer ces résultats à des études conformationnelles antérieures. On démontre que cette approche fournit une vue complète du comportement conformationnel du polypeptide, incluant les structures proposées par des travaux théoriques ou expérimentaux. Afin d'illustrer l'applicabilité de la méthode pour l'identification de conformation d'intérêt biologique, une étude a été menée sur des tripeptides chimiotactiques à géométrie restreinte.

Mots clés : peptides, conformation, prédictions théoriques.

Can. J. Chem. Downloaded from www.nrcresearchpress.com by 92.62.229.171 on 09/08/12
For personal use only.

Introduction

In the past decade, much effort has been made to identify absolute minimum energy structures for peptidic molecules. In such investigations, thousands of energy-minimized molecular conformations have been thrown away, retaining only a few lowest energy structures. Nevertheless, such generated structures constitute an ensemble wherein classes or groups of organisations are expected. In fact, experimental evidence suggests that polypeptides as short as four or five residues can adopt nonrandom conformations in aqueous solutions (1). Strategies based on energy minimization, dynamics, and Monte-Carlo simulations have been used in various studies (2, 3) to simulate the conformational space. The determination of minimum energy conformations of polypeptides by dynamic programming was also recently presented (4). A comparative study of the different methods has been published recently (5).

Here we describe an approach based on energy minimization after random generation of initial conformations. Our purpose is to generate the population of conformations characterizing a particular peptidic sequence. Subsequent analysis of this ensemble of conformers is expected to reveal the intrinsic organization in conformational space. The largest part of the conformational space is sampled by generating a large number of initial random conformations. Subsequently, the conformational energies of the resulting structures are minimized, using the conjugate gradient technique, to the nearest local minimum into the torsional space.

Such a procedure allows us to generate a sample of conformers representative of the conformational behaviour of the peptide of interest. The empirical conformational energy program for peptides (ECEPP) force field (6–8) appeared to be very well suited for such applications, as the use of a rigid geometry reduces the number of variables to only torsional angles. Actually, this force field has proven to be well adapted for applications of molecular mechanics to peptidic structure. Particularly, the procedure of Scheraga, called the "Build-Up" method, allowed reasonable predictions of global minima for small and medium peptides to be made (9). The same energy function was recently applied by Wüthrich and co-workers (10). A population of conformers for Enkephalin was generated, using a systematic search procedure.

During the past decade, the conformation of the endogenous opioid pentapeptide Tyr-Gly-Gly-Phe-Leu-Met **M-Enk**[2] has been extensively investigated. Studies to identify local minima, using theoretical simulations, have proposed conformations that can be classified in four main categories. The first class of structures adopts a β-turn involving residues Gly^3 and Phe^4. Such structures are generated by the existence of a (5 → 2) intramolecular hydrogen bond involving $CO(Gly^2)$ and $NH(Met^5)$. Both theoretical results (10–20) and NMR

[1]Author to whom correspondence may be addressed.

[2]Abbreviations used:
fMLP formyl-Methionine-Leucine-Phenylalanine (this is not in accordance with the usual code but is universally used in the field of chemotactic peptides)
fMAP formyl-Methionine-αAminoisobutyric acid-Phenylalanine
M-Enk Tyr-Gly-Gly-Phe-Leu-Met (Met5 enkephaline)

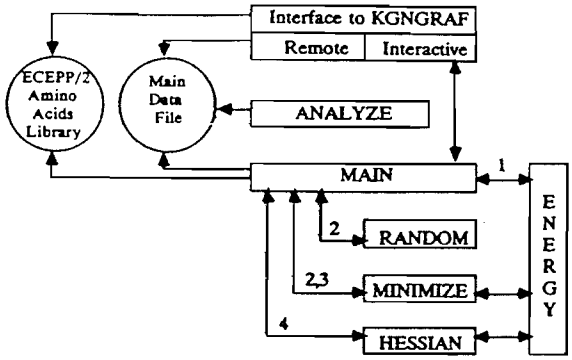

FIG. 1. Flowchart of the PEPSEA program.

studies (21–24) have supported this conformation. The application of recent multi-spin methods has confirmed these results (25, 26). Another group of structures involves β-turns including residues Gly^2 and Gly^3, generated by the existence of a (4 → 1) intramolecular hydrogen bond between $CO(Tyr^1)$ and the terminal $OH(Phe^4)$. Pioneering investigations of DeCoen *et al.* first mentioned this possibility (19), which was also suggested by C.P.K. model studies (27) and confirmed by a systematic conformational search (10). Exclusively extended structures were determined by X-ray diffraction studies (28–30). However, a folded β-turn structure was observed by X-ray diffraction studies of Leu-Enkephalin (31). Finally, a γ-turn involving the three residues Gly^2-Gly^3-Phe^4 was predicted by Scheraga, from simulations based on a statistical mechanical algorithm (32). Our purpose in this study has been to generate a population of conformers for **M-Enk,** and to evaluate its representation of the full conformational space by comparison with previous results.

The investigation of chemotactic peptides has also proven to be very challenging, the most potent agent being the tripeptide formyl-Met-Leu-Phe-OH: **fMLP.**[2] Structure–activity relationships were established, trying to identify the *active* conformer. In a recent publication, we formulated a hypothesis about the structural requirements for chemotactic activity (33). Although more rigid than **fMLP,** the peptide **fMAP,**[2] where the Leu residue has been substituted by the residue **Aib** (α-aminoisobutyric acid), retains the chemotactic activity (34–36). Structural studies by ^1H and ^{13}C NMR (34,37) and infrared spectroscopy (37) inferred that the presence of intramolecular hydrogen bonds suggests a structure involving a β- or γ-turn, with CO(Met) and NH(Phe). To corroborate our model of the *active* conformer for a chemotactic tripeptide, we have investigated the conformational properties of **fMAP.**

Method

Our method of population generation of conformations, based on random search and energy minimization, has been implemented as an interactive molecular modeling package.

Description of the PEPSEA[3] program

The scheme of the program is shown in Fig. 1. The MAIN module assumes the control and data file management, routing the execution following the options chosen by the user. PEPSEA can be used in two different modes. The interactive mode is suitable for data preparation and for single conformation calculations. The remote mode is used for multiple conformation applications and to submit applications to local or remote computers. In its present version, the interactive mode is interfaced with the KGNGRAF molecular modeling package (38). Interactive tools have been implemented to build up specific sequences, using the ECEPP amino-acid library (6–8).

As indicated by the numbers in Fig. 1, the program offers four different options. Option 1 allows us to perform a single ECEPP energy calculation. Route 2 allows us to generate a population of conformers. Random values are assigned to torsional angles and the corresponding energy minimized. This process is repeated a number of times corresponding to the number of conformers one wishes to study. Route 3 allows the minimization of predefined conformers, while option 4 computes the Hessian matrices in order to estimate free energies.

The ENERGY module is similar to the energy function of the ECEPP/2 program (39). It reproduces, exactly, ECEPP calculations for the residues included in the amino-acid library (6–8). The RANDOM module returns a random number between 0 and 1 based on a subtractive method (40). These numbers are converted to values between −180 and 180°, to be assigned to the variable torsional angles as specified by the user. The MINIMIZE module is used to find the minima of the energy function. It uses the conjugate gradient algorithm (41). A subroutine has been implemented to estimate the first derivatives by finite differences. Based on comparative studies described by Fletcher (42), the method of the central derivative was used, and proved to be well adapted for the polynomial function of the energy. The convergence criterion was set to 10^{-4}, terminating the calculation when the module of the vector constituted by the first derivatives becomes less than that value. Step sizes of 0.001 degree are used. The module does not impose any restrictions on the number of iterations. The HESSIAN module calculates the determinant of the Hessian matrix, constituted by the second derivatives of the energy function at the minimum under investigation. This is done for a predefined set of low energy conformers.

The subroutine used to compute second derivatives is similar to the one used for first derivatives. Nevertheless, optimal values for the step size have to be determined by the user. In its present version, the ANALYZE module estimates partition functions and free energy values following well-established methods (43). This program can also sort and manipulate the main data file.

Experimental procedure

In practice, the user needs to decide about the sequence of residues, making sure that the residues are included in the library. Secondly, variable angles must be specified before submitting the process.

For **M-Enk,** the peptidic sequence has been built using the standard residue library of ECEPP (6–8) with the end groups uncharged, $-NH_2$ and -COOH. A dielectric constant of 2 was used in the energy calculations. A total number of 3000 conformers was randomly generated and energy-minimized to the closest minimum, using all 13 possible ϕ, Ψ, $\chi 1$ angles as variables. The resulting population of conformers was sorted by increasing values of the conformational energies. Subsequently, the first 100 conformers of lower energies have

[3]PEPSEA is an abbreviation for Peptidic Search.

Can. J. Chem. Downloaded from www.nrcresearchpress.com by 92.62.229.171 on 09/08/12
For personal use only.

Can. J. Chem. Downloaded from www.nrcresearchpress.com by 92.62.229.171 on 09/08/12
For personal use only.

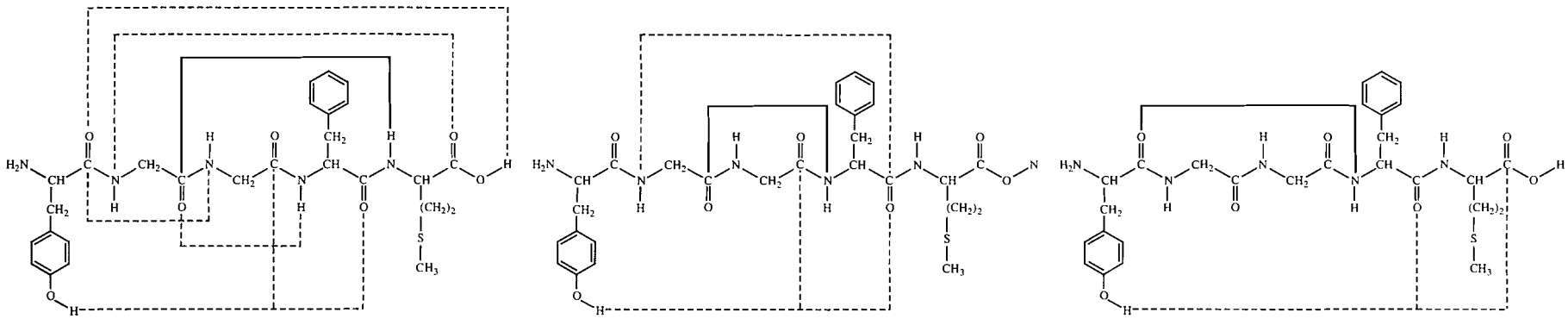

	Class 1					Class 2								Class 3
No.	Code	Type	N	ΔE kcal/mol	ΔG	Tyr[1] OH C′O Gly[3]	Tyr[1] OH C′O Phe[4]	Tyr[1] OH C′O Met[5]	Cly[2] NH C′O Met[5]	Gly[2] NH C′O Phe[4]	Gly[3] NH C′O Tyr[1]	Phe[4] NH C′O Gly[2]	Met[5] OH C′O Tyr[1]
Class 1													
1	GA*C*AE	II′	2	0.00	0.00		*						*
2	FCC*AF	II′	1	1.16	0.16		*		*		*		
3	FDC*AC	II′	4	1.56	−0.98	*			*				
4	FDC*AG	II′	1	2.37	−0.50	*			*				
5	F*DC*AG	II′	1	3.22	0.62	*			*				
9	FAD*AE	IV	1	3.91	0.43	*			*				
10	FDC*BG	II′	1	4.12	1.96	*						*	
17	FHAAG	III	1	5.74	2.22	*			*				
18	FDC*EF*	IV	2	5.78	4.12				*			*	
Class 2													
6	FDC*EC		2	3.43	2.10	*				*			
7	FDC*FA		1	3.88	2.06	*				*			
8	FDC*EA		1	3.88	2.44	*				*			
11	FDC*EE		1	4.13	0.88	*							
20	FEC*EE		1	6.09	1.41		*						
23	F*EC*EG		1	6.47	2.22		*						
Class 3													
12	BC*DAE	IV	1	4.43	1.15			*					
13	BC*DFB	IV	1	4.53	0.82		*						
14	BC*DFC	IV	1	4.68	1.51		*						
19	B*C*DAE	IV	1	5.82	2.91			*					

FIG. 2. Classes of conformers of **M-Enk**. No.: Ranking order by increasing ΔE. Code: Conformational code (43). Type: Type of turn. N: Frequency of occurrence. ΔE: Relative conformational energy. ΔG: Relative conformational free energy. *: Presence of hydrogen bonds.

Can. J. Chem. Downloaded from www.nrcresearchpress.com by 92.62.229.171 on 09/08/12
For personal use only.

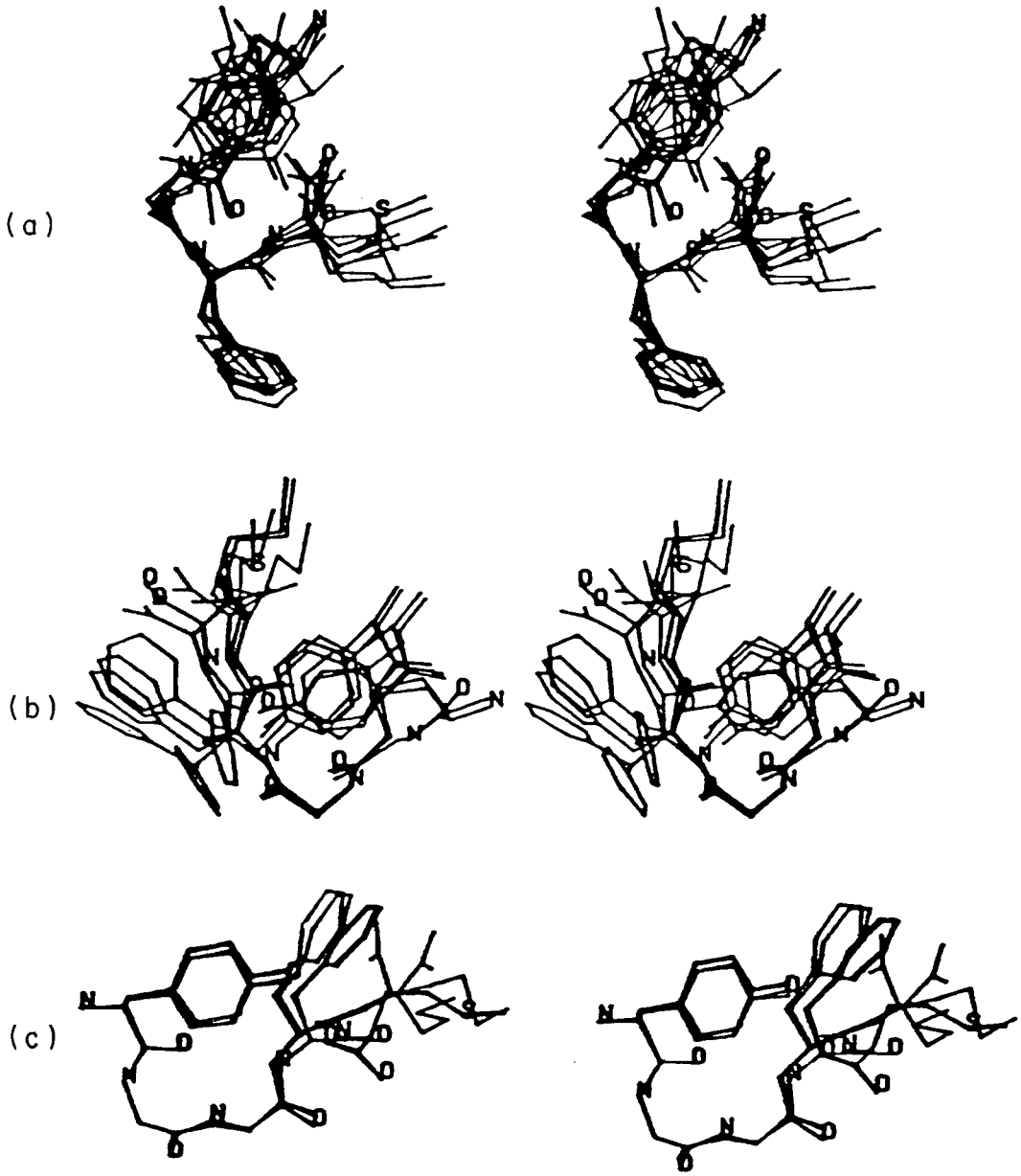

FIG. 3. Stereographic superpositions of conformers of **M-Enk**. (*a*) class 1; (*b*) class 2; (*c*) class 3.

been submitted to energy minimization, allowing all rotatable bonds to be modified.

For **fMAP,** the peptidic sequences were built from the standard library of ECEPP (6–8) updated for the α-aminoisobutyric acid residue **Aib.** Atomic partial charges for this particular residue were computed by CNDO/2 calculations (44). Fifteen hundred starting conformers were randomly generated and energy-minimized to the closest minima. Again, a dielectric constant of 2 was used in the energy calculations. For this generating process, all torsional angles ϕ, Ψ and $\chi 1$'s were allowed to vary. The first 100 conformers of lower energies were submitted to a further energy minimization, allowing all rotatable bonds to be modified. The resulting population of conformers was sorted by increasing values of the conformational energies.

The calculations were performed on IBM RISC/6000 model 520 workstations (Laboratoire de modélisation moléculaire, Université de Sherbrooke), and on an IBM 4381, VM/CMS operating system (Centre de l'informatique, Université de Sherbrooke). The SYBYL molecular modeling system was used for displaying, plotting, and fitting of the molecular structures (45). Dihedral angles are labelled according to the IUPAC–IUB Commission on Biochemical Nomenclature (46).

Results and discussion

Conformational domains of Met-Enkephalin

The corresponding conformations have been identified in accordance with the conventional letter-coded partition of the [ϕ,Ψ] maps (43). The most stable conformers appeared to be distributed into three major classes presented in Fig. 2. For each structure, one finds an identification number (no.), the ranking order by increasing energy, the conformational code, the type of turn, (N) the frequency of occurrence, (ΔE) the relative conformational energy, (ΔG) the relative conformational free energy computed at 300 K, and finally the

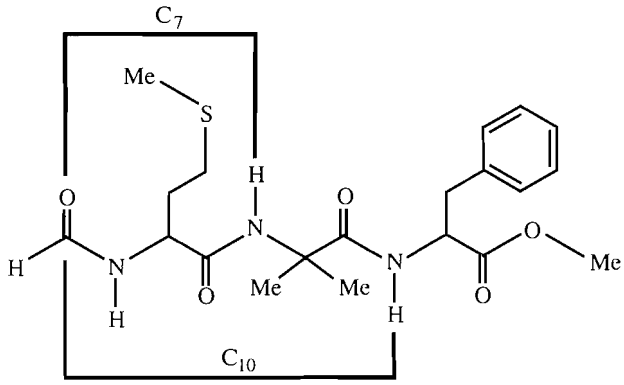

Class 1				Class 2				Class 3			
No.	Code	*N*	ΔE	No.	Code	*N*	ΔE	No.	Code	*N*	ΔE
1	AAD	1	0.00	6	CAE	1	1.14	3	EAE	4	0.47
2	AAE	3	0.41	7	CFE	3	1.15	10	EAE	1	1.38
4	AAE	2	0.55	8	CAE	2	1.18	15	EAF	1	1.50
5	AAE	1	0.56	9	CAE	2	1.33	18	EAE	7	1.56
11	AAE	2	1.40	13	CAE	3	1.44	23	EAE	3	1.96
12	AAE	3	1.43	16	CAE	1	1.54	25	EAE	5	1.98
14	AAE	1	1.48	22	FAE	2	1.96	27	AA*E	4	2.31
17	AAE	1	1.54	24	FAF	1	1.97	28	EAE	4	2.41
19	AAE	3	1.76	26	CAF	2	2.22	29	DAE	1	2.41
20	AAD	1	1.90	33	FAE	1	2.88	30	DAE	3	2.48
21	AAF	2	1.94	35	FAE	2	3.41	31	EAE	2	2.52
				36	CFE	1	3.51	32	DAE	3	2.87
								34	EAF	1	2.96

FIG. 4. Classes of conformers of **fMAP**. No.: Ranking order by increasing ΔE. Code: Conformational code (43). Type: Type of turn. *N*: Frequency of occurrence. ΔE: Relative conformational energy.

presence and nature of possible hydrogen bonds. The different possible hydrogen bonds are also indicated, the thick line indicating the main hydrogen bond, which characterizes the type of structure for a particular class of structures.

The first class is the most populated (14 structures over 30). It is characterized by a β-turn involving residues Gly^3 and Phe^4, with the existence of an (5 → 2) intramolecular hydrogen bond involving $CO(Gly^2)$ and $NH(Met^5)$. The global minima no. 1, coded GA*C*AE (E = −14.20 kcal/mol), and no. 3, coded FDC*AC (ΔG = −0.98 kcal/mol), identical to the global minimum proposed by Wüthrich (10) and similar to the second minimum of Scheraga (9), belong to this group. Interestingly, a frequency of occurrence of 4 was obtained for this most probable structure no. 3. It is important to mention the contribution of the Tyr^1 OH^{η} in the stabilisation of folded structures. Most theoretical (10–20) and experimental (21–26) studies have proposed such conformations. Figure 3*a* gives the superposition of the structures belonging to this group. Another kind of Gly^3-Phe^4 type II′ β-turn was reported by Moskowitz and co-workers (13, 47). In this particular structure, the ω angle of Met^5 differed by 180°; nevertheless, after minimization by PEPSEA, this structure converged exactly to our conformer no. 3 coded and FDC*AC.

Class 2 involves similar structures but with a γ-turn including residue Gly^3 generated by the existence of a (4 → 2) intramolecular hydrogen bond between $CO(Gly^2)$ and the $NH(Phe^4)$. Figure 3*b* gives the superposition of the structures belonging to this group. More flexibility is allowed by this class of conformers, especially for the Tyr and Phe side chains. Recent theoretical studies have also mentioned the probable existence of these structures (32). Again in this group the Tyr^1 OH^{η} contributes to hydrogen bonding in seven cases.

The third class is characterized by the presence of a β-turn with the central residues Gly^2-Gly^3 generated by a (4 → 1) intramolecular hydrogen bond between $CO(Tyr^1)$ and the terminal $OH(Phe^4)$. Interestingly, the similarities between this type of structure and potent rigid opioid compounds led Momany (48) and other groups (49, 50) to suggest a Gly^2-Gly^3 type II′ β-turn as the bioactive conformation for recognition at the opioid receptor. Figure 3*c* shows that the structures differ only by the orientation of the methionine residue, the rest of the molecule adopting a globular shape of structure similar to rigid opioids.

These three groups of structures obtained for **M-Enk** include most of the structures previously reported. Some particular structures are interesting to examine. Structures similar to the extended X-ray structures were found with ΔE higher than 20 kcal/mol. Also the folded structure observed for **Leu-Enk** (31) converged, after energy minimization, to a minimum with a ΔE = 17 kcal/mol.

*The chemotactic peptide f-Met-Aib-Phe **fMAP***

Figure 4 presents the first 100 most stable conformers resulting from the minimization of all torsional angles. Conformational energies are relative to the global minimum no.

Can. J. Chem. Downloaded from www.nrcresearchpress.com by 92.62.229.171 on 09/08/12
For personal use only.

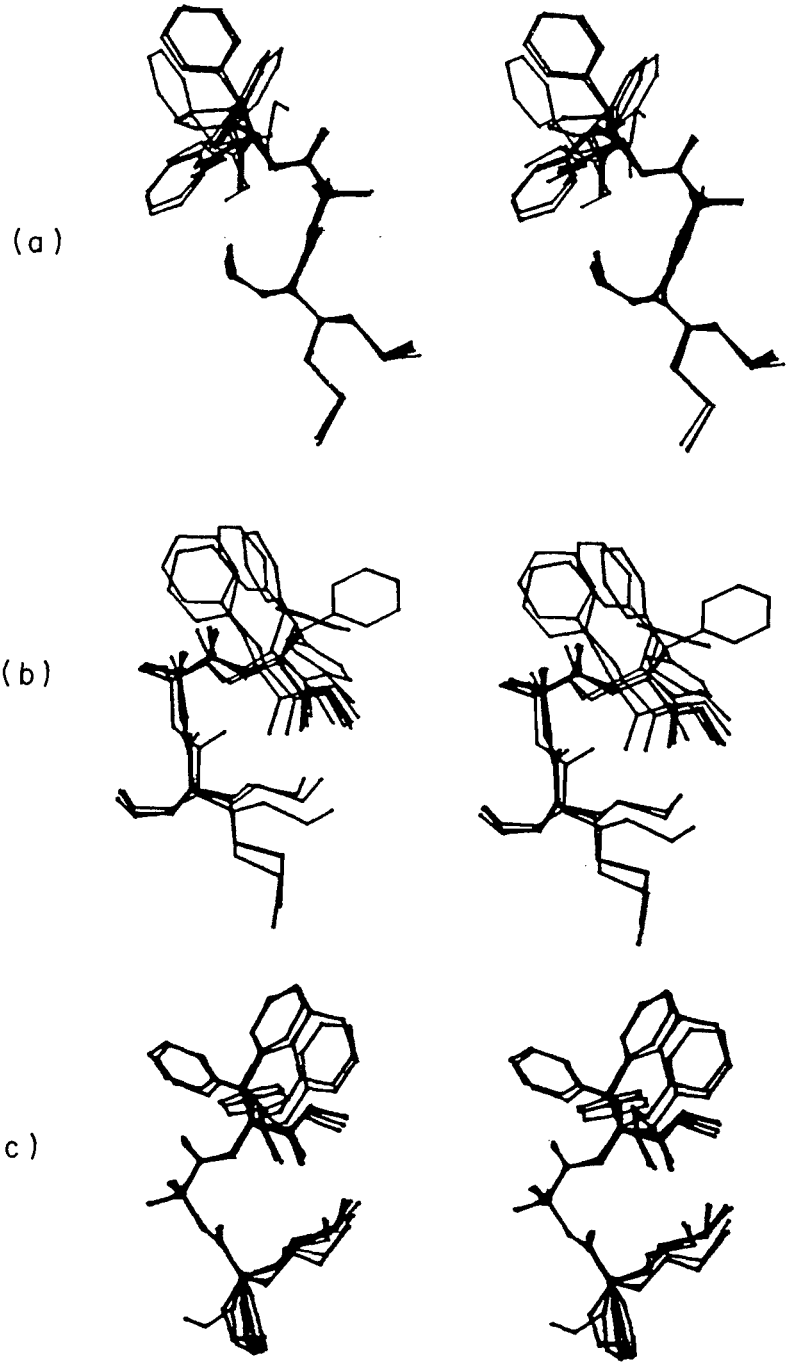

FIG. 5. Stereographic superpositions of conformers of **fMAP**. (*a*) class 1 (*b*) class 2 (*c*) class 3.

Can. J. Chem. Downloaded from www.nrcresearchpress.com by 92.62.229.171 on 09/08/12
For personal use only.

1 (E −2.66 kcal/mol). The table gives the code corresponding to the conformations. The frequency of occurrence is the number of times the conformer was obtained after minimization. Among the 100 conformers, 80 are distributed into three classes. The first two classes are composed of folded structures and the third one includes extended structures. Folded structures can be stabilized by two main hydrogen bonds, one between formyl(CO) and Phe(NH), giving rise to a C_{10} β-turn, and the other, between formyl(CO) and Aib(NH), to form a γ-turn structure.

The first class is characterized by the presence of a type III or III′ β-turn. It includes 20 conformers of relatively low energies (less than 2 kcal/mol) and includes the global minimum (no. 1). Figure 5*a* shows a superposition of these structures and demonstrates the similarity of the members of the class. The variability is due to the possible rotations of the Phe side chain. Previous NMR studies have concluded that the presence of an Aib residue favored the formation of 3_{10} helices characterized by type III or III′ β-turns (51). More specifically, by empirical energy calculations Semus reached the conclusion that **fMAP** adapted a β-turn structure (52).

The second class includes 21 conformers characterized by the presence of the γ-turn. Superpositions of Fig. 5*b* show

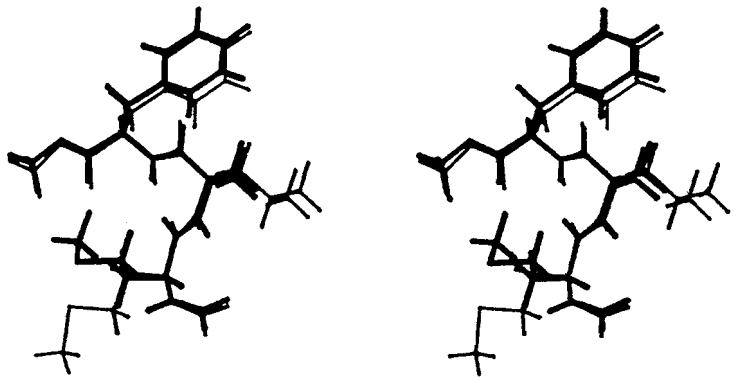

FIG. 6 Superposition of the proposed active conformer of **fMLP** (33) with **fMAP** from class 3 (thick lines).

Can. J. Chem. Downloaded from www.nrcresearchpress.com by 92.62.229.171 on 09/08/12
For personal use only.

that the Met is mainly oriented in two different ways, while the Phe residue can rotate more freely than in class 1.

The third class is composed of 39 conformers of energies lower than 3 kcal/mol. The main structural feature is the extended structure, without hydrogen bond. By examining the superposition of Fig. 5*c*, one observes the proximity between the Met side chain and the backbone. This interaction constitutes the main factor of electrostatic stabilization for this class of compounds. Only 15 among the first 100 structures do not belong to our classes. The structures are extended, and the only conformer no. 43 forms a C_7 hydrogen bond between Met(CO) and Aib(NH) giving rise to a γ-turn structure, also proposed by Antony Raj and Balaram (37) from infrared and ^{1}H NMR studies.

To verify our hypothesis of active structure for this family of compounds (33), we present in Fig. 6 the superposition of our previously proposed active conformer of **fMLP** and **fMAP** (thick lines) as it appears in the third class of structures. It is seen that the only modifications are observed for the Met side chain, while the backbones are similar. Although not stabilized by hydrogen bonds, this third class of peptides appears to be compatible with our hypothesis of active conformer and includes 50% of the population generated. This also indicates that an active chemotactic peptide must have the formyl group free of intramolecular interaction in order to be available for the formation of the complex with the receptor.[4]

In conclusion, the strategy based on random generation of peptidic structures, followed by energy minimization, has been shown to generate relevant populations of conformers. The method appears to be an excellent alternative when a systematic conformational search of conformations is prohibitive. The analysis of such populations led to the conclusion that the structures are organized into domains. Further investigations have already been undertaken in our group to develop methods of analysis based on statistical mechanics, in order to predict physico-chemical properties of ensembles of conformations. Such an approach is expected to give a better understanding of the conformational behaviour of flexible molecules and particularly of polypeptides.

[4]Supplementary material in the form of tables of torsional angles for Met-Enkephalin and for formyl α-aminoisobutyric acid–phenylalanine may be purchased from: The Depository of Unpublished Data, Document Delivery, CISTI, National Research Council Canada, Ottawa, Canada K1A 052.

Acknowledgements

This research was made possible by the support of the I.B.M. Canada Ltée, through the Cooperative Project program, allowing our laboratory to be equiped with state-of-the-art workstations. The TRIPOS company is also acknowledged for a grant that allowed us to use the SYBYL software.

1. G. Fisher and F. X. Schmid. Biochemistry, **29**, 2205 (1990).
2. M. Saunders. J. Am. Chem. Soc. **109**, 3150 (1987).
3. H. Kawai, T. Kikuchi, and Y. Okamoto. Protein Eng. **3**, 85 (1989).
4. S. Vajda and C. Delisi. Biopolymers, **29**, 1755 (1990).
5. A. E. Howard and P. A. Kollman. J. Med. Chem. **31**, 1669 (1988).
6. F. A. Momany, R. F. McGuire, A. W. Burgess, and H. A. Scheraga. J. Phys. Chem. **79**, 2361 (1974).
7. G. Nemethy, M. S. Pottle, and H. A. Scheraga. J. Phys. Chem. **87**, 1883 (1983).
8. F. A. Momany, L. M. Carruthers, R. F. McGuire, and H. A. Scheraga. J. Phys. Chem. **78**, 1595 (1974).
9. M. Vasquez and H. A. Scheraga. Biopolymers, **24**, 1437 (1985).
10. T. Schaumann, W. Braun, and K. Wüthrich. Biopolymers, **29**, 679 (1990).
11. L. B. Morales, R. Garduno-Juarez, and D. Romero. J. Biomol. Struct. Dynam. **8**, 721 (1991).
12. M. R. Pincus, R. P. Carty, J. Chen, J. Lubowsky, M. Avitable, D. Shah, H. A. Scheraga, and R. B. Murphy. Proc. Natl. Acad. Sci. USA, **84**, 4821 (1987).
13. J. W. Moskowitz, K. E. Schmidt, S. R. Wilson, and W. Cui. Int. J. Quantum Chem. Quantum Chem. Symp. **22**, 611 (1988).
14. Y. Y. Balodis, G. V. Nikiforovich, I. V. Grinsteine, R. E. Vegner, and G. I. Chipens. FEBS Lett. **86**, 239 (1978).
15. Z. Li and H. A. Scheraga. Proc. Natl. Acad. Sci. USA, **84**, 6611 (1987).
16. O. Purisima and H. A. Scheraga. J. Mol. Biol. **196**, 697 (1987).
17. D. R. Ripoll and H. A. Scheraga. J. Protein Chem. **8**, 263 (1989).
18. Y. Isogai, G. Nemethy, and H. A. Scheraga. Proc. Natl. Acad. Sci. USA, **74**, 414 (1977).

19. J. L. DeCoen, C. Humblet, and M. H. J. Koch. FEBS Lett. **73**, 38 (1977).
20. S. J. Weiner, P. A. Kollman, D. T. Nguyen, and D. A. Case. J. Comput. Chem. **7**, 230 (1986).
21. C. Garbay-Janeguiberry, B. P. Roques, R. Oberlin, M. Anteunis, and A. K. Lala. Biochem. Biophys. Res. Commun. **71**, 558 (1976).
22. C. R. Jones, W. A. Gibbons, and V. Garsky. Nature, **262**, 779 (1976).
23. B. P. Roques, C. Garbay-Janeguiberry, M. Anteunis, and A. K. Lala. Nature, **262**, 778 (1976).
24. M. A. Khaled, M. M. Long, W. D. Thompson, R. J. Bradley, G. B. Brown, and D. W. Urry. Biochem. Biophys. Res. Commun. **76**, 224 (1977).
25. L. Zetta, A. deMarco, and G. Zannoni. Biopolymers, **25**, 2315 (1986).
26. A. Motta, T. Tancredi, and P. A. Temussi. FEBS Lett. **215**, 215 (1987).
27. A. F. Bradbury, D. G. Smyth, and C. R. Snell. Nature, **260**, 165 (1976).
28. J. F. Griffin, D. A. Langd, G. D. Smith, T. L. Blundell, I. J. Tickle, and S. Bedarkar. Proc. Natl. Acad. Sci. USA, **83**, 3272 (1986).
29. D. Mastropaolo, A. Camerman, L. Y. Y. Ma, and N. Camerman. Life Sci. **40**, 1995 (1987).
30. M. Doi, M. Tanaka, T. Ishida, M. Inoue, T. Fujiwara, K. Tomita, T. Kimura, S. Sakakibara, and G. M. Sheldrick. J. Biochem. **101**, 485 (1987).
31. G. D. Smith and J. F. Griffin. Science, **199**, 1214 (1978).
32. G. H. Paine and H. A. Scheraga. Biopolymers, **26**, 1125 (1987).
33. A. G. Michel, G. Lajoie, and C. Ameziane-Hassani. Int. J. Pept. Protein Res., **36**, 489 (1990).
34. M. Iqbal, P. Balaram, H. J. Showell, R. J. Freer, and E. L. Becker, FEBS Lett. **165**, 171 (1984).
35. M. Sukumar, P. Antony Raj, P. Balaram, and E. L. Becker. Biochem. Biophys. Res. Commun. **128**, 339 (1985).
36. C. Toniolo, M. Crisma, G. Valle, G. M. Bonora, S. Polinelli, E. C. Becker, R. J. Freer, Sudhanand, R. R. Balaji, P. Balaram, and M. Suramar. Pept. Res. **2**, 275 (1989).
37. P. Antony Raj and P. Balaram. Biopolymers, **24**, 1131 (1985).
38. S. Chin, R. Tahliavina, J. P. Prost, and M. Martins-Costa. Visualization techniques and windowing interfaces: KGNGRAF, XWIB and REMOTE. *In* Modern techniques in computational chemistry: MOTECC-90. *Edited by* E. Clementi. ESCOM. Leiden, Netherlands. 1990 Chap. 24, pp. 1021–1090.
39. M. J. Brownman, L. M. Carruthers, K. L. Kashuba, F. A. Momany, M. S. Pottle, S. P. Rosen, and S. M. Rumsey. QCPE, **11**, 286 (1975).
40. D. E. Knuth. *In* "Semi-numerical algorithms." 2nd ed. Vol. 2. The art of computer programming. Addison-Wesley, Reading Mass. 1981, 3.2–3.3.
41. M. J. D. Powell. Math. Program. **12**, 241 (1977).
42. C. A. Fletcher. *In* Computational techniques for fluid dynamics. Vol. 1. Fundamental and general technics. Springer-Verlag, New York. 1988. pp. 55–60.
43. S. S. Zimmerman, M. S. Pottle, G. Nemethy, and H. A. Scheraga. Macromolecules, **10**, 1 (1977).
44. Y. Patterson, S. M. Rumsey, E. Benedetti, G. Nemethy, and H. A. Scheraga. J. Am. Chem. Soc. **103**, 2947 (1981).
45. Sybyl. Molecular modeling software. Version 5.4 (1991). Tripos Associates, Inc. St. Louis, Missouri.
46. IUPAC–IUB Commission on Biochemical Nature. Biochemistry, **9**, 3471 (1970).
47. S. R. Wilson, W. Cui, J. W. Moskowitz, and K. V. Schmidt. Tetrahedron Lett. **29**, 4373 (1988).
48. F. A. Momany. Biochem. Biophys. Res. Commun. **75**, 1098 (1977).
49. G. H. Loew and S. K. Burt. Proc. Natl. Acad. Sci. USA, **75**, 7 (1978).
50. G. H. Loew, G. Hashimoto, L. Williamson, S. K. Burt, and W. Anderson. Mol. Pharmacol. **22**, 2677 (1982).
51. S. F. Semus, E. C. Becker, C. Toniolo, and R. F. Freer. Biochem. Biophys. Res. Commun. **157**, 569 (1988).
52. C. Toniolo. Biopolymers, **28**, 247 (1989).

Can. J. Chem. Downloaded from www.nrcresearchpress.com by 92.62.229.171 on 09/08/12
For personal use only.

On the nature of the anomeric effect in XH_n—CH_2—OH systems, with X = F, O, N, C

F. GREIN
Department of Chemistry, University of New Brunswick, Fredericton, N.B., Canada E3B 6E2

AND

P. DESLONGCHAMPS
Department of Chemistry, University of Sherbrooke, Sherbrooke, Quebec, Canada J1K 2R1

Received May 30, 1991

This paper is dedicated to Professor Sigeru Huzinaga on the occasion of his 65th birthday

F. GREIN and P. DESLONGCHAMPS. Can. J. Chem. **70**, 604 (1992).

Using geometry optimizations at the 6-31G** level, energies, bond distances, and charges were obtained for systems XH_n—CH_2—OH with X = F, O, N, C, for various rotational conformers of the OH group. Conformational analysis shows that systems with X = F and O receive anomeric stabilization due to a partial π-bond forming in the CH_2—OH fragment of the molecule, amplified or diminished by lone pair repulsion (or dipole) energies. For the systems with N and C, no π-bond stabilization is found. However, the e-NH_2—CH_2—OH system is still stabilized due to favourable lone pair repulsion circumstances.

Key words: anomeric effect, *ab initio* studies, π-bonding model.

F. GREIN et P. DESLONGCHAMPS. Can. J. Chem. **70**, 604 (1992).

Utilisant des optimisations de géométrie au niveau 6-31G**, on a déterminé les énergies, les longueurs de liaison et les charges de divers conformères rotationnels du groupe OH des systèmes XH_n—CH_2—OH (X = F, O, N et C). L'analyse conformationnelle montre que les systèmes dans lesquels X = F et O reçoivent de la stabilisation anomérique qui résulte de la formation d'une liaison π partielle dans le fragment CH_2—OH de la molécule, amplifiée ou diminuée par les énergies de répulsion (ou dipolaire) de la paire d'électrons libre. Pour les systèmes avec N et C, on n'a pas observé de stabilisation par liaison-π. Toutefois, le système e-NH_2—CH_2—OH est encore stabilisé à cause des circonstances favorables créées par la répulsion de la paire libre.

Mots clés : effet anomérique, études *ab initio*, modèle de liaison-π.

[Traduit par la rédaction]

Can. J. Chem. Downloaded from www.nrcresearchpress.com by 92.62.229.171 on 09/08/12
For personal use only.

Introduction

Considerable experimental evidence has been found in recent years for "stereoelectronic" effects, which relate the conformation and reactivity of molecules to the orientation of electron pairs in space. Such evidence is summarized in books by Deslongchamps (1) and Kirby (2). The term "anomeric" effect was introduced in 1958 by Lemieux and Chu (3) in connection with the orientation of an alkoxy group in the pyranose ring. As a general rule, a lone pair of electrons (lp) on O oriented antiperiplanar (app) to a polar bond stabilizes the molecule, leading to a shortening of the C—O bond and a lengthening of the polar bond. A simple explanation is given by the partial donation of a lone pair electron into the polar bond resulting in the formation of a partial C—O double bond combined with a lengthening of the polar bond C—Y due to the negative charge on Y. In molecular orbital terms, this electronic stabilization is understood by delocalization of an n_p lone pair of O into the σ* orbital of the adjacent C—Y bond (4, 5). In an earlier interpretation (6), the anomeric effect was considered to be destabilizing due to the electrostatic repulsion of dipoles (or electron pairs) (7).

Molecular orbital studies have been found to reproduce this effect quite well. A large number of theoretical papers have appeared in the literature, considering many different systems and various aspects of the anomeric effect, starting in 1971 with the ground-breaking work by Wolfe *et al.* (8). For recent work see, for example, Reed and Schleyer (9, 10), as well as articles to be cited later on.

As a simple example, which was discussed in detail by

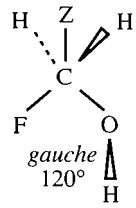

1*a*

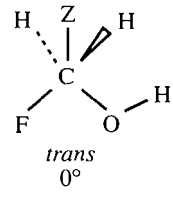

1*b*

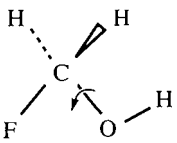

F–CH_2–OH

1*c*

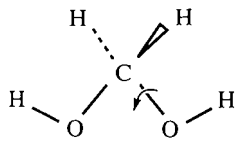

a-OH–CH_2–OH

2

Wolfe *et al.* (8), the lowest energy of fluoromethanol occurs for OH being *gauche* to CF, **1***a*, which is about 5 kcal/mol more stable than the *trans* conformer **1***b*. For the *gauche* conformer, the CO distance is about 0.01 Å shorter, and the CF distance about 0.015 Å longer than for *trans*. Also the OCF angle undergoes change.

While theoretical results obtained for energy and geometry changes are in good agreement with experimental findings, it is considerably more difficult to explain the nature of the anomeric effect, and in particular to decompose the

Can. J. Chem. Downloaded from www.nrcresearchpress.com by 92.62.229.171 on 09/08/12
For personal use only.

calculated energy differences into components corresponding to familiar concepts like steric effects, "electronic" effects, lone pair repulsions, etc.

In the following work, systems of type XH_n—CH_2—OH will be investigated, where in each case the OH hydrogen is being rotated about the CO bond. X will be F, O, and N. For reference purposes, C will also be included. While each of the above systems individually, or in combination with others, has been studied before (see, for example, Wolfe *et al.* (11), Smits *et al.* (12)), in this work a new analysis of energetic and bond distance changes will be presented, allowing us to classify the systems into various categories according to interactions that take place in the course of the OH rotation.

Method

For each of the systems XH_n—CH_2—OH, with X = F, O, N, C, geometry optimizations were performed at the 6-31G** level, using the GAUSSIAN 86 program (13). The Z—C—O—H dihedral angle (denoted briefly as the OH dihedral angle ϕ) was varied from 0° (*anti*), to 60°, to 90°, to 120° (*gauche*), to 180° (*syn*), where Z is defined in **1***a*, and the notations *anti*, *syn*, and *gauche* refer to the orientation of OH relative to the CX bond. Examples are shown in **1***a* and **1***b*. Besides the 60° intervals, ϕ = 90° was included due to its significance in the Fourier analysis to be discussed later. For each choice of OH dihedral angle, a complete geometry optimization of all other parameters, bond distances, bond angles, and remaining dihedral angles, was carried out.

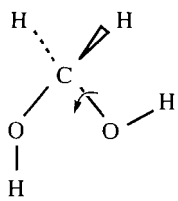

s-OH–CH_2–OH

3

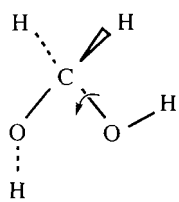

g-OH–CH_2–OH

4

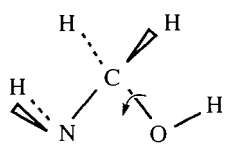

e-NH_2–CH_2–OH

5

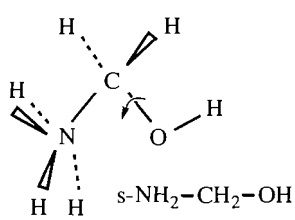

s-NH_2–CH_2–OH

6

For a given series of OH rotations, the dihedral angles of the XH_n hydrogens were fixed. For example, in the *a*-OH—CH_2—OH series, the dihedral angle of the (left) *a*-OH was kept at 0°, *anti*, whereas for *s*-OH—CH_2—OH, *s*-OH was kept at 180°, *syn*. Table 1 and structures **1***c*, **2**–**8** give the XH_n dihedral angles of all systems. For XH_n = OH, the prefixes *a*, *s*, *g* refer to *anti*, *syn*, and *gauche*, respectively, with respect to CX, whereas for XH_n = NH_2 and CH_3, the prefixes e and s refer to eclipsed and staggered, respectively, with respect to CH_2X.

Table 1. Choice of dihedral angles for the XH_n hydrogens of XH_n—CH_2—OH

XH_n—CH_2—OH	$\phi(XH_n)$[a]
a-OH—CH_2—OH	0°
s-OH—CH_2—OH	180°
g-OH—CH_2—OH	120°
e-NH_2—CH_2—OH	±60°
s-NH_2—CH_2—OH	±120°
e-CH_3—CH_2—OH	0, ±120°
s-CH_3—CH_2—OH	±60°, 180°

[a]Given are the dihedral angles Z—C—X—H, where *Z* is defined in **1***a*.

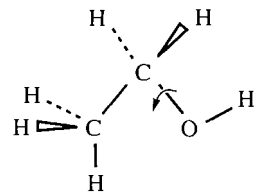

e-CH_3–CH_2–OH

7

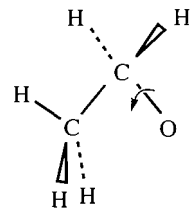

s-CH_3–CH_2–OH

8

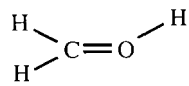

9*a*

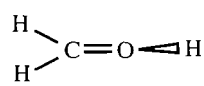

9*b*

Results and Fourier analysis

In Table 2, the calculated energy differences ΔE relative to ϕ = 0 (OH *trans*) are given for all geometry-optimized structures. It is seen that the first four systems, with X = F and O, all have the energy minimum at 120°, *gauche*, as one would expect, or at 90° for *s*-OH—CH_2—OH. (Actually, if ϕ is optimized, the minimum occurs at 127.77° for *a*-OH—CH_2—OH, being 0.06 kcal/mol lower than at 120°, and at 95.44° for *s*-OH—CH_2—OH, being 0.04 kcal/mol lower than at 90°; and so on for the other systems. For the purposes of this work, angles of 90°, 120° will be required.) While e-NH_2—CH_2—OH has its minimum at 180°, the remaining three systems of Table 2 are most stable at 0°. They are examples of the "*gauche* effect," as formulated by Wolfe *et al.* (8, 14, 15), whereby conformations with a maximum number of *gauche* interactions between adjacent electron pairs or polar bonds are most stable. Wolfe *et al.* (8) found that in the case of the anomeric effect conformations with a polar bond between two electron pairs will be destabilized.

Can. J. Chem. Downloaded from www.nrcresearchpress.com by 92.62.229.171 on 09/08/12
For personal use only.

Table 2. Calculated relative energies ΔE, in kcal/mol, for the systems XH_n—CH_2—OH, from 6-31G** geometry optimizations at OH dihedral angles of 0, 60, 90, 120, and 180°

XH_n—CH_2—OH	0°	60°	90°	120°	180°
F—CH_2—OH	0.00	−1.63	−3.89	−4.79	−2.37
a-OH—CH_2—OH	0.00	−0.83	−3.00	−4.49	−3.38
s-OH—CH_2—OH	0.00	−0.42	−1.28	−0.33	5.64
g-OH—CH_2—OH[a]	0.00	−0.44	−2.62	−3.86	0.79
e-NH_2—CH_2—OH	0.00	0.52	−1.20	−3.02	−3.82
s-NH_2—CH_2—OH	0.00	0.91	0.21	0.06	2.28
e-CH_3—CH_2—OH	0.00	1.37	0.68	0.27	2.40
s-CH_3—CH_2—OH	0.00	1.28	0.63	0.13	1.77

[a]$\Delta E(240) = 0.60$, $\Delta E(300) = 0.21$ kcal/mol.

Table 3. Fourier constants V_1–V_3, in kcal/mol, for systems XH_n—CH_2—OH, obtained from the relative energies of Table 2.

XH_n—CH_2—OH	V_1	V_2	V_3
F—CH_2—OH	−3.69	−2.71	1.31
Reference 16[b]	−5.25	−2.20	0.96
a-OH—CH_2—OH	−4.69	−1.29	1.31
Reference 17[b]	−7.65	−0.97	0.88
s-OH—CH_2—OH	3.82	−4.26	1.82
g-OH—CH_2—OH[a]	−0.48	−1.69	1.27
e-NH_2—CH_2—OH	−4.91	0.88	1.09
s-NH_2—CH_2—OH	0.95	−0.87	1.33
e-CH_3—CH_2—OH	0.87	−0.51	1.53
s-CH_3—CH_2—OH	0.41	−0.24	1.36
Reference 16[b]	0.93	−0.05	1.14

[a]$V'_1 = -1.47$, $V'_2 = 1.10$ kcal/mol.
[b]Some signs changed due to opposite convention for 0°.

In summary, judging by the $\phi = 120°$ conformer being more stable than the 0° conformer, the anomeric effect applies to all systems with X = F and O. While the above criterion also applies to e-NH_2—CH_2—OH, it is noted that for this system the 180° conformer is even more stable than the 120° one.

In the following, a Fourier analysis of ΔE will be performed, according to the method given by Radom and coworkers (16, 17). The formula used is

$$[1] \quad \Delta E(\phi) = (V_1/2)(1 - \cos\phi) + (V_2/2)(1 - \cos 2\phi) + (V_3/2)(1 - \cos 3\phi)$$

Additional terms $V'_1\sin\phi + V'_2\sin 2\phi$ will be needed for *g*-OH—CH_2—OH, which is not symmetric about 180°. According to the formula, $V(\phi)$ is zero at 0° and 360°, and therefore $\Delta E(0)$ was chosen as reference energy in Table 2.

From ΔE at 60, 120, and 180°, the V_i values of Table 3 were obtained. Taking $\Delta E(90)$ instead of ΔE at 60 or 120° leads to nearly identical V_i's. An interpretation of the V_i is given by Radom *et al.* (16). However, it is important to restate the important aspects. The V_3 portion of eq. [1] has maxima at 60 and 180°, and is zero at 0° and 120°. V_3 describes the threefold repulsion the rotating OH receives when it is eclipsing the two CH bonds at 60° and 300°, and the CX bond at 180°. V_3 is a strictly steric term, and is always positive. For the rotation of OH in CH_3OH, the energy difference between the staggered and eclipsed positions is 1.29 kcal/mol (6-31G**), and therefore V_3 is expected to be about 1.3 kcal/mol. Table 3 confirms this.

The V_2 part of eq. [1] has a maximum at 90°, and is zero at 0° and 180°. For the X = F, O systems, V_2 is negative, implying that the system is more stable at $\phi = 90$ than at $\phi = 0$, which checks with Table 2. Small negative values of V_2, as seen for the s-NH_2 and the CH_3 systems, are not considered to be significant, as will be explained later.

The V_1 portion of eq. [1] has a maximum at 180°, and a minimum at 0°. Since $\Delta E(180) = V_1 + V_3$, we can estimate $V_1 \cong \Delta E(180) - 1.3$ kcal/mol, or in other words, V_1 is the energy difference between 0 and 180°, corrected for the threefold steric repulsion. Essentially V_1 is negative if the conformation with OH at 180° (*syn*) is more stable than at 0° (*anti*), and positive if less stable. Negative and positive V_1 parameters occur in Table 3. The nature of V_1 and V_2 will be explained in detail later on.

Optimized C—O distances are given in Table 4. C—X distances will not be shown, since they depend on the nature of *X* and the orientation of the XH_n hydrogens, and are therefore not so useful for the comparative studies that follow. For the X = F and O systems, R_{CO} decreases starting with the 0° conformer, going through a minimum at 120°. For the remaining systems, R_{CO} increases between $\phi = 0$ and $\phi = 60°$, decreasing thereafter with a minimum again at 120°. It is known that SCF wavefunctions with polarization functions, such as 6-31G**, give bond distances significantly shorter than experimental values, and that correlated wavefunctions are required to correct this error. However, for our purposes only changes in *R* values are required, which are essentially independent of basis set.

In Table 5, the Mulliken charges on OH and XH_n are given. The charge on CH_2 can be derived as $Q_{CH2} = -Q_{OH} - Q_{XHn}$. A cursory look at Table 5 shows that for the systems with X = F and O, the negative charge on OH decreases as one goes from 0° to 90°, increasing thereafter. The OH charges on the remaining systems change little over the range 0–120°, but become more negative at 180°. The negative XH_n charges increase for all systems as one goes from 0 to 180° (or the positive charges for X = C decrease).

Discussion

For a simple definition of the anomeric stabilization, one may use the energy difference between the *anti* and *gauche* conformers, or $\Delta E(120)$ of Table 2. Accordingly, systems with *X* = *F* and *O*, as well as e-NH_2, have $\Delta E(120)$ negative, and therefore receive anomeric stabilization when OH is rotated from $\phi = 0$ to $\phi = 120°$. The remaining systems are not stabilized. The changes of R_{CO} and of charges mentioned earlier suggest that e-NH_2—CH_2—OH does not fit the same pattern as systems **1**–**4**. This will be discussed in detail later on. Since $\Delta E(120) = 0.75\,V_1 + 0.75\,V_2$, anomeric stabilization in terms of the V_i parameters means that $V_1 + V_2$ has to be negative. If both V_1 and V_2 are negative, such is assured (systems with *F*, *a*-OH, and *g*-OH). If V_1 is positive and V_2 negative, V_2 has to be more negative than $-V_1$. This is the case for *s*-OH—CH_2—OH. At the dihedral angles $\phi = 0°$ and 120°, OH is staggered relative to CH_2X, and the V_3 term is zero. Therefore, the anomeric stabilization depends only on V_1 and V_2, their signs and relative magnitudes.

Let us consider V_2 in more detail. In all cases of anomeric stabilization (omitting the special case of e-NH_2), V_2

Table 4. Optimized C—O distances (in Å) for systems XH_m—CH_2—OH, at various OH dihedral angles. 6-31G** basis set

XH_m—CH_2—OH	0°	60°	90°	120°	180°
F—CH_2—OH	1.3749	1.3689	1.3633	1.3630	1.3742
a-OH—CH_2—OH	1.3815	1.3787	1.3740	1.3727	1.3802
s-OH—CH_2—OH	1.3932	1.3924	1.3875	1.3857	1.3946
g-OH—CH_2—OH	1.3934	1.3912	1.3868	1.3850	1.3939
e-NH_2—CH_2—OH	1.3991	1.3998	1.3950	1.3932	1.3968
s-NH_2—CH_2—OH	1.4082	1.4090	1.4047	1.4029	1.4087
e-CH_3—CH_2—OH	1.4056	1.4088	1.4061	1.4037	1.4064
s-CH_3—CH_2—OH	1.4035	1.4074	1.4050	1.4026	1.4053

Table 5. Mulliken charges for OH (first line) and XH_n (second line), for optimized structures of XH_n—CH_2—OH. 6-31G** basis set

XH_n—CH_2—OH	0°	60°	90°	120°	180°
F—CH_2—OH	−0.279	−0.273	−0.268	−0.269	−0.288
	−0.387	−0.397	−0.405	−0.410	−0.415
a-OH—CH_2—OH	−0.280	−0.278	−0.276	−0.279	−0.294
	−0.280	−0.288	−0.298	−0.306	−0.317
s-OH—CH_2—OH	−0.317	−0.311	−0.306	−0.309	−0.325
	−0.294	−0.301	−0.310	−0.319	−0.325
g-OH—CH_2—OH	−0.306	−0.302	−0.297	−0.299	−0.319
	−0.279	−0.284	−0.291	−0.299	−0.309
e-NH_2—CH_2—OH	−0.291	−0.293	−0.291	−0.293	−0.307
	−0.149	−0.158	−0.168	−0.177	−0.190
s-NH_2—CH_2—OH	−0.318	−0.318	−0.315	−0.318	−0.332
	−0.148	−0.152	−0.161	−0.170	−0.181
e-CH_3—CH_2—OH	−0.312	−0.313	−0.312	−0.314	−0.325
	0.012	0.000	−0.011	−0.021	−0.029
s-CH_3—CH_2—OH	−0.304	−0.307	−0.307	−0.309	−0.316
	0.020	0.009	−0.003	−0.015	−0.033

Can. J. Chem. Downloaded from www.nrcresearchpress.com by 92.62.229.171 on 09/08/12
For personal use only.

is negative. (Small negative V_2, as obtained for s-NH_2 and the CH_3 systems, should be ignored. They are artifacts of the fitting formula.) A negative V_2 means that the system is more stable at $\phi = 90°$ than at 0°.

Such a negative V_2 can be explained by considering the "π-bonding model." If X in XH_n—CH_2—OH is sufficiently electronegative, then partial charges $XH_n^{(-)}$, CH_2—$OH^{(+)}$ are to be expected. CH_2—$OH^{(+)}$ carries a partial double bond, depending on the amount of positive charge. For the extreme case of a full positive charge, we have the cation CH_2=OH^+.

In the following, energies, C—O bond distances and Mulliken charges of CH_2=OH^+ will be compared with the corresponding quantities of the eight systems studied here. If the systems under investigation have ΔE, R_{CO}, and Q_{OH} values following the pattern of CH_2=OH^+ values as OH is being rotated, we invoke the π-bonding model to be valid for the system under consideration.

First, *ab initio* geometry optimizations with the 6-31G** basis set were performed on CH_2=OH^+. At equilibrium, this cation is planar, **9***a*, due to the π-bond. If OH is tilted 90° out of this plane, with a dihedral angle between CH and OH of 90°, **9***b*, an energy of 22.95 kcal/mol has to be expended. Since for planar CH_2=OH^+ V_1 and V_3 are zero, and $\Delta E(90) = 0.5\ V_1 + V_2 + 0.5\ V_3$ according to eq. [1], one finds $V_2 = -22.95$ kcal/mol, where 90° corresponds to the planar conformation. To mimic the CH_2—OH group in XH_n—CH_2—OH, the CH_2 group was pyramidalized, with dihedral angles fixed at ±60° with respect to the plane Z—C—O, **10***a*. OH was rotated about C—O, with $\phi = 0$ when OH is in the Z—C—O plane, **10***b*. This is equivalent to the definition of $\phi = 0$ for the other systems. The ΔE values (relative to $\phi = 0$), C—O distances, and Mulliken charges for OH are given in Table 6. The energy differences are very large, which is not surprising since rotations occur about a double bond.

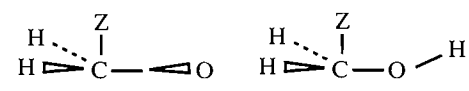

$\phi = 90°$ $\phi = 0°$

10*a* **10***b*

The important point is that for CH_2=OH^+ ΔE is negative

Table 6. 6-31G** results for $CH_2{=}OH^+$ with OH rotating about C—O, and CH_2 held in pyramidal position. For definition of the OH dihedral angle see **10***a* and **10***b*[a]

	0°[b]	60°	90°[c]	120°	180°
ΔE (kcal/mol)	0.00	−24.28	−32.62	−29.89	−13.48
R_{C-O} (Å)	1.2508	1.2370	1.2350	1.2394	1.2425
Q(OH)	0.048	0.126	0.140	0.127	0.085

[a]For $CH_2{=}OH^+$, $V_1 = -12.7$, $V_2 = -27.1$, $V_3 = -0.8$ kcal/mol.
[b]For 0°, the COH angle was fixed at 120°. Without setting this angle, OH would move from *cis* (0°) to *trans* (180°).
[c]The energy minimum occurs at 97.95° with ΔE 0.38 kcal/mol lower than at 90°.

at 60°, the energy reaching a minimum at 90° (or actually 97.95°, see Table 6), and is still close to this value at 120°, rising significantly at 180°, where, however, $\Delta E(180)$ is still negative.

In a similar manner, systems $XH_n{-}CH_2{-}NH_2$ can be compared with $CH_2{=}NH_2^+$, which is also planar at equilibrium. For $F{-}CH_2{-}NH_2$, Irwin *et al.* (18) obtained the global minimum for the N lone pair being antiperiplanar to C—F, 180°, and a local minimum at 0° (lp synperiplanar to CF). The potential curve has a maximum at 101.5°.

For $CH_2{=}OH^+$, the CO distance drops by 0.015 Å when going from 0 to 90°, and is still about 0.01 Å lower at 180° than at 0°. This is understandable since the π-bond is strongest at $\phi = 90°$, and nonexistent at 0 and 180°. Also, the *trans* configuration 180° is more stable than *cis*, 0°. The OH charges, as given in Table 6, also reflect the π-stabilization. Whereas they are close to 0 at 0°, and quite small at 180°, they reach a maximum of +0.140 at 90°, implying that the electrons are maximally involved in bonding and therefore not available as atomic charges. For $CH_2{=}OH^+$, the ΔE values of Table 6 lead to the Fourier parameters $V_1 = -12.7$, $V_2 = -27.1$ (V_2 was −22.9 for the planar cation), and $V_3 = -0.8$ kcal/mol. Due to the lack of threefold symmetry, V_3 is not meaningful. V_1 and V_2 are both negative, V_1 reflecting the fact that 180° is more stable than 0°, and V_2 the fact that 90° is more stable than 0°, as outlined above.

The V_i, ΔE, R_{CO}, and Q_{OH} values of $CH_2{=}OH^+$ will be used for comparison with the corresponding values of the systems under investigation.

The systems $F{-}CH_2{-}OH$ and *a*-OH—CH_2—OH resemble $CH_2{=}OH^+$ in all detail, as far as ΔE, V_i, R_{CO}, and Q_{OH} values are concerned. For example, ΔE is negative at 60°, and still negative at 180°. The shift of the minimum from 90° (actually 98°) to 120° (or thereabouts) is explained by the 90° conformer having a contribution from the destabilizing V_3, and a smaller contribution from V_1 (but a larger one from V_2). This is seen by comparing $\Delta E(90) = 0.5\,V_1 + V_2 + 0.5\,V_3$ with $\Delta E(120) = 0.75\,V_1 + 0.75\,V_2 + 0\,V_3$ (from eq. [1]). For both systems, not only is CH_2 + OH positive, but F is more negative than OH, Table 5, a fact one can readily accept. For *a*-OH—CH_2—OH, there are oxygens on each side of *C*, having the same electronegativity, but Table 5 shows that for the various conformers *a*-OH is more negative than the rotating OH, except at 0° where they are the same by symmetry.

For *s*-OH—CH_2—OH the charge on the rotating OH is more or less negative than on *s*-OH, depending on ϕ. For *g*-OH—CH_2—OH, the rotating OH is always more negative than *g*-OH, except at 120° where they are the same by symmetry. This might imply that for these systems C—X is less polar than CO and that therefore the π-bonding model may not apply. However, as ΔE and R_{CO} values show, the π-bonding model is still working well. Slight differences to the first two systems are that $\Delta E(180)$ is positive, and $R_{CO}(180)$ is larger than $R_{CO}(0)$. The charges Q_{OH} for both systems are least negative at 90°, corresponding to being most positive at 90° for $CH_2{=}OH^+$. Also, the CH_2—OH fragment overall still has a positive charge. This implies that the *s*-OH and *g*-OH systems can also be classified as receiving their stabilization according to the π-bonding model.

All systems in the π-bonding category have a sizeable negative V_2, ranging from −1.29 to −4.26 kcal/mol. It results, as outlined before, from the energy of the system at 90° being more stable than at 0°. A negative V_2 is essential for the π-bonding model to hold.

The remaining systems, with X = N and C, all have $\Delta E(60)$ positive. The ΔE values remain positive except for e-NH_2, for which system they turn increasingly negative, having an energy minimum at 180°. Looking at ΔE values only, the e-NH_2 system might still be considered to follow the π-bonding model. However, a glance at R_{CO} and Q_{OH} values tells otherwise. For this, as well as for the other N and C systems, R_{CO} increases when going from 0 to 60°, decreases to 120°, and increases again to 180°. This pattern is opposite to that calculated for $CH_2{=}OH^+$ (except 120° → 180°) and corresponds closely to the CO distance changes in CH_3—OH, where R_{CO} is about 0.004 Å larger at the eclipsed ($\phi = 60$, 180°) positions than at the staggered ones ($\phi = 0$, 120°).

For both X = N and X = C systems, the OH charges are essentially constant, except that they turn considerably more negative at 180°. For s-NH_2 and the two CH_3 systems, this is due to the stronger H–H repulsion at 180° than at 60°, resulting from the proximity of the rotating hydrogen to the NH_2 or CH_3 hydrogens at 180°, as is also reflected in the higher energies at 180° (and positive V_1). For e-NH_2, the reason is not obvious. For comparison, in CH_3—OH the OH charges at the eclipsed positions (60°, 180°) are 0.004 units more negative than at the staggered positions (0°, 120°), closely resembling the pattern observed for the X = N and C systems.

For both NH_2 systems, the CH_2—OH portion of the molecule is still positive, allowing the π-bonding model to hold in principle. However, contrary to the *s*-OH and *g*-OH systems discussed before, the higher electronegativity of O vs. N is now so dominant that the CH_2—OH fragment of the molecule behaves nearly like CH_3—OH, and no similarities to $CH_2{=}OH^+$ can be found.

For the CH_3 systems, the combined charge on CH_2—OH is negative, as is expected. They were included as reference

Can. J. Chem. Downloaded from www.nrcresearchpress.com by 92.62.229.171 on 09/08/12
For personal use only.

Can. J. Chem. Downloaded from www.nrcresearchpress.com by 92.62.229.171 on 09/08/12
For personal use only.

systems for which the anomeric effect is known not to hold. They follow closely the pattern of CH_3—OH. The system with s-NH_2 will be classified as belonging to the same group.

The reverse anomeric effect is cited as holding for s-NH_2—CH_2—OH by Krol *et al.* (19). Using a 4-21G basis set, they found s-NH_2—CH_2—OCH_3 to be 0.78 kcal/mol more stable at 0° than at 120°, in qualitative agreement with our result for s-NH_2—CH_2—OH (0.06 kcal/mol). On the other hand, Senderowitz *et al.* (20) found for s-NH_2—CH_2—OH the 120° conformation to be more stable than 0° by 1.40 (3-21G), 0.14 (6-31G*), and 0.31 kcal/mol (MP3//6-31G* with partial geometry optimization). While such small energy differences depend on the details of the optimization procedure, the main point made in the present study is that C—O distance changes and charge changes in s-NH_2—CH_2—OH are in contradiction to those pattern established for CH_2=OH^+. Therefore, it is considered better to classify s-NH_2—CH_2—OH as having no anomeric effect rather than invoking the reverse anomeric effect. If the NH_2 and OH dihedral angles of s-NH_2—CH_2—OH are relaxed, not fixed at ±120° as in the present study for reasons of Fourier analysis, then the 6-31G** basis set predicts the most stable conformer of s-NH_2—CH_2—OH to have ϕ = 110.7° and to be 0.17 kcal/mol more stable than the 0° conformer, close to 0.14 as obtained in ref. 20. However, the V_i parameters, calculated using ϕ(120), stay the same.

Obviously, despite some similarities, e-NH_2—CH_2—OH is quite different from its s-NH_2 counterpart. In particular the ΔE values, although positive at 60°, become negative, and are most negative at 180°.

This leads us to a detailed consideration of the remaining Fourier parameter V_1. Radom *et al.* (16) explain V_1 as resulting from dipole interactions. Using e-NH_2—CH_2—OH as example, for ϕ = 0 the dipole moments N → lp and O → lp point in the same direction, **11***a*, and repel each other, whereas for ϕ = 180°, they point in opposite directions and attract each other, **11***b*. An equivalent, but simpler, concept is to talk about lone pair (lp) repulsions. (A form of intramolecular hydrogen bonding may also be included, see below.) At 0°, the lone pairs of N and O repel each other, but at 180° there is no such repulsion (**11***a*, **11***b*). For the systems with e-NH_2, as well as for F and *a*-OH, there is lone pair repulsion at 0°, but none at 180°. Therefore, these systems have negative V_1, with values of −3.91 for F, −4.69 for *a*-OH and −4.91 kcal/mol for e-NH_2. (For *g*-OH—CH_2—OH, a V_1 of −0.48 kcal/mol can be explained on the same basis.) Due to the large negative V_1, and the small (even positive) V_2, the energy pattern of e-NH_2—CH_2—OH is governed by the V_1 term, leading to a large negative energy at 180°. (Since $V_1 + V_2 < 0$, there is still anomeric stabilization at 120°.) As was outlined before, the π-bonding model does not apply.

V_1 can also arise from the repulsion of the OH hydrogen with one of the XH_n hydrogens, in which case it is positive under the conventions adopted in this paper. For *s*-OH—CH_2—OH, at 0° there is no lp–lp repulsion (**12***a*), but at 180° (**12***b*) H–H repulsion is present. For this system, V_1 = 3.82 kcal/mol. The same situation applies also to s-NH_2 and the CH_3 systems. All have positive, if small, V_1 parameters.

In summary, V_1 can have two contributions, one from lone pair repulsions, and one from OH—XH_n H–H repulsion. The former may be considered to be electrostatic, the latter is steric. With our conventions, V_1 is always negative for lp repulsions (since they occur for ϕ = 0), and always positive for H–H repulsions (since they occur for ϕ = 180°).

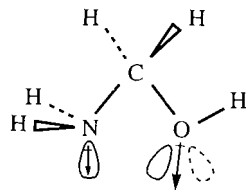

e-NH_2, 0°

11*a*

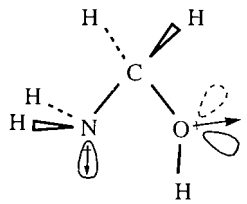

e-NH_2, 180°

11*b*

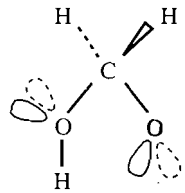

s-OH, 0°

12*a*

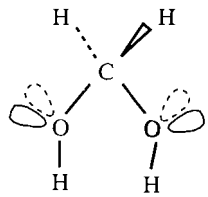

s-OH, 180°

12*b*

Classification of systems

The systems with X = F and O all have sizeable negative V_2 parameters, and follow in all respects the π-bonding model. The main mechanism for anomeric stabilization is the desire of the CH_2—OH portion of the molecule to achieve maximal π-bonding character, which is accomplished between ϕ = 90 and ϕ = 120°. Within this class of π-bonding molecules, two subclasses can be distinguished, according to whether V_1 is negative or positive. If V_1 is negative, then the systems (F, *a*-OH, and *g*-OH) receive additional anomeric stabilization due to the decreasing lone pair repulsions as the OH group is rotated away from the *anti* position. If V_1 is positive (*s*-OH), the relation $V_1 < -V_2$ must be sat-

Can. J. Chem. Downloaded from www.nrcresearchpress.com by 92.62.229.171 on 09/08/12
For personal use only.

isfied; otherwise there is no more anomeric stabilization. For positive V_1, there is increasing H–H repulsion as the OH group moves towards 180°. This energy term opposes the π-bonding stabilization.

The second class consists of molecules for which there is no π-electron stabilization (e-NH_2, s-NH_2, both CH_3 systems). In these cases, V_2 is zero or small. Again, there are two subclasses. For e-NH_2—CH_2—OH, V_1 is negative and large. Since at 120° ΔE (= 0.75 V_1 + 0.75 V_2) is negative, there is formally anomeric stabilization, despite the absence of π-bonding (or very small amount only). For the remaining systems, V_1 is positive and small, and there is no way to achieve anomeric stabilization. The CH_3—CH_2—OH systems, as was mentioned earlier, have been included in this study as reference systems in order to illustrate just this point.

Comparison with other energy decomposition schemes

Earlier, Grein and Deslongchamps (21) proposed a simple model for predicting anomeric stabilization energies for systems XH_m—CH_2—YH_n, where X, Y = N and O. This energy is decomposed into contributions from an electronic effect, operating when a lone pair on X is in antiperiplanar position to CY, represented by the energy parameter a, lp–lp repulsions with energy parameter r_{lp}, 1,3-diaxial H–H repulsions r_{HH}, and intramolecular hydrogen bonding due to the proximity of a lone pair on X and a hydrogen on Y, with parameter h. For example, for a-OH—CH_2—OH, at 0° (**13***a*), $E_{rel}(0) = 2r_{lp}$, and at 120° (**13***b*) $E_{rel}(120) = r_{lp} + h + a$. So the anomeric stabilization energy is $E_{rel}(120) - E_{rel}(0) = h + a - r_{lp}$. Arguments were given for $h \cong -r_{lp} \cong -r_{HH} \cong -1$ kcal/mol, and $a \cong -2$ kcal/mol for O. Therefore, for a-OH—CH_2—OH, $\Delta E(120)$ is predicted to be −4 kcal/mol, compared with the calculated −4.49 kcal/mol, Table 2. With $a_O = -2$ and $a_N = -2.5$ kcal/mol, all anomeric stabilization energies of the systems XH_m—CH_2—YH_n were predicted within 0.5 kcal/mol. The methoxy systems OH—CH_2—OCH_3 and OCH_3—CH_2—OCH_3 were also included.

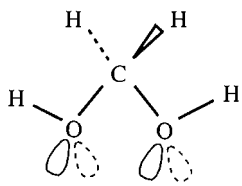

a-OH, 0°

13*a*

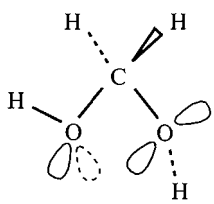

a-OH, 120°

13*b*

Smits *et al.* (12) considered *anti* and *gauche* conformers of the same systems as were studied here. A single determinant of non-orthogonal localized molecular orbitals was used. The energy (4-31G) was decomposed into quasiclassical, interference, and charge transfer terms. Interference terms were found to be most important for stabilizing the *anti* conformer. A direct comparison with the present scheme of energy decomposition is not possible.

For dimethoxymethane (DMM), Wiberg and Murcko (22) calculated and analyzed a conformational energy map. Interesting for our purposes is the energy decomposition for a-OCH_3—CH_2—OCH_3 (our notation). The energy difference between $\phi = 0$ and 120° is 3.3 kcal/mol. To estimate the lp–lp repulsion in the $\phi = 0$ conformer, they found the energy difference between the two corresponding conformers of methyl propyl ether to be 1.4 kcal/mol, with $\phi = 0$ being more stable. From this they obtained the anomeric stabilization of DMM, corrected for lp–lp repulsion, to be 3.3 + 1.4 = 4.7 kcal/mol. According to the present analysis, the reduction in the lone pair repulsion at 120° is already contained in $\Delta E(120)$, and therefore the portion remaining for the electronic effect is the difference between the 120° stabilization and the lp repulsions, rather than the sum.

Summary and conclusion

The anomeric effect predicts the *gauche* conformer to be more stable than the *anti* conformer for the systems XH_n—CH_2—OH studied here, provided the electronegativity of X is sufficiently high. *Ab initio* calculations on conformers with OH dihedral angles from 0° (*anti*) to 180° (*syn*) showed that anomeric stabilization is obtained for XH_n = F, a-OH, g-OH, and s-OH. For these systems, energies, C—O distances and charges on OH follow closely the corresponding values of $CH_2{=}OH^+$, for which OH is rotated in a similar fashion. Anomeric stabilization derives from the tendency to form a π-bond in the CH_2—OH fragment of the molecule. For XH_n = F, a-OH, and g-OH, lone pair repulsions are diminished when rotating the OH group from *anti* to *gauche*, thereby increasing the anomeric stabilization energy. For s-OH—CH_2—OH, however, the OH hydrogens experience increasing repulsion as OH is rotated towards the *syn* position. Therefore, the π-bonding stabilization is diminished by H–H repulsion.

For the X = N systems, the electronegativity of N is insufficient to cause π-bonding stabilization. However, the e-NH_2 system is still stabilized by decreasing lp repulsions as the dihedral angle of OH moves towards 180°. On the other hand, for s-NH_2 there is no such stabilization, and this system behaves in all respects like the reference systems CH_3—CH_2—OH.

The π-bonding model requires the OH hydrogen of XH_n—CH_2—OH to be rotated 90 to 120° out of the X—C—O plane (starting at H *trans* to C—X) for maximal π-bonding and energy lowering. The orientation of lone pairs on oxygen is of no immediate concern and is incidental only. For an angle of 120° (*gauche*), idealized sp^3-type lone pairs happen to be antiperiplanar (app) to the C—X bond. The π-bonding model puts emphasis on the conformation of the OH hydrogen rather than the oxygen lone pairs. The two pictures are intimately connected. For example, consider the n–σ* model. Using $sp^2 + p$ hybridization on O, instead of sp^3, the p-type lone pair on O is parallel to, and overlaps best with, the σ* orbital of the C—X bond when OH has a dihedral angle of 90°. Partial π-bonding character in the SN

bond of *syn*-F—S—NH_2 (the most stable conformer) has been demonstrated by Reed and Schleyer (9).

In forthcoming papers, conformational analysis will be applied to other neutral and to corresponding protonated systems. Also, a more detailed quantitative treatment of the various energetic contributions will be given.

Acknowledgements

A number of undergraduate students from the Chemistry Department at UNB have performed computations on the anomeric effect. For the present paper, the help of Robin Martin and Garn Pomeroy is gratefully acknowledged. We would also like to thank the Natural Sciences and Engineering Research Council of Canada for operating grants, and the University of New Brunswick for the allocation of computer time.

1. P. Deslongchamps. Steroelectronic effects in organic chemistry. Pergamon Press, Oxford. 1983.
2. A. J. Kirby. The anomeric effect and related stereoelectronic effects at oxygen. Springer Verlag, Berlin. 1983.
3. R. U. Lemieux and N. J. Chu. Abstr. Pap. — Am. Chem. Soc. **133**, 31N (1958).
4. C. Altona. Ph.D. Thesis, University of Leiden. 1964.
5. C. Romers, C. Altona, H. R. Buys, and E. Havinga. Top. Stereochem. **4**, 39 (1969).
6. J. T. Edwards. Chem. Ind. (London), **1102** (1955).
7. E. L. Eliel. Acc. Chem. Res. **3**, 1 (1970); Angew. Chem. Int. Ed. Engl. **11**, 739 (1972); Kem. Tidskr. **81**, 22 (1969).
8. S. Wolfe, A. Rauk, L. M. Tel, and I. G. Csizmadia. J. Chem. Soc. B, **136** (1971).
9. A. E. Reed and P. v. R. Schleyer. Inorg. Chem. **27**, 3969 (1988).
10. A. E. Reed and P. v. R. Schleyer. J. Am. Chem. Soc. **109**, 7362 (1987).
11. S. Wolfe, M. H. Whangbo, and D. J. Mitchell. Carbohydr. Res. **69**, 1 (1979).
12. G. F. Smits, M. C. Krol, and C. Altona. Mol. Phys. **65**, 513 (1988).
13. M. J. Frisch, J. S. Binkley, H. B. Schlegel *et al.* Gaussian 86. Carnegie–Mellon Quantum Chemistry Publishing Unit, Pittsburgh, Pa. 1984.
14. S. Wolfe. Acc. Chem. Res. **5**, 102 (1972).
15. S. Wolfe, L. M. Tel, W. J. Haines, M. A. Robb, and I. G. Csizmadia. J. Am. Chem. Soc. **95**, 4863 (1973).
16. L. Radom, W. J. Hehre, and J. A. Pople. J. Am. Chem. Soc. **94**, 2371 (1972).
17. G. A. Jeffrey, J. A. Pople, and L. Radom. Carbohydr. Res. **25**, 117 (1972).
18. J. J. Irwin, T. K. Ha, and J. D. Dunitz. Helv. Chim. Acta, **73**, 1805 (1990).
19. M. C. Krol, C. J. M. Huige, and C. Altona. J. Comput. Chem. **11**, 765 (1990).
20. H. Senderowitz, P. Aped, and B. Fuchs. Helv. Chim. Acta, **73**, 2113 (1990).
21. F. Grein and P. Deslongchamps. Second World Congress of Theoretical Organic Chemists, Toronto, July 1990; to be published.
22. K. B. Wiberg and M. A. Murcko. J. Am. Chem. Soc. **111**, 4821 (1989).

Can. J. Chem. Downloaded from www.nrcresearchpress.com by 92.62.229.171 on 09/08/12
For personal use only.

Relativistic compact effective potentials and efficient, shared-exponent basis sets for the third-, fourth-, and fifth-row atoms

WALTER J. STEVENS[1] AND MORRIS KRAUSS
Center for Advanced Research in Biotechnology, National Institute of Standards and Technology, 9600 Gudelsky Drive, Rockville, MD 20850, U.S.A.

HAROLD BASCH
Department of Chemistry, Bar Ilan University, 52100 Ramat Gan, Israel

AND

PAUL G. JASIEN[2]
Molecular Spectroscopy Division, National Institute of Standards and Technology, Gaithersburg, MD 20899, U.S.A.

Received August 2, 1991

This paper is dedicated to Professor Sigeru Huzinaga on the occasion of his 65th birthday

WALTER J. STEVENS, MORRIS KRAUSS, HAROLD BASCH, and PAUL G. JASIEN. Can. J. Chem. **70**, 612 (1992).

Relativistic compact effective potentials (RCEP), which replace the atomic core electrons in molecular calculations, have been derived from numerical Dirac–Fock atomic wavefunctions using shape-consistent valence pseudo-orbitals and an optimizing procedure based on an energy-overlap functional. Potentials are presented for the third-, fourth-, and fifth-row atoms of the Periodic Table (excluding the lanthanide series). The efficiency of molecular calculations is enhanced by using compact Gaussian expansions (no more than three terms) to represent the radial components of the potentials, and energy-optimized, shared-exponent, contracted-Gaussian atomic orbital basis sets. Transferability of the potentials has been tested by comparing calculated atomic excitation energies and ionization potentials with values obtained from numerical relativistic Hartree–Fock calculations. For the alkali and alkaline earth atoms, core polarization potentials (CPP) have been derived which may be added to the RCEP to make possible accurate molecular calculations without explicitly including core-valence correlating configurations in the wavefunction.

Key words: model potentials, effective core potentials, transition metals, relativistic calculations.

WALTER J. STEVENS, MORRIS KRAUSS, HAROLD BASCH et PAUL G. JASIEN. Can. J. Chem. **70**, 612 (1992).

Faisant appel à des fonctions d'onde atomiques Dirac–Fock numériques et utilisant des pseudo-orbitales de valence cohérentes avec la forme et une procédure d'optimisation basée sur un recouvrement fonctionnel d'énergie, on a déterminé des potentiels efficaces compacts relativistes (RCEP) qui remplacent les électrons atomiques internes dans les calculs moléculaires. On présente les potentiels d'atomes des troisième, quatrième et cinquième lignes du tableau périodique (excluant la série des lanthanides). L'efficacité des calculs moléculaires est rehaussée par l'utilisation d'expansions gaussiennes compactes (pas plus de trois termes) pour représenter les composantes radiales des potentiels ainsi que par l'utilisation d'ensembles de base d'orbitales atomiques gaussiennes contractées, optimisés pour l'énergie et à exposant partagé. On a vérifié la transférabilité de ces potentiels en comparant les énergies d'excitation atomique et les potentiels d'ionisation calculés avec les valeurs obtenues par des calculs numériques relativistes de Hartree–Fock. Pour les atomes des métaux alcalins et alcalino-terreux, on a pu déduire des potentiels de polarisation interne (CPP) qui peuvent être ajoutés au RCEP pour éventuellement obtenir des calculs moléculaires précis sans inclure d'une façon explicite dans la fonction d'onde les corrélations entre les électrons internes et ceux de valence.

Mots clés : potentiels modèles, potentiels internes efficaces, métaux de transition, calculs relativistes.
[Traduit par la rédaction]

Introduction

The use of atomic effective core potentials (ECP) and model potentials (MP) to eliminate chemically inactive atomic core electrons from quantum mechanical calculations has become routine in the past decade. The development of such potentials in the early 1970's and applications through the mid-1980's have been reviewed previously (1). The use of such potentials in molecular calculations has gained widespread acceptance, and sets of effective potentials are included in widely distributed quantum chemistry programs such as HONDO (2), GAMESS (3), and GAUSSIAN (4). We previously published accurate compact effective potentials (CEP) and matching basis sets for the atoms of the first two rows (Li–Ar) of the Periodic Table (5). We designated the potentials "compact" because they are represented analytically by small Gaussian expansions and, therefore, offer significant economy in molecular calculations where the computer time required to construct the electronic integrals is proportional to the complexity of the potentials. In this report, we present effective potentials and basis sets of similar quality for the third, fourth, and fifth rows of the Periodic Table derived from numerical, relativistic, Dirac–Fock atomic wavefunctions. The analytic expansions of these potentials are also limited to a few Gaussian terms (three or less), so we have designated them as "relativistic compact effective potentials" (RCEP).

Recently, several compilations of model potentials and effective core potentials for use in molecular calculations have appeared in the literature. For the heavier atoms, relativistic effects have been incorporated by deriving the potentials from relativistic Hartree–Fock (6) or Dirac–Fock (7) atomic

[1]Author to whom correspondence may be addressed.
[2]NRC–NAS Postdoctoral Fellow, NIST, 1984–1986. Current address: California State University, San Marcos, CA 92096, U.S.A.

Printed in Canada

Can. J. Chem. Downloaded from www.nrcresearchpress.com by 92.62.229.171 on 09/08/12
For personal use only.

Can. J. Chem. Downloaded from www.nrcresearchpress.com by 92.62.229.171 on 09/08/12
For personal use only.

wavefunctions. There are generally two types of potentials that have attained widespread use: the model potentials of Huzinaga and co-workers (8), which retain the nodal characteristics of the valence orbitals in the core region, and effective core potentials, which result in nodeless valence "pseudo-orbitals" (9). The Huzinaga model potentials offer the advantage of valence wavefunctions that resemble those from all-electron calculations and are therefore optimum for calculating valence contributions to molecular properties, but they do not offer the economic advantage of reduced basis set size that can be achieved with the ECP method and corresponding nodeless pseudo-orbitals.

ECPs for most of the atoms in the Periodic Table have been published by several authors. Bachelet *et al.* (10) published potentials based on the method of Hamann *et al.* (11) for use in density functional calculations. Hay and Wadt (12) published a set of *ab initio* ECPs derived from numerical, relativistic Hartree–Fock (6) calculations. Christiansen and co-workers (13) published relativistic potentials derived from numerical Dirac–Fock calculations (7). In the latter two cases the potentials are generated on a numerical grid by inverting Fock equations for pseudo-orbitals derived from numerical atomic wavefunctions. The numerically tabulated potentials are then least-squares fit with analytic Gaussian expansions. Due to the complex shape, accurate fits for each numerical potential can require as many as six or more Gaussian functions. The ECP generation method described in detail below is similar to the Dirac–Fock approach of Christiansen and co-workers (13), but offers an alternative to least-squares fitting that leads to very compact analytic potentials with no loss of accuracy.

Among other sets of potentials being used extensively in molecular calculations, the pseudopotentials reported by Preuss and co-workers (14), and by Durand, Barthelat, and co-workers (15) are most noteworthy. The Preuss potentials have the same form as the ECP, but the parameters in the Gaussian expansions are optimized by minimizing the differences between ECP-computed valence energies of several neutral and ionic atomic states and those obtained from all-electron Hartree–Fock or quasi-relativistic Hartree–Fock calculations. This method makes no explicit use of the all-electron atomic orbitals in the pseudo-potential derivation, and relies on the spectral fit to produce a pseudo-Hamiltonian with the correct properties. The analytic Gaussian expansions used for these pseudopotentials generally contain a small number of terms, due to the limited amount of data being fit. The Durand/Barthelat potentials were also optimized by comparing ECP and all-electron calculations, but a unique functional based on orbital overlap and eigenvalue differences was used (16). The optimized RCEP parameters reported in this paper were determined by the same method.

Before the RCEPs can be used in molecular calculations, atomic orbital basis sets must be specified. In the generation of the Gaussian basis sets reported here, we considered several things. First, the number of primitive Gaussians required to accurately represent the atomic pseudo-orbitals was determined for each type of atom. For efficiency in molecular calculations, the exponents of the s and p primitive Gaussians were required to be the same. Also for efficiency in molecular calculations, a contraction scheme was developed that kept the number of basis functions as small as possible while still predicting accurately the low-lying neutral and ionic states of the atoms.

Method

Background

We briefly review the derivation of relativistic effective potentials, following the formalism first introduced by Lee *et al.* (17). The effective potentials are constructed to reproduce the valence electron orbital energies and densities obtained from numerical solutions of the Dirac–Fock equations for an appropriate atomic configuration (7). It is assumed that the valence electron density is dominated by the large components of the Dirac–Fock spinors and that the small components may be neglected. The Dirac–Fock Hamiltonian for the large components has the general form (18)

$$[1]\qquad \{\boldsymbol{H}_0(r) + \boldsymbol{H}_{\mathrm{m}}(r) + \boldsymbol{H}_{\mathrm{d}}(r) + \boldsymbol{H}_{\mathrm{so}}(r) + \boldsymbol{H}(O[\boldsymbol{\alpha}^4])\}P_{l,j}(r) = \boldsymbol{\varepsilon}_{l,j}P_{l,j}(r)$$

where H_0 is the nonrelativistic Hamiltonian, H_{m} the mass–velocity correction to the kinetic energy, H_{d} the Darwin term, and H_{so} the spin-orbit coupling. $P_{l,j}(r)$ is a spinor depending on the orbital and total angular momentum eigenvalues l,j. In the effective potential derivation, the Dirac–Fock equation for each angular momentum is replaced by

$$[2]\qquad \{\boldsymbol{H}_0^{\mathrm{val}} + \boldsymbol{V}_{l,j}^{\mathrm{REP}}(r)\}\boldsymbol{\chi}_{l,j}(r) = \boldsymbol{\varepsilon}_{l,j}\boldsymbol{\chi}_{l,j}(r)$$

where H_0^{val} is the nonrelativistic part of the valence Fock Hamiltonian, $\chi_{l,j}$ is a nodeless pseudo-spinor constructed from the large component Dirac–Fock spinor, and $V_{l,j}^{\mathrm{REP}}$ is a relativistic effective potential (to be determined) that replaces the relativistic terms in the valence Hamiltonian as well as the core-valence interaction terms. The nonrelativistic part of the valence Fock Hamiltonian for angular momentum, l, is given by

$$[3]\qquad \boldsymbol{H}_0^{\mathrm{val}} = -\frac{1}{2}\nabla^2 - \frac{Z_{\mathrm{eff}}}{r} + \frac{l(l+1)}{2r^2} + \boldsymbol{W}_{\mathrm{val}}^*$$

Z_{eff} is the nuclear charge minus the number of core electrons. $V_{l,j}^{\mathrm{REP}}$ absorbs the remaining nuclear attraction terms, which are canceled by the core-electron coulomb potential at long range. The valence coulomb and exchange term, W_{val}^*, is constructed from valence pseudo-spinors. This means that $V_{l,j}^{\mathrm{REP}}$ also contains the difference between the exact valence coulomb/exchange term, W_{val}, and the effective term, W_{val}^*. This difference is minimized in the valence region through the use of "shape-consistent" pseudo-spinors (19) as discussed in a subsection below.

Once the pseudo-spinors and eigenvalues are available, the REP may be derived by inverting the atomic valence Fock equation:

$$[4]\qquad \boldsymbol{V}_{l,j}^{\mathrm{REP}} = \boldsymbol{\varepsilon}_{l,j} + \frac{Z_{\mathrm{eff}}}{r} - \frac{l(l+1)}{2r^2} + \frac{\left(\frac{1}{2}\nabla^2 - \boldsymbol{W}_{\mathrm{val}}^*\right)\boldsymbol{\chi}_{l,j}}{\boldsymbol{\chi}_{l,j}}$$

Each valence spinor with a given angular momentum generates a unique REP. These j-dependent potentials may be used directly in molecular calculations (17, 20), but it is more common to use averaged relativistic potentials (AREP), as

Can. J. Chem. Downloaded from www.nrcresearchpress.com by 92.62.229.171 on 09/08/12
For personal use only.

defined by Lee *et al.* (17), which eliminate the j-dependence due to spin-orbit coupling

$$[5] \qquad V_l^{\mathrm{AREP}}(r) = \frac{1}{(2l+1)} \times [l V_{l,l-1/2}^{\mathrm{REP}}(r) + (l+1) V_{l,l+1/2}^{\mathrm{REP}}(r)]$$

The total, semi-local, AREP for use at each atomic center in molecular calculations is given by

$$[6] \qquad V^{\mathrm{AREP}}(r) = \sum_l \sum_{m=-l}^{l} V_l^{\mathrm{AREP}}(r) \, |lm\rangle\langle lm|$$

where the projectors ensure that the potentials operate on the proper angular momentum components of the molecular wavefunction.

The sum over angular momentum, l, in eq. [6] formally runs to infinity. For those orbitals that are orthogonal to core orbitals of the same angular momentum, the potentials are repulsive and have shapes that are unique for each angular momentum value. However, for orbitals with angular momentum greater than the maximum orbital angular momentum occurring in the core, there is no orthogonality constraint, and the potentials are attractive and represent the unshielding of the nuclear charge as the core electron density is penetrated. All such attractive potentials are found to have similar shapes, so it is a good approximation to use a finite expansion for the AREP of the form (17)

$$[7] \qquad V^{\mathrm{AREP}} = V_{\mathrm{LMAX}}^{\mathrm{AREP}} + \sum_{l=0}^{\mathrm{LMAX}-1} \sum_{m=-l}^{l} [V_l^{\mathrm{AREP}} - V_{\mathrm{LMAX}}^{\mathrm{AREP}}] \, |lm\rangle\langle lm|$$

where LMAX is one more than the maximum orbital angular momentum in the core. It is common to designate the AREP for a given angular momentum as a difference potential with the notation $V_{l-\mathrm{LMAX}}$.

While the AREP potentials defined by eq. [5] do not contain spin-orbit coupling effects, one can define an effective spin-orbit coupling operator in terms of the difference between the $j = l + \frac{1}{2}$ and $j = l - \frac{1}{2}$ potentials. This was first proposed by Ermler *et al.* (21), and used by Stevens and Krauss (22) to calculate spin-orbit splittings for several diatomic molecules. The form of the spin-orbit coupling operator is

$$[8] \qquad H^{\mathrm{so}} = \sum_{l=1}^{\infty} \Delta V_l^{\mathrm{REP}} \left[\frac{l}{2l+1} \left| l, l+\frac{1}{2} \right\rangle\left\langle l, l+\frac{1}{2} \right| + \frac{l+1}{2l+1} \left| l, l-\frac{1}{2} \right\rangle\left\langle l, l-\frac{1}{2} \right| \right]$$

where the difference potential is defined by

$$[9] \qquad \Delta V_l^{\mathrm{REP}}(r) = V_{l,l+1/2}^{\mathrm{REP}}(r) - V_{l,l-1/2}^{\mathrm{REP}}(r)$$

The exact form of the REP, and thus of the effective spin-orbit operators, depends on the pseudo-spinors that are used to generate the REP. Pacios, Christiansen, and co-workers (13) have recently published analytic fits of effective spin-orbit operators for the atoms Li–Rn. The operators were generated from pseudo-spinors similar to the ones reported below, so they should be compatible with the potentials presented in this work. Wadt (23) has suggested an alternative method for obtaining molecular spin-orbit coupling constants from pseudo-wavefunctions without using effective operators. The spin-orbit integrals are calculated in the usual way, but a scaling parameter is used which is defined by matching calculated atomic spin-orbit coupling constants to *ab initio*, all-electron values. This procedure also could be used in conjunction with the effective potentials presented here.

Shape-consistent pseudo-spinors

The starting point for the REP generation is an atomic Dirac–Hartree–Fock (DHF) wavefunction obtained with the computer program of Desclaux (7). The atomic spinors from such calculations are in numerical form, tabulated on a logarithmic radial grid. The exact DHF atomic configuration and the partitioning of the numerical orbitals into core and valence subgroups are choices that depend on the type of atom being considered, as discussed below.

For all atoms, the large components of the valence j-dependent DHF spinors were used to construct nodeless pseudo-spinors by the shape-consistent procedure of Christiansen *et al.* (19). Shape-consistent construction is not necessary for DHF spinors with orbital angular momenta LMAX or greater, since they are already nodeless. The idea behind the shape-consistent approach is to make the pseudo-spinor match the Dirac–Fock atomic spinor as closely as possible, thereby minimizing the difference between the all-electron and ECP valence interaction terms and maintaining the correct overlap behavior in molecular bond formation. The shape-consistent pseudo-spinors, $\chi_{l,j}$, are defined by

$$[10a] \qquad \chi_{l,j}(r) = \sum_{i=0}^{4} c_i r^{i+N}, \qquad r \le r_{\mathrm{m}}$$

$$[10b] \qquad \chi_{l,j}(r) = P_{l,j}(r), \qquad r \ge r_{\mathrm{m}}$$

$$[10c] \qquad \langle \chi_{l,j} | \chi_{l,j} \rangle = 1$$

where r_{m} is a match point at which a four-term polynomial with leading power N is joined smoothly to the DHF spinor to produce a normalized pseudo-spinor with no nodes, one radial maximum, and two inflection points. The advantage of this procedure is that the pseudo-spinor is identical to the DHF spinor in the chemically important valence region outside the match point. We have modified the Christiansen procedure slightly to simplify the pseudo-spinor generation. In the Christiansen procedure, r_{m} is set as small as possible while still maintaining the nodeless character and a maximum of two inflection points in the pseudo-spinor. In our procedure, r_{m} is chosen as close as possible to the outermost radial density maximum of the DHF spinor. We found that the pseudo-spinors constructed in this way consistently had the desired properties for this choice of r_{m}. Christiansen *et al.* also recommend a leading power of $l + 2$ for the polynomial segment (where l is the orbital angular momentum), to satisfy cusp conditions at $r = 0$. We have used instead a cubic leading term for s, p, and d spinors, and a quartic leading term for f spinors. This causes no problems for atomic and molecular calculations using basis sets, but it could lead to difficulties if the potentials were used in numerical calculations where proper boundary conditions are crucial for numerical integration. Our modified procedure was

Can. J. Chem. Downloaded from www.nrcresearchpress.com by 92.62.229.171 on 09/08/12
For personal use only.

used previously in the successful generation of nonrelativistic effective potentials for lighter atoms (5).

Relativistic compact effective potentials

Once the nodeless pseudo-spinors are defined on the same numerical grid as the DHF spinors, numerical REPs are generated according to eq. [4]. For orbital angular momenta greater than zero, AREPs are then obtained by averaging the two REPs for each l to eliminate the j-dependence, as shown in eq. [5]. At this point one may obtain an analytic representation of the AREP by a least-squares fit to an expansion of suitable functions such as Gaussians. This procedure has been adopted by Hay and Wadt (12) and by Christiansen *et al.* (13). However, the shape of the REPs is often complicated, and a large number of Gaussians (>6) is usually required to obtain a reliable fit. An alternative to direct least-squares fitting is the generation of compact analytic expansions by a method similar to the one used by us previously (5). These compact expansions improve the efficiency of molecular calculations, since the computer time required to calculate electronic integrals over the potentials is proportional to the length of the analytic expansions.

In our method, the numerically tabulated AREPs from eq. [5] are considered to be "exact." They are then used in atomic valence-only Hartree–Fock calculations to generate a set of *j-independent*, "exact" pseudo-orbitals and eigenvalues. This may be accomplished either on a numerical grid or with a basis set expansion for the orbitals. We chose to use large, even-tempered basis sets of Gaussian functions for this purpose. The resulting analytic pseudo-orbitals and eigenvalues are very similar to those derived by Hay and Wadt (12) from j-independent, numerical, relativistic Hartree–Fock orbitals (6). Following our previous compact effective potential procedure [5], analytic, relativistic compact effective potentials (RCEP) are generated that reproduce the "exact" pseudo-orbitals and eigenvalues as closely as possible. The analytic RCEP expansions are written

$$[11] \quad r^2 V_l^{\mathrm{AREP}}(r) = \sum_k A_{l,k} r^{n_{l,k}} \mathrm{e}^{-B_{l,k} r^2}$$

where the number of terms in the expansion is no more than three. For fixed values of $n_{l,k}$, the parameters $A_{l,k}$ and $B_{l,k}$ are directly varied in atomic Hartree–Fock calculations until the variationally determined "trial" pseudo-orbitals and eigenvalues match the "exact" pseudo-orbitals and eigenvalues to within a certain tolerance. Barthelat *et al.* (16) have proposed a useful criterion for optimization. The parameters are varied until the functional $\|\boldsymbol{O}\|$ is minimized, where

$$[12a] \quad \|\boldsymbol{O}\| = [\langle \chi_l | \boldsymbol{O}^2 | \chi_l \rangle]^{1/2}$$

$$[12b] \quad \boldsymbol{O} = \tilde{\varepsilon}_l |\tilde{\chi}_l\rangle\langle\tilde{\chi}_l| - \varepsilon_l |\chi_l\rangle\langle\chi_l|$$

χ_l and ε_l are the "exact" pseudo-orbital and eigenvalue, and $\tilde{\chi}_l$ and $\tilde{\varepsilon}_l$ are calculated by solving the Hartree–Fock equations with the trial analytic potential, $\tilde{V}_l^{\mathrm{AREP}}$, in

$$[13] \quad \left[-\frac{1}{2}\nabla^2 - \frac{Z_{\mathrm{eff}}}{r} + \frac{l(l+1)}{2r^2} + \tilde{V}_l^{\mathrm{AREP}} + W_{\mathrm{val}}^* \right] \tilde{\chi}_l = \tilde{\varepsilon}_l \tilde{\chi}_l$$

with the valence Coulomb and exchange operators, W_{val}^*, constructed from the "exact" pseudo-orbitals, and the trial pseudo-orbital, $\tilde{\chi}_l$, expanded in the same large, even-tempered basis set of Gaussians as the "exact" pseudo-orbital. This procedure converges quite rapidly, and has the advantage that optimized parameters for one atom can be used as initial guesses for the next atom as one moves across rows or down columns of the Periodic Table. The parameters, $n_{l,k}$, were not varied exhaustively, but several sets were tried until values were found that gave sufficiently accurate potentials for each type of atom. For all potentials reported in Tables 1–3 the overlap of the "exact" and calculated pseudo-orbitals is greater than 0.99999, and the difference between the "exact" and calculated eigenvalues is less than 0.001 hartree.

Results and discussion

The relativistic compact effective potentials are presented in Tables 1–3. Energy-optimized basis sets with shared exponents for the s and p primitives are given in Tables 4–6. Enforcing shared exponents in the basis sets could increase the number of primitive Gaussians required for a given level of accuracy, but the speed with which molecular integrals are calculated is significantly enhanced due to the common exponential terms.

The exact procedure used for the RCEP and basis set generation depends on the type of atom being considered. Each unique atom type is discussed separately below.

Alkali and alkaline earth atoms

For the alkali and alkaline earth atoms, the core was taken as all orbitals up to and including the $(n-1)$ shell, where n is the principal quantum number of the outermost s-electron in the ground state. For simplicity, monovalent cations were used for the alkaline earth potential generation. s-Orbitals were obtained from DHF calculations on the ground states, while p-, d-, and f-orbitals were taken from configuration-averaged wavefunctions for the lowest excited states of each angular momentum with fixed, degeneracy-weighted coefficients.

We found that the valence pseudo-orbitals of the alkali and alkaline earths could be represented very accurately by four-term Gaussian sp expansions. The exponents and s-function coefficients were energy-optimized for the ns^1 (^2S) states of the alkalis and the ns^2 (^1S) states of the alkaline earths. The p-function exponents were set equal to the s values and the p coefficients were optimized for the np^1 (^2P) states of the alkalis and the ns^1np^1 (^3P) states of the alkaline earths. Test calculations showed that these basis sets accurately described the lowest S and P states of the neutral atoms and the alkaline earth cations. Double-zeta, 3,1 contractions of these basis sets are given in the tables. Accurate representation of alkali anionic states will require the addition of diffuse s Gaussians to the basis sets.

There are large core-valence correlation effects for these atoms that cannot be included explicitly in molecular calculations if the penultimate shell is absorbed into an effective core potential. The importance of such effects on molecular structure has been noted by several authors (24–26). Core–core correlation can also indirectly affect the valence electrons (27) and lead to errors in atomic excitation energies and ionization potentials. Müller *et al.* (28, 29) have shown that core–valence and core–core correlation energy may be calculated to a high level of accuracy without introducing explicit core–valence correlating configurations into

Can. J. Chem. Downloaded from www.nrcresearchpress.com by 92.62.229.171 on 09/08/12
For personal use only.

TABLE 1. Relativistic compact effective potentials for the third-row atoms. The form of the analytic representation is

$$r^2V_l(r) = \Sigma A_{lk} r^{n_{lk}} e^{-B_{lk}r^2}$$

Z	Atom	N_{core}	RCEP	A_{lk}	n_{lk}	B_{lk}
19	K	18	V_d	−4.30002	1	0.49652
			V_{s-d}	6.71530	0	2.48731
				8.46683	2	0.60190
			V_{p-d}	7.06252	0	0.94170
				2.69868	2	0.33623
20	Ca	18	V_d	−5.81970	1	2.38045
				−2.16548	1	0.40639
			V_{s-d}	8.00522	0	2.10543
				8.94751	2	0.66865
			V_{p-d}	8.66222	0	1.79413
				5.57218	2	0.49323
21	Sc	10	V_d	−3.66956	1	9.95712
			V_{s-d}	3.71885	0	1.46409
				178.26066	2	3.59217
				−161.78394	2	3.32583
			V_{p-d}	3.93048	0	23.53849
				45.69140	2	6.58415
22	Ti	10	V_d	−3.66581	1	11.20971
			V_{s-d}	3.88067	0	1.61172
				172.25051	2	4.00960
				−155.08356	2	3.66406
			V_{p-d}	4.04433	0	31.67782
				53.00048	2	7.45793
23	V	10	V_d	−3.79146	1	12.79659
			V_{s-d}	3.43258	0	1.50439
				178.03957	2	4.27321
				−156.30605	2	3.84121
			V_{p-d}	3.76481	0	30.83720
				58.96503	2	8.34454
24	Cr	10	V_d	−3.64362	1	13.93307
			V_{s-d}	3.59679	0	1.72136
				184.07663	2	4.75681
				−161.41996	2	4.25348
			V_{p-d}	3.68862	0	32.28223
				65.48046	2	9.28137
25	Mn	10	V_d	−3.85254	1	15.88592
			V_{s-d}	3.71264	0	2.05981
				181.67442	2	5.43248
				−156.33704	2	4.79887
			V_{p-d}	4.36804	0	49.76765
				75.53242	2	10.36623
26	Fe	10	V_d	−3.89423	1	17.61910
			V_{s-d}	3.81706	0	2.33150
				172.05349	2	6.08365
				−144.70056	2	5.26659
			V_{p-d}	4.13737	0	49.40456
				82.73696	2	11.40183
27	Co	10	V_d	−3.94746	1	19.44559
			V_{s-d}	3.07705	0	2.25935
				215.48382	2	6.66665
				−174.11816	2	5.76818
			V_{p-d}	3.95321	0	50.28146
				90.90043	2	12.52610
28	Ni	10	V_d	−3.99337	1	21.36373
			V_{s-d}	3.42572	0	2.21817
				218.54146	2	6.71585
				−184.10961	2	5.80856
			V_{p-d}	3.87540	0	56.45353
				99.68289	2	13.66534
29	Cu	10	V_d	−4.00276	1	23.29060
			V_{s-d}	3.32465	0	2.62059
				224.32330	2	7.81082
				−180.30470	2	6.63324
			V_{p-d}	3.42130	0	51.15734
				105.70126	2	14.73406
30	Zn	10	V_d	−3.91648	1	24.88705
			V_{s-d}	3.43082	0	2.79159
				244.31634	2	8.32676
				−199.42711	2	7.09651
			V_{p-d}	4.11473	0	75.70603
				118.29936	2	16.07627
30	Zn	28	V_f	−2.95556	1	0.73655
			V_{s-f}	5.98306	0	0.55756
				−0.81189	2	0.42740
			V_{p-f}	4.63785	0	0.40095
				−0.55769	2	0.32955
			V_{d-f}	2.22461	0	1.05839
				1.79370	2	0.50931
31	Ga	10	V_d	−3.87363	1	26.74302
			V_{s-d}	4.12472	0	3.46530
				260.73263	2	9.11130
				−223.96003	2	7.89329
			V_{p-d}	4.20033	0	79.99353
				127.99139	2	17.39114
31	Ga	28	V_f	−3.54799	1	1.04513
			V_{s-f}	7.24152	0	0.62166
				−1.83000	2	0.58728
			V_{p-f}	4.95321	0	0.45235
				−0.84809	2	0.41215
			V_{d-f}	2.20160	0	1.62891
				3.75397	2	0.78381
32	Ge	28	V_f	−1.26859	1	0.82751
			V_{s-f}	6.77027	0	12.24839
				27.21907	2	2.41291
			V_{p-f}	8.31253	0	15.55556
				15.53292	2	1.82031
			V_{d-f}	1.62360	0	3.06970
				3.20660	2	0.80525
33	As	28	V_f	−4.77028	1	1.64583
			V_{s-f}	13.03398	0	20.76160
				43.12429	2	2.80084
			V_{p-f}	6.44063	0	16.05834
				28.12117	2	2.29432
			V_{d-f}	2.23508	0	1.12086
				4.60721	2	1.12140
34	Se	28	V_f	−5.58498	1	2.09356
			V_{s-f}	13.28081	0	20.55644
				51.00011	2	3.15490
			V_{p-f}	1.79640	0	2.58495
				30.43787	2	2.58526
			V_{d-f}	2.40001	0	1.38290
				6.59948	2	1.42671
35	Br	28	V_f	−4.78206	1	2.12116
			V_{s-f}	2.60190	0	3.21538
				44.15165	2	3.21639
			V_{p-f}	2.09478	0	2.72704
				30.59546	2	2.72762
			V_{d-f}	1.79375	0	1.73168
				10.04660	2	1.73246
36	Kr	28	V_f	−5.61220	1	2.64295
			V_{s-f}	2.36066	0	3.59276
				51.88629	2	3.57933
			V_{p-f}	2.34982	0	3.07132
				35.67029	2	3.07238
			V_{d-f}	2.85459	0	7.08677
				16.29386	2	2.15058

TABLE 2. Relativistic compact effective potentials for the fourth-row atoms. The form of the analytic representation is given in Table 1

Z	Atom	N_{core}	RCEP	A_{lk}	n_{lk}	B_{lk}
37	Rb	36	V_f	−3.23942	1	0.36395
			V_{s-f}	26.37428	0	0.18693
				−21.20813	0	0.40031
				−2.49855	2	0.21048
			V_{p-f}	5.46002	0	0.69850
				2.48839	2	0.26539
			V_{d-f}	28.32654	0	0.08272
				−26.59458	0	0.26365
				−4.38861	2	0.13507
38	Sr	36	V_f	−4.13596	1	0.51676
			V_{s-f}	24.16768	0	0.18029
				−17.38542	0	0.52170
				−3.79121	2	0.23231
			V_{p-f}	10.49841	0	1.30074
				5.46439	2	0.40227
			V_{d-f}	37.43956	0	0.25550
				−36.00393	0	0.28868
				−1.73727	2	0.26949
39	Y	28	V_f	−3.70827	1	3.13323
			V_{s-f}	3.52458	0	0.74734
				141.66551	2	2.37431
				−115.67795	2	2.11046
			V_{p-f}	3.45319	0	0.82924
				85.09453	2	2.20379
				−67.46192	2	1.92973
			V_{d-f}	2.29590	0	9.36770
				20.62182	2	2.83038
40	Zr	28	V_f	−6.11923	1	4.31441
			V_{s-f}	4.57031	0	0.93035
				139.02972	2	2.66632
				−112.55854	2	2.33003
			V_{p-f}	4.04524	0	0.97753
				86.37034	2	2.50892
				−66.64768	2	2.14998
			V_{d-f}	5.64085	0	16.57598
				26.66093	2	3.32079
41	Nb	28	V_f	−5.81695	1	4.64198
			V_{s-f}	4.99937	0	1.07339
				127.21570	2	2.93940
				−100.17856	2	2.51174
			V_{p-f}	3.64794	0	0.99626
				85.80845	2	2.73360
				−62.17437	2	2.28020
			V_{d-f}	2.77206	0	10.48803
				29.05246	2	3.64266
42	Mo	28	V_f	−7.23009	1	5.62507
			V_{s-f}	3.83695	0	1.01907
				129.35214	2	3.27945
				−90.19151	2	2.68386
			V_{p-f}	3.83295	0	1.10957
				89.77478	2	3.04740
				−62.98231	2	2.49708
			V_{d-f}	2.73486	0	9.70400
				32.53231	2	4.03098
43	Tc	28	V_f	−7.54356	1	6.26067
			V_{s-f}	4.31377	0	1.17731
				120.82547	2	3.61432
				−80.61847	2	2.86418
			V_{p-f}	3.38952	0	1.08449
				89.03016	2	3.30452
				−57.06568	2	2.59907
			V_{d-f}	2.86365	0	11.62092
				37.18014	2	4.45900
44	Ru	28	V_f	−7.98448	1	6.98304
			V_{s-f}	4.82384	0	1.29393
				124.36917	2	3.87163
				−81.31936	2	3.04871
			V_{p-f}	3.86590	0	1.20273
				103.67006	2	3.48391
				−72.15048	2	2.82303
			V_{d-f}	3.21083	0	14.33743
				42.07321	2	4.90003
45	Rh	28	V_f	−8.13225	1	7.64968
			V_{s-f}	5.20773	0	1.33777
				90.36859	2	4.39131
				−50.06846	2	2.95308
			V_{p-f}	3.85874	0	1.19468
				106.11615	2	3.67503
				−72.74348	2	2.92434
			V_{d-f}	3.34825	0	17.89248
				47.13883	2	5.34874
46	Pd	28	V_f	−8.33466	1	8.34327
			V_{s-f}	3.97809	0	1.21315
				218.99250	2	4.03301
				−168.44404	2	3.45772
			V_{p-f}	4.14021	0	1.45607
				108.32601	2	4.05510
				−72.83147	2	3.21616
			V_{d-f}	3.30611	0	19.54477
				52.78802	2	5.84664
47	Ag	28	V_f	−8.44669	1	9.01696
			V_{s-f}	6.20634	0	1.51740
				92.40173	2	4.82747
				−56.82624	2	3.23088
			V_{p-f}	3.75637	0	1.21699
				118.86801	2	4.05349
				−80.95335	2	3.18615
			V_{d-f}	3.40895	0	22.94020
				57.10513	2	6.26627
48	Cd	28	V_f	−8.69864	1	9.81325
			V_{s-f}	6.56934	0	1.60476
				93.59610	2	5.08876
				−59.36395	2	3.37727
			V_{p-f}	3.67863	0	1.25171
				145.67316	2	4.21415
				−104.50694	2	3.42592
			V_{d-f}	3.33094	0	22.35337
				62.06616	2	6.75408
49	In	28	V_f	−8.84031	1	10.58987
			V_{s-f}	6.90124	0	1.73883
				101.77272	2	5.30270
				−68.48319	2	3.62806
			V_{p-f}	3.98554	0	1.43045
				171.90487	2	4.47679
				−129.87594	2	3.74447
			V_{d-f}	3.49244	0	29.16072
				68.27816	2	7.26566
50	Sn	46	V_f	−5.60682	1	0.82050
			V_{s-f}	7.18487	0	2.60504
				91.84771	2	1.01356
				−73.06581	2	0.95780
			V_{p-f}	5.07311	0	0.67947
				95.37048	2	0.76292
				−87.03674	2	0.74276
			V_{d-f}	5.10243	0	1.65430
				5.27466	2	0.60301

Can. J. Chem. Downloaded from www.nrcresearchpress.com by 92.62.229.171 on 09/08/12
For personal use only.

TABLE 2 (*concluded*)

Z	Atom	N_{core}	RCEP	A_{lk}	n_{lk}	B_{lk}
51	Sb	46	V_f	−2.90951	1	0.75490
				−12.44921	1	2.83072
			V_{s-f}	7.55592	0	5.86819
				79.99053	2	1.21790
				−53.01395	2	1.10036
			V_{p-f}	8.30360	0	3.51430
				45.56610	2	0.96029
				−29.04708	2	0.86461
			V_{d-f}	9.22182	0	2.45981
				7.92129	2	0.76415
52	Te	46	V_f	−3.95984	1	0.94847
				−13.42871	1	3.94682
			V_{s-f}	12.95665	0	3.49400
				72.77514	2	1.33530
				−47.45882	2	1.21477
			V_{p-f}	8.47921	0	1.37394
				51.93673	2	1.28425
				−39.40684	2	1.27761
			V_{d-f}	11.54663	0	3.66618
				11.23776	2	0.93189
53	I	46	V_f	−3.69639	1	0.97628
				−14.00305	1	4.33343
			V_{s-f}	12.11123	0	4.13071
				70.73761	2	1.49121
				−41.09206	2	1.33375
			V_{p-f}	10.59271	0	3.04692
				65.05047	2	1.14405
				−46.02273	2	1.06339
			V_{d-f}	9.73089	0	3.93063
				13.98880	2	1.06920
54	Xe	46	V_f	−5.10538	1	1.27068
				−14.39873	1	5.90469
			V_{s-f}	13.44278	0	7.15744
				83.21672	2	1.65478
				−45.48918	2	1.45217
			V_{p-f}	12.73758	0	4.36144
				75.57733	2	1.36439
				−49.60137	2	1.25455
			V_{d-f}	17.79041	0	5.89897
				17.25358	2	1.23485

the wavefunction. This is accomplished through the use of a "core polarization" potential (CPP) that interacts with the valence electrons. The CPP recommended by Müller is centered on the atomic nucleus and has the form

$$[14] \qquad \mathbf{V}_{pol} = \sum_i \sum_j \frac{(1 - e^{-\beta r_i^2})\mathbf{r}_i}{r_i^3} \alpha \frac{(1 - e^{-\beta r_j^2})\mathbf{r}_j}{r_j^3}$$

where the indices i and j run over all valence electrons, α is the measured or calculated polarizability of the core electrons, and the electric field is multiplied by a Gaussian cutoff that accounts for the penetration of the polarizable core by the valence electrons. The cutoff exponent, β, is adjusted empirically by matching the calculated ionization potential of the single-valence-electron atom to the experimentally measured value.

Müller *et al.* developed CPP for all-electron alkali and alkaline earth atoms (28) and demonstrated their accuracy in a series of molecular calculations (29). Christiansen (30), Jeung *et al.* (31), Preuss and co-workers (32), and Spiegelman *et al.* (33) have also made use of CPP in effec-

TABLE 3. Relativistic compact effective potentials for the fifth-row atoms. The form of the analytic representation is given in Table 1

Z	Atom	N_{core}	RCEP	A_{lk}	n_{lk}	B_{lk}
55	Cs	54	V_f	−5.01874	1	0.31356
			V_{s-f}	6.79629	0	0.40093
				13.72442	2	0.45384
				−12.27571	2	0.65203
			V_{p-f}	12.30018	0	0.67287
				2.95222	2	0.22290
			V_{d-f}	1.96793	0	0.40835
				2.47096	1	0.24413
				−0.80500	2	0.20154
56	Ba	54	V_f	−4.89584	1	0.37866
				−17.47201	1	3.17423
			V_{s-f}	13.46017	0	0.40687
				8.12634	2	0.46605
				−14.33523	2	0.94266
			V_{p-f}	17.03588	0	1.17727
				4.74706	2	0.28981
			V_{d-f}	12.78807	1	1.00450
				−0.28677	1	0.14394
57	La	46	V_g	−2.85665	1	1.42345
			V_{s-g}	8.85347	0	22.29739
				110.12463	2	1.85122
				−68.41778	2	1.64320
			V_{p-g}	2.98675	0	1.77635
				53.65423	2	2.47524
				−35.51815	2	3.98941
			V_{d-g}	1.67298	0	1.52169
				18.46625	2	1.52182
			V_{f-g}	−4.64430	1	2.67762
				−14.43101	1	10.06608
72	Hf	60	V_g	−2.59020	1	1.14090
			V_{s-g}	5.08602	0	18.98210
				154.12616	2	4.32002
				−76.34646	2	3.92413
			V_{p-g}	3.80263	0	1.11008
				159.39488	2	2.58171
				−133.12772	2	2.38920
			V_{d-g}	5.23486	0	21.00000
				30.09851	2	2.80487
			V_{f-g}	11.03700	0	1.11377
73	Ta	60	V_g	−4.33440	1	1.65262
			V_{s-g}	4.24022	0	3.78450
				89.32811	2	3.95058
				−30.38231	2	3.17838
			V_{p-g}	3.33868	0	1.00580
				171.53349	2	2.58191
				−138.02173	2	2.35390
			V_{d-g}	3.04913	0	24.29129
				41.20515	2	3.18604
			V_{f-g}	7.84634	0	1.13011
74	W	60	V_g	−5.26480	1	2.03828
			V_{s-g}	2.47299	0	0.96514
				113.46745	2	3.62713
				−52.07178	2	2.65502
			V_{p-g}	3.91085	0	1.23902
				172.36976	2	2.80797
				−135.31607	2	2.54122
			V_{d-g}	3.87349	0	27.55935
				49.52511	2	3.51973
			V_{f-g}	6.99471	0	1.20561
75	Re	60	V_g	−6.62225	1	2.51731
			V_{s-g}	3.32067	0	1.00603
				101.83236	2	3.86550
				−39.91860	2	2.52065

Can. J. Chem. Downloaded from www.nrcresearchpress.com by 92.62.229.171 on 09/08/12
For personal use only.

Can. J. Chem. Downloaded from www.nrcresearchpress.com by 92.62.229.171 on 09/08/12
For personal use only.

TABLE 3 (*continued*)

Z	Atom	N_{core}	RCEP	A_{lk}	n_{lk}	B_{lk}
			V_{p-g}	3.83735	0	1.22884
				166.17144	2	3.01686
				−121.99416	2	2.65033
			V_{d-g}	4.57819	0	29.23499
				58.72776	2	3.86422
			V_{f-g}	6.44315	0	1.27456
76	Os	60	V_g	−7.96753	1	3.01084
			V_{s-g}	4.03478	0	1.17006
				148.94410	2	3.82663
				−84.75261	2	2.93435
			V_{p-g}	3.10454	0	1.02178
				172.77128	2	3.10435
				−120.70117	2	2.66013
			V_{d-g}	6.63507	0	31.00000
				66.85726	2	4.17953
			V_{f-g}	6.33120	0	1.38742
77	Ir	60	V_g	−8.98208	1	3.46859
			V_{s-g}	4.83629	0	1.27403
				162.58173	2	3.97153
				−98.47624	2	3.07970
			V_{p-g}	3.80021	0	1.08342
				203.96216	2	3.21008
				−151.65910	2	2.79432
			V_{d-g}	7.96874	0	33.00000
				73.97844	2	4.47188
			V_{f-g}	6.28559	0	1.48524
78	Pt	60	V_g	−9.79854	1	3.90813
			V_{s-g}	5.79843	0	1.36279
				247.96906	2	3.91136
				−187.51594	2	3.34227
			V_{p-g}	3.67055	0	1.07586
				151.55915	2	3.52491
				−93.02055	2	2.80443
			V_{d-g}	13.09353	0	42.63116
				80.29385	2	4.74468
			V_{f-g}	6.13870	0	1.58988
79	Au	60	V_g	−10.72358	1	4.38763
			V_{s-g}	6.35612	0	1.55636
				428.19753	2	4.06792
				−364.44039	2	3.71593
			V_{p-g}	4.41518	0	1.18798
				194.20535	2	3.59588
				−136.57550	2	3.01551
			V_{d-g}	8.88198	0	35.25000
				86.76612	2	5.02307
			V_{f-g}	6.21603	0	1.68881
80	Hg	60	V_g	−11.51618	1	4.85764
			V_{s-g}	4.09547	0	1.17357
				394.68735	2	4.18793
				−310.08898	2	3.70966
			V_{p-g}	3.61202	0	0.95913
				211.83161	2	3.58353
				−148.42850	2	2.99268
			V_{d-g}	8.27074	0	35.54665
				92.85678	2	5.29318
			V_{f-g}	6.28302	0	1.80978
81	Tl	60	V_g	−12.13787	1	5.31294
			V_{s-g}	4.77833	0	1.29566
				337.05349	2	4.43233
				−253.19592	2	3.80665
			V_{p-g}	3.45912	0	0.94782
				238.10901	0	3.73562
				−168.94091	2	3.14378
			V_{d-g}	7.41137	0	33.43080
				98.49883	2	5.55174

TABLE 3 (*concluded*)

Z	Atom	N_{core}	RCEP	A_{lk}	n_{lk}	B_{lk}
			V_{f-g}	6.27606	0	1.91385
82	Pb	78	V_g	−2.76464	1	0.51756
			V_{s-g}	6.94774	0	2.44363
				32.39564	2	0.97662
				−17.72106	2	0.82022
			V_{p-g}	4.94619	0	1.49041
				26.06040	2	0.66916
				−17.16033	2	0.59861
			V_{d-g}	4.99762	0	2.19203
				4.52730	2	0.46937
			V_{f-g}	4.95827	0	0.69081
				125.32798	2	0.20773
				−124.15758	2	0.20680
83	Bi	78	V_g	−5.34991	1	0.77941
			V_{s-g}	5.91224	0	0.58082
				58.30673	2	0.95682
				−46.52354	2	0.86480
			V_{p-g}	7.58772	0	2.41860
				17.65062	2	0.98429
				−1.55133	2	0.51229
			V_{d-g}	8.20935	0	4.10212
				8.38970	2	0.63052
			V_{f-g}	31.99918	0	1.17643
				−31.22481	0	0.57108
				16.82287	2	0.78832
84	Po	78	V_g	−6.91426	1	0.98236
			V_{s-g}	5.38765	0	0.39388
				55.71735	2	0.99601
				−41.35987	2	0.84405
			V_{p-g}	11.84449	0	4.87877
				27.85431	2	1.26544
				−2.29848	2	0.84347
			V_{d-g}	9.51261	0	2.52803
				11.38029	2	0.75864
			V_{f-g}	33.57540	0	0.71317
				−32.32727	0	0.44923
				7.89213	2	0.56249
85	At	78	V_g	−8.22821	1	1.18142
			V_{s-g}	6.65302	0	0.49276
				33.10060	2	1.27555
				−15.98654	2	0.85421
			V_{p-g}	10.73147	0	3.37381
				150.80821	2	0.97488
				−128.82729	2	0.93728
			V_{d-g}	15.83166	0	3.88638
				14.55150	2	0.87679
			V_{f-g}	4.27097	0	1.12284
				−3.39500	2	1.15530
86	Rn	78	V_g	−9.36991	1	1.37920
			V_{s-g}	5.25644	0	0.47169
				62.19287	2	1.26952
				−39.27598	2	1.01268
			V_{p-g}	7.38631	0	3.32534
				71.81385	2	1.11620
				−45.67830	2	0.99950
			V_{d-g}	4.90484	0	0.92214
				12.61598	2	0.92221
			V_{f-g}	2.96924	0	1.61735
				−0.17844	2	0.32150

tive core potential calculations. We have derived CPP similar to Müller's for use with the alkali and alkaline earth RCEP. The parameters and atomic valence energies are re-

Can. J. Chem. Downloaded from www.nrcresearchpress.com by 92.62.229.171 on 09/08/12
For personal use only.

TABLE 4. Contracted Gaussian valence basis sets for the third-row atoms. Expansion coefficients are for normalized basis functions and normalized primitive Gaussians. The *d* basis sets are taken from Rappe *et al.* (37).

Atom(Z)		α_{sp}	C_s	C_p		α_d	C_d
K(19)	1*sp*	0.2201	−0.286027	−0.066245			
		0.04825	0.482050	0.356898			
		0.02242	0.675841	0.704426			
	2*sp*	0.01020	1.0	1.0			
Ca(20)	1*sp*	0.2604	−0.676466	−0.270374			
		0.1439	0.525693	0.407807			
		0.04859	0.960216	0.828129			
	2*sp*	0.02167	1.0	1.0			
Sc(21)	1*sp*	40.07	−0.003296	−0.007753	1*d*	23.24	0.026288
		3.665	−0.655617	−0.615592		6.143	0.142881
		3.047	0.103253	0.780261		2.007	0.398178
		0.9588	1.320199	0.834079		0.6652	0.640201
	2*sp*	0.3557	1.0	1.0	2*d*	0.2021	1.0
	3*sp*	1.264	−0.057596	−0.031779	3*d*	0.05454	1.0
		0.07502	1.016468	1.004065			
	4*sp*	0.02741	1.0				
Ti(22)	1*sp*	51.08	−0.002004	−0.006949	1*d*	28.11	0.025746
		4.180	−0.619686	−0.326613		7.630	0.141260
		2.997	0.156029	0.544254		2.528	0.400607
		1.019	1.248817	0.789631		0.8543	0.634532
	2*sp*	0.3745	1.0	1.0	2*d*	0.2673	1.0
	3*sp*	1.383	−0.072891	−0.025949	3*d*	0.0743	1.0
		0.08128	1.020184	1.003353			
	4*sp*	0.03023	1.0	1.0			
V(23)	1*sp*	48.16	−0.004277	−0.008007	1*d*	33.36	0.025530
		4.685	−0.545554	−0.265673		9.331	0.140336
		3.115	0.131799	0.522944		3.158	0.397933
		1.098	1.218022	0.754434		1.113	0.629027
	2*sp*	0.3936	1.0	1.0	2*d*	0.3608	1.0
	3*sp*	1.5650	−0.085426	−0.022816	3*d*	0.1007	1.0
		0.09409	1.023584	1.003066			
	4*sp*	0.03370	1.0	1.0			
Cr(24)	1*sp*	23.12	−0.005918	−0.018018	1*d*	37.89	0.025910
		5.036	−0.590750	−0.144996		10.58	0.144130
		2.867	0.296120	0.497416		3.603	0.403597
		1.144	1.107646	0.672884		1.270	0.620846
	2*sp*	0.4529	1.0	1.0	2*d*	0.4118	1.0
	3*sp*	1.571	−0.090329	−0.037281	3*d*	0.1126	1.0
		0.09654	1.025164	1.004879			
	4*sp*	0.03492	1.0				
Mn(25)	1*sp*	72.17	−0.002635	−0.007172	1*d*	42.63	0.026095
		5.728	−0.593184	−0.245649		11.97	0.146772
		3.729	0.224656	0.532283		4.091	0.407115
		1.321	1.175342	0.730536		1.450	0.614590
	2*sp*	0.4754	1.0	1.0	2*d*	0.4700	1.0
	3*sp*	1.8270	−0.096146	−0.032600	3*d*	0.1281	1.0
		0.1130	1.026668	1.004376			
	4*sp*	0.03890	1.0	1.0			
Fe(26)	1*sp*	70.28	−0.002611	−0.07940	1*d*	47.10	0.026608
		6.061	−0.692435	−0.290151		13.12	0.152010
		4.134	0.362530	0.591028		4.478	0.413827
		1.421	1.140645	0.719448		1.581	0.605542
	2*sp*	0.5121	1.0	1.0	2*d*	0.5100	1.0
	3*sp*	1.9780	−0.098172	−0.033731	3*d*	0.1382	1.0
		0.1213	1.026957	1.004462			
	4*sp*	0.410	1.0	1.0			
Co(27)	1*sp*	75.68	−0.005271	−0.008085	1*d*	51.69	0.025447
		6.496	−0.705525	−0.390988		14.70	0.149529
		4.791	0.347880	0.680078		4.851	0.425056
		1.594	1.175595	0.729594		1.643	0.605465
	2*sp*	0.5572	1.0	1.0	2*d*	0.5075	1.0
	3*sp*	2.337	−0.089267	−0.015935	3*d*	0.1433	1.0
		0.1269	1.022589	1.001945			
	4*sp*	0.04232	1.0	1.0			

TABLE 4 (*concluded*)

Atom(Z)		α_{sp}	C_s	C_p		α_d	C_d
Ni(28)	1*sp*	89.36	−0.005220	−0.007529	1*d*	58.73	0.026246
		7.265	−0.683993	−0.445862		16.71	0.150334
		5.572	0.251050	0.706364		5.783	0.413385
		1.850	1.236451	0.753606		2.064	0.604114
	2*sp*	0.6594	1.0	1.0	2*d*	0.6752	1.0
	3*sp*	3.235	−0.063418	0.001136	3*d*	0.1825	1.0
		0.1295	1.013237	0.999895			
	4*sp*	0.04327	1.0	1.0			
Cu(29)	1*sp*	83.42	−0.004829	−0.008284	1*d*	65.80	0.025597
		7.970	−0.644799	−0.321895		18.82	0.148609
		5.600	0.265240	0.618133		6.538	0.411786
		1.932	1.189791	0.722184		2.348	0.605507
	2*sp*	0.6874	1.0	1.0	2*d*	0.7691	1.0
	3*sp*	2.866	−0.074774	−0.000541	3*d*	0.2065	1.0
		0.1319	1.017037	1.000058			
	4*sp*	0.04400	1.0	1.0			
Zn(30)	1*sp*	113.5	−0.004280	−0.007429	1*d*	65.99	0.027653
N_{core} = 10		8.308	−0.820232	−0.432605		19.81	0.158794
		6.332	0.425006	0.723451		6.945	0.420971
		2.146	1.198077	0.727217		2.543	0.585277
	2*sp*	0.8116	1.0	1.0	2*d*	0.9165	1.0
	3*sp*	2.906	−0.082356	−0.023001	3*d*	0.3264	1.0
		0.1623	1.021574	1.002824			
	4*sp*	0.05369	1.0	1.0			
Zn(30)	1*sp*	0.9278	−0.277539	−0.055932			
N_{core} = 28		0.1758	0.510462	0.517112			
		0.07976	0.634043	0.548141			
	2*sp*	0.03690	1.0	1.0			
Ga(31)	1*sp*	113.9	−0.001711	−0.008046	1*d*	70.43	0.028877
N_{core} = 10		9.155	−0.823036	−0.357432		21.05	0.166253
		6.633	0.458618	0.663794		7.401	0.427776
		2.278	1.161817	0.713619		2.752	0.570410
	2*sp*	0.8818	1.0	1.0	2*d*	1.026	1.0
	3*sp*	2.123	−0.145506	−0.096261	3*d*	0.3907	1.0
		0.1939	1.051147	1.017573			
	4*sp*	0.07461	1.0	1.0			
Ga(31)	1*sp*	1.634	0.831592	−0.188607			
N_{core} = 28		1.473	−1.161286	0.140880			
		0.2607	0.237640	0.348597			
		0.1461	0.912666	0.682579			
	2*sp*	0.05274	1.0	1.0			
G3(32)	1*sp*	1.834	0.493860	0.006414			
		1.529	−0.857354	−0.086052			
		0.3594	0.410830	0.383232			
		0.1470	0.800378	0.698185			
	2*sp*	0.05598	1.0	1.0			
As(33)	1*sp*	2.709	0.121479	−0.002920			
		1.578	−0.518918	−0.095054			
		0.4358	0.428791	0.424682			
		0.1776	0.808078	0.671290			
	2*sp*	0.06984	1.0	1.0			
Se(34)	1*sp*	3.711	0.055744	−0.006014			
		1.586	−0.510520	−0.121447			
		0.5339	0.480755	0.452607			
		0.2085	0.810292	0.669750			
	2*sp*	0.07821	1.0	1.0			
Br(35)	1*sp*	3.276	0.200570	0.005418			
		2.044	−0.649298	−0.132407			
		0.6398	0.405405	0.430017			
		0.2561	0.872604	0.686022			
	2*sp*	0.09567	1.0	1.0			
Kr(36)	1*sp*	3.081	0.533789	0.035906			
		2.413	−1.001465	−0.169695			
		0.7386	0.415510	0.435080			
		0.2941	0.880103	0.685760			
	2*sp*	0.1095	1.0	1.0			

Can. J. Chem. Downloaded from www.nrcresearchpress.com by 92.62.229.171 on 09/08/12
For personal use only.

TABLE 5. Contracted Gaussian valence basis sets for the fourth-row atoms. Expansion coefficients are for normalized basis functions and normalized primitive Gaussians

Atom(Z)		α_{sp}	C_s	C_p		α_d	C_d
Rb(37)	1*sp*	0.1543	−0.753390	−0.108684			
		0.09892	0.406270	0.055587			
		0.03227	1.112487	1.014168			
	2*sp*	0.01490	1.0	1.0			
Sr(38)	1*sp*	0.1836	−1.075139	−0.955549			
		0.1252	0.947037	0.856447			
		0.03968	0.934226	0.871558			
	2*sp*	0.01840	1.0	1.0			
Y(39)	1*sp*	29.84	−0.006294	−0.003457	1*d*	5.399	0.012020
		3.242	1.436231	−0.097386		1.066	0.342950
		2.694	−2.550213	−0.098933		0.3892	0.739397
		0.8430	1.756065	1.112190			
	2*sp*	0.3015	1.0	1.0	2*d*	0.1300	1.0
	3*sp*	1.324	−0.057976	−0.025891	3*d*	0.04121	1.0
		0.06806	1.014874	1.002833			
	4*sp*	0.02729	1.0				
Zr(40)	1*sp*	30.53	−0.004504	−0.004092	1*d*	6.191	0.012000
		3.518	1.708899	−0.078665		1.320	0.325005
		2.971	−2.918518	−0.140588		0.5359	0.740299
		0.9587	1.822958	1.130526			
	2*sp*	0.3764	1.0	1.0	2*d*	0.1900	1.0
	3*sp*	0.9293	−0.061958	−0.060217	3*d*	0.05900	1.0
		0.06910	1.020739	1.009302			
	4*sp*	0.02759	1.0	1.0			
Nb(41)	1*sp*	38.53	−0.002059	−0.003576	1*d*	7.994	0.010433
		3.907	1.618867	−0.033217		1.550	0.318071
		3.274	−2.830860	−0.185568		0.6666	0.739654
		1.052	1.818465	1.133471			
	2*sp*	0.4165	1.0	1.0	2*d*	0.2462	1.0
	3*sp*	1.057	−0.071919	−0.067815	3*d*	0.07860	1.0
		0.07876	1.023797	1.010254			
	4*sp*	0.03091	1.0	1.0			
Mo(42)	1*sp*	39.67	−0.009716	−0.004015	1*d*	9.051	0.010883
		4.633	0.770126	−0.034146		1.777	0.311829
		3.208	−2.229530	−0.251817		0.7848	0.741802
		1.224	2.046495	1.192347			
	2*sp*	0.4728	1.0	1.0	2*d*	0.2899	1.0
	3*sp*	1.181	−0.075222	−0.071971	3*d*	0.09107	1.0
		0.08489	1.024137	1.010227			
	4*sp*	0.03276	1.0				
Tc(43)	1*sp*	48.87	−0.006485	−0.003492	1*d*	9.451	0.012195
		4.770	1.330930	0.037514		1.887	0.346950
		3.740	−2.698832	−0.297801		0.8506	0.707123
		1.305	1.956263	1.174900			
	2*sp*	0.4940	1.0	1.0	2*d*	0.3258	1.0
	3*sp*	1.744	−0.094275	−0.085401	3*d*	0.1031	1.0
		0.1206	1.028604	1.010946			
	4*sp*	0.04310	1.0	1.0			
Ru(44)	1*sp*	56.00	−0.002837	−0.003198	1*d*	10.30	0.011961
		4.625	1.891661	−0.103766		2.044	0.364575
		3.793	−3.431011	−0.127594		0.8988	0.694316
		1.367	2.074446	1.146533			
	2*sp*	0.5183	1.0	1.0	2*d*	0.3443	1.0
	3*sp*	1.528	−0.069035	−0.072990	3*d*	0.1108	1.0
		0.09673	1.020343	1.008642			
	4*sp*	0.03636	1.0	1.0			
Rh(45)	1*sp*	56.87	−0.003087	−0.003748	1*d*	11.56	0.013519
		5.945	0.700510	−0.014772		2.240	0.370081
		4.078	−2.160867	−0.268975		1.015	0.684936
		1.547	2.029434	1.193604			
	2*sp*	0.5963	1.0	1.0	2*d*	0.3960	1.0
	3*sp*	1.894	−0.081700	−0.071093	3*d*	0.1262	1.0
		0.1179	1.023308	1.008280			
	4*sp*	0.04219	1.0	1.0			

Can. J. Chem. Downloaded from www.nrcresearchpress.com by 92.62.229.171 on 09/08/12
For personal use only.

TABLE 5 (*concluded*)

Atom(Z)		α_{sp}	C_s	C_p		α_d	C_d
Pd(46)	1*sp*	41.82	−0.016522	−0.005555	1*d*	12.40	0.013759
		5.460	2.749478	0.056773		2.404	0.394121
		4.600	−4.457343	−0.388641		1.143	0.655946
		1.752	2.253933	1.231997			
	2*sp*	0.6691	1.0	1.0	2*d*	0.4693	1.0
	3*sp*	2.177	−0.075029	−0.056178	3*d*	0.1513	1.0
		0.1149	1.019049	1.005515			
	4*sp*	0.04219	1.0	1.0			
Ag(47)	1*sp*	63.56	−0.000731	−0.004234	1*d*	14.64	0.013628
		6.390	1.392736	0.061276		2.693	0.372695
		5.022	−2.873102	−0.338746		1.233	0.681294
		1.789	2.017361	1.190832			
	2*sp*	0.6871	1.0	1.0	2*d*	0.5057	1.0
	3*sp*	2.451	−0.072539	−0.049830	3*d*	0.1900	1.0
		0.1561	1.021358	1.006516			
	4*sp*	0.05227	1.0	1.0			
Cd(48)	1*sp*	63.38	−0.000464	−0.004874	1*d*	15.51	0.012065
		6.714	2.292877	0.189630		2.941	0.370168
		5.602	−3.902884	−0.491872		1.379	0.680760
		1.971	2.084604	1.213501			
	2*sp*	0.7689	1.0	1.0	2*d*	0.5782	1.0
	3*sp*	2.696	−0.064866	−0.053338	3*d*	0.2300	1.0
		0.1758	1.019661	1.007102			
	4*sp*	0.05647	1.0	1.0			
In(49)	1*sp*	71.76	0.000733	−0.004513	1*d*	17.16	0.014893
		7.654	1.089781	0.031615		3.127	0.388135
		5.616	−2.731089	−0.338006		1.475	0.662639
		2.104	2.112844	1.213464			
	2*sp*	0.8410	1.0	1.0	2*d*	0.6452	1.0
	3*sp*	2.610	−0.099690	−0.110317	3*d*	0.2754	1.0
		0.1901	1.031230	1.013900			
	4*sp*	0.08267	1.0	1.0			
Sn(50)	1*sp*	2.604	0.031042	−0.005053			
		0.7532	−0.611859	−0.180100			
		0.3191	0.548163	0.370068			
		0.1239	0.849150	0.781334			
	2*sp*	0.04798	1.0	1.0			
Sb(51)	1*sp*	0.9922	0.690076	0.180229			
		0.8089	−1.580495	−0.487093			
		0.4312	0.815248	0.473936			
		0.1498	0.894994	0.804414			
	2*sp*	0.05803	1.0	1.0			
Te(52)	1*sp*	2.364	0.087179	−0.003982			
		0.9769	−0.776826	−0.236900			
		0.4647	0.563250	0.401467			
		0.1771	0.926053	0.793179			
	2*sp*	0.06737	1.0	1.0			
I(53)	1*sp*	2.625	0.073660	−0.008880			
		1.014	−0.836870	−0.257351			
		0.5009	0.656247	0.455368			
		0.2023	0.900744	0.760107			
	2*sp*	0.07800	1.0	1.0			
Xe(54)	1*sp*	1.739	0.349091	−0.005429			
		1.169	−1.197512	−0.277342			
		0.5765	0.758409	0.467189			
		0.2218	0.888699	0.763456			
	2*sp*	0.08486	1.0	1.0			

Can. J. Chem. Downloaded from www.nrcresearchpress.com by 92.62.229.171 on 09/08/12
For personal use only.

TABLE 6. Contracted Gaussian valence basis sets for the fifth-row atoms. Expansion coefficients are for normalized basis functions and normalized primitive Gaussians

Atom(Z)		α_{sp}	C_s	C_p		α_d	C_d
Cs(55)	1*sp*	0.1157	−0.519994	−0.150560			
		0.05317	0.493361	0.221602			
		0.01897	0.872312	0.896486			
	2*sp*	0.007740	1.0	1.0			
Ba(56)	1*sp*	0.1266	−1.560287	−0.686637			
		0.09433	1.482538	0.807346			
		0.03020	0.878917	0.822436			
	2*sp*	0.01531	1.0	1.0			
La(57)	1*sp*	9.173	−0.054833	−0.009798	1*d*	1.238	−0.053797
		3.120	0.676604	0.231262		0.6061	0.380144
		2.104	−1.034429	−0.601215		0.2518	0.720349
		1.320	−0.518907	0.195189			
		0.4960	1.631603	1.076137			
	2*sp*	0.2004	1.0	1.0	2*d*	0.09787	1.0
	3*sp*	0.6182	−0.107095	−0.051869	3*d*	0.03536	1.0
		0.04546	1.033448	1.008108			
	4*sp*	0.01775	1.0	1.0			
Hf(72)	1*sp*	4.711	0.403273	0.013791	1*d*	3.298	−0.005062
		3.331	−0.996540	−0.179991		0.9286	0.427636
		0.9844	0.979338	0.693601		0.3405	0.667943
		0.3587	0.445791	0.461877			
	2*sp*	0.6448	1.0	1.0	2*d*	0.1230	1.0
	3*sp*	0.08568	1.0	1.0	3*d*	0.04268	1.0
	4*sp*	0.03500	1.0	1.0			
Ta(73)	1*sp*	5.544	0.264429	0.016092	1*d*	3.438	−0.010797
		3.436	−0.865843	−0.182862		1.016	0.439474
		1.033	1.008583	0.722442		0.3733	0.658929
		0.3747	0.420826	0.436168			
	2*sp*	0.7315	1.0	1.0	2*d*	0.1351	1.0
	3*sp*	0.09340	1.0	1.0	3*d*	0.04807	1.0
	4*sp*	0.03684	1.0	1.0			
W(74)	1*sp*	4.328	1.973960	0.172752	1*d*	3.653	−0.016297
		3.898	−2.605377	−0.348372		1.112	0.450108
		1.108	1.052920	0.727425		0.4148	0.648857
		0.4047	0.412613	0.434635			
	2*sp*	0.8219	1.0	1.0	2*d*	0.1495	1.0
	3*sp*	0.09776	1.0	1.0	3*d*	0.05255	1.0
	4*sp*	0.03750	1.0				
Re(75)	1*sp*	4.666	1.451709	0.156457	1*d*	3.846	−0.021360
		4.062	−2.101771	−0.342900		1.216	0.456284
		1.188	1.062295	0.738595		0.4585	0.643606
		0.4339	0.416694	0.432092			
	2*sp*	0.9127	1.0	1.0	2*d*	0.1659	1.0
	3*sp*	0.1048	1.0	1.0	3*d*	0.05836	1.0
	4*sp*	0.03981	1.0	1.0			
Os(76)	1*sp*	5.019	1.726729	0.283956	1*d*	3.829	−0.028163
		4.444	−2.364185	−0.462163		1.339	0.457633
		1.230	1.070406	0.763251		0.5165	0.642551
		0.4501	0.391956	0.403944			
	2*sp*	1.0020	1.0	1.0	2*d*	0.1880	1.0
	3*sp*	0.1104	1.0	1.0	3*d*	0.06552	1.0
	4*sp*	0.04101	1.0	1.0			
Ir(77)	1*sp*	5.522	1.052849	0.143988	1*d*	4.393	−0.025391
		4.579	−1.697001	−0.325563		1.403	0.475718
		1.289	1.087609	0.776442		0.5593	0.618182
		0.4734	0.377230	0.398328			
	2*sp*	1.116	1.0	1.0	2*d*	0.2129	1.0
	3*sp*	0.1159	1.0	1.0	3*d*	0.07634	1.0
	4*sp*	0.04276	1.0	1.0			
Pt(78)	1*sp*	6.653	0.282256	0.036575	1*d*	4.658	−0.026327
		3.995	−1.075967	−0.284606		1.487	0.495995
		1.541	1.131255	0.752346		0.6093	0.594877
		0.5599	0.478241	0.476585			

Can. J. Chem. Downloaded from www.nrcresearchpress.com by 92.62.229.171 on 09/08/12
For personal use only.

TABLE 6 (*concluded*)

Atom(Z)		α_{sp}	C_s	C_p		α_d	C_d
	2*sp*	1.200	1.0	1.0	2*d*	0.2527	1.0
	3*sp*	0.1277	1.0	1.0	3*d*	0.09508	1.0
	4*sp*	0.04754	1.0	1.0			
Au(79)	1*sp*	7.419	0.222546	0.019924	1*d*	3.630	−0.087402
		4.023	−1.086045	−0.299997		1.912	0.468634
		1.698	1.156039	0.748919		0.8423	0.654805
		0.6271	0.518061	0.504023			
	2*sp*	1.502	1.0	1.0	2*d*	0.3756	1.0
	3*sp*	0.1515	1.0	1.0	3*d*	0.1544	1.0
	4*sp*	0.04925	1.0	1.0			
Hg(80)	1*sp*	25.54	−0.022041	−0.006068	1*d*	4.204	−0.055849
		8.458	0.309845	0.063000		1.871	0.478221
		4.493	−1.080984	−0.314502		0.8215	0.622006
		1.751	1.093600	0.746398			
		0.6753	0.519202	0.487253			
	2*sp*	1.586	1.0	1.0	2*d*	0.3700	1.0
	3*sp*	0.1520	1.0	1.0	3*d*	0.1674	1.0
	4*sp*	0.04780	1.0	1.0			
Tl(81)	1*sp*	27.72	−0.015939	−0.005281	1*d*	4.284	−0.077432
		8.583	0.307229	0.072455		2.136	0.455402
		4.650	−1.124512	−0.343413		0.9832	0.652892
		1.876	1.114798	0.759620			
		0.7369	0.531758	0.489550			
	2*sp*	1.629	1.0	1.0	2*d*	0.4500	1.0
	3*sp*	0.1600	1.0	1.0	3*d*	0.2040	1.0
	4*sp*	0.06181	1.0	1.0			
Pb(82)	1*sp*	1.534	0.225652	0.028257			
		0.9923	−0.658998	−0.140659			
		0.2241	0.766214	0.428132			
		0.09664	0.500934	0.663422			
	2*sp*	0.03900	1.0	1.0			
Bi(83)	1*sp*	1.746	0.162327	0.016087			
		0.9925	−0.653854	−0.158284			
		0.2642	0.801350	0.460932			
		0.1135	0.516861	0.649770			
	2*sp*	0.04642	1.0	1.0			
Po(84)	1*sp*	1.897	0.132690	0.006796			
		1.000	−0.681546	−0.176142			
		0.3107	0.840179	0.490092			
		0.1273	0.536942	0.645759			
	2*sp*	0.05100	1.0	1.0			
At(85)	1*sp*	2.676	0.068973	−0.002652			
		0.9805	−0.718668	−0.194971			
		0.3598	0.917123	0.506172			
		0.1483	0.546749	0.653171			
	2*sp*	0.05887	1.0	1.0			
Rn(86)	1*sp*	2.489	0.082820	0.004727			
		1.013	−0.803200	−0.231180			
		0.4072	0.983073	0.541354			
		0.1646	0.553051	0.647745			
	2*sp*	0.06500	1.0	1.0			

ported in Table 7. The alkaline earth CPP were derived for singly charged cations, but were found to work quite well for the two-electron ground states as shown in Table 7. Krauss and Stevens have used the alkali RCEP and CPP in studies of alkali cluster polarizabilities (34) and calculations of accurate alkali diatomic potential energy curves (35). In test calculations we have found that the CPP perform well for the P and D excited states of the alkali atoms, but less accurately for the excited states of the neutral alkaline earths. Improved results could be obtained by introducing a unique CPP cutoff exponent for each angular momentum, but this seriously complicates the use of the CPP in molecular calculations and was not done in the work reported here.

One must use the RCEP for the alkali and alkaline earth atoms with caution, especially in strong ionic bonding situations or in calculations of ligands bonding to the monovalent alkali cations or the divalent alkaline earth cations. We have found that the exchange repulsion interaction between the cation core electrons and the ligand electrons is underestimated by the RCEP for small ligand–metal separations.

Can. J. Chem. Downloaded from www.nrcresearchpress.com by 92.62.229.171 on 09/08/12
For personal use only.

TABLE 7. Core polarizabilities ((bohr)^3), Gaussian cutoff exponents, and valence energies (hartree) for the Group IA and Group IIA atoms. The energies were calculated with the uncontracted 4GTO basis sets given in Tables 4–6 and ref. 5. The Group IIB energies are taken from full two-electron configuration interaction calculations. The form of the core polarizability operator is

$$\sum_i \sum_j \frac{(1 - e^{-\beta r_i^2})\,\bar{r}_i}{r_i^3}\,\alpha\,\frac{(1 - e^{-\beta r_j^2})\,\bar{r}_j}{r_j^3}$$

Atom	α	β	E_{val} (calcd.) no core α	E_{val} (calcd.) with core α	E_{val} (expt.)
Li	0.1915	0.600	−0.19604	−0.19773	−0.19814
Na	0.9947	0.642	−0.18160	−0.18833	−0.18886
K	5.354	0.285	−0.14749	−0.15919	−0.15952
Rb	8.020	0.251	−0.13998	−0.15341	−0.15351
Cs	15.15	0.172	−0.12626	−0.14248	−0.14310
Be	0.0519	1.900	−1.00739	−0.01214	−1.01161
Mg	0.4814	0.950	−0.81731	−0.83140	−0.83327
Ca	3.161	0.380	−0.63543	−0.65838	−0.66076
Sr	5.730	0.264	−0.58579	−0.61128	−0.61442
Ba	10.62	0.241	−0.52068	−0.55219	−0.55900

This underestimation will occur for all potentials that do not include the penultimate shell in the valence space. Alkali and alkaline earth effective potentials with the penultimate shell in the valence space have been reported by other authors (12, 13).

Transition metal atoms

Before proceeding with RCEP generation for the transition metal atoms, one must decide which orbitals are to be considered part of the core. This choice has been discussed and tested by a number of authors (1, 12, 13, 36). Certainly, the outermost $(n + 1)s$ orbital (where n is the principal quantum number) and the partially occupied nd orbitals are in the valence space. However, the nd orbitals have large spatial overlap with the ns and np orbitals. Also, the radial shape of the nd orbitals is sensitive to different d occupation numbers in the low-lying excited states and cationic configurations (37). These occupancy-related shape changes can result in significant changes in the ns/nd and np/nd Coulomb and exchange interactions. We have found that placing the ns and np orbitals in the core does not give the correct energy behavior for atomic states of different d occupancy. Other authors have come to similar conclusions (12, 13). Hence, to maximize the transferability of the potentials to various atomic configurations, the transition metal ns and np orbitals are considered to be part of the valence space.

Another question arises concerning the boundary between the transition metals and the main-group elements to the right side of the Periodic Table. For the third-row atoms (first transition series) trial calculations were made for both Zn and Ga with the $3s$, $3p$, and $3d$ orbitals in the core. For Zn, relatively poor results were obtained, particularly for the energies and geometries of ligands interacting with the dication, Zn^{2+}. For Ga, the differences between molecular SCF calculations (e.g., GaH_3 and GaF_3) with three valence electrons versus 21 valence electrons on Ga were about the same size as the differences between RCEP and all-electron results, e.g., ~0.02 Å in bond lengths and 0.005–0.008 hartree in atomization energies (~2%). Consequently, we decided to define Ge, Sn, and Pb as the first group of the main-group elements. For completeness, however, we have included the tested Zn and Ga potentials with the $3s$,$3p$, and $3d$ electrons in the core in Table 3. They should be used only with caution.

For the transition metal V_{LMAX} potentials, the Dirac–Fock atomic spinors and eigenvalues were obtained from atomic ion configurations with the outer nd and $(n + 1)s$ electrons removed to give a ns^2np^6 configuration plus one electron in an orbital with l = LMAX (f for 3rd and 4th row atoms, g for the 5th row atoms). For the 5th row atoms, this procedure was also used to generate the V_{f-g} potentials. For all transition metals, the V_{l-LMAX} potentials for l = 0, 1, and 2 were generated from $ns^2np^6nd^m$ 2+ cation states using multiplet-averaged relativistic atomic wavefunctions.

Energy-optimized, double-zeta quality sp basis sets and triple-zeta quality d basis sets for the transition metal atoms are given in Tables 4–6. The triple-zeta d basis set was found to be necessary to describe the orbital shape changes that accompany changes in the d occupancy. For the third-row atoms, Sc–Cu, Gaussian d basis sets with six primitives were already available from the all-electron energy-optimized sets reported by Rappe *et al.* (37). For consistency we also generated six primitive d sets for Zn and Ga. For all other transition metals, the d basis sets were energy-optimized along with the s and p basis sets according to the following scheme.

Basis sets consisting of five primitives each for s, p, and d were optimized without the outer s-electrons for the $ns^2np^6nd^m$ atomic states with the highest possible spin and angular momentum coupling. The s and p functions were required to have common sets of exponents. The d occupation number, m, was chosen so that neutral atom states were used whenever possible. Since it is not possible to have $m > 10$, cationic configurations were necessarily used for the rightmost atoms in the three series. The five d primitives were contracted triple-zeta, 3,1,1 (4,1,1 in the case of the third row). This triple-zeta contraction was found to adequately handle the change in d-orbital shape that accompanies changing occupation number. The tight s and p primitives were contracted double-zeta, 4,1 using the variationally determined atomic orbital coefficients from the above config-

Can. J. Chem. Downloaded from www.nrcresearchpress.com by 92.62.229.171 on 09/08/12
For personal use only.

Can. J. Chem. Downloaded from www.nrcresearchpress.com by 92.62.229.171 on 09/08/12
For personal use only.

TABLE 8. Calculated energies for the third row atoms using the RCEPs and basis sets reported in Tables 1 and 4. The energies are taken from spin- and space-restricted SCF calculations using the GAMESS code (ref. 3) including six Cartesian components for the *d* basis functions[a]

Atom(Z)	N_{core}	Valence electronic configuration	State	Energy (hartree)
K(19)	18	$4s^1$	^2S	−0.14749
Ca(20)	18	$4s^2$	^1S	−0.60636
Sc(21)	10	$3s^23p^63d^14s^2$	^2D	−46.02825
Ti(22)	10	$3s^23p^63d^24s^2$	^3F	−57.45757
V(23)	10	$3s^23p^63d^34s^2$	^4F	−70.69246
Cr(24)	10	$3s^23p^63d^44s^2$	^5D	−85.85801
Mn(25)	10	$3s^23p^63d^54s^2$	^6S	−103.18913
Fe(26)	10	$3s^23p^63d^64s^2$	^5D	−122.52113
Co(27)	10	$3s^23p^63d^74s^2$	^4F	−144.24904
Ni(28)	10	$3s^23p^63d^84s^2$	^3F	−168.46278
Cu(29)	10	$3s^23p^63d^94s^2$	^2D	−195.28937
Zn(30)	10	$3s^23p^63d^{10}4s^2$	^1S	−224.95040
Zn(30)	28	$4s^2$	^1S	−0.91529
Ga(31)	10	$3s^23p^63d^{10}4s^24p^1$	^2P	−257.13106
Ga(31)	28	$4s^24p^1$	^2P	−1.99065
Ge(32)	28	$4s^24p^2$	^3P	−3.67042
As(33)	28	$4s^24p^3$	^4S	−6.05221
Se(34)	28	$4s^24p^4$	^3P	−9.13353
Br(35)	28	$4s^24p^5$	^2P	−13.12543
Kr(36)	28	$4s^24p^6$	^1S	−18.11747

[a]There is a large overlap between the spherical component of the *d* basis functions and the *s* basis functions in some cases. Thus, different computer programs may produce slightly different energies depending on the threshold for linear dependence and the removal of neary linearly dependent functions.

uration. Attempts to use minimal basis (single-zeta) contractions for these functions resulted in unacceptable energetic errors for states with different *d* occupancies.

For optimization of the outer shell basis sets, different procedures were used depending on the atomic *d* occupancy. For atoms with less than full *d* shells, three *s* primitives were added to the basis set and optimized for the $ns^2np^6nd^{m-1}(n+1)s^1$ state with the highest possible spin and angular momentum coupling. Three *p* primitives were then added with exponents set equal to the corresponding *s* primitives. For the final basis set, these outer *s* and *p* primitives were contracted 2,1 with the *s* contraction coefficients taken from the above state, and the *p* contraction coefficients taken from the $ns^2np^6nd^{m-1}(n+1)p^1$ state. For Zn, Cd, and Hg, with full *d* shells, the three outermost *s* and *p* primitives were optimized and contracted for the $ns^2np^6nd^{10}(n+1)s^1(n+1)p^1$ triplet configuration. For Ga, In, and Tl they were optimized and contracted for the $ns^2np^6nd^{10}(n+1)s^2(n+1)p^1$ doublet configuration. The final transition metal basis sets consist of 34 basis functions (if all six Cartesian *d* components are retained). Reference energies[3] for spin- and space-restricted atomic calculations using the transition metal RCEP and matching basis sets are given in Tables 8–10.

The transferability of the transition metal RCEPs and the adequacy of the optimized basis sets were tested by calculating the relative energies of various atomic and ionic states and comparing the results with all-electron numerical, relativistic Hartree–Fock values (38). The comparisons are presented in Table 11. The RCEP results generally agree with the corresponding all-electron numerical results to well within 0.01 hartree.

[3]M. W. Schmidt. Private communication.

TABLE 9. Calculated energies for the fourth row atoms using the RCEPs and basis sets reported in Tables 2 and 5. See Table 8 for details of the calculations

Atom(Z)	N_{core}	Valence electronic configuration	State	Energy (hartree)
Rb(37)	36	$5s^1$	^2S	−0.13998
Sr(38)	36	$5s^2$	^1S	−0.55952
Y(39)	28	$4s^24p^64d^15s^2$	^2D	−37.74243
Zr(40)	28	$4s^24p^64d^25s^2$	^3F	−46.32647
Nb(41)	28	$4s^24p^64d^35s^2$	^4F	−56.13744
Mo(42)	28	$4s^24p^64d^45s^2$	^5D	−67.26168
Tc(43)	28	$4s^24p^64d^55s^2$	^6S	−79.82802
Ru(44)	28	$4s^24p^64d^65s^2$	^5D	−93.12832
Rh(45)	28	$4s^24p^64d^75s^2$	^4F	−109.21647
Pd(46)	28	$4s^24p^64d^85s^2$	^3F	−126.37789
Ag(47)	28	$4s^24p^64d^95s^2$	^2D	−145.26138
Cd(48)	28	$4s^24p^64d^{10}5s^2$	^1S	−166.01470
In(49)	28	$4s^24p^64d^{10}5s^25p^1$	^2P	−188.23879
Sn(50)	46	$5s^25p^2$	^3P	−3.26771
Sb(51)	46	$5s^25p^3$	^4S	−5.29937
Te(52)	46	$5s^25p^4$	^3P	−7.86239
I(53)	46	$5s^25p^5$	^2P	−11.20997
Xe(54)	46	$5s^25p^6$	^1S	−15.30124

TABLE 10. Calculated energies for the fifth row atoms using the RCEPs and basis sets reported in Tables 3 and 6. See Table 8 for details of the calculations

Atom(Z)	N_{core}	Valence electronic configuration	State	Energy (hartree)
Cs(55)	54	$6s^1$	^2S	−0.12726
Ba(56)	55	$6s^2$	^1S	−0.49607
La(57)	46	$5s^25p^65d^16s^2$	^2D	−31.03204
Hf(72)	60	$5s^25p^65d^26s^2$	^3F	−48.22029
Ta(73)	60	$5s^25p^65d^36s^2$	^4F	−57.05401
W(74)	60	$5s^25p^65d^46s^2$	^5D	−67.00120
Re(75)	60	$5s^25p^65d^56s^2$	^6S	−78.15341
Os(76)	60	$5s^25p^65d^66s^2$	^5D	−90.40131
Ir(77)	60	$5s^25p^65d^76s^2$	^4F	−103.94415
Pt(78)	60	$5s^25p^65d^86s^2$	^3F	−118.81880
Au(79)	60	$5s^25p^65d^96s^2$	^2D	−135.08856
Hg(80)	60	$5s^25p^65d^{10}6s^2$	^1S	−152.84860
Tl(81)	60	$5s^25p^65d^{10}6s^26p^1$	^2P	−171.72024
Pb(82)	78	$6s^26p^2$	^3P	−3.35839
Bi(83)	78	$6s^26p^3$	^4S	−5.32913
Po(84)	78	$6s^26p^4$	^3P	−7.75612
At(85)	78	$6s^26p^5$	^2P	−10.91106
Rn(86)	78	$6s^26p^6$	^1S	−14.72705

Main group atoms

The valence space of the main group atoms to the right of Ga, In, and Tl in the periodic table was taken as the outermost occupied *s* and *p* orbitals. The V_{LMAX} potentials were generated from atomic ion configurations with three electrons outside the core, two in the outermost *s* orbital, and one in an orbital with LMAX angular momentum. The V_{l-LMAX}

TABLE 11. Comparison of selected RCEP and relativistic Hartree–Fock (RHF, ref. 6) term energies (eV)[a] for the third, fourth, and fifth row transition metals and their positive ions

Configuration		Atom	RCEP	RHF	Atom	RCEP	RHF	Atom	RCEP	RHF
d^1s^2	^2D	Sc(21)	0.0	0.0	Y(39)	0.0	0.0	La(57)	0.0	0.0
d^3	^4F		4.65	4.65		3.19	3.32		1.08	1.08
$d^2(+)$	^3F		6.32	6.32		5.91	6.02		4.38	4.37
d^2s^2	^3F	Ti(22)	0.0	0.0	Zr(40)	0.0	0.0	Hf(72)	0.0	0.0
d^4	^5D		4.44	4.48		2.41	2.44		4.38	4.37
$d^3(+)$	^4F		6.15	6.17		5.61	5.65		7.49	7.54
d^3s^2	^4F	V(23)	0.0	0.0	Nb(41)	0.0	0.0	Ta(73)	0.0	0.0
d^5	^6S		3.47	3.55		0.78	0.81		3.06	2.94
$d^4(+)$	^5D		5.99	6.06		5.15	5.19		7.34	7.28
d^4s^2	^5D	Cr(24)	0.0	0.0	Mo(42)	0.0	0.0	W(74)	0.0	0.0
d^6	^5D		6.01	6.07		1.99	1.99		4.19	4.16
$d^5(+)$	^6S		4.89	4.94		3.79	3.86		6.11	6.20
d^5s^2	^6S	Mn(25)	0.0	0.0	Tc(43)	0.0	0.0	Re(75)	0.0	0.0
d^7	^4F		9.43	9.49		3.69	3.69		5.86	5.80
$d^6(+)$	^5D		9.64	9.70		7.04	7.05		9.31	9.35
d^6s^2	^5D	Fe(26)	0.0	0.0	Ru(44)	0.0	0.0	Os(76)	0.0	0.0
d^8	^3F		7.81	7.87		0.28	0.27		3.88	3.85
$d^7(+)$	^5F		8.28	8.33		4.40	4.50		8.13	8.17
d^7s^2	^4F	Co(27)	0.0	0.0	Rh(45)	0.0	0.0	Ir(77)	0.0	0.0
d^9	^2D		7.40	7.53		0.12	0.14		2.64	2.63
$d^8(+)$	^3F		8.11	8.22		4.88	4.93		7.67	7.74
d^8s^2	^3F	Ni(28)	0.0	0.0	Pd(46)	2.36	2.19	Pt(78)	0.0	0.0
d^{10}	^1S		5.92	6.04		0.0	0.0		0.41	0.50
$d^9(+)$	^2D		7.99	8.12		6.45	6.44		7.13	7.26
$d^{10}s^1$	^2S	Cu(29)	0.04	0.06	Ag(47)	0.0	0.0	Au(79)	0.0	0.0
d^9s^2	^2D		0.0	0.0		3.94	3.86		1.83	1.86
$d^{10}(+)$	^1S		6.64	6.62		6.24	6.33		7.59	7.65
$d^9s^1(+)$	^3D		7.48	7.45		10.90	10.88		9.82	9.89
$d^{10}s^2$	^1S	Zn(30)	0.0	0.0	Cd(48)	0.0	0.0	Hg(80)	0.0	0.0
$d^9s^2(+)$	^2D		14.81	14.69		16.53	16.39		14.06	14.00

[a]1 hartree = 27.212 eV.

Can. J. Chem. Downloaded from www.nrcresearchpress.com by 92.62.229.171 on 09/08/12
For personal use only.

potentials for $l > 1$ were also generated from three-valence-electron atomic ion configurations. The $V_{s-\mathrm{LMAX}}$ and $V_{p-\mathrm{LMAX}}$ potentials were generated from multiplet-averaged ns^2np^m neutral atom states. The RCEP for the main group atoms are given in Tables 1–3.

The pseudo-orbitals of the main group elements are accurately represented by shared-exponent, Gaussian *sp* basis sets of five primitives. In the tables, these basis sets are contracted to double-zeta, 4,1. The exponents and contraction coefficients were energy-optimized using the multiplet-averaged ns^2np^m atomic configurations. Reference energies[3] from spin- and space-restricted SCF calculations using the RCEP and matching basis sets are presented in Tables 8–10.

Molecular calculations

The RCEPs and basis sets reported here have been used in a number of quantum mechanical investigations of molecular structures and energetics. The selenium and tellurium potentials were used by Jasien and Stevens (39) in a study of proton affinities of molecules containing Group VIA atoms. Basch *et al.* (40) used the tellurium potential and multiconfiguration self-consistent-field (MCSCF) methods to study the geometry and properties of the low-lying electronic states of TeO_2. The chromium potential and an energy-optimized Slater-type basis set were used by Jasien and Stevens (44) to study the potential energy curves and properties of low-lying states of CrO and CrO^+ using MCSCF and multireference configuration interaction (MRCI) methods. Basch *et al.* used the zinc RCEP along with CEP and basis sets previously published for the lighter elements (5) to study the effect of cations on imidazole hydrogen bonding (42) and on imidazole tautomerism (43). The calcium potential and basis set were used by Krauss and Stevens (44) to study metal binding selectivity by proteins. Krauss and Stevens have used the cesium potential and basis set, along with the core polarization potential, to study the polarizabilities of alkali clusters (34). They also have published very accurate low-lying potential energy curves for several alkali diatomic molecules using the RCEP, CPP, and corresponding basis

sets (35). The Cs potential was also used to characterize the binding of Cs clusters to GaAs surfaces (45). More recently, Garmer and Krauss used the zinc RCEP in a study of the effect of active site ionicity on the transition states for CO_2 hydrolysis by carbonic anhydrase (46), and the cobalt RCEP and basis set in a study of the spectroscopy of cobalt-substituted carbonic anhydrase (47). Gordon and co-workers used the RCEP to study Group IV propellanes (48), Group IV sulfur and oxygen propellane derivatives (49), and high valent transition metal alkylidenes (50) and alkylidene complexes (51). They have also used the RCEP in recent studies of hetroatom analogues of benzene (52), olefin metathesis catalysts (53), and transition metal – silicon double bonds (54).

Concluding remarks

The relativistic compact effective potentials and matching basis sets reported here will improve the efficiency of quantum mechanical calculations on molecules containing heavy atoms. The small number of terms in the analytic expansions of the potentials and the shared-exponent constraint on the basis sets reduce the computer time required to calculate molecular electronic integrals. Since the potentials are generated from Dirac–Fock atomic orbitals and eigenvalues, they account for the effects of relativity on valence electron spatial distribution and energetics. While spin-orbit dependencies have been averaged out during the generation of the potentials, these effects may be reintroduced via effective spin-orbit operators (17) or by scaling the usual spin-orbit integrals over valence orbitals (21).

Acknowledgment

The authors wish to thank Dr. Michael W. Schmidt for carefully reviewing the RCEPs and basis sets, and for providing the tables of spin- and space-restricted reference energies. We also thank him and others in the quantum chemistry group at North Dakota State University for installing the potentials and basis sets in the GAMESS program.

Can. J. Chem. Downloaded from www.nrcresearchpress.com by 92.62.229.171 on 09/08/12
For personal use only.

1. J. C. Berthelat and Ph. Durand. Gazz. Chim. Ital. **108**, 225 (1978); M. Krauss and W. J. Stevens. Annu. Rev. Phys. Chem. **35**, 357 (1984); P. A. Christiansen, W. C. Ermler, and K. S. Pitzer. Annu. Rev. Phys. Chem. **36**, 407 (1985); L. Szasz. Pseudopotential theory of atoms and molecules. John Wiley & Sons, New York, 1983; K. Balasubramanian and K. S. Pitzer. Adv. Chem. Phys. **67**, 287 (1987); P. Durand and J. P. Malrieu. Adv. Chem. Phys. **67**, 321 (1987).
2. M. Dupuis, J. D. Watts, H. O. Villar, and G. J. B. Hurst. HONDO 7.0, QCPE Program No. 544, QCPE Bull. **8**, 79 (1988).
3. M. W. Schmidt, K. K. Baldridge, J. A. Boatz *et al.* QCPE Bulletin **10**, 52 (1990).
4. M. J. Frisch, H. Head-Gordon, G. W. Trucks *et al.* Gaussian 90. Gaussian, Inc. Pittsburgh, Pa. 1990.
5. W. J. Stevens, H. Basch, and M. Krauss. J. Chem. Phys. **81**, 6026 (1984).
6. R. D. Cowan and D. C. Griffin. J. Opt. Soc. Am. **66**, 1010 (1976).
7. J. P. Desclaux. Comput. Phys. Commun. **9**, 31 (1975).
8. V. Bonifacic and S. Huzinaga. J. Chem. Phys. **60**, 2779 (1974); **62**, 1507 (1975); **62**, 1509 (1975); **64**, 956 (1976); **65**, 2322 (1976); Y. Sakai. J. Chem. Phys. **75**, 1303 (1981); Y. Sakai and S. Huzinaga. J. Chem. Phys. **76**, 2537 (1982); **76**, 2552 (1982); Y. Sakai, E. Miyoshi, M. Klobukowski, and S. Huzinaga. J. Comput. Chem. **8**, 226 (1987); **8**, 256 (1987); S. Huzinaga, L. Seijo, Z. Barandiaran, and M. Klobukowski. J. Chem. Phys. **86**, 2132 (1987); S. Huzinaga, M. Klobukowski, and Y. Sakai. J. Phys. Chem. **88**, 4880 (1984); S. Katsuki and S. Huzinaga. Chem. Phys. Lett. **152**, 203 (1988); L. Seijo, Z. Barandiaran, and S. Huzinaga. J. Chem. Phys. **91**, 7011 (1989); **93**, 5843 (1990).
9. W. A. Goddard III. Phys. Rev. **174**, 659 (1968); C. F. Melius and W. A. Goddard III. Phys. Rev. A, **10**, 1528 (1974); L. R. Kahn, P. Baybutt, and D. G. Truhlar. J. Chem. Phys. **65**, 3826 (1976).
10. G. B. Bachelet, D. R. Hamann, and M. Schlüter. Phys. Rev. B, **26**, 4199 (1982).
11. D. R. Hamann, M. Schlüter, and C. Chiang. Phys. Rev. Lett. **43**, 1494 (1979).
12. P. J. Hay and W. R. Wadt. J. Chem. Phys. **82**, 270 (1985); W. R. Wadt and P. J. Hay. J. Chem. Phys. **82**, 284 (1985); P. J. Hay and W. R. Wadt. J. Chem. Phys. **82**, 299 (1985).
13. L. F. Pacios and P. A. Christiansen. J. Chem. Phys. **82**, 2664 (1985); M. M. Hurley, L. F. Pacios, P. A. Christiansen, R. B. Ross, and W. C. Ermler. J. Chem. Phys. **84**, 6840 (1986); L. A. LaJohn, P. A. Christiansen, R. B. Ross, T. Atashroo, and W. C. Ermler. J. Chem. Phys. **87**, 2812 (1987); R. B. Ross, J. M. Powers, T. Atashroo, W. C. Ermler, L. A. LaJohn, and P. A. Christiansen. J. Chem. Phys. **93**, 6654 (1990).
14. H. Preuss, H. Stoll, U. Wedig, and Th. Krüger. Int. J. Quantum Chem. **19**, 113 (1981); U. Wedig, M. Dolg, H. Stoll, and H. Preuss. *In* Quantum chemistry: the challenge of transition metals and coordination chemistry. *Edited by* A. Veillard. NATO ASI Series C, Vol. 176, Reidel, Dordrecht. 1986. pp. 79–89; M. Dolg, U. Wedig, H. Stoll, and H. Preuss. J. Chem. Phys. **86**, 866 (1987); **86**, 2123 (1987); G. Igel-Mann, H. Stoll, and H. Preuss. Mol. Phys. **65**, 1321 (1988); M. Dolg, H. Stoll, A. Savin, and H. Preuss. Theor. Chim. Acta, **75**, 173 (1989); M. Dolg, H. Stoll, and H. Preuss. J. Chem. Phys. **90**, 1730 (1989).
15. Ph. Durand and J. C. Barthelat. Theor. Chim. Acta (Berlin), **38**, 283 (1975); G. F. Pacchioni, P. Fantucci, G. Giunchi, and J. C. Barthelat. Gazz. Chim. Ital. **110**, 183 (1980); G. H. Jeung, J. C. Barthelat, and M. Pelissier. Chem. Phys. Lett. **91**, 81 (1982); Y. Bouteiller, C. Mijoule, M. Nizam, J. C. Barthelat, J. P. Daudey, M. Pelissier, and B. Silvi. Mol. Phys. **65**, 295 (1988).
16. J. C. Barthelat, Ph. Durand, and A. Serafini. Mol. Phys. **33**, 159 (1977).
17. Y. S. Lee, W. C. Ermler, and K. S. Pitzer. J. Chem. Phys. **67**, 5861 (1977); W. C. Ermler, Y. S. Lee, K. S. Pitzer, and N. W. Winter. J. Chem. Phys. **69**, 976 (1978); Y. S. Lee, W. C. Ermler, K. S. Pitzer, and A. D. McLean. J. Chem. Phys. **70**, 288 (1979); W. C. Ermler, Y. S. Lee, and K. S. Pitzer. J. Chem. Phys. **70**, 293 (1979).
18. H. A. Bethe and E. E. Salpeter. Quantum mechanics of one- and two-electron atoms. Academic Press, New York. (1957).
19. P. A. Christiansen, Y. S. Lee, and K. S. Pitzer. J. Chem. Phys. **71**, 4445 (1979).
20. Y. S. Lee, W. C. Ermler, and K. S. Pitzer. J. Chem. Phys. **73**, 360 (1980); P. A. Christiansen and K. S. Pitzer. J. Chem. Phys. **73**, 5160 (1980); **74**, 1162 (1981); K. S. Pitzer and P. A. Christiansen. Chem. Phys. Lett. **77**, 589 (1981).
21. W. C. Ermler, Y. S. Lee, P. A. Christiansen, and K. S. Pitzer. Chem. Phys. Lett. **81**, 70 (1981).
22. W. J. Stevens and M. Krauss. Chem. Phys. Lett. **86**, 320 (1982); J. Chem. Phys. **76**, 3834 (1982).
23. W. R. Wadt. Chem. Phys. Lett. **89**, 245 (1982).
24. S. P. Walch, C. W. Bauschlicher, Jr., H. Partridge, and P. E. M. Siegbahn. Chem. Phys. Lett. **92**, 54 (1982).
25. B. C. Laskowski and S. R. Langhoff. Chem. Phys. Lett. **92**, 49 (1982).

26. H. Partridge, C. W. Bauschlicher, Jr., S. P. Walch, and B. Liu. J. Chem. Phys. **79**, 1866 (1983).
27. L. G. M. Pettersson. Chem. Phys. Lett. **180**, 365 (1991).
28. W. Müller, J. Flesch, and W. Meyer. J. Chem. Phys. **80**, 3297 (1984).
29. W. Müller and W. Meyer. J. Chem. Phys. **80**, 3311 (1984); I. Schmidt-Mink, W. Müller, and W. Meyer. Chem. Phys. **92**, 263 (1985).
30. P. A. Christiansen. Chem. Phys. Lett. **127**, 50 (1986); J. Phys. Chem. **94**, 7865 (1990).
31. J. H. Jeung, J. P. Malrieu, and J. P. Daudey. J. Chem. Phys. **77**, 3571 (1982).
32. P. Fuentealba, H. Preuss, H. Stoll, and L. Von Szentpály. Chem. Phys. Lett. **89**, 418 (1982).
33. F. Spiegelmann, D. Pavolini, and J. P. Daudey. J. Phys. B: At. Mol. Opt. Phys. **22**, 2465 (1989).
34. M. Krauss and W. J. Stevens. Chem. Phys. Lett. **164**, 514 (1989).
35. M. Krauss and W. J. Stevens. J. Chem. Phys. **93**, 4236 (1990).
36. L. F. Pacios and P. G. Calzada. Int. J. Quantum Chem. **34**, 267 (1988).
37. A. K. Rappe, T. A. Smedley, and W. A. Goddard III. J. Phys. Chem. **85**, 2607 (1981).
38. R. L. Martin and P. J. Hay. J. Chem. Phys. **75**, 4539 (1981).
39. P. G. Jasien and W. J. Stevens. J. Chem. Phys. **83**, 2984 (1985).
40. H. Basch, D. Cohen, and M. Albeck. Chem. Phys. Lett. **144**, 450 (1988).
41. P. G. Jasien and W. J. Stevens. Chem. Phys. Lett. **147**, 72 (1988).
42. H. Basch, M. Krauss, and W. J. Stevens. J. Am. Chem. Soc. **107**, 7267 (1985).
43. H. Basch, M. Krauss, and W. J. Stevens. Int. J. Quantum. Chem. **31**, 405 (1987).
44. M. Krauss and W. J. Stevens. J. Am. Chem. Soc. **112**, 1460 (1990).
45. M. Krauss and W. J. Stevens. J. Chem. Phys. **93**, 8915 (1990).
46. D. R. Garmer and M. Krauss. J. Am. Chem. Soc. **113**, 6426 (1991).
47. D. R. Garmer and M. Krauss. Int. J. Quant. Chem. In press.
48. M. S. Gordon, K. A. Nguyen, and M. T. Carroll. Polyhedron, **10**, 1247 (1991).
49. K. A. Nguyen, M. T. Carroll, and M. S. Gordon. J. Am. Chem. Soc. **113**, 7924 (1991).
50. T. R. Cundari and M. S. Gordon. J. Am. Chem. Soc. **113**, 5231 (1991).
51. T. R. Cundari and M. S. Gordon. J. Am. Chem. Soc. **114**, 539 (1992).
52. N. Matsunaga, T. R. Cundari, M. W. Schmidt, and M. S. Gordon. Theor. Chim. Acta. In press.
53. T. R. Cundari and M. S. Gordon. Organometallics. In press.
54. T. R. Cundari and M. S. Gordon. J. Phys. Chem. In press.

Can. J. Chem. Downloaded from www.nrcresearchpress.com by 92.62.229.171 on 09/08/12
For personal use only.

Chemical interpretation: basis set use and the Periodic Table

LELAND C. ALLEN
Department of Chemistry, Princeton University, Princeton, NJ 08544, U.S.A.

Received September 5, 1991

This paper is dedicated to Professor Sigeru Huzinaga on the occasion of his 65th birthday

LELAND C. ALLEN. Can. J. Chem. **70**, 631 (1992).

Examination of contemporary quantum chemistry literature and texts strongly indicates the need for new interpretative measures and indices that have heuristic chemical appeal, but are rigorously defined by physics. A closer look at the Periodic Table in search of such measures leads to *configuration energy* (CE), the average energy of a valence electron, which adds a third intrinsic dimension to the Table itself, and is also strongly correlated with atomic energy level spacings. CE can be translated into a quantum mechanical operator whose expectation value in molecules and solids is the Energy Index, EI_A. Many chemical effects: rotation and inversion barriers, the anomeric and α-effects, hyperconjugation, etc., appear capable of being quantified, unified, and simplified by EI_A, but because it is a one-electron entity, it does not correlate with binding energies or heats of formation. EI_A is *in situ* electronegativity, and systematic release of basis set contraction constraints permits a controlled analysis of bond polarity in terms of radial and angular hybridization changes.

Key words: *ab initio* calculations, basis sets, electronegativity, Periodic Table, bond polarity index.

LELAND C. ALLEN. Can. J. Chem. **70**, 631 (1992).

Un examen de la littérature et des manuels de chimie quantique contemporaine montre la nécessité de nouvelles mesures et d'indices interprétatifs qui auraient un caractère chimique heuristique, mais qui seraient rigoureusement définis par la physique. Un examen plus approfondi du tableau périodique pour trouver de telles measures conduit à l'*énergie de configuration* (EC), l'énergie moyenne d'un électron de valence, qui ajoute une troisième dimension intrinsèque au tableau lui-même et qui est intimement relié aux espacements des niveaux d'énergie. L'EC peut être transformée en un opérateur de la mécanique quantique dont la valeur d'expectative dans les molécules et dans les solides est égale à l'indice d'énergie, IE_A. Il semble l'IE_A puisse aussi permettre de quantifier, d'unifier et de simplifier plusieurs effets chimiques, comme les barrières à la rotation et à l'inversion, les effets α et anomériques, l'hyperconjugaison, etc; toutefois, comme il s'agit d'une entité à un électron, elle ne permet pas d'établir de corrélation avec les énergies de liaison ou les chaleurs de formation. Le fait que l'IE_A donne lieu à une libération *in situ* systématique de l'électronégativité des contraintes des bases de contraction permet de faire une analyse contrôlée de la polarité des liaisons en fonction des changements radiaux et des angles d'hybridation.

Mots clés : calculs *ab initio*, ensembles de base, électronégativité, tableau periodique, index de la polarité des liaisons.

[Traduit par la rédaction]

Levels of chemical interpretation

It is generally acknowledged that present day quantum chemistry calculations are broadly divided into two categories: (1) *ab initio*, all-electron, exact Hamiltonian. These are identified with small molecule chemical physics, the development of new mathematically sophisticated computational techniques, and with detailed electronic structure investigations of medium sized molecules that illustrate the basic physics of a novel or controversial bonding problem. (2) One- and two-electron semiempirical models, e.g., extended Hückel theory, ZINDO, PM3. These are generally applied to large molecules of immediate interest to synthetic organic and inorganic chemists and focus on chemical trends. Although the choice of *ab initio* or semiempirical model is generally attributed to the size of the molecule addressed, more fundamentally it is a question of the style and nature of the interpretation desired. Two contemporary textbooks illustrate these contrasting approaches: *Ab initio molecular orbital theory*, (1)[1] and *Orbital interactions in chemistry* (2*a*).[2] Although both texts are based on molecular orbital concepts, the explanations and interpretative framework of the two are notably different. The application sections of the former are filled with diagrams giving detailed geometries, tables of binding and interaction energies, proton affinities, and dipole moments. There are numerous three-dimensional molecular orbital plots and the applications treated are mostly molecules made from first-row elements with occasional systems involving higher rows and a few with first-row transition elements. In contrast, *Orbital interactions* is based on qualitative/semiquantitative perturbation theory and the text is dominated by valence orbital MO energy level diagrams accompanied by qualitative AO-based MO schematics and HOMO—LUMO interaction arguments. Fragment orbitals and isolobal analogies are employed to derive trends in larger and more complex molecules. Representative element compounds and transition metal complexes from all rows, along with an energy band and density of states diagram treatment of solid state chemistry, puts nearly the whole domain of the Periodic Table on an equal footing. The simplest possible MO concepts are evoked and the patterns characteristic of chemistry are emphasized over the details of the physics, thus making this approach by far the most useful to the vast majority of practicing chemists. However, this approach sometimes leads to oversimplification and explanations are generally more qualitative.

[1]This text is primarily concerned with chemical bonding in medium sized molecules that are of interest to physical organic chemists and to the present article, rather than the high precision solutions for many different expectation values in 1–4 atom systems that are generally of interest to molecular physicists.

[2]The chapter on solids is nicely augmented by ref. 2*b*.

Printed in Canada

Can. J. Chem. Downloaded from www.nrcresearchpress.com by 123.30.183.119 on 09/08/12
For personal use only.

Can. J. Chem. Downloaded from www.nrcresearchpress.com by 123.30.183.119 on 09/08/12
For personal use only.

Even if *ab initio* calculations were easily possible for the largest molecules, the physical variables available: total energies, binding energies, ionization potentials, molecular dipole moments, inner moments such as quadrupole coupling constants, or even (undecomposed) molecular orbital plots, are not often quantities in terms of which chemical trends can be easily discerned or rationalized.

Are there other *ab initio* defined properties that can bridge the gap between these two modes of chemical interpretation? We have found one, atomic *configuration energy* and its associated molecular property, the Energy Index, EI_A, for atom A in a molecule.

A closer look at the Periodic Table[3]

It is obvious that the simplest key to chemical interpretation is the Periodic Table, but it is not clear how to make a quantitative connection between it and atoms in molecules and solids. None of the parameters describing it are continuous variables whose values might be able to reflect changes undergone by an atom when it forms a molecule or solid. A closer look at the Periodic Table also reveals it to be somewhat misleading and incomplete. These shortcomings can be resolved by defining a new variable, configuration energy, which we believe to be the Table's intrinsic third dimension. Configuration energy, in turn, can be translated into a quantum mechanical operator whose expectation value over a molecular wavefunction provides chemically significant information.

In spite of — or because of — its everyday familiarity, the Periodic Table possesses a number of puzzling and infrequently addressed features. (a) What is the origin of its diagonal line separating metals from nonmetals? (b) It is far from periodic: as one descends a group in the *p*-block the increasing metallic character of the elements has long been recognized. The chemistry of carbon is quite different than the chemistry of lead. (c) Why, among all representative atoms (excluding the noble gas atoms) are only N, O, F, Cl, and Br unable to utilize all their valence electrons in bonding? (d) It is our principal guide in anticipating which of the three types of bonding: covalent, metallic, or ionic, will form between atoms. But it provides no definition of these bond types nor a way to differentiate between them. (e) It is the most powerful instrument for organizing chemical phenomena but it does not contain any information about the energy of atoms, even though everyone knows that energy is the central parameter for describing the structure of matter.

It is clear that something is missing, and this appears to be a historical accident dating from the time when Bohr provided the physical underpinning of the Periodic Table by defining electronic configurations (4). In chemical terms, the Periodic Table is a sequence of groups whose atoms have common properties and behavior. Physicists, however, see it as a collection of valence electron configurations that depict the properties of atomic shell structure. The quantum numbers n and l are more than labels for blocks of elements, and more than indicators of atomic size and orbital shape: their primary role is to specify an *energy*, and the obviously relevant quantity is the average energy of a valence electron configuration. Thus, CE, configuration energy, is defined as the average one-electron valence shell energy of a ground state free atom:

$$[1] \quad CE = (a\epsilon_s + b\epsilon_p)/(a + b)$$

where a, b are occupancies and ϵ_s, ϵ_p the s and p ionization potentials for spherical atoms of the representative elements; for the *d*-block transition elements, $\epsilon_p \rightarrow \epsilon_d$ of the $n - 1$ shell and b is its valence region occupancy.[4] CE possesses another energy level related property that is of almost equal importance to that expressed in eq. [1]: it is strongly correlated with the spacings of the one-electron energy levels of the atom in question (3). Large CE goes with large energy level separations, thus making a close connection between the magnitude of CE and the density of states in solids and molecules. This correlation follows immediately from the fact that the effective potential seen by an electron in an atom is funnel shaped: deeper funnels have more widely spaced energy levels (this characteristic is familiar from the textbook example of the hydrogen atom).

CE answers the questions posed earlier. (a) Values generated by eq. [1][4] precisely define the metalloid band (B, Si, Ge, As, Sb, and Te) associated with the metal/nonmetal diagonal line: all elements to the right of the metalloids have higher CEs and are nonmetals, all those to the left have lower CEs and are metals. The band itself is a region of nearly constant CE. (b) Metallization down a group occurs because the size of the atoms is increasing, therefore both the magnitude of the average valence energy level and the spacings of the levels are decreasing. Bonding directionality is being lost because the *s*, *p*, and *d* levels are becoming nearly degenerate, allowing mixing in many combinations. These changes are quantified (3) by CE. (c) The oxidation state limitations of N, O, F, Cl and Br are explained by their CEs: aside from the noble gas atoms He, Ne, Ar, and Kr, these atoms have the highest CEs in the Periodic Table and some of their valence electrons are held too tightly to engage directly in bonding. Because of their high CEs they have a correspondingly large energy gap to the first available unoccupied level, likewise discouraging bonding. (d) The interrelationship between metallic (M), covalent (C), and ionic (I) bonding may be visualized as an equilateral triangle with vertices labeled M, C, and I. The M–C line is a row of the Periodic Table and along it CE quantitatively measures the relative metallic versus covalent nature of an atom in question. The legs M–I and I–C require binary combinations of atoms (e.g., Na_2S, SCl_2) and along these legs the appropriate measure is ΔCE.

Historically, the need for configuration energy has been partially met by the concept of electronegativity, originally defined by Pauling (5) 10 years after Bohr's contribution. This concept has been the subject of much debate over many years, but a survey of textbooks and the research literature since 1932 shows that only two scales, those of Pauling (5, 6) and of Allred and Rochow (7), have been extensively used by experimental scientists. We previously showed (8) that eq. [1] closely matches these two, thus assuring that the information content of electronegativity is subsumed in CE.

[3]This section summarizes a much fuller account, including graphs and data supporting statements, given in ref. 3.

[4]ϵ_s and ϵ_p are obtained from the high resolution atomic energy level data compiled at the National Bureau of Standards. A list of CEs, along with graphs of these numbers as a function of the groups of the Periodic Table, are given in ref. 3.

TABLE 1. Rotational barriers (kcal/mol)

Molecule	ΔE_T	$3/4\Delta(EI_A + EI_B)$
$HOC\text{-}NH_2$	15.7	16.66
$H_3C\text{-}CH_3$	2.98	2.99
$H_3C\text{-}NH_2$	2.39	2.34
$N_3C\text{-}OH$	1.36	1.29

In the 1989 article (8) electronegativity was emphasized and defined by eq. [1]. The new viewpoint presented here is an extension and generalization of that article.

In summary, a closer look at the Periodic Table leads to the definition of a new quantity, configuration energy, that adds a new third dimension to the Table, embodies and goes beyond the usual concept of electronegativity, and can be rigorously defined in atomic physics terms. We now need to transform this characteristic *atomic* quantity into a *molecular* environment. We previously showed how this can be done by projecting an atomic orbital on the vector representation of an LCAO MO and weighting it by the one-electron energy of the MO, thereby obtaining a new one-electron energy for an atom, A, in a molecule (the Energy Index, EI_A) (9):

$$EI_A = \sum_i^N n_i \epsilon_i \sum_j^{M(A)} \sum_k^M C_{ij}^* C_{ik} S_{jk} \Big/ \sum_i^N n_i \sum_j^{M(A)} \sum_k^M C_{ij}^* C_{ik} S_{jk}$$

Applications of the Energy Index, EI_A, and Bond Polarity Index, BPI_{AB}

Range of applications

The Energy Index, EI_A, and the closely related Bond Polarity Index, BPI_{AB}, defined below, are one-electron measures and our experience to date indicates that they may be able to quantify and unify the following chemical phenomena: (a) rotational barriers; (b) inversion barriers; (c) hyperconjugation; (d) Bent's rules; (e) substitution effect on primary, secondary, and tertiary carbon centers; (f) the α-effect; (g) the anomeric effect; (h) hydrogen bond dimerization energies; and (i) group electronegatives.

Barriers

In Table 1 we list results for the rotational barriers in four classic molecules that have long been employed as tests of rotational barrier theories: the large formamide barrier that models rotation around the peptide bond, and the famous ethane, methylamine, and methanol set that approximately obey a 3:2:1 rule (10). A chief virtue of the Energy Index is that it yields a *local* energy measure and these barriers may be simply described by the change in $\Sigma_i EI_i$ summed over those atoms that define the bond around which rotation is taking place. In formamide a partial π bond is being broken and in CH_3CH_3, CH_3NH_2, and CH_3OH a partial π anti-bond is being broken. The 3/4 in front of $\Delta(EI_A + EI_B)$ in Table 1 is the scale factor required to connect the many-electron E_T with our one-electron EI_A. We also have results for the two barriers in fluoromethanol (10), $FH_2C\text{—}OH$, and again the scale factor is 3/4. This latter molecule is especially important because rationalization of its two barriers is tantamount to an explanation of the anomeric effect. The inversion barrier in NH_3 is similarly found to have a 3/4 scale factor.

The Bond Polarity Index, BPI_{AB} (9)

As one would expect, this entity is associated with the *difference*, $EI_A - EI_B$, across a bond, but because any atom exists in a molecular environment the concept of polarity must be precisely defined and, as originally introduced by Pauling (5), this means *ionic character*, therefore requiring that the covalent component be subtracted out:

$$BPI_{AB} = (EI_A - EI_A^{ref}) - (EI_B - EI_B^{ref})$$

For example, for the C—N bond in $H_3C\text{—}NH_2$ we compute (at 6 − 31G*) $EI_C = -0.689$ au and $EI_N = -0.695$ au in $H_3C\text{—}NH_2$, $EI_C^{ref} = 0.665$ au in $H_3C\text{—}CH_3$, $EI_N^{ref} = -0.710$ au in $H_2N\text{—}NH_2$, and then $BPI_{CN} = (-0.689 + 0.665) - (-0.695 + 0.710) = -0.039$ au. Other examples and properties of BPI_{AB} are given in ref. 9. A particularly promising application is to the important, but long discounted, concept of group electronegativity. In this application (11) one chooses a reference system for A (A = CH_3 is the most satisfactory and relevant from a physical organic chemistry standpoint) and then B represents the functional group of interest (e.g., CH_2CH_3, CH_2OH, CCH, CHO, NH_2, PH_2, OH, CF_3, CN, SiH_3, etc.). We have studied 25 groups, compared them with the six other most cited definitions, and also with the three most relevant experimentally determined measurements (Swain F and Taft σ_F, field/inductive effects, and Siegbahn E_B, C 1*s* core electron binding energies). Our BPI_{AB} derived group electronegativities have considerably higher correlation coefficients with the experimental values than any of the others, thus providing encouragement for this scheme.

Hydrogen bond dimerization energies

These have been notoriously difficult to determine, both experimentally and computationally, and we recently carried out an exhaustive *ab initio* study (12) to ascertain what level will reproduce the four dimerization energies that are accurately known experimentally (as well as their geometries and vibrational frequencies). It turns out that calculations at the MO SCF level with the 6 − 31 + G* basis are quite accurate and significantly better than the many other correlated and non-correlated solutions explored. Since this computational level is within the Hartree–Fock approximation, we are investigating whether BPI_{AH} and $EI_B - EI_N$ applied to the atoms A—H ··· B in the hydrogen bonds studied will parallel our *ab initio* results (EI_N is EI for the noble gas atom at the end of the row containing B).

Solid state

There is a solid state chemistry application that we find especially appealing. This is the use of BPI_{AB} as a complement to Roald Hoffmann's ingenious invention, the overlap population weighted density of states (COOP, Crystal Orbital Overlap Population) (2*b*). Hoffmann's concept adds greatly to chemical interpretability by identifying, as far as possible, localizable chemical bonds in solids. In the same manner we propose that the polarity of these bonds be obtained by BPI_{AB}. One can immediately see application to contemporary semiconductor research where many current efforts are centered on extending the traditional Group IV compounds to the III-V and II-VI series.

Advantages of the indices

Given the results discussed here, it is not entirely unreasonable to believe that all nine of the characteristically chemical phenomena listed above may be quantified by EI_A

Can. J. Chem. Downloaded from www.nrcresearchpress.com by 123.30.183.119 on 09/08/12
For personal use only.

Can. J. Chem. Downloaded from www.nrcresearchpress.com by 123.30.183.119 on 09/08/12
For personal use only.

and BPI_{AB} (and maybe even most one-electron representable chemical bonding features might be so encompassed). If so, what advantages would this type of interpretation offer? First, it would accomplish a large measure of unification presently missing from chemistry. The possibility of unification derives ultimately from the fact that configuration energies, EI_A, and BPI_{AB}, are obtained directly from *ab initio* wavefunctions, thus providing the broadest and deepest foundation available for defining such entities. (This connection with *ab initio* theory does not, of course, preclude obtaining actual EI_A and BPI_{AB} values from semiempirical wavefunctions.) Second, if it turns out that EI_A and BPI_{AB} can represent a significant fraction of the one-electron representable chemical bonding rules and concepts, the resulting simplification in interpretation will be substantial. When properly referenced (as in the definition of BPI_{AB}), EI_A is *in situ* electronegativity, and the various chemical bonding phenomena listed and discussed above are a manifestation of electronegativity change due to angular and radial hybridization changes occurring around the bonds in question. For chemical phenomena that have a local origin, interpretation via EI_A can be simpler and less ambiguous than use of orbitals because of its atomic focus and because it avoids selection of orbitals and choice of dominant interactions. It may be noted in passing that EI_A is the first attempt to devise a true *in situ* electronegativity: the frequently discussed "equalization of electronegativity" would not lead to $\Delta(EI_A + EI_B)$ for a rotation barrier such as we obtain, unless some entirely new conformation-dependent feature were added to current discussions of this hypothesis.

Limitations of the indices

The fact that configuration energy, EI_A, and BPI_{AB} are one-electron entities immediately points out their limitation and this is most obvious and severe in their inability to correlate binding energies and heats of formation. However, it will be recalled that Pauling's original definition of electronegativity was expressed as a function of the difference between a heteronuclear bond energy and an average of its homonuclear values (5). Rationalization of the accuracy of Pauling's electronegativity values in the light of his bond energy definition was achieved in a recent study (13).

There have been numerous articles in the J. Phys. Chem. and the J. Am. Chem. Soc. during the last two years in which Y.-R. Luo *et al.* (14) claimed good linear correlations between a simple definition of electronegativity, $V_x = n_x/r_x$, where n_x = number of valence electrons, r_x = a covalent radius obtained from several different sources, and differences in heats of formation. We have made extensive plots of CE, EI_A, and BPI_{AB} against the same experimental data used by Luo and have been unable to find useful or scientifically convincing correlations. We have also found some inconsistencies in tables of data given by Luo. Recent articles by Drago *et al.* (15) support our belief that Luo's electronegativity (or anyone else's definition) does not correlate with binding energy or heats of formation (or differences in heats of formation). Drago has found that at least three parameters are required to correlate bond energy data.[5] (It is also important to note here that the hydrogen bond dimerization energy problem discussed above is a special case arising because this bond is a small perturbation between two closed shell monomers).

Finally, of course, there are subtle chemical effects, both within and outside the Hartree–Fock approximation, which cannot be catalogued by EI_A or BPI_{AB}. These include effects dependent upon multipole moments and polarizabilities of higher order than dipole.

Further developments

The expression for EI_A is readily recognized as an energy-weighted Mulliken population analysis divided by the population analysis itself, and L. H. Reed (to be published) has proposed a generalization that replaces $\bar{P}\bar{S}$ in the Mulliken formulation with $\bar{S}^{\alpha}\bar{P}\bar{S}^{1-\alpha}$. Exploration of α may provide a further reduction in basis set dependence over that already achieved by energy weighting. Another possibility for generalizing the Mulliken overlap assumption is to employ Doggett's formulation (16) of Löwdin's 1953 suggestion (17) for preserving the dipole moment of the overlap charge. Since bond polarity closely parallels bond dipole, this procedure will considerably enlarge the range of BPI_{AB} values and tend to reduce basis set sensitivity.

Basis set contractions as an aid to chemical interpretation

In the sections above we have defined a new *ab initio* index, EI_A, that we believe will help unify and simplify the one-electron concepts used by chemists to categorize chemical observations. EI_A derives its interpretative capability from *in situ* manifestation of the Periodic Table and it is our hypothesis that optimum understanding of the structure of matter and prediction of new materials can be achieved by detailed analysis of how free atoms distort when they form molecules and solids. To carry out this program we need to view basis set choice and contraction in a new light.

The development of basis sets has been governed by the trade-off between size and energy lowering ability. During the last 40 years this topic has become a sophisticated and complex research field often accompanied by good summary reviews, and three excellent recent ones are those of Feller and Davidson (18), Davidson and Feller (19), and Huzinaga (20). Our purpose here is to suggest a new way to use this large body of existing research knowledge.

For a representative element, we start with an established basis that provides a reasonable representation of the atomic Hartree–Fock solution. All linear expansion coefficients used to represent this approximate free atom Hartree–Fock wavefunction are then frozen and this basis is used to calculate a molecular wavefunction. The difference between the free atom CE and the rigid basis EI_A is the "molecular field" effect and it can be either stabilizing or destabilizing. In the next stage of calculation, a splitting of *s* valence functions only is permitted. Then splitting of the p_x, p_y, and p_z's is separately investigated (with the *s* functions returned to their initial frozen set). Splitting of *s* and *p* valence bases is then allowed simultaneously. Returning to the frozen atom basis, we now add a *d* polarization function (the *s* orbitals are also polarized by *p* orbitals and the *ps* by *s* orbitals, but these distortions largely cancel). With *d* orbitals present, the *s* and *p* splittings are successively added in, and at each step the change in EI_A values is recorded. In this process we are cataloguing the electronegativity changes due to changes in ra-

[5]Drago also has a paper in press (J. Phys. Chem.) that specifically illustrates the inadequacies of V_x.

dial and angular hybridization and correlating them with molecular geometry. This will provide rules for assigning true *in situ* electronegativities and bond polarities as a function of atom type and molecular coordinates — a goal that a very great number of papers employing Mulliken valence state orbital electronegativity have unsuccessfully attempted for over 40 years. The problem has been that valence state orbital electronegativities are given for specified *free atom* hybridizations but no method has been devised to accurately determine the needed true *molecular* hybridizations. The method given here does so because it defines a *molecular* expectation value. The price to be paid is availability of a molecular wavefunction.

Finally, a major objective of our chemical interpretation scheme is to unify the analysis of molecular and solid state electronic structure throughout the Periodic Table, and therefore it is to be expected that effective core potential (pseudopotential) methods will be employed. Recent research by Huzinaga on his *ab initio* model potential (21) and effective Hamiltonian (22) methods are important developments related to this usage.

Can. J. Chem. Downloaded from www.nrcresearchpress.com by 123.30.183.119 on 09/08/12
For personal use only.

Acknowledgements

Sigeru Huzinaga is justifiably famous for his sustained efforts in developing basis sets for *ab initio* molecular calculations. His extension of the even-tempered concept to well-tempered Gaussians has significantly advanced the pool of knowledge on this important problem and his MIMI-i, MIDI-i, and MAXi sets generate uniform quality bases for most of the representative and transition metal elements of greatest interest. Huzinaga's more than 20 years of continuous and thoroughly systematic effort in this field provides one of the cornerstones upon which *ab initio* electronic structure theory rests. He has conscientiously recorded his contributions in review articles and in a 1984 book and it continues in the Chicago tradition of Robert Mulliken and Clemens Roothaan which Sigeru experienced as a research associate starting in the late 1950's and where I first met him. He then took his knowledge back to Japan as a professor at Kyushu University where he had been an undergraduate.

In the late 1960's and early 1970's after he had returned to North America, he turned his attention to formal aspects of many-electron theory and wrote major papers on general SCF formalism, separability of many-electron systems, UHF theory, and eigenspace manipulation.

The early 1970's saw the start of his seminal work on his model potential method with its emphasis on correct representation of the Coulomb and Exchange core operators (as opposed to matching AO energies and shapes). Sigeru has also contributed to the development of semiempirical methods (e.g., CNDO) and written programs for the Xα scattered wave scheme.

We hope that he and his collaborators will continue their various useful efforts and that they will enjoy good health.

The author wishes to acknowledge many useful conversations with Eugene T. Knight and the financial assistance of Geo Centers, U.S. Army, ARDEC, Dover, New Jersey, and the ACS/PRF.

1. W. J. Hehre, L. Radom, P. Schleyer, and J. A. Pople. Ab initio molecular orbital theory. John Wiley Interscience, New York. 1986.
2. (*a*) T. A. Albright, J. K. Burdett, and M.-H. Whangbo. Orbital interactions in chemistry. (John Wiley – Interscience, New York. 1985); (*b*) Roald Hoffmann. Solids and surfaces: a chemist's view of bonding in extended structures. VCH Publishing, New York. 1988.
3. L. C. Allen. J. Am. Chem. Soc. In press.
4. N. Bohr. Nature, **112**, 29 (1923).
5. L. Pauling. J. Am. Chem. Soc. **54**, 3570 (1932).
6. A. L. Allred. J. Inorg. Nucl. Chem. **17**, 215 (1961).
7. A. L. Allred, and E. G. Rochow. J. Inorg. Nucl. Chem. **5**, 264 (1958).
8. L. C. Allen. J. Am. Chem. Soc. **111**, 9003 (1989).
9. L. C. Allen, D. A. Egolf, E. T. Knight, and C. Liang. J. Phys. Chem. **94**, 5602 (1990).
10. E. T. Knight and L. C. Allen. J. Am. Chem. Soc. Submitted.
11. L. H. Reed and L. C. Allen. J. Phys. Chem. **96**, 157 (1992).
12. J. Wehbeh and L. C. Allen. J. Am. Chem. Soc. Submitted.
13. L. H. Reed and L. C. Allen. Inorg. Chem. In press.
14. Y.-R. Luo, and S. W. Benson. J. Phys. Chem. **94**, 914 (1990); Y.-R. Luo and P. D. Pacey. J. Am. Chem. Soc. **113**, 1465 (1991), and articles cited.
15. R. S. Drago. Inorg. Chem. **29**, 1379 (1990); R. S. Drago, N. Wong, and D. C. Ferris. J. Am. Chem. Soc. **113**, 1970 (1991).
16. G. Doggett. J. Chem. Soc. (London) A: 229 (1969).
17. P. O. Löwdin. J. Chem. Phys. **21**, 374 (1953).
18. D. Feller and E. R. Davidson. *In* Reviews in computational chemistry. *Edited by* K. B. Lipkowitz and D. B. Boyd. VCH Publishing, New York. 1990. Chap. 1.
19. E. R. Davidson and D. Feller. Chem. Rev. **86**, 681 (1986).
20. S. Huzinaga. Comput. Phys. Rep. **2**, 279 (1985).
21. S. Huzinaga, L. Seijo, Z. Barandiarán, and M. Klobukowski. J. Chem. Phys. **86**, 2132 (1987).
22. S. Katsuki and S. Huzinaga. Chem. Phys. Lett. **152**, 203 (1988).

Computational determination of the relative stabilities of some nitro carbocations

PAUL C. REDFERN, JANE S. MURRAY, AND PETER POLITZER[1]

Department of Chemistry, University of New Orleans, New Orleans, LA 70148, U.S.A.

Received September 19, 1991

This paper is dedicated to Professor Sigeru Huzinaga on the occasion of his 65th birthday

PAUL C. REDFERN, JANE S. MURRAY, and PETER POLITZER. Can J. Chem. **70**, 636 (1992).

The relative stabilities of a group of nitro carbocations (derivatives of the methyl, cyclopropyl, and cyclopropenyl cations) are determined by means of *ab initio* SCF/3-21G calculations, and compared to the corresponding results for other substituent groups, both electron donating and withdrawing. The α-nitro carbocations are generally destabilized relative to the parent cation, but often to a lesser extent than anticipated from the strongly electron-withdrawing nature of NO_2. The optimized structures indicate that this is due to the stabilizing formation of an intramolecular ring involving the nitro group; however, this requires the proximity of a sufficiently positive carbon.

Key words: carbocations, *ab initio* SCF calculations, relative stabilities, nitro derivatives.

PAUL C. REDFERN, JANE S. MURRAY et PETER POLITZER. Can. J. Chem. **70**, 636 (1992).

Utilisant des méthodes *ab initio* SCF/3-21G, on a calculé les stabilités relatives d'un certain nombre de carbocations de dérivés nitrés (dérivés des cations méthyle, cyclopropyle et cyclopropényle) et on les a comparées aux résultats correspondants obtenus avec d'autres substituants, tant électro-attracteurs que électro-donneurs. Les carbocations en α d'un nitro sont généralement déstabilisés par rapport au cation parent; toutefois, ils le sont souvent moins que ce qui avait été anticipé sur la base de la nature très électro-attractive du NO_2. Les structures optimisées indiquent que ce résultat est dû à la formation stabilisante d'un cycle intramoléculaire impliquant le groupe nitro; toutefois, ce cycle nécessite la proximité d'un carbone suffisamment positif.

Mots clés : carbocations, calculs *ab initio* en champ auto-cohérent, stabilités relatives, dérivés nitrés.

[Traduit par la rédaction]

Introduction

In recent years, a number of compounds containing ionic or highly polar C^+C^- linkages have been synthesized (1–6); some examples are **1**(1), **2**(4), and **3**(6):

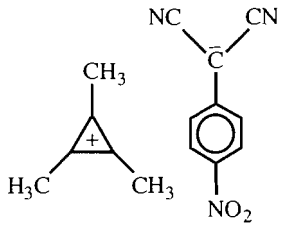

1

$(H_2N)_3C^+ {}^-C(NO_2)_3$

2

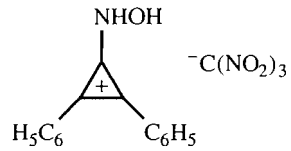

3

The carbocations or positive portions of such systems are stabilized by electron-donating α-substituents, which allow the positive charge to be delocalized (eq. [1]), while electron-withdrawing groups correspondingly stabilize the carbanions or negative portions. These are well-established substituent effects (7–9), fully in agreement with calculations of relative stabilities (10, 11).

[1] 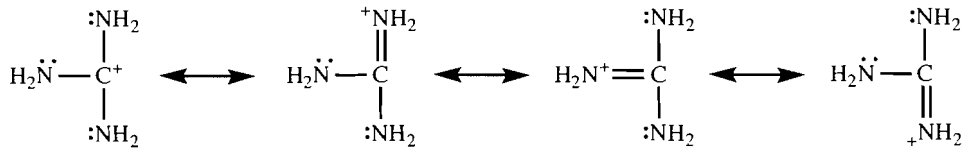

4

The same reasoning suggests that electron-withdrawing groups (e.g., CF_3, CHO, CN, NO_2, etc.) will destabilize carbocations, and indeed this is generally the case. However, numerous studies, both experimental (12–22) and theoretical (23–28), have shown that this destabilizing effect is often much weaker than anticipated, and a variety of carbocations bearing electron-withdrawing α-substituents have been prepared or observed (e.g., **5** (12, 21), **6** (14), **7** (18), and **8** (19)).

In some instances, such as α-cyano and α-keto carbocations, this unexpected level of stability can be attributed to conjugative donation of electronic charge, as shown in eqs.

[1]Author to whom correspondence may be addressed.

Printed in Canada

Can. J. Chem. Downloaded from www.nrcresearchpress.com by 123.30.183.119 on 09/08/12
For personal use only.

[2] and [3] (10, 16, 23, 24, 26); this can presumably be stimulated by the positive center even in groups that are not normally resonance donors (29).

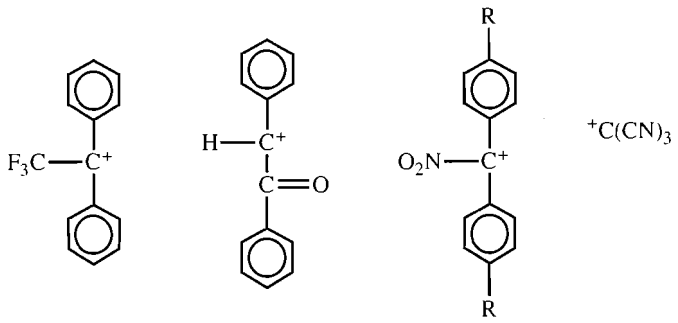

5 6 7*a*: R = H *b*: R = CH_3 8

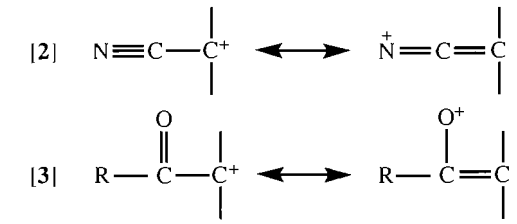

It has been pointed out that α-keto carbocations could also be stabilized through the formation of oxiranyl ions (16, 21, 27):

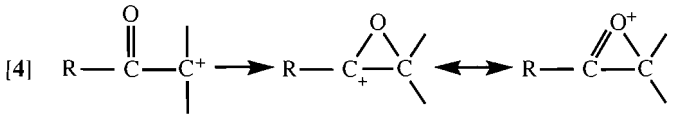

However, this is deemed unlikely on the basis of stereochemical evidence (16, 21).

Despite the considerable activity in the area of carbocations bearing electron-withdrawing α-substituents, we have found relatively little mention of α-nitro carbocations. The NO_2 group is strongly electron withdrawing, through both induction and resonance (29), and the nitrogen bears a formal positive charge:

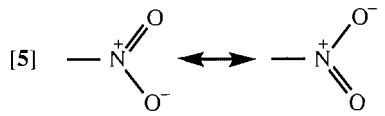

It would therefore be particularly interesting to determine the effect of α-NO_2 upon carbocation stability. Olah *et al.* have reported the preparation of the α-nitrodiphenylmethyl and α-nitro-*p*-tolylmethyl cations (**7***a* and **7***b*) (18); these can of course be expected to benefit from some stabilization through electron donation by the phenyl groups:

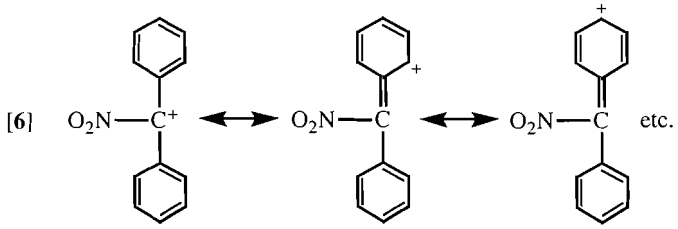

Our objective in this work has accordingly been to determine computationally the relative stabilities of a group of nitro carbocations. The hydrocarbon parents of these are the methyl (**9**), cyclopropyl (**10**), and cyclopropenyl (**11**) cations:

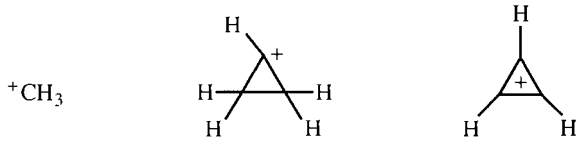

9 **10** **11**

To provide perspective, we shall compare the results for the NO_2 derivatives to those for several other substituents, both electron donating and electron accepting.

Methods

An approach that has been used in the past for determining the relative stabilities of carbocations is to compare their tendencies to interact with the hydride ion, H^-, to form a neutral molecule (9, 10). This can be done by means of the isodesmic reaction shown as eq. [7].

[7] $^+CXYZ + CH_4 \rightarrow H—CXYZ + {}^+CH_3$

ΔE for this reaction can be regarded as a measure of the stability of the carbocation ^+CXYZ relative to that of $^+CH_3$; the more negative is ΔE, the less stable is ^+CXYZ.

We have accordingly used the GAUSSIAN 88 system of programs (30) to compute optimized structures and energies at the *ab initio* SCF/3-21G level for the carbocations and for the corresponding neutral molecules formed by interacting with H^-. (In a few instances, including $^+CH_3/CH_4$, the data required were taken from the Carnegie-Mellon Quantum Chemistry Archive (31).) For each carbocation, the existence of a local energy minimum was confirmed by computing the vibration frequencies and verifying that there are no imaginary values.

Results

Our calculated total energies and the resulting ΔE values for eq. [7] are given in Table 1, and some of the optimized structural properties of the carbocations are in Table 2. The data taken from the Archive (31) are indicated. Most of the cations are found to be planar, either completely or at least in their frameworks (Table 2). The exceptions to this are all among the nitro derivatives.

In Table 1, the carbocations are listed in order of decreasing stability; those with $\Delta E > 0$ are viewed as being more stable than $^+CH_3$, and $\Delta E < 0$ is taken to mean less stable than $^+CH_3$. Since the reactants and products in eq. [7] differ only by the location of a C—H bond, the ΔE values can be expected to benefit from some cancellation of error. For example, Table 1 shows ΔE for the carbocations $^+C_3H_5$ and $^+C_3H_3$ to be 21 and 85 kcal/mol, respectively; at the SCF/6-31G*//6-31G* level, using energies taken from the Archive (31) these are 24 and 93 kcal/mol. Thus, the ΔE values in Table 1 should satisfactorily represent the trend in relative stabilities.

Discussion

Table 1 shows the well-established stabilization of carbocations by α-NH_2 and α-OH (9–11), and Table 2 supports its interpretation in terms of charge delocalization, as

Can. J. Chem. Downloaded from www.nrcresearchpress.com by 123.30.183.119 on 09/08/12
For personal use only.

TABLE 1. Calculated 3-21G energies

Molecule	Energy (hartrees)	Carbocation	Energy (hartrees)	ΔE^a (kcal/mol)
$CH(NH_2)_3$	−204.12574	$^+C(NH_2)_3$	−203.40112	153
CH_3NH_2	−94.68166[b]	$^+CH_2NH_2$	−93.86284[b]	93
C_3H_4	−115.16201[b]	$^+C_3H_3$	−114.32957[b]	85
$CH(CH_3)_3$	−156.43447	$^+C(CH_3)_3$	−155.57274	67
$CH_2NH_2NO_2$	−296.98190	$^+CHNH_2NO_2$	−296.09568	53
CH_3OH	−114.39802[b]	$^+CH_2OH$	−113.51414[b]	53
$C_3H_3NO_2$	−317.45956	$^+C_3H_2NO_2$ (**14**)	−316.55349	39
$C_3H_5NO_2$	−318.69491	$^+C_3H_4NO_2$ (**12**)	−317.78613	37
C_3H_6	−116.40121[b]	$^+C_3H_5$	−115.46705[b]	21
CH_4	−39.97688[b]	$^+CH_3$	−39.00913[b]	0
$C_3H_5NO_2$	−318.69491	$^+C_3H_4NO_2$ (**13**)	−317.72713	0
CH_3NO_2	−242.25586	$^+CH_2NO_2$	−241.28449	−2
CH_3CH	−131.19180[b]	$^+CH_2CN$	−130.21045	−9
$CH_2(CN)_2$	−222.39335	$^+CH(CN)_2$	−221.39984	−16
$CH(CN)_3$	−313.58447	$^+C(CN)_3$	−312.58114	−22
$CH_2(NO_2)_2$	−444.51355	$^+CH(NO_2)_2$	−443.50322	−27
$CH(NO_2)_3$	−646.75587	$^+C(NO_2)_3$	−645.71105	−48

[a]This energy difference is for the reaction given in eq. [7].
[b]These 3-21G energies were taken from ref. 31.

in eq. [1]. Thus the calculated C—N and C—O bond lengths in $^+CH_2NH_2$ are, respectively, 0.205 and 0.188 Å shorter than in CH_3NH_2 and CH_3OH. In $^+C(NH_2)_3$, the decrease is 0.139 Å for each C—N bond; presumably the carbon cannot accept as much electronic charge from each of three NH_2 groups as it can from one alone.

In the case of $^+C(CH_3)_3$, hyperconjugation can be invoked (9):

[8] 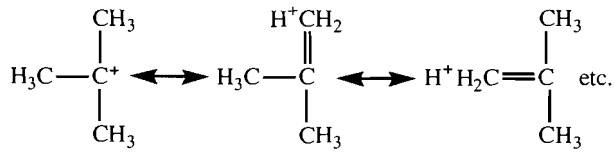

The C—C distances are shortened by 0.066 Å in going from $HC(CH_3)_3$ to $^+C(CH_3)_3$, and the computed average charges on the methyl hydrogens increase from +0.20 to +0.32.

The rather large stabilization observed for the cyclopropenyl cation, **11**, can be attributed, at least in part, to delocalization of its π electrons (9):

[9] 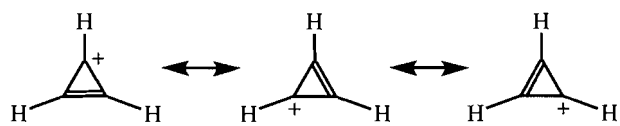

11

The calculated C—C bond length in **11** is 1.361 Å, compared to 1.282 and 1.523 (twice) in cyclopropene. Dewar has suggested that σ conjugation also plays a significant role in **11** (32).

Earlier studies of mono-α-cyano carbocations showed that the CN group is indeed destabilizing, but that some of the delocalization described by eq. [2] does occur, thereby presumably lessening the extent of destabilization (10, 23, 24, 26). Tables 1 and 2 extend these conclusions to di- and tri-α-cyano cations. The shortening of the C—C bond in going from the neutral molecule to the cation is 0.103, 0.089, and 0.079 Å for the mono-, di-, and tricyano systems, respectively; the corresponding lengthening of the C—N bond is 0.017, 0.012, and 0.010 Å.

Proceeding now to the nitro carbocations, and looking first at the simplest member of this group, $^+CH_2NO_2$, it is striking that this cation is nearly as stable as $^+CH_3$ despite the presence of the strongly electron-withdrawing nitro group. (Appearance potential measurements have also indicated a surprising degree of stability for $^+CH_2NO_2$ (7, 33).) Several of the nitro carbocations are considerably *more* stable than $^+CH_3$, and the β-nitrocyclopropyl ion **12** is even stabilized relative to its parent, $^+C_3H_5$ (**10**).

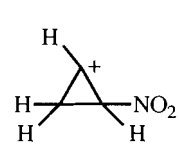

12

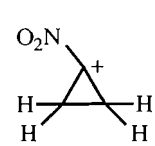

13

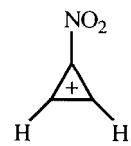

14

The apparent reason for the unexpected stabilities of the NO_2 carbocations can be seen in the structures given in Table 2. Starting again with $^+CH_2NO_2$, it is seen that the NO_2 group forms a three-membered ring involving the "positive" carbon. Formally, the +1 charge thereby shifts to the nitrogen. It should be noted that the bond lengths in the ring are fairly close to their typical values; for example, the 3-21G optimized C—O distance in ethylene oxide is 1.470 Å (17), compared to 1.535 Å calculated for $^+CH_2NO_2$. Since this ring formation is a significant structural rearrangement, which may account for the surprising stability found for this carbocation, we repeated the geometry optimization at the SCF/6-31G* and MP2/6-31G* levels; the latter includes electronic correlation effects. The three-membered ring was formed in both instances. (The MP2/6-31G* geometry is given in Table 2 in parentheses.) It is interesting to note that

Can. J. Chem. Downloaded from www.nrcresearchpress.com by 123.30.183.119 on 09/08/12
For personal use only.

an analogous cyclic structure was proposed as an intermediate in a rearrangement undergone by **7***a* (18).

Table 2 shows that the ring also occurs in the dinitro and trinitro derivatives, $^{+}CH(NO_2)_2$ and $^{+}C(NO_2)_3$. The situation becomes particularly interesting in the case of the nitrocyclopropyl cation because of the two possible isomers,

TABLE 2. Selected 3-21G structural properties of carbocations

Carbocation[a]	Bond length (Å)	Bond angle (degrees)
$^{+}C(NH_2)_3$	C—N: 1.324	N—C—N: 120.0 Planar
$^{+}CH_2NH_2$	C—N: 1.267[b]	Planar[b]
$^{+}C_3H_3$	C—C: 1.361[b]	C—C—C: 60.0[b] Planar[b]
$^{+}C(CH_3)_3$	C—C: 1.474	C—C—C: 120.0
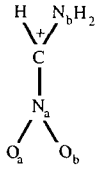	C—N_a: 1.470 C—N_b: 1.251 N_a—O_a: 1.223 N_a—O_b: 1.246	Planar
$^{+}CH_2OH$	C—O: 1.252[b]	Planar[b]
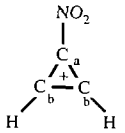 **14**	C_a—N: 1.412 C_a—C_b: 1.347 C_a—C_b: 1.378 N—O: 1.236	N—C_a—C_b: 149.2 C_a—C_b—C_b: 59.2 C_b—C_a—C_b: 61.5 Planar
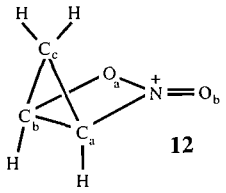 **12**	C_a—C_b: 1.515 C_a—C_c: 1.554 C_b—C_c: 1.475 C_a—N: 1.498 C_b—O_a: 1.521 N—O_a: 1.422 N—O_b: 1.157	C_a—C_b—C_c: 62.6 C_a—C_c—C_b: 60.0 C_a—N—O_a: 94.7 C_a—C_b—O_a: 90.1 C_a—N—O_b: 139.2 O_a—N—O_b: 126.1
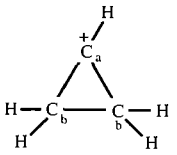	C_a—C_b: 1.453[b] C_b—C_b: 1.522[b]	C_a—C_b—C_b: 58.4[b] C_b—C_a—C_b: 63.2[b]
$^{+}CH_3$	C—H: 1.078[b]	Planar[b]
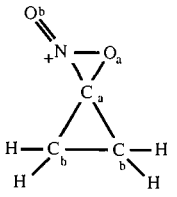 **13**	C_a—C_b: 1.474 C_b—C_b: 1.531 C_a—N: 1.391 N—O_a: 1.405 C_a—O_a: 1.542 N—O_b: 1.155	C_a—C_b—C_b: 58.7 C_b—C_a—C_b: 62.6 C_a—N—O_a: 66.9 C_a—O_a—N: 56.1 C_a—N—O_b: 157.5
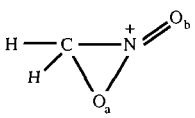	C—N: 1.451 (1.417)[c] C—O_a: 1.535 (1.577)[c] N—O_a: 1.401 (1.300)[c] N—O_b: 1.154 (1.188)[c]	C—N—O_a: 65.1 (70.8)[c] C—O_a—N: 59.0 (58.1)[c] C—N—O_b: 159.3 (153.6)[c]
$^{+}CH_2CN$	C—C: 1.353 C—N: 1.156	C—C—H: 120.0 C—C—N: 180.0 Planar
$^{+}CH(CN)_2$	C—C: 1.372 C—N: 1.150	C—C—C: 122.1 C—C—N: 180.0 Planar
$^{+}C(CN)_3$	C—C: 1.387 C—N: 1.147	C—C—C: 120.0 C—C—N: 180.0 Planar

Can. J. Chem. Downloaded from www.nrcresearchpress.com by 123.30.183.119 on 09/08/12
For personal use only.

TABLE 2 (*concluded*)

Carbocation[a]	Bond length (Å)	Bond angle (degrees)
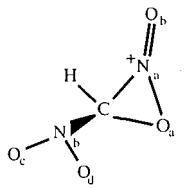	$C—N_a$: 1.446 $C—O_a$: 1.494 $N_a—O_a$: 1.409 $N_a—O_b$: 1.149 $C—N_b$: 1.468 $N_b—O_c$: 1.223 $N_b—O_d$: 1.239	$C—N_a—O_a$: 63.1 $C—O_a—N$: 59.7 $C—N_a—O_b$: 160.9 $C—N_b—O_c$: 113.8 $C—N_b—O_d$: 113.8
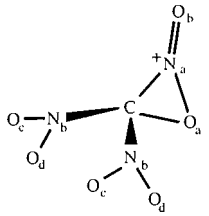	$C—N_a$: 1.439 $C—O_a$: 1.477 $N_a—O_a$: 1.416 $N_a—O_b$: 1.144 $C—N_b$: 1.482 $N_b—O_c$: 1.245 $N_b—O_d$: 1.210	$C—N_a—O_a$: 62.3 $C—O_a—N$: 59.6 $C—N_a—O_b$: 161.4 $C—N_b—O_c$: 110.1 $C—N_b—O_d$: 117.2

[a]The carbocations are listed in the same order as in Table 1.
[b]These structural data were taken from ref. 31.
[c]MP2/6-31G* optimization.

12 and **13**, in which the NO_2 can be β or α to the positive center. Cyclic rearrangement takes place in both cations, but in **12** the inclusion of the positive carbon requires that a four-membered ring be formed. **12** turns out to be considerably more stable than **13**, and (as mentioned earlier) even more stable than the parent cyclopropyl cation. The latter point is especially striking; **12** is the only nitro carbocation in Table 1 for which this is true, that it shows greater stability than its parent hydrocarbon cation.

One factor that may favor **12** or **13** is a lesser degree of strain in the four-membered C—C—N—O ring compared to the three-membered C—N—O. We verified this by computing the strain energies in **15** and **16** using the isodesmic reaction procedure (11, 34); at the 3-21G level, they are 31.0 and 21.5 kcal/mol, respectively. Furthermore, the strain energy in **17** is given as 65 kcal/mol, vs. 57.3 in **18** (35). Thus it seems reasonable to infer that roughly 25% of the

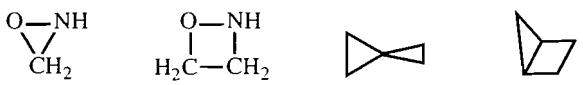

15 **16** **17** **18**

energy difference between **12** and **13** is due to the greater degree of strain in the latter. It also appears that there may be a greater delocalization of charge in **12** than in **13**. This is suggested by the distributions of calculated atomic charges in the two cases, as given by the GAUSSIAN 88 procedure and shown below.

Since the proximity of a sufficiently positive carbon is clearly a key factor in the rearrangement to a ring, the fact that this does *not* occur in the nitrocyclopropenyl cation, **14** (see Table 2), presumably reflects the fact that the positive charge is delocalized through the mechanism shown in eq. [9]. To test this interpretation, we examined the cation $^+CHNH_2NO_2$; the presence of the strong electron donor NH_2 should also significantly delocalize the positive charge and produce a more negative carbon. Indeed, the NO_2 again does *not* form a ring (Table 2). Table 1 shows that the NH_2, NO_2 combination gives an overall cation stability very similar to that of $^+CH_2OH$.

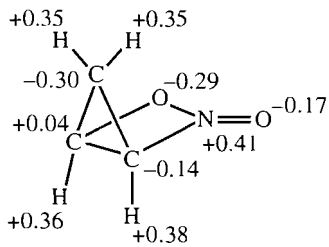

12

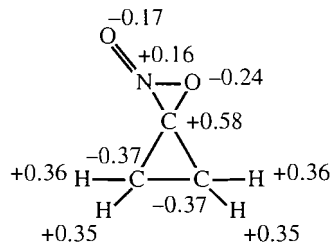

13

Summary

We have found that α-nitro groups do in general destabilize carbocations relative to the parent cations. However, the effect is often much weaker than would be anticipated from the strongly electron-withdrawing nature of NO_2, due to the stabilizing formation of an intramolecular ring involving the NO_2 group. This can occur when the ipso or a neighboring carbon is sufficiently positive.

Acknowledgements

We thank Professor Joseph H. Boyer for suggesting this investigation and for very useful discussions. We greatly appreciate the support provided by the U.S. Army Research Office, and computer resources provided by the Pittsburgh Supercomputer Center.

1. E. M. Arnett, E. B. Troughton, A. T. McPhail, and K. E. Molter. J. Am. Chem. Soc. **105**, 6172 (1983).
2. V. I. P'yankova, K. V. Altukhov, V. V. Perekalin, G. A. Berkova, and V. P. Pozdnyakov. Dokl. Akad. Nauk SSSR, **278**, 885 (1984); Engl. transl. 341.

Can. J. Chem. Downloaded from www.nrcresearchpress.com by 123.30.183.119 on 09/08/12
For personal use only.

3. E. M. Arnett, B. Chawla, K. Molter, K. Amarnath, and M. Healy. J. Am. Chem. Soc. **107**, 5288 (1985).
4. A. M. Krishnan, P. Sjoberg, P. Politzer, and J. H. Boyer. J. Chem. Soc. Perkin Trans. 2, 1237 (1989).
5. K. Okamoto, T. Kitagawa, K. Takeuchi, K. Komatsu, T. Kinoshita, S. Aonuma, M. Nagai, and A. Miyabo. J. Org. Chem. **55**, 996 (1990).
6. A. Gunasekaran and J. H. Boyer. Heteroatom. Chem. Submitted.
7. S. P. McManus and C. U. Pittman, Jr. *In* Organic reactive intermediates. *Edited by* S. P. McManus. Academic Press, New York. 1973. Chap. 4.
8. J. C. Stowell. Carbanions in organic synthesis. Wiley–Interscience, New York. 1979.
9. J. March. Advanced organic chemistry. 3rd ed. Wiley–Interscience, New York. 1985.
10. M. H. Lien and A. C. Hopkinson. J. Mol. Struct. (THEOCHEM), **121**, 1 (1985).
11. W. J. Hehre, L. Radom, P. v. R. Schleyer, and J. A. Pople. Ab initio molecular orbital theory. Wiley–Interscience, New York. 1986.
12. G. A. Olah and C. U. Pittman. J. Am. Chem. Soc. **88**, 3310 (1966).
13. P. G. Gassman and J. J. Talley. J. Am. Chem. Soc. **102**, 1214 (1980).
14. J.-P. Begue and M. Charpentier-Morize. Acc. Chem. Res. **13**, 207 (1980).
15. G. A. Olah, M. Arvanaghi, and G. K. Surya Prakash. J. Am. Chem. Soc. **104**, 1628 (1982).
16. X. Creary and C. C. Geiger. J. Am. Chem. Soc. **104**, 4151 (1982).
17. P. G. Gassman and T. T. Tidwell. Acc. Chem. Res. **16**, 279 (1983).
18. G. A. Olah, G. K. Surya Prakash, M. Arvanaghi, V. V. Krishnamurthy, and S. C. Narang. J. Am. Chem. Soc. **106**, 2378 (1984).
19. R. C. Beaumont, K. B. Aspin, T. J. Demas, J. H. Hoggatt, and G. E. Potter. Inorg. Chim. Acta, **84**, 141 (1984).
20. X. Creary. Acc. Chem. Res. **18**, 3 (1985).
21. L. H. Dao, M. Maleki, A. C. Hopkinson, and E. Lee-Ruff. J. Am. Chem. Soc. **108**, 5237 (1986).
22. X. Creary, M. E. Mehrsheikh-Mohammadi, and M. D. Eggers. J. Am. Chem. Soc. **109**, 2435 (1987).
23. D. A. Dixon, P. A. Charlier, and P. G. Gassman. J. Am. Chem. Soc. **102**, 3957 (1980).
24. M. N. Paddon-Row, C. Santiago, and K. N. Houk. J. Am. Chem. Soc. **102**, 6561 (1980).
25. W. F. Reynolds, P. Dais, D. W. MacIntyre, R. D. Topsom, S. Marriott, E. v. Nagy-Felsobuki, and R. W. Taft. J. Am. Chem. Soc. **105**, 378 (1983).
26. D. A. Dixon, R. A. Eades, R. Frey, P. G. Gassman, M. L. Hendewerk, M. N. Paddon-Row, and K. N. Houk. J. Am. Chem. Soc. **106**, 3885 (1984).
27. M. H. Lien and A. C. Hopkinson. J. Am. Chem. Soc. **110**, 3788 (1988).
28. P.-A. Carrupt and P. Vogel. J. Org. Chem. **55**, 5696 (1990).
29. O. Exner. Correlation analysis of chemical data. Plenum Press, New York. 1988. Tables 1 and 3.
30. M. J. Frisch, M. Head-Gordon, H. B. Schlegel *et al.* GAUSSIAN 88, Gaussian Inc., Pittsburgh, Pa., 1988.
31. R. A. Whiteside, J. S. Binkley, R. Krishnan *et al.* Carnegie-Mellon Quantum Chemistry Archive, Carnegie-Mellon University, Pittsburgh, Pa. 1980.
32. M. J. S. Dewar. J. Am. Chem. Soc. **106**, 669 (1984).
33. J. L. Franklin. *In* Carbonium ions. Vol. I. *Edited by* G. A. Olah and P. v. R. Schleyer. Wiley–Interscience, New York. 1970. Chap. 2.
34. J. S. Murray, P. C. Redfern, J. M. Seminario, and P. Politzer. J. Phys. Chem. **94**, 2320 (1990).
35. A. Greenberg and J. F. Liebman. Strained organic molecules. Academic Press, New York. 1978.

Can. J. Chem. Downloaded from www.nrcresearchpress.com by 123.30.183.119 on 09/08/12
For personal use only.

The electronic structure of small transition metal clusters

HIROSHI TATEWAKI
Computer Center, Nagoya City University, Mizuhoku, Nagoya, Japan

AND

MUTSUMI TOMONARI
Fundamental Research Laborotory, NEC Corporation, Miyagaoka, Tsukuba, Japan

Received July 19, 1991

This paper is dedicated to Professor Sigeru Huzinaga on the occasion of his 65th birthday

HIROSHI TATEWAKI and MUTSUMI TOMONARI. Can. J. Chem. **70**, 642 (1992).

In this paper we report the energy level distributions for transition metal clusters obtained by symmetry-broken and symmetry-constrained SCF methods. Investigated clusters were Fe_4, Ni_4, Cu_4, Zn_4, Fe_6, Ni_6, Cu_6, and Zn_6. Contracted Gaussian-type basis sets of the same size generated by the method of Tatewaki and Huzinaga were used throughout the paper. It will be shown that the *d*-hole localization model as well as the model with a two-electron-like ionization process is essential to discuss the electronic structure of the positive ion states, and the models bring the energy level distribution of the clusters rather close to the density of the state of the corresponding metals. The calculated first ionization potentials agree quite well with those of experiment. For example, the experimental ionization potential for Fe_4 is between 6.3 and 6.5 eV, while calculated values are 5.9 and 6.3 eV for the $3d$ electron ionization (d^{-1}) and $4s$ electron ionization (s^{-1}), respectively. If we define the Fermi level of the clusters as the first ionization potential, the Fermi level for Fe_4 is composed of the d^{-1} or $d^{-1} + s^{-1}$ state. The Fermi level for Ni_4 is found to be s^{-1} or $s^{-1} + d^{-1}$. Those of Cu_4 and Zn_4 are definitely of the s^{-1} state. Further discussion is also presented for larger clusters of M_6 (M = Fe, Ni, Cu, and Zn).

Key words: transition metal clusters, ionization potential, *ab initio* SCF calculations, energy level distributions.

HIROSHI TATEWAKI et MATSUMI TOMONARI. Can. J. Chem. **70**, 642 (1992).

Dans ce travail, on rapporte les distributions des niveaux d'énergie d'agrégats de métaux de transition qui ont été obtenues par des méthodes de champ auto-cohérent avec symétrie brisée et symétrie contrainte. On a étudié les agrégats de Fe_4, Ni_4, Cu_4, Fe_6, Ni_6 et Zn_6. Dans tout ce travail, on a utilisé une base restreinte de type gaussien de la même dimension que celle générée par la méthode de Tatewaki et Huzinaga. On va démontrer que le modèle de localisation du trou-*d* de même que le modèle avec un processus d'ionisation ressemblant à deux électrons sont essentiels pour discuter de la structure électronique des états des ions positifs et que les modèles amènent la distribution du niveau d'énergie des agrégats relativement près de la densité de l'état des métaux correspondants. Les premiers potentiels d'ionisation calculés sont en bon accord avec les valeurs expérimentales. Par exemple, le potentiel d'ionisation expérimental du Fe_4, se situe entre 6,3 et 6,5 eV alors que les valeurs calculées sont de 5,9 et 6,3 eV respectivement pour l'ionisation de l'électron $3d$ (d^{-1}) et l'ionisation de l'électron $4s$ (s^{-1}). Si l'on fait l'hypothèse que le niveau de Fermi des agrégats est égal au potentiel de la première ionisation, le niveau de Fermi du Fe_4 est donc composé de l'état d^{-1} ou de l'état $d^{-1} + s^{-1}$, le niveau de Fermi du Ni_4 est égal à s^{-1} ou $s^{-1} + d^{-1}$. Ceux du Cu_4 et du Zn_4 sont définitivement égaux à s^{-1}. On présente aussi d'autres discussions concernant les agrégats plus importants M_6 (M = Fe, Ni, Cu et Zn).

Mots clés : agrégats de métaux de transition, potentiel d'ionisation, calculs SCF *ab initio*, distributions des niveaux d'énergie.

[Traduit par la rédaction]

Introduction

The properties of transition metal clusters and the chemisorption of gases on them have been experimentally studied extensively with the aid of gas matrix techniques (1–7) as well as supersonic expansion techniques with laser or oven vaporization (8–14). The experimentalist now seems able to produce naked clusters of controlled size.

In this paper we will discuss the electronic structure of Fe_4, Ni_4, Cu_4, Zn_4, Fe_6, Ni_6, Cu_6, and Zn_6. For clusters including Fe, Ni, and Cu, experimental ionization thresholds have been reported (8–10); the uncertainty in the threshold values was smaller than 1.5 eV. The positions of the *d*-band relative to the Fermi level were given for Cu and Zn clusters (6, 7) although precise sizes of the clusters were unknown.

For years we have continuously investigated small transition metal clusters with *ab initio* SCF and CI methods (15–21). For these, the energy level distributions, namely the band structure of the clusters, were investigated. Before we studied transition metal clusters, it was commonly accepted that the energy level distributions predicted by *ab initio* SCF calculations were fairly different from the density of the state of the corresponding metals. The *d*-levels for Ni clusters (22) predicted by *ab initio* SCF calculations began around 5 eV below the Fermi level but for the solid the top of the *d*-band is at the Fermi level. The results were more exaggerated in Cu clusters (23) where the *d*-levels began around 10 eV below the Fermi level and the corresponding value of the solid Cu was only 2 eV. Two studies (22, 23) utilized orbital energies, and discussions developed there were based on the fact that reorganization energies (difference between the absolute value of the orbital energy and the ionization potential calculated by the ΔSCF method) became smaller as the cluster size became greater. Because the positive hole was shared equally by the atoms that constituted the clusters, reorganization energies should be smaller for larger clusters. They (22, 23) actually were able to demonstrate that reorganization energies decreased as the cluster size increased. Schmeisser *et al.* (6), however, using the matrix isolation

Printed in Canada

Can. J. Chem. Downloaded from www.nrcresearchpress.com by 92.62.229.171 on 09/08/12
For personal use only.

Can. J. Chem. Downloaded from www.nrcresearchpress.com by 92.62.229.171 on 09/08/12
For personal use only.

technique, showed that the *d*-band of small Cu clusters began 3 eV below the Fermi level and had its peak 4 eV below the level, which was the same as the solid if we move the peak of the cluster contributed from the *d* electrons 1 eV shallower to the Fermi level. A similar relation between the energy level distribution of the cluster and that of the solid was found for Zn clusters by Schroeder *et al.* (7).

Introducing the *d*-hole localization model that will be described in the present paper, Tatewaki *et al.* (15) showed that the *d*-level energy distribution of small Cu clusters began ca. 2 eV below the Fermi level, which was very close to the value of the solid, as well as to that of Schmeisser *et al.* Many X_α calculations (24–28) have been performed. In many cases they gave parallel results to those of the *d*-hole localization method, but some ambiguity arose, since by this method the *d*-hole localization and *d*-hole delocalization models gave almost the same energy level distributions (28). The X_α methods should be carefully applied to a system in which some types of electrons are strongly localized, when determining the physical or chemical characteristics of the system.

We feel that our interpretation of the energy level distributions of the transition metal clusters has been verified experimentally; the progression of experiments, however, provided many excellent data such as those of Powers *et al.* (8) and Rohlfing *et al.* (9, 10). It is therefore desirable to investigate the mechanism of the ionization more thoroughly. In this paper it will be shown that two-electron-process-like ionization of the *d* electron gives the Fermi level for Fe clusters. Together with a *d*-hole localization model, it will be shown that the calculated first ionization potentials always agree with experiment within an error of 0.5 eV.

Basis sets

To clarify the electronic structure of a sequence of similar molecules, it is desirable to use basis sets of the same quality for the respective molecules, which probably reveals the characteristics of the electronic structure of the sequence and even clarifies the defects or limitations of the calculations or the methods themselves. We used contracted Gaussian type functions (CGTFs) developed by the method of Tatewaki and Huzinaga (29–31) and summarized by Huzinaga *et al.* in ref. 32. The basis sets modified in the present paper are (4333/43/5) (32). Three sets of numbers separated by slashes indicate the number of primitive GTFs in the respective CGTFs of the *s*, *p*, and *d* symmetries. Dividing the outermost *s*- and *d*-type CGTFs into two parts, we generated the sets of (43321/43/41) + p.f. which were used throughout this work. The p.f. in this expression implies a polarization function spanned by two *p*-type GTFs. The exponents and expansion coefficients for the polarization functions were determined in the following way. As an example, Fe $(3d^7 4s^1)\ ^5F$ was chosen as a parent state. By using the CGTFs of (4333/43/5) and adding two primitive *p*-type GTFs, we calculated $(3d^7 4p^1)\ ^5F^o$ where (43345/43/5) was fixed to that of the parent and only the expansion coefficients and the exponents of the augmented *p*-type functions were energetically optimized. The basis set, (4333/43/5), p.f. thus determined, total energies, and orbital energies for the parent state are collected in Table 1. For Ni the parent state was $(3d^9 4s^1)\ ^3D$ and the optimized state was $(3d^9 4p^1)\ ^3P^o$, and for Cu and Zn the parents were $(3d^{10} 4s^1)\ ^2S$ and $(3d^{10} 4s^2)\ ^1S$ and the optimized states were $(3d^{10} 4p^1)\ ^2P^o$ and $(3d^{10} 4s^1 4p^1)\ ^3P^o$, respectively. Results for Ni, Cu, and Zn are also collected in Table 1. It is noted that the differences in the total and orbital energies between the fully contracted basis set of (4333/43/5) and those newly generated are, at most, 0.0024 au, indicating that the optimization of the original CGTFs is almost perfect.

Electronic structure of Fe_4, Ni_4, Cu_4 and Zn_4

(a) Geometry optimization and ground state for Fe_4

The geometry adopted for the M_4 clusters was D_{4h}. We chose Fe_4 and geometry optimization was performed for this cluster, possessing D_{4h} symmetry.

The electronic configurations considered were generated in the following way:

1. We found that the *d* electrons avoided the concentrating intermolecular region for Fe_2 and Fe_3 (21). We determined that Fe_4 has 8 vacancies in the eight molecular orbitals generated from the atomic $d_{x^2-y^2}$ and d_{zx} orbitals, which point toward the intermolecular region (the molecular axis was *z* and four Fe atoms were placed on the *x* and *y* axes); the $d_{x^2-y^2}$'s yielded a_{1g}, b_{1g}, e_{ux}, and e_{uy}, and the d_{zx}'s generated a_{2u}, b_{2u}, e_{gx}, and e_{gy}. Furthermore, we generated another four *d*-holes. They were distributed among α: a_{1g}, b_{1g}, e_{ux}, and e_{uy}, which were generated from $3d_{z^2}$; or among β: a_{1u}, b_{1u}, e_{gx}, and e_{gy}, which were generated from $3d_{yz}$; or among χ: a_{2g}, b_{2g}, e_{ux}, and e_{uy}, which were generated from $3d_{xy}$. The number of holes generated was 12 and it corresponds to three 3*d*-holes per atom. The states generated from α, β, and χ had the same spatial symmetry, B_{1g}.

2. We further assumed high spin states. It was found that the lowest configuration was always β. The electronic states arising from α, β, and χ are expressed as

$$(\alpha)\ \Phi(\alpha;{}^{15}B_{1g}) = \Phi(\beta;\ 7a_{1g},\ 7b_{1g},\ 9e_{ux},\ 9e_{uy} \rightarrow 1a_{1u},\ 1b_{1u},\ 3e_{gx},\ 3e_{gy})$$

$$(\beta)\ \Phi(\beta;{}^{15}B_{1g}) = 6a_{1g}^{\ 1}\ 3a_{2u}^{\ 1}\ 1b_{1u}^{\ 1}\ 3e_{g}^{\ 2}\ 8e_{u}^{\ 2}\ 4e_{g}^{\ 2}\ 3b_{2u}^{\ 1}\ 1a_{1u}^{\ 1}\ 6b_{1g}^{\ 1}\ 3b_{2g}^{\ 2}\ 7a_{1g}^{\ 2}\ 9e_{u}^{\ 4}\ 7b_{1g}^{\ 2}\ 10e_{u}^{\ 4}\ 3a_{2g}^{\ 2}\ 8a_{1g}^{\ 2}\ 11e_{u}^{\ 2}\ {}^{15}B_{1g}$$

$$(\chi)\ \Phi(\chi;{}^{15}B_{1g}) = \Phi(\beta;\ 3a_{2g},\ 3b_{2g},\ 9e_{ux},\ 9e_{uy} \rightarrow 1a_{1u},\ 1b_{1u},\ 3e_{gx},\ 3e_{gy})$$

3. To test the adequacy of the high spin states we calculated the lower spin state of the $^{13}A_{1g}$ and $^{13}B_{1u}$ states where the electron in the highest two half-filled orbitals was deexcited into the lowest half-filled orbital.

$$(\delta)\ \Phi(\alpha;{}^{13}A_{1g}) = \Phi(\beta;\ 6b_{1g} \rightarrow 6a_{1g})$$

$$(\varepsilon)\ \Phi(\alpha;{}^{13}B_{1u}) = \Phi(\beta;\ 1a_{1u} \rightarrow 6a_{1g})$$

Total energies for $\Phi(\alpha;{}^{15}B_{1g})$, $\Phi(\beta;{}^{15}B_{1g})$, and $\Phi(\chi;{}^{15}B_{1g})$ vs. the internuclear bond distance are shown in Fig. 1(*a*). Lower spin states were so high in energy (around 10 eV) that they are shown separately in Fig. 1(*b*). We were able to conclude that the high spin state is plausible. The lowest state takes the minimum at $R = 5.43$ au. We feel the calculated bond distance is too long.

Transition metal dimers give a considerably shorter bond distance than the distance for the bulk metal in almost all cases. Walch and Baushlicher (33, 34), Walch *et al.* (35), and Langhoff (36) showed by theoretical calculations that the difference in bond length between the dimer and the nearest neighbor of the metal is considerable and that the difference

Can. J. Chem. Downloaded from www.nrcresearchpress.com by 92.62.229.171 on 09/08/12
For personal use only.

TABLE 1. Basis sets, polarization functions, total energies, and orbital energies for (*a*) Fe, (*b*) Ni, (*c*) Cu, and (*d*) Zn

(*a*) Basis set (4333/43/5) for the parent: Fe $(3d^74s^1)\ ^5F$

Exponent for *s*-type CGTFs

*s*1	*s*2	*s*3	*s*4
9668.1576	132.89698	10.570868	0.77990721
1457.5243	14.510947	1.6969976	0.09031348
330.13829	5.9863944	0.66231581	0.03305041
88.696266			

Coefficients for *s*-type GTFs

0.0174095	−0.1066641	0.2244466	−0.1107037
0.1219622	0.6356908	−0.7219607	0.6003409
0.4414856	0.4360698	−0.4107245	0.4832512
0.5528922			

Exponent for *p*- and *d*-type CGTFs

*p*1	*p*2	*d*1
389.99465	0.55197634	35.803187
90.887232	3.9875682	9.8223791
27.780589	1.5113603	3.2259611
9.2854136		1.0369955
		0.28598944

Coefficients for *p*- and *d*-type CGTFs

0.0285625	0.2493311	0.0302672
0.1832498	0.3144806	0.1576493
0.5060150	0.5599452	0.3739431
0.4569957		0.4683263
		0.3388954

Polarization functions (p.f.)

Selected state for optimizing p.f.	Expon.	Coeff.
$(3d^74p^1)\ ^5F^0$	0.11319	0.36975
	0.02989	0.73453

Total energies and orbital energies for the parent Fe $(3d^74s^1)\ ^5F$

	(4333/43/5)	(43321/43/41) + p.f.
TE	−1261.1586 au	−1261.1602 au
e_{3d}	−0.3919	−0.3930
e_{4s}	−0.2242	−0.2243

(*b*) Basis set (4333/43/5) for the parent: Ni $(3d^94s^1)\ ^3D$

Exponent for *s*-type CGTFs

*s*1	*s*2	*s*3	*s*4
11337.092	155.40488	12.685906	0.86670537
1707.0566	17.061711	2.0419942	0.09974700
386.08898	7.0514802	0.78996022	0.03577552
103.65456			

Coefficients for *s*-type CGTFs

0.0172075	−0.1076622	0.2247803	−0.1012341
0.1209250	0.6418763	−0.7226563	0.5572668
0.4402247	0.4301887	−0.4109362	0.5243291
0.5550397			

Exponent for *p*- and *d*-type CGTFs

*p*1	*p*2	*d*1
464.97413	0.67447298	45.776211
108.42548	4.8806953	12.661264
33.206047	1.8504007	4.1799761
11.132781		1.3459035
		0.36719566

TABLE 1 (*continued*)

Coefficients for *p*- and *d*-type CGTFs

*p*1	*p*2	*d*1
0.0279662	0.2519563	0.0289570
0.1812634	0.3140962	0.1552632
0.5063194	0.5583456	0.3740010
0.4577327		0.4687862
		0.3412941

Polarization functions (p.f.)

Selected state for optimizing p.f.	Expon.	Coeff.
$(3d^9 4p^1)\ ^3P^0$	0.12540	0.35608
	0.03192	0.75042

Total energies and orbital energies for the parent Ni $(3d^9 4s^1)\ ^3D$

	(4333/43/5)	(43321/43/41) + p.f.
TE	−1505.3975 au	−1505.3991 au
e_{3d}	−0.4354	−0.4363
e_{4s}	−0.2284	−0.2285

(*c*) Basis set (4333/43/5) for the parent: Cu $(3d^{10} 4s^1)\ ^2S$

Exponent for *s*-type CGTFs

*s*1	*s*2	*s*3	*s*4
12089.304	166.95803	13.814849	0.88752228
1823.5302	18.483882	2.2257608	0.10710259
413.53596	7.6641691	0.85906487	0.03799219
111.29899			

Coefficients for *s*-type CGTFs

0.0173351	−0.1082132	0.2248336	−0.0978264
0.1214047	0.6401603	−0.7214133	0.5200087
0.4402931	0.4321033	−0.4124074	0.5616982
0.5542714			

Exponent for *p*- and *d*-type CGTFs

*p*1	*p*2	*d*1
498.58239	0.73410312	47.886771
116.54226	5.3273781	13.346022
35.825982	2.0161455	4.4377998
12.057314		1.4365512
		0.39445901

Coefficients for *p*- and *d*-type CGTFs

0.0282436	0.2498044	0.0317015
0.1824069	0.3174630	0.1651675
0.5072951	0.5574896	0.3819468
0.4548585		0.4630582
		0.3278561

Polarization functions (p.f.)

Selected state for optimizing p.f.	Expon.	Coeff.
$(3d^{10} 4p^1)\ ^2P^0$	0.11348	0.35450
	0.02918	0.75051

Total energies and orbital energies for the parent Cu $(3d^{10} 4s^1)\ ^2S$

	(4333/43/5)	(43321/43/41) + p.f.
TE	−1637.4279 au	−1637.4293 au
e_{3d}	−0.4675	−0.4685
e_{4s}	−0.2309	−0.2310

Can. J. Chem. Downloaded from www.nrcresearchpress.com by 92.62.229.171 on 09/08/12
For personal use only.

TABLE 1 (*concluded*)
(*d*) Basis set (4333/43/5) for the parent: Zn $(3d^{10}4s^2)\ ^1S$

Exponent for *s*-type CGTFs			
*s*1	*s*2	*s*3	*s*4
12854.512	179.29451	15.029977	1.1465861
1941.2826	19.854772	2.4094552	0.13999201
441.21745	8.2314821	0.94607226	0.04851075
119.04900			
Coefficients for *s*-type CGTFs			
0.0174760	−0.1085663	0.2257514	−0.1195371
0.1220601	0.6451868	−0.7292475	0.5881911
0.4408879	0.4271726	−0.4034483	0.5039919
0.5528590			
Exponent for *p*- and *d*-type CGTFs			
*p*1	*p*2	*d*1	
531.52482	0.78814268	58.953297	
124.42461	5.6984920	16.535577	
38.371899	2.1413437	5.5579113	
12.969020		1.8493120	
		0.53793445	
Coefficients for *p*- and *d*-type CGTFs			
0.0286683	0.2262452	0.0271550	
0.1845032	0.3339176	0.1499489	
0.5093271	0.5617786	0.3727743	
0.4500247		0.4742278	
		0.3203486	

Polarization functions (p.f.)		
Selected state for optimizing p.f.	Expon.	Coeff.
$(3d^{10}4s^14p^1)\ ^3P^0$	0.15795	0.49805
	0.04623	0.60480

Total energies and orbital energies for the parent Zn $(3d^{10}4s^2)\ ^1S$

	(4333/43/5)	(43321/43/41) + p.f.
TE	−1776.2167 au	−1776.2191 au
e_{3d}	−0.7644	−0.7655
e_{4s}	−0.2875	−0.2876

becomes much smaller for the trimer. For example R_e of Sc_2 was 5.27 au whereas R_e of the equilateral triangle Sc_3 was 5.74 au. The bond distance for the nearest neighbor in the solid is 6.25 au. We see an abrupt increase of the distance between Sc_2 and Sc_3. Similar results are found for Cu and Ag clusters (36). From the values for Sc and other results (33–36), a plausible bond length for Fe_4 is expected to approximate the value for the nearest neighbor in the solid. Without confirming the conjecture with configuration interaction calculations, we adopted the nearest neighbor value for the solid as the bond distance for calculating the ionization potentials of Fe_4.

We have no doubt that SCF calculations would give a longer bond distance for other clusters. Geometry optimizations were, therefore, not performed for the others and the assumed bond distances for Ni_4, Cu_4, and Zn_4 were set equal to those for the nearest neighbor in the corresponding metal.

(b) Band structure by Koopmans' theorem

The ground state of Fe_4 is $^{15}B_{1g}$ with configuration β, as was discussed, and hereafter we simply denote the state as $^{15}B_{1g}$. The total energy, gross atomic orbital populations (GAOPs) (37), excitation energies, and ionization potentials are shown in Table 2. Except for Fe_4, excited states were not calculated since the ground states are well established. The results for Ni_4 are collected in Table 3. The ground state for Ni_4 was $^7B_{1g}$ as given in refs. 19 and 22 and the orbitals for the open shell, $6a_{1g}{}^18e_u{}^26b_{1g}{}^1$, were mainly composed of $3d_{x^2-y^2}$. The corresponding data for Cu_4, and Zn_4 are listed in Tables 4 and 5, respectively.

The ionization potentials calculated by Koopmans' theorem are shown in the third column of Table 2(*b*) or in the third column of Tables 3, 4, and 5. Results by this theorem are also schematically shown in Figs. 2(*a*) and 2(*b*) together with those of M_6 clusters.

We define the Fermi level of the clusters as the first ionized state. We refer to the *s*-ionized and *d*-ionized state as *s*-level and *d*-level, as in solid state physics.

Koopmans' theorem showed that the Fermi level of Fe_4 is the 4*s* ionized state (hereafter we denote the state by s^{-1}), and the 3*d* ionized state (d^{-1}) lies 3.4 eV below the Fermi level.

Can. J. Chem. Downloaded from www.nrcresearchpress.com by 92.62.229.171 on 09/08/12
For personal use only.

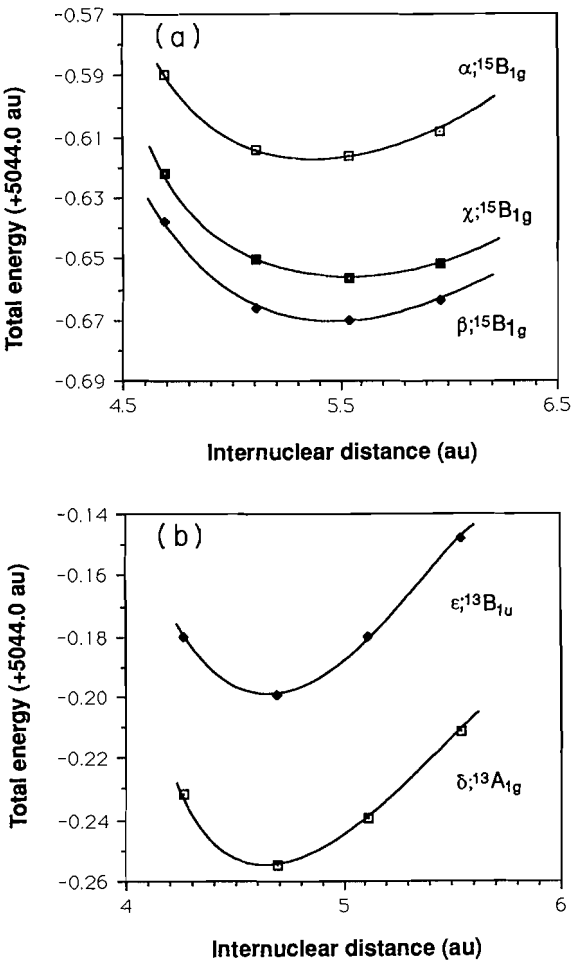

FIG. 1. (*a*) Total energies[a] versus internuclear distance for the lower three $^{15}B_{1g}$ states of Fe_4. (*b*) Total energies versus internuclear distance for the upper two states $^{13}A_{1g}$ and $^{13}B_{1u}$ of Fe_4.

[a]Total energies are in au and +5044.0 au is added to the total energies of the respective states.

In the solid Fe, however, the Fermi level consists of the top of the *s*- and *d*-bands. From Tables 3, 4, and 5 and the figures we see that the Fermi level of the other M_4 clusters also consists of the s^{-1} state so far as Koopmans' theorem is concerned. Except for Zn_4, the Fermi level takes almost the same position relative to the vacuum level. If we proceed from Fe_4 to Zn_4, the top of the *d*-band relative to the Fermi level becomes deeper; it is situated at 5.1 eV below the Fermi level for Ni_4, and at 7.0 and 16.4 eV below the Fermi level for Cu_4 and Zn_4. Corresponding values for solid Ni, Cu, and Zn are 0.0, 2.1, and 9.2 eV, respectively. Koopmans' theorem indicates how the electronic structure of small clusters differs from that of the solid.

(c) Band structure by symmetry-constrained ΔSCF

In this subsection, results given by symmetry-constrained SCF calculations for the ground and ionized states will be discussed. They are displayed in the fourth column of Tables 2(*b*), 3, 4, and 5 for the respective clusters. For Fe_4 we found that the two-electron-process-like *d* ionized state occupied the first ionized state, which lay 4.0 eV below the vacuum level; on the other hand, the first s^{-1}-like state lay 5.1 eV below the vacuum level. For symmetry-constrained ΔSCF, the Fermi level was spanned by the two-electron-process-like *d* ionized state.

[1] $3d^{2.4}\,4p^{0.1} \rightarrow 4s^{1.5}\,\infty^1$

A similar state was found for Ni_4, and was the lowest among the *d* electron ionized states. Contrary to Fe_4, the first d^{-1} for Ni_4 lay 1.5 eV below the Fermi level, namely, the first s^{-1}.

[2] $3d^{2.5} \rightarrow (4s4p)^{1.5}\,\infty^1$

No such state was found for Cu_4 and Zn_4 and the first d^{-1}-like state lay considerably below the Fermi level. An analysis of the two-electron-process-like state will be given in subsection (*d*).

The band structure predicted by the symmetry-constrained ΔSCF method gave a different form from that of Koopmans' theorem for Ni_4 and especially for Fe_4, and similar results for Cu_4 and Zn_4. In the fifth column of Tables 2(*b*), 3, 4, and 5, reorganization energies (RE) are given, where it is shown that reorganization energies (4.8–3.9 eV) of the top of the *d*-band for Fe_4 and Ni_4 are twice as large as those (2.1–1.8 eV) for Cu_4 and Zn_4. The experimental ionization potentials are given in the last column of each table and we see the ionization potential calculated for Fe_4 (4.0 eV) is very small compared with the observed threshold (6.3–6.5 eV) given by Rohlfing *et al.* (9). This disagreement requires further investigation.

(d) Band structure by symmetry-broken ΔSCF

Since the assumed bond distances for the clusters are four to five times greater than the mean values of r for the $3d$ electron, $\langle 3d|r|3d\rangle$, it might be reasonable to assume that when the *d* electron is ionized, the hole created is located at one of the atoms that constitute the clusters. (For example the bond distance is 4.69 au for the solid Fe and $\langle 3d|r|3d\rangle$ is 1.17 au for the Fe atom.) Introducing C_{2v} symmetry, we calculated the *d*-hole states. In actual calculations, orbital populations with an unequal number of *d* electrons with respect to the constituent atoms were prepared for the initial data. If the SCF procedure converges and the resulting solution has a localized *d*-hole at one of the constituents, we succeed in obtaining a localized *d*-hole state. Results are given at the bottom of Tables 2–5.

Hereafter we discuss the case of Fe_4. As expected, the state with the localized *d*-hole appeared to give lower ionization potentials. The calculated ionization potential was as small as 3.53 eV (see the second row from the bottom of Table 2). It will be shown that this state includes the Fermi level. The calculated ionization potential is too small compared with the experimental threshold of 6.3–6.5 eV. The localization of the *d*-hole implies that the atomic ionization process is important in the Fe cluster. If we assume that the relativistic energies for the neutral atom and the ion are the same, the ionization potential of the system is given by

$$\begin{aligned}[3]\quad \mathrm{IP(exptl)} &= \mathrm{TE(SCF,ion)} + \mathrm{CE(ion)} \\ &\quad - \{\mathrm{TE(SCF,neutral)} + \mathrm{CE(neutral)}\} \\ &= \{\mathrm{TE(SCF,ion)} - \mathrm{TE(SCF,neutral)}\} \\ &\quad + \{\mathrm{CE(ion)} - \mathrm{CE(neutral)}\} \\ &= \mathrm{IP(\Delta SCF)} + \Delta\mathrm{CE}\end{aligned}$$

where IP(exptl.) is the atomic ionization potential given by experiment. The TE (SCF) and CE are the atomic (ionic) SCF total and atomic (ionic) correlation energies. IP(ΔSCF) is the

Can. J. Chem. Downloaded from www.nrcresearchpress.com by 92.62.229.171 on 09/08/12
For personal use only.

TABLE 2. (*a*) Excitation energies and (*b*) ionization potentials of Fe_4

Ground state configuration (4*s* and 3*d* electrons); $\Phi(\beta;{}^{15}B_{1g})$
$6a_{1g}^{1}\ 3a_{2u}^{1}\ 1b_{1u}^{1}\ 3e_{g}^{2}\ 8e_{u}^{2}\ 4e_{g}^{2}\ 3b_{2u}^{1}\ 1a_{1u}^{1}\ 6b_{1g}^{1}\ 3b_{2g}^{2}\ 7a_{1g}^{2}\ 9e_{u}^{4}\ 7b_{1g}^{2}\ 10e_{u}^{4}$
$3a_{2g}^{2}\ 8a_{1g}^{2}11e_{u}^{2}\ {}^{15}B_{1g}$
Total energy −5044.63809 au
GAOPs of SCF wavefunctions;

s	*p*	*d*	Total
6.71	12.36	6.93	26.00

(*a*) Excitation energies

State[a]	Excitation energy(eV)
$\Phi(\varepsilon;{}^{13}B_{1u})$	11.94
$\Phi(\delta;{}^{13}A_{1g})$	10.43
$\Phi(\alpha;{}^{15}B_{1g})$	1.31
$\Phi(\chi;{}^{15}B_{1g})$	0.44
$\Phi(\beta;{}^{15}B_{1g})$	0.0

(*b*) Ionization potentials

State	Character	$-\varepsilon_i$(eV)	ΔSCF(eV)	RE(eV)	Exptl.[b] (eV)
D_{4h} (symmetry constrained)					
$(11e_u^{-1})\ {}^{14}E_u$	$4s^{-1}$	5.38	5.13	0.25	6.3–6.5
$(8a_{1g}^{-1})\ {}^{16}B_{1g}$	$4s^{-1}$	7.87	5.76	2.11	
$(3a_{2g}^{-1})\ {}^{16}B_{2g}$	$3d^{-1}$(tepl)[c]	8.77	3.98	4.79	6.3–6.5
$(10e_u^{-1})\ {}^{16}E_u$	$3d^{-1}$(deloc)	9.76	6.50	3.26	
$(7b_{1g}^{-1})\ {}^{16}A_{1g}$	$3d^{-1}$(deloc)	9.78	7.13	2.65	
$(6a_{1g}^{-1})\ {}^{14}B_{1g}$	$3d^{-1}$(deloc)	13.91	12.33	1.57	
C_{2v} or D_{2h} (symmetry broken)					
$(14a_g^{-1})\ {}^{16}A_g$	$3d^{-1}$(tepl)	9.78	2.80	6.98	6.3–6 .5
$(6b_{1g}^{-1})\ {}^{16}B_{1g}$	$3d^{-1}$(tepl)	8.77	3.31	5.46	
$(16b_2^{-1})\ {}^{16}B_2$	$3d^{-1}$(loc)	8.77	3.53	5.24	
$(18a_1^{-1})\ {}^{14}A_1$	$3d^{-1}$(loc)	13.91	7.13	6.78	

[a]The electronic configurations for the excited states are expressed as
$\Phi(\alpha;{}^{15}B_{1g}) = \Phi(\beta;\ 7a_{1g},\ 7b_{1g},\ 9e_{ux},\ 9e_{uy} \rightarrow 1a_{1u},\ 1b_{1u},\ 3e_{gx},\ 3e_{gy})$
$\Phi(\chi;{}^{15}B_{1g}) = \Phi(\beta;\ 7a_{2g},\ 7b_{2g},\ 9e_{ux},\ 9e_{uy} \rightarrow 1a_{1u},\ 1b_{1u},\ 3e_{gx},\ e_{gy})$
$\Phi(\delta;{}^{13}A_{1g}) = \Phi(\beta;\ 6b_{1g} \rightarrow 6a_{1g})$
$\Phi(\varepsilon;{}^{13}B_{1u}) = \Phi(\beta;\ 1a_{1u} \rightarrow 6a_{1g})$
See also the main text.
[b]See ref. 9.
[c]The abbreviation tepl means two-electron-process-like.

ionization potential given by the total energy difference between the ion and the neutral atom. The atomic correlation correction is calculated from the experimental ionization potential and that of ΔSCF.

$$[4] \quad \Delta CE = IP(exptl) - IP(\Delta SCF)$$

ΔCEs are collected in Table 6. For Fe, the atomic correlation correction for the *d* ionization is 2.4 eV, leading to an ionization potential of 5.9 eV, which is close to the experimental ionization threshold of 6.3–6.5 eV given by Rohlfing *et al.* (9).

For the case of 4*s* electron ionization we analogously add the atomic correlation correction of 1.2 eV, leading to an ionization potential of 6.3 eV, which is slightly greater than the ionization potential of the *d*-hole state. One may doubt the validity of the use of the atomic correlation correction for 4*s* electron ionization. In atomic 4*s* ionization of Fe, Ni, and Cu, ΔCE arises mainly from the 4*s*–3*d* electronic correlations, which are included in the neutral systems but are not in the ions. If one 4*s*-like electron is shared with *n* atoms that constitute the clusters, then it might be not unreasonable to assume that the *s*–*d* correlation energy per atom is around $1/n$ of the atomic case. If we deprive the cluster of one 4*s*-like electron we may obtain a more appropriate ionization potential by adding the atomic correlation correction to IP(ΔSCF). Since we disregarded the difference in the correlation energies among the 4*s*-like valence electrons between the ion and the neutral system, the estimated ionization potential (6.3 eV for Fe_4) might be lower bound. The difference in the ionization potentials between the 3*d* and 4*s* ionizations is fairly small (0.4 eV). Taking account of the ambiguity of the correlation correction, we assign the Fermi level of the Fe_4 clusters as d^{-1} or as a mixture of the s^{-1} and d^{-1} states.

Results of the symmetry-broken calculations with the atomic correlation correction and the experimental ionization threshold are schematically shown in Fig. 3(*a*) together

Can. J. Chem. Downloaded from www.nrcresearchpress.com by 92.62.229.171 on 09/08/12
For personal use only.

TABLE 3. Ionization potentials of Ni_4

Ground state configuration ($4s$ and $3d$ electrons)
$6a_{1g}^{1}\ 8e_u^{2}\ 6b_{1g}^{1} \ldots 3a_{2g}^{2}\ 8a_{1g}^{2}\ 11e_u^{2}\ {}^7B_{1g}$
Total energy −6021.64189 au
GAOPs of SCF wavefunctions:

s	p	d	Total
6.74	12.32	8.94	28.00

State	Character	$-\varepsilon_i$(eV)	ΔSCF(eV)	RE(eV)	Exptl.[a] (eV)
D_{4h} (symmetry constrained)					
$(11e_u^{-1})\ {}^8E_u$	$4s^{-1}$	5.35	5.08	0.27	5.6–6.4
$(8a_{1g}^{-1})\ {}^8B_{1g}$	$4s^{-1}$	8.07	6.23	1.84	
$(3a_{2g}^{-1})\ {}^8B_{2g}$	$3d^{-1}$(tepl)[b]	10.44	6.53	3.91	5.6–6.4
$(7b_{1g}^{-1})\ {}^8A_{1g}$	$3d^{-1}$(tepl)	10.92	7.09	3.83	
$(1a_{1u}^{-1})\ {}^8B_{1u}$	$3d^{-1}$(deloc)	12.51	9.05	3.46	
$(6a_{1g}^{-1})\ {}^6B_{1g}$	$3d^{-1}$(deloc)	15.03	13.10	1.93	
C_{2v} or D_{2h} (symmetry broken)					
$(16b_2^{-1})\ {}^8B_2$	$3d^{-1}$(loc)	10.44	4.56	5.88	5.6–6.4
$(6b_{1g}^{-1})\ {}^8B_{1g}$	$3d^{-1}$(tepl)	10.44	5.21	5.23	
$(24a_1^{-1})\ {}^8A_1$	$3d^{-1}$(tepl)	10.92	3.90	7.02	
$(14a_g^{-1})\ {}^8A_g$	$3d^{-1}$(tepl)	10.92	3.89	7.03	
$(18a_1^{-1})\ {}^6A_1$	$3d^{-1}$(loc)	15.03	8.24	6.79	

[a]See ref. 10.
[b]The abbreviation tepl means two-electron-process-like.

TABLE 4. Ionization potentials of Cu_4

Ground state configuration ($4s$ and $3d$ electrons)
$3b_{2g}^{2} \ldots 3a_{2g}^{2}\ 8a_{1g}^{2}\ 11e_u^{2}\ {}^3A_{2g}$
Total energy −6549.75709 au
GAOPs of SCF wavefunctions:

s	p	d	Total
6.76	12.28	9.96	29.00

State	Character	$-\varepsilon_i$(eV)	ΔSCF(eV)	RE(eV)	Exptl.[a] (eV)
D_{4h} (symmetry constrained)					
$(11e_u^{-1})\ {}^2E_u$	$4s^{-1}$	5.41	5.19	0.22	6.4–7.9
$(8a_{1g}^{-1})\ {}^4A_{2g}$	$4s^{-1}$	7.97	6.24	1.73	
$(3a_{2g}^{-1})\ {}^4A_{1g}$	$3d^{-1}$(deloc)	12.45	10.39	2.06	
$(7b_{1g}^{-1})\ {}^4B_{2g}$	$3d^{-1}$(deloc)	12.79	10.87	1.92	
$(3b_{2g}^{-1})\ {}^4B_{1g}$	$3d^{-1}$(deloc)	13.79	11.93	1.86	
C_{2v} (symmetry broken)					
$(16b_2^{-1})\ {}^4A_1$	$3d^{-1}$(loc)	12.45	6.34	6.11	
$(21a_1^{-1})\ {}^4B_2$	$3d^{-1}$(loc)	12.79	6.32	6.47	
$(12b_2^{-1})\ {}^4A_1$	$3d^{-1}$(loc)	13.79	6.34	7.45	

[a]See ref. 8.

with the results for Ni_4, Fe_6, and Ni_6. We immediately recognize the accuracy of the calculations.

When we calculated the Ni_4 cluster with C_{2v} symmetry, the following ionized state was found.

$$[5]\quad (3d,Ni_3)^{0.9}(3d,Ni_4)^{0.9} \rightarrow (4s4p,Ni_1)^{-0.4}(4s4p,Ni_2)^{-0.4}(4s,Ni_3)^{0.8}(4s,Ni_4)^{0.8}\ \infty^{1.0}$$

where Ni_3 and Ni_4 are on the diagonal line and the same stands for Ni_1 and Ni_2. $(4s4p, Ni_1)^{-0.4}$ means that the $4s$- and $4p$-like electrons of Ni_1 decrease by 0.4 and $(4s,Ni_3)^{0.8}$ means that the $4s$-like electrons of Ni_3 increase by 0.8. This relation implies that one of the 1.8 d-like electrons at Ni_3 and Ni_4 is ionized and the remaining 0.8 electrons are excited into $4s$ orbitals of Ni_3 and Ni_4 and, furthermore, the valence electrons distributed around Ni_1 and Ni_2 move in order to

Can. J. Chem. Downloaded from www.nrcresearchpress.com by 92.62.229.171 on 09/08/12
For personal use only.

screen the d-holes. The calculated ionization potential was very small and the electronic configuration was D_{2h}-like; we performed a D_{2h} calculation for Ni_4 to gain confidence and got the same solution as for C_{2v}. We, therefore, performed only D_{2h} calculations for Fe_4 and obtained ionization potentials of 2.80 ($^{6}A_g$) and 3.31 eV ($^{6}B_{1g}$), which are also shown in the bottom part of Table 2. The ionization process for the two states was two-electron-like as for Ni_4.

$$[6]\quad (3d,Fe_3)^{0.9}(3d,Fe_4)^{0.9} \rightarrow (4s4p,Fe_1)^{-0.4}(4s4p,Fe_2)^{-0.4}(4s,Fe_3)^{0.8}(4s,Fe_4)^{0.8}\,\infty^{1.0} \qquad \text{for } {}^{6}A_g$$

and

$$[7]\quad (3d,Fe_3)^{0.9}(3d,Fe_4)^{0.9} \rightarrow (4s4p,Fe_1)^{-0.2}(4s4p,Fe_2)^{-0.2}(3d,Fe_1)^{-0.1}(3d,Fe_2)^{-0.1}(4s4p,Fe_3)^{0.7}(4s4p,Fe_4)^{0.7}\,\infty^{1.0} \qquad \text{for } {}^{6}B_{1g}$$

We divide the process into two parts. First, atomic ionization of $(3d^74s^1) \rightarrow (3d^64s^1)$ arises at one of the Fe_3 and Fe_4, and atomic de-excitation $(3d^74s^1) \rightarrow (3d^64s^2)$ simultaneously arises at the remaining Fe_3 or Fe_4. Second, to screen the positive d-holes, the outer shells are reorganized; the $4s$ and $4p$ electrons from other atomic sites move in. As atomic correlation corrections for the ionization and the de-excitation are 2.4 and 0.9 eV, as shown in Table 6, total ΔCE is 3.3 eV,[1] leading to ionization potentials of 6.1 and 6.6 eV for $^{6}A_g$ and $^{6}B_{1g}$, which are slightly higher than that (5.9 eV) of the Fermi level (see Table 7). If we recall the uncertainty in estimating the correlation correction and the smallness of the difference in the ionization energy, we cannot say which of the two, the d-hole localized state or the two-electron-process-like ionized state, includes the Fermi level.

Information on ionization potentials for the other atoms is also collected in Table 6, together with the atomic correlation correction ΔCE. Ionization potentials for the other clusters of Ni_4, Cu_4, and Zn_4 calculated with symmetry-broken SCF and those with the correlation correction are compared with experimental values in Table 7. The latter are also shown in Figs. 3(*a*) and (*b*).

Let us discuss Ni_4, using the results given in the figure and the tables. The experimental ionization threshold given by Rohlfing *et al.* (10) was 5.6–6.4 eV while the s^{-1} level calculated with the correlation correction gave an ionization potential of 6.5 eV. Agreement is quite good. By the same level of approximation, we found that the state with the localized d-hole lay only 1 eV below the Fermi level of s^{-1}. As the separation of the two levels is fairly small, we assign the Fermi level as s^{-1} or a mixture of s^{-1} and d^{-1} states for the cluster. As before, two-electron-like ionization processes were first found for Ni_4 in both the C_{2v} and D_{2h} symmetries and the lowest two states obtained with the two symmetries were found to be identical (see the bottom part of Table 3). The magnitude of the correlation correction for the state was 4.2 eV and the state corrected lay 1.6 eV below the Fermi level. It is noted that, in Ni_4 and Fe_4, two-electron-like ionization processes bring the two d-hole states near or very near to the Fermi level. Such a state appears only if the atomic $(4s^23d^n)$ state lies near or below the $(4s^13d^{n+1})$ state.

Since the atomic de-excitation energy of $(3d^{n+1}4s^1) \rightarrow (3d^n4s^2)$ is exaggerated in the SCF-level approximation, it makes the ionized states of two-electron-like-processes, which are expressed by relations [1] and [2], stable even in the symmetry-constrained SCF.

We next discuss the case of Cu_4. The calculated ionization potential for Cu_4 is 6.7 eV while the experimental value obtained by Powers *et al.* (8) lies between 6.4 and 7.9 eV. The calculated ionization potential is in the region of the experimental threshold. For Cu clusters Schmeisser *et al.* (6) found that the top of the d-band began 3 eV below the Fermi level. As discussed in the previous subsection, symmetry-constrained ΔSCF results in the position of the top of the d-band relative to the Fermi level having a larger value of 5.2 eV, predicting a different electronic structure between the solid and the clusters. The symmetry-broken ΔSCF with correlation correction gave the top of the d-band 2.4 eV below the Fermi level, which was close to the experimental value of 3 eV. It will be shown that the top of the d-band becomes 2.7 eV below the Fermi level for Cu_6.

For Zn clusters it was found experimentally (7) that the top of the d-band began 10 eV below the Fermi level and that of the solid was 9.2 eV below. The symmetry-constrained ΔSCF gave 14.8 eV (see Table 5) while symmetry-broken ΔSCF with and without correlation correction gave 9.7 and 9.6 eV respectively. In the case of Zn_4 the effects of the correlation correction were small because the corrections for the s^{-1} and d^{-1} states were almost the same.

The positions of the Fermi level relative to the vacuum level and the top of the d-band relative to the Fermi level are

TABLE 5. Ionization potentials of Zn_4

Ground state configuration ($4s$ and $3d$ electrons)
$3b_{2g}^2 \ldots 3a_{2g}^2\, 8a_{1g}^2\, 11e_u^4\, 8b_{1g}^2\, {}^1A_{1g}$
Total energy −7104.79121 au
GAOPs of SCF wavefunctions:

s	p	d	Total
7.72	12.30	9.99	30.00

State	Character	$-\varepsilon_i$(eV)	ΔSCF(eV)	RE(eV)
D_{4h} (symmetry constrained)				
$(8b_{1g}^{-1})\ {}^2B_{1g}$	$4s^{-1}$	4.78	4.58	0.20
$(8a_{1g}^{-1})\ {}^2A_{1g}$	$4s^{-1}$	12.34	11.75	0.59
$(3a_{2g}^{-1})\ {}^2A_{2g}$	$3d^{-1}$(deloc)	21.18	19.36	1.82
$(3b_{2g}^{-1})\ {}^2B_{2g}$	$3d^{-1}$(deloc)	21.79	20.02	1.77
C_{2v} (symmetry broken)				
$(16b_2^{-1})\ {}^2B_2$	$3d^{-1}$(loc)	21.18	(14.3)	(6.9)
$(3a_2^{-1})\ {}^2A_2$	$3d^{-1}$(loc)	21.57	14.67	6.90
$(7b_1^{-1})\ {}^2B_1$	$3d^{-1}$(loc)	21.59	14.63	6.96
$(18a_1^{-1})\ {}^1A_1$	$3d^{-1}$(loc)	21.79	(14.9)	(6.9)

[1]One could take another route to obtain ΔCE for the ionization given by relations [6] and [7]. The ionization processes could be divided into three processes instead of two. Firstly, at Fe_3 and Fe_4 the atomic de-excitation $(3d^74s^1) \rightarrow (3d^64s^2)$ arises; secondly, one-electron ionization for the $4s$-like electrons proceeds at one of the two atoms; and thirdly, reorganization take places with a large movement of the $4s$ and $4p$ electrons, including the other atomic sties. The correlation correction for the first stage might be twice that for the de-excitation (1.8 eV). For the second stage we could use the correlation correction of 1.5 eV for $(3d^64s^2) \rightarrow (3d^64s^1)$ instead of the ΔCE of $(3d^74s^1) \rightarrow (3d^74s^0)$. Total ΔCE is 3.3 eV, which is just the same as mentioned in the main text.

Can. J. Chem. Downloaded from www.nrcresearchpress.com by 92.62.229.171 on 09/08/12
For personal use only.

TABLE 6. Ionization potentials for Fe, Ni, Cu, and Zn atoms

Atom	Character	State	$-\varepsilon_i$(eV)	ΔSCF(eV)	RE(eV)	Exptl.[a](eV)	Correl. correct.(eV)
Fe	R.S.[b]	$4s^13d^7\ ^5F$	0.0	0.0	0.0	0.0	
	G.S.	$4s^23d^6\ ^5D$		−1.76		−0.88	0.9
	s^{-1}	$4s^03d^7\ ^4F$	6.10	6.06	0.04	7.27	1.2
	d^{-1}	$4s^13d^6\ ^6D$	10.69	4.65	6.04	7.02	2.4
	d^{-1}	$4s^13d^6\ ^4G$	10.69	8.34	2.35	10.17	1.8
Ni	G.S.[c]	$4s^13d^9\ ^3D$	0.0	0.0	0.0	0.0	
		$4s^23d^8\ ^3F$		−1.30		0.03	1.3
	s^{-1}	$4s^03d^9\ ^2D$	6.22	6.19	0.03	7.62	1.4
	d^{-1}	$4s^13d^8\ ^4F$	11.87	5.78	6.09	8.70	2.9
	d^{-1}	$4s^13d^8\ ^2G$	11.87	9.13	2.74	11.57	2.4
Cu	G.S.[d]	$4s^13d^{10}\ ^2S$	0.0	0.0	0.0	0.0	
	s^{-1}	$4s^03d^{10}\ ^1S$	6.29	6.26	0.03	7.73	1.5
	d^{-1}	$4s^13d^9\ ^3D$	12.75	7.76	4.99	10.53	2.8
	d^{-1}	$4s^13d^9\ ^1D$	12.75	7.95	4.80	10.98	3.0
Zn	G.S.[e]	$4s^23d^{10}\ ^1S$	0.0	0.0	0.0	0.0	
	s^{-1}	$4s^13d^{10}\ ^2S$	7.83	7.53	0.30	9.39	1.9
	d^{-1}	$4s^23d^9\ ^2D$	20.83	15.47	5.36	17.30	1.8

[a]See ref. 38.
[b]Total energy for the reference state ^5F is −1261.1602 au.
[c]Total energy for the ground state of ^3D is −1505.3990 au.
[d]Total energy for the ground state ^2S is −1637.4293 au.
[e]Total energy for the ground state ^1S is −1776.2191 au.

thus systematically explained for M_4 clusters by symmetry-broken ΔSCF.

Band structure of Fe_6, Ni_6, Cu_6, and Zn_6

In this section the band structure of Fe_6, Ni_6, Cu_6, and Zn_6 will be discussed. We adopted O_h symmetry and the internuclear distances were fixed equal to those of nearest neighbors of the corresponding metals as in the case of the M_4 clusters. We calculated only the candidates for the ground state of the respective clusters. To discuss the band structure of the M_6 clusters we decided to modify the orbital energies of the candidate states by the following equation.

$$[8] \quad IP(M_6) = -\varepsilon_i - RE + \Delta CE$$

where RE is reorganization energy and ΔCE is the atomic correlation correction defined in Eq. [4].

In the previous section we saw that the localized *d*-hole state always consists of the top of the *d*-band, and the state resulting from the two-electron-process-like (tepl) ionization keeps the position very near to the Fermi level for Fe_4. We use the two reorganization energies of M_4 for the modification; we feel that the use of these energies may give smaller reorganization energies of ca. 1 eV or less for both s^{-1} and d^{-1} (19, 21). In Tables 8–11, the total energies, orbital energies, reorganization energies, and ionization potentials with correlation correction are shown for Fe_6, Ni_6, Cu_6, and Zn_6, respectively. The information on ionization potentials is summarized in Table 12 as well as in Figs. 3(*a*) and (*b*) where band widths are those of the orbital energy level distributions (discussed in the next paragraph). The experimental ionization thresholds are 5.8–6.0, 6.4–7.9, and 6.4–7.9 eV for Fe_6, Ni_6, and Cu_6, while the calculated first ionization potentials are 5.7, 6.8, and 6.9 eV for the respective clusters. We can say that the calculated ionization potentials agree well with the experimental values. The top of the *d*-band for Fe_6, which arises from the tepl ionization, consists only of the Fermi level among the M_6 clusters and that for Ni_6 lies 1.7 eV below the Fermi level. The value of 1.7 eV is still small and we leave the assignment of $s^{-1} + d^{-1}$ as the Fermi level with some hesitation. The top of the *d*-band was experimentally found ca. 3 and 10 eV below the Fermi level for Cu and Zn clusters. The corresponding calculated values agree with the experimental values with good accuracy (see Table 12).

We define the *s*(*d*)-band width as the difference between the orbital energy of the highest occupied *s*(*d*)-like orbital and that of the lowest occupied *s*(*d*)-like orbital. We would like to point out the uncertainty in the use of orbital energies to discuss the band width. Using the ΔSCF ionization potentials given in ref. 19, one finds that *s*-band widths provided by the orbital energies are 2.72 and 4.76 eV for Ni_4 and Ni_6, respectively, and those by ΔSCF for Ni_4 and Ni_6 are 1.15 and 4.21 eV; we can, therefore, say that the band width estimated with the orbital energies reflects the same trends as the band width calculated using ΔSCF. As shown in Figs. 2(*a*) and (*b*), the *s*-band width is one-half of the *d*-band width for Fe_4 and Ni_4, which is as wide as that for the corresponding metals (19, 21). The *s*-band width increases twice and becomes as wide as the *d*-band width for Fe_6 and Ni_6. For Cu_6 and Zn_6 the *d*-band width is close to that of the solid. The *s*-band width of Cu_6 is nearly half that of the solid and that of Zn_6 is almost the same as that of solid Zn. The data presented indicate rather rapid convergence of the *s*-band width of the clusters to that of the solid. We recall that the top of the *d*-band relative to the Fermi level is close to that of the corresponding metals for all the clusters under consider-

Can. J. Chem. Downloaded from www.nrcresearchpress.com by 92.62.229.171 on 09/08/12
For personal use only.

Can. J. Chem. Downloaded from www.nrcresearchpress.com by 92.62.229.171 on 09/08/12
For personal use only.

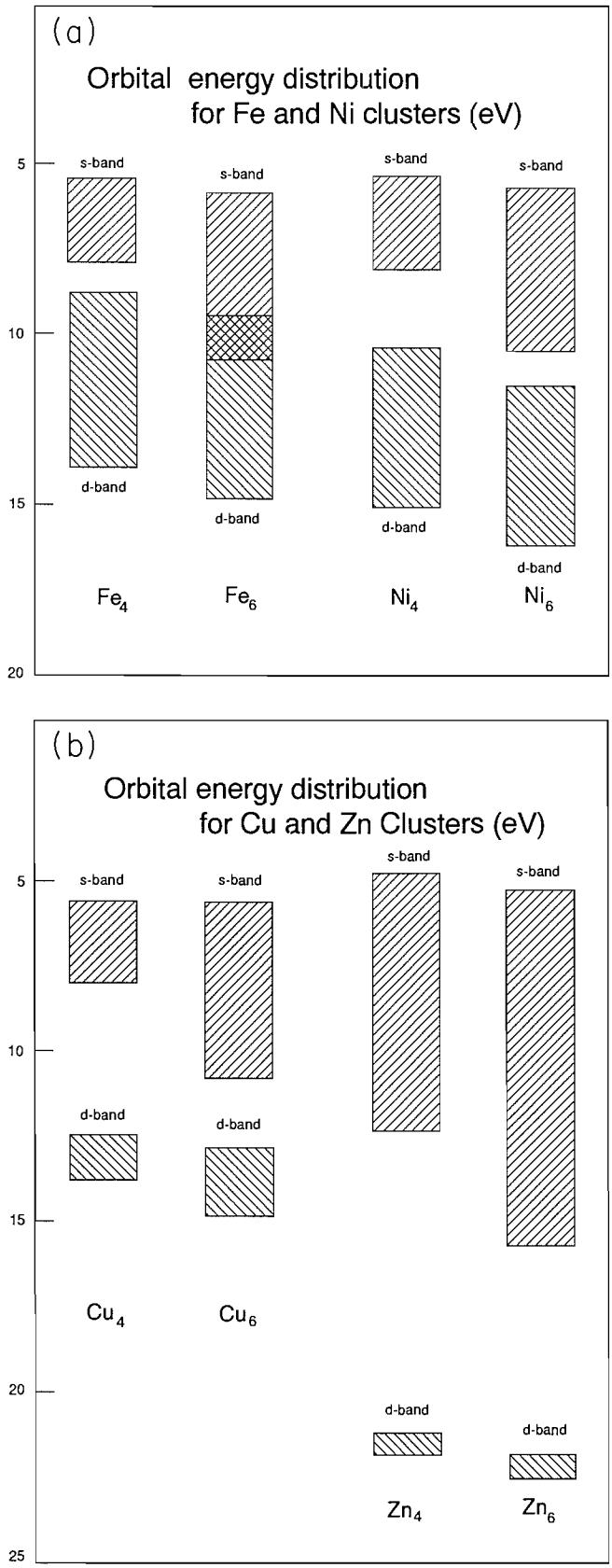

FIG. 2. (*a*) Orbital energy[a] distribution for Fe and Ni clusters. (*b*) Orbital energy distribution for Cu and Zn clusters.
[a]Orbital energies are in eV.

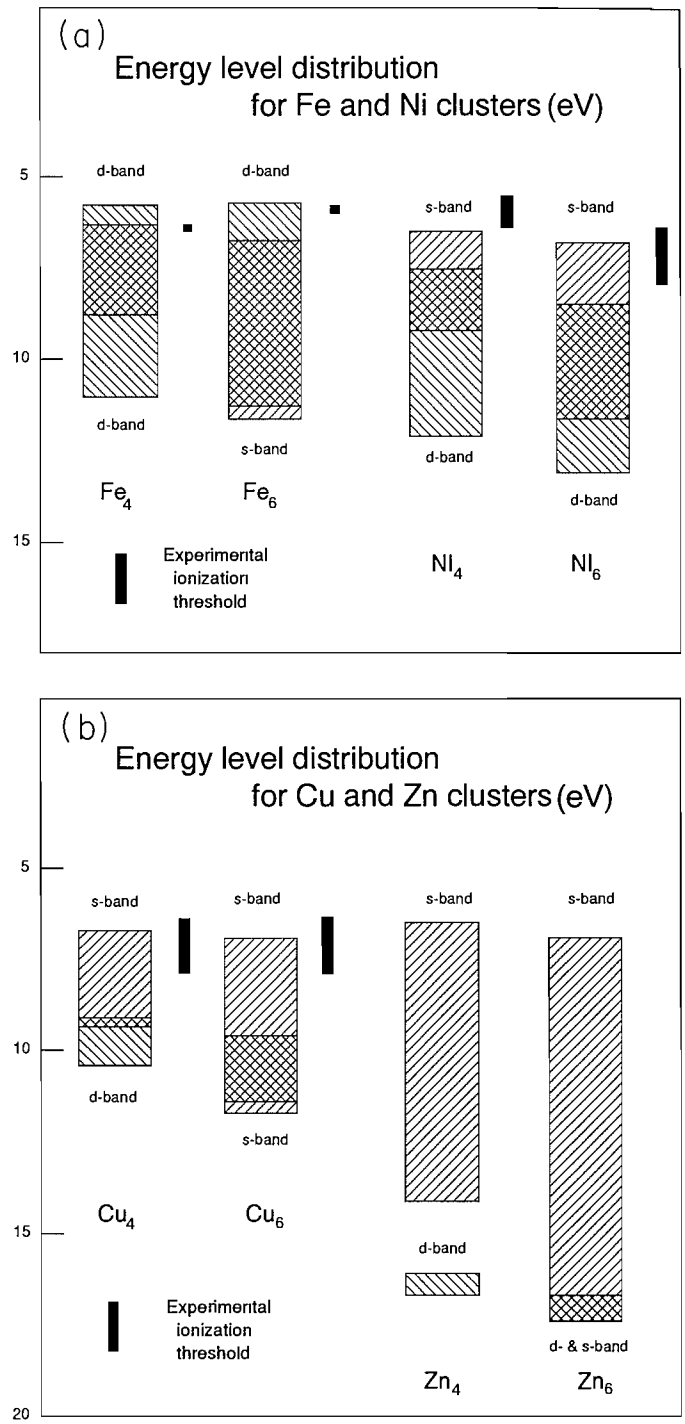

FIG. 3. (*a*) Energy level[a] distribution for Fe and Ni clusters. (*b*) Energy level distribution for Cu and Zn clusters.
[a]Energy levels are in eV. The widths of the energy level distribution are those of the orbital energy distributions. The experimental ionization thresholds for the respective clusters are also included.

ation. We can, therefore, expect that the shape of the energy distributions of the clusters will resemble that of the metals even at smaller cluster size. Making a strong contrast, reasonable agreement between the first ionization potential of the clusters and the work function of the solid seems to require larger cluster size (8–10); for example, see the

TABLE 7. Ionization potentials for Fe_4, Ni_4, Cu_4, and Zn_4

	$-\varepsilon$(eV)	Symmetry broken ΔSCF (d^{-1}) (eV)	Correl. correct. (eV)	Estimated IP (eV)	Exptl. IP (eV)
$Fe_4(s^{-1})$	5.38	5.13	1.2	6.3	6.3–6.5[a]
$(d^{-1}$(loc))	8.77	3.53	2.4	5.9	
$(d^{-1}$(tepl))	9.78	2.80	3.3	6.1	
$(d^{-1}$(tepl))	8.77	3.31	3.3	6.6	
Fermi-L[b]	s^{-1}	d^{-1}		d^{-1} or (d^{-1} and s^{-1})	
d relative to Fermi-L	3.39	0.0		0.0	
$Ni_4(s^{-1})$	5.35	5.08	1.4	6.5	5.6–6.4[c]
$(d^{-1}$(loc))	10.44	4.56	2.9	7.5	
$(d^{-1}$(tepl))	10.92	3.89	4.2	8.1	
Fermi-L	s^{-1}	d^{-1}		s^{-1} or (s^{-1} and d^{-1})	
d relative to Fermi-L	5.09	0.0		1.0 or 0.0	
$Cu_4(s^{-1})$	5.41	5.19	1.5	6.7	6.4–7.9[d]
$(d^{-1}$(loc))	12.45	6.34	2.8	9.1	
Fermi-L	s^{-1}	s^{-1}		s^{-1}	
d relative to Fermi-L	7.04	1.15		2.4	3
$Zn_4(s^{-1})$	4.78	4.58	1.9	6.5	
$(d^{-1}$(loc))	21.18	14.3	1.8	16.1	
Fermi-L	s^{-1}	s^{-1}		s^{-1}	
d relative to Fermi-L	16.40	9.7		9.6	10

[a]See ref. 9.
[b]Fermi-L means Fermi level.
[c]See ref. 10.
[d]See ref. 8.

TABLE 8. Total energies, orbital energies, and ionization potentials for Fe_6

Ground state configuration (4s and 3d electrons)
$\{(5e_g^2\ 11a_{1g}^1\ 1b_{1u}^1\ 10e_u^2\ 3b_{2u}^1\ 8a_{2u}^1\ 6e_g^2\ 1a_{1u}^1\ 6b_{1g}^1\ 11e_u^2\ 12a_{1g}^2$
$3b_{2g}^2\ 7b_{1g}^1\ 4b_{2u}^1\ 7e_g^2\ 12e_u^4\ 13e_u^4\ 8b_{1g}^2\ 2b_{1u}^2\ 9a_{2u}^2\ 4b_{2g}^2\ 14a_{1g}^2$
$3a_{2g}^2)\ ^{19}B_{1u}\ (13a_{1g}^2\ 14e_u^2\ 10a_{2u}^2)\ ^3A_{2g}\}\ ^{21}B_{2u}$
Total energy −7566.90302 au
GAOPs of SCF wavefunctions:

	s	p	d	Total
Plane	6.51	12.56	6.91	25.98
Top	6.83	12.28	6.93	26.03

State	Character	$-\varepsilon_i$ (eV)	Estimated RE (SB)(eV)	Correl. correct.(eV)	Estimated IP(eV)
O_h (symmetry constrained)					
$(10a_{2u}^{-1})$	$4s^{-1}$	5.82	0.3	1.2	6.7
$(13a_{1g}^{-1})$	$(3d + 4s)^{-1}$	10.74	0.3	1.2	11.6
$(3a_{2g}^{-1})$	$3d^{-1}$	9.44	7.0[a]	3.3	5.7
$(3a_{2g}^{-1})$	$3d^{-1}$	9.44	5.2[b]	2.4	6.6
$(5e_g^{-1})$	$3d^{-1}$	14.80	5.2	2.4	12.0

[a]The reorganization energy is that of the symmetry-broken solution calculated for the two-electron-like process (tepl) of Fe_4.
[b]The reorganization energy is that of the symmetry-broken solution for the d-hole localized state calculated for Fe_4.

Can. J. Chem. Downloaded from www.nrcresearchpress.com by 92.62.229.171 on 09/08/12
For personal use only.

TABLE 9. Total energies, orbital energies, and ionization potentials for Ni_6

Ground state configuration (4*s* and 3*d* electrons)
$\{(1a_{2u}{}^1 3t_{2g}{}^3 1e_u{}^2 6e_g{}^4 3t_{2u}{}^6 6a_{1g}{}^2 4t_{2g}{}^6 8t_{1u}{}^6 1a_{2g}{}^2 9t_{1u}{}^6 4t_{2u}{}^6 7e_g{}^4 3t_{1g}{}^6)\ {}^7A_u\ (7a_{1g}{}^2\ 10t_{1u}{}^4)\ {}^3T_{1g}\}\ {}^9T_{2u}$
Total energy −9032.4589 au
GAOPs of SCF wavefunctions:

	s	*p*	*d*	Total
Plane	6.60	12.49	8.91	28.00
Top	6.60	12.49	8.91	28.00

State	Character	$-\varepsilon_i$ (eV)	Estimated RE (SB)(eV)	Correl. correct.(eV)	Estimated IP(eV)
O_h (symmetry constrained)					
$(10t_{1u}{}^{-1})$	$4s^{-1}$	5.73	0.3	1.4	6.8
$(7a_{1g}{}^{-1})$	$4s^{-1}$	10.49	0.3	1.4	11.6
$(3t_{1g}{}^{-1})$	$3d^{-1}$	11.53	5.9[a]	2.9	8.5
$(3t_{1g}{}^{-1})$	$3d^{-1}$	11.53	7.0[b]	4.2	8.7
$(1a_{2u}{}^{-1})$	$3d^{-1}$	16.10	5.9	2.9	13.1

[a]The reorganization energy is that of the symmetry-broken solution for the *d*-hole localized state calculated for Ni_4.
[b]The reorganization energy is that of the symmetry-broken solution calculated for the two-electron-like process (tepl) of Ni_4.

TABLE 10. Total energies, orbital energies, and ionization potentials for Cu_6

Ground state configuration (4*s* and 3*d* electrons)
$6a_{1g}{}^2\ 3t_{2g}{}^6\ 8t_{1u}{}^6\ 1a_{2u}{}^2\ 6e_g{}^4\ 3t_{2u}{}^6\ 9t_{1u}{}^6\ 4t_{2g}{}^6\ 1e_u{}^4\ 7e_g{}^4\ 4t_{2u}{}^6\ 3t_{1g}{}^6$
$1a_{2g}{}^2\ 7a_{1g}{}^2\ 10t_{1u}{}^4\ {}^3T_{1g}$
Total energy −9824.64520 au
GAOPs of SCF wavefunctions:

	s	*p*	*d*	Total
Plane	6.71	12.36	9.94	29.00
Top	6.71	12.36	9.94	29.00

State	Character	$-\varepsilon_i$ (eV)	Estimated RE (SB)(eV)	Correl. correct.(eV)	Estimated IP(eV)
O_h (symmetry constrained)					
$(10t_{1u}{}^{-1})$	$4s^{-1}$	5.63	0.2	1.5	6.9
$(7a_{1g}{}^{-1})$	$4s^{-1}$	10.39	0.2	1.5	11.7
$(1a_{2g}{}^{-1})$	$3d^{-1}$	12.86	6.1	2.8[a]	9.6
$(6a_{1g}{}^{-1})$	$3d^{-1}$	14.78	6.1	2.8[a]	11.5

[a]For 3*d* ionized states ($3d^{-1}$(loc)), the reorganization energy is that of the symmetry-broken solution calculated for Cu_4.

ionization potentials of Fe_4 and Fe_6 in Tables 7 and 12 and compare them with the work function of 4.5 eV for the solid Fe (39).

Effect of different splitting of basis sets

We will consider what happens if we further divide the *d*-type CGTFs, taking Fe and Fe_4 as examples.

In the atomic case (43321/43/41) + p.f. gave a total energy of −1260.1602 and 1260.9893 au for the ground state ^5F and the *d*-electron ionized state ^6D, yielding an ionization potential of 4.65 eV, while (4332/43/311) + p.f. gave −1261.1602 and −1260.9900 au for ^5F and ^6D, yielding an ionization potential of 4.63 eV, which is very close to the result for the smaller splitting set. Since in the localized *d*-hole model the atomic ionization process is dominant, the results given above suggest that splitting causes only negligibly small effects.

For the tepl ionization, the effect of splitting might be larger. With smaller splitting we obtained total energies of −5044.63809 and −5044.53528 au for the ground state of $^{15}B_{1g}$ and the $14a_g{}^{-1}$ tepl ionized state, yielding an ionization potential of 2.80 eV, while larger splitting gave total energies of −5044.63832 and −5044.53776 au for the ground and ionized states respectively, yielding an ionization potential of 2.74 eV. The effects of the splitting are rather small for the total energies as well as for the ionization potentials. Results given in this paper are probably free from the problems that could arise from different ways of splitting the basis sets.

Can. J. Chem. Downloaded from www.nrcresearchpress.com by 92.62.229.171 on 09/08/12
For personal use only.

TABLE 11. Total energies, orbital energies, and ionization potentials for Zn_6

Ground state configuration (4*s* and 3*d* electrons)
$6a_{1g}^2\ 3t_{2g}^6\ 8t_{1u}^6\ 1a_{2u}^6\ 3t_{2u}^6\ 6e_g^4\ 4t_{2g}^6\ 9t_{1u}^6\ 1e_u^4\ 7e_g^4\ 4t_{2u}^6\ 1a_{2g}^2$
$3t_{1g}^6\ 7a_{1g}^2 8e_g^4\ 10t_{1u}^2\ {}^1A_{1g}$
Total energy −10657.12514 au
GAOPs of SCF wavefunctions:

	s	*p*	*d*	Total
Plane	7.65	12.37	9.98	30.00
Top	7.65	12.37	9.98	30.00

State	Character	$-\varepsilon_i$ (eV)	Estimated RE (SB)(eV)	Correl. correct.(eV)	Estimated IP(eV)
O_h (symmetry constrained)					
$(8e_g^{-1})\ {}^1A_{1g}$	$4s^{-1}$	5.16	0.2	1.9	6.9
$(7a_{1g}^{-1})\ {}^2T_{1u}$	$4s^{-1}$	15.68	0.2	1.9	17.4
$(3t_{1g}^{-1})\ {}^2T_{1g}$	$3d^{-1}$	21.83	6.9[a]	1.8	16.7
$(6a_{1g}^{-1})\ {}^2A_{1g}$	$3d^{-1}$	22.57	6.9[a]	1.8	17.5

[a]For 3*d* ionized states ($3d^{-1}$(loc)), the reorganization energy is that of the symmetry-broken solution calculated for Zn_4.

TABLE 12. Ionization potentials for Fe_6,Ni_6, Cu_6, and Zn_6

	$-\varepsilon$ (eV)	Symmetry broken ΔSCF(d^{-1}) (eV)	Correl. correct. (eV)	Estimated IP (eV)	Exptl. IP (eV)
$Fe_6(s^{-1})$	5.82	5.5	1.2	6.7	5.8–6.0[a]
(d^{-1}(tepl))	9.44	2.4	3.3	5.7	
Fermi-L[b]	s^{-1}	d^{-1}		d^{-1} or (d^{-1} and s^{-1})	
d relative to Fermi-L	3.62	0.0		0.0	
$Ni_6(s^{-1})$	5.73	5.4	1.4	6.8	6.4–7.9[c]
(d^{-1}(loc))	11.53	5.6	2.9	8.5	
Fermi-L	s^{-1}	d^{-1}		s^{-1} or (s^{-1} and d^{-1})?	
d relative to Fermi-L	5.80	0.0		1.7 or 0.0	
$Cu_6(s^{-1})$	5.63	5.4	1.5	6.9	6.4–7.9[d]
(d^{-1}(loc))	12.86	6.8	2.8	9.6	
Fermi-L	s^{-1}	s^{-1}		s^{-1}	
d relative to Fermi-L	7.23	1.4		2.7	3
$Zn_6(s^{-1})$	5.16	5.0	1.9	6.9	
(d^{-1}(loc))	21.83	14.9	1.8	16.7	
Fermi-L	s^{-1}	s^{-1}		s^{-1}	
d relative to Fermi-L	16.67	9.9		9.8	10

[a]See ref. 9.
[b]Fermi-L means Fermi level.
[c]See ref. 10.
[d]See ref. 8.

Discussion

We have discussed the electronic structure of Fe_4, Ni_4, Cu_4, Zn_4, Fe_6, Ni_6, Cu_6, and Zn_6. It was found that the experimental ionization thresholds were well explained by the symmetry-broken ΔSCF method with correlation correction. The Fermi level of the clusters consists of d^{-1} or $d^{-1} + s^{-1}$ for Fe clusters, and of s^{-1} or $s^{-1} + d^{-1}$ for Ni clusters, although for Ni_6 we have hesitated to take the assignment of $s^{-1} + d^{-1}$. The Fermi level of the Cu and Zn clusters was definitely the s^{-1} state.

For all the clusters except for Fe_6 the top of the *d*-band holds the localized *d*-hole at one of the constituent atoms. The total wave function for the ion (d^{-1}) has, in essence, the following form:

$$[9]\quad \phi = C_A|\phi_d(A^{-1}BCD\ldots)\phi_k(A^{-1}BCD\ldots)| + C_B|\phi_d(AB^{-1}CD\ldots)\phi_k(AB^{-1}CD\ldots)| + C_C|\phi_d(ABC^{-1}D\ldots)\phi_k(ABC^{-1}D\ldots)| + \ldots$$

Can. J. Chem. Downloaded from www.nrcresearchpress.com by 92.62.229.171 on 09/08/12
For personal use only.

where ϕ_d and ϕ_k symbolically represent all the d and conduction electrons, respectively. The first line implies that the d electron at atom A is ionized and the conduction electrons move to screen the positive hole at A. The other lines have a similar meaning (in the ΔSCF method only one term in eq. [9] was employed). This holds true for the atom, clusters, and the bulk metal and explains why the top of the d-band relative to the Fermi level was not very different from that of the atom. Auger spectra (40, 41) observed for bulk Cu and Zn were found to be atomic-like and are consistent with the present arguments.

In Fe_6 and (Fe_4) we found the tepl ionized state consists of the Fermi level and this type of the ionized state lies near the top of the d-band in Ni_4 and Ni_6. The wave function of the states may be written as

$$[10]\quad \phi = C_A|\phi_d(A^{-1}B^{d\to\kappa}CD\ldots)\phi_k(A^{-1}B^{d\to\kappa}CD\ldots)| + C_B|\phi_d(AB^{-1}C^{d\to\kappa}D\ldots)\phi_k(AB^{-1}C^{d\to\kappa}D\ldots)| + C_C|\phi_d(ABC^{-1}D^{d\to\kappa}\ldots)\phi_k(ABC^{-1}D^{d\to\kappa}\ldots)|$$

As in eq. [9] ϕ_d and ϕ_k represent all the s and d electrons. The first line indicates that the d electron at atomic site A is ionized and the d electron at atomic site B is simultaneously excited into the valence orbitals and that the conduction electrons move to screen the resulting positive holes; very high reorganization energy is released with a shifting of the valence electrons. This type of ionization is especially important when the atomic ground state has an electronic configuration of (s^2d^n) and the average atomic configuration for the solid or the clusters is (s^1d^{n+1}).

Acknowledgements

One of the present authors (H.T.) expresses his sincere thanks to Dr. S. Huzinaga who suggested investigation of the basis sets. Without the studies on the characteristics of the basis sets and without compact basis sets with high accuracy, the present authors could have not performed the investigations presented in this paper.

Computations were carried out on an ACOS 930-10 of the Computer Center of Nagoya City University and on HITAC M680's of the Computer Center of Hokkaido University.

1. A. B. Callear and J. H. Conner. Chem. Phys. Lett. **13**, 245 (1972).
2. T. C. Devore, A. Ewing, H. F. Franzen, and V. Calder. Chem. Phys. Lett. **35**, 78 (1975).
3. H. Huber, E. P. Kundig, M. Moskovitz, and G. A. Ozin. J. Am. Chem. Soc. **97**, 2097 (1975).
4. J. E. Hulse and M. Moskovitz. J. Chem. Phys. **66**, 3988 (1977).
5. G. A. Ozin, Catal. Rev. **16**, 191 (1977); Faraday Symp. Chem. Soc. **14**, 1 (1980).
6. D. S. Schmeisser, K. Jacobi, and D. M. Kolb. J. Chem. Phys. **75**, 5300 (1981).
7. W. Schroeder, H. Wiggerhauser, W. Schrittenlacher, and D. M. Kolb. J. Chem. Phys. **86**, 1147 (1987).
8. D. E. Powers, S. G. Hansen, M. E. Geusic, D. L. Michalopoulos, and R. E. Smalley. J. Chem. Phys. **78**, 2866 (1983).
9. E. A. Rohlfing., D. M. Cox, A. Kaldor, and K. H. Johnson. J. Chem. Phys. **81**, 3846 (1984).
10. E. A. Rohlfing, D. M. Cox, and A. Kaldor. J. Phys. Chem. **88**, 4497 (1984).
11. M. D. Morse, M. E. Geusic, J. R. Heath, and R. E. Smalley. J. Chem. Phys. **83**, 2293 (1985).
12. K. Liu, E. K. Parks, S. C. Richtsmeier, L. G. Pobo, and S. J. Riley. J. Chem. Phys. **83**, 2882 (1985).
13. D. G. Leopold and W. C. Lineberger. J. Chem. Phys. **85**, 51 (1986).
14. M. D. Morse. Chem. Rev. **86**, 1049 (1986).
15. H. Tatewaki, E. Miyoshi, and T. Nakamura. J. Chem. Phys. **76**, 5073 (1982).
16. E. Miyoshi, H. Tatewaki, and T. Nakamura. J. Chem. Phys. **78**, 815 (1983).
17. M. Tomonari, H. Tatewaki, and T. Nakamura. J. Chem. Phys. **80**, 344 (1984).
18. H. Tatewaki, M. Tomonari, and T. Nakamura. J. Chem. Phys. **82**, 5608 (1985).
19. M. Tomonari, H. Tatewaki, and T. Nakamura. J. Chem. Phys. **85**, 2875 (1986).
20. M. Tomonari and H. Tatewaki. J. Chem. Phys. **88**, 1828 (1988).
21. H. Tatewaki, M. Tomonari, and T. Nakamura. J. Chem. Phys. **88**, 6419 (1988).
22. H. Basch, M. D. Newton, and J. W. Moskowitz. J. Chem. Phys. **73**, 4492 (1980).
23. J. Demuynck, M.-M. Rohmer, A. Strich, and A. Veillard. J. Chem. Phys. **75**, 3443 (1981).
24. R. P. Messmer, S. K. Knudson, K. H. Johnson, J. B. Diamond, and C. Y. Yang. Phys. Rev. B, **13**, 1396 (1976).
25. R. P. Messmer, D. R. Salahab, K. H. Johnson, and C. Y. Yang. Chem. Phys. Lett. **51**, 84 (1977).
26. C. Y. Yang, K. H. Johnson, D. R. Salahab, J. Kasper, and R. P. Messmer. Phys. Rev. B, **24**, 5673 (1981).
27. D. P. Post and E. J. Baerends. Chem. Phys. Lett. **86**, 176 (1982).
28. R. P. Messmer, T. C. Caves, and C. M. Kao. Chem. Phys. Lett. **90**, 296 (1982).
29. H. Tatewaki and S. Huzinaga. J. Chem. Phys. **71**, 4339 (1979); **72**, 399 (1980).
30. H. Tatewaki and S. Huzinaga. J. Comput. Chem. **1**, 205 (1980).
31. Y. Sakai, H. Tatewaki, and S. Huzinaga. J. Comput. Chem. **2**, 100 (1981); **2**, 109 (1981).
32. S. Huzinaga, J. Andzelm, M. Klobukowski, E. Radzio-Andzelm, Y. Sakai, and H. Tatewaki. Gaussian basis sets for molecular calculations. Elsevier, Amsterdam and New York. 1984.
33. S. P. Walch and C. W. Bauschlicher, Jr. J. Chem. Phys. **79**, 3590 (1983).
34. S. P. Walch and C. W. Bauschlicher, Jr. J. Chem. Phys. **83**, 5735 (1985).
35. S. P. Walch, C. W. Bauschlicher, Jr., and S. R. Langoff. J. Chem. Phys. **85**, 5900 (1986).
36. S. R. Langoff, C. W. Bauschlicher, Jr., S. P. Walch, and B. C. Laskowski. J. Chem. Phys. **85**, 7211 (1986).
37. R. S. Mulliken. J. Chem. Phys. **23**, 1833 (1955).
38. C. E. Moore. Atomic energy levels. Natl. Stand. Data Circular 467, U.S. GPO, Washington, D.C. Aug. 15, 1952.
39. (*a*) R. A. Tawil and J. Callaway. Phys. Rev. B, **7**, 1242 (1973); (*b*) L.-G. Petersson, R. M. Melander, D. P. Spears, and S. B. M. Hagstrom. Phys. Rev. B, **14**, 4177 (1976).
40. E. Antonides, E. C. Janse, and A. Sawatzky. Phy. Rev. B, **15**, 1669 (1977).
41. E. Antonides, E. C. Janse, and A. Sawatzky. Phy. Rev. B, **15**, 4596 (1977).

Can. J. Chem. Downloaded from www.nrcresearchpress.com by 92.62.229.171 on 09/08/12
For personal use only.

Properties of atoms in molecules: structures and reactivities of boranes and carboranes

R. F. W. BADER AND D. A. LEGARE
Department of Chemistry, McMaster University, Hamilton, Ont., Canada L8S 4M1

Received August 1, 1991

This paper is dedicated to Professor Sigeru Huzinaga on the occasion of his 65th birthday

R. F. W. BADER and D. A. LEGARE. Can. J. Chem. **70**, 657 (1992).

The energies, geometries, and charge distributions of the *closo*-, *nido*-, and *arachno*-boranes and *closo*-carboranes are determined in SCF calculations using a contracted (9*s*,5*p*) basis set of Huzinaga, supplemented with polarization functions. Good agreement is obtained between the experimental and calculated geometries. Molecular structures are assigned on the basis of the bond paths defined by the topology of the charge density using the theory of atoms in molecules. This theory is used to characterize the atomic interactions and to account for the stabilities of these electron-deficient systems. It is shown that their stability is a consequence of the delocalization of charge over the surfaces of the three- and four-membered rings of atoms that result from the formation of bonds of reduced order, a delocalization that is itself essential to the formation of the ring bonds. The Laplacian of the charge density is used to predict the sites of nucleophilic and electrophilic attack in these molecules, predictions that are in agreement with known experimental findings.

Key words: boranes, carboranes, charge density, Laplacian of ρ.

R. F. W. BADER et D. A. LEGARE. Can J. Chem. **70**, 657 (1992).

Faisant appel à des calculs en champ auto-cohérent utilisant l'ensemble de base contracté (9*s*,5*p*) de Huzinaga supplémenté de fonctions de polarisation, on a calculé les énergies, les géométries et les distributions de charge des *closo*-, *nido*- et *arachno*-boranes et des *closo*-carboranes. On a obtenu un bon accord entre les géométries calculées et expérimentales. On a attribué les structures moléculaires en se basant sur les voies de liaisons définies par la topologie de la densité de charge, en utilisant la théorie des atomes dans les molécules. Cette technique est utilisée pour caractériser les interactions atomiques et pour rendre compte des stabilités de ces systèmes électro-déficients. On montre que leur stabilité est une conséquence de la délocalisation de la charge sur les surfaces des atomes des cycles à trois et à quatre chaînons qui est elle-même essentielle à la formation de liaisons dans les cycles. On utilise le laplacien de la densité de charge pour prédire les sites des attaques nucléophiles et électrophiles dans ces molécules; ces prédictions sont en bon accord avec les données expérimentales connues.

Mots clés : boranes, carboranes, densité de charge, laplacien de ρ.

[Traduit par la rédaction]

Introduction

This paper reports the theoretical determination of the geometries and molecular graphs for a series of boranes and carboranes. In addition to determining their molecular structures, the stabilities and reactivities of these structures are related to their atomic properties and to the atomic graphs of the boron and carbon atoms. The molecular graphs determine the atomic connectivities in terms of the topology of the charge density, whereas the atomic graphs determine the reactivity of a molecule towards nucleophilic and electrophilic attack in terms of the topology of the Laplacian of the charge density. All of these properties are defined by quantum mechanics using the theory of atoms in molecules, a theory that extends quantum mechanics to an atom in a molecule (1, 2). In addition to BH and BH_3, the molecules considered here are the *closo* structures (closed structures of *n* atoms in an *n*-atom polyhedral framework) $B_6H_6^{2-}$, $B_7H_7^{2-}$, $B_{12}H_{12}^{2-}$, $C_2B_3H_5$, and $C_2B_4H_6$; the *nido* structures (open structures of *n* atoms in an $n + 1$ atom polyhedral framework) B_2H_6, B_5H_9, and B_6H_{10}; and the single *arachno* structure (open structures of *n* atoms in an $n + 2$ atom polyhedral framework) B_4H_{10}. The reader is referred to the text by Greenwood and Earnshaw (3) for a full discussion of the nomenclature and properties of the boranes and carboranes.

The boranes are of particular interest from the point of view of theories of bonding because of their electron-deficient nature, as judged on the basis of the Lewis electron pair model of the chemical bond. The theory of atoms in molecules leads to an unequivocal assignment of a molecular structure and provides a classification of the bonds so defined (1, 4). This information adds a physical complement to the electron counting models of structure as embodied in Lipscomb's styx rules (5) and in the molecular orbital based rules of Wade (6).

Computations and comparison of calculated and experimental geometries

The results are obtained from single determinant SCF calculations using the program Gaussian 88 (7). The [6,1,1,1/4,1] Dunning contraction (8) of the (9*s*,5*p*) Huzinaga basis (9) was used for boron and carbon, augmented with a single *d* basis function. Exploratory calculations demonstrated the importance of providing an adequate description of the hydrogen atoms, particularly the inclusion of a diffuse function to describe their hydridic nature. The Duijneveldt (10) set of 6*s* functions contracted to [4,1,1] was used, together with a single *p* function with an optimized exponent of 1.0725. The energies and optimized geometries obtained in these calculations are summarized in the Appendix. The numbering of the atoms in each molecule as used throughout the paper is also indicated.

Baudet (11) has compiled the geometries of the neutral boranes based upon experimental data obtained from microwave, electron diffraction, and X-ray diffraction techniques. X-ray data are available for salts of the hexa- (12*a*)

Can. J. Chem. Downloaded from www.nrcresearchpress.com by 123.30.183.119 on 09/08/12
For personal use only.

Can. J. Chem. Downloaded from www.nrcresearchpress.com by 123.30.183.119 on 09/08/12
For personal use only.

and dodecahydroborates (12*b*). The experimentally determined geometrical parameters are compared with the theoretical values in Table 1. The agreement is good, being best when the single molecule calculations are compared with gas phase microwave data. Both experiment and theory support the general observations that B—C distances are shorter than B—B distances in the same molecule and that the angle subtended at a carbon in a three- or four-membered ring in a carborane is larger than 60° or 90° respectively, while the corresponding angles subtended at a boron are less than these values.

The orbital energy of triply degenerate HOMO in $B_6H_6^{2-}$ is found to be positive, and equal to +0.0520 au. Fowler (13) found an even more positive value (by 0.030 au) for this orbital energy, using the 6-31G* basis set, which yields a molecular energy higher by 0.08 au than that obtained here. These results suggest that the free anion may be unstable towards autoionization and is stable only when its negative charge is counterbalanced in a crystalline environment. The doubly degenerate HOMO and HOMO-1 in $B_7H_7^{2-}$ also exhibit positive eigenvalues, 0.017 and 0.013 au, respectively. The eigenvalues of all of the occupied levels in the dodecahydroborate are negative. The fact that the HOMO energy in the hexahydroborate decreased significantly with an increase in the size of the basis set shows that its value is not stable towards an expansion of the basis set, as Fowler suggests might be the case. A calculation approaching the Hartree–Fock limit or one that includes electron correlation could predict the anions to be stable entities in the gas phase.

Structure and bonding in the boranes and carboranes

Molecular structure and molecular graphs

A (3,−1) critical point in the electronic charge density ρ is formed between every pair of interacting atoms. Two gradient vectors of ρ originate there and trace out a line, the atomic interaction line, linking the two nuclei along which the electronic charge density is a maximum with respect to any neighbouring line. In an equilibrium geometry such a line is called a bond path and the associated critical point the bond critical point. The creation of the bond critical point and its associated accumulation of electronic charge in the internuclear region meet the necessary and sufficient conditions for the atoms to be bonded to one another (1, 14). The global behaviour of the gradient vector field of the electronic charge density is illustrated in Fig. 1 for $C_2B_3H_5$. It illustrates the definition of an atom as the union of an attractor and its basin — a region of space bounded by surfaces of zero flux in the gradient vector field of the charge density — together with the definition of a bond path and an interatomic surface.

The collection of bond paths defines the molecular graph for a given nuclear geometry and all geometries possessing equivalent molecular graphs possess the same molecular structure (1, 4). The molecular structures defined by the theory of atoms in molecules have been shown to recover known chemical structures. In addition, the theory predicts changes in structure by giving operational meaning to the concepts of the making and breaking of chemical bonds (1, 4).

The Lewis electron pair model of the chemical bond between pairs of atoms does not apply to the skeletal frameworks of the boranes and carboranes and one is forced to extend the electron pair concept to include three-centre two-electron bonds (15), which in the base of the boranes consist of B—H—B bridges and three-membered boron rings. The ability of theory to define the network of bonds independent of any model, by determining which nuclei are linked by lines of maximum charge density, is of particular importance for these systems. Diborane and pentaborane were used in an early application of the theory to demonstrate its ability to assign structures in systems with unusual bonding situations (16).

The molecular structures determined by theory are shown in Fig. 2. The model of the three-centre B—H—B bridging bond is recovered in the form of a hydrogen linked by bond paths to two borons in the *nido* and *arachno* compounds; however, these same structures do not exhibit linked three-membered boron rings. Only in B_4H_{10} is there a B—B bond path linking two borons that are each linked to two hydrogen bridges. In B_5H_9 and B_6H_{10} such borons are not linked to one another, but are instead linked to the apical boron atom. There is, in the latter compound, an additional bond path linking borons 9 and 10, those which are linked to only a single hydrogen bridge. The styx model (5) represents the structure of pentaborane in terms of four equivalent resonance forms, each of which possesses four hydrogen bridges, one three-membered boron ring, and two single B—B bonds to the apical boron. This corresponds to assigning two-thirds of an electron pair bond to each link with the apical boron and one-twelfth of an electron pair to each link between the borons involved in hydrogen bridging. In B_6H_{10} there are two three-membered boron rings in the styx model, one between the apical boron B2 and boron atoms B4 and B9, the other between B2, B5, and B10. Thus these B—B bonds to the apical boron atom are predicted to be weaker than the two full B—B bonds in this molecule. The *closo* anions, which do not possess any hydrogen bridges, exhibit linked three-membered rings of boron atoms so that a B—B bond path lies along each edge of the corresponding *n*-vertex polyhedron. The structure for the carborane $C_2B_3H_5$ does not exhibit any B—B bond paths and an electron pair may be associated with each bond path in this structure; it is electron precise. There are however, bond paths linking the boron atoms in the electron-deficient $C_2B_4H_6$.

At the midpoint between the basal atoms B9 and B10 in B_6H_{10} and between the adjacent basal boron atoms in $B_7H_7^{2-}$ there are (3,−3) critical points, i.e., local maxima in ρ of very small magnitude, rather than the anticipated (3,−1) bond critical points. These maxima are bounded on either side by (3,−1) critical points that are close to the maxima in position and in value, those in B_6H_{10}, for example, possessing values of ρ only 0.0004 au smaller than that at the maximum and separated from it by 0.38 au. While non-nuclear maxima are possible (1), the use of a larger, more flexible basis set in the present systems would likely cause them to disappear, with each maximum and its adjacent bond critical points being replaced by a single bond critical point, as shown in the molecular graphs of Fig. 2. What is important is that the charge density along these bond paths is very flat in the central region of the bond.

With the exception of BH_3, all of the molecules in Fig. 2 exhibit bonded rings of atoms. The electronic charge density exhibits a critical point in the interior of each ring, a (3,+1) critical point, which possesses two positive curvatures whose axes define the ring surface and a single negative curvature lying along a perpendicular axis, Fig. 1. The charge density attains its minimum value in a ring surface at

TABLE 1. Comparison of experimental and calculated geometries for boranes and carboranes

Molecule	Technique	Experimental	This work
B2H6			
Bond or angle		Baudet	
B1—B5	MW	1.743	1.797
B1—H3(Terminal)		1.1841(3)	1.186
B1—H2(Bridging)		1.314(3)	1.329
H3—B1—H4		121.5(5)	122.4
H2—B1—H8		96.9(5)	94.9
B4H10			
Bond or angle		Baudet	
B1—B5	XR	1.845(2)	1.903
B5—B6		2.786	2.877
B1—B2(B—B bond)		1.75	1.75
B1—H10(Bridging)		1.21(4)	1.26
B5—H10(Bridging)		1.37(10)	1.43
B1—H3(Terminal)		1.14(4)	1.18
B5—H11(Terminal)		1.14(4)	1.19
B5—H13(Terminal)			1.18
H11—B5—H13		126	120
B2—B1—H3		118	116
B2—B1—H10		109	111
H10—B5—H9		135.7	135.7
B1—H10—B5		91.1	90.0
B1—B5—B2		56.6	54.6
B5—B1—B2		61.7	62.7
B5—B1—B2—B6		118.1	116.6
B2—B1—B5—H10		170	173
B5H9			
Bond or angle		Baudet	
B1—B5(Apical bond)	MW	1.690(5)	1.711
B1—B2(Equatorial bond)		1.803(5)	1.822
B5—H14(Terminal apical)		1.181(5)	1.177
B2—H7(Terminal equatorial)		1.186(5)	1.177
B1—H10(Bridging)		1.352(5)	1.354
B1—B5—B2		64.5	64.3
B5—B1—H6		131.0(5)	132.1
B1—B2—B3—H11		116.0	116.8
B5—B2—B3—H11		193.1(29)	167.9
B5—B3—B2—B1		50.9	51.0
B6H10			
Bond or angle		Baudet	
B1—B2	MW	1.774(13)	1.769
B2—B4	MW	1.762(4)	1.772
B2—B9	MW	1.783(11)	1.855
B1—B4	MW	1.818(5)	1.824
B4—B9	MW	1.710(6)	1.768
B9—B10	MW	1.654(3)	1.640
B2—H8	XR	1.25(6)	1.18
B1—H3	XR	1.14(6)	1.18
B4—H11	XR	1.18(4)	1.18
B9—H15	XR	1.28(5)	1.18
B1—H6	XR	1.32(6)	1.30
B4—H6	XR	1.48(5)	1.39
B4—H13	XR	1.31(4)	1.32
B9—H13	XR	1.35(4)	1.35
B5—B1—B4	MW	103.0	103.1

Can. J. Chem. Downloaded from www.nrcresearchpress.com by 123.30.183.119 on 09/08/12
For personal use only.

TABLE 1 (*concluded*)

Molecule	Technique	Experimental	This work
B1—B4—B9	MW	108.2	108.3
B4—B9—B10	MW	110.4	110.1
B1—B2—H3	XR	126.8	126.6
B2—B4—H11	XR	119.4	137.8
B2—B9—H15	XR	136.3	127.9
Dipole moment (debye)	MW	2.50	2.86
B6H6(2—)		Ref. 12*a*	
Bond or angle			
B1—B2		1.69(1)	1.748
B2—B3			2.472
B1—H7		1.11(7)	1.215
B7H7(2—)			
Bond or angle		n/a	
B7—H14(Apical)			1.215
B1—H8(Equatorial)			1.215
B1—B7(Apical)			1.848
B1—B2(Equatorial)			1.666
B1—B7—H14(Apical)			129.9
B1—B2—H9(Equatorial)			126.0
H9—B2—B1—B7			134.1
B7—B1—B2—B6			91.9
B12H12(2—)			
Bond or angle		Ref. 12*b*	
B1—H13		1.07	1.201
B1—B2		1.77	1.799
C2B3H5			
Bond or angle		Baudet	
C1—H6	(ED)	1.071(7)	1.068
B2—H8		1.183(6)	1.179
C1—B2		1.556(2)	1.560
B2—B3		1.853(2)	1.895
C1—C5		2.261(3)	2.225
B2—C1—B3		73.05(1)	74.78
C1—B2—B3		53.48(1)	52.61
C1—B2—C5		93.16(1)	90.96
C2B4H6			
Bond or angle		Baudet	
B1—C6	(ED)	1.633(4)	1.626
B1—B2		1.720(4)	1.716
B1—B3		2.432(6)	2.427
C5—C6		2.179(7)	2.166
B1—H7		1.244(12)	1.172
C5—H11		1.104(22)	1.065
B1—C6—B2		63.55	63.69
C6—B2—B1		58.22	58.16
C5—B1—C6		83.73	83.48
B1—C6—B3		96.26	96.52

the ring critical point. The interiors of the *closo* molecules are enclosed by ring surfaces and they are cage structures. There is a critical point in the interior of each cage structure for which all three curvatures are positive, a (3,+3) or cage critical point, Fig. 1. The charge density is a local minimum at such a critical point. The set of critical points associated with a molecular charge distribution completely determines its chemical topology; N, the number of (pseudo) (3,−3)'s equals the number of nuclei; b, the number of (3,−1)'s, the number of bond paths; r, the number of (3,+1)'s, the number of rings; and c, the number of (3,+3)'s, the number of cages. The set of numbers $\{N,b,r,c\}$, the characteristic set (16), must satisfy the Poincare–Hopf relationship (17)

$$[1] \quad N - b + r - c = 1$$

Can. J. Chem. Downloaded from www.nrcresearchpress.com by 123.30.183.119 on 09/08/12
For personal use only.

Can. J. Chem. Downloaded from www.nrcresearchpress.com by 123.30.183.119 on 09/08/12
For personal use only.

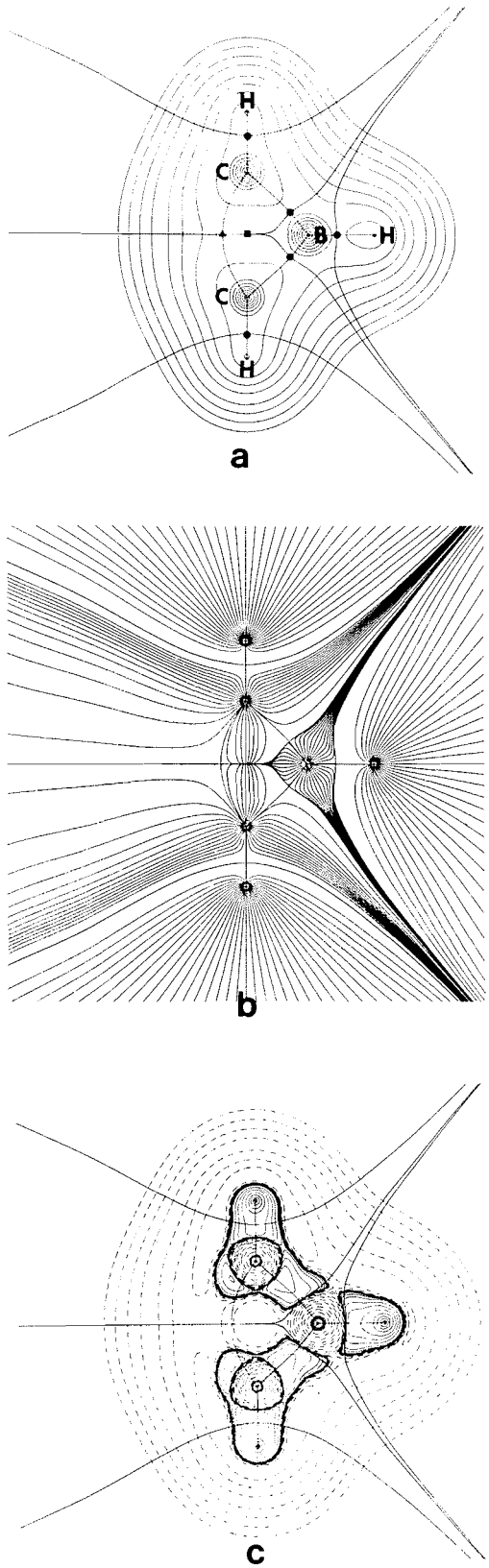

FIG. 1. Contour maps of (*a*) the electronic charge density ρ and (*c*) its Laplacian, and (*b*) a display of the gradient vector field of ρ, all for a symmetry plane of $C_2B_3H_5$ containing the nuclei H—C—B(—H)—C—H. The contour plots are overlaid with bond paths and the atomic boundaries. Bond or (3,−1) critical points are denoted by dots. All of the trajectories of $\nabla\rho$ in the vicinity of a given nucleus terminate at that nucleus, in all three dimensions, thereby defining the basin of the atom. The (3,−1) critical points whose trajectories link the nuclei in this plane appear as (2,0) critical points. The two trajectories defining the bond path originate at each such point and the two trajectories indicating the intersection of the interatomic surface with the plane terminate there. A (3,+1) or ring critical point appears as a (2,0) denoted by a triangle, and a central cage or (3,+3) critical point, which appears as a (2,+2), is denoted by a star. Solid contours denote negative values of the Laplacian, dashed contours positive values. The outer contour value for ρ is 0.001 au and remaining contours increase in the order 2×10^n, 4×10^n, and 8×10^n with n beginning at −3 and increasing in steps of unity. Plus and minus values of the same contour set apply to $\nabla^2\rho$. See Tables 2 and 6 for values of $\nabla^2\rho$ at specific points in this and succeeding diagrams.

The characteristic set for $C_2B_3H_5$ for example is {10,11,3,1}. Equation [1] is brought into correspondence with Euler's expression for a closed polyhedron by associating N with the number of vertices V, b with the number of edges E, r with the number of faces F, and transposing $c = 1$ to the RHS to yield

$$[2] \quad V - E + F = 2$$

Classification of atomic interactions

Bond order, path, ellipticity, and character

The theory, in addition to assigning a structure in terms of a set of bond paths, affords a description and characterization of how the electronic charge density is distributed in each of the atomic interactions so defined. This information is summarized in terms of the properties of the charge density at the bond critical points.

The value of the charge density at the bond critical point, the quantity ρ_b, provides a measure of bond order. For the interaction between a given pair of atoms, its value increases as the bond length decreases and the strength of the interaction increases (18, 19). Unlike C—C and N—N bonds for example, where one can define a bond order–ρ_b relationship for orders one to three, the bonds in the molecules considered here are all of formal order one or less. To allow for a facile comparison of the relative strengths of each type of bond, the values of ρ_b listed in Table 2 are referenced to the value for one such bond to give a bond order n. The B—H_t (H_t is a terminal hydrogen) and B—H_b (H_b is a bridging hydrogen) bonds in diborane are assigned orders of unity in Table 2, as is the B—B bond in B_4H_{10} and the B—C and C—H bonds in $C_2B_3H_5$. Also listed in Table 2 are the values of ρ at the ring (ρ_r) and cage (ρ_c) critical points.

The distances of the bond critical point from the two nuclei define the associated bonded radii of the atoms, r_A and r_B of Table 2. Their relative values reflect the direction of interatomic charge transfer (20). The bond paths associated with the bridging bonds are noticeably bent and, in such cases, the value of the bond path length R_b is greater than the equilibrium or geometrical path length R_e, Table 2.

The curvature of ρ at a given point determines whether electronic charge is locally depleted (curvature positive) or locally concentrated (curvature negative) at that point, in the sense that for a positive curvature the value of ρ at the point is less than its value averaged over neighbouring points, with the reverse being true for a negative curvature. The sum of the three curvatures defines the Laplacian of the electron density, the quantity $\nabla^2\rho$. The curvature of ρ at a bond critical point along the bond path is positive. Thus the charge density attains its minimum value at the critical point along

Can. J. Chem. Downloaded from www.nrcresearchpress.com by 123.30.183.119 on 09/08/12
For personal use only.

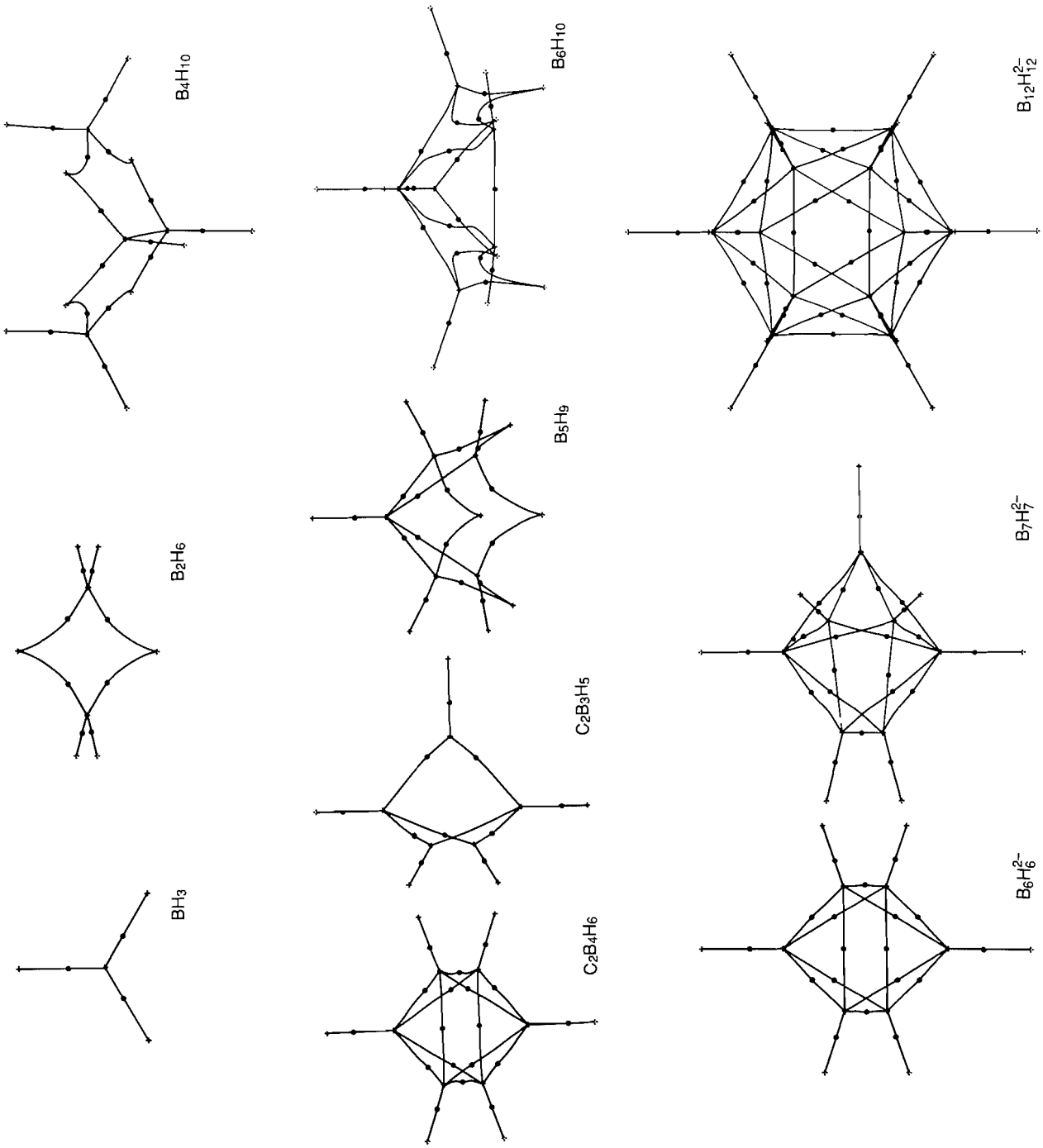

FIG. 2. Molecular graphs for boranes and carboranes with bond critical points denoted by dots. The structures depicted here are predicted by theory in terms of the properties of the observable charge distribution. Note the inwardly curved nature of the bond paths linking the bridging protons.

Can. J. Chem. Downloaded from www.nrcresearchpress.com by 123.30.183.119 on 09/08/12
For personal use only.

TABLE 2. Bond properties for the borane series (reference values for ρ_b are starred)

Formula	Bond	R_e, a_o	R_b, a_o	r_A, a_o	r_B, a_o	n	ρ_b, e/a_o^3	$\nabla^2\rho_b, e/a_o^5$	λ_1, e/a_o^5	λ_2, e/a_o^5	λ_3, e/a_o^5	ϵ	ρ_r and ρ_c, e/a_o^3
BH	B—H_t	2.3322		0.9626	1.3696	0.9724	0.1795	−0.4217	−0.4699	−0.4699	−0.4699	0.0000	
BH_3	B—H_t	2.2508		0.9511	1.2997	0.9897	0.1827	−0.2498	−0.4758	−0.3734	0.5993	0.2741	
B_2H_6	B1—$H3_t$	2.2409	2.2415	0.9539	1.2875	1.0000	*0.1846	−0.2583	−0.4342	−0.4053	0.5812	0.0714	ρ_r = 0.1083
	B1—$H2_b$	2.5123	2.6010	0.9957	1.5792	1.0000	*0.1146	0.1864	−0.1671	−0.1067	0.4602	0.5657	
B_4H_{10}	B1—B2	3.2987	3.3389	1.6513	1.6513	1.0000	*0.1378	−0.3058	−0.1782	−0.1480	0.0204	0.2042	ρ_r = 0.0840
	B1—$H3_t$	2.2291		0.9542	1.2750	0.9919	0.1831	−0.2095	−0.4146	−0.3723	0.5774	0.1134	
	B5—$H11_t$	2.2452	2.2462	0.9564	1.2897	1.0000	0.1846	−0.2614	−0.4240	−0.4038	0.5665	0.0498	
	B5—$H13_t$	2.2374	2.2382	0.9543	1.2838	1.0141	0.1872	−0.2782	−0.4394	−0.4117	0.5729	0.0675	
	B1—$H10_b$	2.3724	2.3915	0.9686	1.4122	1.1764	0.1348	0.1598	−0.2540	−0.1778	0.5917	0.4285	
	B5—$H10_b$	2.7010	2.8674	1.0570	1.7448	0.8264	0.0947	0.0829	−0.1010	−0.0653	0.2493	0.5467	
B_5H_9	B1—B5	3.2330	3.2336	2.1226	1.1108	0.9794	0.1350	−0.1090	−0.1646	−0.0484	0.1039	2.4039	ρ_r = 0.1110
	B1—$H6_t$	2.2248	2.2252	0.9527	1.2724	1.0125	0.1869	−0.2546	−0.4340	−0.3982	0.5776	0.0900	
	B5—$H14_t$	2.2248		0.9520	1.2727	0.9599	0.1772	−0.1363	−0.3724	−0.3724	0.6085	0.0000	
	B1—$H10_b$	2.5584	2.7080	1.0405	1.6446	0.9909	0.1136	0.0787	−0.1822	−0.0229	0.2839	6.9458	
B_6H_{10}	B1—B2	3.3419	3.3443	2.0195	1.3238	0.9154	0.1262	−0.1992	−0.1625	−0.0566	0.0198	1.8728	ρ_r = 0.1071
	B2—B4	3.3478	3.3646	1.2630	2.0869	0.9044	0.1247	−0.1870	−0.1674	−0.0479	0.0283	2.4961	ρ_r = 0.1068
	B2—B9	3.5062	3.7223	1.8332	1.7084	0.7748	0.1068	−0.0928	−0.1319	−0.0075	0.0466	16.6455	ρ_r = 0.1033
	B9—B10	3.0991		1.5529	1.5529	1.2322	0.1698	−0.4595				0.3626	
	B1—$H3_t$	2.2250		0.9537	1.2714	1.0146	0.1873	−0.2543	−0.4273	−0.3976	0.5706	0.0748	
	B2—$H8_t$	2.2291		0.9529	1.2763	0.9821	0.1813	−0.1839	−0.3915	−0.3843	0.5918	0.0187	
	B4—$H11_t$	2.2253		0.9527	1.2730	1.0271	0.1896	−0.2838	−0.4346	−0.4239	0.5747	0.0253	
	B9—$H15_t$	2.2327		0.9537	1.2797	0.9924	0.1832	−0.2204	−0.4279	−0.3817	0.5891	0.1212	
	B1—$H6_b$	2.4543	2.5028	0.9870	1.4994	1.0946	0.1254	0.1507	−0.2232	−0.1155	0.4894	0.9335	
	B4—$H6_b$	2.6232	3.1981	1.2317	1.8511	0.9440	0.1082	−0.0864	−0.1522	−0.0161	0.0818	8.4454	
	B4—$H13_b$	2.4990	2.6314	1.0373	1.5774	1.1346	0.1300	−0.0216	−0.2252	−0.0741	0.2777	2.0396	
	B9—$H13_b$	2.5564	3.5957	1.1516	2.0857	0.9698	0.1111	−0.0550	−0.1261	−0.0111	0.0822	10.3819	
$B_6H_6^{2-}$	B—B	3.3032	3.3114	1.6518	1.6518	0.9076	0.1251	−0.1692	−0.1458	−0.0445	0.0212	2.2759	ρ_r = 0.1159
	B—H_t	2.2953		0.9613	1.3340	0.8294	0.1531	−0.0200	−0.3114	−0.3114	0.6028	0.0000	ρ_c = 0.0642
$B_7H_7^{2-}$	B1—B7	3.4922		1.8076	1.6850	0.7723	0.1065	−0.0940	−0.1261	−0.0156	0.0477	7.0693	ρ_r = 0.1042
	B1—B2	3.1491		1.5747	1.5747	1.0769	0.1484	−0.3164					ρ_c = 0.0485
	B1—$H8_t$	2.2958		0.9627	1.3331	0.8288	0.1530	−0.0134	−0.3320	−0.2773	0.5958	0.1971	
	B7—$H14_t$	2.2964		0.9594	1.3370	0.8570	0.1582	−0.0691	−0.3310	−0.3310	0.5929	0.0000	
$B_{12}H_{12}^{2-}$	B—B	3.3998	3.4033	1.7006	1.7006	0.8553	0.1179	−0.1614	−0.1544	−0.0407	0.0338	2.7918	ρ_r = 0.1097
	B—H_t	2.2695		0.95751	1.3120	0.9068	0.1657	−0.0899	−0.3467	−0.3467	0.6034	0.0000	ρ_c = 0.0136
$C_2B_3H_5$	B—C	2.9483	2.9557	0.9560	1.9987	1.0000	*0.1685	0.0306	−0.2948	−0.2927	0.6181	0.0072	ρ_r = 0.1003
	C—H_t	2.0182		1.2242	0.7940	1.0000	*0.2933	−1.1867	−0.7344	−0.7344	0.2820	0.0000	ρ_c = 0.0908
	B—H_t	2.2270		0.9501	1.2769	1.0043	0.1854	−0.2439	−0.4554	−0.3861	0.5977	0.1794	
$C_2B_4H_6$	B—C	3.0735	3.0757	1.0055	2.0682	0.8577	0.1445	0.0873	−0.2077	−0.0825	0.3775	1.5172	ρ_r = 0.1297
	B—B	3.2433	3.7615	1.6233	1.6233	0.9412	0.1297	−0.1279	−0.1388	−0.0024	0.0133	57.5559	ρ_c = 0.0780
	C—H_t	2.0116		1.2270	0.7846	1.0123	0.2969	−1.1830	−0.7400	−0.7400	0.2970	0.0000	
	B—H_t	2.2146		0.9513	1.0060	1.0166	0.1857	−0.2283	−0.4285	−0.3962	0.5965	0.0814	

TABLE 3. Integrated electron populations, net charges, and energies for atoms in the borane series (atoms by difference are starred)

	Boron atoms				Terminal hydrogen atoms				Bridging hydrogen atoms			
Formula	Atom	N(B), e	q(B), e	E(B), e^2/a_o	Atom	$N(H_t)$, e	$q(H_t)$, e	$E(H_t)$, e^2/a_o	Atom	$N(H_b)$, e	$q(H_b)$, e	$E(H_b)$, e^2/a_o
BH	B1	4.2106	+0.7894	−24.2125	H2	1.7917	−0.7917	−0.9112				
BH_3	B1	2.8385	+2.1615	−23.7544	H2	1.7199	−0.7199	−0.8804				
B_2H_6	B1	2.8764	+2.1236	−23.7300	H3	1.7042	−0.7042	−0.8751	H2	1.7133	−0.7133	−0.9305
B_4H_{10}	B1	3.6095	+1.3905	−24.0085	H3	1.6626	−0.6626	−0.8536	H7	1.7169	−0.7169	−0.9220
	B5	3.0427	+1.9574	−23.8729	H11	1.6936	−0.6936	−0.8777				
					H13	1.7003	−0.7003	−0.8804				
B_5H_9	B1	3.7790	+1.2210	−24.15	H6	1.6828	−0.6828	−0.8609	H10	1.6736	−0.6736	−0.8934
	B5				H14	1.6792	−0.6792	−0.8402				
B_6H_{10}	B1	3.5080	+1.4920	−24.0316	H3	1.6727	−0.6727	−0.8597	H6	1.7008	−0.7008	−0.9128
	B4	3.7793	+1.2207	−24.1363	H8	1.6834	−0.6834	−0.8554	H13	1.7188	−0.7188	−0.9206
	B2	3.9865	+1.0135	−24.2329	H11	1.6886	−0.6886	−0.8713				
	B9				H15	1.7007	−0.7007	−0.8665				
$B_6H_6^{2-}$	B1*	4.5326	+0.4674	−24.4041	H7	1.8008	−0.8008	−0.8403				
$B_7H_7^{2-}$	B1	4.4450	+0.5550	−24.4112	H8	1.7684	−0.7684	−0.8349				
	B7				H14	1.7957	−0.7957	−0.8535				
$B_{12}H_{12}^{2-}$	B1*	4.4274	+0.5726	−24.4198	H13	1.7393	−0.7393	−0.8574				
$C_2B_3H_5$	B2	2.8723	+2.1277	−23.7248	H8	1.7033	−0.7033	−0.8628				
$C_2B_4H_6$	B1*	3.3090	1.6910	−23.9406	H7	1.6947	−0.6947	−0.8514				

this path and electronic charge is locally depleted at the critical point with respect to neighbouring points along the bond path. The two curvatures of ρ perpendicular to the bond path at the bond critical point are negative. Thus ρ is a local maximum in the interatomic surface at the bond critical point and electronic charge is locally concentrated there. The formation of an interatomic surface and a chemical bond is, therefore, the result of a competition between the perpendicular contractions of ρ, which lead to a concentration or contraction of electronic charge towards the bond path, and the parallel expansion of ρ away from the interatomic surface, which leads to its separate concentration in one or both of the atomic basins (1, 14). The sign of $\nabla^2\rho_b$, Table 2, determines which of the two competing effects dominates a given interaction.

As a consequence of the appearance of $\nabla^2\rho$ in the local expression for the virial theorem, it can be shown that the potential energy dominates the local energy and is stabilizing in those regions of space where the Laplacian is negative and electronic charge is concentrated (1). When ρ_b is relatively large in value and $\nabla^2\rho_b$ is negative, electronic charge is accumulated and concentrated in the binding region and the atoms are bound by the charge that is shared between the nuclei. When ρ_b is relatively low in value and $\nabla^2\rho_b$ is positive, electronic charge is separately concentrated in the atomic basins and the interaction is typical of that found between closed-shell systems, such as found in ionic bonds and hydrogen bonds.

In a bond with cylindrical symmetry such as the C—C bond in ethane, the two perpendicular curvatures of ρ at the bond critical point, λ_1 and λ_2, are of equal magnitude. However, if these curvatures are of differing magnitudes, then the density falls off less rapidly along the axis of the curvature with the smaller of the two magnitudes. The resulting elliptical nature of the charge density associated with this preferred accumulation of electronic charge in a given plane containing the bond path, the plane of the π density in ethene for example, is quantitatively measured by the bond ellipticity $\varepsilon = ((\lambda_1/\lambda_2) - 1)$, where λ_2 is the curvature of smallest magnitude.

Charge density along the bond paths

The values of ρ_b and $\nabla^2\rho_b$ for the C—H bonds in the carboranes, Table 2, are typical of a shared or covalent interaction, one that is dominated by a contraction of ρ towards the bond path leading to its accumulation in the internuclear region. Thus $\nabla^2\rho_b < 0$ and ρ_b is relatively large in value for these interactions. The concentration of charge density that links the valence shell charge concentrations (VSCC's) of the carbon and hydrogen atoms and leads to their binding is shown in Fig. 1. The atomic charges are given in Table 3 and the small net charge on a hydrogen bonded to carbon in the carboranes, ±0.02, is indicative of the nearly equal sharing of electronic charge between the carbon and hydrogen atoms.

There is a considerable transfer of electronic charge from boron to a terminal or bridging hydrogen atom, $q(H) = -0.7$ e, Table 3, and the values of ρ_b and $\nabla^2\rho_b$ for the B—H bonds are intermediate in value between those for a shared interaction as found in C–H and a closed-shell or ionic interaction, for which ρ_b is less than 0.1 au and $\nabla^2\rho_b > 0$. The values of ρ_b for the B—H bonds lie within the range 0.1–0.2 and the values of $\nabla^2\rho_b$ lie on either side of zero, the point of change between the two extremes of bonding. The plots of the Laplacian distribution for $C_2B_3H_5$ in Fig. 1 show that, unlike the sharing of the charge concentration between the two atoms as found in C—H, the regions of charge concentration for B–H interactions are largely localized within the basins of the hydrogen atoms.

One anticipates that the bonding between B and a terminal hydrogen will exhibit the least variation throughout the series and the data in Table 2 bear this out. The bond lengths of the terminal B—H bonds in the *nido*- and *arachno*-boranes and carboranes vary by 0.02 au from the value 2.23 au. They have bond orders that vary by only 0.02 from the standard bond of order one in B_2H_6, with the sole exception of the bond to the apical boron in B_5H_9 for which $n = 0.96$. The values of $\nabla^2\rho_b$ are of similar magnitude and are less than zero in each case. The terminal hydrogens in the negatively charged *closo* compounds bear slightly larger negative charges than those in the neutral molecules, an effect that is most pronounced in the hexaborane. Because of

Can. J. Chem. Downloaded from www.nrcresearchpress.com by 123.30.183.119 on 09/08/12
For personal use only.

this shift towards more ionic binding, the bond lengths are somewhat longer, the bond orders smaller, and the values of $\nabla^2\rho_b$ closer to zero for the B—H_t bonds in the *closo* molecules.

The bonds to the bridging hydrogens are, in general, longer than those to the terminal hydrogens, with an average length of 2.55 au. The associated bond paths are strongly curved towards the interiors of the rings formed by the bridging hydrogens (see Fig. 2 and the bridging plane of diborane, Fig. 3). As a consequence, the bond path lengths, R_b, for the bridging hydrogens exceed their geometric lengths, R_e (Table 2). The B—H_b bonding in the *nido*- and *arachno*-boranes is characterized by lower values of ρ_b than are found for their B—H_t bonds, 0.11 compared to 0.18 au, and also by near-zero values of $\nabla^2\rho_b$, which in these cases are mostly positive. The *arachno* molecule B_4H_{10} provides an example of a case in which the two bonds to a bridging hydrogen atom are inequivalent. The values of ρ_b differ from the reference value in diborane by ±0.02 au, with the critical point linked to the boron forming the B—B bond having a large ρ_b value, and the other, linked to a boron in a BH_2 group, having the smaller value. Both have positive values of $\nabla^2\rho_b$, with the first mentioned interaction being slightly more ionic.

The reference B–B interaction is the central B—B bond in B_4H_{10}. Its ρ_b value is intermediate between those for the terminal and bridging B–H interactions. A display of the Laplacian distribution for the B—B bond, Fig. 3, shows that the valence shell charge concentrations of both atoms are joined together to give a contiguous concentration of electronic charge that is shared between them, as evidenced by a $\nabla^2\rho_b$ value of −0.31 au. These borons possess 0.6–0.7 more electrons than borons B5 and B6, which are each linked to four hydrogens. The C—C bond in ethane has a ρ_b value of 0.25 au and a $\nabla^2\rho_b$ value of −0.66 au. Thus the B—B bond in these molecules is a relatively weak shared interaction. The B–B interactions in B_5H_9 are similar to the standard, but with a reduced extent of charge accumulation and charge concentration.

The B–B interactions between the apical and basal borons in B_6H_{10} all have reduced bond orders compared to the standard, and exhibit a smaller degree of charge concentration in the internuclear region. In agreement with the styx

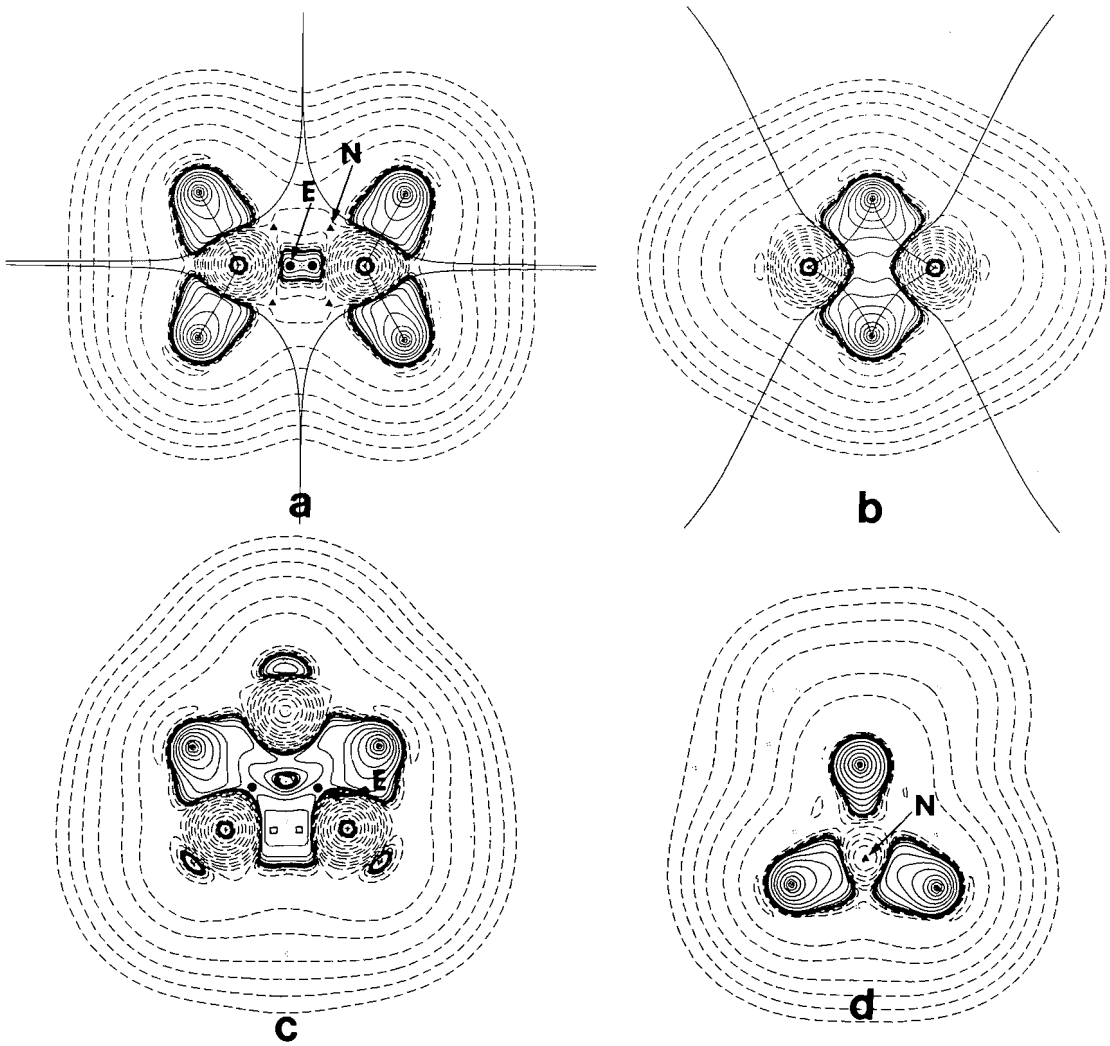

FIG. 3. Contour maps of the Laplacian distributions for *nido*-diborane and *arachno*-tetraborane, the former in the plane of the terminal hydrogens (*a*), and the bridging plane (*b*), the latter in the plane of the bonded borons and two bridging hydrogens (*c*) and in the plane of one bridging and two neighbouring terminal hydrogens (*d*). E and N denote predicted sites of electrophilic and nucleophilic attack, respectively. Note the presence of two bonded maxima in $-\nabla^2\rho$ along the bond path linking the borons in tetraborane that are absent in diborane, which does not possess a B—B bond.

Can. J. Chem. Downloaded from www.nrcresearchpress.com by 123.30.183.119 on 09/08/12
For personal use only.

Can. J. Chem. Downloaded from www.nrcresearchpress.com by 123.30.183.119 on 09/08/12
For personal use only.

model of this molecule outlined above, the weakest of these interactions are found between those atoms that, in the model, are involved in three-centre boron ring bonds, those linking the apical atom to borons 4 and 5 and to borons 9 and 10. The interaction between the two basal borons, B9 and B10, which are not linked by a bridging hydrogen, has an order equal to 1.23 and the largest degree of charge concentration in the internuclear region. The B–B interactions in the carborane $C_2B_4H_6$, which again are predicted by the styx model to be involved in three-centre bonding, have bond orders of 0.94 and a reduced extent of charge concentration compared to the standard.

The bond orders of the B–B interactions in the *closo*-boranes become progressively smaller as the size of the cage increases, from 0.91 in $B_6H_6^{2-}$ to 0.86 in $B_{12}H_{12}^{2-}$. In the heptahydroborate, the bonds to the apical boron have orders less than the standard value while those between the five equivalent borons have orders in excess of unity, to yield an average value of ρ_b that is intermediate between those for the other two *closo* compounds.

There is considerable transfer of electronic charge from boron to carbon in the carboranes, and the C—B bonds, like the B—H bonds, are very polar. The ρ_b values for the C—B bonds in $C_2B_3H_5$ are similar to those observed for the B—H_t bonds, but their values of $\nabla^2\rho_b$ lie on the ionic side of the zero value. The molecule $C_2B_4H_6$ is electron deficient with respect to the number of skeletal bond paths it exhibits and, correspondingly, the value of ρ_b for the C—B bond decreases from that found in $C_2B_3H_5$, which is electron precise.

Charge density in the ring surfaces

Because of their electron-deficient nature, the boranes form ring and cage structures to gain maximum stability from a minimum amount of electronic glue. They do this through a very pronounced delocalization of the charge density over the ring surfaces, an effect that is quantitatively characterized by the values of ρ_r and the ellipticities of the ring bonds. The three-centre model of the two-electron bond is mirrored in the molecular graphs of theory by the presence of four- and five-membered hydrogen-bridged rings and the three-membered rings of boron atoms or of a carbon and two boron atoms in a carborane. In all of these rings the value of ρ_r, the minimum value attained by the charge density in the ring surface, is only slightly less than the value of ρ_b, the minimum value attained by the charge density in the lines of maximum charge density forming the ring's perimeter, Table 2. Correspondingly, the ring bonds exhibit large ellipticities with their major axes oriented in a direction tangent to the surface of the molecule, indicating a delocalization of electronic charge over the surface of the ring. The same charge delocalization is reflected in the Laplacian of the charge density. This distribution is negative over each of the ring surfaces beyond the boron core distributions, and electronic charge is concentrated almost evenly over the entire surface, see Figs. 3–5. The contraction of ρ along the axis perpendicular to the ring surface at the ring critical point is so large it dominates the two positive curvatures of ρ in the ring surface and the Laplacian is negative even at the ring critical points in these systems. That these effects are unique to the electron-deficient systems is illustrated by a comparison of the properties of the two carboranes. The molecule $C_2B_3H_5$ is electron precise. Thus the value of ρ_r for its four-membered rings is considerably less than the values of ρ_b for the peripheral bonds, and their ellipticities are less than 0.01. The molecule $C_2B_4H_6$ is electron deficient. In this case, the value of ρ_r for the three-membered rings is the same as the value of ρ_b for the peripheral B—B bonds to four significant figures and they exhibit extreme ellipticities of 58. The B—B bond paths are inwardly curved away from the perimeter of the ring, another characteristic of the three-centre systems.

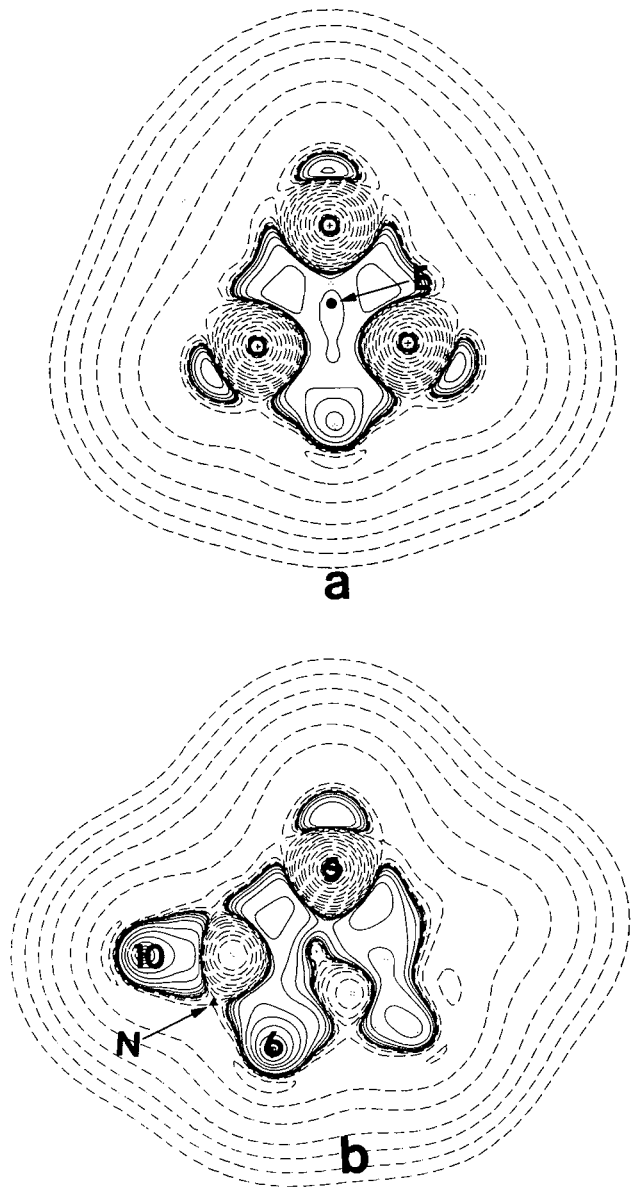

FIG. 4. Contour maps of the Laplacian distributions for *nido*-pentaborane, in a plane containing two basal and the apical boron atoms (*a*) and in a plane containing the apical boron, one bridging, and one neighbouring terminal hydrogen (*b*). The same diagrams apply to *nido*-hexaborane.

These characteristics of the charge density provide a quantitative measure of the extent to which electronic charge is delocalized over and concentrated in the ring surface of electron-deficient molecules where it serves to bind all of the nuclei of the ring. The description of such molecules as globally delocalized by King and Rouvray (21) is particularly apt. The surface delocalization of electronic charge

Can. J. Chem. Downloaded from www.nrcresearchpress.com by 123.30.183.119 on 09/08/12
For personal use only.

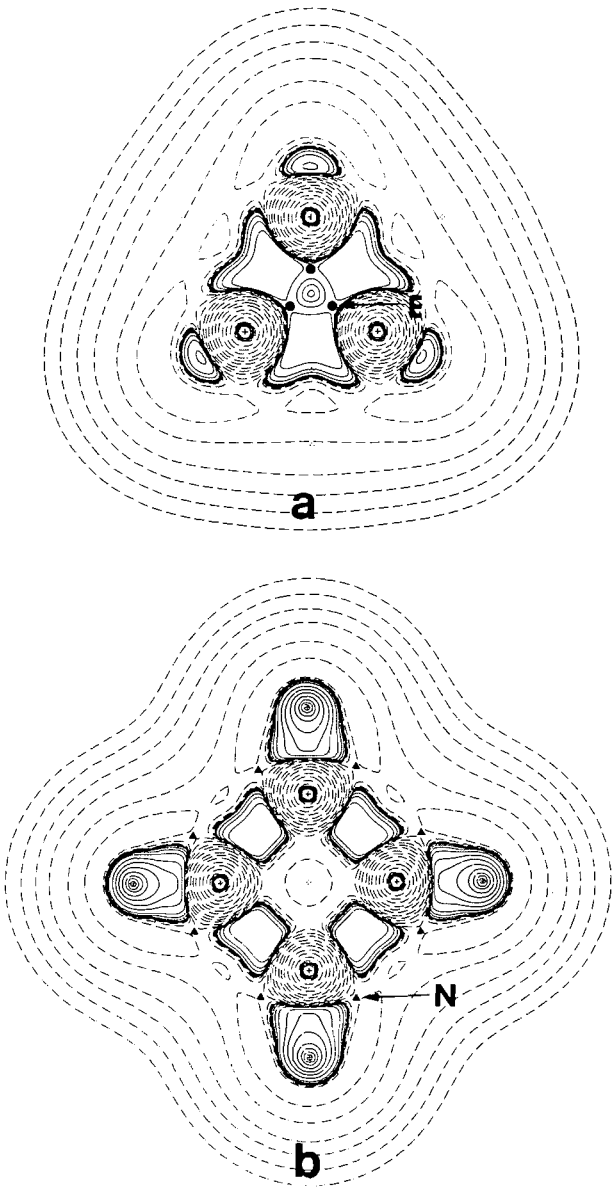

FIG. 5. Contour map of the Laplacian distribution for *closo*-hexahydrohexaborate, for a plane containing a B—B—B face (*a*) and for a plane containing a plane of four boron atoms (*b*). The same diagrams apply to the hepta- and dodecahydroborates.

demonstrated to be present in the *closo* molecules is also consistent with Stone's (22) description of the bonding in polyhedral atomic clusters as a perturbed spherical shell of atoms for which the electronic wave functions are the surface harmonics characterized by the quantum numbers l and m. The effect of this surface delocalization of charge on the energy is discussed below.

Atomic properties

Table 3 lists the atomic populations, charges, and energies, while Table 4 lists the same properties relative to their values in diborane. These atomic properties are obtained using the programs PROAIM (23) and OMEGA (24). The atomic population of atom Ω, $N(\Omega)$, is obtained by an integration of ρ over the basin of the atom. Its net charge $q(\Omega) = Z_\Omega - N(\Omega)$. An atomic energy $E(\Omega)$ is, by the atomic statement of the virial theorem, equal to the negative of the atomic electronic kinetic energy $T(\Omega)$, as obtained through an integration of the kinetic energy density (1, 4). Because of the extremely flat nature of the charge density in certain of the three-membered ring structures commented on above, the program has difficulty following certain of the paths traced out by the gradient vectors of ρ that define the interatomic surfaces for the boron atoms, and it was not possible, in these cases, to integrate the property densities over the atomic basins. There is an internal check on the accuracy of an atomic integration provided by the evaluation of the integral of the Laplacian of the charge density. The atomic value of this integral should vanish, because of the zero flux surface condition defining the atomic boundaries. When the value of this integral is less than 1×10^{-3} au the error in the energy of the atom is less than 0.2 kcal mol^{-1}. Table 5 gives the sums of the atomic populations and energies for four molecules where all the atoms could be integrated within this limit and the integration errors are seen to be 0.006 e or less in the total population and 1 kcal mol^{-1} or less in energy. In $B_6H_6^{2-}$, $B_{12}H_{12}^{2-}$, and $C_2B_4H_6$, all atoms other than the equivalent boron atoms could be integrated within the limit set on the value of the atomic Laplacian, and the boron results were obtained by difference in these cases. In B_5H_9, B_6H_{10}, and $B_7H_7^{2-}$ the average values of the populations and energies of the two borons, which could not be separately integrated, are given in Tables 3 and 4.

The bridging hydrogen atoms possess a negative charge equal to -0.71 ± 0.01 e except for pentaborane where the charge drops to -0.67 e. The bridging hydrogen atom is most stable in diborane, being least stable in pentaborane where its population is significantly less. The relative stabilities, in general, correlate with the bond orders.

Excluding the negatively charged *closo* compounds but including the carboranes, the negative charge on a terminal hydrogen is, in general, somewhat smaller than that on a bridging hydrogen and it is less stable, as reflected in the values for diborane itself. The terminal atoms most similar to the standard are those in the BH_2 groups in B_4H_{10}, the other terminal hydrogens possessing smaller populations and less negative energies. A hydrogen bonded to a boron of a single B—B bond such as H3 in B_4H_{10} and B_6H_{10} possesses the net charge of smallest magnitude. A hydrogen bonded to an apical boron has a net charge of smaller magnitude than one bonded to a basal boron. The bridging hydrogens are more stable than the terminal hydrogens in the same molecule to an extent greater than that anticipated on the basis of a slightly greater electron population. One reason for the increased stability of the bridging hydrogens is their more contracted nature. The volume of a bridging hydrogen atom, measured out to its 0.001 au density envelope, is 59.2 a_0^3 compared to 82.8 a_0^3 for a terminal hydrogen in diborane. This more contracted nature of the charge density results in a potential energy of interaction of the proton of a bridging hydrogen with its own atomic charge distribution that is more negative than that for the more diffuse terminal atom by 16 kcal mol^{-1}. Another factor contributing to the increase in stability is, as discussed in more detail below, the presence of the delocalized charge over the surface of the hydrogen-bridged rings.

The terminal hydrogens in the *closo*-boranes possess the largest electron populations of all the hydrogens. These populations decrease as the size of the cluster increases. In

TABLE 4. Comparison of integrated electron populations and energies for atoms in the borane series (reference atoms are starred)

	Boron atoms				Terminal hydrogen atoms				Bridging hydrogen atoms			
Formula	Atom	ΔN(B), e	ΔE(B), e^2/a_o	ΔE(B), kcal/mol	Atom	$\Delta N(H_t)$, e	$\Delta E(H_t)$, e^2/a_o	$\Delta E(H_t)$, kcal/mol	Atom	$\Delta N(H_b)$, e	$\Delta E(H_b)$, e^2/a_o	$\Delta E(H_b)$, kcal/mol
BH	B1	+1.3342	−0.4825	−302.8	H2	+0.0875	−0.0361	−22.65				
BH_3	B1	−0.0379	−0.0244	−15.31	H2	+0.0156	−0.0053	−3.313				
B_2H_6	B1*	0.0000	0.0000	0.000	H3*	0.0000	0.0000	0.000	H2*	0.0000	0.0000	0.0000
B_4H_{10}	B1	+0.7331	−0.2785	−174.8	H3	−0.0416	+0.0215	+13.47	H7	+0.0036	+0.0085	+5.328
	B5	+0.1662	−0.1429	−89.67	H11	−0.0107	−0.0026	−1.619				
					H13	−0.0040	−0.0053	−3.301				
B_5H_9	B1	+0.9026	−0.4181	−262.4	H6	−0.0215	+0.0142	+8.886	H10	−0.0397	+0.0371	+23.26
	B5				H14	−0.0250	+0.0349	+21.89				
B_6H_{10}	B1	+0.6316	−0.3016	−189.3	H3	−0.0315	+0.0154	+9.657	H6	−0.0125	+0.0176	+11.07
	B4	+0.9029	−0.4063	−254.9	H8	−0.0208	+0.0197	+12.37	H13	+0.0055	+0.0099	+6.212
	B2	+1.1101	−0.5029	−315.6	H11	−0.0157	+0.0038	+2.359				
	B9				H15	−0.0035	+0.0086	+5.409				
$B_6H_6^{2-}$	B1	+1.656	−0.6741	−423.0	H7	+0.0965	+0.0349	+21.87				
$B_7H_7^{2-}$	B1	+1.5686	−0.6812	−427.5	H8	+0.0641	+0.0402	+25.21				
	B7				H14	+0.0915	+0.0216	+13.53				
$B_{12}H_{12}^{2-}$	B1	+1.551	−0.6898	−432.8	H13	+0.0351	+0.0177	+11.11				
$C_2B_3H_5$	B2	−0.0041	+0.0052	+3.263	H8	−0.0010	+0.0123	+7.712				
$C_2B_4H_6$	B1	+0.4326	−0.4474	−280.7	H7	−0.0095	+0.0237	+14.87				

TABLE 5. Comparison of total integrated electron populations and energies with SCF results for molecules in the borane series

Molecule	$\langle N\rangle = \sum_\Omega N(\Omega)$ e	$q = \langle N\rangle - N_{molec}$ e	$\langle E\rangle = \sum_\Omega E(\Omega)$ e^2/a_o	E(SCF) e^2/a_o	$\Delta E = \langle E\rangle - E$(SCF) e^2/a_o	ΔE kcal/mol
BH	6.0023	+0.0023	−25.1237	−25.1242	+0.0005	+0.3138
BH_3	7.9981	−0.0019	−26.3955	−26.3953	−0.0002	−0.1255
B_2H_6	15.9963	−0.0037	−52.8214	−52.8224	+0.001	+0.6275
$C_2B_3H_5$	31.9940	−0.0060	−152.7066	−152.7085	+0.0019	+1.1923

$B_7H_7^{2-}$ a hydrogen bonded to an apical boron has a larger population than one bonded to a basal boron. While the terminal hydrogens in the *closo*-boranes possess larger electron populations, they are less stable than the terminal hydrogens in diborane. The charge distributions of the terminal hydrogens of the *closo*-boranes are the most diffuse of the atoms in the boranes with atomic volumes equal to 104.3 a_0^3 to give an average density of 0.017 e a_0^{-3}.

Since hydrogen withdraws charge from boron, the stability of a boron atom increases with a decrease in the number of bound hydrogen atoms. Thus the least stable boron atoms are those in diborane and the corresponding borons of the BH_2 groups in B_4H_{10}. Boron atoms linked to one other boron by a bond path possess 0.6–0.9 more electrons than does the standard atom in diborane. Boron atoms in the two *nido*-boranes are involved in ring systems over which there is significant charge delocalization and they, like the bridging hydrogens that link them, are stabilized relative to the standard atoms. For the boron atoms, the stabilization is in excess of 200 kcal mol^{-1}.

The borons in $C_2B_3H_5$, which are linked by bond paths to two carbons and a terminal hydrogen, have populations and energies that are nearly identical to those for the standard boron in diborane. In addition, the terminal hydrogen attached to boron has the same population as the standard H_t atom in diborane to within 0.001 e. Thus the boron linked to two carbons appears to a terminal hydrogen to be nearly identical to the standard boron atom in diborane. Each carbon in the dicarbapentaborane has a net charge of −2.103 e. This charge decreases slightly to −2.003 e in dicarbahexaborane and the terminal hydrogens bonded to the borons are again almost unchanged from the standard. Thus the two skeletal electrons of the added BH_t group are donated almost entirely to the borons in $C_2B_4H_6$, and each has 0.43 more electrons than do those in $C_2B_3H_5$. As a result, there is sufficient electronic charge to form bond paths between the borons in dicarbahexaborane, the bond path equivalent of three-centre two-electron bonds for a B_2C ring of atoms. Thus the two skeletal electrons of the added BH_t group initiate the formation of bond paths between the borons that serve to catalyse the delocalization of charge over the surfaces of the resulting three-membered rings. The boron atoms are significantly stabilized, by ≈280 kcal mol^{-1} relative to the standard or to the borons in dicarbapentaborane. The dicarbahexaborane molecule is, therefore, considerably stabilized by the surface delocalization of charge associated with the model of the two-electron three-centre ring of atoms.

The boron atoms in the negatively charged *closo*-boranes have considerably greater electron populations than do the

Can. J. Chem. Downloaded from www.nrcresearchpress.com by 123.30.183.119 on 09/08/12
For personal use only.

boron atoms in diborane, with $\Delta N(B) \cong 1.6$ e, Table 4. While the terminal hydrogens in the *closo* molecules are somewhat less stable than the standard H_t in diborane, each boron atom is stabilized relative to the standard boron atom by an amount in excess of 420 kcal mol^{-1}. The delocalization of charge over the surfaces of the three-membered rings in the *closo* compounds leads to a considerable stabilization of these molecules, as it does in the case of $C_2B_4H_6$.

Reactivity in terms of the Laplacian of the charge density

The Laplacian of the charge density, through its ability to define and locate centres of local charge concentrations and local charge depletions, provides the physical basis for the Lewis concept of the localized electron pair and its associated models of molecular geometry and reactivity (1, 25). Since electronic charge is concentrated in regions where the Laplacian is negative, it is most useful to discuss the topology of the negative of the Laplacian distribution, a maximum in $-\nabla^2\rho$ corresponding to a local concentration of electronic charge.

The Laplacian distribution recovers the electronic shell model of an atom by exhibiting a corresponding number of pairs of shells of charge concentration and charge depletion (25–28). For a spherical atom, the outer shell or valence shell of charge concentration, the VSCC, contains a sphere over whose surface electronic charge is maximally and uniformly concentrated. Upon entering into chemical combination, the VSCC is distorted and local maxima, minima, and saddles appear on the sphere of maximum charge concentration. It has been demonstrated in many systems (25, 29, 30, 31) that the local maxima correspond in number, location, and size to the localized pairs of electrons assumed in the Lewis model. All of the properties postulated in the VSEPR model of molecular geometry (32) for bonded and nonbonded pairs of electrons are recovered by the maxima in the VSCC of the central atom (29, 30).

The Lewis model also encompasses chemical reactivity through the concept of a generalized acid–base reaction. Complementary to the local maxima in the VSCC for the discussion of reactivity are its local minima. A local charge concentration is a Lewis base or a nucleophile, while a local charge depletion is a Lewis acid or an electrophile. A chemical reaction corresponds to the combination of a "lump" in the VSCC of the base with the "hole" in the VSCC of the acid (25). It has been demonstrated in many examples that this matching of extrema in the Laplacian distributions correctly identifies the sites of electrophilic and neucleophilic attack, as well as predicting the relative orientation of approach of the two reactants (25, 33, 34). In an early study of the boranes, using the approximation of partial retention of diatomic differential overlap for the calculation of the wave function, Dixon *et al.* (35) predicted the sites of electrophilic and nucleophilic attack in terms of Mulliken atomic and group charges and the inner shell energy eigenvalues. These same papers compared localized molecular orbitals obtained in these calculations with topologically allowed structures defined by Epstein and Lipscomb (36).

The topology of the Laplacian in the VSCC determines an atom's reactivity and it is summarized in the atomic graph (1, 37). The maxima in $-\nabla^2\rho$ are $(3,-3)$ critical points and they are connected by pairs of lines originating at intervening $(3,-1)$ critical points. These lines are the analogues of the bond paths that link the maxima in ρ and their network produces the atomic graph. For example, in a tetrahedrally bonded carbon atom there are four bonded maxima in the VSCC that are linked by pairs of lines originating at six intervening $(3,-1)$ critical points to generate a tetrahedron with curved faces. In the interior of each face or ring is a $(3,+1)$ or ring critical point. The Laplacian in the VSCC attains its most positive values at these ring critical points and they are the centres of nucleophilic attack. For example, the minimum in the face opposite the bonded maximum with F in the VSCC of carbon in methylfluoride locates the point of nucleophilic attack at a saturated carbon leading to inversion. The nitrogen in ammonia has a similar atomic graph with one bonded maximum being replaced by a nonbonded concentration of charge. Nonbonded charge concentrations generally serve as the nucleophiles. In systems where there are no nonbonded charge concentrations, that is, no unshared pairs of electrons, the $(3,-1)$ critical points serve as the centres of electrophilic attack. They denote the highest concentrations of electronic charge not involved in bonding in the VSCC's of such atoms. This is the situation for a carbon atom in benzene and substituted benzenes (34), for example, and is the situation for the boron and carbon atoms in the boranes and carboranes.

The atomic graphs for boron are unique among those so far encountered because of the extreme degree of charge transfer to both hydrogen and carbon. Bonding to either of these atoms is accompanied by a nearly complete transfer of boron's valence shell of charge concentration and the local maxima in $-\nabla^2\rho$ are found within the boundaries of the hydrogen and carbon atoms. In the case of hydrogen, this corresponds to the presence of the single maximum in $-\nabla^2\rho$, which occurs at the position of the proton. For this reason the $(3,\pm1)$ critical points can occur at distances from the boron nucleus greater than the normal shell radius. The boron atom in diborane will serve to illustrate these features, Fig. 3. The atomic graph of boron is a distorted tetrahedron whose vertices correspond to the maxima in $-\nabla^2\rho$ found at the positions of the protons. The vertices are linked by six intervening $(3,-1)$ critical points and there is one $(3,+1)$ critical point in each of the four faces. The coordinates of the $(3,\pm1)$ critical points, their distances R from the nucleus, and the values of the Laplacian are listed in Table 6. The Laplacian is most negative at the $(3,-1)$ critical point linking the two bridging hydrogens and this is the predicted position of electrophilic attack, Fig. 3. Nucleophilic attack is predicted to occur at either of the two $(3,+1)$ critical points lying on either side of the bonded ring of atoms, that is, in the face of the tetrahedron formed by linking a terminal proton with the two bridging protons.

The atomic graph for boron in BH_3 is particularly simple. The VSCC is reduced to a belt-like distribution lying in the plane of the nuclei, with the maxima at the protons linked by intervening $(3,-1)$ critical points. The sphere of charge concentration is totally absent on either side of this plane and a nucleophile has direct access to the core of the boron atom, as previously illustrated (1). This molecule is a very strong Lewis acid.

In B_4H_{10}, Fig. 3, boron B1 has a bonded charge concentration in its VSCC along the bond path linking it to the other bridgehead boron atom, B2. In a shared interaction, each atom in general exhibits an associated bonded charge concentration, separated one from the other by an intervening

Can. J. Chem. Downloaded from www.nrcresearchpress.com by 123.30.183.119 on 09/08/12
For personal use only.

TABLE 6. Atomic graphs: critical points in $-\nabla^2\rho$ for the borane series (site of electrophilic and nucleophilic attack are starred)

Molecule	n	x	y	z	$\nabla^2\rho$, $e/\mathbf{a}_o$	**R**
BH3–B1						
(3,−1)*	3	1.0689	0.6171	0.0000	0.00488	1.2342
B_2H_6–B1						
(3,−1)	1	−2.9783	0.0000	0.0000	0.03039	1.2801
(3,−1)*	1	−0.3583	0.0000	0.0000	−0.05567	1.3398
(3,−1)	4	−1.3543	−0.8500	0.9502	0.03592	1.3204
(3,+1)*	2	−0.6886	1.0432	0.0000	0.08510	1.4517
(3,+1)	2	−3.2205	0.0000	−0.8132	0.05541	1.7259
B_4H_{10}–B1						
(3,−1)	1	−0.9196	0.0000	−1.9370	−0.00631	1.2652
(3,−1)*	2	−0.9819	0.9483	−0.3222	−0.06434	1.2972
(3,−1)	1	−2.4725	0.0000	0.1048	0.01806	1.3016
(3,−1)	2	−2.6802	−0.7920	−1.0793	0.03604	1.3118
(3,+1)	1	−3.1271	0.0000	−0.5995	0.05369	1.5087
(3,+1)	2	−1.6090	−1.6253	−1.2802	0.08112	1.6689
(3,+1)	1	−1.3813	−0.3311	0.8727	0.10317	1.8265
(3,−3)	1	−0.3565	0.0000	−0.8610	−0.31827	1.2936
B_4H_{10}–B5						
(3,−1)	1	0.0000	3.8246	1.4111	0.02849	1.2754
(3,−1)	2	0.9773	2.1053	1.3717	0.02277	1.2977
(3,−1)	2	−0.9656	2.8191	−0.1130	0.03604	1.3171
(3,−1)	1	0.0000	1.5832	0.0701	−0.04524	1.3369
(3,+1)	1	0.0000	2.4891	−0.6530	0.05672	1.4482
(3,+1)	1	0.0000	1.2965	1.2766	0.06700	1.5067
(3,+1)*	2	1.6272	2.8764	1.4781	0.07366	1.7789
B_5H_9–B1						
(3,−1)	1	0.0000	2.8449	0.9620	0.01557	1.3014
(3,−1)	2	1.0346	1.6209	−0.3955	−0.09403	1.3217
(3,−1)	2	0.7494	3.0942	−1.1481	0.03331	1.3279
(3,−1)	1	0.0000	2.1181	−1.5750	0.03232	1.3400
(3,+1)	1	0.0000	1.1340	−0.8083	0.11179	1.4061
(3,+1)	1	0.0000	2.8879	−1.6370	0.04976	1.4376
(3,+1)*	2	1.5726	2.7768	−0.2299	0.07640	1.6100
(3,−3)	1	0.0000	1.5649	0.6111	−0.30181	1.2397
B_5H_9–B5						
(3,−1)*	4	−0.7298	0.7298	1.0937	−0.13656	1.2824
(3,−1)	4	0.0000	1.2782	2.4374	0.03974	1.4047
(3,+1)	1	0.0000	0.0000	0.5154	0.14894	1.3394
(3,+1)	4	0.9127	−0.9127	2.4286	0.04126	1.4126
(3,+3)	1	0.0000	0.0000	−0.0993	0.18489	1.9541
$B_6H_6^{2-}$–B1						
(3,−1)	4	0.8812	0.8812	−2.9969	0.03550	1.4108
(3,−1)*	4	0.7274	0.7274	−1.6203	−0.14372	1.2530
(3,+1)	1	0.0000	0.0000	−1.0679	0.13340	1.2678
(3,+1)*	4	1.2610	0.0000	−2.9977	0.03690	1.4242
(3,−3)	4	1.0941	0.0000	−1.5362	−0.18827	1.3551
(3,+3)	1	0.0000	0.0000	0.0000	0.25011	2.3357
$C_2B_3H_5$–C1						
(3,−1)*	3	−0.6865	0.3963	1.5026	−0.42393	0.9938
(3,−1)	3	0.0000	0.8965	2.5499	−0.07386	1.0021
(3,+1)	3	−0.7913	0.4569	2.5228	−0.05256	1.0059
(3,−3)	3	0.0000	0.8346	1.5048	−0.64414	1.0263
(3,+3)	1	0.0000	0.0000	0.0000	0.39371	2.1021
$C_2B_3H_5$–B2						
(3,−1)	2	0.0000	2.6271	1.1497	0.02076	1.2788
(3,−1)	2	−1.0393	1.1674	0.0000	0.02972	1.3747
(3,+1)	2	−1.3196	0.7619	0.0000	0.04982	1.8561
(3,+1)*	2	−1.1885	0.6862	0.6036	0.05163	1.9194

Can. J. Chem. Downloaded from www.nrcresearchpress.com by 123.30.183.119 on 09/08/12
For personal use only.

Can. J. Chem. Downloaded from www.nrcresearchpress.com by 123.30.183.119 on 09/08/12
For personal use only.

(3,−1) critical point. (One notes that in diborane, where there is no B—B bond path, each boron exhibits a (3,−1) critical point at the corresponding position along the internuclear axis and they are separated by a (3,+1) critical point.) Atom B1 is also linked to one terminal and two bridging hydrogen atoms and their associated maxima, together with the bonded maximum to B2, again yield a tetrahedral atomic graph for B1 and its complement B2. Reference to Table 6 shows that the most negative set of (3,−1) critical points in these graphs and in those for the other two boron atoms are those that link the bonded maximum on boron with the maximum on a bridging hydrogen on either B1 or B2. They are, therefore, the predicted sites of electrophilic attack, Fig. 3. They are accessible from the back of the molecule, that is, away from the open face, access to which is hindered by the two *endo* hydrogens, H11 and H12.

The (3,+1) critical points with the most positive values of the Laplacian are found within the atomic graphs of B1 and B2, in a face formed by the atoms 2, 7, and 10 for B1, for example. There are four such equivalent positions, each lying within the inner or open face of the molecule, and the approach of a nucleophile is hindered by the proximity of the *endo* hydrogens H11 and H12. These two borons also have (3,+1) critical points with $\nabla^2\rho$ values of 0.081 au on the opposite side of the molecule, in the faces formed by the bonded maximum to the other boron, a terminal hydrogen, and a bridging hydrogen: the face formed by the atoms 2, 3, and 7 for atom B1, for example. The (3,+1) critical points on borons B5 and B6 of the BH_2 groups are smaller by only 0.007 au, Table 6. Each lies in one of the four faces formed by one bridging and two terminal hydrogens. These sites are more accessible than those on B1 and B2 and, in addition, the positive charges on B5 and B6 are 0.6 e greater than those on B1 and B2. Thus nucleophilic attack is predicted to occur at these peripheral borons, Fig. 3. This prediction is in agreement with the statement of Muetterties (38) that cleavage of BH by a nucleophile occurs at these atoms.

There is a single bonded maximum situated between the apical boron atom B5 and each of the basal atoms in *nido*-pentaborane; it is 1.2 au from the basal atom and 2.0 au from B5. Each of these maxima is linked by a (3,−1) critical point to the hydrogen bonded to B5. The bonded maxima are themselves linked by another set of (3,−1) critical points, each of which lies in an exterior face formed by the apical and two basal boron atoms, see Fig. 4. Thus the atomic graph for the apical boron is a four-sided pyramid topped by a terminal hydrogen with a (3,+1) critical point in the bottom face formed by the four bonded maxima. There is a (3,+3) cage critical point along the symmetry axis in the interior of the molecule. The (3,−1) critical points that link the bonded maxima, each of which is 1.28 au from the apical boron atom, represent the largest nonbonded concentrations of electronic charge in this molecule and they are the predicted sites of electrophilic attack. The (3,+1) critical points with the most positive values for the Laplacian lie within the interior of the molecule and are inaccessible to nucleophiles. The most positive (3,+1) holes on the exterior of the molecule lie in a face of the tetrahedral atomic graph for a basal boron atom formed by the bonded maximum shared with the apical boron and the maxima associated with a bridging and a terminal hydrogen, Fig. 4. These predictions are in agreement with the statement (3) that electrophilic attack occurs at borons furthest removed from an open face, and nucleophilic attack occurs at borons involved in bridging.

The other *nido* compound studied here, B_6H_{10}, has a corresponding reaction profile in terms of its atomic graphs. In analogy with the atomic graph for the apical boron in B_5H_9, the largest concentrations of nonbonded charge on the exterior of B_6H_{10} are found at the (3,−1) critical points linking the bonded maxima shared by the apical boron with basal borons 1, 4, and 5. They are found 1.27 au from the apical boron where $\nabla^2\rho = -0.13$ au, compared to corresponding values of 1.28 and −0.14 au for pentaborane. Similarly, nucleophilic attack occurs, as in B_5H_9, at a basal boron, B4 or B5, in the face critical point formed by the links to the apical boron and a terminal and bridging hydrogen. The values of R and $\nabla^2\rho$ are 1.54 and +0.073 au compared to corresponding values of 1.61 and +0.076 au for pentaborane. The distributions are so similar for the two *nido* molecules that Fig. 4 serves equally well for either system.

The atomic graphs for the borons in the *closo*-boranes are similar to those found for the apical boron in the *nido*-boranes. In these molecules there are two bonded charge concentrations along each bond path linking the equivalent borons, as found for the B—B bond path in B_4H_{10}. These maxima are linked by (3,−1) critical points, as illustrated for a triangular face of the hexaborate in Fig. 5. The bonded maxima for a given boron are linked to the maximum charge concentration of its terminal hydrogen to yield a four-sided pyramid in the case of the hexaborate and a five-sided one in the dodecahydrate. There is a (3,+1) critical point in each of the corresponding faces and a (3,+3) or cage critical point at the origin in the interior of the cage, a point shared by the bases of all the boron atomic graphs. The forms of the atomic graphs and the values of the Laplacian at corresponding critical points are similar for all three *closo* compounds, and data are given in Table 6 only for the hexahyroborate.

Electrophilic attack, as in the *nido*-boranes, is predicted to occur at a concentration of nonbonded charge at a (3,−1) critical point linking the bonded maxima located on two different, neighbouring paths in the atomic graph for a given boron, Fig. 5. While the value of the Laplacian is more negative at the intervening (3,−1) critical points linking the bonded maxima along a given bond path, these are tightly bound as they are involved with the distribution of charge between the bonded borons. The values of R and $\nabla^2\rho$ for the reactive critical points are very similar for all three of the *closo* molecules. Their values in au for the hexa-, hepta-, and dodecaborate are, respectively, 1.25 and −0.14; 1.25 and −0.13; 1.26 and −0.15.

Nucleophilic attack occurs at one of the (3,+1) critical points, each of which lies in one of the pyramidal faces of the atomic graph for a boron atom, Fig. 5. The values (in au) of R and $\nabla^2\rho$ at these critical points for the six-, seven-, and 12-membered systems are, respectively, 1.42, +0.037; 1.71, +0.052; 1.40, +0.046. The (3,+1) critical point with a more positive value for the Laplacian, given in Table 6 for $B_6H_6^{2-}$, lies within the interior of the cage and is not accessible to a nucleophile.

In the carboranes there is a single bonded maximum along each B—C bond path within the basin of the carbon atom and another associated with its bond to hydrogen. Thus the atomic graph of a carbon in $C_2B_3H_5$ is tetrahedral in form and, in $C_2B_4H_6$, a pentagonal pyramid. The (3,−1) critical points

Can. J. Chem. Downloaded from www.nrcresearchpress.com by 123.30.183.119 on 09/08/12
For personal use only.

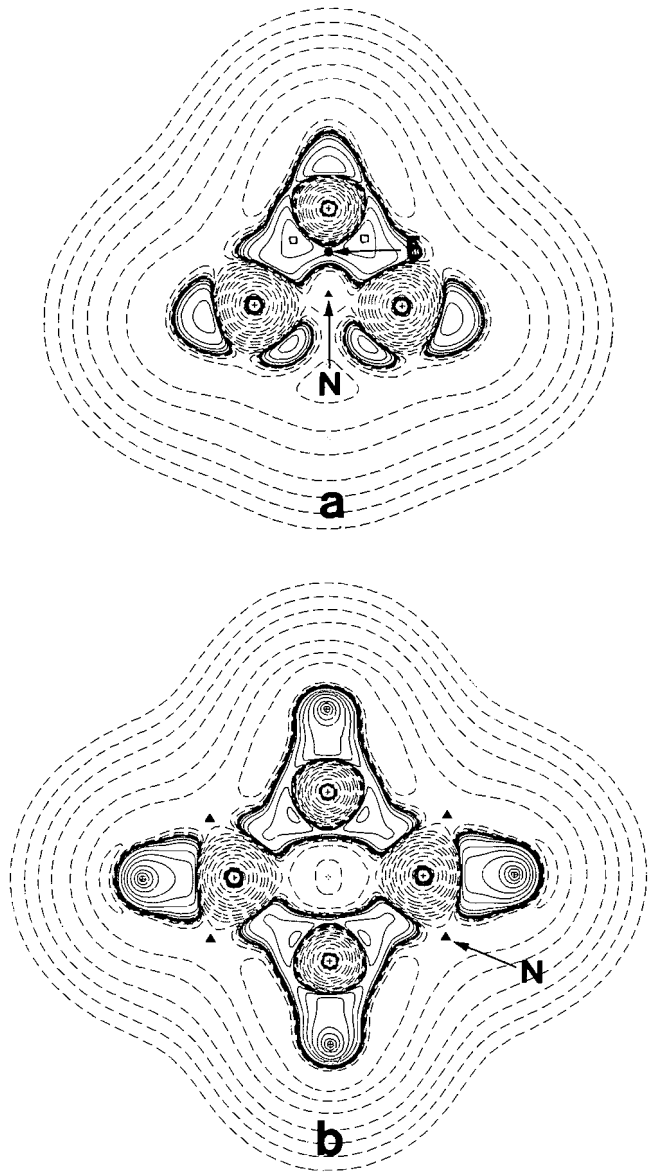

FIG. 6. Contour plots of the Laplacian distributions in a B—C—B face in $C_2B_3H_5$ (*a*) and in a plane containing the two apical carbons and two of the borons in $C_2B_4H_6$ (*b*).

linking the bonded maxima on two neighbouring C—B bond paths represent by far the largest concentrations of charge not involved in bonding and they are the predicted sites of electrophilic attack in both molecules, as illustrated in Fig. 6 for $C_2B_3H_5$. The values of R and $\nabla^2\rho$ for $C_2B_4H_6$ are quite similar, being 0.99 and −0.37 au, respectively, as is its position relative to the nuclei, illustrated in Fig. 6. Nucleophilic attack in $C_2B_3H_5$ is predicted to occur at a (3,+1) critical point close to the centre in a triangular BCB face, 1.92 au from a boron and 2.03 au from carbon, where the Laplacian equals +0.052 au. In $C_2B_4H_6$ there are bond paths between the boron atoms, and their atomic graphs differ from those in the triborane molecule. The (3,+1) critical point with the most positive value of the Laplacian in this system is located in a symmetry plane containing two carbon and two boron nuclei, 1.78 au from a boron where $\nabla^2\rho = +0.061$ au, Fig. 6. This is in agreement with the statement by Onak (39) that conversion of *closo*-dicarbahexaborane to its *nido* form by addition of trimethylamine occurs by nucleophilic attack at boron.

Since the boranes are electron deficient, nucleophilic attack should be more prevalent than electrophilic attack in these molecules. The largest value of $\nabla^2\rho$ for a site of nucleophilic attack in the boranes studied here is +0.09 au for B_2H_6. Ranking these molecules by their $\nabla^2\rho$ values, one finds for susceptibility to nucleophilic attack:

$$B_2H_6 > B_5H_9 > B_4H_{10} > B_6H_{10} > C_2B_4H_6 > B_7H_7^{2-} > C_2B_3H_5 > B_{12}H_{12}^{2-} > B_6H_6^{2-}$$

Similarly, for susceptibility to electrophilic attack:

$$C_2B_3H_5 > C_2B_4H_6 > B_{12}H_{12}^{2-} > B_6H_6^{2-} > B_5H_9 > B_6H_{10} > B_7H_7^{2-} > B_4H_{10} > B_2H_6$$

In summary, the properties of the Laplacian of the charge distributions for the boranes and carboranes lead to the following points regarding their relative reactivities: (1) $B_7H_7^{2-}$ is more susceptible to nucleophilic attack than either of the other two *closo*-boranes. (2) Among the *nido*-boranes, larger species are less reactive with respect to nucleophilic attack, in agreement with observation (3). (3) Electrophilic attack does occur preferentially at apical boron atoms, those furthest removed from an open face, and nucleophilic attack does occur most likely at basal boron atoms that are involved with hydrogen bridging, again in agreement with observation (3). (4) In carboranes, electrophilic attack occurs at carbon, while nucleophilic attack occurs at boron. (5) The *closo* compounds, whether they be boranes or carboranes, are as a group less susceptible to nucleophilic attack than any of the open clusters, and the cage species are the most stable.

Conclusions

The theory of atoms in molecules yields a precise definition of the molecular structures of the boranes and carboranes and a description of the bonded interactions that give rise to these structures in terms of characteristic features of the charge density and the properties of the atoms. The structures demonstrate that the formal electron counting scheme, which associates a bond with a pair of electrons, is not a necessary requirement for the formation of a bond path between a pair of atoms. The lines of maximum charge density, which link the atoms in the electron-deficient three-membered faces and hydrogen-bridged rings, have reduced bond orders compared to the formal electron pair standards. The reduction in bond order is, however, considerably less than that anticipated by taking the ratio of the number of electron pairs to the number of bond paths, a ratio labelled by the letter s. Thus the values of the bond orders n listed in Table 2 are greater than the corresponding s values, as illustrated by the following examples; $s = 0.75$ and $n = 0.98$ for B_5H_9, $s = 0.58$ and $n = 0.91$ for $B_6H_6^{2-}$, $s = 0.43$ and $n = 0.86$ for $B_{12}H_{12}^{2-}$, and $s = 0.58$ and $n = 0.90$ for $C_2B_4H_6$, the latter being the average of the C—B and B—B bond orders. Assigning one pair of electrons to each pair of bridged hydrogen bond paths yields a value of 0.5 for s for the hydrogen-bridged two-electron three-centre bond. Taking the B—H_t value of ρ_b as the unit bond order for a B–H interaction, one obtains n values ranging from 0.62 to 0.65 for the

orders of the bridging hydrogen bond paths. Thus electronic charge is accumulated along the bond paths in the electron-deficient systems to yield bond orders in excess of the fractional orders anticipated on the basis of the model that assigns one electron pair to each chemical bond.

The analysis of the charge density in terms of its critical points and Laplacian distribution has shown that the stabilization of these electron-deficient systems is achieved not only by the accumulation of an excess of electronic charge along the bond paths, but by a concomitant concentration of electronic charge within, and its delocalization over the rings of bonded atoms that result from the formation of the extra interatomic linkages. Thus the atoms linked by bond paths with reduced bond orders are more stable than corresponding atoms in the standard linkages, an example of this being the dramatic increase in the stability of the boron atoms in the electron-deficient $C_2B_4H_6$ compared to those in the electron-precise $C_2B_3H_5$. The stabilization of a ring system through a surface delocalization of charge has been previously discussed and illustrated for three-membered ring systems (14, 40, 41) and in the boranes (14, 42).

Can. J. Chem. Downloaded from www.nrcresearchpress.com by 123.30.183.119 on 09/08/12
For personal use only.

1. R. F. W. Bader. Atoms in molecules — a quantum theory. Oxford University Press, Oxford, U.K. 1990.
2. R. F. W. Bader. Chem. Rev. **91**, 893 (1991).
3. N. N. Greenwood and A. Earhshaw. Chemistry of the elements. Pergamon Press, Oxford. 1984.
4. R. F. W. Bader, T. T. Nguyen-Dang, and Y. Tal. Rep. Prog. Phys. **44**, 893 (1981).
5. W. N. Lipscomb. Boron hydrides. Benjamin, New York. 1963.
6. K. Wade. Chem. Commun. 792 (1971); Nature (London) Phys. Sci. **240**, 71 (1972); Adv. Inorg. Radiochem. **18**, 1 (1976).
7. M. J. Frisch, M. Head-Gordon, H. B. Schlegel *et al.* Gaussian, Inc., Pittsburgh. 1988.
8. T. H. Dunning, Jr. J. Chem. Phys. **53**, 2823 (1970); **55**, 716 (1971).
9. S. Huzinaga. Gaussian basis sets for molecular calculations. Elsevier, Amsterdam. 1984; J. Chem. Phys. **42**, 1293 (1965).
10. J. G. C. M. van Duijneveldt-van de Rijdt and F. B. van Duijneveldt. J. Mol. Struct. (THEOCHEM), **89**, 185 (1982).
11. R. A. Baudet. Advances in boron and the boranes: the molecular structures of boranes and carboranes. VCH Publishers, New York. 1988.
12. (*a*) R. Schaeffer, Q. Johnson, and G. S. Smith. Inorg. Chem. **4**, 917 (1965); (*b*) L. Barton, T. Onak, R. J. Remmel, and S. G. Shore. Gmelin Handbuch. Vol. **54**, Springer-Verlag, Berlin. 1979. p. 20.
13. P. W. Fowler. J. Chem. Soc. Faraday Trans. 2, **82**, 61 (1986).
14. R. F. W. Bader and H. Essen. J. Chem. Phys. **80**, 1943 (1980).
15. H. C. Longuet-Higgins. Q. Rev. Chem. Soc. **11**, 121 (1957).
16. R. F. W. Bader, S. W. Anderson, and A. J. Duke. J. Am. Chem. Soc. **101**, 1389 (1979).
17. K. Collard and G. G. Hall. Int. J. Quantum Chem. **12**, 623 (1977).
18. R. F. W. Bader, T. S. Slee, D. Cremer, and E. Kraka. J. Am. Chem. Soc. **105**, 5061 (1983).
19. R. J. Boyd. Stud. Org. Chem. (Amsterdam), **31**, 485 (1987); R. J. Boyd and S. C. Choi. Chem. Phys. Lett. **120**, 80 (1985); **129**, 62 (1986); R. J. Boyd, O. Knop, and S. C. Choi. J. Am. Chem. Soc. **110**, 7299 (1988).
20. R. F. W. Bader, P. M. Baddall, and P. E. Cade. J. Am. Chem. Soc. **93**, 1831 (1971); S. C. Choi, R. J. Boyd, and O. Knop. Can. J. Chem. **65**, 1109 (1987).
21. R. B. King and D. H. Rouvray. J. Am. Chem. Soc. **99**, 7834 (1977).
22. A. J. Stone. Inorg. Chem. **20**, 563 (1981).
23. F. W. Biegler-Konig, R. F. W. Bader, and T.-H. Tang. J. Comput. Chem. **13**, 317 (1982).
24. F. W. Biegler-König, T. T. Nguyen-Dang, Y. Tal, R. F. W. Bader, and A. J. Duke. J. Phys. B: At. Mol. Phys. **14**, 2739 (1981).
25. R. F. W. Bader, P. J. MacDougall, and C. D. H. Lau. J. Am. Chem. Soc. **106**, 1594 (1984).
26. R. F. W. Bader and P. M. Beddall. J. Chem. Phys. **56**, 3320 (1972).
27. Z. Shi and R. J. Boyd. J. Chem. Phys. **88**, 4375 (1988).
28. R. P. Sagar, A. C. T. Ku, V. H. Smith, and A. M. Simas. J. Chem. Phys. **88**, 4367 (1988).
29. R. F. W. Bader, R. J. Gillespie, and P. J. MacDougall. J. Am. Chem. Soc. **110**, 7329 (1988).
30. R. F. W. Bader, R. J. Gillespie, and P. J. MacDougall. *In* From atoms to polymers. *Edited by* J. F. Liebman and A. Greenberg. VCH Publishers, New York. 1989.
31. P. J. MacDougall, M. B. Hall, R. F. W. Bader, and J. R. Cheeseman. Can. J. Chem. **67**, 1842 (1989).
32. R. J. Gillespie. Molecular geometry. Van Nostrand Reinhold, London. 1972.
33. M. T. Carroll, J. R. Cheeseman, R. Osman, and H. Weinstein. J. Phys. Chem. **93**, 5120 (1989); M. T. Carroll, C. Chang, and R. F. W. Bader. Mol. Phys. **63**, 387 (1988); T.-H. Tang, W.-J. Hu, D.-Y. Yan, and Y. P. Cui. J. Mol. Struct. (THEOCHEM), **207**, 327 (1990); K. E. Laidig and R. F. W. Bader. J. Am. Chem. Soc. **113**, 6312 (1991); Z. Shi and R. J. Boyd. J. Phys. Chem. **95**, 4698 (1991).
34. R. F. W. Bader and C. Chang. J. Phys. Chem. **93**, 2946 (1989).
35. D. A. Dixon, D. A. Kleier, T. A. Halgren, J. H. Hall, and W. N. Lipscomb. J. Am. Chem. Soc. **99**, 6226 (1977); J. H. Hall, D. A. Dixon, D. A. Kleier, T. A. Halgren, L. D. Brown and W. N. Lipscomb. J. Am. Chem. Soc. **98**, 2086 (1976); J. H. Hall, D. S. Marynick, and W. N. Lipscomb. J. Am. Chem. Soc. **96**, 770 (1974).
36. I. R. Epstein and W. N. Lipscomb. Inorg. Chem. **10**, 1921 (1971).
37. R. F. W. Bader and P. J. MacDougall. J. Am. Chem. Soc. **107**, 6788 (1985); R. F. W. Bader and P. L. A. Popelier. J. Mol. Struct. (THEOCHEM). In press.
38. E. L. Muetterties. The chemistry of boron and its compounds. Wiley and Sons, New York. 1967.
39. T. Onak. Advances in boron and the boranes: the molecular structures of boranes and carboranes. VCH Publishers, New York. 1988.
40. K. B. Wiberg, R. F. W. Bader, and C. D. H. Lau. J. Am. Chem. Soc. **109**, 985 (1987); **109**, 1001 (1987).
41. D. Cremer and E. Kraka. J. Am. Chem. Soc. **107**, 3800 (1985); **107**, 3811 (1985); D. Cremer and J. Gauss. J. Am. Chem. Soc. **108**, 7467 (1986).
42. R. F. W. Bader. *In* Chemical applications of topology and graph theory. *Edited by* R. B. King. Elsevier Scientific Publishing, New York. 1983.

Appendix: Borane energies, coordinates

(Energies and atomic coordinates in atomic units)

TABLE A1. BH

BH, $C_{\infty v}$ E(RHF) = −25.124157 au

Atom	x	y	z
B1	0.00000	0.00000	0.22124
H2	0.00000	0.00000	−2.11093

TABLE A2. BH_3

BH_3, D_{3h} E(RHF) = −26.395270 au

Atom	x	y	z
B1	0.00000	0.00000	0.00000
H2	0.00000	2.25084	0.00000
H3	1.94929	−1.12542	0.00000
H4	−1.94929	−1.12542	0.00000

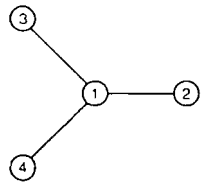

TABLE A3. B_2H_6

B_2H_6, D_{2h} E(RHF) = −52.822442 au

Atom	x	y	z
B1	−1.6982	0.0000	0.0000
H2	0.0000	0.0000	1.8514
H3	−2.7774	1.9639	0.0000
H4	−2.7774	−1.9639	0.0000
B5	1.6982	0.0000	0.0000
H6	2.7774	−1.9639	0.0000
H7	2.7774	1.9639	0.0000
H8	0.0000	0.0000	−1.8514

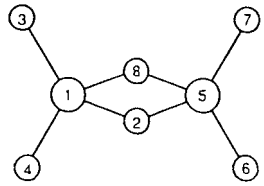

TABLE A4. B_4H_{10}

B_4H_{10}, C_{2v} E(RHF) = −104.477749 au

Atom	x	y	z
B1	−1.64935	0.00000	−0.90345
B2	1.64935	0.00000	−0.90345
H3	−2.61283	0.00000	−2.91360
H4	2.61283	0.00000	−2.91360
B5	0.00000	2.71799	0.77701
B6	0.00000	−2.71799	0.77701
H7	−2.50164	−1.75440	0.44703
H8	2.50164	−1.75440	0.44703
H9	2.50164	1.75440	0.44703
H10	−2.50164	1.75440	0.44703
H11	0.00000	2.73239	3.02214
H12	0.00000	−2.73239	3.02214
H13	0.00000	4.63883	−0.37037
H14	0.00000	−4.63883	−0.37037

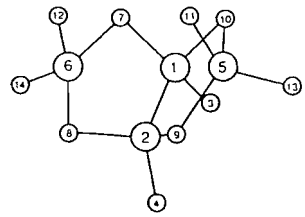

TABLE A5. B_5H_9

B_5H_9, C_{4v} E(RHF) = −128.597863 au

Atom	x	y	z
B1	0.00000	2.43416	−0.27283
B2	2.43416	0.00000	−0.27283
B3	0.00000	−2.43416	−0.27283
B4	−2.43416	0.00000	−0.27283
B5	0.00000	0.00000	1.85481
H6	0.00000	4.64360	−0.01215
H7	4.64360	0.00000	−0.01215
H8	0.00000	−4.64360	−0.01215
H9	−4.64360	0.00000	−0.01215
H10	1.82100	1.82100	−1.96208
H11	1.82100	−1.82100	−1.96208
H12	−1.82100	−1.82100	−1.96208
H13	−1.82100	1.82100	−1.96208
H14	0.00000	0.00000	4.07958

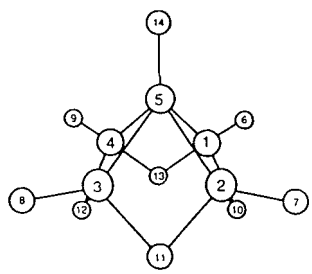

Can. J. Chem. Downloaded from www.nrcresearchpress.com by 123.30.183.119 on 09/08/12
For personal use only.

TABLE A6. B_6H_{10}
B_6H_{10}, C_S E(RHF) = −153.860374 au

Atom	x	y	z
B1	2.84236	−0.11692	0.00000
B2	0.00000	1.64075	0.00000
H3	4.91057	0.70327	0.00000
B4	0.70225	−0.21088	2.69923
B5	0.70225	−0.21088	−2.69923
H6	2.60860	−1.77117	1.79789
H7	2.60860	−1.77117	−1.79789
H8	−0.01128	3.86981	0.00000
B9	−2.43041	−0.35557	1.54956
B10	−2.43041	−0.35557	−1.54956
H11	1.36770	0.34747	4.74802
H12	1.36770	0.34747	−4.74802
H13	−0.92215	−2.10902	2.63832
H14	−0.92215	−2.10902	−2.63832
H15	−3.96890	0.26888	3.04215
H16	−3.96890	0.26888	−3.04215

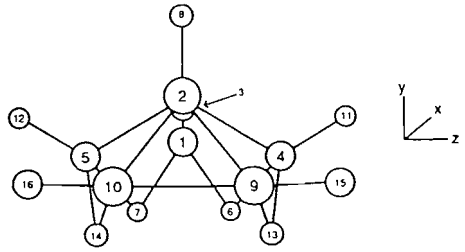

TABLE A7. $B_6H_6^{2-}$
$B_6H_6^{2-}$, O_h E(RHF) = −151.466097 au

Atom	x	y	z
B1	0.00000	0.00000	−2.33569
B2	2.33569	0.00000	0.00000
B3	−2.33569	0.00000	0.00000
B4	0.00000	2.33569	0.00000
B5	0.00000	−2.33569	0.00000
B6	0.00000	0.00000	2.33569
H7	0.00000	0.00000	−4.63096
H8	4.63096	0.00000	0.00000
H9	−4.63096	0.00000	0.00000
H10	0.00000	4.63096	0.00000
H11	0.00000	−4.63096	0.00000
H12	0.00000	0.00000	4.63069

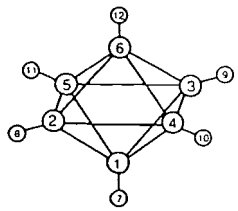

TABLE A8. $B_7H_7^{2-}$
$B_7H_7^{2-}$, D_{5h} E(RHF) = −176.759690 au

Atom	x	y	z
B1	0.82778	2.54763	0.00000
B2	−2.16715	1.57452	0.00000
B3	−2.16715	−1.57452	0.00000
B4	0.82778	−2.54763	0.00000
B5	2.67874	0.00000	0.00000
B6	0.00000	0.00000	−2.24057
B7	0.00000	0.00000	2.24057
H8	1.53721	4.73105	0.00000
H9	−4.02447	2.92395	0.00000
H10	−4.02447	−2.92395	0.00000
H11	1.53721	−4.73105	0.00000
H12	4.97452	0.00000	0.00000
H13	0.00000	0.00000	−4.53698
H14	0.00000	0.00000	4.53698

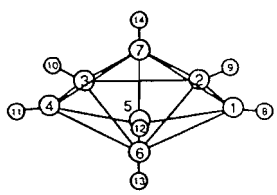

Can. J. Chem. Downloaded from www.nrcresearchpress.com by 123.30.183.119 on 09/08/12
For personal use only.

Can. J. Chem. Downloaded from www.nrcresearchpress.com by 123.30.183.119 on 09/08/12
For personal use only.

TABLE A9. $B_{12}H_{12}^{2-}$

$B_{12}H_{12}^{2-}$, I_h E(RHF) = −303.326804 au

Atom	x	y	z
B1	0.00000	0.00000	3.23340
B2	0.00000	2.89204	1.44602
B3	2.75050	0.89369	1.44602
B4	1.69990	−2.33971	1.44602
B5	−1.69990	−2.33971	1.44602
B6	−2.75050	0.89369	1.44602
B7	0.00000	0.00000	−3.23340
B8	0.00000	−2.89204	−1.44602
B9	2.75050	−0.89369	−1.44602
B10	1.69990	2.33971	−1.44602
B11	−1.69990	2.33971	−1.44602
B12	−2.75050	−0.89369	−1.44602
H13	0.00000	0.00000	5.50294
H14	0.00000	4.92198	2.46099
H15	4.68108	1.52097	2.46099
H16	2.89307	−3.98196	2.46099
H17	−2.89307	−3.98196	2.46099
H18	−4.68108	1.52097	2.46099
H19	0.00000	0.00000	−5.50294
H20	0.00000	−4.92198	−2.46099
H21	4.68108	−1.52097	−2.46099
H22	2.89307	3.98196	−2.46099
H23	−2.89307	3.98196	−2.46099
H24	−4.68108	−1.52097	−2.46099

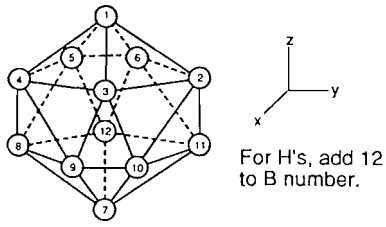

TABLE A10. $C_2B_3H_5$

$C_2B_3H_5$, D_{3h} E(RHF) = −152.708566 au

Atom	x	y	z
C1	0.00000	0.00000	2.10213
B2	0.00000	2.06718	0.00000
B3	−1.79023	−1.03359	0.00000
B4	1.79023	−1.03359	0.00000
C5	0.00000	0.00000	−2.10213
H6	0.00000	0.00000	4.12036
H7	0.00000	0.00000	−4.12036
H8	0.00000	4.29423	0.00000
H9	−3.71891	−2.14711	0.00000
H10	3.71891	−2.14711	0.00000

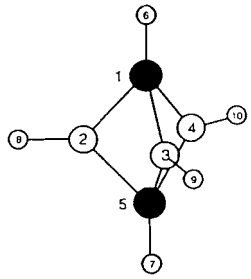

TABLE A11. $C_2B_4H_6$

$C_2B_4H_6$, D_{4h} E(RHF) = −177.939490 au

Atom	x	y	z
B1	−2.29337	0.00000	0.00000
B2	0.00000	−2.29337	0.00000
B3	2.29337	0.00000	0.00000
B4	0.00000	2.29337	0.00000
C5	0.00000	0.00000	−2.04620
C6	0.00000	0.00000	2.04620
H7	−4.50802	0.00000	0.00000
H8	0.00000	−4.50802	0.00000
H9	4.50802	0.00000	0.00000
H10	0.00000	4.50802	0.00000
H11	0.00000	0.00000	−4.05779
H12	0.00000	0.00000	4.05779

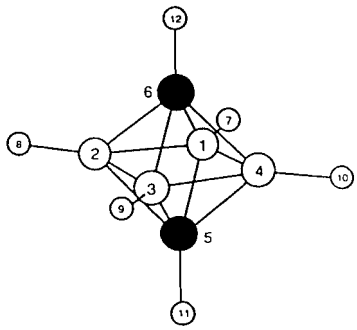

Diagrammatic analysis of nonlinear response properties in time-dependent Hartree–Fock theory

HIDEO SEKINO

Quantum Theory Project, University of Florida, Gainesville, FL 32611, U.S.A.

Received August 23, 1991

This paper is dedicated to Professor Sigeru Huzinaga on the occasion of his 65th birthday

HIDEO SEKINO. Can. J. Chem. **70**, 677 (1992).

Nonlinear response properties in Time-Dependent Hartree–Fock (TDHF) theory are analyzed by diagrammatic techniques and compared with the expression in propagator theory. The term that ensures that the quadratic response function is correct through first order in electron correlation emerges in the coupling term between lower order TDHF amplitudes and causes a violation of particle–hole pair conservation. It is shown diagrammatically that the dynamic hyperpolarizabilities can be expressed by lower order solutions in accordance with the $2n + 1$ rule.

Key words: nonlinear response property, TDHF, diagrammatic.

HIDEO SEKINO. Can. J. Chem. **70**, 677 (1992).

Utilisant une technique faisant appel à des diagrammes, on a analysé les propriétés de réponse non-linéaires de la théorie de Hartree–Fock dépendante du temps (TDHF) et on l'a comparé avec l'expression de la théorie du propagateur. Le terme qui assure que la fonction de réponse quadratique est correcte pour le premier ordre de corrélation électronique émerge dans le terme de couplage entre les amplitudes TDHF d'ordre les plus bas et il provoque une violation de la conservation de la paire trou–particule. On montre par un diagramme que les hyperpolarisabilités dynamiques peuvent être exprimées par des solutions de plus bas ordre, en accord avec la règle $2n + 1$.

Mots clés : propriété de réponse non-linéaire, TDHF, diagrammatique.

[Traduit par la rédaction]

Can. J. Chem. Downloaded from www.nrcresearchpress.com by 92.62.229.171 on 09/08/12
For personal use only.

Introduction

The theoretical investigation of nonlinear optical properties of molecules is one of the most challenging subjects in quantum chemistry. However, because the properties are highly sensitive to the frequency of the applied optical field, theories within a framework of stationary states may not be able to provide meaningful prediction for the experimental situation. High-order Time-Dependent Hartree–Fock (TDHF) theory is one of the methods that provide nonlinear dynamic response properties such as frequency-dependent hyperpolarizabilities. We have formulated the high-order TDHF and implemented it to calculate frequency-dependent hyperpolarizabilities of general molecules in different nonlinear optical processes (1). Recently the method was reformulated using a molecular orbital (MO) based algorithm (2). Performance of the computation employing the new algorithm was dramatically improved and is promising for applications to larger systems. The theories for nonlinear properties have also been formulated by propagator techniques (3, 4) and some applications have been made at the Hartree–Fock level (5, 6). But care must be taken to ensure that the nonlinear response function is correct through first order in electron correlation (3, 5). We present here the nonlinear response properties in a TDHF framework using diagrammatic techniques and make comparison with the expression in propagator theory.

Diagrammatic representation of nonlinear response property

The Time-Dependent Hartree–Fock (TDHF) equation is obtained by projecting Hartree–Fock (HF) differential equations onto a single determinantal wavefunction $|\phi\rangle$ composed of perturbed orbitals.

$$[1] \qquad \left(\hat{f} - \mathrm{i}\frac{\partial}{\partial t}\right)|\phi\rangle = |\phi\rangle\epsilon$$

The space is then spanned by singly excited determinants $|\phi_i\rangle$ with respect to the original determinant composed of original nonperturbed orbitals.

$$[2] \qquad |\phi\rangle = (|\phi_1\rangle, |\phi_2\rangle, \ldots, |\phi_n\rangle)U$$

Here, U is an unitary transformation that back-transforms the perturbed orbitals to the original orbitals and is called the TDHF amplitude. The Lagrangian multiplier ϵ represents the Hartree–Fock manifold of the perturbed system and thus the dimension of the corresponding matrix is equal to the number of the occupied orbitals for all orders. The Fock operator includes the time-dependent perturbation, $\Sigma_j \boldsymbol{E}_j \cdot \boldsymbol{O}_j e^{\pm i\omega t}$, caused by an oscillating external electric field of field strength $|\boldsymbol{E}_j|$ and property under consideration $\boldsymbol{O}_j$. For simplicity, the perturbations considered from now on are assumed to be all of the same kind and the applied electric field is monochromatic with frequency ω. The Fock matrix is expanded in the power series of E.

$$[3] \qquad \mathbf{f}(E) = \mathbf{f}^{(0)} + E\mathbf{f}(\pm\omega)e^{\pm i\omega t} + \frac{E^2}{2}\mathbf{f}(\pm\omega, \pm\omega)e^{\pm i(\omega\pm\omega)t} + \frac{E^3}{6}\mathbf{f}(\pm\omega \pm \omega \pm \omega)e^{\pm i(\omega\pm\omega\pm\omega)t} + \ldots$$

and further decomposed to a pure one-body term $\boldsymbol{O}$ and the Hartree–Fock effective potential

$$[4a] \qquad \mathbf{f}(\pm\omega, \pm\omega, \ldots) = \mathbf{O}\delta_{(n),1} + \mathbf{g}(\pm\omega, \pm\omega, \ldots)$$

where the external perturbation $\mathbf{O}$ appears only in the first order and the effective potential consists of the two-electron integral $\mathbf{v}$ and the density matrix $\mathbf{d}$.

$$[4b] \qquad \mathbf{g}(\pm\omega, \pm\omega, \pm\omega, \ldots) = \mathbf{v}.\mathbf{d}(\pm\omega, \pm\omega, \pm\omega, \ldots)$$

Here, "." means a two-index contraction between the anti-

symmetrized two-electron integral supermatrix $\mathbf{v} = \langle pq\|rs\rangle$ and the density matrix $\mathbf{d}(\pm\omega,\pm\omega,\pm\omega,\ldots)$. The $\boldsymbol{\epsilon}$ matrix,

$$[5]\qquad \boldsymbol{\epsilon}(E) = \boldsymbol{\epsilon}^{(0)} + E\boldsymbol{\epsilon}(\omega)e^{\pm i\omega t} + \frac{E^2}{2}\boldsymbol{\epsilon}(\pm\omega,\pm\omega)e^{\pm i(\omega\pm\omega)t} + \frac{E^3}{6}\boldsymbol{\epsilon}(\omega\pm\omega\pm\omega)e^{\pm i(\omega\pm\omega\pm\omega)t} + \ldots$$

and the amplitudes,

$$[6]\qquad \mathbf{U}(E) = \mathbf{U}^{(0)} + E\mathbf{U}(\pm\omega)e^{\pm i\omega t} + \frac{E^2}{2}\mathbf{U}(\pm\omega,\pm\omega)e^{\pm i(\omega\pm\omega)t} + \frac{E^3}{6}\mathbf{U}(\pm\omega,\pm\omega,\pm\omega)e^{\pm i(\omega\pm\omega\pm\omega)t} + \ldots$$

are also expanded with respect to the field E. In eq. [5], $\boldsymbol{\epsilon}^{(0)}$ is the diagonal canonical zeroth order Hartree–Fock solution and $\mathbf{U}^{(0)} = \mathbf{1}$.

Backprojecting eq. [1] onto the zeroth order Hartree–Fock space, we have

$$[7a]\qquad \mathbf{f}^{(0)}\mathbf{U}^{(0)} = \mathbf{U}^{(0)}\boldsymbol{\epsilon}^{(0)}$$

$$[7b]\qquad \{\pm\omega + \mathbf{f}^{(0)}\}\mathbf{U}(\pm\omega) + \mathbf{f}(\pm\omega)\mathbf{U}^{(0)} = \mathbf{U}(\pm\omega)\boldsymbol{\epsilon}^{(0)} + \mathbf{U}^{(0)}\boldsymbol{\epsilon}(\pm\omega)$$

$$[7c]\qquad \{\pm(\omega\pm\omega) + \mathbf{f}^{(0)}\}\mathbf{U}(\pm\omega,\pm\omega) + \mathbf{f}(\pm\omega,\pm\omega)\mathbf{U}^{(0)} + 2\mathbf{f}(\pm\omega)\mathbf{U}(\pm\omega) = \mathbf{U}(\pm\omega,\pm\omega)\boldsymbol{\epsilon}^{(0)} + 2\mathbf{U}(\pm\omega)\boldsymbol{\epsilon}(\pm\omega) + \mathbf{U}^{(0)}\boldsymbol{\epsilon}(\pm\omega,\pm\omega)$$

$$[7d]\qquad \{\pm(\omega\pm\omega\pm\omega) + \mathbf{f}^{(0)}\}\mathbf{U}(\pm\omega,\pm\omega\pm\omega) + \mathbf{f}(\pm\omega,\pm\omega,\pm\omega)\mathbf{U}^{(0)} + 3\mathbf{f}(\pm\omega,\pm\omega)\mathbf{U}(\pm\omega) + 3\mathbf{f}(\pm\omega)\mathbf{U}(\pm\omega,\pm\omega) = \mathbf{U}(\pm\omega,\pm\omega,\pm\omega)\boldsymbol{\epsilon}^{(0)} + 3\mathbf{U}(\pm\omega,\pm\omega)\boldsymbol{\epsilon}(\pm\omega) + 3\mathbf{U}(\pm\omega)\boldsymbol{\epsilon}(\pm\omega,\pm\omega) + \mathbf{U}^{(0)}\boldsymbol{\epsilon}(\pm\omega,\pm\omega,\pm\omega)$$

All matrices can be divided into several blocks such as occupied-occupied, virtual-occupied, occupied-virtual, and virtual-virtual blocks. The Hartree–Fock condition is thus

$$[8]\qquad \epsilon_{ai}(\pm\omega,\pm\omega,\ldots) = 0$$

for all occupied orbitals, $i,j,\ldots$ and virtual orbitals, $a,b,\ldots$.

From the condition [8] and eq. [7], the TDHF amplitude $\mathbf{U}(\pm\omega,\pm\omega,\pm\omega\ldots)$ is obtained. For example, from $\boldsymbol{\epsilon}_{v-o}(\pm\omega,\pm\omega) = 0$ in eq. [7c], we have the TDHF equation for the virtual-occupied amplitude $\mathbf{U}_{v-o}(\pm\omega,\pm\omega)$,

$$[7c']\qquad \{\pm(\omega\pm\omega) + \mathbf{f}^{(0)}\}\mathbf{U}_{v-o}(\pm\omega,\pm\omega) + \mathbf{f}_{v-o}(\pm\omega,\pm\omega) + 2\mathbf{f}(\pm\omega)\mathbf{U}(\pm\omega) = \mathbf{U}_{v-o}(\pm\omega,\pm\omega)\boldsymbol{\epsilon}^{(0)} + 2\mathbf{U}(\pm\omega)\boldsymbol{\epsilon}(\pm\omega)$$

Here, $\mathbf{f}^{(0)} = \boldsymbol{\epsilon}^{(0)}$ is diagonal. As we will see, a part of $\mathbf{f}_{v-o}(\pm\omega,\pm\omega)$ can be expressed by a two-index contraction of $\mathbf{U}_{v-o}(\pm\omega,\pm\omega)$ and typical RPA-type two-electron integrals. The other terms are simply products of lower order solutions and contribute as constants. Therefore eq. [7c'] is linear in $\mathbf{U}_{v-o}(\pm\omega,\pm\omega)$. The density matrix $\mathbf{d}(\pm\omega,\pm\omega,\pm\omega,\ldots)$

$$[9]\qquad \mathbf{d}(E) = \mathbf{d}^{(0)} + E\mathbf{d}(\pm\omega)e^{\pm i\omega t} + \frac{E^2}{2}\mathbf{d}(\pm\omega,\pm\omega)e^{\pm i(\omega\pm\omega)t} + \frac{E^3}{6}\mathbf{d}(\pm\omega,\pm\omega,\pm\omega)e^{\pm i(\omega\pm\omega\pm\omega)t} + \ldots$$

is then calculated through $\mathbf{d}(E) = \mathbf{U}(E)\mathbf{U}^{\dagger}(E)$. As we have seen in eq. [4], the density matrix is in turn used to create the Fock matrix. Thus the TDHF equation can be solved iteratively. The dynamic nonlinear response properties are given as a contraction of the perturbation property $\boldsymbol{\sigma}$ with the density matrix which comprises the nonlinear perturbation process under consideration. For the Hartree–Fock case, it is given as a contraction between the property corresponding to the perturbation and the one-body density matrix corresponding to the process such as $\mathbf{d}(\pm\omega,\pm\omega)$, $\mathbf{d}(o,\pm\omega)$, $\mathbf{d}(\pm\omega,\pm\omega,\pm\omega)\ldots$ for Second Harmonic Generation (SHG), ElectroOptic Pockels Effect (EOPE), Third Harmonic Generation (THG) ... etc. We now present the TDHF equation and the nonlinear response property diagrammatically. Here, we define the TDHF amplitudes

[D-1] 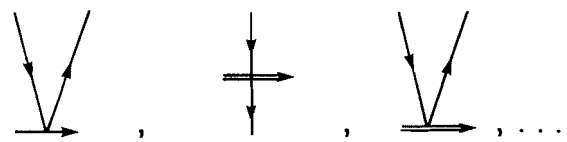

which represent $\mathbf{U}_{v-o}(+\omega)$, $\mathbf{U}_{o-o}(+\omega,+\omega)$, $\mathbf{U}_{o-o}(+\omega,+\omega)\ldots$ and the amplitudes

[D-2] 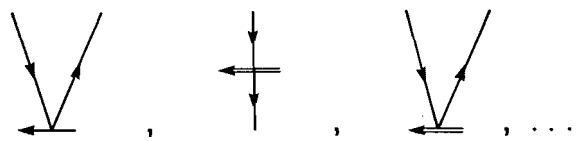

which represent $\mathbf{U}_{v-o}(-\omega)$, $\mathbf{U}_{o-o}(-\omega,-\omega)$, $\mathbf{U}_{v-o}(-\omega,-\omega)\ldots$. The direction of the arrow with respect to the time progression corresponds to the associated time factors such as $e^{+i(\omega_1+\omega_2+\ldots)t}$ or $e^{-i(\omega_1+\omega_2+\ldots)t}$.

The density matrix of Second Harmonic Generation (SHG) $\mathbf{d}(-2\omega;\,\omega,\omega) = \mathbf{U}(+\omega,+\omega) + \mathbf{U}(+\omega)\mathbf{U}^{\dagger}(-\omega) + \mathbf{U}^{\dagger}(-\omega,-\omega)$, for example, is represented as

[D-3a] 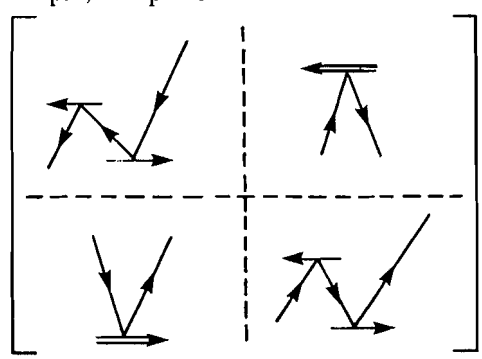

Can. J. Chem. Downloaded from www.nrcresearchpress.com by 92.62.229.171 on 09/08/12
For personal use only.

and

[D-3*b*] 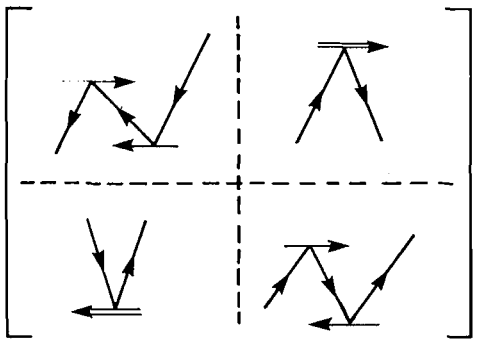

Here we have chosen the occupied-occupied block of $\boldsymbol{U}(\pm\omega,\pm\omega,\ldots)$ to have a symmetric relation $\mathbf{U}_{o-o}(+\omega, +\omega,\ldots) = \mathbf{U}_{o-o}(-\omega,-\omega,\ldots)$. This, together with the orthogonality condition, ensures

[D-4] 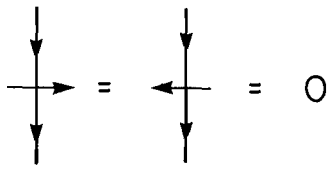

for the first-order amplitude. The occupied-occupied block of the second-order amplitude is determined through the second-order orthogonality condition $\mathbf{U}^{\dagger}_{o-o}(-\omega,-\omega) + \mathbf{U}^{\dagger}(-\omega)\mathbf{U}(+\omega) + \mathbf{U}_{o-o}(+\omega,+\omega) = \mathbf{0}$

[D-5] 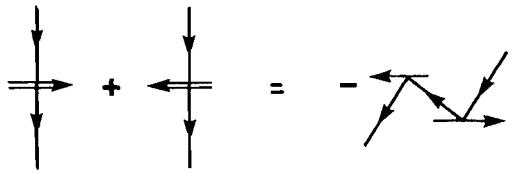

Now we define the Fock matrices diagrammatically. For zeroth order $\mathbf{f}^{(0)} = \mathbf{h}^{(0)} + \mathbf{g}^{(0)}$

[D-6] 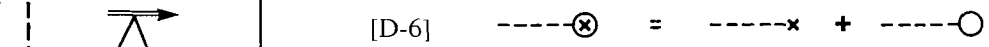

where ---× represents the one-electron part $\mathbf{h}^{(0)}$ and ---○ represents the effective HF potential caused by the two-electron part $\mathbf{g}^{(0)}$. For the first order $\mathbf{f}(\pm\omega) = \mathbf{O} + \mathbf{g}(\pm\omega)$

[D-7*a*]

and

[D-7*b*]

where

[D-8*a*] 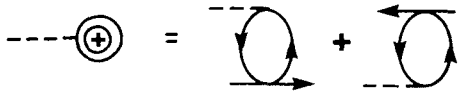

and

[D-8*b*]

The Fock matrices have a one-electron part ---△ and the effective HF potentials ---⊕ and ---⊖ are perturbed once before and once after the interaction ---- by the TDHF amplitudes → and ←. For the second order, the bare one-electron part **O** does not contribute to the Fock matrix and $\mathbf{f}(\pm\omega,\pm\omega) = \mathbf{g}(\pm\omega,\pm\omega)$ for the SHG case. The effective potential $\mathbf{g}(\pm\omega,\pm\omega)$ is now represented as

[D-9*a*] 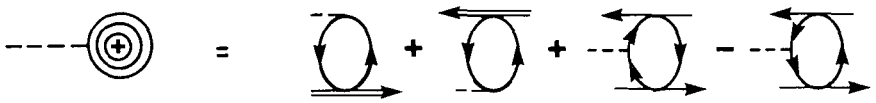

and

[D-9*b*] 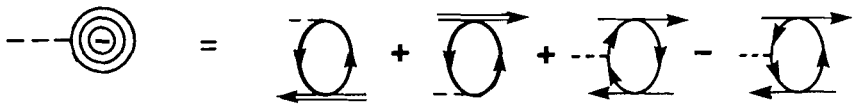

Similarly the occupied-occupied blocks of $\boldsymbol{\epsilon}$ are represented as follows. For $\boldsymbol{\epsilon}^{(0)}$, we have the diagrammatic representation

[D-10] 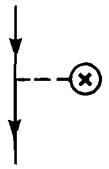

and the incoming and outgoing lines have same indices because the matrix is diagonal for the canonical zeroth order HF orbitals. Since $\boldsymbol{\epsilon}(\pm\omega) = \mathbf{f}(\pm\omega)$ for the same block, $\boldsymbol{\epsilon}(\pm\omega)$ is represented as

[D-11*a*] 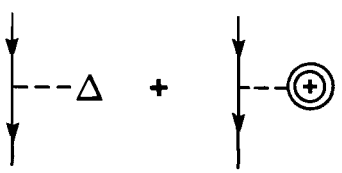

and

Can. J. Chem. Downloaded from www.nrcresearchpress.com by 92.62.229.171 on 09/08/12
For personal use only.

[D-11*b*]

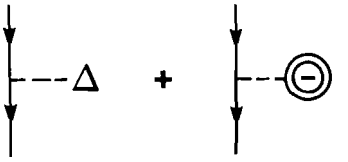

From the condition that the virtual-occupied block of $\epsilon(\pm\omega)$ in eq. [7*b*] must be zero, we obtain the linearized (first-order) TDHF equations for $U(\pm\omega) = \mathbf{U}_{v-o}(\pm\omega)$. This is represented diagrammatically as

[D-12*a*]

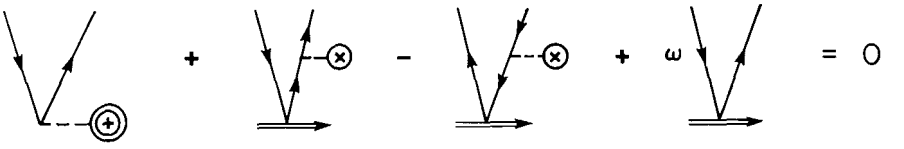

and

[D-12*b*]

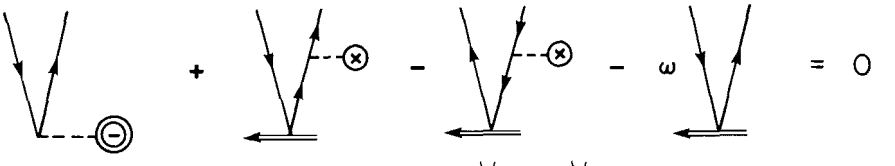

Using eqs. [D-8*a*] and [D-8*b*], we can replace the Fock matrices and by the TDHF amplitudes and and we arrive at the coupled equations for $U(\pm\omega)$.

$$[10] \quad \begin{bmatrix} \mathbf{A} & \mathbf{B} \\ \mathbf{B} & \mathbf{A} \end{bmatrix} \begin{bmatrix} U(+\omega) \\ U(-\omega) \end{bmatrix} \pm \omega \begin{bmatrix} U(+\omega) \\ U(-\omega) \end{bmatrix} + \begin{bmatrix} O \\ O \end{bmatrix} = \begin{bmatrix} \mathbf{0} \\ \mathbf{0} \end{bmatrix}$$

Here, **A** and **B** are ordinary Random Phase Approximation (RPA) matrices.

[D-13*a*]

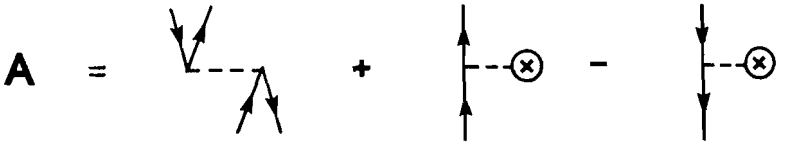

and

[D-13*b*]

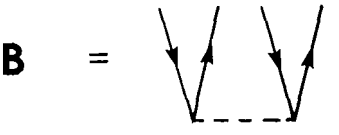

We can formally solve the equations

$$[11] \quad \begin{bmatrix} U(+\omega) \\ U(-\omega) \end{bmatrix} = -\mathbf{P}^{-1}(\omega) \begin{bmatrix} O \\ O \end{bmatrix}$$

where

$$[12] \quad \mathbf{P}(\omega) = \begin{bmatrix} \omega\mathbf{I} + \mathbf{A} & \mathbf{B} \\ \mathbf{B} & -\omega\mathbf{I} + \mathbf{A} \end{bmatrix}$$

From the condition that the virtual-occupied block of $\epsilon(\pm\omega \pm \omega)$ is zero in eq. [7*c*], the second-order TDHF equations are obtained.

[D-14*a*]

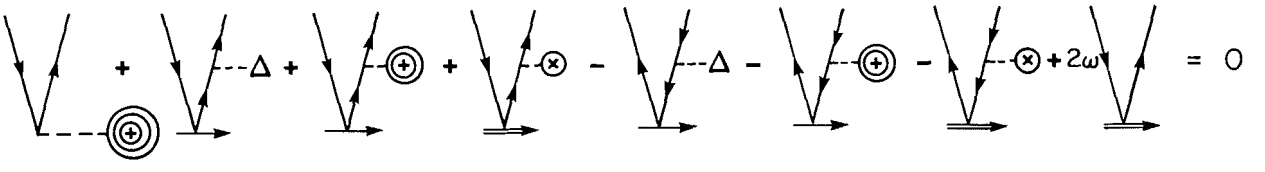

and

Can. J. Chem. Downloaded from www.nrcresearchpress.com by 92.62.229.171 on 09/08/12
For personal use only.

[D-14*b*] 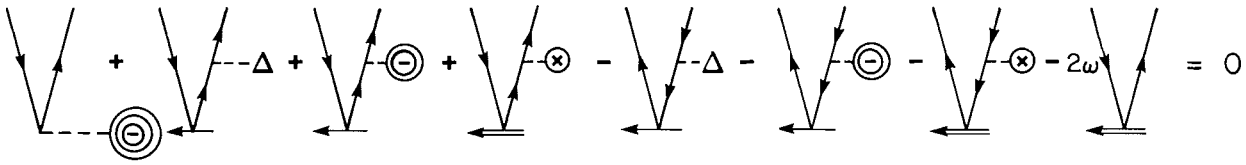

Using eqs. [D-9*a*] and [D-9*b*], we again replace the Fock matrices by the TDHF amplitudes and arrive at the final equations for the amplitudes $U(\pm\omega,\pm\omega) = \mathbf{U}_{v-o}(\pm\omega,\pm\omega)$

$$[13] \quad \begin{bmatrix} \mathbf{A} & \mathbf{B} \\ \mathbf{B} & \mathbf{A} \end{bmatrix} \begin{bmatrix} U(+\omega, +\omega) \\ U(-\omega, -\omega) \end{bmatrix} \pm 2\omega \begin{bmatrix} U(+\omega, +\omega) \\ U(-\omega, -\omega) \end{bmatrix} + \begin{bmatrix} h(+\omega, +\omega) \\ h(-\omega, -\omega) \end{bmatrix} = \begin{bmatrix} \mathbf{0} \\ \mathbf{0} \end{bmatrix}$$

where $\mathbf{h}(\pm\omega,\pm\omega)$ are constant terms composed of lower order terms and represented diagrammatically as:

[D-15*a*] 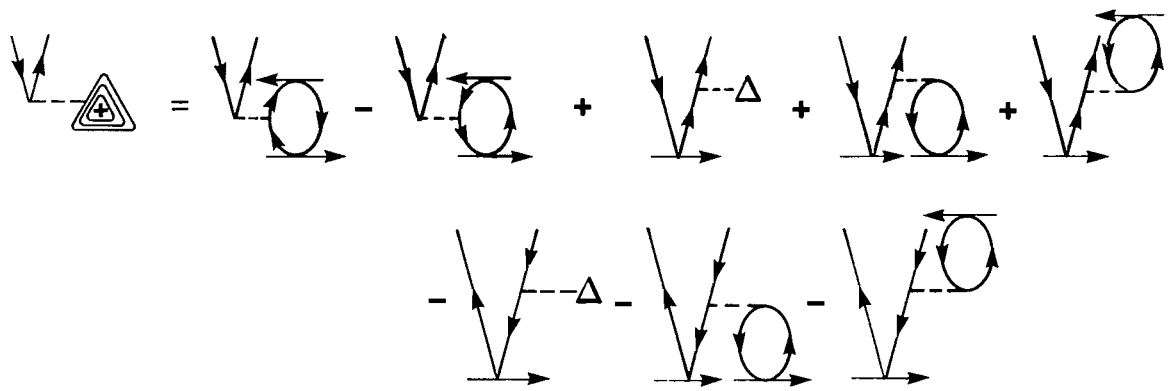

and

[D-15*b*] 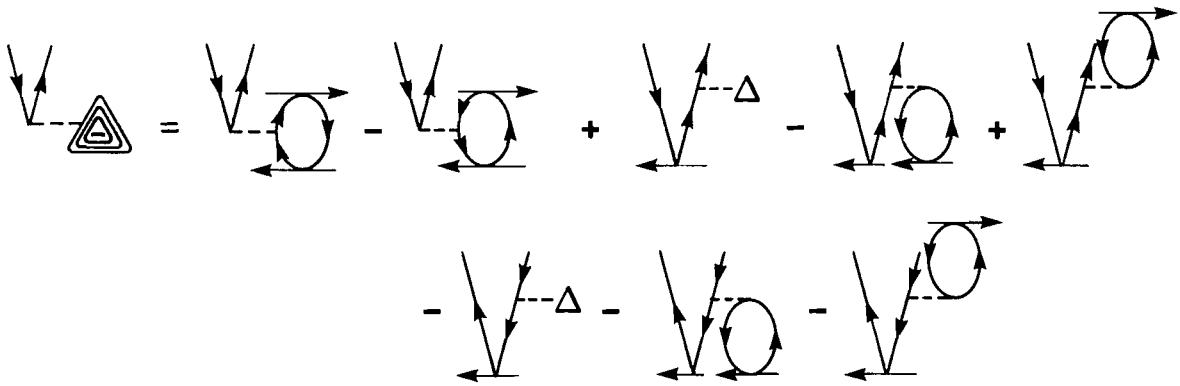

Therefore we can solve the TDHF equations for the second-order amplitudes $\mathbf{U}(\pm\omega,\pm\omega)$ in the same way as in the first-order solutions.

$$[14] \quad \begin{bmatrix} U(+\omega, +\omega) \\ U(-\omega, -\omega) \end{bmatrix} = -\mathbf{P}^{-1}(2\omega) \begin{bmatrix} h(+\omega, +\omega) \\ h(-\omega, -\omega) \end{bmatrix}$$

The **P** matrix has exactly the same form as in eq. [12] except that the frequency is now replaced by 2ω. The form of the **P** matrix is always the same for any order of TDHF equation. Therefore only a single diagonalization of the RPA matrix is sufficient to obtain all order solutions. The third-order response property of SHG is provided by contraction between the perturbation **O** and the density matrix $\mathbf{d}(+\omega,+\omega)$.

[D-16] 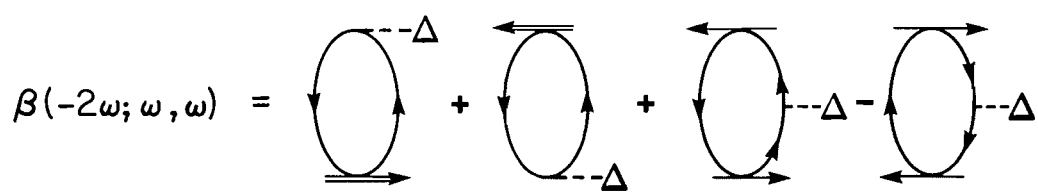

Can. J. Chem. Downloaded from www.nrcresearchpress.com by 92.62.229.171 on 09/08/12
For personal use only.

Inserting the solutions $U(+\omega,+\omega)$ and $U(-\omega,-\omega)$ from eq. [14] for and , and introducing new amplitudes $U(+2\omega)$ = and $U(-2\omega)$ = that satisfy

[15] $$\mathbf{P}(2\omega)\begin{bmatrix} U(2\omega) \\ U(-2\omega) \end{bmatrix} + \begin{bmatrix} O \\ O \end{bmatrix} = \begin{bmatrix} 0 \\ 0 \end{bmatrix}$$

and diagrammatically

[D-17] 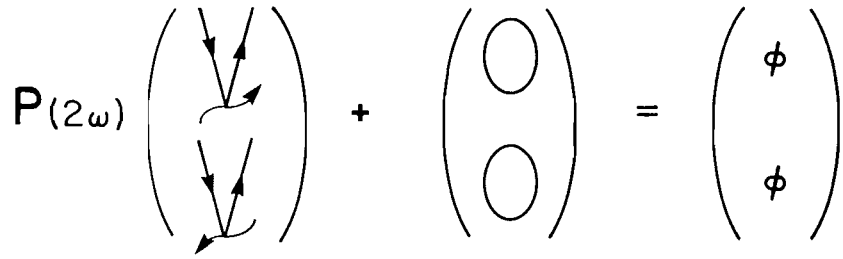

it becomes

[D-18] 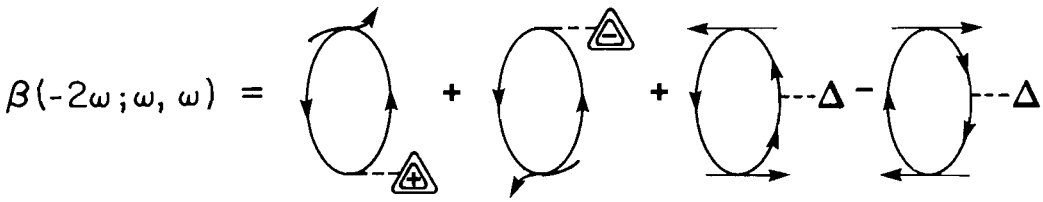

Therefore, the property is expressed by only first-order solutions. Using eqs. [D-15*a*] and [D-15*b*], we finally have

[D-19] 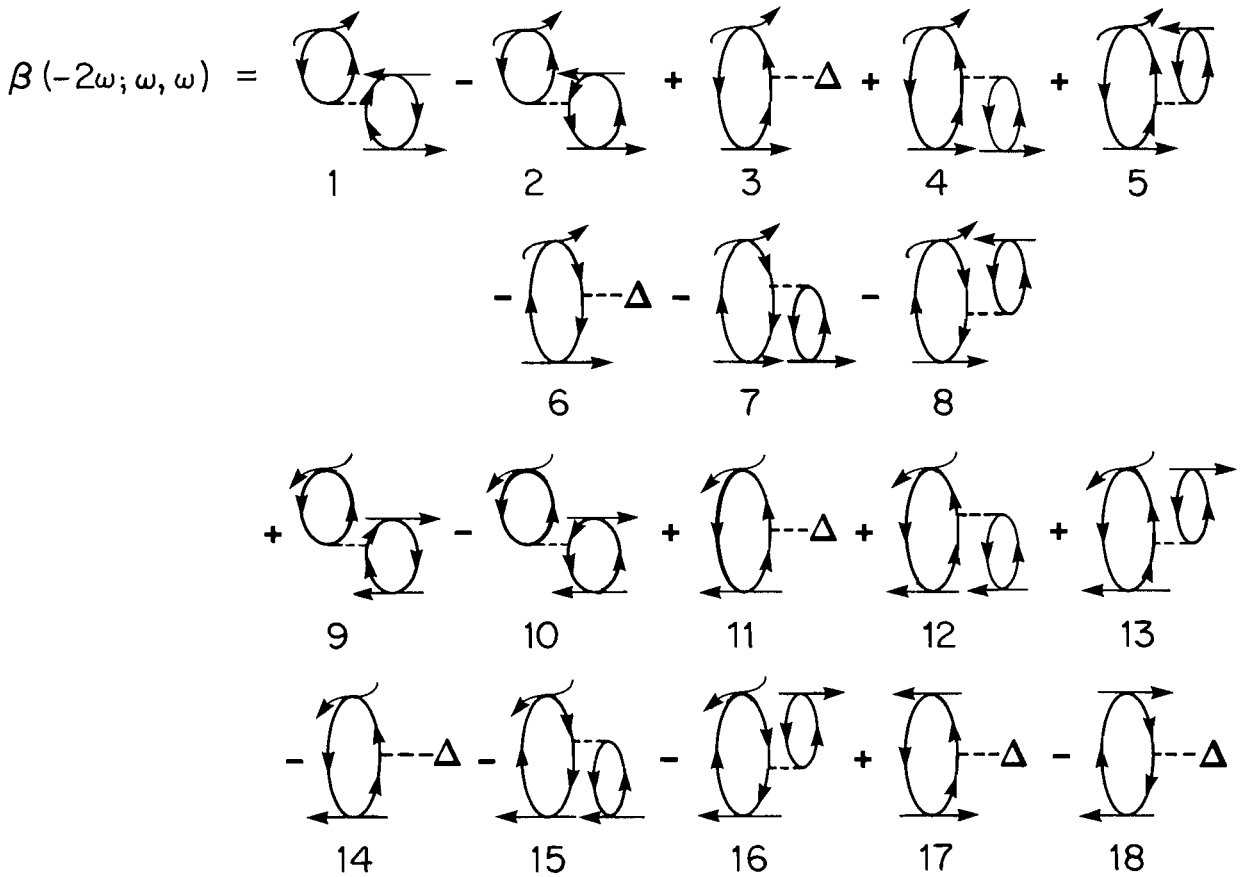

As we have seen above, the nonlinear property $\beta(-2\omega;\omega,\omega)$ can be calculated either from the first- and the second-order amplitudes $U(\pm\omega)$ and $U(\pm\omega,\pm\omega)$ or only from the first-order amplitudes $U(\pm\omega)$ and $U(\pm2\omega)$. The higher order properties such as γ can be expressed by the lower order amplitudes in a similar manner. This is of course a consequence of the $2n + 1$ or $2n$ rule (7).

Can. J. Chem. Downloaded from www.nrcresearchpress.com by 92.62.229.171 on 09/08/12
For personal use only.

Can. J. Chem. Downloaded from www.nrcresearchpress.com by 92.62.229.171 on 09/08/12
For personal use only.

Comparison with the expression in the propagator method

We now introduce a set of excitation and deexcitation operators $\{Q_J^\dagger, Q_J\}$ defined by

$$[16] \quad Q_J^\dagger = \sum_{a,i} (a^\dagger i Z_{ai}^J + i^\dagger a Y_{ai}^J), \qquad J = \pm 1, 2, \ldots, N(M-N)$$

Here M is the size of the basis set and N is the number of the occupied orbitals and $\{Z_{ai}^J, Y_{ai}^J\}$ is an RPA solution.

$$[17] \quad \begin{bmatrix} \mathbf{A} & \mathbf{B} \\ -\mathbf{B} & -\mathbf{A} \end{bmatrix} \begin{bmatrix} \mathbf{Z}^J \\ \mathbf{Y}^J \end{bmatrix} = -\mathrm{sgn}(J)\omega_J \begin{bmatrix} \mathbf{Z}^J \\ \mathbf{Y}^J \end{bmatrix}$$

The amplitudes $U(\pm\omega,\pm\omega,\pm\omega) = \mathbf{U}_{v-o}(\pm\omega,\pm\omega,\ldots)$ and the constant terms $h(\pm\omega,\pm\omega,\pm\omega\ldots) = \mathbf{h}_{v-o}(\pm\omega,\pm\omega,\ldots)$ may be transformed onto the new basis $\{Q_J^\dagger, Q_J\}$,

$$[18a] \quad \Lambda(\omega, \omega, \ldots) \equiv \begin{bmatrix} \tilde{U}(+\omega, +\omega,\ldots) \\ \tilde{U}(-\omega, -\omega,\ldots) \end{bmatrix} = [\mathbf{Z}^\dagger \; \mathbf{Y}^\dagger] \begin{bmatrix} -U(+\omega, +\omega,\ldots) \\ U(-\omega, -\omega,\ldots) \end{bmatrix}$$

and

$$[18b] \quad \begin{bmatrix} \tilde{h}(+\omega, +\omega, \ldots) \\ \tilde{h}(-\omega, -\omega, \ldots) \end{bmatrix} = [\mathbf{Z}^\dagger \; \mathbf{Y}^\dagger] \begin{bmatrix} h(+\omega, +\omega, \ldots) \\ h(-\omega, -\omega, \ldots) \end{bmatrix}$$

The first-order equations, eq. [10], become

$$[19] \quad (\mathbf{D} - \omega\mathbf{I}) \begin{bmatrix} \tilde{U}(+\omega) \\ \tilde{U}(-\omega) \end{bmatrix} + \begin{bmatrix} \tilde{h}(+\omega) \\ \tilde{h}(-\omega) \end{bmatrix} = \begin{bmatrix} \mathbf{0} \\ \mathbf{0} \end{bmatrix}$$

Here the **J**th element of the vector $h(\pm\omega)$ is

$$[20] \quad \tilde{h}(\pm\omega) = -\mathrm{sgn}(J)\langle[\kappa_{-J}, O]\rangle$$

and

$$[21a] \quad \kappa_J = Q_J^\dagger$$

for $J > 0$

$$[21b] \quad \kappa_J = Q_{|J|}$$

for $J < 0$. **D** is a diagonal matrix that contains RPA energies $\{\omega_J\}$ as its diagonal elements. Thus the first-order amplitudes are easily solved as

$$[22] \quad \tilde{U}^J(\pm\omega) = -\frac{\tilde{h}^J(\pm\omega)}{\omega - \mathrm{sgn}(J)\omega_J}$$

The second-order equations, eq. [13], become

$$[23] \quad (\mathbf{D} - 2\omega\mathbf{I}) \begin{bmatrix} \tilde{U}(+\omega, +\omega) \\ \tilde{U}(-\omega, -\omega) \end{bmatrix} + \begin{bmatrix} \tilde{h}(+\omega, +\omega) \\ \tilde{h}(-\omega, -\omega) \end{bmatrix} = \begin{bmatrix} \mathbf{0} \\ \mathbf{0} \end{bmatrix}$$

Here,

$$[24] \quad \tilde{h}(\pm\omega, \pm\omega) = -\mathrm{sgn}(J)\langle[[\kappa_{-J}, O], \Lambda(\omega)]\rangle - \frac{1}{2}\mathrm{sgn}(J)\langle[[[\kappa_{-J}, H^{(0)}], \Lambda(\omega)], \Lambda(\omega)]\rangle$$

and $H^{(0)}$ is a non-perturbed Hamiltonian. The second-order amplitudes are thus

$$[25] \quad \tilde{U}^J(\pm\omega,\pm\omega) = -\frac{\tilde{h}^J(\pm\omega,\pm\omega)}{2\omega - \mathrm{sgn(J)}\omega_J}$$

It is easy to see that the new first-order amplitudes $U(\pm 2\omega)$ introduced in eq. [15] are also expressed on the new basis as

$$[26] \quad \tilde{U}^J(\pm 2\omega) = -\frac{\tilde{h}^J(\pm\omega)}{2\omega - \mathrm{sgn(J)}\omega_J}$$

The terms 3, 6, 11, and 14 in eq. [D-19] are obtained by a contraction of the first-order solutions $U(\pm\omega)$ and $U(\pm 2\omega)$ with the property O, which is represented on the new basis $\{Q^{\dagger}_J, Q_J\}$ as

$$[27] \quad \tilde{O} = \langle [[\kappa_{-J}, O], \kappa_N] \rangle$$

and correspond to

$$[28] \quad \sum_{J,N} \frac{\mathrm{sgn}(JN)\langle O, \kappa_J]\rangle\langle [[\kappa_{-J}, O], \kappa_N]\rangle\langle [\kappa_{-N}, O]\rangle}{(2\omega - \mathrm{sgn}(J)\omega_J)(\omega - \mathrm{sgn}(N)\omega_N)}$$

The terms 17 and 18 correspond to

$$[29] \quad -\sum_{JJ'} \frac{\mathrm{sgn}(JJ')\langle (\kappa_J, O, \kappa_{J'})\rangle\langle [\kappa_{-J}, O]\rangle\langle [\kappa_{-J'}, O]\rangle}{(\omega - \mathrm{sgn}(J)\omega_J)(\omega - \mathrm{sgn}(J')\omega_{J'})}$$

and all the rest of the terms arise from a contraction among two first-order amplitudes $U(\pm\omega)$ and another first-order amplitude $U(\pm 2\omega)$ with unperturbed Hamiltonian $H^{(0)}$, which is represented on the new basis as

$$[30] \quad \tilde{H}^{(0)} = \langle (\kappa_N, [\kappa_{-J}, H^{(0)}], \kappa_M) \rangle$$

and correspond to

$$[31] \quad -\sum_{J,N,M} \frac{\mathrm{sgn}(JNM)\langle [O, \kappa_J]\rangle\langle (\kappa_N, [\kappa_{-J}, H^{(0)}], \kappa_M)\rangle\langle [\kappa_{-N}, O]\rangle\langle [\kappa_{-M}, O]\rangle}{(2\omega - \mathrm{sgn}(J)\omega_J)(\omega - \mathrm{sgn}(N)\omega_N)(\omega - \mathrm{sgn}(M)\omega_M)}$$

Since three amplitudes, two $U(\pm\omega)$ and one $U(\pm 2\omega)$, must contract to $H^{(0)}$, $H^{(0)}$ has a super matrix form such as in eq. [30].

Discussion

Higher order TDHF equations and nonlinear response properties are presented by diagrammatic techniques. As seen above, the third-order property that was originally derived using second-order TDHF amplitudes can be expressed with only first-order terms. This is a consequence of the $2n + 1$ rule (7) for dynamic properties. Klingbeil *et al.* proved this for fourth-order properties (8). Karna and Dupuis have shown it for both third- and fourth-order properties (9). Sekino and Bartlett (2) and Karma *et al.* (10) used the algorithm for calculating dynamic first and second hyperpolarizabilities β and γ. Rice *et al.* (11) and Parkinson and Oddershede (6) employed an equivalent principle for computing the first hyperpolarizability.

To express the Hartree–Fock density matrix in the space spanned by M basis functions, we need an operator manifold of dimension M^2, but only $N(M - N)$ complex variables are necessary to determine the Hartree–Fock energy of each order. Thus we need to solve $2N(M - N)$ real TDHF equations for $U(\pm\omega, \pm\omega, \ldots)$. Using the transformed basis $\{Q^{\dagger}_J, Q_J\}$, we can conveniently decouple the TDHF equations to $\tilde{U}(\pm\omega, \pm\omega, \ldots)$ and we arrive at the sum-over state representation of the nonlinear response function. This formulation is conceptually more appealing and the same formalism provides other related properties such as two-photon transition moments and transition probabilities between excited states (5, 6). However, it has computational disadvantages for calculating hyperpolarizabilities. An expression in supermatrix form, such as $\langle (\kappa_N, [\kappa_J, H^{(0)}], \kappa_M) \rangle$, is not useful in real computation where the size of operator space is not small. In our formalism, which involves Fock matrix formation, all contributions are expressed essentially by one-body terms and no supermatrix appears explicitly. The space required for mapping (ordered two-electron integrals) from density matrix to Fock matrix is $2M^2$. The typical integral lists of this kind are the P and K lists (15), which are commonly used for F matrix formation in AO basis. In contrast with the AO based methods (1, 9), the MO based algorithm presented here can divide the problem into subblocks: the occupied-occupied, virtual-occupied, etc. Only the mapping corresponding to the virtual-occupied block of the density matrix to the virtual-occupied block of the Fock matrix is required to obtain the TDHF amplitude through eqs. [10] and [13]. The mapping involving the virtual-virtual block of the density matrix to the virtual-occupied block of the Fock matrix is required for computation of third-order properties, while mapping that involves the virtual-virtual block of the density matrix to the virtual-virtual block of the Fock matrix is necessary for properties of more than fourth order. However, these mappings are required only for formation of the constant terms $h(\pm\omega, \pm\omega)$ etc., that is, required only once. The size of the space for mapping to solve eq. [10] or eq. [13] is only $2N(M - N)$ and can still be handled in the core memory of computers, even in cases with over 100 basis sets. Although those equations can be solved in a noniterative manner, we chose an iterative solution for the problem since the latter is much more efficient for nontrivial systems (2). Further, we implemented a reduced linear equation scheme (12–14) to accelerate the convergency for solving the equations. Performance of the vectorized program for dynamic hyperpolarizabilities β and γ was dramatic (2), and is promising for applications to larger systems.

It is known that the term shown in eq. [31] is necessary for the response function to be correct through first order in electron correlation (3, 5). In the first-order TDHF equation, the constant contribution is nothing but the external perturbation **O**. The second-order energy expression in Coupled Perturbed Hartree Fock (CPHF) is characterized by particle–hole bubbles. All the particle–hole pairs created at one time disappear together at another time (16). This so-called particle–hole pair conservation is no longer true in the higher order energy diagram as in eq. [D-19]. From the diagrammatic expression [D-14, 15], it is evident that the terms that violate the particle–hole pair conservation come from the coupling between two first-order terms $U(\pm\omega)$ in the second-order constant contribution $h(\pm\omega, \pm\omega)$ and those are

Can. J. Chem. Downloaded from www.nrcresearchpress.com by 92.62.229.171 on 09/08/12
For personal use only.

the terms that correspond to eq. [31]. Since it is a constant contribution, the violation happens only once for third-order properties. In general, nth order nonlinear response properties have terms that violate the particle–hole pair conservation $n - 2$ times. It should be noted, however, that TDHF theory is still one-body theory. There is no possibility to create real double excitation clusters that have no constraint in connecting among each other through two-electron interactions.

Acknowledgment

The author thanks Prof. R. J. Bartlett for useful discussions and Prof. J. Oddershede for providing preprints of his paper.

1. H. Sekino and R. J. Bartlett. J. Chem. Phys. **85**, 976 (1986).
2. H. Sekino and R. J. Bartlett. Int. J. Quantum Chem. (1991).
3. E. Dalgaard. Phys. Rev. A, **26**, 3235 (1982).
4. J. Olsen and P. Jørgensen. J. Chem. Phys. **82**, 3235 (1985).
5. P. W. Sengeløv and J. Oddershede. Chem. Phys. **124**, 371 (1988).
6. W. A. Parkinson and J. Oddershede. J. Chem. Phys. **94**, 7251 (1991).
7. T. S. Nee, R. G. Parr, and R. J. Bartlett. J. Chem. Phys. **64**, 2216 (1976).
8. R. Klingbeil, V. G. Kaveeshwar, and R. P. Hurst. Phys. Rev. A, **4**, 1760 (1971).
9. S. P. Karna and M. Dupuis. J. Comput. Chem. **12**, 487 (1991).
10. S. P. Karna, P. N. Prasad, and M. Dupuis. J. Chem. Phys. **94**, 1171 (1991).
11. J. E. Rice, R. D. Amos, S. M. Colwell, N. C. Handy, and J. Sanz. J. Chem. Phys. **93**, 8828 (1990).
12. J. A. Pople, R. Krishnam, H. B. Schlegel, and J. S. Binkley. Int. J. Quantum Chem. Symp. **13**, 225 (1979).
13. R. J. Bartlett and E. Brandas. J. Chem. Phys. **56**, 5467 (1972); **59**, 2032 (1973); Int. J. Quantum Chem. Symp. **5**, 151 (1971); E. Brandas and R. J. Bartlett. Chem. Phys. Lett. **8**, 153 (1971); R. J. Bartlett, J. C. Bellum, and E. Brandas. Int. J. Quantum Chem. Symp. **7**, 449 (1973).
14. G. D. Purvis III and R. J. Bartlett. J. Chem. Phys. **75**, 1284 (1981).
15. R. C. Raffenetti. Chem. Phys. Lett. **20**, 335 (1973).
16. T. C. Caves and M. Karplus. J. Chem. Phys. **50**, 3649 (1969); **75**, 320 (1981).

Can. J. Chem. Downloaded from www.nrcresearchpress.com by 92.62.229.171 on 09/08/12
For personal use only.

Time-dependent treatment of scattering: potential referenced and kinetic energy referenced modified Cayley approaches to atom–diatom collisions and time-scale separations

OMAR A. SHARAFEDDIN[1] AND DONALD J. KOURI[2]

Department of Chemistry and Department of Physics, University of Houston, Houston, TX 77204-5641, U.S.A.

AND

DAVID K. HOFFMAN

Department of Chemistry and Ames Laboratory,[3] Iowa State University, Ames, IA 50011, U.S.A.

Received June 10, 1991

This paper is dedicated to Professor Sigeru Huzinaga on the occasion of his 65th birthday

OMAR A. SHARAFEDDIN, DONALD J. KOURI, and DAVID K. HOFFMAN. Can. J. Chem. **70**, 686 (1992).

The time-dependent Lippmann–Schwinger equation describing atom–diatom collisions is expressed in terms of a general reference Hamiltonian, H_r, whose dynamics are easily solved in one representation, and a corresponding disturbance Hamiltonian, H_d, whose dynamics are easily solved in a different representation. The wavefunction at time $t + \tau$ is then expressed in terms of its value at a previous time t by means of a simple quadrature approximation. The resulting expression for $\psi(t + \tau)$ has a form similar to that occurring in earlier numerical unitary solutions to the time-dependent Schrodinger equation via a Cayley transformation. The structure of the new equations is made explicit for (a) the choice where H_r is taken to be the kinetic energy and H_d is the potential energy and (b) the choice where H_r is taken to be the potential energy and H_d is the kinetic energy. In addition, we also deal with several alternatives for treating the binding potential of the diatom. Several alternatives for choosing representations are then explored for reducing the equations to a form amenable to computation. The short time structure of the equations is discussed in terms of a multiple time-scales analysis.

Key words: molecular collisions, multiple time scales, quantum dynamics.

OMAR A. SHARAFEDDIN, DONALD J. KOURI et DAVID K. HOFFMAN. Can. J. Chem. **70**, 686 (1992).

L'équation de Lippmann–Schwinger qui est reliée au temps et qui décrit les collisions atome–diatome peut être exprimée en termes d'un Hamiltonien de référence générale, H_r, dont les dynamiques peuvent facilement être résolues par une représentation et un Hamiltonien correspondant de perturbation, H_d, dont les dynamiques peuvent facilement être résolues par une autre représentation. On peut alors exprimer la fonction d'onde au temps $t + \tau$ en termes de sa valeur à un temps antérieur t par le biais d'une approximation quadratique simple. L'expression qui en résulte pour $\psi(t + \tau)$ a une forme semblable à celle que l'on retrouve dans des solutions numériques unitaires antérieures de l'équation de Schroedinger reliée au temps qui sont obtenues par le biais d'une transformation de Cayley. On rend la structure des nouvelles équations explicite en faisant le choix que (a) H_r est l'énergie cinétique et H_d est l'énergie potentiel et (b) H_r est l'énergie potentiel et H_d est l'énergie cinétique. De plus, on tient compte des divers cas possibles pour le traitement du potentiel de liaison du diatome. On explore alors plusieurs options pour le choix des représentations permettant de réduire les équations à une forme que l'on peut traiter par un ordinateur. On discute de la structure de faible temps en fonction d'une analyse d'échelles multiples du temps.

Mots clés : collisions moléculaire, échelles multiples du temps, dynamiques quantique.

[Traduit par la rédaction]

1. Introduction

Recently, time-dependent wavepacket methods have proved to be very useful in treating molecular collisions (1–57).[4] In a series of papers (47 (paper 1), 49, 50), we initiated a systematic study of the time-dependent version of the Lippmann–Schwinger equation for scattering. Our objective is to develop an assortment of efficient methods for treating molecular collisions. The philosophy pursued is to split the Hamiltonian in an exact fashion into a reference piece, H_r, whose dynamics is simple in a certain representation, and a concomitant disturbance, H_d, whose dynamics is also simple in some *different* representation. Then the formal solution to the time-dependent Schrodinger equation is expressed in terms of the wavepacket at an earlier time evolved forward to the current time by an easily calculated evolution operator for the reference dynamics, plus an integral (over time) term that combines the H_r and H_d dynamics in a sequential fashion. The reference dynamics enters in terms of the (infinite order) evolution operator for the reference dynamics, while H_d enters in a linear fashion. There are numerous options available for dealing with the integral term in order to obtain suitable equations for computations. In our earlier work, we explored methods based on the wavefunction and the time-dependent amplitude density (47, 49), and on two different choices for H_r and H_d: the standard one where H_r is the kinetic energy and H_d the potential (49, 50), and a new one where H_r is the potential and H_d is the kinetic energy (49). In ref. 50, we also derived a new computational approach using the standard splitting of the Hamiltonian H into H_r and H_d, and expressing the current

[1]R. A. Welch Predoctoral Fellow under R. A. Welch Foundation Grant E-608.

[2]Supported in part under National Science Foundation Grant CHE89-07429.

[3]Ames Laboratory is operated for the U.S. Department of Energy by Iowa State University under Contract No. 2-7405-ENG-82. This research was supported by the Division of Chemical Sciences, Office of Basic Energy Sciences.

[4]Some recent reviews include ref. 1*a* for molecule-surface scattering, ref. 1*b* for collinear gas phase reactive scattering, and ref. 1*c* for a general review.

Printed in Canada

Can. J. Chem. Downloaded from www.nrcresearchpress.com by 92.62.229.171 on 09/08/12
For personal use only.

Can. J. Chem. Downloaded from www.nrcresearchpress.com by 92.62.229.171 on 09/08/12
For personal use only.

time wavepacket in terms of a modified Cayley transform acting on the earlier time wavepacket. This procedure was applied successfully to a potential modelling elastic electron–atom scattering.

In this paper, we extend the modified Cayley transform equations to the case of atom–diatom scattering, including both rotational and vibrational degrees of freedom. We present the basic equations for an arbitrary choice of H_r and H_d, and then apply them to four specialized cases: (1) H_r is the complete relative kinetic energy and H_d is the complete potential energy; (2) H_r is the complete relative kinetic energy *plus* the diatom binding potential energy, and H_d is the remaining potential energy; (3) H_r is the complete potential energy and H_d is the complete relative kinetic energy; and (4) H_r is the potential energy minus the diatom binding potential energy, and H_d is the complete relative kinetic energy plus the diatom binding potential energy. We explore several possible ways to implement these equations, and study particularly the roles of representations used and the particle masses and range of interactions in the choice of computational method. Of special interest is the possibility of time-scale separations as a means of simplifying the equations. It is also noted that our techniques apply equally well to the symmetric split operator approach (11*a*).[5]

The paper is organized as follows. In Sect. 2 we present the derivation of the modified Cayley method for an atom–diatom system and a general choice of H_r and H_d. Then in Sects. 3 and 4, we apply the choices of H_r and H_d to specialized cases (1) and (2), and cases (3) and (4), respectively, and discuss the choice of representations and the role of time scales for various motions. Finally, in Sect. 5, we indicate some directions for future work.

2. General referenced modified Cayley method

We desire to solve the time-dependent Schrodinger equation

$$[1] \qquad i\hbar \frac{\partial|\psi(t)\rangle}{\partial t} = H|\psi(t)\rangle$$

where the Hamiltonian H may be expressed as

$$[2] \qquad H = H_r + H_d$$

Here, H_r denotes the so-called reference Hamiltonian, and H_d is a disturbance Hamiltonian. In general, H_r and H_d do not commute, so that no representation exists in which both are diagonal. However, in general, some representation will exist in which H_r is diagonal, and some *different* representation will exist in which H_d is diagonal. The solution to eq. [1] may be expressed as

$$[3] \qquad |\psi(t)\rangle = \frac{-i}{\hbar}\int_{t-\tau}^{t} dt' e^{-iH_r(t-t')/\hbar} H_d|\psi(t')\rangle + e^{-iH_r\tau/\hbar}|\psi(t-\tau)\rangle$$

We note that eq. [3] is *exact,* and represents a means of splitting H into H_r and H_d so that each can be evaluated in its eigen-representation. (This is reminiscent of the split operator approach to time-dependent quantum dynamics. *However, in eq. [3] the splitting enters without approximation.* Of course, eventually, some approximations will be introduced in order to carry out calculations to a desired level of accuracy. There are *many* ways to approximate eq. [3] so that considerable flexibility is gained, and the approximate computational expressions will be chosen such that as $\tau \to 0$, the result becomes arbitrarily accurate.)

To obtain the modified Cayley form, we approximate the integral over t' in eq. [3] by the simple trapezoidal rule. This yields

$$[4] \qquad |\psi(t)\rangle = \frac{-i\tau}{2\hbar}\left[H_d|\psi(t)\rangle + e^{-iH_r\tau/\hbar}H_d|\psi(t-\tau)\rangle\right] + e^{-iH_r\tau/\hbar}|\psi(t-\tau)\rangle$$

Rearranging and solving for $|\psi(t)\rangle$ then leads to

$$[5] \qquad |\psi(t)\rangle = \left[1 + \frac{i\tau}{2\hbar}H_d\right]^{-1} e^{-iH_r\tau/\hbar}\left[1 - \frac{i\tau}{2\hbar}H_d\right] \times |\psi(t-\tau)\rangle$$

This is the modified Cayley form referenced to H_r. By way of reminder, the usual Cayley transform (or Crank–Nicholson (58) method leads to the expression (8)

$$[6] \qquad |\psi(t)\rangle = \left[1 + \frac{i\tau}{2\hbar}H\right]^{-1}\left[1 - \frac{i\tau}{2\hbar}H\right]|\psi(t-\tau)\rangle$$

Thus, it requires inverting an operator containing the full Hamiltonian, or more efficiently, solving the set of equations (8, 58)

$$[7] \qquad \left[1 + \frac{i\tau}{2\hbar}H\right]|\psi(t)\rangle = \left[1 - \frac{i\tau}{2\hbar}H\right]|\psi(t-\tau)\rangle$$

We have previously pointed out (50) that the form eq. [5] can be viewed also as being related to the symmetric split operator (11) approach, since for small enough τ,

$$[8] \qquad \left[1 + \frac{i\tau}{2\hbar}H_d\right]^{-1} \cong 1/\exp(i\tau H_d/2\hbar)$$

$$[9] \qquad = \exp(-i\tau H_d/2\hbar)$$

and

$$[10] \qquad \left[1 - \frac{i\tau}{2\hbar}H_d\right] \cong \exp(-i\tau H_d/2\hbar)$$

which leads to

$$[11] \qquad |\psi(t)\rangle = e^{-iH_d\tau/2\hbar}\, e^{-iH_r\tau/\hbar}\, e^{-iH_d\tau/2\hbar}|\psi(t-\tau)\rangle$$

However, even though the symmetric split operator expression contains $(H_d\tau/2\hbar)$ to infinite order, it is *not* necessarily more accurate than eq. [5]. In fact, as τ becomes larger, having $(H_d\tau/2\hbar)$ to infinite order, but not with the correct coefficients of the various commutators, may lead to worse results. The accuracy of eq. [5] is controlled by the degree to which the trapezoidal rule accurately yields the time integral in eq. [3] above, while the accuracy of eq. [11] depends on the size of the commutator, $[H_r,H_d]$. In fact, calculations comparing the two show that for the systems studied, the kinetic referenced modified Cayley is more robust. We shall focus on the modified Cayley version, eq. [5], in this paper, but the same analyses can be made using the symmetric split operator equations. In eq. [5], one may carry

[5]See also the symmetric split operator approach of DeVries (11*b*).

Can. J. Chem. Downloaded from www.nrcresearchpress.com by 92.62.229.171 on 09/08/12
For personal use only.

out the usual procedure of evaluating $[1 + i\tau/2\hbar H_d]^{-1}$, $e^{-iH_r\tau/\hbar}$, and $[1 - i\tau/2\hbar H_d]$ in their respective diagonalizing representations, followed by appropriate transformations between these two representations. There are, however, other interesting options that we shall explore in this paper.

Finally, we note from the structure of eq. [5] that, in some sense, a "natural" representation in which to calculate $|\psi(t)\rangle$ is determined by H_d, since the left-most operator in eq. [5] is diagonal in this representation, and the first operator acting on $|\psi(t-\tau)\rangle$ is $[1 - i\tau/2\hbar H_d]$. The basic procedure then would require transforming $[1 - i\tau/2\hbar H_d]|\psi(t-\tau)\rangle$ from the H_d to the H_r representation, followed by application of $e^{-iH_r\tau/\hbar}$ in the H_r representation. Then one would transform back to the H_d representation for application of $[1 + i\tau/2\hbar H_d]^{-1}$, yielding $|\psi(t)\rangle$ in the H_d representation. Alternatively, one can evaluate $\exp(-iH_r\tau/k)$ in the H_d representation, or $[1 - i\rho/2\hbar H_d]$ and $[1 + i\tau/2\hbar H_d]^{-1}$ in the H_r representation, so that the entire calculation could be done without changing representations (62–64). Since these operators depend only on the time step size (65), rather than on the time itself, they may be evaluated once and stored, thereby saving computational effort if a number of wave-packet propagations are to be done.

3. Kinetic energy referenced modified Cayley method

In this case, we choose H_r to be the total relative kinetic energy operator for the atom–diatom collision system, and H_d is then the full potential energy for the system. The basic equation (eq. [5]) then becomes

$$[12]\quad |\psi^{JM}(n_0 j_0 l_0|t)\rangle = \left[1 + \frac{i\tau}{2\hbar}V\right]^{-1} e^{-i(K_R+K_r)\tau/\hbar} \times \left[1 - \frac{i\tau}{2\hbar}V\right]|\psi^{JM}(n_0 j_0 l_0|t-\tau)\rangle$$

where we choose to work initially in the coupled angular momentum (65) or Arthurs–Dalgarno representation (developed in ref. 59). Then J is the total angular momentum quantum number, $M\hbar$ is the space fixed z-component of total angular momentum, n_0, j_0, and l_0 are the initial vibrational, diatom rotational angular momentum, and orbital angular momentum quantum numbers, $\boldsymbol{R}$ is the vector from the diatom center of mass to the atom, $\boldsymbol{r}$ is the diatom internuclear vector, the symbol K represents a kinetic energy operator for motion in the coordinate occurring as a subscript, and V denotes the complete potential energy operator. It is clear from eq. [12] that a convenient representation for $|\psi^{JM}(n_0 j_0 l_0)|t)\rangle$ will be the coordinate representation, since the potential energy V is diagonal in this representation. It is also, however, convenient to employ the conservation of total angular momentum. We project eq. [12] from the left with $\langle \boldsymbol{R}\boldsymbol{r}|$, and insert resolutions of the identity

$$[13]\quad 1 = \int d\boldsymbol{R}' \int d\boldsymbol{r}' |\boldsymbol{R}'\boldsymbol{r}'\rangle\langle \boldsymbol{R}'\boldsymbol{r}'|$$

and

$$[14]\quad 1 = \frac{4}{\pi^2}\sum_{jlJ'M'}\int_0^\infty dK K^2 \int_0^\infty dk k^2 |Kl\rangle|kj\rangle|\mathcal{Y}_{jl}^{J'M'}\rangle \times \langle \mathcal{Y}_{jl}^{J'M'}|\langle kj|\langle Kl|$$

where

$$[15]\quad \langle \boldsymbol{R}'\boldsymbol{r}'|\boldsymbol{R}\boldsymbol{r}\rangle = \delta(\boldsymbol{R}-\boldsymbol{R}')\delta(\boldsymbol{r}-\boldsymbol{r}')$$

$$[16]\quad \langle R|Kl\rangle = j_l(KR)$$

$$[17]\quad \langle r|kj\rangle = j_j(kr)$$

$$[18]\quad \langle \theta\varphi\chi\xi|\mathcal{Y}_{jl}^{J'M'}\rangle = \sum_{m_j}\langle lM' - m_j jm_j|J'M'\rangle \times Y_{lM'-m_j}(\theta\psi)Y_{jm_j}(\chi\psi)$$

χ, ξ and θ, φ are the polar and azimuthal angles of $\boldsymbol{r}$ and $\boldsymbol{R}$, $j_j(kr)$ and $j_l(KR)$ are the usual spherical Bessel functions, and $\langle lM' - m_j jm_j|J'M'\rangle$ is a Clebsch–Gordan coefficient (60). This yields

$$[19]\quad \psi^{JM}(\boldsymbol{R}\boldsymbol{r}|n_0 j_0 l_0|t) = \left[1 + \frac{i\tau}{2\hbar}V(r R\hat{r}\cdot\hat{R})\right]^{-1} \times \frac{4}{\pi^2}\sum_{jlJ'M'}\int_0^\infty dK K^2 \int_0^\infty dk k^2\, e^{-i(K^2/\mu + k^2/m)\hbar\tau/2} j_l(KR) j_j(kr) \times \mathcal{Y}_{jl}^{J'M'}(\hat{R}\hat{r}) \int d\boldsymbol{R}' \int d\boldsymbol{r}' j_l(KR') j_j(kr') \mathcal{Y}_{jl}^{J'M'*}(\hat{R}'\hat{r}') \times \left[1 - \frac{i\tau}{2\hbar}V(r'R'\hat{r}'\cdot\hat{R}')\right]\psi^{JM}(\boldsymbol{R}'\boldsymbol{r}'|n_0 j_0 l_0|t-\tau)$$

To further simplify, we take advantage of conservation of total angular momentum, and write (for any time t),

$$[20]\quad \psi^{JM}(\boldsymbol{R}\boldsymbol{r}|n_0 j_0 l_0|t) = \sum_\Omega D^J_{\Omega M}(\xi\theta\varphi)\psi^{J\Omega}(Rr\alpha|n_0 j_0 l_0|t)$$

where $D^J_{\Omega M}$ is a Wigner rotation matrix (60), (ξ,θ,φ) are the Eulerian angles of a body frame whose z-axis is along $\hat{R}$, and oriented so that the diatom is in the (x,z) plane. Then α, the angle between $\boldsymbol{r}$ and $\boldsymbol{R}$, is the polar angle of the diatomic axis in the rotating frame. Noting that (61)

$$[21]\quad \mathcal{Y}_{jl}^{JM}(\hat{R}\hat{r}) = \sqrt{\frac{2l+1}{8\pi^2}}\sum_\Omega D^J_{\Omega M}(\phi\theta\varphi)\,\langle l0j\Omega|J\Omega\rangle\, P_{j\Omega}(\cos\alpha)$$

where $P_{j\Omega}(\cos\alpha)$ is a normalized associated Legendre polynomial, we can project eq. [19] with $D^{J*}_{\Omega M}(\xi\theta\varphi)$ to obtain

$$[22]\quad \psi^{J\Omega}(Rr\alpha|n_0j_0l_0|t) = \left[1 + \frac{i\tau}{2\hbar}V(Rr\alpha)\right]^{-1}\frac{4}{\pi^2}\sum_{\substack{jl\\ \Omega'}}\int_0^\infty dKK^2\int_0^\infty dkk^2\, e^{-i(K^2/\mu + k^2/m)\hbar\tau/2}j_l(KR)j_j(kr)\frac{(2l+1)}{(2J+1)}$$
$$\times \langle l0j\Omega|J\Omega\rangle\langle l0j\Omega'|J\Omega'\rangle\, P_{j\Omega}(\cos\alpha)\int_0^\infty dR'R'^2\int_0^\infty dr'r'^2\int_{-1}^1 d(\cos\alpha')j_j(kr')P_{j\Omega'}(\cos\alpha')$$
$$\times\left(1 - \frac{i\tau}{2\hbar}V(R'r'\alpha')\right)\psi^{J\Omega'}(R'r'\alpha'|n_0j_0l_0|t-\tau)$$

We note that the fact that the potential energy depends only on $\hat{r}\cdot\hat{R}$ rather than on $\hat{r}$ and $\hat{R}$ separately has been used in obtaining eq. [22]. This equation can be used to calculate $\psi^{J\Omega}(Rr\alpha|n_0j_0l_0|t)$ at time t from its previous values at time $t-\tau$.

If we include the diatomic binding potential in H_r, so that

$$[23]\quad H_r = K_R + K_r + v(r)$$

the result is easily shown to be

$$[24]\quad \psi^{J\Omega}(Rr\alpha|n_0j_0l_0|t) = \left[1 + \frac{i\tau}{2\hbar}v(Rr\alpha)\right]^{-1}\frac{2}{\pi}\sum_{\substack{jl\\ n\Omega'}}\int_0^\infty dKK^2\, e^{-i(\hbar K^2/2\mu + \epsilon_{nj}/\hbar)\tau}j_l(KR)f_{nj}(r)\left(\frac{2l+1}{2J+1}\right)\langle l0j\Omega|J\Omega\rangle\langle l0j\Omega'|J\Omega'\rangle$$
$$\times P_{j\Omega}(\cos\alpha)\int_0^\infty dR'R'^2\int_0^\infty dr'r'^2\int_{-1}^1 d(\cos\alpha')j_l(KR')f_{nj}(r')P_{j\Omega'}(\cos\alpha')\left[1 - \frac{i\tau}{2\hbar}v(R'r'\alpha')\right]$$
$$\times\psi^{J\Omega'}(R'r'\alpha'|n_0j_0l_0|t-\tau)$$

where $f_{nj}(r)$ is the vibrational eigenstate of the vibrating–rotating diatom, having energy ϵ_{nj}, and

$$[25]\quad v(R'r'\alpha') = V(R'r'\alpha') - v(r')$$

In this case, the summation over the index n replaces the integration over k.

We note that if the symmetric split operator (11) were used, then $\exp(-i\tau V(Rr\alpha)/2\hbar)$ would replace

$$\left[1 + \frac{i\tau}{2\hbar}V(Rr\alpha)\right]^{-1}\quad\text{and}\quad\left[1 - \frac{i\tau}{2\hbar}V(Rr\alpha)\right]$$

in eq. [22], and $\exp(-i\tau v(Rr\alpha)/2\hbar)$ would replace

$$\left[1 + \frac{i\tau}{2\hbar}v(Rr\alpha)\right]^{-1}\quad\text{and}\quad\left[1 - \frac{i\tau}{2\hbar}v(Rr\alpha)\right]$$

in eq. [24].

Equations [22] and [24] are the result of using a total angular momentum (30, 59, 66), rotating body frame (38, 40, 67), coordinate representation, combined with the KRMC equation. We shall use them now to examine the consequences of time-scale separations for the various motions in the atom–diatom system. The natural time scales for each degree of freedom can be determined by examination of the manner in which the time (65) enters the factors $\exp[-i(K^2\tau/\mu + k^2\tau/m)\hbar/2]$ and $[1 \pm (i\tau/2\hbar)V(Rr\alpha)]^{\mp1}$ in eq. [22], and $\exp[-i(\hbar K^2\tau/2\mu + \epsilon_{nj}\tau/\hbar)]$ and $[1 \pm (i\tau/2\hbar)V(Rr\alpha)]^{\mp1}$ in eq. [24]. The terms representing kinetic energy are easy to analyze, and for eq. [22] the ratios τ/μ and τ/m naturally occur (65). There are also natural length scales r_0 associated with the binding potential $v(r)$, and R_0 associated with the scattering potential $v(Rr\alpha)$ (65) (defined by eq. [25]). These are essentially range parameters associated with the distance over which a potential is significant. Thus it is important to understand that the length scales R_0 and r_0 essentially contain the qualitative information about (a) whether the bound motion in r permits large or small excursions (so if r_0 is small, this corresponds to a tightly bound system, and if r_0 is large, denoting large excursions, one has a loosely bound system, such as van der Waals bond); (b) whether the scattering interaction is long ranged (with R_0 large) or short ranged (with R_0 small). We define effective times τ_1' and τ_2' by (65)

$$[26]\quad \tau_1' = \tau/\mu R_0^2$$

and

$$[27]\quad \tau_2' = \tau/mr_0^2$$

It is straightforward then to introduce the natural energy units $\hbar^2/2\mu R_0^2$ and $\hbar^2/2mr_0^2$ associated with the R and r degrees of freedom respectively. If K and k are measured in units $1/R_0$ and $1/r_0$ respectively, then for eq. [22] we will have factors

$$[28]\quad \exp[-i(\hbar\tilde{K}^2\tau_1'/2 + \hbar\tilde{k}^2\tau_2'/2)]$$

and

$$[29]\quad \left[1 \pm i\hbar\left(\frac{\tau_1'}{2}\tilde{v}(Rr\alpha) + \frac{\tau_2'}{2}\tilde{v}(r)\right)\right]^{\mp1}$$

and for eq. [24], the factors are

$$[30]\quad \exp\left[-i\left(\hbar\tilde{K}^2\tau_1'/2 + \frac{\hbar\tau_2'}{2}\tilde{\epsilon}_{nj}\right)\right]$$

Can. J. Chem. Downloaded from www.nrcresearchpress.com by 92.62.229.171 on 09/08/12
For personal use only.

Can. J. Chem. Downloaded from www.nrcresearchpress.com by 92.62.229.171 on 09/08/12
For personal use only.

and

$$[31] \quad \left[1 \pm \frac{i\hbar}{2}\tau_1'\tilde{v}(Rr\alpha)\right]^{\mp 1}$$

Here, all quantities with tildes are dimensionless.

To consider time-scale separations, it is clear that one must consider the relative sizes of the masses μ and m and the lengths R_0 and r_0. The basic condition that must be satisfied by the *physical time step*, τ, is that it be short enough to ensure that an accurate description is obtained in the trapezoidal quadrature evaluation of the time integral in eq. [3]. Typically, one expects this to be governed by the rate at which the wavepacket is moving *and* being distorted by the potential, and this is strongly influenced by the energies included in the construction of the original packet for relative motion, and the initial internal state of the bounded notion. For many systems, the rate of motion will be dominated by the masses μ and m, so that τ must be chosen small enough to follow the motion of the light particle. If, for example, this is taken to be particle 1, with mass μ, then τ must be chosen small enough that τ_1' does not result in so large a change in the average position of particle 1 that the integrand changes too rapidly. We note futher that by construction,

$$[32] \quad \mu R_0^2/mr_0^2 << 1$$

and by eqs. [26] and [27],

$$[33] \quad \tau = \frac{\mu}{R_0^2}\tau_1'$$

and

$$[34] \quad \tau_2' = (\tau_1'\mu R_0^2/mr_0^2)$$

or

$$[35] \quad \tau_2' << \tau_1'$$

Thus, the effective time for the r-motion of the more massive particle is much shorter than that for the lighter particle associated with R-motion. As a result, we expect that for eq. [22], the factor $\exp[-i\hbar\tilde{k}^2\tau_2'/2]$ should be close to one and $\tau_2'\tilde{v}(r)/2$ should be small compared to $\tau_1'\tilde{v}(Rr\alpha)/2$. To see the consequence of this, we can consider the extreme case of $mr_0^2 \rightarrow \infty$, or $\tau_2' \equiv 0$. Then one has that

$$[36] \quad \int_0^\infty dk k^2 \exp(-i\hbar\tilde{k}^2\tau_2'/2) j_l(kr) j_l(kr') = \int_0^\infty dk k^2 j_l(kr) j_l(kr')$$

$$[37] \quad = \frac{\pi}{2}\frac{\delta(r - r')}{r^2}$$

Next we note that the basic parameter τ (or τ_1') is under our control. It can be chosen small enough so that the change in R is also not too great. In a recent paper (62), we showed that for τ_1' not too large, a quadrature evaluation of the integral over K,

$$[38] \quad G_l(R,R'|\tilde{K}_{max},\tau_1') = \frac{2}{\pi}\sum_{p=1}^{N_R} w_p \Delta K j_l(\tilde{K}_p R)\exp(-i\tilde{K}_p^2\hbar\tau_1'/2)\, j_l(\tilde{K}_p R')$$

leads to a strongly peaked function of R and R'. Here, ΔK is the (fixed) step size in wavenumber, Kmax equals $N_R\Delta K$, and trapezoidal weights w_p (with $w_1 = w_N = \frac{1}{2}$) are used. In fact, $G_l(R,R'|K_{max},\tau_1')$ is very weakly dependent on l. It is then possible to do the sum over l in eq. [22]:

$$[39] \quad \sum_l \frac{2l+1}{2J+1}\langle l0j\Omega|J\Omega\rangle\langle l0j\Omega'|J\Omega'\rangle = \delta_{\Omega\Omega'}$$

At this point, the sum over j can then be done:

$$[40] \quad \sum_j P_{j\Omega}(\cos\alpha)\, P_{j\Omega}(\cos\alpha') = \delta(\cos\alpha - \cos\alpha')$$

leading thereby to an equation that is only parametrically dependent on r and α. (It is important to note that eq. [40] follows because the $P_{j\Omega}$ are normalized associated Legendre polynomials.) This is reminiscent of an IOS (69) type reduction to dynamical equations in which the scattering is parametrically a function of the orientation of the target diatom.

Of course, our principal interest is *not* in such an extreme limit. Instead, one expects that for τ such that τ_1' leads to a highly peaked $G_l(R,R'|K_{max},\tau_1')$, the corresponding value of τ_2' will lead to an even more strongly peaked $G_j(r,r'|k_{max},\tau_2')$, given by

$$[41] \quad G_j(r,r'|k_{max},\tau_2') = \frac{2}{\pi}\Delta k\sum_{q=1}^{N_r} w_q j_j(k_q r)\exp(-ik_q^2\hbar\tau_2'/2) j_j(k_q r')$$

with $k_{max} = N_r\Delta k$. This can result in substantial reduction of the computational effort in solving eq. [22], since the peaking property of both G_l and G_j corresponds to their being sparse or banded matrices when R, R' and r, r' are replaced by discrete grids. This should result in a dynamical approach that goes beyond the IOS, in that the slow degrees of freedom *are* permitted to change during the collision. This is because one makes use of the banded structure of the propagator without going to the extreme Dirac delta function limit.

4. Potential referenced modified Cayley method

In this instance, we reverse the roles of the relative kinetic energy and potential energy operators (49). Then eq. [5] reads

$$[42] \quad |\psi^{JM}(n_0 j_0 l_0|t)\rangle = \left[1 + \frac{i\tau}{2\hbar}(K_R + K_r)\right]^{-1} e^{-iV\tau/\hbar} \times \left[1 - \frac{i\tau}{2\hbar}(K_R + K_r)\right]|\psi^{JM}(n_0 j_0 l_0|t - \tau)\rangle$$

Clearly, it is desirable to utilize the momentum representation in this equation due to the appearance of $[1 + (i\tau/2\hbar)(K_R$

$+ K_r)]^{-1}$ as the left-most operator on the RHS. We project eq. [22] with $\langle kj| < Kl| < Y_{jl}^{JM}|$, again insert appropriate resolutions of the identity, and carry through straightforward but tedious manipulations to obtain

$$[43]\quad \psi^J(Kkjl|n_0j_0l_0|t) = \frac{4}{\pi^2}\left[1 + \frac{i\tau\hbar}{4}\left(\frac{K^2}{\mu} + \frac{k^2}{m}\right)\right]^{-1}\int_0^\infty dRR^2\int_0^\infty drr^2\int_{-1}^{1} d(\cos\alpha) j_l(KR)j_l(kr)\sum_{\substack{j'l'\\ \Omega}}\frac{\sqrt{(2l+1)(2l'+1)}}{(2J+1)}$$
$$\times \langle l0j\Omega|J\Omega\rangle\langle l'0j'\Omega|J\Omega\rangle P_{j\Omega}(\cos\alpha)e^{-iV(R\tau\alpha)\tau/\hbar}P_{j'\Omega}(\cos\alpha)\int_0^\infty dK'K'^2\int_0^\infty dk'k'^2$$
$$\times j_l(K'R)j_j(k'r)\left[1 - \frac{i\tau\hbar}{4}\left(\frac{K'^2}{\mu} + \frac{k'^2}{m}\right)\right]\psi^J(K'k'j'l'|n_0j_0l_0|t-\tau)$$

As in the preceding analysis, body frame Euler angles (ξ,θ,φ) were introduced to simplify the equations (taking advantage of the Wigner–Eckart theorem (59)).

Finally, it is straightforward to obtain the resulting equations when the diatomic binding potential $v(r)$ is included in H_d. By use of eq. [21], we obtain

$$[44]\quad \psi^J(Knjl|n_0j_0l_0|t) = \frac{2}{\pi}\left[1 + \frac{i\tau}{2\hbar}\left(\frac{\hbar^2K^2}{2\mu} + \epsilon_{nj}\right)\right]^{-1}\int_0^\infty dRR^2\int_0^\infty drr^2\int_{-1}^{1} d(\cos\alpha)$$
$$\times j_l(KR)f_{nj}(r)\sum_{\substack{n'j'l'\\ \Omega}}\frac{\sqrt{(2l+1)(2l'+1)}}{(2J+1)}\langle l0j\Omega|J\Omega\rangle\langle l'0j'\Omega|J\Omega\rangle P_{j\Omega}(\cos\alpha)e^{-iv(R\tau\alpha)\tau/\hbar}P_{j'\Omega}(\cos\alpha)$$
$$\times \int_0^\infty dK'K'^2 j_{l'}(K'R)f_{n'j'}(r)\left[1 - \frac{i\tau}{2\hbar}\left(\frac{\hbar^2K'^2}{2\mu} + \epsilon_{n'j'}\right)\right]\psi^J(K'n'j'l'|n_0j_0l_0|t-\tau)$$

This completes the choices for H_r and H_d that we wish to consider in the present paper. We remark that one might anticipate that eq. [18] or eq. [20] will be most useful when the kinetic energy or internal energy is much larger than the potential energy. This is reflected in the fact that both eqs. [18] and [20] include the kinetic energy to infinite order. By contrast, eq. [23] and [24] should be most useful when the potential energy is much larger. Of course, we anticipate that hybrid algorithms can be devised that utilize the form most appropriate (depending on which of the energies is larger).

5. Conclusions

We note that the forms eq. [18] and eq. [23] are suitable also for treating the possibility of reactive processes since a bound state approximation to the motion in r has not been made. One possible way to treat reactions is by the use of negative imaginary arrangement decoupling potentials (39, 40, 52). Other ways are also under study. It is also possible to formulate the equations using a body frame (38, 67) description throughout, or to use hyperspherical coordinates (68). One also can use other choices of the reference Hamiltonian, H_r, thereby leading to different disturbances, H_d. Finally, the present methods are ideally suited to parallelization, and we anticipate that extremely efficient algorithms can be devised for solving these equations on parallel architecture computers. All these options are currently under study.

1. (*a*) R. B. Gerber, R. Kosloff, and M. Berman. Comput. Phys. Rep. **5**, 59 (1986); (*b*) V. Mohan and N. Sathymurthy. Comput. Phys. Rep. **7**, 213 (1988); (*c*) R. Kosloff. J. Phys. Chem. **92**, 2087 (1988).
2. J. Mazur and R. J. Rubin. J. Chem. Phys. **31**, 1395 (1959).
3. E. A. McCullough and R. E. Wyatt. J. Chem. Phys. **54**, 3578 (1971); **54**, 3592 (1971).
4. Ch. Zubert, T. Kamal, and L. Zulike. Chem. Phys. Lett. **36**, 396 (1975).
5. E. J. Heller. J. Chem. Phys. **62**, 1544 (1975); **65**, 4979 (1976); K. C. Kulander and E. J. Heller. J. Chem. Phys. **69**, 2439 (1978); G. Drolshagen and E. J. Heller. J. Chem. Phys. **79**, 2072 (1983).
6. A. Askar and A. S. Cakmak. J. Chem. Phys. **68**, 2794 (1978).
7. K. C. Kulander. J. Chem. Phys. **69**, 5064 (1978); J. C. Gray, G. A. Fraser, D. G. Truhlar, and K. C. Kulander. J. Chem. Phys. **73**, 5726 (1980); A. E. Orel and K. C. Kulander. Chem. Phys. Lett. **146**, 428 (1988).
8. C. LeForestier, G. Bergerson, and P. C. Hiberty. Chem. Phys. Lett. **84**, 385 (1981); C. LeForestier. Chem. Phys. **87**, 241 (1984).
9. P. M. Agrawal and L. M. Raff. J. Chem. Phys. **77**, 3946 (1982).
10. E. J. Heller, R. L. Sundberg, and D. J. Tannor. J. Phys. Chem. **86**, 1822 (1982).
11. (*a*) M. D. Feit and J. A. Fleck. J. Chem. Phys. **79**, 301, (1983); **80**, 2578 (1984); (*b*) P. De Vries. NATO ASI Ser. Ser. B: **171**, 113 (1988); A. D. Bandrauk and H. Shen. Chem. Phys. Lett. **176**, 428 (1991).
12. D. Kosloff and R. Kosloff. J. Comput. Phys. **52**, 35 (1983); J. Chem. Phys. **79**, 1823 (1983).
13. C. LeForestier. Chem. Phys. **87**, 241 (1984); *In* Theory of chemical reaction dynamics. *Edited by* D. C. Clary. Reidel, Dordrecht. 1986. p. 235; F. le Quere and C. LeForestier. J. Chem. Phys. **92**, 247 (1990).
14. G. Drolshagen and E. J. Heller. J. Chem. Phys. **79**, 2072 (1983).
15. H. Tal-Ezer and R. Kosloff. J. Chem. Phys. **81**, 3967 (1984).

Can. J. Chem. Downloaded from www.nrcresearchpress.com by 92.62.229.171 on 09/08/12
For personal use only.

16. R. Kosloff and C. Cerjan. J. Chem. Phys. **81**, 3722 (1984).
17. A. T. Yinnon, R. Kosloff, and R. B. Gerber. Surf. Sci. **148**, 148 (1984); R. B. Gerber, A. T. Yinnon, and R. Kosloff. Chem. Phys. Lett. **105**, 523 (1984).
18. D. Imre, J. Kinsey, A. Sinha, and J. Krenos. J. Phys. Chem. **88**, 3956 (1984).
19. R. T. Skodje. Chem. Phys. Lett. **109**, 227 (1984).
20. R. C. Mowrey and D. J. Kouri. Chem. Phys. Lett. **119**, 285 (1985).
21. B. Jackson and H. Metiu. J. Chem. Phys. **83**, 1952 (1985); S. Sawada, R. Heather, B. Jackson, and H. Metiu. J. Chem. Phys. **83**, 3009 (1985).
22. Z. H. Zhang and D. J. Kouri. Phys. Rev. A, **34**, 2687 (1986).
23. B. Jackson and H. Metiu. J. Chem. Phys. **84**, 3535 (1986); **85**, 4192 (1986); **86**, 1026 (1987).
24. R. C. Mowrey and D. J. Kouri. J. Chem. Phys. **84**, 6466 (1986).
25. T. J. Park and J. C. Light. J. Chem. Phys. **85**, 5870 (1986).
26. V. Mohan and N. Sathymurthy. Curr. Sci. **55**, 115 (1986); S. Thareja and N. Sathymurthy. J. Phys. Chem. **91**, 1970 (1987).
27. R. C. Mowrey and D. J. Kouri. J. Chem. Phys. **86**, 6140 (1987).
28. R. Heather and H. Metiu. J. Chem. Phys. **86**, 5009 (1987); **90**, 6116 (1989); **91**, 1596 (1989).
29. D. J. Kouri and R. C. Mowrey. J. Chem. Phys. **87**, 2087 (1987).
30. Y. Sun, R. C. Mowrey, and D. J. Kouri. J. Chem. Phys. **87**, 339 (1987).
31. R. C. Mowrey, H. F. Bowen, and D. J. Kouri. J. Chem. Phys. **86**, 2441 (1987); R. C. Mowrey, H. F. Bowen, T. Yinnon, and R. B. Gerber. J. Chem. Phys. **89**, 3925 (1988).
32. D. Huber and E. J. Heller. J. Chem. Phys. **87**, 5302 (1987); **89**, 4752 (1988); D. Huber, E. J. Heller, and R. G. Littejohn. J. Chem. Phys. **87**, 5302 (1987); D. Huber, S. Ling, D. G. Imre, and E. J. Heller. J. Chem. Phys. **90**, 7317 (1989).
33. Y. Sun and D. J. Kouri. J. Chem. Phys. **89**, 2958 (1988).
34. B. Jackson. J. Chem. Phys. **88**, 1383 (1988); **89**, 2473 (1988); J. Chem. Phys. In press.
35. D. Chaseman, D. J. Tannor, and D. G. Imre. J. Chem. Phys. **89**, 6667 (1988).
36. S. O. Williams and D. J. Imre. J. Phys. Chem. **92**, 6648 (1988).
37. D. J. Tannor and S. A. Rice. Adv. Chem. Phys. **70**, 441 (1988).
38. Y. Sun, R. S. Judson, and D. J. Kouri. J. Chem. Phys. **90**, 241 (1989).
39. D. Neuhauser and M. Baer. J. Chem. Phys. **90**, 4351 (1989); J. Phys. Chem. **93**, 2872 (1989); J. Chem. Phys. **91**, 4651 (1989).
40. D. Neuhauser, M. Baer, R. S. Judson, and D. J. Kouri. J. Chem. Phys. **90**, 5882 (1989); **93**, 312 (1990); Comput. Phys. Commun. **63**, 460 (1991).
41. X.-P. Jiang, R. Heather, and H. Metiu. J. Chem. Phys. **90**, 2555 (1989).
42. M. Jacon, O. Atabek, and C. LeForestier. J. Chem. Phys. **91**, 1585 (1989).
43. J. Zhang and D. G. Imre. J. Chem. Phys. **90**, 1666 (1989).
44. R. N. Dixon. Mol. Phys. **68**, 263 (1989).
45. R. S. Judson, D. J. Kouri, D. Neuhauser, and M. Baer. Phys. Rev. A, **42**, 351 (1990).
46. J. Z. H. Zhang. Chem. Phys. Lett. **160**, 417 (1989); J. Chem. Phys. **92**, 324 (1990).
47. D. K. Hoffman, O. Sharafeddin, R. S. Judson, and D. J. Kouri. J. Chem. Phys. **92**, 4167 (1990).
48. S. Das and D. J. Tannor. J. Chem. Phys. **92**, 3403 (1990).
49. O. A. Sharafeddin, D. J. Kouri, R. S. Judson, and D. K. Hoffman. J. Chem. Phys. **93**, 5580 (1990).
50. R. S. Judson, D. B. McGarrah, O. A. Sharafeddin, D. J. Kouri, and D. K. Hoffman. J. Chem. Phys. **94**, 3577 (1991).
51. D. Neuhauser and R. S. Judson. J. Chem. Phys. In press.
52. D. Neuhauser, R. S. Judson, R. L. Jaffe, M. Baer, and D. J. Kouri. Chem. Phys. Lett. **176**, 546 (1991).
53. O. A. Sharafeddin, H. F. Bowen, D. J. Kouri, and D. K. Hoffman. J. Comput. Phys. (In press).
54. R. Viswanathan, S. Shi, E. Villalonga, and H. Rabitz. J. Chem. Phys. **91**, 2333 (1989).
55. D. Neuhauser. J. Chem. Phys. In press.
56. M. Founargiotakis and J. C. Light. J. Chem. Phys. **93**, 633 (1990).
57. R. N. Dixon, C. C. Marston, and G. G. Balint-Kurti. J. Chem. Phys. **93**, 6520 (1990).
58. W. H. Press, B. P. Flannery, S. A. Teukolsky, and W. T. Vetterling. Numerical recipes: the art of scientific computing. Cambridge Univ. Press, New York. 1986.
59. A. M. Arthurs and A. Delgarno. Proc. R. Soc. London A: **256**, 540 (1960).
60. D. M. Brink and G. R. Satchler. Angular momentum. Clarendon Press, Oxford. 1968.
61. D. J. Kouri, T. G. Heil, and Y. Shimoni. J. Chem. Phys. **65**, 226 (1976).
62. (*a*) O. A. Sharafeddin, D. J. Kouri, N. Nayar, and D. K. Hoffman. J. Chem. Phys. **95**, 3224 (1991); (*b*) N. Makri. Chem. Phys. Lett. **159**, 489 (1989).
63. D. K. Hoffman, N. Nayar, O. A. Sharafeddin, and D. J. Kouri. J. Phys. Chem. **95**, 8299 (1991).
64. J. C. Light, I. P. Hamilton, and J. V. Lill. J. Chem. Phys. **82**, 1400 (1985).
65. O. A. Sharafeddin, H. F. Bowen, D. J. Kouri, S. Das, D. J. Tannor, and D. K. Hoffman. J. Chem. Phys. **95**, 4727 (1991).
66. P. G. Burke and M. J. Seaton. Methods Comput. Phys. **10**, 61 (1971).
67. J. O. Hirshfelder and E. P. Wigner. Proc. Natl. Acad. Sci. (USA) **21**, 113 (1935); C. F. Curtiss, J. O. Hirschfelder, and F. T. Adler. J. Chem. Phys. **18**, 1638 (1950); C. F. Curtiss. J. Chem. Phys. **21**, 1199 (1953); D. J. Kouri and C. F. Curtiss. J. Chem. Phys. **44**, 2120 (1966); C. F. Curtiss. J. Chem. Phys. **48**, 1725 (1968); W. R. Thorson. J. Chem. Phys. **42**, 3878 (1965); R. T Pack and J. O. Hirschfelder. J. Chem. Phys. **49**, 4009 (1968); K. P. Lawley and J. Ross. J. Chem. Phys. **43**, 2930 and 2943 (1965); M. Jacob and G. C. Wick. Ann. Phys. (NY), **7**, 404 (1959); R. T Pack. J. Chem. Phys. **60**, 633 (1974); P. McGuire and D. J. Kouri. J. Chem. Phys. **60**, 2499 (1974); H. Klar. J. Phys. B: At. Mol. Phys. **6**, 2139 (1973); M. Tamir and M. Shapiro. Chem. Phys. Lett. **31**, 166 (1975).
68. A. Kuppermann and P. G. Hipes. J. Chem. Phys. **84**, 5962 (1986); R. T Pack and G. A. Parker. J. Chem. Phys. **87**, 3888 (1987); J. Linderberg, S. Padjkaer, Y. Ohrn, and B. Vessal. J. Chem. Phys. **90**, 6254 (1989); J. M. Launay and B. Lepetit. Chem. Phys. Lett. **144**, 346 (1988); G. C. Schatz. J. Chem. Phys. **90**, 1237 (1989); and references therein.
69. R. B. Bernstein. Atom–molecule collision theory. Plenum Press, New York. 1979. Chap. 9.

Can. J. Chem. Downloaded from www.nrcresearchpress.com by 92.62.229.171 on 09/08/12
For personal use only.

Selenium sulfur dihalides, Ch_nX_2 (n = 1, 2, 3; Ch = Se, S; X = Br, Cl). Raman and ^{77}Se NMR spectroscopic characterization

JOHN B. MILNE

Department of Chemistry, University of Ottawa, Ottawa, Ont. Canada, K1N 6N5

Received July 4, 1991

This paper is dedicated to the memory of Professor Thomas Birchall

JOHN B. MILNE. Can. J. Chem. **70**, 693 (1992).

Solutions of Se_2Cl_2 in S_2Cl_2, Se_2Br_2 in S_2Cl_2, Se in S_2Cl_2, and S in Se_2Cl_2 have been studied by Raman and ^{77}Se NMR spectroscopy. Selenium sulfur dihalides, $SeSCl_2$, $SeSBr_2$, and SeSBrCl, formed in these solutions, have been shown by Raman and ^{77}Se NMR spectroscopy to have chain structures. Solutions of Se_2Cl_2 in S_2Cl_2, S in Se_2Cl_2, and Se in S_2Cl_2 have been shown to contain, in addition to Se_2Cl_2, S_2Cl_2, $SeSCl_2$, Se_3Cl_2, and S_8, trichalcogen dichlorides Se_2SCl_2 and SeS_2Cl_2. Selenium-77 signals corresponding to all seven chain isomers of the expected Se-containing dichalcogen dihalides, Se_2Br_2, Se_2Cl_2, Se_2BrCl, $SeSCl_2$, $SeSBr_2$, BrSeSCl, and ClSeSBr, have been observed in the spectrum of a 1 : 1 molar mixture of S_2Cl_2 and Se_2Br_2. The disulfur dichloride and dibromide, as well as the bromide chloride, are also present. Selenium–bromine and sulfur–chlorine linkages are observed to be preferred over selenium–chlorine and sulfur–bromine bonding in these mixtures. The ^{77}Se chemical shifts correlate well with the electronegativity of the directly bonded neighbour but inversely with that of the next-nearest neighbour.

Key words: selenium halides, sulfur halides, low valent chalcogen halides, ^{77}Se NMR, Raman spectroscopy.

JOHN B. MILNE. Can. J. Chem. **70**, 693 (1992).

Faisant appel à la spectroscopie Raman et à la RMN du ^{77}Se, on a étudié des solutions de Se_2Cl_2 dans le S_2Cl_2, de Se_2Br_2 dans le S_2Cl_2, de Se dans le S_2Cl_2 et de S dans le Se_2Cl_2. En se basant sur la spectroscopie Raman et la RMN du ^{77}Se, on a montré que les dihalogénures de soufre et de sélénium qui se forment dans ces solutions ($SeSCl_2$, $SeSBr_2$ et SeSBrCl) possèdent des structures en chaîne. On a montré que les solutions de Se_2Cl_2 dans le S_2Cl_2, de S dans le Se_2Cl_2 et de Se dans le S_2Cl_2 contiennent des dichlorures de chalcogènes (Se_2SCl_2 et SeS_2Cl_2) en plus du Se_2Cl_2, du S_2Cl_2, du $SeSCl_2$, du Se_3Cl_2 et du S_8. Dans le spectre d'un mélange 1 : 1 molaire du S_2Cl_2 et de Se_2Br_2, on a observé des signaux du ^{77}Se correspondant à tous les sept isomères en chaîne attendus pour les dihalogénures de dichalcogènes contenant du Se (Se_2Br_2, Se_2Cl_2, Se_2BrCl, $SeSCl_2$, $SeSBr_2$, BrSeSCl et ClSeSBr). Le dichlorure et le dibromure de disoufre ainsi que le bromure et le chlorure de disoufre y sont aussi présents. On a observé que, dans ces mélanges, les liaisons sélénium–brome et soufre–chlore sont préférées aux liaisons sélénium–chlore et soufre–brome. Il existe une corrélation entre les déplacements chimiques du ^{77}Se et les électronégativités des atomes qui y sont directement attaché; cette corrélation est toutefois inversée avec les atomes qui se trouvent dans la position suivante.

Mots clés : halogénures de sélénium, halogénures de soufre, halogénures de chalcogènes de basse valence, RMN du ^{77}Se, spectroscopie Raman.

[Traduit par la rédaction]

Introduction

Chloro- and bromosulfanes, S_nX_2, have been extensively studied (1) and shown to consist of sulfur chains like their organic analogues. Recently Se_2Cl_2 and Se_2Br_2 were shown to contain equilibrium amounts of SeX_2, Se_3X_2, and Se_4X_2 (2). The mixed halogen compounds, Se_nBrCl (n = 1,2) have also been reported (2) but mixed chalcogen dihalides have received little attention although sulfur selenium chains in general are currently of great interest (3). Early work, using chemical methods, suggested that $SeSCl_2$ has a trigonal pyramidal structure (4). The two possible isomers, with either selenium or sulfur terminal, were prepared from mixtures of Se in S_2Cl_2 and S in Se_2Cl_2 respectively. However, other work (5) has shown that S_2Cl_2 and Se react quantitatively according to

$$[1] \quad S_2Cl_2 + 2Se = Se_2Cl_2 + 2S$$

with no evidence for $SeSCl_2$ formation.

To clarify the nature of these reactions and characterize some of the mixed chalcogen dihalides, a Raman and ^{77}Se NMR study of mixtures of S_2Cl_2 with Se_2Cl_2, Se_2Br_2, and Se, and Se_2Cl_2 with S was undertaken as part of an ongoing study of low-valent Se halide chemistry (2, 6).

Experimental section

Disulfur dichloride (BDH), sulfur (MCB), and selenium (Baker analyzed) were used directly. Diselenium dichloride was prepared from stoichiometric amounts of Se and $SeCl_4$ (2) and Se_2Br_2 was prepared from HBr (Fisher, 48%), SeO_2 (Aldrich), and Se (Baker analyzed) by the method of Lenher and Kao (5). Moisture sensitive mixtures were made up by weighing in a dry box at ambient temperature. Often 1–3 h of mixing were required to produce homogeneous mixtures and, in the case of the S in the Se_2Cl_2 mixture, heating at 75°C over several minutes was used to achieve solution. Mixing of S_2Cl_2 with Se_2X_2 (X = Br, Cl) was accompanied by marked cooling.

Raman spectra were measured using a Jobin–Yvon monochromator with a PAR photon counting system. The spectra were excited with the 647.1 nm line of a Spectra Physics Kr ion laser.

Selenium-77 NMR spectra were measured with a Varian XL300 spectrometer operating at 57.28 MHz. The probe temperature was 21°C. The spectra were run with an external D_2O lock and referenced to aqueous saturated H_2SeO_3 ($\delta(Me_2Se) = \delta(H_2SeO_3$, satd.) + 1303.7 ppm).[2] A pulse angle of 50° and 2 s recycle time were usually used and 512–1024 transients were collected with a sweep width of 30 000 Hz or less. All samples were degassed by six

[1] A preliminary report of this work will appear in Chemical Communications of the Royal Society of Chemistry.

[2] J. Milne, unpublished.

Can. J. Chem. Downloaded from www.nrcresearchpress.com by 92.62.229.171 on 09/08/12
For personal use only.

Can. J. Chem. Downloaded from www.nrcresearchpress.com by 92.62.229.171 on 09/08/12
For personal use only.

freeze–thaw cycles under vacuum before sealing. The signals were all relatively broad (>21 Hz) and, for this reason and low isotopomer concentrations, no Se–Se couplings (11–65 Hz (7)) were observed.

Results and discussion

Raman spectroscopy

The Raman spectrum of a 1:1 molar mixture of S_2Cl_2 and Se_2Cl_2 is shown in Fig. 1, trace A. The spectrum exhibits peaks corresponding to S_2Cl_2 (540, 449, 243, 209, and 105 cm^{-1} (8)) and Se_2Cl_2 (359, 289, 148, 131, and 85 cm^{-1} (8)). In addition, peaks are observed at 414, 190, and 170 cm^{-1}. The contributions of S_2Cl_2 and Se_2Cl_2 to this spectrum were subtracted by using intensity scaling factors for the non-overlapped peaks of S_2Cl_2 (540, 243, and 209 cm^{-1}) and Se_2Cl_2 (290 cm^{-1}) taken from spectra of the pure compounds run under identical conditions. The resultant spectrum is given as trace B in Fig. 1 and consists of peaks at 441, 414, 369, 190, and 170 cm^{-1}. The peak at 414 cm^{-1} is coincident with ν(SeCl) of $SeCl_2$ but is 4 times stronger than that expected for the equilibrium concentration of $SeCl_2$ present (2). The observation of both SCl (441 cm^{-1}) and SeCl (369 cm^{-1}) stretching bands as well as the SeS (414 cm^{-1}) stretching band is consistent with the formation of the chain isomer of $SeSCl_2$. In addition, the SeSCl deformation modes at 190 and 170 cm^{-1} are nicely bracketed by the comparable modes for Se_2Cl_2 and S_2Cl_2, 148/131 and 243/209 cm^{-1} and show comparable intensity ratios. It should also be noted that no peak corresponding to an SeS double bond stretching mode, expected for the pyramidal isomers and estimated to lie near 560 cm^{-1} (mean of the Se_2 and S_2 diatomic stretching frequencies (9)), is observed. Apparently mixtures of Se_2Cl_2 and S_2Cl_2 are in equilibrium with the mixed chalcogen dichloride,

$$[2] \quad S_2Cl_2 + Se_2Cl_2 \overset{K(SeSCl_2)}{=} 2SeSCl_2$$

where, on the basis of peak intensities, the equilibrium lies to the reactant side. A complete assignment of the Raman spectrum of the $SeSCl_2$ molecule is given in Table 1.

The early claims (4) of the synthesis of the pyramidal isomers of $SeSCl_2$ called for long periods of reflux of Se and S_2Cl_2 for the isomer with Se terminal and of S and Se_2Cl_2 for that with S terminal. The Raman spectra of these two mixtures (initial dissolution of S in Se_2Cl_2 required a brief period of warming) remained unchanged, regardless of the time of heating at 80°C for up to 20 h. The spectrum of a 1:1 molar mixture of Se in S_2Cl_2 is shown in Fig. 1, trace C. The spectrum is similar to that of the Se_2Cl_2/S_2Cl_2 mixture, showing the presence of the reactants and a small amount of the chain isomer of $SeSCl_2$. In addition, however, three peaks at 477, 221, and 152 cm^{-1} are observed, which correspond to the three strongest bands of elemental sulfur, S_8, dissolved in S_2Cl_2, (10), and as discussed below, in Se_2Cl_2. Thus, Se dissolves readily in S_2Cl_2 according to

$$[3] \quad 8Se + 8S_2Cl_2 = 4S_2Cl_2 + 4Se_2Cl_2 + S_8$$

and some $SeSCl_2$ is formed by equilibrium [2]). The spectrum of a 1:1 molar mixture of S in Se_2Cl_2, shown in Fig. 1, trace D, shows the characteristic strong bands of Se_2Cl_2 (2), the three sharp bands due to S_8, and weak peaks due to a trace of S_2Cl_2. Because of the very low concentration of S_2Cl_2 and the fact that equilibrium [2] lies on the reactant side,

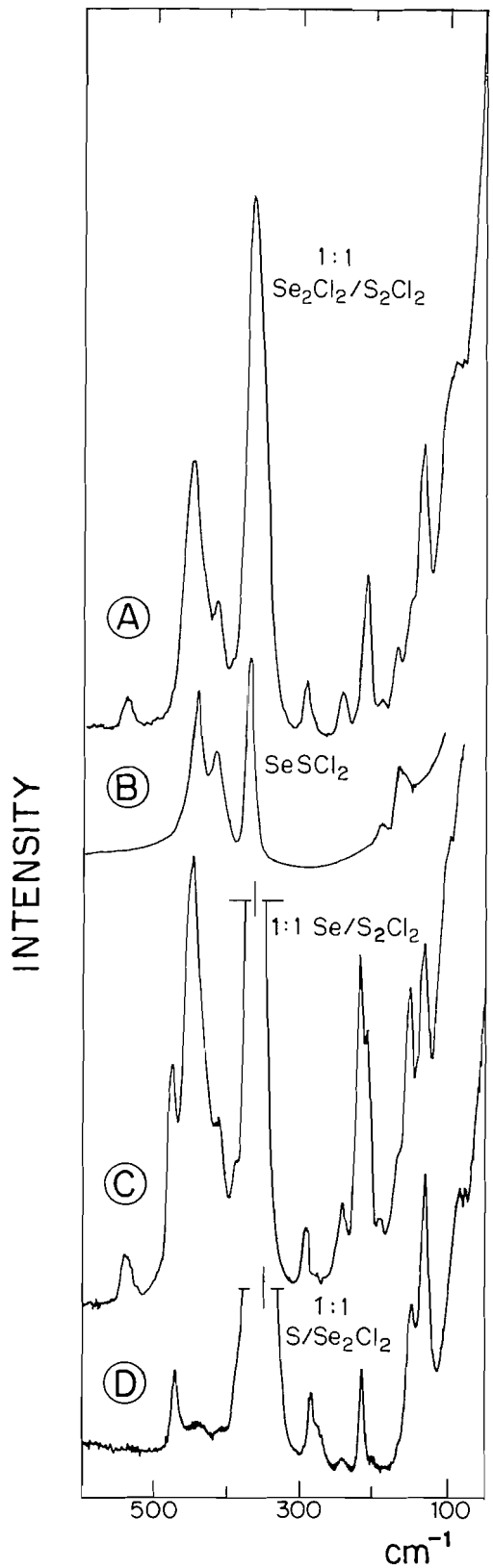

FIG. 1. Raman spectra of selenium sulfur chloride mixtures. Trace A: 1:1 molar ratio Se_2Cl_2/S_2Cl_2; trace B: Spectrum of $SeSCl_2$ determined from trace A by subtraction of Se_2Cl_2 and S_2Cl_2 bands; trace C: 1:1 molar ratio Se/S_2Cl_2; trace D: 1:1 molar ratio S/Se_2Cl_2.

TABLE 1. Vibrational assignment of the Raman spectrum of ClSeSCl

Frequency (cm^{-1})			Mode no.	Description of mode
S_2Cl_2[a]	Se_2Cl_2[a]	$SeSCl_2$		
102	87	—	4	τ
209	131	170	3	δ(ClChX)
243	148	190	6	δ′(ClChX)
449	367	369	2	ν(ChX)
540	289	414	1	ν(ChCh)
436	367	441	5	ν′(ChX)

[a]Reference 18.

the $SeSCl_2$ formed goes undetected in this spectrum. Apparently elemental sulfur dissolves in Se_2Cl_2 as S_8 rings, in the same manner as sulfur does in S_2Cl_2 (10), and only a small amount of oxidation of sulfur occurs to give S_2Cl_2.

The Raman spectrum of a 1:1 molar mixture of Se_2Br_2 and S_2Cl_2 was not very informative. Because of the strong light absorption by the sample, the spectrum was of poor quality and all of the observed peaks were coincident with those of the reactants and Se_2Cl_2 and S_2Br_2. The dominant peaks were those corresponding to Se—Cl and Se—Br stretching modes at 309 and 265 cm^{-1} respectively.

Selenium-77 NMR spectroscopy

The ^{77}Se NMR spectrum of the 1:1 molar mixture of Se_2Cl_2 and S_2Cl_2 is shown in Fig. 2, trace A. The observed chemical shifts and integrated intensities are given in Table 2. The signal due to Se_2Cl_2 is readily identified at 1285.6 ppm as well as those of $SeCl_2$ at 1741.7 ppm and one of the two signals of the Se_3Cl_2 molecule at 1280.1 ppm (2). The half-height linewidth of this latter signal is 21 Hz, compared to that for Se_2Cl_2 itself (35 Hz), which suggests that this peak is due to the central Se (β-Se) of the three-Se chain. The second strongest signal in the spectrum at 1298.4 ppm arises from $SeSCl_2$. On the basis of the integrated peak intensities listed in Table 2, the value of the equilibrium constant for reaction [2] is calculated to be 0.08, assuming that $[Se_2Cl_2] = [S_2Cl_2]$.

The ^{77}Se NMR spectrum of a 1:1 molar mixture of Se and S_2Cl_2 is shown in trace B of Fig. 2 and chemical shifts and integrated intensities are given in Table 2. The same strong signals as for the Se_2Cl_2/S_2Cl_2 mixture are observed, with minor changes in intensities, confirming the conclusion of the Raman experiment that this mixture results in, effectively, an equimolar mixture of Se_2Cl_2 and S_2Cl_2 (containing some S_8), which take part in subsequent equilibria. Evaluation of the equilibrium constant for equilibrium [2] from the signal intensities gives $K(SeSCl_2) = 0.07$, in good agreement with the constant determined from the spectrum of the Se_2Cl_2/S_2Cl_2 mixture.

The ^{77}Se NMR spectrum of a 1:1 molar mixture of S and Se_2Cl_2 is shown in trace C of Fig. 2 and the shifts and intensities are given in Table 2. The signals for the major peaks, $SeCl_2$, Se_2Cl_2, Se_3Cl_2, and $SeSCl_2$, are all observed but two changes are noteworthy; (*a*) the chemical shifts are all 5–11 ppm more shielded than those of the Se_2Cl_2/S_2Cl_2 and Se/S_2Cl_2 mixtures and (*b*) the integrated intensities of the $SeCl_2$, Se_3Cl_2, and $SeSCl_2$ peaks are much lower compared to those in the other solutions. The chemical shifts are close to those reported for pure liquid Se_2Cl_2 (2). Apparently, the presence of a small amount of S_8 as solute has little effect on the chemical shifts in Se_2Cl_2, and the 5–11 ppm negative chemical shift of the same species in Se_2Cl_2/S_2Cl_2 and Se/S_2Cl_2 mixtures results from the presence of S_2Cl_2. Using the equilibrium constant determined for reaction [2] above, $K(SeSCl_2) = 0.08$, and the intensity for Se_2Cl_2 and $SeSCl_2$ for the S/Se_2Cl_2 solution in Table 2, $[S_2Cl_2]$ (in units of relative concentration), is found to be 0.25, which is to be compared to 50 (assuming $[S_2Cl_2] = [Se_2Cl_2]$) for the other mixtures. This low concentration accounts for the failure to observe peaks for S_2Cl_2 in the Raman spectrum and indicates why the chemical shifts for this mixture are different from those of the Se_2Cl_2/S_2Cl_2 and Se/S_2Cl_2 mixtures.

A number of weak signals, which lie slightly to the less shielded side of the $SeSCl_2$ signal, appear in the spectra of all three mixtures. These must arise from the trichalcogen dichlorides, ClSeSSCl, ClSSeSCl, ClSeSSeCl, and ClSeSeSCl, for which five signals are expected. These signals are very weak and poorly defined but a reasonable assignment can be made. If a comparison of the relative intensities of these peaks in the Se/S_2Cl_2 and Se_2Cl_2/S mixtures is made, the most shielded signal (1309.2/1314.8 ppm; peak no. 4, Table 2) and the middle two peaks of the four signals that are slightly less shielded (1329.4/1334.8 ppm, peak no. 6, and 1335.3/1340.4 ppm, peak no. 7, Table 2) are of greater intensity than the remaining weak peaks in the mixtures where the selenium content is highest, indicating that these signals belong to the Se-rich species, ClSeSSeCl and ClSeSeSCl. The broader of the three peaks (1329.4/1334.8 ppm; peak no. 6) is assigned to the α-Se in ClSeSeSCl by comparison with the assignment of the two signals of differing breadths for Se_3Cl_2 (2). Of the remaining two strong signals, peak no. 7 (1335.3/1340.4 ppm, which lies closest to the α-Se signal of ClSeSeSCl) is assigned to the β-Se in this molecule by analogy with the close proximity of the α- and β-Se signals of Se_3Cl_2 (2), and peak no. 4 (1309.2/1314.8 ppm) is assigned to ClSeSSeCl. The remaining weak signals, peak nos. 5 (1327.3/1334.8 ppm) and 8 (1345.2/1350.5 ppm) are then due to the SeS_2Cl_2 species. On the basis of the ^{77}Se chemical shifts in SeS rings (3*a*,*d*), where isolated Se (SSeS) is deshielded relative to Se bound to Se (SeSeS), peak no. 8 may be assigned to ClSSeSCl relative to the shift of the β-Se for ClSeSeSCl (peak no. 7). Only one signal, lying close to the shift observed for Se_4Cl_2 (2) and probably due to a four-chalcogen species, $Se_xS_{4-x}Cl_2$ ($x = 1,2,3$), was observed in the spectra of the Se/S_2Cl_2 and S/Se_2Cl_2 mixtures.

The five chemical shifts arising from trichalcogen species are also observed in the spectrum of the Se_2Cl_2/S_2Cl_2 mixture, Fig. 2, trace A. The relative positions of these peaks remain the same as for the other mixtures.

The ^{77}Se NMR spectrum of a 1:1 molar mixture of Se_2Br_2 and S_2Cl_2 consists of eight strong signals (11), as shown in Fig. 3 and listed in Table 3, along with integrated intensities and linewidths at half-height. Weak peaks, due to Se_3X_2 and other minor species, accounted for <1% of the total area intensity of the spectrum. The eight signals are divided into two groups of four, one group in the region 1223.0–1180.6 ppm, consisting of resonances of ^{77}Se bonded to Br, and another group in the region 1285.6–1313.0 ppm for ^{77}Se bonded to Cl. Complete mixing of chalcogens and halogens to give chain-type dichalcogen dihalides will yield 10 different species, seven of which will carry at least one Se atom. Eight different ^{77}Se chemical shifts are expected, since the

Can. J. Chem. Downloaded from www.nrcresearchpress.com by 92.62.229.171 on 09/08/12
For personal use only.

Can. J. Chem. Downloaded from www.nrcresearchpress.com by 92.62.229.171 on 09/08/12
For personal use only.

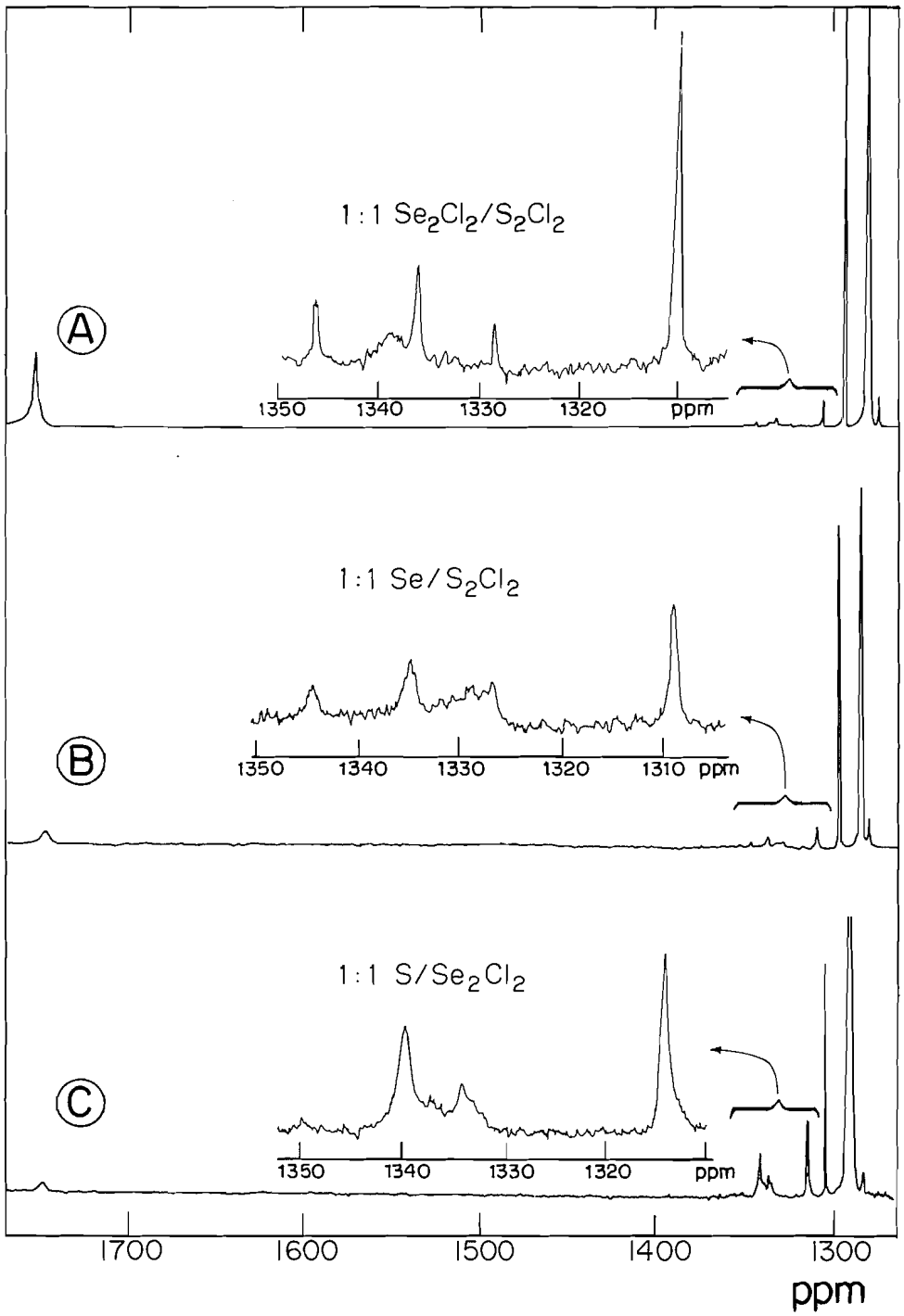

FIG. 2. Selenium-77 NMR spectra of selenium sulfur chloride mixtures. Trace A: 1 : 1 molar mixture Se_2Cl_2/S_2Cl_2; trace B: 1 : 1 molar mixture Se/S_2Cl_2; trace C: 1 : 1 molar mixture S/Se_2Cl_2.

species ClSeSeBr will give two different signals. These species are all listed in Table 3. The chemical shifts are assigned as follows. The two signals expected for ClSeSeBr are easily assigned to the peaks of nearly equivalent integrated intensity in the diselenium dibromide and diselenium dichloride parts of the spectrum (2), 1291.1 ppm (Se on Cl) and 1180.6 ppm (Se on Br). The other strong signals neighbouring these ClSeSeBr peaks are due to the parent dichloride (1285.6 ppm) and dibromide (1186.9 ppm), which lie slightly more shielded than in the pure liquids. The assignment of these four diselenium dihalide signals parallels that observed for mixtures of Se_2Cl_2/Se_2Br_2 in CH_2Cl_2 (6) and suggests that the assignment of the signals for Se attached to Cl for ClSeSeCl and ClSeSeBr in the Se_2Cl_2/Se_2Br_2 mixture (2) may be reversed. From the relative chemical shifts of Se_2Cl_2 and $SeSCl_2$ in the Se_2Cl_2/S_2Cl_2 mixture, the signal at 1298.3 ppm is assigned to $SeSCl_2$ and the remaining peak in the Se bound to Cl part of the spectrum (1313.0 ppm)

TABLE 2. ^{77}Se NMR chemical shifts for selenium sulfur chlorides[a]

Peak no.	1:1 Se_2Cl_2/S_2Cl_2	1:1 Se/S_2Cl_2	1:1 S/Se_2Cl_2	Assignment
0	[b]	700.7	704.7	$Se_{4-x}S_xCl_2$
1	1280.1	1278.9	1284.5	Se_3Cl_2
2	1285.6(100)	1283.6(100)	1291.3(100)	Se_2Cl_2
3	1298.4(14)	1296.7(13.5)	1304.7(2.0)	$SeSCl_2$
4	1310.3(0.9)	1309.2(1.6)	1314.8(1.7)	ClSeSSeCl
5	1328.2(0.3)	1327.3(0.9)	—	ClSeSSCl
6	1336.2(0.5)	1329.4(1.5)	1334.8(1.3)	ClSe*SeSCl
7	1339.1(0.5)	1335.3(1.6)	1340.4(1.8)	ClSeSe*SCl
8	1346.3(0.3)	1345.2(1.2)	1350.5(0.1)	ClSSeSCl
9	1741.7(12.6)	1741.7(9.1)	1730.2(1.4)	$SeCl_2$

[a]The chemical shifts are reported relative to $\delta = 0$ ppm for neat Me_2Se at 21° C. Their precision is estimated to be ±1.5 ppm; Signal intensities are in parentheses and are normalized to $I(Se_2Cl_2) = 100.0$.
[b]Not measured.

must be due to BrSSeCl. Thus, for the six signals assigned up to now, the ^{77}Se signal for the dichalcogen dihalide with Br attached to the remote chalcogen is deshielded relative to the case where Cl is attached to the remote chalcogen (δ(BrSSe*Cl) > δ(ClSSe*Cl); δ(BrSeSe*Cl) > δ(ClSeSe*-Cl); δ(BrSeSe*Br) > δ(ClSeSe*Br)) and in a parallel fashion the remaining peaks are assigned δ(BrSSeBr) (= 1223.0 ppm) > δ(ClSSeBr) (= 1206.1 ppm).

From a comparison of the relative intensities of the signal of Se attached to Br to those of the Se attached to Cl, it is apparent that most of the Se is bound to Br and the S to Cl. On the basis of the known ChX bond dissociation energies (12) the opposite combinations would have been expected. However, the SeX bond dissociation energies are derived from studies of SeX_2 and SeX_4 and not Se_2X_2, and the work on S_2Br_2 is of doubtful accuracy. Moreover, in view of the endothermicity of mixing of S_2Cl_2 and Se_2Br_2, entropy is obviously playing an important role in these reactions.

From the integrated intensities of the various species, their relative concentrations, c_{rel}, may be calculated and these are listed in Table 4. From the $SeSCl_2$ formation constant, calculated above for equilibrium [2], the relative concentration of S_2Cl_2, c_{rel} (S_2Cl_2), may be calculated, assuming that $K(SeSCl_2)$ is little changed by the presence of dichalcogen bromides. Calculation shows that c_{rel} (S_2Cl_2) = 110 (relative to c_{rel} (Se_2Cl_2) = 50). From the bromine and chlorine mass balances for the 1:1 Se_2Br_2/S_2Cl_2 stoichiometry, the relative concentrations of S_2Br_2 and S_2BrCl may also be calculated. The relative concentrations of all species are listed in Table 4.

From these relative concentrations, the constant governing the halogen mixing disproportionation,

$$[4] \quad Se_2Cl_2 + Se_2Br_2 \overset{K(Se_2BrCl)}{=} 2\,Se_2BrCl$$

is found to be 2.8, which is slightly less than that calculated for CH_2Cl_2 solutions, 3.0 (6). The diselenium compounds are less susceptible to the disproportionation than the disulfur species for which the comparable equilibrium constant, $K(S_2BrCl)$, is 4.5.

The linewidths at half-height, $W_{1/2}$, listed in Table 3, are three to four times larger for the diselenium dihalides than for the selenium sulfur species. In addition, while both types of lines broaden with temperature, those of the Se_2X_2 species broaden faster than those of SeX_2 species. Increasing linewidth at half-height with temperature indicates exchange broadening and this has been confirmed by two-dimensional exchange NMR spectroscopy experiments, which indicate a mechanism involving halide exchange (13) that is at least 10 times more rapid for diselenium than for selenium sulfur species. Previously the NMR signals of α- and β-Se in Se_2X_2 and Se_4X_2 were assigned on the basis of dif-

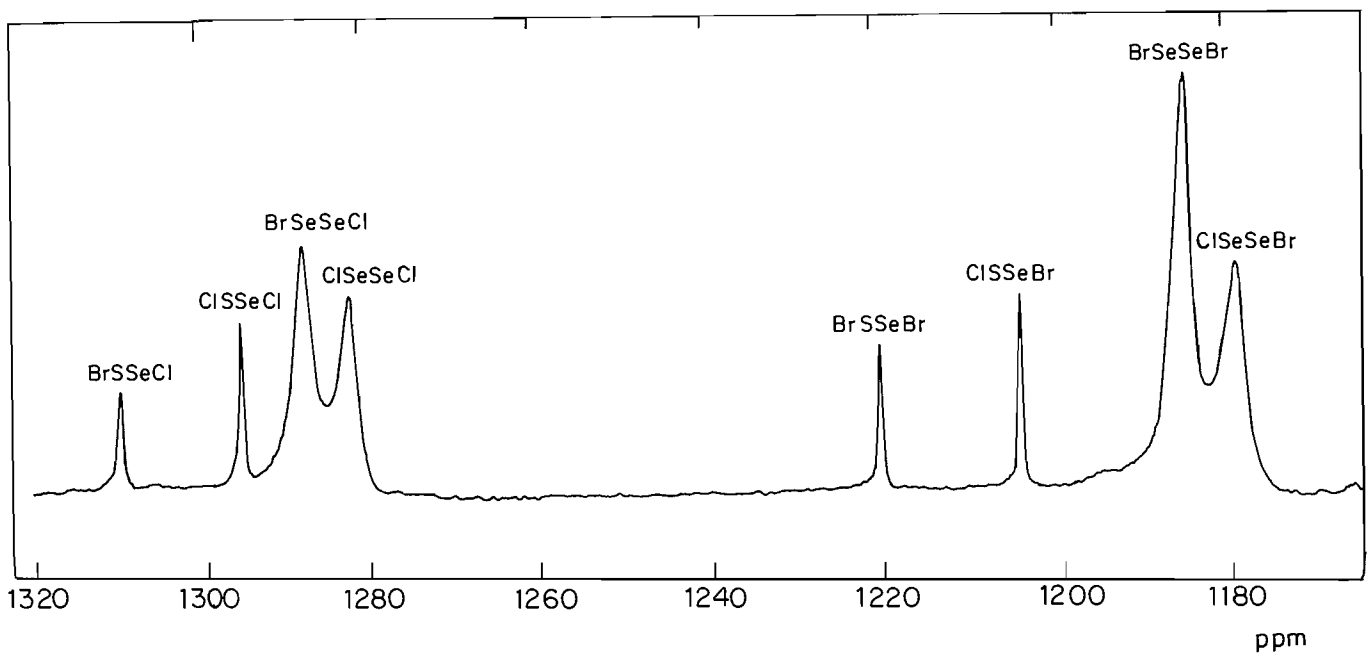

FIG. 3. Selenium-77 NMR spectrum of 1:1 molar mixture of Se_2Br_2 and S_2Cl_2.

Can. J. Chem. Downloaded from www.nrcresearchpress.com by 92.62.229.171 on 09/08/12
For personal use only.

TABLE 3. Peak numbers, chemical shifts (δ), relative integrated intensities (I_{rel}), half-height linewidths ($W_{1/2}$), and assignments for ^{77}Se NMR signals in the spectrum of a 1:1 molar mixture of Se_2Br_2 and S_2Cl_2

Peak no.	δ[a] (ppm)	I_{rel}[b]	$W_{1/2}$ (Hz)	Assignment
1	1313.0	15	37	ClSeSBr
2	1298.3	21	33	ClSeSCl
3	1291.1	133	140	ClSe*SeBr
4	1285.6	100	134	ClSeSeCl
5	1223.0	19	37	BrSeSBr
6	1206.1	21	28	BrSeSCl
7	1186.9	238	147	BrSeSeBr
8	1180.6	124	147	BrSe*SeCl

[a]Reported relative to δ = 0 for neat Me_2Se at 21° C; the precision for these shifts is estimated to be ±1.5 ppm.
[b]Normalized to I_{rel} = 100 for ClSeSeCl.

TABLE 4. Relative concentrations of dichalcogen dihalides, Ch_2X_2, species in the 1:1 molar mixture of Se_2Br_2 and S_2Cl_2

Ch_2X_2	c_{rel}[a]
BrSeSeCl	129
BrSeSeBr	119
BrSeSCl	21
BrSeSBr	19
ClSeSeCl	50
ClSeSCl	21
ClSeSBr	15
ClSSCl	110
BrSSBr	43
BrSSCl	145

[a]Units of relative concentration.

fering signal breadth, which was attributed to the differing proximity of the quadrupole relaxed Cl and Br to the Se nucleus of interest (2). It is now apparent that the greater width at half-height of the signal of α-Se, which is directly bound to Cl or Br, compared to that of the β-Se, with only Se near neighbours, is due to halide exchange.

The ^{77}Se chemical shift, δ(^{77}Se), correlates in general terms with Se oxidation state and electronegativity of the directly bonded near-neighbour atoms (14). The decreased shielding resulting from decreased electron density at the Se nucleus is usually assumed to be dominated by the paramagnetic contribution (14). The chemical shifts of the Se_2X_2 and SeX_2 (X = Br, Cl) follow this rule in general (2, 6). For the same halogens, the signal of the Se(II) species is several hundred ppm deshielded compared to the Se(I) species ($SeCl_2$: 1730.7 ppm; Se_2Cl_2: 1291.3 ppm; $SeBr_2$: 1467.7 ppm; Se_2Br_2: 1192.7 ppm; SeBrCl: 1600.7 ppm; mean of Se_2BrCl: 1248.7 ppm). For the SeX_2 compounds, the more electronegative the halogen, the more deshielded the Se. This applies to the Se_2X_2 (mean signal for Se_2BrCl) chemical shifts as well. For the same halogen or combination of halogens, the $SeSX_2$ is always deshielded relative to the analogous Se_2X_2 species, reflecting the greater Pauling electronegativity, χ_P, of sulfur (χ_P = 2.58), compared to selenium (χ_P = 2.55). However, the influence of the electronegativity of the next-nearest neighbour atom on Se shielding is opposite to that for nearest neighbours. Thus, in all cases, when Cl (χ_P = 3.16), as next-nearest neighbour, is replaced by Br (χ_P = 2.96), the remote Se is deshielded. This trend has been observed for perfluorochloromethyl selenides, diselenides, and thioselenides (7) and alkyl selenides and diselenides (15). Gombler (7) has accounted for the effect using hyperconjugation arguments, which require F—C multiple bonding and greater ionic character in C—Cl bonds, compared to C—F bonds. This present work shows that this anomalous trend occurs even with simple remote atoms (Br and Cl) and not just with $CF_{3-x}Cl_x$ groups. The trend appears to be related to the polarizability of the remote group as was suggested by Luthra *et al.* for the alkyl compounds (15).

Conclusion

Both S_2F_2 and Se_2F_2 exist in trigonal pyramidal and chain stereoforms (16). Early dipole moment studies of benzene solutions suggested that Se_2Cl_2 may also have a pyramidal form (17) but these observations are probably accounted for by the presence of equilibrium amounts of $SeCl_2$, Se_3Cl_2, and Se_4Cl_2 in these solutions (6) and all the evidence supports a chain structure for this molecule (8, 18). Seleninyl chloride, $SeOCl_2$, has a pyramidal form (19) but this work has shown that $SeSCl_2$, prepared by equilibration of S_2Cl_2 and Se_2Cl_2 mixtures, has a chain structure. No evidence for the pyramidal isomers was found even after long periods of heating. While oxygen is often found in terminal positions in compounds and ions, sulfur commonly gives catenated structures and, due to the similar electronegativity of S and Se, $SeSCl_2$ adopts the chain structure, ClSeSCl.

The observation of eight strong signals in the Se(I) part of the ^{77}Se NMR spectrum of a 1:1 molar mixture of Se_2Br_2 and S_2Cl_2 is consistent with the chain structure for all dichalcogen dihalides, Ch_2X_2 (Ch = Se, S; X = Cl, Br). The greater width at half-height of the diselenium dihalide signals indicates more rapid halide exchange for these compounds than for the selenium sulfur dihalides (13) and, by extension of this trend, than for the disulfur dihalides. This is expected, as a result of the weaker halogen bonding to Se (D(SeCl) = 243 kJ mol^{-1}) than to S (D(SCl) = 272 kJ mol^{-1}) (20). The integrated peak intensities show that the combination of Se—Br and S—Cl bonding is favoured over that of Se—Cl and S—Br bonding, indicating that for chalcogen–halogen bonds, overlap of atomic orbitals of like principal quantum number leads to stronger bonding than with unlike principal quantum number.

The ^{77}Se chemical shifts of catenated selenium alkyls (15) and perhaloalkyl derivatives (7) have been interpreted in terms of changes in shielding due to electronegativity changes in the group of atoms bonded to Se (7) and β- and γ-effects (15). Both electronegativity and β-effects are observed for the simple selenium and selenium sulfur dihalides. The greater electronegativity of the directly attached atoms leads to greater ^{77}Se deshielding while increased polarizability of the next nearest neighbour causes increased deshielding of Se.

NOTE ADDED IN PROOF: Since the acceptance of this manuscript, a paper dealing with the characterization of $SeSCl_2$ has come to my attention (Raman, mass and ^{77}Se NMR spectra of $SeSCl_2$ and its reactions with potassium iodide and titanocene pentasulfide to produce cyclic selenium

Can. J. Chem. Downloaded from www.nrcresearchpress.com by 92.62.229.171 on 09/08/12
For personal use only.

sulfides. R. Steudel, B. Plinke, D. Jensen, and F. Baumgart, Polyhedron, **10**, 1037 (1991)). There is good agreement between the two reports with respect to the interpretation and the actual measured chemical shifts and frequencies. Some discrepancies arise, however, in the assignment of the signals that appear to the higher chemical shift side of the Se_2Cl_2 signal (1305–1350 ppm).

Acknowledgement

We dedicate this paper to Tom Birchall, who was the first to use ^{77}Se NMR to study the structural chemistry of selenium compounds. The support of the Natural Sciences and Engineering Research Council of Canada, in the operation of the NMR facility, is acknowledged.

1. K. W. Bagnall. Selenium, Tellurium and Polonium. *In* Comprehensive inorganic chemistry. Vol. 2. *Edited by* J. C. Bailar *et al.* Pergamon Press, Oxford. 1972.
2. M. Lamoureux and J. Milne. Can. J. Chem. **67**, 1936 (1989).
3. (*a*) P. Pekonen, Y. Hiltunen, R. S. Laitinen, and J. Valkonen. Inorg. Chem. **30**, 1874 (1991); (*b*) P. Pekonen, Y. Hiltunen, R. S. Laitinen, and T. A. Pakkanen. Inorg. Chem. **29**, 2770 (1990); (*c*) R. Steudel, D. Jensen, and F. Baumgart. Polyhedron, **9**, 1199 (1990); (*d*) R. S. Laitinen and T. A. Pakkanen. Inorg. Chem. **26**, 2598 (1987).
4. (*a*) A. Baroni. Atti Linc. **16**, 515 (1932); (*b*) Atti Linc. **25**, 720 (1937).
5. V. Lenher and C. H. Kao, J. Am. Chem. Soc. **47**, 772 (1925).
6. M. Lamoureux and J. Milne. Polyhedron, **9**, 589 (1990).
7. (*a*) W. Gombler. Z. Naturforsch. B: Anorg. Chem. Org. Chem. **36**, 535 (1981); (*b*) W. Gombler. Magn. Reson. Chem. **29**, 73 (1991).
8. P. J. Hendra and P. J. D. Park. J. Chem. Soc. (A), 908 (1968).
9. G. Herzberg. Spectra of diatomic molecules. van Nostrand, Toronto. 1957. Table 39. p. 567.
10. F. Feher, K. Naused, and H. Weber. Z. Anorg. Allg. Chem. **290**, 303 (1957).
11. J. Milne. Chem. Commun. 1048 (1991).
12. J. E. Huheey. Inorganic chemistry. Harper and Row, Cambridge, Mas. 1983. Table E-1. p. A-39.
13. J. Milne and A. J. Williams. J. Am. Chem. Soc. In press.
14. H. C. E. McFarlane and W. McFarlane. Selenium-77 and tellurium-125. *In* NMR of newly accessible nuclei. Vol. 2. *Edited by* P. Laszlo. Academic Press, New York, 1983. Chap. 10.
15. N. P. Luthra, A. M. Boccanfuso, R. B. Dunlap, and J. D. Odom. J. Organomet. Chem. **354**, 51 (1988).
16. (*a*) F. Seel. Chimia, **22**, 79 (1968); (*b*) A. Haas and H. Willner. Z. Anorg. Allg. Chem. **454**, 17 (1979).
17. C. P. Smyth, G. L. Lewis, A. J. Grossmann, and F. B. Jennings. J. Am. Chem. Soc. **62**, 1219 (1940).
18. R. Forneris and C. E. Hennies. J. Mol. Struct. **5**, 449 (1970).
19. D. Gregory, I. Hargittai, and M. Kolonits. J. Mol. Struct. **31**, 261 (1976).
20. K. F. Purcell and J. C. Kotz. Inorganic chemistry. W. B. Saunders, Philadelphia. 1977. Table 6-3.

Can. J. Chem. Downloaded from www.nrcresearchpress.com by 92.62.229.171 on 09/08/12
For personal use only.

Long-range shielding and NMR chemical shifts in silicon carbide polytypes

DEQI GUO, J. STEPHEN HARTMAN,[1] AND MARY FRANCES RICHARDSON[1]
Department of Chemistry, Brock University, St. Catharines, Ont. Canada L2S 3A1

Received July 30, 1991

This paper is dedicated to the memory of Professor Thomas Birchall

DEQI GUO, J. STEPHEN HARTMAN, and MARY FRANCES RICHARDSON. Can. J. Chem. **70**, 700 (1992).

Despite an apparently successful empirical correlation, it is incorrect to ascribe variations in ^{29}Si and ^{13}C chemical shifts in silicon carbide polytypes to diamagnetic anisotropy effects.

Key words: silicon carbide, long-range shielding, polytypism, MAS NMR.

DEQI GUO, J. STEPHEN HARTMAN et MARY FRANCES RICHARDSON. Can. J. Chem. **70**, 700 (1992).

L'attribution des variations des déplacements chimiques du ^{29}Si et du ^{13}C dans les polytypes de carbure de silicium à l'effet anisotropique diamagnétique est inexacte en dépit du succès apparent de la corrélation empirique.

Mots clés : carbure de silicium, blindage à longue distance, polytypisme, MAS RMN.

[Traduit par le rédaction]

Can. J. Chem. Downloaded from www.nrcresearchpress.com by 92.62.229.171 on 09/08/12
For personal use only.

Silicon carbide, an important industrial material (1), is known for its remarkable display of polytypism. There are more than 200 known polytypes, which are characterized by having identical Si—C double layers arranged in different stacking sequences (2, 3). Since our initial work on the distinctive ^{29}Si and ^{13}C Magic Angle Spinning (MAS) NMR spectra of the 6H, 3C, and 15R polytypes (4, 5), NMR has become an important characterization tool for silicon carbide (6). All polytypes so far studied other than 3C and 2H, which have only a single silicon (and carbon) site, show several peaks in their MAS NMR spectra (4, 5, 7–9) despite the fact that the immediate-neighbour tetrahedron in SiC is essentially identical for all sites (10). We (4, 5) and others (7, 11) showed that the number of peaks could be correlated with the number and geometrical arrangement of higher neighbours. However, peaks could not be readily assigned to particular atoms in the structures. We undertook the present work as a possible approach to SiC peak assignments.

Calculations

McConnell (12) expressed the relationship between the chemical shielding increment $\Delta\sigma$ and the molar diamagnetic anisotropy $\Delta\chi$ of distant (cylindrically symmetrical) bonds as:

$$[1] \quad \Delta\sigma = \Delta\chi[(1 - 3\cos^2\theta)/3R^3]$$

where $\Delta\chi$ is the difference between the susceptibility parallel to the bond and the susceptibility perpendicular to it, R is the distance between the nucleus of interest and the electrical center of gravity of the distant bond, and θ is the angle between the vector R and the bond vector (Fig. 1).

Expansion of eq. [1] to include all contributions within a certain distance from a central atom gives the shielding increment for that atom:

$$[2] \quad \Delta\sigma = \Delta\chi(G_j)$$

$$[3] \quad G_j = \sum_n [(1 - 3\cos^2\theta_n)/3R_n^3]$$

The chemical shift, in ppm to low field of a reference compound, is related to the shielding by $\delta_{sample} = \sigma_{reference} - \sigma_{sample}$, and can be divided into local and long-range parts, so that

$$[4] \quad \delta_{X(j)} = \delta_i^X - \Delta\chi(G_j)$$

where $\delta_{X(j)}$ is the overall chemical shift of atom $X(j)$ in the structure, δ_i^X is the "intrinsic" chemical shift, i.e., the shift that atom X would have if it were bonded only to its four neighbours, and $(\Delta\chi)(G_j)$ represents the chemical shift due to long-range shielding because of the diamagnetic susceptibility of chemical bonds. G_j, the geometric factor, is a term dependent only upon the crystal structure and the location of the electrical centre of gravity for the bonds, initially taken at the midpoint. The sum is over all bonds n out to a certain radius. Equation [4] allows a value of $\Delta\chi$ to be calculated explicitly and compared to experimental values.

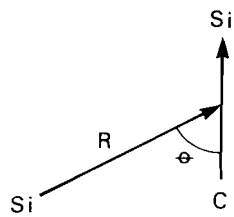

FIG. 1. Definition of parameters used in the McConnell equation for calculating the shielding increment induced by a distant bond.

Bonds to nearest neighbours were eliminated from the sum, both because the point dipole approximation is not valid at such short ranges (12) and because the nearest-neighbour effects are assumed to be accounted for in the intrinsic shift terms. Each crystallographically independent atom in the structure produces an equation. Once the chemical shifts are assigned to particular atoms in the structure, it is straightforward to carry out a least-squares fit to a series of equations and determine $\Delta\chi$ and the intrinsic chemical shifts for carbon and silicon in these structures (13).

Results and discussion

Figure 2 shows typical convergence behaviour for eq. [3] as a function of distance from the central atom. Convergence is barely achieved at a distance of 50 Å: the slowness of convergence is due to the fact that although there is an R^{-3}

[1]Authors to whom correspondence may be addressed.

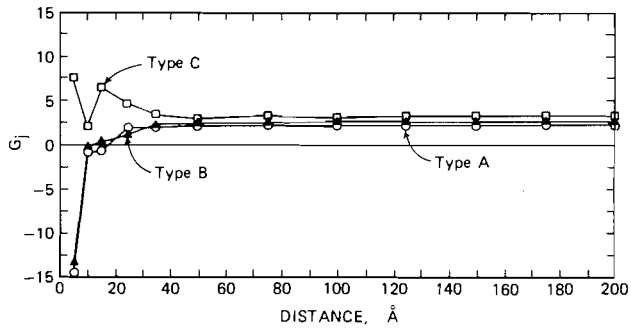

FIG. 2. Convergence behavior of the geometric factor G_j as a function of distance from the central atom for the Types A, B, and C atoms in 6H SiC. The types (5) correspond to the independent atoms.

dependence for the shielding due to one bond, the number of bonds increases as R^3. Others (14) have also noted the necessity of extending calculations out to at least 50 Å in McConnell-type calculations.

The geometric factors for the three independent silicons and carbons in 6H SiC have distinct values (Fig. 2). If these are assigned to the three peaks in the ^{29}Si and ^{13}C NMR spectra of 6H SiC in such a way that the chemical shift is to low field as G_j increases, least-squares solution of eq. [4] yields values of 97.8×10^{-33} m^3/bond (7.78×10^3 ppm A^3/bond) for $\Delta\chi$, and 0.79 and 40.13 ppm for the intrinsic chemical shifts of silicon and carbon, respectively. The intrinsic shifts are in reasonable agreement with the ^{29}Si shift in tetramethylsilane (0 ppm) and the ^{13}C shift of the central carbon in $(Me_3Si)_4C$ (77 ppm relative to TMS) (15). However, the value of $\Delta\chi$ for an Si—C bond is nearly three orders of magnitude larger than the usual values for single bonds (16). In other words, if $\Delta\chi$ for an Si—C bond has a magnitude similar to those for C—H or C—C bonds, the long-range shielding effect should amount to no more than a few tenths of a part per million, an amount similar to that observed, for example, in aryl ethers (17). Variations in the formulation of the long-range shielding (13), e.g., changing the peak assignments, moving the electrical centre of gravity, and shifting the layers (which changes the bond distances), do not alleviate the problem.

The unreasonable $\Delta\chi$ value (7.78×10^3 ppm/A^3) for the Si—C bond shows that long-range diamagnetic shielding cannot be the origin of the variation in ^{29}Si and ^{13}C chemical shifts in SiC polytypes. Furthermore, our recent work on chemical shift tensors for the 6H polytype (18) yielded firm peak assignments that are inconsistent with those based on long-range diamagnetic shielding. The results of the present calculations are consistent with the usual predominance of paramagnetic contributions to the shielding, arising from nonspherical electron density about an atom and calculated from orbital overlaps between a central atom and its successive neighbors (16). Diamagnetic shielding effects normally are a major factor only in ^{1}H NMR (e.g., ref. 19).

Sherriff has carried out diamagnetic shielding calculations based on the McConnell equation, which have successfully correlated ^{29}Si chemical shifts of a wide range of silicate minerals (20). The practical utility of this approach to calculating silicate chemical shifts is undeniable, and it can be applied to Al,Si order/disorder problems (20) and extended from the usual four-coordinate silicon to the relatively rare six-coordinate silicon in silicates (21). However, neighbour anisotropy effects on diamagnetic shielding, which are inherently long range in network solids, cannot be the true basis of the success of these calculations, which deal with atoms only out to the second-neighbour positions. The success may be attributable to an accidental modelling of a paramagnetic contribution to chemical shift, with similar geometric form but falling off much more rapidly with distance. The $\Delta\chi$ for the Si—O bond (20) (-701.6 ppm/A^3, orders of magnitude larger than expected for diamagnetic shielding) seems consistent with inadvertent modelling of a large paramagnetic shielding term.

NMR is potentially more sensitive than X-ray diffraction to local environment (22, 23), and is the analytical tool of choice for amorphous or disordered solids. Thus correlations of the chemical shift with easily calculated structure-dependent functions are becoming increasingly important. However, the diamagnetic shielding term is not the major factor in network solids such as silicon carbide and silicates. Further work is needed to elucidate the factors affecting chemical shift in systems such as these.

Acknowledgements

We thank Mr. T. R. B. Jones for technical assistance, Prof. M. J. McGlinchey of McMaster University for suggesting the long-range shielding calculations, Dr. L. Wolfe and co-workers of General Abrasive, Niagara Falls, for access to production-run silicon carbide samples, and the Natural Sciences and Engineering Research Council of Canada for financial support in the form of operating grants to M. F. R. and J. S. H.

1. F. Aldinger and H.-J. Kalz. Angew. Chem. Int. Ed. Engl. **26**, 371 (1987); D. R. Ulrich. Chem. Eng. News, **68** (January 1), 28 (1990).
2. A. R. Verma and P. Krishna. Polymorphism and polytypism in crystals. John Wiley and Sons, New York. 1966.
3. J. Schlichting, G. Czack, E. Koch-Bienemann, P. Kuhn, and F. Schroder, (*Volume authors*). Gmelin handbook of inorganic chemistry. 8th ed. Springer-Verlag, Berlin/Heidelberg/New York. 1984; Supplement Volume B2, Si-Silicon, Properties of Crystalline Silicon Carbide.
4. G. R. Finlay, J. S. Hartman, M. F. Richardson, and B. L. Williams. J. Chem. Soc. Chem. Commun. 159 (1985).
5. J. S. Hartman, M. F. Richardson, B. L. Sherriff, and B. G. Winsborrow. J. Am. Chem. Soc. **109**, 6059 (1987).
6. G. R. Hatfield and K. R. Carduner. J. Mater. Sci. **24**, 4209 (1989); G. L. Turner, R. J. Kirkpatrick, S. H. Risbud, and E. Oldfield. Am. Ceram. Soc. Bull. **66**, 656 (1987); Z.-F. Zhang, F. Babonneau, R. M. Laine, Y. Mu, J. F. Harrod, and J. A. Rahn. J. Am. Ceram. Soc. **74**, 670 (1991); W. R. Schmidt, L. V. Interrante, R. H. Doremus, T. K. Trout, P. S. Marchetti, and G. E. Maciel. Chem. Mater. **3**, 257 (1991); J. Lipowitz, H. A. Freeman, R. T. Chen, and E. R. Prack. Adv. Ceram. Mater. **2**, 121 (1987); T. Taki, M. Inui, K. Okamura, and M. Sato. J. Mater. Sci. Lett. **8**, 918 (1989); R. F. Davis and J. T. Glass. Adv. Solid-State Chem. **2**, 1 (1991).
7. J. R. Guth and W. T. Petuskey. J. Phys. Chem. **91**, 5361 (1987).
8. D. C. Apperley, R. K. Harris, G. L. Marshall, and D. P. Thompson. J. Am. Ceram. Soc. **74**, 777 (1991).
9. G. W. Wagner, B. K. Na, and M. A. Vannice. J. Phys. Chem. **93**, 5061 (1989).
10. A. H. Gomes de Mesquita. Acta Crystallogr. **23**, 610 (1967).

Can. J. Chem. Downloaded from www.nrcresearchpress.com by 92.62.229.171 on 09/08/12
For personal use only.

11. M. O'Keeffe. Chem. Mater. **3**, 332 (1991).
12. H. M. McConnell. J. Chem. Phys. **27**, 226 (1957).
13. D. Guo. M.Sc. Thesis, Brock University, St. Catharines, Ont. 1988.
14. J. Tegenfeldt, H. Feucht, G. Ruschitzka, and U. Haeberlen. J. Magn. Reson. **39**, 509 (1980).
15. A. I. Al-Mansour, S. S. Al-Showiman, and I. M. Al-Najjan. Spectrochim. Acta, **44A**, 643 (1988).
16. R. K. Harris. Nuclear magnetic resonance spectroscopy. Revised edition. Longman Scientific and Technical, Essex. 1986.
17. N. J. Clayden. Magn. Reson. Chem. **27**, 692 (1989).
18. M. F. Richardson, J. S. Hartman, D. Guo, and B. G. Winsborrow. Chem. Mater. In press.
19. M. J. McGlinchey, R. C. Burns, R. Hofer, S. Top, and G. Jaouen. Organometallics, **5**, 104 (1986).
20. B. L. Sherriff. Ph.D. Thesis, McMaster University, Hamilton, Ont. 1988; B. L. Sherriff and H. D. Grundy. Nature, **332**, 819 (1988); B. L. Sherriff, H. D. Grundy, and J. S. Hartman. Eur. J. Mineral. **3**, 751 (1991).
21. J. F. Stebbins and M. Kanzaki. Science, **251**, 294 (1991).
22. C. A. Fyfe, H. Strobl, G. T. Kokotailo, G. J. Kennedy, and G. E. Barlow. J. Am. Chem. Soc. **110**, 3373 (1988); H. Strobl, C. A. Fyfe, G. T. Kokotailo, and C. T. Pasztor. J. Am. Chem. Soc. **109**, 4733 (1987).
23. J. W. Richardson, Jr., J. J. Pluth, J. V. Smith, W. J. Dytrich, and D. M. Bibby. J. Phys. Chem. **92**, 243 (1988).

Can. J. Chem. Downloaded from www.nrcresearchpress.com by 92.62.229.171 on 09/08/12
For personal use only.

Benzothiarsolium cations: evidence for $p\pi$-bonding between arsenic and sulfur in the first structurally characterized arsenium system

NEIL BURFORD,[1] TRENTON M. PARKS, AND BRUCE W. ROYAN
Department of Chemistry, Dalhousie University, Halifax, N.S., Canada B3H 4J3

JOHN F. RICHARDSON
Department of Chemistry, University of Louisville, Louisville, KY 40292, U.S.A.

AND

PETER S. WHITE[2]
Department of Chemistry, University of New Brunswick, Fredericton, N.B., Canada E3B 6E2

Received July 4, 1991

This paper is dedicated to the memory of Professor Thomas Birchall

NEIL BURFORD, TRENTON M. PARKS, BRUCE W. ROYAN, JOHN F. RICHARDSON, and PETER S. WHITE. Can. J. Chem. **70**, 703 (1992).

Tetrachloroaluminate salts of the benzothiazarsolium and toluodithiarsolium heteronaphthalenic cations have been prepared from the corresponding chloroarsoles by a routine halide ion abstraction procedure. Characterization data are presented, including the X-ray crystal structure of the thiaza derivative. (Crystal data for $C_6H_5AlAsCl_4NS$: monoclinic, space group $P2_1/c$, a = 6.4259(5) Å, b = 23.654(3) Å, c = 8.5859(7) Å, β = 98.203(6)°, V = 1291.7(2) Å^3, Z = 4, R = 0.054.) A planar bicyclic cationic unit is observed, typical of other heteronaphthalenic systems. The crystal structure of 2-chlorobenzo-1,3,2-thiazarsole has been obtained for direct comparison, and also has a close to planar heterobicyclic moiety. (Crystal data for $C_6H_5AsClNS$: monoclinic, space group $P2_1/c$, a = 8.370(3) Å, b = 10.829(3) Å, c = 8.756(2) Å, β = 95.99(2)°, V = 789.2(3) Å^3, Z = 4, R = 0.025.) The planarity and short heterocyclic bond lengths observed in the two compounds imply a significant degree of $p\pi$ bonding, which is unique between sulfur and arsenic. In addition, the cation is a rare example of a structurally characterized cationic dicoordinate arsenic, or arsenium, system.

Key words: arsenic, arsolium, arsenium, $p\pi$-bonding, sulfur, heteronaphthalenic.

NEIL BURFORD, TRENTON M. PARKS, BRUCE W. ROYAN, JOHN F. RICHARDSON et PETER S. WHITE. Can. J. Chem. **70**, 703 (1992).

On a préparé les tétrachloroaluminates des cations hétéronaphtaléniques benzothiazarsolium et toluodithiarsolium en faisant appel à une méthode de routine pour enlever un ion halogénure des chloroarsoles correspondants. On présente les données ayant servi à leur caractérisation, y compris la structure cristalline du dérivé thiaza. (Données cristallographiques du $C_6H_5AlAsCl_4NS$: monoclinique, groupe d'espace $P2_1/c$, a = 6,4259(5), b = 23,654(3) et c = 8,5859(5) Å, β = 98,203(6)°, V = 1291,7(2) Å^3, Z = 4 et R = 0,054.) On a observé la présence d'une unité cationique bicyclique plane, typique d'autres systèmes hétéronaphtaléniques. On a obtenu la structure cristalline du 2-chlorobenzo-1,3,2-thiazarsole par une comparaison directe; elle comporte aussi une portion hétérobicyclique pratiquement plane. (Données cristallographiques du $C_6H_5AsClNS$: monoclinique, groupe d'espace $P2_1/c$, a = 8,370(3), b = 10,829(3) et c = 8,756(2) Å, β = 95,99(2)°, V = 789,2(3) Å^3, Z = 4 et R = 0,025.) Le fait que, dans les deux molécules, la structure est plane et les longueurs des liaisons hétérocycliques sont courtes implique l'existence d'une liaison $p\pi$ importante, mais unique, entre le soufre et l'arsenic. De plus, le cation est un rare exemple d'un système cationique dicoordonné de l'arsenic, ou arsénium, à être caractérisé d'un point de vue structurel.

Mots clés : arsenic, arsolium, arsénium, liaison $p\pi$, soufre, hétéronaphtalénique.

[Traduit par la rédaction]

Introduction

Compounds containing multiple bonds between heavier non-metal elements are now commonplace. While they represent experimentally confirmed contradictions of the "Double Bond Rule",[3] a variety of synthetic innovations are responsible for this significant fundamental development, the most common being steric shielding (2). Nevertheless, $p\pi$ bonding is by no means general throughout the p-block, with the restricted valency and coordination of the more electron-rich elements requiring alternative structural or electronic features to support incorporation into a $p\pi$-bonded system (see, for example, ref. 3).

We recently introduced the cationic heteronaphthalenic framework **1** as a versatile template for the construction of new $p\pi$ bonded units involving pnicogens and chalcogens, including systems containing the first examples of stable $p\pi$ bonding between phosphorus and sulfur (4–6). Compounds of this type apparently benefit from the stabilization associated with accommodation of a Hückel number of π-electrons as well as the molecular positive charge. Here we present the 1,3,2-benzothiazarsolium (**2**) (for a preliminary communication of this work, see ref. 7) and 5-methyl-1,3,2-benzodithiarsolium (**3**) (preliminary communication, ref. 8) cations as the first examples of stable systems containing arsenic–sulfur $p\pi$ bonding. This is illustrated in the crystal structure of **2**$AlCl_4$ and by an inter-

[1]Author to whom correspondence may be addressed.

[2]Present address: Department of Chemistry, University of North Carolina at Chapel Hill, Chapel Hill, NC 27514, U.S.A.

[3]"Elements with a principal quantum number greater than 2 are incapable of forming $p\pi$ interactions." See, for example, ref. 1.

Can. J. Chem. Downloaded from www.nrcresearchpress.com by 92.62.229.171 on 09/08/12
For personal use only.

esting comparison with the structure of the corresponding 2-chloroarsole **4**.

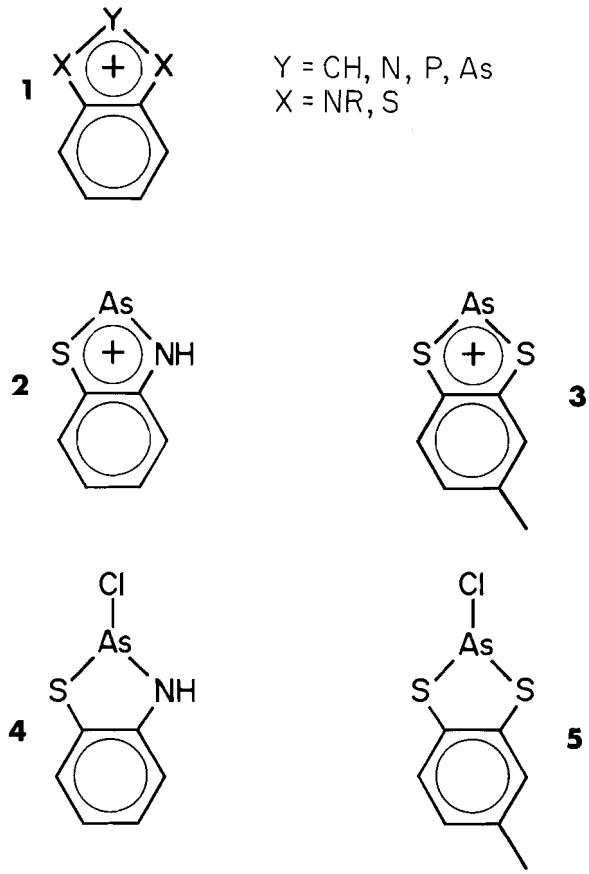

Experimental

General procedures

All compounds reported here are extremely moisture sensitive and are handled under rigorously anaerobic and anhydrous conditions. $AsCl_3$ (AESAR) and Et_3N (BDH) were distilled under N_2 before use. $AlCl_3$ (Aldrich) was sublimed under vacuum before use. 3,4-Toluenedithiol (Aldrich) and *o*-aminothiophenol (Aldrich) were used as received. 2-Chloro-5-methyl-1,3,2-benzodithiarsole **5** was prepared by the literature procedure (9), with minor modifications. CH_2Cl_2 and hexane were dried over P_2O_5 and CaH_2 and stored in evacuated bulbs. $CDCl_3$ was dried over P_2O_5. Solids were manipulated in a Vacuum/Atmospheres nitrogen-filled glove box. Glass equipment was flame dried before use. Reactions were performed in an evacuated (10^{-3} Torr; 1 Torr = 133.3 Pa) dual compartment vessel,[4] unless otherwise indicated. Melting points were recorded on a Fisher–Johns apparatus and are uncorrected. Elemental analyses were performed by Beller Laboratories, Gottingen, Germany. IR spectra were recorded as Nujol mulls on CsI plates using a Perkin–Elmer 283B spectrophotometer. NMR spectra were recorded on a Nicolet NT-360 spectrometer in 5 or 10 mm flame-sealed Pyrex tubes. Chemical shifts are reported in ppm relative to external standards ($[Al(H_2O)_6]^{3+}$ for ^{27}Al) and relative to the internal solvent signal for ^1H and ^{13}C. Mass spectra were obtained by using a CEC model 21-104 mass spectrometer. Crystals suitable for crystallography were obtained as described in text for each compound, and were selected and mounted in Pyrex capillaries in the dry box.

[4]A modification of the H-tube reaction vessel described in ref. 10.

Preparation and characterization data

*$C_6H_4SN(H)AsCl$ **4***

A solution of $AsCl_3$ (1.08 g, 6.0 mmol) in Et_2O (15 mL) was added to a stirred mixture of *o*-aminothiophenol (0.75 g, 6.0 mmol) and Et_3N (1.21 g, 12.0 mmol) in Et_2O (20 mL), and the mixture was stirred at room temperature for 3 h. A yellow solution was decanted from the white precipitate and the solvent was removed *in vacuo* to leave a bright yellow solid, which was recrystallized from CH_2Cl_2 to give yellow/orange crystals of 2-chlorobenzo-1,3,2-thiazarsole (0.92 g, 3.9 mmol, 65%), mp 135–137°C. IR: 3290m, 1450s, 1355m, 1300m, 1250m, 1020m, 850m, 740vs, 580m, 555m, 460m, 420s, 290m, 230vs cm^{-1}. NMR, ^1H: 753–6.99 ppm (ABCD), 6.6 ppm (NH); ^{13}C: 147, 126, 126, 124, 121, 115 ppm. Anal. calcd.: C 30.85, H 2.16, N 6.00%; found: C 30.63, H 2.19, N 5.91%.

*$[C_6H_4SN(H)As]$ **2** $[AlCl_4]$*

A solution of 2-chlorobenzo-1,3,2-thiazarsole (0.332 g, 1.42 mmol) in CH_2Cl_2 (40 g) was added dropwise to a stirred suspension of $AlCl_3$ (0.193 g, 1.45 mmol) in CH_2Cl_2 (40 g) over a period of 25 min. A deep yellow solution initially formed and later produced a bright yellow microcrystalline precipitate. The solution was decanted and the solid was washed by two cold-spot back distillations, and characterized as benzo-1,3,2-thiazarsolium tetrachloroaluminate (0.391 g, 1.07 mmol, 75%), mp 135–137°C. Recrystallization from a dilute CH_2Cl_2 solution by slow removal of solvent produced small pale yellow crystals suitable for crystallography. Larger, higher quality crystals were obtained from a concentrated reaction mixture by slow removal of solvent. IR: 3230m, 1555m, 1545m, 1245m, 1220m, 760vs, 720s, 710s, 540m, 530s, 505vs, 475vs, 450s, 290m cm^{-1}. NMR, ^1H: 8.40–7.60 ppm (ABCD), 8.4 ppm (NH); ^{13}C: 130, 128, 127, 119 ppm (quarternary carbons not observed). Anal. calcd.: C 19.64, H 1.38, N 3.82, S 8.74%; found: C 19.78, H 1.24, N 3.80, S 8.87%.

*$[CH_3C_6H_4S_2As]$ **3** $[AlCl_4]$*

5-Methylbenzo-1,3,2-dithiarsole (0.497 g, 1.88 mmol) in CH_2Cl_2 (25 mL) was added dropwise over 3 h to a vigorously stirred suspension of $AlCl_3$ (0.250 g, 1.88 mmol) in CH_2Cl_2 (25 mL). The red/orange reaction mixture was stirred for 14 h and the solvent was slowly removed until crystallization began. At this point the solid was redissolved and the reaction vessel cooled in an ice water/NaCl bath. A bright orange crystalline solid was isolated and characterized as 5-methylbenzo-1,3,2-dithiarsolium tetrachloroaluminate (0.262 g, 0.66 mmol, 35%), mp 121–123°C. IR: 820s, 540m, 510m, 485vs, 435m cm^{-1}. NMR, ^1H: 8.33 (d), 8.26 (s), 7.75 (d), 2.66 (s) ppm ($^3J_{HH}$ = 8.6 Hz); ^{13}C: 153, 150, 142, 131, 129, 128, 21 ppm. Anal. calcd.: C 21.13, H 1.52, S 16.11, As 18.83%; found: C 20.97, H 1.78, S 15.82, As 18.50%.

X-ray data collection, solution, and refinement

All pertinent crystallographic data are summarized in Table 1. Data were collected at room temperature on an Enraf–Nonius CAD-4 diffractometer (MoK_α, λ = 0.70930 Å, graphite monochromator) using the ω–2θ scan technique. No significant decay of three standard reflections was observed during data collection. Unit cell parameters were obtained from the setting angles of 25 accurately centred reflections. The choice of space groups was based on systematically absent reflections. Data were corrected for Lorentz and polarization effects. Scattering factors were taken from Cromer and Waber (11) and anomalous dispersion effects were included in F_c (12). An empirical absorption correction was applied for $C_6H_4SN(H)AsCl$ **4** based on a series of psi scans. The structures were solved using direct methods (13, 14) to find the heavier elements, and the remaining non-hydrogen atoms were located from a series of difference Fourier maps. Hydrogen atom positional parameters were refined in **4** and included in ideal positions as fixed contributions to the structure. In **2**$AlCl_4$ the thermal parameters for hydrogen atoms were not refined (B_{iso} = 1.2 × B of the bonded atom). The models were refined using full-matrix least-squares techniques based on F, minimizing the function $\Sigma w(|F_o| - |F_c|)^2$,

Can. J. Chem. Downloaded from www.nrcresearchpress.com by 92.62.229.171 on 09/08/12
For personal use only.

TABLE 1. Crystallographic data

Formula	$C_6H_5AsClNS$	$C_6H_5AlAsCl_4NS$	
fw	233.55	366.89	
Space group	$P2_1/c$	$P2_1/c$	
a, Å	8.370 (3)	6.4259 (5)	
b, Å	10.829 (3)	23.654 (3)	
c, Å	8.756 (2)	8.5859 (7)	
β, °	95.99 (2)	98.203 (6)	
V, Å^3	789.2	1291.68	
Z	4	4	
$F(000)$	456	712	
D_{calcd}, g cm^{-1}	1.97	1.887	
Size, mm	0.10 × 0.25 × 0.40	0.69 × 0.35 × 0.35	
μ, cm^{-1}	48.1	36.5	
Max 2θ, °	55	50	
Reflections:			
Measured	2068	2547	
Unique	1832	2264	
Observed	1402	1786	$(I_0 > 3\sigma(I_0))$
Parameters	107	128	
R	0.025	0.042	
R_w	0.026	0.054	
GoF	1.07	1.825	

TABLE 2. Fractional atomic coordinates and isotropic thermal parameters for compound **4**

Atom	x/a	y/b	z/c	B
As	0.01801 (4)	0.44042 (3)	0.22657 (4)	2.686 (5)
Cl	0.2005 (1)	0.38876 (8)	0.04344 (9)	3.65 (2)
S	0.0872 (1)	0.63473 (7)	0.26513 (9)	2.94 (1)
N	0.1350 (3)	0.4017 (2)	0.4036 (3)	2.94 (5)
C1	0.2324 (4)	0.4883 (2)	0.4844 (3)	2.65 (6)
C2	0.3321 (4)	0.4606 (4)	0.6173 (4)	3.66 (7)
C3	0.4222 (4)	0.5530 (4)	0.6902 (4)	4.52 (9)
C4	0.4151 (5)	0.6714 (4)	0.6337 (4)	4.45 (8)
C5	0.3147 (4)	0.7006 (3)	0.5025 (4)	3.66 (7)
C6	0.2235 (4)	0.6089 (3)	0.4283 (3)	2.69 (6)
H(N)1	0.142 (5)	0.339 (4)	0.427 (4)	3.5*
H2	0.336 (5)	0.378 (4)	0.655 (5)	4.3*
H3	0.490 (6)	0.532 (4)	0.776 (5)	5.3*
H4	0.476 (5)	0.728 (4)	0.683 (5)	5.3*
H5	0.310 (5)	0.777 (4)	0.464 (5)	4.3*

Starred atoms were refined with fixed isotropic thermal parameters. Anisotropically refined atoms are given in the form of the isotropic equivalent displacement parameter.

TABLE 3. Fractional atomic coordinates and isotropic thermal parameters for **2**$AlCl_4$

Atom	x/a	y/b	z/c	$B(iso)$
As	0.5554 (1)	0.20848 (2)	0.11401 (7)	0.0464 (3)
S	0.3237 (2)	0.18153 (6)	0.2564 (2)	0.0451 (6)
N	0.6429 (7)	0.1374 (2)	0.1069 (4)	0.041 (2)
C1	0.5500 (8)	0.0943 (2)	0.1809 (5)	0.037 (2)
C2	0.613 (1)	0.0378 (3)	0.1790 (6)	0.049 (3)
C3	0.505 (1)	−0.0011 (2)	0.2518 (7)	0.057 (3)
C4	0.340 (1)	0.0142 (3)	0.3287 (7)	0.060 (3)
C5	0.278 (1)	0.0699 (3)	0.3353 (6)	0.049 (3)
C6	0.3870 (8)	0.1102 (2)	0.2607 (6)	0.038 (2)
Al	1.0285 (2)	0.34815 (6)	0.2554 (2)	0.0314 (6)
Cl1	0.8336 (2)	0.36445 (7)	0.0411 (2)	0.0474 (6)
Cl2	0.9184 (2)	0.27701 (6)	0.3737 (2)	0.0456 (6)
Cl3	1.0271 (2)	0.41836 (6)	0.4114 (2)	0.0452 (6)
Cl4	1.3426 (2)	0.33206 (6)	0.2143 (2)	0.0468 (6)
H(N)1	0.7756	0.1281	0.0470	0.041
H2	0.7413	0.0255	0.1176	0.050
H3	0.5482	−0.0452	0.2478	0.056
H4	0.2577	−0.0177	0.3863	0.058
H5	0.1520	0.0811	0.4007	0.049

$B(iso)$ is the mean of the principal axes of the thermal ellipsoid.

where $w = [\sigma(F)^2 + (0.005F)^2 + 0.4]^{-1}$ for compound **4** (15), and was derived from counter statistics for **2**$AlCl_4$. Positional and isotropic thermal parameters are given in Tables 2 and 3 and selected bond lengths and angles are given in Table 4. Supplementary material (anisotropic thermal parameters and structure factors, 27 pages) is available.[5]

Results and discussion

Preparation and characterization of benzothiarsolium cations

The halide ion abstraction reaction is widely used in inorganic synthesis and has been exploited in the development of non-metal cations. Convenient reagents and high yields (essentially quantitative) are the principal advantages, although the non-metal salts are generally extremely reactive. The new arsolium cations are typical examples. The haloarsoles **4** and **5** react rapidly with $AlCl_3$[6] to give the corresponding tetrachloroaluminate salts of **2** and **3**. As for the phosphorus analogs, good yields and ease of isolation of the salts are only possible if the haloarsole is kept at a low concentration with respect to the acid during the reaction to

[5]These tables may be purchased from: The Depository of Unpublished Data, Document Delivery, CISTI, National Research Council Canada, Ottawa, Canada K1A 0S2.

[6]A number of halide ion abstracting agents have been employed and found to react; however, the products have proven difficult to isolate and characterize.

Can. J. Chem. Downloaded from www.nrcresearchpress.com by 92.62.229.171 on 09/08/12
For personal use only.

TABLE 4. Selected bond lengths (Å) and angles (°)

$C_6H_5AsClNS$		$C_6H_5AlAsCl_4NS$	
As—S	2.1991 (8)		2.1536 (15)
As—N	1.795 (3)		1.776 (4)
C(6)—N	1.388 (4)	C(1)—N	1.382 (7)
C(1)—S	1.755 (3)	C(6)—S	1.736 (5)
C(1)—C(6)	1.394 (4)		1.383 (7)
As—Cl	2.393 (1)		
S—As—N	88.84 (8)		89.27 (14)
C(1)—S—As	96.4 (2)	C(6)—S—As	96.95 (18)
C(6)—N—As	121.4 (3)	C(1)—N—As	121.6 (3)
S—As—Cl	98.65 (3)		
Intermolecular contacts:			
As—Cl(2)	3.399 (2)	As—Cl′	3.3842 (9)
As—Cl(2)′	3.345 (1)	S—Cl′	3.436 (1)
As—Cl(4)	3.637 (2)		
As—Cl(4)′	3.390 (2)		
S—Cl(4)′	3.583 (2)		
NH—Cl(3)	2.389 (2)		
NH—Cl(2)′	2.913 (2)		

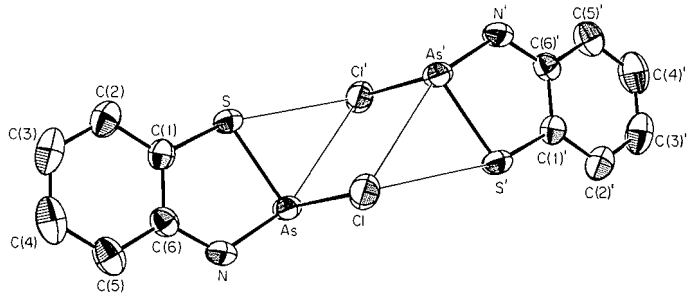

FIG. 1. ORTEP view of the dimeric unit of compound **4**.

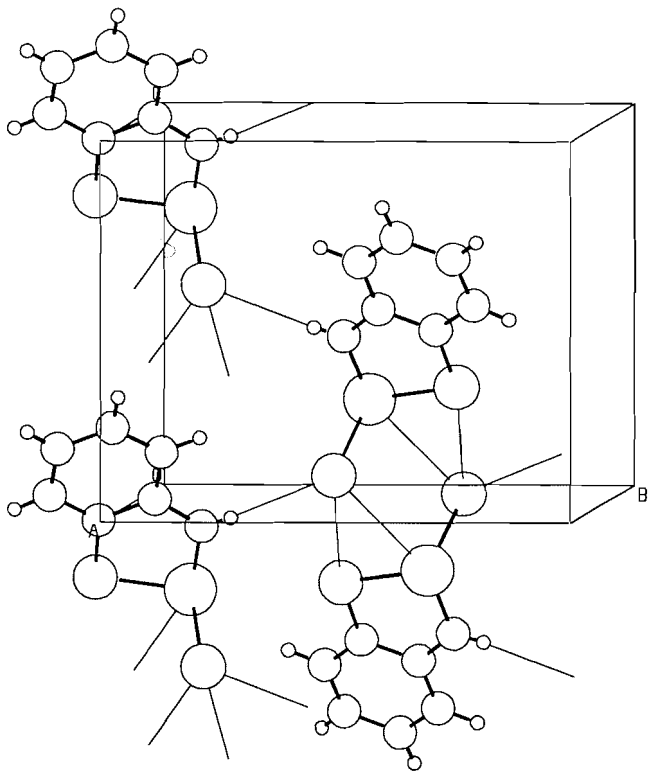

FIG. 2. PLUTO view of the unit cell of compound **4** showing intermolecular contacts that are within the sums of the van der Waals radii for the atoms involved.

prevent aromatic substitution of the benzo moiety by the solvent (5).

The new arsolium salts have been characterized by the usual techniques and exhibit familiar spectroscopic features. A strong absorption around 485 cm^{-1} is observed in the IR spectra and is characteristic of the ν_3 vibration of $AlCl_4^-$ (16). The ^1H and ^{13}C NMR data show a dramatic deshielding of the nuclei in the benzo unit in the cations **2** and **3** with respect to those of the precursor arsoles **4** and **5**. This is consistent with the values obtained for other derivatives of **1** (4–6), as well as those reported for benzo-1,3-dithiolium (17), benzo-1,3-thiazolium (18), and benzo-1,3,2-dithiazolium (19) cations, and can be attributed to effective delocalization of the positive charge throughout the bicyclic framework. A similar feature is observed for the chemical shift of the amine proton of **2** with respect to **4**. For the toluo derivatives **3** and **5**, a larger $^3J_{HH}$ (*ortho*) value is observed for the cation **3**, typical of a naphthalenic system (see, for example, ref. 20).

Structural features of the benzothiazarsolium unit (4 and 2AlCl₄)

2-Chloro-1,3,2-benzothiazarsole **4** exists as dimeric units in the solid state, and is isostructural with the phosphorus analog (6). An As_2Cl_2 parallelogram (As—Cl, 2.293(1) Å; As—Cl′, 3.3842(9) Å) links the two molecules, which are related by a crystallographic centre of inversion (Fig. 1). The heterobicyclic unit is almost planar with the arsenic centre only 0.1439(3) Å from the C_6SN plane, and is essentially perpendicular to the As_2Cl_2 unit. Similar halogen-bridged dimeric arrangements have been reported for a number of non-metal halide systems (e.g., PBr_4^- (21), $As_2I_8^{2-}$ (22), $ArSnCl^+$ (23), Ar_2SnCl^+ (24)), including the chloroarsines (^{t}BuN)(Me_2Si)(^{t}BuN)AsCl (25), and $C_4H_8N_2S \cdot AsCl_3$ (26). The dimer units of **4** are associated by hydrogen bonding between the amino protons and chlorine centres (Fig. 2).

Interestingly, 5-methyl-2-chloro-1,3,2-benzodithiarsole **5** (9), which is closely related to **4**, adopts a very different structure. The molecules are arranged in sheets (Fig. 3) and the contact distances between the molecular units (As—Cl′, 3.81 Å; S—Cl′, 3.69 Å) are substantially longer than those in the dimer of **4** [As—Cl′, 3.3842(9) Å, S—Cl′, 3.436(1) Å). Furthermore, the As—Cl bond (2.236(3) Å) is considerably shorter than the shortest of those in **4** (As—Cl, 2.293(1) Å), and the bicyclic unit is far from planar with the arsenic centre displaced from the C_6S_3 plane by 0.58 Å (cf. 0.1439(3) Å in **4**). As such, the molecular structure of **5** resembles that of the severely folded 5-methyl-2-phenyl-1,3,2-benzodithiaphosphole (4, 5).

1,3,2-Benzothiazarsolium **2** tetrachloroaluminate is isostructural with other structurally characterized derivatives of **1**$AlCl_4$ salts (4, 7). While discrete cationic and anionic units are evident, there are significant (Table 4) cation–anion interactions (distances within the sums of the respective van der Waals radii: As, 2.0; S, 1.8; N, 1.5; Cl, 1.8 Å (values from ref. 27)), consistent with the contact array observed for

Can. J. Chem. Downloaded from www.nrcresearchpress.com by 92.62.229.171 on 09/08/12
For personal use only.

Can. J. Chem. Downloaded from www.nrcresearchpress.com by 92.62.229.171 on 09/08/12
For personal use only.

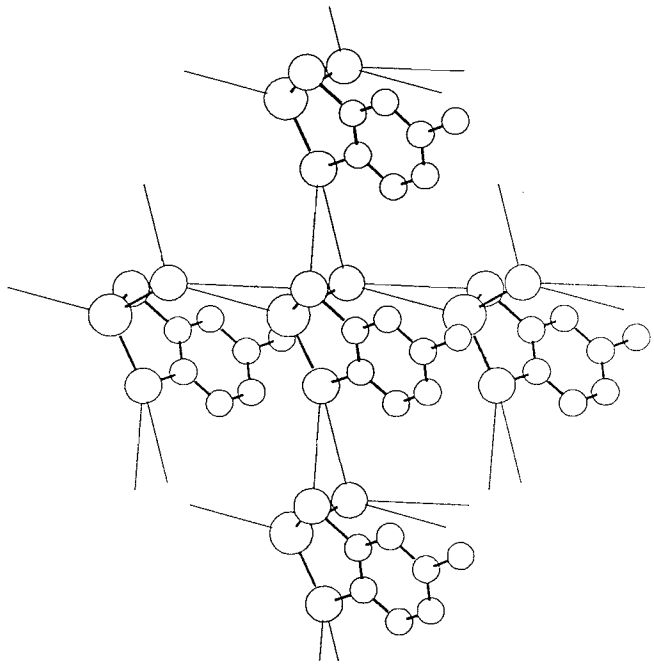

FIG. 3. PLUTO view of the molcular packing in compound **5**, generated from the data provided in ref. 9.

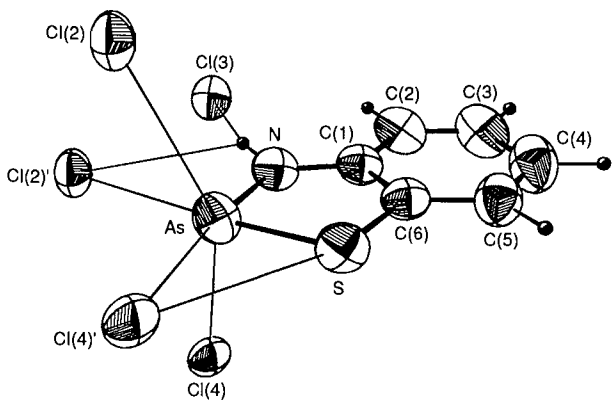

FIG. 4. ORTEP view of the cation **2** showing the cation–anion interactions involving the chlorine atoms of the $AlCl_4^-$ units.

the isostructural series, as illustrated for **2**$AlCl_4$ in Fig. 4. The contacts are similar in length and array to those reported for many Main Group cations (e.g., Ch_4^{2+}, Ch = S, Se, Te (28), which have been investigated theoretically and are envisaged as nucleophilic charge transfer interactions (29)). We believe that the magnitude of these interactions is small and their effect on the electronic structure of the cation is negligible. Identical structural features are observed within the cationic units of the tetrachloroaluminate salts of 1,3,2-benzodithiaphospholium (5) and 5-methyl-1,3,2-benzodithiaphospholium (30) despite their very different packing arrangements. This is corroborated by the regular tetrahedral geometry of the anion, which can be severely distorted in the presence of transition metal/arene cationic complexes (see, for example, refs. 24 and 31) and small polarizing cations, such as Li^+ (32).

The intermolecular interactions between the monomers in compound **4** (and those in the phosphorus analog (6)) can also be considered as contacts. Both Pn–Hal bonds are dramatically longer than standard covalent σ-bonds, and the longer bond (As—Cl′, 3.3842(9) Å) is comparable with the cation–anion interactions mentioned above. Moreover, each chlorine atom of **4** makes a secondary contact with the sulfur centre of the other molecule (3.436(1) Å), reminiscent of the same contact present in the isostructural series of **1**$AlCl_4$ (6) (S—Cl(4) in Fig. 4). On this basis, compound **4** may be regarded as partially ionic (6).

Cation **2** is planar, with a mean deviation of 0.020 Å and a maximum deviation from the best plane of 0.050(8) Å at C(4). The bonds within the heterocyclic moiety of the cation **2** (As—S, 2.1536(15) Å; As—N, 1.776(4) Å; C—S, 1.736(5) Å) are significantly shorter than those of compound **4** (As—S, 2.1991(8) Å; As—N, 1.795(3) Å; C—S, 1.755(3) Å) except for the C—N bonds, which are crystallographically identical. All of the bonds within the bicyclic units are shorter than the corresponding single bonds (As—S (for compilations of As—S bond lengths see refs. 33, 34): $(PhS)_3As$, 2.243(1) Å (35); *cyclo*-$(MeAsS)_{3or4}$: 2.19(2)–2.34(2) Å (36); As—N: (^{t}BuN)(Me_2Si)(^{t}BuN)AsCl, 1.832(3) Å (25); C—S: 1.80 Å (37); C—N: 1.47 Å (38)).

pπ *Bonding between arsenic and sulfur*

Structural studies on arsenic-sulfur compounds show a consistent As—S bond length (2.19–2.34 Å (33–36)), which is viewed as a single bond. A significantly shorter bond (2.173(3) Å) was observed in the $As_3S_4^+$ cation, and rationalized by means of a valence bond model involving a π-bonded resonance contributor (34). Cation **2** exhibits an even shorter As—S bond (2.1536(15) Å), and a dramatic shortening with respect to that of the arsine analog **4**. This bond length comparison is related to the relative planarity of the bicyclic unit in each compound (**2** and **4**), and indicates an enhancement of the heterocyclic π-structure in the cation, a rationale that is supported by ^{1}H and ^{13}C solution NMR (5, 6), MCD (39), and solid state NMR (40) spectroscopic results. This unique As–S π-interaction effects a similar bond shortening to that of the As—N π-interaction and the system shows no indication of As–N π-localization, consistent with the phosphorus analogs (6). Therefore, we conclude that within the heteronaphthalenic environment $4p$–$2p\pi$ bonding can coexist with $4p$–$3p\pi$ bonding.

The formation of the isolated cation **2** is made possible by the low basicity of the anion ($AlCl_4^-$). Nevertheless, the near planarity of the heterobicyclic unit of the neutral chlorothiazarsole **4**, the intermediacy of the bond lengths between those of the cation and typical single bonds, and the long As—Cl "covalent" (partially ionic) bond can also be interpreted in terms of a degree of heterocyclic π-bonding. Such features are completely consistent with the phosphorus analog (6) and are likely imposed by the inherent stability associated with the heteronaphthalenic (10π) framework, which is apparently competitive with the basicity of the chloride anion toward the cation **2** (consider the **2**Cl as the ionic alternative, and **4** as the covalent alternative). The dimeric arrangement is enforced by As–Cl and S–Cl contacts that resemble the anion–cation contacts in the salt and further validate the partial ionic model for the formally covalent chlorothiazarsole. With this in mind, the longer As—S bonds and more severely folded heterocycle observed in the di-

thiarsole **5** (9) can be interpeted in terms of a less effective S—As—S π-network, in comparison to the N—As—S π-network.

Coordinatively unsaturated arsenic centres

The development of π-chemistry for the heavier non-metal elements requires the consequential discovery of stable coordinatively unsaturated environments. Di- and mono-coordination have become common for phosphorus in recent years, and represent one of the most active areas of synthetic phosphorus chemistry. In contrast, systems containing monocoordinate arsenic are extremely rare (41) and dicoordinate arsenic environments are comparatively rare. Imitation of well-established dicoordinate phosphorus systems has provided examples of arsenes (2, 42), arsabenzenes (43), polyarsenides (44), and planar polyarsa homocyclic ligands (45). However, aside from the novel complexes $(C_5Me_5)_2As^+$ (46) and $[C_5Me_5(CO)_2Mn{=}As{=}Mn(CO)_2C_5Me_5]^+$ (47), the new cation **2** represents the first structural characterization of a system containing a dicoordinate cationic arsenium environment, a formal analog of the carbene unit. Phosphenium cations are well known and have an extensive chemistry (see, for example, ref. 48); however, structural studies on the corresponding arsenium systems (few examples have been reported, ref. 49) are limited, and examples have been shown to adopt dimeric structures, which allow for tri-coordination at arsenic (50). Identification of the novel cationic dicoordinate environment in **2** has been made possible by the stabilizing factors associated with the heteronaphthalenic framework (5).

Acknowledgements

We thank the Natural Sciences and Engineering Research Council of Canada and the donors of the Petroleum Research Fund, administered by the American Chemical Society, for financial support (N.B.) and the Atlantic Region Magnetic Resonance Centre for obtaining the NMR spectra.

1. P. Jutzi. Angew. Chem. Int. Ed. Engl. **14**, 232 (1975).
2. A. H. Cowley and N. C. Norman. Prog. Inorg. Chem. **34**, 1 (1986); R. West, M. J. Fink, and J. Michl. Science (Washington D.C.), **214**, 1343 (1981); M. Drager, J. Escudie, C. Couret, H. Ranivonjatova, and J. Satge. Organometallics, **7**, 1010 (1988).
3. N. Burford, J. Passmore, and J. P. Sanders. From atoms to polymers. *In* Molecular structure and energetics. Vol. 11. *Edited by* J. F. Liebman and A. Greenberg. VCH, New York. 1989. p. 53; T. Klapotke and J. Passmore. Acc. Chem. Res. **22**, 234 (1989).
4. (*a*) N. Burford, B. W. Royan, A. Linden, and T. S. Cameron. J. Chem. Soc. Chem. Commun. 842 (1988); (*b*) N. Burford and B. W. Royan. Phosphorus, Sulfur, Silicon, **41**, 37 (1989); (*c*) N. Burford, B. W. Royan, A. I. Dipchand, and P. S. White. Acta Crystallogr. Sect. C: Cryst. Struct. Commun. **C45**, 1485 (1989).
5. N. Burford, B. W. Royan, A. Linden, and T. S. Cameron. Inorg. Chem. **28**, 144 (1989).
6. N. Burford, A. I. Dipchand, B. W. Royan, and P. W. White. Inorg. Chem. **29**, 4938 (1990).
7. N. Burford, B. W. Royan, and P. S. White. J. Am. Chem. Soc. **111**, 3746 (1989).
8. N. Burford and B. W. Royan. J. Chem. Soc. Chem. Commun. 19 (1989).
9. J. M. Kisenyi, G. R. Willey, M. G. B. Drew, and S. O. Wandiga. J. Chem. Soc. Dalton Trans. 69 (1985).
10. A. L. Wayda and J. L. Dye. J. Chem. Educ. **62**, 356 (1985).
11. D. T. Cromer and J. T. Waber. *In* International tables for X-ray crystallography. Vol. IV. Kynoch Press, Birmingham. 1974. Table 2.2B. (Present Distributor: Kluwer Academic Publishers, Dordrecht and Boston.)
12. D. T. Cromer. *In* International tables for X-ray crystallography. Vol. IV. Kynoch Press, Birmingham. 1974. Tables 2.3.1.
13. B. A. Frenz. SDP/VAX. The Enraf–Nonius CAD 4 SDP — a real-time system for concurrent X-ray data collection and crystal structure determination. *In* Computing in crystallography. *Edited by* H. Schenk, R. Olthof-Hazekamp, H. van Koningsveld, and G. C. Bassi. Delft University Press, Delft, Holland. 1978. pp. 64–71.
14. E. J. Gabe, F. L. Lee, and Y. Le Page. The NRCVAX crystal structure system. *In* Crystallographic computing 3: data collection, structure determination, proteins, and databases. *Edited by* G. M. Sheldrick, C. Kruger, and R. Goddard. Clarendon Press, Oxford. 1985. p. 167.
15. R. C. G. Killean and J. L. Lawrence. Acta. Crystallogr. Sect. B: Struct. Crystallogr. Cryst. Chem. **B25**, 1750 (1969).
16. K. Nakamoto. Infrared and Raman spectra of inorganic and coordination compounds. 4th ed. Interscience, Toronto. 1986.
17. G. A. Olah and J. L. Grant. J. Org. Chem. **42**, 2237 (1977); G. Scherowsky and J. Weiland. Liebigs Ann. Chem. 404 (1974).
18. T. Matsumoto, H. Yamamoto, and S. Inoue. J. Am. Chem. Soc. **106**, 4829 (1984).
19. J. L. Morris and C. W. Rees. J. Chem. Soc. Perkin Trans. 1, 217 (1987).
20. L. M. Jackman and S. Sternhill. Applications of nuclear magnetic resonance spectroscopy in organic chemistry. Pergamon Press, Toronto. 1969; N. Jonathon, S. Gordon, and B. P. Dailey. J. Chem. Phys. **36**, 2443 (1962); A. W. Cordes, M. Hojo, H. Koenig, M. C. Noble, R. T. Oakley, and W. T. Pennington. Inorg. Chem. **25**, 1137 (1986).
21. W. S. Sheldrick, A. Schmidpeter, K. B. Dillon, A. W. G. Platt, and T. C. Waddington. J. Chem. Soc. Dalton Trans. 413 (1981).
22. W. S. Sheldrick, H.-J. Hausler, and J. Kaub. Z. Naturforsch. B: Chem. Sci. **43**, 789 (1988).
23. M. S. Weininger, P. F. Rodesiler, and E. L. Amma. Inorg. Chem. **18**, 751 (1979).
24. H. Schmidbauer, T. Probst, B. Huber, O. Steigelmann, and G. Muller. Organometallics, **8**, 1567 (1989).
25. M. Veith and B. Bertsch. Z. Anorg. Allg. Chem. **557**, 7 (1988).
26. D. J. Williams, M. G. Newton, and K. J. Wynne. Cryst. Struct. Commun. **6**, 167 (1977).
27. R. Steudel. Chemistry of the non-metal elements. de Guyter, New York. 1977.
28. G. Cardinal, R. J. Gillespie, J. F. Sawyer, and J. E. Verkis. J. Chem. Soc. Dalton Trans. 765 (1982); R. K. McMullan, D. J. Prince, and J. D. Corbett. Inorg. Chem. **10**, 1749 (1971); T. W. Couch, D. A. Lokken, and J. D. Corbett. Inorg. Chem. **10**, 2319 (1971).
29. R. F. W. Bader, R. J. Gillespie, and P. J. MacDougall. From atoms to polymers. *In* Molecular structure and energetics. Vol. 11. *Edited by* J. F. Liebman and A. Greenberg. VCH, New York. 1989. p. 1.
30. T. S. Cameron and A. Linden. Phosphorus, Sulfur, Silicon. **41**, 75 (1989).
31. R. W. Turner and E. L. Amma. J. Am. Chem. Soc. **88**, 1877 (1966); B. Fan, Q. Shen, and Y. Lin. J. Organomet. Chem. **376**, 51 (1989); M. Cesari, U. Pedritti, A. Zazetta, G. Lugli, and N. Marconi. Inorg. Chim. Acta, **5**, 439 (1971).
32. P. Barbier, G. Mairesse, and J.-P. Wignacourt. Cryst. Struct. Commun. **5**, 633 (1976).
33. M. Draeger. Chem. Ber. **107**, 2601 (1974).
34. B. H. Christian, R. J. Gillespie, and J. F. Sawyer. Inorg. Chem. **20**, 3410 (1981).
35. G. C. Pappalardo, R. Chakravorty, K. J. Irgolic, and E. A.

Can. J. Chem. Downloaded from www.nrcresearchpress.com by 92.62.229.171 on 09/08/12
For personal use only.

Myers. Acta Crystallogr. Sect. C: Cryst. Struct. Commun. **C39**, 1618 (1983).
36. A.-J. Dimaio and A. L. Rheingold. Chem. Rev. **29**, 798 (1990), and references therein.
37. L. Pierce and M. Hayashi. J. Chem. Phys. **35**, 479 (1961).
38. A. F. Wells. *In* Structural inorganic chemistry. 5th ed. Clarendon Press, Oxford. 1984.
39. B. W. Royan, N. Burford, J. Waluk, and J. Michl. Organometallics, **9**, 1085 (1990).
40. R. D. Curtis, B. W. Royan, R. E. Wasylishen, M. D. Lumsden, and N. Burford. Inorg. Chem. Submitted.
41. G. Maerkl and H. Sejpka. Angew. Chem. Int. Ed. Engl. **25**, 264 (1986).
42. P. B. Hitchcock, M. F. Lappert, A. K. Rai, and H. D. Williams. J. Chem. Soc. Chem. Commun. 1633 (1986).
43. A. J. Ashe III. Top. Curr. Chem. **105**, 125 (1982).
44. W. Schmettow and H. G. von Schnering. Angew. Chem. Int. Ed. Engl. **16**, 857 (1977).
45. O. J. Scherer, H. Sitzmann, and G. Wolmershauser. Angew. Chem. Int. Ed. Engl. **28**, 212 (1989).
46. P. Jutzi, T. Wippermann, C. Kruger, and H.-J. Kraus. Angew. Chem. Int. Ed. Engl. **22**, 250 (1985).
47. A. Strube, G. Huttner, and L. Zsolnai. Angew. Chem. Int. Ed. Engl. **27**, 1529 (1988).
48. A. H. Cowley and R. A. Kemp. Chem. Rev. **85**, 367 (1985).
49. M. Veith, B. Bertsch, and V. Huch. Z. Anorg. Allg. Chem. **559**, 73 (1988).
50. N. Burford, B. W. Royan, J. M. Whalen, J. F. Richardson, and R. D. Rogers. J. Chem. Soc. Chem. Commun. 1273 (1990).

Can. J. Chem. Downloaded from www.nrcresearchpress.com by 92.62.229.171 on 09/08/12
For personal use only.

Sulphur–nitrogen anions: ^{14}N and ^{15}N NMR investigations of the deprotonation of cyclic sulphur imides and sulphur–ammonia solutions

T. CHIVERS[1] AND K. J. SCHMIDT

Department of Chemistry, The University of Calgary, Calgary, Alta., Canada T2N 1N4

Received June 11, 1991

This paper is dedicated to the memory of Professor Thomas Birchall

T. CHIVERS and K. J. SCHMIDT. Can. J. Chem. **70**, 710 (1992)

The following systems have been investigated by ^{14}N and (or)^{15}N NMR spectroscopy: (*a*) the deprotonation of S_7NH by *n*-BuLi, (*b*) solutions of S_8, S_7NH, 1,3- and 1,4-$S_6(NH)_2$, and K_2SN_2 in liquid ammonia, (*c*) the reaction of sodium azide with sulphur in hexamethylphosphoramide (HMPA), (*d*) the reactions of S_7NH and $S_4(NH)_4$ with potassium amide in liquid ammonia in various molar ratios, and (*e*) the reaction of $(NSCl)_3$ with potassium amide (1:6 molar ratio) in liquid ammonia. These investigations have provided an NMR characterization of the thermally unstable S_7N^- ($\delta^{15}N$ ca. −324 ppm) and $S_2N_2H^-$ ions ($\delta^{14}N$ +7 and −149 ppm, $^1J(^{14}N-^1H)$ 36 Hz, $^1J(^{15}N-H)$ 55 Hz, $^2J(^{15}N-^{15}N)$ 2.2 Hz) in liquid ammonia, demonstrated the existence of S_7N^-, in addition to $SSNSS^-$, as the major nitrogen-containing ingredient of sulphur–ammonia solutions (SAS), and confirmed the formation of the $SSNSS^-$, but not S_7N^-, from the reaction of sodium azide and sulphur in HMPA. Consistent with previous chemical investigations, the NMR data show that the S_7N^- and $S_2N_2H^-$ ions are thermally unstable with respect to the formation of $SSNSS^-$ and $S_3N_3^-$, respectively, in solution. Solutions of $S_4(NH)_4/4KNH_2$ or $(NSCl)_3/6KNH_2$ show the same two ^{14}N or ^{15}N NMR resonances at ca. +97 and −108 ppm as a solution of NSN^{2-} in liquid ammonia.

Key words: sulphur–nitrogen anions, nitrogen NMR, liquid ammonia.

T. CHIVERS et K. J. SCHMIDT. Can. J. Chem. **70**, 710 (1992)

Faisant appel à la RMN du ^{14}N et (ou) ^{15}N, on a étudié les systèmes suivants : (*a*) la déprotonation du S_7NH par le *n*-BuLi, (*b*) des solutions de S_8, de S_7NH, des 1,3- et 1,4-$(NH)_2S_6$ et du K_2SN_2 dans l'ammoniac liquide, (*c*) la réaction de l'azoture de sodium avec le soufre dans l'hexaméthylphosphoramide (HMPA), (*d*) les réactions du S_7NH et du $S_4(NH)_4$ avec l'amidure de sodium, dans l'ammoniac liquide, à divers rapports molaires et (*e*) la réaction du $(NSCl)_3$ avec l'amidure de potassium (rapport molaire 1 : 6) dans l'ammoniac liquide. Ces études ont permis (*a*) de caractériser par RMN les anions thermiquement instables S_7N^- (δ^{15} environ −324 ppm) et $S_2N_2H^-$ ($\delta^{14}N$ +7 et −149 ppm, $^1J(^{14}N-^1H)$ 36 Hz, $^1J(^{15}N-H)$ 55 Hz, $^2J(^{15}N-^{15}N)$ 2,2 Hz) dans l'ammoniac liquide; (*b*) de démontrer l'existence de l'ion S_7N^-, en plus de l'ion $SSNSS^-$, comme ingrédient majeur contenant de l'azote dans des solutions ammoniacales de soufre (SAS) et (*c*) de confirmer la formation de l'ion $SSNSS^-$, mais pas de l'ion S_7N^-, lors de la réaction de l'azoture de sodium et du soufre dans le HMPA. En accord avec les études chimiques antérieures, les données de la RMN montrent que les ions S_7N^- et $S_2H_2H^-$ sont thermiquement instables par rapport à la formation respectivement des ions $SSNSS^-$ et $S_3N_3^-$ en solution. En RMN du ^{14}N ou du ^{15}N, les solutions de $S_4(NH)_4/4KNH_2$ ou de $(NSCl)_3/6KNH_2$ présentent les mêmes résonances, à environ +97 et −108 ppm, qu'une solution de NSN^{2-} dans l'ammoniac liquide.

Mots clés : anions soufre–azote, RMN de l'azote, ammoniac liquide.

[Traduit par la rédaction]

Introduction

Investigations of binary sulphur–nitrogen (S-N) anions have contributed significantly to the development of S–N chemistry (1). The well-characterized examples include cyclic anions, $S_3N_3^-$ and $S_4N_5^-$ (2, 3), acyclic catenated anions, $SSNSS^-$ and $SSNS^-$ (4, 5), and the dianion NSN^{2-} (6). In addition, there are several S–N anions, e.g., $SNSNH^-$ and $SNSN^{2-}$, which are known only as (chelating) ligands in metal complexes (7, 8). The formation of these anions in solution has been inferred from the preparation of such metal complexes by the deprotonation of $S_4(NH)_4$ in the presence of a metal halide (9, 10). The thermally unstable anion S_7N^-, generated by the deprotonation of S_7NH (11), has also been characterized in metal complexes (12, 13) and its existence as a free anion in solution has been established by the isolation of alkyl (14) and trimethylsilyl (15) derivatives. The formation of the S_7N^- ion in sulphur–ammonia solutions (SAS) has also been the controversial subject of several recent investigations (16–18). Finally, the possible production of the S_2N^- ion from the electrochemical reduction (19) of $SNSS^-$ or the reaction of $SNSS^-$ with amide ion (20) has been suggested on the basis of UV–visible (19,20) and Raman spectroscopic evidence (20).

Several recent publications have demonstrated the value of ^{14}N NMR spectroscopy for monitoring the behavior of small S–N molecules or ions in solution (21–25). The large chemical shift differences (see Table 1) and relatively sharp resonances observed for S–N anions (24) provide a method of analysis for complex mixtures of these anions that is superior to alternatives such as UV–visible or Raman spectroscopy. The latter techniques suffer from the disadvantages of broad, overlapping absorption bands or photoinduced (laser light) decomposition of samples, respectively. As well, the ^{15}N NMR spectra of ^{15}N-enriched samples can provide useful structural information (through the observation of $^{15}N-^{15}N$ coupling) that is not available from the use of other spectroscopic methods (26).

In this investigation we have, therefore, applied the techniques of ^{14}N and ^{15}N NMR spectroscopy to monitor the deprotonation of the cyclic sulphur imides S_7NH, 1,3- and 1,4-$S_6(NH)_2$, and $S_4(NH)_4$, and the formation of S–N anions in SAS. The specific objectives were to (*a*) provide an NMR spectroscopic identification of the S_7N^-, $SNSNH^-$, $SNSN^{2-}$, and S_2N^- ions, (*b*) identify the major nitrogen-

[1]Author to whom correspondence may be addressed.

Can. J. Chem. Downloaded from www.nrcresearchpress.com by 92.62.229.171 on 09/08/12
For personal use only.

TABLE 1. Nitrogen NMR parameters for S–N anions[a]

Anion	Solvent	Nucleus[b]	δ (ppm)[c]	$\nu_{1/2}$ (Hz)[d]
S_7N^-	NH_3(l)	14	−324	280
S_7N^-	THF[e]	15	−319	
$S_4N_5^-$	NH_3(l)	14	−326 (1 N)	160
		14	−240 (4 N)	130
$S_3N_3^-$	NH_3(l)	14	−230	110
$S_3N_3^-$	CH_3CN	14	−230	180
$S_2N_2H^-$	NH_3(l)	14	−149 (1 N)[f]	80
			+7 (1 N)	110
$S_2N_2H^-$	NH_3(l)	15	−148 (1 N)[g]	4
			+9 (1 N)[h]	4
SN_2H^-	NH_3(l)	14	−107[i]	400
SN_2^{2-}	NH_3(l)	14	+98[i]	200
S_4N^-	THF	14	+106	280
S_4N^-	HMPA	15	+107	
S_4N^-	CH_3CN	14	+107	148
S_4N^-	NH_3(l)	14	+107	110
S_3N^-	NH_3(l)	14	+230	110
S_3N^-	CH_3CN	14	+235	180

[a]All the NMR data listed in this table were determined during the course of this work.
[b]Nucleus used (^{14}N or ^{15}N).
[c]Relative to $MeNO_2$(l); positive shifts are to high frequency.
[d]Linewidth at half-height.
[e]At −80°C.
[f]Doublet, $^1J(^{14}N-^1H)$ = 36 Hz.
[g]Doublet, $^1J(^{15}N-^1H)$ = 55 Hz.
[h]Doublet, $^2J(^{15}N-^{15}N)$ = 2.2 Hz.
[i]The assignment of this resonance is tentative, see text for discussion.

containing species in SAS, and (*c*) seek evidence for the existence of novel binary S–N anions that might subsequently be the target of a synthetic investigation (for preliminary communications, see ref. 27). As a prelude to our studies of the deprotonation of cyclic sulphur imides, the ^1H, ^{14}N, and ^{15}N NMR chemical shifts and coupling constants ($^1J(^{15}N-^1H)$) of these ring systems were determined (28).

Experimental

Reagents

The following reagents were prepared by the literature procedures: S_7NH (29), $S_5(NH)_3$ isomers, $S_6(NH)_2$ isomers (30), $S_4(NH)_4$ (31), $PNP^+S_4N^-$(PNP = $(Ph_3P)_2N$) (32), $(NSCl)_3$ (33), $K_2(N_2S)$ (6), 50% ^{15}N-enriched S_7NH (34), and 99% ^{15}N-enriched S_4N_4 (35) (which was converted to $S_4(^{15}NH)_4$ by reduction with $SnCl_2 \cdot 2H_2O$ in 1,2-dichloroethane/methanol) (31).

The following commercial reagents were used as received: *n*-butyllithium in hexanes (2.1 M, Aldrich), potassium amide (ROC/RIC), sodium azide (95% ^{15}N-enriched in one terminal position) and NH_4Cl (99% ^{15}N-enriched) (Stohler Isotopes), PPh_3 (Fisher), and S_8 (sublimed, Fisher). Liquid ammonia and hexamethylphosphoric triamide (HMPA) were distilled from sodium before use. Acetonitrile and DMF were purified as described previously (24).

Instrumentation

NMR spectra were obtained on Bruker AM-400 and AMX-500 standard-bore spectrometers and on a Bruker AM-400 wide-bore instrument. The ^{14}N NMR experiments on the 400 MHz spectrometers were carried out at 28.915 MHz using 12-bit digitizers. Samples in organic solvents were investigated by using a broadband probe and 10 mm NMR tubes.

Samples using NH_3(l) as a solvent required the use of NMR tubes made from thick-walled (1.5 mm) 10 mm o.d. glass tubing, narrowing to $\frac{1}{4}$-in. standard wall tubing at the open end. The solvents were transferred onto samples already in the tubes by using a vacuum line equipped with Teflon J. Young valves. Connections between the tubes and the vacuum line (which was also fitted with $\frac{1}{4}$-in. tubing) were made with valves that used Swagelok connectors containing $\frac{1}{4}$-in. Teflon ferrules. When the appropriate amount of solvent had been transferred into the tube, the solvents were cooled to −196°C, and the tubes were then flame-sealed (in the upper $\frac{1}{4}$-in. section) under vacuum.

Typical acquisition parameters were an acquisition time (AQ) of 0.07 s, a pulse length (PW) of 20 μs (ca. 90° pulse), a relaxation delay (RD) of zero, a sweep width (SW) of 30 000 Hz, and a data collection size (TD) of 4 K (zero-filled to 16 K before transformation). In all cases at least 3000 scans were collected, and most samples were run unlocked. The signal from dissolved N_2 gas ($\delta^{14}N$ −71.5 ppm relative to $MeNO_2$(l) at 0 ppm) (35) was used as an internal standard for all ^{14}N spectra, except for the NH_3(l) samples for which the ammonia signal was used as an internal reference. Care must be taken when using NH_3(l) as a reference if large amounts of NH_4^+ cations are present, since the rapid H^+ exchange between NH_3 and NH_4^+ can significantly alter the ^{14}N chemical shift of NH_3. In this case, external referencing is preferred.

The SAS samples were prepared in 10 mm thick-walled tubes, as described above, and their ^{14}N NMR spectra were obtained at 36.14 MHz on a Bruker AMX-500 spectrometer equipped with a 16-bit digitizer and a 10 mm broadband probe. The acquisition parameters were AQ = 0.13 s, PW = 40 μs (ca. 90° pulse), RD = zero, SW = 30 000 Hz, and TD = 8 K (zero-filled to 64 K before transforming).

The ^{15}N NMR spectra were acquired at 40.557 MHz on the 400 MHz spectrometers. Natural abundance spectra were run on an AM-400 wide-bore spectrometer using a 20 mm broadband probe (total sample volume ca. 12 mL) and acetone-d_6 inserts to obtain a lock. ^{15}N-enriched samples in NH_3(l) were made up as described above and were sealed in thick-walled 16 mm tubes, which were then mounted coaxially within 20 mm tubes containing D_2O to provide a lock signal. The AM-400 wide bore spectrometer and the 20 mm broadband probe were used to obtain these spectra. The acquisition parameters for this spectrometer were PW = 40 μs (ca. 45° pulse), RD = 2.5 s for natural abundance ^{15}N, or RD = 30 s for enriched ^{15}N in NH_3(l), SW = 25 000 Hz, TD = 16 K (zero-filled to 64 K).

The ^{15}N enriched samples in solvents other than NH_3(l) were run on the AM-400 standard-bore spectrometer in 10 mm tubes (D_2O inserts for lock) using a broadband probe and a PW = 16 μs (ca. 45° pulse), RD = 30 s, SW = 35 000 Hz, TD = 16 K (zero-filled to 32 K).

All ^{14}N and ^{15}N NMR chemical shifts are reported with reference to $MeNO_2$(l) at 0 ppm using the downfield positive convention. The ^{14}N and (or) ^{15}N NMR parameters for the S-N anions studied in this investigation are summarized in Table 1.

Results and discussion

NMR characterization of the S_7N^- ion

A variety of bases, including Ph_3CNa (36), Na (14*a*), NaH (14*a*), LiOH (14*a*), KOH (15), *n*-Bu_4NOH (11), EtLi (14*a*), *n*-BuLi (37), $Ph_3P{=}CH_2$ (10), $NaNH_2$ (14*a*), and liquid ammonia (17, 20) have been used for the deprotonation of S_7NH. The available evidence indicates that the yellow S_7N^- ion is thermally stable below −50°C in THF (11, 15), but it decomposes to give the blue $SSNSS^-$ ion above this temperature (11). Consequently, the combination of a base and solvent that remains mobile below −60°C was deemed to be necessary for the NMR characterization of S_7N^-. The use of *n*-BuLi in THF proved to be suitable for this purpose. The initial experiments employed ^{15}N NMR spectroscopy in order to obtain narrow resonances. As indicated in Fig. 1*a*, the natural abundance ^{15}N NMR spectrum of a 1 M solution of S_7NH in THF at −80°C shows a doublet ($^1J(^{15}N-^1H)$ 94 Hz)

Can. J. Chem. Downloaded from www.nrcresearchpress.com by 92.62.229.171 on 09/08/12
For personal use only.

Can. J. Chem. Downloaded from www.nrcresearchpress.com by 92.62.229.171 on 09/08/12
For personal use only.

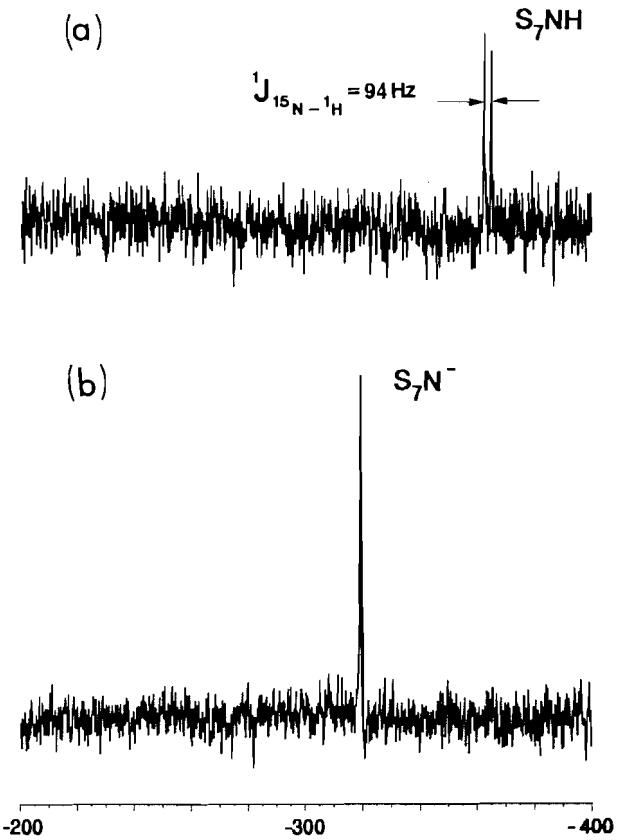

FIG. 1. The ^{15}N NMR spectra (natural abundance) of (*a*) a 1 M solution of S_7NH in THF at −80°C (2.5 h acquisition); (*b*) the same solution at −80°C after the addition of an equimolar amount of Bu^{n}Li in hexane (2 h acquisition).

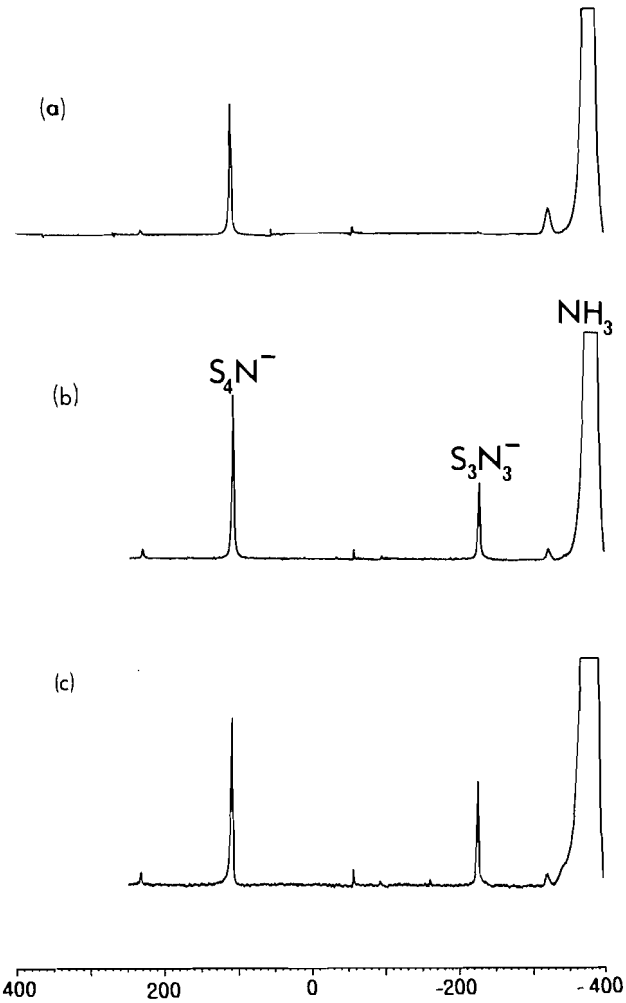

FIG. 2. The ^{14}N NMR spectra of (*a*) a ca. 0.2 M solution of S_7NH in NH_3(l) after 4 h; (*b*) a ca. 0.2 M solution of 1,4-$S_6(NH)_2$ in NH_3(l) after 4 h, (*c*) a 0.2 M solution of 1,3-$S_6(NH)_2$ in NH_3(l) after 3 h.

at −364 ppm. Upon addition of an equimolar amount of Bu^{n}Li in hexane to this solution at −80°C, this doublet disappears completely and instead a singlet at −318.8 ppm is observed (Fig. 1*b*). At this temperature the solution is yellow and there is no evidence for the formation of $SSNSS^-$ ($\delta^{15}N$ +106 ppm) (24). No other resonances are observed with the exception of that of dissolved N_2 at −71.5 ppm (35). Consequently, we assign the resonance at −318.8 ppm to the S_7N^- anion.

We also investigated the deprotonation of S_7NH with *n*-BuLi by ^{14}N NMR spectroscopy. At −80°C the ^{14}N NMR resonance for S_7N^- (generated from S_7NH and Bu^{n}Li) was very broad. However, at 25°C a resonance at ca. −327 ppm ($\nu_{1/2} \sim 1000$ Hz) was observed in addition to the signal for $SSNSS^-$ at +106 ppm. The S_7N^- ion is unexpectedly stable at room temperature in this system. The intensities of the NMR signals for S_7N^- and $SSNSS^-$ are approximately equal after 1 day and an appreciable amount of S_7N^- remains after 1 week. A third weak resonance at −134 ppm, which does not correspond to any known S–N anion (24), was also observed at 25°C.

^{14}N NMR spectra of solutions of S_7NH in liquid ammonia

A solution of S_7NH in liquid ammonia exhibits an UV absorption band at 256 nm (attributed to S_7N^-) with a wide tail extending to 600 nm (17, 20). After 2 h at −35°C this absorption decreases in intensity and bands in the visible region attributed to the formation of $SSNSS^-$(λ_{max} 578 nm) and $SSNS^-$ (λ_{max} 462 nm) are observed (17, 20). The formation of $SSNSS^-$ was confirmed by Raman spectroscopy (20). On the basis of the UV–visible and Raman spectroscopic data, Lelieur and co-workers proposed that the disproportionation of S_7N^- generated in this way is complete and produces $SSNSS^-$ and a neutral sulphur species formulated as S_{am} (am = NH_3) (20).

During the course of this work Woollins and co-workers reported that a solution of S_7NH in NH_3(l) gives rise to ^{14}N NMR signals at 104 ($\nu_{1/2}$ 120 Hz), −232 ($\nu_{1/2}$ 100 Hz), −331 ($\nu_{1/2}$ 440 Hz), and −401 ppm ($\nu_{1/2}$ 500 Hz) in the approximate percentages (sic) 50:20:20:20, which they attribute to $SSNSS^-$, $S_3N_3^-$, S_7NH, and an unidentified species, respectively (25, 38). In the light of our NMR characterization of the S_7N^- ion, we have investigated the S_7NH–NH_3(l) system by ^{14}N NMR spectroscopy in order to monitor the formation of S–N anions and identify them. The ^{14}N NMR spectrum of a deep blue solution of S_7NH in liquid ammonia after 4 h at 25°C (Fig. 2*a*) shows a major resonance attributed to $SSNSS^-$ at +107 Hz ($\nu_{1/2}$ 110 Hz), a weaker resonance at −324 ppm ($\nu_{1/2}$ 270 Hz), which we assign to the S_7N^- ion rather than S_7NH (*vide supra*), and *very weak* signals at −230 ($\nu_{1/2}$ 100 Hz), −34 ($\nu_{1/2}$ 60 Hz), and

Can. J. Chem. Downloaded from www.nrcresearchpress.com by 92.62.229.171 on 09/08/12
For personal use only.

+228 ppm ($\nu_{1/2}$ 110 Hz) attributed to $S_3N_3^-$, an unidentified species, and $SNSS^-$, respectively. The ^{14}N NMR spectrum of this solution showed the same major features after 30 days and again after 1 year. The narrowness of the unassigned resonance at −34 ppm rules out a species containing an N–H group, since one-bond ^{14}N–^1H coupling constants for S–NH species are ≥35 Hz (*vide infra*). Thus it seems likely that this signal belongs to a new binary S–N anion. These NMR results are consistent with previous studies of the deprotonation of S_7NH in which the yellow S_7N^- has been shown to disproportionate to $SSNSS^-$ (and sulphur) (11, 15).

^{14}N NMR spectra of solutions of 1,3- and 1,4-$S_6(NH)_2$ in liquid ammonia

Tingle and Olson have shown that the deprotonation of 1,4- and 1,5-$S_6(NH)_2$ with ethyllithium in THF at 0°C followed by alkylation with methyl iodide produces the corresponding *N*-methyl and *N,N'*-dimethyl derivatives, indicating the formation of the $S_6N_2H^-$ and $S_6N_2^{2-}$ ions, respectively (14*b*). By contrast, the isomer 1,3-$S_6(NH)_2$ produced S_7NMe under similar conditions (14*b*). The solutions of the $S_6(NH)_2$ isomers in THF are intense blue-green after treatment with ethyllithium (14*b*) and, in an earlier study, we showed by UV–visible spectroscopy that a solution of 1,4-$S_6(NH)_2$ in hexamethylphosphoric triamide (containing dimethylamine) produces the blue $SSNSS^-$ anion (11).

In this investigation the ^{14}N NMR spectra of liquid ammonia solutions of 1,3- and 1,4-$S_6(NH)_2$ were determined. As indicated in Figs. 2*b* and 2*c*, the major component of these solutions is the $SSNSS^-$ ion ($\delta^{14}N$ +109 ppm) but, in contrast to solutions of S_7NH in liquid ammonia, significant amounts of $S_3N_3^-$($\delta^{14}N$ −228 ppm) are also present. There are also weak resonances at +232 ($SSNS^-$) and −322 ppm. The latter signal could be attributed to S_7N^-, but the possibility that it is caused by the $S_6N_2^{2-}$ ion or the deprotonated nitrogen atom of $S_6N_2H^-$ cannot be ruled out. Indeed, in the case of 1,3-$S_6(NH)_2$, another signal at −343 ppm can be detected as a weak shoulder on the NH_3(l) resonance. This signal is in the appropriate region of the NH group of the $S_6N_2H^-$ anion. These NMR results are consistent with the previously proposed equilibria between cyclic and $SSNSS^-$ that were invoked to explain the predominant formation of S_7NH in the synthesis of cyclic sulphur imides (eq. [1]) (39).

$$[1] \quad S_7N^- \rightleftharpoons SSNSS^- + \tfrac{3}{8}\,S_8 \rightleftharpoons \tfrac{1}{2}\,S_6N_2^{2-} + \tfrac{1}{2}\,S_8$$

The formation of S_7NMe upon alkylation of deprotonated 1,3-$S_6(NH)_2$ in THF (14*b*) is presumably due to the rapid transformation of 1,3-$S_6N_2^{2-}$ into S_7N^- in THF solution.

^{15}N NMR spectra of the reaction of sodium azide with elemental sulphur

The formation of the S_7N^- and $S_6N_2^{2-}$ ions has also been proposed to account for the synthesis of S_7NH and $S_6(NH)_2$ isomers from sodium azide and sulphur in HMPA (39). In this investigation the formation of S–N anions in the reaction of azide ion (90% ^{15}N-enriched on one terminal nitrogen atom) with sulphur in $(Me_2N)_3PO$ ($\delta^{15}N$ −357.8 ppm, $^1J(^{31}P-^{15}N)$ 32 Hz) was monitored by ^{15}N NMR spectroscopy. As indicated in Fig. 3*a*, the ^{15}N NMR spectrum of the dark blue reaction mixture after 2 days revealed the formation of $SSNSS^-$ and the presence of some unreacted azide ion ($\delta^{15}N$ −284.9 ppm). Consequently, an additional quantity of sulphur was added to the reaction mixture until the total amount was three times that usually used in the synthesis of

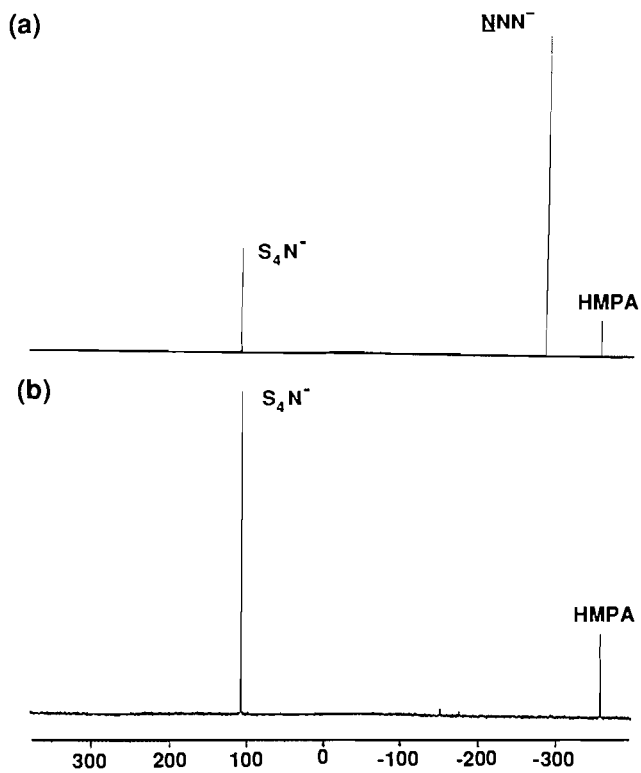

FIG. 3. The ^{15}N NMR spectra of the reaction of $^*NNN^-$ ($^*N$ = 90% ^{15}N) with S_8 in HMPA (*a*) after 2 days; (*b*) after 2 weeks and the addition of more S_8.

S_7NH (29). After 2 weeks the ^{15}N NMR spectrum showed that all the azide ion had been consumed (Fig. 3*b*). There is only one resonance ($\delta^{15}N$ +107 ppm), apart from that of the solvent, and this can be attributed to the $SSNSS^-$ ion. Surprisingly, the S_7N^- ion could not be detected in this solution even though the signal/noise ratio was sufficiently low to reveal its presence in concentrations smaller by a factor of 10^{-2} than that of $SSNSS^-$. We conclude, therefore, that the equilibria represented by eq. [1] strongly favour $SSNSS^-$ in HMPA and only shift to form S_7N^- (and $S_6N_2^{2-}$) upon hydrolysis with aqueous hydrochloric acid (29).

^{14}N NMR spectra of sulphur–ammonia solutions (SAS)

The nature of the species present in dark blue SAS has been studied extensively by UV–visible and Raman spectroscopy (16–18, 20, 40–45). In 1982 we identified the major *nitrogen-containing* species in these solutions as $SSNSS^-$ and suggested that it was formed from S_7N^- (16). Subsequently, two other groups showed that SAS are photosensitive and contain $SSNS^-$ in addition to $SSNSS^-$ (40–42), but there is disagreement about the presence of S_7N^- and the identity of the precursor of $SSNSS^-$ in such solutions. On the basis of an initial investigation by UV–visible spectroscopy, Prestel and Schindewolf claimed that 36 ± 4% of the dissolved sulphur in liquid ammonia is present as S_7N^- (17). However, in a subsequent study by the same group using anion exchange HPLC a species tentatively identified as $S_4NH_2^-$ was observed in addition to $SSNSS^-$ and $SSNS^-$ (45, 47). Lelieur and co-workers maintain that S_7N^- is not present in SAS on the basis of UV–visible and Raman spectroscopic data; they propose the formation of a neutral sulphur

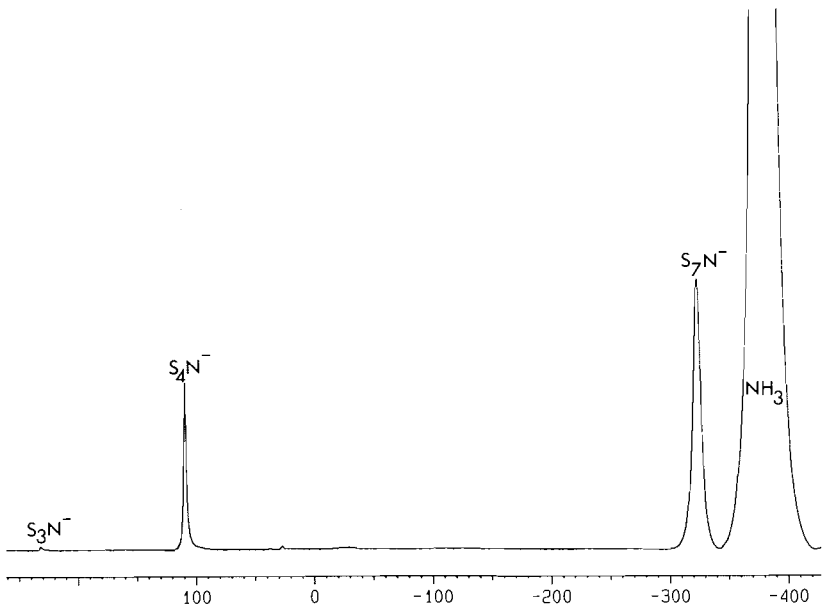

FIG. 4. The ^{14}N NMR spectrum of a 1 M (S atom) solution of S_8 in liquid ammonia after 2 h at 25°C (2 h acquisition).

species tentatively formulated as S_{2am} (am = NH_3) (18). These authors also speculate that the asymmetrical anion SSN^-, which is unknown, is the precursor of $SSNS^-$, and hence $SSNSS^-$, in SAS (18).

In the light of our ^{14}N NMR characterization of S_7N^-, SAS were investigated by ^{14}N NMR spectroscopy in an attempt to reconcile these observations and conclusions. During the course of this work Woollins and co-workers reported resonances at −329 ($\nu_{1/2}$ 350), −38 ($\nu_{1/2}$ 100), +105 ($\nu_{1/2}$ 100), and 192 ($\nu_{1/2}$ 100) (ppm (Hz)) in the approximate percentages 80:5:10:5, which they attributed to S_7NH, an unidentified species, $SSNSS^-$, and NS^+. respectively (25).[2,3] In our work, ^{14}N NMR spectra were recorded at regular intervals over the course of 9 days. A major resonance at −323 and a weaker resonance at +109 ppm attributable to S_7N^- (rather than S_7NH) and $SSNSS^-$, respectively, and a *very weak* resonance at +239 ppm assigned to $SSNS^-$ were observed (Fig. 4) (24). Surprisingly, and in agreement with the results of Woollins and co-workers (25), the resonance at −323 ppm, which we attribute to S_7N^-, accounts for ca. 80% of the nitrogen-containing species in SAS and this increases to 88% after 5 days. During the first 3 days of the experiment a weak, very narrow ($\nu_{1/2}$ 30 Hz) resonance is observed at −34 ppm. It is possible that this unidentified species is the precursor of $SSNSS^-$ in SAS, but the narrow line width rules out a species containing an N–H group. There is no evidence for the presence of any other nitrogen-containing species, e.g., $S_4NH_2^-$ or $S_2(NH_3)$, in SAS, but the resonances for such species could be obscured by the broad signal for the solvent ammonia.

In summary, our ^{14}N NMR spectra of SAS (0.2 M) recorded over a period of 9 days show the same major features as those reported by Woollins and co-workers (25) with the exception of the weak resonance at 192 ppm, which we did not observe. Our interpretation differs from that of Woollins (25), in that the strong resonance at ca. −325 ppm is assigned to the S_7N^- ion rather than S_7NH. This conclusion is consistent with the observation that S_7NH is readily deprotonated by liquid ammonia (*vide supra*). The lack of evidence for the presence of S_7N^- in SAS on the basis of UV–visible and Raman spectra (18) may be due to the lower concentrations of SAS used for these measurements and (or) the thermal and photochemical instability of S_7N^-.

The ^{14}N NMR investigation does not, however, shed any light on the *mechanism* of the formation of S_7N^- in SAS.

Attempted characterization of the S_2N^- ion

Lelieur and co-workers have shown by UV–visible and Raman spectroscopy that the progressive addition of an alkali-metal amide to SAS results in the conversion of $SSNSS^-$ to $SSNS^-$ and, subsequently, a new S–N anion tentatively formulated as the unsymmetrical anion SSN^- (20). The symmetrical SNS^- anion has been proposed to result from the thermal decomposition of $S_3N_3^-$ (4) and the electrochemical reduction of $SSNS^-$ (19). A symmetrical (C_{2v}) arrangement has been shown by Hartree–Fock–Slater self-consistent field calculations to be the most stable form of S_2N^- (47).

The cleavage of an S—S bond in $SSNSS^-$ by triphenylphosphine produces $SSNS^-$ (5) and the conversion of $SSNS^-$ into SNS^- in a similar manner is a reasonable possibility. In an attempt to identify the NS_2^- ion, the reactions of $SSNSS^-$ and $SSNS^-$($(Ph_3P)_2N^+$ salts) with Ph_3P were monitored by ^{14}N NMR spectroscopy. The reactions were carried out in both dimethylformamide and acetonitrile, since these solvents obscure different regions of the ^{14}N NMR window. In both cases, it was found that the addition of one molar equivalent of Ph_3P to a solution of $SSNSS^-$ ($\delta^{14}N$

[2]Nitrogen NMR chemical shifts (in ppm) are quoted here with reference to external $MeNO_2$(l). ^{14}N NMR chemical shifts in ref. 25 were given relative to NH_3(l) ($\delta(NH_3)$(l) = −380 ppm vs. $MeNO_2$(l)).

[3]The existence of the extremely electrophilic NS^+ cation in liquid ammonia solutions is highly unlikely. For example, NS^+ salts react vigorously with alkanes at 0°C (46).

Can. J. Chem. Downloaded from www.nrcresearchpress.com by 92.62.229.171 on 09/08/12
For personal use only.

Can. J. Chem. Downloaded from www.nrcresearchpress.com by 92.62.229.171 on 09/08/12
For personal use only.

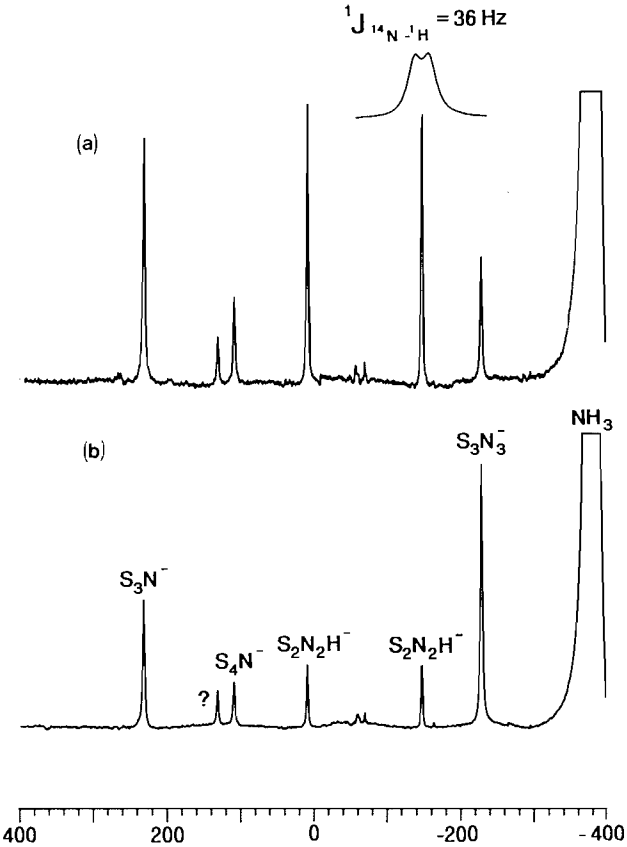

FIG. 5. The ^{14}N NMR spectra of the reaction of S_7NH with KNH_2 in a 1:3 molar ratio after (*a*) 2 h; (*b*) 10 days in NH_3(l) at 25°C.

+107 ppm) produces a new resonance at +235 ppm attributable to $SSNS^-$ (24). However, the complete conversion of $SSNSS^-$ into $SSNS^-$ required more than one molar equivalent of Ph_3P and the addition of greater than two molar equivalents of Ph_3P did not produce any new NMR resonances. Thus there is no evidence for the formation of a stable NS_2^- ion under these conditions.

Characterization of the $S_2N_2H^-$ ion

As an alternative source of the NS_2^- ion the reaction of $SSNSS^-$ (produced by the deprotonation of S_7NH) with potassium amide in liquid ammonia was also investigated. The combination of the low viscosity of liquid ammonia, which contributes to the relatively narrow resonances, the good solubility and stability of S–N anions in this solvent, and the fact that the ^{14}N NMR resonance of liquid ammonia does not obscure the region of interest make this an ideal system for monitoring the formation of S–N anions.

The addition of one molar equivalent of KNH_2 to a solution of S_7NH in liquid ammonia causes very little change in the ^{14}N NMR spectrum compared with that of S_7NH alone. However, the addition of two molar equivalents of potassium amide produces significant changes. Specifically, the relative concentration of S_7N^- is reduced and the $SSNS^-$ ($\delta^{14}N$ +230 ppm) and $S_3N_3^-$ ions ($\delta^{14}N$ −230 ppm) are readily detected as components of the reaction mixture. The addition of a third molar equivalent of potassium amide results in a more dramatic change in composition as indicated in Fig. 5*a*. A comparison of this spectrum with the ^{14}N NMR spectrum of the same solution obtained after 10 days (Fig. 5*b*) indicates that these changes result from the transformation of $SSNSS^-$ into $SSNS^-$, which in turn is converted to a previously unidentified S–N anion with equally intense resonances at +7 and −149 ppm. These resonances are associated with the same species since they grow and decay together (Fig. 5). The signal at −149 ppm is a doublet ($^1J(^{14}N-^1H)$ 36 Hz) indicating that one of the nitrogen atoms is attached to a hydrogen atom. A reasonable candidate for this species is the $S_2N_2H^-$ ion, **1**, which has previously been identified only as a ligand in metal complexes (7, 8). The coordinated $S_2N_2H^-$ ligand exhibits ^{14}N NMR signals at ca. −20 and −150 ppm (25).[3]

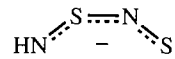

1

Chemical investigations of the deprotonation of $S_4(NH)_4$ indicate that this process also produces the $S_2N_2H^-$ ion (10). Consequently, the reaction of $S_4(NH)_4$ with two molar equivalents of potassium amide in liquid ammonia was also investigated. The ^{14}N NMR spectrum of the red-brown solution so obtained after 1 h at 23°C showed two major resonances at +7 and −148 ppm attributed to the $S_2N_2H^-$ ion (*vide supra*). However, after 24 h this species was partially converted to $S_3N_3^-$ ($\delta^{14}N$ −230 ppm).

To obtain $^{15}N-^{15}N$ (and $^{15}N-^1H$) spin coupling information in support of the proposed structure of **1**, the same experiment was conducted with 99% ^{15}N-enriched $S_4(NH)_4$. The ^{15}N NMR spectrum is displayed in Fig. 6*a*. Two resonances were observed at +9 and −148 ppm ($^1J(^{15}N-^1H)$ 55 Hz) in addition to a weak resonance at −230 ppm for $S_3N_3^-$. The ratio $^1J(^{15}N-^1H)/^1J(^{14}N-^1H)$ is 1.53, cf. $\gamma(^{15}N)/\gamma(^{14}N) = 1.40$ (where γ = magnetogyric ratio). The coupling between the inequivalent nitrogen atoms was determined for the resonance at +9 ppm to be ca. 2.2 Hz by the application of a convolution-difference algorithm. The corresponding coupling constant in neutral S–N rings is 2–3 Hz, while the value for the cation $S_4N_3^+$ is 8.5 Hz (48). These NMR data for the product of the deprotonation of $S_4(^{15}NH)_4$ with two molar equivalents of potassium amide are uniquely consistent with a species containing the -NSNH group and, in view of previous chemical evidence (10), we formulate this product as $SNSNH^-$, **1**.

The NMR experiments also demonstrate that the $S_2N_2H^-$ ion is partially converted into the $S_3N_3^-$ ion in liquid ammonia (Figs. 5*a* and *b*). This finding explains the previously reported observation that the deprotonation of $S_4(NH)_4$ by potassium hydride in THF produces $K^+S_3N_3^-$ as the final product (49). It is also noted that the explosive product of the reaction of $S_4(NH)_4$ with Ph_3CNa (1:2 molar ratio) was tentatively identified as $Na_2N_4S_4H_2$ on the basis of analytical data (36). It seems likely that this product is $Na[S_2N_2H]$, but the use of large cations, e.g., Ph_4As^+ or $(Ph_3P)_2N^+$, will likely be necessary to isolate stable crystalline salts (1).

Attempted characterization of the $S_2N_2^{2-}$ ion

A solution of $S_4(NH)_4$ in the presence of a base, e.g., diazabicycloundecane, has been used to prepare metal complexes of the $S_2N_2^{2-}$ ion (50). Numerous coordination compounds of this S–N ligand are known (7, 8), but it has not been characterized as the free anion. Consequently, the reaction of 99% ^{15}N-enriched $S_4(NH)_4$ with KNH_2 in liquid ammonia in a 1:4 molar ratio was investigated. As indi-

Can. J. Chem. Downloaded from www.nrcresearchpress.com by 92.62.229.171 on 09/08/12
For personal use only.

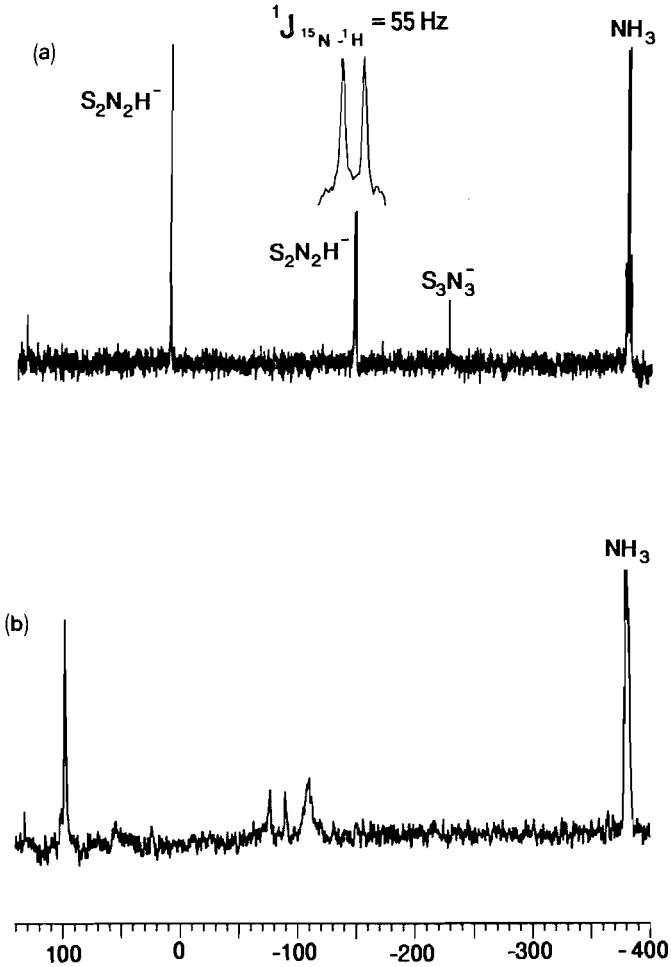

FIG. 6. The ^{15}N NMR spectra of the reaction of 99% ^{15}N-enriched $S_4(NH)_4$ (0.08 M) with KNH_2 in (*a*) a 1:2 molar ratio; (*b*) a 1:4 molar ratio in NH_3(l) at 25°C.

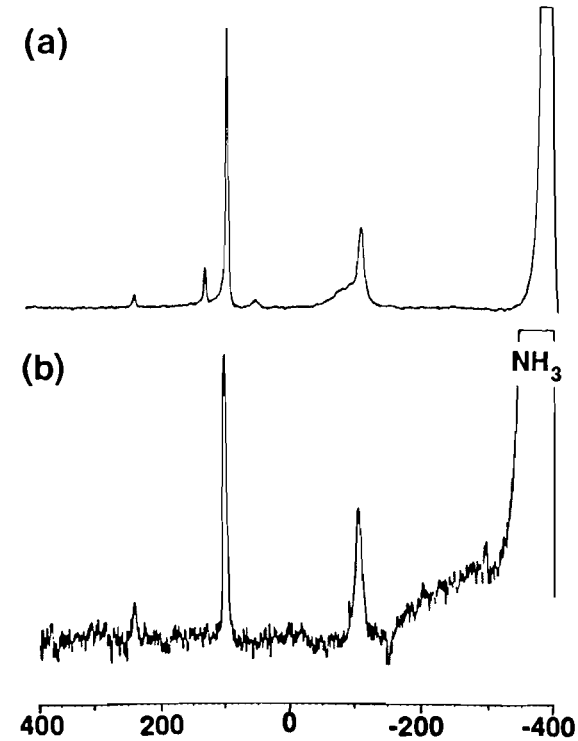

FIG. 7. The ^{14}N NMR spectra of (*a*) a solution of $(NSCl)_3$ and KNH_2 (1:6 molar ratio) after 7 days; (*b*) K_2[NSN] in NH_3(l) at 25°C.

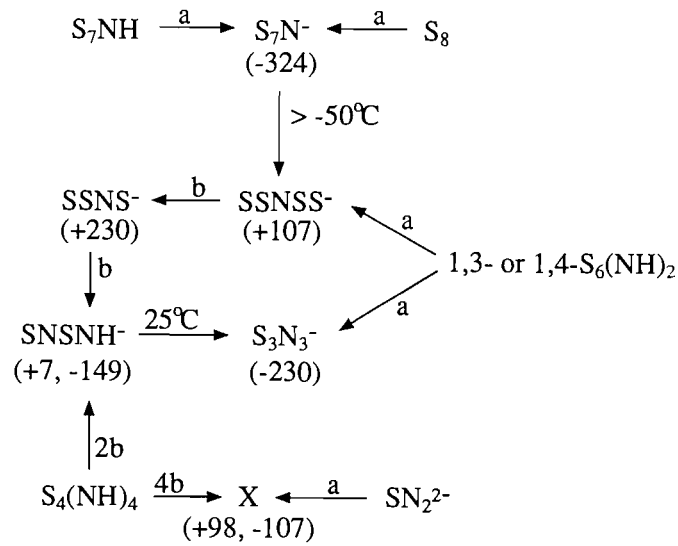

SCHEME 1. Sulphur–nitrogen anions formed in the deprotonation of cyclic sulphur imides by potassium amide in liquid ammonia; a = NH_3(l); b = KNH_2. Nitrogen NMR chemical shifts (ppm) are given in parentheses (ref. $MeNO_2$(l)). See text for a discussion of the identity of X.

cated in Fig. 6*b* the signals at +9 and −148 ppm are replaced completely by two much broader resonances at +98 ($\nu_{1/2}$ 80 Hz) and −110 ppm ($\nu_{1/2}$ 300 Hz). The broadness of the resonances prevents the detection of ^{15}N–^{15}N coupling. Consequently, it is not possible to ascertain whether these two signals belong to a single anion with inequivalent nitrogen, e.g., $S_2N_2^{2-}$ ions, or indicate the formation of two different S–N anions. The latter alternative seems more likely since it is reasonable to expect that the linewidths of the resonances for $S_2N_2^{2-}$ would be comparable to those of $S_2N_2H^-$.

The symmetrical NSN^{2-} ion is a possible product of this deprotonation reaction, but it has not been characterized by NMR spectroscopy (6). Consequently, an ^{14}N NMR spectrum of K_2[NSN] in liquid ammonia was obtained (Fig. 7*b*). This solution exhibits the same two resonances at +98 ($\nu_{1/2}$ 200 Hz) and −107 ppm ($\nu_{1/2}$ 400 Hz) that are observed for the $4KNH_2/S_4(NH)_4$ reaction in liquid ammonia.

The reaction of $(NSCl)_3$ with potassium amide (1:6 molar ratio) in liquid ammonia was also monitored by ^{14}N NMR spectroscopy, since this system provided the first synthesis of K_2[NSN] (51). After 30 min the anions $S_3N_3^-$ ($\delta^{14}N$ −230 ppm) and $S_4N_5^-$ ($\delta^{14}N$ −240 and −326 ppm) are readily identified, but the major product is an unidentified species ($\delta^{14}N$ −4 ppm). During the course of several days these signals disappear and are replaced by resonances at +96 ($\nu_{1/2}$ 110 Hz) and −109 ppm ($\nu_{1/2}$ 330 Hz) (Fig. 7*a*). Thus the same species are produced in liquid ammonia solutions

of either (*a*) $S_4(NH)_4/4KNH_2$, (*b*) $K_2[NSN]$, or (*c*) $(NSCl)_3/6KNH_2$.

An equilibrium between SN_2^{2-} and the $NSNH^-$ ion, formed by deprotonation of ammonia by the highly basic dianion, provides a possible explanation for these observations (eq. [2]).

[2] $SN_2^{2-} + NH_3 \rightleftarrows NSNH^- + NH_2^-$

The relatively sharp resonance at ca. +97 ppm can be attributed to the SN_2^{2-} ion[4] and the much broader resonance at ca. −108 ppm may be due to $NSNH^-$, which is undergoing a rapid 1,3 proton shift between equivalent nitrogen atoms.[5]

Conclusions

The thermally unstable S_7N^- ion has been characterized by ^{14}N and ^{15}N NMR spectroscopy. The NMR investigations support the conclusion, based upon previous chemical and UV–visible spectroscopic evidence, that S_7N^- decomposes to give $SSNSS^-$ and reveal that S_7N^- is the major nitrogen-containing species in solutions of sulphur in liquid ammonia (1 M in S atom). The reaction of $SSNSS^-$ with an excess of amide ion in liquid ammonia produces $SNSS^-$ and, subsequently, the novel anion $S_2N_2H^-$, which decomposes to give $S_3N_3^-$ at room temperature. No evidence was obtained for the formation of S_2N^- in this system. The deprotonation of $S_4(NH)_4$ by two molar equivalents of potassium amide in liquid ammonia also produces $S_2N_2H^-$. Liquid ammonia solutions of $S_4(NH)_4/4KNH_2$ show the same two ^{14}N or ^{15}N NMR resonances as are found for $K_2[NSN]$ or $(NSCl)_3/6KNH_2$ in liquid ammonia. These resonances are *tentatively* attributed to an equilibrium mixture of the NSN^{2-} and $NSNH^-$ ions rather than the $SNSN^{2-}$ ion. The results of these NMR studies are summarized in Scheme 1.

Acknowledgements

We thank the Natural Sciences and Engineering Research Council of Canada for financial support, Mark Edwards for the synthesis of cyclic sulphur imides, and Professor H. Vogel and Dr. D. D. McIntyre (Department of Biological Sciences, The University of Calgary) for assistance with some of the NMR experiments. Ian Drummond, a former student of Professor Tom Birchall, was instrumental in initiating our work on sulphur–nitrogen anions.

1. T. Chivers and R. T. Oakley. Top. Curr. Chem. **102**, 117 (1982).
2. J. Bojes, T. Chivers, W. G. Laidlaw, and M. Trsic. J. Am. Chem. Soc. **101**, 4517 (1979)
3. W. Flues, O. J. Scherer, J. Weiss, and G. Wolmershäuser. Angew. Chem. Int. Ed. Engl. **15**, 379 (1976).
4. T. Chivers, W. G. Laidlaw, R. T. Oakley, and M. Trsic. J. Am. Chem. Soc. **102**, 5773 (1980).
5. J. Bojes, T. Chivers, W. G. Laidlaw, and M. Trsic. J. Am. Chem. Soc. **104**, 4837 (1982).
6. M. Herberhold and W. Ehrenreich. Angew. Chem. Int. Ed. Engl. **21**, 633 (1982).
7. T. Chivers and F. Edelmann. Polyhedron, **5**, 1661 (1986).
8. P. F. Kelly and J. D. Woollins. Polyhedron, **5**, 607 (1986).
9. R. Jones, P. F. Kelly, C. P. Warrens, D. J. Williams, and J. D. Woollins. J. Chem. Soc. Chem. Commun. 711 (1986).
10. T. Chivers, F. Edelmann, U. Behrens, and R. Drews. Inorg. Chim. Acta, **116**, 1509 (1986).
11. T. Chivers and I. Drummond. Inorg. Chem. **13**, 1222 (1974).
12. J. Weiss. J. Anorg. Allg. Chem. **532**, 184 (1986).
13. (*a*) H. G. Heal and R. J. Ramsay. J. Inorg. Nucl. Chem. **36**, 950 (1974); (*b*) R. J. Ramsay, H. G. Heal, and H. Garcia-Fernandez. J. Chem. Soc. Dalton Trans. 237 (1976).
14. (*a*) B. A. Olsen and F. P. Olsen. Inorg. Chem. **8**, 1736 (1969); (*b*) E. M. Tingle and F. P. Olsen. Inorg. Chem. **8**, 1741 (1969).
15. M. H. Mendelsohn and W. L. Jolly. J. Inorg. Nucl. Chem. **35**, 95 (1973).
16. T. Chivers and C. Lau. Inorg. Chem. **21**, 453 (1982).
17. H. Prestel and U. Schindewolf. Z. Anorg. Allg. Chem. **551**, 21 (1987).
18. P. Dubois, J. P. Lelieur, and G. Lepoutre. Inorg. Chem. **28**, 195 (1989).
19. T. Chivers and M. Hojo. Inorg. Chem. **23**, 2738 (1984).
20. P. Dubois, J. P. Lelieur, and G. Lepoutre. Inorg. Chem. **27**, 3032 (1988).
21. P. S. Belton and J. D. Woollins. Magn. Reson. Chem. **24**, 1080 (1986).
22. J. Passmore and M. Schriver. Inorg. Chem. **27**, 2749 (1988).
23. P. S. Belton, I. P. Parkin, D. J. Williams, and J. D. Woollins. J. Chem. Soc. Chem. Commun. 1479 (1988).
24. T. Chivers, K. J. Schmidt, D. D. McIntyre, and H. J. Vogel. Can. J. Chem. **67**, 1788 (1989).
25. I. P. Parkin, J. D. Woollins, and P. S. Belton. J. Chem. Soc. Dalton Trans. 511 (1990).
26. T. Chivers, R. T. Oakley, O. J. Scherer, and G. Wolmershäuser. Inorg. Chem. **20**, 914 (1981).
27. For preliminary communications see, (*a*) T. Chivers, D. D. McIntyre, K. J. Schmidt, and H. J. Vogel. J. Chem. Soc. Chem. Commun. 1341 (1990); (*b*) T. Chivers and K. J. Schmidt. J. Chem. Soc. Chem. Commun. 1342 (1990).
28. T. Chivers, M. Edwards, K. J. Schmidt, D. D. McIntyre, and H. J. Vogel. Magn. Reson. Chem. **30**, 177 (1992).
29. J. Bojes and T. Chivers. Inorg. Synth. **18**, 203 (1978).
30. H. G. Heal and J. Kane. Inorg. Synth. **11**, 184 (1968).
31. G. Brauer. Handbook of preparative inorganic chemistry. Vol. 1. 2nd ed. Academic Press, New York. 1963. p. 411.
32. J. Bojes, T. Chivers, and R. T. Oakley. Inorg. Synth. **25**, 35 (1989).
33. W. L. Jolly and K. D. Maguire. Inorg. Synth. **9**, 102 (1967).
34. R. Steudel. J. Phys. Chem. **81**, 343 (1977).
35. D. D. McIntyre, A. W. Apblett, P. Lundberg, K. J. Schmidt, and H. J. Vogel. J. Magn. Reson. **83**, 377 (1989).
36. M. Becke-Goehring and R. Schwartz. Z. Anorg. Allg. Chem. **296**, 3 (1958).
37. R. B. Bruce, D. W. Stephan, and M. J. McGlinchey. Inorg. Chim. Acta, **53**, 119 (1981).
38. P. S. Belton, I. P. Parkin, D. J. Williams, and J. D. Woollins. J. Chem. Soc. Chem. Commun. 1479 (1988).
39. J. Bojes and T. Chivers. J. Chem. Soc. Dalton Trans. 1715 (1975).
40. L. Bernard, J. P. Lelieur, and G. Lepoutre. Nouv. J. Chim. **9**, 199 (1985).
41. H. Prestel and U. Schindewolf. Ber. Bunsen-ges Phys. Chem. **90**, 150 (1986).
42. H. Prestel, S. Seelert, and U. Schindewolf. Z. Phys. Chem. **148**, 97 (1986).

[4]The ^{14}N NMR chemical shift of NSO^- occurs ca. 125 ppm to high frequency from that of Me_3SiNSO ($\delta^{14}N$ −50 ppm) (24). By analogy, a similar shift to high frequency might be expected for NSN^{2-} compared to $Me_3SiNSNSiMe_3$ ($\delta^{14}N$ −59 ppm).

[5]Although the diprotonated species HNSNH has been characterized by ^1H NMR spectroscopy, no ^{14}N NMR data are available (52).

Can. J. Chem. Downloaded from www.nrcresearchpress.com by 92.62.229.171 on 09/08/12
For personal use only.

43. P. Dubois, J. P. Lelieur, and G. Lepoutre. Inorg. Chem. **26**, 1897 (1987).
44. P. Dubois, J. P. Lelieur, and G. Lepoutre. Inorg. Chem. **28**, 2849 (1989).
45. (*a*) S. Seelert and U. Schindewolf. Phosphorus, Sulphur, Silicon, Relat. Elem. **48**, 275 (1990); (*b*) **55**, 239 (1991).
46. A. Apblett, T. Chivers, and J. F. Fait. Inorg. Chem. **29**, 1643 (1990).
47. (*a*) M. Trsic and W. G. Laidlaw. J. Mol. Struct. **123**, 259 (1985); (*b*) L. Behera, T. Kar, and A. B. Sannigrahi. J. Mol. Struct. (Theochem.), **209**, 111 (1990).
48. T. Chivers. Chem. Rev. **85**, 341 (1985).
49. J. Bojes, T. Chivers, I. Drummond, and G. MacLean. Inorg. Chem. **17**, 3668 (1978).
50. R. Jones, P. F. Kelly, D. J. Williams, and J. D. Woollins. Polyhedron, **6**, 1541 (1987).
51. W. Berg, M. Goehring, and H. Malz. Z. Anorg. Allg. Chem. **283**, 13 (1956).
52. M. Herberhold, W. Jellen, W. Bühlmeyer, and W. Ehrenreich. Z. Naturforsch. B: **40**, 1229 (1985).

Can. J. Chem. Downloaded from www.nrcresearchpress.com by 92.62.229.171 on 09/08/12
For personal use only.

^{77}Se NMR spectroscopic study of the molecular composition of sulfur–selenium melts

TRISTRAM CHIVERS,[1] RISTO S. LAITINEN,[1,2] AND KENNETH J. SCHMIDT
Department of Chemistry, The University of Calgary, 2500 University Drive N.W., Calgary, Alta., Canada T2N 1N4

Received July 12, 1991

This paper is dedicated to the memory of Professor Thomas Birchall

TRISTRAM CHIVERS, RISTO S. LAITINEN, and KENNETH J. SCHMIDT. Can. J. Chem. **70**, 719 (1992).

A series of six sulfur–selenium mixtures containing 0.4, 5, 15, 25, 35, and 45 mol% of selenium were heated in evacuated ampoules at 430°C for 4 h and, keeping the material molten at 135°C, their natural-abundance ^{77}Se NMR spectra were recorded. The equilibrium melt in each case was found to contain both heterocyclic Se_nS_{8-n} species and polymeric material. The most abundant eight-membered selenium sulfide rings were SeS_7, which was the main cyclic component in all melts studied in this work, and 1,2-Se_2S_6, the quantity of which increased with increasing selenium content of the melt. In addition the melts contained smaller amounts of 1,3, 1,4, and 1,5 isomers of Se_2S_6, 1,2,3, 1,2,4, and 1,2,5 isomers of Se_3S_5, 1,2,3,4, 1,2,3,5, and 1,2,5,6 isomers of Se_4S_4, 1,2,3,4,5-Se_5S_3, 1,2,3,4,5,6-Se_6S_2, and Se_8. The relative distribution of the cyclic products as a function of the selenium content in the melt was virtually identical with that obtained earlier in the CS_2 solutions of the quenched melts, implying that the extracted quenched melts actually represent the original melt composition as far as the Se_nS_{8-n} species are concerned. The resonances due to the polymeric material in the melts could best be interpreted by the statistical random distribution of selenium and sulfur in the polymeric chains, the probability of occurrence of the different fragments being governed by the overall composition of the melt. As the selenium content increases, the relative amount of selenium bound in the polymer seems to increase at the expense of heterocyclic selenium sulfides.

Key words: selenium sulfides, sulfur–selenium melt, ^{77}Se NMR spectroscopy.

TRISTRAM CHIVERS, RISTO S. LAITINEN et KENNETH J. SCHMIDT. Can. J. Chem. **70**, 719 (1992).

Une série de six mélanges de soufre–sélénium contenant 0,4, 5, 15, 25, 35 et 45 mol% de sélénium placés dans des ampoules sous vide a été chauffé à 430°C pendant 4 h et on a alors déterminé leurs spectres RMN du ^{77}Se en abondance naturelle, tout en maintenant les produits à l'état fondu à 135°C. Dans chacun des cas, on a trouvé que les produits fondus contiennent des espèces hétérocycliques Se_nS_{8-n} ainsi que des produits polymériques. Les composés cycliques les plus abondants sont le cycle sulfuré du sélénium comportant huit chainons, SeS_7, qui est le composant cyclique principal dans tous les mélanges fondus étudiés, et le 1,2-Se_2S_6 dont la quantité augmente avec une majoration de la quantité de sélénium dans le produit fondu. On retrouve de plus des quantitiés plus faibles des isomères 1,3-, 1,4- et 1,5-Se_2S_6, des isomères 1,2,3-, 1,2,4- et 1,2,5-Se_3S_5, des isomères 1,2,3,4-, 1,2,3,5- et 1,2,5,6-Se_4S_4, du 1,2,3,4,5-Se_5S_3, du 1,2,3,4,5,6-Se_6S_2 et du Se_8. La distribution relative des produits cycliques en fonction de la quantité de sélénium contenue dans le produit fondu est pratiquement identique avec celle qui a été observée antérieurement avec des solutions de CS_2 de produits fondus préalablement soumis à une trempe; ce résultat suggère que, en ce qui a trait aux espèces Se_nS_{8-n}, les extraits des produits fondus soumis à la trempe représentent en fait la composition originale du produit fondu. On peut interpréter les résonances dues à des matériaux polymériques présents dans les produits fondus par une distribution statistique du sélénium et du soufre dans les chaines polymériques, la probabilité de rencontrer divers fragments étant définie par la composition globale du produit fondu. Lorsque la composition en sélénium augmente, les quantités relatives de sélénium présentes dans le polymère semblent augmenter au dépens des sulfures de sélénium hétérocycliques.

Mots clés : sulfures de sélénium, mélange fondu de soufre–sélénium, spectroscopie RMN du ^{77}Se.

[Traduit par la rédaction]

Introduction

In the molten state sulfur and selenium have long been known to mix in all proportions (1). Ringer (2) recorded the phase diagram of the sulfur–selenium binary system as early as 1902 and reported a eutectic point at ca. 105°C for the selenium content of 40 mol% (2). Boctor and Kullerud (3) reinvestigated the phase relations in the Se–S system by using modern thermoanalytical methods and, while they found a temperature minimum of 102°C at a composition of 35 mol% selenium, they questioned the existence of this eutectoid. On the basis of the phase diagram they explained the complete liquid miscibility in the Se–S system in terms of the equilibrium copolymerization theory.

While Ringer's phase diagram gives indications of the formation of binary compounds, it was only with the advent of modern analytical techniques that the existence of selenium sulfides could unequivocally be shown. The first reliable evidence that there are binary compounds in molten mixtures of sulfur and selenium as well as in the vapour over the melt came from vapour pressure measurements (4), even though the authors did not discuss the nature and the structures of these compounds at the time. Fergusson *et al.* (5*a*) and Ward (5*b*) were the first to deduce the existence of heterocyclic Se_nS_{8-n} molecules in crystalline phases that had been formed by quenching molten mixtures of the elements in varying molar ratios. The former based their conclusions on X-ray powder diffraction and absorption spectroscopy, and the latter on Raman spectroscopy. These conclusions were supported by mass and Raman spectroscopic studies as well as by crystal structure determinations (for recent reviews on the efforts on identification and characterization of selenium sulfides, which were prepared from melts or through a variety of other synthetic routes, see ref. 6).

It was soon apparent that the crystalline phases that had

[1]Authors to whom correspondence may be addressed.
[2]Permanent address: Department of Chemistry, University of Oulu, Linnanmaa, SF-90570 Oulu, Finland.

Can. J. Chem. Downloaded from www.nrcresearchpress.com by 92.62.229.171 on 09/08/12
For personal use only.

Can. J. Chem. Downloaded from www.nrcresearchpress.com by 92.62.229.171 on 09/08/12
For personal use only.

been obtained by quenching and recrystallizing sulfur–selenium melts contained complicated mixtures of several molecular species. In fact, only the reactions of titanocene compounds of the type $[Ti(C_5H_5)_2E_5]$ and $[Ti(C_5H_5)_2(\mu\text{-}E_2)_2Ti(C_5H_5)_2]$ (E = S or Se) with dichlorosulfanes or dichlorodiselane are known to result in the formation of pure stoichiometric compounds (7). All crystal structures were disordered (6) and therefore only the overall conformation of the ring molecules could be deduced. Low-temperature Raman spectra indicated the presence of S—S, Se—S, and Se—Se bonds in all samples (8), but did not allow the identification of actual molecular species. It was only with ^{77}Se NMR spectroscopy that individual heterocyclic selenium sulfides could be identified (9). The NMR spectroscopic characterization was based on the comparison of spectra of natural-abundance samples with those of the samples with corresponding chemical composition, but with selenium enriched in the ^{77}Se- isotope (92% enrichment).

It is questionable, however, that the CS_2 solutions and crystalline phases prepared from the quenched sulfur–selenium melt represent the actual melt. The solubility of selenium sulfides rapidly decreases as the selenium content increases. In fact most of the material is insoluble in CS_2 and apparently contains polymeric species. It has indeed been estimated by DSC that the polymerization threshold is lowered with the introduction of selenium in the liquid (3). The present study was initiated in order to establish directly the equilibrium composition of the sulfur–selenium melt and its dependence on the elemental composition.

Experimental section

The preparation of the samples

A series of six samples were prepared by mixing elemental sulfur (Fisher) and selenium (Anachemia) together in various molar ratios. The mass of the resulting mixtures was adjusted to 3.0 g each and they contained 0.4, 5, 15, 25, 35, and 45 mol% selenium. Each sample was sealed in an evacuated ampoule with an external diameter of 8 mm and heated at ca. 430°C for 4 h. The ampoules were allowed to cool to 135°C and were subsequently inserted in 10 mm NMR tubes containing d_5-nitrobenzene (Aldrich) as an external ^2H lock for the NMR measurements. They were immediately lowered into the NMR probe, which was kept at 135°C throughout the acquisition.

NMR spectroscopy

The ^{77}Se NMR spectra were recorded with a Bruker AM-400 spectrometer operating at 76.31 MHz. The spectral width was 71.43 kHz and the resolution 4.36 Hz/data point. The pulse width was 6.0 μs, corresponding to the nuclide tip angle of 45°. The pulse delay was 2.8 s. The accumulations generally contained 15 000–20 000 transients. In the case of the sample containing 25 mol% of selenium 94 000 transients were acquired in order to maximize the signal-to-noise ratio. All spectra were referenced externally to a saturated solution of SeO_2 at room temperature. The chemical shifts (ppm) are reported relative to neat Me_2Se at room temperature ($\delta(Me_2Se) = \delta(SeO_2) + 1302.6$).

Results and discussion

The natural-abundance ^{77}Se NMR spectra of the six sulfur–selenium melts studied in this work are shown in Fig. 1. There are two distinct regions in all spectra: the region at 750–550 ppm is typical for the eight-membered Se_nS_{8-n} ring molecules (9), and that at 1050–850 ppm is inferred to contain resonances from the polymeric material. A more detailed assignment is presented below, after which the composition of the molten mixtures as a function of the selenium content is discussed.

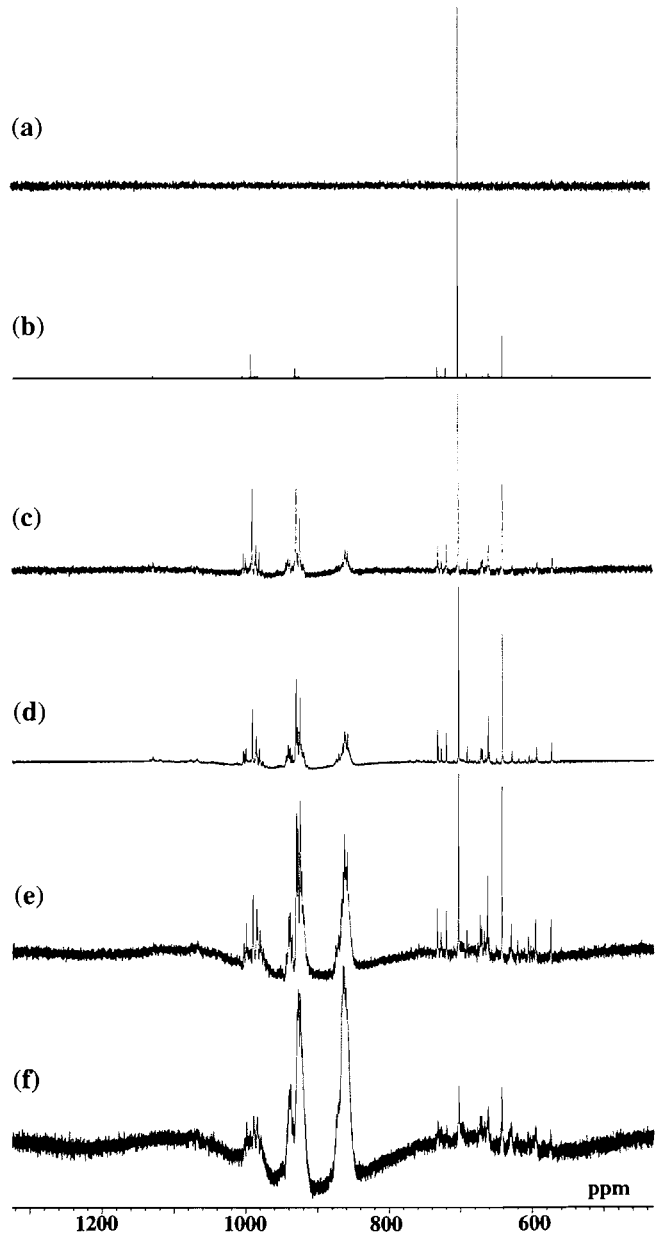

FIG. 1. The natural abundance ^{77}Se NMR spectra of six molten mixtures of sulfur and selenium recorded at 135°C. (*a*) 0.4 mol% Se; (*b*) 5 mol% Se; (*c*) 15 mol% Se; (*d*) 25 mol% Se; (*e*) 35 mol% Se; (*f*) 45 mol% Se.

Se_nS_{8-n} ring molecules

All possible Se_nS_{8-n} ring molecules formed in the melt are shown in Table 1 together with an abbreviated notation used in their designation. The main species observed in the CS_2 solutions of the quenched sulfur–selenium melts are listed in Table 2 together with their chemical shifts (9*b*). This in-

TABLE 1. The abbreviated notation for all possible Se_nS_{8-n} ring molecules[a]

SeS_7	1,2-Se_2S_6	1,2,3-Se_3S_5	1,2,3,4-Se_4S_4	1,2,3,4,5-Se_5S_3	1,2,3,4,5,6-Se_6S_2	Se_7S
A_1	**A_2**	**A_3**	**A_4**	**A_5**	**A_6**	**A_7**
	1,3-Se_2S_6	1,2,4-Se_3S_5	1,2,3,5-Se_4S_4	1,2,3,4,6-Se_5S_3	1,2,3,4,5,7-Se_6S_2	
	B_2	**B_3**	**B_4**	**B_5**	**B_6**	
	1,4-Se_2S_6	1,2,5-Se_3S_5	1,2,3,6-Se_4S_4	1,2,3,5,6-Se_5S_3	1,2,3,4,6,7-Se_6S_2	
	C_2	**C_3**	**C_4**	**C_5**	**C_6**	
	1,5-Se_2S_6	1,3,5-Se_3S_5	1,2,4,5-Se_4S_4	1,2,3,5,7-Se_5S_3	1,2,3,5,6,7-Se_6S_2	
	D_2	**D_3**	**D_4**	**D_5**	**D_6**	
		1,4,6-Se_3S_5	1,2,4,6-Se_4S_4	1,2,4,6,7-Se_5S_3		
		E_3	**E_4**	**E_5**		
			1,2,4,7-Se_4S_4			
			F_4			
			1,2,5,6-Se_4S_4			
			G_4			
			1,3,5,7-Se_4S_4			
			H_4			

[a]Homocyclic S_8 and Se_8 are excluded from the table.

TABLE 2. The chemical shifts (ppm) of Se_nS_{8-n} ring molecules

Species[a]	Chemical shift		
	CS_2 solution[b]	Melt[c]	Difference
SeS_7			
A_1	699.7	705	5
Se_2S6			
A_2	633.9	644	10
B_2	729.1	734	5
C_2	687.3	693	6
D_2	716.9	722	5
Se_3S_5			
A_3	654.2; 560.6	664; 576	10; 16
B_3	727.4; 662.9; 653.0	733; 672; 662	6; 9; 9
C_3	723.7; 662.6; 619.7	729; 672; 630	5; 9; 10
Se_4S_4			
A_4	664.4; 581.6	674; 596	10; 14
B_4	722.4; 669.0; 641.6; 588.9	728; 678; 652; 602	6; 9; 10; 13
D_4	680.8; 655.4	—	
G_4	655.5	666	10
Se_5S_3			
A_5	657.9; 598.2; 591.2	668; 612; 609	10; 14; 18
Se_6S_2			
A_6	690.1; 606.7; 582.9	690; 616; 599	0; 10; 16
Se_8	614.6	621	7

[a]For the abbreviated notation, see Table 1.
[b]See ref. 9*b*.
[c]The chemical shifts of the different molecular species are taken from the spectrum of the melt with 25 mol% of Se. The values of the chemical shifts in other samples were virtually identical.

formation can be used to assign the resonances observed in the actual melts at 750–550 ppm (see Fig. 1). The assignments are indicated in the NMR spectrum of the melt containing 25 mol% selenium, the pertinent region of which is shown in Fig. 2.

The most intense resonance in the region of eight-membered selenium sulfide rings is found at 705 ppm in all spectra (see Figs. 1 and 2). It almost coincides with the room temperature solution resonance of SeS_7 (**A_1**), the reported chemical shift of which is 699.7 ppm (9*b*). It is reasonable to assign the signal at 705 ppm to SeS_7 since, as the most sulfur-rich Se_nS_{8-n} molecule, it can be expected to be the main component in the sulfur-rich melts. Further support is found from the NMR spectrum of the melt containing 0.4 mol% of selenium (see Fig. 1), which shows only this signal.

The second most intense resonance in the spectrum of Fig. 2 is that at 644 ppm. It is assigned to 1,2-Se_2S_6 (**A_2**). This chemical shift is also close to the value of the corresponding species in CS_2 at 633.9 ppm (9*b*). This signal first appears when the melt contains 5 mol% of selenium. Its relative intensity with respect to that of SeS_7 increases with increasing selenium content, in agreement with the solution spectra (9*b*).

Can. J. Chem. Downloaded from www.nrcresearchpress.com by 92.62.229.171 on 09/08/12
For personal use only.

Can. J. Chem. Downloaded from www.nrcresearchpress.com by 92.62.229.171 on 09/08/12
For personal use only.

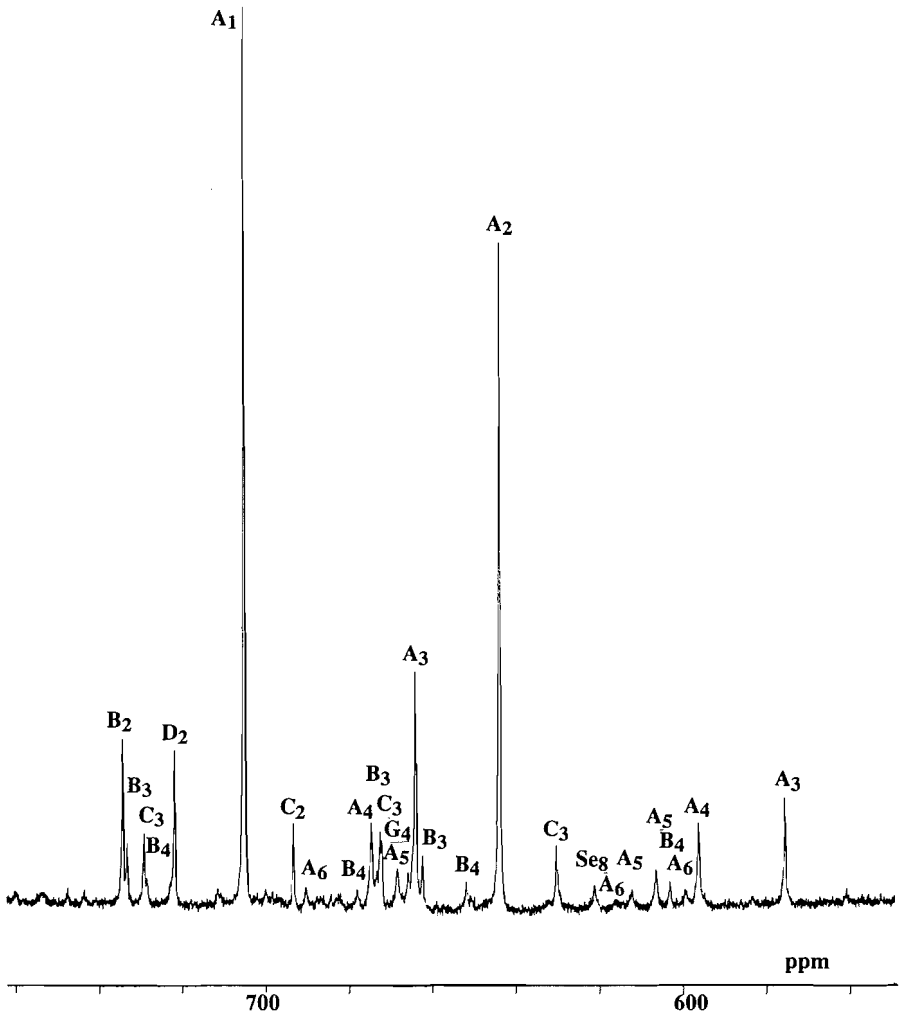

FIG. 2. An expansion of the 750–500 ppm region of the natural abundance ^{77}Se NMR spectrum of the molten mixture of sulfur and selenium containing 25 mol% Se. The assignment of the resonances is indicated in the spectrum. For the notation used in the figure, see Table 1.

Other resonances in the Se_nS_{8-n} region could be assigned by taking into consideration the earlier deductions on the trends in the chemical shifts (9*b*) as well as the relative intensities of the different signals (see Fig. 2).

In addition to the signals assigned in Fig. 2 there are some very weak resonances that remain unassigned. Those at 780–740 ppm probably indicate small concentrations of six-membered selenium sulfide ring molecules and those above 1050 ppm are due to seven-membered Se_nS_{7-n} heterocycles (10).

The comparison between the chemical shifts observed in the melts and the corresponding shifts in the solution spectra at room temperature is shown in Table 2. It is seen that all signals in the melts have been shifted downfield from their solution counterparts. In the case of isolated selenium atoms (structural type -S-Se-S-) the shift is ca. 5 ppm, with one sulfur and one selenium neighbour (-Se-Se-S-) it is ca. 10 ppm, and with two selenium neighbours (-Se-Se-Se-) the shift is 15–20 ppm. The temperature and solvent dependence of the chemical shift seem to correlate inversely with the electronegativity difference between adjacent neighbours.

Polymeric material

The three groups of resonances at 1050–850 ppm are assigned to the polymeric material in the melt (see Fig. 1). Analogously with the trend of the chemical shifts observed for the Se_nS_{8-n} rings (9*b*) it is reasonable to expect that isolated selenium atoms (i.e., selenium atoms with two sulfur neighbours) appear at the lowest field, with one selenium and one sulfur neighbour they resonate at higher field, and with two selenium neighbours at the highest field. Thus the group of signals at 1050–980 ppm implies isolated selenium atoms in the polymer, that at 970–920 ppm implies the structural unit -Se-Se-S-, and the group at 890–850 ppm the structural unit -Se-Se-Se-, i.e., three or more adjacent selenium atoms. This assignment finds support from the relative intensities of these groups as a function of selenium content in the melt (see Fig. 1). With 5 mol% Se in the melt only structural units -S-Se-S- and -Se-Se-S- are found in the melt, with the former more prominent than the latter. As the selenium content of the mixtures increases, the relative abundance of longer selenium fragments increases, as seen in the strengthening of the signals both at 970–920 and 890–850 ppm. Simultaneously the

TABLE 3. The calculated relative intensities of the ^{77}Se resonances in various seven-atom Se_nS_m fragments[a]

Fragment			Se content in the melt (mol%)				
			5	15	25	35	45
(A) -S-Se-S-							
S-S-	**S-Se-S**	-S-S	100	100	100	100	100
Se-S-	**S-Se-S**	-S-S	10	35	67	108	163
S-Se-	**S-Se-S**	-S-S	10	35	67	108	163
Se-Se-	**S-Se-S**	-S-S	—	6	22	58	133
Se-S-	**S-Se-S**	-Se-S	—	6	22	58	133
Se-S-	**S-Se-S**	-S-Se	—	3	11	29	66
S-Se-	**S-Se-S**	-Se-S	—	3	11	29	66
Se-Se-	**S-Se-S**	-Se-S	—	1	7	31	109
Se-Se-	**S-Se-S**	-S-Se	—	1	7	31	109
Se-Se-	**S-Se-S**	-Se-Se	—	—	1	8	45
(B) -Se-Se-S-							
S-S-	**Se-Se-S**	-S-S	100	100	100	100	100
Se-S-	**Se-Se-S**	-S-S	5	18	33	54	81
S-Se-	**Se-Se-S**	-S-S	5	18	33	54	81
S-S-	**Se-Se-S**	-Se-S	5	18	33	54	81
S-S-	**Se-Se-S**	-S-Se	5	18	33	54	81
Se-Se-	**Se-Se-S**	-S-S	—	3	11	29	67
S-S-	**Se-Se-S**	-Se-Se	—	3	11	29	67
Se-S-	**Se-Se-S**	-Se-S	—	3	11	29	67
Se-S-	**Se-Se-S**	-S-Se	—	3	11	29	67
S-Se-	**Se-Se-S**	-S-Se	—	3	11	29	67
S-Se-	**Se-Se-S**	-Se-S	—	3	11	29	67
Se-Se-	**Se-Se-S**	-Se-S	—	—	3	15	55
S-Se-	**Se-Se-S**	-Se-Se	—	—	3	15	55
Se-Se-	**Se-Se-S**	-S-Se	—	—	3	15	55
Se-S-	**Se-Se-S**	-Se-Se	—	—	3	15	55
Se-Se-	**Se-Se-S**	-Se-Se	—	—	1	8	45
(C) -Se-Se-Se-							
S-S-	**Se-Se-Se**	-S-S	100	100	100	100	100
Se-S-	**Se-Se-Se**	-S-S	—	33	65	108	164
S-Se	**Se-Se-Se**	-S-S	—	33	65	108	164
Se-Se-	**Se-Se-Se**	-S-S	—	—	20	58	135
Se-S-	**Se-Se-Se**	-Se-S	—	—	20	58	135
S-Se-	**Se-Se-Se**	-Se-S	—	—	10	29	67
Se-S-	**Se-Se-Se**	-S-Se	—	—	10	29	67
Se-Se-	**Se-Se-Se**	-Se-S	—	—	8	32	111
Se-Se-	**Se-Se-Se**	-S-Se	—	—	8	32	111
Se-Se-	**Se-Se-Se**	-Se-Se	—	—	—	8	45

[a]The middle selenium atom of the seven-atom chain is considered to be observed in the NMR spectrum. This atom and its immediate neighbours are indicated in bold. The computations were based on the probabilities of occurrence of the different fragments in the polymeric selenium sulfide as a function of the selenium content in the melt. The numerical values were scaled by assigning the most sulfur-rich fragment in each group (A)–(C) a reference value 100. The relative intensities <1 are denoted by a dash.

intensities of the resonances implying isolated selenium atoms diminish.

Because sulfur and selenium are distributed statistically in the polymer chains and the chemical shifts are also influenced by longer range effects than just by nearest neighbours, there is only a limited possibility of discussing the origin of the discrete resonances observed in the polymer signals. However, if the statistical distribution is assumed to be governed by the overall composition of the melt and the long-range effects on the chemical shift are arbitrarily limited only to the third adjacent atom from the observed selenium, the following qualitative inferences can be made. The computational details based on the probability of occurrence of different seven-atom fragments are shown in Table 3. In these fragments the selenium nucleus to be observed by NMR is in the middle of the chain with the intensity of its resonance directly proportional to the probability of occurrence of the fragment in question. The fragments have been divided into three groups according to the nearest neighbours to the "observed" selenium atom as indicated in Table 3. The expected relative intensities of the resonances due to different fragments (i.e., the probabilities of occurrence of these fragments) in each group have been scaled by assigning the most sulfur-rich fragment the reference value 100.

Can. J. Chem. Downloaded from www.nrcresearchpress.com by 92.62.229.171 on 09/08/12
For personal use only.

TABLE 4. The relative distribution of Se_nS_{8-n} species as a function of the melt composition

	Molten mixtures of sulfur and selenium, selenium content of the melt (%)[b]					CS_2 solutions of quenched melt,[c] selenium content of the melt (%)[d]			
Species[a]	0.4	5	15	25	35	10	30	35	40
A_1	100	82	61	47	38	70.5	47.0	39.0	40.0
A_2	—	11	15	20	19	17.0	23.5	20.0	20.0
B_2	—	3	4	5	5	2.5	3.5	3.0	2.5
C_2	—	1	2	3	3	2.0	2.5	3.0	2.0
D_2	—	2	5	5	5	3.5	4.0	3.5	3.5
A_3	—	1	5	7	9	4.5	8.0	11.5	10.5
B_3	—	—	3	4	5	—	2.0	3.0	4.0
C_3	—	—	3	4	5	—	2.5	3.5	3.5
A_4	—	—	2	2	4	—	3.5	6.0	5.5
B_4	—	—	—	1	3	—	1.0	2.0	2.0
D_4	—	—	—	—	—	—	0.5	1.0	1.0
G_4	—	—	—	<0.5	1	—	<0.5	1.0	0.5
A_5	—	—	—	<0.5	2	—	1.5	2.5	3.0
A_6	—	—	—	<0.5	1	—	0.5	1.0	1.5
Se_8	—	—	<0.5	<0.5	<0.5	—	<0.5	<0.5	0.5
Total Se[e]	100	100	100	100	100	100.0	100.0	100.0	100.0

[a]For the abbreviated notation; see Table 1.

[b]The data for the melt with the selenium content of 45 mol% are missing, because the signal-to-noise ratio was not sufficient to warrant even a semi-quantitative determination of the relative distribution of the Se_nS_{8-n} rings.

[c]See ref. 9*b*.

[d]The melt composition in this case refers to the composition of the original melt, which was then quenched, extracted with CS_2, crystallized, and redissolved in CS_2.

[e]Total amount of selenium bound in Se_nS_{8-n} rings.

It is seen from Fig. 1 that in the case of the melt with 5 mol% selenium there is only one major signal in the region of isolated selenium atoms (1050–980 ppm) at 1008 ppm with a few minor resonances. Comparison of the observed intensities with those expected from the computations given in Table 3 indicates that this major resonance should be due to a selenium nucleus far separated from other selenium atoms. This of course is reasonable, since in the sulfur-rich melt the frequency of occurrence of selenium in the polymeric chain is not expected to be high. The few minor signals can be assigned to fragments where the second selenium atom is separated by one, two, or at most three sulfur atoms. The relative intensities observed in Fig. 1 are in good agreement with the computations of Table 3. As the selenium content of the melt increases these minor resonances gain in intensity. Simultaneously new signals due to fragments containing more than two selenium atoms in close proximity appear in the spectrum. As a consequence, this group of resonances becomes more complicated with more even distribution of intensities. However, the signal at 1008 ppm due to the most totally isolated selenium is a major resonance in all spectra of Fig. 1. It has the highest intensity up to the melt composition of 25 mol% Se and it is only with higher selenium contents that resonances due to other fragments become more significant. These observations are also in qualitative agreement with the computations of Table 3.

Similar conclusions can be made for the group of resonances in the region implying one selenium and one sulfur neighbour to the observed nucleus (970–920 ppm). In the sulfur-rich melt only one major signal at 943 ppm is observed. According to Table 3 this indicates Se_2 fragments far removed from each other by chains of sulfur atoms. It is only with increasing selenium content in the melt that resonances from other fragments become more prominent, and thus the group of signals is more complicated.

The region for selenium with two selenium neighbours (890–850 pm) is not so well resolved into discrete components. Therefore it is not meaningful to discuss the possible distribution of the selenium-containing fragments even at the approximate level carried out above. The computed intensities of Table 3 can be used, however, to explain why no resonances at 890–850 ppm are observed in the melt containing 5 mol% Se. The only possibility in this region would be Se_3 fragments far removed from each other by long chains of sulfur. At the sulfur-rich end the probability of occurrence of this fragment is very low.

Composition of the melts

Since all sulfur–selenium mixtures were heated well above the polymerization threshold, they contain significant amounts of polymeric material. Steudel *et al.* (11) estimated that the quantity of polymeric sulfur in the equilibrium sulfur melt is ca. 50%. The amount of polymer in sulfur–selenium melts is of similar order of magnitude. With increasing selenium content the relative amount of polymer seems to grow, and more selenium is involved in the polymer. Since only selenium is observable with ^{77}Se NMR spectroscopy, the increasing selenium content in the polymer causes a dramatic change in the spectra of Fig. 1, as discussed above.

The relative distribution of the selenium-containing Se_nS_{8-n} rings as a function of the selenium content in the melt is shown in Table 4. The melts also contain homocyclic sulfur

Can. J. Chem. Downloaded from www.nrcresearchpress.com by 92.62.229.171 on 09/08/12
For personal use only.

molecules, mainly cyclooctasulfur, but it is unobservable in the ^{77}Se NMR spectrum. SeS_7 (A_1) is the main eight-membered heterocyclic component in all melts studied in this work. As seen in Fig. 1, it is the sole component in the melt with 0.4 mol% Se. As expected, its content is lowered as the selenium content of the melt increases. 1,2-Se_2S_6 is another main component in melts with selenium content above 5 mol%. Its abundance steadily increases as the selenium content in the melt increases. In addition to these two main components there are several minor components in the melt. Generally it can be said that the ring molecules with higher selenium content become more abundant as the selenium content of the melt increases.

It is interesting to compare the distribution of Se_nS_{8-n} species in the melt to that observed earlier in CS_2 solutions of the quenched melts (9*b*). The product distributions in both cases are practically identical and behave similarly as a function of total selenium content (see Table 4). The composition of the quenched melts evidently represents that of the melt itself. Upon extracting the quenched amorphous material with CS_2 the Se_nS_{8-n} species dissolve totally, leaving the polymeric material behind as the undissolved residue.

Conclusions

The molecular composition of molten mixtures of sulfur and selenium at different molar ratios has been studied with ^{77}Se NMR spectroscopy at 135°C. The melts have been shown to consist of eight-membered heterocyclic selenium sulfide rings as well as of polymeric material. SeS_7 and 1,2-Se_2S_6 are the main Se_nS_{8-n} species over the whole composition range studied in this work (up to 45 mol% Se in the melt), with a variety of other molecules as minor components. The product distribution is practically identical with that observed in CS_2 solutions of the quenched melts and behaves similarly as a function of the composition of the melt.

The composition of the polymeric material in the equilibrium melt is best explained by the statistical random distribution of sulfur and selenium in the polymeric chains. The polymer resonances in the ^{77}Se NMR spectrum can be interpreted in terms of the probability of occurrence of different fragments based on the total selenium content of the melts.

Acknowledgments

Financial support from the National Sciences and Engineering Research Council of Canada in the form of an International Scientific Exchange Award, from the Academy of Finland, and from The Finnish Cultural Foundation is gratefully acknowledged.

1. Gmelin Handbuch der anorganischen Chemie, Selen B. 8th ed. Springer Verlag, Berlin, Heidelberg, New York. 1949. p. 160.
2. W. E. Ringer. Z. Anorg. Chem. **32**, 183 (1902).
3. N. Z. Boctor and G. Kullerud. J. Solid State Chem. **71**, 513 (1987).
4. (*a*) M. G. Zhuravleva and G. I. Churfarov. Zh. Prikl. Khim. **24**, 28 (1951); (*b*) V. V. Illarionov and L. M. Lapina. Dokl. Akad. Nauk SSSR, **114**, 1021 (1957); (*c*) L. M. Lapina and V. V. Illarionov. Zh. Neorg. Khim. **3**, 1210 (1958); (*d*) L. M. Lapina. Zh. Neorg. Khim. **3**, 1386 (1958); (*e*) G. G. Devyatyk, A. I. Odnesetsev, and V. A. Ulmin. Russ. J. Inorg. Chem. **7**, 996 (1962).
5. (*a*) J. E. Fergusson, G. M. Pratt, G. A. Rodley, and C. J. Wilkins. J. Inorg. Nucl. Chem. **24**, 157 (1962); (*b*) A. T. Ward. J. Phys. Chem. **72**, 4133 (1968).
6. (*a*) R. Steudel and R. Laitinen. Top. Curr. Chem. **102**, 177 (1982); (*b*) Gmelin Handbuch der anorganischen Chemie, Selenium, Suppl. B2. 8th ed. Springer Verlag, Berlin, Heidelberg, New York. 1984. p. 280; (*c*) R. S. Laitinen. Acta Chem. Scand. Ser. A: A**43**, 361 (1987).
7. (*a*) R. Laitinen, N. Rautenberg, J. Steidel, and R. Steudel. Z. Anorg. Allg. Chem. **486**, 116 (1982); (*b*) R. Steudel and E.-M. Strauss. Angew. Chem. **96**, 356 (1984); Angew. Chem. Int. Ed. Engl. **23**, 362 (1984); (*c*) R. Steudel, M. Papavassiliou, E.-M. Strauss, and R. Laitinen. Angew. Chem. **98**, 81 (1986); Angew. Chem. Int. Ed. Engl. **25**, 99 (1986); (*d*) R. Steudel, D. Jensen, and M. Papavassiliou. Phosphorus, Sulfur Silicon Relat. Elem. **41**, 349 (1989); (*e*) D. M. Giolando, M. Papavassiliou, J. Pickardt, T. B. Rauchfuss, and R. Steudel. Inorg. Chem. **27**, 2596 (1988); (*f*) R. Steudel, D. Jensen, and F. Baumgart. Polyhedron, **9**, 1199 (1990).
8. (*a*) R. Laitinen, L. Niinistö, and R. Steudel. Acta Chem. Scand. Ser. A: A**33**, 737 (1979); (*b*) R. Laitinen and R. Steudel. J. Mol. Struct. **68**, 19 (1980); (*c*) R. Laitinen, R. Steudel, and E.-M. Strauss. J. Chem. Soc. Dalton Trans. 1896 (1985).
9. (*a*) R. S. Laitinen and T. A. Pakkanen. J. Chem. Soc. Chem. Commun. 1381 (1986); (*b*) Inorg. Chem. **26**, 2598 (1987); (*c*) R. S. Laitinen, P. Pekonen, Y. Hiltunen, and T. A. Pakkanen. Acta Chem. Scand. **43**, 436 (1989).
10. (*a*) R. Steudel, M. Papavassiliou, D. Jensen, and K. Seppelt. Z. Naturforsch. B: Chem. Sci. **43**, 245 (1988); (*b*) R. Steudel, M. Papavassiliou, and W. Krampe. Polyhedron, **7**, 581 (1988); (*c*) P. Pekonen, Y. Hiltunen, R. S. Laitinen, and T. A. Pakkanen. Inorg. Chem. **29**, 2770 (1990); (*d*) Inorg. Chem. **30**, 3679 (1991).
11. (*a*) R. Steudel, R. Strauss, and L. Koch. Angew. Chem. **97**, 58 (1985); Angew. Chem. Int. Ed. Engl. **24**, 59 (1985); (*b*) R. Steudel and R. Strauss. Z. Naturforsch. B: Anorg. Chem. Org. Chem. **37**, 1219 (1982).

Can. J. Chem. Downloaded from www.nrcresearchpress.com by 92.62.229.171 on 09/08/12
For personal use only.

Preparation and characterization of $Tl(1,2\text{-}C_2H_4Cl_2)B(OTeF_5)_4$: a metal complex of a least coordinating solvent and a least coordinating anion

PAUL K. HURLBURT, OREN P. ANDERSON, AND STEVEN H. STRAUSS[1]

Department of Chemistry, Colorado State University, Fort Collins, CO 80523, U.S.A.

Received July 4, 1991

This paper is dedicated to the memory of Professor Thomas Birchall

PAUL K. HURLBURT, OREN P. ANDERSON, and STEVEN H. STRAUSS. Can. J. Chem. **70**, 726 (1992).

Addition of $B(OTeF_5)_3$ to $TlOTeF_5$ in the weakly coordinating solvents dichloromethane, 1,2-dichloroethane, and 1,1,2-trichlorotrifluoroethane produces solutions of $M(solv)_x^+B(OTeF_5)_4^-$. When the solvent was 1,2-dichloroethane, the crystalline compound $Tl(1,2\text{-}C_2H_4Cl_2)B(OTeF_5)_4$ was isolated and studied by X-ray crystallography: triclinic, space group $P\bar{1}$, a = 9.221 (4), b = 11.396 (5), c = 12.538 (4) Å, α = 110.75 (3)°, β = 101.72 (3)°, γ = 99.74 (3)°, Z = 2, T = −116°C. The $Tl(1,2\text{-}C_2H_4Cl_2)^+$ cation contains a five-membered chelate ring with Tl—Cl distances of 3.138 (4) and 3.179 (3) Å. The metal ion is weakly bonded to four $B(OTeF_5)_4^-$ counterions, with nine Tl—F interactions that range from 2.950 (5) to 3.981 (8) Å. When the solvent is dichloromethane or 1,1,2-trichlorotrifluoroethane, only the unsolvated solid salt $TlB(OTeF_5)_4$ can be isolated by crystallization. This salt is thermally unstable, slowly forming $TlOTeF_5$ and volatile $B(OTeF_5)_3$.

Key words: noncoordinating anion, noncoordinating solvent, metal ion solvation.

PAUL K. HURLBURT, OREN P. ANDERSON et STEVEN H. STRAUSS. Can. J. Chem. **70**, 726 (1992).

Lorsqu'on ajoute du $B(OTeF_5)_3$ a du $TlOTeF_5$, dans des solvants faiblement coordinants comme le dichlorométhane, le 1,2-dichloroéthane et le 1,1,2-trichlorotrifluoroéthane, on obtient des solutions de $M(solv)_x^+B(OTeF_5)_4^-$. Avec du 1,2,-dichloroéthane comme solvant, on a isolé le composé cristallin $Tl(1,2\text{-}Cl_2C_2H_4)B(OTeF_5)_4$ et on l'a étudié par diffraction des rayons-X : triclinique, groupe d'espace $P\bar{1}$, a = 9,221(4), b = 11,396(5) et c = 12,538(4) Å, α = 110,75(3)°, β = 101,72(3)° et γ = 99,74°, Z = 2, T = 116°C. Le cation $Tl(1,2\text{-}Cl_2C_2H_4)^+$ comporte un chélate cyclique à cinq chaînons dans lequel les distances Tl—Cl sont égales à 3,138(4) et 3,179(3) Å. L'ion métallique est faiblement lié à quatre contre-ions $B(OTeF_5)_4^-$ dans lesquels neuf interactions Tl—F se trouvent entre 2,950(5) à 3,981(8) Å. Avec le dichlorométhane ou le 1,1,2-trichlorotrifluoroéthane, la cristallisation ne fournit que le sel solide $TlB(OTeF_5)_4$ non solvaté. Ce sel est thermiquement instable; il forme lentement du $TlOTeF_5$ et du $B(OTeF_5)_3$ qui est volatil.

Mots clés : anion non-coordinant, solvant non-coordinant, solvatation des ions métaux.

[Traduit par la rédaction]

Introduction

There has been increasing interest in recent years to find new anions that are more weakly coordinating than the classical "noncoordinating" anions ClO_4^-, $CF_3SO_3^-$, BF_4^-, SbF_6^-, etc. One term that has been used for such new anions is "least coordinating" anions (1). Examples include $B(OTeF_5)_4^-$ (2), $B_{11}CH_{12}^-$ (1, 3), and BAr_4^- (Ar = C_6H_5 (4) or 3,5-$C_6H_3(CF_3)_2$ (5)). The interest in such species derives in part from a desire to study coordinatively unsaturated cations such as R_3Si^+ (6) and Fe(porphyrin)$^+$ (3*b*), both of which have yet to be prepared and isolated in a condensed phase, and in part from the desire to prepare more active transition metal catalysts (4). Another goal that could be achieved if metal ions (M^{n+}) could be electrostatically decoupled from their counterions (X^-) is that compounds such as $M(L)X_n$, where L is an extremely weak Lewis base such as a chlorocarbon,[2] a chlorofluorocarbon, or a hydrocarbon, could be isolated and characterized in the solid state by X-ray crystallography. With respect to chlorocarbons, this goal has been realized in a limited number of cases.

In this paper we describe the synthesis and characterization of $TlB(OTeF_5)_4$ and $Tl(1,2\text{-}C_2H_4Cl_2)B(OTeF_5)_4$. The former compound is soluble in the "least coordinating" solvents dichloromethane, 1,2-dichloroethane, and 1,1,2-trichlorotrifluoroethane. The latter compound contains a Tl—Cl—C—C—Cl chelate ring. Thallium is only the third metal that has been shown by X-ray crystallography to coordinate to a simple chlorocarbon. Chlorocarbon complexes of Ag (7) and Ru (8) have also been structurally characterized.

Experimental

Dichloromethane, dichloromethane-d_2, 1,2-dichloroethane, 1,2-dichloroethane-d_4, and 1,1,2-trichlorotrifluoroethane were distilled from P_2O_5. The compounds $B(OTeF_5)_3$ (9) and $TlOTeF_5$ (2*b*) were prepared by literature procedures. These two compounds, as well as $TlB(OTeF_5)_4$ and $Tl(1,2\text{-}C_2H_4Cl_2)B(OTeF_5)_4$ (*vide infra*), are very sensitive to traces of moisture. Therefore, all manipulations involving them were performed under a purified dinitrogen atmosphere using standard techniques (10).

Spectroscopic measurements

Samples for IR spectroscopy were Nujol mulls between AgCl windows. Spectra were recorded at room temperature on a Perkin–Elmer 983 spectrometer. Peak positions are ±1 cm^{-1}. Samples of $TlB(OTeF_5)_4$ for ^{19}F NMR spectroscopy were dichloromethane solutions in 5-mm glass tubes. Spectra were recorded at room temperature on a Bruker WP-300 spectrometer operating at 282.4 MHz, after tuning with a separate sample of dichloromethane-d_2. Chemical shifts (δ scale) are relative to $CFCl_3$. The ^{19}F NMR spectrum of $TlB(OTeF_5)_4$ was an AB_4X pattern shielded relative to $CFCl_3$ (X = ^{125}Te, I = 1/2, 7% natural abundance). Chemical shifts and J_{AB} were determined by comparing the experimental spectrum to a simulated spectrum that was calculated using LAOCOON PC (11). The value of J_{BX} was measured directly from the experimental spectrum.

[1]Author to whom correspondence may be addressed.

[2]In this context, a chlorocarbon is defined as a mono- or polychlorinated aliphatic or aromatic hydrocarbon; it contains no other heteroatoms.

Printed in Canada

Can. J. Chem. Downloaded from www.nrcresearchpress.com by 92.62.229.171 on 09/08/12
For personal use only.

Can. J. Chem. Downloaded from www.nrcresearchpress.com by 92.62.229.171 on 09/08/12
For personal use only.

$TlB(OTeF_5)_4$ and $Tl(1,2\text{-}C_2H_4Cl_2)B(OTeF_5)_4$

$TlOTeF_5$ (0.40 g, 0.91 mmol) and $B(OTeF_5)_3$ (0.81 g, 1.1 mmol) were mixed in 1,2-dichloroethane (2 mL). The resulting colorless solution was kept in the freezer (−20°C) for 24 h, at which time the crystalline solid $Tl(1,2\text{-}C_2H_4Cl_2)B(OTeF_5)_4$ was present (stoichiometry established by X-ray diffraction (*vide infra*)). This compound slowly loses the coordinated 1,2-dichloroethane molecule under a dinitrogen atmosphere, making a per cent yield determination and elemental analysis problematic. The unsolvated compound $TlB(OTeF_5)_4$ was prepared by mixing $TlOTeF_5$ (0.26 g, 0.60 mmol) and $B(OTeF_5)_3$ (0.43 g, 0.59 mmol) in dichloromethane (3 mL). The mixture (off-white solid in a colorless solution) was stirred for 25 min, at which point all volatiles were removed under vacuum ($\sim 10^{-5}$ Torr (1 Torr = 133.3 Pa); 2 h). An infrared spectrum (*vide infra*) revealed that none of the starting materials remained. The off-white solid compound is thermally unstable, eventually (days) forming $TlOTeF_5$ and $B(OTeF_5)_3$. ^{19}F NMR of $TlB(OTeF_5)_4$ (CH_2Cl_2): δ_A −38.5, δ_B −45.5, J_{AB} = 190 Hz, J_{BX} = 3588 Hz.

X-ray crystallographic study of $Tl(1,2\text{-}C_2H_4Cl_2)B(OTeF_5)_4$

A Nicolet *R3m* diffractometer equipped with a LT-1 variable-temperature accessory was used. Crystals of $Tl(1,2\text{-}C_2H_4Cl_2)B(OTeF_5)_4$ were examined under an argon atmosphere at <−150°C. A suitable crystal was attached with Dow–Corning silicone grease to the end of a glass fiber and quickly placed into the cold nitrogen stream (−116°C) of the LT-1 unit.

Centering on 25 reflections allowed least-squares calculation of the cell constants, which are listed, along with other experimental parameters, in Table 1. The intensities of control reflections ($\bar{2}00$, $0\bar{1}0$, and 005), monitored every 97 reflections, showed no significant trend during the course of the data collection. An empirical absorption correction, based on intensity profiles for 16 reflections over a range of setting angles (ψ) for the diffraction vector, were applied to the observed data. The transmission factors ranged from 0.205 to 0.436. Although the absolute values of the transmission factors are high, the improvement in R_{merge} after the absorption correction (0.185 before and 0.053 after) indicates that these values are satisfactory. Lorentz and polarization corrections were applied to the data.

The structure was solved using an interpretation of the Patterson map.[3] The refinement involved anisotropic thermal parameters for all non-hydrogen atoms. Hydrogen atoms were included in calculated positions (C—H = 0.96 Å, $U(H) = 1.2U_{iso}(C)$). Neutral atom scattering factors (including anomalous scattering) were taken from ref. 12. The weighted least-squares refinements converged (weights calculated as $(\sigma^2(F) + |g|F_o^2)^{-1})$, with the average shift/esd <0.005 over the last three refinement cycles. In the final difference Fourier maps, the maximum and minimum electron densities were 1.43 and −1.94 e Å^{-3}. Analysis of variance as a function of Bragg angle, magnitude of F_o, reflection indices, etc., showed no significant trends.

Table 2 contains a list of atomic positional and isotropic thermal parameters for all unique non-hydrogen atoms of $Tl(1,2\text{-}C_2H_4Cl_2)B(OTeF_5)_4$. Table 3 contains a list of selected bond distances and angles. Complete lists of bond distances (Table S-1), bond angles (Table S-2), anisotropic thermal parameters (Table S-3), hydrogen atom parameters (Table S-4), and observed and calculated structure factors (Table S-5) are available as supplementary material.[4]

Results and discussion

The formation of $Tl(1,2\text{-}C_2H_4Cl_2)B(OTeF_5)_4$ and $TlB(OTeF_5)_4$ are summarized in the reaction scheme below:

$$TlOTeF_5 + B(OTeF_5)_3 \xrightarrow{\text{solvent}} Tl(\text{solvent})_xB(OTeF_5)_4$$
solvent = CH_2Cl_2, 1,2-$C_2H_4Cl_2$, or 1,1,2-$C_2Cl_3F_3$

$$Tl(\text{solvent})_xB(OTeF_5)_4 \xrightarrow{\text{crystallize}} Tl(1,2\text{-}C_2H_4Cl_2)B(OTeF_5)_4$$
solvent = 1,2-$C_2H_4Cl_2$

$$Tl(\text{solvent})_xB(OTeF_5)_4 \xrightarrow{\text{crystallize}} TlB(OTeF_5)_4$$
solvent = CH_2Cl_2 or 1,1,2-$C_2Cl_3F_3$

$$TlB(OTeF_5)_4 \xrightarrow{\text{vacuum (days)}} TlOTeF_5 + B(OTeF_5)_3$$

The difference in the stoichiometry of the compound isolated upon crystallization is almost certainly due to the ligand strength of the three different solvents. That is, the Tl—Cl(C) bonds in the presumed $Tl(CH_2Cl_2)_x^+$ and $Tl(1,1,2\text{-}C_2Cl_3F_3)_x^+$ cations are sufficiently weak that the coordinated solvent molecules are "squeezed out" of the lattice as it forms. Structural, conductimetric, and ^{13}C NMR spectroscopic data have left little doubt that 1,2-dichloroethane is a stronger ligand for Ag(I) than dichloromethane (7). It is sensible that this order would be preserved for Tl(I). It is also sensible that 1,1,2-trichlorotrifluoroethane would be the weakest donor of all three. In harmony with these expectations, we found that the solubility of $TlOTeF_5$ in 1,2-dichloroethane, 30.2 mM, is considerably greater than in dichloromethane, 1.1 mM. We conclude that this must be due to a difference in the coordinating ability of the two solvents, since the difference in their dielectric constants is small

[3]Calculations for diffractometer operations were performed by using software supplied with the Nicolet *R3m* diffractometer. All structural calculations were performed on the Data General Eclipse S/140 computer in the X-ray laboratory at Colorado State University with the SHELXTL program library written by Professor G. M. Sheldrick and supplied by Nicolet XRD Corporation.

[4]Supplementary Tables S-1–S-5 and supplementary Fig. S-1 may be purchased from the Depository of Unpublished Data, Document Delivery, CISTI, National Reseach Council Canada, Ottawa, Canada K1A 0S2.

Tables S-1, S-2, and S-4 have also been deposited with the Cambridge Crystallographic Data Centre, and can be obtained on request from The Director, Cambridge Crystallographic Data Centre, University Chemical Laboratory, Lensfield Road, Cambridge, CB2 1EW, U.K.

Can. J. Chem. Downloaded from www.nrcresearchpress.com by 92.62.229.171 on 09/08/12
For personal use only.

TABLE 1. Details of the X-ray diffraction study of $Tl(1,2\text{-}C_2H_4Cl_2)B(OTeF_5)_4$

Compound		$Tl(1,2\text{-}C_2H_4Cl_2)B(OTeF_5)_4$
Molecular formula		$C_2H_4BCl_2F_{20}O_4Te_4Tl$
Formula wt., g mol^{-1}		1268.5
Space group		$P\bar{1}$
Unit cell dimensions:	a, Å	9.2210 (39)
	b, Å	11.3963 (52)
	c, Å	12.5377 (44)
	α, deg	110.745 (31)
	β, deg	101.720 (33)
	γ, deg	99.740 (33)
Unit cell volume, $Å^3$		1163.84 (85)
Z		2
Calcd. density, g cm^{-3}		3.62
Crystal dimensions, mm		0.22 × 0.31 × 0.43
Data collection temperature, °C		−116 (1)
Radiation (λ, Å)		Mo K_α (0.7107)
Monochromator		Graphite
Absorption coeff., cm^{-1}		123.13
Scan type		θ–2θ
Scan speed, deg min^{-1}		Variable (4–30)
2θ range, deg		4–50
Reflections		$\pm h, -k, \pm l$
Total no. of reflections measured		5512
No. of obsd. reflections, $\lvert F_o\rvert > 2.5\sigma(F_o)$		3704
Data/parameter ratio		12.03
R		0.0432
R_w		0.0411
GOF		1.505
g (refined)		0.00046
Slope of normal probability plot		1.265

TABLE 2. Atomic coordinates (×10^4) and isotropic thermal parameters ($Å^2$ × 10^3) for $Tl(1,2\text{-}C_2H_4Cl_2)B(OTeF_5)_4$

Atom	x	y	z	U^a
Tl	1871(1)	1054(1)	3193(1)	29(1)
Cl(1)	155(4)	3183(3)	3089(4)	51(2)
Cl(2)	4002(3)	3706(3)	3464(3)	40(1)
C(1)	1390(15)	4370(12)	2825(14)	50(6)
C(2)	2920(15)	4882(11)	3659(14)	51(7)
B	4024(14)	1681(10)	7903(10)	20(4)
Te(1)	3102(1)	−931(1)	5888(1)	20(1)
O(1)	4246(8)	737(6)	6815(6)	27(3)
F(1)	2280(8)	−454(6)	4699(5)	35(3)
F(2)	4664(8)	−1272(6)	5228(6)	46(3)
F(3)	3805(8)	−1593(6)	6950(6)	43(3)
F(4)	1414(7)	−760(5)	6438(5)	29(2)
F(5)	2006(7)	−2580(5)	4879(5)	33(3)
Te(2)	2524(1)	3399(1)	7025(1)	23(1)
O(2)	2721(8)	2190(6)	7650(6)	26(3)
F(6)	1171(8)	2163(7)	5645(6)	45(3)
F(7)	958(8)	3711(7)	7655(6)	44(3)
F(8)	3877(8)	4744(6)	8297(7)	48(3)
F(9)	4036(8)	3143(7)	6264(7)	44(3)
F(10)	2200(10)	4554(7)	6366(7)	54(4)
Te(3)	2663(1)	1130(1)	9733(1)	22(1)
O(3)	3759(8)	962(6)	8671(6)	24(3)
F(11)	828(7)	897(6)	8677(5)	35(3)
F(12)	2983(8)	2879(5)	10250(5)	34(3)
F(13)	4311(8)	1328(7)	10901(6)	45(3)
F(14)	2191(9)	−617(6)	9302(6)	46(3)
F(15)	1584(9)	1209(7)	10821(6)	44(3)
Te(4)	7419(1)	2862(1)	9020(1)	23(1)
O(4)	5398(8)	2754(6)	8462(7)	27(3)
F(16)	7145(7)	1100(5)	8527(6)	35(3)
F(17)	7247(9)	2980(7)	10471(5)	45(3)
F(18)	7845(8)	4614(6)	9507(6)	42(3)
F(19)	7756(9)	2721(8)	7608(7)	53(4)
F(20)	9449(8)	3031(7)	9602(8)	58(4)

[a]Equivalent isotropic U defined as one third of the trace of the orthogonalised U_{ij} tensor.

(the dielectric constants for dichloromethane and 1,2-dichloroethane are 9.08 and 10.65, respectively (13)). Furthermore, we found that $TlOTeF_5$ is not soluble to any detectable extent in 1,1,2-trichlorotrifluoroethane.

The overall structure of $Tl(1,2\text{-}C_2H_4Cl_2)B(OTeF_5)_4$ is shown in Fig. 1. The thallium coordination sphere and the conformation of the Tl—Cl—C—C—Cl chelate ring are shown in Figs. 2 and 3, respectively. A stereoview of the unit cell packing is shown in Fig. S-1, which is available as supplementary material.[4] Selected bond distances and angles are listed in Table 3.

Thallium is only the third metal that has been shown conclusively (i.e., by X-ray crystallography) to coordinate to extremely weakly basic (14) chlorocarbons.[2] Thallium is also the first such metal from Period 6 and the first such metal with a $d^{10}s^2$ electron configuration. Previous structurally characterized examples are dichloromethane complexes of Ag (7) and Ru (8), 1,2-dichloroethane complexes of Ag (7), and a 1,2,3-trichloropropane complex of Ag.[5] Based on IR and NMR spectroscopic data, others have concluded that dichloromethane can coordinate to Mo and W (15) or to Re (16), respectively. Many examples of M—Cl(C) linkages have been reported in compounds in which the chlorine atom is a substituent on a much stronger ligand such as an amine or a phenoxide (17).

The thallium–organochlorine bonds and the Tl—Cl—C—C—Cl chelate ring are the most interesting and significant aspects of the structure. The Tl—Cl distances of 3.138 (4) and 3.179 (3) Å are well within the sum of van der Waals radii for these atoms, which is probably between 3.75 Å (18) and 3.80 Å (19). For comparison, the Tl—Cl distances in the Rock Salt and CsCl modifications of TlCl are 3.15 (2) and 3.32 (2) Å, respectively (20).[6] Despite the fact that 1,2-dichloroethane is extremely weakly coordinated to Tl(I) in this structure, the five-membered Tl—Cl—C—C—Cl chelate ring (see Fig. 3) exhibits the same puckered conformation seen with more traditional and much stronger bidentate ligands such as ethylenediamine (21).

The Tl(I) ion in $Tl(1,2\text{-}C_2H_4Cl_2)B(OTeF_5)_4$ is weakly coordinated via secondary bonds (22) to up to nine fluorine atoms from four different $B(OTeF_5)_4^-$ counterions (see Fig. 2). The nine Tl—F(Te) distances range from 2.950 (5) Å for Tl—F11″ to 3.981 (8) Å for Tl—F3′. The next most distant fluorine atom is F13‴, which is 4.057 (9) Å from Tl. While the sum of van der Waals radii for thallium and fluorine has been reported to be either 3.35 or 3.50 Å (18, 19), we have

[5]D. M. Van Seggen, O. P. Anderson, and S. H. Strauss. Submitted for publication.

[6]The stable form of TlCl at 25°C and 1 atm (101.3 kPa) has the CsCl structure, while TlCl grown by vapor deposition onto a KCl, KBr, or KI substrate has the Rock Salt structure.

TABLE 3. Selected bond distances (Å) and angles (deg) for $Tl(1,2\text{-}C_2H_4Cl_2)B(OTeF_5)_4$

Tl—Cl1	3.138 (4)	Tl—Cl2	3.179 (3)
Tl—F11″	2.950 (5)	Tl—F1	2.980 (8)
Tl—F15‴	3.004 (8)	Tl—F16′	3.049 (6)
Tl—F6	3.129 (7)	Tl—F4″	3.136 (7)
Tl—F2′	3.317 (7)	Tl—F9	3.640 (6)
Tl—F3′	3.981 (8)	C1—C2	1.45 (2)
C1—Cl1	1.78 (2)	C2—Cl2	1.78 (2)
B—O	1.45 (2) – 1.50 (2)	Te—O	1.807 (8) – 1.827 (9)
Te—F	1.803 (7) – 1.850 (9)	Te—F(Tl)	1.814 (8) – 1.850 (9)
Tl—Cl1—C1	107.6 (5)	Tl—Cl2—C2	108.2 (5)
Cl1—C1—C2	113 (1)	Cl2—C2—C1	113 (1)
Cl1-Tl-Cl2	65.1 (1)	O—B—O	106 (1) – 113 (1)
B—O—Te	128.3 (7) – 133.4 (7)	O—Te—F_{ax}	176.0 (4) – 178.0 (3)
O—Te—F_{eq}	89.2 (3) – 96.1 (3)		

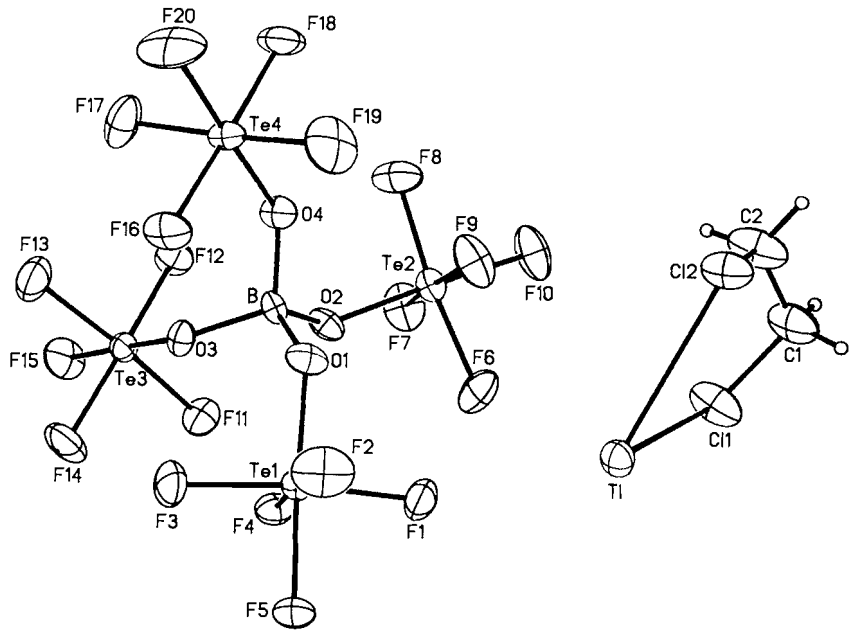

FIG. 1. Drawing of the $Tl(1,2\text{-}C_2H_4Cl_2)B(OTeF_5)_4$ asymmetric unit (50% probability ellipsoids). The separation of the $Tl(1,2\text{-}C_2H_4Cl_2)^+$ cation and the $B(OTeF_5)_4^-$ anion is to scale.

included two fluorine atoms whose Tl—F distances are >3.50 Å in the Tl coordination sphere shown in Fig. 2. This is because Tl—F distances in TlF, which possesses a very distorted Rock Salt structure, range all the way from 2.25 (2) to 3.90 (2) Å (23). Another relevant comparison can be made with $Tl(C_9H_{21}N_3)PF_6$,[7] in which the Tl(I) ion has a N_3F_3 donor set. In this compound, the Tl—F(P) distances are 3.23 (1), 3.27 (1), and 3.54 (2) Å (24).

The structure of the bound 1,2-dichloroethane ligand in $Tl(1,2\text{-}C_2H_4Cl_2)B(OTeF_5)_4$ is not significantly perturbed from the structure of the free molecule. In solid 1,2-dichloroethane at −140°C, which exists as the *anti* conformer, the C—Cl and C—C bond distances and the Cl—C—C bond angle are 1.80 (2) Å, 1.49 (4) Å, and 105.5 (5)°, respectively (25). Only the Cl—C—C bond angle is distinguishable from the values found in $Tl(1,2\text{-}C_2H_4Cl_2)B(OTeF_5)_4$, 113 (1)° and 114 (1)° (see Table 3). A better comparison for our complex would be a 1,2-dichloroethane solvate with a *gauche* conformation; one such example (data obtained at −160°C) has an average C—Cl bond distance, a C—C bond distance, and an average Cl—C—C bond angle of 1.798 (5) Å, 1.467 (5) Å, and 112.6 (4)°, respectively (26). This solvate has a Cl—C—C—Cl torsional angle of 61.6°, while in our complex this angle is 68.9°. In 1,2-dichloroethane complexes of Ag(I), the Cl—C—C—Cl torsional angles range from 65.0° to 70.0° (7*a*). The increase in the Cl—C—C—Cl torsional angle in the complexes relative to the solvate is minor: the change of 4°–8° may allow the ligand to achieve a more optimal Cl—M—Cl bite angle.

The structure of the $B(OTeF_5)_4^-$ counterion (idealized S_4 symmetry, with the S_4 axis bisecting the O1—B—O2 and O3—B—O4 angles) is virtually identical with those found in $Tl(mesitylene)_2B(OTeF_5)_4$ (2*b*), $AgB(OTeF_5)_4$ (2*c*), and $Ag(CO)B(OTeF_5)_4$ (2*a*). As was found in these three other structures, the bonds between Te atoms and F atoms coordinated to Tl in $Tl(1,2\text{-}C_2H_4Cl_2)B(OTeF_5)_4$ are not signifi-

[7] $C_9H_{21}N_3$ = *N*,*N*′,*N*″-trimethyl-1,4,7-triazacyclononane.

Can. J. Chem. Downloaded from www.nrcresearchpress.com by 92.62.229.171 on 09/08/12
For personal use only.

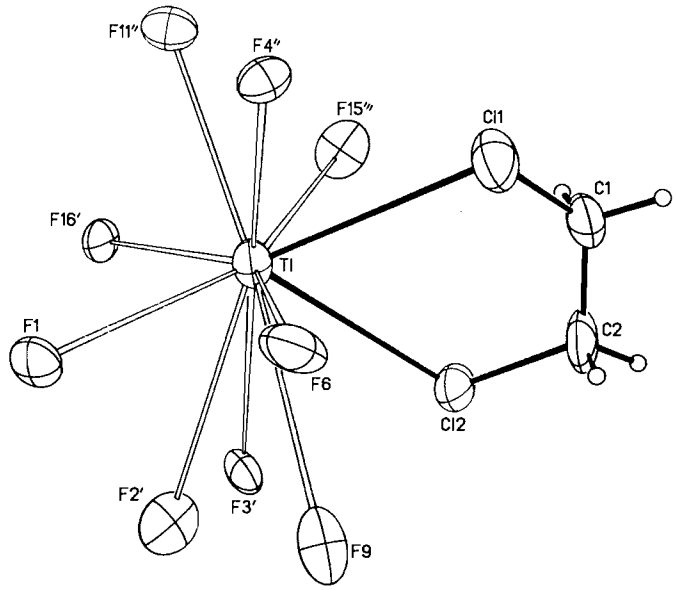

FIG. 2. Drawing of the Tl coordination sphere in $Tl(1,2\text{-}C_2H_4Cl_2)B(OTeF_5)_4$, emphasizing the bidentate coordination of the 1,2-dichloroethane ligand (50% probability ellipsoids).

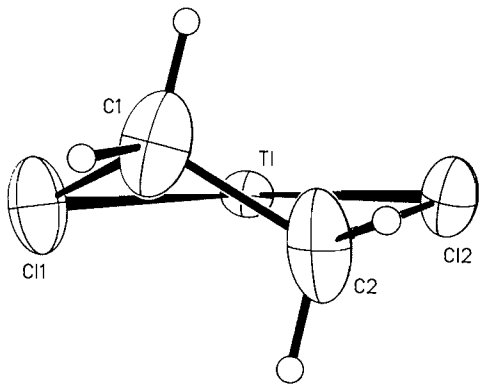

FIG. 3. Drawing of the $Tl(1,2\text{-}C_2H_4Cl_2)^+$ cation in $Tl(1,2\text{-}C_2H_4Cl_2)B(OTeF_5)_4$, showing the conformation of the five-membered chelate ring (50% probability ellipsoids). This asymmetric cation is inversion related to its enantiomer in the unit cell, which contains two asymmetric units.

cantly longer than the other Te—F distances in this compound. Generally, coordination of an anion such as SbF_6^- produces a longer Sb—F bond distance to the bridging F atom (27), but this is not always the case (28).

A solid-state (Nujol mull) IR spectrum of $TlB(OTeF_5)_4$ exhibits bands that are typical of the $B(OTeF_5)_4^-$ anion (2*b*):[8] 980 cm^{-1} (s, bd; ν(BO)), 799 cm^{-1} (w, sp), 723 cm^{-1} (s, sp), and 706 cm^{-1} (s, sp; ν(TeO)), and 664 cm^{-1} (s, sp), 639 cm^{-1} (m, sp), and 621 cm^{-1} (m, sp; ν(TeF)). These are matched by the following bands for $Tl(1,2\text{-}C_2H_4Cl_2)B(OTeF_5)_4$: 983 cm^{-1} (s, bd; ν(BO)), 798 cm^{-1} (w, sp), 721 cm^{-1} (s, sp), and 705 cm^{-1} (s, sp; ν(TeO)), and 664 cm^{-1} (s, sp), 641 cm^{-1} (m, sp), and 625 cm^{-1} (m, sp; ν(TeF)).

In addition, the IR spectrum of $Tl(1,2\text{-}C_2H_4Cl_2)B(OTeF_5)_4$ exhibited bands attributable to the coordinated 1,2-dichloroethane molecule at 1314 and 1282 cm^{-1} (CH_2 wag) and at 878 cm^{-1} (CH_2 rock) (29). Bands attributable to CCl stretching were not observed, presumably because they were buried under the intense Te—O and Te—F stretching bands.[9] However, the spectrum of the deuterated derivative $Tl(1,2\text{-}C_2D_4Cl_2)B(OTeF_5)_4$ exhibited a band at 610 cm^{-1}, which we assign as ν(CCl) for the coordinated chlorocarbon ligand since the *gauche* conformer of 1,2-dichloroethane-d_4 has a CCl stretching band at 616 cm^{-1} (7*a*). Coordination of 1,2-dichloroethane to Tl(I) has lowered ν(CCl) by 6 cm^{-1}, a smaller change than was seen for two 1,2-dichloroethane complexes of Ag(I) (7*a*). For these complexes, $\Delta\nu$(CCl) was 16 cm^{-1}. The larger effect on ν(CCl) is in harmony with the observation that the Ag—Cl bonds in $Ag(1,2\text{-}C_2H_4Cl_2)OTeF_5$ and $Ag_2(1,2\text{-}C_2H_4Cl_2)_4Pd(OTeF_5)_4$, which fall in the range 2.640 (3)–3.000 (3) Å (7*a*), are shorter and presumably stronger than the Tl—Cl bonds in $Tl(1,2\text{-}C_2H_4Cl_2)B(OTeF_5)_4$.

Future reports from this laboratory will detail the further use of $B(OTeF_5)_4^-$ and related highly fluorinated least coordinating anions.

Acknowledgements

This research was supported by grants from the National Science Foundation (CHE-8805788 and CHE-9011610). We thank Professor J. R. Norton for the use of his IR spectrometer, D. M. Van Seggen for measuring the solubility of $TlOTeF_5$, and M. M. Miller for assistance with crystallographic computing. The Siemens *R3m*/E diffractometer and computing system were purchased with a grant from the National Science Foundation (CHE-8103011).

1. K. Shelly, D. C. Finster, Y. J. Lee, W. R. Scheidt, and C. A. Reed. J. Am. Chem. Soc. **108**, 3117 (1986).
2. (*a*) P. K. Hurlburt, O. P. Anderson, and S. H. Strauss. J. Am. Chem. Soc. **113**, 6277 (1991); (*b*) S. H. Strauss, M. D. Noirot, and O. P. Anderson. Inorg. Chem. **26**, 2216 (1987); (*c*) D. M. Van Seggen, P. K. Hurlburt, M. D. Noirot, O. P. Anderson, and S. H. Strauss. To be published.
3. (*a*) D. J. Liston, Y. J. Lee, W. R. Scheidt, and C. A. Reed. J. Am. Chem. Soc. **111**, 6643 (1989); (*b*) G. P. Gupta, G. Lang, Y. J. Lee, W. R. Scheidt, K. Shelly, and C. A. Reed. Inorg. Chem. **26**, 3022 (1987); (*c*) K. Shelly, D. C. Finster, Y. J. Lee, W. R. Scheidt, and C. A. Reed. J. Am. Chem. Soc. **107**, 5955 (1985).
4. R. F. Jordan, C. S. Bajgur, R. Willett, and B. Scott. J. Am. Chem. Soc. **108**, 7410 (1986).
5. H. Nishida, N. Takada, and M. Yoshimura. Bull. Chem. Soc. Jpn. **57**, 2600 (1984).
6. (*a*) J. B. Lambert, W. J. Schulz, Jr., J. A. McConnell, and W. Schilf. J. Am. Chem. Soc. **110**, 2201 (1988); (*b*) G. K. S. Prakash, S. Keyaniyan, R. Aniszfeld, L. Heiliger, G. A. Olah, R. C. Stevens, H.-K. Choi, and R. Bau. J. Am. Chem. Soc. **109**, 5123 (1987).
7. (*a*) M. R. Colsman, T. D. Newbound, L. J. Marshall, M. D. Noirot, M. M. Miller, G. P. Wulfsberg, J. S. Frye, O. P. Anderson, and S. H. Strauss. J. Am. Chem. Soc. **112**, 2349 (1990); (*b*) T. D. Newbound, M. R. Colsman, M. M. Miller, G. P. Wulfsberg, O. P. Anderson, and S. H. Strauss. J. Am. Chem. Soc. **111**, 3762 (1989); (*c*) M. R. Colsman, M. D. Noirot, M. M. Miller, O. P. Anderson, and S. H. Strauss. J. Am. Chem. Soc. **110**, 6886 (1989).
8. M. Brown and J. M. Waters. J. Am. Chem. Soc. **112**, 2442 (1990).

[8]Abbreviations: s, strong; m, medium; w, weak; bd, broad; sp, sharp.

[9]For the *gauche* conformer of 1,2-dichloroethane, the symmetric and antisymmetric C—Cl stretching frequencies are 676 and 654 cm^{-1}, respectively (29).

Can. J. Chem. Downloaded from www.nrcresearchpress.com by 92.62.229.171 on 09/08/12
For personal use only.

9. H. Kropshofer, O. Leitzke, P. Peringer, and F. Sladky. Chem. Ber. **114**, 2644 (1981).
10. D. F. Shriver and M. A. Drezdzon. The manipulation of air-sensitive compounds. Wiley–Interscience, New York. 1986.
11. M. Clark and J. S. Thrasher. J. Chem. Educ. **67**, 235 (1990).
12. International tables for X-ray crystallography. Vol. IV. Kynoch Press, Birmingham, England. 1974.
13. R. C. Weast (*Editor*). Handbook of chemistry and physics. 54st ed. CRC Press, Cleveland, Ohio. 1974. p. E-54.
14. (*a*) T. B. McMahon, T. Heinis, G. Nicol, J. K. Hovey, and P. Kebarle. J. Am. Chem. Soc. **110**, 7591 (1988); (*b*) S. F. Smith, J. Chandrasekhar, and W. L. Jorgensen. J. Phys. Chem. **86**, 3308 (1982); (*c*) R. H. Staley and J. L. Beauchamp. J. Am. Chem. Soc. **97**, 5920 (1975).
15. W. Beck and W. Schloter. Z. Naturforsch. B: Anorg. Chem. Org. Chem. **33**, 1214 (1978).
16. (*a*) J. M. Fernandez and J. A. Gladysz. Organometallics, **8**, 207 (1989); (*b*) C. H. Winter and J. A. Gladysz. J. Organomet. Chem. **354**, C33 (1988).
17. R. J. Kulawiec and R. H. Crabtree. Coord. Chem. Rev. **99**, 89 (1990).
18. A. Bondi. J. Phys. Chem. **68**, 441 (1964).
19. L. Pauling. The nature of the chemical bond. Cornell University Press, Ithaca, N.Y. 1960. p. 257.
20. L. G. Schulz. Acta Crystallogr. **4**, 487 (1951).
21. F. A. Cotton and G. Wilkinson. Advanced inorganic chemistry. 5th ed. Wiley–Interscience, New York. 1988. pp. 53–56.
22. N. W. Alcock. Adv. Inorg. Chem. Radiochem. **15**, 1 (1972).
23. N. W. Alcock and H. D. B. Jenkins. J. Chem. Soc. Dalton Trans. 1907 (1974).
24. K. Wieghardt, M. Kleine-Boymann, B. Nuber and J. Weiss. Inorg. Chem. **25**, 1309 (1986).
25. T. B. Reed and W. N. Lipscomb. Acta Crystallogr. **6**, 45 (1953).
26. T. Chivers, J. F. Richardson, and N. R. M. Smith. Inorg. Chem. **24**, 2453 (1985).
27. K. Shelly, T. Bartczak, W. R. Scheidt, and C. A. Reed. Inorg. Chem. **24**, 4325 (1985).
28. W. H. Hersh. J. Am. Chem. Soc. **107**, 4599 (1985).
29. S. Mizushima. Structure of molecules and internal rotation. Academic Press, New York. 1954. p. 222.

Can. J. Chem. Downloaded from www.nrcresearchpress.com by 92.62.229.171 on 09/08/12
For personal use only.

Structure and magnetic properties of monophenylphosphinate bridged chain polymers of manganese(II), $[ML_2(HPhPO_2)_2]_x$ (where L = $HPhPO_2H$, CH_3CONH_2, H_2O, $HCONH(CH_3)$, and C_5H_5N)

JING-LONG DU, STEVEN J. RETTIG, ROBERT C. THOMPSON,[1] AND JAMES TROTTER
Department of Chemistry, University of British Columbia, 2036 Main Mall, Vancouver, B.C. Canada V6T 1Z1

AND

PETER BETZ AND AVI BINO
Department of Inorganic and Analytical Chemistry, The Hebrew University of Jerusalem, 91904 Jerusalem, Israel

Received July 3, 1991

This paper is dedicated to the memory of Professor Thomas Birchall

JING-LONG DU, STEVEN J. RETTIG, ROBERT C. THOMPSON, JAMES TROTTER, PETER BETZ, and AVI BINO. Can. J. Chem. **70**, 732 (1992).

Crystals of $Mn(CH_3CONH_2)_2(HPhPO_2)_2$ are monoclinic, a = 5.668(2), b = 7.500(2), c = 23.104(2) Å, β = 95.52(2)°, Z = 2, space group $P2_1/c$, and those of $Mn(HPhPO_2H)_2(HPhPO_2)_2$ are monoclinic, a = 23.281(1), b = 5.508(2), c = 20.5489(6) Å, β = 90.424(4)°, Z = 4, space group $C2/c$. The structures were solved by heavy-atom methods and were refined by full-matrix least-squares procedures to R = 0.028 and 0.035 for 2081 and 2117 reflections with $I \geq 3\sigma(I)$, respectively. Both compounds have structures consisting of polymeric chains propagating along the crystallographic b axis; two phosphinate ligands bridge adjacent manganese atoms forming square planar MO_4 units, and six coordination about the metal is achieved by axially O-bonded neutral ligands. Indirect evidence supports similar structures for the other complexes studied here. The complexes are antiferromagnetic and the magnetic susceptibilities have been analyzed according to two Heisenberg models for linear chains. The exchange coupling constants range from -0.30 cm^{-1} for the acetamide complex to -0.06 cm^{-1} for the pyridine complex. Magnetostructural correlations involving these complexes and the previously studied $Mn(HCONH_2)_2(HPhPO_2)_2$, reveal that the magnitude of the magnetic coupling is enhanced by symmetrically bridging O—P—O units and short Mn–O–P–O–Mn pathways for exchange.

Key words: polymeric manganese monophenylphosphinates, crystal structures, magnetic properties.

JING-LONG DU, STEVEN J. RETTIG, ROBERT C. THOMPSON, JAMES TROTTER, PETER BETZ et AVI BINO. Can. J. Chem. **70**, 732 (1992).

Les cristaux de $Mn(CH_3CONH_2)_2(HPhPO_2)_2$ sont monocliniques, groupe d'espace $P2_1/c$, avec a = 5,668(2); b = 7,500(2) et c = 23,104(2) Å, β = 95,52(2)° et Z = 4 alors que ceux de $Mn(HPhPO_2H)_2(HPhPO_2)_2$ sont monocliniques, groupe d'espace $C2/c$, avec a = 23,281(1); b = 5,508(2) et c = 20,5489(6) Å, β = 90,424(2)° et Z = 4. On a résolu les structures par les méthodes des atomes lourds et on les a affinées par la méthode des moindres carrés jusqu'à des valeurs de R = 0,028 et 0,035, respectivement pour 2081 et 2117 réflexions avec $I \geq 3\sigma(I)$. Les deux composés possèdent des structures formées de chaînes de polymères se propageant le long de l'axe cristallographique b; deux coordinats phosphinates établissent des ponts avec les atomes de manganèse adjacents et forment des unités MO_4 plan carré; l'hexacoordination autour du métal est obtenue par des coordinats neutres liés d'une façon axiale par le biais d'oxygènes. Des données indirectes suggèrent des structures semblables pour les autres complexes étudiés ici. Les complexes sont antiferromagnétiques et on a analysé les susceptibilités magnétiques selon deux modèles de Heisenberg pour des chaînes linéaires. Les constantes de couplage d'échange varient de $-0,30$ cm^{-1} pour le complexe de l'acétamide à $-0,06$ cm^{-1} pour le complexe de la pyridine. Des corrélations magnétostructurales impliquant ces complexes et le $Mn(HCONH_2)_2(HPhPO_2)_2$ étudié antérieurement révèlent que l'amplitude du couplage magnétique est rehaussé par la présence d'unités O—P—O formant des ponts symétriques et par de courts chemins Mn–O–P–O–Mn pour les échanges.

Mots clés : monophénylphosphinates de manganèse polymériques; structures cristallines; propriétés magnétiques.
[Traduit par la rédaction]

Introduction

Several single crystal X-ray structure determinations have revealed that the structures adopted by binary metal phosphinates, $M(R_2PO_2)_2$, involve metal ions linked in chains by double phosphinate bridges with MO_4 chromophores ranging from square planar (1) through distorted tetrahedral (2–5) to close to regular tetrahedral (6, 7) geometries, the particular structure adopted depending on both the metal and the composition of the phosphinate ligand. Compounds of composition $ML_2(R_2PO_2)_2$ in which metal ions are linked in chains by double phosphinate bridges forming square planar MO_4 chromophores with axially coordinated L groups are also known (8, 9). The three atom O–P–O bridges in these polymeric materials have been shown to be capable of transmitting magnetic exchange effects and our interest in these compounds has been in investigating how both the sign (antiferromagnetic or ferromagnetic) and magnitude of the exchange is affected by structural changes (10, 11).

We reported, earlier, studies on the formamide complex of manganese(II) monophenylphosphinate, $Mn(HCONH_2)_2(HPhPO_2)_2$, **1** (9). The compound has the double phosphinate bridged chain structure with axially coordinated formamide ligands and exhibits antiferromagnetic coupling between metal centres. With a view to examining how the nature of L, in complexes of the type $ML_2(HPhPO_2)_2$, affects the magnetic coupling we have, in the present work, synthesized and characterized five related complexes where L = CH_3CONH_2 (**2**), $HPhPO_2H$ (**3**), $HCONH(CH_3)$ (**4**), H_2O (**5**), and C_5H_5N (**6**). Compounds **2** and **3** were obtained in crystalline forms suitable for single crystal X-ray diffrac-

[1]Author to whom correspondence should be addressed.

Can. J. Chem. Downloaded from www.nrcresearchpress.com by 92.62.229.171 on 09/08/12
For personal use only.

tion studies and the results of these are reported here. Magnetic susceptibility, infrared spectroscopic, and differential thermal analysis studies are reported on all five compounds.

Experimental

Syntheses

Poly-bis(acetamide)bis(μ-monophenylphosphinato)manganese(II), $Mn(CH_3CONH_2)_2[H(C_6H_5)PO_2]_2$, 2

Manganese(II) chloride tetrahydrate (0.501 g) was dissolved in 40 mL of acetone and the solution was added to a solution prepared by dissolving acetamide (1.82 g) and monophenylphosphinic acid (0.712 g) in 50 mL of acetone. Colorless crystals were collected by filtration, washed with acetone, and air-dried. Anal. calcd. for $MnC_{16}H_{22}O_6N_2P_2$: C 42.21, H 4.87, N 6.15; found: C 42.30, H 4.89, N 6.10.

Poly-bis(monophenylphosphinic acid)bis(μ-monophenylphosphinato)manganese(II), $Mn[H(C_6H_5)PO_2H]_2[H(C_6H_5)PO_2]_2$, 3

Monophenylphosphinic acid (3.13 g) was partially neutralized with sodium hydroxide (0.179 g) in 70 mL of distilled water. The resulting solution was added dropwise to a manganese salt solution prepared by dissolving manganese(II) perchlorate hexahydrate (1.62 g) in 10 mL of distilled water. The resulting solution became cloudy after stirring for about 40 min. The stirring of the solution was continued for ~18 h. The product was collected by filtration, washed with distilled water, and air-dried. Anal. calcd. for $MnC_{24}H_{26}O_8P_4$: C 46.40, H 4.22; found: C 46.48, H 4.25. Single crystals suitable for X-ray diffraction studies were obtained from the above reaction by slow evaporation of a solution in which reagent concentrations were about half those specified above.

Bis(N-methylformamide)bis(monophenylphosphinato)manganese(II), $Mn(HCONHCH_3)_2[H(C_6H_5)PO_2]_2$, 4

Manganese(II) monophenylphosphinate (~1.0 g) prepared as described previously (12), was dissolved in 20 mL of *N*-methylformamide. A white powder was obtained after the solvent was removed under vacuum. The powder was washed with acetone, then left to air-dry. Anal. calcd. for $MnC_{16}H_{22}O_6N_2P_2$: C 42.21, H 4.87, N 6.15; found: C 41.95, H 4.90, N 6.05.

Diaquobis(monophenylphosphinato)manganese(II), $Mn(H_2O)_2[H(C_6H_5)PO_2]_2$, 5

Monophenylphosphinic acid (2.84 g) was neutralized with potassium carbonate (1.39 g) in 50 mL of aqueous methanol solution (50:50 by volume). Manganese(II) sulfate monohydrate (1.69 g) was dissolved in 50 mL distilled water, then added dropwise to the stirring monophenylphosphinate solution. The white precipitate that formed was isolated by filtration, washed with aqueous methanol, and then air-dried. Anal. calcd. for $MnC_{12}H_{16}O_6P_2$: C 38.63, H 4.32; found: C 38.55, H 4.30.

Bis(pyridine)bis(monophenylphospinato)manganese(II), $Mn(C_5H_5N)_2[H(C_6H_5)PO_2]_2$, 6

Manganese(II) monophenylphosphinate (~1.0 g) was mixed with 40 mL of pyridine and 10 mL of 2,2-dimethoxypropane. The mixture was refluxed for 8 h, then a white powder was isolated by filtration, washed with a small portion of diethyl ether, and then dried under vacuum at room temperature for about 2 h. Anal. calcd. for $MnC_{22}H_{22}O_4N_2P_2$: C 53.34, H 4.48, N 5.66; found: C 52.54, H 4.42, N 5.31. This compound appears to contain a small amount of lattice water (approximately 0.5 mol) as evidenced by the microanalysis and the presence of a weak band centered around 3300 cm^{-1} in the infrared spectrum. Repeated syntheses always gave lattice water and attempts to remove it by heating led to the simultaneous dissociation of pyridine.

Experimental techniques

Infrared spectra (4000–250 cm^{-1}) were obtained on samples mulled in Nujol and pressed between KRS-5 plates (Harshaw Chemical Co.) using a Perkin–Elmer model 598 spectrophotometer. Frequencies are considered accurate to within ±3 cm^{-1}. Differential scanning calorimetry (DSC), measurements were made with a Mettler DSC 20 cell and a Mettler TC 10 TA processor operating over the temperature range 35–400°C. Some thermogravimetric analysis information was obtained by weighing the aluminum crucible containing the sample prior to and following a thermal event (accuracy ~±5%). Magnetic susceptibilities from ~80 to ~2 K were measured using a PAR model 155 vibrating sample magnetometer as described previously (5). Measurements were made at a field of 7501 G. The diamagnetic corrections used were (in 10^{-6} cm^3 mol^{-1}): Mn^{2+}, −14; $(C_6H_5)(H)PO_2^-$, −78; $HCONHCH_3$, −26; CH_3CONH_2, −26; H_2O, −12; C_5H_5N, −49; $H(C_6H_5)PO_2H$, −78.

X-ray crystallographic analyses of $Mn(CH_3CONH_2)_2[H(C_6H_5)PO_2]_2$, 2, and $Mn[H(C_6H_5)PO_2H]_2[H(C_6H_5)PO_2]_2$, 3

Crystallographic data for $Mn(CH_3CONH_2)_2[H(C_6H_5)PO_2]_2$ and $Mn[H(C_6H_5)PO_2H]_2[H(C_6H_5)PO_2]_2$ appear in Table 1. The final unit-cell parameters were obtained by least squares on the setting angles for 25 reflections with $2\theta = 29.6°–39.9°$ and 99.6°–118.8°, respectively. The intensities of three standard reflections, measured every 200 reflections throughout the data collections, showed only small random variations. The data were processed[2] and corrected for Lorentz and polarization effects, decay, and absorption (empirical, based on azimuthal scans for four reflections).

The structure analysis of $Mn[H(C_6H_5)PO_2H]_2[H(C_6H_5)PO_2]_2$ was initiated in the centrosymmetric space group $C2/c$ on the basis of the *E*-statistics and the appearance of the Patterson function, this choice being confirmed by the subsequent successful solution and refinement of the structure. Both structures were solved by heavy-atom methods, the coordinates of the Mn and P atoms being determined from the Patterson functions and those of the remaining non-hydrogen atoms from subsequent difference Fourier syntheses. All non-hydrogen atoms of both complexes were refined with anisotropic thermal parameters. All hydrogen atoms of $Mn(CH_3CONH_2)_2[H(C_6H_5)PO_2]_2$ were refined with isotropic thermal parameters and for $Mn[H(C_6H_5)PO_2H]_2[H(C_6H_5)PO_2]_2$ the phosphorus- and oxygen-bound hydrogen atoms were refined with isotropic thermal parameters and the remaining hydrogen atoms were fixed in idealized positions (C—H = 0.98 Å, $B_H = 1.2\ B_{\text{bonded atom}}$). A correction for secondary extinction was applied for $Mn[H(C_6H_5)PO_2H]_2[H(C_6H_5)PO_2]_2$, the final value of the extinction coefficient being 1.10×10^{-6}. Neutral atom scattering factors and anomalous dispersion corrections for the non-hydrogen atoms were taken from the *International Tables for X-Ray Crystallography* (13). Final atomic coordinates and equivalent isotropic thermal parameters, selected bond lengths, and selected bond angles appear in Tables 2–4, respectively. Hydrogen atom parameters, anisotropic thermal parameters, complete tables of bond lengths and bond angles, torsion angles, intermolecular contacts, least-squares planes, and measured and calculated structure factor amplitudes are included as supplementary material.[3]

[2]TEXSAN/TEXRAY structure analysis package (Molecular Structure Corp., 1985), which includes versions of the following: DIRDIF, direct methods for difference structures, by P. T. Beurskens; ORFLS, full-matrix least-squares, and ORFFE, function and errors, by W. R. Busing, K. O. Martin, and H. A. Levy; ORTEP II, illustrations, by C. K. Johnson.

[3]Supplementary material mentioned in the text may be purchased from the Depository of Unpublished Data, Document Delivery, CISTI, National Research Council Canada, Ottawa, Canada K1A 0S2.

Tables of hydrogen atom parameters and bond lengths and angles have also been deposited with the Cambridge Crystallographic Data Centre and can be obtained on request from The Director, Cambridge Crystallographic Data Centre, University Chemical Laboratory, Lensfield Road, Cambridge CB2 1EW, U.K.

Can. J. Chem. Downloaded from www.nrcresearchpress.com by 92.62.229.171 on 09/08/12
For personal use only.

TABLE 1. Crystallographic data*

Compound	$Mn(CH_3CONH_2)_2(HPhPO_2)_2$, **2**	$Mn(HPhPO_2H)_2(HPhPO_2)_2$, **3**
Formula	$C_{16}H_{22}MnN_2O_6P_2$	$C_{24}H_{26}MnO_8P_4$
fw	455.25	621.30
Color, habit	Colorless, prism	Colorless, prism
Crystal size, mm	0.08×0.25×0.40	0.10×0.15×0.20
Crystal system	Monoclinic	Monoclinic
Space group	$P2_1/c$	$C2/c$
a, Å	5.668(2)	23.281(1)
b, Å	7.500(2)	5.508(2)
c, Å	23.104(2)	20.5489(6)
β°	95.52(2)	90.424(4)
V, Å^3	977.4(3)	2635.2(7)
Z	2	4
ρ_{calc}, g/cm^3	1.547	1.255
$F(000)$	470	1276
Radiation	Mo	Cu
μ, cm^{-1}	8.43	68.51
Transmission factors	0.86–1.00	0.80–1.00
Scan type	ω–2θ	ω–2θ
Scan range, deg in ω	1.21+0.35 tan θ	1.10+0.30 tan θ
Scan rate, deg/min	32	16
Data collected	$+h$, $+k$, $\pm l$	$+h$, $+k$, $\pm l$
$2\theta_{max}$, deg	60	155
Crystal decay	Negligible	Negligible
Total reflections	3321	3122
Unique reflections	3043	3042
R_{merge}	0.037	0.018
Reflections with $I \geq 3\sigma(I)$	2081	2117
No. of variables	168	182
R	0.028	0.035
R_w	0.035	0.045
gof	1.20	1.90
Max Δ/σ (final cycle)	0.02	0.04
Residual density e/Å^3	−0.27 to +0.29	−0.39 to +0.30

*Temperature 294 K, Rigaku AFC6S diffractometer, Mo-K_α radiation (λ = 0.71069 Å) or Cu-K_α radiation (λ = 1.54178 Å), graphite monochromator, takeoff angle 6.0°, aperture 6.0 × 6.0 mm at a distance of 285 mm from the crystal, stationary background counts at each end of the scan (scan/background time ratio 2:1, up to 8 rescans), $\sigma^2(F^2) = [S^2(C + 4B) + (0.03F^2)^2]/Lp^2$ (S = scan rate, C = scan count, B = normalized background count), function minimized $\Sigma w(|F_o| - |F_c|)^2$ where $w = 4F_o^2/\sigma^2(F_o^2)$, $R = \Sigma||F_o| - |F_c||/\Sigma|F_o|$, $R_w = (\Sigma w(|F_o| - |F_c|)^2/\Sigma w|F_o|^2)^{1/2}$, and $gof = [\Sigma w(|F_o| - |F_c|)^2/(m - n)]^{1/2}$. Values given for R, R_w, and *gof* are based on those reflections with $I \geq 3\sigma(I)$.

Results and discussion

Structural studies

Crystals of the acetamide complex **2** are isomorphous with those of the previously studied (9) formamide derivative **1**, both belonging to the monoclinic crystal system and space group $P2_1/c$. Crystals of the monophenylphosphinic acid complex **3** are also monoclinic, space group $C2/c$. All three compounds have structures consisting of polymeric chains propagating along the crystallographic b axis; two phosphinate ligands bridge adjacent manganese atoms forming square planar MO_4 units. Six-coordination about the metal is achieved by axially *O*-bonded neutral ligands. Figures 1 and 2 show the structures of **2** and **3**, respectively and give the atom numbering schemes. Stereoscopic views of sections of the polymeric chains of **2** and **3** are shown in Figs. 3 and 4.

Both amide hydrogens in **2** are involved in hydrogen bonding. The interchain N—H(2)···O(1)($1 - x$, $-y$, $1 - z$) interaction gives H(2)···O(1) and N···O(1) distances of 2.11(3) and 3.074(2) Å, respectively, with an N—H(2)···O(1) bond angle of 173(2)°. The intrachain N—H(3)···O(2)($1 + x$, y, z) hydrogen bond gives H(3)···O(2) and N···O(2) distances of 2.23(2) and 2.982(2) Å, respectively, and an N—H(3)···O(2) bond angle of 152(2)°. Inter- and intrachain hydrogen bonding like that described here was reported previously for **1** where both N···O(1) and N···O(2) distances are given as ~2.9 Å (9). There is no interchain hydrogen bonding in **3**; however, this compound has strong intrachain hydrogen bonding involving O(4)—H(3)···O(2) resulting in H(3)···O(2) and O(4)···O(2) distances of 1.62(5) and 2.555(3) Å, respectively, and an O(4)—H(3)···O(2) bond angle of 175(5)°.

The coordination around manganese in **2** and **3** is approximately octahedral with O—Mn—O bond angles ranging from 87.89(5)° to 92.11(5)° in **2** and from 85.67(7)° to 94.32(7)° in **3**. The Mn—O(3) distances involving the terminal ligands are approximately the same in **2** and **3** (2.182(1) and 2.175(2) Å) and are significantly shorter than the corresponding distance in **1** (2.241(3) Å) (9). As in the case of **1** (9), there are two Mn—O distances involving the bridging phosphinate groups in **2** and **3**. The average Mn—O(bridging) distance is the same in **2** and **3** (2.203(1) and 2.204(2) Å) and is significantly greater than the corresponding average distance in **1** (2.175(3) Å) (9). It would

Can. J. Chem. Downloaded from www.nrcresearchpress.com by 92.62.229.171 on 09/08/12
For personal use only.

TABLE 2. Final atomic coordinates (fractional) and B_{eq} (Å^2)[a]

Atom	x	y	z	B_{eq}
		2		
Mn	1/2	1/2	1/2	1.46(1)
P	−0.01495(7)	0.41447(5)	0.42702(2)	1.51(1)
O(1)	0.2292(2)	0.3417(2)	0.44544(6)	1.99(4)
O(2)	−0.2096(2)	0.3624(2)	0.46411(5)	1.89(4)
O(3)	0.4996(2)	0.3006(2)	0.56875(6)	2.62(5)
N	0.7200(3)	0.0658(3)	0.54666(9)	2.98(7)
C(1)	−0.1025(3)	0.3505(2)	0.35282(7)	1.77(6)
C(2)	−0.3257(3)	0.3981(3)	0.32688(8)	2.41(7)
C(3)	−0.3969(4)	0.3498(3)	0.27000(9)	2.91(8)
C(4)	−0.2461(4)	0.2532(3)	0.2386(1)	3.09(8)
C(5)	−0.0258(4)	0.2050(3)	0.2636(1)	3.5(1)
C(6)	0.0469(4)	0.2533(3)	0.32030(9)	2.75(7)
C(7)	0.5469(3)	0.1395(2)	0.57309(8)	2.15(6)
C(8)	0.4081(5)	0.0209(3)	0.6090(1)	3.6(1)
		3		
Mn	1/4	3/4	1/2	1.97(2)
P(1)	0.22827(3)	0.2619(1)	0.40480(3)	2.04(3)
P(2)	0.11822(3)	0.5352(1)	0.52320(3)	2.54(3)
O(1)	0.21788(9)	0.5230(3)	0.42181(9)	2.61(8)
O(2)	0.20834(8)	0.0775(3)	0.45508(8)	2.33(7)
O(3)	0.16899(8)	0.6720(4)	0.5477(1)	2.75(8)
O(4)	0.1246(1)	0.2558(4)	0.5189(1)	3.5(1)
C(1)	0.1945(1)	0.1915(5)	0.3282(1)	2.1(1)
C(2)	0.2000(1)	0.3532(6)	0.2764(1)	2.8(1)
C(3)	0.1752(1)	0.3033(6)	0.2166(1)	3.4(1)
C(4)	0.1445(1)	0.0918(6)	0.2080(2)	3.6(1)
C(5)	0.1386(1)	−0.0702(6)	0.2587(2)	3.3(1)
C(6)	0.1639(1)	−0.0226(5)	0.3190(1)	2.8(1)
C(7)	0.0568(1)	0.5709(6)	0.5739(1)	2.7(1)
C(8)	0.0230(2)	0.7745(7)	0.5682(2)	4.6(2)
C(9)	−0.0242(2)	0.8028(2)	0.6089(2)	5.6(2)
C(10)	−0.0373(2)	0.6353(9)	0.6540(2)	5.0(2)
C(11)	−0.0044(2)	0.433(1)	0.6592(2)	6.3(2)
C(12)	0.0424(2)	0.3999(8)	0.6195(2)	5.2(2)

[a] $B_{eq} = (8/3)\pi^2\Sigma\Sigma U_{ij}a_i^*a_j^*(a_i \cdot a_j)$.

TABLE 3. Bond lengths (Å) with estimated standard deviations

Atom	Atom	Distance	Atom	Atom	Distance
		2			
Mn	O(2)′	2.174(1)	C(1)	C(6)	1.391(3)
Mn	O(3)	2.182(1)	C(1)	C(2)	1.394(2)
Mn	O(1)	2.232(1)	C(2)	C(3)	1.386(3)
P	O(1)	1.510(1)	C(3)	C(4)	1.378(3)
P	O(2)	1.512(1)	C(4)	C(5)	1.372(3)
P	C(1)	1.803(2)	C(5)	C(6)	1.384(3)
O(3)	C(7)	1.240(2)	C(7)	C(8)	1.491(3)
N	C(7)	1.325(3)			
		3			
Mn	O(1)	2.165(2)	C(2)	C(3)	1.382(4)
Mn	O(3)	2.175(2)	C(3)	C(4)	1.377(5)
Mn	O(2)′	2.243(2)	C(4)	C(5)	1.378(5)
P(1)	O(1)	1.500(2)	C(5)	C(6)	1.394(4)
P(1)	O(2)	1.524(2)	C(7)	C(12)	1.372(5)
P(1)	C(1)	1.798(3)	C(7)	C(8)	1.374(4)
P(2)	O(3)	1.487(2)	C(8)	C(9)	1.394(5)
P(2)	O(4)	1.549(2)	C(9)	C(10)	1.345(6)
P(2)	C(7)	1.787(3)	C(10)	C(11)	1.358(6)
C(1)	C(6)	1.389(4)	C(11)	C(12)	1.377(5)
C(1)	C(2)	1.394(4)			

NOTE: The prime refers to the symmetry operation $1 + x, y, z$ for **2** and $x, 1 + y, z$ for **3**.

appear that the weaker manganese-terminal ligand interaction in **1** compared with that in **2** and **3** has resulted in stronger manganese-bridging phosphinate interactions. This has a significant effect on the magnetic properties of these compounds as will be described later.

Consideration of the internal bond parameters of the bridging phosphinate groups in **2** and **3** reveals relatively little difference in bond angles but significant differences in P—O bond distances. While the average P—O bond distance is the same in **2** and **3** (1.511(1) and 1.512(2) Å, respectively) and comparable with that reported for **1** (1.515(4) Å)[4] (9), the O—P—O group is symmetrical in **2** (as is the case for **1**) but asymmetrical in **3** (Δ P–O = 0.024(4) Å). This asymmetry in the bridging O—P—O unit is undoubtedly a consequence of hydrogen-bonding interactions. In **3**, only one of the oxygens (O(2)) is involved in hydrogen-bonding interactions (intrachain). As a result the P—O(2) bond is significantly longer than the P—O(1) bond in this compound. In both **1** and **2** the two phosphinate oxygens are both involved in hydrogen-bonding interactions (O(1) in interchain interactions and O(2) in intrachain interactions) resulting in symmetrical O—P—O groups. This, we believe, also has a significant effect on the magnetic properties of these compounds (see below).

Attempts to obtain **4**, **5** and **6** in crystalline form suitable for single crystal X-ray diffraction studies were unsuccessful and hence our conclusions concerning the structures of these compounds are based on indirect evidence only. These compounds are stoichiometrically equivalent to **1**, **2** and **3** and their properties, to be described here, are at least consistent with their having similar structures in which manganese ions are linked in chains by double phosphinate bridges and different neutral ligands occupy the axial positions. All six of the compounds under consideration here dissolve in water (where dipolar and hydrogen bonding interactions with the solvent likely break up the phosphinate bridged chains) but are insoluble in a wide range of organic solvents including ethanol, chloroform, benzene, carbon tetrachloride, and dichloromethane. Their thermal properties are also very similar. Differential scanning calorimetry studies show that while **1** exhibits loss of formamide in two steps at ~140 and 190°C, the other compounds show loss of both neutral ligands in a single step at 130°C for **2**, **4**, and **5**, at 140°C for **3** and at 123°C for **6**. Compound **6** contains a small amount of lattice water (see experimental section), which appears to be removed along with the pyridine ligands at 123°C. No other thermal events are seen for any of the compounds up to the onset of exothermic decomposition which occurs in the 220–240°C range.

Selected bands in the infrared spectra are given in Table 5. Of the six complexes, five show two bands assigned to the antisymmetric and symmetric PO_2 stretching vibrations of a bridging phosphinate group. The presence of both neutral monophenylphosphinic acid and anionic monophenylphosphinate ligands in **3** accounts for the multiplicity of bands in

[4]Bond lengths and angles for **1** not reported in ref. 9 are calculated using the positional parameters reported earlier (9).

Can. J. Chem. Downloaded from www.nrcresearchpress.com by 92.62.229.171 on 09/08/12
For personal use only.

TABLE 4. Bond angles (deg) with estimated standard deviations[a]

Atom	Atom	Atom	Angle	Atom	Atom	Atom	Angle
			2				
O(2)′	Mn	O(2)″	180.00	P	O(2)	Mn#	135.58(7)
O(2)′	Mn	O(3)	90.35(5)	C(7)	O(3)	Mn	135.4(1)
O(2)′	Mn	O(3)*	89.65(5)	C(6)	C(1)	C(2)	118.5(2)
O(2)′	Mn	O(1)	92.11(5)	C(6)	C(1)	P	121.8(1)
O(2)′	Mn	O(1)*	87.89(5)	C(2)	C(1)	P	119.7(1)
O(3)	Mn	O(3)*	180.00	C(3)	C(2)	C(1)	120.7(2)
O(3)	Mn	O(1)	89.88(5)	C(4)	C(3)	C(2)	119.8(2)
O(3)*	Mn	O(1)	90.12(5)	C(5)	C(4)	C(3)	120.2(2)
O(1)	Mn	O(1)*	180.00	C(4)	C(5)	C(6)	120.3(2)
O(1)	P	O(2)	116.47(7)	C(5)	C(6)	C(1)	120.5(2)
O(1)	P	C(1)	109.43(8)	O(3)	C(7)	N	122.2(2)
O(2)	P	C(1)	108.74(7)	O(3)	C(7)	C(8)	120.3(2)
P	O(1)	Mn	121.92(7)	N	C(7)	C(8)	117.5(2)
			3				
O(1)	Mn	O(1)″	180.00	P(2)	O(3)	Mn	129.6(1)
O(1)	Mn	O(3)	85.68(7)	C(6)	C(1)	C(2)	119.3(2)
O(1)	Mn	O(3)″	94.32(7)	C(6)	C(1)	P(1)	121.5(2)
O(1)	Mn	O(2)′	90.75(7)	C(2)	C(1)	P(1)	119.2(2)
O(1)	Mn	O(2)*	89.25(7)	C(3)	C(2)	C(1)	120.7(3)
O(3)	Mn	O(3)″	180.00	C(4)	C(3)	C(2)	119.7(3)
O(3)	Mn	O(2)′	88.32(7)	C(3)	C(4)	C(5)	120.4(3)
O(3)	Mn	O(2)*	91.68(7)	C(4)	C(5)	C(6)	120.4(3)
O(2)′	Mn	O(2)*	180.00	C(1)	C(6)	C(5)	119.5(3)
O(1)	P(1)	O(2)	115.5(1)	C(12)	C(7)	C(8)	118.4(3)
O(1)	P(1)	C(1)	109.9(1)	C(12)	C(7)	P(2)	121.5(3)
O(2)	P(1)	C(1)	108.4(1)	C(8)	C(7)	P(2)	120.0(3)
O(3)	P(2)	O(4)	116.5(1)	C(7)	C(8)	C(9)	119.6(3)
O(3)	P(2)	C(7)	112.6(1)	C(10)	C(9)	C(8)	121.4(4)
O(4)	P(2)	C(7)	102.7(1)	C(9)	C(10)	C(11)	119.2(3)
P(1)	O(1)	Mn	132.2(1)	C(10)	C(11)	C(12)	120.6(4)
P(1)	O(2)	Mn#	133.0(1)	C(7)	C(12)	C(11)	120.8(4)

[a]NOTE: ′, ″, *, and # refer to the symmetry operations: $1 + x, y, z$; $-x, 1 - y, 1 - z$; $1 - x, 1 - y, 1 - z$; and $x - 1, y, z$; respectively, for **2** and $x, 1 + y, z$; $1/2 - x, 3/2 - y, 1 - z$; $1/2 - x, 1/2 - y, 1 - z$; and $x, y - 1, z$ for **3**.

the PO_2 stretching region for this compound. The similarity in the PO_2 stretching frequencies observed for **1** and **2** is consistent with the nearly identical PO_2 bond parameters for these two compounds; the corresponding bands are shifted to higher frequencies in **4**, **5**, and **6**. It has been suggested that the frequency separation between the two PO_2 stretching vibrations in metal phosphinates provides a measure of the equivalence of the two P—O bonds (10). In **1** and **2** the structure determinations show the P—O bonds to be virtually equivalent and for these compounds the frequency separations are 84 and 89 cm^{-1}, respectively. The much higher separations of 114 and 122 cm^{-1} observed for **4** and **6** may reflect the presence of unsymmetrical O—P—O bridging units in these compounds. In the case of **4** this might be expected since the $HCONHCH_3$ ligand, like the $H(C_6H_5)PO_2H$ ligand in **3**, should be involved in intrachain hydrogen bonding only, resulting in nonequivalent P—O bonds as discussed above for **3**. Employing this criterion, the frequency separation of 84 cm^{-1} in **5** suggests equivalent P—O bonds in this compound.

All compounds except **3** and **6** exhibit one band over the frequency range 2360–2400 cm^{-1} assigned to the P—H stretching vibration. The pyridine complex, **6**, is somewhat unique in this regard in that the P—H band is split and shifted to lower frequencies (2310, 2280 cm^{-1}). The band splitting may reflect the presence of two structurally inequivalent phosphinate groups in this compound while the shift to lower frequency may reflect more weakly coordinated phosphinate ligands. Consistent with the latter suggestion is the fact that **6** exhibits the highest frequency antisymmetric and symmetric PO_2 stretching frequencies of the six compounds under consideration here (Table 5). That pyridine is in fact coordinated in **6** is evidenced by the fact that the 6a and 16b bands (in the notation of Kline and Turkevich (14)), which occur at 601 and 403 cm^{-1}, respectively, in the free base, are seen to exhibit their characteristic shift to higher frequencies upon coordination (15). The observation of two bands in the ν(PH) region for **3** is not unexpected owing to the presence of both neutral monophenylphosphinic acid and bridging phosphinate groups. Bands in the 3100–3400 cm^{-1} region corresponding to ν(NH) vibrations for **1**, **2**, and **4** and ν(OH) for **3** and **5** are very broad, consistent with the presence of strong hydrogen-bonding interactions. The ν(CO) vibrations are at lower

Can. J. Chem. Downloaded from www.nrcresearchpress.com by 92.62.229.171 on 09/08/12
For personal use only.

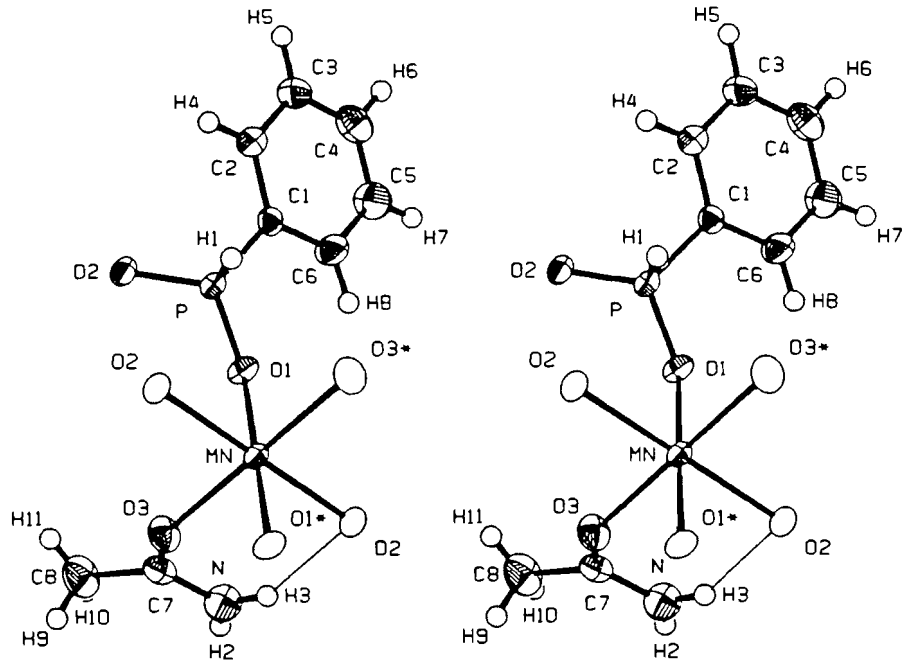

FIG. 1. Stereoscopic view of $Mn(CH_3CONH_2)_2[H(C_6H_5)PO_2]_2$, **2**, showing atom labelling and the coordination about Mn; 50% probability thermal ellipsoids are shown for the non-hydrogen atoms.

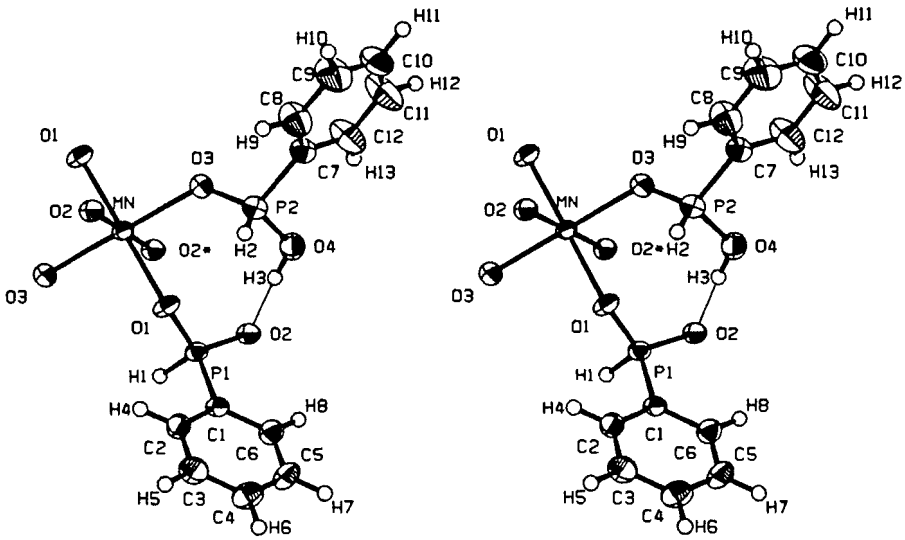

FIG. 2. Stereoscopic view of $Mn[H(C_6H_5)PO_2H]_2[H(C_6H_5)PO_2]_2$, **3** showing atom labelling and the coordination about Mn; 50% probability thermal ellipsoids are shown for the non-hydrogen atoms.

frequencies in **2** and **4** compared with ν(CO) in **1** and this may reflect stronger binding to manganese in **2** and **4**. This is confirmed by the X-ray diffraction results in the case of **1** and **2**.

Magnetic studies

Magnetic susceptibility and magnetic moment data for complexes **2** through **6** are deposited. (see footnote 3) Data for **1** were given previously (9). Plots of magnetic moment versus temperature are given in Fig. 5. The $^6A_{1g}$ ground state for octahedral manganese(II) renders a relatively straightforward interpretation of magnetic properties. In the absence of magnetic exchange effects the magnetic moment should be spin-only (5.92 μ_B) and temperature independent except possibly at very low temperatures where zero-field splitting may impart some temperature dependence. All six complexes under consideration here exhibit decreasing magnetic moments with decreasing temperature (Fig. 5), indicative of antiferromagnetic exchange. Exchange is confirmed for complexes **1**, **2**, and **4** for which maxima in magnetic susceptibility versus temperature plots have been observed at 5.8 K for **1** (9) and at ~3.5 K for **2** and **4**.

As described previously for **1** (9), we have analyzed the magnetic susceptibility data for **2** through **6** according to two isotropic Heisenberg models for linear chains, the scaling model of Wagner and Friedberg with $S = 5/2$ (16) and the Weng model (17) with coefficients generated by Hiller *et al.*

Can. J. Chem. Downloaded from www.nrcresearchpress.com by 92.62.229.171 on 09/08/12
For personal use only.

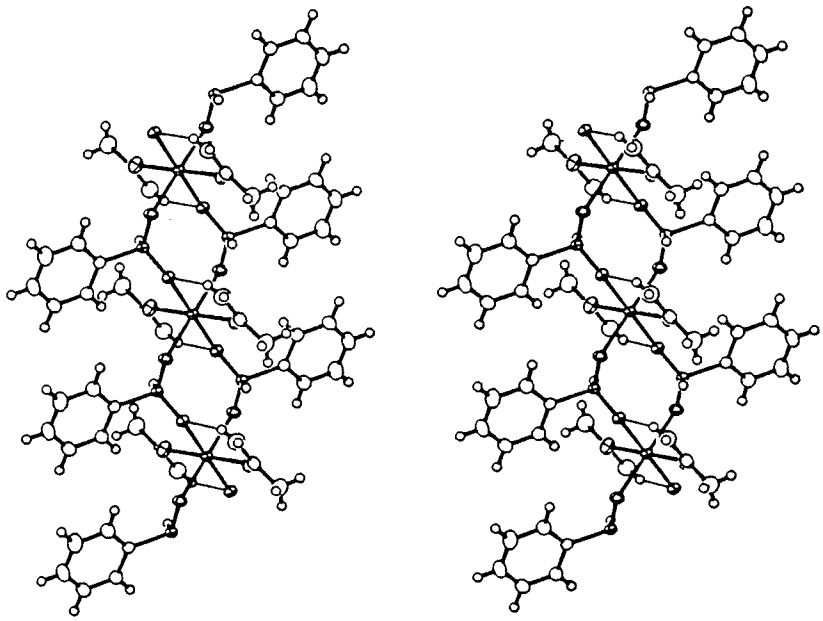

FIG. 3. Stereoscopic view of a portion of the chain structure of $Mn(CH_3CONH_2)_2[H(C_6H_5)PO_2]_2$, **2**, showing hydrogen bonding (fine bonds).

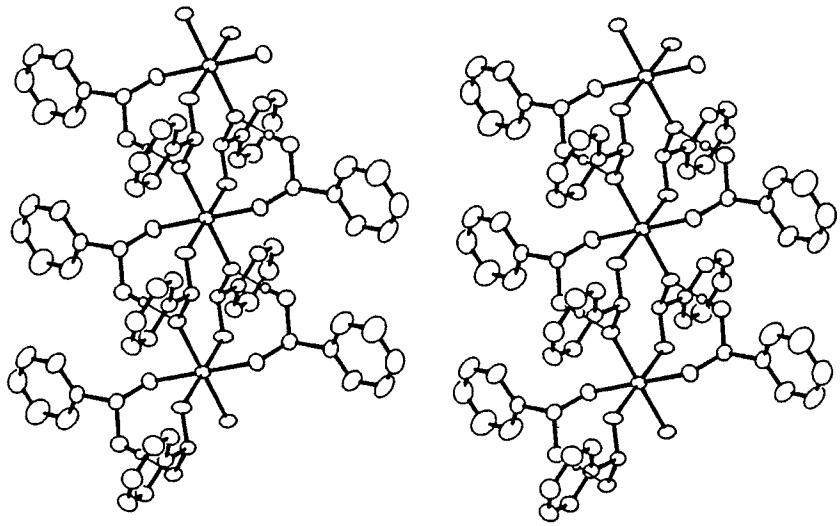

FIG. 4. Stereoscopic view of the chain structure of $Mn[H(C_6H_5)PO_2H]_2[H(C_6H_5)PO_2]_2$, **3**, fine bonds represent hydrogen bonds.

(18) for $S = 5/2$. Within these models the Hamiltonian is $\mathcal{H} = -2J\Sigma\hat{s}_i \cdot \hat{s}_j$. According to the Wagner and Friedberg model,

$$\chi_M = \left[\frac{Ng^2\beta^2S(S+1)}{3kT} \cdot \frac{(1+U)}{(1-U)}\right]$$

where

$$U = \coth K - \frac{1}{K} \qquad \text{and} \qquad K = \frac{2JS(S+1)}{kT}$$

According to the second model,

$$\chi_M = \left[\frac{Ng^2\beta^2}{kT}\right]\left[\frac{(A+BX^2)}{(1+CX+DX^3)}\right]$$

where

$$A = 2.9167, \qquad B = 208.04,$$

$$C = 15.543, \qquad D = 2707.2, \qquad X = \frac{|J|}{kT}$$

Experimental magnetic susceptibility data were analyzed using both models with the exchange coupling constant J as the only fitting parameter. The absence of orbital angular momentum in the ground state of manganese(II) permits g to be fixed at 2.00. Best fits were obtained by minimizing the function

$$F = \left[\left(\frac{1}{n}\right)\Sigma\left(\frac{(\chi_i^{calc} - \chi_i^{obs})}{\chi_i^{obs}}\right)^2\right]^{1/2}$$

where n is the number of data points. The value of F, then, provides a measure of agreement between the experimental data and the model.

Can. J. Chem. Downloaded from www.nrcresearchpress.com by 92.62.229.171 on 09/08/12
For personal use only.

TABLE 5. Selected infrared frequencies[a] for $MnL_2[H(C_6H_5)PO_2]_2$ complexes

Assignment	1[b]	2	3	4	5	6
ν_{anti} PO_2	1130 vs	1134 vs	1174 vs 1144 vs	1162 vs	1144 vs	1192 vs
ν_{sym} PO_2	1046 s	1045 s	1023 s 963 vs	1048 s	1060 s	1070 s
ν CO	1670 s 1690 m sh	1653 vs		1657 vs		
ν PH	2380 m	2380 m	2390 m 2408 m	2379 m	2357 m	2310 m 2280 m
Other bands[c]	3240 m br 3120 m br	3360 m br 3160 m br	3360 w br 3181 w br	3224 m br	3318 s br	624 424

[a]Frequencies in cm^{-1}; vs = very strong, s = strong, m = medium, sh = shoulder, br = broad.
[b]Data from ref. 9.
[c]ν_{NH} for **1**, **2**, and **4**; ν_{OH} for **3** and **5** and 6a and 16b internal vibrations of the pyridine ligand in **6**.

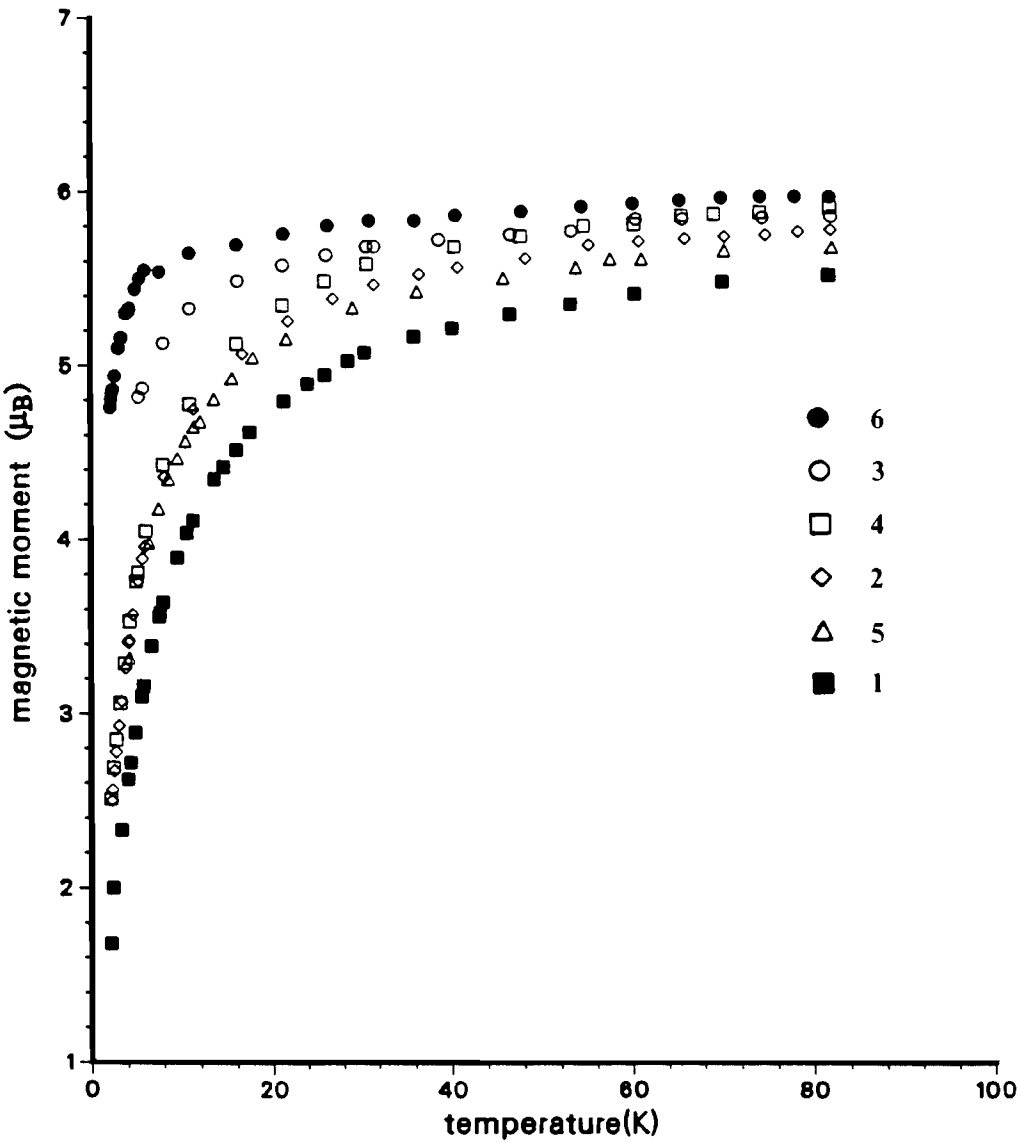

FIG. 5. Plots of magnetic moment versus temperature for compounds **1**–**6**.

Can. J. Chem. Downloaded from www.nrcresearchpress.com by 92.62.229.171 on 09/08/12
For personal use only.

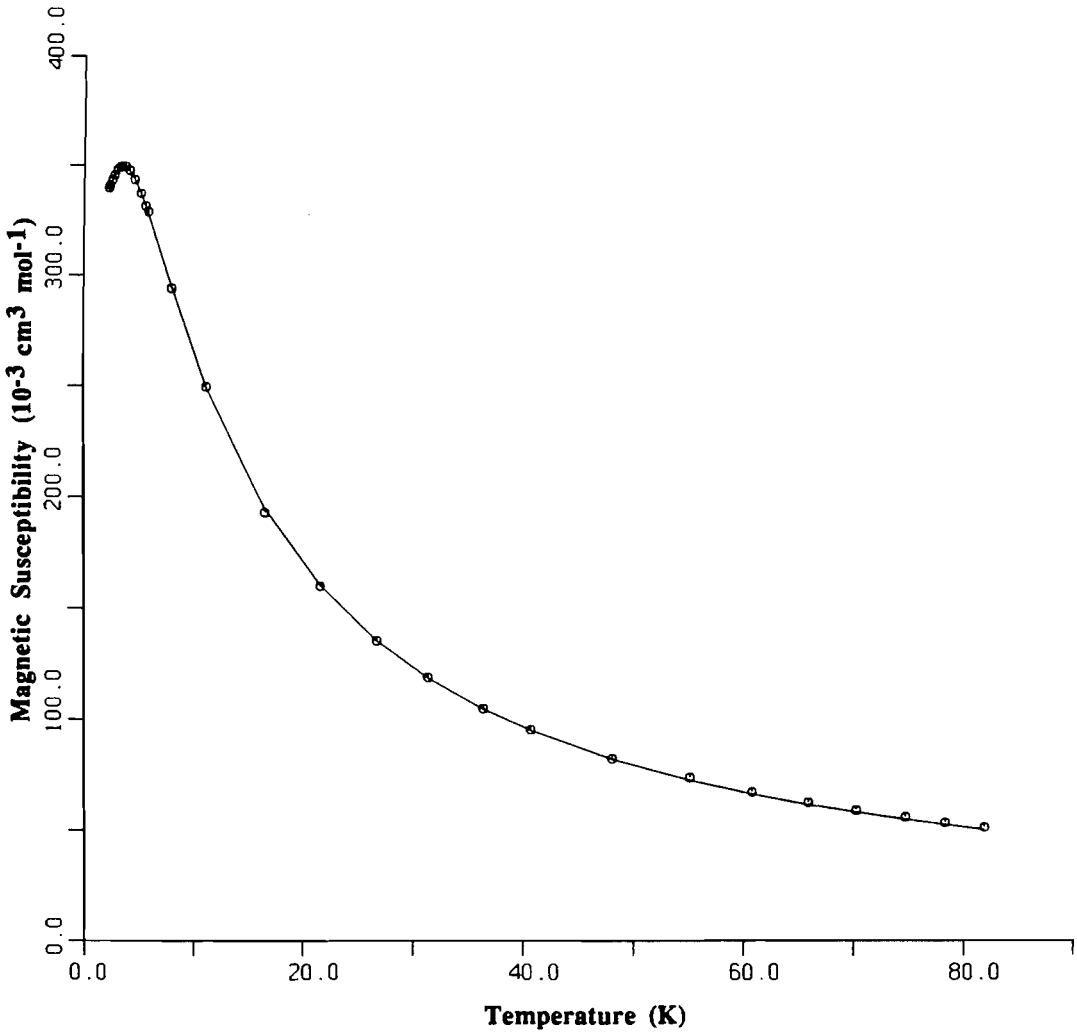

FIG. 6. Plot of magnetic susceptibility versus temperature for compound **2**. The circles are experimental data and the line is calculated using the Wagner–Friedberg model as described in the text.

Figure 6 shows the agreement between experiment and theory for the acetamide complex, **2**, and the magnetic parameters generated for the best fits between experiment and theory are given in Table 6. There is good agreement between experiment and theory using either model as judged by the value of the fitting function F, although the Wagner–Friedberg model seems generally to give better agreement and it reproduces the temperature of the susceptibility maximum in **1**, **2**, and **4** better.

The availability of single crystal X-ray diffraction determined bond parameters for **1**, **2**, and **3** permits a detailed examination of magnetostructural correlations in these complexes. For these complexes the exchange coupling clearly decreases in the order **1** > **2** > **3** (Table 6). This order can be understood if it is assumed that the magnetic exchange increases with decreasing length of the Mn–O–P–O–Mn pathway for exchange and, moreover, is favored by symmetrical O—P—O units. The latter would imply good π delocalization over the phosphinate bridge and should result in an effective π-pathway for exchange. It has been suggested for some time that the π-pathway for exchange is important in antiferromagnetic coupling between metal centres in phosphinate bridged compounds (10). The lengths of the Mn–O–P–O–Mn pathways for **1**, **2**, and **3** are 7.38(1),

TABLE 6. Magnetic parameters[a,b] for $MnL_2[H(C_6H_5)PO_2]_2$ complexes

Compound	L	$-J$[c] (cm^{-1})	F[d]
1[e]	$HCONH_2$	0.51	0.0436
		(0.47)	(0.0402)
2	CH_3CONH_2	0.30	0.0085
		(0.28)	(0.0205)
3	$H(C_6H_5)PO_2H$	0.13	0.0092
		(0.12)	(0.0102)
4	$HCONHCH_3$	0.28	0.0322
		(0.27)	(0.0426)
5	H_2O	0.33	0.0200
		(0.31)	(0.0153)
6	C_5H_5N	0.06	0.0192
		(0.05)	(0.0238)

[a]The data outside the parentheses were obtained using the Wagner–Friedberg model (16) and those inside the parentheses using the Weng model (17, 18).
[b]g was set at 2.00.
[c]The estimated uncertainty in J is ±5%.
[d]The fitting function F is defined in the text.
[e]Data taken from ref. 9.

Can. J. Chem. Downloaded from www.nrcresearchpress.com by 92.62.229.171 on 09/08/12
For personal use only.

7.43(1), and 7.43(1) Å, respectively. The shorter pathway in **1** is due largely to shorter Mn—O distances in this complex as discussed above. Hence the formamide complex, **1**, combines the shorter exchange pathway with symmetrical O—P—O bridges to give the largest $|J|$ of the three complexes. On the other hand, the monophenylphosphinic acid complex, **3**, combines the longer exchange pathway with unsymmetrical O—P—O bridges to give the smallest $|J|$. The intermediate $|J|$ observed for the acetamide complex, **2**, is consistent with the combination of an unfavorable path length with favorable symmetrically bridging O—P—O units.

An examination of bond angles at the bridging atoms reveals the total variation in O—P—O angles over the compounds is 1° with **1** having the intermediate angle (116.0(2)°). The Mn—O—P angles in **1** (Mn—O(1)—P = 129.1(2) and Mn—O(2)—P = 129.0(2)°) are smaller than those in **3** (132.2(1) and 133.0(1)°) while **2** exhibits both the smallest (121.9(1)°) and largest (135.6(1)°) angle of this type amongst the three compounds. The average of the Mn—O—P angles in **2** is the same as that in **1**. There appears to be no simple correlation between the magnitude of the exchange in these compounds and the angles at the bridging atoms.

Detailed magnetostructural correlation studies on **4**, **5**, and **6** are not possible owing to the absence of X-ray determined structures. The *N*-methylformamide complex, **4**, should exhibit only intrachain hydrogen bonding that would result in unsymmetrical O—P—O bridges and this may account for the fact that $|J|$ for this compound is less than that in the formamide complex, **1**. The value of $|J|$ for the pyridine complex, **6**, is quite small. Indeed, the value given in Table 6 for this compound should be considered an upper limit since in cases such as this, where the exchange is clearly very weak, the effect of the zero-field splitting may be contributing significantly to the observed magnetic properties. Since there is no possibility of hydrogen bonding in **6** we conclude the relatively high basicity of the neutral ligand in this case may lead to relatively strong pyridine–manganese interactions and correspondingly weaker manganese–phosphinate interactions and therefore weaker exchange. As discussed above, there is infrared evidence for unsymmetrical O—P—O units in this compound and this too may contribute to weakening the exchange. The aquo complex, **5**, should exhibit both intrachain and interchain hydrogen bonding as has, in fact, been observed previously for the dimethylphosphinate analogue (8). This would be expected to give symmetrical O—P—O bridges in **5**, a result supported by the infrared spectral studies described above. The fact that $|J|$ for **5** is approximately the same as the value obtained for **2** (which has symmetrical O—P—O bridges) suggests the M–O–P–O–M pathway is about the same length in these two complexes.

Acknowledgements

The authors thank the Natural Sciences and Engineering Research Council of Canada for financial support and Mr. P. Borda of this department for C, H, and N microanalyses.

1. A. Bino and L. Sissman. Inorg. Chim. Acta, **128**, L21 (1987).
2. P. Colamarino, P. L. Orioli, W. D. Benzinger, and H. D. Gillman. Inorg. Chem. **15**, 800 (1976).
3. R. Cini, P. Colamarino, P. L. Orioli, L. S. Smith, P. R. Newman, H. D. Gillman, and P. Nannelli. Inorg. Chem. **16**, 3223 (1977).
4. K. W. Oliver, S. J. Rettig, R. C. Thompson, and J. Trotter. Can. J. Chem. **60**, 2017 (1982).
5. J. S. Haynes, K. W. Oliver, S. J. Rettig, R. C. Thompson, and J. Trotter. Can. J. Chem. **62**, 891 (1984).
6. M. Shieh, K. J. Martin, P. J. Squattrito, and A. Clearfield. Inorg. Chem. **29**, 958 (1990).
7. J.-L. Du, S. J. Rettig, R. C. Thompson, and J. Trotter. Can. J. Chem. **69**, 277 (1991).
8. W. V. Cicha, J. S. Haynes, K. W. Oliver, S. J. Rettig, R. C. Thompson, and J. Trotter. Can. J. Chem. **63**, 1055 (1985).
9. P. Betz, A. Bino, J.-L. Du, L. S.-M. Lo, and R. C. Thompson. Inorg. Chim. Acta, **170**, 45 (1990).
10. J. S. Haynes, K. W. Oliver and R. C. Thompson. Can. J. Chem. **63**, 1111 (1985).
11. J.-L. Du, K. W. Oliver, and R. C. Thompson. Inorg. Chim. Acta, **141**, 19 (1988).
12. J.-L. Du and R. C. Thompson. Can. J. Chem. **67**, 1239 (1989).
13. J. A. Ibers and W. C. Hamilton (*Editors*). International tables for X-ray crystallography. Vol. IV. Kynoch Press. Birmingham, U.K. 1974. pp. 99–102 and 149. (Present distributor: Kluwer Academic Publishers, Dordrecht, The Netherlands).
14. C. H. Kline and J. Turkevich. J. Chem. Phys. **12**, 300 (1944).
15. B. F. Little and G. L. Long. Inorg. Chem. **17**, 3401 (1978).
16. G. R. Wagner and S. A. Friedberg. Phys. Lett. **9**, 11 (1964).
17. C. H. Weng. Ph.D. Dissertation. Carnegie-Mellon University, Pittsburgh, Pa. 1968.
18. W. Hiller, J. Strähle, A. Datz, M. Hanack, W. E. Hatfield, L. W. terHaar, and P. Gütlich. J. Am. Chem. Soc. **106** 329 (1984).

Can. J. Chem. Downloaded from www.nrcresearchpress.com by 92.62.229.171 on 09/08/12
For personal use only.

Electron densities and the VSEPR model of molecular geometry

R. J. GILLESPIE
Department of Chemistry, McMaster University, Hamilton, Ont., Canada L8S 4M1

Received August 25, 1991

This paper is dedicated to the memory of Professor Thomas Birchall

R. J. GILLESPIE. Can. J. Chem. **70**, 742 (1992).

This paper reviews the present status of the VSEPR model of molecular geometry in relation to electron densities. The discussion is based on the electron pair domain version of this model. The fundamental postulates of the model are summarized and illustrated by a discussion of the structures of some molecules with five and seven electron pair domains in the valence shell, including the recently discovered ions XeF_5^- and $XeOF_6^-$. The total electron density does not provide any obvious support for the model and although electron density deformation maps do provide some support they are not always reliable. The Laplacian of the electron density, however, shows the presence of valence shell charge concentrations that correspond closely in number and properties to the electron pair domains of the VSEPR model. This correspondence between electron pair domains and valence shell charge concentrations provides a physical basis for a better understanding of the VSEPR model.

Key words: VSEPR model, electron densities, molecular geometry, Laplacian of the electron density, electron pair domain.

R. J. GILLESPIE. Can. J. Chem. **70**, 742 (1992).

Dans ce travail, on examine la situation actuelle du modèle VSEPR de la géométrie moléculaire en regard des densités électroniques. La discussion est basée sur la version de ce modèle liée au domaine de la paire d'électrons. On résume les postulats fondamentaux du modèle et on les illustre par une discussion des structures de quelques molécules comportant des domaines de cinq et sept paires d'électrons dans la couche de valence, y compris les ions XeF_5^- et $XeOF_6^-$ découverts récemment. La densité électronique totale ne fournit pas un support évident pour le modèle; par ailleurs, les cartes de déformation de la densité électronique leur fournissent un léger support, même si elles ne sont pas fiables. Toutefois, le laplacien de la densité électronique montre la présence de concentrations de charges de la couche de valence qui correspondent bien, en nombre et en propriétés, avec les domaines des paires d'électrons du modèle VSEPR. Cette correspondance entre les domaines des paires d'électrons et les concentrations de charges de la couche de valence fournit une base physique pour une meilleure compréhension du modèle VSEPR.

Mots clés : modèle VSEPR, densités d'électrons, géométrie moléculaire, laplacien de la densité électronique, domaine de la paire d'électrons.

[Traduit par la rédaction]

Can. J. Chem. Downloaded from www.nrcresearchpress.com by 92.62.229.171 on 09/08/12
For personal use only.

It is now over 30 years since the Valence Shell Electron Pair Repulsion (VSEPR) model of molecular geometry was first proposed and it continues to be an extremely useful model for the prediction and understanding of the geometry of covalent molecules. Despite its success it is sometimes criticised on the grounds that it is an empirical model that does not have a sound theoretical basis. The purpose of this paper is to review the present status of the model, particularly in relation to the detailed information on the electron densities of molecules that has become available since the VSEPR model was first formulated. We first describe an electron pair domain version of the model and illustrate its application by some recently determined structures of molecules with five or seven valence shell electron pairs. Then we discuss the physical basis of the model. In particular, we consider to what extent the model can be justified by an examination of the electron density and the Laplacian of the electron density. Finally we note that the theoretical basis for the model provided by the Laplacian of the electron density should lead to a better understanding of those molecules that appear to be exceptions to the VSEPR model.

The VSEPR model is a direct development from Lewis's idea that the covalent bond can be represented as a shared pair of electrons. This brilliant idea, which cleared up enormous confusion concerning valence and bonding, and which is still used by every chemist today, had no theoretical basis for many years. We now understand that the fundamental basis of the concept of the electron pair is the Pauli exclusion principle. The VSEPR model, which is a natural extension of the Lewis model, is similarly based on the Pauli exclusion principle, which plays a major role in determining the electron distribution in molecules (1, 2).

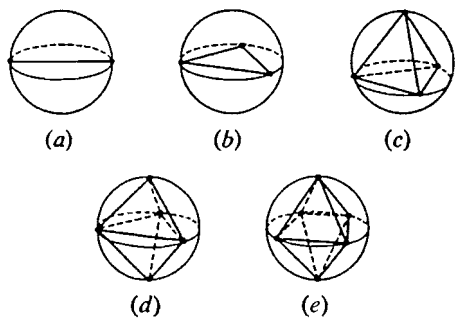

FIG. 1. Arrangements of points on the surface of a sphere that maximize their distance apart.

The electron pair domain version of the VSEPR model

The primary postulate of the VSEPR model is that the electron pairs in the Lewis structure of a molecule are arranged as far apart as possible. These electron pair arrangements are often illustrated by the arrangements of points on the surface of a sphere that maximize the least distance between any pair of points (Fig. 1). However, electron pairs are not very realistically represented by points, so it is pref-

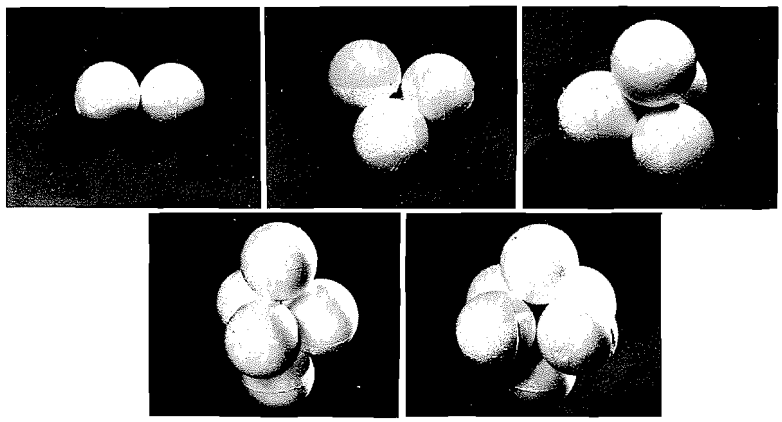

FIG. 2. Arrangements of spherical electron pair domains that minimize their distance from the nucleus.

Can. J. Chem. Downloaded from www.nrcresearchpress.com by 92.62.229.171 on 09/08/12
For personal use only.

erable to think of a valence shell electron pair as a charge cloud composed of two electrons of opposite spin and which occupies as much space as possible while excluding other electrons from this space in accordance with the Pauli exclusion principle. Thus we could consider, as an alternative model, the arrangements adopted by different numbers of circles of equal radii occupying as large a fraction as possible of the surface of a sphere without overlapping. This model leads to exactly the same arrangements as the points-on-a-sphere model. Another variation of the same basic idea that was first proposed by Kimball[1] and which has been extensively developed by Bent (3) is to consider each electron pair charge cloud as having a spherical shape of the same size. Bent called it the tangent-sphere model. I prefer to call it the domain model. The spherical electron pair domains are packed as closely as possible around the core of the atom and again we arrive at the same arrangements (Fig. 2). These basic arrangements of two to six electron pairs were first proposed by Sidgwick and Powell in 1940 (4). They are fundamental to the VSEPR model and they form the basis for the prediction of the molecular shapes.

In our paper in 1957 (5) Nyholm and I went beyond these basic electron pair arrangements by pointing out that not all the electron pairs in a valence shell should be regarded as equivalent. The differences between electron pairs were expressed in the form that lone-pair–lone-pair repulsions are stronger than lone-pair–bond-pair repulsions, which are stronger than bond-pair–bond-pair repulsions. On this basis one can account in a qualitative manner for the many small deviations of real structures from the "ideal" structures predicted on the basis of equivalent electron pairs. However, it is simpler, more realistic, and less liable to the misinterpretation that it is a classical electrostatic model to express the VSEPR model in terms of the sizes and shapes of localized electron pair domains rather than in terms of electron pair repulsions. Indeed there would be some advantage in changing the name to the VSEPD model: the Valence Shell Electron Pair Domain model. In these terms the three basic postulates or rules of the VSEPR (VSEPD) model are as follows.

1. Nonbonding domains are larger than single bond domains; they are more spread out and occupy more space in the valence shell than single bond domains. This is understandable because lone pairs are under the influence of only one positive core rather than two.

2. The size of a single bond domain in the valence shell of a central atom decreases with increasing electronegativity of the ligand.

3. Although it is often convenient to think of double and triple bonds as composed of a σ and one or two π bonds or two or three bent single bonds, respectively, it is simpler in the electron pair domain model to consider a double bond as a two electron pair domain and a triple bond as a three electron pair domain in which the individual electron pairs are not distinguished. These bond domains increase in size from a single to a double to a triple bond.

Application of the VSEPR model to molecules with five or seven valence shell electron pairs

Trigonal bipyramidal AX_5 molecules and the related AX_4E, AX_3E_2, and AX_2E_3 molecules provide particularly interesting applications of the VSEPR model because the five vertices of a trigonal bipyramid are not all equivalent. The axial positions of a trigonal bipyramid are more crowded than the equatorial positions; they have three neighbors at 90° whereas an equatorial position has two neighbors at 90° and two more at 120°. So large domains will prefer the equatorial positions, forcing smaller domains into the axial positions. Thus lone pair domains, double bond domains, and the domains of less electronegative ligands are preferentially found in the equatorial positions (Fig. 3). Moreover, because the axial domains are in a more crowded position, axial bonds are always longer than equivalent equatorial bonds (Fig. 3). No other simple model enables one to make these predictions about the geometry of molecules with a central atom with five valence shell electron pairs.

The recently prepared XeF_5^- ion (6) has a unique planar pentagonal AX_5E_2 structure based on a pentagonal bipyramidal arrangement of seven electron pairs with the two lone pairs in the axial positions (Fig. 4). In contrast to the trigonal bipyramid the lone pairs prefer the axial positions, which are the least crowded positions with all neighbors at 90° whereas each equatorial position has two neighbors at 72°. The prediction of the geometry of molecules in which there are seven electron pairs in the valence shell of the central

[1]G. E. Kimball. References to unpublished work by Kimball and his students are given by H. A. Bent (3).

Can. J. Chem. Downloaded from www.nrcresearchpress.com by 92.62.229.171 on 09/08/12
For personal use only.

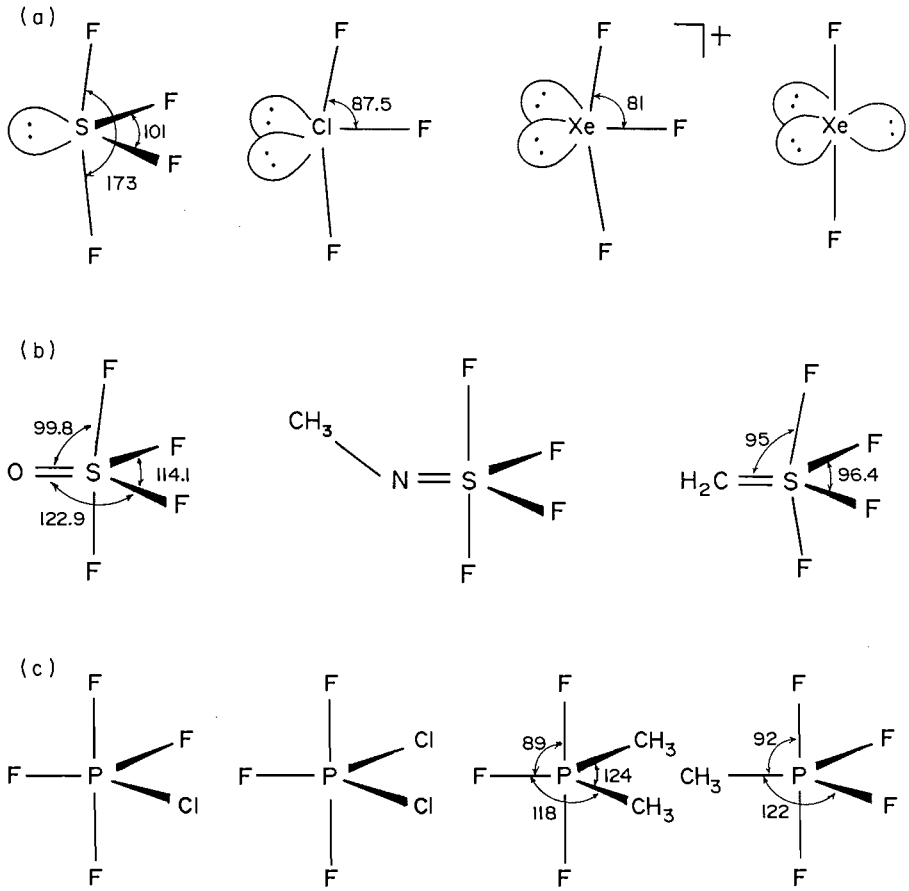

FIG. 3. Molecules with a trigonal bipyramidal arrangement of five electron pair domains in the valence shell of the central atom. (*a*) Lone pair domains always occupy the equatorial positions. (*b*) Double bond domains always occupy the equatorial positions. (*c*) Less electronegative ligands preferentially occupy the equatorial positions.

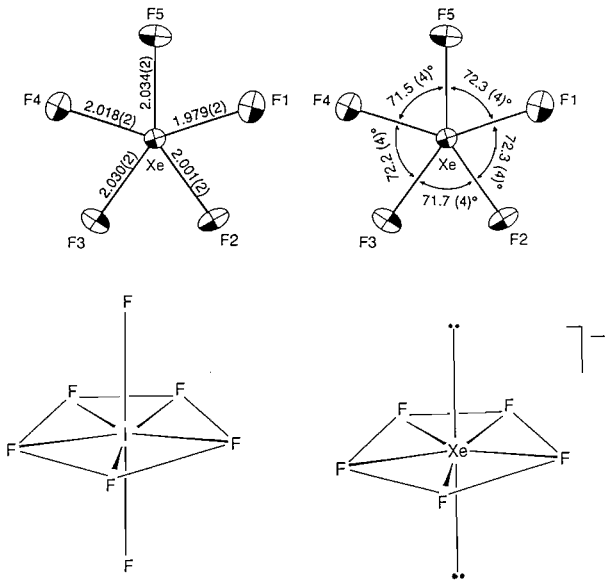

FIG. 4. The structure of the planar pentagonal ion XeF_5^-.

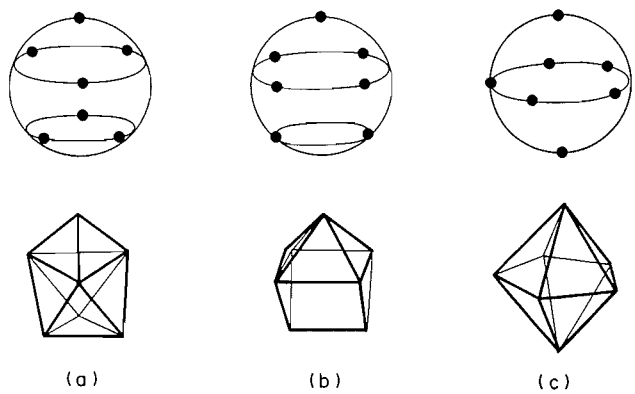

FIG. 5. Possible arrangements for seven points on the surface of a sphere. (*a*) Monocapped octahedron. (*b*) Monocapped trigonal prism. (*c*) Pentagonal bipyramid.

atom A cannot be made with as much certainty as for molecules in which there are six or fewer electron pairs in the valence shell because there are three electron pair arrangements with very similar interpair distances (Fig. 5). However, it is reasonable to assume that the structure will be based on the pentagonal bipyramidal arrangement of seven electron pair domains that we find in the closely related molecule IF_7. Moreover, we expect a structure based on an arrangement in which two lone pairs can occupy two equivalent less crowded positions and this is the pentagonal bipyramid with the lone pair domains in the two axial positions.

The IOF_6^- ion has recently been shown to have a penta-

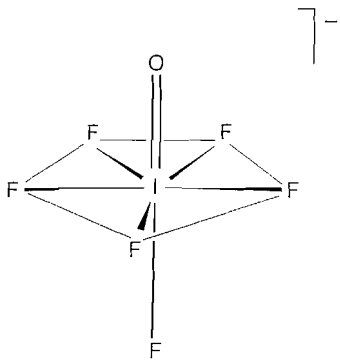

FIG. 6. The structure of the pentagonal bipyramidal ion IOF_6^-.

gonal bipyramid structure in which the doubly bonded oxygen occupies an axial position (7,8) as expected (Fig. 6). Moreover, the I—F bond in the less crowded axial position is, as expected, shorter (182.4 pm) than the equatorial bonds (187.4 pm). In contrast, in trigonal bipyramidal molecules the axial bonds are always longer than the equatorial bonds because the axial positions are the most crowded.

Although we cannot make an absolutely unambiguous prediction of the basic geometry of these seven coordinated molecules they do have one of the three possible predicted geometries. Moreover, the details of their structures are fully consistent with the postulates of the VSEPR model. No other model gives us a better understanding of the geometry of these molecules.

Electron densities

Can we legitimately think of electron pairs as essentially localized nonoverlapping charge clouds representing bonding pairs and lone pairs as the VSEPR model assumes? Many accurate calculations of electron densities in simple molecules have been made and in no case are there any features in the total electron density that represent localized bonding or nonbonding electron pairs. The water molecule provides us with a simple example (9). As we see in Fig. 7 there is no obvious localization of charge corresponding to lone pairs or bonding pairs. A bond is only apparent as a ridge of maximum density between the high concentrations of charge that surround each nucleus. This ridge has been called a bond path (10).

Total electron densities can also be obtained from accurate X-ray crystallographic studies. Again they give no evidence for localized electron pairs, either bonding or nonbonding. Nevertheless the usefulness of the Lewis and VSEPR models has inspired efforts to examine the total electron density in more detail. The total electron density is dominated strongly by the high concentration of electron density surrounding each nucleus and the changes in the

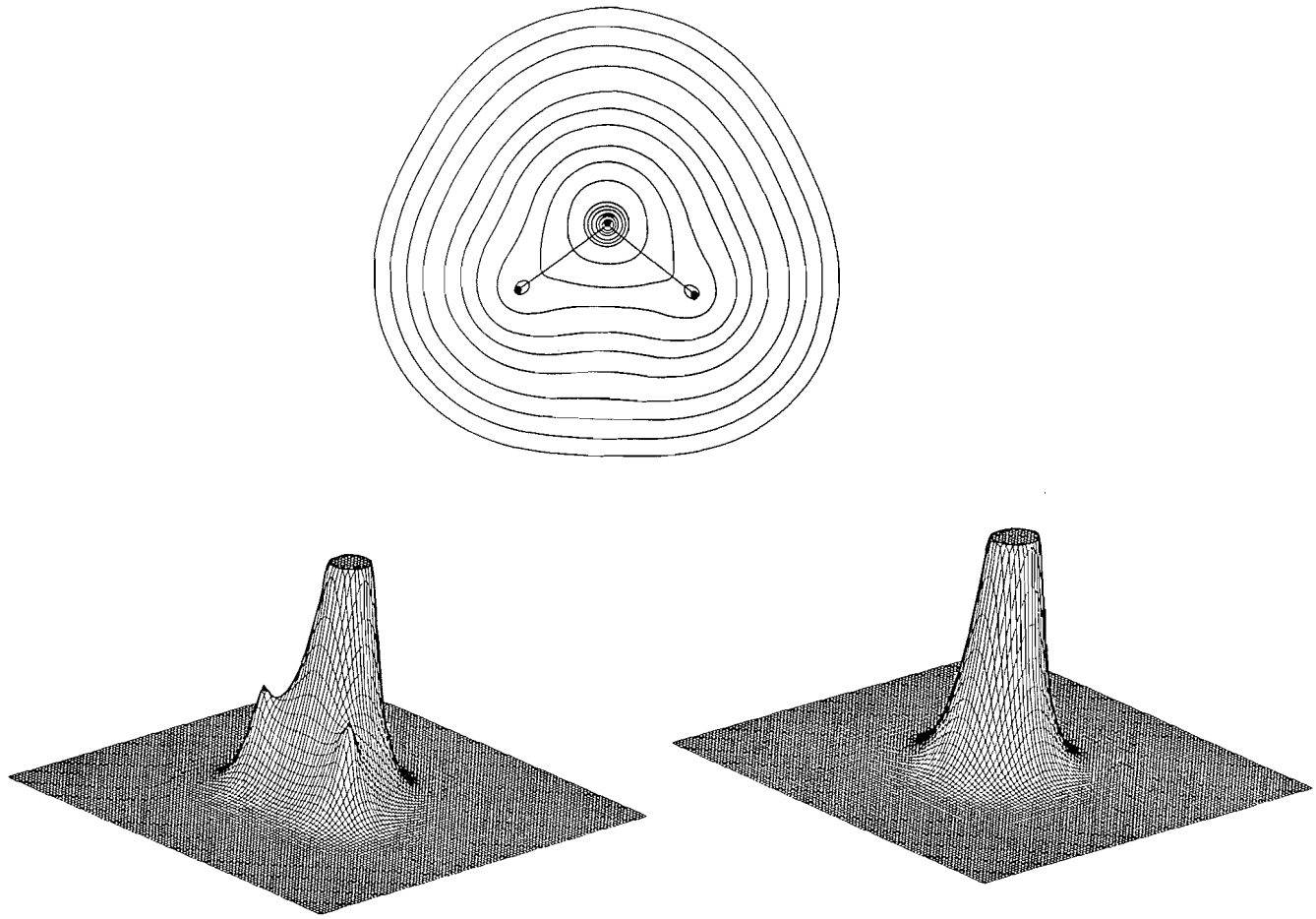

FIG. 7. The electron density distribution in the water molecule. (*a*) Contour plot in the plane of the molecule. (*b*) Relief map in the plane of the molecule. (*c*) Relief map in a plane through the oxygen atom and perpendicular to the plane of the molecule.

Can. J. Chem. Downloaded from www.nrcresearchpress.com by 92.62.229.171 on 09/08/12
For personal use only.

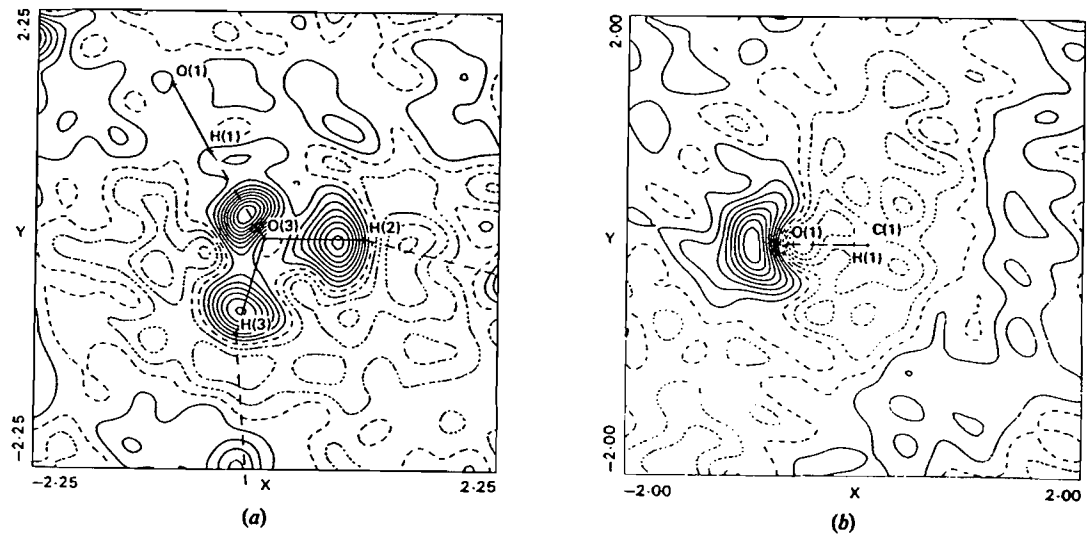

FIG. 8. Electron density difference (deformation) maps for a water molecule in oxalic acid dihydrate, $(COOH)_2.2H_2O$; (*a*) in the plane of the molecule; (*b*) in a plane through the oxygen atom perpendicular to the plane of the molecule. Reproduced by permission from Stevens and Coppens (11).

Can. J. Chem. Downloaded from www.nrcresearchpress.com by 92.62.229.171 on 09/08/12
For personal use only.

electron density that accompany molecule formation are relatively very small. Various attempts have been made to make these small changes in electron density more apparent. One method is by the calculation of electron density difference (deformation) maps, which are obtained by subtracting from the observed total electron density the densities of the isolated spherical atoms. Electron density difference maps for the water molecule in oxalic acid dihydrate are shown in Fig. 8 (11). There is a significant electron density in this difference map corresponding to the bond pairs and the lone pairs of the water molecule although the two lone pairs are not resolved. However, the problems that are sometimes associated with the interpretation of such maps are illustrated by the electron density difference map for tetrafluoroterephthalonitrile in Fig. 9, which shows no density at all in the C—F bond regions (12). These problems arise because the subtraction of the spherical densities of isolated atoms, although apparently reasonable, is an arbitrary procedure that cannot be theoretically justified.

The Laplacian of the electron density

It is only the total electron density that is an unambiguous experimentally determinable property of a molecule and so we must examine the total density and not some arbitrary difference or deformation density if we hope to obtain reliable evidence for bond pairs and lone pairs and to better understand the VSEPR model. Bader *et al.* showed that the Laplacian of the electron density, that is, the second differential of the electron density in three dimensions, provides us with a means of looking at the total electron density in some detail in a useful and informative way (9). For simplicity we first consider the one-dimensional function $f(x)$ shown in Fig. 10. This function decreases rapidly with increasing x and has two weak shoulders but no maxima or minima. The electron density in a free atom along any radius from the nucleus decreases in a somewhat similar manner although much more rapidly. The first differential of this function is everywhere negative because the slope is continually decreasing although not in a uniform manner. The second differential $f''(x)$ exhibits a minimum and $-f''(x)$ a maximum where the function has a larger value than the average of its value at the two neighboring points, in other words where $f(x), > \frac{1}{2}[f(x - dx) + f(x + dx)]$. We see that the weak shoulder in the $f(x)$ function is a much more apparent maximum in $-f''(x)$.

In an atom we have to consider the variation of ρ in three dimensions. Thus we are concerned with the Laplacian of the electron density

$$\nabla^2\rho = \frac{\partial^2\rho}{\partial x^2} + \frac{\partial^2\rho}{\partial y^2} + \frac{\partial^2\rho}{\partial z^2}$$

Wherever $-\nabla^2\rho$ is positive there is a local concentration of charge, that is, the electron density is greater than the average density in the immediate neighborhood. Wherever $-\nabla^2\rho$ is negative there is an analogous local depletion of charge. A plot of $-\nabla^2\rho$ for any plane through a spherical free atom shows maxima and minima corresponding to the electron shells (Fig. 11). For the argon atom there is an inner spike and two concentric shells in which the electron density is locally concentrated, separated by regions of electron density depletion. We can think of these as regions of locally increased and decreased electron density although they are not maxima and minima in the electron density. The outer shell corresponds to the valence shell. In the valence shell there is a spherical surface on which the electronic charge is maximally concentrated. This is called the valence shell charge concentration (VSCC). In general this surface persists when an atom forms part of a molecule but the sphere is distorted and is no longer one of uniform charge concentration.

The Laplacian of the electron density of the water molecule (9) shows two local charge concentrations in the valence shell of oxygen corresponding to the two bonds and two charge concentrations corresponding to the lone pairs (Fig. 12). These four charge concentrations have an ap-

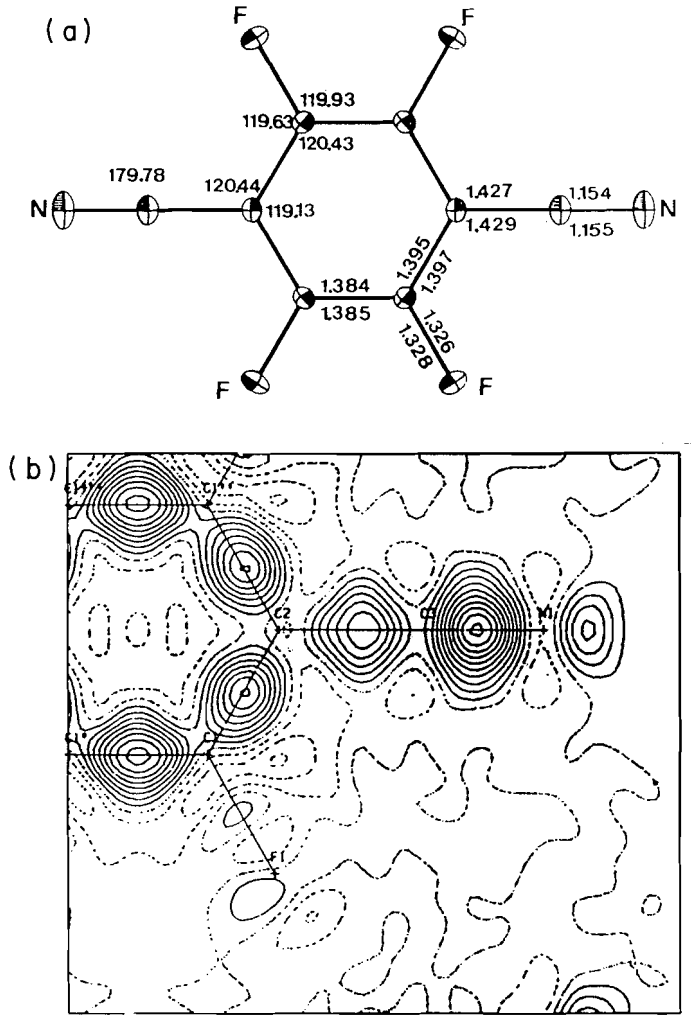

FIG. 9. Tetrafluoroterephthalonitrile. (*a*) Structure and geometrical parameters. (*b*) Electron density difference (deformation) map. This shows bonding density in the CC and CN bonds and lone pair density on nitrogen but almost no bonding density in the CF bond. Reproduced by permission from Dunitz *et al.* (12).

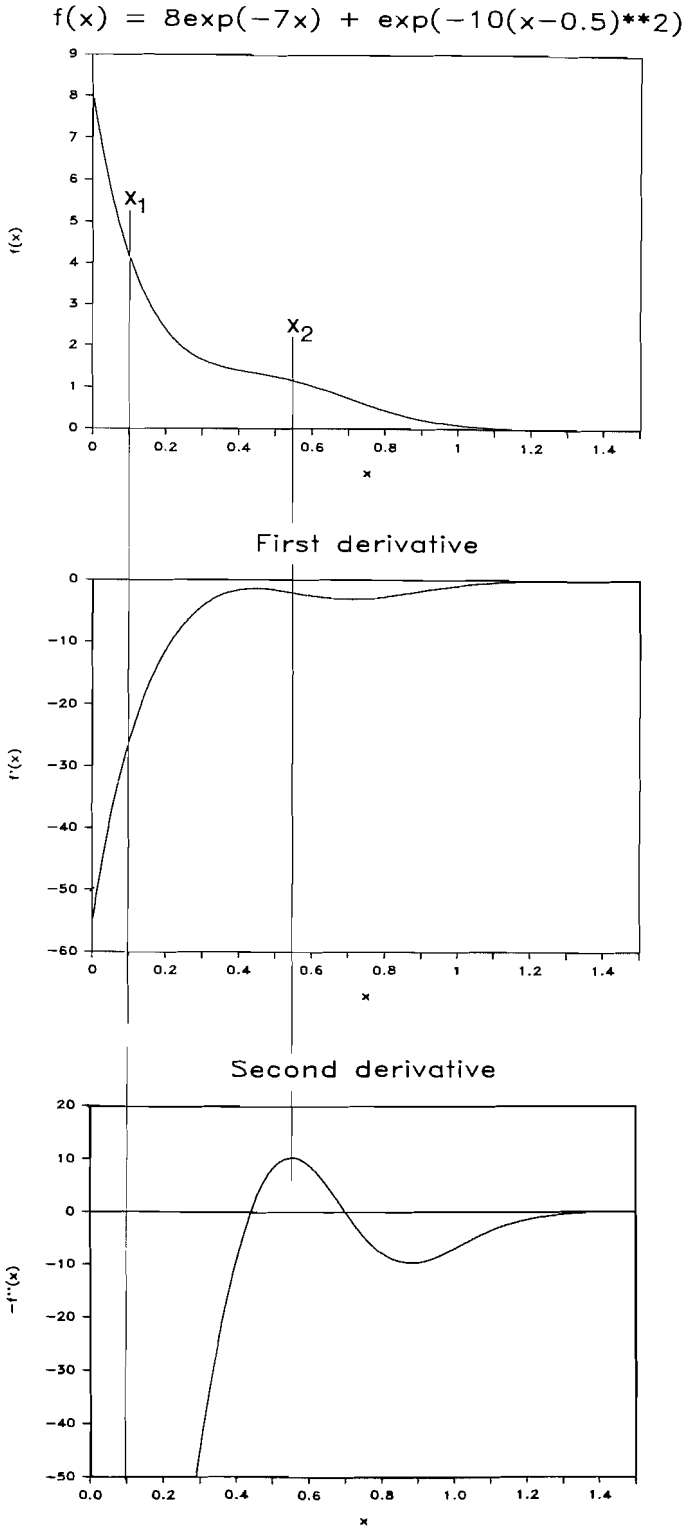

FIG. 10. Plot of a monotonically decreasing function $f(x)$ and its first and second derivatives. The negative of the second derivative is shown here. This has a maximum at x_2 where $f(x)$ has a shoulder, that is, where $f(x) > \frac{1}{2}[f(x - dx) + (x + dx)]$ or where $f(x)$ is locally concentrated.

proximately tetrahedral arrangement and their properties (Table 1) mimic exactly the properties postulated for localized electron pairs in the VSEPR model. For example, the nonbonded charge concentrations are larger and occupy a larger area on the valence shell sphere of charge concentration than the bonding charge concentrations. The nonbonding charge concentrations are closer to the nucleus than the bonding charge concentrations and the angle between the nonbonding charge concentrations is greater than the angle between the bonding charge concentrations.

The Laplacian of the electron density of the ammonia molecule shows three bonding charge concentrations and one nonbonding charge concentration, which also have relative sizes and positions that correspond closely to those postulated for localized electron pairs in the VSEPR model (Table 1).

In the five electron pair molecule ClF_3 the Laplacian of the electron density has five regions of charge concentration with a trigonal bypyramidal arrangement and exactly those properties of size and position predicted for the localized electron pair domains of the VSEPR model (Table 2 and Fig. 13). For example, the nonbonding charge concentrations are in the equatorial positions and the axial charge

Can. J. Chem. Downloaded from www.nrcresearchpress.com by 92.62.229.171 on 09/08/12
For personal use only.

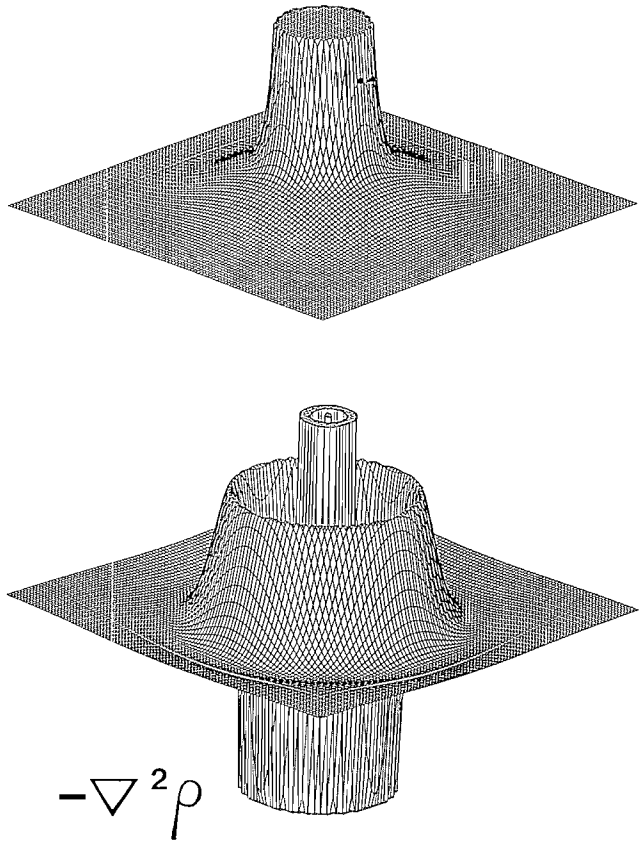

FIG. 11. Relief maps of the charge density and the negative of its Laplacian for a plane containing the nucleus of an argon atom. Function values above an arbitrary maximum are not shown.

TABLE 1. Valence shell charge concentrations[a]

	r (Å)	$-\nabla^2\rho$ (au)	Area (Å^2)	lAl (deg)	lAb (deg)	bAb (deg)
			H_2O			
Lone pairs	0.339	4.138	0.50	134.0	104.4	
Bond pairs	0.441	2.057	0.38		104.4	101.0
			NH_3			
Lone pair	0.338	2.299	0.83		114.2	
Bond pairs	0.510	1.685	0.71		104.4	

[a]Abbreviations: r, distance from maximum of charge concentration to nucleus; $-\nabla^2\rho$, value at maximum of charge concentration; area, approximate area of charge concentration; l, lone pair; b, bond pair.

concentrations are smaller and further from the nucleus than the equatorial charge concentrations.

Similar results have been obtained (13, 14) for SF_4, SOF_4, and ClF_5 (Table 2 and Fig. 14).

The important and interesting result of the study of the Laplacian of the electron density is that although the electrons are not highly localized into pairs as postulated by the VSEPR model there are an equal number of local concentrations of charge (VSCC's) that exhibit all the properties ascribed to the electron pair domains of the VSEPR model. Although the VSEPR model gives a highly exaggerated picture of the extent of localization of electron pairs in a molecule, there is nevertheless a very partial localization of electrons into pairs that gives rise to the small local concentrations of charge that have exactly the properties postulated for the localized electron pairs of the VSEPR model.

Valence shell charge concentrations and the Pauli exclusion principle

The valence shell charge concentrations result from the operation of the Pauli exclusion principle or spin correlation but because spin correlation is opposed by the electrostatic repulsion between the electrons (charge correlation) it is less effective in producing localized pairs than is assumed in the VSEPR model.

Linnett previously discussed the distribution of electrons in a molecule, a consequence of spin and charge correlation in the context of his double-quartet theory (15). According to Linnett we can consider the eight electrons of a neon atom or an oxide ion as consisting of one set of four electrons of α spin and another set of four of β spin. The most probable arrangement in each set as a consequence of both spin and charge correlation is at the corners of a tetrahedron. As a consequence of spin correlation the two sets tend to come into coincidence but this tendency is opposed by charge correlation. Linnett assumes that to a first approximation there is, as a consequence, little or no correlation between the two tetrahedral sets (Fig. 15). The overall electron density of the neon atom or the oxide ion is then spherical. We can think of forming the water molecule by the addition of two protons to an oxide ion. Each proton provides an additional attractive force tending to pull the two tetrahedral sets of electrons more towards coincidence, thus giving a partial localization of the electrons into two bonding pairs and two nonbonding pairs and the formation therefore of four corresponding local charge concentrations with an approximately tetrahedral arrangement (Fig. 15). The lone pair electrons are not as localized as the bonding pair electrons because they are not subject to the attraction of the protons and their localization depends only on spin correlation.

Summary and future developments

Although no complete theoretical justification of the VSEPR model has yet been given we now have a better understanding of its physical basis. Electrons in molecules are not as localized into electron pair domains as the VSEPR model assumes; nevertheless, there is a partial localization of electrons into pairs as a consequence of spin and charge correlation that gives rise to small local charge concentrations that have all the properties ascribed to the localized pairs of the VSEPR model. It seems reasonable to assume that an examination of the Laplacian of the electron density in those molecules that appear to be exceptions to the VSEPR model (2) will improve our understanding of the geometry of these molecules and also of the VSEPR model and its limitations. One such limitation is the assumption that the core of the atom underlying the valence shell is spherical. In the case of the transition metals and atoms with polarizable cores this may not always be the case and a nonspherical shell may have an important influence on the geometry of a molecule (2). Studies of the Laplacian of the electron density in such mol-

Can. J. Chem. Downloaded from www.nrcresearchpress.com by 92.62.229.171 on 09/08/12
For personal use only.

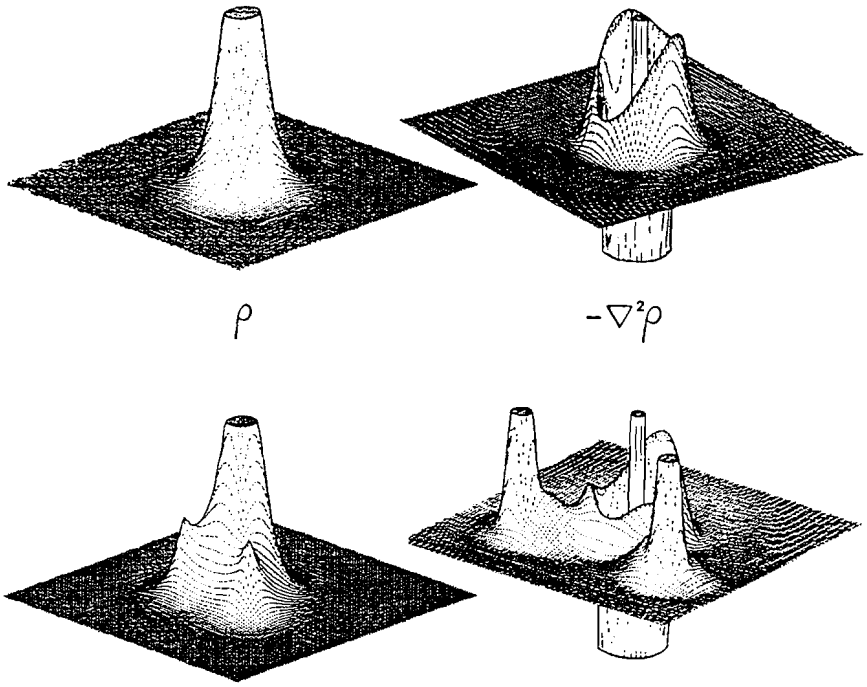

FIG. 12. Relief maps of the charge density and the negative of the Laplacian for the two symmetry planes of the water molecule. Lower maps are for the molecular plane and the upper maps are for the perpendicular plane. There is a spike-like concentration of charge surrounding the oxygen nucleus (which is terminated at an arbitrary value) that corresponds to the inner core. The valence shell charge concentration (VSCC) is not uniform but exhibits maxima and saddles in these two-dimensional relief maps. In the perpendicular (nonbonding) plane the VSCC of oxygen exhibits two maxima and two saddle points in $-\nabla^2\rho$. In the plane of the molecule $-\nabla^2\rho$ exhibits two maxima, one along each bond path to a proton. What appears to be a third maximum is another view of the two nonbonded maxima appearing in the upper diagram.

Can. J. Chem. Downloaded from www.nrcresearchpress.com by 92.62.229.171 on 09/08/12
For personal use only.

TABLE 2. Valence shell charge concentrations[a]

	r (Å)	$-\nabla^2\rho$ (au)	Area (Å^2)	lAl (deg)	lAb(eq) (deg)	b(ax)Ab(eq) (deg)
				ClF_3		
Lone pairs	0.605	1.58	1.52	147.8		
Bond pairs(eq)	0.670	0.595	0.66		96.5	83.6
Bond pair(ax)	0.687	0.319	0.41			83.6
				SF_4		
Lone pair	0.666	0.999	1.90		129.7	
Bond pairs(eq)	0.707	0.342	0.94		129.7	84.5
Bond pairs(ax)	0.726	0.268	0.49			84.5
				SOF_4		
Bond pair(=O)	0.463	1.175	2.06		101.7	
Bond pairs(eq)	0.705	0.381	0.89			83.0
Bond pairs(ax)	0.715	0.381	0.71			83.0
				ClF_5		
Lone pair	0.600	1.900	1.35			
Bond pair(ax)	0.653	0.866	0.78		180.0	
Bond pair(ba)	0.662	0.619	0.64		97.2	

[a] r, distance of maximum of charge concentration from nucleus; $-\nabla^2\rho$, value at maximum of charge concentration; area, approximate area of charge concentration; l, lone pair; b, bond pair.

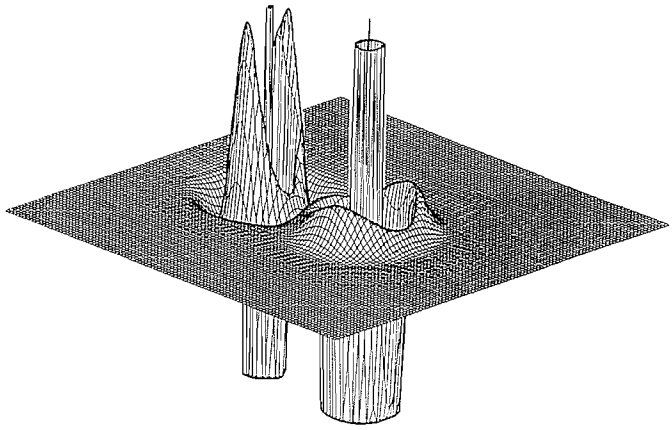

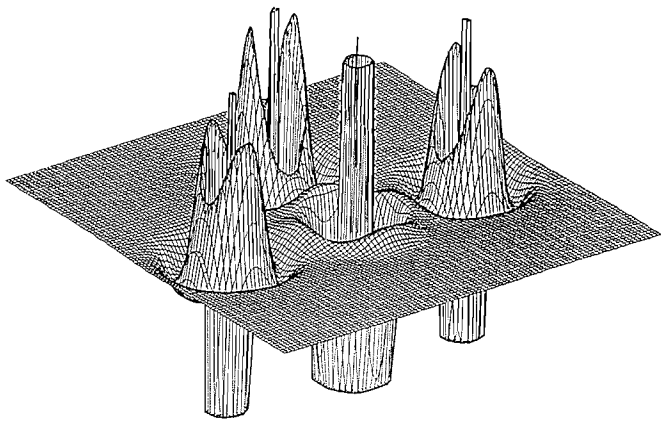

FIG. 13. Relief maps of $-\nabla^2\rho$ for the equatorial (upper) and axial (lower) planes of ClF_3. The chlorine atom exhibits three shells of charge concentration. In the equatorial plane there are two nonbonded and one bonded charge concentration in the valence shell. In the axial plane there are three bonded charge concentrations in the valence shell and a fourth apparent maximum that is another view of the saddle between the two nonbonded maxima in the equatorial plane. Thus the VSCC of the chlorine atom possesses two nonbonded and three bonded concentrations of charge.

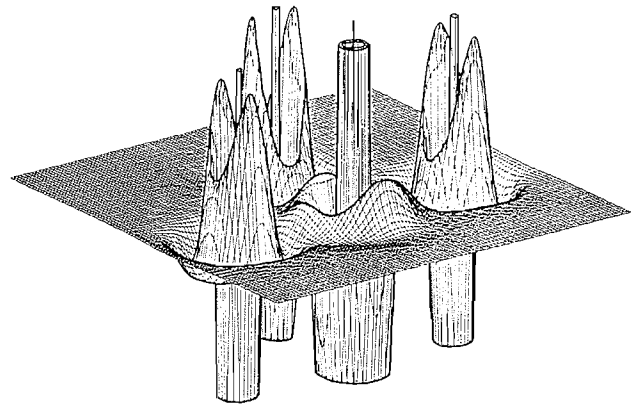

FIG. 14. A relief map of $-\nabla^2\rho$ in a symmetry plane of ClF_5 containing the chlorine, the axial fluorine, and two of the fluorine nuclei in the basal plane of the square pyramid. The figure illustrates the relative sizes of the charge concentrations; nonbonded > axial bonded > basal bonded.

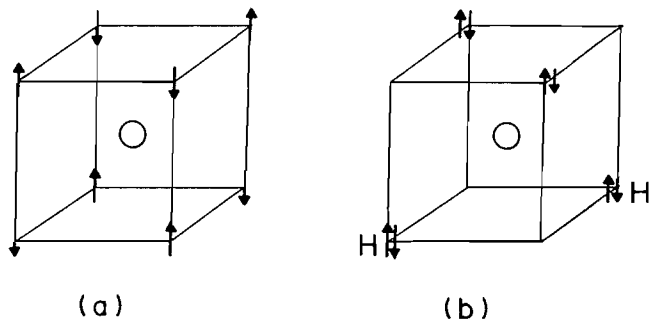

FIG. 15. (*a*) In the oxide ion there are two sets of four electrons with the same spin. In each set the most probable arrangement is tetrahedral as a consequence of spin and charge correlation. There is little correlation between the two sets as a consequence of the opposing effects of spin and charge correlation. The overall charge density in the ion is spherical. (*b*) The effect of adding two protons to the oxide ion to form the water molecule is to attract the two tetrahedra into partial coincidence, thus giving rise to four local charge concentrations, two bonding and two nonbonding.

ecules should help us to understand the effect of a nonspherical core on the geometry of a molecule and enable us to extend the VSEPR model to include such molecules.

1. R. J. Gillespie. Molecular geometry. Van Nostrand Reinhold, London. 1972.
2. R. J. Gillespie and I. Hargittai. The VSEPR model of molecular geometry. Allyn and Bacon, Boston. 1991.
3. H. A. Bent. J. Chem. Educ. **40**, 446 (1963); **40**, 523 (1963); **42**, 302 (1965); **42**, 348 (1965); **44**, 512 (1967); **45**, 768 (1968).
4. N. V. Sidgwick and H. E. Powell. Proc. R. Soc. A: **176**, 153 (1940).
5. R. J. Gillespie and R. S. Nyholm. Q. Rev. Chem. Soc. **11**, 339 (1957).
6. K. O. Christe, E. C. Curtis, D. A. Dixon, H. P. Mercier, J. C. P. Sanders, and G. J. Schrobilgen. J. Am. Chem. Soc. **113**, 3351 (1991).
7. K. O. Christe, J. C. P. Saunders, G. J. Schrobilgen, and W. W. Wilson. J. Chem. Soc. Chem. Commun. 837 (1991).
8. A. H. Mahjoub and K. Seppelt. J. Chem. Soc. Chem. Commun. 840 (1991).
9. R. F. W. Bader, P. J. MacDougall, and C. D. H. Lau. J. Am. Chem. Soc. **106**, 1594 (1984).
10. R. F. W. Bader and H. Essen. J. Chem. Phys. **80**, 1943 (1984).
11. E. D. Stevens and P. Coppens. Acta Crystallogr. Sect. B: Struct. Crystallogr. Cryst. Chem. **B36**, 1864 (1980).
12. J. D. Dunitz, W. B. Schweizer, and P. Seiler. Helv. Chim. Acta, **66**, 123 (1983).
13. R. F. W. Bader. Atoms in molecules: a quantum theory. Clarendon Press, New York. 1990.
14. R. F. W. Bader, R. J. Gillespie, and P. J. MacDougall. J. Am. Chem. Soc. **110**, 7329 (1988); *In* From atoms to polymers: isoelectronic analogies. of Molecular structure and energetics. Vol. 11. *Edited by* J. F. Liebman and A. Greenberg. VCH, New York. 1989.
15. J. W. Linnett. The electronic structure of molecules. Methuen, London. 1964.

Can. J. Chem. Downloaded from www.nrcresearchpress.com by 92.62.229.171 on 09/08/12
For personal use only.

Mono- and dinuclear palladium complexes containing 2-pyridylphosphine ligands, including X-ray characterization of $Pd_2I_2(\mu\text{-}PPh_2py)_2$ and a dimethylacetylenedicarboxylate A-frame complex $Pd_2Cl_2(\mu\text{-}Ppy_3)_2(\mu\text{-}MeO_2C \cdot C{=}C \cdot CO_2Me)$; py = 2-pyridyl

YUN XIE, CHUNG-LI LEE, YEPING YANG,[1] STEVEN J. RETTIG, AND BRIAN R. JAMES[2]
Department of Chemistry, University of British Columbia, Vancouver, B.C., Canada V6T 1Z1

Received July 4, 1991

This paper is dedicated to the memory of Professor Thomas Birchall

YUN XIE, CHUNG-LI LEE, YEPING YANG, STEVEN J. RETTIG, and BRIAN R. JAMES. Can. J. Chem. **70**, 751 (1992).

Dibromo- and diiodo[(2-pyridyl)phosphine]palladium(II) complexes are prepared by metathesis of *cis*-$PdCl_2(PPh_{3-n}py_n)_2$ species (n = 1–3) using the appropriate sodium halide; py = 2-pyridyl. NMR spectroscopy, particularly $^{13}C\{^1H\}$, is used to distinguish *cis* and *trans* isomers. The dinuclear complexes $Pd_2X_2(\mu\text{-}PPh_{3-n}py_n)_2$, X = halide, are synthesized via a conproportionation reaction using $PdX_2(PPh_{3-n}py_n)_2$ and $Pd_2(dba)_3$; dba = dibenzylideneacetone. Both $Pd_2I_2(\mu\text{-}PPh_2py)_2$ and a dimethylacetylenedicarboxylate A-frame complex $Pd_2Cl_2(\mu\text{-}Ppy_3)_2(\mu\text{-}MeO_2C \cdot C{=}C \cdot CO_2Me)$ are characterized crystallographically as head-to-tail isomers. The former crystallizes in the monoclinic space group $C2/c$ with a = 30.992(3), b = 18.764(1), c = 13.100(1) Å, β = 100.676(5)°, and Z = 8; the data were refined to R = 0.035 for 5874 reflections with $I \geq 3\sigma(I)$. The A-frame compound is triclinic of space group $P\bar{1}$ with a = 13.545(2), b = 15.064(2), c = 11.991(2) Å, α = 111.56(1), β = 95.36(1), γ = 97.63(1)°, and Z = 2; R = 0.033 from 7128 reflections with $I \geq 3\sigma(I)$. The $Pd_2X_2(\mu\text{-}PPhpy_2)_2$ complexes exist as a mixture of diastereomers because of chirality induced at the phosphorus atoms. The $Pd_2X_2(\mu\text{-}Ppy_3)_2$ complexes in water generate the $[Pd_2(H_2O)_2(\mu\text{-}Ppy_3)_2]^{2+}$ dication, which is isolated as various salts. The mononuclear complexes in water generate aquo and hydroxo species.

Key words: dimethylacetylenedicarboxylate adducts, palladium complexes (dinuclear), pyridylphosphines.

YUN XIE, CHUNG-LI LEE, YEPING YANG, STEVEN J. RETTIG et BRIAN R. JAMES. Can. J. Chem. **70**, 751 (1992).

On a préparé les complexes dibromo- et diiodo[(2-pyridyl)phosphine]palladium(II) par métathèse d'espèces *cis*-$PdCl_2(PPh_{3-n}py_n)_2$ (n = 1–3) en utilisant l'halogénure de sodium approprié; py = 2-pyridyl. On a utilisé la RMN, particulièrement celle du $^{13}C\{^1H\}$, pour distinguer entre les isomères *cis* et *trans*. On a synthétisé les complexes dinucléaires $Pd_2X_2(\mu\text{-}PPh_{3-n}py_n)_2$, X = halogénure, par le biais d'une réaction de conproportionation impliquant le $PdX_2(PPh_{3-n}py_n)_2$ et le $Pd(dba)_3$; dba = dibenzylidène acétone. Faisant appel à la cristallographie, on a pu établir que le $Pd_2I_2(\mu\text{-}PPh_2py)_2$ ainsi qu'un complexe en forme de A de l'acétylènedicarboxylate de diméthyle, $Pd_2Cl_2(\mu\text{-}Ppy_3)_2(\mu\text{-}MeO_2C \cdot C{=}C \cdot CO_2Me)$, sont des isomères tête à queue. Le premier cristallise dans le groupe d'espace monoclinique $C2/c$, avec a = 30,992(3), b = 18,764(1) et c = 13,100(1) Å, β = 100,676(5)° et Z = 8; on a affiné les données jusqu'à une valeur de R = 0,035 pour 5874 réflexions avec $I \geq 3\sigma(I)$. Le composé en forme de A est triclinique, groupe d'espace $P\bar{1}$, avec a = 13,545(2), b = 15,064(2) et c = 11,991(2) Å, α = 111,56(1), β = 95,36(1) et γ = 97,63(1)°, Z = 2 et R = 0,033 pour 7128 réflexions avec $I \geq 3\sigma(I)$. Les complexes $Pd_2X_2(\mu\text{-}PPhpy_2)_2$ existent sous la forme d'un mélange de diastéréo-isomères provoqués par la chiralité des atomes de phosphore. Dans l'eau, les complexes $Pd_2X_2(\mu\text{-}Ppy_3)_2$ conduisent à la formation du dication $[Pd(H_2O)_2(\mu\text{-}Ppy_3)_2]^{2+}$ que l'on a isolé sous la forme du plusieurs sels. Dans l'eau, les complexes mononucléaires fournissent des espèces aquo et hydroxo.

Mots clés : adduits de l'acétylènedicarboxylate de diméthyle, complexes dinucléaires du palladium, pyridylphosphines.

[Traduit par la rédaction]

Introduction

Our original interest in the well-known complexes of the type $Pd_2X_2(dpm)_2$ (X = anionic ligand)[3] arose because of their potential use in separation of gaseous components, particularly CO and H_2, in coal-gas streams (1). This then led to the discovery that such complexes readily abstract sulfur from H_2S to generate H_2 and the bridged-sulfide coproduct $Pd_2X_2(\mu\text{-}S)(dpm)_2$ (2). To extend such chemistry into aqueous media, we turned our attention to the 2-pyridyl substituted phosphines $PPh_{3-n}py_n$, whose solubility in water increases as n increases from 0 (insoluble) to 3 (3). The use of such phosphines has also rekindled a long-standing interest of this group in metal-complex catalyzed hydration of olefins (4), a topic that is of current interest and one in which both platinum and palladium–phosphine complexes show promise (5–7). To these ends, we are developing further the chemistry of, and catalysis by, complexes containing 2-pyridyl(phosphine) ligands, a subject that in itself is accruing considerable recent literature (8–13), following its instigation in the early 1970s within a PPh_2py system (14); this mono-pyridyl ligand was used extensively by Balch and coworkers (15–17), the studies including a communication on $PdCl_2(PPh_2py)_2$ and $Pd_2Cl_2(PPh_2py)_2$ (17). Newkome *et al.* (18) reported on *cis* and *trans*-$PdCl_2(PPhpy_2)_2$. These Pd complexes are, to our knowledge, the only ones reported within the complete series of $PdX_2(PPh_{3-n}py_n)_2$ and $Pd_2X_2(PPh_{3-n}py_n)_2$ complexes (X = halide).

This present paper reports on all nine mononuclear and all

[1]On leave from Anhui University, Hefei, The People's Republic of China.

[2]Author to whom correspondence may be addressed.

[3]Abbreviations used: dpm = bis(diphenylphosphino)methane; py = 2-pyridyl; dpmMe(monomethylated dpm) = 1,1-bis(diphenylphosphino)ethane; the $PPh_{3-n}py_n$ (n = 1–3) ligands and dpmMe in the dinuclear $Pd_2(I)$ species are always bridging, but for convenience the μ symbol is omitted; DMAD = dimethylacetylenedicarboxylate; dba = dibenzylideneacetone.

Can. J. Chem. Downloaded from www.nrcresearchpress.com by 92.62.229.171 on 09/08/12
For personal use only.

TABLE 1. Characterization of mono- and dinuclear Pd–pyridylphosphine complexes

	Complex	%C (calcd.)	%H (calcd.)	%N (calcd.)	λ_{max} nm ($\varepsilon \times 10^{-3}$ M^{-1} cm^{-1})[a]	$^{31}P\{^1H\}$, δ[b] *cis*	*trans*
1*a*	$PdCl_2(Ppy_3)_2$	50.62 (50.90)	3.34 (3.42)	11.90 (11.87)	338 (3.42)	34.6	—
1*b*	$PdBr_2(Ppy_3)_2$	44.55 (45.22)	3.00 (3.04)	9.94 (10.55)	362 (4.13)	32.1	—
1*c*	$PdI_2(Ppy_3)_2$	39.90 (40.45)	2.65 (2.72)	9.51 (9.44)	428 (3.03)	—	7.0
2*a*	$PdCl_2(PPhpy_2)_2$[c]	54.67 (54.45)	3.99 (3.71)	7.88 (7.94)	337 (6.21)	30.9	17.7
2*b*	$PdBr_2(PPhpy_2)_2$	46.84 (48.36)	3.52 (3.30)	6.71 (7.05)	362 (6.63)	27.9	—
2*c*	$PdI_2(PPhpy_2)_2$	41.85 (43.24)	2.82 (2.95)	6.59 (6.31)	421 (3.62)	—	8.9
3*a*	$PdCl_2(PPh_2py)_2$[d]	57.89 (58.01)	4.27 (4.01)	4.20 (3.98)	340 (13.2)	29.5	23.4
3*b*	$PdBr_2(PPh_2py)_2$	51.42 (51.51)	3.53 (3.56)	3.42 (3.53)	363 (9.73)	26.5	20.5
3*c*	$PdI_2(PPh_2py)_2$	45.94 (46.05)	3.09 (3.18)	2.99 (3.16)	425 (3.11)		9.6
						$^{31}P\{^1H\}$, δ[b]	
4*a*	$Pd_2Cl_2(Ppy_3)_2$	44.28 (44.25)	3.01 (2.97)	10.26 (10.32)	335(12.0), 460(8.43)	6.3	
4*b*	$Pd_2Br_2(Ppy_3)_2$	39.63 (39.90)	2.70 (2.68)	9.00 (9.31)	348(11.6), 475(10.3)	4.35	
4*c*	$Pd_2I_2(Ppy_3)_2$	36.08 (36.14)	2.40 (2.43)	8.20 (8.43)	376(9.70), 525(11.7)	0.55	
5*a*	$Pd_2Cl_2(PPhpy_2)_2$	44.06 (44.17)	3.23 (3.37)	6.27 (6.24)[e]	333(10.8), 462(9.47)	5.2	
5*b*	$Pd_2Br_2(PPhpy_2)_2$	42.30 (42.65)	2.80 (2.91)	6.34 (6.22)	345(15.0), 476(9.90)	3.28	
5*c*	$Pd_2I_2(PPhpy_2)_2$	37.60 (38.62)	2.78 (2.63)	5.29 (5.63)	376(15.3), 530(13.7)	−0.16	
6*a*	$Pd_2Cl_2(PPh_2py)_2$	51.17 (51.40)	3.25 (3.48)	3.73 (3.46)	332(7.57), 466(2.87)	4.4	
6*b*	$Pd_2Br_2(PPh_2py)_2$	45.31 (45.42)	3.15 (3.14)	2.95 (3.11)	348(13.7), 483(7.92)	2.92	
6*c*	$Pd_2I_2(PPh_2py)_2$	41.47 (41.11)	3.07 (2.84)	2.76 (2.82)	379(13.4), 540(10.8)	−0.44	
	DMAD adducts				^1H, δ(Me)[f]	$^{31}P\{^1H\}$, δ[b]	
7	$Pd_2Cl_2(Ppy_3)_2(\mu$-DMAD)	44.87 (45.21)	3.16 (3.16)	8.53 (8.78)	3.03	34.1	
8	$Pd_2Cl_2(PPhpy_2)_2(\mu$-DMAD)	47.59 (47.72)	3.50 (3.38)	5.69 (5.87)	3.15, 3.08, 3.06, 2.47 (4:2:2:1)	35.5, 35.3, 33.8 33.3 (4:2:2:1)	
9	$Pd_2Cl_2(PPh_2py)_2(\mu$-DMAD)	50.68 (50.45)	3.51 (3.60)	3.09 (2.94)	3.10	35.8	
	Bis(aquo)species $[Pd_2(H_2O)_2(Ppy_3)_2]^{2+}2A^-$[g]						
10*a*	A = BF_4	37.37 (37.81)	2.90 (2.96)	8.47 (8.82)		−21.8 (−19.4)[h]	
10*b*	A = PF_6	33.71 (33.70)	2.55 (2.64)	7.72 (7.86)		−22.2	
10*c*	A = BPh_4	66.45 (66.08)	4.78 (4.83)	5.92 (5.93)		−22.6	

[a] In CH_2Cl_2 at ~20°C.

[b] All singlets. Data measured at ~20°C unless otherwise stated: in CD_2Cl_2 at −70°C for **1***a*–**1***c*, **2***b*, **2***c*, **3***b*, **3***c*; in CD_2Cl_2 for **2***a*, **3***a*, **4***a*–**4***c*, **6***c*; in $CDCl_3$ for **5***a*–**5***c*, **6***a*, **7**–**9**; in CD_3CN for **10***a*, **10***b*; in acetone-d_6 for **10***c*.

[c] Characterized by Newkome *et al.* (18), including an X-ray structure of the *cis* isomer.

[d] Reported by Maisonnat *et al.* (17), but with no detail.

[e] % Cl 16.00; calcd. 15.80.

[f] All singlets; in $CDCl_3$ at ~20°C.

[g] IR (Nujol), $\nu(H_2O)$ 1627 cm^{-1}. Λ(MeCN, ohm^{-1} mol^{-1} cm^2): 270 (**10***a*), 255 (**10***b*), 190 (**10***c*). UV/vis: in H_2O 409 nm ($\varepsilon = 9.3 \times 10^3$ M^{-1} cm^{-1}); in MeCN 420 nm ($\varepsilon = 6.1 \times 10^3$ M^{-1} cm^{-1}).

[h] In H_2O at ~20°C.

nine dinuclear complexes; *cis* and *trans* formulations within the mononuclear species are assigned, and a head-to-tail (HT) geometry (implying the two phosphorus atoms are bound to different metals) demonstrated crystallographically for $Pd_2I_2(PPh_2py)_2$, and for the A-frame complex $Pd_2Cl_2(Ppy_3)_2(\mu$-DMAD). The anticipated chirality at the coordinated phosphorus of a bridging $PPhpy_2$ ligand is observed; and finally the solvolysis of two Ppy_3 complexes in water is studied.

Experimental section

The compounds $PdCl_2(PhCN)_2$ (19), $Pd_2(dba)_3 \cdot CHCl_3$ (20), PPh_2py (21), and Ppy_3 (22) were prepared by the literature procedures. $^{31}P\{^1H\}$ (121.4 MHz) and $^{13}C\{^1H\}$ (75.4 MHz) NMR spectra were recorded on a Varian XL-300 instrument. $^{31}P\{^1H\}$ NMR shifts are given relative to the external 85% H_3PO_4, downfield being positive; $^{13}C\{^1H\}$ NMR shifts are relative to external TMS. Infrared spectra were recorded as Nujol mulls on a Nicolet 5DX FT spectrophotometer. Visible absorption spectra were recorded on a Perkin–Elmer 552A spectrophotometer. Conductivity measurements were recorded in aqueous or MeCN solution at 10^{-3} M complex concentration in a cell (Fisher Sci. Co.) connected to a Beckman Serfass conductance bridge. pH titrations were carried out at 25°C in aqueous media under N_2 using a Corning 12 pH-meter and a combination electrode.

The $PPhpy_2$ ligand was prepared by a procedure similar to that reported for Ppy_3 (22). ^{n}BuLi (50 mL, 1.6 M in hexane) was transferred to 50 mL of Et_2O at −100°C, under N_2. 2-Bromopyridine (80 mmol) was added and the mixture stirred vigorously at −100°C until the colour turned to deep red (~4 h). Liquid $PPhCl_2$ (40 mmol in 10 mL Et_2O) was then added dropwise via a syringe with stirring of the reaction solution; this generates a light brown slurry, which is then stirred at −90°C for 2 h. The mixture was then extracted at room temperature with degassed H_2SO_4 (2 M, 2 × 100 mL), and the aqueous layer collected and made alkaline by adding (with stirring) saturated NaOH solution. The deposited yellow crystals were washed with H_2O, and with acetone/H_2O (1:1), recrystallized from acetone/petroleum ether (1:1), and dried *in vacuo*. Yield 60%; mp 96.7–98.3°C. $^{31}P\{^1H\}$ NMR ($CDCl_3$, 20°C) δ: −1.98. Anal. calcd. for $C_{16}H_{13}N_2P$: C 72.71, H 4.96, N 10.60; found: C 72.90, H 4.99, N 10.43. (Despite reported use of $PPhpy_2$, we were unable to find details of its synthesis and characterization; see, for example, ref. 13.)

Can. J. Chem. Downloaded from www.nrcresearchpress.com by 92.62.229.171 on 09/08/12
For personal use only.

Can. J. Chem. Downloaded from www.nrcresearchpress.com by 92.62.229.171 on 09/08/12
For personal use only.

The various Pd complexes (see Table 1) were synthesized routinely under an N_2 atmosphere, but this is probably not essential. Elemental analyses of the complexes (Table 1) were satisfactory except for the C analyses of **2***b*, **2***c*, and **5***c*, which were low by 1.0–1.5% and could not be improved. The samples were "pure" as judged by $^{31}P\{^1H\}$ NMR data; impurities could be the respective sodium halides or occluded solvent; both structures determined reveal solvate molecules (*vide infra*).

*$PdX_2(PPh_{3-n}py_n)_2$ complexes (***1**a–**1**c; **2**a–**2**c; **3**a–**3**c*)*

The chloro species **1***a*, **2***a*, and **3***a* were prepared by dissolving $PdCl_2(PhCN)_2$ (300 mg, 0.78 mmol) in CH_2Cl_2 (20 mL), and adding to this reddish-brown solution 2 equivalents of the pyridylphosphine dissolved in a minimum amount of CH_2Cl_2 (~7 mL). After the solution was stirred at room temperature for 30 min, a yellow solid slowly precipitated; addition of Et_2O (40 mL) completed the precipitation. The complexes were purified by dissolution/reprecipitation twice from CH_2Cl_2/Et_2O, and dried *in vacuo*; yields ~95%. The syntheses follow that given for **3***a* in the literature, but with no details (17). The bromo (**1***b*, **2***b*, **3***b*) and iodo analogues (**1***c*, **2***c*, **3***c*) were prepared from **1***a*, **2***a* and **3***a*, respectively, by addition of 10 equivalents of the appropriate sodium halide dissolved in a minimum amount of water to the chloro complex (~0.3 mmol) dissolved in CH_2Cl_2 (150 mL); MeOH (5 mL) was introduced to homogenize the mixture, which was stirred for 2 h at room temperature. The solution colour changed from yellow to orange (bromo species) or brown (iodo species), and crystals of the product formed on reducing the solution volume to ~20 mL; the complexes were collected, washed with H_2O (100 mL) and then MeOH (100 mL), and dried *in vacuo*; yields 85–95%.

*$Pd_2X_2(PPh_{3-n}py_n)_2$ complexes (***4**a–**4**c; **5**a–**5**c; **6**a–**6**c*)*

To a suspension of $PdX_2(PPh_{3-n}py_n)_2$ complex (0.42 mmol) in CH_2Cl_2 (20 mL) was added slowly $Pd_2(dba)_3 \cdot CHCl_3$ (0.22 g, 0.21 mmol) dissolved in CH_2Cl_2 (20 mL), and the mixture stirred at room temperature for ~1 h until a clear solution resulted. The volume was then reduced to 10 mL and Et_2O (10 mL) added to yield the desired product; the collected solid was precipitated twice from CH_2Cl_2 (15 mL) using Et_2O (10 mL), and vacuum-dried; yields ≥ 80%.

*$Pd_2Cl_2(PPh_{3-n}py_n)_2(\mu\text{-}MeO_2C \cdot C{\equiv}C \cdot CO_2Me)$; n = 3(***7**), 2 (**8**), and 1(**9**)*

Excess DMAD (0.41 g, 2.8 mmol) was added to a CH_2Cl_2 solution (50 mL) containing **4***a* (0.20 g, 0.25 mmol), and the mixture stirred for 1 h at room temperature. The resulting solution was reduced to 30 mL by Rotavap, and Et_2O added (50 mL) to precipitate complex **7** in quantitative yield. **8** and **9** were made similarly from **5***a* and **6***a*, respectively.

*$[Pd_2(H_2O)_2(Ppy_3)_2]^{2+}$ $2A^-$; A = BF_4 (***10**a*), PF_6 (***10**b*), BPh_4 (***10**c*)*

Complex **4***a* (15 mg, 19 μmol) was dissolved in H_2O (100 mL) to form a green solution (~1 h), and 5 equivalents of the appropriate salt solution (5 mL) added with stirring ($NaBF_4$ or KPF_6 in H_2O; $NaBPh_4$ in MeOH). The green solid that precipitated overnight was collected, redissolved in MeCN and reprecipitated by addition of Et_2O, and dried *in vacuo*; yields 80–90%.

Crystallographic characterization of **6**c *as $Pd_2I_2(PPh_2py)_2 \cdot 1/2$(acetone), and* **7** *as $Pd_2Cl_2(Ppy_3)_2(\mu\text{-}DMAD) \cdot 2CH_2Cl_2$*

Crystals were prepared by placing test tubes containing 10 mL of a saturated solution of the complex (**6***c* in acetone, **7** in CH_2Cl_2) in a closed vessel (300 mL) containing 100 mL Et_2O; purple crystals of **6***c* · 0.5 C_3H_6O and yellow crystals of **7** · $2CH_2Cl_2$ were formed over 2 days.

Crystallographic data for both compounds are given in Table 2. Final unit-cell parameters were obtained by least squares on 2 sin θ/λ values for 25 reflections (with 2θ = 40–60° for **6***c* and 34–46° for **7**). The intensities of three check reflections, measured each hour of X-ray exposure time throughout the data collections, showed small random fluctuations. The data were processed, with absorption corrections being applied using the Gaussian integration method (23, 24)[4].

In each structural determination there was a choice between centrosymmetric and noncentrosymmetric space groups, the former being suggested by both the *E*-statistics and the Patterson functions. Both structures were solved by conventional heavy-atom methods, the coordinates of Pd, P, and metal-coordinated halogen atoms being determined from the Patterson functions and those of the remaining non-hydrogen atoms from subsequent difference maps.

In both structures there is disordering of solvent molecules. In **6***c*, an acetone solvate (O(1), C(35–37)) is disordered 1:1 about the twofold axis (1/2, *y*, 1/4). One methyl carbon, C(35), was constrained to be on the twofold axis even though it is obvious from the resulting geometry that this atom must be displaced from the twofold axis by about 0.4 Å. Unfortunately, attempts to refine C(35) in a more realistic position resulted in a singular matrix. The incorrect model employed does account for the electron density in the region and, in view of the relatively minor importance of the solvent molecule, no attempts at more sophisticated treatment were made. In **7**, one of the two independent CH_2Cl_2 molecules (Cl(5–7), C(38)) was disordered in a way such that the two Cl atoms were unequally distributed over three sites. The site occupancies were initially estimated from the relative peak heights on a Fourier map and were subsequently adjusted to result in nearly equal thermal parameters for the three positions. The thermal parameters and occupancy factors could not be simultaneously refined due to high correlations. The thermal parameters of the carbon atom C(38) are indicative of at least twofold disorder of this atom as well, but again no attempt was made to resolve this disorder.

In the final stages of full-matrix least-squares refinement all non-hydrogen atoms were refined with anisotropic thermal parameters, and hydrogen atoms (except those associated with the disordered solvent molecules) were included as fixed atoms in calculated positions (methyl H positions based on observed positions, $C(sp^3)$—H = 0.98 Å, $C(sp^2)$—H = 0.97 Å, $U_H \propto U_{parent}$). Neutral atom scattering factors and anomalous scattering corrections (Pd, I, Cl, P) were taken from ref. 24. Final positional and equivalent isotropic thermal parameters (U_{eq} = 1/3 trace diagonalized U) are given in Table 3. Selected bond lengths, bond angles, and intra-annular torsion angles appear in Table 4. Anisotropic thermal parameters, calculated hydrogen parameters, complete listings of bond lengths, bond angles, torsion angles, and measured and calculated structure factor amplitudes have been deposited (Tables S1–S6).[5]

Results and discussion

The $PdX_2(PPh_{3-n}py_n)_2$ complexes

The four-coordinate, mononuclear complexes all contain monodentate pyridylphosphine ligands bound via the phosphorus and were synthesized from $PdCl_2(PhCN)_2$ using a method published in outline only for **3***a*, $PdCl_2(PPh_2py)_2$ (17).

[4]The computer programs used include locally written programs for data processing and locally modified versions of the following: ORFLS, full-matrix least-squares, and ORFFE, function and errors, by W. R. Busing, K. O. Martin and H. A. Levy; FORDAP, Patterson and Fourier syntheses, by A. Zalkin; ORTEP II, illustrations, by C. K. Johnson.

[5]This supplementary material may be purchased from: The Depository of Unpublished Data, Document Delivery, CISTI, National Research Council Canada, Ottawa, Canada K1A 0S2.

Tables of bond lengths and angles and hydrogen atom parameters have also been deposited with the Cambridge Crystallographic Data Centre and can be obtained on request from The Director, Cambridge Crystallographic Data Centre, University Chemical Laboratory, Lensfield Road, Cambridge CB2 1EW, U.K.

TABLE 2. Crystallographic data[a] for **6c** · 0.5 C_3H_6O and **7** · 2 CH_2Cl_2

Compound	$Pd_2I_2(PPh_2py)_2 \cdot 0.5\ C_3H_6O$	$Pd_2Cl_2(Ppy_3)_2(\mu\text{-DMAD}) \cdot 2\ CH_2Cl_2$
Formula	$C_{34}H_{28}I_2N_2P_2 \cdot 0.5\ C_3H_6O$	$C_{36}H_{30}Cl_2N_6O_4P_2Pd_2 \cdot 2\ CH_2Cl_2$
fw	1022.2	1126.2
Crystal system	Monoclinic	Triclinic
Space group	$C2/c$	$P\bar{1}$[b]
a, Å	30.992(3)	13.545(2)
b, Å	18.764(1)	15.064(2)
c, Å	13.100(1)	11.991(2)
α°	90	111.56(1)
β°	100.676(5)	95.36(1)
γ°	90	97.63(1)
V, Å^3	7486(1)	2228.1(7)
Z	8	2
ρ_{calcd}, g/cm^3	1.814	1.679
$F(000)$	3920	1120
μ(Mo-K_α), cm^{-1}	26.93	12.75
Crystal size, mm	0.26 × 0.26 × 0.58	0.18 × 0.22 × 0.47
Transmission factors	0.438–0.562	0.747–0.822
Scan type	ω–2θ	ω–2θ
Scan range, deg in ω	0.80 + 0.35 tan θ	0.65 + 0.35 tan θ
Scan speed, deg/min	1.68–10.06	1.18–10.06
Data collected	$\pm h, +k, +l$	$\pm h, -k, \pm l$
$2\theta_{max}$, deg	55	55
Crystal decay	Negligible	Negligible
Unique reflections	8081	10217
Reflections with $I \geq 3\sigma(I)$	5874	7128
No. of variables	411	532
R	0.035	0.033
R_w	0.049	0.039
gof	1.956	1.843
Mean Δ/σ (final cycle)	0.04	0.05
Max Δ/σ (final cycle)	0.27	0.31
Residual density e/Å^3	−2.85 to +1.12, both near $I(2)$	−1.92 to +0.855, both near disordered CH_2Cl_2

[a]Temperature 294 K, Enraf–Nonius CAD4-F diffractometer, Mo-K_α radiation ($\lambda K_{\alpha 1}$ = 0.70930, $\lambda K_{\alpha 2}$ = 0.71359 Å), graphite monochromator, takeoff angle 2.7°, aperture (2.0 + tan θ) × 4.0 mm at a distance of 173 mm from the crystal, scan range extended by 25% on both sides for background measurement, $\sigma^2(I) = C + 2B + [p(C - B)]^2$ (C = scan count, B = normalized background count, p = 0.04 for **6c** · 0.5 C_3H_6O, 0.035 for **7** · 2 CH_2Cl_2), function minimized $\Sigma w(|F_o| - |F_c|)^2$ where $w = 4F_o^2/\sigma^2(F_o^2)$, $R = \Sigma||F_o| - |F_c||/\Sigma|F_o|$, $R_w = (\Sigma w(|F_o| - |F_c|)^2/\Sigma w|F_o|^2)^{1/2}$, and gof = $(\Sigma(|F_o| - |F_c|)^2/(m - n))^{1/2}$. Values given for R, R_w, and gof are based on those reflections with $I \geq 3\sigma(I)$.

[b]Reduced cell, Donnay convention.

The *cis* and *trans* forms of the $PdCl_2(PPhpy_2)_2$ complex (**2a**) were synthesized previously from $PdCl_4^{2-}$, and an X-ray structure given for the *cis* isomer (18); the $^{31}P\{^1H\}$ NMR signal is a singlet for either the *cis* or *trans* isomer, and using the structural data Newkome *et al.* (18) were able to assign the lower field signal to the *cis* isomer (Table 1). We have used $^{13}C\{^1H\}$ to distinguish the geometric isomers; in the *trans* complex, $^2J_{PP}$ is usually large (~400 Hz) compared to a value of <50 Hz in the *cis* complex, and hence the C atoms adjacent to a phosphorus appear as a virtual 1:2:1 triplet (as opposed to a doublet in a *cis* isomer) (25, 26). Table 5 lists the $^{13}C\{^1H\}$ data for selected complexes, which show that **1a** is *cis*, while the iodo species **2c** and **3c** are *trans*. The $^{31}P\{^1H\}$ data for **1a** (Table 1) fit well a tentatively suggested correlation (18) of a gradual downfield shift with sequential replacement of Ph by py in the complexes *cis*-$PdCl_2(PPh_{3-n}py_n)_2$ as n varies from 0 to 3. The same trend holds for the series of *cis*-dibromo complexes **3b**–**2b**–**1b**; the opposite trend holds for the diiodo species **3c**–**2c**–**1c**, which, however, have *trans* geometry; the data given for *trans*-**2a** and *trans*-**3a** follow the same trend as for the *trans*-diiodo complexes (Table 1).

The $^{31}P\{^1H\}$ NMR data (Table 1) refer to the dissolved, isolated complexes, but the syntheses of the *trans*-diiodo species by metathesis reactions from the predominantly *cis*-dichloro precursors probably involve an isomerization process. The *trans* geometry is normally preferred in nonpolar solvents, while a π-interaction between pyridyl groups on adjacent phosphine ligands (noted in the structure of *cis*-$PdCl_2(PPhpy_2)_2$) has been suggested as a possible reason for preferred *cis* geometry (18).

It is worth noting also that, for any given pyridyl phosphine ligand within a *cis* or *trans* triad, the $^{31}P\{^1H\}$ singlet shifts to higher field as Cl is replaced successively by Br and then I, consistent with increasing basicity of the halogeno ligand. The UV/vis absorption maximum of the complexes occurs as a charge transfer band at 337–340 nm for the three dichloro species, at 362–363 nm for the dibromo species, and

Can. J. Chem. Downloaded from www.nrcresearchpress.com by 92.62.229.171 on 09/08/12
For personal use only.

TABLE 3. Final positional (fractional × 10^4; I, Pd, P, Cl(1–2) × 10^5) and isotropic thermal parameters ($U \times 10^3$ Å^2) with estimated standard deviations in parentheses

Atom	x	y	z	U_{eq}[a]
$Pd_2I_2(PPh_2py)_2 \cdot 0.5\ C_3H_6O$				
I(1)	41608(1)	3444(2)	21746(3)	47
I(2)	34079(2)	40321(2)	41821(4)	74
Pd(1)	40389(1)	16727(2)	28522(3)	34
Pd(2)	38059(1)	28965(2)	35013(3)	39
P(1)	34572(4)	19500(7)	16602(9)	36
P(2)	39518(4)	22957(8)	49728(10)	40
N(1)	3666(2)	3315(2)	1987(3)	49
N(2)	4535(1)	1513(2)	4183(3)	40
C(1)	3459(2)	2877(3)	1243(4)	41
C(2)	3732(3)	4003(3)	1757(5)	74
C(3)	3580(3)	4277(4)	781(6)	82
C(4)	3357(3)	3848(4)	22(5)	77
C(5)	3300(2)	3139(3)	241(4)	55
C(6)	3352(2)	1517(3)	394(4)	43
C(7)	3702(2)	1394(3)	−117(4)	53
C(8)	3635(2)	1111(4)	−1108(4)	66
C(9)	3217(3)	943(4)	−1595(4)	72
C(10)	2872(2)	1052(4)	−1121(5)	67
C(11)	2938(2)	1342(3)	−126(4)	53
C(12)	2949(2)	1804(3)	2124(4)	41
C(13)	2858(2)	1128(3)	2426(5)	59
C(14)	2467(2)	974(4)	2757(6)	73
C(15)	2169(2)	1506(5)	2795(5)	68
C(16)	2258(2)	2187(4)	2508(5)	66
C(17)	2641(2)	2339(3)	2186(4)	53
C(18)	4444(2)	1743(3)	5101(4)	41
C(19)	4892(2)	1118(3)	4192(4)	48
C(20)	5166(2)	907(3)	5100(5)	52
C(21)	5060(2)	1109(4)	6036(4)	65
C(22)	4704(2)	1541(4)	6030(4)	64
C(23)	4061(2)	2798(3)	6186(4)	51
C(24)	4284(3)	3432(5)	6221(5)	83
C(25)	4374(4)	3820(6)	7144(8)	120
C(26)	4241(4)	3552(7)	8015(6)	114
C(27)	4029(3)	2911(6)	7989(5)	88
C(28)	3937(2)	2544(4)	7091(4)	62
C(29)	3520(2)	1681(3)	5149(4)	42
C(30)	3571(2)	953(3)	5180(5)	51
C(31)	3230(2)	517(3)	5317(5)	58
C(32)	2842(2)	795(4)	5425(5)	59
C(33)	2780(2)	1514(4)	5382(6)	68
C(34)	3120(2)	1965(3)	5242(5)	58
O(1)[1]	4708(5)	2984(10)	934(14)	141
C(35)[1]	5000	3557(16)	2500	277
C(36)[1]	4993(13)	4318(31)	748(35)	268
C(37)[1]	4995(17)	3613(32)	1013(41)	271
$Pd_2Cl_2(Ppy_3)_2(MeO_2CC{=}CCO_2Me) \cdot 2\ CH_2Cl_2$				
Pd(1)	11602(2)	15958(2)	46547(2)	26
Pd(2)	24012(2)	30544(2)	40820(2)	27
Cl(1)	8575(9)	562(7)	30254(10)	54
Cl(2)	25161(8)	25756(8)	19763(9)	49
Cl(3)	−1676(3)	3054(2)	10026(3)	182
Cl(4)	−1755(3)	4547(2)	9067(3)	170
Cl(5)[2]	3696(3)	3393(4)	9432(3)	200
Cl(6)[3]	5236(4)	2233(3)	9528(3)	201
Cl(7)[4]	3557(14)	2340(11)	8994(15)	196
P(1)	36743(7)	24275(7)	46205(9)	30
P(2)	−1279(6)	21429(6)	39597(8)	27
O(1)	1336(3)	2390(2)	7654(3)	55
O(2)	653(3)	3654(2)	7660(3)	60
O(3)	3013(3)	5079(2)	6253(3)	58
O(4)	2884(3)	4661(2)	7824(3)	74
N(1)	2445(2)	1211(2)	5402(3)	30
N(2)	1135(2)	3695(2)	3829(3)	32
N(3)	5265(3)	1975(3)	3399(3)	48
N(4)	−1933(2)	2627(2)	4650(3)	43
N(5)	5121(2)	3998(2)	5337(3)	47
N(6)	−1517(3)	704(3)	2310(3)	49
C(1)	1544(2)	2886(2)	6055(3)	28
C(2)	2224(3)	3497(2)	5832(3)	29
C(3)	1146(3)	3055(3)	7211(3)	34
C(4)	2743(3)	4456(3)	6750(4)	36
C(5)	947(5)	2446(4)	8761(5)	73
C(6)	3506(5)	6043(4)	7064(6)	88
C(7)	3393(3)	1521(3)	5298(3)	31
C(8)	4193(3)	1137(3)	5652(4)	42
C(9)	4011(3)	449(3)	6143(4)	47
C(10)	3033(3)	152(3)	6272(4)	44
C(11)	2282(3)	541(3)	5890(4)	37
C(12)	165(3)	3329(2)	3802(3)	31
C(13)	−607(3)	3761(3)	3537(4)	42
C(14)	−407(3)	4595(3)	3311(4)	46
C(15)	588(3)	4987(3)	3362(4)	42
C(16)	1326(3)	4512(3)	3614(4)	43
C(17)	4290(3)	1691(3)	3384(3)	37
C(18)	3722(3)	852(4)	2522(4)	54
C(19)	4187(4)	271(4)	1620(4)	63
C(20)	5184(4)	554(4)	1629(4)	60
C(21)	5698(4)	1400(4)	2501(5)	58
C(22)	−1154(3)	2214(3)	4877(3)	32
C(23)	−1094(3)	1827(3)	5756(4)	38
C(24)	−1855(3)	1876(3)	6451(4)	50
C(25)	−2635(3)	2332(3)	6263(4)	52
C(26)	−2643(3)	2678(3)	5365(4)	52
C(27)	4675(3)	3348(3)	5739(4)	35
C(28)	4879(3)	3424(3)	6905(4)	52
C(29)	5586(4)	4206(4)	7711(5)	69
C(30)	6054(3)	4870(3)	7315(5)	60
C(31)	5805(3)	4747(3)	6121(5)	54
C(32)	−737(3)	1370(2)	2410(3)	32
C(33)	−326(3)	1461(3)	1423(4)	47
C(34)	−759(4)	807(4)	271(4)	61
C(35)	−1569(4)	99(4)	141(4)	65
C(36)	−1917(4)	77(4)	1180(5)	67
C(37)	−1265(10)	4170(8)	9994(13)	208
C(38)	4357(11)	2715(18)	10170(12)	293

[a] U_{eq} = 1/3 trace U(diag), superscripts 1–4 refer to occupancy factors of 0.5, 0.943, 0.825, and 0.232 respectively.

at 421–428 nm for the diiodo species, without consideration of the presence of *cis* and (or) *trans* forms (Table 1); the trend is indicative of a halogen → metal charge transfer, being of lowest energy for the diiodo complexes.

Attempts to find ν(Pd—X) and ν(Pd—P) stretches in the IR, widely used to distinguish *cis* and *trans* isomers within $PdX_2(PR_3)_2$ complexes (26, 27), were unsuccessful because of strong absorption by the pyridyl phosphine ligands.

The $Pd_2X_2(PPh_{3-n}py_n)_2$ complexes

The phosphorus atoms within the dinuclear Pd(I) complexes are equivalent whether a head-to-tail (HT) geometry exists or an HH arrangement (with the two phosporus atoms

Can. J. Chem. Downloaded from www.nrcresearchpress.com by 92.62.229.171 on 09/08/12
For personal use only.

TABLE 4. Selected bond lengths (Å), bond angles (°), and intra-annular torsion angles (°), with estimated standard deviations in parentheses

$Pd_2I_2(PPh_2py)_2 \cdot 0.5\ C_3H_6O$

I(1)—Pd(1)	2.6958(5)	P(2)—C(18)	1.827(5)
I(2)—Pd(2)	2.6954(6)	P(2)—C(23)	1.824(5)
Pd(1)—Pd(2)	2.5970(5)	P(2)—C(29)	1.813(6)
Pd(1)—P(1)	2.217(1)	N(1)—C(1)	1.344(7)
Pd(1)—N(2)	2.121(4)	N(1)—C(2)	1.350(8)
Pd(2)—P(2)	2.206(1)	N(2)—C(18)	1.355(6)
Pd(2)—N(1)	2.103(4)	N(2)—C(19)	1.332(7)
P(1)—C(1)	1.823(5)	C(1)—C(5)	1.403(7)
P(1)—C(6)	1.821(5)	C(2)—C(3)	1.377(9)
P(1)—C(12)	1.812(5)		
I(1)—Pd(1)—Pd(2)	171.78(2)	C(6)—P(1)—C(12)	102.6(2)
I(1)—Pd(1)—P(1)	97.48(4)	Pd(2)—P(2)—C(18)	113.8(2)
I(1)—Pd(1)—N(2)	90.9(1)	Pd(2)—P(2)—C(23)	118.2(2)
Pd(2)—Pd(1)—P(1)	77.53(4)	Pd(2)—P(2)—C(29)	113.5(2)
Pd(2)—Pd(1)—N(2)	93.4(1)	C(18)—P(2)—C(23)	101.3(2)
P(1)—Pd(1)—N(2)	169.4(1)	C(18)—P(2)—C(29)	104.5(2)
I(2)—Pd(2)—Pd(1)	168.34(2)	C(23)—P(2)—C(29)	103.9(3)
I(2)—Pd(2)—P(2)	98.45(4)	Pd(2)—N(1)—C(1)	116.3(3)
I(2)—Pd(2)—N(1)	89.4(1)	Pd(2)—N(1)—C(2)	123.7(4)
Pd(1)—Pd(2)—P(2)	79.05(4)	C(1)—N(1)—C(2)	119.7(5)
Pd(1)—Pd(2)—N(1)	92.5(1)	Pd(1)—N(2)—C(18)	116.6(3)
P(2)—Pd(2)—N(1)	171.2(1)	Pd(1)—N(2)—C(19)	124.1(3)
Pd(1)—P(1)—C(1)	112.8(2)	C(18)—N(2)—C(19)	118.6(4)
Pd(1)—P(1)—C(6)	121.5(2)	P(1)—C(1)—N(1)	113.2(4)
Pd(1)—P(1)—C(12)	111.9(2)	P(1)—C(1)—C(5)	126.5(4)
C(1)—P(1)—C(6)	99.4(2)	N(1)—C(1)—C(5)	120.1(5)
C(1)—P(1)—C(12)	107.2(2)	P(2)—C(18)—N(2)	113.9(3)
		P(2)—C(18)—C(22)	125.3(4)
P(1)—Pd(1)—Pd(2)—N(1)	−40.5(1)	P(2)—Pd(2)—Pd(1)—N(2)	−37.3(1)
Pd(1)—Pd(2)—N(1)—C(1)	41.2(4)	Pd(2)—Pd(1)—N(2)—C(18)	36.9(4)
Pd(2)—N(1)—C(1)—P(1)	−13.3(5)	Pd(1)—N(2)—C(18)—P(2)	−10.9(5)
N(1)—C(1)—P(1)—Pd(1)	−29.6(4)	N(2)—C(18)—P(2)—Pd(2)	−28.7(5)
C(1)—P(1)—Pd(1)—Pd(2)	44.2(2)	C(18)—P(2)—Pd(2)—Pd(1)	41.6(2)

$Pd_2Cl_2(Ppy_3)_2(MeO_2CC{=}CCO_2Me) \cdot 2\ CH_2Cl_2$

Pd(1)—Cl(1)	2.373(1)	O(1)—C(3)	1.335(4)
Pd(1)—P(2)	2.2434(9)	O(1)—C(5)	1.452(5)
Pd(1)—N(1)	2.128(3)	O(2)—C(3)	1.192(4)
Pd(1)—C(1)	2.010(3)	O(3)—C(4)	1.315(5)
Pd(2)—Cl(2)	2.384(1)	O(3)—C(6)	1.444(6)
Pd(2)—P(1)	2.2260(9)	O(4)—C(4)	1.198(5)
Pd(2)—N(2)	2.127(3)	N(1)—C(7)	1.341(4)
Pd(2)—C(2)	2.003(3)	N(1)—C(11)	1.344(4)
P(1)—C(7)	1.845(4)	N(2)—C(12)	1.349(4)
P(1)—C(17)	1.842(4)	N(2)—C(16)	1.345(5)
P(1)—C(27)	1.831(4)	C(1)—C(2)	1.330(5)
P(2)—C(12)	1.860(3)	C(1)—C(3)	1.481(5)
P(2)—C(22)	1.842(4)	C(2)—C(4)	1.487(5)
P(2)—C(32)	1.832(4)		
Cl(1)—Pd(1)—P(2)	95.71(4)	C(4)—O(3)—C(6)	116.9(4)
Cl(1)—Pd(1)—N(1)	89.04(8)	Pd(1)—N(1)—C(7)	123.5(2)
Cl(1)—Pd(1)—C(1)	175.0(1)	Pd(1)—N(1)—C(11)	117.5(2)
P(2)—Pd(1)—N(1)	174.81(8)	C(7)—N(1)—C(11)	118.6(3)
P(2)—Pd(1)—C(1)	88.85(9)	Pd(2)—N(2)—C(12)	125.9(2)
N(1)—Pd(1)—C(1)	86.3(1)	Pd(2)—N(2)—C(16)	116.3(2)
Cl(2)—Pd(2)—P(1)	98.71(4)	C(12)—N(2)—C(16)	117.8(3)
Cl(2)—Pd(2)—N(2)	89.63(8)	Pd(1)—C(1)—C(2)	112.1(3)
Cl(2)—Pd(2)—C(2)	176.1(1)	Pd(1)—C(1)—C(3)	121.0(2)
P(1)—Pd(2)—N(2)	171.57(8)	C(2)—C(1)—C(3)	126.7(3)
P(1)—Pd(2)—C(2)	85.2(1)	Pd(2)—C(2)—C(1)	113.3(3)
N(2)—Pd(2)—C(2)	86.5(1)	Pd(2)—C(2)—C(4)	122.3(3)
Pd(2)—P(1)—C(7)	117.9(1)	C(1)—C(2)—C(4)	124.2(3)

Can. J. Chem. Downloaded from www.nrcresearchpress.com by 92.62.229.171 on 09/08/12
For personal use only.

TABLE 4 (*concluded*)

Pd(2)—P(1)—C(17)	116.4(1)	O(1)—C(3)—O(2)	123.1(4)
Pd(2)—P(1)—C(27)	112.9(1)	O(1)—C(3)—C(1)	111.2(3)
C(7)—P(1)—C(17)	97.5(2)	O(2)—C(3)—C(1)	125.5(3)
C(7)—P(1)—C(27)	103.7(2)	O(3)—C(4)—O(4)	122.9(4)
C(17)—P(1)—C(27)	106.6(2)	O(3)—C(4)—C(2)	112.2(3)
Pd(1)—P(2)—C(12)	117.3(1)	O(4)—C(4)—C(2)	124.9(4)
Pd(1)—P(2)—C(22)	111.9(1)	P(1)—C(7)—N(1)	121.1(3)
Pd(1)—P(2)—C(32)	114.3(1)	P(1)—C(7)—C(8)	118.0(3)
C(12)—P(2)—C(22)	107.4(2)	N(1)—C(7)—C(8)	120.9(3)
C(12)—P(2)—C(32)	100.3(2)	P(2)—C(12)—N(2)	118.5(3)
C(22)—P(2)—C(32)	104.4(2)	P(2)—C(12)—C(13)	119.8(3)
C(3)—O(1)—C(5)	116.9(3)	N(2)—C(12)—C(13)	121.3(3)
N(1)—Pd(1)—P(2)—C(12)	29.3(9)	C(7)—P(1)—Pd(2)—C(2)	59.0(2)
Pd(1)—P(2)—C(12)—N(2)	15.4(3)	P(1)—Pd(2)—C(2)—C(1)	−94.8(3)
P(2)—C(12)—N(2)—Pd(2)	−1.6(4)	Pd(2)—C(2)—C(1)—Pd(1)	13.1(3)
C(12)—N(2)—Pd(2)—P(1)	−66.8(7)	C(2)—C(1)—Pd(1)—N(1)	85.0(3)
N(2)—Pd(2)—P(1)—C(7)	50.9(6)		
Pd(2)—P(1)—C(7)—N(1)	3.6(3)	C(1)—Pd(1)—P(2)—C(12)	51.2(2)
P(1)—C(7)—N(1)—Pd(1)	6.5(4)	Pd(1)—P(2)—C(12)—N(2)	15.4(3)
C(7)—N(1)—Pd(1)—P(2)	−54.9(11)	P(2)—C(12)—N(2)—Pd(2)	−1.6(4)
		C(12)—N(2)—Pd(2)—C(2)	−74.8(3)
C(1)—Pd(1)—N(1)—C(7)	−76.8(3)	N(2)—Pd(2)—C(2)—C(1)	84.0(3)
Pd(1)—N(1)—C(7)—P(1)	6.5(4)	Pd(2)—C(2)—C(1)—Pd(1)	13.1(3)
N(1)—C(7)—P(1)—Pd(2)	3.6(3)	C(2)—C(1)—Pd(1)—P(2)	−93.0(2)

TABLE 5. $^{13}C\{^1H\}$ NMR data for the $PPh_{3-n}py_n$ ligands, and *trans*-$PdI_2(PPh_2py)_2$ (**3***c*), *trans*-$PdI_2(PPhpy_2)_2$ (**2***c*), and *cis*-$PdCl_2(Ppy_3)_2$ (**1***a*)[a]

Compound	C(1)	C(2)	(C3)	C(4)	C(5)	C(6)	C(7)	C(8)	C(9)
PPh_2py	136.2(d,11.6)	134.2(d,20.0)	128.7(d,7.4)	129.1(s)	164.0(d,3.0)[c]	150.4(d,12.7)	127.9(d,15.2)	122.2(s)	135.8(d,2.1)
$PPhpy_2$	[b]	135.1(d,20.6)	128.9(d,7.8)	129.7(s)	162.9(d,2.8)[c]	150.5(d,11.9)	128.5(d,17.9)	122.6(s)	135.9(d,3.0)
Ppy_3	—	—	—	—	161.9(d,3.6)[c]	150.5(d,11.5)	129.3(d,19.5)	122.9(s)	136.0(d,3.4)
3*c*	—	131.6(t,11.8)	123.6(t,10.2)	126.6(s)	[b]	145.4(t,15.2)	126.3(t,24.6)	119.9(s)	131.0(br.s)
2*c*	—	136.8(t,14.0)	127.6(t,12.2)	131.0(s)	[b]	149.1(t,17.0)	131.5(t,24.0)	124.0(s)	135.1(t,10.0)
1*a*	—	—	—	—	[b]	148.7(d,20.0)	131.5(d,21.7)	124.3(s)	135.5(d,17.4)

[a]In $CDCl_3$ at ~20°C for the ligands; in CD_2Cl_2 at −20°C for the complexes; s = singlet, d = doublet, t = triplet, br = broad; coupling constant given in parentheses is the $|^xJ_{PC} + {}^{x+2}J_{PC}|$ value in Hz, where x = 1–3; labelling of C atoms is depicted below.

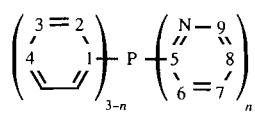

[b]Signal is not detected due to the lack of proton NOE effect.
[c]Very low intensity.

on the same metal). The crystal structure of $Pd_2I_2(PPh_2py)_2$, **6***c*, reveals the HT arrangement (Fig. 1), and thus the singlet in the $^{31}P\{^1H\}$ NMR spectrum (Table 1) is assigned to this isomer. Balch and co-workers had assumed that the corresponding dichloro complex **6***a* had the HT configuration (17), based on this geometry being found for other structurally characterized homo- or hetero-dinuclear analogues, although HH arrangements were later shown to exist (15, 16, 28). The $^{31}P\{^1H\}$ data listed in Table 1 suggest strongly that all the $Pd_2X_2(PPh_{3-n}py_n)_2$ isolated have the HT configuration; there are regular trends in the small chemical shift changes on (*a*) changing halogen within any one pyridylphosphine triad, and (*b*) changing the pyridylphosphine within a fixed halogen triad. The trends are in the same directions observed within the mononuclear complexes. For the platinum analogue $Pt_2I_2(PPh_2py)_2$, which has been isolated in both HT and HH forms, the former (thermodynamically stable) isomer gives a $^{31}P\{^1H\}$ signal at δ −5.7, some 15 ppm to higher field than the HH isomer (15). The more labile nature of the Pd—P bond probably allows the thermodynamically more stable HT form to predominate.

Within the nine dinuclear complexes, the $^{31}P\{^1H\}$ signals at room temperature are broader for the bis(pyridyl)phosphine species **5***a*–**5***c*, and this is attributed to the presence of a mixture of diastereomers because of chirality induced at the P atoms via bridging coordination of one of the two pyridyl groups (see structures, following page).

The P nuclei in **5***a* (*R*, *R*) and **5***a* (*S*, *S*) are all equivalent and should give a singlet in the $^{31}P\{^1H\}$ NMR spectrum; the P nuclei within **5***a* (*S*, *R*), related by an inversion centre located at the centre of the Pd—Pd bond, are enantiotopic and should also give rise to a singlet. At −20 to −85°C, two sharp singlets are observed at δ 2.0 and 6.0 in about a 2:1 intensity ratio; the room temperature singlet is an averaged sig-

Can. J. Chem. Downloaded from www.nrcresearchpress.com by 92.62.229.171 on 09/08/12
For personal use only.

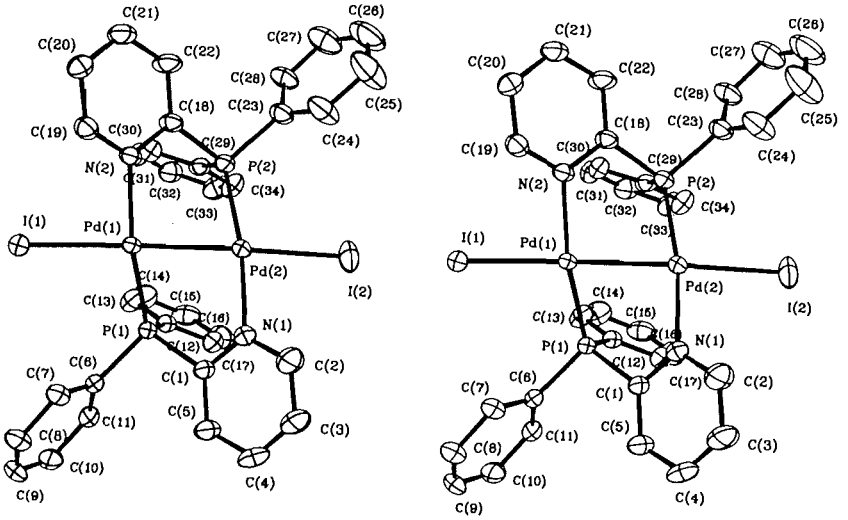

FIG. 1. Stereoview of $Pd_2I_2(PPh_2py)_2$, **6***c*, showing 33% probability thermal ellipsoids.

nal, the inversion at P presumably taking place via dissociation of a pyridyl moiety at a Pd centre, rotation about the Pd—P bond at the other Pd, and recoordination of the second pyridyl moiety. Direct inversion at a P centre is not feasible (29). The $^{31}P\{^1H\}$ room temperature singlet for **5***c*, the iodo analogue, separates into two broad singlets at −20°C (δ + 0.9, −0.2), but the downfield signal then coalesces at −40°C before reappearing at −60°C as an AB quartet centred at the original 0.9 ppm position (these reversible NMR spectral changes are unaffected by addition of NaI in acetone solution, showing that ionic equilibria via loss of iodide are not involved); the inequivalence of the two, now diastereotopic, P atoms of one of the diastereomers (probably the *S*, *R* isomer, judging by signal intensities) could result from a nonplanar structure evident at the lower temperatures (*vide infra*, structure of **6***c*); the J_{PP} coupling (~20 Hz) is characteristic of diagonally positioned P atoms in an HT arrangement (15).

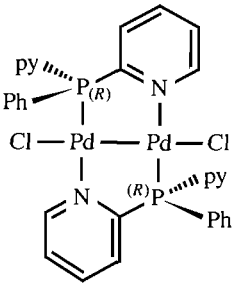

5*a* (*R*, *R*)

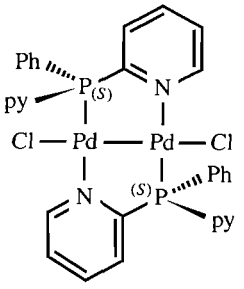

5*a* (*S*, *S*)

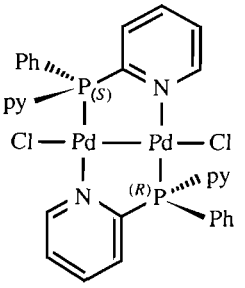

5*a* (*S*, *R*)

Although there are several structures reported with connecting PPh_2py ligands between two metals in an HT arrangement (11, 15, 21, 30),[6] to our knowledge there are none (including the metal–metal bond) containing two four-coordinate metal centres, as in $Pd_2I_2(PPh_2py)_2$, **6***c* (Fig. 1). The structure of **6***c*, which crystallizes with one disordered acetone solvate molecule per two molecules of complex, reveals many distortions, however, from square-planar geometry at the Pd(I) atoms, while there are no unusual intermolecular contacts. The I—Pd—Pd angles at the metal centres are 8–11° from linearity, with the iodine atoms *cisoid* with respect to the Pd—Pd bond. The angles between the Pd–ligand bonds vary from 77.5 to 98.5°, but the coordination at the Pd centres is nonplanar (Table 6), and the dihedral angle between the normals to the two mean planes is 41.3°. The phenyl rings are planar within experimental error, but the pyridyl rings are significantly nonplanar with maximum deviations from the mean planes being 0.015(5) and 0.023(7) Å, respectively, for the N(1) and N(2) rings. The torsion angles (Table 4) show that the five-membered rings are very nonplanar, but the relative orientation of the two bridging ligands still leaves a *trans* arrangement of P and N at each metal. This is found also in $PdCl(PPh_2py)_2$-$RhCl(CO)$, which is four-coordinate at the Pd and six-coordinate at the Rh (15), but in $PdCl(PPh_2py)_2RuCl(CO)_2$, also a four- and six-coordinate system (21), and in $PdCl(PPh_2py)_2(\mu\text{-}CO)MoCl(CO)_2$ (11) the bridging HT pyridylphosphines are *trans* at the Pd and *cis* at the other metal. Within **6***c* and the Pd—Rh complex, the metal–metal bond lengths are 2.597 Å (a single bond) and 2.594 Å, respectively, while those of the Pd—Ru (2.660 Å) and Pd—Mo (2.817 Å) are longer; the accommodation of longer metal–metal bonds by connecting PPh_2py ligands has been dis-

[6]The $Re_2Cl_2(PPh_2py)_4^{2+}$ species has at each Re a *trans*-N and *trans*-P arrangement for the four bridged PPh_2py ligands (12).

Can. J. Chem. Downloaded from www.nrcresearchpress.com by 92.62.229.171 on 09/08/12
For personal use only.

TABLE 6. Deviations (Δ, Å) from mean planes of the ligand atoms at palladium centres for $Pd_2I_2(PPh_2py)_2$, **6***c*, and $Pd_2Cl_2(Ppy_3)_2(\mu$-DMAD), **7**, and at the (=C—C(O)OMe) fragments of **7**[a]

Atom	Deviation	Atom	Deviation
	6*c*		
Pd(1)	0.1353(4)	Pd(2)	−0.1624(4)
I(1)	−0.0194(4)	I(2)	0.0932(5)
Pd(2)	−0.0231(4)	Pd(1)	0.1094(4)
P(1)	0.022(1)	P(2)	−0.102(1)
N(2)	0.021(4)	N(1)	−0.101(5)
	7		
Pd(1)	−0.0388(3)	Pd(2)	−0.0136(3)
Cl(1)	<0.001(1)	Cl(2)	−0.002(1)
P(2)	<0.001(1)	P(1)	0.001(1)
N(1)	<0.001(4)	N(2)	0.015(3)
C(1)	<0.001(4)	C(2)	−0.022(4)
O(1), O(2), C(1), C(3); χ^2 = 67.7; max. Δ = 0.028(4) Å			
O(3), O(4), C(2), C(4); χ^2 = 7.8; max. Δ = 0.010(4) Å			

[a] $\chi^2 = \Sigma(\Delta/\sigma(\Delta))^2$.

cussed by Balch's group, the key factor being freedom of rotation about the P—C(py) bond (30). The Pd—Pd bond length in **6***c* is sufficiently short so that the two PPh_2py ligands can remain *trans* to each other. The Pd—P (av. 2.212 Å) and Pd—N (2.112 Å) distances are close to those reported for the Pd—Rh, Pd—Ru, and Pd—Mo complexes. The Pd—P distances are significantly shorter than those of 2.29 Å found in the P—P connecting ligand systems $Pd_2Br_2(dpm)_2$ (31) and $Pd_2Cl_2(dpmMe)_2$ (32); a similar shortening of the Rh—P bond in the A-frame, HT complex $Rh_2Cl_2(PPh_2py)_2(\mu$-CO) compared to dpm-bridged rhodium A-frame complexes has been rationalized in terms of the relative *trans* effects, P > N (30). The Pd—I bond lengths in **6***c* (2.696 and 2.695 Å) are unusually long for terminal Pd—I bonds, but are essentially the same as found in the unbridged complex $[PdI(MeNC)_2]_2$, which contains a linear I—Pd—Pd—I unit with a metal–metal bond length of 2.533 Å (33), and again the elongation is attributed to the *trans* effect of the Pd—Pd bond.

*The insertion products from dimethylacetylenedicarboxylate (DMAD), $Pd_2Cl_2(PPh_{3-n}py_n)_2(\mu$-$MeO_2CC{=}CCO_2Me)$; n = 3(**7**), 2(**8**), and 1(**9**)*

Studies from Balch's group have established that the molecules CO, SO_2, or MeNC do not insert into the Pd—Pd bond of $Pd_2Cl_2(PPh_2py)_2$, **6***a*, although CO or MeNC reacted to give unbridged Pd—Pd products containing these reagents as terminal ligands (17). This behaviour contrasts with that of $Pd_2Cl_2(dpm)_2$, which gives the familiar A-frame products (17, 34), and was attributed to the limited flexibility of the PPh_2py ligand and the relative lability of the pyridyl nitrogen (17).

We find that **6***a* (and **4***a* and **5***a*) does react readily with DMAD to give the "expected" insertion product (Table 1), a dimetallated olefin, exactly analogous to the $Pd_2Cl_2(dpm)_2$ system (35), and we have determined the structure of the product **7** from $Pd_2Cl_2(Ppy_3)_2$, **4***a*. The coordination at each Pd (Fig. 2) approximates to square planar with the *trans* P and N geometry, a terminal chloride, and a carbon of the bridging olefin; the geometry of the inserted ligand approximates that of a dimetallated olefin, originally determined crystallographically for a hexafluoro-2-butyne adduct, however, and not an isolated DMAD adduct from the dpm system (35). Other closely related, crystallographically characterized, bridging DMAD adducts include complexes such as $Rh_2Cl_2(\mu$-CO)(μ-DMAD)$(dpm)_2$ (36) and $Ir_2Cl_2(CO)_2(\mu$-DMAD)$(dpm)_2$ (37).

A molecule of **7** crystallizes with two solvate molecules of CH_2Cl_2, one of which is disordered. There are some possible interactions between nonbonded atoms (Table 7), but these are weak and not significant in determining the basic molecular geometry just outlined. A projection of the nearly planar $Pd_2C_4Cl_2$ portion of the molecule is shown in Fig. 3. Comparison with a corresponding figure for the structure of $Pd_2Cl_2(dpm)_2(\mu$-$F_3CC{=}CCF_3)$ (35) reveals similarities for the coordinated olefinic moieties except for a remarkable difference in the Pd. . .Pd separation (2.910 Å for **7** and 3.492 Å for the 2-butyne adduct), while the Cl—Pd—C angles are also ~10° smaller in the dpm system; the differences are "compensated for" by a closing up of each of the Pd—C—C bond angles by ~10°, and an increase to 45.2° of the dihedral angle between normals to mean planes comprising Cl(1), P(2), N(1), C(1), Pd(1) (essentially planar), and Cl(2), P(1), N(2), C(2), Pd(2) (somewhat nonplanar) (Table 6).

As mentioned above, the PPh_2py ligand is considered of insufficient bite to accommodate the longer metal–metal bonds while maintaining *trans* disposed PPh_2py ligands at the two metal sites. Nevertheless in **7**, a 2.910 Å metal separation is maintained without recourse to a change to *cis* orientation of the Ppy_3 ligands at one metal site. It is unlikely that Ppy_3 is more flexible than PPh_2py, and thus examples of dinuclear HT species, in which the latter ligand accommodates longer metal–metal bonds while remaining *trans* disposed at both metals, will probably be found. Figure 4 shows how the larger bite of Ppy_3 is accomplished by an opening up of each of the angles of the chelate ring, particularly at the nitrogen atom (Pd—N—C is 116.6° in **6***c* and 125.9° in **7**). As in **6***c*, the pyridyl rings containing the coordinating nitrogen atoms in **7** are nonplanar, but somewhat less so, the maximum deviations from the mean planes being 0.011(4) and 0.009(4) Å, respectively, for the N(1) and N(2) rings; of the other four pyridyl rings, three are planar but, surprisingly, that with N(4) shows the greatest deviation from planarity (0.017(5) Å). The (O(3), O(4), C(2), C(4)) fragment at Pd(2) is planar while the corresponding fragment at Pd(1) is distinctly nonplanar (Table 6), reflecting further the completely unsymmetrical nature of **7**; the dihedral angle (between normals to the mean planes) is 59.0° and the twisting most likely occurs in order to minimize unfavourable nonbonded contacts with the pyridyl groups (e.g., Table 7, C(6)—H(6b). . .N(3)). The geometry of the dimetallated olefin moiety resembles closely that found in $Ir_2Cl_2(CO)_2(\mu$-DMAD)$(dpm)_2$, where again the ester groups are twisted with respect to each other (37). In this Ir_2 complex, however, there is a shorter metal–metal distance of 2.779 Å (corresponding to a single bond), somewhat longer metal–carbon bonds (2.052, 2.133 Å), and a decrease in one of the two Ir—C—C bond angles (107.0, 112.3°), cf. Fig. 3. In **7**, the Ir_2 species, and related Rh_2 species (36, 38),

Can. J. Chem. Downloaded from www.nrcresearchpress.com by 92.62.229.171 on 09/08/12
For personal use only.

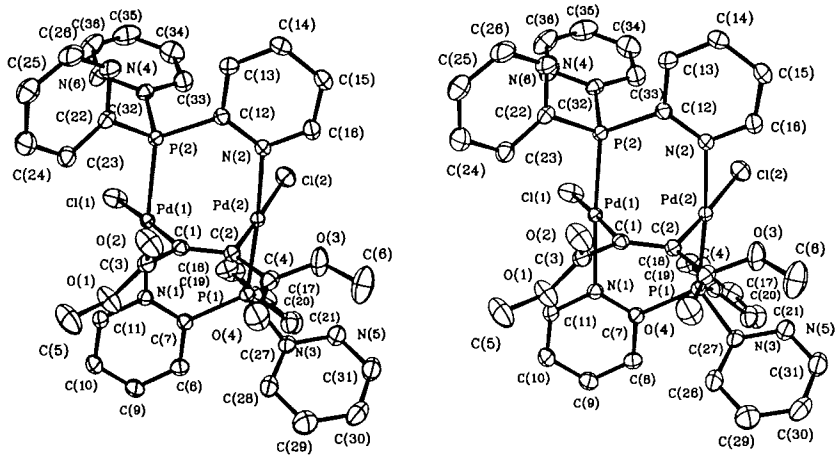

FIG. 2. Stereoview of $Pd_2Cl_2(Ppy_3)_2(\mu\text{-DMAD})$, **7**, showing 33% probability thermal ellipsoids.

TABLE 7. Possible weak interactions between nonbonded atoms in $Pd_2Cl_2(Ppy_3)_2(\mu\text{-DMAD}) \cdot 2CH_2Cl_2$[a]

D—H. . .A	H. . .A (Å)	D. . .A (Å)	D—H. . .A (°)
C(24)—H(24). . .Cl(1)[1]	2.95	3.595(5)	125
C(34)—H(34). . .Cl(1)[2]	2.86	3.661(5)	141
C(28)—H(28). . .Cl(5)[3]	2.93	3.570(5)	125
C(37)—H(37a). . .O(2)[4]	2.53	3.38(1)	145
C(6)—H(6b). . .N(3)[5]	2.61	3.474(6)	147
C(13)—H(13). . .N(4)[3]	2.33	3.038(5)	129
C(10)—H(10). . .N(6)[1]	2.46	3.214(5)	134

[a]All the interactions are intermolecular, except the entry beginning C(13); Cl(5), C(37), and H(37a) refer to the CH_2Cl_2 molecules. Superscripts refer to symmetry operations: [1] $-x$, $-y$, $1-z$; [2] $-x$, $-y$, $-z$; [3] x, y, z; [4] $-x$, $1-y$, $2-z$; [5] $1-x$, $1-y$, $1-z$.

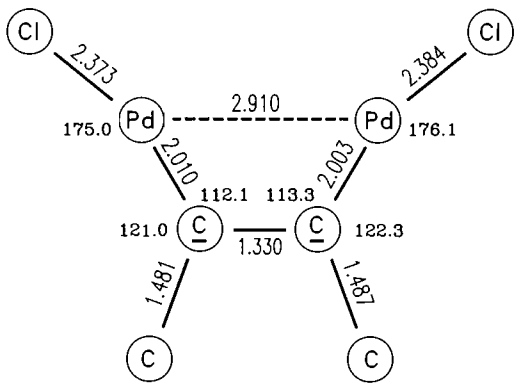

FIG. 3. Projection of the nearly planar $Pd_2C_4Cl_2$ portion of **7** (not drawn to scale).

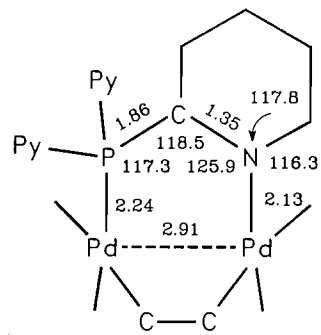

FIG. 4. Diagram showing geometry within one of the 7-membered chelate rings of **7** (not drawn to scale).

containing a bridging DMAD there is a slight twisting of the "parallel" acetylene group with respect to the metal–metal axis, which probably minimizes contacts with the pyridyl/phenyl rings.

Finally, the Pd—N bond lengths in **7** are within ~0.02 Å of those in **6***c* and the other PPh_2py systems mentioned above, Pd—Mo (11), Pd—Rh (15), and Pd—Ru (21), but the Pd—P bond in **7** is the longest observed (by up to 0.05 Å), perhaps reflecting a somewhat more electronegative effect for the pyridyl (*vs.* phenyl) substituent.

There is clearly sufficient flexibility of **7** in solution to result in a structure with equivalent P atoms, the $^{31}P\{^1H\}$ signal at ~20°C appearing as a singlet. Complex **9**, the PPh_2py analogue, similarly gives a singlet $^{31}P\{^1H\}$ signal, while the chiral $PPhpy_2$ system **8** gives rise to four singlets (cf. **5***a*); more detailed studies are required to unravel the NMR behaviour.

Whether the Ppy_3 ligand is sufficiently flexible to stabilize an A-frame, single atom, bridged complex remains to be established. Complex **4***a*, $Pd_2Cl_2(Ppy_3)_2$, in CH_2Cl_2 does react readily with CO at 1 atm (101.3 kPa) even at sub-zero temperatures but attempts to work up the product simply resulted in isolation of only **4***a*; similar behaviour has been reported for $Pd_2Cl_2(PPh_2py)_2$, where the solution product was tentatively suggested to be $[PdCl(CO)(PPh_2py)]_2$, contain-

Can. J. Chem. Downloaded from www.nrcresearchpress.com by 92.62.229.171 on 09/08/12
For personal use only.

ing monodentate PPh_2py bound via phosphorus and no bridging ligands (17).

Other structurally characterized Ppy_3 species are *trans*-$RhCl(CO)(Ppy_3)_2$, which contains monodentate P-bound Ppy_3 (9), and $Ru(Ppy_3)_2^{2+}$ in which octahedral geometry is realized via the six pyridyl N-donors (10).

Aqueous solution chemistry of $PdCl_2(Ppy_3)_2$, **1**a, *and* $Pd_2Cl_2(Ppy_3)_2$, **4**a

The interests in the aqueous solution chemistry of pyridylphosphine complexes were outlined in the Introduction; it should be mentioned also that the dpm analogue of the μ-DMAD species (7–9) is a catalyst for the cyclotrimerization of the acetylene to hexamethyl mellitate (35), and the pyridylphosphine ligand systems have the potential for such catalysis in aqueous media. Qualitatively, the most water-soluble of the complexes listed in Table 1 are $PdCl_2(Ppy_3)_2$, **1***a*, and $Pd_2Cl_2(Ppy_3)_2$, **4***a*, dissolution being accompanied by formation of aquo complexes, eq. [1].

[1] $Pd_2Cl_2(Ppy_3)_2 + 2H_2O \rightleftharpoons Pd_2(H_2O)_2(Ppy_3)_2^{2+} + 2Cl^-$

4*a* (orange) **10** (green)

Complex **4***a* dissolves with replacement of the two terminal chlorides by water, and the bis(aquo) dication has been isolated as salts with BF_4^-, PF_6^-, and BPh_4^- as anions, **10***a*–**10***c* (Table 1). A 1627 cm^{-1} IR band (obscured in **10***c*) of coordinated water is seen, and ν(OH) bands are absent. Reaction [1] is readily reversed by adding LiCl, and an HT configuration is assumed for the ionic green species; the $^{31}P\{^1H\}$ singlet is some 25–30 ppm upfield from that of the dichloro precursor. The complexes **10***a*–**10***c* dissolve in MeCN (or acetone) to give perhaps the respective bis(solvent) cations, and conductivity data in MeCN support a 1:2 electrolyte formulation.

To our knowledge, the only other reported case of a neutral, dinuclear, bridged phosphine being soluble in water is $Pd_2Cl_2(dmpm)_2$, which contains bis(dimethylphosphino)-methane; however, this species dissolves as the neutral $Pd_2(OH)_2(dmpm)_2$ species with liberation of 2 equivalents of HCl (39), implying that the pK_a of each coordinated water ligand is $<<7.0$. Aqueous solutions of **4***a* (present as the dication **10**) surprisingly show no dissociation of protons even at pH 11.0; this non-acidic character of the coordinated water (vs. that of the dmpm system) implies that bridged Ppy_3 is a far more basic ligand to the Pd_2^I unit than is dmpm, and this presumably reflects the much stronger basicity generally of a pyridine versus phosphine ligand.

Complex **1***a*, *cis*-$PdCl_2(Ppy_3)_2$, dissolves in water with immediate loss of both chloride ligands (as estimated by titration with $AgNO_3$); the resulting solution is acidic, however, and the immediate molar conductivity (265 ohm^{-1} mol^{-1} cm^2) may include a contribution from the proton(s) of coordinated water. Indeed, pH-titration data reveal loss of one proton per Pd up to pH 11.00, with 50% titration at pH ~4.8, but the titration does not give the standard S-shape curve; the behaviour is typical of *cis*-bis(aquo)palladium(II) species (40) and is summarized in eq. [2] (L = monodentate, phosphorus-bonded Ppy_3):

$$[2]\quad Pd(H_2O)_2L_2^{2+} \overset{-H^+}{\rightleftharpoons} [Pd(OH)(H_2O)L_2]^+ \overset{-H_2O}{\rightleftharpoons} 1/2[Pd_2(\mu\text{-}OH)_2L_4]^{2+}$$

The titration curve results from a combination of the equilibrium constants for proton dissociation, and dimerization.

Acidification of the aqueous solution of **1***a* to pH 1.5 (using dilute HNO_3) and addition of a methanol solution of $NaBPh_4$ precipitated a yellow powder that is probably mainly $[Pd(H_2O)_2(PPy_3)_2][BPh_4]_2$.(Λ (MeCN): 220 ohm^{-1} mol^{-1} cm^2.) Anal. calcd. for $C_{78}H_{72}N_6B_2O_2P_2Pd$: C 71.43, H 5.23, N 6.41; found: C 70.12, H 5.10, N 6.60. The presence of some hydroxy species would account for the low C analysis. Similar precipitation of a species at pH 5.6 using $NaBPh_4$ gave a more orange product that analyzed well for $[Pd(OH)(H_2O)(PPy_3)_2][BPh_4]$. (Λ (MeCN) 180 ohm^{-1} mol^{-1} cm^2. IR (for the less pure PF_6 salt, Nujol): ν(OH) 3651, 3595; ν(H_2O) 1628 cm^{-1}.) Anal. calcd. for $C_{54}H_{44}N_6BO_2P_2Pd$: C 65.42, H 4.78, N 8.48; found: C 65.39, H 4.60, N 7.72. Salts precipitated out by addition of BPh_4^- or BF_4^- to aqueous solutions of $PdCl_2(Ppy_3)_2$ (e.g., at 3.7 mM, pH = 2.9) analyze well for a 66:34 mixture of the bis(aquo)/aquo(hydroxo) species. The $^{31}P\{^1H\}$ NMR signal in MeCN at 20°C for all the above isolated samples is observed as a singlet around 33.4 ppm, which could be an averaged signal for bis(aquo)/aquo(hydroxo) species, or more likely results from a single species containing coordinated MeCN; the shift is consistent with monodentate, phosphorus-bonded Ppy_3 (cf. Table 1).

At pH 11.00 (following titration of the single proton), addition of $NaBPh_4$ results in precipitation of a purple solid, which can be recrystallized from MeCN/EtOH (1:1) at −15°C to give a complex best formulated as $[Pd_2(\mu\text{-}OH)_2(Ppy_3)_2(MeCN)_2](BPh_4)_2$ (cf. eq. [2], in which one Ppy_3 ligand at each Pd(II) centre has been replaced by MeCN). IR (CH_2Cl_2): ν(OH) 3680 cm^{-1}. NMR (CD_3CN, 20°C): $^{31}P\{^1H\}$ δ 29.1, singlet; ^1H δ 2.35, singlet (MeCN). Anal. calcd. for $C_{82}H_{76}N_8B_2O_2P_2Pd_2$: C 65.77, H 4.85, N 7.48, O 2.14; found: C 65.50, H 4.64, N 7.34, O 2.24.

The $^{31}P\{^1H\}$ NMR spectrum of *cis*-$PdCl_2(Ppy_3)_2$ in D_2O gives two singlets at 27.3 and 21.6 ppm with intensity ratio of ~2:1: the former is attributed to the equilibrium mixture of the bis(aquo)/aquo(hydroxo) species, and the latter to the dinuclear, hydroxo-bridged species; see eq. [2].

Concluding remarks

The paper has described synthesis and characterization of nine mononuclear Pd(II)–, and nine dinuclear Pd_2(I)–pyridylphosphine complexes containing also halide ligands. Some comparisons are made to analogous dpm systems and associated A-frame chemistry, but the major raison d'etre for the work is to develop the aqueous solution chemistry of palladium–phosphine complexes with a view to study their homogeneous catalytic properties in this medium. Preliminary work on some aqueous systems is presented, and a good database generally has been established for Pd–pyridylphosphine chemistry.

Although Tom Birchall worked on phenylamines and phenylphosphines, he had not to our knowledge probed the mysteries of aminophosphines. Thus, the topic of this paper is somewhat remote from his major interests as a main-group chemist, but nevertheless the dedication is of the utmost sincerity toward a most genial friend and colleague within the Canadian inorganic chemistry community.

Acknowledgements

We thank the Natural Sciences and Engineering Research Council of Canada for financial support via an operating grant

Can. J. Chem. Downloaded from www.nrcresearchpress.com by 92.62.229.171 on 09/08/12
For personal use only.

(to B.R.J.), the Isaak Walton Killam Foundation for a postdoctoral fellowship (to C-L.L.) administered by the University of British Columbia, and Johnson Matthey Ltd. for the loan of palladium.

1. C-L. Lee, B. R. James, D. A. Nelson, and R. T. Hallen. Organometallics, **3**, 1360 (1984); S. E. Lyke, M. A. Lilga, D. A. Nelson, B. R. James, and C-L. Lee. Ind. Eng. Chem. Prod. Res. Dev. **25**, 517 (1986); D. A. Nelson, R. T. Hallen, C-L. Lee, and B. R. James. *In* Recent developments in separation science. Vol. IX. *Edited by* N. Li and J. M. Calo. CRC Press, Cleveland, Ohio. 1986. p. 1.
2. A. F. Barnabas, D. Sallin, and B. R. James. Can. J. Chem. **67**, 2009 (1989), and references therein.
3. I. Zay, Y. Xie, and B. R. James. Proc. Int. Conf. Coord. Chem. 28th. Gera, 1990. Abstract 2-105.
4. B. R. James and J. Louie. Inorg. Chim. Acta, **3**, 568 (1969).
5. C. M. Jensen and W. C. Trogler. Science, **233**, 1069 (1986); D. Ramprasad, H. J. Yue, and J. A. Marsella. Inorg. Chem. **27**, 3151 (1988).
6. Y. Xie. Ph.D. Dissertation, University of British Columbia. 1990.
7. S. Ganguly and D. M. Roundhill. J. Chem. Soc. Chem. Commun. 639 (1991).
8. Y. Xie and B. R. James. J. Organomet. Chem. **417**, 277 (1991), and references therein.
9. K. Wajda-Hermanowicz, M. Koralewicz, and F. P. Pruchnik. Appl. Organomet. Chem. **4**, 173 (1990), and references therein; K. Wadja, F. P. Pruchnik, and T. Lis. Inorg. Chim. Acta, **40**, 207 (1980).
10. F. R. Keene, M. R. Snow, P. J. Stephenson, and E. R. T. Tiekink. Inorg. Chem. **27**, 2040 (1988).
11. Z-Z. Zhang, H-K. Wang, H-G. Wang, and R-J. Wang. J. Organomet. Chem. **314**, 357 (1986).
12. T. J. Barder, F. A. Cotton, G. L. Powell, S. M. Tetrick, and R. A. Walton. J. Am. Chem. Soc. **106**, 1323 (1984).
13. M. G. Ehrlich, F. R. Fronczek, S. F. Watkins, G. R. Newkome, and D. C. Hager. Acta Crystallogr. C: Cryst. Struct. Commun. **40**, 78 (1984), and references therein.
14. H. G. Ang, W. E. Kow, and K. F. Mok. Inorg. Nucl. Chem. Lett. **8**, 829 (1972).
15. J. P. Farr, M. M. Olmstead, and A. L. Balch. Inorg. Chem. **22**, 1229 (1983), and references therein; J. P. Farr, F. E. Wood, and A. L. Balch. Inorg. Chem. **22**, 3387 (1983).
16. F. E. Wood, J. Hvoslef, H. Hope, and A. L. Balch. Inorg. Chem. **23**, 4309 (1984), and references therein.
17. A. Maisonnat, J. P. Farr, and A. L. Balch. Inorg. Chim. Acta, **53**, L217 (1981).
18. G. R. Newkome, D. W. Evans, and F. R. Fronczek. Inorg. Chem. **26**, 3500 (1987).
19. M. S. Kharasch, R. C. Seyler, and F. R. Mayo. J. Am. Chem. Soc. **60**, 882 (1938).
20. T. Ukai, H. Kawazura, Y. Ishii, J. J. Bonnet, and J. A. Ibers. J. Organomet. Chem. **65**, 253 (1974).
21. A. Maisonnat, J. P. Farr, M. M. Olmstead, C. T. Hunt, and A. L. Balch. Inorg. Chem. **21**, 3961 (1982).
22. K. Kurtev, D. Ribola, R. A. Jones, D. J. Cole-Hamilton, and G. Wilkinson. J. Chem. Soc. Dalton Trans. 55 (1980).
23. P. Coppens, L. Leiserowitz, and D. Rabinovich. Acta Crystallogr. **18**, 1035 (1965); W. R. Busing and H. A. Levy. Acta Crystallogr. **22**, 457 (1967).
24. International tables for X-ray crystallography. Vol. IV. Kynoch Press, Birmingham. 1974.
25. J. G. Verkade and L. D. Quin (*Editors*). Phosphorus-31 NMR spectroscopy in stereochemical analysis. VCH, Deerfield Beach, Fla. 1987.
26. J. G. Verkade. Coord. Chem. Rev. **9**, 1 (1973).
27. K. Nakamoto. Infrared and Raman spectra of inorganic and coordination compounds. 4th ed. Wiley, New York. 1986. pp. 324, 339.
28. J. P. Farr, M. M. Olmstead, N. M. Rutherford, F. E. Wood, and A. L. Balch. Organometallics, **2**, 1758 (1983).
29. M. J. Gallagher and I. D. Jenkins. Top. Stereochem. **3**, 11 (1968).
30. J. P. Farr, M. M. Olmstead, C. T. Hunt, and A. L. Balch. Inorg. Chem. **20**, 1182 (1981).
31. R. G. Holloway, B. R. Penfold, R. Colton, and M. J. McCormick. J. Chem. Soc. Chem. Commun. 485 (1976).
32. C-L. Lee, Y-P. Yang, S. J. Rettig, B. R. James, D. A. Nelson, and M. A. Lilga. Organometallics, **5**, 2220 (1986).
33. N. M. Rutherford, M. M. Olmstead, and A. L. Balch. Inorg. Chem. **23**, 2833 (1984).
34. R. J. Puddephatt. Chem. Soc. Rev. **12**, 99 (1983).
35. A. L. Balch, C-L. Lee, C. H. Lindsay, and M. M. Olmstead. J. Organomet. Chem. **177**, C22 (1979); C-L. Lee, C. T. Hunt, and A. L. Balch. Inorg. Chem. **20**, 2498 (1981).
36. M. Cowie and T. G. Southern. Inorg. Chem. **21**, 246 (1982).
37. B. R. Sutherland and M. Cowie. Organometallics, **3**, 1869 (1984).
38. J. T. Mague. Inorg. Chem. **22**, 45 (1983).
39. M. L. Kullberg and C. P. Kubiak. Organometallics, **3**, 632 (1984).
40. M. C. Lim and R. B. Martin. J. Inorg. Nucl. Chem. **38**, 1911 (1976); N. N. Chernova and I. G. Kurskii. Zh. Neorg. Khim. **23**, 1014 (1978).

Can. J. Chem. Downloaded from www.nrcresearchpress.com by 92.62.229.171 on 09/08/12
For personal use only.

Physical and structural studies of *N*-carboxymethyl- and *N*-(*p*-methoxyphenyl)-3-hydroxy-2-methyl-4-pyridinone

ZAIHUI ZHANG, STEVEN J. RETTIG, AND CHRIS ORVIG[1]

Department of Chemistry, University of British Columbia, 2036 Main Mall, Vancouver, B.C., Canada V6T 1Z1

Received May 14, 1991

This paper is dedicated to the memory of Professor Thomas Birchall

ZAIHUI ZHANG, STEVEN J. RETTIG, and CHRIS ORVIG. Can. J. Chem. **70**, 763 (1992).

3-Hydroxy-1-carboxymethyl-2-methyl-4-pyridinone (Hcmp) and 3-hydroxy-1-(*p*-methoxyphenyl)-2-methyl-4-pyridine (Hpap) have been prepared and studied by single crystal X-ray diffraction. Crystals of Hcmp are monoclinic, a = 6.340 (2), b = 7.705 (1), c = 16.226 (1) Å, β = 94.74 (1), Z = 4, space group $P2_1/n$ and those for Hpap are monoclinic, a = 10.8435 (9), b = 16.680 (2), c = 13.5665 (6) Å, β = 109.450 (4), Z = 8, space group $C2/c$. Both structures were solved by direct methods and were refined by full-matrix least-squares procedures to R = 0.030 and 0.041 (R_w = 0.039 and 0.058) for 1642 and 1819 reflections with $I \geq 3\sigma(I)$, respectively. Bond lengths and bond angles in the two compounds are normal; however, Hcmp forms as a zwitterion in the solid state. The two compounds were also studied by mass spectrometry, UV, infrared, proton NMR spectroscopies, and potentiometric equilibrium measurements. The protonation constants for Hcmp are log K_1 = 9.76 (1), log K_2 = 3.43 (1), and log K_3 = 2.78 (3) and for Hpap are log K_1' = 9.42 (4) and log K_2' = 3.16 (8).

Key words: 3-hydroxy-4-pyridinone, zwitterion, hydrogen bonding, protonation constant, crystallography, solid state.

ZAIHUI ZHANG, STEVEN J. RETTIG et CHRIS ORVIG. Can. J. Chem. **70**, 763 (1992).

On a préparé la 3-hydroxy-1-carboxyméthyl-2-méthylpyridin-4-one (HCMP) et la 3-hydroxy-1-(*p*-méthoxyphényl)-2-méthylpyridin-4-one (HPAP) et on les a examinés par diffraction des rayons X par un cristal unique. Les cristaux du HCMP sont monocliniques, avec a = 6,340(2), b = 7,705(1) et c = 16,226(1) Å, β = 94,74(1), Z = 4 et groupe d'espace $P2_1/n$ et ceux du HPAP sont monocliniques, avec a = 10.8435(9), b = 16,680(2) et c = 13,5665(6) Å, β = 109,450(4), Z = 8 et groupe d'espace $C2/c$. On a résolu les deux structures par des méthodes directes et on les a affinées par la méthode des moindres carrés (matrice complète) jusqu'à des valeurs de R = 0,030 et 0,041 (R_w = 0,039 et 0,058), respectivement, pour 1642 et 1819 réflexions avec $I \geq 3\sigma(I)$. Les longueurs et les angles de liaisons des deux composés sont normaux; toutefois, le HCMP forme un zwitterion en phase solide. On a étudié les deux composés par spectrométrie de masse, par spectroscopies UV, infrarouge et RMN et par des mesures d'équilibres potentiométriques. Les constantes de protonation du HCMP sont log K_1 = 9,76(1), log K_2 = 3,43(1) et log K_3 = 2,78(3) alors que pour la HPAP log K_1' = 9,42(4) et log K_2' = 3,16(8).

Mots clés : 3-hydroxypyridin-4-one, zwitterion, liaison hydrogène, constantes de protonation, cristallographie, état solide.

[Traduit par la rédaction]

Introduction

As part of our project to examine the coordination chemistry and biochemical properties of aluminum, gallium, and indium complexes, we have been studying tris(ligand) complexes of these metal ions with 3-hydroxy-4-pyrones (1–3) and 3-hydroxy-4-pyridinones (4–7) as bidentate ligands. The preparation and characterization of a series of *N*-alkyl (**1**) and *N*-aryl (**2**) substituted-3-hydroxy-2-methyl-4-pyridinones and their metal complexes have been reported (7, 8). The studies have shown that these complexes have unique properties: reasonable water solubility, variable lipophilicity, high thermodynamic stability, and interesting biological activity (7, 9–11).

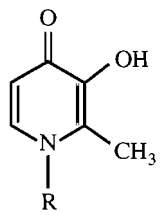

R =		
H	Hmpp,	**1***a*
CH_3	Hdpp,	**1***b*
CH_2CH_3	Hmepp,	**1***c*
CH_2COOH	Hcmp,	**1***d*

1

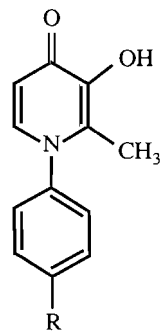

R =		
H	Hppp,	**2***a*
CH_3	Hptp,	**2***b*
OCH_3	Hpap,	**2***c*
NO_2	Hpnp,	**2***d*

2

As these ligands have very high affinity for trivalent metal ions, there is significant interest in using them as chelators for various metal ions. We have studied the solution chemistry and the biochemical properties of tris(ligand) complexes of aluminum(III), gallium(III), and indium(III) with these ligands (4–7, 9–11). Kontoghiorghes and co-workers

[1]Author to whom correspondence may be addressed.

Can. J. Chem. Downloaded from www.nrcresearchpress.com by 92.62.229.171 on 09/08/12
For personal use only.

Can. J. Chem. Downloaded from www.nrcresearchpress.com by 92.62.229.171 on 09/08/12
For personal use only.

have used 3-hydroxy-1,2-dimethyl-4-pyridinone (Hdpp) for iron overload treatment in preliminary clinical trials (12–15). Taylor and Kontoghiorghes also investigated the mobilization of plutonium(IV) and iron(III) from transferrin and ferritin by hydroxypyridinone chelators (16). The *N*-aryl substituted 3-hydroxy-4-pyridinones were also used as selective extractants for various metal ions, e.g., gallium(III) (17, 18), iron(III) (19–21), vanadium(V) (22–24), uranium(VI) (25), thorium(IV) (26), protactinium(V) (26), zirconium(IV) (27), niobium(V) (27), and tantalum(V) (27).

Tautomerism is one of the important features of heterocyclic compounds. For 4-pyridinones, there are two possible tautomers, 4-hydroxypyridine and 4-pyridinone (28). In the equilibrium between these two tautomers, the predominant form in polar solvents is the pyridinone; however, the hydroxypyridine tautomer appears to be more stable in the gas phase (29–31). In the crystal structures of 1-alkyl-3-hydroxy-4-pyridinones (**1***a*, **1***b*) reported in the literature (8), these compounds exist as the pyridinone forms and the ring system of the pyridinones shows some delocalization of the formal double bonds. The effect of the ring nitrogen substituent on the delocalization has also been discussed (32). Herein we report our studies of the 3-hydroxy-4-pyridinones, **1***d* and **2***c*, using various physical techniques including single crystal X-ray crystallography, potentiometric equilibrium measurements, and UV spectrophotometry. The effect on the delocalization of the formal ring double bonds is compared among the three groups of substituents: alkyl, aryl, and carboxyl groups.

Experimental

Materials and methods

All chemicals were reagent grade and were used as received unless specified: maltol (3-hydroxy-2-methyl-4-pyrone, Sigma), *p*-anisidine (Eastman Organic Chemicals), and glycine (Sigma). Water was deionized (Barnstead D8902 and D8904 cartridges) and distilled (Corning MP-1 Megapure still).

Proton NMR spectra of compounds were recorded in $CDCl_3$ or D_2O with a Varian XL-300 or a Bruker AC-200E spectrometer. Mass spectra were obtained with a Kratos MS50 (electron impact ionization, EI) instrument. Infrared spectra were recorded as KBr pellets in the range 4000–200 cm^{-1} with a Perkin–Elmer PE 783 spectrophotometer and were referenced to polystyrene film. Melting points were measured with a Mel-Temp apparatus and are uncorrected. Ultraviolet spectra were recorded in the range 350–200 nm with a Shimadzu UV-2100 spectrophotometer. Analyses for C, H, and N were performed by P. Borda of this department. Potentiometric equilibrium measurements were done as previously described (9, 10).

N-*Carboxymethyl-3-hydroxy-2-methyl-4-pyridinone, Hcmp*

Maltol (4.95 g, 39.2 mmol) and glycine (5.92 g, 78.8 mmol) were dissolved in 100 mL hot distilled water and the pH of the solution was adjusted to about 9 with 8 N NaOH. The mixture was refluxed for 20 h and then decolorized with activated charcoal. The volume of the solution was reduced to 50 mL and 6 N HCl solution was added to this solution to lower the pH to around 3; a yellowish solid precipitated. Recrystallization (twice) of this solid from hot water yielded an off-white crystalline product (3.09 g, 43%); mp 258–260°C. Infrared spectrum (cm^{-1}, KBr disk): 3300–2500 (b, hydrogen bonded), 1650–1600 (b, s), 1545, 1520, 1450, 1380–1350 (b, s), 1270 (b, s), 1210 (w), 1075, 830, and 810. ^1H NMR spectrum (D_2O, 25°C): δ 2.44 (s, 3H, $NC(CH_3)$), 4.87 (s, 2H, NCH_2COOH), 7.02 (d, 1H, 8.0 Hz, $CHC(O)$), 7.93 (d, 1H, 8.0 Hz, $CHCHN$). Mass spectrum (EI): *m/e* 183 (M^+), 165 ($M^+ - H_2O$). Anal. calcd. for $C_8H_9NO_4$: C 52.46, H 4.95, and N 7.65; found: C 52.57, H 4.98, and N 7.63. Single crystals suitable for X-ray diffraction were obtained from a saturated solution by slow evaporation.

1-(p-Methoxyphenyl)-3-hydroxy-2-methyl-4-pyridinone, Hpap

Maltol (4.02 g, 31.9 mmol) and *p*-anisidine (7.93 g, 64.4 mmol) were suspended in 100 mL dilute HCl solution (3 mL concentrated HCl in 100 mL water). This mixture was refluxed for 72 h and then cooled to room temperature. A light grey solid was collected by filtration. It was recrystallized from hot ethanol (after being decolorized with activated charcoal for 30 min) yielding a white crystalline solid (4.27 g, 58% yield), mp 249°C. Infrared spectrum (cm^{-1}, KBr disk): 3180 (b), 1630 (s), 1578 (s), 1530 (w), 1510 (s), 1465, 1400 (w), 1380 (w), 1320 (w), 1300 (s), 1250, 1205, 1170 (s), 1105 (w), 1040 (s), 845, 825. ^1H NMR spectrum ($CDCl_3$, 25°C): δ 2.11 (s, 3H, $NC(CH_3)$), 3.90 (s, 3H, OCH_3), 5.66 (s, 1H, b, *OH*), 6.45 (d, 1H, 7.8 Hz, *CH*C(O)), 6.9–7.3 (m, 5H, C_6H_4 and CHC*H*N). Mass spectrum (EI): *m/e* 231 (M^+), 215 ($M^+ - CH_4$), 199 ($M^+ - OCH_3$). Anal. calcd for $C_{13}H_{13}NO_3$: C 67.52, H 5.67, and N 6.06; found: C 67.51, H 5.71, and N 6.13. Single crystals obtained from an ethanol solution were used for X-ray crystallographic analysis.

X-ray crystallographic analyses

Crystallographic data for Hcmp and Hpap appear in Table 1. The final unit-cell parameters were obtained by least-squares refinements on the setting angles for 25 reflections with 2θ = 42.28°–54.80° for Hcmp and 2θ = 92.53°–108.29° for Hpap. The data were collected at 21 ± 1°C with a Rigaku AFC6S diffractometer. The take-off angle was 6.0° and the detector aperture was 6.0 mm in both horizontal and vertical directions at a distance of 285 mm from the crystal. Reflections with *I* between 1 σ(*I*) and 40 σ(*I*) were rescanned (maximum of 8 scans) and the counts were accumulated to ensure good counting statistics. Stationary background counts were recorded on each side of the reflection. The ratio of peak counting time to background counting time was 2:1. The intensities of three standard reflections, measured every 200 reflections for Hcmp and 150 reflections for Hpap throughout the data collections, remained essentially constant in each case. The data were processed and corrected for Lorentz and polarization effects. An empirical absorption correction, based on azimuthal scans of several reflections for Hpap and using the program DIFABS (applied after isotropic refinement with hydrogen atoms included in the model) for Hcmp, was applied. A correction for secondary extinction was also applied (coefficient = 1.98 (3) × 10^{-5}) for Hpap.

Both structures were solved by direct methods (33). The nonhydrogen atoms were refined anisotropically and hydrogen atoms were refined with isotropic thermal parameters. Neutral atom scattering factors were taken from ref. 34. Anomalous dispersion effects were included in F_{calc} (35); the values for $\Delta f'$ and $\Delta f''$ were chosen from Cromer (36). All calculations were performed using the TEXSAN crystallographic software package of Molecular Structure Corporation (37). Final atomic coordinates and equivalent isotropic thermal parameters B_{eq} appear in Table 2 for Hcmp and Table 3 for Hpap, respectively. Measured and calculated structure factors have been placed in the Depository of Unpublished Data.[2] Bond lengths and bond angles are listed in Table 4 and Table 5, respectively.

Results and discussion

1-Carboxymethyl-3-hydroxy-2-methyl-4-pyridinone and 1-(*p*-methoxyphenyl)-3-hydroxy-2-methyl-4-pyridinone have

[2]Tables of structure factors, anisotropic thermal parameters, and other material mentioned in the text may be purchased from: The Depository of Unpublished Data, Document Delivery, CISTI, National Research Council Canada, Ottawa, Canada K1A 0S2.

Tables of hydrogen atom coordinates and intra- and intermolecular bond distances and angles relating to hydrogen atoms have also been deposited with the Cambridge Crystallographic Data Centre and can be obtained on request from The Director, Cambridge Crystallographic Data Centre, University Chemical Laboratory, Lensfield Road, Cambridge CB2 1EW, U.K.

Can. J. Chem. Downloaded from www.nrcresearchpress.com by 92.62.229.171 on 09/08/12
For personal use only.

TABLE 1. Crystallographic data for Hcmp and Hpap[a]

Compound	Hcmp	Hpap
Formula	$C_8H_9NO_4$	$C_{13}H_{13}NO_3$
fw	183.16	231.25
Crystal system	Monoclinic	Monoclinic
Space group	$P2_1/n$	$C2/c$
a, Å	6.340(2)	10.8435(9)
b, Å	7.705(1)	16.680(2)
c, Å	16.226(1)	13.5665(6)
β°	94.74(1)	109.450(4)
V, Å^3	789.9(3)	2313.7(3)
Z	4	8
ρ_{calc}, g/cm^3	1.540	1.328
$F(000)$	384	976
Radiation	Mo	Cu
λ, Å	0.71069	1.54178
μ, cm^{-1}	1.17	7.43
Crystal size, mm	0.12 × 0.35 × 0.45	0.25 × 0.25 × 0.40
Transmission factors	0.93–1.04	0.74–1.00
Scan type	ω–2θ	ω–2θ
Scan range, deg in ω	1.26 + 0.35 tan θ	0.94 + 0.30 tan θ
Scan speed, deg/min	32	32
Data collected	$+h$, $+k$, $\pm l$	$+h$, $+k$, $\pm l$
$2\theta_{max}$, deg	60	155
Crystal decay	Negligible	Negligible
Total reflections	2640	2477
Total unique reflections	2443	2339
R_{merge}	0.020	0.010
No. of reflections with $I \geq 3\sigma(I)$	1642	1819
No. of variables	154	207
R	0.030	0.041
R_w	0.039	0.058
gof	2.03	2.52
Max Δ/σ (final cycle)	0.01	0.02
Residual density e/Å^3	−0.16 to +0.20	−0.16 to +0.24

[a]Temperature 294 K, Rigaku AFC6S diffractometer, graphite monochromator, takeoff angle 6.0°, aperture 6.0 × 6.0 mm at a distance of 285 mm from the crystal, stationary background counts at each end of the scan (scan/background time ratio 2:1, up to 8 rescans), $\sigma^2(F^2) = [S^2(C + 4B) + (pF^2)^2]/Lp^2$ (S = scan rate, C = scan count, B = normalized background count, $p = 0.02$ for Hcmp and 0.03 for Hpap), function minimized $\Sigma w(|F_o| - |F_c|)^2$ where $w = 4F_o^2/\sigma^2(F_o^2)$, $R = \Sigma||F_o| - |F_c||/\Sigma|F_o|$, $R_w = (\Sigma w(|F_o| - |F_c|)^2/\Sigma w|F_o|^2)^{1/2}$, and gof $= [\Sigma w(|F_o| - |F_c|)^2/(m - n)]^{1/2}$. Values given for R, R_w, and gof are based on those reflections with $I \geq 3\sigma(I)$.

TABLE 2. Final atomic coordinates (fractional) and B_{eq} (Å^2)[a] for Hcmp

Atom	x	y	z	B_{eq}
O (1)	0.2550 (1)	0.1339 (1)	0.55699 (5)	3.3
O (2)	0.6127 (2)	0.2876 (1)	0.62640 (5)	3.3
O (3)	0.6549 (1)	−0.0052 (1)	0.28805 (5)	3.5
O (4)	0.4348 (2)	0.0517 (1)	0.17817 (5)	3.4
N (1)	0.4990 (1)	0.2696 (1)	0.37577 (5)	2.2
C (1)	0.1619 (2)	0.1120 (2)	0.38538 (8)	2.9
C (2)	0.3566 (2)	0.1962 (1)	0.42452 (6)	2.1
C (3)	0.3988 (2)	0.2029 (1)	0.50945 (6)	2.2
C (4)	0.5850 (2)	0.2822 (2)	0.54494 (6)	2.4
C (5)	0.7262 (2)	0.3505 (2)	0.49210 (7)	2.8
C (6)	0.6794 (2)	0.3435 (2)	0.40863 (7)	2.7
C (7)	0.4613 (2)	0.2614 (2)	0.28500 (7)	2.5
C (8)	0.5226 (2)	0.0868 (2)	0.24938 (6)	2.4

[a]$B_{eq} = (8/3)\pi^2\Sigma\Sigma U_{ij}a_i^* a_j^* (\mathbf{a}_i \cdot \mathbf{a}_j)$.

been prepared in fair yields under differing conditions: Hcmp was obtained by maintaining the pH of the solution around 9 while Hpap was synthesized in acidic medium. This is necessitated by the different basicity of the amines.

The structures of Hcmp and Hpap were established by single crystal X-ray diffraction. ORTEP views of the two molecules are shown in Fig. 1. Stereodiagrams of the unit cell packing are shown for Hcmp in Fig. 2 and for Hpap in Fig. 3. In Hcmp, the carboxyl group is deprotonated and the ketone oxygen atom on the pyridinone ring is protonated thus forming a zwitterion. There is an extraordinarily strong O—H···O hydrogen bond (O(2)—H(2)···O(4) ($\frac{1}{2} + x$, $\frac{1}{2} - y$, $\frac{1}{2} + z$), H···O = 1.43 (2) Å, O···O = 2.475 (1) Å, O—H···O = 175 (2)°) between two molecules. Three-dimensional networks of Hcmp molecules are formed by C—H···O hydrogen bonds (C(6)—H(7)···O(4) ($\frac{3}{2} - x$, $\frac{1}{2} + y$, $\frac{1}{2} - z$), H···O = 2.46 (1) Å, C···O = 3.333 (2) Å, C—H···O = 156 (1)° and C(7)—H(8)···O(3) ($\frac{3}{2} - x$, $\frac{1}{2} + y$, $\frac{1}{2} - z$), H···O = 2.41 (2) Å, C···O = 3.322 (2) Å, C—H···O = 162(1)°) plus an additional O—H···O hydrogen bond (O(1)—H(1)···O(3) ($1 - x$, $-y$, $1 - z$),

TABLE 3. Final atomic coordinates (fractional) and B_{eq} (Å^2)[a] for Hpap

Atom	x	y	z	B_{eq}
O (1)	−0.0381 (1)	0.09674 (8)	−0.10482 (9)	4.5
O (2)	0.1571 (1)	0.11469 (7)	−0.19037 (8)	4.3
O (3)	0.3761 (1)	0.15245 (9)	0.55646 (9)	5.4
N (1)	0.2409 (1)	0.13542 (8)	0.1235 (1)	3.7
C (1)	0.0102 (2)	0.1114 (2)	0.1103 (1)	5.1
C (2)	0.1139 (1)	0.1193 (1)	0.0610 (1)	3.6
C (3)	0.0867 (1)	0.1132 (1)	−0.0442 (1)	3.4
C (4)	0.1842 (2)	0.1232 (1)	−0.0937 (1)	3.4
C (5)	0.3104 (2)	0.1434 (1)	−0.0241 (1)	4.2
C (6)	0.3351 (2)	0.1480 (1)	0.0801 (1)	4.2
C (7)	0.2766 (1)	0.1381 (1)	0.2365 (1)	3.5
C (8)	0.3022 (2)	0.2111 (1)	0.2872 (1)	4.1
C (9)	0.3360 (2)	0.2133 (1)	0.3946 (1)	4.4
C (10)	0.3436 (2)	0.1434 (1)	0.4510 (1)	3.9
C (11)	0.3197 (2)	0.0707 (1)	0.3999 (1)	4.1
C (12)	0.2855 (2)	0.0679 (1)	0.2922 (1)	4.1
C (13)	0.3643 (3)	0.0845 (2)	0.6161 (2)	6.5

[a] $B_{eq} = (8/3)\pi^2\Sigma\Sigma U_{ij} a_i^* a_j^* (\mathbf{a}_i \cdot \mathbf{a}_j)$.

TABLE 4. Bond lengths (Å) with estimated standard deviations

Atoms	Compound	
	Hcmp	Hpap
O(1)—C(3)	1.351 (1)	1.357 (2)
O(2)—C(4)	1.320 (1)	1.254 (2)
O(3)—C(8)	1.230 (1)	
O(3)—C(10)		1.363 (2)
O(3)—C(13)		1.423 (3)
O(4)—C(8)	1.269 (1)	
N(1)—C(2)	1.371 (1)	1.383 (2)
N(1)—C(6)	1.348 (2)	1.354 (2)
N(1)—C(7)	1.474 (1)	1.452 (2)
C(1)—C(2)	1.489 (2)	1.492 (2)
C(2)—C(3)	1.383 (1)	1.361 (2)
C(3)—C(4)	1.409 (2)	1.438 (2)
C(4)—C(5)	1.393 (2)	1.420 (2)
C(5)—C(6)	1.363 (2)	1.351 (2)
C(7)—C(8)	1.527 (2)	1.381 (2)
C(7)—C(12)		1.380 (2)
C(8)—C(9)		1.379 (2)
C(9)—C(10)		1.382 (2)
C(10)—C(11)		1.378 (2)
C(11)—C(12)		1.383 (2)

TABLE 5. Bond angles (deg) with estimated standard deviations

Atoms	Compound	
	Hcmp	Hpap
C(10)—O(3)—C(13)		117.9 (2)
C(2)—N(1)—C(6)	121.61 (9)	120.3 (1)
C(2)—N(1)—C(7)	119.91 (9)	121.0 (1)
C(6)—N(1)—C(7)	118.42 (9)	118.7 (1)
N(1)—C(2)—C(1)	119.74 (9)	119.2 (1)
N(1)—C(2)—C(3)	118.5 (1)	118.8 (1)
C(1)—C(2)—C(3)	121.8 (1)	122.1 (1)
O(1)—C(3)—C(2)	118.0 (1)	118.3 (1)
O(1)—C(3)—C(4)	121.29 (9)	118.7 (1)
C(2)—C(3)—C(4)	120.7 (1)	123.0 (1)
O(2)—C(4)—C(3)	117.4 (1)	121.5 (1)
O(2)—C(4)—C(5)	124.4 (1)	124.1 (1)
C(3)—C(4)—C(5)	118.1 (1)	114.4 (1)
C(4)—C(5)—C(6)	119.9 (1)	121.4 (1)
N(1)—C(6)—C(5)	121.2 (1)	122.1 (2)
N(1)—C(7)—C(8)	113.01 (9)	119.5 (1)
N(1)—C(7)—C(12)		119.9 (1)
O(3)—C(8)—O(4)	124.8 (1)	
O(3)—C(8)—O(7)	119.9 (1)	
O(4)—C(8)—C(7)	115.2 (1)	
C(8)—C(7)—C(12)		120.7 (1)
C(7)—C(8)—C(9)		119.2 (2)
C(8)—C(9)—C(10)		120.6 (2)
O(3)—C(10)—C(9)		115.8 (2)
O(3)—C(10)—C(11)		124.4 (2)
C(9)—C(10)—C(11)		119.8 (1)
C(10)—C(11)—C(12)		120.1 (2)
C(7)—C(12)—C(11)		119.6 (2)

H···O = 1.94 (2) Å, O···O = 2.719 (1) Å, O—H···O = 152 (2)°. The bridging carboxyl groups link Hcmp molecules together (Fig. 2). The Hpap structure contains centrosymmetric C—H···O hydrogen bonded dimeric units (C(8)—H(7)···O(2) ($\frac{1}{2} - x, \frac{1}{2} - y, -z$), H···O = 2.34 (2) Å, C···O = 3.279 (2) Å, C—H···O = 160 (1)°). Each dimer is linked to two others by O—H···O hydrogen bonds (O(1)—H(1)···O(2) $-x, y, -\frac{1}{2} - z$), H···O = 1.82 (2) Å, O···O = 2.662 (2) Å, O—H···O = 152 (2)°) to form the three-dimensional network (Fig. 3).

Both structures contain legitimate intermolecular (see above) and intramolecular C—H···O hydrogen bonds (C(1)—H(5)···O(1), H···O = 2.35 (2) Å, C···O = 2.803 (2) Å, C—H···O = 110 (1)° in Hcmp and C(1)—H(4)···O(1), H···O = 2.37 (3) Å, C···O = 2.798 (2) Å, C—H···O = 107 (2)° in Hpap). The formation of legitimate C—H···O bonds has not been observed in the structures of reported 1-alkyl-3-hydroxy-2-methyl-4-pyridinones, **1***a* and **1***b* (8). In addition, there is an intramolecular O—H···O bond observed both in Hcmp (O(1)—H(1)···O(2), H···O = 2.29 (2) Å, O···O = 2.719 (2) Å, O—H···O = 112 (1)°) and in Hpap (O(1)—H(1)···O(2), H···O = 2.36 (2) Å, O···O = 2.749 (2) Å, O—H···O = 106 (2)°) molecules.

The six-membered pyridinone ring systems in both Hpap and Hcmp are slightly, but significantly, nonplanar (maximum deviations from the mean planes being 0.0203 (19) Å in the former and 0.0099 (13) Å in the latter), as noted earlier for 3-hydroxy-2-methyl-4-pyridinone (Hmpp) and 3-hydroxy-1,2-dimethyl-4-pyridinone (Hdpp) (8). The deviation from planarity is towards a N(1), C(4) boat in both molecules. In the Hpap molecule, the phenyl ring is planar to within 0.0063 (15) Å and is oriented roughly at right angles to the pyridinone ring (the dihedral angle between the two planes is 73.7°) to minimize steric interaction with the adjacent C(1) methyl group. In Hcmp, the plane formed by the carboxymethyl substituent on N(1) is also perpendicular to the pyridinone ring (the dihedral angle is 91.0°) and it is planar to within 0.0148 (11) Å.

The pattern of bond lengths within the pyridinone ring in

Can. J. Chem. Downloaded from www.nrcresearchpress.com by 92.62.229.171 on 09/08/12
For personal use only.

Can. J. Chem. Downloaded from www.nrcresearchpress.com by 92.62.229.171 on 09/08/12
For personal use only.

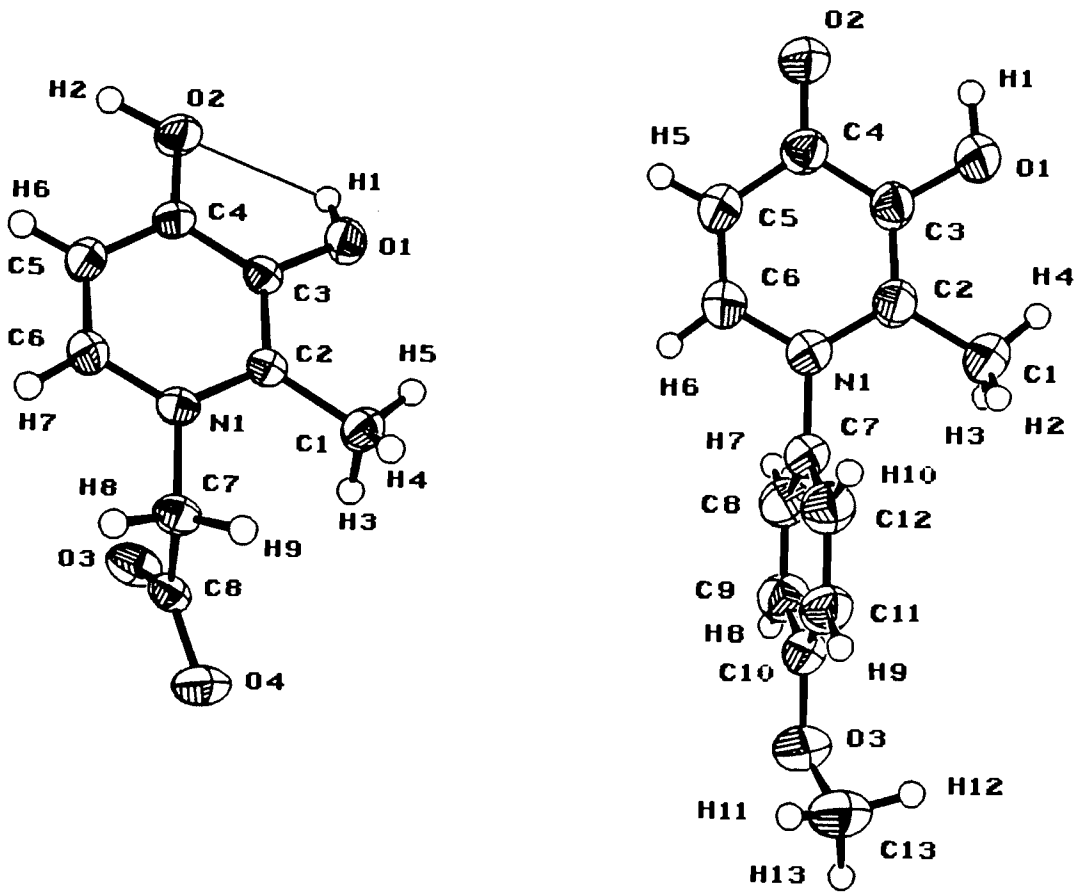

FIG. 1. ORTEP views of the Hcmp (left) and Hpap (right) molecules; 50% probability thermal ellipsoids are shown. Hydrogen atoms have been assigned artificially small thermal parameters for the sake of clarity.

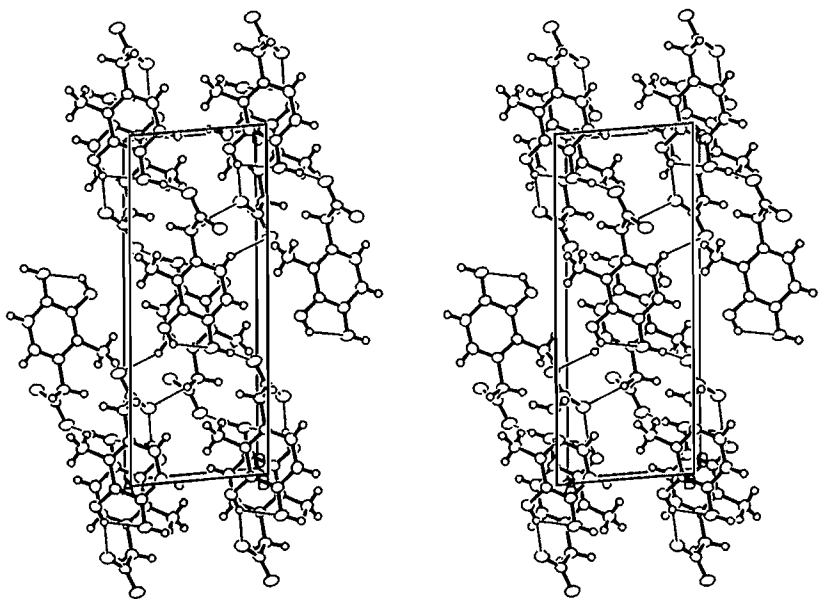

FIG. 2. ORTEP stereoscopic view of the packing arrangement in Hcmp.

Hpap is different from that observed in Hmpp and Hdpp. The most noticeable feature is the more pronounced localization of the formal double bonds in Hpap vs. that in Hmpp and Hdpp. Shorter C(2)—C(3), C(5)—C(6) and ketone C(4)—O(2) bonds, and loner N(1)—C(2) and C(4)—C(5) bonds are observed in Hpap. Also, the C(3)—C(4)—C(5) bond angle in Hpap is about 1° smaller than that in Hmpp and Hdpp and 4° smaller than in Hcmp. In Hcmp, a different

pattern of bond lengths and bond angles in the pyridinone ring is observed. The bond lengths are more averaged than in the other pyridinone systems and the intra-annular bond angles are all within 1° of 120°. A significantly longer ketone O(2)—C(4) bond (1.320 Å) is also observed than in Hpap (1.254 Å), Hmpp (1.280 Å), of Hdpp (1.272 Å). These bond lengths and angles taken together indicate that a delocalized pyridinone ring is obtained in Hcmp and that the positive charge of the zwitterion is distributed throughout the ring rather than concentrated at the nitrogen. In the pyridinone systems, which we have studied crystallographically, the extent of the delocalization of the formal double bonds in the pyridinone ring follows the order: Hcmp >> Hmpp ≈ Hdpp > Hpap. We had previously sought to isolate crystals with the ring-based cation by acidifying Hdpp (and other noncarboxyl substituted 3-hydroxy-4-pyridinones) to make H_2dpp^+ or analogues without success.

The protonation constants of Hcmp and Hpap were determined by potentiometric equilibrium measurements. The results are listed in Table 6. The protonation equilibria for the amphoteric ligands are described by eqs. [1]–[3] for Hcmp (H_2L) and eqs. [4] and [5] for Hpap (HL):

$$[1]\quad H^+ + L^{2-} \rightleftharpoons HL^- \qquad K_1 = \frac{[HL^-]}{[H^+]\,[L^{2-}]}$$

$$[2]\quad H^+ + HL^- \rightleftharpoons H_2L \qquad K_2 = \frac{[H_2L]}{[H^+]\,[HL^-]}$$

$$[3]\quad H^+ + H_2L \rightleftharpoons H_3L^+ \qquad K_3 = \frac{[H_3L^+]}{[H^+]\,[H_2L]}$$

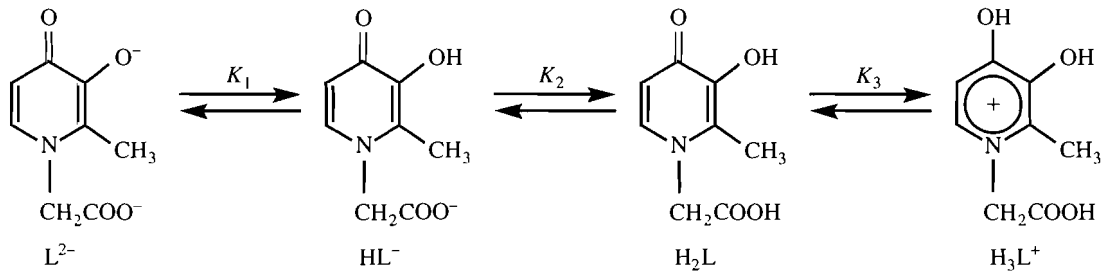

$$[4]\quad H^+ + L^- \rightleftharpoons HL \qquad K_1' = \frac{[HL]}{[H^+]\,[L^-]}$$

$$[5]\quad H^+ + HL \rightleftharpoons H_2L^+ \qquad K_2' = \frac{[H_2L^+]}{[H^+]\,[HL]}$$

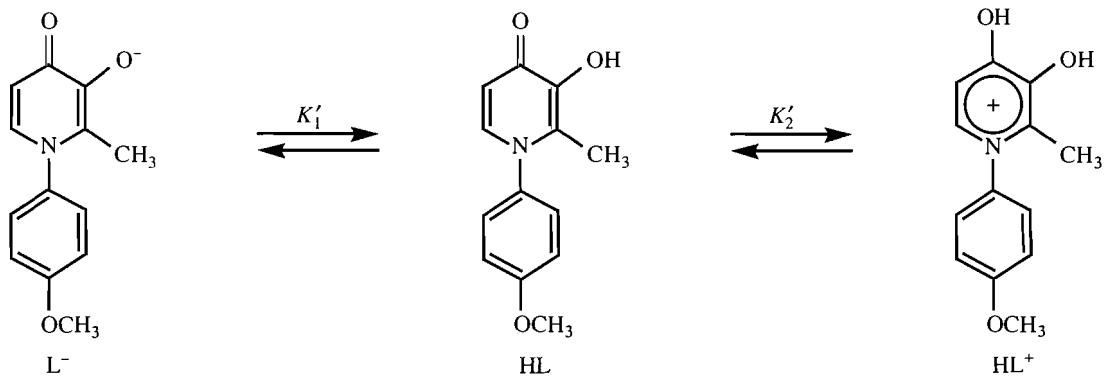

Log K_1 for Hcmp is close to that for other *N*-alkyl-3-hydroxy-2-methyl-4-pyridinones (log K_1 = 9.76 vs. ~9.8) (10). This suggests that the deprotonated carboxyl group at the ring nitrogen in solution does not affect the electron density of the pyridinone ring to any significant extent vs. the *N*-alkyl substituted pyridinones. It is possible for Hcmp to form a zwitterion in solution; therefore, an equilibrium would be established between the neutral ligand, H_2L and the zwitterion species. The protonation processes of the neutral ligand, H_2L, and the zwitterion would then contribute to both of the determined protonation constants K_2 and K_3 for equilibria [2] and [3].

The constants for Hpap are similar to those reported for 3-hydroxy-2-methyl-1-phenyl-4-pyridinone (Hppp) (log K_1 = 9.42 vs. 9.40, log K_2 = 3.16 vs. 3.03) (7) and lower than those for the *N*-alkyl-3-hydroxy-2-methyl-4-pyridinones (log K_1 = 9.42 vs. ~9.8 and log K_2 = 3.16 vs. ~3.7). This suggests that the *p*-methoxyphenyl group and unsubstituted phenyl group have similar electron-withdrawing effects on the pyridinone ring.

Can. J. Chem. Downloaded from www.nrcresearchpress.com by 92.62.229.171 on 09/08/12
For personal use only.

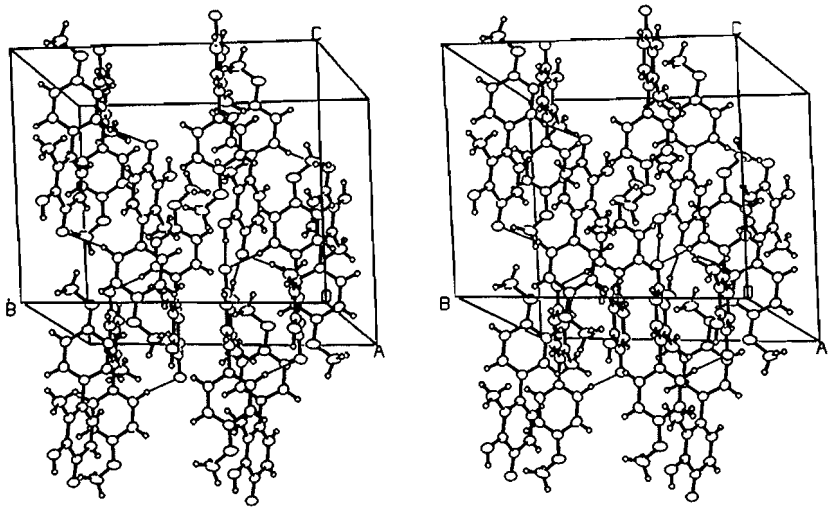

FIG. 3. ORTEP stereoscopic view of the packing arrangement in Hpap.

TABLE 6. Protonation constants (K_1, K_2) for Hcmp and Hpap at 25°C in 0.15 M NaCl[a]

	Hcmp	Hpap
log K_1	9.76 (1)	9.42 (4)
log K_2	3.43 (1)	3.16 (8)
log K_3	2.78 (3)	

[a]Numbers in parentheses represent standard deviations between successive runs.

TABLE 7. Ultraviolet spectral data[a,b] for Hcmp and Hpap

	λ (nm)	ε (M^{-1} cm^{-1})
Hcmp	281	12 900
	218	15 100
	207	10 400
Hpap	283	19 700
	225	38 400 (sh)
	207	62 500

[a]In H_2O, pH = 7.4, 25°C.
[b]sh = shoulder.

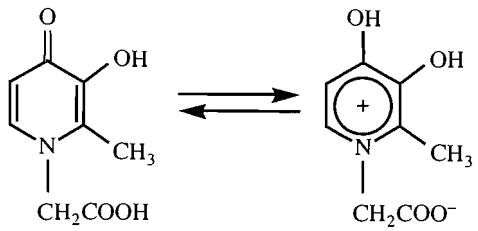

The infrared spectrum of Hpap shows the characteristic four-band pattern in the range 1650–1500 cm^{-1}. This is assigned collectively to $\nu_{C=O}$ and ν_{ring} vibrations, since resolving these two highly mixed modes is extremely difficult (8, 38, 39). The IR spectrum of Hcmp shows a very broad band in the range 3300–2500 cm^{-1}, a result of the strong intermolecular hydrogen bonding of the carboxyl groups (40). The characteristic four-band pattern between 1650–1500 cm^{-1} for pyridinone ring stretching is not obvious in Hcmp because of the formation of zwitterions and the delocalization of the formal ring double bonds. There is a wide strong band from 1650 to 1600 cm^{-1} that is assigned to a mixture of stretchings of the carboxylate anion and the pyridinone ring.

The UV spectral data are shown in Table 7. The bands observed are from $\pi \rightarrow \pi^*$ transitions. E (ethylinic) and B (benzenoid) bands were recorded at 218 and 281 nm for Hcmp and 225 and 283 nm for Hpap, respectively. There was, in addition, a third absorption in each case. The extinction coefficients are much higher for Hpap than for Hcmp, an effect of the *p*-methoxyphenyl substituent. Proton NMR spectrum of Hcmp shows the characteristic doublet of ring proton doublets with a coupling constant of 8 Hz. In the Hpap spectrum, only one ring proton doublet with a coupling constant of 7.8 Hz was resolved; the other one appeared in the envelope of phenyl protons.

In conclusion, the structural studies of Hcmp and Hpap reveal that there is an extensive hydrogen bond network in both structures; hydroxyl and ketone functionalities contribute a number of hydrogen-bonding sites to each of the molecules. The protonated and delocalized pyridinone ring system was finally obtained in the solid state in Hcmp by formation of a zwitterion, and it does indeed show highly averaged bond distances.

Acknowledgments

Acknowledgment is made to the Natural Sciences and Engineering Research Council of Canada and to the U.S. Public Health Service (CA 48964) for operating grants, the University of British Columbia for a University Graduate Fellowship (Z.Z.), and to Professor J. Trotter for the kind use of his crystallographic facilities.

1. M. M. Finnegan, S. J. Rettig, and C. Orvig. J. Am. Chem. Soc. **108**, 5033 (1986).
2. M. M. Finnegan, T. G. Lutz, W. O. Nelson, A. Smith, and C. Orvig. Inorg. Chem. **26**, 2171 (1987).
3. C. A. Matsuba, W. O. Nelson, S. J. Rettig, and C. Orvig. Inorg. Chem. **27**, 3935 (1988).

Can. J. Chem. Downloaded from www.nrcresearchpress.com by 92.62.229.171 on 09/08/12
For personal use only.

4. W. O. Nelson, T. B. Karpishin, S. J. Rettig, and C. Orvig. Inorg. Chem. **27**, 1045 (1988).
5. W. O. Nelson, S. J. Rettig, and C. Orvig. Inorg. Chem. **28**, 3153 (1989).
6. Z. Zhang, T. L. T. Hui, and C. Orvig. Can. J. Chem. **67**, 1708 (1989).
7. Z. Zhang, S. J. Rettig, and C. Orvig. Inorg. Chem. **30**, 509 (1991).
8. W. O. Nelson, T. B. Karpishin, S. J. Rettig, and C. Orvig. Can. J. Chem. **66**, 123 (1988).
9. D. J. Clevette, W. O. Nelson, A. Nordin, C. Orvig, and S. Sjöberg. Inorg. Chem. **28**, 2079 (1989).
10. D. J. Clevette, D. M. Lyster, W. O. Nelson, T. Rihela, G. A. Webb, and C. Orvig. Inorg. Chem. **29**, 667 (1990).
11. Z. Zhang, D. M. Lyster, G. A. Webb, and C. Orvig. Nucl. Med. Biol. **19**, 327 (1992).
12. G. J. Kontoghiorghes, M. A. Aldouri, L. Sheppard, and A. V. Hoffbrand. Lancet, (**i**), 1294 (1987).
13. G. J. Kontoghiorghes, M. A. Aldouri, A. V. Hoffbrand, J. Barr, B. Wonke, T. Kourouclaris, and L. Sheppard. Br. Med. J. **295**, 1509 (1987).
14. G. J. Kontoghiorghes, A. N. Bartlett, A. V. Hoffbrand, J. G. Goddard, L. Sheppard, J. Barr, and P. Nortey. Br. J. Haemat. **76**, 295 (1990).
15. A. N. Bartlett, A. V. Hoffbrand, and G. J. Kontoghiorghes. Br. J. Haemat. **76**, 301 (1990).
16. D. M. Taylor and G. J. Kontoghiorghes. Inorg. Chim. Acta. **125**, L35 (1986).
17. B. Tamhina, M. J. Heark, and K. Jakopcic. J. Less-Common Metals, **33**, 289 (1973).
18. M. J. Herak, B. Tamhina, and K. Jakopcic. J. Inorg. Nucl. Chem. **35**, 1665 (1973).
19. M. J. Heark, M. Janko, and B. Tamhina. Mikrochim. Acta, 783 (1973).
20. B. Tamhina and M. J. Heark. Croat. Chem. Acta, **45**, 603 (1973).
21. M. J. Herak and B. Tamhina. Croat. Chem. Acta, **46**, 237 (1974).
22. C. Vojkovic, B. Tamhina, and M. J. Heark. Z. Anal. Chem. **276**, 377 (1975).
23. B. Tamhina and M. J. Herak. Mikrochim. Acta, 45 (1975).
24. B. Tamhina, V. Vojkovic, and M. J. Herak. Croat. Chem. Acta, **48**, 183 (1976).
25. B. Tamhina and M. J. Herak. J. Inorg. Nucl. Chem. **38**, 1505 (1976).
26. M. J. Herak and M. Janko. J. Inorg. Nucl. Chem. **34**, 2627 (1972).
27. M. Janko and M. J. Herak. Mikrochim. Acta, 198 (1972).
28. J. Elguero, C. Marzin, A. R. Katritzky, and P. Linda. Adv. Heterocycl. Chem. Suppl. 1, Academic Press, New York. p. 86 (1976).
29. C. D. Johnson. Comprehensive heterocyclic chemistry. *Edited by* A. R. Katritzky and C. W. Ress. Pergamon Press, New York. 1984. pp. 148–157.
30. T. L. Gilchrist. Heterocyclic chemistry. Pitman Publishing Ltd., London. 1985. pp. 290–296.
31. A. Maqueatian, Y. van Haverbeke, C. de Meyer, A. R. Katritzky, M. J. Cook, and A. D. Page. Can. J. Chem. **53**, 490 (1975).
32. W. O. Nelson. Ph.D. Thesis, The University of British Columbia. 1988.
33. (*a*) C. J. Gilmore. J. Appl. Crystallogr. **17**, 42 (1984); (*b*) P. T. Beurskens. DIRDIF: Direct methods for difference structures—an automatic procedure for phase extension and refinement of difference structure factors. Technique report 1984/1, Crystallography Laboratory, Toernooiveld 6525 Ed. Nijmegen, Netherlands.
34. International tables for X-ray crystallography. Vol. IV. Kynoch Press, Birmingham, England. Table 2.2A. 1974.
35. J. A. Ibers and W. C. Hamilton. Acta Crystallogr. **17**, 781 (1964).
36. International tables for X-ray crystallography. Vol. IV. Kynoch Press, Birmingham, England. Table 2.3.1. 1974.
37. TEXSAN-TEXRAY Structure analysis package, Molecular Structure Corporation. 1985.
38. B. D. Batts and E. Spinner. Aust. J. Chem. **22**, 2581 (1969).
39. D. Cook. Can. J. Chem. **41**, 2575 (1963).
40. A. Novak. Struct. Bonding (Berlin), **18**, 177 (1974).

Can. J. Chem. Downloaded from www.nrcresearchpress.com by 92.62.229.171 on 09/08/12
For personal use only.

Tris-triphenylsiloxy compounds of aluminium[1]

ALLEN W. APBLETT, ALISON C. WARREN, AND ANDREW R. BARRON[2]

Department of Chemistry and Materials Research Laboratory, Harvard University, Cambridge, MA 02138, U.S.A.

Received July 4, 1991

ALLEN W. APBLETT, ALISON C. WARREN, and ANDREW R. BARRON. Can. J. Chem. **70**, 771 (1992).

The reaction of $AlMe_3$ with three equivalents of $HOSiPh_3$ in THF results in the formation of the solvent complex $Al(OSiPh_3)_3(THF)$ (**1**). Hydrolysis of **1** yields the stable water complex $Al(OSiPh_3)_3(H_2O)(THF)_2$ (**2**) in which the THF molecules are hydrogen bonded to the coordinated water ligand. Compounds **1** and **2** have been fully characterized by ^1H, ^{13}C, ^{17}O, ^{27}Al, and ^{29}Si NMR and IR spectroscopy. In addition, variable temperature ^1H NMR of **2** has been employed to investigate the steric interactions between the phenyl rings of adjacent siloxide ligands. The molecular structures of the solvates **1**·(THF) and **2**·$(THF)_{1.25}$ have been determined by X-ray crystallography. **1**·(THF): monoclinic $P2_1/c$, a = 10.03 (1), b = 23.758 (6), c = 23.294 (7) Å, β = 101.13 (6)°, Z = 4, R = 0.084, R_w = 0.094. **2**·$(THF)_{1.25}$: cubic $Pa\bar{3}$, a = 23.034 (3) Å, Z = 4, R = 0.093, R_w = 0.099.

Key words: aluminium, siloxide, hydrolysis, complex, NMR spectroscopy.

ALLEN W. APBLETT, ALISON C. WARREN et ANDREW R. BARRON. Can. J. Chem. **70**, 771 (1992).

La réaction du $AlMe_3$ avec trois équivalents de $HOSiPh_3$ dans du THF conduit à la formation d'un complexe incorporant le solvant, $Al(OSiPh_3)_3(THF)$ (**1**). L'hydrolyse du composé **1** fournit le complexe aqueux stable, $Al(OSiPh_3)_3(H_2O)(THF)_2$ (**2**) dans lequel les molécules de THF sont coordonnées à l'eau par des liaisons hydrogènes. On a caractérisé complètement les molécules **1** et **2** par la RMN du ^1H, du ^{13}C, du ^{17}O, du ^{27}Al et du ^{29}Si ainsi que par spectroscopie infrarouge. De plus, on a utilisé la RMN du ^1H à température variable pour étudier les interactions stériques entre les noyaux aromatiques des coordinats siloxydes adjacents. Les structures moléculaires des produits solvatés **1**·(THF) et **2**·$(THF)_{1.25}$ ont été déterminées par diffraction des rayons-X. **1**·(THF) : monoclinique, $P2_1/c$, a = 10,03(1), b = 23,758(6) et c = 23,294(7) Å, β = 101,13(6)°, Z = 4, R = 0,084, R_w = 0,094. **2**·$(THF)_{1.25}$: cubique, $Pa\bar{3}$, a = 23,034(3) Å, Z = 4, R = 0,093, R_w = 0,099.

Mots clés : aluminium, siloxyde, hydrolyse, complexe, RMN.

[Traduit par la rédaction]

Introduction

Recent work in our laboratory has been concerned with the synthesis and structural characterization of siloxy-substituted alumoxanes (1–3). While alumoxanes is a term applied to organically substituted aluminium oxygen macromolecules in general, we have determined that siloxy-substituted derivatives all have the empirical formula $[Al(O)_x(OH)_y(OSiR_3)_z]_n$ where $2x + y + z = 3$ (3). These materials were first synthesized in 1958 by Andrianov and Zhadanov via the hydrolysis of trisiloxy compounds of aluminium (eq. [1]) (4).

$$[1]\quad Al(OSiR_3)_3 \xrightarrow[-HOSiR_3]{+H_2O} [Al(O)_x(OH)_y(OSiR_3)_y]_n$$

Since there are only a limited number of stable trialkylsilanols commercially available for use as precursors to these aluminium trisiloxides, we have developed an alternative route to siloxy-alumoxanes based on the hydrolysis of dimeric dimethylaluminium monosiloxides (2), (eq. [2]), which are readily prepared from polydiorganosiloxides (eq. [3]) (5).

$$[2]\quad n[AlMe_2(OSiR_3)]_2 \xrightarrow[-MeH\ -HOSiR_3]{+H_2O} \frac{n}{2}[Al(O)_x(OH)_y(OSiR_3)_z]_n$$

$$[3]\quad n\,AlMe_3 + (R_2SiO)_n \xrightarrow{\Delta} \frac{n}{2}[AlMe_2(OSiR_2Me)]_2$$

While both of the routes outlined in eqs. [1] and [2] lead to high molecular weight siloxy-alumoxanes, we have been unable to isolate any of the proposed intermediates in the hydrolysis reactions, for example, low molecularity species containing either coordinated water or terminal hydroxide groups (eq. [4]).

$$[4]\quad Al(OSiR_3)_3 \xrightarrow{+H_2O} Al(OSiR_3)_3(H_2O) \xrightarrow[-HOSiR_3]{\Delta} [Al(OH)(OSiR_3)_2]_x$$

In an effort to isolate such species we have investigated the hydrolysis of the aluminium siloxide compound derived from the sterically bulky triphenyl silanol, $HOSiPh_3$. The rationale for the choice of this ligand is based on the concept that sterically demanding ligands preclude oligomerization, and thus in the present case the condensation reaction that leads to alumoxane formation is prevented.

Experimental

General

Elemental analyses were performed by Oneida Research Services, Whitesboro, N.Y. Melting points and thermogravimetric analyses were obtained on a Seiko 200 TG/DTA instrument. IR spectra (4000–400 cm^{-1}) were recorded on a Nicolet 5ZDX FTIR as Nujol or Fluorolube mulls on KBr plates. ^1H and ^{13}C NMR spectra were obtained on a Bruker AM-500 spectrometer, and chemical shifts are reported relative to $SiMe_4$ in C_6D_6 unless otherwise stated. ^1H–^1H COSY NMR spectra were collected by use of a standard pulse sequence (6, 7) with 45° mixing pulse, a 1–2 s relaxation delay, and a resolution of ca. 4 Hz per point. The FID's were not weighted before Fourier transformation, and the spectral matrix was symmetrized about the diagonal. ^1H–^{13}C correlated 2D NMR spectra were obtained using a standard pulse sequence (8),

[1]Dedicated to the memory of Tom Birchall, for his many contributions to main group inorganic chemistry.

[2]Author to whom corrrespondence may be addressed.

Printed in Canada

Can. J. Chem. Downloaded from www.nrcresearchpress.com by 92.62.229.171 on 09/08/12
For personal use only.

TABLE 1. Heteroatom NMR chemical shifts[a]

Compound	^{27}Al	^{29}Si	^{17}O
$Al(OSiPh_3)_3(THF)$	57.5 (3400)	−24.6	12.9 (780), THF 7.2 (730), $OSiPh_3$[b]
$Al(OSiPh_3)_3(H_2O)(THF)_2$	58.8 (4380)	−25.7	17.2 (660), THF 14.5 (585), H_2O[c] 8.8 (860), $OSiPh_3$[b]
$[AlMe_2(\mu\text{-}OSiPh_3)]_2$	57.4 (6440)	−10.8	47.8 (780)
$Al(acac)(OSiPh_3)_2$	53.0 (2300)[d]	−24.2[e]	375.0 (2200), acac 12.9 (1400), $OSiPh_3$
$HOSiPh_3$		−12.6	8.9 (414)

[a]$W_{1/2}$ values in Hz are given in parentheses. Unless otherwise stated all spectra were obtained at ambient temperatures, in CH_2Cl_2:$CDCl_3$ (1:1).
[b]22.3% ^{17}O enriched $OSiPh_3$.
[c]22.3% ^{17}O enriched H_2O.
[d]Reference 17, $C_2D_2Cl_4$, 120°C.
[e]Reference 17, $CDCl_3$.

spectral widths of 250 and 300 Hz, and 1000 and 256 data points in the F2 (^{13}C) and F1 (^1H) domains, respectively. The latter domain was zero filled to 512 K and Lorentzian line-broadening functions equal to the digital resolution (ca. 4 Hz) were applied to each axis. ^{17}O, ^{27}Al, and ^{29}Si NMR spectra (see Table 1) were recorded in a Bruker WM-300 spectrometer and chemical shifts were reported versus H_2O, $[Al(H_2O)_6]^{3+}$, and $SiMe_4(CDCl_3)$, respectively. X-ray data were collected on a Nicolet R3m/V four-circle diffractometer equipped with a LT-1 low-temperature device.

$AlMe_3$ as a 2 M solution in hexane (Aldrich), $HOSiPh_3$ (Huls), and $ClSiPh_3$ (Aldrich) were commercial samples and were used without further purification. Unless otherwise stated all manipulations were performed under an atmosphere of dry nitrogen. Solvents were dried, distilled, and degassed before use. Water was doubly distilled and deionized.

*$Al(OSiPh_3)_3(THF)$ (**1**)*

A solution of $AlMe_3$ (10.6 mL, 2 M solution in hexane, 21.2 mmol) in THF (50 mL) was added dropwise to a stirred solution of $HOSiPh_3$ (17.53 g, 63.4 mmol) in THF (50 mL) at 0°C. After 12 h all gas evolution had ceased and the volatiles were removed *in vacuo*, 50°C, to afford a powdery white solid in quantitative yield (21.06 g, 99.9%). Crystals of **1**·(THF) suitable for X-ray structural analysis were obtained by cooling a solution of 40 g of the crude material in 30 mL THF to −25°C; mp 353°C (dec. without melting). IR (Fluorolube and Nujol, cm^{-1}): 3182 (w), 3083 (w), 3064 (m), 3047 (m), 3020 (w), 3010 (w), 2975 (s), 2876 (s), 1588 (w), 1566 (vw), 1428 (s), 1304 (w), 1261 (m), 1187 (w), 1114 (vs), 1070 (vs), 1025 (w), 999 (m), 918 (w), 871 (m), 787 (s), 765 (w), 743 (s), 709 (vs), 701 (vs), 501 (vs), 484 (w), 475 (w), 433 (m). NMR ($CDCl_3$) ^1H: 7.55 (18H, d, J(H–H) = 6.7 Hz, *o*-CH), 7.32 (9H, t, J(H–H) = 7.5 *p*-CH), 7.17 (18H, dd, J(H–H) = 6.7 Hz, J(H–H) = 7.5 Hz, *m*-CH), 3.76 (4H, t, J(H–H) = 6.7 Hz, OCH_2), 1.52 (4H, t, J(H–H) = 6.7 Hz, OCH_2CH_2). ^{13}C: 138.4 (Si-C), 135.0 (*o*-CH), 128.9 (*p*-CH), 127.5 (*m*-CH), 70.5 (OCH_2), 25.1 (OCH_2CH_2). Anal. calcd. for $C_{62}H_{61}AlO_5Si_3$: C 74.66, H 6.16; found: C 74.60, H 5.99.

*$Al(OSiPh_3)_3(H_2O)(THF)_2$ (**2**)*

Degassed water (100 mg, 0.56 mmol) was added to a solution of **1** (5.0 g, 5.01 mmol) in THF (30 mL). The solution was swirled momentarily to mix the reagents. Upon sitting, the solution gradually deposited large, colorless cube-shaped crystals. After 12 h the solution was decanted and the crystals were dried *in vacuo*. A further crop of crystals of **2**·$(THF)_{1.25}$ was obtained upon cooling the mother liquor to −30°C. Drying the crystals (50°C) resulted in the removal of excess solvated THF and the formation of pure **2**. Yield: 5.02 g, 98%; mp 182°C (dec.). IR (Fluorolube and Nujol, cm^{-1}): 3659 (br s, ν O-H), 3071 (m), 3046 (m), 2948 (m), 2926 (s), 2858 (s), 1582 (w), 1478 (m), 1451 (m), 1412 (vs), 1304 (m), 1262 (m), 1186 (m), 1113 (vs), 1071 (vs), 1026 (s), 997 (s), 916 (w), 882 (m), 743 (s), 708 (vs), 644 (m), 606 (m), 517 (vs). NMR ($CDCl_3$) ^1H: 7.72 (6H, d, J(H–H) = 6.7 Hz, *o*-CH), 7.65*(12H, d, J(H–H) = 6.8 Hz, *o*-CH), 7.48 (3H, t, J(H–H) = 7.3 Hz, *p*-CH), 7.43(6H, t, J(H–H) = 7.4 Hz, *p*-CH), 7.36* (6H, dd, J(H–H) = 7.5 Hz, *m*-CH), 7.19* (12H, dd, J(H–H) = 7.6 Hz, *m*-CH), 3.86 (2H, s, OH_2), 3.74 [8H, t, J(H–H) = 6.5 Hz, OCH_2) 1.80 (8H, t, J(H–H) = 6.5 Hz, OCH_2CH_2). ^{13}C: 138.6*, 135.5 (Si-C), 135.0*, 134.9 (*o*-CH), 129.9, 128.8* (*p*-CH), 127.8, 127.4* (*m*-CH), 68.3 (OCH_2), 25.4 (OCH_2CH_2). Anal. calcd. for $C_{62}H_{63}AlO_6Si_3$: C 73.34, H 6.25; found: C 73.42, H 6.28.

Preparation of $H^{17}OSiPh_3$

Water (0.54 g, 40 mmol) enriched in ^{17}O (22.3%) was added dropwise via syringe to a stirred solution of $ClSiPh_3$ (11.79 g, 40 mmol) in THF (20 mL). After 8 h, the volatiles were stripped off, *in vacuo*, to yield a pale-yellow solid. Crystallization from 50 mL of 50:50 ether: pentane, at −25°C, yielded colorless crystals. Isolated yield: 10.17 g, 92%.

Crystallography

A crystal data summary is given in Table 2, and fractional atomic coordinates for **1** and **2** are listed in Tables 3 and 4 respectively.[3] Crystals of **1** and **3** were mounted directly onto the goniometer with silicon grease. Unit-cell parameters and intensity data were obtained by following previously detailed procedures, using a Nicolet R3m/V diffractometer operating in the θ–2θ scan mode. Data collection was controlled by using the Nicolet P3 program (9).

The structure of **1**·(THF) was solved using the direct methods program XS (10), which revealed the position of most of the heavy atoms. Standard difference map techniques were used to find the remaining non-hydrogen atoms. The crystallographic identification of the oxygen atom in the uncoordinated THF molecule was assigned on the basis of the atom thermal parameters. After all the non-hydrogen atoms were located and refined anisotropically, a

[3]Tables of all bond lengths and angles, anisotropic displacement coefficients, hydrogen atom coordinates, and observed and calculated structure factor amplitudes may be puchased from: The Depository of Unpublished Data, Document Delivery, CISTI, National Research Council Canada, Ottawa, Canada K1A OS2.

Tables of bond lengths and angles, and hydrogen atom coordinates, for **1** and **2** have also been deposited with the Cambridge Crystallographic Data Centre, and can be obtained on request from the Director, Cambridge Crystallographic Data Centre, University Chemical Laboratory, Lensfield Road, Cambridge CB2 1EW, U.K.

Can. J. Chem. Downloaded from www.nrcresearchpress.com by 92.62.229.171 on 09/08/12
For personal use only.

TABLE 2. Crystallographic data for **1** and **3**

Parameter	**1**·(THF)	**2**·$(THF)_{1.25}$
Formula	$C_{62}H_{61}AlO_5Si_3$	$C_{70}H_{73}AlO_{7.25}Si_3$
Crystal system	Monoclinic	Cubic
Space group	$P2_1/c$	$Pa\bar{3}$
a, Å	10.03(1)	23.034(3)
b, Å	23.758(6)	23.034(3)
c, Å	23.294(7)	23.034(3)
β, deg	101.13(6)	
V, Å^3	5446(6)	12221(3)
Z	4	4
D(calcd.), g/cm^3	1.216	1.386
Crystal dimens., mm	0.43 × 0.30 × 0.26	0.27 × 0.26 × 0.27
Temp, K	273	273
Radiation	MoK_α(λ = 0.71073 Å, graphite monochromator)	
μ, mm^{-1}	0.146	0.158
2θ limits (deg)	4.0–45.0	4.0–55.0
No. of data collected	8214	11708
No. of unique data	7109	3606
No. of obsd. data	5158	2050
R	0.084	0.093
R_w	0.094	0.099
Final residual, e Å^{-3}	0.45	1.04

Can. J. Chem. Downloaded from www.nrcresearchpress.com by 92.62.229.171 on 09/08/12
For personal use only.

difference map revealed some but not all of the hydrogen atoms. Hydrogens were, therefore, included as fixed atom contributors in the final cycle, d(C—H) = 0.96 Å, U_{eq} = 0.08 Å^3. Refinement was performed to convergence (Δ/δ(max) < 0.001) with this model. The weighting scheme was $w = [\sigma^2(|F_o|) + 0.0274(|F|)^2]^{-1}$.

The structure of **2**·$(THF)_{1.25}$ was solved by direct methods (XS), which revealed the position of the Al, O, and Si atoms. The atoms Al(1) and O(2) lie on a threefold rotation axis at x, y, z, where $x = y = z$; thus their site occupancy factors were fixed at $\frac{1}{3}$, and their positions were allowed to freely refine along the threefold rotation axis. Standard difference map techniques were used to find the remaining non-hydrogen atoms, including the presence of a THF molecule, the site occupancy of which was freely refined to a value of 0.99 and was, therefore, fixed at 1.0 in the final refinement. Attempts to refine the structure with a $\frac{2}{3}$ site occupancy of the THF molecules resulted in a significant increase in the R and R_w. After all the non-hydrogen atoms were located and refined anisotropically, a difference map revealed some but not all of the hydrogen atoms. Hydrogens were therefore included as fixed atom contributors in the final cycle, d(C—H) = 0.96 Å, U_{eq} = 0.08 Å^3. Since the bound H_2O ligand can only be hydrogen bonded to two of the three symmetry-related THF molecules, it is therefore probably disordered, and the site occupancy factor for H(2B) was therefore set at $\frac{2}{3}$. After the $Al(OSiPh_3)_3(H_2O)(THF)_3$ unit was refined a peak of significant electron density remained, which generated a highly distorted six-membered ring by symmetry. Based on NMR and TGA data this is likely a disordered THF molecule. Refinement of this peak as oxygen (site occupancy $\frac{1}{6}$) and carbon (site occupancy $\frac{4}{6}$ with no hydrogens) led to convergence of the entire structure (Δ/δ (max) < 0.001) and a significant lowering of the R factor. The weighting scheme was $w = [\sigma^2(|F_o|) + 0.0124\,(|F|)^2]$.

Although both structures refined to a satisfactory level, the weighted R factor in each case remained high. However, since the bond length and angle esd's are acceptable and atom connectivity is entirely consistent with analytical and NMR spectral characterization the solutions are adequate and undoubtedly correct.

Results and discussion

The interaction of 3 equivalents of triphenylsilanol with trimethylaluminium in THF results in the formation of the solvated trisiloxide complex, Al(OSiPh$_3$)(THF), **1**, with the concomitant liberation of methane (eq. [5]).

$$[5]\quad AlMe_3(THF) + 3\ HOSiPh_3 \xrightarrow[THF]{} \underset{(\mathbf{1})}{Al(OSiPh_3)_3\,(THF)} + 3\ MeH$$

Hydrolysis of a THF solution of **1** does not result in the hydrolytic cleavage of the aluminium–siloxide bonds and the formation of an alumoxane, as is observed for the triethylsiloxide analogue (3), but instead allows for the isolation of the water complex, $Al(OSiPh_3)_3(H_2O)(THF)_2$, **2**, (eq. [6]).

$$[6]\quad Al(OSiPh_3)_3(THF) \xrightarrow[THF]{+H_2O} Al(OSiPh_3)_3(H_2O)(THF)_2$$

The molecular structure of the THF solvates **1**·(THF) and **2**·$(THF)_{1.25}$ have been determined by X-ray crystallography and are shown in Figs. 1 and 2 respectively. Selected bond lengths and angles are given in Tables 5 and 6.

The structure of **1**·(THF) consists of a discrete monomeric $Al(OSiPh_3)_3(THF)$ unit with a second THF present in the crystal lattice as a molecule of solvation; this uncomplexed THF is, however, only removed from the crystal lattice at elevated temperatures, >50°C. The structure of **2**·$(THF)_{1.25}$ consists of an $Al(OSiPh_3)_3(H_2O)$ unit situated on a threefold rotation axis. There are three symmetry-related THF molecules suitably positioned for hydrogen bonding to the coordinated water molecule. Since the site occupancy of these THF molecules is unity but only two can be hydrogen bonded to the H_2O at the same time, the H_2O hydrogens must be disordered over the three symmetry-related sites, and the presence of three, rather than two, THF molecules is a function of the crystal packing. Thus the structure is best considered as consisting of **2** with a molecule of THF present in the crystal lattice. There is no doubt that hydrogen bonding is present between the water and THF molecules, since the O···O distances (2.62 Å) are within the expected

Can. J. Chem. Downloaded from www.nrcresearchpress.com by 92.62.229.171 on 09/08/12
For personal use only.

TABLE 3. Fractional coordinates ($\times 10^4$) and equivalent isotropic thermal parameters ($10^3 \times$ Å^2) of the non-hydrogen atoms in **1**·(THF)

Atom	*x*	*y*	*z*	*U*(eq)[a]
Al(1)	1783(2)	2713(1)	6394(1)	26(1)
O(1)	2618(4)	3116(2)	6950(2)	36(1)
Si(1)	2905(2)	3653(1)	7376(1)	29(1)
C(1)	2190(7)	3509(2)	8043(3)	36(2)
C(2)	1059(7)	3166(3)	8010(3)	50(3)
C(3)	460(8)	3060(4)	8502(4)	64(3)
C(4)	1071(10)	3286(4)	9024(4)	74(4)
C(5)	2200(11)	3625(3)	9082(3)	69(4)
C(6)	2783(8)	3730(3)	8588(3)	49(3)
C(7)	4792(6)	3770(2)	7586(2)	29(2)
C(8)	5337(7)	4293(3)	7809(3)	41(2)
C(9)	6719(7)	4367(3)	7972(3)	44(2)
O(2)	1600(4)	2017(2)	6548(2)	34(1)
Si(2)	1203(2)	1527(1)	6959(1)	30(1)
C(19)	886(6)	858(2)	6529(3)	32(2)
C(20)	1400(8)	770(3)	6027(3)	47(3)
C(21)	1161(8)	267(3)	5710(3)	57(3)
C(22)	413(8)	−151(3)	5902(3)	57(3)
C(23)	−137(8)	−70(3)	6383(3)	59(3)
C(24)	97(7)	425(2)	6702(3)	45(3)
C(25)	2620(7)	1418(2)	7606(2)	34(2)
C(26)	3175(8)	894(3)	7780(3)	51(3)
C(27)	4218(8)	820(3)	8240(3)	61(3)
C(28)	4768(8)	1291(4)	8562(3)	62(3)
C(29)	4284(8)	1813(3)	8393(3)	53(3)
C(30)	3228(7)	1875(3)	7927(3)	46(3)
C(31)	−408(7)	1705(2)	7215(3)	36(2)
C(32)	−1394(8)	2018(3)	6867(3)	49(3)
C(33)	−2677(8)	2103(3)	7014(3)	60(3)
C(34)	−2930(9)	1883(3)	7531(4)	65(3)
C(35)	−1980(9)	1583(3)	7872(4)	68(3)
C(36)	−721(9)	1494(3)	7733(3)	56(3)
O(3)	300(4)	2994(2)	6026(2)	33(1)
Si(3)	−639(2)	3191(1)	5420(1)	29(1)
C(37)	−1389(7)	2552(2)	5011(3)	35(2)
C(38)	−2294(7)	2585(3)	4475(3)	49(3)
C(39)	−2823(9)	2113(4)	4168(3)	69(3)
C(40)	−2479(8)	1575(3)	4410(3)	57(3)
C(41)	−1658(9)	1530(3)	4924(4)	60(3)
C(42)	−1080(7)	2021(3)	5231(3)	45(3)
C(43)	376(6)	3602(2)	4973(3)	35(2)
C(44)	849(6)	3387(3)	4493(2)	35(2)
C(45)	1734(8)	3699(3)	4220(3)	50(3)
C(46)	2169(7)	4222(3)	4435(3)	49(3)
C(47)	1732(8)	4440(3)	4897(3)	54(3)
C(48)	865(7)	4133(3)	5180(3)	44(2)
C(49)	−2004(6)	3671(2)	5571(2)	30(2)
C(50)	−2333(7)	3723(3)	6122(3)	41(2)
C(51)	−3376(7)	4077(3)	6221(3)	47(3)
C(52)	−4148(7)	4362(3)	5764(3)	44(3)
C(53)	−3860(7)	4316(2)	5205(3)	39(2)
C(54)	−2823(7)	3978(2)	5115(3)	35(2)
O(4)	2968(4)	2681(2)	5871(2)	35(1)
C(55)	3023(9)	2227(3)	5465(4)	69(3)
C(56)	3990(12)	2429(4)	5092(5)	100(5)
C(57)	4727(10)	2871(4)	5401(4)	84(4)
C(58)	3913(8)	3136(3)	5786(3)	48(3)
C(13)	2138(6)	4302(2)	7003(2)	33(2)
C(15)	2264(8)	5099(3)	6351(3)	52(3)
C(10)	7606(7)	3943(3)	7905(3)	46(3)
C(14)	2839(7)	4634(3)	6671(3)	44(2)
C(16)	931(8)	5241(3)	6360(3)	53(3)
C(17)	177(8)	4915(3)	6673(3)	57(3)
C(11)	7106(7)	3427(3)	7692(3)	49(3)
O(5)	4553(12)	994(5)	5728(8)	192(8)
C(60)	6310(17)	481(8)	6321(9)	202(12)
C(12)	5681(7)	3346(3)	7529(3)	38(2)
C(18)	788(8)	4460(3)	6987(3)	50(3)
C(61)	6480(21)	508(12)	5771(10)	322(21)
C(59)	5023(19)	691(12)	6270(9)	268(17)
C(62)	5380(25)	807(11)	5474(9)	271(18)

[a]Equivalent isotropic *U* defined as one third of the trace of the orthogonalized U_{ij} tensor.

TABLE 4. Fractional coordinates ($\times 10^4$) and equivalent isotropic thermal parameters ($10^3 \times$ Å^2) of the non-hydrogen atoms in **2**·$(THF)_{1.25}$

Atom	*x*	*y*	*z*	*U*(eq)[a]
Al(1)	1789(1)	1789(1)	1789(1)	32(577)
O(1)	1489(2)	2264(2)	1305(2)	51(2)
Si(1)	1017(1)	2589(1)	923(1)	41(1)
C(1)	602(3)	2068(3)	455(3)	44(2)
C(2)	866(4)	1577(3)	233(3)	64(3)
C(3)	591(4)	1200(4)	−131(4)	76(3)
C(4)	28(4)	1308(3)	−291(3)	65(3)
C(5)	−262(4)	1768(3)	−66(3)	61(3)
C(6)	22(3)	2147(3)	305(3)	50(2)
C(7)	1391(3)	3109(3)	423(3)	49(2)
C(8)	1161(5)	3277(4)	−98(4)	82(4)
C(9)	1442(6)	3656(4)	−466(4)	107(5)
C(10)	1966(5)	3884(3)	−307(4)	77(3)
C(11)	2205(4)	3740(3)	213(4)	72(3)
C(12)	1927(3)	3352(3)	569(4)	64(3)
C(13)	487(3)	2986(3)	1406(3)	50(2)
C(14)	368(4)	2782(4)	1951(4)	69(3)
C(15)	−40(4)	3056(5)	2308(4)	86(4)
C(16)	−342(4)	3520(4)	2108(5)	81(4)
C(17)	−231(4)	3727(4)	1578(5)	77(4)
C(18)	182(3)	3466(3)	1209(4)	61(3)
O(2)	2248(2)	2248(2)	2248(2)	70(577)
O(3)	2831(5)	3107(5)	1786(5)	194(7)
C(19)	2863(7)	3639(4)	2151(7)	139(7)
C(20)	3239(7)	3932(7)	1905(9)	197(12)
C(21)	3720(6)	3520(7)	1439(5)	133(7)
C(22)	3383(7)	3103(8)	1452(6)	167(10)
C(23)	4763	0	562	90
O(4)	4763	0	562	90

[a]Equivalent isotropic *U* defined as one third of the trace of the orthogonalized U_{ij} tensor.

range (11). In addition to the three THF's situated around the water, the electron density map and crystal cell packing indicate the presence of a severely disordered THF molecule in the center of the unit cell. Thus, $3\frac{1}{4}$ THF's are required per aluminium. The thermogravimetric analysis of a freshly crystallized sample of **2** indicates the loss of slightly more than 3 equivalents of THF per aluminium consistent with the presence of a further molecule of solvation. Therefore, a highly disordered THF molecule was included in the final refinement (see Experimental). The excess THF molecules are removed on prolonged drying *in vacuo*, leaving the two

Can. J. Chem. Downloaded from www.nrcresearchpress.com by 92.62.229.171 on 09/08/12
For personal use only.

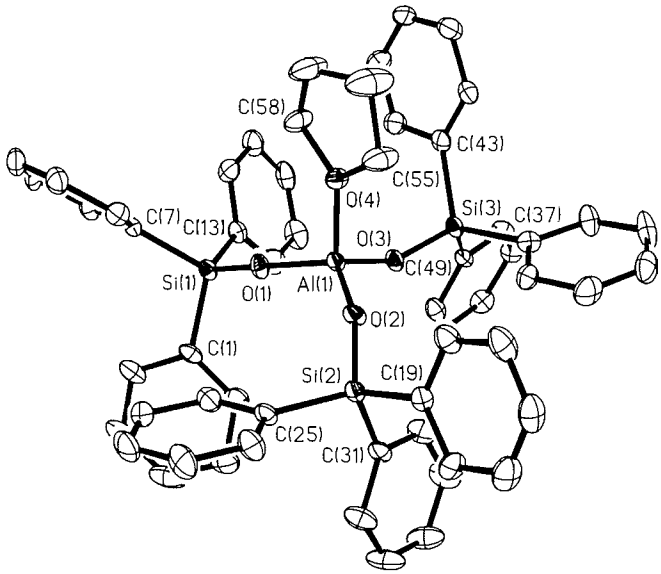

FIG. 1. Structure of $Al(OSiPh_3)_3(THF)$ (**1**) with thermal ellipsoids drawn at the 40% level. The THF of solvation and hydrogen atoms are omitted for clarity.

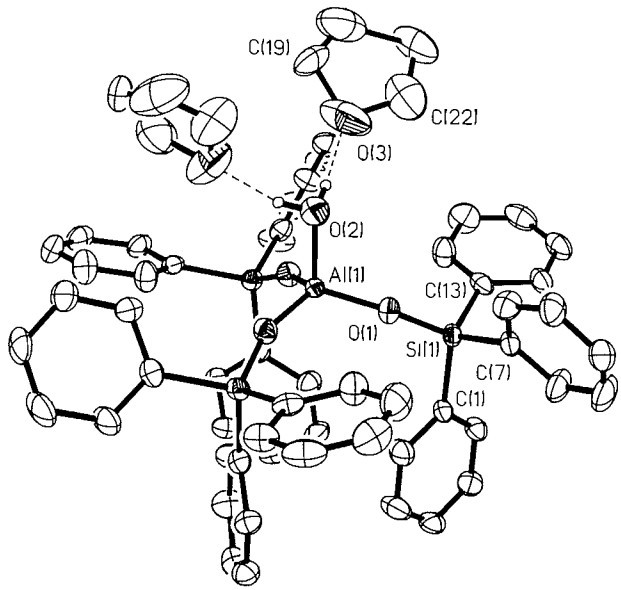

FIG. 2. Structure of $Al(OSiPh_3)_3(H_2O)(THF)_2$ (**2**) with thermal ellipsoids drawn at the 40% level. The THF's of solvation and hydrogen atoms not associated with the water ligand are omitted for clarity.

molecules hydrogen bonded to the coordinated water molecule. Although these hydrogen-bonded THF molecules are, in turn, removed upon high temperature thermolysis of **2**, the water ligand remains complexed.

As is commonly observed for four-coordinate Lewis acid base complexes of aluminium (12, 13) the geometry around each aluminium is distorted from tetrahedral, with the angles associated with the THF (**1**) and H_2O (**2**) ligands being the most acute. The similarity in aluminium coordination geometries in these compounds is illustrated by comparing the sums of interligand angles associated with the siloxide ligands (342.5(2)° (**1**), 343.2(2)° (**2**)). This similarity is perhaps unsurprising since we previously observed that the geometry around aluminum is primarily dependent on the steric bulk of substituent ligands (12, 14), and in the case of compounds **1** and **2** the coordination geometry is dominated by the sterically bulky siloxide ligands.

Whereas the THF (**1**) and H_2O (**2**) Al—O bond distances are within the range usually observed (15–18), the siloxide Al—O distances (1.696 (4)–1.709 (4) Å) are significantly shorter. The latter are, however, close to the values found in $Al(OSiPh_3)_2(acac)$ (19). This shortening was previously ascribed to a possible π-type interaction between the oxygen lone pairs and the σ^* orbitals on aluminum (17, 20). The Si—O bonds in **1** and **2** are also within the range observed for some π-type interaction (21). There appears to be no correlation, however, between the Al—O—Si bond angle and either the Al—O or Si—O bond lengths. A similar lack of correlation was observed previously for both main group and transition metal alkoxide and aryloxide complexes (17, 22).

The IR spectrum of **2** contains a broad resonance at 3659 cm^{-1} consistent with a hydrogen-bonded O-H group. This assignment is confirmed by the observation of an isotope shift for the deuterated analogue of **2**, $Al(OSiPh_3)_3(D_2O)(THF)_2$ (ν(O-D) = 2447 cm^{-1}).

In Table 1, the ^{29}Si, ^{27}Al, and ^{17}O NMR chemical shifts of compounds **1** and **2** are compared with each other, those of the parent silanol, the dimeric monosiloxide $[AlMe_2(\mu\text{-}OSiPh_3)]_2$ (23), and the literature values for $Al(acac)(OSiPh_3)_2$ (acac = acetylacetonate) (19). The ^{27}Al NMR resonances for **1** and **2** are consistent with four-coordinate aluminium complexes with three alkoxide ligands (9). The ^{29}Si and ^{17}O NMR spectra for **1** and **2** (see Table 1) are consistent with terminal siloxides (19) and are distinct from those observed for the bridging siloxides in the dimeric compound $[AlMe_2(\mu\text{-}OSiPh_3)]_2$ (23). It is also interesting to note that the ^{17}O NMR spectral shifts of the terminal siloxides are close to that of the free silanol.

The ^1H NMR signals for both **1** and **2** were sufficiently resolved at 500 MHz that fully interpretable first-order spectra could be obtained. Since the spectra of **2** displayed two sets of phenyl groups in a 1:2 ratio, due to restricted rotation (*vide infra*), it was necessary in this instance to establish ^1H–^1H connectivity using the standard COSY 2D NMR technique (Fig. 3) (6, 7). The assignment of the *ortho*, *meta*, and *para* carbons of the phenyl rings was accomplished with the assistance of a standard heteronuclear-correlated (^1H–^{13}C) experiment (e.g., Fig. 4) using delay times optimized for direct ^1H–^{13}C coupling (8).

Although the four-coordinate geometry about the aluminium center in **1**·(THF) observed in the solid state is retained in solution, as indicated by ^{27}Al NMR, there exists only a single set of resonances for the THF's, indicating the presence of a rapid degenerate exchange between free and coordinated THF (eq. [7]), which does not cease on cooling (−70°C).

[7] $Al(OSiEt_3)_3(THF) + THF^* \rightleftharpoons Al(OSiEt_3)_3(THF^*) + THF$

We previously observed that the dissociative ligand exchange for the sterically hindered aryloxide complexes $AlMe(BHT)_2$ (eq. [8]) (2,6-di-*tert*-butyl-4-methylphenol, BHT-H from the trivial name butylated hydroxytoluene) readily ceases below 0°C, whereas the associative exchange for $AlMe_2(BHT)L$ (eq. [9]) continues down to −80°C (24).

TABLE 5. Selected bond lengths (Å) and angles (°) in **1**·(THF)

Al(1)—O(1)	1.696(4)	Al(1)—O(2)	1.709(4)
Al(1)—O(3)	1.703(4)	Al(1)—O(4)	1.861(5)
O(1)—Si(1)	1.606(4)	O(2)—Si(2)	1.606(4)
O(3)—Si(3)	1.608(4)	O(4)—C(55)	1.444(9)
O(4)—C(58)	1.475(8)	Si(1)—C(1)	1.866(7)
Si(1)—C(7)	1.882(6)	Si(1)—C(13)	1.861(6)
Si(2)—C(19)	1.875(6)	Si(2)—C(25)	1.879(6)
Si(2)—C(31)	1.876(7)	Si(3)—C(37)	1.873(6)
Si(3)—C(43)	1.866(7)	Si(3)—C(49)	1.866(7)
O(1)—Al(1)—O(2)	116.3(2)	O(1)—Al(1)—O(3)	114.7(2)
O(1)—Al(1)—O(4)	103.8(2)	O(2)—Al(1)—O(3)	111.5(2)
O(2)—Al(1)—O(4)	101.9(2)	O(3)—Al(1)—O(4)	107.0(2)
Al(1)—O(1)—Si(1)	157.3(3)	Al(1)—O(2)—Si(2)	151.1(3)
Al(1)—O(3)—Si(3)	149.7(3)	Al(1)—O(4)—C(55)	124.7(5)
Al(1)—O(4)—C(58)	124.5(4)	C(55)—O(4)—C(58)	110.6(6)
O(1)—Si(1)—C(1)	108.4(3)	O(1)—Si(1)—C(7)	109.3(3)
O(1)—Si(1)—C(13)	111.2(2)	C(1)—Si(1)—C(7)	109.8(3)
C(1)—Si(1)—C(13)	110.5(3)	C(7)—Si(1)—C(13)	107.6(3)
O(2)—Si(2)—C(19)	109.4(2)	O(2)—Si(2)—C(25)	110.0(3)
O(2)—Si(2)—C(31)	110.8(2)	C(19)—Si(2)—C(25)	109.6(3)
C(19)—Si(2)—C(31)	107.1(3)	C(25)—Si(2)—C(31)	109.9(3)
O(3)—Si(3)—C(37)	108.6(2)	O(3)—Si(3)—C(43)	110.6(3)
O(3)—Si(3)—C(49)	109.8(2)	C(37)—Si(3)—C(43)	110.4(3)
C(37)—Si(3)—C(49)	110.7(3)	C(43)—Si(3)—C(49)	106.6(3)

TABLE 6. Selected bond lengths (Å) and angles (°) in **2**·$(THF)_{1.25}$

Al(1)—O(1)	1.708(5)	Al(1)—O(2)	1.83(1)
O(1)—Si(1)	1.586(5)	Si(1)—C(1)	1.875(7)
Si(1)—C(7)	1.871(7)	Si(1)—C(13)	1.889(7)
O(3)—C(19)	1.48(1)	O(3)—C(22)	1.48(2)
O(1)—Al(1)—O(2)	104.0(2)	O(1)—Al(1)—O(1A)	114.4(1)
Al(1)—O(1)—Si(1)	160.4(3)	O(1)—Si(1)—C(1)	111.4(3)
O(1)—Si(1)—C(7)	109.3(3)	O(1)—Si(1)—C(13)	110.2(3)
C(1)—Si(1)—C(7)	106.9(3)	C(1)—Si(1)—C(13)	108.6(3)
C(7)—Si(1)—C(13)	110.5(3)	C(19)—O(3)—C(22)	104.3(1)

[8] $AlMe(BHT)_2L + L^* \rightleftharpoons AlMe(BHT)_2L^* + L$

[9] $AlMe_2(BHT)L + L^* \rightleftharpoons AlMe_2(BHT)L^* + L$

The continued exchange at low temperatures between free and coordinated THF in **1**·(THF) suggests an associative ligand exchange is in effect. The solid state structure lends partial credence to this proposal, since the uncomplexed THF is positioned for incipient complexation to the metal. The exchange of excess THF with those hydrogen bonded to the water ligand in a freshly crystallized sample of **2** does not cease at low temperatures. This facile exchange is, however, consistent with the weak hydrogen bonding as opposed to an associative exchange.

As can be seen from ^1H and ^{13}C NMR data (see Experimental) there are two distinct environments for the phenyl groups in **2**, which may be related to the solid state structure (Fig. 2) as those positioned equatorial (six phenyl groups, marked with an asterisk in the Experimental) and axial (three phenyl groups) to the Al(1)—O(2) vector. Thus the presence of a distinct phenyl environment indicates that at room temperature there is no rotation about the Al—O—Si bonds. However, the phenyl groups do exhibit free rotation, since only a single set of resonances is observed for each of the *ortho* and *meta* ring protons.

Heating an NMR sample of **2** results in coalescence of the signals for the phenyl rings (T_c = 60°C). It is possible that this is due to the onset of dissociation of the coordinated water molecule, which in turn results in a planar three-coordinated aluminum, and releases the steric restraint imposed on the siloxide groups. However, the activation energy ($\Delta G^{\ddagger}$) for this exchange is calculated (25) from the NMR data to be 16.5(±0.3) kJ mol^{-1}, which is inconsistent with ligand bond dissociation energies (BDE) previously observed for aluminium complexes, 63–115 kJ mol^{-1} (24, 26). A consideration of the space-filling representation of **2** in Fig. 5 shows that the THF molecules are sufficiently distant from the triphenylsiloxide groups to have no significant steric effects, as can be implied from their fluxional nature in solution while the siloxides remain rigid. However, the $OSiPh_3$ groups are locked together, precluding the rotation around the Al—O—Si bonds. We propose, therefore, that the measured activation barrier is the energy required to overcome this sterically induced rigidity.

If a sample of **2** is cooled below −70°C the ^1H NMR

Can. J. Chem. Downloaded from www.nrcresearchpress.com by 92.62.229.171 on 09/08/12
For personal use only.

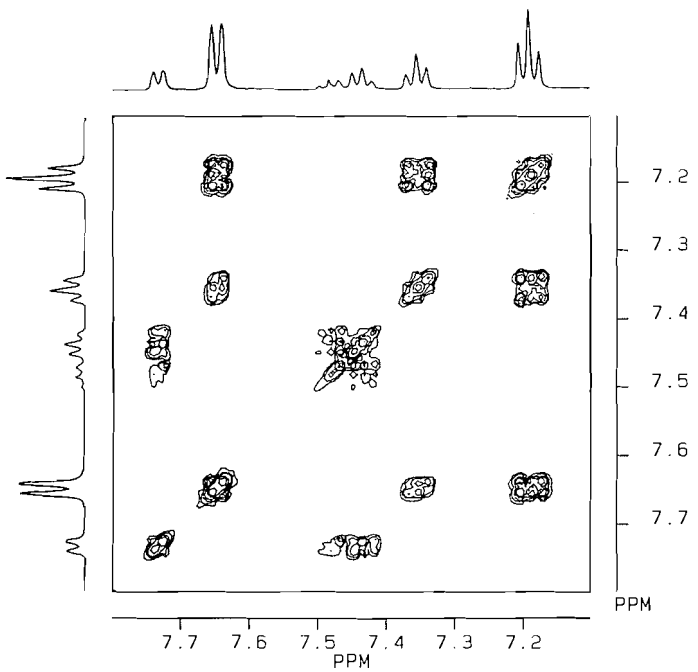

FIG. 3. ^{1}H-^{1}H COSY spectrum of $Al(OSiPh_3)_3(H_2O)(THF)_2$ (**2**).

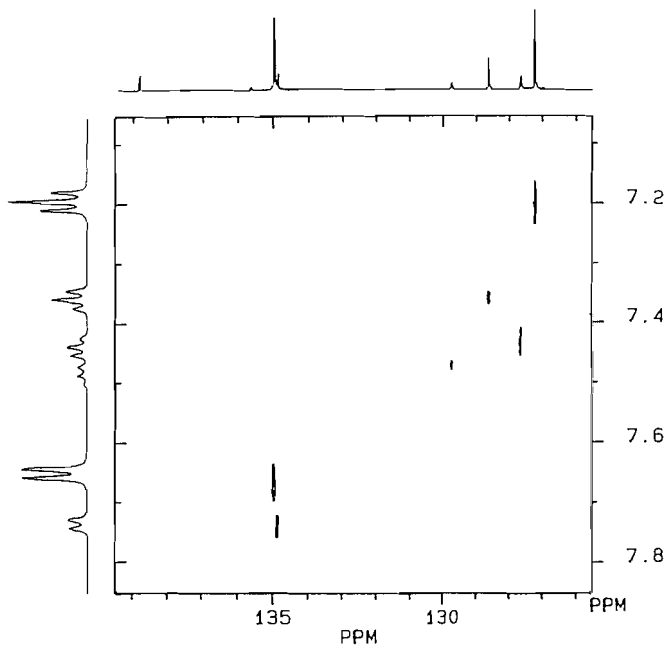

FIG. 4. ^{1}H-^{13}C correlated 2D NMR spectrum of $Al(OSiPh_3)_3(H_2O)(THF)_2$ (**2**).

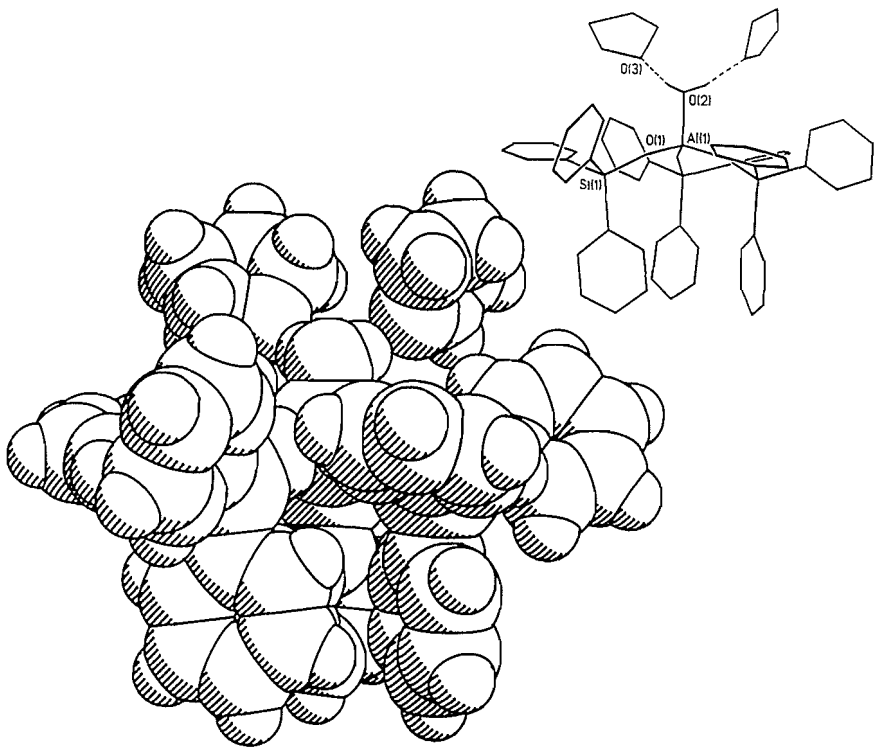

FIG. 5. Space-filling representation of $Al(OSiPh_3)_3(H_2O)(THF)_2$ (**2**), and its equivalent line drawing (inset), viewed perpendicular to the Al(1)—O(2) vector, showing the steric hindrance imposed on the triphenylsiloxide groups.

spectrum indicates that not only are the siloxide groups rigid but the axially disposed phenyl rings have ceased to rotate ($\Delta G^{\ddagger} = 9.7(\pm 0.2)$ kJmol^{-1}), providing two environments for the *ortho* and *meta* ring protons.

We note that both of these processes are rare measures of the steric constraints imposed on an organic substituent within a sterically hindered molecule.

Acknowledgements

Financial support for this work is provided by the Aluminum Research Board (U.S.A.), Dr. R. P. Tooze at Imperial Chemical Industries, Wilton Materials Research Centre (U.K.), and Dr. K. Wynne at the Office of Naval Research. We thank the Natural Sciences and Engineering Research

Can. J. Chem. Downloaded from www.nrcresearchpress.com by 92.62.229.171 on 09/08/12
For personal use only.

Council of Canada for a post-doctoral fellowship (A.W.A.) We are grateful to Dr. A. P. Sattelberger, Isotope and Nuclear Chemistry Division, Los Alamos National Laboratory, for the gift of ^{17}O enriched water. We are indebted to Prof. S. G. Bott, University of North Texas, for insightful discussion concerning the X-ray crystallography.

1. A. W. Apblett and A. R. Barron. 73rd Canadian Chemical Conference, Halifax, Nova Scotia. 1990. Abstract 593 IN-D16.
2. A. W. Apblett and A. R. Barron. The Second International Ceramic Science and Technology Congress, Orlando, Fla. 1990. Abstract 65-SIP-90c.
3. A. W. Apblett, A. C. Warren, and A. R. Barron. Chem. Mater. **4**, 167 (1992).
4. K. A. Andrianov and A. A. Zhadanov. J. Polym. Sci. **30**, 513 (1958).
5. A. W. Apblett and A. R. Barron. Organometallics, **9**, 2137 (1990).
6. W. P. Ave, E. Bartholdi, and R. R. Ernst. J. Chem. Phys. **64**, 2229 (1976).
7. K. Nagayama, A. Kumar, K. Wuthrich, and R. R. Ernst. J. Magn. Reson. **40**, 321 (1980).
8. A. Bax. Two dimensional nuclear magnetic resonance in liquids. D. Reidel, Dordrecht. 1982.
9. P3/R3 Data Collection Manual. Nicolet Instrument Corp., Madison, Wis. 1988.
10. SHELXTL-PLUS Users Manual. Nicolet Instruments Corp., Madison, Wis. 1988.
11. D. A. Wierda, T. L. Feng, and A. R. Barron. Acta Crystallogr. Sect. C: Cryst. Struct. Commun. **C45**, 339 (1989).
12. D. A. Wierda and A. R. Barron. Polyhedron, **8**, 831 (1989).
13. M. D. Healy, J. W. Ziller, and A. R. Barron. J. Am. Chem. Soc. **112**, 2949 (1990).
14. A. R. Barron. J. Chem. Soc. Dalton Trans. 3047 (1988).
15. M. J. Zaworotko, R. D. Rogers, and J. L. Atwood. Organometallics, **1**, 1179 (1982).
16. J. L. Atwood and M. J. Zaworotko. J. Chem. Soc. Chem. Commun. 302 (1983).
17. M. D. Healy, J. W. Ziller, and A. R. Barron. Organometallics, **10**, 597 (1991).
18. J. P. Oliver and R. Kumar. Polyhedron, **9**, 409 (1990).
19. J. H. Wengrovius, M. F. Garbauskas, E. A. Williams, R. C. Going, P. E. Donahue, and J. F. Smith. J. Am. Chem. Soc. **108**, 982 (1986).
20. N. Burford, B. W. Royan, R. E. v.H. Spence, T. S. Cameron, A. Linden, and R. D. Rogers. J. Chem. Soc. Dalton Trans. 1521 (1990).
21. M. D. Healy and A. R. Barron. J. Organomet. Chem. **381**, 165 (1990), and references therein.
22. B. D. Steffey, P. E. Fanwick, and I. P. Rothwell. Polyhedron, **9**, 763 (1990).
23. H. Schmidbaur and F. Schindler. Chem. Ber. **99**, 2178 (1966).
24. J. R. Nash, M. D. Healy, and A. R. Barron. 199th National Meeting of the American Chemical Society, Boston, Mass. 1990. Abstract INOR 175.
25. H. Shanan-Atidi and K. H. Bar-Eli. J. Phys. Chem. **74**, 961 (1970).
26. C. H. Henrickson, D. Duffy, and D. P. Eyman. Inorg. Chem. **6**, 1064 (1968).

Can. J. Chem. Downloaded from www.nrcresearchpress.com by 92.62.229.171 on 09/08/12
For personal use only.

Synthesis, multinuclear magnetic resonance spectra, and chemistry of some complexes $[(\mu\text{-}SR)_6(MX)_4]^{2-}$ (R = alkyl; M = Zn or Cd; X = Cl, Br, or I) and the X-ray structural analysis of $(Et_4N)_2[(\mu\text{-}SPr^i)_6(CdBr)_4]$[1,2]

PHILIP A. W. DEAN,[3] JAGADESE J. VITTAL,[3] AND YUYANG WU
Department of Chemistry, University of Western Ontario, London, Ont., Canada N6A 5B7

Received July 4, 1991

This paper is dedicated to the memory of Professor Thomas Birchall

PHILIP A. W. DEAN, JAGADESE J. VITTAL, and YUYANG WU. Can. J. Chem. **70**, 779 (1992).

The self-assembly method has been used to prepare a wide range of new adamantane-like anions of the type $[(\mu\text{-}SR)_6(MX)_4]^{2-}$ (M = Zn or Cd; R = alkyl or benzyl; X = Cl, Br, or I) as their Et_4N^+ salts. Metal ($^{111\text{ or }113}Cd$) NMR data have been measured for the cadmium complexes, and also for many of the possible mixed-metal complexes $[(\mu\text{-}SR)_6(CdX)_n(ZnX)_{4-n}]^{2-}$. In the complexes with mixed metals, the effects of Zn substitution on the metal chemical shifts are generally larger for the alkyl- and benzyl-thiolate complexes than for related benzenethiolate complexes. However, for $[(\mu\text{-}SPr^i)_6(CdX)_n(CdX')_{4-n}]^{2-}$ (X/X' = Cl/Br, Cl/I, or Br/I), substituent effects are no larger than found in some PhS^--bridged complexes. The reaction of $[(\mu\text{-}SPr^i)_6(CdX)_4]^{2-}$ (X = Cl, Br, or I) with E'_8 (E' = S or Se) in CH_2Cl_2 gives $[Cd_4(\mu_4\text{-}E')(\mu\text{-}SPr^i)_{12}(CdX)_4]^{2-}$ as the major species detectable by metal, ^{13}C, and, where applicable, ^{77}Se NMR. However, the reaction does not occur stoichiometrically. The compound $(Et_4N)_2[(\mu\text{-}SPr^i)_6(CdBr)_4]$ crystallizes in the monoclinic space group $P2_1/c$ with cell dimensions a = 24.079(3) Å, b = 11.365(2) Å, c = 22.561(3) Å, β = 113.89(1), and Z = 4. The structure was refined to $R(R_w)$ = 0.0663(0.0703) with the use of 2669 unique data with $I > 2.5\sigma(I)$. The anion contains an adamantane-type $(\mu_2\text{-}S)_6Cd_4$ cage composed of a nearly regular Cd_4 tetrahedron and a distorted S_6 octahedron, the irregularity of which is caused by 1,3-interactions of the substituent groups on the sulfur atoms. The axial or equatorial dispositions of the six alkyl groups in the four fused M_3S_3 rings are [aae, aae, aee, aee]. For the zinc-group elements, this is the first example of an adamantane-like $(\mu\text{-}Salkyl)_6M_4$ cage that has been characterized crystallographically.

Key words: cadmium complex, cadmium-111/113 NMR, thiolate complex, X-ray analysis, zinc complex.

PHILIP A. W. DEAN, JAGADESE J. VITTAL et YUYANG WU. Can. J. Chem. **70**, 779 (1992).

On a utilisé la méthode d'auto-assemblage pour préparer une grande variété de nouveaux anions ressemblant à l'adamantane, du type $[(\mu\text{-}SR)_6(MX)_4]^{2-}$ (M = Zn ou Cd; R = alkyle ou benzyle; X = Cl, Br ou I), sous forme de sels du Et_4N^+. On a mesuré les spectres RMN des $^{111\text{ ou }113}Cd$ des complexes du cadmium ainsi que ceux de tous les composés métalliques mixtes possibles $[(\mu\text{-}SR)_6(CdX)_nZnX_{4-n}]^{2-}$. Dans les complexes métalliques mixtes, l'effet de la substitution du Zn sur les déplacements chimiques du métal sont généralement plus grands avec les complexes alkyl- et benzylthiolates qu'avec les complexes benzènethiolates apparentés. Toutefois, avec $[(\mu\text{-}SPr^i)^6(CdX)_n(CdX')_{4-n}]^{2-}$ (X/X' = Cl/Br, Cl/I ou Br/I), les effets de substituants ne sont pas plus importants que ceux observés dans quelques complexes comportant un pont PhS^-. La réaction du $[(\mu\text{-}SPr^i)_6(CdX)_4]^{2-}$ (X = Cl, Br ou I) avec E'_8 (E' = S ou Se), dans le CH_2Cl_2, fournit du $[Cd_4(\mu_4\text{-}E')(\mu\text{-}SPr^i)_{12}(CdX)_4]^{2-}$ comme principale espèce détectable par RMN des métaux, du ^{13}C et, lorsque c'est applicable, du ^{77}Se. Toutefois, la réaction n'est pas stoechiométrique. Les cristaux du composé $(Et_4N)_2[(\mu\text{-}SPr^i)_6(CdBr)_4]$ sont monocliniques, groupe d'espace $P2_1/c$, avec a = 24,079(3), b = 11,365(2) et c = 22,561(3) Å, β = 113,89(1) et Z = 4. On a affiné la structure jusqu'à des valeurs de $R(R_w)$ = 0,0663(0,0703) à l'aide de 2669 réflexions indépendantes avec $I > 2{,}5\sigma(I)$. L'anion contient une cage $(\mu_2\text{-}S)_6Cd_4$ du type adamantane composée d'un Cd_4 tétraédrique pratiquement régulier et d'un S_6 octaédrique déformé dont l'irrégularité est causée par des interactions-1,3 des substituants portés par les atomes de soufre. Les arrangements axiaux et équatoriaux des six groupes alkyles dans les quatre cycles M_3S_3 condensés sont [aae, aae, aee, aee]. Pour les éléments du groupe du zinc, il s'agit du premier exemple d'une cage $(\mu\text{-}Salkyl)_6M_4$ du type adamantane à être caractérisé par cristallographie.

Mots clés : complexe du cadmium, RMN des $^{111/113}Cd$, complexe thiolate, diffraction des rayons X, complexe du zinc.

[Traduit par la rédaction]

Introduction

Adamantane-like anions of the general type $[(\mu\text{-}EPh)_6(MX)_4]^{2-}$ are well established for a variety of divalent metal centres, especially for E = S and X = SPh^- or halide (1–5). Of particular relevance to the present paper, some anions of this general type are known for each of the zinc-group elements (1–5). The $(\mu\text{-}SPh)_6M_4$ cages, where they exist for Zn(II)–Hg(II),[4] provide possible models for the cysteinate-bridged tetrametallic cages occurring when some forms of the cysteine-rich metal-binding protein metallothionein are loaded with the divalent d^{10} metal ions.

It seems reasonable to suggest that cages involving alkyl thiolates might provide a better model for the cysteinyl binding sites of metallothionein than cages involving benzenethiolates. However, remarkably little attention has been paid to adamantanoid clusters containing cages of the type $(\mu\text{-}SAlk)_6M^{II}_4$.[5,6] Thus, Hagen and Holm (9) synthesized and

[1]Presented in part at the 74th Canadian Chemical Conference, Hamilton, Ontario. June 2–6, 1991.

[2]No reprints available.

[3]Authors to whom correspondence may be addressed.

[4]For mercury, the $[(\mu\text{-}EPh)_6(HgX)_4]^{2-}$ anions appear to exist for E = Se or Te, but not for E = S (4).

[5]$SAlk^-$ represents alkyl- or benzyl-thiolate.

[6]Several examples of $(\mu\text{-}SAlk)_6M^I_4$ (M = Cu or Ag) have been described (6–8), but these are not directly analogous to the complexes of the divalent metal centres in that they have distorted-planar coordination at the metal centres with no terminal ligands X.

Can. J. Chem. Downloaded from www.nrcresearchpress.com by 92.62.229.171 on 09/08/12
For personal use only.

Can. J. Chem. Downloaded from www.nrcresearchpress.com by 92.62.229.171 on 09/08/12
For personal use only.

fully characterized the $[(\mu\text{-SEt})_6(FeSEt)_4]^{2-}$ anion, while in very recent work from our own laboratory we synthesized $(Et_4N)_2[(\mu\text{-SPr}^n)_6(CdI)_4]$ and characterized this and the Zn(II) and Hg(II) analogues in solution using multinuclear magnetic resonance methods (4). The Zn(II) and Cd(II) complexes are stable at ambient probe temperature, but the Hg(II) complex appears to be stable only at reduced temperature. The ^{113}Cd NMR spectra of the series $[(\mu\text{-SPr}^n)_6(CdI)_n(ZnI)_{4-n}]^{2-}$ were sufficiently different from those reported (10, 11) for $[(\mu\text{-SPh})_6(CdSPh)_n(ZnSPh)_{4-n}]^{2-}$ to warrant further study of alkylthiolate-bridged Cd_nZn_{4-n} cages by metal NMR.

In this paper we describe the synthesis of a much wider series of complexes of the type $[(\mu\text{-SAlk})_6(MX)_4]^{2-}$ (M = Zn or Cd; X = Cl, Br, or I). The multinuclear magnetic resonance spectra of these and related complexes with mixed metals or mixed terminal halides are given. A single crystal X-ray structural analysis of $(Et_4N)_2[(\mu\text{-SPr}^i)_6(CdBr)_4]$ has been carried out to characterize a representative $(\mu\text{-SAlk})_6Cd_4$ cage and to allow comparison with structures containing the $(\mu\text{-SPh})_6Cd_4$ core (3, 9). As well, the reaction of $[(\mu\text{-SPr}^i)_6(CdX)_4]^{2-}$ with elemental sulfur and selenium is reported.

Experimental

Materials and general procedure

All starting materials were from commercial sources and were used as received. The compounds $M(SR)_2$ (M = Zn or Cd; R = Me, Et, 1-Pr, 2-Pr, 1-Bu, 2-Bu, or benzyl) were prepared by an adaptation of the literature synthesis (12) of $Zn(SR)_2$, in which $Me_2CO{:}H_2O$ (1:5) was used instead of water and the metal nitrates instead of the sulphates. The salt $(Et_4N)_2[(\mu\text{-SPr}^n)_6(CdI)_4]$ was prepared as reported earlier (4), and a sample of $(Pr^iS)_2Se$ was also synthesized by the literature method (13). Red selenium was obtained by the reduction of Na_2SeO_3 with $Na_2S_2O_4$ in strongly acidic aqueous solution. The Se_8 was separated by filtration, washed with water, then alcohol, dried *in vacuo*, and stored in the dark in a refrigerator.

All solvents used in synthesis or in the preparation of NMR samples were dried over 3 Å Molecular Sieves and thoroughly deoxygenated by sparging with Ar(g). All syntheses and preparations of NMR samples were carried out under an atmosphere of Ar or N_2.

Synthesis

The tetranuclear anions were all prepared by the self-assembly method and isolated as their Et_4N^+ salts. Within this general procedure there was some variation, as exemplified by the syntheses of the salts of $[(\mu\text{-SPr}^i)_6(CdCl)_4]^{2-}$ and $[(\mu\text{-SEt})_6(CdBr)_4]^{2-}$.

$(Et_4N)_2[(\mu\text{-SPr}^i)_6(CdCl)_4$

The synthesis was generally similar to that reported for $(Et_4N)_2[(\mu\text{-SPr}^n)_6(CdI)_4]$ (4). A mixture of $CdCl_2$ (0.18 g, 0.98 mmol), $Et_4NCl.H_2O$ (0.37 g, 2.0 mmol), and $Cd(SPr^i)_2$ (0.87 g, 3.3 mmol) was stirred in CH_2Cl_2 (20 mL) for 1 h. The small amount of insoluble material was removed by filtration. The volume of the filtrate was reduced to ca. 4 mL by gentle heating under a flow of N_2(g), and then Et_2O (2 mL) was layered on. The mixture was allowed to stand in the refrigerator overnight. The white solid so formed was separated by filtration, washed with Et_2O, and dried *in vacuo* at room temperature. The yield was 1.1 g (84%).

In the same manner were prepared $(Et_4N)_2[(\mu\text{-SR})_6(MX)_4]$ for the following R/M/X combinations: Pr^i/Zn/Cl (81% yield), Br (62%), I (74%); Pr^i/Cd/Br (74%), I (78%); Me/Zn/Br (71%), I (61%); Pr^n/Zn/I (68%); Bu^n/Zn/I (45%); Bu^n/Cd/I (57%). For $(Et_4N)_2[(\mu\text{-SEt})_6(ZnX)_4]$ (X = Cl, Br), the salts prepared in this way gave unsatisfactory elemental analyses, though they appeared pure by ^1H and ^{13}C NMR.[7] For the following R/M/X combinations, the initial three-component mixture remained milky, but the procedure was otherwise the same: Et/Cd/Cl (41%), Br (29%), I (48%); Et/Zn/I (36%). Alternative, higher yield syntheses for R/M/X = Et/Cd/Br, I are given below.

The ether was replaced by pentane to produce the salts with R/M/X = benzyl/Zn/Cl (92%), Br (94%), I (84%). When this adapted procedure was used for salts of $[(\mu\text{-Sbenzyl})_6(CdX)_4]^{2-}$ (X = Cl, Br, I), oily white solids were obtained after the mixtures were refrigerated. These solids were separated by decantation and washed several times with pentane, then dried *in vacuo* to give white foamy solids. Yields for X = Cl, Br, I were 54, 84, 75%, respectively.

$(Et_4N)_2[(\mu\text{-SEt})_6(CdBr)_4]$ (Method 2)

Into a solution of $CdBr_2$ (1.1 g, 4.0 mmol) and Et_4NBr (0.42 g, 2.0 mmol) in EtOH (50 mL) at 40°C was stirred EtSH (0.50 g, 8.1 mmol) followed by Et_3N (0.81 g, 8.0 mmol). A white precipitate formed. This dissolved when MeCN (5 mL) was added to the mixture at room temperature. Cooling the resulting solution to 5°C overnight gave the product as white crystals. The yield was 1.0 g (72%). The analogous iodide can be prepared similarly, in 58% yield.

The salt $(Et_4N)_2[(\mu\text{-SEt})_6(ZnBr)_4]$, pure by ^1H and ^{13}C NMR, was obtained in a similar manner, but with the addition of Et_2O before cooling overnight. However, this salt did not give satisfactory elemental analyses.

Elemental microanalyses

Analyses for C, H, and N were carried out by Guelph Chemical Laboratories Ltd. Analytical data for the new compounds are given in Table 1.

Nuclear magnetic resonance spectra

Proton and ^{13}C NMR spectra of $(Et_4N)_2[(\mu\text{-SR})_6(MX)_4]$ were obtained at ambient probe temperature using a Varian Gemini-200 spectrometer system, with solutions in standard 5 mm o.d. NMR tubes. These spectra have been deposited. Carbon-13 NMR spectra of the reaction mixtures of $[(\mu\text{-SPr}^i)_6(CdX)_4]^{2-}$ with sulfur or selenium were measured at ambient probe temperature in 10 mm o.d. NMR tubes on a Varian XL-200 spectrometer system operating without a ^2D field/frequency lock. The CH_2Cl_2 signal (δ_C = 54.2) was used as an internal reference.

Natural-abundance $^{111/113}Cd$ and ^{77}Se NMR spectra were measured with a Varian XL-200 or -300 spectrometer system again running without a ^2D field-frequency lock; the field drift was <1 Hz/day. On both machines interference obscured part of the ^{113}Cd region, so many spectra were measured using ^{111}Cd, which is almost as sensitive as ^{113}Cd at natural abundance.[8] No primary isotope effect is expected, i.e., chemical shifts should be the same for both ^{111}Cd and ^{113}Cd. External referencing was by sample interchange, using 0.1 M $Cd(ClO_4)_2$(aq) for $^{111/113}Cd$ and pure Me_2Se for ^{77}Se. On the lower and higher field instruments, the reference frequencies were, for ^{113}Cd, 44.37 and 66.53 MHz, respectively; for ^{111}Cd, 42.41 and 63.59 MHz, respectively; for ^{77}Se, 38.15 and 57.20 MHz, respectively. The negative Overhauser effect is significant for $^{111/113}Cd$ in the Cd–Salkyl complexes, therefore inverse gated proton decoupling was used, with the decoupler off for at least 80% of each duty cycle. Most of the $^{111/113}Cd$ NMR spectra were measured using an acquisition time of 1 s, cycle time of

[7]Copies of these data may be purchased from: The Depository of Unpublished Data, Document Delivery, CISTI, National Research Council Canada, Ottawa, Canada K1A 0S2.

Table S5, additional bond distances and angles, has also been deposited with the Cambridge Crystallographic Data Centre and can be obtained on request from The Director, Cambridge Crystallographic Data Centre, University Chemical Laboratory, Lensfield Road, Cambridge CB2 1EW, U.K.

[8]The natural abundances of ^{111}Cd, ^{113}Cd, and ^{77}Se are 12.75, 12.26, and 7.58%, respectively; their relative receptivities, D^C, relative to ^{13}C = 1, are 6.97, 7.67, and 3.01, respectively (14).

TABLE 1. Analytical data for $(Et_4N)_2[(\mu\text{-}SR)_6(MX)_4]$

			C %		H %		N %	
R	M	X	Calcd.	Found	Calcd.	Found	Calcd.	Found
Me	Zn	Br	23.50	23.42	5.20	5.08	2.49	2.87
Me	Zn	I	20.14	20.37	4.46	4.33	2.14	2.47
Et	Cd	Cl	27.60	27.50	5.79	5.57	2.30	2.58
Et	Cd	Br	24.08	24.13	5.05	5.00	2.01	1.85
Et	Zn	I	24.08	23.72	5.05	4.82	2.01	2.16
Et	Cd	I	21.22	20.89	4.45	4.11	1.77	1.34
1-Pr	Zn	I	27.58	27.28	5.58	5.45	1.89	2.06
1-Pr	Cd	I	24.47	24.19	4.95	4.68	1.68	1.64
1-Bu	Zn	I	30.70	30.54	6.06	6.08	1.79	1.79
1-Bu	Cd	I	27.41	27.56	5.41	5.52	1.60	1.96
2-Pr	Zn	Cl	36.63	35.49	7.42	7.47	2.51	2.39
2-Pr	Cd	Cl	31.34	31.60	6.34	6.15	2.15	2.36
2-Pr	Zn	Br	31.59	31.35	6.40	6.53	2.17	2.16
2-Pr	Cd	Br	27.58	27.09	5.58	5.45	1.89	1.60
2-Pr	Zn	I	27.58	27.51	5.58	5.23	1.89	2.04
2-Pr	Cd	I	24.47	24.25	4.95	4.99	1.68	1.61
2-Bu	Zn	Cl	40.07	39.49	7.90	7.82	2.34	2.26
2-Bu	Cd	Cl	34.64	34.87	6.83	6.51	2.02	2.18
2-Bu	Zn	Br	34.90	34.56	6.88	7.17	2.04	1.92
2-Bu	Cd	Br	30.70	30.83	6.06	5.71	1.79	2.08
2-Bu	Zn	I	30.70	30.42	6.06	6.34	1.79	1.50
2-Bu	Cd	I	27.41	27.28	5.41	5.63	1.60	1.69
$PhCH_2$	Zn	Cl	49.65	50.02	5.89	5.87	2.00	2.29
$PhCH_2$	Cd	Cl	43.78	43.44	5.20	4.98	1.76	1.40
$PhCH_2$	Zn	Br	44.07	44.86	5.23	5.29	1.77	1.93
$PhCH_2$	Cd	Br	39.38	40.02	4.67	4.72	1.58	1.56
$PhCH_2$	Zn	I	39.38	39.56	4.67	4.74	1.58	1.75
$PhCH_2$	Cd	I	35.60	35.13	4.22	4.14	1.43	1.40

TABLE 2. Summary of X-ray structure determination

Compound	$C_{34}H_{82}N_2Br_4Cd_4S_6$
Formula weight	1480.646
Crystal system	Monoclinic
Space group	$P2_1/c$ (No. 14)
Cell dimensions (Å)	$a = 24.079(3)$
	$b = 11.365(2)$
	$c = 22.561(3)$
	$\beta = 113.89(1)$
Temperature, °C	23
Cell volume ($Å^{-3}$)	5645(2)
Z	4
Density, g cm^{-3}, obsd; calcd.	1.75(5), 1.743
$F(000)$	2912
Diffractometer, filter	Enraf–Nonius CAD4F; nickel
Radiation, wavelength (Å)	CuKα, 1.5418
Approx. crystal dimensions (mm)	0.15 × 0.23 × 0.34
No. of faces, face indices	12, {100}, {011}, {10$\bar{1}$}, and {110}
Index	$-23 < h < 0$, $0 < k < 11$, $-22 < l < 22$
2θ ranges (deg)	$0 < 2\theta < 100$
Absorption coeff. (cm^{-1})	178.5
Absorption max., min.	0.064, 0.098
$R(F)$ for average, before, after	0.030, 0.024
No. of reflections averaged	173
No. of reflections rejected for systematic absences	399
No. of unique data	5797
No. of observ., variables	2699($I < 2.5\sigma(I)$), 277
Final model; R_1 and R_2	0.0663, 0.0703
Extinction parameter	0.000381(48)
Residual electron density range (e A^{-3})	0.613 to −0.740

Can. J. Chem. Downloaded from www.nrcresearchpress.com by 92.62.229.171 on 09/08/12
For personal use only.

Can. J. Chem. Downloaded from www.nrcresearchpress.com by 92.62.229.171 on 09/08/12
For personal use only.

TABLE 3. Atomic positional ($\times 10^4$) and thermal ($\times 10^3$) parameters for $(Et_4N)_2[(\mu\text{-}SPr^i)_6(CdBr)_4]$

Atom	x	y	z	$U(Å^2)^a$	Occu.
Cd(1)	3217.7(8)	−1351.6(20)	−449.4(9)	79.0(8)*	
Cd(2)	1765.5(9)	−1560.6(21)	32.7(10)	90.2(10)*	
Cd(3)	1955.3(9)	1340.8(20)	−912.7(10)	88.0(9)*	
Cd(4)	3124.4(9)	766.2(20)	955.2(10)	86.1(9)*	
Br(1)	3977.7(14)	−2442.6(31)	−805.7(17)	104.2(16)*	
Br(2)	978.7(16)	−2954.6(37)	177.8(17)	121.8(18)*	
Br(3)	1280.9(16)	2865.7(35)	−1752.0(18)	126.9(18)*	
Br(4)	3817.7(15)	1842.5(35)	2019.5(15)	112.9(16)*	
S(12)	2557(3)	−2774(7)	−166(3)	88(3)*	
S(13)	2615(3)	119(7)	−1315(2)	82(3)*	
S(14)	3803(3)	−687(7)	722(3)	87(3)*	
S(23)	1215(3)	−272(7)	−944(4)	95(4)*	
S(24)	2209(4)	−224(8)	1008(4)	111(4)*	
S(34)	2641(3)	2345(7)	115(3)	87(3)*	
C(121)	2136(12)	−3699(28)	−886(14)	102(10)	
C(122)	2579(14)	−4647(31)	−961(16)	128(12)	
C(123)	1900(13)	−2948(29)	−1504(14)	114(11)	
C(131)	3152(13)	1073(24)	−1492(14)	99(10)	
C(132)	3314(16)	455(32)	−2009(15)	150(14)	
C(133)	3087(28)	2422(24)	−1484(31)	99(21)	0.50
C(133′)	2814(24)	2179(38)	−1858(28)	97(21)	0.50
C(141)	4447(12)	181(26)	737(13)	101(10)	
C(142)	4224(23)	1260(35)	288(22)	104(18)	0.60
C(143)	4936(17)	352(44)	1430(14)	88(15)	0.60
C(142′)	4467(37)	845(69)	150(27)	110(29)	0.40
C(143′)	5044(21)	−440(65)	1168(34)	110(27)	0.40
C(231)	582(15)	484(31)	−920(15)	138(13)	
C(232)	2(17)	−256(37)	−1254(20)	194(18)	
C(233)	648(15)	788(32)	−228(15)	137(13)	
C(241)	2388(17)	−1137(36)	1735(20)	161(15)	
C(242)	2922(23)	−1900(50)	1745(29)	131(22)	0.60
C(243)	2511(31)	−262(51)	2297(27)	165(27)	0.60
C(242′)	2657(42)	−2352(48)	1695(45)	108(36)	0.40
C(243′)	2975(38)	−847(120)	2332(41)	222(53)	0.40
C(341)	2148(13)	3102(26)	455(14)	103(10)	
C(342)	1608(16)	3735(36)	−74(17)	186(17)	
C(343)	2527(17)	4013(32)	965(17)	182(17)	
N(1)	562(12)	4899(26)	1663(14)	127(9)	
C(1)	249(22)	4318(42)	2060(22)	194(5)	
C(2)	1206(21)	5108(44)	2199(21)	194(5)	
C(3)	588(20)	4289(45)	1093(23)	194(5)	
C(4)	289(20)	6096(44)	1385(23)	194(5)	
C(5)	−436(21)	4156(42)	1632(21)	194(5)	
C(6)	1607(20)	5830(41)	1909(21)	194(5)	
C(7)	908(19)	3036(44)	1324(21)	194(5)	
C(8)	343(19)	6821(42)	1989(21)	194(5)	
N(2)	4663(11)	5161(25)	1274(12)	107(8)	
C(11)	5237(21)	5464(45)	1211(21)	194(5)	
C(12)	4795(21)	3919(45)	1432(22)	194(5)	
C(13)	4598(21)	5854(44)	1769(22)	194(5)	
C(14)	4061(20)	5032(43)	625(23)	194(5)	
C(15)	5133(20)	6802(44)	1010(21)	194(5)	
C(16)	5318(20)	3712(41)	2098(22)	194(5)	
C(17)	4012(20)	5696(43)	1815(20)	194(5)	
C(18)	4112(19)	4381(41)	70(22)	194(5)	

[a]Parameters marked with an asterisk were assigned anisotropic thermal parameters given as the isotropic equivalent displacement parameter defined as $U_{eq} = 1/3\Sigma_i\Sigma_j U_{ij} \cdot a^*_i \cdot a^*_j \cdot a_i \cdot a_j$.

5 s, spectral window of 10 kHz, and tip angles of ca. 88° (for spectra at 213 K) and ca. 83° (for spectra at ambient probe temperature). For mixtures of $[(\mu\text{-}SPr^i)_6(CdX)_4]^{2-}$ and sulfur or selenium, the conditions were as follows: acquisition time, 0.6 s; cycle time, 4.6 s; spectral window, 25 kHz; tip angle, 83° (at ambient probe temperature). Selenium-77 NMR spectra were measured using continuous proton decoupling. For $[Cd_4(\mu_4\text{-}Se)(\mu\text{-}SPr^i)_{12}(CdX)_4]^{2-}$, $T_1(^{77}Se)$ appears to be ca. 20 s. In final spectra, measured using the

Can. J. Chem. Downloaded from www.nrcresearchpress.com by 92.62.229.171 on 09/08/12
For personal use only.

TABLE 4. Cadmium chemical shifts[a] of some complexes $[(\mu\text{-}SR)_6(CdX)_n(ZnX)_{4-n}]^{2-}$ in CH_2Cl_2[b]

R	X	Temperature (K)	δ_{Cd}[a] $n = 4$	$n = 3$	$n = 2$	$n = 1$
Et[c]	Cl	293[d]	607			
		233	619			
	Br	292	595	593	590	588
	I	293	568	564	559	554
		256	576	571	566	560
2-Pr	Cl	296	588	584	580	575
		217[e]	602	597	592	585
	Br	294	566	561	556	550
		214[e]	583	574	567	560
	I	295	529	518	509	501
		218[e]	548	533	519	510
2-Bu	Cl	292	588	584	579	573
		215[e]	601[d]			
	Br	293	568	562	556	550
		215[e]	582	573	565	559
	I	292	531	519	510	502
		215[e]	548[d]			
1-Pr	I	294	563	558	554	549
		213[f]	578	571	564	557
1-Bu	I	293	562	557	552	548
		215	578	572	565	558
$PhCH_2$	Cl	292	594[g]			
		215[e]	605	604	603	600
	Br	293	584	582	580	578
		215[e]	596	594	592	590
	I	293	560	556	552	547
		215	576			
Ph	I	260	←——— ≈518[h] ———→			

[a]Relative to external 0.1 M $Cd(ClO_4)_2$ (aq) at 293 ± 1 K, for solutions containing 0.05 mol/L of solvent at ambient temperature, except as noted. Reproducibility ±1 ppm.
[b]Except where noted otherwise.
[c]In MeCN.
[d]Concentration 0.025 mol/L of solvent.
[e]Average position of several closely spaced resonances (see text).
[f]Data from ref. 4, for solutions having 0.06 mol/L of solvent.
[g]Broad unresolved signals occur in Cd_4:Zn_4 mixtures.
[h]Separate signals not resolved.

XL-300 spectrometer, the following conditions were used to obtain the ^{77}Se NMR spectra of these species at ambient probe temperature: acquisition time and cycle time, 1 s; spectral window, 10 kHz; tip angle, 18°. Temperature calibration was made using a calibrated thermocouple probe in a stationary dummy sample. Cadmium-111/113 chemical shifts were found to be reproducible to ±1 ppm and ^{77}Se chemical shifts to 0.1 ppm. In a single spectrum, signal separations could usually be measured more precisely.

NMR spectra were simulated as described earlier (15).

X-ray structure determination

Single crystals of $(Et_4N)_2[\mu\text{-}SPr^i)_6(CdBr)_4]$ were grown by diffusing diethyl ether into an acetone solution of the compound at 5°C. A colorless crystal of suitable quality was mounted in air on a glass fibre with epoxy cement. The crystal density was determined to be 1.75(5) g cm^{-3} by the neutral buoyancy method using a mixture of carbon tetrachloride and hexane.

The data collection was carried out on an Enraf–Nonius CAD4F diffractometer using Cu Kα radiation (16) with nickel filter. Photo and automatic indexing routines, followed by least-squares fits of 20 accurately centered reflections ($35.5 < \theta < 41.5$), gave cell constants and an orientation matrix. Intensity data were recorded in ω–2θ mode, at variable scan speeds (1.27–2.75 deg min^{-1}) and scan width of 0.8 + 0.14 tan θ, with a maximum time per datum of 60 s. Background estimates were made by extending the scan by 25% on each side. Standard reflections 200, 002, and 202 were monitored every 180 min of X-ray exposure time and showed 8.2% decay over the total period of 110.3 h. In all, 6375 reflections and 123 standards were recorded. Corrections were made for Lorentz, monochromator, and crystal polarization, background radiation effects, and decay, using the Structure Determination Package (17) running on a PDP11/23+ computer. Numerical absorption correction was applied using the program AGNOST (18). The cell parameters and the systematic absences (19*a*) indicated that the space group was $P2_1/c$ and the correctness of the choice of the space group was confirmed by successful solution and refinement of the structure.

The structure was readily solved by a combination of MULTAN (20) and difference Fourier techniques. Refinement was by full-matrix least-squares techniques on F, using the SHELX-76 software (21) running on a SUN 3/50 workstation. Scattering factors for neutral, non-hydrogen atoms were taken from ref. 19*b*. Anisotropic thermal parameters were assigned for all the Cd, Br, and S atoms and were refined, while the thermal parameters of all the remaining non-hydrogen atoms were refined isotropically. At this stage, high thermal motions were found for most of the isopropyl methyl carbon atoms, indicating possible disorder. The disorder could be successfully resolved for C133, C142, C143, C242, and C243 while for C232, C233, C342, and C343 the disorder could not be resolved due to smearing of electron density as indicated by the electron density maps. The C—C bond distances were, therefore, constrained to 1.542 Å. For the above reasons the hydrogen atoms were not included in the structure factor calculations. The tetraethylammonium cations also showed the expected high thermal activity, an artifact of unresolvable disorder. A common temperature factor was assigned for all the carbon atoms and refined in the least-squares refinements.

With the use of 2669 observations with $I > 2.5\sigma(I)$, and utilizing weights of the form $w = k/\sigma^2(F_o) + gF^2$, where $k = 1.8849$ and $g = 0.001029$, refinement of 277 variables converged at agreement factors $R = 0.0663$, $R_w = 0.0703$. The top five peaks in the final difference Fourier synthesis had electron density in the range 0.613–0.535 e A^{-3}.

The experimental details and crystal data, and positional and U(equiv) thermal parameters, are given in Tables 2 and 3, respectively. Tables of anisotropic thermal parameters, root-mean-square amplitudes of vibration, and structure amplitudes have been included in the depository materials.

Results and discussion

Synthesis

The self-assembly reaction shown in eq. [1*a*] is a straightforward route to a wide range of new adamantane-like

$$[1a] \quad 3M(SR)_2 + MX_2 + 2X^- \rightarrow [(\mu\text{-}SR)_6(MX)_4]^{2-}$$

complexes of zinc and cadmium containing bridging alkyl- or benzyl-thiolate anions. An alternative route to $[(\mu\text{-}SEt)_6(CdX)_4]^{2-}$ (X = Br or I) is shown in eq. [1*b*]. Twenty-

$$[1b] \quad 4CdX_2 + 6EtSH + 6Et_3N \rightarrow [(\mu\text{-}SEt)_6(CdX)_4]^{2-} + 6Et_3NH^+ + 4X^-$$

eight analytically pure Et_4N^+ salts have been isolated, including all members of the series where R = 2-Pr, 2-Bu, or benzyl, M = Zn or Cd, and X = Cl, Br, or I, and, in addition, salts with the following R/M/X combinations: Me/Zn/Br, I; Et/Zn/I; Et/Cd/Cl, Br, I; 1-Pr/Zn/I; 1-Bu/Zn, Cd/I. Also, spectroscopically but not analytically pure materials were obtained for R/M/X = Et/Zn/Cl, Br.

Can. J. Chem. Downloaded from www.nrcresearchpress.com by 92.62.229.171 on 09/08/12
For personal use only.

All attempts to isolate complexes where R = Me, M = Cd, and X = Cl, Br, or I failed. Neither could we obtain any evidence for these complexes in *in situ* NMR experiments. Nevertheless, it is evident that the $[(\mu\text{-SPr}^n)_6(\text{MI})_4]^{2-}$ (M = Zn, Cd) ions, reported earlier (4), are just two members of a much wider series of zinc and cadmium complexes of the general type $[(\mu\text{-SAlk})_6(\text{MX})_4]^{2-}$.

Previously, the self-assembly method was used to synthesize $[(\mu\text{-SPh})_6(\text{FeX})_4]^{2-}$ (X = Cl or Br) (22) and $[(\mu\text{-EPh})_6(\text{HgX})_4]^{2-}$ (4) as well as $[(\mu\text{-SPr}^n)_6(\text{MI})_4]^{2-}$ (M = Zn, Cd, or Hg) (4). An alternative synthetic method, halogen oxidation of the homoleptic parent anions $[(\mu\text{-EPh})_6(\text{MEPh})_4]^{2-}$, was used for $[(\mu\text{-EPh})_6(\text{MX})_4]^{2-}$ (E = S or Se; M = Zn or Cd; X = Cl, Br, or I) (3). This latter preparative route cannot be applied in the present case because parent ions of the type $[(\mu\text{-SAlk})_6(\text{MAlk})_4]^{2-}$ have not yet been described.

Cadmium-111/113 NMR spectra of complexes with a tetranuclear cage

(i) $[(\mu\text{-SR})_6(\text{CdX})_4]^{2-}$

Cadmium-111/113 NMR chemical shift data for the new complexes, $[(\mu\text{-SAlk})_6(\text{CdX})_4]^{2-}$, are included in Table 4 (n = 4). For a given alkyl group, $^{111/113}$Cd (hereinafter indicated by just Cd) nuclear shielding varies with X in the order I > Br > Cl. This order, that of Normal Halogen Dependence (23), has been observed for $[\text{CdX}_4]^{2-}$ (24) and $[(\mu\text{-EPh})_6(\text{CdX})_4]^{2-}$ (E = S or Se) (3). For a constant halogen, the variation of Cd chemical shift with the substituent on sulfur is primary alkyl ≥ benzyl > secondary alkyl > phenyl.[9] The same order was found previously for $[\text{Cd(SR)}_4]^{2-}$ in water (25).

The complexes $[(\mu\text{-SPr}^i)_6(\text{CdX})_4]^{2-}$ (X = Cl, Br) give particularly narrow lines in their Cd NMR spectra at ambient probe temperature and, for these, two-bond ^{113}Cd–S–^{111}Cd coupling gives rise to clear satellites at this temperature. The corresponding iodide and the series $[(\mu\text{-SCH}_2\text{Ph})_6(\text{CdX})_4]^{2-}$ (X = Cl, Br, I) give satellites at reduced temperature. Values for ^2J are included in Table 5. For comparison, ^2J is 44 – ca. 56 Hz in species with the $(\mu\text{-SPh})_6\text{Cd}_4$ cage (3, 26–28). Only for the iodides does ^2J for the alkyl- and benzyl-thiolate complexes overlap the range of values found for the benzenethiolate complexes. The coupling depends on terminal halogen in the order Cl < Br < I. Thus the halogen dependence of ^2J found previously for $[(\mu\text{-SePh})_6(\text{CdX})_4]^{2-}$ (3, 28) is shown to be general.

In some cases (R = 2-Pr, 2-Bu, or PhCH_2; X = Cl, Br, or I) closely spaced multiple lines are found in the reduced temperature Cd NMR spectrum of $[(\mu\text{-SR})_6(\text{CdX})_4]^{2-}$. For example, the spectrum of $[(\mu\text{-SCH}_2\text{Ph})_6(\text{CdI})_4]^{2-}$ in CH_2Cl_2 at 213 K consists of a major signal at $\delta_{\text{Cd}} = 575._7$, with a strong shoulder at $\delta_{\text{Cd}} = 575._9$. These two lines have identical ^{111}Cd–^{113}Cd satellite splittings. We feel that in these cases the multiple signals are observed at too high a temperature to be due to slowing of inversion at sulfur, and so are more likely to result from restricted S—C bond rotation. We note that the molecular structure of $[(\mu\text{-SPr}^i)_6(\text{CdBr})_4]^{2-}$ (see below) shows evidence of disorder from rotation about most of the S—C bonds.

As can be seen from $\delta_{\text{Cd}}([(\mu\text{-SR})_6(\text{CdX})_4]^{2-})$ in Table 4, these metal chemical shifts show large temperature dependences. The changes of −0.14 to −0.25 ppm/K are of comparable size to the −0.2 ppm/K found (26, 29) for $[(\mu\text{-SPh})_6(\text{CdSPh})_4]^{2-}$.

[9]Solutions of $[(\mu\text{-SPh})_6(\text{MX})_4]^{2-}$ in acetone at 295 K give δ_{Cd} = 551, 535, and 501 for X = Cl, Br, and I, respectively (3).

TABLE 5. Two-bond ^{111}Cd–^{113}Cd coupling constants[a]

Complex	$^2J(^{111}\text{Cd–S–}^{113}\text{Cd})$ (Hz)[b]
$[(\mu\text{-SPr}^i)_6(\text{CdCl})_4]^{2-}$	22[c]
$[(\mu\text{-SPr}^i)_6(\text{CdBr})_4]^{2-}$	28[d]
$[(\mu\text{-SPr}^i)_6(\text{CdI})_4]^{2-}$	44
$[(\mu\text{-SPr}^i)_6(\text{CdBr})_3(\text{ZnBr})]^{2-}$	32
$[(\mu\text{-SPr}^i)_6(\text{CdBr})_2(\text{ZnBr})_2]^{2-}$	36
$[(\mu\text{-SCH}_2\text{Ph})_6(\text{CdCl})_4]^{2-}$	24
$[(\mu\text{-SCH}_2\text{Ph})_6(\text{CdBr})_4]^{2-}$	32
$[(\mu\text{-SCH}_2\text{Ph})_6(\text{CdI})_4]^{2-}$	44
$[(\mu\text{-SCH}_2\text{Ph})_6(\text{CdCl})_3(\text{ZnCl})]^{2-}$	26
$[(\mu\text{-SCH}_2\text{Ph})_6(\text{CdCl})_2(\text{ZnCl})_2]^{2-}$	35

[a]For solutions in CH_2Cl_2 at 215 ± 3 K.
[b]Estimated error ±1 Hz.
[c]^2J = 20 ± 1 Hz at 292 K.
[d]^2J = 26 ± 1 Hz at 293 K.

(ii) $[(\mu\text{-SR})_6(\text{CdX})_n(\text{ZnX})_{4-n}]^{2-}$

When $[(\mu\text{-SAlk})_6(\text{CdX})_4]^{2-}$ and the analogous $[(\mu\text{-SAlk})_6(\text{ZnX})_4]^{2-}$ are mixed in various ratios, the Cd NMR spectra of newly prepared mixtures at, or below, ambient probe temperature show a total of four resonances. An example is shown in Fig. 1. These results show that redistribution of metals (eq. [2]) is rapid on the prepar-

$$[2]\quad [(\mu\text{-SAlk})_6(\text{CdX})_4]^{2-} + [(\mu\text{-SAlk})_6(\text{ZnX})_4]^{2-} \rightleftharpoons [(\mu\text{-SAlk})_6(\text{CdX})_n(\text{ZnX})_{4-n}]^{2-}$$

(equilibrium mixture)

ative time scale but not on the NMR time scale. The observation of four signals confirms the integrity of both the Cd_4 and Zn_4 cages in solution. In addition, it is evident from the spectra of the mixtures (e.g., Fig. 1) that the redistribution occurs close to statistically, unlike the case of $[(\mu\text{-SPh})_6(\text{CdSPh})_4]^{2-}$:$[(\mu\text{-SPh})_6(\text{ZnSPh})_4]^{2-}$ mixtures where $[(\mu\text{-SPh})_6(\text{CdSPh})_n(\text{ZnSPh})_{4-n}]^{2-}$ occurs, but only for n = 3 and 4 in DMF (10) and only for n = 2–4 in acetone (11).

Although separate signals are observed at ambient probe temperature, sharper lines are observed at reduced temperature. There is evidently residual exchange at ambient temperature. Cadmium NMR chemical shifts for $[(\mu\text{-SAlk})_6(\text{CdX})_n(\text{ZnX})_{4-n}]^{2-}$ at ambient and reduced temperature are given in Table 4.

As can be seen from the data in Table 4 for the two complete series $[(\mu\text{-SR})_6(\text{CdX})_n(\text{ZnX})_{4-n}]^{2-}$ (R = Pr^i or PhCH_2), the range $\Delta\delta_{\text{Cd}}(4,1)$ ($= \delta_{\text{Cd}}(n=4) - \delta_{\text{Cd}}(n=1)$) varies with X in the order I > Br > Cl, and increases with decreasing temperature. The pattern of chemical shifts for individual members of a series shows a nonlinear, second-order dependence on the number of Zn atoms in the cage. In general, the values of $\Delta\delta_{\text{Cd}}(4,1)$ for $[(\mu\text{-SAlk})_6(\text{CdX})_n(\text{ZnX})_{4-n}]^{2-}$ have the same sign as, but are significantly larger than, the 1.5 ppm that can be extrapolated from data for $[(\mu\text{-SPh})_6(\text{CdSPh})_n(\text{ZnSPh})_{4-n}]^{2-}$ (10, 11). For mixtures of $[(\mu\text{-SPh})_6(\text{CdI})_4]^{2-}$ and $[(\mu\text{-SPh})_6(\text{ZnI})_4]^{2-}$, separate signals are not observed for different members of the series $[(\mu\text{-SPh})_6(\text{CdI})_n(\text{ZnI})_{4-n}]^{2-}$ (Table 4). This result makes it clear that it is the difference in bridging rather than terminal groups that leads to differences in $\Delta\delta_{\text{Cd}}(4,1)$ between the alkyl- or benzyl-thiolate complexes and the benzenethiolate com-

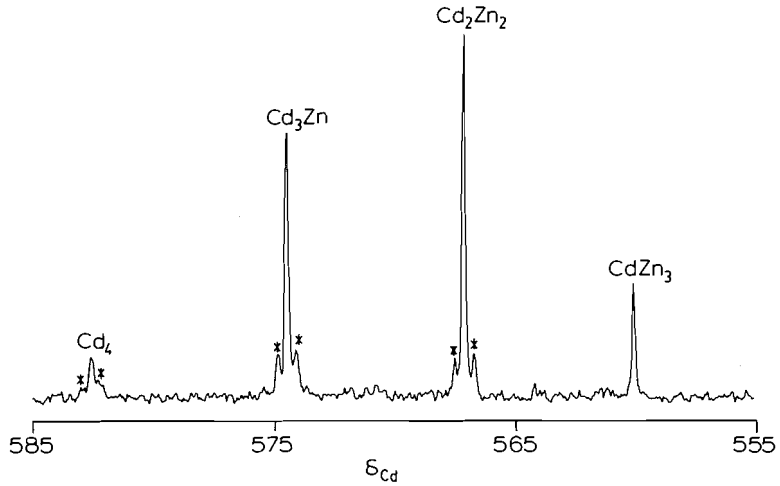

FIG. 1. 44.37 MHz 113-Cd NMR spectrum of a mixture with $[(\mu\text{-}SPr^i)_6(CdBr)_4]^{2-}$:$[(\mu\text{-}SPr^i)_6(ZnBr)_4]^{2-}$ = 1:1 in CH_2Cl_2 at 215 K. *indicates Cd satellite.

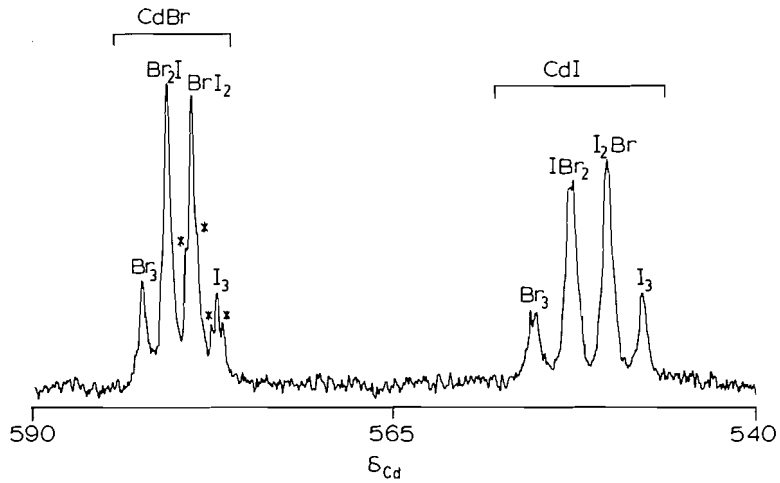

FIG. 2. 42.41 MHz 111-Cd NMR spectrum of a mixture with $[(\mu\text{-}SPr^i)_6(CdBr)_4]^{2-}$:$[(\mu\text{-}SPr^i)_6(CdI)_4]^{2-}$ = 1:1 in CH_2Cl_2 at 215 K. *indicates Cd satellite.

plexes. For Cd NMR spectroscopic purposes, at least, it is clearly dangerous to assume that benzenethiolate typifies all thiolates.

For RS/X = Pr^iS/Br and $PhCH_2S$/Cl, the reduced temperature spectra of $[(\mu\text{-}SR)_6(CdX)_n(ZnX)_{4-n}]^{2-}$ are sufficiently sharp to allow observation of the satellites due to $^2J(^{113}Cd\text{–}S\text{–}^{111}Cd)$ that are expected for n = 2–4 (e.g., Fig. 1). These couplings are given in Table 5. For both series it is found that the magnitude of ^2J varies with n in the order $2 > 3 > 4$.

(iii) $[(\mu\text{-}SPr^i)_6(CdX)_n(CdX')_{4-n}]^{2-}$

In view of the sensitivity of δ_{Cd} to zinc substitution in $[(\mu\text{-}SAlk)_6(CdX)_{4-n}(ZnX)_n]^{2-}$, we thought it of interest to study the sensitivity of the chemical shifts to the more distant changes that occur in series of the type $[(\mu\text{-}SAlk)_6(CdX)_n(CdX')_{4-n}]^{2-}$. Accordingly, we examined the Cd NMR spectra of $[(\mu\text{-}SPr^i)_6(CdX)_4]^{2-}$:$[(\mu\text{-}SPr^i)_6(CdX')_4]^{2-}$ mixtures (X/X' = Cl/Br, Cl/I, Br/I). No such complete series has been studied previously.

At ambient probe temperature, the mixtures show just two broad lines, one in the region expected for Cd attached directly to X, the other in the region expected for Cd attached directly to X'. At reduced temperature, however, additional fine structure becomes evident. As an example, Fig. 2 shows the ^{111}Cd NMR spectrum of a 1:1 mixture of $[(\mu\text{-}SPr^i)_6(CdBr)_4]^{2-}$ and $[(\mu\text{-}SPr^i)_6(CdI)_4]^{2-}$ in CH_2Cl_2 at 215 K. The spectrum clearly does not consist of the superimposed spectra of the two starting complexes, showing that redistribution of the halides has occurred. The region due to ^{111}Cd–Br and that due to ^{111}Cd–I both show four signals. Evidently δ_{Cd} is also sensitive to the nature of the more distant halogens. The individual lines can be assigned using the chemical shifts of the starting complexes and the variation of the intensities of the signals as the ratio of the two starting complexes is changed. Chemical shift assignments for the bromoiodo complexes, as well as the bromochloro and chloroiodo complexes, which were assigned similarly, are given in Table 6. It is noteworthy that in the spectrum of Fig. 2, the Cd NMR signal intensity distribution is close to 1:3:3:1 in both regions of absorption, showing that halide redistribution is a close-to-statistical process. This is true for the other binary mixtures also.

From the data in Table 6, it can be seen that if X'^- is a heavier halide than X^-, then substitution of X'^- for X^- in $[(\mu\text{-}SPr^i)_6(CdX)_4]^{2-}$ causes shielding of Cd attached to X. Con-

Can. J. Chem. Downloaded from www.nrcresearchpress.com by 92.62.229.171 on 09/08/12
For personal use only.

TABLE 6. Cadmium chemical shifts of $[(\mu\text{-}SPr^i)_6(CdX)_n(CdX')_{4-n}]^{2-}$[a] (X, X' = Cl, Br, I)

X	X'	Temperature (K)	n	δ_{Cd}[b] $(\mu\text{-}SR)_3CdX$ kernel	δ_{Cd}[b] $(\mu\text{-}SR)_3CdX'$ kernel
Cl	Br	292[c]		588	570
		215[d]	4	601.1	
			3	600.3	585.8
			2	599.5	584.8
			1	598.6	583.7
			0		582.6
Cl	I	293[c]		587	535
		215[d]	4	601.0	
			3	599.0[e]	560.0,599.7
			2	596.9[f]	555.4
			1	594.4[g]	551.4
			0		547.8
Br	I	294[c]		567	532
		215[d]	4	582.5	
			3	580.7	555.0
			2	578.9[h]	552.5
			1	577.2[h]	550.1
			0		547.7

[a]Produced *in situ* in $[(\mu\text{-}SPr^i)_6(CdX)_4]^{2-}$:$[(\mu\text{-}SPr^i)_6(CdX')_4]^{2-}$ mixtures. $[Cd_4]_{total}$, in mol/L of solvent at ambient probe temperature, were 0.1 for X/X' = Cl/Br, and 0.05 for X/X' = Cl/I and Br/I.

[b]Relative to external 0.1 M $Cd(ClO_4)_2$ (aq) at 293 ± 1 K.

[c]Average values; at ambient probe temperature, additional fine structure is not well resolved.

[d]See text.

[e]^2J(Cd–Cd) ≈ 25 Hz.

[f]^2J(Cl–*Cd*–S–*Cd*–I) = 25 ± 1 Hz.

[g]^2J(Cl–*Cd*–S–*Cd*–I) ≈ 33 Hz.

[h]^2J(Br–*Cd*–S–*Cd*–I) = 34 ± 1 Hz.

versely, X'^- substitution of $[(\mu\text{-}SPr^i)_6(CdX)_4]^{2-}$ causes deshielding if X'^- is lighter than X. The magnitude of the effect observed depends on both X and X'. Not unexpectedly, the largest changes per substitution are found in the series $[(\mu\text{-}SPr^i)_6(CdCl)_n(CdI)_{4-n}]^{2-}$, where introduction of I^- causes an average change in δ_{Cd}(Cd–Cl) of −2.2 ppm/I^- and introduction of Cl^- causes an average change in δ_{Cd}(Cd–I) of 4 ppm/Cl^-.

In contrast to the results found for $[(\mu\text{-}SPr^i)_6(CdBr)_n(CdI)_{4-n}]^{2-}$, only two broad signals were observed for the series $[(\mu\text{-}SePh)_6(CdBr)_n(CdI)_{4-n}]^{2-}$ (3), but the spectra of the less soluble $PhSe^-$ complexes were measured at 260 K, where residual exchange might be a problem. Separate signals were observed at 213 K for several complexes of the type $[(\mu\text{-}EPh)_6(CdEPh)_n(CdNCE')_{4-n}]^{2-}$ (E = S or Se, E' = O or S) (28). In the latter case, the effects of substitution at a distant terminal site range up to 5 ppm in magnitude, comparable to the largest changes observed for the 2-propylthiolate complexes.

Reaction of $[(\mu\text{-}SPr^i)_6(CdX)_4]^{2-}$ with sulfur and selenium

Reaction of $[(\mu\text{-}SPh)_6(MSPh)_4]^{2-}$ (M = Cd or Zn) with E'_8 (E' = S or Se) has been shown to give the decametallic complex $[M_6(\mu_3\text{-}E')_4(\mu_2\text{-}SPh)_{12}(MSPh)_4]^{4-}$ according to eq. [3] (30). It is not at all obvious from this what the course of

[3] $5[(\mu\text{-}SPh)_6(MSPh)_4]^{2-} + E'_8$

$\rightarrow 2[M_6(\mu_3\text{-}E')_4(\mu_2\text{-}SPh)_{12}(MSPh)_4]^{4-} + 16Ph_2S_2 + 2SPh^-$

the reaction with sulfur or selenium might be if the terminal positions of the starting tetranuclear cluster are occupied by halides instead of chalcogenates. The complexes $[(\mu\text{-}SPr^i)_6(CdX)_4]^{2-}$, which give sharp Cd NMR spectra at ambient probe temperature (see above), are ideal starting complexes to investigate this problem.

At room temperature, sulfur or *red* selenium dissolve readily in solutions of $[(\mu\text{-}SPr^i)_6(CdX)_4]^{2-}$ in CH_2Cl_2. The Cd NMR spectral changes that accompany this dissolution are qualitatively similar in each case. As an example, Fig. 3(*a*) shows the ^{111}Cd NMR spectrum of a mixture where $[(\mu\text{-}SPr^i)_6(CdI)_4]^{2-}$:red Se = 1:0.5. The major Cd NMR spectral change caused by addition of selenium is the appearance of two equally intense new resonances. The one significantly less shielded than the line of the starting complex is arbitrarily assigned to a cadmium Cd_A, and the one slightly more shielded is assigned to Cd_B. By comparison with, for example, the data in Table 4, it is evident that both new signals are due to four-coordinate cadmium. The chemical shift of Cd_A shows little sensitivity to change of the terminal halide, but changes significantly if selenium is replaced by sulfur in the mixture. Conversely, $\delta_{Cd}(Cd_B)$ is sensitive to change of the terminal halide but relatively insensitive to change of the chalcogen. Both resonances show satellites. The magnitude of the satellite separation is 40 Hz. By comparison with the data in Table 5, this is clearly a two-bond ^{113}Cd–E–^{111}Cd coupling. Therefore Cd_A and Cd_B must be linked by one or more bridging groups. On the basis of these findings, the high-frequency signal in Fig. 3(*a*) is assigned to the kernel $(\mu\text{-}Se)Cd_A(\mu\text{-}SPr^i)_3$ while the low-frequency signal is assigned to $ICd_B(\mu\text{-}SPr^i)_3$, with corresponding assignments in the other mixtures.

When the mixtures contain red selenium, a ^{77}Se resonance is also found for the new cadmium-containing species. A partial ^{77}Se NMR spectrum of the $[(\mu\text{-}SPr^n)_6(CdI)_4]^{2-}$:red Se mixture is shown in Fig. 3(*b*). (There is an additional signal from $(Pr^iS)_2Se$; see below.) The position of the signal in the region of the ^{77}Se NMR spectrum shown in Fig. 3(*b*) is not very sensitive to the nature of the terminal halide: δ_{Se} = −613.6, −610.6, and −607.4 for X = Cl, Br, and I, respectively. This signal is in the region expected for Se^{2-} in various forms, e.g., δ_{Se} = −511 for 0.5 M $(NH_4)_2Se$ in D_2O (31), δ_{Se} = −490[10] in hexagonal CdSe(s) (32), δ_{Se} = −731 for $[Cd_6(\mu_3\text{-}Se)_4(\mu\text{-}SPh)_{12}(CdI)_4]^{4-}$ in DMF.[11] As exemplified by Fig. 3(*b*), the ^{77}Se signals of the new complexes have $^{111/113}$Cd satellites. The satellite splittings are insensitive to the nature of the halide X: J(ave) = 73 ± 1, 74 ± 1, and 73 ± 1 Hz for X = Cl, Br, and I, respectively. The magnitudes of the satellite splittings puts them in the range observed for $^1J(^{111/113}Cd–^{77}Se)$ in Cd(II)–$PhSe^-$ complexes (3, 30, 34). The ^{77}Se NMR spectra point to a single selenium environment in which the selenium (as selenide) is directly attached to cadmium.

The Cd and ^{77}Se NMR results are consistent with the skeleton **I**.[12] A skeleton like **I** occurs in $[Zn_4(\mu_4\text{-}Cl)(SPh)_{12}$-

[10]The chemical shift reported in ref. 32 has been converted to Me_2Se as reference using δ_{Se} (relative to Me_2Se) = δ_{Se} (relative to Na_2SeO_3(aq)) + 1253 (33).

[11]Unpublished results of P. A. W. Dean and V. Manivannan.

[12]Structure **I** was drawn using the atomic coordinates for $[ClZn_8(SPh)_{16}]^-$ from ref. 35.

Can. J. Chem. Downloaded from www.nrcresearchpress.com by 92.62.229.171 on 09/08/12
For personal use only.

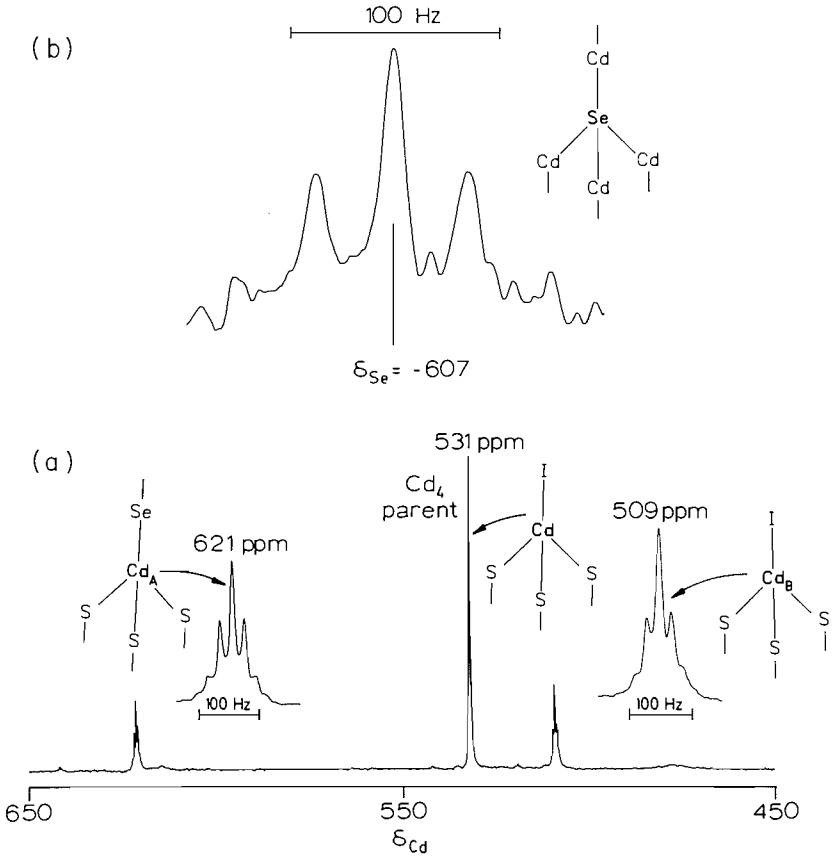

FIG. 3. NMR spectra of Cd/Se-containing species in a 1:0.5 mixture of $[(\mu\text{-SPr}^i)_6(CdI)_4]^{2-}$ and red Se in CH_2Cl_2 at 295 K. (*a*) 42.41 MHz 111-Cd NMR spectrum. (*b*) 57.20 MHz 77-Se NMR spectrum.

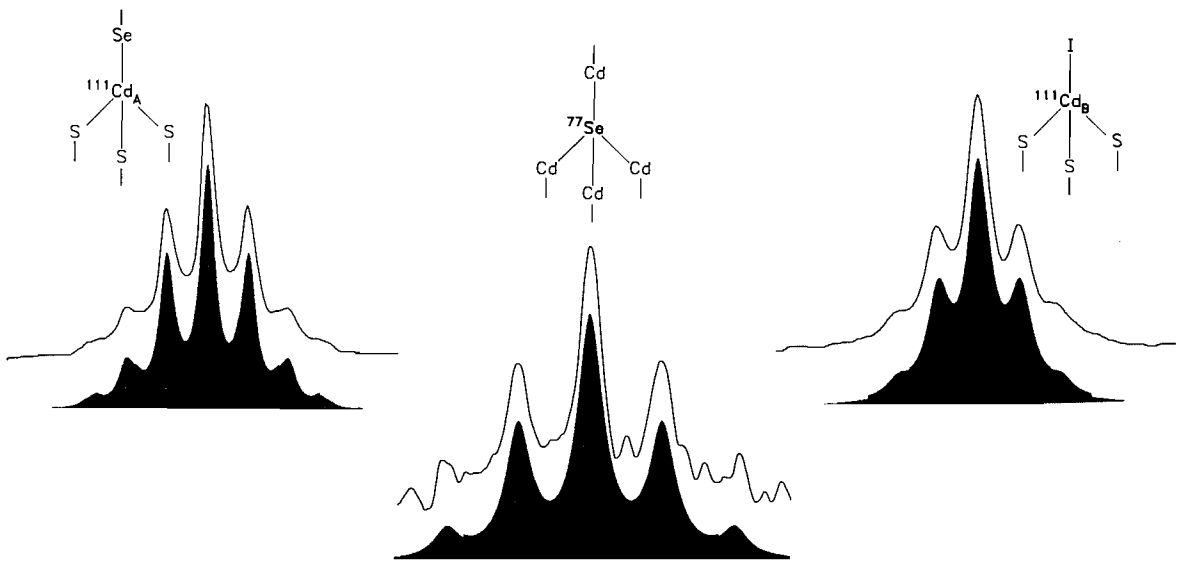

FIG. 4. Observed and (below) simulated NMR spectra of $[(Cd_A)_4(\mu_4\text{-Se})(\mu\text{-SPr}^i)_{12}(Cd_BI)_4]^{2-}$.

$(ZnSPh)_4]^-$ (35). Very lately, while our own study was in progress, the series $[Cd_4(\mu_4\text{-E}')(\mu\text{-EPh})_{12}(CdX)_4]^{2-}$ (E, E' = S, Se, Te; X = halide or EPh^-) was prepared by the self-assembly method and shown to have this structure also (36). As well, the same structure has been found in $^3_\infty[\{SCd_8(S\text{–}2\text{–}Bu)_{12}\}(CN)_{4/2}]$.[13] In **I**, magnetically active Cd in the chemically different A and B sites can be expected to couple

[13] I. G. Dance, R. G. Garbutt, I. Ma, and M. L. Scudder. Unpublished work quoted in ref. 36.

Can. J. Chem. Downloaded from www.nrcresearchpress.com by 92.62.229.171 on 09/08/12
For personal use only.

TABLE 7. Cd and ^{77}Se NMR data for $[(Cd_A)_4(\mu_4\text{-}E')(\mu_2\text{-}SPr^i)_{12}(Cd_BX)_4]^{2-}$ in CH_2Cl_2 at 294 ± 1 K[a]

E′	X	$\delta_{Cd}(Cd_A)$[a,b]	$\delta_{Cd}(Cd_B)$[a,b]	δSe[c]	$^2J(Cd\text{–}Cd)_{ave}$[d,e]	$^1J(Cd\text{–}Se)$[d]
S	Cl[f]	645	570		38	
	Br[f]	645	553		39	
	I[g]	642	518		41	
Se	Cl[h]	628	556	−613.6	35	73
	Br[h]	626	539	−610.6	37	74
	I[i]	621	508	−607.4	40	73

[a]See structure **I** of text for labelling.
[b]Relative to external 0.1 M $Cd(ClO_4)_2$(aq) at 293 ± 1 K.
[c]Relative to external pure Me_2Se at 295 ± 1 K.
[d]Estimated error ±1 Hz.
[e]$^2J(Cd_A\text{–}S\text{–}Cd_B)$ and $^2J(^{111}Cd_A\text{–}S\text{–}^{113}Cd_B)$ were not resolved (see text).
[f]In a mixture where $[Cd_4]_{initial}$ = 0.05 mol/L of solvent and Cd_4:S = 1:1.
[g]In a mixture where $[Cd_4]_{initial}$ = 0.2 mol/L of solvent and Cd_4:S = 1:0.67.
[h]In a mixture where $[Cd_4]_{initial}$ = 0.1 mol/L of solvent and Cd_4:Se = 1:0.5.
[i]In a mixture where $[Cd_4]_{initial}$ = 0.2 mol/L of solvent and Cd_4:Se = 1:0.5.

TABLE 8. ^{13}C NMR data for $[(\mu\text{-}SPr^i)_6(CdX)_4]^{2-}$ and $[(Cd_A)_4(\mu_4\text{-}E')(\mu_2\text{-}SPr^i)_{12}(Cd_BX)_4]^{2-}$ in CH_2Cl_2 at 294 ± 1 K[a]

		$\delta_C(Pr^i$ in $Cd_4)$		$\delta_C(Pr^i$ in $Cd_8)$	
E	X	CH_3	CH	CH_3	CH
S	Cl	30.1	34.5	30.0[b]	34.9[c]
S	Br	30.2	34.9	30.0[d]	35.1[e]
S	I	30.1	35.5	29.9	35.7
Se	Cl	30.1	34.6	30.0	35.0
Se	Br	30.2	34.9	30.0	35.2[f]
Se	I	30.1	35.7	29.9	36.4

[a]The Cd_8 complex was formed *in situ* from the Cd_4 complex and E′ (see text). The starting concentration of Cd_4 complex was 0.05–0.1 mol/L of CH_2Cl_2.
[b]$^3J(C\text{–}Cd)$ = 10.0 ± 0.2 Hz.
[c]$^2J(C\text{–}Cd)$ = 8.0 ± 0.2 Hz.
[d]$^3J(C\text{–}Cd)$ = 9.5 ± 0.2 Hz.
[e]$^2J(C\text{–}Cd)$ = 7.9 ± 0.2 Hz.
[f]$^2J(C\text{–}Cd)$ = 7.8 ± 0.2 Hz.

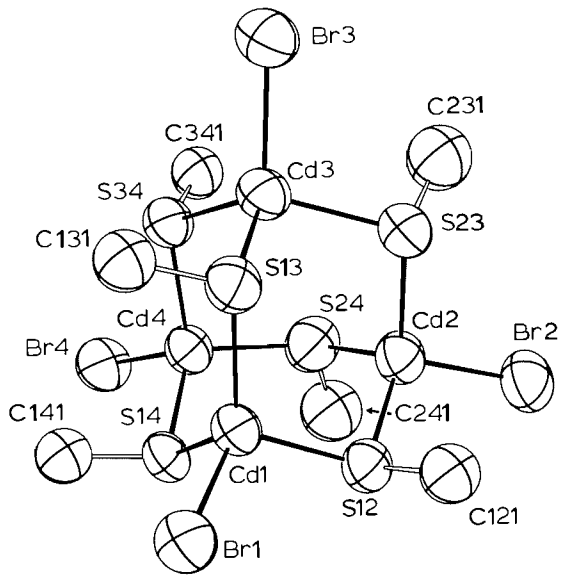

FIG. 5. Perspective view of the anion $[(\mu\text{-}SPr^i)_6(CdBr)_4]^{2-}$. For clarity, the methyl groups of the thiolate have been omitted.

through two bonds. Both ^{113}Cd and ^{111}Cd in site A or B will couple to ^{111}Cd in site B or A, but given the linewidths and the magnitude of ^2J, the separate couplings to $^{111/113}$Cd will not be resolved. Also, we can expect that magnetically different types of Cd in site A will couple with each other. Finally, ^{77}Se is expected to couple to magnetically active Cd in site A, but not to that in the more distant site B. Taking into account appropriate statistics, the ^{111}Cd and ^{77}Se NMR spectra of Fig. 3 can be simulated using structure **I** with $^1J(^{111}Cd\text{–}^{77}Se)$ = 73 Hz, $^2J(^{111}Cd_{A\,or\,B}\text{–}S\text{–}^{111/113}Cd_{B\,or\,A})$ = $^2J(^{111}Cd_A\text{–}S\text{–}^{113}Cd_A)$ = 40 Hz, and the empirical matching of linewidths. The good match between the observed and simulated spectra is shown in Fig. 4. On this basis, we conclude that reaction of $[(\mu\text{-}SPr^i)_6(CdX)_4]^{2-}$] with sulfur or selenium does indeed generate $[Cd_4(\mu_4\text{-}E')(\mu\text{-}SPr^i)_{12}(CdX)_4]^{2-}$ of structure **I**. Cadmium-111 and ^{77}Se NMR data for the various $[Cd_4(\mu_4\text{-}E')(SPr^i)_{12}(CdX)_4]^{2-}$ are given in Table 7.

The complex $[Cd_4(\mu_4\text{-}E')(SPr^i)_{12}(CdX)_4]^{2-}$ was the major product of these reactions that was detected by Cd NMR. However, for E′ = S, X = Cl, Br, I, colourless, crystalline material formed in the mixtures over several hours at ambient probe temperature. When dissolved in CD_3CN, these materials showed only Et_4N^+ by ^{1}H NMR. For the case of E′ = S, X = Br, X-ray analysis[14] showed the product to be $(Et_4N)_2[CdBr_4]$. When E′ = Se, no crystalline material formed, but at high Se/Cd_4 ratios a yellow oil separated that again showed only the ^{1}H NMR spectrum of Et_4N^+.

Carbon-13 NMR confirms that the Cd_4 complexes are converted into one major Cd-containing product. The ^{13}C NMR data of the cadmium complexes are given in Table 8. The ^{13}C NMR spectra also show that when sulfur is used as the oxidant, the oxidized isopropylthiolate is converted not to Pr^iSSPr^i alone, but to an equilibrium mixture of the disulfide (δ_C: 22.3 (CH_3), 41.4 (CH)), Pr^iSSSPr^i (δ_C = 22.2, 41.8), and $Pr^iSSSSPr^i$ (δ_C = 22.4, 42.1), even though $[(\mu\text{-}SPr^i)_6(CdX)_4]^{2-}$ is still present.

The ^{13}C NMR data for the new cadmium complexes formed on oxidation by selenium are included in Table 8. In this case, the thiolate that is released from $[(\mu\text{-}SPr^i)_6(CdX)_4]^{2-}$ appears as $(Pr^iS)_2Se$ (δ_C = 23.5 (CH_3), 41.2 (CH);

[14]P. A. W. Dean, Yuyang Wu, J. J. Vittal, and N. C. Payne, to be submitted for publication.

Can. J. Chem. Downloaded from www.nrcresearchpress.com by 92.62.229.171 on 09/08/12
For personal use only.

TABLE 9. Selected interatomic distances (Å) and angles (deg) for $[(\mu\text{-}SPr^i)_6(CdBr)_4]^{2-}$, **1**

		Cd . . Cd	
Cd(1). . .Cd(2)	4.067(3)	Cd(1). . .Cd(3)	4.138(3)
Cd(1). . .Cd(4)	4.058(3)	Cd(2). . .Cd(3)	4.052(3)
Cd(2). . .Cd(4)	4.064(3)	Cd(3). . .Cd(4)	4.063(3)
		Mean	4.074(32)
		S. . .S	
S(12). . .S(13)	4.224(3)	S(12). . .S(14)	3.711(3)
S(12). . .S(23)	4.124(3)	S(12). . .S(24)	4.231(3)
S(13). . .S(14)	4.416(3)	S(13). . .S(23)	3.812(3)
S(13). . .S(34)	4.081(3)	S(14). . .S(24)	4.172(3)
S(14). . .S(34)	4.297(3)	S(23). . .S(24)	4.073(3)
S(23). . .S(34)	4.438(3)	S(24). . .S(34)	3.919(3)
		Mean	4.12(22)
		Cd—Br	
Cd(1)—Br(1)	2.593(4)	Cd(2)—Br(2)	2.590(4)
Cd(3)—Br(3)	2.595(4)	Cd(4)—B(4)	2.608(4)
		Mean	2.596(8)
		Cd—S	
Cd(1)—S(12)	2.525(7)	Cd(2)—S(12)	2.534(8)
Cd(1)—S(13)	2.533(8)	Cd(3)—S(13)	2.537(8)
Cd(1)—S(14)	2.555(7)	Cd(4)—S(14)	2.523(8)
Cd(2)—S(23)	2.528(8)	Cd(3)—S(23)	2.537(8)
Cd(2)—S(24)	2.527(9)	Cd(4)—S(24)	2.519(8)
Cd(3)—S(34)	2.512(7)	Cd(4)—S(34)	2.526(8)
		Mean	2.53(1)
		Br—Cd—S	
S(12)—Cd(1)—Br(1)	111.6(2)	S(13)—Cd(1)—Br(1)	109.4(2)
S(14)—Cd(1)—Br(1)	107.4(2)	S(12)—Cd(2)—Br(2)	109.3(2)
S(23)—Cd(2)—Br(2)	108.2(2)	S(24)—Cd(2)—Br(2)	109.3(2)
S(13)—Cd(3)—Br(3)	113.7(2)	S(23)—Cd(3)—Br(3)	103.7(2)
S(34)—Cd(3)—Br(3)	110.7(2)	S(14)—Cd(4)—Br(4)	105.8(2)
S(24)—Cd(4)—Br(4)	114.3(2)	S(34)—Cd(4)—Br(4)	106.6(2)
		Mean	109.2(31)
		S—Cd—S	
S(13)—Cd(1)—S(12)	113.2(2)	S(14)—Cd(1)—S(12)	93.8(2)
S(14)—Cd(1)—S(13)	120.4(3)	S(23)—Cd(2)—S(12)	109.1(2)
S(24)—Cd(2)—S(12)	113.4(3)	S(24)—Cd(2)—S(23)	107.3(3)
S(23)—Cd(3)—S(13)	97.4(3)	S(34)—Cd(3)—S(13)	107.8(2)
S(34)—Cd(3)—S(23)	123.1(3)	S(24)—Cd(4)—S(14)	111.7(3)
S(34)—Cd(4)—S(14)	116.7(2)	S(34)—Cd(4)—S(24)	101.9(3)
		Mean	109.6(88)
		Cd—S—Cd	
Cd(2)—S(12)—Cd(1)	107.0(3)	Cd(3)—S(13)—Cd(1)	109.4(2)
Cd(4)—S(14)—Cd(1)	106.1(2)	Cd(3)—S(23)—Cd(2)	106.3(3)
Cd(4)—S(24)—Cd(2)	107.3(3)	Cd(4)—S(34)—Cd(3)	107.5(3)
		Mean	107.3(12)

δ_{Se} = 602), which was identified by comparison of its ^{13}C and ^{77}Se NMR spectra with those of an authentic sample of the Se(II) dithiolate. The Se(II) compound reacts only very slowly with excess $[(\mu\text{-}SPr^i)_6(CdX)_4]^{2-}$ (days to weeks at the concentrations used for ^{13}C NMR (see Table 8)).

On the basis of the preceding information, the reaction stoichiometry is apparently that given in eq. [4].

$$[4]\quad 7[(\mu\text{-}SPr^i)_6(CdX)_4]^{2-} + (\{3 + 3x\}/8)\,E'_8 \rightarrow 3[Cd_4(\mu_4\text{-}E')(\mu\text{-}SPr^i)_{12}(CdX)_4]^{2-} + 3Pr^iSE'_xSPr^i + 4CdX_4^{2-}$$

(X = Cl, Br, I; E′ = S, $x \approx 1$ (ave); E′ = Se, $x = 1$)

A curious feature of these reactions is that they do not, in fact, occur stoichiometrically. The $[Cd_4(\mu_4\text{-}E')(\mu\text{-}SPr^i)_{12}(CdX)_4]^{2-}$ that is initially formed appears to react with additional sulfur or selenium in preference to $[(\mu\text{-}SPr^i)_6(CdX)_4]^{2-}$, so that the octanuclear complex dies away while the starting material still exists. Our attempts to identify the new complexes formed from the octanuclear complex have so far been unsuccessful.

Crystal structure of $(Et_4N)_2[(\mu\text{-}SPr^i)_6(CdBr)_4]$, $(Et_4N)_2$ ***1***

The crystal structure of the salt contains well-separated anions and cations. The structure of the $Cd_4Br_4(S—C_1)_6$ skeleton of the anion **1** is presented in Fig. 5. This is the first example of a $(\mu\text{-}SAlk)_6M_4$ cage that has been characterized

Can. J. Chem. Downloaded from www.nrcresearchpress.com by 92.62.229.171 on 09/08/12
For personal use only.

TABLE 10. Correlation of S. . .S distances and S—Cd—S angles in **1**–**3** with the nature of the 1,3-interaction involved[a]

	1	**2**	**3**
S. . .S distances (Å)			
a–a	4.416, 4.438	4.316, 4.434	4.334
Mean:	4.43(2)	4.38(8)	4.334(0)
a–e	3.919–4.297	3.939–4.224	4.028–4.157
Mean:	4.14(12)	4.11(10)	4.09(9)
e–e	3.711, 3.812	3.695, 3.750	4.046
Mean:	3.76(7)	3.72(4)	4.046(0)
S—Cd—S angles (deg)			
a–a	120.4, 123.1	114.7, 118.4	117.1
Mean:	121.7(19)	116.6(26)	117.1(0)
a–e	101.9–116.7	99.9–110.8	104.5–109.6
Mean:	110.1(46)	107.0(37)	107.4(32)
e–e	93.8, 97.4	91.5, 93.5	105.2
Mean:	95.6(25)	92.5(14)	105.2(0)

[a]See text.

for Zn(II)–Hg(II). Selected interatomic distances and angles are compiled in Table 9.

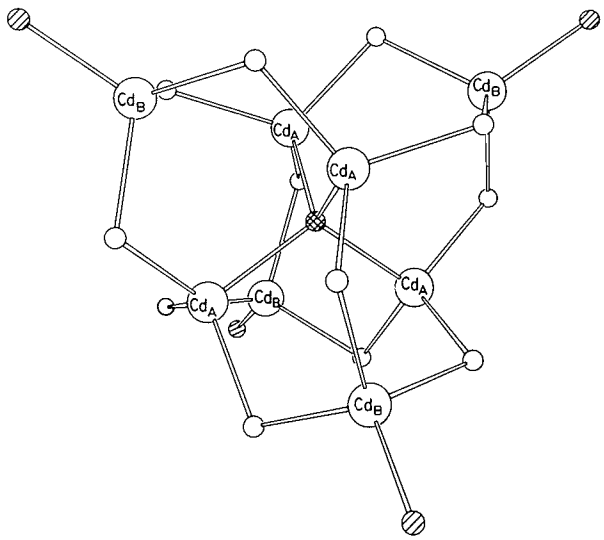

I

(○ = sulfur (of thiolate); ⊘ = halide; ⊗ = chalcogenide)

There is no crystallographically imposed symmetry in **1**. The four cadmium atoms of the $Cd_4Br_4S_6$ core are arranged at the vertices of a nearly regular inner tetrahedron. The range of nonbonded Cd. . .Cd distances is 4.054–4.138 Å, with mean 4.074(32) Å, and the range of Cd—Cd—Cd angles is 59.21°–60.05°, with mean 59.7(4)°. The mean Cd. . .Cd distance is slightly smaller than 4.30(10) Å found for $[(\mu\text{-}SPh)_6(CdSPh)_4]^{2-}$, **2**, as the (Et_4N^+) $(Et_3N)^+$ salt (9), or 4.164(4) Å, reported for $[(\mu\text{-}SPh)_6(CdBr)_4]^{2-}$, **3**, as the Me_4N^+ salt (3). Each edge of the Cd_4 tetrahedron is bridged by one of the six isopropylthiolate ligands. The six bridging sulfur atoms occupy the corners of an octahedron that is highly distorted, as indicated by the large range of S. . .S distances (3.711–4.416 Å). Similar distortions have been observed in all other adamantane-like thiolate-bridged structures (1), and are a consequence of intramolecular interaction between the substituents on the bridging sulfur atoms as discussed further below. Tetrahedral coordination about each Cd is completed by a terminal bromide ligand. The four bromines are arranged at the apices of an irregular outer tetrahedron. The range of Br. . .Br is 8.128–8.486 Å.

The mean value of the Cd—S bond lengths in **1**, 2.53(1) Å, is comparable to the values determined for **2** and **3**, 2.56(2) and 2.545(6) Å, respectively. However, the mean Cd—Br bond length at 2.596(8) Å is larger than 2.564(3) Å observed for **3**. This may be explained in terms of electronic perturbation associated with substitution effects on the sulfur atoms. The Cd—S—Cd angles in **1** range from 106.1° to 109.4°, with a mean of 107.3(12)°. This mean value is less than the means of 113.8(34)° and 109.8(5)° in **2** and **3**, respectively, as expected for a smaller Cd_4 tetrahedron when the Cd—S distances are very similar. A large variation in S—Cd—S angles is observed (93.8°–123.1° with a mean of 109.6(88)°), as has been found for **2** (91.5°–118.8° (mean 106.2°)) and **3** (104.5°–117.1° (mean 109.1°)).

Adamantane-like $[(\mu\text{-}SR)_6M_4]$ can exist as four configurational isomers, depending on the relative orientations of the R substituents at the pyramidal sulfur atoms in the four $M_3(SR)_3$ rings (1, 3). Of the four isomers, two have C_3 symmetry and two have C_1 symmetry. Figure 5 shows that the six isopropyl groups in **1** adopt the configuration of Isomer III (C_1 symmetry). The anion **2** has the same form. In contrast, the benzenethiolate analogue, **3**, occurs as Isomer IV (C_3 symmetry).

In Isomer III, the orientations of the R substituents (axial or equatorial) in the four six-membered M_3S_3 rings are [aae, aae, aee, aee]. (This configuration has two axial–axial interactions, which is the minimum possible number.) Thus, a–a, a–e, and e–e substituent–substituent interactions occur, and accordingly both the S. . .S distances and the S—Cd—S angles should reflect the nature of the interaction involved (1). The S. . .S distances and the S—Cd—S angles for **1**, **2**, and **3** are grouped in Table 10 in terms of 1,3-substituent

Can. J. Chem. Downloaded from www.nrcresearchpress.com by 92.62.229.171 on 09/08/12
For personal use only.

interactions. Both parameters follow the order a–a > a–e > e–e, as expected. It can be seen that the S_{axial}. . .S_{axial} distances and S_{axial}—Cd—S_{axial} angles for **1** are slightly larger than those found in **2** and **3**. This could be attributed to the bulkiness of the substituent in **1**.

Acknowledgments

We are grateful to the Natural Sciences and Engineering Research Council of Canada for funding this work through an operating grant to P.A.W.D. Thanks are due to Prof. N. C. Payne of this Department for providing the diffraction facilities, software, and encouragement to J. J. V., and to Susan England, also of this Department, for expert technical assistance.

1. I. G. Dance. Polyhedron, **5**, 1037 (1986), and references therein.
2. P. J. Blower and J. R. Dilworth. Coord. Chem. Rev. **76**, 121 (1987).
3. P. A. W. Dean, J. J. Vittal, and N. C. Payne. Inorg. Chem. **26**, 1683 (1987).
4. P. A. W. Dean and V. Manivannan. Inorg. Chem. **29**, 2997 (1990).
5. J. J. Vittal, P. A. W. Dean, and N. C. Payne. Can. J. Chem. **70**, 792 (1992).
6. I. G. Dance, G. A. Bowmaker, G. R. Clark, and J. K. Seadon. Polyhedron, **2**, 1031 (1983).
7. J. R. Nicholson, I. L. Abrahams, W. Clegg, and C. D. Garner. Inorg. Chem. **24**, 1092 (1985).
8. G. Henkel, P. Betz, and B. Krebs. Angew. Chem. Int. Ed. Engl. **26**, 145 (1987); Angew. Chem. **99**, 131 (1987).
9. K. S. Hagen and R. H. Holm. Inorg. Chem. **23**, 418 (1984).
10. I. G. Dance. Aust. J. Chem. **38**, 1745 (1985).
11. P. A. W. Dean and J. J. Vittal. Inorg. Chem. **25**, 514 (1986).
12. D. C. Bradley and C. H. Marsh. Chem. Ind. 361 (1967).
13. J. L. Kice, T. W. S. Lee, and S. Pan. J. Am. Chem. Soc. **102**, 4448 (1980); J. L. Kice and H. Slebocka-Tilk. J. Am. Chem. Soc. **104**, 7123 (1982).
14. R. K. Harris. Nuclear magnetic resonance spectroscopy. Pitman, London. 1983. p. 230.
15. P. A. W. Dean, J. J. Vittal, and M. H. Trattner. Inorg. Chem. **26**, 4245 (1987).
16. Enraf–Nonius: CAD4 Diffractometer Manual. Delft, The Netherlands. 1988.
17. Enraf–Nonius Structure Determination Package. SDP-PLUS, Version 3.0. 1985.
18. D. Cahen and J. A. Ibers. J. Appl. Crystallogr. **5**, 298 (1972).
19. International tables for X-ray crystallography. (*a*) Vol. A. D. Reidel Publishing Co., Boston. 1983; (*b*) Vol. IV. Kynoch Press, Birmingham. 1974.
20. P. Main. MULTAN 82 Manual. Department of Physics, University of York, York. July, 1982.
21. G. M. Sheldrick. SHELX-76, Program for crystal structure determination. University of Cambridge, England. 1976.
22. D. Coucouvanis, M. Kanatzidis, E. Simhon, and N. C. Baenziger. J. Am. Chem. Soc. **104**, 1874 (1982).
23. C. J. Jameson and J. Mason. *In* Multinuclear NMR. *Edited by* J. Mason. Plenum Press, New York. 1987. p. 69 et seq., and references therein.
24. R. Colton and D. Dakternieks. Aust. J. Chem. **33**, 2405 (1980).
25. G. K. Carson, P. A. W. Dean, and M. J. Stillman. Inorg. Chim. Acta, **66**, 37 (1982).
26. P. A. W. Dean and J. J. Vittal. J. Am. Chem. Soc. **106**, 6436 (1984).
27. I. G. Dance and J. K. Saunders. Inorg. Chim. Acta, **96**, L71 (1985).
28. P. A. W. Dean and J. J. Vittal. Can. J. Chem. **66**, 2443 (1988).
29. I. G. Dance. Inorg. Chim. Acta, **108**, 227 (1985).
30. I. G. Dance, A. Choy, and M. L. Scudder. J. Am. Chem. Soc. **106**, 6285 (1985).
31. J. D. Odom, W. H. Dawson, and P. D. Ellis. J. Am. Chem. Soc. **101**, 5815 (1979).
32. W. Koch, O. Lutz, and A. Nolle. Z. Phys. A: At. Nucl. **289**, 17 (1978).
33. H. E. Wachli. Phys. Rev. **90**, 331 (1953).
34. G. K. Carson and P. A. W. Dean. Inorg. Chim. Acta, **66**, 37 (1982).
35. I. G. Dance. Aust. J. Chem. **38**, 1391 (1985).
36. G. S. H. Lee, K. J. Fisher, D. C. Craig, M. L. Scudder, and I. G. Dance. J. Am. Chem. Soc. **112**, 6435 (1990).

Can. J. Chem. Downloaded from www.nrcresearchpress.com by 92.62.229.171 on 09/08/12
For personal use only.

Metal-selenolate chemistry: stereochemistry of adamantane-type clusters of formula $[(\mu\text{-SePh})_6(MSePh)_4]^{2-}$ (M = Zn and Cd)

JAGADESE J. VITTAL, PHILIP A. W. DEAN, AND NICHOLAS C. PAYNE[1]

Department of Chemistry, University of Western Ontario, London, Ont., Canada N6A 5B7

Received July 4, 1991

This paper is dedicated to the memory of Professor Thomas Birchall

JAGADESE J. VITTAL, PHILIP A. W. DEAN, and NICHOLAS C. PAYNE. Can. J. Chem. **70**, 792 (1992).

The structures of three tetramethylammonium salts containing anions of formula $[(\mu\text{-SePh})_6(MSePh)_4]^{2-}$ (M = Zn and Cd) were determined by single crystal X-ray diffraction techniques. The Zn salt crystallizes in different space groups depending upon the solvent combination used in the synthesis. Thus crystals of $(Me_4N)_2[Zn_4(SePh)_{10}]$, **1**, grown from a mixture of methanol, acetonitrile, and acetone are triclinic, space group $P\bar{1}$, with cell dimensions a = 13.214(2), b = 23.859(2), c = 13.072(1) Å, α = 91.134(8), β = 113.350(8), γ = 79.865(9)°, and Z = 2. In the absence of acetone, a solvated crystal $(Me_4N)_2[Zn_4(SePh)_{10}] \cdot CH_3CN$, **2**, is formed, which belongs to the monoclinic space group $P2_1/n$ with a = 14.248(1), b = 39.722(2), c = 13.408(1) Å, β = 97.132(5)°, and Z = 4. The Cd salt $(Me_4N)_2[Cd_4(SePh)_{10}]$, **3**, crystallizes in the monoclinic space group $P2_1/c$, with a = 20.830(2), b = 14.282(1), c = 25.872(1) Å, β = 99.626(6)°, and Z = 4. These three salts are the first examples of homoleptic, tetranuclear selenolatometal(II) anions with $(\mu\text{-Se})_6M_4$ cages of adamantane-type stereochemistry. In each case the phenyl substituents of the bridging ligands adopt the configuration [aae, aae, aee, aee], which has the minimum number of two 1,3-axial–axial non-bonding substituent interactions.

Key words: selenolate complexes, synthesis, X-ray crystallography, isomerism, adamantane stereochemistry.

JAGADESE J. VITTAL, PHILIP A. W. DEAN et NICHOLAS C. PAYNE. Can. J. Chem. **70**, 792 (1992).

Utilisant la diffraction des rayons X par un cristal unique, on a déterminé les structures de trois sels tétraméthylammonium contenant des anions $[(\mu\text{-SePh})_6(MSePh)_4]^{2-}$ (M = Zn et Cd). Le sel de zinc cristallise dans divers groupes d'espace suivant la nature de la combinaison de solvants utilisés au cours de la synthèse. Ainsi, les cristaux de $(Me_4N)_2[Zn_4(SePh)_{10}]$, **1**, obtenus par cristallisation dans un mélange de méthanol, acétonitrile et acétone sont tricliniques, groupe d'espace $P\bar{1}$, avec a = 13,214(2), b = 23,859(2) et c = 13,072(1) Å, α = 91,134(8), β = 113,350(8) et γ = 79,865(9)° et Z = 2. En l'absence d'acétone, il se forme un cristal solvaté de $(Me_4)_2[Zn_4(SePh)_{10}] \cdot CH_3CN$, **2**, qui est monoclinique, groupe d'espace $P2_1/n$, avec a = 14,248(1), b = 39,722(2) et c = 13,408(1) Å, β = 97,132(5)° et Z = 4. Le sel de Cd, $(Me_4N)_4[Cd_4(SePh)_{10}]$, **3**, cristallise dans le groupe d'espace monoclinique, groupe d'espace $P2_1/c$, avec a = 20,830(2), b = 14,282(1) et c = 25,872(1) Å, β = 99,626(6) et Z = 4. Ces trois sels représentent les premiers exemples d'anions sélénométalliques(II) tétranucléaires et homoleptiques comportant des cages $(\mu\text{-Se})_6M_4$ avec une stéréochimie de type adamantane. Dans chacun des cas, les substituants phényles des ligands créant un pont adoptent la configuration [aae, aae, aee, aee] qui comporte le nombre minimal de deux interactions 1,3-axiales–axiales non-liantes entre de substituants.

Mots clés : complexes de sélénolate, synthèse, diffraction des rayons X, isomérie, stéréochimie de l'adamantane.

[Traduit par la rédaction]

Introduction

In the chemistry of metal-thiolates, a frequently encountered structural unit is the adamantane-type tetranuclear cluster with a $(\mu\text{-SR})_6M_4$ core (1, 2). To date more than 20 such compounds have been characterized by X-ray structure analyses (3–20). By contrast, the structural chemistry of analogous metal-selenolates is essentially undeveloped. The only well-characterized compound, to our knowledge, is the Cd complex $(Me_4N)_2[(\mu\text{-SePh})_6(CdBr)_4]$ (3). We previously reported (3, 21–27) some chemistry of $[(\mu\text{-SePh})_6(MSePh)_4]^{2-}$ (M = Zn and Cd). To obtain structural data on the selenolate anions $[(\mu\text{-SePh})_6(MSePh)_4]^{2-}$ (M = Zn and Cd), and to examine their relationships with other adamantane-type cages, we determined the crystal structures of $(Me_4N)_2[(\mu\text{-SePh})_6(CdSePh)_4]$ and $(Me_4N)_2[(\mu\text{-SePh})_6(ZnSePh)_4]$ (unsolvated and as an acetonitrile solvate). We present herein our results, which represent the first reported examples of the homoleptic tetranuclear M(II) selenolates of formula $M_4(SePh)_{10}]^{2-}$.

[1]Author to whom correspondence may be addressed.

Experimental

Materials and general manipulative procedures

Starting materials were from commercial sources and were used as received. All manipulations were carried out under an atmosphere of Ar(g). Before use, solvents were dried over 3 Å Molecular Sieves and sparged with Ar(g). The salt $(Me_4N)_2[Cd_4(SePh)_{10}]$, **3**, was synthesized as reported earlier (22).

Syntheses of $(Me_4N)_2[Zn_4(SePh)_{10}]$

A synthesis of **1** in analytically pure form was described earlier (3). It now appears that the formation of **1** by the procedure described must have been serendipitous. We report here that the presence of acetone is necessary to obtain the unsolvated zinc complex. A reproducible synthesis of this material and of the analogous acetonitrile solvate is now given.

$(Me_4N)_2[Zn_4(SePh)_{10}]$, **1**

A solution of sodium benzeneselenolate was prepared by adding benzeneselenol (2.90 g, 18.48 mmol) to a solution of sodium (0.426 g, 18.5 mmol) in methanol (10 mL). Into the solution of NaSePh was stirred $Zn(NO_3)_2 \cdot 6H_2O$ (1.839 g, 6.18 mmol), then, after a wait of 10 min, a solution of $Me_4NC\ell$ (0.365 g, 3.33 mmol) in MeOH (10 mL), which produced a white precipitate. After addition of acetone (20 mL) and acetonitrile (10 mL), the mixture was warmed to 333 K to give a clear, pale yellow so-

Can. J. Chem. Downloaded from www.nrcresearchpress.com by 92.62.229.171 on 09/08/12
For personal use only.

TABLE 1. Summary of X-ray structure determinations

Parameter	1	2	3
Crystal data			
Compound	$C_{68}H_{74}N_2Se_{10}Zn_4$	$C_{68}H_{74}N_2Se_{10}Zn_4 \cdot CH_3CN$	$C_{68}H_{74}N_2Se_{10}Cd_4$
Formula weight	1970.44	2011.49	2158.56
Crystal system, space group	Triclinic, $P\bar{1}$	Monoclinic, $P2_1/n$	Monoclinic, $P2_1/c$
Cell dimensions (Å) a =	13.214(2)	14.248(1)	20.830(2)
b =	23.859(2)	39.722(2)	14.282(1)
c =	13.072 (1)	13.408(1)	25.872(1)
α =	91.134(8)	90	90
β =	113.350(8)	97.132(5)	99.626(6)
γ =	79.865(9)	90	90
cell volume (Å^3), Z	3719(2), 2	7529(2), 4	7588(2), 4
Density, g cm^{-3}, obsd.	1.77(5)	1.78(4)	1.91(5)
calcd.	1.77	1.74	1.89
F(000) electrons	1912	3911	4111
Experimental details			
Radiation, wavelength (Å)	Mo(K$\bar{\alpha}$), 0.71073	Cu(K$\bar{\alpha}$), 1.5418	Cu(K$\bar{\alpha}$), 1.5418
Filter/monochromator	Graphite	Nickel	Nickel
Scan width (°)	0.70 + 0.35 tan θ	0.75 + 0.14 tan θ	0.75 + 0.14 tan θ
No. of data, stds collected	3734, 83; 6349, 152	5055, 112; 5349, 124	8544, 224
Absorption coeff. (cm^{-1})	62.27	74.90	150.7
No. of unique data	3588, 6086	4550, 5152	7792
No. of data averaged	182, 252	716, 214	1064
No. of unique data ($I > 0$)	9088	9580	7792
Refinement details			
No. of observations ($I \geq 3\sigma(I)$)	4709	6462	4440
No. of variables	275	290	272
Extinction coeff.	—	$3.7(5) \times 10^{-4}$	$2.5(3) \times 10^{-4}$
Final model; R_1 and R_2	0.0628, 0.0650	0.0483, 0.0551	0.050, 0.055
Residual Fourier peaks (e Å^{-3})	1.530 to −0.926	0.766 to −0.654	0.863 to −0.659
Max. shift/esd, parameter	−0.042, N2 rot x	0	0.018, C342 rot y

Can. J. Chem. Downloaded from www.nrcresearchpress.com by 92.62.229.171 on 09/08/12
For personal use only.

lution. The warm solution was filtered hot and the filtrate was set aside for 1 day at 278 K for crystallization to occur. The colourless transparent crystals were separated by decantation, washed with a 1:1 (v:v) MeOH:H_2O mixture, then with MeOH, and finally with Et_2O before being dried *in vacuo*. In this way 2.15 g of product were obtained. A second crop of 0.50 g resulted from concentration of the mother liquor, to give a total yield of 88%. The solubility and ^{13}C and ^{77}Se NMR spectra of this product were identical to those of the analytically pure material produced previously (3).

$(Me_4N)_2[Zn_4(SePh)_{10}] \cdot CH_3CN$, **2**

Omission of the acetone in the procedure described above for **1** gave a comparable yield of this acetonitrile solvate as light yellow plate-like crystals. The solvate is significantly less soluble in MeCN or $(CH_3)_2CO$ than is **1**, e.g., the solubility of **1** in acetonitrile at 295 K exceeds 0.05 mol L^{-1}, whereas that of **2** is about 0.025 mol L^{-1}. Proton NMR ($(CD_3)_2CO$, 294 K): 2.86 (s, CH_3CN), 3.76 ($(CH_3)_4N^+$), 6.6–7.8 (aromatic H's). ^{13}C NMR ($(CD_3)_2CO$, 294 K): 6.6 (CH_3CN), 56.0 ($(CH_3)_4N^+$), 112.2 (CH_3CN), 125.5 (C_4), 128.5 ($C_{3,5}$), 130.2 (C_1, bridging), 131.9 (C_1, terminal), 135.6 ($C_{2,6}$). (Except for the resonances due to MeCN, the ^{13}C NMR spectrum is virtually identical to that reported (3) for **1**.) Anal. calcd. for $C_{70}H_{77}N_3Se_{10}Zn_4$: C 41.79, H 3.86, N 2.09; found: C 42.09 and 42.12, H 4.06 and 3.95, N 1.88 and 1.64.

NMR spectroscopy

NMR spectra were obtained as reported previously (3, 25). The reference for ^{77}Se NMR was external pure Me_2Se at 295 K.

X-ray crystallography

Compounds **1**, **2**, and **3** were examined by experimental procedures standard in our laboratory (3). An overview is given below, and crystal data are summarized in Table 1.

Crystals suitable for X-ray diffraction studies were obtained directly from the reaction mixtures. They were colorless, transparent, and fairly stable in air, though on prolonged exposure to air and (or) X-radiation the crystals tended to decompose, changing color to light yellow and becoming opaque. Precession and Weissenberg photographs were taken to establish the space groups and to get preliminary cell dimensions. Crystal densities were determined by the neutral buoyancy method in mixtures of carbon tetrachloride and 1,2-dibromoethane. The data collections were carried out on an Enraf–Nonius CAD4F diffractometer (28) at 296 K. Intensity data were recorded in ω–2θ scan mode at variable scan speeds, so chosen as to optimize counting statistics within a maximum time per datum of 60 s. Background estimates were made by extending the scan by 25% on each side. Standard reflections were monitored every 180 min of X-ray exposure time. For the Zn salts **1** and **2** crystal decay was significant, necessitating data collection from two crystals in each case. Lorentz, polarization, and decay (where applicable) corrections were applied using the Structure Determination Package running on a PDP11/23+ computer (29). A Gaussian absorption correction (30) was made to the data for compounds **1** and **2**, whereas for **3** an analytical correction was applied (31). The data were then merged using scale factors calculated from reflections in the region common to both data

Can. J. Chem. Downloaded from www.nrcresearchpress.com by 92.62.229.171 on 09/08/12
For personal use only.

TABLE 2. Atomic positional ($\times 10^4$) and thermal parameters ($\times 10^3$) for **1**

Atom	x	y	z	U or U_{eq}(Å^2)[a]
Zn(1)	4477.1(18)	2402.7(9)	3365.3(18)	40.6(8)
Zn(2)	2737.6(18)	2244.2(9)	5316.3(19)	43.3(9)
Zn(3)	1169.3(19)	3262.5(9)	2409.0(19)	43.9(9)
Zn(4)	1894.4(18)	1498.0(9)	2245.0(19)	44.2(9)
Se(1)	6261.6(18)	2394.1(11)	3277.8(20)	62.0(10)
Se(2)	2722.2(23)	2005.0(12)	7090.4(20)	72.8(11)
Se(3)	136.4(21)	4166.5(10)	1460.6(22)	70.2(11)
Se(4)	1243.4(21)	668.0(9)	1354.4(20)	63.5(10)
Se(12)	4486.4(16)	2408.8(9)	5255.2(17)	45.9(8)
Se(13)	2958.1(16)	3183.4(8)	2176.9(17)	43.9(8)
Se(14)	3643.3(17)	1670.7(8)	2107.1(18)	45.6(8)
Se(23)	1273.4(17)	3104.7(8)	4333.9(17)	44.1(8)
Se(24)	2285.2(17)	1380.6(8)	4260.7(17)	45.3(8)
Se(34)	419.7(16)	2389.8(8)	1668.3(17)	45.2(8)
C(11)	6892(11)	2975(6)	4202(11)	45(5)
C(12)	7920(11)	3070(6)	4249(11)	64(6)
C(13)	8406(11)	3501(6)	4885(11)	85(8)
C(14)	7865(11)	3837(6)	5474(11)	71(7)
C(15)	6837(11)	3743(6)	5427(11)	74(7)
C(16)	6351(11)	3312(6)	4791(11)	57(6)
C(21)	3760(11)	2361(6)	8239(12)	52(5)
C(22)	3714(11)	2329(6)	9285(12)	66(6)
C(23)	4429(11)	2587(6)	10177(12)	75(7)
C(24)	5189(11)	2877(6)	10022(12)	95(9)
C(25)	5235(11)	2909(6)	8976(12)	78(7)
C(26)	4520(11)	2651(6)	8084(12)	73(7)
C(31)	−1387(12)	4162(6)	1124(11)	64(6)
C(32)	−1710(12)	3918(6)	1882(11)	64(6)
C(33)	−2843(12)	3940(6)	1640(11)	94(9)
C(34)	−3651(12)	4207(6)	641(11)	97(9)
C(35)	−3327(12)	4451(6)	−117(11)	106(10)
C(36)	−2195(12)	4428(6)	125(11)	79(7)
C(41)	1306(9)	691(6)	−93(12)	42(5)
C(42)	388(9)	579(6)	−1011(12)	62(6)
C(43)	389(9)	600(6)	−2077(12)	78(7)
C(44)	1310(9)	733(6)	−2226(12)	78(7)
C(45)	2228(9)	844(6)	−1308(12)	86(8)
C(46)	2227(9)	823(6)	−242(12)	77(7)
C(121)	5603(9)	1754(6)	6006(13)	44(5)
C(122)	5365(9)	1270(6)	6378(13)	74(7)
C(123)	6217(9)	799(6)	6865(13)	76(7)
C(124)	7306(9)	812(6)	6980(13)	83(8)
C(125)	7544(9)	1297(6)	6608(13)	101(9)
C(126)	6693(9)	1768(6)	6121(13)	70(7)
C(131)	3517(11)	3871(5)	2644(11)	44(5)
C(132)	4336(11)	3995(5)	2309(11)	54(5)
C(133)	4784(11)	4487(5)	2654(11)	71(7)
C(134)	4411(11)	4854(5)	3332(11)	84(8)
C(135)	3591(11)	4729(5)	3666(11)	105(10)
C(136)	3144(11)	4237(5)	3322(11)	76(7)
C(141)	4702(13)	977(7)	2671(12)	49(5)
C(142)	5069(13)	736(7)	3749(12)	86(8)
C(143)	5870(13)	234(7)	4082(12)	95(9)
C(144)	6304(13)	−26(7)	3337(12)	104(9)
C(145)	5938(13)	215(7)	2259(12)	153(15)
C(146)	5136(13)	717(7)	1926(12)	104(9)
C(231)	1806(10)	3768(5)	5049(12)	46(5)
C(232)	2871(10)	3720(5)	5896(12)	66(6)
C(233)	3242(10)	4207(5)	6403(12)	79(7)
C(234)	2548(10)	4741(5)	6062(12)	73(7)
C(235)	1484(10)	4789(5)	5215(12)	82(8)
C(236)	1113(10)	4302(5)	4708(12)	59(6)
C(241)	928(11)	1243(5)	4322(12)	42(5)
C(242)	258(11)	1654(5)	4677(12)	66(6)
C(243)	−718(11)	1536(5)	4726(12)	72(7)
C(244)	−1025(11)	1008(5)	4420(12)	78(7)
C(245)	−356(11)	598(5)	4065(12)	97(9)
C(246)	621(11)	715(5)	4016(12)	79(7)
C(341)	−131(11)	2493(5)	74(11)	47(5)
C(342)	−1150(11)	2862(5)	−476(11)	60(6)
C(343)	−1615(11)	2927(5)	−1637(11)	81(7)
C(344)	−1060(11)	2622(5)	−2249(11)	79(7)
C(345)	−41(11)	2253(5)	−1699(11)	95(9)
C(346)	423(11)	2188(5)	−538(11)	62(6)
N(1)	2558(12)	8717(6)	9649(13)	61(5)
C(1)	3787(12)	8687(6)	10224(13)	118(13)
C(2)	1976(12)	9323(6)	9513(13)	129(14)
C(3)	2170(12)	8382(6)	10326(13)	147(15)
C(4)	2299(12)	8476(6)	8534(13)	137(15)
N(1′)	2340(79)	8801(40)	9014(83)	59(25)
C(1′)	1690(79)	9049(40)	9676(83)	59(25)
C(2′)	2166(79)	9220(40)	8106(83)	59(25)
C(3′)	1953(79)	8271(40)	8521(83)	59(25)
C(4′)	3550(79)	8661(40)	9753(83)	59(25)
N(2)	1244(14)	3897(7)	8393(15)	84(6)
C(5)	497(14)	3887(7)	8996(15)	173(15)
C(6)	2401(14)	3907(7)	9211(15)	173(15)
C(7)	1248(14)	3379(7)	7740(15)	173(15)
C(8)	830(14)	4416(7)	7624(15)	173(15)
C(5′)	1399(14)	3561(7)	9408(15)	159(20)
C(6′)	156(14)	4304(7)	8009(15)	159(20)
C(7′)	1251(14)	3503(7)	7496(15)	159(20)
C(8′)	2170(14)	4220(7)	8656(15)	159(20)

[a] Anisotropic thermal parameters are given in the form of isotropic equivalent parameter defined as $U_{eq} = 1/3\ \Sigma_i\Sigma_j U_{ij} \cdot a_i^* \cdot a_j^* \cdot a_i \cdot a_j$.

sets, and averaged to produce three sets of unique data for structure solution and refinement.

All three structures were solved by a combination of MULTAN (32) and difference Fourier syntheses, and refined by full-matrix least-squares techniques on F using the SHELX76 software (33) running on a SUN 3/50 work-station. Scattering factors for Zn and Cd atoms were taken from the International Tables (34). In the refinements, all metal and selenium atoms were assigned anisotropic thermal parameters. The phenyl ring carbon atoms were constrained to regular hexagonal geometry with C—C = 1.392 Å and were allotted isotropic thermal parameters. All phenyl hydrogen atoms were located successfully by difference Fourier methods, placed in calculated positions (C—H = 0.95 Å), and included in the structure factor calculations.

Disorder of the tetramethylammonium cations was present in every structure; it was modelled by refining rigid groups of T_d symmetry, N—C = 1.485 Å, of varying multiplicities deduced from difference Fourier syntheses. The cation hydrogen atoms could not be located reliably owing to the disorder, and all were omitted from structure factor calculations. In compound **1**, both cations have disordered carbon atoms; two groups were included in the model for each ion, with major components of multiplicities 0.90 and 0.60. Individual isotropic thermal parameters were refined for the atoms of the major components, whereas overall group thermal parameters were applied to the minor components. For compound **2**, the carbon atoms of only one cation were disordered; overall group thermal parameters were refined for the two rigid groups of multiplicities 0.60 and 0.40. And in crystals of compound **3**, both cations have disordered carbon atoms; two groups were included in

TABLE 3. Atomic positional (× 10^4) and thermal parameters (× 10^3) for **2**

Atom	x	y	z	U or U_{eq} (Å^2)[a]
Zn(1)	3046.7(10)	3689.1(3)	3667.4(10)	43.4(4)
Zn(2)	5005.3(10)	3799.7(4)	6163.7(9)	42.0(4)
Zn(3)	2228.7(10)	4031.3(3)	6326.3(10)	45.0(4)
Zn(4)	3013.3(10)	3037.0(3)	6105.3(10)	41.6(4)
Se(1)	2659.3(12)	3664.7(4)	1873.9(9)	72.1(5)
Se(2)	6644.2(9)	3941.7(4)	6585.6(10)	67.6(5)
Se(3)	1200.8(11)	4473.1(3)	6743.2(10)	66.4(4)
Se(4)	2513.5(10)	2517.9(3)	6788.0(11)	61.1(4)
Se(12)	4571.1(8)	3944.2(3)	4359.6(7)	39.7(3)
Se(13)	1826.4(8)	3984.3(3)	4485.6(9)	49.8(3)
Se(14)	2654.5(8)	3113.7(3)	4238.3(8)	43.9(3)
Se(23)	3894.5(8)	4097.1(3)	7107.1(8)	44.2(3)
Se(24)	4718.7(8)	3183.0(3)	6388.6(8)	43.9(3)
Se(34)	2065.4(8)	3451.6(3)	6969.4(8)	40.8(3)
C(11)	3249(5)	4038(2)	1308(5)	45(3)
C(12)	3300(5)	4354(2)	1765(5)	56(3)
C(13)	3734(5)	4620(2)	1327(5)	73(4)
C(14)	4117(5)	4571(2)	432(5)	87(4)
C(15)	4067(5)	4256(2)	−25(5)	76(4)
C(16)	3632(5)	3990(2)	413(5)	67(3)
C(21)	6715(6)	4018(2)	8012(6)	54(3)
C(22)	6480(6)	4333(2)	8360(6)	71(4)
C(23)	6589(6)	4400(2)	9388(6)	89(4)
C(24)	6934(6)	4151(2)	10067(6)	92(5)
C(25)	7170(6)	3836(2)	9719(6)	85(4)
C(26)	7060(6)	3769(2)	8692(6)	73(4)
C(31)	756(4)	4313(2)	7955(6)	47(3)
C(32)	1361(4)	4171(2)	8739(6)	61(3)
C(33)	1006(4)	4062(2)	9604(6)	74(4)
C(34)	46(4)	4094(2)	9687(6)	83(4)
C(35)	−560(4)	4235(2)	8903(6)	77(4)
C(36)	−205(4)	4345(2)	8037(6)	62(3)
C(41)	3525(7)	2195(2)	6762(6)	53(3)
C(42)	4211(7)	2162(2)	7591(6)	95(5)
C(43)	4883(7)	1907(2)	7617(6)	110(6)
C(44)	4867(7)	1684(2)	6815(6)	103(5)
C(45)	4181(7)	1716(2)	5986(6)	105(5)
C(46)	3510(7)	1972(2)	5960(6)	75(4)
C(121)	5499(5)	3728(2)	3634(4)	34(2)
C(122)	6220(5)	3528(2)	4118(4)	54(3)
C(123)	6886(5)	3384(2)	3571(4)	64(3)
C(124)	6831(5)	3440(2)	2541(4)	73(4)
C(125)	6110(5)	3639(2)	2057(4)	66(3)
C(126)	5444(5)	3783(2)	2603(4)	53(3)
C(131)	1964(5)	4436(2)	4004(5)	49(3)
C(132)	2632(5)	4657(2)	4481(5)	63(3)
C(133)	2722(5)	4979(2)	4096(5)	83(4)
C(134)	2144(5)	5080(2)	3234(5)	87(4)
C(135)	1475(5)	4859(2)	2758(5)	84(4)
C(136)	1385(5)	4537(2)	3142(5)	65(3)
C(141)	3548(5)	2826(2)	3684(6)	45(3)
C(142)	4247(5)	2952(2)	3147(6)	59(3)
C(143)	4824(5)	2732(2)	2691(6)	66(3)
C(144)	4702(5)	2386(2)	2771(6)	77(4)
C(145)	4004(5)	2260(2)	3308(6)	106(6)
C(146)	3427(5)	2480(2)	3764(6)	85(4)
C(231)	4111(5)	4574(2)	7044(5)	43(2)
C(232)	3683(5)	4780(2)	7697(5)	58(3)
C(233)	3819(5)	5127(2)	7683(5)	81(4)
C(234)	4382(5)	5268(2)	7015(5)	75(4)
C(235)	4810(5)	5062(2)	6362(5)	60(3)
C(236)	4674(5)	4715(2)	6377(2)	60(3)
C(241)	5062(6)	3107(2)	7812(6)	43(2)
C(242)	4724(6)	3309(2)	8537(6)	74(4)
C(243)	4987(6)	3243(2)	9553(6)	90(5)
C(244)	5587(6)	2975(2)	9844(6)	71(4)
C(245)	5925(6)	2772(2)	9120(6)	98(5)
C(246)	5662(6)	2838(2)	8104(6)	86(4)
C(341)	751(5)	3368(2)	6540(5)	43(2)
C(342)	437(5)	3180(2)	5686(5)	71(4)
C(343)	−529(5)	3135(2)	5402(5)	81(4)
C(344)	−1179(5)	3278(2)	5971(5)	74(4)
C(345)	−865(5)	3465(2)	6825(5)	66(3)
C(346)	100(5)	3510(2)	7109(5)	53(3)
N(1)	1296(8)	5719(3)	5829(9)	75(3)
C(1)	874(13)	5967(5)	6479(14)	117(6)
C(2)	1292(15)	5866(5)	4808(15)	136(8)
C(3)	750(13)	5392(5)	5744(14)	113(6)
C(4)	2282(15)	5652(5)	6258(16)	141(8)
N(2)	2938(6)	7745(2)	4822(6)	76(3)
C(5)	3221(6)	7403(2)	5191(6)	129(4)
C(6)	3593(6)	7997(2)	5343(6)	129(4)
C(7)	2980(6)	7763(2)	3722(6)	129(4)
C(8)	1958(6)	7816(2)	5031(6)	129(4)
C(5′)	1891(6)	7713(2)	4685(6)	129(4)
C(6′)	3210(6)	8073(2)	5304(6)	129(4)
C(7′)	3292(6)	7727(2)	3828(6)	129(4)
C(8′)	3357(6)	7467(2)	5471(6)	129(4)
C(9)	3530(15)	−31(6)	5133(16)	144(8)
N(3)	3953(16)	391(6)	6561(18)	180(9)
C(10)	3727(15)	185(6)	5986(17)	116(6)

[a] Anisotropic thermal parameters are given in the form of the isotropic equivalent parameter defined as $U_{eq} = 1/3\ \Sigma_i\Sigma_j U_{ij} \cdot a_i^* \cdot a_j^* \cdot a_i \cdot a_j$.

the model for each, with major component multiplicities of 0.70 and 0.60.

The final cycles of refinement were based on those unique data with $I > 3\sigma(I)$. Selected experimental details of the analyses are given in Table 1, while the remaining data are listed in Table S1. Secondary extinction corrections were applied to the data for **2** and **3**. The analyses of variance suggested that the weighting schemes were appropriate. Final positional parameters for **1** are given in Table 2, for **2** in Table 3, and for **3** in Table 4. Hydrogen atom parameters, anisotropic thermal parameters, and root-mean-square amplitudes of vibration have been deposited as Tables S2, S3, and S4.[2]

Results and discussion

The synthesis of the Cd salt $(Me_4N)_2[Cd_4(SePh)_{10}]$, **3**, was described previously (22). The preparations of the Zn salts **1** and **2** involve the use of $Zn(NO_3)_2 \cdot 6H_2O$, $NaSeC_6H_5$, and

[2] Copies of supplementary experimental details, hydrogen atom parameters, anisotropic thermal parameters, root-mean-square amplitudes of vibration, supplementary dimensions, selected least-squares planes, selected torsion angles, and structure amplitudes for **1**, **2**, and **3** may be purchased from: The Depository of Unpublished Data, Document Delivery, CISTI, National Research Council Canada, Ottawa, Canada K1A 0S2.

The tables of supplementary experimental details, hydrogen atom parameters, and supplementary dimensions have also been deposited with the Cambridge Crystallographic Data Centre and can be obtained on request from The Director, Cambridge Crystallographic Data Centre, University Chemical Laboratory, Lensfield Road, Cambridge CB2 1EW, U.K.

Can. J. Chem. Downloaded from www.nrcresearchpress.com by 92.62.229.171 on 09/08/12
For personal use only.

TABLE 4. Atomic positional ($\times 10^4$) and thermal parameters ($\times 10^3$) for **3**

Atom	x	y	z	U or U_{eq}(Å^2)[a]
Cd(1)	1311.9(6)	6817.5(10)	3475.8(5)	68.4(5)
Cd(2)	3158.9(6)	7764.6(9)	4357.6(5)	60.4(4)
Cd(3)	3085.3(6)	5200.0(9)	3354.3(5)	69.3(5)
Cd(4)	2251.6(6)	5172.4(10)	4832.8(5)	71.8(5)
Se(1)	292.5(10)	7294.3(18)	2800.1(8)	93.4(9)
Se(2)	3895.9(10)	9111.9(15)	4777.4(8)	80.6(8)
Se(3)	3714.6(12)	4139.2(17)	2809.3(8)	100.4(9)
Se(4)	1882.4(13)	4092.1(22)	5531.8(10)	125.9(12)
Se(12)	2082.1(9)	8300.2(14)	3734.5(7)	66.4(7)
Se(13)	1914.5(10)	5705.0(14)	2881.5(8)	74.1(7)
Se(14)	1124.3(10)	5695.4(18)	4245.6(9)	94.8(9)
Se(23)	3827.4(9)	6525.1(14)	3889.4(7)	67.6(7)
Se(24)	2847.5(9)	6765.5(14)	5146.4(7)	68.2(7)
Se(34)	2890.7(9)	4194.3(14)	4194.8(7)	71.8(7)
C(11)	−281(7)	7900(9)	3208(6)	78(6)
C(12)	−334(7)	7563(9)	3704(6)	114(8)
C(13)	−767(7)	7978(9)	3990(6)	134(9)
C(14)	−1148(7)	8731(9)	3780(6)	132(9)
C(15)	−1096(7)	9069(9)	3284(6)	163(11)
C(16)	−662(7)	8653(9)	2998(6)	124(8)
C(21)	3803(6)	10024(10)	4233(5)	77(6)
C(22)	3196(6)	10389(10)	4021(5)	103(7)
C(23)	3151(6)	11121(10)	3662(5)	132(9)
C(24)	3713(6)	11489(10)	3515(5)	127(8)
C(25)	4320(6)	11124(10)	3728(5)	161(11)
C(26)	4364(6)	10392(10)	4087(5)	119(8)
C(31)	3527(6)	4698(9)	2130(6)	65(5)
C(32)	2902(6)	4618(9)	1842(6)	115(8)
C(33)	2760(6)	4999(9)	1341(6)	137(9)
C(34)	3243(6)	5461(9)	1127(6)	127(8)
C(35)	3868(6)	5541(9)	1415(6)	116(8)
C(36)	4010(6)	5159(9)	1916(6)	105(7)
C(41)	2554(7)	4074(8)	6130(5)	81(6)
C(42)	3004(7)	4795(8)	6248(5)	95(6)
C(43)	3480(7)	4739(8)	6694(5)	124(8)
C(44)	3506(7)	3961(8)	7021(5)	146(10)
C(45)	3056(7)	3240(8)	6903(5)	158(11)
C(46)	2580(7)	3297(8)	6457(5)	142(9)
C(121)	1616(6)	9012(9)	4170(4)	72(5)
C(122)	970(6)	9242(9)	3981(4)	86(6)
C(123)	620(6)	9786(9)	4283(4)	119(8)
C(124)	916(6)	10100(9)	4775(4)	158(10)
C(125)	1561(6)	9869(9)	4965(4)	132(9)
C(126)	1911(6)	9325(9)	4663(4)	105(7)
C(131)	2088(6)	6527(10)	2353(6)	69(5)
C(132)	1634(6)	6607(10)	1895(6)	149(10)
C(133)	1771(6)	7161(10)	1484(6)	154(10)
C(134)	2362(6)	7634(10)	1531(6)	131(9)
C(135)	2816(6)	7554(10)	1989(6)	149(10)
C(136)	2679(6)	7000(10)	2400(6)	104(7)
C(141)	725(8)	6446(10)	4703(7)	110(7)
C(142)	156(8)	6130(10)	4861(7)	153(10)
C(143)	−120(8)	6637(10)	5227(7)	155(10)
C(144)	173(8)	7461(10)	5436(7)	152(10)
C(145)	743(8)	7776(10)	5279(7)	161(11)
C(146)	1019(8)	7269(10)	4912(7)	152(10)
C(231)	4148(5)	7230(9)	3359(5)	71(5)
C(232)	4008(5)	8181(9)	3302(5)	84(6)
C(233)	4277(5)	8710(9)	2940(5)	118(8)
C(234)	4685(5)	8289(9)	2635(5)	122(8)
C(235)	4826(5)	7338(9)	2691(5)	122(8)
C(236)	4557(5)	6808(9)	3053(5)	108(7)
C(241)	3718(6)	6445(7)	5474(5)	57(5)

Can. J. Chem. Downloaded from www.nrcresearchpress.com by 92.62.229.171 on 09/08/12
For personal use only.

TABLE 4 (*concluded*)

Atom	*x*	*y*	*z*	*U* or U_{eq}(Å^2)[a]
C(242)	4007(6)	6958(7)	5909(5)	98(7)
C(243)	4628(6)	6724(7)	6165(5)	110(7)
C(244)	4961(6)	5978(7)	5987(5)	113(7)
C(245)	4672(6)	5464(7)	5552(5)	118(8)
C(246)	4051(6)	5698(7)	5296(5)	88(6)
C(341)	2236(7)	3341(11)	3934(5)	89(6)
C(342)	1956(7)	2796(11)	4283(5)	130(8)
C(343)	1460(7)	2169(11)	4095(5)	183(12)
C(344)	1244(7)	2087(11)	3558(5)	156(10)
C(345)	1524(7)	2633(11)	3209(5)	232(16)
C(346)	2020(7)	3260(11)	3397(5)	171(11)
N(1)	4040(5)	12759(8)	463(5)	95(5)
C(1)	4439(5)	13465(8)	794(5)	141(7)
C(2)	4024(5)	11876(8)	765(5)	141(7)
C(3)	3367(5)	13119(8)	307(5)	141(7)
C(4)	4330(5)	12573(8)	−14(5)	141(7)
C(1′)	3412(5)	12870(8)	100(5)	157(20)
C(2′)	4005(5)	13251(8)	963(5)	157(20)
C(3′)	4168(5)	11748(8)	569(5)	157(20)
C(4′)	4574(5)	13165(8)	220(5)	157(20)
N(2)	1327(12)	10040(18)	2215(9)	189(10)
C(5)	913(12)	9701(18)	1727(9)	189(10)
C(6)	1930(12)	9471(18)	2323(9)	189(10)
C(7)	1498(12)	11037(18)	2151(9)	189(10)
C(8)	963(12)	9950(18)	2660(9)	189(10)
N(2′)	890(18)	9716(28)	1939(14)	189(15)
C(5′)	1499(18)	9160(28)	2054(14)	189(15)
C(6′)	1026(18)	10622(28)	1697(14)	189(15)
C(7′)	397(18)	9188(28)	1571(14)	189(15)
C(8′)	637(18)	9895(28)	2434(14)	189(15)

[a]Anisotropic thermal parameters are given in the form of the isotropic equivalent parameter defined as $U_{eq} = 1/3\ \Sigma_i\Sigma_j U_{ij} \cdot a_i^* \cdot a_j^* \cdot a_i \cdot a_j$.

Can. J. Chem. Downloaded from www.nrcresearchpress.com by 92.62.229.171 on 09/08/12
For personal use only.

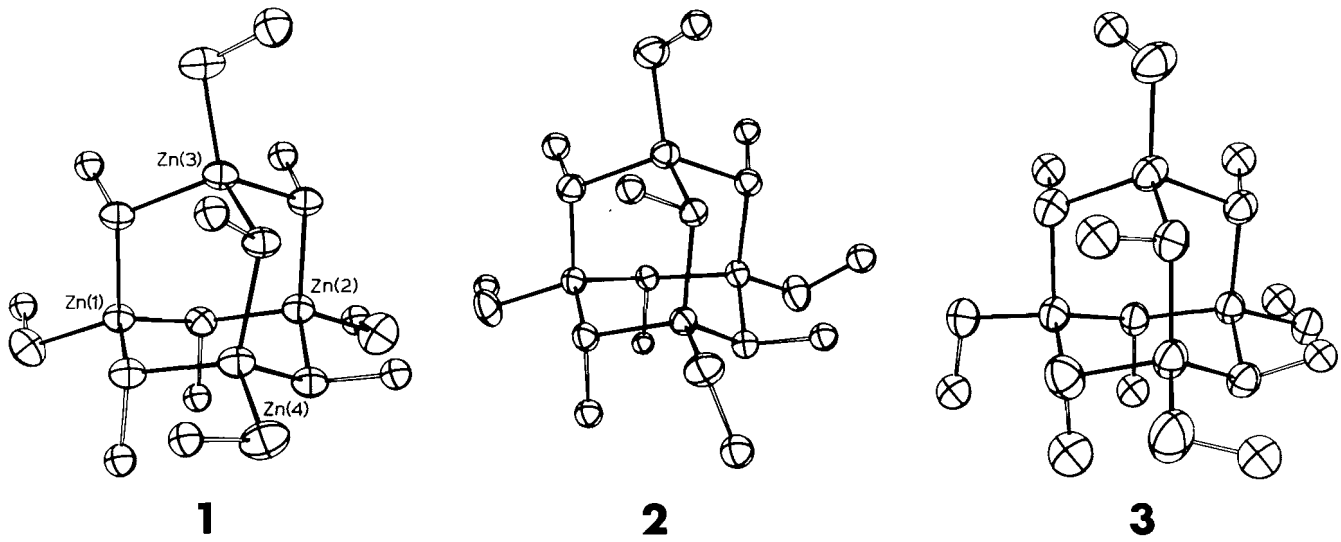

FIG. 1. The adamantane-like skeleton of the anions in compounds **1**, **2**, and **3**. Thermal ellipsoids are drawn at the 50% probability level.

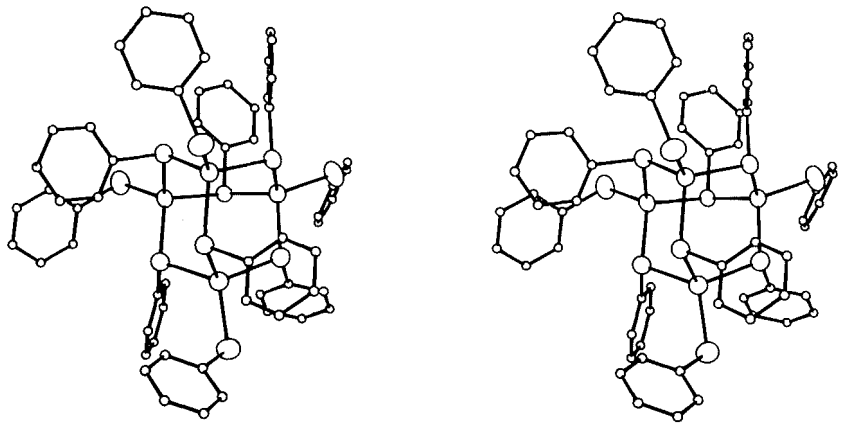

FIG. 2. A stereoview of the anion in **2**.

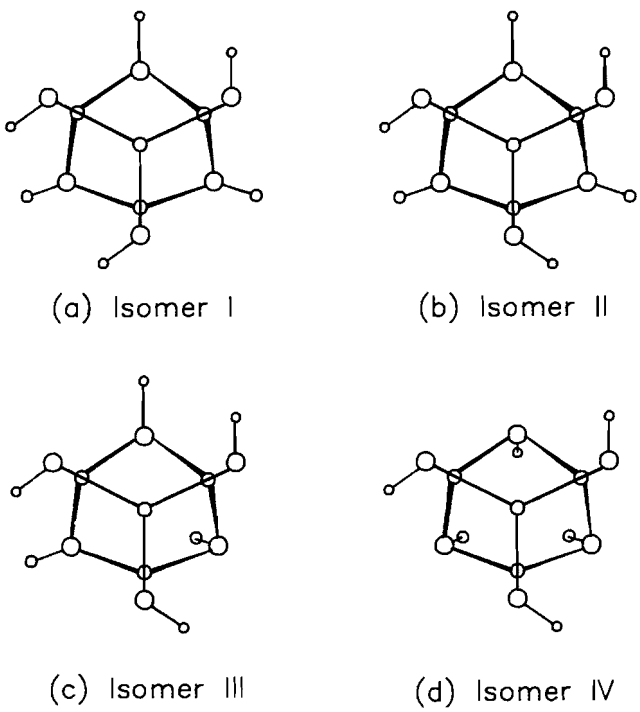

FIG. 3. The four possible configurational isomers for a $[(\mu\text{-SePh})_6(\text{MSePh})_4]^{2-}$ anion.

$(CH_3)_4NC\ell$ in the ratios 2:3–3.5:1 under anaerobic conditions. When the reaction mixture contains only acetonitrile, methanol, and water, the solvated crystals **2** are formed. If acetone is added to the above mixture, the product crystallized from solution is **1**. The syntheses of **1** and **2** are quite reproducible. It is noteworthy that the two products differ significantly in solubility in acetone and acetonitrile, **2** being less soluble than **1**. Also interesting is the finding that **2** gives sharper ^{77}Se NMR signals than **1**. At 295 K a solution having 0.025 mol of **2** per litre of MeCN has the expected two ^{77}Se resonances, at $\delta_{Se} = 37.2$ for terminal ligands ($PhSe_t$) and -10.3 for bridging ligands ($PhSe_{br}$), with line widths of ca. 33 and 24 Hz, respectively. For 0.05 mol of **1** per litre of MeCN, the corresponding values are $\delta_{Se} = 38.0$ ($PhSe_t$), and -8.8 ($PhSe_{br}$), with line widths of 75 and 55 Hz, respectively (23). The most likely explanation for the difference is a higher purity of the less soluble compound.

The crystal structures of the three compounds consist of well-separated cations and anions. The closest cation–anion and anion–anion distances of approach are given in Table S5. Cation and solvate molecule structures are unexceptional and will not be discussed further. The cage skeletons of the anions **1**, **2**, and **3** are depicted in Fig. 1, while a stereoview of the anion in **2** is shown in Fig. 2. The same numbering scheme was used consistently for all three anions, and the ligand atoms are numbered according to their connectivity; thus Se(1) and C(11) through C(16) form the terminal phenylselenolato ligand on Zn(1), Se(12) and C(121) through C(126) form the ligand bridging Zn(1) and Zn(2), and so forth.

The common structural features in these $[(\mu\text{-SePh})_6(\text{MSePh})_4]^{2-}$ anions are now briefly summarized. The metal atoms are located at the vertices of a tetrahedron, with selenolate ligands bridging the six edges. The Se atoms thus occupy the corners of a highly distorted octahedron, and each metal atom is bonded to one terminal and three bridging SePh groups. Each face of the tetrahedron is composed of a six-membered $M_3(\mu\text{-Se})_3$ ring in chair conformation, to give an adamantane-like overall stereochemistry. Unlike adamantane, isomerism occurs in these cluster anions due to the difference between the lone pair and phenyl substituents upon the selenium atoms. The phenyl groups are positioned either axially (a) or equatorially (e) in each ring (1). However, where two rings share a common edge formed by a bridging selenolate ligand, the adoption of an axial disposition with respect to one ring *ipso facto* defines this group as equatorially disposed with respect to the other; there are thus always six axial and six equatorial substituents.

In all, four geometric isomers of $M_4(\mu\text{-Se})_6$ are possible, I–IV, Fig. 3, which differ in the number of energetically disfavored 1,3-axial,axial phenyl group nonbonded interactions (3). For example, isomer I has a (3-2-1-0) axial pattern corresponding to aaa,aae,aee,eee substituent dispositions, and point symmetry C_1. Similarly isomer II has (2-2-2-0), with higher point symmetry C_3. Isomer III has (2-2-1-1), again point symmetry C_1, while (3-1-1-1), point symmetry C_3, may be assigned to Isomer IV. Isomers I and III are asymmetric, II and IV are dissymmetric, and all four can exist

Can. J. Chem. Downloaded from www.nrcresearchpress.com by 92.62.229.171 on 09/08/12
For personal use only.

TABLE 5. Selected distances (Å) and angles (deg)

M =	Zn in **1**	Zn in **2**	Cd in **3**
M—Se_t			
M(1)—Se(1)	2.398(3)	2.401(2)	2.605(2)
M(2)—Se(2)	2.401(3)	2.400(2)	2.585(2)
M(3)—Se(3)	2.397(3)	2.396(2)	2.573(2)
M(4)—Se(4)	2.393(3)	2.409(2)	2.590(3)
Mean	2.397(3)	2.401(5)	
M—Se_b			
M(1)—Se(12)	2.457(3)	2.471(2)	2.673(2)
M(2)—Se(12)	2.440(3)	2.488(2)	2.647(2)
M(1)—Se(13)	2.492(3)	2.465(2)	2.666(2)
M(3)—Se(13)	2.468(3)	2.470(2)	2.639(2)
M(1)—Se(14)	2.473(3)	2.496(2)	2.636(2)
M(4)—Se(14)	2.477(3)	2.513(2)	2.681(2)
M(2)—Se(23)	2.511(3)	2.449(2)	2.665(2)
M(3)—Se(23)	2.490(3)	2.486(2)	2.678(2)
M(2)—Se(24)	2.481(3)	2.508(2)	2.658(2)
M(4)—Se(24)	2.482(3)	2.456(2)	2.653(2)
M(3)—Se(34)	2.477(3)	2.480(2)	2.693(2)
M(4)—Se(34)	2.507(3)	2.519(2)	2.680(2)
Se—C			
Se(1)—C(11)	1.902(13)	1.909(7)	1.927(16)
Se(2)—C(21)	1.896(14)	1.927(8)	1.904(15)
Se(3)—C(31)	1.884(15)	1.925(7)	1.911(14)
Se(4)—C(41)	1.923(13)	1.934(10)	1.905(14)
Se(12)—C(121)	1.913(13)	1.937(6)	1.901(14)
Se(13)—C(131)	1.906(12)	1.924(8)	1.883(16)
Se(14)—C(141)	1.910(16)	1.928(7)	1.890(19)
Se(23)—C(231)	1.919(13)	1.923(7)	1.911(14)
Se(24)—C(241)	1.909(13)	1.935(8)	1.925(13)
Se(34)—(C341)	1.918(13)	1.919(8)	1.869(15)
Mean	1.908(12)	1.926(8)	1.903(18)
M. . .M nonbonded			
M(2). . .M(1)	4.098(3)	4.106(2)	4.347(2)
M(3). . .M(1)	4.172(3)	4.117(2)	4.412(2)
M(4). . .M(1)	4.124(3)	4.173(2)	4.402(2)
M(3). . .M(2)	4.115(3)	4.094(2)	4.447(2)
M(4). . .M(2)	4.164(3)	4.128(2)	4.423(2)
M(4). . .M(3)	4.156(3)	4.133(2)	4.458(2)
Se_b. . .Se_b nonbonded			
a:a Se(14). . .Se(12)	4.241(3)	4.273(2)	4.522(2)
Se(23). . .Se(13)	4.235(3)	4.320(2)	4.536(2)
a:e Se(13). . .Se(12)	4.022(3)	3.938(2)	4.298(2)
Se(23). . .Se(12)	3.964(3)	3.969(2)	4.395(2)
Se(24). . .Se(12)	3.949(3)	4.055(2)	4.329(2)
Se(34). . .Se(13)	3.965(3)	3.924(2)	4.245(2)
Se(24). . .Se(14)	3.994(3)	3.864(2)	4.225(2)
Se(34). . .Se(14)	4.095(3)	4.084(2)	4.279(2)
Se(24). . .Se(23)	4.091(3)	3.971(2)	4.133(2)
Se(34). . .Se(24)	3.863(3)	4.095(2)	4.430(2)
e:e Se(14). . .Se(13)	3.558(3)	3.682(2)	4.136(2)
Se(34). . .Se(23)	3.690(3)	3.644(2)	4.003(2)
M—Se_b—M			
M(2)—Se(12)—M(1)	113.58(11)	111.80(6)	109.60(8)
M(3)—Se(13)—M(1)	114.52(10)	113.05(6)	112.54(8)
M(4)—Se(14)—M(1)	112.82(11)	112.85(6)	111.79(9)
M(3)—Se(23)—M(2)	110.71(10)	112.10(6)	113.83(8)
M(4)—Se(24)—M(2)	114.08(10)	112.51(6)	112.79(8)
M(4)—Se(34)—M(3)	112.98(10)	111.53(6)	112.13(8)

Can. J. Chem. Downloaded from www.nrcresearchpress.com by 92.62.229.171 on 09/08/12
For personal use only.

TABLE 5 (*concluded*)

M =	Zn in **1**	Zn in **2**	Cd in **3**
Se_b—M—Se_b			
a:a Se(14)—M(1)—Se(12)	118.66(11)	118.70(6)	116.81(8)
Se(23)—M(3)—Se(13)	117.33(11)	121.30(6)	117.08(8)
a:e Se(13)—M(1)—Se(12)	108.71(10)	105.87(6)	107.20(7)
Se(23)—M(2)—Se(12)	106.37(10)	106.99(6)	111.66(7)
Se(24)—M(2)—Se(12)	106.70(11)	108.52(6)	109.39(7)
Se(24)—M(2)—Se(23)	110.04(11)	106.49(6)	101.86(7)
Se(34)—M(3)—Se(13)	106.58(10)	104.89(6)	105.53(8)
Se(24)—M(4)—Se(14)	107.29(10)	102.08(6)	104.77(9)
Se(34)—M(4)—Se(14)	110.46(10)	108.52(6)	105.92(8)
Se(34)—M(4)—Se(24)	101.50(10)	110.78(6)	112.34(8)
e:e Se(14)—M(1)—Se(13)	91.55(10)	95.86(6)	102.53(8)
Se(34)—M(3)—Se(23)	95.94(10)	94.42(6)	96.39(7)

in enantiomeric forms. Indeed, a spontaneous resolution of one hand has been reported (3) for $(Me_4N)_2[(\mu\text{-}EPh)_6(CdBr)_4]$ (E = S or Se), the only known example of isomer IV. All the other reported examples, with the exception of $[(\mu\text{-}TeR)_6Ag_4]^{2-}$ (20), have crystallized in centrosymmetric space groups as racemic modifications. Interestingly, in the two cases where there is crystallographically imposed symmetry (3) or geometric constraints imposed by the backbones of the bridging ligands (18, 19), the configurations of isomers II or IV (with C_3 symmetry and three 1,3-axial–axial pairs) are observed. The stereochemistry of isomer I (which has the maximum possible of four axial pairs of interactions) is found most often in Fe-thiolate cages; why this is so is not clear. Although crystallizing in different lattices, the anions in **1**, **2**, and **3** all adopt the stereochemistry of isomer III. This isomer has only two axial–axial pairs of interactions, and occurs in 12 of the 21 reported $(\mu\text{-}SR)_6M_4$ cages (3–20). For the anions of **1**, **2**, and **3** both enantiomers are present in the crystal lattice, since all crystallized in centrosymmetric space groups.

Selected interatomic distances and angles for **1**, **2**, and **3** are given in Table 5. Compound **1** is isomorphous and isostructural with $(Me_4N)_2[M_4(SPh)_{10}]$, where M = Mn (4), Co (9), or Zn (14). A comparison of interatomic distances and angles with those in the corresponding isomorphous compounds and their sulfur analogs reveals the trend expected for the change in size of metal atoms and E atoms. The ranges of nonbonded M. . .M distances of 4.098(3)–4.172(3) in **1**, 4.094(2)–4.173(2) in **2**, and 4.347(2)–4.477(2) Å for **3** imply slightly distorted T_d geometries for the metal atoms. Compound **3** contains the same $(\mu\text{-}Se)_6M_4$ cage as the only example of isomer IV, though $PhSe_t$ ligands have replaced the Br atoms, and the Cd. . .Cd distances for **3** are significantly larger than the mean value of 4.251(6) Å found in the $[\mu\text{-}(SePh)_6(CdBr)_4]^{2-}$ anion (3).

There is no significant variation in the Zn—Se_t distances in **1** and **2**, though the Cd—Se_t distances range from 2.573(2) to 2.605(2) Å. The M—Se_{br} distances vary more, from 2.440(3) to 2.511(3) in **1**, from 2.449(2) to 2.519(2) in **2**, and from 2.636(2) to 2.693(2) Å in **3**. A similar degree of variation is seen in the M—Se—M angles. It is noteworthy that the M—Se_{br} distances are all significantly longer than the M—Se_t values in each of the three anions. A mean Zn—Se_t distance of 2.471(13) Å was found in the anion $[Zn(Se_4)_2]^{2-}$ (35), and a mean Cd—Se_t value of 2.643(9) Å in the $[Cd(Se_4)_2]^{2-}$ anion (36).

There are, however, large differences in Se_{br}—M—Se_{br} angles and Se_{br}. . .Se_{br} distances. We attribute these variations to intramolecular interactions between the axial phenyl substituents on the $(\mu\text{-}SePh)_3M_3$ rings. These are also reflected in the Se_{br}—M—Se_{br} angles. A correlation between pairwise substituent orientation for Se_{br}—M—Se_{br} angles and Se_{br}. . .Se_{br} distances listed in Table 5 can be derived, and it is clearly apparent that the skeleton distorts to minimize the unfavourable repulsive interactions between axially disposed substituents.

	Se_{br}. . .Se_{br} range/values (Å)	Se_{br}—M—Se_{br} range/values (deg)
M = Zn (compounds **1** and **2**)		
aa	4.235(3)–4.320(2)	117.3(1)–121.3(1)
ae	3.863(3)–4.095(3)	101.5(1)–110.8(1)
ee	3.558(3)–3.690(3)	91.5(1)–95.9(1)
M = Cd (compound **3**)		
aa	4.522(2), 4.536(2)	116.8(1), 117.1(1)
ae	4.113(2)–4.430(2)	101.9(1), 112.3(1)
ee	4.003(2), 4.136(2)	96.4(1), 102.5(1)
M = Cd (ref. 3, isomer IV)[3]		
aa	4.582(3)	121.2(1)
ae	4.226(3), 4.351(3)	106.3(1), 111.0(1)
ee	4.108(3)	102.0(1)

Although all three anions adopt the configuration of isomer III, there are differences in the arrangements of the phenyl rings on the selenolato ligands. These arise from rotations about the metal—Se_t and the Se_{br}—C bonds. Thus the dihedral angles between the planes of the phenyl rings with 1,3-axial–axial interactions are different:

[3]The nonbonded Se_{br}. . .Se_{br} distances in the anion $[(\mu\text{-}SePh)_6(CdBr)_4]^{2-}$, compound **2** in ref. 3, were interchanged in Table III; they should read E(1) . . . E(2) 4.226(3) Å and E(1) . . . E(2)′ 4.108(3) Å.

Can. J. Chem. Downloaded from www.nrcresearchpress.com by 92.62.229.171 on 09/08/12
For personal use only.

Compound	Phenyl rings:	Dihedral angles (deg) 12 and 14	13 and 23
1		63.8(6)	70.3(4)
2		63.7(3)	79.1(2)
3		54.5(5)	83.9(4)

However, it can be seen from Fig. 1 that the major differences are in the relative orientations of the phenyl rings attached to the terminal Se atoms. Torsion angles describing these variations have been collected in Table S7. Since there is no obvious systematic reason for these differences, we suppose that they may be due to packing effects in the crystal lattice.

Acknowledgements

We thank the Natural Sciences and Engineering Research Council of Canada for financial support of this work, in the form of operating grants to P.A.W.D. and N.C.P.

1. I. G. Dance. Polyhedron, **5**, 1037 (1986).
2. P. J. Blower and J. R. Dilworth. Coord. Chem. Rev. **76**, 121 (1987).
3. P. A. W. Dean, J. J. Vittal, and N. C. Payne. Inorg. Chem. **26**, 1683 (1987).
4. T. Costa, J. R. Dorfman, K. S. Hagen, and R. H. Holm. Inorg. Chem. **22**, 4091 (1983).
5. K. S. Hagen, D. W. Stephan, and R. H. Holm. Inorg. Chem. **21**, 3928 (1982).
6. K. S. Hagen and R. H. Holm. Inorg. Chem. **23**, 418 (1984).
7. D. Coucouvanis, M. Kanatzidis, E. Simhon, and N. C. Baenziger. J. Am. Chem. Soc. **104**, 1874 (1982).
8. M. A. Whitener, J. K. Bashkin, K. S. Hagen, J.-J. Girerd, E. Gamp, N. Edelstein, and R. H. Holm. J. Am. Chem. Soc. **108**, 5607 (1986).
9. (*a*) I. G. Dance. J. Am. Chem. Soc. **101**, 6264 (1979); (*b*) I. G. Dance and J. C. Calabrese. J. Chem. Soc. Chem. Commun. 762 (1975).
10. D. Fenske, J. Meyer, and K. Merzweiler. Z. Naturforsch. **42**, 1207 (1987).
11. J. L. Hencher, M. A. Khan, F. F. Said, and D. G. Tuck. (*a*) Polyhedron, **4**, 1263 (1985); (*b*) Inorg. Nucl. Chem. Lett. **17**, 287 (1981).
12. I. G. Dance. Inorg. Chem. **20**, 2155 (1981).
13. I. G. Dance. J. Am. Chem. Soc. **102**, 3445 (1980).
14. I. G. Dance, personal communication.
15. K. S. Hagen and R. H. Holm. Inorg. Chem. **22**, 3171 (1983).
16. I. G. Dance, G. A. Bowmaker, G. R. Clark, and J. K. Seadon. Polyhedron, **2**, 1031 (1983).
17. D. Coucouvanis, C. N. Murphy, and S. K. Kanodia. Inorg. Chem. **19**, 2993 (1980).
18. J. R. Nicholson, I. L. Abrahams, W. Clegg, and C. D. Garner. Inorg. Chem. **24**, 1092 (1985).
19. G. Henkel, P. Betz, and B. Krebs. Angew. Chem. Int. Ed. Engl. **26**, 145 (1987).
20. J. Zhao, D. Adcock, W. T. Pennington, and J. W. Kolis. Inorg. Chem. **29**, 4358 (1991).
21. P. A. W. Dean and J. J. Vittal. Inorg. Chem. **24**, 3722 (1985).
22. P. A. W. Dean and J. J. Vittal. Inorg. Chem. **25**, 514 (1986).
23. P. A. W. Dean and J. J. Vittal. Inorg. Chem. **26**, 278 (1987).
24. P. A. W. Dean, J. J. Vittal, and M. H. Trattner. Inorg. Chem. **25**, 4245 (1986).
25. P. A. W. Dean and J. J. Vittal. Can. J. Chem. **66**, 2343 (1988).
26. P. A. W. Dean and V. Manivannan. Inorg. Chem. **29**, 2997 (1990).
27. P. A. W. Dean and V. Manivannan. Can. J. Chem. **68**, 214 (1990).
28. Enraf–Nonius: Enraf–Nonius CAD4F Users Manual. Delft, The Netherlands. 1982.
29. Enraf–Nonius Structure Determination Package, SDP-PLUS, Version 3.0. 1985.
30. P. Coppens, L. Leiserowitz, and D. Rabinovich. Acta Crystallogr. **18**, 1035 (1965).
31. D. Cahen and J. A. Ibers. J. Appl. Crystallogr. **5**, 298 (1972).
32. P. Main *et al.* MULTAN 82 Manual. Department of Physics, University of York, York, England. 1982.
33. G. M. Sheldrick. SHELX-76, Program for crystal structure determination. University of Cambridge, England. 1976.
34. International tables for X-ray crystallography. (*a*) Vol. A. D. Reidel Publishing Co., Boston. 1983; (*b*) Vol. IV. Kynoch Press, Birmingham. 1974.
35. M. A. Ansari, C. H. Mahler, G. S. Chorghade, Y.-J. Lu, and J. A. Ibers. Inorg. Chem. **29**, 3832 (1990).
36. R. M. H. Banda, J. Cusick, M. L. Scudder, and I. G. Dance. Polyhedron, **8**, 1995 (1989).

Can. J. Chem. Downloaded from www.nrcresearchpress.com by 92.62.229.171 on 09/08/12
For personal use only.

Cycloaddition de la *C*-*p*-anisyl-*N*-phénylnitrilimine sur deux énamines cycliques dérivées de la 1,2-dihydro-6,7-diméthoxyisoquinoléine-3-carboxylate d'éthyle. Régiochimie, stéréochimie et évolution des cycloadduits

KHADIJA MOUSTAID, NGUYEN DINH AN ET BERNARD LAUDE[1]
Laboratoire de chimie organique, Université de Franche-Comté, 16 Route de Gray, 25030 Besancon, France

MARIE-FRANCE MERCIER
Centre de spectrométrie, Université de Franche-Comté, 16 Route de Gray, 25030 Besancon, France

ET

AHMED SEDQUI
Département de chimie, Faculté des sciences, BP 2121, Université de Tetouan, Maroc

Reçu le 22 mai 1991

KHADIJA MOUSTAID, NGUYEN DINH AN, BERNARD LAUDE, MARIE-FRANCE MERCIER et AHMED SEDQUI. Can. J. Chem. **70**, 802 (1992).

La synthèse de deux dérivés du 1,2-dihydro-6,7-diméthoxyisoquinoléine-3-carboxylate d'éthyle est décrite. Ces énamines cycliques portant un groupe ester sur le carbone énaminique réagissent de façon régio- et stéréospécifique avec une diarylnitrilimine. La régiochimie est spécifiée par voies chimique et spectroscopique. Le détermination radiocristallographique de la structure d'un cycloadduit permet de préciser la stéréochimie de la réaction et de la comparer avec celle qui avait été décrite lorsque le dipolarophile initial ne comporte pas de groupe ester sur le carbone énaminique.

Mots clés : cycloaddition dipolaire-1,3, diarylnitrilimine, énamine cyclique, régiochimie, stéréochimie.

KHADIJA MOUSTAID, NGUYEN DINH AN, BERNARD LAUDE, MARIE-FRANCE MERCIER, and AHMED SEDQUI. Can. J. Chem. **70**, 802 (1992).

Two ethyl-1,2-dihydro-6,7-dimethoxyisoquinoline-3a-carboxylate derivatives were synthesized. These cyclic enamines in which the enaminic carbon atom was bonded with an ester group react regio- and stereospecifically with a diarylnitrilimine. The regiochemistry was specified by chemical and spectroscopic methods. The radiocrystallographic structure of one cycloadduct allows us to determine the stereochemistry of the reaction and to compare it with that of the reaction of a diarylnitrilimine with a 1,2-dihydro-1,2-dialkylisoquinoline without an ester group at the enaminic carbon atom.

Key words: 1,3-dipolar cycloaddition, diarylnitrilimine, cyclic enamine, regiochemistry, stereochemistry.

Introduction

Dans un article récent (1) nous avons décrit la synthèse et l'utilisation comme précurseurs d'ylures d'azométhine des dérivés de type **4** (figure 1) de la 3,4-dihydro-6,7-diméthoxyisoquinoléine portant un groupement ester en position -3. Ayant noté que leur aromatisation en dérivés de l'isoquinoléine **5** s'effectue par simple chauffage dans l'éthanol, nous avons envisagé de transformer ces composés **5** en dérivés **7** de la 1,2-dihydro-6,7-diméthoxy-3-éthoxycarbonyl isoquinoléine. Ces derniers composés sont des dipolarophiles et il nous a semblé intéressant d'étudier le rôle joué par le groupe ester en -3 dans leur comportement vis-à-vis d'une diarylnitrilimine **8** et de la comparer du double point de vue régio- et stéréochimique, avec celui déjà décrit dans le cas des 1,2-dihydro-1,2-dialkylisoquinoléines non substituées en position -3 (2).

Synthèse des dérivés de la 1,2-dihydro-6,7-diméthoxy-2-méthyl-3-éthoxycarbonylisoquinoléine 7

Les différentes étapes de cette synthèse sont rassemblées sur la figure 1. La méthode d'accès aux composés **4** depuis le bromure de 3,4-diméthoxybenzyle a été décrite dans notre mémoire précédent (1). Ici nous avons préféré préparer l'ester éthylique pour limiter le nombre de signaux correspondant à un groupe méthoxy en rmn ^{1}H. L'oxydation des composés **4** en isoquinoléines **5** s'effectue par simple chauffage dans l'éthanol dans le cas de **5***a*. Par contre, il faut catalyser cette oxydation par une trace d'éthylate de sodium dans le cas de **5***b* (cf. partie expérimentale). Traités par l'iodure de méthyle, les composés **5** donnent les sels d'isoquinolinium **6**, mais le mode opératoire diffère selon que R = H ou CH_3 (cf. partie expérimentale).

La réduction de ces sels **6** par $NaBH_4$ selon une adaptation du mode opératoire décrit par Dyke *et al.* (3) conduit aux dipolarophiles **7***a*,*b*.

Réactions de cycloaddition et transformation d'un cycloadduit

Les composés **7** réagissent aisément avec la *C*-*para*anisyl-*N*-phénylnitrilimine formée *in situ* selon la méthode de Huisgen *et al.* (4). Les rendements sont convenables et la réaction est régio- et stéréospécifique puisqu'elle ne conduit qu'à un seul cycloadduit **9** dérivé du 1-*para*-anisyl-7,8-diméthoxy-4-méthyl-3-phényl-3a,4,5,9b-tetrahydropyrazolo[3,4-*c*]isoquinoleine-3a-carboxylate d'éthyle (figure 1).

La régiochimie est précisée à l'aide des paramètres de rmn ^{13}C des cycloadduits puisque le carbone quaternaire C−3a a un déplacement chimique de l'ordre de 90 ppm, ce qui permet d'affirmer qu'il est lié à deux atomes d'azote. Ce résultat est en accord avec plusieurs travaux antérieurs (5, 6) concernant l'orientation de la cycloaddition des diarylnitrilimines sur des sites dipolarophiliques portant un groupement ester. Ces travaux montrent que d'une manière générale,

[1]Auteur à qui adresser toute correspondance.

Printed in Canada

Can. J. Chem. Downloaded from www.nrcresearchpress.com by 92.62.229.171 on 09/08/12
For personal use only.

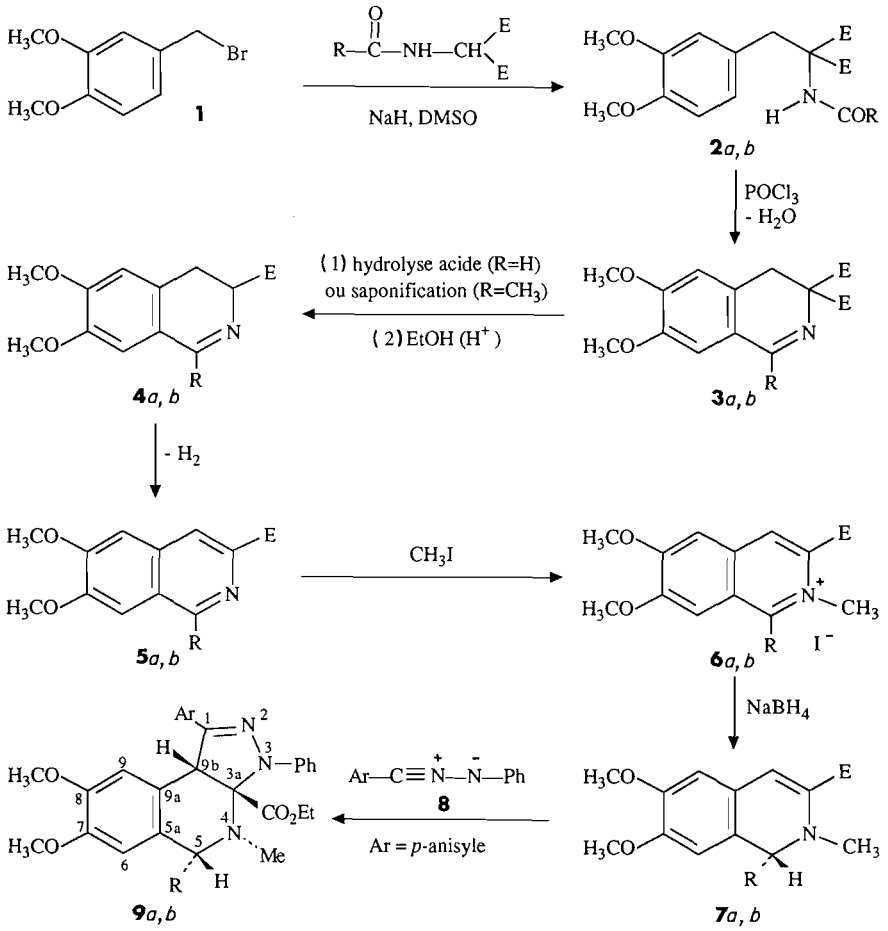

E = CO_2Et, *a* : R = H, *b* : R = CH_3

FIG. 1

l'extrémité azotée du dipôle se fixe sur le carbone portant la fonction ester.

Cependant, une inversion de cette régiochimie a été récemment décrite par Daou et Soufiaoui (7) dans le cas du 2-éthoxycarbonyl-*N*-méthylindole. Aussi, nous a-t-il semblé nécessaire de vérifier par voie chimique la régiochimie de la cycloaddition du dipôle **8** sur les composés **7**.

Dans ce but, nous avons transformé le cycloadduit **9***a* selon les réactions représentées sur la figure 2.

Une première tentative de saponification du cycloadduit **9***a* ne permet pas d'isoler l'acide correspondant mais conduit à l'azépinone **10***a*. La saponification s'accompagne de l'ouverture de l'hétérocycle hexagonal qui se referme ensuite par réaction intramoléculaire entre les fonctions acide et amine secondaire. Cette transformation avait également été décrite par Daou et Soufiaoui (7) dans le cas d'un cycloadduit issu de l'action d'une diarylnitrilimine sur le 2-éthoxycarbonyl-*N*-méthylindole homologue inférieur de nos dipolarophiles.

Le traitement du cycloadduit **9***a* par l'acide acétique conduit après protonation et ouverture au pyrazole **11***a*.

L'analyse quantitative élémentaire du composé **11***a* est en accord avec sa structure qui est celle d'un isomère de **9***a*. Le spectre d'absorption ir présente une bande ν(N—H) = 3400 cm^{-1} et un abaissement de la fréquence ν(C=O) du groupe ester qui passe de 1730 cm^{-1} dans **9***a* à 1710 cm^{-1} dans **11***a* par suite de la conjugaison de ce groupe ester avec le cycle pyrazolique. Les paramètres de rmn ^1H et ^{13}C sont également en accord avec la structure proposée.

Mais ces propriétés spectroscopiques ne seraient pas en opposition avec une structure résultant de la transformation du régioisomère inverse du cycloadduit **9***a*. Nous avons donc cherché à transformer le groupement ester du produit **11***a* en hydrogène afin de déterminer avec certitude la structure du cycloadduit. La saponification directe du pyrazole **11***a* conduit à la même azépinone **10***a* obtenue par saponification du cycloadduit. Il convenait donc d'éviter toute réaction entre le groupe NH avec le reste ester et dans ce but nous avons acétylé le groupe NH du pyrazole **11***a* par action du chlorure d'acétyle en milieu pyridinique. Le produit acétylé **12***a* est ensuite saponifié et l'acide **13***a* obtenu est décarboxylé par chauffage. Il est alors facile de confirmer la structure du pyrazole **14***a* en examinant le spectre de rmn ^1H qui présente un singulet à 7,9 ppm caractéristique d'un proton H-5 pyrazolique alors qu'un proton H-4 pyrazolique résonne vers 6,7–6,8 ppm (8, 9).

Ces transformations confirment la régiochimie proposée pour les cycloadduits **9** sur la base du déplacement chi-

Can. J. Chem. Downloaded from www.nrcresearchpress.com by 92.62.229.171 on 09/08/12
For personal use only.

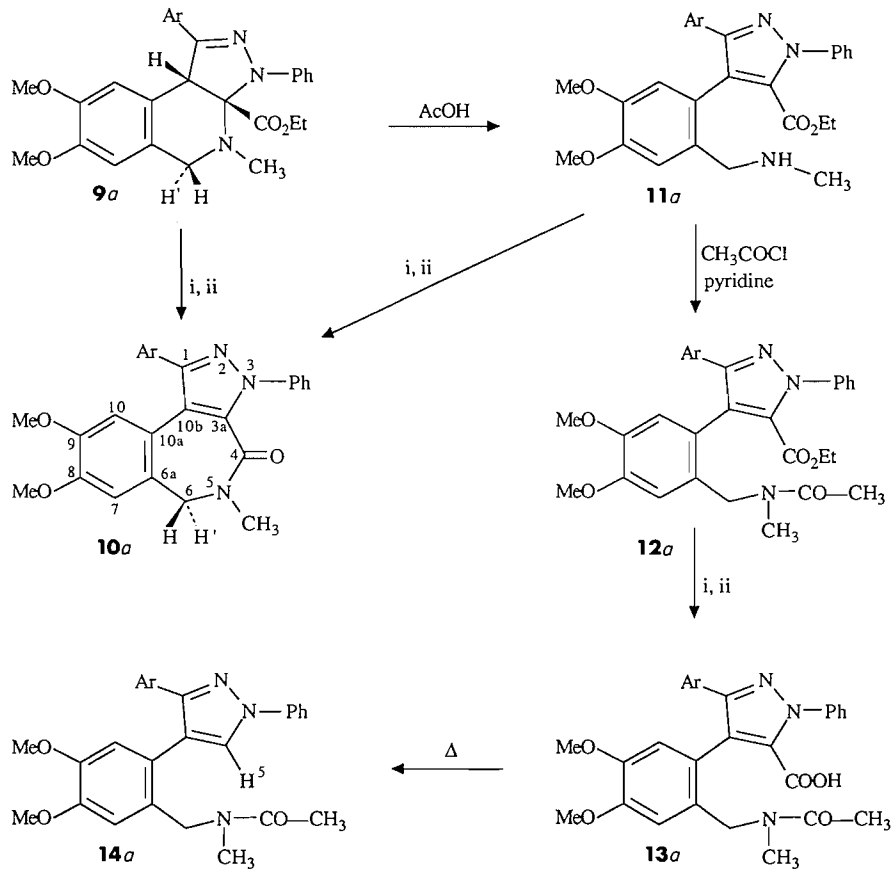

Ar = *p*-anisyle, i: KOH méthanolique 2 N, ii : HCl

FIG. 2

mique du carbone C-3a et elles invalident la régiochimie proposée initialement pour les cycloadduits issus de l'action des diarylnitrilimines sur le 2-éthoxycarbonyl-*N*-méthylindole (7) et rectifiée par la suite (10).

Stéréochimie de la cycloaddition

Les paramètres de rmn ^1H et ^{13}C des cycloadduits ne permettant pas d'accéder à leur stéréochimie, nous avons fait appel à une détermination radiocristallographique de la structure du 1-*para*-anisyl-7,8-diméthoxy-4,5-diméthyl-3-phényl-3a,4,5,9b-tétrahydropyrazolo[3,4-*c*]isoquinoléine-3a-carboxylate d'éthyle **9***b* (11).

Cette structure permet de relever les caractéristiques suivantes : (*i*) les deux groupes méthyles en N-4 et C-5 se situent de même côté du cycle diméthoxybenzo dans une disposition *cis* avec une position pseudo-axiale pour le groupe *N*-méthyle et pseudo-équatoriale pour le groupe méthyle en -5; (*ii*) le groupe *N*-méthyle en -4 et le groupe ester en -3a sont dans une disposition pseudo-*trans* diaxiale avec un angle de torsion entre les deux groupes méthyle et ester : CH_3–N–4–C–3a–CO_2Et = 156,8°.

Cette structure appelle quelques commentaires notamment par comparaison avec les résultats décrits par Kitane *et al.* (2) et Mercier *et al.* (12) dans le cas de la cycloaddition des diarylnitrilimines sur diverses 1-alkyl-*N*-méthyl-1,2-dihydroisoquinoléines **15** (figure 3).

Dans cette étude, Kitane *et al.* (2) ont montré que la stéréochimie des dipolarophiles **15** était telle que le groupe *N*-méthyle et le groupe alkyle en -1 étaient dans une disposition pseudo-*trans*-diaxiale. Ceci impose alors une approche du dipôle en *anti* du groupement le plus encombrant à savoir le groupe *N*-méthyle plus proche du site dipolarophilique. C'est effectivement ce qui est observé sur le diagramme PLUTO (figure 3) obtenue par détermination radiocristallographique de la structure de **16** (R = isopropyle). On y voit nettement que le cycloadduit s'est développé en *trans* du reste *N*-méthyle et en *cis* du groupement isopropyle, ces deux groupes étant en disposition pseudo-*trans*-diaxiale sur l'hétérocycle hexagonal azoté.

Dans le cas de notre dipolarophile **7***b*, on peut penser que sa conformation est analogue à celle proposée par Kitane *et al.* (2) pour le composé **15**. C'est d'ailleurs celle qui éloigne le plus les deux groupes *N*-méthyle en -2 et ester en -3. Dans ces conditions, on peut donc attendre la même stéréochimie pour l'approche du dipôle, à savoir en *anti* du groupe *N*-méthyle et en *syn* du groupe méthyle en -1.

Le diagramme PLUTO (figure 3) de la structure du cycloadduit **9***b* montre bien que le dipôle s'est approché en *syn* du méthyle en -1 mais il apparaît que le reste *N*-méthyle se

Can. J. Chem. Downloaded from www.nrcresearchpress.com by 92.62.229.171 on 09/08/12
For personal use only.

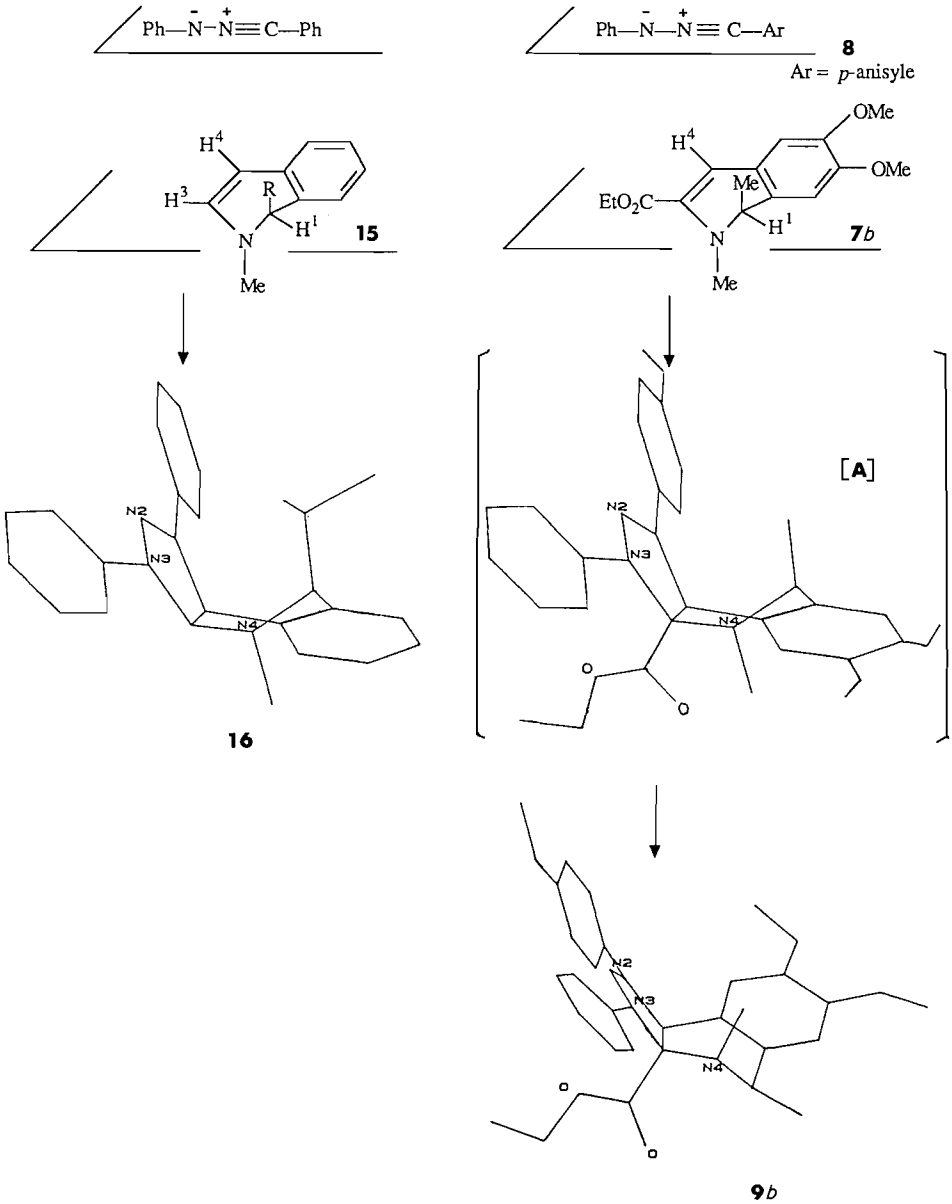

FIG. 3

retrouve dans une disposition *cis* du cycle pyrazolinique et du groupe méthyle en -5.

Nous pensons pouvoir lever cette contradiction apparente en faisant appel à une épimérisation de l'atome d'azote N-4 lors de la cycloaddition. Cette épimérisation assure alors la décompression stérique qui interviendrait si le groupe ester en -3a et le reste *N*-méthyle en -4 se retrouvaient dans une disposition *cis* comme indiqué sur l'intermédiaire **[A]** (figure 3).

Conclusion

Nous avons pu préparer des énamines cycliques dérivées du 1,2-dihydro-6,7-diméthoxy-*N*-méthylisoquinoléine-3-carboxylate d'éthyle. Ces dipolarophiles réagissent de façon régio- et stéréospécifique avec une diarylnitrilimine. La régiochimie de la réaction déterminée par voies spectroscopique et chimique correspond à l'union de l'atome de carbone du dipolarophile portant le groupe ester avec l'extrémité azotée du dipôle. Le résultat semble général.

Si la stéréochimie de la cycloaddition s'effectue de façon que le dipôle approche le dipolarophile en *syn* du substituant fixé en β du site dipolarphilique et en *anti* du groupe *N*-méthyle situé en α du site dipolarophilique, il apparaît que la présence du groupe ester fixé sur l'atome de carbone voisin du reste *N*-méthyle exerce un encombrement stérique tel que la cycloaddition s'accompagne d'une épimérisation de l'atome d'azote qui renvoie le groupe *N*-méthyle en disposition *trans* par rapport au groupe ester dans le cycloadduit.

Partie expérimentale

Les points de fusion déterminés sur banc Kofler ne sont pas corrigés. Les spectres d'absorption ir ont été obtenus avec un spectrophotomètre Beckman IR 33, les produits étant pastillés dans KBr. Les spectres de rmn ont été obtenus avec un spectomètre

Can. J. Chem. Downloaded from www.nrcresearchpress.com by 92.62.229.171 on 09/08/12
For personal use only.

Can. J. Chem. Downloaded from www.nrcresearchpress.com by 92.62.229.171 on 09/08/12
For personal use only.

Bruker–Spectrospin AC 200 (200 MHz pour le proton et 50 MHz pour le ^{13}C), les échantillons étant dissous dans $CDCl_3$ (sauf indication contraire) avec le tétraméthylsilane comme référence interne. Les microanalyses ont été assurées par le Service d'Analyses du CNRS à Vernaison.

Le précurseur de la *C-para*-anisyl-*N*-phénylnitrilimine est préparé selon la méthode de Huisgen *et al.* (4).

Dérivés du 3,4-dihydro-6,7-diméthoxyisoquinoléine-3-carboxylate d'éthyle ***4***

Le mode opératoire est calqué sur celui décrit par Lakhlifi *et al.* (1) pour l'obtention des esters méthyliques. La seule différence intervient lors de la dernière étape où le méthanol est remplacé par de l'éthanol absolu. On opère à partir de 0,01 mol de diester **3**. En fin de réaction, le résidu est repris sans chauffer par un mélange d'hexane et de propan-1-ol (4 : 1). Les produits **4** cristallisés sont essorés et chacun d'eux est décrit ci-après.

*3,4-Dihydro-6,7-diméthoxyisoquinoléine-3-carboxylate d'éthyle (****4****a)*

On obtient 1,76 g de produit (Rdt. 67%), *F* 138–140°C; ir, ν_{max} : 1725 (ester); rmn ^1H, δ : 1,32 (t, 3H, $^3J_{CH_3-CH_2}$ = 7,10 Hz, CH_3 de éthyle), 2,96 (d, 2H, $^3J_{CH_2-4-H-3}$ = 10,20 Hz, CH_2-4), 3,91 (s, 3H, OCH_3), 3,94 (s, 3H, OCH_3), 4,25 (dt, 1H, ^3J = 10,20 Hz, $^4J_{H-3-H-1}$ = 2,90 Hz, H-3), 4,32 (q, 2H, ^3J = 7,10 Hz, CH_2 de éthyle), 6,80 (s, 1H, H-5), 6,95 (s, 1H, H-8), 8,35 (d, 1H, $^4J_{H-1-H-3}$ = 2,90 Hz, H-1). Anal. calc. pour $C_{14}H_{17}NO_4$: C 63,84, H 6,51, N 5,32; tr. : C 63,92, H, 6,43, N 5,46.

*3,4-Dihydro-,6,7-diméthoxy-1-méthyl-isoquinoléine-3-carboxylate d'éthyle (****4****b)*

On obtient 2,14 g de produit (Rdt. 77%), *F* 100°C; ir, ν_{max} : 1730 (ester); rmn ^1H, δ : 1,30 (t, 3H, $^3J_{CH_3-CH_2}$ = 7,10 Hz, CH_3 de éthyle), 2,40 (d, 3H, $^5J_{CH_3-H-3}$ = 1,90 Hz, CH_3-1), 2,90 (d, 2H, $^3J_{CH_2-4-H-3}$ = 10,60 Hz, CH_2-4), 3,90 (s, 6H, OCH_3), 4,20 (tq, 1H, $^3J_{H-3-CH_2-4}$ = 10,60 Hz, $^5J_{H-3-CH_3-1}$ = 1,90 Hz, H-3), 4,30 (q, 2H, ^3J = 7,10 Hz, CH_2 de éthyle), 6,80 (s, 1H, H-5), 7,0 (s, 1H, H-8). Anal. calc. pour $C_{15}H_{19}NO_4$: C 64,96, H 6,91, N 5,05; tr. : C 65,07, H 6,83, N 5,17.

Dérivés du 6,7-diméthoxyisoquinoléine-3-carboxylate d'éthyle ***5***

*6,7-Diméthoxyisoquinoléine-3-carboxylate d'éthyle (****5****a)*

On dissout 0,01 mol de composé ***4****a* dans 40 mL d'éthanol contenus dans un bécher de forme haute de 250 mL. Cette solution est maintenue un quart d'heure à très légère ébullition sur une plaque chauffante installée sous la hotte. La solution est ensuite concentrée jusqu'à 10 mL et par refroidissement le composé ***5****a* cristallise (Rdt. quantitatif), *F* 181°C; ir, ν_{max} : 1710 (ester); rmn ^1H, δ : 1,46 (t, 3H, $J_{CH_3-CH_2}$ = 7,10 Hz, CH_3 de éthyle), 4,05 (s, 6H, OCH_3), 4,53 (q, 2H, *J* = 7,10 Hz, CH_2 de éthyle), 7,20 (s, 1H, H-5 ou H-8), 7,30 (s, 1H, H-8 ou H-5), 8,45 (s, 1H, H-4), 9,15 (s, 1H, H-1). Anal. calc. pour $C_{14}H_{15}NO_4$: C 64,35, H, 5,79, N, 5,36; tr. : C, 64,24, H 5,87, N 5,47.

*6,7-Diméthoxy-1-méthyl-isoquinoléine-3-carboxylate d'éthyle (****5****b)*

On dissout 0,01 mol de composé ***4****b* dans 40 mL d'éthanol absolu et ajoute une pointe de spatule d'éthylate de sodium et opère comme précédemment. Après départ de tout le solvant par évaporation sous vide de la trompe à eau, le résidu solide est repris par 20 mL d'acétone. Seul le composé ***4****b* y est soluble. Le produit ***5****b* insoluble est essoré et séché. Le rendement de la réaction est limité à 50%, mais le composé de départ ***4****b* non oxydé est récupéré et réengagé dans une nouvelle expérience. On peut ainsi par opérations successives obtenir un rendement global d'environ 80% en produit ***5****b*, *F* 170°C, ir, ν_{max} : 1710 (ester); rmn ^1H, δ : 1,48 (t, 3H, $J_{CH_3-CH_2}$ = 7,10 Hz, CH_3 de éthyle), 2,98 (s, 3H, CH_3-1), 4,02 (s, 3H, OCH_3), 4,05 (s, 3H, OCH_3), 4,51 (q, 2H, $J_{CH_2-CH_3}$ = 7,10 Hz, CH_2 de éthyle), 7,20 (s, 1H, H-5 ou H-8 , 7,35 (s, 1H, H-8 ou H-5), 8,32 (s, 1H, H-4). Anal. calc. pour $C_{15}H_{17}NO_4$: C65,44, H 6,22, N 5,09; tr. : C 65,35, H 6,36, N 5,12.

Sels d'isoquinoliniums ***6***

*Iodure de 6,7-diméthoxy-3-éthoxycarbonyl-*N*-méthylisoquinolinium (****6****a)*

Un mélange de 1,3 g (5 mmol) de composé ***5****a*, 15 mL d'acétone et 5 mL d'iodure de méthyle est agité à température ambiante pendant 12 h. Le précipité obtenu est filtré, lavé plusieurs fois à l'acétone et essoré. On obtient 1,1 g de produit (Rdt. 76%), *F* > 250°C; ir, ν_{max} : 1725 (ester); rmn ^1H (DMSO-d_6), δ : 1,42 (t, 3H, $J_{CH_3-CH_2}$ = 7,10 Hz, CH_3 de éthyle), 4,05 (s, 3H, OCH_3), 4,09 (s, 3H, OCH_3), 4,48 (q, 2H, $J_{CH_2-CH_3}$ = 7,10 Hz, CH_2 de éthyle), 4,58 (s, 3H, N-CH_3), 7,90 (s, 1H, H-5 ou H-8), 8,05 (s, 1H, H-8 ou H-5), 9,00 (s, 1H, H-4), 9,80 (s, 1H, H-1). Produit non analysé.

*Iodure de 6,7-diméthoxy-1-méthyl-3-éthoxycarbonyl-*N*-méthylisoquinolinium (****6****b)*

Dans un tube en verre épais de 100 mL, on introduit 2,75 g (0,01 mol) de composé ***5****b* et 20 mL d'iodure de méthyle. Le tube est scellé et chauffé à 140°C dans un bain d'huile pendant 12 h. Après refroidissement, on ouvre le tube, filtre, lave le solide plusieurs fois à l'acétone et essore. On obtient 3,67 g de produit (Rdt. 88%), *F* > 250°C; ir, ν_{max} : 1720 (ester); rmn ^1H, δ : 1,45 (t, 3H, $J_{CH_3-CH_2}$ = 7,10 Hz, CH_3 de éthyle), 3,30 (s, 3H, CH_3-1), 4,10 (s, 3H, OCH_3), 4,15 (s, 3H, OCH_3), 4,40 (s, 3H, N-CH_3), 4,50 (q, 2H, $J_{CH_2-CH_3}$ = 7,10 Hz), 7,90 (s, 1H, H-5 ou H-8), 7,95 (s, 1H, H-8 ou H-5), 8,70 (s, 1H, H-4). Produit non analysé.

*Réduction des sels d'isoquinolinium (****6****). Obtention des dérivés du 1,2-dihydro-6,7-diméthoxy-*N*-méthylisoquinoléine-3-carboxylate d'éthyle* **7**

Mode opératoire : On dissout 0,01 mol de composé **6** dans 100 mL d'une solution aqueuse d'éthanol à 50%. Sous agitation magnétique, on ajoute par petites portions 0,04 mol de $NaBH_4$. L'agitation est ensuite prolongée durant 4 h, puis l'éthanol est chassé par évaporation sous vide. Le résidu est repris par 100 mL d'une solution aqueuse à 10% d'acide acétique puis neutralisé par du carbonate de sodium et extrait trois fois avec 50 mL de chloroforme. Les extraits chloroformiques sont réunis, lavés à l'eau salée, séchés sur sulfate de sodium et évaporés sous vide. Le résidu huileux est repris par de l'éthanol dans lequel le produit **7** cristallise.

*1,2-Dihydro-6,7-diméthoxy-*N*-méthylisoquinoleine-3-carboxylate d'éthyle (****7****a)*

On obtient 2,54 g de produit (Rdt. 92%), *F* 152–153°C; ir, ν_{max} : 1725 (ester); rmn ^1H, δ : 1,45 (t, 3H, $J_{CH_3-CH_2}$ = 7,10 Hz, CH_3 de éthyle), 3,70 (s, 3H, N-CH_3), 4,00 (s, 3H, OCH_3), 4,05 (s, 3H, OCH_3), 4,10 (centre d'un syst. AB, 2H, J_{AB} = 15,9 Hz, CH_2-1), 4,40 (q, 2H, *J* = 7,10 Hz, CH_2 de éthyle), 6,70 (s, 1H, H-8), 6,90 (s, 1H, H-5), 7,80 (s, 1H, H-4). Anal. calc. pour $C_{15}H_{19}NO_4$: C 64,96, H 6,91, N 5,05; tr. : C 64,83, H 5,05, N 5,12.

*1,2-Dihydro-6,7-diméthoxy-1,2-diméthylisoquinoleine-3-carboxylate d'éthyle (****7****b)*

On obtient 2,76 g de produit (Rdt. 96%), *F* 80–82°C; ir, ν_{max} : 1720 (ester); rmn ^1H, δ : 1,40 (t, 3H, $J_{CH_3-CH_2}$ = 7,20 Hz, CH_3 de éthyle), 1,20 (d, 3H, J_{CH_3-H-1} = 6,80 Hz, CH_3-1), 2,80 (s, 3H, N-CH_3), 3,90 (s, 3H, OCH_3), 3,93 (s, 3H, OCH_3), 4,20 (q, 1H, *J* = 6,80 Hz, H-1), 4,30 (partie AB d'un système ABX_3 avec J_{AB} = 3,60 Hz et ^3J = 7,20 Hz, 2H, CH_2 de éthyle), 6,60 (s, 1H, H-8), 6,75 (s, 1H, H-5), 6,95 (s, 1H, H-4). Anal. calc. pour $C_{16}H_{21}NO_4$: C 65,96, H 7,27, N 4,81; tr. : C 65,83, H 7,32, N 4,91.

Réactions de cycloadditions

Dans un erlenmeyer bicol de 100 mL, on introduit 5 mmol de dipolarophile **7**, 5 mmol d'α-chloro-*para*-anisylidène-phénylhydrazone (précurseur de la nitrilimine **8**) et 30 mL de benzène anhydre. On chauffe ce mélange à reflux sous agitation magnétique en additionnant, en 15 min, 5 mL de triéthylamine. Le reflux est maintenu 24 h. Après retour à la température ambiante, on ajoute 20 mL de benzène, filtre le chlorhydrate de triéthylamine et chasse

Can. J. Chem. Downloaded from www.nrcresearchpress.com by 92.62.229.171 on 09/08/12
For personal use only.

le solvant à l'évaporateur rotatif. Le résidu est repris par de l'éthanol et le cycloadduit cristallise.

1-para-*Anisyl-7,8-diméthoxy-4-méthyl-3-phényl-3a,4,5,9b-tétrahydropyrazolo[3,4-c]isoquinoléine-3a-carboxylate d'éthyle (**9**a)*

On obtient 1,33 g de cycloadduit (Rdt. 53%), *F* 100°C; ir, ν_{max} : 1730 (ester); rmn ^{1}H, δ : 0,98 (t, 3H, $J_{CH_3-CH_2}$ = 7,10 Hz, CH_3 de éthyle), 2,42 (s, 3H, N-CH_3), 3,52 (s, 3H, OCH_3), 3,61 (d, 1H, ^2J = 16 Hz, H-5), 3,81 (s, 3H, OCH_3), 3,84 (s, 1H, OCH_3), 4,02 (q, 2H, *J* = 7,10 Hz, CH_2 de éthyle), 4,59 (d, 1H, ^2J = 16 Hz, H'-5), 5,12 (s, 1H, H-9b), 6,50–7,80 (m, 11H arom.); rmn ^{13}C, δ : 13,55 (q, *J* = 127 Hz, CH_3 de éthyle), 37,85 (q, *J* = 135,1 Hz, N-CH_3), 45,55 (d, *J* = 140,1 Hz, C-9b), 51,55 (t, *J* = 137,5 Hz, C-5), 52,25 (q, *J* = 144 Hz, OCH_3), 55,45 (q, *J* = 144,1 Hz, OCH_3), 55,65 (q, *J* = 144,5 Hz, OCH_3), 61,40 (t, *J* = 149,5 Hz, CH_2 de éthyle), 91,95 (s, C-3a), 110–160,15 (15 signaux de carbones aromatiques), 168 (s, C=O ester). Anal. calc. pour $C_{29}H_{31}N_3O_5$: C69,44, H 6,23, N 8,38; tr. : C 69,36, H 6,32, N 8,29.

1-para-*Anisyl-7,8-diméthoxy-4,5-diméthyl-3-phényl-3a,4,5,9b-tétrahydropyrazolo[3,4-c]isoquinoléine-3a-carboxylate d'éthyle (**9**b)*

On obtient 1,88 g de cycloadduit (Rdt. 73%), *F* 137°C; ir, ν_{max} : 1740 (ester); rmn ^{1}H, δ : 0,94 (t, 3H, $J_{CH_3-CH_2}$ = 7,10 Hz, CH_3 de éthyle), 1,62 (d, 3H, $J_{CH_3-H\text{-}5}$) = 6,95 Hz, CH_3-5), 2,05 (s, 3H, N-CH_3), 3,51 (s, 3H, OCH_3), 3,87 (s, 3H, OCH_3), 3,90 (s, 3H, OCH_3), 4,04 (partie AB d'un système ABX_3, 2H, J_{AB} = 2,9 Hz, ^3J = 7,10 Hz, CH_2 de éthyle), 4,12 (q, 1H, *J* = 6.95 Hz, H-5), 4,85 (s, 1H, H-9b), 6,70–7,80 (m, 11H arom.); rmn ^{13}C, δ : 13,60 (q, *J* = 127 Hz, CH_3 de éthyle), 18,30 (q, *J* = 127,1 Hz, CH_3-5), 33,15 (q, *J* = 135,2 Hz, N-CH_3), 50,75 (d, *J* = 136,2 Hz, C-9b), 55,75 (d, *J* = 135,8 Hz, C-5), 55,20 (q, *J* = 144 Hz, OCH_3), 55,30 (q, *J* = 144,2 Hz, OCH_3), 55,70 (q, *J* = 143,9 Hz, OCH_3), 61,40 (t, *J* = 145 Hz, CH_2 de éthyle), 90,25 (s, C-3a), 108,9–160 (15 signaux de carbones aromatiques), 169,9 (s, C=O ester). Anal. calc. pour $C_{30}H_{33}N_3O_5$: C 69,88, H 6,45, N 8,15; tr. : C 71,02, H 6,37, N 8,22.

*Saponification du cycloadduit **9**. Obtention de la 1*-para-*anisyl-8,9-diméthoxy-5-méthyl-3-phényl-5,6-dihydro-4H-pyrazolo[3,4-c]benzo(e)azepin-4-one (**10**a)*

On dissout 0,5 g (1 mmol) de cycloadduit **9***a* dans 30 mL d'une solution méthanolique de potasse 2 N. Le mélange est porté à reflux pendant 1 h. On laisse refroidir et verse dans 200 mL d'eau. Le précipité est filtré, lavé à l'eau, essoré et recristallisé dans l'éthanol. On obtient 0,26 g de produit (Rdt. 58%), *F* 234°C; ir, ν_{max} : 1635 (lactame); rmn ^{1}H, δ : 3,15 (s, 3H, N-CH_3), 3,49 (s, 3H, OCH_3), 3,83 (s, 3H, OCH_3), 3,94 (s, 3H, OCH_3), 4,05 (d, 1H, ^2J = 14,20 Hz, H-6), 4,75 (d, 1H, ^2J = 14,20 Hz, H'-6), 6,90–7,70 (m, 11H arom.). Anal. calc. pour $C_{27}H_{25}N_3O_4$: C 71,19, H 5,53, N 9,23; tr. : C 71,27, H 5,47, N 9,05.

*Hydrolyse acide du cycloadduit **9**a. Obtention du 4-(4,5-diméthoxy-2-*N*-méthylaminométhylphényl)-3-*para*-anisyl-1-phényl-pyrazole-5-carboxylate d'éthyle (**11**a)*

Une solution de 1 g (2 mmol) de cycloadduit **9***a* dans 20 mL d'acide acétique est portée à léger reflux durant 1 h. Après refroidissement, la solution est versée dans 250 mL d'eau, neutralisée par du bicarbonate de sodium solide puis extraite trois fois avec 50 mL de chloroforme. Les phases organiques sont réunies, laveés à l'eau et séchées sur Na_2SO_4. Après évaporation le résidu est cristallisé dans l'éthanol. On obtient 0,55 g de produit (Rdt. 55%), *F* 200°C; ir, ν_{max} : 3400 (NH), 1710 (ester); rmn ^{1}H, δ : 0,90 (t, 3H, $J_{CH_3-CH_2}$ = 7,10 Hz, CH_3 de éthyle), 2,25 (s, 3H, N-CH_3), 3,90–4,10 (m, 4H, CH_2 de éthyle et N-CH_2), 3,76 (s, 3H, OCH_3), 3,87 (s, 3H, OCH_3), 4,05 (s, 3H, OCH_3), 6,70–7,70 (m, 11 H arom.). Anal. calc. pour $C_{29}H_{31}N_3O_5$: C 69,44, H 6,23, N 8,38; tr. : C 69,52, H 6,37, N 8,26.

La saponification de ce composé **11***a* dans les mêmes conditions que celles décrites pour le cycloadduit **9***a* conduit à l'azépinone **10***a* avec un rendement de 65%.

*Acétylation du composé **11**a. Obtention du 4-(2-*N*-acétyl-N-méthylaminométhyl-4,5-diméthoxyphényl)-3-*para*-anisyl-1-phényl-pyrazole-5-carboxylate d'éthyle (**12**a)*

À un mélange de 1 mmol (0,5 g) de composé **11***a* et 1 mmol de pyridine, on ajoute lentement et sous agitation 1 mmol de chlorure d'acétyle. L'agitation est ensuite prolongée pendant 12 h à température ambiante et on ajoute de la glace sur le mélange réactionnel. On additionne ensuite du bicarbonate de sodium pour atteindre pH 10 et laisse reposer 24 h. Le solide formé est filtré, lavé à l'eau, essoré et purifié par cristallisation dans l'éthanol. On obtient 0,43 g de produit (Rdt. 79%), *F* 90°C; ir, ν_{max} : 1720 (ester), 1640 (amide); rmn ^{1}H (certains signaux sont dédoublés par suite de l'existence de deux rotamères), δ : 0,90 (t, 3H, $J_{CH_3-CH_2}$ = 7,00 Hz, CH_3 de éthyle), 1,83 et 1,98 (2s pour 3H, $COCH_3$), 2,54 et 2,73 (2s pour 3H, N-CH_3), 3,77, 3,86 et 3,92 (3s pour 9H, 3 groupes OCH_3), 4,05 (partie AB d'un système ABX_3, 2H, J_{AB} = 16 Hz et ^3J = 7 Hz, CH_2 de éthyle), 4,30 (centre d'un système AB, 2H, J_{AB} = 16,70 Hz, N-CH_2), 6,60–7,60 (m, 11H arom.). Anal. calc. pour $C_{31}H_{33}N_3O_6$: C 68,49, H 6,12, N 7,73; tr. : C 68,58, H 5,96, N 7,67.

*Saponification du composé **12**a. Obtention de l'acide 4-(2-*N*-acétyle-N-méthylaminométhyl-4,5-diméthoxyphényl)-3-*para*-anisyl-1-phénylpyrazole-5-carboxylique (**13**a)*

À une solution de 1 mmol de composé **12***a* (0,545 g) dans 20 mL de méthanol, on ajoute 10 mL d'une solution méthanolique de potasse 2 N. Le mélange est porté à reflux pendant 1 h. Après élimination du solvant à l'évaporateur rotatif, on reprend à l'eau et acidifie par HCl à 10%. Le précipité est filtré, lavé et séché. On obtient 0,51 g de produit (Rdt. quantitatif), *F* >250°C; ir, ν_{max} : 1710 (acide), 1640 (amide); rmn ^{1}H (certains signaux sont dédoublés par suite de l'existence de deux rotamères), δ : 1,75 et 1,90 (2s pour 3H, $COCH_3$), 2,50 et 2,70 (2s pour 3H, N-CH_3), 3,80, 3,86 et 3,90 (3s pour 9H, 3 groupes OCH_3), 3,95–4,45 (m pour 2 syst. AB imbriqués, N-CH_2), 6,50–7,60 (m, 11H arom.), 8,80 (sl, OH de CO_2H). Anal. calc. pour $C_{29}H_{29}N_3O_6$: C 67,55, H 5,65, N 8,15; tr. : C 67,73, H 5,88, N 8,23.

*Décarboxylation de l'acide **13**a. Obtention du 4-(2-*N*-acétyl-N-méthylaminométhyl-4,5-diméthoxyphényl)-3-*para*-anisyl-1-phénylpyrazole (**14**a)*

Dans un ballon à fond rond de 20 mL, on place 0,51 g d'acide **13***a* (1 mmol) et à l'aide de la flamme d'un bec Bunsen, on le porte à fusion et chauffe (avec attention pour éviter tout charbonnement) jusqu'à cessation du dégagement de dioxyde de carbone. Le produit restant est repris par de l'éthanol après refroidissement et cristallise. On obtient 0,335 g de produit (Rdt. 71%); ir, ν_{max} : 1635 (amide); rmn ^{1}H (certains signaux sont dédoublés par suite de l'existence de deux rotamères), δ : 1,80 et 2,05 (2s pour 3H, $COCH_3$), 2,60 et 2,75 (2s pour 3H, N-CH_3), 3,80, 3,85 et 3,95 (3s pour 9H, 3 groupes OCH_3), 4,15 et 4,40 (2s pour 2H, N-CH_2), 6,60–7,80 (m, 11H arom.), 7,90 (s, 1H, H-5). Anal. calc. pour $C_{28}H_{29}N_3O_4$: C 71,32, H 6,20, N 8,91; tr. : C 71,47, H 6,02, N 8,78.

1. T. Lakhlifi, A. Sedqui, B. Laude, Nguyen Dinh An et J. Vebrel. Can. J. Chem. **69**, 1156 (1991).
2. S. Kitane, K. Tshiamala, B. Laude, J. Vebrel et E. Cerutti. Tetrahedron, **41**, 3737 (1985).
3. S. F. Dyke, M. Sainsbury et J. R. Evans. Tetrahedron, **29**, 213 (1973).
4. R. Huisgen, M. Seidel, G. Wallbillich et H. Knupfer. Tetrahedron, **17**, 3 (1962).

5. K. Tshiamala, S. Kitane, J. Vebrel et B. Laude. Bull. Soc. Chim. Belg. **95**, 1083 (1986).
6. K. N. Houk et K. Yamaguchi. *Dans* 1,3-Dipolar cycloaddition chemistry. Vol. 2. *Editeur*: A. Padwa. J. Wiley and Sons, New-York. 1984. p. 440.
7. B. Daou et M. Soufiaoui. Tetrahedron, **45**, 3351 (1989).
8. J. Elguero, R. Jacquier et J. L. Imbach. J. Chem. Phys. **62**, 643 (1965).
9. J. Elguero, R. Jacquier et G. Tarrago. Bull. Soc. Chim. Fr. 2981 (1966).
10. K. Moustaid, Nguyen Dinh An, J. Vebrel, B. Laude, B. Daou et M. Soufiaoui. C.R. Acad. Sci. Paris, Ser. 2, **312**, 1129 (1991).
11. F. Theobald, N. Rodier, K. Moustaid, Nguyen Dinh An et B. Laude. Acta Crystallogr. Sous presse.
12. R. Mercier, S. Kitane, K. Tshiamala, J. Vebrel, B. Laude et G. M. Sheldrick. Acta Crystallogr. Sect. C: Cryst. Struct. Commun. **C42**, 1844 (1986).

Can. J. Chem. Downloaded from www.nrcresearchpress.com by 92.62.229.171 on 09/08/12
For personal use only.

Structure cristalline et moléculaire d'un composé tricyclique contenant le cycle à dix chaînons dioxo diaza diphosphécine

BRIGITTE DUTHU, KARIM EL ABED, DOURAID HOUALLA[1] ET ROBERT WOLF
Unité de recherche associée au Centre National de la recherche scientifique n° 454, Université Paul Sabatier, 31062 Toulouse CEDEX, France

ET

JOËL JAUD
Centre d'élaboration des matériaux et d'études structurales du Centre National de la Recherche Scientifique, 29 rue Jeanne Marvig, 31400 Toulouse, France

Reçu le 6 mars 1991[2]

BRIGITTE DUTHU, KARIM EL ABED, DOURAID HOUALLA, ROBERT WOLF et JOËL JAUD. Can. J. Chem. **70**, 809 (1992).

La sulfuration de l'organophosphoré tricyclique dimère **2** conduit facilement au dérivé tricyclique disoufré **3**. Ce dernier a été caractérisé par RMN ^{31}P, ^{1}H et ^{13}C, analyse élémentaire et spectrométrie de masse. Sa structure cristalline et moléculaire a été établie par diffraction des rayons X et comparée à celle de **2** qui avait été déterminée précédemment. L'utilisation conjointe des données de RMN et de diffraction des rayons X a permis de bien préciser la structure moléculaire des deux composés. Une estimation chiffrée de l'ouverture du cône d'anisotropie de la double liaison P═S est proposée.

Mots clés : phosphécine, RMN, rayons X, tricycle.

BRIGITTE DUTHU, KARIM EL ABED, DOURAID HOUALLA, ROBERT WOLF, and JOËL JAUD. Can. J. Chem. **70**, 809 (1992).

The sulfuration of the tricyclic organophosphorus dimer **2** leads easily to the dithiotricyclic derivative **3**, which has been characterized by ^{31}P, ^{1}H, and ^{13}C NMR, elemental analysis, and mass spectroscopy. Its crystal and molecular structure has been established by X-ray diffraction and compared to that of **2**, which was previously determined. The comparative analysis of X-ray diffraction and NMR parameters gives accurate information about the molecular structure of both compounds. A numerical value of the anistropy cone of the P═S double bond is proposed.

Key words: phosphecine, NMR, X-ray, tricycle.

Can. J. Chem. Downloaded from www.nrcresearchpress.com by 92.62.229.171 on 09/08/12
For personal use only.

Introduction

Dans un article précédent, nous avons décrit la structure cristalline et moléculaire de l'octahydro-2,2,6,6,10,10,14,14-octaméthyl bis-1,2,3-oxazaphospholo[2,3-*b* : 2′,3′-*g*]-1,6,3,8,2,7-dioxadiazadiphosphécine **2** (1) qui résulte de la dimérisation, par rupture–fermeture d'une liaison P—O, du bicyclophosphane[3] **1**.

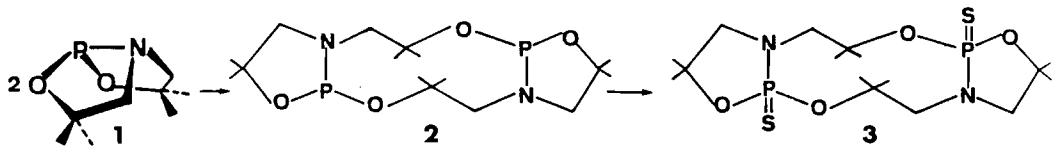

La formation spontanée, à la température ambiante, de ce dimère traduit, à notre sens, le relâchement de la contrainte inhérente à la géométrie en forme de toit à double pente adoptée par le bicyclophosphane **1** ainsi que par tous les composés de cette famille (2, 3).

Parmi les différentes réactions (alcoolyse, acidolyse . . .) conduites avec le composé **2** la sulfuration donne très facilement le dérivé soufré **3** dont nous avons établi la structure cristalline et moléculaire par diffraction des rayons X.

Dans cet article nous décrivons cette structure et la comparons à celle de **2**. Nous présentons également une étude comparative des données de diffraction des rayons X et des paramètres de RMN (^{1}H et ^{13}C) des deux composés qui nous permet de compléter notre connaissance de leurs structures moléculaires.

Résultats et discussion

L'action du soufre élémentaire, en quantité équimoléculaire, sur le dimère **2** a lieu en solution dans le toluène. Dès la dissolution totale du soufre, le spectre de RMN ^{31}P de cette solution montre la disparition du signal à $\delta\ ^{31}P = 140$ ppm dû au dimère **2** et son remplacement par un pic unique à $\delta = 71{,}5$ ppm. Une légère concentration de la solution laisse déposer un solide incolore dont le spectre de masse (ionisation chimique par NH_3) montre la présence du pic parent à $m/e^+ = 443$ MH^+ qui est également le pic de base (100%). Ce solide a été, en outre, entièrement caractérisé par analyse élémentaire et RMN (^{1}H et ^{13}C). Une recristallisation soignée dans le toluène sec nous a fourni des cristaux convenables pour l'étude cristallographique par diffraction des rayons X.

Structure

La maille cristalline de **3** contient deux types de molécules cristallographiquement indépendantes dans le rapport de 2 : 1. L'entité majoritaire **3***a* ne possède aucun élément de symétrie; les paramètres structuraux comme les longueurs et

[1]Auteur à qui adresser toute correspondance.

[2]Révision reçue le 25 septembre 1991.

[3]La nomenclature correcte de ce composé est : 3,3,7,7-tétraméthyl-2,8-dioxa-5-aza-1-phospha^{III}bicyclo[3.3.0]octane. Pour des raisons de commodité nous l'appellerons bicyclophosphane.

Can. J. Chem. Downloaded from www.nrcresearchpress.com by 92.62.229.171 on 09/08/12
For personal use only.

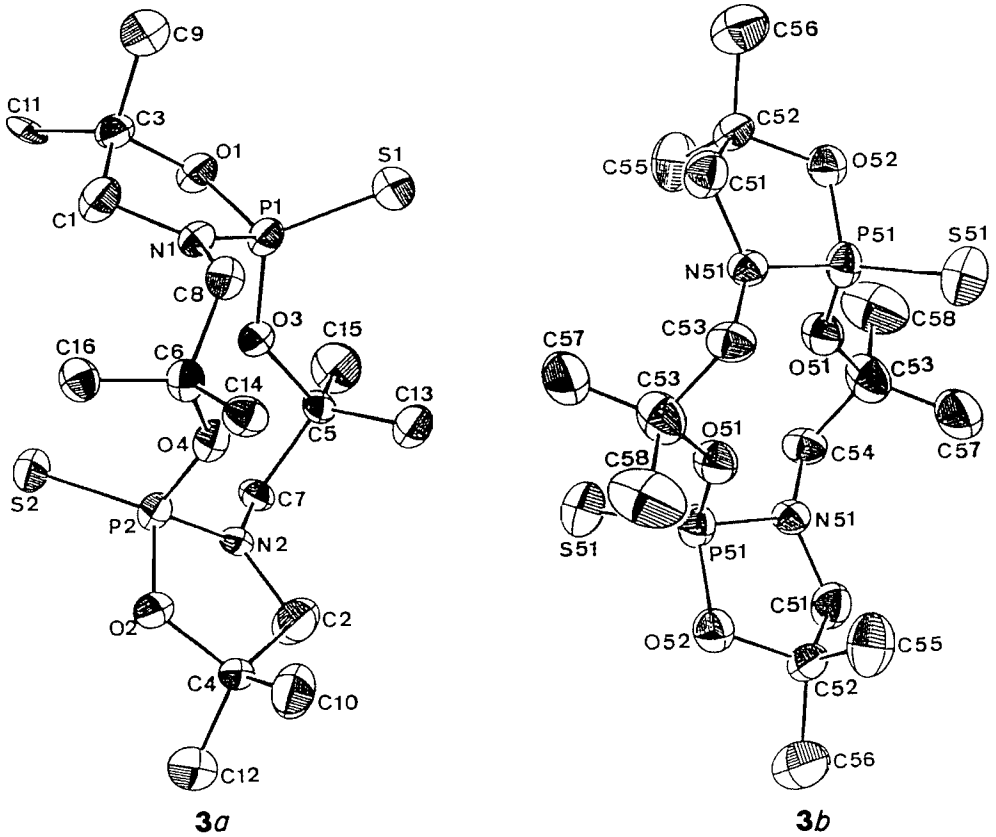

FIG. 1. Représentation ORTEP des 2 molécules présentes dans la maille cristalline de **3**. **3***a* : molécule sans aucune symétrie. **3***b* : molécule centrosymétrique. Pour des raisons de clarté les atomes d'hydrogène ont été omis.

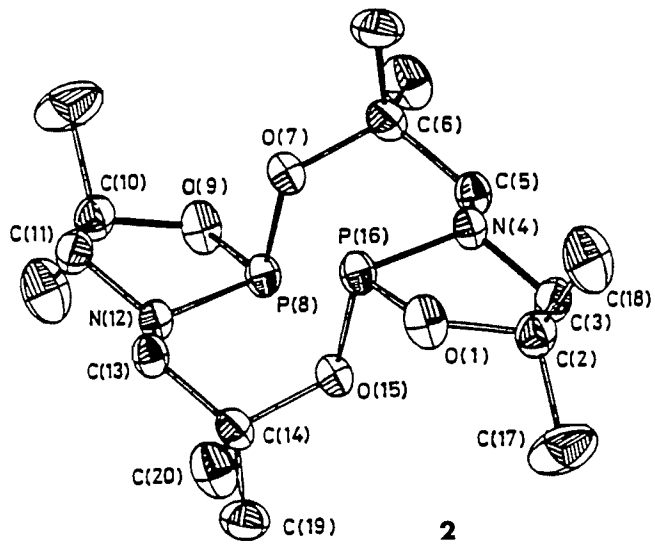

FIG. 2. Représentation ORTEP du dimère **2** extraite de la référence 1.

les angles des liaisons sont tous singuliers. En revanche, l'entité minoritaire **3***b* est, comme le dimère **2** (1), centrosymétrique et s'organise autour d'un centre de symétrie cristallographique. La figure 1 montre une vue perspective de ces deux molécules, les atomes d'hydrogène ayant été omis pour des raisons de clarté. Dans la figure 2, nous avons reproduit une vue perspective du dimère **2**; elle nous permettra de suivre les transformations intervenues suite à la sulfuration.

Les cycles à cinq chaînons P(1)O(1)C(3)C(1)N(1) et P(2)O(2)C(4)C(2)N(2) de **3***a* et les deux cycles analogues P(51)O(52)C(52)C(51)N(51) de **3***b* adoptent tous une forme enveloppe. Dans le premier et les troisièmes, les atomes de carbone en α de l'atome d'oxygène, à savoir C(3) et C(52), sont à la pointe des rabats alors que dans le second, c'est l'atome de carbone C(2) en α de l'atome d'azote qui occupe cette position. Rappelons que dans le composé **2**, les cycles à cinq chaînons homologues adoptent eux aussi une forme enveloppe avec l'atome de carbone C(3) en α de l'atome d'azote à la pointe de rabat (1). Le cycle à dix chaînons N(1)P(1)O(3)C(5)C(7)N(2)P(2)O(4)C(6)C(8) de **3***a* ne peut être décrit par aucune forme géométrique simple alors que celui de **3***b* formé par les atomes N(51)P(51)O(51)C(53)C(54) et leurs homologues cristallographiques adopte, comme dans le dimère **2**, une forme bateau–chaise–bateau.

La sulfuration de **2** se traduit par une augmentation sensible de la somme des trois angles intracycliques des liaisons autour du phosphore en pont : cette valeur passe de 293,7° dans **2** (1) à 315,3° autour de P(1), 314,5° autour de P(2) et 311,4° autour de P(51). Cette modification est tout à fait conforme à ce qui est attendu quand la coordination de l'atome de phosphore passe de 3 à 4. Dans le même temps, la somme des angles des liaisons autour de l'atome d'azote, qui était de 344,7° dans **2** (1) atteint 359,9° autour de N(1), 360° autour de N(2) et 353,9° autour de N(51). Par comparaison avec la valeur de 322,4° trouvée dans le double ad-

TABLEAU 1. Paramètres de RMN ^1H des composés **2** et **3**. Solvant : C_6D_6; 250 MHz

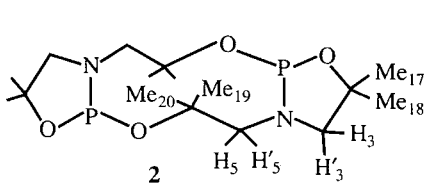

2

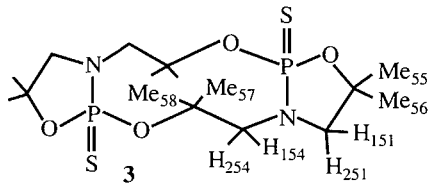

3

2			**3**		
Proton	δ (ppm)	*J* (Hz)	Proton	δ (ppm)	*J* (Hz)
Me(17)	1,36 (s)		Me(55) ou(56)	1,40 (s)	
Me(18)	1,44 (s)		Me(56) ou(55)	1,35 (s)	
Me(20)	1,61 (s)		Me(57) ou(58)	1,47 (s)	
Me(19)	1,62 (d)	$^4J_{H\text{-}C\text{-}C\text{-}O\text{-}P}$ = 1,8	Me(58) ou(57)	1,83 (s)	
H(3)	2,63 (dd)	$^2J_{H(3)H'(3)}$ = 8,2 $^3J_{H(3)P}$ = 12,4	H(151)	2,7 (dd)	$^2J_{H(151)H(251)}$ = 8,7 $^3J_{H(151)P}$ = 8,7
H'(3)	3,23 (dd)	$^3J_{H'(3)P}$ = 1,7	H(251)	3,20 (dd)	$^3J_{H(251)P}$ = 13,9
H(5)[a]	3,00	$^2J_{H(5)H'(5)}$ = 13 $^3J_{H(5)P}$ = 16,8	H(154)	2,12 (ddd)	$^3J_{H(154)P}$ = 12,7 $^4J_{J(154)P}$ = 7,1
H'(5)[a]	3,25	$^3J_{H'(5)P}$ = 10,6 $^4J_{H'(5)P}$ = 1,5	H(254)	3,81 (dd)	$^2J_{H(254)H(154)}$ = 14,7 $^3J_{H(254)P}$ = 10,6

[a]H(5) et H'(5) constituent la partie AB d'un système ABX (X = P).

duit **4** (4) on voit bien que le relâchement de la contrainte due à la double cyclisation a permis à l'atome d'azote de retrouver la conformation plane qu'il a généralement quand il est directement lié à l'atome de phosphore.

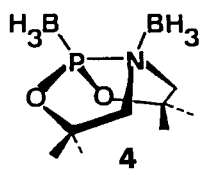

4

Étude RMN

RMN ^1H

Les spectres de RMN ^1H de **2**[4] et de **3** correspondent à des molécules symétriques : dans les deux composés les huit substituants CH_3 et les quatre groupements N-CH_2 donnent respectivement naissance à quatre et deux signaux seulement. Dans le cas de **2**, ceci veut dire qu'à la température d'enregistrement des spectres (24°C) la conformation moyenne, vue en RMN, est compatible avec la structure moléculaire déterminée par diffraction des rayons X. Il en est de même pour **3**. En effet, la conformation asymétrique **3***a*, présente dans la maille cristalline, diffère très peu de la conformation centrosymétrique **3***b*. Sa distorsion est très probablement due à l'asymétrie de l'empilement, laquelle va disparaître lors du passage en solution.

L'analyse complète des ces spectres fournit les paramètres rassemblés dans le tableau 1. Un examen comparatif de ces données permet les remarques et commentaires suivants :

(*i*) Parmi les quatre groupes CH_3 du dimère **2**, il en existe un (δ = 1,62 ppm) qui présente un couplage $^4J_{H\text{-}C\text{-}C\text{-}O\text{-}P}$ de 1,8 Hz avec le phosphore. L'examen d'un modèle moléculaire montre que la conformation enveloppe du cycle à cinq chaînons avec l'atome de carbone C(3) à la pointe du rabat (1) ne permet à aucun substituant CH_3 de ce cycle de se trouver dans la position spatiale communément requise (planéité des quatre liaisons concernées, règle de M), pour qu'un tel couplage existe. En revanche un des substituants CH_3 du cycle à dix chaînons peut très bien occuper cette position spatiale compte tenu de la forme bateau–chaise–bateau de ce cycle. Cette analyse est confirmée par l'exploitation des données de diffraction des rayons X qui montre que les quatre atomes P(16), O(15), C(14) et C(19) se trouvent dans un plan qui contient un des protons portés par C(19). Il nous paraît raisonnable d'attribuer le signal à δ = 1,61 ppm au second substituant CH_3 du carbone C(14). Il en résulte que les pics à δ = 1,36 ppm et δ = 1,44 ppm sont attribuables aux deux groupes CH_3 portés par l'atome de carbone C(2).

Dans le dimère **3**, les 4 groupes CH_3 donnent naissance à 4 signaux dont aucun n'est dédoublé par couplage lointain avec le phosphore. Par comparaison avec **2**, nous attribuons les pics les plus déblindés à δ = 1,47 ppm et δ = 1,83 ppm aux substituants CH_3 du cycle à 10 chaînons et, par conséquent, les pics à δ = 1,40 ppm et δ = 1,35 ppm aux substituants CH_3 du cycle à 5 chaînons.

(*ii*) Il existe dans chacun des composés **2** et **3**, un seul groupe de protons NCH_2 dans lequel un des deux protons présente un couplage supplémentaire, à travers quatre liaisons, avec le phosphore : H'(5) pour **2**, $^4J_{H\text{-}C\text{-}C\text{-}O\text{-}P}$ = 1,5 Hz; H(154) pour **3**, $^4J_{H\text{-}C\text{-}C\text{-}O\text{-}P}$ = 7,1 Hz. Il est évident que ce groupe appartient obligatoirement au cycle à dix chaînons. En effet, les protons NCH_2 du cycle à cinq chaînons ne peu-

[4]L'étude détaillée des spectres de RMN (^1H et ^{13}C) de **2** n'avait pas été effectuée lors de la description de sa structure cristalline et moléculaire (1).

Can. J. Chem. Downloaded from www.nrcresearchpress.com by 92.62.229.171 on 09/08/12
For personal use only.

TABLEAU 2. Paramètres de RMN ^{13}C des composés **2** et **3**. Solvant : C_6D_6; 62,89 MHz

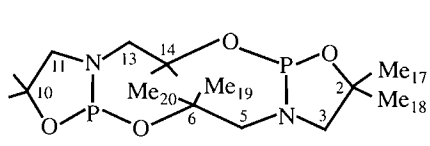

2

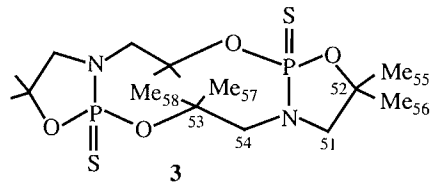

3

2			**3**		
Carbone	δ (ppm)	*J* (Hz)	Carbone	δ (ppm)	*J* (Hz)
C(19)	28,0 (d)	$^3J_{C\text{-}C\text{-}O\text{-}P}$ = 22,3	C(57)	25,6(d)	$^3J_{C\text{-}C\text{-}O\text{-}P}$ = 2,3
C(20)	28,9 (d)	$^3J_{C\text{-}C\text{-}O\text{-}P}$ = 4,3	C(55) ou(58)	27,7 (s)	
C(17) ou(18)	30,0 (s)		C(58) ou(55)	28,1 (s)	
C(18) ou(17)	30,2 (s)		C(56)	28,3 (d)	$^3J_{C\text{-}C\text{-}O\text{-}P}$ = 7,6
C(5)C(13)	59,5 (dd)	$^2J_{C\text{-}N\text{-}P}$ = 7,5 $^3J_{C\text{-}C\text{-}O\text{-}P}$ = 9,8	C(54)	58,2 (dd)	$^2J_{C\text{-}N\text{-}P}$ = 7,5 $^3J_{C\text{-}C\text{-}O\text{-}P}$ = 8,2
C(3)C(11)	62,9 (d)	$^2J_{C\text{-}N\text{-}P}$ = 4,5[a]	C(51)	62,2 (d)	$^2J_{C\text{-}N\text{-}P}$ = 14,3[a]
C(6)C(14)	76,7 (d)	$^2J_{C\text{-}O\text{-}P}$ = 6,1	C(53)	82,1 (d)	$^2J_{C\text{-}O\text{-}P}$ = 4
C(2)C(10)	83,4 (d)	$^2J_{C\text{-}O\text{-}P}$ = 9,4[b]	C(52)	84,8 (d)	$^2J_{C\text{-}O\text{-}P}$ = 10,2[b]

[a]Ces valeurs sont, en fait, la moyenne des constantes de couplage $^2J_{C\text{-}N\text{-}P}$ et $^3J_{C\text{-}C\text{-}O\text{-}P}$.
[b]De même ces valeurs sont la moyenne de $^2J_{C\text{-}O\text{-}P}$ et de $^3J_{C\text{-}C\text{-}N\text{-}P}$.

vent pas avoir d'autre couplage que $^3J_{H\text{-}C\text{-}N\text{-}P}$ car le nombre de liaisons qui les séparent du second noyau de phosphore est égal à six. En fait les données de rayons X montrent que les quatre atomes P(51), O(51), C(53) et C(54) se trouvent bien dans un plan qui contient un des protons liés à C(54) alors que les atomes analogues de **2**, à savoir P(16), O(15), C(14) et C(13), ne sont pas coplanaires. Toutefois il faut signaler que la détermination de la structure de **2** par diffraction des rayons X a été effectuée à −50°C alors que celle de **3** l'a été à la température ambiante. Il est vraisemblable qu'à la température d'enregistrement des spectres de RMN (24°C) la flexibilité du cycle à dix chaînons de **2** soit telle que les quatre atomes P(16), O(15), C(15) et C(13) puissent se trouver en moyenne dans un plan qui contienne un des protons liés à C(13), ce qui expliquerait le couplage $^4J_{H\text{-}C\text{-}C\text{-}O\text{-}P}$ observé.

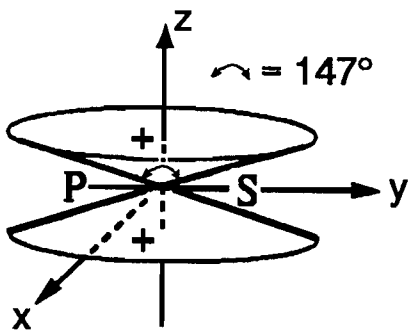

Le passage du dimère **2** à son dérivé soufré **3** se traduit par des variations importantes des déplacements chimiques des substituants CH_3 et des protons NCH_2 du cycle à dix chaînons. Pour les deux groupements CH_3 nous assistons à un blindage de 0,14 ppm de l'un (δ passe de 1,61 ppm à 1,47 ppm) et à un déblindage de 0,21 ppm de l'autre (δ passe de 1,62 ppm à 1,83 ppm). Le même phénomène s'observe avec les protons NCH_2 : celui qui est couplé à travers quatre liaisons avec le phosphore, H(154), subit un blindage de 1,13 ppm (δ passe de 3,25 ppm à 2,12 ppm) alors que l'autre proton NCH_2 est déblindé de 0,81 ppm (δ passe de 3,00 ppm à 3,81 ppm). Il est clair que ces variations sont attribuables aux effets d'anisotropie résultant du remplacement du doublet libre du phosphore dans **2** par la double liaison P═S. Connaissant les positions spatiales des protons H(154) et H(254) qui subissent ces effets, nous pouvons estimer à 147° ± 12[5] la valeur de l'ouverture de la zone de blindage du cône P═S.

RMN ^{13}C

L'analyse des spectres de RMN ^{13}C de **2** et de **3** apporte quelques précisions complémentaires.

Dans chaque composé les signaux correspondant aux quatre groupes CH_3 se présentent comme deux doublets et deux singulets (voir tableau 2). Pour l'attribution de ces signaux, nous nous sommes appuyés sur les données structurales fournies par la diffraction des rayons X. En effet, il est connu que la constante de couplage $^3J_{C\text{-}C\text{-}O\text{-}P}$ obéit à une loi comparable à la loi de Karplus relative à la constante de couplage $^3J_{H\text{-}C\text{-}C\text{-}H}$ (5). Dans le dimère **2**, les quatre angles dièdres concernés sont : P(16)—O(1)—C(2)—C(17) = 124,6°(8), P(16)—O(1)—C(2)—C(18) = 115,4°(8), P(16)—O(15)—C(14)—C(19) = −177,9°(8) et P(16)—O(15)—C(14)—C(20) = −59.6°(8). L'attribution de la grande constante de couplage 22,3 Hz au carbone C(19) (δ = 28,0 ppm) paraît cohérente. Le fait qu'en RMN ^1H les

[5]Les valeurs extrêmes de cet angle ont été obtenues en calculant l'angle entre la perpendiculaire à la liaison P—S menée en son milieu I et la droite IH(154) d'une part, et la droite IH(254) d'autre part.[6]

[6]À notre connaissance, il n'existe, dans la littérature, aucune valeur chiffrée de l'ouverture du cône d'anisotropie de la double liaison P═S.

Can. J. Chem. Downloaded from www.nrcresearchpress.com by 92.62.229.171 on 09/08/12
For personal use only.

TABLEAU 3. Données cristallographiques et conditions de mesure pour **3**

Données cristallographiques

Formule brute : $C_{16}H_{32}N_2O_4P_2S_2$ — Masse molaire : 442,5
Système cristallin : monoclinique — Groupe d'espace : $P2_1/C$
a = 17,953 Å — V = 3363 Å^3
b = 12,832 Å β = 115,00° — Z = 6
c = 16,11 Å — $F(000)$ = 1416
ρ_m = 1,31 g cm^{-3} — μ(MoK$\bar{\alpha}$) = 0,39 cm^{-1}

Enregistrement des données

Température : 20°C
Radiation : MoK$\bar{\alpha}$ λ = 0,71069 Å; monochromateur : graphite
Distance cristal–détecteur : 207 mm
Fenêtre détecteur; hauteur : 4 mm, largeur : 4 mm
Angle de fuite : 3,2°
Mode de balayage : $\theta/2\theta$
Angle de Bragg maximum : 27°. Indice $0 \leq h \leq 21$, $0 < k \leq 8$, $-18 \leq l \leq 18$
Largeur de balayage : (0,8 + 0,347 tg θ)°
Paramètres pour la détermination de la vitesse de balayage (12) :
SIGPRE = −7; SIGMA = −0,15; VPRE = 10 min^{-1}; TMAX = 80 s
Contrôles : intensité, orientation
Périodicité : 3600 s 100 réflexions

Affinement

Nombre de réflexions pour affinement des paramètres cristallins : 25
Nombre de réflexions indépendantes : 4773
Nombre de réflexions observées : $2716 > 2\sigma(I)$
Nombre de paramètres affinés : 353
Facteurs de convergence finaux : R = 0,057; R_w = 0,062 S = 1,62
Fonction de minimisation : $\Sigma w(|F_o| - |F_c|)^2$
$R = \Sigma(|F_o| - k|F_c|)/\Sigma|F_o|$
$S = [\Sigma w(|F_o| - |F_c|)^2/(m - n)]^{1/2}$
m = nombre de réflexions
n = nombre de paramètres affinés
w = schéma de pondération avec poids unitaire

déplacements chimiques des substituants CH_3 portés par le même cycle soient voisins (voir tableau 2) nous incite à considérer qu'il en est de même en RMN ^{13}C. Il en résulte que le signal à δ = 28,9 ppm avec $^3J_{C\text{-}C\text{-}O\text{-}P}$ = 4,3 Hz peut être attribué au noyau de carbone C(20). Dans le composé **3**, les angles dièdres homologues sont : P(51)—O(52)—C(52)—C(55) = −91,1°(8), P(51)—O(52)—C(52)—C(56) = −147,6°(8), P(51)—O(51)—C(53)—C(57) = 43,7°(8) et P(51)—O(51)—C(53)—C(58) = 78,7°(8). Nous attribuons la constante de couplage de 7,6 Hz au carbone C(56) et celle de 2,3 Hz au carbone C(57). On peut remarquer que dans le dimère **2**, les deux noyaux de carbone méthyliques couplés avec le phosphore appartiennent tous les deux au cycle à cinq chaînons, alors que dans son dérivé soufré **3**, l'un appartient au cycle à cinq chaînons, l'autre au cycle à dix chaînons. Il est probable que cette différence est liée à la modification de la position du rabat du cycle à cinq chaînons en passant de **2** à **3** : dans **2** le rabat de l'enveloppe est situé sur l'atome de carbone en α de l'atome d'azote alors que dans **3** il est situé sur l'atome de carbone tertiaire en α de l'atome d'oxygène.

La forme doublet de doublet des signaux à δ = 59,5 ppm dans le spectre de **2** et δ = 58,2 ppm dans celui de **3**, permet d'attributer ces pics aux noyaux de carbone en α de l'atome d'azote des cycles à dix chaînons. Il en résulte que les doublets à δ = 62,9 et 62,2 ppm sont respectivement attribuables aux noyaux de carbone C(3) C(11) de **2** et C(51) de **3**. Le blindage observé en passant du cycle à cinq chaînons au cycle à dix chaînons permet de parachever cette analyse. Les doublets à δ = 76,7 ppm et δ = 83,4 ppm dans le spectre de **2** sont respectivement attribuables aux noyaux C(6) C(14) et C(2) C(10). De même, les doublets à δ = 82,1 ppm et δ = 84,8 ppm dans celui de **3** sont respectivement attribuables aux noyaux de carbone C(53) et C(52). Les déplacements chimiques des noyaux de carbone des cycles à cinq chaînons sont en accord avec les valeurs relevées pour les mêmes noyaux de carbone dans le monomère **1** (6).

Conclusion

Au cours de ce travail nous avons effectué une étude comparative du dimère **2** et de son dérivé soufré **3** à l'aide de la diffraction des rayons X et de la RMN (^{31}P, ^1H et ^{13}C). Le rapprochement des données fournies par ces deux méthodes nous a permis d'avoir une connaissance très précise des structures moléculaires de ces deux composés. Nous avons pu, en particulier, fournir une appréciation chiffrée de l'ouverture du cône d'anisotropie lié à la liaison double P═S.

Partie expérimentale

Méthodes spectroscopiques

Les spectres de RMN ^{31}P, ^1H et ^{13}C ont été enregistrés avec différents spectromètres Bruker : AC 80, WM 250 et AM 300 WB. Les déplacements chimiques, exprimés en parties par million du champ inducteur (ppm), sont mesurés avec une précision de ±0,02

Can. J. Chem. Downloaded from www.nrcresearchpress.com by 92.62.229.171 on 09/08/12
For personal use only.

Can. J. Chem. Downloaded from www.nrcresearchpress.com by 92.62.229.171 on 09/08/12
For personal use only.

TABLEAU 4. Coordonnées atomiques et déviations standards de **3**

Atome	x	y	z	B_{eq} (Å^2)[a]
S1	0,2191(2)	−0,2218(3)	0,2141(2)	4,9
S2	0,1525(1)	0,2181(3)	0,3499(1)	4,0
S51	0,5169(2)	0,1777(4)	0,8432(2)	6,6
P1	0,2166(1)	−0,1115(3)	0,2928(1)	3,2
P2	0,1198(1)	0,1894(3)	0,2224(1)	3,1
P51	0,4774(2)	0,1574(3)	0,9361(2)	4,1
O1	0,2710(3)	−0,1283(6)	0,3991(3)	3,7
O2	0,0597(3)	0,2734(6)	0,1544(3)	3,6
O3	0,2446(3)	−0,0023(6)	0,2747(3)	3,3
O4	0,0772(3)	0,0824(6)	0,1853(3)	3,5
O51	0,4312(4)	0,0535(7)	0,9331(4)	4,7
O52	0,4204(4)	0,2490(7)	0,9407(4)	4,4
N1	0,1298(4)	−0.0938(7)	0,3012(4)	2,9
N2	0,1909(4)	0,1947(7)	0,1837(4)	2,6
N51	0,5438(4)	0,1646(8)	1,0444(5)	3,5
C1	0,1400(5)	−0.084(1)	0,3955(6)	4,5
C2	0,1571(6)	0,236(1)	0,0908(6)	5,9
C3	0,2212(5)	−0,140(1)	0,4521(5)	3,3
C4	0,0815(5)	0,299(1)	0,0779(5)	3,3
C5	0,2867(5)	0,0416(9)	0,2215(5)	2,5
C6	0,0127(5)	0,023(1)	0,1954(5)	3,5
C7	0,2770(5)	0,1573(9)	0,2309(5)	2,9
C8	0,0492(5)	−0.087(1)	0,2230(5)	3,5
C9	0,2106(6)	−0,254(1)	0,4621(7)	5,7
C10	0,0087(7)	0,271(1)	−0,0102(7)	5,9
C11	0.2668(6)	−0.088(1)	0,5437(7)	5,8
C12	0,0966(7)	0,415(1)	0,0839(7)	5,7
C13	0,2474(6)	0,004(1)	0,1220(6)	4,5
C14	−0,0567(5)	0,012(1)	0,0999(6)	4,2
C15	0,3773(6)	0,014(1)	0,2696(7)	5,3
C16	−0,0188(5)	0,067(1)	0,2610(6)	3,9
C51	0,5321(6)	0,260(1)	1,0857(6)	5,0
C52	0,4405(5)	0,283(1)	1,0355(6)	4,1
C53	0,6267(7)	0,017(1)	1,1349(7)	5,9
C54	0,6239(6)	0,112(1)	1,0803(6)	4,3
C55	0,3881(7)	0,220(1)	1,0704(7)	6,8
C56	0,4224(8)	0,398(1)	1,0308(9)	7,5
C57	0,6033(9)	0,036(1)	1,2128(8)	8,2
C58	0,7113(9)	−0.033(1)	1,167(1)	9,2

[a]Les atomes affinés anisotropiquement sont donnés sous la forme d'équivalents isotropiques définis ainsi au moyen des paramètres de la maille : $B_{eq} = 4/3[a^2B(1,1) + b^2B(2,2) + c^2B(3,3) + ab(\cos\gamma)B(1,2) + ac(\cos\beta)B(1,3) + bc(\cos\alpha)B(2,3)]$.

ppm pour ^{1}H et ±0,03 ppm pour ^{31}P et ^{13}C (références : tétraméthylsilane, TMS, ^{1}H et ^{13}C; H_3PO_4 à 85% pour ^{31}P). Les constantes de couplage, exprimées en Hz, sont mesurées avec une précision de ±0,2 Hz pour ^{1}H et ±0,5 Hz pour ^{13}C. La résolution complète des spectres a été parachevée par des expériences de découplage homonucléaire proton–proton et hétéronucléaire proton–phosphore, carbone–proton et carbone–phosphore. Le spectre de masse a été obtenu avec un spectromètre Nermag R10 utilisant l'ionisation chimique par NH_3.

Données cristallographiques

Les paramètres et le groupe spatial du composé **3** ont été déterminés à l'aide d'un diffractomètre automatique quatre cercles Enraf–Nonius du type CAD 4, également utilisé pour la collection des données (25 réflexions situées dans une couronne de 12° à 14° en angle de Bragg ont servi à déterminer la maille du cristal mesuré).

Les données cristallographiques et les conditions de mesure et d'affinement sont regroupées dans le tableau 3.

Aucune correction de décroissance d'intensité n'a été nécessaire, les taches choisies comme étalons étant restées stables au cours du temps (variation moyenne inférieure à 3%). Les données ont été corrigées des facteurs de Lorentz et de la polarisation. L'examen des taches azimuthales n'ayant pas montré de variation significative lors de la rotation autour du vecteur de diffusion, la correction d'absorption a été négligée.

La structure a été déterminée par utilisation des méthodes directes (7) (MULTAN 1982). L'ensemble des calculs cristallographiques a été effectué sur VAX 730 de Digital en utilisant la chaîne SDP de Frenz (8). Cette détermination montre la présence dans la maille de six molécules; deux d'entre elles s'organisent autour d'un centre de symétrie (la notation appliquée commence par l'atome P(51)) tandis que les quatre autres molécules sont situées en position générale dans la maille (la numérotation débute par l'atome P(1)).

L'affinement des paramètres d'agitation thermique et des positions de l'ensemble des atomes a été effectué, avant de localiser les atomes d'hydrogène, par séries de Fourier différence. Après avoir été recalculée afin de fixer les distances C—H à 0,97 Å, l'agitation thermique des atomes d'hydrogène a été prise telle que $B_{iH} = 1{,}2\ B_{iC}$. Les positions et l'agitation thermique de ces atomes ont alors été fixées, leurs contributions étant seulement introduites dans le calcul. Dans ces conditions la valeur du facteur d'accord est de 0,057.

Pour tous les atomes, les facteurs de diffusion sont ceux mentionnés par Cromer et Waber (9). La diffusion anomale des atomes de phosphore, soufre, oxygène et azote utilise les valeurs des tables internationales (Cromer et Liberman (10)). À l'issue du dernier affinement la série différence finale n'a montré aucun résidu significatif, les valeurs extrêmes des densités électroniques étant de −0,4 et de +0,3 électron.

Au dernier tour d'affinement la valeur maximum du rapport Δ/σ est de 0,075 et la moyenne est d'environ 0,03.

Les coordonnées atomiques et les facteurs d'agitation thermique équivalents des atomes semi-lourds sont regroupés dans le tableau 4,[7] tandis que la numérotation de ces mêmes atomes est indiquée sur les représentations perspectives des molécules (ORTEP) (11). Les distances et angles interatomiques sont regroupés dans les tableaux 5 et 6.

Préparation de **3**

L'octahydro-2,2,6,6,10,10,14,14-octaméthyl bis-1,2,3 thiooxazaphospho[2,3-*b* : 2′,3′-*g*]-1,6,3,8,2,7 dioxadiazadiphosphécine **3** a été obtenu de la façon suivante.

À une solution de 95 mg ($2{,}5 \times 10^{-4}$ mol) du dimère **2** dans 2 mL de toluène, on ajoute 16 mg (5×10^{-4} mol) de fleur de soufre. La dissolution totale de ce dernier nécessite 30 min de chauffage à 40°C. Le spectre de RMN ^{31}P du mélange réactionnel montre alors la présence d'un signal unique à $\delta\ ^{31}P = 71{,}5$ ppm correspondant au dérivé soufré **3**. Une légère concentration de la solution laisse déposer un solide blanc qui a été lavé à l'hexane et séché sous vide. PF = 180°C. La pureté du produit a été vérifiée par RMN (voir les tableaux 1 et 2), spectrométrie de masse (ionisation chimique NH_3) et analyse élémentaire. SM (intensité relative) : 445 (10,9), 444 (24,4), 443 (100) MH^+. Anal. calcd. pour $C_{16}H_{32}N_2O_4P_2S_2$: C 43,4; H 7,29; N 6,33; trouvé : C 43,42; H 7,34; N 6,26. Une recristallisation dans le toluène a fourni les cristaux qui ont servi à la diffraction des rayons X.

[7]Les tableaux des amplitudes des facteurs de structure, des facteurs d'agitation thermique et des équations des principaux plans moyens sont disponibles. On peut les acheter de : Dépôt de données non publiées, Service de fourniture de documents, ICIST, Conseil national de recherches Canada, Ottawa, Canada K1A OS2.

Les coordonnées atomiques, distances et angles de liaisons sont également disponibles au Cambridge Crystallographic Data Centre. On peut les obtenir en s'adressant au directeur, Cambridge Crystallographic Data Centre, University Chemical Laboratory, Lensfield Road, Cambridge CB2 1EW, Royaume-Uni.

Can. J. Chem. Downloaded from www.nrcresearchpress.com by 92.62.229.171 on 09/08/12
For personal use only.

TABLEAU 5. Distances de liaisons en Å et déviations standards estimées (entre parentheses) pour le composé **3**

Atome 1	Atome 2	Distance	Atome 1	Atome 2	Distance
P1	S1	1,920(5)	N2	C7	1,49(1)
P1	O1	1,593(6)	N51	C51	1,46(2)
P1	O3	1,562(8)	N51	C54	1,47(1)
P1	N1	1,632(8)	C1	C3	1,53(1)
P2	S2	1,922(3)	C2	C4	1,53(2)
P2	O2	1,595(7)	C3	C9	1,50(2)
P2	O4	1,569(9)	C3	C11	1,51(1)
P2	N2	1,637(8)	C4	C10	1,52(1)
P51	S51	1,923(5)	C4	C12	1,51(2)
P51	O51	1,564(9)	C5	C7	1,52(2)
P51	O52	1,583(9)	C5	C13	1,53(1)
P51	N51	1,652(6)	C5	C15	1,52(1)
O1	C3	1,48(1)	C6	C8	1,55(2)
O2	C4	1,49(1)	C6	C14	1,53(2)
O3	C5	1,47(1)	C6	C16	1,51(2)
O4	C6	1,45(1)	C51	C52	1,52(1)
O51	C53	1,46(1)	C52	C55	1,51(2)
O52	C52	1,49(1)	C52	C56	1,52(2)
N1	C1	1,47(1)	C53	C54	1,50(2)
N1	C8	1,467(8)	C53	C57	1,50(2)
N2	C2	1,47(1)	C53	C58	1,52(2)

TABLEAU 6. Angles de liaisons (en degrés) du composé **3**

Atome 1	Atome 2	Atome 3	Angle	Atome 1	Atome 2	Atome 3	Angle
S1	P1	O1	115,9(3)	N2	C2	C4	107,3(9)
S1	P1	O3	116,6(3)	O1	C3	C1	105,2(7)
S1	P1	N1	116,4(3)	O1	C3	C9	107,0(9)
O1	P1	O3	102,9(4)	O1	C3	C11	108,2(8)
O1	P1	N1	96,0(3)	C1	C3	C9	113,0(8)
O3	P1	N1	106,4(4)	C1	C3	C11	111(1)
S2	P2	O2	114,9(3)	C9	C3	C11	111,7(9)
S2	P2	O4	117,3(3)	O2	C4	C2	107,3(8)
S2	P2	N2	117,5(2)	O2	C4	C10	107,7(8)
O2	P2	O4	104,8(3)	O2	C4	C12	105,8(9)
O2	P2	N2	96,8(4)	C2	C4	C10	111,5(9)
O4	P2	N2	102,9(4)	C2	C4	C12	113,5(9)
S51	P51	O51	117,0(4)	C10	C4	C12	110,8(9)
S51	P51	O52	112,9(4)	O3	C5	C7	102,2(8)
S51	P51	N51	118,6(3)	O3	C5	C13	111,5(8)
O51	P51	O52	107,3(4)	O3	C5	C15	108,2(7)
O51	P51	N51	102,7(4)	C7	C5	C13	113,0(8)
O52	P51	N51	95,8(5)	C7	C5	C15	108,6(8)
C1	N1	C8	122,5(7)	C13	C5	C15	112,7(9)
C2	N2	C7	112,6(8)	O4	C6	C8	105,0(7)
C51	N51	C54	120,9(8)	O4	C6	C14	106,5(8)
N1	C1	C3	104,7(8)	O4	C6	C16	115,2(9)
C8	C6	C14	106,2(9)	C51	C52	C56	112(1)
C8	C6	C16	112,7(8)	C55	C52	C56	113(1)
C14	C6	C16	110,8(8)	O51	C53	C54	103,2(8)
N2	C7	C5	113,9(7)	O51	C53	C57	112(2)
N1	C8	C6	116,4(9)	O51	C53	C58	107(1)
N51	C51	C52	104,3(8)	C54	C53	C57	114(1)
O52	C52	C51	103,6(8)	C54	C53	C58	109(1)
O52	C52	C55	107,9(9)	C57	C53	C58	112(2)
O52	C52	C56	106,4(9)	N51	C54	C53	113(1)
C51	C52	C55	113,5(9)				

Remerciements

Les différentes analyses spectroscopiques ainsi que l'analyse élémentaire ont été effectuées dans les services spécialisés du Groupe Régional de Mesures Physiques de Toulouse. Les responsables et le personnel de ces services : Mme Bon, MM. Commenges, Dall'ava, Pelletier, Servin et Tran Le Trang (RMN), Mme Richelme (SM), M. Mila et Mme Bourdil (analyses élementaires) sont chaleureusement remerciés.

1. C. Bonningue, D. Houalla, R. Wolf et J. Jaud. J. Chem. Soc. Perkin Trans. 2, 773 (1983).
2. D. Houalla, F. H. Osman, M. Sanchez et R. Wolf. Tetrahedron Lett. 3041 (1977).
3. C. Bonningue, D. Houalla, M. Sanchez et R. Wolf. J. Chem. Soc. Perkin Trans. 2, 19 (1981).
4. D. Grec, L. G. Hubert-Pfalzgraf, J. G. Riess et A. Grand. J. Am. Chem. Soc. **102**, 7133 (1980).
5. D. Gorenstein. Phosphorus-31 NMR. Principles and applications. Academic Press, New York. 1984. pp. 43–51.
6. B. Duthu, D. Houalla et R. Wolf. Can. J. Chem. **66**, 2965 (1988).
7. P. Main, S. E. Hull, L. Lessinger, G. Germain, J. P. Declerq et M. M. Woolfson. MULTAN (1982), a system of computer programs for the automatic solution of crystal structures from X-ray diffraction data. Universities of York and Louvain.
8. B. A. Frenz *et al.* Structure Determination Package, College Station, Texas; and Enraf–Nonius, Delft, The Netherlands. 1985.
9. D. T. Cromer and J. T. Waber. International tables for X-ray crystallography. Vol. IV. Kynoch Press, Birmingham. 1974. Table 2.2 A.
10. D. T. Cromer and D. Liberman. International tables for X-ray crystallography. Vol. IV. Kynoch Press, Birmingham. 1974. Table 2.3.1
11. C. K. Johnson, ORTEP II, Rep. ORNL-5138, Oak Ridge National Laboratory, Tennessee. 1976.
12. A. Mosset, J. J. Bonnet et J. Galy. Acta Crystallogr. Sect. B: Struct. Crystallogr. Cryst. Chem. **B33**, 2639 (1977).

Can. J. Chem. Downloaded from www.nrcresearchpress.com by 92.62.229.171 on 09/08/12
For personal use only.

Synthesis of torrentin, dihydrosantamarine, and saussurea lactone from santonin

GONZALO BLAY, LUZ CARDONA, BEGOÑA GARCÍA, AND JOSÉ R. PEDRO[1]

Department of Organic Chemistry, Faculty of Chemistry, University of Valencia, E-46100 Burjassot, Valencia, Spain

Received July 22, 1991

GONZALO BLAY, LUZ CARDONA, BEGOÑA GARCÍA, and JOSÉ R. PEDRO. Can. J. Chem. **70**, 817 (1992).

The synthesis of the eudesmanolide torrentin (**1**) by sensitized photooxygenation of synthetic dihydrosantamarine (**3**) is reported. Both dihydrosantamarine and dihydroreynosin (**11**) were obtained from the 1,2-epoxide **9**, which, in turn, was prepared from the diselenide **7**. An improved procedure for the synthesis of the elemanolide saussurea lactone (**4**) is also reported.

Key words: eudesmanolide, elemanolide, santonin, torrentin, saussurea lactone.

GONZALO BLAY, LUZ CARDONA, BEGOÑA GARCÍA et JOSÉ R. PEDRO. Can. J. Chem. **70**, 817 (1992).

On rapporte la synthèse de l'eudesmolide de torrentine (**1**) par une photo-oxygénation de la dihydrosantamarine de synthèse (**3**). On a obtenu à la fois la dihydrosantamarine et la dihydroreynosine (**11**) à partir de l'époxyde **9** qui a par ailleurs été préparé à partir du disélénure **7**. On rapporte aussi une méthode améliorée de synthèse de l'élémanolide lactone de saussurea (**4**).

Mots clés : eudesmanolide, élémanolide, santonine, torrentine, lactone saussurea.

[Traduit par la rédaction]

Torrentin is an eudesmanolide isolated a few years ago (1) from *Artemisia herba-alba* subsp. *valentina*, and whose structure has been revised recently (2). This paper reports on the synthesis of torrentin (**1**) from santonin (**2**) via a multistep reaction sequence involving dihydrosantamarine (**3**) as an intermediate product. It also contributes an improved procedure for the synthesis of saussurea lactone (**4**) from santonin (**2**). The sesquiterpene lactones, which constitute an important group of natural compounds widely distributed in the family Compositae, have received much attention because of their biological activities (3).

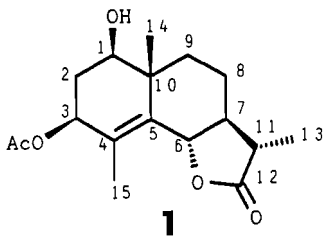

1

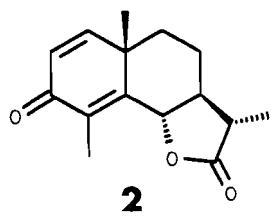

2

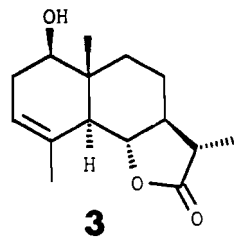

3

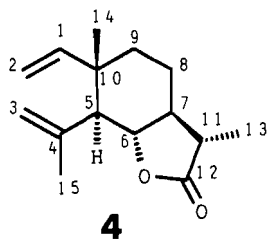

4

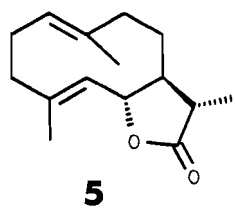

5

Dihydrosantamarine (**3**) was synthesized previously (4) from the dihydrocostunolide (**5**) and, more recently, by an 11-step refunctionalization (5) of the A ring of santonin (**2**). We synthesized dihydrosantamarine (**3**) via a shorter synthetic pathway by applying a new selective transformation of diselenide **7** to the 1,2-epoxide **9**. The conversion of dihydrosantamarine (**3**) into torrentin (**1**) involved the sensitized photooxygenation of the 3,4-double bond of the former as a key step (6).

We used the diol-lactone **6** as starting product, which was prepared from santonin (**2**) according to Grieco (7), i.e., by hydrogenation and epimerization (8) at C4, formation of the corresponding tosylhydrazone and a Shapiro reaction (9), and, finally, the ozonolysis of the 2,3-double bond followed by reduction with sodium borohydride.

Our strategy was based on the synthesis of the 1,2-epoxide **9** from the diol **6** by oxidation–elimination of the diselenide **7** and the simultaneous epoxidation of the resulting double bond. Inasmuch as the elimination of the C2 selenoxide should be faster (10) than that of the C3 selenoxide, the yield of epoxide **9** must be more favourable than that of **10** in relation to those obtained by epoxidation (3) of saussurea lactone (**4**).

With the above ideas in mind, we addressed the synthesis

[1]Author to whom correspondence may be addressed.

Printed in Canada

Can. J. Chem. Downloaded from www.nrcresearchpress.com by 92.62.229.171 on 09/08/12
For personal use only.

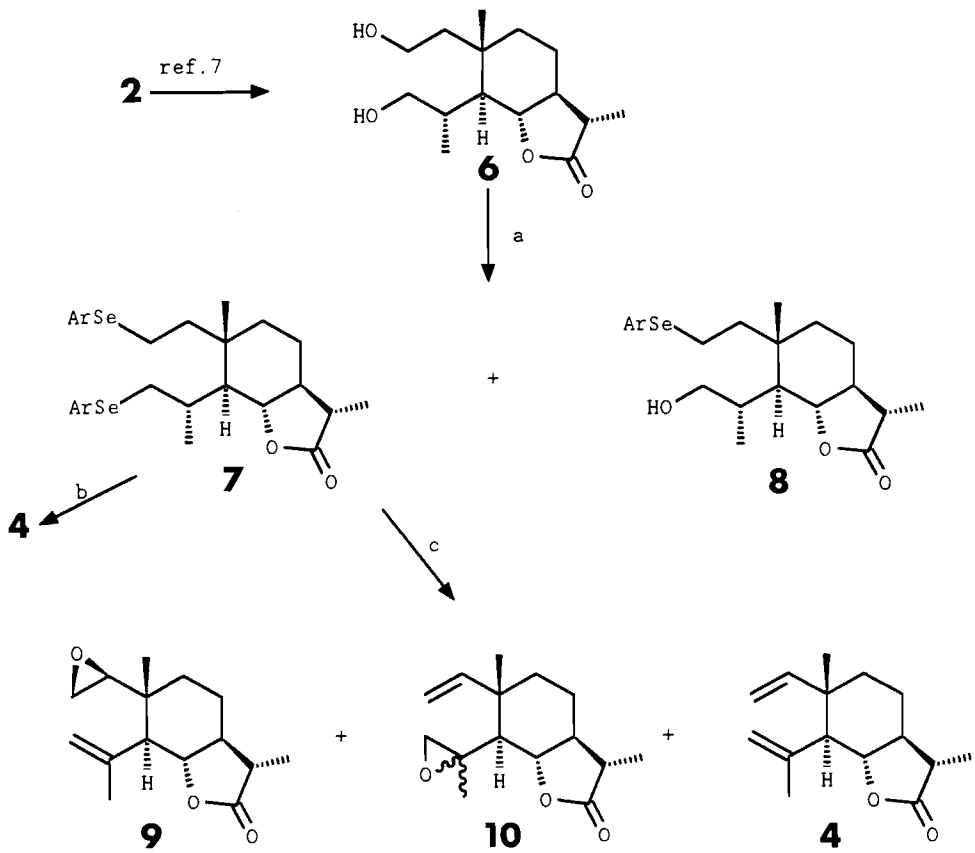

Reagents: (a) 4.8 eq. ArSeCN, *n*-Bu_3P; (b) 30% H_2O_2; (c) *m*-CPBA; Ar = *o*-$NO_2C_6H_4$-

SCHEME 1

of the diselenide **7** from the diol **6** by reaction with *o*-nitrophenylselenocyanate-tri-*n*-butylphosphine. Despite Grieco's explicit claim that **7** cannot be synthesized (7), our past experience with similar substrates (11, 12) told us that the synthesis in question should pose no problem. In fact, the diselenide **7** was obtained with a yield of 72% by reaction of the diol **6** with 4.8 equivalents of *o*-nitrophenylselenocyanate–tri-*n*-butylphosphine in THF–pyridine. Diselenide **7** was subjected to various simultaneous oxidation–elimination and epoxidation procedures with epoxidizing reagents such as sodium perborate/acetic anhydride (13), *p*-nitroperoxybenzoic acid (14), trifluoroacetic anhydride/H_2O_2 (15), and trichloroacetonitrile/H_2O_2 (16) at temperatures between 0 and 4°C and for long reaction times (7 days), which yielded mainly the divinyl compound **4**. However, the use of hexafluoroacetone/H_2O_2 (17) under identical reaction conditions provided the 1,2-epoxide **9** with a yield of 25%, together with the 3,4-epoxide **10** (19%) and the divinyl compound **4** (34%), while shorter reaction times and room temperature conditions yielded preferentially the 3,4-epoxide **10**. Finally, the best yields of the 1,2-epoxide **9** were secured with *m*-chloroperoxybenzoic acid. After 8 days at 0–4°C, the said epoxide was obtained with a yield of 44%, together with 11% of the 3,4-epoxide **10** and 10% of the divinyl compound **4**. Even though the yield of the 1,2-epoxide **9** obtained by oxidation of the diselenide **7** was somewhat low, it is interesting to note the selectivity of the reaction, since the epoxides **9** and **10** were obtained in a 4:1 ratio, while direct epoxidation of divinyl compound **4** yielded the same epoxides in a 1:4 ratio (4) (Scheme 1).

On the other hand, by oxidation of the diselenide **7** with H_2O_2/THF (18) saussurea lactone (**4**) was obtained with a yield of 90%. This synthesis of saussurea lactone (**4**) from santonin (**2**), through the diselenide **7**, improves remarkably those previously reported (7).

On treatment with boron trifluoride etherate, the compound **9** underwent an intramolecular Prins reaction, through the nucleophilic attack of the olefin on the coordinate form of the epoxide, and yielded a mixture of two eudesmanolides that were resolved by column chromatography (Scheme 2). The less polar compound was obtained with a yield of 59% and was identified as dihydrosantamarine (**3**) consistent with its ^1H NMR spectrum (δ_H 5.30 (brs, 3-H), 3.93 (dd, J = 9.8 and 11.1 Hz, 6-H), 3.62 (dd, J = 6.7 and 9.8 Hz, 1α-H), 1.79 (brs, 15-H)). The more polar component, which was obtained with a yield of 25%, was identified as dihydroreynosin **11**. Its ^1H NMR spectrum included two broad singlets (δ_H 4.95 and 4.80) corresponding to the protons of the exocyclic methylene group, in addition to the signals corresponding to 6-H (δ_H 4.03, t, J = 10.5 Hz) and 1α-H (δ_H 3.48, dd, J = 4.6 and 11.4 Hz).

Once dihydrosantamarine (**3**) had been synthesized it was transformed into torrentin (**1**). The introduction of an oxygenated function at C3 was thought to be feasible by sensitized photooxygenation of the 3,4-double bond (6). However, as such an oxygenated function of torrentin was an acetate

Can. J. Chem. Downloaded from www.nrcresearchpress.com by 92.62.229.171 on 09/08/12
For personal use only.

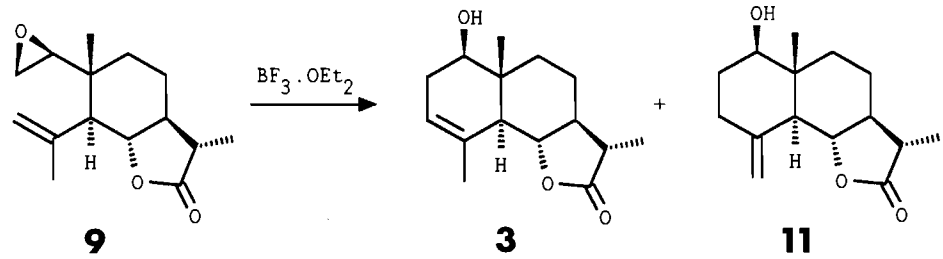

SCHEME 2

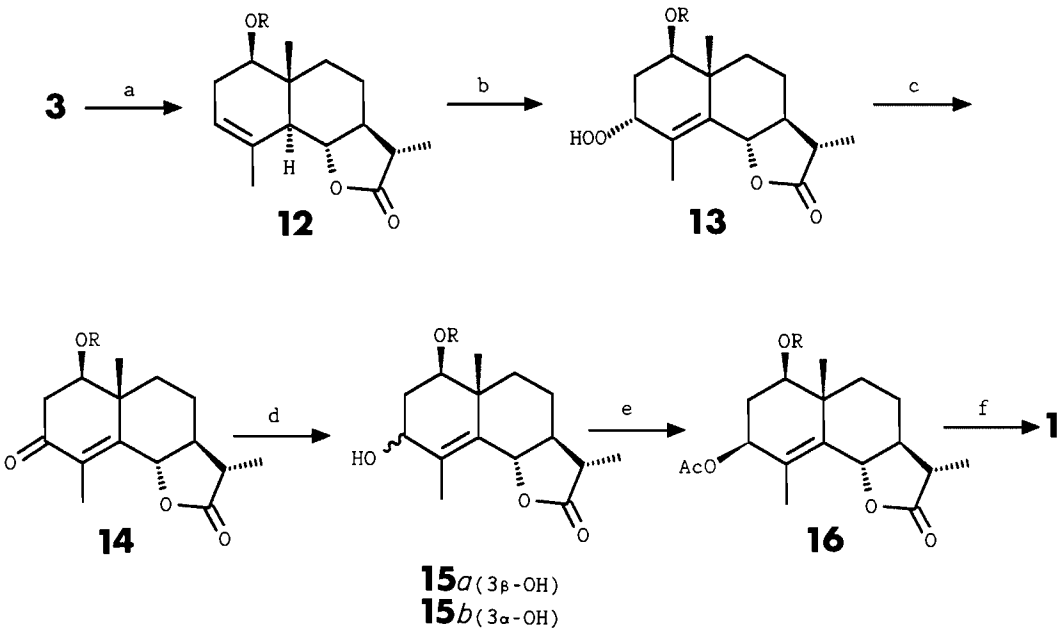

SCHEME 3

group, it required the hydroxyl group at C1 to be protected. Therefore, the first reaction involved was the treatment of dihydrosantamarine (**3**) with *tert*-butyldimethylsilyl chloride in DMF/imidazole (19) in order to protect the hydroxyl function as a silyl ether. Protected dihydrosantamarine, **12**, was converted into the corresponding 3α-hydroperoxide **13**, by bubbling oxygen through an ethanol solution sensitized by means of methylene blue and irradiated with two 400-W lamps. On treatment with acetic anhydride in pyridine (20), the hydroperoxide **13** yielded the α,β-unsaturated ketone **14**, which, by reduction with $LiAlH(O\text{-}t\text{-}Bu)_3$ in THF at 0°C, provided a mixture of the desired 3β-alcohol **15***a* (65%) and its 3α-epimer **15***b* (26%). Finally, on acetylation of **15***a* and cleavage of the silyl ether with $n\text{-}Bu_4NF$, torrentin (**1**) was obtained and was found to be identical with its natural counterpart (2) (Scheme 3).

Experimental

Melting points were determined in capillary tubes with a Büchi melting point apparatus and were used uncorrected. IR spectra were recorded on a Perkin–Elmer 281 spectrometer. ^1H and ^{13}C NMR were run on a Bruker AC-200 instrument (200.1 MHz for ^1H NMR and 50.3 MHz for ^{13}C) by using $CDCl_3$ solutions (Tables 1 and 2). Mass spectra were recorded at 70 eV on a Hewlett–Packard GC/MS system 5988A, with an ULTRA-2 GC column (25 m, cross-linked diphenyl 5% phenylmethyl silicone gum phase). Optical

TABLE 1. ^{13}C NMR data of compounds **4**, **6–10** (50.3 MHz, $CDCl_3$, δ)

C	6	7[a]	8[a]	9	10	4
1	45.5	37.9[b]	37.7[b]	58.8	147.9	147.8
2	58.8	20.0	19.9	44.6[b]	111.7	111.3
3	69.1	35.3	68.2	116.1	52.5	115.1
4	35.0	29.9	33.5	140.4	55.5	140.9
5	48.0	49.6	45.2	53.5[c]	54.5[b]	55.7
6	83.3	81.4	81.7	80.8	80.6	81.2
7	53.7	52.2	52.2	51.8[c]	52.1[b]	52.2
8	24.4	23.4	23.4	22.9	23.5	23.5
9	39.6	39.7[b]	40.0[b]	34.1[b]	40.8	39.4
10	40.0	40.5	40.4	39.3	42.3	42.6
11	41.8	40.7	40.8	41.4	41.2	41.6
12	182.0	179.2	179.5	178.9	178.8	179.1
13	12.7	12.4	12.4	12.5	12.5	12.5
14	13.7[b]	17.7[c]	13.1[c]	23.2[d]	18.3[c]	23.9[b]
15	22.1[b]	21.3[c]	21.9[c]	15.3[d]	21.8[c]	18.3[b]

[a]Aromatic carbons for compound 7: 125.4, 125.5, 126.4, 126.6, 128.7, 128.8, 132.6, 133.6, 133.7, 146.4, and 146.7; compound **8**: 125.3, 126.3, 129.1, 133.6, and 146.6;

[b–d]The signals with these superscripts may be interchanged within the corresponding spectrum.

Can. J. Chem. Downloaded from www.nrcresearchpress.com by 92.62.229.171 on 09/08/12
For personal use only.

TABLE 2. ^{13}C NMR of compounds **1**, **3**, **11–16** (50.3 MHz, $CDCl_3$, δ)

C	3	11	12	13	14	15*a*	15*b*	16[a]	1[a]
1	75.0	78.2	75.6	73.2	74.8	75.2	73.2	74.7	74.1
2	32.6[b]	31.2[b]	33.7[b]	31.0	43.1	36.6	36.3	33.4	32.9
3	121.1	36.0[b]	121.6	86.0	197.4	71.0	71.9	72.8	72.8
4	133.3	142.8	133.3	121.6	129.4	128.1[b]	126.2[b]	124.8[b]	125.0[b]
5	53.5[c]	52.4[c]	53.7[c]		152.8	132.0[b]	134.2[b]	134.1[b]	133.9[b]
6	81.2	79.3	81.5	82.6	82.0	82.7	82.5	82.7	82.5
7	50.4[c]	52.3[c]	50.7[c]	52.6	52.0	52.8	52.6	52.4	52.5
8	22.7	23.0	22.9	24.3	24.4	24.6	24.3	24.5	24.5
9	34.4[b]	33.5[b]	35.3[b]	38.4	38.3	38.5	38.5	38.6	38.1
10	40.6	42.8	41.2	42.9	44.2	43.4	42.9	43.1	42.6
11	40.5	41.2	40.7	41.0	41.1	41.3	41.0	41.1	41.1
12	179.6	179.3	179.7	178.5	177.6	178.6	178.6	178.4	178.3
13	12.3	12.5	12.5	12.4	12.4	12.4	12.4	12.3	12.4
14	10.9[d]	11.6	11.3[d]	18.4[b]	11.1[b]	14.6[c]	17.6[c]	14.2[c]	14.4[c]
15	23.1[d]	110.3	23.3[d]	18.0[b]	17.8[b]	19.0[c]	17.8[c]	18.5[c]	18.4[c]
MeSi			−4.8	−4.8	−5.0	−4.9	−4.8	−5.0	
MeSi			−4.0	−4.0	−4.0	−4.1	−3.9	−4.0	
Me_3CSi			18.0	17.7	17.9	18.0	18.0	18.0	
Me_3CSi			25.8	25.8	25.7	25.8	25.8	25.7	

[a]Acetate carbons 21.1 and 170.8.
[b–d]The signals with these superscripts may be interchanged within the corresponding spectrum.

Can. J. Chem. Downloaded from www.nrcresearchpress.com by 92.62.229.171 on 09/08/12
For personal use only.

rotations were taken on a Perkin–Elmer 241 polarimeter. Reaction solvents were purified and dried by standard methods (20). THF was distilled from Na–benzophenone prior to use. *o*-Nitrophenylselenocyanate was prepared by Bauer's procedure as described by Hori and Sharples (21) and had a melting point of 140–142°C.

*2,3-Di-*o*-nitrophenylseleno-5,7*α*H,4,6,11*β*H-eleman-6,12-olide* **7**

To a solution of diol **6** (35 mg, 0.127 mmol) and *o*-nitrophenylselenocyanate (141 mg, 0.62 mmol) in THF–pyridine 1:1 (1.4 mL) at room temperature under argon, was added, via syringe, tri-*n*-butylphosphine (195 μL, 0.778 mmol) and the mixture stirred for 5 h. To this reaction mixture was added, also via syringe, the resulting solution from *o*-nitrophenylselenocyanate (35 mg, 0.15 mmol), pyridine (0.5 mL), and tri-*n*-butylphosphine (48 μL, 0.19 mmol). Then the reaction mixture was stirred for 20 h. After solvent removal, the residue was chromatographed on silica gel (dichloromethane–methanol 100:1). The first eluted product was diselenide **7** (60 mg, 72%) and the second one was the monoselenide **8** (13 mg, 23%). Compound **7** was a yellow solid, mp 157–158°C (hexane–acetone); ν_{max} (KBr)/cm^{-1}: 3080, 3060, 1770, 1590, 1560, 1505, 1330, 1000, and 735; δ_H: 8.26(1H, dd, *J* 1.4 and 8.3, Ar-H), 8.14(1H, d, *J* 8.0, Ar-H), 7.50–7.20(6H, m, Ar-H), 4.04(1H, t, *J* 10.7, 6-H), 3.10–3.00(2H, m, 3-H), 2.94 (1H, td, *J* 5.5 and 12.0, 2-H), 2.75(1H, td, *J* 4.7 and 12.0, 2′-H), 2.26(1H, 2q, *J* 6.9 and 12.2, 11-H), 1.26 and 1.23 (6H, two d, *J* 6.9, 13-H and 15-H), and 1.00(3H, s, 14-H) Anal. calcd. for $C_{27}H_{32}N_2O_6Se_2$: C 50.79, H 5.05; found: C 50.8, H 5.0. Compound **8** was a yellow oil; ν_{max}/cm^{-1} (NaCl): 3540–3300, 1760, 1580, 1555, 1500, 1330, 1000, and 725; δ_H: 8.24(1H, dd, *J* 1.5 and 8.0, Ar-H), 7.56 (1H, dd, *J* 1.5 and 8.0, Ar-H), 7.49(1H, td, *J* 1.5 and 8.0, Ar-H), 7.27(1H, td, *J* 1.5 and 8.0, Ar-H), 3.99(1H, t, *J* 10.7, 6-H), 3.60–3.50(2H, m, 3-H), 3.16 (1H, td, *J* 4.5 and 12.0, 2-H), 2.82(1H, td, *J* 4.3 and 12.0, 2′-H), 2.25(1H, dq, *J* 6.9 and 12.1, 11-H), 1.20(3H, d, *J* 6.9, 13-H), 1.00(3H, s, 14-H), and 0.99(3H, d, *J* 7.0, 15-H).

*1,2β-Epoxy-5,7*α*H,6,11*β*H-elem-3-en-6,12-olide* **9** *from* **7**

To a solution containing diselenide **7** (184 mg, 0.288 mmol) in CH_2Cl_2 (7 mL), 85% *m*-chloroperbenzoic acid (439 mg, 2.16 mmol) was added at 0°C and the resulting mixture stirred at 0–4°C for 9 days. The product was treated by the usual procedure and chromatographed on silica gel (increasing polarity of hexane–ether) to afford compound **4** (7 mg, 10%), compound **9** (32 mg, 44%), and compound **10** (9 mg, 11%). Their physical and spectral features were as follows: compound **9**, mp 145–147°C (hexane–dichloromethane); ν_{max} (KBr)/cm^{-1}: 3060, 1765, 1630, 1010, 890, 860, and 800; δ_H: 5.07(1H, brs, 3-H), 4.83(1H, brs, 3′-H), 4.04(1H, dd, *J* 10.2 and 11.6, 6-H), 2.86(1H, t, *J* 3.5, 1-H), 2.64 (2H, m, 2-H), 2.42(1H, d, *J* 11.6, 5-H), 2.31(1H, dq, *J* 6.9 and 12.1, 11-H), 1.82(3H, s, 15-H), 1.20(3H, d, *J* 6.9, 13-H), and 0.86(3H, s, 14-H); *m/z* (EI): 250 (M^+, 1%), 235 ($M^+ - CH_3$, 5), 219 (2), 151 (10), 149 (21), 147 (11), 137 (15), 121 (30), 107 (38), 93 (43), 83 (58), and 55 (100). Compound **10**, mp 109–110°C (hexane–dichloromethane); ν_{max}(KBr)/cm^{-1}: 3100, 1770, 1015, 995, and 810; δ_H: 5.81(1H, dd, *J* 10.8 and 17.5, 1-H), 5.04(1H, d, *J* 17.5, 2-H), 5.02(1H, d, *J* 10.8, 2′-H), 4.01(1H, t, *J* 10.9, 6-H), 2.73(1H, d, *J* 4.4, 3-H), 2.50(1H, d, *J* 4.4, 3′-H), 2.31(1H, dq, *J* 7.0 and 12.0, 11-H), 1.37(3H, s, 15-H), 1.21(3H, d, *J* 7.0, 13-H), and 1.19(3H, s, 14-H); *m/z* (EI): 250 (M^+, 1%), 235 ($M^+ - CH_3$, 15), 221 (3), 207 (3), 193 (7), 181 (12), 167 (16), 149 (27), 137 (20), 123 (33), 109 (54), 93 (57), and 55 (100).

*5,7*α*H,6,11*β*H-Elema-1,3-dien-6,12-olide* **4** *from* **7**

A solution of diselenide **7** (26 mg, 0.041 mmol) in THF (0.3 mL) was treated with 30% aqueous hydrogen peroxide (45 μL, 0.04 mmol) at 0°C for 20 h. The reaction mixture was extracted with ethyl acetate and filtered through a short plug of silica gel to afford compound **4** (8.8 mg, 90%) with the following features: mp 149–152°C (hexane–dichloromethane); ν_{max}(KBr)/cm^{-1}: 3090, 1765, 1640, 1005, 1000, 910, and 890, δ_H: 5.78(1H, dd, *J* 10.9 and 17.3, 1-H), 5.01(1H, m, 3-H), 4.96(1H, dd, *J* 0.8 and 10.9, 2-H), 4.92(1H, dd, *J* 0.8 and 17.3, 2′-H), 4.67(1H, brs, 3′-H), 4.10(1H, dd, *J* 10.2 and 11.5, 6-H), 2.31(1H, dq, *J* 7.0 and 12.0 11-H), 2.21(1H, d, *J* 11.5, 5-H), 1.76(3H, s, 15-H), 1.21(3H, d, *J* 7.0, 13-H), and 1.06(3H, s, 14-H); *m/z* (EI): 234 (M^+, 4%), 220 (2), 219 ($M^+ - CH_3$, 11), 206 (1), 199 (1), 177 (11), 167 (16), 156 (74), 149 (48), 141 (33), and 139 (100).

*1β-Hydroxy-5,7*α*H,6,11*β*H-eudesm-3-en-6,12-olide* **3** *and 1β-hydroxy-5,7*α*H,6,11*β*H-eudesm-4(15)-en-6,12-olide* **11** *from* **9**

To a solution of epoxide **9** (71 mg, 0.287 mmol) in benzene (4 mL), $BF_3 \cdot OEt_2$ (81 μL, 0.287 mmol) was added. The mixture was stirred at room temperature for 30 min, after which it was worked up in the usual manner. By flash chromatography (increasing polarity of hexane – ethyl acetate), compounds **3** (43 mg, 59%) and **11** (18 mg, 25%) were separated. Compound **3** was a

Can. J. Chem. Downloaded from www.nrcresearchpress.com by 92.62.229.171 on 09/08/12
For personal use only.

solid melting at 130–132°C (hexane–dichloromethane); ν_{max}(KBr)/cm^{-1}: 3500, 3020, 1745, 1180, 1125, 1040, and 850; δ_H: 5.30 (1H, brs, 3-H), 3.93 (1H, dd, *J* 9.8 and 11.1, 6-H), 3.62 (1H, dd, *J* 6.7 and 9.8, 1-H), 2.50–2.30 (1H, m, 2-H), 2.27 (1H, dq, *J* 6.8 and 12.2, 11-H), 2.19(1H, brd, *J* 11.1, 5-H), 1.79(3H, brs, 15-H), 1.20(3H, d, *J* 6.8, 13-H), and 0.86(3H, s, 14-H); *m/z* (EI): 250 (M^+, 14%), 235 ($M^+ - CH_3$, 1), 232 ($M^+ - H_2O$, 1), 222 (1), 217 (1), 167 (35), and 149 (100). Compound **11** was a solid melting at 138–139°C; ν_{max}(KBr)/cm^{-1}: 3490, 3090, 1750, 1650, 1150, 1135, 1045, 995, and 890; δ_H: 4.95(1H, brs, 15-H), 4.80(1H, brs, 15′-H), 4.03(1H, t, *J* 10.5, 6-H), 3.48(1H, dd, *J* 4.6 and 11.4, 1-H), 2.40–2.25(2H, m, 3-H and 11-H, overlapped signals), 2.02(1H, brd, *J* 10.5, 5-H), 1.20(3H, d, *J* 6.9, 13-H), and 0.80(3H, s, 14-H); *m/z* (EI): 250 (M^+, 1.4%), 233 (M^+ − OH, 3), 232 ($M^+ - H_2O$, 19) 217 (2), 206 (2), 191 (3), 177 (5), 165 (23), 147 (14), 121 (33), 107 (32), and 55 (100).

*1*β-tert-*Butyldimethylsilyloxy-5,7*α*H,6,11*β*H-eudesm-3-en-6,12-olide* ***12*** *from* ***3***

To a solution of dihydrosantamarine **3** (70 mg, 0.28 mmol) in DMF (2.4 mL), *tert*-butyldimethylsilyl chloride (182 mg, 1.17 mmol) and imidazol (229 mg, 3.37 mmol) were added. The temperature of the reaction was raised to 35–40°C, with stirring for 24 h. The reaction product, extracted with ethyl acetate, was chromatographed on silica gel, from which hexane – ethyl acetate (9:1) eluted compound **12** (90 mg, 88%), mp 123–126°C from hexane–ether; ν_{max}(KBr)/cm^{-1}; 3025, 1775, 1250, 1175, 1090, 860, 830, and 770; δ_H: 5.28(1H, brs, 3-H), 3.91(1H, dd, *J* 9.8 and 11.0, 6-H), 3.55(1H, dd, *J* 6.7 and 9.4, 1-H), 2.25(1H, dq, *J* 6.7 and 12.1, 11-H), 2.15(1H, brd, *J* 11.0, 5-H), 2.35–2.10(1H, m, 2-H, overlapped with 11-H and 5-H), 2.1–1.8(3H, m, 2′-H, 8-H, and 9-H), 1.77(3H, brs, 15-H), 1.65–1.40(2H, m, 7-H and 8′-H), 1.20(3H, d, *J* 6.7, 13-H), 1.12(td, 1H, *J* 3.7, 13.0, 9′-H), and 0.85 (12H, s, 14-H and Me-C-Si); *m/z* (CI, methane): 365 [$(M + H)^+$, 19%)], 307 [$(M + H)^+ - C_4H_{10}$, 39], 233 (100), 187 (27), 158 (12), and 157 (74). Anal. calcd. for $C_{21}H_{36}O_3Si$: C 69.18, H 9.95; found: C 69.2, H 9.9.

*1*β-tert-*Butyldimethylsilyloxy-3*α*-hydroperoxy-7*α*H,6,11*β*H-eudesm-4-en-6,12-olide* ***13*** *from* ***12***

Compound **12** (102 mg, 0.281 mmol) was dissolved in absolute ethanol (23 mL) and methylene blue (2.3 mg) was added. Oxygen was gently bubbled through the solution. The reaction tube was submerged in a water bath (17°C) thermostated by an external flow of cold methanol and irradiated by two lamps (HOSRAM HQL, 400 W each) for 7 h. The product was isolated by evaporating the solution to dryness, then dissolving the residue in dichloromethane and passing it through a short column of silica gel using ethyl acetate as solvent. After solvent removal, the residue was chromatographed on silica gel (increasing polarity of hexane – ethyl acetate) to afford unreacted starting material (6 mg, 6%), compound **14** (5 mg, 5%), and compound **13** (65 mg, 58%); ν_{max}(KBr)/cm^{-1}: 3500–3120, 1790, 1745, 1100, 1030, 985, 830, and 775; δ_H: 8.24(1H, s, OOH), 4.54 (1H, brd, *J* 10.5, 6-H), 4.20(1H, brs, 3-H), 3.72(1H, dd, *J* 3.6 and 12.5 Hz, 1-H), 2.3–2.2(2H, m, 2-H and 11-H), 1.95(3H, s, 15-H), 1.18(3H, d, *J* 6.8, 13-H), 1.03(3H, s, 14-H), 0.87(9H, s, Me-C-Si), 0.10(3H, s, Me-Si), and 0.03(3H, s, Me-Si).

*1*β-tert-*Butyldimethylsilyloxy-3-oxo-7*α*H,6,11*β*H-eudesm-4-en-6,12-olide* ***14*** *from* ***13***

A solution of hydroperoxide **13** (58 mg, 0.147 mmol) in pyridine (0.6 mL) was treated with acetic anhydride (3 drops) for 1 h. The reaction mixture was dissolved in ethyl acetate (100 mL), washed with diluted aqueous HCl and brine, and dried. Evaporation of the solvent yielded pure ketone **14** (55 mg, 99%), mp 146–148°C from hexane–ether; ν_{max}(KBr)/cm^{-1}: 1775, 1660, 1610, 1090, 1020, 980, 830, and 770; δ_H: 4.72(1H, dd, *J* 1.5 and 11.6, 6-H), 3.77(1H, t, *J* 8.8, 1-H), 2.53(2H, d, *J* 8.8, 2-H), 2.32(1H, dq, *J* 7.0 and 11.6, 11-H), 2.12(1H, dt, *J* 3.0 and 13.5, 9-H), 2.1–1.9(1H, m, 8-H), 1.96(3H, d, *J* 1.5, 15-H), 1.85(1H, qd, *J* 3.0 and 12.3, 8′-H), 1.29(1H, td, *J* 4.4 and 13.3, 9′-H), 1.23(3H, d, *J* 7.0, 13-H), 1.22(3H, s, 14-H), 0.86(9H, s, Me-C-Si), 0.05(3H, s, Me-Si), and 0.02(3H, s, Me-Si); *m/z* (CI, methane): 379 [$(M + H)^+$, 39%], 321 [$(M + H)^+ - C_4H_{10}$, 60], and 247 (100). Anal. calcd. for $C_{21}H_{34}O_4Si$: C 66.62, H 9.05; found: C 66.6, H 9.0.

*1*β-tert-*Butyldimethylsilyloxy-3*β*-hydroxy-7*α*H,6,11*β*H-eudesm-4-en-6,12-olide* ***15****a from* ***14***

A solution of compound **14** (38 mg, 0.101 mmol) in THF (1.3 mL) was treated at 0°C with LiAlH(O-*t*-Bu)$_3$ (142 mg, 0.50 mmol) in THF (1.3 mL) for 2 h. The reaction mixture was worked up in the usual way. Two products were separated by flash chromatography: the 3α-alcohol ***15****b* (9.9 mg, 26%) and the 3β-alcohol ***15****a* (24.9 mg, 65%). Compound ***15****b*, an oil; ν_{max} (NaCl)/cm^{-1}: 3520–3300, 1760, 1250, 1100, 1025, 980, 830, and 770; δ_H: 4.55(1H, brd, *J* 11.3, 6-H), 3.94(1H, brs, 3-H), 3.76(1H, dd, *J* 4.8 and 11.4, 1-H), 2.25(1H, dq, *J* 6.8 and 11.8, 11-H), 1.97(3H, s, 15-H), 1.03(3H, s, 14-H), 1.46(1H, qd, *J* 3.4 and 12.2, 8-H), 1.20(1H, d, *J* 6.8, 13-H), 1.03(3H, s, 14-H), 0.87(9H, s, Me-C-Si), 0.08(3H, s, Me-Si), and 0.04(3H, s, Me-Si); *m/z* (CI, methane): 363 [$(M + H)^+ - H_2O$, 16], 277 (9), 249, (100), 231 (35), 175 (15). Anal. calcd. for $C_{21}H_{36}O_4Si$: C 66.27, H 9.53; found: C 66.3, H 9.5. Compound ***15****a*, mp 155–157°C (hexane–ether); ν_{max}(KBr)/cm^{-1}: 3500, 1760, 1085, 1030, 1010, 980, 830, and 730; δ_H: 4.58(1H, dt, *J* 1.3 and 10.9, 6-H), 4.03(1H, ddd, *J* 1.3, 6.3 and 8.4, 3-H), 3.47(1H, dd, *J* 3.1 and 11.4, 1-H), 2.24(1H, dq, *J* 7.0 and 11.8, 11-H), 2.03(1H, ddd, *J* 3.1, 6.3, and 12.6, 2-H), 1.93(3H, s, 15-H), 2.00–1.60(1H, m, 7-H), 1.74(1H, ddd, *J* 8.4, 11.4, and 12.6, 2′-H), 1.49(1H, qd, *J* 3.2 and 12.0, 8′-H), 1.21(3H, d, *J* 7.0, 13-H), 1.12(3H, s, 14-H), 0.87(9H, s, Me-C-Si), 0.07(3H, s, Me-Si), and 0.03(3H, s, Me-Si); *m/z* (CI, methane): 3.63 [$(M + H)^+ - H_2O$, 19%], 277 (9), 249, (100), 231 (29), and 175 (20). Anal. calcd. for $C_{21}H_{36}O_4Si$: C 66.27, H 9.53; found: C 66.3, H 9.4.

*1*β-tert-*Butyldimethylsilyloxy-3*β*-acetoxy-7*α*H,6,11*β*H-eudesm-4-en-6,12-olide* ***16*** *from* ***15****a*

Compound ***15****a* (28 mg, 0.074 mmol) was treated with acetic anhydride (0.18 mL) in pyridine (0.25 mL) containing a catalytic amount of 4-dimethylaminopyridine for 3 h. Usual work-up yielded compound **16** (28 mg, 89%) as a colorless oil; ν_{max}(NaCl)/cm^{-1}: 1780, 1740, 1250, 1235, 1020, 835, and 770; δ_H 5.31(1H, brt, *J* 8.5, 3-H), 4.57(1H, dt, *J* 1.4 and 11.0, 6-H), 3.47(1H, dd, *J* 3.3 and 12.7, 1-H), 2.24(1H, dq, *J* 7.0 and 11.8, 11-H), 2.05(3H, s, MeCOO-), 2.1–1.9 (1H, m, 2-H), 1.75(3H, s, 15-H), 1.8–1.6 (2H, m, 2′-H and 7-H), 1.47(1H, qd, *J* 3.2 and 12.7, 8′-H), 1.20(3H, d, *J* 7.0, 13-H), 1.12(3H, s, 14-H), 0.85(9H, s, Me-C-Si), 0.05(3H, s, Me-Si), and 0.01(3H, s, Me-Si); *m/z* (CI, methane): 363 [$(M + H)^+ - CH_3COOH$, 42%], 277 (11), 249 (100), 231 (40), 185 (17), 157 (29), and 117 (32). Anal. calcd. for $C_{23}H_{38}O_5Si$: C 65.36, H 9.06); found: C 65.4, H 9.0.

*1*β-*Hydroxy-3*β*-acetoxy-7*α*H,6,11*β*H-eudesm-4-en-6,12-olide (torrentin)* ***1*** *from* ***16***

Compound **16** (20 mg, 0.048 mmol), dissolved in THF (0.35 mL), was treated for 5 min with *n*-$Bu_4NF \cdot 3H_2O$ (57 mg, 0.18 mmol), dried overnight *in vacuo*, then over P_2O_5. The reaction mixture was worked up in the usual way and chromatographed on silica gel (flash, hexane–ether 4:6) affording torrentin (**1**) (14 mg, 92%) as a solid of melting point 202–204°C (hexane–ether); $[\alpha]_D^{24}$ +36.0 (*c* 0.67, $CHCl_3$); ν_{max}(KBr)/cm^{-1}: 3500, 3300–3200, 1780, 1760, 1705, 1660, 1260, 1240, 1170, 1020, and 980; δ_H: 5.31(1H, brt, *J* 8.2, 3-H), 4.60(1H, dt, *J* 1.5 and 11.1, 6-H), 3.53 (1H, brd, *J* 3.0 and 12.3, 1-H), 2.26 (1H, dq, *J* 7.0 and 11.8, 11-H), 2.16(1H, ddd, *J* 3.0, 6.7, and 12.0, 2α-H), 2.06(3H, s, CH_3COO-), 2.1–2.0(1H, m, 9β-H), 2.0–1.8(1H, m, 8α-H), 1.78(3H, s, 15-H), 1.8–1.6(2H, m, 2β-H and 7-H, overlapped signals), 1.53(1H, qd, *J* 3.4 and 12.1, 8β-H), 1.25(1H, td, *J* 3.8 and 13.2, 9α-H), 1.21(3H, d, *J* 6.9, 13-H), and 1.16(3H, s, 14-H); *m/z* (EI): 308 (M^+, 2%), 290 ($M^+ - H_2O$, 0.1), 266 (1.2), 248 ($M^+ - CH_3COOH$, 100), and 233 (16). Anal. calcd. for $C_{17}H_{24}O_5$: C 66.21, H 7.84); found: C 66.2, H 7.8.

Acknowledgements

Financial support from Dirección General de Investigación Científica y Técnica (DGICYT, Grant PB 87-0039) is gratefully acknowledged. One of us (G. Blay) is specially thankful to Conselleria de Cultura, Educació i Ciència (Generalitat Valenciana) for a grant.

1. J. Delgado, J. A. Marco, J. R. Pedro, J. Sánchez, J. M. Sendra, and E. Seoane. Phytochemistry, **18**, 1523 (1979).
2. J. A. Marco, J. F. Sanz, and M. Carda. Phytochemistry, **28**, 2505 (1989).
3. J. S. Roberts and I. Bryson. Nat. Prod. Rep. **1**, 105 (1984); B. M. Fraga. Nat. Prod. Rep, **2**, 147 (1985); **3**, 237 (1986); **4**, 473 (1987); **5**, 497 (1988); **7**, 61 (1990), **7**, 515 (1990).
4. N. S. Bankar and G. H. Kulkarni. Indian J. Chem. **13**, 744 (1975).
5. R. S. Harapanhalli. J. Chem. Soc. Perkin Trans. 1, 2633 (1988); M. Ando, K. Tajima, and K. Takase. Bull. Chem. Soc. Jpn. **52**, 2737 (1979); M. Ando, A. Akahane, and K. Takase. Bull. Chem. Soc. Jpn. **51**, 283 (1978).
6. F. S. El-Feraly, D. A. Benigni, and A. T. McPhail. J. Chem. Soc. Perkin Trans. 1, 355 (1983).
7. P. A. Grieco and M. Nishizawa. J. Org. Chem. **42**, 1717 (1977).
8. J. B. Hendrickson and T. L. Bogard. J. Chem. Soc. 1678 (1962).
9. R. H. Shapiro. Org. React. **23**, 405 (1976).
10. H. J. Reich, S. Wollowitz, J. E. Trend, F. Chow, and D. F. Wendelborn. J. Org. Chem. **43**, 1697 (1978).
11. M. Arnó, B. García, J. R. Pedro, and E. Seoane. Tetrahedron, **40**, 5243 (1984).
12. G. Blay, I. Fernández, B. García, and J. R. Pedro. Tetrahedron, **45**, 5925 (1989).
13. G. Xie, L. Xu, J. Hu, S. Ma, W. Hou, and F. Tao. Tetrahedron Lett. **29**, 2967 (1988).
14. G. Balme, M. Malacria, and J. Goré. J. Chem. Res. (M), 2869 (1981).
15. P. A. Bartlett and L. A. McQuaid. J. Am. Chem. Soc. **106**, 7854 (1984).
16. L. A. Arias, S. Adkins, C. J. Nagel, and R. D. Bach. J. Org. Chem. **48**, 888 (1983).
17. R. P. Heggs and B. Ganem. J. Am. Chem. Soc. **101**, 2484 (1979).
18. C. Paulmier. Selenium reagents and intermediates in organic synthesis. Pergamon Press, Oxford. 1986.
19. E. J. Corey and A. Ventakeswarlu. J. Am. Chem. Soc. **94**, 6190 (1972).
20. D. D. Perrin and W. L. F. Armarego. Purification of laboratory chemicals. 3rd ed. Pergamon Press, Oxford. 1988.
21. T. Hori and K. B. Sharpless. J. Org. Chem. **43**, 1689 (1978).

Can. J. Chem. Downloaded from www.nrcresearchpress.com by 92.62.229.171 on 09/08/12
For personal use only.

Prototropic equilibria of 2-pyridylbenzimidazoles in aqueous solution

MERCEDES NOVO, MANUEL MOSQUERA,[1] AND FLOR RODRÍGUEZ PRIETO[1]

Universidad de Santiago, Dpto. Química Física, Facultad de Química, E-15706 Santiago de Compostela, Spain

Received August 15, 1991

MERCEDES NOVO, MANUEL MOSQUERA, and FLOR RODRÍGUEZ PRIETO. Can. J. Chem. **70**, 823 (1992).

In this paper we report the acid–base behaviour of 2-(*n'*-pyridyl)benzimidazoles (*n'* = 2,3,4) and some methyl derivatives in aqueous solution over a wide range of acidity, involving interesting features with respect to competition in protonation between the benzimidazole N3 and the pyridyl N, with the existence of the corresponding two monocations in equilibrium in the case of *n'* = 4. The influence of pH on the electronic absorption spectra of all compounds has been studied in order to identify the ground-state species present as a function of acidity and to obtain the acidity constants of the various prototropic equilibria occurring in the wide range of acidity studied.

Key words: 2-pyridylbenzimidazoles, prototropic equilibria, protonation, acidity constants.

MERCEDES NOVO, MANUEL MOSQUERA et FLOR RODRÍGUEZ PRIETO. Can. J. Chem. **70**, 823 (1992).

Dans ce travail, on a examiné le comportement acide–base de 2-(*n'*-pyridyl)benzimidazoles (*n'* = 2, 3, 4) et des quelques-uns de leurs dérivés méthylés en solutions aqueuses, sur une grande plage d'aciditiés; les comportements considérés comprennent des caractéristiques intéressantes concernant la compétition lors de la protonation entre les positions N3 du benzimidazole et le N du pyridyle et l'existence de deux monocations correspondants en équilibre dans le cas où *n'* = 4. Dans le but d'identifier les espèces présentes dans l'état fondamental en fonction de l'acidité et pour obtenir les constantes d'acidité des divers équilibres prototropiques se produisant aux acidités très variées qui ont été examinées, on a étudié l'influence du pH sur les spectres d'absorption électronique de tous les composés.

Mots clés : 2-pyridylbenzimidazoles, équilibre prototropique, protonation, constantes d'acidité.

[Traduit par la rédaction]

Can. J. Chem. Downloaded from www.nrcresearchpress.com by 92.62.229.171 on 09/08/12
For personal use only.

Introduction

The pH dependence of the photophysical behaviour of benzimidazole has been studied by a number of authors in relation to the effect of substitution on the ground- and excited-state acidity constants of this compound (1–3). The introduction of aromatic 2-substituents with heteroatoms brings additional protonation possibilities (4–7) and in some cases, e.g., those of 2-(2′-hydroxyphenyl)benzimidazole (8) and 2-(2′-aminophenyl)benzimidazole (9), the formation of intramolecular hydrogen bonds.

2-Pyridylbenzimidazoles are particularly interesting because the separate parent compounds have nitrogen atoms of very similar basicity: the pK_a values of the pyridinium ion and the N3-protonated benzimidazole cation are 5.25 and 5.532 respectively (10), which suggests that these atoms may compete for protons in pyridylbenzimidazoles. In the work described here we investigated the acid–base behaviour of 2-pyridylbenzimidazoles in order (*a*) to clarify the situation as regards such competition, and (*b*) to determine the ground-state species present at various acidities as a necessary preliminary step towards subsequent research on photoemission by these compounds (11).

Experimental

2-(2′-Pyridyl)benzimidazole (2PBI) was purchased from Aldrich Chemical Co. and purified by recrystallization from ethanol/water. 2-(3′-Pyridyl)benzimidazole (3PBI) and 2-(4′-pyridyl)benzimidazole (4PBI) were prepared by high-temperature condensation of *o*-phenylenediamine with nicotinic and isonicotinic acids respectively (12) and were purified by repeated recrystallization in ethanol/water. 1-Methyl-2-(2′-pyridyl)benzimidazole (M2PBI) was prepared by a published procedure (13), as was the quaternary salt 2-[4′-(*N*-methylpyridinylium)]benzimidazole iodide (4PBIQS) (14). The identity and purity of the prepared products was supported by measurements of their melting points and ^{1}H NMR spectra.

Acidity was varied using perchloric acid and sodium hydroxide, and sodium perchlorate was used to control ionic strength, 0.1 M in most of the series of experiments, except in those performed with $[HClO_4] > 0.1$ M, in which the ionic strength was the concentration of acid. In experiments with 4PBIQS, acidity was controlled over the range pH 6–9 by 0.01 M sodium dihydrogenphosphate buffer. All these chemicals were Merck p.a. products.

UV absorption spectra were recorded in a Kontron Uvikon 820 spectrophotometer at 25°C. Except for experiments at $[HClO_4] > 0.1$ M, for which the acidity function H_+ was calculated (15), pH was measured using a Radiometer PHM82 pH-meter with a Type B combined electrode.

Theoretical equations were fitted to the experimental data using a weighted least-squares nonlinear optimization program based on Marquardt's algorithm (16).

Results and discussion

Prototropic forms

The influence of pH on the absorption spectrum of 2PBI has been reported previously (11). The behaviour of 3PBI observed in the work described here was very similar (Fig. 1), and is interpreted identically, as follows.

The shift of the low-energy band to smaller wavenumbers upon increasing pH from neutral to pH 13 is attributed to the formation of the monoanion A by deprotonation of the neutral species N. Since a similar shift in the spectrum of 2-phenylbenzimidazole (PhBI) is due to loss of the benzimidazole N1 proton (17), we assume that it is likewise this proton that is lost by 2PBI and 3PBI. This hypothesis is supported by the behaviour of the absorption spectrum of the methyl derivative M2PBI, in which the low-energy band is independent of pH at pH > 7.

Upon increasing acidity from pH 7 to pH 3, the low-energy band of 3PBI hardly changes but isosbestic points appear in the high-energy band, reflecting acid–base equilibrium between the neutral species and a monoprotonated cation C. The change in the spectrum is nevertheless very slight, and the fact that it is a similarly slight spectral change

[1]Authors to whom correspondence may be addressed.

Printed in Canada

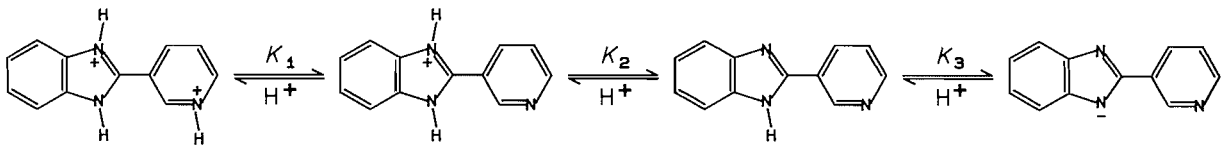

SCHEME 1. Acid–base equilibria for 3PBI.

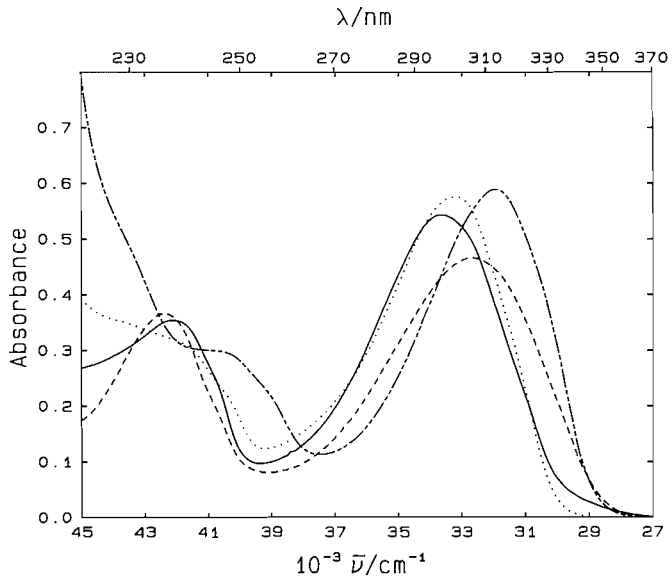

FIG. 1. Absorption spectra of 3PBI in aqueous solutions of pH 13.16 (——), pH 7.14 (· · ·), pH 3.07 (——), and $H_+ = -0.27$ (– – –). [3PBI] = 3.7×10^{-5} mol dm^{-3}.

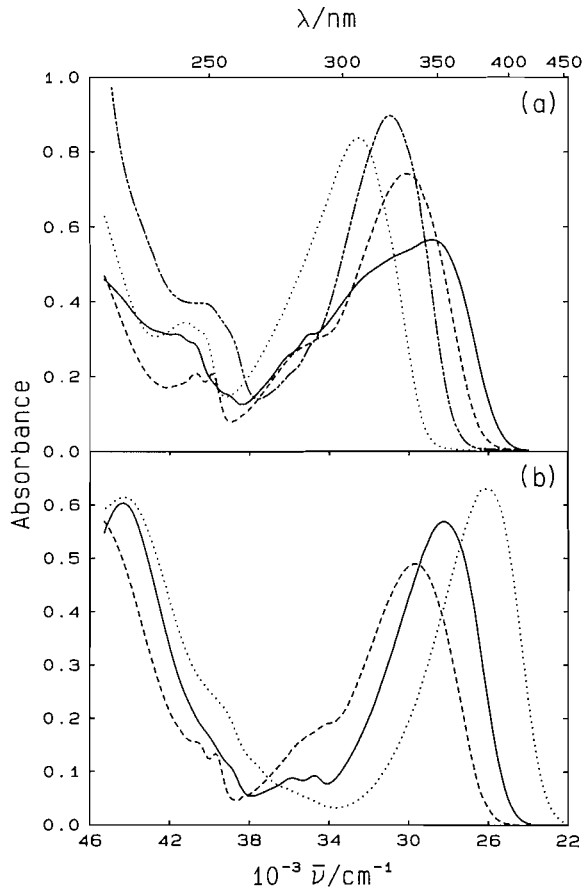

FIG. 2. (*a*) Absorption spectra of 4PBI in aqueous solutions of pH 12.94 (——), pH 6.85 (· · ·), pH 3.02 (——), and $H_+ = -0.11$ (– – –). [4PBI] = 3.7×10^{-5} mol dm^{-3}. (*b*) Absorption spectra of 4PBIQS in aqueous solutions of pH 11.90 (· · ·), pH 5.92 (——), and $H_+ = -0.27$ (– – –). [4PBIQS] = 2.1×10^{-5} mol dm^{-3}.

that is observed upon protonation of PhBI (17), whose only basic nitrogen atom is the benzimidazole N3, suggests that it is N3 that is protonated in C as well.

At higher acidities ([$HClO_4$] > 1 M for 2PBI and pH < 2 for 3PBI), the low-energy band undergoes a shift back to smaller wavenumbers, which is due to the formation of the dication D. This process involves protonation of the pyridyl nitrogen, which causes a greater modification of the spectrum than protonation at N3. As expected, in acid media M2PBI behaved like the unmethylated species,[2] the monocation being protonated at N3 and the dication being formed in the presence of proton concentrations greater than 1 M.

Scheme 1 shows the four prototropic forms of 3PBI that exist at the different pH values; the pattern for 2PBI is the same.

The influence of pH on the absorption spectrum of 4PBI (Fig. 2*a*) resembles that observed on the absorption spectra of its isomers as regards neutral-to-basic media and highly acid media. Thus, the spectrum of 4PBI at neutral pH is similar to those of 2PBI and 3PBI, being attributed to the neutral species N, and shifts to smaller wavenumbers upon increasing pH from neutral to basic due to the formation of the anion A (Scheme 2). At high acidities ([$HClO_4$] ≃ 1 M), the low-energy band of the 4PBI absorption spectrum is again shifted towards smaller wavenumbers as observed in 2PBI and 3PBI, being likewise explicable in terms of the formation of a dication D, protonated at the benzimidazole N3 and at the pyridyl N.

However, the spectrum of 4PBI at pH 3 is very different from those of its isomers, with an extremely broad, irregular low-energy band shifted considerably towards smaller wavenumbers (Fig. 2*a*). The morphology of this band suggests that it is contributed to by two different species obtained by protonation of the neutral species N. Taking into account the above-mentioned possibility that the benzimidazole N3 and the pyridyl N may compete for protons in pyridylbenzimidazoles, a feasible interpretation of the observed spectrum would be the presence of both the N3-protonated cation, C_b, and the cation protonated at the pyridyl N, C_p, in equilibrium at pH 3 (Scheme 2).

[2]Low-energy absorption maxima for M2PBI at pH 7.21, pH 2.42, and $H_+ = -3.24$ are at 34 000, 34 000, and 32 200 cm^{-1}, respectively.

Can. J. Chem. Downloaded from www.nrcresearchpress.com by 92.62.229.171 on 09/08/12
For personal use only.

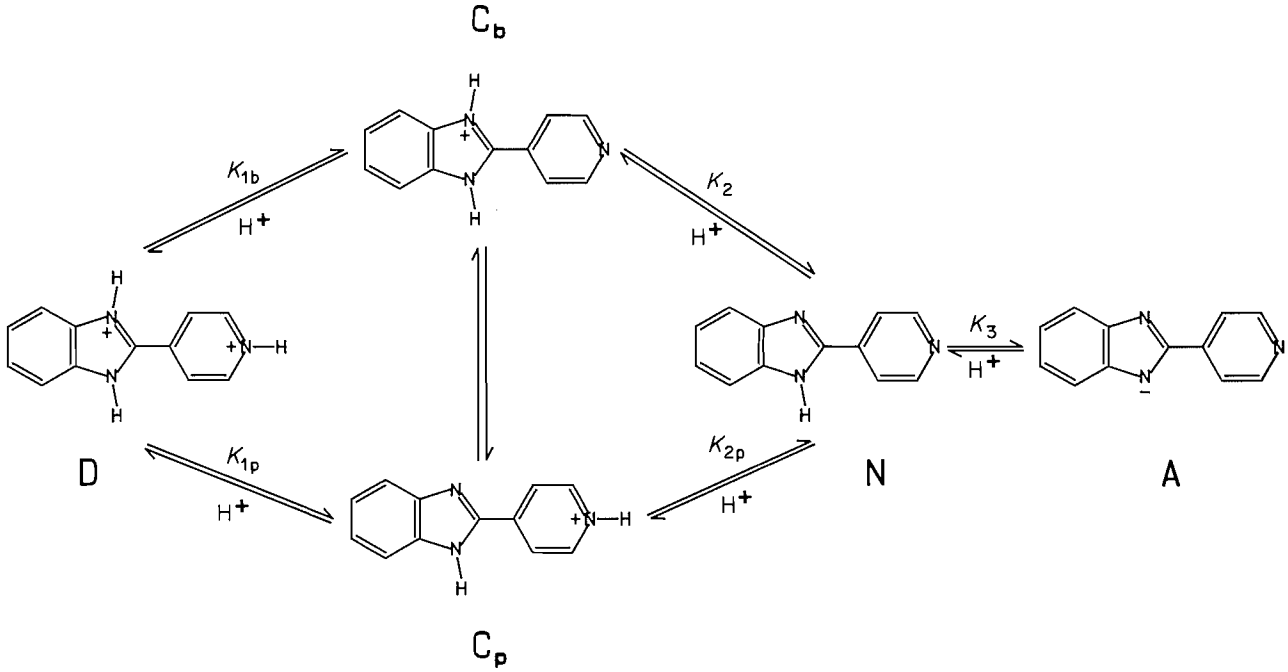

SCHEME 2. Acid–base equilibria for 4PBI.

To verify the above hypothesis, the absorption spectrum of the quaternary salt 4PBIQS was studied. Since 4PBIQS differs from the 4PBI C_p cation only in having a methyl group where C_p has its additional hydrogen, it is thought to be a most suitable molecule for our purpose.

The absorption spectrum of 4PBIQS at pH 4–7 (Fig. 2*b*) has an apparently non-composite low-energy band whose peak lies at 28 300 cm^{-1} and must be attributed to the monocation M (Scheme 3). The position of that band with respect to those of the neutral species N of 2-pyridylbenzimidazoles confirms that the presence of a positive charge on the pyridyl N results in a large shift towards smaller wavenumbers, as observed for the dications of all the compounds studied. At higher acidities, the protonation of M at the benzimidazole N3 yields the dication D, whose low-energy absorption is slightly shifted to greater wavenumbers, being almost identical to that of the 4PBI dication.

Nevertheless, the behaviour of 4PBIQS in neutral-to-basic media is quite different from that of the unmethylated pyridylbenzimidazoles: the low-energy band of the spectrum undergoes a very large shift towards smaller wavenumbers, that shift beginning to be apparent in the neighbourhood of pH 8. This behaviour can be explained by the formation of a new species, the zwitterion Z, by loss of the proton from the benzimidazole N1 in 4PBIQS (Scheme 3). The structural differences of this neutral species Z with respect to the neutral species N of the related compounds account for the great differences in the spectra. Note that an uncharged resonant form can be written for Z but, according to the results of a structural study of species Z by Alcalde *et al.* (18), the dipolar form makes the main contribution to its structure.

On the basis of the simpler behaviour of 4PBIQS, we now return to 4PBI in order to verify the hypothesis that the irregular low-energy band of the 4PBI spectrum at pH 3 was contributed to by both cations C_b and C_p, species that must be in equilibrium at that acidity (Scheme 2). Since the C_p spectrum must be very similar to that of species M of 4PBIQS and the C_b spectrum may be assumed to differ very little from that of the neutral species N of 4PBI, as observed in 2PBI and 3PBI, the sum of contributions of both spectra of M and N should account for the observed spectrum of 4PBI at pH 3. A spectrum very similar to the experimental one is indeed obtained when one assumes a 50% contribution of each species. That leads to the conclusion that the benzimidazole N3 and the pyridyl N must have very similar basicities in 4PBI. Results concerning acidity constants in the next section will give further support to this conclusion.

On the other hand, it is interesting to note that a zwitterionic species like that of 4PBIQS might exist for 4PBI, being obtainable from C_p from loss of the proton from the benz-

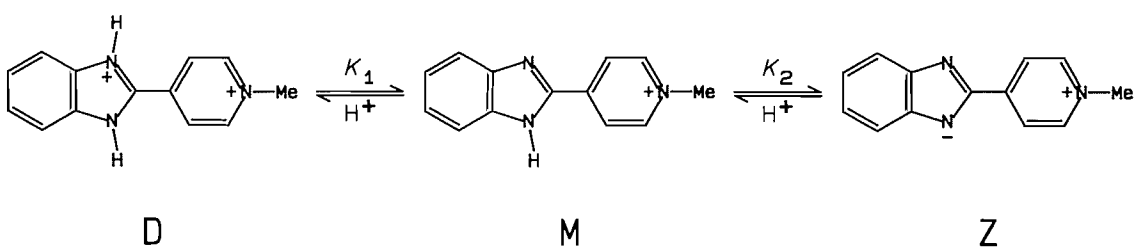

SCHEME 3. Acid–base equilibria for 4PBIQS.

Can. J. Chem. Downloaded from www.nrcresearchpress.com by 92.62.229.171 on 09/08/12
For personal use only.

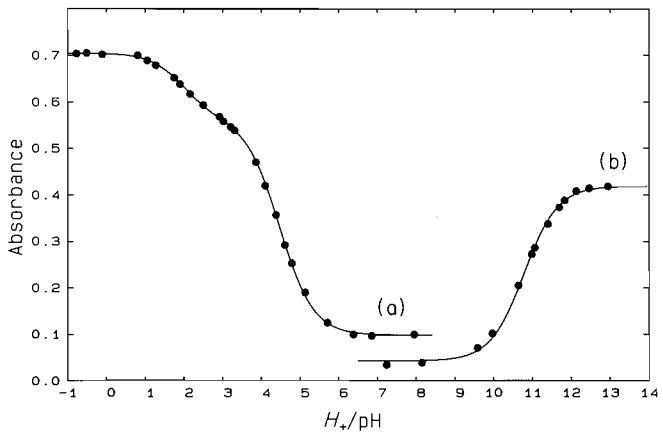

FIG. 3. Plot of absorbance against H_+/pH for 4PBI in aqueous solution: (*a*) at 340 nm in neutral-to-acid media; (*b*) at 346 nm in neutral-to-basic media. Curves are the result of fitting the corresponding theoretical equations (see text) to the experimental data. [4PBI] = 3.7×10^{-5} mol dm^{-3}.

imidazole N1. Nevertheless, no absorption is observed at the corresponding small wavenumbers for 4PBI in neutral media, so that the existence of such a species must be ruled out.

Acidity constants

Quantitative analysis of the dependence of absorbance on pH or H_+ at a fixed wavelength allows calculation of the acidity constants[3] of the various acid–base processes occurring in the acidity range studied. The most complex case is that of 4PBI: not only do four different species of 4PBI occur in the range pH 0–7 (see Scheme 2), but the proximity of the acidity constants for the first and second protonation processes means that both processes must be analyzed together (see Fig. 3).

The equilibria of Scheme 2 imply the following theoretical equation for the acidity range pH 0–7:

$$[1] \quad A^{\lambda} = \frac{A^{\lambda}_{N}K_1K_2 + A^{\lambda}_{C}K_2H + A^{\lambda}_{D}H^2}{K_1K_2 + K_2H + H^2}$$

where A^{λ} is the absorbance at wavelength λ (with subscripts N, C, and D indicating absorbance by the neutral species, the monocations, and the dication respectively), H is defined either as 10^{-pH} for pH > 1 or as 10^{-H_+} for greater acidities, and K_1 and K_2 are the macroscopic acidity constants for the equilibria between dication and monocation and between monocation and neutral species respectively.

The relationships between the macroscopic constants and the microscopic constants defined in Scheme 2 (K_{1b}, K_{1p}, K_{2b}, and K_{2p}) are given by

$$[2] \quad K_1 = K_{1b} + K_{1p}$$

[3]Note that pH, measured at ionic strength no greater than 0.1 M, gives hydrogen ion activity while the acidity function H_+ also includes the activity coefficients of both base and acid of the indicator used to determine H_+ (15). Therefore, our acidity constants, calculated from pH values and the spectrophotometrically measured concentrations of acid and base without activity corrections, are those usually called "mixed" or "practical" acidity constants for a certain ionic strength (19), and those in which H_+ was used are thermodynamic acidity constants on the assumption that the activity coefficients of base and acid are the same for both the species under study and the indicator.

TABLE 1. pK_a values obtained by spectrophotometric titration for the various acid–base equilibria of the species studied

Compound	pK_1	pK_2	pK_3
2PBI	−1.59 ± 0.05[a]	4.41 ± 0.03[b]	12.05 ± 0.05[c]
M2PBI	−1.27 ± 0.04[a]	4.47 ± 0.03[b]	—
3PBI	1.56 ± 0.03[c]	4.53 ± 0.03[c]	11.21 ± 0.03[c]
4PBI	1.96 ± 0.02[c]	4.47 ± 0.01[c]	10.78 ± 0.02[c]
4PBIQS	2.26 ± 0.02[d]	8.89 ± 0.01[e]	—
PhBI[f]	—	5.23	11.91
MPhBI[g]	—	5.2	—

[a]Based on the acidity function H_+ (15).
[b]Ionic strength $I = 4 \times 10^{-3}$ M.
[c]I = 0.1 M.
[d]I = 0.5 M.
[e]I = 0.05 M.
[f]Reference 17.
[g]Reference 2.

$$[3] \quad \frac{1}{K_2} = \frac{1}{K_{2b}} + \frac{1}{K_{2p}}$$

and

$$[4] \quad K_1K_2 = K_{1b}K_{2b} = K_{1p}K_{2p}$$

The absorbances corresponding to each species are given by

$$[5] \quad A^{\lambda}_{N} = c_0\, l\, \epsilon^{\lambda}_{N}$$

$$[6] \quad A^{\lambda}_{C} = \frac{c_0\, l\, (\epsilon^{\lambda}_{Cb}K_{1b} + \epsilon^{\lambda}_{Cp}K_{1p})}{K_{1p} + K_{1b}}$$

$$[7] \quad A^{\lambda}_{D} = c_0\, l\, \epsilon^{\lambda}_{D}$$

where c_0 is the total concentration of pyridylbenzimidazole, l is the cell length, and ϵ^{λ}_{i} is the molar absorption coefficient of species i at wavelength λ.

Equation [1] is also valid for the compounds with only one form of monocation, K_1 and K_2 then being identical to the microscopic constants. When a given acidity constant is sufficiently different from the neighbouring constants that it is possible to consider the corresponding equilibrium in isolation over an appreciable acidity range, eq. [1] can be simplified to

$$[8] \quad A^{\lambda} = \frac{A^{\lambda}_{ac}H + A^{\lambda}_{bas}K_a}{K_a + H}$$

where K_a is the acidity constant in question and A^{λ}_{ac} and A^{λ}_{bas} are the absorbances of the corresponding acid and base at wavelength λ.

Figure 3 shows the experimental absorbance–pH/H_+ data for 4PBI over the acidity range studied, together with the curves fitted in accordance with eq. [1] for pH < 7 and eq. [8] for pH > 7. Table 1 lists the corresponding acidity constants together with those obtained for the other compounds studied by the same procedure. In all cases both acidity constants and absorbances by the various species were fitted, a good agreement of the latter values with the experimental ones being obtained. On the other hand, the values listed for the acidity constants are the means of those obtained from several series of data at different wavelengths.

Can. J. Chem. Downloaded from www.nrcresearchpress.com by 92.62.229.171 on 09/08/12
For personal use only.

Table 1 likewise shows the published acidity constants for PhBI (17) and 1-methyl-2-phenylbenzimidazole (MPhBI) (2).

The value of pK_3 for PhBI agrees well with that of 2PBI, but is about one unit greater than those of 3PBI and 4PBI. This suggests that the benzimidazole NH group is more acid with a pyridyl ring present than with a phenyl ring, the discrepancy for 2PBI being explicable in terms of a greater lone pair – lone pair repulsion in its corresponding anion with respect to the anions of 3PBI and 4PBI, in which benzimidazole N1 and pyridyl N are farther away.

The value of pK_2, for those cases in which it refers to the monocation ↔ neutral species N equilibrium, is practically the same for all the compounds studied; in particular, the basicity of the benzimidazole N3 is virtually the same for all the PBI isomers, and in the case of 4PBI that of the pyridyl N must be very similar. As deduced from Table 1, the benzimidazole N3 is rather less basic in the 2-pyridylbenzimidazoles than in PhBI. For 4PBIQS, pK_2 refers to the monocation ↔ zwitterion equilibrium, which is a process of different nature than those of the related compounds as it involves protonation at the benzimidazole N1. Note that a similar value may be assumed to hold for the hypothetical equilibrium C_p ↔ zwitterion of 4PBI. Since the value of that pK_a is about four units higher than the value of pK_2 for 4PBI, this result confirms our earlier conclusion that no zwitterionic species is formed for 4PBI.

K_1 varies quite widely from one compound to another. In particular, it is about 1000 times greater for 2PBI than for 3PBI and 4PBI; if in these compounds the two aromatic rings are coplanar, as in PhBI (17), this can be attributed to steric hindrance of diprotonation in 2PBI. This interpretation does not necessarily contradict M2PBI (which might be expected to suffer greater steric hindrance, having a value of K_1 about two times less than that of 2PBI), for comparison (2) of data for PhBI and MPhBI suggests that methylation results in loss of ring coplanarity and hence less steric hindrance; reduction of conjugation is apparent, for example, in the fact that methylation shifts the low-energy bands of 2PBI and PhBI to rather greater wavenumbers.

Analysis of the change in absorbance with acidity only allows calculation of the macroscopic acidity constants, which in the case of 4PBI are not identical to the microscopic constants (see eqs. [2], [3], and [4]). The microscopic constants cannot be obtained spectrophotometrically, because the absorption spectra of C_p and C_b cannot be recorded separately. It is nevertheless possible to estimate these constants on the not unreasonable assumption that the value of K_{1p} for 4PBI is very similar to the value of K_1 for 4PBIQS. This hypothesis implies the values of 2.26 for pK_{1p} and pK_{1b}, and 4.17 for pK_{2p} and pK_{2b}. These estimates confirm that the pyridyl N and the benzimidazole N3 are almost equally basic in 4PBI, and that C_p and C_b should therefore be present in roughly equal proportions, in accordance with the interpretation given above to the spectrum of 4PBI at pH 3. The fact that the benzimidazole N3 and the pyridyl N have equal basicities in 4PBI, not observed in 2PBI and 3PBI, is a curious feature since the presence of two atoms of identical basicities in the same molecule is rare.

Acknowledgements

We thank the Xunta de Galicia and the Rectorado de la Universidad de Santiago for financial support. M. N. thanks the C.I.C.Y.T. for a postgraduate training grant.

1. M. Kondo and H. Kuwano. Bull. Chem. Soc. Jpn. **43**, 1433 (1969).
2. M. Krishnamurthy, P. Phaniraj, and S. K. Dogra. J. Chem. Soc. Perkin Trans. 2, 1917 (1986).
3. P. C. Tway and L. J. Cline Love. J. Phys. Chem. **86**, 5227 (1982).
4. A. K. Mishra and S. K. Dogra. Indian J. Phys. **58B**, 480 (1984).
5. A. K. Mishra and S. K. Dogra. Indian J. Chem. **24A**, 364 (1985).
6. A. K. Mishra and S. K. Dogra. Bull. Chem. Soc. Jpn. **58**, 3587 (1985).
7. H. K. Sinha and S. K. Dogra. J. Photochem. **36**, 149 (1987).
8. H. K. Sinha and S. K. Dogra. Chem. Phys. **102**, 337 (1986).
9. A. K. Mishra and S. K. Dogra. J. Photochem. **31**, 333 (1985).
10. R. C. Weast (*Editor*). CRC Handbook of chemistry and physics. 66th ed. CRC Press, Boca Raton, Fla. 1985.
11. F. Rodriguez Prieto, M. Mosquera, and M. Novo. J. Phys. Chem. **94**, 8536 (1990).
12. Y. Sasaki and T. Shigematsu. Bull. Chem. Soc. Jpn. **46**, 3438 (1973).
13. M. Kondo. Bull. Chem. Soc. Jpn. **51**, 3027 (1978).
14. C. Marzin, M. E. Peek, J. Elguero, H. P. Figeys, and N. Defay. Heterocycles, **6**, 911 (1977).
15. M. W. Lovell, B. S. Vogt, and S. M. Schulman. J. Phys. Chem. **88**, 1885 (1984).
16. D. W. Marquardt. J. Soc. Ind. Appl. Math. **2**, 431 (1963).
17. A. K. Mishra and S. K. Dogra. Spectrochim. Acta, Part A, **39**, 609 (1983).
18. E. Alcalde, I. Dinares, J. Frigola, J. Rius, and C. Miravitlles. J. Chem. Soc. Chem. Commun. 1086 (1989).
19. A. Albert and E. P. Serjeant. *In* The determination of ionization constants. Chapman and Hall, London. 1971. pp. 75–84.

Can. J. Chem. Downloaded from www.nrcresearchpress.com by 92.62.229.171 on 09/08/12
For personal use only.

Polyether carboxylic acids incorporating a benzodioxinic subunit: synthesis and complexing ability of sodium and potassium

PASCAL BOSSERAY, GÉRARD COUDERT, AND GÉRALD GUILLAUMET

Laboratoire de chimie bioorganique et analytique, Unité de recherche associée du Centre national de recherche scientifique, n° 499, Université d'Orléans, BP 6759, 45067 Orléans CEDEX 2, France

AND

GEORGES JEMINET, MADELEINE TISSIER, AND JEAN JUILLARD[1]

Laboratoires de chimie organique biologique et de chimie physique des solutions, Unité de recherche associée du Centre national de recherche scientifique, n^{os} 485 et 434, Université Blaise Pascal (Clermont 2), 63177 Aubière CEDEX, France

Received July 15, 1991

PASCAL BOSSERAY, GÉRARD COUDERT, GÉRALD GUILLAUMET, GEORGES JEMINET, MADELEINE TISSIER, and JEAN JUILLARD. Can. J. Chem. **70**, 828 (1992).

We report here the synthesis of new polyoxygenated macrocyclic derivatives with a benzodioxinic subunit and a carboxylic side chain (**2**, **3**), along with some of their corresponding acyclic polyethers (**1**). Formation constants of sodium and potassium complexes with both the acid and anion forms of these compounds were obtained from potentiometric measurements. The enhancement of both complexing ability and selectivity afforded by the presence of a carboxylic side chain is discussed.

Key words: polyether carboxylic acids, macrocycles, benzo-1,4-dioxin, sodium and potassium complexes, solvent methanol.

PASCAL BOSSERAY, GÉRARD COUDERT, GÉRALD GUILLAUMET, GEORGES JEMINET, MADELEINE TISSIER et JEAN JUILLARD. Can. J. Chem. **70**, 828 (1992).

Nou avons réalisé la synthèse de nouveaux dérivés macrocycliques polyoxygénés porteurs d'un bras carboxylique (**2**, **3**) et de composés ouverts correspondants (**1**). Toutes ces molécules comportent un motif benzodioxinique 1-4. Les constantes de formation dans le méthanol des complexes des ions sodium et potassium avec les deux formes, acide et anion, de ces composés ont été obtenues par des mesures potentiométriques. On discute des améliorations des propriétés de complexation et de sélectivité déterminées par la présence du bras carboxylique.

Mots clés : acides carboxyliques de polyéthers, macrocycles, benzo-1,4-dioxine, complexes du sodium et du potassium, méthanol comme solvant.

Can. J. Chem. Downloaded from www.nrcresearchpress.com by 92.62.229.171 on 09/08/12
For personal use only.

Introduction

In previous work, some of us developed synthetic methods that enabled us to prepare benzodioxinic macrocyclic polyethers bearing a side chain on the carbon next to the benzodioxinic subunit (1–3). In a recent paper (3) we reported data on sodium and potassium ion interactions with some lariat-ethers obtained in this manner. Both their complexing ability and potassium–sodium selectivity were disappointing. These properties might be expected to improve with the introduction of side chains bearing a carboxylic group. For example, the preparation and testing of carboxylic acyclic and macrocyclic polyethers that are more or less efficient in extracting alkali-metal and alkaline-earth cations selectively have been reported by Wieranga *et al.* (4), Nakahama and co-workers (5), Hiratani (6), and Bartsch and co-workers (7). Such substances can be used for modeling the activity of naturally occurring carboxylic polyether ionophores such as monensin, nigericin, grisorixin, lasalocid, calcimycin, and their derivative compounds, which have been studied in Clermont for years. The compounds synthesized here were of three types, as shown in Fig. 1. They were tested for their complexing efficiency and selectivity for potassium and sodium cations in methanol. Preliminary extraction experiments in a biphasic system were also carried out in order to evaluate them as potential ionophores. Comparisons were made with analogs not bearing a carboxylic side chain (3).

Methods and results

Synthesis

The preparation of polyether compounds **1** has been described previously (2). The key intermediate **6** in the synthesis of **2** and **3** was prepared from 2-carboxy-benzo-1,4-dioxin **4** (8) in three steps (Scheme 1).

The first step was the functionalization of the heterocycle at C_3, which was achieved by treatment of 5-benzyloxy-2-pentanone (2) with the dianion of **4** (9). The lactone **5**, which was obtained after treatment with hydrochloric acid in aqueous dioxan, was then easily converted to diol **6** by reduction with lithium aluminium hydride. The syntheses of macrocycles **2** and **3** from diol **6** are shown in Schemes 2 and 3. Macrocyclic derivatives **7** were prepared by treatment of **6** with excess sodium hydride in tetrahydrofuran or in a tetrahydrofuran–hexamethylphosphoramide mixture (9:1) followed by reaction with the bistosylates of tetra-, penta-, and hexaethylene glycols (10). When potassium hydride was used as base the yield fell dramatically (20%). Diols **6**, in the presence of bis(2-chloroethyl) ether, tetrabutylammonium hydrogen sulfate, and 50% aqueous sodium hydroxide (11), were converted to the benzodioxinic dichloro polyethers **10**, which were subsequently cyclized with catechol and dry sodium hydroxide in *n*-butanol (12) to give compounds **11**.

[1]Author to whom correspondence may be addressed.

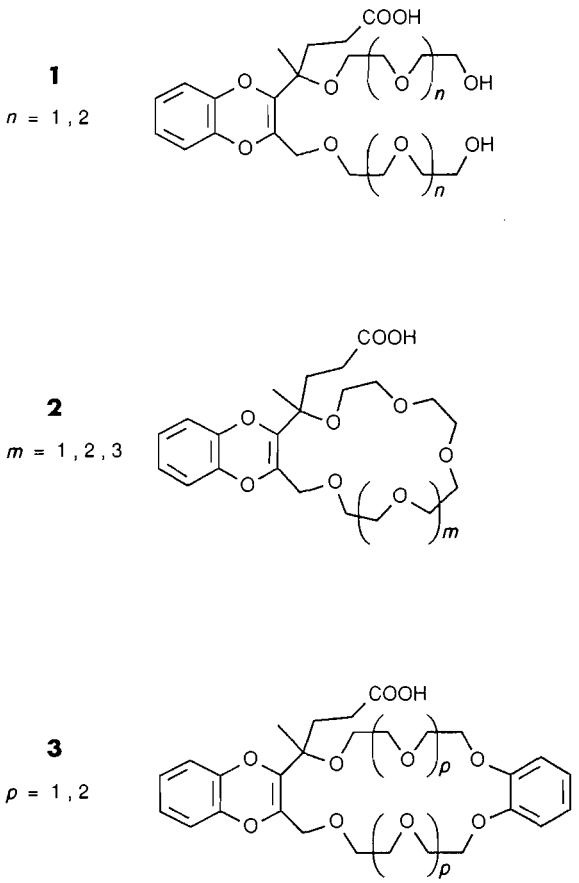

FIG. 1. Carboxylic polyether with a benzodioxinic subunit; here considered **1***a*, $n = 1$; **1***b*, $n = 2$; **2***a*, $m = 1$; **2***b*, $m = 2$; **2***c*, $m = 3$; **3***a*, $p = 1$; **3***b*, $p = 2$.

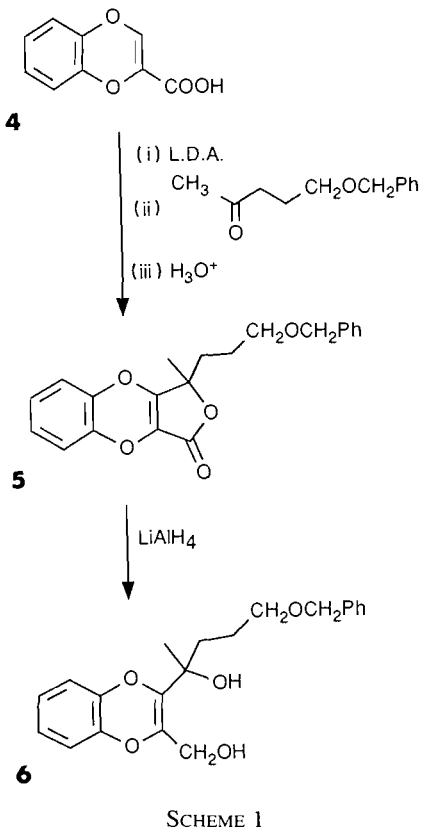

SCHEME 1

Hydrogenolysis of the benzyl protecting group of derivatives **7** and **11**, which was performed in ethyl acetate using a palladium-on-carbon catalyst (13), led to primary alcohols **8** and **12**.

Despite several attempts, the direct oxidation of **8** and **12** to the corresponding carboxylic acids failed. However, Swern oxidation (14) of **8** and **12** gave aldehydes **9** and **13**, which were then subjected to alkaline oxidation with silver nitrate (15) to afford the required acid derivatives **2** and **3**.

Complex formation in methanol

It has been shown (16) that polyether carboxylic ionophores (AH) are able to form both charged and neutral complexes with a cation M^+ in methanol: AHM^+ and AM. The presence of AHM^+ was therefore expected here and so the two formation equilibria [1] and [2]:

[1] $AH + M^+ \rightleftarrows AHM^+$

[2] $A^- + M^+ \rightleftarrows AM$

were included to take this into account, along with the corresponding deprotonation equilibria [a] and [a′]:

[a] $AH \rightleftarrows A^- + H^+$

[a′] $AHM^+ \rightleftarrows AM + H^+$

This system was studied by potentiometry using concurrently two sensitive glass electrodes, one responsive to H^+, the other to M^+, i.e., Na^+ or K^+. The pK_a's of the acidic polyethers were first determined using the usual procedures. Formation constants β_1 and β_2 were then obtained by measuring the activities of H^+ and M^+ when successive amounts of a basic solution of tetrabutylammonium methylate in methanol were added to a solution of the ligand and the alkali metal chloride at equimolar concentration. Procedures and processing of the data using Leden formation functions have been described elsewhere (16). Results thus obtained are set out in Table 1. With some of the non-carboxylic benzodioxinic polyoxygenated macrocycles previously studied, formation of A_2K^+ was observed (3). Formation of 2-ligand–1-cation complexes, i.e., $A_2H_2M^+$ or A_2M^-, is improbable here since good fits were obtained assuming formation of only AHM^+ and AM. Acid dissociation constants of the AHM^+ species in columns 2 and 3 of Table 1 were obtained by combining equilibrium constants for reactions [1], [2], and [a] according to eq. [3]:

[3] $pK_{a'} = pK_a - \log \beta_2 + \log \beta_1$

For comparison, previous data (16–18) for naturally occurring carboxylic polyether ionophores are given in Table 1. Also, some pK_a values of simple carboxylic acids obtained under the conditions described here are given in Table 2.

Complex formation in biphasic water – organic solvent system

The purpose of these measurements was to access the heterogeneous formation constants for reaction [4] in which the overlined species are in the organic phase and the others in the aqueous phase.

[4] $\overline{AH} + M^+ \rightleftarrows \overline{AM} + H^+$

Can. J. Chem. Downloaded from www.nrcresearchpress.com by 92.62.229.171 on 09/08/12
For personal use only.

Can. J. Chem. Downloaded from www.nrcresearchpress.com by 92.62.229.171 on 09/08/12
For personal use only.

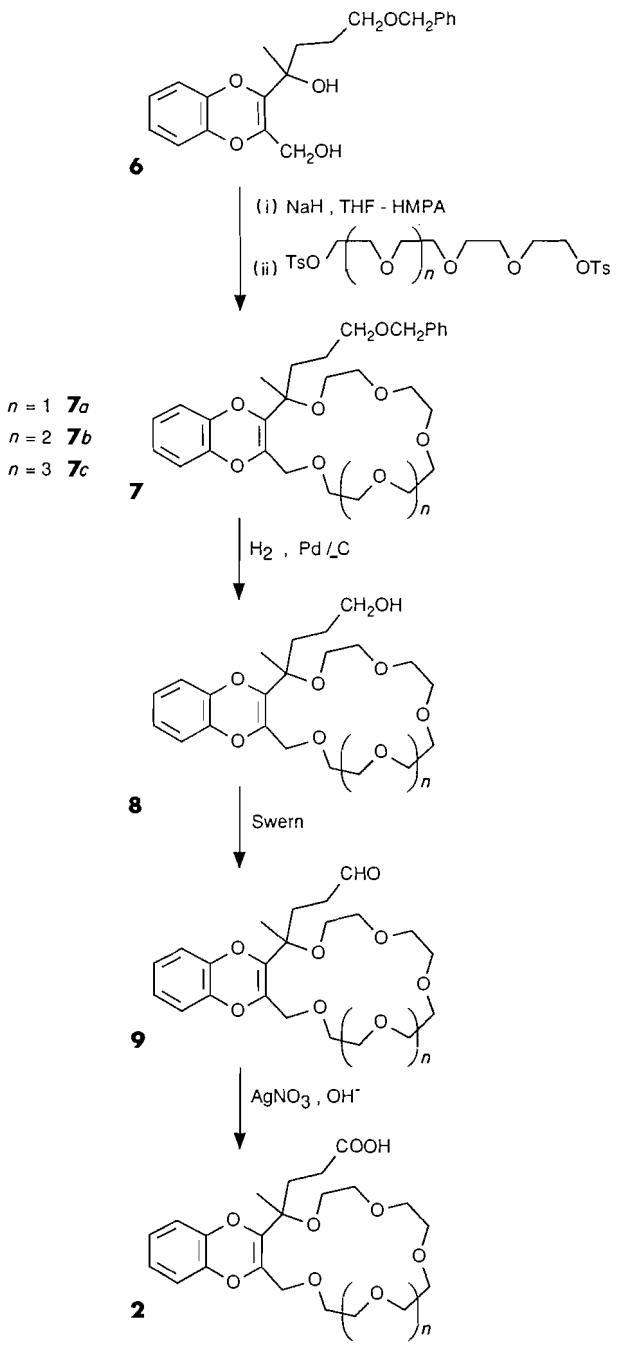

SCHEME 2

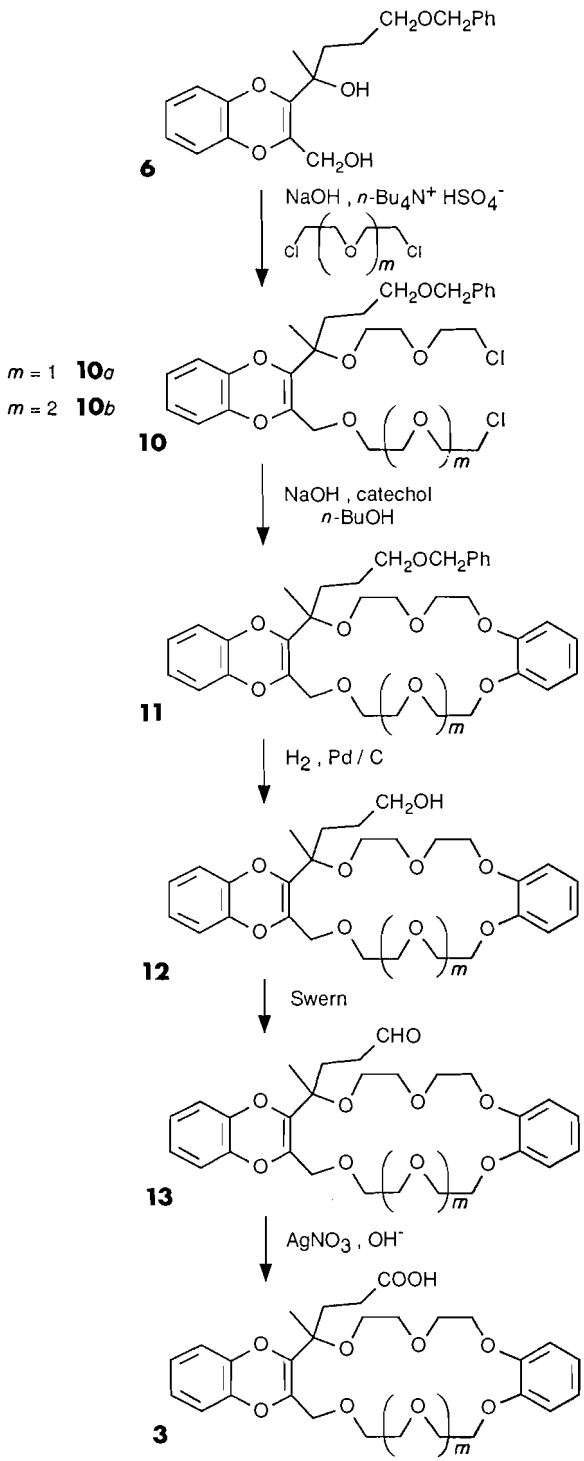

SCHEME 3

This was achieved by extracting the cation from the aqueous phase at variable pH by the ligand in the organic phase, using as the organic phase the *n*-butanol–toluene 30–70% mixture, according to a method first proposed by Pressman *et al.* (19) and developed by Pfeiffer and Lardy (20).

Experiments were limited to the 5–8 pH range. Under these conditions the distribution coefficient was rather small for all the products studied. This may be attributed to an observed partition in favor of water for most of the complex salts formed. Since they do not provide useful information, numerical data are not reported here for the sake of brevity.

Discussion

Synthesis

A new class of polyethers incorporating a benzodioxinic subunit and bearing a side chain with a terminal carboxylic acid group has been described. These compounds were obtained using a synthetic scheme with a limited number of steps, which should allow further developments to be made.

TABLE 1. Formation constants of acid, AHM^+, and neutral, AM, complexes of polyether carboxylic acid, AH, and metal cation, M^+, and acid dissociation of AH and AHM^+ in methanol at 25.0°C (molar scale of concentration)

Compound	pK_a (AH)	$pK_{a'}$ ($AHNa^+$)	$pK_{a'}$ (AHK^+)	log β_0 ($AHNa^+$)	log β_1 (ANa)	log β_0 (AHK^+)	log β_1 (AK)
1*a*	9.75	—	—	<<1	≅1.9	<<1	≅1.9
1*b*	9.87	8.6	8.92	0.9	2.16	1.32	2.27
2*a*	10.14	8.99	8.84	1.26	2.41	1.30	2.60
2*b*	9.62	8.86	8.81	2.30	3.06	2.73	3.54
2*c*	9.82	8.92	9.18	1.74	2.64	3.10	3.74
3*a*	9.86	—	8.07	—	—	2.33	4.12
3*b*	9.81	—	9.19	—	—	2.76	3.38
m[a]	10.24	6.23	5.00	2.29	6.30	2.40	5.24
n[a]	10.32	7.85	8.27	2.19	4.66	3.59	5.64

[a]m: monensin (18); n: nigericin (16).

TABLE 2. pK_a of model carboxylic acids in methanol at 25.0°C (molar scale of concentration, accuracy ±0.01)

Acid	pK_a	Acid	pK_a
Acetic acid	9.63[a]	Isovaleric acid	9.88
Propionic acid	9.82[a]	3,3-Dimethylbutyric acid	10.15
Butyric acid	9.84[a]	Methoxyacetic acid	8.51
Valeric acid	9.90	Ethoxyacetic acid	8.61
Isobutyric acid	10.03	β-Ethoxypropionic acid	9.51

[a]From reference 17.

Acid dissociation in methanol

In light of data on simple carboxylic acids, the acidity constants obtained for compounds **1–3** (Table 1) are within the expected range. In particular, judging from the large pK_a change from ethoxyacetic to β-ethoxypropionic acid, the inductive effect of the ethoxy group probably vanishes totally beyond four carbons. However, given that polyethers **1–3** are structurally similar in the vicinity of the carboxylic acid group, the significant variations observed in acid dissociation are a little surprising. The differences observed could be related to variations in the preferential conformation of the crown ring, which may or may not facilitate the interaction of the carboxylic hydroxyl with one of the oxygens of the ring through hydrogen bonding, thus more or less increasing the stability of the acid form. Such lowering of the acidity of a carboxylic group by the presence of a crown ether moiety in the molecule has already been observed (7*c*, 21).

The specificity of the interactions between the carboxylic acid and the oxygens of the crown should vanish on complexation with an alkali-metal cation. This is borne out by observation: the acidity differences are generally smooth; most of the $pK_{a'}$ values lie near 8.9, except in some particular cases. In addition, as expected, from AH to AHM^+ acidity is increased, but less than for the naturally occurring carboxylic ionophores, monensin and nigericin.

Complexation of Na^+ and K^+

As has been noted earlier (results) both the acid and anionic forms of the carboxylic polyethers are able to act as ligands of alkali-metal cations. Complexes of the neutral acid molecules can be compared to complexes of analogous benzodioxinic crown ethers without a carboxylic acid (3). This is done in Table 3 for compounds **2** and **3***a*. For complexation with potassium, differences are rather small, the trend being that the stabilization of the complex by the presence of the carboxylic acid increases as the size of the crown increases; the strongest complexation previously observed (3) for the seven-oxygen ring is probably retained. The same is not true for the sodium complexes, for which the presence of the carboxylic acid strengthens the complexation noticeably for the five-oxygen ring and even more so for the six-oxygen ring. The maximum observed with a simple crown ether, substituted or not, then recurs for the six-oxygen ring as shown in Fig. 2. Two of us have shown (25) that for one-chain polyethers, complexation increases with the number of oxygens, mainly for statistical reasons, this effect being more efficient for potassium than sodium cation as shown clearly in Fig. 1 from ref. 25. Table 1 shows that this is also true for **1**.

The complexation of a cation by polyethers possessing an anionic ligand is clearly more efficient than its complexation by polyethers with an acid ligand or by analogous monocarboxylic crown compounds. Differences in complexing ability range from 0.6 to 1.8 in terms of the logarithm of the formation constants. Such differences are smaller than those observed for natural polyether carboxylic ionophores, which range from to 2 to 4. With the latter substances the ionization of the carboxylic function corresponds mainly to the stabilization of the pseudo-ring and incidentally to the participation of this function in the coordination of the cation. Here, the carboxylate group acts mainly in coordinating the cation but also in creating a more closed space around the cation. This hemi-cage effect is more efficient in the case of small-size crown ether as observed for compound **3***a*, for example.

Conclusions

The complexing ability of some of these substances may then be considered as satisfactory but preliminary extraction experiments have shown that their lipophilic properties would have to be increased through appropriate chemical

Can. J. Chem. Downloaded from www.nrcresearchpress.com by 92.62.229.171 on 09/08/12
For personal use only.

TABLE 3. Comparison of data concerning formation of sodium and potassium charged complexes of compounds **2** previously studied (3) and compounds here noted **2*** and resulting from substituting a methyl group for the carboxylic acid (log β_1, methanol 25.0°C, molar scale of concentration, estimated accuracy ±0.02)

Cation	2*a*	2*a**	2*b*	2*b**	2*c*	2*c**	3*a*	3*a**
Na^+	1.26	0.95	2.30	1.54	1.74	1.64		
K^+	1.30	1.40	2.73	2.70	3.10	2.85	2.33	2.28

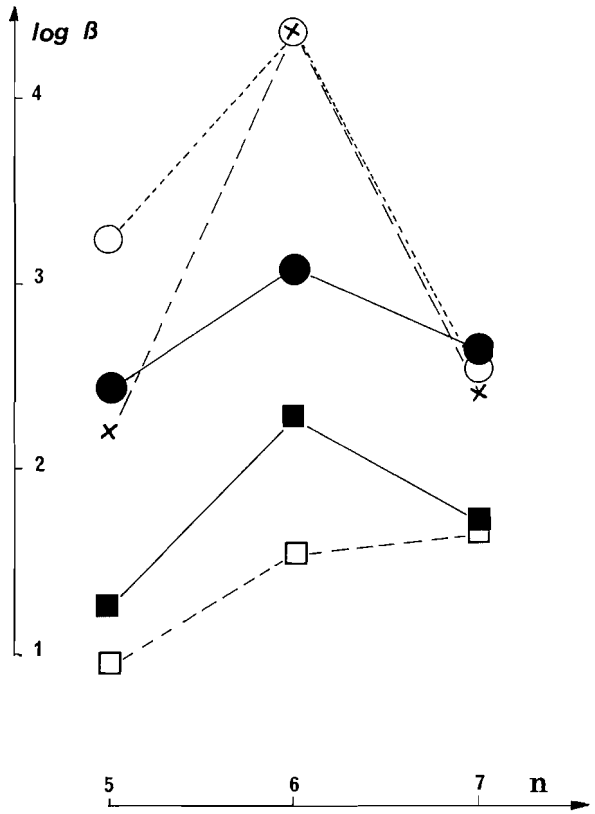

FIG. 2. Formation constant of complexes of crown ether with sodium ion in methanol (in terms of log β) as a function of the number *n* of oxygens in the crown. ○, simple crown ether (22); ×, dibenzocrown ether (23, 24); ■, compounds **2**, reaction [1]; ●, compounds **2**, reaction [2]; □ compounds **2*** resulting from substitution of a methyl group for the carboxylic arm (3).

modifications to obtain efficient ionophoric systems. The synthetic scheme used in this study can be easily adapted for such a purpose.

Experimental

Synthesis and purification

Infrared (ir) spectra were recorded on a Perkin Elmer 297 spectrometer. Nuclear magnetic resonance (nmr) spectra were obtained in $CDCl_3$ solution on Hitachi Perkin R 24 (60 MHz) and Bruker AM 300 (300 MHz) instruments. All samples that contained an OH group were back-exchanged in D_2O before analysis. Tetramethylsilane was used as an internal standard. Low-resolution mass spectra were recorded on a Nermag R 10.10 C mass spectrometer using a 70 eV ionization potential. Column chromatography was performed with 230–400 (flash chromatography) and 70–230 (gravity chromatography) mesh silica gel (E. Merck). Analytical thin-layer chromatography (tlc) was carried out on cut sections of E. Merck precoated aluminium sheets of silica gel 60 F_{254}. Chromatography solvents were distilled before use. Tetrahydrofuran (THF) was distilled from sodium benzophenone ketyl immediately prior to use. All reactions involving air- or moisture-sensitive reagents were performed under an argon atmosphere. Analyses of all new compounds, indicated by the symbols of the elements, were within ±0.4% of the theoretical values.

3-Methyl-3 [3-(phenylmethoxy)propyl]furo[3,4-b][1,4]benzodioxin-1-(3H)-one **5**

To a stirred solution of diisopropylamine (1.8 g, 17.6 mmol) in 8 mL of tetrahydrofuran was added *n*-butyllithium (11 mL, 17.6 mmol, 1.6 M in hexane) at −5°C. The pale yellow solution was stirred for 20 min at the same temperature. The reaction mixture was cooled to −78°C and a solution of 2-carboxy-benzo-1,4-dioxin **4** (8) (1.42 g, 8 mmol) in 7.5 mL of tetrahydrofuran was then added dropwise. The reaction mixture was stirred for a further 5 h at −78°C. 5-Benzyloxy-2-pentanone(2) (2.3 g, 12 mmol) dissolved in 3 mL of THF was added and the resulting solution was stirred at −78°C for 2 h. The reaction was quenched with water, and the mixture was warmed up to room temperature and extracted with Et_2O (2 × 20 mL). The aqueous layer was acidified with 10% HCl and extracted with CH_2Cl_2 (4 × 20 mL). This organic phase was dried over anhydrous $MgSO_4$, filtered, and evaporated.

A solution of the oily residue in dioxane (30 mL) and 10% HCl (30 mL) was stirred at room temperature. The reaction was monitored by tlc. After hydrolysis and extraction with CH_2Cl_2 (4 × 20 mL), the organic phase was washed with 5% aqueous sodium hydrogen carbonate solution (30 mL), with 10% HCl (10 mL), dried over anhydrous $MgSO_4$, and evaporated. The oily residue was chromatographed to give **5** as a colorless oil (87%); ir (film): 1780, 1710 cm^{-1}; ^1H nmr ($CDCl_3$) δ: 1.3 (s, 3H, CH_3), 1.8 (m, 4H, CH_2), 3.3 (t, J = 6.5 Hz, 2H, CH_2O), 4.3 (s, 2H, OCH_2Ph), 6.7–6.8 (m, 4H, aromatic), 7.05 (s, 5H, aromatic). Anal. ($C_{21}H_{20}O_5$) C, H.

α-Methyl-2 [3-(phenylmethoxy)propyl]-benzo-1,4-dioxin-2,3-dimethanol **6**

To a solution of the lactone **5** (1.35 g, 4 mmol) in 20 mL of anhydrous ether was added an excess of hydride reagent ($LiAlH_4$) and the reaction was stirred for 2 h at room temperature. The reaction was monitored by tlc. Cold water was added cautiously; the salts were filtered through Celite and washed with ether. The organic phase was dried over anhydrous $MgSO_4$, filtered, and evaporated. The residue was purified by filtration through a short column of silica gel (petroleum ether – ether, 6:4) to leave **6** as a colorless oil (91%); ir (film): 3600–3100, 1680 cm^{-1}; ^1H nmr ($CDCl_3$) δ: 1.4 (s, 3H, CH_3), 1.7–1.9 (m, 4H, CH_2), 3.7–3.5 (m, 2H, CH_2O), 4.2 (s, 2H, =C-CH_2O), 4.5 (s, 2H, OCH_2Ph), 6.5–7.0 (m, 4H, aromatic), 7.3 (s, 5H, aromatic). Anal. ($C_{21}H_{24}O_5$) C, H.

Synthesis of macrocycles 7

A suspension of sodium hydride (25.7 mmol, 50% dispersion in mineral oil, washed three times with dry tetrahydrofuran) in 40 mL of anhydrous tetrahydrofuran was refluxed and diols **6** (1.93 g, 5.8 mmol) dissolved in 48 mL of anhydrous tetrahydrofuran were added dropwise with stirring. The reaction mixture was

Can. J. Chem. Downloaded from www.nrcresearchpress.com by 92.62.229.171 on 09/08/12
For personal use only.

Can. J. Chem. Downloaded from www.nrcresearchpress.com by 92.62.229.171 on 09/08/12
For personal use only.

refluxed for 2 h and a solution of bistosylate (5.8 mmol) of the relevant poly(ethylene glycol) in 48 mL of dry solvent was added. The heating and stirring were continued for another 36 h. After cooling, the reaction mixture was poured into water and extracted with ether (4 × 30 mL). The organic layer was dried over anhydrous $MgSO_4$ and concentrated *in vacuo* to give an oil, which was purified by flash chromatography. For the synthesis of **7***a* and **7***b*, the solvent used was a THF–HMPA mixture (9:1).

6,8,9,11,12,14,15,17,18,20-Decahydro-6-methyl-6-[3-(phenylmethoxy)propyl][1,4] benzodioxino[2,3-c] - [1,6,9,12,15]-pentaoxacycloheptadecin **7***a* (40%); oil; ir (film): 1680,1100 cm^{-1}; ^1H nmr ($CDCl_3$) δ: 1.4 (s, 3H, CH_3), 1.7 (m, 4H, CH_2), 3.5–3.8 (m, 18H, CH_2O), 4.3 (s, 4H, CH_2O), 6.5–6.7 (m, 4H, aromatic), 7.1 (s, 5H, aromatic). Anal. ($C_{29}H_{38}O_8$) C, H.

6,8,9,11,12,14,15,17,18,20,21,23-Dodecahydro-6-methyl-6-[3-(phenylmethoxy)propyl]-[1,4]benzodioxino[2,3c]-[1,6,9,12,15,18]-hexaoxacycloeicosin **7***b* (43%); oil; ir (film): 1680, 1100 cm^{-1}; ^1H nmr ($CDCl_3$) δ: 1.4 (s, 3H, CH_3), 1.7 (m, 4H, CH_2), 3.5–3.8 (m, 22H, CH_2O), 4.2 (s, 2H, =C-CH_2O), 4.35 (s, 2H, OCH_2Ph), 6.5–6.7 (m, 4H, aromatic), 7.1 (s, 5H, aromatic). Anal. ($C_{31}H_{42}O_9$) C, H.

6,8,9,11,12,14,15,17,18,20,21,23,24,26-Tetrahydro-6-methyl-6-[3-(phenylmethoxy)propyl]-[1,4]benzodioxino[2,3-c]-[1,6,9,12,15,18,21]-heptaoxacyclotricosin **7***c* (35%); oil; ir (film): 1680,1100 cm^{-1}; ^1H nmr ($CDCl_3$) δ: 1.4 (s, 3H, CH_3), 1.7 (m, 4H, CH_2), 3.5–3.8 (m, 26H, CH_2O), 4.2 (s, 2H, =C-CH_2O), 4.35 (s, 2H, OCH_2Ph), 6.5–6.7 (m, 4H, aromatic), 7.1 (s, 5H, aromatic). Anal. ($C_{33}H_{46}O_{10}$) C, H.

Synthesis of benzodioxinic dichloro polyethers ***10***

A general procedure for the synthesis of these compounds has already been described (1).

2-[1-[2-(2-Chloroethoxy)ethoxy]-1-methyl-4-(phenylmethoxy) butyl]-3-[[2-(2-chloroethoxy)ethoxy]methyl]benzo-1,4-dioxin **10***a* was already described (1).

2-[1-[2-[2-(2-Chloroethoxy)ethoxy]ethoxy]-1-methyl-4-(phenylmethoxy)butyl]-3-[[2-[2-(2-chloroethoxy)ethoxy]ethoxy]methyl]-benzo-1,4-dioxin **10***b*; oil (20%); ir (film): 1680,1100 cm^{-1}; ^1H nmr ($CDCl_3$) δ: 1.4 (s, 3H, CH_3), 1.8 (m, 4H, CH_2) 3.5–3.7 (m, 26H, CH_2O and CH_2Cl), 4.3 (s, 2H, =C-CH_2O), 4.5 (s, 2H, Ph-CH_2-O), 6.6–6.7 (m, 4H, aromatic), 7.3 (s, 5H, aromatic). Anal. ($C_{33}H_{46}Cl_2O_9$) C, H.

Synthesis of macrocyclic polyethers ***11***

A typical procedure for the cyclization of the derivatives **10** with catechol has already been described (1).

6,8,9,11,12,19,20,22,23,25-Decahydro-6-methyl-6-[3-(phenylmethoxy-propyl] - [1, 4]benzodioxino[2, 3-i]-[1, 4, 7, 12, 15, 18]-benzohexaoxacycloeicosin **11***a* has already been described (1).

6,8,9,11,12,14,15,22,23,25,26,28,29,31 - Tetradecahydro-6-methyl-6-[3-(phenylmethoxy)propyl]-[1,4]benzodioxino[2,3-i]-[1,4,7,10,15,18,21,24]-benzooctaoxacyclohexacosin **11***b*; oil (37%); ir (film): 1680,1100 cm^{-1}; ^1H nmr ($CDCl_3$) δ: 1.4 (s, 3H, CH_3), 1.7 (m, 4H, CH_2), 3.3–4.3 (m, 3OH, CH_2O), 6.3–6.6 (m, 8H, aromatic), 7.0 (s, 5H, aromatic). Anal. ($C_{39}H_{30}O_{11}$) C, H.

Hydrogenolysis of ***7*** *and* ***11***

A mixture of **7** or **11** (0.73 mmol) and 10% palladized charcoal (25 mg) in ethyl acetate (12 mL) was reduced with stirring under a hydrogen atmosphere at ambient conditions for 3 h. The reaction mixture was filtered to remove catalyst and the filtrate was concentrated *in vacuo*. The compound **8** or **12** was obtained quantitatively as a colorless oil.

1,3,4,6,7,9,10,12,13,15-Decahydro-1-methyl-[1,4,7,10,13]-pentaoxacycloheptadecino[16,17-b]-[1,4]benzodioxin-1-propanol **8***a*; ir (film): 3700–3100, 1680,1100 cm^{-1}; ^1H nmr ($CDCl_3$) δ: 1.3 (s, 3H, CH_3), 1.7 (m, 4H, CH_2), 3.4–3.8 (m, 18H, CH_2O), 4.3 (dd, J_{AB} = 12 Hz, 2H, =C-CH_2O), 6.5–6.7 (m, 4H, aromatic). Anal. ($C_{22}H_{32}O_8$) C, H.

1,3,4,6,7,9,10,12,13,15,16,18-Dodecahydro-1-methyl-[1,4,7,10,13,16]-hexaoxacycloeicosano[19,20-b]-[1,4]benzodioxin-1-propanol **8***b*; ir (film): 3700–3100, 1680,1100 cm^{-1}; ^1H nmr ($CDCl_3$) δ: 1.35 (s, 3H, CH_3), 1.7 (m, 4H, CH_2), 3.4–3.8 (m, 22H, CH_2O), 4.35 (s, 2H, =CH-CH_2O), 6.4–6.8 (m, 4H, aromatic). Anal. ($C_{24}H_{36}O_9$) C, H.

1,3,4,6,7,9,10,12,13,15,16,18,19,21-Tetradecahydro-1-methyl-[1,4,7,10,13,16,19]-heptaoxacyclotricosano[22,23-b]-[1,4]benzodioxin-1-propanol **8***c*; ir (film): 3700–3100, 1680,1100 cm^{-1}; ^1H nmr ($CDCl_3$) δ: 1.35 (s, 3H, CH_3), 1.7 (m, 4H, CH_2), 3.4–3.8 (m, 26H, CH_2O), 4.8 (s, 2H, =C-CH_2O), 6.4–6.8 (m, 4H, aromatic). Anal. ($C_{26}H_{40}O_{10}$) C, H.

6,8,9,11,12,19,20,22,23,25-Decahydro-6-methyl-[1,4]benzodioxino[2,3-i]-[1,4,7,12,15,18-]-benzohexaoxacycloeicosin-6-propanol **12***a* (98%); oil; ir (film): 3700–3100, 1680, 1200 cm^{-1}; ^1H nmr ($CDCl_3$;) δ: 1.3 (s, 3H, CH_3), 1.8 (m, 4H, CH_2), 3.5–4.3 (m, 2OH, CH_2-O), 6.5–6.8 (m, 8H, aromatic). Anal. ($C_{28}H_{36}O_9$) C, H.

6,8,9,11,12,14,15,22,23,25,26,28,29,31-Tetradecahydro-6-methyl-[1,4]benzodioxino[2,3-i]-[1,4,7,10,15,18,21,24]-benzooctaoxacyclohexacosin-6-propanol **12***b* (98%); oil; ir (film: 3700–3100,1680,1200 cm^{-1}; ^1H nmr ($CDCl_3$) δ: 1.3 (s, 3H, CH_3), 1.8 (m, 4H, CH_2) 2.5, 3.5–4.3 (m, 28H, CH_2O), 6.5–6.8 (m, 8H, aromatic). Anal. ($C_{32}H_{44}O_{11}$).

Preparation of aldehydes ***9*** *and* ***13***

To a solution of dimethyl sulfoxide (0.546 g, 7 mmol) in dichloromethane (10 mL) at −60°C was added a solution of oxalyl chloride (0.4879 g, 4.1 mmol) in dichloromethane (10 mL) and the mixture stirred at −60°C for 30 min. A solution of alcohol **8** or **12** (2.6 mmol) in dichloromethane (10 mL) was then added to this mixture at −60°C. After stirring for 1 h, triethylamine (3 mL) was added. The stirring was continued at −60°C for another 10 min. The mixture was then allowed to warm up slowly to room temperature, quenched with saturated ammonium chloride, and extracted with dichloromethane (4 × 15 mL). The organic layer was washed with water, dried ($MgSO_4$), and evaporated to dryness. The product was purified by flash chromatography with ether – petroleum ether as eluent to yield pure **9** or **13**.

1,3,4,6,7,9,10,12,13,15-Decahydro-1-methyl-[1,4,7,10,13]-pentaoxacycloheptadecino[16,17-b]-[1,4]benzodioxin-1-propanal **9***a* (79%); oil; ir (film)-: 2720,1710 cm^{-1}; ^1H nmr ($CDCl_3$) δ: 1.4 (s, 3H, CH_3), 2.0–2.2 (m, 2H, CH_2), 2.3–2.5 (m, 2H, CH_2-CHO), 3.5–3.7 (m, 16H, CH_2O), 4.3 (s, 2H, =C-CH_2O), 6.5–6.7 (m, 4H, aromatic), 9.4 (m, 1H, CHO). Anal. ($C_{22}H_{30}O_8$) C, H.

1,3,4,6,7,9,10,12,13,15,16,18-Dodecahydro-1-methyl-[1,4,7,10,13,16]-hexaoxacycloeicosano[19,20-b]-[1,4]benzodioxin-1-propanal **9***b* (78%); oil; ir (film): 2720,1710 cm^{-1}; ^1H nmr ($CDCl_3$) δ: 1.4 (s, 3H, CH_3), 2.0–2.2 (m, 2H, CH_2), 2.3–2.5 (m, 2H, CH_2-CHO), 3.4–3.6 (m, 2OH, CH_2O), 4.4 (s, 2H, =C-CH_2O), 6.5–6.7 (m, 4H, aromatic), 9.4 (m, 1H, CHO). Anal. ($C_{24}H_{34}O_9$) C, H.

1,3,4,6,7,9,10,12,13,15,16,18,19,21-Tetradecahydro-1-methyl-[1,4,7,10,13,16,19]- heptaoxacyclotricosano[22,23-b]-[1,4] benzodioxin-1-propanal **9***c* (61%); oil; ir (film): 2720,1710 cm^{-1}; ^1H nmr ($CDCl_3$) δ: 1.4 (s, 3, CH_3), 2.0–2.2 (m, 2H, CH_2), 2.3–2.5 (m, 2H, CH_2-CHO), 3.4–3.6 (m, 2H, CH_2O), 4.3 (s, 2H, =C-CH_2O), 6.5–6.7 (m, 4H, aromatic), 9.4 (m, 1H, CHO). Anal. ($C_{26}H_{38}O_{10}$) C, H.

6,8,9,11,12,19,20,22,23,25-Decahydro-6-methyl-[1,4]benzodioxino[2,3-i] - [1,4,7,12,15,18] - benzohexaoxacycloeicosin - 6-propanal **13***a* (66%); oil; ir (film): 2720, 1720, 1680, 1100 cm^{-1}, ^1H nmr ($CDCl_3$) δ: 1.3 (s, 3H, CH_3), 1.9–2.1 (m, 2H, CH_2), 2.3–2.6 (m, 2H, CH_2-CHO), 3.5–4.4 (m, 18H, CH_2O), 6.6–6.9 (m, 8H, aromatic), 9.5 (m, 1H, CHO). Anal. ($C_{28}H_{34}O_9$) C, H.

6,8,9,11,12,14,15,22,23,25,26,28,29,31-tetradecahydro-6-methyl-[1,4]benzodioxino[2,3-i]-[1,4,7,10,15,18,21,24]benzooctaoxacyclohexacosin-6-propanal **13***b* (40%); oil; ir (film): 2720, 1720,

1680, 1100 cm^{-1}, ^1H nmr ($CDCl_3$) δ: 1.3 (s, 3H, CH_3), 1.9–2.1 (m, 2H, CH_2), 2.3–2.6 (m, 2H, CH_2-CHO), 3.5–4.4 (m, 26H, CH_2O), 6.6–6.9 (m, 8H, aromatic), 9.5 (m, 1H, CHO). Anal. ($C_{32}H_{42}O_{11}$) C, H.

Preparation of acids **2** and **3**

To a solution of silver nitrate (0.1275 g, 0.75 mmol) in distilled water (6 mL) was slowly added a solution of aldehyde **9** or **13** (0.37 mmol) in ethanol (16.5 mL) and the mixture stirred at room temperature. A solution of sodium hydroxide (0.0596 g, 1.49 mmol) in distilled water (11 mL) was then added to this mixture at room temperature. The formation of a black precipitate was observed. The progress of the reaction was followed by tlc. After 30 min, the reaction mixture was filtered through Celite and the filter cake was washed with water and ether. The aqueous layer was separated, extracted with ether (1 × 10 mL), brought to pH 2 (pH paper), and reextracted with dichloromethane (4 × 15 mL). The combined organic extracts were dried ($MgSO_4$) and evaporated *in vacuo* to afford **2** or **3** as a syrup. Pure acids **2** and **3** were obtained by a rapid filtration through a short silica gel column.

1,3,4,6,7,9,10,12,13,15-Decahydro-1-methyl-[1,4,7,10,13]-pentaoxacycloheptadecino[16,17-b][1,4]benzodioxin-1-propanoic acid **2***a* (98%); oil; ir (film): 3600–2400, 1780,1270,1100 cm^{-1}; ^1H nmr ($CDCl_3$) δ: 1.4 (s, 3H, CH_3), 2.0–2.3 (m, 2H, CH_2), 2.4–2.7 (m, 2H, CH_2-COOH), 3.5–3.8 (m, 16H, CH_2O), 4.25 and 4.7 (2d, J = 13 Hz, 2H, =C-CH_2O), 6.6–6.9 (m, 4H, aromatic); ms(m/z): 439 (M^+ + 1). Anal. calcd. for $C_{22}H_{30}O_9$: C 60.27, H 6.85; found: C 60.69, H 6.93.

1,3,4,6,7,9,10,12,13,15,16,18-Dodecahydro-1-methyl-[1,4,7,10,13,16]-hexaoxacycloeicosano[19,20-b][1,4]benzodioxin-1-propanoic acid **2***b* (96%); oil; ir (film): 3600–2400,1710,1270,1100 cm^{-1}; ^1H nmr ($CDCl_3$) δ: 1.4 (s, 3H, CH_3), 2.0–2.2 (m, 2H, CH_2), 2.4–2.6 (m, 2H, CH_2-COOH), 3.5–3.8 (m, 2OH, CH_2O), 4.3 and 4.55 (2d, J = 11.9 Hz, 2H, =C-CH_2O), 6.6–6.9 (m, 4H, aromatic); ms (m/z): 483 (M^+ + 1). Anal. calcd. for $C_{24}H_{34}O_{10}$: C 59.75, H 7.05; found: C 60.14, H 7.17.

1,3,4,6,7,9,10,12,13,15,16,18,19,21-Tetradecahydro-1-methyl-[1,4,7,10,13,16,19]-heptaoxacyclotricosano[22,23-b][1,4]benzodioxin-1-propanoic acid **2***c* (99%); oil; ir (film): 3600–2400,1720,1270,1100 cm^{-1}; ^1H nmr ($CDCl_3$) δ: 1.4 (s, 3H, CH_3), 2.0–2.2 (m, 2H, CH_2), 2.4–2.6 (m, 2H, CH_2-COOH), 3.5–3.8 (m, 24H, CH_2O), 4.25 and 4.60 (2d, J = 13, 9 Hz, 2H, =C-CH_2O), 6.6–6.9 (m, 4H, aromatic); ms (m/z): 527 (M^+ + 1). Anal. calcd. for $C_{26}H_{38}O_{11}$: C 59.31, H 7.22; found: C 59.72, H 7.33.

6,8,9,11,12,19,20,22,23,25-Decahydro-6-methyl-[1,4]benzodioxino[2,3-i]-[1,4,7,12,15,18]-benzohexaoxacycloeicosin-6-propanoic acid **3***a* (80%); oil; ir (film): 3600–2400,1710,1100 cm^{-1}; ^1H nmr ($CDCl_3$) δ: 1.4 (s, 3H, CH_3), 2.0–2.1 (m, 2H, CH_2), 2.4–2.5 (m, 2H, CH_2-COOH), 3.5–4.5 (m, 18H, CH_2O), 6.5–6.9 (m, 8H, aromatic); ms (m/z): 531 (M^+ + 1). Anal. calcd. for $C_{28}H_{34}O_{10}$: C 63.39, H 6.41; found: C 63.67, H 6.50.

6,8,9,11,12,14,15,22,23,25,26,28,29,31-Tetradecahydro-6-methyl-[1,4]benzodioxino[2,3-i]-1,4,7,10,15,18,21,14]-benzooctaoxacyclohexacosin-6-propanoic acid **3***b* (90%); oil; ir (film): 3600–2400, 1710, 1100 cm^{-1}; ^1H nmr ($CDCl_3$) δ: 1.4 (s, 3H, CH_3), 2.0–2.1 (m, 2H, CH_2), 2.4–2.5 (m, 2H, CH_2-COOH), 3.5–4.5 (m, 26H, CH_2O), 6.5–6.9 (m, 8H, aromatic); ms (m/z): 619 (M^+ + 1). Anal. calcd. for $C_{32}H_{42}O_{12}$: C 62.95, H 5.57; found: C 63.17, H 5.71.

Potentiometric measurement

Two glass indicator electrodes were used, one specific for the alkali-metal ion, either sodium (Jena er Glass) or potassium (Solea type pKV3), the other specific to hydrogen ion (Orion 91-01). The reference electrode was a two-stage model of the following type, the double junction being meant to prevent any contamination of the solution by potassium cations.

Hg, Hg_2Cl_2	KCl, Hg_2Cl_2 saturated in methanol	ClO_4NEt_4 8×10^{-2} M in methanol	Experimental solution

Potentials were recorded using an Orion research millivoltmeter model 701/A. Standardization of both electrodes was performed before measurements. For the pH standardization, buffers in methanol prepared according to De Ligny *et al.* (26) were used. Solutions of tetrabutylammonium methylate in methanol were prepared as previously described (27). All the data were obtained at 25.0°C.

Extraction measurement

These were conducted using procedures previously described (28).

Acknowledgments

We are indebted to Professor R. Blankespoor, on leave from Calvin College, Grand Rapids, who read this paper and recommended changes in the usage of the English language.

1. G. Coudert, G. Guillaumet, and M. Mpassi. Synthesis, 111 (1985).
2. P. Bosseray, G. Guillaumet, G. Coudert, and H. Wasserman. Tetrahedron Lett. **30**, 1387 (1989).
3. M. Mpassi, G. Guillaumet, G. Coudert, M. Tissier, and J. Juillard. Can. J. Chem. **67**, 1132 (1989).
4. W. Wieranga, B. R. Evans, and J. A. Wolterson. J. Am. Chem. Soc. **101**, 1334 (1979).
5. H. Kuboniwa, S. Nagami, K. Yamaguchi, A. Hirao, S. Nakahama, and N. Yamazaki. J. Chem. Soc. Chem. Commun. 1468 (1985).
6. K. Hiratani. Chem. Lett. 21 (1981); Bull. Soc. Chim. Jpn. **55**, 1963 (1982).
7. (*a*) G. S. Heo, R. A. Bartsch, L. Schlobonm, and J. G. Lee. J. Org. Chem. **46**, 3574 (1981); (*b*) R. A. Bartsch, G. S. Heo, S. I. Kang, Y. Liu, and J. Strzelbicki. J. Org. Chem. **47**, 457 (1982); (*c*) J. Strzelbicki and R. A. Bartsch. Anal. Chem. **53**, 1984 (1981); **53**, 2277 (1981); **53**, 2251 (1981); (*d*) W. Walkowiak, W. A. Charewicz, S. I. Kang, I. W. Yang, M. J. Pugia, and R. A. Bartson. Anal. Chem. **62**, 2018 (1990); (*e*) W. Walkowiak, S. I. Kang, L. E. Stewart, G. Ndip, and R. A. Bartson. Anal. Chem. **62**, 2022 (1990).
8. L. Lalloz, V. Loppinet, G. Coudert, G. Guillaumet, B. Loubinoux, C. Labrid, M. Beaughard, G. Dureng, and J. C. Lamar. J. Med. Chem. **24**, 994 (1981).
9. G. Guillaumet, G. Coudert, and B. Loubinoux. Tetrahedron Lett. 4379 (1979).
10. J. M. Timko, S. S. Moore, D. M. Walba, P. C. Huberty, and D. J. Cram. J. Am. Chem. Soc. **99**, 4207 (1977).
11. P. D. Cesare and B. Gross. Synthesis, 458 (1979).
12. S. Kopolov, T. E. H. Esch, and J. Smid. Macromolecules, **6**, 133 (1973).
13. C. H. Heathcock and R. Ratcliffe. J. Am. Chem. Soc. **93**, 1746 (1971).
14. A. J. Mancuso, J. L. Huang, and D. Swern. J. Org. Chem. **43**, 2480 (1978).
15. M. Shamma and H. R. Rodriguez. Tetrahedron, **24**, 6583 (1968).
16. Y. Pointud, C. Tissier, and J. Juillard. J. Solution Chem. **12**, 473 (1983).
17. Y. Pointud, J. Juillard, G. Jeminet, and L. David. J. Chem. Soc. Faraday Trans. 1, **77**, 1 (1981).
18. Y. Pointud, C. Pierzo, C. Tissier, and J. Juillard. J. Chim. Phys. **82**, 891 (1985).

Can. J. Chem. Downloaded from www.nrcresearchpress.com by 92.62.229.171 on 09/08/12
For personal use only.

19. B. C. Pressman, E. J. Harris, W. S. Jagger, and J. H. Johnson. Proc. Natl. Acad. Sci. (U.S.A.), **58**, 1949 (1967).
20. D. R. Pfeiffer and H. A. Lardy. Biochemistry, **15**, 935 (1976).
21. M. Newcomb and D. Cram. J. Am. Chem. Soc. **97**, 1257 (1977).
22. G. W. Gokel, D. M. Goli, C. Mingati, and L. Echegoyen. J. Am. Chem. Soc. **105**, 6786 (1983).
23. H. K. Frensdorf. J. Am. Chem. Soc. **93**, 600 (1971).
24. D. G. Parsons, M. R. Truter, and J. N. Wingfield. Inorg. Chim. Acta, **27**, 81 (1980).
25. G. Chaput, G. Jeminet, and J. Juillard. Can. J. Chem. **53**, 2240 (1975).
26. C. L. De Ligny, P. M. M. Luikx, M. Rehbach, and A. A. Wienecke. Recl. Trav. Chim. (Pays-Bas), **79**, 699 (1960).
27. J. Woźnicka, C. Lhermet, N. Morel-Desrosiers, J. P. Morel, and J. Juillard. J. Chem. Soc. Faraday Trans. 1, **85**, 1709 (1989).
28. C. Gaboyard, G. Dauphin, and G. Jeminet. Agric. Biol. Chem. **54**, 1149 (1990).

Can. J. Chem. Downloaded from www.nrcresearchpress.com by 92.62.229.171 on 09/08/12
For personal use only.

Electrosynthesis of thiocyanato and mixed ligand thiocyanato complexes of transition metals by the sacrificial dissolution of metal anodes

M. C. CHAKRAVORTI[1] AND GAMPA V. B. SUBRAHMANYAM

Department of Chemistry, Indian Institute of Technology, Kharagpur-721 302, India

Received June 27, 1991

M. C. CHAKRAVORTI and GAMPA V. B. SUBRAHMANYAM. Can. J. Chem. **70**, 836 (1992).

A general method for the electrosynthesis of anionic and mixed ligand nonelectrolytic thiocyanato complexes of transition metals has been developed by the oxidation of sacrificial metal anodes in aqueous, or aqueous ethanolic, medium containing ammonium thiocyanate at room temperature and at an applied potential of 2–7 V. The method is rapid and gives good yield with high purity.

Key words: electrosynthesis, thiocyanato complexes, mixed ligand thiocyanato complexes.

M. C. CHAKRAVORTI et GAMPA V. B. SUBRAHMANYAM. Can. J. Chem. **70**, 836 (1992).

On a mis au point une méthode générale d'électrosynthèse de complexes thiocyanato anioniques et de complexes thiocyanato non-électrolytiques à ligands mixtes de métaux de transition; cette méthode fait appel à une oxydation d'anodes métalliques suicidaires, en solutions aqueuses ou dans un milieu éthanolique aqueux contenant du thiocyanate d'ammonium, à la température ambiante et à un potential appliqué de 2 à 7 V. La méthode est rapide et elle donne de bons rendements et les produits sont d'une grande pureté.

Mots clés : électrosynthèse, complexes thiocyanato, complexes thiocyanato à ligands mixtes.

[Traduit par la rédaction]

Introduction

In recent years there has been a growing interest in the synthesis of coordination compounds starting directly from metals (1–4). Electrochemical synthesis in which a sacrificial metal anode is dissolved in the presence of an electrolyte containing an appropriate ligand is an established way for the electrolytic synthesis of a variety of metal complexes in a single step (1). The process uses the metals directly and thus contamination of the product by the anions, which is often encountered in chemical methods using the metal salts, is absent. The method is rapid and highly selective. Oldham *et al.* recently reported the electrosynthesis of the anionic thiocyanato complexes of Zn, Cd, Ga, Co, and Au from a nonaqueous solution of thiocyanic acid using the metals as anode (5). In the present communication we describe a general method for the rapid and direct electrochemical synthesis of transition metal thiocyanato complexes and also mixed ligand thiocyanato complexes by the dissolution of sacrificial metal anodes in an aqueous (or aqueous ethanolic) solution of ammonium thiocyanate (also containing the appropriate ligand when mixed complexes are to be prepared).

Experimental

The metals were in the form of rods, lumps, chips, or foils and were mostly 99.8% pure. Other chemicals were of AR/GR quality from reputable manufacturers.

The electric power was supplied by a dc power supply (Aplab, India). The current was recorded from the scale of the power supply and checked by connecting a separate ammeter or milliammeter into the circuit. The electrolytic cell was a tall form of beaker (100 cm^3) fitted with a rubber stopper through which four holes were made. The appropriate metal rods (iron and molybdenum) formed the anode and were inserted through a hole. Other metals were used as lumps, foils, or chips. These were tied with a platinum wire, which was inserted through the hole. Chromium and manganese were previously deposited on a platinum foil sealed to a platinum wire that served as the anode. In all cases a platinum foil (about 1 × 1 × 0.15 cm) connected to a platinum wire served as the cathode and was introduced through the second hole. Two glass tubes were introduced through the other two holes. These allowed input and exit of nitrogen where it was necessary to carry out electrolysis in the absence of air.

Metals were analysed by standard titrimetric or gravimetric methods. Sulphur was determined gravimetrically as $BaSO_4$ after decomposing the complexes with nitric acid (6). Nitrogen was determined by the micro Dumas method. Reflectance spectra were recorded using a Shimadzu UV spectrophotometer (no. 3100) against $BaSO_4$. Infrared spectra were recorded in KBr pellet using a Perkin Elmer instrument (no. 883). Magnetic susceptibility was measured by the Gouy method using $Hg[Co(NCS)_4]$ as calibrant. Diamagnetic corrections were taken from standard sources (7).

Preparation of the complexes

$[(CH_3)_4N]_2[M(NCS)_4]$ where M = Mn, Fe, Co, Cu, Zn, and Cd; $[(CH_3)_4N]_3[Cr(NCS)_6]$; $[(CH_3)_4N]_4[Ni(NCS)_6]$ and $[(CH_3)_4N]_4[Mo_2O_4(NCS)_6]$

The electrolysis was carried out using 10 cm^3 of an aqueous solution containing 1 g NH_4SCN. The details of the experimental conditions are given in Table 1. After the electrolysis, the complexes were precipitated by adding a slight excess of tetramethylammonium chloride (or thiocyanate) dissolved in the minimum volume of water. The complexes were separated by filtering under suction within 30 min. These were dried by pressing between the folds of filter paper and then keeping in a desiccator over sulphuric acid.

Electrolysis using iron as anode was carried out in a stream of nitrogen. In all other cases electrolysis was carried out in air.

$[(CH_3)_4N]_3[Fe(NCS)_6]$

This was prepared by a two-step electrolysis. In the first step $[Fe(NCS)_4]^{2-}$ was generated *in situ* as described above, after which the iron anode was replaced by a platinum foil electrode and the electrolysis was continued in air for one more hour. Finally, the tetramethylammonium salt was obtained by the addition of a concentrated solution of tetramethylammonium chloride.

$[M(py)_4(NCS)_2]$, where M = Mn, Fe, Co, and Ni; $[M(py)_2(NCS)_2]$, where M = Cu, Zn and Cd; $[Mo_2O_4(py)_4(NCS)_2]$

The electrolysis was carried out using 10 cm^3 of an aqueous solution containing 3–4 cm^3 pyridine and 1 g NH_4SCN. Except for

[1]Author to whom correspondence may be addressed.

Can. J. Chem. Downloaded from www.nrcresearchpress.com by 92.62.229.171 on 09/08/12
For personal use only.

TABLE 1. Experimental conditions for the electrosynthesis of the anionic thiocyanato complexes

Compound	Voltage, V	Current, A	Amount of metal oxidised, g	Yield g	Yield %	E_F, mol F^{-1}
$(Me_4N)_3[Cr(NCS)_6]$	3	0.25	0.149	1.50	84	0.31
$(Me_4N)_2[Mn(NCS)_4]$	2	0.15	0.140	0.85	78	0.48
$(Me_4N)_2[Fe(NCS)_4]$	2	0.10	0.100	0.60	71	0.52
$(Me_4N)_2[Co(NCS)_4]$	2	0.20	0.211	1.25	76	0.49
$(Me_4N)_4[Ni(NCS)_6]$	2	0.10	0.100	0.50	62	0.48
$(Me_4N)_2[Cu(NCS)_4]$	2	0.10	0.100	0.50	68	0.46
$(Me_4N)_2[Zn(NCS)_4]$	5	0.35	0.411	1.65	61	0.48
$(Me_4N)_2[Cd(NCS)_4]$	4	0.10	0.210	0.65	71	0.51
$(Me_4N)_4[Mo_2O_4(NCS)_6]$	5	0.35	0.220	1.30	63	0.18
$(Me_4N)_3[Fe(NCS)_6]$	3(4)[a]	0.2(0.3)[a]	0.212	1.75	74	

Time of electrolysis in each case was 1 h.
[a]Values in parentheses refer to the subsequent electrolytic oxidation of the initially formed Fe complex.

TABLE 2. Experimental conditions for the electrosynthesis of the mixed ligand thiocyanato complexes

Compound	Voltage, V	Current, A	Amount of metal oxidised, g	Yield g	Yield %	E_F, mol F^{-1}
$[Mn(bipy)_2(NCS)_2]$	6	0.10	0.090	0.60	80	0.44
$[Fe(bipy)_2(NCS)_2]$	6	0.10	0.095	0.60	73	0.46
$[Co(bipy)_2(NCS)_2]$	7	0.10	0.100	0.65	75	0.45
$[Ni(bipy)_2(NCS)_2]$	6	0.10	0.096	0.55	67	0.44
$[Cu(bipy)(NCS)_2]$	7	0.10	0.098	0.45	71	0.41
$[Zn(bipy)(NCS)_2]$	7	0.10	0.104	0.35	63	0.43
$[Cd(bipy)(NCS)_2]$	6	0.05	0.110	0.30	79	0.52
$[Mo_2O_4(bipy)_2(NCS)_2]$	6	0.10	0.072	0.40	75	0.20

Time of electrolysis in each case was 1 h.

molybdenum, in all cases the complexes precipitated during the electrolysis. The molybdenum complex was precipitated on concentrating the solution in a desiccator over dry $CaCl_2$. The complexes were separated by filtration under suction, washed with ethanol, and dried over sulphuric acid.

$[ML_2(NCS)_2]$, where M = Mn, Fe, Co, Ni, Zn, and Cd;
$[ML(NCS)_2]$, where M = Cu, Zn, and Cd; and
$[Mo_2O_4L_2(NCS)_2]$ where L = 2,2′-bipyridyl and 1,10-phenanthroline

The electrolysis was carried out in 60–70% aqueous ethanolic medium (10–12 cm^3) containing 1 g NH_4SCN and 0.2–0.3 g 2,2′-bipyridyl or 1,10-phenanthroline hydrate. The precipitates of the complexes appeared during the electrolysis. These were separated and dried as in the previous case. Electrolysis using iron as an anode was carried out in a stream of nitrogen. While zinc and cadmium gave $[ML(NCS)_2]$ with 0.2–0.3 g of the ligand, the complexes $[ML_2(NCS)_2]$ were obtained using 0.5 g of 2,2′-bipyridyl and 1,10-phenathroline hydrate.

All the mixed ligand complexes could also be prepared by first electrolysing in the presence of an aqueous solution of NH_4SCN (as in the case of the preparation of the anionic complexes), followed by the addition of the appropriate ligand (3–4 cm^3 pyridine as such, or 2,2′-bipyridyl or 1,10-phenanthroline hydrate in amounts as mentioned above and dissolved in a minimum volume of ethanol).

The experimental conditions along with the yields, etc. for the preparation of the 2,2′-bipyridyl complexes from aqueous ethanolic medium containing the ligand bipyridyl are given in Table 2. The same apply (with slight change in some cases) for the preparation of the pyridine and the 1,10-phenanthroline complexes.

Results and discussion

Our studies show that anionic thiocyanato complexes and also nonelectrolytic mixed ligand thiocyanato complexes of many transition metals can be easily and quickly prepared in a single step by anodic dissolution of the metals in aqueous or mixed solvent at room temperature. The applied voltage is low (2–5 V in aqueous medium and 5–7 V in mixed solvent) and the yield is very good (60–90% based on the amount of the metal oxidized). The main reactions taking place at the electrodes are

$$2H^+ + 2e \rightarrow H_2 \text{ (at cathode)}$$

$$M - ne \rightarrow M^{+n} \text{ (at anode)}$$

which is evident from the observed electrochemical efficiency. A slight deviation of the electrochemical efficiency (Tables 1 and 2) from the theoretical value of $1/n$ is ascribed to slight fluctuation of the current during the electrolysis and some other reactions taking place at the anode. In almost all cases a feeble foul smell was noted during electrolysis; this may be due to partial oxidation of thiocyanate at the anode.

An obvious advantage of the present method is the absence of any contamination of the products by the anions, which is often encountered in chemical methods using the metal salts. It was checked that tetramethylammonium chloride and tetramethylammonium thiocyanate gave the same product and there is no occlusion of chloride in the

Can. J. Chem. Downloaded from www.nrcresearchpress.com by 92.62.229.171 on 09/08/12
For personal use only.

product while using tetramethylammonium chloride. Another advantage of the method is that it uses an aqueous or mixed solvent at room temperature, while the common methods for the preparation of thiocyanato complexes often use nonaqueous solvents and sometimes involve reactions in the melt.

The compounds were characterized by chemical analysis and the measurement of the magnetic moments, ir spectra, and electronic spectra. The magnetic moments (8–13) and the important band positions in the ir spectra (9, 14–24) of most of the complexes are available in the literature. In all such cases our values agreed with the literature values. For other compounds also, these were as expected. The electronic spectral band positions of only a few compounds are available in the literature (9, 25–28) and our values are in agreement with these. For other compounds our data are in accordance with expectation.

All the analytical data have been deposited as Supplementary Material.[2]

1. V. A. Konev, V. Yu. Kukushkin, and Yu. N. Kukushkin. Russ. J. Inorg. Chem. **31**, 838 (1986).
2. P. L. Timms. Adv. Inorg. Radiochem. **14**, 121 (1972).
3. G. A. Ozin and A. Van der Voet, Prog. Inorg. Chem. **19**, 105 (1975).
4. D. G. Tuck. Pure Appl. Chem. **51**, 2005 (1979).
5. C. Oldham, M. J. Taylor, and D. G. Tuck. Inorg. Chim. Acta, **100**, L9 (1985).
6. W. G. Palmer. Experimental inorganic chemistry. Cambridge University Press, Cambridge. 1954 p. 421.
7. J. Lewis and R. G. Wilkins. Modern coordination chemistry. Interscience, New York. 1960 p. 403.
8. J. J. Salzmann and H. H. Schmidtke. Inorg. Chim. Acta, **2**:**3**, 207 (1969).
9. D. Forster and D. M. L. Goodgame. Inorg. Chem. **4**, 268 (1965); **4**, 823 (1965).
10. B. F. Little and G. J. Long. Inorg. Chem. **17**, 3401 (1978).
11. W. A. Baker, Jr. and H. M. Bononich. Inorg. Chem. **3**, 1184 (1964).
12. Th.I. Pirtea. Rev. Chim (Bucharest), **12**, 223 (1961).
13. C. M. Harris and E. D. McKenzie. J. Inorg. Nucl. Chem. **19**, 372 (1961).
14. A. Sabatini and I. Bertini. Inorg. Chem. **4**, 959 (1965).
15. D. Forster and M. L. Goodgame. J. Chem. Soc. **4**, 715 (1965).
16. D. Forster and W. Dew. Horrocks, Jr. Inorg. Chem. **6**, 339 (1967).
17. J. Lewis, R. S. Nyholm, and P. W. Smith. J. Chem. Soc. 4590 (1961).
18. R. J. H. Clark and A. D. J. Goodwin. Spectrochim. Acta, **26A**, 323 (1970).
19. I. S. Ahuja and A. Garg. J. Inorg. Nucl. Chem. **34**, 1929 (1972).
20. K. König, K. Madeja, and K. J. Watson. J. Am. Chem. Soc. **90**, 1146 (1968).
21. A. A. Schilt and K. Fritsch. J. Inorg. Nucl. Chem. **28**, 2677 (1966).
22. W. P. Griffith. J. Chem. Soc. (A), 211 (1969).
23. Porai-Koshits. Kristollagrafiva, **3**, 686 (1958).
24. M. C. Chakravorti and D. Bandyopadhaya. Synth. React. Inorg. Met.-Org. Chem. **15**, 1 (1985).
25. C. K. Jorgenson. Adv. Chem. Phys. **5**, 33 (1963).
26. F. A. Cotton, D. M. L. Goodgame, M. Goodgame, and A. Sacco. J. Chem. Soc. **83**, 4157 (1961).
27. S. M. Nelson and T. M. Shepherd. J. Chem. Soc. 3276 (1965).
28. E. König and K. Madeja. Inorg. Chem. **6**, 48 (1967).

[2]These data may be purchased from: The Depository of Unpublished Data, Document Delivery, CISTI, National Research Council Canada, Ottawa, Canada K1A 0S2.

Can. J. Chem. Downloaded from www.nrcresearchpress.com by 92.62.229.171 on 09/08/12
For personal use only.

Ion chemistry of aluminum and boron in methane–oxygen flames

PIERRE N. CROVISIER, J. HUGH HORTON, CARL S. HASSANALI, AND JOHN M. GOODINGS[1]

Department of Chemistry and Centre for Research in Earth and Space Science, York University, 4700 Keele Street, North York, Ont., Canada M3J 1P3

Received August 2, 1991

PIERRE N. CROVISIER, J. HUGH HORTON, CARL S. HASSANALI, and JOHN M. GOODINGS. Can. J. Chem. **70**, 839 (1992).

The ion chemistry of aluminum and boron, primarily in the +3 oxidation state, was studied by doping premixed, methane–oxygen flames of both fuel-rich and fuel-lean (oxygen-rich) composition with 1×10^{-6} mol fraction of $AlCl_3$ and 5×10^{-4} mol fraction of $B(OC_2H_5)_3$. Ions were observed by sampling the flames at atmospheric pressure through a nozzle into a mass spectrometer. At this low concentration level, aluminum exhibits two cation series: (*a*) $AlO^+.nH_2O$ (n = 2, 3) formed by proton transfer to AlO(OH) and $Al(OH)_3$ in which hydration reactions are involved; and (*b*) $Al^+.nH_2O$ (n = 0, 1) by protonation of AlOH with hydration/dehydration steps. At the higher concentration of the boron additive, four cation series were observed: (*a*) $B(OC_2H_5)_3H^+.nH_2O$ (n = 0, 1) based on proton transfer to the $B(OC_2H_5)_3$ additive; (*b*) $BO^+.nH_2O$ (n = 1–4) similar to aluminum; (*c*) $HB_2O_3^+.nH_2O$ (n = 1–3) involving the protonated dimer of metaboric acid, BO(OH); and (*d*) $B_3O_4^+.nH_2O$ (n = 2, 3) involving the protonated trimer of BO(OH) whose structures might be cyclic or linear. Other series members are formed by subsequent hydration or dehydration of the parent cations. The anions BO_2^- and BO^- previously studied by D. E. Jensen were also observed. The formation chemistry and probable structures of these ions are discussed, and compared with similar results obtained previously for flames doped with transition metals; notably Sc, Ti, V, and Cr in the +3 oxidation state.

Key words: aluminum, boron, ions, flame, gas phase.

PIERRE N. CROVISIER, J. HUGH HORTON, CARL S. HASSANALI et JOHN M. GOODINGS. Can. J. Chem. **70**, 839 (1992).

On a étudié la chimie ionique de l'aluminium et du bore, principalement dans leur état d'oxydation +3, en dopant des flammes prémélangées de méthane et d'oxygène, de compositions tant riches que pauvres (riches en oxygène) en combustibles, avec des fractions molaires de 1×10^{-4} de $AlCl_3$ et de 5×10^{-4} de $B(OC_2H_5)_3$. On a observé les ions en effectuant un échantillonnage des flammes, à pression atmosphérique, à l'aide d'un bec relié à un spectromètre de masse. À ces basses concentrations, l'aluminium présente deux séries de cations : (*a*) $AlO^+.nH_2O$ (n = 2, 3) formé par un transfert de proton vers le AlO(OH) et le $Al(OH)_3$ dans lequel des réactions d'hydratation sont impliquées; et (*b*) $Al^+.nH_2O$ (n = 0, 1) formés par la protonation du AlOH avec des étapes d'hydratation et de déshydratation. Aux concentrations plus élevées de l'additif de bore, on a observé quatre séries de cations : (*a*) $B(OC_2H_5)_3H^+.nH_2O$ (n = 0, 1) qui provient d'un transfert de proton à l'additif $B(OC_2H_5)_3$; (*b*) $BO^+.n(H_2O)$ (n = 1–4) semblables à ceux de l'aluminium; (*c*) $HB_2O_3^+.nH_2O$ (n = 1–3) impliquant le dimère protoné de l'acide métaborique, BO(OH); et (*d*) $B_3O_4.nH_2O$ (n = 2, 3) impliquant le trimère protoné du BO(OH) dont les structures peuvent être soit cycliques ou linéaires. D'autres membres de la série se forment par des réactions subséquentes d'hydratation ou de déshydratation des cations parents. On a aussi observé la présence des anions BO_2^- et BO^- qui avaient été étudiés antérieurement par D. E. Jensen. On discute de la chimie de la formation et des structures probables de ces ions et on les compare avec des résultats semblables obtenus antérieurement pour des flammes dopées avec des métaux de transitions, principalement le Sc, Ti, V et Cr dans leur état d'oxydation +3.

Mots clés : aluminium, bore, ions, flamme, phase gazeuse.

[Traduit par la rédaction]

Introduction

The motivation for this work on aluminum and boron arose out of our previous studies of the ion chemistry of the first row of 10 transition metals (Sc–Zn) in a hydrocarbon flame (1, 2). In these studies, the nude metallic oxide ion was observed for the first time in flames (2); i.e., AO^+, where A is the metal atom. Most of these metals form compounds with the metal in multiple oxidation states, including the +3 state for seven of them (Sc, Ti, V, Cr, Fe, Co, and Ni); it is the only state known for Sc. The oxide ion signals observed were large for VO^+ but considerably smaller for ScO^+, TiO^+, and CrO^+. However, members of the hydrated oxide ion series $AO^+.nH_2O$ (n = 0–3) accounted for 99% of the metallic flame ions observed for Sc and 81% for V, but only 6% for Ti and 0.2% for Cr.

The probable formation of these oxide ions in the flame is straightforward, involving the neutral trihydroxide, $A(OH)_3$, and oxide-hydroxide, AO(OH), which differ by a single water molecule

[1] $$A(OH)_3 + M \rightleftarrows AO(OH) + H_2O + M$$

where M is any other flame species. Oxide ion formation is initiated by proton transfer to these species followed by dehydration reactions

[2] $$HX^+ + A(OH)_3 \rightleftarrows X + A(OH)_3H^+$$
$$\text{or } A(OH)_2(H_2O)^+ \text{ or } AO^+.2H_2O$$

[3] $$A(OH)_2(H_2O)^+ + M \rightleftarrows H_2O + M + A(OH)_2^+$$
$$\text{or } AO^+.H_2O$$

[4] $$HX^+ + AO(OH) \rightleftarrows X + A(OH)_2^+ \quad \text{or } AO^+.H_2O$$

[5] $$A(OH)_2^+ \quad \text{or } AO^+.H_2O + M \rightleftarrows H_2O + M + AO^+$$

Here, HX^+ is a naturally occurring flame ion of the general type $C_xH_yO_z^+$ which functions as a proton donor for the chemical ionization of metallic species. From the promi-

[1]Author to whom correspondence may be addressed.

Can. J. Chem. Downloaded from www.nrcresearchpress.com by 92.62.229.171 on 09/08/12
For personal use only.

Can. J. Chem. Downloaded from www.nrcresearchpress.com by 92.62.229.171 on 09/08/12
For personal use only.

nence of the signals observed for the oxide ion series, evidently the +3 oxidation state is emphasized for V, like Sc, but not for Ti nor Cr. These considerations provided our motivation for this study of Al and B, both main group III elements in the +3 oxidation state, in order to find out the degree to which their flame-ion chemistry is similar to that of Sc and V. We are not aware of any previous study of aluminum ions in flames. With regard to boron, Jensen (3, 4) studied the formation of alkali metal metaborates in fuel-rich, H_2–O_2–N_2 flames; he observed BO_2^- and BO^- mass spectrometrically and measured the corresponding electron affinities of BO_2 and BO. In similar fuel-rich hydrogen flames with added acetylene and doped with a trace of trimethylborate, $B(OCH_3)_3$, Burdett and Hayhurst (5) identified a "series of hydrates $H_2BO_2^+(H_2O)_n$," and "sets of borate and mixed borate/hydrate clusters, i.e., $H_2BO_2^+(HBO_2)_m$ and $H_2BO_2^+(H_2O)_x(HBO_2)_y$, with n, m, x, and y up to 5, were also found. In addition, borate clustering to H_3O^+ was observed in ions of the type $H_3O^+(HBO_2)_p(H_2O)_q$." However, there is no discussion of these ions beyond this statement of observations.

In this work, we studied primarily the cation chemistry of Al and B in the same, fuel-rich, CH_4–O_2 flame employed for the ion chemistry of transition metals. The ions were observed by sampling the flame at atmospheric pressure through a nozzle into a mass spectrometer. The nature of Al and B imposed limitations on the range of experimental conditions that could be examined. Thus, Al was added to the flame at the low concentration level of 10^{-6} mol fraction. Under this condition, no Al anions were observed, nor were any Al cations or anions seen in a fuel-lean (i.e., oxygen-rich) CH_4–O_2 flame. When B was admitted to the fuel-rich flame at the higher concentration of 5×10^{-4} mol fraction, an interesting variety of B_2 and B_3 cations as well as B_1 species was observed. In common with Jensen (3, 4), the anion chemistry revealed just BO_2^- and BO^-. Only very crude qualitative observations of B cations were made in the fuel-lean flame, however, because the nozzle of the mass spectrometer quickly clogged with solid boron oxides under fuel-lean conditions, and the results were not properly reproducible.

Experimental

The flame used in these experiments was a premixed, laminar, methane–oxygen flame of fuel-rich composition whose bulk characteristics are given in Table 1. It was conical in shape, ca. 3.5 mm in base diameter and 5 mm in height with a rounded tip, and with a bright blue reaction zone approximately 0.3 mm thick. It was stabilized at atmospheric pressure on a quartz capillary burner of inner diameter 2.3 mm, and surrounded by a flowing argon shield to minimize the entrainment of atmospheric air. The gases used were Matheson CP grade (CH_4 > 99.0%, O_2 > 99.6%, Ar > 99.9%) added directly from high-pressure cylinders without further purification.

With regard to the additives, all of the organometallic aluminum compounds that are commercially available and reasonably volatile are pyrophoric. In any case, the concentration of aluminum in the flame had to be kept low to avoid the excessive production of solid aluminum oxide (corundum), Al_2O_3, which would clog the orifice in the sampling nozzle of the mass spectrometer. Therefore, aluminum was added by spraying a 0.500 molar aqueous solution of $AlCl_3$ using a small part of the flame's oxygen supply to operate a tiny atomizer (6). It gave a small concentration of aluminum of 1×10^{-6} mol fraction in the equilibrium burnt-gas region of the flame. The presence of aluminum did not change the bulk characteristics of the flame nor its colour.

TABLE 1. Bulk characteristics of the fuel-rich flame

Flame parameter	
Equivalence ratio ϕ	2.15
Unburnt gas flow rates (mL s^{-1})	
CH_4	13.0
O_2	12.1
Adiabatic flame temperature (K)	2456
Measured flame temperature (K)	2200
Burnt-gas rise velocity (m s^{-1})	2.0
Equilibrium burnt-gas composition at 2200 K (mol fractions)	
H_2O	0.25144
H_2	0.41195
O_2	0.00000049
CO	0.29781
CO_2	0.034872
H	0.0036255
OH	0.00030488
O	0.00000191

Boron was added to the flame by flowing part of the flame's oxygen supply through a glass wool plug saturated with triethylborate, $B(OC_2H_5)_3$. This compound had a convenient vapour pressure at room temperature to provide a concentration of 5×10^{-4} mol fraction of boron in the equilibrium burnt gas. We have commented previously that this technique using a glass wool plug gives a much more even flow of the additive than bubbling oxygen through the liquid additive in a conventional gas saturator equipped with a glass frit (7). Although the concentration of boron is much higher than that of aluminum, a still higher boron concentration was avoided; a concentration of 1×10^{-3} mol fraction produced enough solid boron oxides to cause appreciable clogging of the orifice in the sampling nozzle. The addition of the boron additive imparted a bright green colour to the flame.

As an addition to the work done with the fuel-rich flame described in Table 1, some experiments were attempted using a similar fuel-lean, methane–oxygen flame (i.e., oxygen-rich) of equivalence ratio $\phi = 0.216$ whose bulk characteristics have been given previously (8). At the low aluminum concentration level of 1×10^{-6} mol fraction, no aluminum ions of any kind were unambiguously identified. Although boron ions were observed at the higher boron concentration of 5×10^{-4} mol fraction, the clogging problem of the nozzle with solid boron oxides was much more severe, such that stable quantitative measurements could not be made.

The flame-ion mass spectrometer has been described previously (9), and only a brief summary will be given here. The flame burner was mounted on a motorized carriage that provided accurate alignment of the flame axis with the sampling nozzle. A conical sampling nozzle of orifice diameter ca. 0.10 mm was employed, mounted in a water-cooled flange. The nozzle tip was an electron microscope lens made of platinum–iridium alloy described previously (10). Concentration profiles of individual or total ions as a function of axial distance, z, were traced out by advancing the flame onto the sampling nozzle of the mass spectrometer. Inside the nozzle, the sampled ions were focussed into a beam by an ion lens, and passed through two stages of differential pumping into a quadrupole mass filter. The mass-analyzed ions were detected with a parallel-plate Faraday collector connected to a vibrating reed electrometer having a grid-leak resistance of 10^{10} Ω.

The ion signal magnitudes in the profile figures are quoted in volts based on the detected ion current passing through 10^{10} Ω. A reproducible zero on the distance scale of the ion profiles, $z = 0$, was obtained from a fairly sharp minimum on the profile of pressure versus distance, z; pressure was measured by an ionization gauge mounted in the vacuum chamber housing the mass filter. The

pressure minimum corresponded to the downstream edge of the flame's bright, luminous reaction zone. The ion signal magnitudes reported below were corrected for mass discrimination in the ion lens and mass filter against ions of high mass number M (i.e., mass/charge ratio) measured at high resolving power. The correction procedure was given previously (11). The upper limit to the mass range of the mass spectrometer is 165 u.

The ion signals can be subject to distortion because the sampled flame gas is cooled in passing through the cold boundary layer surrounding the sampling orifice, and also in the adiabatic expansion to supersonic velocity that occurs downstream of the nozzle throat. These effects have been described in a series of papers by Hayhurst and co-workers, all of which are referenced in the latest work (5). Ion–molecule reactions having large rates can shift in the exothermic direction in response to the cooling during sampling. The effect is most likely to occur for hydrate formation because the rate involves the reagent water, a major product of combustion. Although this sampling effect may enhance certain hydrate ion signals to some extent, it is unlikely to falsify their existence.

Neutral aluminum and boron species

The background neutral aluminum and boron chemistry in the flame should be examined before considering the ion chemistry in detail. Although aluminum and boron are added as $AlCl_3$ and $B(OC_2H_5)_3$, respectively, these compounds will decompose to give a number of neutral species whose final equilibrium concentrations in the burnt gas will be independent of the chemical nature of the original additive. To calculate the concentrations of these species in the flame, ΔG_f^0 values at 2200 K for those aluminum and boron species listed in the JANAF tables were used (12). The ΔG^0 values and corresponding equilibrium constants for a number of reactions involving aluminum or boron species and the major neutral species present in the burnt gas of the fuel-rich flame could then be evaluated, again using data from the JANAF tables. Finally, the concentrations of the aluminum or boron species were calculated using the concentration data for the major flame species given in Table 1. The results of these calculations for the most important aluminum and boron species appear in Table 2, with concentrations given as fractions of the total aluminum or boron concentration in the flame. The AO_2^- anions are included since thermodynamic data are available.

In the case of the aluminum calculations, an important consideration arises because solid aluminum oxide, Al_2O_3, is stable under flame conditions. This was indicated by the formation of a solid white deposit, presumably aluminum oxide, which built up on the sampling plate when $AlCl_3$ was added to the flame. Since the activity for any solid is essentially unity, the equilibrium of Al_2O_3 with respect to its elements sets the concentration of gaseous atomic Al, and hence the concentrations of all other gaseous aluminum species in any particular flame (see, for example, ref. 13). Thus, no matter how much aluminum is added, the flame will contain constant concentrations of aluminum species at any given temperature provided the threshold for solid Al_2O_3 formation is exceeded. Such a result has implications for calibrating species concentrations or, conversely, for measuring flame temperatures. That is, the determination of the concentration of a major aluminum species such as AlO(OH) or AlOH in the flame can give a direct measure of the flame temperature, since the concentration is a function of the temperature only; the total amount of aluminum added is unimportant.

TABLE 2. Relative concentrations of aluminum and boron species present in the fuel-rich flame at equilibrium

Compound A = Al, B	Fraction of total additive present	
	Al[a]	B[b]
AO(OH)	0.726	0.977
AOH	0.267	[c]
HAO	3.93×10^{-6}	0.0172
AO	0.00520	0.00190
AO_2	8.16×10^{-6}	0.00153
A_2O	0.00241	2.53×10^{-11}
$(AO)_2$	2.92×10^{-4}	3.20×10^{-6}
A_2O_3	[c]	0.00119
A	3.02×10^{-5}	5.74×10^{-5}
AH	2.41×10^{-5}	[c]
$A(OH)_3$	[c]	8.80×10^{-4}
AO_2^-	4.76×10^{-8}	1.35×10^{-5}
Total	1.000	1.000

[a]Added as $AlCl_3$ to give 1×10^{-6} mol fraction in the burnt gas.

[b]Added as $B(OC_2H_5)_3$ to give 5×10^{-4} mol fraction in the burnt gas.

[c]Data were not available for these species in the gas phase.

The equilibrium calculations based on the JANAF tables (12) indicate that the aluminum chemistry is dominated by the oxide–hydroxide AlO(OH) with a significant contribution from the monohydroxide AlOH. The isomer of the latter, HAlO, is much less important. However, there are a number of gaps in the JANAF data. From emission spectra of Al and AlO in fuel-rich H_2–O_2–N_2 flames, Jensen and Jones (14) infer by an indirect method that the dominant neutral species is the radical dihydroxide $Al(OH)_2$; their conclusion is endorsed by Newman and Page (15). That the dominant neutral species involves aluminum in the +2 oxidation state is surprising. Unfortunately, the aluminum ions that were observed neither substantiate nor negate this conclusion. Also, no data are available for the trihydroxide $Al(OH)_3$ although the observed ions do imply the presence of this species in the flame.

In the boron case, the calculations given in Table 2 indicate that the oxide-hydroxide, metaboric acid BO(OH), accounts for nearly 98% of the boron present in the flame. No data are available for the mono- or dihydroxide or hydride, but the trihydroxide, orthoboric or boracic acid $B(OH)_3$, is given. The presence of neutral species based on the dimer and trimer of metaboric acid is implied by the ion chemistry. The dimer, $[BO(OH)]_2$, could rearrange to a stable linear structure, $O{=}BOB(OH)_2$. The trimer, $[BO(OH)]_3$, could lead to a linear structure, $O{=}BOB(OH)OB(OH)_2$, or a cyclic structure having a six-membered OBOBOB ring with each boron coordinated to an OH group. This latter structure is similar to that of metaboric acid in the solid phase (16).

Results and discussion

Aluminum ions

Only a low concentration level of 1×10^{-6} mol fraction of aluminum in the burnt gas of the fuel-rich flame was introduced by spraying a 0.500 molar aqueous solution of $AlCl_3$ using an atomizer. A total of four aluminum cations was

Can. J. Chem. Downloaded from www.nrcresearchpress.com by 92.62.229.171 on 09/08/12
For personal use only.

Can. J. Chem. Downloaded from www.nrcresearchpress.com by 92.62.229.171 on 09/08/12
For personal use only.

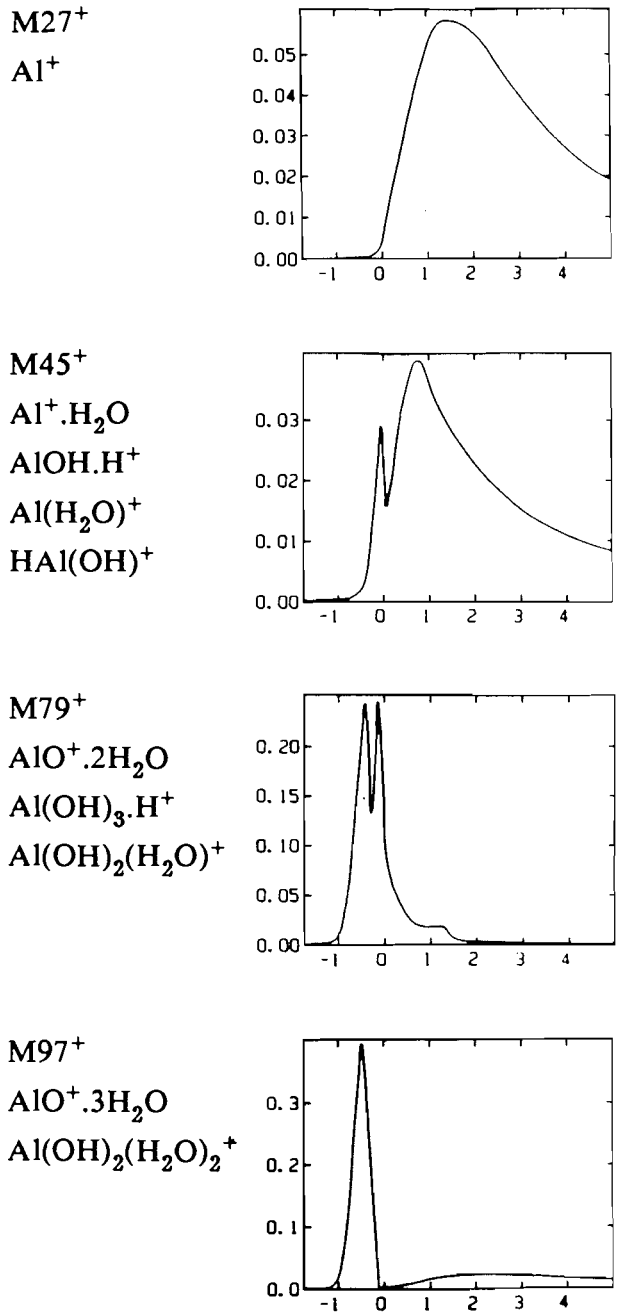

FIG. 1. Mass numbers, chemical assignments, and concentration profiles of aluminum cations observed in the fuel-rich flame below 165 u. The mass number of each cation is given first, then an empirical formula that identifies it as a member of a particular series, followed by its probable structural formula(e). All profile magnitudes are given in volts, plotted against distance along the flame axis, z, in mm. The reaction zone is located upstream of $z = 0$ (negative z).

observed, whose concentration profiles are given in Fig. 1 as a function of distance along the flame axis, z. They can be grouped as members of two cation series, $AlO^+.nH_2O$ and $Al^+.nH_2O$. The aluminum ion chemistry will be discussed in the following order: total ion profiles, anion chemistry, the two cation series, and fuel-lean flame considerations.

Total ion profiles

The total ion profiles for the fuel-rich flame did not differ, within experimental error, from those observed in the undoped flame (presented with the total ion profiles for boron in Fig. 2). Thus, aluminum does not appear to contribute any significant new ion source or sink to the naturally occurring ions already present in the undoped flame.

Aluminum anion chemistry

In marked contrast to the boron anions discussed later, no aluminum anions of any kind were identified in the fuel-rich flame. Assuming AlO_2^- to be the dominant anion, failure to observe it at this low concentration level of aluminum is not surprising in view of the small equilibrium concentration for AlO_2^- in Table 2. The fraction of total aluminum additive given as 4.76×10^{-8} corresponds to an AlO_2^- concentration of 1.6×10^5 ions cm^{-3}, just below the detection limit of the mass spectrometer. The experimental observation is consistent with the theoretical prediction.

$AlO^+.nH_2O$ series (n = 2, 3)

Unlike the Sc, Ti, and V cases where the ions $AO^+.nH_2O$ ($n = 0$–3) were identified (2), only the $n = 2$, 3 ions were observed unambiguously in the case of Al. Protonation of the oxide-hydroxide, the major aluminum neutral species listed in Table 2, would give $Al(OH)_2^+$ or $AlO^+.H_2O$ with $n = 1$ by reaction [4]. This ion at $M61^+$ was observed, but not reproducibly. A very small signal was seen in the burnt-gas region by increasing the voltage on the ion lens downstream of the sampling nozzle. Increasing the lens voltage imparts extra kinetic energy to the ions after they enter the mass spectrometer, and could cause hydrated molecules to break up. Thus, $AlO^+.H_2O$ is probably not a genuine flame ion but could appear if $AlO^+.2H_2O$ loses a water molecule on collision, as in reaction [3]. Failure to observe a regular signal for $AlO^+.H_2O$ could occur either if it rapidly hydrates to form $AlO^+.2H_2O$ at $M79^+$, or if it loses a water of hydration to form AlO^+ at $M43^+$ according to reaction [5]. However, if AlO^+ were present, it would probably have been masked by the very large signal due to protonated ketene, CH_3CO^+, a natural flame ion at the same mass number (9).

No signal was observed at $M62^+$ corresponding to the protonation of the radical dihydroxide $Al(OH)_2$ which Jensen and Jones (14) believe to be the dominant aluminum neutral species present in the flame. Alternatively, if the odd electron were weakly bound, it might ionize by electron transfer to give $Al(OH)_2^+$ at $M61^+$ (indistinguishable from the protonated oxide-hydroxide). If endothermic, this ionization process might also be enhanced by increased kinetic energy from the high voltage applied to the ion lens. Under the regular condition of the ion lens, however, the dihydroxide could be chemically ionized by the reaction

[6] $$H_3O^+ + Al(OH)_2 \rightarrow H + Al(OH)_2(H_2O)^+$$
$$\text{or } AlO^+.2H_2O$$

for the direct formation of the series member with $n = 2$ at $M79^+$. The large signal at $M79^+$ could also be produced by proton transfer to the trihydroxide $Al(OH)_3$ according to reaction [2]. Furthermore, $M79^+$ might arise by dehydration of the series member with $n = 3$ at $M97^+$, the largest signal observed with aluminum

[7] $$Al(OH)_2(H_2O)_2^+$$
$$\text{or } AlO^+.3H_2O + M \rightleftarrows M + H_2O + AlO^+.2H_2O$$

Certainly the profile at $M79^+$ in Fig. 1 is complex; it exhibits twin peaks in the reaction zone and a further one

Can. J. Chem. Downloaded from www.nrcresearchpress.com by 92.62.229.171 on 09/08/12
For personal use only.

downstream near $z = 1.3$ mm, indicative of several ion formation processes.

The $AlO^+.3H_2O$ ions at $M97^+$ could be produced from $Al(OH)_3$ in a three-body process

[8] $H_3O^+ + Al(OH)_3 + M \rightleftarrows M + Al(OH)_2(H_2O)_2^+$ or $AlO^+.3H_2O$

where the central Al atom is surrounded by a stable electron octet. Reaction [8] might be responsible for the maximum in the profile shown in Fig. 1, which occurs downstream where H_3O^+ is the major source ion. The three-body process would also be enhanced by any drop in temperature resulting from the entrainment of atmospheric air. The peak in the reaction zone could arise by proton transfer to neutral $Al(OH)_3(H_2O)$ having an electron octet if this species exists in the flame, or by hydration via the back reaction [−7]. In any case, the profile shape for $M97^+$ is indicative of two or more formation reactions. Much of this cation chemistry for aluminum could be clarified by measurements of the proton affinities for $Al(OH)_3$ and AlO(OH), and the ionization energy of $Al(OH)_2$.

$Al^+.nH_2O$ series (n = 0, 1)

The two ions in this series exist only downstream. The profile peak in the reaction zone at $M45^+$ in Fig. 1 is presumed to arise from protonated acetaldehyde, $CH_3CHO.H^+$, at the same mass number. The first hydrate, $Al^+.H_2O$ at $M45^+$, can be formed by protonation of the second-most important neutral aluminum species listed in Table 2, AlOH

[9] $H_3O^+ + AlOH \rightleftarrows Al(H_2O)^+ + H_2O$

A second isomer of $M45^+$, $HAl(OH)^+$, is also possible. Presumably this isomer would be formed by protonation of HAlO whose concentration in the flame is much lower, as seen in Table 2. In either case, the major proton source should be H_3O^+ since this is the dominant ion in the downstream portion of the fuel-rich flame.

Formation of the Al^+ ion at $M27^+$ could occur by dehydration of $M45^+$

[10] $Al(H_2O)^+ + M \rightleftarrows Al^+ + H_2O + M$

This mechanism is particularly attractive because it can be seen from the profiles in Fig. 1 that $M27^+$ appears to form after $M45^+$. However, it is also possible that a charge transfer mechanism previously invoked for the ionization of alkali metals is operative (17)

[11] $H_3O^+ + Al \rightarrow Al^+ + H_2O + H$

which is exothermic by 8.6 kJ mol^{-1} (12).

The Al^+ and $Al^+.H_2O$ ions account for 7.9% and 5.4% respectively, of the aluminum ions observed in the flame. As such, they are of greater importance than members of the same series for scandium and vanadium (2); as will be seen below, no boron members of this series were observed at all. Apparently the +3 oxidation state is, surprisingly, somewhat less emphasized in aluminum compared with scandium and vanadium.

Fuel-lean flame considerations

The fuel-lean flame (i.e., oxygen-rich) described in the experimental section was similarly doped with aluminum using the same atomizer techniques. However, no cations or anions of aluminum were observed with the mass spectrometer at the low concentration of aluminum obtainable. Calculations similar to those given in Table 2 were carried out for the fuel-lean flame, and revealed that AlO(OH) was the only important gas-phase species. Since the protonated form of this species, $Al(OH)_2^+$, was not observed in the fuel-rich flame under regular conditions, it is perhaps not surprising that it was not observed in the fuel-lean flame either. Thus, chemical ionization in the fuel-lean flame did not produce measurable ion signals.

Boron ions

Boron was added as $B(OC_2H_5)_3$ vapour to give 5×10^{-4} mol fraction of boron species in the burnt gas of the fuel-rich flame, a concentration 500 times greater than that used with aluminum. In this case, many more cations were observed, which can be organized into four cation series: $B(OC_2H_5)_3H^+.nH_2O$, $BO^+.nH_2O$, $HB_2O_3^+.nH_2O$, and $B_3O_4^+.nH_2O$. Clearly, a new dimension is added by the observation of B_2 and B_3 ions. The presentation of the results and discussion for boron will follow the same order employed for aluminum: total ion profiles, anion chemistry, the four cation series, and fuel-lean flame considerations.

Total ion profiles

Total ion profiles for the fuel-rich flame with and without the $B(OC_2H_5)_3$ additive are found in Fig. 2. The addition of boron to the flame results in a large increase in the total positive ion concentration, and an even larger relative increase in the total negative ion concentration. Since the flame is a quasi-neutral plasma, the difference between the total positive and negative ion signals gives the free electron concentration at any point on the flame axis. Thus, boron is an effective electron scavenger in the reaction zone; the total positive and negative ion concentrations are nearly equal there, such that the free electron concentration is effectively zero. On the other hand, boron is not an effective electron scavenger downstream. The initial large increase of both positive and negative ions upstream was observed previously with other additives (7, 8, 10, 18). It does not imply any new ion production process, but rather a decreased rate of ion loss. This occurs because relatively fast cation–electron recombination has been replaced by slower cation–anion recombination, resulting in a higher, steady-state level of ionization.

Boron anion chemistry

In the fuel-rich flame, only the BO_2^- and BO^- anions were detected, whose profiles are shown in Fig. 3. Our results for boron anions in a CH_4–O_2 flame clearly parallel those of Jensen in a H_2–O_2–N_2 flame (3, 4). The anions are derived from dissociative electron attachment to BO(OH) in the reaction zone

[12a] $e^- + BO(OH) \rightleftarrows BO_2^- + H$

[12b] $\rightleftarrows BO^- + OH$

The similarity in shape of the BO_2^- and BO^- profiles in Fig. 3 suggests that the two ions are equilibrated or nearly so

[13] $BO_2^- + H_2 \rightleftarrows BO^- + H_2O$

albeit with BO_2^- present in large excess. Reaction [13] mentioned by Jensen (4), in combination with the balanced flame radical reaction

[14] $H + H_2O \rightleftarrows OH + H_2$

would be indistinguishable from the reaction

[15] $BO_2^- + H \rightleftarrows BO^- + OH$

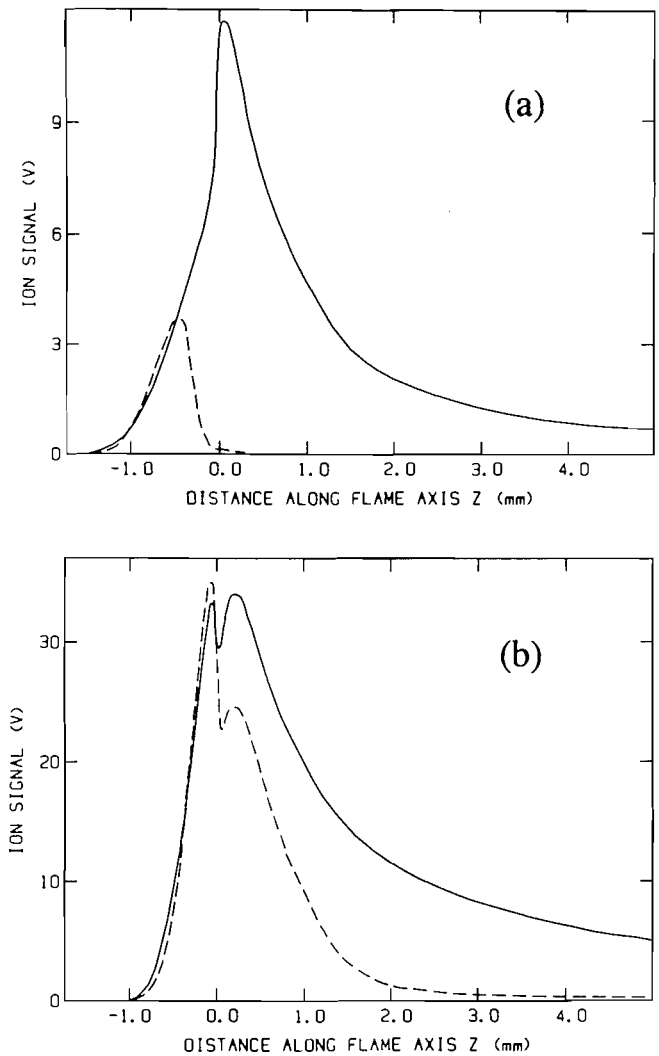

FIG. 2. Concentration profiles for the total ion signals (*a*) in the undoped fuel-rich flame and (*b*) in the fuel-rich flame doped with $B(OC_2H_5)_3$. Total positive ion signal is indicated by the solid line and total negative ion signal by the broken line. The flame reaction zone is located upstream of $z = 0$ (negative z).

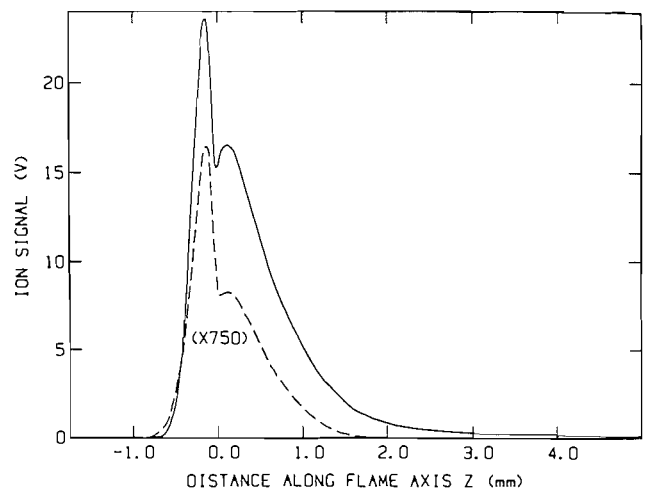

FIG. 3. Concentration profiles for the boron anions BO_2^- at $M43^-$ (solid line) and BO^- at $M27^-$ (broken line). The BO^- signal is multiplied by a factor of 750 in the figure. The reaction zone is located upstream of $z = 0$ (negative z).

It is also not surprising that the BO_2^- and the total negative ion profiles have similar shapes. Downstream in the fuel-rich flame where [H] becomes large, BO_2^- is destroyed by the back reaction [−12*a*] involving associative electron detachment. The signal minimum near $z = 0$ is caused by "H-atom overshoot" above its equilibrium concentration before [H] is reduced by the slow, neutral, three-body recombination reactions H + H + M and H + OH + M.

$B(OC_2H_5)_3H^+.nH_2O$(n = 0, 1)

Profiles for all 11 boron cations observed within the range of the mass spectrometer (165 u) are given in Fig. 4. It is clear from the mass numbers that two of the ions stem from protonation of the $B(OC_2H_5)_3$ additive, namely $B(OC_2H_5)_3H^+$ at $M147^+$ and its first hydrate, $B(OC_2H_5)_3H^+.H_2O$ at $M165^+$. It is just possible that the latter ion could also form directly by protonation of the hydrated additive, $(H_2O)B(OC_2H_5)_3$, with a filled valence shell around the B atom. As would be expected, both profiles exhibit a large peak in the flame reaction zone.

There are two aspects to this ion series that are somewhat surprising. The first is that both ion profiles show a tiny maximum near $z = 4$ mm downstream in the burnt gas; it is difficult to see in the $M165^+$ diagram, but it is definitely present in the original profile data. This would seem to indicate that a small amount of the additive survives into the burnt-gas region. The second aspect concerns the breakdown of the additive in the reaction zone. Initially, it might be expected to given orthoboric acid $B(OH)_3$ by three successive nucleophilic substitution (S_N2) reactions of OH for OC_2H_5 of the type

[16] $$B(OC_2H_5)_3 + OH \rightarrow B(OC_2H_5)_2(OH) + OC_2H_5$$

However, the protonated intermediates $B(OC_2H_5)_x(OH)_{3-x}H^+$ ($x = 2, 1$) were never observed. It would appear that the substitutions occur too rapidly to allow significant steady-state concentrations of the intermediates to build up.

$BO^+.nH_2O$ series (n = *1–4*)

Profiles for the four members of this series are given in Fig. 4 at $M45^+$, $M63^+$, $M81^+$, and $M99^+$. The BO^+ ion was not observed. This is perhaps not too surprising, given that boron is an electron-deficient element; BO^+ might be expected to be a strong Lewis acid, satisfying its empty valence orbitals by coordinating water molecules.

The ion signal for the first member of the series, $B(OH)_2^+$ at $M45^+$, is small and exists only in the downstream region; the peak in the reaction zone in Fig. 4 is due to protonated acetaldehyde, as mentioned in connection with $Al^+.H_2O$. Presumably $B(OH)_2^+$ is formed by proton transfer as in reaction [4] to the oxide-hydroxide or metaboric acid, BO(OH). From Table 2 it is the major boron species present in the flame at equilibrium. The *downstream* portions of the remaining members of the series are probably made by successive hydrations of this electron-deficient species, as in the back reaction [−3]. This is borne out by the fact that the downstream maxima occur progressively later in the flame as one goes down the series to the higher hydrates. Apparently $BO^+.2H_2O$ or $B(OH)_2(H_2O)^+$ at $M63^+$ is the preferred hydrate, since this signal is at least twice as large as that for any other member of the series in the downstream region. The shoulder on the downstream peak at $z = 0.5$ mm is due to a

Can. J. Chem. Downloaded from www.nrcresearchpress.com by 92.62.229.171 on 09/08/12
For personal use only.

Can. J. Chem. Downloaded from www.nrcresearchpress.com by 92.62.229.171 on 09/08/12
For personal use only.

$M45^+$
$BO^+.H_2O$
$BO(OH).H^+$
$B(OH)_2^+$

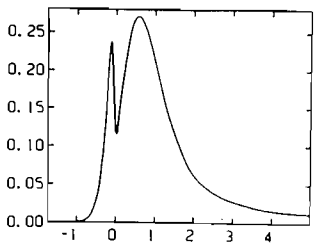

$M63^+$
$BO^+.2H_2O$
$B(OH)_3.H^+$
$B(OH)_2(H_2O)^+$

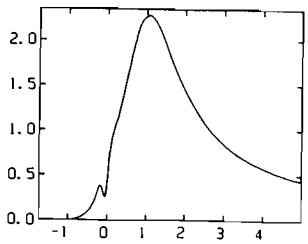

$M81^+$
$BO^+.3H_2O$
$B(OH)_2(H_2O)_2^+$

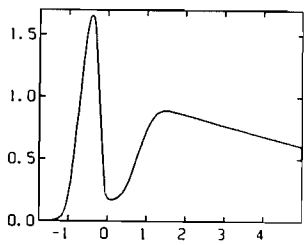

$M89^+$
$HB_2O_3^+.H_2O$
$[BO(OH)]_2H^+$
$(HO)BOB(OH)_2^+$

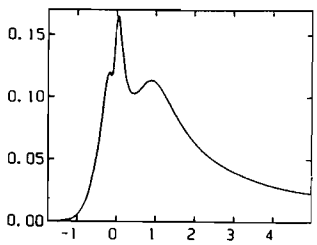

$M99^+$
$BO^+.4H_2O$
$B(OH)_2(H_2O)_2^+.H_2O$

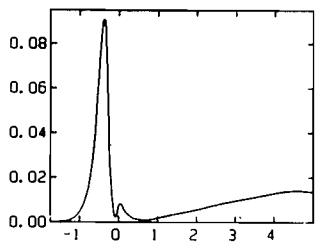

$M107^+$
$HB_2O_3^+.2H_2O$
$[BO(OH)]_2H^+.H_2O$
$(H_2O)(HO)BOB(OH)_2^+$

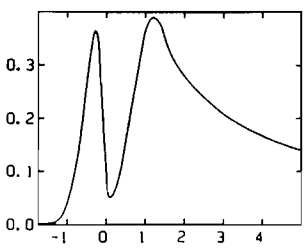

$M125^+$
$HB_2O_3^+.3H_2O$
$[BO(OH)]_2H^+.2H_2O$
$(H_2O)(HO)BOB(OH)_2(H_2O)^+$

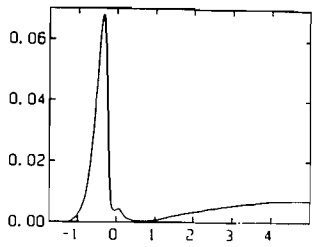

$M133^+$
$B_3O_4^+.2H_2O$
c-$[BO(OH)]_3H^+$
ℓ-$[BO(OH)]_3H^+$

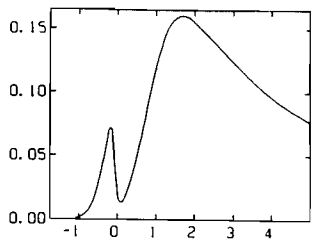

$M147^+$
$B(OC_2H_5)_3H^+$

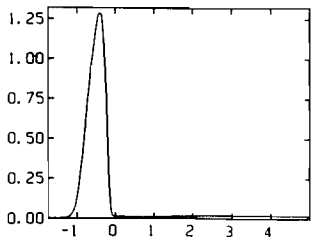

$M151^+$
$B_3O_4^+.3H_2O$
c-$[BO(OH)]_3H^+.H_2O$
ℓ-$[BO(OH)]_3H^+.H_2O$

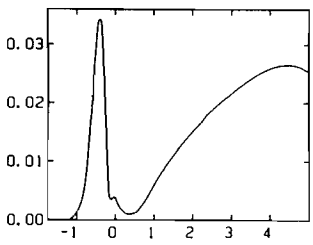

$M165^+$
$B(OC_2H_5)_3H^+.H_2O$

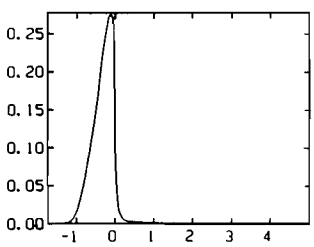

FIG. 4. Mass numbers, chemical assignments, and concentration profiles of boron cations observed in the fuel-rich flame at or below 165 u. The mass number of each cation is given first, then an empirical formula that identifies it as a member of a particular series, followed by its probable structural formula(e). All profile magnitudes are given in volts, plotted against distance along the flame axis, z, in mm. The reaction zone is located upstream of $z = 0$ (negative z).

naturally occurring flame ion at the same mass number. The final member of the series, $BO^+.4H_2O$ at $M99^+$, has a much smaller profile magnitude. A reasonable structure would be the true hydrate $B(OH)_2(H_2O)_2^+.H_2O$, with the water hydrogen-bonded in the outer coordination sphere to the two OH groups. It is probably not a true flame ion but arises due to cooling during sampling.

There is also signal present in the *reaction zone* for all these ions except possibly $BO^+.H_2O$, although naturally occurring flame ions at the same mass numbers may distort the peak magnitudes. In the reaction zone, formation of the series could well be initiated by protonation of orthoboric acid, $B(OH)_3$, formed by nucleophilic substitution of the additive as described in the previous section. Subsequent hydration could then form the remaining members of the series. This suggests that $B(OH)_3$ might be an important species in the reaction zone before its concentration drops off to a low equilibrium value in the downstream region of the flame. All of the ion chemistry of the $BO^+.nH_2O$ series, as well as that of the next two boron cation series, is summarized in Fig. 5.

$HB_2O_3^+.nH_2O$ series (n = *1–3*)

Both this ion series and the next one involving $B_3O_4^+.nH_2O$ represent ions arising from the polymerization of the additive in the flame. The relatively large concentration of boron additive in the flame must be responsible for this phenomenon. The first ion in the series, $HB_2O_3^+.H_2O$ at $M89^+$ shown in Fig. 4, has peaks in the reaction zone and downstream. The peak at $z = 0$ is again caused by a naturally occurring flame ion. The most reasonable structure involves a protonated form of the dimer, either $[BO(OH)]_2$ or $O{=}BOB(OH)_2$, to give $(HO)BOB(OH)_2^+$. The multiple peaks in the ion signal suggest that more than one ionization process is occurring. Thus, formation of the ion could take place by direct protonation of a dimer if it exists in the flame

[17] $HX^+ + [BO(OH)]_2$ or $O{=}BOB(OH)_2 \rightleftarrows (HO)BOB(OH)_2^+ + X$

or by an addition reaction with the first member of the $BO^+.nH_2O$ series

[18] $B(OH)_2^+ + BO(OH) + M \rightleftarrows (HO)BOB(OH)_2^+ + M$

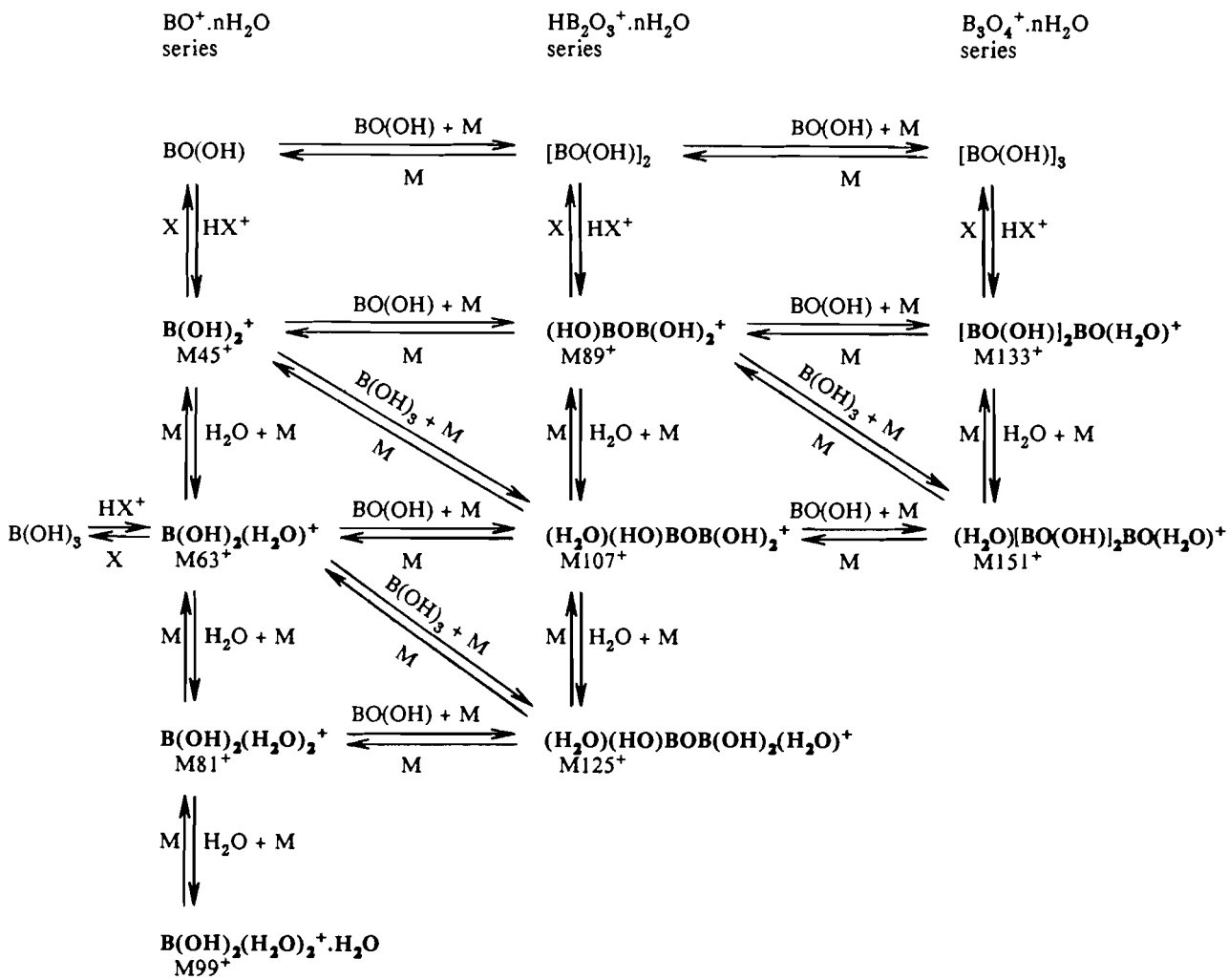

FIG. 5. Reaction flow diagram, which summarizes the boron cation chemistry leading to the three ionic series shown across the top of the figure. Probable structural formulae for the ions are given in bold, with their mass numbers written underneath. The ions of the $B_3O_4^+.nH_2O$ series could have either a linear or a cyclic structure. The symbols HX^+ and X represent flame species that are proton donors or proton receptors, respectively.

Can. J. Chem. Downloaded from www.nrcresearchpress.com by 92.62.229.171 on 09/08/12
For personal use only.

This latter reaction would not appear to be important in the reaction zone, since $B(OH)_2^+$ was not observed there.

The next two ions in this series at $M107^+$ and $M125^+$ could be formed by successive hydrations of the parent ion at $M89^+$. The water molecules would tend to coordinate at the more electron-deficient B site, so that the ion at $M107^+$ would have a structure $(H_2O)(HO)BOB(OH)_2^+$, and the ion at $M125^+$ might be $(H_2O)(HO)BOB(OH)_2(H_2O)^+$. There are other possible structures such as ones in which the bridging O is protonated. The ion at $M107^+$ could also be formed from the $BO^+.nH_2O$ series, either by addition of metaboric acid or, in the reaction zone, orthoboric acid

[19] $B(OH)_2(H_2O)^+ + BO(OH) + M \rightleftarrows (H_2O)(HO)BOB(OH)_2^+ + M$

[20] $B(OH)_2^+ + B(OH)_3 + M \rightleftarrows (H_2O)(HO)BOB(OH)_2^+ + M$

Analogous reactions involving $B(OH)_2(H_2O)_2^+$ and $B(OH)_2(H_2O)^+$ could also form the ion at $M125^+$. All of this ion chemistry is summarized in Fig. 5.

$B_3O_4^+.nH_2O$ series (n = 2, 3)

Profiles of the two members of this cation series at $M133^+$ and $M151^+$ are given in Fig. 4. They show signals in the downstream region, and also in the reaction zone. The first ion may be derived by protonation of the trimer of metaboric acid

[21] $HX^+ + [BO(OH)]_3 \rightleftarrows B_3O_4^+.2H_2O + X$

As previously discussed in the section on neutral boron species, the neutral parent species could have a linear or a cyclic form, giving rise to two possible structures for $M133^+$; a linear one, *l*-$(HO)BOBO(OH)B(OH)_2^+$, or the protonated cyclic structure, *c*-$BO(OH)BO(OH)BO(H_2O)^+$. Protonation could occur either on one of the OH sites or possibly on a bridging O atom.

The other member of the series at $M151^+$ could arise by hydration of $M133^+$. Alternatively, it could be formed from the $HB_2O_3^+$ cation series, by addition either of metaboric or of orthoboric acid

[22] $(H_2O)(HO)BOB(OH)_2^+ + BO(OH) + M \rightleftarrows B_3O_4^+.3H_2O + M$

[23] $(HO)BOB(OH)_2^+ + B(OH)_3 + M \rightleftarrows B_3O_4^+.3H_2O + M$

Obviously, there are a number of structural possibilities for this ion, whether it is cyclic or linear. The ion chemistry of this series is also summarized in Fig. 5.

Clearly, the three boron cation series are strongly interlinked, chemically. The ion chemistry is interesting because it involves the formation of species that are precursors to the deposits of solid boron oxides that were eventually seen to coat the sampling plate of the mass spectrometer. Essentially all of these cations agree with those reported by Burdett and Hayhurst in their brief, four-line statement (5) quoted in our Introduction. Their "series of hydrates $H_2BO_2^+(H_2O)_n$" can be rewritten as $BO^+.(n + 1)H_2O$, the same as our B_1 series. Similarly, members of their other series are equivalent to ours: e.g., their "mixed borate/hydrate clusters . . . $H_2BO_2^+(H_2O)_x(HBO_2)_y$" give our $HB_2O_3^+.2H_2O$ with $x = 1$, $y = 2$; $HB_2O_3^+.3H_2O$ with $x = 2$, $y = 1$; and $B_3O_4^+.3H_2O$ with $x = 1$, $y = 2$. Their various series overlap to some extent, and they have not considered structure. Nevertheless, the agreement of their observations with ours is gratifying.

Fuel-lean flame considerations

It was not possible to measure quantitative profiles for boron ions in the fuel-lean flame (i.e., oxygen-rich) described in the experimental section. Solid boron oxides tended to clog the orifice in the sampling nozzle in the space of a few minutes. Nevertheless, a number of boron ions were detected qualitatively. With regard to the anions, evidence was obtained for both BO_2^- and BO^-, and also for BO_4^- and BO_6^-. The latter anion would require the coordination of at least two oxygen molecules at the B site. With regard to the cations, $M45^+$, $M63^+$, $M81^+$, $M107^+$, and $M133^+$ were all detected. Possibly the boron ion chemistry in the fuel-lean flame and fuel-rich flame has much in common.

Conclusions

The ion chemistry of aluminum and boron was studied by doping methane–oxygen flames with $AlCl_3$ and $B(OC_2H_5)_3$ to give 1×10^{-6} and 5×10^{-4} mol fraction, respectively, in the burnt gas. Measurements were made by sampling the flame through a nozzle into a mass spectrometer. The ions observed for both Al and B, elements in the +3 oxidation state, have aspects in common with ions observed previously for transition metals exhibiting the same oxidation state (1, 2), primarily Sc, Ti, V, and Cr.

A common theme for all of these elements is chemical ionization by proton transfer of their oxide-hydroxides, AO(OH), and trihydroxides, $A(OH)_3$, where A is the elemental atom. Subsequent hydration/dehydration of these ions gives rise to an oxide ion series $AO^+.nH_2O$ (n = 2, 3 for Al and 1–4 for B; large oxide ion signals were observed previously for Sc and V (n = 0–3), and small ones for Ti (n = 0–3) and Cr (n = 0, 1). The absence of AO^+ with Al and B probably reflects the electron-deficient nature of their valence shells.

The atomic ion series $A^+.nH_2O$ was not present with B but was observed with Al (n = 0, 1), arising by proton transfer to the monohydroxide, AOH, with subsequent dehydration. It was the dominant ion series observed with Cr (n = 0–3), major with Ti (n = 1–4), but minor with Sc (n = 1, 4) and V (n = 0, 1). It was also a dominant series with five other transition metals, Mn, Fe, Co, Ni, and Cu, but different chemical ionization mechanisms are possible, not necessarily associated with AOH.

Upper limits to the additive concentration in the flames for both Al and B were imposed by the formation of solid oxides that tended to clog the orifice in the sampling nozzle. This prevented the observation of Al ions in a fuel-lean flame; only qualitative measurements were possible in the flame doped with B. In a fuel-rich flame with the relatively high concentration of B additive, however, two polymeric ion series were observed: $HB_2O_3^+.nH_2O$ (n = 1–3) and $B_3O_4^+.nH_2O$ (n = 2, 3). These are formed by ion–molecule addition reactions of BO(OH) to single B ions, or proton transfer reactions to dimers and trimers of BO(OH). The B_3 series of ions can involve both cyclic and linear structures. A further ion series for boron, $B(OC_2H_5)_3H^+.nH_2O$ (n = 0, 1), arises by proton transfer to the additive with subsequent hydration. The ion chemistry of boron reveals a sequence in

Can. J. Chem. Downloaded from www.nrcresearchpress.com by 92.62.229.171 on 09/08/12
For personal use only.

the underlying neutral chemistry in which the $B(OC_2H_5)_3$ additive first converts to $B(OH)_3$ in the flame reaction zone by nucleophilic substitution (S_N2), and then to BO(OH) as the dominant species downstream in the burnt gas. The anion chemistry revealed only a very large BO_2^- signal and a much smaller one for BO^-, in line with the previous studies of Jensen (3, 4). As a general statement about the ion chemistry, boron had more in common with Si (19) than with the metallic elements, reflecting the nonmetallic character of B; its strong affinity for oxygen produces B—O—B structures in rings and chains.

Acknowledgement

Partial support of this work by the Natural Sciences and Engineering Research Council of Canada under Grant No. A-1604 is acknowledged.

1. Q. Tran, N. S. Karellas, and J. M. Goodings. Can. J. Chem. **66**, 2210 (1988).
2. J. M. Goodings, Q. Tran, and N. S. Karellas. Can. J. Chem. **66**, 2219 (1988).
3. D. E. Jensen. Trans. Faraday Soc. **65**, 2123 (1969).
4. D. E. Jensen. J. Chem. Phys. **52**, 3305 (1970).
5. N. A. Burdett and A. N. Hayhurst. J. Chem. Soc. Faraday Trans. I, **78**, 2997 (1982).
6. J. M. Goodings, S. M. Graham, and W. J. Megaw. J. Aerosol Sci. **14**, 679 (1983).
7. J. M. Goodings and C. S. Hassanali. Int. J. Mass Spectrom. Ion Processes, **101**, 337 (1990).
8. J. M. Goodings, N. S. Karellas, and C. S. Hassanali. Int. J. Mass Spectrom. Ion Processes, **89**, 205 (1989).
9. J. M. Goodings, D. K. Bohme, and C.-W. Ng. Combust. Flame, **36**, 27 (1979).
10. N. S. Karellas and J. M. Goodings. Int. J. Mass Spectrom. Ion Processes, **87**, 187 (1989).
11. J. M. Goodings, K. Elguindi, and D. K. Bohme. Can. J. Chem. **61**, 1703 (1983).
12. M. W. Chase, C. A. Davies, J. R. Downey, D. J. Frurip, R. A. MacDonald, and A. N. Syverud. JANAF thermochemical tables. 3rd ed. J. Phys. Chem. Ref. Data, **14**, Suppl. No. 1, 1985.
13. P. A. Rock. *In* Chemical thermodynamics. University Science Books, Mill Valley, Calif. 1983. p. 286.
14. D. E. Jensen and G. A. Jones. J. Chem. Soc. Faraday Trans. I, **68**, 259 (1972).
15. R. N. Newman and F. M. Page. Combust. Flame, **17**, 149 (1971).
16. F. A. Cotton and G. Wilkinson. *In* Advanced inorganic chemistry. 5th ed. John Wiley & Sons, New York. 1988. p. 169.
17. A. N. Hayhurst and N. R. Telford. Trans. Faraday Soc. **66**, 2784 (1970).
18. N. S. Karellas, C. S. Hassanali, J. M. Goodings, and A. N. Hayhurst. Int. J. Mass Spectrom. Ion Processes, **93**, 115 (1989).
19. J. H. Horton and J. M. Goodings. Can. J. Chem. In press.

Can. J. Chem. Downloaded from www.nrcresearchpress.com by 92.62.229.171 on 09/08/12
For personal use only.

Nuclear magnetic resonance studies of the methylammonium hexahalotellurates

MARK R. MACINTOSH, MARCO L. H. GRUWEL, KATHERINE N. ROBERTSON, AND RODERICK E. WASYLISHEN[1]

Department of Chemistry, Dalhousie University, Halifax, N.S., Canada B3H 4J3

Received May 28, 1991

MARK R. MACINTOSH, MARCO L. H. GRUWEL, KATHERINE N. ROBERTSON, and RODERICK E. WASYLISHEN. Can. J. Chem. **70**, 849 (1992).

A ^2H and ^{14}N NMR study of the solid methylammonium hexahalotellurates, $(MA)_2TeX_6$ (MA = $CH_3ND_3^+$ or $CD_3NH_3^+$, X = Cl, Br, and I), has been undertaken to characterize the dynamics of the methylammonium (MA) ion as a function of temperature. At room temperature, the MA ion in the hexachlorotellurate (solid II) is confined to C_3 jumps about the C—N axis while a small angle libration of the C—N axis is occurring. In the room temperature phase, solid I, of $(MA)_2TeBr_6$ and $(MA)_2TeI_6$ the MA ions are performing overall reorientations on the ps time scale, averaging the ^2H nuclear quadrupolar interactions to zero. Variable temperature ^2H NMR spin-lattice relaxation times, T_1, indicate an activation energy, E_A, for "isotropic" reorientations of the $CH_3ND_3^+$ ion of 5.2 ± 0.5 and 2.6 ± 0.3 kJ mol^{-1} for X = Br and I, respectively. Deuterium T_1 values for C-deuterated MA ion in the hexaiodotellurate indicate an E_A for whole-ion reorientation of 3.1 ± 0.3 kJ mol^{-1}. At any given temperature, the correlation time, τ_c, derived from the T_1 results was found to be the same for the two deuterium-labelled hexaiodotellurates. The similarity of both the E_A and the τ_c values implies correlated motion of the methyl and ammonium groups. The ^{14}N T_1 results for solid I of $(MA)_2TeI_6$ indicate that C—N axis motions, with an E_A = 5.6 ± 0.6 kJ mol^{-1}, are more hindered than N—D or C—D bond dynamics. The ^2H NMR spectra for $(MA)_2TeI_6$ (solid II) and $(MA)_2TeBr_6$ (solids II, III, and IV) are characterized by a Pake doublet line shape. The measured peak-to-peak splittings are less than what is predicted by C_3 motion about the molecular symmetry axis. It is possible to model these line shapes by postulating that C_3 rotations of the methyl and ammonium groups occur as the C—N axis librates in an effective cone about the position of the static molecular axis. For $(CH_3ND_3)_2TeBr_6$ and $(CD_3NH_3)_3TeBr_6$ the peak-to-peak splittings in the ^2H NMR spectra were measured as a function of temperature in solid phases II, III, and IV and were found to be similar. Finally, the ^2H NMR line shape relaxation for $(MA)_2TeBr_6$ (solid III) displays an orientation dependence indicating that rotations about the C—N axis are discrete rather than diffusive in nature. For solid phase II of $(MA)_2TeCl_6$, the line shape is observed to relax isotropically, implying that continuous C_3 rotations are taking place.

Key words: ^2H and ^{14}N NMR, methylammonium hexahalotellurates, molecular motion.

MARK R. MACINTOSH, MARCO L. H. GRUWEL, KATHERINE N. ROBERTSON et RODERICK E. WASYLISHEN. Can. J. Chem. **70**, 849 (1992).

On a réalisé une étude RMN du ^2H et du ^{14}N d'hexatellurates de méthylammonium solides, $(MA)_2TeX_6$ (MA = $CH_3ND_3^+$ ou $CD_3NH_3^+$, X = Cl, Br ou I), dans le but de caractériser la dynamique d l'ion méthylammonium (MA) en fonction de la température. À la température ambiante, l'ion MA présent dans l'hexachlorotellurate (solide II) est limité à des sauts C_3 autour de l'axe C—N alors qu'on note un faible angle de libration de l'axe C—N. Dans la phase présente à la température ambiante, solide I, des sels $(MA)_2TeBr_6$ et $(MA)_2TeI_6$, les ions MA subissent, à l'échelle de temps de la ps, des réorientations globales qui ramènent la moyenne des interactions quadrupolaires nucléaires du ^2H à zéro. Les temps de relaxation spin-réseau, T_1, en RMN du ^2H, à température variable, permettent de déterminer que l'énergie d'activation, E_A, pour les réorientations «isotropiques» de l'ion $CH_3ND_3^+$ sont égales à 5,2 ± 0,5 et 2,6 ± 0,3 kJ mol^{-1} respectivement pour X = Br et I. Les valeurs des T_1 du deutérium pour l'ion MA C-deutéré de l'hexaiodotellurate indiquent que la valeur de E_A pour la réorientation globale de l'ion est égale à 3,1 ± 0,3 kJ mol^{-1}. À n'importe quelle température donnée, on a trouvé que le temps de corrélation, τ_c, obtenu à partir des valeurs de T_1 est le même pour les deux hexaiodotellurates marqués au deutérium. La similarité des valeurs de E_A et de τ_c implique qu'il existe une corrélation entre les mouvements des groupes méthyle et ammonium. Les valeurs des T_1 obtenues par RMN du ^{14}N du solide I du $(MA)_2TeBr_6$ indiquent que les mouvements le long de l'axe C—N, avec une E_A = 5,6 ± 0,6 kJ mol, sont plus empêchés que ceux autour des liaisons N—D et C—D. Les spectres RMN du ^2H du $(MA)_2TeI_6$ (solide II) et du $(MA)_2TeBr_6$ (solides II, III et IV) sont caractérisés par une raie en forme de doublet de Pake. Les couplages entre sommets qui ont été mesurées sont plus faibles que ceux que l'on peut prédire sur la base du mouvement C_3 autour de l'axe de symétrie moléculaire. Il est possible de créer un modèle de la forme de ces raies en faisant l'hypothèse que les rotations C_3 des groupes méthyle et ammonium se produisent alors que l'axe C—N est en libration dans un cône effectif autour de la position de l'axe moléculaire statique. Pour les sels $(CH_3ND_3)_2TeBr_6$ et $(CD_3NH_3)TeBr_6$, on a mesuré les couplages entre sommets dans les spectres RMN du ^2H, déterminés en fonction de la température, pour les phases II, III et IV; on a trouvé qu'ils sont semblables. Enfin, la forme de raie de relaxation du spectre RMN du ^2H du $(MA)_2TeBr_6$ (solide III) présente une dépendance sur l'orientation qui indique que les rotations autour de l'axe C—N sont de nature discrète plutôt que diffuse. Pour le solide de la phase II du $(MA)_2TeCl_6$, on a observé que la forme de la raie subit une relaxation isotropique qui implique qu'il se produit des rotations C_3 continues.

Mots clés : RMN du ^2H et du ^{14}N, méthylammonium hexahalotellurates, mouvement moléculaire.

[Traduit par la rédaction]

Introduction

Several studies have been completed in an effort to characterize the dynamic, structural, and thermodynamic properties of the methylammonium hexahalotellurates, $(MA)_2TeX_6$ (X = Cl, Br, and I) (1–5). These complexes are all solids at room temperature and undergo solid–solid phase transitions as they are cooled. These phase transitions were first revealed by differential thermal analysis (DTA) and

[1]Author to whom correspondence may be addressed.

Can. J. Chem. Downloaded from www.nrcresearchpress.com by 92.62.229.171 on 09/08/12
For personal use only.

nuclear quadrupole resonance (NQR) studies of the halogen nuclei (1). More recently, investigators also used NQR (2) and DTA (4) as well as adiabatic calorimetry (3) to demonstrate the existence of additional phases. A summary of the transition temperatures and the corresponding molar entropy changes with provisional phase designations is given below. Notice the dramatic temperature decrease of the solid I ↔ II phase transition on going from $(MA)_2TeCl_6$ to

$(MA)_2TeCl_6$	VI	$\xleftrightarrow[0.77\,R]{73\text{ K}}$	V	$\xleftrightarrow[1.79\,R]{137\text{ K}}$	IV	$\xleftrightarrow[0.30\,R]{\sim 155\text{ K}}$	III	$\xleftrightarrow[0.20\,R]{226\text{ K}}$	II	$\xleftrightarrow[1.18\,R]{439\text{ K}}$	I
$(MA)_2TeBr_6$					IV	$\xleftrightarrow[1.56\,R]{129\text{ K}}$	III	$\xleftrightarrow[0.65\,R]{164\text{ K}}$	II	$\xleftrightarrow[1.91\,R]{289\text{ K}}$	I
$(MA)_2TeI_6$							III	$\xleftrightarrow[0.73\,R]{66\text{ K}}$	II	$\xleftrightarrow[2.66\,R]{116\text{ K}}$	I

$(MA)_2TeBr_6$ ($\Delta T_{I\leftrightarrow II}$ = 150 K) and from $(MA)_2TeBr_6$ to $(MA)_2TeI_6$ ($\Delta T_{I\leftrightarrow II}$ = 173 K). In each case, the high-temperature phase transition, from solid I to solid II, involves a change from a cubic crystal structure to a less symmetric lattice, i.e., a structural phase transition takes place.

Proton NMR second moments, $M_2(^1H)$, provide a measure of the motional averaging of the ^1H dipolar interaction and were reported for the $(MA)_2TeX_6$ salts by Kume *et al.* (1). For temperatures between 77 and about 300 K, $M_2(^1H)$ for $(MA)_2TeCl_6$ was essentially independent of temperature ($\approx 6\ G^2$). This value is much less than the calculated static intramolecular $M_2(^1H)$ value of 30 G^2 and is in fair agreement with the value calculated (7.8 G^2) using a model that assumes rapid C_3 jumps about the C—N axis of an isolated MA ion. For the other $(MA)_2TeX_6$ salts (X = Br and I), $M_2(^1H)$ is approximately 0.5 G^2 at 300 K, implying that at this temperature there is substantially more rotational freedom for the MA ions than is present in the hexachlorotellurate. Note that at 300 K the hexabromo- and hexaiodotellurates are in the high-temperature phase, solid I, where the MA ions effectively occupy crystal sites of spherical symmetry. The small observed $M_2(^1H)$ values indicate that the C—N axis is performing effectively "isotropic" rotations or jumps at a rate that is much faster than the ^1H–^1H dipolar interaction in Hz. At temperatures below the solid I ↔ II phase transition, the ^1H second moment of $(MA)_2TeBr_6$ steadily increases from 3.8 G^2 in solid II to a value of 7.8 G^2 in solid IV. A similar trend is observed for the MA ion in the hexaiodotellurate. This increase in $M_2(^1H)$ reflects an increased hindrance of C—N axis reorientations and is consistent with the continued presence of rapid C_3 rotations about the C—N axis.

The high-temperature cubic solid phase I of the $(MA)_2TeX_6$ distinguishes them from the other methylammonium hexahalometallates, $(MA)_2MX_6$ (M = tetravalent Sn, Pt, Se, Pd, and Pb; X = Cl, Br, and I), which are all rhombohedrally distorted from cubic crystal symmetry (6). As a result of the structural differences among the $(MA)_2MX_6$, the dynamics of the cation in the $(MA)_2TeX_6$ are predictably different than for the other $(MA)_2MX_6$ salts. The MA ions in the rhombohedral $(MA)_2MX_6$ have been or are predicted to be characterized by anisotropic motion (7) and do not undergo "isotropic" rotations as they do in the $(MA)_2TeX_6$ salts. The unique variation of the MA ion dynamics in the $(MA)_2TeX_6$ is deserving of further investigation by the NMR of spin-one nuclei (8). Both ^2H and ^{14}N NMR spin-lattice relaxation and line-shape studies have been used to probe the motional characteristics of the MA cation in the $(MA)_2TeX_6$ salts as a function of temperature. The use of two different NMR-active nuclei as probes allows for the separation of the C—D or N—D bond dynamics and the C—N bond reorientations (*vide infra*). Where possible, line-shape simulations have been included to model the experimental results.

Theory

Deuterium and ^{14}N are quadrupolar nuclei (I = 1) and their solid-state NMR spectra are dominated by nuclear quadrupolar interactions (9–15). These interactions arise from coupling between the nuclear quadrupole moment, eQ, and the electric field gradient (efg) at that nucleus. In general, the spin-one NMR spectrum of a polycrystalline sample in a strong magnetic field, $\boldsymbol{B}_0$, is characterized by a Pake powder pattern that is symmetric about the isotropic resonance frequency, ν_0 ($\nu_0 \approx \gamma\boldsymbol{B}_0/2\pi$). The observed line shape is the resultant superposition of doublets corresponding to all possible orientations of crystallites in the applied field, $\boldsymbol{B}_0$. The doublet splittings are given in frequency units by eq. [1]

$$[1]\quad \Delta\nu(\theta,\phi) = \left(\frac{3}{2}\right)\chi\left[\frac{(3\cos^2\theta - 1)}{2} - \frac{(\eta\sin^2\theta\cos^2 2\phi)}{2}\right]$$

where χ is the nuclear quadrupolar coupling constant, $eq_{zz}eQ/h$, q_{zz} is the largest component of the efg tensor, θ and ϕ orient $\boldsymbol{B}_0$ in the principal axis system of the efg tensor, and η is the asymmetry parameter. For η = 0, the ϕ-dependence vanishes and eq. [1] is reduced to

$$[2]\quad \Delta\nu(\theta) = \left(\frac{3}{2}\right)\chi\left(\frac{3\cos^2\theta - 1}{2}\right)$$

where θ is the angle between q_{zz} and $\boldsymbol{B}_0$. Typically, the spectral asymmetry for the N—D and C—D bonds of the methylammonium ion is $\leq$0.1, which indicates that eq. [2] is a reasonable approximation of eq. [1] for the purposes of this study.

The ^2H NMR time scale is defined with respect to the quadrupolar coupling constant, χ. Dynamics are considered fast when τ_c, the correlation time that describes q_{zz} vector dynamics, is much shorter than the reciprocal of the coupling constant, χ^{-1}. Fast motion of appropriate symmetry can average the traceless quadrupolar interaction to zero. This is generally observed in the liquid state and also in solids for nuclei at crystal sites of high symmetry. Fast exchange involving three or more sites about one symmetry axis will attenuate the breadth of the observed line shape, producing an

Can. J. Chem. Downloaded from www.nrcresearchpress.com by 92.62.229.171 on 09/08/12
For personal use only.

Can. J. Chem. Downloaded from www.nrcresearchpress.com by 92.62.229.171 on 09/08/12
For personal use only.

effective efg tensor with axial symmetry even if $\eta_{static} \neq 0$. The appropriate scaling factor, S, is given by eq. [3],

$$[3] \quad S = \left(\frac{3\cos^2\beta - 1}{2}\right)$$

where β is the angle between q_{zz} and the axis of fast rotation. Thus, for either $CD_3NH_3^+$ or $CH_3ND_3^+$, rapid C_3 jumps or diffusion about the C—N bond axis lead to $S = 1/3$ assuming an NCD or CND bond angle of 109.5°. If an additional motion about a C_n axis ($n \geq 3$) is present the reductive effect of the two motions on the spectral width is multiplicative.

The NMR spin-lattice relaxation time constant, T_1, can also provide useful dynamical information (12–16). For quadrupolar nuclei such as ^2H and ^{14}N, the quadrupolar mechanism is the dominant relaxation mechanism and is given by eq. [4]

$$[4] \quad \frac{1}{T_1} = \left(\frac{3}{10}\right)\pi^2\chi^2\left(1 + \frac{\eta^2}{3}\right)f(\omega_0,\tau_c)$$

where $\omega_0 = 2\pi\nu_0$ and $f(\omega_0,\tau_c)$ describes the ω_0 and τ_c dependence of the rate of spin-lattice relaxation. If isotropic reorientation is occurring and the dynamics of the observed nucleus can be adequately described by one effective correlation time, τ_c, $f(\omega_0,\tau_c)$ is given by eq. [5].

$$[5] \quad f(\omega_0,\tau_c) = \frac{\tau_c}{(1 + \omega_0^2\tau_c^2)} + \frac{4\tau_c}{(1 + 4\omega_0^2\tau_c^2)}.$$

In the extreme narrowing regime $\tau_c << \omega_0^{-1}$, and $f(\omega_0,\tau_c)$ is $5\tau_c$. Generally, the temperature dependence of τ_c exhibits simple Arrhenius behaviour (eq. [6]), thus,

$$[6] \quad \tau_c = \tau_0 \exp\left(\frac{E_A}{RT}\right)$$

where τ_0 corresponds to the correlation time at infinite temperature and E_A is the effective barrier to the motion described by τ_c.

Spin-lattice relaxation experiments on powder line shapes can also discern free diffusion (continuous rotation) from rotational jumps. Torchia and Szabo (16) have described rigorous T_1 relaxation expressions for both three-site jumps and continuous diffusion. In the extreme narrowing limit, their expressions predict an orientational dependence of the relaxation for the "jump" model. Specifically, there is a $\cos^2\theta$ dependence to the relaxation; T_1 increases from $\theta = 0°$ to 90°. In contrast, there is no T_1 anisotropy expected for continuous diffusive motions; that is, all parts of the powder pattern relax synchronously. This analysis is complicated by spectral overlap of the two transitions that are possible for an $I = 1$ nucleus. For example, the singularities at the $\theta = 90°$ orientations overlap with the $\theta = 35.3°$ orientations from the other subspectrum. As a result, the observed difference in line-shape anisotropy between the $\theta = 0°$ and "90°" orientations is less than predicted by theory but is still discernible. In general, any fast flipping motion that occurs is expected to produce an orientational dependence of the spin-lattice relaxation, which can be observed by examining partially relaxed spectra.

Experimental

The $(MA)_2TeX_6$ salts (X = Cl, Br, and I) were prepared by dissolving tellurium dioxide in a solution of aqueous hydrogen halide and adding to this the appropriate aqueous methylammonium halide solution (17). The solids were recovered from the reaction mixture and dried under vacuum. Deuteration of the ammonium group was achieved by successive recrystallization of the complexes from deuterium oxide (99.9%). The methyl deuterated hexachlorotellurate salt was prepared from aqueous CD_3NH_3Cl. For X = Br and I, the corresponding CD_3NH_3X salts were prepared by neutralizing CD_3NH_3Cl, isolating the methylamine, and then adding the appropriate hydrogen halide, prior to reaction with TeO_2 and HX.

Once the solids were recovered under vacuum, the samples were allowed to dry further in a vacuum desiccator before they were sealed in NMR tubes. These methylammonium salts fit the literature description (3) (yellow crystals for $(MA)_2TeCl_6$, deep orange crystals for $(MA)_2TeBr_6$, and shiny black crystals for $(MA)_2TeI_6$) and were observed via NMR line-shape studies to undergo reversible phase transitions at temperatures very close to those established in previous studies (1, 3).

NMR measurements for ^2H and ^{14}N were recorded at 55.4 and 26.1 MHz, respectively, on a Nicolet 360 NB spectrometer ($\boldsymbol{B}_0$ = 8.48 T). The deuterium $\pi/2$ pulse lengths were 7.2–8.2 μs. A Bruker MSL-200 spectrometer was used to perform some of the ^2H NMR measurements on the noncubic phases of the $(MA)_2TeX_6$. The ^2H NMR frequency is 30.7 MHz ($\boldsymbol{B}_0$ = 4.70 T) and $\pi/2$ pulse lengths of 4.5 μs were used with a quadrupole echo pulse sequence to measure line shapes and relaxation times (18). Spin-lattice relaxation times were measured using the inversion–recovery technique with either a compensating one-pulse or a quadrupole echo pulse program (19). Typically, ten variable delays were used. A three-parameter fit of the intensity of a peak at a particular delay was used to determine T_1 values.

The peak-to-peak or quadrupolar splitting, $\Delta\nu_{pp}$, in the ^2H NMR spectra was measured directly from the spectrum or with a peak picking routine. This splitting represents the frequency difference between the two most intense points in a ^2H NMR line shape. In the limit of zero line broadening, $\Delta\nu_{pp} = \Delta\nu$ provided there is axial symmetry of the efg tensor (20). The effect of artificial or natural line broadening is to change the line shape such that $\Delta\nu_{pp} < \Delta\nu$. This implies that values of χ derived from the apparent quadrupolar splitting will be underestimated in cases where line broadening is considerable.

The experimental spectra were simulated using the FORTRAN program, MXQET (21), which ran on a VAX 8800 main-frame computer.

Results and discussion

NMR line shapes

In the cubic phase (solid I) of $(MA)_2TeI_6$ a single "isotropic" peak is observed for both ^2H and ^{14}N NMR spectra with line widths at half height, $\Delta\nu_{1/2}$, of <1 and 3 kHz, respectively. Typical line shapes are shown in Fig. 1 and indicate an effectively cubic reorientation potential for each of the observed nuclei. Both rapid C_3 exchange about the molecular symmetry axis and fast overall reorientation of the C—N axis must be taking place in order to observe the isotropic line shapes.

Similar ^2H NMR spectra were observed for the solid I phase of $(MA)_2TeBr_6$. Nitrogen-14 NMR spectra of the hexabromotellurate salt were not observed, probably because of dipolar coupling to $^{79/81}Br$, which broadens the line shape relative to those observed for $(MA)_2TeI_6$ (solid I). Note that NQR transitions are observed for both the TeI_6^{2-} and $TeBr_6^{2-}$ salts; therefore, it is unlikely that either of the halides would be self-decoupled from ^{14}N. We do not believe

Can. J. Chem. Downloaded from www.nrcresearchpress.com by 92.62.229.171 on 09/08/12
For personal use only.

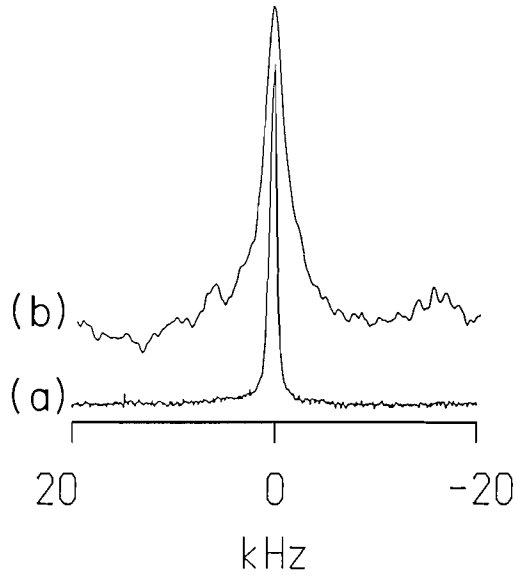

FIG. 1. NMR spectra for $(MA)_2TeI_6$ (solid I): (*a*) ^2H spectrum at 153 K ($\Delta\nu_{1/2} < 1$ kHz), which is similar to line shapes for $(MA)_2TeBr_6$ (solid I); (*b*) the ^{14}N NMR spectrum at 174 K ($\Delta\nu_{1/2} < 3$ kHz).

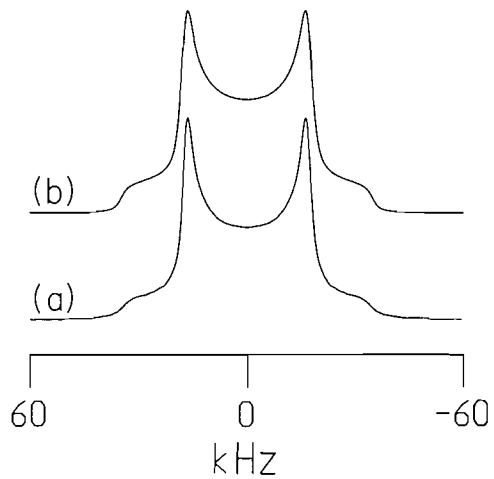

FIG. 2. Experimental (*a*) and simulated (*b*) ^2H NMR lines shapes for $(MA)_2TeCl_6$ at 293 K. The simulation was based on a model assuming C_3 jumps about the C—N axis with diffusion of the symmetry axis about a cone with a half angle of 22 ± 1° and the following input parameters: χ = 170 kHz, β = 109.5°, η = 0, $\pi/2$ = 4.5 μs, echo delay = 40 μs, and Lorentzian and Gaussian line broadening of 2.0 and 1.0 kHz, respectively.

that the increased ^{14}N NMR line width results from restricted motion of the C—N axis. Instead, the inability to obtain a spectrum is a manifestation of the relatively weak ^{14}N $\boldsymbol{B}_1$ radio frequency pulses available on the Nicolet 360 NB spectrometer which are incapable of uniformly exciting spectral lines with $\Delta\nu_{1/2} > 5$ kHz. In addition, long probe dead times at 26.1 MHz using the Nicolet high resolution "liquids" probe preclude observation of broad peaks.

The experimental ^2H NMR spectrum for $(MA)_2TeCl_6$ at 293 K (solid II) is shown in Fig. 2. The line shape has a peak-to-peak splitting, $\Delta\nu_{pp}$, of 32.8 kHz. This line shape is similar to those obtained for the solid phases II, III, and IV of $(MA)_2TeBr_6$ and solid phase II of $(MA)_2TeI_6$. The MA ions no longer experience the isotropic potential of solid I and are

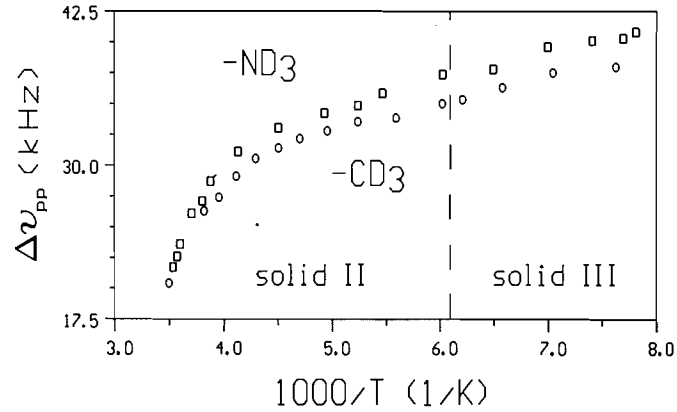

FIG. 3. The $\Delta\nu_{pp}$ for the N- and C-deuterated $(MA)_2TeBr_6$ (solids II and III) as a function of inverse temperature.

characterized by a nonzero reduction factor ($S \neq 0$). Assuming tetrahedral geometry about the C and N atoms of the MA ion, eq. [3], with β = 109.47°, gives S = 1/3 for pure C_3 rotations. From the observed quadrupolar splitting of 32.8 ± 1 kHz, eq. [2] predicts a static quadrupolar coupling constant of 131 ± 4 kHz. This value of χ is smaller than the expected static value, e.g., ≈175 kHz from ref. 22, indicating that the C—N axis is not static in the solid II phase of $(MA)_2TeCl_6$.

The observed peak-to-peak splittings, $\Delta\nu_{pp}$, were measured for the ^2H NMR line shapes of $CH_3ND_3^+$ and $CD_3NH_3^+$ in the hexabromotellurate as a function of temperature below the solid I ↔ II phase transition. The temperature dependence of these splittings is shown in Fig. 3. For the N-deuterated $(MA)_2TeBr_6$, $\Delta\nu_{pp}$ varies from 21.7 ± 1 to 42.5 ± 1 kHz for temperatures between 280 and 99 K. In the case of the carbon-labelled salt, $CD_3NH_3^+$, $\Delta\nu_{pp}$ increases from 20.4 kHz at 286 K to 36.6 kHz at 122 K. This variation in splitting with temperature demonstrates the gradual onset of C—N axis reorientational freedom with increasing temperature. The temperature dependence of the splittings for the N- and C-deuterated MA in $(MA)_2TeBr_6$ (solids II and III) is not quite the same at low temperatures. At any given temperature, the peak-to-peak splitting, $\Delta\nu_{pp}$, arising from the ND_3^+ group is slightly larger than $\Delta\nu_{pp}$ due to the CD_3 moiety. This difference could result if one end of the MA ions was undergoing librational motion to a greater extent than the other. Our results suggest that the amplitude of the librational motion of the ND_3^+ group is smaller than that of the CD_3 group at any given temperature. This is entirely reasonable since the ammonium groups are expected to hydrogen-bond more strongly with the neighbouring TeX_6^{2-} anions. Alternatively, the larger peak-to-peak splittings observed for the ammonium-labelled $(MA)_2TeBr_6$ could imply that its static value of the quadrupolar coupling constant, χ, is larger than for $(CD_3NH_3^+)_2TeBr_6$. This second explanation is less likely, since it has been determined (22, 23) that the value of χ decreases as the strength of the hydrogen bonding increases.

The anisotropy of the solid II NMR line shapes indicates that some of the motions present in the solid phase I have become slow on the ^2H NMR time scale. Intuitively, whole-ion (C—N axis) reorientations are expected to be more hindered than the C_3 rotational motion. Solid II ^2H NMR line shapes are consistent with a slowing of the C—N axis reorientations while the C_3 rotations of the methyl and ammo-

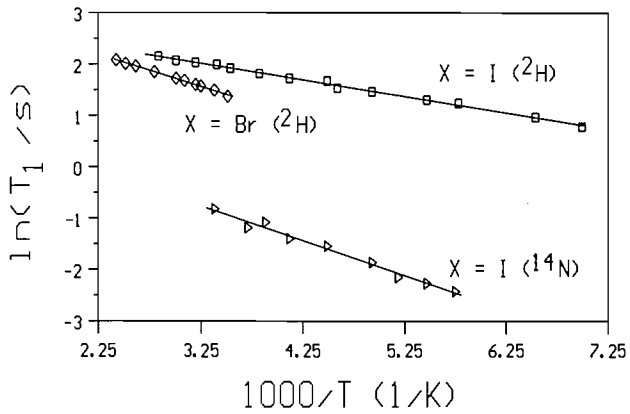

FIG. 4. The ^2H and ^{14}N NMR spin-lattice relaxation times for solid I of some N-deuterated $(MA)_2TeX_6$ (X = Br and I) as a function of inverse temperature.

nium groups continue. That is, the motion of the C—N axis in solid II is highly hindered relative to that in the solid I phase. The observed ^2H NMR line shapes for solid II of $(MA)_2TeCl_6$ and solids II and III of $(MA)_2TeBr_6$ can be simulated with a model based on C_3 jumps of the methyl and ammonium groups about the C—N axis while the C—N axis is librating. Figure 2 shows the line shape simulated for the spectrum of $(MA)_2TeCl_6$ at 293 K. The simulation was performed assuming C_3 rotations take place while the C—N axis diffuses around a cone with a half angle of 22 ± 1°. Other details of the simulation are given in the figure caption.

This model of a wobbling C_3 axis tracing out a cone is a practical physical model making it convenient to quantify the extent of the librational motion. As the temperature is increased, the C—N axis gains motional freedom, which can be measured by the simulation-derived angle of the effective librational axis about which C_3 rotations continue to occur. As the temperature is increased the effective cone made by the wobbling C—N axis also increases. As a result, this model is consistent with the observed quadrupolar splittings and the ^1H NMR second moment results (1). As the temperature is decreased the angle of the half-cone decreases and $\Delta\nu_{pp}$ and $M_2(^1H)$ increase.

NMR spin-lattice relaxation results

The ^2H and ^{14}N NMR spin-lattice relaxation results for $(MA)_2TeI_6$ (solid I) and the ^2H NMR spin-lattice relaxation of $(MA)_2TeBr_6$ (solid I) are displayed in Fig. 4. The results given are for the N-deuterated methylammonium salts. A ^2H NMR T_1 study of $(CD_3NH_3)_2TeI_6$ (solid I) was also performed but is not shown as it displayed essentially the same temperature dependence as the corresponding N-deuterated analogue. The negative slope of the $\ln(T_1)$ versus reciprocal temperature plots indicates "extreme narrowing" conditions, validating the use of $f(\omega_0,\tau_c) = 5\tau_c$ in eq. [4]. Equation [4] may be used to establish the time scale of the motions effective in relaxing the ^2H and ^{14}N nuclei, respectively. However, note that for the methylammonium ion, the ^2H and ^{14}N nuclear relaxation times will probe different motions. The ^{14}N nuclei relax by the motion of the C—N bond axis since the largest principal component of the nitrogen efg tensor lies along this axis. For the same reason ^2H nuclei are relaxed by motion of the C—^2H or N—^2H bond; hence, the effective deuterium correlation time, τ_c (^2H), reflects internal motions of the $CD_3(ND_3)$ group as well as the overall motion of the C—N axis. At 183 K, the ^2H and ^{14}N T_1 values are 3.7 ± 0.4 and 0.10 ± 0.02 s, respectively. Substitution of the respective T_1 values in eq. [4] along with the quadrupolar coupling constants for methylammonium chloride ($\chi(^2H)$ = 175 kHz and $\chi(^{14}N)$ = 900 kHz from ref. 22) results in correlation times of 0.60 ps for ^2H and 0.80 ps for ^{14}N. These are incredibly short correlation times for the methylammonium cation in the solid state at 183 K. The slightly longer effective correlation time for motion of the C—N bond is intuitively what one would anticipate. As temperature increases our results indicate that the bond vector dynamics for ^2H and ^{14}N occur at comparable rates. We suspect the ^2H correlation times are more reliable than the corresponding ^{14}N values because the value of $\chi(^2H)$ is probably more reliable than $\chi(^{14}N)$. Any uncertainty in χ strongly influences the accuracy of a calculated correlation time as a result of the χ^2 dependence of τ_c (eq. [4]). Despite these uncertainties in the value of χ the error in the ^{14}N correlation times is probably less than 50%.

The ^2H spin-lattice relaxation times for the N- and C-deuterated $(MA)_2TeI_6$ are the same within experimental error. Again it is difficult to make precise comparisons of the correlation times when accurate values of χ are not known. Considering the similarity of the T_1 temperature dependence, the correlation times describing C—D and N—D bond dynamics will be the same if the two quadrupolar coupling constants are comparable. This will be assumed for two reasons. First, the values of χ for MA ions in other compounds show only a small dependence on the site of deuteration. For example, Jurga and Spiess (24) studied methylammonium perchlorate using ^2H NMR spectroscopy. They examined motionally averaged spectra and found χ for $CH_3ND_3^+$ and $CD_3NH_3^+$ to be 168 and 166 kHz, respectively.[2] Also the $\Delta\nu_{pp}$ dependence on reciprocal temperature shown in Fig. 3 demonstrates the similarity of χ for the differently deuterium-labelled $(MA)_2TeBr_6$ salts. As a result, the values of χ for the two $(MA)_2TeI_6$ should be similar and support a model based on correlated motion of the ammonium and methyl groups.

An activation barrier to the motion described by τ_c (eq. [6]) can be obtained from the T_1 dependence on inverse temperature. Such Arrhenius plots are shown in Fig. 4 from which E_A for N—D, C—D, and C—N dynamics can be determined. Table 1 lists the E_A values determined in this study. For the sake of comparison the results from the ^1H NMR (2) and the infrared spectroscopy (3) studies are included in Table 2. Several comments can be made about these derived activation energies. First, the E_A values for ND_3^+ and CD_3 overall reorientation in $(MA)_2TeI_6$ (solid I) are small (≈ 3 kJ mol^{-1}) and are the same within the estimated error of this analysis (±10%). These activation energies correspond closely to the values obtained in previous studies (2, 3). The E_A for internal rotations of the methyl and ammonium groups of a MA ion is expected[3] to be about 10 kJ mol^{-1}, implying that the much smaller values derived for $(MA)_2TeI_6$ (solid I) do not describe the independent motion of the labelled groups. This suggests that there is correlated motion of the two groups,

[2]We obtained motionally averaged spectra for methylammonium chloride at 293 K to provide another comparison; $\Delta\nu_{pp}$ = 32.6 ± 1 and 34.1 ± 1 kHz for CH_3ND_3Cl and CD_3NH_3Cl, respectively.

[3]The potential barrier to internal rotation of ethane is determined by infrared spectroscopy to be 12.25 kJ mol^{-1} (25).

Can. J. Chem. Downloaded from www.nrcresearchpress.com by 92.62.229.171 on 09/08/12
For personal use only.

TABLE 1. Regression analysis of NMR relaxation results for $(MA)_2TeX_6$ (solid I)

$(MA)_2TeX_6$	Nucleus	Cation	$\ln(T_1)$ = constant + $[E_A$ (kJ mol^{-1})$/RT]$
X = Br	^2H	$CH_3ND_3^+$	$\ln(T_1) = 3.6 - [(5.2 \pm 0.5)/RT]$
I	^2H	$CH_3ND_3^+$	$\ln(T_1) = 3.1 - [(2.6 \pm 0.3)/RT]$
I	^2H	$CD_3NH_3^+$	$\ln(T_1) = 3.3 - [(3.1 \pm 0.3)/RT]$
I	^{14}N	$CH_3ND_3^+$	$\ln(T_1) = 1.4 - [(5.6 \pm 0.6)/RT]$

TABLE 2. The E_A (kJ mol^{-1}) for the solid I phase of $(MA)_2TeX_6$ salts from previous studies

$(MA)_2TeX_6$	C_3 motion	Whole ion reorientation	Reference
X = Cl	—	7.0	2
Br	—	3.7	2
Br	—	3.9	3
I	6.1	2.7	2
I	—	3.1	3

TABLE 3. Spin-lattice relaxation times (s) for $(MA)_2TeCl_6$

Cation	Temperature (K)	$T_1(\theta = 0°)$ (s)	$T_1(\theta$ = "90°") (s)
$CH_3ND_3^+$	298	5.7 ± 0.3	5.8 ± 0.3
$CH_3ND_3^+$	325	6.6 ± 0.3	6.6 ± 0.3
$CD_3NH_3^+$	325	9.6 ± 0.5	9.8 ± 0.5

i.e., both sets of T_1 results seem to describe the same motion. Correlated motion of the two groups is further supported by the previous comparison of correlation times derived from the ^2H NMR T_1 results for the N- and C-deuterated MA ions. The near identity of the correlation times implies that the dynamics of the two groups occur at the same rate. Secondly, the "isotropic" reorientation of the MA ion is more restricted in the $TeBr_6^{2-}$ lattice compared to the TeI_6^{2-} as a result of two considerations: (1) the void between the hexabromotellurate complex anions is slightly smaller, allowing less volume for the MA ion to move about, and (2) the ND_3^+ moiety should hydrogen-bond more strongly to the $TeBr_6^{2-}$ ions than to the TeI_6^{2-} ions as a result of the relative electronegativities of the two halide atoms. Lastly, within the $(MA)_2TeI_6$ lattice, the deuterium bond vector dynamics are shown to be energetically less demanding than the C—N motions. This reflects the relative ease with which the C_3 motion about the C—N axis occurs compared with whole-ion reorientation. However, as previously mentioned, it should be emphasized that relaxation of the ^2H nuclei occurs by C_3 rotations of the methyl and ammonium groups and through C—N axis reorientations while the ^{14}N nuclei are relaxed only by whole-ion motion. Note that $q_{zz}(^{14}N)$ lies along the C—N axis. As a result, it is expected that the E_A values derived from ^2H T_1 studies will always be less than or equal to those determined from the analogous ^{14}N results.

Finally, it is determined from the ^2H NMR relaxation spectra for $(MA)_2TeBr_6$ (solid III) at 150 K that the motion the MA ion performs consists of jumps between three equivalent sites. For nuclei that relax by rotational jumps the two orientational extremes provide the largest difference in the T_1 values of the line shape. If the T_1 values for these two positions are determined experimentally to be different, then

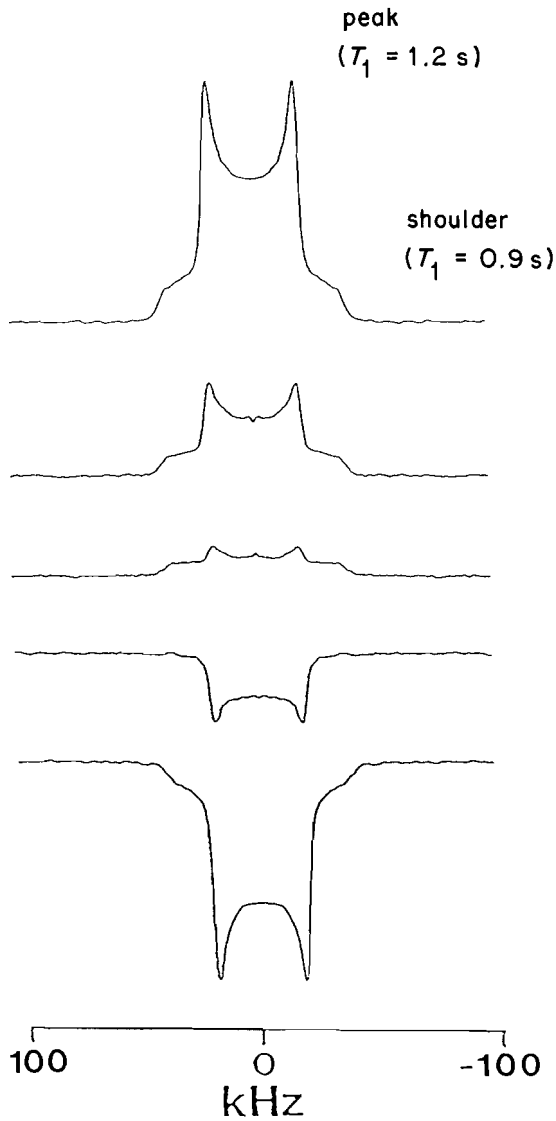

FIG. 5. A stacked plot of partially relaxed ^2H NMR spectra for $(MA)_2TeBr_6$ at 150 K (solid III) demonstrating T_1 anisotropy and establishing that the MA ions are undergoing discrete motions. The variable delays from the bottom to the top of the figure are: 0.01, 0.4, 0.8, 1.2, and 3.0 s; the respective T_1 values for $\theta = 0°$ and "90°" are 0.9 and 1.2 s.

discrete motion is occurring. By inspecting the recovery of the signal intensity for the shoulder and peak positions of the spectra in Fig. 5 the orientational dependence of the relaxation of the MA ion in $(MA)_2TeBr_6$ can be observed. As expected for jump motions, the shoulders ($\theta = 0°$) relax more efficiently than the peaks (θ = "90°"). The respective T_1 values are approximately 0.9 and 1.2 s.

The T_1 anisotropy observed for solid III of the hexabro-

Can. J. Chem. Downloaded from www.nrcresearchpress.com by 92.62.229.171 on 09/08/12
For personal use only.

motellurate salt contrasts with the result obtained for solid phase II of $(MA)_2TeCl_6$ (Table 3). The line shape in this case does not display an orientational dependence to the relaxation. As a result, the rotational motion about the molecular axis is diffusive rather than discrete in nature. Note that the T_1 values increase with increasing temperature, indicating extreme narrowing conditions apply ($\tau_c << \omega_0^{-1}$).

Conclusions

Both ^2H and ^{14}N NMR line-shape and relaxation studies are shown to be useful probes of the dynamics of the MA ion in the $(MA)_2TeX_6$ as a function of temperature. In summary, room temperature $(MA)_2TeCl_6$ (solid II) is characterized by an anisotropic line shape that is typical of C_3 rotation about a librating C—N axis. The other $(MA)_2TeX_6$ (X = Br and I) have a room temperature phase (solid I) characterized by "isotropic" line shapes. Both the ^2H and ^{14}N NMR results clearly demonstrate that the cation is performing overall reorientations on the ps time scale. The activation energies for the MA ion reorientation for X = Br and I are different, possibly due to both hydrogen bonding and steric effects. Both N- and C-deuterated $(MA)_2TeI_6$ have the same E_A and τ_c within experimental error, indicating that rotations of the ammonium and methyl groups are probably strongly coupled and are not two independent motions. Also the E_A values derived are much less than would be expected for the internal rotation of the methyl and ammonium groups. Nitrogen-14 NMR relaxation results for the iodotellurate indicate the E_A value for C—N axis reorientation is higher than the corresponding E_A value obtained from ^2H NMR relaxation results. This implies that the dynamics of the C—D and N—D bond vectors are energetically more favourable than reorientation of the C—N axis. In the lower-temperature phases of the hexahalotellurates the motion of the C—N axis gradually becomes more restricted resulting in an anisotropic ^2H NMR line shape. The quadrupolar splitting increases as the temperature is decreased. These spectra are simulated with coupled C_3 jumps of the methyl and ammonium groups that occur while the C—N axis librates. Finally, the orientational dependence of the T_1 measurements for $(MA)_2TeBr_6$ at 150 K (solid III) demonstrates that the C_3 motion of the MA ion involves three-site jumps rather than continuous diffusion about the molecular symmetry axis. In solid II of $(MA)_2TeCl_6$, the partially relaxed NMR line shapes do not show an orientational dependence, implying that the C_3 motion is diffusive.

Can. J. Chem. Downloaded from www.nrcresearchpress.com by 92.62.229.171 on 09/08/12
For personal use only.

Acknowledgements

We would like to acknowlege the financial support of the Natural Sciences and Engineering Research Council of Canada (NSERC). The authors also thank Professor O. Knop for continued interest and helpful discussions. Mr. B. Macdonald is thanked for his assistance in teaching one of the authors (M.R.M.) the operation of the Nicolet 360 NB spectrometer. Professor M. A. White is acknowledged for editorial comments. Finally, the authors of ref. 21 are thanked for making the program MXQET available.

1. Y. Kume, R. Ikeda, and D. Nakamura. J. Phys. Chem. **82**, 1927 (1978).
2. Y. Furukawa, H. Kiriyama, and R. Ikeda. Bull. Chem. Soc. Jpn. **54**, 103 (1981).
3. N. Onoda, T. Matsuo, and H. Suga. J. Phys. Chem. Solids, **47**, 211 (1986).
4. N. Onoda, T. Matsuo, and H. Suga. Philos. Mag. A: **57**, 245 (1988).
5. K. Kitahama and H. Kiriyama. Acta. Crystallogr. **34**, S302 (1978).
6. (*a*) R. W. G. Wyckoff. Am. J. Sci. **16**, 349 (1928); (*b*) Y. Kume, R. Ikeda, and D. Nakamura. J. Magn. Reson. **33**, 331 (1979); (*c*) K. Kitahama, H. Kiriyama, and Y. Baba. Bull. Chem. Soc. Jpn. **52**, 324 (1979).
7. (*a*) R. Ikeda, Y. Kume, D. Nakamura, Y. Furukawa, and H. Kiriyama. J. Magn. Reson. **24**, 9 (1976); (*b*) W. I. F. David, W. T. A. Harrison, R. C. Ward, A. J. Leadbetter, T. Matsuo, and H. Suga. Physica B (Amsterdam): **156** and **157**, 96 (1989).
8. (*a*) R. E. Wasylishen, O. Knop, and J. B. Macdonald. Solid State Commun. **56**, 581 (1985); (*b*) R. E. Wasylishen. Can. J. Chem. **64**, 773 (1986); (*c*) M. L. H. Gruwel and R. E. Wasylishen. Z. Naturforsch A: Phys. Sci. **45**, 55 (1990); (*d*) O. Knop, R. E. Wasylishen, M. A. White, T. S. Cameron, and M. J. M. Van Oort. Can. J. Chem. **68**, 412 (1990).
9. A. Abragam. Principles of nuclear magnetism. Oxford University Press, Oxford. 1961. pp. 159–170.
10. H. W. Spiess. *In* NMR basic principles and progress. Vol. 15. *Edited by* P. Diehl, E. Fluck, and R. Kosfeld. Springer-Verlag, Berlin. 1978. pp. 55–214.
11. C. P. Slichter. Principles of magnetic resonance. Springer-Verlag, Berlin. 1990. pp. 485–500.
12. K. R. Jeffrey. Bull. Magn. Reson. **3**, 69 (1980).
13. H. C. Jarrel and I. C. P. Smith. *In* The multinuclear approach to nmr spectroscopy. *Edited by* J. B. Lambert and F. G. Riddell. D. Reidel Publishing Company, Holland. 1983. pp. 151–168.
14. J. H. Davis. Biochim. Biophys. Acta, **737**, 117 (1983).
15. R. G. Griffin, K. Beshah, R. Eblehäuser, T. H. Huang, E. T. Olejniczak, D. M. Rice, D. J. Siminovitch, and R. J. Wittebort. *In* The time domain in surface and structural dynamics. *Edited by* G. J. Long and F. Grandjean. Kluwer Academic Publishers, Boston. 1988. pp. 81–105.
16. D. A. Torchia and A. Szabo. J. Magn. Reson. **49**, 107 (1982).
17. H. Marshall. *In* Inorganic syntheses. *Edited by* W. C. Fernelius. McGraw–Hill, New York. 1946. p. 188.
18. J. H. Davis, K. R. Jeffrey, M. Bloom, M. I. Valic, and T. P. Higgs. Chem. Phys. Lett. **42**, 390 (1976).
19. R. Freeman, S. P. Kempsell, and M. H. Levitt. J. Magn. Reson. **38**, 453 (1980).
20. (*a*) J. Seelig. Q. Rev. Biophys. **10**, 353 (1977); (*b*) R. Dietrich and L. Trahms. J. Magn. Reson. **71**, 337 (1987).
21. M. S. Greenfield, A. D. Ronemus, R. L. Vold, R. R. Vold, P. D. Ellis, and T. E. Raidy. J. Magn. Reson. **78**, 89 (1987).
22. M. J. Hunt and A. L. MacKay. J. Magn. Reson. **15**, 402 (1974).
23. G. Soda and T. Chiba. J. Chem. Phys. **50**, 439 (1969).
24. S. Jurga and H. W. Spiess. Z. Naturforsch. A: Phys., Phys. Chem. Kosmophys. **40a**, 602 (1985).
25. D. G. Lister, J. N. Macdonald, and N. L. Owen. Internal rotation and inversion. An introduction to large amplitude motions in molecules. Academic Press, London. 1978. p. 132.

Transformation of 1-methyluracils and uridine to respective, 4-substituted pyrimdin-2(1*H*)-ones via pyridinium salts

GRAZYNA WENSKA AND BOHDAN SKALSKI[1]
Faculty of Chemistry, A. Mickiewicz University, 60-780 Poznan, Poland

AND

ZOFIA GDANIEC
Institute of Bioorganic Chemistry, Polish Academy of Sciences, Poznan, Poland

Received September 28, 1990[2]

GRAZYNA WENSKA, BOHDAN SKALSKI, and ZOFIA GDANIEC. Can. J. Chem. **70**, 856 (1992).

1-Methyluracil and 1-methylthymine are converted into *N*-(1-methylpyrimidin-2-one-4-yl)- and *N*-(1,5-dimethylpyrimidin-2-one-4-yl)-pyridinium chlorides, respectively. The pyrimidinyl-pyridinium salts were then reacted with various nucleophiles under very mild conditions to give high yields of the desired 4-substituted pyrimidinones. In a similar manner 2′,3′,5′-tri-*O*-acetyluridine is efficiently converted into new 4-substituted pyrimidinone nucleosides.

GRAZYNA WENSKA, BOHDAN SKALSKI et ZOFIA GDANIEC. Can. J. Chem. **70**, 856 (1992).

On a transformé respectivement le méthyl-1-uracile et la méthyl-1-thymine en chlorure de *N*-(méthyl-1-pyrimidinone-2-yl-4-)-pyrimidinium et en chlorure de *N*-(diméthyl-1,5-pyrimidinone-2-yl-4)-pyrimidinium. Les sels de pyrimidinyl-pyrimidinium, par réaction subséquente avec divers nucléophiles, dans des conditions très douces, donnent avec des rendements élevés, les pyrimidinones substituées en position 4 attendues. D'une façon analogue, on a transformé efficacement la tri-*O*-acétyl-2′,3′,5′-uridine en des nouveaux nucléosides contenant la pyrimidinone substituée en position 4.

[Traduit par la rédaction]

Can. J. Chem. Downloaded from www.nrcresearchpress.com by 92.62.229.171 on 09/08/12
For personal use only.

Introduction

The conversion of 1-alkyluracils and uridine to various 4-substituted 2-pyrimidinone derivatives requires activation of the C-4 position and is often achieved with 4-chloro or thio derivatives (1). The C-4 position can also be activated by trimethylsilylation (2) or by treatment with various phosphorylating or condensing agents in the presence of 1-methylimidazole (3), 1,2,4-triazole (4), or 3-nitro-1,2,4-triazole (5) to give appropriate, reactive 4-(3-methyl-imidazolium), 4-(1,2,4-triazol-1-yl), and 4-(3-nitro-1,2,4-triazol-1-yl) derivatives. The latter method was developed in recent studies of oligonucleotide synthesis by Reese and Ubasawa (6) and is now the most frequently used method in the conversion of uridines to cytidines (4, 7, 8). Recently, the synthesis of 4-substituted pyrimidine nucleosides involving a displacement of the 4-*O*-triisopropylphenylsulfonyl group in uridine and thymidine with malonate-type nucleophiles was reported (9).

Adamiak *et al.* showed previously (10, 11) that nucleosides having per-*O*-acetylated sugar residues, such as uridine, thymidine, guanosine, and inosine, undergo quantitative transformation into the corresponding water-soluble, fluorescent pyrimidin-4-yl and purin-6-yl pyridinium salts, when treated with 4-chlorophenylphosphorodichloridate in the presence of pyridine. The purinyl-pyridinium salts have already proven very useful as intermediates in purine nucleoside chemistry (12, 13). A preliminary study in the case of pyrimidinyl-pyridinium salts has demonstrated that they can serve as intermediates in various side processes during oligonucleotide synthesis using the phosphotriester method, including formation of the 4-triazolyl derivatives mentioned above (11).

In this work the reactivity of pyrimidyn-4-yl pyridinium salts towards various *O*-, *N*-, or *S*-nucleophiles was tested by using 1-methyl derivatives **2***a*,*b* and tri-*O*-acetyl riboside **2***c*. Based on the results of these experiments the synthetic procedures yielding new 4-substituted pyrimidin-2(1*H*)-ones from 1-methyluracils (**1***a*,*b*) and uridine (**1***c*) have been developed.

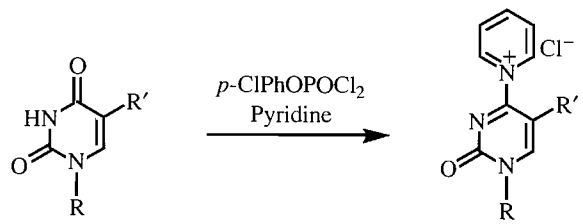

1*a*, *b*, *c* **2***a*, *b*, *c*

a: R = CH_3 R′ = H
b: R = CH_3 R′ = CH_3
c: R = 2′,3′,5′-tri-*O*-acetyl-β-D-ribofuranosyl R′ = H

SCHEME 1

Results and discussion

1-Methyluracil (**1***a*), 1-methylthymine (**1***b*), and 2′,3′,5′-tri-*O*-acetyluridine (**1***c*) were converted to the respective *N*-(pyrimidin-2-one-4-yl)-pyridinium chlorides **2***a*, **2***b*, and **2***c*, respectively, by treatment with 4-chlorophenylphosphorodichloridate in the presence of pyridine (Scheme 1), i.e., under conditions used previously for similar transformations in purine and pyrimidine nucleosides (10, 11). Pure salts were obtained either as concentrated aqueous solutions (**2***a* and **2***c*) or as lyophilizates (**2***b*). The samples were stable when stored at 0°C for several weeks.

The salts **2***a*,*b* were subjected to reaction with imidazole, histidine, 1-methylimidazole, 4,5-diphenylimidazole, in-

[1]Author to whom correspondence may be addressed.
[2]Revision received November 22, 1991.

TABLE 1. Reactivity of pyridinium salts **2***a–c* towards nucleophiles.

	Pyridinium salt	Nucleophile	Solvent[a]	Time (h)	% Conversion of **2**	% Product[b]
1	**2***a*	Imidazole	a	22	100	**3***a* (81)
2	**2***b*	Imidazole	a	24	96	**3***b* (93)
3	**2***c*	Imidazole	a	18	98	**3***c* (82)
4	**2***a*	Histidine	a	22	66	**4***a* (45)
5	**2***b*	Histidine	a	24	38	**4***b* (38)
6	**2***a*	1-Methylimidazole	a	18	100	**5***a* (51), **6***a*(34)
7	**2***b*	1-Methylimidazole	a	20	93	**5***b* (75), **6***b*(15)
8	**2***a*	3-Chlorophenol	b	1.5	95	**7***a* (94)
9	**2***b*	3-Chlorophenol	b	1.5	95	**7***b* (92)
10	**2***c*	3-Chlorophenol	b	1.5	100	**7***c* (85)
11	**2***a*	7-Hydroxycoumarin	c	24	80	**8***a* (69)
12	**2***b*	7-Hydroxycoumarin	c	24	78	**8***b* (61)
13	**2***a*	Mercaptoethanol	a	0.5	100	**9***a* (72)
14	**2***b*	Mercaptoethanol	a	0.5	100	**9***b* (60)
15	**2***c*	Mercaptoethanol	a	0.5	100	**9***c* (87)
16	**2***a*	Sodium azide	d	0.25	100	**10***a* (90)
17	**2***b*	Sodium azide	d	0.25	100	**10***b* (93)
18	**2***c*	Sodium azide	a	0.25	100	**10***c* (82)

[a]Solvents were a: water, b: water/chloroform (1:1, v:v); c: water/dioxane (1:4; v:v); d: dimethylformamide.
[b]Yields of isolated products.

Can. J. Chem. Downloaded from www.nrcresearchpress.com by 92.62.229.171 on 09/08/12
For personal use only.

dole, glycine, 3-chlorophenol, 7-hydroxycoumarin, mercaptoethanol, and azide ions. The reactions were carried out at room temperature in water or in a mixture of water and organic solvent (1,4-dioxane or chloroform) at pH ca. 6, i.e., the natural pH of the solutions. In the case of 7-hydroxycoumarin the pH of the reaction medium had to be adjusted to 7.5 in order to make the reaction go to completion (Table 1; entries 11, 12). The extent of the reactions was monitored by measuring the loss of pyridinium salts using a sensitive, spectrophotometric Zincke reaction test (11, 14). Among the nucleophiles listed above, 4,5-diphenylimidazole, indole, and glycine appeared to be unreactive towards **2***a,b*, whereas all the others reacted with **2***a,b* to give the appropriate C-4 substituted pyrimidine derivatives **3***a,b*–**10***a,b*. The products **3***a,b*–**10***a,b* were isolated by a combination of extraction and (or) chromatography on silica gel and identified by means of ^1H and ^{13}C NMR and mass spectral techniques. The synthetic procedures developed for the preparation of **3***a,b*–**10***a,b* were then applied to similar transformations of uridine. Thus, the pyridinium salt **2***c* derived from uridine was treated with some of the above-listed nucleophiles, imidazole, 3-chlorophenol, mercaptoethanol, and sodium azide, to give 4-substituted nucleoside derivatives **2***c*, **7***c*, **9***c*, and **10***c*, respectively. The results are summarized in Table 1, and the structures of the products are shown in Scheme 2. Some of the products are fluorescent. In these cases the emission parameters (λ_{max} and fluorescence quantum yield) are included in the experimental section.

In the case of the reaction of **2***a* with imidazole a quantitative conversion into **3***a* was also achieved with dimethylformamide or 1,4-dioxane as solvents instead of water or a water – organic solvent mixture, indicating that a broad range of solvents can be used in these transformations.

Attempts were also made to introduce the imidazol-1-yl substituent into the C-4 position of uridine as well as the synthesis of **3***a*, **4***a*, and **8***a* according to the method described by Matsuda *et al.* (3) as a possible alternative to our method. However, all these attempts were unsuccessful. The HPLC analyses of the reaction mixtures after 3 h revealed almost exclusive presence of the methylimidazolium salts instead of the expected substitution products. Prolongation of the reaction time (18 h) had no effect on the progress of the reactions, except for significant deacetylation in the case of the per-*O*-acetylated nucleoside salt.

Reactions of **2***a,b* with histidine (Table 1; entries 4, 5) were less efficient than those with other nucleophiles. They are of interest, however, since they may offer the possibility of selective, chemical modification of histidine residues in proteins.

In the case of the reaction of **2***a,b* with 1-methylimidazole (Table 1; entries 6, 7) products derived from the imidazole ring opening, **6***a,b*, were isolated in addition to the expected 1-methylimidazolium salts **5***a,b*. This observation and the fact that 1-methylimidazolium salts derived from pyrimidine nucleosides were previously identified as potential side products in oligonucleotide synthesis when the 2,4,6-triisopropylbenzenesulfonyl chloride/1-methylimidazole system was used as condensing reagent (11) prompted us to examine the chemical stability of salts **5***a,b* in acidic and basic conditions. They appeared to be stable in acidic media (0.05 N HCl, room temperature, 24 h) whereas, at pH > 7 a partial transformation into ring-opened products **6***a,b* occurred as a result of hydrolytic opening of the imidazolium ring of **5***a,b* (cf. Scheme 3). In the case of **5***a* the ring opening reaction occurred to a small extent (4%, HPLC) at pH 7.1 (TRIS buffer, room temperature, 24 h). When more basic conditions (TRIS, pH = 9.0, 24 h) were applied, the HPLC analysis revealed the presence of **5***a* (19%), **6***a* (75%), and **1***a* (6%). The ratio of **6***a*/**1***a* (14:1) remained unchanged after almost all of **5***a* disappeared (3 days), indicating that **5***a* also undergoes a nucleophilic attack of hydroxide ion at C-4 under these conditions to give **1***a*. 5-Methyl derivative **5***b* appeared to be less susceptible towards hydrolytic opening of

Can. J. Chem. Downloaded from www.nrcresearchpress.com by 92.62.229.171 on 09/08/12
For personal use only.

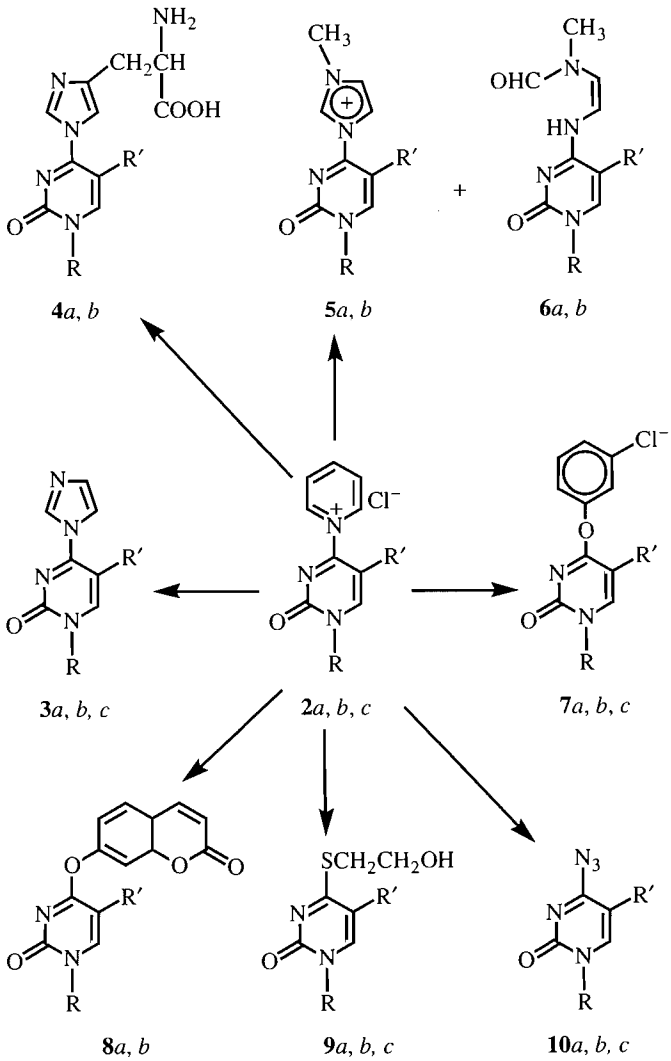

a: R = CH_3, R′ = H
b: R = CH_3, R′ = CH_3
c: R = 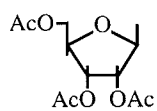 , R′ = H

SCHEME 2

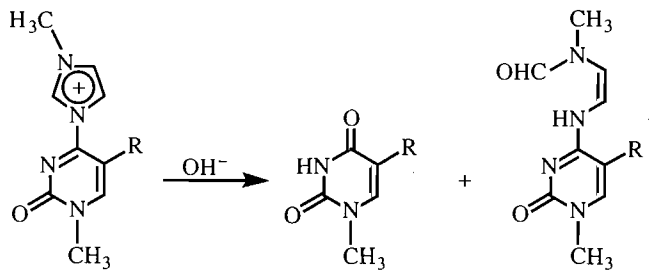

SCHEME 3

the imidazolium ring, reflecting its diminished electron deficiency compared with **5***a*. Under analogous conditions of pH and temperature only 49% of **5***b* disappeared, after 24 h, to give **6***b* (27%) and **1***b* (22%). Both **6***a* and **6***b* were stable within the pH range $1 < pH < 9$. Thus, one can conclude that formation of imidazolium salts during oligonucleotide synthesis and their further transformation into relatively stable analogs of **6***a*,*b* may result in a point mutation in the synthetic oligomer.

The structures of the compounds **6***a*,*b* were unequivocally determined with the aid of ^1H and ^{13}C NMR spectrometry. The signal assignments based on the conventional one-dimensional technique (chemical shifts and decoupling) were confirmed by two-dimensional ^1H–^1H COSY spectra. In the case of **6***a*,*b* all the resonances except for N-CHO and pyrimidine C6-H and N1-CH_3 are doubled indicating the existence of an amide *cis–trans* equilibrium due to restricted N-C=O bond rotation (15). As could be expected, increasing temperature resulted in significant broadening of these signals. However, coalescence did not occur within the temperature range studied (298–373 K).

The mode of methylimidazolium ring opening, determining the site of attachment of the formyl group to the methylamino nitrogen in **6***a*,*b*, was deduced from the following observations. In the long-range ^1H–^1H COSY spectrum of **6***a* in DMSO the formyl proton signal (δ 8.06 ppm) is coupled with N-CH_3 proton signals (δ 3.26 and 3.10 ppm). Moreover, the N-H signals (δ 9.33 and 8.77 ppm) were correlated with C=C-H proton resonances whereas no correlation with the N-CH_3 signal was observed. The resonance of the N-CH_3 group of the opened imidazolium ring appears as a singlet in ^1H spectra measured in aprotic solvents ($CDCl_3$, CD_3CN, DMSO-d_6) in which H/D exchange does not occur. These observations are consistent with the proposed structures of **6***a*,*b*.

Aryl groups were proposed by Reese and Skone for protection of uracil on O-4 in oligoribonucleotide synthesis and several 4-*O*-phenyl derivatives were synthesized via 4-triazolyl derivatives (16). We found that similar derivatives can be obtained via pyrimidinyl-pyridinium salts. Treatment of **2***a*,*b*,*c* with 3-chlorophenol in a chloroform–water two-phase system gave the desired 4-*O*-(3-chlorophenyl) derivatives **7***a*,*b*,*c* with 94, 92, and 85% yields, respectively.

Mercaptoethanol and azide ion appeared to be the most reactive among all the nucleophiles used. Addition of mercaptoethanol to aqueous solutions of **2***a*,*b*, and **2***c* caused complete loss of pyridinium salts after ca. 30 min, whereas in the case of sodium azide the reaction was completed within 15 min to give, respectively, 4-(2-hydroxythioethyl) derivatives **9***a*,*b*,*c* and 4-azido derivatives **10***a*,*b*,*c* with excellent yields (cf. Table 1; entries 13–18). The 4-(2-hydroxyethylthio) derivative **9***c* was also obtained directly from *O*-protected uridine in a one-pot manner with an overall yield 78% (*vide infra*).

It has been observed previously that 4-azido substituted pyrimidine (3, 17) and 6-azido substituted purine (18) nucleosides tend to form tetrazolo structures in solution. In the purine series the azidoazomethine–tetrazole equilibrium was shown to be influenced by the nature of the solvent (18). In the case of **10***a*,*b*,*c* the infrared spectra in DMSO exhibit the presence of an absorption at ca. 2230 cm^{-1} due to the azido group while no such absorption could be observed in chloroform solutions. The ^1H and ^{13}C NMR spectra, on the other

hand, show the existence of a single tautomeric form in each of these solvents. Thus, one can conclude that in DMSO **10***a*,*b*,*c* exist in the azido form whereas in chloroform the tautomeric tetrazolo form exists, exclusively.

In conclusion, we have demonstrated that pyrimidin-4-yl pyridinium salts are highly reactive towards various nucleophiles to give the appropriate, 4-substituted derivatives. The very mild conditions required for both the activation and substitution steps and the high yields of the products make these compounds attractive intermediates for modification of uracils.

Experimental

Pyridine and dioxane were purified and dried as described previously (10). 1-Methyluracil and 1-methylthymine were synthesized according to the reported procedure (19). Synthesis of **2***c* was described previously (11). All the other reagents (Merck, Aldrich, and Fluka) were used as received. Thin-layer chromatography was performed on Merck F_{254} and Merck RP silica gel plates. Merck PSC 60-F_{254} silica gel plates were used for preparative separations. Column chromatography was performed on H60, MN 100–200 mesh, and RP silica gels (Merck) and NM 300 cellulose (Macherey Nagel). The following solvent systems were used for TLC: chloroform/methanol, 30:1 (A); chloroform/methanol, 20:1 (B); chloroform/methanol, 10:1 (C); ethyl acetate (D); ethyl acetate/methanol, 15:1 (E); water (F); ethanol (G); ethanol/30% aqueous acetic acid, 2:1 (H); ethanol/water, 3:1 (I); all v/v.

HPLC separations in the case of the stability studies of **5***a*,*b* were performed on a Waters 600E instrument using an ODS column eluted isocratically with a mixture of $CH_3CN/H_2O/CH_3COOH$, 25:74.9:0.1 (v:v:v). Melting points were taken on a Boetius apparatus and are uncorrected. UV-absorption and fluorescence emission spectra were measured on a Zeiss UV–VIS M-40 spectrophotometer and a Perkin Elmer MPF 44 spectrofluorometer. Fluorescence quantum yields were determined relative to quinine bisulfate (ϕ = 0.55, 1 N H_2SO_4) (20). Mass spectra were obtained by using a Jeol JMS-D-100 mass spectrometer. A Varian Gemini 300 VT instrument was used to obtain ^1H and ^{13}C NMR spectra. The chemical shifts δ_H and δ_C are reported in ppm relative to TMS and dioxane as internal standards. Microanalyses were performed on a Perkin Elmer 2400 CHN analyser.

N-[1-Methylpyrimidin-2(1H)-one-4-yl]pyridinium chloride, **2**a *and N-[1,5-dimethylpyrimidin-2(1H)-one-4-yl]pyridinium chloride,* **2**b

A dry sample of 1-methyluracil or 1-methylthymine (3 mmol) was dissolved in anhydrous pyridine (50 mL) and treated with 4-chlorophenylphosphorodichloridate (0.73 mL, 4.5 mmol). The mixture was stirred for 18 h. The precipitate formed was filtered, dissolved in ice-cold water, and neutralized to pH ca. 6.2–6.5 with Dowex-1 resin (HCO_3^-). The resin was filtered, and the filtrate concentrated under vacuum to ca. 10 mL and passed through a Dowex-1 (Cl^-) column. The eluates were concentrated (<30°C) to give ca. 0.1 M aqueous solutions of **2***a* and **2***b*. In the case of the more stable **2***b* the solution was lyophilized to give a yellow solid (86% yield). Some selected spectral data for **2***a*,*b* are presented below.

2*a*: UV (H_2O) λ_{max}: 268 nm, 310 nm; ^1H NMR (D_2O) δ: 9.53 (m, 2, pyridine Cα-H), 8.91 (m, 1, pyridine Cγ-H), 8.73 (d, J = 6.9 Hz, 1, C6-H), 8.34 (m, 2, pyridine Cβ-H), 7.34 (d, J = 6.9 Hz 1, C5-H), 4.68 (s, 3, N-CH_3); ^{13}C NMR δ: 163.24, 157.61, 151.64, 142.60, 129.21, 98.82, 40.31.

2*b*: UV (H_2O) λ_{max}: 263 nm (ϵ 5300), 334 nm (ϵ 5000); ^1H NMR (D_2O) δ: 9.18 (m, 2, pyridine Cα-H), 8.93 (m, 1, pyridine Cγ-H), 8.61 (s, 1, C6-H), 8.36 (m, 2, pyridine Cβ-H), 4.75 (s, 3, N-CH_3), 2.13 (s, 3, C-CH_3); ^{13}C NMR δ chemical shifts were identical with those reported previously (21).

General procedure for the syntheses of ***3–10***

Water was used as a solvent unless otherwise specified. 0.1 M aqueous solutions of **2***a*,*b* or **2***c* (aliquots corresponding to 1–5 mmol samples of the salts) were treated with the appropriate nucleophile (3 equiv.) and the reaction mixture kept at room temperature until almost complete loss of pyridinium salt was detected by the Zincke test (14). The reaction times and yields are summarized in Table 1. Isolation procedures and spectral data for the products are presented below.

1-Methyl-4-(imidazol-1-yl)pyrimidin-2(1H)-one, **3**a *(Table 1; entry 1)*

Water was removed under reduced pressure. The solid residue was chromatographed twice on SiO_2 (systems D and A) and the product crystallized from isopropanol: mp > 260°C; UV (H_2O) λ_{max}: 304 nm (ϵ 9400), 239 nm (ϵ 8800); fluorescence emission λ_{max}: 363 nm (ϕ = 0.002); ^1H NMR (TFA-*d*/acetone-d_6) δ: 9.66 (m, 1, imidazole C2-H), 8.55 (d, J = 7.1 Hz, 1, C6-H), 8.27, 7.72 (2m, 2, imidazole C4-H and C5-H), 7.30 (d, J = 7.1 Hz, 1, C5-H), 3.91 (s, 3, N-CH_3); ^{13}C NMR (TFA-*d*/acetone-d_6) δ: 160.15, 159.31, 150.67, 136.48, 123.53, 120.93, 97.68, 41.12; MS *m*/*z* (relative intensity): M^+ 176(88), 175(100), 149(10), 134(18), 107(9). Anal. calcd. for $C_8H_8N_4O$: C54.53, H 4.58, N 31.80; found: C 54.47, H 4.54, N 31.84.

1,5-Dimethyl-4-(imidazol-1-yl)pyrimidin-2(1H)-one, **3**b *(Table 1; entry 2)*

The aqueous solution was extracted with chloroform. The organic layer was dried and the solvent evaporated. The crude product was chromatographed (SiO_2, system D) and then recrystallized from isopropanol; mp 151–153°C (dec.); UV (H_2O) λ_{max}: 316 nm (ϵ 8700), 238 nm (ϵ 7000); fluorescence emission λ_{max}: 376 nm (ϕ = 0.002); ^1H NMR ($CDCl_3$) δ: 8.27 (s, 1, imidazole C2-H), 7.73 (s, 1, C6-H), 7.65 and 7.16 (2m, 2, imidazole C4-H and C5-H), 3.60 (s, 3, N-CH_3), 2.31 (s, 1, C5-CH_3); ^{13}C NMR ($CDCl_3$) δ: 159.34, 155.49, 151.05, 137.02, 130.41, 118.16, 104.35, 38.46; MS *m*/*z* (relative intensity): M^+ 190(69), 189(100), 163(6), 148(8), 140(6). Anal. calcd. for $C_6H_{10}N_4O$: C 56.83, H 5.30, N 29.45; found: C 56.67, H 5.27, N 29.32.

1-(2′,3′,5′-Tri-O-acetyl-β-D-ribofuranosyl)-4-(imidazol-1-yl)-pyrimidin-2-(1H)-one, **3**c *(Table 1; entry 3)*

The aqueous solution was extracted with chloroform. The organic layer was dried and then concentrated under reduced pressure. The residue was chromatographed on SiO_2 (system D). Fractions containing pure product were collected and evaporated under vacuum to give **3***c* as a foam. UV (H_2O) λ_{max}: 305 nm (ϵ 7800), 242 nm (ϵ 8700); fluorescence emission λ_{max}: 374 nm (ϕ = 0.002); ^1H NMR ($CDCl_3$) δ: 8.41 (br s, 1, imidazole C2-H), 8.13 (d, J = 7.3 Hz, 1, C6-H), 7.70 and 7.19 (2s, 2, imidazole C4, C5-H), 6.58 (d, J = 7.3 Hz, 1, C5-H), 6.14 (d, 1, Cl′-H), 5.51–5.26 (m, 2, sugar C-H), 4.53–4.42 (m, 3, sugar C-H), 2.15, 2.13 and 2.12 (3s, 9, $COCH_3$); ^{13}C NMR ($CDCl_3$) δ: 170.12, 169.53, 158.96, 154.41, 145.57, 131.82, 128.35, 116.32, 94.60, 89.72, 80.35, 73.85, 70.00, 62.85, 20.75, 20.42; high resolution MS, *m*/*z*: M^+ 420.12781 ($C_{18}H_{20}N_4O_8$ requires 420.12796 amu).

Reaction of **2**a *with histidine (Table 1; entry 4)*

The reaction mixture was concentrated and chromatographed on a reversed phase silica gel column (system F). The fractions containing **4***a* were collected, the solvent evaporated to dryness, and the solid residue recrystallized from a mixture of isopropanol–water: mp 233–240°C (dec.); UV (H_2O) λ_{max}: 305 nm (ϵ 8700), 238 nm (sh); fluorescence emission λ_{max}: 363 nm (ϕ = 0.0007); ^1H NMR (D_2O) δ: 7.80 (br s, 1, histidine C2-H), 7.23 (d, J = 7.3 Hz, 1, C6-H), 6.93 (br s, 1, histidine C5-H), 5.78 (d, J = 7.3 Hz, 1, C5-H), 3.57 (m, 1, CH-CO), 3.19 (s, 3, N-CH_3), 3.07 (m, 2, CH_2); ^{13}C NMR (D_2O) δ: 174.99, 164.98, 159.94, 154.03, 137.07, 135.88, 118.60, 97.05, 55.69, 38.40, 29.52. Anal. calcd. for $C_{11}H_{13}N_5O_3$: C 50.18, H 4.97, N 26.60; found: C 49.87, H 4.85, N 26.33.

Can. J. Chem. Downloaded from www.nrcresearchpress.com by 92.62.229.171 on 09/08/12
For personal use only.

Can. J. Chem. Downloaded from www.nrcresearchpress.com by 92.62.229.171 on 09/08/12
For personal use only.

Reaction of **2**b *with histidine (Table 1; entry 5)*

A work-up utilizing the same procedure as for **2***a* (see above) gave a crystalline sample of **4***b*: mp 194–197°C; UV (H_2O) λ_{max}: 318 nm (ϵ 8800), 240 nm (sh); fluorescence emission λ_{max}: 376 nm (ϕ = 0.0007); ^{1}H NMR (D_2O) δ: 8.22 (s, 1, histidine C2-H), 8.15 (s, 1, C6-H), 7.55 (s, 1, histidine C5-H), 4.00 (m, 1, CH-CO), 3.55 (s, 3, N-CH_3), 3.12 (m, 2, CH_2), 2.21 (s, 3, C-CH_3); ^{13}C NMR (D_2O) δ: 174.18, 159.99, 158.04, 154.68, 138.86, 137.40, 117.95, 108.46, 55.37, 39.44, 29.42, 15.38. Anal. calcd. for $C_{12}H_{15}N_5O_3$: C 51.98, H 5.45, N 25.25; found: C 51.67, H 5.41, N 25.11.

Reaction of pyridinium salt **2**a *with 1-methylimidazole (Table 1; entry 6)*

The reaction mixture was extracted with $CHCl_3$. The organic layer was dried, concentrated under vacuum, and chromatographed on an SiO_2 column (B) to yield a pure sample of **6***a*: mp 200°C; UV (H_2O) λ_{max}: 301 nm (ϵ 20 700), 225 nm (sh); ^{1}H NMR ($CDCl_3/CD_3OD$, 5:1) δ: 8.09 (s, 1, CHO), 7.55 (d, J = 7 Hz, 1, C6-H), 7.15 and 6.88 (2m, total 1, C=CH), 6.08 and 5.94 (2d, J = 7.1 and 7.3 Hz, total 1, C5-H), 5.50 and 5.26 (2d, J = 7.1 and 6.6 Hz, total 1, C=CHO), 3.44 (s, 3, N-CH_3), 3.19 and 3.03 (2s, total 3H, *cis* and *trans* CO-N-CH_3); ^{13}C NMR ($CDCl_3/CD_3OD$) δ: 164.16 and 162.48 (aldelhyde C=O), 162.11 and 160.96 (C4), 157.82 (C=O), 147.09 (C6), 121.36 and 116.38 (C=C), 110.74 and 109.38 (C=C), 95.51 (C5), 37.87 (N-CH_3), 37.49 and 31.89 (N-CH_3); MS m/z (relative intensity): M^+ 208(37), 180(18), 164(25), 151(15), 150(100), 144(20), 138(29), 136(12), 126(6). Anal. calcd. for $C_9H_{12}N_4O_2$: C 51.91, H 5.80, N 26.90; found: 51.84, H 5.79, N 26.85.

The aqueous layer remaining after extraction with $CHCl_3$ was concentrated and chromatographed on cellulose (systems G, I). The fractions containing imidazolium salt **5***a* were concentrated to remove ethanol and then passed through a Dowex (Cl^-) column. The aqueous eluate was treated with charcoal and evaporated to dryness. The sample of **5***a* was stored at 5°C and was stable for over 2 weeks: UV (H_2O) λ_{max}: 313 nm (ϵ 4800), 242 nm (sh); fluorescence emission λ_{max}: 371 nm (ϕ = 0.14); ^{1}H NMR (D_2O) δ: 9.56 (s, 1, imidazole C2-H), 8.32 (d, J = 7.3 Hz, 1, C6-H), 8.04 and 7.53 (2d, 2, imidazole C4-H and C5-H), 6.90 (d, J = 7.3 Hz, 1, C5-H), 3.88 (s, 3, N-CH_3), 3.48 (s, 3, N-CH_3); ^{13}C NMR (D_2O) δ: 158.20 (C4), 156.25 (imidazole C3), 137.02 (C2), 126.02 (C6), 120.60 (imidazole C4 and C5), 96.71 (C5), 40.10 (N-CH_3), 37.60 (N-CH_3). Anal. calcd. for $C_9H_{11}N_4OCl{\cdot}xH_2O$: C 44.17, H 5.35, N 22.89; found: C 41.10, H 5.27, N 22.71.

Reaction of pyridinium salt **2**b *with 1-methylimidazole (Table 1; entry 7)*

Extraction of the reaction mixture with chloroform and column chromatography of the organic layer over SiO_2 (C) gave **6***b*: mp 192°C; UV λ_{max} (H_2O): 308 nm (ϵ 18 700), 224 nm (sh); ^{1}H NMR ($CDCl_3/CD_3OD$ 5:1) δ: 8.10 (s, 1, CHO), 7.41 (d, J = 1 Hz, 1, C6-H), 6.84 and 6.98 (2d, J = 7.5 and J = 7.2 Hz, total 1, C=CH), 5.20 and 5.70 (dd, J = 5.7 Hz and J = 1 Hz; and d, J = 7.2 Hz, total 1, C=CH), 3.41 (s, 3, N-CH_3), 3.22 and 3.09 (2s, total 3, CO-N-CH_3), 1.99 and 2.05 (2d, total 3, C-CH_3); ^{13}C NMR ($CDCl_3/CD_3OD$ 5:1) δ: 161.99, 159.9, 157.66, 144.33, 115.62, 109.60, 103.05, 38.02, 37.54, 12.40; MS m/z (relative intensity): M^+ 222(27), 194(19), 178(16), 164(100), 163(25), 152(21), 150(11), 140(10). Anal. calcd. for $C_{10}H_{14}N_4O_2$: C 54.04, H 6.34, N 25.10; found: C 53.97, H 6.26, N 25.02.

The aqueous layer obtained after extraction with $CHCl_3$ was concentrated under vacuum and chromatographed over cellulose (systems G, I). Fractions containing **5***b* were concentrated and passed through a Dowex (Cl^-) column. The eluate was evaporated to dryness under vacuum to give **5***b* as a white solid: UV (H_2O) λ_{max}: 324 nm (ϵ 4700); fluorescence emission λ_{max}: 387 nm (ϕ = 0.104); ^{1}H NMR (D_2O) δ: 9.27 (s, 1, imidazole C2-H), 8.24 (s, 1, C6-H), 7.86 and 7.51 (2m, 2, imidazole C4-H and C5-H), 3.87 (s, 3, N-CH_3), 3.48 (s, 3, N-CH_3), 2.11 (s, 3, C-CH_3); ^{13}C NMR (D_2O) δ: 156.58, 144.93, 137.81, 125.10, 122.33, 108.90, 39.87, 37.43, 14.30. Anal. calcd. for $C_{10}H_{13}N_4OCl{\cdot}xH_2O$: C 46.42, H 5.84, N 21.65; found: C 46.27, H 5.83, N 21.49.

*1-Methyl-4-(3-chlorophenoxy)pyrimidin-2(1*H*)-one,* **7**a *(Table 1; entry 8)*

3-Chlorophenol (0.933 g, 7.26 mmol) and triethylamine (0.35 mL, 2.5 mmol) were added to a two-phase system composed of an aqueous solution of pyridinium salt **2***a* (20 mL, 2.42 mmol) and chloroform (20 mL). The mixture was stirred vigorously for 2 h in the absence of light. The chloroform layer was separated and fractionated on a silica gel column (system E) to give **7***a*: mp 146–148°C; UV (H_2O) λ_{max}: 280 nm (ϵ 7800); ^{1}H NMR ($CDCl_3$) δ: 7.61 (d, J = 7.1 Hz, 1, C6-H), 7.15 (m, 4, aromatic H), 6.04 (d, J = 7.1 Hz, 1, C5-H), 3.48 (s, 3, N-CH_3); ^{13}C NMR ($CDCl_3$) δ: 171.04, 156.31, 152.29, 149.37, 134.80, 130.30, 126.13, 122.44, 120.28, 94.81, 38.08; high resolution MS m/z: 236.03518 ($C_{11}H_9N_2O_2Cl$ requires 236.03519 amu). Anal. calcd. for $C_{11}H_9N_2O_2Cl$: C 55.82, H 3.83, N 11.84; found: C 55.80, H 3.85, N 11.63.

*1,4-Dimethyl-4-(3-chlorophenoxy)pyrimidin-2(1*H*)-one,* **7**b *(Table 1; entry 9)*

This compound was obtained according to the procedure described for **7***a*. Fractions from a silica-gel column (system E) were collected and evaporated to dryness. The residue was dissolved in methanol and decolorized with charcoal. Crystallization from ethyl acetate gave **7***b* as white needles: mp 211°C; UV (H_2O) λ_{max}: 289 nm (ϵ 7300); ^{1}H NMR (DMSO-d_6/$CDCl_3$) δ: 7.99 (d, J = 1.0 Hz, 1, C6-H), 7.30 (m, 4, aromatic H), 3.34 (s, 3, N-CH_3), 2.03 (d, J = 1.0 Hz, 3, C-CH_3); ^{13}C NMR (DMSO-d_6/$CDCl_3$) δ: 169.31, 155.22, 152.57, 148.61, 133.28, 130.62, 125.53, 122.39, 120.87, 101.96, 36.89, 11.43; high resolution MS, m/z: 250.05066 ($C_{12}H_{11}N_2O_2Cl$ requires 250.05083 amu). Anal. calcd. for $C_{12}H_{11}N_2O_2Cl$: C 57.49, H 4.42, H 11.18; found: C 57.46, H 4.42, N 11.21.

*1-(2′,3′-5′-Tri-*O*-acetyl-*β*-D-ribofuranosyl)-4-(3-chlorophenoxy)pyrimidin-2(1*H*)-one,* **7**c (Table 1; entry 10)

The pyridinium salt **2***c* was reacted with 3-chlorophenol under conditions analogous to those used for synthesis of **7***a*. The chloroform layer was separated and chromatographed on SiO_2 ($CHCl_3$ and system A). Appropriate fractions were collected and the solvent evaporated to give **7***c* as an oil. UV (H_2O) λ_{max}: 278 nm (ϵ 7700); ^{1}H NMR ($CDCl_3$) δ: 7.91 (d, J = 7.4 Hz, 1, C6-H), 7.20 (m, 4, aromatic H), 6.18 (d, J = 7.4 Hz, 1, C5-H), 6.11 (d, 1, C1′-H), 5.39, 5.32, and 4.38 (3m, 5, sugar C-H), 2.15, 2.14, and 2.10 (3s, 9, $COCH_3$); ^{13}C NMR ($CDCl_3$) δ: 170.88. 169.94, 169.37, 154.85, 151.51, 143.58, 134.52, 130.09, 126.18, 122.07, 120.00, 96.00, 89.00, 79.74, 73.49, 69.68, 62.75, 20.76, 20.46. High resolution MS m/z: M^+ 480.09340 ($C_{21}H_{21}N_2O_9Cl$ requires 480.09313 amu).

*1-Methyl-4-(coumarin-7-oxy)pyrimidin-2(1*H*)-one,* **8**a *(Table 1; entry 11)*

The reaction of **2***a* with 7-hydroxycoumarin was carried out in a mixture of dioxane/water 4:1 (v/v) at pH 7.5 adjusted with $NaHCO_3$. Crystals of pure **8***a*, precipitated from the reaction mixture, were filtered: mp 161°C; UV (CH_3OH) λ_{max}: 305 nm (ϵ 13 100, sh), 285 nm (ϵ 16 500); fluorescence emission λ_{max}: 378 nm (ϕ = 0.002); ^{1}H NMR (TFA-*d*/acetone-d_6) δ: 8.67 (d, J 7.6 Hz, 1, C6-H), 8.15 (d, J = 9.4 Hz, 1, coumarin C3-H), 7.9 (m, 1, aromatic H), 7.42 (m, 2, aromatic H), 6.75 (d, J = 9.4 Hz, 1, coumarin C4-H), 6.45 (d, J = 7.6 Hz, 1, C5-H), 3.86 (s, 3, N-CH_3); ^{13}C NMR (TFA-*d*/acetone-d_6) δ: 173.36, 166.06, 161.13, 156.14, 154.19, 151.27, 146.93, 132.90, 121.36, 119.63, 118.05, 111.56, 94.97, 40.41; MS m/z (relative intensity): M^+ 270(100), 200(8), 188(19), 187(97), 159(43), 149(8), 109(6). Anal. calcd. for $C_{14}H_{10}N_2O_4$: C 62.22, H 3.72, N 10.37; found: C 62.07, H 3.69, N 10.18.

Can. J. Chem. Downloaded from www.nrcresearchpress.com by 92.62.229.171 on 09/08/12
For personal use only.

1,5-Dimethyl-4-(coumarin-7-oxy)pyrimidin-2(1H)one, **8**b *(Table 1; entry 12)*

The solvent and pH were the same as for synthesis of **8***a*. The reaction mixture was concentrated under vacuum, and the crystalline product was filtered off and separated from unreacted 7-hydroxycoumarin by chromatography on SiO_2 plates (system E): mp 238°C; UV (CH_3OH) λ_{max}: 307 nm (ε 12 700), 288 nm (ε 12 600); fluorescence emission λ_{max} 376 nm (φ = 0.001); ^{1}H NMR (TFA-*d*/acetone-d_6) δ: 8.34 (s, 1, C6-H), 8.13 (d, *J* = 9.5 Hz, 1, coumarin C3-H), 7.86 (m, 1 aromatic H), 7.38 (m, 2, aromatic H), 6.71 (d, *J* = 9.5 Hz, 1, coumarin C4-H), 3.89 (s, 3, N-CH_3), 2.40 (s, 3, C-CH_3); ^{13}C NMR (TFA-*d*/acetone-d_6) δ: 171.93, 166.45, 157.38, 155.94, 155.03, 153.66, 147.19, 132.05, 120.56, 117.30, 114.29, 112.07, 40.53, 11.94; MS *m/z* (relative intensity): (M^+ + 1) 285(18), M^+ 284(100), 270(6), 214(7), 187(19), 159(15), 149(10), 146(7), 134(9). Anal. calcd. for $C_{15}H_{12}N_2O_4$: C 63.37, H 4.25, N 9.85. Found: C 63.14, H 4.21, N 9.73.

1-Methyl-4-(2-hydroxyethylthio)pyrimidin-2(1H)one, **9**a *(Table 1; entry 13)*

The reaction mixture was extracted with $CHCl_3$. The extract was chromatographed on silica gel plates (system E). Product **9***a* was obtained as an oil that solidified upon addition of ethyl acetate: mp 70–72°C; UV (H_2O) λ_{max}: 301 nm (ε 20 700), 225 nm (sh); ^{1}H NMR ($CDCl_3/CH_3OD$) δ: 7.46 (d, *J* = 6.9 Hz, 1, C6-H), 6.30 (d, *J* = 6.9 Hz, 1, C5-H), 3.70 (t, *J* = 6.5 Hz, 2, CH_2), 3.49 (s, 3, N-CH_3), 3.30 (t, *J* = 6.5 Hz, 2, CH_2); ^{13}C NMR ($CDCl_3/CH_3OD$) δ: 177.87, 156.04, 145.47, 104.46, 61.11, 32.35, 32.02. MS *m/z* (relative intensity): M^+ (186(1), 166(4), 156(18), 142(45), 141(35), 127(12), 126(100). Anal. calcd. for $C_7H_{10}N_2O_2S$: C 45.14, H 5.41, N 15.04; found: C 45.03, H 5.37, N 14.94.

1,5-Dimethyl-4-(2-hydroxyethylthio)pyrimidin-2(1H)one, **9**b *(Table 1; entry 14)*

The reaction mixture was extracted with $CHCl_3$ and the organic layer was dried and concentrated under reduced pressure. The residue was separated on an SiO_2 column (system E): mp 110°C; UV (H_2O) λ_{max}: 308 nm (ε 18 700), 224 nm (sh); ^{1}H NMR ($CDCl_3/CD_3OD$) δ: 7.29 (d, *J* = 0.8 Hz, 1, C6-H), 3.76 (t, 2, CH_2), 3.48 (s, 3, N-CH_3), 3.33 (t, 2, CH_2), 2.04 (d, *J* = 0.8 Hz, 3, C-CH_3); ^{13}C NMR ($CDCl_3/CD_3OD$) δ: 178.19, 155.92, 143.30, 113.07, 61.11, 38.08, 32.02, 13.81; MS *m/z* (relative intensity): M^+ 200(5), 183(5), 170(13), 156(100), 155(64), 140(11). Anal. calcd. for $C_8H_{12}N_2O_2S$: C 47.98, H 6.04, N 13.99; found: C 47.76, H 5.98, N 13.87.

*1-(2′,3′,5′-Tri-*O*-acetyl-β-D-ribofuranosyl)-4-(2-hydroxyethylthio)-pyrimidin-2(1H)one,* **9**c *(Table 1; entry 15)*

The product was isolated as described above. System E was used for chromatography. UV (H_2O) λ_{max}: 301 nm (ε 19 600); ^{1}H NMR $CDCl_3$) δ: 7.64 (d, *J* = 7.0 Hz, 1, C6-H), 6.44 (d, *J* = 7.0 Hz, 1, C5-H), 6.19 (d, 1, C1′-H), 5.42, 5.35, and 4.38 (3m, 5, sugar C-H), 3.73 (t, *J* = 6.5 Hz, 2, CH_2), 3.30 (t, *J* = 6.5 Hz, 2, CH_2), 2.16, 2.14, and 2.10 (3s, 9, $COCH_3$); ^{13}C NMR δ: 177.56, 169.96, 169.59, 169.50, 156.82, 146.12, 103.81, 88.89, 80.06, 73.36, 69.88, 62.77, 61.13, 32.47, 20.67, 20.36, 20.23; high resolution MS, *m/z*: M^+ 430.10427 ($C_{17}H_{22}N_2O_9S$ requires 430.10444 amu).

One-pot synthesis of **9**c

The solution of 2′,3′,5′-tri-*O*-acetyluridine (1 mmol) in dry pyridine (10 mL) was treated with 4-chlorophenylphosphorodichloridate (1.5 mmol) and left overnight at room temperature followed by addition of mercaptoethanol (7 mmol). The Zincke test indicated 9% conversion of the pyridinium salt after ca. 1 h. The reaction mixture was evaporated to dryness, and the residue was dissolved in aqueous sodium bicarbonate and then extracted with chloroform. Chromatography on SiO_2 (system E) gave **7***c* in 78% overall yield.

1-Methyl-4-azidopyrimidin-2(1H)-one, **10**a *(Table 1; entry 16)*

The aqueous solution containing 2 mmol of **2***a* was evaporated (<30°C) to dryness. The solid residue was dissolved in dry dimethylformamide (20 mL) and sodium azide (0.195 g, 3 mmol) was added. The resulting mixture was stirred for 15 min and then the solvent was evaporated under vacuum at 35°C. The residue was treated with water (30 mL) and the aqueous solution extracted with chloroform. The organic layer was dried over Na_2SO_4, concentrated, and treated with hexane to give crystals of **10***a*: mp 206–208°C; UV (H_2O) λ_{max}: 270 nm (ε 8500, sh), 258 nm (ε 10 000); ^{1}H NMR (DMSO-d_6) δ: 7.73 (d, *J* = 7.3 Hz, 1, C6-H), 6.94 (d, 1, C5-H), 3.73 (s, 3, N-CH_3); ^{13}C NMR (DMSO-d_6) δ: 151.42, 143.62, 141.52, 92.26, 36.62; high resolution MS, *m/z*: 151.04932 ($C_5H_5N_5O$ requires 151.04936 amu). Anal. calcd. for $C_5H_5N_5O$: C 39.73, H 3.33, N 46.34; found: C 39.60, H 3.28, N 46.49.

1,5-Dimethyl-4-azidopyrimidin-2(1H)-one, **10**b *(Table 1; entry 17)*

This compound was obtained according to the procedure described for **10***a*. The crude product was chromatographed on an SiO_2 column (system B): mp 178–180°C; UV (H_2O) λ_{max}: 273 nm (ε 7500, sh), 257 nm (ε 9500); ^{1}H NMR (DMSO-d_6) δ: 7.76 (d, *J* = 1.2 Hz, 1, C6-H), 3.56 (s, 3, N-CH_3), 2.28 (d, *J* = 1.2 Hz, 3, C-CH_3); ^{13}C NMR (DMSO-d_6) δ: 152.19, 143.30, 138.05, 101.64, 36.46, 12.19; high resolution MS, *m/z*: 165.06494 ($C_6H_7N_5O$ requires 165.06498 amu). Anal. calcd. for $C_6H_7N_5O$: C 43.63, H 4.27, N 42.40; found: C 43.41, H 4.25, N 42.27.

*1-(2′,3′,5′-Tri-*O*-acetyl-β-D-ribofuranosyl)-4-azidopyrimidin-2(1H)-one,* **10**c *(Table 1; entry 18)*

The aqueous solution of **2***c* was treated with sodium azide. Pure **10***c*, which precipitated from the reaction mixture, was filtered off. An additional amount of the product was isolated from the filtrate by extraction ($CHCl_3$) and chromatography on SiO_2 (system D). UV (H_2O/CH_3OH, 9:1) λ_{max}: 265 nm (ε 7000, sh), 251 nm (ε 7600); ^{1}H NMR ($CDCl_3$) δ: 7.71 (d, *J* = 7.8 Hz, 1, C6-H), 6.98 (d, *J* = 7.8 Hz, 1, C5-H), 6.29 (d, 1 C1′-H), 5.45, 5.39, and 4.39 (3m, 5, sugar C-H), 2.17, 2.14, and 2.09 (3s, 9, $COCH_3$); ^{13}C NMR ($CDCl_3$) δ: 169.99, 169.59, 169.50, 150.53, 142.58, 133.85, 94.70, 88.78, 80.69, 73.24, 69.95, 62.75, 20.68, 20.37, and 20.23; high resolution MS, *m/z*: M^+ 395.10757 ($C_{15}H_{17}N_5O_8$ requires 395.10749 amu).

Acknowledgments

This work was supported by the Polish Ministry of Education (Grant R.P.II.13.2.15). We thank Prof. S. Paszyc and Dr. R. W. Adamiak for their interest in this work.

1. T. Ueda. *In* Chemistry of nucleosides and nucleotides. *Edited by* L. B. Townsend. Plenum Press, New York. 1988.
2. H. Vorbruggen and U. Niedballa. Angew. Chem. **83**, 729 (1975).
3. A. Matsuda, K. Obi, and T. Miyasaka. Chem. Pharm. Bull. **33**, 2575 (1985).
4. K. J. Divakar and C. B. Reese. J. Chem. Soc. Perkin Trans. 1, 1171 (1982).
5. S. S. Jones, B. Rayner, C. B. Reese, A. Ubasawa, and M. Ubasawa. Tetrahedron, **36**, 3075 (1980).
6. C. B. Reese and A. Ubasawa. Tetrahedron Lett. **21**, 2265 (1980).
7. W. L. Sung. Nucleic Acids Res. **9**, 6139 (1981).
8. B. Skalski, G. Wenska, S. Paszyc, and Z. Stefaniak. Can. J. Chem. **66**, 1027 (1988).
9. N. Bischofberger. Tetrahedron Lett. **28**, 2821 (1987).
10. R. W. Adamiak, E. Biala, and B. Skalski. Nucleic Acids Res. **13**, 2989 (1985).
11. R. W. Adamiak, E. Biala, Z. Gdaniec, S. Mielewczyk, and B. Skalski. Chem. Scr. **26**, 3 (1986); **26**, 7 (1986).
12. R. W. Adamiak, E. Biala, and B. Skalski. Angew Chem. Int. Ed. Engl. **24**, 1024 (1985).
13. S. Mielewczyk, Z. Gdaniec, G. Bobrowska, and R. W. Adamiak. Nucleosides and Nucleotides, **6**, 273 (1987).

14. Th. Zincke. Liebigs Ann. Chem. 330 (1903); 331 (1903); F. Krohnke. Angew. Chem. **75**, 371 (1963).
15. W. E. Stewart and T. H. Siddall. Chem. Rev. **70**, 517 (1970).
16. C. B. Reese and P. Skone. J. Chem. Soc. Perkin Trans. 1, 1263 (1984).
17. J. J. Fox, D. van Praag, I. Wempen, I. L. Doerr, L. Cheong, J. E. Knoll, M. L. Eidinoff, A. Bendich, and G. B. Brown. J. Am. Chem. Soc. **81**, 178 (1959).
18. C. Temple, Jr., C. L. Kussner, and J. A. Montgomery. J. Org. Chem. **31**, 2210 (1966).
19. H. Schollhorn and U. Thewalt. J. Heterocycl. Chem. **26**, 1499 (1989).
20. D. F. Eaton. Pure Appl. Chem. **60**, 1107 (1988).
21. Z. Gdaniec, S. Mielewczyk, R. W. Adamiak, and B. Skalski. Heterocycles, **27**, 2807 (1988).

Can. J. Chem. Downloaded from www.nrcresearchpress.com by 92.62.229.171 on 09/08/12
For personal use only.

A phosphorus-31 NMR study of solid carbonylhydridotris(triphenylphosphine)rhodium(I). Unusual MAS sideband intensities in second-order NMR spin systems

GANG WU, RODERICK E. WASYLISHEN,[1] AND RONALD D. CURTIS
Department of Chemistry, Dalhousie University, Halifax, N.S., Canada B3H 4J3

Received July 25, 1991

GANG WU, RODERICK E. WASYLISHEN, and RONALD D. CURTIS. Can. J. Chem. **70**, 863 (1992).

The CP/MAS ^{31}P NMR spectrum of carbonylhydridotris(triphenylphosphine)rhodium(I), $RhH(CO)(PPh_3)_3$ (**1**), can be described as a tightly coupled ABMX spin system (X = ^{103}Rh). In contrast to the solution ^{31}P NMR spectrum, the three equatorial phosphorus nuclei are nonequivalent in the solid state and this structural feature allows us to measure the two-bond spin–spin couplings, $^2J(^{31}P,^{31}P)$. A new method is proposed for extracting the principal components of the chemical shift tensor from slow MAS NMR spectra in a tightly *J*-coupled two-spin system. For compound **1**, the principal components of the ^{31}P chemical shift tensors calculated using this method are in good agreement with those obtained from NMR spectra of a static sample. The principal components of the ^{31}P chemical shift tensors determined for **1** are compared with those reported previously for Wilkinson's catalyst, $RhCl(PPh_3)_3$. The δ_{22} component of the ^{31}P chemical shift tensors in **1** shows the largest variation with structure. This is ascribed to differences in the orientation of the P—C_{ipso} bond about the equatorial plane of the trigonal bipyramidal structure.

Key words: rhodium–phosphine compounds, AB spin system, ^{31}P chemical shift tensor, magic-angle spinning, molecular structure.

GANG WU, RODERICK E. WASYLISHEN et RONALD D. CURTIS. Can. J. Chem. **70**, 863 (1992).

On peut décrire le spectre RMN CP/MAS du ^{31}P du carbonylhydrido (triphénylphosphine)rhodium(I), $RhH(CO)(PPh_3)_3$ (**1**), par un système de spin ABMX (X = ^{103}Rh) fortement couplé. Contrairement à ce qui a été observé dans le spectre RMN du ^{31}P en solution, les trois noyaux des phosphores équatoriaux ne sont pas équivalents à l'état solide et cette caractéristique structurale nous a permis de mesurer les couplages spin–spin à travers deux liaisons, $^2J(^{31}P,^{31}P)$. On propose une nouvelle méthode pour extraire les principales composantes du tenseur du déplacement chimique à partir de spectres RMN, mesurés lentement par la technique de rotation à l'angle technique, dans un système *J* à deux spin couplés. Pour le composé **1**, les principales composantes des tenseurs du déplacement chimique du ^{31}P, calculées par cette méthode, sont en bon accord avec celles obtenues à partir de spectres RMN d'un échantillon statique. On a comparé les principales composantes des tenseurs du déplacement chimique du ^{31}P du composé **1** avec celles rapportées antérieurement pour le catalyseur de Wilkinson, $RhCl(PPh_3)_3$. La composante δ_{22} des tenseurs du déplacement chimique du ^{31}P du composé **1** est celle qui varie le plus avec la structure. On attribue cette propriété aux différences dans l'orientation de la liaison P—C_{ipso} autour du plan équatorial de la structure trigonale bipyramidale.

Mots clés : composés rhodium–phosphine, système de spin AB, tenseur du déplacement chimique du ^{31}P, rotation à l'angle technique, structure moléculaire.

[Traduit par la rédaction]

Introduction

Carbonylhydridotris(triphenylphosphine)rhodium(I), $RhH(CO)(PPh_3)_3$ (**1**), is one of the most important commercial homogeneous catalysts (1–3). In solution, ^{31}P NMR studies indicate that **1** is capable of undergoing dissociation to generate $RhH(CO)(PPh_3)_2$ as indicated in eq. [1].

$$[1] \quad RhH(CO)(PPh_3)_3 \underset{-PPh_3}{\overset{+PPh_3}{\rightleftharpoons}} RhH(CO)(PPh_3)_2$$

The latter species is an active catalyst for alkene hydrogenation and hydroformylation (4). The dissociation of a triphenylphosphine ligand from **1** is apparent from ^{31}P NMR ligand exchange studies in toluene solution (5). For example, when a large excess of triphenylphosphine is added to a toluene solution of **1**, the doublet at $\delta(^{31}P)$ = 39.8 ppm ($^1J(^{103}Rh,^{31}P)$ = 155 Hz) arising from $RhH(CO)(PPh_3)_3$ broadens and shifts to a lower frequency ($\delta(^{31}P) = -7.2$ ppm for free triphenylphosphine ligands). Typical exchange rates for dissociation are on the order of 50 s^{-1} at 25°C for a solution containing a 6:1 excess of PPh_3. The observation of a simple doublet in the ^{31}P NMR spectrum of **1** in toluene solution suggests that all three PPh_3 groups are chemically equivalent and that they occupy the equatorial sites of a trigonal bipyramid as deduced from X-ray diffraction studies (6).

The yellow crystals of $RhH(CO)(PPh_3)_3$ are monoclinic and belong to the space group $P2_1/n$ (C_{2h}^5). Examination of the X-ray diffraction results indicates that each of the three PPh_3 ligands is nonequivalent due to slight variations in structure (see Fig. 1). One of the primary objectives of the present study is to demonstrate that the ^{31}P cross-polarization (CP) magic-angle spinning(MAS) NMR spectrum of **1** is sensitive to these subtle structural differences. As well, we describe a general procedure for analyzing the AB portion of a slow MAS NMR spectrum to obtain average principal components of the A and B spin chemical shift tensors. The CP/MAS ^{31}P NMR spectrum of **1** is analyzed as the ABM portion of a general ABMX spectrum where X = ^{103}Rh ($I = \frac{1}{2}$). The NMR parameters obtained from our solid-state study are compared with corresponding solution NMR studies (5) and with related solid-state NMR studies on Wilkinson's catalyst, $RhCl(PPh_3)_3$ (7).

Theory

For an isolated or uncoupled spin-1/2 nucleus, it is well-known that the analysis of slow MAS NMR spectra is ca-

[1]Author to whom correspondence may be addressed.

Can. J. Chem. Downloaded from www.nrcresearchpress.com by 92.62.229.171 on 09/08/12
For personal use only.

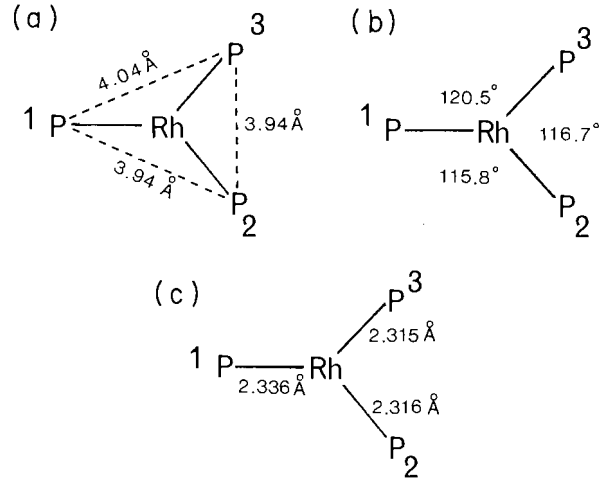

FIG. 1. Selected structural parameters of the RhP_3 moiety in **1**. Phosphorus sites are numbered as in ref. 6.

pable of yielding the principal components of the chemical shift (CS) tensor and, hence, the chemical shift anisotropy (8–14). Such techniques are particularly attractive in cases where the MAS spectrum consists of several isotropic peaks, making the analysis of the corresponding static powder NMR spectrum very difficult. The most widely used procedure for analyzing slow MAS NMR spectra is the well-known Herzfeld–Berger technique (9). In cases where the spin under observation is coupled to a heteronuclear spin through direct dipole–dipole and indirect spin–spin (J) interactions, the relative intensity of the peaks in the J-coupled multiplet in each spinning sideband is modulated by the dipolar and J interactions as well as the chemical shift anisotropy (10, 15). If the dipolar coupling and the anisotropy in J (ΔJ) are negligible, then the heteronuclear J-coupled multiplet observed with MAS NMR will show regular fine structure similar to that observed in solution NMR spectra. However, this is not generally true if two nuclei are strongly J-coupled, i.e., an AB spin pair. In such a case, even if the dipolar coupling and ΔJ are zero, it is still possible to have AB multiplets with different relative intensity in each spinning sideband because the mixing between the $|\alpha\beta\rangle$ and $|\beta\alpha\rangle$ states becomes orientation dependent in an AB spin system.

Consider a strongly J-coupled spin pair, A and B, each with anisotropic chemical shift and isotropic J coupling (the dipolar interaction between the two spins is assumed to be negligible). The resulting four transitions, ν_i, and their relative intensities, P_i, are given by eq. [2]:

$$[2a] \quad \nu_1 = \frac{1}{2}(\nu_A + \nu_B) - \frac{1}{2}J - \frac{1}{2}D, \qquad P_1 = 1 - J/D$$

$$[2b] \quad \nu_2 = \frac{1}{2}(\nu_A + \nu_B) + \frac{1}{2}J - \frac{1}{2}D, \qquad P_2 = 1 + J/D$$

$$[2c] \quad \nu_3 = \frac{1}{2}(\nu_A + \nu_B) - \frac{1}{2}J + \frac{1}{2}D, \qquad P_3 = 1 + J/D$$

$$[2d] \quad \nu_4 = \frac{1}{2}(\nu_A + \nu_B) + \frac{1}{2}J + \frac{1}{2}D, \qquad P_4 = 1 - J/D$$

where $D = [(\nu_A - \nu_B)^2 + J^2]^{1/2}$. If (θ_A, ϕ_A) and (θ_B, ϕ_B) are used to define the orientation of the applied magnetic field B_0 in the principal axis system of the two chemical shielding tensors, A and B, respectively, then ν_A and ν_B are

$$[3a] \quad \nu_A = \nu_0[1 - (\sigma_{11}{}^A \sin^2\theta_A \cos^2\phi_A + \sigma_{22}{}^A \sin^2\theta_A \sin^2\phi_A + \sigma_{33}{}^A \cos^2\theta_A)]$$

$$[3b] \quad \nu_B = \nu_0[1 - (\sigma_{11}{}^B \sin^2\theta_B \cos^2\phi_B + \sigma_{22}{}^B \sin^2\theta_B \sin^2\phi_B + \sigma_{33}{}^B \cos^2\theta_B)]$$

It is clear from eqs. [2] and [3] that because of the term D each transition characterizes a more complicated powder line shape than that of an isolated nucleus with anisotropic chemical shift. Therefore, the previous method of analyzing spinning sidebands in a slow MAS NMR spectrum (9) is not directly applicable to a tightly J-coupled AB spin pair, since in this case the envelope of spinning sidebands associated with each transition cannot be characterized by three distinct principal components of a chemical shift tensor.

Fortunately, if we take the average of the four transitions in eq. [2], the term D can be removed and the expressions of both transition frequency and intensity become very simple:

$$[4a] \quad \nu_0 = \frac{1}{4}(\nu_1 + \nu_2 + \nu_3 + \nu_4) = \frac{1}{2}(\nu_A + \nu_B)$$

$$[4b] \quad P_0 = \frac{1}{4}(P_1 + P_2 + P_3 + P_4) = 1$$

The transition ν_0 is not observable, but can be easily constructed in a slow MAS NMR spectrum. Its calculated position appears at the centre of a J-coupled AB multiplet and its intensity is the average of all four peaks. It should be noted, however, that the intensity distribution of such constructed spinning sidebands still cannot be characterized by a single chemical shift tensor, since each constructed sideband equals the average of sidebands due to the two different CS tensors of spin A and B. Only when the magnitudes of the principal components of the two CS tensors are approximately the same (not necessarily in their orientations) can one analyze the constructed sidebands with the usual methods (9, 11, 12) and recover the elements of the chemical shift tensor.

Theoretical justification of the above procedure can be made by applying the Floquet Hamiltonian theory to a homonuclear spin-1/2 pair in rotating solids (16). Assuming that the sample spinning rate is much greater than the isotropic J coupling between the two nuclei of an AB spin pair, one can rewrite eq. 17 in ref. 16 and obtain the intensities of the four transitions in the ith order spinning sideband, P^i, as follows (dipolar interactions and ΔJ are ignored):

$$[5a] \quad P_1^i = Y_1 I_A^i + Y_4 I_B^i$$

$$[5b] \quad P_2^i = Y_2 I_B^i + Y_3 I_A^i$$

$$[5c] \quad P_3^i = Y_2 I_A^i + Y_3 I_B^i$$

$$[5d] \quad P_4^i = Y_1 I_B^i + Y_4 I_A^i$$

where

Can. J. Chem. Downloaded from www.nrcresearchpress.com by 92.62.229.171 on 09/08/12
For personal use only.

$$Y_1 = \frac{1}{2}(1 - \cos\Psi - \sin\Psi)$$

$$Y_2 = \frac{1}{2}(1 + \cos\Psi + \sin\Psi)$$

$$Y_3 = \frac{1}{2}(1 - \cos\Psi + \sin\Psi)$$

$$Y_4 = \frac{1}{2}(1 + \cos\Psi - \sin\Psi)$$

and $\sin\Psi = J/D$. I_A^i and I_B^i are the intensities of the ith order spinning sideband due to the chemical shift tensors of spin A and spin B, respectively, in the absence of any spin–spin interaction. From eq. [5], it is easy to show that the average intensity of the J-coupled multiplet in the ith order spinning sideband becomes independent of the J interaction, i.e.,

$$[6] \quad \frac{1}{4}(P_1^i + P_2^i + P_3^i + P_4^i) = \frac{1}{2}(I_A^i + I_B^i)$$

Furthermore, it is interesting to note in eq. [5] that the relative intensity of peaks in the J-coupled multiplet deviates from that obtained in solution NMR studies. For example, the relative intensity of P_1^i and P_2^i is given as

$$[7] \quad \frac{P_1^i}{P_2^i} = \frac{(1 - \sin\Psi)(I_A^i + I_B^i) - \cos\Psi(I_A^i - I_B^i)}{(1 + \sin\Psi)(I_A^i + I_B^i) - \cos\Psi(I_A^i - I_B^i)}$$

Obviously, if $I_A^i \neq I_B^i$, this ratio is different from $(1 - \sin\Psi)/(1 + \sin\Psi)$, which is the ratio expected for an AB spin pair in the solution NMR spectrum.

Inspection of eqs. [5] and [7] reveals the following general features regarding the MAS NMR spectrum of two tightly J-coupled spins: (1) the relative intensities of the four peaks in an AB multiplet vary depending on the order of the spinning sidebands, (2) the relative intensities of the AB multiplets become distorted in comparison with those obtained in solution NMR studies, and (3) only in the case where the spinning rate is so high that all spinning sidebands are of negligible intensity (i.e., $I_A = I_B = 1$ for the isotropic peaks) do the MAS spectra restore the normal AB patterns observed in solution.

Experimental

Carbonylhydridotris(triphenylphosphine)rhodium(I), **1**, was purchased from Aldrich Chemical Company and was used for the present NMR study without further purification. The yellow crystals of **1** were ground and packed into a zirconium oxide rotor (7 mm o.d.). Phosphorus-31 CP/MAS NMR spectra were obtained on a Bruker MSL-200 NMR spectrometer (B_0 = 4.70 T) operating at 81.033 MHz. All spectra were acquired at 20°C with high-power proton decoupling during data acquisition. Cross polarization was accomplished under the Hartmann–Hahn match condition using 90° pulses of 4 μs. Typical values of the contact time were 2–5 ms and the recycle time was 10 s. Sample spinning rates ranged from 2 to 4 kHz. The magic angle was adjusted by examining the ^{79}Br NMR signal of KBr (17). All ^{31}P spectra were referenced to 85% H_3PO_4(aq) by using solid $NH_4H_2PO_4$ as a secondary reference. The latter compound has a chemical shift of +0.81 ppm with respect to 85% H_3PO_4(aq). The acquisition time was 106 ms and the 8 K FID was zero-filled to 16 K prior to Fourier transformation. The line widths at half-height in the MAS NMR spectra were approximately 25 Hz. No improvement in the line width was observed by using longer acquisition times.

The static ^{31}P NMR spectrum of a powdered sample of **1** was obtained on a Varian Unity-400 NMR spectrometer (B_0 = 9.40 T) using a slightly modified Varian 7-mm MAS probehead. Proton and phosphorus 90° pulse lengths for cross polarization were 5 μs with a decoupling field strength in excess of 90 kHz. The contact time was 2.5 ms with an acquisition time of 35 ms and a recycle time of 20 s. The audiofrequency filters were opened to their maximum values, 100 kHz, in order to observe the ^{31}P NMR signal approximately 12 μs after the cross-polarization period. This was found to help alleviate spectral distortions associated with a loss of information in the first few data points. A sensitivity enhancement corresponding to 50 Hz of line broadening was applied to the FID prior to Fourier transformation.

The phosphorus-31 NMR spectrum of a toluene solution of **1** (50 mg in 2.0 mL) was obtained at 146.12 MHz on a Nicolet 360 NB NMR spectrometer with broadband proton decoupling. The solution sample was prepared under a nitrogen environment and sealed in a 10-mm NMR tube. The NMR spectrum was recorded at room temperature (20°C) and was referenced to external 85% H_3PO_4(aq).

Simulation of the isotropic portion of the MAS NMR spectra was accomplished by the LAME8 program (18). All the spinning sideband analyses were performed using a Simplex program based on the Herzfeld–Berger method (9). The static powder line shape was calculated by simply overlapping three independent CS powder patterns.

Results and discussion

The ^{31}P CP/MAS NMR spectra of **1** is shown in Fig. 2. The presence of intense first and second-order spinning sidebands indicates that the ^{31}P chemical shift anisotropies are large compared with the sample spinning frequency, 4.0 kHz. The isotropic portion of the ^{31}P CP/MAS spectrum of **1** is given in Fig. 3*a*. Since the three ^{31}P nuclei are nonequivalent in the solid state, all the possible J couplings between ^{31}P–^{31}P and ^{31}P–^{103}Rh are readily resolved in the high-resolution, solid-state NMR spectrum. The calculated spectrum is also shown in Fig. 3*b* and best-fit parameters are summarized in Table 1. The resultant pattern suggests an ABMX spin system in **1** (A, B, and M represent the three ^{31}P nuclei; X = ^{103}Rh). The three isotropic chemical shifts were determined to be 45.35, 34.34, and 33.84 ppm compared to the single chemical shift (41.15 ppm) obtained from a solution NMR spectrum. The assignment of three phosphorus chemical shifts to P1, P2, and P3 shown in Fig. 1 is based on arguments regarding the relative magnitudes of the principal components of the chemical shift tensors (*vide infra*). It is readily seen from Fig. 3 that, although all the observed line positions are well reproduced (rms deviation < 0.8 Hz), the intensities of the outer peaks of the AB portion in the simulated spectrum are significantly smaller than the observed intensities. As discussed in the theory section, this is due to the strong J coupling and the orientation-dependent chemical shifts in the solid state, so that the AB pattern in the MAS spectrum of **1** differs from that expected in solution.

The one-bond ^{103}Rh–^{31}P coupling constants, $^1J(^{103}\text{Rh},^{31}\text{P})$, in **1** fall in the normal range reported for related rhodium(I) compounds (19, 20) and agree well with the value observed for the same compound in toluene solution. The three essentially equal $^1J(^{103}\text{Rh},^{31}\text{P})$ values confirm that the three phosphorus atoms are at equatorial sites, since $^1J(^{103}\text{Rh},^{31}\text{P}_{ax})$ has been found to be smaller than $^1J(^{103}\text{Rh},^{31}\text{P}_{eq})$ (19). Following previous solution NMR investiga-

Can. J. Chem. Downloaded from www.nrcresearchpress.com by 92.62.229.171 on 09/08/12
For personal use only.

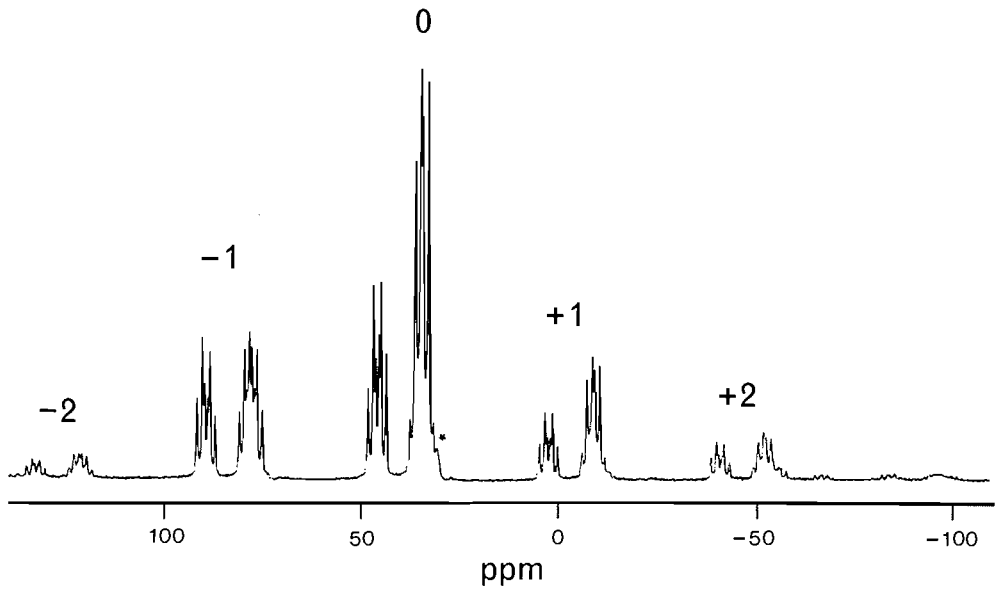

FIG. 2. The CP/MAS ^{31}P NMR spectrum of **1**. Sample spinning frequency was 4.0 kHz. The orders of the spinning sidebands are numbered by the usual convention, i.e., positive signs refer to the low-frequency sidebands relative to the isotropic peaks. A small impurity peak is indicated by *.

Can. J. Chem. Downloaded from www.nrcresearchpress.com by 92.62.229.171 on 09/08/12
For personal use only.

tions of rhodium(I) complexes (21), the sign of $^1J(^{103}Rh,^{31}P)$ in **1** is assigned as negative.

Since the three triphenylphosphine ligands in **1** are equivalent in solution, $^2J(^{31}P,^{31}P)$ cannot be measured. The values of $^2J(^{31}P,^{31}P)$ in solid **1** are comparable to those reported for five-coordinate rhodium(I) compounds (22). This two-bond coupling was intermediate between the magnitudes of $^2J(^{31}P,^{31}P)_{cis}$ and $^2J(^{31}P,^{31}P)_{trans}$ reported for four-coordinate rhodium(I) compounds (19, 20) where $^2J(^{31}P,^{31}P)_{cis} < {}^2J(^{31}P,^{31}P)_{trans}$. Similar to the discussion of $^1J(^{103}Rh,^{31}P)$, the values of $^2J(^{31}P,^{31}P)$ also provide evidence that the three phosphorus atoms are at approximately equivalent equatorial sites; otherwise a much smaller $^2J(^{31}P,^{31}P)$, characteristic of a $^2J(^{31}P_{ax},^{31}P_{eq})$, would be observed (23). The sign of $^2J(^{31}P,^{31}P)$ was assumed to be positive (19), although no difference could be introduced in the simulated spectrum by varying the relative sign of $^2J(^{31}P,^{31}P)$ and $^1J(^{103}Rh,^{31}P)$.

In addition to the isotropic peaks, several spinning sidebands also appear in the MAS NMR spectrum of **1**, as shown in Fig. 2. Inspection of the relative intensities of the *J*-coupled multiplet in each spinning sideband indicates that both heteronuclear ($^{103}Rh,^{31}P$) and homonuclear ($^{31}P,^{31}P$) dipolar interactions are small. Based on the X-ray crystal structure (6), the direct dipolar coupling constants

$$R_{AX} \equiv \left(\frac{\mu_0}{4\pi}\right) r_{AX}^{-3} \gamma_A \gamma_X \left(\frac{\hbar}{2\pi}\right)$$

are as follows: $^1R_{P-Rh} \leq 125$ Hz and $^2R_{P-P} \leq 325$ Hz. These values are small with respect to the sample spinning frequency (ca. 4 kHz), confirming that the relative intensities of the spinning sidebands are primarily governed by the anisotropic chemical shift and the J_{AB} coupling.

Unusual AB patterns also appear in the different order spinning sidebands as observed in the isotropic part of the slow MAS NMR spectrum. In Fig. 4 several spinning sidebands are shown for easy comparison. It is clear that the relative intensities of peaks within the high-frequency multiplet (M spin) remain essentially unchanged in the different order spinning sidebands, while the relative intensities of peaks within the AB part vary dramatically.[2]

It is straightforward to recover the principal components of the CS tensor for the M spin. The relative intensities of the central peak of the high-frequency triplet were measured at three different sample spinning rates and the three principal components of the CS tensor were obtained by implementing the Herzfeld–Berger method (9). For the A and B spins, the intensity of the AB multiplet due to the strong $^{31}P-^{31}P$ *J* coupling was averaged in each spinning sideband, as described in the theory section. Assuming that the chemical shift anisotropies at the two tightly *J*-coupled spins are approximately the same, the principal components of the two CS tensors can be recovered by using the averaged intensities. If the two CS tensors differ, then the averaged principal components are obtained, provided that the difference between the corresponding principal components of the two CS tensors is small compared to their anisotropies.

The principal components of phosphorus CS tensors in **1**, obtained from analysis of the MAS NMR spectrum, are given in Table 2. To confirm the accuracy of these values, a static powder spectrum was obtained at a high magnetic field (B_0 = 9.40 T). Analysis of the static powder spectrum (shown in Fig. 5*a*) permits the determination of the principal components for all three ^{31}P chemical shift tensors in **1**. Since the dipolar couplings and *J* couplings (ca. 150 Hz) are much

[2]In fact, the relative intensities of peaks within the M-spin multiplet do change very slightly, presumably due to the small deviation from first-order *J* coupling between the M spin and the other two spins, or due to the residual homonuclear dipolar interactions among the ^{31}P nuclei in **1**.

Can. J. Chem. Downloaded from www.nrcresearchpress.com by 92.62.229.171 on 09/08/12
For personal use only.

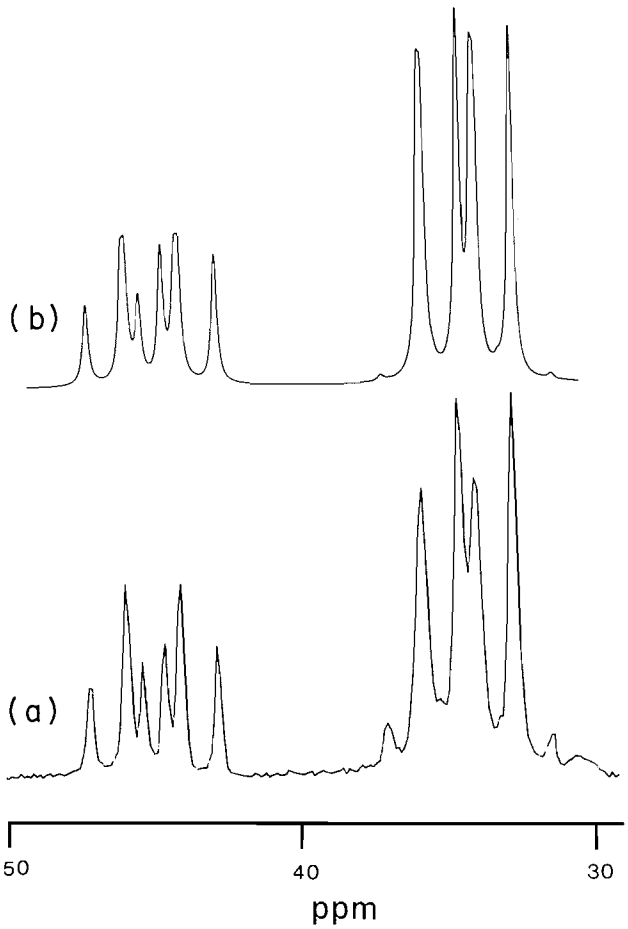

FIG. 3. (*a*) The isotropic part of the CP/MAS ^{31}P NMR spectrum of **1**. (*b*) Calculated spectrum with parameters given in Table 1. A Lorentzian line shape with the half-height width of 20 Hz was used.

smaller than the chemical shift anisotropies in Hz ($\Delta\nu = \nu_{11} - \nu_{33} \approx 24$ kHz at $B_0 = 9.40$ T), it is reasonable to analyze the static powder line shape by simple overlapping of the three independent chemical shift powder patterns. The calculated ^{31}P NMR static powder line shape is also shown in Fig. 5*b*. It is evident that all of the main shoulders of the experimental line shape are reproduced in the calculated spectrum. The anomalous features at the low-frequency end of the static line shape were also observed at $B_0 = 4.70$ T. These features may be attributed to the second-order J coupling effect between P1 and P3, or to the homonuclear dipolar coupling between the three ^{31}P nuclei. Nonetheless, the effect is small and does not influence the determination of the principal components in the present case. The results obtained from analysis of the static powder line shape (also shown in Table 2) clearly indicate that analysis of the MAS NMR spectrum gives reasonable estimates of the principal components for P2 (M spin), while for P1 and P3 (A and B spins) it yields the averaged values of the corresponding principal components. Also, it is clear that the principal components of the CS tensors for P1 and P3 differ by less than 15 ppm.

In Table 2 the values of the chemical shift anisotropy ($\Delta\delta = \delta_{11} - \delta_{33}$) observed for the three ^{31}P nuclei of **1** are comparable to those reported previously (7) for the mutually *trans* phosphorus nuclei in the approximately square planar $RhCl(PPh_3)_3$, Wilkinson's catalyst, the only rhodium–phosphine complex for which complete ^{31}P shielding data are available (24). It is interesting to note that the variation of the δ_{33} components of the three ^{31}P chemical shift tensors in **1** is relatively small: furthermore, the three δ_{33} components in **1** are similar to the corresponding components at the mutually *trans* ^{31}P nuclei in $RhCl(PPh_3)_3$. Since the orientation of δ_{33} has been determined to be almost parallel to the Rh—P bond in $RhCl(PPh_3)_3$ (7), it is reasonable to expect that δ_{33} of the ^{31}P chemical shift tensor also lies along the Rh—P bond for each ^{31}P nucleus in **1**. Thus, the chemical shieldings along the Rh—P bond in compound **1** are probably similar to those at the two mutually *trans* phosphorus nuclei in $RhCl(PPh_3)_3$. Also, the three δ_{11} components in **1** have approximately the same values as those of the mutually *trans* ^{31}P nuclei in $RhCl(PPh_3)_3$.

In contrast to δ_{11} and δ_{33}, the δ_{22} component of the ^{31}P CS tensors in **1** shows large variations and all three δ_{22} components deviate from the corresponding values in $RhCl(PPh_3)_3$. From Table 2 it is readily seen that the unique high-frequency isotropic chemical shift at P2 in **1** is mainly due to the significant deshielding of the δ_{22} component. From a solution ^{31}P NMR study, significantly different isotropic chemical shifts have been found in different conformers associated with rotation of the phenyl groups about the Rh—P bond in *trans*-$[RhX(CO)L_2]$ complexes (X = halogen; L = tertiary phosphine) (25). Therefore, two distinct isotropic shifts (ca. 45 and 34 ppm) observed in **1** may also reflect the local orientation of the phenyl groups with respect to the trigonal bipyramidal structure in the solid state. Since the unique

TABLE 1. Best-fit parameters from the ^{31}P CP/MAS NMR spectrum of $RhH(CO)(PPh_3)_3$[a]

Isotropic chemical shift[b] (ppm)		
δ(P1)	δ(P2)	δ(P3)
34.34	45.35	33.84
Coupling constant,[c] J (Hz)		
$^1J(^{103}Rh,^{31}P_1) = -156$,	$^1J(^{103}Rh,^{31}P_2) = -154$,	$^1J(^{103}Rh,^{31}P_3) = -156$
$^2J(^{31}P_1,^{31}P_2) = +109$,	$^2J(^{31}P_1,^{31}P_3) = +113$,	$^2J(^{31}P_2,^{31}P_3) = +111$

[a]The $^{31}P\{^1H\}$ NMR spectrum of **1** in toluene solution at room temperature consists of a doublet arising from the coupling of three ^{31}P nuclei with ^{103}Rh nucleus (δ = 41.15 ppm, $^1J(^{103}Rh,^{31}P) = 154$ Hz).
[b]The estimated error in the chemical shifts is ±0.12 ppm.
[c]The estimated error in the spin–spin coupling constants is ±5 Hz.

Can. J. Chem. Downloaded from www.nrcresearchpress.com by 92.62.229.171 on 09/08/12
For personal use only.

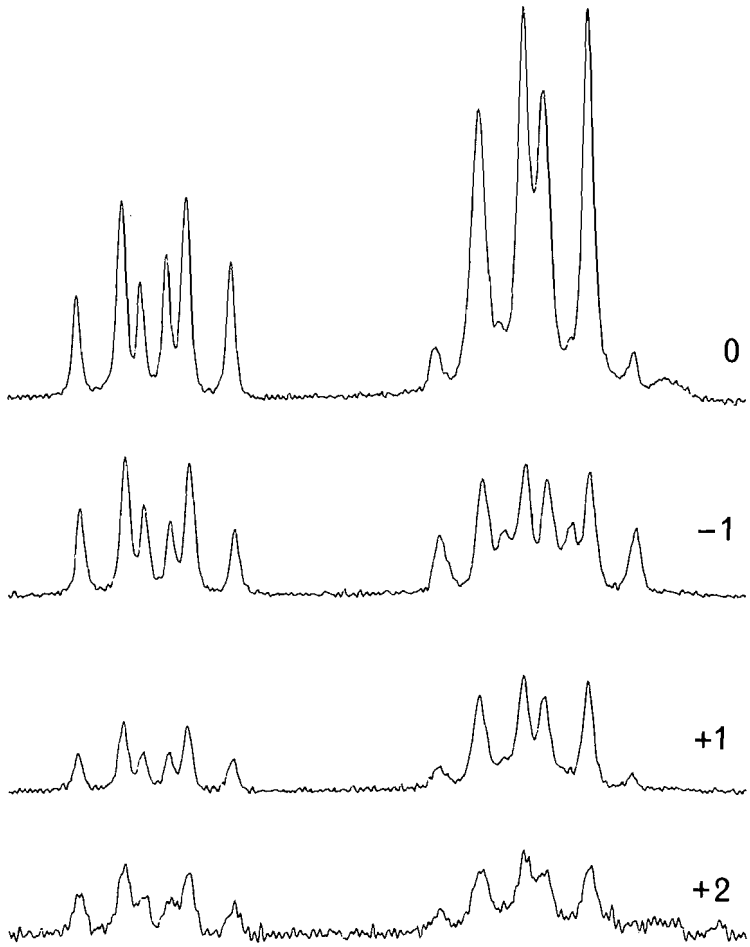

FIG. 4. Selected spinning sidebands from the slow MAS NMR spectrum of **1**. The vertical scale of the +2 spinning sideband has been expanded by a factor of two.

TABLE 2. Principal components of the ^{31}P chemical shift tensors in $RhH(CO)(PPh_3)_3$ and $RhCl(PPh_3)_3$

	$RhH(CO)(PPh_3)_3$					$RhCl(PPh_3)_3$		
	MAS[a]		Static[b]			Single crystal[c]		
	P1,P3	P2	P1	P3	P2	P1	P3	P2
δ_{11}	107	109	98	110	110	91	110	171
δ_{22}	52	89	52	52	84	38	37	73
δ_{33}	−57	−62	−47	−61	−61	−52	−59	−100
$\Delta\delta = \delta_{11} - \delta_{33}$	164	171	145	171	171	143	169	271

[a]All principal components are in ppm and estimated errors are less than ±5 ppm.
[b]All principal components are in ppm and estimated errors are ±2 ppm.
[c]From ref. 7.

isotropic shift at 45.15 ppm results from deshielding of the δ_{22} component that is perpendicular to the Rh—P bond, it is reasonable to associate the variations in δ_{22} with the different orientations of the P—C_{ipso} bonds at each of the three phosphorus sites. This argument is supported by the X-ray crystal structure of **1** where the dihedral angles of (OC)—Rh—P—C_{ipso} for the three phosphorus sites are P1(−64, +55, +176), P2(+7, +129, −112), and P3(−177, −54, +64) (6). The relative orientation of the phenyl groups is unique at P2. Since the principal components of the ^{31}P CS tensors at P1 and P3 are similar, the assignment of P1 and P3 remains ambiguous.

It is worth noting that in a recent ^{31}P NMR study of a series of solid cyclic and acyclic phosphorus–metal complexes, δ_{22} was reported to be much more sensitive to the local geometry at the phosphorus atoms than δ_{11} and δ_{33} (26). Similarly, we have found evidence that the δ_{22} component of the ^{31}P chemical shift tensors in **1** is sensitive to the local orientation of the phenyl groups. However, work on ^{31}P chemical shielding in phosphine–metal complexes is just

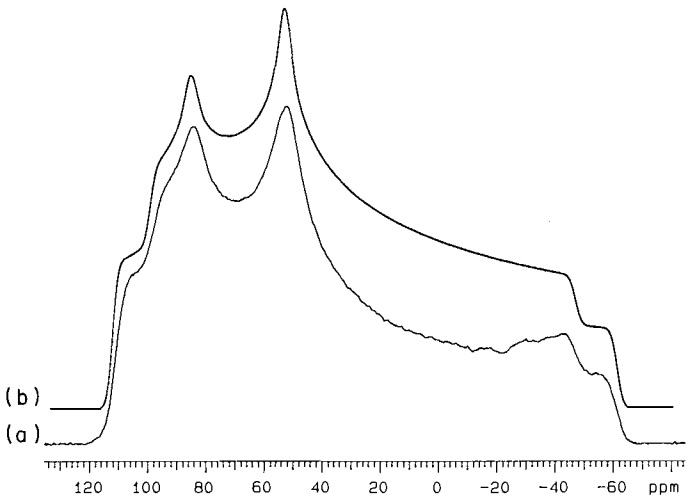

FIG. 5. (*a*) Observed static powder spectrum of **1** at B_0 = 9.40 T. (*b*) Calculated static powder line shape of **1** using the parameters listed in Table 2.

beginning and details of how the principal components of chemical shift tensors correlate with the structural parameters are still not fully understood. Therefore, our assignment must be regarded as tentative. Further investigations of phosphorus shift tensors in metal phosphine compounds are in progress in our laboratory.

Summary

We have shown that the relative intensities of the NMR transitions observed for tightly coupled spin systems in the high-resolution MAS NMR spectra of solids do not correspond to those calculated using the conventional high-resolution Hamiltonian applicable to second-order spectra in isotropic solutions. The Herzfeld–Berger method cannot be used directly to recover the principal components of a chemical shift tensor when one of the spins is a part of an AB spin system. Here, we have proposed and successfully applied a simple procedure to recover the average ^{31}P chemical shift tensors for the AB spin pair in $RhH(CO)(PPh_3)_3$. The δ_{11} and δ_{33} components are similar to those obtained for the two mutually *trans* ^{31}P nuclei in the square planar complex, $RhCl(PPh_3)_3$. The intermediate components of the ^{31}P chemical shift tensors in $RhH(CO)(PPh_3)_3$, $RhCl(PPh_3)_3$, and related compounds (26) show the largest variation with molecular structure and it is this component that is mainly responsible for variations of δ_{iso} in these compounds.

Acknowledgements

We are grateful to the Natural Sciences and Engineering Research Council of Canada for financial support. We thank Mr. Bill Kenny of Varian for making it possible for us to obtain ^{31}P NMR spectra of **1** at 9.40 T, and Dr. F. Morin, McGill University, for obtaining ^{31}P NMR spectra at 7.05 T. Finally, we thank Professors T. S. Cameron and O. Knop for helpful discussions concerning the reported X-ray results of compound **1**.

1. R. L. Pruett. Adv. Organomet. Chem. **17**, 1 (1979).
2. F. E. Paulik. Catal. Rev. **6**, 49 (1972).
3. F. H. Jardine. Polyhedron, **1**, 569 (1982).
4. (*a*) G. Yagupsky, C. K. Brown, and G. Wilkinson. J. Chem. Soc. A, 1392 (1970); (*b*) C. K. Brown and G. Wilkinson. J. Chem. Soc. A, 2753 (1970).
5. R. V. Kastrup, J. S. Merola, and A. A. Oswald. Adv. Chem. Ser. **196**, 43 (1982).
6. S. J. La Placa and J. A. Ibers. Acta. Crystallogr. **18**, 511 (1965).
7. A. Naito, D. L. Sastry, and C. A. McDowell. Chem. Phys. Lett. **115**, 19 (1985).
8. M. M. Maricq and J. S. Waugh. J. Chem. Phys. **70**, 3300 (1979).
9. J. Herzfeld and A. E. Berger. J. Chem. Phys. **73**, 6021 (1980).
10. R. K. Harris, K. J. Packer, and A. M. Thayer. J. Magn. Reson. **62**, 284 (1985).
11. N. J. Clayden, C. M. Dobson, L.-Y. Lian, and D. J. Smith. J. Magn. Reson. **69**, 476 (1986).
12. D. Fenzke, B. Maeß, and H. Pfeifer. J. Magn. Reson. **88**, 172 (1990).
13. M. H. Levitt, D. P. Raleigh, F. Creuzet, and R. G. Griffin. J. Chem. Phys. **92**, 6347 (1990).
14. H. J. M. De Groot, S. O. Smith, A. C. Kolbert, J. M. L. Courtin, C. Winkel, J. Lugtenburg, J. Herzfeld, and R. G. Griffin. J. Magn. Reson. **91**, 30 (1991).
15. P.-J. Chu, J. H. Lunsford, and D. J. Zalewski. J. Magn. Reson. **87**, 68 (1990).
16. A. Kubo and C. A. McDowell. J. Chem. Phys. **92**, 7156 (1990).
17. J. S. Frye and G. E. Maciel. J. Magn. Reson. **48**, 125 (1982).
18. C. W. Haigh. Annu. Rep. NMR Spectrosc. **4**, 311 (1971).
19. P. S. Pregosin and R. W. Kunz. *In* NMR basic principles and progress. Vol. 16. *Edited by* P. Diehl, E. Fluck, and R. Kosfeld. Springer-Verlag, Berlin. 1979.
20. J. G. Verkade and J. A. Mosbo. *In* Phosphorus-31 NMR spectroscopy in stereochemical analysis. *Edited by* J. G. Verkade and L. D. Quin. VCH Publishers Inc., Deerfield Beach, Fla. 1987.
21. E. M. Hyde, J. D. Kennedy, B. L. Shaw, and W. McFarlane. J. Chem. Soc. Dalton Trans. 1571 (1977).
22. O. R. Hughes and D. A. Young. J. Am. Chem. Soc. **103**, 6636 (1981).
23. T. Yoshida, D. L. Thorn, T. Okano, S. Otsuka, and J. A. Ibers. J. Am. Chem. Soc. **102**, 6451 (1980).
24. T. M. Duncan. A compilation of chemical shift anisotropies. The Farragut Press, Chicago. 1990.
25. C. H. Bushweller, S. Hoogasian, A. D. English, J. S. Miller, and M. Z. Lourandos. Inorg. Chem. **20**, 3448 (1981).
26. E. Lindner, R. Fawzi, H. A. Mayer, K. Eichele, and K. Pohmer. Inorg. Chem. **30**, 1102 (1991).

Can. J. Chem. Downloaded from www.nrcresearchpress.com by 92.62.229.171 on 09/08/12
For personal use only.

Modelisation de la bromation au moyen de $TBABr_3$ de matrices organiques complexes : suivi de la bromation de carbazoles à l'aide de la voltampérométrie et de la chromatographie liquide hautes performances

ANNIE DESBENE-MONVERNAY

Institut de topologie et de dynamique des systèmes, Laboratoire associé au Centre national de la recherche scientifique, Université Paris VII, 1 rue Guy de la Brosse, 75005 Paris, France

OUZAMA KARAZOUN ET JACQUES BERTHELOT

Laboratoire de Chimie Organique Structurale, Unité de recherche associée n° 455 Université P. et M. Curie, 4 Place Jussieu, 75230 Paris CÉDEX 05, France

ET

PAUL-LOUIS DESBENE[1]

Laboratoire d'analyse des systèmes organiques complexes, Université de Rouen, 43 rue Saint-Germain, 27000 Evreux, France

Reçu le 19 juin 1991

ANNIE DESBENE-MONVERNAY, OUZAMA KARAZOUN, JACQUES BERTHELOT et PAUL-LOUIS DESBENE. Can. J. Chem. **70**, 870 (1992).

En vue de déterminer le degré de substitution de matrices complexes, la bromation de différents carbazoles par le tribromure de tétrabutylammonium a été envisagée en tant que modèle de réaction de substitution. Elle nous a permis de tester la validité d'une méthode de dosage voltampérométrique des ions tribromures et des espèces libérées, les ions Br^- et H^+. Les résultats obtenus pour différents rapports substrat/réactif sont en excellent accord avec ceux obtenus en chromatographie liquide hautes performances. La technique électrochimique constitue une méthode fiable, rapide et facile à mettre en oeuvre pour suivre la cinétique de la bromation ou déterminer le degré de substitution de matrices organiques complexes.

Mots clés : bromation, tribromure de tétrabutylammonium, dosage voltampérométrique (Br_3^-, Br^-, H^+), degré de substitution.

ANNIE DESBENE-MONVERNAY, OUZAMA KARAZOUN, JACQUES BERTHELOT, and PAUL-LOUIS DESBENE. Can. J. Chem. **70**, 870 (1992).

To determine the degree of substitution of complex matrices, the bromination of various carbazoles by tetrabutylammonium tribromide has been used as a model of a substitution reaction. This has allowed us to test the validity of the voltamperometric titration of tribromide ions and species formed (Br^- and H^+ ions). The results obtained for various substrate/reagent ratios are in excellent agreement with those of high performance liquid chromatography. The electrochemical titration can be considered as reliable, fast, and very easy to use. It permits us to follow the bromination kinetics and to determine the degree of substitution of complex organic matrices.

Key words: bromination, tetrabutylammonium tribromide, voltamperometric titration (Br_3^-, Br^-, H^+), degree of substitution.

Introduction

Le tribromure de tetrabutylammonium ($TBABr_3$) a déjà été utilisé comme nouvel agent de bromation des doubles et triples liaisons (1, 2) ainsi que comme réactif pour substituer un atome de brome à un hydrogène dans les aromatiques activés (phénols (3) et amines (4)). Les avantages de $TBABr_3$ comme réactif de bromation sont nombreux : caractère non toxique et non corrosif; composé très stable à degré de brome constant; produit donnant lieu à une réaction douce, à température ordinaire.

Par ailleurs le dosage des ions Br_3^- et Br^-, mis au point dans le cas de la bromation d'alcènes (5, 6), a permis d'appréhender pour la première fois l'indice de brome d'un milieu complexe : les résidus lourds des pétroles (7).

Afin de poursuivre notre modélisation de la bromation par $TBABr_3$ de cette matrice organique complexe, l'usage de ce réactif, associé à la technique de dosage électrochimique précédemment élaborée, est maintenant appliqué à une réaction de substitution, la bromation de carbazoles, ce type de composé offrant l'avantage de présenter plusieurs sites d'attaque électrophile.

Le degré de substitution déterminé électrochimiquement est comparé avec celui obtenu en chromatographie liquide à hautes performances, technique qui permet en outre de préciser le nombre, la nature et les proportions des composés formés.

Partie expérimentale

Réactifs

Un certain nombre des composés étudiés sont des produits commerciaux utilisés directement : c'est le cas du perchlorate de tétrabutylammonium (TBAP) puriss Fluka, du bromure et du tribromure de tétrabutylammonium (TBABr et $TBABr_3$) Janssen Chimica et de l'acide perchlorique normapur 70% Prolabo. Le carbazole, le *N*-éthyl-carbazole et le *N*-éthyl, 3-carboxaldéhyde-carbazole provenant de chez Aldrich ont été recristallisés avant usage. Le *N*-méthyl, le 3-chloro, le 3-bromo, le 3,6-dibromo et le 3,6-dichloro-carbazoles ont été synthétisés selon le processus décrit dans la référence 8.

En ce qui concerne les solvants, le chloroforme Spectrosol SDS, l'acétonitrile, le nitrométhane, le diméthylformamide et le diméthylsulfoxyde, qui sont de qualité spectroscopique et pro-

[1]Auteur à qui adresser toute correspondance.

Printed in Canada

Can. J. Chem. Downloaded from www.nrcresearchpress.com by 92.62.229.171 on 09/08/12
For personal use only.

Can. J. Chem. Downloaded from www.nrcresearchpress.com by 92.62.229.171 on 09/08/12
For personal use only.

viennent de chez Aldrich, ont été utilisés sans purification ultérieure. Le carbonate de propylène Aldrich a été distillé sous vide avant usage. Enfin pour la chromatographie liquide nous avons utilisé du *n*-heptane et de l'acétate d'éthyle Chromasol SDS.

Électrochimie

L'étude voltampérométrique a été effectuée à l'aide d'électrodes à disque de Pt (diamètre = 2 mm), Au (diamètre = 5 mm) et C Vitreux (diamètre = 3 mm), de type Tacussel EM-EDI, commandées par une unité d'asservissement Contravit Tacussel et tournant à la vitesse de 500 t/min. La cellule contenant 25 mL de solvant 0,1 M en perchlorate de tétrabutylammonium comprend, outre l'électrode tournante, une grille de Pt cylindrique comme électrode auxiliaire et se trouve reliée par l'intermédiaire d'un pont électrolytique à une électrode de référence de type $Ag–Ag^+$ 10^{-2} M dans l'acétronitrile.

Les courbes *i–E* enregistrées à l'aide d'une table traçante Ifelec (IF 3802) ont été obtenues avec un potentiostat Par EGG 173 piloté par un générateur de signaux Par EGG 175.

Bromation

La bromation des composés a été réalisée à température ambiante en faisant réagir sous agitation magnétique 5 mL d'une solution de chloroforme contenant 0,5 mmol de carbazole avec 5 mL d'une solution de chloroforme 0,1 M en $TBABr_3$. Les prises d'essais, opérées à la seringue (250 μL), ont été transférées directement du mélange réactionnel dans la cellule électrochimique.

Les produits de bromation du carbazole, 3-bromo et 3,6-dibromo carbazole ont été identifiés par comparaison de leurs caractéristiques physiques (point de fusion) et spectrales (IR, RMN ^1H et masse) avec celles d'un échantillon authentique.

Chromatographie

L'analyse du milieu réctionnel a été effectuée en chromatographie de partage en phase normale sur une installation Beckman comportant deux pompes 112 gérées par un controleur modèle 421, un injecteur Altex équipé d'une boucle de 20 μL et un détecteur UV modèle 165. La séparation des carbazoles est obtenue en moins de 10 min sur une colonne de silice (300 × 4,6 mm; dp = 7 μm) avec comme phase mobile un mélange *n*-heptane/acétate d'éthyle 85 : 15, et pour un débit de 1 mL/min. La longueur d'onde de détection est fixée à 254 nm. Dans ces conditions les temps de rétention du carbazole, du 3-bromo et du 3,6 dibromo-carbazole sont respectivement de 4,8, 6,0 et 8,0 min.

Résultats et discussion

$TBABr_3$ est un agent de bromation qui peut donner lieu soit à des réactions d'addition dans le cas de composés insaturés :

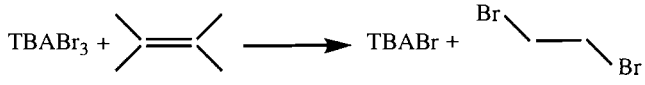

soit à des réactions de substitution sur des composés aromatiques :

$$x\ TBABr_3 + \text{substrat} \rightarrow x\ TBABr + \text{substrat bromé} + x\ HBr \quad (x \text{ fois})$$

Dans les réactions d'addition il y a libération d'un ion Br^- par double liaison ou par ion Br_3^- consommé, alors que pour les réactions de substitution il se forme deux ions Br^- pour un atome de brome fixé ou encore pour un ion tribromure disparu. De plus, dans ce dernier cas, chaque atome de brome fixé se substitue à un atome d'hydrogène entrainant l'apparition d'un proton en solution. Aussi le dosage des ions Br_3^-, Br^- et H^+ doit-il permettre de suivre la réaction de substitution lors de la bromation par $TBABr_3$ de composés aromatiques. En outre, dans le cas plus complexe d'une compétition entre les réactions d'addition et de substitution, il apparait possible d'opérer la discrimination entre ces deux types de réaction.

Étude voltampérométrique des espèces considérées

Le comportement voltamétrique en milieu organique des halogénures a été considéré depuis longtemps (9), notamment celui des ions qui nous intéressent à savoir, Br^- (10–12) et Br_3^- (11, 13). Afin d'optimiser le dosage de ces ions au sein de matrices complexes, nous avons reconsidéré leur comportement en voltamétrie stationnaire, dans plusieurs solvants organiques, en opérant avec des microélectrodes tournantes de Pt, d'Au et de C vitreux. Les courbes intensité–potentiel obtenues dans l'acétonitrile avec ces différents matériaux d'électrode sont représentées sur la figure 1 pour le bromure de tétrabutylammonium (TBABr) et le tribromure de tétrabutylammonium ($TBABr_3$). C'est avec une électrode à disque de Pt, qui présente le domaine d'électroactivité le plus étendu et le courant résiduel le plus faible, que les vagues sont les mieux définies et les processus d'oxydoréduction :

$$6\ Br^- \underset{I}{\overset{I'}{\rightleftharpoons}} 2\ Br_3^- + 4e^-$$

$$2\ Br_3^- \underset{II,II'}{\rightleftharpoons} 3\ Br_2 + 2e^-$$

les plus réversibles.

Par ailleurs la hauteur des paliers de diffusion est proportionnelle à la concentration en ion pour les différentes vagues I, II, I′ et II′. Les pentes des droites de calibration qui représentent la sensibilité *S* de la réponse de l'électrode à la concentration en espèce électroactive varient sensiblement d'un métal à l'autre (tableau 1). Le Pt offre la sensibilité maximum pour l'oxydation des ions Br^- (vagues I et II) et l'oxydation des ions Br_3^- (vague II′), tandis que l'Au est le plus favorable pour la réduction des ions tribromure (vague I′).

L'influence du solvant sur la sensibilité de la réponse en courant a été considérée uniquement dans le cas du Pt, matériau qui offre les meilleures performances. Le choix des solvants est limité du fait des conditions à remplir simultanément : conductivité élevée, caractère aprotique, domaine d'électroactivité étendu, inertie chimique vis à vis de $TBABr_3$. La nature du solvant influe sur la hauteur des paliers de diffusion, qui néanmoins varie proportionellement à la concentration en espèce électroactive dans tous les milieux considérés. La sensibilité de la réponse *S* évolue avec la viscosité (η) du solvant et s'avère maximum dans l'acétonitrile (tableau 2). Si on se réfère à l'expression du courant limite atteint en régime stationnaire :

$$i_l = \text{const} \cdot n \cdot A \cdot D^{2/3} \cdot \omega^{1/2} \cdot \nu^{-1/6} \cdot C$$

n : nombres d'électrons échangés
A : surface de l'électrode
ω : vitesse de rotation de l'électrode
D : coefficient de diffusion de l'espèce électroactive
C : concentration de l'espèce électroactive
ν : viscosité cinématique du milieu ($\nu = \eta/d$; d : densité)

En considérant *D* inversemment proportionnel à η, ce qui semble vérifié pour les ions Br^- et Br_3^-, i_l s'avère proportionnel à $\eta^{-5/6}$, ce qui est effectivement observé (fig. 2).

Par ailleurs les réactions de bromation à l'aide de $TBABr_3$

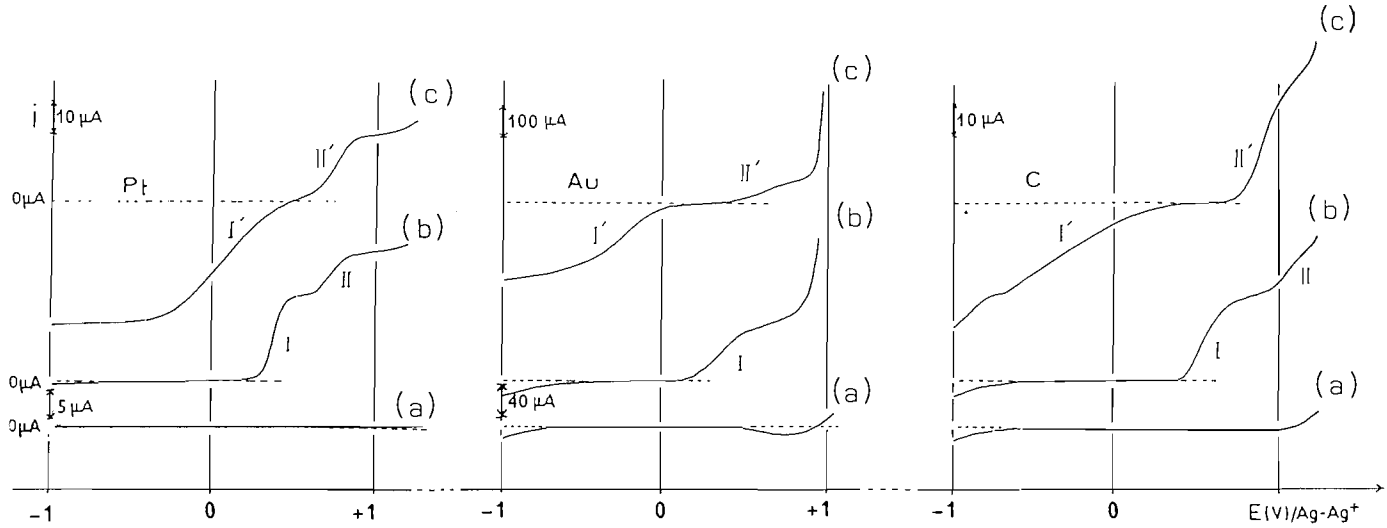

FIG. 1. Voltammogrammes obtenus sur électrode tournante à disque de Pt, Au et C vitreux en milieu CH_3CN perchlorate de tetrabutylammonium (TBAP) 0,1 M (ω = 500 t/min; V = 100 mV/s). (*a*) courbe support; (*b*) TBABr 8×10^{-4} M; (*c*) $TBABr_3$ 8×10^{-4} M.

TABLEAU 1. Pente des droites de calibration $i_D = f(\text{conc})$ pour différents matériaux d'électrode

Ion	Matériau	Pente (mA cm^{-2} $mmol^{-1}$ L)	[coefficient de régression]
Br^-		Vague I	Vague II
	Pt	0,53[0,999]	0,26[0,998]
	Au	0,36[0,999]	—
	C vitreux	0,49[0,999]	—
Br_3^-		Vague I'	Vague II'
	Pt	1,45[0,999]	0,78[0,999]
	Au	1,53[0,999]	0,38[0,995]
	C vitreux	0,53[0,997]	0,67[0,999]

sont effectuées préferentiellement dans le chloroforme, où elles sont rapides et totales. Malheureusement ce solvant de faible constante diélectrique, solubilisant mal les sels supports, est difficilement utilisable en électrochimie. Aussi avons nous considéré l'évolution de la sensibilité de la réponse d'une électrode à disque de Pt dans CH_3CN en fonction de la quantité de chloroforme ajoutée (tableau 3). On observe une décroissance linéaire de la sensibilité avec la concentration en chloroforme pour les vagues I et I'. Néanmoins en présence de 90% de $CHCl_3$ la sensibilité n'est divisée que par 2, ce qui permet des ajouts importants de mélange réactionnel dans la cellule électrochimique, sans diminution considérable du signal relatif à l'oxydation des ions Br^- et à la réduction des ions Br_3^-.

En conclusion le dosage des ions Br^- et Br_3^- présente une sensibilité optimale en milieu CH_3CN, avec une électrode de Pt. Il est à souligner que la présence d'oxygène ne modifie pas les différentes vagues considérées et que le dosage peut avoir lieu sous air. Par contre l'état de surface de l'électrode et le sens de balayage du potentiel influent de façon sensible sur l'allure, la position et la hauteur de la vague de réduction des ions tribromures et doivent être contrôlés.

En ce qui concerne les carbazoles, ils s'oxydent dans les mêmes conditions d'analyse aux environs de 1 volt, à des potentiels qui varient légèrement en fonction de leur structure (tableau 4). Le potentiel de demi-vague des carbazoles augmente dans l'ordre *N*-alkyl carbazole, carbazole, 3-halogénocarbazole, carbazoles 3,9-disubstitués et carbazoles 3,6-disubstitués, c'est à dire avec le caractère inductif accepteur du ou des substituants. L'oxydation du carbazole est représentée à titre d'exemple sur la figure 3*a*.

Quant aux protons, ils présentent une vague de réduction caractérisée par un potentiel de demi-vague de −200 mV/$Ag-Ag^+$ (Fig. 3*c*), qui se déplace vers les potentiels plus négatifs en présence d'ions tribromures. Ainsi pour les carbazoles disubstitués il est impossible d'opérer une quantification à partir du signal obtenu en réduction.

La courbe intensité–potentiel obtenue après bromation du

TABLEAU 2. Pente des droites de calibration $i_D = f(\text{conc})$ dans différents solvants

Solvant	$\epsilon^{25°C}$	$\eta^{25°C}$	Pente (μA $mmol^{-1}$ L) TBABr		[coefficient de régression] $TBABr_3$	
			Vague I	Vague II	Vague I'	Vague II'
Acétonitrile	38,0	0,37	17,5[0,999]	8,7[0,995]	40,0[0,999]	23,0[0,999]
Nitrométhane	35,9	0,67	12,5[0,999]	6,0[0,997]	30,0[0,999]	14,5[0,999]
Diméthylformamide	36,7	0,90	9,0[0,999]	—	17,5[0,999]	13,0[0,994]
Diméthylsulfoxyde	46,5	2,24	7,5[0,999]	—	12,5[0,999]	—
Carbonate de propylène	69,0	2,5	5,0[0,991]	3,0[0,991]	8,5[0,998]	7,5[0,986]

Can. J. Chem. Downloaded from www.nrcresearchpress.com by 92.62.229.171 on 09/08/12
For personal use only.

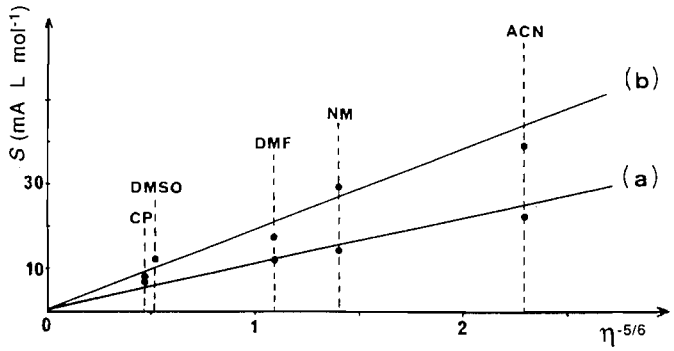

FIG. 2. Variation de la sensibilité de la réponse d'une électrode de Pt (S) à l'oxydation des ions Br^- (a) et à la réduction des ions Br_3^- (b) en fonction de la viscosité (η) du solvant.

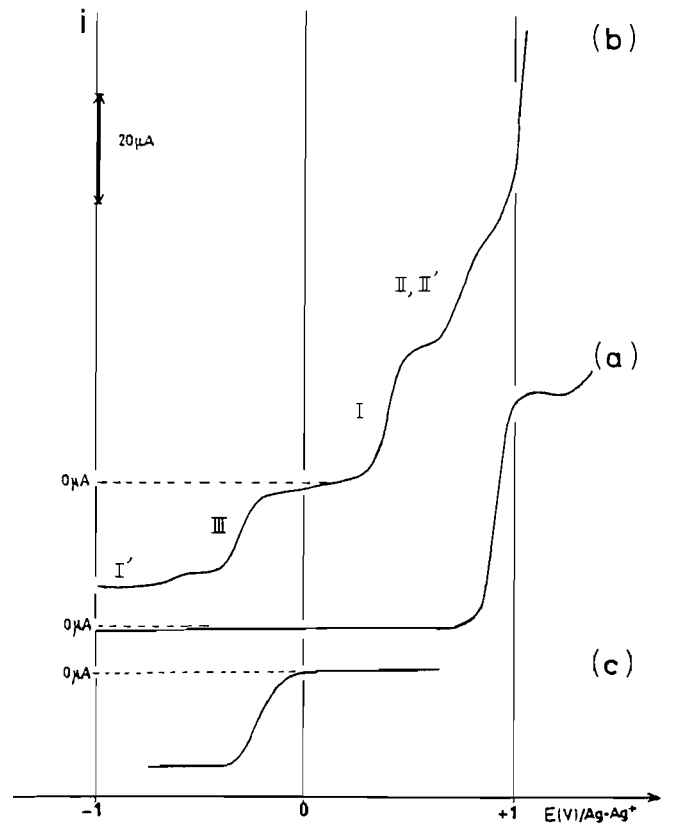

FIG. 3. Voltammogrammes obtenus sur électrode tournante à disque de Pt en milieu CH_3CN + TBAP 0,1 M (ω = 500 t/min; V = 100 mV/s). (a) carbazole $1{,}5 \times 10^{-3}$ M; (b) mélange réactionnel (carbazole 5×10^{-2} M + $TBABr_3$ 5×10^{-2} M) (250 μL) après 3 min de réaction; (c) $HClO_4$ $0{,}95 \times 10^{-3}$ M.

carbazole par $TBABr_3$ est représentée sur la figure 3*b*. L'étude voltampérométrique des différentes espèces mises en jeu permet à partir d'une telle courbe d'évaluer le degré d'avancement de la réaction de substitution d'un atome d'hydrogène par un atome de brome en exploitant : (*i*) l'évolution de la vague de réduction de Br_3^- (I'), qui diminue au fur et à mesure de la consommation du réactif $TBABr_3$; (*ii*) l'évolution de la vague d'oxydation de Br^- (I), qui augmente lors de la libération d'ions Br^- à raison de 2 Br^- formés par Br_3^- consommé; (*iii*) l'évolution de la vague de réduction des ions H^+ (III), qui sont libérés à la suite de la substitution sur le substrat d'un atome d'hydrogène par un atome de brome.

La vague située à +700 mV/Ag–Ag^+ qui résulte des vagues d'oxydation de Br_3^- (II') et de Br^- (II), s'avère moins nette pour les composés s'oxydant plus facilement, c'est à dire les carbazoles *N*-alkyl substitués. Elle peut néanmoins être utilisée pour déterminer la teneur en ions tribromure dans les cas délicats, où la vague de réduction des protons interfère avec celle des ions Br_3^-, comme c'est le cas notamment avec les carbazoles disubstitués.

Bromation des carbazoles

La bromation des carbazoles par $TBABr_3$ a été réalisée dans le chloroforme, solvant donnant des réactions rapides et complètes. Les résultats obtenus en voltampérométrie avec des carbazoles différemment substitués sont rassemblés dans le tableau 4.

En ce qui concerne le carbazole, il ressort que :

(*i*) La réaction du carbazole avec $TBABr_3$ en mélange équimoléculaire (10^{-1} M) est une réaction quasi instantanée et totale comparable à celle des amines aromatiques (4).

(*ii*) Pour deux équivalents de $TBABr_3$, la bromation est rapide mais pas tout à fait totale puisqu'il reste 13% de réactif. Une évolution se manifeste après une demi-heure, se traduisant par une diminution des concentrations en ions H^+ et Br^-, due vraisemblablement en partie à la libération de HBr dans l'atmosphère.

(*iii*) Avec 3 équivalents de $TBABr_3$ la réaction de bromation est rapide mais s'avère limitée à la fixation de deux atomes de brome par mole de substrat. On note également une diminution des pourcentages en ions H^+ et Br^- correspondant à un dégagement de HBr, par ailleurs mis en évidence par piégeage et dosage acido basique.

Pour les carbazoles substitués il s'avère que :

(*i*) La substitution de l'azote par un groupe alkyle (Me ou Et) ralentit légèrement la réaction de bromation par rapport au carbazole non substitué puisqu'après 3 min il reste encore, dans le cas du *N*-méthyl et du *N*-ethyl carbazole, respectivement 27 et 24% de tribromure qui n'a pas réagi au lieu de 6% dans le cas du carbazole. La réaction apparaît cependant totale au bout d'une demi-heure. L'attaque de Br_3^-, se faisant par les atomes de brome terminaux chargés négativement (14), est rendue plus difficile dans le cas des carbazoles *N*-alkyl substitués pour lesquels la densité électronique en position 3 est augmentée. On conçoit que, dans de telles conditions, la cinétique de bromation des *N*-alkyl carbazoles soit ralentie par rapport à celle du carbazole.

(*ii*) Avec un substituant halogène en position 3, cas du 3-chloro ou du 3-bromo carbazole, la bromation du carbazole est instantanée et complète.

(*iii*) Enfin, la disubstitution en position 3,6 (cas du 3,6-dichloro ou du 3,6-dibromo carbazole) et en position 3,9 (cas du 9-éthyl 3-formyl carbazole) limite la réaction de bromation à environ 15%.

Ce dernier résultat qui peut paraître surprenant, les carbazoles, 3,9-disubstitués conservant un hydrogène en position 6 dégagé du point de vue stérique, doit trouver son origine au niveau des densités électroniques.

On doit de plus noter que le degré de substitution calculé à partir de la concentration en protons (tableau 4 colonne 5) est généralement inférieur à celui déterminé à partir des ions Br^- (tableau 4 colonne 9) lui même inférieur à celui obtenu

Can. J. Chem. Downloaded from www.nrcresearchpress.com by 92.62.229.171 on 09/08/12
For personal use only.

TABLEAU 3. Pente des droites de calibration $i_D = f(\text{conc})$ dans différents mélanges $CH_3CN/CHCl_3$

	Pente (μA mmol^{-1} L) TBABr	[coefficient de régression]		Pente (μA mmol^{-1} L) $TBABr_3$	[coefficient de régression]
% $CHCl_3$	Vague I	Vague II	% $CHCl_3$	Vague I′	Vague II′
0	17,5[0,999]	8,7[0,995]	0	40,0[0,999]	23,0[0,999]
5	15,5[0,999]	8,0[0,994]	10	40,0[0,999]	20,0[0,999]
25	13,7[0,999]	7,4[0,993]	20	37,2[0,999]	18,8[0,999]
50	11,2[0,998]	6,5[0,998]	40	35,0[0,999]	17,5[0,999]
70	10,0[0,998]	5,4[0,995]	50	29,1[0,998]	15,0[0,998]
90	8,7[0,994]	4,4[0,989]	60	27,2[0,999]	13,7[0,999]
			70	25,2[0,999]	12,5[0,998]
			90	20,2[0,997]	10,0[0,994]

TABLEAU 4. Analyse en voltampérométrie de la bromation de carbazoles par $TBABr_3$

Composé	Potentiel de demi-vague $E_{1/2}$ (mV/Ag–Ag$^+$)	Rapport $TBABr_3$/substrat M/M	Temps (min)	Dosages des différentes espèces H^{+a} (%)	Br^{-b} (%)	Br_3^{-c} (%)	Bilan global (%)^d	Degré de substitution à partir de Br^{-e} (%)	Degré de substitution à partir de Br_3^{-f} (%)
Carbazole	900	1	3	80	170	6	91	85	94
			30	82	195	0	98	98	100
		2	3	143	298	41	190	149	159
			30	172	375	13	201	188	187
			60	152	337	13	182	169	187
		3	3	168	337	119	288	169	181
			30	193	381	98	289	191	202
			60	172	362	100	281	181	200
			120	168	350	100	275	175	200
NMe carbazole	770	1	3	73	148	27	101	74	73
			30	87	188	0	94	94	100
NEt carbazole	850	1	3	69	134	24	91	67	76
			30	89	187	0	94	94	100
3-Cl carbazole	910	1	3	96	200	2	102	100	98
			30	81	175	0	88	88	100
3-Br carbazole	920	1	3	84	166	7	90	83	93
			30	92	190	0	95	95	100
3,6-DiCl carbazole	1140	1	3	[g]	24	82[h]	94	12	18
			30	[g]	24	87[h]	99	12	13
			90	[g]	28	87[h]	101	14	13
3,6-DiBr carbazole	1150	1	3	[g]	6	82[h]	85	3	18
			30	[g]	8	82[h]	86	4	18
			90	[g]	11	82[h]	88	6	18
9-Et 3-CHO carbazole	1050	1	3	[g]	22	85[h]	96	11	15
			30	[g]	27	82[h]	96	14	18

[a] $[H^+]/[\text{Carb.}]_{\text{initiale}} \times 100$.
[b] $[Br^-]/[\text{Carb.}]_{\text{initiale}} \times 100$.
[c] $[Br_3^-]/[\text{Carb.}]_{\text{initiale}} \times 100$.
[d] $([Br^-]/2 + [Br_3^-])/[\text{Carb.}]_{\text{initiale}} \times 100$.
[e] $[Br^-]/2/[\text{Carb.}]_{\text{initiale}} \times 100$.
[f] $([Br_3^-]\text{initiale} - [Br_3^-])/[\text{Carb.}]_{\text{initiale}} \times 100$.
[g] Les vagues des ions H^+ et Br_3^- sont confondues.
[h] % déterminés à partir des vagues d'oxydation (II) et (II′).

à partir des ions tribromures (tableau 4 colonne 10). Ces écarts s'expliquent principalement par le fait que la vague de réduction des protons se situe à proximité de la vague de réduction des ions Br_3^- et en raison du dégagement de HBr.

Afin de valider les résultats de l'étude électrochimique, la bromation du carbazole non substitué à été suivie par chromatographie liquide à hautes performances. Les courbes d'étalonnage établies, en chromatographie de partage en phase normale, pour chacun des composés ont permis l'analyse quantitative du milieu réactionnel après bromation du carbazole par $TBABr_3$ et conduit, pour différents rapports molaires $TBABr_3$/carbazole, aux résultats rassemblés dans le tableau 5.

Ces résultats appellent les commentaires suivants :

(*i*) Dans le cas d'un mélange équimoléculaire, la bromation est terminée après 30 min du fait de la consommation

Can. J. Chem. Downloaded from www.nrcresearchpress.com by 92.62.229.171 on 09/08/12
For personal use only.

TABLEAU 5. Analyse en chromatographie liquide à hautes performances de la bromation du carbazole par $TBABr_3$

Rapport $TBABr_3$/carbazole M/M	Temps de réaction (min)	% des différents produits[a]			Substitution[b] (%)
		Carbazole	Bromo carbazole	Dibromo carbazole	
1/1	30	21	62	17	96
	60	20	63	17	97
2/1	30	2	4	93	190
	60	2	7	91	189
3/1	30	0	0	100	200
	60	0	0	100	200

[a] [Produit]/[carb.]$_{initiale}$ × 100.
[b] (% bromo carbazole) + (2 × % dibromo carbazole).

TABLEAU 6. Degré de substitution du carbazole déterminé par différentes techniques analytiques à l'issue de sa bromation par $TBABr_3$

$TBABr_3$/carbazole M/M	Voltampérométrie			CLHP[d]
	à partir de H^+[a]	à partir de Br^-[b]	à partir de Br_3^-[c]	
1/1	82	98	100	96
1/2	172	188	187	190
1/3	193	191	202	200

[a] [H^+]/[carb.]$_{initiale}$ × 100.
[b] 0,5 × [Br^-]/[carb.]$_{initiale}$ × 100.
[c] [Br_3^-] consommé/[carb.]$_{initiale}$ × 100.
[d] ([Bromo carb.]/[carb.]$_{initiale}$ + 2[Dibromocarb.]/[carb.]$_{initiale}$) × 100.

totale de $TBABr_3$, mais il reste 21% de carbazole. La monosubstitution s'avère majoritaire par rapport à la disubstitution. Le degré de substitution global atteint 96%, en bon accord avec ceux déterminés électrochimiquement (cf. tableau 4).

(*ii*) Pour un mélange correspondant à des proportions $TBABr_3$/carbazole égales à 2 : 1, la réaction de bromation est pratiquement complète, puisqu'il ne subsiste plus qu'une faible proportion de carbazole (2%). On observe une faible quantité de carbazole monobromé à côté du dibromocarbazole largement majoritaire. Le degré de substitution s'élève à 190%, c'est à dire à une valeur comparable à celles obtenues à l'aide du dosage électrochimique.

(*iii*) Avec un gros excès de $TBABr_3$ (3 : 1), la bromation est totale et conduit exclusivement au dibromocarbazole. Le degré de substitution atteint 200%, résultat à rapprocher de ceux calculés par la technique électrochimique à partir de la teneur du milieu réactionnel en ions Br^-, Br_3^- et H^+.

Conclusion

La bromation du carbazole par $TBABr_3$ est une réaction rapide, qui sous certaines conditions peut être totale. Elle conduit préférentiellement au dérivé monosubstitué dans le cas d'un mélange équimoléculaire et exclusivement au composé disubstitué en présence d'un excès égal ou supérieur à deux équivalents de $TBABr_3$. Les atomes de brome se fixent en positions 3 et 6, reconnues depuis longtemps comme étant les plus réactives. En effet les densités électroniques sur le noyau carbazolyle calculées à l'aide des coefficients (C^2) des orbitales atomiques obtenues à partir de la théorie de Hückel (15) indiquent que les sites réactifs sont les positions 1, 3, 6, 8 et 9.

Il est à noter que les positions 1 et 8 sont défavorisées stériquement. Quant à l'azote il doit être protoné par les H^+ libérés par la réaction de substitution. Ces deux remarques expliquent que la substitution se limite à deux atomes de brome fixés en positions 3 et 6 sur la molécule de carbazole.

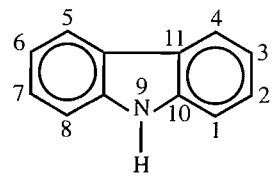

1	0,133
2	0,001
3	0,118
4	0,073
9	0,202
10	0,051
11	0,024

En présence d'un halogène en position 3, la réaction de substitution est également instantanée et totale alors qu'elle se trouve ralentie du fait de l'existence d'un groupement alkyle sur l'azote.

Pour les dérivés disubstitués son rendement diminue et s'annule quasiment lorsque les positions 3 et 6 ne sont pas disponibles, ce qui confirme que ces pôles 3 et 6 sont bien les sites de la substitution électrophile.

D'un point de vue analytique on note un bon accord entre l'analyse en chromatographie liquide et les différentes possibilités offertes par les dosages voltampérométriques pour la détermination du degré de substitution (cf. tableau 6). La technique électrochimique ne donne pas d'indication sur les produits formés. Elle ne différencie pas la mono, la di, la trisubstitution et ne précise pas les sites réactionnels. Néanmoins elle permet de suivre facilement le degré d'avancement de la réaction de bromation par $TBABr_3$ et de faire rapidement un bilan global de la substitution. Rappelons également qu'elle est apte à discriminer entre réaction d'addition et de substitution. Aussi cette approche simple, d'application générale, semble particulièrement appropriée au cas des matrices complexes pour lesquelles les constituants exacts ne sont pas connus et qui ne peuvent donner lieu qu'à un bilan global.

On se propose donc d'appliquer cette méthode fiable,

Can. J. Chem. Downloaded from www.nrcresearchpress.com by 92.62.229.171 on 09/08/12
For personal use only.

rapide et facile à mettre en oeuvre, que constitue la réaction de bromation par $TBABr_3$ associée au dosage voltampérométrique des ions Br_3^- et Br^-, à des cas plus complexes : composés donnant lieu à la fois à des réactions d'addition et de substitution, composés se trouvant au sein de matrices complexes, dans la mesure où celles-ci ne donnent pas de vagues d'oxydo-réduction dans le domaine de potentiel [−1 V; +1 V], films polymères, dérivés notamment du carbazole, pour préciser, à partir du degré de substitution, leur état de réticulation.

1. M. Fournier, F. Fournier et J. Berthelot. Bull. Soc. Chim. Belg. **93**, 157 (1984).
2. J. Berthelot et M. Fournier. Can. J. Chem. **64**, 603 (1986).
3. J. Berthelot, C. Guette, M. Ouchefoun, P-L. Desbene et J-J. Basselier. J. Chem. Res. 381 (1986).
4. J. Berthelot, C. Guette, M. Essayegh, P-L. Desbene et J-J. Basselier. Synth. Commun. **16**, 1641 (1986).
5. A. Desbene-Monvernay, J. Berthelot et P-L. Desbene. J. Chem. Educ. **64**, 86 (1987).
6. J. Berthelot, J-J. Basselier, P-L. Desbene et A. Desbene-Monvernay. Analusis, **15**, 22 (1987).
7. P-L. Desbene, J. Berthelot, M. Ouchefoun, C. Guette, J-J. Basselier, R. Boulet et A. Desbene-Monvernay. Talanta, **34**, 645 (1987).
8. J. F. Ambrose, L. L. Carpenter et R. F. Nelson. J. Electrochem. Soc. **122**, 876 (1975).
9. C. K. Mann et K. K. Barnes (*Éditeurs*). *Dans* Electrochemical reactions in nonaqueous systems. Marcel Dekker, New York. 1970. pp. 498–508.
10. I. M. Kolthoff et J. F. Coetzee. J. Am. Chem. Soc. **79**, 1852 (1957).
11. A. I. Popov et D. H. Geske. J. Am. Chem. Soc. **80**, 5346 (1958).
12. H. E. Zittel et F. J. Miller. Anal. Chim. Acta, **37**, 141 (1967).
13. M. C. Cheney et K. S. Fletcher. Anal. Chem. **51**, 807 (1979).
14. J. Berthelot, C. Guette, P-L. Desbene, J-J. Basselier, P. Chaquin et D. Masure. Can. J. Chem. **68**, 464 (1990).
15. J. F. Ambrose et R. F. Nelson. J. Electrochem. Soc. **115**, 1159 (1968).

Can. J. Chem. Downloaded from www.nrcresearchpress.com by 92.62.229.171 on 09/08/12
For personal use only.

A stability and equilibrium study on Cd – salicylidene tris(hydroxymethyl) methylamine – chloride binary and ternary complexes

REFAT ABDEL-HAMID[1] AND MOHAMED T. EL-HATY[2]
Department of Chemistry, Faculty of Science, Sohag, Egypt

Received June 19, 1991

REFAT ABDEL-HAMID and MOHAMED T. EL-HATY. Can. J. Chem. **70**, 877 (1992).

Binary and ternary complexes of Cd(II) with salicylidene tris(hydroxymethyl) methylamine and chloride ion at 298 K were studied polarographically at I = 0.1 mol dm^{-3} $NaClO_4$ in 30% (v/v) DMF – aqueous medium at pH 10.2. The overall formation constants were found to be, for the binary system, log β_1 = 3.55 ± 0.03 and log β_2 = 5.40 ± 0.07 and, for the ternary one, log β_{11} = 7.64 ± 0.06 and log β_{12} = 9.56 ± 0.06.

Key words: formation constants, binary and ternary complexes of Cd(II).

REFAT ABDEL-HAMID et MOHAMED T. EL-HATY. Can. J. Chem. **70**, 877 (1992).

Faisant appel à la polarographie et opérant à 298 K, à un pH de 10,2, à I = 0,1 mol dm^{-3} de $NaClO_4$, dans un milieu à 30% (v/v) de DMF/eau, on a étudié les complexes binaires et ternaires du Cd(II) avec le salicylidène tris(hydroxyméthyl) méthylamine et l'ion chlorure. On a trouvé que les constantes globales de formation du système binaire sont log β_1 = 3,55 ± 0,03 et log β_2 = 5,40 ± 0,07 alors que celles du système ternaire sont log β_{11} = 7,64 ± 0,06 et log β_{12} = 9,56 ± 0,06.

Mots clés : constantes de formation, complexes binaires et ternaire du Cd(II).

[Traduit par la rédaction]

Introduction

In view of the confusing results of Sreenivasulu *et al.* (1) for the cadmium(II) – salicylidene tris(hydroxymethyl) methylamine binary system in different supporting electrolytes it was thought worthwhile to undertake a further polarographic study of these complexes using a more sophisticated computerized analysis (2) for the estimation of the stability constants. The investigation was extended to include a study of ternary complexes of Cd(II) with the title Schiff base and chloride.

Experimental

Salicylidene tris(hydroxymethyl) methylamine was synthesized following the method described elsewhere (3), and purified by repeated crystallization from methanol or ethanol (mp 134°C). The results of the elemental microanalysis of the compound were in agreement with its structure ($C_{11}H_{15}O_4N$; calcd.(found)%: C 58.66(58.72), H 6.71(6.60), N 6.22(6.31)).

All reagents used were of analytical (B.D.H. or Merck) grade. Fresh 0.10 mol dm^{-3} $NaClO_4$/30% dimethylformamide – aqueous stock solution was prepared by dissolving sodium perchlorate in carbon dioxide free bidistilled water. Fresh Schiff base stock solution (2.00 mol dm^{-3}) was prepared from the fresh electrolyte solution (0.10 mol dm^{-3} $NaClO_4$) on the same day that measurements were performed. The stock solution (0.10 mol dm^{-3}) of cadmium(II) was prepared using cadmium chloride, and standardized (4).

All experiments were performed in 30%(v/v) dimethylformamide – aqueous medium at 298 K. A 0.01% Triton-X100 was used as a maximum suppressor.

DC and cyclic polarograms were performed using an EG & G PAR model 364A polarographic analyzer. The measurements were carried out using a conventional three-electrode configuration. An EG & G PAR model SMDE 303 mercury-drop system in small dropping mode was used as working electrode. The electrode area was 1.05 mm^2. The reference electrode was a $Ag/AgNO_3$ (0.01 mol dm^{-3}) electrode in 0.10 mol dm^{-9} sodium perchlorate/30%(v/v) dimethylformamide – aqueous solution. A 1.0 cm^2 platinum sheet auxilliary electrode was used throughout. Solutions were purged with pure nitrogen before measurements and an atmosphere of nitrogen was maintained above the working solution.

Calculations were performed using the POLAG computer program on a CROMEMCO CS 500 computer.

Results and discussion

The most common method of extracting stability constants from polarographic data is that of DeFord and Hume (5, 6). The method is based on the following equations:

$$[1] \quad F = \exp\left[nF/RT\,(E_{1/2(s)} - E_{1/2(c)})\right] + \ln\,(I_{ds}/I_{dc})$$

$$[2] \quad F = 1 + C_L\beta_1 + C_L^2\beta_2 + \ldots C_L^n\beta_N$$

where $E_{1/2(s)}$ and $E_{1/2(c)}$ are the half-wave potentials for the uncomplexed and complexed metal ion, respectively, I_{ds} and I_{dc} are the diffusion currents of the uncomplexed and complexed metal ion, C_L is the analytical concentration of the ligand, and β_N is the overall stability constant of the Nth complex.

If a second ligand is present, the method of Schaap and McMasters (7, 8) is used.

POLAG is a nonlinear least-squares iterative program that seeks to minimize U, the sum of squares of the residual, i.e.,

$$[3] \quad U = \sum_{1}^{K} (F_{calc} - F_{obs})^2$$

where K is the number of data points; F_{obs} is given by eq. [1] and represents the experimental data; F_{calc} is obtained from eq. [2].

A solution of 1.0 mmol dm^{-3} cadmium(II) in 0.10 mol dm^{-3} $NaClO_4$/30% dimethylformamide – aqueous medium exhibits a reversible cyclic voltammetric two-electron diffusion-controlled wave at a peak current potential, E_p, of 0.586 volt versus Ag/Ag^+. The reduction of Cd(II) binary and ternary complexes of the system under investigation in the pH range 7–12 gives a cyclic voltammetric two-electron reversible diffusion-controlled wave as revealed from the

[1]Author to whom correspondence may be addressed.
[2]Department of Chemistry, Faculty of Science, Aswan, Egypt.

Can. J. Chem. Downloaded from www.nrcresearchpress.com by 92.62.229.171 on 09/08/12
For personal use only.

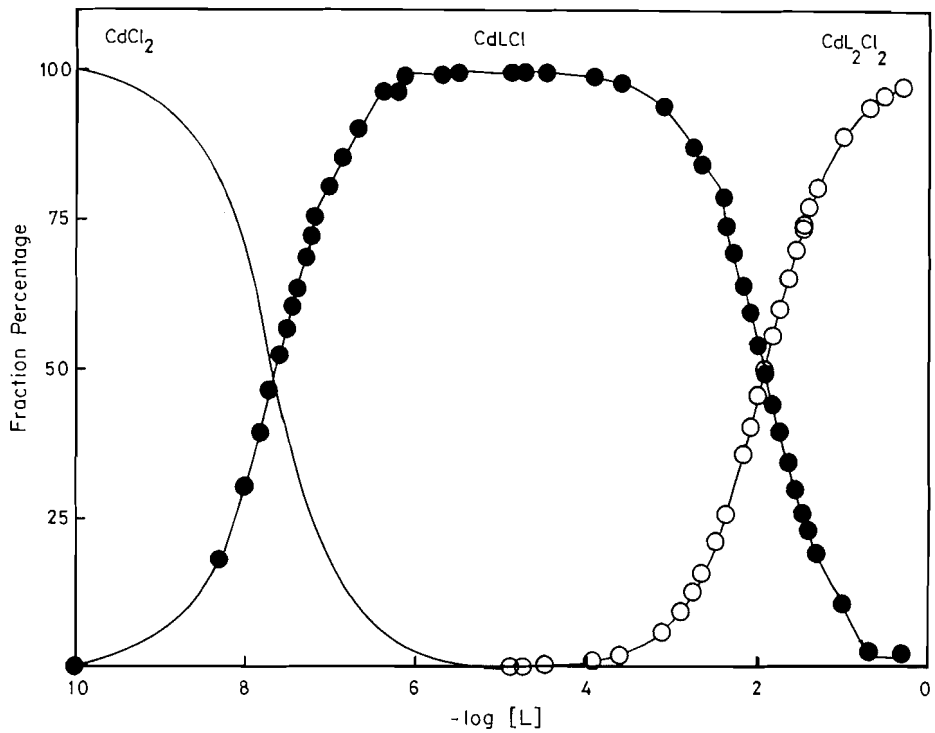

FIG. 1. Distribution diagram for the ternary system.

TABLE 1. Cyclic voltammetric data for Cd(II) – Schiff base binary system in 0.1 mol dm^{-3} $NaClO_4$/30%(v/v) DMF – aqueous medium at pH 10.2, [Cd(II)] = 1.0 mmol dm^{-3}, [Schiff base] = 0.05 mol dm^{-3}

Scan rate (mV s^{-1})	$-E_p^c$ (V)	$-E_p^a$ (V)	i_p^c (μA)	$E_p - E_{p/2}$ (mV)	i_p^a/i_p^c
20	0.704	0.674	5.85	28.0	1.00
50	0.702	0.676	6.70	28.5	1.02
100	0.705	0.672	7.66	29.0	0.98
200	0.706	0.673	9.01	29.0	0.96
500	0.706	0.677	11.70	29.5	0.98

cyclic voltammetric data obtained (cf. Table 1). These anodic and cathodic peak current potentials, E_p^a and E_p^c, were independent of scan rate (9), $E_p^a - E_p^c$ and $E_p - E_{p/2}$ were 30 ± 2 and 29 ± 2 mV, respectively, and the anodic to cathodic peak current ratio, i_p^a/i_p^c, approaches unity. The diffusion-controlled nature is confirmed by the linear dependence of the peak current, i_p^c, on the square root of the scan rate, $\nu^{1/2}$.

Binary system

The stability constants of binary complexes of Cd(II) with the title Schiff base were evaluated separately prior to those of the ternary complexes. Identical conditions were maintained in both binary and ternary systems.

A plot of $-E_{1/2}$ versus log C (logarithm of concentration of the Schiff base) gives a smooth curve, suggesting the formation of overlapping complexes. The POLAG computer program data suggest that the most likely model corresponds to the presence of ML and ML_2 species with overall stability constants, log β, of 3.55 ± 0.03 and 5.40 ± 0.07, respectively. These values are in good agreement with those previously reported for this system (1).

TABLE 2. DC polarographic data for the Cd(II) – Schiff base binary and ternary systems in 0.1 mol dm^{-3} $NaClO_4$/30%(v/v) DMF – aqueous medium at pH 10.2, [Cd(II)] = 1.0 mmol dm^{-3}

Binary system			Ternary system	
[Ligand] (mol dm^{-3})	$-E_{1/2}$ (V)	i_d (μA)	$-E_{1/2}$ (V) [KCl] = 0.1 mol dm^{-3}	i_d (μA) [KCl] = 0.1 mol dm^{-3}
0.00	0.586	6.25	0.600	6.22
0.02	0.657	6.23	0.740	6.20
0.03	0.659	6.17	0.741	6.20
0.04	0.660	5.95	0.742	6.19
0.05	0.662	5.86	0.744	5.91
0.06	0.667	5.79	0.746	5.84
0.08	0.692	5.76	0.751	5.40
0.10	0.692	5.53	0.757	5.30
0.20	0.705	5.22	0.770	5.10
0.40	0.716	4.68	0.782	3.82
0.60	0.725	3.44	0.791	3.43
0.80	0.728	2.54	0.796	2.77
1.00	0.733	2.02	0.799	2.10

Ternary system

The ternary system was studied by keeping the concentration of the weaker ligand (chloride) constant (0.1 mol dm^{-3}) while varying the concentration of the subject Schiff base (cf. Table 2).The shift in the half-wave potentials is greater in the presence of chloride than in its absence, indicative of formation of a mixed ligand complex. From the data obtained, the most likely model shows the presence of both CdLCl and $CdLCl_2$ with stability constants, log β_{11} = 7.64 ± 0.06 and log β_{12} = 9.56 ± 0.06, respectively.

A typical species-distribution graph for the ternary system is shown in Fig. 1.

Can. J. Chem. Downloaded from www.nrcresearchpress.com by 92.62.229.171 on 09/08/12
For personal use only.

Acknowledgment

The authors are grateful to Prof. D. J. Leggett, Department of Chemistry, University of Houston, Houston, Texas, for providing us with a copy of the POLAG program.

1. R. Sreenivasulu, V. S. Ragnavendra Rao, and J. Sreeramulu. J. Electrochem. Soc. India, **36**, 131 (1987).
2. D. J. Leggett. Talanta, **27**, 787 (1980).
3. S. C. Rustagi and G. N. Rao. Indian J. Chem. **13**, 702 (1975).
4. A. I. Vogel. A text book of qualitative inorganic analysis, including elementary instrumental analysis. Longman, London. 1978.
5. D. D. DeFord and D. V. Hume. J. Am. Chem. Soc. **73**, 5321 (1951).
6. D. N. Hume, D. D. DeFord, and G. C. B. Cave. J. Am. Chem. Soc. **73**, 5323 (1951).
7. D. L. McMasters and W. B. Schaap. Proc. Indiana Acad. Sci. **67**, 111 (1958).
8. W. B. Schaap and D. L. McMasters. J. Am. Chem. Soc. **83**, 4699 (1961).
9. R. S. Nicholson and I. Shain. Anal. Chem. **36**, 706 (1964).

Can. J. Chem. Downloaded from www.nrcresearchpress.com by 92.62.229.171 on 09/08/12
For personal use only.

Studies of the effect of hydrogen bonding on the absorption and fluorescence spectra of all-*trans*-retinal at room temperature

S. ALEX, H. LE THANH, AND D. VOCELLE[1]

Département de chimie, Université du Québec à Montréal, C.P. 8888, Succ. A, Montréal (Québec), Canada H3C 3P8

Received June 18, 1991

S. ALEX, H. LE THANH, and D. VOCELLE. Can. J. Chem. **70**, 880 (1992).

Ultraviolet (UV)–visible and fluorescence spectra were obtained for complexes of ATR and TFA at different ratios and in four different solvents: hexane, chloroform, dichloromethane, and methanol. In the first three solvents, a large excess of TFA generates retinylic cations that absorb from 459 to 600 nm. Also, in $CHCl_3$, Raman spectroscopy and fluorescence indicate that some aggregated species like ATR:$(TFA)_n$, with a λ_{max} of ca. 470 nm, are present. In methanol, TFA protonates the solvent and it is $CH_3O^+H_2$ which interacts with ATR so that only blue-shifted H-bonded ATR is present. From these results, it is shown that in the tautomeric equilibrium C=O. . .HOOC-(1) ⇋ C=O$^+$H. . .$^-$O$_2$C-(2), form (1) is always favored in the ground state whatever the solvent. In the excited state in hexane and in methanol, (1) is rapidly transformed into (2). In CH_2Cl_2 and $CHCl_3$, this transformation is absent so that there is no energy dissipation, with the result that the retinal complexes become more unstable.

Key words: all-*trans*-retinal, fluorescence, H-bonds, trifluoroacetic acid, UV–vis spectroscopy.

S. ALEX, H. LE THANH et D. VOCELLE. Can. J. Chem. **70**, 880 (1992).

Les spectres UV–visible et de fluorescence ont été obtenus pour des complexes d'ATR et de TFA à des concentrations variées et dans quatre solvants différents : l'hexane, le chloroforme, le dichlorométhane et le méthanol. Dans les trois premiers solvants, un grand excès de TFA génère des cations rétinyliques qui absorbent de 459 à 600 nm. Aussi, dans le $CHCl_3$ la spectroscopie Raman et la fluorescence indiquent que des espèces associées du genre ATR : $(TFA)_n$ sont présentes. Dans le méthanol, TFA protonne le solvant et c'est $CH_3O^+H_2$ qui interagit avec ATR de telle sorte que seulement de l'ATR lié par des liaisons hydrogènes et absorbant dans le bleu, est présent. De ceci, il est démontré que dans l'équilibre tautomérique C=O. . .HOOC-(1) ⇋ C=O$^+$H. . .$^-$O$_2$C-(2), la forme (1) est toujours privilégiée dans l'état fondamental quel que soit le solvant. Dans l'hexane et le méthanol, dans l'état excité, (1) se transforme rapidement en (2). Dans le CH_2Cl_2 et $CHCl_3$, cette dernière transformation est absente ce qui empêche la dissipation de l'énergie absorbée avec pour conséquence de rendre les complexes de rétinal plus instables.

Mots clés : rétinal tout *trans*, fluorescence, liaisons hydrogènes, acide trifluoroacétique, spectroscopie UV–visible.

Introduction

This paper relates to room-temperature absorption and fluorescence spectra of H-bonded all-*trans*-retinal (see formula below), a polyene aldehyde of photochemical interest in the field of vision (1, 2, and refs. cited therein).

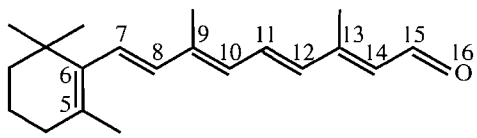

It is also important because of the unique properties of the electronic excited states of polyene analogs (1–9), properties that have often been used by nature in pigments (1, 2). For many years, the excited singlet state manifold of retinal has provided a challenging system because it can occupy three low-lying states (viz. $^1B_u^+$, $^1A_g^-$, and $^1n\pi^*$), which are very close in energy (1, 5, 8). Generally speaking, it is admitted now that the strongly allowed $^1B_u^+$–^1A_g and the weaker $^1n\pi^*$ electronic transition required a higher energy than the symmetry forbidden $^1A_g^-$–^1A_g electronic transition (1, 4, 8, 9). However, there are examples to demonstrate that this relative level ordering is dependent on the solvent, the temperature, and the conformation of retinal (3–6), these conferring on this molecule unusual fluorescence properties (10–12).

Hydrogen-bonding interactions between an acid such as trifluoroacetic acid (TFA hereafter) and all-*trans*-retinal (ATR hereafter) can be of different types depending on the polarity of the solvents in which the systems are studied and may lead to a simple hydrogen bond or (and) a hydrogen-bonded ion pair (13–15). In other words, this can be summarized by the following tautomeric equilibrium (eq. [1]) between a hydrogen-bonded and a proton transfer complex, written using a symbolic notation as:

$$\underset{\text{(hydrogen-bonded complex)}}{C{=}O\ldots HOOC} \rightleftharpoons \underset{\text{(hydrogen-bonded ion pair)}}{C{=}OH^+\ldots {}^-OOC} \quad [1]$$

In general, the potential representing the motion of the proton betwen the C=O and the $^-$OOC ends is unsymmetrical and is regulated by two minima (14). The proton populations of these two minima are determined by the acid and base strength of the proton donor and acceptor, the polarity of the medium, and by other factors such as the specific solvation of the species, etc. (14, 15). In addition, these molecules are generally differently H-bonded in the ground and in the excited states and it is believed that the nature of these H-bonds may govern their photochemical behavior.

To determine the exact nature of these H-bonds in the ground and excited states, the absorption and emission spectra of all-*trans*-retinal mixed with increasing amounts of TFA were measured in various solvents. This study was carried out at room temperature rather than at low temperatures in order to provide a model system that can be used to understand the photochemistry of Schiff bases in visual and bacterial pigments. Also, at this temperature, one can take advantage of the fact that all-*trans*-retinal does not fluoresce unless it is strongly hydrogen-bonded (10, 11) or aggregated (16).

[1]Author to whom correspondence may be addressed.

Can. J. Chem. Downloaded from www.nrcresearchpress.com by 92.62.229.171 on 09/08/12
For personal use only.

Can. J. Chem. Downloaded from www.nrcresearchpress.com by 92.62.229.171 on 09/08/12
For personal use only.

Materials and methods

All-*trans*-retinal was purchased from Aldrich Chemical Company (Milwaukee, Wis.) and used without further purification. All solvents were spectrograde (Fisher-Canada, Ont.) and were dried over molecular sieves. The formation of the hydrogen-bonded system was carried out by simply adding the desired amount of trifluoroacetic acid (Aldrich Chemical Company) to the stock solution of all-*trans*-retinal dissolved in the proper solvent. In this work, the simple association of hydrogen with the oxygen of the C=O link in eq. [1] (viz. C=O + HOOC $\leftrightharpoons$ C=O . . .HOOC) was not considered, its association constant K being 5000 M^{-1} in hexane (K has been calculated using the Chignell and Gratzer approach (13)). It is worth noting that this reaction is complete as in similar H-bonded Schiff bases (17). This was one reason to select TFA (pK_a = 0.23 in water) since the association ability abides by a linear relationship to the pK_a of the H-bonder in both states (2, 9). ATR:TFA complexes with a molecular ratio ranging from 1:1 to 1:∞ were made and tested in four solvents, which were hexane (C_6H_{14}, dielectric constant D = 1.89), chloroform ($CHCl_3$, D = 4.81), dichloromethane (CH_2Cl_2, D = 9.08), and methanol (MeOH, D = 32.80). The initial ATR concentration selected was in the range of $2 \times 10^{-5} - 2 \times 10^{-4}$ M for UV measurements and about ten times more dilute for emission measurements. It should be noted that a phase separation occurred between hexane and TFA for large concentrations of the latter, therefore measurements reported here correspond only to the organic phase. No fluorescence is detected in chloroform and dichloromethane if the starting ATR concentration is below ca. 10^{-5} M and in these solvents the complexes form aggregates and (or) carbocations. Time-resolved fluorescence experiments were also done for an ATR:TFA molecular ratio equal to 1:50 and in the same four solvents using a 45° illumination–collection geometry and an average accumulation time of 2 h. Raman spectra of these compounds were collected using a 488 nm excitation wavelength in order to take advantage of the preresonance effect.

The absorption spectra were collected on a Cary 2200 UV–visible spectrometer set at a 2-nm resolution. The fluorescence measurements were acquired on a Perkin–Elmer MPF-44 fluoremeter using a 8 nm bandpass slit. The spectra were not corrected for the spectral response of the detection system. The fluorescence lifetime of retinal complexes was measured using Photochemical Research Associates Inc. International model 3000 fluorescence lifetime, single photon counting equipment (PRA, London, Ont.). The excitation light was generated by nitrogen flash lamp PRA model 510. Fluorescence excitation and emission were detected using appropriate band pass interference filters. Data were analyzed by a PRA statistical deconvolution program. The Raman spectra were recorded on a Spex Triplemate spectrograph coupled to an EG & G Princeton Applied Research detector, model 1422, and samples were excited with 20 mW of the 488.8 nm laser line (Spectra-Physics CW Ar^+ laser, model 2016). The sealed capillary was mounted on a thermally regulated sample holder and maintained at a temperature of 5°C. The spectra were recorded with a 5 cm^{-1} slit width during 15 min. The ATR concentration used for these experiments was ca. 10^{-4} M.

Results and discussion

UV–visible

UV–visible spectra were obtained for complexes of ATR and TFA at different ratios. The spectra of these products were collected in four different solvents and the electronic transition positions are quoted, *vide supra,* in Figs. 1 and 2. Depending on the nature of the solvent, the complexes are differently affected by the hydrogen-bonding agent TFA. Two types of results are noted: (*i*) those obtained in hexane and in methanol where the maximum of the absorption band

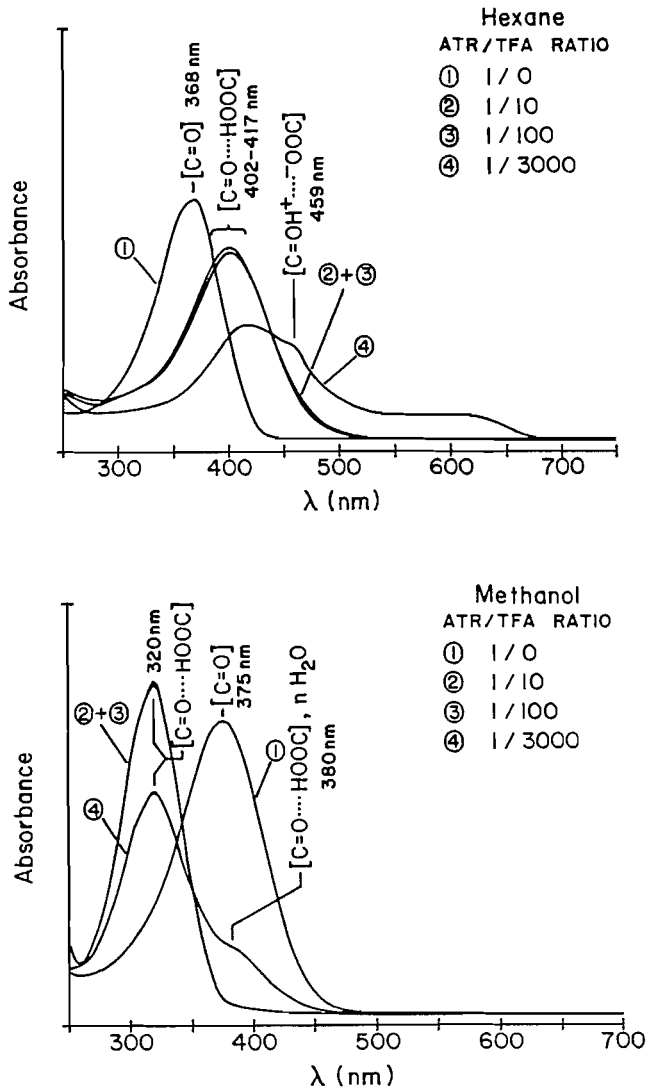

FIG. 1. UV–visible spectra of all-*trans*-retinal (2×10^{-4} M) mixed with various quantities of trifluoroacetic acid in hexane and methanol.

is shifted and the absorbance modified while these two parameters remain almost independent of the TFA quantity over a wide range of concentrations (see Fig. 1); (*ii*) those obtained in dichloromethane and chloroform where the maximum of the absorption band is also shifted and the absorbance modified but these are a direct function of the TFA concentration (Fig. 2).

In hexane and methanol solutions, both the π–π^* and the n–π^* transitions of ATR appear as one band, which is centered at ca. 368 nm in hexane and 375 nm in methanol (see Fig. 1). In hexane solutions, upon addition of TFA in ratios of 1:10–1:100 (Fig. 1), the band is red shifted to 402–417 nm. This band must be due to some H-bonded complexes of ATR and TFA and the shift is explained by a better stabilization of the π^* excited state. When a very large excess of TFA is used (1:3000), Fig. 1 shows that the spectrum is now composed of at least two bands, the first one being ca. 417 nm with an apparent shoulder at 459 nm and the second appearing at ca. 600 nm. The band at 417 nm is attributed to ATR–TFA complexes as previ-

Can. J. Chem. Downloaded from www.nrcresearchpress.com by 92.62.229.171 on 09/08/12
For personal use only.

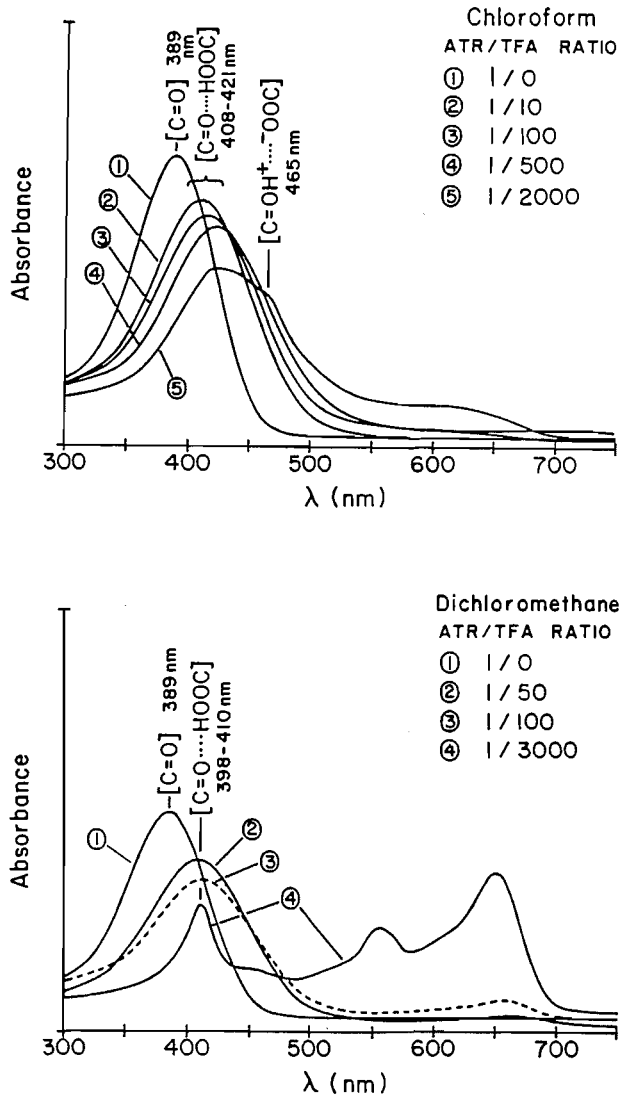

FIG. 2. UV–visible spectra of all-*trans*-retinal (2×10^{-4} M) mixed with various quantities of trifluoroacetic acid in chloroform and dichloromethane.

ously indicated, while the others at ca. 459 and ca. 600 nm must be due to protonated forms of ATR. In the 600-nm region, the spectra obtained here show a close resemblance to those acquired by Blatz *et al.* (18, 19) using retinol and acids. Hence, the spectral features are assigned to cationic forms of retinal since Blatz *et al.* (18, 19) invoked the presence of retinylic cations to explain the bands at ca. 600 nm (viz.: C=C—C=C—$\overset{+}{C}$H$_2$). In the present study, it is possible to obtain two kinds of charged species. First, by simple protonation of the retinal carboxyl function as indicated in eq. [2] and previously in eq. [1], where Ret indicates the polyenic part of retinal:

$$\text{Ret—CHO} + \text{HO}_2\text{CCF}_3 \rightleftharpoons \text{Ret—}\overset{\text{H}}{\underset{|}{\text{C}}}\text{=}\overset{+}{\text{O}}\text{H}\cdots{}^{-}\text{O}_2\text{CCF}_3 \quad [2]$$

$$\text{other resonance forms} \longleftrightarrow \text{Ret—}\overset{\text{H}}{\underset{|}{\overset{|}{\underset{+}{\text{C}}}}}\text{—OH}\cdots{}^{-}\text{O}_2\text{CCF}_3$$

Being in hexane, the counterion must remain close to the retinylic carbocation and thus forms an ion pair that absorbs at ca. 459 nm, as seen with protonated Schiff bases (17).

The second form of protonated retinal could come from a reaction of protonated retinal with a trifluoroacetate anion as shown in eq. [3].

$$\text{Ret—}\overset{\text{H}}{\underset{|}{\text{C}}}\text{=}\overset{+}{\text{O}}\text{H} + {}^{-}\text{O}_2\text{CCF}_3 \rightleftharpoons \left[\text{Ret—}\overset{\text{H}}{\underset{|}{\overset{|}{\text{C}}}}\text{—O}_2\text{CCF}_3 \atop \text{OH}\right]$$

$$\Big\Updownarrow \text{TFA} \qquad [3]$$

$$\text{Ret—}\overset{\text{H}}{\underset{+}{\overset{|}{\text{C}}}}\text{—O}_2\text{CCF}_3 \rightleftharpoons \left[\text{Ret—}\overset{\text{H}}{\underset{|}{\overset{|}{\text{C}}}}\text{—O}_2\text{CCF}_3 \atop \overset{+}{\text{O}}\text{H}_2\right]$$

$$\Big\Updownarrow$$

other resonance forms

This of course follows the same line of reasoning used by Blatz *et al.* (18), who advocated the following reaction (eq. [4]):

$$\text{Ret—CH}_2\text{OH} + \text{HO}_2\text{C-} \rightleftharpoons \text{Ret—}\overset{+}{\text{C}}\text{H}_2\text{OH}_2\cdots{}^{-}\text{O}_2\text{C-} \quad [4]$$

$$\Big\downarrow$$

$$\text{Ret—}\overset{+}{\text{C}}\text{H}_2\cdots{}^{-}\text{O}_2\text{C-}$$

Hence, a species like Ret—$\overset{+}{\text{C}}$H—O_2CCF_3 could also absorb at ca. 600 nm since it is structurally close to Ret—CH_2^{+}. . .$^{-}$O$_2$C-. It does not preclude the possibility that the bands at 459 and 600 nm could belong to the same entity. However, if this was indeed the case, the fluorescence results (see below) would be difficult to explain. As indicated in Materials and methods, there is a phase separation occurring at such a high ratio of TFA and the spectrum was taken in the phase containing ATR, TFA, and hexane.

In methanol, with ratios of 1:10 and 1:100, the ATR:TFA systems present a band at 320 nm (Fig. 1) that is blue-shifted relative to the 375-nm band of ATR. This band must represent some H-bonded ATR complexes, but of a different kind since it is blue-shifted. Since the hydroxyl function is a better acceptor than the oxygen of the carbonyl group, methanol must be partly protonated by TFA. This protonated methanol ($\text{CH}_3\text{O}^{+}\text{H}_2$) could then form effective H-bonds with ATR (viz.: Ret—CHO. . .H$_2^{+}$OCH$_3$). Papanikolas *et al.* (9) noted a similar blue-shifted system in using decatetraenal hydrogen-bonded to hexafluoroisopropyl alcohol, and this was explained by a better stabilization of the ground state. The shape of the absorption band (see Fig. 1) partly confirms that, as there might exist a better coincidence between the n–π^* and π–π^* electronic transitions, as a consequence of the well-established blue shift of the n–π^* transition upon H-bonding (20).

In the presence of a very large excess of TFA, Fig. 1 shows that the band at 320 nm is still there but quite reduced in intensity and there is a new band at ca. 380 nm, almost coincidental with the band obtained for retinal alone in methanol.

However, this does not seem to be an equilibrium since no isobestic point is detected in the spectra. This new band probably indicates that the H-bonded retinal is now surrounded by trifluoroacetate ions; this can be illustrated as follows:

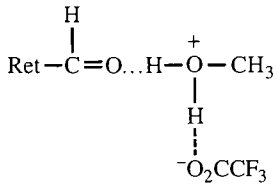

The large excess of TFA must make the presence of its anion around the retinal moiety more likely and, in doing so, it would neutralize the positive charge on the oxonium ion, consequently restoring a kind of "neutral" methanol. That this could indeed be the case is inferred by the following experiment. When different amounts of water are added to the methanolic solutions of ATR and TFA, the spectra are altered and a new band grows at 375–380 nm. This means that $CH_3OH_2^+$ is replaced in part by H_3O^+, which implies that retinal is now mostly solvated by neutral methanol molecules (CH_3OH) that are in very large excess compared to the water molecules.

In chloroform, the spectra presented in Fig. 2 show a marked similarity to those obtained in hexane. Upon addition of TFA, a red shift occurs and the band slowly moves first to 402 nm (ATR:TFA, 1:10), then to 421 nm (1:500). During this red shift the band intensity decreases and broadens, probably indicating that aggregates are formed. In a very large excess of TFA (1:2000), as previously seen in hexane, the spectrum exhibits two bands: one at ca. 410 nm with a shoulder at 465 nm, the other at 600 nm. The bands at 465 and 600 nm are ascribed to the same cations as described for hexane solutions.

These similarities between the results obtained in hexane and chloroform could be an oversimplification of the results in chloroform, which are, in fact, more complex. This stems from the following experiment. It is well known that the carbon–carbon double-bond stretching mode ($\nu_{C=C}$) of retinal can be related to the wavelength of its electronic transition by the following expression (eq. [5]) (21).

$$[5] \quad \lambda_{max} = 7002.22 - 4.20 \times \nu_{C=C}$$

where λ_{max} is the maximum absorption wavelength and $\nu_{C=C}$ the carbon–carbon stretching mode frequency observed in the Raman spectrum. This equation has already been tested by us on similar systems (22). When Raman measurements of $\nu_{C=C}$ were conducted on ATR alone in all four solvents (hexane, methanol, $CHCl_3$, and CH_2Cl_2), the λ_{max} calculated using eq. [5] was the same, within experimental error, as those actually found by means of UV–visible spectroscopy. The same applies for ATR:TFA complexes in hexane and methanol. However, in $CHCl_3$, eq. [5] no longer holds. For instance, for a ATR:50 TFA system, application of eq. [5] gives a λ_{max} of ca. 470 nm, which does not correspond with the actual value of 410 nm found in the UV–visible spectrum. This lack of agreement must be attributed to a difference in the nature of the hydrogen bonds in chloroform. Two explanations can be given. As suggested by a referee, it could arise from modifications of relative energies and ordering in the excited state since the ground state frequency of the C=C stretching vibration is also a function of these electronic states.[2] The second explanation implies the formation of new hydrogen-bonded complexes with a λ_{max} of 470 nm, which is not seen clearly by UV–vis spectroscopy but which resonates fully with the 488-nm laser line and is probably more Franck–Condon active. The structure of the new species could be a trimer such as described below:

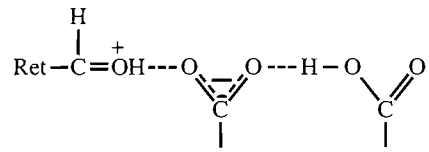

With Schiff bases of retinal, this trimer has effectively been seen to exist at room and low temperatures (22–24) and consequently, in these cases, eq. [5] also did not hold. Whichever explanation is right, both demonstrate that the hydrogen bonds in chloroform are different from those in the other solvents.

In dichloromethane, the UV–vis results are similar to those found in chloroform (see Fig. 2) for a low molar ratio of ATR:TFA. When the TFA concentration is large, more than one band appears in the 550–700 nm region, indicating that several cationic complexes are present. Equation [5] remains valid for Raman measurements of a 1 ATR:50 TFA molecular ratio, but at higher TFA concentrations laser-induced fluorescence becomes intense and makes Raman measurements impossible to achieve.

From these results it is possible to elucidate the role played by the intermolecular hydrogen bonds and their influence on the stability of these systems. For instance, it is seen from the absorption measurements that as long as the TFA concentrations are kept moderately low (i.e., 1–100 TFA for 1 ATR), the equilibrium between the molecular associated species and the ionic one in eq. [1] is displaced to the left. When large excesses of TFA are used, some proton transfer is observed in three solvents, C_6H_{14}, $CHCl_3$, and CH_2Cl_2, but not in methanol. The lack of evidence of proton transfer in methanol solutions is ascribed to the fact that, in such a solvent, the proton may retain some association with its environment, meaning that the medium competes quite effectively against ATR. In addition, from Raman data, there are indications that, at least in $CHCl_3$, some aggregations do occur in the ground state. Finally, it appears that the equilibrium of eq. [1] must be governed by a strongly asymmetric double well, where the H-bonded species are in the deeper well while the protonated species, always in the minority, are in the higher well.

Fluorescence

The fluorescence results behave somewhat the same way as those obtained in UV–visible spectroscopy except that it is more practical to present and discuss the results for each solvent.

In hexane

Stationary fluorescence results of ATR–TFA complexes are presented in Fig. 3 and Table 1. They show the excitation and emission spectra for a mixture of one molecular equivalent of ATR to 50 molecular equivalents of TFA. Such

[2]For a more recent review of this question see G. Orlandi, F. Zerbetto, and M. Z. Zgierski. Chem. Rev. **91**, 867 (1991).

Can. J. Chem. Downloaded from www.nrcresearchpress.com by 92.62.229.171 on 09/08/12
For personal use only.

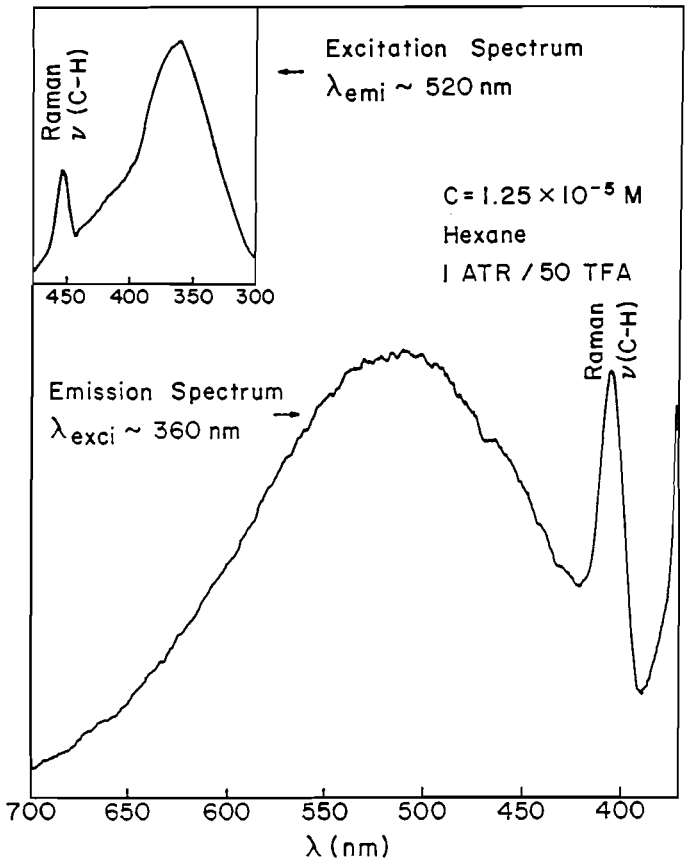

FIG. 3. Emission and excitation spectra of a 1 ATR:50 TFA complex in hexane (concentration 1.25×10^{-5} M).

a ratio has been selected in order to prevent the complexed retinal being significantly dissociated in dilute solutions. The excitation spectrum is displayed in the upper left corner in Fig. 3. The quantum yield at room temperature is about 4.0×10^{-4} (determined by using quinine sulfate as internal standard, assuming a quantum yield of 0.55 (25)), and this is consistent with previously published quantum yields (3, 10, 17). Strong Raman interferences are seen in both spectra and are pointed out, *vide supra*, in Fig. 3. The excitation wavelengths fall at 360–370 nm while the emission is seen at 520–530 nm, leading to an average Stokes shift of ca. 8200 cm^{-1}. The emission bandshape is almost independent of the ATR:TFA molecular ratio provided that this ratio remains below 1:100. For higher ratios, the spectra are characterized by a profile that suggests the presence of unresolved components, which yield a broad band between 500 and 620 nm. These emissions cannot be related to precise excitation wavelengths due to a strong inner filter effect.

For a very large ratio of ATR:TFA (viz. 1:∞), a new fluorescence band is detected at ca. 670 nm, which is associated with a maximum excitation energy of 620 nm (more precisely, the excitation band appears as a continuum with a maximum located at 620 nm) and is assigned to retinylic cations as quoted before in the UV–visible section. Time-resolved experiments were also carried out in hexane for a mixture of ATR:TFA with a ratio of 1:50 and the fluorescence decay curves can be fitted by using a biexponential model that is characterized by two time constants equal to 5.72 and 1.33 nanoseconds (ns). The relative intensities related to the slow and the fast components are 43 and 57% respectively. These results are summarized in Table 1.

Upon isotopic substitution using deuterated TFA, the fluorescence decreases by a factor of 1.7–1.8 and this cannot be explained by a simple difference between the H and D bond strength in the ground state (26, 27). This fact, combined with the large Stokes shift, suggests that the emission may originate from another species generated in the excited state rather than from the radiative relaxation of the excited hydrogen-bonded species.

In methanol

The data obtained in methanol resemble, to a certain point, those recorded in hexane solutions. For an excitation wavelength centered at ca. 320–325 nm, an emission spectrum is obtained for the 1 ATR:50 TFA system with a maximum at ca. 490 nm, affording a Stokes shift of ca. 10 800 cm^{-1}. This is similar to what was observed in hexane and the spectrum shows little dependence on the variations of the concentration of ATR or of TFA or of their respective ratios. Upon a large addition of TFA, fluorescence quenching occurs and no emission is detected even if the excitation wavelength is shifted to 380 nm. It is believed that quenching is due to some water molecules (almost always associated with TFA) present in the solution. That this could be the case is indicated by the following experiment: when water is purposely added to the methanol solution of ATR:TFA, quenching is considerably amplified. As expected, no evidence of the presence of highly emitting retinylic cations was found whatever the experimental conditions chosen. As in hexane, time-resolved experiments were done and the fluorescence decay curves are also biexponential, with two time constants at 3.60 and 0.56 ns associated with relative intensities of 38 and 62% respectively (see Table 1).

In chloroform

In this solvent, the excitation and emission spectra are very sensitive to the concentration of ATR, and a concentration of ca. 2×10^{-5} M was found most useful. Under this condition, for an ATR:TFA ratio of 1:50, the excitation spectrum looks like a continuum with a maximum located at ca. 460–470 nm while the emission spectrum has its maximum at ca. 640–650 nm. No fluorescence is detected following the excitation in the absorption band of the H-bonded complex whatever the concentration chosen. When the concentration of TFA is increased, the spectra become rather complex since there are continua for both the excitation and the emission spectra.

The red-shifted band that absorbs at ca. 470 nm and leads to emission is probably the same one that was already identified by resonance Raman spectroscopy. Nevertheless, the complexity of the excitation emission spectra cannot be explained by invoking the presence of only a single molecular association ATR:TFA but rather by a multitude of forms, which could be polymeric forms such as either ATR:$(TFA)_n$ or $(ATR)_n$:TFA. In these adducts the proton can be located anywhere between the carboxylic and the C=O aldehyde ends. In addition, chloroform may participate in these structures since its hydrogen atom could also form hydrogen bonds. Time-resolved fluorescence measurements carried out on these systems are characterized by a biexponential model having two time constants equal to 3.85 and 0.22 ns, the faster component explaining 94% of the decay curve (Table 1). This leads to quite distinct data, when compared to previous solvents.

Can. J. Chem. Downloaded from www.nrcresearchpress.com by 92.62.229.171 on 09/08/12
For personal use only.

TABLE 1. Fluorescence data of ATR/TFA mixtures in different solvents

Solvents	ATR/TFA ratio	Wavelength (nm) Excitation	Wavelength (nm) Emission	Lifetime (ns)	Fractionnal intensity (%)
Hexane	1/0	*	*	(—)	(—)
D = 1.89	1/50	360–370	520–530		
	1/∞	Continuum (400–640)	640–670	5.72[a] (1.33)[b]	43[c] (57)[d]
Chloroform	1/0	*	*	(—)	(—)
D = 4.81	1/50	Continuum (400–550)	640–650	3.85 (0.22)	6 (94)
	1/∞	Continuum (400–640)	640–680	(—)	(—)
Dichloromethane	1/0	*	*	(—)	(—)
D = 9.08	1/50	Continuum (420–680)	640–700	4.24 (0.31)	9 (91)
	1/∞	Continuum (400–700)	640–700	(—)	(—)
Methanol	1/0	*	*	(—)	(—)
D = 32.63	1/50	320–325	490	3.60 (0.56)	38 (62)
	1/∞	*	*	(—)	(—)

*No fluorescence detected.
(—)No data available.
[a,b]Correspond respectively to the slow and the fast time constants of the biexponential fluorescence decay.
[c,d]The fractional intensities for the slow (c) and the fast (d) components of the fluorescence decay.

In dichloromethane

The results are very similar to those obtained in chloroform: visualize an emission maximum at ca. 640–700 nm with an excitation maximum at ca. 460–470 nm for the same ATR:TFA ratio and concentration. The only difference is that in dichloromethane, fluorescence at 690–700 nm, which was only occasionally seen in chloroform (for high ratios of TFA to ATR), is now almost always present and dominant. The signal at 690–700 nm is optimal for an excitation wavelength centered between 620 and 660 nm. This feature, which dominates the spectrum, is assigned to retinylic cations, is quite intense, and must probably hide the fluorescence coming from other entities. All the results are displayed in Table 1. Also, contrary to the other three solvents, in dichloromethane the ATR:TFA complexes are less stable and more time-sensitive. This generates secondary products of unknown structures, which are unfortunately difficult to identify. This comment can be verified in the following experiment: when ATR is dissolved in neat TFA, at least three different electronic transitions (at 418, 616, and 660 nm) are seen just after TFA addition and, within 1 h, five new and relatively sharp bands grow and replace the previous ones. The new bands are located at 410, 464, 506, 555, and 608 nm and the spectrum possesses a large number of excitation/emission pairs. This must result from the high proportion of retinylic cations formed in chlorinated solvents, compared to hexane where it was minimal and to methanol where it was completely absent. Fluorescence decays are modelized with two time constants: 4.24 and 0.31 ns, the faster component being the dominant part of the decay curve as seen previously in chloroform (see Table 1).

Therefore, depending on the solvents, two fluorescence regimes describe the behavior of these complexes. From these results and theoretical considerations, the data can be understood as follows: recent experiments carried out on similar systems (9) unambiguously demonstrated that the fluorescence detected in a long polyene aldehyde has a $^1B_u^+$ character. This implies that the two low-lying $^1A_g^-$ and $^1n\pi^*$ states need to be inverted with respect to the $^1B_u^+$ state and protonation could be the simplest way to achieve this requirement. Protonation will convert the n orbital to a bonding orbital and, therefore, the n–π^* transition is blue-shifted in vacuum (1). Also, protonation is known to stabilize the "*ionic*" $^1B_u^+$ energy level (1, 4, 9, 28), and, concomitantly, it can destabilize the "*covalent*" $^1A_g^-$ state, thus providing the changes necessary for state inversion in going from the free (or H-bonded) to the protonated adduct (1, 4, 9, 28). It should be noted that the simple association of the aldehyde with hydrogen does not induce a state inversion even if the resulting $^1B_u^+$–$^1n\pi^*$ and $^1B_u^+$–$^1A_g^-$ energy gaps are somehow narrowed. Since no protonated complexes are observed in the ground state, fluorescence in hexane and methanol has to originate from the protonated form induced after an H-transfer in the excited state. A reverted potential in this state is conceivable, as ATR molecules are known to be more basic in the excited state (29) and therefore should favor the right-hand side of eq. [1].

Incidentally, the excited state lifetimes for complexed or protonated ATR are in the nanosecond range and therefore sufficiently long to allow proton transfer since this reaction occurs on a shorter time scale (26, 27). In that sense, these two arguments support evidence for a reverted potential in the excited state. Furthermore, the influence of isotopic substitution and the quenching phenomenon corroborate this hypothesis. This is also consistent with the large Stokes shift observed in these systems. However, care should be taken because large Stokes shifts are not a priori sufficient proof to support this hypothesis according to previous work done

Can. J. Chem. Downloaded from www.nrcresearchpress.com by 92.62.229.171 on 09/08/12
For personal use only.

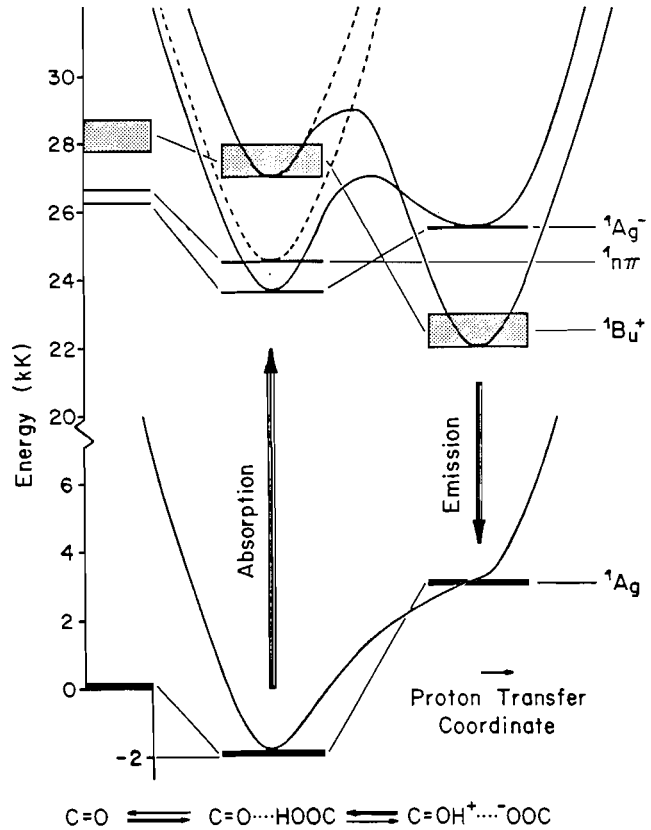

FIG. 4. Potential energy curves as a function of the proton position for the ground and the lowest excited states of H-bonded all-*trans*-retinal.

in this field on retinal or its analogs (3, 5, 12, 17), and the observed lifetimes may only derive from a solvent relaxation effect.

A *qualitative* energy diagram giving an illustration of the level ordering for the H-bonded and protonated ATR:TFA complexes is shown in Fig. 4. The values used in the graph are adapted from refs. 1, 4, 9, and 28 and completed by experimental data collected in this work. The potential energy surface curves are hypothetical, as are also some stabilization and destabilization energies for the ground and the excited states.

In chloroform, no proton transfer is detected, either because it is not favored in both states or simply because the emission from the protonated species is self-absorbed by the absorption band of the red-shifted species seen at ca. 470 nm, or else fluorescence is quenched due to extensive ground state complexation. So far, the so-called red-shifted species has not been identified, but the formation of a complex like $ATR(TFA)_2$ is strongly suspected since this structure is rather common with these types of compounds (22–24, 30, 31) and by the tendency of organic acids to self-associate in organic solvents (32). Coordination using a polymeric acid as a proton source should generate a more "acidic" proton (22, 30, 31), which then could form a protonated or a more tightly H-bonded system, both of them being able to fluoresce. This hypothesis is supported by the fact that when the TFA concentration is gradually increased, the excitation spectrum becomes broader and broader, meaning that successive equilibria may be present in the medium, such as:

[6] $ATR(TFA)_n \leftrightharpoons ATR(TFA)_{n+1} \leftrightharpoons ATR(TFA)_{n+2}$ with $n > 2$

This concept is not new as Blatz *et al.* (30) and Baasov *et al.* (31) came to the same conclusions in other studies. Emission deriving after excitation of the main electronic transition shows that the medium is complex. This applies for chloroform and also for dichloromethane, except that in the latter case the situation deteriorates rapidly due to the irreversible conversion of ATR into carbocations.

Therefore the only question left unanswered is why these complexes are so sensitive to solvent properties. In a first approximation, this has nothing to do with their respective polarity and another reason has to be found. In alkane solvents, it is seen that an H-transfer in the excited state takes place, and this is understandable as it is generally admitted that this case resembles the kinetics of unsolvated molecules, which are well known to induce ultrafast H-atom translocations (see ref. 26 and refs. therein) because the barrier to H-transfer is zero. In methanol, the 10 000 cm^{-1} Stokes shift is also explained by a proton transfer occurring in the excited state, from the associated species ([Ret—CHO. . .HOOC]*) to the protonated species ([Ret—CHO^+-H. . .^-O_2C-]*). Then fluorescence occurs from the excited protonated form into the protonated form in the ground state, which immediately reverts to the most stable associated species (see Fig. 4). However, this holds as long as the TFA concentration is not too large and in the absence of water, since then a large decrease of H-transfer is found due to H-intermolecular competition between all molecules present.

In chloroform and dichloromethane, TFA is present in polymeric form and they therefore generate a certain number of ATR H-complexes, depending on the concentration of the H-donor and the solvent. The H-complexes show more instability towards illumination and are easily converted into red-shifted species. The formation of carbocations is easier in these solvents since the absence of proton transfer in the excited state reduces its rate of relaxation and, in consequence, produces an energy buildup making these complexes more susceptible to photochemical transformations (26, 27).

Conclusion

H-bonded ATR complexes have unique optical properties and are stable when a proton transfer reaction occurs in the excited state. This may answer questions about the mechanism of vision, as it involves wavelength regulation in photointermediates for visual and bacterial pigments. But it mainly demonstrates that the H-bond strength is a critical parameter defining the stability of H-bonded retinal, and this cannot be predicted by simply looking at the solvent polarity but rather by measuring the solvent ability to favor an even distribution of the acceptor–donor molecules in the medium.

Acknowledgments

We wish to thank Dr. F. Boucher and B. Zelent (Centre de recherche en biophysique de Trois-Rivières (Qué.)) for recording of the time-resolved fluorescence data. We are also grateful to the National Research Council of Canada and to l'Université du Québec à Montréal for financial support.

Can. J. Chem. Downloaded from www.nrcresearchpress.com by 92.62.229.171 on 09/08/12
For personal use only.

1. R. R. Birge. Annu. Rev. Biophys. Bioeng. **10**, 315 (1981); Biochem. Biophys. Acta, **1016**, 213 (1990).
2. C. Sandorfy and D. Vocelle. Can. J. Chem. **64**, 2251 (1986).
3. R. S. Becker, G. Hug, P. K. Das, A. M. Schaffer, T. Takemura, N. Yamamoto, and W. Waddell. J. Phys. Chem. **80**, 2265 (1976).
4. R. R. Birge, J. A. Bennett, L. M. Hubbard, H. L. Fang, B. M. Pierce, D. S. Kliger, and G. E. Leroi. J. Am. Chem. Soc. **104**, 2519 (1982).
5. R. R. Birge, J. A. Bennett, B. M. Pierce, and T. M. Thomas. J. Am. Chem. Soc. **100**, 1533 (1978).
6. P. K. Das and R. S. Becker. J. Phys. Chem. **86**, 921 (1982).
7. R. Snyder, E. Arvidson, C. Foote, L. Harrigan, and R. S. Christensen. J. Am. Chem. Soc. **107**, 4117 (1985).
8. L. P. Murray and R. R. Birge. Can. J. Chem. **63**, 1967 (1985).
9. J. Papanikolas, G. C. Walker, V. A. Shamamian, R. L. Christensen, and J. Clayton Baum. J. Am. Chem. Soc. **112**, 1912 (1990).
10. T. Takemura, P. K. Das, G. Hug, and R. S. Becker. J. Am. Chem. Soc. **98**, 7099 (1976).
11. T. Takemura, P. K. Das, G. Hug, and R. S. Becker. J. Am. Chem. Soc. **100**, 2626 (1978).
12. S. Hotchandani, P. Paquin, and R. M. Leblanc. Can. J. Chem. **56**, 1985 (1978).
13. D. A. Chignell and W. B. Gratzer. J. Phys. Chem. **72**, 2934 (1968).
14. R. Scott and S. Vinogradov. J. Phys. Chem. **73**, 1890 (1969).
15. T. K. Pal, G. K. Mallik, T. Ganguly, and S. B. Banerjee. Bull. Chem. Soc. Jpn. **62**, 3315 (1989).
16. T. Takemura, G. Hug, P. K. Das, and R. S. Becker. J. Am. Chem. Soc. **100**, 2631 (1978).
17. P. K. Das, G. Kogan, and R. S. Becker. Photochem. Photobiol. **30**, 689 (1979).
18. P. E. Blatz, N. Baumgartner, V. Balasubramaniyan, P. Balasubramaniyan, and E. Stedman. Photochem. Photobiol. **14**, 531 (1971).
19. P. E. Blatz and D. L. Pippert. Chem. Commun. 176 (1978).
20. G. J. Brealey and M. Kasha. J. Am. Chem. Soc. **77**, 4462 (1955).
21. H. Kakitani, T. Kakitani, H. Rodman, B. Honig, and R. Callender. J. Phys. Chem. **87**, 3620 (1983).
22. S. Alex, C. Sandorfy, and D. Vocelle. J. Phys. Chem. **95**, 3121 (1991).
23. H. Le-Thanh and D. Vocelle. Can. J. Chem. **68**, 1909 (1990).
24. D. Larouche, A. Gélinas, H. Le Thanh, C. Sandorfy, and D. Vocelle. Photochem. Photobiol. **53**, 153 (1991).
25. R. F. Chen, G. G. Uvrek, and N. Alexander. Science, **156**, 949 (1967).
26. P. F. Barbara, P. K. Walsh, and L. E. Brus. J. Phys. Chem. **93**, 29 (1989).
27. D. L. Williams and A. Heller. J. Phys. Chem. **74**, 4473 (1970).
28. R. R. Birge, L. P. Murray, R. Zidovetzki, and H. M. Knapp. J. Am. Chem. Soc. **109**, 2090 (1987).
29. J. P. Corsetti and B. E. Kolher. J. Chem. Phys. **67**, 5237 (1977).
30. P. E. Blatz, R. H. Johnson, J. H. Mohler, D. K. Al-Dilaimi, S. Dewhurst, and J. O. Erickson. Photochem. Photobiol. **13**, 237 (1971).
31. T. Baasov, N. Friedman, and M. Sheves. Biochemistry, **26**, 3210 (1987).
32. Y. Fujii, H. Yamada, and M. Mizuta. J. Phys. Chem. **92**, 6768 (1988).

Can. J. Chem. Downloaded from www.nrcresearchpress.com by 92.62.229.171 on 09/08/12
For personal use only.

Kinetic analysis of thermal decomposition reactions. VII. Effect of radiation and doping on the thermal decomposition of $BaCO_3$–TiO_2 and $SrCO_3$–TiO_2 crystalline mixtures

SULIMAN N. BASAHEL AND EL-HUSSIENY M. DIEFALLAH[1]

Department of Chemistry, Faculty of Science, King Abdulaziz University, Jeddah, Saudi Arabia

Received April 2, 1991

SULIMAN N. BASAHEL and EL-HUSSIENY M. DIEFALLAH. Can. J. Chem. **70**, 888 (1992).

DTA–TG techniques were applied to study the thermal decomposition and reactivity in intimately mixed powders of barium or strontium carbonate and titanium dioxide. The results showed that the temperature for the thermal decomposition of $BaCO_3$–TiO_2 mixtures precedes the decomposition of pure $BaCO_3$ by about 250°C, whereas the decomposition of $SrCO_3$–TiO_2 mixtures precedes the decomposition of pure $SrCO_3$ by about 60°C. Kinetic analysis of the isothermal data in view of various solid-state reaction models showed that the reaction is best described by the phase boundary models. The effects of ^{60}Co γ irradiation and of doping the metal oxide with Li^+ or Cu^{2+} ions on the thermal decomposition reactions were investigated.

Key words: titanates, thermal decomposition, doping, irradiation effects.

SULIMAN N. BASAHEL et EL-HUSSIENY M. DIEFALLAH. Can. J. Chem. **70**, 888 (1992).

On a appliqué les techniques de l'ATD–TG à l'étude de la décomposition thermique et de la réactivité de poudres intimement mélangées de carbonates de baryum ou de strontium et de dioxyde de titane. Les résultats montrent que la température de décomposition thermique de mélanges de $BaCO_3$–TiO_2 précède celle de la décomposition du $BaCO_3$ pur par environ 250°C; par ailleurs, la décomposition de mélanges de $SrCO_3$–TiO_2 ne précède la décomposition du $SrCO_3$ pur que par 60°C. Une analyse cinétique des données isothermiques en relation avec les divers modèles de réactions à l'état solide montrent que les meilleurs modèles pour décrire la réaction sont les phases limites. On a aussi examiné les effets d'irradiation par des rayons γ du ^{60}Co et du dopage de l'oxyde métallique par des ions Li^+ ou Cu^{2+} sur les réactions de décompositions thermiques.

Mots clés : titanates, décomposition thermique, dopage, effets d'irradiation.

[Traduit par la rédaction]

Introduction

Processes involving the chemical transformations of solids play an increasingly important role in modern technology, as sophisticated and costly solids can be produced by reaction of other, precursory solids (1). Solid state reactions between metal carbonates and metal oxides are carried out to obtain more important solids and to gain understanding of some of the factors influencing these reactions (1–7). The processes of forming titanates in crystalline mixtures have become very important in the ceramic industry and other technologies (2, 3). The thermoanalytical behaviour of $CaSO_4$ – metal oxide and $CaCO_3$ – metal oxide systems was discussed by Ishii *et al.* (4). The formation of $CaTiO_3$ in the $CaSO_4$–TiO_2 system was shown to proceed in two steps (5). The role of CO_2 removal in the $BaCO_3$–TiO_2 system was described by Dell (6) and the effects of dispersion and mixing conditions of reactant particles on reactivity in this system was studied by Yamaguchi *et al.* (7).

The chemical and catalytic reactivity of a solid depends on its method of preparation, so that structural and electronic imperfections may have important effects on the behaviour of a solid state reaction. Irradiation of a solid might alter the kinetics of a reaction and help to clarify the reaction mechanism (1, 8). Doping with metal ions or other pretreatment of samples may have important effects on the reactivity of solids (1).

In the present study, the reactivity in $BaCO_3$–TiO_2 and $SrCO_3$–TiO_2 systems, which are potentially suitable for conversion to $BaTiO_3$ and $SrTiO_3$, were investigated. The kinetics of the thermal decomposition of $BaCO_3$–TiO_2 and $SrCO_3$–TiO_2 reactions were studied and compared with the kinetic equations that give the best fit to the experimental data to find out whether the reaction is phase boundary or transport controlled. The effects of increasing γ radiation dose and of doping the metal oxide with Li^+ or Cu^{2+} ions, on the kinetics and the activation parameters of the solid state reactions, were investigated.

Experimental

Analar barium carbonate (BDH Chemicals Ltd.), C.P. grade strontium carbonate (Fluka AG), and titanium dioxide (Hering–Kahlbaum AG) were used in this study. Mixtures of metal carbonate – TiO_2 (each with particle size less than 125 μm) were prepared by thoroughly mixing the powders in a 1:1 molar ratio by first tumbling the dry powders together for 3 h and then grinding them with a mortar and pestle. The mixtures were dried in a thermostated oven at 120°C for few hours.

DTA–TG behaviour of the $BaCO_3$–TiO_2 and $SrCO_3$–TiO_2 systems was investigated using a Shimadzu model 30 thermal analyzer. The kinetics of the isothermal decomposition and formation of titanate were studied in the temperature range 820–950°C under 1 atm (101.3 kPa) pressure in air flow (50 mL/min). The X-ray diffraction patterns for samples calcined at selected temperatures were performed using a Philips instrument model 1700, with nickel-filtered Cu Kα radiation.

Samples were irradiated using ^{60}Co-Gammacell and were exposed to successively increasing doses at a dose rate of 1.01 ± 0.05 kGy h^{-1}.

Doping of TiO_2 with Li^+ or Cu^{2+} ions was carried out using the impregnation technique at dopant metal ion concentrations of 0.5

[1]Author to whom correspondence may be addressed. Present address: Department of Chemistry, Faculty of Science, Benha, Egypt.

Printed in Canada

Can. J. Chem. Downloaded from www.nrcresearchpress.com by 92.62.229.171 on 09/08/12
For personal use only.

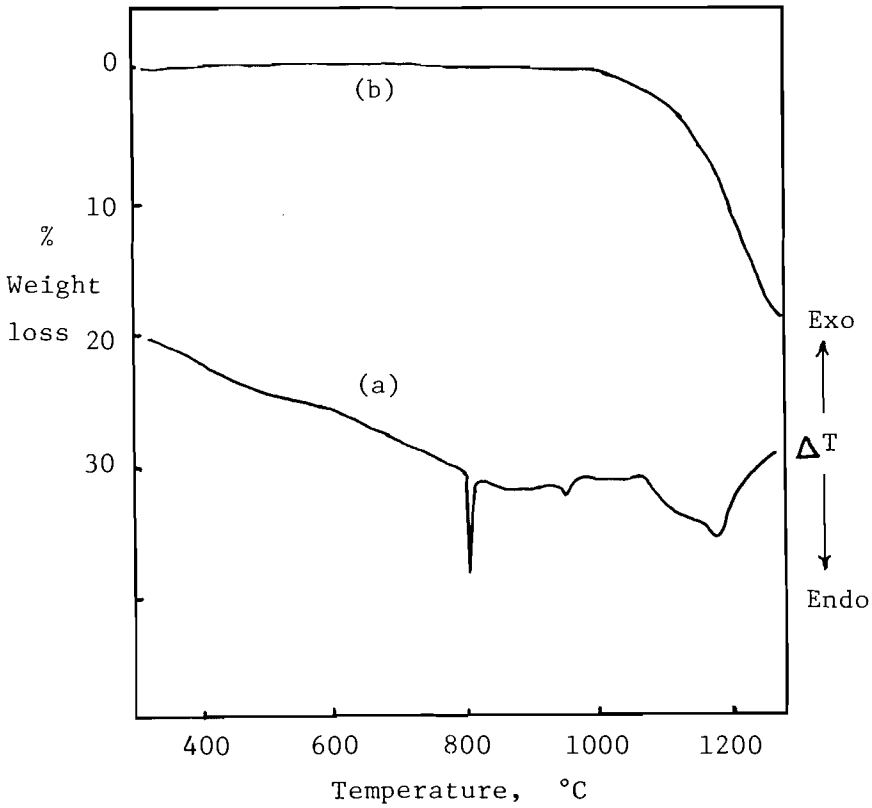

FIG. 1. (*a*) DTA and (*b*) TG curves of barium carbonate; 9.3 mg sample heated at 20°C/min.

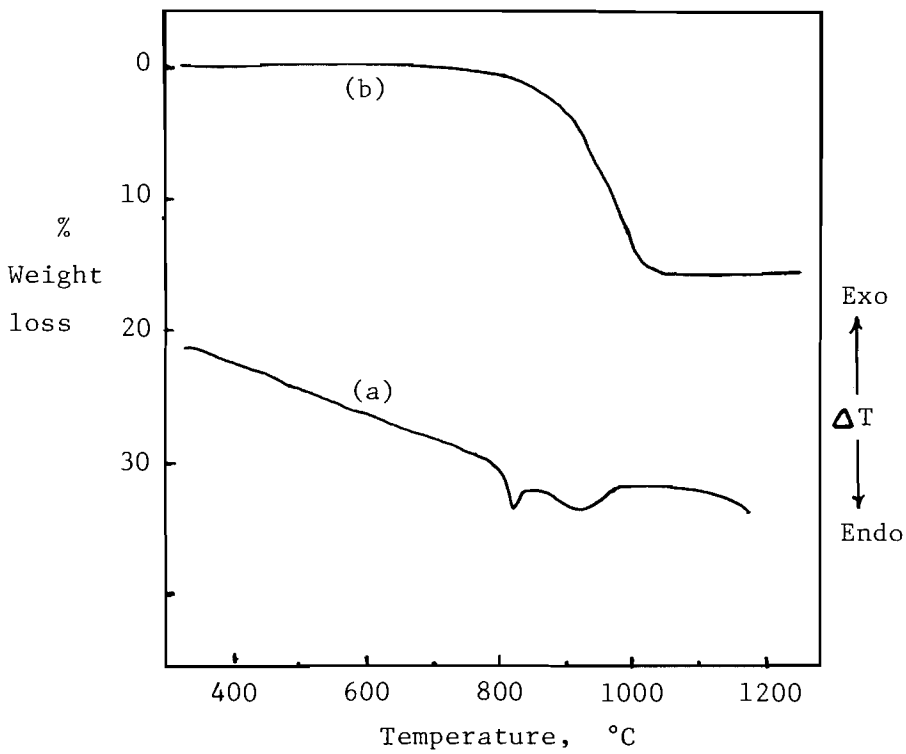

FIG. 2. (*a*) DTA and (*b*) TG curves of barium carbonate – anatase mixture (1:1 molar ratio); 9.3 mg sample heated at 20°C/min.

and 5.0 metal atom %, using standard solutions of lithium nitrate or copper acetate. The impregnated oxide was dried in an oven at 250°C for 1 h, then heated in a muffle furnace at 400°C for 3 h.

DTA–TG analysis of the initial and calcined samples showed that the lithium and copper present in the calcined doped TiO_2 are in the form of their oxides, Li_2O and CuO respectively.

Can. J. Chem. Downloaded from www.nrcresearchpress.com by 92.62.229.171 on 09/08/12
For personal use only.

Can. J. Chem. Downloaded from www.nrcresearchpress.com by 92.62.229.171 on 09/08/12
For personal use only.

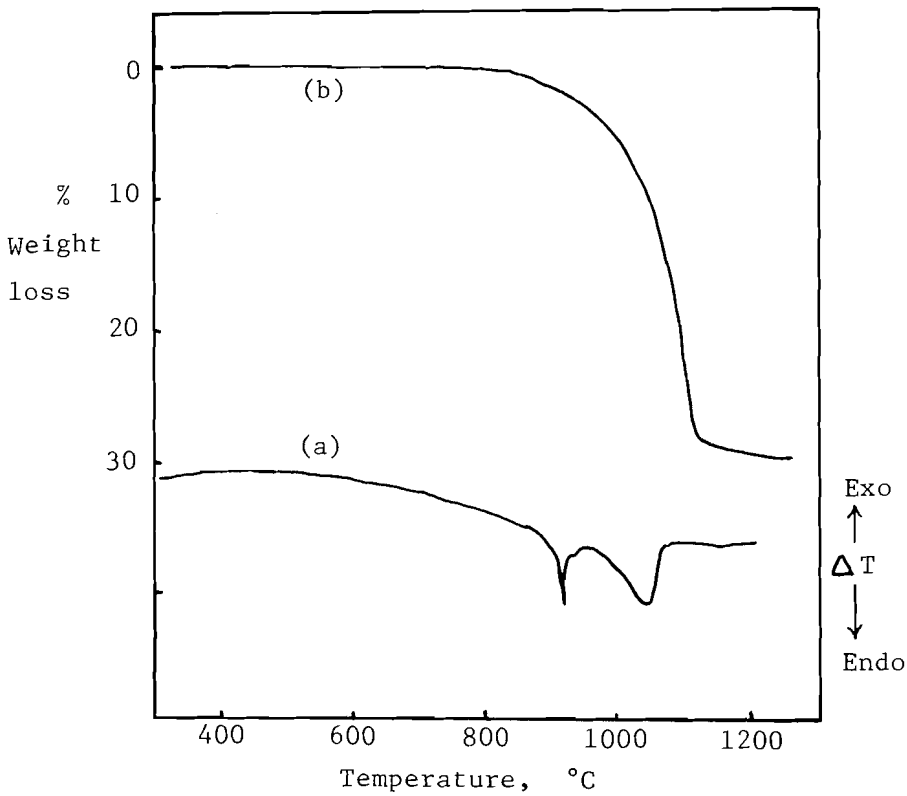

FIG. 3. (*a*) DTA and (*b*) TG curves of strontium carbonate; 8.5 mg sample at a heating rate of 20°C/min.

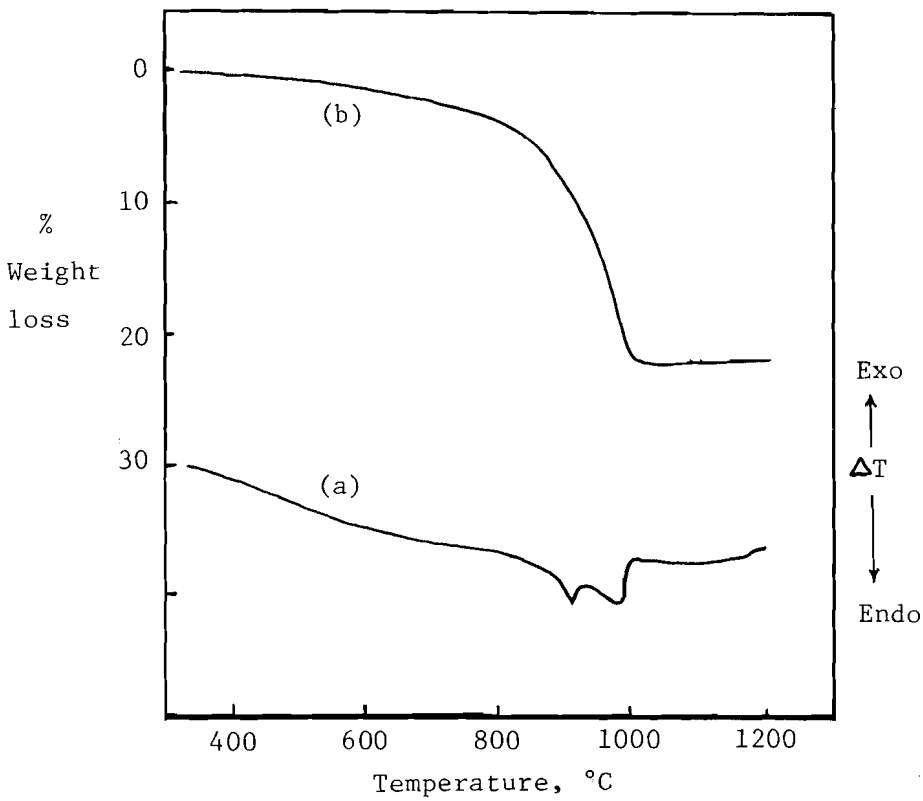

FIG. 4. (*a*) DTA and (*b*) TG curves of strontium carbonate anatase mixture (1:1 molar ratio); 9.1 mg sample heated at 20°C/min.

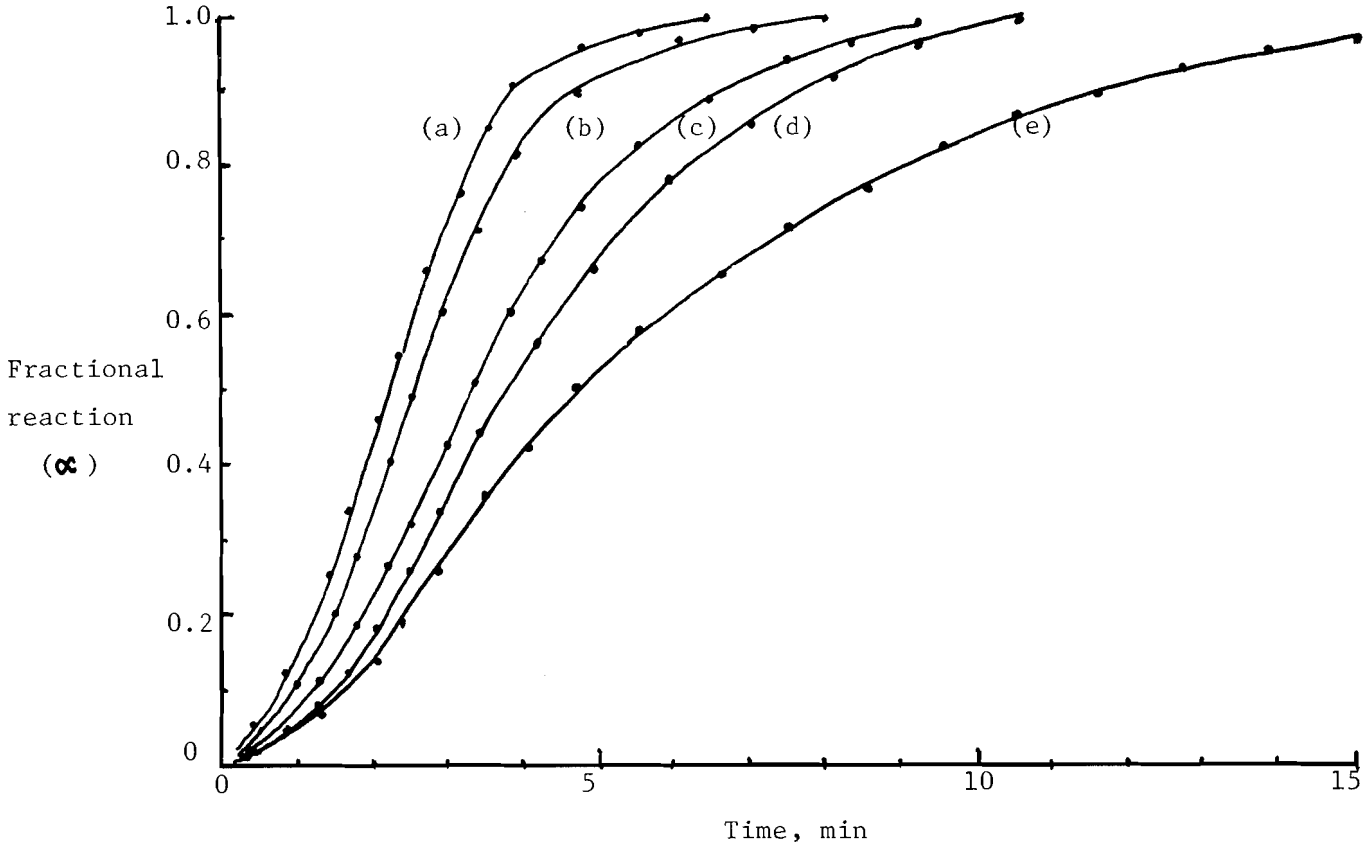

FIG. 5. Isothermal α/t curves for the formation of barium titanate in a crystalline mixture of barium carbonate and anatase; (*a*) 934; (*b*) 915; (*c*) 893; (*d*) 874; and (*e*) 858°C.

Results and discussion

Figures 1 and 2 show the DTA–TG curves obtained for the $BaCO_3$ and $BaCO_3$–TiO_2 (anatase) system, respectively. At room temperature, barium carbonate belongs to the orthorhombic system and high-temperature X-ray analysis (9) has shown that at 805°C it undergoes transformation to the hexagonal form and, at 976°C, it transforms to the cubic form. The DTA curve of $BaCO_3$ (Fig. 1) shows, in addition to the two endothermic peaks corresponding to these two phase transitions, a third highly endothermic and broad peak at 1100–1200°C due to the decomposition of $BaCO_3$. In the $BaCO_3$–anatase system (Fig. 2) the DTA curve shows two endothermic peaks, the first at 805°C due to the first phase transition of $BaCO_3$ and a second, relatively more broad endothermic peak, at about 900°C, which results from the overlap of the second phase transition in $BaCO_3$ and the endothermic peak due to the decomposition of $BaCO_3$ and the formation of $BaTiO_3$. The titanate formation reaction starts at a temperature that is about 250°C below that required to start the decomposition of pure $BaCO_3$.

At room temperature $SrCO_3$ belongs to the orthorhombic system and it undergoes transformation to the hexagonal system at 912°C. Figure 3 shows the DTA–TG curves for pure $SrCO_3$. The DTA curve shows, in addition to the peak at 912°C due to phase transition, a peak at 1030°C due to decomposition of $SrCO_3$. The DTA–TG curves obtained for the $SrCO_3$–anatase system (Fig. 4) showed that the phase transition peak remains at 912°C, but the decomposition peak is shifted to lower temperatures due to the formation of strontium titanate.

The remarkable decrease in the decomposition temperature of the metal carbonate – metal oxide mixtures could be attributed to the formation of the single phase product. It is also evident that the TG traces of the intimately mixed powders do not reveal intermediate curve breaks either at the fast or at the slow heating rates. X-ray diffraction patterns for $BaCO_3$–TiO_2 and $SrCO_3$–TiO_2 mixtures (in 1:1 molar ratio) calcined at 950°C for 15 min showed the formation of $BaTiO_3$ and $SrTiO_3$, respectively. Yamaguchi *et al.* (7) pointed out that the particle size ratio of $BaCO_3$ to TiO_2 in the reaction mixture is closely related to the formation of intermediate phases. It was suggested that the reaction between $BaCO_3$ and coarse TiO_2 to form $BaTiO_3$ proceeds in three steps with the formation of Ba_2TiO_4 during the reaction, whereas in equimolar mixtures of $BaCO_3$ – fine TiO_2, the reaction leads directly to $BaTiO_3$.

Reaction isotherms were obtained by isothermal gravimetry in air and the degree of reaction was calculated from the weight loss of the mixtures. Figures 5 and 6 show typical fractional reaction (α) vs. time (t) curves obtained for the isothermal decomposition of a 1:1 molar ratio of crystalline powdered mixtures of $BaCO_3$–TiO_2 and $SrCO_3$–TiO_2, with the formation of barium titanate and strontium titanate, respectively. It is evident that the α/t curves are not sigmoidal and that the formation reactions do not follow the exponential growth model.

The fractional reaction – time curves obtained under var-

Can. J. Chem. Downloaded from www.nrcresearchpress.com by 92.62.229.171 on 09/08/12
For personal use only.

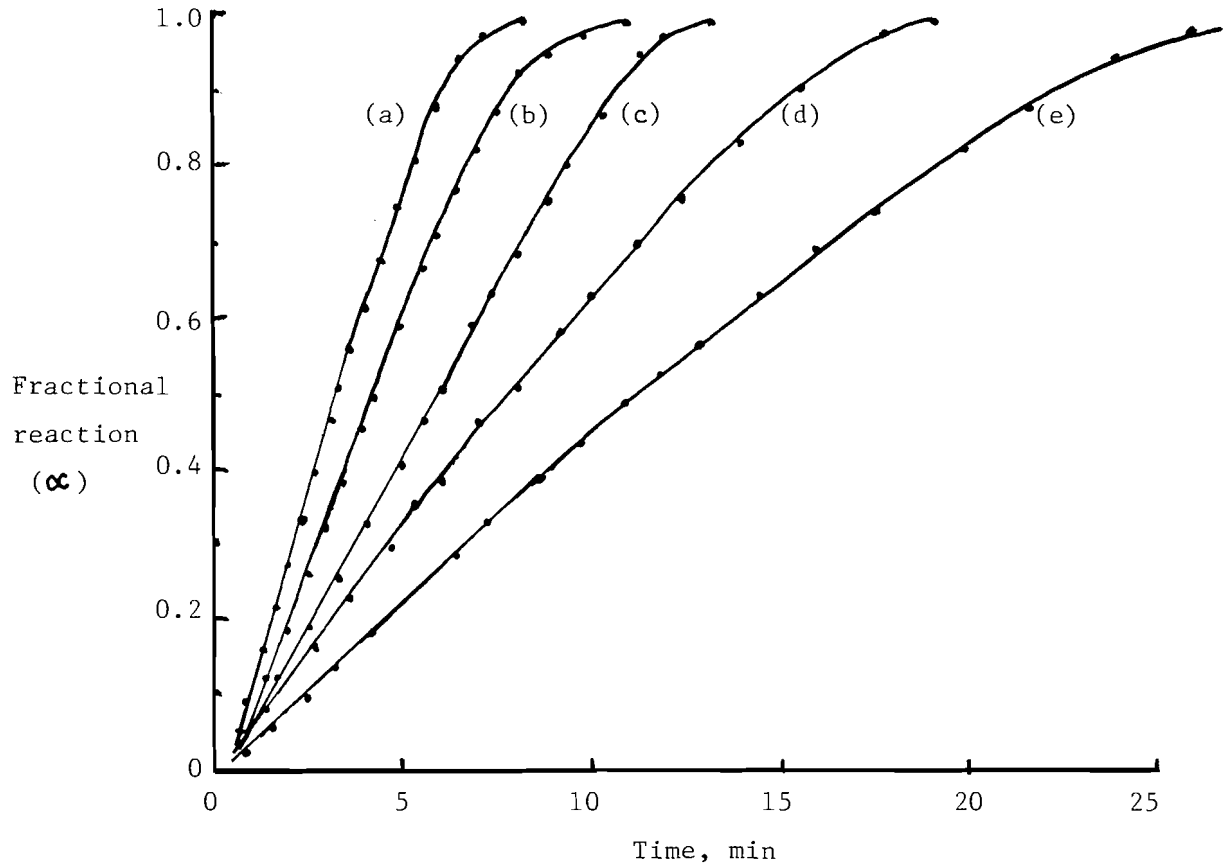

FIG. 6. Isothermal α/t curves for the formation of strontium titanate in a crystalline mixture of strontium carbonate and anatase; (*a*) 935; (*b*) 915; (*c*) 897; (*d*) 874; and (*e*) 857°C.

TABLE 1. Activation parameters of the isothermal reaction in $BaCO_3$–TiO_2 and $SrCO_3$–TiO_2 systems

System	log *A* (min^{-1})	*E* (kJ mol^{-1})
$BaCO_3$–TiO_2	7.9 ± 0.7	196 ± 14
$SrCO_3$–TiO_2	8.7 ± 0.2	221 ± 5

TABLE 2. Effect of γ irradiation on the activation parameters of the isothermal reaction in the barium carbonate – anatase system

Radiation dose (MGy)	log *A* (min^{-1})	*E* (kJ mol^{-1})
Non-irradiated	7.9 ± 0.7	196 ± 14
0.60	9.2 ± 1	226 ± 20
1.17	8.6 ± 0.6	212 ± 14
1.64	8.2 ± 1	201 ± 25
2.26	7.3 ± 0.8	183 ± 18

ious conditions were analyzed by linear regression (LR) analysis according to the different heterogeneous solid state reaction models (10–14). The results of the kinetic data analysis showed that the phase boundary models and the first-order kinetics give the best fit. The reactivities of the $CaSO_4$–TiO_2 and $BaSO_4$–TiO_2 systems (5) examined by isothermal TG studies were found to fit Jander's diffusion equation. However, analysis of the results obtained under the present experimental conditions in $BaCO_3$–TiO_2 and $SrCO_3$–TiO_2 systems have shown that the diffusion functions give a much less satisfactory fit to the experimental data. Rate constants calculated for the solid state reaction between $BaCO_3$ and ZnO according to the diffusion models showed a pronounced drift with time, indicating that these models are invalid for analyzing the reaction (10). The results obtained here show that the phase boundary models give the best representation of the reaction.

TABLE 3. Effect of doping on the activation parameters of the isothermal reaction in the barium carbonate – anatase system

% M-doped TiO_2	log *A* (min^{-1})	*E* (kJ mol^{-1})
Non-doped TiO_2	7.9 ± 0.7	196 ± 14
0.5% Li-doped	7.8 ± 0.6	194 ± 14
5.0% Li-doped	8.0 ± 0.9	197 ± 21
0.5% Cu-doped	7.0 ± 0.6	174 ± 13
5.0% Cu-doped	11.1 ± 1.4	264 ± 32

The activation energies of solid state reactions could vary between relatively large limits depending on the nature and the method of preparing the starting materials (15, 16). Table 1 shows the activation energies and frequency factors ob-

Can. J. Chem. Downloaded from www.nrcresearchpress.com by 92.62.229.171 on 09/08/12
For personal use only.

tained for the solid state reactions in MCO_3–TiO_2 calculated according to the Arrhenius equation by LR analysis using rate constants calculated on the basis of the phase boundary contracting area model. The results show that the titanate formation reaction has higher activation energy and frequency factor with $SrCO_3$ than with $BaCO_3$. The radius of Ba^{2+} (1.35 Å) is higher than that of Sr^{2+} (1.13 Å) and, based on Coulombic attractions, the Sr^{2+} ions will have a stronger oxygen-to-carbon bond than the Ba^{2+} ions. This should increase the energy needed to liberate CO_2 and thus increase the activation energy for the reaction. It was reported that in the $BaCO_3$–TiO_2 system the activation energy could change between 200 and 280 kJ/mol depending on particle size and method of mixing (7).

The results of the kinetic data analysis of the thermal decomposition of irradiated mixtures of $BaCO_3$–TiO_2 showed that radiation did not introduce a change in the reaction model and mechanism. The effects of radiation dose on the activation energy and the frequency factor of the reactions are shown in Table 2. Although the changes in the activation parameters are within experimental errors, there is a regular decrease in both the activation energy and the frequency factor of the reaction with increasing radiation dose. However, the values in the non-irradiated mixtures are lower than those obtained for mixtures having low radiation doses, which may be due to the effects of small dose radiation annealing. Since radiation introduces defects into the solid and at crystal surfaces (8), and these defects may act as important sites for reaction nucleation and initiation of decomposition, this could result in a lowering of activation energy at the higher doses where internal radiolytic reactions and the generation of defects and their catalytic effects compete with radiation annealing.

The results for thermal decomposition and titanate formation reaction of doping the anatase with Li^+ or Cu^{2+} ions showed that doping did not change the model for the reaction interface. Table 3 summarizes the results of the effects of doping on the activation parameters calculated by LR analysis. Doping with Li^+ seems not to have a significant effect on the activation parameters of the reaction, whereas doping with Cu^{2+} causes a lowering in the activation parameters at low concentration and an increase at the higher concentration. At low concentration Cu^{2+} facilitates electron transfer reactions in the solid and the release of CO_2. At the higher dopant concentration, copper titanate could form in high enough yield and this may lead to an increase in the activation parameters. The results here showed that Cu^{2+} dopant effects are not additive but are interactive for the system studied, and that more detailed investigation of the effects of copper is required to confirm the kinetic consequences of the presence of the additive.

1. V. V. Boldyrev, M. Bulens, and B. Delmon. The control of the reactivity of solids. Elsevier, Amsterdam. 1979.
2. P. P. Budnikov and M. M. Ginstling. Principles of solid state chemistry. *Translated and edited by* K. Shaw. Gordon and Breach Science Publishers, Inc., New York. 1968.
3. A. R. West. Solid state chemistry and its applications. J. Wiley & Sons Ltd., New York. 1987.
4. T. Ishii, R. Furuichi, H. Matsusato and T. Okutani. *In* Therm. Anal. Proc. Int. Conf. 5th, Kyoto. *Edited by* H. Chihara. Heyden, Tokyo. 1977. p. 440.
5. T. Ishii. *In* React. Solids, Proc. Int. Symp. 9th. Vol. 2. *Edited by* K. Dyrek, J. Haber, and T. Nowotny. Elsevier, Amsterdam. 1982. p. 427.
6. R. M. Dell. Inst. Chem. Eng. Symp. Ser. **27**, 3 (1968).
7. T. Yamaguchi, S. H. Cho, H. Nagai and H. Kuno. React. Solids Proc. Int. Symp. 8th. Plenum, New York. 1977. p. 701.
8. P. J. Herley and P. W. Levy. React. Solids Proc. Int. Symp. 7th. *Edited by* J. S. Anderson, M. W. Roberts, and F. S. Stone. Chapman and Hall, London. 1972. p. 387.
9. T. Nishino, T. Sakurai, and E. Yamanchi. *In* React. Solids Proc. Int. Symp. 9th. Vol. 2. *Edited by* K. Dyrek, J. Haber, and J. Nowotny. Elsevier, Amsterdam. 1982. p. 663.
10. S. F. Hulbert and J. J. Klawitter. Am. Ceram. Soc. **50**, 484 (1967).
11. W. W. Wendlandt. Thermal methods of analysis. J. Wiley & Sons, New York. 1975.
12. M. E. Brown, D. Dollimore, and A. K. Galwey. Comprehensive chemical kinetics. Vol. 22, Elsevier, Amsterdam. 1980.
13. A. M. M. Gadalla. Thermochim. Acta, **74**, 255 (1984).
14. M. E. Brown. Introduction to thermal analysis. Chapman and Hall, London. 1988. Chap. 13.
15. Z. A. Omran, M. A. Mousa, A. A. Abdel-Fattah, and El-H. M. Diefallah. Thermochim. Acta, **145**, 271 (1989).
16. A. A. El-Bellihi, A. M. Abdel-Badei, and El-H. M. Diefallah. Thermochim. Acta, **165**, 147 (1990).

Can. J. Chem. Downloaded from www.nrcresearchpress.com by 92.62.229.171 on 09/08/12
For personal use only.

The structure of the pyranosyl nucleoside 1-(2′,3′-dideoxy-β-D-*erythro*-hex-2′-enopyranosyl)thymine and a comparison with AZT

LESLIE W. TARI AND ANTHONY S. SECCO[1]

Department of Chemistry, University of Manitoba, Winnipeg, Man., Canada R3T 2N2

Received July 5, 1991

LESLIE W. TARI and ANTHONY S. SECCO. Can. J. Chem. **70**, 894 (1992).

Pyranosyl nucleosides are among the most recent modifications of natural nucleosides to receive attention as potential HIV inhibitors. As part of our studies involving modified nucleosides, the crystal structure of 1-(2′,3′-dideoxy-β-D-*erythro*-hex-2′-enopyranosyl)thymine was determined and its molecular structure and conformation compared with AZT in an effort to assess the title compound's potential activity against HIV. The compound crystallizes in the monoclinic space group $P2_1$ with cell dimensions a = 7.966(3), b = 18.004(3), c = 8.346(3) Å, β = 91.29(3)°. The crystal structure, solved by direct methods and refined to R = 0.032 and wR = 0.041 for 1285 observed data, contains two independent molecules in the asymmetric unit, each displaying different torsion angles, χ (64.5(6)° and 72.7(6)°) and γ (62.0(7)° and 178.6(5)°). Molecular conformations, described as slightly distorted chairs with O5′ *endo* and C5′ *exo* and with equatorial substituents, are stabilized by a network of hydrogen bonds throughout the crystal. Despite the substantial difference in χ values with respect to AZT in the solid state, molecules appear to exhibit sufficient structural overlap with AZT to expect a similar capacity for binding to the active site of phosphorylation; the barrier to rotation about the *N*-glycosidic bond is only slightly greater for the title compound. The significant difference, on comparison with AZT, appears at the primary hydroxyl, which is so oriented as to probably preclude activity of this pyranosyl compound as an anti-HIV agent. The conformational parameters given are in accordance with the IUPAC–IUC Joint Commmission on Biochemical Nomenclature (Pure Appl Chem. **55**, 1273 (1983)).

Key words: crystal structure, modified nucleoside, pyranosyl nucleoside, anti-HIV drugs.

LESLIE W. TARI et ANTHONY S. SECCO. Can. J. Chem. **70**, 894 (1992).

Les nucléosides de pyranosyle font partie des plus récentes modifications des nucléosides naturels à recevoir de l'attention comme inhibiteurs potentiels du HIV. Dans le cadre de nos études impliquant des nucléosides modifiés et dans le but d'évaluer l'activité potentielle du composé mentionné dans le titre contre l'HIV, on a déterminé la structure cristalline de la 1-(2′,3′-didésoxy-β-D-*erythro*-hex-2′-énopyranosyl)thymine et on a comparé sa structure moléculaire ainsi que sa conformation avec celles de l'AZT. Le composé cristallise dans le groupe d'espace monoclinique, groupe d'espace $P2_1$, avec a = 7,966(3), b = 18,004(3) et c = 8,346(3) Å et β = 91,29(3)°. On a résolu la structure par des méthodes directes et on l'a affinée jusqu'à des valeurs de R = 0,032 et R_w = 0,041 pour 1285 réflexions observées; elle contient deux molécules indépendantes par unité asymétrique et chacune présente des angles de torsion χ (64,5(6) et 72,7°) et γ (62,0(7) et 178,6(5)°) différents. Les conformations moléculaires, que l'on peut décrire comme des chaises légèrement déformées avec l'O5′ *endo*, le C5′ *exo* et les substituants équatoriaux, sont stabilisées par un réseau de liaisons hydrogènes dans tout le cristal. Malgré des différences substantielles, par rapport à l'AZT, dans les valeurs de χ à l'état solide, les molécules semblent présenter des recouvrements structuraux suffisants avec l'AZT pour s'attendre à une capacité similaire à se lier au site actif de phosphorylation; la barrière à la rotation autour de la liaison *N*-glycosidique n'est que légèrement supérieure pour le composé mentionné dans le titre. Lorsqu'on le compare à l'AZT, la seule différence importante se rapporte à l'hydroxyle primaire qui est orienté d'une façon telle qu'une activité de ce composé pyranosyle comme agent anti-HIV est peu probable. Les paramètres conformationnels sont conformes aux recommendations de la commission conjointe de l'UICPA et de l'UIC relativement à la nomenclature biochimique (Pure Appl. Chem. **55**, 1273 (1983)).

Mots clés : structure cristalline, nucléoside modifié, nucléoside de pyranosyle, médicaments anti-HIV.

[Traduit par la rédaction]

Introduction

As part of our ongoing studies of modified nucleosides, we have synthesized the title compound. The compound was first synthesized by Yamazaki, Matsudo, Sugiyama, Seto, and Yamaoka (1) to demonstrate a new method of preparing 2′,3′-unsaturated pyranosyl nucleosides. Several hexeno- and hexano-pyranosyl nucleosides, like their pento-furanosyl analogs, have long been known to exhibit significant biological activity. Only in the past year have the pyranosyl compounds been investigated as potential anti-Human Immunodeficiency Virus (HIV) drugs (2). Presently, the most effective acquired immunodeficiency syndrome (AIDS) chemotherapy involves 3′-azido-3′deoxythymidine (AZT), the structural characteristics of which have been well documented (3–5) and their relationship to its activity been inferred (4–6). However, the adverse side effects of AZT have necessitated the search for drugs with an equal or greater efficacy but lower toxicity. The difficulty in designing nucleosides as therapeutic agents for AIDS patients is the lack of detailed structural knowledge of the active sites of (*i*) the cellular kinases responsible for phosphorylation and of (*ii*) the viral reverse transcriptase that incorporates the resulting nucleotide into the growing DNA strand. Using AZT as the best available model, we may be able to effectively screen the pyranosyl compounds for anti-HIV activity by comparing the structural parameters of these strategically modified nucleosides with those of AZT. In this context, we have undertaken the present crystallographic study in an attempt to investigate the conformational features of the title compound for

[1]Author to whom correspondence may be addressed.

Can. J. Chem. Downloaded from www.nrcresearchpress.com by 92.62.229.171 on 09/08/12
For personal use only.

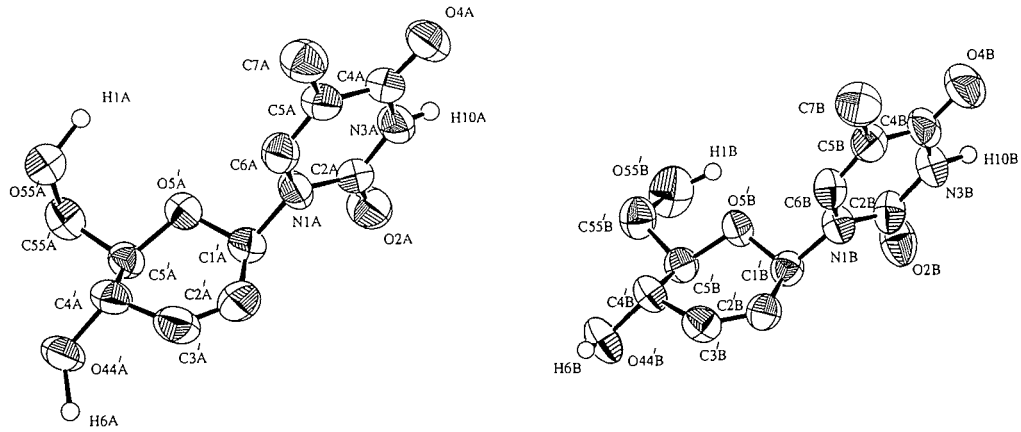

FIG. 1. An ORTEPII (21) plot of the two molecules (**I** and **II**) in the asymmetric unit with 50% probability anisotropic thermal ellipsoids for the non-H atoms (nominal isotropic for H's) and atomic numering scheme. Some hydrogens have been omitted for clarity.

comparison with those of AZT, as a predictive tool for its activity.

Crystal data

$C_{12}H_{14}O_5N_2$ fw = 254.24

Monoclinic, a = 7.966(3), b = 18.004(3), c = 8.346(3) Å, β = 91.29(3)°, V = 1196.6(6) Å^3, Z = 4, D_x = 1.411, Mg m^{-3}, μ = 9.13 cm^{-1}, $F(000)$ = 536(298 K; CuKα,λ = 1.54178 Å), space group $P2_1$ (from absent reflections condition and structure analysis).

Experimental

The title compound was synthesized by condensation of the pertrimethylsilylated thymine with the 3,4,6-tri-*O*-acetyl-D-glucal according to the method reported by Kondo, Nakai, and Goto (7) for uracil. Crystals were obtained by slow evaporation of a methanol/ethyl acetate solution of the compound. Data were collected using a colorless crystal of dimensions 0.30 × 0.25 × 0.40 nm on a Rigaku AFC6S diffractometer equipped with an evacuated beam collimator and detector tunnel. Graphite monochromated CuKα radiation was employed with the intensities measured 400 mm from the crystal. Measured data to 2θ = 106° included reflections h (0–8), k (0–18), l (−8–8). Scans were of the ω–2θ type, where the ω scan speed was 32° min^{-1}. The scan width in ω was (1.57 + 0.30 tan θ)° and weak reflections were rescanned up to four times and the counts accumulated. Of the 1582 reflections measured, 1460 were considered unique; for averaged data R_{int} = 0.035; 1285 reflections (88%) were classified as observed, having $F^2 \geq 3\sigma(F^2)$. Three standard reflections monitored throughout data collection showed less than 1% change in their intensities over the period of the experiment, indicating no decay correction was required. Lorentz–polarization corrections were applied and an empirical absorption correction was included in the data processing step (transmission factors, 0.875–1.000, based on ψ-scans of three reflections).

The structure was solved by direct methods.[2] The phase set with the highest combined figure of merit yielded an E-map showing the complete heavy-atom framework of two independent molecules in the asymmetric unit. The non-H atoms were refined to conver-

TABLE 1. Final fractional positional parameters and equivalent isotropic thermal parameters (Å^2) with esd's in parentheses

Atom	x	y	z	B_{eq}[a]
O2A	0.4172(5)	0.8913	−0.1269(5)	5.9
O4A	0.4109(5)	0.7177(3)	0.2637(5)	6.4
O5'A	0.7029(4)	1.0151(3)	0.0974(4)	4.5
O44'A	0.6890(6)	1.2131(3)	0.1910(5)	5.4
O55'A	1.0093(4)	1.0647(3)	0.2253(5)	5.6
N1A	0.4987(5)	0.9260(3)	0.1254(5)	4.6
N3A	0.4175(6)	0.8061(4)	0.0740(6)	4.9
C1'A	0.5295(7)	1.0030(4)	0.0760(8)	5.1
C2A	0.4426(6)	0.8753(4)	0.0137(7)	4.6
C2'A	0.4242(7)	1.0572(5)	0.1637(8)	6.0
C3'A	0.4885(8)	1.1176(4)	0.2303(8)	5.7
C4A	0.4412(7)	0.7823(4)	0.2297(7)	4.8
C4'A	0.6694(7)	1.1350(4)	0.2195(6)	4.5
C5A	0.5033(6)	0.8379(4)	0.3388(6)	4.7
C5'A	0.7474(6)	1.0925(4)	0.0847(6)	4.1
C6A	0.5277(7)	0.9063(4)	0.2834(7)	4.9
C7A	0.5378(8)	0.8168(4)	0.5101(8)	6.1
C55'A	0.9347(7)	1.0959(4)	0.0874(7)	5.2
O2B	0.0621(6)	0.7493(3)	0.5914(5)	6.5
O4B	0.0613(6)	0.9131(4)	0.1812(6)	7.0
O5'B	0.0367(4)	0.5965(3)	0.3438(4)	4.2
O44'B	−0.1744(6)	0.4184(3)	0.3568(5)	5.9
O55'B	0.3196(5)	0.5150(4)	0.4040(6)	7.4
N1B	−0.0670(5)	0.7148(4)	0.3567(5)	4.5
N3B	0.0531(6)	0.8313(3)	0.3848(6)	5.1
C1'B	−0.0919(6)	0.6385(4)	0.4140(6)	4.1
C2B	0.0206(7)	0.7637(4)	0.4544(7)	5.1
C2'B	−0.2608(7)	0.6096(4)	0.3739(6)	4.5
C3'B	−0.2825(7)	0.5419(4)	0.3208(7)	4.7
C4B	0.0194(7)	0.8515(4)	0.2278(8)	5.1
C4'B	−0.1391(6)	0.4901(4)	0.2945(7)	4.2
C5B	−0.0717(7)	0.7976(4)	0.1306(7)	4.9
C5'B	0.0174(6)	0.5191(4)	0.3780(7)	4.4
C6B	−0.1058(7)	0.7334(4)	0.2001(7)	4.7
C7B	−0.1125(9)	0.8161(5)	−0.0391(8)	7.1
C55'B	0.1783(7)	0.4835(5)	0.3224(8)	5.4

[a] $B_{eq} = \frac{8\pi^2}{3} \sum_{i=1}^{3} \sum_{j=1}^{3} U_{ij} a_i^* a_j^* \vec{a}_i \cdot \vec{a}_j$.

[2] All computation was carried out using the TEXSAN software package (an integrated system of crystal structure solution, refinement, and analysis programs available from Molecular Structure Corporation, The Woodlands, Texas 77381). Package contains versions of MITHRIL (8), ORFLS (9), and ORFFE (10).

Can. J. Chem. Downloaded from www.nrcresearchpress.com by 92.62.229.171 on 09/08/12
For personal use only.

Can. J. Chem. Downloaded from www.nrcresearchpress.com by 92.62.229.171 on 09/08/12
For personal use only.

gence and subsequent difference Fourier maps revealed 21 of the hydrogens. Full-matrix least-squares refinement continued to convergence with all non-H atoms assigned anisotropic thermal parameters, and available H's assigned isotropic temperature factors. At this stage, a difference map indicated positions for four of the six methyl H's, but attempts to refine them were unsuccessful. However, these positions were used in orienting all six methyl hydrogens in ideal positions. The H of O44′A was difficult to locate. Difference maps showed two very small peaks, both in chemically reasonable positions to be the hydrogen of O44′A. When each peak position was refined individually as the hydrogen, the refinement tended to shift the hydrogen toward the other peak coordinates. This difficulty in refining the H position, in combination with the development of a large temperature factor associated with the atom, suggested the possibility that the hydrogen was disordered. Therefore, the H6A occupancy was assigned 0.5 at each of the two observed peak positions on the difference map and refined along with all other atoms. Their coordinates and isotropic temperature factors were allowed to vary in subsequent refinement cycles. No attempt to determine the occupancies of the disordered hydrogen was made. From this point, convergence of the entire structure was reached within three cycles and yielded $R = 0.0322$ and $wR = 0.0413$ for 1285 observed data where $R = \Sigma||F_o| - |F_c||/\Sigma|F_o|$ and $wR = \Sigma w||F_o| - |F_c||^2/\Sigma w|F_o|^2$. The maximum parameter shift was 0.16σ on the final cycle of refinement and the standard deviation in an observation of unit weight was 1.831 for 417 variables. The function minimized was $\Sigma w(|F_o| - |F_c|)^2$, where $w = 4F_o^2/\sigma^2(F_o^2)$; a weighting analysis confirmed the suitability of the chosen weights by showing uniform average values of $\Sigma w(|F_o| - |F_c|)^2$ over ranges of index classes, F_o, and sin θ/λ. Following convergence, the peaks on the difference Fourier map had densities corresponding to ± 0.16 e Å^{-3} randomly scattered throughout the cell. When the complete data set was used $R = 0.0387$ and $wR = 0.0486$. The enantiomer refined was chosen on the basis of the chirality of the starting sugar (*vide supra*). Scattering factors and anomalous dispersion corrections for non-hydrogen atoms were from ref. 11, and from ref. 12 for the scattering factors of hydrogen. Final atomic positional parameters and equivalent isotropic thermal parameters are given in Table 1.[3] Molecules in the asymmetric unit are displayed in Fig. 1 along with the atom labels.

Results and discussion

Molecular geometry

Bond lengths and bond angles are given in Table 2. The two independent molecules in the asymmetric unit possess similar molecular dimensions, with bond lengths and angles that are within the normal range (13). The two molecules differ, most notably, in their *N*-glycosidic torsion angles (23) (χ, O5′—C1′—N1—C6), which are 64.5(6)° (+*sc*) in **I** and 72.7(6)° (+*sc*) in **II**, as well as in the values of their torsion angles (γ) C4′—C5′—C55′—O55′, which are 62.07(7)° (+*sc*) in **I**, and 178.6(5)° (+*ap*) in **II**. The value of γ adopted by **I** represents a more sterically hindered (close O55′A···C4′A contact), thus less energetically favorable, conformation than the value found in **II**, the attainment of which may be ascribed to the fact that the O55′A hydrogen, H1A, is involved in an intermolecular hydrogen bond (Table 3). The γ torsion angle in **II** is stabilized by an intramolecular hydrogen bond between H1B and O5′B (Table 3).

The O5′—C1′ bond differs in length from the O5′—C5′ bond in **I**, with the O5′—C5′ bond length being shorter by 0.04(1) Å. An analogous trend is observed in other pyranosyl nucleosides, e.g., amicetin (14), cytosamine triacetate (15), and 1-(2′,3′-dideoxy-β-D-*erythro*-hexopyranosyl)thymine (16). However, the same is not true in **II**, where the O5′—C1′ and O5′—C5′ bond lengths are not significantly different (at $p > 0.05$). The C1′—N1 glycosyl bond distances for **I** and **II** are identical within experimental error, with values of 1.468(8) and 1.470(7) Å, respectively.

The dimensions of the thymine moiety in **I** and **II** are in good agreement with those of 1-methyl thymine (17), thymidine (18), and 1-(2-hydroxyethyl)thymine (19). The thymine rings in both **I** and **II** are essentially planar, with average deviations of ±0.005 Å and ±0.013 Å from their respective mean planes through N1, C2, N3, C4, C5, and C6.

Puckering parameters (20) for the pyrenose rings were found to be $\varphi = 80.2°$, $\theta = 129.1°$, $Q = 0.485$ Å in **I** and $\varphi = 88.6°$, $\theta = 130.9°$, $Q = 0.494$ Å in **II**. These parameters are structurally manifested in both molecules as slightly distorted half-chair conformations (distorted toward twist boats), with O5′ *endo* and C5′ *exo*. The three substituents on the pyrenose rings adopt the less sterically hindered equatorial positions.

Molecules of the title compound form an extensive network of intermolecular hydrogen bonds (Table 3). A packing diagram is given in Fig. 2, in which the disordered hydrogen bonded to O44′A is shown at only one position, viz. H6A′. It is interesting to note (although not shown in Fig. 2) that in both positions H6A and H6A′ the disordered hydrogen is involved in hydrogen bonding interactions (Table 3). The ability to bond in both environments provides an explanation for the observed disorder in H6A. Despite the apparent overlap of the thymine rings in the asymmetric unit, their interplanar spacing of 3.65 Å and their 9.8° dihedral angle indicate that π–π stacking interactions do not have a significant influence on the crystal packing.

Biological implications

Currently, AZT has the highest therapeutic index of the nucleoside analogs that are known to inhibit the replication of HIV-I in vivo. AZT has a well-defined mode of action. It becomes activated, like natural nucleosides, through phosphorylation by cellular kinases, and is subsequently combined with the HIV's reverse transcriptase, resulting in either blockage of the active site as a competitive inhibitor of natural nucleotides, or incorporation into viral DNA leading to premature chain termination. The structural features of AZT, implicated as crucial in recognition by phosphorylating enzymes, are twofold. Firstly, the relative position of the electron-rich terminus of the azido group with respect to the thymine moiety is deemed important (4, 5) from the perspective of hydrogen bonding and potential electrostatic interactions within the active site. Secondly, it is important that the rotation of the base about the *N*-glycosyl bond be energetically feasible, so that the potential for hydrogen bonding interactions between the base and the cognate enzyme can be fully realized, while maintaining the integrity

[3]Supplementary material includes tables of anisotropic thermal parameters, refined H-atom positional and isotropic thermal parameters, bond distances and angles involving H atoms, torsion angles, least-squares planes, and structure factors. This material may be purchased from the Depository of Unpublished Data, Document Delivery, CISTI, National Research Council Canada, Ottawa, Canada K1A 0S2.

Tables of H-atom parameters, bond distances, and bond angles have also been deposited with the Cambridge Crystallograpic Data Centre and can be obtained on request from The Director, Cambridge Crystallographic Data Centre, University Chemical Laboratory, Lensfield Road, Cambridge CB2 1EW, U.K.

TABLE 2. Bond lengths (Å) and angles (°) for non-hydrogen atoms

Bond	Length	Bond	Length
O2A—C2A	1.221(6)	O2B—C2B	1.211(6)
O4A—C4A	1.221(7)	O4B—C4B	1.223(7)
O5′A—C1′A	1.405(6)	O5′B—C1′B	1.411(6)
O5′A—C5′A	1.444(6)	O5′B—C5′B	1.431(6)
O44′A—C4′A	1.436(6)	O44′B—C4′B	1.423(7)
O55′A—C55′A	1.401(7)	O55′B—C55′B	1.421(7)
N1A—C1′A	1.468(8)	N1B—C1′B	1.470(7)
N1A—C2A	1.373(7)	N1B—C2B	1.379(7)
N1A—C6A	1.380(7)	N1B—C6B	1.378(7)
N3A—C2A	1.360(7)	N3B—C2B	1.376(8)
N3A—C4A	1.377(7)	N3B—C4B	1.381(7)
C1′A—C2′A	1.490(9)	C1′B—C2′B	1.475(8)
C2′A—C3′A	1.320(9)	C2′B—C3′B	1.306(8)
C3′A—C4′A	1.480(8)	C3′B—C4′B	1.494(8)
C4A—C5A	1.435(9)	C4B—C5B	1.449(8)
C4′A—C5′A	1.505(7)	C4′B—C5′B	1.508(7)
C5A—C6A	1.330(8)	C5B—C6B	1.324(8)
C5A—C7A	1.499(8)	C5B—C7B	1.484(9)
C5′A—C55′A	1.493(8)	C5′B—C55′B	1.516(8)

Bonds	Angle	Bonds	Angle
C1′A—O5′A—C5′A	112.5(4)	C1′B—O5′B—C5′B	110.9(4)
C1′A—N1A—C2A	119.4(5)	C1′B—N1B—C2B	118.3(5)
C1′A—N1A—C6A	119.1(5)	C1′B—N1B—C6B	120.5(5)
C2A—N1A—C6A	121.5(5)	C2B—N1B—C6B	120.4(5)
C2A—N3A—C4A	128.0(5)	C2B—N3B—C4B	126.9(5)
O5′A—C1′A—N1A	106.3(4)	O5′B—C1′B—N1B	105.2(4)
O5′A—C1′A—C2′A	113.5(5)	O5′B—C1′B—C2′B	112.5(5)
N1A—C1′A—C2′A	112.4(5)	N1B—C1′B—C2′B	112.7(5)
O2A—C2A—N1A	122.7(5)	O2B—C2B—N1B	123.1(6)
O2A—C2A—N3A	123.3(5)	O2B—C2B—N3B	122.5(6)
N1A—C2A—N3A	114.0(5)	N2B—C2B—N3B	114.3(5)
C1′A—C2′A—C3′A	122.0(6)	C1′B—C2′B—C3′B	121.3(6)
C2′A—C3′A—C4′A	121.2(6)	C2′B—C3′B—C4′B	122.4(6)
O4A—C4A—N3A	119.5(5)	O4B—C4B—N3B	119.5(6)
O4A—C4A—C5A	125.7(6)	O4B—C4B—C5B	124.4(6)
N3A—C4A—C5A	114.8(5)	N3B—C4B—C5B	116.0(5)
O44′A—C4′A—C3′A	109.1(5)	O44′B—C4′B—C3′B	110.8(5)
O44′A—C4′A—C5′A	109.0(4)	O44′B—C4′B—C5′B	108.3(4)
C3′A—C4′A—C5′A	110.9(5)	C3′B—C4′B—C5′B	110.1(5)
C4A—C5A—C6A	118.4(5)	C4B—C5B—C6B	116.4(5)
C4A—C5A—C7A	118.8(5)	C4B—C4B—C7B	118.7(6)
C6A—C5A—C7A	122.8(6)	C6B—C5B—C7B	124.8(6)
O5′A—C5′A—C4′A	109.2(4)	O5′B—C5′B—C4′B	109.6(4)
O5′A—C5′A—C55′A	106.6(5)	O5′B—C5′B—C55′B	104.8(4)
C4′A—C5′A—C55′A	113.4(5)	C4′B—C5′B—C55′B	114.1(5)
N1A—C6A—C5A	123.2(6)	N1B—C6B—C5B	125.7(6)
O55′A—C55′A—C5′A	113.7(4)	O55′B—C55′B—C5′B	110.5(5)

TABLE 3. Distances and angles for hydrogen bonds

			Distances (Å)		Angles (°)
D	A	A *at*	D···A	H···A	D—H···A
O55′A—H1A···O4B	$1 + x, y, z$	2.79(7)	1.6(1)	170(7)
O44′A—H6A···O2A	$1 - x, 1/2 + y, -z$	3.35(7)	2.5(3)	124(15)
O44′A—H6A′···O2B	$1 - x, 1/2 + y, 1 - z$	2.74(6)	1.7(1)	165(10)
N3A—H10A···O44′A	$1 - x, -1/2 + y, -z$	2.89(6)	2.07(6)	165(5)
O44′B—H6B···O2A	$-x, -1/2 + y, -z$	2.74(6)	1.90(7)	167(7)
N3B—H10B···O44′B	$-x, 1/2 + y, 1 - z$	2.82(6)	1.91(8)	154(6)
O55′B—H1B···O5′B	x, y, z	2.726(6)	2.30(7)	104(5)

Can. J. Chem. Downloaded from www.nrcresearchpress.com by 92.62.229.171 on 09/08/12
For personal use only.

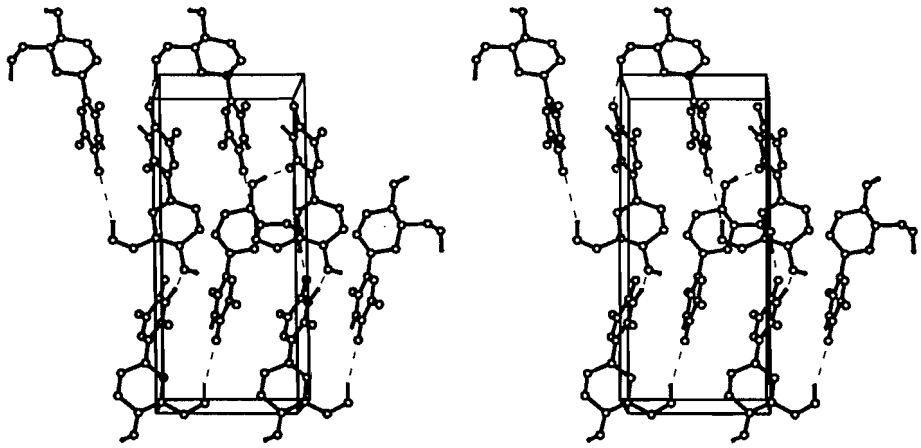

FIG. 2. Stereoscopic view using PLUTO (22) of molecular packing in the unit cell. Some of the hydrogen bonds are indicated by dotted lines. The directions of axes are x ($-a\leftarrow + a$), y ($\uparrow + b$), and z ($+c$ into the page).

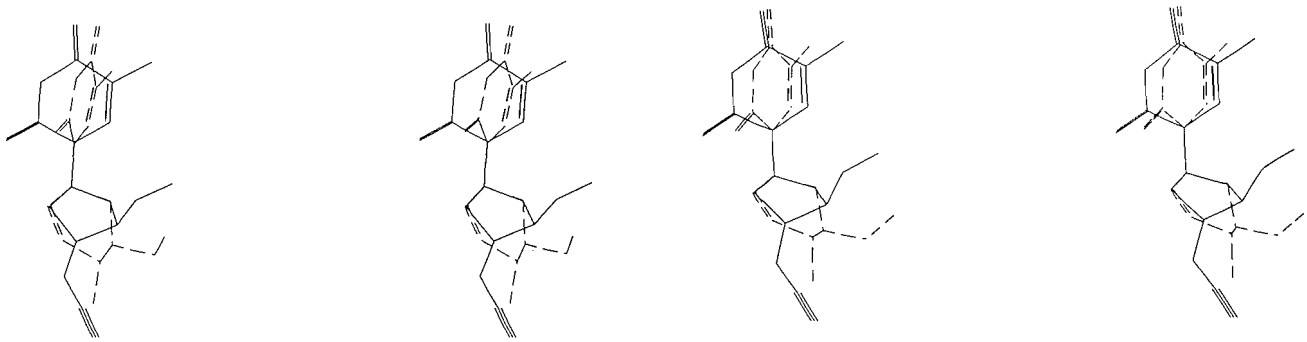

I II

FIG. 3. Stereoscopic views of the crystal structure conformations of the two independent molecules of the title compound (-----) shown with N1, C1′, and C2′ superimposed on N1, C1′, and C2′ of the purported active conformer of AZT (——) (5). Molecule **I** (left). Molecule **II** (right).

TABLE 4. Selected intramolecular distances (Å) for the title compound and AZT (5)

Molecule **I**	Molecule **II**	AZT
O2A—O44′A···6.712(6)	O2B—O44′B···6.535(6)	O2—N3′γ···7.373(3)
N3A—O44′A···7.697(7)	N3B—O44′B···7.654(6)	N3—N3′γ···8.836(4)
O4A—O44′A···9.213(6)	O4B—O44′B···9.227(6)	O4—N3′γ···10.625(4)

of the interaction between the terminal azido nitrogen and the enzyme (5).

It may be suggested that any active analog of AZT must display similar structural features. The structure of the title compound, in both forms **I** and **II**, has been compared to the structure of the purported active conformer of AZT (4, 5), as illustrated in Fig. 3. The relative position of the O44′ hydroxyl (the azido counterpart) and the thymine moiety in the title compound is described by the intramolecular distances listed in Table 4; analogous distances in AZT are included in the table for comparison. Considering the results in Table 4, and the fact that the *inter*atomic distances (Fig. 3) from the terminal azido nitrogen to O44′ in the title structure are only 1.30(1) Å (**I**) and 1.16 (1) Å (**II**), it appears that the title compound exhibits enough structural similarity with AZT to possess a similar capacity for binding within the active site of enzymatic phosphorylation. Although a spatial correspondence between the title compound and AZT exists, the *N*-glycosidic torsion angle χ differs by approximately 70° and 79° when comparing AZT with **I** and **II**, respectively. To ascertain the importance of the differences in χ, the energy required to rotate the base 360° around the *N*-glycosyl bond was calculated at 10° intervals (for both the title compound and AZT), and found to be less than 1 kcal/mol higher for

Can. J. Chem. Downloaded from www.nrcresearchpress.com by 92.62.229.171 on 09/08/12
For personal use only.

the title compound than for AZT.[4] Furthermore, the energy/χ-angle profile is virtually identical in both systems. As this small difference in rotational energy would indicate, the relative values in the crystal of the *N*-glycosidic torsion angle, χ, in AZT and the title structure are not important features in this comparison.

The completion of the enzymatic phosphorylation process requires that at least the following two conditions be met. Firstly, recognition of and binding to the active site must occur. Secondly, it is critical that, once bound, the nucleoside analog presents the oxygen atom to be phosphorylated to the appropriate enzymatic site with positional specificity. Phosphorylation will not likely occur in any nucleoside analog that has its phosphorylation site oriented significantly differently from that in AZT. Figure 3 clearly shows that the sites of phosphorylation in AZT (O5′) and in the title compound (O55′) are oriented quite differently in the superimposed structures. These oxygens, i.e., O5′ and O55′, can only be brought into proximity with each other by having the pyrenose ring undergo the unlikely ring-flip to an alternative conformation with O5′A (or B) *exo* and C5′A (or B) *endo*, which would result in severe steric clashes between the thymine and the C6′ hydrogens. The distances between O5′ in AZT and O55′ in the title structure are 2.336(9) Å **I** and 4.02 (1) Å **II** in the respective comparisons.

On the basis of the above structural comparisons with AZT, the inference is that the title compound would not effectively inhibit the HIV virus. As corroborating evidence for this conclusion, it is interesting to note that, while this work was in progress, the study cited as ref. 2 appeared in the literature indicating that the title compound possesses little activity against the HIV-1 virus in vitro.

Acknowledgement

We gratefully acknowledge financial support by the University of Manitoba and the Natural Sciences and Engineering Research Council of Canada.

[4]All energy calculations were carried out on a Silicon Graphics IRIS 4D70/GT workstation using the program PCMODEL v. 4.0 (Serena Software, Box 3076, Bloomington, Indiana (1990)) with default parameters. Calculations involved rotating χ through 360° in steps of 10° and minimizing the energy of the remainder of the molecule at each step (i.e., allowing the molecule to relax).

1. T. Yamazaki, K. Matsuda, H. Sugiyama, S. Seto, and N. Yamaoka. J. Chem. Soc. Perkin Trans. 1, 1654 (1977).
2. M. Bessodes, M.-J. Egron, J. Filippi, and K. Antonakis. J. Chem. Soc. Perkin Trans. 1, 3035, (1990).
3. I. Dyer, J. N. Low, P. Tollin, H. R. Wilson, and R. A. Howie. Acta Crystallogr. Sect. C: Cryst. Struct. Commun. **C44**, 767 (1988).
4. A. Camerman, D. Mastropaolo, and N. Camerman. Proc. Natl. Acad. Sci. U.S.A. **84**, 8239 (1987).
5. G. I. Birnbaum, J. Giziewicz, E. J. Gabe, T.-S. Lin, and W. H. Prusoff. Can. J. Chem. **65**, 2135 (1987).
6. P. Van Roey, J. M. Salerno, C. K. Chu, and R. F. Schinazi. Proc. Natl. Acad. Sci. U.S.A. **86**, 3929 (1989).
7. T. Kondo, H. Nakai, and T. Goto. Agric. Biol. Chem. **35**, 1990 (1971).
8. G. J. Gilmore. MITHRIL. J. Appl. Crystallogr. **17**, 42 (1984).
9. W. R. Busing, K. O. Martin, and H. A. Levy. ORFLS. Report ORNL-TM-305. Oak Ridge National Laboratory, Tenn. 1962.
10. W. R. Busing, K. O. Martin, and H. A. Levy. ORFFE. Report ORNL-TM-306. Oak Ridge National Laboratory, Tenn. 1964.
11. D. T. Cromer and J. T. Waber. *In* International tables for X-ray crystallography. Vol. IV. Kynoch Press, Birmingham. 1974. pp. 99–102 and 149.
12. R. F. Stewart, E. R. Davidson, and W. T. Simpson. J. Chem. Phys. **42**, 3175 (1965).
13. F. H. Allen, O. Kennard, D. G. Watson, L. Brammer, A. G. Orpen, and R. Taylor. J. Chem. Soc. Perkin Trans. 2, S1 (1987).
14. J. L. Smith and M. Sundralingam. Acta Crystallogr. Sect B: Struct. Crystallogr. Cryst. Chem. **B37**, 1095 (1981).
15. J. Sygusch, F. Brisse, and S. Hannessian. Acta Crystallogr. Sect. B: Struct. Crystallogr. Cryst. Chem. **B30**, 40 (1974).
16. H. L. De Winter, N. M. Blaton, O. M. Peeters, C. J. De Ranter, A. Van Aerschot, and P. Herdewijn. Acta Crystallogr. Sect. C: Cryst. Struct. Commun. **C47**, 838 (1991).
17. K. Hoogsteen. Acta Crystallogr. **16**, 28 (1963).
18. D. W. Young, P. Tollin and H. R. Wilson. Acta Crystallogr. Sect. B: Struct. Crystallogr. Cryst. Chem. **B25**, 1423 (1969).
19. M. Shibata, A. Takenaka, Y. Sasada, and M. Ohki. Acta Crystallogr. Sect. C: Cryst. Struct. Commun. **C41**, 1356 (1985).
20. D. Cremer and J. A. Pople. J. Am. Chem. Soc. **97**, 1354 (1975).
21. C. K. Johnson, ORTEPII. Report ORNL-5138. Oak Ridge National Laboratory, Tenn. (1976).
22. S. Motherwell and W. Clegg. PLUTO. Program for plotting molecular and crystal structures, University of Cambridge, England. (1978).
23. IUPAC–IUC Joint Commission on Biochemical Nomenclature. Pure Appl. Chem. **55**, 1273 (1983).

Can. J. Chem. Downloaded from www.nrcresearchpress.com by 92.62.229.171 on 09/08/12
For personal use only.

Structural study in the oligomethylene dithiobenzoate series, *n*DBS, where *n*, the number of methylene groups, is odd

CLAUDE LEBLANC AND FRANÇOIS BRISSE[1]

Département de chimie, Université de Montréal, C.P. 6128, Succ. A, Montréal (Que.), Canada H3C 3J7

Received December 21, 1989[2]

CLAUDE LEBLANC and FRANÇOIS BRISSE. Can. J. Chem. **70**, 900 (1992).

Model compounds of the poly(oligomethylene thioterephthalates) have been synthesized and characterized by X-ray diffraction analyses. The pink *n*-methylenedithiobenzoates, obtained for $n = 3, 5, 7$, and 9, all have a low melting point of about 320–330 K. They all crystallize in the monoclinic system, space group $P2_1/c$. The *a* and *b* unit cell dimensions vary little while the *c* dimension increases monotonically as *n* changes from 3 to 9. The crystal structure of the four compounds were established from low-temperature X-ray intensities. Except for the lengthening of the methylenic sequence, the four molecules studied here are isostructural. One of the thiobenzoate groups of the molecules is coplanar with all the methylenic carbons, while the other thiobenzoate group is at 90° from the above plane of atoms. The methylenic sequence has the same conformation. It may be described by $g^+(t)_n$, where *n* is the number of methylene groups. Thus, the four compounds belong to a crystallographically homologous series. The molecules form centrosymmetric "dimers," which, in turn, are herring-bone packed in their respective unit cells. In each "dimer" two aromatic rings are across from one another while being mutually perpendicular. On the basis of the above results, one proposes three potentially acceptable structures for the parent poly(oligomethylene thioterephthalates).

Key words: dithiobenzoate, methylene sequence, crystal structure, poly(oligomethylene thioterephthalate).

CLAUDE LEBLANC et FRANÇOIS BRISSE. Can. J. Chem. **70**, 900 (1992).

On a synthétisé des composés modèles des poly(thiotéréphtalates d'oligométhylène) et on les a caractérisés par diffraction des rayons X. Les points de fusion des dithiobenzoates de *n*-méthylène, $n = 3, 5, 7$ et 9, sont tous relativement bas (320–330 K). Ils cristallisent tous dans le système monoclinique, groupe d'espace $P1/c$. Les dimensions *a* et *b* de la maille varient très peu, mais la valeur de *c* augmente d'une façon monotone alors que *n* passe de 3 à 9. On a déterminé les structures cristallines des quatre composés à partir d'intensités mesurées à basse température. À l'exception de l'allongement de la séquence méthylénique, les quatre molécules étudiées sont isostructurales. L'un des groupes thiobenzoates des molécules est coplanaire avec les carbones méthyléniques, alors que l'autre groupe thiobenzoate fait un angle de 90° avec le plan mentionné plus haut. La conformation de la séquence méthylénique est la même dans toutes les molécules. Elle peut être décrite par $g^+(t)_n$, où *n* est le nombre de groupes méthyléniques. D'un point de vue cristallographique, les quatre composés appartiennent donc tous à une série homologue. Les molécules forment des «dimères» centrosymétriques qui s'entassent en chevron dans leurs mailles respectives. Dans chaque «dimère» deux noyaux aromatiques se trouvent placés face à face, tout en étant perpendiculaires l'un à l'autre. Sur la base de ces résultats, on propose trois structures potentiellement acceptables pour les poly(thiotéréphtalates d'oligométhylène) parents.

Mots clés : dithiobenzoate, séquence méthylénique, structure cristalline, poly(thiotéréphtalate d'oligométhylène).

[Traduit par la rédaction]

Introduction

To establish what the geometrical and conformational characteristics of a linear polymer are, we analyzed the constancies and the variations of the bond distances and the bond and torsion angles of small molecules that are chemically and, presumably, structurally related to the parent polymer. This was done by X-ray diffraction from single crystals. We chose this approach since polymer single crystals, suitable for an X-ray structural determination, cannot usually be obtained. However, X-rays interact with a partially crystalline, or ordered, polymer to produce a fiber diffraction pattern containing a limited amount of information. Thus, the structural data derived from the model compounds is very useful in the interpretation of the fiber pattern.

The structures of the poly(*n*-methylene terephthalates) or *n*GT's were investigated in this laboratory for $n = 2$–6 through the use of their model compounds, the oligomethylene dibenzoates and their di-*para*-substituted analogs: 3 GT(1), 4 GT(2), 6 GT(3, 4).

However, very little has been reported so far on the synthesis or the structure of dicarboxylic dithiol polyesters (5). We have undertaken a systematic study of such polymers where the diacid is terephthalic acid. The present work deals with model compounds of the poly(*n*-methylene thioterephthalates), the sulfur relatives of the above-mentioned *n*GT's. The model compounds chosen to represent the poly(*n*-methylene thioterephthalates) are the *n*-methylene dithiobenzoates (or *n*DBS). It is the synthesis and the analysis of the properties of the odd members of this series (3 DBS, 5 DBS, 7 DBS, and 9 DBS) which are reported here.

Experimental

The *n*-methylene dithiobenzoates are prepared in a two-step process. First, potassium thiobenzoate is obtained by reacting thiobenzoic acid and KOH at 0°C in the presence of MeOH. In the second step, the potassium salt is made to react with the dibromoalkane of interest, in the presence of MeOH, and refluxed for 6 h at 65°C.

$$2C_6H_5COS^- K^+ + Br(CH_2)_nBr \rightarrow C_6H_5COS(CH_2)_nSCOC_6H_5 + 2KBr$$

At the end of the reaction the product precipitates. It is filtered and purified by recrystallization in MeOH. All the compounds

[1]Author to whom correspondence may be addressed.

[2]Revision received September 23, 1991.

Can. J. Chem. Downloaded from www.nrcresearchpress.com by 92.62.229.171 on 09/08/12
For personal use only.

TABLE 1. Crystal data of interest for *n*DBS, where *n* is odd

Parameter	3 DBS	5 DBS	7 DBS	9 DBS
Molecular formula	$C_{17}H_{16}O_2S_2$	$C_{19}H_{20}O_2S_2$	$C_{21}H_{24}O_2S_2$	$C_{23}H_{28}O_2S_2$
Molecular weight	316.44	344.50	372.55	400.59
Melting point (K)	328	320	332	328
Unit cell	Monoclinic	Monoclinic	Monoclinic	Monoclinic
a (Å)	9.008(3)	9.170(5)	9.307(3)	9.381(5)
b	5.865(3)	5.787(4)	5.682(2)	5.604(3)
c	30.659(7)	33.553(10)	36.796(11)	40.496(24)
β (deg)	106.56(2)	100.78(3)	95.62(3)	91.47(4)
$c \sin \beta$	29.386	32.921	36.619	40.483
V (Å^3)	1552.7	1749.1	1936.5	2128.2
d_o (g cm^{-3})	1.30	1.24	1.23	1.20
d_c	1.354	1.308	1.278	1.250
Z	4	4	4	4
Space group	$P2_1/c$	$P2_1/c$	$P2_1/c$	$P2_1/c$
F(000)	664	728	792	856
μ(radiation) (cm^{-1})	3.29 (Mo)	2.98 (Mo)	2.74 (Mo)	23.3 (Cu)
T (K)	163	143	143	178

prepared in this manner are pink and are obtained in high yields (80–90%).

Crystals, in the form of thin platelets suitable for X-ray analysis, were obtained by slow evaporation of their respective methanolic solutions. The unit-cell dimensions were obtained with the Enraf–Nonius CAD4 diffractometer by least-squares analysis of the diffractometer setting angles of 25 well-centered reflections in the range $30° < 2\theta < 44°$ for 3 DBS, 5 DBS, and 7 DBS, and $40° < 2\theta < 45°$ for 9 DBS. The low temperature required for the X-ray data collection of all four compounds was maintained using a modified Nonius cooling system. The temperature achieved was stable to ±4°. The crystal data of interest are given in Table 1. The intensity data were recorded using the $\omega/2\theta$ scan technique with a scan range calculated by $\Delta\omega = (1.00 + 0.35 \tan \theta)°$ and the graphite monochromatized Mo radiation, $\lambda(\text{MoK}\bar{\alpha}) = 0.71069$ Å. For 9 DBS, the X-ray intensities were obtained with the graphite monochromatized copper radiation, $(\text{CuK}\bar{\alpha}) = 1.54178$ Å, while the scan range was calculated by $\Delta\omega = (0.80 + 0.14 \tan \theta)°$. The intensities of seven reference reflections were monitored every hour and showed no significant decay of the crystals. The orientation of the crystals was verified every 100 measurements. The intensity data were reduced to a common scale using standard procedures.[3] Lorentz and polarization corrections, as well as an absorption correction based on the geometrical description of the crystal, were applied in all cases.

The structures were solved by direct methods. All the non-hydrogen atoms were found on E-maps calculated with the set of phases having the highest combined figure of merit. The structures were refined at first by a full-matrix least-squares procedure minimizing $\Sigma w(|F_o| - |F_c|)^2$. The weights applied were derived from the counting statistics of the measured intensities. After all H atoms were localized, the final refinements proceeded in the block-diagonal approximation, with anisotropic temperature factors for the non-hydrogen atoms and isotropic for H atoms. The refinements all converged satisfactorily. The details of the data collection and least-squares refinements are summarized in Table 2. The scattering curves for the non-hydrogen atoms were taken from ref. 9 and those for H atoms from ref. 10. The anomalous scattering contributions of the S atoms were included in the structure factor calculations (11). The atomic coordinates are listed in Tables 3 (*a*)–(*d*) while the structure factor tables have been deposited as part of the Supplementary Material.[4]

Results and discussion

All the *n*DBS compounds remain pink even after four recrystallizations. Their melting points are low and in a relatively narrow range of temperatures, 320–330 K. The melting points do not seem to be correlated with either the methylene chain length or its parity, as these values are also in the neighbourhood of those found when the number of methylene groups is even.[5] The unit-cell dimensions (a, b, c, β, V) vary regularly with n, the number of methylene groups (see Table 1 and Fig. 1). The two dimensions a and b change only slightly while c, the product $c \sin \beta$, and the unit-cell volume, V, increase significantly as n changes from 3 to 9. These linear variations have been parametrized, as follows, as a function of n:

$$a(\text{Å}) = 6.280 \times 10^{-2}\, n + 8.840 \quad (\sigma = 0.032)$$

$$b(\text{Å}) = -4.440 \times 10^{-2}\, n + 6.001 \quad (\sigma = 0.008)$$

$$c(\text{Å}) = 1.6377\, n + 25.550 \quad (\sigma = 0.286)$$

$$c \sin \beta\ (\text{Å}) = 1.8517\, n + 23.738 \quad (\sigma = 0.111)$$

$$V\ (\text{Å}^3) = 95.710\, n + 1267.4 \quad (\sigma = 2.67)$$

As will be seen later, such a regular evolution of the unit-cell parameters is an indication that the molecules are very sim-

[3]The programs used here are modified versions of the NRC set of programs (NRC-2, data reduction; NRC-3, absorption correction; NRC-10, bond distances and angles; NRC-22, mean planes), MULTAN80, and ORTEP (6–8).

[4]Tables of hydrogen atom positional parameters, anisotropic temperature factors, and the observed and calculated structure amplitudes are available. Copies may be purchased from the Depository of Unpublished Data, Document Delivery, CISTI, National Research Council Canada, Ottawa, Canada K1A 0S2.

Tables of H-atom fractional coordinates have also been deposited with the Cambridge Crystallographic Data Centre and can be obtained on request from The Director, Cambridge Crystallographic Data Centre, University Chemical Laboratory, Lensfield Road, Cambridge CB2 1EW, U.K.

[5]C. Leblanc and F. Brisse. To be published.

Can. J. Chem. Downloaded from www.nrcresearchpress.com by 92.62.229.171 on 09/08/12
For personal use only.

TABLE 2. Summary of data collections and least-squares refinements

Parameter	3 DBS	5 DBS	7 DBS	9 DBS
h, k, l ranges	$0 \le h \le 11$ $0 \le k \le 7$ $-37 \le l \le 37$	$0 \le h \le 11$ $0 \le k \le 7$ $-40 \le l \le 40$	$0 \le h \le 11$ $0 \le k \le 7$ $-44 \le l \le 44$	$0 \le h \le 11$ $0 \le k \le 7$ $-49 \le l \le 49$
$2\theta_{max}$ (deg)	50.0	50.0	50.0	140.0
Maximum fluctuation of standard reflections (%)	1.8	3.1	3.9	5.5
Number of reflections measured	2718	3056	3373	4044
Number of observed reflections	1717	1878	2452	3273
when $I \ge k\sigma(I)$, k	1.96	1.96	1.96	1.96
Range of transmission factor (%)	91–98	92–98	88–97	47–89
Crystal size (mm)	0.07 × 0.30 × 0.41	0.06 × 0.30 × 0.44	0.10 × 0.32 × 0.52	0.05 × 0.27 × 0.38
$R = \Sigma\|\|F_o\| - \|F_c\|\|/\Sigma\|F_o\|$	0.054	0.052	0.045	0.068
$R_w = [\Sigma w\Delta F^2/\Sigma wF_o^2]^{1/2}$	0.035	0.040	0.043	0.056
$S = [\Sigma w\Delta F^2/(m - n)]^{1/2}$	1.82	1.50	1.95	4.50
Displacement/σ, average	0.07	0.025	0.07	0.06
Extreme fluctuations of residual electron density (e Å^{-3})	−0.30, 0.29	−0.31, 0.36	−0.28, 0.26	−0.26, 0.38

TABLE 3(*a*). Final atomic coordinates and their esd's (S × 10^5, O, C × 10^4) and U_{eq} (×10^4) for 3 DBS

$$U_{eq} = \frac{1}{3}\sum_i \sum_j U_{ij}\, a_i^* a_j^* a_i \cdot a_j$$

Atom	x	y	z	U_{eq}
S(1)	68560(12)	21438(17)	49239(4)	401
S(1′)	119523(13)	−16585(21)	61610(4)	523
O(1)	7500(3)	6407(4)	4814(1)	518
O(1′)	10417(3)	−692(4)	6747(1)	481
C(1)	5143(4)	5218(6)	4293(1)	306
C(1′)	12056(4)	−3931(6)	6957(1)	324
C(2)	4018(4)	3552(6)	4153(1)	405
C(2′)	13138(4)	−5380(6)	6862(1)	387
C(3)	2732(5)	3942(7)	3794(1)	473
C(3′)	13740(4)	−7188(7)	7148(1)	496
C(4)	2552(5)	5981(7)	3554(1)	477
C(4′)	13235(5)	−7573(7)	7528(1)	514
C(5)	3674(5)	7646(7)	3696(1)	478
C(5′)	12166(4)	−6140(7)	7626(1)	467
C(6)	4959(4)	7271(6)	4059(1)	423
C(6′)	11569(4)	−4329(7)	7343(1)	422
C(7)	6564(4)	4907(6)	4679(1)	352
C(7′)	11343(4)	−1965(6)	6659(1)	387
C(8)	8688(4)	2635(6)	5344(1)	401
C(8′)	10908(5)	874(7)	5917(1)	491
C(9)	9344(4)	429(6)	5584(1)	395

TABLE 3(*b*). Final atomic coordinates and their esd's (S × 10^5; C, O × 10^4) and U_{eq} (×10^4) for 5 DBS

Atom	x	y	z	U_{eq}
S(1)	−24007(11)	76854(21)	−13056(3)	483
S(1′)	41381(10)	20095(18)	3553(3)	354
O(1)	−687(3)	6691(5)	−1826(1)	428
O(1′)	3294(3)	−2209(4)	477(1)	421
C(1)	−2233(4)	9959(6)	−2019(1)	271
C(1′)	5510(4)	−1153(6)	926(1)	280
C(2)	−3357(4)	11406(7)	−1941(1)	348
C(2′)	6612(4)	467(7)	1045(1)	347
C(3)	−3838(4)	13234(7)	−2202(1)	432
C(3′)	7776(4)	−21(7)	1360(1)	420
C(4)	−3214(4)	13637(7)	−2534(1)	423
C(4′)	7836(4)	−2091(7)	1562(1)	438
C(5)	−2102(4)	12221(8)	−2615(1)	418
C(5′)	6732(4)	−3692(7)	1450(1)	416
C(6)	−1619(4)	10380(7)	−2359(1)	364
C(6′)	5572(4)	−3229(6)	1135(1)	361
C(7)	−1635(3)	7984(7)	−1750(1)	319
C(7′)	4234(4)	−747(6)	588(1)	301
C(8)	−1439(4)	5141(7)	−1081(1)	429
C(8′)	2463(4)	1592(6)	−18(1)	334
C(9)	−15(4)	5599(7)	−787(1)	387
C(9′)	2000(4)	3784(6)	−254(1)	352
C(10)	566(4)	3445(7)	−556(1)	363

ilar in conformation and in crystal packing. A similar pattern was reported (12) in the *N,N′*-oligomethylene bisbenzamide series when, however, the number of methylene groups is even.

Structural results

The atomic numbering of the *n*DBS molecules is reported in Fig. 2 while drawings of the molecules are shown in Fig. 3. It is apparent that the molecules in the series have the same conformation. The main feature of these molecules, which are chemically symmetrical, is their lack of symmetry in the solid state. An examination of Fig. 3 reveals that the two thiobenzoate groups of a given molecule have totally different orientations with respect to the methylenic sequence. To establish this quantitatively, the bond distances, bond angles, and torsion angles are compared in Tables 4 and 5. In each aromatic ring, the average value of the intracyclic bond angles is 120°. However, the usual narrowing of the bond angle at C(1), due to the conjugation between the thioester group and the aromatic ring, is observed (13). Indeed, the average value of the C(6)—C(1)—C(2) angles is 118.9°, while the individual values are in the range of 118.3(3)°–119.6(3)°. Concurrently the C(1)—C(7) bond distance is slightly shorter; its average is 1.493 Å. The average C(sp^2)—C(sp^2) distance is 1.383(3) Å in 3 DBS, 1.380(5) Å in 5 DBS, 1.385(4) Å in 7 DBS, and 1.386(8) Å in 9 DBS,

Can. J. Chem. Downloaded from www.nrcresearchpress.com by 92.62.229.171 on 09/08/12
For personal use only.

Can. J. Chem. Downloaded from www.nrcresearchpress.com by 92.62.229.171 on 09/08/12
For personal use only.

TABLE 3(*c*). Final atomic coordinates and their esd's (S × 10^5; C, O × 10^4) and U_{eq} (×10^4) for 7 DBS

Atom	*x*	*y*	*z*	U_{eq}
S(1)	127369(9)	87341(17)	64254(2)	436
S(1′)	51258(8)	11457(14)	44175(2)	357
O(1)	10899(2)	7703(4)	6897(1)	395
O(1′)	6061(2)	−3094(4)	4293(1)	408
C(1)	12364(3)	11019(5)	7075(1)	292
C(1′)	3971(3)	−2122(5)	3903(1)	274
C(2)	13516(3)	12449(6)	7012(1)	334
C(2′)	2850(3)	−598(5)	3820(1)	367
C(3)	13920(3)	14305(6)	7244(1)	389
C(3′)	1778(3)	−1157(6)	3543(1)	450
C(4)	13182(3)	14743(6)	7544(1)	381
C(4′)	1840(3)	−3227(6)	3349(1)	397
C(5)	12038(3)	13341(6)	7612(1)	389
C(5′)	2971(3)	−4758(6)	3430(1)	393
C(6)	11622(3)	11487(6)	7380(1)	334
C(6′)	4035(3)	−4213(5)	3704(1)	344
C(7)	11859(3)	9023(5)	6829(1)	308
C(7′)	5141(3)	−1656(5)	4202(1)	295
C(8)	11872(3)	6149(6)	6221(1)	408
C(8′)	6701(3)	784(6)	4740(1)	373
C(9)	10524(3)	6618(5)	5965(1)	370
C(9′)	6989(3)	2978(6)	4977(1)	359
C(10)	10084(3)	4467(5)	5732(1)	363
C(10′)	8338(3)	2670(6)	5239(1)	364
C(11)	8724(3)	4818(6)	5477(1)	362

TABLE 3(*d*). Final atomic coordinates and their esd's (S × 10^5; C, O × 10^4) and U_{eq} (×10^4) for 9 DBS

Atom	*x*	*y*	*z*	U_{eq}
S(1′)	104249(10)	1979(17)	57677(2)	468
S(1)	20003(10)	96748(19)	34697(3)	510
O(1′)	9413(2)	−4032(4)	5883(1)	509
O(1)	3959(2)	8632(4)	3045(1)	452
C(1′)	11415(3)	−3097(6)	6230(1)	348
C(1)	2537(3)	11970(6)	2884(1)	317
C(2′)	12535(4)	−1562(6)	6303(1)	457
C(2)	1354(3)	13402(6)	2944(1)	397
C(3′)	13520(4)	−2141(7)	6554(1)	546
C(3)	1003(3)	15268(6)	2730(1)	441
C(4′)	13390(4)	−4214(7)	6731(1)	487
C(4)	1828(3)	15712(7)	2460(1)	446
C(5′)	12259(4)	−5724(6)	6660(1)	477
C(5)	3001(3)	14299(7)	2396(1)	450
C(6′)	11284(3)	−5167(6)	6411(1)	432
C(6)	3353(3)	12415(6)	2608(1)	397
C(7′)	10335(3)	−2601(6)	5962(1)	388
C(7)	2980(3)	9964(6)	3108(1)	393
C(8′)	8915(4)	−108(6)	5481(1)	443
C(8)	2821(4)	7054(7)	3655(1)	480
C(9′)	8731(4)	2061(7)	5267(1)	448
C(9)	4066(4)	7560(6)	3891(1)	452
C(10′)	7481(4)	1797(7)	5025(1)	452
C(10)	4424(3)	5402(6)	4104(1)	426
C(11′)	7233(4)	3948(7)	4803(1)	459
C(11)	5687(3)	5764(6)	4339(1)	451
C(12)	5982(4)	3641(7)	4561(1)	459

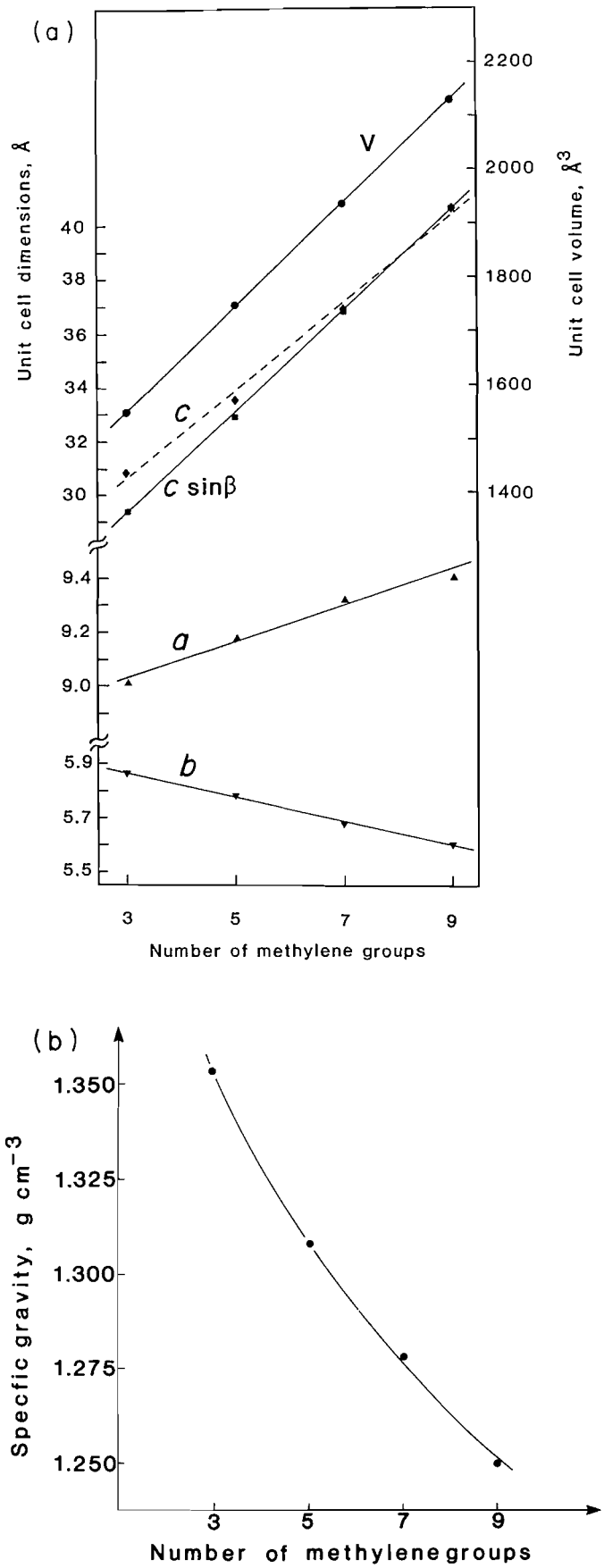

FIG. 1. Variation of the unit-cell parameters (*a*) and the specific gravity (*b*) with *n* the number of methylene groups in the odd *n*DBS.

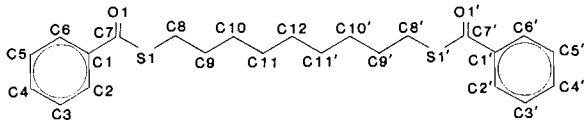

FIG. 2. Atomic numbering adopted for the *n*DBS molecules.

in good agreement with the compilation found in *Molecular structures and dimensions* (14). The thioester groups are planar. However, the bond angles show the same deviation from 120° as was reported for the ester groups. The C(1)—C(7)—O, O—C(7)—S, C(1)—C(7)—S bond angles have average values of 122.5(4), 121.5(3), and 115.9(3)° respectively. The C(sp^2)—S and C(sp^3)—S distances, with averages of 1.769(4) and 1.808(5) Å, agree well with their respective published values of 1.76 and 1.80 Å (14). The two S—C(8)—C(9) bond angles behave unusually since they systematically take significantly different values depending upon which end of the molecule is considered (Table 5). At the unprimed end, the S—C(8)—C(9) angles average 114.9(3)°, while at the primed end of the molecules the average is 111.4(3)°. In the methylenic sequence itself, the C—C bond distances vary over a large interval, from 1.499(5) to 1.530(4) Å, and average 1.515 Å. The C—C—C bond angles behave in a similar way: average 112.7°, range 109.8(3)°–114.9(3)°. It should be pointed out that the first and the last angles in the sequence, C(8)—C(9)—C(10), are always smaller than any of the others and show little variation. Their range is only from 109.8(3)° to 111.7(3)°. In other words, it seems that the central part of the chain is a bit more flexible or deformable than its ends, which are attached to S atoms. The torsion angles within the aliphatic sequence are all *trans*. However, the unusual behavior noted for the θ = S—C(8)—C(9) angles is also reflected in the τ = C(7)—S—C(8)—C(9) torsion angles. The primed values are in the range 173.8°–179.8°, while the unprimed ones range from 89.6° to 91.8°. Thus, at the unprimed end of the molecule, a "pseudo" *gauche* torsion angle corresponds to a large θ = S—C(8)—C(9) bond angle, while at the primed end a *trans* conformation is associated with a smaller value of θ. This observation may be rationalized when one compares the schematic representation and the Newman projections, along the C(8)—S bond, of the two ends of the molecules (Fig. 4). At the primed end of the molecule, the carbonyl group is *gauche* to two hydrogen atoms and the C(8′)—C(9′) bond is in the ester plane, τ′ = C(7′)—S′—C(8′)—C(9′) ~ 180°, and thus does not interact with the p_z orbital on the sulphur atom. However, at the other end (the unprimed end) of the molecule, the carbonyl is "pseudo" *gauche* to the first bond of the aliphatic segment, and also "pseudo" *gauche* to one hydrogen atom. It can be seen that in this case the C(8)—C(9) bond is in the plane containing the large p_z orbital of sulphur (τ =

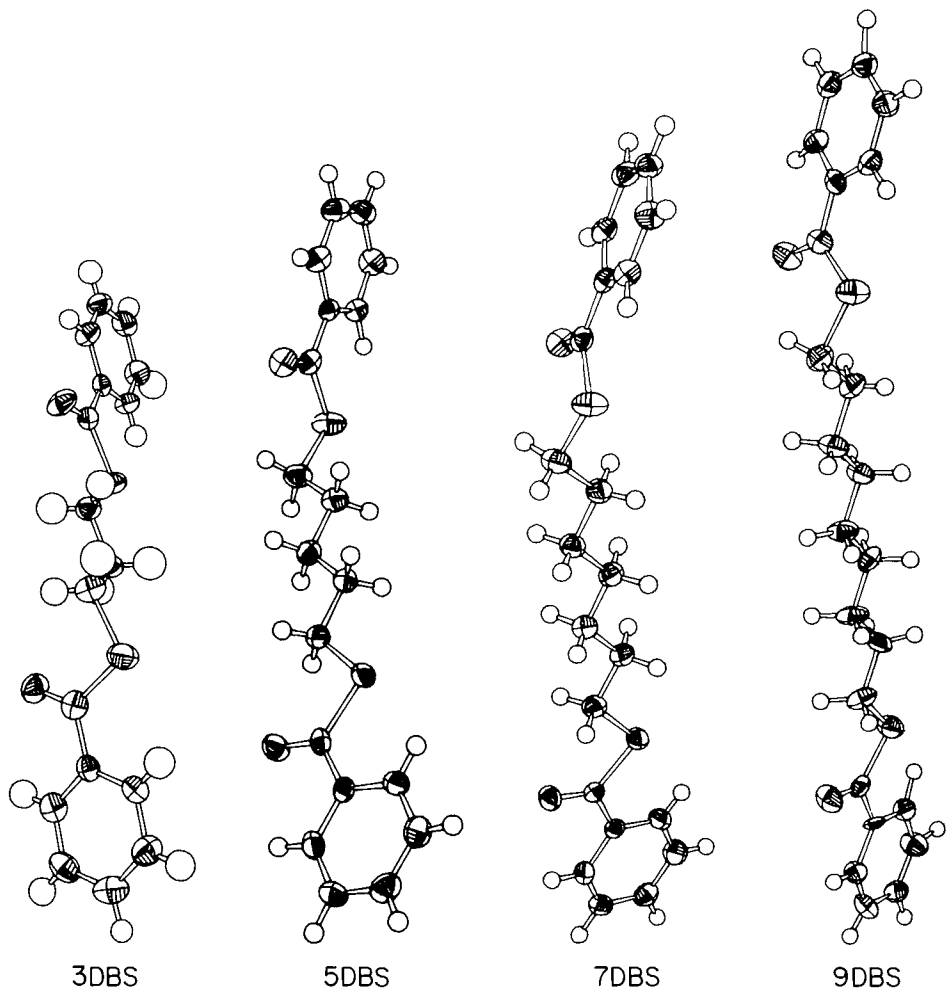

FIG. 3. The *n*DBS molecules shown side by side in the order: 3 DBS, 5 DBS, 7 DBS, 9 DBS.

Can. J. Chem. Downloaded from www.nrcresearchpress.com by 92.62.229.171 on 09/08/12
For personal use only.

TABLE 4. Comparison of the bond distances (Å) and angles (deg) of the aromatic rings and thioester groups in the *n*DBS

	3 DBS		5 DBS		7 DBS		9 DBS	
	1[a]	2[a]	1	2	1	2	1	2
Aromatic ring:								
Distances								
C(1)—C(2)	1.386(5)	1.385(5)	1.390(5)	1.382(5)	1.383(4)	1.367(4)	1.397(5)	1.384(5)
C(2)—C(3)	1.385(6)	1.370(6)	1.391(6)	1.384(5)	1.385(4)	1.391(4)	1.392(5)	1.392(5)
C(3)—C(4)	1.383(6)	1.389(6)	1.364(5)	1.372(6)	1.379(4)	1.380(4)	1.381(6)	1.372(5)
C(4)—C(5)	1.375(6)	1.383(6)	1.374(6)	1.372(6)	1.372(4)	1.376(4)	1.385(5)	1.381(5)
C(5)—C(6)	1.380(6)	1.376(6)	1.388(6)	1.378(5)	1.387(4)	1.377(4)	1.396(5)	1.380(5)
C(6)—C(1)	1.394(5)	1.387(5)	1.385(5)	1.387(5)	1.400(4)	1.400(4)	1.391(5)	1.380(5)
Angles								
C(6)—C(1)—C(2)	119.1(3)	118.9(3)	118.3(3)	118.9(3)	118.3(3)	119.4(3)	119.6(3)	119.0(3)
C(1)—C(2)—C(3)	120.5(4)	120.5(4)	119.9(3)	120.0(3)	120.8(3)	119.7(3)	119.9(3)	119.9(3)
C(2)—C(3)—C(4)	119.7(4)	120.9(4)	120.8(4)	120.6(4)	120.3(3)	120.7(3)	120.0(4)	120.7(3)
C(3)—C(4)—C(5)	120.2(4)	118.5(4)	120.0(4)	119.6(4)	119.8(3)	119.8(3)	120.6(4)	119.3(3)
C(4)—C(5)—C(6)	120.4(4)	120.8(4)	119.9(4)	120.2(4)	120.2(3)	119.8(3)	119.6(3)	120.2(3)
C(5)—C(6)—C(1)	120.1(4)	120.4(4)	120.9(3)	120.6(3)	120.5(3)	120.6(3)	120.2(3)	120.9(3)
Thioester group:								
Distances								
C(1)—C(7)	1.498(5)	1.486(5)	1.495(5)	1.488(5)	1.498(4)	1.494(4)	1.497(5)	1.491(5)
C(7)—O	1.206(5)	1.207(4)	1.210(4)	1.216(4)	1.211(4)	1.207(4)	1.216(4)	1.216(4)
C(7)—S	1.772(4)	1.774(4)	1.771(3)	1.771(4)	1.771(3)	1.779(3)	1.757(4)	1.758(4)
Angles								
C(1)—C(7)—O	122.9(3)	122.9(3)	122.8(3)	122.4(3)	122.6(3)	122.0(2)	122.3(3)	122.2(3)
C(1)—C(7)—S	114.8(3)	116.1(3)	115.1(2)	116.4(2)	115.7(2)	116.7(2)	115.6(3)	116.2(3)
O—C(7)—S	122.3(3)	121.0(3)	122.0(3)	121.0(3)	121.7(2)	121.2(2)	122.2(3)	120.9(3)

[a]1: unprimed atoms; 2: primed atoms.

TABLE 5. Bond distances (Å), bond angles, and torsion angles (deg) in the aliphatic sequence of the *n*DBS

	3 DBS		5 DBS		7 DBS		9 DBS	
Aliphatic sequence	1[a]	2[a]	1	2	1	2	1	2
Distances								
S—C(8)	1.803(4)	1.804(4)	1.807(4)	1.808(4)	1.804(3)	1.805(3)	1.812(4)	1.817(4)
C(8)—C(9)	1.508(6)	1.522(5)	1.506(5)	1.513(5)	1.517(4)	1.530(4)	1.517(5)	1.499(5)
C(9)—C(10)			1.511(5)	1.515(5)	1.526(4)	1.516(4)	1.519(5)	1.517(5)
C(10)—C(11)					1.513(4)	1.524(4)	1.513(5)	1.518(5)
C(11)—C(12)							1.512(5)	1.519(5)
Angles								
θ = S—C(8)—C(9)	114.5(3)	111.0(3)	115.2(3)	111.7(2)	115.1(2)	111.6(2)	114.9(3)	111.6(3)
C(8)—C(9)—C(10)	109.8(3)		111.7(3)	111.4(3)	111.6(2)	110.9(2)	111.4(3)	111.7(3)
C(9)—C(10)—C(11)			114.5(3)		113.9(2)	114.0(2)	114.2(3)	114.2(3)
C(10)—C(11)—C(12)					112.7(2)		113.3(3)	113.3(3)
C(11)—C(12)—C(13)							114.9(3)	
Torsion angles								
τ = C(7)—S—C(8)—C(9)	91.8(3)	173.8(3)	91.4(3)	175.5(2)	89.8(2)	−179.8(2)	91.0(6)	−178.8(5)
ϕ_1 = S—C(8)—C(9)—C(10)	170.8(3)	−177.4(3)	169.4(3)	−178.0(2)	165.4(2)	−178.4(2)	164.2(5)	179.3(5)
ϕ_2 = C(8)—C(9)—C(10)—C(11)			180.0(3)	176.7(3)	178.7(2)	−178.2(2)	178.3(6)	179.5(6)
ϕ_3 = C(9)—C(10)—C(11)—C(12)					178.1(2)	−179.3(2)	177.2(6)	−179.7(6)
ϕ_4 = C(10)—C(11)—C(12)—C(13)							−179.3(6)	179.1(6)
C(2)—C(1)—C(7)—S	−6.0(5)	−1.5(5)	−2.9(5)	−2.9(5)	−5.1(4)	−6.6(4)	−4.9(9)	−6.5(9)
C(2)—C(1)—C(7)—O	176.1(4)	179.0(4)	177.8(3)	177.6(3)	175.9(3)	173.9(3)	175.6(7)	174.7(7)
C(6)—C(1)—C(7)—S	179.0(4)	177.1(3)	176.1(3)	175.6(3)	173.8(3)	173.8(2)	174.5(5)	173.3(5)
C(6)—C(1)—C(7)—O	−4.9(5)	−2.5(6)	−3.2(5)	−3.8(5)	−5.2(4)	−5.8(4)	−5.1(10)	−5.4(10)

[a]1: unprimed atoms; 2: primed atoms.

Can. J. Chem. Downloaded from www.nrcresearchpress.com by 92.62.229.171 on 09/08/12
For personal use only.

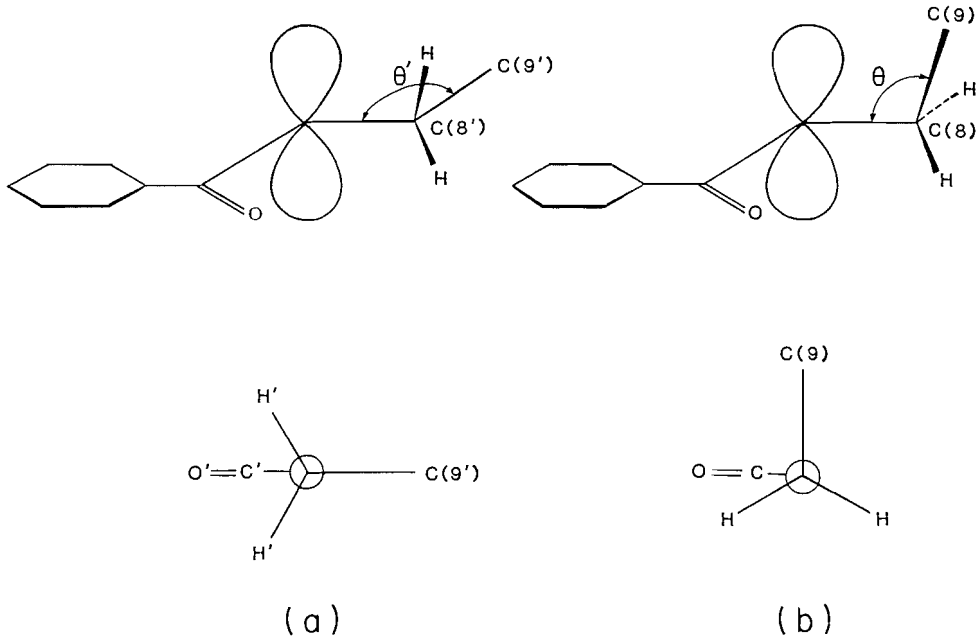

FIG. 4. Schematic representation and Newman projections along the C(8)—S bond of (*a*) the primed end of the molecules, and (*b*) the unprimed end.

TABLE 6. Dihedral angles (deg) of interest

	3 DBS		5 DBS		7 DBS		9 DBS	
Dihedral angle	A[a]	B[a]	A	B	A	B	A	B
1/2 (or ε and ε')	6.1	8.5	3.6	3.6	6.3	5.4	5.3	6.2
2/3	6.5	87.3	5.5	84.8	2.2	80.5	0.3	80.5
1/1'	82.5		78.3		72.8		70.6	

[a]A: unprimed atoms; B: primed atoms.

C(7)—S—C(8)—C(9) ~ 90°). As a consequence there is a strong interaction, which results in an enlargement of the θ = S—C(8)—C(9) bond angle. Experimentally we observe that for τ ~ 90° the angle θ is 110°–111° while for τ' ~ 180°, θ' is 114°–115°.

The conformation of the C(7)-S-C(8)...C(8')-S'-C(7') sequence of atoms is the same for all the odd *n*DBS compounds. It may be described as g^+ttt for 3 DBS, g^+tttt for 5 DBS, and so on, or abbreviated as $g^+(t)_n$, (*g* = *gauche*, $g^+ \approx +60°$, *t* = *trans* ≈ 180°).

As a first approximation the molecules can be seen (Fig. 3) as made up of two nearly planar groups of atoms. The first group is the unprimed thiobenzoate; the second group includes the primed thiobenzoate group, all of the methylenic C atoms, and S. This is clearly appreciated when one compares the primed and unprimed values of the τ = C(7)—S—C(8)—C(9) torsion angles (Table 5). At the unprimed end, this angle is close to 90° while at the primed end its value is nearly 180°, a difference of about 90°. Energetically these two conformations must be very similar. Since there is no chemical reason for this behavior, it is attributed to packing effects. On closer inspection, the previous planes of atoms may be subdivided again since the aromatic rings (plane **1**, made up of C(1) → C(6)) and the thioester groups (plane **2**, C(1), C(7), O, S) are not exactly coplanar although each is individually planar. The dihedral angle, ε, between planes **1** and **2** is small and varies between 2° and 6° and is of the same order of magnitude as that reported in benzoates (15). The methylenic C atoms, between the primed and unprimed thiobenzoates, are nearly coplanar (plane **3**). The dihedral angles between all these planes are given in Table 6 for all odd *n*DBS.

Packing of the molecules

Stereopairs are shown in Fig. 5 (*a*)–(*d*). In all *n*DBS molecules, two centrosymmetrically related molecules adopt a head-to-tail type of disposition (Fig. 6). These "nonbonded dimers" form a layer parallel to the *ab* plane in which the individual molecules are at about 45° from *ab*. In the next layer, observed at *c*/2, the molecules are at −45° from *ab*. Thus when seen in the *bc* projection, the molecules form a herring-bone pattern. This type of packing is reminiscent of that adopted by the *N*,*N*'-oligomethylene dibenzamides with an even number of methylene groups. However, in the latter case, each molecule was H-bonded to two neighboring ones (12). Since the *n*DBS molecules with *n* odd have comparable unit cell dimensions, belong to the same space group, have the same conformation and the same mode of packing,

Can. J. Chem. Downloaded from www.nrcresearchpress.com by 92.62.229.171 on 09/08/12
For personal use only.

Can. J. Chem. Downloaded from www.nrcresearchpress.com by 92.62.229.171 on 09/08/12
For personal use only.

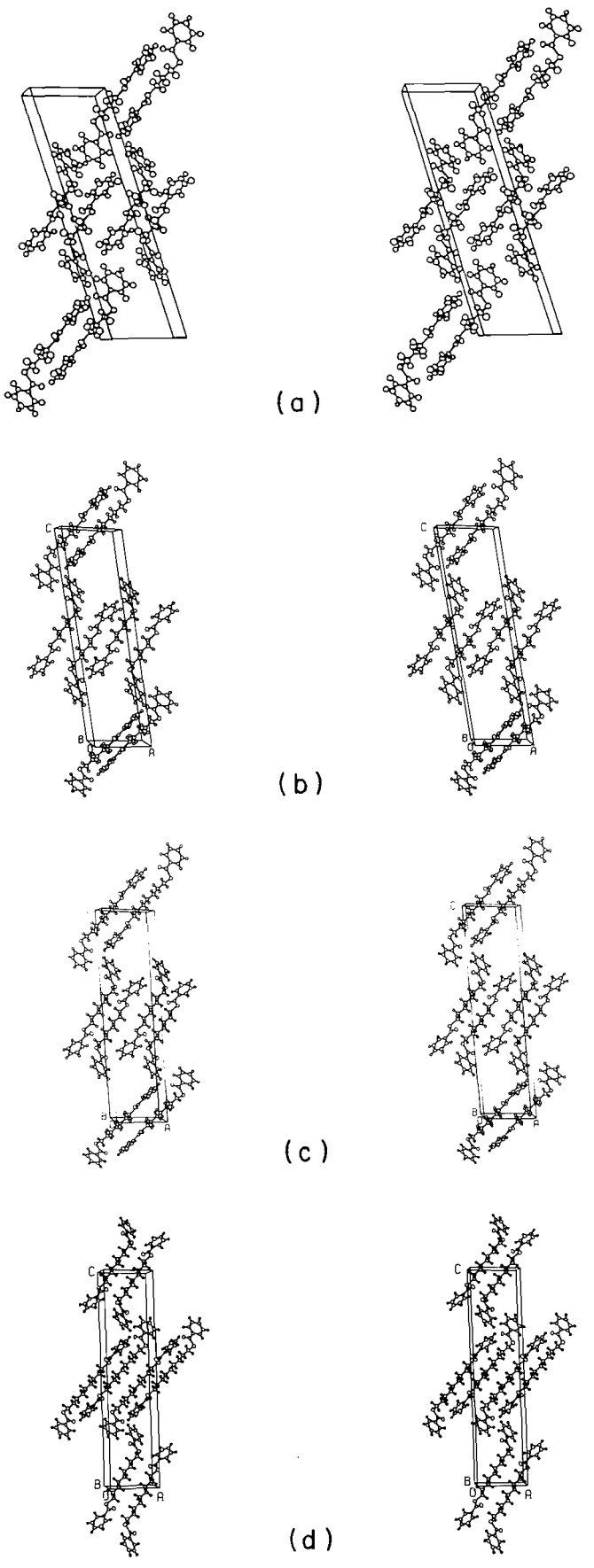

FIG. 5. Packing of the *n*DBS molecules in their respective unit cells. (*a*) 3 DBS; (*b*) 5 DBS; (*c*) 7 DBS; (*d*) 9 DBS.

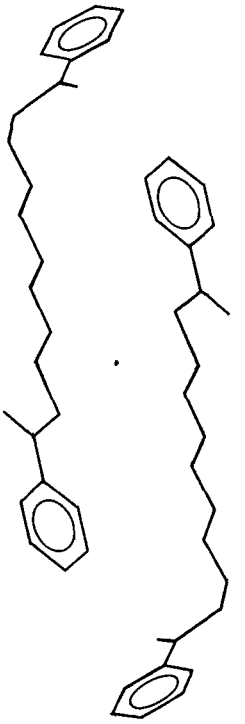

FIG. 6. Head-to-tail disposition of two centrosymmetrically related molecules

they constitute a crystallographically homologous series. Surprisingly there is no such relationship among the *n*DBS molecules with *n* even (see footnote 5).

Extension to the parent polythioester

A reasonably sound structure for the parent polymers, the poly(oligomethylene thioterephthalates), may be proposed using the information derived from the present study of their model compounds. The relation between the polythioester and its model compound is shown in Fig. 7. The fiber repeat, p_o, which is the distance measured along the chain axis between two consecutive crystallographically equivalent units, may be experimentally accessible from measurements of an X-ray fiber pattern of the oriented polymer. Thus, if a polymer and its model compound have the same conformation, the polymer's fiber repeat is also the distance between the centers of the aromatic rings in the model compound. It is expected that the reverse is also true. Many crystal structures of non-chiral synthetic polymers belong to centrosymmetric space groups and, quite often, the polymer chain itself is crystallographically centrosymmetric (3, 16). Assuming that this situation applies here and that the number of methylene groups is odd, the only centers of symmetry will be found in the middle of each terephthaloyl group. However, if the aliphatic segment possesses an even number of methylenes, a further center of symmetry will be found at the mid-point of the central CH_2—CH_2 bond. Consequently, the polymer's fiber repeat is the distance between the centers of two consecutive aromatic rings for an even number of methylenes in the model compounds. It is twice that distance when there is an odd number of methylenes (Fig. 7).

Can. J. Chem. Downloaded from www.nrcresearchpress.com by 92.62.229.171 on 09/08/12
For personal use only.

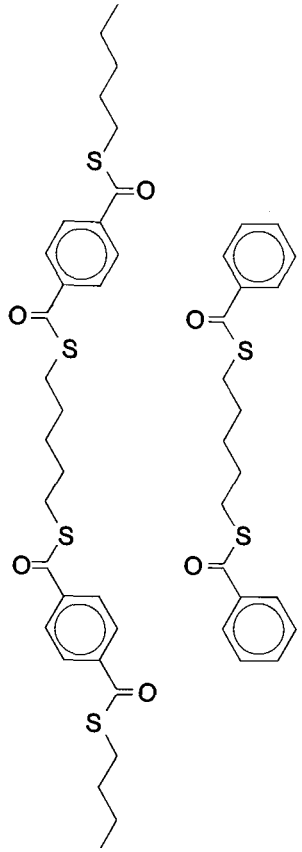

FIG. 7. Relation between a polymer, poly(pentamethylene thioterephthalate), and its model compound, pentamethylene dithiobenzoate.

TABLE 7. Values of the fiber repeat, p_0 (Å), calculated for the three possible conformations of the poly(oligomethylene thioterephthalates)

	n			
	3	5	7	9
Case I[a]	25.08	30.82	34.83	40.50
Case II	26.90	31.96	37.24	42.24
Case III	25.99	31.39	36.03	41.37

[a]See text and Fig. 8.

Since in the *n*DBS molecules two conformations are equally represented ($\tau \approx 90°$ and $\tau \approx 180°$), it is reasonable to expect that the parent polymer will adopt one or the other or even a combination of the two. For an ordered polymer, i.e., a crystalline one, only a few combinations need to be considered. These are schematically described in Fig. 8. Apart from the bond distances and angles, three types of torsion angles are required to describe the conformation of the poly(oligomethylene thioterephthalates). The torsion angles to be specified are ε, τ, and ϕ_i's. In the model compounds the angle ε is always small and stays in the range of 2°–6°, while τ may be either 90° or 180° and the ϕ_i's are all 180°. The fiber repeat may be evaluated according to the schemes shown in Fig. 8. Assuming that the methylenic sequence remains in the fully extended conformation three cases are possible:

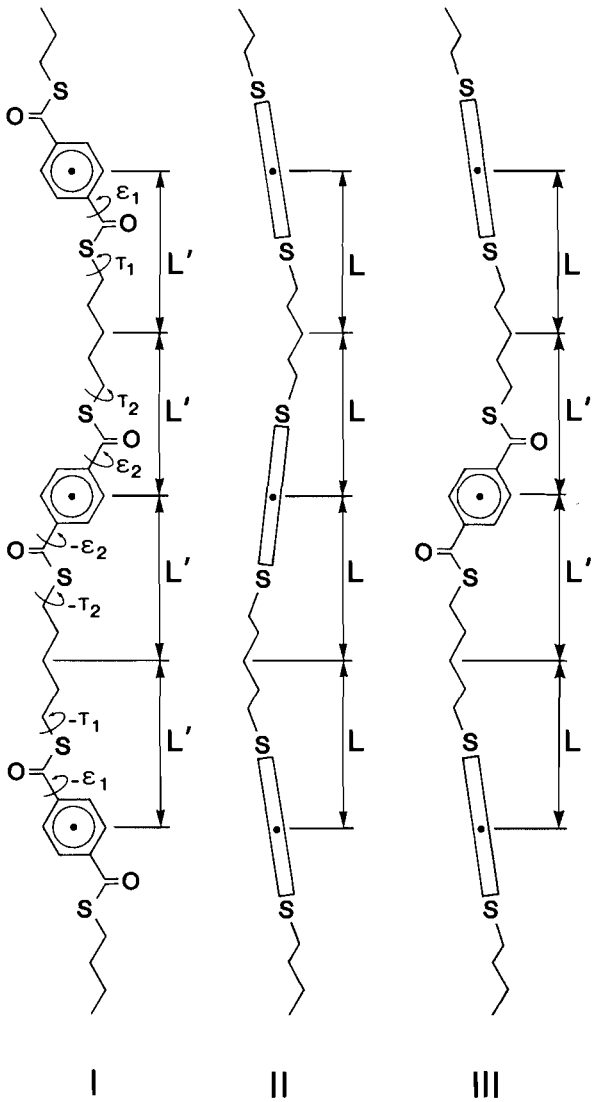

FIG. 8. Three possible conformations of poly(pentamethylene thioterephthalate). The τ torsion angle may take the values of ~90° or ~180° while all the ε and ϕ_i torsion angles are kept equal to 0° and 180° respectively. Thus the terephthaloyl groups are shown either in the plane of the page or perpendicular to it (long rectangles), while the S-$(CH_2)_5$-S sequence is only in the plane of the page. The black dots indicate the centers of symmetry.

Case I. All τ's are 180°. This corresponds to the all-*trans* conformation, then the fiber repeat, $p = 4L'$.

Case II. All the τ's are 90°. Because of the centers of symmetry $\tau_1 = \tau_2 = 90°$ and $\tau_1' = \tau_2' = -90°$, then $p = 4L$.

Case III. Here $\tau_1 = -\tau_1' = 90°$ while $\tau_2 = \tau_2' = 180°$. The fiber repeat is $p = 2L + 2L'$.

The quantities L and L' are the distances from the central atom to the center of the unprimed and primed aromatic rings corresponding to $\tau = 90°$ and $\tau' = 180°$ respectively. The fiber repeats calculated for each situation are given in Table 7.

Acknowledgements

We thank the Natural Sciences and Engineering Research Council of Canada for its financial support. We also thank Dr. M. Simard for collecting the X-ray data.

1. S. Poulin-Dandurand, S. Pérez, J.-F. Revol, and F. Brisse. Polymer, **20**, 419 (1979).
2. A. Palmer, S. Poulin-Dandurand, and F. Brisse. Can. J. Chem. **63**, 3079 (1985).
3. A. Palmer, S. Poulin-Dandurand, J.-F. Revol, and F. Brisse. Eur. Polym. J. **20**, 783 (1984).
4. F. Brisse, A. Palmer, B. Moss, D. Dorset, W. A. Roughead, and D. P. Miller. Eur. Polym. J. **20**, 791 (1984).
5. E. Mack and H. R. Thoennessen. Ger. Patent 2 016 631; 21 oct. 1971.
6. F. R. Ahmed, S. R. Hall, M. E. Pippy, and C. P. Huber. J. Appl. Crystallogr. **6**, 309 (1973).
7. P. Main, S. J. Fiske, S. E. Hull *et al.* MULTAN80. A system of computer programs for the automatic solution of crystal structures from X-ray diffraction data. Universities of York, England, and Louvain, Belgium.
8. C. K. Johnson. ORTEP. Report ORNL-3794. Oak Ridge National Laboratory, Tenn. 1965.
9. D. T. Cromer and J. B. Mann. Acta Crystallogr. Sect. A: Cryst. Phys. Diffr. Theor. Gen. Crystallogr. **A24**, 321 (1968).
10. R. F. Stewart, E. R. Davidson, and W. T. Simpson. J. Chem. Phys. **42**, 3175 (1965).
11. D. T. Cromer and D. A. Liberman. J. Chem. Phys. **53**, 1891 (1970).
12. J. Brisson and F. Brisse. Can. J. Chem. **63**, 3390 (1985).
13. A. Domenicano and A. Vaciago. Acta Crystallogr. Sect. B: Struct. Crystallogr. Cryst. Chem. **B31**, 221 (1975).
14. Molecular structures and dimensions. Vol. A1. International Union of Crystallography, Cambridge. 1972.
15. F. Brisse and S. Pérez. Acta Crystallogr. Sect. B: Struct. Crystallogr. Cryst. Chem. **B32**, 2110 (1976).
16. B. Rémillard and F. Brisse. Polymer, **23**, 1960 (1982).

Can. J. Chem. Downloaded from www.nrcresearchpress.com by 92.62.229.171 on 09/08/12
For personal use only.

Crystal and molecular structures of 1,4-dibromo- and 1,4-diiodocubane

N. T. KAWAI, D. F. R. GILSON,[1] J. F. BRITTEN,[2] I. S. BUTLER,[1] AND P. G. FARRELL
Department of Chemistry, McGill University, 801 Sherbrooke St. W., Montreal, Que., Canada H3A 2K6

Received June 21, 1991

N. T. KAWAI, D. F. R. GILSON, J. F. BRITTEN, I. S. BUTLER, and P. G. FARRELL. Can. J. Chem. **70**, 910 (1992).

The crystal structure of 1,4-dibromocubane has been determined by X-ray diffraction. The crystal is monoclinic, $P2_1/n$, a = 6.878(1), b = 6.960(7), c = 8.793(2) Å, β = 113.08(2)°, Z = 2, R = 0.055. The C—Br bond length, at 1.926 Å, is shorter than usual and the carbon framework is probably distorted by longer bonds along the edges. The direct dipole coupling constants between protons, obtained from the partially oriented NMR spectrum, show that a distortion of the proton positions from the ideal cube occurs in the bromo compound but not in diiodocubane, presumably because of the higher strain energy in the former.

Key words: halocubanes, crystal structures, NMR spectroscopy, molecular modelling calculations.

N. T. KAWAI, D. F. R. GILSON, J. F. BRITTEN, I. S. BUTLER et P. G. FARRELL. Can. J. Chem. **70**, 910 (1992).

On a déterminé la structure cristalline du 1,4-dibromocubane par diffraction des rayons X. Les cristaux sont monocliniques, groupe d'espace $P2_1/n$, avec a = 6,878(1), b = 6,960(7) et c = 8,793(2) Å, β = 113,08(2)°, Z = 2 et R = 0,055. La longueur de la liaison C—Br, à 1,926 Å, est plus courte que d'habitude et la structure carbonée fondamentale est probablement déformée par des liaisons plus longues à la périphérie. Les constantes de couplage dipolaires directes entre les protons, obtenues à partir de spectres RMN partiellement orientés, montrent que, dans le composé bromé, il existe une déformation de la position des protons par rapport à un cube idéal; cette situation n'existe pas dans le diiodocubane, probablement à cause de l'énergie de tension plus élevée dans le premier.

Mots clés : halocubanes, structures cristallines, spectroscopie RMN, calculs par modélisation moléculaire.

[Traduit par la rédaction]

Introduction

The possibility of distortions of the cubic framework of substituted cubanes was first examined by Tracey (1), who studied the proton magnetic resonance spectra of the mono- and 1,4-dicarboxylic acid derivatives oriented in lyotropic liquid crystal solutions. The protons vicinal to the carboxylic acid groups were displaced in the direction of the substituent such that the HCCH dihedral angle is non-zero, suggesting that the cage structure was elongated along the symmetry axis. The crystal structures of several derivatives of cubane (pentacyclo[4.2.0^{2,5}.0^{3,8}.0^{4,7}]octane) have now been reported (2–6). The differences in carbon–carbon bond lengths in these compounds has become a topic of considerable interest, in particular, the changes in the exocyclic bond lengths. The crystal structure of cubane-1,4-dicarboxylic acid showed that these bonds were shorter than normal, when compared with analogous bonds in bicyclooctane and adamantane carboxylic acid derivatives (4). The cage–cage bond lengths found for cubylcubane and 2-*tert*-butylcubylcubane, 1.458 and 1.474 Å, respectively, are significantly shorter, by 0.114 Å, than the average value of C—C bonds derived from the Cambridge Crystallographic Database for connected carbon atoms each bonded to three other carbons (5). In related, but much earlier, studies, a comparison of the bond lengths of carbon–halogen compounds (7, 8) showed that there is a significant shortening of the carbon–halogen bond length in the adamantyl halides compared with *tert*-butyl analogues.

In the present study we report the results of a crystal structure investigation of 1,4-dibromocubane, and of the hydrogen atom positions derived from the analysis of the dipole–dipole coupling constants of the proton magnetic resonance spectra of the dibromo and diiodo compounds, oriented in a nematic liquid crystal solvent. A crystallographic study of 1,4-diiodocubane was discontinued when the structure of this compound was reported (6). The results obtained, however, were in agreement with the published study.

Experimental

Preparation

Pentacyclo[4.2.0.0^{2,5}.0^{3,8}.0^{4,7}]octane-1,4-dicarboxylic acid (0.9 g) and mercuric oxide (2.6 g) were stirred together in refluxing dibromomethane (50 mL). A solution of bromine (2.0 g) in dibromomethane (25 mL) was added dropwise over 30 min and the mixture refluxed overnight. After cooling and filtering, the solvent was removed to leave a solid material, which was extracted several times with hot hexanes. Evaporation yielded the crude dibromocubane, which was purified by recrystallization from hexanes followed by sublimation, mp 196–198°C (0.90 g, 72%). For the diiodo derivative, the dicarboxylic acid (0.9 g), (diacetoxyiodo)benzene (3.3 g), and iodine (2.5 g) were stirred together in refluxing carbon tetrachloride (150 mL) under irradiation from a 200-W tungsten lamp for 8 h. A second addition of the same amounts of (diacetoxyiodo)benzene and iodine was then made and the reaction continued for a further 24 h. After cooling, the reaction mixture was thoroughly washed with sodium thiosulphate solution, dried, and the solvent removed to leave a solid that was purified as described above for the dibromo derivative, mp 225°C (dec.) (0.75 g, 42%).

X-ray crystallography

Diffraction data on a single crystal of dibromocubane, approximately 0.2 mm in all directions, were collected at room temperature on an Enraf–Nonius CAD4 diffractometer with Mo-Kα radiation ($K\alpha_1$ = 0.70930, $K\alpha_2$ = 0.71359) using θ/2θ scans. Unit cell parameters were refined with 24 reflections (2θ = 40–50°). Crystal data are

$C_8H_6Br_2$ f.w. = 261.94

Monoclinic, a = 6.878(1), b = 6.960(7), c = 8.793(2) Å, β = 113.08(2); V = 387.2(1) Å^3; Z = 2; D_{calc} = 2.247 Mg m^{-3}; F(000) = 247.96; μ = 102.8 cm^{-1}. The density determined by flotation

[1]Authors to whom correspondence may be addressed.

[2]Present address: Department of Chemistry, McMaster University, 1280 Main St. W., Hamilton, Ont., Canada L8S 4M1.

Can. J. Chem. Downloaded from www.nrcresearchpress.com by 92.62.229.171 on 09/08/12
For personal use only.

TABLE 1. Atomic coordinates and equivalent isotropic temperature factors (B_{iso} in Å^3) for dibromocubane

Atom	x	y	z	B_{iso}
Br	0.2758(2)	0.3117(2)	0.1522(2)	4.52(9)
C1	0.411(2)	0.126(2)	0.063(1)	2.7(6)
C2	0.518(2)	0.180(2)	−0.054(2)	3.4(7)
C3	0.292(2)	−0.046(2)	−0.050(1)	3.2(6)
C4	0.595(2)	−0.007(2)	0.168(2)	3.4(7)
H1	0.49(2)	0.32(2)	−0.09(1)	5(3)
H2	0.14(2)	−0.14(2)	−0.04(1)	6(3)
H3	0.65(1)	−0.00(1)	0.28(1)	1(2)

in aqueous zinc bromide solutions was 2.13 Mg m^{-3}. Systematic absences occurred at: $h,0,1$: $h + 1 = 2n + 1$; $0,k,0$:$k = 2n + 1$, indicating the space group $P2_1/n$ ($P2_1/c$ with an alternate choice of cell, no. 14), with molecules located at special positions. Intensity data were collected using the $\theta/2\theta$ scan mode up to $2\theta = 44.7°$. Two octants were measured within the index range $h,k,l = -6$ to 6, 0 to 6, and 0 to 9. Three standard reflections, measured 46 times during the data collection, showed a maximum instability of 2.83%, and were used to make corrections in the data reduction. Of the 475 unique reflections measured, 415 had intensities greater than $2.5\sigma(I)$.

The structure was solved by Patterson methods using the NRCVAX software (9). Halogen positions were determined from a Patterson map, and the carbon atoms were positioned from an electron density difference map. Hydrogen positions were initially located according to the carbon atom framework. Spherical absorption corrections were performed. Refinement of the non-hydrogen atoms was made with anisotropic temperature factors, while the hydrogen atoms were refined with isotropic factors. Final atomic coordinates are given in Table 1, and the thermal parameters are listed in Table 2. The lowest and highest peaks in the final difference map were −1.4 e Å^{-3} and 0.65 e Å^{-3}. The final extinction coefficient was 0.1867. Convergence was reached at $R = 0.055$, $R_W = 0.063$, for the 415 significant reflections, where $R = \Sigma(F_o - F_c)/\Sigma F_o$, $R_W = [\Sigma(K(F_o - F_c)^2)/\Sigma(KF_o^2)]^{1/2}$. Refinement was based on 59 variables, weight based on counting statistics with a modifier K in KF_o^2 of 0.00005. Bond lengths and angles are presented in Table 3.

Nuclear magnetic resonance

The NMR spectra were obtained on a Varian XL-300 spectrometer for dilute solutions (about 3 mol%) of dibromo- and diiodocubane in the solvent 1132, a mixture of phenylcyclohexylcyanides (Merck). The spectra were analyzed using a version of the LAOCOON program modified for dipolar coupling.

Results and discussion

The molecular structure and numbering system is shown in Fig. 1, and the packing diagram in Fig. 2. The structure is isomorphous with 1,4-diiodocubane (6) and also with the 1,4-dinitro derivative (3).

The search for substituent-induced variations in the carbon–carbon bond lengths in cubane derivatives is complicated by the observation that the crystallographically inequivalent C—C bond lengths show considerable variation. The average "edge" bond distance, C2—C3, in five cubane derivatives is 1.556 ± 0.006 Å (5), and dibromocubane at 1.567 Å is at the longer limit but within the error. The average bond length at C1 appears to be slightly shorter than the edge distance, and the bond angles at C1 are slightly larger, at 91.8°. In the diiodo compound, the averaged C—C distances were the same, and the bond angles closer to 90°. Thus the cage structure of dibromocubane may be slightly compressed along the symmetry axis. Recently, the gas phase structure of cubane itself was studied by electron diffraction (10). A vibrationally averaged C—C distance, r_g, of 1.573 Å was obtained. The value reported from the crystal structure determination (2) was 1.551 Å (averaged over the different distances in the crystal).

To accommodate the ring strain in the cubyl system, the C—C bonds become more p in character and the exocyclic bonds acquire more s-character. Thus these bonds are usually shorter than expected. The carbon–halogen bond lengths in the cubanes can be compared with those reported (7, 8) for *tert*-butyl and adamantyl derivatives, Table 4. The expected trend is observed.

The structures of the dibromo- and diodocubanes were calculated using the MM2 method (11) and the results for dibromocubane are included in Table 3. Interestingly, the deviations from a symmetric structure are in the same direction as observed in the X-ray study, but much larger; the edge C—C distance is much longer than the bonds to C1 and the angles at C1 greater than 90°. The predicted structure of diiodocubane is very close to the reported structure, i.e., the angles in the ring are close to 90° and the C—C bond lengths are the same. In both cases, however, the calculated C1–halogen bond lengths are even shorter than observed, 1.913 and 2.105 Å, for the dibromo and diiodo compounds, respectively.

To fit the results of the oriented NMR spectra to the structure, it is necessary to adopt coordinates for the carbon

TABLE 2. Temperature factors for dibromocubane[a]

Atom	u_{11}	u_{22}	u_{33}	u_{12}	u_{13}	u_{23}
Br	0.064(1)	0.050(1)	0.081(1)	−0.0036(8)	0.0525(9)	−0.0103(5)
C1	0.041(7)	0.038(8)	0.033(7)	−0.003(6)	0.025(6)	−0.007(5)
C2	0.047(8)	0.034(8)	0.061(9)	−0.003(7)	0.034(7)	0.006(7)
C3	0.038(7)	0.049(8)	0.041(7)	−0.003(6)	0.023(6)	0.000(7)
C4	0.042(8)	0.06(1)	0.037(8)	−0.007(6)	0.024(7)	−0.002(7)
H1	0.06(4)[b]					
H2	0.07(4)					
H3	0.02(3)					

[a]Anisotropic temperature factors are of the form:

$$T = -2\pi^2(h^2u_{11}(a^*)^2 + k^2u_{22}(b^*)^2 + l^2u_{33}(c^*)^2 + 2hku_{12}(a^*b^*) + 2hlu_{13}(a^*c^*) + 2klu_{12}(b^*c^*))$$

[b]Isotropic temperature factors, U, are given for the hydrogen atoms.

Can. J. Chem. Downloaded from www.nrcresearchpress.com by 92.62.229.171 on 09/08/12
For personal use only.

Can. J. Chem. Downloaded from www.nrcresearchpress.com by 92.62.229.171 on 09/08/12
For personal use only.

TABLE 3. Bond lengths (Å) and angles (deg) for dibromocubane

Bond(s)	X-ray	MM2
Br—C1	1.93(1)	1.9131
C1—C2	1.54(2)	1.5486
C1—C3	1.56(2)	
C1—C4	1.55(2)	
C2—C3′	1.57(2)	1.5640
C2—C4′	1.56(2)	
C3—C2′	1.57(2)	
C3—C4′	1.57(2)	
C4—C2′	1.56(2)	
C4—C3′	1.57(2)	
C2—H1	1.0(1)	1.1140
C3—H2	1.3(1)	
C4—H3	0.9(1)	
Br—C1—C2	123.1(8)	122.97
Br—C1—C3	123.9(8)	122.97
Br—C1—C4	125.0(8)	122.97
C2—C1—C3	91.5(8)	93.19
C2—C1—C4	92.6(9)	93.18
C3—C1—C4	91.2(9)	93.18
C1—C2—C3′	88.5(9)	87.4
C1—C2—C4′	89.5(9)	87.4
C1—C2—H1	111(7)	125.0
C3′—C2—C4′	90.4(9)	92.0
C3′—C2—H1	139(7)	126.44
C4′—C2—H1	122(7)	126.44
C1—C3—C2′	88.8(9)	87.4
C1–C3–C4′	88.5(8)	87.4
C1—C3—H2	126(5)	125.0
C2′—C3—C4′	90.9(9)	92.00
C2′—C3—H2	101(5)	126.44
C4′—C3′H2	142(5)	126.44
C1—C4—C2′	89.7(9)	87.4
C1—C4—C3′	88.3(9)	87.4
C1—C4—H3	121(5)	125.0
C2′—C4—C3′	90.5(9)	92.01
C2′—C4—H3	129(6)	126.44
C3′—C4—H3	125(5)	126.44

TABLE 4. Comparison of carbon–halogen bond distances (Å) (7, 8)

	Bromo-	Iodo-
tert-Butyl-	1.975	2.19
Adamantyl-	1.947	2.160
Cubyl-	1.926	2.133

cage and this was done for those averaged from the X-ray data and those derived from the MM2 calculations.

For a molecule with threefold molecular symmetry the dipole–dipole coupling constants (12) are given by eq. [1],

$$[1]\quad D_{ij} = -k\left\{C_{3z^2-r^2}\left[-2\frac{(\Delta z_{ij})^2}{r^5_{ij}} + \frac{(\Delta x_{ij})^2}{r^5_{ij}} + \frac{(\Delta y_{ij})^2}{r^5_{ij}}\right]\right\}$$

where $k = -\hbar\gamma_i\gamma_j/2\sqrt{5}\pi$. Assuming C_3 axial symmetry, there are three different proton–proton distances in the 1,4-dihalocubane structure, along the cube edge, across the face, and across the cube diagonal, and the oriented NMR spectrum is determined by three direct dipole coupling constants, three indirect couplings, and a single order parameter describing the orientation. For a perfect cube, the angle between the H-H direction along the edge of the cube and the C_3 axis, which is assumed to be the axis of orientation in the liquid crystal solvent, is 54.7°, which reduces this direct di-

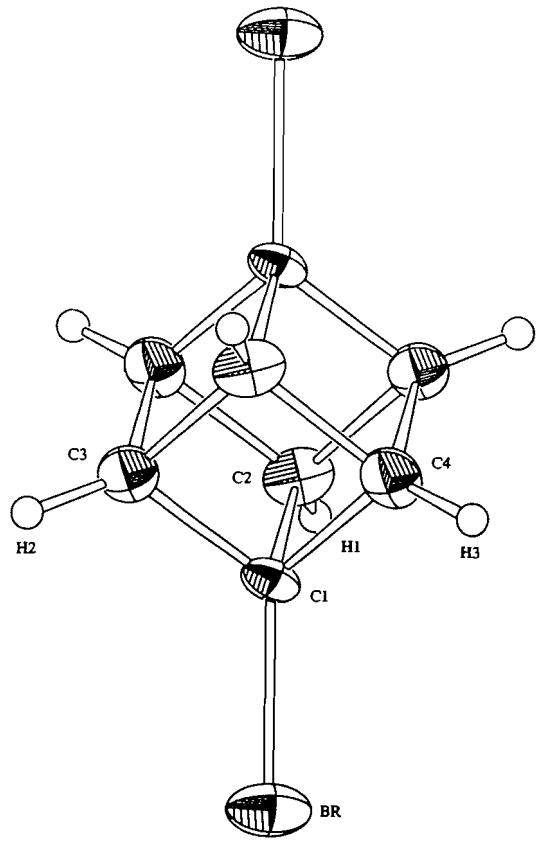

FIG. 1. ORTEP diagram (13) of 1,4-dibromocubane. Thermal ellipsoids are represented at 30% probability for carbon and bromine atoms, and as arbitrary spheres for the hydrogen atoms

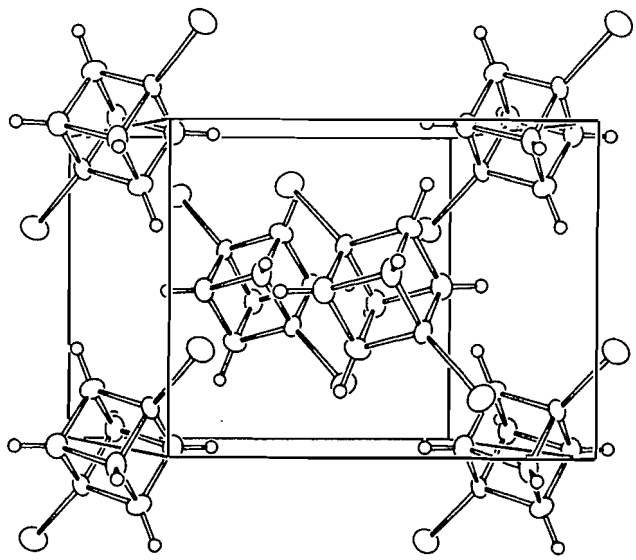

FIG. 2. Packing diagram of the monoclinic unit cell viewed down the a^* axis, with the c axis horizontal.

Can. J. Chem. Downloaded from www.nrcresearchpress.com by 92.62.229.171 on 09/08/12
For personal use only.

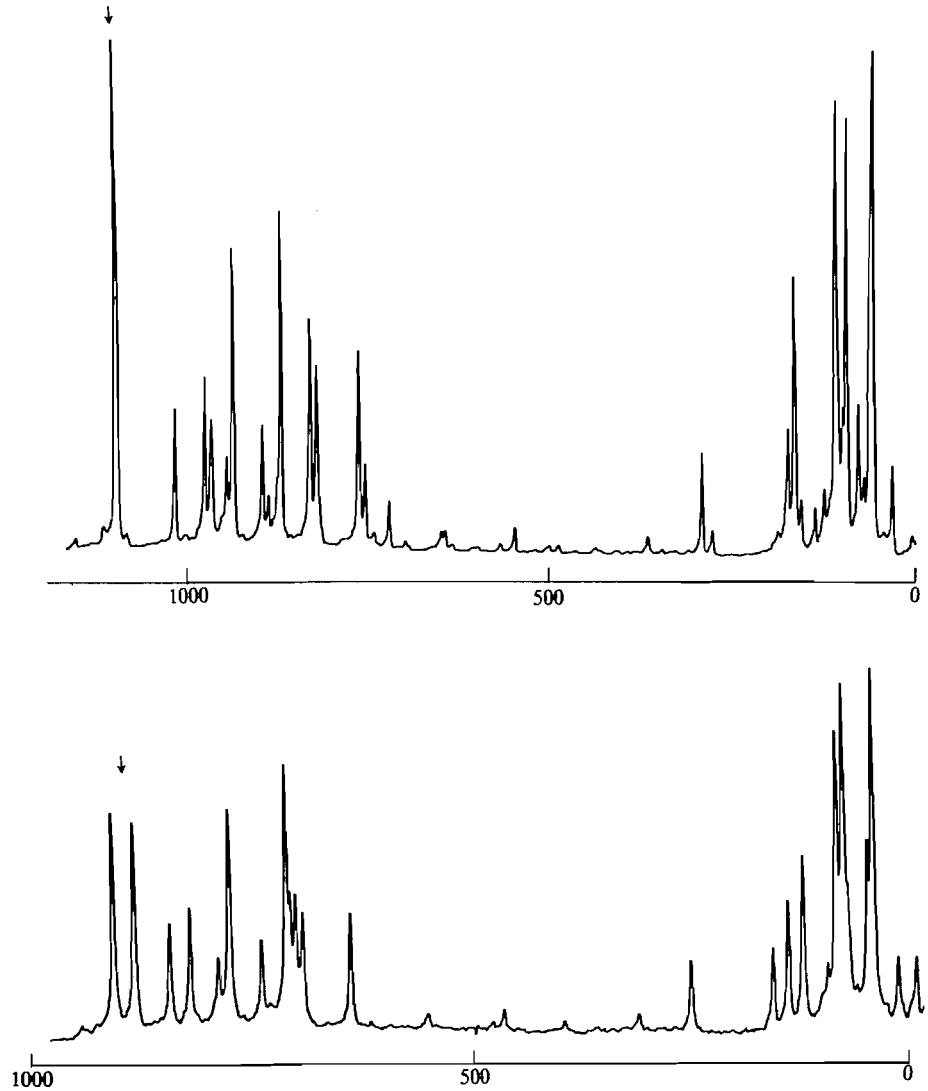

FIG. 3. Oriented NMR spectra of diiodocubane (upper) and dibromocubane (lower). The spectra are symmetrical about their centres and only half the spectra are shown. The arrows indicate the major line splitting for the finite value of D_{12} in the dibromo compound.

TABLE 5. Dipolar coupling constants, D_{ij} (Hz), in 1,4-dibromo- and 1,4-diiodocubane[a]

	Dibromocubane		Diiodocubane	
	Expt.	Calcd.	Expt.	Calcd.
D_{22}	513.64	513.64	620.74	620.70
D_{14}	−12.00	−12.01	1.17	1.16
D_{16}	184.97	184.97	225.28	225.38
J_{12}		3.13		1.03
J_{14}		6.23		5.48
J_{16}		−1.84		0.74
C_{3z-r}		0.6137		0.7348
rms error (Hz)		0.19		0.36

[a] $D_{12} = D_{13} = D_{23} = D_{45} = D_{46} = D_{56}$
$D_{14} = D_{15} = D_{24} = D_{26} = D_{35} = D_{36}$
$D_{16} = D_{25} = D_{34}$

TABLE 6. Proton coordinates in 1,4-dibromocubane and 1,4-diiodocubane obtained by fitting the D_{ij} values to carbon coordinates based on the average values from the X-ray structures and on the calculated MM2 coordinates

	Dibromocubane		Diiodocubane	
	X-ray	MM2	X-ray	MM2
x_1	0.000	0.000	0.000	0.000
y_1	2.3115	2.3148	2.3044	2.3084
z_1	0.8223	0.8235	0.8143	0.8157
x_2	2.0018	2.0047	1.9957	1.9991
y_2	1.1558	1.1574	1.1522	1.1542
z_2	0.8223	0.8235	0.8143	0.8157

$x_2 = x_4; x_3 = x_5; y_2 = y_3 = -y_1/2; y_4 = y_5 = y_1/2; y_6 = -y_1; z_2 = z_3 = z_1; z_4 = z_5 = z_6 = -z_1.$

pole coupling constant to zero. If a displacement of the proton positions occurs, then a small coupling constant results and the effect upon the spectrum is to produce a slight splitting of certain lines, shown in Fig. 3. The results of the spectral analysis are given in Table 5. The absence of the splitting (or a splitting small enough to be within the line width) in the case of the diiodo derivative indicates that little or no distortion occurs for this compound.

With the assumption of C_3 symmetry, the geometric relationships between the coordinates are; $x_1 = 0.0$, $x_2 = \sqrt{3}/2\ y_1$, $y_2 = -y_1/2$, thus the y_1 and z_1 coordinates and the motional constant $C_{3z^2-r^2}$ remain to be fitted to the three dipole–dipole coupling constants. To fit the structure to the carbon framework, the adjustable parameters were modified so that $y_1 = y(\mathrm{C1}) + r_H \cdot \sin(\alpha)$, and $z_1 = z(\mathrm{C1}) + r_H \cdot \cos(\alpha)$, where r_H is the C—H bond length and α is the angle made by the C—H bond to the z-axis. The carbon coordinates derived by (*i*) averaging the crystal coordinates and (*ii*) from the MM2 calculations were then used for y(C1) and z(C1). C—H bond lengths of 1.096 and 1.093 Å were obtained for the dibromo and diiodo compounds, respectively, and the angles α were identical at 70.3°. The proton coordinates are listed in Table 6. The occurrence of non-zero dipolar couplings in the case of dibromocubane results from a distortion of the cubic carbon framework and not as a result of a displacement of the proton positions. It should be emphasized, however, that comparisons of structural information derived by different experimental methods should include vibrational corrections. The MM2 calculations do show that the strain energy in the dibromo compound is about 66 kJ mol^{-1} higher than in the diiodo compound. The two main contributions to this increased strain energy are the C—C—Br bend and the C—C—C—Br torsion and, in attempting to relieve this extra strain, the dibromo molecule distorts.

Acknowledgements

This work was supported by grants from the Natural Sciences and Engineering Research Council of Canada (NSERC) and le Fonds pour la formation de chercheurs et l'aide à la recherche (FCAR) (D.F.R.G. and I.S.B.). N.T.K. also acknowledges the award of a postgraduate scholarship by NSERC. C. T. Yim is thanked for the Pascal version of the modified LAOCOON program. The authors are grateful to E. J. Gabe and Y. Lepage (X-Ray Diffraction Laboratory, National Research Council of Canada, Ottawa) for the X-ray diffraction data collection.

1. A. S. Tracey. Can. J. Chem. **62**, 101 (1984).
2. E. B. Fleischer. J. Am. Chem. Soc. **86**, 3889 (1964).
3. P. E. Eaton, B. K. R. Shankar, G. D. Price, J. J. Pluth, E. E. Gilbert, J. Alster, and O. Sandus. J. Org. Chem. **49**, 185 (1984).
4. O. Ermer and J. Lex. Angew. Chem. Int. Ed. Engl. **28**, 447 (1987).
5. R. Gilardi, M. Maggini, and P. E. Eaton. J. Am. Chem. Soc. **110**, 7232 (1988).
6. H. L. Ammon, C. S. Choi, and S. Reddy. Acta Crystallogr. Sect. C: Cryst. Struct. Commun. **C44**, 1671 (1988).
7. D. Chadwick, A. C. Legon, and D. J. Millen. J. Chem. Soc. Faraday Trans. 2, **68**, 2064 (1972).
8. A. C. Legon, D. J. Millen, and A. Samsam-Baktiari. J. Mol. Struct. **52**, 71 (1979).
9. E. J. Gabe, F. L. Lee, and Y. Lepage. J. Appl. Crystallogr. **22**, 384 (1989).
10. L. Hedberg, K. Hedberg, P. E. Eaton, N. Nodari, and A. G. Robiette. J. Am. Chem. Soc. **113**, 1514 (1991).
11. N. L. Allinger. J. Am. Chem. Soc. **99**, 8127 (1977).
12. L. C. Snyder. J. Chem. Phys. **43**, 4041 (1965).
13. C. K. Johnson. ORTEP-II, Report ORNL-5138, Oak Ridge National Laboratory, Oak Ridge, Tenn. 1976.

Can. J. Chem. Downloaded from www.nrcresearchpress.com by 92.62.229.171 on 09/08/12
For personal use only.

Electron thermalization distance distribution and ion mobility in n-C_6F_{14}

TAKEHISA YOSHINARI[1] AND GORDON R. FREEMAN
Chemistry Department, University of Alberta, Edmonton, Alta., Canada T6G 2G2

Received July 16, 1991

TAKEHISA YOSHINARI and GORDON R. FREEMAN. Can. J. Chem. **70**, 915 (1992).

Electron thermalization distances in liquid n-C_6F_{14} were estimated from the electric field dependence of the free-ion yields at $0.3 \leq E$ (MV/m) ≤ 3.7 and densities $1564 \leq d$ (kg/m^3) ≤ 1951; the latter correspond to $335.4 \geq T$ (K) ≥ 191.3. The distance distribution function that best fits the data has a Gaussian body and power tail (*YGP*), the same as in n-alkanes and in C_6F_6 and SF_6, but different from those in the liquids N_2, CO, and CS_2. The latter apparently capture electrons at higher energies than do the fluorine compounds. The static relative permittivity of liquid n-C_6F_{14} was measured as a function of temperature and compared with the square of the refractive index and the Debye and Clausius–Mosotti equations. Atomic polarization appears to contribute 6% to the refractive index in the far infrared. Cation mobilities at temperatures $335.4 \geq T$ (K) ≥ 191.2 are fitted by the free volume model, with $v_0 = 1.71 \times 10^{-4}$ m^3/mol and $E_v = 3.24$ kJ/mol.

Key words: electron, ion, liquid density, permittivity, mobility, n-C_6F_{14}, thermalization distance.

TAKEHISA YOSHINARI et GORDON R. FREEMAN. Can. J. Chem. **70**, 915 (1992).

En se basant sur la relation entre le champ électrique et les rendements en ions libres à $0,3 \leq E$ (MV/m) $\leq 3,7$ et à des densités de $1564 \leq d$ (kg/m^3) ≤ 1951 (qui correspondent à $335,4 \geq T$ (K) $\geq 191,3$), on a évalué les distances de thermalisation des électrons dans le n-C_6F_{14}. La fonction de la distribution de la distance qui caractérise le mieux les données possède un corps gaussien et un queue en puissance (*YGP*); il s'agit de la même distribution que pour les n-alcanes, le C_6F_6 et le SF_6, mais elle est différente de celle observée dans le N_2, le CO et le CS_2 liquides. Ces derniers liquides semblent capturer les électrons à des énergies plus élevées que les composés fluorés. On a mesuré la permittivité relative statique du n-C_6F_{14} en fonction de la température et on l'a comparée au carré de l'indice de réfraction et aux équations de Debye et de Clausius–Mosotti. Il semble que, dans l'infrarouge lointain, la polarisation atomique fasse une contribution de 6% à l'indice de réfraction. On a justé les mobilités cationiques aux températures $335,4 \geq T$ (K) $\geq 191,2$ avec le modèle du volume libre, avec $v_0 = 1,71 \times 10^{-4}$ m^3/mol et $E_v = 3,24$ kJ/mol.

Mots clés : électron, ion, densité de liquide, permittivité, mobilité, n-C_6F_{14}, distance de thermalisation.
[Traduit par la rédaction]

Introduction

The shape of the electron thermalization distance distribution depends on the electron scattering (1) and capture (2) properties of the liquid. In the present work the search for different distribution functions was continued by studying a liquid that captures electrons to form anions, perfluoro-n-hexane (3, 4). The electron-capturing efficiency of n-C_6F_{14} is greater than that of C_6F_6 (3*b*), which was studied earlier (5).

Experimental

Materials

Perfluoro-n-hexane (Aldrich, 99%) was further purified by putting Davison molecular sieves 3A into it for 4 days, then transferring it onto phosphorus pentoxide (2–5 mm mesh, Baker, Granusic) where it was stored for about 2 months before being transferred into the conductance cell. All treatments and transfers were done under vacuum. The molecular sieves had been heated at 210°C under vacuum for 6 days, then cooled before transferring the fluorocarbon onto it. The phosphorus pentoxide had been evacuated for 2 weeks at room temperature, then for 3 min at 100°C, then cooled.

The liquid was degassed by trap-to-trap distillation while pumping on the receiver at 77 K, during each transfer.

Measurements

A conductance cell for low-pressure liquids (6) was used, with 2.97-mm electrode spacing.

The free-ion yield at a given applied field strength was determined by dividing the integrated ion current from the sample by that from the accelerator target, and multiplying by an appropriate factor that included the electron density of the sample (7). A 100-ns pulse of 1.7 MeV X-rays deposited ~1 μJ/kg in the fluorocarbon.

The cooling (8) and heating (9) systems and temperature measurement were as described in the references cited. The temperature uncertainty was 0.3 K.

Ion mobilities were measured by time of flight (10). The mobilities were independent of applied field strength up to the highest field used, 2.7 MV/m. Each reported mobility value is the average of six measurements, three made with different positive applied voltages and three with different negative voltages.

Liquid permittivities, densities, and viscosities

Values of the static relative permittivities ϵ of n-C_6F_{14} were obtained from the measured capacitance of the empty conductance cell at 295 K and of the filled cell at various temperatures (11). They are plotted in Fig. 1.

Values of the liquid density d at 273–323 K are reported in ref. 12. At $273 < T/\text{K} < 323$ the densities were calculated from ϵ and the Clausius–Mosotti equation (13)

$$[1] \quad P\frac{(\epsilon - 1)M}{(\epsilon + 2)d}$$

where $P = 40.2 \times 10^{-6}$ m^3/mol is the molar polarization, calculated from the values of ϵ and d at 294.6 K, and $M = 0.338$ kg/mol is the molar mass. Values of ϵ and d are listed in Table 1.

The value $\epsilon = 1.759$ at 293.2 K is much larger than $n_D^2 = 1.566$ (12). The low value of the refractive index was confirmed by measurements here. The difference is not due to a permanent dipole moment (it would have to be 2.1×10^{-30} C m, or 0.64 D), because the measured temperature dependence of ϵ is much smaller than that calculated from the Debye equation (13) and the measured values of d (12). We suggest that the refractive index at far-

[1]Permanent address: Department of Physics, Faculty of Science, Yamagata University, 4-12, 1-chome, Koshirakawa-Machi, Yamagata, Japan 990.

Can. J. Chem. Downloaded from www.nrcresearchpress.com by 92.62.229.171 on 09/08/12
For personal use only.

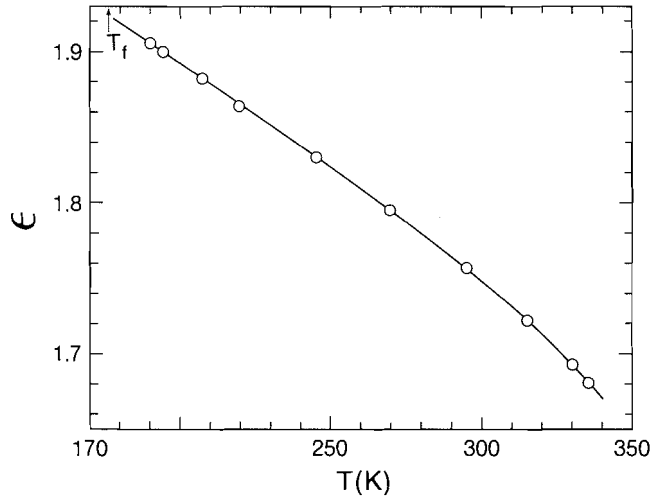

FIG. 1. Temperature dependence of static relative permittivity of n-C_6F_{14}. T_f = freezing point.

TABLE 1. Static relative permittivity and density of n-C_6F_{14}

T (K)	ϵ^a	d^b (kg/m^3)	d^c (kg/m^3)
335.4	1.681	1556	
330.1	1.693	1578	
323.22	1.708	1603	1607
315.2	1.722	1631	
313.21	1.726	1637	1638
303.25	1.744	1669	1669
295.0	1.757	1693	
294.61	1.758	1694	1695
283.25	1.774	1725	1727
273.15	1.790	1752	1756
269.5	1.795	1761	
245.3	1.830	1820	
219.6	1.864	1880	
207.1	1.882	1908	
194.2	1.900	1938	
191.2	1.904	1945	

[a]Static relative permittivity calculated from capacitance measurements.
[b]Density calculated from ϵ and the Clausius–Mosotti equation, using $P = 40.2 \times 10^{-6}$ m^3/mol.
[c]Reference 12.

infrared frequencies (10^{12}–10^{13} cy/s) contains a 6% contribution from atomic polarization.

Viscosity values are from ref. 12.

Results and discussion

Free-ion yields and electron thermalization distances

The electric field strength dependences of free-ion yields in n-C_6F_{14} at temperatures from 191.3 to 335.4 K are shown in Fig. 2; G_{fi}^E is the number of pairs of free ions formed per 16 aJ (100 eV) of energy absorbed by the sample when the electric field strength across it is E.

The competition between geminate recombination of the initial electron–ion pairs, driven by mutual Coulombic attraction, and free-ion formation, driven by thermal energy and the external electric field, is a stochastic process (14).

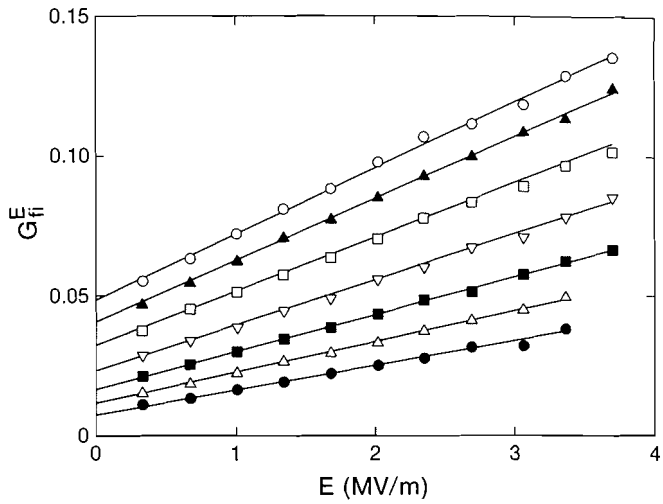

FIG. 2. Electric field strength dependence of free ion yields in n-C_6F_{14} at T(K): ○, 335.4; ▲, 315.3; □, 295.2; ▽, 269.7; ■, 245.3; △, 220.3; ●, 191.3. The curves were calculated from eqs. [2]–[5], using the parameter values in Table 2.

The free-ion yields and their field and temperature dependences can be calculated from an extended (14) model of Onsager's (15). The probability ϕ_{fi}^E of free-ion formation is

$$[2]\quad \phi_{fi}^E = G_{fi}^E/G_{tot} = \int_0^\infty \phi_{fi}^0(y)[1 + f(E,y,T)]F(y)dy$$

where G_{tot} is the total yield of initial ionization, and

$$[3]\quad \phi_{fi}^0(y) = \exp(-\xi^2/4\pi\epsilon_0\epsilon k_B T y) = \exp(-r_c/y)$$

where $-\xi$ is the electron charge, ϵ_0 is the permittivity of vacuum, k_B is Boltzmann's constant, T is the temperature, r_c is the "critical" Onsager radius, and the fractional increase of $\phi_{fi}^0(y)$ caused by the field E is

$$[4]\quad f(E,y,T) = e^{-\beta y}\sum_{n=1}^{\infty}\frac{(\beta y)^n}{(n+1)!}\sum_{j=0}^{n-1}(n-j)\frac{(r_c/y)^{j+1}}{(j+1)!}$$

where $\beta = \xi E/k_B T = 11\ 600\ E/T$ in SI units, and $F(y)dy$ is the fraction of electrons that have thermalization distances between y and $y + dy$.

The distribution function $F(y)$ in many liquids has a 3-dimensional Gaussian body and a power tail (14), and is designated YGP:

$$[5]\quad F(y) = \begin{cases} 0.96\ \mathrm{YG}, & y < 2.4\ b_{GP} \\ 0.96\ \mathrm{YG} + 0.48\ (b_{GP}^2/y^3), & y > 2.4\ b_{GP} \end{cases}$$

where 0.96 is a normalization factor and $\mathrm{YG} = (4y^2/\pi^{1/2}b_{GP}^3)\exp(-y^2/b_{GP}^2)$, and b_{GP} is the dispersion parameter and the most probable value of y. Other types of distribution function that have been tried are given in refs. 2 and 14.

For n-C_6F_{14} the value $G_{tot} = 3.0$ was taken to be the same as that for C_6F_6 (5). The best fitting $F(y)$ for n-C_6F_{14} over

Can. J. Chem. Downloaded from www.nrcresearchpress.com by 92.62.229.171 on 09/08/12
For personal use only.

TABLE 2. Electron thermalization distances b_{GP} in n-C_6F_{14}

T (K)	ϵ^a	d (kg/m^3)	$10^2\ G_{fi}^{0\,b}$	$b_{GP}{}^c$ (nm)	$b_{GP}d$ (10^{-7} kg/m^2)
335.4	1.683	1556	4.8	4.5	70
330.0[d]	1.694	1578	4.6	4.5	71
315.3	1.723	1631	4.1	4.4	72
295.2	1.757	1693	3.2	4.2	71
269.7	1.794	1760	2.3	4.0	70
245.3	1.830	1820	1.6	3.8	69
220.3	1.865	1888	1.14	3.6	68
207.0	1.883	1908	0.95	3.5	67
191.3[e]	1.904	1945	0.73	3.4	66

[a]Static relative permittivity.
[b]Zero-field free-ion yield. Calculated using $F(y)$ = YGP and G_{tot} = 3.0.
[c]Most probable thermalization distance.
[d]Normal bp = 330.3 K.
[e]Normal fp = 186.06 K.

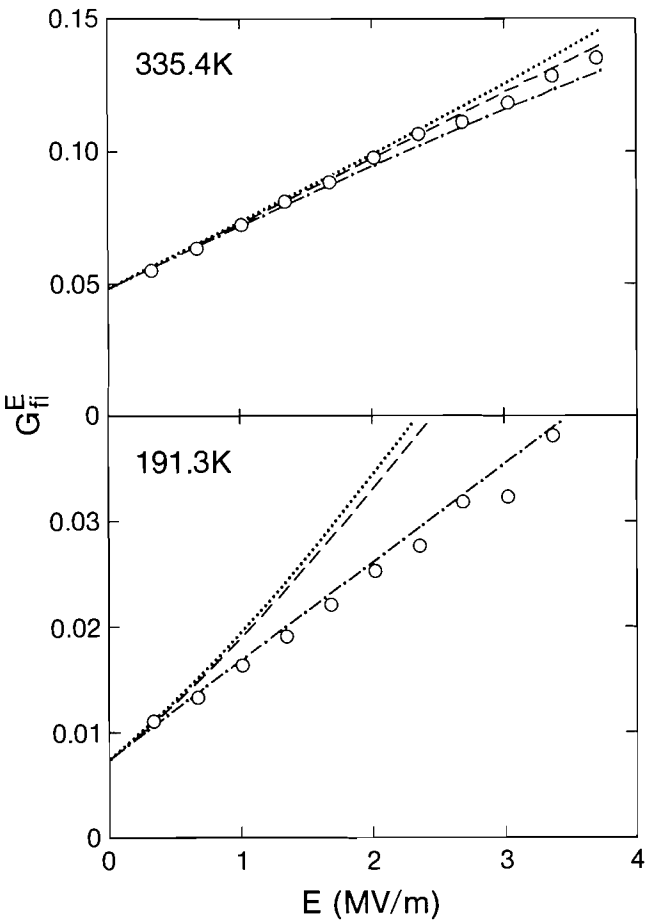

FIG. 3. Free ion yields (O) at 335.4 and 191.3 K compared to those calculated for $F(y)$ = YEP (–·–), YE (– – –), and YEC (····), using the parameter values in Table 3.

the ranges of d and E used was YGP, and this function was used to calculate the curves in Fig. 2. The parameter values are listed in Table 2. The value of $b_{GP}d$ is nearly constant over the 25% variation of liquid density.

The distribution YGP fits the G_{fi}^E data in liquid C_6F_6 and SF_6 (5) as well as that in n-C_6F_{14}, in spite of the fact that these compounds attach electrons to form anions. This distribution is characteristic of most liquids such as n-alkanes, which do not attach electrons (14). On the other hand, data for the liquids N_2 (2), CO (16), and CS_2 (5) cannot be fitted by YGP, but require the modified exponential function YEP:

TABLE 3. Electron thermalization distance distribution parameters for the curves in Fig. 3[a]

	b_{Ex} (nm)[b]	
	335.4 K	191.3 K
YEP	3.0	2.0
YE	3.9	3.2
YEC	2.6	2.2

[a]G_{tot} = 3.0, y_0 = 1 nm, ϵ as in Table 2.
[b]Attenuation coefficient.

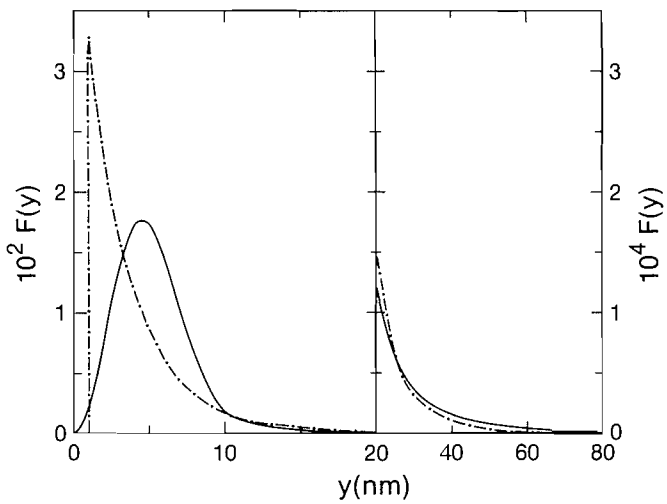

FIG. 4. Electron distribution functions. $F(y)$ = YGP (—) and YEP (–·–), for T = 335.4 K.

$$[6]\quad F(y) = \begin{cases} 0.97\ \mathrm{YE}, & 0 < (y - y_0) < 3.5\ b_{EP} \\ 0.97\ \mathrm{YE} + 0.72\ [b_{EP}^2/(y - y_0)^3], & \end{cases}$$

$$(y - y_0) > 3.5\ b_{EP}$$

where 0.97 is a normalization factor, $\mathrm{YE} = b_{EP}^{-1} \exp[(y - y_0)/b_{EP}]$, y_0 is taken as 1 nm, and b_{EP} is the attenuation coefficient. It appears that the liquids N_2, CO, and CS_2 capture electrons well before thermalization, and that n-C_6F_{14}, C_6F_6, and SF_6 capture electrons at a later, lower energy stage.

The extents to which YE and YEP fail to fit the n-C_6F_{14} data at 335.4 K and 191.3 K are shown in Fig. 3. Another modification of an exponential function, designated YEC (2), was also tried. None fits the data as well as does YGP. The parameter values for the curves in Fig. 3 are listed in Table 3.

The shapes of the distribution functions YGP and YEP are compared in Fig. 4. Both functions have a y^{-3} tail, which extends the distributions to larger separation distances. The tail is an artifact of the single-pair microzone model, attributed to the single ion–electron pairs that survive after the rapid neutralization of the innermost $(n - 1)$ pairs in micro-

Can. J. Chem. Downloaded from www.nrcresearchpress.com by 92.62.229.171 on 09/08/12
For personal use only.

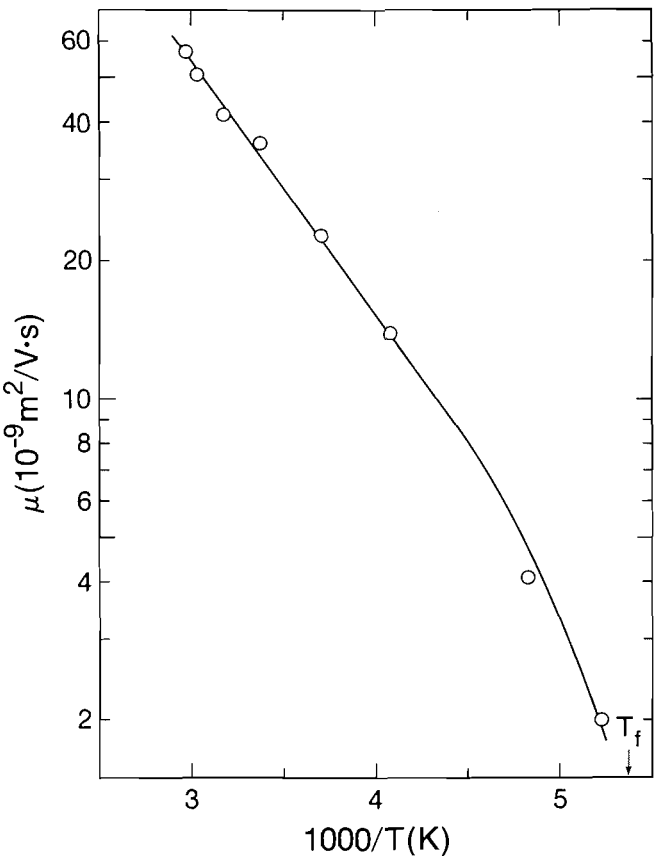

FIG. 5. Arrhenius plot of cation mobilities μ in n-C_6F_{14}. The full curve was calculated from the free volume eq. [7], using $v_0 = 1.71 \times 10^{-4}$ m^3/mol and $E_v = 3.2$ kJ/mol.

TABLE 4. Cation mobilities in n-C_6F_{14}

T (K)	η^a (10^{-6} Pa s)	μ (10^{-9} m^2 V^{-1} s^{-1})	$\mu\eta$ (10^{-12} N/V)
335.4	393	57	22
330.0	426	51	22
315.3	520	42	22
295.7	684	36	25
269.9	1040	23	24
245.3		13.9	
207.0		4.1	
191.2		2.0	

[a]Liquid viscosity (12).

zones (spurs) that initially contain n pairs (14). A y^{-3} distribution by itself gives a reasonable fit to the data at 191.3 K, but not those at the higher temperatures. The core of the distribution contributes progressively more to the free-ion yields at higher fields (Fig. 5 in ref. 17) and at higher temperatures (Figs. 7 and 8 in ref. 2).

A Gaussian core is attributed to randomization of the direction of motion of the slowing-down electrons by the scattering in the final stages of de-energization. An exponential core is attributed to capture of the electrons by molecules before the electrons have become thermalized, and before the ion–electron separation distances have been Gaussianized.

Cation mobility

An Arrhenius plot of the cation mobilities μ is given in Fig. 5. The curve is not linear at $T \leq 230$ K, but it is adequately fitted by the free volume model (10, 18):

$$[7] \quad \mu = \frac{A}{T^{1/2}}\left(\frac{v - v_0}{v_0}\right)\exp(-E_v/RT)$$

where A is a constant, v is the molar volume, v_0 is the molar volume at which diffusion ceases, and R is the gas constant. The best fitting values are $E_v = 3.24$ kJ/mol and $v_0 = 1.71 \times 10^{-4}$ m^3/mol.

The product of the mobility and the liquid viscosity, μη, is nearly constant over the temperature region for which viscosity values are available (Table 4).

Acknowledgement

We thank the staff of the Radiation Research Center for assistance. The value of n_D^2 was checked here by Prof. J. E. Bertie and Mr. D. Keefe.

1. T. Yoshinari, N. Gee, and G. R. Freeman. Can. J. Chem. **70**, 327 (1992).
2. G. Ramanan and G. R. Freeman. J. Chem. Phys. **87**, 319 (1987).
3. L. A. Rajbenbach. (*a*) J. Am. Chem. Soc. **88**, 4275 (1966); (*b*) J. Phys. Chem. **73**, 356 (1969).
4. W. F. Schmidt and A. O. Allen. J. Chem. Phys. **52**, 2345 (1970).
5. N. Gee and G. R. Freeman. Can. J. Phys. **68**, 930 (1990).
6. J.-P. Dodelet, K. Shinsaka, U. Kortsch, and G. R. Freeman. J. Chem. Phys. **59**, 2376 (1973).
7. N. Gee, P. C. Senanayake, and G. R. Freeman. J. Chem. Phys. **89**, 3710 (1988).
8. M. A. Floriano and G. R. Freeman. J. Chem. Phys. **85**, 1603 (1986).
9. N. Gee and G. R. Freeman. Phys. Rev. A, **32**, 525 (1985).
10. N. Gee and G. R. Freeman. J. Chem. Phys. **90**, 5399 (1989).
11. N. Gee, K. Shinsaka, J.-P. Dodelet, and G. R. Freeman. J. Chem. Thermodyn. **18**, 221 (1986).
12. V. E. Stiles and G. H. Cady. J. Am. Chem. Soc. **74**, 3771 (1952).
13. P. W. Atkins. Physical chemistry. 4th ed. Freeman, New York. 1990. pp. 650–653.
14. G. R. Freeman. *In* Kinetics of nonhomogeneous processes. *Edited by* G. R. Freeman. Wiley–Interscience, New York. 1987. Chap. 2.
15. L. Onsager. Phys. Rev. **54**, 554 (1938).
16. G. Ramanan and G. R. Freeman. Can. J. Chem. **66**, 1304 (1988).
17. J.-P. Dodelet, P.-G. Fuochi, and G. R. Freeman. Can. J. Chem. **50**, 1617 (1972).
18. N. Gee and G. R. Freeman. Can. J. Chem. (*a*) **67**, 27 (1989); (*b*) **68**, 1527 (1990).

Can. J. Chem. Downloaded from www.nrcresearchpress.com by 92.62.229.171 on 09/08/12
For personal use only.

Mono- and difunctional furan-based 1,2,3,5-dithiadiazolyl radicals; preparation and solid state structures of 2,5-[$(S_2N_2C)OC_4H_2(CN_2S_2)$] and 2,5-[$(S_2N_2C)OC_4H_2(CN)$]

A. WALLACE CORDES

Department of Chemistry and Biochemistry, University of Arkansas, Fayetteville, AR 72701, U.S.A.

CHARLES M. CHAMCHOUMIS, ROBIN G. HICKS, RICHARD T. OAKLEY,[1] KELLY M. YOUNG

Guelph–Waterloo Centre for Graduate Work in Chemistry, Guelph Campus, Department of Chemistry and Biochemistry, University of Guelph, Guelph, Ont., Canada N1G 2W1

AND

ROBERT C. HADDON

AT&T Bell Laboratories, Murray Hill, NJ 07974, U.S.A.

Received September 6, 1991

A. WALLACE CORDES, CHARLES M. CHAMCHOUMIS, ROBIN G. HICKS, RICHARD T. OAKLEY, KELLY M. YOUNG, and ROBERT C. HADDON. Can. J. Chem. **70**, 919 (1992).

The preparation and solid state characterization of the bifunctional radical furan-2,5-bis(1,2,3,5-dithiadiazolyl) 2,5-[$(S_2N_2C)OC_4H_2(CN_2S_2)$] and the related monofunctional radical 2-cyanofuran-5-(1,2,3,5-dithiadiazolyl) 2,5-[$(S_2N_2C)OC_4H_2(CN)$] are described. The crystal structure of 2,5-[$(S_2N_2C)OC_4H_2(CN_2S_2)$] is orthorhombic, space group $Pna2_1$, and consists of interleaved arrays of dimers, for which the mean interannular S···S contact is 3.137 Å. The crystal structure of the monofunctional radical 2,5-[$(S_2N_2C)OC_4H_2(CN)$] is monoclinic, space group $P2_1/n$, and consists of a ribbon-like network of dimers (mean interannular S···S = 3.126 Å) interconnected by close head-to-tail CN···S contacts. The dimer units form stacks parallel to z, with a mean interdimer S···S separation of 3.956 Å. The similarities and differences between these two crystal structures and those of related benzene-substituted systems are discussed.

Key words: dithiadiazolyl radicals, furan-based diradicals, cyanofuran-based radicals, radical dimers, crystal structures.

A. WALLACE CORDES, CHARLES M. CHAMCHOUMIS, ROBIN G. HICKS, RICHARD T. OAKLEY, KELLY M. YOUNG et ROBERT C. HADDON. Can. J. Chem. **70**, 919 (1992).

On décrit la préparation et la caractérisation à l'état solide du radical bifonctionnel furane-2,5-bis(1,2,3,5-dithiadiazolyl) 2,5-[$(S_2N_2C)OC_4H_2(CN_2S_2)$] et du radical monofonctionnel apparenté 2-cyanofurane-5-((1,2,3,5-dithiadiazolyl) 2,5-[$(S_2N_2C)OC_4H_2(CN)$]. La structure cristalline du 2,5-[$(S_2N_2C)OC_4H_2(CN_2S_2)$] est orthorhombique, groupe d'espace $Pna2_1$ et elle comporte des arrangements intercalés de dimères pour lesquels le contact interannulaire S···S moyen est de 3,137 Å. La structure cristalline du radical monofonctionnel 2,5-[$(S_2N_2C)OC_4H_2(CN)$] est monoclinique, groupe d'espace $P2_1/n$ et elle est formée d'un ensemble en forme de ruban de dimères (distance S···S interannulaire moyenne = 3,126 Å) reliés par des contacts tête à queue CN···S rapprochés. Les unités de dimère s'empilent d'une façon parallèle à z et la séparation S···S interdimère moyenne est de 3,956 Å. On discute des similarités et des différences entre ces deux structures cristallines et celles de systèmes apparentés comportant des benzènes substitués.

Mots clés : radicaux dithiadiazolyles, diradicaux de dérivés furaniques, radicaux de cyanofuranes, dimères radicalaires, structures cristallines.

[Traduit par la rédaction]

Introduction

Our interest in the design of molecular conductors based on neutral heterocyclic thiazyl and selenazyl building blocks (1) led us to investigate the solid state properties of 1,3- and 1,4-phenylene bridged 1,2,3,5-dithiadiazolyl and 1,2,3,5-diselenadiazoyl biradicals [$(E_2N_2C)C_6H_6(CN_2E_2)$] **1** (2, 3) and **2** (4) (E = S, Se). These bifunctional radicals associate in the solid state, but both the packing patterns and the mode of association are significantly different. The 1,4-derivatives **2** (E = S, Se) form dimers that adopt a herring-bone-like packing pattern, while in the α-phase of the 1,3-derivatives (E = S, Se) the molecules stack in vertical arrays, with association occurring through alternate ends of sequential diradical units (2). The selenium-based 1,3-phenylene system also crystallizes in a second (or β) phase, in which the crescent-shaped dimers link together in chain-like arrays (3). All the structures, particularly the selenium

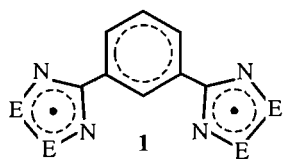

1

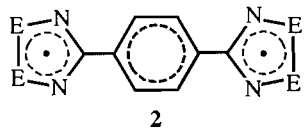

2

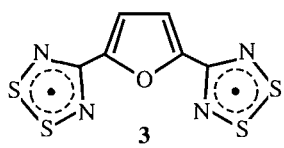

3

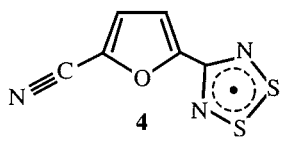

4

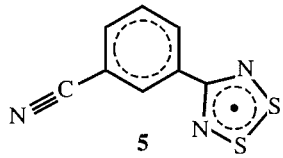

5

derivatives, are characterized by short inter-radical E···E

[1]Author to whom correspondence may be addressed.

Printed in Canada

Can. J. Chem. Downloaded from www.nrcresearchpress.com by 92.62.229.171 on 09/08/12
For personal use only.

Can. J. Chem. Downloaded from www.nrcresearchpress.com by 92.62.229.171 on 09/08/12
For personal use only.

contacts. The results of variable temperature single-crystal conductivity studies on both phases of the selenium-based 1,3-derivatives are consistent with intrinsic semiconductor behaviour (3).

As a continuation of this work we are constructing diradical systems that are similar in shape to the phenylene-bridged systems already studied. As a first step we synthesized and structurally characterized the furan-bridged diradical system 2,5-[$(S_2N_2C)OC_4H_2(CN_2S_2)$] **3**, in the hope that this system would opt for a packing pattern similar to that found for the 1,3-phenylene bridged material (2). In addition we also prepared and characterized a monofunctional radical possessing a 5-cyanofuryl substituent, i.e., **4**, to see if the crystal structure of this system would resemble that found in the α-phase of the recently reported 3-cyanophenyl compound (5). Herein we provide a full account of the preparation and crystal structures of **3** and **4**.

Results and discussion

Preparation of radicals

Our synthetic methodology for generating both mono- and bifunctional dithia- and diselenadiazolyls is now well established (2–5). The condensation of a persilylated amidine with sulphur (or selenium) dichloride affords the corresponding dithiadiazolium (or diselenadiazolium) chloride, which can then be reduced, typically by triphenylantimony, to the radical. In the present paper we extend this approach to include both the monofunctional and bifunctional furan-substituted dithiadiazolyls **3** and **4** (Scheme 1). As before, purification and crystal growth can be effected by vacuum sublimation methods (see Experimental).

Crystal structure of 3

Dark, blue-black blocks of **3**, grown by sublimation at 160°C/10^{-2} Torr (1 Torr = 133.3 Pa), are not isomorphous with crystals of the 1,3-phenylene-bridged diradical **1** (E = S) (tetragonal, space group $I4_1/a$); instead they belong to the orthorhombic space group $Pna2_1$. In contrast to the vertical columns of diradicals found in the structure of **1** (E = S), the crystal structure of **3** consists of discrete dimer units linked internally at both ends, as found in **2**. An ORTEP drawing, showing the atom numbering scheme, is given in Fig. 1. Non-hydrogen atom coordinates are given in Table 1. The internal bond lengths and angles summarized in Table 2 are typical of those seen in dithiadiazolyls (6, 7). The mean intradimer S····S separation, 3.137 Å, is also similar to those seen in the related bifunctional dimers, e.g., **1** (3.140 Å) and **2** (3.121 Å). As in the structure of 1,4-phenylene derivative **2**, there is a slight bowing of the dimer units, so that the mean centroid-to-centroid distance between the two furan rings (3.388 Å) is significantly longer than the terminal S····S links.

Within the unit cell (Fig. 2) the dimers generate a herring-bone network in the *xz* plane, with four dimers per unit cell. As such the packing pattern is reminiscent of that observed for **2** but, as a result of the reduction of the (approximate) D_{2h} symmetry of the molecular unit found in **2**, the "ribs" within each herring-bone assembly curve inwards or outwards with respect to the plane of the network. The space group propagates this alternation of curvatures along sets of "ribs" in both the *x* and *z* directions. Within each sheet there are three interdimer S····S interactions d_1–d_3 (Table 2) that are closer than the expected van der Waals contact (8). Of these, the two perpendicular approaches d_2 and d_3 (mean 3.221 Å) are remarkably close, significantly more so than

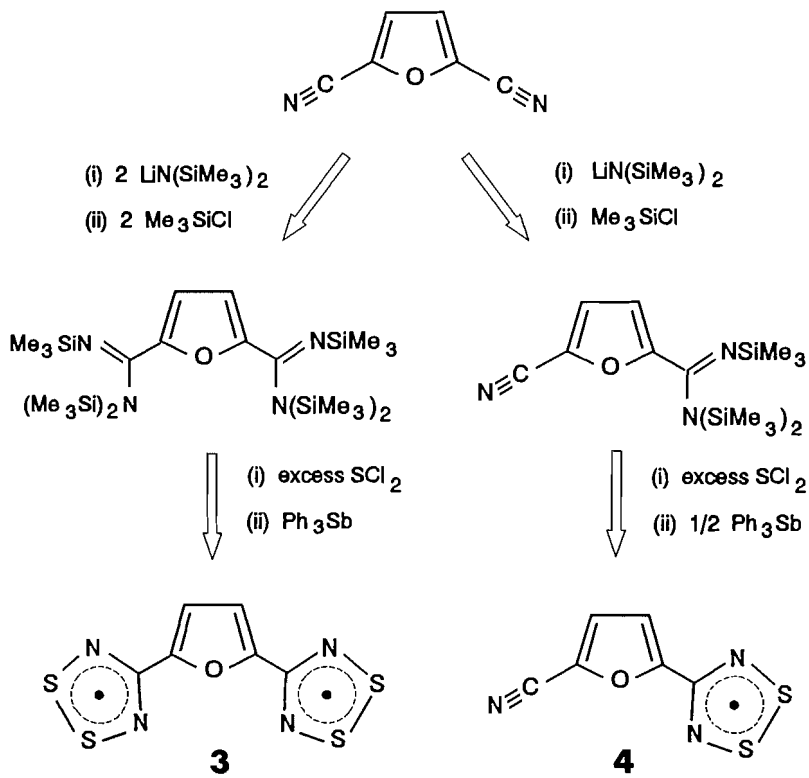

SCHEME 1

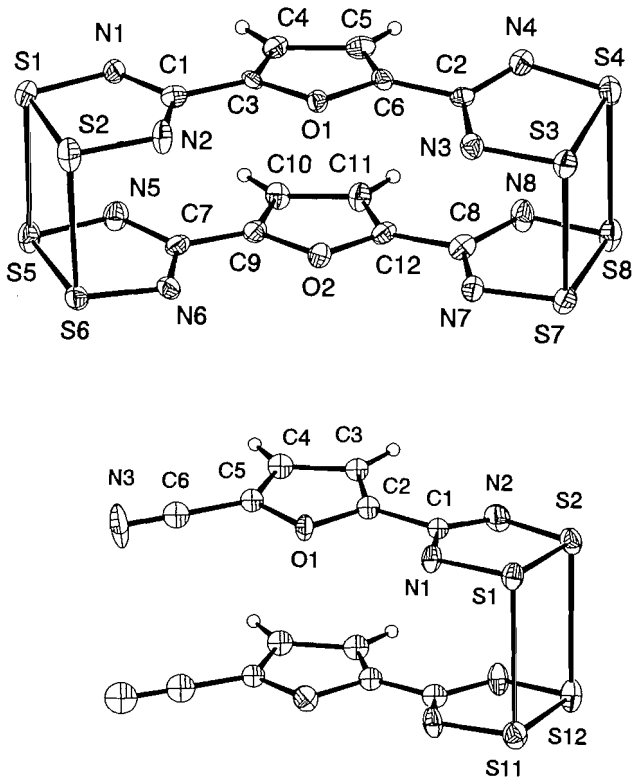

FIG. 1. ORTEP drawing of dimers of **3** and **4**, showing atom numbering.

TABLE 1. Non-hydrogen atom coordinates in **3**

Atom	*x*	*y*	*z*	B(Å^2)
S(1)	0.1356(1)	0.1413(4)	0.000	3.12(4)
S(2)	0.1784(1)	−0.1790(4)	0.0105(2)	3.51(5)
S(3)	0.4974(1)	−0.1709(4)	0.3549(1)	2.75(4)
S(4)	0.5004(1)	0.1387(4)	0.4169(1)	3.48(5)
S(5)	0.2416(1)	0.2962(4)	−0.1327(1)	3.13(4)
S(6)	0.2872(1)	−0.0224(4)	−0.1191(1)	2.81(4)
S(7)	0.5978(1)	−0.0019(4)	0.2242(1)	2.71(4)
S(8)	0.6070(1)	0.3165(4)	0.2795(2)	3.16(4)
O(1)	0.3182(2)	0.0634(8)	0.2079(3)	2.0(1)
O(2)	0.4328(2)	0.2505(8)	0.0626(3)	2.2(1)
N(1)	0.1852(3)	0.256(1)	0.0693(4)	2.9(1)
N(2)	0.2312(3)	−0.109(1)	0.0843(4)	3.0(1)
N(3)	0.4326(3)	−0.103(1)	0.2963(4)	2.4(1)
N(4)	0.4350(3)	0.245(1)	0.3673(4)	3.0(1)
N(5)	0.2918(3)	0.421(1)	−0.0667(4)	2.8(1)
N(6)	0.3454(3)	0.067(1)	−0.0540(4)	2.7(1)
N(7)	0.5381(3)	0.076(1)	0.1608(4)	2.4(1)
N(8)	0.5485(3)	0.434(1)	0.2216(4)	3.2(1)
C(1)	0.2283(4)	0.110(1)	0.1049(5)	2.3(2)
C(2)	0.4101(4)	0.107(1)	0.3102(4)	1.9(1)
C(3)	0.2740(4)	0.206(1)	0.1653(4)	1.8(1)
C(4)	0.2832(4)	0.420(1)	0.1877(5)	2.3(2)
C85)	0.3370(4)	0.419(1)	0.2484(5)	2.6(2)
C(6)	0.3554(3)	0.205(1)	0.2583(4)	1.9(1)
C(7)	0.3394(4)	0.287(1)	−0.0341(5)	2.3(2)
C(8)	0.5208(4)	0.294(1)	0.1668(5)	2.4(2)
C(9)	0.3868(4)	0.388(1)	0.0230(5)	2.3(2)
C(10)	0.3944(4)	0.605(1)	0.0471(5)	2.4(2)
C(11)	0.4471(4)	0.606(1)	0.1047(5)	2.7(2)
C(12)	0.4696(4)	0.393(1)	0.1127(5)	2.3(2)

the corresponding contacts in the structure of **2** (mean 3.500 Å).

Although the contacts d_1–d_3 between dimers are strong, indeed more so than in **2** (E = S), the curvature of the molecular skeleton leads to an isolation of neighbouring sheets. As illustrated in Fig. 3, the outside edge of one furan ring is forced into the pocket formed by the curvature of its neighbour; this eliminates the possibility of any close intersheet S----S contacts (along *y*) of any consequence.

Crystal structure of ***4***

Crystals of **4**[2] belong to the monoclinic space group $P2_1/n$, and consist of radical dimers linked in a cofacial manner through S----S contacts (mean 3.126 Å). An ORTEP drawing, showing the atom numbering scheme, is given in Fig. 1. Non-hydrogen atom coordinates are given in Table 3 and internal structural parameters summarized in Table 2. In many ways the crystal structure closely resembles that of the α-phase of the 3-cyanophenyl-substituted dithiadiazolyl **5** (5). As in this latter structure, which is also monoclinic, $P2_1/n$, with a = 7.295(3), b = 20.488(2), c = 11.367(2) Å, β = 95.54(2)°, the dimers form snake-like ribbons connected by head-to-tail CN----S contacts (mean 3.048 Å, cf. 3.075 Å in α-**5**) (Fig. 4).

Despite the similarity in the ribbon-like networks there are subtle but important differences between the structures of **4** and α-**5**. As in **5**, individual dimers of **4** form stacks running parallel to *z* (in α-**5** the stacking direction is *x*, which is equivalent to *z* in these $P2_1/n$ cells), but the interdimer S----S separation of 3.956 Å (mean of d_1 and d_2) is much shorter (4.26(5) Å in α-**5**). Also, while the benzene and CN_2S_2 rings in **5** display a significant torsion about the phenyl–CN_2S_2 bond (12(4)°),[3] the furan and CN_2S_2 rings in **4** are more nearly coplanar (mean furyl–CN_2S_2 torsion angle = 7(5)°).[3] The origins of this difference may arise from the greater size of the benzene ring in α-**5**, which forces the observed twisting in order to allow adjacent ribbons to approach one another. This point can be better appreciated after consideration of the fact that the angle between the 2,5-substituents on a furan ring (144° in a pentagon) is substantially larger than between the 1,3-substituents on a benzene core (120° in a hexagon). This difference forces a more severe curvature on the ribbon-like backbone of α-**5**, which, when coupled with greater peripheral spread of the phenyl group, induces a twisting of the phenyl rings about the ligand–CN_2S_2 linkage. The twisting also introduces a sheer effect between the two phenyl groups in a dimer unit, which reduces intradimer phenyl–phenyl contacts.

Perhaps as a consequence of the features noted above, the stacking patterns of the ribbons in **4** and α-**5**, and the number and nature of inter-stack contacts are very different. The principal differences are illustrated in Figs. 5 and 6, which show the stacking of the dimer S_4 subunits in the two structures, as viewed parallel to the *y* axis. In **4** adjacent S_4 stacks are out of register (Fig. 5), so that there are significant S----S

[2]We have not observed any tendency of **4** to form a second crystalline phase, as does **5**.

[3]This is the mean of the four 4-atom 3-bond torsion angles; the number in parentheses is the range.

Can. J. Chem. Downloaded from www.nrcresearchpress.com by 92.62.229.171 on 09/08/12
For personal use only.

TABLE 2. Summary of distances (Å) in **3** and **4**

		3		**4**	
Mean intradimer (range)					
S—S		2.089 (2.077–2.096)		2.077 (2.074–2.080)	
S—N		1.633 (1.623–1.641)		1.638 (1.639–1.656)	
CN		1.336 (1.329–1.350)		1.33 (1.30–1.36)	
C—C(*exo*)		1.455 (1.440–1.479)		1.47 (1.42–1.52)	
Intradimer					
S1····S5		3.127(4)	S1····S11		3.164(5)
S2····S6		3.133(3)	S2····S12		3.087(5)
S3····S7		3.058(3)			
S4····S8		3.228(4)			
Interdimer					
S1····S3′	d_1	3.681(3)	S1····S11′	d_1	3.920(5)
S6····S7′	d_2	3.399(3)	S2····S12′	d_2	3.999(5)
S6····S8′	d_3	3.164(3)	S2····S2′	d_3	4.030(5)
			S1····S1′	d_4	3.732(5)
			S12····S12′	d_5	3.881(5)
			S11····S11′	d_6	3.920(5)
			S1····S11′	d_7	4.104(5)
			S2····S12′	d_8	4.001(5)

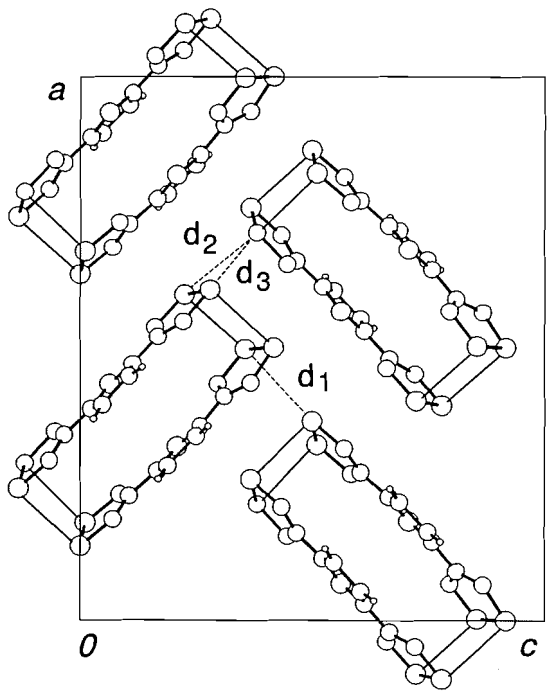

FIG. 2. Packing of dimers of **3** in *xz* plane, showing close interdimer contacts.

TABLE 3. Non-hydrogen atom coordinates in **4**

Atom	*x*	*y*	*z*	B(Å^2)
S(1)	0.1363(3)	0.0425(1)	0.9227(4)	2.68(6)
S(2)	0.3111(3)	−0.0096(1)	1.0163(5)	2.91(7)
S(11)	0.1650(3)	0.0429(2)	0.4871(5)	3.24(7)
S(12)	0.3403(3)	−0.0074(2)	0.5919(5)	3.40(7)
O(1)	0.3485(6)	0.2266(3)	1.064(1)	2.6(2)
O(11)	0.3746(6)	0.2283(4)	0.596(1)	3.1(2)
N(1)	0.2049(8)	0.1139(4)	0.974(1)	2.5(2)
N(2)	0.4022(8)	0.0551(5)	1.083(1)	3.3(2)
N(3)	0.365(1)	0.3912(5)	1.076(2)	5.8(3)
N(11)	0.2344(8)	0.1154(4)	0.525(1)	2.9(2)
N(12)	0.4315(8)	0.0567(4)	0.641(1)	3.0(2)
N(13)	0.390(1)	0.3925(6)	0.604(2)	4.8(3)*
C(1)	0.3328(9)	0.1079(5)	1.056(1)	1.9(2)*
C(2)	0.412(1)	0.1696(5)	1.116(2)	2.5(2)*
C(3)	0.537(1)	0.1789(5)	1.220(2)	2.5(2)*
C(4)	0.556(1)	0.2472(6)	1.233(2)	3.0(2)*
C(5)	0.439(1)	0.2732(6)	1.140(2)	2.5(2)*
C(6)	0.397(1)	0.3406(5)	1.104(2)	3.1(3)*
C(11)	0.364(1)	0.1134(6)	0.597(2)	2.8(2)*
C(12)	0.441(1)	0.1701(5)	0.646(2)	2.5(2)*
C(13)	0.570(1)	0.1823(6)	0.733(2)	2.9(2)*
C(14)	0.586(1)	0.2503(5)	0.749(2)	3.0(2)*
C(15)	0.469(1)	0.2746(5)	0.659(2)	2.4(2)*
C(16)	0.426(1)	0.3394(6)	0.628(2)	3.7(3)*

Note: starred atoms were refined isotropically.

contacts between the dimers both above and below to either side. By contrast, the S_4 stacks in α-**5** (Fig. 6) are in register, so that only S····S contacts d_3 (4.170 Å) and d_4 (4.168 Å), which are notably longer than those in **4**, are maintained between neighbours immediately to either side.

Summary and conclusions

The seemingly minor differences in the molecular structures of 2,5-furan- and 1,3-benzene-based dithiadiazolyl radicals lead to major differences in crystal structure. In the case of the bifunctional system **3**, the relatively wide angle (in comparison to the 1,3-phenylene structure **1**) between the two radical rings forces the crystal structure into a pseudo 1,4-phenylene instead of a pseudo α-1,3-phenylene packing pattern. The same issues work to advantage in the cyano-substituted derivative **4**. The smaller (than cyanobenzene) cyanofuran ring, coupled with a more obtuse angle between

Can. J. Chem. Downloaded from www.nrcresearchpress.com by 92.62.229.171 on 09/08/12
For personal use only.

Can. J. Chem. Downloaded from www.nrcresearchpress.com by 92.62.229.171 on 09/08/12
For personal use only.

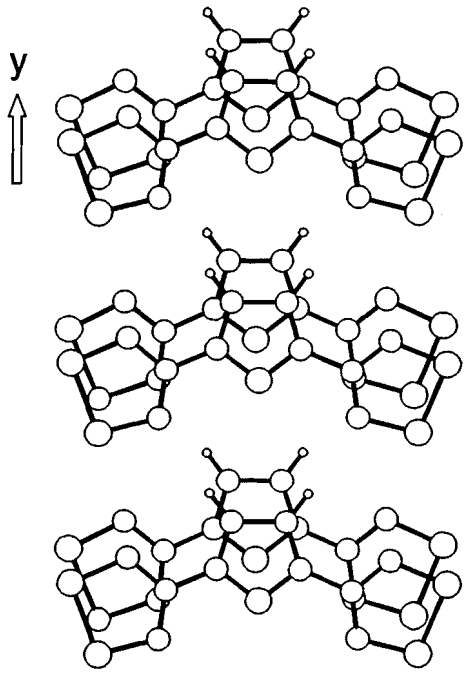

FIG. 3. Packing of dimers of **3** parallel to *y*.

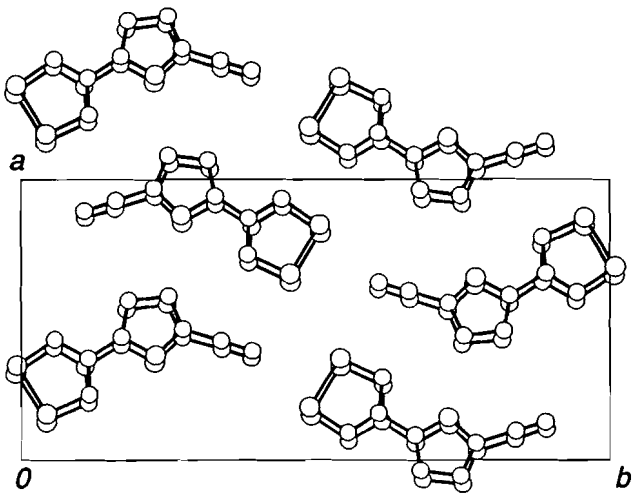

FIG. 4. Ribbon-like network of dimers of **4** in the *xy* plane.

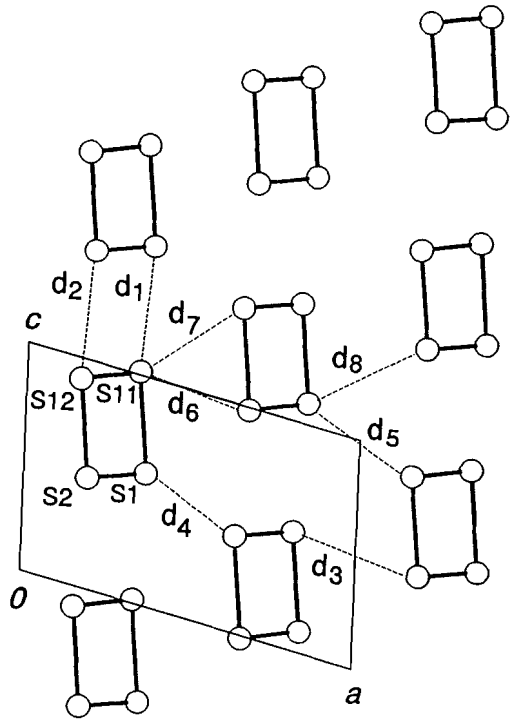

FIG. 5. Stacking of dimer S_4 units in **4**, viewed parallel to *y*.

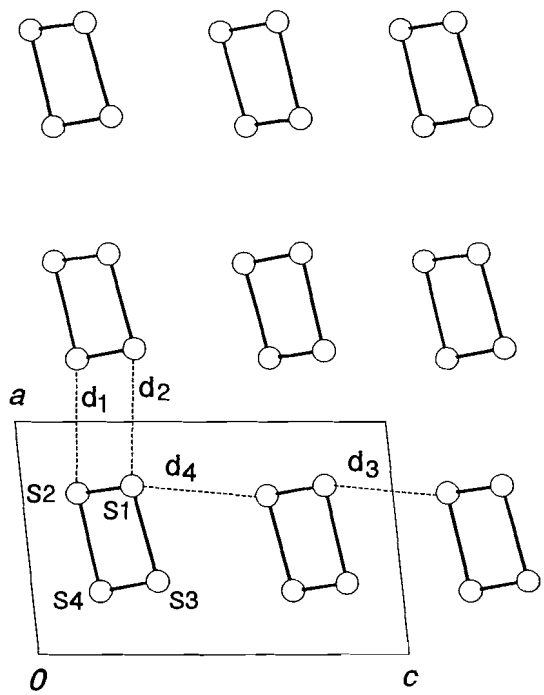

FIG. 6. Stacking of dimer S_4 units in the α-phase of **5**, viewed parallel to *y*.

the 2- and 5-substituents, produces flatter, less-ruffled ribbons, that can stack in a pseudo-interleaved (out-of-register) manner, thereby producing a much more tightly packed (in terms of S····S contacts) arrangement than in the 3-cyanophenyl-substituted system **5**. The selenium analogue to **4** should have conductivity characteristics significantly greater than that of the selenium counterpart of **5**.

Experimental

Starting materials and general procedures

Furan-2,5-dimethanol, lithium bis(trimethylsilyl)amide, sulphur dichloride, and triphenylantimony were all obtained commercially (Aldrich). Sulfur dichloride was distilled (at 1 atm (= 101.3 kPa)) before use and $LiN(SiMe_3)_2$ was converted into its diethyl etherate in order to facilitate amidine synthesis (9). Acetonitrile (Fisher HPLC grade) was purified by distillation from P_2O_5. All reactions were performed under an atmosphere of nitrogen. 2,5-Dicyanofuran was prepared by oxidation of furan-2,5-dimethanol to the corresponding dialdehyde (10) and conversion of the latter to the dioxime (11); subsequent dehydration with acetic anhydride (12) then afforded the dinitrile. Selenium tetrachloride was prepared by direct oxidation of selenium with chlorine gas (13). Mass spectra were recorded on a Kratos MS890 mass spectrometer. ^1H NMR spectra were recorded at 200 MHz on a Varian Gemini 200 MHz spectrometer. Infrared spectra (CsI optics, Nujol mulls) were obtained on a Nicolet

Can. J. Chem. Downloaded from www.nrcresearchpress.com by 92.62.229.171 on 09/08/12
For personal use only.

20XS/C FTIR instrument. Elemental analyses were performed by MHW laboratories, Phoenix, Arizona.

*Preparation of furan-2,5-bis(*N,N,N′*-tris(trimethylsilylamidine), DIFURADS*

A solution of 2,5-dicyanofuran (6.02 g, 0.51 mmol) in 30 mL diethyl ether was added dropwise to a slurry of $LiN(SiMe_3)_2 \cdot Et_2O$ (25.0 g, 10.3 mmol) in 100 mL diethyl ether and the resulting dark-brown solution stirred under nitrogen for 16 h. The solvent was then removed *in vacuo* to leave a dark-brown solid, to which was added Me_3SiCl (1.6. mL, 12.7 mmol) in 100 mL of toluene. This mixture was heated at reflux for 5 h, then filtered to remove LiCl, and the solvent distilled off to leave a dark-brown solid, which was crystallized from hot acetonitrile/toluene to give colourless needles of furan-2,5-bis(*N,N,N′*-tris(trimethylsilylamidine),DIFURADS (12.7 g, 2.2 mmol, 43%), mp 112–115°C. ^1H NMR (δ, $CDCl_3$): 0.14 (Me_3Si, 54H, s), 6.56 (H_2C_4O, 2H, s). Anal. calcd. for $C_{24}H_{56}N_4OSi_6$: C 49.43, H 9.33, N 9.61; found: C 49.53, H 9.35, N 9.65.

Preparation of 2,5-[$(S_2N_2C)OC_4H_2(CN_2S_2)$], 3

An excess of SCl_2 (1.6 mL, 25 mmol) was injected via syringe into a slurry of DIFURADS (2.94 g, 5.00 mmol) in 60 mL acetonitrile, and the resulting red/orange slurry stirred and heated to gentle reflux for 1 h. The mixture was filtered to remove the crude product 2,5-[$(S_2N_2C)OC_4H_2(CN_2S_2)]Cl_2$ (a brick-red solid). This material was dried *in vacuo*, then reduced with triphenylantimony (1.8 g, 5.2 mmol) in a slurry of 50 mL acetonitrile for 6 h at room temperature. The mixture was filtered, and the residual black solid washed with 2 × 20 mL acetonitrile and pumped dry *in vacuo*. This crude product was purified by sublimation at 160°C/10^{-2} Torr to give lustrous black (green to reflected light) blocks of 2,5-[$(S_2N_2C)OC_4H_2(CN_2S_2)$] **3** (E = S) (0.60 g, 2.2 mmol, 44%), mp 275–278°C. IR (1600–250 cm^{-1} region): 1355 (br, s), 1259 (m), 1166 (s), 1044 (w), 1037 (w), 978 (m), 818 (m), 799 (m), 771 (s), 695 (w), 597 (w), 520 (w), 505 (s), 429 (w), 379 (w) cm^{-1}. Mass spectrum (EI, *m/e*): 274 (M^+, 80%) 228 ($(M - NS)^+$, 28%), 196 ($(M - S_2N)^+$, 57%), 150 ($(NC(C_4H_2O)CNS)^+$, 15%), 118 ($(NC(C_4H_2O)CN)^+$, 12%), 78 ($(S_2N)^+$, 33%), 64 (S_2^+, 100%). Anal. calcd. for $C_6H_2N_4OS_4$: C 26.27, H 0.73, N 20.42; found: C 26.25, H 0.90, N 20.39.

*Preparation of 5-cyanofuran-2-(*N,N,N′*-tris(trimethylsilylamidine),CNFURADS*

Powdered $LiN(SiMe_3)_2 \cdot Et_2O$ (12.08 g, 50.0 mmol) was slowly added to a solution of 2,5-dicyanofuran (5.90 g, 50.0 mmol) in 100 mL diethyl ether, producing a dark-brown solution. The mixture was stirred overnight under nitrogen, and the solvent removed *in vacuo* to leave a dark-brown solid. A solution of Me_3SiCl (8.0 mL, 6.3 mmol) in 100 mL toluene was then added, and the mixture heated at reflux for 5 h. Filtration of the mixture, and removal of the solvent from the filtrate, afforded a dark-brown oil that was distilled *in vacuo* to give 5-cyanofuran-2-(*N,N,N′*-tris(trimethylsilylamidine), CNFURADS (11.0 g, 31.3 mmol, 63%), as a colourless waxy solid, bp 114–116°C/10^{-2} Torr, which was recrystallized from acetonitrile as colourless flakes, mp 68–70°C. ^1H NMR (δ, $CDCl_3$): 0.13 (Me_3Si, 27H, s), 6.50 and 7.07 (H_2C_4O, 2H, J_{AB} 3.6 Hz). Anal. calcd. for $C_{15}H_8N_3OSi_3$: C 51.23, H 8.31, N 11.95; found: C 51.43, H 8.28, N 12.15.

Preparation of 2,5-[$(S_2N_2C)OC_4H_2(CN)$], 4

Sulphur dichloride (2.5 mL, 39 mmol) was injected into a slurry of CNFURADS (3.55 g, 10.0 mmol) in 50 mL acetonitrile, and the resulting mixture stirred and heated to gentle reflux under nitrogen for 30 min. The resulting red precipitate was filtered off and dried *in vacuo*. This crude dithiadiazolium chloride was then reduced wth Ph_3Sb (1.8 g, 5.0 mmol) in 50 mL acetonitrile to give a khaki-brown solid (1.60 g), which was purified by vacuum sublimation at 160°C to give blue-black crystals of 2,5-[(S_2N_2C)-$OC_4H_2(CN)$] **6** (E = S) (1.60 g, 81%), mp > 244°C (dec.). IR: ν(CN) 2234 cm^{-1} and (1600–250 cm^{-1} region) 1346 (s), 1298 (s), 1219 (m), 1155 (m), 1023 (m), 986 (m), 964 (m), 833 (w), 812 (m), 804 (m), 773 (s), 696 (w), 596 (w), 588 (w), 558 (w), 504 (s), 463 (w), 448 (w) cm^{-1}. Mass spectrum (EI, *m/e*): 196 (M^+, 100%), 150 ($(M - NS)^+$, 30%), 132 ($(M - S_2)^+$, 20%), 118 ($(NC(C_4H_2O)CN)^+$, 42%), 94 (70%), 78 (S_2N^+, 90%). Anal. calcd. for $C_6H_2N_3OS_2$: C 24.85, H 0.70, N 14.49; found: C 25.00, H 0.55, N 14.41.

X-ray measurements

All X-ray data were collected on an ENRAF–Nonius CAD-4 at 293 K with monochromated Mo K_α (λ = 0.71073 Å radiation). Crystals were mounted on glass fibers coated with epoxy. Crystals of **3** belong to the orthorhombic space group $Pna2_1$, and have unit cell parameters a = 19.545(4), b = 5.913(2), c = 16.242(2) Å. Crystals of **4** are monoclinic, space group $P2_1/n$, with a = 10.455(5), b = 20.645(3), c = 7.060(4) Å, β = 104.44(4)°. Data were collected using a θ/2θ technique with a scan width of (1.0 + 0.3 tan θ). Both structures were solved using MULTAN and refined by full-matrix least squares which minimized $\Sigma w(\Delta F)^2$. The final R and R_w values of 0.034 and 0.036 (for **3**) and 0.049 and 0.051 (for **4**) were based respectively on refinements of 270 and 152 parameters with 1164 and 767 unique data with $F_o^2 > 3\sigma(F_o^2)$. Crystals of **4** were extremely thin plates (the data crystal was 0.03 mm thick), which led to a low number of $I > 3\sigma(I)$ reflections, and the consequent need to refine carbon atoms isotropically. Data collection, structure solution, and refinement parameters for all structures have been deposited.[4]

Acknowledgements

Financial support at Guelph was provided by the Natural Sciences and Engineering Research Council of Canada, and at Arkansas by the National Science Foundation (EPSCOR program) and the State of Arkansas.

1. A. W. Cordes, R. C. Haddon, and R. T. Oakley. *In* The chemistry of inorganic ring systems. *Edited by* R. Steudel. Elsevier, Amsterdam. 1992. p. 295.
2. M. P. Andrews, A. W. Cordes, D. C. Douglass, R. C. Haddon, P. Marsh, R. T. Oakley, T. T. M. Palstra, L. F. Schneemeyer, G. W. Trucks, R. Tycko, J. V. Waszczak, K. M. Young, and N. M. Zimmerman. J. Am. Chem. Soc. **113**, 3359 (1991).
3. A. W. Cordes, R. C. Haddon, R. G. Hicks, R. T. Oakley, T. T. M. Palstra, L. F. Schneemeyer, and J. V. Waszczak. J. Am. Chem. Soc. **114**, 1729 (1992).
4. A. W. Cordes, R. C. Haddon, R. T. Oakley, L. F. Schneemeyer, J. V. Waszczak, K. M. Young, and N. M. Zimmerman. J. Am. Chem. Soc. **113**, 582 (1991).
5. A. W. Cordes, R. C. Haddon, R. G. Hicks, R. T. Oakley, and T. T. M. Palstra. Inorg. Chem. In press.

[4]Tables of crystal data, structure solution and refinement (S1), hydrogen atom coordinates (S2), bond lengths and angles (S3 and S4), and anisotropic thermal parameters (S5 and S6) (10 pages), along with tables of observed and calculated structure factors (29 pages) for both structures may be purchased from: The Depository of Unpublished Data, Document Delivery, CISTI, National Research Council Canada, Ottawa, Canada, K1A OS2.

Tables S1–S4 have also been deposited with the Cambridge Crystallographic Data Centre and can be obtained on request from The Director, Cambridge Crystallographic Data Centre, University Chemical Laboratory, Lensfield Road, Cambridge CB2 1EW, U.K.

6. A. J. Banister, M. I. Hansford, Z. V. Hauptmann, A. W. Luke, S. T. Wait, W. Clegg, and K. A. Jørgensen. J. Chem. Soc. Dalton Trans. 2793 (1990).
7. A. W. Cordes, J. D. Goddard, R. T. Oakley, and N. P. C. Westwood. J. Am. Chem. Soc. **111**, 6147 (1989).
8. A. Bondi. J. Phys. Chem. **68**, 441 (1964).
9. R. T. Boeré, R. T. Oakley, and R. W. Reed. J. Organomet. Chem. **331**, 161 (1987).
10. A. F. Oleinik and K. Yu Novitskii. Zh. Org. Chim. **6**, 2632 (1970).
11. T. El Hajj, A. Masroua, J.-C. Martin, and G. Descotes. Bull. Soc. Chim Fr. 855 (1987).
12. S. Morikiwa and S. Teratake. Jpn. Kohai Tokkyo Koho, 79,19,963; Chem. Abstr. **91**, 39301c (1979).
13. G. Brauer. Handbook of preparative chemistry. Vol. 1. Academic, New York. 1963. p. 423.

Can. J. Chem. Downloaded from www.nrcresearchpress.com by 92.62.229.171 on 09/08/12
For personal use only.

Sorption of magnesium–picolinate complexes on a macroporous styrene–divinylbenzene copolymer containing immobilized 8-hydroxyquinoline and on the copolymer itself

GOCOOL PERSAUD AND FREDERICK F. CANTWELL[1]

Department of Chemistry, University of Alberta, Edmonton, Alta., Canada T6G 2G2

Received July 31, 1991

GOCOOL PERSAUD and FREDERICK F. CANTWELL. Can. J. Chem. **70**, 926 (1992).

The sorbent XAD-OXINE was prepared by covalently binding 8-hydroxyquinoline onto the surface of the macroporous copolymer Amberlite XAD-2 to give about 20% surface coverage. Sorption, onto both XAD-2 and XAD-OXINE, of the magnesium-containing species that are present in solutions of magnesium ion and picolinic acid was studied by the column equilibration/atomic absorption technique at solution pH of 6.00 and 7.50 and ionic strength of 0.25. By using solutions containing various amounts of added magnesium and picolinic acid, in which the ratio of the two metal–ligand complex species, MgP^+/MgP_2, varied greatly (P^- is the ligand picolinate), it was shown that neither the species Mg^{2+} nor the species MgP^+ sorb to an appreciable extent onto the parent polymer XAD-2, but the neutral species MgP_2 sorbs strongly and exhibits a linear isotherm. Then, by measuring the sorption isotherm of the species Mg^{2+} on XAD-OXINE in the absence of picolinic acid, by measuring the overall sorption of magnesium-containing species on XAD-OXINE in the presence of picolinic acid, and by assuming that the sorption of the species MgP_2 onto XAD-OXINE was about the same as it was on XAD-2, it was possible to show that the species MgP^+ sorbs strongly onto XAD-OXINE, and exhibits linear sorption isotherms. Thus, XAD-OXINE sorbs all three species Mg^{2+}, MgP^+, and MgP_2.

Key words: Amberlite XAD-2, immobilized oxine, magnesium ion.

GOCOOL PERSAUD et FREDERICK F. CANTWELL. Can. J. Chem. **70**, 926 (1992).

On a préparé l'adsorbant XAD-OXINE en liant d'une façon covalente de la 8-hydroxyquinoléine sur la surface du copolymère macroporeux Amberlite XAD-2 de manière à couvrir environ 20% de la surface. Faisant appel à la technique de l'équilibration sur colonne/absorption atomique et opérant à un pH de 6,00 et 7,50 et à une force ionique de 0,25, on a étudié la sorption, sur du XAD-2 ainsi que sur du XAD-OXINE, d'espèces contenant du magnésium contenues dans des solutions d'ion magnésium et d'acide picolinique. Utilisant des solutions contenant diverses quantités de magnésium et d'acide picolinique ajoutés, dans lesquelles les rapport des deux espèces métalliques/complexes ligands, MgP^+/MgP_2, varient beaucoup (P = ligand picolinate), on a montré que ni l'espèce Mg^{2+} ni l'espèce MgP^+ ne s'adsorbe d'une manière appréciable sur le polymère parent XAD-2; toutefois, l'espèce neutre MgP_2 s'adsorbe fortement et elle présente une isotherme linéaire. En mesurant l'isotherme de sorption des espèces Mg^{2+} sur le XAD-OXINE en l'absence d'acide picolinique, en mesurant la sorption globale des espèces contenant du magnésium sur le XAD-OXINE en présence d'acide picolinique et en faisant l'hypothèse que la sorption du MgP_2 sur le XAD-OXINE est pratiquement égale à celle observée sur le XAD-2, il est alors possible de démontrer que l'espèce MgP^+ s'adsorbe fortement sur le XAD-OXINE et qu'elle présente des isothermes d'adsorption linéaires. Le XAD-OXINE adsorbe donc les trois espèces Mg^{2+}, MgP^+ et MgP_2.

Mots clés : Amberlite XAD-2, oxine immobilisé, ion magnésium.

[Traduit par la rédaction]

Macroporous copolymers of styrene and divinylbenzene (DVB) find many uses in analytical chemistry. They are routinely used to concentrate trace components from both biological and environmental samples (1, 2). They have been used as packings for moderate efficiency liquid chromatography columns (3, 4) and, in the form of microparticles, as reverse-phase packings for high-efficiency liquid chromatography columns (5–7). These polymers are essentially nonionic and tend to strongly adsorb hydrophobic, nonionic sample molecules from aqueous solution. However, they also sorb ionic sample species (8). They have been used as HPLC packings for "dynamic ion exchange" chromatography of lanthanide ions (9). In this latter type of application a large surfactant ion is reversibly sorbed onto the surface of all of the packing in the column and lanthanide sample ions are chromatographed on this reversibly modified packing.

Macroporous styrene–DVB copolymers have also been derivatized by covalently attaching various groups to the polymer surface. Low-capacity cation and anion exchangers have been prepared by attaching sulfonate or quaternary ammonium groups. They have been used as liquid chromatographic column packings for separating both organic and inorganic ions (10, 11). A physico-chemical model has been developed to explain the retention of organic ions on such low-capacity ion exchangers (12, 13). Ligands have also been covalently bound to macroporous styrene–DVB copolymers in order to prepare "chelating sorbents" suitable for preconcentrating trace-metal ions from aqueous sample solutions (14–17).

Chelating sorbents have been used not only to preconcentrate metal ions but also to achieve metal ion "speciation" measurements, in which the concentration of a free (hydrated) metal ion species M^{n+} is measured in solutions containing metal–ligand complexes of the ion M^{n+}, even when the complexes are kinetically labile (18). These measurements of free-metal ion concentration are made by the column equilibration/atomic spectroscopy method in which a sample solution is equilibrated with a small bed of chelating sorbent and then the sorbed metal ion M^{n+} is eluted into an atomic absorption spectrophotometer. The underlying principles of the method have been presented in detail (18–21). An essential requirement of the method is that, of all the M^{2+} containing species that are present, the sorbent will se-

[1]Author to whom correspondence may be addressed.

Can. J. Chem. Downloaded from www.nrcresearchpress.com by 92.62.229.171 on 09/08/12
For personal use only.

Can. J. Chem. Downloaded from www.nrcresearchpress.com by 92.62.229.171 on 09/08/12
For personal use only.

lectively sorb M^{n+} but will not sorb its metal–ligand complexes. Recently a chelating sorbent, XAD-OXINE, which was prepared by covalently binding the ligand oxine (8-hydroxyquinoline) to the macroporous styrene–DVB copolymer Amberlite XAD-2, was investigated for use in measuring free magnesium ion concentration (22). It was found that in the presence of ligands that form rather hydrophilic complexes with Mg^{2+}, such as EDTA and oxalate, it is possible to measure accurately the concentration of the species Mg^{2+} at concentrations as low as 10^{-6} M, even though the complexes are kinetically labile and even when the species Mg^{2+} represents only a few percent of total dissolved magnesium in solution. However, in contrast, it was found that in the presence of the ligand picolinate, P^-, which forms more hydrophobic complexes with Mg^{2+} because of the presence of an aromatic ring on the ligand, the measured values of $[Mg^{2+}]$ were erroneously high. Preliminary studies suggested that this is because one or both of the magnesium–picolinate complexes, MgP^+ and MgP_2, is sorbed by XAD-OXINE (Table V, ref. 22).

In the present work, sorption of the species Mg^{2+}, MgP^+, and MgP_2 onto XAD-OXINE and onto the parent copolymer XAD-2 is investigated quantitatively. Because macroporous styrene–DVB copolymers and their derivatives are used extensively for chromatography, for preconcentration of both organic and metal ions, and for speciation studies, the resultant quantitative description is broadly relevant in analytical chemistry.

Experimental section

Reagents

Sodium chloride (BDH), which was used to adjust ionic strength, piperazine *N,N'* bis(2-ethanesulfonic acid) (PIPES; Sigma Chemical Co.), which was used to prepare the buffers, oxalic acid (Fisher), disodium ethylenediamine tetraacetic acid (EDTA; Fisher), and picolinic acid (2-pyridinecarboxylic acid; Sigma) were all reagent grade and were used as received. Magnesium stock solutions were prepared by dissolving the metal powder in 6 M nitric acid and diluting.

Purified water, prepared by passing the laboratory distilled water through a mixed-bed ion exchange resin column (Amberlite MB-1; Rohm and Haas) was used in preparing all solutions. The 1 M NaCl stock solution was passed through a 16 cm × 2.5 cm bed of Dowex Chelating Resin (Sigma) to reduce the level of trace Mg^{2+} before using this solution in the preparation of samples and standards.

All solutions containing Mg^{2+}, both standards and samples, were buffered with 0.0010 M PIPES, a noncomplexing buffer (22), to pH 6.00 or 7.50 and all had their ionic strengths adjusted to 0.25_0 M with NaCl. Complexation of Mg^{2+} by Cl^- is small enough to be neglected (22).

Sorbents

The sorbent "XAD-2" is the parent polymer. It is the macroporous styrene–DVB copolymer Amberlite XAD-2 (Rohm and Haas). The 100–200 mesh (75–150 μm) cut was used. It was obtained by grinding and sieving. Fines were removed by sedimentation and decantation in methanol, and soluble impurities were removed by cycling it through washes with 1.2 M HCl, water, 1 M NaOH, water, and methanol.

The chelating sorbent "XAD-OXINE" was prepared from XAD-2 by covalently binding oxine to its surface via a methylene group linkage, as described elsewhere (22, 23). It has a complexing capacity, based on Cu^{2+} uptake, of 264 ± 2 μmol/g of dry sorbent (22).

Apparatus

The column equilibration/atomic absorption apparatus is described elsewhere (22). The column design was the same for both XAD-2 and XAD-OXINE and was similar to that used previously (20). For each sorbent the column consisted of a 1.0-cm length bed packed in a 1.5-mm i.d. Teflon tube with small sintered glass frits inserted into the tube at each end of the sorbent bed. The weight of sorbent was 5.2 mg in each case.

Due to space restrictions imposed by efforts to minimize the holdup volume of the system, it was not practical to thermostat the column. However, experiments were run at ambient temperature in a controlled temperature room (25 ± 2°C) and calibrating standards of Mg^{2+}, containing no ligand, were always run along with sample solutions containing ligand so that operating at ambient temperature introduced minimal errors.

Column equilibration procedure

Sample and standard solutions were pumped via the peristaltic pump through the small column of XAD-2 or XAD-OXINE at a constant flow rate (±0.1 mL/min) at nominal values of 4.5–5.0 mL/min.

In a typical experiment the solution of interest was pumped through the column for 20 min in the "loading" step, in order to bring the sorbent to equilibrium with the solution. Next the column was eluted for 2.0 min with 1.0 M HNO_3 and the eluate was directed into the nebulizer of an atomic absorption spectrophotometer (Perkin–Elmer, model 4000). The measured atomic absorption signal was a peak, the area of which, $(P.A.)_{total}$, was proportional to the sum of magnesium-containing species sorbed and magnesium-containing species in the solution present in the holdup volume of the system. The holdup volume was measured experimentally (22). The peak area associated with magnesium-containing species sorbed, $(P.A.)_{sorbed}$, in a particular experiment was then calculated from $(P.A.)_{total}$ and from the peak area associated wtih the holdup of the particular magnesium-containing solution of interest, $(P.A.)_{holdup}$, using the expression:

$$[1] \quad (P.A.)_{sorbed} = (P.A.)_{total} - (P.A.)_{holdup}$$

For both the standard solution and the sample solution a correction was made for the presence of a very small amount of magnesium impurity that had not been removed by the Dowex Chelating Resin column cleanup. Details of this small correction were previously given (22). For comparison with results reported in ref. 22, it may be noted that all experiments in the present report were performed by the "without washing" procedure described in that reference.

Results and discussion

Picolinic acid has three conjugate acid–base species, H_2P^+ (pK_{a1} = 1.03), HP (pK_{a2} = 5.21), and P^-, the picolinate anion. The pK_a values are from the critical compilation of Martell and Smith (24) at 25°C and c = 0.1. The ligand species is P^-.

Because peak area (P.A.) is the quantity obtained directly from the atomic absorption spectrophotometer and because P.A. is directly proportional to the total moles of all of the magnesium-containing species sorbed on the column and is therefore proportional to the total adsorbed concentration (mol/kg) on that column, it is convenient to plot P.A. as the vertical-axis variable in the measured isotherms reported below.

Sorption of Mg^{2+}

Sorption isotherms are plots of concentration sorbed versus concentration in solution, at equilibrium. Sorption isotherms of the species Mg^{2+} on XAD-OXINE (not shown) have been measured in the absence of added picolinate at c = 0.25_0 for pH 6.00 and 7.50 (23). The isotherm obtained

TABLE 1. Fractional distribution of magnesium-containing species in solution as a function of pH and total picolinic acid concentration added ($C_{\text{picolinic acid}}$), for ionic strength 0.25 and $C_{Mg} << C_{\text{picolinic acid}}$

		α_i			
$C_{\text{picolinic acid}}$	i	pH = 5.00	pH = 6.00	pH = 7.00	pH = 7.50
0.001	Mg^{2+}	0.95	0.90	0.89	0.89
0.01	Mg^{2+}	0.63	0.40	0.37	0.36
0.05	Mg^{2+}	0.17	0.058	0.048	0.047
0.001	MgP^+	0.047	0.095	0.105	0.106
0.01	MgP^+	0.31	0.42	0.43	0.43
0.05	MgP^+	0.42	0.31	0.28	0.28
0.001	MgP_2	0.001	0.004	0.005	0.005
0.01	MgP_2	0.062	0.18	0.20	0.20
0.05	MgP_2	0.41	0.64	0.67	0.67

at pH 7.50 is about four times steeper than that obtained at pH 6.00, consistent with a greater degree of ionization of the immobilized ligand oxine at higher pH, and both isotherms exhibit a slight concavity toward the [Mg^{2+}] axis, which is generally similar to that seen in Fig. 1 of ref. 22.

When the parent polymer, XAD-2, was used as the sorbent in the absence of picolinate, it was found that no sorption of Mg^{2+} was detectable on XAD-2 in these experiments. This is consistent with the view that the sorption of Mg^{2+} on XAD-OXINE results from complexation of Mg^{2+} by immobilized oxinate ligand.

Picolinate complexes

Picolinate forms the complex species MgP^+ and MgP_2, with stepwise formation constants of 1.6×10^2 (at $c = 0.1$) and 8.9×10^3 (at $c = 0$) (24). Evaluation of the experimental sorption data requires theoretical calculation of the concentrations of the magnesium-containing species Mg^{2+}, MgP^+, and MgP_2. These multiple-equilibrium calculations were performed with the aid of the speciation program COMICS (23, 25). In the calculations the acidity constants and metal–ligand formation constants were corrected to ionic strength $c = 0.25_0$ using activity coefficients obtained with the Davies equation (26), and uncertainties in theoretically calculated species concentrations were obtained by error propagation (23).

Results of these theoretical species distribution calculations at pH 5.00, 6.00, 7.00, and 7.50, for added picolinic acid concentrations, $C_{\text{picolinic acid}}$, of 0.001 M, 0.01 M, and 0.05 M, are presented in Table 1. In the table are shown values of α_i, the fraction of the total magnesium in solution that is present as species i, where i is either Mg^{2+}, MgP^+, or MgP_2. Since these calculations were performed assuming a very small added magnesium concentration, the α_i values in Table 1 are independent of C_{Mg} and will apply to other added magnesium concentrations provided that $C_{Mg} << C_{\text{picolinic acid}}$. Information from Table 1 is needed to determine which of the complex species MgP^+ and MgP_2 is sorbed, and to what extent.

Sorption on XAD-2

Examination of Table 1 reveals two important relationships. First, examination of any horizontal row shows that, for a constant $C_{\text{picolinic acid}}$ and for pH $\geq$ 6, the fraction of magnesium that is present in the form of any particular species is nearly constant, independent of pH. Second, examination of the vertical columns shows that the relative fractional contribution of any species varies markedly with $C_{\text{picolinic acid}}$ and, more importantly, the ratio $(\alpha_{MgP_2}/\alpha_{MgP^+})$ also changes markedly. At any pH $\geq$ 6 this ratio has values of approximately 0.05, 0.4_5, and $2._5$ for $C_{\text{picolinic acid}}$ of 0.001, 0.01, and 0.05, respectively.

Study of the sorption of magnesium–picolinate complexes on the parent polymer XAD-2 is aided by the above relationships and is simplified even more by the fact that the species Mg^{2+} does not sorb significantly on XAD-2. Thus, any magnesium sorbed on XAD-2 will be due to only MgP^+ and (or) MgP_2. Furthermore, the fact that the ratio $(\alpha_{MgP_2}/\alpha_{MgP^+})$ varies so greatly with $C_{\text{picolinic acid}}$ makes it possible to determine the extent to which each of these two species is adsorbed on XAD-2 by studying the amount of magnesium sorbed for constant C_{Mg} and varied $C_{\text{picolinic acid}}$. The results of these two studies, one at pH 6.00 and the other at pH 7.50, are presented in Table 2.

Interpretation of the information in Table 2 is achieved by making plots of $(P.A.)_{sorbed}$ versus the concentrations of individual magnesium–picolinate complex species at a particular pH. Such plots were made for $(P.A.)_{sorbed}$ versus [MgP_2] at pH 6.00 and at pH 7.50. The former is shown in Fig. 1. Linear regression yields a slope of 0.13 ± 0.01, intercept of -0.01 ± 0.04, and correlation coefficient of 0.997 for the plot at pH 6.00 and a slope of 0.14 ± 0.02, intercept of -0.02 ± 0.03, and correlation coefficient of 0.989 for the plot at pH 7.50. In contrast to the linearity of these plots, plots of $(P.A.)_{sorbed}$ versus [MgP^+] (not shown) are nonlinear. Correlation coefficients of 0.37 and 0.78 were obtained at pH 6.00 and 7.50, respectively. These results reveal the following: (*i*) The neutral species MgP_2 is sorbed on the hydrophobic surface of the parent polymer XAD-2 while the cationic species MgP^+ either is not sorbed or is sorbed to a much smaller extent than MgP_2. This is shown by the good linearity of the plots of $(P.A.)_{sorbed}$ versus [MgP_2]. (*ii*) The sorption of MgP_2 on the polymer surface is independent of pH. This is shown by the fact that the slopes of the plots of $(P.A.)_{sorbed}$ versus [MgP_2] at pH 6.00 and pH 7.50 are equal to one another. Since XAD-2 is a nonionic polymer with very few acid–base groups (27) this lack of pH dependence is consistent with expectations.

Sorption on XAD-OXINE

If XAD-OXINE sorbs all three species, Mg^{2+}, MgP^+, and MgP_2, then when a solution containing magnesium and picolinate is equilibrated with XAD-OXINE the measured peak area $(P.A.)_{sorbed}$ will be the sum of peak areas due to three sorbed species:

$$[2] \quad (P.A.)_{sorbed} = (P.A.)_{sorbed,Mg^{2+}} + (P.A.)_{sorbed,MgP^+} + (P.A.)_{sorbed,MgP_2}$$

Since sorption isotherms for the species Mg^{2+} have been measured on XAD-OXINE, as discussed above, and since [Mg^{2+}] can be theoretically calculated for a sample solution containing both magnesium and picolinate, then it is a simple matter to read, from the appropriate Mg^{2+} sorption isotherm, the value of $(P.A.)_{sorbed,Mg^{2+}}$ to be used in eq. [2].

In addition, the value of $(P.A.)_{sorbed,MgP_2}$ to be used in eq. [2] for sorption on XAD-OXINE can be estimated from the sorption of MgP_2 on the parent polymer XAD-2. The sorbent XAD-OXINE has a relatively small fraction of its sur-

Can. J. Chem. Downloaded from www.nrcresearchpress.com by 92.62.229.171 on 09/08/12
For personal use only.

TABLE 2. Effect of varying $C_{\text{picolinic acid}}$ at constant C_{Mg} on the theoretical species distribution of magnesium-containing species and on the peak area due to the total amount of magnesium-containing species sorbed on the parent polymer XAD-2, for two different pH

pH	$C_{Mg} \times 10^6$ M	$C_{\text{picolinic acid}} \times 10^3$ M	$[Mg^{2+}] \times 10^6$ M	$[MgP^+] \times 10^6$ M	$[MgP_2] \times 10^6$ M	$(P.A.)_{\text{sorbed}}$
6.00	10.0	1.00	9.1	9.1	0.040	0.021 ± 0.003
6.00	10.0	10.0	4.2	4.2	1.7	0.168 ± 0.015
6.00	10.0	50.0	0.62	3.1	6.2	0.80 ± 0.08
7.50	4.78	6.00	2.5	1.8	0.51	0.077 ± 0.001
7.50	4.78	10.0	1.7	2.1	0.98	0.112 ± 0.001
7.50	4.78	20.0	0.85	2.0	1.9	0.23 ± 0.01
7.50	4.78	50.0	0.23	1.4	3.2	0.46 ± 0.03

TABLE 3. Effect of varying C_{Mg} at constant $C_{\text{picolinic acid}} = 0.050_0$ M on peak areas due to sorption of magnesium-containing species on the sorbents XAD-OXINE and XAD-2, for two different pH

pH	$C_{Mg^{2+}} \times 10^6$ M	$(P.A.)_{\text{sorbed}}$ on XAD-OXINE	$(P.A.)_{\text{sorbed},Mg^{2+}}$ on XAD-OXINE	$(P.A.)_{\text{sorbed},MgP_2}$ on XAD-2	$(P.A.)_{\text{sorbed},MgP^+}$[a] on XAD-OXINE	$[MgP^+]$[b] $\times 10^6$ M
6.00	0.82	0.118 ± 0.001	0.015 ± 0.001	0.042 ± 0.004	0.061 ± 0.005	0.257
6.00	4.39	0.683 ± 0.007	0.034 ± 0.003	0.261 ± 0.003	0.388 ± 0.009	1.37
6.00	7.98	1.18 ± 0.01	0.065 ± 0.005	0.48 ± 0.04	0.63 ± 0.04	2.50
6.00	11.5	1.72 ± 0.03	0.086 ± 0.007	0.72 ± 0.02	0.91 ± 0.03	3.60
7.50	1.04	0.379 ± 0.001	0.060 ± 0.005	0.075 ± 0.001	0.24 ± 0.01	0.248
7.50	2.14	0.79 ± 0.04	0.090 ± 0.007	0.171 ± 0.008	0.53 ± 0.04	0.509
7.50	3.62	1.25 ± 0.04	0.127 ± 0.010	0.32 ± 0.02	0.81 ± 0.04	0.862
7.50	5.18	1.78 ± 0.06	0.182 ± 0.015	0.43 ± 0.02	1.16 ± 0.06	1.23

[a] From eq. [2]: $(P.A.)_{\text{sorbed},MgP^+} = (P.A.)_{\text{sorbed}} - (P.A.)_{\text{sorbed},Mg^{2+}} - (P.A.)_{\text{sorbed},MgP_2}$.
[b] $[MgP^+]$ calculated from theory using COMICS program.

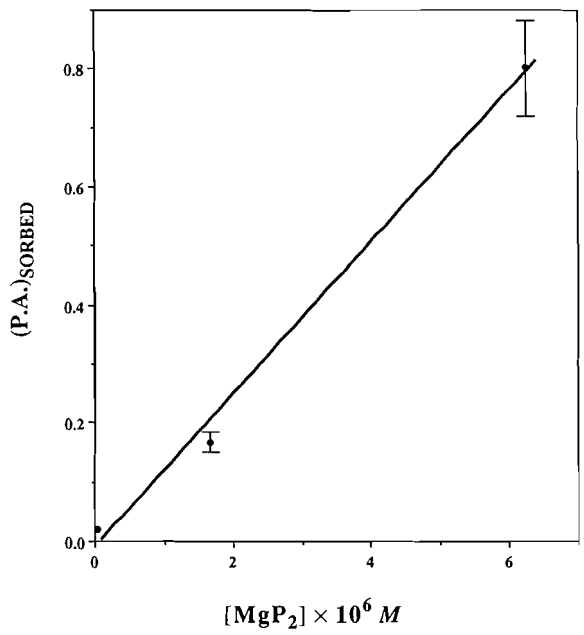

FIG. 1. Sorption of magnesium-containing species, as peak area (P.A.) of sorbed magnesium, on the parent polymer XAD-2 as a function of the concentration of the species MgP_2 in solution, at pH = 6.00 and ionic strength 0.25_0.

face occupied by covalently attached oxine groups, (i.e., for a complexing capacity of 264 μmol/g, only about 20% of the benzene rings at the surface of the styrene–DVB copolymer have attached oxine). Therefore, in terms of its adsorption of the neutral species MgP_2, the XAD-OXINE is expected to behave quantitatively much like XAD-2 (12, 13). As a consequence, if identical sample solutions containing magnesium and picolinate are passed through columns of XAD-OXINE and XAD-2, containing the same amount of sorbent, then the value of $(P.A.)_{\text{sorbed},MgP_2}$ to be used in eq. [2] for XAD-OXINE can be taken to be the same as the value found for XAD-2, because the latter sorbs MgP_2 but not MgP^+ or Mg^{2+}.

Since it is possible, independently, to know the values of $(P.A.)_{\text{sorbed, } Mg^{2+}}$ and $(P.A.)_{\text{sorbed},MgP_2}$ to be used in eq. [2], then it is possible to know whether and to what extent the species MgP^+ is sorbed on XAD-OXINE. Presented in column 3 of Table 3 are experimentally measured values of $(P.A.)_{\text{sorbed}}$ that were obtained at two different pH's when solutions containing constant $C_{\text{picolinic acid}} = 0.050_0$ M and varied C_{Mg} were equilibrated with XAD-OXINE; presented in column 4 are values of $(P.A.)_{\text{sorbed},Mg^{2+}}$ that were read from the experimentally measured Mg^{2+} isotherms on XAD-OXINE at the appropriate $[Mg^{2+}]$; and presented in column 5 are values of $(P.A.)_{\text{sorbed},MgP_2}$ that were obtained by equilibrating the sample solution with the XAD-2 column. The sixth column presents values of $(P.A.)_{\text{sorbed},MgP^+}$ obtained by subtracting $(P.A.)_{\text{sorbed},Mg^{2+}}$ and $(P.A.)_{\text{sorbed},MgP_2}$ from $(P.A.)_{\text{sorbed}}$, as per eq. [2]. The last column shows $[MgP^+]$ values for the solution, obtained by theoretical calculations. Plots were made of $(P.A.)_{\text{sorbed},MgP^+}$ versus $[MgP^+]$ at pH 6.00 and 7.50, respectively. The former plot is shown in Fig. 2. These plots correspond to sorption isotherms for the species MgP^+ on XAD-OXINE.

Both isotherms for MgP^+ are linear. At pH 6.00 the slope is 0.25 ± 0.01 (intercept 0.01 ± 0.02; $r = 0.998$) and at pH

Can. J. Chem. Downloaded from www.nrcresearchpress.com by 92.62.229.171 on 09/08/12
For personal use only.

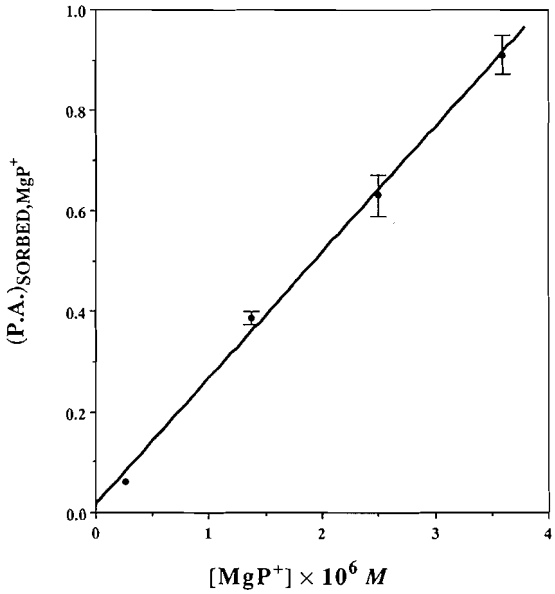

FIG. 2. Sorption of MgP^+, as peak area (P.A.) due to sorbed MgP^+ on XAD-OXINE as a function of the concentration of MgP^+ in solution, at pH 6.00 and ionic strength 0.25_0.

7.50 it is 0.92 ± 0.04 (intercept 0.03 ± 0.03; r = 0.998). A greater slope for the isotherm at higher pH means that the cationic species MgP^+ is sorbed more strongly on XAD-OXINE as a result of an increase in the degree of ionization of the covalently bound oxine to form its anion oxinate. Increased sorption of a cationic sample species as the result of an increase in negative surface-charge density is qualitatively consistent with the theoretical predictions of the "double-layer ionic adsorption and exchange model" (13, 28, 29). *Quantitative* evaluation of the sorption of MgP^+ on XAD-OXINE in terms of this theoretical model is not possible at this time because it was not possible accurately to measure the surface-charge density on XAD-OXINE (22).

Conclusions

On the parent polymer, XAD-2, the hydrophobic, neutral species MgP_2 is sorbed (undoubtedly by the process of surface adsorption) while the charged species Mg^{2+} and MgP^+ are not significantly sorbed compared to MgP_2.

On the derivatized polymer, XAD-OXINE, all three magnesium-containing species Mg^{2+}, MgP^+, and MgP_2 are sorbed. Sorption of the hydrophilic metal ion Mg^{2+} on XAD-OXINE is likely the result of complexation by the bound ligand oxinate. Sorption of the hydrophobic, neutral species MgP_2 is very likely due to the process of surface adsorption on the extensive styrene–DVB polymer surface that is available in XAD-OXINE. Sorption of the hydrophobic cationic species MgP^+ on XAD-OXINE is probably due to a combination of adsorption on the polymer surface and cation exchange in the diffuse part of the electrical double layer (13, 28, 29). However, the possibility of sorption of MgP^+ as a result of the formation of a mixed-ligand complex of magnesium with picolinate and bound oxine cannot be ruled out.

The relative strengths of sorption on XAD-OXINE for the species Mg^{2+}, MgP^+, and MgP_2 at ionic strength c = 0.25 and pH 6.00 and 7.50 can be seen from the relative (P.A.) values in Table 3. Sorption strength for MgP_2 will be relatively independent of c and pH but sorption strength for both Mg^{2+} and MgP^+ will increase markedly with increasing pH and with decreasing ionic strength.

Acknowledgements

This work was supported by the Natural Sciences and Engineering Research Council of Canada and by the University of Alberta.

1. G. Lebel, D. T. Williams, B. R. Hollebone, C. Shewchuk, L. T. Brownlee, H. Tosine, R. Clement, and S. Suter. Int. J. Environ. Anal. Chem. **38**, 21 (1990).
2. M. Salvadori, P. Dolara, E. Bertini, and C. Coppi. Toxicol. Lett. **45**, 241 (1989).
3. J. L. Robinson, W. J. Robinson, M. A. Marshall, A. D. Barnes, K. J. Johnson, and D. S. Salas. J. Chromatogr. **189**, 145 (1980).
4. H. Y. Mohammed and F. F. Cantwell. Anal. Chem. **50**, 491 (1978).
5. R. G. Baum, R. Saetre, and F. F. Cantwell. Anal. Chem. **52**, 15 (1980).
6. D. P. Lee. J. Chromatogr. Sci. **20**, 203 (1982).
7. M. J. Cope and J. E. Davidson. Analyst, **112**, 417 (1987).
8. F. F. Cantwell and S. Puon. Anal. Chem. **51**, 623 (1979).
9. C. H. Knight, R. M. Cassidy, B. M. Recoski, and L. W. Green. Anal. Chem. **56**, 474 (1984).
10. D. T. Gjerde, G. Schmuckler, and J. S. Fritz. J. Chromatogr. **187**, 35 (1980).
11. D. J. Pietrzyk, Z. Iskandarani, and G. L. Schmitt. J. Liquid Chromatogr. **9**, 2633 (1986).
12. S. Afrashtehfar and F. F. Cantwell. Anal. Chem. **54**, 2422 (1982).
13. R. A. Hux and F. F. Cantwell. Anal. Chem. **56**, 1258 (1984).
14. F. Vernon and H. Eccles. Anal. Chim. Acta, **63**, 403 (1973).
15. S. N. Willie, R. E. Sturgeon, and S. S. Berman. Anal. Chim. Acta, **149**, 59 (1983).
16. J. R. Parrish. Anal. Chem. **54**, 1890 (1982).
17. G. V. Myasoedova and S. B. Savvin. Chelating sorbents in analytical chemistry; CRC critical reviews in analytical chemistry. Vol. 17(1). CRC Press, Cleveland. 1987.
18. P. Y. T. Chow and F. F. Cantwell. Anal. Chem. **60**, 1569 (1988).
19. F. F. Cantwell, J. S. Nielsen, and S. E. Hrudey. Anal. Chem. **54**, 1498 (1982).
20. J. Treit, J. S. Nielsen, B. Kratochvil, and F. F. Cantwell. Anal. Chem. **55**, 1650 (1983).
21. J. A. Sweileh, D. Lucyk, B. Kratochvil, and F. F. Cantwell. Anal. Chem. **59**, 586 (1987).
22. G. Persaud and F. F. Cantwell. Anal. Chem. **64**, 89 (1992).
23. G. Persaud. Ph.D. Thesis, University of Alberta, 1990.
24. A. E. Martell and R. M. Smith. Critical stability constants. Vol. 1. Plenum Press, New York. 1974.
25. D. D. Perrin and I. G. Sayce. Talanta, **14**, 833 (1967).
26. C. W. Davies. Ion association. Butterworth, Toronto. 1962.
27. S. Puon and F. F. Cantwell. Anal. Chem. **49**, 1256 (1977).
28. F. F. Cantwell. *In* Advances in ion exchange and solvent extraction. Vol. 9. *Edited by* J. A. Marinsky and Y. Marcus. Marcel Dekker, New York. 1985. Chap. 6.
29. H. Liu and F. F. Cantwell. Anal. Chem. **63**, 2032 (1991).

Can. J. Chem. Downloaded from www.nrcresearchpress.com by 92.62.229.171 on 09/08/12
For personal use only.

The $\tilde{a}^3A'' \leftarrow \tilde{X}^1A'$ electronic spectra of acetaldehyde-h_4 and -d_4

N. N. YAKOVLEV AND I. A. GODUNOV[1]

The Laboratory of Molecular Spectroscopy, Department of Chemistry, Moscow M. Lomonosov State University, Moscow W-234, 119899, Russia

Received July 11, 1991

N. N. YAKOVLEV and I. A. GODUNOV. Can. J. Chem. **70**, 931 (1992).

The $\tilde{a}^3A'' \leftarrow \tilde{X}^1A'$ electronic absorption spectra of acetaldehyde-h_4 and -d_4 were recorded in the vapour phase at room temperature. The major experimental requirement was a high pressure × path length (650 Torr × 140 m). The vibrational structure of these electronic transitions was interpreted in terms of the torsional modes ν'_{15} and ν''_{15} attached to the ν'_{14} out-of-plane bending mode. The main CH_3CHO results agreed with those obtained earlier (Moule and Ng); the values of the 0_0^0 transition and torsional barrier height were 27240.1 and 590 cm^{-1} respectively. Three inversion (out-of-plane bending) energy levels in the excited $\tilde{a}^3A''$ state were found and the inversion potential function was determined with a barrier height of 1110 cm^{-1}. The CD_3CDO spectrum confirmed the CH_3CHO analysis. The values of the 0_0^0 transition and torsional barrier height were equal to 27270 and 610 cm^{-1}.

Key words: vibronic spectrum, acetaldehyde, molecular structure.

N. N. YAKOVLEV et I. A. GODUNOV. Can. J. Chem. **70**, 931 (1992).

Opérant à la température ambiante, on a déterminé les spectres d'absorption électronique $a^3A'' \leftarrow X^1A'$ des acétaldéhydes-h_4 et -d_4 en phase gazeuse. La condition expérimentale principale est une valeur élevée de la pression × longueur de parcours (650 Torr × 140 m). On a interpréte la structure vibrationnelle de ces transitions électroniques en fonction des modes de torsion ν'_{15} et ν''_{15} attachés au mode de déformation hors-plan ν'_{14}. Les principales caractéristiques du spectre du CH_3CHO sont en bon accord avec celles obtenues antérieurement (Moule et Ng); les valeurs de la transition 0_0^0 et la hauteur de la barrière de torsion sont respectivement égales à 27240,1 et 590 cm^{-1}. On a observé trois niveaux d'inversion de l'énergie (déformation hors-plan) dans l'état excité a^3A'' et on a trouvé que le hauteur de la barrière de la fonction du potentiel d'inversion est égale à 1110 cm^{-1}. Le spectre du CD_3CDO confirme l'analyse du spectre du CH_3CHO. Les valeurs de la transition 0_0^0 et de la hauteur de la barrière de torsion sont égales à 27270 et 610 cm^{-1}.

Mots clés : spectre de vibration, acétaldéhyde, structure moléculaire.

[Traduit par la rédaction]

Introduction

The $\tilde{a}^3A'' \leftarrow \tilde{X}^1A'$ electronic absorption spectrum of acetaldehyde-h_4 in the vapour phase at room temperature was investigated earlier by Moule and Ng (1). This spectrum was interpreted in terms of the torsional modes ν'_{15} and ν''_{15} attached to the ν'_{14} out-of-plane C—H bending mode. Both modes were highly Franck–Condon active and their intensity distributions suggested that: (*i*) the methyl group undergoes a rotation from an $\tilde{X}^1A'$ eclipsed conformation to an $\tilde{a}^3A''$ staggered conformation and (*ii*) the aldehyde -CHO group is nonplanar in the $\tilde{a}^3A''$ state. The 0_0^0 band at 27240.4 cm^{-1} was not directly observed because of low intensity.

However Moule and Ng (1) failed to determine the inversional potential because of insufficient experimental data. Because they used a cell with a large volume, it was not possible for them to record the spectra of the isotopic species. Therefore we have investigated the $\tilde{a}^3A'' \leftarrow \tilde{X}^1A'$ spectra of both CH_3CHO and CD_3CDO.

Experimental

The CH_3CHO and CD_3CDO used were of 99.0 and 99.5% purity, respectively. CD_3CDO contained ≥98% of deuterium. Both samples were purified by vacuum trap-to-trap distillation.

The spectra were photographically recorded on a DFS-452 spectrograph in the 1st order of holographic grating (2400 lines per mm) at a modest resolution of 120 000. Pathlengths of up to 140 m at 20°C were obtained with a 2.5 m stainless steel Whytetype multipath cell for vapour pressures up to 650 Torr (1 Torr = 133.3 Pa). A XBO-250 W xenon arc was the light source and a BS-10 glass filter was used to isolate the far-UV radiation. Calibration was made with the iron lines of an iron–neon hollow cathode lamp. Absorption intensities were estimated from tracings of the spectra recorded with a IFO-451 microdensitometer. Line positions were directly measured on spectograms with a IZA comparator. The accuracy of the measurements was ~0, 5 cm^{-1} for CH_3CHO and ~1.0 cm^{-1} for CD_3CDO. The CH_3CHO bands are fairly sharp and single-headed. The CD_3CDO bands are less intense, broader, and double-headed with a separation of ~7 cm^{-1}. The heads of the lower frequency components were measured.[2]

Results and discussion

The key to the analysis of the acetaldehyde-h_4 and -d_4 spectra was the same as in ref. 1. Using the torsional transitions in $\tilde{X}^1A'$ states from microwave and far infrared (2, 3) spectra, we assigned selected bands to the torsional $15^0_{v''}$ vibronic transitions. Then taking into account the results of the analyses of acetaldehyde $-h_4$ and $-d_4$ $\tilde{A}^1A'' \leftarrow \tilde{X}^1A'$ spectra (4, 5) we assigned some bands to the torsional $15_0^{v'}$ and $15^{v'}_{v''}$ transitions. After that we established the 0_0^0 transition wavenumbers of acetaldehyde-h_4 and -d_4 as 27240.1 and 27270 cm^{-1}, respectively, using the 15^{0A}_{2A}, 15^{2A}_{2A}, and 15^{2A}_{0A} transitions for CH_3CHO and also the 15^{0E}_{1E}, 15^{1E}_{1E}, and 15^{1E}_{0E} transitions for CD_3CDO (the 0_0^0 transitions were not directly observed). Thus for each isotopic species we found the group of strong bands ("pattern") that accompanied the "origin"

[1]Author to whom correspondence may be addressed.

[2]Tables A and B list the main vibrational assignments in the 350–370 nm region for acetaldehyde-h_4 and -d_4, respectively, and may be purchased from: The Depository of Unpublished Data, Document Delivery, CISTI, National Research Council Canada, Ottawa, Canada K1A 0S2.

Can. J. Chem. Downloaded from www.nrcresearchpress.com by 92.62.229.171 on 09/08/12
For personal use only.

TABLE 1. Vibrational "pattern" accompanying the "origin" (0_0^0) of the $\tilde{a}^3A'' \leftarrow \tilde{X}^1A'$ electronic transition

	CH_3CHO		CD_3CDO		
cf. Fig. 1	$\nu(cm^{-1})$	$\Delta\nu(cm^{-1})$	$\nu(cm^{-1})$	$\Delta\nu(cm^{-1})$	Assignment
1	26897.2	342.9	—	—	15_{3E}^{0E}
2	26963.8	276.3	—	—	15_{2E}^{0E}
3	26983.0	257.1	27060	210	15_{2A}^{0A}
4	27096.5	143.6	27161	109	15_{1E}^{0E}
5	27141.5	98.6	27196	74	15_{2E}^{1E}
6	(27240.1)	0.0	(27270)	0.0	0_0^0
7	27275.4	35.3	27298	28	15_{1A}^{1A}
8	27300.5	60.4	—	—	15_{2E}^{2E}
9	27315.7	75.6	27324	54	15_{2A}^{2A}
10	27348.5	108.4	27343	73	15_{3E}^{3E}
11	27414.2	174.1	—	—	15_{2E}^{3E}
12	27418.8	178.7	27407	137	15_{0E}^{1E}
13	27428.5	188.4	27425	155	15_{1E}^{2E}
14	27544.7	304.6	—	—	15_{1E}^{3E}
15	27572.8	332.7	27536	266	15_{0A}^{2A}
16	27689.2	449.1	27648	378	15_{0E}^{3E}

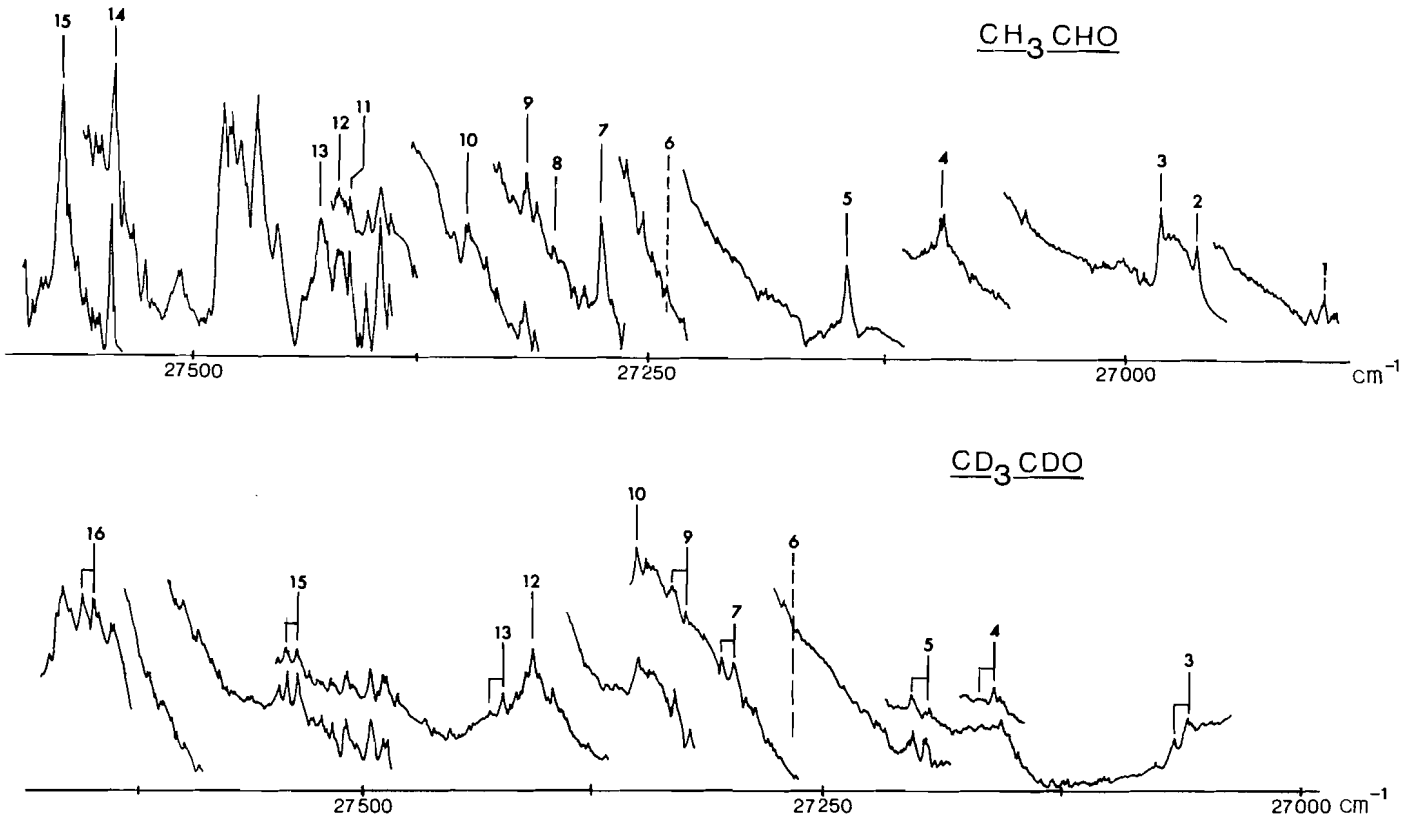

FIG. 1. The UV absorption spectra of acetaldehyde-h_4 and -d_4 near the 0_0^0 transitions. (Band numbers are the same as in Table 1)

(0_0^0) of the electronic $\tilde{a}^3A'' \leftarrow \tilde{X}^1A'$ transition (see Table 1 and Fig. 1). The figure shows that the most intensive bands correspond to the 15_{0A}^{2A} transition in the CH_3CHO spectrum and the 15_{0E}^{1E} transition in the CD_3CDO spectrum.

We also found several of the same patterns that accompany the "pseudoorigins" listed in Table 2 with their possible assignments. One can see from Table 2 that three inversion energy levels in the excited triplet electronic state have been found for CH_3CHO and it is rather difficult to assign these "pseudoorigins" differently (the possibility of their assignments to the $A^1A'' \leftarrow \tilde{X}^1A'$ system has also been considered).

Can. J. Chem. Downloaded from www.nrcresearchpress.com by 92.62.229.171 on 09/08/12
For personal use only.

TABLE 2. "Pseudoorigins" in CH_3CHO and CD_3CDO spectra and their possible assignments[a]

CH_3CHO			CD_3CDO		
$\nu(cm^{-1})$	$\Delta\nu(cm^{-1})$	Assignment	$\nu(cm^{-1})$	$\Delta\nu(cm^{-1})$	Assignment
27603.9	363.8	ν_{10} (1)	27610	340	ν_{10}
27743.5	503.4	$2\nu_{14}$ (1)	27711	441	$2\nu_{14}$
27771.9	531.8	$3\nu_{14}$	27935	665	$2\nu_{10}$
27965.1	725.0	$2\nu_{10}$	27997	727	ν_8; ν_9
28128.5	888.4	$4\nu_{14}$	28269	999	ν_{12}; ν_{13}
28145.2	905.1	ν_8; ν_{13}			

[a]Mode descriptions are taken from ref. 6.

TABLE 3. Observed and calculated inversion energy levels and barrier heights (b) of formaldehyde and acetaldehyde (in cm^{-1})

	H_2CO		D_2CO		CH_3CHO			CD_3CDO		
					A^1A''	$\tilde{a}^3A''$		A^1A''	$\tilde{a}^3A''$	
Levels of energy[a]	A^1A_2	$\tilde{a}^3A_2$	A^1A_2	$\tilde{a}^3A_2$		This work			This work	
	Ref. 9		Ref. 9		Ref. 4	obsd.	calcd.[b]	Ref. 4	obsd.	calcd.
0^-	124.5	36	67.0	(9.9)	33	—	1.3	11	—	0.3
1^+	542.3	538.2	386.0	448.8	487	503.4	503.6	350	441	437.9
1^-	947.9	777.2	667.1	(569.5)	—	531.8	531.7	—	—	445.6
2^+	1429.3	1175.0	1015.0	889.4	—	888.4	888.5	—	—	792.3
2^-	(1949.8)	(1572.8)	1397.0	(1183.8)	—	—	1043.4	—	—	864.0
3^+	—	—	—	1533.9	—	—	1322.6	—	—	1105.5
b	350.3	775.6	333.2	769.0	685[c]	1110		565[c]	1110	
$\angle\Theta$[d]	34.0°	41.1°	33.3°	43.0°	37.5°	45.0°		37.5°	45.0°	

[a]The notation is that of ref. 10.
[b]$K_1 = 855.36\ cm^{-1}\ Å^{-2}$, $k_1 = 2688.69\ cm^{-1}$, $k_2 = 1.31\ Å^{-2}$, see potential, eq. [1].
[c]Calculated with the data from ref. 4 using the method presented in ref. 10.
[d]The out-of-plane angle Θ corresponds to the minima of the potential, eq. [1].

The parameters of the inversional potential

$$[1] \quad V(Z) = K_1Z^2 + k_1 \exp(-k_2Z^2)$$

where Z is the out-of-plane oxygen displacement, have been determined by the method of Ueda and Shimanouchi (7) for this molecule. Strictly speaking, the -CHO group has a pyramidal structure in the acetaldehyde equilibrium configuration in the lowest excited singlet S_1 and triplet T_1 electronic states. Such -CHO group "deformation" of the planar structure in the ground S_0 electronic state of acetaldehyde was approximated by an out-of-plane C—H bond displacement (1, 4). In this case the CCH angle was decreased and the CCO angle was fixed. But we could not obtain the rotational constants listed in ref. 4 for acetaldehyde-h_4 in the S_1 state with geometric parameters from "model *ii*" (4). Instead of $A' = 1.649$, $B' = 0.338$, and $C' = 0.300\ cm^{-1}$ (4) we obtained $A' = 1.842$, $B' = 0.317$, and $C' = 0.288\ cm^{-1}$, but the rotational contours of the acetaldehyde-h_4 vibronic bands 0_0^0, 14_0^1 (A_1, E), 15_0^2 (A_1, E) calculated with these rotational constants were far from the experimental ones listed in ref. 4. However, calculated and experimental vibronic band rotational contours of CH_3CHO and CH_3CDO spectra (4) agree well if we use the geometric parameters derived from the microwave spectrum (8), except r(C=O) = 1.316 Å and the out-of-plane C=O bond displacement angle $\Theta = 37.5°$ (with $\angle CCO = 116.2°$). In fact, only the planar $CCH_{ald.}$ and CCO angles differ from those of "model *ii*" (4).

For acetaldehyde in the T_1 state, we assume the geometric parameters to be the same as in the S_1 state, except for the Θ angle. We take this angle as the minimum of the potential, eq. [1]. The calculated parameters of the potential, eq. [1], are listed in Table 3. The inversion potentials of acetaldehyde-h_4 and -d_4 in the S_1 state and those of formaldehyde-h_2 and -d_2 in the S_1 and T_1 states (9) are also listed in Table 3. We assume that the inversion potentials of acetaldehyde-h_4 and -d_4 in the T_1 state are approximately the same, and we calculate the inversion energy levels of CD_3CDO, Table 3. Using the data, we assign the 441 cm^{-1} frequency found in the CD_3CDO spectrum (Table 2) to the inversion level 14^{1+} or 14^{1-}. Taking into account that the 14_0^{1+} transition is more intense than the 14_0^{1-} transition in the CH_3CHO spectrum, we tentatively assigned the CD_3CDO 441 cm^{-1} frequency to the 14^{1+} level. Because of low intensity, we could not observe the transitions to higher inversional levels in the CD_3CDO spectrum and thus could not assign this frequency definitely.

One can see from Table 3 that the acetaldehyde inversion barrier in the T_1 state is approximately twice that in the S_1 state

Can. J. Chem. Downloaded from www.nrcresearchpress.com by 92.62.229.171 on 09/08/12
For personal use only.

TABLE 4. Experimental and calculated torsional energy levels and internal rotation potentials of acetaldehyde-h_4 and -d_4 molecules (in cm^{-1})

Torsional transitions and potential parameters	CH_3CHO					CD_3CDO			
			$\tilde{a}^3A''$					$\tilde{a}^3A''$	
	$\tilde{X}^1A$	A^1A''		This work		$\tilde{X}^1A$	A^1A''	This work	
	(ref. 3)	(ref. 4)	(ref. 1)	obsd.	calcd.	Calcd. in ref. 2	(ref. 4)	obsd.	calcd.
$1E \leftarrow 0E^a$	141.9	195	181	178.7	179.9	109.8	147	137	137.4
$1A_2 \leftarrow 0A_1$	143.7	—	—	—	180.2	109.9	—	—	137.4
$2A_1 \leftarrow 0A_1$	255.5	345	334	332.7	332.4	211.5	277	266	264.3
$2E \leftarrow 0E$	269.4	—	—	—	336.5	213.0	—	—	264.4
$3E \leftarrow 0E$	—	478	—	449.1	449.5	298.7	391	378	378.1
$3A_2 \leftarrow 0A_1$	—	—	—	—	479.2	310.6	—	—	379.7
F	7.575	6.65	6.81	6.95		4.44	3.70	3.95	
V_3	408.3	660	624.8	590		415.0[b]	665	610	
V_6	−12.6	—	—	15.5		−22.3[b]	—	−0.4	
0°	—	29771	27240.4	27240.1		—	29808	27270	

[a]The selection rules for optical transitions are : $A_1 \leftrightarrow A_1$; $A_2 \leftrightarrow A_2$; and $E \leftrightarrow E$.
[b]Assumed.

and the Θ equilibrium value in the T_1 state is about 8° larger than in the S_1 state. Similar relations are observed for formaldehyde, see Table 3.

We mentioned above that the vibronic bands in the CD_3CDO spectrum were double-headed with a separation of about 7 cm^{-1}. Such contours seem to be part of the vibronic band rotational contours. We also investigated the possibility of assigning the 7 cm^{-1} frequency to the inversion splitting $14^{0-}(0^{0-}) - 0^{0+}$. From the T_1 inversion potentials for CH_3CHO and CD_3CDO and the assignment of the 503 cm^{-1} frequency in the CH_3CHO spectrum to the 14^{1+} level (Table 2), we calculate an inversion splitting of 41–45 cm^{-1} for CH_3CHO by the method of Coon *et al.* (10). As such intervals are not observed in the CH_3CHO spectrum, this hypothesis has been rejected.

Using the torsional levels obtained from the spectral analysis, we determined the T_1 internal rotation potential functions

$$[2] \quad V(\varphi) = \frac{1}{2}[V_3(1 - \cos 3\varphi) + V_6(1 - \cos 6\varphi)]$$

for acetaldehyde-h_4 and -d_4 by the method of Lewis *et al.* (11), Table 4. The reduced rotational constants F listed in Table 4 are calculated with the help of geometric parameters obtained for the inversional potential (microwave parameters (7) but r(C=O) = 1.316 Å, ∠ Θ = 45° with ∠CCO = 113.2°). One can see from Table 4 that these internal rotational potentials are in good agreement both with each other and with the potential determined for CH_3CHO by Moule and Ng (1).

Conclusions

The results of the $\tilde{a}^3A'' \leftarrow \tilde{X}^1A'$ spectral analysis for acetaldehyde-h_4 and -d_4 agree well with each other and confirm the earlier analysis (1) reported for acetaldehyde-h_4. We obtain three inversion levels and determine the inversion potential of CH_3CHO in the excited T_1 triplet state. The T_1 state inversion barrier is approximately twice that of the S_1 state. A similar result was obtained earlier for formaldehyde (9).

1. D. C. Moule and K. H. K. Ng. Can. J. Chem. **63**, 1378 (1985).
2. J. S. Crighton and S. Bell. J. Mol. Spectrosc. **112**, 315 (1985).
3. I. Kleiner, M. Goodfroid, M. Hermann, and A. R. W. McKellar. J. Mol. Spectrosc. **142**, 238 (1990).
4. M. Noble and E. K. C. Lee. J. Chem. Phys. **81**, 1632 (1984).
5. M. Baba, I. Hanazaki, and U. Nagashima. J. Chem. Phys. **82**, 3938 (1985).
6. K. B. Wiberg, V. Walters, and S. D. Colson. J. Phys. Chem. **88**, 4723 (1984).
7. T. Ueda and T. Shimanouchi. J. Chem. Phys. **47**, 4042 (1967).
8. R. W. Kilb, C. C. Lin, and E. B. Wilson. J. Chem. Phys. **26**, 1695 (1957).
9. D. J. Clouthier and D. A. Ramsay. Annu. Rev. Phys. Chem. **34**, 31 (1983).
10. J. B. Coon, N. W. Naugle, and R. D. McKenzie. J. Mol. Spectrosc. **20**, 107 (1966).
11. J. D. Lewis, T. B. Malloy, T. O. Chao, and J. Laane. J. Mol. Struct. **12**, 427 (1972).

Can. J. Chem. Downloaded from www.nrcresearchpress.com by 92.62.229.171 on 09/08/12
For personal use only.

Study of the dissociation of the products of some proton transfer reactions in acetonitrile solvent

WLODZIMIERZ GALEZOWSKI[1] AND ARNOLD JARCZEWSKI
Faculty of Chemistry, A. Mickiewicz University, Grunwaldzka 6, 60-780 Poznan, Poland

Received April 17, 1991

WLODZIMIERZ GALEZOWSKI and ARNOLD JARCZEWSKI. Can. J. Chem. **70**, 935 (1992).

The conductometric study of the products of the proton transfer reactions of C-acids (nitriles, nitroalkanes, and 2,4,6-trinitrotoluene) with the strong amine bases (1,1,3,3-tetramethylguanidine (TMG), 1,8-diazabicyclo[5.4.0]undec-7-ene (DBU), 1,8-bis(dimethylamino)naphthalene (DMAN), and piperidine) in acetonitrile shows their large degree of dissociation into free ions. The dissociation constant values have been estimated at 25°C to be larger than 1×10^{-4} M. This weakens the formalism commonly accepted in spectrophotometric kinetic studies of these systems of reactions, based on the assumption that the product is an ion pair. Spectrophotometric equilibrium and kinetic measurements provided evidence that reverse reaction is a second-order process (pseudo-first order because cation concentration is controlled by side reactions). The influence of the common cation ($TMGH^+$) on the equilibria of the proton abstraction from 2-methyl-1-(4-nitrophenyl)-1-nitropropane and 4-nitrophenylcyanomethane with TMG base in acetonitrile at 25°C was examined and was found to be compatible with the assumption of large dissociation of the reaction product for free ions. "Equilibrium constants" estimated by the Benesi and Hildebrand method (which assumes an ion-pair product) decreased with increasing concentration of added $TMGH^+$ cation, but these "equilibrium constants" multiplied by $[TMGH^+]$ are constant. The observed pseudo-first-order rate constants of the proton transfer reaction, measured at large excess of the base over C-acid, grow with the cation concentration due to the increase of the backward reaction rate. The concentration of added common cation shows a negligible influence on the observed rate constants of deuteron transfer reaction. Thus, as a result of side reactions, in which extra amounts of cation are formed, some second-order rate constants k_f^H and also kinetic isotope effects (KIEs) (k_f^H/k_f^D) that have been measured in acetonitrile can be substantially overestimated.

Key words: ion-pair dissociation, proton transfer reactions, kinetic isotope effects.

WLODZIMIERZ GALEZOWSKI et ARNOLD JARCZEWSKI. Can. J. Chem. **70**, 935 (1992).

Une étude conductométrique des produits de réactions de transfert de protons d'acides C (nitriles, nitroalcanes et 2,4,6-trinitrotoluène) avec des bases fortes aminées (1,1,3,3-tétraméthylguanidine (TMG), 1,8-diazabicyclo[5.4.0]undéc-7-ène (DBU), 1,8-bis(diméthylamino)naphtalène (DMAN) et pipéridine) dans l'acétonitrile montre qu'ils sont fortement dissociés en ions libres. À 25°C, on a évalué que les constantes de dissociation sont plus grandes que 1×10^{-4} M. Ces résultats affaiblissent le formalisme généralement accepté dans les études cinétiques spectrophotométriques de ces systèmes de réactions, qui est basé sur l'hypothèse que le produit est une paire d'ions. L'équilibre spectrophotométrique et les mesures cinétiques fournissent des données suggérant que la réaction inverse est du deuxième ordre (pseudo-premier ordre parce que la concentration des cations est contrôlée par des réactions parasites). Opérant à 25°C, dans l'acétonitrile, on a examiné l'influence du cation commun ($TMGH^+$) sur l'équilibre de la réactions d'enlèvement du proton du 2-méthyl-1-(4-nitrophényl)-1-nitropropane et du 4-nitrophénylcyanométhane par la base TMG et on a trouvé que cette influence est compatible avec l'hypothèse d'une importante dissociation des produits de réaction en ions libres. Les «constantes d'équilibre» évaluées par la méthode de Benesi et Hildebrand (qui fait l'hypothèse que le produit est une paire d'ions) diminuent avec une augmentation de la concentration de cation $TMGH^+$ ajoutée; toutefois, ces «constantes d'équilibre» multipliées par $[TMGH^+]$ sont constantes. Les constantes de vitesse du pseudo-premier-ordre observées pour la réaction de transfert de proton, mesurées avec un grand excès de base par rapport à l'acide C, augmentent avec la concentration de cation; ce résultat est dû à l'augmentation de la vitesse de la réaction en retour. La concentration du cation commun ajouté ne présente qu'une influence négligeable sur les constantes de vitesse observées pour la vitesse de transfert de deutéron. À cause de réactions secondaires dans lesquelles il se forme des quantités supplémentaires de cations, il est donc possible que les constantes de vitesse du deuxième ordre, k_f^H, qui ont été mesurées ainsi que les effets isotropiques cinétiques (EIC) (k_f^H/k_f^D) qui ont été mesurés dans l'acétonitrile soient substantiellement surestimées.

Mots clés : dissociation de paires d'ions, réactions de transfert de proton, effets isotropiques cinétiques.

[Traduit par la rédaction]

Introduction

The proton transfer reactions between C-acids of various structures and strong amines in aprotic solvents have been extensively studied for many years (1–10). The kinetics of these systems of reactions were mostly carried out spectrophotometrically, taking advantage of the fact that the ionic products formed after abstraction of the proton have large absorption coefficients in the visible range of the spectrum. The particularly important parameter obtained from these kinetic studies was the primary deuterium kinetic isotope effect (KIE), which appeared to be a useful tool in determining the mechanism of the proton transfer and also the magnitude of the tunnel effect (2, 3, 10, 11).

The kinetic studies of these reactions were performed in a variety of solvents, mostly aprotic solvents, of different polarity (2, 10–13), since Caldin and Mateo predicted that the value of KIE is strongly dependent on the polarity of the solvent in which the proton transfer reaction has been carried out (2, 12). They predicted that in high-polarity solvents the proton transfer was coupled with the motion of the molecules of the solvent, which reduced the effective deuteron/proton mass ratio, consequently decreasing the KIE value (2). Therefore, low-polarity solvents seemed to fa-

[1]Author to whom correspondence may be addressed at: Department of Chemistry, Rice University, Box 1892, Houston, TX 77251, U.S.A.

Can. J. Chem. Downloaded from www.nrcresearchpress.com by 92.62.229.171 on 09/08/12
For personal use only.

vour large KIE values by the "uncoupled mechanism" (14, 15). Consequently for comparison, kinetic experiments were performed in both low- and high-polarity aprotic solvents (10, 14, 16). However, very frequently, the equilibrium constants for the ionogenic proton transfer reactions were too small in low-polarity solvents, constraining kinetic measurements to high-polarity solvents, mostly acetonitrile (8–10).

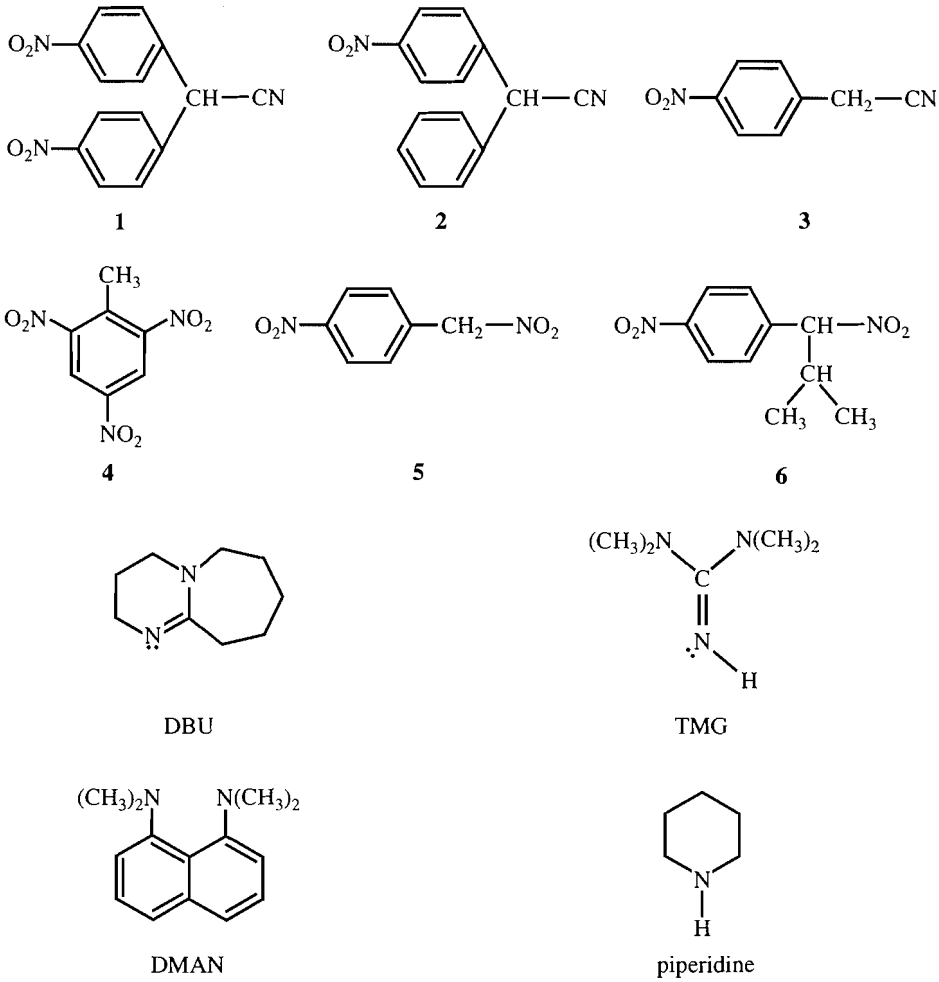

On the basis of the fit of the experimental equilibrium data to the Benesi and Hildebrand equation (1) the products were claimed to be ion pairs, unexpectedly for both groups of low- and high-polarity solvents (1, 2). However, in our previous paper (14) we proved that the products of some proton transfer reactions between 1-(4-nitrophenyl)-1-nitroalkanes and DBU or TMG carried out in acetonitrile solvent are dissociated to free ions, showing that the Benesi and Hildebrand method is frequently not reliable in these systems of reactions.

The estimation of the degree of dissociation of the product for a reaction of a C-acid with a strong organic base in acetonitrile is crucial for determining the kinetic equation. This is of particular importance for the reactions of nitrophenylcyanoalkanes, which have relatively large pK_a values in comparison with nitrophenylnitroalkanes, reacting with a similar rate constant (8–10, 17). The reactions of nitriles, with small equilibrium constants, present an interesting system in which the KIE values are close to a maximum around $\Delta G_0 = 0$.

The use of the correct kinetic equation has a fundamental significance for the results of kinetic experiments and their interpretation. Therefore, the intention of this work is to estimate the degree of dissociation of the products of some proton transfer reactions for a larger number of C-acids and bases in acetonitrile solvent, and also to discuss the possible implications on the results of spectrophotometric equilibrium and kinetic measurements, as we believe that the effect of the common cation derived from the reacting base has a considerable impact on kinetic and equilibrium parameters.

Results and discussion

Conductometric measurements

Proton transfer reactions between C-acids and amines give ion-pair products that can dissociate to free ions depending

Can. J. Chem. Downloaded from www.nrcresearchpress.com by 92.62.229.171 on 09/08/12
For personal use only.

$$AH + B \underset{}{\overset{K_r}{\rightleftharpoons}} A^-, BH^+ \overset{K_d}{\rightleftharpoons} A^- + BH^+$$

SCHEME 1

TABLE 1. Results of conductance studies of proton transfer between various C-acids and amine bases in acetonitrile at 25°C showing very large ionization and dissociation of the reaction product

System	$10^2 C_B$ (mol dm^{-3})	Onsager slope	Λ_0 (Ω^{-1} cm^2 mol^{-1})
1 + DBU	2.67–9.64	293–394	134–138
1 + TMG	2.58–9.33	329–414	145–150
1 + piperidine	2.58–9.33	357–448	139–145
2 + DBU	2.67–9.64	407–735	140–155
2 + TMG	2.62–9.48	560–659	155–160
4 + DBU	2.67–9.64	294–363	149–155
4 + TMG	2.63–9.48	376–525	160–164

on the polarity of the solvent used (1, 16) (Scheme 1),[2] where AH = C-acid, B = base, A^-, BH^+ = ion pair, A^- and BH^+ are free ions. Kinetic measurements on these reactions are always carried out in a large excess of the base concentration over the reacting C-acid, to assure pseudo-first-order conditions (1–10, 12–14). Therefore in the present work conductometric experiments were performed under similar conditions.

For all reactions of **1**, **2**, and **4** with DBU and TMG and the reaction of **1** with piperidine in a given concentration range (Table 1) the plots of Λ vs. $C_{AH}^{1/2}$ gave reasonable values of Λ_0. As an example, for the reaction of **4** with TMG the Λ_0 ranging between 160 and 164 is close to that of tetramethylguanidinium picrate, which is equal 161 (18). The experimental Onsager slopes (18) shown in Table 1 are not far from theoretical values, indicating both a very extensive ionization of C-acid and dissociation of the resulting salt into free ions. (Those theoretical Onsager slopes in acetonitrile at 25°C vary from 320 to 380 depending on particular Λ_0.)

No correction for conductivity of contaminants or solvolysis products of amine bases was applied. A simple subtraction of the conductivity of the base solution was not satisfactory, leading in some cases even to a slight increase in Λ with C-acid concentration. The specific conductivity κ_0 of the solutions of the bases in MeCN solvent increases with base concentration and is larger for the stronger bases DBU (pK_a in acetonitrile at 25°C = 23.9 (19), $\kappa_0 = (5–10) \times 10^{-6}$ Ω^{-1} cm^{-1} in the concentration range 0.02–0.08 M) and TMG (pK_a = 23.3 (20); $(2–4) \times 10^{-6}$ Ω^{-1} cm^{-1}, 0.03–0.1 M) and smaller for weaker bases DMAN (pK_a = 18.3;[3] $(2–3) \times 10^{-7}$ Ω^{-1} cm^{-1}, 0.05–0.18 M) and piperidine (pK_a = 18.9 (21); $(4–10) \times 10^{-7}$ Ω^{-1} cm^{-1}, 0.04–0.13 M)).

Conductometric measurements in the solutions of strong amine bases in acetonitrile show poor reproducibility due to unavoidable contaminants (22). We also found in our study

[2]The alternative scheme, in which free ions are initially formed from reactants (with following ion-pairing), is experimentally indistinguishable from Scheme 1 presented in this paper and leads to basically the same conclusions.

[3]K. T. Leffek and P. Pruszynski, personal communication.

TABLE 2. Results of conductance studies of proton transfer reactions between various C-acids and amine bases in acetonitrile at 25°C

System	$10^2 C_B$ (mol dm^{-3})	Λ_0 (Ω^{-1} cm^2 mol^{-1})	$10^3 K_{ef}$ (mol dm^{-3})
1 + DMAN	2.38–8.62	137–133[a]	3.1–7.1[b]
2 + piperidine	1.86–62.3	140–118[a]	0.01–5.1[b]
2 + DMAN	5.04–18.2	140[c]	0.003–0.011[b]
3 + DBU	2.20–9.74	154[c]	2.8–7.3[b]
3 + TMG	2.58–9.33	154[c]	0.24–1.08[b]
4 + piperidine	3.68–13.3	160–140[a]	0.009–0.11[b]
5 + piperidine	17.2–62.3	158–151[a]	0.14–0.30[b]
5 + DMAN	2.38–8.62	200–157[a]	0.03–0.16[b]

[a]Decreasing monotonically with base concentration.
[b]Increasing monotonically with base concentration.
[c]An average value.

that, despite of all precautions taken, these specific conductivities varied with a new batch of solvent or amine base used (the κ_0 values shown above are the lowest we achieved). Therefore, although a correction for solvolysis of amine bases could be made by employing pK_a values of amine base and the autoprotolysis constant of acetonitrile (22), it is hard to account for variable amounts of unknown impurities, that unfortunately affect the conductivity of the systems under study quite strongly.

Accordingly, for data analysis of systems behaving like weak electrolytes, not listed in Table 1, a simple treatment was applied in which effects of interionic forces on mobility and thermodynamic potential were neglected. Under these assumptions the conductivity of the reaction products is described by eq. [1], which is analogous to the Kraus and Bray equation (14, 23):

$$[1] \quad 1/\Lambda = 1/\Lambda_0 + C_{AH}\,\Lambda/(K_{ef}\Lambda_0^2)$$

where C_{AH} is the total concentration of C-acid, Λ is the equivalent conductivity, and Λ_0 is the limiting equivalent conductance. The effective equilibrium constant, K_{ef}, is described by eq. [2]:

$$[2] \quad 1/K_{ef} = 1/K_d + 1/(K_r K_d C_B)$$

where K_r and K_d are defined in Scheme 1, and C_B is the base concentration in large excess over C_{AH}. From eq. [2], K_d and K_r values can be estimated using the relation $1/K_{ef}$ vs. $1/C_B$.

The K_{ef} values obtained from the Kraus and Bray formalism (plot $1/\Lambda$ vs. $C_{AH}\Lambda$) are collected in Table 2. They represent the lower limit of dissociation constants of the ion pairs, K_d (14).

The values of K_r and K_d for the reaction of **3** with DBU (Table 3) were estimated using the relation $1/K_{ef}$ vs. $1/C_B$. In the case of the reactions of **2** and **5** with DMAN the plot of $1/(K_{ef}\Lambda_0^2)$ vs. $1/C_B$ was used (eq. [3]), due to the large standard deviations of Λ_0 affecting the accuracy of K_{ef}.

$$[3] \quad 1/(K_{ef}\Lambda_0^2) = 1/(K_d\Lambda_0^2) + 1/(K_d\Lambda_0^2 K_r C_B)$$

The experimental data fitted to eq. [3] showed excellent correlation coefficients. The K_d values were then calculated from the initial intercepts and the mean values of Λ_0.

The reactions of **2** and **4** with piperidine (Table 2) show some irregularities as compared to other systems, since their

Can. J. Chem. Downloaded from www.nrcresearchpress.com by 92.62.229.171 on 09/08/12
For personal use only.

$$AH + B \rightleftharpoons \underset{ip}{A^-, BH^+} \rightleftharpoons A^- + BH^+ \overset{B}{\rightleftharpoons} A^- + BHB^+ \rightleftharpoons \underset{ip'}{A^-, BHB^+}$$

SCHEME 2

TABLE 3. Estimated values of K_d and K_r for the products of some reactions between C-acids and amine bases in acetonitrile at 25°C

System	$10^3 K_d$ (mol dm^{-3})	K_r (mol^{-1} dm^3)
2 + DMAN	0.067 ± 0.002	1.91 ± 0.03
3 + DBU	30 ± 20	4 ± 3
5 + DMAN	1.3 ± 0.3	1.36 ± 0.07

effective constants K_{ef} increase considerably faster than could be expected from the increase of the base concentration, which is not consistent with eq. [2]. This is particularly evident for the reaction of **2** over a wide range of piperidine concentration.

The simplest explanation of this phenomenon seems to be the interaction of the second molecule of piperdine with the cation, as shown in Scheme 2.

The formation of BHB^+ ions, known as a homoconjugation, is favoured by two factors: the low steric demands of the base, and by hydrogens available for hydrogen bonding (24). From the set of amines under investigation, piperidine demonstrates the strongest tendency to form homoconjugates. The homoconjugation constant for piperidinium cation, which is 25 M^{-1} (25), indicates that in the range of piperidine concentration (0.0186–0.623 M, Table 2) used, the equilibrium between piperidinium cation and its homoconjugated form can be observed. Both forms exist in comparable amounts for a concentration of piperidine equal to 1×10^{-2} M. With increasing concentration of piperidine above 10^{-2} M, the bulk of the piperidinium cation exists as the homoconjugate. Collaterally, the increase of the equilibrium constant and also a larger extent of dissociation of the ion pairs formed in the proton transfer reactions have been observed (Scheme 2) (24). Homoconjugation was a reason to omit the K_r and K_d values for the reactions of piperidine base with C-acids (Table 3). However, in these cases the considerable dissociation of the ion-pair product can be deduced from the K_{ef} values shown in Table 2.

The examination of the results leads to the conclusion that the smallest value of dissociation constant K_d found in this study is equal to 6.7×10^{-5} M (Table 3), which is comparable with the largest values of C-acid concentrations commonly used in kinetic or equilibrium experiments carried out by means of spectrophotometric methods (1–17, 26). Hence, the assumption that the products of these proton transfer reactions in acetonitrile solvent are ion pairs in the spectrophotometric range of C-acid concentration is not justified.

We would like to emphasize here that direct kinetic measurements are suitable only for reactions with fairly large equilibrium constants, which means the systems involving a rather strong C-acid and a strong base, such as those shown in Tables 1–3.

We believe that in acetonitrile solvent most proton transfer reactions from nitro or cyano group activated C-acids give products that are mostly dissociated into free ions; however, in the cases where the ability of charge delocalization is smaller, comparable amounts of both forms (ions and ion pairs) exist in equilibrium. This last case is particularly difficult with respect to interpretation of kinetic data. Both extreme cases, with the product fully dissociated to free ions or entirely in the form of ion pairs, are worthy of study.

Effect of common cation on the equilibria and kinetics of proton transfer reactions

Equilibria

The equilibrium data for the reaction of C-acids with amines (in a large excess over C-acid) in acetonitrile often fulfill the Benesi and Hildebrand eq. [4] (14).

$$[4] \quad C_{AH}/A = 1/\epsilon + 1/(\epsilon K_{Ben} C_B)$$

where A is the absorbance of the product (optical path length 1 cm), ϵ the molar absorptivity of the product, and K_{Ben} the "equilibrium constant" estimated by the Benesi and Hildebrand method. This agreement suggests that the product of the proton transfer reaction exists mainly as the ion pair, in contrast to the conclusions derived from conductometric measurements.

We partly discussed the possible reason for this discrepancy (14), indicating the effect of the common cation BH^+, which was formed in side reactions of strong amines with acetonitrile solvent and its acidic contaminants or brought in with amine base. In the present paper the spectrophotometric results supporting our assumptions are presented.

The concentration of BH^+ cations of a strong amine base (B) in acetonitrile solution increases with the concentration of the amine as can be seen from conductometric measurements of solutions of amines (κ_0 values quoted in preceding paragraph). However, it is difficult to estimate the real concentration of the BH^+ cations under conditions of spectrophotometric equilibrium or kinetic measurements. Therefore, the addition of a well-dissociated salt of the BH^+ cation allows control of its concentration over the whole range of measurements. For this purpose we used 1,1,3,3-tetramethylguanidinium picrate ($TMGH^+$ Pi^-) which is well dissociated in acetonitrile solvent (18).

As a working model we chose the reaction between 2-methyl-1-(4-nitrophenyl)-1-nitropropane (**6**) and TMG due to its moderate rate and the great resistance of the product to oxidation. The conductometric measurements show a large degree of dissociation of the product of this reaction in acetonitrile solvent.[4]

The equilibrium data for reactions of TMG with both **6** and **3**, with and without additions of tetramethylguanidinium picrate, fulfilled fairly well the Benesi and Hildebrand equation [4] (Tables 4 and 5), which could, as already mentioned, suggest a small degree of dissociation of the product into free ions. However, the resulting "equilibrium constants" K_{Ben} decreased considerably with increasing

[4]W. Galezowski, unpublished results.

Can. J. Chem. Downloaded from www.nrcresearchpress.com by 92.62.229.171 on 09/08/12
For personal use only.

TABLE 4. Common cation effect on equilibria of 2-methyl-1-(4-nitrophenyl)-1-nitropropane (**6**) (C_{AH} = 2.5 × 10^{-5} M) with TMG reaction in acetonitrile at 25°C

10^3C_{TMG} (M)	$10^4C_{TMGH^+Pi^-}$ (M)	K_{Ben} (M^{-1})	ϵ_{515} (cm^{-1} mol^{-1} dm^3)	r	$K = K_{Ben}[TMGH^+]$
9.28–46.4	0	100 ± 4	17200 ± 300	0.998	—
9.28–46.4	1	21.4 ± 0.8	18500 ± 700	0.9997	(2.1 ± 0.1) × 10^{-3}
4.64–116	2	11 ± 2	19000 ± 3000	0.9992	(2.2 ± 0.4) × 10^{-3}

TABLE 5. Common cation effect on equilibria of 4-nitrophenylcyanomethane (**3**) (C_{AH} = 2.5 × 10^{-5} M) with TMG reaction in acetonitrile at 25°C

10^3C_{TMG} (M)	$10^4C_{TMGH^+Pi^-}$ (M)	K_{Ben} (M^{-1})	ϵ_{532} (cm^{-1} mol^{-1} dm^3)	r	$K = K_{Ben}[TMGH^+]$
2–10	0	420 ± 3	36 100	0.99995	—
2–10	0.5	190 ± 20	32 500	0.996	—
2–100	1	73 ± 3	40 200	0.9991	(7.3 ± 0.3) × 10^{-3}
2–100	2	35 ± 3	39 400	0.9999	(7.0 ± 0.6) × 10^{-3}
20–100	4	18.4 ± 0.7	43 800	0.9992	(7.4 ± 0.3) × 10^{-3}

[TMGH$^+$]. It is worthy of notice that the product of K_{Ben} and $C_{TMGH^+Pi^-}$ is constant. This result is in excellent agreement with the assumption of full dissociation of the ion pairs since in this case K and K_{Ben} are

$$[5] \quad K = \frac{[BH^+][A^-]}{[AH][B]}$$

and

$$[6] \quad K_{Ben} = \frac{K}{[BH^+]} = \frac{[A^-]}{[AH][B]}$$

The reason that eq. [6] is also fulfilled without the addition of common cation is that [BH$^+$] (the sum of BH$^+$ concentrations derived from both sources: the measured reaction, and from the environment) changes relatively slowly with the concentration of the base.

Employing the pK_a of TMG and K values from Tables 4 and 5, pK_a for **3** and **6** can be calculated. They are 25.4 and 25.9, respectively.

Kinetic experiments

Kinetics of the proton transfer reaction between **6** and TMG in acetonitrile without additions of tetramethylguanidinium picrate, for different concentrations of the TMG base (Table 6), fulfill the following equation:

$$[7] \quad k^H_{obs} = (k^H_f)_{app}C_{TMG} + k^*_b$$

where k^H_{obs} is the pseudo-first-order rate constant and $(k^H_f)_{app}$ the apparent second-order rate constant. The relation of k^H_{obs} against C_{TMG} showed relatively large intercepts, k^*_b; on the other hand the plots of k^D_{obs} vs. C_{TMG} for the deuteron transfer reaction (Table 7) pass through the origin, indicating that the A$^-$,TMGD$^+$ is a short-lived intermediate (Scheme 3) and D/H exchange in the C-acid is irreversible (k^D_b is much smaller than the sum of rate constants of all protonation reactions of the carbanion).

The reaction medium contains a sufficient excess of exchangeable protons over concentration of deuterated C-acid (C_{AD} = 2.5 × 10^{-5} M) to make the D/H exchange in C-acid

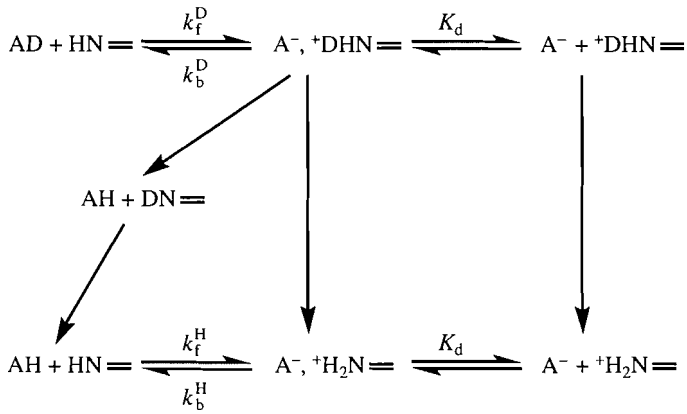

SCHEME 3

irreversible (27). There exist a number of sources of exchangeable protons, taking into account that well-dried TMG base still contains ca. 1% of water (28), and that the TMG molecule itself has an easily exchangeable proton, and also that well-dried acetonitrile solvent still contains 0.001% of water, which makes the concentration of exchangeable protons equal to ca. 1 × 10^{-3} M.

The assumption that the D/H isotopic exchange is much faster than internal return seems to be well justified, since the rate constants of internal return for the ion-pair products of the reactions of nitrophenylnitroalkanes in low-polarity solvents are relatively small, e.g., for the reaction of **6** with DBU in THF and chlorobenzene solvents they are about 1 s^{-1} (16). Since the rate constants of the reactions of C-acids with amines, as well as the equilibrium constant for ion-pair formation, are poorly dependent on the polarity of the solvent (14, 16), we can assume that the rate constant k^D_b(Scheme 3) of the reaction of **6** with TMG is of the same order of magnitude. Furthermore, when thermodynamic barriers are low, dissociation of the ion pairs, as well as D/H exchange in the TMGD$^+$ cation, are very fast processes (11). Therefore we can expect that the kinetics of the reaction of **6**-*d* with

Can. J. Chem. Downloaded from www.nrcresearchpress.com by 92.62.229.171 on 09/08/12
For personal use only.

Can. J. Chem. Downloaded from www.nrcresearchpress.com by 92.62.229.171 on 09/08/12
For personal use only.

TABLE 6. Common cation effect on observed and second-order rate constants for proton transfer reactions between 2-methyl-1-(4-nitrophenyl)-1-nitromethane (**6**) and TMG in acetonitrile at 25°C

$10^3 C_{TMG}$ (M)	$10^2 k^H_{obs}$ (s^{-1})	$(k^H_f)_{app}$ ($dm^3\ mol^{-1}\ s^{-1}$)	k^*_b (s^{-1})
(*a*) $C_{TMGH^+Pi^-} = 0$			
4.64	1.62		
9.28	2.44		
13.92	2.69	1.10 ± 0.05	0.012 ± 0.001
18.56	3.26		
23.20	3.77		
32.50	4.80		
(*b*) $C_{TMGH^+Pi^-} = 1 \times 10^{-4}$ M			
4.64	5.8		
9.28	6.0		
13.92	6.1		
18.56	6.6	0.87 ± 0.06	0.051 ± 0.002
23.20	7.0		
32.50	8.2		
46.40	9.2		
(*c*) $C_{TMGH^+Pi^-} = 2 \times 10^{-4}$ M			
4.64	9.5		
9.28	9.5		
13.92	10.0	0.56 ± 0.05	0.0914 ± 0.0009
18.56	10.2		
23.20	10.4		
32.50	11.0		

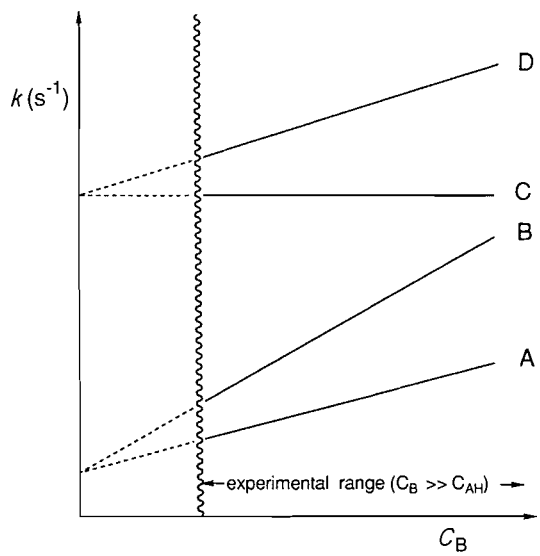

FIG. 1. The influence of BH^+ cations originating from side reactions on the measured values of second-order rate constants. A: $k = k_b = k^H_b K_d^{-1}[BH^+]$, eq. [10], no addition of common cation BH^+; $[BH^+]$ increases considerably with C_B (an arbitrary chosen linear function); B: $k = k^H_{obs} = k^H_f C_B + k_b$, eq. [9], otherwise as in A; slope = $(k^H_f)_{app} > k^H_f$; C: $k = k_b$, $[BH^+]$ = const. (the common cation BH^+ added, and assuming that side reactions contribute negligibly to $[BH^+]$ as a result of full suppression of dissociation of their products); D: $k = k^H_{obs} = k^H_f C_B + k_b$, otherwise as in C; slope = k^H_f.

TMG follows the scheme described by Melander and Saunders (27), with the Guggenheim or end-point method plots curved initially.

These small curved parts were discarded, and the resulting k^D_{obs} values plotted against C_B gave good straight lines with slopes k^D_f, fulfilling the following equation:

$$[8] \quad k^D_{obs} = k^D_f C_{TMG}$$

Melander and Saunders (27) assumed that $[BH^+]$ does not vary with time. This condition was fulfilled in our experiments with the addition of $TMGH^+Pi^-$ and was approximately true for experiments without this addition, since the common cation BH^+ is formed not only in the reaction between C-acids and TMG base, but also in the reaction of strong TMG base with acetonitrile solvent and acidic contaminants (22).

The effect of the common cation $TMGH^+$ on the kinetics of the proton transfer reaction

The data presented in Tables 6 and 7 support our assertion of a large dissociation of the products of proton transfer reactions in acetonitrile into free ions. The values of the apparent rate constants for backward reaction k^*_b increase with $C_{TMGH^+Pi^-}$ (Table 6). The increase of $C_{TMGH^+Pi^-}$ from 1×10^{-4} M to 2×10^{-4} M caused almost twofold increase of k^*_b, as was expected for complete dissociation of the ion pairs into free ions. Therefore, when k^H_{obs} is now described in terms of true, not apparent, rate constants, eq. [9] is valid:

$$[9] \quad k^H_{obs} = k^H_f C_{TMG} + k_b$$

where k^H_f is the second-order rate constant, and the rate constant of the reverse reaction k_b varies with $[BH^+]$ according to eq. [10]

$$[10] \quad k_b = k^H_b K_d^{-1}[TMGH^+]$$

where k^H_b is the rate constant of internal return within the ion pair (see Scheme 3). It is noteworthy that k_b depends on C_{TMG}, in contrast to k^*_b. The latter is simply an experimental initial intercept (eq. [7]), which has been erroneously considered to be equal to k^H_b.

The lack of a significant dependence of the second-order rate constant for the forward, deuteron transfer reaction, k^D_f, on $C_{TMGH^+Pi^-}$ (Table 7) suggests that the concentration of the salt does not particularly influence the rate constants. However, the data collected in Table 6 show that estimated rate constants $(k^H_f)_{app}$ decrease with increasing $C_{TMGH^+Pi^-}$.

This phenomenon seems to be a consequence of the salt effect on the rate of the backward reaction. The rate constant $(k^H_f)_{app}$ measured as a slope of the plot of k^H_{obs} against C_B without addition of $TMGH^+Pi^-$ is overestimated since $[TMGH^+]$ increases with the increase of TMG base concentration, amplifying k_b (Fig. 1).

As a consequence of too large values of $(k^H_f)_{app}$, and no influence of the backward reaction on the measured value of the rate constant of the deuteron transfer reaction, k^D_f, the values of the kinetic isotope effects $(k^H_f)_{app}/k^D_f$, entry for $C_{TMGH^+Pi^-} = 0$ in Table 7, are too large. The addition of $TMGH^+Pi^-$ reduces the error in k^H_f because dissociation of the side-reaction products is suppressed.

In conclusion, the spectrophotometrically measured equilibrium and rate constants for proton transfer reactions in acetonitrile show definite dependence upon the $TMGH^+$ cation concentration, which is in good agreement with our

TABLE 7. Common cation effect on observed and second-order rate constants for deuteron transfer reactions between 2-methyl-1-(4-nitrophenyl)-1-nitromethane-1-*d* and TMG in acetonitrile solvent at 25°C

$10^2 C_{TMG}$ (M)	$10^3 k^D_{obs}$ (s^{-1})	k^D_f ($dm^3\ mol^{-1}\ s^{-1}$)	10^3 intercept (s^{-1})	$(k^H_f)_{app}/k^D_f$
(*a*) $C_{TMGH^+Pi^-} = 0$				
2.0	2.05 ± 0.05			
4.0	3.91 ± 0.03			
6.0	5.85 ± 0.04	0.093 ± 0.001	0.20 ± 0.06	11.8 ± 0.6
8.0	7.57 ± 0.24			
10.0	9.51 ± 0.17			
(*b*) $C_{TMGH^+Pi^-} = 1 \times 10^{-4}$ M				
2.0	1.63 ± 0.12			
4.0	3.79 ± 0.08			
6.0	5.65 ± 0.07	0.094 ± 0.004	0.0 ± 0.3	9.3 ± 0.8
8.0	7.71 ± 0.02			
10.0	9.02 ± 0.08			
(*c*) $C_{TMGH^+Pi^-} = 2 \times 10^{-4}$ M				
2.0	2.14 ± 0.03			
4.0	3.79 ± 0.08			
6.0	5.50 ± 0.11	0.090 ± 0.003	0.3 ± 0.2	6.2 ± 0.6
8.0	7.68 ± 0.08			
10.0	9.20 ± 0.19			

previous assumption of a large degree of dissociation of the product for free ions (14). In the case of a proton transfer reaction characterized by a moderate equilibrium constant, the large excess of the base over C-acid is applied; then $[BH^+]$ from sources other than the examined reaction is dependent upon the concentration of the base. Hence, the measured second-order rate constants k^H_f can be overestimated. Since $[BH^+]$ does not affect significantly the estimated rate constants for the deuteron transfer reaction, k^D_f, the primary deuterium kinetic isotope effects k^H_f/k^D_f are overestimated.

The addition of the common cation BH^+ should make the rate constant of the backward reaction virtually independent of the concentration of the base. However, the resulting large increase in the rate constant of the reverse reaction is not very favourable to the accuracy of the k^H_f estimation. On the other hand, if the proton transfer reaction is characterized by a very large equilibrium constant, then the addition of a common cation is redundant, since in this case the backward reaction has a negligible influence on the observed rate constant k^H_{obs}.

Experimental

Acetonitrile

The commercial product, purchased from Apolda, was purified by the O'Donnell method (29) with a final, fractional distillation over P_2O_5. The distillation apparatus was flushed with argon to eliminate air. The quality of the solvent was characterized by the following parameters: absorbance at 200 nm < 0.1 (optical path length 1 cm), $\kappa < 1 \times 10^{-7}\ \Omega^{-1}\ cm^{-1}$.

C-acids

Bis(4-nitrophenyl)cyanomethane (**1**), 4-nitrophenylphenylcyanomethane (**2**), 2,4,6-trinitrotoluene (**4**), 4-nitrophenylnitromethane (**5**), and 2-methyl-1-(4-nitrophenyl)-1-nitropropane (**6**) were synthesized according to procedures already described (8, 17, 26, 14, respectively); 4-nitrophenylcyanomethane (**3**) was a commercial product from Eastman. The melting points and the spectra after recrystallization from ethanol were in accordance with the literature, except for bis(4-nitrophenyl)cyanomethane, mp 96.5–98°C, which was recrystallized from 1,2-dichloroethane/hexane mixture (lit. (8) mp 93–94.5°C).

2-Methyl-1-(4-nitrophenyl)-1-nitropropane-1-*d* was prepared as described earlier (16). The deuteration was completed to at least 99%, as judged from the NMR spectrum.

Amines

1,8-Diazabicyclo[5.4.0]undec-7-ene (DBU), 1,1,3,3-tetramethylguanidine (TMG), and piperidine, commercial products (Aldrich), were dried over KOH pellets and then distilled in the apparatus flushed with argon. Both DBU and TMG were distilled under vacuum. 1,8-Bis(dimethylamino)naphthalene (DMAN), a commercial product (Aldrich), was recrystallized from ethanol; mp 48–49°C.

1,1,3,3-Tetramethylguanidinium picrate ($TMGH^+Pi^-$) was prepared according to a procedure described by Leffek *et al.* (19) (mp 128.5–129.5°C). The solutions of both C-acid and base were prepared from freshly purified reagents just before measurements. In the kinetic and equilibrium experiments $TMGH^+\ Pi^-$ was added to the C-acid solutions.

Conductivity measurements were carried out using a Tesla BM-484 semiautomatic conductivity bridge operating at 1592 Hz with a conventional, calibrated cell with platinum electrodes. The cell constant was 0.8744 cm^{-1}, determined in normal way (14). The cell was sealed to exclude atmospheric moisture and gases. The temperature was maintained at 25.0 ± 0.1°C. For each concentration of base, conductivity was typically measured for six concentrations of C-acid in the concentration range $(4–24) \times 10^{-4}$ M.

Spectrophotometric measurements of equilibria were performed at 515 and 532.5 nm for **6** and **3** respectively with the solutions of $TMGH^+Pi^-$ as a reference. Each K_{Ben} value resulted from absorbance values for at least five base concentrations.

Kinetic measurements were performed with a stopped flow spectrophotometer using a C-acid concentration of ca. 2.5×10^{-5} M and base concentrations shown in Tables 6 and 7. The observed first-order rate constants were calculated according to the Guggenheim method. In the case of the deuteron transfer reaction, the initial curved part of the Guggenheim plot, corre-

Can. J. Chem. Downloaded from www.nrcresearchpress.com by 92.62.229.171 on 09/08/12
For personal use only.

sponding to a time less than 0.2 half-life, was discarded (27). The second-order rate constants were calculated according to eqs. [7] and [8]. The addition of $TMGH^+$ Pi^- to the products of the proton transfer reactions did not change the λ_{max}, molar absorptivity ϵ, or the shape of absorption band of the anion of C-acid under investigation.

Acknowledgements

Financial support of this work from the CPBP 01.19.04.16. program and Grant No. 2 0762 91 01 is gratefully acknowledged. We also thank Professor K. T. Leffek and Professor E. S. Lewis for helpful discussions.

1. E. F. Caldin, A. Jarczewski, and K. T. Leffek. Trans Faraday Soc. **67**, 1110 (1971).
2. E. F. Caldin and S. Mateo. J. Chem. Soc. Faraday Trans. 1, **71**, 1876 (1975).
3. E. F. Caldin and S. Mateo. J. Chem. Soc. Faraday Trans. 1, **72**, 112 (1976).
4. M. Sasaki, N. Sugimoto, and J. Osugi. Chem. Lett. 887 (1980).
5. N. Sugimoto, M. Sasaki, and J. Osugi. Bul. Inst. Chem. Res. Kyoto Univ. **59**, 163 (1981).
6. K. T. Leffek and P. Pruszynski. Can. J. Chem. **60**, 1692 (1982).
7. A. Jarczewski and P. Pruszynski. Polish J. Chem. **58**, 1175 (1984).
8. M. Hojatti and K. T. Leffek. Can J. Chem. **64**, 2365 (1986); **62**, 2653 (1984).
9. K. T. Leffek and P. Pruszynski. Can. J. Chem. **66**, 1454 (1988).
10. P. Pruszynski and A. Jarczewski. J. Chem. Soc. Perkin Trans. 2, 1117 (1986).
11. R. P. Bell. The proton in chemistry. Chapman and Hall, London. 1973.
12. E. F. Caldin, D. M. Parboo, F. A. Walker, and C. R. Wilson. J. Chem. Soc. Faraday Trans. 1, **72**, 1856 (1976).
13. A. Jarczewski, P. Pruszynski, M. Kazi, and K. T. Leffek. Can. J. Chem. **62**, 954 (1984).
14. W. Galezowski and A. Jarczewski. J. Chem. Soc. Perkin Trans. 2, 1647 (1989).
15. J. L. Kurz and L. C. Kurz. J. Am. Chem. Soc. **90**, 4451 (1972).
16. W. Galezowski and A. Jarczewski. Can. J. Chem. **68**, 2242 (1990).
17. A. Jarczewski, P. Pruszynski, and K. T. Leffek. Can. J. Chem. **61**, 2029 (1983).
18. I. M. Kolthoff and M. K. Chantooni. J. Am. Chem. Soc. **91**, 2875 (1969).
19. K. T. Leffek, P. Pruszynski, and K. Thanapaalasingham. Can. J. Chem. **67**, 590 (1989).
20. I. M. Kolthoff, M. K. Chantooni, and S. Bhowmik. J. Am. Chem. Soc. **90**, 23 (1968).
21. J. F. Coetzee and G. R. Padmanabhan. J. Am. Chem. Soc. **87**, 5005 (1965).
22. I. M. Kolthoff and M. K. Chantooni. J. Phys. Chem. **72**, 2270 (1968).
23. C. A. Kraus and W. C. Bray. J. Am. Chem. Soc. **35**, 1315 (1913).
24. Th. Zeegers-Huyskens and P. Huyskens. *In* Molecular interactions. Vol. 2. *Edited by* H. Ratajczak and W. J. Orville-Thomas. Wiley, Chichester, New York. 1980. Chap. 1.
25. J. F. Coetzee, G. R. Padmanabhan, and G. P. Cumingham. Talanta, **11**, 93 (1964).
26. A. Jarczewski, P. Pruszynski, and K. T. Leffek. Can. J. Chem. **57**, 669 (1979).
27. L. Melander and W. H. Saunders, Jr. Reaction rates of isotopic molecules. John Wiley and Sons, New York. 1980. Chap. X. pp. 287–291.
28. E. F. Caldin, S. Mateo, and P. Warrick. J. Am. Chem. Soc. **103**, 202 (1981).
29. J. F. O'Donnell, J. T. Ayers, and C. K. Mann. Anal. Chem. **37**, 1161 (1961).

Can. J. Chem. Downloaded from www.nrcresearchpress.com by 92.62.229.171 on 09/08/12
For personal use only.

Preparation and structure of silver complexes with 4-nitroimidazole

ISABELLE SÉGALAS AND ANDRÉ L. BEAUCHAMP[1]

Département de chimie, Université de Montréal, C.P. 6128, Succ. A, Montréal (Québec), Canada H3C 3J7

Received June 25, 1991

ISABELLE SÉGALAS and ANDRÉ L. BEAUCHAMP. Can. J. Chem. **70**, 943 (1992).

The reaction of 4-nitroimidazole (NO_2ImH) with $AgNO_3$ and $AgBF_4$ in neutral or weakly acidic aqueous media yielded the insoluble [$Ag(NO_2Im)$] compound, whose infrared and ^{13}C NMR spectra are consistent with a polymeric chain of deprotonated ligands bridging silver atoms via the endocyclic nitrogen atoms. In strongly acidic solution, [$Ag(NO_2ImH)_2$]X salts (X = NO_3, BF_4) were obtained and their crystal structures were determined. [$Ag(NO_2ImH)_2$]NO_3: monoclinic, $P2/n$, a = 14.214(1), b = 12.571(2), c = 14.222(1) Å, β = 111.38(7)°, Z = 8, R = 0.021, 3443 observed reflections; [$Ag(NO_2ImH)_2$]BF_4: monoclinic, $P2_1/c$, a = 9.543(4), b = 6.478(2), c = 20.869(9) Å, β = 90.84(3)°, Z = 4, R = 0.027, 1646 observed reflections. In both compounds, the two-coordinated metal forms roughly collinear bonds to two neutral ligands via the endocyclic nitrogen atom adjacent to the nitro group. One oxygen of each nitro group makes a secondary Ag—O bond near the equatorial plane. The anions are hydrogen bonded to the ligand N—H groups and do not directly interact with the metal. Solution ^1H and ^{13}C NMR spectra show that the cationic complexes dissociate in DMSO. The infrared and CP-MAS ^{13}C NMR spectra are discussed in connection with the coordination patterns observed.

Key words: silver, imidazole, crystal structure, infrared spectroscopy, nuclear magnetic resonance.

ISABELLE SÉGALAS et ANDRÉ L. BEAUCHAMP. Can. J. Chem. **70**, 943 (1992).

Le 4-nitroimidazole (NO_2ImH) réagit avec $AgNO_3$ et $AgBF_4$ en solution aqueuse neutre ou peu acide pour former le composé insoluble [$Ag(NO_2Im)$], dont les spectres infrarouge et RMN ^{13}C sont en accord avec une chaîne polymère constituée du ligand déprotoné pontant deux atomes d'argent par l'intermédiaire des atomes d'azote endocycliques. En solution très acide, les sels [$Ag(NO_2ImH)_2$]X (X = NO_3, BF_4) sont obtenus et leur structure cristalline a été determinée. [$Ag(NO_2ImH)_2$]NO_3 : monoclinique, $P2/n$, a = 14,214(1), b = 12,571(2), c = 14,222(1) Å, β = 111,38(7)°, Z = 8, R = 0,021, 3443 réflexions observées; [$Ag(NO_2ImH)_2$]BF_4 : monoclinique, $P2_1/c$, a = 9,543(4), b = 6,478(2), c = 20,869(9) Å, β = 90,84(3)°, Z = 4, R = 0,027, 1646 réflexions observées. Dans les deux cas, la métal bicoordonné est lié de façon à peu près linéaire à deux ligands neutres par l'atome d'azote endocyclique adjacent au groupe nitro. L'un des oxygènes de chaque groupe nitro forme une liaison secondaire Ag—O près du plan équatorial. Les anions établissent des liaisons hydrogène avec les groupes N—H des ligands, sans interagir directement avec le métal. Les spectres RMN ^1H et ^{13}C montrent que les complexes cationiques se dissocient dans DMSO. Les spectres infrarouges et RMN ^{13}C à l'état solide sont discutés en relation avec les modes de coordination observés.

Mots clés : argent, imidazole, structure cristalline, spectroscopie infrarouge, résonance magnétique nucléaire.

Can. J. Chem. Downloaded from www.nrcresearchpress.com by 92.62.229.171 on 09/08/12
For personal use only.

Introduction

Nitroimidazoles are known to be effective radiosensitizers and chemotherapeutic agents both as free molecules (1–3) and when coordinated to metals like Pt, Ru, and Rh (4–6). The role played by the nitro groups in the coordination of these molecules has so far attracted little attention. As part of our current interest for metal complexes of nitroimidazoles, we recently described the structure of a CH_3Hg^+ complex with 4-nitroimidazole (7), in which the nitro oxygens, although only weakly bonded to the metal, had a determining influence on the overall structure. We wish to report here on the interaction of this ligand with the Ag^+ ion, another soft, low-coordinated, Lewis acid. The endocyclic N donors are anticipated to be the preferred target for this metal (8), but coordination with the neutral ligand could in principal take place with either of the two tautomeric forms (Scheme 1).[2] Even though the 4-nitro tautomer has been shown to be present in the solid state (9) and to predominate in water solution (10), coordination to the 5-nitro tautomer could be favoured in systems where the nitro group would create steric hindrance. On the other hand, nitro groups could exhibit weak donor properties and directly participate in bonding with silver, as do the carbonyl-like oxygens adjacent to the main nitrogen coordination sites in complexes with thymine (11), cytosine (12), succinimide (13), and glutarimide (14). Thus, it was of interest to determine if the nitro oxygens in 4-nitroimidazole would bind to silver and if the ligand geometry would be affected by coordination.

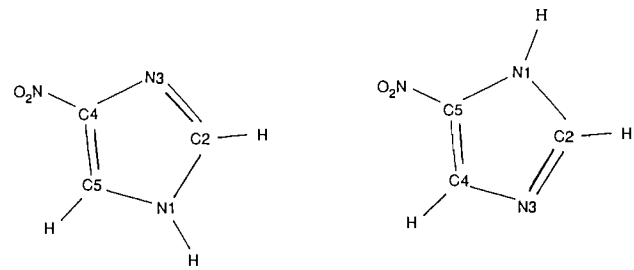

SCHEME 1

Experimental

Reagents and methods

$AgNO_3$ (BDH), Ag_2CO_3 (Alfa), 4-nitroimidazole (Aldrich), and HBF_4 (48% aqueous solution, Alfa) were used as received.

The infrared spectra (4000–250 cm^{-1}) were recorded on a

[1]Author to whom correspondence may be addressed.

[2]Ring numbering conventionally starts with the N—H(R) position and the tautomers are usually referred to as the 4-nitro and 5-nitro forms, respectively.

Can. J. Chem. Downloaded from www.nrcresearchpress.com by 92.62.229.171 on 09/08/12
For personal use only.

Perkin–Elmer 783 spectrophotometer. KBr pellets were used for the free ligand and $[Ag(NO_2Im)]$. Since the $[Ag(NO_2ImH)_2]X$ compounds reacted with KBr, the spectra were taken with Nujol and hexachlorobutadiene mulls between KRS-5 windows.

The NMR spectra were recorded with a Varian VXR-300 spectrometer at 300 MHz for ^1H and 75.43 MHz for ^{13}C. The solution spectra were taken in $(CD_3)_2SO$ and referenced to the residual solvent signal. The chemical shifts were converted to the standard TMS scale by assigning $\delta = 2.49$ (^1H) or 39.6 ppm(^{13}C) to these signals. The solid-state ^{13}C CP/MAS spectra were obtained under the following conditions: spin rate ~4100 Hz, contact time = 2.5 ms, relaxation delay = 25 s, 150–250 scans. The aromatic signal of hexamethylbenzene powder at 132.0 ppm was used to calibrate the chemical shifts.

Preparations

$[Ag(NO_2Im)]$

To 0.68 g (6.0 mmol) of 4-nitroimidazole dissolved in hot water (50 mL) was added 1.02 g (6.0 mmol) of $AgNO_3$. The yellowish precipitate immediately formed was filtered from the cooled solution and dried *in vacuo*. Yield: 1.20 g, 91%. Anal. (Guelph Microanalytical Lab.) calcd. for $C_3H_2AgN_3O_2$: C 16.38, H 0.92, N 19.11; found: C 16.65, H 1.08, N 19.89.

$[Ag(NO_2ImH)_2]NO_3$

To a hot solution of 4-nitroimidazole (0.68 g, 6.0 mmol) in water (60 mL) was added $AgNO_3$ (1.02 g, 6.0 mmol) dissolved in a minimum of warm water. The $[Ag(NO_2Im)]$ precipitate initially formed was redissolved by adding a minimum of concentrated HNO_3 to the hot solution. The complex started to precipitate while the mixture was cooling down to room temperature. After 2 days at room temperature, colourless platelets were filtered and dried *in vacuo*. Yield: 0.74 g, 63%. Crystals from this homogeneous batch were used for X-ray work. When the reaction was conducted under stoichiometric conditions (M:L = 1:2), the infrared spectrum of the product indicated substantial contamination by free ligand.

$[Ag(NO_2ImH)_2]BF_4$

Ag_2CO_3 (0.41 g, 1.5 mmol) was added to 0.44 mL (3.3 mmol) of 48% HBF_4. After evolution of CO_2, the greyish, syrupy solution of $AgBF_4$ was poured into a solution of 0.68 g (6.0 mmol) of 4-nitroimidazole in 60 mL of hot water. The yellowish precipitate initially formed was redissolved with a minimum of concentrated HBF_4 solution. Air-stable needles were isolated as above. Yield: 0.65 g, 52%. Crystals from this homogeneous batch were used for X-ray work. The sample obtained from a 1:1 M:L mixture showed the same infrared spectrum, but the solid was sticky and more difficult to isolate, probably because it could not be completely freed from small amounts of hygroscopic HBF_4 and (or) $AgBF_4$.

Crystallographic measurements and structure determination

The crystallographic work was done with an Enraf–Nonius CAD-4 diffractometer, following similar procedures for the two compounds. The reduced cell was determined from 25 randomly distributed reflections ($13° < \theta < 18°$) generated by the automatic search routine of the CAD-4 software and centered in the counter aperture. Indexing yielded in both cases a primitive monoclinic cell, which was checked with axial photographs taken about each of the axes. These oscillation photographs showed the expected layer–line separations, and a Laue mirror was present for oscillations about *b*. The crystal data are provided in Table 1.

$[Ag(NO_2ImH)_2]BF_4$

The Niggli matrix was not consistent with a symmetry higher than monoclinic. Space group $P2_1/c$ was uniquely defined from the systematic absences ($h0l$, $l \neq 2n$; $0k0$, $k \neq 2n$) revealed by the full data set.

The intensity data were collected by using the $\omega/2\theta$ scan mode, over a $\Delta\omega$ range of $(0.80 + 0.35 \tan\theta)°$. Five standard reflections were monitored for crystal decay every hour and for misorientation every 200 reflections. A complete sphere of data ($2\theta \leq 50°$, MoK$\bar{\alpha}$) was collected. An absorption correction based on crystal geometry was applied (Gaussian integration, grid $10 \times 10 \times 10$). Averaging equivalent reflections yielded a standard two-octant (hkl, $hk\bar{l}$) data set consisting of 2263 unique reflections, of which 1646 had intensity above background. These data were corrected for the effects of Lorentz and polarization.

The Ag atom was located from a Patterson map. The remaining non-hydrogen atoms were then found from a difference Fourier (ΔF) map. The structure was first refined isotropically by full-matrix least-squares procedures. The function minimized was $\Sigma w(|F_o| - |F_c|)^2$, with weights w based on counting statistics. The hydrogen atoms were fixed at idealized positions ($U_{iso} = 0.05$ Å^2). Their parameters were not refined, but their coordinates were recalculated after each cycle. All non-hydrogen atoms were finally refined anisotropically. The final ΔF map showed a general background below ± 0.52 e Å^{-3}.

$[Ag(NO_2ImH)_2]NO_3$

The auto-indexing procedure yielded a reduced cell with parameters corresponding to a primitive monoclinic lattice: $a = 14.214(1)$, $b = 12.571(2)$, $c = 14.223(1)$ Å, $\alpha = 90.01(1)$, $\beta = 111.38(1)$, and $\gamma = 90.00(1)°$. The Laue mirror on the oscillation photograph about *b* was consistent with this cell. The systematic absences ($h0l$, $h + l \neq 2n$) noted in a fast precollection suggested Pn and $P2/n$ as possible space groups. However, since *a* and *c* were roughly equal, an orthorhombic cell with one face centred would also fit the lattice. Oscillation photographs about the potential orthorhombic axes failed to reveal the extra mirror planes. Thus, a primitive monoclinic lattice was used to collect the data. Nevertheless, a whole sphere of data ($2\theta < 50°$, MoK$\bar{\alpha}$) was collected as above. Before starting the structure resolution, the Laue symmetry was checked on the full data set. The intensities were first corrected for absorption. An orthorhombic *C*-centred cell was then defined from the *P*-monoclinic cell: $\mathbf{a}_0 = -\mathbf{a}_m - \mathbf{c}_m$, $\mathbf{b}_0 = \mathbf{a}_m - \mathbf{c}_m$, $\mathbf{c}_0 = -\mathbf{b}_m$. The Laue mirror already found in the monoclinic cell (now perpendicular to c_0) was confirmed by the low *R* factor (0.01) and mean Δ/σ value (0.6) when the $hkl/hk\bar{l}$ pairs were compared. Orthorhombic Laue symmetry was clearly ruled out by the *R* and Δ/σ values for the $hkl/\bar{h}kl$ (0.26, 16.9) and $hkl/\bar{h}k\bar{l}$ pairs (0.25, 16.6). A *C*-centred monoclinic cell with β accidentally equal to 90° was also rejected as inconsistent with the systematic absences: beside the *C*-centring condition (hkl, $h + k \neq 2n$), absences were noted for the $hk0$ reflections with $h \neq 2n$ and $k \neq 2n$, indicating that a glide plane was present *perpendicular* to *c*. In a *C*-centred monoclinic cell (space groups Cc or $C2/c$), only a *c* glide plane (perpendicular to *b*) is allowed, with an extinction condition $h0l$, $l \neq 2n$. The glide plane detected is actually the *n* plane of the $P2/n$ or P/n cell.

The data set obtained after averaging the equivalent reflections consisted of 4153 independent hkl and $hk\bar{l}$ reflections, of which 3443 had intensities significantly above background. These data were corrected for the effects of Lorentz and polarization.

The asymmetric unit of the $P2/n$ cell corresponds to two formula units. The two Ag atoms were located from a Patterson map. The remaining non-hydrogen atoms were then positioned from a ΔF map. Refinement was carried out as above. Atomic coordinates showed no correlation coefficients >0.5. Hydrogens were handled as in the previous case. The general background in the final ΔF map was below $\pm$ 0.29 e Å^{-3}. This model showed no abnormally large thermal motion or artificial disorder that could indicate that the space group would be Pn instead of $P2/n$.

TABLE 1. Crystallographic data

	$[Ag(NO_2ImH)_2]NO_3$	$[Ag(NO_2ImH)_2]BF_4$
Formula	$C_6H_6AgN_7O_7$	$C_6H_6AgBF_4N_6O_4$
Formula weight	396.02	420.82
F(000)	1552	816
Crystal system	Monoclinic	Monoclinic
Space group	$P2/n$	$P2_1/c$
a, Å	14.214(1)	9.543(4)
b, Å	12.571(2)	6.478(2)
c, Å	14.222(1)	20.869(9)
β, deg	111.38(7)	90.84(3)
V, Å^3	2366.4(4)	1290.0(8)
Z	8	4
d_{cal}, g cm^{-3}	2.223	2.167
d_{obs}, g cm^{-3}	2.18	2.08
Crystal size, mm (faces)	0.14 (001–00$\bar{1}$)	0.56 (001–00$\bar{1}$)
	0.42 (010–0$\bar{1}$0)	0.23 (011–0$\bar{1}$1)
	0.50 (10$\bar{1}$–$\bar{1}$01)	0.05 (101–$\bar{1}$01)
μ, cm^{-1}	17.36	16.22
Transmission range	0.49–0.79	0.69–0.93
Temperature	293 K	293 K
Radiation	MoKᾱ	MoKᾱ
Wavelength, Å	0.71069	0.71069
2θ max, deg	50.0	50.0
Fluctuation of standards, %	±0.51	±0.70
Number of independent reflections	4153	2263
Rejection criterion, $I/\sigma(I) <$	3.0	3.0
Number of independent observed reflections	3443	1646
$R = \Sigma\|\|F_o\| - \|F_c\|\|/\Sigma\|F_o\|$	0.021	0.027
$R_w = [\Sigma w(\|F_o\| - \|F_c\|)^2/\Sigma w\|F_o\|^2]^{1/2}$	0.025	0.028
Goodness-of-fit ratio	1.54	1.52

The scattering curves used were from Cromer and Mann (15), except for hydrogen (16). Anomalous dispersion was taken into account for Ag (17). The refined coordinates for the NO_3^- and the BF_4^- salts are listed in Tables 2 and 3, respectively.[3]

Results and discussion

Unsubstituted imidazole (ImH) has been known for many years to form a very stable silver imidazolate [Ag(Im)]

[1] $Ag^+ + LH \rightleftharpoons AgL\downarrow + H^+$

[2] $H^+ + LH \rightleftharpoons LH_2^+$

[3] $Ag^+ + 2LH \rightleftharpoons AgL\downarrow + LH_2^+$

(8). This insoluble compound precipitates when the pH of an equimolar mixture of ligand and $AgNO_3$ is raised to ~10 with NaOH (18). The very low solubility of the product and the addition of OH^- help to remove the weakly acidic proton (pK_a = 14.4) (19) of imidazole, displacing equilibrium [1] to the right. Since imidazole is also a Brønsted base (eq. [2], pK_a of ImH_2^+ = 7.0) (19), it can also act as proton quencher, leading to disproportionation reaction [3]. Thus, without added NaOH, half of the ligand in a 1:1 Ag:imidazole mixture would be used to neutralize the released proton and the yield in [Ag(Im)] would probably not exceed 50%.

With 4-nitroimidazole, the corresponding insoluble $[Ag(NO_2Im)]$ complex is formed essentially quantitatively without adding NaOH. The electron-attracting nitro group increases ligand acidity (pK_a = 9.3) (19) and makes the proton easier to displace in aqueous media. On the other hand, because of its very low Brønsted basicity (pK_a of $NO_2ImH_2^+$ = 0.0) (19), the ligand does not efficiently bind the expelled proton and has no levelling effect on the yield. Thus, large excess of ligand should be avoided, since its low solubility in water would result in samples contaminated with unreacted ligand.

The $[Ag(ImH)_2]NO_3$ complex containing the formally neutral ligand was obtained from a mixture of $AgNO_3$ and excess imidazole, by addition of HNO_3 to reduce the pH to 5.5 (20) or 4 (21). The pH was kept low enough to avoid reaction [1], but not so low as to completely displace equilibrium [2] toward LH_2^+. With 4-nitroimidazole, the preparation of the NO_3^- and BF_4^- salts of $[Ag(NO_2ImH)_2]^+$ required much higher (1–2 M) acid concentrations to prevent the formation of $[Ag(NO_2Im)]$ via reaction [1].

[3]The supplementary material includes tables of refined temperature factors, distances and angles in the ligands, distances and angles for hydrogen bonds, least-squares plane calculations, and structure factor amplitudes for both structures, as well as a table of infrared wavenumbers for 4-nitroimidazole, its *N*-deuterated derivative, and the three Ag complexes (39 pages). Complete set of data may be purchased from the Depository of Unpublished Data, Document Delivery, CISTI, National Research Council Canada, Ottawa, Canada K1A 0S2.

The tables of hydrogen atom coordinates and geometry of the hydrogen bonds have also been deposited with the Cambridge Crystallographic Data Centre and can be obtained on request from The Director, Cambridge Crystallographic Data Centre, University Chemical Laboratory, Lensfield Road, Cambridge CB2 1EW, U.K.

Can. J. Chem. Downloaded from www.nrcresearchpress.com by 92.62.229.171 on 09/08/12
For personal use only.

Can. J. Chem. Downloaded from www.nrcresearchpress.com by 92.62.229.171 on 09/08/12
For personal use only.

TABLE 2. Refined coordinates ($\times 10^4$, Ag $\times 10^5$) and equivalent isotropic temperature factors ($Å^2 \times 10^3$) for [Ag(4-nitroimidazole)$_2$]NO_3[a]

Atom	x	y	z	U_{eq}
Ag(A)	13313(2)	4442(2)	12517(2)	42
Ag(B)	37527(2)	56769(2)	14296(2)	43
O(1A)	8995(2)	6882(1)	706(1)	47
O(2A)	9175(2)	6897(1)	2276(1)	49
O(3A)	8648(2)	5479(1)	1386(1)	51
O(11A)	2433(2)	2474(2)	1428(2)	63
O(21A)	3897(2)	2943(2)	1425(2)	65
O(12A)	254(1)	2302(1)	1303(2)	51
O(22A)	−1161(1)	2705(1)	1459(1)	47
O(1B)	6341(1)	9409(1)	1310(2)	53
O(2B)	7004(1)	7928(2)	1107(2)	52
O(3B)	5400(1)	8036(2)	767(1)	48
O(11B)	3323(1)	7425(1)	106(1)	48
O(21B)	3518(1)	7794(1)	−1298(1)	50
O(12B)	3608(1)	7633(1)	2579(1)	47
O(22B)	3664(1)	7946(1)	4095(1)	47
N(1A)	8931(2)	6416(2)	1458(1)	34
N(11A)	4186(2)	−271(2)	1077(2)	42
N(31A)	2812(1)	396(2)	1212(2)	32
N(41A)	3247(2)	2273(2)	1374(2)	43
N(12A)	−1501(2)	−536(2)	1391(2)	37
N(32A)	−140(1)	195(2)	1290(2)	34
N(42A)	−551(2)	2055(2)	1379(1)	35
N(1B)	6251(1)	8458(2)	1070(1)	37
N(11B)	3793(2)	4553(2)	−1406(1)	36
N(31B)	3703(1)	5340(2)	−63(1)	32
N(41B)	3490(1)	7169(2)	−648(2)	36
N(12B)	3724(2)	4692(2)	4283(2)	35
N(32B)	3734(1)	5497(2)	2914(1)	31
N(42B)	3650(1)	7337(2)	3413(2)	34
C(21A)	3269(2)	−473(2)	1101(2)	38
C(41A)	3481(2)	1192(2)	1258(2)	31
C(51A)	4338(2)	784(2)	1178(2)	42
C(22A)	−605(2)	−704(2)	1309(2)	40
C(42A)	−792(2)	961(2)	1366(2)	29
C(52A)	−1639(2)	518(2)	1433(2)	35
C(21B)	3797(2)	4421(2)	−464(2)	37
C(41B)	3646(2)	6072(2)	−789(2)	29
C(51B)	3702(2)	5601(2)	−1628(2)	35
C(22B)	3754(2)	4576(2)	3352(2)	37
C(42B)	3686(2)	6225(2)	3607(2)	28
C(52B)	3677(2)	5738(2)	4461(2)	32

[a]The first digit in the atomic symbols indicates the position in the 4-nitroimidazole unit or nitrate ion, the second digit corresponds to ligand number, and letters A and B are used to distinguish the two symmetry-independent formulae in the asymmetric unit.

TABLE 3. Refined coordinates ($\times 10^4$, Ag $\times 10^5$) and equivalent isotropic temperature factors ($Å^2 \times 10^3$) for [Ag(4-nitroimidazole)$_2$]BF_4[a]

Atom	x	y	z	U_{eq}
Ag	22290(4)	11423(5)	24644(2)	53
F(1)	1179(2)	1075(4)	5277(1)	74
F(2)	2848(3)	1309(4)	6040(1)	73
F(3)	3344(3)	−147(5)	5096(1)	86
F(4)	2944(3)	3309(4)	5158(1)	80
O(11)	2822(4)	5527(5)	2424(1)	84
O(21)	4340(3)	7544(5)	2870(2)	69
O(12)	47(3)	3580(5)	1977(1)	67
O(22)	−1590(3)	3267(6)	1263(2)	88
N(11)	4996(3)	2592(5)	4044(2)	50
N(31)	3522(3)	2390(5)	3238(1)	41
N(41)	3726(4)	5897(5)	2827(2)	51
N(12)	304(3)	−2232(5)	888(2)	49
N(32)	1092(3)	−234(5)	1662(1)	39
N(42)	−548(3)	2624(6)	1548(2)	53
C(21)	4102(4)	1395(6)	3715(2)	47
C(41)	4094(4)	4311(6)	3272(2)	37
C(51)	5010(4)	4479(6)	3768(2)	45
C(22)	1250(4)	−1998(6)	1360(2)	46
C(42)	−32(4)	652(6)	1361(2)	38
C(52)	−543(4)	−520(6)	882(2)	49
B	2586(5)	1395(8)	5392(2)	47

[a]Atomic position numbering as described in footnote to Table 2.

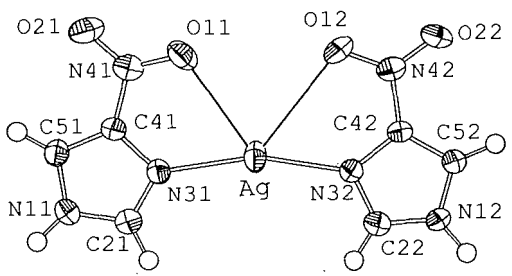

FIG. 1. ORTEP drawing of the [Ag(4-nitroimidazole)$_2$]$^+$ ion in the NO_3^- salt (cation B). Cation A is almost identical. Ellipsoids correspond to 50% probability. Hydrogens are shown as spheres of arbitrary size. Lines correspond to Ag—O secondary bonds.

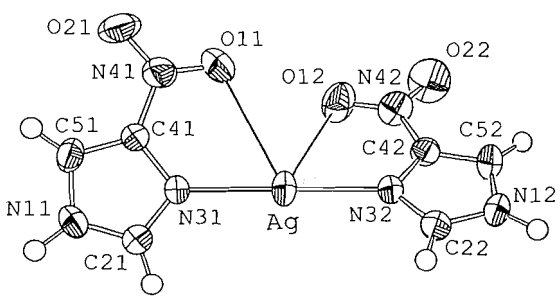

FIG. 2. ORTEP drawing of the [Ag(4-nitroimidazole)$_2$]$^+$ ion in the BF_4^- salt. Conditions as in Fig. 1.

[Ag(NO_2Im)] is a powdery, probably polymeric, material, from which single crystals could not be grown. The [Ag(NO_2ImH)$_2$]$^+$ salts were isolated as suitable crystalline solids and their structures were determined by X-ray diffraction.

X-ray diffraction

The NO_3^- and the BF_4^- salts contain the roughly linear two-coordinate [Ag(NO_2ImH)$_2$]$^+$ cation shown in Figs. 1 and 2, respectively. The ligand retains its N1—H proton[4] and binds to the metal via the ring nitrogen atom N3 adjacent to the nitro group, whereas one of the nitro oxygens, directed toward the equatorial plane (perpendicular to N—Ag—N), forms secondary Ag—O bonds. The two symmetry independent cations present in the NO_3^- salt (one shown in Fig. 1) have very similar conformations: the imidazole rings are

[4]When the ligands are discussed collectively, the atoms are represented by the unparenthesized one-digit symbols shown for the 4-nitro tautomer in Scheme 1. To designate one particular ligand, the individual parenthesized symbols of Tables 2 or 3 are used in the text.

TABLE 4. Selected interatomic distances (Å) and bond angles (°)

(*a*) $[Ag(NO_2ImH)_2NO_3$

Ag(A)—N(31A)	2.127(2)	Ag(B)—N(31B)	2.140(2)
Ag(A)—N(32A)	2.135(2)	Ag(B)—N(32B)	2.133(2)
Ag(A)—O(11A)	2.956(2)	Ag(B)—O(11B)	2.812(2)
Ag(A)—O(12A)	2.808(2)	Ag(B)—O(12B)	3.001(2)
N(1A)—O(1A)	1.252(3)	N(1B)—O(1B)	1.237(3)
N(1A)—O(2A)	1.243(3)	N(1B)—O(2B)	1.245(3)
N(1A)—O(3A)	1.237(3)	N(1B)—O(3B)	1.245(3)
N(31A)—Ag(A)—N(32A)	169.9(1)	N(31B)—Ag(B)—N(32B)	162.3(1)
N(31A)—Ag(A)—O(11A)	61.8(1)	N(31B)—Ag(B)—O(11B)	64.5(1)
N(31A)—Ag(A)—O(12A)	125.4(1)	N(31B)—Ag(B)—O(12B)	135.9(1)
N(32A)—Ag(A)—O(11A)	128.2(1)	N(32B)—Ag(B)—O(11B)	131.9(1)
N(32A)—Ag(A)—O(12A)	64.7(1)	N(32B)—Ag(B)—O(12B)	61.3(1)
O(11A)—Ag(A)—O(12A)	63.7(1)	O(11B)—Ag(B)—O(12B)	71.5(1)
Ag(A)—N(31A)—C(21A)	124.5(2)	Ag(B)—N(31B)—C(21B)	129.2(2)
Ag(A)—N(31A)—C(41A)	131.0(2)	Ag(B)—N(31B)—C(41B)	126.1(2)
Ag(A)—N(32A)—C(22A)	129.1(2)	Ag(B)—N(32B)—C(22B)	123.9(2)
Ag(A)—N(32A)—C(42A)	126.6(2)	Ag(B)—N(32B)—C(42B)	131.7(2)
Ag(A)—O(11A)—N(41A)	107.6(2)	Ag(B)—O(11B)—N(41B)	108.5(2)
Ag(A)—O(12A)—N(42A)	109.1(2)	Ag(B)—O(12B)—N(42B)	106.9(1)
O(1A)—N(1A)—O(2A)	119.3(2)	O(1B)—N(1B)—O(2B)	120.3(2)
O(1A)—N(1A)—O(3A)	119.9(2)	O(1B)—N(1B)—O(3B)	119.8(2)
O(2A)—N(1A)—O(3A)	120.8(2)	O(2B)—N(1B)—O(3B)	119.9(2)

(*b*) $[Ag(NO_2ImH)_2]BF_4$

Ag—N(31)	2.173(3)	Ag—N(32)	2.173(3)
Ag—O(11)	2.898(4)	Ag—O(12)	2.793(3)
Ag—O(12)[a]	2.984(3)	B—F(2)	1.373(5)
B—F(1)	1.376(5)	B—F(4)	1.377(6)
B—F(3)	1.384(6)		
N(31)—Ag—N(32)	175.2(1)	O(12)—Ag—O(12)[a]	85.0(1)
N(31)—Ag—O(11)	63.1(1)	Ag—N(31)—C(21)	127.9(3)
N(31)—Ag—O(12)	118.2(1)	Ag—N(31)—C(41)	127.0(2)
N(31)—Ag—O(12)[a]	109.0(1)	Ag—N(32)—C(22)	131.8(3)
N(32)—Ag—O(11)	118.4(1)	Ag—N(32)—C(42)	124.3(2)
N(32)—Ag—O(12)	65.8(1)	Ag—O(11)—N(41)	108.0(3)
N(32)—Ag—O(12)[a]	73.4(1)	Ag—O(12)—N(42)	108.4(2)
O(11)—Ag—O(12)	65.2(1)	Ag—O(12)[a]—N(42)[a]	103.6(2)
O(11)—Ag—O(12)[a]	134.4(1)	Ag—O(12)[a]—Ag[a]	135.7(1)
F(1)—B—F(2)	109.2(4)	F(1)—B—F(3)	109.2(4)
F(1)—B—F(4)	108.7(4)	F(2)—B—F(3)	108.8(4)
F(2)—B—F(4)	110.1(4)	F(3)—B—F(4)	110.9(4)

[a] $-x, -\frac{1}{2} + y, \frac{1}{2} - z$.

nearly coplanar, making dihedral angles of 4.9(2)° (molecule A) and 3.4(2)° (molecule B). In the BF_4^- compound (Fig. 2), the rings are 44.2(4)° apart. The nitro groups have mutually *syn* orientations in these three independent complex cations.

An analogous two-coordinate species was found in $[Ag(imidazole)_2]NO_3$ (20, 21) whereas a more complex hexanuclear pattern was observed for the perchlorate (22). The Ag—N distances observed here (Table 4) (mean 2.135 Å, NO_3^-; 2.172 Å, BF_4^-) are slightly longer than those found by these authors (2.075(3) and 2.089(3) for ClO_4^-, 2.120(8) and 2.132(8) Å for NO_3^-), but comparable with those reported for silver atoms bonded to similar rings in purines (23).

Departure from linearity is significant (Table 4), but not uncommon for Ag(I). In the NO_3^- salt (cation A), the O(11A)···O(12A) separation (3.044(3) Å) is just above the normal van der Waals distance (3.0 Å). Therefore, the N(31A)—Ag(A)—N(32A) unit (169.9(1)°) could not be made more linear without producing steric hindrance between the nitro groups, *if the ligands were kept coplanar*. On the other hand, the greater departure from linearity for cation B (162.3(1)°) cannot be ascribed to O(11B)···O(12B) steric hindrance, since the separation is 3.400(3) Å. At any rate, there should be free rotation about the Ag—N bonds in solution, and the *syn*-nitro coplanar arrangement found for the nitrate salt is probably due to crystal packing, because the ligands are not coplanar in the BF_4^- salt, where the N—Ag—N angle is 175.2(1)°.

Since the sum of the van der Waals radii is 3.2 Å (24), the intramolecular Ag···O distances (2.7–3.0 Å, Table 4) should correspond to some bonding, but much weaker than a normal covalent bond, for which distances <2.45 Å are expected (11, 25). As the ligand is not flexible, the Ag—O distance is directly correlated with the Ag—N3—C angles, which should be equal if coordination took place along the

Can. J. Chem. Downloaded from www.nrcresearchpress.com by 92.62.229.171 on 09/08/12
For personal use only.

Can. J. Chem. Downloaded from www.nrcresearchpress.com by 92.62.229.171 on 09/08/12
For personal use only.

TABLE 5. Distances (Å) and angles (°) in the ligands

	Ag complexes[a]	Free ligand (9)
N(1)—C(2)	1.340(6)	1.348(3)
N(1)—C(5)	1.351(9)	1.349(3)
C(2)—N(3)	1.311(5)	1.318(3)
N(3)—C(4)	1.364(3)	1.363(3)
C(4)—C(5)	1.357(9)	1.361(3)
C(4)—N(4)	1.422(3)	1.420(3)
N(4)—O(1)	1.222(4)	1.229(2)
N(4)—O(2)	1.226(4)	1.227(3)
C(5)—N(1)—C(2)	108.2(3)	108.0(2)
N(1)—C(2)—N(3)	111.6(3)	112.0(2)
C(2)—N(3)—C(4)	104.3(2)	103.4(2)
N(3)—C(4)—C(5)	111.4(6)	112.1(2)
C(4)—C(5)—N(1)	104.6(5)	104.4(2)
N(3)—C(4)—N(4)	121.5(4)	120.8(2)
C(5)—C(4)—N(4)	127.2(9)	126.9(2)
C(4)—N(4)—O(1)	118.4(6)	118.5(2)
C(4)—N(4)—O(2)	117.7(5)	118.4(2)
O(1)—N(4)—O(2)	123.8(4)	123.0(2)

[a]Mean values for the six symmetry-independent ligands in the NO_3^- and BF_4^- salts. Details in the supplementary material, Table S-11.

expected N3 lone-pair direction. For the six independent ligands in these two structures, the differences between Ag—N3—C4 and Ag—N3—C2 are large and of different signs: +6.5° (ligand 1A), −2.5° (2A), −3.1° (1B), and +7.8° (2B) for NO_3^-, −0.9° (ligand 1) and −7.3° (ligand 2) for BF_4^-. This shows again that secondary bonding, although providing stabilization, does not impose strict structural requirements to the "chelate" ring and to the metal coordination geometry.

Details on the distances and angles in the individual ligands are provided in the supplementary material. The ligand geometry is not appreciably perturbed by coordination, as shown in Table 5, where the mean values for the complexes are compared with the data for free 4-nitroimidazole (9). There are no appreciable differences in bond lengths. Angles are usually more sensitive to coordination, but only two angles are possibly affected here. The mean C2—N3—C4 angle of 104.3° (range 103.9–104.6°) in the complexes, slightly greater than in the free ligand (103.4(2)°), would be consistent with the usual increase resulting from the smaller size of the N3 "lone pair" after coordination. The other difference is found for C4—N4—O2 (complexes: 117.7°, range 116.8–118.2°; free ligand: 118.4°). This angle involves external nitro oxygens, and it should be sensitive to intermolecular effects. Details on the weighted least-squares planes are also given in the supplementary material. The five-membered rings are planar within 1.2 σ (0.005 Å). As previously noted in the structure of $[Ag(imidazole)_2]NO_3$ (20), displacement of the metal from this plane is usually large, reaching 0.29 Å in the BF_4^- compound. Combination of torsion about C4—N4 and out-of-plane bending of the NO_2 unit leads to the following dihedral angles between the nitro groups and their respective rings: 0.9(3) and 0.7(3)° (NO_3^-, molecule A), 8.2(3) and 3.9(3)° (NO_3^-, B), 3.8(4), and 2.7(4)° (BF_4^-). Most of these distortions are highly significant, but still small compared with the ~45° twist about the C2—NO_2 bond observed in $PtCl_2L_2$ complexes with 2-nitroimidazole derivatives (4).

The unit cell of the BF_4^- salt is shown in Fig. 3. The anions lie close to planes parallel to the *ab* face at $z = 0$ and $\frac{1}{2}$. Between these planes are found the complex cations, with their N—Ag—N direction roughly parallel to the *ac* plane and making a ~45° angle with the *a* and the *c* axes. Within the cationic regions, cohesion is achieved by normal van der Waals contacts and by an intermolecular Ag···O(12) interaction of 2.984(3) Å. Both ends of each cation are anchored to BF_4^- ions in different layers by means of hydrogen bonding with the N1—H groups. F(3) takes part in a standard N(11)—H···F(3) bond (N···F separation = 2.856(4) Å), whereas F(1) is involved in a bifurcated hydrogen bond with two different N(12)—H groups (N···F = 2.924(4) and 3.003(4) Å).

A different packing pattern is found for the nitrate salt (Fig. 4). There are no intermolecular Ag···O contacts in this case. Furthermore, in contrast with $[Ag(imidazole)_2]NO_3$ (20), the anions have no direct interactions with the metal. The building units of the structure are infinite ribbons in which flat complex cations are bridged by NO_3^- ions forming hydrogen bonds with ligand N1—H groups. One such ribbon contains cations of type A, roughly parallel to the *ab* plane, with their N(31A)—Ag(A)—N(32A) direction parallel to the *a* axis at $y \sim 0$ (or 1). The N1—H groups at both ends of the cation form strong hydrogen bonds to two symmetry equivalent nitrate ions of type B:N(11A)···O(3B) = 2.873(3) Å and N(12A)···O(2B) = 2.790(3) Å. The crystallographic twofold axis generates a second ribbon, next to the first and running in the same direction, thereby optimizing van der Waals contacts between parallel planar components. Similar ribbon pairs, oriented along *c*, centred at $y = \frac{1}{2}$, and parallel to the *bc* face, contain cations B and anions A, also linked by N1—H···O(nitrate) hydrogen bonds: N(11B)···O(2A) = 2.806(3) Å and N(12B)···O(1A) = 2.755(3) Å. The nitro groups do not participate in hydrogen bonding. The only intermolecular contacts of the nitro groups occur with the C2—H region of ligands in the other type of ribbons.

Infrared spectroscopy

The frequencies are provided in Table S-12 (supplementary material) for 4-nitroimidazole, the *N*-deuterated derivative, and the three silver complexes.

The spectrum of the 4-nitro compound contains most of the bands of unsubstituted imidazole with only small shifts. Our assignments are made by comparison with those deduced from systematic studies on imidazole (26) and 4-methylimidazole derivatives (27). In the present case, one set of ν, δ, and γ(C—H) modes should be replaced by nine vibrations involving the nitro group. Four internal modes are located in well-defined regions identified for nitrobenzenes (28–30): ν_{as}, 1510; ν_s, 1375; δ, 860; γ, 745 cm^{-1}. The normally weak ρ(NO_2) vibration, observed at ~530 cm^{-1} for nitrobenzenes, could produce the very weak feature at 470 cm^{-1}. The torsion mode is not expected to lie above 200 cm^{-1}. The ν(C—NO_2) mode probably corresponds to the strong band at 982 cm^{-1}, which replaces the imidazole δ(C—H) mode at 1050 cm^{-1} in this region. The δ(C—NO_2) mode is tentatively assigned to a clear band at 435 cm^{-1}, absent from the spectrum of imidazole.

The two δ(C—H) bands are readily recognized, since they are not appreciably shifted from their positions in imidazole (26). The γ(C—H) bands are more difficult to locate. One of these modes gives rise to a doublet at 819/811 cm^{-1}, close to the position found for imidazole. The 920 cm^{-1} region, where one such mode is found for imidazole, retains only the

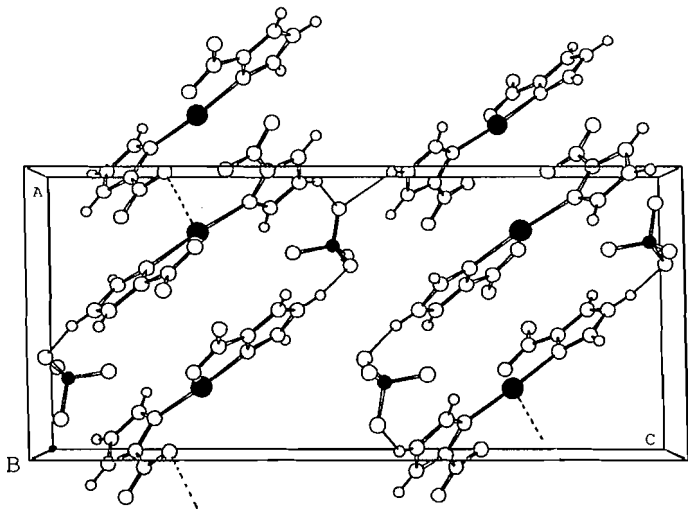

FIG. 3. Unit cell of $[Ag(4\text{-nitroimidazole})_2]BF_4$. Atoms are shown as spheres of arbitrary sizes: Ag (black) < C ~ N ~ O ~ F < B (black) < H. Full lines correspond to hydrogen bonds, and dashed lines to intermolecular Ag···O contacts. The unit cell origin is indicated by a black dot.

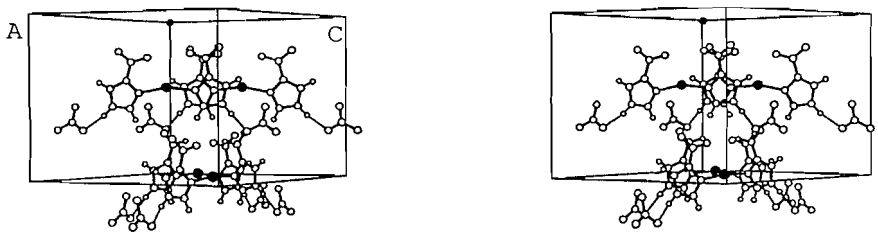

FIG. 4. Stereoview of molecular packing for $[Ag(4\text{-nitroimidazole})_2]NO_3$. Conditions as for Fig. 3.

922 and 906 cm^{-1} components, which are likely due to ring vibrations. Similarly, the γ(C—H) doublet of imidazole at 749/730 cm^{-1} is replaced here by the single 749 cm^{-1} feature assigned to the $\gamma(NO_2)$ vibration. The best candidate for the second γ(C—H) vibration of 4-nitroimidazole is found at 834 cm^{-1}, next to the other.

The spectral regions sensitive to N—H motion are identified by comparison with the *N*-deuterated derivative. The broad ν(N—H) massif centred at 2800 cm^{-1} is replaced by a less complex feature for ν(N—D) near 2180 cm^{-1}. Deuteration gives rise to new bands at 888/873 and 668 cm^{-1}, also found for imidazole (26, 27) and assigned to δ(N—D) and γ(N—D), respectively. The corresponding N—H vibrations can thus be identified at 1240 (δ) and 950 (γ) cm^{-1}, respectively. Deuteration removes the 1150/1135 cm^{-1} doublet, which is possibly shifted to 1210 cm^{-1} with considerable loss of intensity: this doublet originates from a ring mode found to be sensitive to ring substitution in imidazole derivatives (26, 27). The $\nu(C—NO_2)$ mode, also expected to be coupled with the ring, is displaced from 982 to 1003 cm^{-1}. Both of these effects could be related to loss of coupling with δ(N—H) motion upon deuteration.

The most obvious spectral changes for the $[Ag(NO_2ImH)_2]X$ complexes arise from anion bands. They are found at the typical wavenumbers for uncoordinated anions (31), and low site symmetry imparts some intensity to certain IR-forbidden bands: for NO_3^-, 1360 (vs, br), 1035 (vw), 710 (m), 830 cm^{-1} (masked); BF_4^-: 1020 (vs, br), 512 (m). Among the ligand bands, the ν(N—H) mode in the BF_4^- salt is shifted from 2800 to 3320 cm^{-1}, probably because of weaker H-bonding. This band remains unshifted in the nitrate, where the crystallographic work shows that hydrogen bonding is stronger. As the ligand stays formally neutral in these compounds, the remaining ligand modes do not undergo drastic changes. The following bands are found to undergo appreciable shifts: 1510 (+10), 1330 (+10), 982 (+14), 435 (+10) cm^{-1}.

As expected, the spectrum of $[Ag(NO_2Im)]$ contains no anion bands and ligand deprotonation introduces drastic spectral changes. The strong ν(N—H) massif near 2800 cm^{-1} is completely washed out. Loss of coupling with N—H motion and changes in ring bond orders displace many of the ligand vibrations. The high wavenumber ring band at 1565 cm^{-1} is probably displaced to ~1500 cm^{-1} and overlaps with the $\nu(NO_2)$ band. The 1150/1135 cm^{-1} doublet for the ring mode sensitive to deuteration moves toward 1200 cm^{-1}. Other bands undergo large changes: 1075 (+43), 982 (+35), 922 (+36), 906 (−43), 599 (−47) cm^{-1}. The shift from 435 to ~460 cm^{-1} with considerable loss of intensity of the low-frequency band assigned to $\delta(C—NO_2)$ seems to be another good diagnostic for complexation of 4-nitroimidazole in the anionic form.

Nuclear magnetic resonance

No solvent could be found to dissolve the $[Ag(NO_2Im)]$ compound. DMSO is the only common solvent in which the $[Ag(NO_2ImH)_2]X$ complexes were soluble enough to obtain ^1H and ^{13}C NMR spectra. In both kinds of spectra, the chemical shifts were found to coincide with those reported

Can. J. Chem. Downloaded from www.nrcresearchpress.com by 92.62.229.171 on 09/08/12
For personal use only.

TABLE 6. CP/MAS ^{13}C NMR data

	C2	C4	C5	Reference
NO_2ImH	138.2	147.4	121.5	
$[Ag(NO_2ImH)_2]NO_3$	141.3	144.9	121.5	
$[Ag(NO_2Im)]$	145.2	147.6	130.8	
Imidazole	136.3	126.8	115.3	36
$[(NiR)_2(imidazolate)]^+$	142.1	125.1	125.1	35[a]

[a]Solution in $(CD_3)_2CO$; R = 7-amino-4-methyl-5-aza-3-hepten-2-one.

for free 4-nitroimidazole in this solvent (32–34), indicating that the ligands had been displaced from the coordination sphere.

The solid-state ^{13}C spectra (Table 6) proved to be more informative. Since the solid (9) contains the tautomeric form found to be highly dominant in solution (10), the assignments proposed for solution spectra are used directly (32–34).

In $[Ag(NO_2ImH)_2]NO_3$, coordination to the N3 lone pair of a formally neutral ligand induces relatively small shifts of 3.1 ppm downfield on C2 and 2.5 ppm upfield on C4, whereas C5 is not displaced. For $[Ag(NO_2Im)]$, the shifts are larger for C2 and C5 (+7.0 and +9.3 ppm, respectively), whereas C4 is displayed by only +0.2 ppm. For comparison, Table 6 includes data for a complex containing two uniligating square-planar RNi^+ units (R = 7-amino-4-methyl-5-aza-3-hepten-2-one) bonded to N1 and N3 of a deprotonated imidazole ring (35). To determine the peak shifts produced by this type of binding, comparison with the solution spectrum of imidazole would not be informative, since fast tautomeric exchange of the N—H proton between N1 and N3 renders C4—H4 and C5—H5 equivalent on the NMR time scale. The data from the solid-state spectrum (36) are more appropriate, since fast exchange does not occur in the crystal. Table 6 reveals that for this complex containing an imidazole monoanion bridging two metal atoms, large downfield shifts of 5.8 and 9.8 ppm are noted for C2 and C5, respectively, whereas C4 does not move very much. Considering the similitude of the $\Delta\delta$ values, it can safely be concluded that 4-nitroimidazole in $[Ag(NO_2Im)]$ also plays a bridging role via N1 and N3.

Conclusion

Under neutral or weakly acidic conditions, 4-nitroimidazole forms the insoluble $[Ag(NO_2Im)]$ compound, in which the ligand is shown to be bridging via N1 and N3 by solid-state ^{13}C NMR. Since the metal exhibits a marked preference for linear two-coordination, this compound likely consists of metal atoms and ligand monoanions alternating along an infinite chain. The formation of this compound can be opposed by using very high concentrations of acid. Then, discrete $[Ag(NO_2ImH)_2]^+$ salts, containing two-coordinate silver and neutral imidazole ligands, are isolated. In these compounds, the metal has a linear N—Ag—N coordination, and since the heterocyclic N atom used to coordinate is the one adjacent to the nitro group, the latter is in a suitable position to close a loose chelate ring by weaker Ag···O semi-bonding near the metal equatorial plane. The latter interaction is not very strong, but it contributes to binding and helps stabilizing the 4-nitro tautomer in the complex.

The particular effects of the nitro group in this system can be related to two main points. Its electron-attracting effects decreases the pK_a of both the neutral ligand and its conjugated acid, increasing the domain of existence of the neutral complex $[Ag(NO_2Im)]$, which does not have to compete with the protonation equilibrium of the free ligand, as was the case for the complex with unsubstituted imidazole. On the other hand, the polar NO_2 group of free 4-nitroimidazole participates in dipolar interactions in the solid state, which considerably reduces water solubility compared to unsubstituted imidazole and renders the preparation of pure, ligand-free, samples more difficult.

Acknowledgments

We wish to thank the Natural Sciences and Engineering Research Council of Canada for financial support, and M. Simard and F. Bélanger-Gariépy for assistance in collecting the X-ray diffraction data and solving the structures.

1. N. Farrell. Transition metal compounds as drugs and chemotherapeutic agents. Kluwer, Dordrecht. 1989. Chap. 6.
2. G. E. Adams, E. D. Clarke, I. R. Flockhart, R. S. Jacobs, D. H. Sehmi, I. J. Stratford, P. Wardman, M. E. Watts, J. Parrick, R. G. Wallace, and C. E. Smithen. Int. J. Radiat. Biol. **35**, 133 (1979).
3. J. M. Brown, N. Y. Yu, D. M. Brown, and W. W. Lee. Int. J. Radiat. Oncol. Biol. Phys. **7**, 695 (1984).
4. J. R. Bales, M. A. Mazid, P. J. Sadler, A. Aggarwal, R. Kuroda, S. Neidle, D. W. Gilmour, B. J. Peart, and C. A. Ramsden. J. Chem. Soc. Dalton Trans. 795 (1985); N. Farrell, T. M. G. Carneiro, F. W. B. Einstein, T. Jones, and K. A. Skov. Inorg. Chim. Acta **92**, 61 (1984).
5. P. K. L. Chan, K. A. Skov, B. R. James, and N. P. Farrell. Int. J. Radiat. Oncol. Biol. Phys. **12**, 1059 (1986).
6. D. M. L. Goodgame, A. S. Lawrence, A. M. Z. Slawin, D. J. Williams, and I. J. Stratford. Inorg. Chim. Acta, **125**, 143 (1986).
7. A. R. Norris, R. Kumar, and A. L. Beauchamp. Inorg. Chim. Acta, **162**, 139 (1989).
8. R. J. Lancashire. *In* Comprehensive coordination chemistry. *Edited by* G. Wilkinson, R. D. Gillard, and J. A. McCleverty. Pergamon Press, Oxford. 1987. Chap. 54.
9. I. Ségalas, J. Poitras, and A. L. Beauchamp. Acta Crystallogr. Sect. C: Cryst. Struct. Commun. **C48**, 295 (1992).
10. P. Jimenez, J. Laynez, R. M. Claramunt, D. Sanz, J. P. Fayet, M. C. Vertut, J. Catalán, J. L. G. de Paz, G. Pfister-Guillouzo, C. Guimon, R. Flammang, A. Maquestiau and J. Elguero. New J. Chem. **13**, 151 (1989).
11. F. Guay and A. L. Beauchamp. J. Am. Chem. Soc. **101**, 6260 (1979).
12. L. G. Marzilli, T. J. Kistenmacher, and M. Rossi. J. Am. Chem. Soc. **99**, 2797 (1977).
13. J. Perron and A. L. Beauchamp. Inorg. Chem. **23**, 2853 (1984).
14. J. Perron and A. L. Beauchamp. Can. J. Chem. **62**, 1287 (1984).
15. D. T. Cromer and J. B. Mann. Acta Crystallogr. Sect. A: Cryst. Phys. Diffr. Theor. Gen. Crystallogr. **A24**, 321 (1968).
16. R. F. Stewart, E. R. Davidson, and W. T. Simpson. J. Chem. Phys. **42**, 3175 (1965).
17. D. T. Cromer and D. Liberman. J. Chem. Phys. **53**, 1891 (1970).
18. J. E. Bauman, Jr. and J. C. Wang. Inorg. Chem. **3**, 368 (1964).
19. J. Reedijk. *In* Comprehensive coordination chemistry. *Edited by* G. Wilkinson, R. D. Gillard, and J. A. McCleverty. Pergamon Press, Oxford. 1987. Chap. 13.2.
20. C.-J. Antti and B. K. S. Lundberg. Acta Chem. Scand. **25**, 1758 (1971).

Can. J. Chem. Downloaded from www.nrcresearchpress.com by 92.62.229.171 on 09/08/12
For personal use only.

21. C. B. Acland and H. C. Freeman. J. Chem. Soc. Chem. Commun. 1016 (1971).
22. G. W. Eastland, M. A. Mazid, D. R. Russell, and M. C. R. Symons. J. Chem. Soc. Dalton Trans. 1682 (1980).
23. F. Bélanger-Gariépy and A. L. Beauchamp. J. Am. Chem. Soc. **102**, 3461 (1980); C. Gagnon, J. Hubert, R. Rivest, and A. L. Beauchamp. Inorg. Chem. **16**, 2469 (1977); C. Gagnon and A. L. Beauchamp. Acta Crystallogr. Sect. B: Struct. Crystallogr. Cryst. Chem. **B33**, 1448 (1977).
24. J. E. Huheey. Inorganic chemistry, principles of structure and reactivity. 3rd ed. Harper & Row, New York. 1983. p. 258.
25. R. G. Griffin, J. D. Ellett, Jr., M. Mehring, J. G. Bullitt, and J. S. Waugh. J. Chem. Phys. **57**, 2147 (1972); P. Coggon and A. T. McPhail. J. Chem. Soc., Chem. Commun. 91 (1972); E. T. Blues, M. G. B. Drew, and B. Femi-Onadeko. Acta Crystallogr. Sect. B: Struct. Crystallogr. Cryst. Chem. **B33**, 3965 (1977); N.-O. Björk and A. Cassel. Acta Chem. Scand. **A30**, 235 (1976).
26. A.-M. Bellocq, C. Perchard, A. Novak, and M.-L. Josien. J. Chim. Phys. **62**, 1334 (1965); C. Perchard, A.-M. Bellocq, and A. Novak. J. Chim. Phys. **62**, 1344 (1965).
27. A.-M. Bellocq and C. Garrigou-Lagrange. J. Chim. Phys. **66**, 1511 (1969).
28. C. Garrigou-Lagrange, M. Chehata, and G. Sourisseau. J. Chim. Phys. **62**, 261 (1965).
29. J. H. S. Green and D. J. Harrison. Spectrochim. Acta, **26A**, 1925 (1970).
30. N. S. Sundar. Spectrochim. Acta, **41A**, 905 (1985).
31. K. Nakamoto. Infrared and Raman spectra of inorganic and coordination compounds. Wiley, New York. 1986.
32. H. A. Staab, H. Irngartinger, A. Mannschreck, and M.-T. Wu. Ann. Chem. **695**, 55 (1966).
33. E. Lippmaa, M. Mägi, S. S. Novikov, L. I. Khmelnitski, A. S. Prihodko, O. V. Lebedev, and L. V. Epishina. Org. Magn. Reson. **4**, 153 (1972).
34. A. McKillop, D. E. Wright, M. L. Podmore, and R. K. Chambers. Tetrahedron, **39**, 3797 (1983).
35. J.-P. Costes, G. Commenges, and J.-P. Laurent. Inorg. Chim. Acta, **134**, 237 (1987).
36. J. Elguero, A. Fruchier, and V. Pellegrin. J. Chem. Soc. Chem. Commun. 1207 (1981).

Can. J. Chem. Downloaded from www.nrcresearchpress.com by 92.62.229.171 on 09/08/12
For personal use only.

Electron ionization mass spectrometry of cobalt(III) β-diketonates and monothio-β-diketonates possessing aryl and fluorinated alkyl substituents

MARK L. J. REIMER[1] AND JOHN B. WESTMORE[2]
Department of Chemistry, University of Manitoba, Winnipeg, Manitoba R3T 2N2

AND

MANORANJAN DAS[3]
School of Chemistry, University of New South Wales, P.O. Box 1, Kensington, N.S.W. 2033, Australia

Received July 23, 1991

MARK L. J. REIMER, JOHN B. WESTMORE, and MANORANJAN DAS. Can. J. Chem. **70**, 952 (1992).

Electron ionization positive ion mass spectra of 15 substituted cobalt(III) β-diketonates and monothio-β-diketonates, $Co^{III}L_3$, where L = RCXCHCOR′, R = phenyl, 2-thienyl, or 2-naphthyl; X = O or S; and R′ = CHF_2, CF_3, C_2F_5, or n-C_3F_7, show a marked dependence on the ligand. Molecular ions, $[Co^{III}L_3]^{+\bullet}$, are observed only for some of the more highly fluorinated complexes (R′ = C_2F_5 or n-C_3F_7). The $[Co^{III}L_2]^{+\bullet}$ ion, possibly generated by ionization of $Co^{II}L_2$ formed by thermal degradation, or by electron ionization of $Co^{III}L_3$, typically decomposes by elimination of a radical, i.e., $L^{\bullet}$ or $R'^{\bullet}$, to yield ions containing Co(II); subsequent decompositions proceed preferentially by loss of even-electron neutral species, also to yield ions containing Co(II). Cobalt-containing ions in which fluorine has rearranged to the metal decrease in variety and abundance for the ligands with higher fluorine content. When metal-bonded oxygen is replaced by sulfur, fluorine migration to Co(III), rather than to Co(II), is preferred. These trends are consistent with a combination of several different concepts including the ability of the metal to undergo valency change, the principle of Hard and Soft Acids and Bases, and the inductive capabilities of the ligand donor atoms and of the R and R′ groups. Ion decomposition pathways are proposed.

Key words: mass spectrometry, cobalt complexes, β-diketonates, fluorinated chelate complexes.

MARK L. J. REIMER, JOHN B. WESTMORE et MANORANJAN DAS. Can. J. Chem. **70**, 952 (1992).

Les spectres de masse des ions positifs obtenus par ionisation électronique de 15 β-dicétonates et de monothio-β-dicétonates de cobalt(III) substitués, $Co^{III}L_3$ [L = RCXCHCOR′, R = phényle, 2-thiényle ou 2-naphtyle, X = O ou X et R′ = CHF_2, CF_3, C_2F_5 ou n-C_3F_7], dépendent grandement de la nature du ligand. On n'observe les ions moléculaires $[Co^{III}L_3]^{+\bullet}$ que pour quelques-uns des complexes les plus fluorés (R′ = C_3F_5 ou n-C_3F_7). L'ion $[Co^{III}L_3]^{+\bullet}$ qui provient peut-être d'une ionisation du $Co^{II}L_3$ formé par une dégradation chimique ou par une ionisation électronique du $Co^{III}L_3$ se décompose d'une façon typique par l'élimination d'un radical, soit $L^{\bullet}$ ou $R'^{\bullet}$, pour fournir des ions contenant du Co(II); les dégradations subséquentes se produisent préférentiellement par la perte d'espèces neutres avec un nombre pair d'électrons et elles conduisent aussi à des ions contenant du Co(II). La variété et l'abondance des ions contenant du cobalt dans lesquels le fluor s'est déplacé vers le métal diminuent avec une augmentation du contenu en fluor. Lorsqu'on remplace de l'oxygène lié à un métal par un soufre, la migration du fluor vers le Co(III) est préférée à une migration vers le Co(II). Ces tendances sont en accord avec une combinaison de plusieurs concepts différents comprenant : l'habilité du métal à subir un changement de valence, le principe des acides et des bases dures et molles et les capacités inductives des atomes du ligand donneur et des groupements R et R′. On propose des voies de décompositions pour les ions.

Mots clés : spectrométrie de masse, complexes du cobalt, β-dicétonates, complexes de chélates fluorés.

[Traduit par la rédaction]

Introduction

The significant volatility and stability of metal β-diketonates and their derivatives make them suitable for gas chromatography (1). When this technique is combined with mass spectrometry, analytical methods, based upon the use of isotopic tracers, can be devised for metals. Recently, metal β-diketonates were used as precursors for chemical vapor deposition (2–4), a promising technique for the preparation of thin films of high T_c superconducting oxides (5), and the application of mass spectrometry to characterize the alkaline earth complexes for this purpose has been described (6).

The mass spectra of these complexes are of interest in their own right because their wide variety permits assessment of the influence exerted by bonding and structure factors, i.e., (*i*) the central metal atom, (*ii*) the ligand donor atoms, and (*iii*) the wide variety of organic substituents attached to the ligand. Conversely, because of this, the mass spectra can often be used to draw conclusions about the condensed phase chemistry of the metals. Much of the early mass spectral work starting from the first extended study (7), has been reviewed (8–11).

In the electron ionization (EI) mass spectrum of an organic compound an odd-electron positive ion ($OE^{+\bullet}$) typically decomposes to an even-electron positive ion (EE^{+}) and an odd-electron neutral ($OE^{\bullet}$) (or, occasionally, to $OE^{+\bullet}$ and an even-electron neutral (EE^{0})), but an even-electron cation preferentially decomposes to another EE^{+} and an EE^{0} (ref. 12, or other texts on mass spectrometry). Many exceptions to this generalization are known, the majority being explicable by aromatic stabilization of the radical cations formed in the reaction: $EE^{+} \rightarrow OE^{+\bullet} + OE^{\bullet}$ (13). To interpret the mass spectra of metal complexes, which also frequently violate this generalization, it is useful to invoke the concept of metal valency change (14, 15) to alter the "odd" or "even" electron character of a metal-containing ion. This character is controlled by the capacity of the complexed metal atom

[1]Present address: Biomedical Mass Spectrometry Unit, McGill University, 1130 Pine Ave. W., Montreal, Que., H3A 1A3 Canada.
[2]Author to whom correspondence may be addressed.
[3]Present address: 435 New Sitaramdera, P.O. Agrico, Jamshedpur 9, Bihar, India 831009.

Can. J. Chem. Downloaded from www.nrcresearchpress.com by 92.62.229.171 on 09/08/12
For personal use only.

Can. J. Chem. Downloaded from www.nrcresearchpress.com by 92.62.229.171 on 09/08/12
For personal use only.

either to accept one or more electrons from the ligands (valence decrease in metal) or to donate one or more electrons to the ligands (valence increase in metal). The mass spectra of metal complexes are often best explained if valence changes in the bonded metal are assumed to occur during some ion dissociation reactions, while metal valence is maintained during others. In fact, many ion decompositions appear to depend upon the oxidation states normally accessible to the metal. This is true of the mass spectra of metal β-diketonates and monothio-β-diketonates, which can be understood, in part, from the dependence of ion stability upon relative stabilities of metal oxidation states (10).

Rearrangements involving transfer of an atom (or group of atoms) to the metal in the formation of a metal-containing fragment ion or neutral species are also observed (16). A plausible explanation for such rearrangements, and the reasons behind the bonding preferences shown by various metals towards the migrating species, is given by the principle of Hard and Soft Acids and Bases (HSAB) (17–21), an empirically derived relationship that correlates the relative affinities of acceptor metals (ions or atoms: Lewis acids) for donor atoms (ligands: Lewis bases) on the basis of their respective electronic properties. This principle has been extended to the mass spectra of fluorinated β-diketonate complexes to explain the rearrangement of fluorine to the metal (22). Formation of ions or neutrals containing Met—F bonds (Met = metal) occurs for Co(II), Fe(III), Fe(II), Cr(III), Al(III), Zn(II), Ni(II), and Mn(II) complexes of 1,1,1,5,5,5-hexafluoro-2,4-pentanedione. All of these metal ions can be considered as hard, or borderline-hard, acids while fluorine can be considered as a hard base. Fluorine migration to these centres is therefore in keeping with HSAB predictions (the two electron-withdrawing CF_3 groups on the ligand would be expected to harden the borderline-hard metals, making them more receptive to a fluorine transfer). Fluorine rearrangement is notably absent, however, in the spectrum of the copper(I) complex with this ligand; Cu(I) is considered to be a soft acid and so would not be expected to bind with fluorine. A comparison (22) of these results with those obtained when a CF_3 group is replaced by methyl, ethyl, isopropyl, *tert*-butyl, phenyl, or 2-thienyl revealed a striking dependence of the abundances of the rearrangement ions on the substituent. Thus, replacement of a CF_3 group by a more electron-releasing species softens the metal, so fluorine rearrangement becomes less prevalent. This phenomenon was also noted for reactions in which HF is eliminated. When one of the CF_3 groups is replaced by a methyl or phenyl group, the relative abundances of the ions resulting from HF loss increase dramatically; softening the metal environment decreases its ability to compete for fluorine.

In the present study we examine the positive ion EI mass spectra of a series of fluorinated cobalt(III) complexes, CoL_3, having the general form $Co^{III}(RCXCHCOR')_3$, where R = phenyl, 2-thienyl, or 2-naphthyl; X = O or S; and R′ = CHF_2, CF_3, C_2F_5, or *n*-C_3F_7, as listed in Table 1. Except for **3***a*, mass spectral studies of these complexes have not been reported previously. The complexes are of interest because of the accessibility of the (III), (II), and (I) valence states of cobalt, which have varying hard/soft acid character. Furthermore, both the X = O, and X = S series of complexes are stable and easily prepared (this is not so for several other metal ions). We relate the trends in observed ion abundances to the ability of the metal to undergo change in valency, to the HSAB principle, and to the inductive effects of the ligand donor atoms and of the R and R′ groups, in a more comprehensive way than has been reported heretofore.

TABLE 1. The cobalt chelates examined and their molar masses

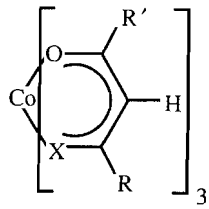

Complex	X	R	R′	M_r
1*a*	O	$-C_6H_5$	$-CHF_2$	650
2*a*	O	$-C_4H_3S$	$-CHF_2$	668
3*a*	O	$-C_6H_5$	$-CF_3$	704
4*a*	O	$-C_4H_3S$	$-CF_3$	722
5*a*	O	$-C_{10}H_7$	$-CF_3$	854
6*a*	O	$-C_6H_5$	$-C_2F_5$	854
6*b*	S	$-C_6H_5$	$-C_2F_5$	902
7*a*	O	$-C_4H_3S$	$-C_2F_5$	872
7*b*	S	$-C_4H_3S$	$-C_2F_5$	920
8*b*	S	$-C_{10}H_7$	$-C_2F_5$	1052
9*a*	O	$-C_6H_5$	$-C_3F_7$	1004
9*b*	S	$-C_6H_5$	$-C_3F_7$	1052
10*a*	O	$-C_4H_3S$	$-C_3F_7$	1022
10*b*	S	$-C_4H_3S$	$-C_3F_7$	1070
11*b*	S	$-C_{10}H_7$	$-C_3F_7$	1202

Experimental

Mass spectrometry

All mass spectra were acquired on a VG 7070E-HF double-focusing (EB) mass spectrometer (VG Analytical Ltd.; Manchester, England) equipped with a DEC Micro PDP-11/73 data system (Digital Equipment Corp.; Maynard, Mass.). Reproducible mass spectra were obtained by introducing samples on a direct insertion probe, which was heated to produce an even rate of volatilization. The low resolution EI conditions were as follows: accelerating voltage, 6 kV; ionizing energy, 70 eV; trap current, 200 μA; source temperature, 200°C; scan rate, 1.0 s/decade; resolution, 1400 (10% valley definition).

Ion decomposition spectra were recorded by linked scanning as follows: (*a*) product ion spectra at constant magnetic field/electric field ratio (i.e., B/E constant; accelerating voltage (V) fixed), and (*b*) constant neutral loss spectra ($B[1 - (E/E_0)]^{1/2}/E$ constant; V fixed), on selected ions in the spectra of **4***a* and **7***b* at a scan rate of 5.0 s/decade. Parent ions were collisionally activated in the first field-free region of the instrument by adjusting the helium pressure in the collision cell to attenuate the parent ion signal by approximately 50%.

Ligand syntheses

The fluorinated β-diketones used in the syntheses of **3***a* and **4***a* were purchased from Aldrich Chemical Co. (Milwaukee, Wis.), and of **5***a* from Eastman Kodak Co. (Rochester, N.Y.). The remaining β-diketones were synthesized by a Claisen condensation of the appropriate methyl ketone ($RCOCH_3$) with the fluorinated ethyl ester ($R'COOC_2H_5$), as previously described (23, 24). The fluorinated monothio-β-diketones were synthesized from their corresponding β-diketones (24–28).

Syntheses of cobalt(III) β-diketonates

These syntheses were based on the procedure of Fay and Piper (29). Sodium tris-carbonatocobaltate(III) trihydrate (0.3 mmol; prepared as described below) and 6 M nitric acid (0.15 mL) were

Can. J. Chem. Downloaded from www.nrcresearchpress.com by 92.62.229.171 on 09/08/12
For personal use only.

added to a solution of the ligand (0.9 mmol) in 1.5 mL of aqueous alcohol (40% ethanol). After refluxing the mixture for 30 min, the precipitated green product was filtered off under suction, washed with cold water, and air dried. Its purity was monitored by TLC and, if warranted, it was further purified by column chromatography (30% methylene chloride/petroleum ether on silica gel).

Following a reported procedure (30), sodium tris-carbonatocobaltate(III) trihydrate, $Na_3[Co(CO_3)_3] \cdot 3H_2O$, was prepared by adding 50 mL of an aqueous solution of cobalt(II) nitrate hexahydrate (0.10 mol) and 30% hydrogen peroxide (10 mL) dropwise, with stirring, to an ice-cold slurry of sodium bicarbonate (0.50 mol) in water (50 mL). The mixture was stirred in an ice bath for 1 h. The precipitated green product was filtered off under suction, washed with 30 mL of cold water, then washed with cold absolute ethanol and allowed to air dry.

Syntheses of cobalt(III) monothio-β-diketonates

As reported previously (28), cobalt (II) acetate tetrahydrate (4 mmol) in absolute ethanol (150 mL) was added to a solution of the ligand (12 mmol) in ethanol (50 mL). After aerating the brown solution for 4 h the resulting precipitate was filtered off and washed with ethanol. (In the cases of **6***b* and **9***b* a solid did not form after aeration, so the solution volume was reduced to 75 mL by evaporation and then cooled. After addition of 5 mL of water, the mixture was refrigerated overnight to obtain a precipitate of the desired product. This was filtered off and washed with cold ethanol.)

Results and discussion

Discussion will focus on the major cobalt-containing ions observed; metal-free fragments will be referred to only when necessary to elucidate decompositions involving metal-containing species.

Co(III) β-diketonates

Mass spectra of the nine Co(III) β-diketonates are given in Table 2, with representative spectra depicted in Fig. 1. (Except where the mass spectral peaks were too small to measure accurately, the isotopic patterns were consistent with the ion assignments proposed in Tables 2 and 4.) The mass spectrum of **3***a* is in good agreement with a previous report (31). To assist in assignment of fragmentation pathways, collisionally activated decompositions of selected ions obtained from **4***a* are listed in Table 3.

Difluoromethyl-substituted ligands (R′ = CHF_2)

In the mass spectra of complexes **1***a* and **2***a*, $[Co^{III}L_3]^{+\bullet}$ ions, or ions unequivocally formed from them, were not detected. The observed ion of highest m/z is the EE^+ species $[Co^{III}L_2]^+$. Since we could not tell from these results whether $[Co^{III}L_2]^+$ is formed by loss of a ligand radical from $[Co^{III}L_3]^{+\bullet}$ or by ionization of $Co^{II}L_2$ formed by thermal degradation of $Co^{III}L_3$, we operated the ion source under ammonia chemical ionization (NH_3CI) conditions for complex **1***a*. Strong signals corresponding to $[CoL_2+H]^+$ and $[CoL_2+NH_4]^+$ were obtained, but the analogous signals for $[CoL_3+H]^+$ and $[CoL_3+NH_4]^+$ could not be detected. This result is consistent with thermal decomposition of CoL_3. Thus, ion decomposition pathways originating from $[Co^{III}L_2]^+$ are shown in Scheme 1. Initially, elimination of a radical, either $R'^{\bullet}$ to give $[Co^{II}L(L - R')]^+$ or $L^{\bullet}$ to give $[Co^{II}L]^+$, suggests reduction of cobalt(III). Subsequently, the relative stability of cobalt(II) towards reduction results, predominantly (but not exclusively), in EE^0 losses (i.e., (L − R′), (L − R), (L − F), CO, CHF), each leading to a fragment ion containing Co(II). Observation of a low yield of $[Co^I]^+$ confirms that further reduction of cobalt is, indeed, possible. (Linked scanning indicates that, for **4***a* at least, $[Co^I]^+$ can form through loss of (L − R′) plus $F^{\bullet}$ from $[Co^{II}F(L - R')]^+$.) Reduction of cobalt(II) is entirely in keeping with the established chemistry of cobalt. With the exception of copper, the +1 oxidation state is better known for cobalt than for any other first transition series metal (32).

A number of decompositions involving fluorine transfer to cobalt are inferred by analogy with results for **4***a* and **7***b*. Thus, losses of the neutral species $Co^{II}F_2$ in the fragmentations $[Co^{II}F(L - COF]^+ \rightarrow [L - COF_2]^+$, and $[Co^{II}L]^+ \rightarrow [L - 2F]^+$ confirm that fluorine rearrangement to cobalt has, in fact, taken place. (The decompositions $[Co^{II}L]^+ \rightarrow [L - COF_2]^+ + Co^{II}F_2 + CO$, and $[Co^{II}L]^+ \rightarrow [L - 2F]^+ + Co^{II}F_2$, were confirmed by linked scanning for **4***a* and **7***b*, respectively. The first of these is probably the sum of the two steps: $[Co^{II}L]^+ \rightarrow [Co^{II}F(L - COF]^+ \rightarrow [L - COF_2]^+$. These conclusions are also consistent with those noted in the introduction.)

Elimination of (L − F) from $[Co^{II}L(L - R')]^+$ to give $[Co^{II}F(L - R')]^+$ also requires fluorine transfer, as do losses of :CHF from $[Co^{III}L_2]^+$ and $[Co^{II}L]^+$. (Corresponding losses of (L − F) and of CF_2 from $[Co^{II}L(L - R')]^+$ and $[Co^{II}L]^+$, respectively, were confirmed by linked scanning for the trifluoromethyl analogue **4***a*.)

Finally, migration of the aryl (R) group to the metal in $[Co^{II}L]^+$ results in the loss of the EE^0 species (L − R) and the formation of the EE^+ fragment $[Co^{II}R]^+$. Concerted mechanisms based on four- and six-membered transition states have been suggested for this process (33).

Trifluoromethyl-substituted ligands (R′ = CF_3)

As above, $[Co^{III}L_3]^{+\bullet}$ ions were not detected in the mass spectra of **4***a* and **5***a*, though a small peak was observed for this ion in the spectrum of **3***a*. The most abundant cobalt-containing fragment ions are $[Co^{III}L_2]^+$ and $[Co^{II}L(L - R')]^+$. Many of the fragmentation pathways proposed in Scheme 2 have been confirmed by linked scanning. Some are similar to those discussed for Scheme 1 and, subsequently, will be referred to only in passing. Eliminations of the EE^0 species CO_2, RC_2H, and CF_2 occur in the decomposition sequence: $[Co^{II}L(L - R')]^+ \rightarrow [LCo^{II}CHCR]^+ \rightarrow [Co^{II}L]^+ \rightarrow [FCo^{II}(L - R')]^+ \rightarrow [FCo^{II}CHCR]^+$. (Note: the 44 dalton neutral fragment eliminated was identified as CO_2 in the very similar mass spectrum of the perdeuterated Fe(III) analogue of **3***a*. The proposed 1,3 shift of an oxygen to carbon of the other, electron-deficient, carbonyl group imparts to the product ion vinyl ion character that "is compensated by the aromatic group α to the charge" (34).) Specifically, for the present complexes, resonance stabilization by the adjacent aromatic group could promote formation of the $[LCo^{II}CHCR]^+$ and $[FCo^{II}CHCR]^+$ ions:

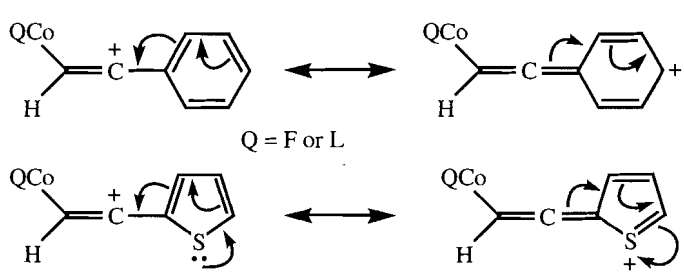

It is also conceivable to regard these species as QCo^+ bonded to the π system of HC≡CR.

Two routes to the ion $[Co^{II}R]^+$ from $[Co^{II}L]^+$ are shown

TABLE 2. EI mass spectra, m/z (%RA), of β-diketonates of cobalt(III)

Ion R,R′→	**1***a* C_6H_5,CHF_2	**2***a* C_4H_3S,CHF_2	**3***a* C_6H_5,CF_3	**4***a* C_4H_3S,CF_3	**5***a* $C_{10}H_7$,CF_3	**6***a* C_6H_5,C_2F_5	**7***a* C_4H_3S,C_2F_5	**9***a* C_6H_5,C_3F_7	**10***a* C_4H_3S,C_3F_7
$[CoL_3]^+$	650 (—)	668 (—)	704 (0.2)	722 (—)	854 (—)	854 (9.3)	872 (1.9)	1004 (5.3)	1022 (0.1)
$[CoL_2(L - 32)]^+$									990 (3.3)
$[CoL_2]^+$	453 (45)	465 (27)	489 (45)	501 (57)	589 (46)	589 (20)	601 (37)	689 (15)	701(34)
$[CoL(L - F)]^+$									682 (2.1)
$[CoL(L - 32)]^+$							569 (11.6)	657 (20)	669 (41)
$[CoFL(L - R')]^+$	421 (2.8)								
$[CoFL(L - CF_3)]^+$						539 (1.5)			
$[CoL(L - R')]^+$	402 (51)	414 (27)	420 (34)	432 (42)	520 (24)	470 (19)	482 (36)	520 (14.3)	532 (35)
$[LCoCHCR]^+$			376 (1.7)	388 (3.3)			438 (1.3)		488 (1.9)
$[CoRL]^+$				363 (1.1)					
$[CoL]^+$	256 (5.6)	262 (5.0)	274 (6.9)	280 (20)	324 (2.7)	324 (4.1)	330 (13.9)	374 (2.6)	380 (14.3)
$[CoF(L - COF)]^+$	228 (8.0)	234 (5.4)		252 (1.6)			302 (2.3)		352 (2.1)
$[CoF(L - R')]^+$	224 (6.3)	230 (3.2)	224 (8.0)	230 (16)	274 (8.9)	224 (2.2)	230 (3.4)		
$[Co(L - CF_2 - HF)]^+$				210 (2.7)					
$[FCoCHCR]^+$				186 (2.0)					
$[CoR]^+$	136 (2.5)	142 (3.0)	136 (1.9)	142 (7.6)	186 (2.5)	136 (2.1)	142 (11.1)	136 (0.8)	142 (7.7)
$[Co]^+$	59 (3.5)		59 (2.1)	59 (2.1)	59 (2.0)	59 (0.8)	59 (1.7)		
Co-free ions:									
$[HL]^+$	198 (3.4)	204 (26)	216 (26)	222 (17)	266 (20)	266 (0.4)	272 (7.4)	316 (5.8)	322 (16)
$[L]^+$			215 (3.0)		265 (3.9)	265 (0.2)			
$[L - S]^+$				189 (4.7)			239 (1.8)		289 (1.1)
$[L - F]^+$	178 (10.5)	184 (1.6)							
$[L - 2F]^+$	159 (3.8)	165 (2.6)							
$[HL - R']^+$	147 (24)	153 (61)	147 (32)	153 (17)	197 (20)	147 (4.6)	153 (15.4)	147 (34)	153 (33)
$[L - COF_2]^+$	131 (4.0)	137 (3.6)		155 (1.3)	199 (1.2)	199 (1.3)	205 (2.6)		255 (2.1)
$[HL - 95]^+$						171 (1.1)	177 (3.1)	221 (1.3)	227 (3.9)
$[RC_3O]$			129 (2.3)	135 (1.4)			135 (1.3)		
$[RCO]^+$	105 (100)	111 (100)	105 (100)	111 (100)	155 (100)	105 (100)	111 (100)	105 (100)	111 (100)
$[RCCH]^+$	102 (30)	108 (4.7)	102 (2.1)	108 (1.8)	152 (6.6)	102 (0.3)	108 (2.0)	102 (1.8)	108 (2.7)
$[R]^+$	77 (51)	83 (13.5)	77 (52)	83 (6.1)	127 (75)	77 (25)	83 (7.4)	77 (27)	83 (8.4)
$[R']^+$	51 (15)		69 (57)	69 (33)	69 (62)				
$[CF_3]^+$	69 (26)	69 (61)				69 (8.7)	69 (27)	69 (33)	69 (42)
$[HL - R']^{2+}$				76.5 (1.8)	98.5 (2.7)				76.5 (3.1)
$\%\Sigma_{50}$, base peak	25.5	29.9	26.7	29.8	26.3	50.0	35.0	38.4	28.4

in Scheme 2. A direct route invokes migration of the ligand aryl group to cobalt, followed by loss of (L − R), as discussed above for **1***a* and **2***a*. The second route, established for **4***a* by linked scanning, proceeds by elimination of the EE^0 species CF_2, HF, and C_3O_2 in the fragmentation sequence: $[Co^{II}L]^+ \rightarrow [Co^{II}F(L - R')]^+ \rightarrow [[Co^{II}(L - CF_2 - HF)]^+ \rightarrow [Co^{II}R]^+$. (Deuterated Fe(III) analogues of **3***a* and **4***a* were used to establish the origin of hydrogen in HF as the central CH position of the ligand (31). After loss of HF the aryl group migrates to the positive cobalt centre, accompanied by expulsion of the neutral fragment C_3O_2.

Complex **4***a* (R = 2-thienyl) gives a low abundance ion of m/z 363, of a type observed only for this compound; linked scanning confirms that its parent is $[Co^{III}L_2]^+$. Two assignments, i.e., $[Co^{II}L_2 - 2R']^+$ or $[Co^{III}RL]^+$, appear possible. Successive losses of two R′· radicals seem unlikely, because the second loss involves the energetically unfavorable elimination of an $OE^{\cdot}$ species ($CF_3^{\cdot}$) from the EE^+ species ($[Co^{II}L(L - R')]^+$). In contrast, the decomposition $[Co^{III}L_2]^+ \rightarrow [Co^{III}RL]^+$, by elimination of (L − R), has a parallel in the reaction $[Co^{II}L]^+ \rightarrow [Co^{II}R]^+$, discussed in the previous paragraph. The very low abundance of $[Co^{III}RL]^+$ in the spectrum of **4***a* is probably a reflection of the greater ease of reduction of cobalt(III) relative to cobalt(II), which opens up alternative decomposition channels for cobalt(III) species. The assignment as $[Co^{III}RL]^+$ is supported by the following measurement. The mass difference, 2.4 mmu, between the alternative assignments requires an instrumental resolution, $M/\Delta M$, of ~150 000 to separate them, about 5–10 times greater than the specified resolution of our mass spectrometer. By software peak matching, at a nominal resolution of 6,300, the mass of the ion was determined as 362.9167 u compared to calculated masses of 362.9172 u for $[Co^{III}RL]^+$ and 362.9196 u for $[Co^{II}L_2 - 2R']^+$. This result, coupled with no detectable broadening of the ion peak, suggests that the contribution of $[Co^{II}L_2 - 2R']^+$ to the signal is minimal, at best.

Pentafluoroethyl- and n-*heptafluoropropyl-substituted ligands (R′ = C_2F_5 and* n-C_3F_7)

Whereas the abundances of $[Co^{III}L_3]^{+\cdot}$ have been very small or not observable for all complexes discussed so far, these ions are all detectable in the spectra of complexes **6***a*, **7***a*, **9***a*, and **10***a* (Table 2). (Despite this, the NH_3 CI mass spectrum of **6***a* is also consistent with extensive thermal decomposition to CoL_2.) Thus, increasing fluorine content increases the abundance of $[Co^{III}L_3]^{+\cdot}$ but, interestingly, the

Can. J. Chem. Downloaded from www.nrcresearchpress.com by 92.62.229.171 on 09/08/12
For personal use only.

Can. J. Chem. Downloaded from www.nrcresearchpress.com by 92.62.229.171 on 09/08/12
For personal use only.

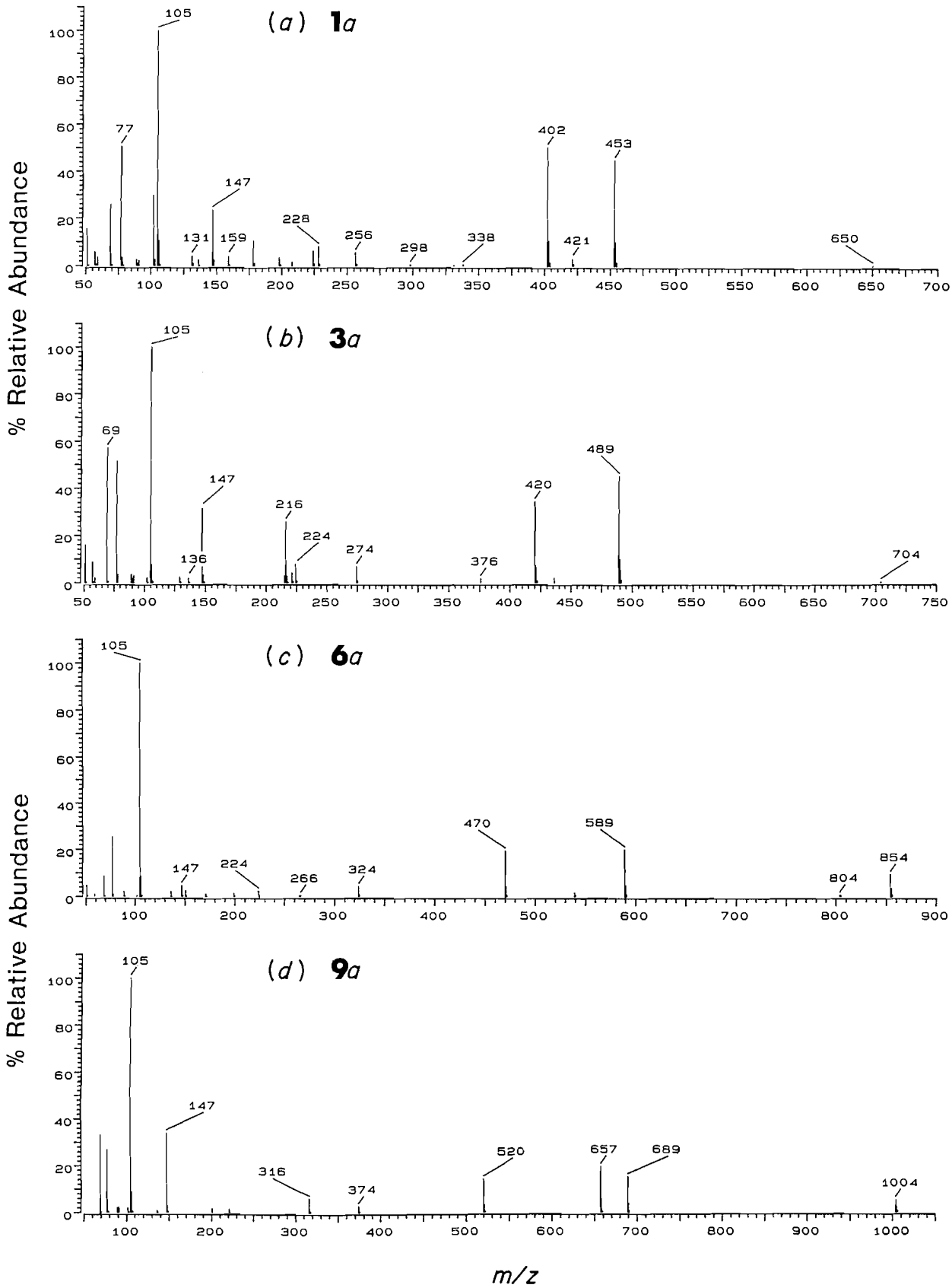

FIG. 1. Low-resolution EI mass spectra of (*a*) tris(1,1-difluoro-4-phenyl-2,4-butanedionato)cobalt(III), **1***a*; (*b*) tris(1,1,1-trifluoro-4-phenyl-2,4-butanedionato)cobalt(III), **3***a*; (*c*) tris(1,1,1,2,2-pentafluoro-5-phenyl-3,5-pentanedionato)cobalt(III), **6***a*; and (*d*) tris(1,1,1,2,2,3,3-heptafluoro-6-phenyl-4,6-hexanedionato)cobalt(III), **9***a*.

TABLE 3. Collisionally activated ion decompositions

(*a*) Product ion spectra

Parent ion (*m*/*z*)		Product ions (*m*/*z*)
4*a*	501	432,418,388,363,294,280,252,230,210,201,189,173,155,142,111
	432	388,362,353,294,280,261,252,230,211,210,186,183,174,155,142,135,111,103
	280	252,230,186,155,142,116,111,103,69
	230	210,186,161,155,154,128,122,112,111,103,83,78,69,59
7*b*	633	514,346,287,255,249
	514	486,346
	486	363,346
	346	255,249

(*b*) Constant neutral loss spectra

Neutral lost		Parent ion (*m*/*z*)
4*a*	44 u	432,230,210,160,155,141,127,113,109,107,103,97,83
7*b*	32 u	287

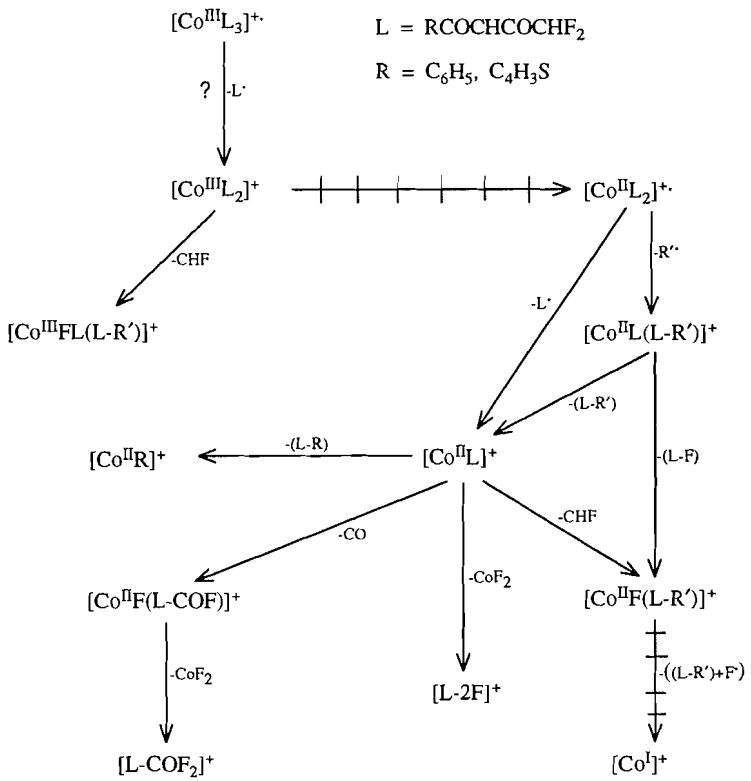

SCHEME 1. Fragmentation pathways proposed for β-diketonates **1***a* and **2***a* (R′ = CHF_2).

abundance is smaller when R′ = C_3F_7 than when R′ = C_2F_5. Also, the abundance of $[Co^{III}L_3]^{+\cdot}$ is greater when R = phenyl than when R = 2-thienyl. The net effect of the various substituents is probably not simple. Up to a point, increasing fluorine content decreases polar interactions between molecules of the complexes (depending upon how they are packed in the solid), and increases the volatility. Beyond this point, increasing molecular mass and dispersion forces decrease the volatility. If the rate of thermal decomposition of CoL_3 is comparable to the sublimation rate at the temperature of the probe, then the observed spectrum could be sensitive to the probe temperature required for volatilization of the complexes. Perhaps these competing effects are optimized when R′ = C_2F_5. As noted above, these observations

Can. J. Chem. Downloaded from www.nrcresearchpress.com by 92.62.229.171 on 09/08/12
For personal use only.

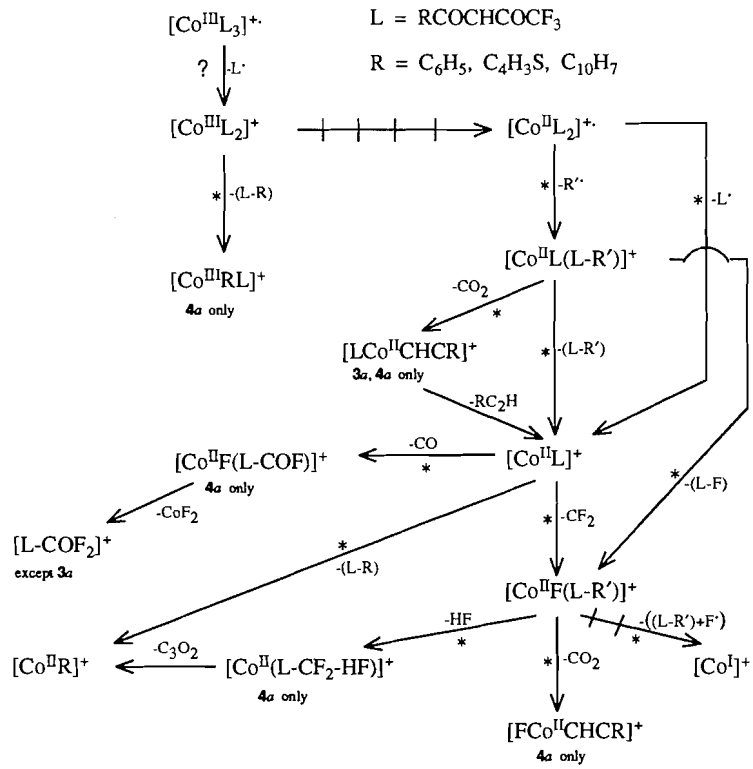

* process confirmed by collisional-activation/linked-scanning for **4***a*

⟶ reaction step for which reduction of cobalt is proposed

SCHEME 2. Fragmentation pathways proposed for β-diketonates **3***a*, **4***a*, and **5***a* (R′ = CF_3).

may also be influenced by the stability of $[Co^{III}L_3]^{+\bullet}$, if it is formed.

The ions $[Co^{III}L_2]^+$, $[Co^{III}L(L - 32)]^+$ (except for **6***a*), $[Co^{II}L(L - R')]^+$, and $[Co^{II}L]^+$ are prominent metal-containing ions. Since loss of the 32 dalton neutral fragment is not confined to sulfur-containing complexes its composition is probably :CHF, rather than S, in all cases.

Almost all of the fragmentation routes proposed in Scheme 3 are similar to those discussed above. Though still observed, ions formed by fluorine transfer to cobalt have declined in both number and significance, but the elimination of C_2F_4 (or 2 :CF_2 by analogy with the spectra of **7***b* and **8***b*, see below), observed only when R′ = C_2F_5 (**6***a* and **7***a*) in the decomposition $[Co^{II}L]^+ \rightarrow [Co^{II}F(L - R')]^+$, is a new reaction here.

Co(III) Monothio-β-diketonates

Mass spectra of the six monothio-β-diketonates **6***b*, **7***b*, **8***b* (R′ = C_2F_5), **9***b*, **10***b*, and **11***b* (R′ = *n*-C_3F_7) are given in Table 4, and representative spectra are shown in Figure 2. To aid in elucidation of fragmentation pathways, the results of collisionally assisted decompositions of selected ions obtained from **7***b* are listed in Table 3.

The low abundance of $[Co^{III}L_3]^{+\bullet}$ ions in the mass spectra of analogues of these complexes having a CF_3 substituent and various aryl substituents was attributed to thermal degradation to reduced complexes, $Co^{II}L_2$ (27, 35). However, we detected low abundances of $[Co^{III}L_3]^{+\bullet}$ and $[Co^{III}L_2(L - F)]^+$ for several of these more highly fluorinated complexes indicating, as above, that increasing fluorine content increases the yield of $[Co^{III}L_3]^{+\bullet}$.

Decomposition pathways observed for these complexes are shown in Scheme 4. Reduction of the metal in $[Co^{III}L_2]^+$ results in the $OE^{+\bullet}$ species $[Co^{II}L_2]^{+\bullet}$, which in turn can lose either F·, to yield $[Co^{II}L(L - F)]^+$, or R′· to give $[Co^{II}L(L - R')]^+$. (These processes are confirmed by linked scanning.) The EE^0 species CO and $R(C_2S)H$ are eliminated from $[Co^{II}L(L - R')]^+$ in the fragmentation sequence $[Co^{II}L(L - R')]^+ \rightarrow [Co^{II}L(L - R'CO)]^+ \rightarrow [Co^{II}L]^+$. Alternative decomposition routes originating from $[Co^{II}L(L - R')]^+$ and leading to $[Co^{II}L]^+$ proceed either by the stepwise elimination of the EE^0 species COS and RC_2H, or by direct loss of (L − R′). From a mechanistic viewpoint, the loss of COS corresponds to the loss of CO_2 in the mass spectra of Co(III) β-diketonates, as discussed above. Loss of the OE· species R′CO· from $[Co^{I}L]^{+\bullet}$ (assuming a further reduction of cobalt) results in the EE^+ species $[Co^{I}SC(R)CH]^+$, which can then eliminate sulfur to give $[Co^{I}CHCR]^+$.

The only ion resulting from fluorine-to-metal transfer that is common to all complexes of this group is $[Co^{III}FL(L - CF_3)]^+$ formed by elimination of :CF_2 from $[Co^{III}L_2]^+$. In addition, for **7***b* and **8***b*, this ion decomposes further by loss of :CF_2 to yield $[Co^{III}FL(L - C_2F_5)]^+$. (This result does not exclude a competing elimination of C_2F_4 from $[Co^{III}L_2]^+$.) We note that fluorine transfer to cobalt(III) is involved in this reaction. In contrast, transfer of fluorine to cobalt(II) is not observed.

All observed spectra of the monothio-β-diketonates ex-

Can. J. Chem. Downloaded from www.nrcresearchpress.com by 92.62.229.171 on 09/08/12
For personal use only.

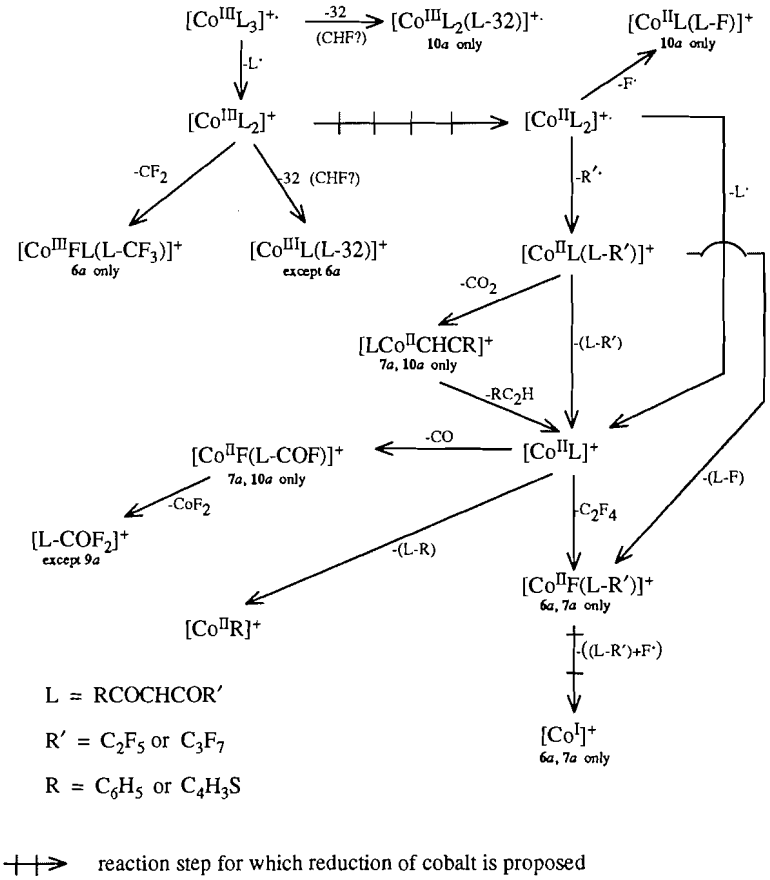

SCHEME 3. Fragmentation pathways proposed for β-diketonates **6***a*, **7***a* (R′ = C_2F_5), **9***a*, and **10***a* (R′ = C_3F_7). Pathways are common to all complexes, except where noted.

hibit metal-free ions that have no analogues in the spectra of the β-diketonates. We attribute their formation to the respective losses of CoS and S in the sequence: $[Co^{II}L(L - R'CO)]^+ \rightarrow [2L - S - R'CO]^+ \rightarrow [2L - 2S - R'CO]^+$. We could confirm only the second step by linked scanning, but the corresponding loss of MetS has been documented previously in the mass spectra of trifluoromethyl-substituted monothio-β-diketonates of Ni(II), Pd(II), Pt(II), Fe(III), Ru(III), Co(III), and Rh(III) (27, 36).

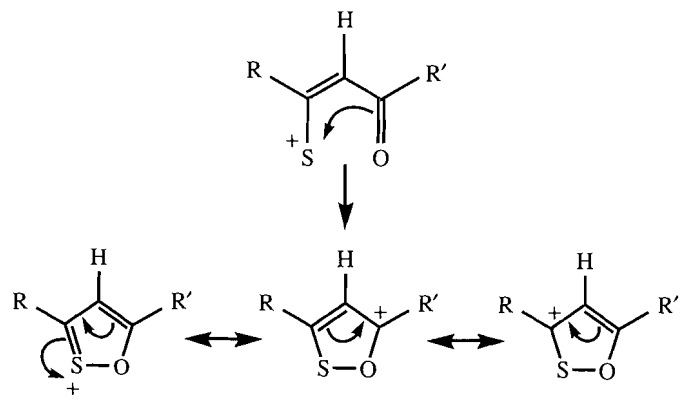

The high abundance of $[L]^+$ observed here also occurs generally for monothio-β-diketonates (27, 36)[4] suggesting that it has a very stable structure, perhaps the resonance-stabilized cyclic structure shown in the diagram.

Influence of ligands and metal on the mass spectra

Effect of fluorine content on ions formed by fluorine-to-metal transfer

Ions attributable to formation by fluorine-to-metal transfer reactions decline in both number and significance in the sequence $CF_3 > CHF_2 > C_2F_5 > n\text{-}C_3F_7$. This is best illustrated by the mass spectra of the β-diketonates, for which the Σ%TIC carried by these ions (i.e., the sum of the %TIC values for $[Co^{II}F(L - COF)]^+$, $[Co^{II}FL(L - R')]^+$, $[Co^{II}F(L - R')]^+$, $[FCo^{II}CHCR]^+$, $[L - 2F]^+$, and $[L - COF_2]^+$, where %TIC is the current for an ion expressed as a percentage of the total metal-containing ion current) when R = phenyl and 2-thienyl (the common aryl groups) has a striking dependence on the R′ group. (The respective Σ%TIC values for CF_3 : CHF_2 : C_2F_5 : C_3F_7 substituents are 6.4 : 6.3 : 2.4 : 0 and 6.3 : 4.3 : 2.9 : 1.2 for R = C_6H_5 and C_4H_3S substituents.) Probably there are several energetic and kinetic factors influencing the extent of the fluorine transfer reactions, including (*a*) hardness of the metal centre, (*b*) relative hardness of each carbon atom of the fluoroalkyl group, (*c*) relative stabilities of the products, and (*d*) conformational/steric factors. If we argue, for simplicity, that the inductive effect of CF_3 is similar to that of F then we predict the hardening effect of the fluoroalkyl groups on cobalt to be $CHF_2 < CF_3 \cong C_2F_5 \cong n\text{-}C_3F_7$, and the relative hardness of their carbon atoms to be $\alpha(CHF_2) < \alpha(CF_3, C_2F_5,$

[4]M. L. J. Reimer, J. B. Westmore, and M. Das. Unpublished results.

Can. J. Chem. Downloaded from www.nrcresearchpress.com by 92.62.229.171 on 09/08/12
For personal use only.

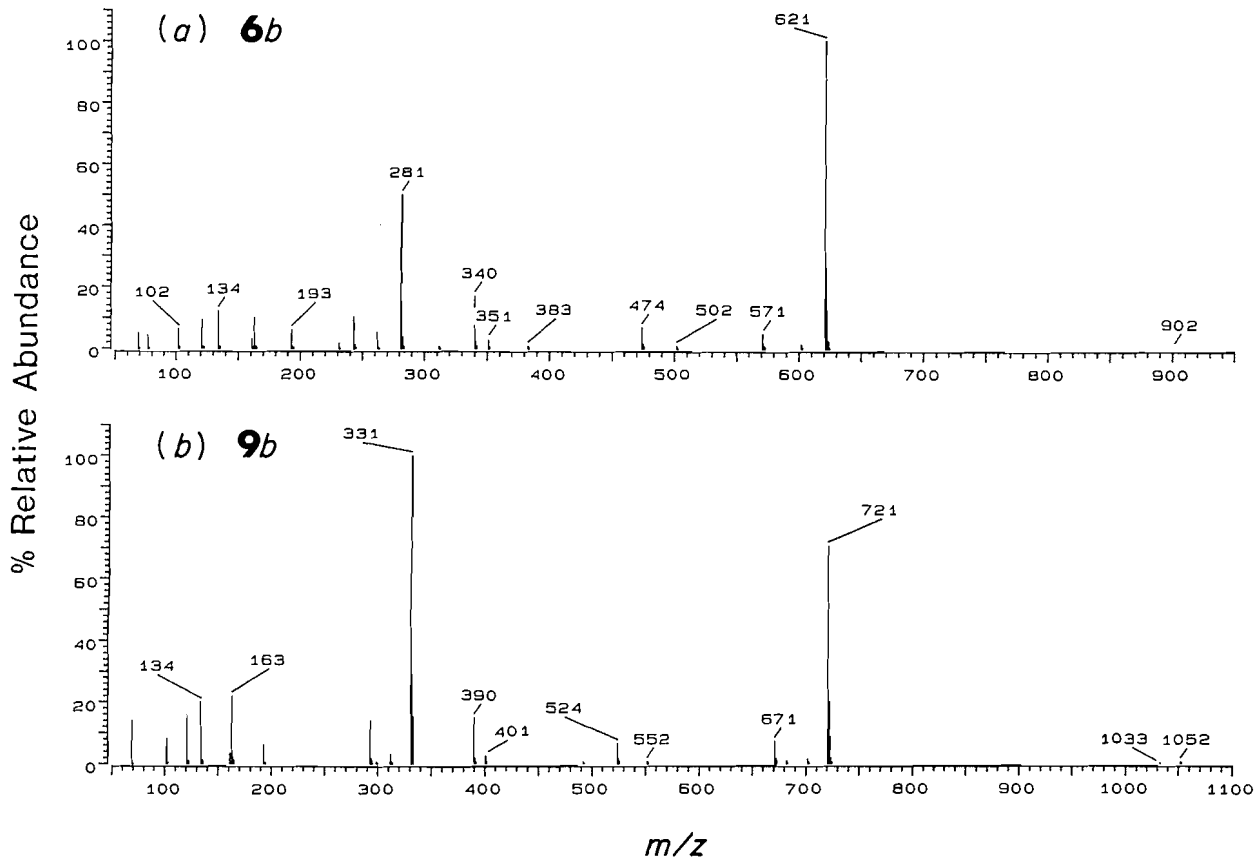

FIG. 2. Low-resolution EI mass spectra of (*a*) tris(1,1,1,2,2-pentafluoro-5-mercapto-5-phenyl-pent-4-en-3-onato)cobalt(III), **6***b*; and (*b*) tris(1,1,1,2,2,3,3-heptafluoro-6-mercapto-6-phenyl-hex-5-en-4-onato)cobalt(III), **9***b*.

n-C_3F_7) < β(C_2F_5, n-C_3F_7) ≅ γ(n-C_3F_7). A variety of neutral species can be lost. For example, considering fluorocarbon and hydrofluorocarbon species only, the possibilities are the following: from CHF_2, loss of :CHF; from CF_3, loss of :CF_2; from CF_2CF_3, loss of α-F gives :$CFCF_3$, loss of β-F gives CF_2:CF_2 or two :CF_2; from $CF_2CF_2CF_3$, loss of α-F gives :$CFCF_2CF_3$, loss of β-F gives CF_2:$CFCF_3$ or CF_2 + :$CFCF_3$, loss of γ-F gives :CF_2 + CF_2:CF_2 or three :CF_2. From factors (*a*)–(*c*) we predict the relative ease of fluorine transfer to cobalt from carbon to be: (*a*) n-C_3F_7 ≅ C_2F_5 ≅ CF_3 > CHF_2, (*b*) CHF_2 > CF_3 ≅ C_2F_5 ≅ n-C_3F_7 (in the competition for fluorine between carbon and cobalt, transfer from the softest carbon should be easiest), (*c*) CF_3 > (CHF_2, C_2F_5, n-C_3F_7) (because :CF_2 has a strongly resonance stabilized structure (23)). To assess factor (*d*) we note that transfer of α, β, or γ fluorines involve five-, six-, or seven-membered cyclic transition states, respectively, with the probability of fluorine being in the correct place for transfer decreasing with increasing ring size. The results suggest that factors (*c*) and (*d*) are the most important, but it is clear that the observance (or absence) of metal–fluorine bonded fragments in the mass spectra of these compounds is highly susceptible to the electronic environment associated with each chelate structure.

Effect of the aryl group on ions formed by fluorine-to-metal transfer

The influence of the aryl (R) substituents can be tentatively assessed from the abundances of ions arising from fluorine-to-metal transfer. (The total abundance of these ions is small owing to the low tendency for fluorine migration, an observation consistent with HSAB theory, which predicts a minimal attraction between a borderline-hard acid, such as Co(II), and a hard base, such as F.) Nevertheless, in the mass spectra of the CF_3-substituted β-diketonates, the ion current carried by $[Co^{II}F(L - R')]^+$ (the only fluorine-transfer ion common to all three complexes studied) is greater for **4***a* (R = 2-thienyl) than for **3***a* (R = phenyl) or **5***a* (R = 2-naphthyl). The respective %TIC values are 4.8 (R = 2-thienyl) > 2.1 (R = phenyl) ≈ 2.3 (R = 2-naphthyl), which we have taken as an approximate ordering of ease of fluorine transfer to cobalt. This is consistent with the greater variety of ions formed by fluorine-to-cobalt transfer (i.e., $[Co^{II}F(L - COF)]^+$, $[Co^{II}F(L - R')]^+$, and $[FCo^{II}CHCR]^+$) in the spectrum of **4***a*, compared to only $[Co^{II}F(L - R')]^+$ in those of **3***a* and **5***a*. The 2-thienyl substituent is known to be more electron releasing than is phenyl because thiophene reacts approximately three orders of magnitude faster than does benzene with electrophilic reagents (37). However, it can release electron density not only to cobalt but also efficiently to the CF_3 substituent in the same ligand through the conjugated system. These results suggest that the latter release is more effective.

Effect of cobalt oxidation state on ions formed by fluorine-to-metal transfer

An examination of metal–fluorine bond formation in the mass spectra of the monothio-β-diketonates reveals an interesting dichotomy. While fluorine transfer in the reaction $[Co^{III}L_2]^+ \rightarrow [Co^{III}FL(L - CF_3)]^+$ can be rationalized on the

Can. J. Chem. Downloaded from www.nrcresearchpress.com by 92.62.229.171 on 09/08/12
For personal use only.

TABLE 4. EI mass spectra, m/z (%RA), of monothio-β-diketonates of cobalt(III)

Ion R,R′ →	**6***b* C_6H_5,C_2F_5	**7***b* C_4H_3S,C_2F_5	**8***b* $C_{10}H_7,C_2F_5$	**9***b* C_6H_5,C_3F_7	**10***b* C_4H_3S,C_3F_7	**11***b* $C_{10}H_7,C_3F_7$
$[CoL_3]^+$	902 (0.6)	920 (—)	1052 (—)	1052 (0.5)	1070 (0.4)	1202 (—)
$[CoL_2(L - F)]^+$				1033 (0.1)	1051 (0.1)	
$[CoL_2]^+$	621 (100)	633 (63)	721 (100)	721 (71)	733 (44)	821 (100)
$[CoL(L - F)]^+$	602 (1.3)	614 (1.5)	702 (2.0)	702 (1.4)	714 (1.1)	802 (1.7)
$[CoFL(L - CF_3)]^+$	571 (4.9)	583 (13.0)	671 (16)	671 (7.3)	683 (0.8)	771 (5.1)
$[CoFL(L - R')]^+$	521 (—)	533 (1.0)	621 (2.8)			
$[CoL(L - R')]^+$	502 (0.9)	514 (1.6)	602 (1.2)	552 (0.7)	564 (1.1)	652 (1.2)
$[CoL(L - R'CO)]^+$	474 (6.8)	486 (2.5)	574 (3.5)	524 (6.5)	536 (1.5)	624 (4.6)
$[LCoCHCR]^+$				492 (0.5)	504 (0.5)	592 (1.3)
$[CoL]^+$	340 (17.0)	346 (29)	390 (12.0)	390 (15)	396 (17)	440 (8.8)
$[CoSC(R)CH]^+$	193 (5.9)	199 (8.1)	243 (12.0)	193 (6.2)	199 (2.9)	243 (9.8)
$[CoCHCR]^+$	161 (3.1)	167 (5.8)	211 (5.0)	161 (3.5)	167 (3.3)	211 (2.9)
Co-free ions:						
$[2L - S - R'CO]^+$	383 (0.9)	395 (1.6)	483 (3.1)			
$[2L - 2S - R'CO]^+$	351 (2.8)	363 (6.8)	451 (2.3)	401 (2.6)	413 (3.6)	501 (2.6)
$[HL]^+$	282 (8.5)	288 (13.0)	332 (23)	332 (15)	338 (5.2)	382 (13.0)
$[L]^+$	281 (50)	287 (100)	331 (78)	331 (100)	337 (100)	381 (33)
$[L - F]^+$	262 (5.3)	268 (5.0)	312 (7.0)	312 (3.2)	318 (1.7)	362 (3.8)
$[L - S]^+$	249 (—)	255 (88)	299 (4.7)	299 (0.5)	305 (37)	349 (3.3)
$[L - 2F]^+$	243 (10.3)	249 (20)	293 (15.0)	293 (14.0)	299 (15)	343 (15)
$[L - CF_2]^+$	231 (1.9)	237 (11.0)	281 (—)			
$[HL - R']^+$	163 (9.9)	169 (15)	213 (25)	163 (22)	169 (7.1)	213 (12.0)
$[R(C_2S)H]^+$	134 (12.0)	140 (18)	184 (29)	134 (20)	140 (12.0)	184 (20)
$[RCS]^+$	121 (9.4)	127 (18)	171 (19)	121 (16)	127 (9.6)	171 (15)
$[RCCH]^+$	102 (6.3)	108 (17)	152 (46)	102 (8.1)	108 (9.0)	152 (26)
$[R]^+$	77 (4.3)	83 (34)	127 (18)			
$[CF_3]^+$	69 (5.0)	69 (12.0)	69 (31)	69 (14.0)	69 (6.2)	69 (7.5)
$\%\Sigma_{50}$, base peak	37.3	20.5	21.9	30.4	35.7	34.8

basis of the hard-acid character of Co(III), the process is otherwise suppressed. HSAB theory rationalizes this behavior: (*i*) after metal reduction, fluorine transfer to the borderline-hard acid Co(II) center is less favored, (*ii*) the replacement of metal-bonded oxygen by sulfur in the chelate ring results in further softening of the cobalt center and a further lowered probability for fluorine migration.

Effect of donor heteroatom

The replacement of oxygen by sulfur in the chelate ring has a marked effect. For example, ions retaining Co—S bonds are observed more frequently than are ions retaining Co—O bonds in the mass spectra of the respective complexes. Typically, $[Co^{II}Aryl]^+$ ions are present in the spectra of β-diketonates and are absent in the spectra of monothio-β-diketonates; this reflects the stronger Co—S interaction since the mechanism proposed for the formation of $[Co^{II}R]^+$ involves breaking of metal–donor bonds.

Summary

Cobalt(III) chelates generally fragment by elimination of two OE$^\bullet$ radicals from $[CoL_3]^{+\bullet}$. Reduction of cobalt upon loss of the second radical species is presumed. Subsequent decomposition occurs through loss of either an EE^0 neutral without reduction of cobalt(II) (preferred) or loss of a third OE$^\bullet$ radical, indicating a further reduction to cobalt(I). In contrast, molecular ions of complexes of these ligands with metals that are resistant to change in oxidation state (e.g., Al(III), Ga(III), Pd(II), and Zn(II)) fragment by elimination of an OE$^\bullet$ species, followed by losses of one or more EE^0 species (37).

The HSAB principle provides a rationale for variations in abundance and variety of ions arising from fluorine-to-metal migration, based on the prediction that a hard base such as fluorine should bind preferentially with a hard acid. Cobalt is difficult to categorize; although Co(III) is a hard acid and as such should bind with fluorine, it is so readily reduced to the softer Co(II) state that relatively few ions involving F—Co(III) bonding are observed. Other results[4] have shown that fluorine migration is widespread in generation of fragment ions from Al(III) and Ga(III) β-diketonates (both metal ions are classified as hard acids), but is suppressed in generation of ions from chelates of Pd(II), a soft acid.

Fluorine transfer is much less significant in the fragmentation of ions from monothio-β-diketonates. The presence of the sulfur donor presumably softens the metal, thereby making the migration of fluorine a less-favored process.

Resonance stabilization by proximate aryl groups is also crucial to the formation of $[LCo^{II}CHCR]^+$ and $[FCo^{II}CHCR]^+$ ions for several of the Co(III) β-diketonates; the lone pair resonance provided by the heterocyclic 2-thienyl group appears to be particularly important.

Acknowledgements

We thank Mr. Wayne Buchannon for assistance in the operation and maintenance of the mass spectrometer, Dr. Gary Stern for his review of the manuscript, and the Natural Sciences and Engineering Research Council of Canada

Can. J. Chem. Downloaded from www.nrcresearchpress.com by 92.62.229.171 on 09/08/12
For personal use only.

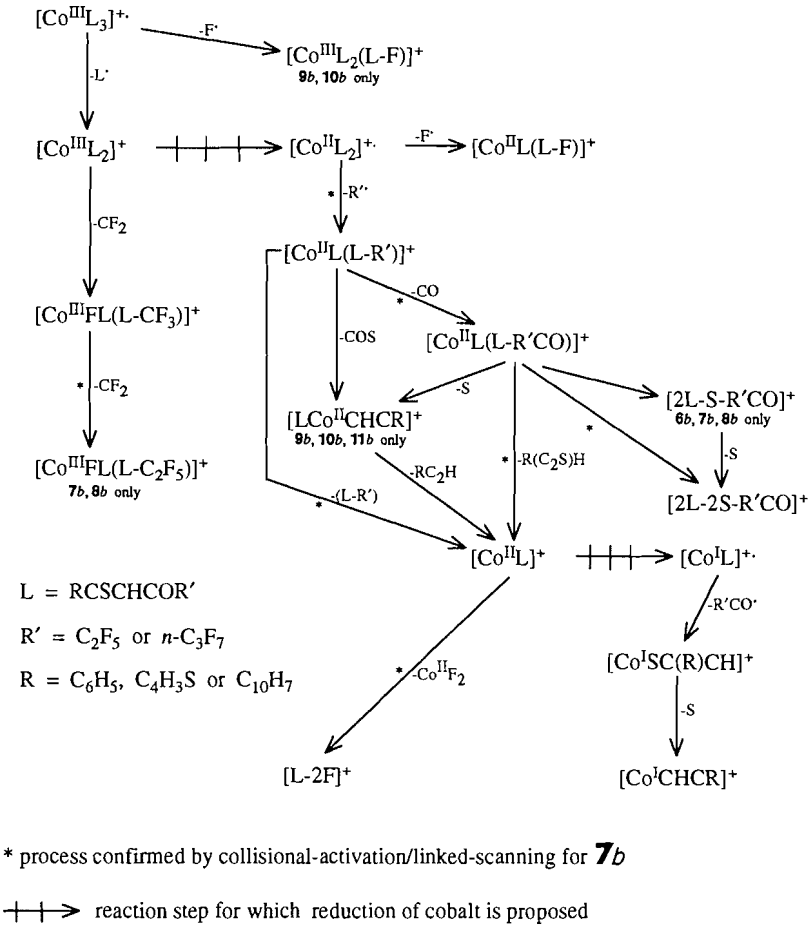

SCHEME 4. Fragmentation pathways proposed for monothio-β-diketonates **6***b*, **7***b*, **8***b* (R′ = C_2F_5), **9***b*, **10***b*, and **11***b* (R′ = C_3F_7). Pathways are common to all complexes, except where noted.

Can. J. Chem. Downloaded from www.nrcresearchpress.com by 92.62.229.171 on 09/08/12
For personal use only.

(NSERC) for financial support. We also thank NSERC and the University of Manitoba for grants to purchase the mass spectrometer.

1. R. W. Moshier and R. E. Sievers. Gas chromatogoraphy of metal chelates. Pergamon Press, Oxford. 1965.
2. J. Zhao, K. H. Dahmen, H. O. Marcy, L. M. Tonge, T. J. Marks, B. W. Wessels, and C. R. Kannewurf. Appl. Phys. Lett. **53**, 1750 (1988).
3. D. S. Richeson, L. M. Tonge, J. Zhao, J. Zhang, H. O. Marcy, T. J. Marks, B. W. Wessels, and C. R. Kannewurf. Appl. Phys. Lett. **54**, 2154 (1989).
4. A. J. Panson, R. G. Charles, D. N. Schmidt, J. R. Szedon, G. J. Machiko, and A. I. Braginski. Appl. Phys. Lett. **53**, 1756 (1988).
5. A. R. Barron. *In* The Strem Chemiker. Vol XIII. No. 1. Strem Chemicals, Inc., Newburyport, Mass. 1990. p. 1.
6. S. B. Turnipseed, R. M. Barkley, and R. E. Sievers. Inorg. Chem. **30**, 1164 (1991).
7. C. G. Macdonald and J. S. Shannon. Aust. J. Chem. **19**, 1 (1966).
8. R. C. Mehrotra, R. Bohra, and D. P. Gaur. Metal β-diketonates and allied derivatives. Academic Press, London. 1978.
9. K. C. Joshi and V. N. Pathak. Coord. Chem. Rev. **22**, 37 (1977).
10. J. B. Westmore. *In* Mass spectrometry of metal compounds. *Edited by* J. Charalambous. Butterworths, London. 1975. Chap. 9.
11. I. K. Gregor and M. Guilhaus. Mass Spectrom. Rev. **3**, 39 (1984).
12. F. W. McLafferty. Interpretation of mass spectra. 3rd ed. University Science Books, Mill Valley, Calif. 1980.
13. K. Karni and A. Mandelbaum. Org. Mass Spectrom. **15**, 53 (1980).
14. J. S. Shannon and J. M. Swan. Chem. Commun. 33 (1965).
15. M. J. Lacey and J. S. Shannon. Org. Mass Spectrom. **6**, 931 (1972).
16. J. M. Miller and G. L. Wilson. Adv. Inorg. Chem. Radiochem. **18**, 229 (1976).
17. S. Ahrland, J. Chatt, and N. R. Davies. Q. Rev. (London), **12**, 265 (1958).
18. R. G. Pearson. J. Am. Chem. Soc. **85**, 3533 (1963).
19. R. G. Pearson. Science, **151**, 172 (1966).
20. R. G. Pearson. Chem. Br. **3**, 103 (1967).
21. R. G. Pearson. J. Chem. Educ. **45**, 581 (1968).
22. M. L. Morris and R. D. Koob. Inorg. Chem. **20**, 2737 (1981).
23. M. Das. Trans. Met. Chem. **5**, 17 (1980).
24. M. Das and S. E. Livingstone. Org. Mass Spectrom. **9**, 781 (1974).
25. R. K. Y. Ho and S. E. Livingstone. Aust. J. Chem. **21**, 1781 (1968).
26. M. Das. Inorg. Chim. Acta, **36**, 79 (1979).
27. S. E. Livingstone and D. S. Moore. Aust. J. Chem. **29**, 283 (1976).
28. M. Das. Inorg. Chim. Acta, **48**, 33 (1981).
29. R. C. Fay and T. S. Piper. J. Am. Chem. Soc. **85**, 500 (1963).

30. H. F. Bauer and W. C. Drinkard. J. Am. Chem. Soc. **82**, 5031 (1960).
31. A. L. Clobes, M. L. Morris, and R. D. Koob. Org. Mass Spectrom. **5**, 633 (1971).
32. F. A. Cotton and G. Wilkinson. Advanced inorganic chemistry. 5th ed. Wiley, New York. 1988. p. 724.
33. M. J. Lacey, C. G. Macdonald, and J. S. Shannon. Org. Mass. Spectrom. **1**, 115 (1968).
34. A. L. Clobes, M. L. Morris, and R. D. Koob. Org. Mass Spectrom. **3**, 1255 (1970).
35. M. Das and S. E. Livingstone. Aust. J. Chem. **27**, 1177 (1974).
36. S. E. Livingstone and N. Saha. Aust. J. Chem. **28**, 1249 (1975).
37. S. Gronowitz. *In* Advances in heterocyclic chemistry. Vol. 1. *Edited by* A. R. Katritzky. Academic Press, New York. 1963. pp. 2ff, and references therein.

Can. J. Chem. Downloaded from www.nrcresearchpress.com by 92.62.229.171 on 09/08/12
For personal use only.

α-Oxosulfines: reactions with alkenes and alkynes[1,2]

IAN W. J. STILL[3] AND DONNA KAYE T. WILSON[4]

J. Tuzo Wilson Research Laboratories, Erindale Campus, University of Toronto, Mississauga, Ont., Canada L5L 1C6

Received April 26, 1991

IAN W. J. STILL and DONNA KAYE T. WILSON. Can. J. Chem. **70**, 964 (1992).

Thiochroman-4-one 1,1-dioxide has been successfully converted into 3-sulfinylthiochroman-4-one 1,1-dioxide and the reactions of this α-oxosulfine with a series of alkenes have been carefully investigated. The α-oxosulfine was found to react as a Diels–Alder diene with 2-methylpropene, *Z*- and *E*-2-butene, 2-ethyl-1-butene, 1-pentene, *Z*-2-pentene, and cyclopentene and cyclohexene to produce a new group of heterocyclic compounds, the 2,3-dihydro-5*H*-1,4-oxathiino[3,2-*c*][1]benzothiopyrans, in yields ranging from 21 to 42%. In all cases, formation of the Diels–Alder adduct was accompanied by a second type of product, identified as the product of electrophilic addition (EA) of a sulfenium species to the alkene, in lesser yields, ranging from 9 to 18%. When the trapping dienophile used was 3,3-dimethyl-1-butene, only the EA adduct was obtained, in 28% yield. Formation of only the EA type of adduct was also observed in reactions of the α-oxosulfine with 2-butyne (21%) and with the thione 2,2,4,4-tetramethylpentane-3-thione (di-*tert*-butyl thioketone) (16%). Attempts to prepare the α-oxosulfines corresponding to the following ketones are also described: thiochroman-4-one 1-oxide, isothiochromanone and isothiochromanone 2,2-dioxide, tetrahydrothiophen-3-one 1,1-dioxide, 3,3,5,5-tetramethylcyclohexanone, and 2-indanone.

Key words: Diels–Alder, electrophilic addition, sulfenic acid.

IAN W. J. STILL et DONNA KAYE T. WILSON. Can. J. Chem. **70**, 964 (1992).

On a transformé avec succès le 1,1-dioxyde de thiochroman-4-one en 1,1-dioxyde de 3-sulfinylthiochroman-4-one et on a examiné avec soin les réactions de cette α-oxosulfine avec une série d'alcènes. On a trouvé que l'α-oxosulfine réagit comme un diène de Diels–Alder avec le 2-méthylpropène, les (*Z*)- et (*E*)-but-2-ènes, le 2-éthylbut-1-ène, le pent-1-ène, le (*Z*)-pent-2-ène, le cyclopentène et le cyclohexène pour conduire à la formation d'un nouvel ensemble de composés hétérocycliques, les 2,3-dihydro-5*H*-1,4-oxathiino[3,2-*c*][1]benzothiopyranes, avec des rendements allant de 21 à 42%. Dans tous les cas, la formation de l'adduit de Diels–Alder est accompagnée par un second type de produit, identifié comme le produit d'addition électrophilique (AE) d'une espèce sulfénium sur l'alcène, avec des rendements plus faibles, allant de 9 à 18%. Lorsqu'on a utilisé le 3,3-diméthylbut-1-ène comme diénophile, on n'a obtenu que du produit d'AE, avec un rendement de 28%. On n'a aussi observé que la formation du produit d'AE dans les réactions de l'α-oxosulfine avec le but-2-yne (rendement de 21%) et avec la thione 2,2,4,4-tétraméthylpentane-3-thione (di-*tert*-butyl thiocétone) (rendement 16%). On décrit aussi les essais effectués dans le but de préparer les α-oxosulfines correspondant aux cétones suivantes : 1-oxyde de la thiochroman-4-one, isothiochromanone et 2,2-dioxyde de l'isothiochromanone, 1,1-dioxyde de la tétrahydrothiophèn-3-one, 3,3,5,5-tétraméthylcyclohexanone et indan-2-one.

Mots clés : Diels–Alder, addition électrophilique, acide sulfénique.

[Traduit par la rédaction]

Introduction

In our earlier study (1) of the reactivity of α-oxosulfines we reported that the α-oxosulfines **1***a* and **2***a*, derived from cyclohexanone and thiochroman-4-one respectively, did not react as heterodienes in Diels–Alder trapping reactions with alkenes and alkynes. This represented behaviour quite in contrast to our preliminary finding (2) that the related α-oxosulfine **2***b* did act as a diene in Diels–Alder reactions, with both 2-methylpropene and norbornene. We were anxious to further investigate this apparent dichotomy and to seek to identify the electronic, steric, or other factors responsible, as well as to establish the generality of such inverse electron-demand Diels–Alder reactions as a potential synthetic route to various heterocyclic compounds.

Generally, α-oxosulfines are unstable, with a few notable exceptions reported by Zwanenburg and co-workers (3), and thus are generated *in situ*. They are conveniently prepared by reaction of the trimethylsilyl enol ether of the parent ketone with thionyl chloride, usually in the presence of a non-nucleophilic base such as 2,6-lutidine or 2,2,6,6-tetramethylpiperidine (1, 3). Interestingly, two alternative procedures for generating α-oxosulfines, using a completely different approach, have been reported very recently (4, 5). The role of the C=S bond in simple sulfines in Diels–Alder reactions is well documented (6, 7). In our present study, it was our intention initially to synthesize a series of α-oxosulfines of different structural types in order to explore their reactivity as (hetero) dienes in the Diels–Alder reaction with standard alkene or alkyne trapping agents. Later, we explored the reactivity of the model α-oxosulfine diene **2***b* towards a variety of structural types of alkene and alkyne. We now present the results of these studies.

Results and discussion

We decided to initiate this part of our study of the reactivity of α-oxosulfines with alkenes and alkynes by reexamining the reactivity of the oxosulfine system **2***b* with a wider range of trapping agents. This, we felt, would be important not only from the point of view of establishing the scope of the Diels–Alder reaction of α-oxosulfines but also in illuminating the rather puzzling dichotomy of behaviour between **2***a* and **2***b* already alluded to in the Introduction.

The starting point for **2***b* involved initial preparation of the keto-sulfone **3***c* by oxidation of **3***a* with peroxyacetic acid (8),

[1]Part II. For previous work see ref. 1.

[2]Taken in part from the Ph.D. thesis of D. K. T. Hutchinson, University of Toronto, 1990.

[3]Author to whom correspondence may be addressed.

[4]Formerly Hutchinson.

Can. J. Chem. Downloaded from www.nrcresearchpress.com by 92.62.229.171 on 09/08/12
For personal use only.

followed by conversion to the trimethylsilyl enol ether **4***c* (9), in an overall yield of 80%. As described earlier (1, 2) the silyl enol ether is converted into the α-oxosulfine **2***b* at low temperatures, via the intermediate β-oxosulfinyl chloride **5** and subsequent loss of HCl. Thionyl chloride was used for many of the sulfinylation reactions but on occasion was replaced with the milder *N*-(chlorosulfinyl)imidazole (10). The loss of HCl to produce **2***b* occurred even in the absence of added base, although addition of 2,6-lutidine was often effective.

The reaction of **2***b* with the isomeric alkenes *Z*-2-butene and *E*-2-butene will be described in detail and serves as a model for the analogous reactions of **2***b* with 2-methylpropene, 2-ethyl-1-butene, 1-pentene, *Z*-2-pentene, cyclopentene and cyclohexene, and 3,3-dimethyl-1-butene, the results of which are summarized in Table 1. The existence of **2***b* as an intermediate in the Diels–Alder trapping reactions was verified using 2,3-dimethyl-1,3-butadiene to afford the adduct **6** (2). Two alkene trapping agents that were totally without success in the trapping of **2***b* were the enol ether systems 2,5-dihydrofuran and ethyl vinyl ether.

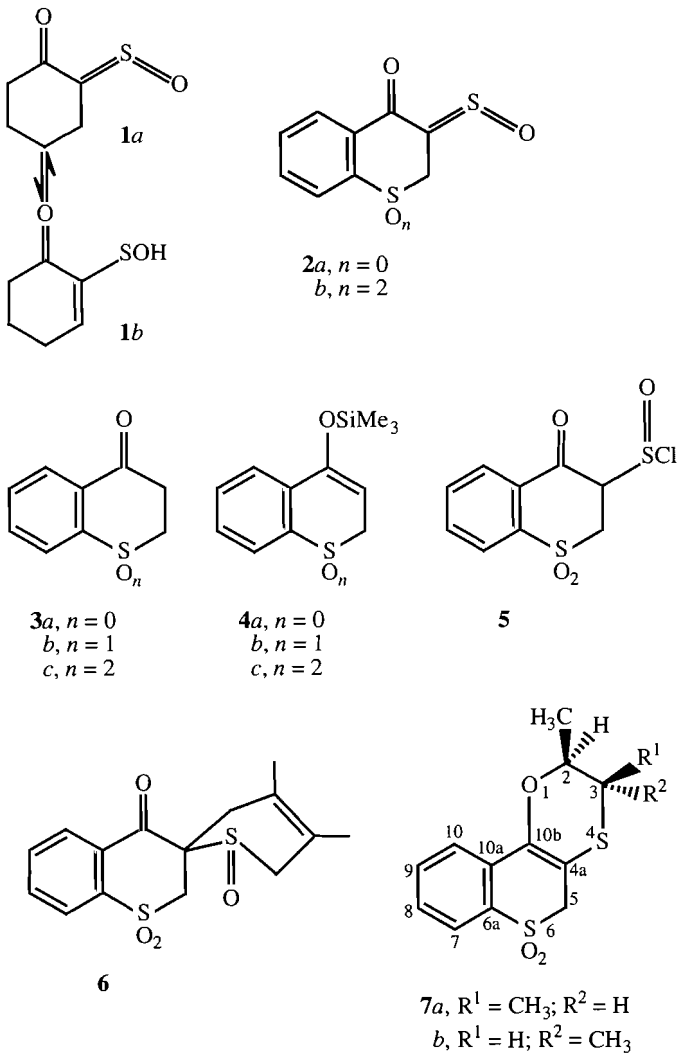

Before describing our results with **2***b* in detail, it is very important to emphasize that, as observed in our preliminary communication (2) but in contrast to the results obtained by Zwanenburg and co-workers (3), *all* of the Diels–Alder adducts (**7***a*,*b*, **10***a*–*c*, **12***a*–*d*) obtained from the reaction of

TABLE 1. Trapping reactions of **2***b* with alkenes and alkynes

Alkene/alkyne	Isolated yield of Diels–Alder adduct (%)	Isolated yield of EA adduct (%)
Z-2-Butene	(**7***a*) 30	(**8***a*) 14
E-2-Butene	(**7***b*) 26	(**8***b*) 10
Cyclopentene	(**12***a*) 42	(**13***a*) 18
Cyclohexene	(**12***b*) 24	(**13***b*) 13
Z-2-Pentene	(**12***c*,*d*) 30[a]	(**8***c*,*d*) 11[a]
1-Pentene	(**10***c*) 21	(**8***e*,*f*) 11[a]
3,3-Dimethyl-1-butene	—	(**8***g*) 28[b]
2-Methylpropene	(**10***b*) 37	(**8***i*) 9
2-Ethyl-1-butene	(**10***a*) 25	(**8***h*) 14
2-Butyne	—	(**14**) 21

[a]Obtained as a mixture of regioisomers.
[b]*anti*-Markovnikov adduct only.

2*b* as a (hetero) diene had suffered deoxygenation at the 1,4-oxathiin sulfur atom. We think that this arises from the fact that **2***b* has not proved to be isolable and therefore that all such Diels–Alder reactions were carried out as *in situ* trapping experiments. Inevitably, this means that thionyl chloride, and the by-product chlorotrimethylsilane, are present in such reaction mixtures, either agent being capable of effecting the deoxygenation of sulfoxides (11, 12). The facile deoxygenation is a consequence of the fact that the *S*-oxides of **7** and its cogeners are expected to be strongly activated towards electrophilic attack by such reagents, due to conjugative electron release from the oxathiin ring oxygen atom. Deoxygenation by $SOCl_2$ probably proceeds via electrophilic attack to produce intermediates such as **9***a*,*b*, with subsequent reduction being effected by the Cl^- counterion. It should be noted that no deoxygenation of **6** was ever observed. Compound **6** is, for both electronic and steric reasons, expected to be much less reactive towards such electrophilic deoxygenation than the 1,4-oxathiin *S*-oxides corresponding to **7***a*,*b* and their analogues.

Reaction of **2***b* with *Z*-2-butene *in situ* was conducted at −23°C in CH_2Cl_2 solution, with the reaction mixture finally being allowed to warm to 25°C. Two products were isolated after careful chromatography, along with some ketosulfone **3***c*, as was generally observed in this series. The first product (30%) was a beige solid and showed a C=C stretching vibration in the IR at 1608 and sulfone bands at 1314 and 1151 cm^{-1}. The ^1H NMR spectrum (400 MHz) showed the expected two doublets of doublets and two triplets of doublets for the aromatic ring protons. The C-5 CH_2 appeared as a very characteristic doublet of doublets at δ 3.78 and 3.86. Two quartets of doublets at δ 3.30 and 4.51 are assigned to the C-3 and C-2 methine hydrogens, respectively. Doublets were observed at δ 1.35 and 1.38 for the two methyl groups. The presence of a molecular ion at m/z = 282, the ^{13}C NMR data (see Table 2), and elemental analysis confirmed the formula $C_{13}H_{14}O_3S_2$ and led us to assign the (deoxygenated) Diels–Alder adduct structure **7***a* to this product.

The second product (14%) was also obtained as a (yellow) solid with a carbonyl stretching band in the IR at 1675 and SO_2 bands at 1295 and 1154 cm^{-1}. A molecular ion was detected at m/z = 317 and elemental analysis confirmed the composition $C_{13}H_{13}ClO_3S_2$. The most characteristic feature

Can. J. Chem. Downloaded from www.nrcresearchpress.com by 92.62.229.171 on 09/08/12
For personal use only.

Can. J. Chem. Downloaded from www.nrcresearchpress.com by 92.62.229.171 on 09/08/12
For personal use only.

in the ^{1}H NMR spectrum of this product was a singlet at δ 6.85, assigned to the lone vinylic proton in structure **8***a*. This structural assignment was further confirmed by the ^{13}C NMR data listed in Table 3. Compound **8***a* represents the electrophilic addition (EA) mode of reaction that was observed in the cyclohexanone and thiochroman-4-one series described previously (1) but which we now encountered for the first time from the α-oxosulfine **2***b*, albeit as a minor product.[5]

We were interested to discover if the Diels–Alder reaction so observed with *Z*-2-butene was stereospecific with respect to the alkene. Accordingly, a trapping experiment was carried out on **2***b*, under identical reaction conditions, using *E*-2-butene. Products analogous to **7***a* and **8***a* were again obtained. The Diels–Alder adduct **7***b* (26%) was very similar to, but clearly not identical with, **7***a*. In particular, **7***b* showed two very characteristic *quintets* in the ^{1}H NMR spectrum at δ 3.16 and 4.08 (J = 6.8, 6.4 Hz, respectively), assigned to the C-3 and C-2 protons. Clearly the much smaller (C-2)H/(C-3)H vicinal coupling constant of 2 Hz found in **7***a* is in accord with the *cis* adduct, with **7***b* as the *trans* isomer.[6] Only a single diastereomer was detected in each case and hence the Diels–Alder addition does show the expected stereospecificity. A second product (10%) obtained from the trapping experiment with *E*-2-butene was shown to have a structure consistent with the EA adduct **8***b*. Once again, this was a single diastereomer and thus, as predicted by the mechanism proposed earlier (1), the electrophilic addition must also proceed by a stereospecific pathway. ^{13}C NMR data for both adducts are listed in Tables 2 and 3.

In using 2-ethyl-1-butene (1,1-diethylethylene) as a dienophile we wished to investigate the regiochemical aspect of the above reactions. While the regiochemistry predicted for the Diels–Alder reaction can be predicted from bond polarities in the ground and transition states and would presumably follow the pattern already observed for 2-methylpropene (2), the situation may not be so clear-cut in the electrophilic addition pathway, where an intermediate (thiiranium ion) species **11** is presumed to be formed (1). Two adducts were again obtained. The Diels–Alder adduct (25%) was assigned structure **10***a* on the basis of IR, ^{1}H NMR, ^{13}C NMR, mass spectral, and elemental analysis and confirmed unambiguously by a single-crystal X-ray structure determination.[7] The minor product (14%), again a single isomer, had spectral properties consistent with the EA product **8***h*. The determination in favour of **8***h*, rather than its regioisomer, is based on the analysis of the ^{1}H and ^{13}C NMR spectra and comparative data from model compounds such as *tert*-butyl chloride and *tert*-butyl mercaptan and from similar adducts in the series derived from α-oxosulfine **2***a* (1). This result suggests that in the (presumed) intermediate thiiranium ion **11** there is a considerable degree of "open" or carbocation-like character, leading normally to nucleophilic trapping by Cl^- at the (more hindered) tertiary site and hence to the Markovnikov regioisomer actually observed. When we reexamined the reaction of **2***b* with 2-methylpropene as trapping agent, a small amount of the minor EA adduct **8***i* (9%) could be isolated, accompanying the expected Diels–Alder addition product **10***b* (37%) (2). The spectral similarities between the EA adducts **8***h*,*i* derived from these two 1,1-disubstituted ethylenes, and in particular the ^{13}C NMR data (Tables 2, 3), are quite striking. Regiochemical results from the EA pathway were not always so clear-cut, however (see

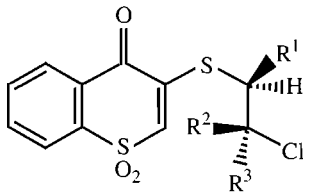

8*a*, $R^1 = R^2 = CH_3$; $R^3 = H$
b, $R^1 = R^3 = CH_3$; $R^2 = H$
c, $R^1 = CH_3$; $R^2 = C_2H_5$; $R^3 = H$
d, $R^1 = C_2H_5$; $R^2 = CH_3$; $R^3 = H$
e, $R^1 = R^3 = H$; $R^2 = n\text{-}C_3H_7$
f, $R^1 = n\text{-}C_3H_7$; $R^2 = R^3 = H$
g, $R^1 = t\text{-}C_4H_9$; $R^2 = R^3 = H$
h, $R^1 = H$; $R^2 = R^3 = C_2H_5$
i, $R^1 = H$; $R^2 = R^3 = CH_3$

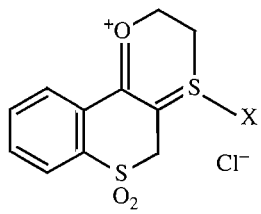

9*a*, X = OS(O)Cl
b, X = Cl

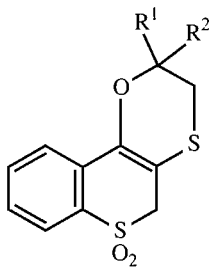

10*a*, $R^1 = R^2 = C_2H_5$
b, $R^1 = R^2 = CH_3$
c, $R^1 = n\text{-}C_3H_7$; $R^2 = H$

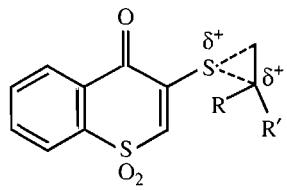

11

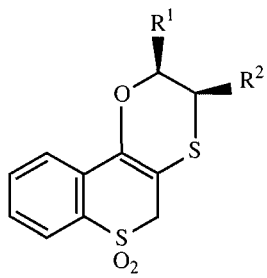

12*a*, $R^1, R^2 = -(CH_2)_3-$
b, $R^1, R^2 = -(CH_2)_4-$
c, $R^1 = CH_3$; $R^2 = C_2H_5$
d, $R^1 = C_2H_5$; $R^2 = CH_3$

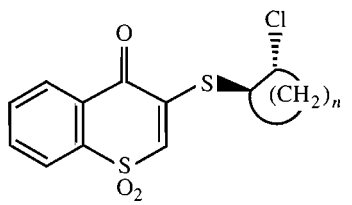

13*a*, $n = 3$
b, $n = 4$

[5]An alternative route to the electrophilic addition product via an intermediate α-chlorosulfenyl chloride cannot be ruled out, cf. ref. 13.

[6]Molecular models show that the 1,4-oxathiin ring probably adopts a boat conformation although a half-chair conformation is also possible.

[7]Crystals of **10***a* were obtained by recrystallization from ethyl acetate/hexane as pale yellow needles. All work was performed on an Enraf–Nonius CAD4 diffractometer using graphite monochromatized MoKα radiation, λ = 0.71073 Å. A crystal of dimensions 0.24 × 0.36 × 0.28 gave the following data: $C_{15}H_{18}O_3S_2$, M_r = 310.4, triclinic, space group $P\bar{1}$ with a = 9.127(2), b = 10.330 (2), c = 8.972(1) Å, α = 106.36(2), β = 112.04(1), γ = 81.11(2)°, V = 751.2 Å^3, D_x = 1.37 g cm^{-3} for Z = 2, μ = 3.4 cm^{-1}, F(000) = 328, room temperature. Full details of the crystallographic structure will be published elsewhere.

TABLE 2. ^{13}C NMR data for Diels–Alder adducts **7***a*,*b*, **10***a*,*c*, **12***a*–*d*

Compound	Type of carbon	δ, ppm
7*a*	C	99.03 (C-4a); 131.87 (C-10b); 134.54 (C-10a); 139.26 (C-6a)
	CH	38.69 (C-3); 74.07 (C-2); 123.06 (C-7/10); 123.37 (C-7/10); 128.01 (C-8); 133.24 (C-9)
	CH_2	52.89 (C-5)
	CH_3	15.39 (C-3 CH_3); 17.35 (C-2 CH_3)
7*b*	C	100.06 (C-4a); 131.78 (C-10b); 134.58 (C-10a); 139.59 (C-6a)
	CH	38.98 (C-3); 76.15 (C-2); 123.07 (C-7/10); 123.35 (C-7/10); 127.99 (C-8); 133.23 (C-9)
	CH_2	52.62 (C-5)
	CH_3	17.99 (C-3 CH_3); 18.94 (C-2 CH_3)
10*a*	C	77.32 (C-2); 98.22 (C-4a); 132.49 (C-10b); 134.84 (C-10a); 138.87 (C-6a)
	CH	123.06 (C-7/10); 123.28 (C-7/10); 127.96 (C-8); 133.27 (C-9)
	CH_2	28.28 (C-2 CH_2CH_3); 32.69 (C-3); 52.82 (C-5)
	CH_3	7.60 (C-2 CH_2CH_3)
10*c*	C	99.51 (C-4a); 131.98 (C-10b); 134.62 (C-10a); 140.42 (C-6a)
	CH	74.58 (C-2); 123.05 (C-7/10); 123.09 (C-7/10); 128.05 (C-8); 133.28 (C-9)
	CH_2	18.68 (C-2′); 30.98 (C-1′); 37.01 (C-3); 52.77 (C-5)
	CH_3	13.98 (C-3′)
12*a*	C	100.68 (C-4a); 131.85 (C-10b); 134.51 (C-10a); 139.97 (C-6a)
	CH	42.87 (C-3a); 77.8 (C-11a); 123.06 (C-7/10); 123.27 (C-7/10); 127.92 (C-8); 133.23 (C-9)
	CH_2	20.82 (C-2); 31.06 (C-1/3); 31.17 (C-1/3); 52.69 (C-5)
12*b*	C	98.59 (C-5a); 131.87 (C-11b); 134.48 (C-11a); 139.07 (C-7a)
	CH	40.98 (C-4a); 73.28 (C-12a); 123.01 (C-8/11); 123.25 (C-8/11); 127.89 (C-9); 133.21 (C-10)
	CH_2	20.03 (C-2); 25.08 (C-3); 29.59 (C-1/4); 31.39 (C-1/4); 52.74 (C-6)
12*c*	C	99.18 (C-4a); 131.98 (C-10b); 134.59 (C-10a); 139.39 (C-6a)
	CH	46.78 (C-3); 73.61 (C-2); 123.06 (C-7/10); 123.35 (C-7/10); 127.98 (C-8); 133.24 (C-9)
	CH_2	22.68 (C-3 CH_2CH_3); 52.90 (C-5)
	CH_3	11.97 (C-3 CH_2CH_3); 16.82 (C-2 CH_3)
12*d*	C	99.32 (C-4a); 131.85 (C-10b); 134.59 (C-10a); 139.39 (C-6a)
	CH	37.78 (C-3); 79.78 (C-2); 123.10 (C-7/10); 123.23 (C-7/10); 127.98 (C-8); 133.28 (C-9)
	CH_2	25.24 (C-2 CH_2CH_3); 52.79 (C-5)
	CH_3	10.45 (C-2 CH_2CH_3); 15.54 (C-3 CH_3)

1-pentene and *Z*-2-pentene cases, in Table 1), suggesting that, as noted by others (14–16), nucleophilic opening of thiiranium species is sensitive to many factors that may override simple structural considerations.

The pattern of results already described is followed, for the most part, by the remaining trapping experiments summarized in Table 1. For example, the symmetrically substituted cycloalkenes cyclopentene and cyclohexene gave the analogous Diels–Alder adducts (**12***a*,*b*) and EA adducts (**13***a*,*b*), again in a roughly 2:1 ratio. When the unsymmetrically disubstituted alkene *Z*-2-pentene was used, regioisomeric mixtures of both the Diels–Alder (**12***c*,*d*) and EA adducts (**8***c*,*d*), the latter in almost equal amounts, were obtained. This is a not unexpected outcome. With the unsymmetrically substituted alkene, 1-pentene, the expected product **10***c* was the sole Diels–Alder adduct isolated but, interestingly, *two* regioisomeric EA adducts (**8***e*,*f*) were again obtained, although the Markovnikov adduct **8***e* was predominant (2.5:1). The exclusive formation of the expected regioisomeric Diels–Alder adducts **10***a*,*b* and Markovnikov-governed EA adducts **8***h*,*i* from the strongly disymmetric alkenes 2-ethyl-1-butene and 2-methylpropene has already

Can. J. Chem. Downloaded from www.nrcresearchpress.com by 92.62.229.171 on 09/08/12
For personal use only.

TABLE 3. ^{13}C NMR data for EA adducts **8***a–i*, **13***b*, **14**

Compound	Type of carbon	δ, ppm
8*a*	C	127.76 (C-4a); 140.98 (C-8a); 146.00 (C-3); 176.08 (C-4)
	CH	46.07 (C-1′); 58.06 (C-2′); 123.47 (C-8); 127.86 (C-2); 129.27 (C-5); 133.11 (C-7); 135.22 (C-6)
	CH_3	14.97 (C-1′ CH_3); 20.36 (C-3′)
8*b*	C	127.89 (C-4a); 140.97 (C-8a); 146.15 (C-3); 176.10 (C-4)
	CH	46.97 (C-1′); 60.06 (C-2′); 123.43 (C-8); 128.03 (C-2); 129.31 (C-5); 133.11 (C-7); 135.15 (C-6)
	CH_3	15.91 (C-1′ CH_3); 22.70 (C-3′)
8*c*	C	127.81 (C-4a); 140.99 (C-8a); 146.13 (C-3); 176.12 (C-4)
	CH	45.79 (C-1′); 66.08 (C-2′); 123.46 (C-8); 127.63 (C-2); 129.28 (C-5); 133.11 (C-7); 135.20 (C-6)
	CH_2	27.52 (C-3′)
	CH_3	11.71 (C-4′); 15.90 (C-1″)
8*d*	C	127.81 (C-4a); 140.99 (C-8a); 146.64 (C-3); 176.15 (C-4)
	CH	53.71 (C-1′); 57.18 (C-2′); 123.49 (C-8); 127.63 (C-2); 129.28 (C-5); 133.11 (C-7); 135.20 (C-6)
	CH_2	22.31 (C-1″)
	CH_3	12.18 (C-2″); 20.68 (C-3′)
8*e*	C	127.68 (C-4a); 141.08 (C-8a); 146.79 (C-3); 175.93 (C-4)
	CH	58.34 (C-2′); 123.50 (C-8); 127.35 (C-2); 129.25 (C-5); 133.11 (C-7); 135.25 (C-6)
	CH_2	19.54 (C-4′); 38.95 (C-3′); 39.66 (C-1′)
	CH_3	13.39 (C-5′)
8*f*	C	127.77 (C-4a); 141.08 (C-8a); 146.13 (C-3); 176.07 (C-4)
	CH	46.19 (C-1′); 123.50 (C-8); 127.93 (C-2); 129.25 (C-5); 133.11 (C-7); 135.25 (C-6)
	CH_2	19.87 (C-3′); 33.18 (C-2′); 45.39 (CH_2Cl)
	CH_3	13.75 (C-4′)
8*g*	C	35.94 ($(CH_3)_3C$); 129.96 (C-4a); 141.06 (C-8a); 147.05 (C-3); 176.28 (C-4)
	CH	59.08 (C-1′); 123.45 (C-8); 128.51 (C-2); 129.29 (C-5); 133.07 (C-7); 135.15 (C-6)
	CH_2	44.92 (CH_2Cl)
	CH_3	28.04 ($(CH_3)_3C$)
8*h*	C	74.94 (C-2′); 127.69 (C-4a); 141.08 (C-8a); 147.09 (C-3); 175.91 (C-4)
	CH	123.47 (C-8); 127.22 (C-2); 129.24 (C-5); 133.06 (C-7); 135.21 (C-6)
	CH_2	41.19 (C-1′); 33.86 (C-3′)
	CH_3	8.7 (C-4′)
8*i*	C	66.66 (C-2′); 127.73 (C-4a); 141.09 (C-8a); 146.93 (C-3); 175.95 (C-4)
	CH	123.47 (C-8); 127.42 (C-2); 129.26 (C-5); 133.07 (C-7); 135.20 (C-6)
	CH_2	46.46 (C-1′)
	CH_3	32.23 (C-3′)
13*b*	C	127.86 (C-4a); 140.99 (C-8a); 146.14 (C-3); 176.15 (C-4)
	CH	49.52 (C-1′); 60.69 (C-2′); 123.43 (C-8); 127.90 (C-2); 129.26 (C-5); 133.06 (C-7); 135.16 (C-6)
	CH_2	22.84 (C-4′/5′); 23.70 (C-4′/5′); 29.57 (C-6′); 34.16 (C-3′)
14	C	118.80 (C-1′); 127.75 (C-4a); 141.46 (C-8a); 142.95 (C-2′); 145.10 (C-3); 176.32 (C-4)
	CH	123.60 (C-8); 127.94 (C-2); 129.10 (C-5); 133.10 (C-7); 135.32 (C-6)
	CH_3	21.72 (C-1′CH_3); 24.70 (C-3′)

Can. J. Chem. Downloaded from www.nrcresearchpress.com by 92.62.229.171 on 09/08/12
For personal use only.

Can. J. Chem. Downloaded from www.nrcresearchpress.com by 92.62.229.171 on 09/08/12
For personal use only.

been described. Thus, a well-marked trend towards regiospecificity of both Diels–Alder adduct and EA adduct formation is revealed in Table 1 as the disymmetry of the trapping alkene is increased.

The other results in Table 1 deserve brief comment. With 3,3-dimethyl-1-butene (*tert*-butylethylene) *only* the EA adduct **8***g* was isolated, in almost 30% yield. The failure to form a Diels–Alder adduct in this instance may simply be due to failure to achieve the necessary coplanarity in the transition state, due to the presence of the bulky *tert*-butyl unit. The *anti*-Markovnikov regiospecificity in the EA adduct is more surprising in the light of other data in Table 1. It is possible, however, that in the presumed intermediate thiiranium ion **11** (R = *tert*-butyl, R′ = H) there is very little "open" carbocation character, because this would involve only a *secondary* carbocation, in contrast to those situations where R and R′ are both methyl (or ethyl) groups. Accordingly, attack of Cl^- on **11** (R = *tert*-butyl, R′ = H) may occur by the S_N2, rather than S_N1, mode, leading to preferred attack at the CH_2 site and hence to the *anti*-Markovnikov adduct observed. The failure of the one alkyne trapping agent used (2-butyne) to lead to any Diels–Alder adduct may be due to the (expected) lower reactivity of alkynes as dienophiles in the inverse electron-demand Diels–Alder reaction. Again in this case a reasonable yield (21%) of the EA adduct **14** was, however, observed.

An alternative approach to the synthesis of α-oxosulfines that had not yet been examined for their Diels–Alder reactivity emphasized the creation of α-oxosulfine units that would be *incapable* of undergoing tautomerization to the corresponding vinylsulfenic acids and hence would not be capable of undergoing the competing electrophilic addition (EA) reaction. For this reason, we selected as target molecules isothiochromanone **15***a* and its 2,2-dioxide **15***b*, tetrahydrothiophen-3-one 1,1-dioxide, 3,3,5,5-tetramethylcyclohexanone, and 2-indanone.

Isothiochromanone was readily prepared by the Friedel–Crafts cyclization of 2-benzylthioacetic acid (17). Reaction of the trimethylsilyl enol ether of **15***a* with thionyl chloride, followed by trapping with 2,3-dimethyl-1,3-butadiene, however, gave no conclusive evidence for the presence of the expected α-oxosulfine. We reasoned that the analogous sulfone **15***b* might be a better choice, particularly since the presence of the sulfone group should enhance the electron deficiency of the α-oxosulfine and hence its ability to undergo inverse electron-demand Diels–Alder reactions. Surprisingly, all attempts to prepare the trimethylsilyl enol ether of **15***b* by any of the methods we had employed previously met with utter lack of success, the ketone **15***b* being recovered in all cases. Since it seemed unlikely that either steric or electronic factors could account for this failure, we suspected that the silyl enol ether had actually formed but was extremely labile to hydrolysis. This view was subsequently confirmed by the conversion of **15***b* into its stable *tert*-butyldimethylsilyl enol ether in 79% yield. Unfortunately, this more hindered silyl enol ether did not react with thionyl chloride to produce the desired α-oxosulfine, even when anhydrous caesium fluoride was used in an attempt to cleave the O—Si bond. Tetrahydrothiophen-3-one 1,1-dioxide was next synthesized from 2,5-dihydrothiophene 1,1-dioxide by a three-step literature procedure (18). Like **15***b*, this compound is a β-ketosulfone, however, and when preliminary attempts to make its trimethylsilyl enol ether were unsuccessful, based upon our experience with **15***b*, we elected not to pursue this avenue farther.

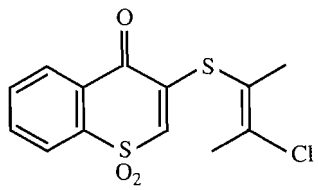

14

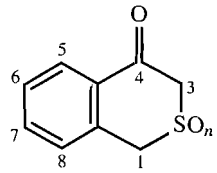

15*a*, *n* = 0
b, *n* = 2

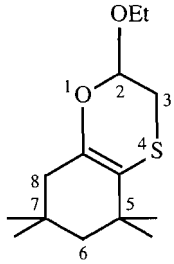

16

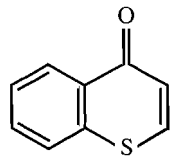

17

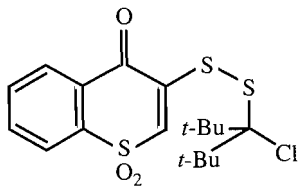

18

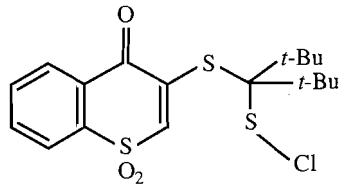

19

We next turned our attention to the α-oxosulfine derived from 3,3,5,5-tetramethylcyclohexanone. Formation of the trimethylsilyl enol ether was readily accomplished and, following reaction with *N*-(chlorosulfonyl)-imidazole, trapping experiments were conducted with 2-methylpropene, 2,3-dimethyl-2-butene, ethyl vinyl ether, and 2-butyne. Only in the case of ethyl vinyl ether was spectroscopic evidence obtained for the formation of the expected Diels–Alder adduct **16**, albeit in only 10% yield. In addition to other expected spectral features, the mass spectrum of **16** showed the presence of both a molecular ion (m/z = 256) and a major fragment ion (m/z = 184) corresponding to retro-Diels–Alder cleavage.

Zwanenburg and co-workers (19) showed that 2-sulfinyl-1-indanone is one of a very small number of stable, isolable α-oxosulfines and that it reacts with ethyl vinyl ether to produce the 1,4-oxathiin type of Diels–Alder adduct. We accordingly prepared 2-inandone from 1-indene (20), in 35% yield. Although the methylene protons in this case are also acidic ($pK_a \sim 12$; see discussion above), the trimethylsilyl enol ether could be readily prepared, contaminated by a small amount of the starting ketone. Reaction of the enol silyl ether with thionyl chloride, however, followed by attempted trapping with ethyl vinyl ether, gave none of the desired Diels–Alder adduct.

One other α-oxosulfine system that we wished to examine was that derived from thiochroman-4-one 1-oxide **3***b*. Since we have observed quite different patterns of reactivity for the α-oxosulfines derived from the corresponding sulfide (1) and sulfone it was important to establish where

Can. J. Chem. Downloaded from www.nrcresearchpress.com by 92.62.229.171 on 09/08/12
For personal use only.

the α-oxosulfine derived from **3***b* fitted in this series. The sulfoxide **3***b* was readily prepared from thiochroman-4-one by oxidation with peroxyacetic acid (21). Unfortunately, all attempts to convert **3***b* into its trimethylsilyl enol ether failed, producing only starting material accompanied by varying amounts of thiochromone, **17**. Several Pummerer-type dehydration reactions of sulfoxides using chlorotrimethylsilane have been described previously (22, 23). This reaction in our case presumably results from preferential *O*-silylation of the (more nucleophilic) sulfoxide site, followed by loss of $HOSiMe_3$ and deprotonation. Attempts to selectively oxidize the enol silyl ether **4***a* with *m*-chloroperoxybenzoic acid (*m*-CPBA) in buffered solution led only to complex mixtures of the ketones **3***a* and **3***b*, accompanied by their respective trimethylsilyl enol ethers. One final attempt to prepare the trimethylsilyl enol ether **4***b* was made, by treating the 3-bromo analogue of **3***b* (24), with zinc and chlorotrimethylsilane by the method of Joshi and Pande (25). Since this procedure again gave no useful result we reluctantly abandoned our attempt to prepare the α-oxosulfine in the sulfoxide series.

Attempts were also made to carry out Diels–Alder type reactions on the α-oxosulfine **2***b*, using heterodienophiles in place of alkenes or alkynes. In some cases (6), neutral imines were found to react with electron-deficient dienes via the inverse electron-demand Diels–Alder reaction. *N*-Methylbenzaldimine was accordingly prepared by a literature procedure (26). In the course of several attempts, however, to react the aldimine with **2***b* under our usual conditions no Diels–Alder adduct could be obtained and only traces of benzaldehyde and the keto-sulfone **3***c* were recovered. In similar trapping experiments using di-*tert*-butyl thioketone (27) a yellow solid adduct (16%) was isolated. The product showed a strong C=O band in the IR at 1653 cm^{-1} characteristic of an EA adduct and was established from ^1H and ^{13}C NMR and mass spectral evidence to have the structure **18** or **19**. The available evidence does not allow us to distinguish between these two possibilities. Disappointingly, when we attempted to extend this reaction to the aryl thioketone 4,4′-dimethoxythiobenzophenone no adduct of either the Diels–Alder or the EA type could be obtained and only **3***c* and unreacted thioketone were recovered.

Experimental

Infrared spectra were recorded using KBr pellets (if solid) or NaCl discs (if liquid), on a Nicolet 5DXB FTIR spectrometer. The ^1H NMR spectra were obtained on a Varian EM-360L spectrometer in $CDCl_3$ solution, unless otherwise indicated. High-field ^1H NMR spectra were obtained on a VXR 400 spectrometer and ^{13}C NMR spectra on a Varian XL-400 spectrometer, operating at 100.53 MHz. The ^{13}C NMR spectra were recorded in $CDCl_3$ solution. High- and low-resolution mass spectra were recorded on a VG-70-250S mass spectrometer. Column chromatography was carried out on grade 60, 60 Å silica gel supplied by Toronto Research Chemicals. Elemental analyses were performed by the Scandinavian Microanalytical Laboratory, Box 25, 2730 Herlev, Denmark.

Dichloromethane and chloroform were dried by distillation over phosphorus pentoxide and stored over 3 Å molecular sieves. Diethyl ether was dried by distillation from sodium benzophenone ketyl. Triethylamine was dried by distillation over calcium hydride and thionyl chloride was purified by distillation over triphenyl phosphite. Potassium iodide was dried at ~140°C for 3 h.

X-ray crystallography[7,8]

Unit cell dimensions based on 25 reflections ($10 < \Theta < 19°$). Intensity data collection (ω–2Θ scans, ω scan width $(0.60 + 0.35 \tan \Theta)°$, max. scan time = 60 s, octants $\pm h$, $\pm k$, l with $2 < 2\Theta < 54°$) gave a total of 3266 data. Variable scan rates (1.65–5.4°/min). Intensities of three standard reflections measured every 2 h showed no evidence of crystal decay.

Data are corrected for Lorentz and polarization effects but not for absorption. Exclusion of 345 zero F_{obs} data gave a final data set of 2921 reflections. The structure was solved by direct methods. Refinement was by full-matrix least-squares calculations, initially with isotropic and then with anisotropic thermal parameters for non-hydrogen atoms. The hydrogen atoms were positioned on geometric grounds and a general hydrogen thermal parameter was refined (final $U_{iso} = 0.057(3)$ Å^2). Final rounds of least-squares refinement included 182 parameters, $R = 0.040$, $wR = 0.043$ for 2131 reflections with $I > 3\sigma(I)$ and weights $(w) + 1/(\sigma^2(F_o) + 0.00036 (F_o)^2)$. Max. shift/esd in final refinement cycle 0.01; density in final difference map in range ±0.45 e/Å^3; there were no chemically significant features.

General procedure for the preparation of trimethylsilyl enol ethers

Dry chloroform (60 mL) was added to potassium iodide (65.70 g, 0.40 mol) with stirring under nitrogen. The mixture was cooled to 0°C and chlorotrimethylsilane (18.0 mL, 0.14 mol) was added. A solution of the ketone (0.059 mol) and triethylamine (33.1 mL, 0.24 mol) in dry chloroform (50 mL) was then added dropwise. The mixture was allowed to warm to room temperature, the flask was covered with foil paper, and the solution refluxed in the dark for 16 h. The reaction mixture was diluted with diethyl ether and the precipitated solid was removed by vacuum filtration and the filtrate dried ($MgSO_4$). Removal of the solvents on the rotary evaporator yielded the crude silyl enol ether, which was distilled (Kugelrohr) or used without further purification.

1-Trimethylsilyloxy-3,3,5,5-tetramethylcyclohexene

The crude silyl enol ether (98%) was obtained as a pale yellow oil. ^1H NMR, δ: 0.2 (s, 9H), 1.0 (br s, 12H), 1.3 (s, 2H), 1.8 (s, 2H), 4.7 (s, 1H).

*cis-2,3-Dihydro-2,3-dimethyl-[5H]-1,4-oxathiino[3,2-c-][1]-benzothiopyran 6,6-dioxide, 7*a

(+/−)-(1′S, 2′S*)-3-(2′-Chloro-1′-methylpropylthio)thiochromone 1,1-dioxide, 8*a

A solution of **4***c* (0.60 g, 2.23 mmol) in dry dichloromethane (5 mL) was stirred at −23°C under nitrogen. A solution of thionyl chloride (0.16 mL, 2.23 mmol) in dichloromethane (1 mL) was added dropwise and *Z*-2-butene was bubbled into the reaction mixture for 5 min. The mixture was stirred at −23°C for 2–3 h and then allowed to warm to 25°C and stirred for a further 16 h. The reaction mixture was washed (satd. $NaHCO_3$) and dried ($MgSO_4$). After filtration and removal of the solvent, a dark oil was obtained as the crude product.

Column chromatography on silica gel using dichloromethane/diethyl ether (99:1) as the eluent produced a brown oil (14%). Crystallization from dichloromethane/pentane yielded **8***a* as yellow needles, mp 137–138°C. IR, ν: 1675 (C=O), 1295, 1154 (SO_2)

[8]A complete set of tables comprising positional and thermal parameters, bond distances, and bond angles for **10***a* may be purchased from: The Depository of Unpublished Data, Document Delivery, CISTI, National Research Council Canada, Ottawa, Canada K1A 0S2.

These tables have also been deposited with the Cambridge Crystallographic Data Centre and can be obtained on request from The Director, Cambridge Crystallographic Data Centre, University Chemical Laboratory, Lensfield Road, Cambridge CB2 1EW, U.K.

Can. J. Chem. Downloaded from www.nrcresearchpress.com by 92.62.229.171 on 09/08/12
For personal use only.

cm^{-1}; ^1H NMR, δ: 1.51 (d, J = 7.0 Hz, 3H), 1.58 (d, J = 6.7 Hz, 3H), 3.42 (qd, J = 7.0, 3.1 Hz, 1H), 4.26 (qd, J = 6.7, 3.1 Hz, 1H), 6.85 (s, 1H), 7.75 (td, J = 7.7, 1.2 Hz, 1H), 7.87 (td, J = 7.6, 1.3 Hz, 1H), 8.02 (dd, J = 7.9, 1.1 Hz, 1H), 8.21 (dd, J = 8.0, 1.3 Hz, 1H); MS, m/z (% rel. int.): 317 (14), 280 (67), 253 (35), 227 (31), 215 (39), 201 (100), 153 (52), 136 (65), 104 (52), 76 (70), 55 (82). Anal. calcd. for $C_{13}H_{13}ClO_3S_2$: C 49.28, H 4.13, Cl 11.19, S 20.24; found: C 49.28, H 4.22, Cl 11.33, S 19.99.

Compound **7***a* was also eluted from the column as a brown oil (30%). Crystallization from acetone/water gave a beige solid, mp 142–143°C. IR, ν: 1608 (C=C), 1314, 1151 (SO_2), cm^{-1}; ^1H NMR, δ: 1.35 (d, J = 7.0, 3H), 1.38 (d, J = 6.5 Hz, 3H), 3.30 (qd, J = 7.0, 2.0 Hz, 1H), 3.78, 3.86 (ABq, J = 16.2 Hz, 2H), 4.51 (qd, J = 6.4, 2.0 Hz, 1H), 7.41 (td, J = 7.6, 1.2 Hz, 1H), 7.58 (td, J = 7.7, 1.3 Hz, 1H), 7.69 (dd, J = 8.0, 1.2 Hz, 1H), 7.85 (dd, J = 7.7, 1.3 Hz, 1H); MS, m/z (% rel. int.): 282 (100), 162 (67), 134 (79), 76 (18), 58 (18). High resolution MS, Exact Mass calcd. for $C_{13}H_{14}O_3S_2$: 282.0384; found: 282.0327. Anal. calcd. for $C_{13}H_{14}O_3S_2$: C 55.30, H 5.00; found: C 55.07, H 5.15.

trans-*2,3-Dihydro-2,3-dimethyl-[5*H*]1,4-oxathiino[3,2-c][1]-benzothiopyran 6,6-dioxide,* **7**b

*(+/−)-(1′*S*, 2′*R*)-3-(2′-Chloro-1′-methylpropylthio)thiochromone 1,1-dioxide,* **8**b

The dienophile *E*-2-butene was bubbled into the reaction mixture obtained as in the previous experiment for 8 min. A dark oil obtained as the crude product was purified by column chromatography on silica gel. Dichloromethane eluted a brown solid (10%). Recrystallization from dichloromethane/pentane yielded **8***b* as a yellow solid, mp 172–173°C. IR (CH_2Cl_2), ν: 1674 (C=O), 1305, 1151 (SO_2) cm^{-1}; ^1H NMR, δ: 1.51 (d, J = 6.8 Hz, 3H), 1.63 (d, J = 6.8 Hz, 3H), 3.35 (qd, J = 6.8, 4.2 Hz, 1H), 4.30 (qd, J = 6.8, 4.2 Hz, 1H), 6.86 (s, 1H), 7.74 (td, J = 7.8, 1.3 Hz, 1H), 7.86 (td, J = 7.6, 1.3 Hz, 1H), 8.03 (dd, J = 7.9, 1.2 Hz, 1H), 8.22 (dd, J = 7.9, 1.2 Hz, 1H); MS, m/z (% rel. int.): 317 (MH^+) (14), 280 (30), 253 (8), 201 (100), 136 (48), 76 (48), 55 (66). High resolution MS, Exact Mass calcd. for $C_{13}H_{12}O_3S_2$ (M − HCl): 280.0228; found; 280.0241.

Compound **7***b* was obtained as a yellow solid (26%). Recrystallization from ethyl acetate/hexane gave beige crystals, mp 137–138°C. IR (CH_2Cl_2), ν: 1618 (C=C), 1317, 1150 (SO_2) cm^{-1}; ^1H NMR, δ: 1.35 (d, J = 6.8 Hz, 3H), 1.46 (d, J = 6.3 Hz, 3H), 3.16 (quintet, J = 6.8 Hz, 1H), 3.80, 3.84 (ABq, J = 16.2 Hz, 2H), 4.08 (quintet, J = 6.4 Hz, 1H), 7.40 (td, J = 7.6, 1.2 Hz, 1H), 7.58 (td, J = 7.7, 1.4 Hz, 1H), 7.67 (dd, J = 8.0, 1.2 Hz, 1H), 7.87 (dd, J = 7.8, 1.3 Hz, 1H); MS, m/z (% rel. int.): 282 (82), 162 (38), 134 (100), 55 (41). High resolution MS, Exact Mass calcd. for $C_{13}H_{14}O_3S_2$: 282.0384; found: 282.0383.

*2,3-Dihydro-2,2-diethyl-[5*H*]-1,4-oxathiino[3,2-c][1]-benzothiopyran 6,6-dioxide,* **10**a

3-(2′-Chloro-2′-ethylbutylthio)thiochromone 1,1-dioxide, **8**h *(use of* N*-(chlorosulfonyl)imidazole (10) in place of $SOCl_2$)*

A solution of imidazole (0.58 g, 8.60 mmol) in dry dichloromethane (15 mL) was stirred under nitrogen at −15°C (CO_2(s) + ethylene glycol). Thionyl chloride (0.16 mL, 2.15 mmol) was added and the mixture was stirred at 25°C for 10 min. The white solid that precipitated was allowed to settle and the supernatant was transferred via a double-tipped needle to a three-necked flask equipped with a magnetic stirrer, gas-inlet adapter, and addition funnel. The solution was stirred under nitrogen at −15°C before adding more thionyl chloride (0.16 mL, 2.15 mmol). The mixture was then stirred at 25°C for 10 min and finally cooled to −23°C. A solution of **4***c* (1.05 g, 3.91 mmol) in dichloromethane (10 mL) was added dropwise to the solution of *N*-chlorosulfinylimidazole (4.30 mmol). 2-Ethyl-1-butene (1.0 mL, 8.19 mmol) was then added and the reaction mixture was stirred at −23°C for 4 h, allowed to warm to 25°C, and stirred an additional 15 h. The reaction mixture was washed (water, 5% $NaHCO_3$) and dried ($MgSO_4$). Filtration and removal of the solvent yielded a dark oil, which was purified by column chromatography. Dichloromethane eluted a yellowish-brown solid, **10***a* (25%), which on recrystallization from ethyl acetate/hexane yielded tan crystals, mp 115–116°C. IR, ν: 1610 (C=C), 1306, 1140 (SO_2) cm^{-1}; ^1H NMR, δ: 0.95 (t, J = 7.5 Hz, 6H), 1.8 (m, 4H), 2.91 (s, 2H), 3.85 (s, 2H), 7.40 (td, J = 7.6, 1.2 Hz, 1H), 7.57 (td, J = 7.7, 1.3 Hz, 1H), 7.68 (dd, J = 8.0, 1.2 Hz, 1H), 7.87 (dd, J = 7.7, 1.3 Hz, 1H); MS, m/z (% rel. int.): 310 (100), 228 (43), 162 (63), 134 (42), 83 (72), 55 (58). Anal. calcd. for $C_{15}H_{18}O_3S_2$: C 58.04, H 5.84, S 20.66; found: C 57.92, H 5.87, S 20.58.

Another yellowish-brown solid, **8***h* (14%) was eluted by dichloromethane and, on recrystallization from dichloromethane/pentane, gave light yellow crystals, mp 178–179°C. IR, ν: 1676 (C=O), 1288, 1153 (SO_2) cm^{-1}; ^1H NMR, δ: 1.01 (t, J = 7.3 Hz, 6H), 1.94 (qd, J = 7.3, 2.7 Hz, 4H), 3.10 (s, 2H), 6.84 (s, 1H), 7.74 (td, J = 7.7, 1.2 Hz, 1H), 7.86 (td, J = 7.7, 1.3 Hz, 1H), 8.01 (dd, J = 7.9, 1.2 Hz, 1H), 8.22 (dd, J = 7.9, 1.3 Hz, 1H); MS, m/z (% rel. int.): 344 (17), 308 (85), 293 (61), 229 (55), 215 (63), 178 (45), 140 (66), 104 (48), 83 (76), 69 (59), 55 (100).

3-(2′-Chloro-2′-methylpropylthio)thiochromone 1,1-dioxide, **8**i

An excess of *N*-chlorosulfinylimidazole (2.53 equiv.) (cf. previous procedure) was used in this experiment. The trapping reagent, 2-methylpropene, was bubbled into the reaction mixture for 10 min. The crude product was isolated as a dark brown liquid and column chromatographed on silica gel. Dichloromethane/carbon tetrachloride (75:25) eluted a yellow solid (9%). Recrystallization from dichloromethane/petroleum ether (30–60°C) yielded a yellow solid (**8***i*), mp 189–190°C. IR, ν: 1663 (C=O), 1287, 1156 (SO_2) cm^{-1}; ^1H NMR, δ: 1.76 (s, 6H), 3.16 (s, 2H), 6.87 (s, 1H), 7.74 (td, J = 7.7, 1.2 Hz, 1H), 7.86 (td, J = 7.7, 1.3 Hz, 1H), 8.02 (dd, J = 7.9, 1.2 Hz, 1H), 8.22 (dd, J = 7.9, 1.3 Hz, 1H); MS, m/z (% rel. int.): 318 (1), 316 (2), 282 (24), 280 (100), 227 (31), 201 (41), 153 (41), 136 (42), 104 (43), 76 (58), 55 (72). High resolution MS, Exact Mass calcd. for $C_{13}H_{13}ClO_3S_2$: 315.9994; found: 315.9971.

cis-*1,2,3,4,4a,12a-Hexahydrocyclohexa[*b*]-[5*H*]-12,5-oxathiino[3,2-c][1]-benzothiopyran 7,7-dioxide,* **12**b

trans-*3-(2′-Chlorocyclohexylthio)thiochromone 1,1-dioxide,* **13**b

A solution of **4***c* (0.60 g, 2.23 mmol) in dry dichloromethane (5 mL) was stirred at 0°C under nitrogen. A solution of thionyl chloride (0.16 mL, 2.23 mmol) in dichloromethane (1 mL) was added dropwise, followed by cyclohexene (1.0 mL, 9.87 mmol). The mixture was stirred at 0°C for 3 h and then allowed to warm to 25°C and stirred for a further 16 h. The reaction mixture was washed (satd. $NaHCO_3$) and dried ($MgSO_4$). Filtration and removal of the solvent gave a dark liquid (0.50 g) that was column chromatographed on silica gel. Dichloromethane/diethyl ether (99:1) eluted **13***b* as a brown liquid (0.10 g, 13%). Crystallization from hexane gave a yellow solid, mp 184–185°C. IR, ν: 1670 (C=O), 1297, 1156 (SO_2) cm^{-1}; ^1H NMR, δ: 1.50 (m, 2H), 1.68 (m, 2H), 1.84 (m, 2H), 2.31 (m, 2H), 3.28 (m, 1H), 4.09 (m, 1H), 6.92 (s, 1H), 7.74 (td, J = 7.7, 1.2 Hz, 1H), 7.86 (td, J = 7.7, 1.3 Hz, 1H), 8.02 (dd, J = 7.9, 1.2 Hz, 1H), 8.20 (dd, J = 7.9, 1.3 Hz, 1H); MS, m/z (% rel. int.): 308 (5), 306 (40), 241 (13), 213 (28), 136 (77), 81 (100).

The same eluent gave another compound **12***b* as a brown oil (0.16 g, 24%). Further purification by HPLC yielded a pale yellow oil. IR, ν: 1616 (C=C), 1316, 1155 (SO_2) cm^{-1}; ^1H NMR, δ: 1.20–2.26 (m, 8H), 3.23 (t, J = 7.0 Hz, 1H), 3.77, 3.90 (ABq, J = 16.2 Hz, 2H), 4.4 (m, 1H), 7.40 (td, J = 7.7, 1.2 Hz, 1H), 7.59 (td, J = 7.8, 1.2 Hz, 1H), 7.71 (dd, J = 8.1, 1.0 Hz, 1H), 7.88 (dd, J = 7.7, 1.3 Hz, 1H); MS m/z (% rel. int.): 310 (25),

Can. J. Chem. Downloaded from www.nrcresearchpress.com by 92.62.229.171 on 09/08/12
For personal use only.

309 (34), 308 (93), 164 (58), 162 (100), 134 (90), 81 (85), 67 (48). High resolution MS, Exact Mass calcd. for $C_{15}H_{16}O_3S_2$: 308.0541; found: 308.0533.

cis-*1,2,3,3a,5,11a-Hexahydrocyclopenta*[b]*-11,4-oxathiino[3,2-c][1]-benzothiopyran 6,6-dioxide,* ***12***a

trans-*3-(2'-Chlorocyclopentylthio)thiochromone 1,1-dioxide,* ***13***a

Cyclopentene (0.60 mL, 7.0 mmol) was used as the trapping reagent. A dark solid (mp 90–103°C) was obtained as the crude product. Flash chromatography on silica gel, using dichloromethane as the eluent, yielded a dark oil, **13***a* (18%). ^{1}H NMR, δ: 2.0 (m, 6H), 3.5 (m, 1H), 4.2 (m, 1H), 6.8 (s, 1H), 7.8 (m, 4H).

Further elution with dichloromethane yielded a brown oil, **12***a* (42%). Crystallization from chloroform/hexanes yielded colourless plates, mp 136–137°C. IR, ν: 1617 (C=C), 1310, 1144 (SO_2) cm^{-1}; ^{1}H NMR, δ: 1.8 (m, 2H), 2.0 (m, 2H), 2.2 (m, 2H), 3.35 (m, 1H), 3.79, 3.99 (ABq, J = 16.2 Hz, 2H), 4.3 (m, 1H), 7.42 (td, J = 7.6, 1.2 Hz, 1H), 7.61 (td, J = 7.7, 1.3 Hz, 1H), 7.72 (dd, J = 8.0, 1.1 Hz, 1H), 7.89 (dd, J = 7.8, 1.2 Hz, 1H); MS, *m/z* (% rel. int.): 294 (54), 162 (35), 134 (29), 67 (35), 58 (22). High resolution MS, Exact Mass calcd. for $C_{14}H_{14}O_3S_2$: 294.0385; found: 294.0376. Anal. calcd. for $C_{14}H_{14}O_3S_2$: C 57.12, H 4.79; found: C 57.08, H 4.86.

cis-*2,3-Dihydro-3-ethyl-2-methyl-[5*H*]-1,4-oxathiino[3,2-c][1]-benzothiopyran 6,6-dioxide,* ***12***c

cis-*2,3-Dihydro-2-ethyl-3-methyl-[5*H*]-1,4-oxathiino[3,2-c][1-]-benzothiopyran 6,6-dioxide,* ***12***d

3-(2'-Chloro-1'-methylbutylthio)thiochromone 1,1-dioxide, ***8***c

3-(2'-Chloro-1'-ethylpropylthio)thiochromone 1,1-dioxide, ***8***d

cis-2-Pentene (0.5 mL) was used as the trapping reagent. The crude product was obtained as a dark liquid that was column chromatographed on silica gel. Dichloromethane/diethyl ether (99:1) eluted a brown oil (11%), which was a mixture of **8***c,d* (1.1:1) (11%). Crystallization from dichloromethane/pentane afforded a pale yellow solid, mp 128.5–130°C. IR, ν: 1676 (C=O), 1289, 1157 (SO_2) cm^{-1}; ^{1}H NMR[9] (**8***c,d*), δ: 1.08 (t, 6H), 1.56 (m, 7H), 1.78 (m, 1H), 1.96 (m, 1H), 2.12 (m, 1H), 3.10 (**8***d*) (ddd, J = 9.4, 4.7, 2.9 Hz, 1H), 3.44 (**8***c*) (qd, J = 7.0, 3.0 Hz, 1H), 3.96 (**8***c*) (dt, J = 10.2, 3.1 Hz, 1H), 4.30 (**8***d*) (qd, J = 6.6, 2.8 Hz, 1H), 6.83, 6.84 (s, 2H), 7.74 (m, 2H), 7.86 (t, J = 7.7 Hz, 2H), 8.03 (d, J = 7.9 Hz, 2H), 8.21 (m, 2H); MS, *m/z* (% rel. int.): 333 (1), 331 (4), 294 (100), 279 (61), 215 (83), 201 (88), 136 (60), 76 (64), 69 (10).

Another brown oil (30%), a mixture of **12***c* and **12***d* (2.8:1.0), was also eluted from the column. Crystallization from ethyl acetate/petroleum ether (30–60°C) gave initially a pale yellow solid and later a white solid, mp 183–184°C, was obtained. IR, ν: 1610 (C=C), 1314, 1153 (SO_2) cm^{-1}; ^{1}H NMR[10] (**12***c*), δ: 1.08 (t, J = 7.4 Hz, 3H), 1.39 (d, J = 6.5 Hz, 3H), 1.54 (m, 2H), 3.18 (ddd, J = 10.1, 4.3, 2.3 Hz, 1H), 3.84 (s, 2H), 4.59 (qd, J = 6.5, 2.2 Hz, 1H), 7.40–7.87 (m, 4H); ^{1}H NMR[10] (**12***d*), δ: 1.08 (t, J = 7.4 Hz, 3H), 1.36 (d, J = 7.0 Hz, 3H), 1.74 (m, 2H), 3.30 (qd, J = 7.0, 1.8 Hz, 1H), 3.78, 3.89 (ABq, J = 16.2 Hz, 2H), 4.20 (ddd, J = 9.0, 4.6, 1.8 Hz, 1H), 7.40–7.87 (m, 4H); MS, *m/z* (% rel. int.): 296 (82), 164 (30), 162 (100), 134 (91), 76 (30), 69 (51), 55 (38). High resolution MS, Exact Mass calcd. for $C_{14}H_{16}O_3S_2$: 296.0541; found: 296.0534. Anal. calcd. for $C_{14}H_{16}O_3S_2$: C 56.73, H 5.44; found: C 56.44, H 5.69.

[9]The number of assigned protons is doubled because of the presence of the two regioisomers. Many of the splitting patterns could not be ascertained because of the resulting overlapping. Signals that were clearly distinguishable are underlined.

[10]Serious overlapping of signals for **12***c,d* occurred only in the aromatic region.

*2,3-Dihydro-2-propyl-[5*H*]-1,4-oxathiino[3,2-c][1]-benzothiopyran 6,6-dioxide,* ***10***c

3-(2'-Chloropentylthio)thiochromone 1,1-dioxide, ***8***e

3-(1'-Chloromethylbutylthio)thiochromone 1,1-dioxide, ***8***f

The enol silyl ether **4***c* (0.60 g, 2.23 mmol) in dry dichloromethane (4 mL) was stirred at −78°C under nitrogen. A solution of thionyl chloride (0.16 mL, 2.23 mmol) in dichloromethane (4 mL) was added dropwise over 5 min and 1-pentene (1.2 mL) was added in one portion. The mixture was stirred at −78°C for 2 h, then allowed to warm to room temperature and stirred for a further 16 h. The reaction mixture was washed (satd. $NaHCO_3$) and dried ($MgSO_4$). The crude product was obtained as a dark oil.

Column chromatography on silica gel using dichloromethane yielded a brown oil (**8***e,f*) (2.5:1, 11%). Crystallization from dichloromethane/pentane gave pale yellow crystals, mp 116–117°C. IR, ν: 1669 (C=O), 1296, 1151 (SO_2) cm^{-1}; ^{1}H NMR,[9] δ: 0.9 (t, 6H), 1.4–2.8 (m, 8H), 3.14 (**8***e*) (m, 2H), 3.22 (**8***f*) (m, 1H), 3.58 (**8***f*) (dd, J = 11.6, 8.4 Hz, 1H), 3.73 (**8***f*) (dd, J = 11.6, 3.9 Hz, 1H), 4.11 (**8***e*) (m, 1H), 6.81 (s, 1H), 6.86 (s, 1H), 7.74 (td, J = 7.7, 1.2Hz, 2H), 7.87 (td, J = 7.8, 1.3 Hz, 2H), 8.02 (dd, J = 7.9, 1.1 Hz, 2H), 8.22 (m, 2H); MS, *m/z* (rel. int.): 294 (86), 265 (69), 227 (48), 201 (72), 153 (70), 76 (90), 69 (100).

Further elution with dichloromethane yielded a brown oil (**10***c*) (21%). Crystallization from ethyl acetate/hexanes gave tan crystals, mp 119.5–120.5°C. IR, ν: 1615 (C=C), 1317, 1147 (SO_2) cm^{-1}; ^{1}H NMR, δ: 0.98 (t, J = 7.2 Hz, 3H), 1.5–1.9 (m, 4H), 3.02 (d, J = 5.8 Hz, 2H), 3.79, 3.91 (ABq, J = 16.1 Hz, 2H), 4.23 (m, 1H), 7.41 (td, J = 7.6, 1.2 Hz, 1H), 7.56 (td, J = 7.7, 1.3 Hz, 1H), 7.66 (dd, J = 8.0, 1.1 Hz, 1H), 7.87 (dd, J = 7.8, 1.2 Hz, 1H); MS, *m/z* (% rel. int.): 296 (75), 162 (100), 134 (89), 76 (29), 58 (38). High resolution MS, Exact Mass calcd. for $C_{14}H_{16}O_3S_2$: 296.0541; found: 296.0540.

3-(1'-Chloromethyl-2',2'-dimethylpropylthio)thiochromone 1,1-dioxide, ***8***g

3,3-Dimethyl-1-butene (1.0 mL) was used as the trapping reagent for **2***b*. The crude product, a dark oil, was column chromatographed on silica gel. Dichloromethane eluted a yellowish-brown solid (28%). Recrystallization from dichloromethane/pentane yielded **8***g* as a yellow solid, mp 164–165°C. IR, ν: 1668 (C=O), 1300, 1157 (SO_2) cm^{-1}; ^{1}H NMR, δ: 1.14 (s, 9H), 3.08 (dd, J = 6.4, 5.3 Hz, 1H), 3.59 (dd, J = 12.1, 6.5 Hz, 1H), 3.97 (dd, J = 12.2, 5.3 Hz, 1H), 7.07 (s, 1H), 7.74 (td, J = 7.7, 1.2 Hz, 1H), 7.86 (td, J = 7.7, 1.3 Hz, 1H), 8.02 (dd, J = 7.9, 1.2 Hz, 1H), 8.21 (dd, J = 7.9, 1.3 Hz, 1H); MS, *m/z* (% rel. int.): 347 (49), 345 (100), 227 (32), 137 (25), 136 (21), 107 (13). High resolution MS, Exact Mass calcd. for $C_{15}H_{18}ClO_3S_2$ (MH^+): 345.0385; found: 345.0385.

E-*3-(2'-Chloro-1'-methyl-1'-propenylthio)thiochromone 1,1-dioxide,* ***14***

2-Butyne (0.50 mL) was used as the trapping reagent for **2***b*. The crude product was obtained as a dark brown oil (0.48 g). Column chromatography on silica gel, using dichloromethane, yielded a yellow solid (0.15 g, 21%). Recrystallization from dichloromethane/pentane gave green crystals of **14**, mp 189.5–190.5°C. IR, ν: 1665 (C=O), 1307, 1156 (SO_2) cm^{-1}; ^{1}H NMR, δ: 2.19 (m, 3H), 2.38 (m, 3H), 6.68 (s, 1H), 7.75 (td, J = 7.7, 1.2 Hz, 1H), 7.87 (td, J = 7.7, 1.3 Hz, 1H), 8.03 (dd, J = 7.9, 1.2 Hz, 1H), 8.22 (dd, J = 7.9, 1.2 Hz, 1H); MS, *m/z* (% rel. int.): 316 (24), 314 (53), 279 (100), 215 (61), 162 (23), 136 (35), 76 (47), 59 (61). High resolution MS, Exact Mass calcd. for $C_{13}H_{11}ClO_3S_2$: 313.9838; found: 313.9834. Anal. calcd. for $C_{13}H_{11}ClO_3S_2$: C 49.60, H 3.52, Cl 11.26, S 20.37; found: C 49.32, H 3.62, Cl 11.26, S 20.26.

Isothiochroman-4-one 2,2-dioxide, ***15***b

A solution of isothiochromanone (0.35 mmol) in dry dichloromethane (5 mL) was stirred at 25°C under nitrogen. A solution of *m*-CPBA (0.79 mmol) in dichloromethane (5 mL) was added

dropwise to the solution, which was stirred at 25°C for 20 h. The organic phase was then washed (10% Na_2SO_3, 10% $NaHCO_3$, satd. NaCl) before being dried ($MgSO_4$). Filtration and subsequent removal of the solvent gave **15***b* as a pale yellow solid (60%). Recrystallization from 95% EtOH afforded pale yellow crystals, mp 157–158°C. IR, ν: 1686 (C=O), 1315, 1119 (SO_2) cm^{-1}; ^1H NMR (acetone-d_6), δ: 4.5 (m, 2H), 4.8 (br s, 2H), 7.4 (m, 3H), 8.2 (m, 1H).

*4-*tert*-Butyldimethylsilyloxyisothiochrom-3-ene 2,2-dioxide*

Diisopropylamine (0.11 mL, 0.76 mmol) and 2.5 M *n*-butyllithium in hexanes (0.32 mL, 0.81 mmol) were added to dry THF (3 mL) with stirring under nitrogen at −78°C. The mixture was stirred for 30 min. A solution of **15***b* (0.15 g, 0.75 mmol) in dry THF (6 mL) was added dropwise over 15 min to the LDA solution. The mixture was stirred for 30 min at −78°C and 4-*tert*-butyldimethylchlorosilane (0.49 g, 3.25 mmol) in THF (5 mL) was then added. After stirring at −78°C for 30 min and then at room temperature for 1.5 h, the solution was concentrated and a light brown solid was obtained. The solid was washed with diethyl ether and the mixture was filtered. Concentration of the yellow filtrate gave a yellow solid (0.19 g, 79%), mp 96–100°C. ^1H NMR, δ: 0.3 (s, 6H), 1.0 (s, 9H), 4.4 (s, 2H), 6.0 (s, 1H), 7.5 (m, 4H).

*2,3-Dihydro-2-ethoxy-5,5,7,7-tetramethylcyclohexeno [1,2-*b*]-1,4-oxathiin,* ***16***

N-(Chlorosulfinyl)imidazole (10) prepared as before from imidazole (0.30 g, 4.40 mmol) and thionyl chloride (0.16 mL, 2.20 mmol) in dry dichloromethane (10 mL) was added dropwise under nitrogen to a cooled solution (−23°C) of 1-trimethylsilyloxy-3,3,5,5-tetramethylcyclohexene (0.50 g, 2.21 mmol), 2,2,6,6-tetramethylpiperidine (0.37 mL, 2.21 mmol), and ethyl vinyl ether (1.0 mL, 10.5 mmol) in dry dichloromethane (5 mL). The mixture was stirred at −23°C for 5 h and then at 25°C for a further 16 h. The reaction mixture was diluted with diethyl ether and filtered. The filtrate was washed (satd. $NaHCO_3$, water) and dried ($MgSO_4$). After filtration and removal of the solvent, a yellow oil (0.42 g) was obtained. Purification by flash chromatography on silica gel (CH_2Cl_2/CCl_4 70:30) yielded **16** as a colourless oil (0.069 g, 10%). IR, ν: 1646 (C=C), 1124 (C—O) cm^{-1}; ^1H NMR, δ: 1.3 (m, 15H), 1.5 (s, 2H), 2.0 (s, 2H), 2.9 (d, J = 3 Hz, 2H), 3.8 (m, 2H), 5.2 (m, 1H); MS, m/z (% rel. int.): 256 (66), 241 (30), 211 (9), 184 (30), 72 (18).

*3-(1'-Chloro-2',2'-dimethyl-1'-*tert*-butylpropyldithio)thiochromone 1,1-dioxide,* ***18****/ 3-(1'-chlorosulfenyl-2',2'-dimethyl-1'-*tert*-butylpropylthio)thiochromone 1,1-dioxide,* ***19***

Di-*tert*-butylthioketone (0.8 mL) was used as the trapping reagent for **2***b*. The crude product was isolated as a reddish-brown oil (1.22 g). Dichloromethane eluted a yellow solid (0.15 g, 16%). Recrystallization from dichloromethane/pentane gave yellow crystals of **18/19**, mp 177–179°C. IR, ν: 1653 (C=O), 1309, 1153 (SO_2) cm^{-1}; ^1H NMR, δ: 1.4 (s, 18H), 8.0 (m, 5H); MS, m/z (% rel. int.): 416 (1), 384 (1), 258 (17), 194 (7), 161 (8), 57 (100). High resolution MS, Exact Mass calcd. for $C_{18}H_{23}O_3S_3$ (M − Cl): 383.0809, found: 383.0782.

Acknowledgements

We thank Dr. Alan Lough of the Department of Chemistry, University of Toronto, for the X-ray crystallographic structure determination. We also acknowledge helpful comments by the two referees.

1. I. W. J. Still, D. V. Frazer, D. K. T. Hutchinson, and J. F. Sawyer. Can. J. Chem. **67**, 369 (1989).
2. I. W. J. Still and F. J. Ablenas. J. Chem. Soc. Chem. Commun. 524 (1985).
3. B. G. Lenz, H. Regeling, H. L. M. van Rozendaal, and B. Zwanenburg. J. Org. Chem. **50**, 2930 (1985).
4. F. Bourdon, J.-L. Ripoll, Y. Vallée, S. Lacombe, and G. Pfister-Guillouzo. J. Org. Chem. **55**, 2596 (1990).
5. K.-P. Pfeifer and G. Himbert. Tetrahedron Lett. **31**, 5725 (1990).
6. D. L. Boger and S. M. Weinreb. *In* Hetero Diels–Alder methodology in organic synthesis. Academic Press Inc., New York. 1987. pp. 137–141.
7. B. Zwanenburg. Recl. Trav. Chim. Pays-Bas, **101**, 1 (1982), and references therein.
8. I. W. J. Still and M. T. Thomas. J. Org. Chem. **33**, 2730 (1968).
9. I. W. J. Still and F. J. Ablenas. Can. J. Chem. **62**, 2535 (1984).
10. Y. H. Kim and J. M. Shin. Tetrahedron Lett. **26**, 3821 (1985).
11. J. S. Pizey. *In* Synthetic reagents. Vol. 1. Ellis Horwood Ltd., Chichester, England. 1974. p. 321.
12. J. Drabowicz, H. Togo, M. Mikolajczyk, and S. Oae. Org. Prep. Proced. Int. **16**, 171 (1984).
13. K. Oka. Synthesis, 661 (1981), and references therein.
14. W. A. Thaler, W. H. Mueller, and P. E. Butler. J. Am. Chem. Soc. **90**, 2069 (1968).
15. G. H. Schmid and V. J. Nowlan. Can. J. Chem. **54**, 695 (1976).
16. W. A. Smit, N. S. Zefirov, I. V. Bodrikov, and M. Z. Krimer. Acc. Chem. Res. **12**, 282 (1979).
17. C. C. Price, M. Hori, T. Parasaran, and M. Polk. J. Am. Chem. Soc. **85**, 2278 (1963).
18. J. L. Belletire and E. G. Spletzer. Synth. Commun. **13**, 269 (1983).
19. B. G. Lenz, H. Regeling, and B. Zwanenburg. Tetrahedron Lett. **25**, 5947 (1984).
20. M.-S. Lin. Ph.D. Thesis, University of Toronto. 1967.
21. A. G. Harrison, M. T. Thomas, and I. W. J. Still. Org. Mass Spectrom. **3**, 899 (1970).
22. R. D. Miller and R. Hässig. Tetrahedron Lett. **26**, 2395 (1986).
23. S. Lane, S. J. Quick, and R. J. K. Taylor. Tetrahedron Lett. **25**, 1039 (1984).
24. I. W. J. Still, P. C. Arora, and S. N. Sokolowsky. Org. Prep. Proced. Int. **7**, 159 (1975).
25. G. C. Joshi and L. M. Pande. Synthesis, 450 (1975).
26. N. H. Cromwell, R. D. Babson, and C. E. Harris. J. Am. Chem. Soc. **65**, 312 (1943).
27. A. Ohno, K. Nakamura, Y. Nakazima, and S. Oka. Bull. Chem. Soc. Jpn. **48**, 2403 (1975).

Can. J. Chem. Downloaded from www.nrcresearchpress.com by 92.62.229.171 on 09/08/12
For personal use only.

Synthesis of bicyclic diones and thiones. Facile methylation of the enolates of bicyclo[2.2.1]heptane-2,5-dione and bicyclo[2.2.2]octane-2,5-dione. An AM1 computational study of bicyclic enolates

N. H. WERSTIUK,[1] S. YEROUSHALMI, AND HONG GUAN-LIN
Department of Chemistry, McMaster University, Hamilton, Ont., Canada L8S 4M1

Received August 15, 1991

N. H. WERSTIUK, S. YEROUSHALMI, and HONG GUAN-LIN. Can J. Chem. **70**, 974 (1992).

A group of bicyclic ketones and thiones have been synthesized for homenolization studies. Bicyclo[2.2.1]heptane-2,5-dione (**6**) undergoes unusually rapid tetramethylation giving 3,3,6,6-tetramethylbicyclo[2.2.1]heptane-2,5-dione (**1**) in good yield. Treatment of **1** with P_2S_5 in xylene gave 3,3,6,6-tetramethylbicyclo[2.2.1]heptane-2,5-dithione (**2**) and 3,3,6,6-tetramethyl15-oxo-bicyclo[2.2.1]heptane-2-thione (**3**), which was converted into **4** with Raney nickel. Bicyclo[2,2,2]octane-2,5-dione (**7**), prepared via a Diels–Alder reaction between 2-trimethylsilyloxy-1,3-cyclohexadiene and and α-acetoxyacrylonitrile followed by a one-step desilylation/hydrolysis, also undergoes facile tetramethylation giving 3,3,6,6-tetramethylbicyclo[2.2.2]octane-2,5-dione (**5**) in good yield. AM1 calculations were carried out on the α-enolates of bicyclo[2.2.1]heptan-2-one, **6**, 5-methylidenebicyclo[2.2.1]heptan-2-one, and 4-acetylbicyclo[2.2.1]-heptan-2-one in an attempt to gain information on the source of the enhanced acidity of the C-3 hydrogens of **6** and **7**.

Key words: bicyclic ketones, thiones, synthesis.

N. H. WERSTIUK, S. YEROUSHALMI et HONG GUAN-LIN. Can. J. Chem. **70**, 974 (1992).

Dans le but d'étudier leur homo-énolisation, on a synthétisé une série de cétones et de thiones bicycliques. La bicyclo[2.2.1]heptane-2,5-dione (**6**) subit une tétraméthylation inhabituellement rapide pour conduire à la 3,3,6,6-tétramethylbicyclo[2.2.1]heptane-2,5-dione (**1**) avec un bon rendement. Soumise à l'action du P_2S_5 dans le xylène, la cétone **1** fournit la 3,3,6,6-tétraméthylbicyclo[2.2.1]heptane-2,5-dithione (**2**) et la 3,3,6,6-tétraméthyl-5-oxo-bicyclo[2.2.1]heptane-2-thione (**3**) qui a été transformée en cétone **4** par action du nickel de Raney. La bicyclo[2.2.2]octane-2,5-dione (**7**), préparée par une réaction de Diels–Alder entre le 2-triméthylsilyloxycyclohexa-1,3-diène et l'α-acétoxyacrylonitrile suivie par une réaction combinée de désilylation et d'hydrolyse, subit aussi une réaction facile de tétraméthylation conduisant à la 3,3,6,6-tétraméthylbicyclo[2.2.2]octane-2,5-dione (**5**) avec un bon rendement. On a effectué des calculs AM1 sur les énolates α des bicyclo[2.2.1]heptan-2-one (**6**), 5-méthylidènebicyclo[2.2.1]heptan-2-one et 4-acétylbicyclo[2.2.1]heptan-2-one dans le but de déterminer la source de l'acidité accrue des protons en C-3 des composés **6** et **7**.

Mots clés : cétones bicycliques, thiones, synthèse.

[Traduit par la rédaction]

Introduction

Our interest in determining the rate enhancement of α-enolization and homoenolization (β- and γ-enolization) by carbonyl and thiocarbonyl groups positioned β and γ to α-enolizable and homenolizable C-H's (1–7) necessitated the synthesis of a group of bicyclic ketones and their thione analogues. To this end, we undertook the synthesis of 3,3,6,6-tetramethylbicyclo[2.2.1]heptane-2,5-dione (**1**), 3,3,6,6-tetramethylbicyclo[2.2.1]heptane-2,5-dithione (**2**), 3,3,6,6-tetramethyl-5-oxo-bicyclo[2.2.1]heptane-2-thione (**3**), 3,3,6,6-tetramethylbicyclo[2.2.1]heptan-2-one (**4**), and 3,3,6,6-tetramethylbicyclo[2.2.2.]octane-2,5-dione (**5**), compounds required for a study of H/D exchange under homoenolization conditions (1 M KO*t*Bu/*t*BuOD, 150–180°C).

In the case of **1**, all C—H bonds are located either α, β, or γ to at least one activating carbonyl group. The hydrogens at C-7 are β to two carbonyl groups; the bridgehead hydrogens at C-1 and C-4 are α and β, and the hydrogens of the *exo* and *endo* methyls are β and γ to these groups. In this latter case, a two-site, through-space interaction with two carbonyl groups is only possible for the carbanion derived from an *endo* methyl. In **2**, the C-H's are activated by two thiocarbonyl groups. In this series of compounds, **3** is an ideal substrate to study because the relative activating effects of carbonyl and thiocarbonyl groups can be determined directly by intramolecular competitive H/D exchange. To establish the degree to which a second carbonyl group exhances the acidity of the C-H's at C-1 (C-4), C-7, and the methyl groups relative to the parent monoketone, it was also necessary to synthesize and study H/D exchange of 3,3,6,6-tetramethylbicyclo[2.2.1]heptan-2-one (**4**). Studies on [2.2.2]-dione **5** would establish the degree to which introduction of a second carbonyl group enhances homoenolization and bridgehead α-enolization relative to the monoketone 3,3-dimethylbicyclo[2.2.2]octan-2-one (8). In the case of **5**, the second carbonyl group is γ to a β-enolizable methylene and β to an α bridgehead hydrogen; the C-7 and C-8 methylenes are identical as are the bridgehead hydrogens and the pairs of *exo* and *endo* methyls.

Our plan was to synthesize and tetramethylate diones **6** and **7**, convert **1** into **2** and **3**, and desulfurize **3** to prepare **4**. This approach would also establish whether methylation of 2,5-diones **6** and **7** is enhanced over the corresponding bicyclic monoketones, which would require repeated treatments with $NaNH_2/CH_3I$ in order to be dimethylated (8).

In this publication, we document the preparation of **1**, **2**, **3**, **4**, and **5**, describe an improved three-step synthesis of **7**, and report on the facile methylation of **6** and **7**. The results of AM1 (9, 10) calculations on **1**–**7**, bicyclo[2.2.1]heptan-2-one (**BH**), 5-methylidenebicyclo[2.2.1]heptan-2-one-(**MBH**), and 4-acetylbicyclo[2.2.1]heptan-2-one (**ABH**) and the enolates of **6**, **BH**, **MBH**, and **ABH** are presented and

[1]Author to whom correspondence may be addressed.

Can. J. Chem. Downloaded from www.nrcresearchpress.com by 92.62.229.171 on 09/08/12
For personal use only.

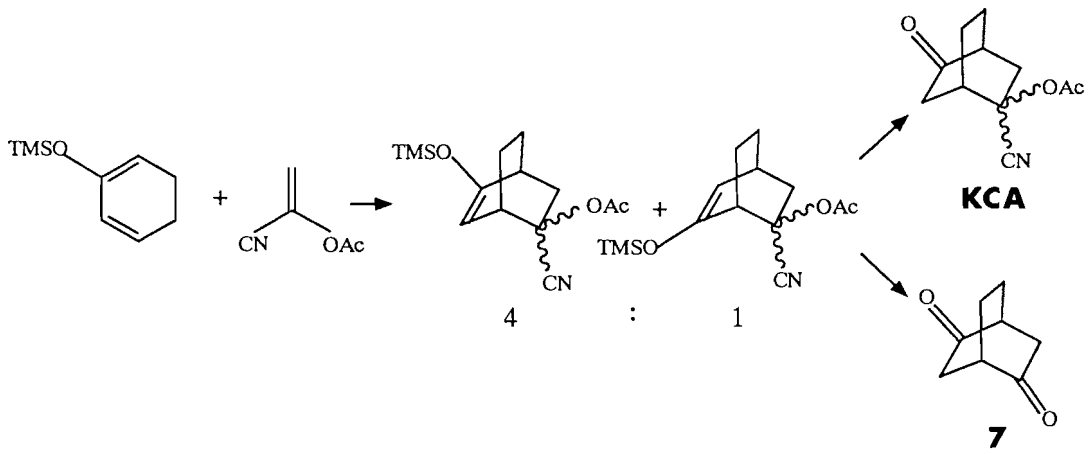

SCHEME 1

discussed. The ^1H and ^{13}C nmr spectra of **1**, **2**, **3**, **4**, **5**, and **7** are interpreted and resonances are assigned. These spectral assignments are important because nmr spectroscopy is the best way to determine the selectivity of H/D exchange in these compounds.

Results and discussion

Synthesis and methylation of **6**

Dione **6** was prepared from norbornadiene by the method of Meinwald *et al.* (11). When dione **6** was reacted with KO*t*Bu/CH_3I in ether at ambient temperature, tetramethylation was complete in 3 h; tetramethyldione **1** was isolated from several reactions in yields that ranged between 55 and 60%. Analysis of the reaction mixtures by gc showed that only minor amounts (<10%) of lower-retention-time products, assumed to be di- and trimethylated diones, were present. This facile tetramethylation contrasts the low reactivity of bicyclo[2.2.1]heptan-2-one, which must be treated several times with fresh $NaNH_2/CH_3I$ to achieve full dimethylation. That **6** is alkylated more readily than the monoketone is certainly due to the enhanced acidity of the hydrogens α to the carbonyl groups. In fact, previous studies established that **6** undergoes H/D exchange in NaOD/D_2O/dioxane faster (the H_{exo} and H_{endo} enhancements are 1200 and 600, respectively) than bicyclo[2.2.1]heptan-2-one (3). In our view, the enhanced acidity of **6** leads to a higher equilibrium concentration of the potassium enolate, relative to the monketone, and this results in an increase in the rate of methylation.

Synthesis and methylation of **7**

Although the synthesis of **7** was reported previously (12), a Diels–Alder reaction between 2-trimethylsilyloxy-1,3-cyclohexadiene (13, 14) and α-acetoxyacrylonitrile was used to construct the [2.2.2] skeleton (15). We reasoned that if the D–A reaction proceeded with good regioselectivity as indicated in Scheme 1, hydrolysis of the D–A adduct would yield **7** in an efficient three-step synthesis (Scheme 1). In fact, this was realized. Nuclear magnetic resonance analysis of the D–A product showed that there was a 4:1 preference for formation of the 2,5-substituted [2.2.2] adduct. In our initial studies, the D–A adduct was desilylated with KF and the ketocyanoacetate (**KCA**), identified on the basis of its ms, nmr, and ir spectra, was isolated as the major product. The **KCA** was hydrolyzed to **6** with aqueous NaOH. To simplify this synthesis, the D–A adduct was desilylated and converted to the ketone with 1 M $NaOCH_3/CH_3OH$ at ambient temperature. This one-pot desilylation–hydrolysis gave **6** in good yield and purity. Any 2,6-dione formed from the regioisomeric D–A adduct presumably was ring-opened to the keto ester, which was separated from **6** by crystallization. This three-step synthesis, which gave **6** in 25% overall yield from the cyclohexadiene and α-cyanovinyl acetate, is an improvement over the route described by Hill *et al.* (12) who used a five-step synthesis that began with a D–A reaction of maleic anhydride and hydroquinone. Dione **7**, like **6**, was readily tetramethylated with KO*t*Bu/CH_3I at ambient temperature; **5** was obtained in 55–60% yield from a number of reactions. This facile tetramethylation of **7** is in accord with the enhanced kinetic acidities of the α hydrogens relative to bicyclo[2.2.2]octan-2-one. Initial H/D exchange studies of **7** in NaOD/D_2O/dioxane have established that the rate enhancements of exchange of H_{exo} and H_{endo} relative to the monoketone are 20 and 15, respectively.[2]

Computational studies

Full geometry optimizations were carried out on **1**, **2**, **3**, **4**, **5**, **6**, and **7** with AM1 (9, 10) and the keyword PRECISE was used to tighten the covergence criteria. The computed geometrical structures of these compounds are given in Fig. 1. Enthalpies of ionization of **BH**, **MBH**, and **6** obtained by computing the heat of formation of the corresponding enolates (16) are given in Table 1. In each case, the enolates were found to be planar. The increase in acidity of the *exo* and *endo* hydrogens of **6** over the monoketone predicted from the computed ΔH_i's is seen in the relative rates of H/D exchange at the α C-3 sites. The second carbonyl group of **6** can enhance the acidity of these C-H's by polar (through-space and through-bond) and homoconjugative effects. It appears from the nature of the HOMO (Fig. 2) of the enolate of **6** that a π-type homoconjugative interaction does not occur although hyperconjugation with the C4—C5 bond is indicated by orbital contributions at C5—O9. The low *exo*

[2]The rates of *exo* and *endo* H/D exchange relative to the *endo* hydrogen of bicyclo[2.2.1]heptan-2-one are 10 400 and 7800, respectively. These experiments were carried out by W. Gunn at McMaster University, 1990.

Can. J. Chem. Downloaded from www.nrcresearchpress.com by 92.62.229.171 on 09/08/12
For personal use only.

Can. J. Chem. Downloaded from www.nrcresearchpress.com by 92.62.229.171 on 09/08/12
For personal use only.

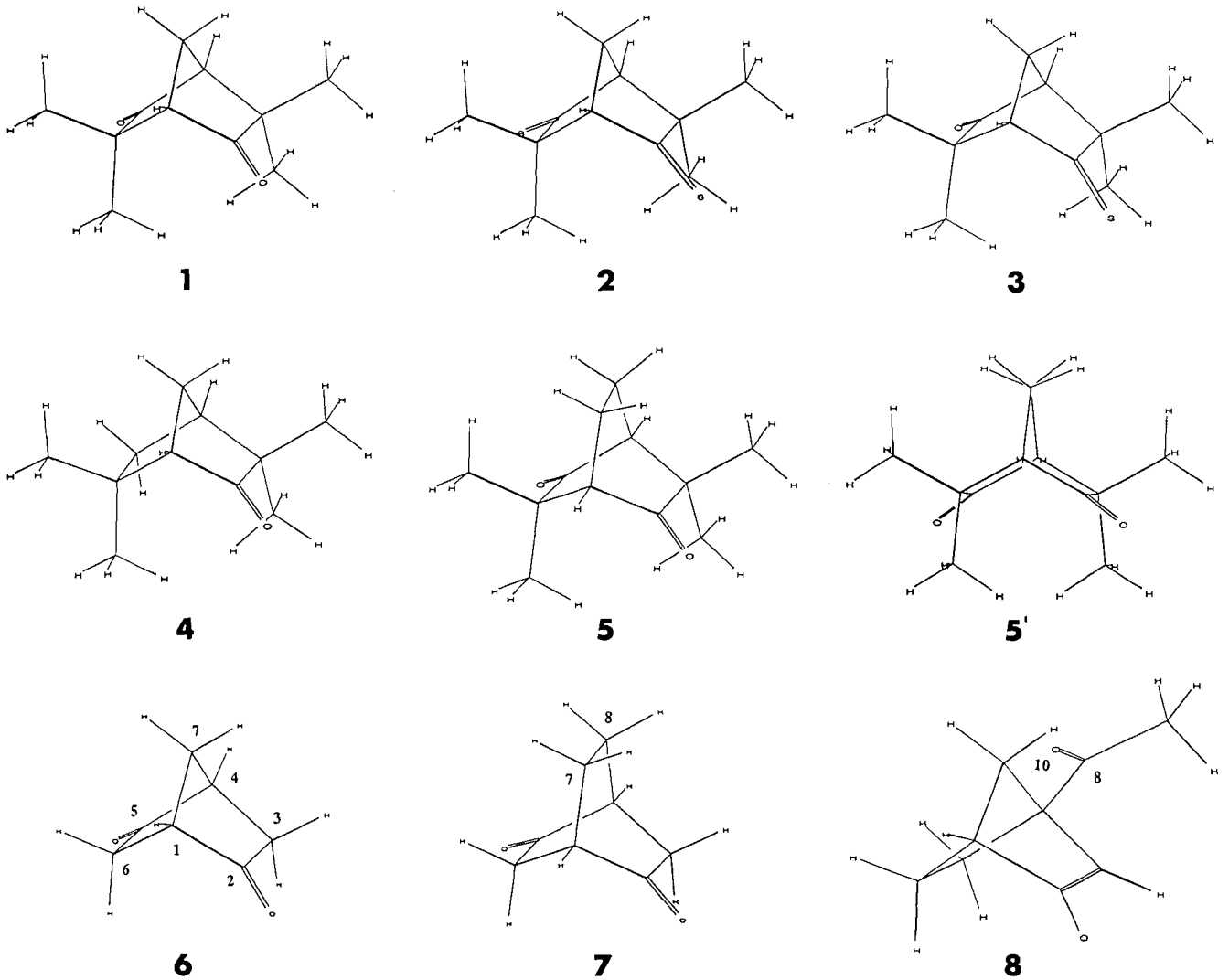

FIG. 1. Fully optimized geometrical structures of **1**, **2**, **3**, **4**, **5**, **6**, **7** and **8** obtained with AM1.

TABLE 1. Computed enthalpies of ionization and kinetic acidities of ketones

Compound	ΔH_f[a] Ketone	ΔH_f[a] Enolate	$\Delta H_i'$[b]	Relative rates of H/D exchange[c]
Bicyclo[2.2.1]heptan-2-one	−39.0	−34.4	368.8	*exo*; 650 *endo*; 1
5-Methylidene bicyclo[2.2.1]heptan-2-one	−13.91	−11.95	366.2	*exo*; 3720 *endo*; 2.1
Compound **6**	−62.1	−68.5	357.8	*exo*; 780 000 *endo*; 600
ABH; 0° conformer	−72.1	−72.0	364.1	—
135° conformer	−72.2	−76.2	360.2	—
180° conformer	−72.1	−75.9	360.4	—

[a] In kcal/mol.
[b] $\Delta H_i = [\Delta H_f(R^-) + \Delta H_f(H^+)] - \Delta H_f(R - H)$; $\Delta H_f(H^+)$ taken as 364.2 kcal/mol.
[c] See refs. 2 and 3.

selectivity[2] observed for H/D exchange of **7** shows that this is the case for the [2.2.2] system as well. If the transition state is achieved early, a larger *exo* selectivity would be expected if homoconjugative stabilization of the enolate was important because *exo* deprotonation would lead to better orbital overlap between the incipient anion at C-3 and the π-system of the carbonyl group at C-5.

To probe possible ring strain and hybridization effects of

Can. J. Chem. Downloaded from www.nrcresearchpress.com by 92.62.229.171 on 09/08/12
For personal use only.

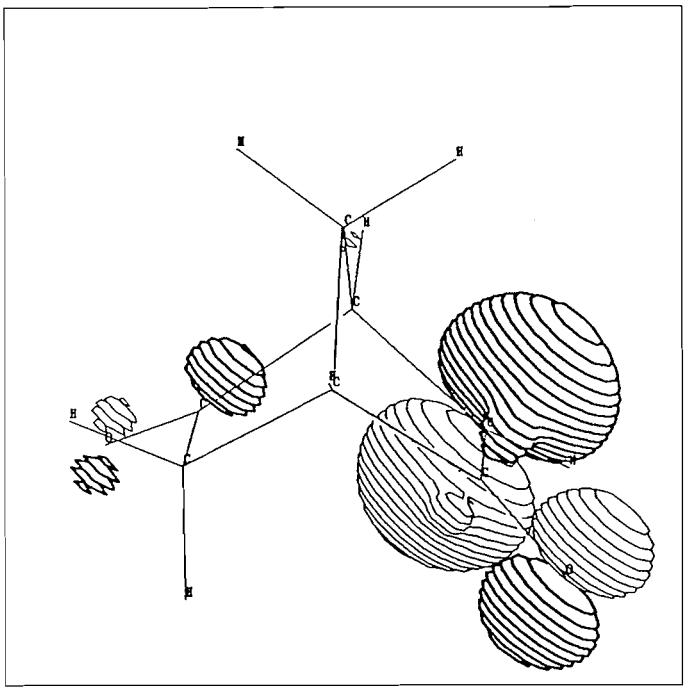

FIG. 2. Plot of the 0.2 au contours of the HOMO of the α-enolate of **6** obtained with AM1/DEN3D calculations.

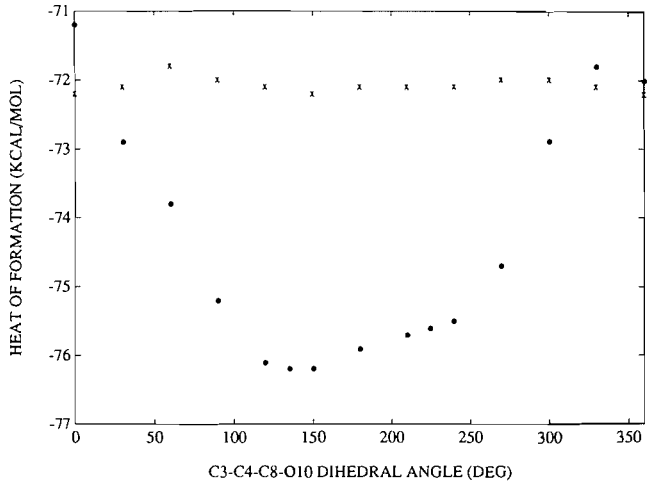

FIG. 3. Plot of the heats of formation of **ABH**(x) and its enolate **8** (·) versus the C3—C4—C5—O10 dihedral (twist) angle.

an sp^2 center at C5 of **BH**, ΔH_i of **MBH** was also computed. As seen from the data in Table 1, introduction of a carbon–carbon double bond at C5 results in a decrease ($\Delta\Delta H_i$ = 2.6 kcal) in the computed ΔH_i, but the decrease is considerably smaller than $\Delta\Delta H_i$ (11.0 kcal) computed for **BH** and **6**. Since the double bond is expected to stabilize the enolate through an inductive/field effect, the calculations suggest that these effects, if present, must be small. It is important to note that the computational results on **MBH** and its enolate are in accord with H/D exchange studies on **MBH** that established that the *exo*-H and *endo*-H rate enhancement are 8.9 and 2.1, respectively, relative to **BH** (2).

To establish how the spatial orientation of a β-carbonyl group affects the stability of an α-enolate, an AM1 computational study was carried out on 4-acetylbicyclo[2.2.1]-heptan-2-one (**ABH**) and its α-enolate. Structure **8** is the most stable geometry of this enolate. Figure 3 shows how the computed ΔH_f of **ABH**(X) and its enolate **8**(·) changes as the C3—C4—C8—O10 dihedral angle is driven through 360° beginning with an angle of 0°. Since the computed ΔH_f of the parent dione **ABH** is essentially independent of this dihedral angle, the computed enthalpy of ionization, ΔH_i, exhibits a dependence on angle nearly identical to ΔH_f of the enolate. On the basis of these results, maximum stabilization of an enolate derived from a 1,4-diketone should be expected when this dihedral angle lies between 105° and 240°. It is noteworthy that this dihedral angle is 110.9° for the enolate of **6**, and **6** exhibits an enhanced kinetic acidity over the parent monoketone. It is also interesting to note that on the basis of the ΔH_i's (Table 1) computed for **6** and 4-acetylbicyclo[2.2.1]heptan-2-one(**ABH**), **6** should show a higher acidity than **ABH**. Although H/D exchange of **ABH** has not yet been studied, Casadevall and co-workers have published the results of a study of 4-acetylcamphor(4-acetyl-1,7,7-trimethylbicyclo[2.2.1]heptan-2-one) and its 4-methyl, 4-chloro, 4-bromo, and 4-nitro analogues (17). The rate enhancements of H/D exchange of H-3-*exo* and H-3-*endo* of 4-acetylcamphor over camphor are 16.4 and 32.3, respectively. These enhancements are significantly lower than those observed for *exo* (1200) and *endo* (600) exchange of **6**, in keeping with the predictions made on the basis of the ΔH_i's computed for **6** and **ABH**. It should be pointed out here that since there is no conformational preference for the acetyl group of **ABH** (*vide supra*), a lower reactivity, relative to **6**, than that expected on the basis of the computed ΔH_i of the 135° conformer should be seen for **ABH**. If homoconjugative stabilization of the α-enolate **6** is not important, the question of why **6** is more acidic than **ABH** arises. If a field effect of the β-carbonyl group is important in stabilizing this α-enolate, then the C3, C=O distance may be the determining factor. That these distances for the α-enolates derived from **6** and **ABH** are 2.39 and 2.54 Å, respectively, is in accord with this hypothesis.

Nuclear magnetic resonance spectral assignments of ketones and thiones

^{13}C spectra

Table 2 documents the assignments of the ^{13}C resonances of **1**, **2**, **3**, **4**, **5**, **6**, and **7**.

^1H spectra

To assign the ^1H resonances of **1**, **2**, **3**, **5**, and **7**, nOe difference spectra were obtained and analyzed. Table 3 lists the resonances irradiated and the assignments made on the basis of the observed enhancements. In the case of **1**, irradiation of the signal at 1.18 ppm resulted in the enhancement of signals at 2.60 and 2.22 ppm. Irradiation of the signal at 1.02 ppm resulted in enhancement of only the signal at 2.60 ppm due to the bridgehead hydrogens. In the case of **2**, irradiation of the signals at 1.33 and 1.10 ppm again led to the assignment of all ^1H resonances. The resolution-enhanced spectrum of **3** showed a multiplet — an AB quartet split into triplets — for the hydrogens at C-7 (Fig. 4). That the upfield portion of this signal, as well as the one at 2.73 ppm, were enhanced when the singlet at 1.29 ppm (the *exo* methyl adjacent to the C=S group) was irradiated, established with certainty the assignment of the resonance of C7-H *syn* to the C=S group and the bridgehead C-H adja-

TABLE 2. ^{13}C chemical shifts of bicyclic ketones and thione analogues[a]

Compound	C1	C2	C3	C4	C5	C6	C7	C8	*exo*-CH_3	*endo*-CH_3	*exo*-CH_3	*endo*-CH_3
1	60.12	217.80	45.93	60.12	217.80	45.93	31.01		23.50	22.33	23.50	22.33
2	74.09	268.64	56.07	74.09	268.64	56.07	35.02		29.52	25.56	29.52	25.56
3	72.72	269.41	55.23	61.84	217.52	45.97	32.68		28.93 (C6)	25.72 (C6)	23.59 (C3)	21.54 (C3)
4	62.42	222.04	46.49	47.20	34.33	36.80	38.75		30.80 (C6)	27.44 (C6)	24.45 (C3)	20.81 (C3)
5	55.99	217.16	44.32	55.99	217.16	44.32	17.93	17.93	24.95	23.47	24.95	23.47
6	47.40	213.70	36.40	47.40	213.70	36.40	33.80					
7	44.91	211.47	40.30	44.91	211.47	40.30	22.10	22.10				

[a]Spectra were obtained in $CDCl_3$ and the chemical shifts were measured relative to internal TMS.

TABLE 3. Nuclear Overhauser enhancements of ^1H resonances

Compound	Resonances irradiated[a]	Resonances enhanced and assignments
1	1.18 (*exo*-CH_3's)	2.60 (H1, H4), 2.22 (H7)
	1.02 (*endo*-CH_3's)	2.60 (H1, H4)
2	2.33 (*exo*-CH_3's)	3.47 (H1, H4), 2.33 (H7)
	1.10 (*endo*-CH_3's)	3.47 (H1, H4)
3	1.29 (*exo*-3-CH_3)	2.73 (H4), 2.28 (H7 *syn* to C=S)
	1.22 (*exo*-6-CH_3)	3.33 (H1, 2.24 (H7 *anti* to C=S)
	1.14 (*endo*-3-CH_3)	2.73 (H4)
	0.99 (*endo*-6-CH_3)	3.33 (H1)
5	1.22 (*exo*-CH_3's)	2.36 (H1, H4), 2.18 (H7(8)-*anti*)
	1.06 (*endo*-CH_3's)	2.36 (H1, H4)
7	2.06 (H7(8)-*syn*)	2.74 (H1, H4), 2.53 (H3(6)-*exo*)
	1.94 (H7(8)-*anti*)	2.74 (H1, H4)

[a]Spectra were obtained at 500 MHz ($CHCl_3$) and chemical shifts are quoted in ppm downfield from internal TMS.

Can. J. Chem. Downloaded from www.nrcresearchpress.com by 92.62.229.171 on 09/08/12
For personal use only.

cent to the C=O group. Irradiation of the singlet at 1.22 ppm due to *exo* methyls adjacent to the C=O group led to an enhancement of the signals of C7-H *syn* to the C=O group (*anti* to C=S) and the bridgehead C-H adjacent to the C=S group. That the resonances due to the C7-H's *syn* and *anti* to the C=S group are separated and assignable at 500 MHz will facilitate the determination of the selectivity of H/D exchange under homoenolation conditions. Irradiation of the singlets at 0.99 and 1.14 ppm due to the *endo* methyls resulted in enhancement of only one signal, the bridgehead hydrogen, in each case and corroborated both the methyl group and bridgehead assignments. Irradiation of the singlet at 1.06 ppm of **5** resulted in an enhancement of only the resonance at 2.36 ppm, the bridgehead hydrogens, and established that this singlet at 1.06 ppm is due to the *endo* methyls at C-3 and C-6. That the resonances at 2.36 and 2.18 are enhanced when the *exo* methyls (1.22 ppm) are irradiated established that the multiplet at 2.18 is due to the hydrogens at C-7 and C-8 that are *anti* to the carbonyl groups at C-2 and C-5, respectively. In this case, the signal due to the *syn*-H's is also enhanced but only one-third the amount that the bridgehead and *anti* hydrogens are enhanced. These results are in accord with the distances between the *exo*-methyl carbon(s) and the bridgehead hydrogen(s) (2.37 Å), the *anti* C7 (C8)-H (2.82 Å) and the *syn* C7(C8)-H (3.28 Å) obtained from the AM1 optimized geometry of **5**. It is interesting to note that, according to AM1, dione **5**, unlike its parent **7**, is twisted (see **5'**). Presumably this is due to a steric interaction of the *endo* methyls. In the case of **7**, irradiation of the multiplet at 2.05 ppm resulted in enhancement of signals at 2.74 and 2.52 ppm. When the resonance at 1.94 was irradiated, only the broad singlet at 2.74 ppm was enhanced. These two experiments led to a definitive assignment of the resonances at 2.74 (bridgehead C-H's), centered at 2.53 (*exo* C3(C6)-H's), centered at 2.47 (*endo* C3(C6)-H's), 2.05 (C7(C8)-H's *syn* to the carbonyl groups at C2 and C5), and 1.94 (C7(8)-H's *anti* to the carbonyl groups) ppm of **7**.

Experimental

General

Melting points were measured with a Kofler Hot-Stage apparatus and all uncorrected nuclear magnetic resonance (nmr) spectra were recorded on Varian EM-390 and Bruker WM-250 and AM-500 spectrometers with $CDCl_3$ or CCl_4 as solvents. Tetramethylsilane (TMS) was used as an internal standard and chemical shifts are reported as parts per million downfield from internal TMS. Mass spectra were recorded on CEC-21-110B, VG Micromass 7070F, and VG ZAB spectrometers. Elemental analyses were carried out by Gailbraith Laboratories Inc., Knoxville, Tenn. Preparative gas–liquid chromatographic separations were performed on Varian Associates A-90-P and A-700 gas chromatographs. Helium was used as a carrier gas and samples were collected manually.

Can. J. Chem. Downloaded from www.nrcresearchpress.com by 92.62.229.171 on 09/08/12
For personal use only.

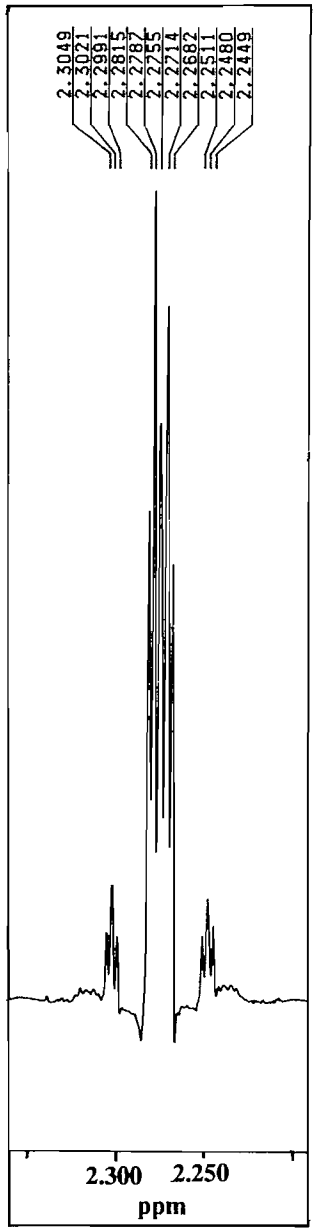

FIG. 4. A section (*syn*- and *anti*-C7-H's) of the resolution-enhanced 500 MHz ^{1}H nmr spectrum of **3**.

Preparation of 3,3,6,6-tetramethylbicyclo[2.2.1]heptane-2,5-dione (1)

Bicyclo[2.2.1]heptane-2,5-dione (5.28 g, 42.5 mmol) prepared by the method of Meinwald *et al.* (11) was placed in a round-bottom flask (1500 mL) containing dry ether (800 mL) and potassium-*tert*-butoxide (30.4 g, 270 mmol) was added. This solution was stirred for 0.5 h and CH_3I (60 mL) in an equal volume of ether was slowly aded over 0.5 h. After the solution was stirred for 3 h, analysis by analytical gc showed that the methylation was complete; only traces of the dione remained and only one major peak was evident. The solid was filtered off and solvent was removed by distillation. Recrystallization of the residue from ether gave **1** (4.2 g, 56%), mp 114–115°C; ^{1}H nmr ($CDCl_3$) δ: 2.60 (t, 2H, bridgehead H-1,H,4), 2.20 (t, 2H, H-7) 1.15 (s, 6H, *exo* CH_3) 1.10 (s, 6H, *endo* CH_3); ^{13}C nmr ($CDCl_3$) δ: 217.8 (C-2, C-5), 70.1 (C-1, C-4), 45.9 (C-3, C-6) 23.5 (*exo* CH_3's, C-9, C-11) 22.3 (C-10, C-12 *endo* CH_3's). Anal. calcd. for $C_{11}H_{12}O_2$: C 73.23, H 8.95; found: C 73.58, H 8.89.

Preparation of bicyclo[2.2.2]octane-2,4 dione (7)

2-Trimethylsiloxy-1,3-cyclohexadiene (1.81 g, 10.7 mmol), prepared by the method of Rubottom and Gruber (14), and 1-cyanovinyl acetate (1.11 g, 10 mmol) were combined in a dry Pyrex tube. The tube was sealed under vacuum and heated at 150°C for 15 h. The viscous product was dissolved in 1 N sodium methoxide/methanol (30 mL); the solution was stirred at room temperature for 3 h and poured into 150 mL of ice-water. The aqueous solution was extracted with methylene chloride, the combined extracts were dried over anhydrous $MgSO_4$, and the solvent was removed by rotoevaporation to yield 1.1 g of crude **7**. Recrystallization from benzene gave 0.70 g of **7** (51%), mp 203–205°C (lit. (10) mp 203–205°C); ^{1}H nmr ($CDCl_3$) δ: 2.75 (bm, 2H, H-1, H-4), 2.52 (q, 4H, H-3 *exo*, H-3 *endo*, H-6 *exo*, H-6 *endo*), 2.06 (bm, 2H, H-7(8) *syn*) 1.94 (bm, 2H, H-7(8) *anti*).

Preparation of 3,3,6,6-tetramethylbicyclo[2.2.2]octane-2,5-dione (5)

Dione **7** (0.83 g, 6.0 mmol) and potassium-*tert*-butoxide (5.38 g, 48.0 mmol) were mixed in dry ether (160 mL) in 3-necked flask (500 mL) fitted with a condenser, drying tube, and dropping funnel. After this mixture was stirred for 30 min, CH_3I (10 mL, 22.8 g, 161 mmol) dissolved in an equal volume of dry ether was added dropwise over a 10-min interval. The mixture was stirred at room temperature for 3 h, then filtered. Removal of the solvent by rotoevaporation gave 0.91 g of crude **5**. Recrystallization from pentane yielded 0.67 g of **5** (58%), mp 69–70°C; ^{1}H nmr ($CDCl_3$) δ: 2.36 (2H, H-1, H-4), 2.18 (m, 2H, H7(8) *anti*), 1.86 (m, 2H, H-7(8) *syn*), 1.22 (s, 6H, *exo* CH_3's), 1.06 (s, 6H, *endo* CH_3's). Mol. Wt. (high resolution ms), calcd. for $C_{12}H_{18}O_2$: 194.1313; found: 194.1312.

Preparation of 3,3,6,6-tetramethylbicyclo[2.2.1]heptane-2,-5-dithione (2) and 3,3,6,6-tetramethyl-5-oxo-bicyclo[2.2.1]heptane-2-thione (3)

A round-bottom flask (250 mL) containing 100 mL of xylene was fitted with a Soxhlet extractor, a condenser, and a drying tube. The extractor was charged with 10.0 g of P_2S_5 in the thimble. After the xylene was refluxed for 2 h to obtain a solution saturated with P_2S_5, dione **1** (3.0 g, 16.7 mmol) was added and the mixture was stirred, refluxed, and monitored by analytical gc. After 5.5 h the solution was cooled, the P_2S_5 removed by filtration, and the xylene distilled under reduced pressure. The concentrate was extracted (5 × 75 mL) with ether/petroleum ether (30–60°C) (50:50 v/v). The combined extracts were filtered and concentrated by distillation. Compounds **1**, **2**, and **3** were separated by column chromatography on neutral alumina (activity 7, mesh size 80–200) beginning with petroleum ether (30–60°C) as the solvent and gradually increasing the polarity by addition of ether. The chromatography was monitored by analytical gc and the appropriate fractions were combined. The order of elution was **2**, **3**, and **1**. Thione **2**, mp 25–30°C; ir (CCl_4) ν_{max}: 1167 (C=S) cm^{-1}; ^{1}H nmr ($CDCl_3$) δ: 3.42 (s, 2H, H-1, H-4), 2.30 (s, 2H, H-7 *syn* and *anti*), 1.27 (s, 6H, *exo* CH_3's), 1.06 (s, 6H, *endo* CH_3's); ^{13}C ($CDCl_3$) δ; 2.68.6 (C-2, C-5), 74.1 (C-1, C-4), 56.1 (C-3, C-6), 35.6 (C-7), 29.5 (*exo* CH_3's), 25.6 (*endo* CH_3's); Mol. Wt. (high resolution ms) calcd. for $C_{11}H_{12}S_2$: 212.0704O; found: 212.06930. **3**, mp 50–53°C; ^{1}H nmr ($CDCl_3$) δ: 3.23 (1H, H-1), 2.70 (1H, H-4), 2.23 (2H, H-7 *syn* and *anti*), 1.21 (s, 3H, *exo* 3-CH_3), 1.21 (s, 3H, *exo* 6-CH_3), 1.06 (s, 3H, *endo* 3-CH_3), 0.94 (s, 3H, *endo* 6-CH_3). ^{13}C nmr ($CDCl_3$) δ: 268.4 (C=S), 217.5 (C=O), 72.7 (C-1), 61.8 (C-4), 55.2 (C-3), 33.7 (C-7), 46.0 (C-6), (*exo* and *endo* CH_3's), 28.9, 25.7, 23.6, and 21.5. Mol. Wt. (high resolution ms) calcd. for $C_{11}H_{16}O_2S$: 196.09320; found: 196.09210.

Preparation of 3,3,6,6-Tetramethylbicyclo[2.2.1]heptan-2-one (4)

Monothione **3** (1.47 g, 7.5 mmol) was dissolved in super dry ethanol (25 mL) in a round-bottom flask (100 mL) fitted with a condenser and a drying tube, and Raney nickel W-2 (10 g) was added. This mixture was stirred and refluxed for 10 h and moni-

tored by analytical gc. The catalyst was filtered off using a sintered-glass funnel containing Celite and washed with ethanol (10 mL). After most of the ethanol was removed by distillation, 0.86 g of ketone **4** was isolated from the concentrate by preparative gc on a 15% Carbowax on Chromosorb W (60–100 mesh) column maintained at 195°C. **4**, ^{1}H nmr (CCl_4) δ: 2.13 (m, 1H, H-4, $J_{4,5x}$ = 4.4 Hz, $J_{4,5n}$ ~0.3 Hz, $J_{4,7a}$ 1.3 Hz, $J_{4,7s}$ = 0.4 Hz), 2.01 (dd, 1H, H-1, $J_{1,7a}$ = 0.8 Hz), 1.96 (m, 1H, H-7 *syn*, $J_{7s,7a}$ = 10.8 Hz, $J_{7s,5n}$ = 2.6 Hz, $J_{7s,4}$ = 0.7 Hz, $J_{7s,1}$ = 1.3 Hz), 1.85 (m, 1H, H-7 *anti*, $J_{7a,7s}$ = 10.8 Hz, $J_{7a,1}$ = 0.8 Hz, $J_{7a,4}$ = 1.8 Hz), 1.63 (bdd, 1H, H-5 *endo*, $J_{5n,5x}$ = 12.8 Hz, $J_{5n,7s}$ = 2.6, $J_{5n,4}$ ~0.3), 1.42 (dd, H-5 *exo*, $J_{5x,5n}$ = 12.8, $J_{5x,4}$ = 4.4), 1.11 (s, 3H, CH_3), 1.04 (s, 3H, CH_3), 1.00 (s, 3H, CH_3), 0.97 (s, 3H, CH_3); ^{13}C nmr ($CDCl_3$) δ: 222.0 (C=O), 62.4 (C-4), 47.2 (C-1), 46.5 (C-3), 36.8 (C-6), 38.7 (C-7), 34.3 (C-5), 30.9 (CH_3), 27.4 (CH_3), 20.8 (CH_3). Anal. calcd. for $C_{11}H_{14}O$: C79.46, H 10.91; found: C 79.27, H 11.03.

Computational studies

RHF calculations were carried out with AM1, Version 2.1, of the general purpose molecular orbital computational package AMPAC (10) that was ported to IBM RT, IBM RS/6000, and MIPS 2030 workstations. Optimizations were carried out with the AM1 default parameters and the keyword PRECISE was used to tighten the convergence parameters. The MO density plot was obtained with the package AM1/DEN3D/DRAW3D (18) and printed as a SUN 3/60 rasterfile on a Laser Jet II printer.

Acknowledgements

We thank the Natural Sciences and Engineering Research Council of Canada for financial support. The IBM RT and PS/2 computers used in this study were obtained under the auspices of an IBM Canada – McMaster University cooperative project.

1. N. H. Werstiuk. Can. J. Chem. **53**, 2211 (1975).
2. N. H. Werstiuk, R. Taillefer, and S. Banerjee. Can. J. Chem. **56**, 1140 (1978).
3. N. H. Werstiuk, R. Taillefer, and S. Banerjee. Can. J. Chem. **56**, 1148 (1978).
4. N. H. Werstiuk and S. Yeroushalmi. Can. J. Chem. **53**, 1601 (1980).
5. N. H. Werstiuk and S. Yeroushalmi. Can. J. Chem. **58**, 1603 (1980).
6. N. H. Werstiuk, S. Yeroushalmi, and G. Timmins. Can. J. Chem. **61**, 1945 (1983).
7. N. H. Werstiuk, G. I. Wade, and P. J. J. Martin. Can. J. Chem. **63**, 2582 (1985).
8. A. K. Cheng, J. B. Stothers, and T. C. Tan. Can. J. Chem. **55**, 447 (1977).
9. M. J. S. Dewar, E. G. Zoebisch, E. F. Healy, and J. J. P. Stewart. J. Am. Chem. Soc. **107**, 3902 (1985).
10. Dewar Research Group and J. J. P. Stewart. QCPE Bull. **6**, 2 (1986).
11. J. Meinwald, J. K. Crandall, and P. G. Gassman. Tetrahedron, **18**, 815 (1962).
12. R. K. Hill, G. H. Morton, J. R. Peterson, J. A. Walsh, and L. A. Paquette. J. Org. Chem. **50**, 5528 (1985), and references therein.
13. C. Girard and J. M. Conia. Tetrahedron Lett. 3327 (1974).
14. G. M. Rubottom and J. M. Gruber. J. Org. Chem. **42**, 1051 (1977).
15. S. Ranganathan, D. Ranganathan, and A. K. Mehrota. Synthesis, 289 (1977).
16. N. H. Werstiuk. Can. J. Chem. **66**, 2958 (1988).
17. F. C. Brown, E. Casadevall, P. Metzger, and D. G. Morris. J. Chem. Research (S), 335 (1977).
18. A. Elmer and M. A. Brook. Tetrahedron Comput. Methodol. **2**, 223 (1989).

Can. J. Chem. Downloaded from www.nrcresearchpress.com by 92.62.229.171 on 09/08/12
For personal use only.

Stereochemistry of crown ethers. X-ray crystallographic structures, solid phase ^{13}C NMR, and solution conformational equilibria in *cis-syn-cis* dicyclohexano-15-crown-5 ether and its sodium thiocyanate complex

G. W. BUCHANAN[1] AND S. MATHIAS

Ottawa–Carleton Chemistry Institute, Department of Chemistry, Carleton University, Ottawa, Ont., Canada K1S 5B6

AND

C. BENSIMON AND J. P. CHARLAND

Division of Chemistry, National Research Council of Canada, Ottawa, Ont., Canada K1A 0R9

Received January 9, 1991[2]

G. W. BUCHANAN, S. MATHIAS, C. BENSIMON, and J. P. CHARLAND. Can. J. Chem. **70**, 981 (1992).

The structures of the title materials have been determined via X-ray crystallography. In the free crown ether, there is effectively a plane of symmetry that bisects the molecule. In the NaNCS complex, ring inversion of one of the cyclohexane moieties has occurred, giving a distorted pentagonal pyramidal coordination geometry about the sodium ion. For the free crown, two conformers, whose free energies differ by ca. 0.5 kJ/mol in solution can be detected via ^{13}C NMR at 168 K. Limiting low-temperature solution spectra are compared to those which have been obtained in the solid phase using the ^{13}C CPMAS technique.

Key words: crown ethers, stereochemistry, X-ray, NMR.

G. W. BUCHANAN, S. MATHIAS, C. BENSIMON et J. P. CHARLAND. Can. J. Chem. **70**, 981 (1992).

On a déterminé les structures des produits mentionnés dans le titre par diffraction des rayons X. Dans l'éther couronne à l'état libre, il existe un plan de symétrie qui bissecte la molécule. Dans le complexe NaNCS, il se produit une inversion des cycles des portions cyclohexaniques; il s'ensuit que la coordination autour du sodium est de type pyramide pentagonale déformée. Pour la couronne libre, à 168 K, la RMN du ^{13}C permet de détecter deux conformères dont les énergies libres diffèrent par environ 0,5 kJ/mol, en solution. On a comparé les spectres obtenus à la limite inférieure de température supportée par la solution avec ceux qui ont été obtenus en phase solide à l'aide de la technique du CPMAS du ^{13}C.

Mots clés : éthers couronnes, stéréochimie, rayons X, RMN.

[Traduit par la rédaction]

Introduction

In crown ether chemistry, the 15-crown-5 system is of interest because of its efficiency for internal encapsulation of the sodium ion. For benzo-15-crown-5, the structures of the free crown as well as the hydrated NaI complex have been determined via X-ray crystallography (1, 2). The solid phase ^{13}C NMR spectrum of the free crown has also been published (3). Recently we reported the X-ray structures, ^{13}C CPMAS NMR, and solution NMR behaviour of dibenzo-15-crown-5 and its NaNCS complex (4). With respect to the derived dicyclohexano 15-crown-5 systems, however, nothing has appeared in the literature to date.

Presently, we report the synthesis, X-ray structures, and solution conformational dynamics for the *cis-syn-cis* isomer of dicyclohexano-15-crown-5 and its NaNCS complex. The limiting low-temperature solution spectra of these materials are compared to solid phase ^{13}C spectra. Results are discussed with respect to those for the analogous dicyclohexano-14-crown-4 molecules (5, 6) and *cis*-cyclohexano-15-crown-5 (7).

Results and discussion

The structures and numbering schemes for the systems examined are presented in Fig. 1. The dispositions of the cyclohexane rings are consistent with those determined via X-ray crystallography. Bond lengths and angles are listed in

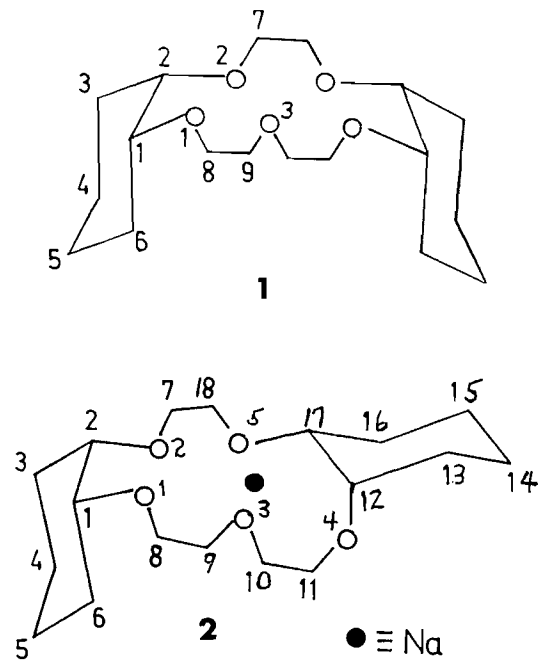

FIG. 1. Structures and numbering schemes for *cis-syn-cis*-dicyclohexano-15-crown-5, **1**, and its NaNCS complex **2**.

[1]Author to whom correspondence may be addressed.

[2]Revision received September 20, 1991.

Can. J. Chem. Downloaded from www.nrcresearchpress.com by 92.62.229.171 on 09/08/12
For personal use only.

Can. J. Chem. Downloaded from www.nrcresearchpress.com by 92.62.229.171 on 09/08/12
For personal use only.

TABLE 1. Bond lengths (Å) and angles (°) (*a*) for **1**; (*b*) for **2**

(*a*)

Bond	Length	Bond	Length
O1—C1	1.4225(24)	C1—C6	1.508(3)
O1—C8	1.416(3)	C2—C3	1.521(3)
C8—C9	1.487(3)	C3—C4	1.511(4)
O2A—C2	1.216(5)	C4—C5	1.512(3)
O2A—C7A	1.422(6)	C5—C6	1.516(3)
O2B—C2	1.628(5)	C7A—C7B′	1.482(6)
O3—C9	1.4070(23)		
C1—C2	1.514(3)		

Bonds	Angle	Bonds	Angle
C1—O1—C8	113.22(14)	C4—C5—C6	111.67(16)
O2B—O2A—C2	117.7(8)	C1—C6—C5	110.40(18)
C2—O2A—C7A	119.0(4)	O2A—C7A—C7B′	107.9(4)
C2—O2B—C7B	115.2(4)	C9—O3—C9′	114.15(19)
O1—C1—C2	112.33(14)		
O1—C1—C6	109.84(16)	C2—C1—C6	110.76(17)
O2B—C7B—C7A′	113.1(5)	O2A—C2—C1	121.4(3)
O2A—C2—C3	106.9(3)	O2B—C2—C1	102.20(25)
O2B—C2—C3	110.1(3)	C1—C2—C3	109.96(17)
O1—C8—C9	110.40(19)	C2—C3—C4	111.52(22)
O3—C9—C8	108.13(18)	C3—C4—C5	111.44(19)

′*x*, *y*, 1.5-*z*

(*b*)

Bond	Length	Bond	Length
S—C19	1.623(6)	N—C19	1.140(7)
Na—O1	2.401(3)	C1—C2	1.508(7)
Na—O2	2.515(3)	C1—C6	1.498(7)
Na—O3	2.412(3)	C2—C3	1.518(7)
Na—O4	2.494(3)	C3—C4	1.520(8)
Na—O5	2.343(3)	C4—C5	1.511(8)
Na—N	2.347(5)	C5—C6	1.513(8)
O1—C1	1.435(6)	C7—C18	1.502(7)
O1—C8	1.418(7)	C8—C9	1.489(10)
O2—C2	1.437(5)	C10—C11	1.481(9)
O2—C7	1.426(5)	C12—C13	1.527(6)
O3—C9	1.433(7)	C12—C17	1.506(6)
O3—C10	1.424(7)	C13—C14	1.518(8)
O4—C11	1.435(6)	C14—C15	1.499(10)
O4—C12	1.425(5)	C15—C16	1.519(7)
O5—C17	1.442(5)	C16—C17	1.507(6)
O5—C18	1.422(5)		
O1····O5	4.288(7)	O1····O4	4.561(7)
O2····O4	4.586(7)	O2····O3	4.185(7)
O3····O5	3.855(7)		

Bonds	Angle	Bonds	Angle
O1—Na—O2	68.64(11)	C17—O5—C18	115.5(3)
O1—Na—O3	69.82(12)	Na—N—C19	154.8(4)
O1—Na—O4	137.38(12)	O1—C1—C2	112.0(4)
O1—Na—O5	129.35(12)	O1—C1—C6	108.1(4)
O1—Na—N	97.41(15)	C2—C1—C6	110.9(4)
O2—Na—O3	116.30(12)	O2—C2—C1	106.5(4)
O2—Na—O4	132.57(11)	O2—C2—C3	112.2(4)
O2—Na—O5	68.09(10)	C1—C2—C3	110.7(4)
O2—Na—N	117.19(14)	C2—C3—C4	110.7(5)
O3—Na—O4	67.56(11)	C3—C4—C5	112.0(5)
O3—Na—O5	108.34(11)	C4—C5—C6	112.2(5)
O3—Na—N	114.14(15)	C1—C6—C5	112.0(5)

TABLE 1 (*concluded*)

Bonds	Angle	Bonds	Angle
O4—Na—O5	66.46(10)	O2—C7—C18	107.4(4)
O4—Na—N	99.81(15)	O1—C8—C9	107.3(6)
O5—Na—N	125.31(15)	O3—C9—C8	109.0(5)
Na—O1—C1	113.4(3)	O3—C10—C11	108.5(5)
Na—O1—C8	113.3(3)	O4—C11—C10	108.4(5)
C1—O1—C8	115.2(4)	O4—C12—C13	112.5(4)
Na—O2—C2	114.11(25)	O4—C12—C17	107.2(3)
Na—O2—C7	112.20(23)	C13—C12—C17	110.0(4)
C2—O2—C7	114.9(3)	C12—C13—C14	110.9(4)
Na—O3—C9	110.6(3)	C13—C14—C15	111.1(5)
Na—O3—C10	105.1(3)	C14—C15—C16	110.7(5)
C9—O3—C10	114.2(4)	C15—C16—C17	110.3(4)
Na—O4—C11	113.9(3)	O5—C17—C12	105.8(3)
Na—O4—C12	116.08(22)	O5—C17—C16	112.1(3)
C11—O4—C12	114.0(4)	C12—C17—C16	112.3(4)
Na—O5—C17	112.51(23)	O5—C18—C7	107.0(4)
Na—O5—C18	113.3(3)	S—C19—N	179.7(4)

Table 1 for the free crown ether **1** and its NaNCS complex **2**. Torsion angles involving ring skeletal atoms are provided in Table 2 while the crystallographic data are collected in Table 3. Atomic parameters are reported in Table 4 and ^{13}C NMR chemical shifts are collected in Table 5. Figure 2 shows stereoviews of **1** and **2**.

For **1** and **2** the initial point of interest from the X-ray data concerns the conformations of the cyclohexane rings. In **1**, since there is disorder present at the C7 site, the molecule effectively possesses a plane of symmetry as depicted below.

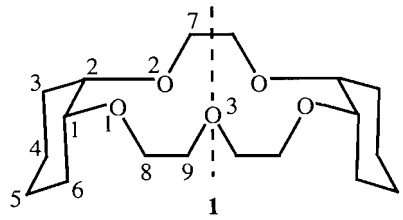

1

In contrast, for the NaNCS complex **2** one of the cyclohexane rings has undergone an inversion process (below).

This behaviour is opposite to that found by X-ray crystallography for the analogous dicyclohexano-14-crown-4 system (5), where the free crown ether lacks any true symmetry element while the LiNCS complex has a plane of symmetry. Further discussion of X-ray structures will be presented in Sect. (*iii*).

(i) Solid phase ^{13}C NMR spectra

Figure 3 contains the solid phase ^{13}C spectra of **1** and **2**. For a system such as **1**, which possesses a plane of symmetry, nine resonances are expected in the solid phase ^{13}C spectrum in the absence of crystal packing effects, multiple conformations, or non-identical molecular environments in the unit cell (3). Indeed the spectrum of solid **1** is consistent with expectations, there being four non-oxygenated resonances of approximately equal intensity in the range of 20–30 ppm and five oxygenated resonances in the range of 69–80 ppm.

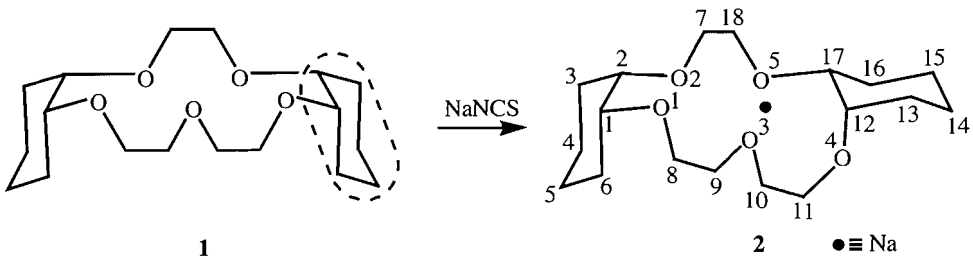

1 **2** ●≡ Na

By analogy with our earlier work (5, 6) and the known influence of axial and equatorial oxygen on chemical shifts of cyclohexyl carbons (8, 9), assignments of the six clearly resolved lines can be made with some confidence. The largest shift difference is apparent for the methine carbons bearing oxygen, where C2, bearing an axial oxygen, is shielded by 7.66 ppm relative to C1 bearing an equatorial moiety. A 4.51 ppm difference is apparent between the resonance for C4 (γ-*gauche* to O2) relative to C5 (γ-*trans* to O1), with C4 being the more shielded. The C3 and C6 sites, being β to oxygen, show only a minor shift difference (28.70 vs. 29.89 ppm) with the C3 site, which is β to axial oxygen, being the more shielded. The three closely spaced CH_2O resonances (69.90–70.82 ppm) cannot be assigned unambiguously.

In the case of **2**, the lack of symmetry in the crystal structure is reflected in the appearance of the solid phase ^{13}C spectrum, there being six clearly discernible resonances in the oxygenated carbon region as well as highly skewed intensities for the four resolved aliphatic carbon lines present in the range of 20–30 ppm.

Can. J. Chem. Downloaded from www.nrcresearchpress.com by 92.62.229.171 on 09/08/12
For personal use only.

TABLE 2. Torsion angles (°) involving C and O atoms of the crown ether

1				2	
	15-membered ring				15-membered ring
C8—O1—C1—C2	92.8(2)			C8—O1—C1—C2	85.5(4)
O1—C1—C2—O2B	64.7(2)	O1—C1—C2—O2A	55.8(3)	O1—C1—C2—O2	56.8(3)
C7B—O2B—C2—C1	−144.2(4)	C7A—O2A—C2—C1	−77.4(3)	C7—O2—C2—C1	−170.4(5)
C2—O2B—C7B—C7A′	78.1(6)			C2—O2—C7—C18	169.8(5)
O2B—C7B—C7A′—O2A′	168.3(6)			O2—C7—C18—O5	−61.3(3)
C7B—C7A′—O2A′—C2′	157.0(5)			C17—O5—C18—C7	−171.5(5)
				C18—O5—C17—C12	166.0(5)
				O4—C12—C17—O5	55.8(3)
				C11—O4—C12—C17	−162.4(5)
				C12—O4—C11—C10	156.5(6)
				O3—C10—C11—O4	−58.4(4)
				C9—O3—C10—C11	−171.8(7)
C9′—O3—C9—C8	177.4(2)			C10—O3—C9—C8	−166.2(7)
O1—C8—C9—O3	73.7(2)			O1—C8—C9—O3	61.8(4)
C1—O1—C8—C9	−166.9(2)			C1—O1—C8—C9	−177.2(6)
	Cyclohexyl rings				Cyclohexyl rings
C6—C1—C2—C3	58.4(2)			C6—C1—C2—C3	58.1(4)
C1—C2—C3—C4	−56.2(2)			C1—C2—C3—C4	−56.9(4)
C2—C3—C4—C5	54.1(2)			C2—C3—C4—C5	53.8(4)
C3—C4—C5—C6	−53.8(2)			C3—C4—C5—C6	−51.6(4)
C4—C5—C6—C1	55.8(1)			C4—C5—C6—C1	52.7(4)
C2—C1—C6—C5	−58.2(2)			C2—C1—C6—C5	−55.8(4)
O1—C1—C2—C3	−178.4(3)			O1—C1—C2—C3	179.1(6)
O1—C1—C6—C5	177.1(2)			O1—C1—C6—C5	−179.1(6)
C8—O1—C1—C6	−143.5(2)			C8—O1—C1—C6	−151.9(5)
O2A—C2—C3—C4	77.4(3)	O—2B—C2—C3—C4	55.6(2)	O2—C2—C3—C4	62.0(4)
C6—C1—C2—O2A	−67.4(3)	C6—C1—C2— 2B	−58.6(2)	C6—C1—C2—O2	−64.1(4)
C7A—O2A—C2—C3	155.4(5)	C7B—O2B—C2—C3	99.0(4)	C7—O2—C2—C3	68.3(4)
C6′—C1′—C2′—C3′	−58.4(2)			C13—C12—C17—C16	55.8(3)
C1′—C2′—C3′—C4′	56.2(2)			C17—C12—C13—C14	−55.2(4)
C2′—C3′—C4′—C5′	−54.1(2)			C12—C13—C14—C15	56.8(4)
C3′—C4′—C5′—C6′	53.8(2)			C13—C14—C15—C16	−57.3(4)
C4′—C5′—C6′—C1′	−55.8(1)			C14—C15—C16—C17	56.7(4)
C2′—C1′—C6′—C5′	58.2(2)			C15—C16—C17—C12	−56.6(4)
C6′—C1′—C2′—O2A′	67.4(3)	C6′—C1′—C2′—O2B′	58.6(2)	C13—C12—C17—O5	178.4(5)
O2A′—C2′—C3′—C4′	−77.4(3)	O2B′—C2′—C3′—C4′	−55.6(2)	C15—C16—C17—O5	−175.6(6)
C7A′—O2A′—C2′—C3′	−155.4(5)	C7B′—O2B′—C2′—C3′	−99.0(4)	C18—O5—C17—C16	−71.2(3)
O1′—C1′—C6′—C5′	−177.1(2)			O4—C12—C13—C14	64.2(4)
O1′—C1′—C2′—C3′	178.4(3)			O4—C12—C17—C16	−66.8(3)
C8′—O1′—C1′—C6′	143.5(2)			C11—O4—C12—C13	76.6(4)

One notable difference in the chemical shifts for solid **1** vs. **2** concerns the CH_2-O carbons. In **2**, the resonances for C8, 9, 10, and 11 are all shielded by at least 3.6 ppm relative to C8 and C9 of **1**. Examination of the torsional angles present in the X-ray structures provides an explanation based on the O—C—C—O networks. For **2**, these angles are 58.4° for the O4—C11—C10—O3 network and 61.8° for the O3—C9—C8—O1 case. In **1**, however, the O3—C9—C8—O1 network has a dihedral angle of 73.7°. Based on the known experimental (8, 9) and theoretical (10, 11) angular dependence of the γ-*gauche* effect in ^{13}C NMR, one expects the expansion of the O—C—C—O dihedral angle from ca. 60° to 75° to lead to substantial deshielding in **1** as observed.

From the spectrum of **2** it is evident that one of the methine carbons bearing axial oxygen appears at 74.32 ppm and the other is part of the overlapping broad signal centered at 70.85 ppm. Comparison of the torsional angle environ-

Can. J. Chem. Downloaded from www.nrcresearchpress.com by 92.62.229.171 on 09/08/12
For personal use only.

TABLE 3. Crystal data for dicyclohexyl-15-crown-5 ether (**1**) and the NaSCN-dicyclohexyl-15-crown-5-ether complex (**2**)

Parameter	Values (**1**)	Values (**2**)
Empirical formula	$NaSNC_{19}H_{32}O_5$	$C_{18}H_{32}O_5$
Formula weight	409.51	328.45
Crystal size, mm	0.12 × 0.23 × 0.35	0.20 × 0.20 × 0.30
Crystal system	Monoclinic	Orthorhombic
Space group	$P2_1/n$ (no. 14, $P2_1/c$)	*Pbnm* (no. 62, *Pnma*)
Z (molecules/cell)	4	4
a, Å	11.0602(6)	7.1720(6)
b, Å	15.1331(8)	10.6311(10)
c, Å	13.3430(6)	23.756(3)
β, deg	100.24(1)	
Cell volume, Å^3	2197.7(2)	1811.3(3)
D_{calc}, g cm^3	1.238	1.204
μ, mm^{-1}	0.19	0.66
Accurate cell parameters from:		
No. of reflections	19	26
2θ range	30–37	100–120
λ, Å	0.70930 (MoKα$_1$)	1.54056 (CuKα$_1$)
$2\theta_{max}$, deg	49.9	119.8
Octants measured	$+h,k,l$; $-h,k,l$; $-h,-k,-l$*	hkl; $-h,-k,-l$*
h range	−12–12	0–7
k range	0–17	0–11
l range	0–15	0–26
Reflections measured	4262	2214
Unique reflections	3839	1366
Reflections observed	1753	1130
$I_{net}/\sigma(I_{net})$ ratio	2.5	2.5
No. of parameters	373	195
R_f (significant reflections)	0.045	0.041
R_w (significant reflections)	0.043	0.055
Goodness-of-fit	1.3	2.3
Weighting scheme	$w^{-1} = \sigma^2(F_o) + 0.0003F_o^2$	$w^{-1} = \sigma^2(F_o) + 0.0003F_o$
Maximum Δ/σ (last cycle)	0.04	0.01
Final D-map background, e/Å^3	<0.19	<0.15
Secondary extinction coefficient	0.6(1)	0.12(6)

*A portion of the $-h,-k,-l$ data segment was collected.

ments for C2 vs. C12 shows that there are two pairs of networks in which significant dihedral angle differences exist. In the C8—O1—C1—**C2** case, θ = 85.5°, while for C18—O5—C17—**C12**, θ = 166.0°. For the C7—O2—**C2**—C3 case, θ = 68.3°, while for C11—O4—**C12**—C13, θ = 76.6°. Based on the aforementioned angular dependencies of ^{13}C steric shifts (8–11), and considering these geometrical differences, the expectation is that C12 would be the more deshielded of this pair of carbons and is thus assigned the resonance at 74.32 ppm.

(ii) Solution ^{13}C spectra

For **1** at 298 K, nine resonances are observed, in accord with the effective twofold symmetry of the molecule induced by rapid cyclohexane inversion on the NMR timescale. Two closely spaced methine carbon resonances appear at 77.90 and 77.72 ppm, since C1 and C2 remain in slightly different environments even in the presence of rapid ring inversion. For the CH_2-O carbons, three lines are observed, as expected, in the range of 68–71 ppm. Due to extensive overlap in the ^1H spectrum of **1** (even at 500 MHz) one cannot use COSY methods for clear distinction between CH_2-O resonances and hence the HETCOR experiment for ^{13}C assignments cannot be employed. For the C3,6 sites again a closely spaced pair of ^{13}C resonances is present, in this case at 27.91 and 27.76 ppm. Finally, two resonances are seen for the C4 and C5 sites at 22.87 and 22.05 ppm, in agreement with its effective symmetry at 298 K in solution.

It is of interest to compare the solid state conformation with that in solution under conditions where cyclohexane ring inversion is slow on the NMR timescale. Reduction of the temperature of the CD_2Cl_2 solution of **1** induced broadening followed by the emergence of a much more complex spectrum at the slow exchange limit of 168 K (Fig. 4). A closer examination of the methine carbon region (Fig. 5) gives an

Can. J. Chem. Downloaded from www.nrcresearchpress.com by 92.62.229.171 on 09/08/12
For personal use only.

Can. J. Chem. Downloaded from www.nrcresearchpress.com by 92.62.229.171 on 09/08/12
For personal use only.

TABLE 4. Atomic coordinates of non-H atoms of dicyclohexyl-15-crown-5 ether, **1**, and its NaSCN complex, **2**

Atom	x	y	z	B_{iso}
		1		
O1	1.10464(19)	0.77422(12)	0.85595(5)	4.19(6)
O2A*	0.7390 (8)	0.6763 (4)	0.82499(21)	4.17(19)
O2B*	0.7883 (8)	0.6245 (4)	0.82507(21)	3.92(20)
O3	1.1786 (3)	0.89990(18)	3/4	4.24(9)
C1	0.9516 (3)	0.75703(16)	0.89324(7)	3.42(7)
C2	0.7668 (3)	0.75184(23)	0.86252(8)	4.49(10)
C3	0.6083 (4)	0.7371 (3)	0.90456(10)	5.40(12)
C4	0.6352 (3)	0.62255(19)	0.94132(8)	4.12(9)
C5	0.8234 (3)	0.62399(21)	0.96994(8)	4.58(10)
C6	0.9807 (3)	0.63986(21)	0.92790(9)	4.55(10)
C7A*	0.8159 (8)	0.6997 (5)	0.77083(14)	4.38(20)
C7B*	0.7040 (8)	0.6290 (4)	0.77097(14)	4.34(20)
C8	1.1537 (3)	0.90212(21)	0.84837 (9)	4.49(9)
C9	1.2825 (3)	0.9160 (3)	0.79971(8)	4.73(11)
		2		
S	−0.10452(14)	0.22259(9)	0.63449(11)	6.47(7)
NA	0.27594(15)	0.39590(10)	0.62068(12)	4.42(8)
O1	0.3625 (3)	0.34192(20)	0.78720(23)	5.28(17)
O2	0.27706(24)	0.51361(17)	0.75395(19)	3.78(13)
O3	0.4694 (3)	0.32355(20)	0.6170 (3)	5.56(17)
O4	0.3319 (3)	0.39752(19)	0.44770(21)	4.39(14)
O5	0.28393(24)	0.53812(17)	0.55282(19)	3.72(13)
N	0.1052 (5)	0.3013 (3)	0.5902 (4)	7.3 (3)
C1	0.3319 (5)	0.3952 (3)	0.8681 (4)	4.7 (3)
C2	0.3507 (5)	0.4923 (3)	0.8509 (3)	4.4 (3)
C3	0.3155 (6)	0.5468 (4)	0.9369 (4)	5.3 (3)
C4	0.1834 (6)	0.5285 (4)	0.9478 (5)	5.3 (3)
C5	0.1597 (6)	0.4310 (4)	0.9595 (5)	5.9 (3)
C6	0.2011 (5)	0.3764 (4)	0.8767 (5)	5.3 (3)
C7	0.2974 (5)	0.5995 (3)	0.7163 (3)	4.11(25)
C8	0.4884 (6)	0.3189 (5)	0.7973 (5)	6.5 (4)
C9	0.5031 (7)	0.2682 (5)	0.7046 (5)	7.1 (4)
C10	0.4521 (7)	0.2774 (4)	0.5225 (5)	6.7 (4)
C11	0.4357 (5)	0.3431 (4)	0.4388 (5)	5.4 (3)
C12	0.3336 (4)	0.4820 (3)	0.4008 (3)	3.94(23)
C13	0.2976 (5)	0.4775 (4)	0.2850 (4)	5.3 (3)
C14	0.1656 (6)	0.4470 (6)	0.2538 (5)	6.9 (4)
C15	0.0793 (6)	0.5062 (5)	0.2972 (4)	6.4 (4)
C16	0.1135 (4)	0.5099 (4)	0.4126 (4)	4.5 (3)
C17	0.2447 (4)	0.5400 (3)	0.4439 (3)	3.58(22)
C18	0.2313 (5)	0.6039 (4)	0.6079 (4)	4.2 (3)
C19	0.0187 (5)	0.2689 (3)	0.6087 (3)	4.54(24)

B_{iso} is the mean of the principal axes of the thermal ellipsoid

*Occupancy factor = 0.5.

insight into the conformational processes that have occurred with respect to the cyclohexane moieties.

From the aforementioned doublet near 77.8 ppm have emerged six CH-O resonances in the range of 79.92–73.13 ppm. We attribute the high-intensity pair at 79.33 and 74.51 ppm to the C1 and C2 sites, respectively, of the symmetrical conformation of **1** illustrated above. The two minor lines of equal intensity at 79.92 and 78.56 ppm are attributed to methine carbons bearing equatorial oxygen in an asymmetric conformation of **1**. Similarly, the pair of lines at 75.60 and 73.13 ppm is deemed to arise from methine carbons bearing axial oxygen in the asymmetric conformation of **1**. Such a conformation could arise as a result of a single cyclohexane inversion depicted below.

Such a duality of conformations has previously been elucidated in the dicyclohexyl-14-crown-4 ether series (12). From the integrated intensities one can calculate K_{eq} and hence the ground state free energy difference ($-\Delta G^0$) between the symmetric and the asymmetric conformations at 168 K using the equation $-\Delta G^0 = RT \ln K_{eq}$. The result is that the symmetric conformation is calculated to be more stable by only 0.50 ± 0.20 kJ/mol.

For **2**, the ^{13}C spectrum at 298 K again shows nine resonances, consistent with rapid conformational averaging on

the NMR timescale. From $^1H-^{13}C$ HETCOR and $^1H-^1H$ COSY spectra at 500 MHz, assignment of the ^{13}C CH_2-O lines is possible in this case since there is less resonance overlap in the ^1H spectrum than is the case for **1**. It is useful to note that all geminal protons are magnetically nonequivalent in these systems, so that rather complex ^1H spectra are observed. Figure 6 shows a HETCOR spectrum.

The low-temperature ^{13}C spectra of **2** also exhibit decoalescence phenomena and the number of resonances increases markedly from the nine observed at 298 K. One cannot rule out the existence of multiple conformations here as well; however, sufficient peak resolution is not present to enable unravelling of the nature of the conformational processes that are occurring.

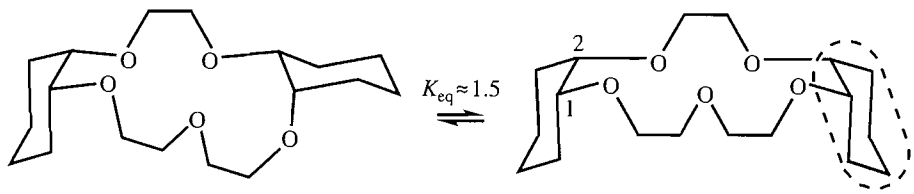

(iii) X-ray crystallographic structures

The ORTEP diagram for **1** is presented in Fig. 2*a*. In this depiction there are no symmetry elements. In fact, however, there is disorder (as illustrated below) at the C7 and O2 sites, with the disordered sites C7A, C7B, O2A, and O2B being equally populated. The crystallographic mirror plane passes through the mid-point of the C7A—C7B′ and C7A′—C7B bonds and the O3 site.

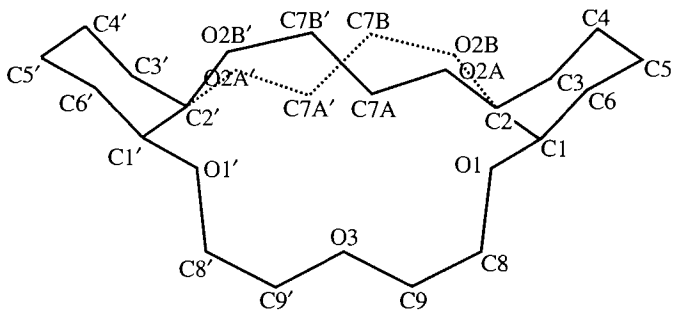

1

The solid phase ^{13}C NMR spectrum of **1** (Fig. 3), which contains nine lines, is consistent with the presence of this symmetry plane. Although there is some overlap of the three CH_2-O resonances near 70 ppm, there are six other clearly resolved resonances observed.

Normal torsion angles in crown ethers are such that O—C—C—O networks are *gauchoid* (dihedral angle ca. 60°) and all other four-atom moieties (ignoring hydrogens) are *transoid* (dihedral angle ca. 180°). In the case of **1**, the C8—O1—C1—C2 angle of 92.8° represents a major deviation, as do the C7A—O2A—C2—C3 and C7B—O2B—C2—C3 angles of 155.4° and 99.0° respectively. Other notable differences from "ideal" geometry are the C8—O1—C1—C6 network (143.5°), C7A—O2A—C2—C1 (77.4°), and C7B—O2B—C2—C1 (144.2°). For the O—C—C—O networks, the O1—C8—C9—O3 case shows significant expansion from pure *gauche* to 73.7°.

In the NaNCS complex **2**, the sodium ion is hexacoordinated to the five oxygen atoms of the crown ether and to the N atom of the SCN anion, resulting in a distorted pentagonal pyramidal coordination polyhedron. The five oxygens are not coplanar, the mean deviation from the least-squares plane connecting them being 0.27 Å. The cross-ring diagonal distances between "opposite" oxygens range from 3.855 to 4.586 Å, the average being 4.295 Å. As expected, the binding cavity is smaller than that found in the X-ray structure of the NaNCS · H_2O · 18-crown-6 complex (13), where the diagonal O—O distances in the 18-membered ring are ca. 5.100 Å on the average.

Data in Table 2 show that there is some distortion in the 15-membered ring from "ideal" conformations of crown ethers. This is particularly evident in the C8—O1—C1—C2 network where the torsion angle of 85.5° departs significantly from the "normal" value of near 180°. Similar types of distortions were observed in the LiNCS complexes of a related dicyclohexano-13-crown-4 system (14).

Figure 2*b* shows that the five ether oxygens are pointing towards the concave side of the crown ether, with the cyclohexane rings and the SCN^- side by side or with the anion coming in the concave side of the 15-membered ring. Hence the Na^+ appears to complex preferentially from the concave direction. Again there is similarity in the orientations of the anion and alkaline cation in the present case with that observed for LiNCS complexes in the analogous 13-crown-4 series (14).

TABLE 5. ^{13}C NMR chemical shifts (δ_C from TMS ± 0.01)

Carbon	**1** (solid)	**1** (solution)*	**2** (solid)	**2** (solution)
C1	73.32	(77.66)[b]	(78.85)[e]	(78.30)[i]
C2	80.98	(77.82)[b]	70.85	(77.47)[i]
C3	28.70	27.82	(26.89)[f]	(26.83)[j]
C4	21.22	(21.96)[c]	19.99	(22.67)[k]
C5	25.73	(22.75)[c]	(25.32)[g]	(20.66)[k]
C6	29.89	27.82	(26.89)[f]	(26.38)[j]
C7	(69.90)[a]	(68.17)[d]	(70.05)[h]	67.13
C8	(70.32)[a]	(68.78)[d]	66.34	66.57
C9	(70.66)[a]	(71.06)[d]	66.34	69.22
C10			66.34	
C11			66.34	
C12			74.32	
C13			(26.89)[f]	
C14			19.99	
C15			(25.10)[g]	
C16			(28.02)[f]	
C17			(80.02)[e]	
C18			(67.98)[h]	

*0.1 M in CD_2Cl_2 at 298 K.
[a-k]Indicate possible interchange of assignments.

Can. J. Chem. Downloaded from www.nrcresearchpress.com by 92.62.229.171 on 09/08/12
For personal use only.

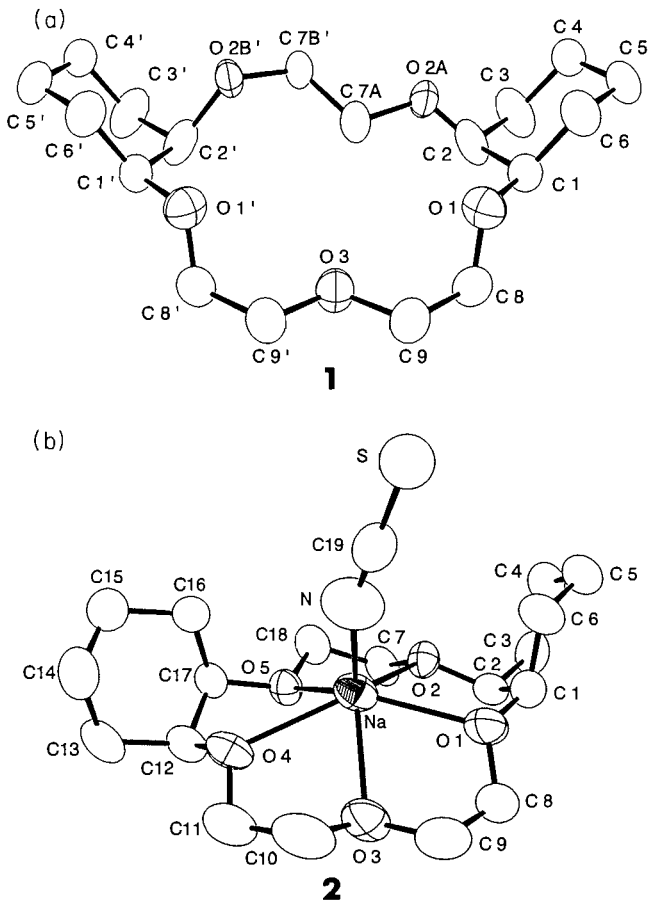

FIG. 2. (*a*) ORTEP diagram of **1**. (*b*) ORTEP diagram of **2**.

As noted earlier, the average diagonal distance between opposite oxygen atoms of **2** is 4.295 Å. By subtraction of twice the van der Waals radius of O (i.e., 2 × 1.4 Å) one can obtain the adjusted diameter of the binding cavity, 1.495 Å. Since the effective diameter of the Na^+ ion is 1.9–2.4 Å (15), the cavity is clearly too small to accommodate the Na^+ ion and hence this cation is found 0.84 Å out of the least-squares plane. By contrast, in the 18-crown-6 complex (13) the longer O—O distances result in an enlarged binding cavity diameter (ca. 2.3 Å) and hence the Na^+ lies only 0.27 Å out of the least-squares plane.

Finally, the Na—O distances listed in Table 1 are shorter when involving equatorial O's than when axial oxygens are bound (2.401 and 2.342 Å vs. 2.515 and 2.494 Å respectively). The Na—O3 distance of 2.412 Å falls in between. In the present 6-coordinate case, the average Na—O bond length of 2.433 Å is somewhat shorter than that in the 7-coordinate $NaNCS \cdot H_2O \cdot$ 18-crown-6 system (13).

Experimental

Crystallographic measurements, structure solution and refinement

Single crystals of **1** and **2** were mounted on glass fibres and measured on a Nonius CAD-4 diffractometer. Accurate cell parameters and intensity data were obtained at room temperature using graphite-monochromated CuKα radiation for **1** and MoKα radiation for **2**. Crystal data are provided in Table 3.

The space group $P2_1/n$ (alternate setting of $P2_1/c$) was uniquely defined from the systematic absences noted in the data of **2**. The intensity data for **1** revealed systematic absences consistent with two possible space groups. These are *Pbnm* (alternate setting *Pnma*) and $Pbn2_1$ (alternate setting of $Pna2_1$). Intensity data were corrected in the usual fashion for Lorentz and polarization-ratio factors but not for absorption. Other details pertaining to the data reduction step are listed in Table 3.

The positions of the non-H atoms of **2** were determined by direct methods with MULTAN (16). At this stage, isotropic refinement of all non-H atoms was carried out by full-matrix least squares. A subsequent difference map revealed the positions of the H atoms. They were included and refined isotropically while non-H atoms were refined anisotropically. The structures were refined to convergence by full-matrix least squares; $\Sigma w(|F_o| - |F_c|)^2$ was minimized with $w^{-1} = \sigma^2(F_o) + 0.0003F_o^2$. Details of the structure refinement of **2** and final *D*-map are given in Table 3.

The structure of **1** was solved in the space group $Pbn2_1$. As in **2**, positions of non-H atoms were derived from direct methods. A close inspection of the electron density maps based on the two possible space groups revealed positional disorder in the $-O-CH_2-CH_2-O$ bridge linking the two cyclohexane rings. Refinement of the occupancy factors of the disordered positions confirmed that this bridge was disordered over two equally populated positions. Least-squares refinement was continued with half-occupied C positions for the disordered bridge and isotropic thermal parameters for C and O atoms. There was further evidence of disorder. Results of refinement at this stage showed O atoms of the disordered bridge with thermal amplitudes much larger than the other non-H atoms of **1**. C—O and C—C distances in the disordered group were similar to those for analogous crown ethers (13, 14). However, two of the four $C_{cyclohexyl}—O—CH_2$ angles were unusually large (ca. 135°), which are highly improbable values.

The refinement of **1** in space group $Pbn2_1$, including H atoms at calculated positions and non-H atoms refined with anisotropic thermal parameters, would have made the number of reflections per refined parameter unacceptably low. As the space group of **1** could be *Pbnm*, cell symmetry was checked with the program MISSYM, which finds all metric symmetry elements from the atomic coordinates of any crystal structure and builds the generators in the unit cell (17). In addition to the *b* and *n* glide planes perpendicular to the *a* and *b* axes respectively, MISSYM detected mirror symmetry perpendicular to the *c* axis of the unit cell. Refinement of **1** was pursued in space group *Pbnm*.

H atoms bonded to non-disordered C atoms were added at calculated positions (C—H bond of 1.08 Å, sp^3 hybridized). Non-H atoms were defined anisotropically and H atoms isotropically. H atoms next to disordered positions C7A and C7B were successfully located in the next *D*-map and refined in the next least-squares cycles. At this stage, the *R* and R_w factors were ca. 1% higher than the final values quoted in Table 3. As the anisotropic thermal parameters of O2 described a highly and abnormally elongated 3D shape, this atom was removed from the structure and relocated in a subsquent *D*-map. The map revealed two positions. These were refined anisotropically as O atoms with half occupancies. This attempted refinement led to the lower residuals listed in Table 3. The high bond angle of ca. 135° centered at the formerly nondisordered O2 site has been replaced by more reasonable values averaging ca. 117°. However, the previous C2—O2 distance of ca. 1.4 Å is now showing systematically short and long C2—O2A and C2—O2B distances (see Table 1). Despite these geometrical distortions, the latter structural description with two partially (and equally) occupied $-O-CH_2-CH_2-O$ bridges linking the two cyclohexane rings has been used. It is of interest to note that similar structural distortions have been found in the X-ray structure of a related dicyclohexano-13-crown-4 ether (14). Details of the structure refinement of **1** and *D*-map are given in Table 3.

All computations were performed with the NRCVAX crystal package (17). The scattering curves were from the International Tables for X-ray Crystallography (18). Bond lengths and angles involving non-H atoms are presented in Table 1 while torsion angles involving ring skeletal atoms are given in Table 2. Refined coordinates of the non-H atoms of **1** and **2** are reported in Table 4.

Can. J. Chem. Downloaded from www.nrcresearchpress.com by 92.62.229.171 on 09/08/12
For personal use only.

Can. J. Chem. Downloaded from www.nrcresearchpress.com by 92.62.229.171 on 09/08/12
For personal use only.

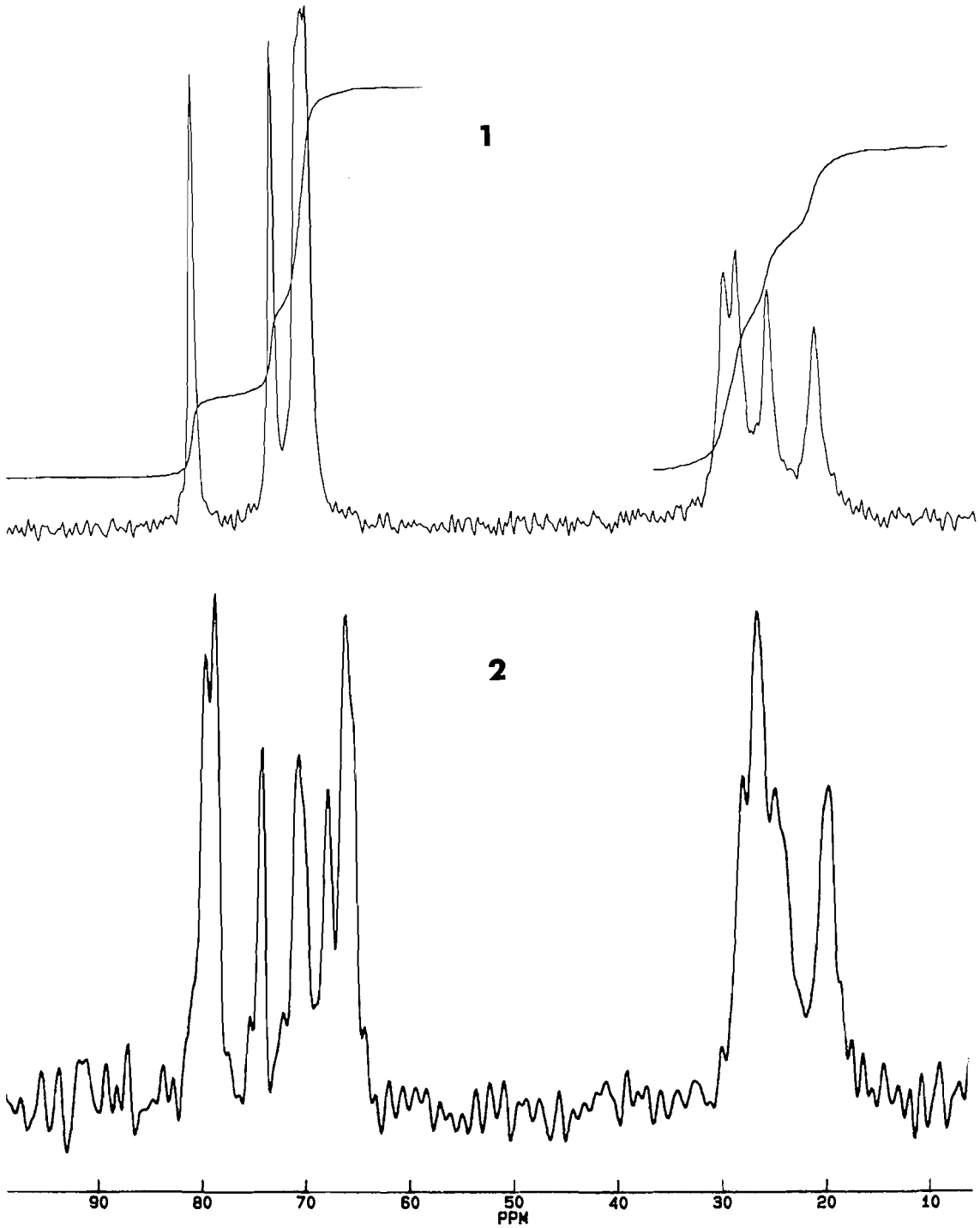

FIG. 3. 45.3 MHz solid phase ^{13}C NMR spectra.

Lists of anisotropic temperature factors, H atomic parameters, all bond lengths and angles, all torsion angles, and calculated, observed, and unobserved structure factors are deposited as Supplementary Material.[3]

[3]These data may be purchased from: The Depository of Unpublished Data, Document Delivery, CISTI, National Research Council Canada, Ottawa, Canada K1A 0S2.

Tables of hydrogen atom parameters and bond lengths and angles have also been deposited with The Cambridge Crystallographic Data Centre and can be obtained on request from The Director, Cambridge Crystallographic Data Centre, University Chemical Laboratory, Lensfield Road, Cambridge CB2 1EW, U.K.

Spectra

The ^{13}C CPMAS NMR spectra were recorded at 45.3 MHz on a Bruker CXP-180 spectrometer using techniques described previously (5). Chemical shifts were measured relative to external solid hexamethylbenzene (HMB) and converted to the TMS scale by the factor of 16.9 ppm, the chemical shift of the CH_3 group of HMB. The solution phase ^{13}C spectra were recorded at 100.6 MHz on a Bruker AM 400 system using conditions of complete ^1H noise decoupling. Typical spectral widths were 10 kHz with 32K data points for acquisition and zero filling to 64K. Normal pulse widths were 30° with a pulse delay of 2 s. Samples were ca. 0.1 M in CD_2Cl_2 solutions. The $^1H^{13}C$ HETCOR spectra were obtained on a Bruker AM 500 spectrometer using low decoupler power in the CW mode

Can. J. Chem. Downloaded from www.nrcresearchpress.com by 92.62.229.171 on 09/08/12
For personal use only.

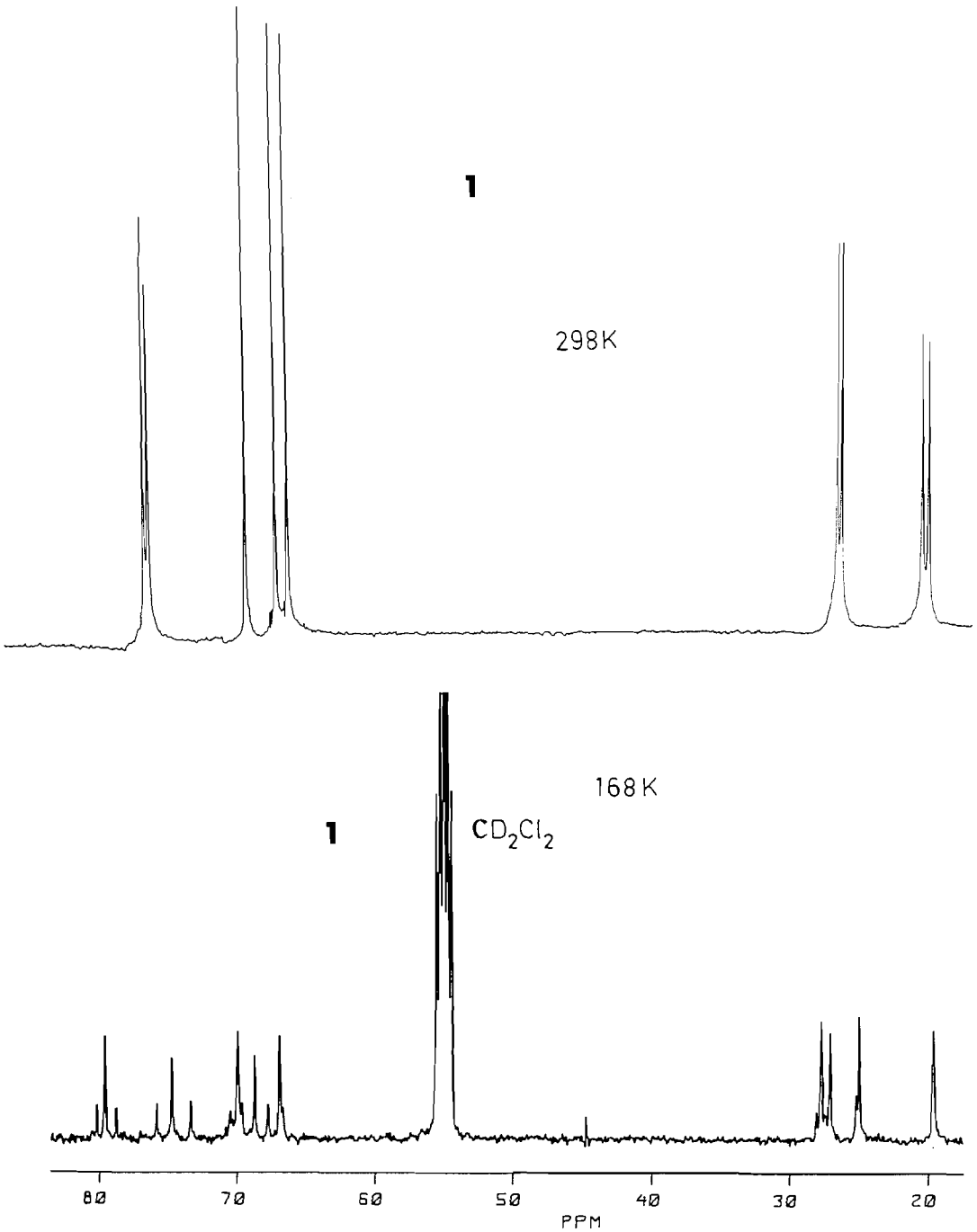

FIG. 4. 100.6 MHz ^{13}C solution spectra of **1** at 298 and 168 K.

(composite phase decoupling), with polarization transfer from ^{1}H to ^{13}C.

The FID's were acquired over 4096 data points for each of the 128 or 256 values of the evolution time, with digital resolution of 7 Hz/point in $F2$ and 5–10 Hz/point in $F1$. The raw data were zero-filled in $F1$ prior to Fourier transformation using the sine bell window function. Proton relaxation delays of 3–5 s were utilized.

Materials

Dibenzo-15-crown-5 was prepared as previously described (4). Hydrogenation of this material to a mixture of **1** and the *cis-anti-cis* isomer was accomplished using an American Instrument Co. 50 000 psi (1 psi = 6.9 kPa) maximum pressure high-pressure apparatus. In 60 mL of 1-butanol were dissolved 2.2 g (0.007 mol) of dibenzo-15-crown-5 and 0.40 g of 5% ruthenium on alumina catalyst. A pressure of 1200 psi was used and the reaction was allowed to proceed for 12 h at a temperature of 120°C. The catalyst was removed via filtration and the butanol by rotary evaporation to yield 2.1 g of a viscous yellow oil. From ^{13}C NMR there appeared to be two configurational isomers present in the ratio of ca. 2:1. Separation of these isomers was accomplished via column chromatography on activated silica gel of mesh size 100–200 using as initial eluent a mixture of 60:40 CH_2Cl_2–hexanes and a ratio of 50:1 silica gel to crude crown ether. Gradual introduction of diethyl ether in place of hexanes yielded **1** as the first isomer eluted, with 5% diethyl ether, 35% hexanes, and 60% CH_2Cl_2. Recrystallization from hexanes yielded the pure *cis-syn-cis* isomer **1**, as subsequently determined by X-ray crystallography, mp 67–68°C. The latter column fractions contained the minor, presumably *cis-anti-cis*, isomer, which remained an oil.

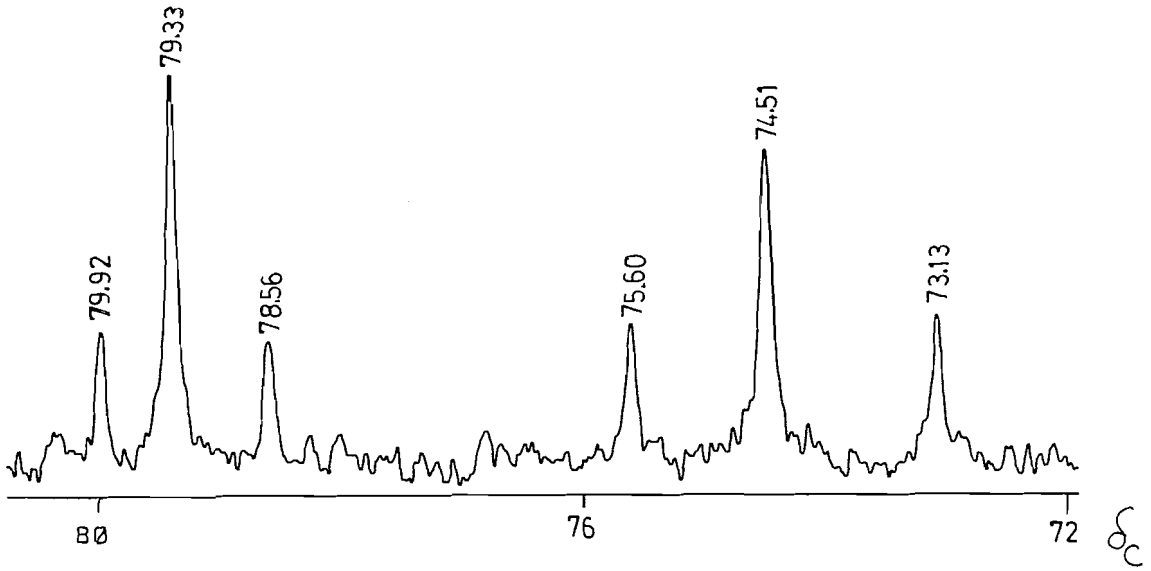

FIG. 5. Methine carbon region of 100.6 MHz spectrum of **1** at 168 K.

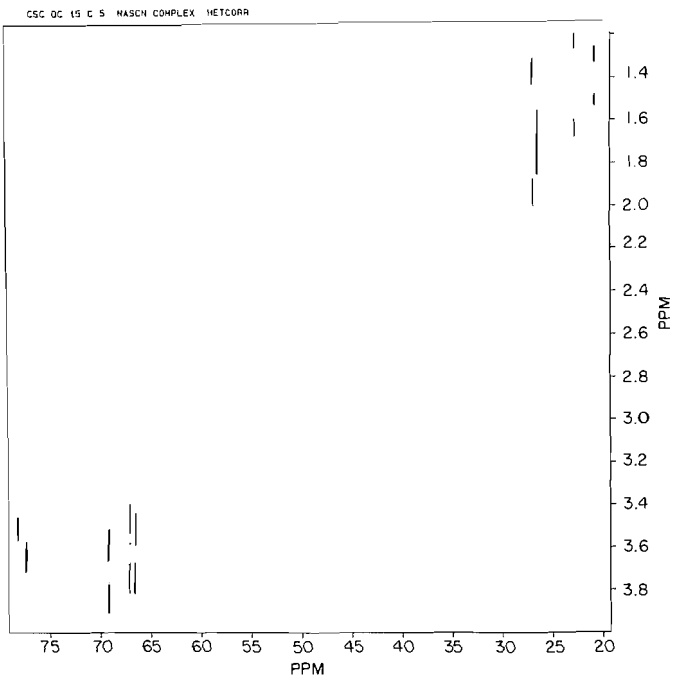

FIG. 6. $^{1}H^{13}C$ HETCOR spectrum of **2** at 500 MHz.

For preparation of the complex **2**, equimolar amounts of **1** and NaNCS were dissolved in a minimum volume of dry methanol. After allowing the mixture to stand for 2–3 h, the solvent was removed by rotary evaporation. Subsequent recrystallization from ethanol–hexanes yielded pure **2**, mp 140–141°C.

Acknowledgements

The continuing financial support of the Natural Sciences and Engineering Research Council of Canada via Operating Grants to G. W. B. is gratefully acknowledged. We thank Drs. J. A. Ripmeester and C. I. Ratcliffe for providing access to the solid phase NMR facilities and Dr. S. Brownstein and J. Bornais for access to the 400 MHz instrument at NRC. The 500 MHz spectra were obtained at Agriculture Canada, courtesy of Dr. B. Blackwell and J. Nikiforuk.

1. M. A. Bush and M. R. Truter. J. Chem. Soc. Perkin Trans. 2, 341 (1972).
2. I. R. Hansen. Acta Crystallogr. Sect. B: Struct. Crystallogr. Cryst. Chem. **B34**, 1026 (1978).
3. P. S. Belton, S. F. Tanner, K. M. Wright, M. P. Payne, M. R. Truter, and J. N. Wingfield. J. Chem. Soc. Perkin Trans. 2, 1307 (1985).
4. G. W. Buchanan, S. Mathias, Y. Lear, and C. Bensimon. Can. J. Chem. **69**, 404 (1991).
5. G. W. Buchanan, R. A. Kirby, and J. P. Charland. J. Am. Chem. Soc. **110**, 2477 (1988).
6. G. W. Buchanan, R. A. Kirby, K. Bourque, and C. Morat. Can. J. Chem. **66**, 2204 (1988).
7. G. W. Buchanan, K. Bourque, G. K. Diedrich, and M. Z. Khan. Magn. Reson. Chem. **25**, 65 (1987).
8. N. K. Wilson and J. B. Stothers. Top. Stereochem. **8**, 1 (1973).
9. H.-J. Schneider and V. Hoppen. Tetrahedron Lett. 579 (1974).
10. K. Seidman and G. E. Maciel. J. Am. Chem. Soc. **99**, 659 (1977).
11. G. W. Buchanan, C. Morat, R. A. Kirby, and J. S. Tse. Can. J. Chem. **69**, 1964 (1991).
12. G. W. Buchanan and R. A. Kirby. Tetrahedron Lett. **28**, 1507 (1987).
13. M. Dobler, J. D. Dunitz and P. Seiler. Acta Crystallogr. Sect. B: Struct. Crystallogr. Cryst. Chem. **B30**, 2741 (1974).
14. G. W. Buchanan, R. A. Kirby, and J. P. Charland. Can. J. Chem. **68**, 49 (1990).
15. J. E. Huheey. Inorganic chemistry: principles of structure and reactivity. 2nd ed. Harper and Row, New York. 1978.
16. G. Germain, P. Main, and M. M. Woolfson. Acta. Crystallogr. Sect A: Cryst. Phys. Diffr. Theor. Gen. Crystallogr. **A27**, 368 (1971).
17. E. J. Gabe, Y. Le Page, J. P. Charland, F. L. Lee, and P. S. White. J. Appl. Crystallogr. **22**, 384 (1989).
18. International tables for X-ray crystallography. Vol. 4. 2nd ed. Kynoch Press, Birmingham. 1974.

Can. J. Chem. Downloaded from www.nrcresearchpress.com by 92.62.229.171 on 09/08/12
For personal use only.

Stereochemistry of crown ethers. X-ray crystallographic structures, solid phase ^{13}C NMR, and solution conformational equilibria in *cis-syn-cis* dicyclohexano-15-crown-5 ether and its sodium thiocyanate complex

G. W. BUCHANAN[1] AND S. MATHIAS

Ottawa–Carleton Chemistry Institute, Department of Chemistry, Carleton University, Ottawa, Ont., Canada K1S 5B6

AND

C. BENSIMON AND J. P. CHARLAND

Division of Chemistry, National Research Council of Canada, Ottawa, Ont., Canada K1A 0R9

Received January 9, 1991[2]

G. W. BUCHANAN, S. MATHIAS, C. BENSIMON, and J. P. CHARLAND. Can. J. Chem. **70**, 981 (1992).

The structures of the title materials have been determined via X-ray crystallography. In the free crown ether, there is effectively a plane of symmetry that bisects the molecule. In the NaNCS complex, ring inversion of one of the cyclohexane moieties has occurred, giving a distorted pentagonal pyramidal coordination geometry about the sodium ion. For the free crown, two conformers, whose free energies differ by ca. 0.5 kJ/mol in solution can be detected via ^{13}C NMR at 168 K. Limiting low-temperature solution spectra are compared to those which have been obtained in the solid phase using the ^{13}C CPMAS technique.

Key words: crown ethers, stereochemistry, X-ray, NMR.

G. W. BUCHANAN, S. MATHIAS, C. BENSIMON et J. P. CHARLAND. Can. J. Chem. **70**, 981 (1992).

On a déterminé les structures des produits mentionnés dans le titre par diffraction des rayons X. Dans l'éther couronne à l'état libre, il existe un plan de symétrie qui bissecte la molécule. Dans le complexe NaNCS, il se produit une inversion des cycles des portions cyclohexaniques; il s'ensuit que la coordination autour du sodium est de type pyramide pentagonale déformée. Pour la couronne libre, à 168 K, la RMN du ^{13}C permet de détecter deux conformères dont les énergies libres diffèrent par environ 0,5 kJ/mol, en solution. On a comparé les spectres obtenus à la limite inférieure de température supportée par la solution avec ceux qui ont été obtenus en phase solide à l'aide de la technique du CPMAS du ^{13}C.

Mots clés : éthers couronnes, stéréochimie, rayons X, RMN.

[Traduit par la rédaction]

Introduction

In crown ether chemistry, the 15-crown-5 system is of interest because of its efficiency for internal encapsulation of the sodium ion. For benzo-15-crown-5, the structures of the free crown as well as the hydrated NaI complex have been determined via X-ray crystallography (1, 2). The solid phase ^{13}C NMR spectrum of the free crown has also been published (3). Recently we reported the X-ray structures, ^{13}C CPMAS NMR, and solution NMR behaviour of dibenzo-15-crown-5 and its NaNCS complex (4). With respect to the derived dicyclohexano 15-crown-5 systems, however, nothing has appeared in the literature to date.

Presently, we report the synthesis, X-ray structures, and solution conformational dynamics for the *cis-syn-cis* isomer of dicyclohexano-15-crown-5 and its NaNCS complex. The limiting low-temperature solution spectra of these materials are compared to solid phase ^{13}C spectra. Results are discussed with respect to those for the analogous dicyclohexano-14-crown-4 molecules (5, 6) and *cis*-cyclohexano-15-crown-5 (7).

Results and discussion

The structures and numbering schemes for the systems examined are presented in Fig. 1. The dispositions of the cyclohexane rings are consistent with those determined via X-ray crystallography. Bond lengths and angles are listed in

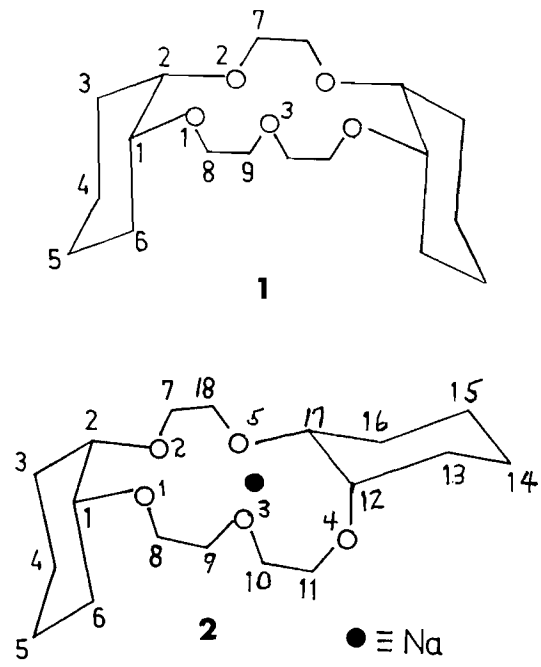

FIG. 1. Structures and numbering schemes for *cis-syn-cis*-dicyclohexano-15-crown-5, **1**, and its NaNCS complex **2**.

[1]Author to whom correspondence may be addressed.

[2]Revision received September 20, 1991.

Can. J. Chem. Downloaded from www.nrcresearchpress.com by 92.62.229.171 on 09/08/12
For personal use only.

Can. J. Chem. Downloaded from www.nrcresearchpress.com by 92.62.229.171 on 09/08/12
For personal use only.

TABLE 1. Bond lengths (Å) and angles (°) (*a*) for **1**; (*b*) for **2**

(*a*)

Bond	Length	Bond	Length
O1—C1	1.4225(24)	C1—C6	1.508(3)
O1—C8	1.416(3)	C2—C3	1.521(3)
C8—C9	1.487(3)	C3—C4	1.511(4)
O2A—C2	1.216(5)	C4—C5	1.512(3)
O2A—C7A	1.422(6)	C5—C6	1.516(3)
O2B—C2	1.628(5)	C7A—C7B′	1.482(6)
O3—C9	1.4070(23)		
C1—C2	1.514(3)		

Bonds	Angle	Bonds	Angle
C1—O1—C8	113.22(14)	C4—C5—C6	111.67(16)
O2B—O2A—C2	117.7(8)	C1—C6—C5	110.40(18)
C2—O2A—C7A	119.0(4)	O2A—C7A—C7B′	107.9(4)
C2—O2B—C7B	115.2(4)	C9—O3—C9′	114.15(19)
O1—C1—C2	112.33(14)		
O1—C1—C6	109.84(16)	C2—C1—C6	110.76(17)
O2B—C7B—C7A′	113.1(5)	O2A—C2—C1	121.4(3)
O2A—C2—C3	106.9(3)	O2B—C2—C1	102.20(25)
O2B—C2—C3	110.1(3)	C1—C2—C3	109.96(17)
O1—C8—C9	110.40(19)	C2—C3—C4	111.52(22)
O3—C9—C8	108.13(18)	C3—C4—C5	111.44(19)

′*x*, *y*, 1.5-*z*

(*b*)

Bond	Length	Bond	Length
S—C19	1.623(6)	N—C19	1.140(7)
Na—O1	2.401(3)	C1—C2	1.508(7)
Na—O2	2.515(3)	C1—C6	1.498(7)
Na—O3	2.412(3)	C2—C3	1.518(7)
Na—O4	2.494(3)	C3—C4	1.520(8)
Na—O5	2.343(3)	C4—C5	1.511(8)
Na—N	2.347(5)	C5—C6	1.513(8)
O1—C1	1.435(6)	C7—C18	1.502(7)
O1—C8	1.418(7)	C8—C9	1.489(10)
O2—C2	1.437(5)	C10—C11	1.481(9)
O2—C7	1.426(5)	C12—C13	1.527(6)
O3—C9	1.433(7)	C12—C17	1.506(6)
O3—C10	1.424(7)	C13—C14	1.518(8)
O4—C11	1.435(6)	C14—C15	1.499(10)
O4—C12	1.425(5)	C15—C16	1.519(7)
O5—C17	1.442(5)	C16—C17	1.507(6)
O5—C18	1.422(5)		
O1····O5	4.288(7)	O1····O4	4.561(7)
O2····O4	4.586(7)	O2····O3	4.185(7)
O3····O5	3.855(7)		

Bonds	Angle	Bonds	Angle
O1—Na—O2	68.64(11)	C17—O5—C18	115.5(3)
O1—Na—O3	69.82(12)	Na—N—C19	154.8(4)
O1—Na—O4	137.38(12)	O1—C1—C2	112.0(4)
O1—Na—O5	129.35(12)	O1—C1—C6	108.1(4)
O1—Na—N	97.41(15)	C2—C1—C6	110.9(4)
O2—Na—O3	116.30(12)	O2—C2—C1	106.5(4)
O2—Na—O4	132.57(11)	O2—C2—C3	112.2(4)
O2—Na—O5	68.09(10)	C1—C2—C3	110.7(4)
O2—Na—N	117.19(14)	C2—C3—C4	110.7(5)
O3—Na—O4	67.56(11)	C3—C4—C5	112.0(5)
O3—Na—O5	108.34(11)	C4—C5—C6	112.2(5)
O3—Na—N	114.14(15)	C1—C6—C5	112.0(5)

TABLE 1 (*concluded*)

Bonds	Angle	Bonds	Angle
O4—Na—O5	66.46(10)	O2—C7—C18	107.4(4)
O4—Na—N	99.81(15)	O1—C8—C9	107.3(6)
O5—Na—N	125.31(15)	O3—C9—C8	109.0(5)
Na—O1—C1	113.4(3)	O3—C10—C11	108.5(5)
Na—O1—C8	113.3(3)	O4—C11—C10	108.4(5)
C1—O1—C8	115.2(4)	O4—C12—C13	112.5(4)
Na—O2—C2	114.11(25)	O4—C12—C17	107.2(3)
Na—O2—C7	112.20(23)	C13—C12—C17	110.0(4)
C2—O2—C7	114.9(3)	C12—C13—C14	110.9(4)
Na—O3—C9	110.6(3)	C13—C14—C15	111.1(5)
Na—O3—C10	105.1(3)	C14—C15—C16	110.7(5)
C9—O3—C10	114.2(4)	C15—C16—C17	110.3(4)
Na—O4—C11	113.9(3)	O5—C17—C12	105.8(3)
Na—O4—C12	116.08(22)	O5—C17—C16	112.1(3)
C11—O4—C12	114.0(4)	C12—C17—C16	112.3(4)
Na—O5—C17	112.51(23)	O5—C18—C7	107.0(4)
Na—O5—C18	113.3(3)	S—C19—N	179.7(4)

Table 1 for the free crown ether **1** and its NaNCS complex **2**. Torsion angles involving ring skeletal atoms are provided in Table 2 while the crystallographic data are collected in Table 3. Atomic parameters are reported in Table 4 and ^{13}C NMR chemical shifts are collected in Table 5. Figure 2 shows stereoviews of **1** and **2**.

For **1** and **2** the initial point of interest from the X-ray data concerns the conformations of the cyclohexane rings. In **1**, since there is disorder present at the C7 site, the molecule effectively possesses a plane of symmetry as depicted below.

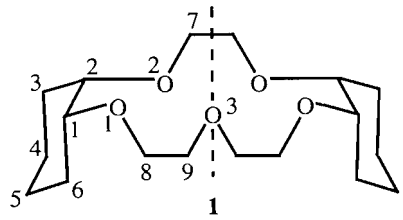

1

In contrast, for the NaNCS complex **2** one of the cyclohexane rings has undergone an inversion process (below).

This behaviour is opposite to that found by X-ray crystallography for the analogous dicyclohexano-14-crown-4 system (5), where the free crown ether lacks any true symmetry element while the LiNCS complex has a plane of symmetry. Further discussion of X-ray structures will be presented in Sect. (*iii*).

(i) Solid phase ^{13}C NMR spectra

Figure 3 contains the solid phase ^{13}C spectra of **1** and **2**. For a system such as **1**, which possesses a plane of symmetry, nine resonances are expected in the solid phase ^{13}C spectrum in the absence of crystal packing effects, multiple conformations, or non-identical molecular environments in the unit cell (3). Indeed the spectrum of solid **1** is consistent with expectations, there being four non-oxygenated resonances of approximately equal intensity in the range of 20–30 ppm and five oxygenated resonances in the range of 69–80 ppm.

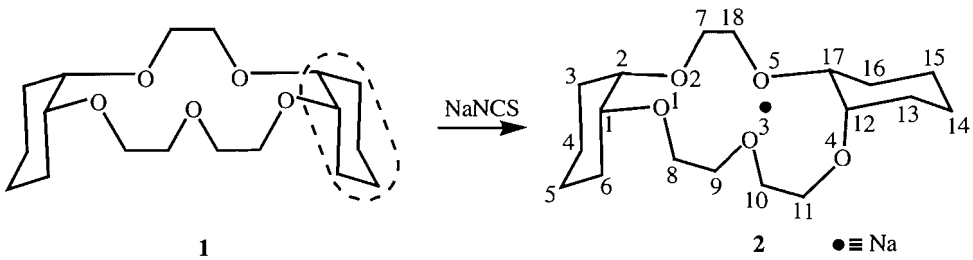

1 **2** ●≡ Na

By analogy with our earlier work (5, 6) and the known influence of axial and equatorial oxygen on chemical shifts of cyclohexyl carbons (8, 9), assignments of the six clearly resolved lines can be made with some confidence. The largest shift difference is apparent for the methine carbons bearing oxygen, where C2, bearing an axial oxygen, is shielded by 7.66 ppm relative to C1 bearing an equatorial moiety. A 4.51 ppm difference is apparent between the resonance for C4 (γ-*gauche* to O2) relative to C5 (γ-*trans* to O1), with C4 being the more shielded. The C3 and C6 sites, being β to oxygen, show only a minor shift difference (28.70 vs. 29.89 ppm) with the C3 site, which is β to axial oxygen, being the more shielded. The three closely spaced CH_2O resonances (69.90–70.82 ppm) cannot be assigned unambiguously.

In the case of **2**, the lack of symmetry in the crystal structure is reflected in the appearance of the solid phase ^{13}C spectrum, there being six clearly discernible resonances in the oxygenated carbon region as well as highly skewed intensities for the four resolved aliphatic carbon lines present in the range of 20–30 ppm.

Can. J. Chem. Downloaded from www.nrcresearchpress.com by 92.62.229.171 on 09/08/12
For personal use only.

TABLE 2. Torsion angles (°) involving C and O atoms of the crown ether

1				2	
	15-membered ring				15-membered ring
C8—O1—C1—C2	92.8(2)			C8—O1—C1—C2	85.5(4)
O1—C1—C2—O2B	64.7(2)	O1—C1—C2—O2A	55.8(3)	O1—C1—C2—O2	56.8(3)
C7B—O2B—C2—C1	−144.2(4)	C7A—O2A—C2—C1	−77.4(3)	C7—O2—C2—C1	−170.4(5)
C2—O2B—C7B—C7A′	78.1(6)			C2—O2—C7—C18	169.8(5)
O2B—C7B—C7A′—O2A′	168.3(6)			O2—C7—C18—O5	−61.3(3)
C7B—C7A′—O2A′—C2′	157.0(5)			C17—O5—C18—C7	−171.5(5)
				C18—O5—C17—C12	166.0(5)
				O4—C12—C17—O5	55.8(3)
				C11—O4—C12—C17	−162.4(5)
				C12—O4—C11—C10	156.5(6)
				O3—C10—C11—O4	−58.4(4)
				C9—O3—C10—C11	−171.8(7)
C9′—O3—C9—C8	177.4(2)			C10—O3—C9—C8	−166.2(7)
O1—C8—C9—O3	73.7(2)			O1—C8—C9—O3	61.8(4)
C1—O1—C8—C9	−166.9(2)			C1—O1—C8—C9	−177.2(6)
	Cyclohexyl rings				Cyclohexyl rings
C6—C1—C2—C3	58.4(2)			C6—C1—C2—C3	58.1(4)
C1—C2—C3—C4	−56.2(2)			C1—C2—C3—C4	−56.9(4)
C2—C3—C4—C5	54.1(2)			C2—C3—C4—C5	53.8(4)
C3—C4—C5—C6	−53.8(2)			C3—C4—C5—C6	−51.6(4)
C4—C5—C6—C1	55.8(1)			C4—C5—C6—C1	52.7(4)
C2—C1—C6—C5	−58.2(2)			C2—C1—C6—C5	−55.8(4)
O1—C1—C2—C3	−178.4(3)			O1—C1—C2—C3	179.1(6)
O1—C1—C6—C5	177.1(2)			O1—C1—C6—C5	−179.1(6)
C8—O1—C1—C6	−143.5(2)			C8—O1—C1—C6	−151.9(5)
O2A—C2—C3—C4	77.4(3)	O—2B—C2—C3—C4	55.6(2)	O2—C2—C3—C4	62.0(4)
C6—C1—C2—O2A	−67.4(3)	C6—C1—C2— 2B	−58.6(2)	C6—C1—C2—O2	−64.1(4)
C7A—O2A—C2—C3	155.4(5)	C7B—O2B—C2—C3	99.0(4)	C7—O2—C2—C3	68.3(4)
C6′—C1′—C2′—C3′	−58.4(2)			C13—C12—C17—C16	55.8(3)
C1′—C2′—C3′—C4′	56.2(2)			C17—C12—C13—C14	−55.2(4)
C2′—C3′—C4′—C5′	−54.1(2)			C12—C13—C14—C15	56.8(4)
C3′—C4′—C5′—C6′	53.8(2)			C13—C14—C15—C16	−57.3(4)
C4′—C5′—C6′—C1′	−55.8(1)			C14—C15—C16—C17	56.7(4)
C2′—C1′—C6′—C5′	58.2(2)			C15—C16—C17—C12	−56.6(4)
C6′—C1′—C2′—O2A′	67.4(3)	C6′—C1′—C2′—O2B′	58.6(2)	C13—C12—C17—O5	178.4(5)
O2A′—C2′—C3′—C4′	−77.4(3)	O2B′—C2′—C3′—C4′	−55.6(2)	C15—C16—C17—O5	−175.6(6)
C7A′—O2A′—C2′—C3′	−155.4(5)	C7B′—O2B′—C2′—C3′	−99.0(4)	C18—O5—C17—C16	−71.2(3)
O1′—C1′—C6′—C5′	−177.1(2)			O4—C12—C13—C14	64.2(4)
O1′—C1′—C2′—C3′	178.4(3)			O4—C12—C17—C16	−66.8(3)
C8′—O1′—C1′—C6′	143.5(2)			C11—O4—C12—C13	76.6(4)

One notable difference in the chemical shifts for solid **1** vs. **2** concerns the CH_2-O carbons. In **2**, the resonances for C8, 9, 10, and 11 are all shielded by at least 3.6 ppm relative to C8 and C9 of **1**. Examination of the torsional angles present in the X-ray structures provides an explanation based on the O—C—C—O networks. For **2**, these angles are 58.4° for the O4—C11—C10—O3 network and 61.8° for the O3—C9—C8—O1 case. In **1**, however, the O3—C9—C8—O1 network has a dihedral angle of 73.7°. Based on the known experimental (8, 9) and theoretical (10, 11) angular dependence of the γ-*gauche* effect in ^{13}C NMR, one expects the expansion of the O—C—C—O dihedral angle from ca. 60° to 75° to lead to substantial deshielding in **1** as observed.

From the spectrum of **2** it is evident that one of the methine carbons bearing axial oxygen appears at 74.32 ppm and the other is part of the overlapping broad signal centered at 70.85 ppm. Comparison of the torsional angle environ-

Can. J. Chem. Downloaded from www.nrcresearchpress.com by 92.62.229.171 on 09/08/12
For personal use only.

TABLE 3. Crystal data for dicyclohexyl-15-crown-5 ether (**1**) and the NaSCN-dicyclohexyl-15-crown-5-ether complex (**2**)

Parameter	Values (**1**)	Values (**2**)
Empirical formula	$NaSNC_{19}H_{32}O_5$	$C_{18}H_{32}O_5$
Formula weight	409.51	328.45
Crystal size, mm	0.12 × 0.23 × 0.35	0.20 × 0.20 × 0.30
Crystal system	Monoclinic	Orthorhombic
Space group	$P2_1/n$ (no. 14, $P2_1/c$)	*Pbnm* (no. 62, *Pnma*)
Z (molecules/cell)	4	4
a, Å	11.0602(6)	7.1720(6)
b, Å	15.1331(8)	10.6311(10)
c, Å	13.3430(6)	23.756(3)
β, deg	100.24(1)	
Cell volume, Å^3	2197.7(2)	1811.3(3)
D_{calc}, g cm^3	1.238	1.204
μ, mm^{-1}	0.19	0.66
Accurate cell parameters from:		
No. of reflections	19	26
2θ range	30–37	100–120
λ, Å	0.70930 (MoKα$_1$)	1.54056 (CuKα$_1$)
$2\theta_{max}$, deg	49.9	119.8
Octants measured	$+h,k,l$; $-h,k,l$; $-h,-k,-l$*	hkl; $-h,-k,-l$*
h range	−12–12	0–7
k range	0–17	0–11
l range	0–15	0–26
Reflections measured	4262	2214
Unique reflections	3839	1366
Reflections observed	1753	1130
$I_{net}/\sigma(I_{net})$ ratio	2.5	2.5
No. of parameters	373	195
R_f (significant reflections)	0.045	0.041
R_w (significant reflections)	0.043	0.055
Goodness-of-fit	1.3	2.3
Weighting scheme	$w^{-1} = \sigma^2(F_o) + 0.0003F_o^2$	$w^{-1} = \sigma^2(F_o) + 0.0003F_o$
Maximum Δ/σ (last cycle)	0.04	0.01
Final D-map background, e/Å^3	<0.19	<0.15
Secondary extinction coefficient	0.6(1)	0.12(6)

*A portion of the $-h,-k,-l$ data segment was collected.

ments for C2 vs. C12 shows that there are two pairs of networks in which significant dihedral angle differences exist. In the C8—O1—C1—**C2** case, θ = 85.5°, while for C18—O5—C17—**C12**, θ = 166.0°. For the C7—O2—**C2**—C3 case, θ = 68.3°, while for C11—O4—**C12**—C13, θ = 76.6°. Based on the aforementioned angular dependencies of ^{13}C steric shifts (8–11), and considering these geometrical differences, the expectation is that C12 would be the more deshielded of this pair of carbons and is thus assigned the resonance at 74.32 ppm.

(ii) Solution ^{13}C spectra

For **1** at 298 K, nine resonances are observed, in accord with the effective twofold symmetry of the molecule induced by rapid cyclohexane inversion on the NMR timescale. Two closely spaced methine carbon resonances appear at 77.90 and 77.72 ppm, since C1 and C2 remain in slightly different environments even in the presence of rapid ring inversion. For the CH_2-O carbons, three lines are observed, as expected, in the range of 68–71 ppm. Due to extensive overlap in the ^1H spectrum of **1** (even at 500 MHz) one cannot use COSY methods for clear distinction between CH_2-O resonances and hence the HETCOR experiment for ^{13}C assignments cannot be employed. For the C3,6 sites again a closely spaced pair of ^{13}C resonances is present, in this case at 27.91 and 27.76 ppm. Finally, two resonances are seen for the C4 and C5 sites at 22.87 and 22.05 ppm, in agreement with its effective symmetry at 298 K in solution.

It is of interest to compare the solid state conformation with that in solution under conditions where cyclohexane ring inversion is slow on the NMR timescale. Reduction of the temperature of the CD_2Cl_2 solution of **1** induced broadening followed by the emergence of a much more complex spectrum at the slow exchange limit of 168 K (Fig. 4). A closer examination of the methine carbon region (Fig. 5) gives an

Can. J. Chem. Downloaded from www.nrcresearchpress.com by 92.62.229.171 on 09/08/12
For personal use only.

Can. J. Chem. Downloaded from www.nrcresearchpress.com by 92.62.229.171 on 09/08/12
For personal use only.

TABLE 4. Atomic coordinates of non-H atoms of dicyclohexyl-15-crown-5 ether, **1**, and its NaSCN complex, **2**

Atom	x	y	z	B_{iso}
		1		
O1	1.10464(19)	0.77422(12)	0.85595(5)	4.19(6)
O2A*	0.7390 (8)	0.6763 (4)	0.82499(21)	4.17(19)
O2B*	0.7883 (8)	0.6245 (4)	0.82507(21)	3.92(20)
O3	1.1786 (3)	0.89990(18)	3/4	4.24(9)
C1	0.9516 (3)	0.75703(16)	0.89324(7)	3.42(7)
C2	0.7668 (3)	0.75184(23)	0.86252(8)	4.49(10)
C3	0.6083 (4)	0.7371 (3)	0.90456(10)	5.40(12)
C4	0.6352 (3)	0.62255(19)	0.94132(8)	4.12(9)
C5	0.8234 (3)	0.62399(21)	0.96994(8)	4.58(10)
C6	0.9807 (3)	0.63986(21)	0.92790(9)	4.55(10)
C7A*	0.8159 (8)	0.6997 (5)	0.77083(14)	4.38(20)
C7B*	0.7040 (8)	0.6290 (4)	0.77097(14)	4.34(20)
C8	1.1537 (3)	0.90212(21)	0.84837 (9)	4.49(9)
C9	1.2825 (3)	0.9160 (3)	0.79971(8)	4.73(11)
		2		
S	−0.10452(14)	0.22259(9)	0.63449(11)	6.47(7)
NA	0.27594(15)	0.39590(10)	0.62068(12)	4.42(8)
O1	0.3625 (3)	0.34192(20)	0.78720(23)	5.28(17)
O2	0.27706(24)	0.51361(17)	0.75395(19)	3.78(13)
O3	0.4694 (3)	0.32355(20)	0.6170 (3)	5.56(17)
O4	0.3319 (3)	0.39752(19)	0.44770(21)	4.39(14)
O5	0.28393(24)	0.53812(17)	0.55282(19)	3.72(13)
N	0.1052 (5)	0.3013 (3)	0.5902 (4)	7.3 (3)
C1	0.3319 (5)	0.3952 (3)	0.8681 (4)	4.7 (3)
C2	0.3507 (5)	0.4923 (3)	0.8509 (3)	4.4 (3)
C3	0.3155 (6)	0.5468 (4)	0.9369 (4)	5.3 (3)
C4	0.1834 (6)	0.5285 (4)	0.9478 (5)	5.3 (3)
C5	0.1597 (6)	0.4310 (4)	0.9595 (5)	5.9 (3)
C6	0.2011 (5)	0.3764 (4)	0.8767 (5)	5.3 (3)
C7	0.2974 (5)	0.5995 (3)	0.7163 (3)	4.11(25)
C8	0.4884 (6)	0.3189 (5)	0.7973 (5)	6.5 (4)
C9	0.5031 (7)	0.2682 (5)	0.7046 (5)	7.1 (4)
C10	0.4521 (7)	0.2774 (4)	0.5225 (5)	6.7 (4)
C11	0.4357 (5)	0.3431 (4)	0.4388 (5)	5.4 (3)
C12	0.3336 (4)	0.4820 (3)	0.4008 (3)	3.94(23)
C13	0.2976 (5)	0.4775 (4)	0.2850 (4)	5.3 (3)
C14	0.1656 (6)	0.4470 (6)	0.2538 (5)	6.9 (4)
C15	0.0793 (6)	0.5062 (5)	0.2972 (4)	6.4 (4)
C16	0.1135 (4)	0.5099 (4)	0.4126 (4)	4.5 (3)
C17	0.2447 (4)	0.5400 (3)	0.4439 (3)	3.58(22)
C18	0.2313 (5)	0.6039 (4)	0.6079 (4)	4.2 (3)
C19	0.0187 (5)	0.2689 (3)	0.6087 (3)	4.54(24)

B_{iso} is the mean of the principal axes of the thermal ellipsoid

*Occupancy factor = 0.5.

insight into the conformational processes that have occurred with respect to the cyclohexane moieties.

From the aforementioned doublet near 77.8 ppm have emerged six CH-O resonances in the range of 79.92–73.13 ppm. We attribute the high-intensity pair at 79.33 and 74.51 ppm to the C1 and C2 sites, respectively, of the symmetrical conformation of **1** illustrated above. The two minor lines of equal intensity at 79.92 and 78.56 ppm are attributed to methine carbons bearing equatorial oxygen in an asymmetric conformation of **1**. Similarly, the pair of lines at 75.60 and 73.13 ppm is deemed to arise from methine carbons bearing axial oxygen in the asymmetric conformation of **1**. Such a conformation could arise as a result of a single cyclohexane inversion depicted below.

Such a duality of conformations has previously been elucidated in the dicyclohexyl-14-crown-4 ether series (12). From the integrated intensities one can calculate K_{eq} and hence the ground state free energy difference ($-\Delta G^0$) between the symmetric and the asymmetric conformations at 168 K using the equation $-\Delta G^0 = RT \ln K_{eq}$. The result is that the symmetric conformation is calculated to be more stable by only 0.50 ± 0.20 kJ/mol.

For **2**, the ^{13}C spectrum at 298 K again shows nine resonances, consistent with rapid conformational averaging on

the NMR timescale. From $^1H-^{13}C$ HETCOR and $^1H-^1H$ COSY spectra at 500 MHz, assignment of the ^{13}C CH_2-O lines is possible in this case since there is less resonance overlap in the ^1H spectrum than is the case for **1**. It is useful to note that all geminal protons are magnetically nonequivalent in these systems, so that rather complex ^1H spectra are observed. Figure 6 shows a HETCOR spectrum.

The low-temperature ^{13}C spectra of **2** also exhibit decoalescence phenomena and the number of resonances increases markedly from the nine observed at 298 K. One cannot rule out the existence of multiple conformations here as well; however, sufficient peak resolution is not present to enable unravelling of the nature of the conformational processes that are occurring.

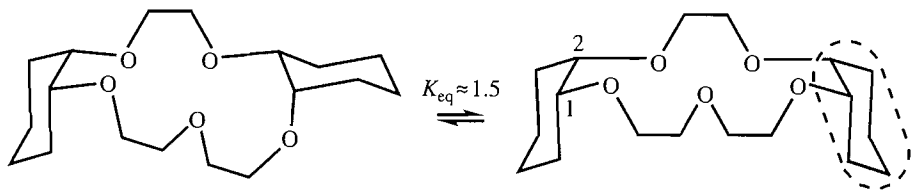

(iii) X-ray crystallographic structures

The ORTEP diagram for **1** is presented in Fig. 2*a*. In this depiction there are no symmetry elements. In fact, however, there is disorder (as illustrated below) at the C7 and O2 sites, with the disordered sites C7A, C7B, O2A, and O2B being equally populated. The crystallographic mirror plane passes through the mid-point of the C7A—C7B′ and C7A′—C7B bonds and the O3 site.

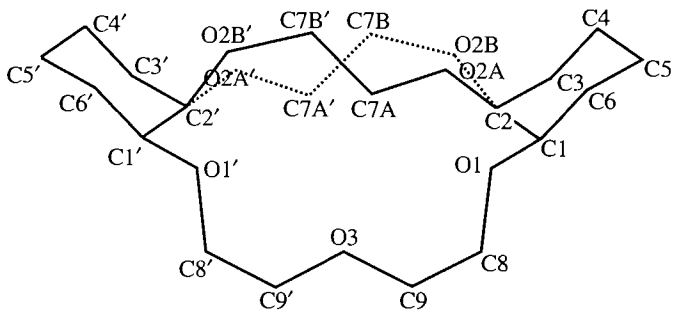

1

The solid phase ^{13}C NMR spectrum of **1** (Fig. 3), which contains nine lines, is consistent with the presence of this symmetry plane. Although there is some overlap of the three CH_2-O resonances near 70 ppm, there are six other clearly resolved resonances observed.

Normal torsion angles in crown ethers are such that O—C—C—O networks are *gauchoid* (dihedral angle ca. 60°) and all other four-atom moieties (ignoring hydrogens) are *transoid* (dihedral angle ca. 180°). In the case of **1**, the C8—O1—C1—C2 angle of 92.8° represents a major deviation, as do the C7A—O2A—C2—C3 and C7B—O2B—C2—C3 angles of 155.4° and 99.0° respectively. Other notable differences from "ideal" geometry are the C8—O1—C1—C6 network (143.5°), C7A—O2A—C2—C1 (77.4°), and C7B—O2B—C2—C1 (144.2°). For the O—C—C—O networks, the O1—C8—C9—O3 case shows significant expansion from pure *gauche* to 73.7°.

In the NaNCS complex **2**, the sodium ion is hexacoordinated to the five oxygen atoms of the crown ether and to the N atom of the SCN anion, resulting in a distorted pentagonal pyramidal coordination polyhedron. The five oxygens are not coplanar, the mean deviation from the least-squares plane connecting them being 0.27 Å. The cross-ring diagonal distances between "opposite" oxygens range from 3.855 to 4.586 Å, the average being 4.295 Å. As expected, the binding cavity is smaller than that found in the X-ray structure of the NaNCS · H_2O · 18-crown-6 complex (13), where the diagonal O—O distances in the 18-membered ring are ca. 5.100 Å on the average.

Data in Table 2 show that there is some distortion in the 15-membered ring from "ideal" conformations of crown ethers. This is particularly evident in the C8—O1—C1—C2 network where the torsion angle of 85.5° departs significantly from the "normal" value of near 180°. Similar types of distortions were observed in the LiNCS complexes of a related dicyclohexano-13-crown-4 system (14).

Figure 2*b* shows that the five ether oxygens are pointing towards the concave side of the crown ether, with the cyclohexane rings and the SCN^- side by side or with the anion coming in the concave side of the 15-membered ring. Hence the Na^+ appears to complex preferentially from the concave direction. Again there is similarity in the orientations of the anion and alkaline cation in the present case with that observed for LiNCS complexes in the analogous 13-crown-4 series (14).

TABLE 5. ^{13}C NMR chemical shifts (δ_C from TMS ± 0.01)

Carbon	**1** (solid)	**1** (solution)*	**2** (solid)	**2** (solution)
C1	73.32	(77.66)[b]	(78.85)[e]	(78.30)[i]
C2	80.98	(77.82)[b]	70.85	(77.47)[i]
C3	28.70	27.82	(26.89)[f]	(26.83)[j]
C4	21.22	(21.96)[c]	19.99	(22.67)[k]
C5	25.73	(22.75)[c]	(25.32)[g]	(20.66)[k]
C6	29.89	27.82	(26.89)[f]	(26.38)[j]
C7	(69.90)[a]	(68.17)[d]	(70.05)[h]	67.13
C8	(70.32)[a]	(68.78)[d]	66.34	66.57
C9	(70.66)[a]	(71.06)[d]	66.34	69.22
C10			66.34	
C11			66.34	
C12			74.32	
C13			(26.89)[f]	
C14			19.99	
C15			(25.10)[g]	
C16			(28.02)[f]	
C17			(80.02)[e]	
C18			(67.98)[h]	

*0.1 M in CD_2Cl_2 at 298 K.
[a-k]Indicate possible interchange of assignments.

Can. J. Chem. Downloaded from www.nrcresearchpress.com by 92.62.229.171 on 09/08/12
For personal use only.

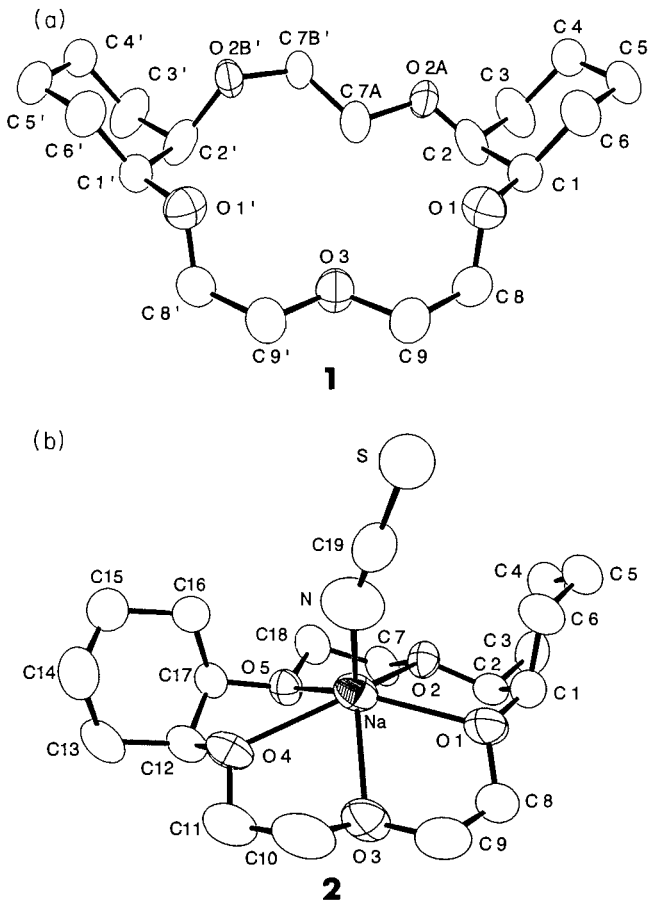

FIG. 2. (*a*) ORTEP diagram of **1**. (*b*) ORTEP diagram of **2**.

As noted earlier, the average diagonal distance between opposite oxygen atoms of **2** is 4.295 Å. By subtraction of twice the van der Waals radius of O (i.e., 2 × 1.4 Å) one can obtain the adjusted diameter of the binding cavity, 1.495 Å. Since the effective diameter of the Na^+ ion is 1.9–2.4 Å (15), the cavity is clearly too small to accommodate the Na^+ ion and hence this cation is found 0.84 Å out of the least-squares plane. By contrast, in the 18-crown-6 complex (13) the longer O—O distances result in an enlarged binding cavity diameter (ca. 2.3 Å) and hence the Na^+ lies only 0.27 Å out of the least-squares plane.

Finally, the Na—O distances listed in Table 1 are shorter when involving equatorial O's than when axial oxygens are bound (2.401 and 2.342 Å vs. 2.515 and 2.494 Å respectively). The Na—O3 distance of 2.412 Å falls in between. In the present 6-coordinate case, the average Na—O bond length of 2.433 Å is somewhat shorter than that in the 7-coordinate $NaNCS \cdot H_2O \cdot$ 18-crown-6 system (13).

Experimental

Crystallographic measurements, structure solution and refinement

Single crystals of **1** and **2** were mounted on glass fibres and measured on a Nonius CAD-4 diffractometer. Accurate cell parameters and intensity data were obtained at room temperature using graphite-monochromated CuKα radiation for **1** and MoKα radiation for **2**. Crystal data are provided in Table 3.

The space group $P2_1/n$ (alternate setting of $P2_1/c$) was uniquely defined from the systematic absences noted in the data of **2**. The intensity data for **1** revealed systematic absences consistent with two possible space groups. These are *Pbnm* (alternate setting *Pnma*) and $Pbn2_1$ (alternate setting of $Pna2_1$). Intensity data were corrected in the usual fashion for Lorentz and polarization-ratio factors but not for absorption. Other details pertaining to the data reduction step are listed in Table 3.

The positions of the non-H atoms of **2** were determined by direct methods with MULTAN (16). At this stage, isotropic refinement of all non-H atoms was carried out by full-matrix least squares. A subsequent difference map revealed the positions of the H atoms. They were included and refined isotropically while non-H atoms were refined anisotropically. The structures were refined to convergence by full-matrix least squares; $\Sigma w(|F_o| - |F_c|)^2$ was minimized with $w^{-1} = \sigma^2(F_o) + 0.0003F_o^2$. Details of the structure refinement of **2** and final *D*-map are given in Table 3.

The structure of **1** was solved in the space group $Pbn2_1$. As in **2**, positions of non-H atoms were derived from direct methods. A close inspection of the electron density maps based on the two possible space groups revealed positional disorder in the $-O-CH_2-CH_2-O$ bridge linking the two cyclohexane rings. Refinement of the occupancy factors of the disordered positions confirmed that this bridge was disordered over two equally populated positions. Least-squares refinement was continued with half-occupied C positions for the disordered bridge and isotropic thermal parameters for C and O atoms. There was further evidence of disorder. Results of refinement at this stage showed O atoms of the disordered bridge with thermal amplitudes much larger than the other non-H atoms of **1**. C—O and C—C distances in the disordered group were similar to those for analogous crown ethers (13, 14). However, two of the four $C_{cyclohexyl}—O—CH_2$ angles were unusually large (ca. 135°), which are highly improbable values.

The refinement of **1** in space group $Pbn2_1$, including H atoms at calculated positions and non-H atoms refined with anisotropic thermal parameters, would have made the number of reflections per refined parameter unacceptably low. As the space group of **1** could be *Pbnm*, cell symmetry was checked with the program MISSYM, which finds all metric symmetry elements from the atomic coordinates of any crystal structure and builds the generators in the unit cell (17). In addition to the *b* and *n* glide planes perpendicular to the *a* and *b* axes respectively, MISSYM detected mirror symmetry perpendicular to the *c* axis of the unit cell. Refinement of **1** was pursued in space group *Pbnm*.

H atoms bonded to non-disordered C atoms were added at calculated positions (C—H bond of 1.08 Å, sp^3 hybridized). Non-H atoms were defined anisotropically and H atoms isotropically. H atoms next to disordered positions C7A and C7B were successfully located in the next *D*-map and refined in the next least-squares cycles. At this stage, the *R* and R_w factors were ca. 1% higher than the final values quoted in Table 3. As the anisotropic thermal parameters of O2 described a highly and abnormally elongated 3D shape, this atom was removed from the structure and relocated in a subsquent *D*-map. The map revealed two positions. These were refined anisotropically as O atoms with half occupancies. This attempted refinement led to the lower residuals listed in Table 3. The high bond angle of ca. 135° centered at the formerly nondisordered O2 site has been replaced by more reasonable values averaging ca. 117°. However, the previous C2—O2 distance of ca. 1.4 Å is now showing systematically short and long C2—O2A and C2—O2B distances (see Table 1). Despite these geometrical distortions, the latter structural description with two partially (and equally) occupied $-O-CH_2-CH_2-O$ bridges linking the two cyclohexane rings has been used. It is of interest to note that similar structural distortions have been found in the X-ray structure of a related dicyclohexano-13-crown-4 ether (14). Details of the structure refinement of **1** and *D*-map are given in Table 3.

All computations were performed with the NRCVAX crystal package (17). The scattering curves were from the International Tables for X-ray Crystallography (18). Bond lengths and angles involving non-H atoms are presented in Table 1 while torsion angles involving ring skeletal atoms are given in Table 2. Refined coordinates of the non-H atoms of **1** and **2** are reported in Table 4.

Can. J. Chem. Downloaded from www.nrcresearchpress.com by 92.62.229.171 on 09/08/12
For personal use only.

Can. J. Chem. Downloaded from www.nrcresearchpress.com by 92.62.229.171 on 09/08/12
For personal use only.

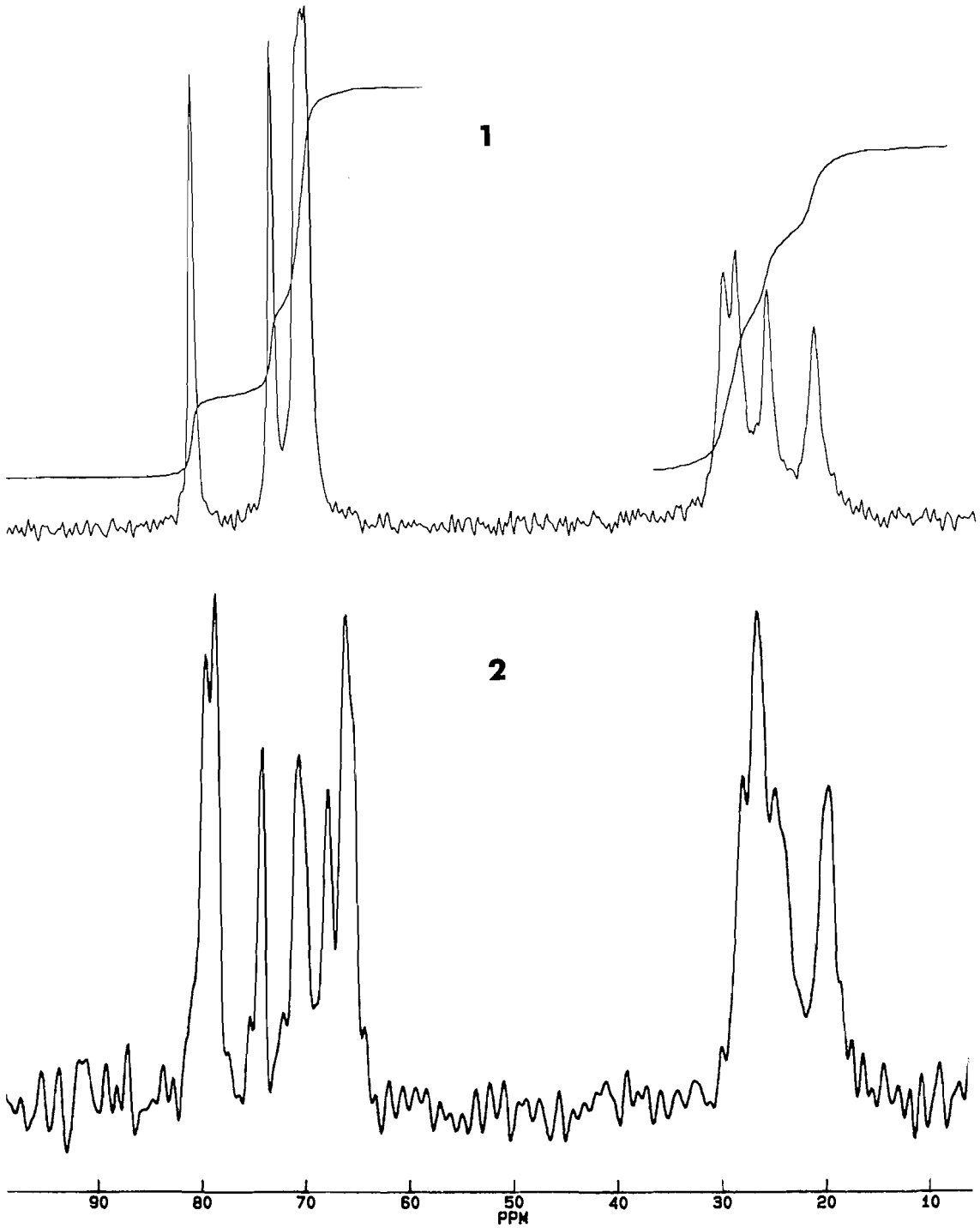

FIG. 3. 45.3 MHz solid phase ^{13}C NMR spectra.

Lists of anisotropic temperature factors, H atomic parameters, all bond lengths and angles, all torsion angles, and calculated, observed, and unobserved structure factors are deposited as Supplementary Material.[3]

[3]These data may be purchased from: The Depository of Unpublished Data, Document Delivery, CISTI, National Research Council Canada, Ottawa, Canada K1A 0S2.

Tables of hydrogen atom parameters and bond lengths and angles have also been deposited with The Cambridge Crystallographic Data Centre and can be obtained on request from The Director, Cambridge Crystallographic Data Centre, University Chemical Laboratory, Lensfield Road, Cambridge CB2 1EW, U.K.

Spectra

The ^{13}C CPMAS NMR spectra were recorded at 45.3 MHz on a Bruker CXP-180 spectrometer using techniques described previously (5). Chemical shifts were measured relative to external solid hexamethylbenzene (HMB) and converted to the TMS scale by the factor of 16.9 ppm, the chemical shift of the CH_3 group of HMB. The solution phase ^{13}C spectra were recorded at 100.6 MHz on a Bruker AM 400 system using conditions of complete ^1H noise decoupling. Typical spectral widths were 10 kHz with 32K data points for acquisition and zero filling to 64K. Normal pulse widths were 30° with a pulse delay of 2 s. Samples were ca. 0.1 M in CD_2Cl_2 solutions. The $^1H^{13}C$ HETCOR spectra were obtained on a Bruker AM 500 spectrometer using low decoupler power in the CW mode

Can. J. Chem. Downloaded from www.nrcresearchpress.com by 92.62.229.171 on 09/08/12
For personal use only.

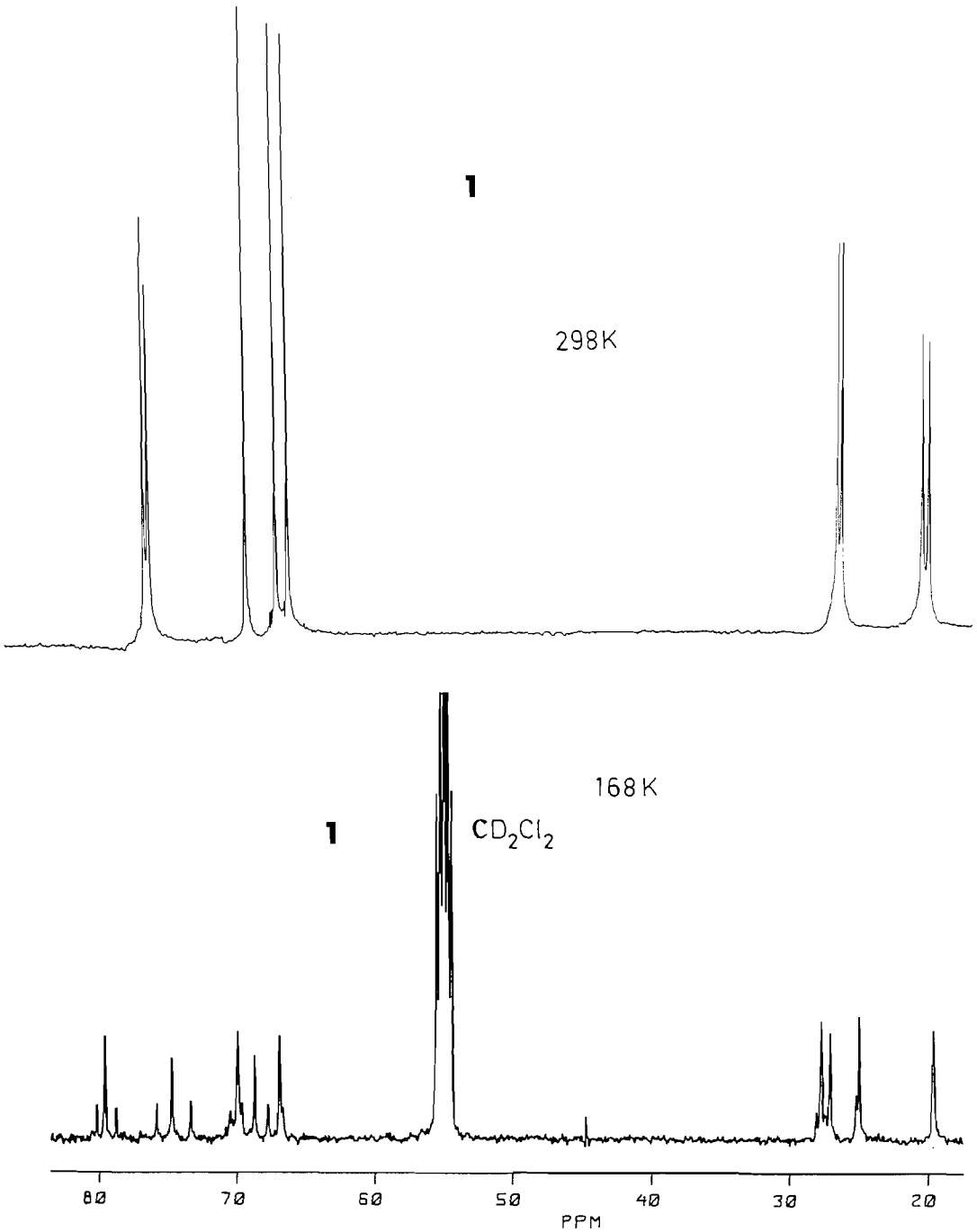

FIG. 4. 100.6 MHz ^{13}C solution spectra of **1** at 298 and 168 K.

(composite phase decoupling), with polarization transfer from ^{1}H to ^{13}C.

The FID's were acquired over 4096 data points for each of the 128 or 256 values of the evolution time, with digital resolution of 7 Hz/point in $F2$ and 5–10 Hz/point in $F1$. The raw data were zero-filled in $F1$ prior to Fourier transformation using the sine bell window function. Proton relaxation delays of 3–5 s were utilized.

Materials

Dibenzo-15-crown-5 was prepared as previously described (4). Hydrogenation of this material to a mixture of **1** and the *cis-anti-cis* isomer was accomplished using an American Instrument Co. 50 000 psi (1 psi = 6.9 kPa) maximum pressure high-pressure apparatus. In 60 mL of 1-butanol were dissolved 2.2 g (0.007 mol) of dibenzo-15-crown-5 and 0.40 g of 5% ruthenium on alumina catalyst. A pressure of 1200 psi was used and the reaction was allowed to proceed for 12 h at a temperature of 120°C. The catalyst was removed via filtration and the butanol by rotary evaporation to yield 2.1 g of a viscous yellow oil. From ^{13}C NMR there appeared to be two configurational isomers present in the ratio of ca. 2:1. Separation of these isomers was accomplished via column chromatography on activated silica gel of mesh size 100–200 using as initial eluent a mixture of 60:40 CH_2Cl_2–hexanes and a ratio of 50:1 silica gel to crude crown ether. Gradual introduction of diethyl ether in place of hexanes yielded **1** as the first isomer eluted, with 5% diethyl ether, 35% hexanes, and 60% CH_2Cl_2. Recrystallization from hexanes yielded the pure *cis-syn-cis* isomer **1**, as subsequently determined by X-ray crystallography, mp 67–68°C. The latter column fractions contained the minor, presumably *cis-anti-cis*, isomer, which remained an oil.

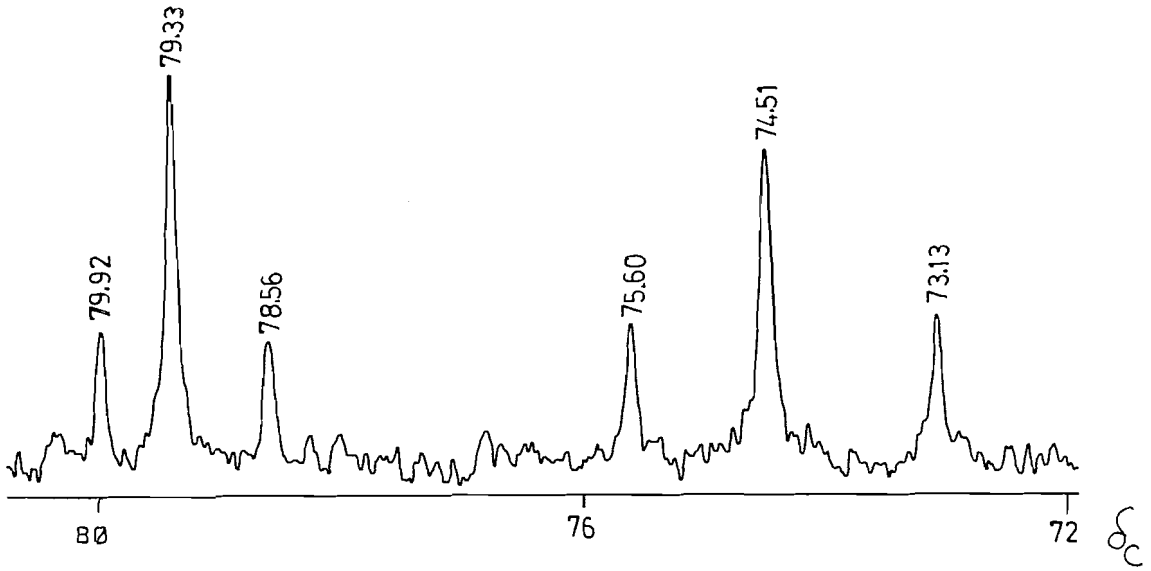

FIG. 5. Methine carbon region of 100.6 MHz spectrum of **1** at 168 K.

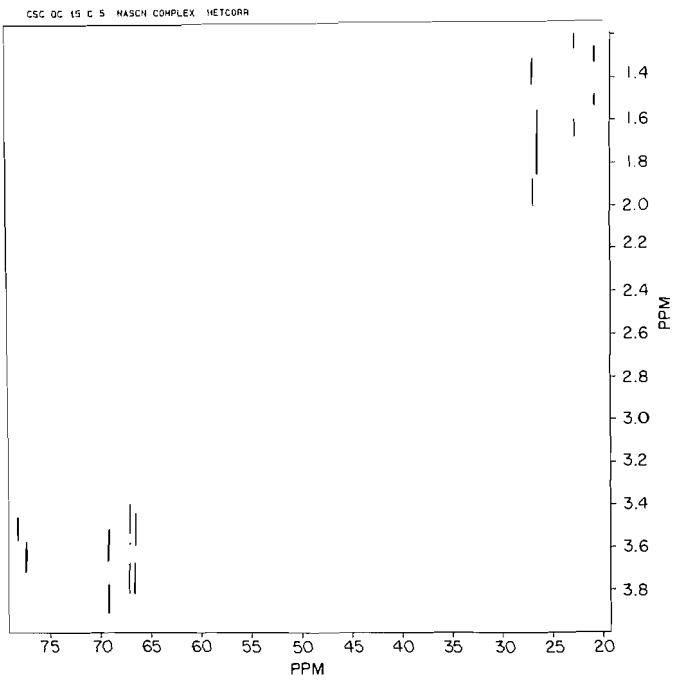

FIG. 6. $^{1}H^{13}C$ HETCOR spectrum of **2** at 500 MHz.

For preparation of the complex **2**, equimolar amounts of **1** and NaNCS were dissolved in a minimum volume of dry methanol. After allowing the mixture to stand for 2–3 h, the solvent was removed by rotary evaporation. Subsequent recrystallization from ethanol–hexanes yielded pure **2**, mp 140–141°C.

Acknowledgements

The continuing financial support of the Natural Sciences and Engineering Research Council of Canada via Operating Grants to G. W. B. is gratefully acknowledged. We thank Drs. J. A. Ripmeester and C. I. Ratcliffe for providing access to the solid phase NMR facilities and Dr. S. Brownstein and J. Bornais for access to the 400 MHz instrument at NRC. The 500 MHz spectra were obtained at Agriculture Canada, courtesy of Dr. B. Blackwell and J. Nikiforuk.

1. M. A. Bush and M. R. Truter. J. Chem. Soc. Perkin Trans. 2, 341 (1972).
2. I. R. Hansen. Acta Crystallogr. Sect. B: Struct. Crystallogr. Cryst. Chem. **B34**, 1026 (1978).
3. P. S. Belton, S. F. Tanner, K. M. Wright, M. P. Payne, M. R. Truter, and J. N. Wingfield. J. Chem. Soc. Perkin Trans. 2, 1307 (1985).
4. G. W. Buchanan, S. Mathias, Y. Lear, and C. Bensimon. Can. J. Chem. **69**, 404 (1991).
5. G. W. Buchanan, R. A. Kirby, and J. P. Charland. J. Am. Chem. Soc. **110**, 2477 (1988).
6. G. W. Buchanan, R. A. Kirby, K. Bourque, and C. Morat. Can. J. Chem. **66**, 2204 (1988).
7. G. W. Buchanan, K. Bourque, G. K. Diedrich, and M. Z. Khan. Magn. Reson. Chem. **25**, 65 (1987).
8. N. K. Wilson and J. B. Stothers. Top. Stereochem. **8**, 1 (1973).
9. H.-J. Schneider and V. Hoppen. Tetrahedron Lett. 579 (1974).
10. K. Seidman and G. E. Maciel. J. Am. Chem. Soc. **99**, 659 (1977).
11. G. W. Buchanan, C. Morat, R. A. Kirby, and J. S. Tse. Can. J. Chem. **69**, 1964 (1991).
12. G. W. Buchanan and R. A. Kirby. Tetrahedron Lett. **28**, 1507 (1987).
13. M. Dobler, J. D. Dunitz and P. Seiler. Acta Crystallogr. Sect. B: Struct. Crystallogr. Cryst. Chem. **B30**, 2741 (1974).
14. G. W. Buchanan, R. A. Kirby, and J. P. Charland. Can. J. Chem. **68**, 49 (1990).
15. J. E. Huheey. Inorganic chemistry: principles of structure and reactivity. 2nd ed. Harper and Row, New York. 1978.
16. G. Germain, P. Main, and M. M. Woolfson. Acta. Crystallogr. Sect A: Cryst. Phys. Diffr. Theor. Gen. Crystallogr. **A27**, 368 (1971).
17. E. J. Gabe, Y. Le Page, J. P. Charland, F. L. Lee, and P. S. White. J. Appl. Crystallogr. **22**, 384 (1989).
18. International tables for X-ray crystallography. Vol. 4. 2nd ed. Kynoch Press, Birmingham. 1974.

Can. J. Chem. Downloaded from www.nrcresearchpress.com by 92.62.229.171 on 09/08/12
For personal use only.

Photolysis of the 1-naphthylmethyl ester of substituted phenylacetic acids: intramolecular charge transfer and rates of decarboxylation of arylacyloxy radicals

JAMES W. HILBORN AND JAMES A. PINCOCK[1]

Department of Chemistry, Dalhousie University, Halifax, N.S., Canada B3H 4J3

Received July 24, 1991

JAMES W. HILBORN and JAMES A. PINCOCK. Can. J. Chem. **70**, 992 (1992).

The photolysis of esters **6** and **8** in methanol leads to products resulting from both naphthylmethyl cations and radicals. The product distribution is nearly independent of X for the esters **6** except when X equals methoxy. A mechanism involving initial homolytic cleavage of the carbon–oxygen bond in the excited singlet state of the ester is proposed. Competition between electron transfer in the radical pair to form the ion pair and decarboxylation of the arylacyloxy radical allows calculations of the rates for this decarboxylation process. The ρ value versus σ is close to zero. When X equals methoxy, intramolecular electron transfer occurs with the naphthalene ring serving as the acceptor and the methoxyaromatic as the donor. This exciplex fragments to carbon dioxide and 1-(1-naphthyl)-2-arylethane.

Key words: acyloxy radical, decarboxylation, photolysis of benzylic esters.

JAMES W. HILBORN et JAMES A. PINCOCK. Can. J. Chem. **70**, 992 (1992).

La photolyse des esters **6** et **8** dans le méthanol conduit à la formation de produits résultant à la fois de cations et de radicaux naphtylméthyles. Pour les esters **6**, la distribution des produits est indépendante de la nature de X, excepté lorsque X est un groupe méthoxyle. On propose un mécanisme impliquant un clivage initial homolytique de la liaison carbone–oxygène dans l'état singulet excité de l'ester. Une compétition entre le transfert d'électrons dans la paire de radicaux pour former la paire d'ions et la décarboxylation du radical arylacyloxy permet de calculer les vitesses de ce processus de décarboxylation. La valeur de ρ versus σ s'approche de zéro. Lorsque X est un groupe méthoxyle, il se produit un transfert intramoléculaire d'électrons avec le noyau naphtalénique servant de accepteur et le fragment méthoxyaromatique agissant comme donneur. Cet exciplexe se fragmente en dioxyde de carbone et 1-(1-naphtyl)-2-aryléthane.

Mots clés : radical acyloxy, décarboxylation, photolyse des esters benzyliques.

[Traduit par la rédaction]

Introduction

Benzylic substrates occupy a central place in the study of electronic effects on organic reactions. This is because variation of substituents along with application of linear free energy relationships (i.e., Hammett correlations) is an excellent probe of the charge changes that occur going from starting material to transition state. Moreover, the usual *meta* and *para* substituents are remote enough from the reaction site that steric effects are generally negligible. Even for radical reactions where charged intermediates are not involved, the decision of which σ scale to use and the sign and magnitude of the small, but measurable, ρ values have been valuable probes of reaction mechanism (1).

Recently, we showed (2) that the singlet photochemistry of 1-naphthylmethyl esters, **1**, in methanol solvent leads to the formation of three major products, as shown in eq. [1].

[1] $$\underset{\mathbf{1}}{ACH_2{-}O_2C{-}R} \xrightarrow[CH_3OH]{h\nu} \underset{\mathbf{2}}{ACH_2{-}OCH_3} + \underset{\mathbf{3}}{H{-}O_2C{-}R} + \underset{\mathbf{4}}{ACH_2{-}R}$$

The mechanism proposed to rationalize the product yields as a function of substituents on the naphthalene ring and changes in the structure of R is outlined in Scheme 1. The ether **2** and the acid **3** are formed by trapping of the 1-naphthylmethyl cation and carboxylate anion respectively. The hydrocarbon is formed from the radical pair that results after loss of carbon dioxide from the alkanoyloxy radical. Since mass balance for the reactions was excellent and only very small amounts of other radical derived products were detectable, essentially all the radical chemistry is occurring in-cage.

There has been considerable recent interest in the partitioning between heterolytic and homolytic pathways in benzylic photochemistry (3, 4). We have been able to rationalize the product yields for substrates **1** by a mechanism involving initial excited-state carbon–oxygen bond cleavage to form a singlet radical pair (i.e., $k_R^X >> k_I^X$). The product partitioning is then controlled by competition between k_{ET}^X, the electron transfer rate that converts the radical pair to the ion pair, and k_{CO_2} as a function of R. This is a quite different suggestion from the usual one that product yields are controlled, at least in part, by competition between k_R^X and k_I^X. Although there is no reason, in principle, why this would not also be true for substrates **1**, the simpler mechanism rationalizes all the cases that we have examined.

We now report results that allow a determination of the effect of substitutents on the rates of decarboxylation of the series of arylacetyloxy radicals, **5**, obtained by photolysis of the corresponding esters, **6**. In addition, we have examined the esters, **8**, in order to assess the effect of substituents directly attached to the developing radical center that results from decarboxylation of **7**.

[1]Author to whom correspondence may be addressed.

Can. J. Chem. Downloaded from www.nrcresearchpress.com by 92.62.229.171 on 09/08/12
For personal use only.

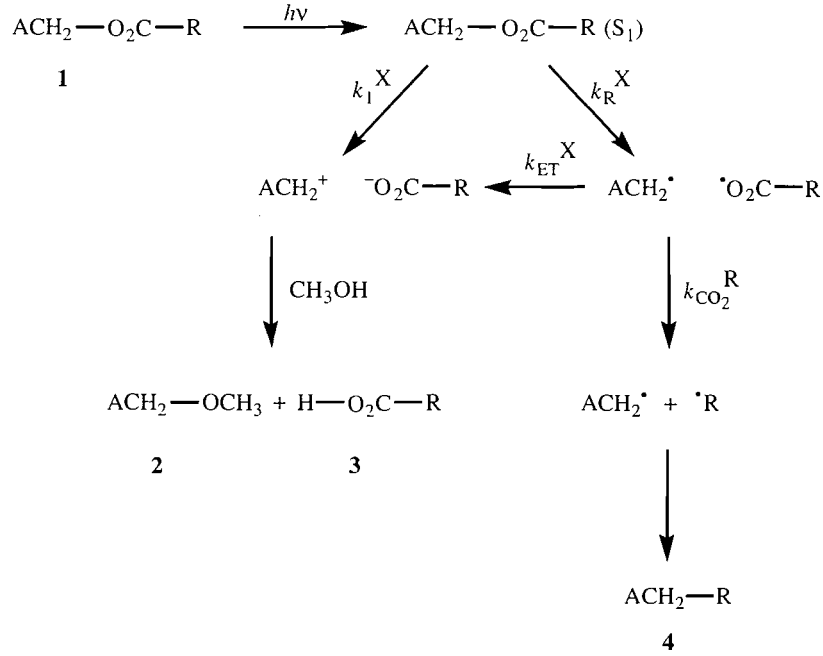

SCHEME 1. Mechanism of the photolysis of 1-naphthylmethyl esters in methanol solvent.

Results

The esters **6** and **8** were all synthesized by reaction of the corresponding acid chloride with 1-naphthylmethanol. Details of the procedure and data for characterization of the compounds are given in the experimental section.

Photolysis of the esters in methanol with a 200-W Hanovia medium-pressure Hg lamp using a Pyrex filter led to clean conversion to the products shown in eq. [1]: A = $C_{10}H_7$; R = X-$C_6H_4CH_2$ and R = X-CH_2. Reactions were monitored by HPLC and taken to completion for preparative scale runs. Photoproducts were isolated, purified, and used to make calibration standards for quantitative runs, which were run to lower conversion (<50%). No changes in product ratios as a function of photolysis time were detected and dark samples taken before and during irradiation were stable. No attempt was made to quantify the yield of the carboxylic acids, **9** (**3**, R = X-$C_6H_4CH_2$) and **10** (**3**, R = X-CH_2), but they could be cleanly isolated by acidification of basic extracts of the reaction mixture. Details of the photolysis procedure are in the experimental section. Values for the product yields in calibrated runs are shown in Table 1.

Also included in Table 1 are values for the quantum yield of fluorescence and the singlet lifetime for all the substrates in methanol.

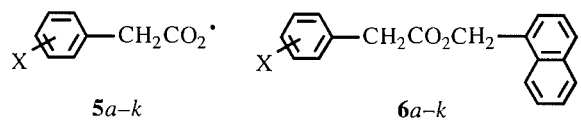

X

a: H
b: 4-OCH_3
c: 3-OCH_3
d: 4-CH_3
e: 3-CH_3
f: 4-F
g: 3-F
h: 4-CF_3
i: 3-CF_3
j: 4-CN
k: 3-CN

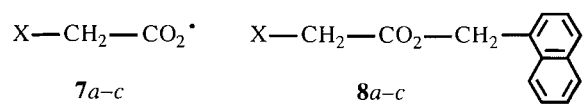

a: CH_3O
b: CN
c: CH_2=CH

Discussion

As the results in Table 1 indicate, the products shown in eq. [1] (i.e., the ether **2** and the coupling products, **11** (**4**, R = X-$C_6H_4CH_2$) or **12** (**4**, R = X-CH_2)), are formed and the mass balance is excellent. Since the yield of the ether is the easiest to quantify, we again (6) made the simplifying approximation that all starting material not accounted for by its formation has formed products from the radical pathway. Therefore, according to Scheme 1, k_{CO_2}/k_{ET}^X = yield of **2**/(100 − yield of **2**). As in our previous work (2, 6), we assume that k_{ET}^X is independent of the structure of the acyloxy radical and only dependent on the structure of the naphthalene ring. This assumption about k_{ET}^X is very reasonable for these substituted phenylacetyloxy radicals. A value of ρ = 0.5 has been measured (7) for the equilibrium acidities of substituted phenylacetic acids. If the substituent effect for the development of negative charge on the phenylacetyloxy radical as it is reduced to the corresponding anion is similar to this, then a ρ value equal to 30 mV/σ can be calculated for the reduction potentials. This gives a range in the reduction potentials of only 28 mV going from the best electron-donating group (4-CH_3O) to the best electron-withdrawing one (4-CN). The plot (2) of log k_{ET}^X as a

Can. J. Chem. Downloaded from www.nrcresearchpress.com by 92.62.229.171 on 09/08/12
For personal use only.

TABLE 1. Photophysical properties and product yields for the photolysis of ester series **6** and **8** in methanol

Compound	X	ϕ_F^a	τ_s (ns)	**2**[b] (%)	**11**[b] (%)	$k_{CO_2}^X \times 10^{-9}$ [c,d] (s^{-1})
6*a*	H	0.14	39	84	16	5.0 (0.8)
6*b*	4-OCH_3	0.08	15	25	54	78 (10)[e]
6*c*	3-OCH_3	0.07	18	16	71	135 (19)[e]
6*d*	4-CH_3	0.15	40	76	23	8.1 (1.1)
6*e*	3-CH_3	0.12	37	71	29	10.5 (1.5)
6*f*	4-F	0.13	40	72	25	10.0 (1.4)
6*g*	3-F	0.13	40	79	23	6.8 (0.9)
6*h*	4-CF_3	0.14	40	72	24	9.0 (1.2)
6*i*	3-CF_3	0.15	39	65	32	13.8 (2.0)
6*j*	4-CN	0.12	37	77	24	7.7 (1.1)
6*k*	3-CN	0.14	38	78	26	7.2 (1.0)
					12[b]	
8*a*	CH_3O	0.14	37	89	10	3.5 (0.5)
8*b*	CN	0.15	39	88	6	3.2 (0.4)
8*c*	CH_2=CH	0.16	39	77	14	7.7 (1.1)

[a]Relative to a value of 0.21 for 1-methylnaphthalene (5).
[b]Estimated error ±2% as determined by calibrated HPLC.
[c]Assuming $k_{ET}^H = 2.6 \times 10^{10}$ s^{-1}.
[d]Errors in parentheses are estimated assuming ±2% error in determination of product yields and ±10% error in the rate of decarboxylation of **15**.
[e]These values are not the correct rates of decarboxylation because the competing intramolecular electron transfer pathway leads to high yields of the decarboxylation product.

function of the oxidation potential change going from the radical pair to the ion pair indicates that this would only lead to a 20% change in k_{ET}^X, which is almost within the expected experimental error for determining k_{CO_2}. Of course, for the compounds studied here, the naphthalene side is constant so k_{ET}^X will equal k_{ET}^H. Using our previously estimated value (2) of 2.6×10^{10} s^{-1} for k_{ET}^H allows calculation of k_{CO_2} as a function of R. These values are listed in Table 1.

Turning first to the benzylic substrates, **6**, the values for k_{CO_2} are all clustered around 9.9×10^9 s^{-1} with the exception of the radicals **5***b* (X = 4-CH_3O) and **5***c* (X = 3-CH_3O) derived from substrates **6***b* and **6***c* respectively. This is made more obvious by the Hammett plot in Fig. 1, which shows that, within experimental error, the slope is close to zero if the two methoxy compounds are excluded. They have estimated rates of decarboxylation that are 10–20 times faster than the others. Clearly, then, the results for the arylacetate esters present two points for discussion: first, the lack of substituent effect for the rates of decarboxylation of the arylacetyloxy radicals, **5**, for all cases except the methoxy-substituted ones and, second, the anomalous behaviour of the methoxy compounds. The first point will be discussed next.

In general, of course, radical reactions have smaller substituent effects then ionic reactions. However, benzylic radicals certainly often have measurable ρ values, indicating the polarity of the transition state. In fact, there have been many quite successful correlations with σ^+ of benzylic rate data for abstraction of hydrogen from toluenes with various electronegative radicals (1, 8). Attempts to assess true radical stabilizing effects in benzylic systems (i.e., σ scales) have relied on studying reactions that have no polarity in the transition state (1*b*) or by measuring ESR hyperfine coupling constants of substituted benzyl radicals (1*a*). These scales indicate that even in completely nonpolar cases, substituents can stabilize benzyl radicals significantly, particularly by conjugation from the *para* position. Our observation of no measurable effect on the rate of loss of carbon dioxide from the arylacetyloxy radicals, **5**, was therefore a surprise.

Two closely related reactions deserve discussion for comparison. The first of these, oxidative decarboxylation of arylacetyl anions by persulfate gave a Hammett correlation with a $\rho^+ = -0.43$, suggesting, as expected, positive charge on the benzylic carbon as in **13** (9). However, later work (10) demonstrated that the electron transferred during the oxidation was probably from the aromatic ring, giving the expected high $\rho^+ = -2.9$. The second example involves the pyrolysis of substituted *tert*-butyl phenyl peracetates (11). Here, the evidence indicates that the cleavage of the O—O bond and the C—C bonds is concerted, producing benzyl and *tert*-butoxy radicals and carbon dioxide in one activated step. The transition state was drawn as in **14** and the reaction again

$$ArCH_2CO_2^- SO_4^{\bullet -} \longleftrightarrow ARCH_2CO_2^{\bullet} SO_4^{2-} \longleftrightarrow ArCH_2^+CO_2^{\bullet -}SO_4^{2-}$$

13

$$PhCH_2 \text{---} CO_2 \text{---} OC(CH_3)_3 \longleftrightarrow PhCH_2^+ \text{---} CO_2 \text{---} {}^-OC(CH_3)_3$$

14

Can. J. Chem. Downloaded from www.nrcresearchpress.com by 92.62.229.171 on 09/08/12
For personal use only.

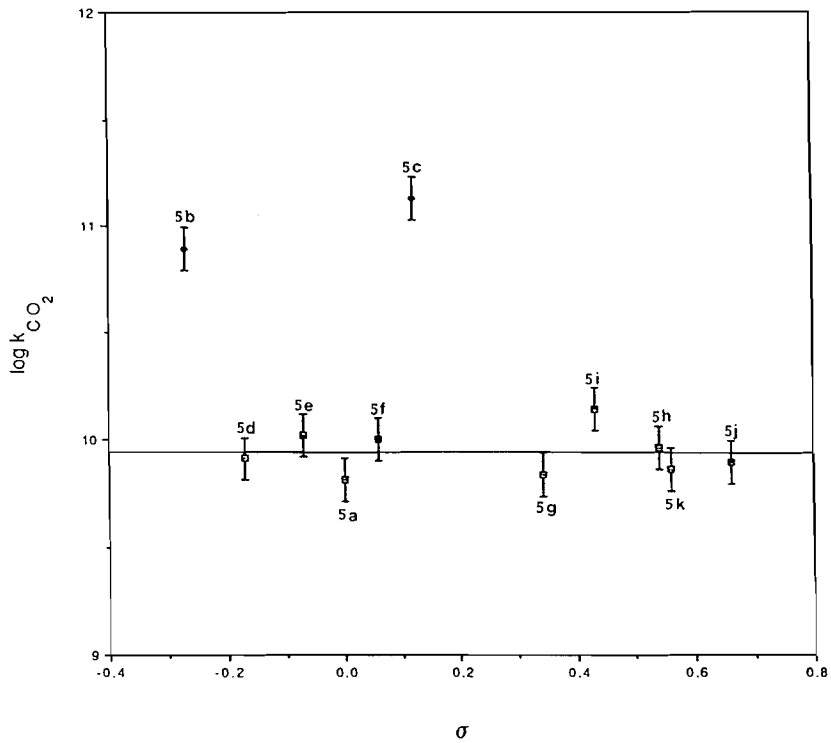

FIG. 1. Hammett plot of log k_{CO_2} versus σ for the decarboxylation of arylacyloxy radicals.

correlates with $\rho^+ = -1.0$ to -1.2 depending on temperature. A suggestion was made that perhaps arylacetyloxy radicals were too reactive to have a discrete lifetime. However, the observation that the 9-methylfluorenylcarboxylate radical, **15**, has a short but measurable lifetime (55 ps) at room temperature (12) makes this unlikely.

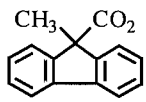

15

There are several differences between our method of determining rates of decarboxylation of arylacetyloxy radicals and that of Bartlett and Rüchardt (11). First, our results are obtained at 20°C as opposed to the higher temperatures (55–100°C) required for the perester decomposition. Thus, the radical has a better chance of having a discrete existence in the shallow energy well that separates it from the arylmethyl radical and carbon dioxide. Second, the counter radical is the carbon-centered radical, 1-naphthylmethyl, so that the polarity in the transition state should be minimized relative to **14** above. Finally, we presented evidence previously (6) that the loss of carbon dioxide from the arylacetyloxy radical may be controlled by the entropy rather than enthalpy of activation. This is true because the stabilization of the incipient benzyl radical requires a freezing of the conformation of the benzene ring to allow overlap with the breaking σ bond. Such entropic effects have been observed before for the much slower loss of carbon monoxide from phenylacetyl ($PhCH_2CO$) radicals (13). For the arylacetyloxy radical, where the enthalpic barrier will be extremely low, this entropic effect may dominate the activation process. If this is true, substituent effects would be expected to be small, i.e., radical stability effects are unimportant in determining the rate of loss of carbon dioxide.

The second major feature in the decarboxylation rates of the arylacetyloxy radicals, **5**, is the enhanced rate of decarboxylation for **5***b*, X = 4-OCH_3 and **5***c*, X = 3-OCH_3. This effect is easily explained when it is also noted that the quantum yield of fluorescence, ϕ_f, and the singlet excited state lifetime, τ_s, are also significantly different for these two substrates. As shown in Table 1, both values for both substrates are about a factor of two lower than for all the other substrates. This is true even though the chromophore and excited-state energy results from the same structural unit, the naphthalene ring. Clearly, another excited singlet-state process has been added to the mechanism for these methoxy-substituted substrates. Our suggestion is that this additional pathway is intramolecular exciplex formation by electron transfer from the methoxy aromatics to the naphthalene ring (Scheme 2). This process, with rate constant k_E, competes with the normal homolytic cleavage pathway, k_R, as well as with fluorescence, k_F. Therefore, both ϕ_F and τ_s will be decreased.

There are many examples of intramolecular exciplexes of this type and many, though not all, are emissive (14). We have looked carefully for excimer emission and have not been able to observe any in either methanol or cyclohexane solvent. However, the Rehm–Weller relationship (15), eq. [2], provides a convincing argument for exciplex formation. Values for the oxidation potential of anisole (1.76 V vs. SCE in CH_3CN) (16), the reduction potential of naphthanlene (−2.6 V vs. SCE in CH_3CN) (16), and the singlet excitation energy, $E_{0,0}$, for these substrates (376 kJ mol^{-1} from the wavelength of the 0,0 band in CH_3OH) gives ΔG_E = 43 kJ mol^{-1}. The electrostatic term in eq. [2] is less certain because the distance between the two charged rings is un-

Can. J. Chem. Downloaded from www.nrcresearchpress.com by 92.62.229.171 on 09/08/12
For personal use only.

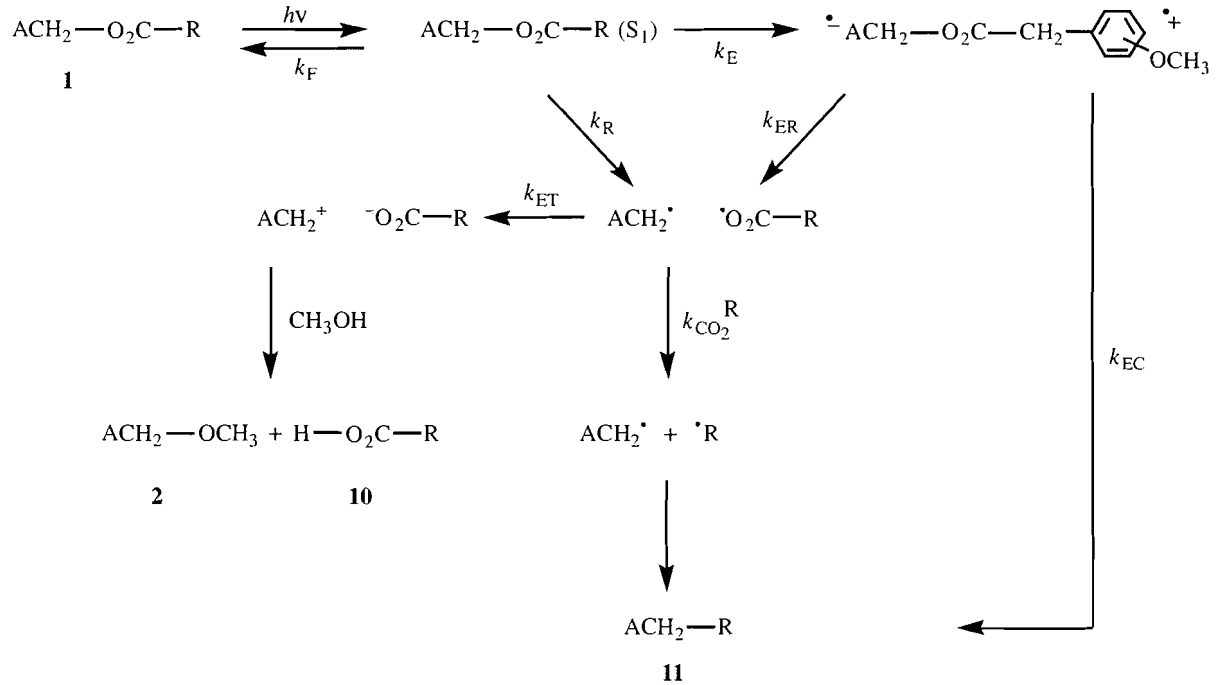

SCHEME 2. Mechanism of the photolysis of 1-naphthylmethyl esters including the intramolecular electron transfer pathway.

[2] $\Delta G_E = E^0(D/D^+) + E^0(A^-/A) - e_0^2/\epsilon r - \Delta E_{0,0}$

known. If the two aromatics interact strongly, they could be quite close. Molecular models indicate that if the rings are coplanar in the exciplex, the maximum distance of separation is 5 Å with no geometric inhibition to shorter distances. Assuming the dielectric constant to be used is that of the bulk medium, methanol, the value of this term is 9 kJ mol^{-1} at 5 Å and 22 kJ mol^{-1} at 2 Å. Thus ΔG_E is probably somewhere between 34 kJ mol^{-1} and 21 kJ mol^{-1}. Using the graph produced by Rehm and Weller (15) for intermolecular charge transfer a value of k_E around 10^7 s^{-1} can be estimated.

The conclusion of this discussion is that intramolecular exciplex formation in **6***b* and **6***c* can compete with the normal singlet excited rate processes: $1/\tau_s = 1/40$ ns $= 2.5 \times 10^7$ s^{-1}.

From the fluorescence data, an estimate of the rate constant of exciplex formation can be made. Equation [3] indicates that the ratio of either lifetimes of the singlet excited states or fluorescence quantum yields for those substrates that do not form exciplexes relative to those that do is simply re-

[3] $\tau_F/\tau_F^E = \phi_F/\phi_F^E = 1 + k_E\tau_F$

lated to the required rate constant. This equation assumes that τ_F^E is the same as τ_F except for the addition of k_E, eq. [4]. On the average, the values of τ_F/τ_F^E and δ_F/ϕ_F^E are about 2.

[4] $1/\tau_F^E = k_F + k_D + k_R + k_E$

Therefore the product of $k_E\tau_F$ is close to unity or in other words, $k_E \approx k_F + k_D + k_R = 2.5 \times 10^7$ s^{-1} as required for exciplex formation to compete with but not dominate other singlet-state processes.

Finally, a value for the oxidation potential of toluene (2.28 V vs. SCE in CH_3CN) (16) used in eq. [2] leads to a value for ΔG_E for electron transfer (without including the electrostatic term) in the methyl-substituted esters **6***d* and **6***e* of +188 kJ mol^{-1}. This is obviously too endoergonic to lead to a rate that would be competitive with other excited singlet-state chemistry.

From the product ratios in Table 1, it is clear that the two methoxy-substituted substrates, **6***b* and **6***c*, give lower yields of the cation-derived product, the methyl ether **2**, and corresponding higher yields of the radical-derived coupling product **11**. The previous discussion suggests strongly that the formation of the intramolecular exciplex is creating another pathway of reactivity for the singlet excited state. The obvious conclusion is that this exciplex then gives preferentially the coupling product **11**. The electronic structure of the charge transfer complex represented by a contributor like **16**, eq. [5], seems ideal for concerted bond cleavage involv-

[5] 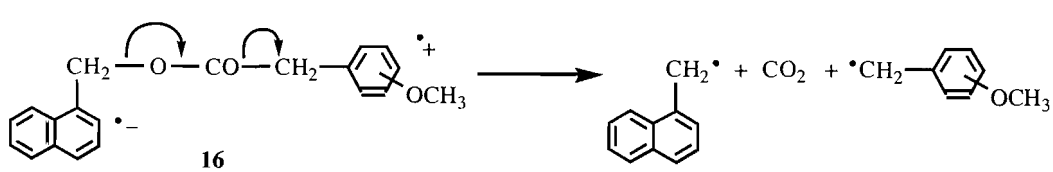

Can. J. Chem. Downloaded from www.nrcresearchpress.com by 92.62.229.171 on 09/08/12
For personal use only.

Can. J. Chem. Downloaded from www.nrcresearchpress.com by 92.62.229.171 on 09/08/12
For personal use only.

ing loss of CO_2 and formation of the precursors required for coupling. Note that the decarboxylation must be concerted in order to avoid formation of the arylacyloxy radical, which would then lead to the normal chemistry of the radical pair. In Scheme 2, as shown, $k_{EC} >> k_{ER}$. In conclusion, the calculated rates of decarboxylation in Table 1 for **5***b* and **5***c*, which are based on the ratio of the products **2** and **11** (**4**, R = X-$C_6H_4CH_2$), are clearly incorrect because an alternate pathway for formation of **11** is occurring.

The effect of substituents on the rates of decarboxylation of the arylacetyloxy radicals, **5**, are negligibly small. We therefore chose to look briefly at the effect of substituents more closely attached. The substrates **8** generate the radicals **7**. Since the fluorescence is normal (Table 1), the yield of **2** (eq. [1]) is now a measure of the decarboxylation rate again. The rates of decarboxylation of $RCO_2^{\cdot}$ are now significantly changed: R, $k_{CO_2} \times 10^{-9}$; H-CH_2, <1.3; NC-CH_2, 3.2; CH_3O-CH_2, 3.5; Ph-CH_2, 5.0; CH_2=$CHCH_2$, 7.7. With the obvious caution that these reactions are so fast that any rate–substituent correlation will be highly compressed, this order does make sense based on radical stability or bond-strength arguments. Clearly, since both the cyano and methoxy substituents give a rate increase relative to hydrogen, polar effects cannot be too important. However, the fact that methoxy is slightly faster than cyano is not in agreement with most scales of radical stabilizing effects (17). This may indicate a slight amount of polar character in the transition state for decarboxylation with the carboxyl oxygens negative and the methylene carbon positive.

Experimental

General

Ultraviolet (UV) spectra were obtained in methanol on a Varian Cary 219 spectrophotometer. Proton (^{1}H NMR) and carbon (^{13}C NMR) nuclear magnetic resonance spectra were obtained in $CDCl_3$ with TMS as an internal standard on a Nicolet NB 360 spectrometer. Mass spectra were obtained on a Hewlett Packard 5890 GC/MS using a 5% phenylsilicone capillary column. Infrared spectra were obtained on a Pye Unicam SP 1000 spectrophotometer. Fluorescence spectra were obtained on a Perkin Elmer MPF 66 spectrophotometer using samples in methanol that were degassed by three freeze–pump–thaw cycles; the optical density of the samples was always less than 0.2 and quantum yields were obtained relative to a value of 0.21 for 1-methylnaphthalene (5). Fluorescence lifetimes were obtained on the same samples using a PRA System 3000 instrument with a hydrogen flash lamp of pulse width 0.8 ns. Microanalysis were by Canadian Microanalytical Service Ltd., Delta, B.C., Canada.

Irradiations

Irradiations were done with a 200-W medium-pressure Hanovia mercury lamp in a standard immersion well with a Pyrex filter. Solutions were degassed with a slow nitrogen stream. Progress of the reaction was monitored by HPLC using a Waters system, operating in isocratic conditions (80:20 methanol:water), equipped with a Brownlee Spheri-10 reverse-phase column (25 × 0.46 cm). Detection was at 280 nm. Complete conversion of 200 mg of the esters took approximately 3 h for the most reactive esters while the unreactive esters took approximately 24 h. Product ratios remained constant throughout the course of the irradiation and dark samples taken either before or during the irradiation showed no conversion. Yields were obtained by calibrating the HPLC detector with samples of the products of known concentration in methanol. For preparative runs the photolyzed solution was concentrated under vacuum to approximately 10 mL and then 30 mL of water and 30 mL of CH_2Cl_2 were added. The CH_2Cl_2 layer was separated and extracted with 2 × 15 mL of a 5% aqueous NaOH solution. The CH_2Cl_2 layer was dried ($MgSO_4$), filtered, and rotoevaporated to give an oil that was subjected to flash chromatography through silica gel using 80:20 hexane:CH_2Cl_2 as the eluent. The aqueous alkaline layer was acidified with concentrated HCl, and extracted with 2 × 25 mL of CH_2Cl_2. Evaporation of this CH_2Cl_2 layer gave products that were identified as the corresponding acids.

Methoxyacetyl chloride, phenylacetyl chloride, 1-naphthylmethanol, cyanoacetic acid, 3-butenoic acid, 4-methoxyphenylacetic acid, 3-methoxyphenylacetic acid, 4-methylphenylacetic acid, 3-methylphenylacetic acid, 4-fluorophenylacetic acid, 3-fluorophenylacetic acid, 4-α,α,α-trifluorophenylacetic acid, 3-α,α,α-trifluorophenylacetic acid, were purchased from the Aldrich Chemical Company. All solvents were distilled prior to use. The acid chlorides were obtained by refluxing three molar equivalent of thionyl chloride with the acid (18). Cyanoacetyl chloride was prepared from cyanoacetic acid using the method of Ireland and Chaykovsky (19). The 4- and 3-cyanophenylacetic acids were obtained by the method of Richter *et al.* (20). The esters generated were hydrolyzed in aqueous base to give the corresponding acids. 1-Methoxymethylnaphthalene, **2**, was obtained by the previous procedure (6).

*Synthesis of substituted and 1-naphthylmethyl phenylacetates (**6**a–k) and 1-naphthylmethyl acetates (**8**a–c)*

To a well-stirred solution of 1-naphthylmethanol (1.56 g, 0.01 mol) and 1 mL of pyridine in 50 mL of dry benzene was slowly added the corresponding acid chloride (0.01 mol) in 30 mL of benzene at room temperature. The pyridinium hydrochloride salt precipitated and after all of the acid chloride was added the solution was stirred overnight. Then 50 mL of water was added and the two layers were separated. The benzene layer was washed twice with 10% aqueous HCl, once with 5% aqueous NaOH, and finally with water. The organic layer was dried ($MgSO_4$), filtered, and rotoevaporated to yield the crude esters. The ester was then column chromatographed over silica gel using 50:50 hexane:methylene chloride as the eluent. The ester fractions were identified by TLC, then combined and concentrated. The esters that were oils were distilled under vacuum and those that were solids were recrystallized from hexane for purification.

Characterization of esters

*1-Naphthylmethyl phenylacetate (**6**a)*: yield 62%; bp 196–200°C at 0.5 Torr[2] (lit. (21) bp 212°C at 4–5 Torr); UV: λ_{max} 265 (ϵ 6.37 × 10^3), 275 (7.39 × 10^3), 284 (5.29 × 10^3); IR (neat): 3010, 2930, 1740 (C=O), 1600, 1520, 1495, 1455, 1240, 1145, 940, 785, 765 cm^{-1}; ^{1}H NMR δ: 7.73–7.75 (m, 1H), 7.62–7.68 (m, 2H), 7.30–7.33 (m, 3H), 7.22 (t, 1H, J = 7.6 Hz), 7.09 (s, 5H), 5.39 (s, 2H, CH_2O), 3.47 (s, 2H, CH_2C(=O)); ^{13}C NMR δ: 171.4 (s, C=O), 133.8 (s), 133.6 (s), 131.5 (s), 131.2 (s), 129.2, 128.6, 128.5, 127.4, 127.0, 126.4, 125.9, 125.2, 123.5, 65.0 (t, CH_2O, J = 147.8 Hz), 41.3 (t, CH_2C(=O), J = 129.8 Hz); GC/MS: 277 (7, M + 1), 276 (39, M^+), 142 (18), 141 (100), 115 (24), 91 (24).

*1-Naphthylmethyl 4-methoxyphenylacetate (**6**b)*: yield 48%; bp 118–120°C at 0.5 Torr; UV: λ_{max} 266 (ϵ 8.16 × 10^3), 275 (8.52 × 10^3), 286 (5.15 × 10^3); IR (neat): 3080, 2980, 1740 (C=O), 1615, 1515, 1250, 1150, 1040, 980, 795, 780 cm^{-1}; ^{1}H NMR δ: 7.89–7.91 (m, 1H), 7.79–7.85 (m, 2H), 7.46–7.49 (m, 3H), 7.40 (t, 1H, J = 7.6 Hz), 7.16 (d, 2H, J = 8.4 Hz), 6.81 (d, 2H, J = 8.4 Hz), 5.55 (s, 2H, CH_2O), 3.74 (s, 3H, OCH_3), 3.57 (s, 2H, CH_2C(=O)); ^{13}C NMR δ: 171.4 (s, C=O), 158.8 (s), 133.7 (s), 131.6 (s), 131.4 (s), 130.1 (d, J = 153.3 Hz), 129.1, 128.5, 127.1, 126.3, 126.0 (s), 125.7, 125.1, 123.5, 114.0 (d, J = 158.7 Hz), 64.7 (t, CH_2O, J = 148.2 Hz), 55.2 (q, OCH_3, J = 143.5 Hz), 40.4 (t, CH_2C(=O), J = 130.0 Hz); GC/MS: 307 (6, M + 1), 306 (29, M^+), 142 (8), 141 (58), 121 (100), 115 (16), 78 (8). Anal. calcd. for $C_{20}H_{18}O_3$: C 78.41, H 5.92; found: C 78.16, H 5.82.

[2] 1 Torr = 133.32 Pa.

Can. J. Chem. Downloaded from www.nrcresearchpress.com by 92.62.229.171 on 09/08/12
For personal use only.

*1-Naphthylmethyl 3-methoxyphenylacetate (**6**c)*: yield 46%; bp 112–114°C at 0.5 Torr; UV: λ_{max} 266 (ϵ 9.17 × 10^3), 275 (9.25 × 10^3), 286 (5.24 × 10^3); IR (neat): 3020, 2930, 1735 (C=O), 1600, 1490, 1255, 1140, 1040, 970, 780, 760 cm^{-1}; ^1H NMR δ: 7.89–7.91 (m, 1H), 7.79–7.85 (m, 2H), 7.46–7.48 (m, 3H), 7.39 (t, 1H, J = 7.6 Hz), 7.18 (t, 1H, J = 8.4 Hz), 6.77–6.84 (m, 3H), 5.55 (s, 2H, CH_2O), 3.67 (s, 3H, OCH_3), 3.60 (s, 2H, $CH_2C(=O)$); ^{13}C NMR δ: 171.3 (s, C=O), 159.6 (s), 135.2 (s), 133.6 (s), 131.5 (s), 131.2 (s), 129.5, 129.3, 128.6, 127.4, 126.5, 125.9, 125.2, 123.5, 121.6, 114.6, 112.9, 65.0 (t, CH_2O, J = 147.7 Hz), 55.1 (q, OCH_3, J = 143.8 Hz), 41.4 (t, $CH_2C(=O)$, J = 129.5 Hz); GC/MS:307 (9, M + 1), 306 (42, M^+), 142 (13), 141 (100), 121 (11), 115 (17), 91 (6), 78 (5). Anal. calcd. for $C_{20}H_{18}O_3$: C 78.41, H 5.92; found: C 78.67, H 6.00.

*1-Naphthylmethyl 4-methylphenylacetate (**6**d)*: yield 55%; mp 41–42°C; UV: λ_{max} 265 (ϵ 5.49 × 10^3), 275 (7.54 × 10^3), 284 (4.46 × 10^3); IR (Nujol): 1730 (C=O), 1505, 1285, 1250, 1125, 965, 785, 760 cm^{-1}; ^1H NMR δ: 7.91–7.94 (m, 1H), 7.82–7.88 (m, 2H), 7.48–7.51 (m, 3H), 7.42 (t, 1H, J = 7.5 Hz), 7.15 (d, 2H, J = 8.0 Hz), 5.56 (s, 2H, CH_2O), 3.62 (s, 2H, $CH_2C(=O)$), 2.32 (s, 3H, CH_3); ^{13}C NMR δ: 171.6 (s, C=O), 136.6 (s), 133.6 (s), 131.5 (s), 131.3 (s), 130.7 (s), 129.2, 128.6, 127.3, 126.4, 125.8, 125.1, 123.5, 64.9 (t, CH_2O, J = 148.4 Hz), 40.9 (t, $CH_2C(=O)$, J = 129.9 Hz), 21.0 (q, CH_3, J = 126.0 Hz); GC/MS: 291 (12, M + 1), 290 (49, M^+), 142 (20), 141 (100), 115 (24), 105 (49), 77 (11). Anal. calcd. for $C_{20}H_{18}O_2$: C 82.73, H 6.25; found: C 82.72, H 6.21.

*1-Naphthylmethyl 3-methylphenylacetate (**6**e)*: yield 41%; mp 30–31°C; UV: λ_{max} 265 (ϵ 5.64 × 10^3), 275 (6.56 × 10^3), 284 (4.60 × 10^3); IR (Nujol): 1730 (C=O), 1605, 1245, 1135, 970, 780, 760 cm^{-1}; ^1H NMR δ: 7.90–7.93 (m, 1H), 7.81–7.87 (m, 2H), 7.48–7.50 (m, 3H), 7.41 (t, 1H, J = 7.9 Hz), 7.04–7.06 (m, 3H), 5.57 (s, 2H, CH_2O), 3.61 (s, 2H, $CH_2C(=O)$), 2,28 (s, 3H, CH_3); ^{13}C NMR δ: 171.5 (s, C=O), 138.1 (s), 133.7 (s), 131.5 (s), 131.3 (s), 130.0, 129.2, 128.9 (s), 128.6, 128.4, 127.8, 127.4, 126.4, 126.3, 125.9, 125.2, 123.6, 65.0 (t, CH_2O, J = 126.6 Hz), 41.3 (t, $CH_2C(=O)$, J = 130.1 Hz), 21.3 (q, CH_3, J = 125.1 Hz); GC/MS:291 (11, M + 1), 290 (49, M^+), 142 (12), 141 (100), 115 (20), 105 (12). Anal. calcd. for $C_{20}H_{18}O_2$: C 82.73, H 6.25; found: C 82.56, H 6.29.

*1-Naphthylmethyl 4-fluorophenylacetate (**6**f)*: yield 57%; mp 57–58°C; UV: λ_{max} 265 (ϵ 6.10 × 10^3), 275 (6.82 × 10^3), 284 (4.68 × 10^3); IR (Nujol):1735 (C=O), 1595, 1505, 1290, 1220, 1125, 970, 785, 760 cm^{-1}; ^1H NMR δ: 7.83–7.92 (m, 3H), 7.48–7.52 (m, 3H), 7.42 (t, 1H, J = 7.6 Hz), 7.19–7.24 (m, 2H), 6.97 (t, 2H, J = 8.7 Hz), 5.57 (s, 2H, CH_2O), 3.62 (s, 2H, $CH_2C(=O)$); ^{13}C NMR δ: 171.2 (s, C=O), 162.0 (d, CF, J = 245.2 Hz), 133.7 (s), 131.5 (s), 131.1 (s), 130.9, 129.5 (s), 129.3, 128.7, 127.5, 126.5, 125.9, 125.2, 123.5, 115.1 (dd, J_{CH} = 162.1 Hz, J_{CCF} = 21.3 Hz), 65.1 (t, CH_2O, J = 148.4 Hz), 40.5 (t, $CH_2C(=O)$, J = 129.5 Hz); GC/MS:295 (6, M + 1), 294 (30, M^+), 142 (13), 141 (100), 115 (15), 109 (16). Anal. calcd. for $C_{19}H_{15}FO_2$: C 77.54, H 5.14; found: C 77.32, H 5.24.

*1-Naphthylmethyl 3-fluorophenylacetate (**6**g)*: yield 40%; mp 55–57°C; UV: λ_{max} 264 (ϵ 6.49 × 10^3), 276 (7.03 × 10^3), 285 (4.97 × 10^3); IR (Nujol): 1730 (C=O), 1585, 1485, 1280, 1250, 1230, 1135, 970, 865, 790, 770 cm^{-1}; ^1H NMR δ: 7.82–7.92 (m, 3H), 7.48–7.51 (m, 3H), 7.41 (t, 1H, J = 7.6 Hz), 7.20–7.26 (m, 1H), 6.91–7.02 (m, 3H), 5.57 (s, 2H, CH_2O), 3.63 (s, 2H, $CH_2C(=O)$); ^{13}C NMR δ: 170.8 (s, C=O), 165.0 (d, CF, J = 245.0 Hz), 133.7 (s), 131.5 (s), 131.1 (s), 130.0 (s), 129.9, 129,4, 128.7, 127.5, 126.5, 125.9, 125.2, 125.0, 123.5, 116.3 (dd, J_{CH} = 162.8 Hz, J_{CCF} = 21.7 Hz), 114.1 (dd, J_{CH} = 162.9 Hz, J_{CCF} = 20.8 Hz), 65.2 (t, CH_2O, J = 148.1 Hz), 41.0 (t, $CH_2C(=O)$, J = 130.1 Hz); GC/MS: 295 (23, M + 1), 294 (100, M^+), 158 (24), 142 (41), 141 (100), 128 (12), 127 (18), 115 (79), 109 (48), 83 (23). Anal. calcd. for $C_{20}H_{15}FO_2$: C 77.54, H 5.14; found: C 77.52, H 5.15.

*1-Naphthylmethyl 4-trifluoromethylphenylacetate (**6**h)*: yield 35%; mp 64–65°C; UV: λ_{max} 265 (ϵ 5.61 × 10^3), 275 (7.54 × 10^3), 284 (4.33 × 10^3); IR (Nujol): 1730 (C=O), 1325, 1280, 1250, 1160, 1140, 1060, 970, 815, 790, 765 cm^{-1}; ^1H NMR δ: 7.83–7.89 (m, 3H), 7.53 (d, 2H, J = 8.1 Hz), 7.47–7.51 (m, 3H), 7.42 (t, 1H, J = 7.6 Hz), 7.34 (d, 2H, J = 8.1 Hz), 5.58 (s, 2H, CH_2O), 3.70 (s, 2H, $CH_2C(=O)$); ^{13}C NMR δ: 170.6 (s, C=O), 137.7 (s), 133.7 (s), 131.5 (s), 131.0 (s), 129.7, 129.4, 128.7, 127.7, 126.5, 126.3 (s), 126.0, 125.7, 125.4 (CF_3), 125.2, 123.4, 65.3 (t, CH_2O, J = 147.8 Hz), 41.1 (t, $CH_2C(=O)$, J = 130.5 Hz); GC/MS: 345 (18, M + 1), 344 (84, M^+), 159 (16), 158 (18), 142 (18), 141 (100), 139 (12), 115 (24), 109 (9). Anal. calcd. for $C_{20}H_{15}F_3O_2$: C 69.76, H 4.39; found: C 69.57, H 4.64.

*1-Naphthylmethyl 3-trifluoromethylphenylacetate (**6**i)*: yield 41%; mp 61–63°C; UV: λ_{max} 265 (ϵ 6.61 × 10^3), 275 (7.24 × 10^3), 283 (5.17 × 10^3); IR (Nujol): 1730 (C=O), 1325, 1290, 1245, 1170, 1105, 1065, 965, 790, 765 cm^{-1}; ^1H NMR δ: 7.87–7.90 (m, 1H), 7.79–7.84 (m, 2H), 7.46–7.51 (m, 5H), 7.32–7.41 (m, 3H), 5.56 (s, 2H, CH_2O), 3.66 (s, 2H, $CH_2C(=O)$); ^{13}C NMR δ: 170.6 (s, C=O), 134.7 (s), 133.7 (s), 132.7, 131.5 (s), 131.0 (s), 129.4, 128.9, 128.7, 127.6, 126.5, 126.3, 126.1, 126.0 (d, CF_3, J = 281.8 Hz), 125.5 (s), 125.2, 124.0, 123.4, 65.3 (t, CH_2O, J = 151.2 Hz), 41.0 (t, $CH_2C(=O)$, J = 129.7 Hz); GC/MS:345 (37, M + 1), 344 (100, M^+), 159 (46), 158 (42), 142 (43), 141 (100), 139 (25), 128 (16), 127 (19), 115 (77), 109 (21). Anal. calcd. for $C_{20}H_{15}F_3O_2$: C 69.76, H 4.39; found: C 69.97, H 4.50.

*1-Naphthylmethyl 4-cyanophenylacetate (**6**j)*: yield 35%; mp 116–118°C; UV: λ_{max} 265 (ϵ 6.24 × 10^3), 275 (7.07 × 10^3), 284 (4.65 × 10^3); IR (Nujol): 2120 (C≡N), 1740 (C=O), 1340, 1215, 1175, 1155, 945, 775 cm^{-1}; ^1H NMR δ: 7.84–7.91 (m, 3H), 7.38–7.54 (m, 5H), 7.16–7.26 (m, 1H), 7.12 (d, 2H, J = 8.3 Hz), 5.57 (s, 2H, CH_2O), 3.60 (s, 2H, $CH_2C(=O)$); ^{13}C NMR δ: 170.1 (s, C=O), 139.1 (s), 133.7 (s), 132.2, 131.5 (s), 130.8 (s), 130.1, 129.5, 128.7, 127.8, 126.5, 126.0, 125.2, 123.4, 118.6 (s, C≡N), 111.2 (s, CCN), 65.5 (t, CH_2O, J = 145.8 Hz), 41.3 (t, $CH_2C(=O)$, J = 130.6 Hz); GC/MS: 302 (7, M + 1), 301 (33, M^+), 142 (12), 141 (100), 116 (11), 115 (18). Anal. calcd. for $C_{20}H_{15}NO_2$: C 79.72, H 5.02, N 4.65; found: C 79.36, H 4.90, N 4.69.

*1-Naphthylmethyl 3-cyanophenylacetate (**6**k)*: yield 43%; mp 92–93°C; UV: λ_{max} 266 (ϵ 6.32 × 10^3), 275 (7.10 × 10^3), 284 (4.65 × 10^3); IR (Nujol): 2100 (C≡N), 1730 (C=O), 1310, 1240, 1215, 1130, 970, 790, 760 cm^{-1}; ^1H NMR δ: 7.84–7.89 (m, 3H), 7.36–7.53 (m, 8H), 5.59 (s, 2H, CH_2O), 3.66 (s, 2H, $CH_2C(=O)$); ^{13}C NMR δ: 170.2 (s, C=O), 135.2 (s), 133.9, 133.7 (s), 132.8, 131.5 (s), 130.9, 129.5, 129.4 (s), 129.3, 128.7, 127.8, 126.6, 126.0, 125.2, 123.3, 118.5 (s, C≡N), 112.6 (s, CCN), 65.4 (t, CH_2O, J = 148.1 Hz), 40.7 (t, $CH_2C(=O)$, J = 130.6 Hz); GC/MS: 302 (7, M + 1), 301 (35, M^+), 142 (15), 141 (100), 116 (12), 115 (26). Anal. calcd. for $C_{20}H_{15}NO_2$: C 79.72, H 5.02, N 4.65; found: C 79.35, H 4.95, N 4.70.

*1-Naphthylmethyl methoxyacetate (**8**a)*: yield 72%; bp 90–92°C at 0.5 Torr; UV: λ_{max} 264 (ϵ 5.61 × 10^3), 276 (6.73 × 10^3), 286 (4.49 × 10^3); IR (neat): 3070, 3010, 2960, 2840, 1760 (C=O), 1520, 1195, 1145, 805, 795, 780 cm^{-1}; ^1H NMR δ: 8.00 (d, 1H, J=8.2 Hz), 7.87 (t, 2H, J = 7.9 Hz), 7.42–7.58 (m, 4H), 5.66 (s, 2H, CH_2O), 4.06 (s, 2H, CH_2OCH_3), 3.43 (s, 3H, OCH_3); ^{13}C NMR δ: 170.1 (s, C=O), 133.6 (s), 131.5 (s), 130.8, 129.5, 128.7, 127.8, 126.6, 125.9, 125.2, 123.3, 69.7 (t, CH_2OCH_3, J = 143.8 Hz), 64.7 (t, $CH_2OC(=O)$, J = 148.0 Hz), 59.4 (q, OCH_3, J = 141.4 Hz); GC/MS: 231 (6, M + 1), 230 (46, M^+), 142 (39), 141 (100), 139 (24), 128 (12), 127 (16), 115 (49). Anal. calcd. for $C_{14}H_{14}O_3$: C 73.03, H 6.13; found: C 72.78, H 6.05.

*1-Naphthylmethyl cyanoacetate (**8**b)*: yield 51%; mp 42–43°C; bp 110–112°C at 0.5 Torr; UV: λ_{max} 266 (ϵ 6.68 × 10^3), 275 (7.22 × 10^3), 286 (4.88 × 10^3); IR (Nujol): 3060, 2280 (C≡N), 1745 (C=O), 1520, 1340, 1230, 1210, 800, 790, 770 cm^{-1}; ^1H NMR δ: 7.98 (m, 1H), 7.86–7.90 (m, 2H), 7.53–7.58 (m, 3H), 7.43–7.47 (m, 1H), 5.67 (s, 2H, CH_2O), 3.44 (s, 2H, CH_2CN); ^{13}C NMR

δ: 162.9 (s, C═O), 133.6 (s), 131.4 (s), 129.9, 129.8 (s), 128.8, 128.1, 126.9, 126.1, 125.2, 123.2, 112.9 (s, C≡N), 66.7 (t, CH_2O, J = 149.3 Hz), 24.7 (t, CH_2CN, J = 136.8 Hz); GC/MS: 226 (7, M + 1), 225 (47, M^+), 158 (17), 142 (13), 141 (100), 140 (26), 129 (13), 128 (12), 127 (13), 115 (27). Anal. calcd. for $C_{14}H_{11}NO_2$: C 74.65, H 4.92, N 6.22; found: C 74.60, H 4.84, N 6.19.

1-Naphthylmethyl 3-butenoate (8c): yield 35%; bp 112–116°C at 0.5 Torr; UV: λ_{max} 265 (ϵ 6.56 × 10^3), 275 (7.48 × 10^3), 286 (5.09 × 10^3); IR (neat): 3030, 2990, 2940, 1740 (C═O), 1325, 1250, 1170, 785, 765 cm^{-1}; ^1H NMR δ: 7.96 (d, 1H, J = 8.1 Hz), 7.78–7.84 (m, 2H), 7.38–7.53 (m, 4H), 5.88–5.95 (m, 1H, CH═CH_2), 5.55 (s, 2H, CH_2O), 5.08–5.15 (m, 2H, CH═CH_2), 3.11 (d, 2H, CH_2CH═C, J = 6.9 Hz); ^{13}C NMR δ: 171.3 (s, C═O), 133.6 (s), 131.5 (s), 131.2 (s), 130.0, 129.2, 128.6, 127.4, 126.4, 125.8, 125.1, 123.4, 118.6 (t, CH═CH_2, J = 156.8 Hz), 64.7 (t, CH_2O, J = 147.8 Hz), 39.0 (t, C(═O)CH_2, J = 129.2 Hz); GC/MS: 227 (7, M + 1), 226 (44, M^+), 158 (21), 142 (13), 141 (100), 140 (15), 139 (10), 115 (15). Anal. calcd. for $C_{15}H_{14}O_2$: C 79.62, H 6.24; found: C 79.63, H 6.25.

Synthesis of the hydrocarbons

1-(2-Methoxyethyl)naphthalene was prepared by the method of Todesco and Put (22). 1-Naphthalenepropanenitrile was synthesized from 2-(1′-naphthyl)ethanol. The alcohol was converted to the mesylate, which was then reacted with potassium cyanide in DMF. The ^1H NMR of these compounds were consistent with the those reported earlier (22, 23). The hydrocarbons (**11***a–k*, **12***c*) were isolated from preparative photolysis and had ^1H NMR that were consistent with their structure.

Acknowledgements

We thank the Natural Sciences and Engineering Research Council of Canada for financial support, and J.W.H. thanks the Sumner Foundation for financial assistance in the form of a graduate fellowship.

1. (*a*) D. R. Arnold. *In* Substituent effects in radical chemistry. *Edited by* H. G. Viehe, Z. Janousek, and R. Merényi. Reidel, Dordrecht. 1986. p. 171; (*b*) X. Creary. *In* Substituent effects in radical chemistry. *Edited by* H. G. Viehe, Z. Janousek, and R. Merényi. Reidel, Dordrecht. 1986. p. 245.
2. D. P. De Costa and J. A. Pincock. J. Am. Chem. Soc. **111**, 8948 (1986).
3. S. J. Cristol and T. H. Bindle. Organic photochemistry. Vol. 6. Marcel Dekker, New York. 1983. p. 327.
4. B. Foster, B. Gaillard, N. Mathur, A. L. Pincock, J. A. Pincock, and C. Sehmbey. Can. J. Chem. **65**, 1599 (1987).
5. P. Lenz, H. Blunre, and D. Schutte-Frohlinde. Ber. Bunsen-Ges. Phys. Chem. **74**, 484 (1970).
6. J. W. Hilborn and J. A. Pincock. J. Am. Chem. Soc. **113**, 2683 (1991).
7. A. Fischer, B. R. Mann, and J. Vaughan. J. Chem. Soc. 1093 (1961).
8. G. A. Russell. *In* Free Radicals. Vol. 1. *Edited by* J. K. Kochi. Wiley and Sons, New York. 1973. p. 275.
9. D. D. Tanner and S. A. A. Osman. J. Am. Chem. Soc. **90**, 6572 (1968).
10. R. M. Dessau and E. I. Heiba. J. Org. Chem. **40**, 3647 (1975).
11. P. D. Bartlett and C. Rüchardt. J. Am. Chem. Soc. **82**, 1756 (1960).
12. D. E. Falvey and G. B. Schuster. J. Am. Chem. Soc. **108**, 7419 (1960).
13. H. Fischer and H. Paul. Acc. Chem. Res. **20**, 200 (1987).
14. F. C. De Schryver, P. Collart, J. Vandensiressche, R. Goedeweeck, A. M. Swinnen, and M. Van der Auweraer. Acc. Chem. Res. **20**, 159 (1987).
15. D. Rehm and A. Weller. Isr. J. Chem. **8**, 259 (1970).
16. L. Meites and P. Zuman. *In* CRC handbook series in organic electrochemistry. Vol. 1. Boca Raton, Fla. 1977.
17. R. Merényi, Z. Janousek, and H. G. Viehe. *In* Substituent effects in radical chemistry. *Edited by* H. G. Viehe, Z. Janousek, and R. Merényi. Reidel, Dordrecht. 1986. p. 301.
18. S. S. Pizey. Synthetic methods. Vol. 1. Wiley and Sons, New York. 1974. 333.
19. R. E. Ireland and M. Chaykovsky. Org. Synth. Vol. 41. Wiley and Sons, London. 1961. p. 5.
20. P. Richter, C. H. Garbe, and G. Wagner. Pharmazie, **29**, 256 (1974).
21. R. N. Chakravarti and R. C. Dhar. Indian Chem. Soc. **30**, 751 (1953).
22. R. V. Todesco and J. Put. J. Photochem. **34**, 305 (1986).
23. S. Indaba and R. D. Rieke. Synthesis, **10**, 842 (1984).

Can. J. Chem. Downloaded from www.nrcresearchpress.com by 92.62.229.171 on 09/08/12
For personal use only.

Characterization, by two-dimensional NMR spectroscopy, of a complex tetrasaccharide glycoside isolated from *Ipomoea stans*

RAUL G. ENRIQUEZ, ISMAEL LEON, FIDEL PEREZ, AND FERNANDO WALLS
Instituto de Quimica, Universidad Nacional Autonoma de Mexico, Mexico, D.F., Mexico 04510

AND

KATHERINE A. CARPENTER, FRANK V. PUZZUOLI, AND WILLIAM F. REYNOLDS[1]
Department of Chemistry, University of Toronto, Toronto, Ont., Canada M5S 1A1

Received July 18, 1991

RAUL G. ENRIQUEZ, ISMAEL LEON, FIDEL PEREZ, FERNANDO WALLS, KATHERINE A. CARPENTER, FRANK V. PUZZUOLI, and WILLIAM F. REYNOLDS. Can. J. Chem. **70**, 1000 (1992).

A mixture of glycosidic acids, each of which consisted of a tetrasaccharide unit linked by an anomeric carbon to 11-hydroxypalmitic acid and containing short-chain fatty acids ester-linked to the sugar units, was isolated from *Ipomoea stans*. Basic hydrolysis allowed isolation of a single compound whose structure was determined by two-dimensional NMR methods to be (*S*)-11-hydroxypalmitic acid 11-*O*-β-quinovopyranosyl-(1-4)-α-rhamnopyranosyl-(1,2)-β-glycopyranosyl-(1-2)-β-quinovopyranoside. Further HPLC separation of the original mixture allowed separation of a compound that was shown, by 2D NMR, to have 2-methylbutanoic acid molecules linked to C-4 of the terminal quinovose and C-2 of rhamnose, 3-hydroxy-2-methyl butanoic acid linked to C-6 of glucose, and with the palmitic acid forming a lactone at C-3 of rhamnose. Closer inspection revealed that this compound was actually a mixture of diastereomers involving different ((2*R*,3*R*) and (2*S*,3*S*)) enantiomers of 3-hydroxy-2-methylbutanoic acid bonded to the chiral tetrasaccharide core.

Key words: tetrasaccharide, two-dimensional NMR.

RAUL G. ENRIQUEZ, ISMAEL LEON, FIDEL PEREZ, FERNANDO WALLS, KATHERINE A. CARPENTER, FRANK V. PUZZUOLI et WILLIAM F. REYNOLDS. Can. J. Chem. **70**, 1000 (1992).

À partir de l'*Ipomoea stans*, on a isolé un mélange d'acides glycosidiques qui contiennent chacun une unité tétrasaccharide liée par un carbone anomérique à l'acide 11-hydroxypalmitique et qui contiennent des esters d'acides gras à chaines plus courtes liés à des unités de sucre. De leur hydrolyse basique on a pu isoler qu'un seul composé dont on a déterminé la structure par des méthodes de RMN bidimensionnelles; il s'agit du 11-*O*-β-quinovopyranosyl-(1,4)-α-rhamnopyranosyl-(1,2)-β-glucopyranosyl-(1,2)-β-quinovopyranoside de l'acide (*S*)-11-hydroxypalmitique. Une séparation plus poussée du mélange original par CHLP a permis de séparer un composé qui, selon la RMN en 2D, contiendrait des molécules d'acide 2-méthylbutanoique liées au C-4 du quinovose terminal et au C-2 du rhamnose, de l'acide 3-hydroxy-2-méthylbutanoique lié au C-6 du glucose et de l'acide palmitique formant une lactone en C-3 du rhamnose. Un examen plus minutieux a révélé que ce composé est en réalité un mélange de diastéréoisomères impliquant différents ((2*R*,3*R*) et (2*S*,3*S*)) énantiomères de l'acide 3-hydroxy-2-méthylbutanoique liés à un noyau tétrasaccharide chiral.

Mots clés : tétrasaccharide, RMN bidimensionnelle.

[Traduit par la rédaction]

Introduction

During the course of a phytochemical investigation of *Ipomoea stans* (Convulvulaceae), a plant used in Mexican traditional medicine for treatement of epileptic seizures (1), we isolated two polysaccharide samples from the roots of this plant. Preliminary characterization indicated that each sample was an oligosaccharide linked to a hydroxylated long-chain fatty acid via an acetal linkage at an anomeric center. Other short-chain fatty acids were ester-linked to the oligosaccharide core. The major difference between the two samples appeared to be the extent of esterification, with the more polar compound containing fewer ester linkages. However, the ^{13}C spectra suggested that neither sample was pure. Instead, each sample appeared to be a mixture of several compounds that apparently were isomers involving different sites of esterification and (or) different short-chain fatty acids. Initial attempts at further chromatographic separation were unsuccessful. Consequently, a portion of each sample was subjected to mild basic hydrolysis to cleave the ester linkages. After purification, the two new compounds were found to be identical. The characterization of this compound, primarily by two-dimensional NMR spectroscopy, is reported below. In addition, subsequent purification via high-pressure liquid chromatography allowed isolation of one pure compound from the less polar fraction. Characterization of this compound is also reported.

Results and discussion

Initial characterization

Initial characterization of the hydrolyzed glycosidic acid was carried out using normal ^1H NMR and normal and DEPT-edited (2) ^{13}C NMR. Measurements were carried out in CD_3OD since this solvent gave the best-resolved ^1H spectrum. The observation of four methine ^{13}C peaks in the region expected for anomeric carbons (δ100–105) suggested that the compound was a tetrasaccharide. Consistent with this, 17 additional methine ^{13}C peaks were observed in the region δ67–84, one of which was assumed to be the oxygen-bearing carbon of the fatty acid. Only one methylene carbon was observed in the sugar region. However, there were four methyl ^{13}C peaks in the region δ14–19. Inspection of the ^1H spectrum also revealed four methyl signals, three showing doublet splitting and a fourth appearing as a broadened triplet. This indicated that three of the four monosaccharides were 6-deoxy (e.g., 6-methyl) sugars. Finally, the ^{13}C spectrum showed a CO_2H signal and 13 further CH_2 signals (the latter in the region δ21–37). Combined with the previously mentioned

[1]Author to whom correspondence may be addressed.

Printed in Canada

Can. J. Chem. Downloaded from www.nrcresearchpress.com by 92.62.229.171 on 09/08/12
For personal use only.

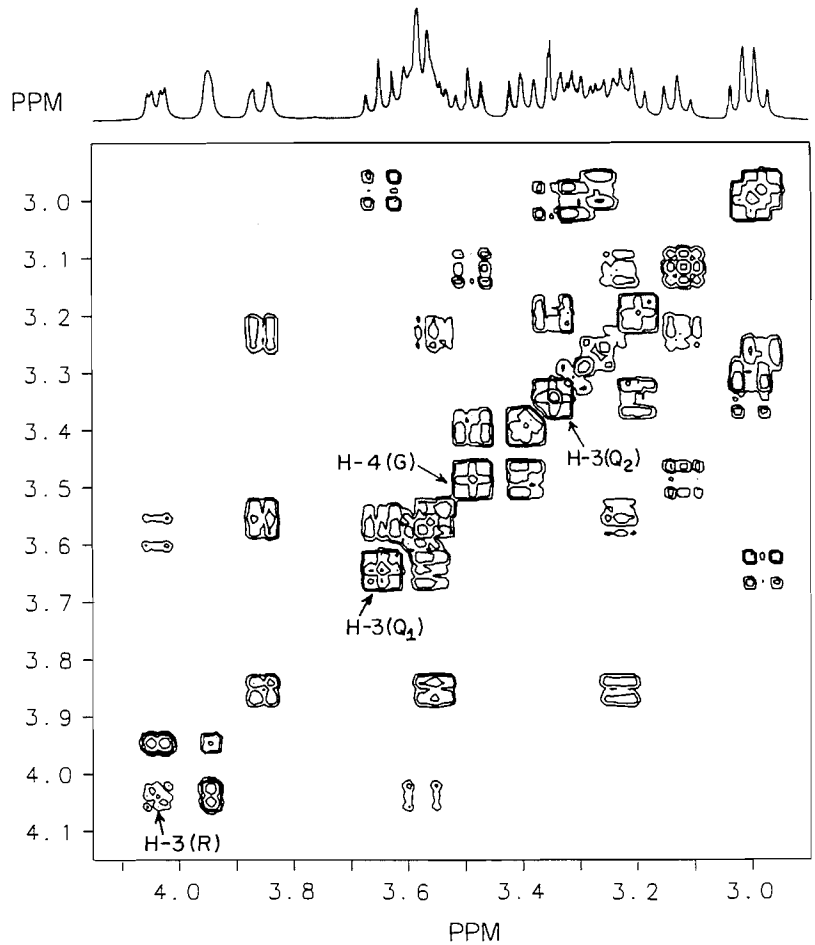

FIG. 1. Expansion of COSY-90 spectrum of **1** in CD_3OD. Resolved H-3 or H-4 protons of individual monosaccharide protons are labeled.

Can. J. Chem. Downloaded from www.nrcresearchpress.com by 92.62.229.171 on 09/08/12
For personal use only.

-CHO- and $-CH_3$ signals, this suggested that the fatty acid was a hydroxypalmitic acid isomer. The ^1H spectrum showed a triplet at δ2.22 characteristic of a CH_2 group adjacent to CO_2H and coupled to another CH_2 group, ruling out C-2 and C-3 as sites of hydroxylation. Similarly the observation of a broadened CH_3 triplet, suggesting virtual coupling to more than one CH_2 group, rules out C-14 to C-16 as the site of hydroxylation. No further conclusions could be drawn at this point since the remaining methylene ^1H signals appeared as a broad, poorly resolved envelope in the range δ1.1–1.7.

Assignment of individual monosaccharide units

Initial assignments were carried out by obtaining a COSY spectrum (3). This allowed tentative assignment of the protons of the four monosaccharide units. Inspection of the one-dimensional NMR spectrum then allowed determination of the individual $^1H-^1H$ coupling constants. The latter data suggested that the four monosaccharide units were one β-glucose unit, G, two β-quinovose units, Q_1 and Q_2, and probably one α-rhamnose unit, R. However, there was some ambiguity on the latter point since the equatorial orientation of H-2 in rhamnose makes it difficult to distinguish α and β anomers of rhamnose on the basis of coupling between H-1 and H-2.

Some of the individual ^1H assignments were unclear due to partial spectral overlap. However, expansion of the COSY spectrum for the region δ2.9–4.3 (see Fig. 1) showed that, for each monosaccharide unit, a peak assigned as either H-3 or H-4 was resolved. This suggested the possibility of using a homonuclear relayed coherence transfer experiment (4) to confirm ^1H assignments. Results of this experiment are illustrated in Fig. 2. This shows f_1 cross sections through peaks assigned as H-3 or H-4 for each monosaccharide. In effect, they provide a low-resolution edited ^1H spectrum with each monosaccharide unit appearing as a separate subspectrum.

The spectra in Fig. 2 are somewhat surprising in that they show relay of information along sequences of four protons on different carbons. Normally the basic relay sequence (4) only transmits information along a three-proton sequence (5). However, Otter and Kotovych have observed similar long-range relay peaks in spectra of polypeptides (6). Multi-exponential relaxation effects may contribute to long-range relay peaks involving methyl protons (7) and this may partially account for our observations for Q_1, Q_2, and R. Strong coupling effects can also cause long-range relay peaks (8) but this is unlikely to be important in this case since most monosaccharide protons are only weakly coupled. The fact that there is only one proton per carbon in most cases and usually similar vicinal $^1H-^1H$ coupling constants should promote the efficiency of at least the original relay stage (5, 9). In any case, regardless of the origins of the long-range peaks, they are obviously very helpful for spectral assignments.

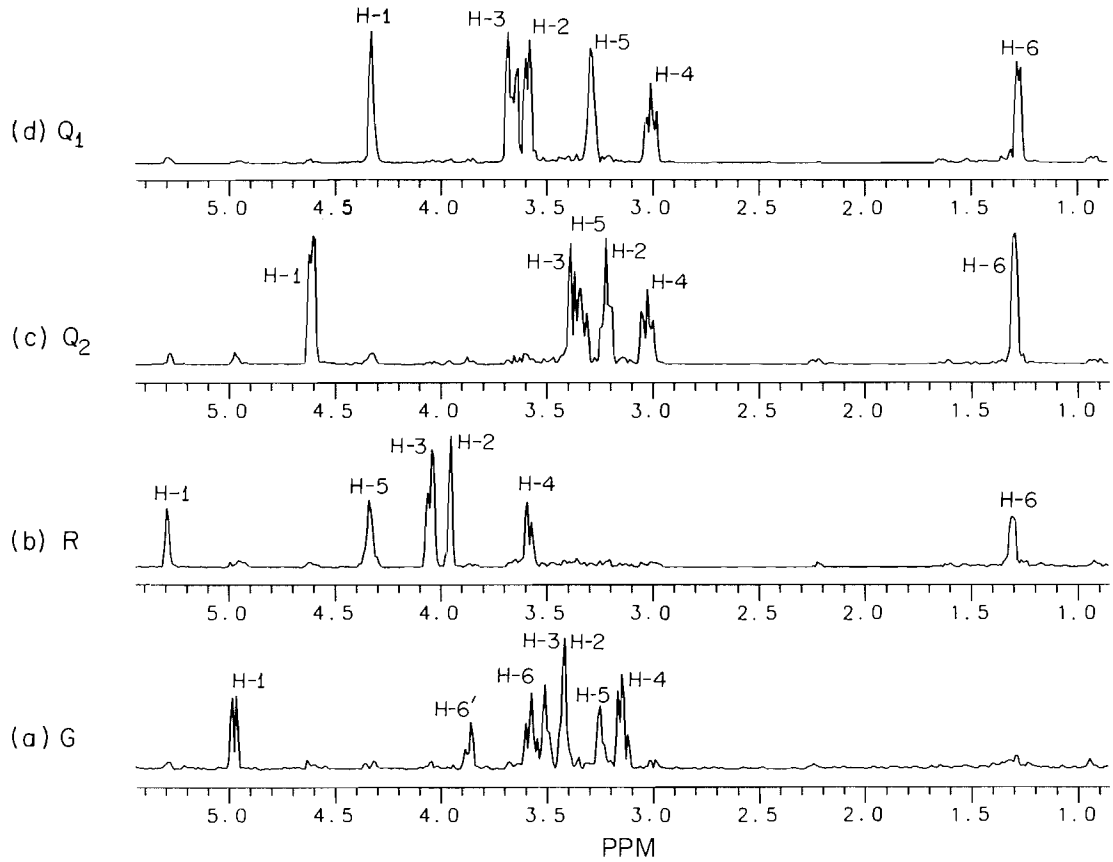

FIG. 2. Edited subspectra of individual monosaccharide units obtained from relay spectrum.

One-bond $^{13}C-^{1}H$ shift-correlated spectra (10) were used to assign ^{13}C chemical shifts, based on the ^{1}H assignments. Complete assignments of sugar protons and carbons are given in Table 1.

Assignment of linkage sites between different monosaccharide units and to the hydroxypalmitic acid chain

The first approach used to determine this information was to obtain nuclear Overhauser effect (nOe) difference spectra with and without irradiation of individual anomeric protons. However, there were three problems with this approach. First and most serious, the molecule is fortuitously tumbling at a rate almost corresponding to the cross-over from positive to negative nOe effects, resulting in very small intensity changes. Second, partial overlap of H-1 of Q_1 and H-5 of R complicated the interpretation of the results of irradiating the former hydrogen. Finally, strong spectral overlap near δ3.6 also hindered interpretation of some of the results. Nevertheless, the nOe results suggested inter-ring nOe's between H-1 of Q_2 and H-4 of R, H-1 of R and H-2 of G, and H-1 of G and H-2 of Q_1, plus an nOe between H-1 of Q_1 and the -CHO- proton assigned to the hydroxylated fatty acid.

To confirm these assignments, $^{13}C-^{1}H$ shift correlation spectra between indirectly bonded carbons and hydrogens (INCH) were measured, using our XCORFE sequence (11). The actual spectra were obtained on a peracetylated sample of the tetrasaccaride in $(CD_3)_2CO$. This was chosen because ^{13}C and ^{1}H relaxation times were significantly longer in the peracetylated compound, minimizing signal loss due to relaxation during the lengthy fixed delays necessary in INCH experiments. ^{1}H and ^{13}C spectra for the peracetylated sample were assigned in the same way as discussed above (see Table 1). Key cross-sectional spectra from the INCH experiment are shown in Fig. 3. Spectra 3*a*–3*g* show all six $^{1}H—C—O—^{13}C$ inter-ring connectivities plus the three-bond connectivity between H-1 of Q_1 and the methine carbon of the fatty acid. Many of the cross sections also show two-bond ($^{1}H—C—^{13}C$) connectivities, which are usually easily recognized by the presence of vicinal $^{1}H-^{1}H$ coupling. Three-bond intra-ring ($^{1}H—C—C—^{13}C$) cross-peaks are generally not observed, presumably because $^{3}J_{CH}$ coupling involving an axial hydrogen is relatively small due to the *gauche* dihedral angle (12). However, a strong three-bond connectivity is observed between the equatorial H-2 and C-4 of R (Fig. 3*e*), reflecting the larger *anti* $^{3}J_{CH}$ coupling (12). This suggests a method for determining the anomeric configuration of R, since C-3 and C-5 of R should show strong cross-peaks with H-1 only if H-1 is equatorial. In fact, these cross-peaks are observed (see Figs. 3*h*, 3*i*), confirming that R exists as its α-anomer. Alternatively, the same information could have been obtained by measuring anomeric $^{1}J_{CH}$ coupling constants (13).

Characterization of fatty acids

Two short-chain fatty acids were isolated from the hydrolysis of each of the two original samples. These were identified from their ^{1}H and ^{13}C spectra as 2-methylbutanoic acid and 3-hydroxy-2-methylbutanoic acid. The former was

Can. J. Chem. Downloaded from www.nrcresearchpress.com by 92.62.229.171 on 09/08/12
For personal use only.

TABLE 1. ^{13}C and ^{1}H chemical shifts and $^{1}H-^{1}H$ coupling constants for the tetrasaccharide unit after basic hydrolysis and (in parentheses) after peracetylation

Monosaccharide	Carbon	δ_C[a]	δ_H[b]	J_{HH}[c]
G	1[d]	101.84(100.74)	4.96(4.84)	$J_{1,2}$ = 7.6
	2[d]	77.90(76.52)	3.39(3.62)	$J_{2,3}$ = 9.1
	3	79.28(75.47)	3.49(5.24)	$J_{3,4}$ = 9.2
	4	72.53(69.82)	3.13(4.90)	$J_{4,5}$ = 9.2
	5	77.95(71.85)	3.22(3.92)	$J_{5,6}$ = 2.4
	6	63.61(62.72)	3.55(4.06)	$J_{5,6'}$ = 4.8
	6′		3.85(4.28)	$J_{6,6'}$ = 12.2
R	1[d]	101.09(98.75)	5.28(4.86)	$J_{1,2}$ = 1.2
	2	72.03(70.85)	3.93(5.02)	$J_{2,3}$ = 3.2
	3	72.06(71.75)	4.03(5.26)	$J_{3,4}$ = 9.2
	4[d]	83.43(77.17)	3.59(3.72)	$J_{4,5}$ = 9.4
	5	67.93(67.55)	4.33(4.12)	$J_{5,6}$ = 6.2
	6	18.43(18.04)	1.30(1.28)	
Q_1	1[d]	103.08(101.55)	4.31(4.48)	$J_{1,2}$ = 8.0
	2[d]	79.19(76.68)	3.58(3.80)	$J_{2,3}$ = 9.1
	3	78.77(75.85)	3.65(5.11)	$J_{3,4}$ = 9.0
	4	77.28(74.38)	2.99(4.61)	$J_{4,5}$ = 8.8
	5	72.99(69.76)	3.29(3.64)	$J_{5,6}$ = 6.2
	6	18.17(17.64)	1.26(1.21)	
Q_2	1[d]	105.11(100.93)	4.59(4.94)	$J_{1,2}$ = 8.0
	2	76.08(69.76)	3.21(4.90)	$J_{2,3}$ = 9.2
	3	77.68(73.67)	3.36(5.16)	$J_{3,4}$ = 9.3
	4	76.93(74.09)	3.02(4.77)	$J_{4,5}$ = 8.8
	5	73.28(70.21)	3.34(3.75)	$J_{5,6}$ = 6.2
	6	18.20(17.71)	1.28(1.15)	

[a] ^{13}C chemical shifts (relative to internal $(CH_3)_4Si$) for **1** in CD_3OD and (in parentheses) for the peracetylated derivative of **1** in $(CD_3)_2CO$.

[b] ^{1}H chemical shifts (relative to internal $(CH_3)_4Si$) for **1** in CD_3OD and (in parentheses) for the peracetylated derivative of **1** in $(CD_3)_2CO$.

[c] Vicinal $^{1}H-^{1}H$ couplings (in Hz) for **1** in CD_3OD.

[d] Denotes a carbon that is a linkage site to another monosaccharide or to hydroxypalmitic acids. Note that the ^{1}H chemical shifts for the attached protons generally show smaller shifts between **1** and its peracetylated derivative than protons attached to carbons whose hydroxyl groups are peracetylated.

the major component (ca. 60%) of the mixture in each case. Based on a comparison of coupling constants with those previously reported (14), the 3-hydroxy-2-methylbutanoic acid is apparently the (2*S*,3*S*) isomer or its (2*R*,3*R*) enantiomer.

Identification of the hydroxypalmitic acid isomer proved more difficult. From ^{13}C chemical shifts and T_1 relaxation times, it seemed improbable that the hydroxyl group was attached to a carbon that was within five carbons of either chain end. However, this still left six possible isomers. To determine the actual structure, the hydroxypalmitic acid was isolated from the glycosidic acid by mild acid hydrolysis. It was esterified (as the methyl ester), then converted to the trimethylsilyl ether. Gas chromatography/mass spectrometry indicated that the compound was 11-hydroxypalmitic acid and the observed rotation indicated that it was the *S* enantiomer (see Experimental). Thus the isolated pure compound has the structure (*S*)-11-hydroxypalmitic acid 11-*O*-β-quinovopyranosyl-(1-4)-α-rhamnopyranosyl-(1,2)-β-glucopyranosyl-(1-2)-β-quinovopyranoside. By analogy with earlier results (14), the quinovose and glucose units are assumed to have the D configuration while the rhamnose unit has the L configuration.

Assigned ^{13}C and ^{1}H chemical shifts and relaxation times for the hydroxypalmitic acid group are given in Table 2.

Determination of the complete structure of one component of the less polar fraction

With the aid of HPLC, a single, apparently pure, component was isolated from the less polar mixture. The ^{1}H spectrum of this compound is exceedingly complicated even at 500 MHz (Fig. 4). Nevertheless, by a combination of COSY, relay, and one-bond and long-range $^{13}C-^{1}H$ shift-correlation spectra it was possible to assign the entire structure and ^{1}H and ^{13}C spectra. The only difference in technique was that we used our recently developed FLOCK sequence (15) for the long-range $^{13}C-^{1}H$ shift correlation experiment, since this sequence gives a wider range of cross-peaks from a single experiment. These experiments indicated that one 2-methylbutanoic acid molecule was attached at C-4 of Q_2, a second 2-methylbutanoic acid was attached at C-2 of R, while a 3-hydroxy-2-methylbutanoic acid molecule was attached at the methylene group of G (C-6). Finally, the carboxylic acid function of the hydroxypalmitic acid formed a lactone ring at C-3 of R. This leads to the final structure **2**. However, one puzzling feature was

Can. J. Chem. Downloaded from www.nrcresearchpress.com by 92.62.229.171 on 09/08/12
For personal use only.

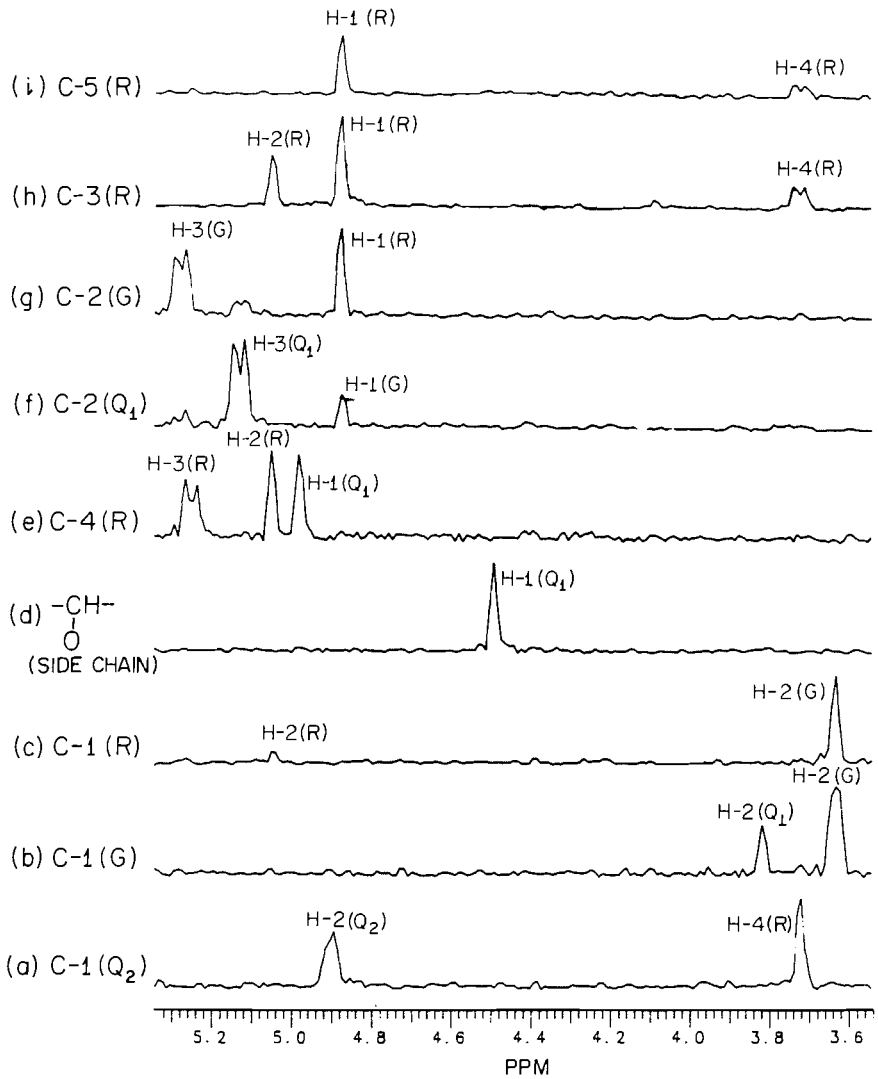

FIG. 3. f_1 cross-sectional spectra through indicated carbon (f_2) frequencies. The sample is a peracetylated sample of **1** in $(CD_3)_2CO$ and spectra were obtained with the XCORFE sequence.

an apparent doubling of ^{13}C peaks for all carbons of G, as well as carbons 1–3 of R and carbons 1, 2, and 5 of Q_1. The chemical shift difference was typically very small (0.03–0.06 ppm) with C-6 of G showing a splitting of 0.10 ppm. The carbons of the 3-hydroxy-2-methylbutanoic acid also showed splittings. This led us to suspect that the apparently pure compound was actually an almost equimolar mixture of two diastereomers, involving bonding of either of a pair of enantiomers ((2*R*,3*R*) or (2*S*,3*S*)) of 3-hydroxy-2-methylbutanoic acid to the chiral tetrasaccharide core. In fact, further very careful HPLC separation allowed isolation of a mixture that was approximately 85:15 in favour of one component. The data in Tables 3 and 4 correspond to the major component of this mixture. In view of the very small amount of sample available, no attempt was made to hydrolyze off the short-chain fatty acids and to determine the chirality of these acids. However, based on previous work on similar compounds (16), the 2-methylbutanoic acid is most likely present as the *S* enantiomer.

^{13}C spin-lattice relaxation times were also determined for **2**, mainly as an aid for assigning as many of the hydroxypalmitic acid carbons as possible. However, they also provide some useful information about mobility within the tetrasaccharide. The shortest relaxation times, corresponding to the slowest molecular motions, are observed for Q_1 and R. This is logical because these groups are linked to opposite ends of the hydroxypalmitic acid. The longest relaxation times are observed for the carbons of Q_2, the terminal quinovose unit. This is also logical since this is the only group that has linkages at C-1 and C-4, allowing for considerable freedom for rotation about the C-1/C-4 axis.

Comparison with related structures

After completion of the characterization of **1**, search of the literature revealed that Miyahara and co-workers had reported the isolation, from *Ipomoea orizabensis* (Convolvulaceae), of a series of four tetrasaccharide derivatives whose core structure differed from our core structure by replacement of Q_1 by a D-fucose unit (14). They also differed from our structure in that all four compounds had a tiglic acid group forming an ester link to the hydroxyl group at C-2 of rhamnose. Each of them contained two additional short-chain fatty acids with each containing a 3-hydroxy-1-meth-

Can. J. Chem. Downloaded from www.nrcresearchpress.com by 92.62.229.171 on 09/08/12
For personal use only.

Can. J. Chem. Downloaded from www.nrcresearchpress.com by 92.62.229.171 on 09/08/12
For personal use only.

TABLE 2. Assignments of ^{13}C and ^{1}H chemical shifts and ^{13}C T_1 relaxation times for 11-hydroxypalmitic acid component of **1**

Carbon	δ_C[a]	δ_H[b]	T_1[c]
1	179.15	—	—
2	36.76	2.22	0.42
3	26.77	1.60	0.52
4[d]	30.48	1.33	0.54
5[d]	30.43	1.33	0.52
6[d]	30.75	1.32	0.48
7	30.88	1.30	0.43
8	31.14	1.29	0.34
9[e]	25.84	1.39	(0.34)
10	35.46	(1.51)[f]	0.19
11	83.50	3.60	0.31
12	35.80	1.48,1.66	0.23
13[e]	25.87	1.39	(0.34)
14	32.96	1.27	0.84
15	23.63	1.33	1.72
16	14.43	0.91	2.91

[a] ^{13}C chemical shift (in CD_3OD), relative to internal $(CH_3)_4$ Si.
[b] ^{1}H chemical shift (in CD_3OD), relative to internal $(CH_3)_4$ Si.
[c] ^{13}C spin-lattice relaxation time (s). Estimated error ±5%.
[d] Assignments could be interchanged.
[e] Assignments could be interchanged. T_1 values are average for the two peaks.
[f] Average chemical shift for slightly nonequivalent CH_2 protons.

ylbutanoic acid group linked to C-6 of glucose (as we observed in **2**) plus an additional short-chain acid (either 3-hydroxy-2-methylbutanoic acid, 2-methylbutanoic acid, or methylpropanoic acid) at either C-3 or C-4 of the terminal quinovose group. The same group has reported a series of other tetrasaccharide derivatives (17, 18) but these differ even more in their monosaccharide units from the structure of the compound that we isolated. However, after our completion of the structure elucidation of **2** (other than the separation of diastereomers), Miyahara and co-workers reported a pair of compounds, isolated from the roots of *Convolvulus scammonia*, which had the identical core structure, **1** (16). However, these differed from our compound in having only one or two short-chain fatty acids. Both compounds have a 2-methylbutanoic acid group at C-2 of R (as in our case) while one of the compounds has a tiglic acid group at C-4 of Q_2. It should be noted that Miyahara and co-workers generally relied on indirect evidence (e.g., ^{1}H shifts after ester hydrolysis) to assign sites of esterification while we have unambiguous evidence from INCH experiments. We have also provided much more complete assignments for the acid carbons and protons. The observation of two compounds differing only in the stereochemistry of an ester-linked fatty acid also is a new observation. Overall, this investigation has provided further support for earlier work demonstrating the great power of 2D NMR for investigations of polysaccharide structures (19).

Based on the results of this and earlier investigations, there appears to be a wide variety of related compounds containing a tetrasaccharide unit linked by an anomeric carbon to 11-hydroxypalmitic acid. However, there appears to be considerable diversity in both the individual monosaccharide units as well as in the numbers, positions, and types of ester-linked short-chain fatty acids. In our case, the basic hydrolysis of both original samples yielded only 3-hydroxy-2-methylbutanoic acid and 2-methylbutanoic acid with no evidence of either tiglic acid or methylpropanoic acid. Furthermore, all compounds from these samples seemed to have the same basic core structure, **1**, although it cannot be absolutely ruled out that one or more of the very minor components from the two samples might have different monosaccharide units and (or) other short-chain fatty acids. However, based on the HPLC traces, there appear to be at least eight major components in the two samples that must have the basic core structure and with one or more molecules of 3-hydroxy-2-methylbutanoic acid and (or) 2-methylbutanoic acids ester-linked to the core. One of these could possibly be the compound of Miyahara and co-workers containing only 2-methylbutanoic acid ester-linked to C-2 of R in structure **1** (16). However, the others must be new compounds. Further investigations are being undertaken to isolate and characterize these additional compounds.

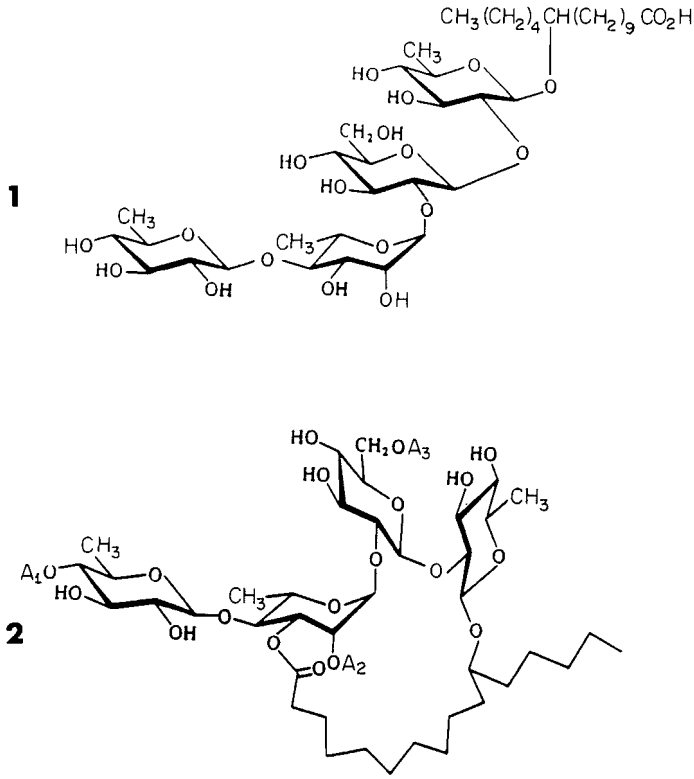

Experimental

Isolation

Plant material was obtained through a local market in Mexico City and identified as *Ipomea stans* by Dr. Miguel Martinez (Instituto de Biologia (UNAM)). Dried roots (1 kg) were defatted with hexane by maceration at room temperature. The material was then macerated three times with three litres of ethyl acetate. About 70 g of a white resinous powder was obtained as the overall residue from the latter treatment. Preliminary inspection of the residue by TLC showed two major spots on SiO_2 eluted with $CHCl_3$:CH_3OH (86:14) with R_f about 0.35 and 0.37. The less polar spot was ca. ten times as abundant as the more polar one. Preparative column chromatography of the crude residue afforded 9.2 g

Can. J. Chem. Downloaded from www.nrcresearchpress.com by 92.62.229.171 on 09/08/12
For personal use only.

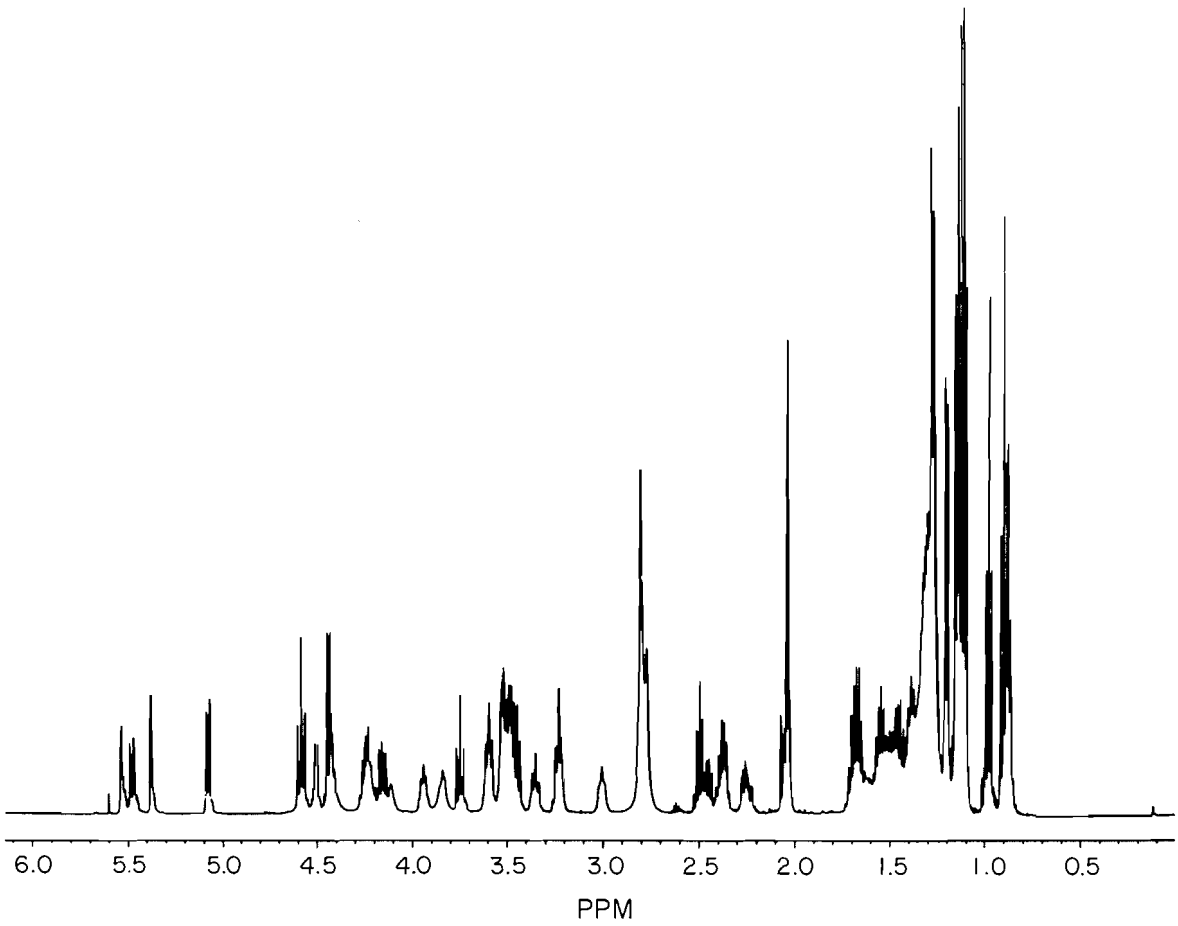

FIG. 4. The 500 MHz ^1H spectrum of **2** in $(CD_3)_2CO$.

of the less polar compound (A) and 0.8 g of the more polar compound (B). Their IR and 90 MHz ^1H NMR spectra indicated that both possessed glycolipid structures. However, more detailed characterization by 400 MHz ^1H NMR and 100 MHz ^{13}C NMR spectra indicated that each product was a mixture of isomers. Neither product would crystallize.

Basic hydrolysis

A (300 mg) was refluxed with 50 mL of ethanolic 0.1 N NaOH for 30 min. The solution was neutralized with dilute acid and extracted with ether. Evaporation of the ether layer yielded an oily liquid, which, on the basis of 90 MHz ^1H NMR, GC–FTIR, and GC–MS was identified as a ca. 60:40 mixture of 2-methylbutanoic acid ethyl ester and 3-hydroxy-2-methylbutanoic acid ethyl ester. The aqueous layer was lyophilized, the residue was extracted with ethanol, and a white crystalline solid, **1**, was isolated.

Treatment of B gave the same fatty acid products in roughly similar proportions.

Acid hydrolysis

A (200 mg) was refluxed for 2 h in 3 N HCl. After neutralization with 0.1 N NaOH the solution was alternatively extracted with $(CH_3CH_2)_2O$ and $CHCl_3$. The organic layers were dried and combined. After evaporation of the solvent, the residue was derivatized with $CH_3OH:BF_3$ prior to GC–MS analysis. The derivative was identified as the methyl ester of 11-hydroxypalmitic acid by comparison with previously reported mass spectral fragmentation patterns for this compound (20). The observed rotation ($[\alpha]_D^{25}$ = +0.42) is very similar to that previously reported for the *S* enantioner of this ester ($[\alpha]_D^{25}$ = +0.45 (16)). As a further confirmation, this compound was converted to its trimethylsilyl ether. Three major fragment ions with *m/z* (relative intensity) of 173(100), 287(70), and 327(13) were observed, respectively consistent with fragments $[CH_3(CH_2)_4CHOSi(CH_3)_3]^+$, $[(CH_3)_3SiOCH(CH_2)_9CO_2CH_3]^+$, and $CH_3(CH_2)_4CH(OSi(CH_3)_3)(CH_2)_9CO]^+$, as expected for the derivatized 11-hydroxypalmitic acid.

Peracetylation of the tetrasaccharide glycoside isolated from basic hydrolysis

1 (40 mg) was repeatedly dissolved in pyridine (3 mL, 5 times) and evaporated to dryness on a rotoevaporator in order to remove traces of water from the sample. After further drying of the sample *in vacuo* over P_2O_5 overnight, 200 μL each of pyridine and acetic acid was added and the mixture heated with stirring at 100°C for 30 min. After 0.5 mL of water was added to the sample, the resultant cloudy mixture was stirred at room temperature for 15 min and then evaporated to dryness. The dried sample was taken up in 4 mL of $CHCl_3$, then washed with 0.1 M sodium carbonate followed by 0.01 M HCl. The organic solution was evaporated to dryness, first with a rotoevaporator, then a vacuum pump, yielding 42 mg of a slightly yellow solid (mp 119–120°C).

HPLC purification

HPLC separation of sample A was carried out on a Varian liquid chromatograph model 8500 equipped with a reverse-phase, cyano-bonded analytical column (Econosphere 250 × 4.6 mm, particle diameter = 5 μm) with an Altex refractive index detector and a Varian integrator model 4270. The eluent was a gradient of CH_3CN/H_2O going from 80:20 to 50:50 respectively, flow at 1.0 mL/min at a pressure of 100 atm (1 atm = 101.3 kPa). The initial chromatogram revealed at least six fractions of which the major (slowest moving) fraction was collected. By repeated injections about 60 mg of the major component was obtained at ca. 90% purity. Further purification by the same procedure gave about

TABLE 3. Assignments of ^{13}C and ^{1}H chemical shifts and ^{13}C relaxation times for the tetrasaccharide core of **2**

Monosaccharide	Carbon	δ_C[a]	δ_H[b]	T_1[c]
G	1[d,e]	100.34	5.07	0.41
	2[d,e]	79.06	3.44	0.41
	3[e]	77.21	3.59	0.46
	4[e]	72.11	3.35	0.39
	5	74.50	3.48	0.42
	6[e,f]	64.53	4.15	0.23
	6′	—	4.43	
R	1[d,e]	96.73	5.38	0.40
	2[e,f]	69.75	5.54	0.32
	3[e,f]	71.73	5.48	0.34
	4[d]	78.31	3.74	0.33
	5	68.60	4.24	0.34
	6	18.32	1.28	0.55
Q_1	1[d,e]	100.45	4.49	0.33
	2[d,e]	79.21	3.52	0.35
	3	78.17	3.51	0.31
	4	77.03	2.99	0.40
	5[e]	72.14	3.23	0.39
	6	18.17	1.20	0.64
Q_2	1[d]	104.39	4.44	0.42
	2	75.33	3.22	0.46
	3	75.10	3.50	0.53
	4[f]	76.10	4.58	0.45
	5	70.54	3.47	0.44
	6	17.97	1.13	0.76

[a] ^{13}C chemical shifts (relative to $(CH_3)_4Si$) in $(CD_3)_2CO$.
[b] ^{1}H chemical shifts (relative to $(CH_3)_4Si$) in $(CD_3)_2CO$.
[c] ^{13}C spin-lattice relation times (s).
[d] Denotes a carbon that is a linkage site to another monosaccharide or to hydroxypalmitic acid.
[e] Carbons that appeared as doublets in the initial sample of **2**.
[f] Denotes a carbon that is a site of esterification.

TABLE 4. ^{13}C and ^{1}H chemical shifts and ^{13}C T_1 relaxation times for fatty acids in **2**

Acid	Carbon	δ_C[a]	δ_H[b]	T_1[c]
11-Hydroxypalmitic acid	1	173.81	—	—
	2	34.36	2.24,2.38	0.25
	3	25.89	1.29,1.48	0.30
	4	29.91	1.26,1.34	0.38
	5	29.07	⟨1.32⟩[e]	0.36
	6[d]	28.77	1.25,1.40	0.32
	7	28.50	⟨1.33⟩[e]	0.30
	8	27.98	⟨1.28⟩[e]	0.32
	9	23.82	1.52,1.70	0.21
	10	34.27	1.44,1.62	0.27
	11	79.51	3.59	0.44
	12	35.22	⟨1.50⟩[e]	0.34
	13	25.39	1.39	0.57
	14	32.64	1.26	1.03
	15	23.34	1.30	2.10
	16	14.11	0.87	3.65
A_1[f]	1	175.91	—	—
	2	41.97	2.37	1.27
	3	27.25	1.44,1.66	0.76
	4	11.87	0.89	⟨2.37⟩[g]
	5	17.02	1.11_5	1.21
A_2[h]	1	175.55	—	—
	2	41.61	2.45	1.09
	3	27.65	1.54,1.67	0.72
	4	11.88	0.97	⟨2.37⟩[g]
	5	17.15	1.15	1.22
A_3[i]	1[j]	175.39	—	—
	2[j]	48.47	2.49	0.91
	3	69.53	3.94	0.91
	4	20.68	1.14_5	0.97
	5	13.41	1.11	1.08

[a] ^{13}C chemical shifts (relative to internal $(CH_3)_4Si$) in $(CD_3)_2CO$.
[b] ^{1}H chemical shifts (relative to internal $(CH_3)_4Si$) in $(CD_3)_2CO$.
[c] ^{13}C spin-lattice relaxation times (s).
[d] Assignment of carbons C-4 to C-8 is uncertain.
[e] Average chemical shift for slightly nonequivalent CH_2 protons.
[f] 2-Methylbutanoic acid ester-linked to C-4 of Q_2. C-5 is the 2-methyl group.
[g] Average relaxation time for partially overlapped carbons.
[h] 2-Methylbutanoic acid ester-linked to C-2 of R.
[i] 3-Hydroxy-2-methylbutanoic acid ester-linked to C-6 of G.
[j] Carbons that appeared as doublets in the initial sample of **2**.

25 mg of product at ca. 97% purity. When the NMR spectrum indicated that the sample was actually a mixture of diastereomers, the whole process was repeated with a new sample of A, but only sampling the leading edge of the major peak. After repeated runs, ca. 30 mg of compound was isolated containing an approximately 85:15 ratio of the two diastereomers. The isolated material was an amorphous white solid, mp = 103°C.

NMR spectra

Preliminary NMR spectra were obtained on a Varian EM-390 spectrometer. All subsequent spectra (including 2D spectra) were obtained on a Varian XL-400 spectrometer. Typically, COSY spectra were obtained using f_1 and f_2 spectral windows of 2000 Hz, 512 time increments (zero-filled to 1024), 16 transients per time increment, 1024 data points for each f.i.d., and a 1 s relaxation delay. Spectra were processed using pseudo-echo weighting in both domains followed by symmetrization by triangular folding. Relay spectra were similar except that they used 64 transients per time increment and a relay delay of 0.5 s. Relay spectra were obtained using the sequence described by Bain and co-workers (21). $^{1}H-^{13}C$ shift correlation spectra were obtained using the Bax modification (10*b*) of the standard shift correlation sequence (10*a*). Typical parameters involved a $^{13}C(f_2)$ spectral window of 10 000 Hz with 2048 data points (zero-filled to 4096), an ^{1}H (f_1) spectral window of 2000 Hz with 192 time increments (zero-filled to 512), 128 transients per time increment, and a relaxation delay of 0.6 s. Modified pseudo-echo processing (similar to shifted-sine-bell processing) was used in both domains.

The XCORFE spectrum was obtained using an f_2 spectral window of 10 000 Hz with 2048 data points zero-filled to 4096. The f_1 spectral window was 2000 Hz and 360 time increments (zero-filled to 1024) were collected with 128 transients per increment. The fixed time prior to polarization transfer was 0.090 s with a refocussing delay of 0.032 s after polarization transfer and a relaxation delay of 0.6 s. Delays in the BIRD pulses were optimized for J_{CH} = 155 Hz. The FLOCK parameters were generally similar except that 160 time increments were used with 256 transients per time increment and a delay prior to polarization transfer of 0.064 s. A separate FLOCK spectrum was run for the ^{13}C carbonyl region with an f_2 spectral width of 600 Hz and 256 data points (zero-filled to 1024).

Acknowledgements

Financial support from the Natural Sciences and Engineering Research Council of Canada (W.F.R.) and CoNaCyT

Can. J. Chem. Downloaded from www.nrcresearchpress.com by 92.62.229.171 on 09/08/12
For personal use only.

(R.G.E.) is gratefully acknowledged. We thank Dr. V. V. Krishnamurthy of Varian Associates for providing the 500 MHz ^{1}H NMR spectrum shown in Fig. 4.

1. J. L. Diaz. Usos de las Plantas Medicinales de Mexico. Monografias Cientificas II, INEPLAM, Mexico. 1976. p. 329.
2. D. M. Doddrell, D. T. Pegg, and M. R. Bendall. J. Magn. Reson. **48**, 323 (1982).
3. A. Bax and R. Freeman. J. Magn. Reson. **44**, 542 (1981).
4. (*a*) G. Eich, G. Bodenhausen, and R. R. Ernst. J. Am. Chem. Soc. **104**, 3731 (1982); (*b*) P. H. Bolton. J. Magn. Reson. **48**, 336 (1982).
5. A. Bax and G. Drobny. J. Magn. Reson. **61**, 306 (1985).
6. A. Otter and G. Kotovych. J. Magn. Reson. **69**, 187 (1986).
7. N. Muller, G. Bodenhausen, K. Wurthrich, and R. R. Ernst. J. Magn. Reson. **65**, 531 (1985).
8. L. E. Kay, P. J. Jones, and J. H. Prestegard. J. Magn. Reson. **72**, 397 (1987).
9. D. W. Hughes. Magn. Reson. Chem. **26**, 214 (1988).
10. (*a*) A. Bax and G. A. Morris. J. Magn. Reson. **42**, 501 (1981); (*b*) A. Bax. J. Magn. Reson. **53**, 517 (1983).
11. W. F. Reynolds, D. W. Hughes, M. Perpick-Dumont, and R. G. Enriquez. J. Magn. Reson. **63**, 413 (1985).
12. K. Bock and C. Pedersen. J. Chem. Soc. Perkin. Trans. 2, 293 (1974).
13. P. E. Hansen. Prog. NMR Spectrosc. **14**, 175 (1981).
14. N. Noda, M. Odo, K. Miyahara, T. Kawasaki, and M. Okabe. Tetrahedron, **43**, 3839 (1987).
15. W. F. Reynolds, S. McLean, M. Perpick-Dumont, and R. G. Enriquez. Magn. Reson. Chem. **27**, 162 (1989).
16. N. Noda, H. Kogitsu, T. Kawasaki, and K. Miyahara. Phytochemistry, **29**, 3565 (1990).
17. N. Noda, H. Kobayashi, K. Miyahara, and T. Kawasaki. Chem. Pharm. Bull. **36**, 920 (1988).
18. N. Noda, M. Nishi, K. Miyahara, and T. Kawasaki. Chem. Pharm. Bull. **36**, 1707 (1988).
19. (*a*) L. Lerner and A. Bax. Carbohydr. Res. **166**, 35 (1987); (*b*) H. van Halbeck. Frontiers of NMR in molecular biology. Alan R. Liss, Inc., New York. 1990. p. 195.
20. H. Wagner and G. Schwarting. Phytochemistry, **16**, 715 (1977).
21. D. W. Hughes, R. A. Bell, T. Neilson, and A. D. Bain. Can. J. Chem. **63**, 3133 (1985).

Can. J. Chem. Downloaded from www.nrcresearchpress.com by 92.62.229.171 on 09/08/12
For personal use only.

Unique electrochemical response of a polyaniline-film coated electrode to several dissolved organic species

JUN YANO[1] AND KOTARO OGURA
Department of Applied Chemistry, Faculty of Engineering, Yamaguchi University, Tokiwadai, Ube, Yamaguchi 755, Japan

AND

AKIRA KITANI AND KAZUO SASAKI
Department of Applied Chemistry, Faculty of Engineering, Hiroshima University, Saijo, Higashihiroshima, Hiroshima 724, Japan

Received April 11, 1991[2]

JUN YANO, KOTARO OGURA, AKIRA KITANI, and KAZUO SASAKI. Can. J. Chem. **70**, 1009 (1992).

Electrode reactions of dissolved inorganic redox species on a polyaniline (PAN) film did not take place when the film was in media of low acidity (pH >3.5 (pK_a of PNA)) and (or) was held at the potential region where PAN itself was not redox active. Redox waves of several dissolved organic species, however, were clearly observed on such an electroinactive PAN film. Further, the organic species transformed the electroinactive PAN film into electrically conducting film.

Key words: electroinactive polyaniline, electrode reaction, organic species.

JUN YANO, KOTARO OGURA, AKIRA KITANI et KAZUO SASAKI. Can. J. Chem. **70**, 1009 (1992).

Aucune réaction d'électrode des espèces redox inorganiques dissoutes n'a eu lieu sur le film polyaniline (PAN), lorsque celui-ci était dans un milieu peu acide (pH > 3.5 (pK_a de PAN)) et (ou) était maintenu dans la région potentielle où le PAN n'était pas redox. Par contre, les ondes redox de plusieurs espèces organiques dissoutes étaient constatées sur le même film PAN électro-inactif. En plus, on a pu voir les espèces organiques transformer le film électro-inactif en film électriquement conductible.

Mots clés : polyaniline électro-inactif, réaction d'électrode, espèces organiques.

Although many studies of the properties of polyaniline (PAN) have been driven by the wide variety of possible applications, little attention has been paid to the electrochemical response of the PAN film to dissolved species. Papers dealing with the response to dissolved *organic* species are especially limited. The PAN film does not respond to any dissolved inorganic species over the potential region where PAN itself is not redox active (1) and (or) in less acidic media (pH >3.5 (pK_a of PAN)) (2). In this communication, we wish to focus our attention on such electroinactive PAN films and examine whether or not the films respond to certain organic species.

Even in the electroinactive potential region (Fig. 1(*b*)), the redox wave of *p*-dimethoxybenzene is evident (Fig. 1(*a*)). Those of *p*-dihydroxydiphenyl and *p*-methoxyphenol were also observed. On the other hand, the PAN film does respond to hydroquinone (Fig. 1(*c*)), although the film itself is electroinactive (Fig. 1(*d*)). It also responded to other quinones such as *o*-benzoquinone, duroquinone, and chloranil. Moreover, it is interesting to find that the film also responded to I^-, in spite of it being one of the inorganic species.

Electroinactive PAN films do not catalyze the electrode reactions of *p*-dimethoxybenzene and hydroquinone (Fig. 1(*a*) and (*c*)). The reason is that the films have few redox-active sites near the film/solution interface and do not work as electron-transfer-mediating catalysts. Two mechanisms of the charge transport are, therefore, proposed for the electrochemical response: (*i*) dissolved species pass through the film smoothly and then reach the electrode substrate; and (*ii*) the film is transformed into an electron conductor by the contact with the species. Ohnuki *et al.* found that the PAN film was hardly permeable to species having a Stokes radii (γ_S) of more than 2 Å (3). This explains the fact that the film responds not to $Fe(CN)_6^{3-}$ (γ_S = 2.7 Å), etc., but to I^- (γ_S = 1.2 Å) in the pH 5 solution. Such permeability also suggests that the film blocks the passage of bulky organic species such as hydroquinone, whose size is roughly equal to that of $Fe(CN)_6^{3-}$. To confirm this, a PAN pellet electrode was employed. The electrode was prepared by compressing PAN powder obtained by potentiostatic electrolysis, as described previously (4). The geometric area of the PAN pellet was 0.32 cm^2 and that of the platinum wire inside the pellet was 0.025 cm^2. The steady-state current–potential (*i*–*E*) curves for the oxidation of 10 mM *p*-dimethoxybenzene in 0.1 M H_2SO_4 and of 10 mM hydroquinone in the pH 5 solution were measured by using both the pellet electrode and a platinum wire electrode having an area of 0.025 cm^2. The limiting oxidative currents of *p*-dimethoxybenzene and hydroquinone were 0.34 and 0.28 mA, respectively. These values were at least 10 times greater than those obtained with the platinum wire electrode. This result strongly supports mechanism (*ii*) as reasonable for the charge transport of the film.

On the PAN film coated electrode experiencing the response of hydroquinone, the redox current of $Fe(CN)_6^{3-}/Fe(CN)_6^{4-}$ was observed, although it was about one tenth smaller than that measured with a bare platinum electrode. This also leads to mechanism (*ii*). To obtain direct evi-

[1]Author to whom correspondence may be addressed.
[2]Revision received November 20, 1991.

Printed in Canada

Can. J. Chem. Downloaded from www.nrcresearchpress.com by 92.62.229.171 on 09/08/12
For personal use only.

Can. J. Chem. Downloaded from www.nrcresearchpress.com by 92.62.229.171 on 09/08/12
For personal use only.

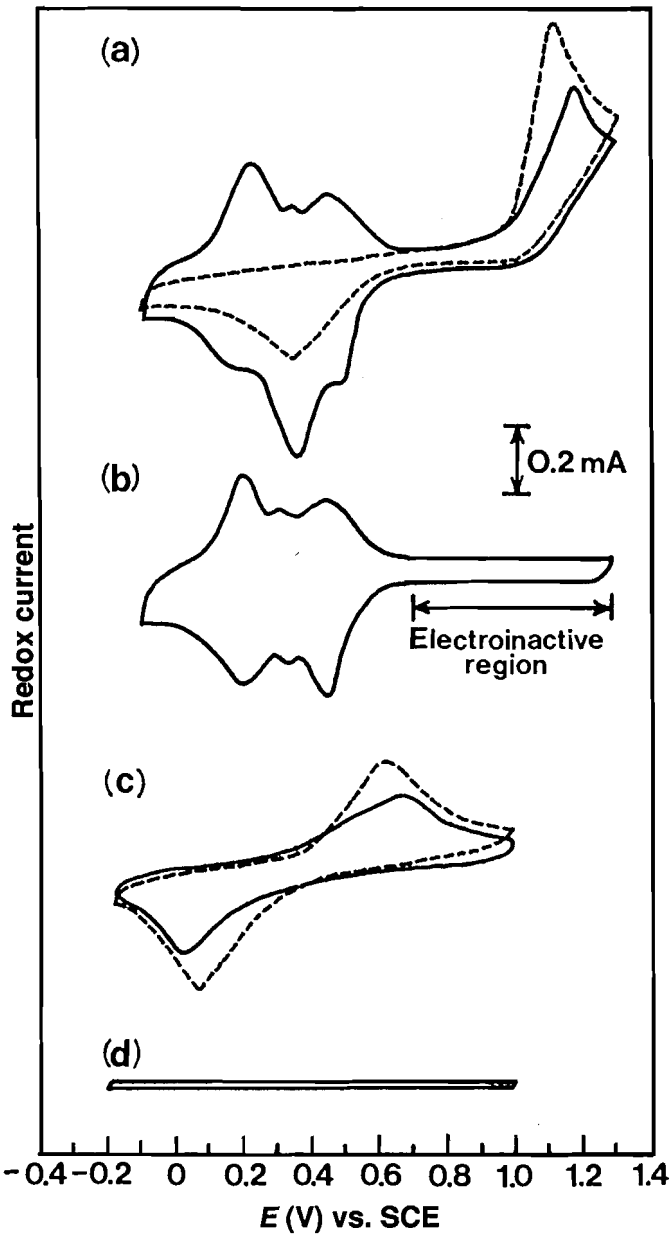

FIG. 1. (*a*) Cyclic voltammograms of *p*-dimethoxybenzene on a bare platinum electrode (broken line) and on the PAN film coated electrode (solid line). Solution: 5 mM *p*-dimethoxybenzene + 0.1 M H_2SO_4. (*b*) Voltammogram showing the redox wave of the PAN film itself on the platinum electrode. Solution: 0.1 M H_2SO_4. (*c*) Voltammograms of hydroquinone on the platinum electrode (broken line) and the PAN film coated electrode (solid line). Solution: McIlvaine buffer solution containing 10 mM hydroquinone (pH 5). (*d*) Voltammogram showing the electroactivity of the PAN film in a McIlvaine buffer solution of pH 5.

dence, the conductivity of the PAN pellet was measured before and after measurements of the steady-state *i*–*E* curves described previously. The conductivity of the pellets equilibrated with 0.1 M H_2SO_4 and the pH 5 solution were 0.87 S cm^{-1} and 8.2×10^{-9} S cm^{-1}, respectively: that of the latter pellet was almost recovered when the pellet was returned to a 0.1 M H_2SO_4 solution. After the measurements, the values became 1.8 S cm^{-1} and 3.5×10^{-6} S cm^{-1}, respectively. The increase is probably caused by interactions between PAN and the species. PAN releases dopant anions over the electroinactive potential region because of the deprotonation of the PAN nitrogens that accompanies oxidation to the imine form (5). The release also occurs in less acidic media (pH >3.5) due to deprotonation of amine and (or) imine forms (6). In both cases, the limited dopant anions that exist near the film/solution interface are expected to be released from the films due to their small diffusion coefficient of about 10^{-13} cm^2 s^{-1} (7), and the redox-active sites still remain inside the film. The organic species used probably have affinities for the films and permeate through the films to reach the oxidized sites. They are oxidized to give the films their oxidized products, quinones. The quinones are incorporated into the parts containing the deprotonated nitrogens within the films. They play the role of the dopant anions and promote electron hopping between the redox-active sites within the films, since they are π-electron-rich species.

1. N. Oyama, Y. Ohnuki, K. Chiba, and T. Ohsaka. Chem. Lett. 1759 (1983).
2. J. Yano, A. Kitani, R. E. Vasquez, and K. Sasaki. Nippon Kagaku Kaishi, 1124 (1985).
3. Y. Ohnuki, H. Matsuda, T. Ohsaka, and N. Oyama. J. Electroanal. Chem. **158**, 55 (1983).
4. A. Kitani, J. Izumi, J. Yano, Y. Hiromoto, and K. Sasaki. Bull. Chem. Soc. Jpn. **57**, 2254 (1984).
5. D. Orata and D. A. Buttry. J. Am. Chem. Soc. **109**, 3574 (1987).
6. J. Chiang and A. G. MacDiarmid. Synth. Met. **13**, 193 (1986).
7. K. Takei, K. Ishihara, T. Iwahori, and T. Tanaka. Denki Kagaku, **59**, 138 (1991).

All voltammograms were measured at 100 mV s^{-1}. The McIlvaine buffer solution of pH 5 was a solution of 0.1 M Na_2HPO_4 and 0.1 M citric acid containing 0.1 M Na_2SO_4 in the ratio of 50:49 (volume). The PAN film about 0.7 μm in thickness was formed on the platinum wire electrode (diameter = 1 mm, length = 10 mm, area = ca. 0.3 cm^2) by repeated potential cycling between −0.2 and 0.8 V vs. SCE at 100 mV s^{-1} in 0.1 M H_2SO_4 containing 0.1 M aniline.

0193C009

Reactions of ferrocene and nickelocene with some stable carbonium ions[1]

SYDNEY K. BROWNSTEIN,[2] ERIC J. GABE, AND ROSEMARY C. HYNES
Institute for Environmental Chemistry, National Research Council of Canada, Ottawa, Ont., Canada K1A 0R6

Received April 23, 1991

SYDNEY K. BROWNSTEIN, ERIC J. GABE, and ROSEMARY C. HYNES. Can. J. Chem. **70**, 1011 (1992).

The reaction of ferrocene and tropylium hexafluorophosphate yields ferrocenyltropylium PF_6, which crystallizes in the monoclinic space group $P2_1/C$ (a = 9.7858(10) Å, b = 16.3692(24) Å, c = 10.901(4) Å, β = 113.030(18)°, Z = 4, T = 27°C, V = 1607.0(7) Å^3, R_f = 0.091, R_w = 0.040) for 102 parameters and 929 observed ($I > 2.5\ \sigma(I)$) out of 2087 total measured reflections. The reaction of nickelocene and triphenylmethyl tetrafluoroborate yields triphenylmethylcyclopentenyl cyclopentadienyl nickel tetrafluoroborate, which crystallizes in the monoclinic space group $P2_1/n$ (a = 11.0306(19) Å, b = 14.078(4) Å, c = 17.117(4) Å, β = 101.134(18)°, Z = 4, T = 27°C, V = 2608.0(11) Å^3, R_f = 0.091, R_w = 0.035) for 147 parameters and 1334 out of 3361 measured reflections.

SYDNEY K. BROWNSTEIN, ERIC J. GABE et ROSEMARY C. HYNES. Can. J. Chem. **70**, 1011 (1992).

La réaction du ferrocène et de l'hexafluorophosphate de tropylium conduit au PF_6 de ferrocényltropylium qui cristallise dans le groupe d'espace monoclinique $P2_1/C$ (a = 9,7858(10), b = 16,3692(24) et c = 10,901(4) Å, β = 113,030(18)°, Z = 4, T = 27°C, V = 1607,0(7) Å^3, R_f = 0,091 et R_w = 0,040) pour 102 paramètres et 929 réflexions observées ($I > 2{,}5\ \sigma(I)$) tirées de 2087 réflexions totales mesurées. La réaction du nickelocène et du tétrafluoroborate de triphénylméthyle fournit tétrafluoroborate de triphénylméthylcyclopentényl cyclopentadiényl nickel qui cristallise dans le groupe d'espace monocyclique $P2_1/n$ (a = 11,0306(19), b = 14,078(4) et c = 17,117(4) Å, β = 101,134(18)°, Z = 4, T = 27°C, V = 2608,0(11) Å^3, R_f = 0,091 et R_w = 0,035) pour 147 paramètres et 1334 réflexions d'un ensemble de 3361 mesurées.

[Traduit par la rédaction]

Introduction

In the first characterization of the structure of ferrocene, its aromatic character was shown by acylation under Friedel–Crafts conditions (1). However, the reaction with triphenylmethylchloride was reported to yield ferriciniuim tetrachloroferrate (2). Therefore, it appeared of interest to study the reaction of ferrocene with stable carbonium ions. The ferrocenylcarbenium ion has been isolated in a few cases (3, 4). A second type of reaction frequently observed with metallocenes under acylation or alkylation conditions is the addition of the organic group to one of the cyclopentadienyl rings (5). Another reaction of metallocenes is as electron donors in charge transfer complexes (6, 7). The stable carbonium ion tropylium acts as an electron acceptor in charge transfer complexes with aromatic hydrocarbons (8). The reactions of tropylium hexafluorophosphate and triphenylmethyl tetrafluoroborate with ferrocene and nickelocene were investigated to determine to which of the three preceding categories they might belong.

Experimental section

Ferrocene, $Fe(C_5H_5)_2$, was recrystallized from hexane. Nickelocene, triphenylmethyl tetrafluoroborate, and tropylium hexafluorophosphate were used as supplied (Aldrich). Acetonitrile was shaken with P_2O_5 and transferred under vacuum to a container on the preparative vacuum line. Methylene chloride was successively shaken with H_2SO_4, $AlCl_3$, and H_2O, then dried successively with $CaCl_2$ and P_2O_5 and transferred under vacuum to the preparative apparatus. Benzene was dried over 5Å molecular sieve and similarly transferred. Sulfur dioxide was stored as a liquid, over P_2O_5, in a container closed with a pressure/vacuum stopcock on the preparative vacuum line. All manipulations of solids were performed in a vacuum glove box under a dry nitrogen atmosphere.

$Fe(C_5H_5)(C_5H_4\text{-}C_7H_6)PF_6$ was prepared from 107.3 mg (0.577 mmol) ferrocene and 49.8 mg (0.211 mmol) $C_7H_7PF_6$ dissolved in 2.4 g acetonitrile. During 48 h at room temperature the colour of the solution changed from orange to a very deep blue-green and some brown solid precipitated. The supernatant liquid was decanted into a second container and the solvent removed under vacuum. The solid residue was washed three times with benzene to remove unreacted ferrocene. It was extracted with CH_2Cl_2 to give a blue solution and a dark residue. The CH_2Cl_2 was evaporated to give 39.3 mg (0.094 mmol) of a deep blue microcrystalline solid whose identity was established by UV, IR, ^{1}H NMR, and a single crystal X-ray structure determination. IR (cm^{-1}) (KBr pellet): 1494 s, 1270 s, 836 vs. UV (CH_2Cl_2 soln.) (λ_{max} Å, log ε): 2600, 4.26; 2640, 4.27; 3300, 3.64; 4010, 4.35; 7000, 3.73. The ^{1}H NMR spectrum in CD_3CN showed multiple resonances at 8.29 (2H), 5.37 (2H), and single lines at 4.30 (2H) and 2.50 (broad, 9H). Single crystals were grown from $CHCl_3$ solution. The dark CH_2Cl_2 insoluble residue was recrystallized from acetonitrile to give, in part, crystals of unreacted tropylium hexafluorophosphate.

$Ni(C_5H_5)(C_5H_5\text{-}C(C_6H_5)_3)BF_4$ was prepared from 17.0 mg nickelocene (0.090 mmol) and 29.0 mg (0.118 mmol) triphenylmethyl tetrafluoroborate dissolved in sulfur dioxide in one arm of an H-shaped reactor. The clear, very dark solution was carefully decanted from some solid into the other arm of the reactor and an equal volume of CH_2Cl_2 condensed with it. At room temperature, solvent was slowly distilled back into the original reactor arm by a slight temperature differential. When some blue-black crystals had formed from the solution the remaining liquid was also decanted back. All volatiles were removed under vacuum and the blue-black crystals were characterized by a single crystal structure determination.

Proton magnetic resonance spectra were obtained at 400 MHz on a Bruker AM 400 spectrometer. Infrared spectra were obtained for KBr pellets on a Nicolet 520 FT-IR spectrometer and UV–visible spectra on CH_2Cl_2 solutions with a Cary 210 spectrophotometer. X-ray diffraction intensities were collected at room temperature on an Enraf–Nonius CAD-4 diffractometer controlled by NRCCAD (9) software, with graphite monochromatized MoK_α radiation, λ = 0.70932 Å, using the θ/2θ scan technique with profile analysis (10). The crystal data are listed in Table 1. The structures were solved by direct methods and refined by full-matrix least-squares calculations. Scattering factors were taken from the *International tables* (11).

[1]Issued as NRCC No. 32968.

[2]Author to whom correspondence may be addressed.

Can. J. Chem. Downloaded from www.nrcresearchpress.com by 92.62.229.171 on 09/08/12
For personal use only.

Can. J. Chem. Downloaded from www.nrcresearchpress.com by 92.62.229.171 on 09/08/12
For personal use only.

TABLE 1. X-ray crystallography parameters for $Fe(C_5H_5)(C_5H_4\text{-}C_7H_6)PF_6$, $(C_7H_7)PF_6$, and $Ni(C_5H_5)(C_5H_5\text{-}C(C_6H_5)_3)BF_4SO_2$

Formula	$FeC_{17}H_{15}PF_6$	$C_7H_7PF_6$	$NiC_{29}H_{25}BF_4SO_2$
Formula wt.	420.116	236.095	583.094
Space group	$P2_1/c$	$R3m$	$P2_1/n$
a, Å	9.7858(10)	9.4831(7)	11.0306(19)
b, Å	16.3692(24)		14.078(4)
c, Å	10.901(4)	8.5960(7)	17.117(4)
β, deg	113.030(18)		101.134(18)
V, Å^3	1,607.0(7)	669.46(7)	2,608.0(11)
Setting angles, no.	25	30	19
2θ range	30 to 35	40 to 50	25 to 34
Z	4	3	4
ρ (calc), g cm^{-3}	1.737	2.157	1.485
Crystal size, mm	0.4 × 0.05 × 0.05	0.3 × 0.3 × 0.1	0.05 × 0.1 × 0.2
Absorption coeff. (μ), cm^{-1}	10.9		7.9
Temperature, °C	27	27	27
$2\theta_{max}$, deg.	44.8		44.8
Measured reflections	2533		3555
Unique reflection	2087		3351
Significant reflections [I net > 2.5σ (I net)]	929		1334
h, k, l ranges	−10–9, 0–17, 0–11		−11–11 −14–0, −18–0
Number of parameters	102		147
R_f significant reflections	0.091		0.091
R_w significant reflections	0.040		0.035
S	2.26		2.41
Residual electron density, Å^3	−0.57, 0.67		−0.56, 0.53

$$R_f = \frac{\Sigma\|F_o| - |F_c\|}{\Sigma|F_o|}$$

$$R_w = \frac{\Sigma w(F_o - F_c)^2}{\Sigma w F_o^2}$$

$$S = \frac{\sqrt{\Sigma w(F_o - F_c)^2}}{n - 1}$$

All computing was performed using the NRCVAX program system (12). Three reference reflections were collected every 100 reflections and their fluctuation was insignificant. No absorption correction was made.

The cation of the tropylium ferrocene compound appeared well defined, but the PF_6 anion was disordered. It was modelled as two rigid groups with fluorine occupancies of 0.7 and 0.3. The major component was fitted as a regular octahedron wtih central phosphorus, P—F = 1.58 Å. The minor component was fitted as an octahedron with no central atom and fluorines 1.58 Å from the centre. Rigid groups were refined anisotropically, as was the iron atom (carbons left isotropic). Hydrogen atoms were included in calculated positions. A weighting scheme based on counting statistics was used.

Results

In the reaction of ferrocene and tropylium hexafluorophosphate, the tropyplium ring bonds to one of the cyclopentadienyl (Cp) rings with the loss of two hydrogen atoms. The structure of the cation is shown in Fig. 1. The reaction proceeds slowly and is significantly incomplete after two days at room temperature. This is shown by the recovery of tropylium hexafluorophosphate even though ferrocene was present in excess. The structure of tropylium hexafluorophosphate was found to be isomorphous with that reported for the perchlorate (13). Key parameters are listed in Table 1.

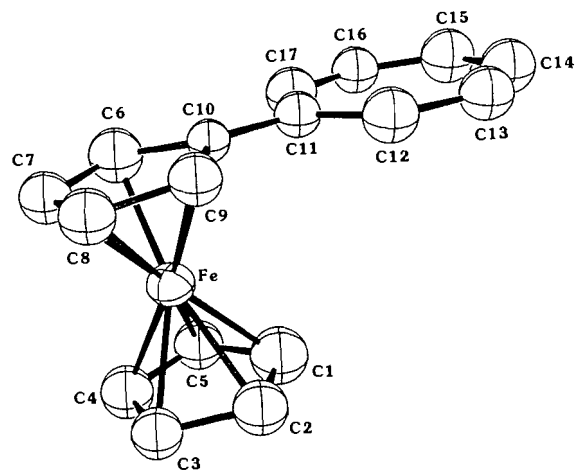

FIG. 1. ORTEP plot of tropylferrocene cation.

The structure of the tropylium ferrocene cation has a planar 7-membered ring bonded to one Cp ring of ferrocene. The ferrocene moiety has almost parallel Cp rings (dihedral angle

Can. J. Chem. Downloaded from www.nrcresearchpress.com by 92.62.229.171 on 09/08/12
For personal use only.

TABLE 2. Atomic parameters x, y, z and B_{iso} for $FeC_{17}H_{15}PF_6$; esd's refer to the last digit printed

Atom	x	y	z	B_{iso}[a]
Fe	0.27526(22)	0.91340(12)	0.16319(17)	3.28(11)
C1	0.3655 (13)	0.9217 (8)	0.0222 (10)	5.5 (3)
C2	0.3368 (13)	0.8404 (7)	0.0400 (10)	4.4 (3)
C3	0.1794 (13)	0.8374 (7)	0.0066 (10)	4.1 (3)
C4	0.1205 (12)	0.9161 (8)	−0.0261 (10)	4.7 (3)
C5	0.2352 (13)	0.9695 (7)	−0.0129 (11)	4.5 (3)
C6	0.2595 (13)	1.0016 (7)	0.2873 (10)	4.6 (4)
C7	0.1646 (12)	0.9381 (7)	0.2855 (10)	4.3 (4)
C8	0.2454 (13)	0.8663 (6)	0.3267 (11)	4.2 (3)
C9	0.3975 (13)	0.8833 (7)	0.3569 (10)	3.9 (3)
C10	0.4105 (12)	0.9692 (6)	0.3325 (9)	2.8 (3)
C11	0.5373 (12)	1.0114 (7)	0.3296 (10)	3.3 (3)
C12	0.6685(13)	0.9653 (7)	0.3621 (10)	4.5 (3)
C13	0.8082 (12)	0.9893 (7)	0.3674 (10)	4.4 (4)
C14	0.8586 (13)	1.0644 (7)	0.3445 (10)	4.9 (4)
C15	0.7799 (13)	1.1329 (7)	0.3093 (11)	5.1 (4)
C16	0.6313 (13)	1.1454 (7)	0.2840 (10)	4.1 (3)
C17	0.5281 (12)	1.0947 (8)	0.2931 (10)	4.5 (3)

[a] B_{iso} is the mean of the principal axes of the thermal ellipsoid.

of 3°), with Fe—C distances ranging from 2.018(10) to 2.054(12) Å. The 7-membered ring is not quite coplanar with the bonded Cp ring (dihedral angle of 8°). The C—C inter-ring bond is 1.459(16) Å, slightly short for a single C—C bond, implying some delocalization throughout both rings. The Fe is equidistant from the two Cp rings at 1.646(2) Å. The Fe—C and Fe—Cp ring distances are in excellent agreement with those for ferrocene itself (14, 15), and shorter than those for the ferricenium ion (16). The packing arrangement is illustrated in Fig. S1.[3] The atomic coordinates are listed in Table 2. Tables of bond lengths and angles, least-squares planes, atomic positions for phosphorus, fluorine, and hydrogen atoms, thermal parameters, and structure factors are found in Table S1–S5 respectively (supplementary material).[3]

There was no evidence for reaction between ferrocene and triphenylmethyl tetrafluoroborate.

Triphenylmethyl tetrafluoroborate adds to one of the cyclopentadienyl rings of nickelocene to give a compound for which the structure of the cation is shown in Fig. 2, and its key X-ray parameters are listed in Table 1. The atom positions for those atoms which were independently refined are listed in Table 3, and the positions of the phenyl carbon atoms, which were refined as rigid groups, are listed in Table S6.[3]

The unsubstituted cyclopentadienyl ring of the nickelocene moiety is planar with a maximum deviation for C10 of 0.039 Å from the best plane. C1 of the substituted cyclo-

[3]Supplementary material mentioned in the text, including Figs. S1 and S2, may be purchased from: The Depository of Unpublished Data, Document Delivery, CISTI, National Research Council Canada, Ottawa, Canada K1A 0S2.

Tables of atomic parameters, bond lengths and angles, and copies of Figs. S1 and S2 have also been deposited with the Cambridge Crystallographic Data Centre and can be obtained on request from The Director, Cambridge Crystallographic Data Centre, University Chemical Laboratory, Lensfield Road, Cambridge CB2 1EW, U.K.

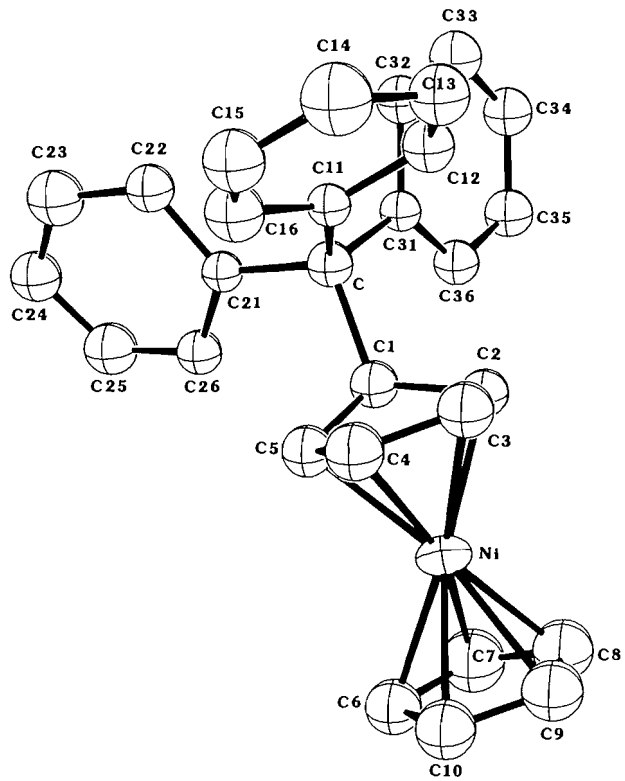

FIG. 2. ORTEP plot of triphenylmethylnickelocene cation.

TABLE 3. Atomic parameters x, y, z and B_{iso} for $NiC_{29}H_{25}BF_4SO_2$; esd's refer to the last digit printed

Atom	x	y	z	B_{iso}[a]
Ni	0.57271(19)	0.66603(15)	0.90331(13)	3.25(11)
S	0.2897 (6)	0.0637 (4)	0.8220 (3)	7.5 (4)
F1	0.2924 (11)	0.2691 (7)	0.8386 (8)	11.4 (10)
F2	0.2169 (11)	0.3792 (8)	0.7555 (6)	11.1 (9)
F3	0.2525 (9)	0.4065 (7)	0.8836 (6)	8.5 (7)
F4	0.4094 (8)	0.3936 (7)	0.8240 (6)	7.5 (7)
O1	0.1645 (10)	0.0614 (9)	0.8334 (7)	8.4 (9)
O2	0.3911 (11)	0.0413 (9)	0.8921 (7)	9.0 (9)
B	0.289 (3)	0.3646 (18)	0.8246 (14)	5.5 (17)
C	0.7887 (12)	0.4905 (8)	0.8047 (8)	2.5 (3)
C1	0.6782 (11)	0.5376 (9)	0.8390 (8)	2.5 (3)
C2	0.6453 (12)	0.6347 (10)	0.8031 (7)	3.4 (4)
C3	0.7100 (12)	0.7063 (9)	0.8527 (8)	3.4 (4)
C4	0.7562 (11)	0.6678 (11)	0.9290 (8)	3.5 (3)
C5	0.7218 (12)	0.5718 (9)	0.9268 (8)	2.9 (3)
C6	0.3921 (14)	0.7043 (11)	0.8607 (9)	4.8 (4)
C7	0.4458 (13)	0.7734 (10)	0.9185 (9)	4.0 (4)
C8	0.4913 (15)	0.7363 (11)	0.9909 (10)	5.3 (4)
C9	0.4612 (14)	0.6375 (11)	0.9820 (9)	5.0 (4)
C10	0.3958 (14)	0.6200 (10)	0.9045 (10)	4.2 (4)

[a] B_{iso} is the mean of the principal axes of the thermal ellipsoid.

pentadienyl ring is tetrahedrally surrounded by four substituents and is 0.426 Å from the plane of the other four ring atoms. The two cyclopentadienyl rings are nearly coplanar (dihedral angle of 4.7°) with nickel–ring distances of 1.656 and 1.697 Å. Tables of selected bond lengths and angles, least-squares planes, hydrogen atom positions, thermal pa-

rameters and structure factors for $NiC_{29}H_{25}BF_4SO_2$ are found in Tables S7–S11 respectively (supplementary material).[3] A stereo depiction of the packing is shown in Fig. S2.[3]

There was no evidence for reaction between nickelocene and tropylium hexafluorophosphate, nor was their any reaction of either cation with cobaltocene or bis(benzene) chromium.

Discussion

No charge transfer complex formation was observed between the stable cations triphenylmethyl or tropylium and ferrocene or nickelocene, nor was a normal acylation reaction observed. Addition of the triphenylmethyl cation to nickelocene, but not ferrocene, was observed and is consistent with results reported under normal alkylating conditions (3). The reaction of tropylium and ferrocene is not a normal alkylation with respect to tropylium although it is for ferrocene. The loss of a hydrogen from one of the carbon atoms of the tropylium ring is rather unusual but unfortunately we could not isolate other reaction products to elucidate the overall reaction.

1. R. B. Woodward, M. Rosenblum, and M. C. Whiting. J. Am. Chem. Soc. **74**, 3458 (1952).
2. I. J. Spilners. J. Organomet. Chem. **11**, 381 (1968).
3. L. Zhan-Ru, K. Gonsalves, R. W. Lenz, and M. D. Rausch. J. Polym. Sci. Part A: Polym. Chem. **24**, 347 (1986).
4. C. Zou and M. S. Wrighton. J. Am. Chem. Soc. **112**, 7578 (1990).
5. U. Kolle and F. Khouzami. Angew. Chem. **92**, 658 (1980).
6. J. S. Miller, D. T. Glatzhofer, D. M. O'Hare, W. M. Reiff, A. Chakraborty, and A. J. Epstein. Inorg. Chem. **28**, 2930 (1989).
7. J. S. Miller, J. C. Calabrese, R. L. Harlow, D. A. Dixon, J. H. Zang, W. M. Reiff, S. Chittipeddi, M. A. Selover, and A. J. Epstein. J. Am. Chem. Soc. **112**, 5496 (1990).
8. M. Feldman and S. Winstein. J. Am. Chem. Soc. **83**, 3338 (1961).
9. Y. Le Page, P. S. White, and E. J. Gabe. NRCCAD — An enhanced CAD-4 Control Program. Abstr. Am. Crystallogr. Assoc. Annual Meeting, 1986, p. 24.
10. D. F. Grant and E. J. Gabe. J. Appl. Crystallogr. **11**, 114 (1978).
11. International tables for X-ray crystallography. Vol. IV. Kynoch Press, Birmingham. 1974.
12. E. J. Gabe, Y. Le Page, J. P. Chartrand, F. L. Lee, and P. S. White. J. Appl. Crystallogr. **22**, 384 (1989).
13. A. I. Kitaigorodskii, Yu T. Struchkov, T. L. Khotsyanova, M. E. Volpin, and D. N. Kursanov. Izv. Akad. Nauk SSSR, 39 (1960).
14. P. Seiler and J. D. Dunitz. Acta Crystallogr. Sect. B: Struct. Crystallogr. Cryst. Chem. **B35**, 1068 (1979).
15. F. Takusagawa and T. Koetzle. Acta Crystallogr. Sect. B: Struct. Crystallogr. Cryst. Chem. **B35**, 1074 (1979).
16. N. J. Mammano, A. Zalkin, A. Landers, and A. L. Rheingold. Inorg. Chem. **16**, 297 (1977).

Can. J. Chem. Downloaded from www.nrcresearchpress.com by 92.62.229.171 on 09/08/12
For personal use only.

Straining strained molecules. III.[1] The spectral and mutagenic properties and an alternate synthesis of diaceperylene and dicyclopenta[1,2,3-*cd*:1′,2′,3′-*lm*]perylene

REGINALD H. MITCHELL,[2] MAHIMA CHAUDHARY, RICHARD VAUGHAN WILLIAMS,[3] ROBERT FYLES, JACK GIBSON, MICHAEL J. ASHWOOD-SMITH,[4] AND ALBERT J. FRY[5]

Department of Chemistry, University of Victoria, Box 3055, Victoria, B.C., Canada V8W, 3P6

Received July 15, 1991

REGINALD H. MITCHELL, MAHIMA CHAUDHARY, RICHARD VAUGHAN WILLIAMS, ROBERT FYLES, JACK GIBSON, MICHAEL J. ASHWOOD-SMITH, and ALBERT J. FRY. Can. J. Chem. **70**, 1015 (1992).

The synthesis of diaceperylene (**1**) from 5,6-dilithioacenaphthene via nickel or cobalt catalysed couplings proceeded in better yield than a multistep synthesis involving formation of 5,5′-diacenaphthene first. Dehydrogenation of **1** to dicyclopenta[1,2,3-*cd*:1′,2′,3′-*lm*]perylene (**2**) proved a better route than coupling of 5,6-disubstituted acenaphthylene derivatives. Ultraviolet, proton, and carbon nuclear magnetic resonance spectra and electrode reduction potential data of **1** and **2** are discussed with respect to molecular mechanics calculations of strain in these and related bridged naphthalenes. Both **1** and **2** were found to be weakly mutagenic in an Ames microsome test, in contrast to cyclopenta[*cd*]pyrene.

REGINALD H. MITCHELL, MAHIMA CHAUDHARY, RICHARD VAUGHAN WILLIAMS, ROBERT FYLES, JACK GIBSON, MICHAEL J. ASHWOOD-SMITH et ALBERT J. FRY. Can. J. Chem. **70**, 1015 (1992)

La synthèse du diacéperylène (**1**), utilisant le 5,6-dilithioacénaphtène comme produit de départ et des couplages catalysés par le nickel ou le cobalt, donne de meilleurs rendements qu'une synthèse en plusieurs étapes impliquant une formation préliminaire du 5,5′-diacénaphtène. La déshydrogénation du composé **1** en dicyclopenta[1,2,3-*cd*:1′,2′,3′-*lm*]pérylène (**2**) est une meilleure voie d'accès à cet hydrocarbure que le couplage d'acénaphtylènes substitués en positions 5 et 6. On discute des spectres UV et RMN du proton et du carbone et des données relatives aux potentiels de réduction à l'électrode des composés **1** et **2** en fonction de calculs de mécanique moléculaire de la tension dans ces composés et dans des dérivés naphtaléniques pontés apparentés. On a trouvé que, contrairement au cyclopenta[*cd*]pyrène, les composés **1** et **2** sont légèrement mutagènes dans un essai microsomique d'Ames.

[Traduit par la rédaction]

Introduction

In the previous paper (1), we discussed strain in acenaphthenes and how further substitution of acenaphthene in the peri positions increases the overall strain of the substituted system. In this paper we investigate straining the perylene nucleus by synthesis and study of diaceperylene (**1**), and dicyclopenta[1,2,3-*cd*:1′,2′,3′-*lm*]perylene ("diaceperylylene")[6] (**2**). The latter is of especial interest in that in the same way that pyracylene (**3**) is a perturbed [12]annulene (2), **2** is formally a perturbed [20]annulene. Moreover, synthesis of cyclopenta aromatics has been attracting unusual interest (3–9) in recent years with the discovery that cyclopenta[*cd*]pyrene ("acepyrylene") **4** is a widespread mutagen (10), despite the fact that pyrene itself is not.

Syntheses

The most logical approach to **1** and **2** is from the commercially available dianhydride **5**. We envisioned reduction of **5** to a tetra-alcohol, followed by conversion to 3,4,9,10-tetrakis(bromomethyl)perylene, and then ring closure using either PhLi (2) or Ph_3P (11). However, we were not able to reduce **5** to the tetra-ol **6** using either $LiAlH_4$/THF or *i*-Bu_2AlH/PhH with conditions that work well for naphthalic anhydride. Conversion of **5** to the tetra-ester **7** proved equally frustrating; MeOH/*p*-TsOH, $(MeO)_3P{=}O$/NaOH (12), MeI/HMPA (13), and diazomethane each yielded only traces of **7**. Dimethyl sulphate/NaOH/dioxane (14) did yield some **7**, but again reduction to **6** failed.

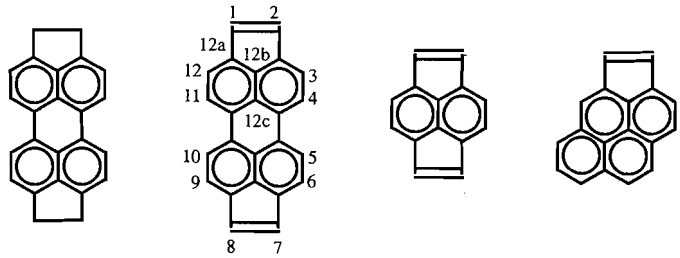

1 **2** **3** **4**

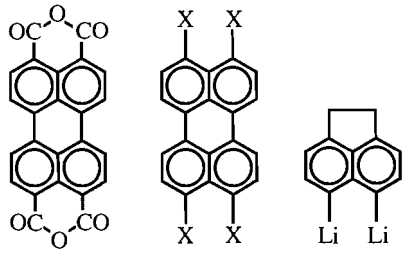

5 **6** X = CH_2OH **8**
7 X = CO_2Me

Coupling of 5,6-dilithioacenaphthene (**8**) (1) was thus attempted next. Numerous coupling procedures (for an extensive list, see ref. 15) are suitable for biaryl preparation, and indeed $Ni(Ph_3P)_2$, $CuCl_2$, TlBr, $Ni(acac)_2$, and $CoCl_2$ all produced pale yellow **1** from **8**. However, the best yields (20–

[1]For part II, see ref. 1.

[2]Author to whom correspondence may be addressed.

[3]Department of Chemistry, University of Idaho, Moscow, Idaho, 83843 U.S.A.

[4]Department of Biology, University of Victoria.

[5]Department of Chemistry, Wesleyan University, Middletown, Conn. 06457, U.S.A.

[6]Acenaphthene → acenaphthylene; pyracene → pyracylene; phenanthrene → phenanthrylene, *thus* perylene → perylylene.

Can. J. Chem. Downloaded from www.nrcresearchpress.com by 92.62.229.171 on 09/08/12
For personal use only.

35%) were obtained with the last two catalysts. Tanaka and Kasai (16) also reported the formation of **1**, but as a red by-product, obtained from the TMEDA complex of **8** on reaction with quinones. Indeed, as obtained from the coupling reactions, **1** is always accompanied by some **2**, which is red, and is extremely difficult to separate from **1**. However, using HPLC, pure **1** can be obtained as yellow crystals, mp 333–335°C (dec.). Very recently, Jaworek and Vögtle (17) reported a different synthesis of **1**. We also investigated stepwise coupling to **1**, by first coupling 5-bromoacenaphthene (**9**) with *n*-BuLi/$CoCl_2$ to give the bi-acenaphthenyl **10**, bromination with NBS/DMF (18) to give dibromide **11**, and coupling of this with *n*-BuLi/$CoCl_2$ to give **1**, but the overall yield was not better, and the product was harder to purify.

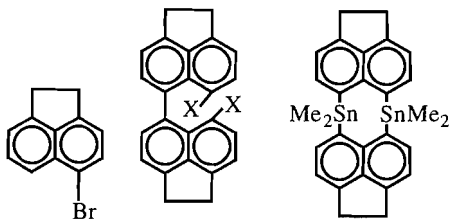

9 **10** X = H, **11** X = Br **12**

Reaction of the dilithio compound **8** with Me_2SnCl_2 gave 26% of the stannocin **12**, mp 277–279°C, which on irradiation in benzene gave less than 5% of **1**. The analogous case in which 1,8-dilithionaphthalene was used to prepare perylene went in 60% yield (19). Dehydrogenation of **1** with DDQ in refluxing benzene yielded 60% of **2** as a dark red compound, mp >350°C (argon). This proved in our hands to be the only useful route to **2** (see also ref. 17), since coupling (*n*-BuLi/$CoCl_2$) of both 5,6-dibromoacenaphthylene (**13**) (obtained by DDQ dehydrogenation of 5,6-dibromacenaphthene (**14**)), and 5-bromoacenaphthylene (15) (obtained from **9** both by DDQ dehydrogenation and NBS-bromination/KI-debromination(2)) proceed to be extremely dirty, producing more than a dozen products each. These coupling reactions were monitored by HPLC for authentic **2** and 5,5′-diacenaphthylene (**16**) (prepared by DDQ dehydrogenation of **10**), and in each case, although some product was observed, it was only in minor amount, and not isolable by us. Clearly, the additional unsaturation of the ace bridge had a dramatic effect on the coupling reactions.

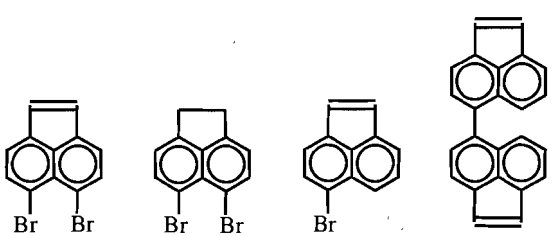

13 **14** **15** **16**

Results and discussion

Ultraviolet spectra

We have discussed the effects of strain on the ultraviolet spectra of aromatic hydrocarbons in our previous paper (1). Introduction of a strained bridge usually results in a bathochromic shift of the *p*-band (the intense, log ε 3–4, long wavelength bands associated with the HOMO–LUMO transition), which is somewhat greater than the effect of the corresponding dimethyl derivative (20). For example the *p*-band of naphthalene (275 nm) is shifted by 1762 cm^{-1} in acenaphthene (289 nm), but only by 1276 cm^{-1} in 1,8-dimethylnaphthalene (285 nm). These are not directly proportional to strain, however, since molecular mechanics calculations (21) indicate that acenaphthene has about 12 kcal/mol more strain than naphthalene, while for 1,8-dimethylnaphthalene the value is only about 3 kcal/mol. Addition of the second bridge to acenaphthene to form pyracene (**17**) (295 nm) substantially increases the strain in the mole-

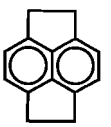

17

cule, some 36 kcal/mol more than in naphthalene, yet causes a considerably smaller bathochromic shift of 704 cm^{-1} than addition of two more methyl groups to 1,8-dimethylnaphthalene to give 1,4,5,8-tetramethylnaphthalene (296 nm), 1304 cm^{-1}. From naphthalene, the total shift for the latter is 2580 cm^{-1}, which is then very similar to that for pyracene at 2466 cm^{-1}, despite the rather different calculated strains of 12 and 36 kcal/mol, respectively, relative to naphthalene. The recent synthesis (17) of 3,4,9,10-tetramethylperylene now permits comparison with **1**. From perylene (434 nm) (22), the tetramethyl compound (451 nm) is shifted 869 cm^{-1}, while the diace compound **1** (455 nm) is shifted 1015 cm^{-1}, which thus suggests that **1** is more similar (in strain) to acenaphthene than to pyracene. This is borne out by molecular mechanics calculations (21), which indicate that addition of two ace bridges to perylene only increases the strain energy by about 19 kcal/mol. As well, it is interesting to note that when two acenaphthenes are joined to form **1**, the calculated increase in strain is only about 5 kcal/mol, while when two naphthalenes are joined to perylene, strain increases by about 9 kcal/mol. This suggests that the pinching caused by the ace bridge is counteracted somewhat by the union to form the perylene nucleus. Unfortunately calculations are not at a stage where λ_{max} values of sufficient accuracy to be of use here can be predicted (23).

Addition of unsaturated bridges to both naphthalene and perylene has, as would be expected, a considerably greater effect on $\Delta E_{HOMO-LUMO}$, and thus λ for the *p*-band is strongly bathochromically shifted. However, since the resultant molecules (**2** and **3**) are non-alternate hydrocarbons, the Streitwieser (24) correlations between ν and Δm (the HMO energy difference between the highest occupied and lowest unoccupied orbitals) do not hold well. For example λ_{max} predicted for acenaphthylene and pyracylene are 357 and 544 nm, respectively, whereas those found are 323 and 385 nm. The perturbation on naphthalene (275 nm) to form pyracylene (385 nm) at 10 390 cm^{-1} is, however, considerably greater than that, 2989 cm^{-1}, on perylene (435 nm) to form diaceperylylene (**2**) (500 nm). Again strain calculations (21) indicate that pyracylene is about 40 kcal/mol more strained than naphthalene, while diaceperylylene is about 30 kcal/mol more strained than perylene.

Can. J. Chem. Downloaded from www.nrcresearchpress.com by 92.62.229.171 on 09/08/12
For personal use only.

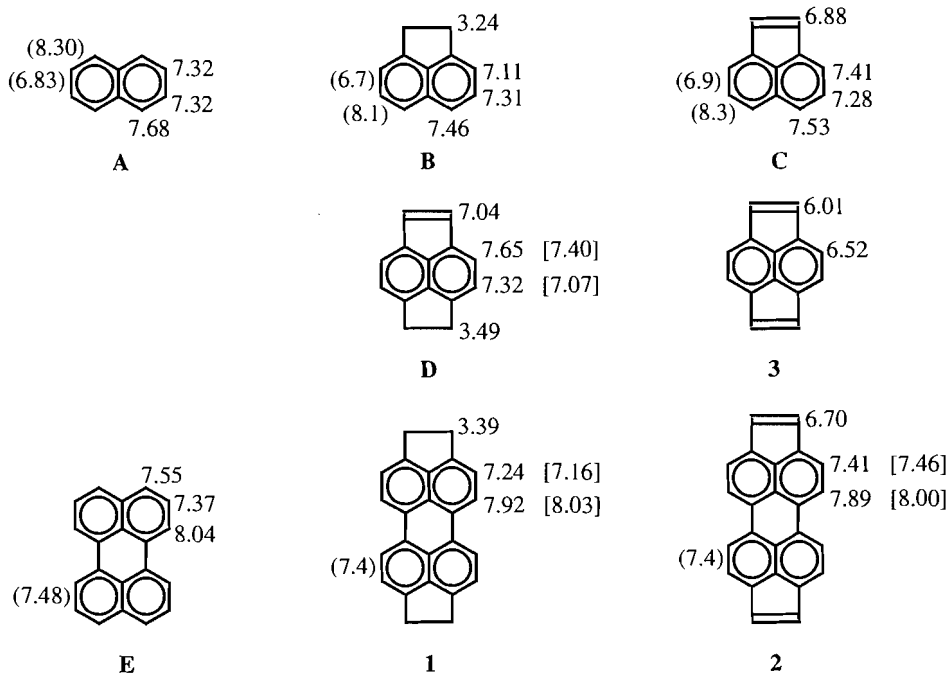

CHART 1. ^{1}H NMR chemical shifts, δ, and (coupling constants) for napthalene (25), acenapthene (26), acenaphthylene (26), pyracylene (2), dihydropyracylene (2), perylene (25), and **1** and **2** [with calculated shifts].

Proton magnetic resonance spectra

The chemical shifts and coupling constants (in parentheses) for compounds **1**, **2**, and several reference compounds are given in Chart 1. The ^{1}H NMR spectrum quoted (17) for **2** must have been misprinted, since it is not consistent with the proposed structure or our data. Comparison of naphthalene, **A**, and acenaphthene, **B**, in Chart 1, indicates that introduction of the saturated bridge shields the adjacent β-H (H-3,8) by ca. 0.2 ppm while leaving the distant β-H (H-4,7) almost unchanged. Introduction of the unsaturated bridge as in acenaphthylene, **C**, however, deshields the adjacent β-H by ca. 0.1 ppm. In perylene, **E**, the bay protons (H-1,6,7,12) are deshielded by 0.7 ppm from those of naphthalene. Summation of these effects would lead to predicted (27–30) chemical shifts of 8.03 and 7.16 for the aryl protons of **1**, very close to those found. Unfortunately the ^{1}H NMR spectrum of pyracene, **17**, does not appear to have been reported, and thus the direct effect of the second five-membered ring is not known; however, fusion of the second five-membered ring to acenaphthylene as in **D** yields chemical shifts of 7.32 and 7.65 ppm, whereas 7.07 and 7.40 might have been expected. The differences could be attributed to the additional strain, but they are rather small. The closer agreement in the case of **1** might indicate that it is less strained than **D**, which is reasonable. Introduction of a double bond into the second bridge of **D** to give **3** markedly shields both the aryl (1.13 ppm) and bridge (1.03 ppm) protons. This has been ascribed (2) to a paramagnetic ring current in the [12]annulene perimeter. The chemical shifts predicted (on the basis of **A**, **C**, **E**) for H-3 (δ 7.46) and for H-4 (δ 8.00) of **2** agree closely with those found, δ 7.41 and 7.89, respectively. They are, however, both marginally shielded (0.05–0.09 ppm), as is the bridge proton by 0.18 ppm, and collectively this may indicate a very weak paramagnetic ring current due to the [20]annulene perimeter of **2**. However, the effect is certainly much weaker than for pyracylene **3**.

Carbon magnetic resonance spectra

The well-known additivity (30, 31) of carbon chemical shifts is used in Chart 2 to predict the chemical shifts of **1** and **2** based on the reference compounds shown. Thus data for **1** are derived by combining the shift data for naphthalene-acenaphthene and naphthalene-perylene and those for **2** are derived from naphthalene-acenaphthylene and naphthalene-perylene. The experimental results are surprisingly close to those calculated, the largest difference occurring for carbons of type 12d, and this may reflect the additional strain of the double pinching of the five-membered rings, which is known (32) to manifest itself most at the 5,6 positions of acenaphthene by a scissoring effect. In pyracylene **3**, the paratropism of the molecule manifests itself mostly in a difference of about 8 ppm, in the downfield shift for the internal carbons C-8a,b, from that calculated (30). Unfortunately, due to the low solubility of **2**, we were not able to see these carbons; however, Jaworek and Vögtle (17) recently reported them at δ 124.5, 130.5, 131.4, and 140.8 in excellent agreement with our calculations, thus indicating very little paratropism. Similar calculations were made to assign the other carbon spectra reported in the experimental section.

Electrode reduction potentials

The hydrocarbons **1** and **2** can be reduced at the dropping mercury electrode and give reproducible (±0.003 V) half-wave potentials. Compound **2** also gives a second wave, corresponding to addition of two electrons to the compound. The measurements were recorded in 85 and 95% aqueous dioxane relative to the standard calomel electrode and are shown, together with those for reference compounds, in Table 1.

Can. J. Chem. Downloaded from www.nrcresearchpress.com by 92.62.229.171 on 09/08/12
For personal use only.

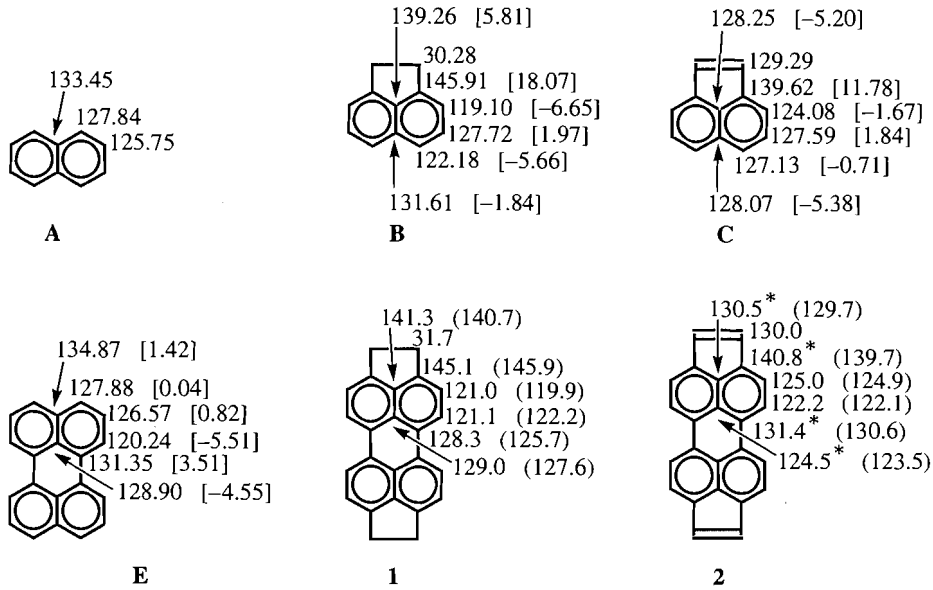

*See ref. 17

CHART 2. ^{13}C NMR chemical shifts, δ, [additivity constants from naphthalene], and (calculated shifts). Data for **A**, **B**, **C**, and **E** are from ref. 37.

TABLE 1. Half-wave electrode reduction potentials (in aqueous dioxane (D)) and molecular orbital energies

	$-\epsilon_{1/2}$ vs. SCE (V)						
	75% D (ref. 33)	85% D	95% D	$-m_{m+1}$	ν, p-band (cm^{-1})	Δm	m_m
A	2.50			0.666	36 364	1.359	0.693
B	2.61	2.58		0.712	34 602	1.266	0.554
E	1.67	1.63	1.70	0.315	23 042	0.658	0.343
1	—	1.76	1.825	0.353	22 026	0.605	0.252
C	1.65	1.62	1.68	0.307	30 960	1.075	0.768
2	—	0.88	0.86	−0.019	20 000	0.498	0.517
2	—	1.19	1.19	(Second wave)			

The literature values and the 85% dioxane values were then used to calculate the experimental values of the LUMO, $\epsilon_{m+1} = \alpha + m_{m+1}\beta$, and the HOMO, $\epsilon_m = \alpha + m_m\beta$, using the previously (1) derived relationships. The values of m_{m+1} and m_m obtained should be equal and of opposite sign (e.g., for naphthalene (**A**) and perylene (**E**)), and give an indication of the accuracy of the method, when compared to the normal Hückel values of 0.618 and 0.347, respectively. Similarly the value obtained (−0.307) for m_{m+1} of acenaphthylene can be compared with the calculated value of −0.285. Fry and Fox (33) have recently shown that an improved correlation between $\epsilon_{1/2}$ and LUMO energies can be obtained using a modified (OMEGAMO) HMO calculation. In the case of **2**, the Hückel value for m_{m+1} is changed from 0 to 0.119, which changes the calculated values of $\epsilon_{1/2}$ from −0.868 to −0.918 V. The observed value of 0.88[2] falls between these. Clearly, however, for **2** the LUMO is close to α in value. Addition of an ace bridge to naphthalene makes reduction more difficult by 0.11 V. However, addition of the two ace bridges to perylene to give **1** makes reduction more difficult by only 0.13 V, somewhat smaller than might be expected. This is consistent with our previous results (1) in the acenaphth[1,2-*a*]acenaphthylene series where each ace bridge added 0.06 V rather than the 0.11 V expected, and thus may give some indication of strain in the system.

Mutagenicity results

The method for detecting mutagenicity was the Salmonella/mammalian microsome test described by Ames *et al.* (34). The *Salmonella typhimurium* strain used was TA 98 (1538 plus an R factor plasmid), kindly provided by Professor B. N. Ames (Berkeley). The microsomal fractions were obtained from rat liver homogenates as described by us previously (35). Without microsomes neither **1** or **2** produced any revertant colonies with TA 98. With microsomes, however, at 100 μg/plate both **1** and **2** gave 20 revertant colonies per plate, while the positive control at 2 μg/plate (2-aminoanthracene) gave 105 revertant colonies/plate after subtraction for negative control. Even at 10 μg/plate, **1** and **2** showed 4 and 16 revertant colonies/plate respectively. Thus both **1** and **2** are very weakly mutagenic, with **2** probably stronger than **1**. They are, however, totally different from **4**,

Can. J. Chem. Downloaded from www.nrcresearchpress.com by 92.62.229.171 on 09/08/12
For personal use only.

Can. J. Chem. Downloaded from www.nrcresearchpress.com by 92.62.229.171 on 09/08/12
For personal use only.

which is a strong mutagen (10). This should be of interest to theoreticians concerned with models of chemical carcinogenicity.

Conclusions

This synthesis of **1** and **2** has made available important members of the cyclopenta-fused aromatics. We have documented their UV, ^{1}H, and ^{13}C NMR spectra, and $\epsilon_{1/2}$ values, and have discussed these relative to strain calculations of structurally similar molecules, to provide data suitable for more detailed study by competent theoreticians.

Experimental

Melting points were determined on a Kofler hot stage and are uncorrected. ^{1}H NMR spectra were determined in $CDCl_3$ (unless otherwise stated) on a Perkin–Elmer R12B (60 MHZ), R32 (90 MHz), or Bruker WM-250 (250 MHz) spectrometer. ^{13}C NMR spectra were recorded either on a Nicolet TT-14 (15.1 MHz) or Bruker WM-250 (62.9 MHz) spectrometer. All chemical shifts are reported in ppm downfield from tetramethylsilane as internal standard. Mass spectra were determined on a Finnigan 3300 mass spectrometer at 70 eV (EI) or using methane chemical ionization (CI). UV spectra were recorded on a Beckman DU-8 spectrometer using cyclohexane as solvent. Microanalyses were carried out by this department or by Canadian Microanalytical Services Ltd. (Vancouver, B.C.). All evaporations were carried out under reduced pressure on a rotary evaporator at about 40°C, and all organic layers were washed with water (unless otherwise stated) and dried with anhydrous $MgSO_4$. The samples for which spectroscopic data are reported were checked for purity by HPLC.

3,4,9,10-Tetrakis(carbomethoxy)perylene **7**

Dimethyl sulphate (20 g, 150 mmol) was added to a stirred solution of the dianhydride **5** (5.6 g, 14 mmol) in aqueous NaOH (25%, 80 mL) and dioxane (400 mL). The mixture was heated under reflux for 24 h, and then was neutralized with aqueous HCl and extracted with dichloromethane–ether (70:30). The extract was washed, dried, and evaporated to give crude **7** (340 mg, 5%). Chromatography over silica gel using dichloromethane–ether (1:1) as eluant gave pure **7** as a pale orange powder, mp 272–275°C. ^{1}H NMR, δ (90 MHz): 8.31, 8.06 (d, J = 7 Hz, 4H each, ArH), 3.95 (s, 12H, -OMe); ^{13}C NMR, δ: 167.8, 140.9, 129.8, 128.1, 124.1, 120.9, 108.2, and 51.1; MS (CI) m/e: 485 (MH^+, 19%), 453 (M − OMe), 100%). Anal. calcd. for $C_{28}H_{20}O_8$: C 69.42, H 4.16; found: C 69.35, H 4.05.

Diaceperylene (1,2,7,8-tetrahydrodicyclopenta[1,2,3-cd:1′,2′,3′-lm]perylene) **1**

n-BuLi (65 mmol in 35 mL hexane) was injected into a stirred solution of 5,6-dibromoacenaphthene (1) (10 g, 32 mmol) in anhydrous ether (1 L) at −10 to −30°C. After 30 min the reaction mixture was cooled to −78°C and $Ni(acac)_2$ (14.4 g, 60 mmol) or anhydrous $CoCl_2$ (dried under vacuum at 110°C for 4 h) (7.8 g, 60 mmol) was added. The mixture was stirred at −78°C for 1 h, then at room temperature for 1 h, and then was heated under reflux for 1 h. The suspended solids were filtered. The ether was washed with water and was evaporated. The residue was combined with the filtered solids and was washed with water, and then thoroughly extracted with hot benzene. The benzene extract was evaporated and chromatographed over basic alumina (activity 2–3) using benzene as eluant. The vividly fluorescent eluant gave a red-orange product on evaporation, crude **1** (>95% pure by NMR) (0.9–1.7 g, 20–35%). Recrystallization from benzene (charcoal) gave a yellow-orange product, mp 333–335°C, with extensive previous darkening even under argon (lit. (16) mp 345–346°C (dec. argon); lit. (17) mp 332–334°C). Preparative HPLC was required to produce a pale yellow sample. UV (cyclohexane) λ_{max} (log ϵ_{max}): 455 nm (4.76), 450sh (4.62), 444sh (4.39), 426 (4.58), 402 (4.22), 380 (3.75), 259 (4.46), 252 (4.41), 246 (4.39), 229 (4.49), and 222 (4.63); ^{1}H NMR, δ (250 MHz) (CD_2Cl_2–CS_2): 7.92, 7.24 (AB, J = 7.4 Hz, 4H each, ArH) and 3.39 (s, 8H, -CH_2-); ^{13}C NMR, δ (63 MHz) (CD_2Cl_2–CS_2): 145.1(C-12a), 141.3(C-12b), 129.0(C-12d), 128.3(C-12c), 121.1(C-3(4)), 121.0(C-4(3)), and 31.7(C-1,2); MS m/e: 304 ($M^{+\cdot}$, 100%). Anal. calcd. for $C_{24}H_{16}$: C 94.70, H 5.30; found: C 95.03, H 5.05.

Diaceperylylene, (dicyclopenta[1,2,3-cd:1′,2′,3′-lm]perylene) **2**

DDQ (2,3-dichloro-5,6-dicyanoquinone) (317 mg, 1.4 mmol) was added to a solution of diaceperylene **1** (170 mg, 0.56 mmol) in dry, argon-degassed benzene (250 mL), and the mixture was heated under reflux for 3 h under argon. After cooling, the mixture was filtered, and the benzene evaporated to give crude product. This was chromatographed over water (4%) deactivated silica gel using benzene–pentane (3:7) as eluant to give the product **2** (102 mg, 60%), which on recrystallization from benzene gave dark red crystals, mp >350°C (argon). UV (cyclohexane) λ_{max} (log ϵ_{max}): 500 nm (4.62), 466 max (4.40), 437 (4.00), 412 (3.55), 336 (3.87), 322 (3.66), 246 (4.50), and 220 (4.67); ^{1}H NMR, δ (250 MHz): 7.89, 7.41 (AB, J = 7.4 Hz, 4H each, ArH) and 6.70 (s, 4H, -CH=CH-); ^{13}C NMR, δ (63 MHz) (CS_2): 130.0(C-1,2,7,8), 125.0(C-3,6,9,12), and 122.2(C-4,5,10,11) (only =CH carbons could be observed, see text); MS m/e 300: ($M^{+\cdot}$, 100%), 150 (100%). Anal. calcd. for $C_{24}H_{12}$: C 95.97, H 4.03; found: C 95.99, H 4.01.

5,5′-Diacenaphthene **10**

n-BuLi (43 mmol) in hexane (27 mL) was injected under argon into a stirred solution of 5-bromoacenaphthene **9** (1) (10.0 g, 43 mmol) in dry ether (100 mL) at 0°C. After 2 h, anhydrous (see **1** above) $CoCl_2$ (13 g, 100 mmol) was added, and the mixture was heated under reflux for 12 h. After cooling, the mixture was poured onto ice, acidified with aqueous 2 M HCl, and the organic layer was washed with water, dried, and evaporated. The crude product was then chromatographed on alumina (activity 2–3) using pentane as eluant and gave, after elution of unchanged **9** and some acenaphthene, 5,5′-diacenaphthene **10** (4.86 g, 74%), which in recrystallization from dichloromethane–hexane gave very pale yellow crystals of **10**, mp 179–180°C (lit. (36) mp 176–178°C). ^{1}H NMR (250 MHz), δ: 7.51 (AB, J = 7.2 Hz, 2H, H-4,4′), 7.41 (AB, J = 7.2 Hz, 2H, H-3,3′), 7.39–7.31 (m, 6H, H-6,6′,7,7′,8,8′), and 3.50 (s, 8H, -CH_2-); ^{13}C NMR (15 MHz), δ: 146.0(C-8a), 145.4(C-2a), 139.4(C-8b), 133.5(C-5), 131.0(C-8c), 129.5(C-4), 127.7(C-7), 121.5(C-6), 119.2(C-3), 119.0(C-8), 30.6(C-2), and 30.1(C-1).

6,6′-Dibromo-5,5′-diacenpahthene **11**

N-Bromosuccinimide (9.75 g, 55 mmol) in DMF (50 mL) was added to a stirred solution of the diacenaphthene **10** (8.4 g, 27 mmol) in DMF (170 mL) at 70–80°C. After 12 h, the reaction mixture was cooled, poured into water, and extracted with dichloromethane. The extract was washed well with water, saturated aqueous NaCl, dried, and evaporated. The residue was chromatographed over silica gel using dichloromethane–pentane (3:7) as eluant to give 7.9 g (62%) of yellow dibromide **11**, mp 180–188°C, which was used directly in the next reaction. ^{1}H NMR (90 MHz), δ: 7.61 (d, J = 8 Hz, 2H, H-4,4′ or 7,7′), 7.5–7.0 (m, 6H, ArH), 3.45 and 3.41 (s, 4H each, -CH_2-); MS (CI) m/e: 463,465,467 (MH, 1:2:1 ratio).

Coupling of **11**

n-BuLi (8.6 mmol) in hexane (3.6 mL) was injected under argon to a stirred solution of the crude dibromide **11** (2.0 g, 4.3 mmol) in dry ether (120 mL) at −10 to 0°C. After 2 h, anhydrous $CoCl_2$ (2.2 g, 17 mmol) was added, and the mixture was heated under reflux for 12 h. The reaction was then worked up as described for **1** above. HPLC indicated that **1** was present, but that the reaction was much dirtier than the direct coupling to **1** described above; moreover, the isolation of **1** was only achieved with difficulty using HPLC (reverse phase C18 with methanol).

5,5,12,12-Tetramethyldiacenaphtho[5,6-bc:5′,6′-fg]-(1,5)distannocin **12**

n-BuLi (6.4 mmol) in hexane (4.3 mL) was injected into a stirred solution of 5,6-dibromoacenaphthene (1) (1.0 g, 3.2 mmol) in dry ether (50 mL) at 20°C. After stirring for 1 h, dimethyltindichloride (0.705 g, 3.21 mmol) was added, and the mixture was then stirred for a further hour before collecting the white precipitate. This was extracted with boiling benzene, and the extract was evaporated and recrystallized from benzene–hexane to yield pale yellow needles of **12** (500 mg, 26%), mp 277–279°C. ^{1}H NMR (90 MHz), δ: 7.72, 7.27 (d, J = 7 Hz, 4H each, ArH), 3.32 (s, 8H, -CH_2-), and 0.54 (s, 12H, -CH_3); MS (CI) m/e: 6.05 (MH^+ for Sn^{120}, correct isotope pattern), intense M − CH_3 peaks. Anal. calcd. for $C_{28}H_{28}Sn_2$: C 55.87, H 4.69; found: C 56.03, H 4.85.

Photolysis of **12** *to give* **1**

A solution of the stannocin **12** (0.4 g) in dry benzene (200 mL) was irradiated in a quartz Hanovia reactor (medium pressure) for 48 h. After filtration, the filtrate was evaporated and chromatographed over basic alumina (activity 2–3) using benzene–hexane (1:5) as eluant. The eluate contained a 3–5% yield of **1** (confirmed by HPLC and UV). However, this sample was difficult to crystallize.

5,6-Dibromoacenaphthylene **13**

DDQ (1.09 g, 4.8 mmol) was added to a stirred solution of 5,6-dibromoacenaphthene (1) (1.0 g, 3.2 mmol) in dry benzene (35 mL), and the mixture was heated under reflux for 30 h. After cooling, pentane (175 mL) was added and the mixture was filtered. The filtrate was passed through a short column of basic alumina (activity 2–3), and the eluate on evaporation yielded 740 mg (75%) of product, which on recrystallization from hexane gave deep yellow crystals of 5,6-dibromoacenaphthylene, mp 132–133°C. ^{1}H NMR (250 MHz), δ: 7.86, (AB, J = 7.35 Hz, 2H, H-4,7), 7.40 (AB, J = 7.35 Hz, 2H, H-3,8), and 6.85 (s, 2H, -CH=CH-); ^{13}C NMR (15 MHz) δ: 140.3(C-2a,8a), 135.8(C-8c), 135.4(C-4), 129.1(C-1,2), 125.7(C-8b), 125.1(C-3,8), and 121.0(C-5,6); MS m/e (CI): 309, 311, 313 (MH^+, 1:2:1 ratio, 100%). Anal. calcd. for $C_{12}H_6Br_2$: C 46.50, H 1.95; found: C 46.87, H 2.03.

Attempted coupling of 5,6-dibromoacenaphthylene

n-BuLi (0.6 mmol) was added to a solution of 5,6-dibromoacenaphthylene (100 mg, 0.3 mmol) in dry THF (30 mL) at 0°C (also at −78°C) under nitrogen. After 30 min, anhydrous $CoCl_2$ (167 mg, 1.3 mmol) was added, and the mixture was then heated under reflux for 14 h. After addition of water and extraction into ether, HPLC indicated that 13 products had formed. No **2** could be isolated.

5-Bromoacenaphthylene **15**

(i) By dehydrogenation

DDQ (1.16 g, 5.1 mmol) was added to a stirred solution of 5-bromoacenaphthene (1) (1.0 g, 4.3 mmol) in dry benzene (25 mL) and the mixture was heated under reflux for 14 h. After cooling, pentane (125 mL) was added and the mixture was filtered. The filtrate was passed through a short column of basic alumina (activity 2–3) to yield 600 mg (60%) of the product, which on recrystallization from ethanol gave yellow crystals, mp 53–55°C. ^{1}H NMR (60 MHz), δ: 7.9–7.0 (m, 5H, ArH) and 6.78 (s, 2H, -CH=CH-); ^{13}C NMR (15 MHz), δ: 140.0(C-2a), 139.4(C-8a), 130.8(C-4), 129.5(C-1), 129.1(C-2), 128.7(C-6), 128.3(C-8b or 8c), 126.4(C-7), 124.9(C-3), 124.7(C-8), and 122.9(C-5); MS m/e (CI): 231, 233 (MH^+, 100%). Anal. calcd. for $C_{12}H_7Br$: C 62.37, H 3.05; found: C 62.09, H 3.22.

(ii) By bromination/dehydrobromination

N-bromosuccinimide (30 g, 0.172 mol) was divided into six portions, and one was added to a stirred solution of 5-bromoacenaphthene (20 g, 0.086 mol) in dry CCl_4 (500 mL), which was then heated to reflux under a bright incandescent light, at which point benzoyl peroxide (100 mg) was added. At approximately 15 min intervals, the remaining portions of NBS were added, and reflux continued with irradiation until nearly all the succinimide product floated. The reaction mixture was then cooled, and the succinimide removed by filtration. The filtrate was evaporated, and the residue recrystallized from ethanol to give 1,2,5-tribromoacenaphthene (24 g, 72%), mp 88–90°C. ^{1}H NMR (90 MHz), δ: 8.0–7.1 (m, 5H, ArH) and 5.95 (bs, 2H, -CHBr-). This tribromide (22 g, 56 mmol) was dissolved in acetone (400 mL), and KI (93 g, 0.56 mmol) and $Na_2S_2O_3.5H_2O$ (112 g, 0.45 mol) were added with stirring. The reaction mixture was stirred under reflux for 14 h, cooled, and filtered. The filtrate was evaporated, and the residue extracted into ether, washed, dried, and evaporated and then chromatographed over silica gel using pentane as eluant to give, after recrystallization from ethanol, yellow crystals of 5-bromoacenaphthylene (7.0 g, 35% overall), identical to the sample obtained in (*i*).

5,5′-Diacenaphthylene **16**

DDQ (185 mg, 0.81 mmol) was added to a stirred solution of 5,5′-diacenaphthene **10** (100 mg, 0.33 mmol) in dry benzene (30 mL) and the mixture was heated under reflux for 14 h. After cooling, pentane (150 mL) was added and the mixture was filtered. The filtrate was passed through a short column of alumina (activity 2–3) to yield the yellow product, which was further purified by HPLC (MCH-10, reverse phase, methanol) to a yellow waxy product. ^{1}H NMR (90 MHz), δ: 7.9–7.1 (m, 10H, ArH) and 7.03 (s, 4H, -CH=CH-); ^{13}C NMR (15 MHz), δ: 139.6(C-8a), 139.3(C-2a), 138.1(C-8b), 130.3(C-2), 129.7(C-1), 129.1(C-4), 128.3(C-5), 128.2(C-8c), 127.7(C-7), 126.8(C-6), 124.1(C-3), and 123.6(C-8); MS m/e (CI): 303 (MH^+, 100%).

Attempted coupling of 5-bromoacenaphthylene

n-BuLi (13 mmol) in hexane (5.4 mL) was added to a stirred solution of 5-bromoacenaphthylene (**15**) (3.0 g, 13 mmol) in dry ether (75 mL) under nitrogen at 0°C. After 3 h, anhydrous $CoCl_2$ (3.4 g, 26 mmol) was added, and then the reaction was heated under reflux for 14 h. After coolling, the ether was washed, dried, and evaporated. The residue consisted of 18 products by HPLC (MCH-10, reverse phase, methanol), one of which was 5,5′-diacenaphthylene (**16**) as about 7% of the mixture.

Measurement of electrode reduction potentials

The values quoted in Table 1 were measured on a Metrohm–Polarecord 626 as 0.0005 M solutions of hydrocarbon in 90% aqueous dioxane, which was 0.175 M in tetra-*n*-butylammonium iodide using a dropping mercury electrode relative to a standard calomel electrode.

Mutagenicity tests

These were carried out using DMSO solutions of **1** and **2** (0.1 mg/mL) on *Salmonella typhimurium* TA 98 (with and without microsomes) as described by us previously (35).

Acknowledgements

We thank Imperial Oil for a University Research Grant, and the University of Victoria and the Natural Sciences and Engineering Research Council of Canada for financial support.

1. R. H. Mitchell, T. Fyles, and L. M. Ralph. Can. J. Chem. **55**, 1480 (1977).
2. B. M. Trost, G. M. Bright, C. Frihart, and D. Brittelli. J. Am. Chem. Soc. **93**, 737 (1971).
3. C. Tintel, J. Cornelisse, and J. Lugtenburg. Recl. Trav. Chim. Pays-Bas, **102**, 14 (1983).
4. H. Lee and R. G. Harvey. J. Org. Chem. **47**, 4364 (1982).
5. L. T. Scott, G. Reinhardt, and N. Roelofs. J. Org. Chem. **50**, 5886 (1985).
6. R. Sangaiah and A. Gold. Org. Prep. Proced. Int. **17**, 53 (1985).
7. H. D. Becker, L. Hansen, and K. Andersson. J. Org. Chem. **50**, 277 (1985).

Can. J. Chem. Downloaded from www.nrcresearchpress.com by 92.62.229.171 on 09/08/12
For personal use only.

8. B. F. Plummer, Z. Y. Al-Saigh, and M. Arfan. J. Org. Chem. **49**, 2069 (1984).
9. R. Sangaiah, A. Gold, and G. E. Toney. J. Org. Chem. **48**, 1632 (1983).
10. E. Eisenstadt and A. Gold. Proc. Nat. Acad. Sci. U.S.A. **75**, 1667 (1978).
11. H. J. Bestmann, R. Hartl, and H. Haberlein. Liebigs Ann. Chem. **718**, 33 (1968).
12. M. M. Harris and P. K. Patel. Chem. Ind. 1002 (1973).
13. J. E. Shaw, D. C. Kunerth, and J. J. Sherry. Tetrahedron Lett. **14**, 689 (1973).
14. J. Grundy, B. G. James, and G. Pattenden. Tetrahedron Lett. **13**, 757 (1972).
15. R. H. Mitchell, M. Chaudhary, T. W. Dingle, and R. V. Williams. J. Am. Chem. Soc. **106**, 7776 (1984).
16. N. Tanaka and T. Kasai. Bull. Chem. Soc. Jpn. **54**, 3026 (1981).
17. W. Jaworek and F. Vögtle. Chem. Ber. **124**, 347 (1991).
18. R. H. Mitchell, Y. H. Lai, and R. V. Williams. J. Org. Chem. **44**, 4733 (1979).
19. J. Meinwald, S. Knapp, and T. Tatsuoka. Tetrahedron Lett. **18**, 2247 (1977).
20. R. N. Jones. J. Chem. Soc. 1 (1942).
21. PCMODELPI (V.3.2), Serena Software, Bloomington, Ind.
22. A. D. Campbell, R. A. Elder, and G. W. Emerson. J. Chem. Soc. 3526 (1959).
23. M. J. S. Dewar. J. Chem. Soc. 3532 (1952).
24. A. Streitweiser. Molecular orbital theory. John Wiley, New York. 1961. p. 217.
25. M. A. Cooper and S. L. Manatt. J. Am. Chem. Soc. **91**, 6325 (1969).
26. M. J. S. Dewar and R. C. Fahey. J. Am. Chem. Soc. **85**, 2704 (1963).
27. J. S. Martin and B. P. Dailey. J. Chem. Phys. **39**, 1722 (1963).
28. K. N. Scott. J. Magn. Reson. **6**, 55 (1972).
29. J. D. Memory and N. K. Wilson. NMR of aromatic compounds. John Wiley, New York. 1982. pp. 64–67.
30. B. M. Trost and W. B. Herdle. J. Am. Chem. Soc. **98**, 4080 (1976).
31. G. J. Martin, M. L. Martin, and S. Odiot. Org. Magn. Reson. **7**, 2 (1975).
32. V. Balasubramaniyan. Chem. Rev. **66**, 567 (1966).
33. A. J. Fry and P. C. Fox. Tetrahedron, **42**, 5255 (1986).
34. B. N. Ames, W. E. Durston, E. Yamasaki, and F. D. Lee. Proc. Nat. Acad. Sci. U.S.A. **70**, 2281 (1973).
35. E. L. Grant, R. H. Mitchell, P. R. West, L. Mazuch, and M. J. Ashwood-Smith. Mutat. Res. **40**, 225 (1976).
36. L. A. Jones and R. Watson. Can. J. Chem. **51**, 1833 (1973).
37. K. Hayamizu and O. Yamamoto. ^{13}C NMR spectra of polycyclic aromatic compounds. Japan Industrial Tech. Assoc., Tokyo. 1982.

Can. J. Chem. Downloaded from www.nrcresearchpress.com by 92.62.229.171 on 09/08/12
For personal use only.

Curve crossing analysis of LFER data in Michael addition reactions[1]

ZEEV GROSS AND SHMARYAHU HOZ[2]
Department of Chemistry, Bar-Ilan University, Ramat-Gan, Israel 52900

Received July 5, 1991

ZEEV GROSS and SHMARYAHU HOZ. Can. J. Chem. **70**, 1022 (1992).

Rate constants for the Michael addition of CN^- in water, aqueous sulfolane, and DMSO, and MeO^- in MeOH to eight mono- and disubstituted 1,1-diaryl-2,2-dinitroethylenes were measured. The ρ values are in the range 0.7 (CN^-/H_2O) – 1.6 (MeO^-/MeOH). For each of the four systems a correlation was found between log *k* and the ^{13}C chemical shift of the carbon that undergoes the nucleophilic attack. However, the quality of the correlation as well as the slope decreases with decreasing ρ values. Analysis of the electronic configuration of the transition state using the curve crossing model shows that the traditional interpretation of the location of the transition state should be reversed. This analysis provides a rationale for the observed dependence of the chemical shift – rate correlation on the ρ value.

ZEEV GROSS et SHMARYAHU HOZ. Can. J. Chem. **70**, 1022 (1992).

On a mesuré les constantes de vitesse pour l'addition de Michael du CN^- (dans l'eau, en solutions aqueuses de sulfolane et dans le DMSO) et du MeO^- (dans le méthanol) sur huit 1,1-diaryl-2,2-dinitroéthylènes mono- et disubstitués. Les valeurs de ρ varient de 0,7 (CN^-/H_2O) à 1,6 (MeO^-/MeOH). Pour chacun des quatre systèmes, on a pu établir une corrélation entre le log *k* et le déplacement chimique (en RMN du ^{13}C) du carbone qui subit l'attaque nucléophile. Toutefois, la qualité de la corrélation ainsi que la pente diminuent avec une diminution des valeurs de ρ. Une analyse de la configuration électronique de l'état de transition à l'aide du modèle du croisement des courbes montre que l'interprétation traditionnelle de la position de l'état de transition doit être renversée. Cette analyse fournit une explication rationnelle pour la relation qui a été observée entre la corrélation déplacement chimique/vitesse et la valeur de ρ.

[Traduit par la rédaction]

Introduction

Although the Ritchie equation was originally designed for anion–cation combination reactions (1), we have shown that after inclusion of a selectivity parameter (eq. [1]), it can also accommodate nucleophilic additions to some activated olefins (2).

[1] $\log k/k_0 = S_+N_+$

The equation was found to be valid for systems having the framework of 9-methylenefluorene (eq. [2]) with various activating groups on the α carbon.

To examine the effect of substitution on the β carbon in these reactions, we have studied the analogous diphenyl system where the aromatic rings can be relatively easily substituted. Since the 9-dinitromethylenefluorene system (eq. [2], X=Y=NO_2, FDN) gave an excellent fit (2) to the Ritchie equation, the diaryl system chosen for the present study was also activated by two nitro groups on the α carbon (DArDN).

As will be shown later, the results of this study seem to imply a contradiction between basic principles and postulates in the field of reaction mechanism. A resolution of this apparent contradiction is advanced using the curve crossing model for nucleophilic attacks on Low LUMO compounds.

[2] 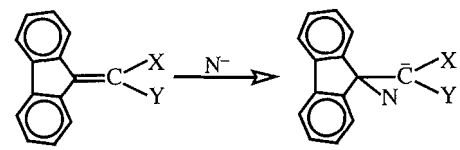

Results

Rate constants for the reactions of various nucleophilic systems (nucleophile/solvent) with a series of substituted 1,1-diaryl-2,2-dinitroethylenes (DArDN, eq. [3]) were determined at 25°C.

[3] 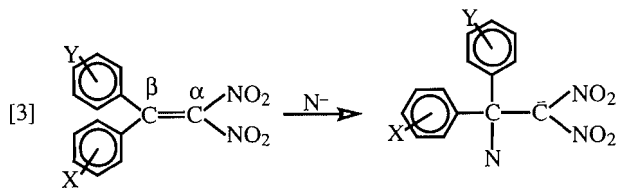

	DADN	MADN	DTDN	DPDN	DFDN	MClDN	DClDN	MNDN
A	OMe	OMe	Me	H	F	Cl	Cl	NO_2
B	OME	H	Me	H	F	H	Cl	H

The reactions were followed spectroscopically by monitoring the disappearance of the absorption of the olefin at its λ_{max}. Occasionally the reactions were also monitored by following the formation of the products. Identical rate constants were obtained by both methods. The concentrations of the substrate were in the range 10^{-5}–10^{-4} M. Concentrations lower than 10^{-5} M were used only for the reactions in water to avoid zero-order kinetics due to aggregation (3). In

[1]Preliminary communication: Tetrahedron Lett. **32**, 5163 (1991).
[2]Author to whom correspondence may be addressed.

Can. J. Chem. Downloaded from www.nrcresearchpress.com by 79.173.37.17 on 09/08/12
For personal use only.

TABLE 1. Second-order rate constants for nucleophilic addition to DArDN and FDN (λ_{max}), nucleophilicity parameter N_+, and ^{13}C chemical shifts

		k (M^{-1} s^{-1})								
Nu/solvent	N_+	DADN	MADN	DTDN	DPDN	MClDN	DFDN	DClDN	MNDN	FDN[a]
CN^-/H_2O	3.67	1.96 ±0.08 (420)	3.08 ±0.49 (420)	1.96 ±0.23 (340)	4.82 ±0.28 (320)	5.96 ±0.36 (325)	6.28 ±0.35 (325)	9.32 ±0.65 (325)	17.19 ±1.4 (331)[b]	0.27 ±0.03
CN^-/25% sulfolane	5.65	2.49 ±0.45 (420)	5.3 ±0.54 (420)	5.18 ±0.66 (340)	8.9 ±1 (320)	12.4 ±1.5 (325)	11.6 ±0.4 (325)	21.1 ±2.1 (325)	34.1 ±5.4 (331)[b]	71 ±2.6
MeO^-/MeOH	6.27	0.6 ±0.06 (372)	1.02 ±0.09 (383)	0.93 ±0.06 (333)	1.87 ±0.14 (320)	6.03 ±0.18 (320)	9.25 ±0.87 (320)	19.5 ±0.2 (320)	31.1[c] ±4.1 [d]	426 ±43
CN^-/DMSO	8.6	0.23[d] ±0.04 (420)	0.57[d] ±0.07 (420)	0.59[d] ±0.09 (340)	1.46[d] ±0.08 (320)	3.41[d] ±0.07 (320)	4.08[d] ±0.19 (320)	8.54[d] ±0.88 (320)	11.7[d] ±1.7 (272)[e]	3.78[d] ±0.45
		^{13}C chemical shift (ppm)								
C_α		148.5	148.9	149.2	149.4	149.4	149.4	149.4	149.5	
C_β		145.08	144.56	144.5	143.86	142.5	141.74	141.37	140.92	

[a]Reference 2.
[b]Shoulder.
[c]Measurements were performed at 272, 335, 380, and 400 nm.
[d]$k \times 10^{-5}$.
[e]Measurements were also performed at 366 nm (λ_{max} of the product).

TABLE 2. ρ and ρ^0 values for the reactions of DarDN with various nucleophilic systems and log k – $^{13}C_\beta$ NMR chemical shift correlation

					$^{13}C_\beta$	
Nu/solvent	ρ	r	ρ^0	r	Slope	r
CN^-/water	0.74 ± 0.05	0.9855	0.8 ± 0.06	0.9826	−0.19	0.886
CN^-/25% sulfolane	0.82 ± 0.04	0.9909	0.87 ± 0.03	0.9709	−0.21	0.895
MeO^-/MeOH	1.44 ± 0.14	0.9676	1.60 ± 0.08	0.9918	−0.4	0.991
CN^-/DMSO	1.36 ± 0.12	0.9750	1.44 ± 0.12	0.9764	−0.37	0.965

all cases the nucleophile concentration was at least ten times higher than that of the substrate. In protic solvents the cyanide anion is partly protonated. The concentration of the free CN^- was calculated from its pK_a and the dissociation constant of the solvent (see experimental section). Usually the free [CN^-] was in the range 0.002–0.01 M. All reactions went to completion. In aqueous solutions, hydrolysis due to the presence of OH^- was observed for the two most reactive derivatives. For these substrates, the reactions were conducted in borax buffered solutions at pH 9.2, thereby minimizing the competing hydrolytic reaction.

Second-order rate constants and λ_{max} for the various derivatives are given in Table 1.

The ^{13}C NMR chemical shifts of C_α and C_β were measured for each of the substrates. The data are given in Table 1.

Discussion

Hammett vs. Ritchie equations

Variation of the nucleophilic system (nucleophile/solvent) in combination with a variation of substituents on the aromatic ring enables a simultaneous analysis of two LFER's: the Ritchie and the Hammett equations. Both equations contradict the reactivity–selectivity principle and cannot coexist unless the ρ values remain constant for all nucleophilic systems. Thus, in the present case the ρ in DMSO, for example, must be equal to that in water.

The question at hand is therefore whether the two LFER's do coexist for DArDN at the price of the severe restriction of having ρ constant for all nucleophilic systems and, in case they do not, which LFER will supersede the other. It should be pointed out that in spite of the severe requirement, cases of simultaneous coexistence of the two equations are known (4).

The reactions of the four nucleophilic systems with the various substituted substrates were found to obey the Hammett equation (Table 2 and Fig. 1). In aqueous solutions the data are best correlated with σ, whereas in nonaqueous media a slightly better correlation is obtained with σ^0 (5). However, as shown in Table 2, the use of one type of σ or the other does not affect the actual ρ values. It should also be pointed out that the σ values of the disubstituted substrates are additive with no apparent deviation (see, however, ref. 6). On the other hand, the Ritchie equation is

Can. J. Chem. Downloaded from www.nrcresearchpress.com by 79.173.37.17 on 09/08/12
For personal use only.

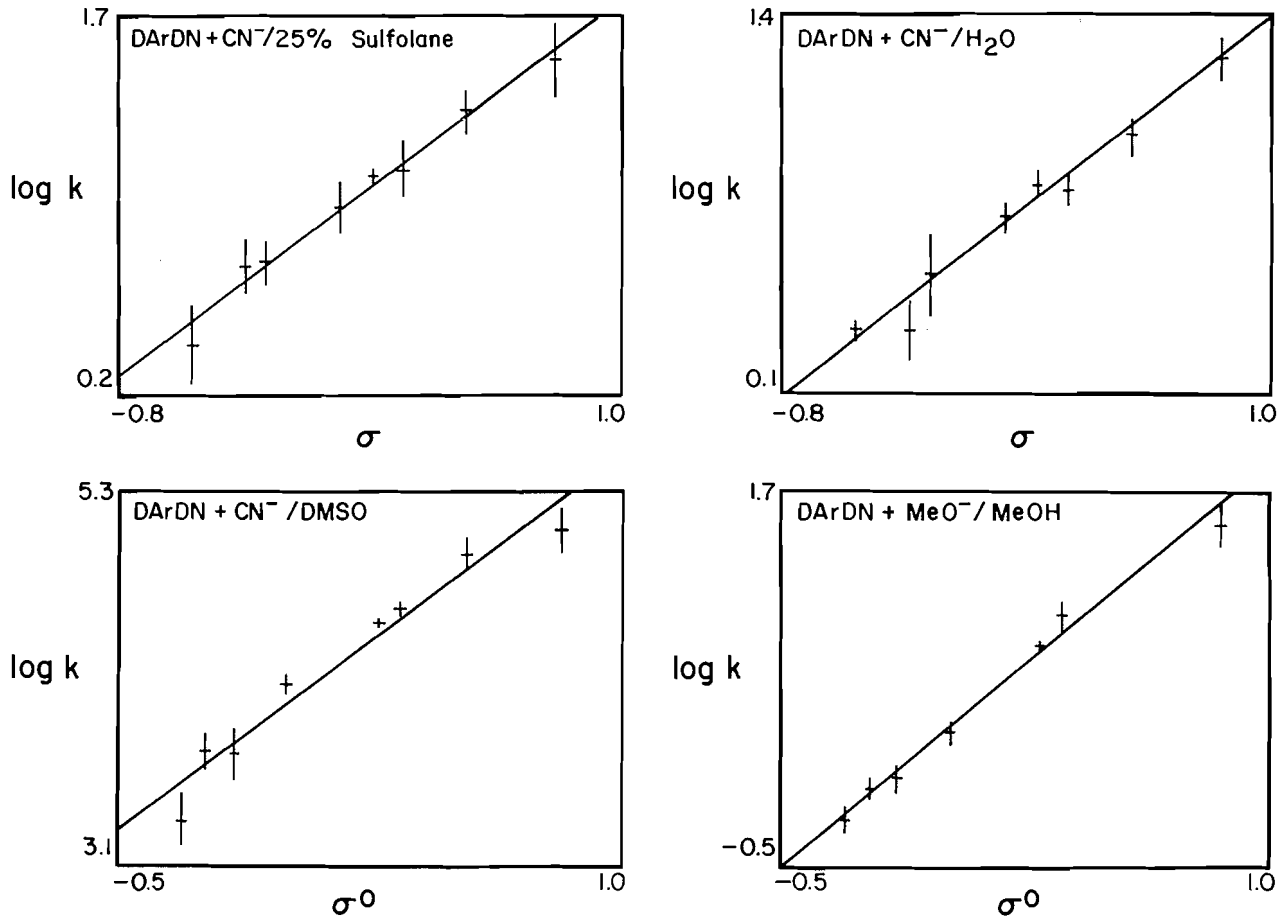

FIG. 1. Hammett plots for nucleophilic additions to 1,1-diaryl-2,2-dinitroethylenes.

not obeyed (Fig. 2). Most probably the requirements of the latter are more stringent, leading thus to a limited range of applicability.

In light of the difference between the Ritchie (N_+) (1) and the Swain–Scott (7) (n) nucleophilicity scales, we have suggested that substrates participating in nucleophilic reactions should be classified according to their LUMO energies (2*a*, 8–10). High LUMO (HL) substrates will obey the Swain–Scott equation (7), whereas low LUMO (LL) substrates will obey the Ritchie N_+ equation (1). The question, in terms of LUMO energy, is: where is the border line between these two classes of substrates? If LUMO energies are the only major factor affecting the behavior of a substrate, then the border line lies (at least within the activated double bond series) between FDN and DArDN derivatives. In a more quantitative way, using half-wave reduction potentials as a measure for the energy of the LUMO, the aforementioned border line lies between −0.2 and −0.94 V, which are the half-wave reduction potentials of DPDN and FDN respectively.[3] Substrates with LUMO energies close to that of FDN are expected to obey both the Hammett and the Ritchie equations, whereas those nearing DPDN will probably obey only the Hammett equation.

[3]The half-wave potentials of the first cathodic wave were determined in methylene chloride with tetrabutylamonium perchlorate as the supporting electrolyte and a platinum rotating disk electrode. We are grateful to Dr. Y. Liftman for the electrochemical measurements.

General description of TS structure in Michael addition reaction (MAR)

Let us first briefly discuss our model for nucleophilic attacks on low-lying LUMO (LL) substrates (8–10). Phenomenologically, substrates of low electrophilicity, i.e., high LUMO substrates, form covalent bonds in their reactions with nucleophiles. On the other hand, increasing the electrophilicity of a substrate will eventually lead to an electron transfer reaction. The radical pair formed may either collapse to the covalent bond or dissociate to the free radicals. Our model assumes continuity between these two extreme cases. That is, in any TS there is a partial covalent bonding as well as a partial diradical character. The relative contributions of these features vary with the LUMO height. Hence, nucleophilic attacks on low LUMO substrates are characterized by a transition state (TS) in which both the nucleophile and the substrate acquire a relatively large radical character. A similar conclusion was reached by Fukuzumi and Kochi for electrophilic aromatic substitution (11). Shaik and Pross have rigorously developed, with a similar outcome, a valence bond model for a large variety of reactions (12, 13). The model is best demonstrated by using the curve crossing method for the construction of the MAR profile (14) (Fig. 3). The profile is constructed by overlaying potential energy curves of the reactants and the products (I and II, Fig. 3). The two curves differ from each other by a transfer of a single electron from N^- to the substrate. Thus, motion from the ionic state of the reactants at the right to form the covalent bond at the left *must involve a partial electron transfer*. The TS

Can. J. Chem. Downloaded from www.nrcresearchpress.com by 79.173.37.17 on 09/08/12
For personal use only.

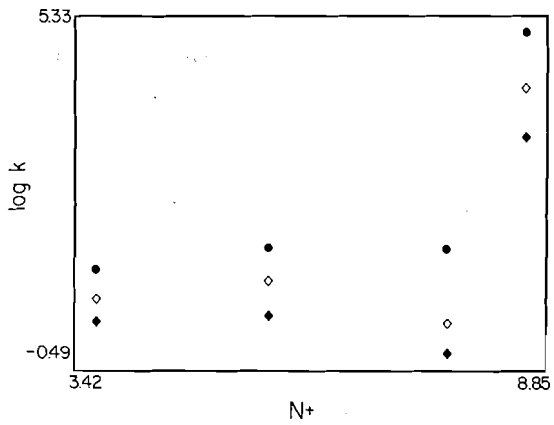

FIG 2. A Ritchie type diagram for selected substrates: MNDN ●; DPDN ◇; DADN ◆.

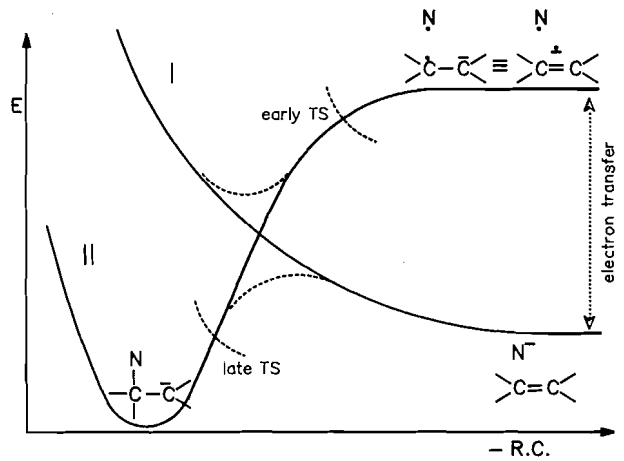

FIG. 3. Construction of a reaction profile for the Michael addition reaction.

is achieved in the region of the avoided crossing. At this point the two configurations are of equal energy and hence the state function at this point has *equal contributions* from the two configurations. Therefore, as was already pointed out (12), about *half an electron* has been transferred from the nucleophile to the substrate at the TS.[4] It should be emphasized that this process does not lead to the formation of two distinct radicals since the TS decays to the covalent product.

Another important feature of this system is that the balance between the diradical and the covalent character varies as one progresses along the Morse type curve. An early TS, that is, an early crossing of the two curves, will result in a larger contribution from the diradical character, whereas a late TS will cause covalent bonding to be highly advanced at the expense of the diradicaloid character.

Thus, although the same amount of charge is transferred from the nucleophile to the substrate regardless of the position of the TS, the actual charge sensed by substituents on the aromatic rings (the probe) depends on the extent to which covalent bond formation has progressed, i.e., on the location of the TS. In a very early TS, the negative charge (the odd electron at the LUMO of the substrate) can be almost freely delocalized onto the aromatic rings and their substituents, leading to a relatively high ρ value (structure **A**). In a very late TS, covalent bond formation becomes dominant, disrupting the probe – negative charge interaction with the latter being now confined mainly to the remote location of the activating group region (structure **B**). Such a separation of the charge from the substituent will lower the ρ value. Thus, contrary to the traditional interpretation, *there is an inverse relationship between the* ρ *and the location of the TS. A relatively small* ρ *corresponds to a late TS and vice versa.*

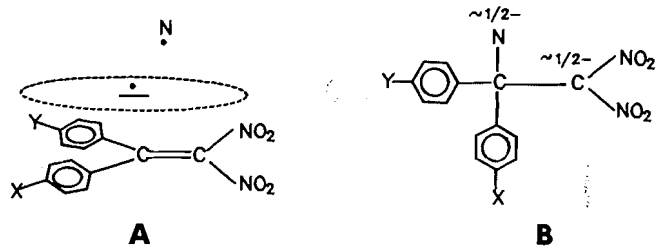

In a previous paper we showed how this model accommodates various observations made in the analogous 1,1-diaryl-2-nitroethylene system (10). In the present paper we will show how this model is further supported by the ^{13}C chemical shift – rate correlation observed in the present system.

^{13}C chemical shift – rate correlation

Variations in reaction rate constants can be correlated with variations in a property of the substrate that is related to the equilibrium energy of the reaction. Assuming a monotonic variation of this property between the reactants and the products, one would expect a linear correlation (LFER) between the rate and that property (both given in energy-related units). The effect on the rate, expressed as a fraction of the equilibrium-related effect, can be used as a measure for the location of the TS along the reaction coordinate (15). However, if the given property is not an equilibrium-related property but is rather an intrinsic property of the reactants, then one would expect to observe such a correlation only for an early TS where the reactants retain this property to a given extent. Thus, for example, the LUMO energy of a substrate does not necessarily have any relation to the equilibrium of the reaction. It becomes energetically meaningful only when interacting with the HOMO of the nucleophile. Thus, in a very early TS, a rate – LUMO energy correlation can be observed. However, in a late TS, since the substrate has undergone significant geometric and electronic changes, the relevancy of the interaction between the HOMO and the original substrate's LUMO to the activation energy is diminished (the relevant LUMO in this case would be that of the deformed substrate).

As can be seen from Fig. 4, log *k* for each of the four reaction sets can be correlated with the ^{13}C NMR chemical shift of the carbon atom that undergoes the nucleophilic attack. The chemical shift of $^{13}C_\alpha$ (where the charge will eventually reside) is insensitive to variation of substituents on the aryl groups. The ^{13}C NMR chemical shift is another property of the reactants that is not related to the reaction equilibrium energy. It may be related to the rate effect through a possible connection with the LUMO energy. In a similar manner, since ^{13}C chemical shift is related to the charge on the

[4]This approximation is valid at the two-configuration approximation level. In reality, the mixing of higher energy configurations as well as the skewing effect may somewhat shift the actual amount of the transferred charge from 0.5 e^-.

Can. J. Chem. Downloaded from www.nrcresearchpress.com by 79.173.37.17 on 09/08/12
For personal use only.

Can. J. Chem. Downloaded from www.nrcresearchpress.com by 79.173.37.17 on 09/08/12
For personal use only.

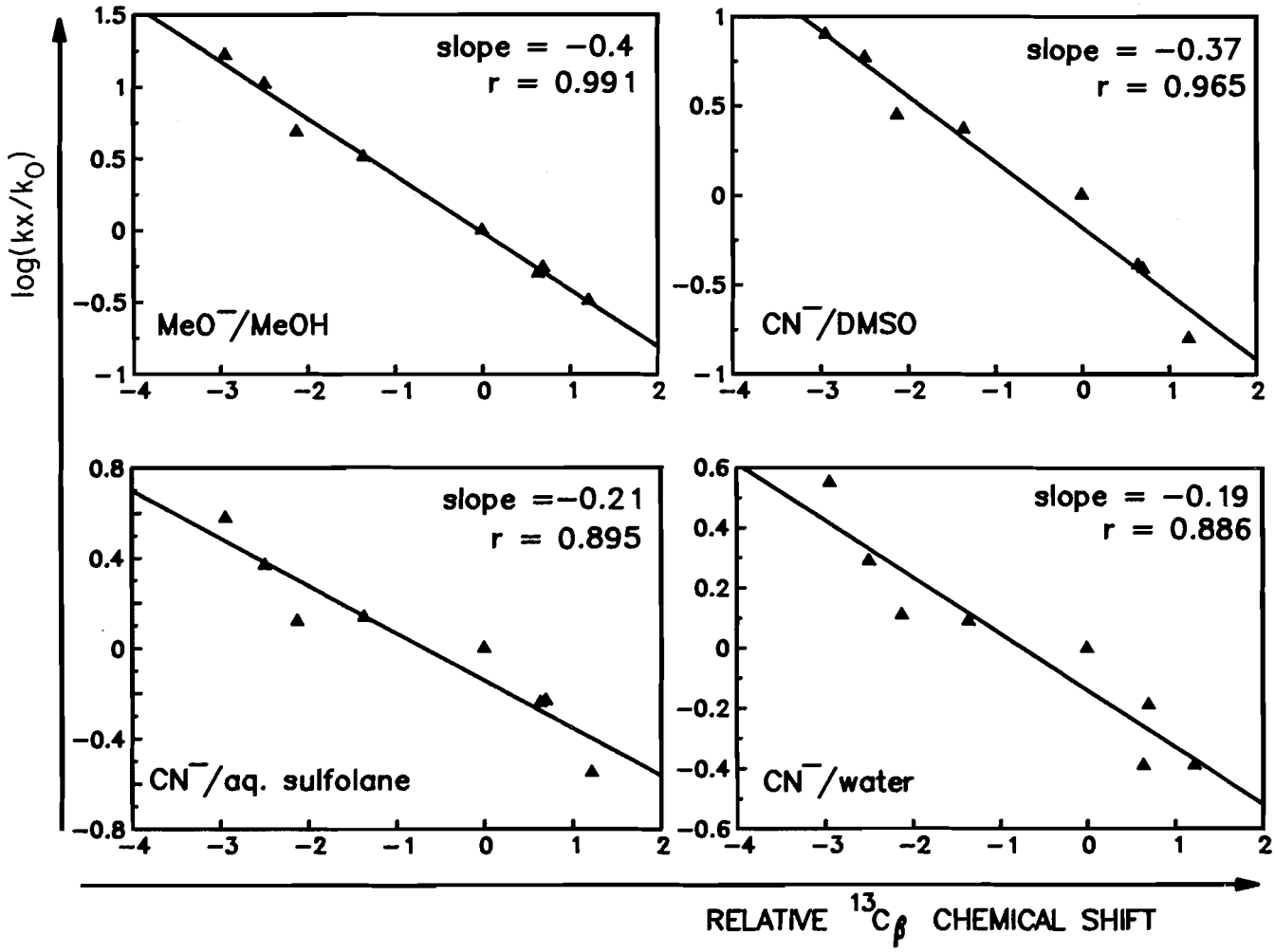

FIG. 4. Log k vs. relative $^{13}C_\beta$ chemical shift.

nucleus (16), it may reflect the electrostatic interaction at the TS. In both cases, it is clear that the later the TS, the less relevant this property is to the rate. Thus, both the quality of the correlation and the slope are expected to decrease as the TS becomes later. Examination of the data in Table 2 and Fig. 4 suggest therefore that the earliness of the TS increases in the order $MeO^-/MeOH > CN^-/DMSO > CN^-/$ aqueous sulfolane $> CN^-/H_2O$. This result is in excellent agreement with our model since the reactions with $MeO^-/$ MeOH and with $CN^-/DMSO$ have larger ρ values and are therefore indeed predicted to have a TS earlier than the reactions with CN^-/aqueous sulfolane and CN^-/H_2O, whose ρ values are smaller. It should be noted that this conclusion also concurs with the Hammond postulate (17), which predicts that the more reactive system has an earlier TS.

Summary and conclusions

The major conclusions of this study, in which the reactivities of four nucleophilic systems (nucleophile/solvent) towards a series of dinitro activated olefins (DArDN) were determined, are (*a*) unlike the analogous fluorenyl system, the DArDN system does not obey the Ritchie N_+ equation. It is suggested that, at least within the realm of activated olefins, the border line between the N_+ and the n (Swain–Scott) behavior lies with substrates having LUMO's with energy between that of DArDN and FDN. In terms of half-wave reduction potentials of substrates, the border line lies between −0.2 and −0.9 V; (*b*) the TS has a structure (radical anionic) that is not an intermediate one between that of reactants and products; (*c*) in the present case, a large ρ value is indicative of an early TS and vice versa; (*d*) the above conclusion provides a rationale for the unexpected behavior of rate – ^{13}C chemical shift correlation as a function of ρ values.

Experimental section

Instrumentation

Kinetic measurements were performed on Uvikon 810-820, Gilford 2400, and Durrum 110 stopped-flow spectrophotometers that were equipped with an Apple II microcomputer for data acquisition. pH measurements were taken with a Radiometer PHM-52 digital pH-meter. ^1H and ^{13}C NMR spectra were recorded on a Bruker AM 300 spectrometer.

Substrates and products

1,1-Diphenyl-2,2-dinitroethylene (DPDN) and 1,1-di(4-methoxyphenyl)-2,2-dinitroethylene (DADN) are known compounds (18). In general, the preparation of the DArDN substrates involved dinitration of the parent 1,1-diarylethylenes according to the following procedure. To a stirred solution of 20 mL glacial acetic acid containing 20 mmol of 1,1-diarylethylene, 3.5 mL red fuming nitric acid in 16.5 mL AcOH was added. The reaction mixture

Can. J. Chem. Downloaded from www.nrcresearchpress.com by 79.173.37.17 on 09/08/12
For personal use only.

was refluxed for 1 h. After cooling, chloroform and ice water were added and the aqueous phase was washed three times with chloroform. The combined chloroform solution was rapidly washed with a 5% $NaHCO_3$ solution, dried over $MgSO_4$, and evaporated. The residue was chromatographed on a silica column (CH_2Cl_2:hexane 2:1). The dinitration products were collected and recrystallized from hexane. The structure of the products was verified by NMR spectroscopy (data will be reported in a separate paper) and elemental analyses (satisfactory elemental analysis was obtained for all elements; oxygen was not analyzed). In this procedure no ring nitrations were observed. The preparation of 1-(4-nitrophenyl)-1-phenyl-2,2-dinitroethylene (MNDN) involved ring nitration of 1,1-diphenyl-2,2-dinitroethylene (DPDN) using the following procedure. To an ice-cold stirred mixture of DPDN (0.27 g, 1 mmol), 15 mL CF_3COOH, and 0.2 g H_2SO_4, 0.11 g red fuming nitric acid in 1 mL CF_3COOH was added over 1 min. After stirring for 15 min at 0–5°C and an additional 20 min at room temperature, the reaction mixture was treated with water and ether. The aqueous phase was washed with three portions of ether, and the combined ethereal solution was treated similarly to the above chloroform solution. No attempt was made to optimize yields. Yields obtained (mp, °C): MADN 37% (107); DTDN 25% (122); MClDN 20% (135); DClDN 21% (132); DFDN 14% (97); MNDN 57% (109). 2,2-Diaryl-3,3-dinitropropionitrile, the adduct of DPDN, is known (18). The general procedure for the preparation of the adducts was as follows: to a mixture of 0.065 g KCN (1 mmol) and 1 mmol DArDN, dry DMSO (10 mL) was added all at once with vigorous stirring. After a few minutes all the solids dissolved and the mixture was poured into a mixture of crushed ice and 50 mL 5% HCl solution. The solids were filtered, and the filtrate was extracted three times with $CHCl_3$, which was dried over $MgSO_4$ and evaporated. Up to this stage the yield was quantitative (NMR and TLC). Attempts were made to crystallize these compounds from hexane, ether, ethanol, acetic acid, trifluoroacetic acid, 5% aqueous HCl, and various mixtures of these solvents, without success. The oils decomposed on standing for several days. Only with 2,2-di-(4-chlorophenyl)-3,3-dinitropropionitrile was a solid product obtained (crystallized from ethanol, acidified with trifluoroacetic acid, mp 127°C; satisfactory C, H, N, Cl elemental analysis was obtained).

Kinetic measurements

The solvents for the kinetic measurements were prepared as follows: double distilled water was boiled prior to use; sulfolane was vacuum-distilled three times, twice over NaOH and once from CaH_2. The middle fraction boiling at 130°C (6.5 Torr; 1 Torr = 133.3 Pa) was collected (19). MeOH was refluxed over Mg + I_2 for 1 h and distilled (20); DMSO, stored for a week over NaOH, was distilled from BaO (21). The concentrations of free CN^- were calculated from the pK_a value of HCN (9.2 (22) and 9.13) (23)) and pK_w (14 and 14.47) (24) of water and a solution of 25% sulfolane in water (v/v). The pK_a of HCN in the aqueous sulfolane was determined by measuring the hydroxide concentration of several KCN solutions using a calibrated pH–KOH profile. Prior to each set of kinetic runs the pH of the freshly prepared cyanide stock solution was determined. The pH measurements were in excellent agreement with the calculated hydroxide concentration. For the relatively slow reactions, the nucleophilic solutions were incubated in the thermostated spectrophotometer until the temperature of 25 ± 0.2°C was reached. The substrate was then injected into the cells (ca. 2.5 μL into 2.5 mL ethanolic solution for the reaction in water). The concentration of the substrate was usually in the range of 10^{-4}–10^{-5} M. The nucleophile concentration was always at least 10 times larger than that of the substrate. In each case first-order rate constants were determined for 3–5 different concentrations of nucleophile. The reactions were usually followed by monitoring the disappearance of the substrate's absorption at its λ_{max}.

1. C. D. Ritchie. Acc. Chem. Res. **5**, 348 (1972); Pure Appl. Chem. **50**, 1281 (1978); Can. J. Chem. **64**, 2239 (1986).
2. (*a*) S. Hoz and D. J. Speizman. J. Org. Chem. **48**, 2904 (1983); (*b*) Tetrahedron Lett. 1775 (1978).
3. S. Hoz, Z. Gross, and D. J. Speizman. Chem. Soc. Perkin Trans. **2**, 1143 (1985).
4. C. D. Ritchie and P. O. I. Virtanen. J. Am. Chem. Soc. **94**, 1589 (1972); M. L. Hertz, D. Feldman, and E. M. Healy. J. Org. Chem. **41**, 221 (1976).
5. O. Exner. *In* Advances in linear free energy relationships. *Edited by* N. B. Chapman and J. Shorter. Plenum Press, London. 1972. Chap. 1.
6. J-E. Dubois, M-F. Ruasse, and A. J. Argile. J. Am. Chem. Soc. **108**, 4840 (1986).
7. G. C. Swain and C. B. Scott. J. Am. Chem. Soc. **75**, 141 (1953).
8. S. Hoz. J. Org. Chem. **47**, 3545 (1982).
9. S. Hoz. *In* Nucleophilicity. *Edited by* J. M. Harris and S. P. McManus. Adv. Chem. Ser. American Chemical Society, Washington, D.C. 1987. Chap. 12.
10. Z. Gross and S. Hoz. J. Am. Chem. Soc. **110**, 7489 (1988).
11. S. Fukuzumi and J. K. Kochi. J. Am. Chem. Soc. **103**, 7240 (1981).
12. S. S. Shaik. Prog. Phys. Org. Chem. **15**, 197 (1985); A. Pross and S. S. Shaik. Acc. Chem. Res. **16**, 363 (1983).
13. A. Pross. Adv. Phys. Org. Chem. **21**, 99 (1985); Acc. Chem. Res. **18**, 212 (1985).
14. E. Buncel, S. S. Shaik, Ik-Hwan Um, and S. Wolfe. J. Am. Chem. Soc. **110**, 1275 (1988).
15. J. E. Leffler and E. Grunwald. Rates and equilibria of organic reactions. Wiley, New York. 1963.
16. J. B. Stothers. Carbon 13 NMR spectroscopy. Academic Press, New York. 1972.
17. G. S. Hammond. J. Am. Chem. Soc. **77**, 334 (1955).
18. M. Albeck, S. Hoz, and Z. Rappoport. J. Chem. Soc. Perkin Trans. 2, 628 (1975).
19. N. Latif and N. Mirinsky. Can. J. Chem. **44**, 1271 (1966).
20. A. I. Vogel. *In* Practical organic chemistry. Longmans, London. (1964). p. 169.
21. J. A. Riddic and W. B. Bunger. *In* Techniques of chemistry. Vol. 2. *Edited by* A. Weissberger. Wiley, New York. 1970. p. 857.
22. R. M. Izatt, J. J. Christensen, R. T. Pack, and R. Bench. Inorg. Chem. **1**, 828 (1962).
23. Z. Gross. Ph.D. Thesis, Bar-Ilan University. 1987.
24. E. M. Wooley and R. E. George. J. Solution Chem. **3**, 119 (1974).

Fragmentation pathways in the mass spectra of isomeric phenylazoxypyridine-*N*-oxides

NIGEL J. BUNCE,[1] H. STEWART MCKINNON, AND RANDY J. SCHNURR
Department of Chemistry and Biochemistry, University of Guelph, Guelph, Ont., Canada N1G 2W1

AND

SAM R. KEUM AND ERWIN BUNCEL
Department of Chemistry, Queen's University, Kingston, Ont., Canada K7L 3N6

Received June 25, 1991

NIGEL J. BUNCE, H. STEWART MCKINNON, RANDY J. SCHNURR, SAM R. KEUM, and ERWIN BUNCEL. Can. J. Chem. **70**, 1028 (1992).

The mass spectral fragmentation pathways of a series of phenylazoxypyridine-*N*-oxides have been studied under electron impact conditions using tandem mass spectrometry. Besides simple C—N cleavages, the azoxypyridine-*N*-oxides undergo deep-seated rearrangements directly from the molecular ion. In addition, the spectra are complicated by a purely chemical reduction of the N—O functionalities that occurs in the ion source prior to ionization.

NIGEL J. BUNCE, H. STEWART MCKINNON, RANDY J. SCHNURR, SAM B. KEUM et ERWIN BUNCEL. Can. J. Chem. **70**, 1028 (1992).

Faisant appel à la spectrométrie de masse en tandem, dans des conditions d'impact électronique, on a déterminé les spectres de masse d'une série de *N*-oxydes de phénylazoxypyridines et on a examiné leurs modes de fragmentation. En plus des simples clivages C—N, les *N*-oxydes d'azoxypyridines subissent des transpositions profondes directement de l'ion moléculaire. De plus, les spectres sont compliqués par une réduction purement chimique des fonctions N—O qui se trouve dans la source ionique avant le processus d'ionisation.

[Traduit par la rédaction]

Can. J. Chem. Downloaded from www.nrcresearchpress.com by 79.173.37.17 on 09/08/12
For personal use only.

Introduction

The mass spectra of aromatic azoxy compounds have received relatively little study. In the 1960s, Bowie *et al.* (1) examined the electron impact (EI) spectra of a wide variety of azoxybenzene derivatives and established the major fragmentation pathways. In addition, they noted that the ratio of the ions Ar^+/Ar'^+ offered a method of distinction between the isomers Ar-N(O)=N-Ar′ and Ar-N=N(O)-Ar′; fragmentation occurred preferentially adjacent to the Ar-N(O) group, so that the ratio Ar^+/Ar'^+ was greater for the isomer Ar-N(O)=N-Ar′ than for Ar-N=N(O)-Ar′

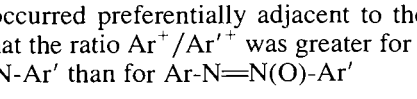

1 **2**

This finding had analytical potential, because the distinction between these isomers has been a difficult problem in the chemistry of aromatic azoxy compounds (2), even with modern spectroscopic techniques.

A more recent study by Waddell *et al.* (3) confirmed most of the conclusions of Bowie *et al.*, but with two important extensions. First, the ratio of the ions Ar^+/Ar'^+ was found to depend upon the sample size introduced into the ion source; the relationship between this ratio and the structure of the azoxy compound was more reliable at high sample sizes as, for example, under direct insertion conditions. Second, it was found that the ion appearing at m/z 182 in the EI spectrum of azoxybenzene, i.e., $(M - 16)^+$, does not originate by loss of an oxygen atom from the molecular ion, as presumed by Bowie *et al.*, but rather arises through a chemical reduction of azoxybenzene in the ion source. This observation is significant in that $(M - O)^+$ is commonly found in the EI spectra of aromatic azoxy compounds, sometimes at high intensities. If a substantial proportion of the substrate undergoes this pre-ionization reaction, then the observed EI spectrum is not simply that of the original azoxy compound, but is the superimposed spectra of two different substances, the azoxy compound and the corresponding azo compound. This could undermine the conclusion of Bowie *et al.* that the ratio of the ions Ar^+/Ar'^+ provides a method of distinguishing between positional isomers of aromatic azoxy compounds, because Ar^+ and Ar'^+ are prominent fragments in the mass spectra of both aromatic azo compounds and aromatic azoxy compounds.

Waddell *et al.* noted that pre-ionization chemical reduction could be expected for any aromatic compounds containing oxygen bonded to nitrogen. We previously described the preparation (4) and acid-catalyzed rearrangements (5) of a series of phenylazoxypyridine-*N*-oxides. These compounds contain two *N*-oxide functionalities: the azoxy bridge and the pyridine-*N*-oxide. Thus one or both N—O functions may undergo pre-ionization chemical reduction in the ion source. In this paper, we report the mass spectra of four isomeric phenylazoxypyridine-*N*-oxides, and show that they do indeed undergo pre-ionization chemical reduction. This study has been greatly aided by the use of tandem mass spectrometry, which allows one to determine unambiguously the parent–daughter relationships between pairs of ions.

Methodology

The azoxy compounds were available from previous studies in our laboratories (6). The mass spectrometer was a Kratos model MS 890, which is a double-focussing mass spectrometer of conventional geometry, i.e., with the electric sector preceding the magnetic sector. Samples were introduced into the mass spectrometer by direct insertion, with an ion source temperature in the neighbourhood of 200°C. The electron beam in the ion source had an energy of 70 eV. The composition of each ion was obtained by

[1]Author to whom correspondence may be addressed.

Can. J. Chem. Downloaded from www.nrcresearchpress.com by 79.173.37.17 on 09/08/12
For personal use only.

comparing the observed mass at high resolution with the calculated mass. In cases where more than one ion of the same nominal mass was detected, peak matching (a scan between two reference peaks of a perfluorokerosene standard) was used to obtain the composition of each of the ions. Spectra were obtained either as conventional electron impact (EI) scans at 70 eV or as linked scans with B/E constant, a scan which identifies all the daughter ions from a given parent.

Results and discussion

Tandem mass spectrometry

The conventional EI spectrum records low-energy ions that survive to the detector without undergoing any fragmentation (molecular ions), and ions initially having much higher energies that undergo single or multiple unimolecular decompositions within the ion source (fragment ions). Tandem mass spectrometry takes advantage of the additional information that can be gleaned from a study of ions of intermediate energy when they fragment in the field-free regions of the spectrometer. The following possibilities exist: (*i*) detect all the daughter ions of a given parent, whether the parent is the molecular ion or is itself a fragment ion; (*ii*) detect all the parents that give rise to a given daughter; (*iii*) detect all the parent ions that cleave to give a particular neutral fragment.

In the present experiments we were interested in detecting all the daughter ions of a given parent ion. For an instrument of conventional geometry, the following scan laws all detect daughter ions arising from parent ions that fragment in the first field-free region (7):

1. V, fixed; Scan B and E, keeping the ratio B/E constant
2. E, fixed; Scan B and V, keeping the ratio B^2/V constant
3. B, fixed; Scan E and V, keeping the ratio E^2/V constant

Scan 1 is the most convenient, because the ion optics in the ion source are inevitably defocussed whenever the accelerating voltage is changed. The Kratos model 890 allows scan 1 to be performed under computer control, i.e., B and E are automatically scanned from low to high values such that their ratio is held constant.

Azoxybenzene

Azoxybenzene had been thoroughly studied by Waddell *et al.* and was included in this work as a standard for comparison. The compositions of all major ions in the EI spectrum were confirmed: see Table 1. Peak matching on the ion at m/z 170 showed this peak to be somewhat asymmetrical. While the chief contributor to this ion is clearly $(M - CO)^+$: m/z 170.0794, there was also a small contribution from an ion having mass ca. m/z 170.06–170.07, possibly $(M - CH_2N)^+$: see Fig. 1.

Tandem mass spectrometry provided evidence in support of the fragmentation scheme previously proposed (Scheme 1). The significant omission from Scheme 1 is m/z 182, $C_{12}H_{10}N_2$. This ion is formed by chemical reduction prior to ionization, and hence represents the molecular ion of azobenzene. Thus m/z is absent from the EI spectrum of azoxybenzene, showing that loss of an oxygen atom is not a reaction of the azoxybenzene cation radical.

The daughter ion scan of m/z 182 is very similar to the EI spectrum of azobenzene.

m/z 182 → 170; 142; 105; 77

TABLE 1. Major ions in the EI spectrum of azoxybenzene

m/z (%)	Composition
198.0795 (28.7)	$C_{12}H_{10}N_2O$
197.0714 (2.8)	$C_{12}H_9N_2O$
182.0839 (3.2)	$C_{12}H_{10}N_2$
170.0825 (6.6)	$C_{11}H_{10}N_2$
169.0748 (9.2)	$C_{11}H_9N_2$
142.0772 (3.1)	$C_{11}H_{10}$
141.0711 (6.7)	$C_{11}H_9$
115.0548 (3.2)	C_9H_7
105.0462 (19.9)	$C_6H_5N_2$
93.0442 (6.4)	C_6H_5O (major)
91.0410 (28.2)	C_6H_5N
78.0436 (8.1)	C_6H_6
77.0403 (100)	C_6H_5

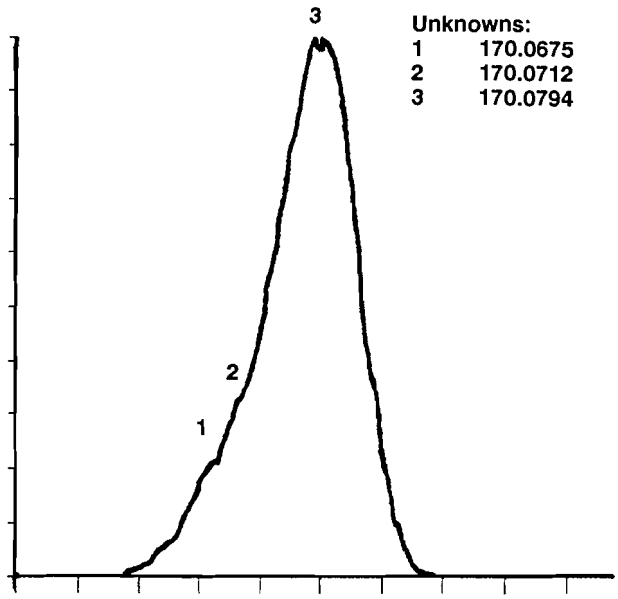

FIG. 1. High resolution peak matching scan of m/z 170 in azoxybenzene.

m/z 198 → 170; 142; 105; 77
169; 142; 141; 115; 93; 91; 77
142; 141; 115; 93; 91; 77

SCHEME 1

Thus m/z 170, 142, 105, and 77 are prominent ions in the mass spectra of both azoxybenzene and azobenzene, as shown by the daughter ion fragment scans on both m/z 198 and 182. By contrast, m/z 91, C_6H_5N, appears to be truly characteristic of azoxybenzene, since it is absent from the spectrum of azobenzene.

Phenylazoxypyridine-N-oxides

The four isomers studied were Ph-N=N(O)-3-PyO, **3**; Ph-N(O)=N-3-PyO, **4**; Ph-N=N(O)-4-PyO, **5**; and Ph-N(O)=N-4-PyO, **6**. Their EI spectra are summarized in Table 2, and a representative EI spectrum is shown in Fig. 2.

Can. J. Chem. Downloaded from www.nrcresearchpress.com by 79.173.37.17 on 09/08/12
For personal use only.

TABLE 2. Major ions in the EI spectra of phenylazoxypyridine-*N*-oxides, **3–6**

		Intensity (%)			
m/z	Composition	**3**[b]	**4**	**5**[c]	**6**
215.0694	$C_{11}H_9N_3O_2$	98.2	9.3	100	76.3
199.0744	$C_{11}H_9N_3O$	24.3	13.6	14.8	12.9
198.0668	$C_{11}H_8N_3O$	6.7	5.2	2.0	2.6
183.0793	$C_{11}H_9N_3$	3.3	2.2	1.7	1.4
172.0641	$C_{10}H_8N_2O$	—	32.5	—	—
(171)	[a]	12.8	10.8	2.9	4.6
170.0682	$C_{10}H_8N_3$	8.5	5.2	3.5	3.0
142.0653	$C_{10}H_8N$	4.7	—	—	1.4
121.0406	$C_6H_5N_2O$	19.3	—	11.0	5.2
115.0546	C_9H_7	5.1	2.0	2.2	2.0
108.0351	$C_5H_4N_2O$	—	—	52.8	19.1
105.0457	$C_6H_5N_2$	10.4	13.2	8.1	10.4
94.0317	C_5H_4NO	19.2	7.2	35.7	10.0
93.0421	$C_5H_5N_2$	30.0	2.8	9.7	8.3
92.0404	$C_5H_4N_2$	12.2	11.7	8.3	4.2
91.0422	C_6H_5N	33.9	20.7	24.5	19.8
78.0364	C_6H_6	55.8	15.0	31.4	23.1
77.0402	C_6H_5	81.6	100	72.4	100

[a]See text.

[b]Base peak *m/z* 65. Other ions (>3%): 150.9985 (5.0), 113.0011 (4.5), 95.0363 (19.1).

[c]Other ions (>3%): 187.0749 (14.8), 185.1071 (6.7), 158.0616 (5.8), 137.0245 (3.6), 122.0365 (9.5), 109.0392 (10.1), 82.0119 (17.3), 81.0284 (13.8).

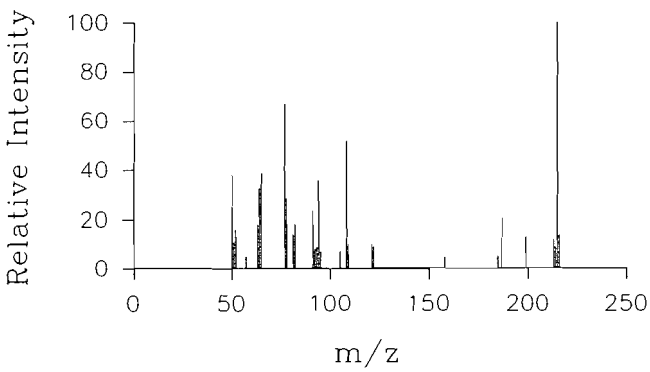

FIG. 2. EI spectrum of compound **5**.

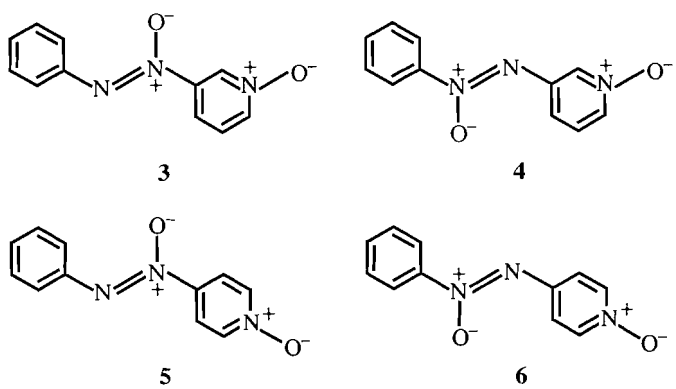

3 **4**

5 **6**

All four isomers show strong molecular ions and significant $[M - O]^+$ peaks, leading us to anticipate the occurrence of pre-ionization chemical reduction. In addition to $[M - O]^+$ peaks (*m/z* 199), $[M - O_2]^+$ peaks were observed at lower intensity at *m/z* 183. Linked scans showed that *m/z* 199 and 183 were both, in all cases, chemical reduction products, since they were absent from the daughter ion spectrum of *m/z* 215; likewise *m/z* 183 did not appear in the daughter ion spectrum of *m/z* 199. Thus both the pyridine-*N*-oxide function and the azoxy bridge *N*-oxide are subject to chemical reduction in the ion source. Tandem mass spectrometry showed that by contrast the appearance of *m/z* 198 $[M - OH]^+$ does result from direct fragmentation of the molecular ion, and is not loss of H from *m/z* 199.

As for azoxybenzene and its derivatives, strong Ar^+ and Ar'^+ ions were observed for the phenylazoxypyridine-*N*-oxides, with *m/z* 77 frequently the base peak of the EI spectrum. The ratio Ar^+/Ar'^+ was obtained for all isomers.

Isomer	Intensity ratio, *m/z* 77: 94
3	4.2
4	14.
5	2.0
6	10.

Although all isomers had much greater intensity at *m/z* 77 ($C_6H_5^+$) than 94 ($C_5H_4NO^+$), these four phenylazoxypyridine-*N*-oxides conform to the rule proposed by Bowie *et al.* that fragmentation tends to be favoured, in a relative sense, at the Ar—N bond closer to the azoxy N—O function. Thus compounds **3** and **5** showed a relatively greater extent of fragmentation to give $C_5H_4NO^+$ than their positional isomers **4** and **6**. However, it would be necessary to have both isomers available to distinguish them on this basis. The Bowie *et al.* "rule of thumb" holds true for these azoxy compounds despite the incursion of pre-ionization chemical reduction.

An ion at nominal mass *m/z* 171 was observed as a direct fragmentation product of the molecular ions of all four phenylazoxypyridine-*N*-oxides, but in no case was there a good match between the experimental mass and the calculated mass of any likely fragment. Peak matching indicated that these ions were actually composites of $C_{10}H_9N_3^+$ and $C_{10}H_7N_2O^+$, although in very different ratios. $C_{10}H_9N_3^+$ is clearly a product of deep-seated rearrangement of the molecular ion, since its composition implies $[M - CO_2]^+$; $C_{10}H_7N_2O^+$ requires the loss of CH_2NO from the molecular ion.

	Composition of *m/z* 171
Isomer	Intensity ratio $C_{10}H_9N_3^+/C_{10}H_7N_2O^+$
3	0.6
4	0.1
6	12

Isomer **5** gave too weak a signal at *m/z* 171 to allow the peak matching experiment to be done. Another difference in the mass spectral behaviour of **5** compared with the other isomers was that **5** was the only one to show evidence of the secondary fragment $[M - CHN_2O]$ at *m/z* 158, corresponding to *m/z* 141 in azoxybenzene.

In the case of the *m/z* 171 ion observed from isomer **4**, the $[M - CH_2NO]$ pathway was the predominant one. In

addition, the EI spectrum of isomer **4** showed a distinctive ion at *m/z* 172, which was identified as the related species $(C_{10}H_8N_2O)^+$, i.e., $[M - HCNO]^+$. It is tempting to ascribe this ion to extrusion of HCNO from the pyridine-*N*-oxide ring, but there is no experimental evidence to support this speculation.

In some respects there were differences in the mass spectroscopic behaviour of the pair of pyridine-3-*N*-oxides compared with the 4-*N*-oxide isomers. For example, both **5** and **6**, the pyridine-4-*N*-oxides, had prominent fragment ions at *m/z* 108 $(C_5H_4N_2O)^+$, i.e., $[M - C_6H_5N]$, which were absent in the EI spectra of the pyridine-3-*N*-oxide isomers. Isomer **5** was the only phenylazoxypyridine-*N*-oxide to show an ion at *m/z* 187 (M − CO), corresponding to *m/z* 170 in the spectrum of azoxybenzene. The daughter ion scan on the molecular ion of the azoxy compound **5** afforded *m/z* 187 (M − CO), 131, and 122, although in the presence of helium as collision gas *m/z* 187 and 108 $(C_5H_4N_2O)$ were the most intense fragments. Similarly, *m/z* 187 yielded *m/z* 170, 158, 109, and 108 (Fig. 3). Fragmentation of the molecular ion $\mathbf{6}^+$ also gave chiefly *m/z* 187 and 108, even though *m/z* 187 was of very low intensity in the EI spectrum.

The daughter ion mass spectrum of the molecular ion $\mathbf{3}^+$ afforded *m/z* 198 $(M - OH)^+$, 171, and 121. The ions at *m/z* 105 and 93, which are prominent in the EI spectrum of **3**, were absent from the daughter ion mass spectrum of the molecular ion $\mathbf{3}^+$. Instead, they are fragmentation products of *m/z* 199, thus explaining their presence in the EI spectrum of **3** as due to the chemical reduction product [M − O]. However, it is not possible to tell which *N*-oxide function of the parent ion had been reduced to afford *m/z* 199. A fragment ion scan of *m/z* 171 also failed to produce ions at *m/z* 105; instead, *m/z* 143 and 115 were the most abundant products.

The fragment ion spectrum of $\mathbf{4}^+$ (*m/z* 215) included *m/z* 198 (M − OH), 186 (M − CHO), 172 (M − HCNO), 147, 143, 105, 91, and 77. In turn, *m/z* 172 afforded *m/z* 143 and 117, while the chemical reduction product at *m/z* 199 gave rise to *m/z* 182, 170, 147, and 105. Once again, some of these ions could therefore be associated fairly unambiguously with either the azoxy compound or its chemical reduction product, but others were common to both spectra.

In the case of **5**, the most abundant fragment from *m/z* 199 appeared at *m/z* 121, while *m/z* 183 fragmented into several species (*m/z* 168, 142, 140, 130, 109, 105, and 92), many of which were of extremely low intensity in the original EI spectrum. The behaviour of the chemical reduction products of compound **6** was more like that of **3**: the most abundant fragment from *m/z* 199 appeared at *m/z* 105, with less intense peaks at m+/z 171 and 122, while *m/z* 183 fragmented rather cleanly into *m/z* 105.

Conclusions

The present results represent the first mass spectrometric study of azoxypyridine derivatives. They show that phenylazoxypyridine-*N*-oxides undergo pre-ionization chemical reduction in the ion source of the mass spectrometer, and hence that their EI spectra are a superposition of the spectra of the substrate and its singly and doubly deoxygenated products. Tandem mass spectrometry is currently the preeminent method for establishing which mass spectral peaks belong to the substrate and which to impurities including, as in this study, impurities introduced through chemical reduction in the ion source of the mass spectrometer.

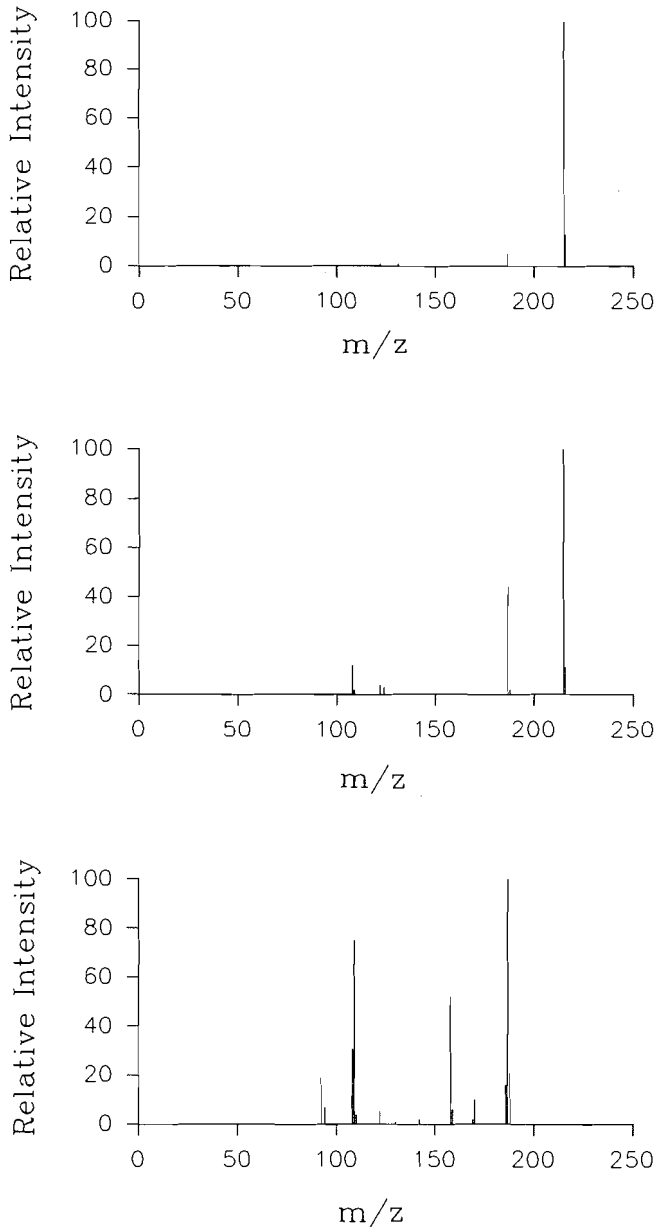

FIG. 3. Daughter ion (B/E) spectra of compound **5**; (top) from the molecular ion without collision gas; (middle) from the molecular ion with helium collision gas; (bottom) from *m/z* 187.

From the analytical perspective, the incursion of pre-ionization chemical reduction implies that the relative intensities of ions in the EI spectra of aromatic azoxy compounds and other *N*-oxides will depend on the conditions in the ion source, and hence upon the operating parameters and also on the instrument used. This would be important in library searching of the spectra of aromatic azoxy compounds and other *N*-oxides, where the exactness of the match between the experimental and the library spectra depends upon relative peak intensities. However, despite this caveat, the dominant fragmentation pathway into Ar^+ ions still permits some distinction of the position of the azoxy oxygen atom on the azo bridge in this series of compounds.

The structure of one of these compounds was previously

Can. J. Chem. Downloaded from www.nrcresearchpress.com by 79.173.37.17 on 09/08/12
For personal use only.

unambiguously determined by X-ray crystallography (6). However, it is not possible to draw structural inferences for several reasons. Comparative X-ray analyses are not available for the complete series of compounds. Even if they were, it would not be profitable to compare the structures of high-energy gas-phase cations based on information obtained from their crystalline neutral counterparts. Despite differences in the detailed pathways and the presence or absence of specific ions in the spectra of the individual phenylazoxypyridine-*N*-oxides, the picture that emerges from the EI spectra as reported in Table 2 is that the mass spectra of these isomers are broadly similar. Differences are more easily visualized in the fragment ion spectra, as shown by the summary scheme below:

Ions formed directly from the molecular ions (m/z 215) of phenylazoxypyridine-*N*-oxides

3: 171; 170; 142; 121
4: 172; 143; 117; 105
5: 187; 131; 122
6: 187; 108

Acknowledgement

N.J.B. and E.B. thank the Natural Sciences and Engineering Research Council of Canada for financial support through operating grants.

1. J. H. Bowie, R. G. Cooks, and G. E. Lewis. Aust. J. Chem. **20**, 1601 (1967).
2. E. Buncel. *In* Mechanisms of molecular migrations. *Edited by* B. S. Thyagarajan. Wiley–Interscience, New York. 1968; A. J. Dolenko and E. Buncel. *In* The chemistry of hydrazo, azo, and azoxy groups. *Edited by* S. Patai. Wiley–Interscience, New York. 1975; R. A. Cox and E. Buncel. *In* The chemistry of hydrazo, azo, and azoxy groups. *Edited by* S. Patai. Wiley–Interscience, New York. 1975.
3. D. S. Waddell, N. J. Bunce, and R. K. Boyd. Org. Mass Spectrom. **23**, 469 (1988).
4. E. Buncel and S. R. Keum. Heterocycles, **20**, 1751 (1983).
5. E. Buncel and S. R. Keum. J. Chem. Soc. Chem. Commun. 578 (1983).
6. E. Buncel, S. R. Keum, M. Cygler, K. I. Varughese, and G. I. Birnbaum. Can. J. Chem. **62**, 1628 (1984).
7. K. L. Busch, G. L. Glish, and S. A. McLuckey. Mass spectrometry/mass spectrometry. VCH Publishers, New York. 1988.

Can. J. Chem. Downloaded from www.nrcresearchpress.com by 79.173.37.17 on 09/08/12
For personal use only.

The 18-crown-6.2 chloroacetonitrile complex. X-ray crystal structure and solid phase motions of guest and host as studied by variable temperature ^{13}C CPMAS NMR spectroscopy

G. W. BUCHANAN[1] AND A. RODRIGUE

Ottawa–Carleton Chemistry Institute, Department of Chemistry, Carleton University, Ottawa, Ont., Canada K1S 5B6

AND

C. BENSIMON AND C. I. RATCLIFFE

Steacie Institute for Molecular Sciences, National Research Council of Canada, Ottawa, Ont., Canada K1A OR6

Received June 18, 1991

G. W. BUCHANAN, A. RODRIGUE, C. BENSIMON, and C. I. RATCLIFFE. Can. J. Chem. **70**, 1033 (1992).

The title complex has two distinct 18-crown-6 moieties of approximate D_{3d} symmetry in the unit cell. The 45.3 MHz ^{13}C CPMAS spectra have two regions of broadening for the crown ether carbons. At high temperatures a dipolar washout mechanism is operative, leading to broadening when molecular motion has a correlation time approximately equal to the inverse of the decoupling field. At lower temperatures broadening occurs when the motional correlation time is equal to the inverse of the chemical shift difference. The activation energy for 18-crown-6 reorientation in this solid is calculated to be ca. 48 kJ/mol. For the chloroacetonitrile, the CH_2 carbon also shows dipolar washout, but at a temperature much lower than the 18-crown-6. The activation energy for reorientation for this "guest species" is ca. 42 kJ/mol.

G. W. BUCHANAN, A. RODRIGUE, C. BENSIMON et C. I. RATCLIFFE. Can. J. Chem. **70**, 1033 (1992).

L'unité asymétrique du complexe mentionné dans le titre comprend deux portions distinctes d'éthers 18-couronnes-6 de symétrie se rapprochant de D_{3d}. Les spectres RMN du ^{13}C, à 45,3 MHz, par la technique de la polarisation croisée avec rotation à l'angle technique, présentent deux régions d'élargissement pour les carbones de l'éther couronne. À température élevée, il existe un mécanisme de déplacement dipolaire qui conduit à un élargissement lorsque le temps de corrélation d'un mouvement moléculaire est approximativement égal à l'inverse du champ de découplage. À des températures plus faibles, l'élargissement se produit lorsque le temps de corrélation du mouvement est égal à l'inverse de la différence du déplacement chimique. On a calculé que l'énergie d'activation de la réorientation de l'éther 18-couronne-6 est d'environ 48 kJ/mol. Pour le chloroacétonitrile, le carbone du CH_2 présente aussi un déplacement dipolaire; on l'observe à une température beaucoup plus faible que pour l'éther 18-couronne-6. L'énergie d'activation pour la réorientation de cette «espèce invitée» est d'environ 42 kJ/mol.

[Traduit par la rédaction]

Can. J. Chem. Downloaded from www.nrcresearchpress.com by 92.62.229.171 on 09/08/12
For personal use only.

Introduction

Dynamic stereochemical phenomena in solid 18-crown-6 ether and several complexes were observed previously via variable temperature ^{13}C CPMAS NMR spectroscopy in these laboratories (1–4). In the case of the 1:1 complex of 18-crown-6 with benzenesulfonamide, independent motions for guest and host species can be detected (3). Recently, we became interested in the ability of 18-crown-6 to complex small neutral halogenated molecules, and isolated and characterized via X-ray crystallography the 2:1 fluoroacetonitrile–18-crown-6 complex (5). In the present work, we report the X-ray structure and the ^{13}C solid phase NMR spectra as a function of temperature for the 2:1 complex of chloroacetonitrile with 18-crown-6 ether, a material whose preparation was previously reported (6) but for which no detailed structural data are available. Evidence is presented for independent reorientational motion in the 18-crown-6 and the chloroacetonitrile moieties. At 230 K, the observed ^{13}C chemical shift pattern for the crown ether carbons is rationalized in terms of torsional angle influences on ^{13}C shieldings.

Results and discussion

NMR spectra

Figure 1 contains the complete 45.3 MHz ^{13}C CPMAS spectra of the 2:1 chloroacetonitrile–18-crown-6 complex **1**, over the temperature range of 335–270 K. In Fig. 2 are presented the spectra of the crown ether carbon region for temperatures ranging from 260 to 230 K.

At 290 K, the ^{13}C solid phase spectrum of **1** shows three resonances at 119.1, 70.0, and 27.2 ppm respectively. In $CDCl_3$ solution at the same temperature there are also three resonances in the ^{13}C NMR spectrum with shifts of 116.7, 70.7, and 25.8 ppm, corresponding to the CN, CH_2O, and CH_2CN carbons respectively. Hence there appear to be no major chemical shift differences between the solution and solid phase spectra for this material at ambient temperature. In CD_2Cl_2, the ^{13}C NMR spectrum of **1** is essentially independent of temperature over the range of 300–173 K.

By contrast, the solid phase spectra show substantial temperature dependence (Figs. 1 and 2). As one proceeds up in temperature from 290 K, the resonance for the CH_2O carbon of the crown ether moiety essentially disappears at 310 K, to reappear with increasing intensity and sharpness as the high-temperature limit of 335 K is reached. This behaviour is reminiscent of that found in the 18-crown-6 moiety of the 1:1 benzenesulfonamide complex (3) and can be attributed to a "dipolar washout" phenomenon (7). When molecular motion has a rate such that the correlation time for the C–H vector, τ_C, is the inverse of the ^1H decoupling field amplitude, then the decoupler is rendered ineffective because of destructive interference between the incoherent spatial modulation due to motion and the coherent spin-space modulation provided by the rf of the ^1H decoupler. This results in a very broad dipolar coupled ^{13}C spectrum.

[1]Author to whom correspondence may be addressed.

Can. J. Chem. Downloaded from www.nrcresearchpress.com by 92.62.229.171 on 09/08/12
For personal use only.

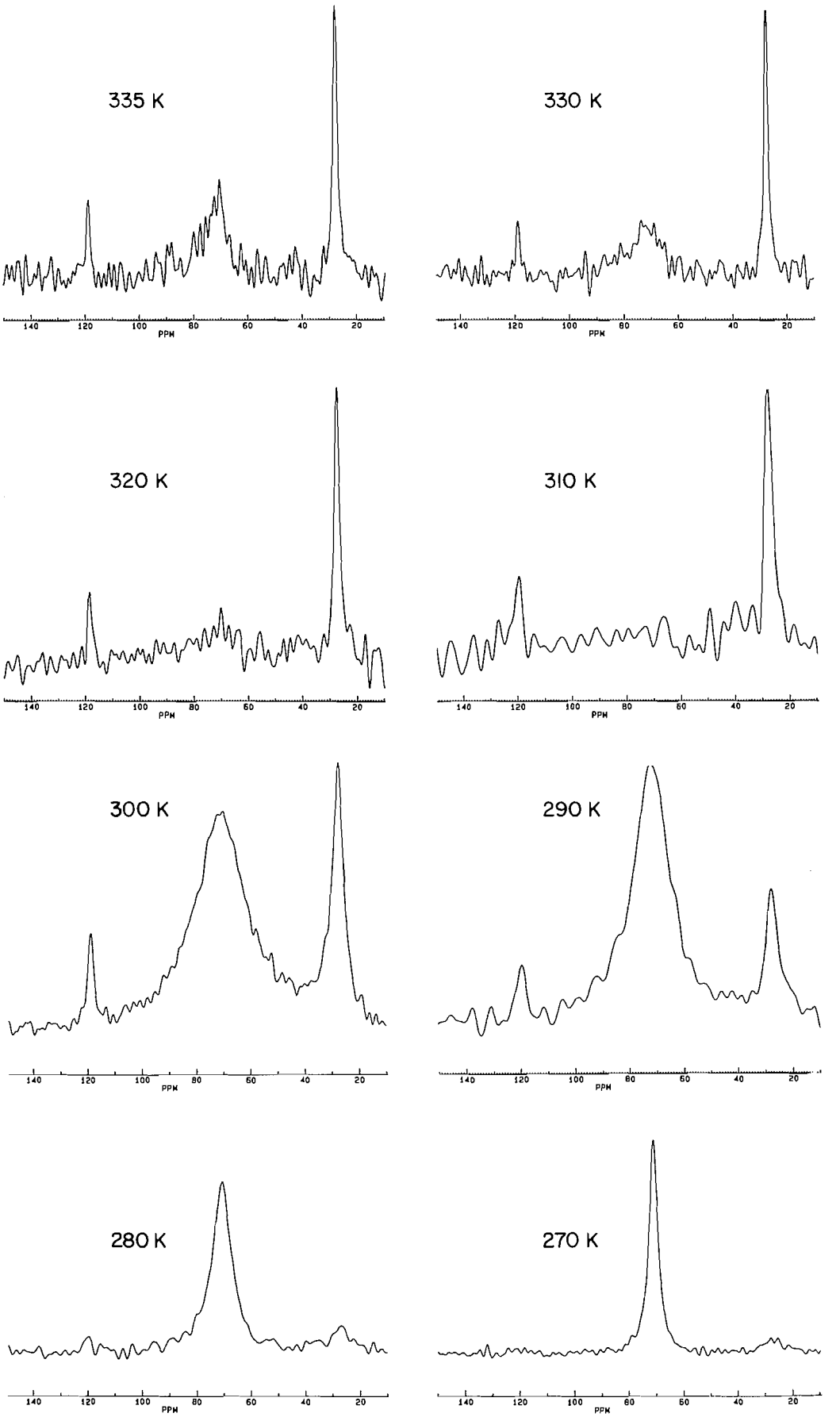

FIG. 1. Complete 45.3 MHz ^{13}C CPMAS NMR spectrum of **1** as a function of temperature.

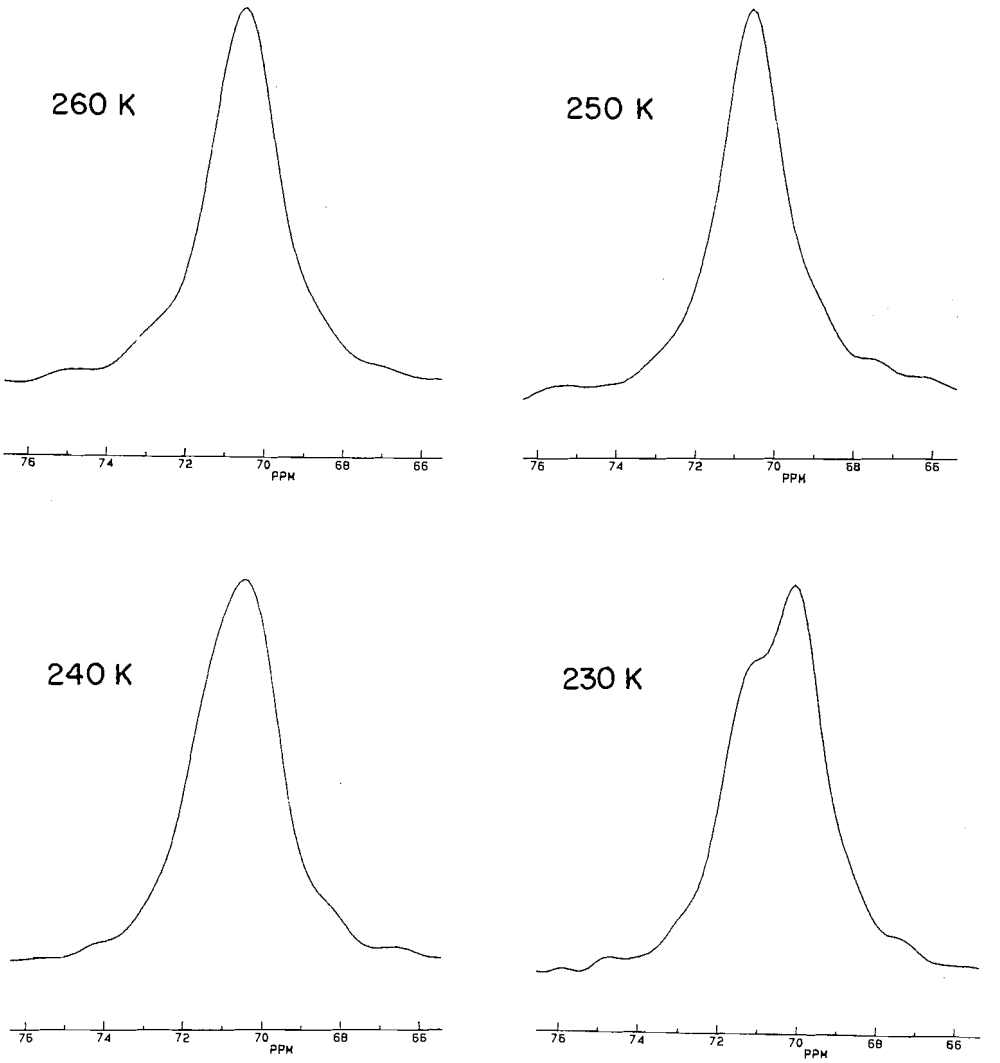

FIG. 2. Expanded crown ether carbon region of ^{13}C CPMAS NMR of **1**.

In the present experiment, the decoupling field amplitude is 60 kHz, so that $\tau_C = \frac{1}{2}\pi\gamma H_1 = \frac{1}{2}\pi \times 60$ kHz $= 2.7 \times 10^{-6}$ s. An estimate of the barrier for this process can be obtained by application of the Waugh–Fedin approximation (8). Employing a temperature of 310 K, the value obtained is ca. 48 kJ/mol.

Below 240 K, a more subtle broadening of the 18-crown-6 carbon resonance occurs (Fig. 2), until two discernible resonances are observed with shifts of 70.0 and 71.1 ppm, at the low-temperature limit of 230 K. Below this temperature, the rate of interconversion between conformations of the solid 18-crown-6 is slow relative to the chemical shift difference (in Hz) between conformationally nonequivalent carbons.

From Fig. 1 it is evident that the CH_2 carbon of the chloroacetonitrile moiety undergoes a dipolar washout near 270 K. Application of the Waugh–Fedin approximation in this case leads to a barrier for reorientation of the $ClCH_2CN$ part of the complex of ca. 42 kJ/mol.

X-ray crystallographic structure

The ORTEP plot and numbering scheme for the unit cell of **1** are depicted in Fig. 3. Table 1 contains the atomic parameters, while bond distances and bond angles are collected in Tables 2 and 3 respectively. There are two different 2:1 complexes present in this unit, both of which possess effectively D_{3d} symmetry in the 18-crown-6 ether ring. The torsion angles for the asymmetric units of the upper and lower complexes (as depicted in Fig. 3) are listed in Table 4. From these data it is evident that all the C—O—C—C networks are within 5° of a pure *transoid* geometry with the exception of C8—O5—C9—C10 where the dihedral angle contracts to 164.2°. All the O—C—C—O networks are *gauchoid*, with angles ranging from 64.0° to 76.5°.

It is of interest to compare the intermolecular C—H---O distances found in **1** to those for related complexes. With the exception (5) of the fluoroacetonitrile complex where these distances are very long (2.89 Å) relative to the sum of the van der Waals radii (2.6 Å) (9), the usual range is from 2.2 to 2.7 Å. For the 2:1 malononitrile–18-crown-6 complex (10), the distances are 2.23 and 2.69 Å respectively, while for the 2:1 acetonitrile–18-crown-6 case (11), the values are 2.43, 2.53, and 2.67 Å. For **1** the intermolecular C—H---O distances are listed in Table 5. The strongest interaction in **1** is between H15B and O6 where the distance is only

Can. J. Chem. Downloaded from www.nrcresearchpress.com by 92.62.229.171 on 09/08/12
For personal use only.

Can. J. Chem. Downloaded from www.nrcresearchpress.com by 92.62.229.171 on 09/08/12
For personal use only.

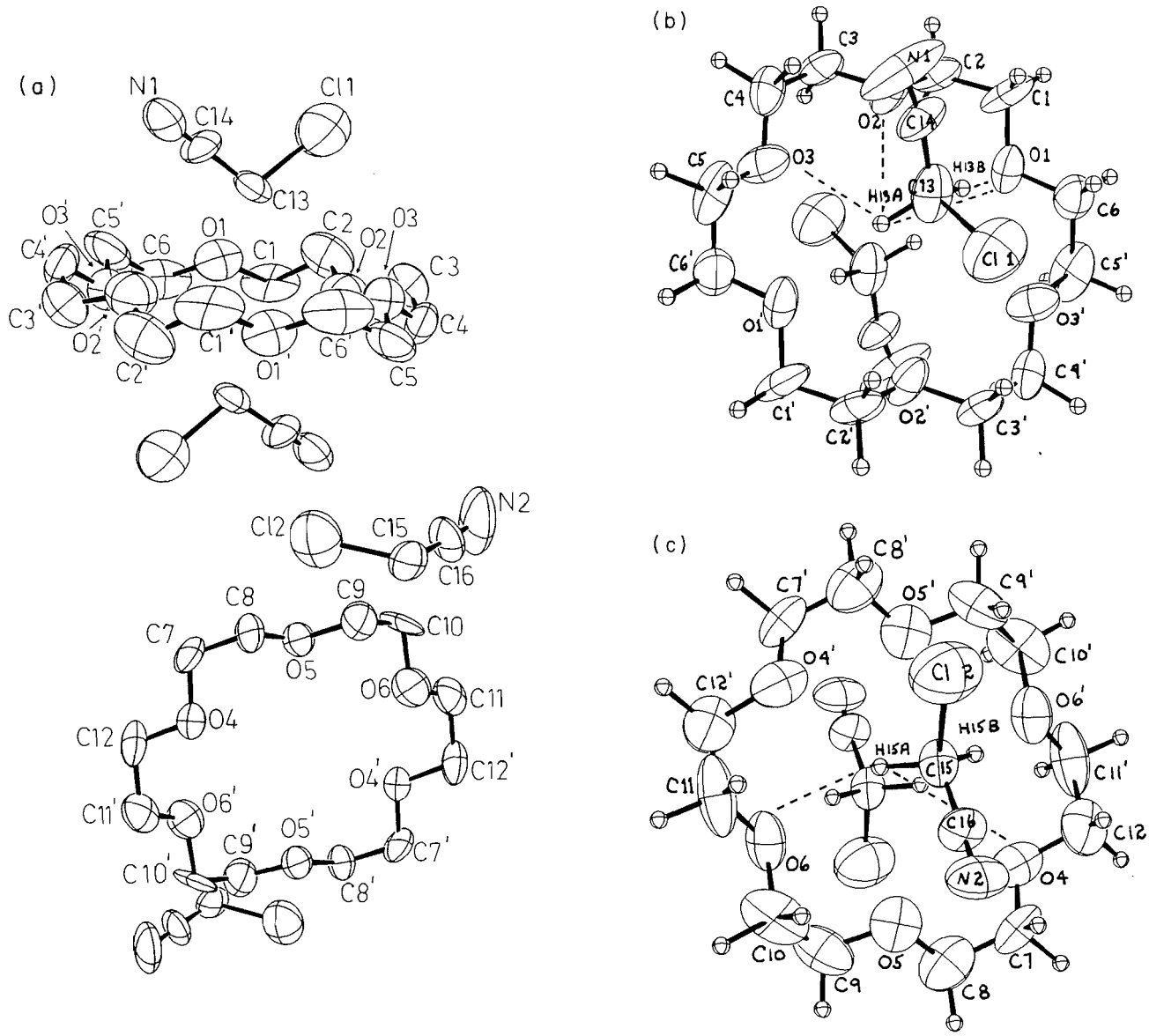

FIG. 3. (*a*) ORTEP plot of X-ray crystallographic structure of **1**. (*b*) ORTEP plot of one half of the asymmetric unit of **1**, showing short intermolecular O---H distances. (*c*) ORTEP plot of the second half of the asymmetric unit of **1**, showing the short intermolecular O---H distances.

2.288 Å. By contrast, the weakest interaction is between H13A and O2 where the distance is found to be 2.787 Å.

To discuss the limiting low-temperature ^{13}C NMR spectrum of the crown ether carbons, it is instructive to examine the torsional environments for each carbon on an individual basis. Each carbon will be present in four networks (ignoring hydrogens), which can be denoted as O—C*—C—O, C*—O—C—C, C—O—C*—C, and C—O—C—C*. Table 6 lists the torsional environments for the individual carbons described via this procedure.

In Figs. 4 and 5 are presented results of GIAO (12–14) calculations of the dihedral angle dependence of ^{13}C NMR shieldings for the above four structural units using ethylene glycol as a model for the O—C*—C—O network and ethylmethyl ether as a model for the other three structural entities. In these calculations, the absolute scale is used wherein chemical shifts increase with increased shielding. On this scale, methane occurs at 221.0 ppm, whereas on the usual TMS scale it appears at −2.1 ppm.

Examination of these figures indicates that expansion of the O—C*—C—O angle above 60° leads to deshielding until an angle of ca. 90° is reached. Also contraction of the C—O—C—C angle below 180° leads to deshielding at all three carbons until an angle of ca. 120° is obtained. Thus by examining the relative deviations from 60° and 180° for each carbon and the calculated shielding change, one can obtain an order of anticipated deshielding for the crown ether carbons in the limiting low-temperature ^{13}C spectrum of solid **1**. Using this method, one concludes that C8, C9, C10, C11, and C12 should be slightly (1–2 ppm) deshielded relative to the other seven carbons. Hence the appearance of the broad doublet of relative component intensity (from peak heights)

TABLE 1. Atomic parameters x,y,z and B_{iso}; esd's refer to the last digit printed

Atom	x	y	z	B_{iso}[a]
Cl1	0.2336(5)	0.15490(25)	0.3679(5)	9.3(4)
Cl2	0.5892(5)	0.3216 (3)	0.7503(6)	10.9(4)
O1	0.0997(10)	0.1287 (5)	0.8301(8)	5.3(6)
O2	−0.2404(10)	0.0658 (5)	0.7228(10)	6.2(7)
O3	0.3246(10)	0.0334 (5)	1.0471(9)	5.9(7)
O4	0.8030(10)	0.5557 (5)	0.8254(10)	7.1(7)
O5	0.7834(11)	0.4582 (5)	0.5279(10)	7.4(8)
O6	0.4747(11)	0.3701 (5)	0.2444(9)	6.4(7)
N1	−0.1657(13)	0.1840 (7)	0.1900(15)	11.5(11)
N2	0.1953(12)	0.3504 (6)	0.6309(12)	6.6(9)
C1	−0.0262(15)	0.1338 (7)	0.6680(14)	6.2(11)
C2	−0.1712(17)	0.1471 (7)	0.6862(15)	7.3(12)
C3	−0.3804(15)	0.0662 (7)	0.7374(13)	5.5(11)
C4	−0.4429(15)	−0.0222 (8)	0.7850(14)	5.9(11)
C5	0.3709(14)	0.1167 (7)	1.0032(15)	5.7(11)
C6	0.2510(15)	0.1219 (7)	0.8228(15)	6.6(11)
C7	0.9350(15)	0.5573 (7)	0.7915(14)	6.1(10)
C8	0.9176(17)	0.4724 (8)	0.6930(15)	7.7(12)
C9	0.7474(18)	0.3732 (8)	0.4281(16)	8.5(13)
C10	0.6371(16)	0.3772 (8)	0.2452(16)	7.9(14)
C11	0.3490(19)	0.3702 (8)	0.0783(14)	8.7(14)
C12	0.8101(17)	0.6417 (7)	0.9106(15)	8.1(12)
C13	0.0313(15)	0.1048 (7)	0.1815(13)	5.9(11)
C14	−0.0833(15)	0.1511 (7)	0.2009(14)	5.5(10)
C15	0.4535(15)	0.3912 (7)	0.6254(13)	4.3(10)
C16	0.2990(14)	0.3653 (7)	0.6276(14)	4.6(10)
H1A	−0.058	0.075	0.575	7.5
H1B	0.014	0.192	0.617	7.5
H2A	−0.203	0.210	0.699	6.4
H2B	−0.259	0.128	0.546	7.6
H3A	−0.485	0.082	0.630	6.6
H3B	−0.356	0.115	0.856	6.6
H4A	−0.567	−0.035	0.770	5.7
H4B	−0.452	−0.077	0.682	5.7
H5A	0.364	0.172	1.095	5.8
H5B	0.495	0.133	1.025	5.8
H6A	0.226	0.057	0.743	7.5
H6B	0.291	0.174	0.769	7.5
H7A	0.952	0.612	0.722	8.0
H7B	1.053	0.575	0.924	8.0
H8A	0.916	0.420	0.777	7.0
H8B	1.043	0.475	0.693	7.0
H9A	0.864	0.404	0.407	8.2
H9B	0.812	0.320	0.489	7.1
H10A	0.657	0.390	0.137	7.9
H10B	0.605	0.303	0.211	9.3
H11A	0.332	0.315	−0.018	6.6
H11B	0.371	0.432	0.028	6.6
H12A	0.919	0.654	1.040	6.7
H12B	0.825	0.692	0.838	6.7
H13A	0.002	0.033	0.190	6.1
H13B	0.040	0.111	0.064	6.1
H15A	0.518	0.462	0.679	6.0
H15B	0.441	0.383	0.489	6.0

[a] B_{iso} is the mean of the principal axes of the thermal ellipsoid.

Can. J. Chem. Downloaded from www.nrcresearchpress.com by 92.62.229.171 on 09/08/12
For personal use only.

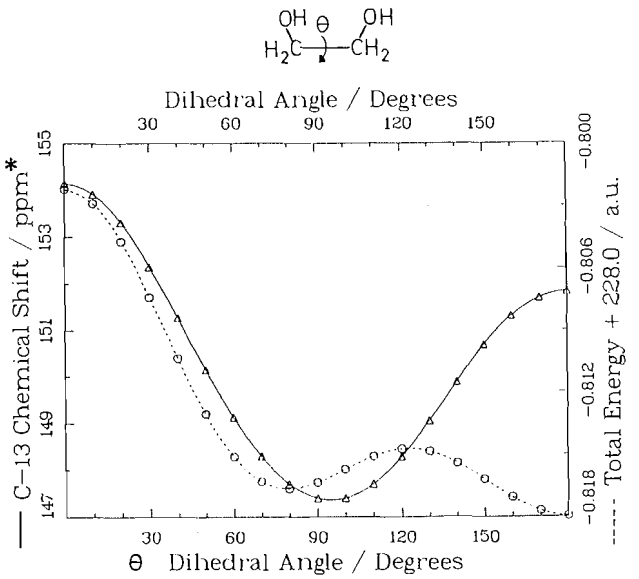

FIG. 4. GIAO calculated angular dependence of the isotropic ^{13}C NMR chemical shift of ethylene glycol (—). Total conformational energy as a function of dihedral angle (····).
*Absolute scale (CH_4 221 ppm) GIAO calcd.

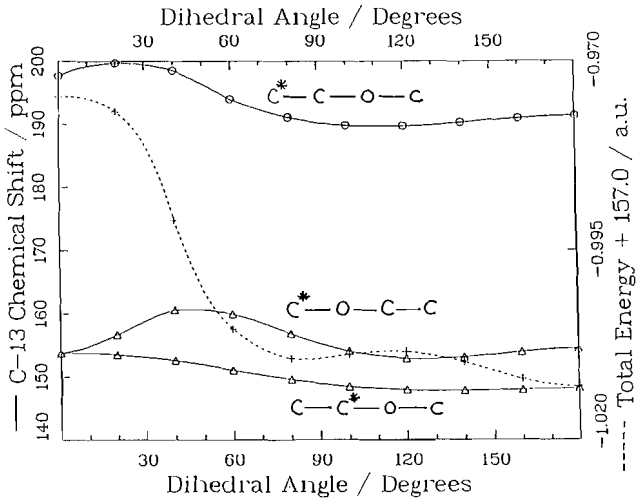

FIG. 5. GIAO calculated angular dependence of the isotropic ^{13}C NMR chemical shifts of the three carbons of ethylmethyl ether (—). Total conformational energy (····).

of 5:7, at 71.2 and 70.0 ppm respectively at 230 K, is in accord with expectations. The observed chemical shift difference of 1.2 ppm in **1** is similar to that found in other 18-crown-6 complexes that possess D_{3d} or pseudo D_{3d} symmetry (1). The relative intensities differ in each case, however, depending on the number of carbons in each type of environment.

Clearly, the relatively broad resonances in the ^{13}C CPMAS spectrum preclude a more detailed analysis of the data. Although we have analysed the shielding trends in terms of torsion angle influences, it is possible that steric and electronic effects of the chloroacetonitrile may also play a role in determining the observed ^{13}C chemical shift differences of the crown ether carbons.

The activation parameters obtained for the $ClCH_2CN$ and 18-crown-6 motions must of course represent averages of the values for the two different components of the unit cell of the crystal. Based on the geometries of the structures obtained, however, it is reasonable to suggest that the motional parameters do not vary substantially for the two different molecules of the complex present in the unit cell.

TABLE 2. Bond distances in angstroms

Bond	Distance	Bond	Distance
Cl(1)—C(13)	1.831(11)	C(5)—C(6)	1.478(16)
Cl(2)—C(15)	1.827(11)	C(5)—H(5A)	1.166(12)
O(1)—C(1)	1.390(13)	C(5)—H(5B)	1.061(12)
O(1)—C(6)	1.465(16)	C(6)—H(6A)	1.108(12)
O(2)—C(2)	1.418(13)	C(6)—H(6B)	1.043(12)
O(2)—C(3)	1.370(16)	C(7)—C(8)	1.466(17)
O(3)—C(4)	1.424(13)	C(7)—H(7A)	1.091(11)
O(3)—C(5)	1.405(13)	C(7)—H(7B)	1.151(11)
O(4)—C(7)	1.387(16)	C(8)—H(8A)	1.120(12)
O(4)—C(12)	1.459(14)	C(8)—H(8B)	1.160(15)
O(5)—C(8)	1.387(14)	C(9)—C(10)	1.468(17)
O(5)—C(9)	1.426(15)	C(9)—H(9A)	1.195(15)
O(6)—C(10)	1.496(16)	C(9)—H(9B)	1.124(12)
O(6)—C(11)	1.393(14)	C(10)—H(10A)	1.062(11)
N(1)—C(14)	0.974(16)	C(10)—H(10B)	1.110(12)
N(2)—C(16)	0.966(16)	C(11)—C(12)	1.509(22)
C(1)—C(2)	1.482(20)	C(11)—H(11A)	1.096(12)
C(1)—H(1A)	1.082(12)	C(11)—H(11B)	1.094(11)
C(1)—H(1B)	1.100(11)	C(12)—C(11)	1.509(22)
C(2)—H(2A)	1.084(11)	C(12)—H(12A)	1.101(12)
C(2)—H(2B)	1.105(12)	C(12)—H(12B)	1.053(11)
C(3)—C(4)	1.530(16)	C(13)—C(14)	1.457(18)
C(3)—H(3A)	1.085(11)	C(13)—H(13A)	1.103(11)
C(3)—H(3B)	1.155(11)	C(13)—H(13B)	1.073(12)
C(4)—O(3)	1.424(13)	C(15)—C(16)	1.431(17)
C(4)—H(4A)	1.082(13)	C(15)—H(15A)	1.106(10)
C(4)—H(4B)	1.162(12)	C(15)—H(15B)	1.135(11)

Experimental

Spectra

The ^{13}C CPMAS solid phase spectra were recorded at 45.3 MHz on a Bruker CXP-180 instrument. Cross polarization (CP) times were typically 3 ms with the radio frequency field amplitude being 60 kHz. Normally 400 accumulations were collected. The sweep width was 20 kHz with a recycle time of 4–8 s. 2K data points were collected with zero filling to 8K before Fourier transformation. Magic angle spinning (MAS) rates of ca. 3 kHz were obtained using Kel-F spinners of the Andrew–Beams type. Chemical shifts were measured relative to external solid hexamethylbenzene (HMB) and converted to the TMS scale via the factor of 16.9 ppm, which is the chemical shift for the CH_3 group of HMB.

Crystallographic measurements and structure solutions

A summary of the crystal data is given in Table 7. Diffraction intensities were collected on a Rikagu diffractometer using MoKα

Can. J. Chem. Downloaded from www.nrcresearchpress.com by 92.62.229.171 on 09/08/12
For personal use only.

TABLE 3. Bond angles in degrees

Bonds	Angle	Bonds	Angle
C(1)—O(1)—C(6)	112.3(9)	C(8)—C(7)—H(7B)	112.3(10)
C(2)—O(2)—C(3)	114.3(9)	H(7A)—C(7)—H(7B)	103.7(9)
C(4)a—O(3)—C(5)	112.1(8)	O(5)—C(8)—C(7)	110.3(10)
C(7)—O(4)—C(12)	113.2(9)	O(5)—C(8)—H(8A)	116.5(11)
C(8)—O(5)—C(9)	114.3(9)	O(5)—C(8)—H(8B)	114.1(11)
C(10)—O(6)—C(11)	111.7(9)	C(7)—C(8)—H(8A)	107.0(10)
O(1)—C(1)—C(2)	109.6(10)	C(7)—C(8)—H(8B)	106.9(10)
O(1)—C(1)—H(1A)	110.9(10)	H(8A)—C(8)—H(8B)	101.3(10)
O(1)—C(1)—H(1B)	109.8(9)	O(5)—C(9)—C(10)	107.9(9)
C(2)—C(1)—H(1A)	111.5(10)	O(5)—C(9)—H(9A)	86.1(9)
C(2)—C(1)—H(1B)	107.0(10)	O(5)—C(9)—H(9B)	121.2(10)
H(1A)—C(1)—H(1B)	107.8(10)	C(10)—C(9)—H(9A)	89.6(9)
O(2)—C(2)—C(1)	107.1(9)	C(10)—C(9)—H(9B)	130.5(11)
O(2)—C(2)—H(2A)	125.2(13)	H(9A)—C(9)—H(9B)	87.7(10)
O(2)—C(2)—H(2B)	91.3(8)	O(6)—C(10)—C(9)	102.3(9)
C(1)—C(2)—H(2A)	126.4(11)	O(6)—C(10)—H(10A)	123.9(11)
C(1)—C(2)—H(2B)	94.9(10)	O(6)—C(10)—H(10B)	88.8(8)
H(2A)—C(2)—H(2B)	94.8(9)	C(9)—C(10)—H(10A)	133.4(13)
O(2)—C(3)—C(4)	111.1(9)	C(9)—C(10)—H(10B)	91.5(9)
O(2)—C(3)—H(3A)	119.1(10)	H(10A)—C(10)—H(10B)	94.9(10)
O(2)—C(3)—H(3B)	112.8(9)	O(6)—C(11)—C(12)	107.7(10)
C(4)—C(3)—H(3A)	107.8(10)	O(6)—C(11)—H(11A)	112.8(11)
C(4)—C(3)—H(3B)	100.3(9)	O(6)—C(11)—H(11B)	112.4(10)
H(3A)—C(3)—H(3B)	103.9(10)	C(12)b—C(11)—H(11A)	107.0(11)
O(3)a—C(4)—C(3)	110.0(9)	C(12)b—C(11)—H(11B)	109.6(12)
O(3)a—C(4)—H(4A)	112.5(10)	H(11A)—C(11)—H(11B)	107.3(10)
O(3)a—C(4)—H(4B)	108.6(9)	O(4)—C(12)—C(11)	105.7(9)
C(3)—C(4)—H(4A)	116.7(10)	O(4)—C(12)—H(12A)	105.8(9)
C(3)—C(4)—H(4B)	104.7(10)	O(4)—C(12)—H(12B)	109.9(11)
H(4A)—C(4)—H(4B)	103.6(9)	C(11)b—C(12)—H(12A)	112.4(11)
O(3)—C(5)—C(6)	109.8(9)	C(11)b—C(12)—H(12B)	112.8(11)
O(3)—C(5)—H(5A)	108.3(9)	H(12A)—C(12)—H(12B)	109.9(11)
O(3)—C(5)—H(5B)	114.1(10)	Cl(1)—C(13)—C(14)	105.8(7)
C(6)—C(5)—H(5A)	106.9(9)	Cl(1)—C(13)—H(13A)	106.9(7)
C(6)—C(5)—H(5B)	112.7(11)	Cl(1)—C(13)—H(13B)	108.7(9)
H(5A)—C(5)—H(5B)	104.6(9)	C(14)—C(13)—H(13A)	112.0(11)
O(1)—C(6)—C(5)	105.5(10)	C(14)—C(13)—H(13B)	114.7(10)
O(1)—C(6)—H(6A)	108.1(9)	H(13A)—C(13)—H(13B)	108.3(10)
O(1)—C(6)—H(6B)	111.7(9)	N(1)—C(14)—C(13)	168.5(14)
C(5)—C(6)—H(6A)	106.5(9)	Cl(2)—C(15)—C(16)	109.2(7)
C(5)—C(6)—H(6B)	114.5(10)	Cl(2)—C(15)—H(15A)	108.6(7)
H(6A)—C(6)—H(6B)	110.1(11)	Cl(2)—C(15)—H(15B)	107.5(8)
O(4)—C(7)—C(8)	111.9(10)	C(16)—C(15)—H(15A)	114.0(10)
O(4)—C(7)—H(7A)	112.1(10)	C(16)—C(15)—H(15B)	113.3(9)
O(4)—C(7)—H(7B)	107.1(9)	H(15A)—C(15)—H(15B)	103.8(9)
C(8)—C(7)—H(7A)	109.5(10)	N(2)—C(16)—C(15)	177.7(13)

Can. J. Chem. Downloaded from www.nrcresearchpress.com by 92.62.229.171 on 09/08/12
For personal use only.

radiation at room temperature. The $\Theta/2\Theta$ scan technique with profile analysis (15) was employed at a speed of $4°/\Omega$. The space group was determined by systematic absences. Unit cell parameters were obtained by refinement of the setting angles of 24 reflections with 2Θ angles in the range of 30–47°. Lorentz and polarization factors were applied but no correction for absorption was made.

Structures were solved by direct methods plus Fourier maps and were refined by full-matrix least-squares analysis with weights based on counting statistics. The last least-squares cycle was calculated with 54 atoms, 236 parameters, and 856 out of 2007 reflections. Non-H atoms were refined anisotropically. H atoms were calculated. All calculations were performed using the NRC VAX Crystal Structure programs (16). Anisotropic thermal parameters are available as supplementary data.[2]

Materials

The 2:1 chloroacetonitrile–18-crown-6 complex **1** was prepared via the following procedure. To 18-crown-6 (1.06 g, 4.0 mmol) dissolved in 15 mL of ethyl acetate was added 1.0 mL of chloroacetonitrile followed by 40 mL of 30–60°C petroleum

[2]These data may be purchased from: The Depository of Unpublished Data, Document Delivery, CISTI, National Research Council, Ottawa, Canada K1A 0S2.

Can. J. Chem. Downloaded from www.nrcresearchpress.com by 92.62.229.171 on 09/08/12
For personal use only.

TABLE 4. Torsion angles (deg) in the asymmetric units of **1**

Bonds	Angle
C6—O1—C1—C2	−176.10(10)
O1—C1—C2—O2	−70.6(7)
C3—O2—C2—C1	−177.8(10)
C2—O2—C3—C4	−177.4(10)
O3—C4—C3—O2	64.0(6)
C3—C4—O3—C5	−175.5(10)
C4—O3—C5—C6′	−175.5(9)
O3—C5—C6′—O1′	71.0(7)
C1—O1—C6—C5′	−179.9(10)
Cl1—C13—C14—N1	127.5(11)
C12—O4—C7—C8	−175.2(10)
C8—O5—C9—C10	−164.2(11)
O4—C7—C8—O5	65.6(7)
C9—O5—C8—C7	−174.5(11)
C11—O6—C10—C9	−178.4(11)
O5—C9—C10—O6	−76.5(8)
C10—O6—C11—C12′	177.3(10)
O6—C11—C12′—O4′	75.0(8)
C11—C12′—O4′—C7′	−174.9(10)
Cl2—C15—C16—N2	125.2(11)

TABLE 5. Intermolecular distances (Å)

Atoms	Distance
H13A···O1	2.461(7)
H13B···O1	2.347(8)
H13A···O2	2.787(8)
H13A···O3	2.745(7)
H15A···O4	2.469(8)
H15A···O6	2.615(7)
H15B···O6	2.288(8)

TABLE 6. Torsional environments for individual carbons

Carbon	O-C*-C-O	C*-O-C-C	C-O-C*-C	C-O-C-C*
C1	70.6	179.9	176.1	177.8
C2	70.6	177.4	177.8	176.1
C3	64.0	177.8	177.4	175.5
C4	64.0	175.5	175.5	177.4
C5	71.0	175.5	175.5	179.9
C6	71.0	176.1	179.9	175.5
C7	65.6	174.9	175.2	174.5
C8	65.6	164.2	174.5	175.2
C9	76.5	174.5	164.2	178.4
C10	76.5	177.3	178.4	164.2
C11	75.0	178.4	177.3	174.9
C12	75.0	175.2	174.9	177.3

ether. The white solid **1** was then filtered off and washed with petroleum ether to yield 1.28 g (77%) of crystalline material, mp 78.5–80.0°C (lit. (6) mp 78°C).

TABLE 7. Crystal data for **1**

Parameter	Value
Empirical formula	$Cl_{12}O_6C_{16}H_{28}N_2$
Formula weight	415.31
Crystal size, mm	0.20 × 0.20 × 0.20
Space group	$P\bar{1}$, triclinic
Z (molecules/cell)	2
a, Å	9.3399
b, Å	15.4226
c, Å	8.6874
α, deg	93.002
β, deg	116.70
γ, deg	100.960
V, Å^3	1083.85(0)
D_{calc}, Mg m^{-3}	1.273
μ, mm^{-1}	0.20
Cell dimensions from:	
number of reflections	24
2θ range, deg	40.00–50.00
λ, Å	0.70930
$2\theta_{max}$, deg	40.0
$F(000)$, electrons	407.95
Reflections measured	2177
Unique reflections	2007
No. of reflections with $I_{net} > 2.5\sigma(I_{net})$	856
h range	−8–8
k range	0–14
l range	−8–8
R_f (significant reflections)	0.095
R_w (significant reflections)	0.035
Goodness-of-fit	4.10
R_f (all reflections)	0.229
R_w (all reflections)	0.037
Maximum Δ/σ	0.083
σ	0.010431
Final D-map:	
deepest hole, e/A^3	−0.350
highest peak, e/A^3	0.360
Secondary extinction coefficient	0.172131

Acknowledgements

We thank the Natural Sciences and Engineering Research Council of Canada and the Department of National Defence for financial support of this work.

1. G. W. Buchanan, R. A. Kirby, J. A. Ripmeester, and C. I. Ratcliffe. Tetrahedron Lett. **28**, 4783 (1987).
2. G. W. Buchanan, M. Z. Khan, J. A. Ripmeester, J. W. Bovenkamp, and A. Rodrigue. Can. J. Chem. **65**, 2564 (1987).
3. G. W. Buchanan, C. Morat, J. P. Charland, C. I. Ratcliffe, and J. A. Ripmeester. Can. J. Chem. **67**, 1212 (1989).
4. G. W. Buchanan, C. Morat, C. I. Ratcliffe, and J. A. Ripmeester. J. Chem. Soc. Chem. Commun. 1306 (1989).
5. A. Rodrigue, G. W. Buchanan, C. Bensimon, and J. W. Bovenkamp. Acta Crystallogr. Sect. C: Cryst. Struct. Commun. **48**, 474 (1992).
6. A. Elbasyouny, H. J. Brugge, K. von Deuten, M. Dickel, A.

Knochel, K. U. Koch, J. Kopf, D. Melzer, and G. Rudolph. J. Am. Chem. Soc. **105**, 6568 (1983).
7. W. P. Rothwell and J. S. Waugh. J. Chem. Phys. **74**, 2721 (1981).
8. J. S. Waugh and E. I. Fedin. Sov. Phys. Solid State (Engl. Trans.), **4**, 1633 (1963).
9. L. Pauling. The nature of the chemical bond. Cornell Univ. Press, New York. (1960).
10. R. Kaufmann, A. Knochel, J. Kopf, J. Oehler, and G. Rudolph. Chem. Ber. **110**, 2249 (1977).
11. F. Weller, H. Borgholte, H. Stenger, S. T. Vogler, and K. Dehnicke. Z. Naturforsch. B: Chem. Sci. **44**, 1524 (1989).
12. R. Ditchfield. *In* MTP international review of science, physical chemistry series I. Molecular structure and properties. Vol. II. Butterworths, London. 1972.
13. C. McMichael Rohlfing, L. C. Allen, and R. Ditchfield. Chem. Phys. **87**, 9 (1984).
14. G. W. Buchanan, C. Morat, R. A. Kirby, and J. S. Tse. Can. J. Chem. **69**, 1964 (1991).
15. D. F. Grant and E. J. Gabe. J. Appl. Crystallogr. **11**, 114 (1978).
16. E. J. Gabe, F. L. Lee, and Y. LePage. J. Appl. Crystallogr. **22**, 384 (1989).

Can. J. Chem. Downloaded from www.nrcresearchpress.com by 92.62.229.171 on 09/08/12
For personal use only.

A group equivalents scheme for free energies of formation of organic compounds in aqueous solution

J. PETER GUTHRIE
Department of Chemistry, University of Western Ontario, London, Ont., Canada N6A 5B7

Received February 13, 1991[1]

J. PETER GUTHRIE. Can. J. Chem. **70**, 1042 (1992).

Group contributions have been determined allowing the calculation of free energies of formation in aqueous solution for organic compounds containing carbon, hydrogen, and oxygen. The system works well for monofunctional compounds. The available literature data for 198 compounds can be accommodated using 79 parameters with an rms deviation of 0.74 kcal/mol.

J. PETER GUTHRIE. Can. J. Chem. **70**, 1042 (1992).

On a déterminé les contributions de groupes permettant de calculer les énergies libres de formation, en solution aqueuse, de composés organiques contenant du carbone, de l'hydrogène et de l'oxygène. Le système fonctionne bien avec les composés monofonctionnels. Utilisant 79 paramètres, on peut accommoder les données disponibles dans la littérature pour 198 composés avec un écart tmr de 0,74 kcal/mol.

[Traduit par la rédaction]

Can. J. Chem. Downloaded from www.nrcresearchpress.com by 79.173.37.17 on 09/08/12
For personal use only.

Introduction

We have made frequent use of thermodynamics calculations as a tool in investigating organic reaction mechanisms (1–13). The traditional way of carrying out these calculations is to determine, experimentally or by estimation, $\Delta H_f^0(g)$, $S^0(g)$, and ΔG_t, and then from these to calculate $\Delta G_f^0(aq)$. ΔG_t is the free energy of transfer of a compound from the gas at 1 atm (101.3 kPa) to 1 M aqueous solution. We will use as standard states the ideal gas at 1 atm and 1 M aqueous solution with an infinitely dilute reference state. Estimation by Benson's group additivity scheme (14) is generally reliable for $\Delta H_f^0(g)$ and $S^0(g)$ of simple compounds, and parameters reported by Hine and Mookerjee (15) allow calculation of ΔG_t. We have found it extremely convenient to generate group contribution parameters allowing direct estimation of $\Delta G_f^0(aq)$. Such parameters would allow direct calculation of equilibrium constants in solution. The present paper reports a set of these parameters for compounds of carbon, hydrogen, and oxygen, tested against the available data base of monofunctional compounds for which experimental values are available. An advantage of parameterizing for $\Delta G_f(aq)$ directly is that equilibrium constants in solution can be used as additional sources of information permitting calculation of new parameters (16). This approach will be employed in a few cases in this work, although exploiting its full potential will be a major undertaking.

At present this treatment is restricted to monofunctional compounds, because in polyfunctional compounds there are important distant polar interactions (15) that require more elaborate treatment.

Results

We began by calculating contributions to $\Delta G_f^0(aq)$ for all groups for which contributions to $\Delta H_f^0(g)$, $S^0(g)$, and ΔG_t were available from the literature. These lead to the values found in Table 1. In a number of cases we could fill in missing group equivalents by use of recent thermochemical data for compounds containing groups for which contributions have not been reported; these group equivalents are also found in Table 1, and the thermodynamic data upon which they are based are found in Table 2. Table 2 is a compilation of free energies of formation in aqueous solution for monofunctional compounds. In several cases we could, by measuring ΔG_t values or calculating them from data in the literature, fill in missing terms and calculate contributions to $\Delta G_f^0(aq)$; such values are also found in Table 1. The ΔG_t values used are found in Table 2. Then we estimated entropy contributions where this was the only thing missing, and where standard estimation procedures looked reasonable, and so filled in more missing terms; these values as well are in Table 1, with suitable cautionary indications. Still more terms could be added by making use of equilibrium constant data. The equilibrium constants are found in Table 3, and led to free energies of formation in aqueous solution, which are found in Table 2. Table 2 also includes values calculated using the parameters in Table 1.

We now turn to a detailed description of the calculations required to complete these tables.

We assume that the heat of vaporization of 3-hexanol will be very similar to that of 2-hexanol, based on their very similar boiling points, 134.5–135.5 and 136 respectively, and the known relationship between boiling point and heat of vaporization (17, 18), and use the value for 2-hexanol (19) as an approximation.

Entropy estimations

The standard entropy of gaseous trans-*2-heptene* was estimated from the value reported for *trans*-2-pentene (20) by adding twice the contribution for $[CH_2(C)_2]$. For *1,5-hexadiene, 2,3-dimethyl-1,3-butadiene, 1-methylcyclohexene, 2-methyl-1-propanol, 2-methyl-1-butanol, 3-methyl-1-butanol, 4-methyl-2-pentanol, 4-methyl-3-pentanol, cyclopentanol,* and *cycloheptanol* values were estimated using Benson's additivity scheme (14). Entropies for *propanoic, butanoic, pentanoic, hexanoic,* and *heptanoic acids* were estimated from the value for acetic acid, by adding increments of $[CH_2(C)(CO)]$ and $[CH_2(C)_2]$. It is distressing that the one literature value, that for pentanoic acid, deviates seriously from expectation, being 105.12 (21) where the estimated value is 95.9 cal deg^{-1} mol^{-1}. The literature value is calorimetric. We feel that it is more likely that the additivity derived value is correct, but clearly there is a need for

[1]Revision received October 10, 1991.

TABLE 1. Group contributions for the calculation of free energies of formation in aqueous solution[a]

Group	ΔH_f^0(g)	S^0(g)	ΔG_f^0(g)	ΔG_t	ΔG_f^0(aq)
$CH_3(C)$	−10.08	30.41	−4.78	0.85	−3.93
$CH_2(C)_2$	−4.95	9.42	1.95	0.21	2.16
$CH(C)_3$	−1.90	−12.07	6.76	−0.33	6.43
$C(C)_4$	0.50	−35.10	11.37	−0.97	10.40
C_dH_2	6.26	27.61	7.74	0.56	8.30
$C_dH(C)$	8.59	7.97	11.27	−0.30	10.97
$C_d(C)_2$	10.34	−12.70	14.53	−0.92	13.61
$C_dH(C_d)$	6.78	6.38	9.94	−0.25	9.69
$C_d(C)(C_d)$	8.88	−14.6	13.64	−1.18	12.46
$CH_2(C)(C_d)$	−4.76	9.80	2.03	0.32	2.35
$CH_2(C_d)_2$	−4.29	10.2	2.38	0.42	2.80
$CH(C)_2(C_d)$	−1.48	−11.69	7.06	−0.13[b]	6.93
$C(C)_3(C_d)$	1.68	−34.72	12.44	−1.27[c]	11.17
C_BH	3.30	11.53	4.92	−0.15	4.77
$C_B(C)$	5.51	−7.69	8.21	−0.96	7.25
$C_B(C_d)$	5.68	−7.80	8.24	−0.77[d]	7.47
$C_B(C_B)$	4.96	−8.64	7.94	−0.57[e]	7.37
$CH_2(C)(C_B)$	−4.86	9.34	2.07	0.26	2.33
$CH_2(C_B)_2$	−6.45[f]	8.41[g]	0.75	0.60[h]	1.35
$CH(C)_2(C_B)$	−0.98	−12.15	7.70	−0.40	7.30
$CH(C_B)_3$	−1.21[i]	−24.36[j]	10.99	−1.35[k]	9.64
$C(C)_3(C_B)$	2.81	−35.18	12.57	−1.27	11.30
$C(C_B)_4$	7.04[l]	−34.42[m]	17.71	−2.49[n]	15.22
$C_{BF}(C_B)_2(C_{BF})$	4.80	−5.00	6.70	−0.64	6.06
$C_{BF}(C_B)(C_{BF})_2$	3.70	−5.00	5.60	−0.64	4.96
$C_{BF}(C_{BF})_3$	1.50	1.40	1.49	−0.64	0.85
$C_dH(C_B)$	6.78	6.38	9.94	−0.25[o]	9.69
$C_d(C)(C_B)$	8.64	−14.6	13.40	−2.00[p]	11.40
C_tH	26.93	24.7	24.63	0.00	24.63
$C_t(C)$	27.35	6.35	26.06	−1.31	24.75
$C_t(C_d)$	29.20	6.43	27.69	−0.31[q]	27.38
$C_dH(C_t)$	6.78	6.38	5.28	−0.25[r]	5.03
$CH_3(O)$	−10.08	30.41	−4.80	0.85	−3.95
$CH_2(C)(O)$	−8.1	10.3[s]	−1.46	0.18	−1.28
$CH(C)_2(O)$	−7.2	−11.0	1.14	−0.16	0.98
$C(C)_3(O)$	−6.6	−33.56	3.81	−1.07	2.74
$CH_2(O)_2$	−16.1	7.81[t]	−8.71	4.07	−4.65
$CH(C)(O)_2$	−16.3	−13.85[u]	−7.11	1.85	−5.26[u]
$C(C)_2(O)_2$	−18.6	−38.3[v]	−6.78	1.51[w]	−5.30
$CH(O)_3$	−27.29[x]	−12.1[y]	−18.63	5.03[z]	−13.59
$C(C)(O)_3$	−27.96[aa]	−35.1[ab]	−17.09	4.26[ac]	−12.83
$CH_2(C_B)(O)$	−8.1	4.97[ad]	0.13	1.46[ae]	1.59
$CH(C_B)(O)_2$					−0.83[af]
$C(C)(C_B)(O)_2$					−2.82[ag]
$C(C_B)(O)_3$	−24.8[ah]	−35.2[ai]	−13.9	7.15[aj]	−6.75
$CH_2(C_d)(O)$	−6.5	8.86[ak]	0.56	0.78	1.34
$C_dH(O)$					4.83[al]
$C_d(C)(O)$					7.39[am]
$C_d(C_B)(O)$					6.49[an]
$C_B(O)$	−0.9	−10.2	2.55	0.59	3.14
OH(C)	−37.9	29.07	−34.61	−6.10	−40.71
$OH(C_d)$	−37.9[ao]	29.1[ao]	−34.61	−6.10[ao]	−40.71[ao]
$OH(C_B)$	−37.9[ao]	29.1[ao]	−34.61	−6.10[ao]	−40.71[ao]
$O(C)_2$	−23.2	8.68	−18.48	−4.01	−22.49
$O(C)(C_d)$					−22.45[ap]
$O(C)(C_B)$	−23.0	9.02[aq]	−18.38	−3.13[ar]	−21.51
$O(C_B)_2$	−21.1	12.96[as]	−17.66	−5.22[at]	−22.88

Can. J. Chem. Downloaded from www.nrcresearchpress.com by 79.173.37.17 on 09/08/12
For personal use only.

TABLE 1 (*continued*)

Group	$\Delta H_f^0(g)$	$S^0(g)$	$\Delta G_f^0(g)$	ΔG_t	$\Delta G_f^0(aq)$
$CH_3(CO)$	−10.08	30.41	−4.78	0.85	−3.93
$CH_2(C)(CO)$	−5.2	9.6	1.65	0.21	1.86
$CH(C)_2(CO)$	−1.7	−12.0	6.97	−0.26[au]	6.71
$C(C)_3(CO)$	1.4	−33.03[av]	11.65	−1.10[aw]	10.55
CHO(C)	−29.1	34.93	−27.15	−4.43	−31.58 total
				−4.06[ax]	−31.21 free
$CHO(C_d)$	−29.1[ay]	34.93[ay]	−27.15	−4.06[ay]	−31.21[ay]
$CHO(C_B)$	−29.1[ay]	34.93[ay]	−27.15	−4.06[ay]	−31.21[ay]
$C_dH(CO)$	5.0	3.58[az]	8.99	−0.75	8.24
$C_d(C)(CO)$	7.5	−24.48[ba]	15.20	0.01[bb]	15.21
$C_B(CO)$	3.7	−10.92[bc]	7.36	0.78	8.14
$CO(C)_2$	−31.4	15.01	−28.17	−5.52	−33.69
$CO(C)(C_d)$	−30.6	17.53[bd]	−28.11	−4.99[be]	−33.10
$CO(C)(C_B)$	−30.9	15.55[bf]	−27.82	−5.47	−33.29
CHO(O)	−32.1	34.93	−30.15	−4.08[bg]	−34.23
CO(C)(O)	−35.1	14.78	−31.80	−5.60	−37.40
$CO(C_d)(O)$	−32.0	18.86[bh]	−29.91	−4.63[bi]	−34.54
$CO(C_B)(O)$	−32.55	18.32[bj]	−30.30	−5.57[bk]	−35.87
OH(CO)	−58.1	24.52	−53.45	−1.99	−55.44
O(C)(CO)	−43.1	8.39	−38.30	0.73	−37.57
$O(C_d)(CO)$	−45.2				
$O(C_d)(CO) + C_d(C)(CO)$				0.54[bl]	
$O(C_B)(CO)$	−36.7				−31.47[bm]
$O(CO)_2$	−46.5	8.57[bn]	−41.75	−4.53[bo]	−37.22[bp]

"All at 25°C; enthalpies and free energies are in kcal mol^{-1}, entropies are in cal deg^{-1} mol^{-1}, standard states are the ideal gas at 1 atm and 1 M aqueous solution with an infinitely dilute reference state. Unless otherwise noted, group contributions to $\Delta H_f^0(g)$ and $S^0(g)$ are from ref. 14, group contributions to ΔG_t are calculated from the contributions to log(γ) in ref. 15, and group contributions to $\Delta G_f^0(g)$ and $\Delta G_f^0(aq)$ are calculated from other values in this table. Symbols identifying the groups are as used by Benson (14). C_d is a doubly bonded carbon, C_t is a triply bonded carbon, C_B is a carbon that is part of one aromatic ring, C_{BF} is a carbon that is at the ring fusion of a fused ring aromatic system.

[b] Based on ΔG_t for 3-methyl-1-butene (22).

[c] Provisionally taken as equal to $[C(C)_3(C_B)]$.

[d] Based on ΔG_t for styrene (8).

[e] Based on ΔG_t for diphenyl (22).

[f] Based on $\Delta H_f^0(g)$ for diphenymethane (24).

[g] Based on $S^0(g)$ for diphenylmethane, Table 2.

[h] Based on ΔG_t for diphenylmethane (22).

[i] Based on ΔH_f^0 for triphenylmethane (24).

[j] Based on $S^0(g)$ for triphenylmethane, Table 2.

[k] Based on ΔG_t for triphenylmethane, this work.

[l] Based on ΔH_f^0 for tetraphenylmethane (24).

[m] Based on $S^0(g)$ for tetraphenylmethane, Table 2.

[n] Based on ΔG_t for tetraphenylmethane, Table 2.

[o] Assigned, as $[C_dH(C_B) \equiv [C_dH(C_d)]$, after Benson (55).

[p] Based on ΔG_t for α-methylstyrene (8).

[q] Based on ΔG_t for butenyne (22).

[r] Assigned, as $[C_dH(C_t)] \equiv [C_dH(C_d)]$, after Benson (55).

[s] This value (55) differs from that in Benson's book (14), but it is not clear what the origin of the more recent value is. The older value seems to give better agreement with experiment and is used here.

[t] Based on S^0 for dimethoxymethane (20).

[u] Based on equilibrium constants for acetal formation, Table 3.

[v] Based on equilibrium constants for ketal formation, Table 3.

[w] Based on ΔG_t for 2,2-dimethoxypropane, evaluated in this work.

[x] Based on ΔH_f^0 for trimethyl orthoformate (24).

[y] Provisionally assumed to be equal to $[CH(C)_3]$. No entropy data could be found to allow evaluation.

[z] Based on ΔG_t for trimethyl orthoformate (1).

[aa] Based on ΔH_f^0 for trimethyl orthoacetate (24), including allowance for two *gauche* interactions (14).

[ab] Provisionally assumed to be equal to $[C(C)_4]$. No entropy data could be found to allow evaluation.

[ac] Based on ΔG_t for trimethyl orthoacetate (1).

[ad] Based on $S^0(g)$ for benzyl alcohol, calculated from S^0 (l) (20), ΔH_{vap} (24), and the vapor pressure, estimated as described in the text.

[ae] Based on ΔG_t for benzyl alcohol (62).

[af] Based on the equilibrium constant for benzaldehyde dimethyl acetal, Table 3.

[ag] Based on the equilibrium constant for acetophenone dimethyl ketal, Table 3.

Can. J. Chem. Downloaded from www.nrcresearchpress.com by 79.173.37.17 on 09/08/12
For personal use only.

TABLE 1 (*concluded*)

[ah] Based on ΔH_f^0(g) for trimethyl orthobenzoate (5).
[ai] Provisionally assumed to be equal to $[C(C_B(C)_3]$. No entropy data could be found to allow evaluation.
[aj] Based on ΔG_t for trimethyl orthobenzoate (5).
[ak] Based on S^0(g) for allyl alcohol (20).
[al] Revised value: the value in ref. 16 is incorrect as a result of a computer programming error.
[am] Based on fitting ΔG_f^0(aq) for enols (16).
[an] Based on the equilibrium constant for 1-phenyl-1-ethenol formation, Table 3.
[ao] Assigned, as $[OH(C_d)] \equiv [OH(C_B)] \equiv [OH(C)]$, after Benson (55, 63). As previously discussed (16), Benson's treatment of enols and enol ethers is not internally consistent. We have based our contributions to ΔG_f^0(aq) on the assignment of $[OH(C_d)]$, and have calculated $[C_dH(O)]$ and $[C_d(C)(O)]$ from experimental data (16).
[ap] Based on the equilibrium constant for formation of α-methoxystyrene (64).
[aq] Based on S^0(g) for anisole, Table 2.
[ar] Based on ΔG_t for anisole (22) and phenetole (62).
[as] Based on S^0 (l) (20) and a vapor pressure for diphenyl ether extrapolated from data in ref. 26.
[at] Based on ΔG_t for diphenyl ether, calculated from the solubility (65) and the vapor pressure (26).
[au] Based on ΔG_t values for isobutyraldehyde (62), corrected for hydration (66), for methyl isopropyl ketone (22), and for diisopropyl ketone (22).
[av] Based on S^0(g) of pivaldehyde (S^0 (l) (32), ΔH_v estimated (18) from the boiling point (26), and the vapor pressure estimated (18) from the vapor pressure, ΔH_v, and ΔC_p (27)) and pinacolone (S^0 (l) (67), ΔH_v estimated (18) from the boiling point (26), and the vapor pressure estimated (18) from the vapor pressure, ΔH_v, and ΔC_p (27, 68)).
[aw] Based on ΔG_t for pinacolone (67).
[ax] Based on ΔG_t for acetaldehyde, propanal, butanal, and methylpropanal, corrected for hydration as described in the text.
[ay] Assigned, as $[CHO(C_d)] \equiv [CHO(C_B)] \equiv [CHO(C)]$ after Benson (55, 63).
[az] Based on S^0(g) for acrolein.
[ba] Based on S^0(g) for methyl methacrylate, Table 2.
[bb] Based on ΔG_t for methyl methacrylate, evaluated in this work.
[bc] Based on S^0(g) for benzaldehyde (69).
[bd] Based on S^0(g) for methyl vinyl ketone.
[be] Based on ΔG_t for methyl vinyl ketone, 3-penten-2-one, mesityl oxide, and benzalacetone (8). Higher weights were given to the values for 3-penten-2-one and mesityl oxide.
[bf] Based on S^0(g) for acetophenone (20).
[bg] Assigned, as $[CHO(O)] \equiv [CHO(C)]$ after Benson (55, 63).
[bh] Based on S^0(g) for acrylic acid (20).
[bi] Based on ΔG_t for acrylic acid, crotonic acid, and cinnamic acid (8).
[bj] Based on S^0(g) for benzoic acid (20).
[bk] Based on ΔG_t for benzoic acid (5) and methyl benzoate (5).
[bl] Based on ΔG_t for isopropenyl acetate, this work; until a more precise value of ΔG_t for an enol is available it is not practical to separate $[O(C_d)(CO)] + [C_d(C)(CO)]$.
[bm] Based on the equilibrium constant for formation of phenyl acetate in solution (70).
[bn] Based on S^0(g) for acetic anhydride (20).
[bo] Calculated from the group contributions to ΔG_f^0(g) and ΔG_f^0(aq).
[bp] Based on the equilibrium constant for formation of acetic anhydride in solution (71).

more experimental values for carboxylic acids. The entropies of *2-pentanol* and *3-hexanol* were estimated from that for 2-butanol (20) by adding increments for $[CH_2(C)_2]$. The entropy of *3-pentanol* was estimated from that for 2-propanol (20) by adding twice the increment for $[CH_2(C)_2]$. The entropies of *2-methyl-2-butanol* and *2-methyl-2-pentanol* were estimated from that for 2-methyl-2-propanol (20) by adding increments for $[CH_2(C)_2]$ and correcting for the loss of symmetry. The entropy for *1-ethoxypropane* was estimated from that for diethyl ether (20) by adding the increment for $[CH_2(C)_2]$ and correcting for the loss of symmetry. The entropy for *ethyl vinyl* ether was calculated from the value for methyl vinyl ether (this work, *vide infra*) by adding the increment for $[CH_2(C)(O)]$. Similarly the entropy for *phenetole* was calculated from that of anisole.

The directly measured free energy of transfer for aliphatic aldehydes refers to the process: gas to equilibrium mixture of aldehyde and covalent hydrate. Since aliphatic aldehydres are appreciably hydrated this means that the observed values are significantly different from those for the free aldehyde, which are generally the quantities of interest. We have revised the literature contributions to refer to the process: free aldehyde in the gas phase to free aldehyde in aqueous solution. To so do we used the observed free energies of transfer (22) for acetaldehyde, propanal, butanal, and 2-methylpropanal, −1.60, −1.54, −1.28, and −0.97 kcal mol^{-1} respectively, and the equilibrium constants for covalent hydration (23), K_h = [hydrate]/[free aldehyde], 1.06, 0.85, 0.65, and 0.62 respectively. ΔG_t(free) = ΔG_t(obs) + RT ln(1 + K_h), so we calculate ΔG_t(free) values of −1.23, −1.18, −0.98, −0.68 respectively. From these values we deduce $[CHO(C)_{free}] = -4.08 \pm 0.09$.

Entropy data in some cases had not been reported for the gas but had been reported for the liquid or solid. In such cases: *benzyl alcohol, diphenyl ether, tetrahydrofuran, anthracene, phenanthrene, pyrene, methacrylic acid, methyl methacrylate, methyl acrylate, diphenylmethane, triphenylmethane,* and *tetraphenylmethane,* we used the heat of vaporization at 25°C, the vapor pressure at 25°C, and the entropy of the liquid to calculate the entropy of the gas. For *benzyl alcohol,* we used the heat of vaporization (24), and a vapor pressure calculated from the Antoine parameters (25). For *diphenyl ether,* we used the entropy of the liquid (20) and

Can. J. Chem. Downloaded from www.nrcresearchpress.com by 79.173.37.17 on 09/08/12
For personal use only.

TABLE 2. Thermodynamic quantities leading to free energies of formation in aqueous solution[a]

Compound	ΔH_f(g)	$\sigma_{\Delta H}$	S(g)	ΔGf(g)	ΔGt(kcal)	ΔGf(aq) obsd.	$\sigma_{\Delta G}$	ΔG_f(aq) calcd.	error
Methane	−17.78	0.10	44.52	−12.04	3.90	−8.14	0.16		
Ethane	−20.03	0.10	54.85	−7.66	3.73	−3.93	0.16	−4.25	0.32
Propane	−25.02	0.12	64.51	−5.83	3.86	−1.97	0.18	−2.09	0.11
Butane	−30.02	0.17	74.12	−3.98	3.98	−0.00	0.21	0.07	−0.08
2-Methylpropane	−32.07	0.17	70.42	−4.94	4.22	−0.72	0.21	−0.85	0.14
Pentane	−35.11	0.22	83.4	−2.13	4.23	2.10	0.25	2.23	−0.13
2-Methylbutane	−36.74	0.24	82.12	−3.38	4.28	0.91	0.27	1.45	−0.55
2,2-Dimethylpropane	−40.18	0.19	73.23	−4.17	4.40	0.23	0.23	0.66	−0.43
Hexane	−39.94	0.19	92.83	−0.07	4.39	4.32	0.23	4.39	−0.07
2-Methylpentane	−41.78	0.24	90.95	−1.35	4.45	3.10	0.27	3.61	−0.51
3-Methylpentane	−41.13	0.24	90.77	−0.65	4.41	3.76	0.27	4.41	−0.65
2,2-Dimethylbutane	−44.48	0.24	85.62	−2.46	4.49	2.04	0.27	3.60	−1.56
Heptane	−44.86	0.31	102.27	1.90	4.52	6.42	0.34	6.55	−0.13
2,4-Dimethylpentane	−49.21	0.36	94.8	−0.22	4.78	4.56	0.38	5.82	−1.26
Octane	−49.86	0.33	111.55	3.85	4.79	8.64	0.36	8.71	−0.07
2,2,4-Trimethylpentane	−53.54	0.36	101.15	3.27	4.75	8.02	0.38	7.55	−0.47
2,2,5-Trimethylhexane	−60.53[b]	0.36	109.96	3.36	4.62	7.98	0.38	9.71	−1.73
3,3-diethylpentane	−55.52	0.41	110.31	8.26	4.12[c]	12.38	0.43	15.70	−3.32
Cyclopropane	12.74	0.14	56.74	24.95	2.65	27.60	0.20	27.77	−0.18
Cyclopentane	−18.26	0.19	70.00	9.41	3.10	12.51	0.23	12.23	0.28
Cyclohexane	−29.49	0.19	71.28	7.50	3.13	10.63	0.23	10.32	0.31
Methylcyclopentane	−25.38	0.19	81.24	8.64	3.50	12.14	0.23	11.85	0.29
Cycloheptane	−28.23	0.24	81.82	15.33	2.70	18.03	0.27	18.68	−0.65
Methylcyclohexane	−36.97	0.24	82.06	6.51	3.61	10.12	0.27	9.59	0.52
Cyclooctane	−29.73	0.24	87.66	21.79	2.76	24.55	0.27	25.39	−0.85
cis-1,2-Dimethylcyclohexane	−41.13	0.43	89.51	9.84	3.48	13.32	0.45	12.84	0.48
Ethene	12.55	0.10	52.45	16.33	3.17	19.50	0.16	19.32	0.18
1-Propene	4.78	0.19	63.80	14.89	3.17	18.05	0.23	17.89	0.16
1-Butene	0.02	0.24	73.04	17.08	3.28	20.36	0.27	20.24	0.12
2-Methyl-1-propene	−4.04	0.22	70.17	13.87	3.06	16.94	0.25	17.66	−0.73
1-Pentene	−5.09	0.24	82.65	18.81	3.56	22.37	0.27	22.40	−0.03
trans-2-Pentene	−7.62	0.26	81.36	16.66	3.24	19.90	0.30	19.63	0.26
2-Methyl-2-butene	−9.99	0.26	80.92	14.42	3.21	17.63	0.30	17.64	−0.01
3-Methyl-1-butene	−6.60	0.19	79.70	18.18	3.73	21.91	0.23	21.54	0.37
1-Hexene	−10.40	0.38	91.93	20.44	3.58	24.02	0.41	24.56	−0.54
2-Methyl-1-pentene	−14.20	0.31	91.34	16.82	3.37	20.19	0.34	21.76	−1.57
4-Methyl-1-pentene	−12.26	0.43	87.89	19.78	3.81	23.59	0.45	23.39	0.20
1-heptene	−14.89	0.24	101.24	22.88	3.55[c]	26.43	0.27	26.72	−0.29
trans-2-Heptene	−17.57[d]	0.22	100.2[e]	20.51	3.56	24.07	0.51	23.95	0.12
1-Octene	−19.46	0.29	110.55	25.25	4.07	29.32	0.32	28.88	0.44
Cyclopentene	8.10	0.33	69.23	26.70	2.46	29.16	0.36	29.32	−0.16
Cyclohexene	−1.20	0.17	74.27	25.61	2.27	27.88	0.21	28.26	−0.39
1-Methylcyclohexane	−10.35	0.19	83.43[e]	23.43	2.57	26.00	0.50	27.21	−1.21
1,3-Butadiene	26.29	0.26	66.62	35.96	2.51	38.47	0.30	38.29	0.18
1,4-Pentadiene	25.24	0.29	79.7	40.72	2.84	43.56	0.32	43.65	−0.09
2-Methyl-1,3-butadiene	18.04	0.26	75.44	34.79	2.58	37.37	0.30	37.37	0.00
1,5-Hexadiene	20.10	0.22	89.38[e]	42.40	2.91	45.31	0.51	45.55	−0.24
2,3-Dimethyl-1,3-butadiene	10.78	0.26	84.89[e]	34.42	2.30	36.71	0.53	37.27	−0.56
1,3,5-Cycloheptatriene	43.24	0.50	75.44	60.79	0.91	61.70	0.52	61.73	−0.03
Ethyne	54.54	0.17	48.00	50.35	1.89	52.24	0.21	51.57	0.67
1-Propyne	44.19	0.19	59.30	46.34	1.59	47.93	0.23	48.00	−0.07
1-Butyne	39.48	0.22	69.51	48.29	1.74	50.03	0.25	49.62	0.41
1-Pentyne	34.50[f]	1.00	78.82	50.24	1.91	52.15	1.01	51.78	0.37
1-Hexyne	29.55[f]	1.00	88.13	52.22	2.19	54.41	1.01	53.94	0.47
1-Heptyne	24.62[f]	1.00	97.44	54.22	2.50	56.72	1.01	56.10	0.62
1-Octyne	19.70[f]	1.00	106.75	56.23	2.61	58.84	1.01	58.26	0.58
1-Nonyne	14.77[f]	1.00	116.06	58.24	2.95	61.19	1.01	60.42	0.77
1-Buten-3-yne	72.80[f]	1.00	66.77	73.12	1.94	75.07	1.01	71.90	3.17
Benzene	19.74	0.17	64.34	30.90	1.03	31.94	0.21	31.99	−0.06
Methylbenzene	12.05	0.14	76.64	29.25	1.01	30.26	0.20	30.13	0.13
Ethylbenzene	7.15	0.26	86.15	31.22	1.10	32.32	0.30	32.46	−0.14
1,2-Dimethylbenzene	4.57	0.26	84.31	29.19	1.00	30.18	0.30	29.33	0.85

Can. J. Chem. Downloaded from www.nrcresearchpress.com by 79.173.37.17 on 09/08/12
For personal use only.

TABLE 2 (*continued*)

Compound	ΔH_f(g)	$\sigma_{\Delta H}$	S(g)	ΔGf(g)	ΔGt(kcal)	ΔGf(aq) obsd.	$\sigma_{\Delta G}$	ΔG_f(aq) calcd.	ΔG_f(aq) error
1,3-Dimethylbenzene	4.13	0.19	85.49	28.40	1.06	29.47	0.23	29.33	0.13
1,4-Dimethylbenzene	4.30	0.24	84.23	28.95	1.09	30.04	0.27	29.75	0.30
Propylbenzene	1.89	0.19	95.76	32.80	1.37	34.17	0.23	34.62	−0.45
(1-Methylethyl)benzene	0.96	0.24	92.87	32.73	1.60	34.33	0.27	34.15	0.18
1,2,4-Trimethylbenzene	−3.30	0.24	94.59	27.69	1.04	29.00	0.27	29.17	−0.17
1,2,3-trimethylbenzene	−2.27	0.29	91.98	29.77	0.92[c]	30.69	0.32	30.22	0.47
1,3,5-trimethylbenzene	−3.80	0.31	92.15	28.19	1.21[c]	29.40	0.34	29.19	0.21
Butylbenzene	−3.13	0.26	105.04	34.72	1.50	36.23	0.30	36.78	−0.56
(1-Methylpropyl)benzene	−4.16	0.29	102.33[g,h]	34.50	1.45	35.95	0.54	36.31	−0.36
(1,1-Dimethylethyl)benzene	−5.40	0.29	94.93[g,h]	35.17	1.46	36.63	0.54	36.66	−0.03
n-Amylbenzene	−8.23[f]	1.00	114.47	36.52	1.66[c]	38.18	1.01	38.94	−0.76
n-Hexylbenzene	−13.15[f]	1.00	123.78	38.53	1.85[c]	40.38	1.01	41.10	−0.72
Styrene	35.30	0.36	82.48	51.08	0.69[j]	51.77[i]	0.38	51.62	0.15
α-Methylstyrene	28.27[j]	0.34	91.7	51.11	−0.21[i]	50.90[i]	0.38	50.05	0.85
Ph-Ph	43.51[k]	0.19	93.02[k]	67.16[k]	−0.74	66.42	0.23	65.57	0.44
Diphenylmethane	33.22	0.43	89.60[l]	67.59	−0.92[c]	66.68	0.45	66.68	−0.00
Triphenylmethane	64.82	0.33	119.16[l]	111.41	−5.48[m]	106.83	0.13	106.72	0.11
Tetraphenylmethane	95.08	1.17	154.96[l]	152.04	−6.47[n]	145.57	0.13	144.64	0.93
Naphthalene	35.92	0.36	80.22	53.27	−0.49	52.78	0.38	53.00	−0.22
1-Methylnaphthalene	27.93[f]	1.00	90.21	52.01	−0.47	51.54	1.01	51.38	0.16
1-Ethylnaphthalene	23.10[f]	1.00	99.94	53.98	−0.49	53.49	1.01	53.71	−0.22
1,3-Dimethylnaphthalene	19.55[f]	1.00	97.86	51.01	−0.57	50.48	1.01	50.58	−0.10
1,4-Dimethylnaphthalene	19.72[f]	1.00	95.86	51.82	−0.92	50.90	1.01	50.99	−0.09
2,3-Dimethylnaphthalene	19.97[f]	1.00	98.22	51.37	−0.88	50.49	1.01	50.99	−0.51
2,6-Dimethylnaphthalene	19.72[f]	1.00	97.68	51.28	−0.73	50.55	1.01	50.99	−0.44
Anthracene	55.19	0.53	93.91[o]	79.38	−2.33	77.05	0.54	74.66	2.39
Phenanthrene	49.59	0.41	92.41[o]	74.23	−2.05	72.18	0.43	72.05	0.13
Pyrene	53.94	0.29	97.73[o]	77.84	−2.56	75.24	0.32	76.36	−1.12
Methanol	−48.16	0.07	57.29	−38.92	−3.21	−42.14	0.15	−42.09	−0.05
Ethanol	−56.21	0.10	67.54	−40.33	−3.11	−43.44	0.16	−43.37	−0.07
1-Propanol	−60.97	0.12	77.63	−38.38	−2.93	−41.31	0.18	−41.21	−0.10
2-Propanol	−65.20	0.12	74.07	−41.55	−2.86	−44.41	0.18	−44.39	−0.02
1-Butanol	−65.73	0.10	86.8	−36.17	−2.82	−38.98	0.16	−39.05	0.07
2-Methyl-1-propanol	−67.85	0.22	83.25[c]	−37.24	−2.62	−39.86	0.51	−40.22	0.36
2-Butanol	−70.00	0.17	85.81	−40.15	−2.68	−42.83	0.21	−42.23	−0.60
2-Methyl-2-propanol	−74.69	0.19	77.98	−42.50	−2.61	−45.12	0.23	−45.25	0.14
1-Pentanol	−70.43	0.12	96.21	−33.97	−2.57	−36.55	0.18	−36.89	0.34
3-Methyl-1-butanol	−72.01	0.33	92.67	−34.50	−2.52	−37.02	0.36	−37.26	0.24
2-Pentanol	−74.74	0.41	95.23	−37.98	−2.49	−40.48	0.43	−40.07	−0.41
3-Pentanol	−75.81	0.36	92.91	−38.37	−2.45	−40.82	0.38	−40.07	−0.75
2-methyl-1-butanol	−72.18	0.33	92.67[e]	−34.66	−2.53[c]	−37.19	0.36	−37.26	0.07
2-Methyl-2-butanol	−79.06	0.33	89.65	−40.65	−2.53	−43.18	0.36	−42.95	−0.23
1-Hexanol	−75.48	0.14	105.52	−32.09	−2.46	−34.55	0.20	−34.73	0.18
3-Hexanol	−79.78[p]	0.25	104.65[q]	−36.13	−2.18	−38.30	0.28	−37.91	−0.39
1-Heptanol	−80.40	0.24	114.83	−30.08	−2.34	−32.42	0.27	−32.57	0.15
1-Octanol	−84.97	0.19	124.14	−27.71	−2.19	−29.91	0.23	−30.41	0.50
1-Nonanol	−89.94	0.33	133.45	−25.75	−1.99[c]	−27.74	0.36	−28.25	0.51
1-Decanol	−94.74	0.38	142.76	−23.62	−1.75[c]	−25.37	0.41	−26.09	0.72
Cyclopentanol	−57.98	0.41	83.05	−26.90	−3.59	−30.50	0.43	−31.03	0.53
Cyclohexanol	−68.40	0.50	83.28[cm]	−27.66	−3.58	−31.26	0.52	−32.64	−1.38
2-Propen-1-ol	−29.76	0.43	73.51	−15.24	−3.13	−18.38	0.45	−18.20	−0.18
Benzyl alcohol	−24.00	0.31	82.62[r]	−1.28	−4.45[c]	−5.73	0.34	−5.71	−0.02
Phenol	−23.04	0.22	75.43	−7.88	−4.72	−12.60	0.25	−11.41	−1.19
2-Methylphenol	−30.74	0.31	85.47	−8.87	−4.00	−12.86	0.34	−12.21	−0.66
4-Methylphenol	−29.97	0.38	83.09	−7.39	−4.24	−11.63	0.41	−12.21	0.58
Ethenol						−24.84[s]	0.21[t]	−25.68	0.84
2-Methyl-1-propenol						−25.18[s]	0.60[t]	−24.35	−0.83
1-Propen-2-ol						−27.02[s]	0.21[t]	−26.40	−0.62
1-Buten-2-ol						−24.98[s]	0.33[t]	−24.05	−0.93
2-Buten-2-ol						−26.19[s]	0.33[t]	−26.01	−0.18
2-Penten-3-ol						−23.84[s]	0.51[t]	−23.66	−0.18
3-Methyl-1-buten-2-ol						−22.60[s]	0.59[t]	−22.75	0.15

Can. J. Chem. Downloaded from www.nrcresearchpress.com by 79.173.37.17 on 09/08/12
For personal use only.

TABLE 2 (*continued*)

Compound	ΔH_f(g)	$\sigma_{\Delta H}$	S(g)	ΔGf(g)	ΔGt(kcal)	ΔGf(aq) obsd.	$\sigma_{\Delta G}$	ΔG_f(aq) calcd.	ΔG_f(aq) error
3-Methyl-2-buten-2-ol						−24.35[s]	0.59[t]	−24.07	−0.28
3,3-Dimethyl-1-buten-2-ol						−20.27[s]	0.72[t]	−21.13	0.86
1-Hydroxycyclopentene						−14.98[s]	0.79[t]	−15.38	0.40
1-Hydroxycyclohexene						−15.89[s]	0.70[t]	−16.44	0.55
1-Phenylethen-1-ol						8.68[s]	0.43[t]	8.68	−0.00
Dimethyl ether	−44.00	0.12	63.83	−27.01	0.00	−27.00	0.18	−26.74	−0.27
1,1′-Oxybisethane	−60.25	0.19	81.9	−29.23	0.27	−28.97	0.23	−29.30	0.33
1-Methoxypropane	−56.93	0.17	83.52	−26.39	0.24	−26.16	0.21	−26.27	0.11
2-Methoxypropane	−60.23	0.24	80.86	−28.90	−0.11	−29.01	0.27	−29.45	0.44
1-Ethoxypropane	−65.06	0.26	92.70[e]	−27.55	0.09	−27.46	0.53	−27.55	0.09
2-Methoxy-2-methylpropane	−67.76	0.26	84.36	−27.77	−0.31	−28.08	0.30	−28.51	0.43
1,1′-Oxybispropane	−70.00	0.26	100.98	−25.26	0.75	−24.51	0.30	−24.98	0.46
2,2′-Oxybispropane	−76.29	0.38	93.27	−29.25	1.37	−27.88	0.41	−27.83	−0.05
1,1′-Oxybisbutane	−79.68	0.33	119.6	−21.08	1.07	−20.01	0.36	−20.66	0.65
Tetrahydrofuran	−44.02	0.19	62.78[u]	−16.61	−1.57	−18.18	0.23	−20.66	0.69
Methyl vinyl ether			70.69[v]						
Ethyl vinyl ether	−33.63[w]	0.20	79.53[x]	−11.20	1.21[w]	−9.99[w]	0.51	−11.98	−1.99
2-Methoxypropene	−35.79[w]	1.01	81.06[w,h]	−13.81	1.26[w]	−12.55[w]	1.11	−11.42	−1.13
2-Ethoxypropene					1.31[w]				
1-Methoxypropene					1.02[w]				
1-Methoxy-2-methylpropene					2.17[w]				
1-Methoxycyclohexene	−39.43[w]	1.06	93.13[w,h]	−1.22	0.36[w]	−0.86[w]	1.18	−1.46	0.60
1-Phenyl-1-methoxyethene	−4.00[w]	1.04	99.62[w,h]	23.78	−0.56[w]	23.22[w]	1.14		
1-Phenyl-1-methoxyethene						23.49[y]	0.46	22.79	0.70
Methoxybenzene	−16.23	0.22	83.31[z]	6.29	−0.56[c]	5.67	0.25	4.51	1.16
Ethoxybenzene	−24.28	0.14	93.81[e]	4.81	−0.33[c]	4.48	0.48	3.23	1.25
Diphenyl ether	12.43		103.7[aa]	40.20	−3.64[ab]	36.56	0.13	34.23	2.33
2-Propanone	−51.94	0.17	70.49	−36.52	−1.95	−38.48	0.21	−37.94	−0.54
2-Butanone	−57.05	0.19	80.81	−35.01	−1.74	−36.74	0.23	−36.94	−0.26
2-Pentanone	−61.90	0.24	89.91	−32.86	−1.63	−34.49	0.27	−34.33	−0.17
3-Pentanone	−61.64	0.19	88.44	−32.16	−1.51	−33.68	0.23	−34.22	0.54
3-Methyl-2-butanone	−62.74	0.22	88.5[g]	−33.28	−1.34	−34.62	0.25	−34.78	0.16
2-Hexanone	−66.87	0.26	96.9[ac]	−30.21	−1.39	−31.60	0.30	−32.17	0.57
3,3-Dimethyl-2-butanone	−69.48		91.77[y]	−31.29	−1.32[s]	−31.61	0.13	−33.08	0.47
2,4-Dimethyl-3-pentanone	−74.40	0.29	99.07[ac]	−28.68	−0.84	−29.52	0.32	−30.79	1.27
Cyclohexanone	−54.04	0.50	77.00	−20.75	−3.02[c]	−23.77	0.52	−24.84	1.07
Methyl vinyl ketone			76.94[z]		−3.07[i]			−17.94	
4-Methyl-3-penten-2-one						−18.95[i,ad]		−18.19	−0.76
Benzalacetone						17.94[i,ad]			
						17.92[ae]		15.18	2.74
Cinnamaldehyde						22.16[af]		20.35	1.81
Acetophenone	−20.72	0.38	89.12	0.47	−2.68	−2.22[s]	0.41	−2.12	−0.10
Acetaldehyde	−39.70	0.12	63.15	−31.80	−1.60	−33.41	0.18		
					−1.17[ag]	−32.97[ag]		−32.60	−0.37
Propanal	−44.36	0.22	72.83	−29.64	−1.54	−31.19	0.25		
					−1.18[ag]	−30.82[ag]		−30.74	−0.08
Butanal	−48.95	0.33	82.44	−27.39	−1.28	−28.67	0.36		
					−0.98[ag]	−28.37[ag]		−28.58	0.21
2-Methylpropanal	−51.58	0.22	79.38[e]		−0.97[c]	−30.08	0.51		
					−0.68[ag]	−29.79[ag]		−29.03	−0.76
Pentanal	−54.61	0.41	91.53	−26.06	−1.13	−27.19	0.43	−26.42	−0.77
Heptanal	−63.05	0.96	110.34	−20.69	−0.77	−21.46	0.97	−22.10	0.64
Acrolein			66.12[z]					−12.77	
trans-2-Butenal	−24.04	0.33	77.05[ah,h]	−10.16	−2.33	−12.58[q]	0.57	−13.38	0.80
Benzaldehyde	−8.77	0.69	80.28[ad]	5.35	−2.12	3.21[i]	0.71	3.45	−0.24
Formic Acid	−90.49[f]		59.45	−83.89	−4.94[ai]	−88.83[ai]		−87.77	−1.06
Acetic Acid	−103.44	0.36	67.52	−89.55	−4.80	−94.35	0.38	−94.22	−0.13
Propanoic Acid	−108.39	0.12	77.1[e]	−87.64	−4.57	−92.22	0.47	−92.36	0.14
Butanoic Acid	−113.72	0.98	86.5[e]	−86.07	−4.46	−90.52	1.08	−90.20	−0.32
Pentanoic Acid	−117.57	0.72	95.9[e]	−83.01	−4.28[c]	−87.29	0.85	−88.04	0.75
Hexanoic acid	−122.35	0.55	105.3[e]	−80.89	−4.33[c]	−85.22	0.72	−85.88	0.66

Can. J. Chem. Downloaded from www.nrcresearchpress.com by 79.173.37.17 on 09/08/12
For personal use only.

TABLE 2 (*continued*)

Compound	ΔH_f(g)	$\sigma_{\Delta H}$	S(g)	ΔGf(g)	ΔGt(kcal)	ΔGf(aq) obsd.	$\sigma_{\Delta G}$	ΔG_f(aq) calcd.	error
Heptanoic acid	−128.15	0.50	114.7[e]	−79.79	−4.27[c]	−84.06	0.68	−83.72	−0.34
Acrylic Acid	−80.51[i]	0.55	75.29[h]	−68.52	−4.31[i]	−73.83[i]	0.72	−71.54	−2.29
Methacrylic acid			69.34[aj]						
Benzoic Acid	−70.29	0.52	88.19	−51.22	−5.80[ak]	−57.02[s]	0.55	−57.01	−0.01
Formic acid methyl ester	−84.97	0.19	72.	−72.41	−0.88	−73.29	0.23	−73.18	−0.11
Acetic acid methyl ester	−98.45	0.38	76.45[ai]	−77.51	−1.42	−78.92	0.60	−79.63	0.71
Acetic acid ethyl ester	−106.14	0.14	86.7	−78.55	−1.20	−79.75	0.20	−80.91	1.16
Methyl propanoate	−104.19[ak]		89.25[ak,h]	−77.34	−1.03	−78.43[s]	0.13	−77.77	−0.66
Methyl acrylate	−79.59	0.19	82.28[v]						
Methyl methacrylate			86.83[aj]		−0.46[m]				
Benzoic acid methyl ester	−64.37[ak]	1.23	95.14[v]	−37.67	−1.88[ak]	−39.55	1.24	−42.42	2.87
Phenyl acetate	−66.85	0.29				−42.87[y]	0.48	−42.85	−0.02
Isopropenyl acetate					−0.90[m]				
Dimethoxymethane	−83.27	0.19	80.24	−54.16	−1.03	−55.19	0.23	−54.47	−0.72
1,1-Dimethoxyethane	−93.14	0.19				−58.92[al]	0.31	−58.85	−0.07
2,2-Dimethoxypropane	−102.68	0.55				−58.50[al]	0.33	−57.75	−0.75
2,2-Dimethoxybutane						−56.03[al]	0.34	−56.00	−0.03
2,2-Dimethoxypentane						−53.51[al]	0.37	−53.84	0.33
2,2-Dimethoxy-3-methylbutane						−53.04[al]	0.36	−53.41	0.37
1,1-Diethoxyethane						−61.00[al]	0.31	−60.76	−0.24
1,1-Diethoxypropane						−58.58[al]	0.36	−58.60	−0.02
1,1-Dimethoxybutane						−54.05[al]	0.44	−53.88	0.17
1,1-Diethoxybutane						−55.87[al]	0.44	−56.34	0.57
1,1-Diethoxy-2-methylpropane						−56.19[al]	0.57	−57.10	0.91
Dimethoxyphenylmethane						−19.00[al]	0.75	−18.96	−0.04
1,1-Dimethoxyl-1-phenylethane						−20.36[al]	0.48	−20.36	0.00
Trimethyl orthoformate	−127.13	0.67	94.57[ai,h]	−85.28	−2.52[ai]	−87.80	0.81	−89.55	1.75
Trimethyl orthoacetate	−136.88	0.55	99.70[ai,h]	−86.86	−2.48[ai]	−89.34	0.72	−91.46	2.12
Trimethyl orthobenzoate	−102.62[ak]	1.24	121.95[ak,h]	−47.90	−2.14[ak]	−50.04[ak]	1.32	−49.99	−0.05
Acetic anhydride	−136.83	0.36	93.2	−113.18		−116.31[y]	0.56	−116.27	−0.04

[a]All at 25°C; enthalpies and free energies are in kcal mol^{-1}, entropies are in cal deg^{-1} mol^{-1}, standard states are the ideal gas at 1 atm and 1 M aqueous solution with an infinitely dilute reference state. Unless otherwise noted, enthalpies of formation are from ref. 24, entropies are from ref. 20, and free energies of transfer are from ref. 22.

[b]Calculated from the values of ΔH_f^0 (l) (24) and ΔH_{vap} (72).

[c]Reference 62.

[d]Calculated from the values of ΔH_f^0 (l) (24) and ΔH_{vap} (73).

[e]Estimated as described in the text.

[f]Reference 20.

[g]Reference 74.

[h]Estimated value.

[i]Reference 8.

[j]Calculated from the values of ΔH_f^0 (l) (24) and ΔH_{vap} (75).

[k]Reference 76.

[l]Calculated from S^0 (l) (20), ΔH_v (24), and vp (25).

[m]This work.

[n]Calculated from the solubility (77) and the vapor pressure (25).

[o]Reference 78.

[p]Estimated as described in the text.

[q]Reference 79.

[r]Calculated from S^0 (l) (20), ΔH_v (24), and vp (25).

[s]Reference 16.

[t]Calculated from the uncertainty in ΔG_f^0(aq) for the keto tautomer (16), assuming an uncertainty of 0.1 kcal mol^{-1} in $\Delta G^0_{enol'n}$.

[u]Calculated from S^0 (l) (29), ΔH_v (24), and vp (30).

[v]Calculated from spectroscopic data as described in the text.

[w]Reference 12; these values must be regarded as provisional, because they are based on an assumed value of [C_d(C)(O)], and a similar assumption for [C_dH(O)] was inconsistent with the spectroscopic entropy of methyl vinyl ether.

[x]Calculated from the value for methyl vinyl ether by adding [CH_2(C)(O)].

[y]Calculated from S^0 (l) (67), ΔH_v (19), and vp estimated (18) from the vp (26), ΔH_v, and ΔC_p (27, 68).

[z]Calculated from structural and spectroscopic parameters as described in the text.

[aa]Calculated from S^0 (l) (20), ΔH_v (24), and vp (26).

[ab]Calculated from the solubility (65) and vp (26).

[ac]Calculated from S^0 (l) (67), ΔH_v (19), and vp (26).

[ad]Reference 69.

[ae]Calculated from the measured equilibrium constant (59).

Can. J. Chem. Downloaded from www.nrcresearchpress.com by 79.173.37.17 on 09/08/12
For personal use only.

TABLE 2 (*concluded*)

[af] Based on the equilibrium constant for cinnamaldehyde formation (60), Table 3.
[ag] Calculated for the free aldehyde as described in the text.
[ah] Reference 80.
[ai] Reference 1.
[aj] Calculated from S^0 (l) (20), an estimated ΔH_v, and vp (26).
[ak] Reference 5.
[al] Calculated from the equilibrium constants in Table 3.
[am] Calculated from S^0 (l) (20), ΔH_v (24), and vp (25).
[an] The entropy value given is based on spectroscopic data as described by the text, but leads to a free energy of formation that is not in good agreement with the prediction of our group additivity scheme, nor in good agreement with expectation based on the equilibrium free energy (86) and free energies of formation of benzoic acid and methanol. The group additivity parameters for entropy give a value of 100.28 cal deg^{-1} mol^{-1}. MM3 calculations (81) gave a value of 107.26 cal deg^{-1} mol^{-1}; MM3 gives values in good agreement with experiment for methyl acetate, benzaldehyde, and acetophenone. Using the MM3 entropy gives ΔG_f^0(aq) = −43.65 kcal mol^{-1} in satisfactory agreement with our group contribution prediction. A reinvestigation of the experimental bases for the entropy of methyl benzoate appears to be in order.

TABLE 3. Equilibrium constants leading to group contributions to free energy of formation[a]

Reaction	log K	ΔG^0
C_6H_5-CO-CH_3 + $CH_3OH \leftrightharpoons C_6H_5$-C($OCH_3$)=$CH_2$ (+H_2O)	−8.17	11.16[b]
CH_3COOH + $CH_3COOH \leftrightharpoons CH_3CO$-O-$COCH_3$ (+H_2O)		15.70[c]
C_6H_5-OH + $CH_3COOH \leftrightharpoons C_6H_5$-O-$COCH_3$ (+ H_2O)		7.39[d]
CH_3-CO-CH_3 + 2$CH_3OH \leftrightharpoons$ (CH_3)$_2$C(OCH_3)$_2$ (+H_2O)	−5.54	7.57[e]
CH_3CH_2-CO-CH_3 + 2$CH_3OH \leftrightharpoons$ (CH_3)(CH_3CH_2)C(OCH_3)$_2$ (+H_2O)	−6.07	8.30[e]
$CH_3CH_2CH_2$-CO-CH_3 + 2$CH_3OH \leftrightharpoons$ (CH_3)($CH_3CH_2CH_2$)C(OCH_3)$_2$ (+ H_2O)	−6.27	8.57[e]
(CH_3)$_2$CH-CO-CH_3 + 2$CH_3OH \leftrightharpoons$ (CH_3)((CH_3)$_2$CH)C(OCH_3)$_2$ (+H_2O)	−6.62	9.04[e]
CH_3CHO + 2$CH_3OH \leftrightharpoons CH_3CH$($OCH_3$)$_2$ (+H_2O)	−1.52	2.08[f]
CH_3CHO + 2$CH_3CH_2OH \leftrightharpoons CH_3CH$($OCH_2CH_3$)$_2$ (+H_2O)	−1.90	2.60[f]
CH_3CH_2CHO + 2$CH_3CH_2OH \leftrightharpoons CH_3CH_2CH$($OCH_2CH_3$)$_2$ (+H_2O)	−2.04	2.80[f]
$CH_3CH_2CH_2CHO$ + 2$CH_3OH \leftrightharpoons CH_3CH_2CH_2CH$($OCH_3$)$_2$ (+H_2O)	−1.40	1.91[f]
$CH_3CH_2CH_2CHO$ + 2$CH_3CH_2OH \leftrightharpoons CH_3CH_2CH_2CH$($OCH_2CH_3$)$_2$ (+H_2O)	−1.97	2.69[f]
(CH_3)$_2$CHCHO + 2$CH_3CH_2OH \leftrightharpoons$ (CH_3)$_2$CHCH(OCH_2CH_3)$_2$ (+H_2O)	−2.77	3.79[f]
C_6H_5-CO-H + 2$CH_3OH \leftrightharpoons C_6H_5$-CH($OCH_3$)$_2$ (+H_2O)	−3.94	5.38[g]
C_6H_5-CO-CH_3 + 2$CH_3OH \leftrightharpoons C_6H_5$-C($OCH_3$)$_2CH_3$ (+H_2O)	−6.95	9.45[h]
C_6H_5-CHO + CH_3-CO-$CH_3 \leftrightharpoons C_6H_5$-CH=CH-CO-$CH_3$ (+H_2O)	2.56	−3.50[i]
C_6H_5-CHO + CH_3-CHO $\leftrightharpoons C_6H_5$-CH=CH-CHO (+$H_2O$)	3.17	4.33[j]

[a] All in aqueous solution at 25°C. The standard state for all species except water is the ideal solution at 1 M with an infinitely dilute reference state. The standard state for water is the pure liquid with unit activity.
[b] Reference 64.
[c] Reference 71.
[d] Reference 70.
[e] Reference 82.
[f] Calculated from the overall equilibrium constants (83, 84) correcting for hemiacetal formation (23).
[g] Calculated from equilibrium constants in methanol (85), assuming that the mole fraction equilibrium constant will be the same in methanol and in water.
[h] Calculated from the equilibrium constants (64) for the conversion of ketone to enol ether and acetal to enol ether.
[i] Reference 59.
[j] Reference 60.

extrapolated the vapor pressure from that at 1 Torr[2] (26), using the heat of vaporization of the liquid (24), an estimated heat capacity of vaporization (27), and a method based on that of Prausnitz (18, 28). For *tetrahydrofuran* we used the entropy of the liquid (29), the heat of vaporization (24), and a vapor pressure calculated from Antoine parameters (30). For *anthracene, phenanthrene,* and *pyrene* we used entropies for the solid (20), heats of sublimation (31), and vapor pressures calculated from Antoine parameters (25). For *methacrylic acid* and *methyl methacrylate* we used the entropies of the liquids (32), heats of vaporization estimated from the boiling points (18), and vapor pressures extrapolated from literature data (26). For *diphenylmethane* we used the entropy of the liquid (20), the heat of vaporization (33), and a vapor pressure calculated from Antoine parameters (25). For *triphenylmethane* we used the entropy of the solid (20), the heat of sublimation (24), and a vapor pressure calculated from Antoine parameters (25). For *tetraphenylmethane* we used the entropy of the solid (20), the heat of sublimation (24), and a vapor pressure calculated from Antoine parameters (25). In this case the Antoine parameters were derived for higher temperatures, so there will be an additional error from extrapolating beyond the range where they apply.

In a number of cases, no entropy value had been reported, but sufficient data were available in the literature to allow a calculation of the entropy from statistical mechanics, using structural and spectroscopic information (14, 34, 35). This was done for *acrolein, methyl vinyl ketone, anisole, methyl benzoate, methyl acrylate,* and *methyl vinyl*

[2] 1 Torr = 133.3 Pa.

Can. J. Chem. Downloaded from www.nrcresearchpress.com by 79.173.37.17 on 09/08/12
For personal use only.

Can. J. Chem. Downloaded from www.nrcresearchpress.com by 79.173.37.17 on 09/08/12
For personal use only.

ether. For *acrolein* we calculated the moments of inertia using MM2 (36) and then used vibrational frequencies (37), and the potential barrier for internal rotation (38), and calculated the reduced moments of inertia for this rotation following Benson (14) using the geometries calculated by MM2. These data lead to $S_{tr} = 37.99$, $S_{rot} = 23.19$, $S_{vib} = 2.90$, $S_{hr} = 4.03$, and $S^0(g) = 68.12$ cal deg^{-1} mol^{-1}. S_{hr} was calculated using tables for a symmetric rotor (14), but the rotor in acrolein is asymmetric, so $R \ln(n)$ must be added to the entropy (39). This correction is needed for all compounds discussed here except anisole. For *methyl vinyl ketone* we used moments of inertia based on microwave spectroscopy (40), vibrational frequencies (38), and the potential barrier for internal rotation (38) and calculated the reduced moments of inertia for this rotation following Benson (14) using the geometries calculated by MM2. These data lead to $S_{tr} = 38.66$, $S_{rot} = 25.47$, $S_{vib} = 4.81$, $S_{hr} = 8.01$, and $S^0(g) = 76.94$ cal deg^{-1} mol^{-1}. For *anisole* we used overall moments of inertia from microwave spectroscopy (41), and reduced moments of inertia for methyl and methoxyl rotation calculated from the MM2 structure. A literature value was used for the barrier to methyl rotation, 4.59 kcal mol^{-1} (42) (theoretical calculation, in good agreement with the observed frequency), and that for methoxyl rotation was derived from microwave spectroscopy, 3.26 kcal mol^{-1} (41). Vibrational frequencies were taken from Owen and Hester (43). These data lead to $S_{tr} = 39.95$, $S_{rot} = 27.92$, $S_{vib} = 9.94$, $S_{hr} = 5.68$, and $S^0(g) = 83.50$ cal deg^{-1} mol^{-1}. For *methyl vinyl ether* we used overall moments of inertia from microwave spectroscopy (44) and reduced moments of inertia for molecular fragments from the literature (methyl (45)) or calculated from the MM2 structure (methoxyl). Literature values were used for the barrier to methyl rotation, 4.07 kcal mol^{-1} (45), and methoxyl rotation, 5.24 kcal mol^{-1} (46). Longer wavelength frequencies were taken from Owen and Sheppard (47). These data lead to $S_{tr} = 38.10$, $S_{rot} = 23.86$, $S_{vib} = 2.77$, $S_{hr} = 5.96$, and $S^0(g) = 70.69$ cal deg^{-1} mol^{-1}. For *methyl acrylate* we used moments of inertia for the whole molecule and the methyl group from microwave spectroscopy (48) and moments of inertia for methoxyl and carbomethoxyl calculated from the MM2 structure. The literature value was used for the barrier to methyl rotation, 1.22 kcal mol^{-1} (48). Barriers for methoxyl and carbomethoxyl rotation were calculated (49) from the torsional vibration frequencies, 175 cm^{-1} (not reported for methyl acrylate; this value is an average for similar compounds (48)) and 160 cm^{-1} (value for methyl crotonate; not observed for methyl acrylate (50)) respectively, as 13.73 kcal mol^{-1} and 10.16 kcal mol^{-1} respectively. Vibrational frequencies were taken from several studies (50–52). These data lead to $S_{tr} = 38.66$, $S_{rot} = 26.35$, $S_{vib} = 6.12$, $S_{hr} = 11.15$, and $S^0(g) = 82.28$ cal deg^{-1} mol^{-1}. For *methyl benzoate* we used moments of inertia for the whole molecule and fragments subject to hindered internal rotation calculated from the MM2 structure. Barriers for methyl, methoxyl, and carbomethoxyl rotation were calculated (49) from the torsional vibration frequencies, 170 cm^{-1}, 100 cm^{-1}, and 58 cm^{-1} (53) respectively, as 2.03, 6.58, and 4.97 kcal mol^{-1} respectively. These frequencies were assigned as mixtures of torsion and skeletal vibration, so they are not an ideal basis for evaluating the potential barriers. The barrier for methyl rotation is in fair agreement with that for CH_3-OCHO, 1.2 kcal mol^{-1} (48). The barrier for methoxyl rotation is quite different from that for CH_3-$COOCH_3$, 13 kcal mol^{-1} (14), but the difference would amount to only 0.7 cal deg^{-1} mol^{-1} in overall entropy. Vibrational frequencies were taken from several studies (53, 54). These data lead to $S_{tr} = 40.64$, $S_{rot} = 29.28$, $S_{vib} = 13.50$, $S_{hr} = 12.20$, and $S^0(g) = 95.14$ cal deg^{-1} mol^{-1}.

We have a particular interest in acetals and ortho esters (13), and therefore have tried to estimate values for the group contributions to entropies, which are the only missing quantities for thermodynamic calculations. The problem is the shortage of entropy values for these types of compounds. Benson has suggested (14) that contributions to entropy would be approximately the same for groups differing only in the attached non-hydrogen atoms so that $[C(C)_4]$ would be a reasonable approximation for $[C(C)_2(O)_2]$ or $[C(C)(O)_3]$. We can examine the quality of this approximation for three series: $[CH_2(C)_2] = 9.42$ (55), $[CH_2(O)_2] = 10.30$ (55), $[CH_2(O)_2] = 7.81$ (this work); $[CH(C)_3] = -12.07$ (55), $[CH(C)_2(O)] = -11.0$ (55), $[CH(C)(O)_2] = -14.1$ (this work); and $[C(C)_4] = -35.10$ (55), $[C(C)_3(O)] = -33.56$ (55), $[C(C)_2(O)_2] = -38.3$ (this work). There is clearly variation, suggesting that the approximation is imperfect. There may be a pattern; one oxygen replacement gives a more positive value than all carbons, two oxygen replacements gives a more negative value. When one notes that only the hydrocarbon groups and $[CH_2(C)(O)]$ are based on more than one experimental entropy, and both $[CH(C)(O)_2]$ and $[C(C)_2(O)_2]$ are based on equilibrium constants in solution, it seems clear that for the moment the best approximation for the groups that must be estimated is to use the corresponding hydrocarbon group, i.e., $[CH(O)_3] \approx [CH(C)_3] = -12.07$, and $[C(O)_4] \approx [C(C)(O)_3] \approx [C(C)_4] = -35.10$.

It was necessary to derive the appropriate enthalpy and entropy ring corrections for cyclohexanone in Benson's scheme (14); these are for an exocyclic double bond to a six-membered ring. We assume that these will be the same as for methylenecyclohexane. The equilibrium constant for isomerization of methylenecyclohexane to 1-methylcyclohexene (56), and the enthalpies of formation of methylenecyclohexane (57) and 1-methylcyclohexene (24) are available. From the equilibrium constant, [1-methylcyclohexene]/[methylenecyclohexane] = 43.2, gas, 180°C (56), we obtain $\Delta G^0 = -3.40$ at 180°C. From the heats of formation of gaseous 1-methylcyclohexene (24) and methylenecyclohexane (57), $\Delta H^0 = -4.28$, and thus $\Delta S^0 = -1.95$ for the conversion of methylenecyclohexane to 1-methylcyclohexene. Since the entropy of 1-methylcyclohexene is available by well-established estimation procedures, Table 2, we can calculate the entropy of methylenecyclohexane as 85.38. We can now evaluate the ring compound corrections as 3.49 kcal mol^{-1} for ΔH and 23.99 cal deg^{-1} mol^{-1} for S^0. For comparison the corrections for cyclohexene are 1.4 kcal mol^{-1} and 21.5 cal deg^{-1} mol^{-1} (14). These corrections were used to calculate ΔG_f^0 for cyclohexanone.

We wished to calculate uncertainties in the $\Delta G_f^0(aq)$ values based on the uncertainties in the data from which they were derived. Although it is common to give uncertainty limits for $\Delta H_f^0(g)$, it is less common to report uncertainties for $S^0(g)$ or ΔG_t. Uncertainties in $\Delta H_f^0(g)$ are the major contributions to uncertainties in $\Delta G_f^0(aq)$, so it seemed acceptable to make rather arbitrary assignments of uncertainties as follows. Experimentally derived entropy values were assigned uncertainties of 0.3 cal deg^{-1} mol^{-1}; estimated values (using group contributions) were assigned uncertainties

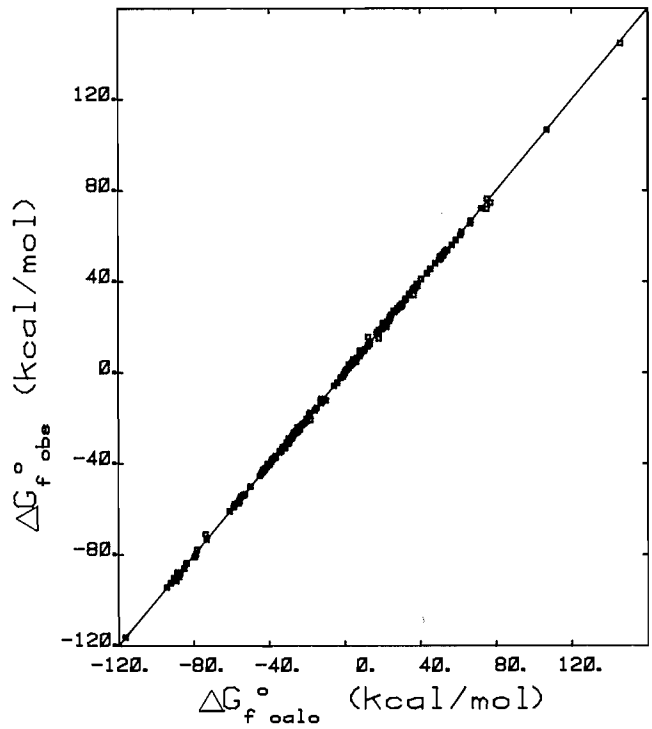

FIG. 1. Free energy of formation in aqueous solution: calculated vs. experimental values.

of 1.5 cal deg^{-1} mol^{-1}. Values of ΔG_t were assigned errors of 0.1 kcal mol^{-1}, as were ΔG^0 values based on equilibria. Uncertainties in ΔG_f^0(aq) values calculated from the ΔG^0 were then derived from the uncertainties in ΔG^0 and in ΔG_f^0(aq) values for the reactants and products.

Discussion

The available body of free energy of formation data for monofunctional organic compounds in aqueous solution is found in Table 2. This table does not include some multifunctional biochemical molecules, for which the simple approach given here is unlikely to give useful estimates, nor various polyfunctional compounds for which ΔG_f^0(aq) has been reported. Monofunctional has been loosely interpreted to mean the absence of strongly interacting polar groups, where the interactions fall outside the group equivalents scheme. Thus ortho esters are included because the interactions of the three oxygens are allowed for by the new groups [$CH(O)_3$], $C(C)(O)_3$], and [$C_B(C)(O)_3$]. Similarly for benzyl or allyl alcohols the groups [$CH_2(C_B)(O)$] and [$CH_3(C_d)(O)$] incorporate the interaction. We exclude compounds such as $CH_3OCH_2CH_2OCH_3$, where there is an important interaction (15) that is not recognized in the group contributions scheme. We also excluded compounds that would otherwise qualify but where there was no experimentally based entropy if the entropy could not be estimated by well-tested procedures. We do not claim to have done an exhaustive literature search, but believe that this is a relatively complete set of data as of this moment. Figure 1 shows a plot of calculated vs. experimental values of ΔG_f^0(aq) for all compounds in Table 2. The rms deviation of calculated from experimental values is 0.74 kcal mol^{-1} for 198 compounds.

Cyclic compounds require additional corrections to both ΔH_f^0(g) and S^0(g), which are listed in Benson's book (14). We have used these corrections unchanged, except for cycloheptatriene, as noted in Table 2, and do not reproduce them here.

We encountered particular problems in picking the best values for the entropies of the polyphenylmethanes. Although there is a recent paper devoted to this topic (58) the situation is still unsettled. Marcus and Loewenschuss estimated entropies for di-, tri-, and tetraphenylmethanes based on estimated frequencies. Frequencies for torsional modes were treated as vibrations and not as hindered rotations. Since the vibrational contribution is dominated by the low-frequency torsional modes, for which there is the least information, it is not clear how reliable these estimates can be. We used the literature values for condensed phase entropies (20), heats of vaporization (33), or sublimation (24), and vapor pressures calculated from Antoine equations (25). Our values differ appreciably from the calorimetric values of Marcus and Loewenschuss (58), in part because of different vapor pressure values, and partly because of a sign error in the calculations which they report. Our values appear to be internally consistent and lead to group contributions that fall into reasonable patterns relative to related groups; attempts to use the entropies reported by Marcus and Lowenschuss did not give such consistent values.

We have examined the data for those compounds where the difference between experimental and calculated values is more than 1 kcal mol^{-1}. In some cases we can see that the problem is probably the simple way in which corrections for crowding have been made: clearly more elaborate steric effects calculations are needed once these corrections become appreciable. This appears to be the situation for 3,3-diethylpentane, and possibly 2,2,5-trimethylhexane. For a number of compounds the discrepancy arises in ΔH_f^0(g) for which we can calculate a value from the parameters in Table 1, even though there is not a large steric correction. It is not clear whether this indicates a defect in the parameterization or a problem with the experimental data. This situation arises for 2,2-dimethylbutane, 1-methylcyclohexene, butenyne, 2-methyl-1-pentene, anthracene, pyrene, anisole, acrylic acid, and perhaps 2,2,5-trimethylhexane. For 2,4-dimethyl-3-pentanone the discrepancy appears to arise in the entropy, since the estimated value is 3.5 cal deg^{-1} mol^{-1} larger than the experimental value. This might imply reduced freedom for internal rotation because of gearing of the two isopropyl groups. For benzalacetone and cinnamaldehyde, where the experimental values are based on equilibrium constants for the aldol condensations (59, 60), we find that the calculated values are in error by 2 kcal mol^{-1}, the compounds being less stable than predicted. This suggests an interaction across the double bond of the conjugated phenyl and carbonyl groups, which is contrary to standard intuition.

For aldehydes we have revised the parameter reported by Hine and Mookerjee (15) to refer only to the free aldehyde in aqueous solution, i.e., we have corrected for covalent hydration. Since Hine and Mookerjee assumed the same value for all [CHO(X)] contributions, and had very few data for unsaturated aldehydes, ketones, and carboxylic acid derivatives, this has serious implications for a number of other groups. For aliphatic ketones the problem is not important because the standard assumption of the same value for all [CH_3(X)] groups leads to a well-defined value for [$CO(C)_2$]. We have calculated new values for the contribu-

Can. J. Chem. Downloaded from www.nrcresearchpress.com by 79.173.37.17 on 09/08/12
For personal use only.

tions [$C_dH(CO)$], [$C_d(C)(O)$], [$C_B(CO)$], [$CO(C)(C_d)$], [$CO(C)(C_B)$], [$CO(C_d)(O)$], and [$CO(C_B)(O)$]. The first three values change in the opposite sense to [CHO(X)], and the last four in the same sense. The net effect of these changes should be zero for the unsaturated carbonyl compounds, since all that has been changed is the way certain combinations of contributions have been split up.

In attempting to devise a predictive scheme such as that described here, the major problem encountered is the shortage of data. This is particularly severe for entropies. Although entropy is the most readily estimated thermodynamic quantity, largely because it is, for small molecules, largely determined by molecular weight and size through the translational and rotational contributions, and although relatively satisfactory estimates can be made by a variety of methods (14), a fully satisfactory parameterization scheme should be based on solid experimental values, with each parameter derived from several independent data values. This happy state has not yet been achieved.

It must be recognized that in the long run and broad perspective any hope of a general group additivity scheme is doomed by the combinatorial explosion of possible groups. This has been recognized, and attempts are being made to derive more efficient schemes (61). In the short run, group additivity schemes can be enormously useful and practical in providing estimates for a limited range of compounds while we wait for better methods. It must also be observed that it is still very rare for quantum mechanical calculations to be carried out to a level permitting usefully accurate absolute enthalpies or entropies of gaseous molecules, and that until such calculations become routinely practical, there will be a need for additivity schemes.

Our conclusion, based upon the results shown in Fig. 1 and Table 2, is that direct estimation of $\Delta G_f^0(aq)$ is a useful procedure, and that further elaboration to accommodate polyfunctional compounds would be a worthwhile endeavor.

Experimental

Materials

2,2-Dimethoxypropane, methyl methacrylate (BDH), and isopropenyl acetate (Eastman) were commercial samples redistilled before use. Triphenylmethane (Aldrich) was used without further purification.

Methods

Samples of the organic compounds were added to portions of suitable aqueous buffers (0.1 N NaOH for 2,2-dimethoxypropane; pH 7 phosphate buffer, ionic strength 0.1 M, for methyl methacrylate and isopropenyl acetate, and distilled water for triphenylmethane) and agitated vigorously at intervals during equilibration in a water bath at 25°C. After a suitable equilibration period (at least 1 h for 2,2-dimethoxypropane, methyl methacrylate, or isopropenyl acetate, 10 days for triphenylmethane) samples of the aqueous solutions were removed after centrifuging, if necessary, to obtain phase separation. Precautions were taken to avoid including any undissolved organic compound, and the samples were analyzed by ^1H nmr (2,2-dimethoxypropane, methyl methacrylate, and isopropenyl acetate) or uv spectroscopy (triphenylmethane). For nmr spectroscopic analysis a suitable amount of *tert*-butyl alcohol was added to a known volume of aqueous solution to act as an internal concentration standard.

Acknowledgments

I thank the Natural Sciences and Engineering Research Council of Canada for financial support of this work, and Jonathon Barker and Xiao-Ping Wang for measuring solubilities.

1. J. P. Guthrie. J. Am. Chem. Soc. **95**, 6999 (1973).
2. J. P. Guthrie. J. Am. Chem. Soc. **96**, 3608 (1974).
3. J. P. Guthrie. J. Am. Chem. Soc. **99**, 3991 (1977).
4. J. P. Guthrie. J. Am. Chem. Soc. **100**, 5892 (1978).
5. J. P. Guthrie and P. A. Cullimore. Can. J. Chem. **58**, 1281 (1980).
6. J. P. Guthrie. Can. J. Chem. **55**, 3562 (1977).
7. J. P. Guthrie. Can. J. Chem. **54**, 202 (1976).
8. J. P. Guthrie. Can. J. Chem. **56**, 962 (1978).
9. J. P. Guthrie. Can. J. Chem. **57**, 454 (1979).
10. J. P. Guthrie. Can. J. Chem. **57**, 236 (1979).
11. J. P. Guthrie and D. C. Pike. Can. J. Chem. **65**, 1951 (1987).
12. J. P. Guthrie and P. A. Cullimore. Can. J. Chem. **57**, 240 (1979).
13. J. P. Guthrie. Acc. Chem. Res. **16**, 122 (1983).
14. S. W. Benson. Thermochemical kinetics. Wiley, New York. 1976.
15. J. Hine and P. K. Mookerjee. J. Org. Chem. **40**, 292 (1975).
16. J. P. Guthrie. *In* The chemistry of enols. *Edited by* Z. Rappoport. Wiley, New York. 1990.
17. I. Wadso. Acta Chem. Scand. **20**, 544 (1966).
18. J. P. Guthrie. Can. J. Chem. **64**, 635 (1986).
19. V. Majer and V. Svoboda. Enthalpies of vaporization of organic compounds. Blackwell, Oxford. 1985.
20. D. R. Stull, E. F. Westrum, Jr., and G. C. Sinke. The chemical thermodynamics of organic compounds. Wiley, New York. 1967.
21. L. A. McDougall and J. E. Kilpatrick. J. Chem. Phys. **42**, 2307 (1965).
22. S. Cabani, P. Gianni, V. Mollica, and L. Lepori. J. Solution Chem. **10**, 563 (1981).
23. J. P. Guthrie. Can. J. Chem. **53**, 898 (1975).
24. J. B. Pedley, R. D. Naylor, and S. P. Kirby. Thermochemical data of organic compounds. 2nd ed. Chapman and Hall, London. 1986.
25. R. M. Stephenson and S. Malinowski. Handbook of thermodynamics of organic compounds. Elsevier, Amsterdam. 1987.
26. R. C. Weast (*Editor*). Handbook of chemistry and physics. 48th ed. Chemical Rubber Co., Cleveland, Ohio. 1967.
27. J. P. Guthrie and K. F. Taylor. Can. J. Chem. **62**, 363 (1984).
28. D. S. Abrams, H. A. Massaldi, and J. M. Prausnitz. Ind. Eng. Chem. Fundam. **13**, 259 (1974).
29. B. V. Lebedev, V. Y. Lityagov, T. I. Krentsina, and V. I. Milov. Russ. J. Phys. Chem. **53**, 152 (1979).
30. J. A. Dean (*Editor*). Lange's handbook of chemistry. 12th ed. New York, N.Y. 1978.
31. J. S. Chickos. Molecular structure and enegetics. Vol. 2. VCH Publishers, Deerfield Beach, Fla. 1987. p. 67.
32. I. A. Vaisilev and V. M. Petrov. Thermodynamic properties of oxygen containing organic compounds. Handbook. Leningrad. 1984. *Referred to in* E. S. Domalski and E. D. Hearing. J. Phys. Chem. Ref. Data, **19**, 881 (1990).
33. E. Morawetz. J. Chem. Thermodyn. **4**, 455 (1972).
34. K. B. Wiberg. Physical organic chemistry. Wiley, New York. 1964.
35. G. N. Lewis and M. Randall. Thermodynamics. *Revised by* K. S. Pitzer and L. Brewer. 2nd ed. McGraw–Hill, New York. 1961.
36. U. Burkert and N. L. Allinger. Molecular mechanics. ACS Monograph 177, 1982.
37. P. Pulay, G. Fogarasi, G. Pongor, J. E. Boggs, and A. Vargha. J. Am. Chem. Soc. **105**, 7037 (1983).
38. J. R. Durig and T. S. Little. J. Chem. Phys. **75**, 3660 (1981).
39. K. S. Pitzer. J. Chem. Phys. **14**, 239 (1946).
40. P. D. Foster, V. M. Rao, and R. F. Curl. J. Chem. Phys. **43**, 1064 (1965).

Can. J. Chem. Downloaded from www.nrcresearchpress.com by 79.173.37.17 on 09/08/12
For personal use only.

41. M. Onda, A. Toda, S. Mori, and I. Yamaguchi. J. Mol. Struct. **144**, 47 (1986).
42. H. Konschin, H. Tylli, and C. Grundfelt-Forsius. J. Mol. Struct. **77**, 51 (1981).
43. N. L. Owen and R. E. Hester. Spectrochim. Acta, **25A**, 343 (1969).
44. P. Cahill, L. P. Gold, and N. L. Owen. J. Chem. Phys. **48**, 1620 (1968).
45. B. Cadioli, E. Gallinella and U. Pincelli. J. Mol. Struct. **78**, 215 (1982).
46. J. R. Durig and D. A. C. Compton. J. Chem. Phys. **69**, 2028 (1978).
47. N. L. Owen and N. Sheppard. Trans. Faraday Soc. **60**, 634 (1964).
48. G. Williams, N. L. Owen, and J. Sheridan. Trans. Faraday Soc. **67**, 922 (1971).
49. A. V. Cunliffe. *In* Internal rotation in Molecules. *Edited by* W. J. Orville-Thomas. Wiley–Interscience, London. 1974.
50. W. O. George, D. V. Hassid, W. C. Harris, and W. F. Maddams. J. Chem. Soc. Perkin Trans. 2, 392 (1975).
51. A. J. Bowles, W. O. George, D. B. Cunliffe-Jones. J. Chem. Soc. (B) 1070 (1970).
52. P. Carmona and J. Moreno. J. Mol. Struct. **82**, 177 (1982).
53. P. Caillet and M.-T. Forel. J. Chim. Phys. **72**, 522 (1975).
54. J. H. S. Green and D. J. Harrison. Spectrochim. Acta, **33A**, 583 (1977).
55. S. W. Benson, F. R. Cruickshank, D. M. Golden, G. R. Haugen, H. E. O'Neal, A. S. Rodgers, R. Shaw, and R. Walsh. Chem. Rev. **69**, 279 (1969).
56. M. Peereboom and J. L. Meijering. J. Catal. **59**, 45 (1979).
57. R. Fuchs and L. A. Peacock. Can. J. Chem. **57**, 2302 (1979).
58. Y. Marcus and A. Loewenschuss. J. Chem. Soc. Faraday Trans. 1, **82**, 993 (1986).
59. J. P. Guthrie, J. Cossar, and K. F. Taylor. Can. J. Chem. **62**, 1958 (1984).
60. J. P. Guthrie, K. J. Cooper, J. Cossar, B. A. Dawson, and K. F. Taylor. Can. J. Chem. **62**, 1441 (1984).
61. S. W. Benson. Chemtech, 121 (1980).
62. M. H. Abraham, G. S. Whiting, R. Fuchs, and E. J. Chambers. J. Chem. Soc. Perkin Trans. 2, 291 (1990).
63. H. K. Eigenmann, D. M. Golden, and S. W. Benson. J. Phys. Chem. **77**, 1687 (1973).
64. J. Toullec and M. El-Alaoui. J. Org. Chem. **51**, 4054 (1986).
65. H. S. Booth and H. E. Everson. Ind. Eng. Chem. **40**, 1491 (1948).
66. J. Hine, J. G. Houston, and J. H. Jensen. J. Org. Chem. **30**, 1184 (1965).
67. R. J. L. Andon, J. F. Counsell, E. B. Lees, and J. F. Martin. J. Chem. Soc. (A), 833 (1970).
68. G. Geisler, K. Quitsch, H. P. Hofmann, and R. Pfestorf. Z. Phys. Chem. **252**, 170 (1972).
69. D. Ambrose, J. E. Connett, J. H. S. Green, J. L. Hales, A. J. Head, and J. F. Martin. J. Chem. Thermodyn. **7**, 1143 (1975).
70. J. Gerstein and W. P. Jencks. J. Am. Chem. Soc. **86**, 4655 (1964).
71. W. P. Jencks, F. Barley, R. Barnett, and M. Gilchrist. J. Am. Chem. Soc. **88**, 4464 (1966).
72. B. D. Smith and R. Srivastava. Thermodynamic data for organic compounds. Part A. Hydrocarbons and ketones. Elsevier, Amsterdam. 1986.
73. R. C. Wilhoit and B. J. Zwolinski. Handbook of vapor pressures and heats of vaporization of hydrocarbons and related compounds. Thermodynamics Research Center, College Station, Tex. 1971.
74. S. W. Benson, F. R. Cruickshank, D. M. Golden, G. R. Haugen, H. E. O'Neal, A. S. Rodgers, R. Shaw, and R. Walsh. Chem. Rev. **69**, 279 (1969).
75. K. E. Coulter, H. Kehde, and B. F. Hiscock. *In* Vinyl and diene monomers. Vol. 24. Part 2. *Edited by* E. C. Leonard. Wiley, New York. 1971. p. 558.
76. R. D. Chirico, S. E. Knipmeyer, A. Nguyen, and W. V. Steele. J. Chem. Thermodyn. **21**, 1307 (1989).
77. B. G. Cox and A. J. Parker. J. Am. Chem. Soc. **94**, 3674 (1972).
78. S. E. Stein, D. M. Golden, and S. W. Benson. J. Phys. Chem. **81**, 314 (1977).
79. American Petroleum Institute. Research Project 44. Selected values of properties of hydrocarbons and related compounds. Thermodynamics Research Center, Dept. of Chemistry, Texas A&M University, College Station, Tex. 1973.
80. J. P. Guthrie. Can. J. Chem. **52**, 2037 (1974).
81. N. L. Allinger, Y. H. Yuh, and J. H. Lii. J. Am. Chem. Soc. **111**, 8551 (1989).
82. K. B. Wiberg and R. R. Squires. J. Am. Chem. Soc. **101**, 5512 (1979).
83. H. Adkins and E. W. Adams. J. Am. Chem. Soc. **47**, 1368 (1925).
84. R. E. Dunbar and H. Adkins. J. Am. Chem. Soc. **56**, 442 (1934).
85. J. M. Bell, D. G. Kubler, P. Sartwell, and R. G. Zepp. J. Org. Chem. **30**, 4284 (1965).
86. J. P. Guthrie, D. C. Pike, and Y. C. Lee. Can. J. Chem. In press.

Can. J. Chem. Downloaded from www.nrcresearchpress.com by 79.173.37.17 on 09/08/12
For personal use only.

The aldol condensation of acetone with acetophenone

J. PETER GUTHRIE[1] AND XIAO-PING WANG
Department of Chemistry, University of Western Ontario, London, Ont., Canada N6A 5B7

Received March 8, 1991[2]

J. PETER GUTHRIE and XIAO-PING WANG. Can. J. Chem. **70**, 1055 (1992).

The kinetics and equilibria involved in the aldol condensation of acetone, acting as carbon acid, and acetophenone have been studied in aqueous alkaline solution. The enone isolated is the *E* isomer. The reactions are all first order in hydroxide, with rate and equilibrium constants (defined for *E*-enone as initial compound) of: $k_{12} = (5.55 \pm 0.17) \times 10^{-6}$ M^{-1} s^{-1}, $k_{21} = (8.00 \pm 0.40) \times 10^{-6}$ M^{-1} s^{-1}, $K_{21} = (1.44 \pm 0.55)$ (ketol to *E*-enone), $K_{24} = 0.160 \pm 0.033$ (ketol to *Z*-enone), $K_{32} = (1.89 \pm 0.26) \times 10^{-3}$ M^{-1} (acetone plus acetophenone to ketol), $k_{23} = 0.180 \pm 0.005$ M^{-1} s^{-1}, $k_{32} = (3.41 \pm 0.49) \times 10^{-4}$ M^{-2} s^{-1}. There is an equilibration of the two enones in base that is faster than hydration to the ketol: $k_{14} = (3.14 \pm 0.84) \times 10^{-5}$ M^{-1} s^{-1}; $k_{41} = (2.81 \pm 0.61) \times 10^{-4}$ M^{-1} s^{-1}; $K_{14} = 0.112 \pm 0.019$. To analyze the behavior of the enone:ketol equililbrium system in acid we simultaneously fitted analytical data for all three species (*E*-enone, *Z*-enone, and ketol) to a kinetic model, so that the rate constants were determined by the best fit to all of the data for an experiment.

J. PETER GUTHRIE et XIAO-PING WANG. Can. J. Chem. **70**, 1055 (1992).

Opérant en solution aqueuse alcaline, on a étudié les cinétiques et les équilibres impliqués dans la condensation aldolique de l'acétone, agissant comme acide carboné, et l'acétophénone. L'énone isolée est l'isomère *E*. Les réactions sont toutes du premier ordre en ion hydroxyde alors que les constantes de vitesse et d'équilibre (définies pour l'énone *E* comme produit initial) sont : $k_{12} = (5{,}55 \pm 0{,}17) \times 10^{-6}$ M^{-1} s^{-1}, $k_{21} = (8{,}00 \pm 0{,}40) \times 10^{-6}$ M^{-1} s^{-1}; $K_{21} = 1{,}44 \pm 0{,}55$ (cétol de l'énone *E*), $K_{24} = 0{,}160 \pm 0{,}033$ (cétol de l'énone *Z*), $K_{32} = (1{,}89 \pm 0{,}26) \times 10^{-3}$ M^{-1} (acétone plus acétophénone conduisant au cétol), $k_{23} = 0{,}180 \pm 0{,}005$ M^{-1} s^{-1} et $k_{32} = (3{,}41 \pm 0{,}49) \times 10^{-4}$ M^{-2} s^{-1}. En milieu basique, il existe un équilibre qui est plus rapide que l'hydratation en cétol : $k_{14} = (3{,}14 \pm 0{,}84) \times 10^{-5}$ M^{-1} s^{-1}, $k_{41} = (2{,}81 \pm 0{,}61) \times 10^{-4}$ M^{-1} s^{-1}; $K_{14} = 0{,}112 \pm 0{,}019$. Dans le but d'analyser le comportement de l'équilibre céto–énolique en milieu acide, on a ajusté les données analytiques obtenues pour les trois espèces (énones *E* et *Z* et cétol) à un modèle cinétique; on a ainsi pu déterminer les constantes de vitesse qui correspondent le mieux avec l'ensemble des données pour une expérience.

[Traduit par la rédaction]

Can. J. Chem. Downloaded from www.nrcresearchpress.com by 79.173.37.17 on 09/08/12
For personal use only.

Introduction

We recently reported on the aldol condensation of acetophenone, acting as carbon nucleophile, with acetone (1). This was, in part, background information for ongoing studies of elimination reactions catalyzed by steroidal imidazoles (2, 3). In the course of this investigation we became aware that there was a concurrent condensation in the opposite sense, with acetone, acting as carbon nucleophile, attacking acetophenone. The reactions involved are described in Scheme 1. The kinetic analysis is from the perspective of the retroaldol reaction, since this is the direction that gives the more accurate rate constants. This reaction turned out to be somewhat more difficult to sort out, but we have now completed the kinetic analysis, and wish to report it in turn. This provides another example of a fully analyzed aldol condensation, to add to those we (1, 4–10) and others (11–14) have previously reported. To complete the analysis we had to develop computer programs allowing us to fit simultaneously multiple sets of data described by equations with common parameters.

Results

Preparation

When we set out to make 3-hydroxy-3-methyl-1-phenyl-1-butanone we found that directed aldol condensation using the preformed lithium enolate of acetophenone gave mixtures consisting mainly of the desired product with small amounts of 4-hydroxy-4-phenyl-2-pentanone. These were essentially impossible to separate on a preparative scale, and we had to use an alternative synthesis (1). 4-Hydroxy-4-phenyl-2-pentanone could be prepared in pure form by reaction of phenyl magnesium bromide with 2,4-pentanedione (15), and 4-phenyl-3-penten-2-one could be obtained by dehydration of the ketol. The enone so obtained was the *E* isomer, based on comparison of its ^1H NMR spectrum with literature values for the two isomers. The diagnostic signals are those for the CH_3-C=C signal, which appears at 2.09δ (16*a*), *Z* isomer, or 2.35δ (16*a*), 2.47δ (16*b*), *E* isomer, and the vinyl hydrogen, for which the signals are at 6.94δ (16*a*), *Z* isomer, or 6.21δ (16*a*), 6.34δ (16*b*), *E* isomer, all in CCl_4. We observed signals at 2.45δ and 6.35δ in CCl_4.

Overall kinetics

We studied the retroaldol kinetics of both *E*-enone and ketol in dilute alkaline solution, and discovered that the two compounds reacted on markedly different time scales, with apparent second-order rate constants of 0.180 ± 0.005 M^{-1} s^{-1} for disappearance of the ketol and $(9.99 \pm 0.25) \times 10^{-6}$ M^{-1} s^{-1} for disappearance of the *E*-enone; see Figs. 1 and 2. The data for the *E*-enone also showed a small amplitude kinetic phase with an apparent second-order rate constant of $(3.12 \pm 0.68) \times 10^{-4}$ M^{-1} s^{-1}; because of the small amplitude of this phase it is not well defined by the data, but appears to be real. We attribute this behavior to isomerization of the enones prior to conversion to the ketol and retroaldol cleavage. This isomerization will be considered in more detail later. The experimental results are found in Table 1. The observed behavior is interpreted in terms of rapid, essentially complete, breakdown of ketol to acetone and

[1]Author to whom correspondence may be addressed.
[2]Revision received October 23, 1991.

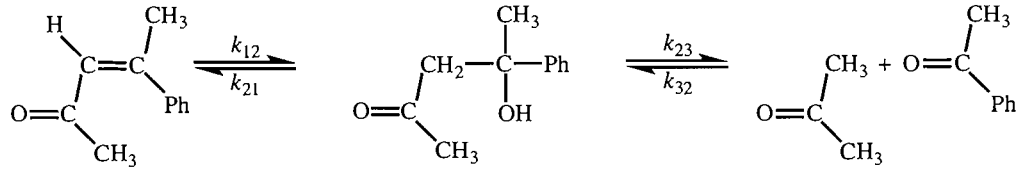

SCHEME 1

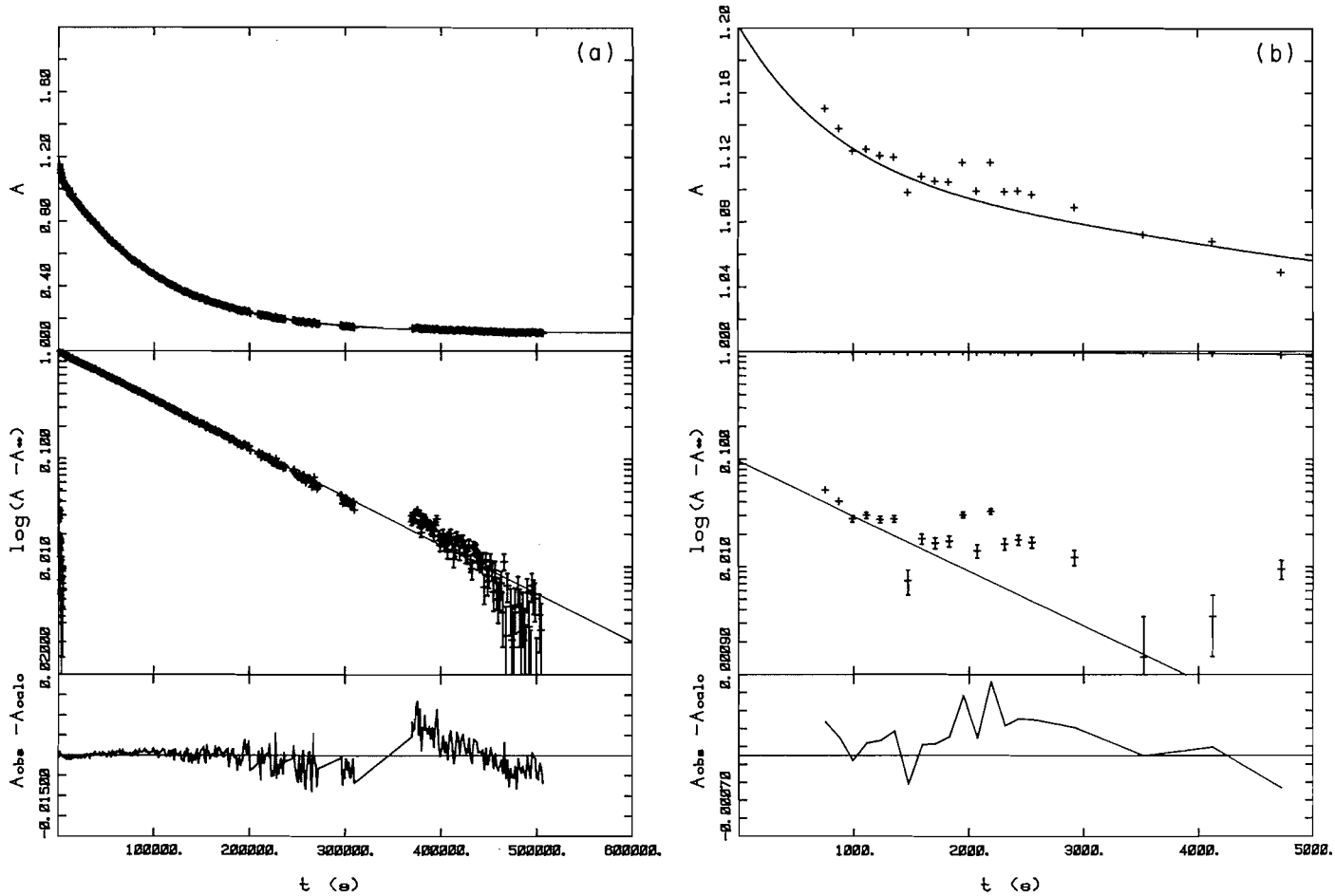

FIG. 1. Kinetics of retroaldol reaction of *E*-enone; 8.89×10^{-6} M enone in 1.0 M aqueous NaOH at 25°C. The lines are calculated using the parameters evaluated by least squares.

acetophenone, with hydration of the enone as rate-determining step for reaction starting with the enone. Had dehydration of the ketol occurred at a rate competitive with breakdown, one would have observed buildup of enone, followed by slow decay. Although some enone doubtless forms, the amounts are very small, as shown by the essential absence of a second exponential decay term in the rate law. This suggests that the apparent rate constants may be simply interpreted since, in terms of Scheme 1, the apparent rate constant for disappearance of enone is k_{12}, and the apparent rate constant for disappearance of ketol is k_{23}. The attractive simplicity of this analysis is marred by the clear signs of deviations from simple first-order behavior for the retroaldol cleavage of the *E*-enone at short reaction times mentioned above. We would like to evaluate all four rate constants in Scheme 1. To carry out a complete analysis of the kinetics it is necessary to measure the equilibrium constants for hydration and the overall aldol condensation. Then with two rate constants from the overall kinetics and two equilibrium constants it should be possible to extract the four rate constants we want.

Rate and equilibrium constants for hydration in acid

To measure K_{12}, the equilibrium constant for covalent hydration of the *E*-enone, we studied equilibration in acid solution, where we expect, based on analogy with other systems (17–19), that hydration–dehydration can be studied without interference by retroaldol cleavage. This proved to be the case, but a complicating factor intervened. Whether one started with *E*-enone or ketol, HPLC analysis of equilibrating solutions in acid showed the presence of three species: the ketol, the *E*-enone, and a third species which we

Can. J. Chem. Downloaded from www.nrcresearchpress.com by 79.173.37.17 on 09/08/12
For personal use only.

TABLE 1. Kinetics of the retroaldol cleavage of PPEO in base[a]

10^6C_0	$[OH^-]$	a_1	a_2	10^4a_3	a_4	10^4a_5
(*a*) Reaction starting with the *E*-enone[b]						
7.77	1.029	0.147	0.116	10.4(7.4)	1.063	0.102(0.001)
9.06	1.778	0.126	0.126	6.51(0.37)	1.219	0.176(0.0002)
9.06	2.038	0.112	0.118	7.18(0.61)	1.255	0.208(0.0002)
9.06	1.488	0.130	0.105	3.61(0.30)	1.199	0.144(0.0002)
8.888	1.0	0.113	0.096	11.75(2.02)	0.993	0.103(0.0003)
				$a_3/[OH^-] = (3.12 \pm 0.68) \times 10^{-4}\ M^{-1}\ s^{-1}$		
				$a_5/[OH^-] = (9.99 \pm 0.25) \times 10^{-6}\ M^{-1}\ s^{-1}$		
(*b*) Reaction starting with the ketol[c]						
16.38	0.0097	1.393	−1.298	22.45(0.41)		
16.38	0.0048	0.926	−0.872	8.69(0.034)		
16.38	0.00285	1.033	−0.980	5.11(0.014)		
16.38	0.0285	0.935	−0.832	48.2(0.67)		
				$a_3/[OH^-] = 0.180 \pm 0.005\ M^{-1}\ s^{-1}$		

[a]In aqueous solution at 25°C, ionic strength 1.0 M (KCl) for runs with [NaOH] less than 1.0 M. Data were fitted by least squares to: absorbance = $a_1 + a_2 \exp(-a_3 t) + a_4 \exp(-a_5 t)$. Averages are weighted means.
[b]Followed at 280 nm.
[c]Followed at 258 nm.

Can. J. Chem. Downloaded from www.nrcresearchpress.com by 79.173.37.17 on 09/08/12
For personal use only.

believe is the geometrical isomer of the enone, i.e., *Z*-4-phenyl-3-penten-2-one. The results of these experiments are found in Table 2. The actual experimental data are given in Table S1.[3] The final proportions of these three species are independent of the starting conditions. A striking feature of the kinetics was that when reaction started with the *E*-enone, the concentration of the *Z*-enone first rose and then fell. This requires that the ketol not be an intermediate on the reaction path from *E*-enone to *Z*-enone, but rather that the *Z*-enone be in a sense an intermediate species that can be formed by a more rapid path and accumulate to levels higher than for the equilibrium state, to which it will relax by a slower path. Thus the reaction system cannot be:

$$E\text{-enone} \leftrightharpoons \text{ketol} \leftrightharpoons Z\text{-enone}$$

Two mechanisms were considered to account for this behavior. In the first we assume that the enol intermediate in hydration–dehydration undergoes loss of water faster than protonation at carbon. This mechanism is shown in Scheme 2; the corresponding reaction coordinate diagram is shown in Fig. 3. If, as seems highly reasonable, the enol were a steady-state intermediate, then this scheme would be equivalent to a simple triangular reaction system:

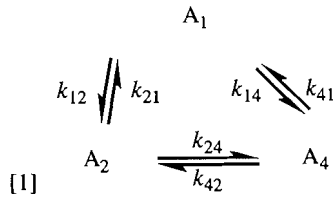

[1]

$A_1 = E$–enone
A_2 = ketol
$A_4 = Z$–enone

For this system, starting with *E*-enone, we can derive, following Ikai and Tanford (20),[4] the equations

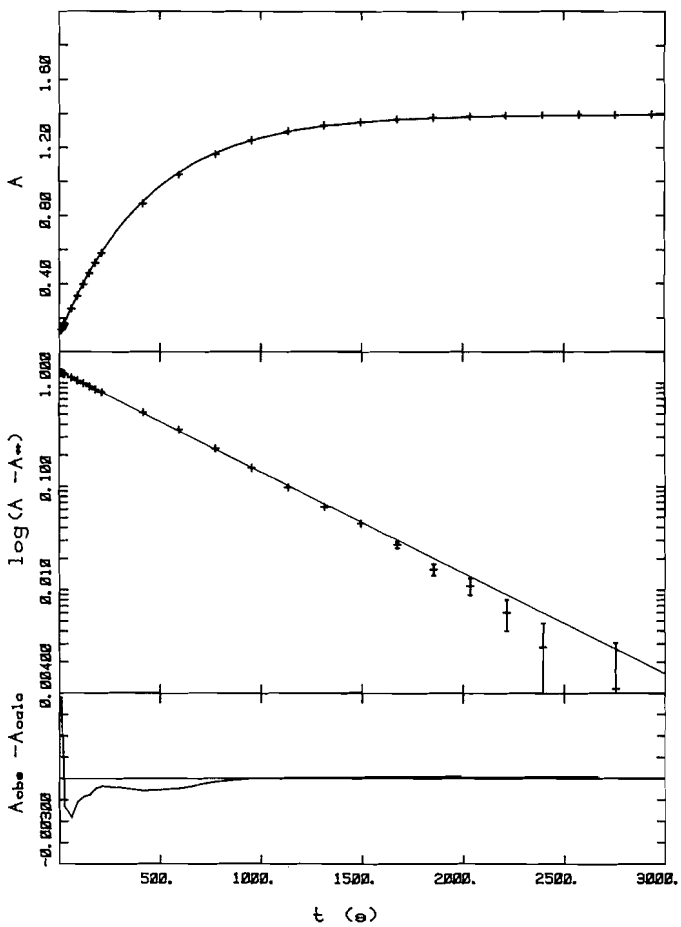

FIG. 2. Kinetics of retroaldol reaction of ketol; 1.64×10^{-5} M ketol in 0.0097 M aqueous NaOH at 25°C. The lines are calculated using the parameters evaluated by least squares.

[3]Copies of the Supplementary Tables may be purchased from the Depository of Unpublished Data, Document Delivery, CISTI, National Research Council Canada, Ottawa, Canada K1A 0S2.

[4]There is an error on page 161 of Ikai and Tanford (20): $C_1(0) = 0$ should be $C_1(0) = C_0$.

$$[E\text{-Enone}] = C_0k_{21}k_{41}/(k_{21}k_{41} + k_{12}k_{41} + k_{14}k_{21}) + \{C_0(\lambda_2(k_{12} + k_{14}) - (\gamma_2 + \gamma_3))/\lambda_2(\lambda_2 - \lambda_3)\} \exp(-\lambda_2 t) - \{C_0(\lambda_3(k_{12} + k_{14}) - (\gamma_2 + \gamma_3))/\lambda_3(\lambda_2 + \lambda_3)\} \exp(-\lambda_3 t)$$

[2] $$[\text{Ketol}] = C_0k_{12}k_{42}/(k_{21}k_{42} + k_{12}k_{42} + k_{12}k_{24}) + \{C_0(\gamma_2 - k_{12}\lambda_2)/\lambda_2(\lambda_2 - \lambda_3)\} \exp(-\lambda_2 t) - \{C_0(\gamma_2 - k_{12}\lambda_3)/\lambda_3(\lambda_2 - \lambda_3)\} \exp(-\lambda_2 t)$$

$$[Z\text{-Enone}] = C_0k_{14}k_{24}/(k_{24}k_{41} + k_{14}k_{42} + k_{14}k_{24}) + \{C_0(\gamma_3 - k_{14}\lambda_2)/\lambda_2(\lambda_2 - \lambda_3)\} \exp(-\lambda_2 t) - \{C_0(\gamma_2 - k_{12}\lambda_3)/\lambda_3(\lambda_2 - \lambda_3)\} \exp(-\lambda_2 t)$$

and for the case of starting with ketol:

$$[E\text{-Enone}] = C_0k_{21}k_{41}/(k_{12}k_{41} + k_{21}k_{41} + k_{21}k_{14}) + \{C_0(\gamma_2 - k_{21}\lambda_2)/\lambda_2(\lambda_2 - \lambda_3)\} \exp(-\lambda_2 t) - \{C_0(\gamma_2 - k_{21}\lambda_3)/\lambda_3(\lambda_2 - \lambda_3)\} \exp(-\lambda_2 t)$$

[3] $$[\text{Ketol}] = C_0k_{12}k_{42}/(k_{12}k_{42} + k_{21}k_{42} + k_{12}k_{24}) + \{C_0(\lambda_2(k_{21} + k_{24}) - (\gamma_2 + \gamma_3))/\lambda_2(\lambda_2 - \lambda_3)\} \exp(-\lambda_2 t) - \{C_0(\lambda_3(k_{21} + k_{24}) - (\gamma_2 + \gamma_3))/\lambda_3(\lambda_2 + \lambda_3)\} \exp(-\lambda_3 t)$$

$$[Z\text{-Enone}] = C_0k_{14}k_{24}/(k_{24}k_{41} + k_{14}k_{42} + k_{14}k_{24}) + \{C_0(\gamma_3 - k_{24}\lambda_2)/\lambda_2(\lambda_2 - \lambda_3)\} \exp(-\lambda_2 t) - \{C_0(\gamma_3 - k_{24}\lambda_3)/\lambda_3(\lambda_2 - \lambda_3)\} \exp(-\lambda_2 t)$$

where

$$p = k_{12} + k_{21} + k_{14} + k_{41} + k_{24} + k_{42} \qquad q = (p^2 - 4)(\gamma_1 + \gamma_2 + \gamma_3))^{1/2}$$

$$\gamma_1 = k_{21}k_{41} + k_{21}k_{42} + k_{24}k_{41} \qquad \lambda_2 = (p + q)/2;$$

$$\gamma_2 = k_{12}k_{41} + k_{12}k_{42} + k_{14}k_{42} \qquad \lambda_3 = (p - q)/2$$

$$\gamma_3 = k_{12}k_{24} + k_{14}k_{21} + k_{14}k_{24}$$

When we attempted to fit the data to the integrated rate law derived for this mechanism, we found that two of the rate constants, describing the interconversion of ketol and the *Z*-enone, were only marginally defined by the data, with uncertainties large relative to the values assigned by least squares. At the 95% confidence level, neither k_{24} nor k_{42} is distinguishable from zero. Thus the first mechanism was rejected.

Since the facts require that the enones interconvert, but that the *Z*-enone *not* be directly converted to ketol, we had to consider possibilities that at first glance seemed implausible. The mechanism that worked is that shown in Scheme 3, which assumes that only the *E*-enone can undergo hydration, so that the *Z*-enone must first isomerize before it can hydrate. We will here show that this mechanism is consistent with the facts. In the discussion we will attempt to justify it in structural terms. The mechanism in Scheme 3, making the plausible steady-state assumption for all intermediates, is equivalent to the simple reaction system:

[4] $$Z\text{-enone} \underset{k_{14}}{\overset{k_{41}}{\leftrightharpoons}} E\text{-enone} \underset{k_{21}}{\overset{k_{12}}{\leftrightharpoons}} \text{ketol}$$

This system is described by the reaction coordinate diagram shown in Fig. 4, and we may derive an integrated rate law, for the case of starting with *E*-enone,

$$[Z\text{-Enone}] = [E\text{-enone}]^0\{k_{14}k_{21}/\lambda_2\lambda_3 + [k_{14}(k_{21} - \lambda_2)/\lambda_2(\lambda_2 - \lambda_3)] \exp(-\lambda_2 t) + [k_{14}(\lambda_3 - k_{21})/\lambda_3(\lambda_2 - \lambda_3)] \exp(-\lambda_3 t)\}$$

[5] $$[E\text{-Enone}] = [E\text{-enone}]^0\{k_{41}k_{21}/\lambda_2\lambda_3 + [(k_{21} - \lambda_2)(k_{41} - \lambda_2)/\lambda_2(\lambda_2 - \lambda_3)] \exp(-\lambda_2 t) - [(k_{21} - \lambda_3)(k_{41} - \lambda_3)/\lambda_3(\lambda_2 - \lambda_3)] \exp(-\lambda_3 t)\}$$

$$[\text{Ketol}] = [E\text{-enone}]^0\{k_{41}k_{12}/\lambda_2\lambda_3 + [k_{12}(k_{41} - \lambda_2)/\lambda_2(\lambda_2 - \lambda_3)] \exp(-\lambda_2 t) - [k_{12}(k_{41} - \lambda_3)/\lambda_3(\lambda_2 - \lambda_3)] \exp(-\lambda_3 t)\}$$

and for the case of starting with ketol,

$$[Z\text{-Enone}] = [\text{ketol}]^0\{k_{41}k_{12}/\lambda_2\lambda_3 + [k_{12}k_{41}/\lambda_2(\lambda_2 - \lambda_3)] \exp(-\lambda_2 t) - [k_{41}k_{12}/\lambda_3(\lambda_2 - \lambda_3)] \exp(-\lambda_3 t)$$

[6] $$[E\text{-Enone}] = [\text{ketol}]^0\{k_{41}k_{21}/\lambda_2\lambda_3 + k_{41}(k_{21} - \lambda_2)/\lambda_2(\lambda_2 - \lambda_3)] \exp(-\lambda_2 t) + k_{41}(\lambda_3 - k_{21})/\lambda_3(\lambda_2 - \lambda_3)] \exp(-\lambda_3 t)\}$$

$$[\text{Ketol}] = [\text{ketol}]^0\{k_{14}k_{21}/\lambda_2\lambda_3 + [k_{41}(\lambda_2 - k_{12} - k_{21})/\lambda_2(\lambda_2 - \lambda_3)] \exp(-\lambda_2 t) + k_{41}(k_{12} + k_{21} - \lambda_3)/\lambda_3(\lambda_2 - \lambda_3)] \exp(-\lambda_3 t)\}$$

Can. J. Chem. Downloaded from www.nrcresearchpress.com by 79.173.37.17 on 09/08/12
For personal use only.

TABLE 2. Equilibration of enones and ketol in acid[a]

10^6k_{21}	10^6k_{12}	10^6k_{14}	10^6k_{41}	10^6k_{24}	10^6k_{42}	$10^{-5}\epsilon_1$	$10^{-5}\epsilon_2$	$10^{-5}\epsilon_3$	$10^4[A_1]_0$	$10^4[A_2]_0$
Fitted to eqs. [2] and [3]:										
2.08	1.16	10.5	93.3	0.577	2.87	4.45	3.74	9.70	3.07	2.91
(0.44)	(0.24)	(3.5)	(16.1)	(0.46)	(2.11)	(0.11)	(0.09)	(2.58)	(0.07)	(0.06)
Observed values:						4.76	3.26		3.41	2.48
1.84	1.03	14.2	84.6	0.927	3.10	4.49	3.87	6.69	4.10	2.98
(0.54)	(0.30)	(4.3)	(21.6)	(0.57)	(1.84)	(0.12)	(0.10)	(1.01)	(0.10)	(0.07)
Observed values:						4.76	3.26		4.42	2.49
Fitted to eqs. [5] and [6]:										
2.96	1.99	13.96	109.			4.35	3.51	9.33	3.18	2.64
(0.09)	(0.08)	(3.16)	(16.)			(0.08)	(0.08)	(1.65)	(0.06)	(0.06)
Observed values:						4.76	3.26		3.41	2.48
3.29	2.33	16.8	166.			4.54	3.37	11.84	4.14	2.61
(0.09)	(0.09)	(5.3)	(42.)			(0.08)	(0.07)	(2.05)	(0.07)	(0.05)
Observed values:						4.76	3.26		4.42	2.49
Average values for fits to eqs. [5] and [6]:										
3.13	2.14	14.7	116.			4.45	3.43	10.3		
(0.23)	(0.17)	(1.8)	(27.)			(0.13)	(0.10)	(1.7)		

Equilibrium constants:

K_{21} = [*E*-enone]/[Ketol] = 1.44 ± 0.55
K_{24} = [*Z*-enone]/[Ketol] = 0.160 ± 0.033
K_{14} = [*Z*-enone]/[*E*-enone] = 0.112 ± 0.019

A_1 is the ketol, A_2 is the *E*-enone, and A_4 is the *Z*-enone.

[a]In aqueous solution at 25°C; $[H^+]$ = 1.0 M. Reaction was followed by HPLC, monitoring at 220 nm. Data were fitted to the kinetic models of Schemes 2 or 3, fitting six sets of peak height vs. time data at once as described in the text. Values in parentheses are standard deviations estimated by the least-squares program. Values of "extinction coefficient" = peak height/concentration and initial concentration were treated as parameters in the fitting process but constrained to be close to the observed values. These observed values are given in the table to allow comparison of fitted and measured values.

Can. J. Chem. Downloaded from www.nrcresearchpress.com by 79.173.37.17 on 09/08/12
For personal use only.

where

$$\lambda_2 = (p + q)/2$$

$$\lambda_3 = (p - q)/2$$

$$p = k_{41} + k_{14} + k_{12} + k_{21}$$

$$q = (p^2 - 4(k_{41}k_{12} + k_{14}k_{21} + k_{41}k_{21}))^{1/2}$$

When we attempted to fit the data to the integrated rate law derived for this mechanism, we found that a satisfactory set of rate constants could be obtained, and that the uncertainties for each rate constant were less than for the corresponding rate constants when we fitted to the mechanism of Scheme 2.

For both models we fitted all the data at once, including HPLC peak heights for three species as a function of time for experiments beginning with enone and with ketol. We used the initial concentrations in the two experiments, and the "extinction coefficients" derived from calibrations as adjustable parameters, but imposed constraints upon the values of these concentrations and the extinction coefficients for enone and ketol by adding extra conditions to the program, minimizing the deviations between the adjusted parameters and the measured values. This allows some variation in these values to optimize the fit, but constrains them to remain close to the directly measured value. Since measurement is subject to error, it would be improper to treat the measured values as absolute. The quality of the final fit is shown in Fig. 5.

At this stage we have a mechanism that is consistent with the data and requires only rate constants that were defined by the data. With this we can fit the experimental points and be confident that we have parameters defining the thermodynamic equilibrium, which we have approached but not quite attained in our experiments.

From the analysis of the equilibrations in acid, we derive K_{24} = [*Z*-enone]/[ketol] = 0.160 ± 0.033; K_{21} = [*E*-enone]/[ketol] = 1.44 ± 0.55; K_{14} = [*Z*-enone]/[*E*-enone] = 0.112 ± 0.019. These equilibrium constants are weighted averages of the values from fits to two pairs of experiments, for each of which the uncertainties were calculated using the full covariance matrix calculated by the least-squares procedure (21).

Equilibrium constant for aldol condensation

To determine the overall equilibrium constant for the aldol condensation, K_{31}, we studied the rate of approach to equilibrium in base, for solutions containing 1.1 M acetone and 0.01 M acetophenone, with or without *E*-enone. The results of least-squares fitting to these data are found in Table 3, and the quality of the fit is shown in Fig. 6. The actual experimental data are found in Table S2.[3] We also examined the initial stages of retroaldol reactions of both *E*-enone and ketol using HPLC analysis. To obtain maximum sensitivity, in

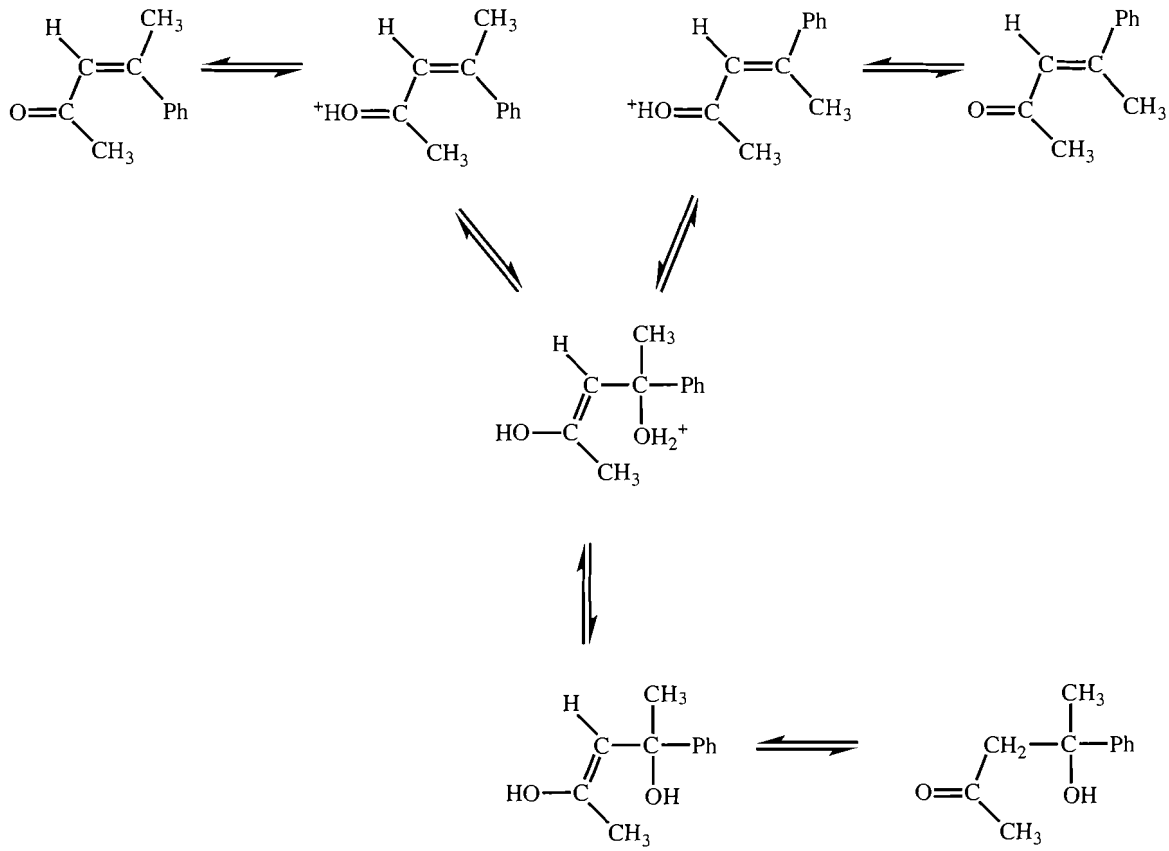

SCHEME 2

these experiments a wavelength optimized for *E*-enone was chosen that meant low sensitivity for ketol, which in any case would have been difficult to see because it eluted close to the acetophenone peak. In these experiments equilibration of the isomeric enones could be seen accompanying the approach to aldol equilibrium. Detailed interpretation of this behavior is not possible because of an unexpected problem in the analysis. Samples taken from the reaction were quenched with phosphoric acid to give near neutral solutions, which were stored for some days before HPLC analysis. Later we realized that isomerization continued even in these quenched solutions, so that relative proportions of the two enones are not meaningful. This unexpected reaction was discovered during the study of acid-catalyzed equilibration, and the experiments reported there are based on analyses carried out immediately after withdrawing and quenching samples of the reaction solution. The experiments in base are sufficient to give the information we require, and so were not repeated, but cannot be analyzed to give rates of isomerization. The data were fitted to a double exponential rate law, which allows us to determine infinity points for use in calculating the equilibrium constant. All four data sets, starting with or without *E*-enone present, and following both *E*- and *Z*-enone, were fitted simultaneously with the same apparent rate constants for all four, but with individual preexponential and constant terms. This allows all available information to be used to obtain the apparent rate constants and the infinity values needed to calculate equilibrium constants.

Analysis of the results of equilibration experiments in basic solutions containing acetone and acetophenone shows that $K_{overall}$ = [*E*-enone]/[acetone] [acetophenone] = K_{32}/K_{12} $(2.73 \pm 0.37) \times 10^{-3}$ M^{-1}, and consequently $K_{32} = (1.89 \pm 0.26) \times 10^{-3}$, and $k_{32} = (3.41 \pm 0.49) \times 10^{-4}$ M^{-2} s^{-1}.

Partitioning of the ketol in base

When the ketol is injected into 1 M NaOH, it is essentially completely converted into acetophenone (observed) and acetone (presumed), with only very small amounts of enones. The proportions, by HPLC analysis, were [acetophenone]/[*E*-enone] = $6.8 \times 10^{-3}/6.4 \times 10^{-7} = 1.1 \times 10^{4}$. This qualitatively confirms the simple interpretation of the UV kinetics presented above, namely that the ketol is converted essentially exclusively to acetone and acetophenone, whereas the *E*-enone reacts with rate-limiting hydration followed by rapid retroaldol cleavage. Since a peak of comparable size is seen for the *Z*-enone, and an unknown amount of equilibration has occurred after quenching, further analysis is pointless. When the *E*-enone is injected into 1 M NaOH, no ketol is seen at any time, but acetophenone is slowly formed, and *Z*-enone is formed by a more rapid equilibration process.

Detailed analysis of the kinetics of retroaldol reactions

For retroaldol reactions starting with the *E*-enone in base we now know that breakdown of the ketol to acetone and acetophenone is much faster than dehydration, by a factor of around 10 000. When the retroaldol reaction is followed by UV spectroscopy, a process is observed with a small amplitude, about 100 times faster than the major reaction

Can. J. Chem. Downloaded from www.nrcresearchpress.com by 79.173.37.17 on 09/08/12
For personal use only.

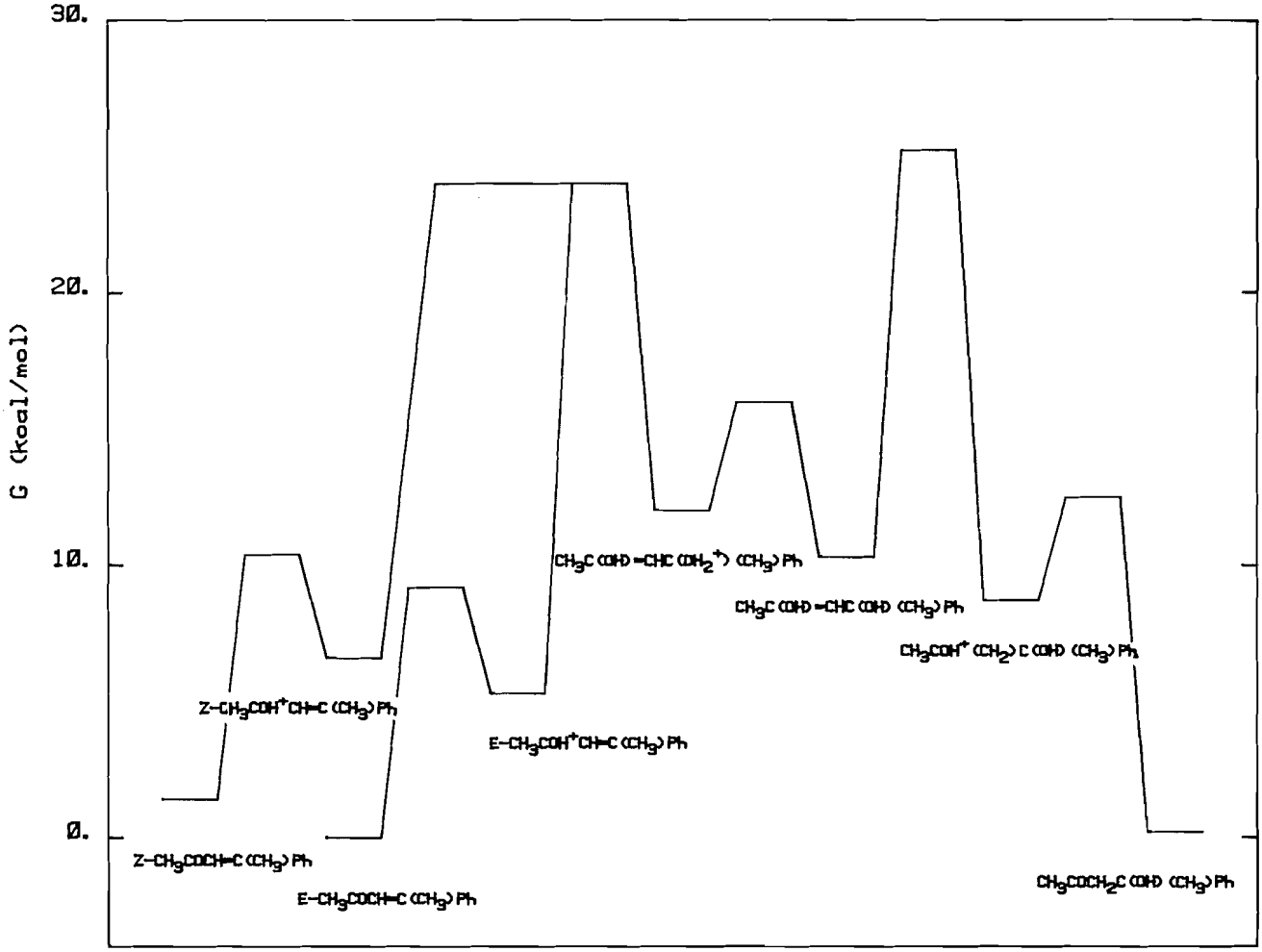

FIG. 3. Reaction coordinate diagram for equilibration of ketol and enones, using the mechanism of Scheme 2. There is an ambiguity since we do not know which of the activation barriers to dehydration from the enol of the ketol by way of the O-protonated form to *E*- or *Z*-enone is higher or if they are coincidentally the same. We have shown them both at the same level. There should be two different rotamers of the protonated enol, since deprotonation is almost certainly faster than rotation of this species, but this could clutter the diagram without there being any additional facts to add. We have assumed that proton transfers are diffusion controlled in the thermodynamically favored direction, and used estimated pK_a values of -4 for the carbonyl protonated enones (assumed to act like vinylogous acetophenone), -6.2 for the carbonyl protonated ketol (assumed to act like acetone), and -1.3 for the protonated enol; the enol content was assumed to be the same as for acetone.

process. This is now attributed to isomerization of the *E*-enone to the *Z*-enone. This must occur without intervention of the ketol. One possibility is that addition of hydroxide ion to the *E*-enone to give the enolate ion corresponding to ketol is most often followed by reversal, expulsion of hydroxide ion to give one or the other enone, and only at a lower rate followed by protonation at carbon to give the ketol. Formation of ketol constitutes essentially irrevocable commitment to cleavage. Thus the system of reactions, shown in Scheme 4, corresponds to a simplified version of the triangular reaction system discussed above for the equilibration in acid, but now $k_{21} = k_{24} = 0$, and species 2 is not the ketol but acetophenone (plus acetone). A kinetically equivalent alternative would be base-catalyzed removal of a γ-proton to give a dienolate, which could then isomerize.[5] Furthermore, since the two phases of the reaction differ by a factor of 100 in rate, we may make the further approximation: k_{14}, $k_{41} >> k_{12}$, k_{42}. Making these substitutions in the equations derived above we now obtain:

$$p = k_{12} + k_{14} + k_{41} + k_{42} \approx k_{14} + k_{41}$$

$$\gamma_1 = 0$$

$$\gamma_2 = k_{12}k_{41} + k_{12}k_{42} + k_{14}k_{42} \approx k_{12}k_{41} + k_{14}k_{42}$$

$$\gamma_3 = 0$$

$$q = (p^2 - 4\gamma_2)^{1/2}$$

$$\lambda_2 = (p + q)/2 \approx p \approx k_{14} + k_{41}$$

$$\lambda_3 = (p - q)/2 \approx \gamma_2/p \approx (k_{12}k_{41} + k_{14}k_{42})/(k_{14} + k_{41})$$

$$\lambda_2\lambda_3 = \gamma_2$$

[5]We thank a referee for suggesting this alternative mechanism.

Can. J. Chem. Downloaded from www.nrcresearchpress.com by 79.173.37.17 on 09/08/12
For personal use only.

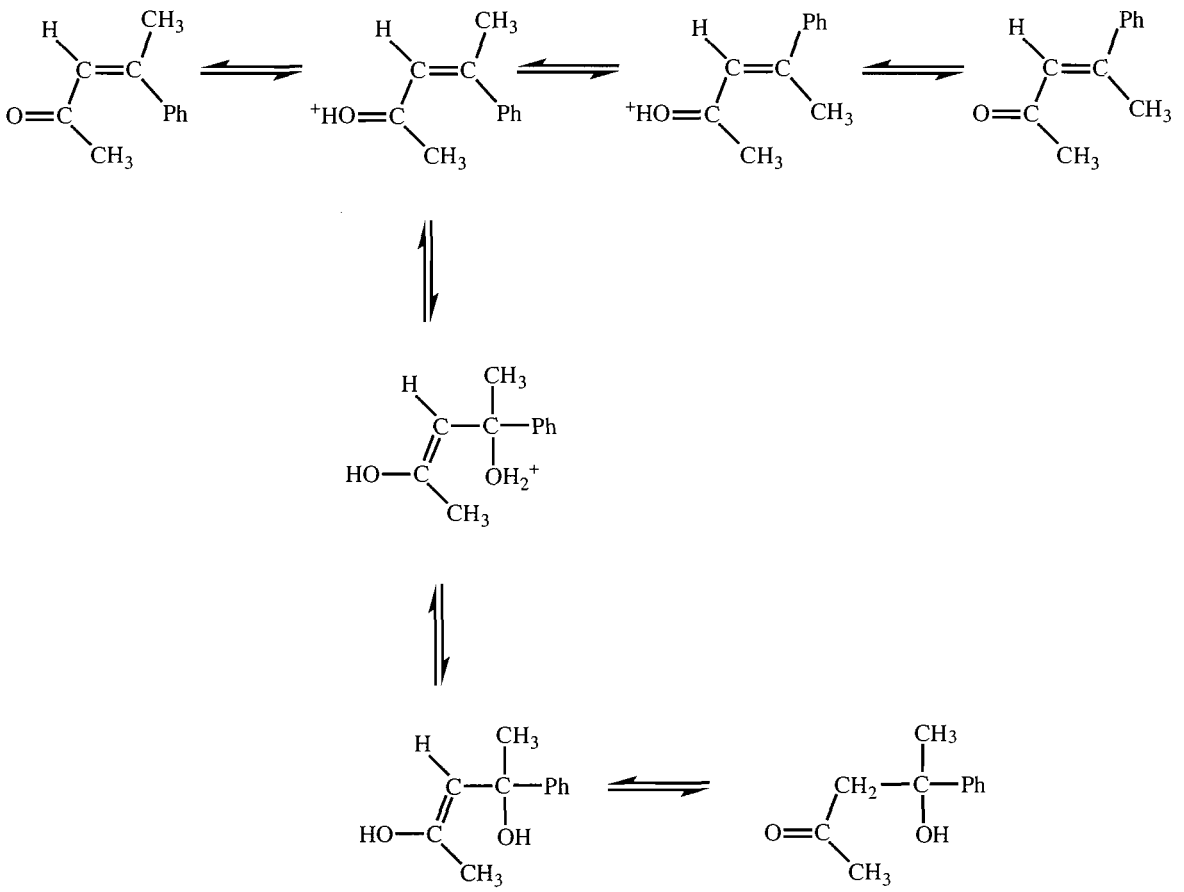

SCHEME 3

$$[E\text{-enone}] = \{C_0(k_{14} - \lambda_3)/(\lambda_2 - \lambda_3)\} \exp(-\lambda_2 t) - \{C_0(k_{14} - \lambda_2)/(\lambda_2 + \lambda_3)\} \exp(-\lambda_3 t)$$
$$\approx \{C_0 k_{14}/(k_{14} + k_{41})\} \exp(-\lambda_2 t) + \{C_0 k_{41}/(k_{14} + k_{41})\} \exp(-\lambda_3 t)$$

[7] $$[\text{Acetophenone}] = C_0 + \{C_0(\lambda_3 - k_{12})/(\lambda_2 - \lambda_3)\} \exp(-\lambda_2 t) - \{C_0(\lambda_2 - k_{12})/(\lambda_2 - \lambda_3)\} \exp(-\lambda_2 t)$$
$$\approx C_0 + \{C_0 k_{14}(k_{42} - k_{12})/(k_{14} + k_{41})^2\} \exp(-\lambda_2 t) - \{C_0\} \exp(-\lambda_2 t)$$

$$[Z\text{-Enone}] = -\{C_0 k_{14}/(\lambda_2 - \lambda_3)\} \exp(-\lambda_2 t) + \{C_0 k_{14}/(\lambda_2 - \lambda_3)\} \exp(-\lambda_2 t)$$
$$\approx -\{C_0 k_{14}/(k_{14} + k_{41})\} \exp(-\lambda_2 t) + \{C_0 k_{14}/(k_{14} + k_{41})\} \exp(-\lambda_2 t)$$

Then the absorbance at any time is given by:

$$\text{Absorbance} = \epsilon_1[E\text{-enone}] + \epsilon_2[\text{acetophenone}] + \epsilon_4[Z\text{-enone}]$$
$$= C_0\epsilon_2 + \{C_0 k_{14}/(k_{14} + k_{41})\}\{\epsilon_1 + \epsilon_2(k_{42} - k_{12})/(k_{14} + k_{41}) - \epsilon_4\} \exp(-\lambda_2 t)$$
$$+ \{C_0/(k_{14} + k_{41})\}\{\epsilon_1 k_{41} - \epsilon_2(k_{14} - k_{41}) + \epsilon_4 k_{14}\} \exp(-\lambda_3 t) = C_0\epsilon_2 + \alpha \exp(-\lambda_2 t) + \beta \exp(-\lambda_3 t)$$

Since $\epsilon_2 \approx \epsilon_1/10$, and $k_{42} \approx 10k_{12}$, and $k_{12} \approx k_{14}/100$, and $\alpha \approx \beta/10$, we may conclude that $\alpha \approx \{C_0 k_{14}/(k_{14} + k_{41})\}(\epsilon_1 - \epsilon_4)$, which means that the two geometrical isomers have rather similar extinction coefficients, that for the *E*-enone being somewhat larger.

The analysis so far leads to the reaction coordinate diagram shown in Fig. 7. This figure is drawn for the addition–elimination mechanism for isomerization. If isomerization occurs by a deprotonation–reprotonation mechanism, then an additional pair of dienolate intermediates, and three transition states, all *lower* than G_{45}* or G_{15}* would have to be added to the diagram. There would be no change to the analysis that follows. It is possible to derive a relationship between k_{42} and k_{12}; this is most readily done using free energies, and referring to Fig. 7. If species 5 is the enolate of the ketol, then

$$\Delta G^{\ddagger}_{12} = G_{52} - G_1$$
$$\Delta G^{\ddagger}_{42} = G_{52} - G_4$$
$$\Delta G^{0}_{14} = G_4 - G_1$$

Can. J. Chem. Downloaded from www.nrcresearchpress.com by 79.173.37.17 on 09/08/12
For personal use only.

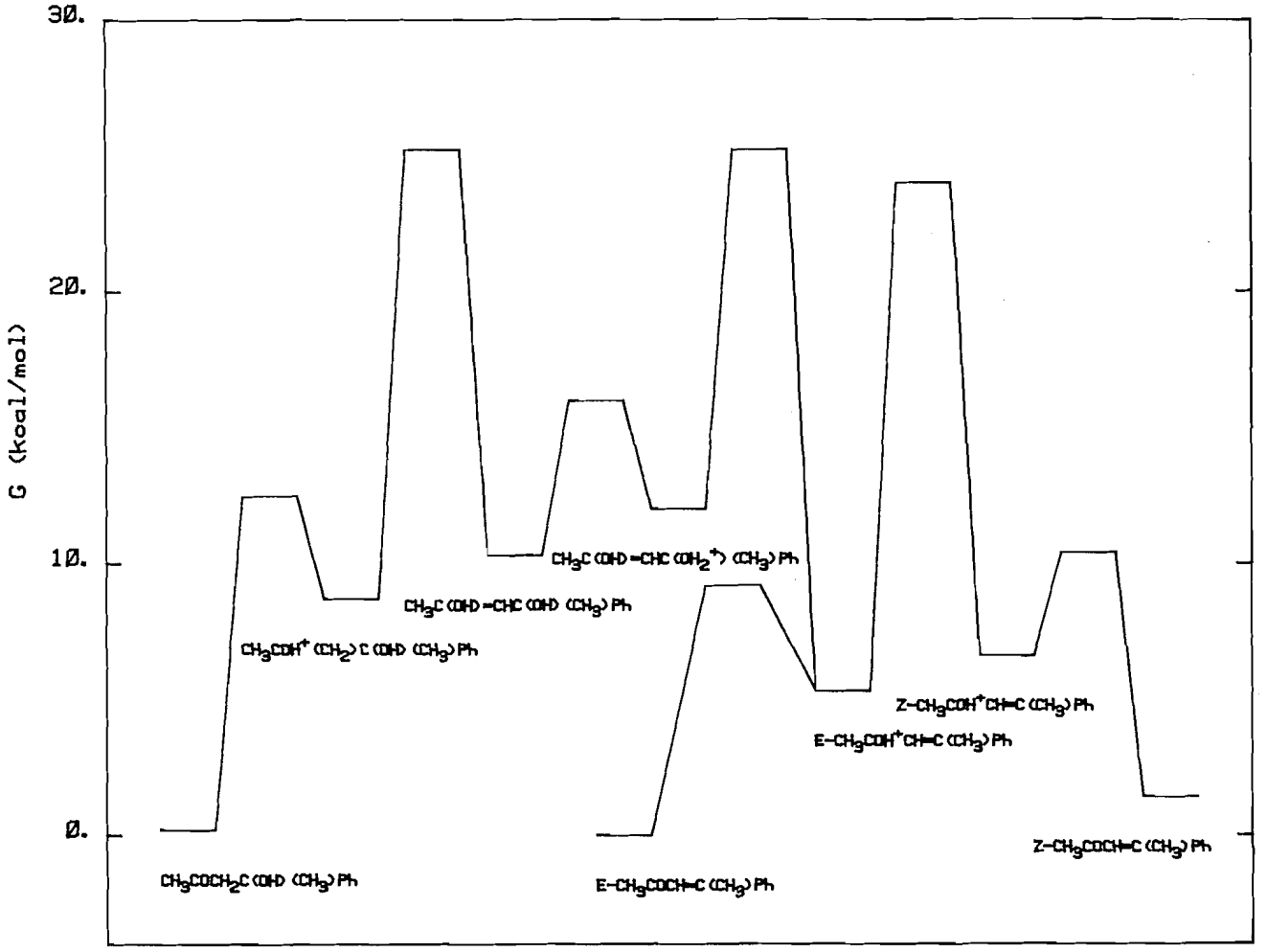

FIG. 4. Reaction coordinate diagram for equilibration of ketol and enones, using the mechanism of Scheme 3. There is an ambiguity because we do not know whether conversion of carbonyl protonated *E*-enone to the enolized ketol or ketonization of the ketol is rate limiting; we have drawn both transition states at the same level. The same assumptions were made concerning basicity of reactants as for Fig. 3.

$$\Delta G^{\ddagger}_{12} - \Delta G^{\ddagger}_{42} = G_4 - G_1 = \Delta G^{0}_{14}$$

$$k_{12}/k_{42} = K_{14}$$

$$k_{42} = k_{12}/K_{14}$$

Now we can simplify the expression for λ_3:

$$\lambda_3 \approx (k_{12}k_{41} + k_{14}k_{42})/(k_{14} + k_{41})$$

$$= k_{12}/(1 + k_{14}/k_{41}) + k_{42}(k_{14}/k_{41})/(1 + k_{14}/k_{41})$$

$$= k_{12}/(1 + K_{14}) + k_{12}(1/K_{14})K_{14}/(1 + K_{14})$$

$$= 2k_{12}/(1 + K_{14})$$

This result is at first surprising, but simply means that if two rapidly interconverting species can both go to product, there are in effect two reaction channels, and reaction is twice as fast as if there were only one. Since the observed value for $\lambda_3 = (9.99 \pm 0.25) \times 10^{-6}\ M^{-1}\ s^{-1}$, and $K_{14} = 0.112 \pm 0.019$, we may now calculate $k_{12} = (9.99 \pm 0.25) \times 10^{-6}\ M^{-1}\ s^{-1}\ (1 + 0.112 \pm 0.019)/2 = (5.55 \pm 0.17) \times 10^{-6}\ M^{-1}\ s^{-1}$. It follows that $k_{42} = k_{12}/K_{14} = (4.96 \pm 0.93) \times 10^{-5}\ M^{-1}\ s^{-1}$.

With k_{12} and k_{42} now determined, and K_{12} and K_{42} known from the analysis of the kinetics of equilibration in acid, we may calculate k_{21} and k_{24}, as $(8.00 \pm 0.40) \times 10^{-6}\ M^{-1}\ s^{-1}$ and $(7.93 \pm 2.22) \times 10^{-6}\ M^{-1}\ s^{-1}$ respectively.

We have now completed the kinetic analysis to the point of having all of the rate and equilibrium constants for the rate-limiting processes for the two principal stages of the aldol condensations leading to the *E*- and *Z*-enones.

The accuracy of the λ_2 values is low, because these parameters are determined by a small amplitude process at short times, but we can extract approximate estimates of k_{14} or k_{41}. $\lambda_2/[OH^-]$ has a weighted average value of $(3.12 \pm 0.68) \times 10^{-4}\ M^{-1}\ s^{-1}$. Since K_{14} is known from both kinetics in base, $K_{14} = 0.159 \pm 0.033$, and kinetics in acid, $K_{14} = 0.112 \pm 0.019$ (values which agree within their estimated standard deviations, we will use the more accurate value from kinetics in acid, and can calculate that $k_{14} = (3.14 \pm 0.84) \times 10^{-5}\ M^{-1}\ s^{-1}$ and $k_{41} = (2.81 \pm 0.61) \times 10^{-4}\ M^{-1}\ s^{-1}$.

Discussion

In the course of the work described in this paper we have developed computer programs written in FORTRAN that

Can. J. Chem. Downloaded from www.nrcresearchpress.com by 79.173.37.17 on 09/08/12
For personal use only.

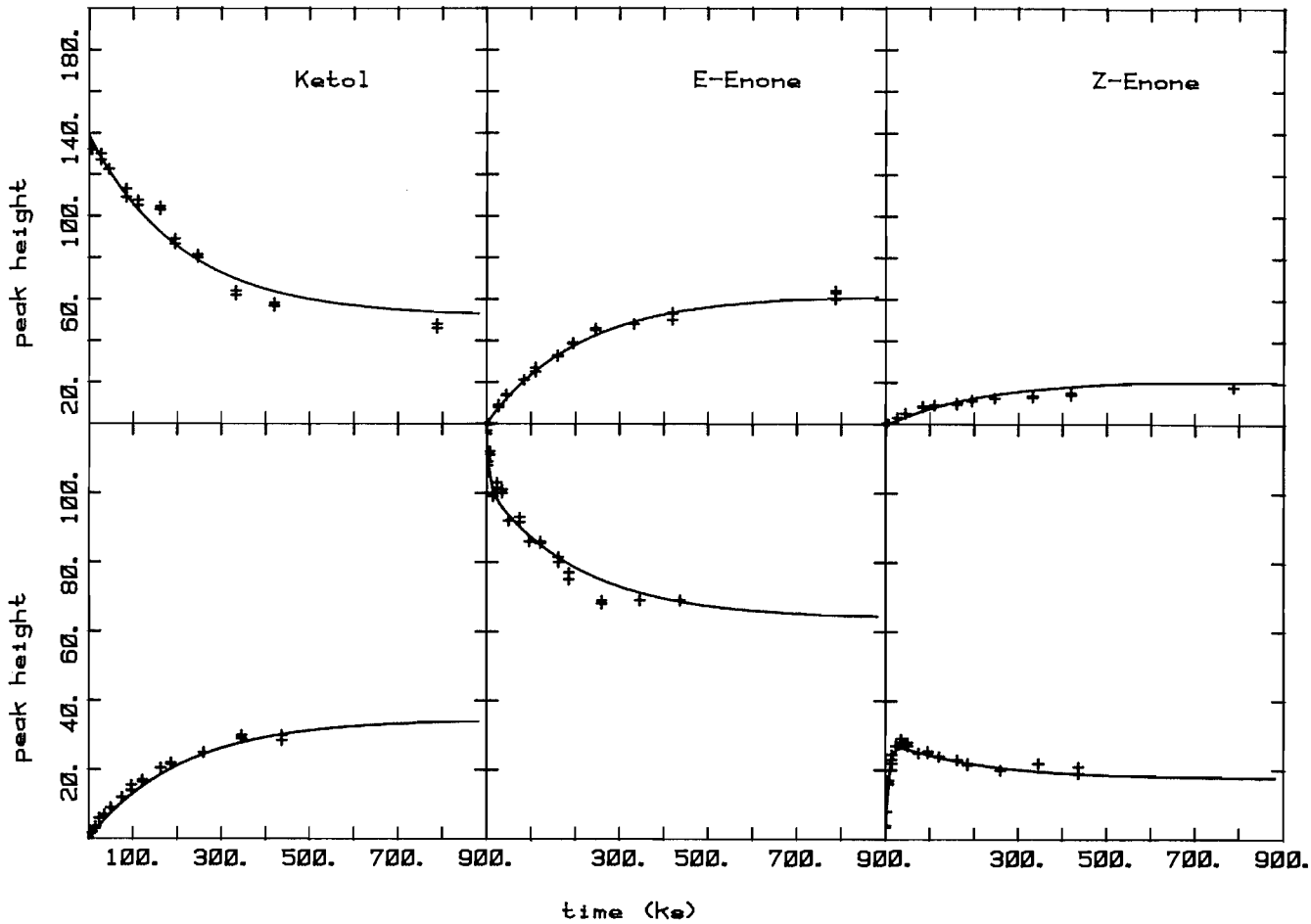

FIG. 5. Equilibration in acid; concentration of the ketol, *E*-enone, and *Z*-enone as a function of time, starting with ketol or *E*-enone. The lines are calculated using the parameters given in Table 2.

TABLE 3. Equilibrium in the aldol condensation of acetone and acetophenone by HPLC[b]

Species analyzed	[AcPh]	[Acetone]	[OH]	a_1	a_2	$10^3 a_3$	a_4	$10^6 a_5$
(*a*) Experiment starting with no enone present:								
[*E*-Enone]	0.01	1.086	0.887	221 ± 10	27 ± 30	1.86 ± 0.43	−238 ± 17	6.38 ± 0.43
[*Z*-Enone]	0.01	1.086	0.887	29 ± 9	−16 ± 29	1.86 ± 0.43	−21 ± 17	6.38 ± 0.43
Equilibrium constant = $[\text{Enone2}]_f/[\text{AcPh}]_f[\text{Acetone}]_f = 3.09 \times 10^{-3}\ \text{M}^{-1}$								
(*b*) Experiment starting with [*E*-enone] = 1.0×10^{-4} M:								
[*E*-Enone]	0.01	1.086	0.887	246 ± 15	221 ± 24	1.86 ± 0.43	677 ± 21	6.38 ± 0.43
[*Z*-Enone]	0.01	1.086	0.887	5 ± 12	−143 ± 22	1.86 ± 0.43	390 ± 19	6.38 ± 0.43
Equilibrium constant = $[\text{Enone2}]_f/[\text{AcPh}]_f[\text{Acetone}]_f = 2.36 \times 10^{-3}\ \text{M}^{-1}$								
Average value of the equilibrium constant = $(2.73 \pm 0.37) \times 10^{-3}\ \text{M}^{-1}$								

[a]In aqueous solution at 25°C, followed by HPLC analysis monitoring absorbance at 280 nm. To obtain convenient peak heights the volume injected and the absorbance scales were adjusted; for ease of comparison the peak heights have been corrected to a common basis, even though this corresponds to peaks over a meter high in some cases. Peak heights vs. time data were fitted to peak height = $a_1 + a_2(\exp(-a_3 t) + a_4 \exp(-a_5 t)$, with a_1, a_2, a_4 specific to the particular data set, while a_3 and a_5 were the same for all data sets, and all four data sets were fitted simultaneously.

allow us to fit several sets of data simultaneously with some parameters common to all sets and some specific to a particular set. Two variations on this theme were used. In the first we fitted the exact integrated rate law, using theoretical expressions for both the exponential terms (apparent rate constants) and the preexponential terms. In favorable cases, including the present example of fitting equilibration data for the two isomeric enones and the ketol in acidic solution, this

Can. J. Chem. Downloaded from www.nrcresearchpress.com by 79.173.37.17 on 09/08/12
For personal use only.

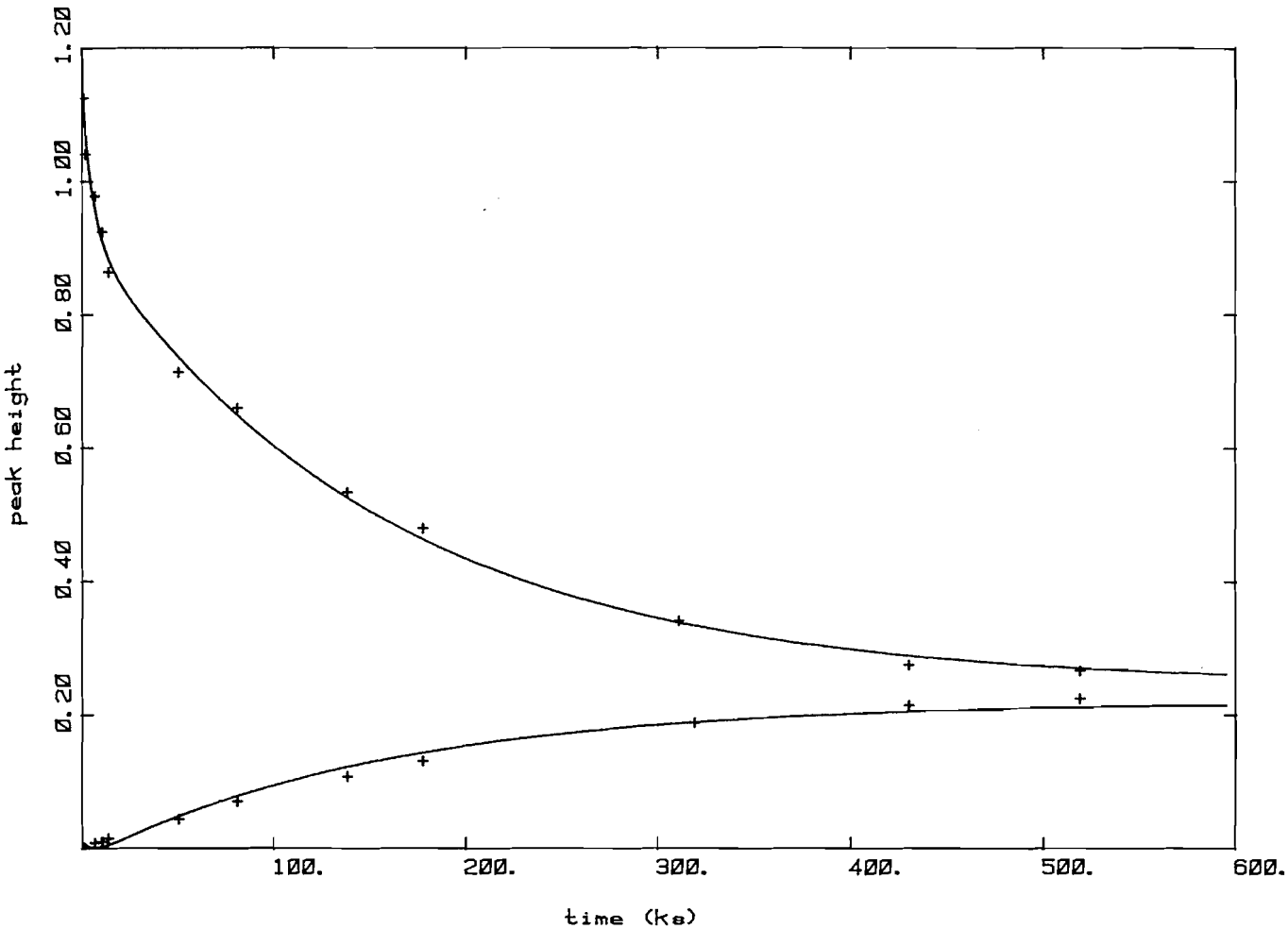

FIG. 6. Equilibration in base: the concentration of *E*-enone as a function of time (as measured by HPLC analysis), starting with either no enone present or 1.0×10^{-4} M enone present. In both cases the solution contained 1.086 M acetone and 0.010 M acetophenone, and 0.887 M NaOH.

allows direct calculation of the relevant rate constants. In the second, used where the data were less precise and we knew there were experimental problems precluding detailed interpretation, we simply fitted all sets of peak heights vs. time data to the same form of integrated rate law, with common apparent rate constants and individual preexponential terms. This allows satisfactory fitting to all the data, even when an individual data set would not give a satisfactory fit because the least-squares program could not converge. It is of course essential to be sure that all data sets used do in fact belong to a single reaction system, so that it is legitimate to apply this procedure. If this precondition is not met, then fitting in this way will provide a new way to mislead oneself.

With the ready availability of HPLC apparatus, it will become increasingly common to use this technique for reaction kinetics. The advantage is that one follows individual species (assuming satisfactory analytical conditions with good resolution); the disadvantage is that the precision is less than can be obtained by UV spectrophotometric kinetics. By treating data for all species involved in a reaction, and for sets of reaction that must have the same values for pseudo first-order rate constants, we can obtain the best possible precision, as well as having the greater accuracy inherent in having a more specific analytical technique.

The second mechanism, shown in Scheme 3, assumes that only the original isomer of the enone undergoes hydration to ketol, while the second isomer does not. This seems peculiar at first glance, but can be rationalized in terms of the conformations of the cations obtained by protonation at the carbonyl oxygen. The *E* isomer can be planar, as is required for maximum conjugative stabilization of the positive charge, although this incurs some destabilizing steric interactions. The *Z* isomer cannot be planar, and may plausibly be assumed to have the phenyl ring nearly orthogonal to the plane of the protonated enone. This avoids steric interactions of the *ortho* hydrogens with the *cis* acetyl group, but imposes interference by these *ortho* hydrogens to the attack of water on the C=C double bond. Thus acid-catalyzed interconversion of the geometrical isomers by way of the protonated enone can lead to addition of water only to the protonated *E* enone.

Further logical implications of the above mechanisms are that acid-catalyzed rotation about the C_3—C_4 bond occurs because the bond order is decreased in the cation, even though the phenyl group can provide little or no conjugative stabilization for the *Z* isomer of the cation. This seems to require that rotation from the *Z* cation to the *E* cation entails only a modest energy barrier because loss of conjugation to

Can. J. Chem. Downloaded from www.nrcresearchpress.com by 79.173.37.17 on 09/08/12
For personal use only.

Can. J. Chem. Downloaded from www.nrcresearchpress.com by 79.173.37.17 on 09/08/12
For personal use only.

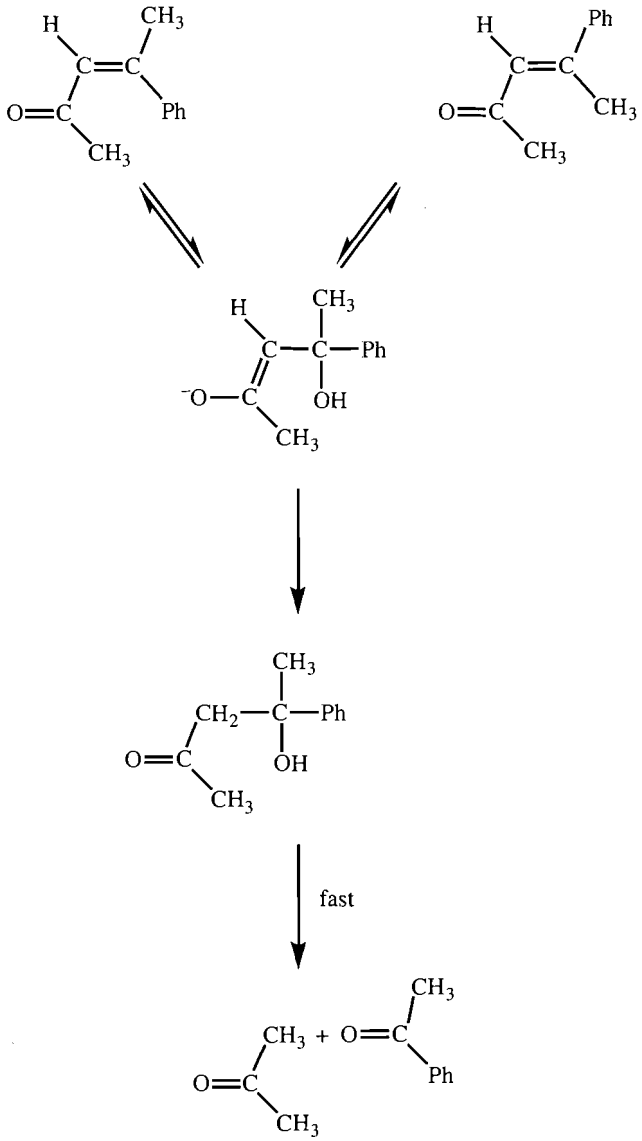

SCHEME 4

the OH can be compensated by gain of conjugation to the phenyl, which rotates as C_3—C_4 rotation occurs.

It is striking that in base, where the form of the overall kinetics followed by UV demands that the ketol undergo retroaldol much faster than dehydration to enone, equilibration of the two enones nonetheless occurs at rates competitive with retroaldol cleavage. Since our principal interest was in determining rate constants for the aldol condensation, we have not settled the mechanism of this isomerization. If it occurs by addition–elimination, then it must follow that the enolate, which is the immediate product of hydroxide addition to either enone, can rotate and expel hydroxide faster than it undergoes reprotonation. If isomerization occurs by deprotonation–reprotonation, then this must be fast relative to ketol formation.

The kinetics of equilibration were fitted to a double exponential integrated rate law. In the present case, since we did not have a sample of the *Z*-enone, and could not apply mass balance constraints, we could not determine a calibration constant for the *Z*-enone. Instead of the more elaborate procedure used for the equilibrations in acid, we simply imposed the requirement that the same apparent rate constants, for both exponentials, apply to all of the species whose reaction could be followed for a given hydroxide concentration. We could then fit four sets of peak height vs. time data (for the two isomeric enones, starting from solutions with identical hydroxide, acetone, and acetophenone concentrations, but initially zero or finite *E*-enone content) and fit simultaneously to obtain the best values of the apparent rate constants. The values so obtained are found in Table 3. Naturally, in these experiments we also observed the formation of the alternative aldol condensation product, 3-methyl-1-phenyl-2-buten-1-one.

The data in Table 4 show that there is a linear free energy relationship between the equilibrium constant for aldol addition reactions with acetone as carbon nucleophile and the equilibrium constant for the addition of water. This is illustrated in Fig. 8. Although the correlation is not exact, it is enough to suggest that there is a useful way to obtain approximate predictions.

Perhaps unsurprisingly there is much less pattern discernible in the equilibrium constants for the dehydration step. Clearly a phenyl group on the β-position of the enone favors dehydration relative to a hydrogen, as does a methyl group, and a phenyl is much more effective ($\delta \log K = +2.75$ for phenyl, +0.52 for methyl). A methyl forced to be *cis* to the acetyl group in the enone is detrimental, although the effect on $\log K_{21}$ is not uniform, $\delta \log K$ being −1.22 when the first β substituent is phenyl, and −0.35 when the first β substituent is methyl. As significant steric effects develop, the magnitude of the effect becomes specific to the particular compound, and is not susceptible to back-of-the-envelope calculations. Molecular mechanics calculations may in time be the best way to predict these effects.

When we compare the two modes of reaction possible for the crossed aldol of acetone and acetophenone we find that the reaction studied in the present work is considerably more favorable than might have been expected. As we have just shown, there is generally a correlation between the equilibrium constant for an aldol addition and that for the addition of water. The two nucleophiles, acetone and acetophenone, have very similar inherent tendencies to add to carbonyls, as measured by their γ values (4, 22), and the equilibrium constants for hydration differ by a factor of 208, favoring acetone. Thus it is disconcerting to find that the equilibrium constants for the two alternative modes of crossed aldol addition differ only by a factor of 2, favoring addition of acetophenone to acetone. Because we had expected a factor more like 200 to disfavor addition of acetone to acetophenone, we were surprised when the synthetic experiments showed that the two reactions were competitive. After the encouraging signs of predictable behavior that we had found, it is perhaps salutary to be reminded that the aldol reaction still has surprises.

Experimental

Materials

4-Hydroxy-4-phenyl-2-pentanone

Bromobenzene (11.8 g, 75 mmol) in 30 mL dry THF was dropped into magnesium turnings (1.8 g, 75 mmol) in 20 mL dry THF under nitrogen in a 100 mL round-bottomed flask with a reflux condenser over a period of 1 h and left to react at room temperature for an additional 0.5 h. A solution of 2.5 g (25 mmol) of

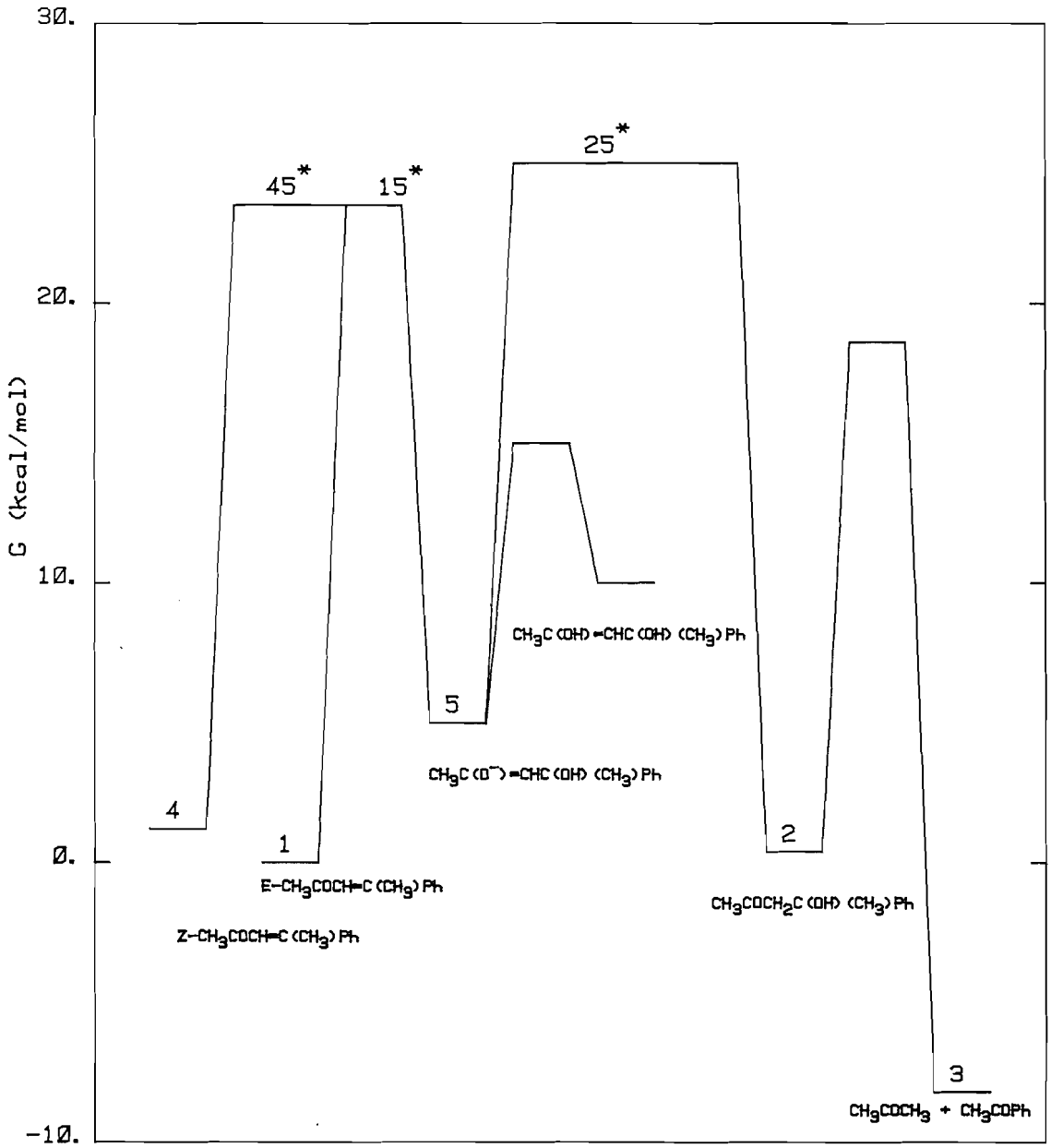

FIG. 7. Reaction coordinate diagram for equilibration of ketol and enones, using the mechanism of Scheme 4. There is an ambiguity because we do not know whether the activation barrier for conversion of the enolate of the ketol to the *E*- or *Z*-enone is higher; consequently we have drawn them both the same, equal to the observed value. As before the enol content of the ketol was assumed the same as for acetone, and a pK_a of 10 was assumed for this enol. Proton transfers to and from oxygen were assumed to be diffusion controlled in the thermodynamically favored direction.

Can. J. Chem. Downloaded from www.nrcresearchpress.com by 79.173.37.17 on 09/08/12
For personal use only.

2,4-pentanedione in 20 mL dry THF was added dropwise to the stirred solution of the Grignard reagent. After all the diketone solution was added, the reaction mixture was stirred overnight (13 h), and poured gradually into 100 mL of a stirred, ice-cold, saturated solution of ammonium chloride in water. The organic layer was separated, dried over anhydrous magnesium sulfate, filtered, and evaporated to dryness, yielding 14 g. The crude product, 1 g, from above, was chromatographed on a column of silica G, 40 g, eluted with a linear gradient (0–30%) of ethyl acetate in hexane. The eluates were pooled according to TLC analysis and evaporated separately to dryness. The fraction that had the same retention time as authentic $PhC(OH)(CH_3)CH_2COCH_3$ was pumped for a half hour to remove residual solvents, yielding 0.7 g. The proton NMR indicated that it was mainly $PhC(OH)(CH_3)CH_2COCH_3$, with some $PhC(CH_3)=CHCOCH_3$ and other impurities.

Pure 4-hydroxy-4-phenyl-2-pentanone was obtained by crystallizing relatively purified ketol at 0°C from 1:1 diethyl ether/hexane and washing with cold hexane. UV (MeOH), λ_{max}:258 nm, ϵ_{max} 187, ϵ_{280} 51. NMR ($CDCl_3$, 200 MHz), δ: 1.51 (s, 3H), 2.06 (s, 3H), 2.83, 3.19 (dd, J = 17.1 Hz, 2H), 4.54 (s, 1H), 7.22–7.45 (m, 5H); lit. (23) ($CDCl_3$, 60 MHz) δ: 8.66–7.30 (m, C_6H_5), 4.73 (s, OH), 3.43, 2.43 (dd, J = 18 Hz, 2H), 2.16 (s, CH_3-C-O), 1.60 (s, CH_3). Exact Mass calcd.: 178.0994; found: 178.0993 ± 0.00009.

4-Phenyl-3-penten-2-one

The crude product (mainly $PhC(OH)(CH_3)CH_2COCH_3$), 0.5 g, from above was added to a crucible containing a small amount of silica gel G. Three drops of 6 N HCl and a small amount of methanol were added. The entire mixture of solid and liquid was mixed

TABLE 4. Equilibrium constants for aldol addition and hydration of various carbonyl compounds[a]

Carbonyl acceptor	log K_{H_2O}	log K_{32}	log K_{21}	log K_{31}
CH_2O	1.6	6.67	−1.37	5.30
CH_3CHO	−1.72	1.59	−0.85	0.74
PhCHO	−2.83	1.07	1.38	2.45
CH_3COCH_3	−4.60	−1.41	−1.20	−2.61
$PhCOCH_3$	−6.92	−2.72	0.16	−2.56

[a]All in aqueous solution at 25°C. Equilibrium constants for addition of water taken from ref. 4; equilibrium constants for aldol addition, aldol dehydration, and aldol condensation from refs. 4 and 25 and this work.

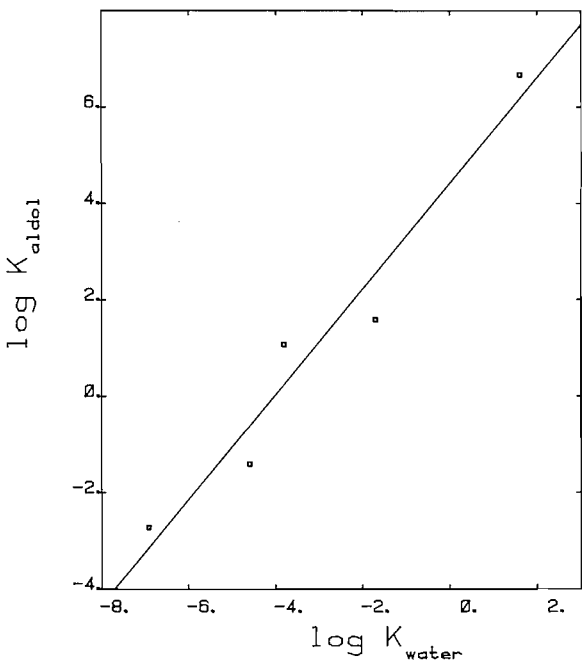

FIG. 8. Correlation between log K_{aldol} for the aldol addition of acetone as nucleophile reacting with formaldehyde, acetaldehyde, benzaldehyde, acetone, and acetophenone, and log K_{H_2O} for the addition of water. Both equilibrium constants are expressed with units of M^{-1}. The correlation line, fitted by least squares, is log K_{aldol} = 4.42 ± 0.94 + 1.09 ± 0.15 log K_{H_2O}.

completely and heated on a steam bath for 1 h. The reaction mixture was washed through filter paper, using solvent ethyl acetate. The filtrate was evaporated to dryness and loaded on a column of silica G, 40 g, eluted with a linear gradient (0–30%) of ethyl acetate in hexane. The eluates were evaporated separately to dryness according to TLC analysis.

Pure 4-phenyl-3-penten-2-one was obtained by crystallizing relatively purified enone at 0°C from 1:1 diethyl ether/hexane and washing with cold hexane. UV(MeOH), λ_{max}:280 nm, ϵ_{max} 18 300; lit. (24) (EtOH), λ_{max}: 280 nm, ϵ_{max} 19 000. NMR ($CDCl_3$, 200 MHz), δ: 2.30 (s, 3H), 2.54 (d, J = 1.3 Hz, 3H), 6.51 (m, J = 1.2 Hz, 1H), 7.26–7.50 (m, 5H); lit. (16) (CCl_4, 60 MHz), δ: 2.06 (s, 3H), 2.35 (d, J = 1 Hz, 3H), 6.21 (m, 1H), 7.10 (br s, 5H). Exact Mass calcd.: 160.0888; found: 160.0911 ± 0.0030.

Methods

Kinetics

The procedure for kinetics was as described (16). Reactions followed by UV spectroscopy were carried out in 10-cm cells holding 25 mL of solution at 25°C. Reactions that were followed by HPLC analysis were carried out in suitable vessels, thermostatted in a water bath, and samples were taken at intervals. For reactions in base, the samples were quenched with 1 M H_3PO_4; for reactions in acid the samples were quenched with 1 M Na_2HPO_4. At first quenched samples were stored and analyzed together, but it was discovered that slow equilibration of the enones was occurring in the quenched samples. For the experiments in Table 2, analysis was carried out immediately after quenching. For the experiments in Table 3, analysis was delayed, and thus no detailed interpretation of enone concentrations can be meaningful except at the end of the equilibration. The solvents used were different mixtures of methanol and water flowing at 2.0 mL/min through a C18 Radial Pak column.

Stock solutions were prepared by weighing purified compounds into volumetric flasks and diluting with solvents (spectrophotometric grade methanol or acetonitrile) to the mark. Sodium hydroxide solutions were titrated against standardized hydrochloride solution using two indicators (phenolphthalein and methyl red) and correcting for carbonate. The extinction coefficients of various compounds were measured by adding measured amounts (Hamilton syringe) of a stock solution in methanol to 25 mL of a solvent (either methanol, ethanol, water, or aqueous potassium chloride solution).

Acknowledgments

We thank the Natural Sciences and Engineering Council of Canada for financial support of this work.

1. J. P. Guthrie and X.-P. Wang. Can. J. Chem. **69**, 339 (1991).
2. J. P. Guthrie and S. O'Leary. Can. J. Chem. **53**, 2150 (1975).
3. J. P. Guthrie, J. Cossar, and B. A. Dawson. Can. J. Chem. **64**, 2456 (1986).
4. J. P. Guthrie. Can. J. Chem. **56**, 962 (1978).
5. J. P. Guthrie. Can. J. Chem. **52**, 2037 (1974).
6. J. P. Guthrie. Can. J. Chem. **59**, 45 (1981).
7. J. P. Guthrie and B. A. Dawson. Can. J. Chem. **61**, 171 (1983).
8. J. P. Guthrie, J. Cossar, P. A. Cullimore, N. M. Kamkar, and K. F. Taylor. Can. J. Chem. **61**, 2621 (1983).
9. J. P. Guthrie, K. J. Cooper, J. Cossar, B. A. Dawson, and K. F. Taylor. Can. J. Chem. **62**, 1441 (1984).
10. J. P. Guthrie, J. Cossar, and K. F. Taylor. Can. J. Chem. **62**, 1958 (1984).
11. A. de Blic and P. Maroni. Bull. Soc. Chim. Fr. 512 (1975).
12. D. S. Noyce and W. L. Reed. J. Am. Chem. Soc. **81**, 624 (1959).
13. C. C. French. J. Am. Chem. Soc. **51**, 3215 (1929).
14. K. Koelichen. Z. Phys. Chem. **33**, 129 (1900).
15. T. J. Leitereg and D. J. Cram. J. Am. Chem. Soc. **90**, 4019 (1968).
16. (*a*) J. Klein and R. Levene. J. Chem. Soc. Perkin Trans. 2, 1971 (1973); (*b*) K. Takai, M. Sato, K. Oshina, and H. Nozaki. Bull. Chem. Soc. Jpn. **57**, 108 (1984).
17. D. S. Noyce, W. A. Pryor, and P. A. King. J. Am. Chem. Soc. **81**, 5423 (1959).
18. J. L. Jensen and D. J. Carre. J. Org. Chem. **39**, 2103 (1974).
19. Y. K. Kim and J. D. Hatfield. J. Chem. Eng. Data, **30**, 149 (1985).
20. A. Ikai and C. Tanford. J. Mol. Biol. **73**, 145 (1973).
21. P. R. Bevington. Data reduction and error analysis for the physical sciences. McGraw–Hill, New York. 1969.
22. E. G. Sander and W. P. Jencks. J. Am. Chem. Soc. **90**, 6154 (1968).
23. I. Stahl, B. Schramm, R. Manske, and J. Gosselck. Liebigs Ann. Chem. 1158 (1982).
24. J. P. Phillips and F. C. Nachod (*Editors*). Organic electronic spectral data. Vol. IV. Wiley, New York. 1963. p. 340.
25. J. P. Guthrie. J. Am. Chem. Soc. **113**, 7249 (1991).

Can. J. Chem. Downloaded from www.nrcresearchpress.com by 79.173.37.17 on 09/08/12
For personal use only.

Silicon cation and anion chemistry in a fuel-rich, methane–oxygen flame

J. Hugh Horton and John M. Goodings[1]

Department of Chemistry, York University, 4700 Keele Street, North York, Ont., Canada M3J 1P3

Received July 26, 1991

J. Hugh Horton and John M. Goodings. Can. J. Chem. **70**, 1069 (1992).

Silicon cations and anions in a fuel-rich, premixed, methane–oxygen flame at atmospheric pressure doped with 0.01 mol% of trimethylsilane were observed by sampling the flame through a nozzle into a mass spectrometer. Twelve cations were observed which can be grouped into five series: $SiOH^+.nH_2O$ (n = 0–2); $SiOCH_3^+.nH_2O$ (n = 0–2); $Si(OH)_3^+.nH_2O$ (n = 0–2); cations by nucleophilic substitution (e.g., $Si(OH)(CH_3)_2(H_2O)^+$); and carbonaceous aromatic cations (c-$HSiCH{=}CH^+$ and c-$HSiCH{=}CCH_3^+$). Similarly, five anions were observed as members of two series: $H_xSiO_3^-$ (x = 0, 1) and $H_xSiO_4^-$ (x = 1–3). The chemical ionization reactions for the formation of these ions are discussed in detail, including proton transfer and also methyl cation transfer, three-body addition, nucleophilic substitution (S_N2) of both the ions themselves and also their neutral silicon precursors, and H-atom abstraction reactions. The neutral silicon chemistry in the flame is dominated by SiO, but evidence was obtained from both the cation and the anion chemistry for the presence of HSiO(OH), silanoic acid; $SiO(OH)_2$, metasilicic acid; and $Si(OH)_4$, orthosilicic acid. The silicon ion chemistry differs markedly from the normal carbon ion chemistry that occurs naturally in the undoped methane–oxygen flame; the silicon ions show a strong tendency towards Si—O bond formation. Consideration is given to the probable structures of the various silicon cations and anions observed.

J. Hugh Horton et John M. Goodings. Can. J. Chem. **70**, 1069 (1992).

On a observé des anions et des cations siliciés dans la flamme de prémélange d'un mélange de méthane–oxygène riche en méthane à la pression atmosphérique et dopé avec 0,1% de triméthylsilane, en injectant, à l'aide d'une buse, des échantillons de flamme dans un spectromètre de masse. On a observé 12 cations que l'on peut regrouper en cinq catégories : $SiOH^+.nH_2O$ (n = 0–2); $SiOCH_3^+.nH_2O$ (n = 0–2); $Si(OH)_3^+.nH_2O$ (n = 0–2); des cations obtenus par substitution nucléophile (par exemple : $Si(OH)(CH_3)_2(H_2O)^+$); et des cations carbonés aromatiques (c-$HSiCH{=}CH^+$ et c-$HSiCH{=}CCH_3^+$). D'une façon analogue, on a observé cinq anions appartenant à deux séries : $H_xSiO_3^-$(x = 0, 1); et $H_xSiO_4^-$ (x = 1–3). On discute en détail des réactions d'ionisation chimique conduisant à ces ions. Ces réactions comprennent : le transfert de proton et de cation méthyle, l'addition a trois espèces, la substitution nucléophile (S_N2) des deux anions eux-mêmes et de leur précurseur silicié et les réactions d'abstraction d'hydrogène. La chimie du silicium neutre, dans la flamme, est dominée par le SiO, mais on a obtenu des preuves de la présence de l'acide silanoique, HSiO(OH), de l'acide métasilicique, $SiO(OH)_2$, et de l'acide orthosilicique, $Si(OH)_4$, à partir de la chimie des cations et des anions. La chimie du silicium diffère nettement de la chimie d l'ion carbone normal qui se forme naturellement dans la flamme du mélange méthane–oxygène non dopé; les ions silicium exhibent une forte tendance vers la formation de liaison Si—O. On formule des hypothèses sur les structures probables des différents cations et anions siliciés observés.

[Traduit par la rédaction]

Introduction

The ion chemistry of carbon in flames has been studied for many years by sampling a flame into a mass spectrometer. A general review article is available (1), and detailed statements of both the carbon cation (2) and anion (3) chemistry have been given for the same flame employed in the present work. However, there have been very few studies of silicon ion chemistry in flames. Silicon is of interest for several reasons. One objective is a comparison with the flame-ion chemistry of carbon; that is, the extent to which the chemistry of carbon and silicon are parallel or different from one another, as well as the extent to which the two elements compete. Since silicon is found as an impurity in coal, silicon compounds are released into the atmosphere when coal is burnt. These compounds have also been observed in the Arctic haze (4). A study of the flame-ion chemistry of silicon can provide information about what silicon compounds are formed during combustion and might suggest mechanisms for their formation. Finally, several silicon compounds, especially SiO, have been implicated in the chemistry of interstellar gas clouds (5, 6).

The few studies of silicon ion chemistry in a flame which have been performed (7, 8) were primarily intended to survey the effects of various Group IV elements on flame ionization detectors. Here, we describe a more detailed study of the silicon ion chemistry taking place in a premixed hydrocarbon flame of fuel-rich composition, using trimethylsilane (TrMS) as the silicon source. Complete profiles of the ion concentrations as a function of distance along the flame axis are presented, rather than isolated measurements at a fixed point in a flame. Also, silicon anions as well as cations have been observed in this work.

Reactions of a large number of silicon ions, especially cations, have been studied using flowing afterglow and selected ion flow tube (SIFT) techniques at room temperature (9–11). These experiments encompass measurements of the kinetics of silicon ion reactions, as well as attempts to formulate mechanisms. In addition, a number of structural calculations have been carried out (5, 12). Of greatest applicability to silicon flame-ion chemistry are the studies of the structure and reactions of $SiOH^+$, and the formation and structure of $SiOCH_3^+$ (13, 14). In many ways, the flame work is complementary to the SIFT studies; our observations of ions that were also seen in the SIFT demonstrate that these ions exist in real systems such as flames. The observed flame ions also suggest that some unexplored mechanisms of silicon ion formation such as methyl cation transfer are possible.

[1]Author to whom correspondence may be addressed.

Can. J. Chem. Downloaded from www.nrcresearchpress.com by 217.78.4.112 on 09/08/12
For personal use only.

Can. J. Chem. Downloaded from www.nrcresearchpress.com by 217.78.4.112 on 09/08/12
For personal use only.

TABLE 1. Bulk characteristics of the fuel-rich flame

Flame parameter	Value
Equivalence ratio ϕ	2.15
Unburnt gas flow rates (mL s^{-1})	
CH_4	13.0
O_2	12.1
Adiabatic flame temperature (K)	2456
Measured flame temperature (K)	2200
Burnt-gas rise velocity (m s^{-1})	2.0
Equilibrium burnt-gas composition at 2200 K (mol fractions):	
H_2O	0.25144
H_2	0.41195
O_2	0.00000049
CO	0.29781
CO_2	0.034872
H	0.0036255
OH	0.00030488
O	0.00000191

When silicon compounds burn, silicon oxides are produced that are deposited on the sampling orifice of the flame-ion mass spectrometer and interfere with the sampling of the flame ions. This effect limited our experiments to low concentrations of TrMS additive in fuel-rich flames. The observation of ions in fuel-lean (i.e., oxygen-rich) flames, in which even more silicon oxides are formed, was ruled out.

Experimental

The flame used in these experiments was a premixed, laminar, fuel-rich, methane–oxygen flame at atmospheric pressure. Bulk characteristics are given in Table 1. The flame was conical in shape, ca. 3.5 mm in base diameter and 5 mm in height with a rounded tip. It was stabilized on a quartz capillary burner of inner diameter 2.3 mm, and was surrounded by a Pyrex tube of diameter 25 mm through which cold Ar flowed to minimize entrainment of ambient air. Gases used were Matheson CP-grade (CH_4 > 99.0%, Ar > 99.9%, and O_2 > 99.6%). All were added directly from high-pressure cylinders without further purification. The flame had a distinct bluish colour, and a bright blue reaction zone of thickness ca. 0.3 mm. Upon adding TrMS, the flame appeared to become slightly more purple in colour.

Silicon was added to the flame as trimethylsilane, $HSi(CH_3)_3$ (TrMS), to give a silicon concentration in the burnt gas of 0.01 mol%. The TrMS (Petrarch, 97%) was added directly from its cylinder into the oxygen gas flow feeding the burner without further purification. Since TrMS has a boiling point of about 7°C, the vapour pressure inside the cylinder (>1 atm; 1 atm = 101.3 kPa) could be readily controlled by immersion in a cooled water bath. The very small and uniform flow rate of TrMS required (0.0024 mL s^{-1}) was achieved by use of a variable leak valve (Granville–Phillips, type C).

The addition of silicon produced SiO_2 in the flame. It caused a buildup of a quartz-like deposit around the sampling orifice of the mass spectrometer, which eventually became blocked. The very small concentration level of 0.01 mol% was chosen to minimize this problem. Silicon ions could only be studied in a fuel-rich flame since a fuel-lean flame would have led to even greater SiO_2 formation. Also, a large sampling orifice of diameter ca. 0.18 mm was used. Even so, experiments could be run for only 3 h at a time before the orifice became clogged with quartz. After each run, the quartz had to be mechanically removed using a steel needle ground to a very fine point.

The burner was mounted on a motorized carriage with the flame in a vertical position to avoid distortion of axial symmetry due to buoyancy effects. The burner drive was calibrated to provide spatial resolution of ±0.02 mm when sampling ion concentrations along the flame axis, z. The burner could be positioned to provide accurate alignment of the conical flame axis with the sampling nozzle of a mass spectrometer. The nozzle itself was made by modifying a platinum electron microscope lens in the form of a "top hat" (J.B. EM Services Inc.), which was swaged into a water-cooled plate in a manner previously described (15). The lens was initially supplied with an orifice diameter of 0.15 mm that was subsequently opened up to 0.18 mm.

The flame-ion mass spectrometer has been described elsewhere in detail (2). Briefly, the sampled ions pass through two stages of differential pumping into a quadrupole mass filter. The mass-analyzed ions are detected with a parallel-plate Faraday collector connected to a vibrating reed electrometer having a grid-leak resistance of 10^{10} Ω. The data are presented below as profiles of ion signal measured in volts versus distance z along the flame axis. Cations or anions can be sampled by reversing the polarity on all electrodes. Also, total cations or total anions can be measured by switching off the dc electric voltages supplied to the quadrupole rods. However, the sensitivity for total ion signals is not the same as that for the individual ion signals, so the profile magnitudes are not directly comparable.

A method has been described (2) for locating a reproducible origin (z = 0) in the flame. It corresponds to the downstream tip of the luminous reaction zone. Thus, negative z refers to the reaction zone of the flame and positive z to the downstream region. The ion signal magnitudes given in the data below have been corrected for mass discrimination present in the filter against ions of high mass number by a method previously described (16). One problem encountered when calibrating peak magnitudes was that signal strengths would slowly decrease as the orifice became clogged by quartz deposits. Thus, peak heights were measured in the first half hour of run-time over a period of several days, and gave reproducible results.

The flame gas is cooled in passing through the thermal boundary layer surrounding the sampling orifice, and also during the expansion to supersonic velocity that proceeds inside the nozzle downstream of the orifice throat. Some ion signals can be subject to distortion during sampling by the mass spectrometer since an ion–molecule reaction having a high kinetic rate can shift in the exothermic direction (17). An example might be the formation of an ion hydrate. However, the enhancement of ion hydrates in the cold boundary layer around the sampling orifice has been minimized in the present experiments by the use of a relatively large orifice 0.18 mm in diameter.

Neutral silicon species

Before proceeding with the silicon ion chemistry, it is first necessary to consider the neutral silicon species likely to be present in the flame. Although silicon is added as trimethylsilane (TrMS), it will decompose and oxidize to give a variety of neutral species whose final equilibrium concentrations are determined by the composition of the burnt gas at 2200 K given in Table 1; at equilibrium, the chemical nature of the original additive is irrelevant. Using ΔG_f^0 values at 2200 K taken from the JANAF tables (18), a series of bimolecular reactions was chosen to encompass all of the silicon species listed in the JANAF tables of any importance, and the major neutral species present in the equilibrium burnt gas of the fuel-rich flame; the burnt-gas composition was also determined using data from JANAF tables (18). Unfortunately, thermochemical data are not available for several silicon species of interest such as silanoic acid, HSiO(OH):

TABLE 2. Equilibrium concentrations of neutral silicon species in the fuel-rich flame

Species	ΔG_f^{0a} 2200 K (kJ mol^{-1})	Reaction	ΔG_{rxn}^0 2200 K (kJ mol^{-1})	Equilibrium concentration[b] (mol fraction)
Si	144.382	$SiO + H_2 \rightarrow Si + H_2O$	286.385	5.16×10^{-10}
Si_2	219.682	$2SiH \rightarrow Si_2 + H_2$	98.788	1.16×10^{-17}
Si_3	249.366	$Si_2 + SiH \rightarrow Si_3 + H$	−34.839	3.14×10^{-24}
SiC	316.922	$SiH + CO \rightarrow SiC + OH$	466.821	1.18×10^{-18}
SiC_2	187.219	$2SiC \rightarrow SiC_2 + Si$	−302.243	4.06×10^{-20}
Si_2C	155.136	$SiC + SiH \rightarrow Si_2C + H$	−226.309	1.13×10^{-20}
SiO	−265.908	$SiO_2(g) + H_2 \rightarrow SiO + H_2O$	−97.663	1.98×10^{-3}
$SiO_2(g)$	−292.150	$SiO_2(l) \rightarrow SiO_2(g)$	220.522	5.81×10^{-6}
SiH	159.235	$Si + H_2 \rightarrow SiH + H$	109.565	1.47×10^{-10}

[a]All values of ΔG_f^0 are taken from JANAF tables (18).
[b]Equilibrium pressures of H_2, H_2O, H, CO, and OH used to calculate the partial pressures of the silicon species are given in Table 1.

metasilicic acid, $SiO(OH)_2$; and orthosilicic acid $Si(OH)_4$. The former two species have been observed using infrared spectroscopy by reacting O atoms with SiH_4 in a frozen Ar matrix (19, 20), and their presence in the flame is implied by the ions observed there. For the common silicon species, however, equilibrium constants K for the above-mentioned reactions were calculated and, ultimately, the concentration of the neutral silicon species could be determined. The calculated equilibrium concentrations are given in Table 2.

There is an interesting and important consideration for these silicon calculations in the flame context. For silicon dioxide, $SiO_2(l)$ is in equilibrium with its vapour, $SiO_2(g)$. Since the activity, a, for any liquid is essentially unity, this sets the concentration of $SiO_2(g)$ and hence the concentration of all other silicon species in a given flame (see, for example, ref. 21). Thus, no matter how much silicon is added, so long as the total concentration exceeds the maximum allowed in the gas phase given by the sum of the concentrations of all silicon gas-phase species, the rest of the silicon should exist as $SiO_2(l)$. Here, the total amount in the gas phase is approximately 0.002 mol fraction, little more than the concentration of the one dominant neutral species, SiO(g). This gives the interesting conclusion that, above a lower limit, the amount of gas-phase silicon is independent of the amount added. If less than 0.002 mol fraction were to be added, as was the case in this experiment (0.0001 mol fraction), then presumably no $SiO_2(l)$ will form. All this assumes that a normal liquid–vapour equilibrium exists for SiO_2 in the flame. If the liquid were to form as tiny droplets in the flame, there might well be surface-energy effects that were not explored in this model.

At *equilibrium*, it can be seen that SiO is by far the dominant gaseous silicon species present in the flame. This agrees well with observations of a silicon/oxygen system in a graphite furnace (22) in which SiO was found to form in the range of 1800–2200 K independent of the partial pressure of oxygen, and to dominate in this temperature region at high oxygen partial pressures. Calculations on a fuel-rich, acetylene–oxygen flame doped with silicon (8) also show SiO(g) as the dominant neutral species, with a concentration of 0.0013 mol fraction. Also, it is clear that adding massive amounts of silicon has only detrimental effects; the ion signals will not be enhanced, and the orifice will clog up with quartz more rapidly. Virtually all of the SiO_2, liquid or vapour, will eventually be deposited as quartz on the much cooler surfaces of the sampling plate.

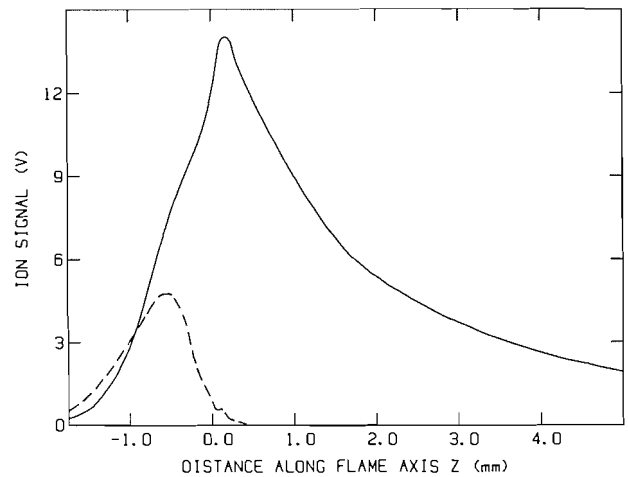

FIG. 1. Concentration profiles for the total positive ion signal (solid line) and total negative ion signal (broken line). The flame reaction zone is located upstream of $z = 0$ (negative z).

Results

All of the results presented refer to measurements made in the fuel-rich, methane–oxygen flame doped with 0.01 mol% of TrMS in the burnt gas. Total positive ion (TPI) and total negative ion (TNI) profiles are presented in Fig. 1, measured with the dc voltages to the quadrupole rods switched off. Within experimental error, these total ion profiles were unchanged when the additive was not present. Profiles for all of the individual cations containing Si observed below 160 u are given in Fig. 2. The 12 measured profiles are listed by increasing mass number and can be divided into five series on the basis of chemical similarity. These series consist of cations of the form $SiOH^+.nH_2O$ (n = 0–2); $Si(OH)_3^+.nH_2O$ (n = 0–2); $SiOCH_3^+.nH_2O$ (n = 0–2); $SiC_xH_y^+$ (x,y = 2,3 and 3,5); and the methylated cation $Si(OH)_2(CH_3)_2^+$.

Profiles for all anions containing Si observed below 160 u are presented in Fig. 3. The five measured anion profiles are similarily grouped into two series of the form $H_xSiO_3^-$ (x = 0, 1) and $H_xSiO_4^-$ (x = 1–3). In addition to

Can. J. Chem. Downloaded from www.nrcresearchpress.com by 217.78.4.112 on 09/08/12
For personal use only.

Can. J. Chem. Downloaded from www.nrcresearchpress.com by 217.78.4.112 on 09/08/12
For personal use only.

$M45^+$
$SiOH^+$
$HSiO^+$

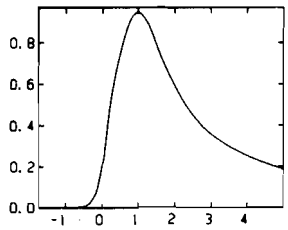

$M79^+$
$Si(OH)_3^+$
$HSi(CH_3)(OH)(H_2O)^+$

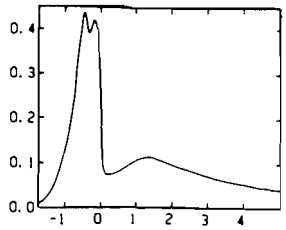

$M55^+$
$SiC_2H_3^+$
c-$HSiCH{=}CH^+$

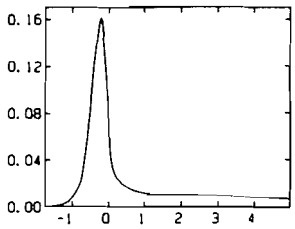

$M81^+$
$SiOH^+.2H_2O$
$HSi(OH)_2^+.H_2O$
$HSi(OH)_2(H_2O)^+$

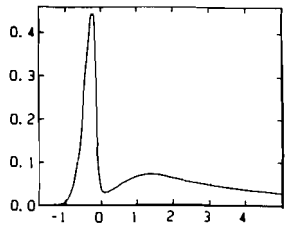

$M59^+$
$SiOCH_3^+$
$SiO(CH_3)^+$
$HSi(CH_3)_2^+$

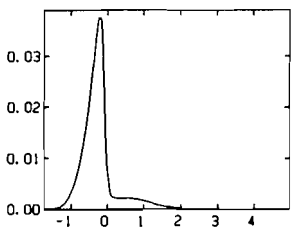

$M93^+$
$Si(OH)_2(OCH_3)^+$
$Si(CH_3)_2(OH)(H_2O)^+$
$HSi(CH_3)(OCH_3)(H_2O)^+$

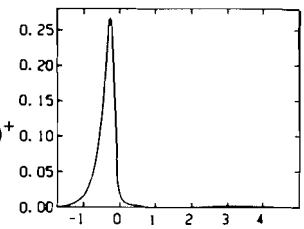

$M63^+$
$SiOH^+.H_2O$
$Si(OH)(H_2O)^+$
$HSi(OH)_2^+$

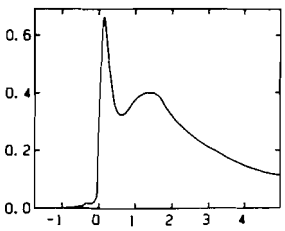

$M95^+$
$SiOCH_3^+.2H_2O$
$HSi(OH)(OCH_3)^+.H_2O$
$HSi(OH)(OCH_3)(H_2O)$
$Si(CH_3)(OH)_2(H_2O)^+$

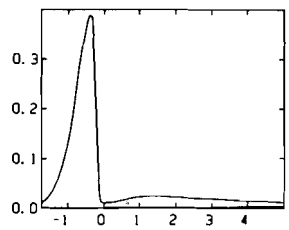

$M69^+$
$SiC_3H_5^+$
c-$HSiCH{=}CCH_3^+$

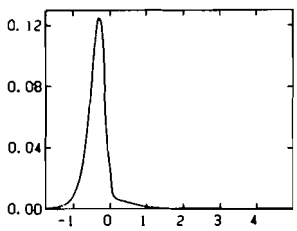

$M97^+$
$Si(OH)_3^+.H_2O$
$Si(OH)_3(H_2O)^+$

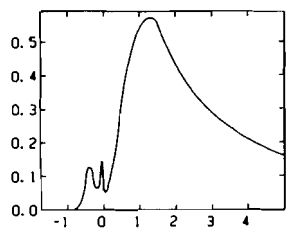

$M77^+$
$SiOCH_3^+.H_2O$
$Si(OCH_3)(H_2O)^+$
$HSi(OH)(OCH_3)^+$
$Si(CH_3)(OH)_2^+$
$SiO(CH_3)(H_2O)^+$
$HSi(CH_3)_2(H_2O)^+$

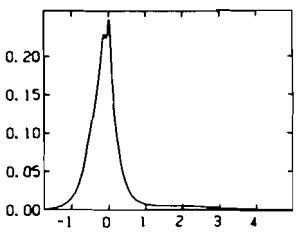

$M115^+$
$Si(OH)_3^+.2H_2O$
$Si(OH)_3(H_2O)^+.H_2O$

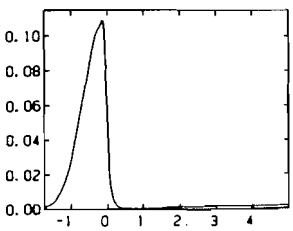

FIG. 2. Mass numbers, chemical assignments, and concentration profiles of silicon cations observed in the fuel-rich flame below 160 u. The mass number of each cation is given first, then an empirical formula that identifies it as a member of a particular series, followed by its probable structural formula(e). All profile magnitudes (see Table 3) are given in volts, plotted against distance z along the flame axis in mm. The reaction zone is located upstream of $z = 0$ (negative z).

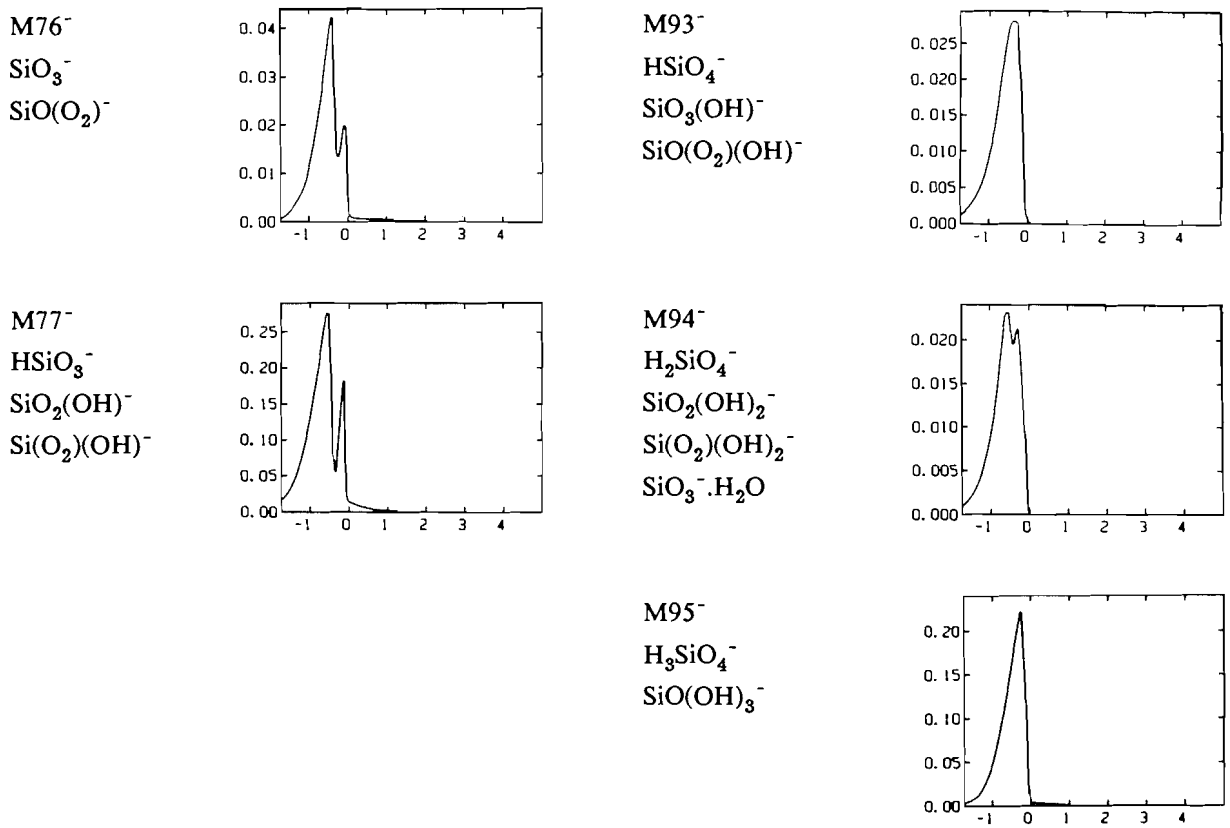

FIG. 3. Mass numbers, chemical assignments, and concentration profiles of silicon anions observed in the fuel-rich flame below 160 u. The mass number of each cation is given first, then an empirical formula that identifies it as a member of a particular series, followed by its probable structural formula(e). All profile magnitudes (see Table 3) are given in volts, plotted against distance z along the flame axis in mm. The reaction zone is located upstream of $z = 0$ (negative z).

these data, which represent profiles of ^{28}Si ions (natural abundance 92.23%), several much smaller peaks were found corresponding to the isotopes ^{29}Si (4.67%) and ^{30}Si (3.10%).

The profile labels give the mass number M of the ion and the sign of its charge, followed by an "empirical" formula and then by possible structural formulae. The empirical formula emphasizes the relationship between various families of ions, and provides an easy reference to the ion in question. Except for $M55^+$ and $M69^+$, which will be discussed later, all of the ionic structures are assumed to have Si as the central atom with hydrogen (H), hydroxy (OH), methoxy (OCH_3), and (or) methyl (CH_3) groups attached directly. The designation (H_2O) indicates a water molecule that is coordinated onto the Si atom, while $.H_2O$ indicates a hydrate formed by hydrogen bonding to the molecule's outer coordination sphere. The designation (O_2) represents an oxygen molecule coordinated onto Si, while O_x indicates x O atoms bonded individually to the Si atom.

All of the profile data are summarized in Table 3 in which the various ions are listed by empirical formula. The profiles exhibit, at most, three maxima; one or two relatively sharp peaks associated with the reaction zone near $z = 0$ (designated Reaction zone (1) and Reaction zone (2) in Table 3) and a broader peak further downstream with $z > 0$. The peak heights are measured in volts, referring to the collected ion current passing through a grid-leak resistor of 10^{10} Ω in the electrometer input circuit. Those peaks attributed to naturally occurring flame ions are noted. These were identified by comparison with profiles of the same mass number without any additive present, as well as by comparing profiles of the same chemical identity but of a different Si isotope.

Discussion

Total ion profiles

The profiles for the total positive and negative ions in the silicon-doped flame shown in Fig. 1 did not differ from those observed in the undoped flame (23). This suggests that the addition of silicon does not introduce new source or sink reactions for ions of any significance involving chemi-ionization or enhanced electron-ion recombination. Also, the very small amount (0.01 mol%) of silicon added would not be sufficient for the silicon chemistry to compete significantly with the normal hydrocarbon chemistry of the flame. For both reasons, the total ion profiles were unaffected.

The silicon additive did have an interesting effect on the *relative* peak heights of the total positive ion (TPI) and total negative ion (TNI) signals, although it was not a chemical effect. During any experimental run, the sampling orifice would clog with silicon oxides over the course of several hours. The TPI signal was affected in the expected manner; it fell from 14 to 11 V over about 3 h as the orifice clogged with SiO_2, thereby allowing less flame gas to be sampled. The TNI signal, however, became larger as time passed, climbing from 4–5 V to about 8 V over the 3-h period. Presumably this was due to the fact that three-body electron attachment, initially to O_2 molecules, is promoted in the cool boundary layer surrounding the orifice. As the orifice di-

Can. J. Chem. Downloaded from www.nrcresearchpress.com by 217.78.4.112 on 09/08/12
For personal use only.

TABLE 3. Summary of peak heights for all silicon ions below 160 u observed in the fuel-rich flame

Ion		Peak height (V)		
Mass no.	Formula	Reaction zone (1)[a]	Reaction zone (2)[a]	Downstream
45^+	$SiOH^+$	—	—	0.951
55^+	$SiC_2H_3^+$	0.161	—	0.0115
59^+	$SiOCH_3^+$	0.0376	—	0.00215
63^+	$SiOH^+.H_2O$	0.663[b]	—	0.402
69^+	$SiC_2H_5^+$	0.125	—	0.00043
77^+	$SiOCH_3^+.H_2O$	0.230	0.249[b]	0.00348
79^+	$Si(OH)_3^+$	0.438[b]	0.420	0.112
81^+	$SiOH^+.2H_2O$	0.445[b]	—	0.0701
93^+	$Si(CH_3)_2(OH)(H_2O)^+$	0.267	—	0.00112
95^+	$SiOCH_3^+.2H_2O$	0.388	—	0.0253
97^+	$Si(OH)_3^+.H_2O$	0.126[b]	0.147	0.571
115^+	$Si(OH)_3^+.2H_2O$	0.109	—	0.00172
76^-	SiO_3^-	0.0423[b]	0.0200	—
77^-	$HSiO_3^-$	0.276[b]	0.182	—
93^-	$HSiO_4^-$	0.0281	—	—
94^-	$H_2SiO_4^-$	0.0232[b]	0.0213	—
95^-	$H_3SiO_4^-$	0.222	—	—
TPI	Total +ve ions	14.0[c]	—	—
TNI	Total −ve ions	4.75[c]	—	—

[a]Refers to the profile peaks in the flame reaction zone, 1 being further upstream and 2 being closer to $z = 0$.

[b]Indicates peaks in the reaction zone that are probably due to $C_xH_yO_z^+$ ions at the same mass number.

[c]The peak heights of the total positive and total negative ions are not directly comparable to the heights of the individual ion peaks.

Can. J. Chem. Downloaded from www.nrcresearchpress.com by 217.78.4.112 on 09/08/12
For personal use only.

ameter shrinks, the effect of the boundary layer is enhanced, so that the TNI signal increases.

Positive ion chemistry

It is logical to begin discussion of the cation chemistry with those ions which are derived from the major neutral silicon species in the flame, SiO. These are ions of the $SiOH^+.nH_2O$ series and possibly also the $SiOCH_3^+.nH_2O$ series.

$SiOH^+.nH_2O$ series (n = 0–2)

The ion found at $M45^+$ is protonated SiO, formed mainly by proton transfer from H_3O^+ downstream

[1] $$SiO + H_3O^+ \rightleftarrows SiOH^+ + H_2O$$

The SiO molecule could protonate on either the O or Si site giving rise to the ions $SiOH^+$ or $HSiO^+$, respectively. *Ab initio* calculations (24) give the proton affinity (PA) at the Si site as 131.8 kcal mol^{-1} and at the O site as 192.4 kcal mol^{-1}, while an experimental value of 189.3 kcal mol^{-1} has been obtained (24). This strongly suggests that $SiOH^+$ is predominant. Either structure places a positive charge density on Si, an effect that seems to be common to many Si cations (12). In contrast, the carbon analogue, CO, protonates mainly on C instead of on O.

The $SiOH^+$ ion has been seen in a premixed acetylene–oxygen flame (8) but not in hydrogen diffusion flames (7). The profile shape shown in Fig. 2 is significant since it closely resembles that of H_3O^+ (2), although it is only about one third as high. This suggests that $SiOH^+$ is maintained primarily by the equilibrium in reaction [1]. The lack of any significant signal in the reaction zone (negative z) does not mean that SiO is not present in that region; it is more likely that other species with higher PA's compete more effectively for protons than SiO in this region.

The next two ions in this series at $M63^+$ and $M81^+$ may be thought of as the first and second hydrates of $SiOH^+$. To the best of our knowledge, neither has been observed previously in a flame. Both exist primarily in the downstream region; the peaks in the reaction zone seen in Fig. 2 are due to naturally occurring $C_xH_yO_z^+$ flame ions. The relative peak heights decrease on going from parent ion to first to second hydrate, and the peak maxima move progressively further downstream. These features suggest that three-body collisions could be responsible for their formation

[2] $$SiOH^+ + H_2O + M \rightleftarrows SiOH^+.H_2O + M$$

[3] $$SiOH^+.H_2O + H_2O + M \rightleftarrows SiOH^+.2H_2O + M$$

where M is a third body. The first hydrate at $M63^+$ has been observed in a selected ion flow tube (SIFT) experiment (13). The pseudo-second-order rate constant k for reaction [2] has been found to be 1×10^{-11} cm^3 $molecule^{-1}$ s^{-1} at 296 K and a helium pressure of 0.35 Torr (1 Torr = 133.3 Pa). The reactions of $SiOH^+$ with ethanol, formic acid, and acetic acid were also found to form $M63^+$ with a rate constant about 10 times larger. However, the concentrations of these neutral species are extremely low in the downstream region of the flame, so that such reactions are not expected to be a significant source of $M63^+$. The ion at $M63^+$ can be formed by S

insertion of $SiOH^+$ into the O—H bond of water (13). This would result in the structure $HSi(OH)_2^+$, which is simply protonated silanoic acid. Alternatively, if silanoic acid itself exists in the flame, $M63^+$ could be formed by proton transfer.

The second hydrate at $M81^+$ has been seen to form by reaction [3] (13) but no rate constant has been measured. There are two possibilities for this structure. The first is a true hydrate of $M63^+$, $HSi(OH)_2^+.H_2O$, in which the water is hydrogen-bonded to the oxygen atoms of the OH groups. The other is one in which water coordinates directly onto the silicon site, represented by $HSi(OH)_2(H_2O)^+$. This second structure is favoured because it maximizes the number of strong Si—O bonds. All of this ion chemistry is summarized in Fig. 4.

$SiOCH_3^+.nH_2O$ series (n = 0–2)

The next series involving $SiOCH_3^+.nH_2O$ can again be derived from SiO. Methyl cation transfer from protonated ketene, CH_3CO^+, the main ion seen in the reaction zone of fuel-rich flames (2), is one possible source for the $SiOCH_3^+$ ion at $M59^+$

$$[4] \quad SiO + CH_3CO^+ \rightleftarrows SiOCH_3^+ + CO$$

Extensive *ab initio* calculations have been carried out in order to determine the structure of this ion (14). These indicate that the structure in which SiO is methylated at the O site has the lowest energy. It is 25.8 kcal mol^{-1} lower in energy than H_3SiCO^+, the second most stable isomer, and 30.3 kcal mol^{-1} lower than the Si-methylated CH_3SiO^+ ion.

While $SiOCH_3^+$ has not, to the best of our knowledge, been observed in a flame, it has been studied in a SIFT experiment where it was seen to form by two mechanisms (13). The first was the reaction of methanol with Si^+

$$[5a] \quad Si^+ + CH_3OH \rightarrow SiOCH_3^+ + H_2O$$

$$[5b] \quad \rightarrow SiOH^+ + CH_3$$

which has a global rate constant k of 2.2×10^{-9} cm^3 $molecule^{-1}$ s^{-1} at 296 K, and a product distribution of 0.25 $SiOCH_3^+$ and 0.75 $SiOH^+$. This seems an unlikely mechanism in our case, as no Si^+ was observed in the flame. A more likely reaction might be

$$[6a] \quad SiOH^+ + CH_3OH \rightarrow SiOCH_3^+ + H_2O$$

$$[6b] \quad \xrightarrow{M} SiOH^+.CH_3OH$$

where the global rate constant k is 1.15×10^{-9} cm^3 $molecule^{-1}$ s^{-1} at 296 K and a helium pressure of 0.35 Torr, giving a product distribution of 0.9 $SiOCH_3^+$ and 0.1 $SiOH^+.CH_3OH$. However, it can be seen from Fig. 2 that $SiOCH_3^+$ exists mainly in the flame reaction zone where $SiOH^+$ is absent; conversely, $SiOH^+$ is prominent downstream where $SiOCH_3^+$ is disappearing. Methanol has been

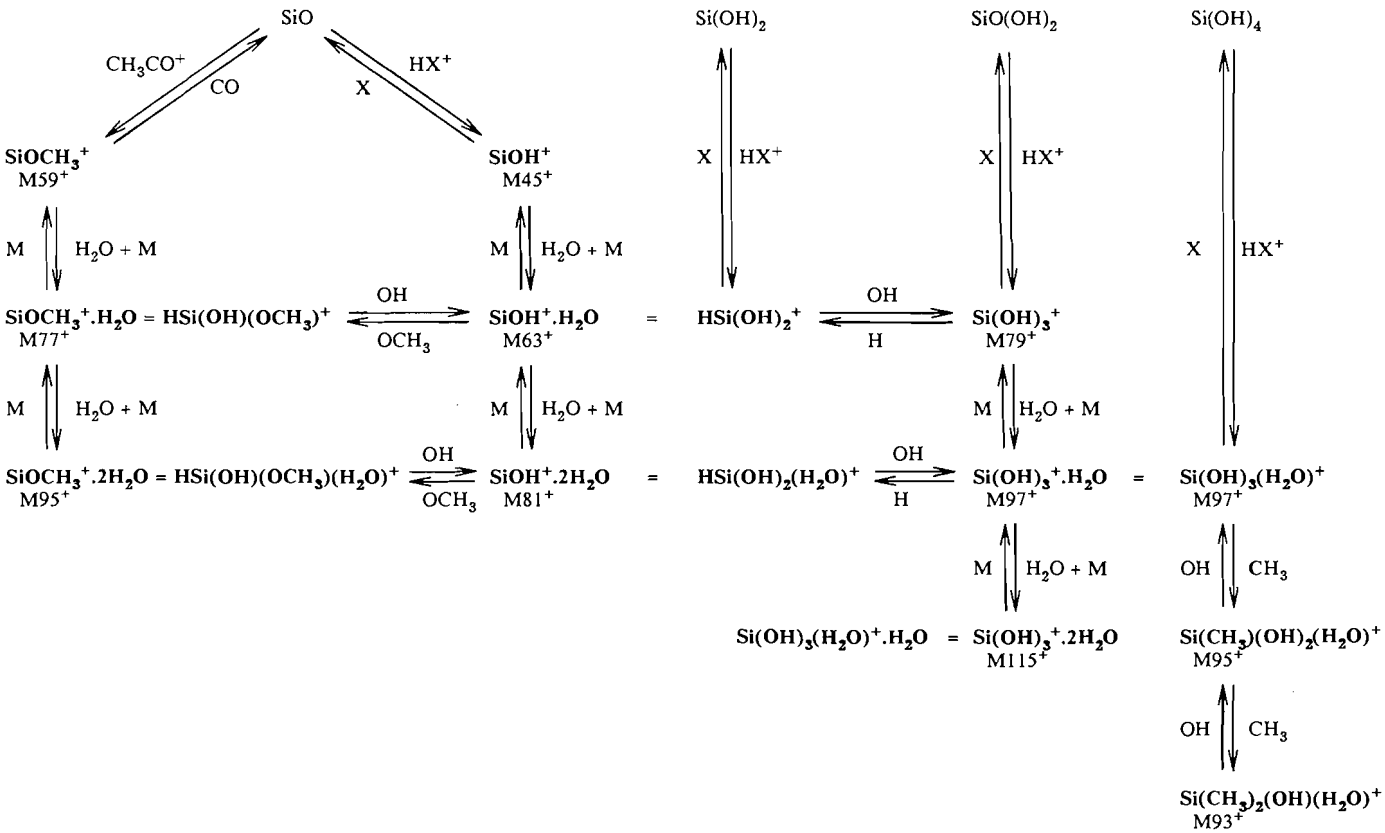

FIG. 4. Reaction flow diagram that summarizes the silicon cation chemistry leading to the ionic series $SiOH^+.nH_2O$, $SiOCH_3^+.nH_2O$, $Si(OH)_3^+.nH_2O$, and some cations formed by nucleophilic substitution. Empirical formulae and probable structural formulae for the cations are given in bold, with their mass numbers written underneath. Equivalent empirical and structural formulae are indicated with an equals sign (=). The symbols HX^+ and X represent other flame species, which are proton donors or proton receptors, respectively. Relevant silicon neutral species in the flame appear across the top of the figure.

Can. J. Chem. Downloaded from www.nrcresearchpress.com by 217.78.4.112 on 09/08/12
For personal use only.

Can. J. Chem. Downloaded from www.nrcresearchpress.com by 217.78.4.112 on 09/08/12
For personal use only.

observed in the reaction zone but not downstream in fuel-lean and stoichiometric methane–oxygen flames at 40 Torr (25). It must be present in the reaction zone of the fuel-rich flame but was not detected at a concentration level above 10^{-5} mol fraction (26). This means that the two reagents used to produce $SiOCH_3^+$ in reaction [6*a*] both exist in the flame, but in the wrong places. Thus, this mechanism, although initially attractive, appears to be a poor one in the flame context.

Ruling out the two mechanisms observed in the SIFT experiments leaves the methyl cation transfer of reaction [4]. In analogy with proton transfer reactions, methyl cation transfer has an associated methyl cation affinity (MCA) defined as the negative ΔH^0 of

$$[7] \quad B + CH_3^+ \rightarrow BCH_3^+$$

Neither the rate constant for reaction [4] nor the MCA of SiO has yet been measured. However, using empirical rules developed by McMahon *et al.* (27), one can say that for a base B of high PA (PA > 170 kcal mol^{-1}), PA(B) − MCA(B) ≈ 100 kcal mol^{-1}, giving a rough value of about 89 kcal mol^{-1} for MCA(SiO). The MCA of CO is calculated to be 80 kcal mol^{-1} (28–30). Using these numbers, reaction [4] should be exothermic by approximately 9 kcal mol^{-1}. A rate constant for reaction [4] is not easy to estimate; methyl cation transfer reactions have very variable rate coefficients that are dependent on both the nature of the methyl cation receptor B and the exoergicity of the reaction (27). The results of McMahon *et al.* suggest that if reaction [4] has a ΔG^0 value of about −27 kcal mol^{-1} or less (a reasonable expectation if ΔH^0 is approximately −9 kcal mol^{-1}), the rate constant should be in the range of $(0.5–1) \times 10^{-9}$ cm^3 $molecule^{-1}$ s^{-1}. This value is typical of many bimolecular ion–molecule reactions in the flame (31, 32).

Further evidence that reaction [4] is the source of $SiOCH_3^+$ comes from a comparison of the profile of $SiOCH_3^+$ in Fig. 2 with that of the protonated ketene ion, CH_3CO^+, at $M43^+$ (2). The shapes are very similar with a fairly sharp peak in the reaction zone and a small downstream maximum, which slowly tails off. This similarity suggests a relationship between the two ions.

The remaining two ions in this series at $M77^+$ and $M95^+$ seen in Fig. 2 can again be formed by successive hydration of the parent ion, $SiOCH_3^+$. The resultant structures should be analogous to those discussed for $SiOH^+.nH_2O$ (n = 1, 2) except that a methoxy group replaces one of the hydroxy groups. Thus, $M77^+$ is the silicon equivalent of protonated methyl formate; i.e., protonated methyl silanoate. Unlike the $SiOH^+.nH_2O$ hydrate series, however, the peak heights increase with increasing n for $SiOCH_3^+.nH_2O$. This suggests that more than simple hydration reactions are occurring.

One possibility is that ions in the $SiOCH_3^+.nH_2O$ series undergo nucleophilic substitution (S_N2) by OH radicals to yield ions of the $SiOH^+$ series; for example

$$[8] \quad HSi(OH)(OCH_3)^+ + OH \rightleftarrows HSi(OH)_2^+ + OCH_3$$

Since [OH] is much greater than [OCH_3] in the flame, such reactions would favour the production of ions of the $SiOH^+.nH_2O$ series. All of this ion chemistry is summarized in Fig. 4.

Nucleophilic substitution (S_N2) reactions

Another possible explanation for the large signals seen for the ions at $M77^+$ and $M95^+$ involves contributions by different isomers to the ion signal. This follows from the fact that there is another source of methylated silicon ions in the flame; namely, the additive TrMS. Figure 5 shows a series of neutral silicon species that may be formed by one or more nucleophilic displacements (S_N2) of CH_3 or H by OH or OCH_3 on TrMS. For example, the first neutral species in the figure, $HSi(CH_3)_2(OH)$, may be formed by the reaction

$$[9] \quad HSi(CH_3)_3 + OH \rightleftarrows HSi(CH_3)_2(OH) + CH_3$$

From Fig. 5, it is evident that there are a number of other possibilities for ions at $M59^+$, $M77^+$, and $M95^+$. A second possible isomer of $M59^+$, protonated $Si(CH_3)_2$ having the formula $HSi(CH_3)_2^+$, can be formed by protonation of $HSi(CH_3)_2(OH)$ to give $HSi(CH_3)_2(H_2O)^+$ at $M77^+$, which can then form $HSi(CH_3)_2^+$ by loss of water. In another series of reactions, $M95^+$ is formed by protonation of $Si(CH_3)(OH)_3$ to yield $Si(CH_3)(OH)_2(H_2O)^+$. Dehydration of this species then yields $Si(CH_3)(OH)_2^+$ at $M77^+$. Since all of these ions are derived by neutral nucleophilic substitution of the additive TrMS, they would be expected to contribute to the ion signal mainly in the reaction zone. Finally, if some of the $M59^+$ signal is present as the higher energy isomer $SiO(CH_3)^+$, hydration of this species would yield a further possible form of $M77^+$, $SiO(CH_3)(H_2O)^+$.

Protonation of additive products formed by nucleophilic substitution could also be responsible for the ion observed at $M93^+$. There are several possible structures at this mass number. One form is $Si(OH)_2(OCH_3)^+$, which would seem the most likely amongst the three listed in Fig. 2, since this structure maximizes the number of strong Si—O bonds. Other possibilities are $HSi(CH_3)(OCH_3)(H_2O)^+$, and $Si(CH_3)_2(OH)(H_2O)^+$. This last ion is very interesting, since it can undergo two successive nucleophilic substitutions with OH as shown in Fig. 4

$$[10] \quad Si(CH_3)_2(OH)(H_2O)^+ + OH \rightleftarrows Si(CH_3)(OH)_2(H_2O)^+ + CH_3$$

$$[11] \quad Si(CH_3)(OH)_2(H_2O)^+ + OH \rightleftarrows Si(OH)_3(H_2O)^+ + CH_3$$

to yield ions at $M95^+$ and $M97^+$. The latter ion is the second member of the $Si(OH)_3^+.nH_2O$ series discussed in the next section. All of the ion chemistry stemming from nucleophilic substitution (S_N2) reactions is summarized in Fig. 5.

$Si(OH)_3^+.nH_2O$ series (n = 0–2)

Profiles of a third series of ions involving $Si(OH)_3^+.nH_2O$ are given in Fig. 2 and their ion chemistry is summarized in Fig. 4. Members of this series have been observed, both in hydrogen diffusion flames doped with tetramethylsilane (TMS) (7), and in a premixed oxygen–acetylene flame (8). In the diffusion flame, all three ions in the series were found; $Si(OH)_3^+.H_2O$ had the largest signal, while in the premixed flame only the first two ions in the series were observed. These experiments provide data at only one fixed point downstream in the flame. The continuous ion profiles measured along the flame axis presented in Fig. 2 give a much more complete picture.

Unlike the $SiOH^+$ series, this cation series has peaks in both the reaction zone and downstream regions. The peaks *in the reaction zone* in Fig. 2 decrease in height with increasing n; in all cases where there is more than one peak in

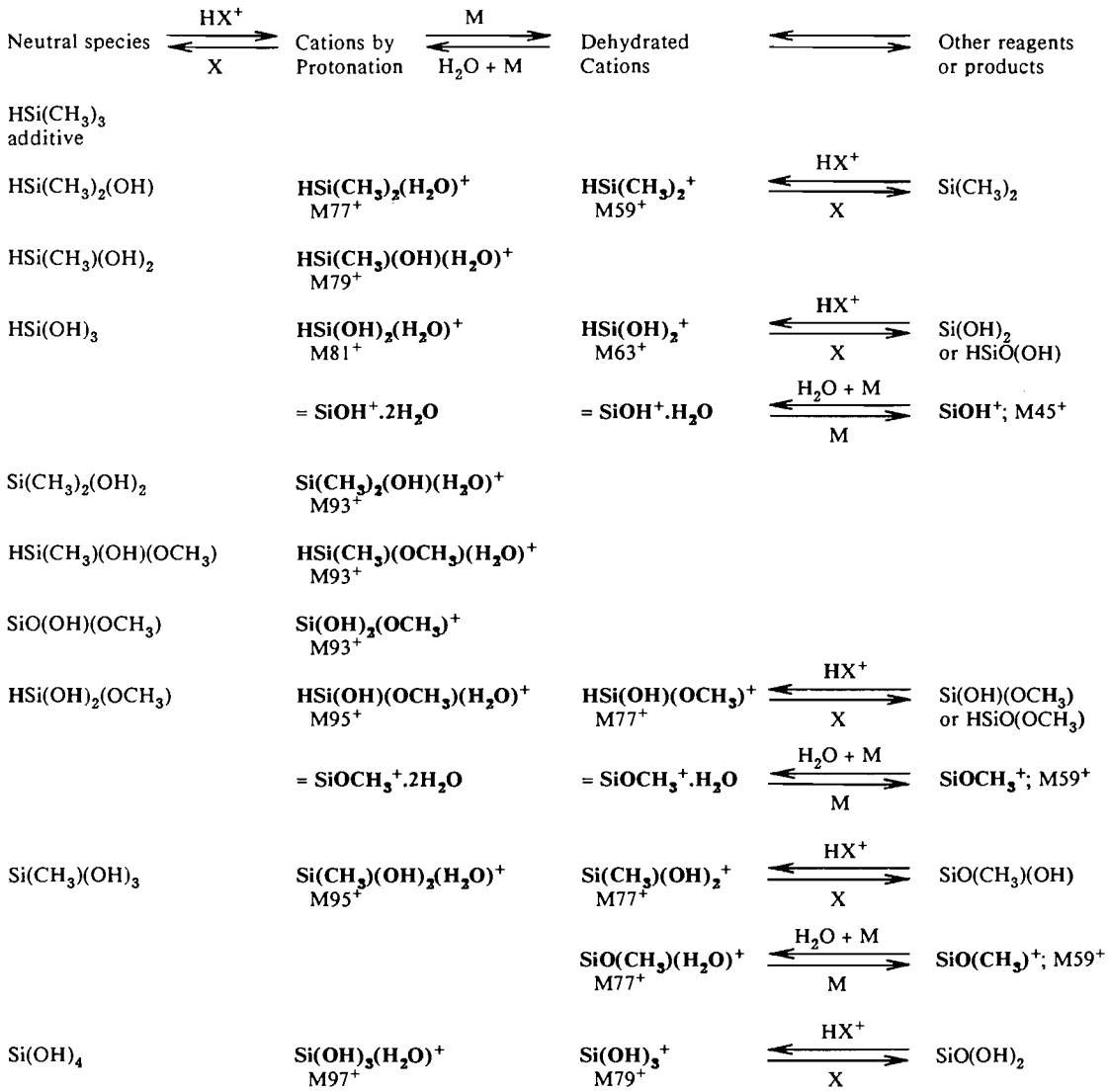

FIG. 5. Reaction flow diagram that summarizes the silicon cation chemistry initiated by neutral products arising from nucleophilic substitution (S_N2) of the trimethylsilane additive. Probable structural formulae and, in some cases, empirical formulae of the cations are given in bold with their associated mass numbers. Equivalent structural and empirical formulae are indicated with an equals sign (=). The figure indicates the formation of the primary cations by proton transfer to the substitution products, then secondary cations formed by dehydration, followed by possible tertiary steps in the reaction sequences. The symbols HX^+ and X represent other flame species, which are proton donors or proton receptors, respectively.

the reaction zone, the one associated with Si ions is closer to $z = 0$. The downstream maxima follow a different pattern; first hydrate ($M97^+$) > nude ion ($M79^+$) >> second hydrate ($M115^+$).

This difference in behaviour suggests that there are different routes to formation of the ions in the downstream region and reaction zone. In the downstream region, $M97^+$ is probably the parent ion, formed by proton transfer to neutral orthosilicic acid, $Si(OH)_4$

$$[12] \quad Si(OH)_4 + H_3O^+ \rightleftarrows Si(OH)_3(H_2O)^+ + H_2O$$

Further evidence for the presence of $Si(OH)_4$ in the flame is provided by deprotonated $Si(OH)_4$ observed in the anion chemistry discussed below. Once formed, the ion at $M97^+$ can then either gain or lose a water molecule to form $M115^+$ or $M79^+$, respectively

$$[13] \quad Si(OH)_3(H_2O)^+ + M + H_2O \rightleftarrows Si(OH)_3(H_2O)^+.H_2O + M$$

$$[14] \quad Si(OH)_3(H_2O)^+ + M \rightleftarrows Si(OH)_3^+ + H_2O + M$$

Since $Si(OH)_3^+$ is dominant in the reaction zone where $Si(OH)_4$ is presumably less abundant, another formation pathway must be found. Protonation of metasilicic acid is a possible source for this ion as indicated in Fig. 4

$$[15] \quad SiO(OH)_2 + HX^+ \rightleftarrows Si(OH)_3^+ + X$$

where the proton donor is written as HX^+ since there are a number of proton sources in the reaction zone. Once $M79^+$ is formed, it can undergo successive hydrations to form $M97^+$ and $M115^+$. Although the proton affinity of metasilicic acid is not known, the reaction is probable since protonation would remove the Si=O double bond to form a highly symmetric molecule. This mechanism is also attractive since deprotonated metasilicic acid is observed in the anion chemistry in the flame reaction zone discussed below. It might also be noted that $M79^+$ could be written as $SiO_2H^+.H_2O$, or the first hy-

Can. J. Chem. Downloaded from www.nrcresearchpress.com by 217.78.4.112 on 09/08/12
For personal use only.

drate of protonated SiO_2. However, SiO_2H^+ at $M61^+$ was not observed.

Another possible formation mechanism for ions of this series involves nucleophilic substitution of other ions already discussed

[16] $SiOH^+.H_2O$ or $HSi(OH)_2^+ + OH \rightleftarrows H + Si(OH)_3^+$

[17] $SiOH^+.2H_2O$ or $HSi(OH)_2(H_2O)^+ + OH \rightleftarrows H + Si(OH)_3(H_2O)^+$ or $Si(OH)_3^+.H_2O$

This mechanism is attractive since it links ions of the $SiOH^+$ and the $Si(OH)_3^+$ hydrate series in the downstream region, as shown in Fig. 4. The profiles of these ions given in Fig. 2 tend to suggest this link; all six profiles have similar shapes for their downstream maxima.

The structures of these ions are fairly straightforward. The $Si(OH)_3^+$ ion amounts to protonated metasilicic acid H_2SiO_3, the silicon analogue of carbonic acid. There is no known carbon analogue for this species in the flame, nor is carbonic acid itself thought to be an important flame species. The $Si(OH)_3^+.H_2O$ ion has two possible structures. First, the water molecule might be hydrogen-bonded to O atoms in the outer coordination sphere of the parent ion. However, the second possibility in which the water molecule is coordinated directly to the central silicon atom to give $Si(OH)_3(H_2O)^+$ is preferable; it is a highly symmetric tetrahedral structure that maximizes the number of Si—O bonds. In the final member of the series at $M115^+$, one water molecule must be hydrogen-bonded to give a structure represented by $Si(OH)_3(H_2O)^+.H_2O$. It is probably not a true flame ion, and arises due to cooling of the flame gas during sampling.

Carbonaceous silicon cations

The last two cations at $M55^+$ and $M69^+$ assigned to $SiC_2H_3^+$ and $SiC_3H_5^+$, respectively, are unlike the other cations previously discussed. Significantly, empirical formulae that include oxygen do not appear to be possible. The formation of numerous carbonaceous silicon ions by reaction of Si^+ with various hydrocarbons has been studied using the SIFT technique (11), and $M55^+$ is one of them. The SIFT experiments indicate that carbonaceous silicon ions are reasonably stable and many are well known. In the flame context, $M55^+$ and $M69^+$ might be expected to have rather special structures.

In our fuel-rich flame, the largest ion signal occurs at $M39^+$(2), and is attributed to $C_3H_3^+$ in which all three carbon atoms are equivalent. A similar structure involving a three-membered ring is proposed for the silicon ion observed at $M55^+$; namely, the silacyclopropenyl cation or *c*-$HSiCH{=}CH^+$, which would be aromatic with two π electrons. Writing the structure with a C=C double bond places the positive charge predominantly on the silicon atom. The ion at $M69^+$ would have a similar structure with one carbon methylated; this is the 2-methylsilacyclopropenyl cation or *c*-$HSiCH{=}CCH_3^+$.

Ab initio calculations are not available for either of these two structures although the *c*-$HSiCH{=}CH^+$ structure has been proposed (11). However, the neutral cyclic SiC_2H_4 species in which two hydrogens are attached to the Si site has been modelled (33) and found to be the second most stable structure, 15.4 kcal mol^{-1} higher in energy than the linear $H_3SiC{\equiv}CH$ isomer, the global minimum. This demonstrates that a cyclic structure for the cation, especially if it is stabilized by π delocalization, is not unreasonable.

A mechanism for the formation of these ions can be suggested, based on a possible mechanism for the formation of the naturally occurring flame ion $C_3H_3^+$ in the undoped flame (34)

[18] $CH_3CO^+ + C_2H_2 \rightarrow C_3H_3^+ + H_2CO$

Although it may take place in more than one step, the mechanism involves the reaction of protonated ketene, the major ion in the flame reaction zone, with acetylene, an important neutral intermediate in fuel-rich combustion.

By analogy, using $SiOCH_3^+$ at $M59^+$ as a precursor

[19] $SiOCH_3^+ + C_2H_2 \rightarrow SiC_2H_3^+ + H_2CO$

[20] $SiOCH_3^+ + C_3H_4 \rightarrow SiC_3H_5^+ + H_2CO$

where C_3H_4 is methylacetylene. Such a reaction would explain why $M59^+$ is such a weak signal compared with its hydrates if much of it is consumed in the formation of these carbonaceous silicon species. Clearly, however, the detailed mechanisms of reactions [18] and [19] are different from the $C_3H_3^+$ case since CH_3 is predominantly attached to the O atom in $SiOCH_3^+$ but not in the case of CH_3CO^+. While the carbonaceous silicon ions exhibit large signals in the flame reaction zone, they also survive downstream, indicating that they are stable against chemical attack in the burnt-gas region.

Anion chemistry

$H_xSiO_3^-$ series (x = 0, 1)

Profiles of the two ions of the $H_xSiO_3^-$ anion series at $M76^-$ and $M77^-$ are shown in Fig. 3. They are interesting because they are the silicon analogues of two major carbon anions, CO_3^- and HCO_3^-, seen previously in this fuel-rich flame (3). To the best of our knowledge, neither SiO_3^- nor $HSiO_3^-$ has been observed previously in a flame. However, they have been studied in a SIFT experiment (9), formed by reaction of $HSiO^-$ with various neutral reagents. For both these species, the silicon ion signal is identified with the peak closer to $z = 0$ in the profiles of Fig. 3. In each case, the larger peak further upstream arises from a naturally occurring flame ion at the same mass number.

The most likely structure for $M77^-$ is that of deprotonated metasilicic acid involving a hydroxy group attached to the Si, with the negative charge delocalized over the two individually bonded O atoms. The ion at $M76^-$ is a free radical. The first possible structure is one in which there are three individually bonded O atoms with the negative charge and unpaired electron delocalized over all three, giving SiO_3^-. The other structure is one in which O_2 is coordinated directly onto the silicon to give $SiO(O_2)^-$.

The SiO_3^- and $HSiO_3^-$ anions may be formed by a mechanism analogous to that proposed for the formation of CO_3^- and HCO_3^- in the undoped flame with CO replaced by SiO (3)

[21] $O_2^- + SiO + M \rightleftarrows SiO_3^- + M$

[22] $SiO_3^- + HY \rightleftarrows HSiO_3^- + Y$

where HY could be such flame species as H_2, OH, or H_2O.

Can. J. Chem. Downloaded from www.nrcresearchpress.com by 217.78.4.112 on 09/08/12
For personal use only.

Can. J. Chem. Downloaded from www.nrcresearchpress.com by 217.78.4.112 on 09/08/12
For personal use only.

This mechanism requires the radical anion SiO_3^- to form first. The corresponding carbon anions have peak heights that are relatively the same size, with CO_3^- always somewhat larger than HCO_3^-. In the silicon case the signal for the radical SiO_3^- is one tenth the magnitude of the $HSiO_3^-$ signal. However, it is also possible that $HSiO_3^-$ is the source of SiO_3^- and not the other way around.

An alternative mechanism is one in which $HSiO_3^-$ is formed directly from neutral metasilicic acid. The fact that protonated metasilicic acid $Si(OH)_3^+$ was also seen in the flame is good evidence that the neutral exists, and could be deprotonated by a strong base such as OH^-

[23] $OH^- + SiO(OH)_2 \rightleftarrows SiO_2(OH)^- + H_2O$

Indeed, delocalization of the Si=O double bond in metasilicic acid by formation of the negative ion might be quite favourable. Then, SiO_3^- anions could be formed by an H-atom stripping reaction in the flame

[24] $SiO_2(OH)^- + H,OH \rightleftarrows SiO_3^- + H_2, H_2O$

which is the reverse of reaction [22]. All of this ion chemistry is summarized in the reaction flow diagram given in Fig. 6.

$H_xSiO_4^-$ series (x = 1–3)

Profiles of the members of the final ion series, $H_xSiO_4^-$, at $M93^-$, $M94^-$, and $M95^-$ are given in Fig. 3. These ions have not, to the best of our knowledge, been previously observed in a flame. Again, there is an analogy to the carbon chemistry in that the ions HCO_4^- and CO_4^- have been observed in the undoped fuel-rich flame (3). These carbon ions are formed by the addition of O_2^- to CO_2, a mechanism analogous to that proposed for CO_3^- and HCO_3^- formation with CO replaced by CO_2 (3). In the silicon case with CO_2 replaced by SiO_2, the addition of SiO_2 to O_2^- could result in the analogous silicon anions. The silicon anion chemistry probably has a very different origin, however, since SiO_4^- was not observed at all, although $H_2SiO_4^-$ and $H_3SiO_4^-$ were present in the flame.

The structure of $H_3SiO_4^-$ at $M95^-$ is fairly straightforward. It is almost certainly a deprotonated $Si(OH)_4$ molecule, $SiO(OH)_3^-$, with a negative charge residing on the O atom. The $H_2SiO_4^-$ ion at $M94^-$ is more difficult to specify, and is a free radical. It is possible that the unpaired electron and negative charge are delocalized over two individually bonded O atoms with two hydroxy groups attached to Si, to give $SiO_2(OH)_2^-$. Another possible structure is one in which an oxygen molecule is coordinated to the Si centre as are the hydroxy groups, giving $Si(O_2)(OH)^-$. Also, $M94^-$ might be a hydrate of $M76^-$, $SiO_3^-.H_2O$.

The final $HSiO_4^-$ ion at $M93^-$ has two possible structures. The first is one in which three O atoms are individually bonded to Si along with one hydroxy group, $SiO_3(OH)^-$. A more reasonable structure would be an oxygen molecule coordinated to the Si centre along with an O atom and hydroxy group, giving $SiO(OH)(O_2)^-$.

The fact that neutral orthosilicic acid, $Si(OH)_4$, has already been proposed as a logical source for a flame cation, $Si(OH)_3(H_2O)^+$ at $M97^+$, and that the major ion in this series at $M95^-$ amounts to deprotonated $Si(OH)_4$, strongly suggests that orthosilicic acid must be present in the flame. It can then function as the primary source of $H_3SiO_4^-$, which can go on to produce the other series members by H-atom stripping

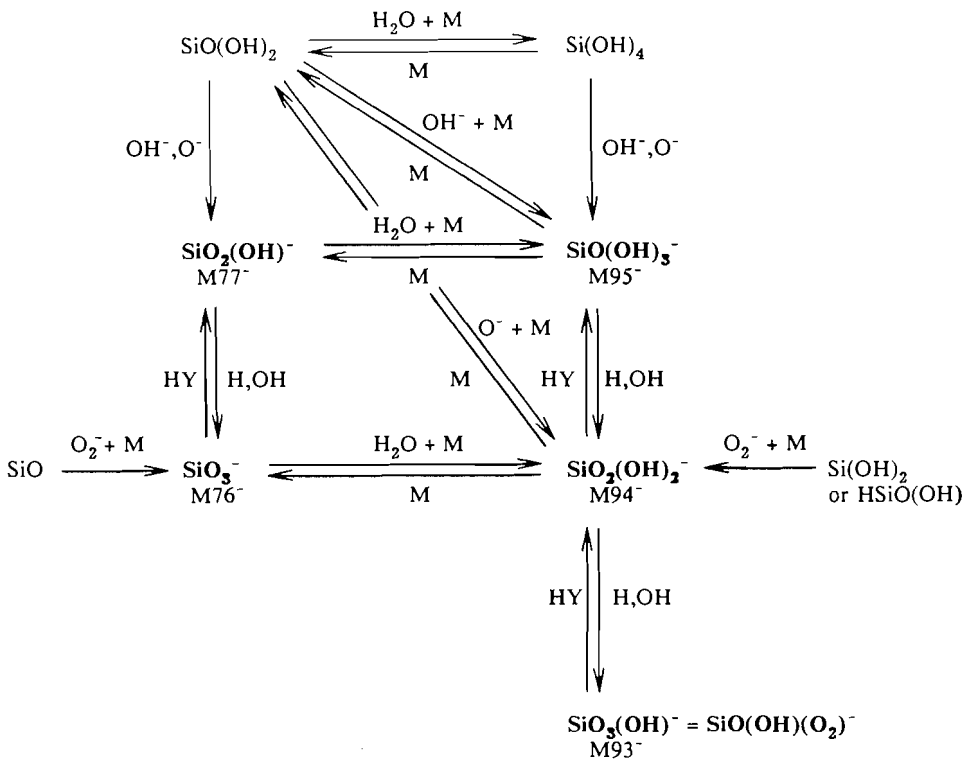

FIG. 6. Reaction flow diagram that summarizes the silicon anion chemistry leading to the ionic series $H_xSiO_3^-$ (x= 0, 1) and $H_xSiO_4^-$ (x = 1–3). Structural formulae for the anions are given in bold, with their mass numbers written underneath. The symbol HY represents an H-atom donor such as H_2 or H_2O. Relevant silicon neutral species in the flame appear around the periphery of the figure.

Can. J. Chem. Downloaded from www.nrcresearchpress.com by 217.78.4.112 on 09/08/12
For personal use only.

[25] $OH^- + Si(OH)_4 \rightleftarrows H_3SiO_4^- + H_2O$

[26] $H_3SiO_4^- + H,OH \rightleftarrows H_2SiO_4^- + H_2,H_2O$

[27] $H_2SiO_4^- + H,OH \rightleftarrows HSiO_4^- + H_2,H_2O$

This is essentially the same mechanism as that proposed in reactions [23] and [24] based on metasilicic acid for the formation of SiO_3^- and $HSiO_3^-$ in the previous section.

Hydrogen-atom abstraction from $M95^-$ is not the only possible source for $M94^-$, however. This ion could be formed by the addition of O_2^- to metasilicic acid

[28] $O_2^- + HSiO(OH) + M \rightleftarrows SiO_2(OH)_2^- + M$

or by the addition of O^- to metasilicic acid

[29] $O^- + SiO(OH)_2 + M \rightleftarrows SiO_2(OH)_2^- + M$

Metasilicic acid could also be the source of $M95^-$ by the addition of OH^-

[30] $OH^- + SiO(OH)_2 + M \rightleftarrows SiO(OH)_3^- + M$

Finally, it is also possible that $M94^-$ and $M95^-$ can be formed by three-body hydrations of $M76^-$ and $M77^-$ since the former two ions can be written as hydrates of the latter two

[31] $SiO_3^- + H_2O + M \rightleftarrows M + H_2SiO_4^-$ or $SiO_3^-.H_2O$

[32] $HSiO_3^- + H_2O + M \rightleftarrows M + H_3SiO_4^-$ or $HSiO_3^-.H_2O$

All of this ion chemistry is summarized in Fig. 6. Clearly, the anion chemistry is very interlinked. Also, it reinforces the cation chemistry with regard to the presence in the flame of the neutral silicon species SiO, $HSiO(OH)$, $SiO(OH)_2$, and $Si(OH)_4$.

Summary and conclusions

The silicon ion chemistry of a fuel-rich methane–oxygen flame doped with 0.01 mol% trimethylsilane has been studied using a flame-ion mass spectrometer. Addition of silicon to the flame did not have any observable effect on the total ion profiles, either positive or negative.

A total of 12 silicon cations was observed in the flame below 160 u. For organizational purposes, they can be grouped into five series: $SiOH^+.nH_2O$ (n = 0–2); $SiOCH_3^+.nH_2O$ (n = 0–2); $Si(OH)_3^+.nH_2O$ (n = 0–2); cations formed by nucleophilic substitution (e.g., $Si(OH)(CH_3)_2(H_2O)^+$); and carbonaceous cations, $SiC_2H_3^+$ and $SiC_3H_5^+$. The various groups overlap to some extent, particularly the cations formed by nucleophilic substitution. Similarily, five anions were observed, which are members of two series: $H_xSiO_3^-$ (x = 0, 1) and $H_xSiO_4^-$ (x = 1–3). The anions are strongly interlinked, chemically.

A number of fairly general conclusions can be drawn as a result of this work.

1. The ion chemistry of silicon differs markedly from the carbon ion chemistry that occurs naturally in the flame.

2. Silicon shows a strong preference towards Si—O bonding as opposed to Si—C bonding. Practically every ion observed contains at least one Si—O bond. The exceptions to this rule are c-$HSiCH{=}CH^+$ and c-$HSiCH{=}CCH_3^+$.

3. As has been well documented (35), silicon tends to avoid the formation of multiple bonds.

4. The silicon flame ions observed favour the coordination number 4 where possible. However, major signals were obtained for species with lower coordination numbers such as $SiOH^+$ and $Si(OH)_3^+$.

5. While most silicon cations gave signals in the flame reaction zone, every cation persisted into the burnt gas region downstream to some degree, in particular, the carbonaceous ions $SiC_2H_3^+$ and $SiC_3H_5^+$. This downstream trend is much less noticeable for the naturally occurring carbon cations in the undoped flame. Also, the downstream persistence is much less pronounced with the silicon anions, which are probably destroyed by associative electron detachment reactions with H atoms.

6. Relatively few reaction mechanisms are required to explain the silicon ion chemistry observed. These include: proton transfer to (cation formation) or from (anion formation) silicon neutral species present in the flame, and also methyl cation transfer; three-body addition reactions involving H_2O (cation chemistry) and O_2^- or O^- (anion chemistry); nucleophilic substitution (S_N2) reactions involving OH, OCH_3, H, and CH_3 on the ions themselves, but principally on the TrMS additive, which provides a variety of species as neutral reagents for chemical ionization processes; and also H-atom abstraction reactions in the anion chemistry.

7. In addition to the dominant neutral species SiO, evidence was obtained from both the cation and the anion chemistry for the presence in the flame of $HSiO(OH)$ (silanoic acid), $SiO(OH)_2$ (metasilicic acid), and $Si(OH)_4$ (orthosilicic acid). However, no direct evidence was obtained for $SiO_2(g)$.

Acknowledgements

Support of this work by the Natural Sciences and Engineering Research Council of Canada under Grant No. A-1604 is acknowledged. The authors are grateful to Professors A. C. Hopkinson and T. Carrington for helpful discussions.

1. H. F. Calcote. *In* Ion–molecule reactions. Vol. 2. *Edited by* J. L. Franklin. Plenum Press, New York, N.Y. 1972. pp. 673–706.
2. J. M. Goodings, D. K. Bohme, and C.-W. Ng. Combust. Flame, **36**, 27 (1979).
3. J. M. Goodings, D. K. Bohme, and C.-W. Ng. Combust. Flame, **36**, 45 (1979).
4. P. J. Sheridan. Atmos. Environ. **23**, 2371 (1989).
5. G. Berthier, F. Pauzat, and Y. Q. Tao. Astron. Astrophys. **135**, L1 (1984).
6. S. Wlodek and D. K. Bohme. J. Chem. Soc. Faraday Trans. **85**, 1643 (1989).
7. N. S. Ham and T. McAllister. Aust. J. Chem. **38**, 347 (1985).
8. N. S. Ham and T. McAllister. Spectrochim. Acta, **42B**, 459 (1987).
9. S. Gronert, R. A. J. O'Hair, S. Prodnuk, D. Sülzle, R. Damrauer, and C. H. DePuy. J. Am. Chem. Soc. **112**, 997 (1990).
10. D. K. Bohme. Int. J. Mass Spectrom. Ion Processes, **100**, 719 (1990).
11. S. Wlodek, A. Fox, and D. K. Bohme. J. Am. Chem. Soc. **113**, 4461 (1991).
12. A. C. Hopkinson and M. H. Lien. Can. J. Chem. **67**, 991 (1989).
13. S. Wlodek, A. Fox, and D. K. Bohme. J. Am. Chem. Soc. **109**, 6663 (1987).
14. M. H. Lien and A. C. Hopkinson. J. Org. Chem. **53**, 2150 (1988).

15. N. S. Karellas and J. M. Goodings. Int. J. Mass Spectrom. Ion Processes, **87**, 187 (1989).
16. J. M. Goodings, K. Elguindi, and D. K. Bohme. Can. J. Chem. **61**, 1703 (1983).
17. A. N. Hayhurst and D. B. Kittelson. Combust. Flame, **28**, 137 (1977).
18. M. W. Chase, C. A. Davies, J. R. Downey, D. J. Frurip, R. A. MacDonald, and A. N. Syverud. JANAF thermochemical tables. 3rd ed. J. Phys. Chem. Ref. Data, **14**, Suppl. No. 1, 1985.
19. R. Withnall and L. Andrews. J. Am. Chem. Soc. **107**, 2567 (1985).
20. R. Withnall and L. Andrews. J. Phys. Chem. **89**, 3261 (1985).
21. P. A. Rock. *In* Chemical thermodynamics. University Science Books, Mill Valley, Calif. 1983. p. 286.
22. W. Frech and A. Cedergren. Anal. Chim. Acta, **113**, 227 (1980).
23. J. M. Goodings, N. S. Karellas, and C. S. Hassanali. Int. J. Mass. Spectrom. Ion Processes, **89**, 205 (1989).
24. A. Fox, S. Wlodek, A. C. Hopkinson, M. H. Lien, M. Sylvain, C. Rodriguez, and D. K. Bohme. J. Phys. Chem. **93**, 1549 (1989).
25. J. Peeters and G. Mahnen. Symp. (Int.) Combust. (Proc.) 14th, 1973. Combustion Institute, Pittsburgh, Pa. p. 133.
26. J. W. Hastie. Combust. Flame, **21**, 187 (1973).
27. T. B. McMahon, T. Heinis, G. Nicol, J. K. Hovey, and P. Kebarle. J. Am. Chem. Soc. **110**, 7591 (1988).
28. J. C. Traeger and R. G. McLoughlin. J. Am. Chem. Soc. **103**, 3647 (1981).
29. J. C. Traeger, R. G. McLoughlin, and A. J. C. Nicholson. J. Am. Chem. Soc. **104**, 5318 (1982).
30. D. D. Wagman, W. H. Evans, V. P. Parker, R. H. Schumm, I. Halow, S. M. Bailey, K. L. Churney, and R. L. Nuttall. J. Phys. Chem. Ref. Data, **11**, Suppl. No. 1, 1982.
31. D. E. Jensen and G. A. Jones. Combust. Flame, **32**, 1 (1978).
32. D. L. Albritton. Atom. Data Nucl. Data Tables, **22**, 1 (1978).
33. M. H. Lien and A. C. Hopkinson. Chem. Phys. Lett. **80**, 114 (1981).
34. J. M. Goodings, D. K. Bohme, and T. M. Sugden. Symp. (Int.) Combust. (Proc.) 16th. 1977. Combustion Institute, Pittsburgh, Pa. 1977. p. 891.
35. A. C. Hopkinson and M. H. Lien. J. Chem. Soc. Chem. Commun. 107 (1980).

Can. J. Chem. Downloaded from www.nrcresearchpress.com by 217.78.4.112 on 09/08/12
For personal use only.

Synthesis of non-enolizable α- and β-peltatins

TONY DURST[1] AND LESLIE DONALD BEHNIA
Ottawa–Carleton Chemistry Institute, Department of Chemistry, University of Ottawa, Ottawa, Ont., Canada K1N 6N5

Received August 28, 1991

TONY DURST and LESLIE DONALD BEHNIA. Can. J. Chem. **70**, 1082 (1992).

The preparation of non-enolizable derivatives of both α- and β-peltatins via reaction of the lactone enolates of the corresponding TBDMS derivatives with CH_3I and hexachloroethane is described. These derivatives are considerably less toxic than the precursor peltatins but show, at best, only marginal activity in in vivo tests against P 388 leukemia.

TONY DURST et LESLIE DONALD BEHNIA. Can. J. Chem. **70**, 1082 (1992).

On décrit la préparation de dérivés non-énolisables des α- ainsi que β-peltatines par l'intermédiaire d'une réaction des énolates de la lactone des dérivés TBDMS correspondants avec le CH_3I et l'hexachloroéthane. Ces dérivés sont beaucoup moins toxiques que les peltatines qui leur donnent naissance; lors d'essais in vivo, ils ne présentent toutefois qu'une activité marginale contre la leucémie P388.

[Traduit par la rédaction]

Introduction

α- and β-Peltatin **1** and **2** are members of the lignan family of compounds (1). These compounds were first isolated and characterized by Hartwell in 1956 from North American podophyllin (*podophyllum peltatum L*) (2). Like the closely related podophyllotoxin, **3**, both peltatins show considerable antineoplastic activity. Clinical use of these compounds was briefly investigated in the 1950's by Greenspan but abandoned due to their high toxicity, unfavourable therapeutic ratios, and their inability to effect more than short-term tumor remissions (3).

In the case of podophyllotoxin it was eventually possible to obtain clinically important derivatives such as Etoposide and Teniposide. No therapeutically useful derivatives have been prepared from either **1** or **2** (1).

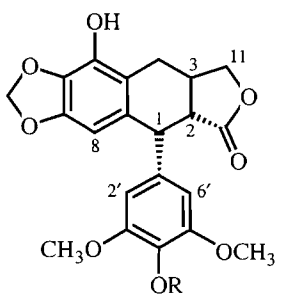

1 R = H
2 R = CH_3

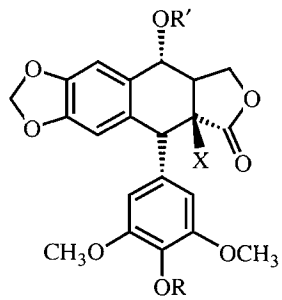

3 R = CH_3, R′ = H
X = H

In 1986 we reported the preparation of several non-enolizable podophyllotoxin derivatives, that is, compounds in which the hydrogen α to the lactone carbonyl group had been replaced by substituents such as CH_3, Cl, Br, and SCH_3 (4). In general, those compounds in which the podophyllotoxin geometry (*trans*-fused lactone, structure **3**) had been retained showed comparable or better in vivo activity against P 388 (T/C = 167 for the chloro derivative (X = Cl) at 40 mg/kg vs. 110 for podophyllotoxin) compared to podophyllotoxin itself. In addition, these derivatives were considerably less toxic. Not surprisingly, those compounds that had the picropodophyllotoxin geometry (*cis*-fused lactone) were inactive and nontoxic at the levels tested. We therefore decided to prepare the analogous derivatives of both α- and β-peltatins to see if a reduction in toxicity might allow one to observe useful anticancer activity.

Results and discussion

The peltatins were isolated from commercially available podophyllin resin. We found that further separation of the crude chromatography fractions containing both peltatins was facilitated by conversion of the phenolic hydroxyl groups to TBDMS ethers. Using this approach, we were able to isolate the TBDMS derivatives **4** and **5**. The amounts obtained are equivalent to a recovery of 8.9 and 7.6% of **1** and **2** from the commercial resin. These compare favourably with the 6.4 and 6.0% yield of these compounds obtained by Hartwell and Detty (2*b*). Further details of the isolation procedure are given in the experimental section.

The protection of the phenolic groups in **1** and **2** was also useful for the subsequent enolate formation. This proceeded smoothly for both **4** and **5** with LDA in THF at −78°C. Protonation of the enolates of **4** and **5** with H_2O at −78°C resulted in their regeneration accompanied by the *cis*-fused isomers **6** and **7**, respectively, in roughly 1:3 ratios. These ratios can be compared with the 45:55 podo- to picropodophyllotoxin ratio obtained upon protonation of the enolate of the THP of podophyllotoxin with acetic acid (5).

Reaction of the enolate of **4** with CH_3I afforded the 2-methyl *trans*-lactone **8** and the isomeric *cis*-fused lactone **9** in 38 and 56% isolated yields, respectively. Similar reaction of the enolate derived from **5** gave the methylated products **10** and **11** in 52 and 46% yields. Chlorination of these enolates with hexachloroethane was considerably more selective. Thus, the enolate of **4** gave 92% of the *trans*-lactone **12** and only 4% of the *cis*-lactone **13**, while 83% of **14** and 6% of **15** were obtained from the enolate of **5**. Similar trends in the ratios of *cis*- to *trans*-fused lactone products were observed in the podophyllotoxin series (4).

The structure and stereochemistry of the 2-substituted products were readily assigned on the basis of their ^1H NMR spectra. The relevant data are summarized in Table 1 and compared with the unsubstituted and isomerized peltatins.

Substitution at C-2 was clearly indicated by the presence of a sharp singlet due to the remaining doubly benzylic hydrogen at C-1. This signal was found in the δ = 4.2 range

[1]Author to whom correspondence may be addressed.

Can. J. Chem. Downloaded from www.nrcresearchpress.com by 92.62.229.171 on 09/08/12
For personal use only.

TABLE 1. Key chemical shifts and coupling constants in the TBDMS protected α- and β-peltatins

Compound	γ-Lactone fusion	Chemical shifts (δ) H-1	H-8	C-2′,6′	Coupling constant H3–H11 (Hz)
4	*trans*	4.57	6.27	108.4	10.1
6	*cis*	4.35	6.32	105.0	3.4
5	*trans*	4.59	6.26	108.2	10.2
7	*cis*	4.36	6.31	104.9	3.4
8	*trans*	4.22	6.23	109.1	11.0
9	*cis*	4.18	6.35	106.9	2.9
10	*trans*	4.24	6.23	108.8	11.3
11	*cis*	4.20	6.34	106.8	3.1
12	*trans*	4.73	6.26	109.1	9.7
13	*cis*	4.48	6.36	—	0
14	*trans*	4.75	6.25	108.9	9.7
15	*cis*	4.51	6.34	—	0

for the methylated compounds **8–11** and δ 4.5–4.7 for the chlorinated derivatives **12–15**.

The *cis*- or *trans*-fusion of the lactone ring was assigned on the basis of J_{H3-11}. As has been noted for the corresponding podophyllotoxins (4), *trans* ring fusion results in >9 Hz coupling constants while the *cis*-fused isomers have J_{H3-11} < 3. Several other consistent trends can be noted from Table 1. The C-1 proton of the isomer having the *trans*-fused lactone is always shifted further downfield than that of the corresponding *cis* isomer. The opposite effect is observed for H-8. In the latter case the aromatic ring at C-1 is essentially perpendicular to the other rings when the lactone fusion is *trans* and thus should have little anisotropy effect on H-8. In the case of the *cis*-fused lactones the half-chair conformation places H-8 in an aromatic ring deshielding zone. Finally, the ^{13}C chemical shifts for C-2′, C-6′ in the *trans*-fused isomers were typically found in the δ = 108–109 ppm range; these were consistently deshielded relative to the corresponding *cis* isomer by at least 2 ppm.

Desilylation of the compounds **8–15** was carried out with either 4 equivalents of tetrabutylammonium fluoride (TBAF) in THF at 0°C for 1 min followed by quenching with saturated NH_4Cl solution or, in the case of the more sensitive chloro compounds, with the same reagents in acetic acid. The proton spectra of the desilylated products were consistent with the structure assignments. See Table 1 and experimental section. Again the size of the J_{H3-11} was crucial in confirming the stereochemistry of the lactone ring junction.

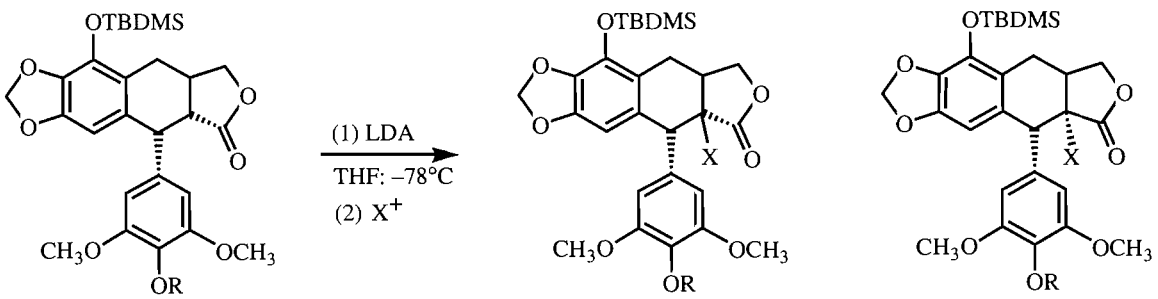

4 R = CH_3
5 R = TBDMS

8 R = CH_3, X = CH_3
10 R = TBDMS, X = CH_3
12 R = CH_3, X = Cl
14 R = TBDMS, X = Cl

6 R = TBDMS, X = H
7 R = CH_3, X = H
9 R = CH_3, X = CH_3
11 R = TBDMS, X = CH_3
13 R = CH_3, X = Cl
15 R = TBDMS, X = Cl

Biological screening results

Testing against leukemia P 388 was performed on the peltatins, all four methylated isomers, and the two *trans*-fused chloro isomers at the Anti-Tumor Division of Bristol Laboratories using the following protocol (6). Ascitic fluid containing 10^6 cancer cells was implanted interperitoneally in female CDF1 mice (4 mice per test group). Treatment began 24 h after implant. The results are given in Table 2.

Under these conditions, α- and β-peltatins are toxic (the majority of the test animals died within 5 days of the administration of the compounds, compared to the 9-day life expectancy of the control group) at levels of 4 and 16 mg/kg. The *cis*-2-methyl derivatives of both α- and β-peltatins were inactive at dosages up to 64 mg/kg. All of the *trans*-fused derivatives were considerably less toxic than the parent peltatins, but only the *trans*-2-methyl-β-peltatin showed any marginal anti-cancer activity (T/C = 133 at 64 mg/kg) at the levels tested. The possibility that some of these com-

Can. J. Chem. Downloaded from www.nrcresearchpress.com by 92.62.229.171 on 09/08/12
For personal use only.

Can. J. Chem. Downloaded from www.nrcresearchpress.com by 92.62.229.171 on 09/08/12
For personal use only.

TABLE 2. In vivo effect of peltatins on P388 leukemia

Compound	Dosage (mg/kg)	T/C[a]
α-Peltatin **4**	4	toxic
	0.4	110
2-Methyl-α-peltatin (*trans*) **8**	4	100
	16	111
	64	128
2-Methyl-α-peltatin (*cis*) **9**	16	100
	64	106
2-Chloro-α-peltatin **12**	4	110
	8	100
β-Peltatin **5**	4	toxic
	1	125
2-Methyl-β-peltatin (*trans*)	4	100
	16	122
	64	133
2-Methyl-β-peltatin (*cis*)		
	16	100
	64	100
2-Chloro-β-peltatin	0.8	100
	1.6	90
	3.2	90
Etoposide[b]	30	270

[a]Lifespan, after implantation of cancer cells of treated (T) animals/that of the control (c) group × 100.

[b]Determined at Bristol Laboratories using the standard procedure (6).

pounds might show improved biological activity after glycosylation remains to be investigated.

Experimental section

General comments

^1H and ^{13}C NMR spectra were recorded on Varian XL200 and Varian FT-80 spectrometers, respectively, using $CDCl_3$ as solvent and TMS as internal standard. Melting points were determined on a Gallenkamp apparatus and are uncorrected. Optical rotations were recorded as $CHCl_3$ solution (c = 1.0) unless otherwise indicated, using a Perkin Elmer 241 polarimeter. Preparative thin-layer chromatography (PTLC) was carried out on glass plates coated with a 1.0 mm layer of Kieselgel 60GF 254. High-performance liquid chromatography was carried out using PrePak-500 silica gel cartridges on a Waters 500 instrument. Typical work-up refers to quenching the reaction mixture with saturated NH_4Cl solution, several extractions with either ethyl acetate or CH_2Cl_2, drying, and evaporating the organic solvents on a rotatory evaporator. All yields refer to isolated, chromatographically homogeneous products.

Preparation of the TBDMS derivatives of α- and β-peltatin from crude podophyllin resin

Podophyllin resin (10.2 g, U.S. Biochemicals) was stirred overnight with 50 mL of $CHCl_3$. The solution was filtered and the residue was similarly treated two more times. Evaporation of the $CHCl_3$ afforded 5.86 g of yellow-brown foam.

The chloroform soluble material (6.0 g) was further fractionated by placing it on 30 g of silica and eluting with 200 mL each of (1) hexanes; (2) 20% CH_2Cl_2 – 80% hexanes; (3) 40% CH_2Cl_2 – 60% hexanes; (4) 60% CH_2Cl_2 – 40% hexanes; (5) 80% CH_2Cl_2 – 20% hexanes; (6) CH_2Cl_2; (7)–(10) fractions contain 2, 4, 6, and 8% ethyl acetate in CH_2Cl_2. The last 5 fractions were combined and evaporated to yield 3.5 g of crude peltatin mixture.

The above mixture (2.38 g), imidazole (16.1 g), and *tert*-butyldimethylsilyl chloride (1.71 g) were combined in 11 mL of DMF, heated overnight at 50°C, and then worked up in the usual manner to yield 3.30 g of a yellow-brown foam. Purification by HPLC (1:9 ethyl acetate – hexanes) afforded 987 mg (14%) of the bis-TBDMS of α-peltatin and 630 mg (9%) of the TBDMS derivative of β-peltatin after recrystallization from hexanes.

*α-Peltatin-bis-TBDMS (**4**):* mp 172–174°C; $[\alpha]_D = -106$; ^1H NMR, δ (ppm): 0.10 (s, 6H), 0.24 (s, 3H), 0.29 (s, 3H), 0.99 (s, 9H), 1.03 (s, 9H), 2.41 (dd, J = 11.2, 16.0 Hz, 1H), 2.68–2.72 (m, 2H), 3.10–3.24 (m, 1H), 3.68 (s, 6H), 3.92 (dd, J = 8.9, 10.1 Hz, 1H), 4.46 (dd, J = 6.2, 8.4 Hz, 1H), 4.56 (d, J = 3.4 Hz, 1H), 5.89 (d, J = 1.4 Hz, 1H), 5.91 (d, J = 1.4 Hz, 1H), 6.26 (s, 1H), 6.30 (s, 2H); ^{13}C NMR, δ (ppm): −4.56 (q), −4.04 (q), 18.67 (s), 18.7 (s), 25.8 (q), 25.9 (q), 28.2 (t), 32.3 (d), 43.8 (d), 47.4 (d), 55.9 (q), 72.4 (t), 100.8 (t), 104.3 (d), 108.4 (d), 122.17 (s), 132.0 (s), 133.2 (s), 133.4 (s), 135.5 (s), 136.5 (s), 147.5 (s), 150.8 (s), 175.1 (s). Anal. calcd. for $C_{33}H_{48}O_8Si_2$: C 63.02, H 7.69; found: C 62.93, H 8.05.

*β-Peltatin TBDMS (**5**):* mp 172–174°C; $[\alpha]_D = -106$; ^1H NMR, δ (ppm): 0.24 (s, 3H), 0.29 (s, 3H), 1.03 (s, 9H), 2.42 (dd, J = 11.6, 15.8 Hz, 1H), 2.5–2.7 (m, 2H), 3.18 (dd, J = 4.1, 15.5 Hz, 1H), 3.75 (s, 6H), 3.80 (s, 3H), 3.948 (dd, J = 8.8, 10.2 Hz, 1H), 4.49 (dd, J = 6.3, 8.5 Hz, 1H), 4.596 (d, J = 3.8 Hz, 1H), 5.90 (d, J = 1.4 Hz, 1H), 5.91 (d, J = 1.4 Hz, 1H), 6.27 (s, 1H), 6.35 (s, 2H); ^{13}C NMR, δ (ppm): −4.04 (q), 18.6 (s), 25.9 (q), 28.1 (t), 32.4 (d), 43.9 (d), 47.3 (d), 56.2 (q), 60.7 (q), 72.4 (t), 100.9 (t), 104.2 (d), 108.2 (d), 122.1 (s), 131.6 (s), 135.6 (s), 136.4 (s), 136.5 (s), 137.0 (s), 147.6 (s), 152.5 (s), 175.0 (s). Anal. calcd. for $C_{28}H_{36}O_8Si$: C 63.61, H 6.86; found: C 63.47, H 7.00.

*Preparation of the lactone enolates derived from **4** and **5** and subsequent reaction with electrophiles*

Representative procedure

TBDMS derivative **4** (510 mg, 0.81 mmol) was dissolved in 5 mL of dry THF and added slowly to a −78°C solution of 0.85 mmol of LDA in 10 mL of dry THF. The solution (bluish color) was stirred for 15 min at −78°C and 0.5 mL of CH_3I was added. The reaction mixture was allowed to warm to room temperature and stirred for a further 10–20 h. Usual work-up afforded a crude product that was separated via preparative TLC (1:7 ethyl acetate – hexane) to afford 200 mg (38%) of the *trans*-fused, less polar isomer **8** and 292 mg (56%) of the methylated *cis*-fused lactone **9**.

*Isomer **8**:* mp 78–83°C; $[\alpha]_D = -102$; ^1H NMR, δ (ppm): 0.10 (s, 6H), 0.24 (s, 3H), 0.27 (s, 3H), 0.98 (s, 9H), 1.03 (s, 9H), 1.22 (s, 3H), 2.36 (dd, J = 12.6, 16.2 Hz, 1H), 2.69–2.92 (m, 1H), 3.01 (dd, J = 5.3, 16.3 Hz, 1H), 3.68 (s, 6H), 3.98 (dd, J = 8.4, 11.0 Hz, 1H), 4.22 (s, 1H), 4.28–4.40 (m, 1H), 5.90 (s, 2H), 6.23 (s, 1H), 6.30 (s, 2H); ^{13}C NMR, δ (ppm): −4.55 (q), −4.06 (q), 16.4 (q), 18.7 (s), 23.1 (t), 25.8 (q), 25.9 (q), 34.3 (d), 46.1 (s), 52.3 (d), 56.0 (q), 70.1 (t), 100.8 (t), 105.2 (d), 109.1 (d), 120.9 (s), 131.3 (s), 133.4 (s), 135.4 (s), 136.3 (s), 147.8 (s), 150.6 (s), 178.6 (s). Anal. calcd. for $C_{34}H_{50}O_8Si_2$: C 63.52, H 7.84; found: C 63.46, H 7.81.

2-Methylated cis*-fused lactone (**9**):* mp 69–75°C; $[\alpha]_D = -106$; ^1H NMR, δ (ppm): 0.11 (s, 6H), 0.21 (s, 3H), 0.24 (s, 3H), 0.99 (s, 9H), 1.03 (s, 9H), 1.19 (s, 3H), 2.63–2.75 (m, 1H), 2.99–3.09 (m, 2H), 3.71 (s, 6H), 3.99 (dd, J = 2.9, 9.1 Hz, 1H), 4.16 (s, 1H), 4.48 (dd, J = 6.9, 9.1 Hz, 1H), 5.85 (s, 2H), 6.30 (s, 2H), 6.35 (s, 1H); ^{13}C NMR, δ (ppm): −4.58 (q), −4.17 (q), 18.5 (s), 18.7 (s), 22.9 (q), 25.8 (q), 27.0 (t), 39.7 (q), 47.0 (s), 51.3 (d), 55.8 (q), 73.5 (t), 100.6 (t), 103.6 (d), 106.9 (d), 119.6 (s), 132.3 (s), 132.6 (s), 135.7 (s), 136.29 (s), 147.3 (s), 151.2 (s), 169.3 (s), 181.4 (s). Anal. calcd. for $C_{34}H_{50}O_8Si_2$: C 63.52, H 7.84; found: C 63.45, H 7.95.

*Preparation of the 2-methylated derivatives of β-peltatin (**10** and **11**)*

From 544 mg (1.03 mmol) of **5** was obtained 292 mg (52%) of the methylated *trans*-fused isomer **10** and 258 mg (46%) of the *cis*-fused product **11**.

*Compound **10**:* mp 76–82°C; $[\alpha]_D = -107$; ^1H NMR, δ (ppm): 0.25 (s, 3H), 0.28 (s, 3H), 1.04 (s, 9H), 1.24 (s, 3H), 2.38 (dd, J = 12.4, 16.2 Hz, 1H), 2.70–2.92 (m, 1H), 3.04 (dd, J = 5.4, 16.4 Hz, 1H), 3.75 (s, 6H), 3.80 (s, 3H), 4.01 (dd, J = 8.6, 11.3

Can. J. Chem. Downloaded from www.nrcresearchpress.com by 92.62.229.171 on 09/08/12
For personal use only.

Hz, 1H), 4.24 (s, 1H), 4.37 (dd, J = 7.4, 8.2 Hz, 1H), 5.90 (s, 2H), 6.23 (s, 1H), 6.35 (s, 2H); ^{13}C NMR, δ (ppm): −4.1 (q), 16.4 (q), 18.6 (s), 23.1 (t), 25.9 (q), 34.4 (d), 45.9 (s), 52.4 (d), 56.6 (q), 60.7 (q), 70.1 (t), 100.9 (t), 105.1 (d), 108.8 (d), 120.9 (s), 130.9 (s), 135.5 (s), 136.4 (s), 136.5 (s), 136.9 (s), 147.8 (s), 152.2 (s), 178.5 (s). Anal. calcd. for $C_{25}H_{38}O_8Si$: C 64.18, H 7.06; found: C 59.19, H 6.47. The low carbon and hydrogen values appear to be due to occluded halocarbons, which were difficult to remove from the foamy solid even under high vacuum.

Compound 11: foam, mp 71–75°C; $[\alpha]_D$ = −107; ^{1}H NMR, δ (ppm): 0.21 (s, 3H), 0.24 (s, 3H), 1.03 (s, 9H), 1.23 (s, 3H), 2.64–2.77 (m, 1H), 3.02 (d, J = 5.4 Hz, 2H), 3.79 (s, 6H), 3.81 (s, 3H), 4.01 (dd, J = 3.1, 9.3 Hz, 4.21 (s, 1H), 4.51 (dd, J = 6.9, 9.3 Hz, 1H), 5.85 (s, 2H), 6.35 (s, 3H); ^{13}C NMR, δ (ppm): −4.17 (q), 18.5 (s), 22.8 (q), 25.9 (q), 26.9 (t), 39.6 (d), 47.0 (s), 51.4 (d), 56.1 (q), 60.8 (q), 73.4 (t), 100.7 (t), 103.4 (d), 106.8 (d), 119.6 (s), 132.2 (s), 135.5 (s), 135.8 (s), 136.3 (s), 137.0 (s), 147.4 (s), 152.9 (s), 181.2 (s). Anal. calcd. for $C_{29}H_{38}O_8Si$: C 64.18, H 7.06; found: C 61.19, H 6.57. The low C and H values appear to be due to occluded halocarbon solvents, which could not be removed from the foamy solid even after prolonged high vacuum.

*Reaction of the enolates of **4** and **5** with hexachloroethane*

The enolate prepared as above from 426 mg (0.68 mmol) of **4** was allowed to react with 1.29 (5.5 mmol) of hexachloroethane, first at −78°C, then at room temperature for 22 h. Usual work-up and purification by PTLC (1:6 ethyl acetate – hexanes) afforded the 2-chloro-*trans* derivative **12** (414 mg, 92%) and 2-chloro-*cis* product **13** (19 mg, 4%).

*2-Chloro-*trans *isomer **12**:* mp 79–86°C; ^{1}H NMR, δ (ppm): 0.10 (s, 6H), 0.26 (s, 3H), 0.29 (s, 3H), 0.98 (s, 9H), 1.04 (s, 9H), 2.65 (dd, J = 10.9, 15.7 Hz, 1H), 2.82–3.00 (m, 1H), 3.08 (dd, J = 5.6, 15.6 Hz, 1H), 3.68 (s, 6H), 4.16 (dd, J = 8.5, 9.7 Hz, 1H), 4.40 (dd, J = 6.7, 8.5 Hz, 1H), 4.73 (s, 1H), 5.90 (d, J = 1.4 Hz, 1H), 5.93 (d, J = 1.4 Hz, 1H), 6.26 (s, 1H), 6.34 (s, 2H); ^{13}C NMR, δ (ppm): −4.54 (q), −4.02 (q), 18.7 (s), 23.5 (t), 25.8 (q), 25.9 (q), 36.7 (d), 53.3 (d), 56.0 (q), 70.6 (t), 71.5 (s), 101.0 (t), 104.6 (d), 109.1 (d), 120.3 (s), 129.5 (s), 131.0 (s), 134.2 (s), 135.8 (s), 136.3 (s), 148.0 (s), 150.9 (s), 170.9 (s). Anal. calcd. for $C_{33}H_{47}O_8Si_2Cl$: C 59.75, H 7.14; found: C 59.21, H 7.38.

*2-Chloro-*cis *isomer **13**:* foam; ^{1}H NMR, δ (ppm): 0.115 (s, 6H), 0.207 (s, 3H), 0.235 (s, 3H), 0.994 (s, 9H), 1.014 (s, 9H), 2.95–3.40 (m, 3H), 3.725 (s, 6H), 4.171 (d, J = 9.0 Hz, 1H), 4.475 (s, 1H), 4.738 (dd, J = 4.9, 8.9 Hz, 1H), 5.881 (s, 2H), 6.358 (s, 1H), 6.421 (s, 2H). This material was not characterized further.

Preparation of the 2-chloro derivatives of TBDMS-protected β-peltatin

The lactone enolate derived from 465 mg (0.88 mmol) of **5** was reacted with excess (1.63 g) of hexachloroethane as above. Work-up and purification (PTLC, 1:5 ethyl acetate – hexanes) afforded 409 mg (83%) of the *trans*-2-chloro isomer **14** and 27 mg (60%) of the *cis* isomer **15**.

trans-*2-Chloro isomer **14**:* mp 212–215°C; $[\alpha]_D$ (c = 1.0) = −133; ^{1}H NMR, δ (ppm): 0.26 (s, 3H), 0.29 (s, 3H), 1.04 (s, 9H), 2.67 (dd, J = 11.0, 15.6 Hz, 1H), 2.80–3.04 (m, 1H), 3.10 (dd, J = 5.5, 15.7 Hz, 1H), 3.75 (s, 6H), 3.80 (s, 3H), 4.19 (dd, J = 8.7, 9.7 Hz, 1H), 4.43 (dd, J = 6.6, 8.4 Hz, 1H), 4.75 (s, 1H), 5.91 (d, J = 1.4 Hz, 1H), 5.93 (d, J = 1.4 Hz, 1H), 6.25 (s, 1H), 6.39 (s, 2H); ^{13}C NMR, δ (ppm): −4.03 (q), 18.6 (s), 23.4 (t), 25.9 (q), 36.8 (d), 53.4 (d), 56.3 (q), 60.7 (q), 70.6 (t), 71.2 (s), 101.0 (t), 104.5 (d), 108.9 (d), 120.3 (s), 129.1 (s), 134.1 (s), 135.9 (s), 136.3 (s), 137.6 (s), 148.0 (s), 152.6 (s), 163.9 (s), 170.9 (s). Anal. calcd. for $C_{28}H_{35}O_8SiCl$: C 59.72, H 6.26; found: C 59.78, H 6.36.

cis-*2-Chloro derivative **15**:* foam; ^{1}H NMR, δ (ppm): 0.21 (s, 3H), 0.24 (s, 3H), 1.02 (s, 9H), 2.97–3.36 (m, 3H), 3.80 (s, 6H), 3.83 (s, 3H), 4.18 (d, J = 9.0 Hz, 1H), 4.51 (s, 1H), 4.75 (dd, J = 5.2, 9.0 Hz, 1H), 4.86 (d, J = 1.4 Hz, 1H), 5.88 (d, J = 1.4 Hz, 1H), 6.35 (s, 1H), 6.47 (s, 2H); M^+ = 562 (calcd. for $C_{28}H_{35}O_8Si$; ^{35}Cl 562. This material was not further characterized.

Desilylation experiments. Method A. Typical procedure

To a solution of 575 mg (0.90 mmol) of **9** in 5 mL of dry THF at 0°C was added 4 equivalents of TBAF (3.6 mL, 1.0 M in THF). The solution was stirred for 1 min and then quenched with saturated NH_3Cl solution. Usual work-up followed by PTLC separation (2:1 ethyl acetate – hexane) afforded 319 mg (86%) of 2-methyl-α-peltatin (*cis*) as fine beige needles, mp 108–111°C; $[\alpha]_D$ (CH_3OH, c = 1.0) = −104; ^{1}H NMR, δ (ppm): 1.20 (s, 3H), 2.81–3.25 (m, 3H), 3.79 (s, 6H), 4.09 (dd, J = 2.2, 9.4 Hz, 1H), 4.14 (s, 1H), 4.58 (dd, J = 6.2, 9.2 Hz, 1H), 5.62 (s, 2H), 5.84 (d, J = 1.0 Hz, 1H), 5.85 (d, J = 1.2 Hz, 1H), 6.29 (s, 1H), 6.54 (s, 2H). Anal. calcd. for $C_{22}H_{22}O_8$: C 63.76, H 5.35; found: C 64.08, H 4.92.

*2-Methyl-α-peltatin (*trans*)*

Treatment of 220 mg (0.34 mmol) of **8** with equivalents of TBAF according to method A above afforded 100 mg (71%) of 2-methyl-α-peltanin (*trans*) after PTLC (2:1 ethyl acetate – hexanes), mp 228–233°C; $[\alpha]_D$ (CH_3OH, c = 0.97) = −123; ^{1}H NMR, δ (ppm): 1.25 (s, 3H), 2.46 (dd, J = 12.4, 16.2 Hz, 1H), 2.70–2.96 (m, 1H), 3.08 (dd, J = 5.4, 16.2 Hz, 1H), 4.25 (s, 1H), 4.30–4.40 (m, 1H), 5.37 (s, 1H), 5.44 (s, 1H), 5.94 (s, 2H), 6.36 (s, 2H). Anal. calcd. for $C_{22}H_{22}O_8$: C 63.76, H 5.35; found: C 63.48, H 5.28.

*2-Methyl-β-peltatin (*trans*)*

Prepared in 75% yield from 169 mg (0.31 mmol) of **10** and 2 equivalents of TBAF following procedure A, mp 242–244°C; ^{1}H NMR, δ (ppm): 1.26 (s, 3H), 2.48 (dd, J = 12.4, 16.4 Hz, 1H), 2.75–2.98 (m, 1H), 3.08 (dd, J = 5.3, 16.1 Hz, 1H), 3.75 (s, 6H), 3.801 (s, 3H), 4.02 (dd, J = 8.7, 11.3 Hz, 1H), 4.26 (s, 1H), 4.31–4.45 (m, 1H), 5.48 (bs, 1H), 5.92 (s, 1H), 6.19 (s, 1H), 6.36 (s, 1H). Anal. calcd. for $C_{23}H_{24}O_8$: C 64.48, H 5.65; found: C 64.59, H 5.82.

*2-Methyl-β-peltatin (*cis*)*

This compound was obtained in 67% yield as yellowish prisms, mp 127–130°C (from CH_2Cl_2–hexanes) from **11** following the desilylation procedure A; $[\alpha]_D$ ($CHCl_3$) = −113; ^{1}H NMR, δ (ppm): 1.24 (s, 3H), 2.67–3.11 (m, 3H), 3.79 (s, 6H), 3.82 (s, 3H), 4.08 (dd, J = 2.8, 9.4 Hz, 1H), 4.20 (s, 1H), 4.52 (dd, J = 6.7, 9.1 Hz, 1H), 5.30 (s, 1H), 5.85 (dd, J = 1.4 Hz, 1H), 5.87 (d, J = 1.4 Hz, 1H), 6.31 (s, 1H), 6.36 (s, 2H). Anal. calcd. for $C_{23}H_{24}O_8$: C 64.48, H 5.65; found: C 64.01, H 5.57.

*2-Chloro-α-peltatin (*trans*)*

A solution of 60 mg (0.091 mmol) of **12** was dissolved in 5 mL of dry THF at 0°C. Acetic acid (0.1 mL) was added followed by 4 equivalents of TBAF (0.35 mL, 1.0 M in THF). After several minutes the reaction mixture was quenched with saturated NH_4Cl solution and then washed with sodium bicarbonate. Further work-up followed by PTLC (3:2 ethyl acetate – hexanes) afforded 38 mg (96%) of 2-chloro-α-peltatin (*trans*) as pale yellow prisms, mp 208–210°C; $[\alpha]_D$ (CH_3OH, c = 0.97) = −136; ^{1}H NMR, δ (ppm): 2.74 (dd, J = 11.0, 15.4 Hz, 1H), 2.84–3.06 (m, 1H), 3.157 (dd, J = 5.4, 15.6 Hz, 1H), 3.784 (s, 6H), 4.19 (dd, J = 8.5, 9.7 Hz, 1H), 4.41 (dd, J = 6.8, 8.4 Hz, 1H), 4.75 (s, 1H), 5.93 (d, J = 1.4 Hz, 1H), 5.96 (d, J = 1.4 Hz, 1H), 6.22 (s, 1H), 6.41 (s, 2H). Anal. calcd. for $C_{21}H_{19}O_8Cl$: C 58.01, H 4.40; found: C 57.70, H 4.41.

*2-Chloro-β-peltatin (*trans*)*

This compound was prepared from the monosilylated chloro derivative **14** using 2 equivalents of TBAF in THF/acetic acid, as above. The yield of product was 91%; mp 182–184°C (pale yellow flakes); $[\alpha]_D$ (CH_3OH, c = 1.01) = −129; ^{1}H NMR, δ (ppm): 2.76 (dd, J = 11.1, 15.7 Hz, 1H), 2.85–3.05 (m, 1H), 3.16 (dd, J = 5.3, 15.7 Hz, 1H), 3.76 (s, 6H), 3.81 (s, 3H), 4.20 (dd, J = 8.7, 9.5 Hz, 1H), 4.43 (dd, J = 6.7, 8.5 Hz, 1H), 4.77 (s, 1H), 5.97 (d, J = 1.4 Hz, 1H), 5.95 (d, J = 1.4 Hz, 1H), 6.22 (s, 1H), 6.40 (s, 2H). Anal. calcd. for $C_{22}H_{21}O_8Cl$: C 58.87, H 4.72; found: C 58.85, H 4.67.

*Reaction of the enolate of **4** with saturated NH_4Cl solution*

The enolate prepared from 202 mg of **4** was prepared as usual at −78°C and then quenched with saturated NH_4Cl solution. Work-up followed by PTLC chromatography (1:6 ethyl acetate – hexanes) afforded 39 mg (19%) of α-peltatin-bis-TBDMS and 158 mg (78%) of the less mobile *cis*-fused isomer **6** as a pale yellow foam, mp 140–142°C; ^{1}H NMR, δ: 0.11 (s, 6H), 0.18 (s, 3H), 0.21 (s, 3H), 0.99 (s, 9H), 1.00 (s, 9H), 2.63–2.71 (m, 2H), 2.92–3.05 (m, 1H), 3.33 (dd, J = 2.8, 9.6 Hz, 1H), 3.69 (s, 6H), 3.89 (dd, J = 3.4, 9.0 Hz, 1H), 4.35 (d, J = 2.6 Hz, 1H), 4.42 (dd, J = 7.6, 9.2 Hz, 1H), 5.86 (d, J = 1.4 Hz, 1H), 5.90 (d, J = 1.4 Hz, 1H), 6.27 (s, 2H), 6.33 (s, 1H); ^{13}C NMR, δ (ppm): −4.6 (q), −4.2 (q), 1.85 (s), 18.7 (s), 24.8 (t), 25.8 (q), 32.6 (d), 45.4 (d), 46.3 (d), 55.9 (q), 73.1 (t), 100.7 (t), 103.9 (d), 105.0 (d), 121.0 (s), 131.6 (s), 133.1 (s), 134.9 (s), 136.0 (s), 136.7 (s), 147.3 (s), 151.6 (s), 178.6 (s). Anal. calcd. for $C_{33}H_{48}O_8Si_2$: C 63.02, H 7.69; found: C 63.06, H 7.49.

*Reaction of the enolate of **5** with saturated NH_4Cl solution. Preparation of **7***

The enolate of **5** was quenched at −78°C with NH_4Cl solution as above. Work-up and PTLC (1:6 ethyl acetate – hexanes) afforded 40 mg (20%) of β-peltatin and 130 mg (64%) of the slightly less polar *cis* isomer **7**; mp 55–60°C; ^{1}H NMR, δ (ppm): 0.21 (s, 3H), 0.27 (s, 3H), 1.01 (s, 9H), 2.71 (dd, J = 1.5, 5.9 Hz, 2H), 2.92–3.10 (m, 1H), 3.32 (dd, J = 2.8, 9.6 Hz, 1H), 3.78 (s, 6H), 3.83 (s, 3H), 3.93 (dd, J = 3.4, 9.0 Hz, 1H), 4.36 (d, J = 3.0, 1H), 4.43 (dd, J = 7.3, 9.3 Hz, 1H), 5.87 (d, J = 1.4 Hz, 1H), 5.92 (d, J = 1.4 Hz, 1H), 6.31 (s, 1H), 6.34 (s, 2H); ^{13}C NMR, δ (ppm): 4.24 (q), 18.5 (s), 24.8 (t), 25.8 (q), 32.6 (d), 45.5 (d), 46.4 (d), 56.2 (d), 60.9 (d), 73.0 (t), 100.7 (t), 103.8 (d), 104.9 (d), 121.0 (s), 131.1 (s), 136.1 (s), 136.7 (s), 136.8 (s), 138.4 (s), 153.3 (s), 178.4 (s). Anal. calcd. for $C_{28}H_{36}O_8Si$: C 63.61, H 6.86; found: 63.89, H 6.69.

Acknowledgements

Financial support by the Natural Sciences and Engineering Research Council of Canada and the biological screening experiments by Bristol Laboratories, Syracuse, are gratefully acknowledged.

1. (*a*) D. C. Ayres and J. D. Loike. Lignans. Chemical, biological and clinical properties. Cambridge University Press, London 1990; (*b*) I. Jardine. Med. Chem. (Academic Press), **16**, 319 (1980); (*c*) T. W. Doyle. *In* Etoposide (VP-16). Current status and new developments. Academic Press, New York, 1984.
2. (*a*) J. L. Hartwell, A. W. Schrecker, and G. Y. Greenberg. J. Am. Chem. Soc. **74**, 6285 (1952); (*b*) J. L. Hartwell and W. E. Detty. J. Am. Chem. Soc. **72**, 246 (1950).
3. (*a*) E. M. Greenspan, J. Colsky, E. M. Schoenbach, and J. M. Shear. J. Natl. Cancer Inst. **14**, 1257 (1954); (*b*) E. M. Greenspan, M. Leiter, and M. J. Setir. J. Natl. Cancer Inst. **10**, 1295 (1950).
4. M. B. Glinski, J. C. Freed, and T. Durst. J. Org. Chem. **52**, 2749 (1987).
5. W. J. Gensler and C. D. Gatsonis. J. Org. Chem. **31**, 3224, 4004 (1956).
6. R. I. Geran, N. H. Greenberg, M. M. MacDonald, A. M. Schumacher, and B. J. Abbot. Cancer Chemother. Rep. Part 3, **3**, 1 (1972).

Can. J. Chem. Downloaded from www.nrcresearchpress.com by 92.62.229.171 on 09/08/12
For personal use only.

A microcolumn method for hexazinone and metabolite residues in soil and vegetation

JOSEPH C. FENG

Forestry Canada, Northern Forestry Centre, 5320-122 Street, Edmonton, Alta., Canada T6H 3S5

Received July 17, 1991

JOSEPH C. FENG. Can. J. Chem. **70**, 1087 (1992).

A soil cleanup method using a disposable microcolumn and a modified capillary gas chromatographic method is described for the analysis of hexazinone (3-cyclohexyl-6-(dimethylamino)-1-methyl-1,3,5-triazine-2,4(1*H*,3*H*)-dione) and two primary metabolites, 3-(4-hydroxycyclohexyl)-6-(dimethylamino)-1-methyl-1,3,5-triazine-2,4(1*H*,3*H*)-dione (metabolite A) and 3-cyclohexyl-6-(methylamino)-1-methyl-1,3,5-triazine-2,4(1*H*,3*H*)-dione (metabolite B). The limits of detection (LOD) were 7, 18, and 36 ng g^{-1} for hexazinone, metabolite B, and metabolite A, respectively; limits of quantitation (LOQ) were 22, 52, and 99 ng g^{-1}, respectively. The mean recoveries were 94 ± 3% and 94 ± 5% for hexazinone and the phytotoxic metabolite B fortified above LOQ and ranging from 0.03 to 6.25 and 0.06 to 12.5 μg g^{-1}, respectively. The recoveries from the non-phytotoxic metabolite A above LOQ increased with concentrations from 0.125 to 25 μg g^{-1}, but were consistent at each level. The final product of cleanup was stable for at least 6 months, and no derivatization was needed before gas chromatography. The use of toluene as the final solvent and the modification of the injection system of the gas chromatograph improved the stability of peak responses. The method is three times more efficient than conventional methods. The cleanup method for soils was modified for the analysis of vegetation samples. Efficient removal of chlorophyll enabled quantitation of hexazinone by gas chromatography. Recoveries of hexazinone ranged from 73 to 96% for forest litter and four different plant species.

JOSEPH C. FENG. Can. J. Chem. **70**, 1087 (1992).

On décrit une méthode de nettoyage du sol qui utilise une microcolonne jetable et une méthode modifiée de chromatographie gazeuse capillaire et qui permet d'analyser l'hexazinone (3-cyclohexyl-6-(diméthylamino)-1-méthyl-1,3,5-triazine-2,4-(1*H*,3*H*)-dione) et deux de ses métabolites primaires, la 3-(4-hydroxycyclohexyl)-6-(diméthylamino)-1-méthyl-1,3,5-triazine-2,4(1*H*,3*H*)-dione (métabolite A) et la 3-cyclohexyl-6-(méthylamino)-1-méthyl-1,3,5-triazine-2,4(1*H*,3*H*)-dione (métabolite B). Les limites de détection (LDD) sont respectivement 7, 18 et 36 ng g^{-1} pour l'hexazinone, le métabolite B et le métabolite A; les limites de quantification (LDQ) sont respectivement 22, 52 et 99 ng g^{-1}. Les récupérations moyennes sont respectivement de 94 ± 3% et de 94 ± 5% pour l'hexazinone et le métabolite phytotoxique B fortifié au-dessus de la LDQ et elles varient respectivement de 0,03 à 6,25 et de 0,06 à 12,5 μg g^{-1}. Les récupérations du métabolite non-toxique A au-dessus de la LDQ augmentent avec les concentrations de 0,125 à 25 μg g^{-1}, mais elles sont cohérentes à chaque niveau. Le produit final du nettoyage est stable pour au moins 6 mois et il n'est pas nécessaire de préparer des dérivés avant d'effectuer la chromatographie gazeuse. L'utilisation de toluène comme solvant final et la modification du système d'injection du chromatographe en phase gazeuse augmentent la stabilité des réponses des pics. La méthode est trois fois plus efficace que les méthodes conventionnelles. La méthode de nettoyage a été modifiée pour l'analyse d'échantillons de végétation. L'élimination efficace de la chlorophylle a permis de quantifier l'hexazinone par chromatographie gazeuse. Les récupérations d'hexazinone s'établissent entre 73 et 96% pour la litière de la forêt et pour quatre espèces différentes de plantes.

[Traduit par la rédaction]

Introduction

Hexazinone is a triazine herbicide registered for forestry use in Canada. Two of its formulations, Pronone 10G (granular) and Velpar L (liquid), have been used in forest site preparation and conifer release (1–5), and are being tested in strip thinning of aspen in mixedwoods (ref. 6, and Sidders[1]).

Because of environmental concerns and pesticide regulations, sensitive analytical methods are required for monitoring this chemical in treated forest areas. Holt's method (7) provides a basic analytical approach for the determination of residues of hexazinone and two primary and two minor metabolites (moderately polar compounds) named as metabolites A, B, D,[2] and E,[3] respectively. Another minor metabolite (metabolite C[4]) is treated as a separate compound and requires a different method in residue analysis, i.e., isolation and gas chromatography, due to its highly polar nature (7). Among these metabolites, only metabolite B is phytotoxic and is about 1% as potent as the parent compound in inhibiting photosynthesis of loblolly pine (*Pinus taeda* L.) (8). A liquid/liquid partitioning procedure followed by derivatization with trifluoroacetic anhydride is employed in Holt's method (7), which is sensitive to a detection limit of 40 ng g^{-1} for hexazinone and metabolites A and B in soils, when analyzed with a packed column gas chromatograph (GC) equipped with a nitrogen–phosphorus detector (NPD). However, the derivatized final product is unstable and has a shelf life of less than 8 h. Feng (9) modified Holt's (7) method by eliminating the derivatization process to increase the shelf life and by using direct[5] gas chromatography to simplify the sample handling. The mod-

[1]D. Sidders. 1990. Personal communication. Forestry Canada, Northwest Region, Saskatchewan District Office, Prince Albert, Sask.

[2]Metabolite D: 3-cyclohexyl-1-methyl-1,3,5-triazine-2,4,6(1*H*,3*H*,5*H*)-trione.

[3]Metabolite E: 3-(4-hydroxycyclohexyl)-1-methyl-1,3,5-triazine-2,4,6(1*H*,3*H*,5*H*)-trione.

[4]Metabolite C: 3-(4-hydroxycyclohexyl)-6-(methylamino)-1-methyl-1,3,5-triazine-2,4(1*H*,3*H*)-dione.

[5]S. Stupp. Personal communication. A&S environmental Testing, Temple, Pa.

Can. J. Chem. Downloaded from www.nrcresearchpress.com by 79.173.37.17 on 09/08/12
For personal use only.

Can. J. Chem. Downloaded from www.nrcresearchpress.com by 79.173.37.17 on 09/08/12
For personal use only.

ified method has a detection limit similar to the latter and has been adopted by researchers in several major forestry studies on the environmental fate of hexazinone (5, 10, 11). The method was further modified by using capillary GC to improve peak resolution (12). The capillary GC method has been adopted in the evaluation of an applicator (13), a soil sampling method (14), the chemical release rate (12), and the chemical movement in soil leachate (15). During the course of development of the analytical method for hexazinone and metabolite residues, the basic concept of extraction and isolation developed by Holt (7) has not changed.

The difficulties experienced in the application of the conventional methods lie in the lack of compatibility of their final products of cleanup with the current available GC–NPD systems. Stringent control of peak fluctuation must be included by analyzing a standard solution alternately with each field sample (5, 9–14). Their isolation processes are labour intensive, time consuming, and costly. Furthermore, the conventional methods are not effective in removing the chlorophyll of vegetation samples. This paper describes a simple, effective isolation method using a disposable microcolumn and a modified GC analysis for hexazinone and metabolite residues in soils, and a further modified isolation method for vegetation.

Experimental

Soil preparation and fortification

Bulk quantity of uncontaminated soil was obtained from a northern Alberta forest and air-dried in an insulated dark room with a portable dehumidifier running at high speed for several days until soil moisture contents stabilized at about 3% oven-dry weight. The air-dried soil was then homogenized, sifted through a 2-mm mesh sieve, and mixed thoroughly (16). Soil was loamy clay containing 10% organic matter. Sixty 20-g aliquots of soil were weighed into separate 250-mL Nalgene polymethylpentene centrifuge bottles (Nalge 2107). Twenty aliquots were extracted and cleaned using the microcolumn method and analyzed separately by GC–NPD to determine the limit of detection (LOD) and limit of quantitation (LOQ) (17, 18). The sensitivity and analyte recovery of the method were determined using fortified soil samples as follows. Three aliquots of soil were reserved as controls. Thirty-six aliquots were fortified as triplicates or sextets with 10 different concentrations of mixture solutions (in toluene) of analytical grade[6] hexazinone, metabolite B, and metabolite A at a weight-ratio of 1:2:4 ranging from 0.001 to 1.25, 0.002 to 2.5, and 0.004 to 5.0 $\mu g\ g^{-1}$, respectively; the last sample was fortified at the highest concentrations of 6.25, 12.5, and 25.0 $\mu g\ g^{-1}$, respectively, without replication, because large amounts of analytical standards were needed. All treated samples were shaken horizontally for 15 min on an Eberbach reciprocating shaker at 280 excursions per minute and allowed to stand in a refrigerator (−5°C) for 40 h.

Crude soil extracts and precolumn sample preparation

Each bottle of soil (20 g) was wetted with 4 mL HPLC grade water and shaken horizontally for 5 min on an Eberbach shaker as described above. The sample was then treated with 200 mL accurately measured methanol, shaken horizontally for 15 min, and allowed to stand overnight in a refrigerator. The next morning, the sample was shaken for another 15 min and was centrifuged at 800 × *g* for 10 min to separate soil and the supernatant, which was designated as "crude extracts." About 170 mL of crude extracts were carefully poured, without disturbing the soil precipitate, through a Millipore Assembly consisting of a 47-mm Teflon-faced glass filter holder assembly, a 0.45-μm HVLP Durapore membrane filter, and a layer of anhydrous sodium sulfate (to remove moisture). A 150-mL aliquot of filtrate (equivalent to 15 g soil) was accurately measured with a 250-mL graduated cylinder and quantitatively transferred with triplicated 5-mL methanol rinse of the cylinder into a 500-mL round bottom flask. The neck of the flask was rinsed with small amounts of methanol. The volume of filtrate was reduced to about 3 mL by using a rotary evaporator at 45°C under reduced pressure. The concentrated filtrate was transferred quantitatively with triplicated 3-mL methanol rinse (or more, if necessary) into a 15-mL graduated conical tube with Teflon-lined cap (17 mL max. capacity). The sample volume was again reduced to 5 mL under a stream of nitrogen by using a 45°C N-Evap (Organomation Assoc. Inc., South Berlin, Mass).

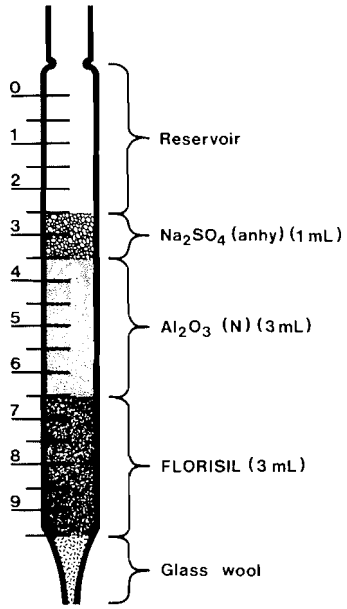

FIG. 1. Schematic illustrating the packing components of a microcolumn made of a 10-mL disposable volumetric pipet for the cleanup of hexazinone and metabolite residues in soil and vegetation.

Disposable microcolumn and cleanup for soil

Isolation of hexazinone and metabolites A and B from the filtered "crude extracts" of soils was accomplished using a homemade disposable microcolumn (Fig. 1).

(i) Preparation of disposable microcolumn

The bottom end of a 10-mL disposable glass volumetric pipet was plugged with glasswool prewashed by Soxhlet extraction in methanol (Fig. 1). A 3-mL bedding of anhydrous Florisil was packed into the glass pipet by lightly tapping on the pipet wall. A second 3-mL bedding of anhydrous, neutral aluminum oxide (Al_2O_3) was added on top by tapping and was followed with a 1-mL layer of anhydrous sodium sulfate (Na_2SO_4) prewashed by Soxhlet extraction in methanol. A dry-packing technique was used and no prewashing of the microcolumn was required before sample loading. The liquid-retaining capacity of the column packing was about 3 mL. An identical microcolumn was also prepared for the vegetation samples.

(ii) Microcolumn cleanup

The concentrated crude extract (5 mL) was loaded on the dry-packed microcolumn followed with triplicated 1-mL methanol rinse of the sample tube. The microcolumn was eluted with 12 mL of methanol (the eluent was the same solvent as in crude extracts). All eluates were collected into a fresh 15-mL graduated conical tube and evaporated to dryness with a stream of nitrogen in a 45°C N-Evap. Toluene (2.5 mL or predetermined volume between 1 and

[6]Analytical grade (100% pure) hexazinone and metabolites A, B, D, and E were supplied by E.I. Du Pont de Nemours, Wilmington, Del. via Du Pont Canada Inc., Mississauga, Ont.

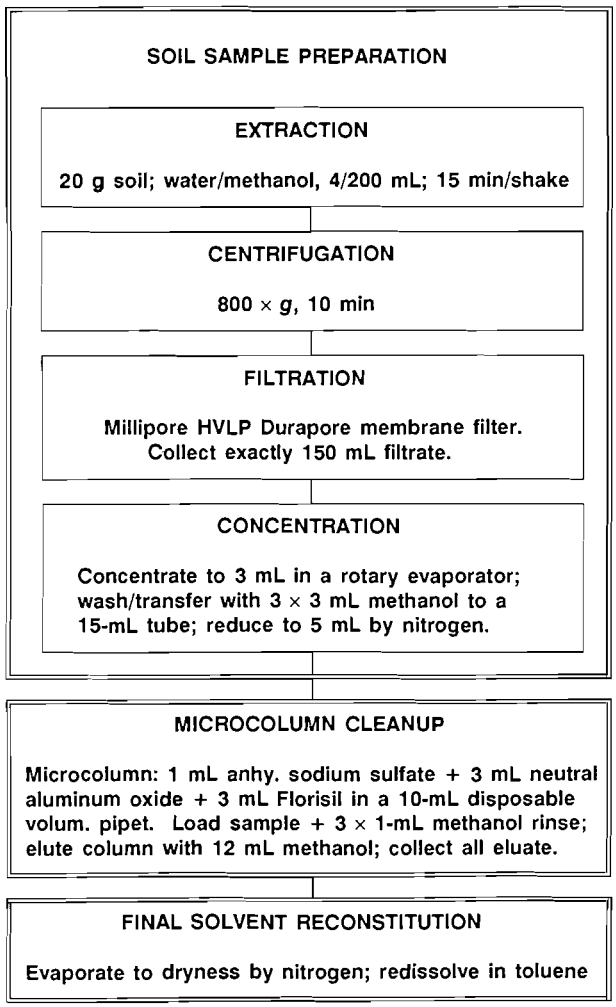

FIG. 2. Flow chart of the sample preparation and the microcolumn cleanup method for determination of hexazinone and metabolite residues in soils.

10 mL depending on the predicted residue concentration in a field sample) was added to the sample tube to redissolve residues before GC analysis. For the calculation of residue concentrations, the total weight of soil sample was 15 g. A flow chart of the foregoing procedure is presented in Fig. 2.

Vegetation sample preparation and fortification

Representative dominant species of tree, shrub, herbaceous, and grass plants or foliage with fine twigs as well as fresh forest litter were collected from the uncontaminated area of a northern Alberta forest. These vegetation species were trembling aspen (*Populus tremuloides* Michx.), willow (*Salix* spp.), showy aster (*Aster conspicuus* Lindl.), and reed grass (*Calamagrostis canadensis* Nutt.). Fresh-frozen vegetation samples were used in this method for better extraction efficiency. Broadleaf foliage and grasses were cut with scissors into 1-cm strips; twigs and fine stems were cut into 0.5-cm lengths. Dry weight and moisture content were determined from 10-g aliquots of samples oven-dried at 105°C for 48 h (16). Duplicate 15-g aliquots of vegetation samples were weighed into 250-mL Nalgene polymethylpentene centrifuge bottles and fortified with 1 μg g^{-1} hexazinone on a dry weight basis. Duplicates of non-spiked samples of each species were analyzed as controls.

Extraction and precolumn cleanup for vegetation

Each bottle of vegetation sample (15 g fresh weight) was treated with 60 mL methanol (accurately measured) and homogenized for 2 min using a Polytron PT-10 homogenizer. The entire bottle contents were filtered as described for soils. The filtrate was collected into a 50-mL graduated conical centrifuge tube with Teflon-lined cap (60 mL total capacity). A 30-mL aliquot of the filtrate (equivalent to extracts of 7.5-g samples) was kept in the tube by removing the excess amounts with a Pasteur pipet or by aspiration. The chlorophyll contents of the filtrate were reduced by partitioning five times with 25 mL hexane and shaking each time for 30 s. The upper phase of the hexane wash was discarded by aspiration. Twenty-five mL of the lower methanol phase (extracts of a 6.25-g sample) were retained by removing the excess amounts with a Pasteur pipet or by aspiration. The volume of sample was reduced to 5 mL with a stream of nitrogen in a 45°C N-Evap.

Microcolumn cleanup for vegetation

A disposable microcolumn identical to that described for soil was used in the isolation of hexazinone and metabolites A and B from the partially cleaned vegetation extracts. The concentrated sample (5 mL) was loaded into the dry-packed microcolumn followed with triplicated 1-mL methanol rinse of the sample tube. Methanol (14 mL) was also used as the eluent to elute hexazinone and metabolites from the adsorbents of the microcolumn. All eluates were collected into a 15-mL graduated conical tube and concentrated to exactly 5 mL with a stream of nitrogen in a 45°C N-Evap. The sample was then partitioned four times, with 10-mL hexane each time. The hexane upper phase of each partitioning and the excess amounts of the lower methanol phase of the last partitioning were removed with a Pasteur pipet or by aspiration and were discarded. Exactly 4 mL of the lower methanol phase was retained in the tube and evaporated to dryness with a stream of nitrogen in a 45°C N-Evap (small amounts of oily residue may remain in the tube). Toluene (2.5 mL or predetermined volume between 1 and 10 mL depending on the predicted concentration of residues in a field sample) was added to the sample tube to redissolve residues of hexazinone and metabolites before GC analysis. For calculating the recovery rate of residues, the total sample fresh weight was 5 g, and the moisture content was used to obtain the oven-dry weight of each sample. A flow chart of this method is presented in Fig. 3. To report the residue level of a field sample, the concentration of herbicide on a dry weight basis should be used.

Capillary gas chromatography

A modified capillary GC was used to determine concentrations of residues of hexazinone and the two primary metabolites A and B. The specific GC conditions were as follows.

(i) Gas chromatograph

A Varian model 3500 Capillary GC was equipped with a specially fitted megabore injector, a Thermionic Specific Detector (NPD), a model 8035 autosampler, a Varian DS 654 data system, and a NEC Pinwriter P6 printer-plotter.

(ii) Chromatographic column

A 15-m J&W fused silica DB-17 capillary column; 0.325 mm i.d.; 0.25 μm film thickness. A 1-m fused silica guard column (phenylmethyl siloxane deactivated, uncoated, megabore tubing of 0.53 mm i.d.) was installed between the megabore injector and the analytical column.

(iii) Temperatures

Injector, 250°C; detector, 300°C; oven temperature program, 80°C (held for 2 min) to 250°C (at 30°C min^{-1}; held for 7.3 min); total run time, 15 min.

(iv) Gases

All gases were supplied by Alberta Oxygen, Edmonton, Alberta. Carrier gas, helium (ultra pure grade) 4.3 mL min^{-1} at 80°C; linear velocity, 57 cm s^{-1} at 80°C; head pressure, 110 kPa; make-up gas, nitrogen (ultra pure grade) 30 mL min^{-1}; plasma gases, air (zero gas grade) 175 mL min^{-1} and hydrogen (ultra pure grade) 4.5 mL min^{-1}.

Can. J. Chem. Downloaded from www.nrcresearchpress.com by 79.173.37.17 on 09/08/12
For personal use only.

Can. J. Chem. Downloaded from www.nrcresearchpress.com by 79.173.37.17 on 09/08/12
For personal use only.

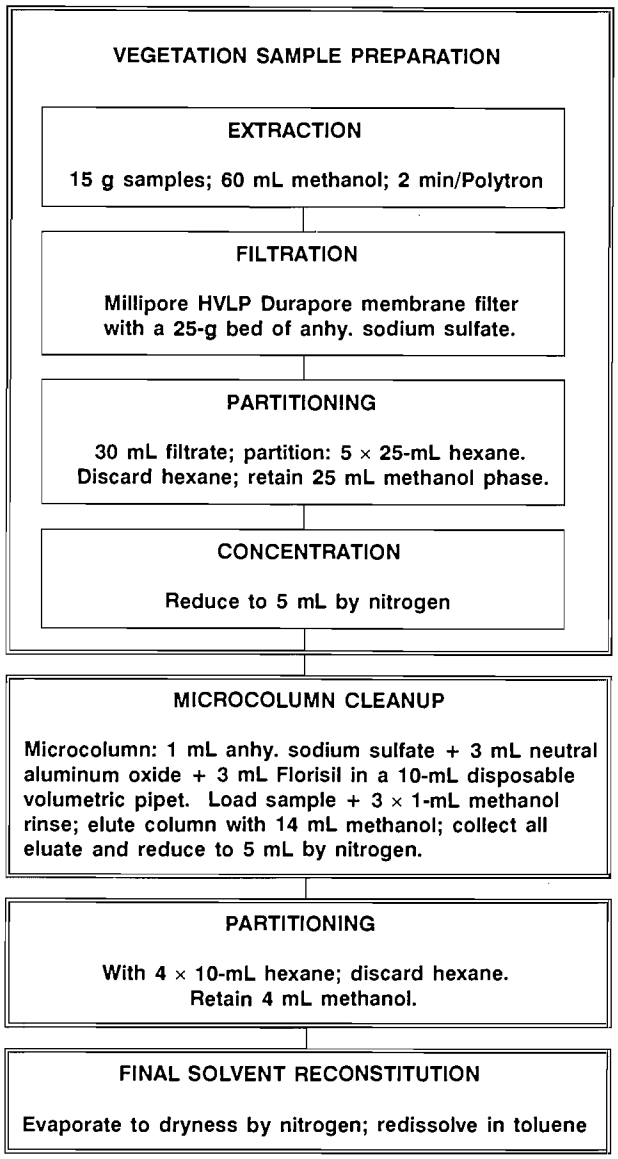

FIG. 3. Flow chart of the sample preparation and the microcolumn cleanup method for determination of hexazinone and metabolite residues in vegetation.

(v) Residue peak quantitation

Use of reference standards[5] in peak height quantitation was reported earlier (9) and can be summarized as follows. A mixture standard solution containing 2.5, 5.0, and 10.0 μg g^{-1} of hexazinone, metabolites B and A, respectively, was analyzed immediately before and after each sample analysis. When a sample showed twice or more the concentration of standard solution, the sample was diluted to near the concentration of standard solution and reanalysed. The average height of two corresponding peaks of the mixture standard solution, analyzed before and after a sample was measured, was used proportionally in calculating the residue concentration of the sample.

Results and discussion

Microcolumn cleanup for soils

The LOD and LOQ were calculated from the gross signals of the analytes (the slope of calibration curve ranging from 0.025 to 2.5 μg mL^{-1}), the mean signal value of field blanks (N = 20) at the retention time of the analyte, and three (LOD) or 10 (LOQ) times the standard deviation of the field blank signals (17, 18). The LOD's were 0.044, 0.110, and 0.218 μg mL^{-1} for hexazinone and metabolites B and A, respectively; LOQ's were 0.132, 0.312, and 0.594 μg mL^{-1}, respectively. The theoretical LODs of three analytes in soils, respectively, were 0.007, 0.018, and 0.036 μg g^{-1}; LOQ's were 0.022, 0.052, and 0.099 μg g^{-1}, respectively, when calculated at full recovery rate (100%) of each analyte using the described analytical method.

The actual recoveries of hexazinone and metabolites A and B from the microcolumn cleanup were tested at 11 concentration levels with a 1:6250 ratio between the lowest and the highest levels of each compound (Table 1). The recoveries of the two phytotoxic compounds, hexazinone and metabolite B, immediately above LOQ at 0.0313 and 0.0625 μg g^{-1}, respectively, were reliable at 94 ± 4 and 89 ± 7%, respectively. Recoveries of both analytes at higher levels were similar to that at 0.0313 and 0.0625 μg g^{-1}, respectively. The overall mean recovery for hexazinone ranging from 0.0313 to 6.25 μg g^{-1} (six levels of concentration) was 94 ± 3%. For metabolite B ranging from 0.0625 to 12.5 μg g^{-1} (six concentration levels), the mean recovery was 94 ± 5%.

Recoveries of the non-phytotoxic metabolite A increased steadily with the increase of concentrations (Table 1). Although the overall recovery for metabolite A above LOQ was relatively lower at 77 ± 21% between 0.125 and 25 μg g^{-1} (six concentration levels), the recovery rates were greater than 50% and were reasonably consistent at each concentration level. Correction factors may be established for several concentration ranges above 0.125 μg g^{-1} and used in calculating the concentration of metabolite A in a field sample.

Total amount of solvents used for the extraction and cleanup of each soil sample in this method was 225 mL. This was less than 30% of the amount required in conventional methods (765 mL) (7, 9). Although rewetting the air-dried sample with 10–20% water (w/w) is necessary in desorbing residues,[7] the initial air-drying of soil is essential in preparing a homogenous sample for subsampling (10). The use of methanol as the extracting solvent made possible the complete desorption of hexazinone and metabolite A and B residues from the soil particles. An aliquot of the crude extract can be taken, with a volume correction, to represent the product of an exhaustive extraction as in the conventional method. The extraction process was further simplified using methanol rather than an acetone–water solution (7, 9), where acetone must be completely evaporated from the aqueous solution followed by separate triplicate partitions with hexane, acetonitrile, and chloroform. Hexazinone and its metabolites A and B are not adsorbed strongly on the microcolumn packing compared with most of coextractives. Therefore, the same solvent, methanol, can be used as the eluent of the microcolumn. Because the fully activated Florisil and aluminum oxide are used in this method, loss of hexazinone and its metabolites to the absorbents would occur if the mixture solution of pure standards[5] is used alone, causing a lack of coextractives to occupy the active sites of the absorbents. Because there was no need to change the solvent phase, the column eluting time was greatly reduced. The final sample dissolved in toluene was stable for

[7]G. Bruns. 1990. Personal communication. Enviro-Test Laboratories, Edmonton, Alta.

TABLE 1. Individual and overall mean recoveries of added hexazinone and metabolites A and B in air-dried soil after microcolumn cleanup

Hexazinone		Metabolite B		Metabolite A		
μg g^{-1}	% recovery	μg g^{-1}	% recovery	μg g^{-1}	% recovery	*N*
0.0010	0	0.0020	0	0.0040	0	3
0.0030	29 ± 25	0.0060	0	0.0120	20 ± 45	3
0.0050	51 ± 4	0.0100	11 ± 19	0.0200	28 ± 43	3
LOD						
0.0100	68 ± 6	0.0200	69 ± 31	0.0400	40 ± 11	3
0.0200	83 ± 3	0.0400	97 ± 17	0.0800	51 ± 10	3
LOQ						
0.0313	94 ± 4	0.0625	89 ± 7	0.125	55 ± 8	6
0.0625	91 ± 11	0.125	95 ± 15	0.25	62 ± 19	3
0.125	97 ± 4	0.25	97 ± 11	0.5	65 ± 8	6
0.625	92 ± 2	1.25	90 ± 5	2.5	79 ± 4	3
1.25	91 ± 5	2.5	89 ± 6	5.0	90 ± 11	3
6.25	96	12.5000	102	25	111	1
Overall mean						
0.031–6.25	94 ± 3	0.063–12.5	94 ± 5	0.125–25	77 ± 21	

TABLE 2. Mean recoveries of added hexazinone at a level of 1 μg g^{-1} dry weight in different vegetation species from the microcolumn cleanup method

Vegetation species	Mean recovery (%)
Trembling aspen (*Populus tremuloides* Michx.)	76.1
Willow (*Salix* spp.)	72.9
Showy aster (*Aster conspicuus* Lindl.)	96.4
Reed grass (*Calamagrostis canadensis* Nutt.)	92.3
Fresh litter	81.5

at least 6 months at 5°C. Due to the simplicity of this method, 20 soil samples can be cleaned up as one batch by one person in 1 day and that is three times or more efficient than the conventional methods. The cost for waste disposal and the risk in environmental and health hazards are also reduced.

Microcolumn cleanup for vegetation

The original method of Holt (7) and its modification (9) were tested using fresh aspen foliage. The end product of sample cleanup showed a dense, dark-green color and high viscosity and was impossible to analyze by either the packed column GC or the capillary GC. Neither was the microcolumn method for soil sample cleanup described above capable of removing chlorophyll from the foliage extracts. The microcolumn method for soils was modified for the cleanup of vegetation samples by using hexane partitioning both before and after microcolumn cleanup to remove chlorophyll from the methanol extracts. Further cleanup was achieved in the final step of the method by changing the solvent from methanol to toluene (final solvent reconstitution) (Fig. 3). The end product was clear or a pale amber color and produced a clean chromatogram. Mean recoveries of hexazinone were the highest for understory species (92–96% for grass and aster), followed by fresh litter (82%) and tree species (73–76% for willow and aspen) (Table 2). The lower limit of detectability for hexazinone using this cleanup method was determined in a separate study and was similar to the soil method described above (19). Total amount of solvents needed for the cleanup of a 15-g vegetation sample was 245 mL. Twelve samples could be processed as one batch by one person in 2.5 days.

Gas chromatography

Earlier reports indicated that both methanol and ethyl acetate seemed to cause fluctuations in peak responses in the Varian GC and that stringent control of peak fluctuation using alternated analyses of reference standard and samples was required for quantifying hexazinone and its metabolites (5, 9–13, 15). The stability of the Varian model 3500 GC was improved by replacing the split/splitless capillary GC injector with a megabore injector fitted with a 1-m-long megabore fused silica guard column and using toluene[8] (20) as the sample solvent. The frequency of analysis of the standard solution may be reduced to once for every 10 field samples for the purpose of "good laboratory practice (GLP)."

In analyzing the toluene solution of reference standards of hexazinone and four metabolites, i.e., metabolites A, B, D, and E, the responses of all peaks were consistent and sensitive. When using toluene in the analysis of both soil and vegetation samples, however, the responses of metabolites A, D, and E were reduced. These losses occurred during the final solvent reconstitution after the microcolumn cleanup when the sample in methanol was evaporated to dryness and redissolved in toluene. Some of these residues tended to adsorb on the coextractive, which adhered on the glass and became less soluble in toluene. Although recoveries of hexazinone and its demethylated derivative, metabolite B, were good when the sample was redissolved in toluene, the recovery of its hydroxylated derivative, metabolite A, was relatively low at lower concentration levels (Table 1). The

[8]Use of toluene for better stability in GC was recommended and supported by the analysis of hexazinone (analytical grade[5]) by C. Jennison, Varian Canada Inc., Georgetown, Ont.

Can. J. Chem. Downloaded from www.nrcresearchpress.com by 79.173.37.17 on 09/08/12
For personal use only.

recoveries of both minor trione metabolites D and E were the lowest among the five tested compounds and were unreliable (data are not shown). When analyzing for metabolites D and E, the final solvent reconstitution should be omitted and the method of residue peak quantitation described above should be followed.

The GC analysis time was shortened by 25% per sample, when the shorter (15 m) than conventional (30 m) DB-17 fused silica capillary column was used. Peaks of hexazinone and four metabolites were well resolved. Retention times were 6.7, 7.7, 9.0, 9.5, and 11.5 min for metabolites D and E, hexazinone, and metabolites B and A, respectively; peak widths at half-height were 3.5, 3.3, 2.9, 6.2, and 8.3 s, respectively. The introduction and frequent replacement of a 1-m fused silica guard column extended the lifetime of the analytical column by about a factor of five for the analyses of foliage samples.

The combined use of the modified capillary GC method and the microcolumn cleanup technique is recommended as an efficient, reliable, and less labour-intensive substitute for conventional methods in analyzing residues of hexazinone and two primary metabolites, A and B, in soil and vegetation.

Acknowledgments

This research was supported by the Northern Forestry Centre, Forestry Canada, and was partially financed under the Canada–Alberta Forest Resource Development Agreement. The author acknowledges the professional advice of Dr. G. Hillman (research scientist), C. Feng (herbicide chemist), and Y. Kalra (soil chemist), and the technical assistance of J. Hudson. The figure was prepared by D. Lee.

1. E. J. Dimock II, T. F. Beebe, and E. B. Collard. Weed Sci. **31**, 215 (1983).
2. N. Malik and W. H. Vanden Born. Can. For. Serv. Inf. Rep. NOR-X-282 (1986).
3. J. C. Feng, V. Stornes, and R. Rogers. J. Environ. Sci. Health Part B: **B23**, 267 (1988).
4. J. Drouin. For. Can. Inf. Rep. NOR-X-306 (1989).
5. R. Prasad and J. C. Feng. Weed Technol. **4**, 371 (1990).
6. R. F. Sutton. For. Chron. **62**, 226 (1986).
7. R. F. Holt. J. Agric. Food Chem. **29**, 165 (1981).
8. S. S. Sung, D. B. South, and D. H. Gjerstad. Weed Sci. **33**, 440 (1985).
9. J. C. Feng. J. Environ. Sci. Health Part B: **B22**, 221 (1987).
10. J. C. Feng and C. C. Feng. Can. For. Serv. Inf. Rep. FPM-X-81 (1988).
11. D. N. Roy, S. K. Konar, D. A. Charles, J. C. Feng, R. Prasad, and R. A. Campbell. J. Agric. Food Chem. **37**, 443 (1989).
12. J. C. Feng, C. C. Feng, and S. S. Sidhu. Can. J. For. Res. **19**, 378 (1989).
13. J. C. Feng, G. B. Ehrentraut, and T. J. Drew. J. Environ. Sci. Health Part B: **B24,** 525 (1989).
14. J. C. Feng and S. Navratil. Can. J. For. Res. **20**, 1549 (1990).
15. J. C. Feng, S. S. Sidhu, C. C. Feng, and V. Servant. J. Environ. Sci. Health Part B: **B24**, 131 (1989).
16. J. C. Feng and H. D. Klassen. Can. For. Serv. Inf. Rep. FPM-X-72 (1986).
17. G. L. Long and J. D. Winefordner. Anal. Chem. **55**, 712A (1983).
18. Guidelines for data acquisition and data quality evaluation in environmental chemistry. Anal. Chem. **52**, 2242 (1980).
19. S. S. Sidhu, J. C. Feng, and C. C. Feng. Expert Comm. Weeds, West Can. Sect. 1989 Res. Rep. **3**, 221 (1989).
20. C. Jennison and J. Jennison. Am. Lab., Chromatography Supplement, 40W (1990).

Can. J. Chem. Downloaded from www.nrcresearchpress.com by 79.173.37.17 on 09/08/12
For personal use only.

^1H and ^{13}C NMR study of the pyrazolo[1,5-*a*]pyrimidine system

STEFANO CHIMICHI[1] AND BARBARA COSIMELLI

Dipartimento di Chimica Organica e Centro CNR sulla Chimica e la Struttura dei Composti Eterociclici e loro Applicazioni, Via Gino Capponi 9, I-50121 Firenze, Italy

AND

FABRIZIO BRUNI AND SILVIA SELLERI

Dipartimento di Scienze Farmaceutiche, Via Gino Capponi 9, I-50121 Firenze, Italy

Received August 29, 1991

STEFANO CHIMICHI, BARBARA COSIMELLI, FABRIZIO BRUNI, and SILVIA SELLERI. Can. J. Chem. **70**, 1093 (1992).

The ^{13}C and ^1H NMR spectra of some pyrazolo[1,5-*a*]pyrimidine derivatives are discussed. All ^{13}C resonances were unambiguously assigned by means of both 2D experiments and gated decoupled spectra from which one-bond and long-range ^{13}C–^1H coupling constants were determined. The literature assignments for H-5 and H-7 in the parent system have been revised and a simple method for distinguishing between 5-methyl and 7-methyl compounds is suggested, based on the carbon chemical shift of the methyl group or on its fine structure in the ^1H NMR spectrum. Regioselective syntheses for all the reported methyl derivatives are also described.

STEFANO CHIMICHI, BARBARA COSIMELLI, FABRIZIO BRUNI et SILVIA SELLERI. Can J. Chem. **70**, 1093 (1992).

On discute des spectres RMN du ^1H et du ^{13}C de quelques dérivés pyrazolo[1,5-*a*]pyrimidine. On a attribué toutes les raies de spectres ^{13}C d'une façon non-ambiguë à l'aide d'expériences en 2D et de spectres découplés à connexion intermittente à partir desquels on a déterminé les constantes de couplage ^{13}C–^1H à travers une et plusieurs liaisons. On a révisé les attributions faites dans la littérature pour les H-5 et H-7 et on suggère une méthode simple pour distinguer les composés portant des méthyles en 5 ou en 7; elle est basée sur le déplacement chimique du carbone des groupes méthyles ou sur la structure fine dans les spectres RMN du ^1H. On décrit aussi des synthèses régiospécifiques pour tous les dérivés méthyles examinés.

[Traduit par la rédaction]

Introduction

As part of our continuing interest in hetero-condensed five-membered heterocycles (1–3), we recently reported a new synthetic pathway to pyrazolo[1,5-*a*]pyrimidines (4). During this work, we noticed the lack of carbon-13 NMR data for this class of compound, some members of which show interesting biological properties (5–7).

We report here a detailed ^{13}C and ^1H NMR study of some pyrazolo[1,5-*a*]pyrimidines, including the parent ring system, carried out by means of gated decoupled, hetero- and homonuclear correlation spectroscopy techniques. We also demonstrate that NMR spectroscopy can be valuable for distinguishing the isomeric 7-methyl and 5-methyl derivatives, this not being easily achieved by other common spectroscopic techniques.

Experimental

Chemicals

3(5)-Aminopyrazole and 4,4-dimethoxybutan-2-one (acetylacetaldehyde dimethyl acetal) are commercially available (Aldrich); 5-amino-3-phenylpyrazole and compounds **1**, **4**, **5**, and **8** were synthesized according to published procedures (8–12, respectively).

5-Methylpyrazolo[1,5-a]pyrimidine (2)

The procedure reported by Bajwa and Sykes (13) was modified by adding 4,4-dimethoxybutan-2-one (1.00 g, 7.6 mmol) to a solution of 3(5)-aminopyrazole (0.57 g, 6.9 mmol) in EtOH (3.5 mL). The solution was then refluxed for 30 min; removal of the solvent left a yellow solid (0.86 g, 94%) mainly consisting (90%, TLC and ^1H NMR spectrum) of compound **2**, together with a very small quantity of the 7-methyl isomer. An analytical sample (colorless plates) obtained by recrystallization from petroleum ether melted at 122–123°C (lit. (13) mp 122–124°C).

7-Methylpyrazolo[1,5-a]pyrimidine (3)

A solution of 3(5)-aminopyrazole (0.57 g, 6.9 mmol) in EtOH (3.5 mL) was added to a solution of the β-keto-acetal (1.00 g, 7.6 mmol) in concentrated HCl (0.3 mL). The solution was refluxed for 30 min and then poured into water (20 mL) and extracted exhaustively with diethyl ether. The ethereal extracts were washed with water (50 mL) and dried on Na_2SO_4. Evaporation to dryness left a yellow solid (0.66 g, 80%) containing the isomeric 7- and 5-methyl derivatives in the ratio 87:13. The mixture was resolved by flash chromatography with ethyl acetate/petroleum ether (bp 40–70°C) (1:1 v/v) as eluent; the faster band gave compound **3** (77%), mp 58–59°C (from petroleum ether) (lit. (13) mp 59–60°C). The second compound was easily recognized (TLC, ^1H NMR spectrum) as 5-methylpyrazolo[1,5-*a*]pyrimidine (**2**) (10%).

5-Methyl-1-phenylpyrazolo[1,5-a]pyrimidine (6)

Operating as for compound **2** employing 5-amino-3-phenylpyrazole, a pink solid (0.62 g, 95%) consisting mainly (96%, TLC and ^1H NMR spectrum) of compound **6** was obtained. An analytical sample (colorless plates) melted at 177–178°C (from ethyl acetate). Anal. calcd. for $C_{13}H_{11}N_3$: C 74.62, H 5.3, N 20.08; found: C 74.26, H 5.21, N 20.27.

7-Methyl-2-phenylpyrazolo[1,5-a]pyrimidine (7)

Operating as for compound **3** starting from 5-amino-3-phenylpyrazole, a yellow solid (0.61 g, 94%) containing the two isomeric 7- and 5-methyl derivatives (93:7) was obtained. Recrystallization from ethanol/water (1:1 v/v) afforded compound **7** as yellow needles, mp 93–94°C (lit. (14) mp 95–96°C).

Instruments

All melting points were determined on a Gallenkamp melting point apparatus and are uncorrected. Carbon-13 and proton NMR spectra were recorded on a Varian VXR-300 instrument in the Fourier transform mode. All carbon spectra were recorded in 10-mm o.d. tubes at 25 ± 0.5°C for 0.5 M solutions in $CDCl_3$, proton coupled spectra were obtained in the "gated decoupling" mode; proton spectra were recorded in 5-mm o.d. tubes at the same temperature. Chemical shifts are reported in ppm high frequency from

[1]Author to whom correspondence may be addressed.

Printed in Canada

Can. J. Chem. Downloaded from www.nrcresearchpress.com by 79.173.37.17 on 09/08/12
For personal use only.

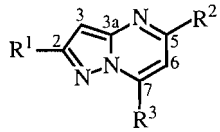

1 $R^1 = R^2 = R^3 = H$ **5** $R^1 = C_6H_5$, $R^2 = R^3 = H$

2 $R^1 = R^3 = H$, $R^2 = CH_3$ **6** $R^1 = C_6H_5$, $R^2 = CH_3$, $R^3 = H$

3 $R^1 = R^2 = H$, $R^3 = CH_3$ **7** $R^1 = C_6H_5$, $R^2 = H$, $R^3 = CH_3$

4 $R^1 = H$, $R^2 = R^3 = CH_3$ **8** $R^1 = C_6H_5$, $R^2 = R^3 = CH_3$

SCHEME 1

TMS as secondary reference standard and coupling constants in Hz. Silica gel plates (Merck F_{254}) and silica gel 60 (Merck 230–400 mesh) were used for analytical TLC and for flash chromatographies, respectively. Solvents were removed under reduced pressure.

Results and discussion

The carbon chemical shifts of the examined compounds **1**–**8** (Scheme 1) are given in Table 1; spectra were analyzed on a first-order basis, the necessary assumptions being fulfilled. Coupling constants are assembled in Table 2; the assignments of carbon resonances (see below) are based on chemical shift arguments, on ^1J(CH) values, and on the fine splitting pattern caused by long-range couplings as well as on HETCOR spectra.

Chemical shift considerations did not always allow an unambiguous assignment; as regards compound **1**, apart from the singlet attributable to the quaternary carbon atom C-3a, the five methine ring carbons appear as doublets with further long-range couplings. The signals at lower frequencies (δ 96.86 and 107.66) are easily attributed to C-3 and C-6, respectively, because the former appears as a doublet of doublets ($^2J_{C3-H2}$ = 9.7 Hz) whereas the latter is a doublet of doublets of doublets due to the long-range couplings both to H-5 and H-7 ($^2J_{C6-H5}$ = 9.9 Hz and $^2J_{C6-H7}$ = 3.0 Hz). Assignment of C-2, C-5, and C-7 resonances is more difficult, their chemical shifts being very close, and was achieved on the following basis.

First, we attempted to assign all the proton resonances of compound **1** (Table 3) by a COSY-90 experiment, which would then be useful in rationalizing the heteronuclear correlation (HETCOR) spectrum. Unfortunately, the COSY spectrum, besides confirming the assignment of H-3 and H-6, allowed us only to attribute the signal at δ 8.166 to H-2; as regards H-7 and H-5 an unambiguous assignment was not attained. Moreover, the HETCOR spectrum shows that the most deshielded carbon atom is not connected with the most deshielded proton but with the signal at δ 8.461; this finding, together with chemical shifts considerations and the fine splitting pattern, suggested that the highest frequency signal in the ^{1}H NMR spectrum should be attributed to H-7 instead of H-5, contrary to the report of Lynch *et al.* (9). To reach a definitive assignment, we synthesized the methyl derivatives **2**, **6** and **3**, **7**. As for the preparation of these compounds, a synthetic pathway leading to a mixture of compounds **2** and **3** was reported in the literature (13) starting from 4,4-dimethoxybutan-2-one. A simple change in the experimental procedure (see Experimental) allowed us to make the synthesis highly regioselective also employing 3-

TABLE 1. ^{13}C NMR ($CDCl_3$, 75 MHz) chemical shifts (δ, ppm) of compounds **1**–**8**[a]

Compound	C-2	C-3	C3a	C-5	C-6	C-7	5-CH_3	7-CH_3	C-*ipso*	C-*ortho*	C-*meta*	C-*para*
1	145.04(dd)	96.86(dd)	148.54(m)	149.02(ddd)	107.66(ddd)	135.01(dm)	—	—	—	—	—	—
2	145.00(dd)	95.65(dd)	148.22[b](ddd)	158.93[c](ddq)	108.75[d](ddq)	134.41(dd)	24.79(qd)	—	—	—	—	—
3	144.34(dd)	96.93(dd)	148.82[b](ddd)	148.57(dd)	107.40(ddq)	146.04(m)	—	17.22(qd)	—	—	—	—
4	144.29(dd)	95.71(dd)	148.52[e](dd)	158.32(qd)	108.35[f](dqq)	145.16(qd)	24.59(qd)	17.04(qd)	—	—	—	—
5	156.03[g](dt)	93.28(d)	149.39(ddd)	148.75(ddd)	107.34(ddd)	134.37(ddd)	—	—	131.33	128.48	126.21	128.74
6	156.35[g](dt)	92.55(d)	149.37(dd)	159.01[c](ddq)	108.73[d](ddq)	134.17(dd)	24.82(qd)	—	132.80	128.77	126.44	128.93
7	155.68[g](dt)	93.65(d)	149.98(dd)	148.57(dd)	107.40(ddq)	146.03[c](ddq)	—	17.24(qd)	133.05	128.75	126.60	128.89
8	155.55[g](dt)	92.51(d)	149.66(d)	158.30(qd)	108.29[f](dqq)	145.17(qd)	24.60(qd)	17.04(qd)	133.22	128.70	126.51	128.73

[a] Multiplicity (s = singlet, d = doublet, t = triplet, q = quartet, m = multiplet).
[b] Appears as doublet of triplets.
[c] Appears as quintet of doublets.
[d] Appears as doublet of quintets.
[e] Appears as triplet.
[f] Appears as doublet of septuplets.
[g] Appears as quartet.

Can. J. Chem. Downloaded from www.nrcresearchpress.com by 79.173.37.17 on 09/08/12
For personal use only.

Can. J. Chem. Downloaded from www.nrcresearchpress.com by 79.173.37.17 on 09/08/12
For personal use only.

TABLE 2. Selected $^{n}J_{C,H}$ (Hz) of compounds **1–8**

Compound	C-2	C-3	C-3a	C-5	C-6	C-7	5-CH_3	7-CH_3
1	$^{1}J_{C\text{-}2,H\text{-}2}$ = 185.3 $^{2}J_{C\text{-}2,H\text{-}3}$ = 5.6	$^{1}J_{C\text{-}3,H\text{-}3}$ = 181.1 $^{2}J_{C\text{-}3,H\text{-}2}$ = 9.7	m[a]	$^{1}J_{C\text{-}5,H\text{-}5}$ = 183.7 $^{3}J_{C\text{-}5,H\text{-}7}$ = 6.2 $^{2}J_{C\text{-}5,H\text{-}6}$ = 2.6	$^{1}J_{C\text{-}6,H\text{-}6}$ = 171.1 $^{2}J_{C\text{-}6,H\text{-}5}$ = 9.9 $^{2}J_{C\text{-}6,H\text{-}7}$ = 3.0	$^{1}J_{C\text{-}7,H\text{-}7}$ = 186.3	—	—
2	$^{1}J_{C\text{-}2,H\text{-}2}$ = 184.6 $^{2}J_{C\text{-}2,H\text{-}3}$ = 5.6	$^{1}J_{C\text{-}3,H\text{-}3}$ = 180.4 $^{2}J_{C\text{-}3,H\text{-}2}$ = 9.7	$^{2}J_{C\text{-}3a,H\text{-}3}$ = 6.7 $^{3}J_{C\text{-}3a,H\text{-}2}$ = 6.7 $^{3}J_{C\text{-}3a,H\text{-}7}$ = 3.3	$^{2}J_{C\text{-}5,5CH_3}$ = 6.4 $^{3}J_{C\text{-}5,H\text{-}7}$ = 6.4 $^{2}J_{C\text{-}5,H\text{-}6}$ = 1.8	$^{1}J_{C\text{-}6,H\text{-}6}$ = 169.2 $^{2}J_{C\text{-}6,H\text{-}7}$ = 3.4 $^{3}J_{C\text{-}6,5CH_3}$ = 3.4	$^{1}J_{C\text{-}7,H\text{-}7}$ = 185.5 $^{2}J_{C\text{-}7,H\text{-}6}$ = 3.0	$^{1}J_{5CH_3}$ = 127.8 $^{3}J_{5CH_3,H\text{-}6}$ = 1.7	—
3	$^{1}J_{C\text{-}2,H\text{-}2}$ = 184.8 $^{2}J_{C\text{-}2,H\text{-}3}$ = 5.6	$^{1}J_{C\text{-}3,H\text{-}3}$ = 180.5 $^{2}J_{C\text{-}3,H\text{-}2}$ = 9.8	$^{3}J_{C\text{-}3a,H\text{-}5}$ = 13.9 $^{2}J_{C\text{-}3a,H\text{-}3}$ = 6.9 $^{3}J_{C\text{-}3a,H\text{-}2}$ = 6.9	$^{1}J_{C\text{-}5,H\text{-}5}$ = 181.8 $^{2}J_{C\text{-}5,H\text{-}6}$ = 2.2	$^{1}J_{C\text{-}6,H\text{-}6}$ = 168.4 $^{2}J_{C\text{-}6,H\text{-}5}$ = 9.6 $^{3}J_{C\text{-}6,7CH_3}$ = 4.6	m[a]	—	$^{1}J_{7CH_3}$ = 130.5 $^{3}J_{7CH_3,H\text{-}6}$ = 3.5
4	$^{1}J_{C\text{-}2,H\text{-}2}$ = 184.2 $^{2}J_{C\text{-}2,H\text{-}3}$ = 5.6	$^{1}J_{C\text{-}3,H\text{-}3}$ = 179.9 $^{2}J_{C\text{-}3,H\text{-}2}$ = 9.9	$^{2}J_{C\text{-}3a,H\text{-}3}$ = 6.9 $^{3}J_{C\text{-}3a,H\text{-}2}$ = 6.9	$^{2}J_{C\text{-}5,5CH_3}$ = 7.0 $^{2}J_{C\text{-}5,H\text{-}6}$ = 2.0	$^{1}J_{C\text{-}6,H\text{-}6}$ = 166.6 $^{3}J_{C\text{-}6,5CH_3}$ = 4.0 $^{3}J_{C\text{-}6,7CH_3}$ = 4.0	$^{2}J_{C\text{-}7,7CH_3}$ = 6.3 $^{2}J_{C\text{-}7,H\text{-}6}$ = 3.0	$^{1}J_{5CH_3}$ = 127.6 $^{3}J_{5CH_3,H\text{-}6}$ = 1.8	$^{1}J_{7CH_3}$ = 130.4 $^{3}J_{7CH_3,H\text{-}6}$ = 3.8
5	$^{2}J_{C\text{-}2,H\text{-}3}$ = 4.5 $^{3}J_{C\text{-}2,H\text{-}ortho}$ = 4.5	$^{1}J_{C\text{-}3,H\text{-}3}$ = 179.4	$^{3}J_{C\text{-}3a,H\text{-}5}$ = 13.7 $^{2}J_{C\text{-}3a,H\text{-}3}$ = 6.7 $^{3}J_{C\text{-}3a,H\text{-}7}$ = 3.4	$^{1}J_{C\text{-}5,H\text{-}5}$ = 183.6 $^{3}J_{C\text{-}5,H\text{-}7}$ = 6.2 $^{2}J_{C\text{-}5,H\text{-}6}$ = 2.6	$^{1}J_{C\text{-}6,H\text{-}6}$ = 171.1 $^{2}J_{C\text{-}6,H\text{-}5}$ = 9.9 $^{2}J_{C\text{-}6,H\text{-}7}$ = 3.0	$^{1}J_{C\text{-}7,H\text{-}7}$ = 186.0 $^{3}J_{C\text{-}7,H\text{-}5}$ = 6.4 $^{2}J_{C\text{-}7,H\text{-}6}$ = 3.6	—	—
6	$^{2}J_{C\text{-}2,H\text{-}3}$ = 4.0 $^{3}J_{C\text{-}2,H\text{-}ortho}$ = 4.0	$^{1}J_{C\text{-}3,H\text{-}3}$ = 178.8	$^{2}J_{C\text{-}3a,H\text{-}3}$ = 6.5 $^{3}J_{C\text{-}3a,H\text{-}7}$ = 3.2	$^{2}J_{C\text{-}5,5CH_3}$ = 6.4 $^{3}J_{C\text{-}5,H\text{-}7}$ = 6.4 $^{2}J_{C\text{-}5,H\text{-}6}$ = 2.1	$^{1}J_{C\text{-}6,H\text{-}6}$ = 169.1 $^{2}J_{C\text{-}6,H\text{-}7}$ = 3.4 $^{3}J_{C\text{-}6,5CH_3}$ = 3.4	$^{1}J_{C\text{-}7,H\text{-}7}$ = 185.3 $^{2}J_{C\text{-}7,H\text{-}6}$ = 3.3	$^{1}J_{5CH_3}$ = 127.8 $^{3}J_{5CH_3,H\text{-}6}$ = 1.7	—
7	$^{2}J_{C\text{-}2,H\text{-}3}$ = 4.2 $^{3}J_{C\text{-}2,H\text{-}ortho}$ = 4.2	$^{1}J_{C\text{-}3,H\text{-}3}$ = 178.8	$^{3}J_{C\text{-}3a,H\text{-}5}$ = 13.7 $^{2}J_{C\text{-}3a,H\text{-}3}$ = 6.7	$^{1}J_{C\text{-}5,H\text{-}5}$ = 181.7 $^{2}J_{C\text{-}5,H\text{-}6}$ = 2.6	$^{1}J_{C\text{-}6,H\text{-}6}$ = 168.5 $^{2}J_{C\text{-}6,H\text{-}5}$ = 9.5 $^{3}J_{C\text{-}6,7CH_3}$ = 4.6	$^{2}J_{C\text{-}7,7CH_3}$ = 6.5 $^{3}J_{C\text{-}7,H\text{-}5}$ = 6.5 $^{2}J_{C\text{-}7,H\text{-}6}$ = 3.1	—	$^{1}J_{7CH_3}$ = 130.6 $^{3}J_{7CH_3,H\text{-}6}$ = 3.6
8	$^{2}J_{C\text{-}2,H\text{-}3}$ = 4.0 $^{3}J_{C\text{-}2,H\text{-}ortho}$ = 4.0	$^{1}J_{C\text{-}3,H\text{-}3}$ = 177.9	$^{2}J_{C\text{-}3a,H\text{-}3}$ = 6.6	$^{2}J_{C\text{-}5,5CH_3}$ = 6.4 $^{2}J_{C\text{-}5,H\text{-}6}$ = 2.1	$^{1}J_{C\text{-}6,H\text{-}6}$ = 166.5 $^{3}J_{C\text{-}6,5CH_3}$ = 4.0 $^{3}J_{C\text{-}6,7CH_3}$ = 4.0	$^{2}J_{C\text{-}7,7CH_3}$ = 6.4 $^{2}J_{C\text{-}7,H\text{-}6}$ = 3.0	$^{1}J_{5CH_3}$ = 127.6 $^{3}J_{5CH_3,H\text{-}6}$ = 1.8	$^{1}J_{7CH_3}$ = 130.5 $^{3}J_{7CH_3,H\text{-}6}$ = 3.8

[a]Not resolved.

Can. J. Chem. Downloaded from www.nrcresearchpress.com by 79.173.37.17 on 09/08/12
For personal use only.

TABLE 3. Selected ^{1}H NMR ($CDCl_3$, 300 MHz) chemical shifts (δ, ppm) of compounds **1**–**8**[a]

Compound	H-2	H-3	H-5	H-6	H-7	5-CH_3	7-CH_3
1	8.17(d,$J_{3,2}$2.2)	6.69(dd,$J_{3,2}$2.2,$J_{3,7}$0.9)	8.46(dd,$J_{5,6}$4.0,$J_{5,7}$1.8)	6.79(dd,$J_{6,7}$7.0,$J_{6,5}$4.0)	8.67(ddd,$J_{7,6}$7.0,$J_{7,5}$1.8,$J_{7,3}$0.9)	—	—
2	8.06(dd,$J_{2,3}$2.4,$J_{2,7}$0.7)	6.55(dd,$J_{3,2}$2.4,$J_{3,7}$0.9)	—	6.67(d,$J_{6,7}$7.2)	8.53(ddd,$J_{7,6}$7.2,$J_{7,3}$0.9,$J_{7,2}$0.7)	2.60(s)	—
3	8.14(d,$J_{2,3}$2.4)	6.71(d,$J_{3,2}$2.4)	8.37(d,$J_{5,6}$4.1)	6.68(dq,$J_{6,5}$4.1,$J_{6,7CH_3}$0.9)	—	—	2.79(d,$J_{7CH_3,6}$0.9)
4	8.07(d,$J_{2,3}$2.4)	6.56(d,$J_{3,2}$2.4)	—	6.55(q,$J_{6,7CH_3}$0.9)	—	2.55(s)	2.73(d,$J_{7CH_3,6}$0.9)
5	—	7.00(d,$J_{3,7}$0.9)	8.46(dd,$J_{5,6}$4.1,$J_{5,7}$1.8)	6.79(dd,$J_{6,7}$7.0,$J_{6,5}$4.1)	8.68(ddd,$J_{7,6}$7.0,$J_{7,5}$1.8,$J_{7,3}$0.9)	—	—
6	—	6.84(d,$J_{3,7}$0.8)	—	6.65(d,$J_{6,7}$7.1)	8.53(dd,$J_{7,6}$7.1,$J_{7,3}$0.8)	2.60(s)	—
7	—	7.00(s)	8.36(d,$J_{5,6}$4.2)	6.67(dq,$J_{6,5}$4.2,$J_{6,7CH_3}$0.9)	—	—	2.85(d,$J_{7CH_3,6}$0.9)
8	—	6.85(s)	—	6.52(q,$J_{6,7CH_3}$0.9)	—	2.55(s)	2.77(d,$J_{7CH_3,6}$0.9)

[a]Multiplicity (s = singlet, d = doublet, q = quartet), $J_{H,H}$ (Hz).

TABLE 4. Substituent coupling constants (CH_3-SCC) for the pyrazolo[1,5-*a*]pyrimidines (Hz)

Compound	(5,6)[a]	(5,7)	(7,5)	(7,6)
2	−1.9	−0.8	—	—
3	—	—	−1.9	−2.7
6	−2.0	−0.7	—	—
7	—	—	−1.9	−2.6

[a]The numbering system (*m*,*n*) is referred to the pyrazolo[1,5-*a*]pyrimidine ring.

phenyl-5-aminopyrazole as starting material, thus obtaining the requisite 5- (compounds **2** and **6**) and 7-methyl derivatives (**3** and **7**). The regioisomers can be easily distinguished on the basis of the carbon chemical shift of the methyl group without a detailed analysis of the other spectral data. This substituent exhibits a diagnostic low-frequency shift (δ 24.8–24.6 vs. 17.2–17.0 ppm, respectively) on going from position 5 to 7. Moreover, as regards the proton spectrum, the methyl group in position 5 does not show coupling to H-6; on the contrary, a small coupling of 0.9 Hz between 7-CH_3 and H-6 is always present in the spectra of derivatives **3**, **4** and **7**, **8** (see Table 3). Because the C-5 and C-7 resonances are easily recognizable in the model compounds **3**, **4** and **7**, **8**, the attribution of signals for the corresponding atoms in compound **1** becomes straightforward. Once the carbon resonances have been established, the HETCOR spectrum allows an unambiguous assignment of H-5 and H-7 signals, thus showing that the previously reported one (9) must be reversed.

Comparison of ^1J(CH) values for pyrazolo[1,5-*a*]pyrimidines and pyrimidine (15) shows that the pyrazole ring fusion is responsible for an increase in all one-bond coupling constants with respect to pyrimidine, thus confirming the electron-withdrawing effect of the fused five-membered ring (1, 2). The methyl-substituted pyrazolo[1,5-*a*]pyrimidines show, as recently reported for other heterocycles (15, 16), additivity of substituent effects upon ^1J(CH). The substituent coupling constant (SCC) for the methyl group in the pyrazolo[1,5-*a*]pyrimidines (Table 4) is defined as the change that occurs in the value of ^1J(CH) at C-*n* upon substitution at a pyrimidine ring carbon, C-*m*($m \neq n$), by a methyl group. The ^1J(CH) values observed for the dimethyl derivatives **4** and **8** agree well with those calculated by using the CH_3-SCC values (166.5 vs. 166.6 Hz and 166.5 vs. 166.5 Hz, respectively).

Finally, it is interesting to note that the general rules outlined for other heterocyclic compounds (1, 17) hold for this ring system too. For example, ^2J(C-β,H-α), in which the coupled proton is geminal to an sp^2 nitrogen atom, and ^3J(CH) through an heteroatom are larger in comparison with other geminal or vicinal couplings, respectively, as well as ^3J(C, CH_3) being smaller than ^2J(C, CH_3) (15).

1. S. Chimichi, P. Tedeschi, A. Camparini, and F. Ponticelli. Org. Magn. Reson. **20**, 141 (1982).
2. S. Chimichi, P. Tedeschi, R. Nesi, and F. Ponticelli. Magn. Reson. Chem. **23**, 86 (1985).
3. S. Chimichi, R. Nesi, F. Ponticelli, and P. Tedeschi. J. Chem. Soc. Perkin Trans. 1, 1477 (1990).
4. F. Bruni, S. Chimichi, B. Cosimelli, A. Costanzo, G. Guerrini, and S. Selleri. Heterocycles, **31**, 1141 (1990).

5. *Edited by* K. T. Potts. Pergamon, Oxford. 1984. Part 4A. Chap. 4.05.
6. M. H. Elnagdi, M. R. H. Elmoghayar, and G. E. H. Elgemeie. *In* Adv. Heterocycl. Chem. Vol. 41. *Edited by* A. R. Katritzky and A. J. Boulton. Academic Press, New York. 1987. p. 319.
7. W. E. Kirkpatrick, T. Okabe, I. W. Hillyard, R. K. Robins, A. T. Dren, and T. Novinson. J. Med. Chem. **20**, 386 (1977), and references therein.
8. A. Takamizawa and Y. Hamashima. Yakugaku Zasshi, **84**, 1113 (1964); Chem. Abstr. **62**, 5276b (1965).
9. B. M. Lynch, M. A. Khan, S. C. Sharma, and H. C. Teo. Can. J. Chem. **53**, 119 (1975).
10. Y. Makisumi. Chem. Pharm. Bull. **10**, 612 (1962).
11. L. Pecori-Vettori, L. Cecchi, A. Costanzo, G. Auzzi, and F. Bruni. Farmaco Ed. Sci. **36**, 441 (1981).
12. S. Checchi, M. Ridi, and P. Papini. Gazz. Chim. Ital. **85**, 1558 (1955).
13. J. S. Bajwa and P. J. Sykes. J. Chem. Soc. Perkin Trans. 1, 3085 (1979).
14. G. Auzzi, L. Cecchi, A. Costanzo, L. Pecori-Vettori, F. Bruni, R. Pirisino, and G. B. Ciottoli. Farmaco Ed. Sci. **34**, 478 (1979).
15. J. Riand and M. T. Chenon. Org. Magn. Reson. **15**, 18 (1981).
16. Y. Takeuchi and K. Aoki. J. Chem. Soc. Perkin Trans. 2, 285 (1979).
17. (*a*) G. Miyajima, K. Takahashi, and H. Sugiyama. Org. Magn. Reson. **6**, 181 (1974); (*b*) Y. Takeuchi. Org. Magn. Reson. **7**, 181 (1975); (*c*) G. W. H. Cheeseman, C. J. Turner, and D. J. Brown. Org. Magn. Reson. **12**, 212 (1979); (*d*) C. J. Turner and G. W. H. Cheeseman. Org. Magn. Reson. **8**, 357 (1976).

Can. J. Chem. Downloaded from www.nrcresearchpress.com by 79.173.37.17 on 09/08/12
For personal use only.

Comportement photoélectrochimique de $ZnIn_2S_4$(n) dans l'obscurité et sous éclairement en solution électrolytique aqueuse

O. SAVADOGO

Département de métallurgie et de génie des matériaux, École polytechnique de Montréal, C.P. 6079, succ. A, Montréal (Québec), Canada H3C 3A7

Reçu le 9 février 1990[1]

O. SAVADOGO. Can. J. Chem. **70**, 1098 (1992).

Les caractéristiques photoélectrochimiques du $ZnIn_2S_4$(n) ont été étudiées à l'aide de techniques potentiodynamiques et de mesures de capacité d'interface. La variation de la densité de courant anodique (i_a) en fonction de $[OH^-]$ et $[H_3O^+]$ a été étudiée dans l'obscurité. Le courant dans l'obscurité est faible (~ 1 μA cm^{-2}) et il a été attribué à la dissolution anodique du matériau. Les résultats expérimentaux montrent que le processus n'est pas limité par la diffusion en surface des espèces en solution. Ce comportement a été interprété par un transfert d'électrons par effet tunnel à travers des états de surface localisés. La dissolution du matériau a été déterminée sous éclairement. Cette dissolution utilise huit porteurs minoritaires p. La variation du coefficient de stabilisation S (i_{ox}/i_t) en fonction du potentiel redox (V_{redox}) et de la concentration en S^{2-} a été déterminée. L'influence de $[S^{2-}]$ et de l'éclairement sur la valeur du potentiel de bandes plates a été déterminée.

O. SAVADOGO. Can. J. Chem. **70**, 1098 (1992).

Photoelectrochemical characteristics of $ZnIn_2S_4$(n) have been studied by potentiodynamic methods and capacity measurements. The variation of the anodic current density (i_a) as a function of $[OH^-]$ and $[H_3O^+]$ has been studied under darkness. This darkness current is small (~ 1 μA cm^{-2}) and it has been attributed to the anodic dissolution of the material. This process is not diffusion controlled. This behaviour was attributed to electron transfer by tunnel effect via localized interface states. The dissolution of the material under illumination has been determined. Its dissolution requires eight holes. The variation of the stabilisation coefficient S (i_{ox}/i_t) with the redox potential (V_{redox}) and the S^{2-} species concentration (C_t) has been studied. The effects of $[S^{2-}]$ and illumination on the flat band potential of the electrode have been determined.

1. Introduction

Les réactions de transfert de charge à l'interface semiconducteur/électrolyte peuvent être effectuées par les électrons de la bande de conduction ou par les trous de la bande de valence (1–4). Les deux types de porteurs ne sont pas tous situés près du niveau de Fermi mais ils sont séparés par la largeur de la bande interdite du semiconducteur. Comme, de plus, la concentration de ces porteurs dans les semiconducteurs est relativement faible, chaque type de porteurs peut être traité comme étant un réactif individuel lors de la réaction interfaciale. Ainsi, selon la nature du composé semiconducteur utilisé, la composition de l'électrolyte, les conditions de polarisation et la présence ou l'absence de l'éclairement, il est possible de mettre en évidence le type de proteurs qui est impliqué dans la réaction de transfert de charge. Ceci n'est pas le cas pour l'électrode métallique où la densité des états au voisinage du niveau de l'énergie de Fermi est très éleveé et où la concentration des électrons y est très importante. En conséquence, contrairement au métal, il semble intéressant et peut-être important de déterminer le type de porteurs (électrons ou trous) qui sont impliqués dans les réactions de transfer de charge à l'interface semiconducteur/électrolyte. Pour mieux comprendre cette différence, il est important d'étudier les réactions de transfert de charge à l'interface semiconducteur/électrolyte pour de nouveaux composés afin de déterminer le rôle exact du matériau sur ces réactions.

Ce travail porte sur l'étude du transfert de charge à l'interface $ZnIn_2S_4$ (n)/solution électrolytique aqueuse dans l'obscurité et sous éclairement. L'effet de $[OH^-]$ sur la densité de courant anodique est étudié à l'aide de l'électrode à disque tournant. Il a été déterminé le nombre de porteurs mis en jeu lors du processus de dissolution anodique de $ZnIn_2S_4$(n) et la variation du courant dû à l'oxydation de l'espèce réductrice (S) en solution en fonction du couple oxydoréducteur. La variation de S en fonction de la composition de l'électrolyte redox et de la densité de courant totale (i_t) est aussi étudiée. Une étude du mécanisme de transfert de charge à l'interface, par l'intermédiaire des états de surface est proposée.

2. Techniques expérimentales

Les cristaux de $ZnIn_2S_4$(n) ont été obtenus par sublimation sous vide ou par transport à l'iode (5, 6). Le taux de porteurs n a été déduit des mesures de capacité d'interface : $n \approx 10^{18}$ cm^{-3}. Les échantillons utilisés ont été préparés suivant une méthode analogue à celle utilisée pour $CdIn_2Se_4$ (7). Une face plane est obtenue par polissage mécanique à la pâte diamant puis à l'alumine «12 heures». Il est procédé ensuite à un décapage chimique par un mélange HNO_3–HCl (1:4) pendant 10 s puis KCN 10% pendant 1 min. Ce traitement est complété par un décapage photoélectrochimique de 15 min ($V_E = 1$ V/E.C.S.; $i = 10^{-3}$ A cm^{-2}). Une surface polie est ainsi obtenue. Une cellule à trois compartiments a été utilisée.

Le montage classique à trois électrodes a été utilisé. L'électrode de référence est une électrode au calomel saturé (E.C.S.), la contre-électrode est une feuille de platine de grande surface (12 cm^2) et l'électrode de travail est $ZnIn_2S_4$(n). Les caractéristiques courant-potentiel de l'interface $ZnIn_2S_4$/solution électrolytique ont été déterminées à l'aide d'un potentiostat PAR 273 et une interface électrolytique (modèle 176). Le capacité de l'interface a été mesurée à l'aide de l'analyseur de réponse en fréquence type PAR 5208 conecté au potentiostat 273 et piloté par le programme PAR 378.

3. Résultats

3.1 Mesure de capacités d'interface

La détermination de la disposition relative des bandes de valence et de conduction à la surface du matériau est possi-

[1]Révision reçue le 11 novembre 1991.

Can. J. Chem. Downloaded from www.nrcresearchpress.com by 79.173.37.17 on 09/08/12
For personal use only.

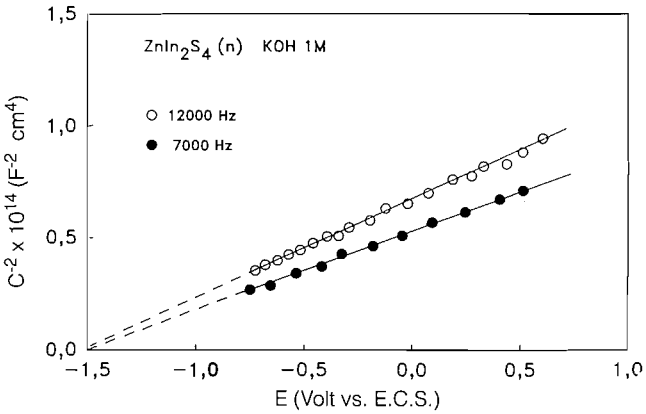

FIG. 1. $C^{-2} = f(V)$ de $ZnIn_2S_4$/KOH 1 M.

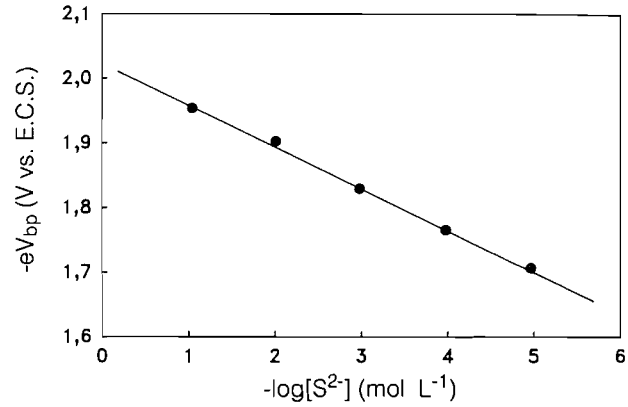

FIG. 2. Variation du potentiel de bandes plates de $ZnIn_2S_4$ en fonction de$[S^{2-}]$ dans KOH 1M.

ble grâce à la connaissance de son potentiel de bandes plates (V_{bp}). V_{bp} peut être obtenu (figure 1) à partir des courbes $C^{-2} = f(V_E)$ qui sont linéaires dans un domaine étendu de potentiel (~1 V) pour les deux fréquences de mesures. Alors, l'équation suivante est vérifiée pour cette interface pour chaque fréquence de mesure :

$$\frac{1}{C^2} = \frac{2}{e\epsilon_0\epsilon n}\left(V_{bp} - V_E - \frac{kT}{e}\right)$$

C est la capacité d'interface par unité de surface, e la charge de l'électron (1.6×10^{-19} C), ϵ la constante diélectrique du semi-conducteur, ϵ_0 la permittivité du vide et n, la densité du nombre de donneurs. V_{bp} a été déterminé à ± 0,100 V près. Les pentes des deux droites sont différentes pour les deux fréquences (figure 1). La pente est plus élevée pour la fréquence la plus importante. Les sens de variation des pentes correspond à un matériau de type n. La valeur de n est de $n \sim 10^{18}$ cm^{-3}. L'extrapolation des droites $C^{-2} = f(V)$ jusqu'à la valeur $C^{-2} = 0$ conduit à la même valeur du potentiel de bandes plates pour les deux fréquences de mesures utilisées :

$$V^{(n)}_{bp} = -1.50 \text{ V/E.C.S.}$$

L'influence des ions sulfures sur les caractéristiques d'impédance a été étudiée dans KOH 1 M parce que dans ce milieu l'addition de quantités variables des ions sulfures $[S^{2-}]$ ne modifient pas le pH du milieu. Les caractéristiques des courbes $C^{-2} = f(V)$ ne sont pas modifiées par $[S^{2-}]$ sauf pour le potentiel de bandes plates dont la variation avec $p[S^{-2}]$ est linéaire avec une pente de 0.057 V (figure 2). Cette variation est identique à celle observée sur $CdIn_2S_4$ (5, 6) et CdS (7, 8) et est attribuée à l'adsorption de HS^- à la surface du matériau. Sous éclairement, l'allure des caractéristiques $C^{2-} = f(V)$ n'est pas modifiée : variation linéaire des courbes avec des pentes identiques à celles obtenues à l'obscurité.

3.2. Courbes courant–potentiel

La figure 3 représente les caractéristiques courant–potentiel dans l'obscurité et sous éclairement. La solution électrolytique d'étude est KOH 1 M. Cette figure présente deux parties distinctes. La région I est caractérisée par une forte variation de courant en fonction de V. Sous éclairement ($I_{h\nu}$), elle est voisine d'un régime de Tafel entre 2 mA cm^{-2} et 5×10^{-1} mA cm^{-2}. Elle s'étend du potentiel de transition V_{tr} à une tension voisine de 0,2 V. Elle est très peu

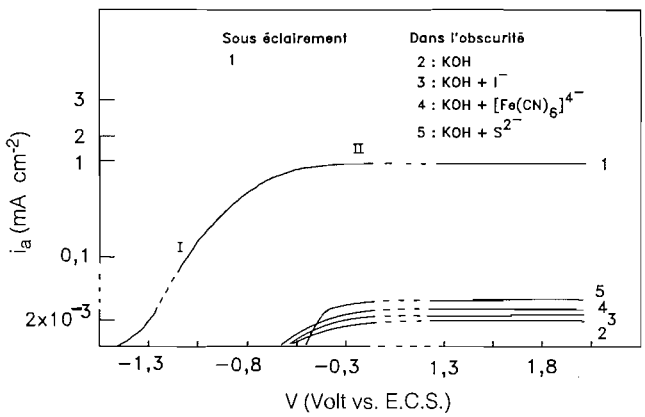

FIG. 3. Caractéristiques V vs. log i de $ZnIn_2S_4$ dans l'obscurité et sous éclairement en présence de plusieurs couples oxydo-réducteurs dans KOH 1M.

étendue dans l'obscurité. Dans la région II, le courant varie peu en fonction du potentiel. Il varie linéairement en fonction de l'intensité lumineuse incidente lorsqu'il est supérieur au courant d'obscurité qui est très faible (10^{-6} A cm^{-2}). Dans l'obscurité, les courbes sont parfaitement reproductibles, le courant de saturation a été étudié en fonction du pH et de la nature des ions. La variation du courant de saturation peut être représentée par les deux lois suivantes :

[2] en milieu acide : $i_a = k_a[H_3O^+]^1$

[3] en milieu basique : $i_a = k_b[OH^-]^{1/2}$ (fig. 4)

Les attaques observées pour un même pH (~14) dans les milieux RbOH, KOH, NaOH et LiOH montrent que le courant de saturation varie en fonction de la nature du cation. Il est d'autant plus faible que le cation est plus petit. La variation de i_a avec la mobilité du cation est linéaire (fig. 5) Pour un milieu donné (RbOH, KOH, NaOH ou LiOH), le courant de saturation varie linéairement avec la concentration du cation. De plus le courant de saturation dû à la réaction dans un milieu contenant plusieurs cations est égal à la somme des densités de courant dûes aux réactions dans les milieux contenant respectivement chacun des cations. Le potentiel de transition anodique–cathodique ne varie pratiquement pas avec la taille du cation. En présence des ions I^-, $[Fe(CN)_6]^{4-}$ ou S^{2-} dans KOH 1 M, une densité de

Can. J. Chem. Downloaded from www.nrcresearchpress.com by 79.173.37.17 on 09/08/12
For personal use only.

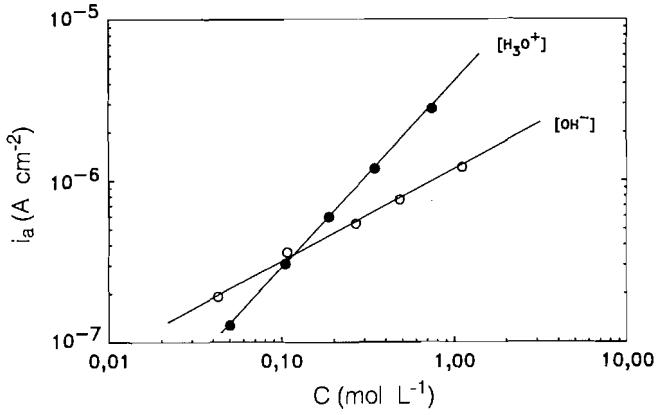

FIG. 4. Cinétique de dissolution anodique de $ZnIn_2S_4$ dans l'obscurité en milieu acide et basique.

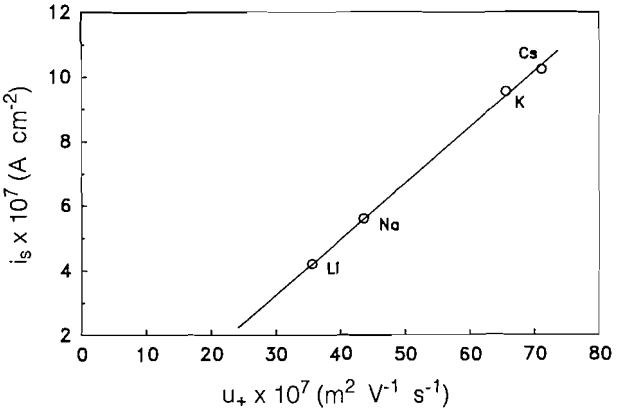

FIG. 5. Variation de i_a en fonction de la mobilité du cation dans l'obscurité pour V = 1 V/ECS en milieu basique.

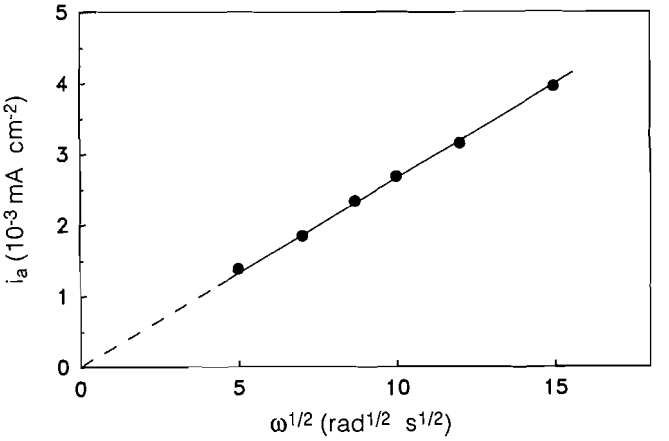

FIG. 6. $i_a = f(\omega^{1/2})$ dans l'obscurité pour $V_E \geq 1{,}8$ V/ECS. ω : vitesse de rotation de l'électrode dans KOH 1 M.

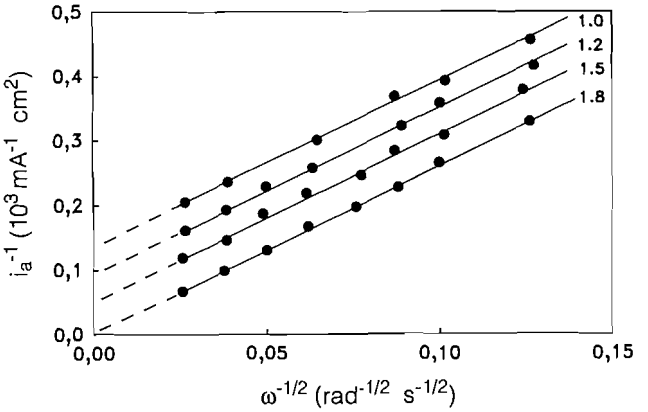

FIG. 7. $i_a^{-1} = f(\omega^{-1/2})$ dans KOH 1 M.

courant de saturation supplémentaire apparaît par rapport à KOH seul. Le courant le plus élevé est observé en présence des ions S^{2-}. Le potentiel de transition anodique–cathodique (V_{tr}) se déplace de 0,1 V/E.C.S. et +0,15 V/E.C.S. vers les valeurs anodiques, en présence de 5×10^{-3} M I^- et $[Fe(CN)_6]^{4-}$ respectivement. Par contre, en présence de 5×10^{-3} M S^{2-}, V_{tr} diminue de 0,1 V. Dans le domaine I, lorsque l'on passe de I^- à $[Fe(CN)_6]^{4-}$ et à S^{2-}, la variation du courant en fonction de V est de plus en plus rapide. Pour une concentration donnée en ions OH^-, la valeur de la vitesse de rotation de l'électrode (ω) influe sur le régime de saturation. La variation de la densité de courant limite (i_a) dans KOH 1 M en fonction de la vitesse de rotation montre que la courbe $i_a = f(\omega^{1/2})$ (fig. 6) est une droite passant par l'origine pour $V_E \geq 1{,}8$ V/E.C.S. Le critère de Levich (9–11) est donc vérifié pour cette électrode, donc le courant serait limité par la diffusion. La variation de la densité de courant (i_a) en fonction de ω permet de séparer le courant qui serait dû à la diffusion et le courant qui serait dû à l'influence de la réaction d'activation pure (i_a^*) :

$$[4] \qquad \frac{1}{i_a} = \frac{1}{i_a^*} + \frac{1}{i_d}$$

i_d est de la forme

$$[5] \qquad \frac{1}{i_d} = A\,\omega^{-1/2}$$

d'où

$$[6] \qquad \frac{1}{i_a} = \frac{1}{i_a^*} + A\,\omega^{-1/2}$$

A est une constante. Les courbes $1/i_a = f(\omega^{-1/2})$ sont des droites parallèles pour différents potentiels du régime de saturation. Seule la droite obtenue pour $V_E \geq 1{,}8$ V passe par l'origine des axes. Pour ces potentiels, la réaction qui proviendrait de la diffusion masque l'influence de la réaction qui serait due à l'activation. Pour les potentiels inférieurs, l'ordonnée à l'origine notée $1/i_a^*$ n'est pas nulle. Par exemple si V_E = 1,5 V/E.C.S., $i_a^* = 12{,}5 \times 10^{-3}$ mA cm^{-2}. i_a^* augmente avec le potentiel (fig. 7). On vérifie ainsi que plus le potentiel est élevé, plus le courant qui proviendrait de l'activation pure est élevé. La variation de i_a en fonction de la température nous a permis de déterminer l'énergie d'activation de la réaction; E_a = 2,2 kcal/mol.

Sous éclairement et pour un pH donné en milieu basique, le potentiel de transition anodique–cathodique se déplace vers les valeurs négatives lorsque l'intensité lumineuse augmente. La variation de V_{tr} en fonction de log $i_{h\nu}$ est linéaire. De même V_{tr} varie linéairement en fonction du pH de 60 mV/

Can. J. Chem. Downloaded from www.nrcresearchpress.com by 79.173.37.17 on 09/08/12
For personal use only.

TABLEAU 1. Valeurs du nombre de charges élémentaires par unité formulaire $ZnIn_2S_4$ pour différents temps de dissolution dans KOH 1 M.

Temps (min)	60	100	140	180	400	420
Nombre de charge	8,0	7,9	8,1	7,9	7,8	7,9

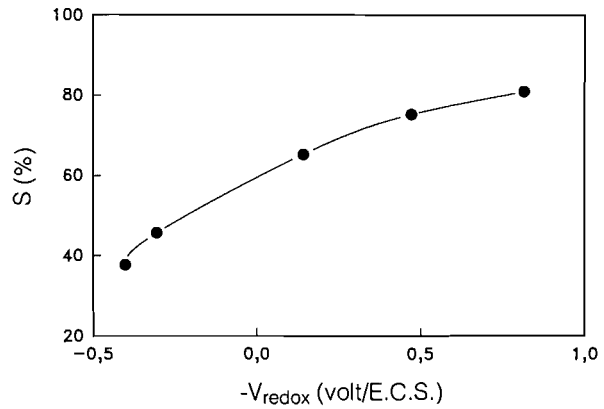

FIG. 8. Variation de S (i_{ox}/i_t) en fonction du potentiel d'oxydo-réduction (V_{redox}) dans KOH 1 M.

unité pH. En présence des ions sulfures, V_{tr} a une variation opposée en fonction de l'intensité lumineuse : il augmente de 60 mV/décade en courant. En plus, il est indépendant de $[S^{2-}]$ pour des concentrations supérieures à 0,25 M. La densité de courant anodique (i_t) est indépendente de la concentration (OH^-). La présence des ions I^-, $[Fe(cn)_6]^{4-}$ ou S^{2-} ne modifie pratiquement pas la valeur de i_t. La dissolution du matériau est étudiée dans KOH 1 M par la mesure de la perte de masse de l'électrode sous éclairement permanent. Le courant a été maintenu pendant un temps à une valeur constante $i_t = 10^{-3}$ A cm^{-2} correspondant au palier de saturation. Avant et après chaque cycle d'attaque, l'électrode est pesée après avoir été rincée et séchée sous un courant d'air chaud. Le tableau 1 montre les résultats obtenus. La dissolution anodique met en jeu huit charges élémentaires par unité formulaire $ZnIn_2S_4$. Dans les conditions de travail utilisées, $V \sim 1$ V, les charges arrivant sur l'interface sont essentiellement constituées par les porteurs p crées dans le région de charge d'espace, draînés par le champ électrique, et le courant i_{ox} est négligeable. La dissolution d'une unité formulaire consomme huit porteurs p. Le bilan des réactions chimiques et électrochimiques à l'électrode a été également établi en présence d'espèces réductrices en solution. Pour ce faire, la mesure de la perte de masse a été réalisée pendant 4 h environ. Pour la même polarisation anodique (~ 1 V), le courant d'oxydo-réduction est indiquée sur la figure 8. D'autre part, pour le même potentiel de polarisation, i_{ox}/i_t varie en fonction de la concentration des ions sulfures (fig. 9). Il a été vérifié expérimentalement que i_{ox}/i_t varie très peu avec i_t pour des concentrations élevées en S^{2-} alors que i_{ox}/i_t diminue avec i_t pour de faibles concentrations en S^{2-} (fig. 10).

Le déplacement de V_{tr} vers les valeurs négatives avec l'augmentation de l'intensité lumineuse indique une dégradation du matériau sous éclairement due aux porteurs p. En présence de fortes concentrations d'ions sulfures, le déplacement de V_{tr} vers les valeurs positives indique une

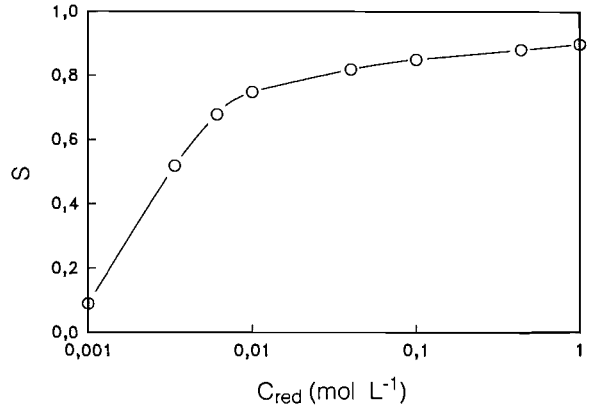

FIG. 9. Variation de S (i_{ox}/i_t) en fonction de la concentration en ions sulfures dans KOH 1 M.

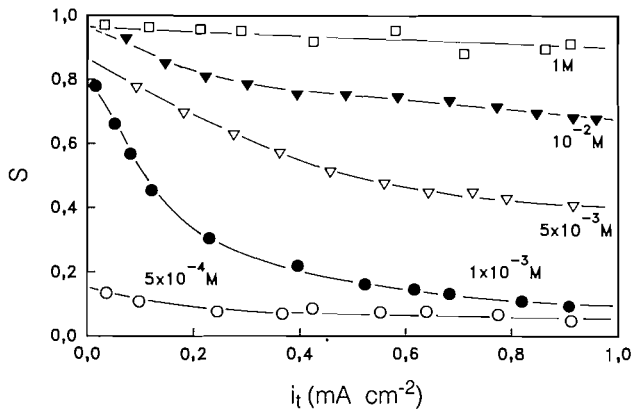

FIG. 10. Variation de S (i_{ox}/i_t) en fonction de i_t dans KOH 1 M.

stabilisation de l'interface, les porteurs étant essentiellement utilisés pour l'oxydation des ions sulfures et non pour la décomposition du matériau.

4. Discussion

L'interprétation des résultats porte sur l'ensemble de ceux obtenus en milieu basique. En milieu acide, à part la cinétique de dissolution, l'ensemble des autres résultats ne sont pas intéressants et ne sont pas indiqués dans ce travail.

4.1 Dans l'obscurité

Les mesures de capacité d'interface ont permis de déterminer la densité de porteurs du matériau $n \sim 10^{18}$ cm^{-3}. La largeur de la bande interdite est de 2,6 eV (12–14) et dans l'obscurité la densité de porteurs p dans la masse est négligeable. Ainsi, le mécanisme de transfert de charge qui utiliserait les porteurs p ne peut donc se produire. L'effet des espèces en solution sur la pseudo-saturation observée aux potentiels élevés pourrait être attribué à un phénomène de diffusion décrit par le modèle de Levich. C'est à dire que la variation linéaire observée entre i_a et $\omega^{1/2}$. Un palier de saturation est interprété de façon classique par la diffusion des ions qui est considérée comme étape lente de la réaction. Un certain nombre de faits seraient favorables à cette interprétation : en effet, la variation du courant de saturation (i_a) en fonction de $\omega^{1/2}$ est linéaire et passe par l'origine des axes pour $V_E \geq 1{,}8$ V/E.C.S. L'établissement des courbes classiques $i_a^{-1} = f(\omega^{-1/2})$ pour différents potentiels a per-

Can. J. Chem. Downloaded from www.nrcresearchpress.com by 79.173.37.17 on 09/08/12
For personal use only.

Can. J. Chem. Downloaded from www.nrcresearchpress.com by 79.173.37.17 on 09/08/12
For personal use only.

mis la séparation des composantes dues à la réaction en surface et à la diffusion et a montré que la composante qui serait due à la diffusion, qui est l'étape la plus lente de la réaction, joue un rôle d'autant plus important que le potentiel est plus élevé. D'autres résultats expérimentaux seraient également en faveur avec cette interprétation : (*i*) l'énergie d'activation E_a est compatible avec une cinétique limitée par la diffusion; (*ii*) l'influence de la mobilité des cations sur i_a est également favorable à cette interprétation.

Cependant, plusieurs faits expérimentaux montrent l'insuffisance d'interpréter les résultats obtenus ici par des phénomènes de diffusion dans l'électrolyte : (*i*) la valeur de la densité de courant de pseudo-saturation obtenue dans ce travail ($\sim 10^{-6}$A cm^{-2}) est bien inférieure à celle requise pour une densité de courant due à la diffusion des ions. Par exemple, la détermination de la densité de courant de pseudo-saturation correspondant à l'électrode de platine dans les mêmes conditions expérimentales effectuées dans ce travail donne une valeur de i_a de l'ordre de 10^{-2}A cm^{-2}; (*ii*) la proportionnalité de i_a avec $(OH^-)^{1/2}$ et non avec $(OH^-)^1$. Dans le cas d'une électrode de platine, les résultats obtenus dans ce travail montrent que i_a est proportionnel à $(OH^-)^1$ et non à $(OH^-)^{1/2}$.

Ces considérations montrent qu'une interprétation cohérente des résultats dans l'obscurité n'est pas possible pour l'instant. D'autres hypothèses d'interprétation sont présentement étudiées. En particulier, l'hypothèse selon laquelle i_a serait dû à la formation des sites superficiels nécessaires à l'attaque du matériau est considérée et l'établissement d'un modèle mathématique lié à cette hypothèse est actuellement étudié.

La variation de i_a avec la mobilité du cation peut être attribuée à la contribution de chaque espèce ionique j à la densité de courant selon la relation classique (15, 16) :

$$[7] \quad i_{aj} = Z_j F C_j U_{+j} E$$

où Z_jF est la charge du cation, C_j sa concentration, U_{+j} sa mobilité et E le champ électrique unitaire exercé sur le cation. Nous avons aussi verifié que la densité de courant totale due à la contribution de l'ensemble des cations se trouvant dans un électrolyte est la somme des contributions partielles des courants dûs aux différents cations. En plus pour un cation donné, la variation linéaire de la densité de courant avec la concentration de l'espèce dans l'électrolyte est favorable à cette interprétation.

Les variations de i_a en fonction de $[OH^-]^{1/2}$ et de $[H_3O^+]^1$ sont linéaires. Elles sont différentes de celles observées sur GaAs (6) où i_a varie comme $[OH^-]$ et $[H_3O^+]^{1/2}$. Dans le cas du germanium, Beck *et al.* (17) ont montré que sa dissolution anodique est une réaction du premier ordre en $[OH^-]$ et en porteurs p^+. Selon le mécanisme proposé, l'étape qui détermine la vitesse de la réaction est la rupture d'une des deux liaisons covalentes du germanium après capture d'un porteur p. Les résultats expérimentaux obtenus dans ce travail favorisent l'idée que l'apparition du courant dans l'obscurité est liée à un transfert d'électrons à travers la charge d'espace par effet tunnel. Ainsi, des électrons qui proviennent d'états superficiels quittent la surface laissant derrière eux des trous dont les niveaux d'énergie sont situés à l'intérieur de la bande interdite du matériau. Le transfert d'électrons à travers la charge d'espace par effet tunnel est possible parce que, dans le régime de pseudo-saturation, la différence de potentiel de charge d'espace (ΔV_{ce}) est comprise entre 2,8 et 3,4 V, la largeur de la bande interdite étant de 2,6 V, les électrons situés à la surface dans la bande de valence ont une énergie supérieure à l'énergie E_{bc} du bas de la bande de conduction du matériau dans le volume. Ainsi ces électrons doivent traverser une barrière dont l'épaisseur est de 1000 Å et qui est pratiquement opaque. Il a été montré que (18, 19) pour les barrières métal/semiconducteur, qui constituent des dispositifs semblables, en première approximation, à l'interface semiconducteur/électrolyte, le transfert d'électrons par effet tunnel devient le mécanisme dominant lorsque le champs électrique devient supérieur à 10^7 V/m. Si $\Delta V_{ce} = 3$ V, $n \geq 10^{24}$ m^{-3}, le champ à la surface est supérieur à 10^8 V/m, et un transfert par effet tunnel peut être envisagé. Si nous appelons S_m un site «potentiel» de fixation de OH^- à la surface du matériau, les réactions de formation, de dissociation et de réaction par oxydation du site pourraient s'écrire :

$$[8a] \quad S_m + OH^- \rightleftharpoons S_m + e^- \text{ (lente)}$$

$$[8b] \quad «e» \qquad S_m + OH^- + p^+ \rightleftharpoons S_m - OH \text{ (lente)}$$

$$[8c] \quad S_m - OH \Rightarrow \text{produits d'oxydation (rapide)}$$

En présence d'une espèces comme Br^-, $[Fe(CN)_6]^{4-}$, I^-, ..., et dans le cas où cette espèce n'est pas encore oxydée, il y a empêchement de la réaction des sites avec OH^- par réaction de ces sites avec cette espèce. Il y a donc compétition entre cette espèce et OH^- pour réagir avec les sites. Dans le cas où cette espèce est Br^- la réaction pourraît être :

$$[9a] \quad S_m + Br^- \rightleftharpoons S_m - Br + e^- \text{ (lente)}$$

$$[9b] \quad «e» \qquad S_m + Br^- + p^+ \rightleftharpoons S_m - Br \text{ (lente)}$$

$$[9c] \quad S_m - Br \rightleftharpoons \text{produits de réaction (rapide)}$$

En plus, la valeur trouvée de l'énergie d'activation thermique de la dissolution anodique du matériau (E_a = 2,2 kcal/mol) favorise l'interprétation selon laquelle les réactions d'interface dans l'obscurité procèdent par des états de surface intermédiaires. Cette interprétation est également en accord avec celle obtenue sur $GaAs_{1-x}P_x$ (x = 0,39) en contact avec KOH 1 M (20).

4.2 Sous éclairement

Sous éclairement, l'absence de variation de i_a avec $[H_3O^+]$ et $[OH^-]$ montre que les phénomènes des réactions sont différents par rapport à celles observées dans l'obscurité. C'est donc l'arrivée des porteurs p à l'interface qui limite la réaction anodique. Ceci est confirmé par le fait que le courant est proportionnel à l'intensité lumineuse lorsque la différence de potentiel de charge d'espace est notable. Les porteurs p^+ générés par les photons sont alors drainés vers la surface et les courants dus à leurs réactions d'interface constituent l'essentiel du courant anodique. La réaction de dissolution met en jeu huit charges élémentaires. En milieu basique, elle peut s'écrire :

$$[10] \quad ZnIn_2S_4 + 11OH^- + 8\,p^+ \rightarrow HZnO_2^- + 2\,InO_2^- + 4\,S(surf) + 5\,H_2O$$

Un dépôt de soufre a été effectivement observé sur la surface de l'électrode. Un résultat analogue a été obtenu pour CdS (18–21, 22). Comme dans les cas de CdS (22) et GaAs (23), la dissolution sous éclairement a lieu par l'arrivée des porteurs p^+ au sommet de la bande de valence. Les dispositions relatives des niveaux d'énergie des bandes de va-

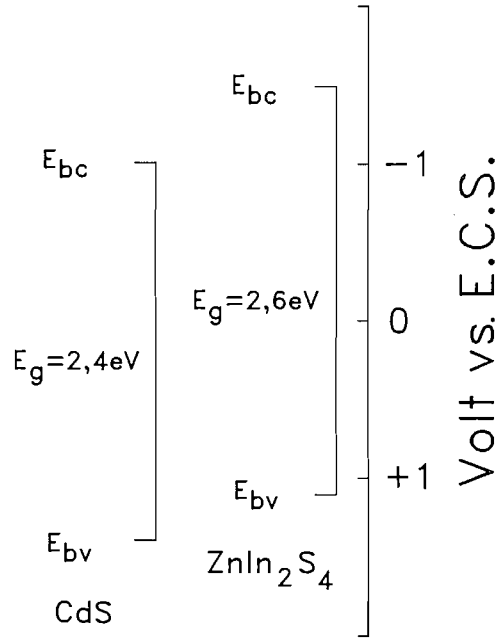

FIG. 11. Dispositions relatives des niveaux d'énergies aux interfaces $ZnIn_2S_4$/KOH 1 M et CdS/KOH 1 M.

lence et de conduction sont représentées sur la figure 11. Elles ont été déterminées à partir du potentiel de bandes plates et de la largeur de la bande interdite. En comparaison, il a été également porté la position des niveaux dans CdS selon les données des références 24 et 25. La bande de valence est profonde dans l'échelle des énergies et les échanges isoénergétiques avec la solution sont peu probables. Il est donc possible d'admettre que la dissolution de ces matériaux s'effectuent par l'intermédiaire d'états de surface ou sites superficiels ayant des niveaux énergétiques situés dans la bande interdite.

Les étapes suivantes peuvent être impliquées dans le mécanisme de dégradation.

[11] $Zn{:}In_2S_4 + p^+ \underset{k_{-1}}{\overset{k_1}{\rightleftharpoons}} Zn.In_2S_4$

[12] $Zn.In_2S_4 + p^+ \xrightarrow{k_d}$ produits de décomposition

[13] $Red + p^+ \xrightarrow{k_{ox}} Ox^+$

[14] $Red + Zn.In_2S_4 \xrightarrow{k_1'} Ox^+ + Zn{:}In_2S_4$

Il est également possible de considérer que si l'intermédiaire de surface $Zn.In_2S_4$ est mobile, alors des réactions d'oxydation irréversibles avec les espèces $Zn.In_2S_4$ peuvent apparaître

[15] $2\ Zn.In_2S_4 \xrightarrow{k_2} A_2$

[16] $A_2 + Zn.In_2S_4 \xrightarrow{k_3} A_3$

---

[17] $A_{n-1} + Zn.In_2S_4 \xrightarrow{k_n}$ produits de réactions

Les courants liés aux différentes réactions peuvent être déterminées : Pour la réaction [11]

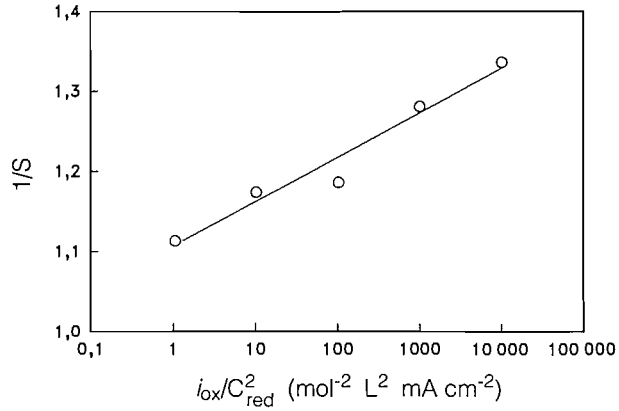

FIG. 12. Variation de S (i_{ox}/i_t) en fonction de $1/C^2_{red}$ dans KOH 1 M.

[18] $i_1 = k_1 p^+$

[19] $i_{-1} = k_{-1}\,[Zn.In_2S_4]$

Pour la réaction [12]

[20] $i_d = k_d\, p^+\, [Zn.In_2S_4]$

Pour la réaction [13]

[21] $i_{ox} = k_{ox}\, C_r\, p^+$

Pour la réaction [14]

[22] $i_1' = k_1'\, C_r\, [Zn.In_2S_4]$

Pour la réaction [17]

[23] $i_n = k_2[Zn.In_2S_4]^2 = k_3[Zn.In_2S_4][A_1] = k_n[A_{n-1}][Zn.In_2S_4]$

Le densité de courant i_d peut être mise sous la forme (26)

[24] $$i_d = \frac{k_1\, k_d\, p^{2+}}{k_{-1} + k_{ox}\, p^+}$$

si $k_{ox}p^+ << k_{-1}$, l'utilisation de l'équation [21] permet de mettre l'équation [24] sous la forme

[25] $$i_d = \frac{k_1\, k_d\, i_{ox}^2}{k_{-1}\, k_{ox}^2\, C_r^2}$$

Comme : $i_t = i_d + i_{ox}$ et $S = i_{ox}/i_t$, alors avec $\alpha = k_1\, k_d/k_{-1}\, k_{ox}$

[26] $$1/S = 1 + \frac{\alpha i_{ox}}{C_r^2}$$

L'utilisation des relations [23] et [24] en tenant compte des équations [21] et [22] permettent également d'avoir une expression identique à la relation [26].

Ainsi la variation linéaire de $1/S$ en fonction de i_{ox}/C_r^2 observée sur la figure 12 est bien expliquée par l'équation [26]. Ainsi S dépend de C_r^2 et de la densité de courant, ce qui est en accord avec l'interprétation selon laquelle que les réactions à l'interface $ZnIn_2S_4$/électrolyte sous éclairement sont limitées essentiellement par la quantité des porteurs p qui arrivent à l'interface. Ainsi, l'interprétation des résultats expérimentaux de ce travail peut être réalisée en utilisant les réactions [12] et [13] ou les réactions [14] et [17].

Can. J. Chem. Downloaded from www.nrcresearchpress.com by 79.173.37.17 on 09/08/12
For personal use only.

La variation de $1/S$ avec i_{ox}/C_r^2 est analogue avec les résultats expérimentaux obtenus sur les systèmes GaAs/Fe(II)–EDTA, GaP/Fe(II)–EDTA, InP/Fe(II)–EDTA et GaP/Fe $(CN)_6^{4-}$ (27–30) pour lesquels une variation linéaire de $S^2/(1 - S)$ en fonction de C_r^2/i_{ox} a été obtenue. Par contre le résultat est différent de celui obtenu sur n-GaP/Fe^{2+} (31) pour lequel une variation linéaire de S en fonction de C_r/i_{ox} a été obtenue.

L'influence du pH et de la température sur la valeur de S sera déterminée ultérieurement et comparée à celle de ZnS et In_2S_3 afin d'étudier l'effet de la transition de ZnS à $ZnIn_2S_4$ et à In_2S_3 sur la valeur de S.

Conclusion

Les réactions à l'interface $ZnIn_2S_4$/electrolyte aqueux ont été étudiées dans l'obscurité et sous éclairement. Dans l'obscurité, le passage du courant serait donc dû à un transfert d'électrons par effet tunnel à travers la barrière de charge d'espace; les électrons issus d'un état superficiel dû à l'interaction entre la solution et la surface laissant derrière eux des trous qui contribuent à la dissolution anodique du matériau. Sous éclairement, le coefficient de stabilisation (S) varie avec la concentration de l'espèce réductrice en solution [C_r] suivant la relation $1/S$ en fonction de i_{ox}/C_r^2. Ces réactions procèdent par l'intermédiaire d'états de surface situés à l'intérieur de la bande interdite et elles sont limitées par l'arrivée des porteurs p en surface.

1. F. Beck et H. Gerischer. Z. Electrochem. 63, 500 (1959).
2. J. F. Dewald. *Dans* Semiconductors. *Editeur* : N. B. Hanney. ACS Monograph No. 140. Reinhold, New York. 1959. p. 727.
3. H. Gerischer. Z. Phys. Chem. Munich, **27**, 48 (1961).
4. H. Gerischer. J. Phys. Chem. **95**, 1356 (1991).
5. O. Savadogo, J. Yazbeck. G. Allais et A. Deschanvres. Rev. Chim. Miner. **3**, 292 (1984).
6. O. Savadogo. Thèse de doctorat, Université de Caen. 1985.
7. R. Tenne, Y. Mirowsky, Y. Greenstrin et D. Cahen. J. Electrochem. Soc. **129**, 1506 (1982).
8. D. S. Ginley et M. A. Butler. J. Electrochem. Soc. **125**, 1968 (1978).
9. O. Savadogo et A. Deschanvres. Bull. Soc. Chim. Fr. **11**, 283 (1983).
10. B. Levich. Acta Physicochim. URSS, **1**, 257 (1942).
11. J. Besson et J. Guitton. Manipulations d'électrochimie. Masson, Paris. 1972. p. 191.
12. L. Baldassarre, V. Cappozzi, G. Maggipinto et A. Minafra. Phys. Status Solidi, **46**, 589 (1978).
13. A. N. Anagnostopoulos, C. Manolikas et D. Papadopolous. Phys. Status Solidi, **77**, 595 (1983).
14. C. Paorici et N. Romeo. J. Jpn. Soc. Appl. **43**, 112 (1974).
15. J. O'M Bockris et A. K. N. Reddy. *Dans* Modern aspects of electrochemistry. Vol. 1. Plenum Publishing Corporation, New York. 1977. p. 372.
16. F. Coeuret et A. Storck. *Dans* Elements de génie électrochimiques. Lavoisier, Paris. 1984. p. 45.
17. F. Beck et H. Gerischer. Z. Elektrochem. **63**, 943 (1959).
18. H. Gerischer et J. Gobrecht. Ber. Bunsen-ges. Phys. Chem. **82**, 520 (1978).
19. S. M. Sze. Physics of semiconductors devices. Wiley–Interscience, New York. 1969.
20. F. El Halouani, G. Allais et A. Deschanves. Electrochem. Acta, **25**, 1065 (1980).
21. H. Minoura, M. Tsuiki et T. Oki. Ber. Bunsen-ges Phys. Chem. **81**, 588 (1977).
22. A. B. Ellis, S. W. Kaiser et M. S. Wrighton. J. Am. Chem. Soc. **98**, 6855 (1976).
23. R. Memming. *Dans* Semiconductor liquid junction solar cells. A. Heller, New York. 1977. p. 38.
24. C. Hollan, J. C. Tranchart et R. Memming. J. Electrochem. Soc. 126, 855 (1979).
25. W. P. Gomes et F. Cardon. *Dans* Semiconductor liquid junction solar cells. A. Heller, New York. 1977. p. 120.
26. K. W. Frese, M. J. Madou et S. R. Morrison. J. Electrochem. Soc. **128**, 1527 (1981).
27. F. Van Overmeire, F. Vanden Kerchove, W. P. Gomes et F. Cardon. Bull. Soc. Chim. Belg. **89**, 181 (1980).
28. K. W. Frese, M. J. Madou et S. R. Morrisson. J. Phys. Chem. **84**, 3172 (1980).
29. W. P. Gomes, F. Van Overmeire, D. Vanmaeckelbergh, F. Vanden Kerchove et F. Cardon. ACS Symp. Ser. **146**, 119 (1981).
30. F. Cardon, W. P. Gomes, F. Vanden Kerchove, D. Vanmaekelbergh et F. Van Overmeire. Faraday Disc. **70**, 153 (1980).
31. D. Vanmaekelbergh, W. P. Gomes et F. Cardon. J. Electrochem. Soc. **546**, 129 (1982).

Can. J. Chem. Downloaded from www.nrcresearchpress.com by 79.173.37.17 on 09/08/12
For personal use only.

Phosphoranes et thio-oxazaphospholidines d'aldohexoses protégés. Synthèses et études stéréochimiques

ZOUHAIR BOUNJA, DOURAID HOUALLA,[1] MONIQUE REVEL ET ROBERT WOLF

Unité de recherche associée au Centre national de la recherche scientifique n° 454, Université Paul Sabatier, 118 Route de Narbonne, 31062 Toulouse CEDEX, France

Reçu le 4 juillet 1991

ZOUHAIR BOUNJA, DOURAID HOUALLA, MONIQUE REVEL et ROBERT WOLF. Can. J. Chem. **70**, 1105 (1992).

Les alcoxybicyclophosphoranes **1**–**5** ont été obtenus par l'action du bicyclophosphane **6** sur les cinq alcools suivants : 1,2,3,4-di-*O*-isopropylidène α-D-galactopyranose **7**, 1,2,5,6-di-*O*-isopropylidène α-D-glucofuranose **8**, méthanol, isopropanol et tertio-butanol. La sulfuration de **1**–**5** fournit les thio-oxazaphospholidines correspondantes : **1**(P═S)–**5**(P═S). Les formes tautomères phosphocines intermédiaires: **1**(P═S)*–**5**(P═S)* sont observées dans tous les cas. Une étude stéréochimique détaillée, basée sur les résultats de RMN de ^{1}H, ^{13}C et ^{31}P est présentée pour les huit composés **1**–**4** et **1**(P═S)–**4**(P═S). En solution, on observe le passage quantitatif du thio-oxazaphospholidine **4**(P═S) au dérivé oxo correspondant **4**(P═O) par la méthode à l'anhydride trifluoroacétique.

ZOUHAIR BOUNJA, DOURAID HOUALLA, MONIQUE REVEL, and ROBERT WOLF. Can. J. Chem. **70**, 1105 (1992).

The alkoxyphosphoranes **1**–**5** have been obtained by the reaction between the bicyclophosphane **6** and the five following alcohols: 1,2,3,4-di-*O*-isopropylidene-α-D-galactopyranose **7**, 1,2,5,6-di-*O*-isopropylidene-α-D-glucofuranose **8**, methanol, isopropanol, and tertiobutanol. The sulfuration of **1**–**5** yields to the corresponding thio-oxazaphospholidines: **1**(P═S)–**5**(P═S). In each case the intermediate tautomeric form **1**(P═S)*–**5**(P═S)*, with an eight-membered ring, is observed. A detailed stereochemical study, based on ^{1}H, ^{13}C, and ^{31}P NMR results is presented for eight compounds: **1**–**4** and **1**(P═S)–**4**(P═S). In solution we observed the quantitative transformation of **4**(P═S) into the corresponding oxo derivative **4**(P═O) by the trifluoroacetic anhydride method.

1. Introduction

L'addition oxydante des alcools et polyols sur les bicyclophosphanes[2] **I** conduit facilement aux alcoxybicyclophosphoranes[2] **II** (1)

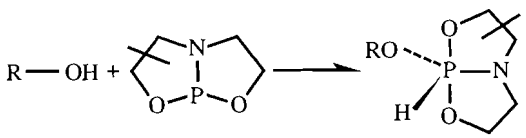

I **II**

Nous avons récemment utilisé cette réaction avec le myo-inositol. L'oxydation des polybicyclophosphoranes qui en dérivent suivie de l'hydrolyse des produits obtenus nous a permis d'accéder, d'une façon simple et rapide, à quelques myo-inositol phosphates biologiquement intéressants (2, 3).

Poursuivant l'étude de la phosphoranylation comme moyen d'accéder à des produits d'intérêt biologique, nous avons préparé cinq bicyclophosphoranes du type **II**, **1**–**5**. Deux dérivent d'aldohexoses protégés : le galactopyranose **7** et le glucofuranose **8**, les trois autres sont issus respectivement du méthanol, de l'isopropanol et du tertio-butanol. C'est le bicyclophosphane **6** qui est utilisé dans tous les cas.

Dans ce travail, nous nous sommes attachés à l'obtention de dérivés soufrés. En effet, parmi les réactions explorées sur **II**, nous avons montré que la sulfuration conduit à un

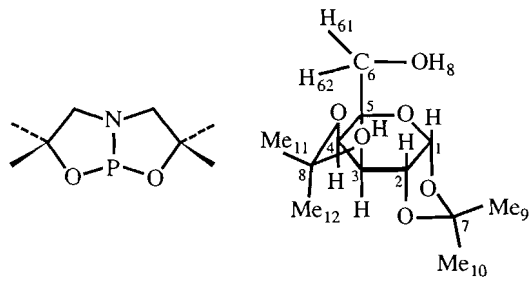

6 **7**

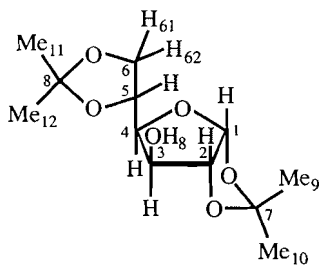

8

mélange de thio-oxazaphospholidine **II** (P═S) et de thiodioxaphosphocine **II** (P═S)*.

Le premier est l'isomère stable et il est pratiquement seul présent après un délai de 24 h. Le fait qu'il comporte une fonction alcool permet d'envisager, par une répétition du schéma réactionnel, de fixer plusieurs restes thio-oxazaphospholidines sur le même substrat hydroxylé.

Le même comportement est observé avec les polybicyclophosphoranes de polyols : partant du glycol (4), du

[1]Auteur à qui adresser toute correspondance.

[2]Nomenclature correcte : (1) pour les bicyclophosphanes (**I**) : 2,8-dioxa 5-aza 1-phospha^{III}bicyclo[3,3,0]octane; (2) pour les bicyclophosphoranes (**II**) : 1-alcoxy 2,8-dioxa 5-aza 1-phospha^{V}-bicyclo[3,3,0]octane.

Can. J. Chem. Downloaded from www.nrcresearchpress.com by 92.62.229.171 on 09/08/12
For personal use only.

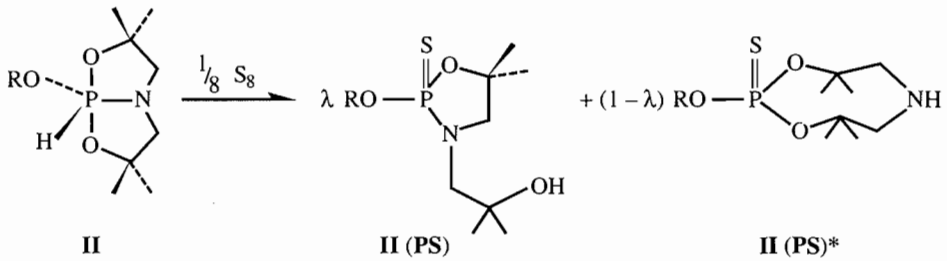

II II (PS) II (PS)*

glycerol[3] ou encore du myo-inositol (2) nous avons pu observer le même déroulement dans les réactions de perphosphoranylation et de sulfuration. Dans les cas du glycol (4), et du glycérol,[3] nous avons pu caractériser, toujours en utilisant le bicyclophosphane tétraméthylé **6**, les deux polythio-oxazaphospholidines **9** et **10** :

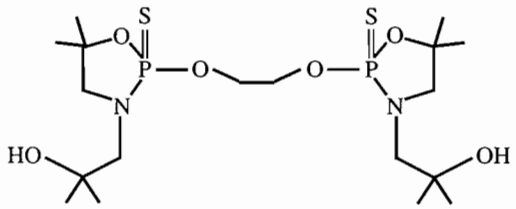

9

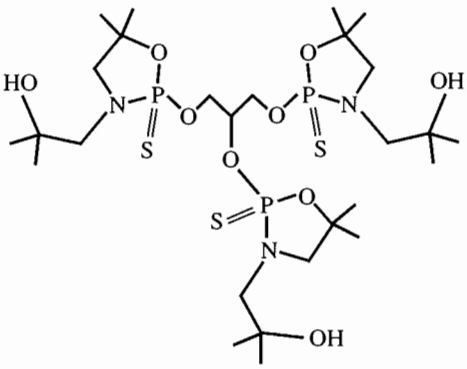

10

Dans les nouveaux dérivés présentés dans ce travail la présence des cycles pyranose ou furanose pourrait conférer aux produits obtenus des propriétés utiles, les sucres jouant le rôle de vecteur du fragment thio-oxazaphospholidine. On sait que des insecticides très actifs appartiennent à cette famille de composés, en particulier l'énantiomère $(R)_C(R)_P$5-phényl thio-oxazaphospholidine **11** (5):

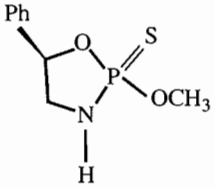

11

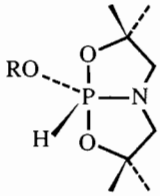

1-5

1 R = galactopyranosyl
2 R = glucofuranosyl
3 R = methyl
4 R = isopropyl
5 R = *tert*-butyl

C'est pour mettre en évidence un éventuel effet dû aux restes aldohexoses que nous avons jumelé à cette étude celle de trois alcoxybicyclophosphoranes **3**, **4**, **5** et des trois dérivés soufrés correspondants **3**(P=S), **4**(P=S), **5**(P=S).

2. Résultats et discussion

2.1. Synthèses

La préparation des cinq bicyclophosphoranes de départ **1**–**5** à partir des cinq alcools choisis et du bicyclophosphane **6** ne présente pas de difficultés particulières (voir partie expérimentale). Elle nous a permis d'établir le tableau qui suit :

Phosphoranes obtenus	ROH	^{31}P	$^{1}J_{H-P}$
1	Galactopyranose **7**	−36,9	804,4
2	Glucofuranose **8**	−41,3	812
3	CH_3OH	−33,8	791,5
4	$(CH_3)_2CHOH$	−36,9	798
5	$(CH_3)_3COH$	−34,7	779

Pour chacune de ces préparations, suivie par RMN de ^{31}P la disparition rapide du signal à δ = 163 ppm correspondant au bicyclophosphane **6** est accompagnée par l'apparition concomitante d'un doublet à champ fort entre −34 et −42 ppm, le couplage $^{1}J_{H-P}$ étant de l'ordre de 800 Hz. Après enlèvement du solvant les phosphoranes **1** et **2** se présentent comme des liquides très visqueux alors que **3** est distillable.

La sulfuration est réalisée par action du soufre élémentaire S_8 en proportion stoechiométrique. À la température ambiante la solubilisation totale de ce dernier dans la solution toluènique utilisée marque la fin de la réaction. Elle nécessite quelques heures dans les cas défavorables de **1** et **2**, mais elle est beaucoup plus rapide avec **3**–**5**. Dans le tableau qui suit nous avons sélectionné un certain nombre de données expérimentales concernant la sulfuration.

Phosphoranes soumis à sulfuration	Temps après l'addition du soufre (h)	Phosphorane restant (%)	**1**–**5**(P=S) (%)	**1**–**5**(P=S)* (%)
1	2	43	48	9
	20	0	97	3
	100	0	98	2
2	1	65	29	6
	4	22	75	3
	100	0	98	2
3	1	0	75	25
	24	0	ca. 100	Traces
4	1	0	70	30
	24	0	ca. 100	Traces
5	1	0	55	45
	24	0	ca. 100	Traces

[3]Résultats non publiés.

Can. J. Chem. Downloaded from www.nrcresearchpress.com by 92.62.229.171 on 09/08/12
For personal use only.

Can. J. Chem. Downloaded from www.nrcresearchpress.com by 92.62.229.171 on 09/08/12
For personal use only.

Les résultats obtenus montrent que l'équilibre étant atteint, les thio-oxazaphospholidines **1**(P=S)–**5**(P=S) sont très largement majoritaires sinon les produits uniques de la réaction. Dans **1**(P=S) et **2**(P=S), l'atome de phosphore étant chiral il y a formation de deux diastéréoisomères. L'induction asymétrique est pratiquement nulle dans **1**(P=S) : les deux pics de RMN ^{31}P à 85,0 ppm et 84,7 ppm ont quasiment la même intensité alors qu'elle est significative dans **2**(P=S), les deux pics à 84,7 et 83,5 ppm sont sensiblement inégaux, respectivement comme 65 et 35%. Ce résultat doit être relié au fait que dans **1**(P=S) le premier atome de carbone chiral est en position γ par rapport au phosphore alors que dans **2**(P=S) il est en position β.

Le tableau qui suit regroupe les valeurs de δ ^{31}P des dix composés soufrés caractérisés :

1(P=S)	**2**(P=S)	**3**(P=S)	**4**(P=S)	**5**(P=S)
85 et 84,7	84,7 et 83,5	86,8	83,5	86,8
1(P=S)*	**2**(P=S)*	**3**(P=S)*	**4**(P=S)*	**5**(P=S)*
52,5	50	54,1	51,0	42,4

2.2. Stéréochimie

Aucun des produits étudiés au cours de ce travail n'a été obtenu à l'état cristallin. Aussi aucune détermination de structure par diffraction des rayons X n'a pu être réalisée. L'étude stéréochimique des ces composés repose donc sur l'analyse de leurs paramètres de RMN. Cependant les résultats conformationnels que nous présentons sont fortement étayés par la connaissance des structures moléculaires de composés analogues **12** (7) et **13** (8).

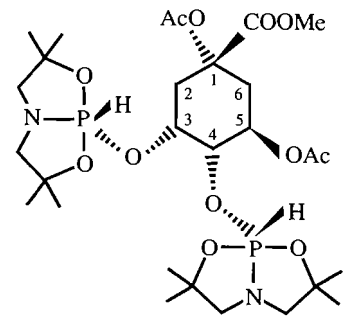

12

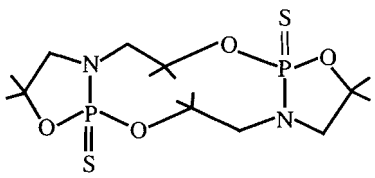

13

*2.2.1. Les bicyclophosphoranes **1–4***

Comme nous venons de le dire nous disposons depuis peu de la structure moléculaire établie par diffraction des rayons X du même reste bicyclophosphoranique dans le dérivé **12** issu de l'acide quinique (7). Comme il s'agit précisement du même fragment, nous pouvons admettre que dans les quatre dérivés **1–4** la géométrie du squelette bicyclophosphoranique est la même. Il s'agit d'une bipyramide trigonale avec une annelation axiale-équatoriale-axiale : les deux atomes d'oxygène occupent les positions axiales et l'atome d'azote une position équatoriale. Afin de compléter cette donnée stéréochimique il nous reste à préciser la conformation des cycles pentagonaux, les modifications qu'ils subissent quand les composés sont en solution, et déterminer l'influence de la phosphoranylation sur la conformation des ensembles galactopyranose de **1** et glucofuranose de **2**.

2.2.1.1. Conformation des cycles pentagonaux. Dans les bicyclophosphoranes présentés, la double substitution sur l'atome de carbone en α de l'oxygène (deux groupements méthyles) nous prive des constantes de couplage $^3J_{H-C-O-P}$, qui suivent une loi de Karplus (9) et apportent des informations sur les angles dièdres correspondants. Cet handicap est en partie levé par la connaissance de la conformation des cycles pentagonaux qui nous est fournie par les rayons X de **12** : c'est une forme enveloppe avec l'atome de carbone en α de l'oxygène à la pointe du rabat (7). Nous conviendrons, avec peu de risques, que cette conformation reste privilègiée en solution pour les composés **1–4**. Les constantes de couplage $^3J_{H-C-N-P}$ (tableau 1) constituent également une sonde intéressante pour l'étude conformationnelle de ces cycles à cinq chainons. L'examen du tableau 1 montre qu'il existe quelques différences entre les quatre composés étudiés.

Dans les dérivés **3** et **4** les constantes de couplage $^3J_{H-C-N-P}$ sont très voisines : 16,2 et 11,2 Hz pour **3**, 15 et 12,8 Hz pour **4**. Nous en concluons que la libration des cycles pentagonaux peut se faire librement. Il est intéressant de noter à ce propos que les mêmes cycles pentagonaux des bicyclophosphoranes (**III**) (R=alkyl ou aryl)

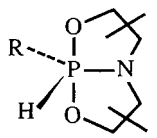

III

sont bloqués en solution : les deux constantes de couplage $^3J_{H-C-N-P}$ ont des valeurs très contrastées comme 24 et 3 Hz (10). Dans **1** et **2** la chiralité des groupements galactopyranose et glucofuranose discrimine tous les sites protoniques des restes bicyclophosphoranes : ainsi aux quatre substituants CH_3 et aux quatre hydrogènes des deux groupements N-CH_2 correspondent des signaux distincts. Dans **1** les couples de constantes de couplage observées pour les deux groupements N-CH_2 sont peu différentes : 12,6 et 14,3 Hz d'une part, 13–14,1 Hz d'autre part. Dans **2** ces paires de constantes de couplage deviennent 19 et 11,3 Hz d'un coté, 21,4 et 11 Hz de l'autre. L'examen d'un modèle moléculaire montre que cette dernière discrimination est interprêtable. En effet, dans **1** l'attachement du groupe bicyclophosphorane à la fonction alcool primaire exocyclique l'éloigne de toute gêne stérique et la libration des cycles pentagonaux peut s'effectuer librement. Il n'en est plus de même dans **2**. Cette fois le bicyclophosphorane est porté par une fonction alcool secondaire directement liée au cycle, ce qui le place à proximité du groupement glucofuranose, lui même encombré par les substituants protecteurs isopropylidènes. On conçoit que la position d'équilibre puisse être telle que l'un des cycles pentagonaux est loin du groupement furanose permettant la libration du cycle alors que l'autre est stériquement gêné et conserve des valeurs contrastées des constantes de couplage $^3J_{H-C-N-P}$.

TABLEAU 1. Paramètres de RMN ^1H des protons N-CH_2 et des substituants CH_3 des groupements bicyclophosphoraniques

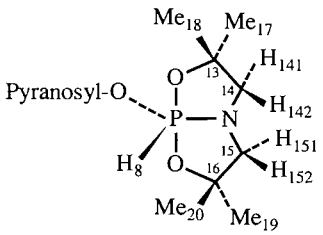

1

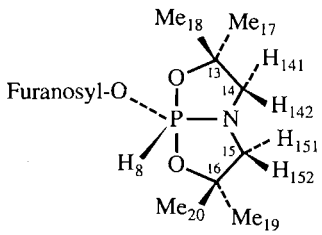

2

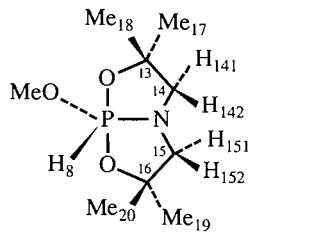

3

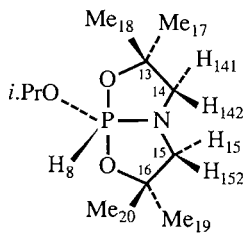

4

	δ, ppm	*J*, Hz	δ, ppm	*J*, Hz	δ, ppm	*J*, Hz	δ, ppm[a]	*J*, Hz[a]
H(8)	7,17	$^1J_{H-P}$ 804	7,34	$^1J_{H-P}$ 811	7,04	$^1J_{H-P}$ 794,9	7,14	$^1J_{H-P}$ 790
H(141)	2,47	$^2J_{H-H}$ −8,2	2,45	$^2J_{H-H}$ −8	2,48[b]	$^2J_{H-H}$ −8,2	2,50	$^2J_{H-H}$ −8,2
		$^3J_{H-P}$ 12,6		$^3J_{H-P}$ 21,4		$^3J_{H-P}$ 16,2		$^3J_{H-P}$ 15
H(142)	2,55	$^3J_{H-P}$ 14,3	2,52	$^3J_{H-P}$ 11	2,52[b]	$^3J_{H-P}$ 11,2	2,57	$^3J_{H-P}$ 12,8
H(151)	2,47	$^2J_{H-H}$ −8	2,45	$^2J_{H-H}$ −8	2,48[b]	$^2J_{H-H}$ −8,2	2,50	$^2J_{H-H}$ − 8,2
		$^3J_{H-P}$ 13		$^3J_{H-P}$ 10,9		$^3J_{H-P}$ 16,2		$^3J_{H-P}$ 15
H(152)	2,54	$^3J_{H-P}$ 14,1	2,52	$^3J_{H-P}$ 12,3	2,52[b]	$^3J_{H-P}$ 11,2	2,57	$^3J_{H-P}$ 12,8
Me(17)	1,29		1,06		1,19		1,21	
Me(18)	1,19		1,19		1,26		1,29	
Me(19)	1,32		1,19		1,19		1,21	
Me(20)	1,19		1,27		1,26		1,29	

[a] Valeurs extraites de la référence 4.

[b] H(141) et H(142) sont respectivement équivalents à H(151) et H(152). Ils constituent la partie AB d'un système ABX (X = P).

2.2.1.2. Influence de la phosphoranylation sur les cycles galactopyranose et glucofuranose. L'examen du tableau 2 qui rassemble les paramètres de RMN ^1H des protons cycliques et des groupements CH_3 protecteurs permet de faire les remarques suivantes :

1. En passant du galactopyranose **7** à son dérivé phosphoranylé **1** les déplacements chimiques des protons H(1), H(2) et H(3) et les constantes de couplage entre eux n'ont pratiquement pas changé. Les seules modifications observées concernent les protons H(5), H(61), H(62) et H(4). Dans **7** les trois premiers donnent naissance à un multiplet ABC entre 3,80 et 3,89 ppm nettement séparé du signal de H(4) à 4,07 ppm. La phosphoranylation se traduit par un déblindage de tous ces protons qui donne naissance à un multiplet ABCD entre 4,18 et 4,36 ppm. Les signaux dus aux groupements CH_3 ne présentent que des variations mineures. En bref la conformation de l'ensemble galactopyranose s'est maintenue lors de la phosphoranylation.

2. La phosphoranylation du glucofuranose **8** a des effets nettement plus marqués. Dans **8** les protons H(2), H(3), H(4) et H(5) forment un multiplet complexe de type ABCD entre 4,35 et 4,45 ppm. Les mêmes protons du dérivé phosphoranylé **2** conduisent à des signaux bien séparés en raison des déblindages qu'ils subissent. Compte tenu du fait que les protons deviennent distinguables à partir d'un système ABCD, nous pouvons estimer les déblindages minima qui interviennent : 0,12 ppm pour H(4), 0.29 ppm pour H(5), 0,36 ppm pour H(2), enfin 0,93 ppm pour H(3). Il en est de même des groupements CH_3 des cycles protecteurs. Ceux qui sont en position *exo*, notés 9 et 11, sur les dessins des molécules **1**, **2**, **7**, **8** subissent des déplacements sensiblement plus importants (0,11 et 0,19 ppm) que les méthyles *endo*, notés 10 et 12 (déblindages respectifs : 0,04 et 0 ppm). Toutes ces observations convergent. Elles permettent de constater que le groupement bicyclophosphorane induit dans son environnement proche un effet de déblindage marqué.

2.2.2. Les thio-oxazaphospholidines **1**(P=S)–**4**(P=S)

Comme nous l'avons dit plut haut, nous connaissons l structure moléculaire du dérivé tricyclique **13** (8) qui com porte deux fois le motif thio-oxazaphospholidine que nou étudions ici : le cycle pentagonal adopte une forme enve loppe avec l'atome de carbone en α de l'oxygène à la point du rabat.[4]

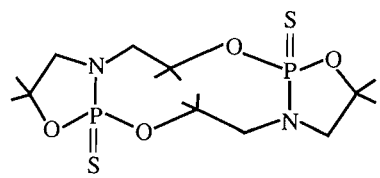

13

Nous admettrons qu'il en sera de même pour les com posés **1**(P=S)–**4**(P=S). L'analyse des paramètres de RMI ^1H des protons diastéréotopes NCH_2, seuls sites commun aux quatre dérivés qui permettent une étude comparative fournira l'essentiel de l'information stéréochimique. Le ta bleau 3 rassemble ces paramètres ainsi que ceux de l'oxo oxazaphospholidine **4** (P=O). Ce dernier a été spécialemen prépare pour cette étude. Il dérive du composé **4** (P=S) dan lequel l'atome de soufre a été remplacé par un atom d'oxygène.

(*a*) Les deux constantes de couplage $^3J_{P-N-C-H}$ des deu groupes de protons diastéréotopes N-CH_2 présentent de

[4] En fait la maille cristalline de ce composé comporte deux en tités, une centrosymétrique et une dépourvue de toute symétrie Dans cette dernière les cycles pentagonaux adoptent tous les deu une forme enveloppe mais se différencient par la position du rabat Dans l'un c'est l'atome de carbone en α de l'oxygène qui occup cette position; dans l'autre c'est celui en α de l'azote (8).

Can. J. Chem. Downloaded from www.nrcresearchpress.com by 92.62.229.171 on 09/08/12
For personal use only.

TABLEAU 2. Comparaison des paramètres de RMN ^1H des cycles galactopyranosique et glucofuranosique dans le galactopyranose **7**, le glucofuranose **8** et dans leurs produits de phosphoranylation **1** et **2**

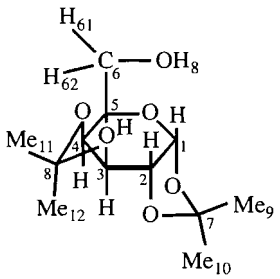

7

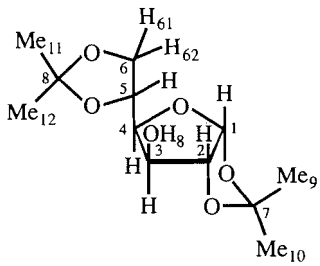

8

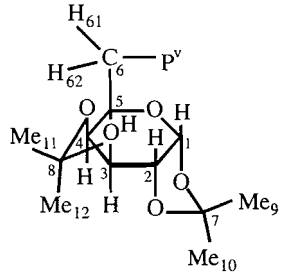

1

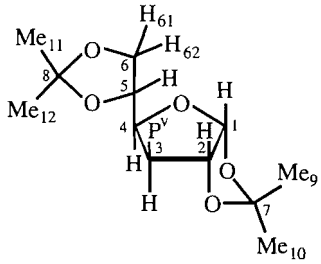

2

	δ, ppm	*J*, Hz	δ, ppm	*J*, Hz	δ, ppm	*J*, Hz	δ, ppm	*J*, Hz
H(1)	5,47	$^3J_{1-2}$ 5[a]	5,46	$^3J_{1-2}$ 5	5,98	$^3J_{1-2}$ 3,5	6,0	$^3J_{1-2}$ 3,6
H(2)	4,19	$^3J_{2-3}$ 2,3[a]	4,16	$^3J_{2-3}$ 2,3	Multiplet ABCD		4,75	$^3J_{2-3}$ 0
H(3)	4,48	$^3J_{3-4}$ 7,9[a]	4,49	$^3J_{3-4}$ 7,9	entre 4,34		5,32	$^3J_{3-4}$ 2,9
								$^3J_{3-P}$ 10
H(4)	4,07	$^3J_{4-5}$ 1,1	Multiplet ABCD		et 4,45 ppm		4,51	$^3J_{4-5}$ 7,6
								$^3J_{4-P}$ 3
H(5)	Multiplet ABC		entre 4,18				4,68	
H(61)	entre 3,8		et 4,36 ppm		4,06	$^3J_{61-5}$ 5	4,24	$^3J_{61-5}$ 4,9
						$^2J_{H-H}$ −8,6		$^2J_{H-H}$ −8
H(62)	et 3,89 ppm				4,1	$^3J_{62-5}$ 6	4,3	$^3J_{62-5}$ 4,4
H(8)	3,43				2,55	$^3J_{8-3}$ 4,2		
Me(9) *exo*	1,09[b]		1,06		1,19[b]		1,38	
Me(10) *endo*	1,44[b]		1,43		1,44[b]		1,48	
Me(11) *exo*	1,16[b]		1,13		1,31[b]		1,42	
Me(12) *endo*	1,39		1,40		1,50[b]		1,50	

[a]Valeurs identiques à celles relevées dans la littérature (11).
[b]Valeurs compatibles avec les données de la littérature (12).

TABLEAU 3. Paramètres de RMN ^1H des protons N-CH_2 des restes thio-oxazaphospholidines (**1(PS)**, **2(PS)**, **3(PS)** et **4(PS)**) et du groupement oxo-oxazaphospholidine (**4(PO)**)

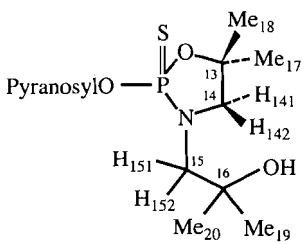

1(PS)

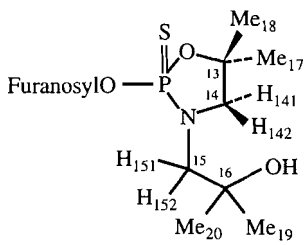

2(PS)

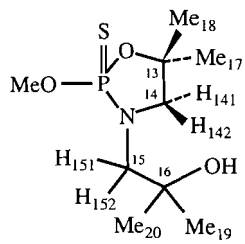

3(PS)

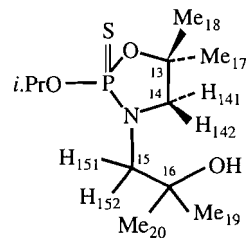

4(PS)

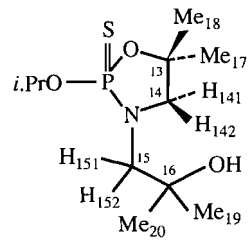

4(PO)

	δ, ppm	*J*, Hz	δ, ppm	*J*, Hz	δ, ppm	*J*, Hz	δ, ppm	*J*, Hz	δ, ppm	*J*, Hz
H(141)	dd 2,78[a]	$^2J_{H-H}$ −14,6	dd 2,70[a]	$^2J_{H-H}$ −14,5	dd 2,70	$^2J_{H-H}$ −14,5	dd 2,69	$^2J_{H-H}$ −14,6		
		$^3J_{H-P}$ 12,3		$^3J_{H-P}$ 12,6		$^3J_{H-P}$ 12,4		$^3J_{H-P}$ 12,2		
	dd 2,69	$^2J_{H-H}$ −14,6	dd 2,64	$^2J_{H-H}$ −14,6					3,08[b]	$^2J_{H-H}$ −15,5
		$^3J_{H-P}$ 12,5		$^3J_{H-P}$ 12,2						$^3J_{H-P}$ 9,8
H(142)	dd 3,31[a]	$^3J_{H-P}$ 7,6	dd 3,42[a]	$^3J_{H-P}$ 11,3	dd 3,24	$^3J_{H-P}$ 11,5	dd 3,25	$^3J_{H-P}$ 11,8		
	dd 3,35	$^3J_{H-P}$ 7,7	dd 3,34	$^3J_{H-P}$ 11,7					3,20[b]	$^3J_{H-P}$ 9,8
H(151)	dd 2,90[a]	$^2J_{H-H}$ −9,2	dd 2,86[a]	$^2J_{H-H}$ −9,5	2,91[c]	$^2J_{H-H}$ −9,6	2,88[c]	$^2J_{H-H}$ −9,2		
		$^3J_{H-P}$ 7,4		$^3J_{H-P}$ 15,2		$^3J_{H-P}$ 13,5		$^3J_{H-P}$ 11,7		
	dd 2,85	$^2J_{H-H}$ −9,3	dd 2,80	$^2J_{H-H}$ −9,3						
		$^3J_{H-P}$ 7		$^3J_{H-P}$ 14,8					3,16[d]	$^3J_{H-P}$ 9,7
H(152)	dd 3,12[a]	$^3J_{H-P}$ 0	dd 3,14[a]	$^3J_{H-P}$ 1,2	3,12[c]	$^3J_{H-P}$ 9,9	3,04[c]	$^3J_{H-P}$ 12,7		
	dd 3,17	$^3J_{H-P}$ 0	dd 3,09	$^3J_{H-P}$ 1,4						

[a]Diastéréoisomère majoritaire.
[b]H(141) et H(142) constituent la partie AB d'un système ABX (X = P).
[c]H(151) et H(152) constituent la partie AB d'un système ABX (X = P.
[d]H(151) et H(152) apparaissent comme équivalents.

Can. J. Chem. Downloaded from www.nrcresearchpress.com by 92.62.229.171 on 09/08/12
For personal use only.

TABLEAU 4. Paramètres de RMN ^{13}C des groupements bicyclophosphoraniques des composés **1**, **2**, **3** et **4**

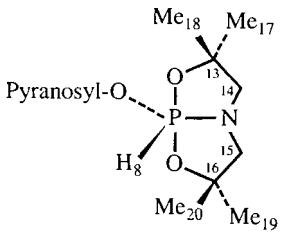

1

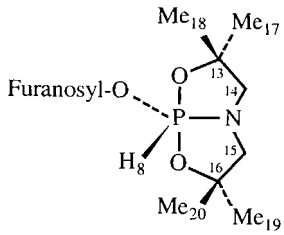

2

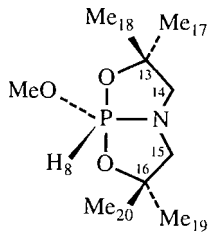

3

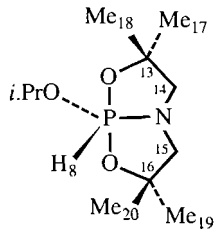

4

	δ, ppm	*J*, Hz	δ, ppm	*J*, Hz	δ, ppm	*J*, Hz	δ, ppm	*J*, Hz
C(13)	d 70,3	^2J 5,3[a]	d 70,7	^2J 5,2[a]	d 70,1	^2J 5,6[a]	d 70,1	^2J 5,6[a]
C(14)	d 55,2	^2J 18,9[b]	d 55,0	^2J 18,9[b]	d 55,4	^2J 18,9[b]	d 55,5	^2J 18,9[b]
C(15)	d 55,2	^2J 18,9[b]	d 55,1	^2J 18,9[b]	d 55,4	^2J 18,9[b]	d 55,5	^2J 18,9[b]
C(16)	d 70,4	^2J 5,3[a]	d 70,9	^2J 5,4[a]	d 70,1	^2J 5,6[a]	d 70,1	^2J 5,6[a]
C(17)	s 29,6		s 29,4		d 29,6	^3J 5,5	d 29,7	^3J 4,9
C(18)	s 29,1		s 29,3		s 29,0		s 29,1	
C(19)	s 29,6		s 29,5		d 29,6	^3J 5,5	d 29,7	^3J 4,9
C(20)	s 28,9		s 28,8		s 29,0		s 29,1	

[a]Ces valeurs sont, en fait, les moyennes des constantes de couplage $^2J_{C\text{-}O\text{-}P}$ et $^3J_{C\text{-}C\text{-}N\text{-}P}$.
[b]De même ces valeurs sont les moyennes de $^2J_{C\text{-}N\text{-}P}$ et de $^3J_{C\text{-}C\text{-}O\text{-}P}$.

différences significatives d'un composé à l'autre. Pour les protons N-CH_2 cycliques elles sont identiques dans **4** (P=O), voisines dans les deux diastéréosiomères de **2** (P=S) ainsi que dans **3** (P=S) et **4** (P=S) (de l'ordre de 11–12 Hz) mais sensiblement différentes dans les deux diastéréoisomères de **1** (P=S) (de l'ordre de 7 et 12 Hz). En utilisant pour les constantes de couplage $^3J_{P\text{-}N\text{-}C\text{-}H}$ et les angles dièdres que font les quatre atomes correspondants une relation de Karplus (9), ces observations peuvent refléter une vitesse de basculement du rabat des cycles pentagonaux différente selon le composé. Rapide jusqu'à moyenner les angles dièdres P—N—C—H dans **4** (P=O) elle est quelque peu ralentie dans **2** (P=S), **3** (P=S) et **4** (P=S), et suffisamment faible dans **5** (P=S) pour qu'une forme enveloppe du cycle pentagonal puisse être observée en solution.

(*b*) La comparaison des paramètres de **4** (P=S) et de **4** (P=O) montre que le remplacement du groupement thiophosphoryle P=S par le groupe phosphoryle P=O a des effets significatifs sur les déplacements chimiques des protons N-CH_2 cycliques et acycliques. Pour les premiers nous assistons à un déblindage de 0,39 ppm de l'un (passage de 2,69 à 3,08 ppm) et un blindage de 0,05 ppm pour l'autre (de 3,25 à 3,20 ppm). Quant aux protons N-CH_2 acycliques il sont tous deux déblindés mais avec des amplitudes différentes : 0,28 ppm pour l'un (de 2,88 à 3,16 ppm) et 0,12 ppm pour l'autre (de 3,16 à 3,04). Ces observations sont à rapprocher de celles que nous avons présentées pour le composé **14** et son dérivé soufré **13** (8).

2.3. RNM ^{13}C

Nous terminerons cette étude par quelques commentaires sur les paramètres de RMN ^{13}C de ces composés, en nous limitant à la partie organo-phosphorée de nos molécules. Le tableau 4 rassemble les données concernant les groupements bicyclophosphoranes, le tableau 5 concerne les hétérocycles thio-oxazaphospholidines.

(*a*) L'examen du tableau 4 montre comme attendu, que la chiralité des ensembles galactopyranose et glucofuranose, dans **1** et **2**, conduit à la discrimination de tous les noyaux de carbones des restes bicyclophosphoraniques. Quatre signaux correspondant aux quatre groupements méthyles, deux pour N-CH_2 et deux pour les carbones O-C. Notons qu'aucun carbone méthylique de **1** et **2** n'est couplé avec l'atome de phosphore alors qu'un tel couplage existe

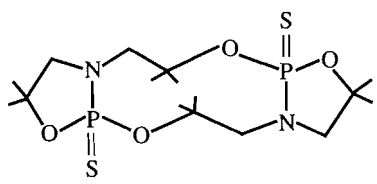

13

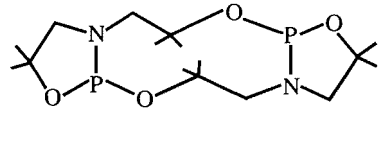

14

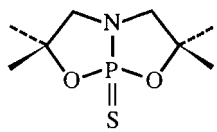

15

Can. J. Chem. Downloaded from www.nrcresearchpress.com by 92.62.229.171 on 09/08/12
For personal use only.

TABLEAU 5. Déplacements chimiques et constantes de couplage avec le phosphore des noyaux de carbone des restes thio-oxazaphospholidines

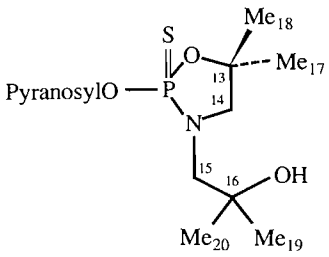

1(PS)

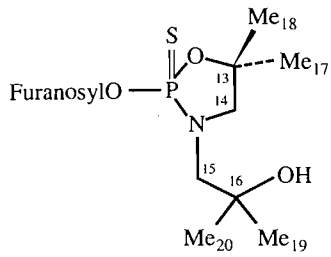

2(PS)

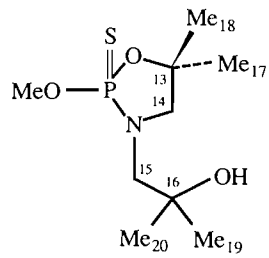

3(PS)

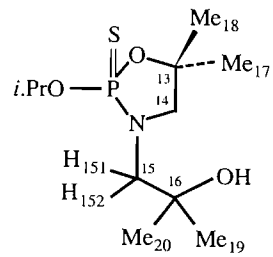

4(PS)

	δ, ppm	*J*, Hz	δ, ppm	*J*, Hz	δ, ppm	*J*, Hz	δ, ppm	*J*, Hz
C(13)	d 82,7	^2J 3,4[a]	d 83,2[b]	^2J 2,6[a]	d 82,6	^2J 2,8[a]	d 82,3	^2J 3,2[a]
	d 82,7	^2J 3,4[a]	d 83,4	^2J 2,8[a]				
C(14)	d 62,1	^2J 11,4[c]	d 62,2[b]	^2J 10,8[c]	d 62,3	^2J 11,0[c]	d 61,8	^2J 11,2[c]
	d 62,5	^2J 11,3[c]	d 62,4	^2J 10,8[c]				
C(15)	d 57,7	^2J 5,5	d 58,6[b]	^2J 5,2	d 58,0	^2J 5,2	d 57,6	^2J 5,1
	d 58,3	^2J 5,3	d 58,4	^2J 5,1				
C(16)	d 71,5	^3J 3,4	d 71,2[b]	^3J 5,0	d 71,7	^3J 4,4	d 71,8	^3J 4,5
	d 71,7	^3J 4,6	d 71,4	^3J 4,5				
C(17) ou C(18)	s 27,8		s 27,4		s 27,9		d 27,8	^3J 5,4
	s 27,9		s 27,4					
C(18) ou C(17)	s 27,9		s 27,7		s 27,9		s 27,9	
	s 28,0		s 27,7					
C(19)	s 27,5		s 27,5		s 27,5		s 27,6	
	s 27,4		s 27,5					
C(20)	s 27,6		s 27,5		s 27,5		s 27,6	
	s 27,7		s 27,5					

[a]Ces valeurs sont, en fait, les moyennes des constantes de couplage $^2J_{C-O-P}$ et $^3J_{C-C-N-P}$.
[b]Diastéréoisomère majoritaire.
[c]Ces valeurs sont les moyennes de $^2J_{C-N-P}$ et de $^3J_{C-C-O-P}$.

pour un groupement CH_3 dans **3** et **4**. Comme il est admis que les constantes de couplages $^3J_{C-C-O-P}$ suivent une relation du type Karplus (9) cette observation traduit, à notre sens, une différence de conformation des cycles pentagonaux dans **1** et **2** d'une part, **3** et **4** d'autre part.

(*b*) Le passage des bicyclophosphoranes **1**, **2**, **3**, **4** aux thio-oxazaphospholidines **1** (P=S), **2** (P=S), **3** (P=S) et **4** (P=S) conduit à un dédoublement de tous les signaux des atomes de carbone. En effet le fragment -O-C$(CH_3)_2$-CH_2-N-CH_2-C$(CH_3)_2$-O, symétrique au départ, se trouve en fin de compte partagé entre un hétérocycle et une chaine linéaire. Les attributions qui figurent dans le tableau 5 résultent de la comparaison des paramètres obtenus avec ceux de composés proches étudiés au laboratoire : **13** (8) et **15**.[5]

3. Conclusion

Au cours de ce travail, nous avons montré que la phosphoranylation d'aldohexoses monohydroxylés constitue un excellent moyen d'accès aux thio-oxazaphospholidines correspondantes. L'analyse des paramètres de RMN ^1H et ^{13}C de ces deux types de composés a permis de mettre en évidence plusieurs particularités stéréochimiques.

[5]Résultats non publiés.

4. Partie expérimentale

4.1. Résonance magnétique nucléaire

Les spectres de RMN ^{31}P, ^1H et ^{13}C ont été enregistrés avec différents spectromètres Bruker : AC 80, AC 200, AC 250 et WM 250. Les déplacements chimiques, exprimés en parties par millions (ppm), sont mesurés avec une précision de ±0,005 ppm pour ^1H et ±0,03 ppm pour ^{31}P et ^{13}C (références tétraméthylsilane, TMS, pour ^1H et ^{13}C, H_3PO_4 pour ^{31}P). Les constantes de couplages, exprimées en Hz, sont mesurées avec une précision de 0,2 Hz pour ^1H et 0,5 Hz pour ^{13}C et ^{31}P. La résolution complète des spectres a été parachevée par des expériences de découplage homonucléaire proton–proton et hétéronucléaire proton–phosphore et carbone–phosphore. Les données expérimentales citées dans le texte ou les tableaux ne sont pas reprises dans ce qui suit.

4.2. Préparations

*4.2.1. Les bicyclophosphoranes : **1–4***

4.2.1.1. Le 3,3,7,7-tétraméthyl 1-[1,2,3,4-di-O-*isopropylidène* α-D-*galactopyranosyloxyl*]*2,8-dioxa 5-aza 1-phospha*^{V} *bicyclo[3.3.0]octane*, ***1***. Quantités utilisées : galactopyranose **7** 541 mg (2,08 × 10^{-3} mol), bicyclophosphane **6** 393 mg (2,08 × 10^{-3} mol), toluène 3 mL. L'enlèvement du solvant après la fin de la réaction conduit à un liquide incolore très visqueux que nous avons caractérisé à l'aide des spectres de RMN de trois noyaux ^1H, ^{31}P et ^{13}C et analyse élémentaire. Parmi les données expérimentales qui n'apparaissent pas dans l'article ajoutons celles concernant la RMN de $^{13}C\{H\}$ (62,89 MHz benzène-d_6) : 24,4 ppm

Can. J. Chem. Downloaded from www.nrcresearchpress.com by 92.62.229.171 on 09/08/12
For personal use only.

Can. J. Chem. Downloaded from www.nrcresearchpress.com by 92.62.229.171 on 09/08/12
For personal use only.

(s, C(10), *endo*), 25,0 ppm (s, C(12), *endo*), 26,3 ppm (s, C(9), *exo*), 64,9 ppm (d, C(6), $^2J_{C-P}$ = 6,1 Hz), 67,7 ppm (d, C(5), $^3J_{C-P}$ = 10 Hz), 71,1–71,2 et 71,3 (3s, C(2), C(3), C(4)), 96,8 ppm (s, C(1)); 108,4 et 109,2 ppm (2s, C(7), C(8)). Anal. calc. pour $C_{20}H_{36}NO_8P$: C 53,44; H 8.07; N 3,11; trouvé C 52,34; H 7,9; N 3,22.

*4.2.1.2. Le 3,3,7,7-tétraméthyl 1-[1,2,5,6-di-*O*-isopropylidène-α-D-glucofuranosyloxy] 2,8-dioxa 5-aza 1-phospha^V bicyclo[3.3.0]octane,* **2**. Quantités utilisées : glucofuranose **8** 463 mg (1,78 × 10^{-3} mol), bicyclophosphane **6** 336 mg (1,78 × 10^{-3} mol) toluène 3 mL. Le composé **2** est un liquide incolore très visqueux. RMN $^{13}C\{H\}$(62,89 MHz benzène-d_6) : 25,7 ppm (s, C(9), *exo*), 26,4 ppm (s, C(10), *endo*), 27,2 ppm (s, C(11), *exo* et C(12) *endo*), 67,9 ppm (s, C(6)), 73,4 ppm (s, C(5)), 79,1 ppm (d, C(3), $^2J_{C-P}$ = 7,9 Hz), 85,3 ppm (d, C(2), $^3J_{C-P}$ = 2,3 Hz), 105,8 ppm (s, C(1)), 109,1 et 111,6 (2s, C(7) et C(8)). Anal. calc. pour $C_{20}H_{36}NO_8P$: C 53,44; H 8,07; N 3,11; trouvé : C 52,23; H 7,9; N 2,97.

4.2.1.3. Le 3,3,7,7-tétraméthyl 1-méthoxy 2,8-dioxa 5-aza 1-phospha^V bicyclo[3.3.0]octane, **3**. Quantités utilisées : méthanol fraichement redistillé 169,5 mg (5,29 × 10^{-3} mol), bicyclophosphane **6** 1000 mg (5,29 × 10^{-3} mol), toluène 3 mL. Après enlèvement du solvant le phosphorane a été purifié par distillation sous pression réduite. Eb.$_{0,05}$: 40°C. Le composé **3** a été caractérisé par RMN et analyse élémentaire. RMN ^1H (250 MHz, benzène-d_6) : 3,45 ppm (d, 3H, CH_3O, $^3J_{H-P}$ = 14,9 Hz), 7,04 ppm (d, 1H, H(8), $^1J_{H-P}$ = 794,9 Hz). RMN $^{13}C\{^1H\}$ (62,89 MHz, benzène-d_6) : 53,3 ppm (d, C(21), $^2J_{C-P}$ = 6 Hz). Anal. calc. pour $C_9H_{20}NO_3P$: C 48,87; H 9,12; N 6,33; trouvé : C 48,67; H 9,3; N 6.75. La synthèse et les caractéristiques du composé **4** ont été publiées par ailleurs (4).

4.3. Les thio-oxazaphospholidines : ***1****(P═S)–****4****(P═S)*

Ces composés ont été obtenus par action du soufre élémentaire sur les bicyclophosphoranes **1**–**4**.

*4.3.1. Le 5,5-diméthyl 3-[(2-méthyl 2-hydroxypropyl] 2-[1,2,3,4-di-*O*-isopropylidéne α-D-galactopyranosyloxy] 2-thio 1,3,2- oxazaphospholidine* ***1*** *(P═S)*

Quantités utilisées : bicyclophosphorane **1**, 330 mg (0,73 × 10^{-3} mol) benzène 4 mL, soufre élémentaire 23,3 mg (0,72 × 10^{-3} atome). Quelques particularités sur l'évolution de la réaction sont dans le texte. Le mélange des deux diastéréoisomères est caractérisé par RMN et analyse élémentaire. RMN ^1H (250 MHz, benzène-d_6) : entre 1,03 et 1,55 ppm (14 s, 48 H, correspondant aux 16 groupements CH_3 attendus, chaque diastéréoisomère comportant 8 groupements méthyles), entre 3,7 et 3,9 ppm (multiplet complexe, 2H, correspondant aux protons H(61) et H(62) des 2 diastéréoisomères; ces protons forment avec H(5) et P un système du type ABXY), 4,23 ppm (dd, 1H, H(2), $^3J_{H(2)-H(1)}$ = 5 Hz, $^3J_{H(2)-H(3)}$ = 2,4 Hz), 4,24 ppm (dd, 1H, H(2) second diastéréoisomère, $^3J_{H(2)-H(1)}$ = 5 Hz, $^3J_{H(2)-H(3)}$ = 2,4 Hz), entre 4,3 et 4,5 ppm (multiplet complexe, 3H, H(3), H(4), et H(5) des deux diastéréoisomères), 5,44 ppm (d, 1H, H(1) des deux diastéréoisomères). Quant aux protons N-CH_2, leurs paramètres se trouvent dans le tableau 3. RMN $^{13}C\{^1H\}$ (62,89 MHz, benzène-d_6) : entre 23 et 28 ppm (15 s correspondant aux 16 carbones méthyliques attendus), 67,2 ppm (d, C(6), premier diastéréoisomère, $^2J_{C-P}$ = 5,4 Hz), 67,4 ppm (d, C(6), 2ième diastéréoisomère, $^2J_{C-P}$ = 5,4 Hz), 67,4 ppm (d, C(5), 1er diastéréoisomère, $^3J_{C-P}$ = 6,9 Hz), 67,8 ppm (d, C(5), 2ième diastéréoisomère, $^3J_{C-P}$ = 6,9 Hz), entre 70,8 et 71,3 ppm (5s correspondant aux 6 carbones C(2), C(3) et C(4) attendus), 96,7 ppm (s, C(1), premier diastéréoisomère), 96,8 ppm (s, C(1), 2ième diastéréoisomère), 108,7 et 109,5 ppm (2s, correspondant aux 2 carbones C(7) et 2 carbones C(8) attendus). Quant aux paramètres des noyaux de carbone C(13), C(14), C(15) et C(16) ils sont rassemblés dans le tableau **5**. Anal. calc. pour $C_{20}H_{36}NO_8PS$: C 49,88; H 7,54; N 2,9; trouvé : C 48,1; H 7,6; N 2,9.

*4.3.2. Le 5,5-diméthyl 3-(2-méthyl 2-hydroxypropyl) 2-[1,2,5,6-di-*O*-isopropylidène α-D-glucofuranosyloxy] 2-thio 1,3,2-oxazaphospholidine,* ***2****(P═S)*

Quantités utilisées : bicyclophosphorane **2** 654,6 mg (1,34 × 10^{-3} mol), benzène 4 mL, soufre élémentaire 43,1 mg (1,3(10^{-3} atome). À la différence du cas précédent la forme thiophosphate **2** (P═S)* à δ ^{31}P = 50 ppm est pratiquement indétectable au bout de 4 jours. Les deux diastéréoisomères de **2** (P═S) ont été caractérisés par RMN et analyse élémentaire. RMN ^1H (250 MHz benzène-d_6) : entre 0,99 et 1,39 ppm (12 s 48H, correspondant aux 16 groupements CH_3), entre 3,97 et 4,17 ppm (multiplet, 2H H(61), H(62), ou H(4), H(5) des deux diastéréoisomères), entre 4,39 et 4,48 ppm (multiplet, 2H, H(4), H(5) ou H(61), H(62) des deux diastéréoisomères), 5,03 ppm (d, 0,35H, H(2) minoritaire $^3J_{H(2)-H(1)}$ = 3,7 Hz), 5,14 ppm (d, 0,65H, H(2) majoritaire $^3J_{H(2)-H(1)}$ = 3,7 Hz), 5,2 ppm (dd, 0,35H, H(3) minoritaire $^3J_{H(3)-H(4)}$ = 2,4 Hz, $^3J_{H-P}$ = 9 Hz), 5,37 ppm (dd, 0,65H, H(3) majoritaire $^3J_{H(3)-H(4)}$ = 2,4 Hz, $^3J_{H-P}$ = 9 Hz), 5,89 ppm (d, 0,35H H(1) minoritaire), 5,85 ppm (d, 065H, H(1) majoritaire). RMN $^{13}C\{^1H\}$ (62,89 MHz benzène-d_6) : entre 25,5 et 27,5 ppm (6s correspondant aux 16 carbones méthyliques attendus), 67,4 ppm (s C(6) minoritaire), 67,8 ppm (s, C(6) majoritaire), 72,6 ppm (s, C(5) minoritaire), 72,9 ppm (s, C(5) majoritaire), 80,8 ppm (d, C(4) majoritaire et minoritaire, $^3J_{C-P}$ = 5,4 Hz), 81 ppm (d, C(3) majoritaire et minoritaire $^2J_{C-P}$ = 10 Hz), 84,5 ppm (s, C(2) minoritaire), 84,6 ppm (s, C(2) majoritaire), 105,4 ppm (s, C(1 majoritaire), 105,5 ppm (s, C(1), minoritaire), 109,5 ppm (s, C(7 ou C(8) minoritaire), 109,6 ppm (s, C(7) ou C(8) majoritaire) 112,1 ppm (s, C(8) ou C(7) minoritaire), 112,3 ppm (s, C(8) ou C(7) majoritaire). Anal. calc. pour $C_{20}H_{36}NO_8PS$: C49,88; H 7,54 N 2,9; trouvé : C 50,5; H 7,6; N 2,9.

4.3.3. Le 5,5-diméthyl 3-[2-méthyl 2-hydroxypropyl] 2-méthoxy 2-thio 1,3,2-oxazaphospholidine, ***3*** *(P═S)*

Quantités utilisées : bicyclophosphorane **3** 279 mg (1,26 × 10^{-3} mol) toluène 3 mL, soufre élémentaire 40,4 mg (1,28 × 10^{-3} atome). Le solvant est enlevé 48 h après la fin de la réaction après avoir vérifié l'absence de **3** (P═S)* tautomère. **3** (P═S) est un liquide jaunâtre et visqueux caractérisé par RMN et analyse élémentaire. RMN ^1H (200 MHz, benzène-d_6) : 1,09; 1,10; 1,1 et 1,18 ppm (4s, 12H, CH_3(17), CH_3(18), CH_3(19) et CH_3(20)) 3,47 ppm (d, 3H, CH_3-O, $^3J_{H-P}$ = 14,4 Hz). RMN $^{13}C\{^1H$ (50,32 MHz, benzène-d_6) : 54,6 ppm (d, C(21), $^2J_{C-P}$ = 5,6 Hz Anal. calc. pour $C_9H_{20}NO_3PS$: C 42,67; H 7,96; N 5,72; trouvé C 41,4; H 8,1; N 5,7.

4.3.4. Le 5,5-diméthyl 3-[2-méthyl 2-hydroxypropyl] 2-isopropyloxy 2-thio 1,3,2-oxazaphospholidine, ***4*** *(P═S)*

Quantités utilisées : bicyclophosphorane **4** 305 mg (1,22 × 10^{-3} mol), toluène 2,5 mL, soufre élémentaire 39,2 mg (1,22 × 10^{-3} atome). Le composé **4** (P═S) est une huile jaunâtre très visqueuse que nous n'avons pas réussi à cristalliser. Il a été caractérisé par RMN et analyse élémentaire. RMN ^1H (200 MHz benzène-d_6) : entre 1,10 et 1,17 ppm (3s, 18H, CH_3(17), CH_3(18) CH_3(19), CH_3(20), CH_3(22) et CH_3(23)), 4,9 ppm (heptuple dédoublé, 1H, H(21), $^3J_{H-H}$ = 6,2 Hz, $^3J_{H-P}$ = 10,6 Hz). RMN $^{13}C\{^1H\}$ (50,3 MHz, benzène-d_6) : 23,2 ppm (d, C(22), $^3J_{C-P}$ = 8,2 Hz), 23,4 ppm (d, C(23), $^3J_{C-P}$ = 2,5 Hz, 72,8 ppm (d, C(21) $^2J_{C-P}$ = 5,6 Hz). Anal. calc. pour $C_{11}H_{24}NO_3PS$: C 46,95; H 8,59 N 4,98; trouvé : C 46,6; H 8,63; N 5,69.

4.4. Le 5,5-diméthyl 3-[2-méthyl 2-hydroxypropyl] 2-isopropyloxy 2-oxo 1,3,2-oxazaphospholidine, ***4*** *(P═O)*

Nous avons suivi la méthode récemment décrite par Helinski *et al.* (13). À une solution de 359 mg (1,28 × 10^{-3} mol) de **4** dans 2 mL de dichlorométhane on ajoute 1 mL de pyridine, puis, en une fois, 321 mg (1,53 × 10^{-3} mol) d'anhydride trifluoroacétique. Le mélange, agité à la température ambiante, est suivi dans sa composition par RMN de ^{31}P. Le remplacement du soufre par l'oxygène c'est à dire la disparition du pic à δ = 83,1 ppm au profit d'un nouveau pic de résonance se trouvant à δ = 18,6 ppm, est terminé

en 2 h. Une évaporation sous pression réduite des produits volatils permet d'isoler un liquide sirupeux qui est extrait plusieurs fois au pentane. L'enlèvement de ce dernier conduit à un liquide visqueux jaunâtre, caractérisé par RMN. RMN ^{31}P (32,44 MHz, $CDCl_3$) : 19,9 ppm (s). RMN ^1H (250 MHz, $CDCl_3$) : 1,23 ppm (d, 3H, CH_3(22), $^3J_{H-H}$ = 6,3 Hz), 1,26 ppm (d, 3H, CH_3(23), $^3J_{H-H}$ = 6,3 Hz), 1,39 ppm (s, 3H, CH_3(17)), 1,41 ppm (s, 3H, CH_3(18)), 1,56 ppm (s, 6H, CH_3(19), CH_3(20)), 4,58 ppm (heptuplet dédoublé, 1H, H(21), $^3J_{H-P}$ = 7,3 Hz). RMN $^{13}C\{^1H\}$ (62,89 MHz, $CDCl_3$) : 22,9 ppm (s, C(22), C(23)), 23,5 ppm (s, C(19), C(20)), 27,3 ppm (s, C(17)), 27,8 ppm (s, C(18)), 54,8 ppm (d, C(15), $^2J_{C-P}$ = 4,5 Hz), 61,1 ppm (d, C(14), 1/2 ($^2J_{C-P}$ + $^3J_{C-P}$ = 13,9 Hz), 72,5 ppm (d, C(21), $^2J_{C-P}$ = 6,4 Hz), 81,1 ppm (s, C(16)), 89,4 ppm (d, C(13), 1/2 ($^2J_{C-P}$ + $^3J_{C-P}$ = 4,2 Hz).

Remerciements

Les auteurs tiennent à remercier les responsables et personnels techniques des services de RMN du Groupe Régional de Mesures Physiques de Toulouse, MM Commenges, Dall'Ava, Pelletier et T. L. Trang, pour l'enregistrement des spectres de RMN utilisés dans ce travail.

1. (*a*) D. Houalla, F. H. Osman, M. Sanchez et R. Wolf. Tetrahedron Lett. 3041 (1977); (*b*) D. Houalla, A. Munoz, H. Ramdane et R. Wolf. Tetrahedron Lett. **26**, 2003 (1985); (*c*) B. Duthu, D. Houalla, M. C. Duriez et R. Wolf. Phosphorus Sulfur, **30**, 319 (1987).
2. B. Duthu, D. Houalla et R. Wolf. Can. J. Chem. **66**, 2965 (1988).
3. B. Duthu, D. Houalla et R. Wolf. Phosphorus, Sulfur Silicon, **51/52**, 81 (1990).
4. B. Duthu, D. Houalla et R. Wolf. Phosphorus, Sulfur Silicon, **51/52**, 61 (1990).
5. M. Eto. Pesticides and alternatives: innovative chemical and biological approaches to pest control. Proceedings of an International Conference. Orthodox Academy of Crete, Kolymbari, Crete, Greece. 1990. pp. 33–44.
6. M. Eto et S. Go. Jpn. Kokai Tokyo Koho JP 01, 199, 986; Chem. Abstr. **112**, 56290 t (1990).
7. M. Baltas, L. Chahoua, L. Gorrichon, P. Tisnes, D. Houalla, R. Wolf et J. Jaud. Can. J. Chem. **69**, 300 (1991).
8. B. Duthu, K. El Abed, D. Houalla, R. Wolf et J. Jaud. Can. J. Chem. **70**, 809 (1992).
9. D. G. Gorenstein. Phosphorus 31 NMR — principles and applications. Academic Press, New York. 1984. pp. 43–51.
10. (*a*) J. Devillers, D. Houalla, J. Roussel et R. Wolf. Org. Magn. Reson. **8**, 500 (1976); (*b*) J. Devillers, D. Houalla, T. Mouheich et R. Wolf. Org. Magn. Reson. **8**, 558 (1976); (*c*) C. Bonningue, J. F. Brazier, D. Houalla et F. H. Osman. Phosphorus Sulfur **5**, 291 (1979).
11. C. Cone et L. Hough. Carbohydr. Res. **1**, 1 (1965).
12. J. C. Jochims et G. Taigel. Chem. Ber. **103**, 448 (1970).
13. J. Helinski, Z. Skrzypczynski, J. Wasiak et J. Michalski. Tetrahedron Lett. **31**, 4081 (1990).

Can. J. Chem. Downloaded from www.nrcresearchpress.com by 92.62.229.171 on 09/08/12
For personal use only.

The synthesis and structural characterization of a series of pentacoordinate diorganotin(IV) *N*-arylidene-α-amino acid complexes

F. E. SMITH[1]

Chemistry Department, Laurentian University, Sudbury, Ont., Canada P3E 2C6

ROSEMARY C. HYNES

Chemistry Department, McGill University, Montreal, Que., Canada H3A 2T5

T. T. ANG AND L. E. KHOO

School of Chemical Sciences, Universiti Sains Malaysia, Penang, Malaysia

AND

G. ENG

Chemistry Department and D.C. Agricultural Experiment Station, University of the District of Columbia, Washington, DC 20005, U.S.A.

Received May 31, 1991

Can. J. Chem. Downloaded from www.nrcresearchpress.com by 79.173.37.17 on 09/08/12
For personal use only.

F. E. SMITH, ROSEMARY C. HYNES, T. T. ANG, L. E. KHOO, and G. ENG. Can. J. Chem. **70**, 1114 (1992).

Eight new diorganotin complexes formulated as $R_2Sn(OArCR''{=}NCHR'COO)$ were prepared and characterized by ^1H and ^{13}C NMR, IR, and elemental analysis. A single crystal X-ray diffraction study of the dibutyltin *N*-salicylidenevaline complex, $Bu_2Sn(OC_6H_4CH{=}NCH(i\text{-}Pr)COO)$, determines the molecular structure. The crystals are orthorhombic, space group $P2_12_12_1$ with a = 9.187(2) Å, b = 10.003(2) Å, c = 23.482(4) Å, V = 2157.8(6) Å^3, Z = 4, and D_c = 1.392 g cm^{-3}. The final discrepancy factors are R_F = 0.040, and R_W = 0.021 for 1131 significant reflections. The tin atom has a distorted trigonal bipyramidal coordination, with no short intermolecular contacts. The two axial Sn—O bonds of 2.078(10) and 2.151(8) Å and the equatorial Sn—N bond of 2.158(8) Å are among the shortest found in related complexes. The fact that the closest intermolecular Sn—O distance is 4.511(8) Å indicates a nonbridging carbonyl group.

F. E. SMITH, ROSEMARY C. HYNES, T. T. ANG, L. E. KHOO et G. ENG. Can. J. Chem. **70**, 1114 (1992).

On a préparé huit nouveaux complexes diorganostanniques de formule $R_2Sn(OArCR''{=}NCHR'COO)$ et on les a caractérisés par RMN du ^1H et du ^{13}C, par IR et par analyses élémentaires. Une étude par diffraction des rayons X réalisée sur un cristal unique du complexe dibutylétain de la *N*-salicylidènevaline, $Bu_2Sn(OC_6H_4CH{=}NCH(i\text{-}Pr)COO)$, a permis de déterminer sa structure. Les cristaux sont orthorhombiques, groupe d'espace $P2_12_12_1$, avec a = 9,187(2), b = 10,003(2) et c = 23,482(4) Å, V = 2157,8(6) Å^3, Z = 4, D_c = 1,392 g cm^{-3}, R_F = 0,040 et R_W = 0,021 pour 1131 réflexions significatives. La coordination de l'atome d'étain correspond à une bipyramide trigonale déformée qui ne comporte pas de contacts intermoléculaires courts. Les longueurs des deux liaisons Sn—O axiales, 2,078(10) et 2,151(8) Å, et de la liaison Sn—N équatoriale, 2,158(8) Å, sont les plus courtes du genre pour des complexes apparentés. Le fait que la distance Sn—O intermoléculaire la plus courte soit égale à 4,511(8) Å indique que le groupe carbonyle n'agit pas comme pont.

[Traduit par la rédaction]

Introduction

A variety of organotin complexes structurally related to *cis*-platin and its derivatives (1, 2) have been investigated for antitumour properties (3–5). Recent reports of the activity of certain diorganotin derivatives of pyridine 2,6-dicarboxylic acid and some related compounds (6, 7) against the P388 lymphocytic leukemia tumour, both in vitro and in vivo, led us to report the synthesis and characterization of a series of diorganotin iminodiacetates (8). As a continuation of these studies we now wish to report the results of an investigation into the synthesis and characterization of a series of diorganotin(IV)–*N*-arylidene-α-amino acid complexes. In this study, eight diorganotin complexes were prepared by condensing diorganotin oxides R_2SnO with the ligands **1**–**4**:

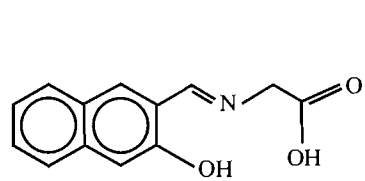

1

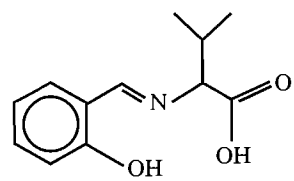

2

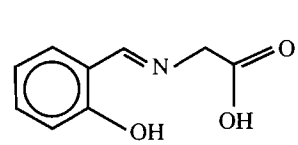

3

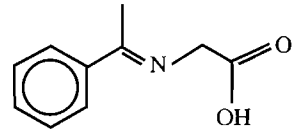

4

A full X-ray structural analysis of the dibutyltin complex of ligand **2** has been carried out (compound **10** in the tables) and

[1]Author to whom correspondence may be addressed.

TABLE 1. Analytical, physical, and IR data of diorganotin–*N*-2-hydroxyarylidene-α-amino acid complexes

(OArCR″=NCHR′CO_2)SnR_2					Preparation	Yield	Melting point	Elemental analysis (%), found (calcd.)			IR (cm^{-1})		
												ν(C—Sn—C)	
Compound	Ar	R″	R′	R	method	(%)	(°C)	C	H	N	ν(C=O)	asym	sym
5	C_6H_4	H	H	CH_3	B	65	184–185	40.11 (40.53);	4.25 (4.03);	4.50 (4.30)	1610, 1580	580	520
6	C_6H_4	H	H	C_4H_9	B	70	118–120	49.39 (49.77);	6.13 (6.15);	3.57 (3.42)	1640, 1590		
7	C_6H_4	CH_3	H	CH_3	B	60	219–220	42.34 (42.39);	4.77 (4.46);	4.17 (4.12)	1580 (br)	560	510
8	C_6H_4	CH_3	H	C_4H_9	B	65	81–83	49.11 (50.97);	6.64 (6.43);	3.46 (3.30)	1600, 1580		
9	C_6H_4	H	Me_2CH	CH_3	A	75	200–202	45.81 (45.69);	5.29 (5.21);	3.78 (3.81)	1650, 1600	580	520
10	C_6H_4	H	Me_2CH	C_4H_9	A	80	148–149	53.09 (53.12);	6.70 (6.93);	2.90 (3.10)	1660, 1610		
11	$C_{10}H_6$	H	H	CH_3	A	70	222–224	47.45 (47.01);	4.06 (4.03);	3.59 (3.73)	1620 (br)	580	510
12	$C_{10}H_6$	H	H	C_4H_9	A	80	120–122	54.91 (54.81);	5.85 (5.93);	3.08 (3.04)	1640, 1590		

TABLE 2. Chemical shifts and coupling constants obtained from the ^1H NMR spectra of compounds **5–12**

Compound	-CH=N- [^3J(Sn=CH)]Hz	Aromatic (δ ppm)	-NCH_2COO (δ ppm)	R_2Sn [^2J($SnCH_3$)]Hz	Other proton δ ppm (*J*) Hz		
					CH_3-C=N-	-NCHRCOO-	-$CH(CH_3)_2$
5	8.29 [36.0]	6.6–7.4	4.33	0.8[84]			
6	8.35 [44.7]	6.6–7.5	4.29	0.8–1.6			
7		6.6–7.5	4.30	0.75 [80]	2.7(s)		
8		6.7–7.5	4.25	0.8–1.6	2.6(s)		
9	8.29 [51.7]	6.7–7.5		0.96 [82]		4.0(d), 2.3–2.5(m)	1.3d [6.9]
				0.58 [78]			1.5d [6.9]
10	8.21 [47.0]	6.7–7.4		0.7–1.8		3.9(d), 2.3–2.5(m)	1.00d [6.8]
							1.07d [6.8]
11	9.14 [57.8]	6.8–7.9	4.40	0.8 [81]			
12	9.14 [52.8]	6.8–7.9	4.38	0.8–1.6			

(s) singlet; (m) multiplet; (d) doublet.

Can. J. Chem. Downloaded from www.nrcresearchpress.com by 79.173.37.17 on 09/08/12
For personal use only.

the results are reported along with a variety of spectroscopic data for both the dimethyltin and dibutyltin derivatives of these ligands.

Experimental

Chemicals and reagents

Dimethyltin and dibutyltin oxides were purchased from Alfa Inorganics and other chemicals were purchased from the Aldrich Chemical Company. All were used without further purification except for salicylaldehyde, which was distilled before use.

IR spectra

These were obtained on a Nicolet instrument with the samples as Nujol mulls or in KBr discs. Results are summarized in Table 1.

NMR spectra

The ^1H and ^{13}C NMR spectra were recorded in $CDCl_3$ on a CFT-20 or Bruker AC-P300 spectrometer. NMR results are summarized in Tables 2 and 3.

*Preparation of ligands **1** and **2** (refs. 9–11)* (Note: ligands **3** and **4** could not be isolated, and so were prepared *in situ*)

A mixture of free (*dl*) α-amino acid (0.1 mol) and the corresponding aldehyde (0.15 mmol) in 300 mL of absolute ethanol and 30 mL of methanol was stirred overnight before refluxing for 3–4 h. After cooling in the refrigerator, a crystalline precipitate formed, which was filtered, washed with petroleum ether (60–80°C), dried, and recrystallized from methanol to give the pure product in 50–60% yield. Microanalyses were carried out at the School of Chemical Sciences, Universiti Sains Malaysia, using an elemental analyzer (model 240-XA). Analytical data for ligands:

N-2-Hydroxynaphthalidieneglycine (**1**), mp 206–208°C (dec.). Anal. calcd. for $C_{13}H_{11}NO_3$: C 68.10, H 4.85; N, 6.11; found: C 68.34, H 4.87; N 6.24.

N-Salicylidenevaline (**2**), mp 160–162°C. Anal. calcd. for $C_{12}H_{15}NO_3$: C 65.15, H 6.85, N 6.33; found: C 64.72, H 6.87, N 6.59.

Preparation of diorganotin–N-2-hydroxyarylidene-α-amino acid complexes

Method A

The diorganotin–*N*-2-hydroxyarylidene-α-amino acid carboxylates can be prepared via the condensation reaction of R_2SnO with either **1** or **2**. An equimolar amount (10 mmol) of either **1** or **2** and R_2SnO (R = CH_3 or *n*-Bu) was mixed with 100 mL of toluene. The mixture was refluxed and the water formed removed azeotropically using a Dean–Stark apparatus. After all the water had been removed from the reaction mixture (about 4 h) the solvent was evaporated with a rotary evaporator and the solid recrystallized from toluene to give the diorganotin carboxylate in high yield. Melting point and analytical data are summarized in Table. 1.

Method B

As ligands **3** and **4** could not be isolated (10, 11), the diorganotin complexes were synthesized by refluxing a mixture of glycine (in excess), R_2SnO, and either salicylaldehyde or 2-hydroxyacetophenone in absolute ethanol.

TABLE 3. Chemical shifts (ppm) from TMS obtained from ^{13}C NMR spectra of compounds **5–12** in $CDCl_3$

Compound	CH=N	NCH_2COO	Me_2Sn/Bu_2Sn	Aromatic	Other
5[a]	172.62	56.93 170.46	4.39	167.45; 135.66; 117.75 136.39; 121.73; 116.27	J(SnC) = 775 Hz
6	172.64	57.63 170.59	26.85 22.17 26.56 13.47	169.51; 135.34; 117.11 137.88; 127.64; 116.98	
7	170.20	52.0 182.0	0.00	166.00; 130.26; 121.09 135.80; 123.20; 117.09	CH_3 \ C=N 22.19(CH_3) / CH_3
8	170.59	53.51 181.34	26.95 22.75 26.58 13.47	166.93; 130.26; 121.09 137.73; 123.63; 117.57	CH_3 \ C=N 21.09(CH_3) / CH_3
9	172.96	74.13 172.78	1.68 0.29	169.06; 135.66; 117.59 137.71; 122.67; 117.26	-$C(Me)_2$ 18.96 / 18.26 ; 35.98
10[b]	172.44	74.78 173.00	27.04 22.56 26.63 13.48	169.51; 135.53; 117.37 137.69; 122.84; 117.37	-$C(Me_2)$ 19.12 / 18.45 ; 35.98 ; 34.65
11	166.42	57.91 172.26	0.69	170.99; 133.87; 129.01; 124.69; 118.44 139.83; 129.66; 127.13; 124.01; 108.77	
12[a]	167.69	57.36 171.18	26.57 22.56 25.78 13.40	170.78; 134.02; 128.23; 124.36; 119.48 138.20; 128.97; 126.32; 123.05; 108.37	

[a]Spectra obtained from Varian Gemini 300 in DMSO.
[b]An extra peak was observed at 20.98 in Bu_2Sn region.

Can. J. Chem. Downloaded from www.nrcresearchpress.com by 79.173.37.17 on 09/08/12
For personal use only.

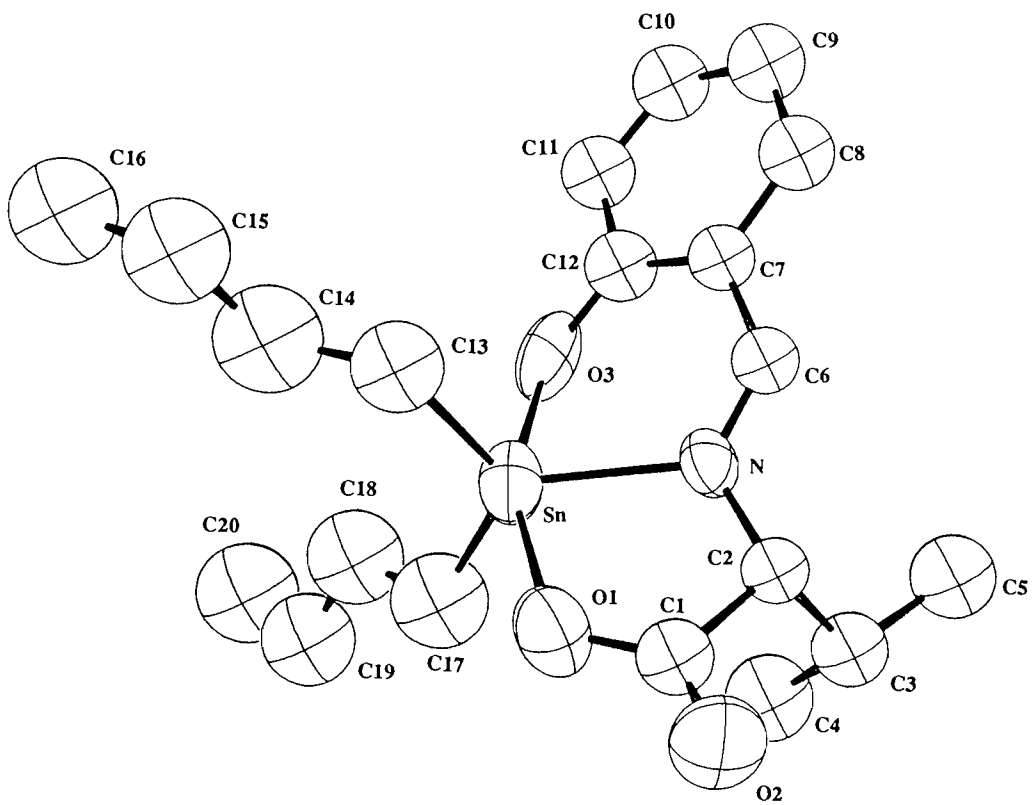

FIG. 1. An ORTEP (18) plot of $Bu_2Sn(OC_6H_4CH{=}NCH(i\text{-}Pr)COO)$ (ellipsoids are shown at 50% probability).

$$H_2NCH_2COOH + R_2SnO + 2HO\text{-}C_6H_4CR'{=}O \rightarrow (OC_6H_4CR'{=}NCH_2CO_2)SnR_2$$

(R′ = H, CH_3; R = CH_3, *n*-Bu)

To a suspension of glycine (20 mmol) in 40 mL of absolute ethanol was added 10 mmol of R_2SnO (R = CH_3; *n*-Bu) followed by salicylaldehyde or 2-hydroxyacetophenone (10 mmol). The mixture was stirred under nitrogen and refluxed for 7–8 h. The excess gly-

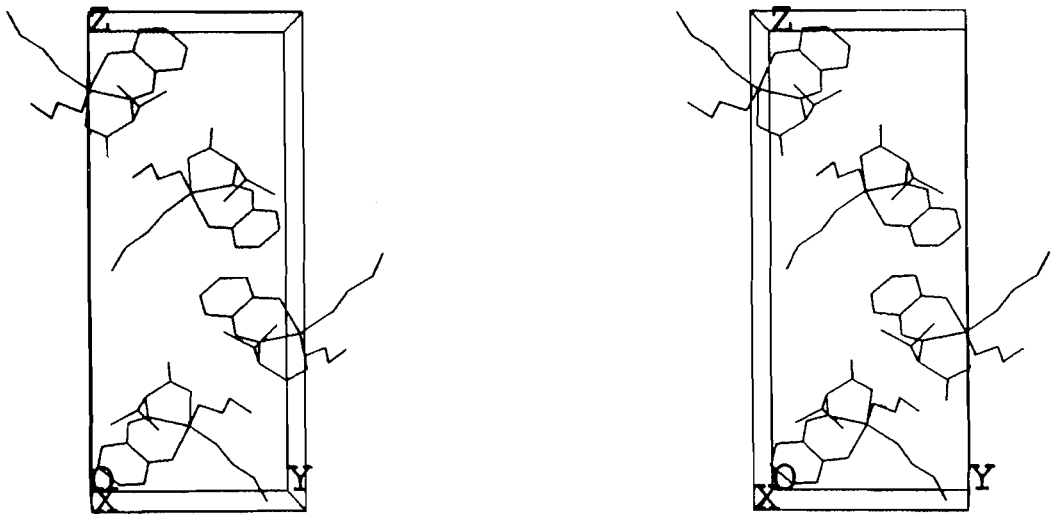

FIG. 2. A stereo plot of the unit cell, showing the packing arrangement.

TABLE 4. Atomic parameters x, y, z, and B_{eq}; esd's refer to the last digit printed

Atom	x	y	z	B_{eq}[a]
Sn	0.16047(9)	0.49528(11)	0.14644(3)	5.65(5)
O1	0.0144(9)	0.5116(11)	0.2177(3)	6.8 (5)
O2	−0.1364(10)	0.4081(8)	0.2768(3)	7.3 (5)
O3	0.2551(9)	0.4042(8)	0.0761(3)	6.7 (5)
N	0.0892(10)	0.2931(8)	0.1624(4)	4.1 (5)
C1	−0.0552(15)	0.4103(13)	0.2361(5)	5.3 (8)
C2	−0.0348(13)	0.2804(11)	0.2018(4)	4.1 (6)
C3	−0.1783(15)	0.2462(12)	0.1689(5)	5.4 (7)
C4	−0.2222(12)	0.3552(12)	0.1242(5)	7.8 (9)
C5	−0.1689(15)	0.1084(10)	0.1386(5)	7.2 (8)
C6	0.1648(14)	0.1894(10)	0.1519(5)	4.4 (6)
C7	0.2853(13)	0.1804(13)	0.1125(5)	4.6 (7)
C8	0.3570(14)	0.0575(11)	0.1086(5)	5.4 (7)
C9	0.4648(15)	0.0381(13)	0.0699(6)	6.6 (8)
C10	0.4947(17)	0.1405(17)	0.0316(5)	7.3 (10)
C11	0.4287(17)	0.2606(15)	0.0339(5)	6.3 (8)
C12	0.3205(16)	0.2847(14)	0.0740(6)	5.6 (8)
C13	0.3495(16)	0.5327(16)	0.1971(6)	9.3 (10)
C14	0.4417(17)	0.6382(17)	0.1789(6)	10.2 (12)
C15	0.5725(19)	0.6662(16)	0.2167(7)	10.5 (12)
C16	0.6723(21)	0.7581(17)	0.1916(7)	12.9 (14)
C17	0.0473(14)	0.6375(12)	0.0978(5)	8.5 (9)
C18	0.1266(18)	0.7218(15)	0.0614(6)	9.8 (10)
C19	0.0391(20)	0.8270(15)	0.0298(6)	11.4 (12)
C20	0.1118(20)	0.8914(14)	−0.0146(6)	12.6 (13)

[a] B_{eq} is the mean of the principal axes of the thermal ellipsoid.

cine was filtered off after cooling and the filtrate concentrated to dryness. The solid was recrystallized from toluene.

The dimethyltin derivative of **4** is insoluble in absolute ethanol so the excess glycine was removed during recrystallization. The yield of these complexes is 60–80% and is comparable to the yield using Method A. Melting points, yields, and analytical and IR data are summarized in Table 1.

X-ray data

Space group and cell dimensions

Empirical formula: $SnC_{20}H_{31}O_3N$ FW = 452.16

Orthorhombic $P2_12_12_1$, a = 9.187(2) Å, b = 10.003(2) Å, c = 23.482(4) Å, volume = 2157.8(6) Å^3. Cell dimensions were obtained from 24 reflections with 2θ in the range 28.00°–33.00°. Crystal dimensions: 0.20 × 0.30 × 0.10 mm, Z = 4, $F(000)$ = 924.86, D_{calc} = 1.392 Mg m^{-3}, μ = 1.20 mm^{-1}, λ = 0.70930 Å (Mo Kα), $2\theta_{max}$ = 44.7°.

Data collection, structure solution and refinement

The intensity data were collected at 295 K on a Nonius diffractometer run by the NRCCAD diffractometer control program (12), using the θ/2θ scan mode and profile analysis (13); 1759 reflec-

Can. J. Chem. Downloaded from www.nrcresearchpress.com by 79.173.37.17 on 09/08/12
For personal use only.

Can. J. Chem. Downloaded from www.nrcresearchpress.com by 79.173.37.17 on 09/08/12
For personal use only.

TABLE 5. Bond distances in angstroms

Bond	Distance	Bond	Distance
Sn—O(1)	2.151(8)	C(6)—C(7)	1.446(18)
Sn—O(3)	2.078(10)	C(7)—C(8)	1.397(19)
Sn—N	2.158(8)	C(7)—C(12)	1.419(20)
Sn—C(13)	2.138(14)	C(8)—C(9)	1.358(20)
Sn—C(17)	2.100(12)	C(9)—C(10)	1.391(22)
O(1)—C(1)	1.273(17)	C(10)—C(11)	1.346(24)
O(2)—C(1)	1.213(16)	C(11)—C(12)	1.389(22)
O(3)—C(12)	1.338(17)	C(13)—C(14)	1.419(22)
N—C(2)	1.472(15)	C(14)—C(15)	1.519(24)
N—C(6)	1.273(15)	C(15)—C(16)	1.425(25)
C(1)—C(2)	1.540(17)	C(17)—C(18)	1.404(18)
C(2)—C(3)	1.565(17)	C(18)—C(19)	1.519(23)
C(3)—C(4)	1.566(17)	C(19)—C(20)	1.395(21)
C(3)—C(5)	1.554(16)		

tions were measured, of which 1632 were unique. Of these, 1131 had $I_{net} > 2.5\sigma(I_{net})$. No correction was made for absorption. The structure was solved by direct methods, followed by a difference Fourier. All non-hydrogen atoms were refined anisotropically. Hydrogen atoms were included in calculated positions. Secondary extinction was refined as in Larson (14) as 0.0558(22). The refined parameter is the average length of a mosaic block in microns. The final least-squares cycle was calculated with 228 parameters and 1131 out of 1632 reflections. Weights based on counting statistics were used. Final residuals are $R_F = 0.040$, $R_W = 0.021$ for data with $I_{net} > 2.5\sigma(I_{net})$, $R_F = 0.006$, $R_W = 0.023$ for all data. The goodness of fit was 1.87. Maximum shift/error was 0.012. In the last *D*-map, the top peak was 0.54 e/Å^3, and the deepest hold was -0.55 e/Å^3. The absolute configuration refined to an η value of 0.82. Scattering factors were taken from the International tables for X-ray crystallography, Vol. IV (15). All computation was performed using the NRCVAX system of crystal structure solving programs (16).

Results and discussion

Organotin carboxylates frequently have di- or polymeric structures resulting from intermolecular bridging by carbonyl oxygen atoms (8, 17). It was anticipated that this series of complexes would exhibit this characteristic, and be six-coordinate. However, the X-ray structural investigation of $Bu_2Sn(OC_6H_4CH{=}NCH(i\text{-}Pr)COO)$ shows that this compound has a five-coordinate monomeric structure. An ORTEP (18) plot of the organotin complex is given in Fig. 1. A stereo pair showing the packing arrangement of the molecules in the unit cell is shown in Fig. 2. The final fractional coordinates of non-hydrogen atoms with equivalent isotropic thermal parameters are listed in Table 4 while the bond lengths and bond angles for the complex are in Tables 5 and 6 respectively. Calculated and observed structure factors, calculated hydrogen atom parameters, and anisotropic thermal parameters have been deposited as Tables S-1, S-2, and S-3, respectively.[2]

The ligand behaves as a tridentate chelating agent via the phenolic oxygen, the imino nitrogen, and a carboxylate oxygen. The two butyl groups and the imino nitrogen take up the equatorial positions and the two oxygens the axial sites in a distorted trigonal bipyramidal arrangement around the tin. The tin atom lies in the ligand plane and forms a five-membered and a six-membered chelate ring with the ligand. There are no close contacts beween the complex entities, and thus no intermolecular tin–oxygen bridging. The closest Sn—O distance between the complexes is 4.511(8) Å (i.e., O(2) at $-x, \frac{1}{2} + y, \frac{1}{2} - z$). Further evidence for the fact that the free carbonyl group on the ligand is not involved in coordination with another tin atom can be deduced from the short C—O distance of 1.213(16) Å. A similar C—O bond length of 1.179(13) Å was reported for a corresponding nonbridging carbonyl group in the compound $Ph_3SnCl{:}2HOC_6H_4CH{=}NCH_2CO_2Et$ (19). The similarities of the spectroscopic data indicate that five-coordinate structures should be proposed for all the organotin compounds studied in this series.

The IR carbonyl stretching vibrations for these diorganotin derivatives are normal and range from 1650 to 1580 cm^{-1} (Table 1). However, the almost equal intensity observed for the asymmetric and symmetric Sn—Me stretching vibrations indicates a bent C—Sn—C moiety for the dimethyltin complexes. This would be consistent with a trigonal bipyramidal configuration for the tin atom, with the methyl groups taking up two of the equatorial positions. The ^{1}H and ^{13}C NMR data are shown in Tables 2 and 3 respectively. Very little shift for the proton and ^{13}C signals was observed for the ligands upon complex formation. However spin–spin coupling between the azomethine proton and the tin nucleus, ^3J(SnN=CH), was detected in all the complexes. This type of spin–spin coupling where the tin nuclei are located in a *trans* position to the azomethine proton has previously been reported (20, 21). It thus confirms the presence of nitrogen–tin coordination in all the complexes. In addition the values of the coupling constant for the diorganotin derivatives, 36–58 Hz for ^3J(SnN=CH) and 78–84 Hz for $^2J(SnCH_3)$ (Table 2), are in agreement with the values reported for the dimethyltin dichloride complexes of a range of Schiff bases (20) obtained from substituted salicylaldehydes and *ortho*-aminophenols (^3J(SnN=CH) = 46–70 Hz; $^2J(SnCH_3)$ = 77–81 Hz). Furthermore the $^2J(SnCH_3)$ values for the dimethyltin derivatives were found to correspond (22) to a C—Sn—C angle range of 120–143°. Similarly the ^1J(SnC) of 774 Hz for **5** is calculated to correspond (22) to a C—Sn—C angle of 145°. This would indicate that the bent C—Sn—C moiety forms part of the trigonal plane of these pentacoordinate complexes. In Tables 2 and 3, it will be noticed that two Sn—Me signals are detected for compound **9** ($Me_2Sn(OC_6H_4CH{=}NCH(i\text{-}Pr)COO)$). This occurs because the underlined proton is enantiotropic and causes the methyl groups bound to the tin, and the *i*-Pr group, to be diastereotopic. These groups thus give two NMR peaks (23).

Some of the Sn—N, Sn—O, and Sn—C bond distances found in this and related complexes are listed in Table 7. It is noteworthy that the Sn—N bond of 2.158(8) Å observed in the present study is the second shortest of the Sn—N bonds listed in Table 7. In addition, the Sn—O and Sn—C bonds

[2]These tables may be purchased from: The Depository of Unpublished Data, Document Delivery, CISTI, National Research Concil Canada, Ottawa, Canada K1A 0S2.

The calculated hydrogen atom parameters have also been deposited with the Cambridge Crystallographic Data Centre and can be obtained on request from The Director, Cambridge Crystallographic Data Centre, University Chemical Laboratory, Lensfield Road, Cambridge CB2 1EW, U.K.

TABLE 6. Bond angles in degrees

Bonds	Angle	Bonds	Angle
O(1)—Sn—O(3)	155.9(3)	C(2)—C(3)—C(4)	113.3(9)
O(1)—SN—N	75.3(4)	C(2)—C(3)—C(5)	111.9(10)
O(1)—Sn—C(13)	93.5(5)	C(4)—C(3)—C(5)	108.9(9)
O(1)—Sn—C(17)	93.6(4)	N—C(6)—C(7)	126.3(10)
O(3)—Sn—N	81.6(3)	C(6)—C(7)—C(8)	117.3(11)
O(3)—Sn—C(13)	100.3(5)	C(6)—C(7)—C(12)	122.5(12)
O(3)—Sn—C(17)	94.1(4)	C(8)—C(7)—C(12)	119.8(12)
N—Sn—C(13)	108.3(5)	C(7)—C(8)—C(9)	120.9(11)
N—Sn—C(17)	125.4(4)	C(8)—C(9)—C(10)	118.1(12)
C(13)—Sn—C(17)	125.9(6)	C(9)—C(10)—C(11)	122.8(13)
Sn—O(1)—C(1)	121.1(9)	C(10)—C(11)—C(12)	120.3(13)
Sn—O(3)—C(12)	127.5(8)	O(3)—C(12)—C(7)	122.0(13)
Sn—N—C(2)	115.1(6)	O(3)—C(12)—C(11)	120.1(13)
Sn—N—C(6)	124.4(8)	C(7)—C(12)—C(11)	117.9(13)
C(2)—N—C(6)	118.3(9)	Sn—C(13)—(C14)	116.6(10)
O(1)—C(1)—O(2)	126.2(12)	C(13)—C(14)—C(15)	115.7(13)
O(1)—C(1)—C(2)	115.7(11)	C(14)—C(15)—C(16)	112.8(14)
O(2)—C(1)—C(2)	118.1(11)	Sn—C(17)—C(18)	118.8(10)
N—C(2)—C(1)	110.5(9)	C(17)—C(18)—C(19)	116.0(14)
N—C(2)—C(3)	111.1(8)	C(18)—C(19)—C(20)	115.6(15)
C(1)—C(2)—C(3)	109.8(10)		

TABLE 7. Comparison of Sn—N, Sn—O, and Sn—C bond lengths in $Bu_2Sn(OC_6H_4CH{=}NCH(i\text{-}Pr)COO)$ with those in other pentacoordinated diorganotin(IV) compounds

Compound	Sn—N (Å)	Sn—O (Å)	Sn—C (Å)	Reference
$Ph_2Sn(OC_6H_4CH{=}NC_6H_4O)$	2.241(13)	2.085(8) 2.103(8)	2.125(11) 2.124(10)	24
$Ph_2Sn(OC_6H_4CH{=}NC_6H_4S)$	2.217(3)	2.093(2)	2.120(2) 2.120(3)	25
$Me_2Sn(OC_6H_4CH{=}NC_6H_4O)$	2.229(11)	2.105(8) 2.118(9)	2.091(14) 2.142(14)	26
$Ph_2Sn(OC_6H_4CHN_2C(O)C_6H_4NH_2)$	2.143(7)[a]	2.076(6) 2.119(9)	2.120(9) 2.122(9)	27
$Bu_2Sn(OC_6H_4CH{=}NCH(i\text{-}Pr)COO)$	2.158(8)	2.078(10) 2.151(8)	2.100(12) 2.138(14)	This work

[a]This figure is the average of two independent determinations (2.163(7) Å and 2.123(6) Å) as suggested by the authors (27).

in this complex are also among the shortest so far observed in pentacoordinated diorganotin complexes of this type.

Acknowledgements

Financial support from the Universiti Sains Malaysia (R & D) fund and the Laurentian University Research Fund (LURF) is gratefully acknowledged.

1. B. Rosenberg, L. Van Camp, and T. Krigas. Nature, **205**, 698 (1965).
2. J. L. van der Veer and J. Reedijk. Chem. Br. **20**, 775 (1988).
3. A. J. Crowe and P. J. Smith. Chem. Ind. 200 (1980).
4. A. J. Crowe, P. J. Smith, and G. Atassi. Chem.-Biol. Interact. **32**, 171 (1980).
5. A. J. Crowe, P. J. Smith, C. J. Cardin, H. E. Parge, and F. E. Smith. Cancer Lett. **24**, 45 (1984).
6. G. Ruisi, A. Silvestri, M. T. LoGludice, R. Barbieri, G. Atassi, F. Huber, K. Gratz, and L. Lamartina. J. Inorg. Biochem. **25**, 229 (1985).
7. M. Gielen, E. Joosen, T. Mancilla, K. Jurkschat, C. Roobol, J. Bernheim, G. Atassi, F. Huber, E. Hoffmann, H. Perut, and B. Mahieu. Main Group Met. Chem. **10**, 148 (1987).
8. F. L. Lee, E. J. Gabe, L. E. Khoo, W. H. Leong, G. Eng, and F. E. Smith. Inorg. Chim. Acta, **166**, 257 (1989).
9. B. Halpern and A. P. Hope. Aust. J. Chem. **27**, 2047 (1974).
10. F. C. McIntire. J. Am. Chem. Soc. **69**, 1377 (1947).
11. J. C. Shechan and V. J. Grenda. J. Am. Chem. Soc. **84**, 2417 (1962).
12. Y. Le Page, P. S. White, and E. J. Gabe. Abstr. Annu. Meeting Am. Crystallogr. Assoc. 1986. p. 24.
13. D. F. Grant and E. J. Gabe. J. Appl. Crystallogr. **11**, 114 (1978).
14. A. C. Larson. *In* Crystallographic computing. *Edited by* F. R. Ahmed. Munksgaard, Copenhagen. 1970. p. 291.
15. International tables for X-ray crystallography. Vol. IV. 2nd ed. Kynoch Press, Birmingham. 1974. p. 99.
16. E. J. Gabe, Y. Le Page, J-P. Charland, F. L. Lee, and P. S. White. J. Appl. Crystallogr. **22**, 384 (1989).

Can. J. Chem. Downloaded from www.nrcresearchpress.com by 79.173.37.17 on 09/08/12
For personal use only.

17. S. W. Ng, C. Wei, and V. G. Kumar Das. J. Organomet. Chem. **345**, 59 (1988).
18. C. K. Johnson. ORTEP-II. Report ORNL-5138, Oak Ridge National Laboratory, Tennessee. 1976.
19. F. L. Lee, E. G. Gabe, L. E. Khoo, G. Eng, and F. E. Smith. Polyhedron, **9**, 653 (1990).
20. K. Kawkami and T. Tanaka. J. Organomet. Chem. **49**, 409 (1973).
21. G. Matsubayashi, T. Tanaka, S. Nisbigaki, and N. Nakatsu. J. Chem. Soc. Dalton Trans. 501 (1979).
22. T. P. Lockhart and F. Davidson. Organometallics, **6**, 2471 (1987).
23. G. van Koten and J. G. Noltes. J. Am. Chem. Soc. **98**, 5393 (1976).
24. H. Preut, F. Huber, R. Barbieri, and N. Bertazzi. Z. Anorg. Allg. Chem. **423**, 75 (1976).
25. H. Preut, H. J. Haupt, F. Huber, R. Cefalu, and R. Barbieri. Z. Anorg. Allg. Chem. **407**, 257 (1974).
26. H. Preut, F. Huber, H. J. Haupt, R. Cefalu, and R. Barbieri. Z. Anorg. Allg. Chem. **410**, 88 (1974).
27. J. Wang, F. Q. Liu, Y. Zhang, R. Wang, H. G. Wang, and X. K. Yao. J. Organometal. Chem. **375**, 173 (1989).

Can. J. Chem. Downloaded from www.nrcresearchpress.com by 79.173.37.17 on 09/08/12
For personal use only.

Metal pyrazolate polymers. Part 3. Synthesis and study of Cu(I) and Cu(II) complexes of 4-Xdmpz (where X = H, Cl, Br, I, and CH_3 for Cu(I) and X = H, Cl, Br, and CH_3 for Cu(II); dmpz = 3,5-dimethylpyrazolate)

MARTIN K. EHLERT, ALAN STORR,[1] AND ROBERT C. THOMPSON[1]

Department of Chemistry, University of British Columbia, 2036 Main Mall, Vancouver, B.C., Canada V6T 1Z1

Received October 11, 1991

MARTIN K. EHLERT, ALAN STORR,[1] and ROBERT C. THOMPSON. Can. J. Chem. **70**, 1121 (1992).

The copper(I) complexes $[Cu(4\text{-}Xdmpz)]_3$ (where X = H, Cl, Br, I and CH_3; dmpz = 3,5-dimethylpyrazolate) and the copper(II) complexes $[Cu(4\text{-}Xdmpz)_2]_x$ have been synthesized and characterized. Qualitative solubility, infrared spectroscopic, and differential scanning calorimetric studies are reported for all complexes. Mass spectra support trimeric formulations for the copper(I) complexes. Scanning electron micrographs and powder X-ray diffractograms have been recorded for the copper(II) compounds. Electronic and EPR spectroscopic studies as well as magnetic susceptibility studies from 2 to 300 K are also reported for the copper(II) compounds, which are proposed to have polymeric chain structures. The magnetic data reveal strong antiferromagnetic interactions in all four of the copper(II) compounds. The data have been analysed employing an isotropic Heisenberg model for antiferromagnetic coupling in extended chain polymers. Values of the exchange coupling constant, J, are determined as -58, -61, -66, and -66 cm^{-1} for the X = H, CH_3, Cl, and Br complexes respectively. The X = Cl compound exhibits an abrupt decrease in magnetic susceptibility below 40 K and possible causes of this anomalous behaviour are discussed.

MARTIN K. EHLERT, ALAN STORR et ROBERT C. THOMPSON. Can. J. Chem. **70**, 1121 (1992).

On a synthétisé et caractérisé les complexes de cuivre(I) $[Cu(Xdmpz\text{-}4)]_3$ (ou X = H, Cl, Br, I et CH_3; dmpz = pyrazolate de diméthyl-3,5) et les complexes de cuivre(II) $[Cu(Xdmpz\text{-}4)_2]_x$. Pour tous ces complexes, on rapporte des études relatives á la solubilité qualitative, à la spectroscopie infrarouge et à la colorimétrie par balayage différentiel. Les spectres de masse confirment les structures trimères proposées pour les complexes de cuivre(I). On a enregistré les micrographiques obtenus par balayage électronique, et les diffractogrammes obtenus par diffraction de rayons X sur les poudres des complexes de cuivre(II). On rapporte également les études spectrospiques et de RPE ainsi que les succeptibilités magnétiques réalisées à des températures allant de 2 à 300 K sur les complexes de cuivre(II) pour lesquels on propose une structure sous forme de chaînes polymérisées. Les données magnétiques révèlent de fortes interactions antiferromagnétiques dans tous les composés de cuivre(II). On a analysé les données obtenues en utilisant un modèle d'Heisenberg isotropique pour le couplage antiferromagnétique dans les longues chaines de polymères. On a déterminé les valeurs de la constante de couplage d'échange, J. Elles sont respectivement de -58, -61, -66 et -66 cm^{-1} pour les complexes où X = H, CH_3, Cl et Br. Le composé où X = Cl montre une brusque diminution de la succeptibilité magnétique en-dessous de 40 K et on discute des causes possibles de ce comportement anormal.

[Traduit par la rédaction]

Introduction

Previous papers in this series have described the synthesis and study of the binary copper(II) pyrazolates $[Cu(4\text{-}Xpz)_2]_x$ (where X = H, Cl, Br, and CH_3; pz = pyrazolate) (1, 2). Two forms of the X = Cl compound (green and brown) were characterized. These compounds all appear to have polymeric chain structures in which adjacent copper ions, with distorted tetrahedral CuN_4 chromophores, are doubly bridged by pyrazolate ligands. This structure was confirmed by single crystal X-ray diffraction studies on the X = H, CH_3, and Cl (green form) materials. Magnetic susceptibility studies over the temperature range 2–300 K revealed relatively strong antiferromagnetic exchange in all the compounds. The magnetic data were successfully analyzed employing an anisotropic Heisenberg model for antiferromagnetic exchange in extended chain polymers, yielding values of the exchange coupling constant, J, in the range -81 to -105 cm^{-1}. A consideration of the relationship between the observed magnitude of exchange and structural considerations led to the suggestion that an important factor in determining the magnitude of exchange in these complexes is the overlap between the pyrazolate π-orbital systems and the metal's magnetic orbital (2). To further investigate the effects of structural change on magnetic exchange in these systems we have synthesized and characterized the four new binary copper(II) pyrazolates, $[Cu(4\text{-}Xdmpz)_2]_x$, where X = H, Cl, Br, and CH_3 and dmpz = 3,5-dimethylpyrazolate. As a group these compounds differ from those previously studied in that they have bulky methyl substituents in the more sterically sensitive 3,5-positions. Otherwise they form an analogous series with H, Cl, Br, and CH_3 substituents in the 4-position.

The syntheses of the $[Cu(4\text{-}Xdmpz)_2]_x$ complexes presented some technical problems. While the 4-X = H compound could be obtained from the molten ligand–metal reaction employed earlier in the preparation of $[Cu(4\text{-}Hpz)_2]_x$ (1), this reaction led to impure products for the other 4-X complexes. This led to the development of a successful route to the required compounds via the copper(I) derivatives, $[Cu(4\text{-}Xdmpz)]_3$. Some characterization of these latter complexes is included in this report. Repeated attempts to obtain samples of the $[Cu(4\text{-}Xdmpz)_2]_x$ compounds in crystalline form suitable for single crystal X-ray diffraction studies were unsuccessful; consequently, it was necessary to resort to indirect methods to obtain structural information on these compounds.

Experimental

3,5-Dimethylpyrazole was purchased from Aldrich and used without further purification.

[1]Authors to whom correspondence may be addressed.

Can. J. Chem. Downloaded from www.nrcresearchpress.com by 92.62.229.171 on 09/08/12
For personal use only.

Can. J. Chem. Downloaded from www.nrcresearchpress.com by 92.62.229.171 on 09/08/12
For personal use only.

Syntheses

3,4,5-Trimethylpyrazole

The procedure of Chambers *et al.* was employed (3). ^{1}H NMR ($CDCl_3$ solution), δ: 1.85 (s, 3, CH_3), 2.15 (s, 6, CH_3), 10.45 (br s, 1, NH). Anal. calcd. for $C_6H_{10}N_2$: C 65.4, H 9.2, N 25.5; found: C 65.2, H 9.0, N 25.5.

4-Chloro-3,5-dimethylpyrazole

The method of Hüttel, Schäfer, and Welzel (4) for the synthesis of 4-chloropyrazole was adopted for use here. 3,5-Dimethylpyrazole (9.23 g, 0.0960 mol) was dissolved in 100 mL of water and glacial acetic acid (15 mL, 0.26 mol) was added to the solution. NaOCl (aq) (200 mL of 0.482 M, 0.0964 mol) was added to the solution and it was stirred at room temperature for 2 h. The mixture was then neutralized with Na_2CO_3 and made slightly basic with a few drops of concentrated ammonia (aq). The resulting mixture was cooled to 5°C and suction filtered. The collected solid was washed with cold water and dried under vacuum at room temperature for 4 h, yielding 10.9 g (87%) of 4-chloro-3,5-dimethylpyrazole. ^{1}H NMR ($CDCl_3$ solution), δ: 2.26 (s, 6, CH_3), 9.93 (br s, 1, NH). Anal. calcd. for $C_5H_7ClN_2$: C 46.0, H 5.4, N 21.4; found: C 45.8, H 5.3, N 21.5.

4-Bromo-3,5-dimethylpyrazole

3,5-Dimethylpyrazole (9.6 g, 0.10 mol) was dissolved in 300 mL of water. Bromine (5.2 mL, 0.10 mol) was added to the solution dropwise, with stirring; the bromine decolourized almost immediately and a small amount of pale yellow oil separated. The resulting mixture was neutralized with concentrated NaOH (aq) and then allowed to settle. The aqueous supernatant was cooled to 5°C overnight and a white solid that precipitated was collected by suction filtration, washed with cold water, and air-dried. The oily component was dried under vacuum, yielding a tan coloured solid. Both solid fractions were combined, recrystallized from toluene, suction filtered, washed with ice-cold petroleum ether, and dried under vacuum at room temperature, yielding 11.2 g (64%) of 4-bromo-3,5-dimethylpyrazole as a white solid. ^{1}H NMR ($CDCl_3$ solution), δ: 2.21 (s, 6, CH_3), 11.2 (br s, 1, NH). Anal. calcd. for $C_5H_7BrN_2$: C 34.3, H 4.0, N 16.0; found: C 34.6, H 4.1, N 16.3.

4-Iodo-3,5-dimethylpyrazole

A variation of the method of Morgan and Ackerman was employed (5). 3,5-Dimethylpyrazole (9.0 g, 0.094 mol) and Na_2CO_3 (0.53 g, 0.050 mol) were dissolved in 500 mL of water and the solution was heated to reflux with stirring. To this solution was added dropwise a solution of KI (31.0 g, 0.186 mol) and I_2 (23.0 g, 0.0905 mol) dissolved in 80 mL of water. When addition of the KI_3 solution was complete, the reaction was cooled to 5°C and left overnight. The precipitate was suction filtered and washed with 300 mL of ice-cold water. The filtercake was dissolved in 200 mL of CH_2Cl_2 and extracted with an equal volume of a dilute aqueous solution of Na_2CO_3 to remove any remaining HI. The CH_2Cl_2 phase was collected, flash evaporated, and dried at room temperature under vacuum for 5 h, yielding 19.0 g (94%) of 4-iodo-3,5-dimethylpyrazole as a white solid. ^{1}H NMR ($CDCl_3$ solution), δ: 2.23 (s, 6, CH_3), 11.65 (br s, 1, NH). Anal. calcd. for $C_5H_7IN_2$: C 27.0, H 3.2, N 12.6; found: C 27.1, H 3.2, N 12.6.

[(Cu(tmpz)]$_3$

This was the first of the Cu(I) pyrazolates prepared in this study and, at the time, it was not recognised that these compounds are air-sensitive when in contact with solvents. $[Cu(tmpz)]_3$, unlike the other compounds in this series, was prepared in air, so the yield of this compound is lower than those for the other copper(I) pyrazolates described here. A variation of the method of Ardizzoia *et al.* was employed (6). Cuprous iodide (1.90 g, 10.0 mmol) was dissolved in 70 mL of acetonitrile. To this was added a solution of 3,4,5-trimethylpyrazole (2.20 g, 20.0 mmol) dissolved in 60 mL of acetone. Within a few minutes the solution had turned brown. Triethylamine (2.8 mL, 20 mmol) was added to the solution and a white solid immediately precipitated. The mixture was allowed to stir for 1 h and then suction filtered, resulting in a white filtercake and green filtrate. The filtercake was washed with acetone and petroleum ether and dried in air at 110°C for 15 min, yielding 1.13 g (66%) of $[Cu(tmpz)]_3$ as a white powder. Anal. calcd. for $C_{18}H_{27}Cu_3N_6$: C 41.7, H 5.2, N 16.2; found: C 41.3, H 5.2, N 16.0.

The preparation of X-ray diffraction quality single crystals of $[Cu(tmpz)]_3$ is described elsewhere (7).

[Cu(4-Xdmpz)]$_3$(where X = H, Cl, Br, I)

These compounds were prepared as white solids in high yields by similar routes. The method is given in detail for the X = Cl compound. Cuprous iodide (1.90 g, 10.0 mmol) was dissolved in 80 mL of deoxygenated acetonitrile under a dinitrogen atmosphere. 4-Chloro-3,5-dimethylpyrazole (1.30 g, 10.0 mmol) was added to the solution and a flocculent white precipitate formed immediately. More white precipitate formed upon addition of triethylamine (1.6 mL, 11 mmol). The mixture was stirred for 2 h, suction filtered, and the filtercake washed with acetonitrile and acetone. The filtercake was dried for 30 min at 110°C in air, yielding 1.81 g (94%) of $[Cu(4\text{-}Cldmpz)]_3$ as a white solid. Anal. calcd. for $C_{15}H_{18}Cl_3Cu_3N_6$: C 31.1, H 3.1, N 14.5; found: C 31.1, H 3.2, N 14.4. Anal. calcd. for $C_{15}H_{18}Br_3Cu_3N_6$: C 25.3, H 2.5, N 11.8; found: C 25.1, H 2.5, N 11.8. Anal. calcd. for $C_{15}H_{18}Cu_3I_3N_6$: C 21.1, H 2.1, N 9.8; found: C 21.3, H 2.2, N 9.7. Anal. calcd. for $C_{15}H_{21}Cu_3N_6$: C 37.8, H 4.4, N 17.6; found: C 38.0, H 4.4, N 17.8.

[Cu(4-Hdmpz)$_2$]$_x$

$[Cu(4\text{-}Hdmpz)_2]_x$ was synthesized via two different routes. The first employed the molten ligand–metal reaction described previously (1). Copper metal shot (3.15 g, 49.6 mmol), washed with 12 M HCl, water, acetone, and dried, and 3,5-dimethylpyrazole (11.0 g, 114 mmol) were combined in a small reaction vessel and heated in air at 115°C, with stirring, for 4 days. The mixture was then cooled to room temperature and extracted from the flask with CH_2Cl_2. The mixture was then suction filtered and the filtercake was washed with petroleum ether, and dried in air at 110°C for 4 h. This yielded approximately 0.5 g of $[Cu(4\text{-}Hdmpz)_2]_x$ as a reddish-brown powder. Anal. calcd. for $C_{10}H_{14}CuN_4$: Cu 25.0, C 47.3, H 5.6, N 22.1; found: Cu 25.2, C 47.1, H 5.4, N 22.3.

In the second method $[Cu(4\text{-}Hdmpz)]_3$ (0.319 g, 2.01 mmol Cu(I)) and 3,5-dimethylpyrazole (1.92 g, 20.0 mmol) were combined in a small vessel and heated under a dioxygen atmosphere at 124°C for 3 h (reaction was probably complete after 1 h). The mixture was then cooled to room temperature and extracted with dry tetrahydrofuran (THF) and suction filtered. The filtercake was washed with more THF and dried in a desiccator at room temperature. This yielded 0.509 g (99%) of $[Cu(4\text{-}Hdmpz)_2]_x$. Anal. calcd. for $C_{10}H_{14}CuN_4$: C 47.3, H 5.6, N 22.1; found: C 47.3, H 5.6, N 22.2.

[Cu(tmpz)$_2$]$_x$ and [Cu(4-Xdmpz)$_2$]$_x$ (where X = Cl, Br)

These compounds were prepared as brown solids (dark brown for X = Br) by similar routes. The method, which gave high yields in all cases, is described in detail for $[Cu(tmpz)_2]_x$. $[Cu(tmpz)]_3$ (0.345 g, 2.00 mmol) and 3,4,5-trimethylpyrazole (1.76 g, 16.0 mmol) were combined in a small vessel and the mixture was heated to 140°C, with stirring, under a dioxygen atmosphere for 2 h and then cooled to room temperature and dried under vacuum for 10 h. The mixture was extracted from the flask under dinitrogen with dry, deoxygenated, THF and then suction filtered under dinitrogen, the filtercake washed with THF, and dried at room temperature under vacuum for 5 h. This yielded 0.540 g (96%) of $[Cu(tmpz)_2]_x$ as a brown powder. Anal. calcd. for $C_{12}H_{18}CuN_4$: Cu 22.5, C 51.1, H 6.4, N 19.9; found: Cu 22.5, C 51.0, H 6.4, N 20.1. Anal. calcd. for $C_{10}H_{12}Cl_2CuN_4$: Cu 19.7, C 37.2, H 3.8, N 17.4; found: Cu 19.7, C 37.2, H 3.7, N 17.4. Anal. calcd. for $C_{10}H_{12}Br_2CuN_4$: Cu 15.4, C 29.2, H 2.9, N 13.6; found: Cu 15.5, C 29.3, H 3.0, N 13.7.

Can. J. Chem. Downloaded from www.nrcresearchpress.com by 92.62.229.171 on 09/08/12
For personal use only.

Attempted preparation of $[Cu(4\text{-}Idmpz)_2]_x$

Attempts to prepare $[Cu(4\text{-}Idmpz)_2]_x$ from the corresponding copper(I) complex were unsuccessful. The temperature and prolonged reaction time required caused significant decomposition of the molten ligand, liberating I_2 (this was visible as purple vapour above the reaction mixture). Presumably, liberated iodide caused partial reduction of the copper(II) formed, preventing the formation of pure product.

Physical characterization

^1H NMR spectra were recorded using a Bruker AC-200 FT-NMR spectrometer equipped with a Bruker B-ACS 120 sample exchanger. Residual $CHCl_3$ in the $CDCl_3$ solvent was used as the internal standard for calibration.

Differential scanning calorimetry (DSC) measurements were made with a Mettler DSC 20 standard cell and TC 10 TA processor as described previously (8).

X-Ray powder diffractograms were collected with a Rigaku Rotaflex RU-200BH rotating anode X-ray powder diffractometer (nickel-filtered or graphite monochromated Cu-K_α radiation). Diffractograms for the copper(II) pyrazolates have been deposited.[2]

Scanning electron micrographs of samples were recorded with a Hitachi S-570 scanning electron microscope. Samples were prepared by applying a thin suspension of the sample in ethanol or petroleum ether to a stainless steel stub, allowing the suspension to dry, and then sputter coating the stub with a thin layer of gold.

Mass spectra were recorded using a Kratos MS 50 mass spectrometer employing the electron impact ionization technique.

Infrared spectra (250–4000 cm^{-1}) were obtained using a Perkin–Elmer model 598 spectrometer. The samples were mulled in hexachlorobutadiene and sandwiched between KRS-5 plates (Harshaw Chemical Co.) and (or) mulled in Nujol and sandwiched between KBr plates.

Electronic spectra (200–2500 nm) were recorded using a Cary 5 UV/visible/NIR spectrophotometer. Samples were mulled in Nujol and pressed between quartz plates.

EPR spectra were recorded using an X-band homodyne spectrometer, which was described previously (2). Samples were measured as polycrystalline powders placed in sealed quartz tubes and measurements were performed at ~90 K.

Magnetic susceptibilities were measured over the temperature range 2–300 K using a Quantum Design (MPMS) SQUID magnetometer (field = 10 kOe). Temperature measurement with this instrument was achieved using a combination of Ge and Pt resistance thermometers. Susceptibility calibration was performed using high purity Ni and Bi standards. The samples were packed as powders into a specially constructed sample holder made from polyvinylchloride (PVC). The sample holder possessed a constant cross-sectional area, thus minimizing its contribution to the SQUID signal. Magnetic susceptibilities were corrected for diamagnetism: copper, −11; $C_5H_7N_2$, −62; $C_6H_9N_2$, −74; $C_5H_6ClN_2$, −76; $C_5H_6BrN_2$, −87 (values in 10^{-6} cm^3 mol^{-1}). A correction of 60×10^{-6} cm^3 mol^{-1} was applied for temperature-independent paramagnetism of the copper(II) ion.

C, H, and N analyses were performed by P. Borda of this department. Cu analyses were performed using iodometric titration.

Results and discussion

Copper(I) complexes, $[Cu(4\text{-}Xdmpz)]_3$

The failure of the molten ligand–metal reaction to yield pure copper(II) complexes of the type $[Cu(4\text{-}Xdmpz)_2]_x$, where X = Cl, Br, and CH_3, led to the development of a clean route to these compounds employing the corresponding copper(I) analogues. These latter complexes may be obtained by the reaction of CuI with the appropriate pyrazole in acetonitrile. The method follows that described by Ardizzoia *et al.* for the synthesis of $[Cu(4\text{-}Hdmpz)]_3$ (6). These compounds are insoluble (or at best, sparingly soluble) in common organic solvents. They are colourless solids and are stable towards O_2 when dry; however, in water-containing solvents they are oxidized to yellow-green soluble species. Ardizzoia *et al.* characterized a cyclic, octameric, copper(II) complex bridged by 4-Hdmpz and hydroxide as the aerial oxidation product of $[Cu(4\text{-}Hdmpz)]_3$ in wet CH_2Cl_2, pyridine, or nitrobenzene (9).

Prior to our recent X-ray diffraction study of $[Cu(4\text{-}Hdmpz)]_3$, which showed a trimeric ring structure (10), the copper(I) pyrazolates were thought to be polymeric (11). We more recently determined by single crystal X-ray diffraction methods that $[Cu(4\text{-}CH_3dmpz)]_3$ also has a trimeric ring structure (7). We conclude that all of the copper(I) pyrazolates prepared in this study have a trimeric structure similar to those mentioned above. In support of this, all of the copper(I) compounds studied here exhibit electron impact mass spectra in which the most intense peak is that due to the molecular ion expected for the trimer. The isotopic patterns are in excellent agreement with those predicted. Further support for the conclusion that the compounds are trimeric comes from the observation that, with the exception of the compound hexakis(μ-3,5-diphenylpyrazolato-*N*,*N*′)hexagold(I) (12), all other structurally characterized univalent coinage metal pyrazolates are trimers (12–14). The copper(I) compounds are all thermally robust. The X = CH_3 compound melts at 308°C and thermally decomposes at 365°C. The X = Cl, Br, and I compounds decompose, without melting, at 350°C, 300°C, and 300°C respectively.

Copper(II) compounds, $[Cu(4\text{-}Xdmpz)_2]_x$: structural studies

Powder X-ray diffractograms of the copper(II) 4-Xdmpz derivatives have been deposited.[2] They indicate that the compounds are crystalline; however, attempts to obtain single crystals were unsuccessful. Nonetheless, based on indirect evidence and comparisons with the structurally characterized $[Cu(4\text{-}Xpz)_2]_x$ complexes (1, 2) we conclude that the compounds are polymeric. The empirical formulae of the 4-Xdmpz compounds do not support monomeric species, unless one assumes either the unlikely coordination number of two for copper(II) or the equally unlikely formation of three-membered chelate rings. Polymeric structures for the compounds are supported by their lack of solubility in a wide range of polar and nonpolar common organic solvents. The X = CH_3, Cl, and Br compounds dissolve with decomposition in water and wet solvents, yielding green soluble species and small amounts of greyish-green insoluble species. The soluble hydrolysis products do not crystallize, but form amorphous films upon drying. These films have not been characterized further. The X = H compound is stable towards water and water-containing organic solvents. Structurally characterized binary copper(II) pyrazolates have extended chain structures and scanning electron micrographs of the 4-Xdmpz complexes studied here show their microcrystals to be long fibres, consistent with such a structure. A scanning electron micrograph of $[Cu(4\text{-}Hdmpz)_2]_x$ is shown in Fig. 1. Furthermore, the similarity in the thermal properties of the compounds studied here and those of the structurally characterized analogues is consis-

[2]Supplementary material mentioned in the text may be purchased from the Depository of Unpublished Data, Document Delivery, CISTI, National Research Council Canada, Ottawa, Canada, K1A 0S2.

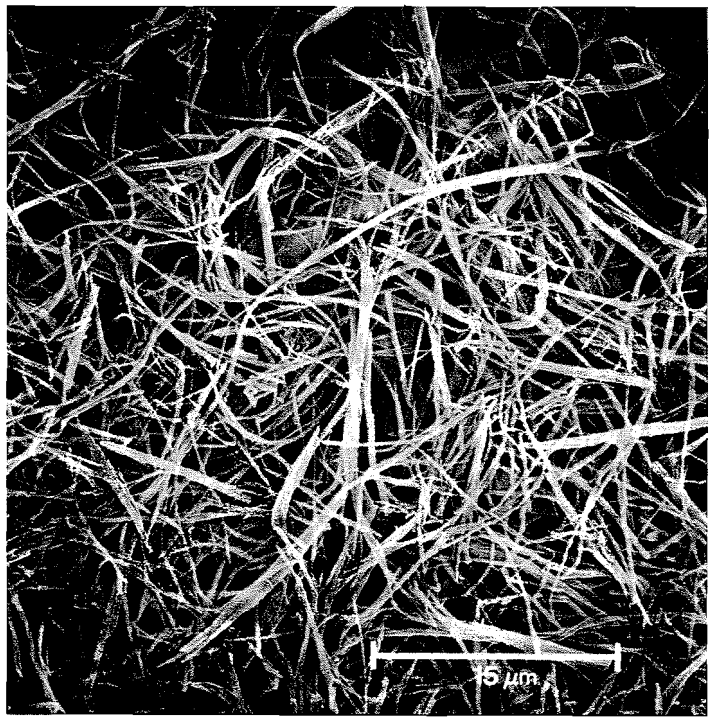

FIG. 1. Scanning electron micrograph of $[Cu(4\text{-}Hdmpz)_2]_x$.

Can. J. Chem. Downloaded from www.nrcresearchpress.com by 92.62.229.171 on 09/08/12
For personal use only.

tent with similar structures. DSC studies show the 4-Xdmpz complexes decompose without melting at 245°C, 233°C, 245°C, and 245°C for the X = H, CH_3, Cl, and Br derivatives. The 4-Xpz compounds also decompose without melting, albeit at 25–45°C higher in temperature. Finally, as discussed in the next section, the magnetic properties of the 4-Xdmpz complexes have been successfully analysed, employing models for magnetically coupled linear chains as reported previously for the 4-Xpz analogues. We conclude that the complexes under investigation here most likely have structures involving extended chains of copper ions linked by double pyrazolate bridges as seen in the single crystal X-ray determined structures of the complexes $[Cu(4\text{-}Xpz)_2]_x$, where X = H, CH_3, and Cl (1, 2). While the presence of sterically hindering methyl groups in the $[Cu(4\text{-}Xdmpz)_2]_x$ complexes does not appear to prevent the formation of extended chain polymers, spectroscopic evidence to be presented next indicates they do have an effect on the geometry of the CuN_4 chromophore.

The 4-Xdmpz complexes are reddish-brown to dark brown in colour; their UV–visible–NIR spectra are shown in Fig. 2. In the visible region, two band maxima are observed for each of the compounds as follows: X = H, 19 000 and 23 100 cm^{-1} (sh); X = CH_3, 18 300 and 21 700 cm^{-1} (sh); X = Cl, 17 800 (sh) and 20 700 cm^{-1}; X = Br, 19 000 (sh) and 21 700 cm^{-1}. In addition, all four compounds show the presence of strong bands in the UV region, presumably charge transfer in origin (Fig. 2), as well as a weak band in the NIR region at 10 500 cm^{-1}. The bands in the visible region, which likely arise from *d–d* transitions, are at significantly higher energies than the corresponding bands reported previously for the analogous $[Cu(4\text{-}Xpz)_2]_x$ compounds. These latter compounds have compressed tetrahedral CuN_4 chromophores and *d–d* bands centred around 15 500 cm^{-1} (2). According to Hathaway (15), complexes with CuN_4

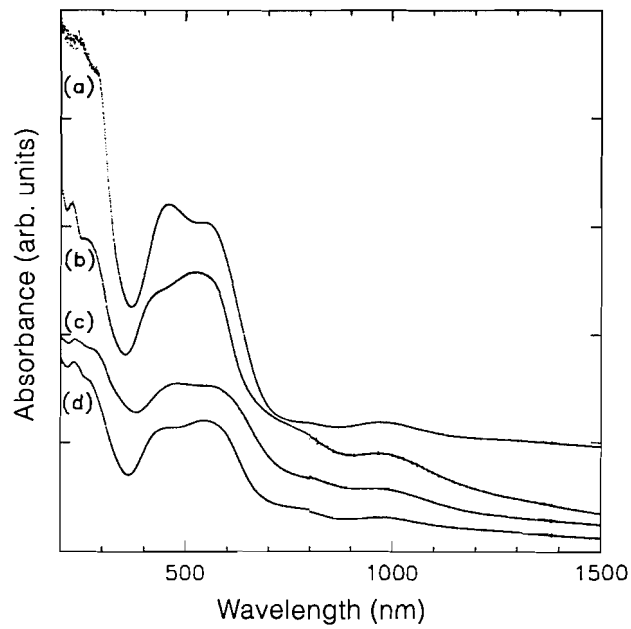

FIG. 2. Electronic spectra for the $[Cu(4\text{-}Xdmpz)_2]_x$ compounds: (*a*) X = Br, (*b*) X = H, (*c*) X = Cl, (*d*) X = CH_3.

chromophores that exhibit *d–d* bands in the 18 000–20 000 cm^{-1} region, as observed in the present study, are likely to have square-coplanar stereochemistries. This spectroscopic criterion of stereochemistry has previously been successfully applied to pyrazolate complexes (16). The mononuclear complexes $[Me_2Ga(4\text{-}Hdmpz)_2]_2Cu$ and $[Me_2Ga(4\text{-}Hpz)_2]_2Cu$ have CuN_4 chromophores with compressed tetrahedral coordination in the former and square-coplanar coordination in the latter (17). The former complex exhibits *d–d* bands at 9 400 cm^{-1} and 12 000 cm^{-1} (sh) while the

corresponding bands in the latter complex are in the 17 000–20 000 cm^{-1} region (16).

Steric crowding involving the methyl substituents in the 3- and 5-positions of the pyrazolate ring may be alleviated in the chain polymer either by a distortion of the $[Cu(4\text{-}Hpz)_2]_x$ structure (1) towards a more regular tetrahedral CuN_4 chromophore or, alternatively, by adopting a polymeric structure like that shown in **1**, which is based on the structures of $[(ON)Ni(4\text{-}Hdmpz)_2]_2Ni$ and $[(C_3H_5)Ni(4\text{-}Hdmpz)_2]_2Ni$ (18, 19) in which the central Ni ions possess square-planar coordination. The spectroscopic evidence presented above supports a structure of the type shown in **1** for the $[Cu(4\text{-}Xdmpz)_2]_x$ compounds.

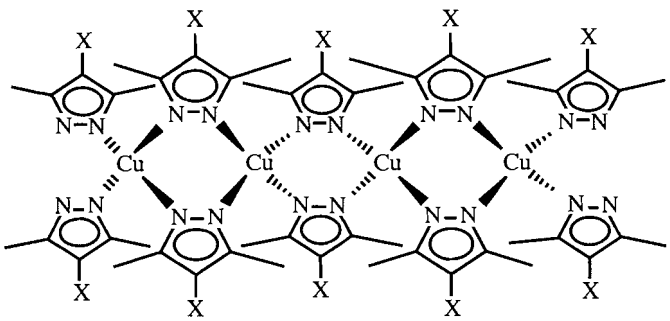

1

To further study the geometries of the CuN_4 chromophores in these complexes we examined their powder EPR spectra at 90 K. As reported previously (2), all of the $[Cu(4\text{-}Xpz)_2]_x$ complexes, except one, exhibit two g-value spectra at ~90 K with $g_\parallel$ values in the range 2.22–2.24 and $g_\perp$ values of ~2.08. The brown form of the X = Cl compound exhibited an isotropic spectrum with $g_0 = 2.084$. The $[Cu(4\text{-}Xdmpz)_2]_x$ complexes, on the other hand, give broad, asymmetric, single resonance lines that lack the features necessary for the determination of g-values directly from the spectra. There appears to be less exchange narrowing here, in comparison to the $[Cu(4\text{-}Xpz)_2]_x$ analogues, due to weaker antiferromagnetic coupling (discussed below). Although these powder EPR spectra do not permit an unequivocal assignment of the CuN_4 chromophore geometry, the fact that they are significantly different from those of the $[Cu(4\text{-}Xpz)_2]_x$ compounds (2) is not inconsistent with a change in chromophore geometry.

Infrared spectra were recorded for all the complexes, primarily as a preliminary test of product purity. In the 4-H, 4-CH_3, 4-Cl, and 4-Brdimethylpyrazolates, a sharp band observed between 700 and 800 cm^{-1} in the copper(I) compounds shifts 10–15 cm^{-1} lower in energy in the corresponding copper(II) compounds. This band was used as a check of whether conversion of the copper(I) to copper(II) compound was complete in the synthesis of the latter. No other particularly useful structural information was obtainable from the infrared spectra. Tabulated band frequencies have been deposited.[2]

$[Cu(4\text{-}Xdmpz)_2]_x$ compounds: magnetic susceptibilities

Magnetic susceptibilities of the four $[Cu(4\text{-}Xdmpz)_2]_x$ compounds were measured from 2.0 to 300 K employing a SQUID magnetometer. Tabulated magnetic susceptibility data for the $[Cu(4\text{-}Xdmpz)_2]_x$ compounds are deposited[2] and plots of χ_M versus temperature are shown in Fig. 3 for $[Cu(4\text{-}Hdmpz)_2]_x$ and $[Cu(4\text{-}Cldmpz)_2]_x$. All four compounds exhibit maxima in their susceptibility versus temperature plots (in the range 105–120 K) indicative of antiferromagnetic exchange coupling. In all cases an increase in susceptibility is observed as the temperature decreases at the lowest temperatures studied. This is not uncommon in strongly antiferromagnetically coupled copper(II) systems and was observed previously for the $[Cu(4\text{-}Xpz)_2]_x$ compounds where it was ascribed to the presence of small amounts of paramagnetic impurities (1, 2). In analysing the magnetic data we employed the isotropic Heisenberg model for exchange coupled linear chains developed by Hall and Estes *et al.* (20, 21). In addition, as in our previous work (1, 2), allowance was made for the paramagnetic impurity by modelling it as a Curie paramagnet with a g-value equal to that of the bulk sample. The expressions used in the fitting procedure are presented below and the symbols have their usual meanings (22). Reasonable fits between experimental data and theory were obtained for the X = H, CH_3, and Br compounds and best-fit

$$\chi_{chain} = \frac{Ng^2\mu_B^2}{kT} \times \left[\frac{0.25 + 0.14995\,x^{-1} + 0.30094\,x^{-2}}{1 + 1.9862\,x^{-1} + 0.68854\,x^{-2} + 6.0626\,x^{-3}}\right]$$

where

$$x = kT/|J|$$

$$\chi_{para} = \frac{Ng^2\mu_B^2 S(S+1)}{3kT}$$

$$\chi = [1 - P]\chi_{chain} + P\chi_{para}$$

values of the J, g, and percent paramagnetic impurity parameters are given for these in Table 1. Better agreement between experiment and theory, particularly in the region of the susceptibility maximum, is obtained when only data at and above 40 K are used in the fitting procedure. Values of J and g obtained from these high-temperature data fits are also given in Table 1. The paramagnetic impurity contributes more to the low-temperature data and the improvement in fit on using the high-temperature data probably reflects inadequacies in modelling the paramagnetic component as was discussed previously (1, 2). Pursuing this further, we examined fits of the experimental susceptibilities for the X = H, CH_3, and Br compounds to theory over the whole temperature range, modelling the paramagnetic component as a Curie–Weiss paramagnet. This adds a fourth parameter, θ,

$$\chi_{para} = \frac{Ng^2\mu_B^2 S(S+1)}{3k(T-\theta)}$$

to the fitting procedure and produces an excellent fit over the entire temperature range studied. The J and g-values obtained with this model agree well with those obtained using fits to the high temperature data only (Table 1).

$[Cu(4\text{-}Cldmpz)_2]_x$ exhibits somewhat unique magnetic properties. Above 40 K it behaves much like the other complexes studied here, exhibiting a broad maximum in its susceptibility versus temperature plot at 120 K. The magnetic data above 40 K are reasonably well modelled according to the isotropic Heisenberg model for exchange coupled linear chains and the best-fit values of J and g obtained using this

Can. J. Chem. Downloaded from www.nrcresearchpress.com by 92.62.229.171 on 09/08/12
For personal use only.

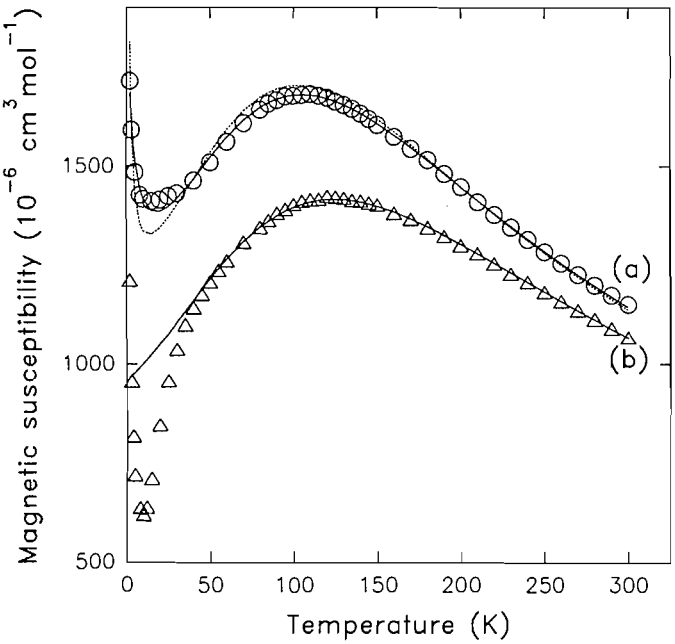

FIG. 3. Plot of magnetic susceptibility versus temperature for (*a*) $[Cu(4\text{-}Hdmpz)_2]_x$ and (*b*) $[Cu(4\text{-}Cldmpz)_2]_x$. The broken curve for (*a*) represents the best fit to theory with a Curie paramagnetic component and the solid curve represents the best fit to theory with a Curie–Weiss paramagnetic component. The solid curve in (*b*) represents the best fit of the data to theory from 40 to 300 K.

model and ignoring paramagnetic impurity are comparable to the values obtained for the other 4-Xdmpz compounds (Table 1). Below 40 K, however, the susceptibility drops abruptly until about 8 K, below which the effects of paramagnetic impurity are seen. The magnetic properties for this compound cannot be modelled well below 40 K using the linear chain model with or without paramagnetic impurity. The abrupt decrease in susceptibility below 40 K is behaviour similar to that observed for $CuSb_2O_6$ (23), which possesses the trirutile structure and behaves magnetically as a linear chain antiferromagnet above 9 K. Nakua *et al.* attributed the rapid decrease in susceptibility below 9 K in $CuSb_2O_6$ as a transition to long-range antiferromagnetic order. One of the pieces of evidence they used to support this conclusion was an examination of the field dependence of $CuSb_2O_6$. Nakua *et al.* found that the magnetization of the compound at 2 K (below T_c) over the applied field range 0–30 kOe exhibited two linear regimes with a transition region between. This behaviour is characteristic of a spin flop transition in polycrystalline antiferromagnets. At 11 K (above T_c) they found the magnetization to be completely linear over the same field range, which is characteristic of the paramagnetic state.

Noting the similarity between the temperature dependence of the susceptibility of $CuSb_2O_6$ and $[Cu(4\text{-}Cldpmz)_2]_x$, we undertook a study of the magnetic field dependence of $[Cu(4\text{-}Cldmpz)_2]_x$. The compound's applied field dependence was examined in the range 0–55 kOe at 5, 10, 15, and 20 K. The results of this study are depicted in Fig. 4. It is apparent that the magnetization data for $[Cu(4\text{-}Cldmpz)_2]_x$ do not exhibit the spin flop transition evident in the data for $CuSb_2O_6$. The magnetization plots at 10 K and especially 5 K for $[Cu(4\text{-}Cldmpz)_2]_x$ show some deviation from linearity at the highest fields. This is most likely due to magnetic saturation effects as the Brillouin function η value at 5 K and 55 kOe is 1.65 for this compound. Even though $[Cu(4\text{-}Cldmpz)_2]_x$ does not exhibit field dependence indicative of a spin flop transition in the range studied, this does not rule out the possibility of such a transition occurring in the compound. The molecular field theory (24) description of spin flop in antiferromagnets predicts that the transition field, H_{SF}, at $T = 0$ K is dependent on both the anisotropy field and the antiferromagnetic exchange energy. If the anisotropy fields for $CuSb_2O_6$ and $[Cu(4\text{-}Cldmpz)_2]_x$ are similar, then the H_{SF} would be expected to be greater for the compound with the larger antiferromagnetic exchange. $[Cu(4\text{-}Cldmpz)_2]_x$ ex-

TABLE 1. Derived magnetic parameters for the $[Cu(4\text{-}Xdmpz)_2]_x$ compounds

Compound	Temperature range (K)	$-J$ (cm^{-1})	g	$100P$	$-\theta$ (K)	F^a
X = H	2–300	56(1)[b]	2.22(2)	0.28(1)	—	0.023
	2–300	58(1)	2.24(2)	0.75(6)	4.4(4)	0.0078
	40–300	58(1)	2.24(1)	0.55(4)	—	0.0018
X = CH_3	2–300	61(1)	2.26(2)	0.31(1)	—	0.012
	2–300	61(1)	2.26(2)	0.33(2)	0.1(2)	0.012
	40–300	60(1)	2.25(2)	0[c]	—	0.0040
X = Cl	40–300	67(1)	2.24(1)	0[c]	—	0.0048
X = Br	2–300	65(1)	2.21(2)	0.50(2)	—	0.014
	2–300	66(1)	2.22(2)	0.65(2)	0.9(1)	0.0072
	40–300	67(1)	2.22(1)	0.67(4)	—	0.0023

[a] The fitting function:

$$F = \left[\frac{1}{n}\sum_{i=1}^{n}\frac{(\chi_i^{obs} - \chi_i^{calc})^2}{(\chi_i^{obs})^2}\right]^{1/2}$$

[b] Numbers in parentheses are the estimated standard deviations in the last digit of the value.

[c] $100P$ set at zero. Measured susceptibilities at the lower temperatures are slightly lower than predicted by the model and including P as a variable parameter here generates small, unrealistic, negative values.

Can. J. Chem. Downloaded from www.nrcresearchpress.com by 92.62.229.171 on 09/08/12
For personal use only.

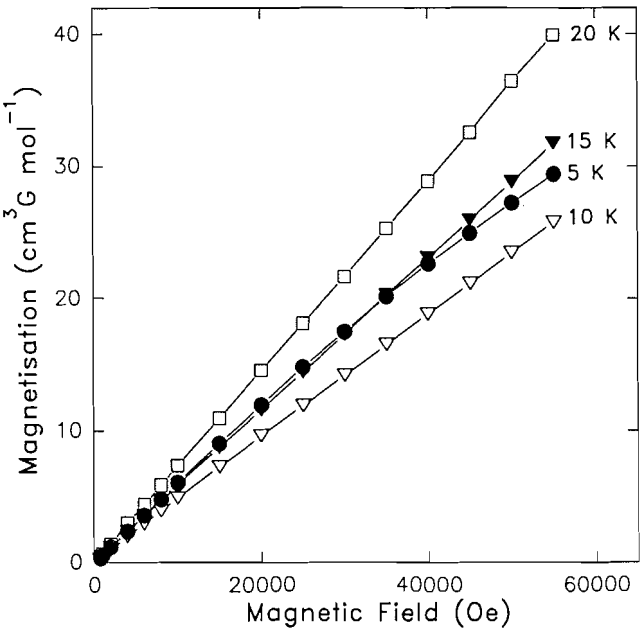

FIG. 4. Magnetization vs. applied magnetic field plot at various temperatures for $[Cu(4\text{-}Cldmpz)_2]_x$. The solid lines are merely a guide to the eye.

hibits its anomalous decrease in susceptibility for an antiferromagnetically coupled linear chain in the range 30–40 K, whereas $CuSb_2O_6$ exhibits this feature between 8 and 9 K. This would imply that if long-range antiferromagnetic ordering is occurring in $[Cu(4\text{-}Cldmpz)_2]_x$, then the magnitude of the interaction is much larger in this compound than in $CuSb_2O_6$ and, as discussed above, one would expect H_{SF} to be higher in the former compound than in the latter, perhaps beyond our experimentally accessible field range.

Our field-dependence studies do not preclude the possibility of long-range order accounting for the unusual susceptibility data for $[Cu(4\text{-}Cldmpz)_2]_x$, but neither do they support such a conclusion. Other possibilities that might account for the behaviour of this compound are a transition to two-dimensional ordering or a structural phase transition that facilitates much stronger one-dimensional antiferromagnetic exchange.

Turning now to a consideration of the magnitude of the exchange coupling in these $[Cu(4\text{-}Xdmpz)_2]_x$ complexes, some interesting comparisons can be made with the $[Cu(4\text{-}Xpz)_2]_x$ analogues. We note that in both sets of compounds the $|J|$ values for the 4-Cl and 4-Br derivatives are the same within experimental uncertainty and are slightly, but significantly, greater than the values for the 4-H and 4-CH_3 derivatives. This variation does not correlate with simple ideas based on relative ligand basicities since the halo-substituted pyrazolates should be expected to be the least basic, form the weakest bonds to copper, and therefore provide the poorest, rather than the most efficient, pathways for exchange. As discussed previously (2), the exchange in these systems appears to be affected more by detailed structural differences between compounds that affect the overlap between the pyrazolate π-orbital system and the metal's magnetic orbital. The effects of structural differences on the magnitude of exchange can be seen by comparing the $|J|$ values of the $[Cu(4\text{-}Xpz)_2]_x$ compounds as a group with the $|J|$ values of the $[Cu(4\text{-}Xdmpz)_2]_x$ compounds. Although all of the compounds under consideration are considered to have extended chain structures, the geometry of the CuN_4 chromophore in the former group is compressed tetrahedral while, as discussed above, the geometry of the chromophore in the latter group is almost certainly different and likely square planar. This basic structural difference probably accounts for the fact that the $[Cu(4\text{-}Xpz)_2]_x$ complexes exhibit $|J|$ values (range 81–105 cm^{-1}) that are consistently higher than those of the $[Cu(4\text{-}Xdmpz)_2]_x$ complexes (range 58–67 cm^{-1}).

Clearly, a better understanding of magneto-structural correlations in the $[Cu(4\text{-}Xdmpz)_2]_x$ complexes will require more detailed structural information. Thus far, we have been unable to obtain crystals large enough for single crystal X-ray diffraction studies. Their lack of solubility and the fact that the compounds decompose without melting have ruled out crystallization approaches. We have had some success in the past in obtaining suitable single crystals of $[Cu(4\text{-}Xpz)_2]_x$ complexes by altering the conditions of synthesis so as to obtain a very slow rate of polymer formation. Unfortunately, we have found that applying such conditions to the synthesis of 4-Xdmpz complexes leads to the decomposition of the pyrazolate ligand, specifically oxidation of the methyl substituents. Investigations of some of these reactions has led to the isolation and structural characterization of some new carboxyl-substituted pyrazolate complexes. These studies will be presented in a subsequent communication.

Acknowledgements

The Natural Sciences and Engineering Research Council of Canada is thanked for operating funds and for an equipment grant for the purchase of the Cary 5 spectrophotometer. We thank F. G. Herring and P. S. Phillips of this department for use of their EPR spectrophotometer and J. F. Carolan and W. N. Hardy, Department of Physics, U.B.C., for use of the SQUID magnetometer.

1. M. K. Ehlert, S. J. Rettig, A. Storr, R. C. Thompson, and J. Trotter. Can. J. Chem. **67**, 1970 (1989).
2. M. K. Ehlert, S. J. Rettig, A. Storr, R. C. Thompson, and J. Trotter. Can. J. Chem. **69**, 432 (1991).
3. D. Chambers, W. A. Denny, J. S. Buckleton, and G. R. Clark. J. Org. Chem. **50**, 4736 (1985).
4. R. Huttel, O. Schafer, and G. Welzel. Justus Liebigs Ann. Chem. **598**, 186 (1956).
5. G. T. Morgan and I. Ackerman. J. Chem. Soc. **123**, 1308 (1923).
6. G. Ardizzoia, G. La Monica, M. A. Angaroni, and F. Cariati. Inorg. Chim. Acta, **158**, 159 (1989).
7. M. K. Ehlert, S. J. Rettig, A. Storr, R. C. Thompson, and J. Trotter. Can. J. Chem. Accepted.
8. J. S. Haynes, K. W. Oliver, and R. C. Thompson. Can. J. Chem. **63**, 1111 (1985).
9. G. A. Ardizzoia, M. A. Angaroni, G. La Monica, F. Cariati, M. Moret, and N. Masciocchi. J. Chem. Soc. Chem. Commun. 1021 (1990).
10. M. K. Ehlert, S. J. Rettig, A. Storr, R. C. Thompson, and J. Trotter. Can. J. Chem. **68**, 1444 (1990).
11. C. B. Singh, S. Satpathy, and B. Sahoo. J. Inorg. Nucl. Chem. **35**, 3947 (1973).
12. H. H. Murray, R. G. Raptis, and J. P. Fackler, Jr. Inorg. Chem. **27**, 26 (1988).
13. R. G. Raptis and J. P. Fackler, Jr. Inorg. Chem. **27**, 4179 (1988).

Can. J. Chem. Downloaded from www.nrcresearchpress.com by 92.62.229.171 on 09/08/12
For personal use only.

14. B. Bovia, F. Bonati, and G. Banditelli. Inorg. Chem. Acta, **87**, 25 (1984).
15. B. J. Hathaway. J. Chem. Soc. Dalton Trans. 1196 (1972).
16. F. G. Herring, D. J. Patmore, and A. Storr. J. Chem. Soc. Dalton Trans. 711 (1975).
17. D. J. Patmore, D. F. Rendle, A. Storr, and J. Trotter. J. Chem. Soc. Dalton Trans. 718 (1975).
18. K. S. Chong, S. J. Rettig, A. Storr, and J. Trotter. Can. J. Chem. **57**, 3090 (1979).
19. K. S. Chong, S. J. Rettig, A. Storr, and J. Trotter. Can. J. Chem. **59**, 996 (1981).
20. J. W. Hall. Ph.D. Thesis, University of North Carolina. 1977.
21. W. E. Estes, W. E. Hatfield, J. A. C. van Ooijen, and J. Reedijk. J. Chem. Soc. Dalton Trans. 2121 (1980).
22. W. E. Hatfield, W. E. Estes, W. E. Marsh, M. W. Pickens, L. W. ter Haar, and R. W. Weller. *In* Extended linear chain compounds. Vol. 3. *Edited by* J. S. Miller. Plenum Press, New York. 1983. Chap. 2.
23. A. Nakua, H. Yun, J. N. Reimers, J. E. Greedan, and C. V. Stager. J. Solid State Chem. **91**, 105 (1991).
24. L. J. de Jongh and A. R. Miedema. Adv. Phys. **23**, 1 (1974).

Can. J. Chem. Downloaded from www.nrcresearchpress.com by 92.62.229.171 on 09/08/12
For personal use only.

Flame photometric detection of some transition metals. I. Calibrations and spectra[1]

XUN-YUN SUN, BRIAN MILLIER, AND WALTER A. AUE[2]
Department of Chemistry, Dalhousie University, Halifax, N.S., Canada B3H 4J3

Received May 10, 1991[3]

XUN-YUN SUN, BRIAN MILLIER, and WALTER A. AUE. Can. J. Chem. **70**, 1129 (1992).

After gas-chromatographic separation as volatile organometallics, some transition elements were found to respond with analytically relevant sensitivities in the flame photometric detector. Their minimum detectable amounts, in mole of metal per second at an $S/N_{p\text{-}t\text{-}p}$ ratio of 2, were 1×10^{-14} for nickel and 6×10^{-13} for rhenium, as well as a less sensitive 2×10^{-12} for molybdenum and 3×10^{-12} for cobalt. (When divided by 3.7, these values yield the $S/\sigma = 3$ limit of detection as recommended by IUPAC.) Calibration curves were established for these elements in comparison with transition metals already known to respond in the flame photometric detector. Their chemiluminescent spectra, together with that of chromium, were measured in the detector at analytically (as opposed to spectroscopically) optimized conditions. Atomic lines, molecular bands, and continua were all present. Also, the spectra produced by several types of carbon compounds were recorded for a definition of potential spectral interferences from hydrocarbonaceous sample matrices. The atomic lines and the massive continua displayed by certain metals are discussed in some detail. Atomic lines appear up to a limiting energy level of 3.6 eV above ground state. It is suggested that continua could arise from small, perhaps catalytically active particles. Also discussed, in accordance with a reviewer's request, are the analytical performance of the FPD compared to ICP and MIP sources, and the definition and influence of noise on measured performance criteria.

XUN-YUN SUN, BRIAN MILLIER et WALTER A. AUE. Can. J. Chem. **70**, 1129 (1992).

On a trouvé que certains éléments de transition, séparés par chromatographie gazeuse sous le forme d'organométalliques volatils, peuvent répondre avec des sensibilités analytiquement acceptables dans un détecteur photométrique à flamme. Les quantités minimales détectables, en mole de métal par seconde, à un rapport de $S/N_{p\text{-}t\text{-}p}$ de 2, sont de 1×10^{-14} pour le nickel et de 6×10^{-13} pour le rhénium alors que des sensibilités plus faibles de 2×10^{-12} et 3×10^{-12} ont été déterminées respectivement pour le molybdène et le cobalt. (Lorsqu'on divise ces valeurs par 7, on obtient la limite de détection $S/\sigma = 3$ recommandée par l'UICPA.) On a établi des courbes de calibration de ces éléments et on les a comparé avec celles de métaux de transitions déjà connus pour donner une réponse dans le détecteur photométrique à flamme. Opérant dans des conditions analytiquement (par opposition à spectroscopiquement) optimisées, on a mesuré leur spectre de chimiluminescence ainsi que celui du chrome dans le détecteur. Des raies atomiques, des bandes moléculaires et des continua sont présents dans tous les cas. De plus, dans le but de définir les interférences spectrales potentielles dues à des matrices d'échantillons contenant des hydrocarbures, on a aussi enregistré les spectres de plusieurs types de composés carbonés. On discute en détail des raies atomiques et des continua importants observés avec certains métaux. Les raies atomiques apparaissent jusqu'à un niveau limite d'énergie de 3,6 eV au-dessus de l'état fondamental. On suggère que les continua sont dûs à des petites particules qui seraient peut-être catalytiquement actives. On discute aussi, à la suggestion d'un arbitre, de la performance de la DPF par comparaison avec les sources ICP et MIP ainsi que la définition et l'influence du bruit sur les critères de la performance mesurée.

[Traduit par la rédaction]

Introduction

The flame photometric detector (FPD) is extensively used in the gas chromatography (GC) of phosphorus and (or) sulfur containing biocides and pollutants (1). In its GC version (and only this version will be considered here) it is a rather simple and comparatively inexpensive device that, beyond P and S, can also detect compounds of B, Ge, Sn, Pb, N, As, Sb, Bi, Se, Te, Cl, Br, and I (the latter three indirectly, e.g., as indium halides). All of these analytes are, of course, *main group* elements.

In contrast, transition elements are rarely determined in the FPD. This is not surprising. The device has a long history (2) and, in its conjunction with GC, was originally developed for organic compounds such as nerve gases (3). Typical applications occur in such related areas as sulfur-containing air pollutants, phosphorus-containing insecticides, and tin-containing antifouling paints. The best-known chemiluminescent emissions from the FPD (from S_2, HPO, and SnH) are molecular in nature. The flame is hydrogen-rich and cool (typically 300–600°C). It is monitored by a combination of interference filter and photomultiplier tube.

In contrast, the typical determination of transition metals by emission spectrometry involves thermal excitation of atomic lines, starting from aqueous solutions of inorganic ions. The high-temperature sources are monitored by monochromators or polychromators. In many instances, such sources, e.g., oxyhydrogen flames, have also been used with gas chromatographic effluents. High-energy sources are well suited for the atomic emission and absorption spectrometry of transition metals.

In the FPD, the situation seems reversed. The only transition metal for which, over the years, the FPD has provided analytical trace methodology is chromium (as the trifluoroacetylacetonate (4, 5)). Recently, we reported on the use of the FPD for metallocenes of the iron group (6–8) and for the determination of manganese (as methylcyclopentadienylmanganesetricarbonyl) in gasolines (9). Unexpectedly, some of the pertinent chemiluminescent emissions turned out to be not molecular but atomic in nature.

The fact that a "cool" source produces strong emission from a very few, highly selective atomic lines, is obviously

[1]Excerpts from this study were presented at the 72nd CIC Conference (Victoria, B.C., June 1989) and the 20th Ohio Valley Chromatography Symposium (Hueston Woods, Ohio, June 1989). This material forms part of the doctoral thesis requirements of X.Y.S.

[2]Author to whom correspondence may be addressed.

[3]Revision received November 29, 1991.

Can. J. Chem. Downloaded from www.nrcresearchpress.com by 92.62.229.171 on 09/08/12
For personal use only.

Can. J. Chem. Downloaded from www.nrcresearchpress.com by 92.62.229.171 on 09/08/12
For personal use only.

of fundamental interest. But it may also prove analytically important. Transition metals occur in a wide variety of biochemical, industrial, and environmental key compounds. While few of these are amenable to gas chromatography, some can be converted into volatile derivatives. More importantly, the flame photometric detector is no longer restricted to conventional gas chromatographic effluents, but is increasingly being used with capillary liquid chromatography and supercritical fluid chromatography. Both techniques are capable of dealing with analytes of low volatility.

It would seem profitable, therefore, to find further transition elements that respond in the FPD with analytically interesting sensitivities. Given the low temperature of the FPD flame, chemical (as opposed to thermal) excitation is a virtual precondition. This brings up some salient points. For one, there exists so far no logical basis on which to predict (*a*) whether a particular element will or will not emit light and (*b*) whether the emission, if any, will be atomic or molecular in nature. However, chemiluminescent emitters can be expected to be much fewer in number and their spectra hence much cleaner in appearance. Also, the presence or absence of spectra, as well as their intensity, should be strongly dependent on detector conditions.

This can be of paramount importance for the FPD's analytical performance. For instance, iron compounds produce mainly atomic lines at low temperature (less oxygen) but mostly molecular bands at high temperature (more oxygen) (6). This is, in a formal sense, contrary to their behavior in high-energy flames or plasmas. Furthermore, the Fe lines occur in the UV, the bands in the visible, making the choice of a monitoring wavelength highly condition-dependent. A related problem is detector cleanliness. Particularly the spectra of weak emitters depend to an inordinate degree on other compounds present in the detector environment. For example, response from different carbon compounds (matrix components, column bleed, the organic part of the analyte) appears to vary over time in overall intensity, wavelength dependence, and even direction (regular vs. inverted peaks). If, say, an FPD has a persistent background of residual sulfur, carbon compounds will produce inverted peaks and the "carbon" spectrum will roughly conform to the (inverted) S_2 bands. Similar effects can be observed from other elements of low FPD response.

All this mandates that spectra can be obtained *at the analytical operating conditions* of the detector. While many of the flame colors (blue S_2, violet Se_2, greenish HPO, red SnH, green BO and BO_2, etc.) are strong enough to be discerned by the dark-adapted eye, the absolute light output is still so weak that only the most prominent of spectra can be measured by a grating monochromator, and then only with wide slits and the most sensitive of phototubes. In many cases, and this study is no exception, the spectra of the FPD's diffuse luminescence phenomena can be picked up only by a variable interference filter ("filter monochromator") that, while allowing much more of the faint light to be collected, is of very low resolution and hence inadequate for most spectral assignments (e.g., the question of whether a particular emission is a molecular band or an atomic line). This is the reason why the spectra of certain elements are often not measured in the FPD, or, worse, why measurements from flames of higher energy are substituted. Occasionally, the luminescent features from low vs. high temperature, and hydrogen-rich vs. air-rich flames do coincide; more often they do not. The FPD is particularly prone to strong changes in the relative intensity of different spectra with just minor changes in operating conditions, much more so than typical high-energy sources. Also, analytically relevant emissions in the FPD cover an enormous range of intensity. On a molar, elemental basis, tin will for instance produce radiation more than eight orders of magnitude stronger than carbon/hydrogen (carbon compounds are common FPD interferents) and more than six orders of magnitude stronger than boron (boron compounds are common FPD analytes).

Yet, without knowledge of the actual spectral mix under particular analytical circumstances, a rational choice of detector conditions, especially for increasing the selectivity of one species over another, is difficult and time-consuming to make. This applies not only to the organometallic analytes, but also to the carbonaceous materials that provide the bulk of many a biological or environmental sample. In this report we shall therefore concentrate on the spectra and calibration curves of some transition elements, and shall add some speculations regarding excited states. In a subsequent report (10) we shall demonstrate how such information can be used to improve the selectivity of the FPD.

Experimental

This study used a basic gas chromatograph with a dual-channel flame photometric detector (Shimadzu GC-4BMPF). Unless otherwise indicated, a packed column (100 × 0.3 cm i.d. glass, 5% OV-101 on Chromosorb W, 100/120 mesh) was kept under a nitrogen flow of between 13 and 27 mL/min. Injection port and detector base temperatures were set at least 30° higher (between 160 and 200°C) than that of the column. The detector, with its quartz chimney removed, was run with 300 mL/min hydrogen and 55–60 mL/min air (depending on the analyte), and an additional 18–24 mL/min of nitrogen was added to the air supply. An efficient exhaust duct was positioned directly above the FPD flue. The photomultipliers were Hamamatsu tubes R 268 (bialkali, 300–650 nm, maximum response at 420 nm) and R 1104 (multialkali, 180–850 nm, maximum response at 420 nm) as indicated in the legends. Their output was amplified by two electrometers and displayed on a dual-channel strip chart recorder (all Shimadzu).

To obtain spectra from the detector, its flow conditions were first optimized for each element in the open (= no interference filter) mode. Then one of the FPD photomultiplier tubes was replaced by a Jarrell–Ash model 82-415 quarter-meter monochromator with a 1180 grooves/mm grating blazed for 500 nm, a pair of (usually) 2.1-mm slits, and the Hamamatsu R 1104 photomultiplier tube. When called for, a 500-nm cut-on filter was inserted into the optical path (at wavelength settings above 600 nm) in order to prevent second-order spectral interference. If the emission was too weak to be detected by the grating monochromator, a variable interference filter (Oriel model 7155 filter monochromator, range 400–700 nm) was used behind an infrared absorbing filter (Oriel 7165). Analytes in amounts corresponding to the upper end of their linear range were repeatedly injected while the wavelength drive was being manually advanced. The measurement of some weak spectra, particularly those of three different types of carbon compounds, was repeated a couple of months after the initial experiment, and again some time after that, to assess and assure adequate reproducibility.

Results and discussion

The responses of some easily available and sufficiently volatile and stable transition metal compounds were measured in the FPD. Several produced luminescence that was substantially more intense than could be expected from the analytes' carbon content. These analytes were the simple

Can. J. Chem. Downloaded from www.nrcresearchpress.com by 92.62.229.171 on 09/08/12
For personal use only.

bis(cyclopentadienyl) derivatives of nickel and cobalt, and carbonyls of rhenium and molybdenum. The metals are thus joining the roster of chromium (4), manganese (9), iron (6), ruthenium (7), and osmium (8), whose responses in the FPD had been previously described.

A variety of other transition metals produced only negligible response. (For this study, "negligible response" is roughly defined as less than ten times the expected carbon response.) We consider such negative results, obtained from compounds of Y, V, W, Zn, Cd, Hg, and Zr, much less conclusive than the positive results on which this study focusses. Conditions in the FPD may not have been suitable for these elements. Or some of the organometallics may have decomposed before reaching the detector. While the latter is immediately obvious when the expected peak *fails* to appear, the opposite effect, i.e., the presence of a peak commensurate with the carbon portion of the molecule, is ambiguous. Such a peak could have been caused by the formation of a non-metallic product from the decomposing analyte. Note that the lack of response from certain transition elements, as mentioned here, refers only to their behaviour in the cool and hydrogen-rich flame of the typical FPD. By no means does it imply that these metals would also fail to respond in, say, a conventional oxyhydrogen flame (which has occasionally been reviewed together with the FPD proper (1)).

Calibration curves

The most sensitive of the new analytes is nickel. This fact commands interest since nickel is an element of economic, environmental, and medical importance. Industrially as well as analytically, it is easily transformed into its highly volatile (and highly toxic) tetracarbonyl (11, 12). Figure 1 shows the calibration curve of bis(cyclopentadienyl)nickel, a compound that is less stable but safer to handle under exploratory circumstances.

Figure 1 also includes the calibration curves of the other new transition metal analytes. Each is the result of an individual, coarse optimization of flow conditions. All measurements are made in the non-dispersive mode. (Data on *dispersive* modes will be given in the companion manuscript (10)). In most cases, and particularly when the spectrum consists of broad bands of low intensity that stretch over an extended wavelength region, the open mode produces higher signal/noise ratios than the use of an interference filter.

(Note that an important criterion here seems to be the amount of light that reaches the phototube. This flux is obviously larger in the non-dispersive than in any dispersive mode, with the implication that types of noise other than that caused by the flame do play a role. To our knowledge, a thorough study of the origins and characteristics of noise in the FPD has never been done, despite the basic interest and potential benefit it would seem to offer.)

Minimum detectable limits can be read directly from this graph: at an ordinate value of 2 for the conventional measurement, at an ordinate value of 0.54 for the IUPAC definition, $S/\sigma = 3$. (The ordinate term "noise" refers here to the short-term peak-to-peak fluctuation of the baseline. For a more precise definition of noise and the detection limit, as well as for a discussion of the pros and cons of using "signal/noise" as the ordinate, refer to the later Note Added in Revision.) Since the GC column temperature was so chosen that each analyte eluted at about 2 min with a $2\sigma_{peak}$ close to 10 sec, these minimum detectable amounts (really: flows), at the more conservative $S/N = 2$ definition, vary from 1×10^{-14} mol/s for nickel to 3×10^{-12} mol/s for cobalt. Table 1 lists these values together with column temperatures and detector conditions. Included in Table 1 are also data for typical carbon compounds, as well as literature references to other transition elements. The assumption inherent in accepting as *elemental* detection limits numbers that were determined using only one compound of a thermally and (or) chemically labile nature, is that no significant decomposition occurred during gas chromatography. A further assumption is that the non-metal part of the analyte molecule did not significantly detract from, or contribute to, the response of the metal.

To allow a visual comparison without repeating information already in the literature, as well as to avoid cluttering up Fig. 1, the relative positions of Ru (7), Mn (9), Fe (6), and Os (8) responses are indicated at the bottom of the graph. The calibration curve for $Cr(CO)_6$ is shown in dashed form, since the flame photometric detection of chromium, as $Cr(tfa)_3$, was described in the literature many years ago. Our measurements are somewhat more sensitive than those found in the seminal work of Ross and Shafik (2.5 ng Cr at $S/N = 6.0$ (4)). However, they fall short by about a factor of two when compared with the minimum detectable amount reported by Burgett and Green (79 pg Cr at $S/N = 12.6$ (5)): in the units used by these authors, our minimum detectable amount is 24 pg Cr at $S/N = 2$.

The calibration curves for $Mo(CO)_6$ and $Co(C_5H_5)_2$ are barely beyond our working definition of significant metal response in the FPD, i.e., that of ten times the response expected from the molecule-sans-metal. Analytically, they are thus of only marginal interest. Here they are shown in dotted lines, for reasons that will become obvious during the later discussion of their spectra.

Spectra

The spectra will be considered in the order of overall intensity (innate sensitivity), i.e., following the calibration curves of Fig. 1 from left to right.

Nickel

One of the definitely interesting transition metal spectra is that of nickel (nickelocene). It is shown in Fig. 2. Unfortunately, most of its features must remain unassigned at this stage. This is due, in part, to the limited resolution available from an FPD emitter of only moderate strength. For reasons discussed earlier, the use of flame conditions optimized for spectral (as opposed to analytical) purposes, was considered inappropriate to this study.

The spectral feature centered at 345 nm, which appears to be slightly broader than the optical bandpath (6.7 nm), is, in our opinion, due to an accumulation of atomic lines. Many prominent Ni lines occur between, say, 335 and 355 nm (13), among them the strongest ones known from emission, absorption, and fluorescence spectrophotometry (14). If preference is given to strong transitions from/to the *ground* state, including states that exceed the ground state by no more than the ambient thermal (kinetic) energy, then the roster includes such lines as 341.476 nm (205–29481 cm^{-1}), 352.454 nm (205–28569 cm^{-1}), 346.165 nm (205–29084 cm^{-1}), 336.957 nm (0–29669 cm^{-1}), 339.105 nm (0–29481 cm^{-1}), and 343.728 nm (0–29084 cm^{-1}). The upper

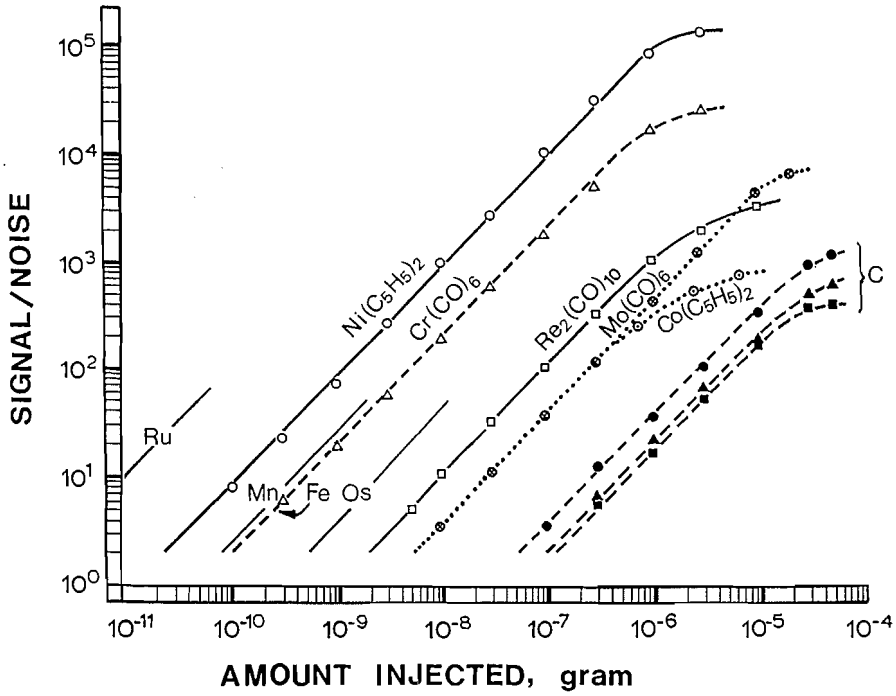

FIG. 1. Calibration curves of compounds containing transition elements, as well as carbon compounds without metals. The position in this graph of earlier reported curves is indicated only by a short section of their lower range: Ru = dicyclopentadienylruthenium (7); Mn = methylcyclopentadienylmanganesetricarbonyl (9); Fe = dicyclopentadienyliron (6) (coincident here with chromiumhexacarbonyl); Os = dicyclopentadienylosmium (8). Other organometallics are indicated by formula. C = carbon compound standards. From left to right: naphthalene, dodecane, di-*n*-hexyl ether. All spectra non-dispersive (no interference filter). Hamamatsu R 268 photomultiplier. Flow conditions as given in the experimental section and in Table 1.

TABLE 1. Transition metals and carbon compounds in the FPD[a]

Element	Compound	Column temperature	Hydrogen (mL/min)	Air (mL/min)	MDA[b] (mol/s)	Filter (nm)	Reference[c]
Ru	$Ru(C_5H_5)_2$	155	300	80	1×10^{-15}	None	7
Cr	$Cr(tfa)_3$	?	70	50 + 50 O_2	2×10^{-13d}	520	5
		160	180	35 O_2	2×10^{-11d}	425.4	4
Cr	$Cr(CO)_6$	60	300	55	5×10^{-14}	None	TP
Ni	$Ni(C_5H_5)_2$	130	300	55	1×10^{-14}	None	TP
Mn	$C_5H_4CH_3Mn(CO)_3$	130	300	55	5×10^{-14}	405	9
Fe	$Fe(C_5H_5)_2$	130	300	60	5×10^{-14}	None	6
		?	140[e]	60 + 27 O_2	8×10^{-12d}	None	26
Os	$Os(C_5H_5)_2$	170	300	60	2×10^{-13}	None	8
Re	$Re_2(CO)_{10}$	132	300	55	6×10^{-13}	None	TP
Mo	$Mo(CO)_6$	52	300	55	2×10^{-12}	None	TP
Co	$Co(C_5H_5)_2$	120	300	55	3×10^{-12}	None	TP
C	Naphthalene	130	300	60	4×10^{-10}	None	TP
C	Dodecane	130	300	60	7×10^{-10}	None	TP
C	Di-*n*-hexyl ether	130	300	60	8×10^{-10}	None	TP

[a]Shimadzu FPD without quartz chimney unless otherwise indicated.

[b]Minimum detectable amount in mole of element per second, at a signal/noise ratio of 2, where noise is the short-term peak-to-peak fluctuation of the baseline. Divide by 3.7 for a rough MDL estimate according to the S/σ (noise) = 3 IUPAC definition. Note that some literature values, marked by *d*, are given in mol (rather than in mol/s). Divide these values by the typical 2σ (peak) value of 10 s for a rough comparison with other data.

[c]TP = this paper.

[d]MDA given in moles (peak width not retrievable from the literature).

[e]Melpar (Tracor) FPD.

Can. J. Chem. Downloaded from www.nrcresearchpress.com by 92.62.229.171 on 09/08/12
For personal use only.

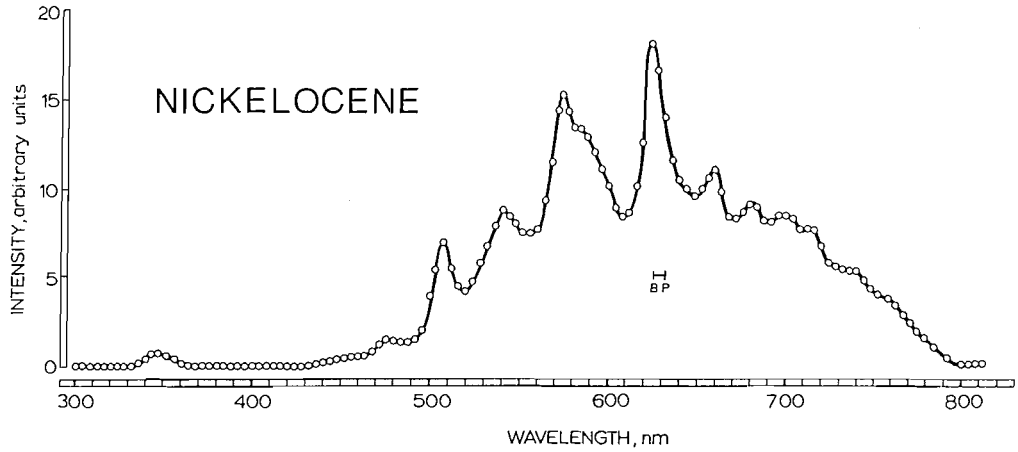

FIG. 2. Spectrum obtained by repeatedly injecting 500 ng of nickelocene under *analytically* optimized gas flows (300 mL/min H_2 and 55 mL/min air). Grating monochromator bandpass: 6.7 nm; photomultiplier tube: R 1104.

state energies are 3.66 and 3.54 eV for the two first-cited lines, as well as 3.68 eV for the line of highest energy whose presence could not be reasonably excluded. (Chemical exitation, for which these numbers are of interest, will be discussed later.)

The much more intense emission(s) between about 450 and 800 nm are puzzling. The literature lists several systems of NiO that occur in that region. The 0,0 transitions of NiO systems V and VI are given as 509.83 and 473.0 nm (15), i.e., at values that appear close to two of the maxima shown in Fig. 2. Judged from the spectrum, the 0,1 transition of System IV at 540.77 nm may be present (but then why not the 0,0 transition at 517.45 nm ?). Similarly, other bands representing these systems fail to appear in the low-resolution spectrum. Also, the overall appearance is quite different from, for instance, the NiO spectrum produced by the chemiluminescent reaction of $Ni(CO)_4$ with O_3 (12).

A quite plausible emitter for some of the sharper bands is NiH. Pearse and Gaydon list several systems. One of these, the "6257 Å system" (NiH $^2\Delta_{2\,1/2} \rightarrow {}^2\Delta_{2\,1/2}$), has strong 0,0 and 1,0 transitions that are close to the maxima of Fig. 2 at 626 and 574 nm (15). And the band shown at 507 nm may correspond to a NiH band mentioned by R. E. Smith (16). While no definitive assignment can be made under the circumstances, we believe that NiH and (with less justification) NiO should be considered as candidates for producing much of the emission in the visible.

Chromium

The spectrum from chromium (chromium hexacarbonyl) was checked because, even though the FPD response of chromium compounds had been known for quite some time and had been claimed to be "specific" with the use of a 425.4-nm interference filter (4), the corresponding FPD spectrum has, to our knowledge, never been reported. Even if it had, the fact that earlier studies were carried out on a Melpar FPD, while this study used a Shimadzu FPD, would have mandated a re-measurement of the chromium spectrum to serve the envisioned experiments on selectivity. The choice of the 425.4-nm interference filter in the seminal FPD paper (4) was obviously based on chromium's strongest emission line at 425.435 nm (actually, on the triplet at 425.435, 427.480, and 428.972 nm, given the bandpass typical of interference filters). This wavelength had been used previously for monitoring Cr emission from an oxyhydrogen torch (i.e., from a hot, oxygen-rich flame of 5.7 L/min H_2 and 39 L/min O_2) connected to a gas chromatograph (17). The choice of a 520-nm filter in the most sensitive FPD determination of Cr reported to date (5) may have been aimed at the strongest emission line in an air–hydrogen flame (520.604 nm (14)). Note, however, that this atomic transition (7593–26796 cm^{-1}), together with its triplet companions, does *not* involve the ground state and that, based on arguments made in this report, it is therefore unlikely to produce strong response in the FPD. (It is interesting to note, nevertheless, that its upper-level energy of 26796 cm^{-1} is *lower* than that of the most energetic line seen, i.e., 27935 cm^{-1} for the 357.869-nm line.)

The upper half of Fig. 3 displays the spectrum obtained under regular operating conditions of our FPD. As expected, it does *not* show the 520-nm line, but it does indeed include a distinct maximum centered at about 427 nm. This peak represents the earlier mentioned triplet, which is also easily observed in the conventional air–hydrogen flame (14). Another combination of three strong emission lines occurs at 357.869, 359.349, and 360.533 nm, with the resulting peak centered in our spectrum at 359 nm (the CrH bands around 368 do not seem to show up). There are no clearly assignable lines at higher energy.

Aside from these atomic emissions, the spectrum is dominated by some broad features of unknown origin. Not surprisingly, then, the minimum detectable limit of chromium hexacarbonyl is considerably better when using the "open" (non-dispersive) mode than when using an interference filter at 427 nm. Indeed, the most prominent spectral feature is located far away, i.e., between 670 and 750 nm (as seen by the red-extended phototube).

Aware of the case of iron (6), we became interested in possible spectral changes resulting from shifts in flame conditions. If such changes occur, the *individual* optimization of disparate emission features can serve purposes both analytical (e.g., increase selectivity) and spectral (e.g., yield information on the identity of the emitters).

In the case of chromium, however, the overall distribu-

Can. J. Chem. Downloaded from www.nrcresearchpress.com by 92.62.229.171 on 09/08/12
For personal use only.

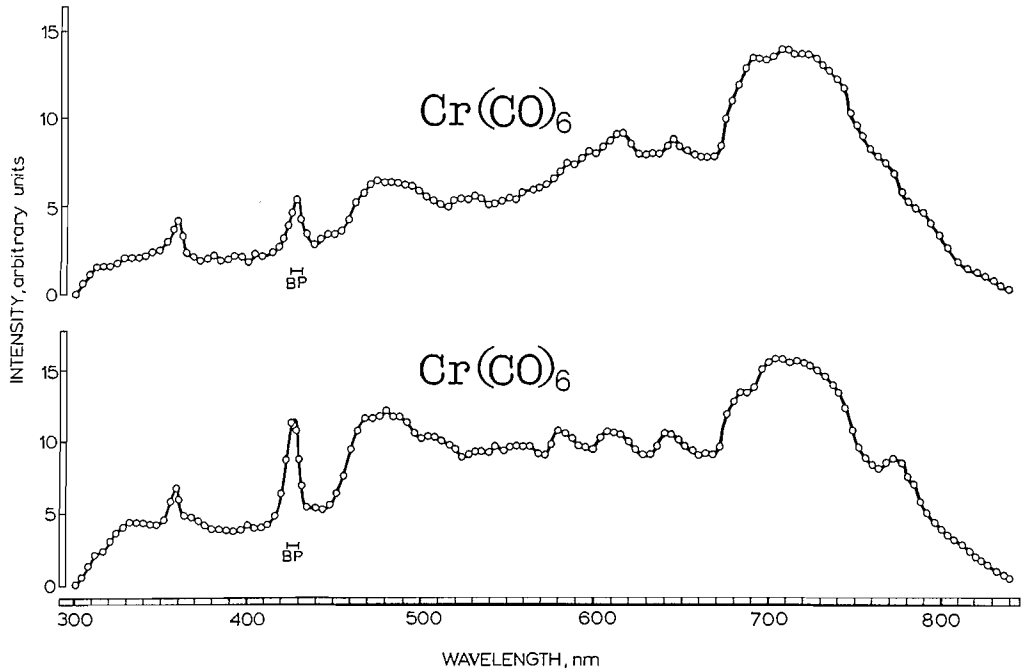

FIG. 3. Spectra obtained from chromium hexacarbonyl with R 1104 PMT and 2.1-mm slits (6.7 nm bandpass). A 500-nm cut-on filter was placed in front of the grating monochromator from 600 nm on to exclude the second order. Upper half: spectrum at regular flame condition (300 mL/min H_2 and 55 mL/min air); lower half: spectrum at stoichiometric flame conditions (50 mL/min H_2 and 125 mL/min air).

tion of the spectrum changes but little, and that within a very wide range of flame conditions. To document this with one out of several runs, the spectrum shown in the lower part of Fig. 3 was obtained from a stoichiometric flame. Not shown here, but in agreement with the conclusion given above, were runs with (*a*) a flame much hotter than usual, though still hydrogen-rich, and (*b*) a flame much cooler and so starved of oxygen as to hover near extinction. (The latter spectrum, because of its very low light level, had to be obtained within the much shorter range and lower dispersion of a filter monochromator.)

It may be mentioned that some of the smaller features, particularly in the hotter and more oxygen-rich flame, could possibly be attributed to CrO. The relevant heads are 579.44 (1,0), 605.16 (0,0), and 639.43 (0,1) nm (15).

The benefits of having available an FPD spectrum valid at *analytically* relevant conditions (top of Fig. 3) are obvious. It alone allows a reasonable choice of wavelength for optimization of response and, much more importantly, for optimization of selectivity vis-a-vis other FPD-active species (10). In this context, the initial literature choice of 425.4 nm as the central wavelength of an interference filter for chromium (with a presumed bandpass around 10 nm) is interesting in light of the fact that the largest response of carbon compounds also occurs in that spectral window (*vide infra*). The "specific" response for chromium at 425.4 nm (4) against the background, presumably mainly carbon compounds, relies therefore on the innate difference in luminescence intensity rather than on the wavelength at which the two emissions are compared. In fact, in our system — and different FPD's can differ greatly in this regard — the open mode produces a higher selectivity for chromium against aliphatic carbon than if that analysis had been carried out with the 425-nm interference filter in place. The reason is obvious from the two spectra obtained at analytical operating conditions.

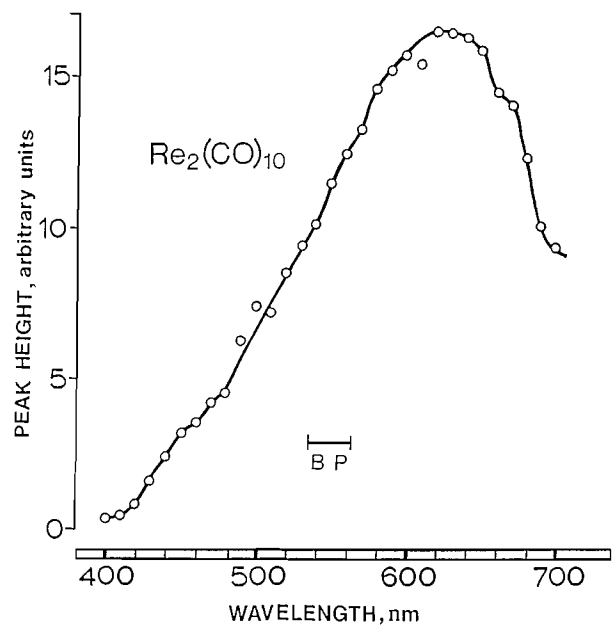

FIG. 4. Spectrum obtained from dirheniumdecacarbonyl at regular flame conditions. Filter monochromator with 4-mm slit and R 1104 PMT. Bandpass (specification) = 28 nm at 550 nm.

Rhenium

The spectrum of rhenium (dirheniumdecacarbonyl) under regular operating conditions is shown in Fig. 4. Rhenium is

Can. J. Chem. Downloaded from www.nrcresearchpress.com by 92.62.229.171 on 09/08/12
For personal use only.

Can. J. Chem. Downloaded from www.nrcresearchpress.com by 92.62.229.171 on 09/08/12
For personal use only.

not a particularly strong emitter in the FPD and, furthermore, its spectrum is essentially continuous: two characteristics that necessitate use of the more sensitive but less versatile filter monochromator. The spectrum differs from rhenium spectra found in the literature. It is known, for instance, that Re is a "flame-greening" element (2) (whereas Fig. 4 suggests red). There is also little similarity between it and the continuum seen in a low-temperature hydrogen diffusion flame (18).

For reasons discussed in the cases of chromium and iron, and for the chance to use the higher resolution and wider wavelength range of the grating monochromator, a variety of hotter flames were tried that, while still hydrogen-rich, contained less hydrogen and more oxygen than the analytically optimized setting. Figure 5 shows the case for Re. Not surprisingly for such a heavy atom (cf. Os (8)), identifying features tend to be submerged in the broad continuum.

The resonant line of Re at 346.047 nm (3.58 eV) is not seen in the spectrum. (Note that the region from 300 to 400 nm was included in the measurement but proved blank.) Either there are too few free atoms present in the first place, or they fail to undergo chemical excitation, or excited atoms are not formed in chemiluminescent processes from di- or triatomic species, or molecular excitation pathways are energetically favored. The only known atomic transitions from *less* than 3.58 eV to/from the ground state, are located at 488.914 nm (2.54 eV) and 527.556 nm. Both are characterized as "cw" (complex and wide) in an arc (13), but are the strongest lines seen in emission from an oxyhydrogen flame (14). Both are absent from this spectrum; however, yet another spectrum from a still hotter flame (not shown here) contained, superimposed on the continuum, some very minor features at these two wavelengths.

The spectrum shown in Fig. 5 for Re is similar in general appearance to that shown in Fig. 3 for Cr, and to those reported earlier for Os (8) and perhaps also for Fe (6). Similar to these other elements, the case can be made here as well that oxides may be involved (for instance, a series of ReO bands is known to occur between 606 and 609 nm (15)). However, the main contribution to response originates from the unassigned continuum.

Molybdenum

Figures 6 and 7 show the spectra obtained from repeatedly injecting $Mo(CO)_6$ and $Co(C_5H_5)_2$. In the calibration curves presented in Fig. 1, response from these two analytes is displayed by dotted lines. The reason for that visual caveat is that we question whether the recorded spectra are, in fact, due to emission from species containing these metals. Our scepticism is based not only on the weakness of response, which is relatively close to the response of carbon compounds, but also on certain spectral features.

The most prominent feature of the molybdenum spectrum shown in Fig. 6 is the relatively sharp peak around 420 nm. There are two prominent atomic lines for Mo in the vicinity, i.e., at 414.355 and 418.832 nm. However, the energy levels for these transitions are apparently in question (13), and it is thus unlikely that they represent transitions to/from the ground state. Also, MoO is very refractory. Owing to the prevailing low light level, we did not separately check for the possible presence of, for instance, the prominent lines 386.411 nm (0–25872 cm^{-1}, 3.21 eV) and 390.296 nm (0–25614 cm^{-1}).

A look at the calibration curves shows that, on a weight basis, the molybdenum compound is only about one order of magnitude larger in response than a typical aromatic carbon compound. However, the spectral measurements demonstrate that the luminescence from molybdenum hexacarbonyl at 420 nm is about ten times stronger than the luminescence obtained from a commensurate amount of naphthalene. Thus it appears that the spectrum shown does indeed contain most of the luminescence that established the calibration curve (note the difference in wavelength range between the calibration curve and the spectrum!). Our own preference is that response is indeed provided by a Mo-containing emitter. However, the formal possibility of carbonaceous emission being enhanced (catalyzed) by the presence of molybdenum is not precluded by the experiment.

Cobalt

Similar arguments can be made in the case of Co (here in the form of dicyclopentadienylcobalt) whose spectrum is shown in Fig. 7. It is even more suggestive of an aromatic

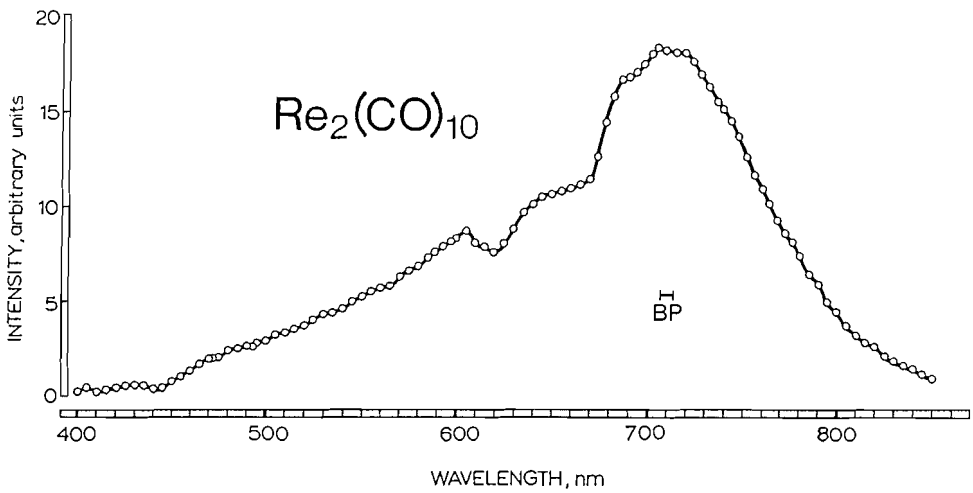

FIG. 5. Spectrum obtained from dirheniumdecacarbonyl in a hotter but still hydrogen-rich flame. Hydrogen: 120 mL/min; air: 125 mL/min. Grating monochromator bandpass: 6.7 nm; PMT: R 1104.

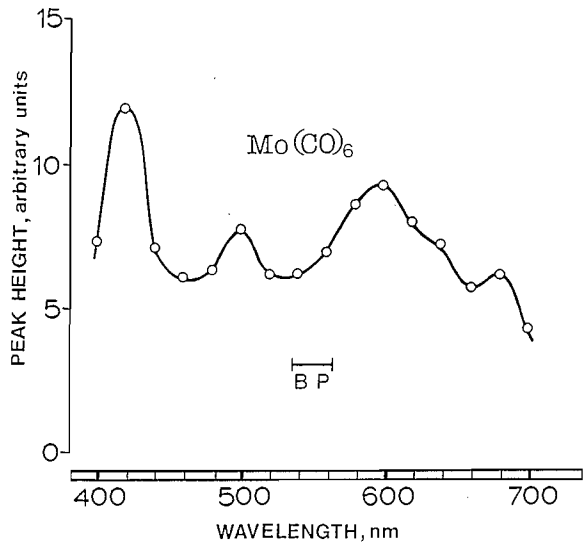

FIG. 6. Spectrum obtained from molybdenum hexacarbonyl at regular flame conditions through a filter monochromator equipped with 4-mm slit and R 1104 photomultiplier.

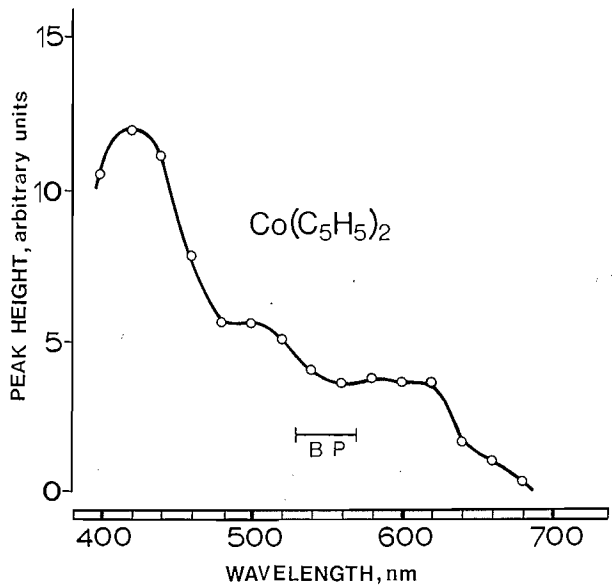

FIG. 7. Spectrum obtained from dicyclopentadienylcobalt under regular flame conditions. Filter monochromator with R 1104 PMT and 6-mm slit.

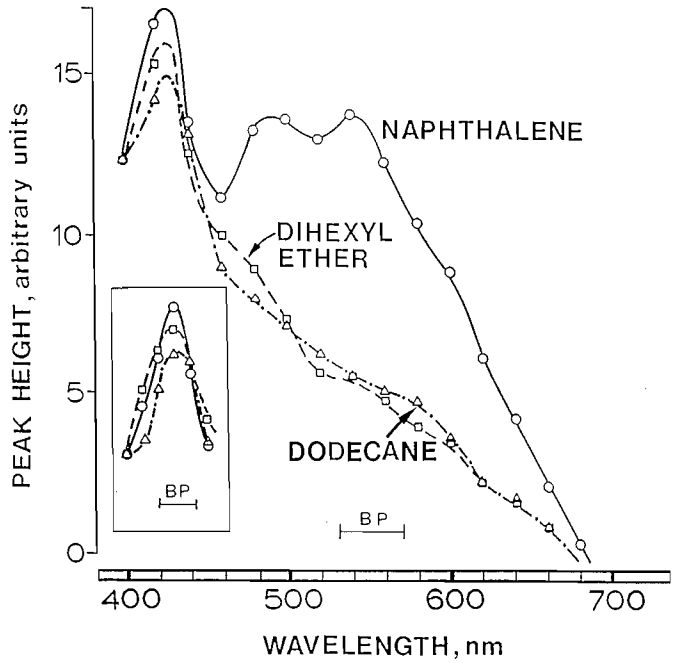

FIG. 8. Spectra obtained from naphthalene (solid line), di-*n*-hexyl ether (dashes), and dodecane (dashes and dots) with a filter monochromator using a 6-mm slit and an R 1104 photomultiplier. Flame conditions: 300 mL/min H_2 and 60 mL/min air. Bandpass: 30 nm at 550 nm. Rectangular insert: Same conditions but 4-mm slit.

hydrocarbon (see below) than that of molybdenum. In the region of the blue maximum there are two cobalt lines involving the ground state, namely 419.071 nm (0–23856 cm^{-1}) and 423.400 nm (0–23612 cm^{-1}) (13). However, these lines are very weak in other systems and, furthermore, one would have expected that, if atomic excitation were occurring, the very strong lines around 350 nm (13, 14) should have been observed in the form of a stronger overall response for Co (the lines are outside the range of the filter monochromator but are included in the open mode of the FPD calibration curve). It may also be mentioned that one of the R heads of CoH is situated at 419.45 nm (but the other, for the 0,0 transition, is located at 448.19 nm!) (16). More reasonable than invoking such spectral features may be to assume that the emission observed within the 400–700 nm range of the filter monochromator is dominated by carbon-based response. If so, this would suggest either that there occurs significant luminescence from cobalt-containing species outside this range, or that the presence of cobalt somehow stimulates carbonaceous emission(s). A comparison of the absolute magnitude of suitable spectra suggests, but does not prove, the former alternative, i.e., that there may indeed exist further uncharted Co emissions.

Both cobalt- and molybdenum-derived emissions could be further investigated. However, because of their low sensitivity and hence minor analytical importance in the FPD, the matter was dropped.

Carbon compounds

Of greater interest are the spectra obtained from carbon compounds themselves, since the latter constitute the major components of many samples wherein trace amounts of organometallics need to be determined. To our knowledge, no literature source describes such spectra as obtained from an FPD at conventional operating conditions. (Spectra from carbon-containing emitters in much hotter and oxygen-rich H_2/O_2 and H_2/air flames are, however, discussed in various papers (e.g., refs. 20–25).) Besides, weak FPD responses are particularly likely to vary with differences in detector construction, condition, and contamination. And, until the *analytically* relevant spectra are known, it is difficult to establish conditions for optimal selectivity (other than by a rather time-consuming trial-and-error approach).

Figure 8 shows the luminescence spectra obtained from three standard carbon compounds (an alkane, an aliphatic ether, and an aromatic) at regular FPD operating conditions. The three compounds were injected *as a mixture* in order to keep the relative amounts precisely the same. Sim-

Can. J. Chem. Downloaded from www.nrcresearchpress.com by 92.62.229.171 on 09/08/12
For personal use only.

Can. J. Chem. Downloaded from www.nrcresearchpress.com by 92.62.229.171 on 09/08/12
For personal use only.

ilar spectra were obtained from experiments repeated over the course of several months.

It is well-known that aromatics respond stronger in the FPD than aliphatics. The data shown in Fig. 8 demonstrate that this is due to a partly different (not just a proportionally enhanced) spectrum. There is little agreement between these spectra and the carbon-based emissions from oxyhydrogen flames (20–25), except for the seemingly common peak at 430 nm. In the oxyhydrogen flames this peak clearly represents CH, with the 0,0 transition of $CH(A^2\Delta–X^2\pi)$ located at 431.42 nm (15). As shown in Fig. 8, the peak apex was rescanned, at the highest resolution obtainable at this low light level. Within the considerable error limits of such a measurement, the maximum is indeed located at that wavelength. Our motivation for rechecking the region was related not only to its obvious analytical importance, but also to our suspicion that some or all of the FPD luminescence found there may originate from excited formaldehyde ("Emeleus's cool flame spectrum," occurring "in the cool flame of ether, acetaldehyde, hexane and other organic substances" (15)). However, the very low light level characteristic of typical FPD settings prevents an experimental assessment of the relevant contributions from CH and CH_2O.

In oxyhydrogen flames, the second most common spectral feature is C_2 ($A^3\pi_g–X'^3\pi_u$), i.e., the Swan bands (15). Prominently visible is usually the 0,0 transition (head at 516.52 nm), accompanied by the 0,1 (563.55 nm) and 1,0 (473.71 nm) transitions. Aside from the measurement shown in Fig. 8, a larger number of spectra were obtained at different times and with different compounds. In none of these did the Swan bands show up unambiguously, although they could, of course, be present. The low light levels involved, and the differences between different carbon structures at wavelengths longer than, say, 460 nm, make this a difficult question to investigate. Aside from CH, and perhaps CH_2O and C_2, the luminescence does not appear to fit any other known carbonaceous emitters. While thus not overly revealing in a spectroscopic context, knowledge of the carbon-related spectra is of considerable value for improving analytical selectivity (10).

Speculations

Some response patterns do appear to show up among the well-responding transition metals. We shall speculate on two of these: the apparent energy limitation of atomic lines, and the ostensible similarity of spectral continua.

Atomic lines

Of the elements covered in this study, only chromium shows clear evidence of atomic lines. For nickel the evidence is, literally, much weaker, and there is no experimental basis for assuming lines to be present in the spectrum from rhenium (or in the ambiguous spectra from molybdenum and cobalt). Table 2 lists the relevant wavelengths of Cr and Ni, together with data of Mn, Fe, and Ru from earlier studies. The atomic lines are particularly pronounced in the cases of Mn and Fe, where they even represent the spectral feature preferred for analysis.

Unfortunately, the extremely low light levels from an FPD run at conventional conditions prevent conclusive high-resolution measurements to be made. Therefore, the case for atomic lines must rest primarily on the agreement of experimental wavelengths with literature values. Given (*a*) the typical condition of a low-temperature FPD flame; (*b*) the experimental evidence that most of the presumedly atomic emissions increase but little in intensity with large increases in flame temperature; and (*c*) the fact that, in contrast to high-temperature AES sources, some metals emit very strongly while others emit only very weakly (if indeed at all), it follows that the excitation cannot simply be ascribed to a thermal process. Furthermore, the reasonable alternative, i.e., the occurrence of chemiluminescence, is consistent with the presence of very *few* lines and, more revealingly, with the detector's preference for those lines that represent transitions from/to the ground state (perhaps including easily accessible levels within the prevailing thermal (kinetic) energy of about 0.1 eV).

TABLE 2. Evidence for atomic lines in FPD spectra

Element	Wavelength (nm)	Reference
Ni	340–355	This paper
Cr	357–360, 425–430	This paper
Mn	403, (540)	9
Fe	344, 373, 387	6
Ru	350, 373, 380	7

If so, then the question arises as to the amount of energy that is being provided by the chemiluminescent process. Just for reference, the (in the context of luminescence) often invoked recombination of hydrogen atoms yields 4.5 eV, while the formation of water from H and OH produces 5.1 eV.

The following comparison will list the shortest wavelengths at which emission from atomic lines is still manifest in the spectra, together with "reasonable" lines of slightly higher energy where it is not. Our criteria for calling a line "reasonable" are strong response in other systems (arc, oxyhydrogen flame, etc.) and the involvement of the ground state. Individually, any one of the deductions resulting from such vague criteria is highly questionable. Cumulatively, however, their similarities enhance one another and thus confer some credibility on the results.

The better responding metals that do display atomic response are Mn (9), Fe (6), Cr, Ru (7), and Ni; the ones that do not are Re and Os (8). Although the FPD-active metals are too few to be definitively classified in terms of their excitation/emission processes and the associated intensity of luminescence, it appears that the strongest responding metals display dominant molecular bands (Ru, Ni), followed by those that show prevailing atomic lines (Mn, Fe, and to a lesser extent Cr), followed by those that produce massive continua (Re, Os, and again, Cr).

Which are the lines of highest energy that do show up, and which are the (reasonable) ones of still higher energy that do not? Manganese emits at 403 nm (3.1 eV), but the next prominent line at 280 nm (4.4 eV) is not seen (and neither is a weak ground-state transition at 322 nm, i.e., at 3.9 eV) (9). Iron emits strongly at 344 nm (3.6 eV), but a weak line at 319 nm (3.9 eV) and a much stronger one at 302 nm (4.1 eV) are not present (6). The most energetic chromium line in the FPD spectrum occurs at 358 nm (3.5 eV), with no reasonably strong lines expected in its vicinity. In ruthenium, the 350-nm line is in evidence but the 343-nm line is not (7). Given that resolution and calibration in that particular experiment were of sufficient quality, this means that 3.55 eV shows up but 3.61 eV does not (there are no

Can. J. Chem. Downloaded from www.nrcresearchpress.com by 92.62.229.171 on 09/08/12
For personal use only.

prominent ground-state transitions close by at higher energies). The most energetic line of nickel that cannot be excluded on spectral evidence is at 355 nm (3.7 eV), but it occurs close to the edge of a broader spectral feature that is preferably assigned to the 341- and 352-nm lines (3.6 and 3.5 eV). The closest reasonable line that clearly fails to appear is that at 323 nm (3.8 eV).

It thus seems that, where atomic lines do show up, *3.6 eV is the approximate energy limit*. Several cases of metals mentioned above argue for that limit and none clearly contradicts it. However, to assume the same upper limit for all metals is tantamount to suggesting that a single particular reaction may drive the various atomic excitation processes (or that some very efficient reaction quenches all emissions above it). No prominent flame gas reaction yielding 3.6 eV comes immediately to mind. The recombination of hydrogen atoms, a prime candidate considering the type of flame and the evidence of the literature on a variety of flame systems, produces 4.5 eV. But why, then, is none of the possible lines in evidence between 340 and 300 nm, a region that was scanned for all strongly responding elements? Of course this could be happenstance: too little is known about excitation process(es) to predict whether or not a particular line could or should show up. Also, the formation of refractory species may have depleted the free atom concentration of certain metals. Or, the recombination of hydrogen atoms may have occurred not via the most straightforward route

$$H + H + Me \rightarrow H_2 + Me^*$$

but via such routes as

$$MeH + H \rightarrow H_2 + Me^*$$

(but note the differing MeH bond energies!). Other high-energy radical recombinations could be involved. Obviously, though, these are not the only scenarios possible.

Continua

Apparent similarities among elements show up not only in atomic emissions but also in the extended continua that figure prominently in the spectra obtained from Re, Cr, Os (8), and, perhaps, Fe (6) compounds. To illustrate this similarity, Fig. 9 repeats and compares spectra involving three elements monitored by the same, red-extended phototube (though at slightly different flame conditions).

In the earlier discussion of these spectra, we mentioned cases that possibly involved oxide bands. However, MeO emissions alone could hardly explain these commanding continua that peak in the red and near infrared (and may reach beyond the photomultiplier's upper wavelength limit).

The process by which these spectra were procured (i.e., by measuring the peak height of compounds injected into the gas chromatograph) circumvents any influence of the solvent or the flame itself, unless, of course, the analyte were so massive in amount or so catalytic in nature that it could seriously alter the general chemistry of the flame.

Hence, if one is to speculate on the origin of these continua, metal-containing species are prime suspects. Although, and because, there is no hard evidence available on this question, we would like to mention the possible presence of small aggregates of metal atoms (with or without other atoms such as O and H). Continua involving various elements in the flame have been repeatedly ascribed to hot oxide particles (27). It is true that blackbody radiation, at temperatures typical of the FPD, is very weak and that its maximum occurs at considerably longer wavelengths. Yet very *small* particles can reportedly shift that spectrum toward the blue. Furthermore, the luminescence of solid bodies can be driven or enhanced by flame radicals. A well-known example of this is the Welsbach mantle, which involves (additional) heating of a solid surface by the recombination of hydrogen atoms (19).

It would thus be conceivable that *small, analyte-derived aggregates,* perhaps acting as catalysts for flame processes and hence offering higher temperatures for excitation, could produce the observed continua. A possible argument against this scenario is the linearity of the calibration curve: considering the low concentration and the short residence time of the analyte in the flame, the size of (and hence the light yield per metal atom from) the very small particles should vary considerably within the wide concentration range covered by the calibration curves. (Obviously, this argument ignores the influence that parameters other than concentration could exert on particle size. As well, it neglects the possible recycling of particles by eddies in the detector chamber, the conceivable temporary coating of detector walls, and a host of other easily imaginable processes.) Consequently, any significant role for the emission of light from small particles must remain an object of speculation: a more conventional interpretation of the obtained spectra is certainly possible.

NOTE ADDED IN REVISION:

One reviewer of this manuscript requested (*a*) that "a perspective of the current usage of ICP's and MIP's as detectors for GC should be presented and briefly compared to the FPD capability presented here," and (*b*) that the term "noise" be closer defined and the use of the "signal/noise" ordinate in Fig. 1 be justified. Both requests touch on topics that range more widely and are of a more basic nature than the current manuscript. We are therefore pleased to comply.

(a) A comparison of the FPD with ICP's and MIP's as GC detectors

This comparison juxtaposes instruments not only of a very different level of complexity, but also of a very different nature. In attempting to correlate that nature to their analytical utility (a correlation necessary because practical experience is incomplete on both sides) we shall consider only transition elements, particularly those mentioned in this paper and its companion (10). Also, since the referee's request was limited to the ICP and MIP, we will not compare atomic absorption (cf. ref. 28), mass spectrometry, or any other type of detection device.

The combination of gas chromatography with various instruments of atomic spectroscopy has been reviewed in considerable detail (28). Both the microwave-induced plasma (MIP) and the inductively coupled plasma (ICP) are high-energy sources in which excitation temperatures exceed the already high kinetic temperatures. Consequently they are very bright — capable, it seems safe to predict, of exciting atomic lines from *all* the transition elements. In the ICP, the detection limits of most transition metals are contained within only two orders of magnitude [cf. ref. 29]. In contrast, FPD response to transition metals varies over at least five orders of magnitude ("at least" because the chromatographically necessary presence of carbon limits the experimental determination of that number). In practice that means that the FPD can be considered *un*responsive to many of the transitior

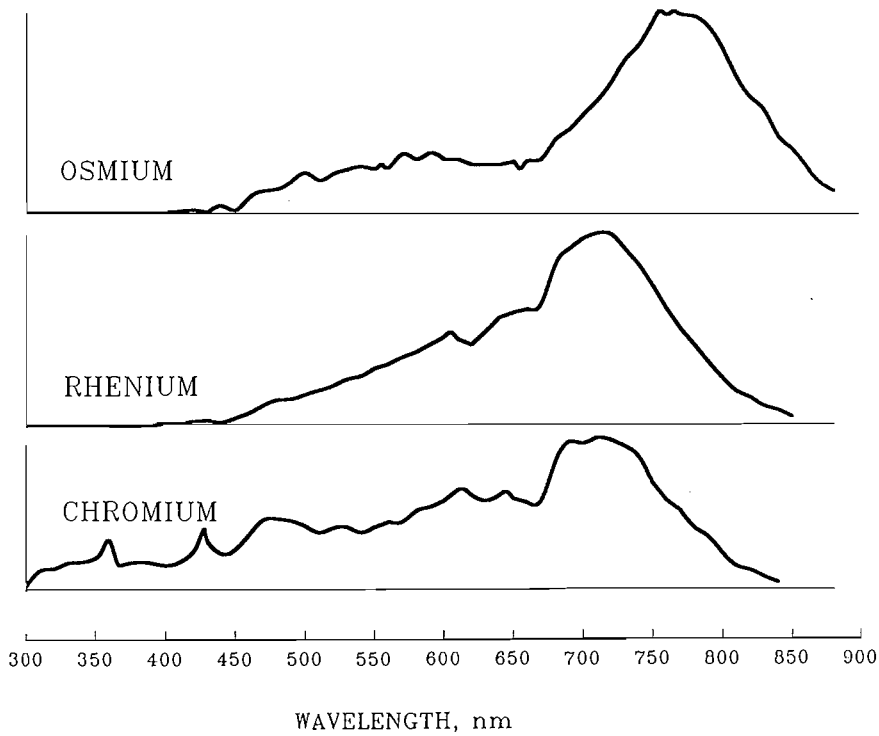

FIG. 9. Similarity of three continua: vertically offset spectra from compounds of osmium (8), rhenium (Fig. 5), and chromium (upper part of Fig. 3).

Can. J. Chem. Downloaded from www.nrcresearchpress.com by 92.62.229.171 on 09/08/12
For personal use only.

elements. This is not surprising: for response in the low-temperature FPD, a suitable chemiluminescent excitation mechanism has to exist. The FPD is hence far more limited (selective) in the choice of suitable analytes.

The transition elements to which the FPD has been shown to respond reasonably well are Ru (7), Ni, Mn (9), Fe (6), Cr (4, 5), Os (8), and Re. Their detection limits still vary (under the same analytical conditions) by three orders of magnitude (see Fig. 1). The priority of performance criteria must depend on the task and training of the analyst, but it can be argued that in this area "sensitivity may rightly be seen as the major problem" (28).

The most popular and, it seems, overall most sensitive of the plasma techniques is the MIP. This is also the one technique by which transition metal analytes similar to ours have been tested (30), and where a commercial instrument has recently become available (31).

Ruthenium, the best responding transition element in the FPD, has an S/N = 2 detection limit of 7.8 pg/s in the MIP (30). In comparison, the FPD detection limit is 0.1 pg/s at the optimized conditions of the original study (7), and 0.4 pg/s at the generalized conditions of the present work (10). Among the transition elements first described as FPD-active in this manuscript, the best responding and probably most important one is nickel. Its detection limit in the FPD is 0.4 pg/s (10), as compared to 2.6 pg/s in the MIP (30). In similar comparisons, chromium appears to respond more strongly in the FPD, manganese response is comparable, and iron responds clearly more weakly than in the MIP (30). The plasma techniques would also be decidedly more sensitive to osmium (30) and, we presume, rhenium (no GC–MIP data available). That ends the current list of reasonable analytes in the FPD. There do exist more transition elements that have been shown to respond well in the GC–MIP but apparently fail to do so in the GC–FPD, such as Co, Cu, and Zn (28). Many more would obviously respond if suitable test compounds were to be injected into a GC–MIP.

In other words, the elements that respond best in the FPD also display greater sensitivity there than in the MIP (as well as in the ICP and DCP); a few more elements are comparable in sensitivity in the two instruments, and for the rest the FPD response is either clearly inferior, or practically non-existent, or unexplored. This typically "selective" behaviour of the FPD vis-a-vis the "general" behaviour of MIP and ICP concurs with our perception of their respective excitation modes.

For the group of elements where the FPD can reasonably compete (Ru, Ni, Mn, Cr, Fe), the selectivity ratios against carbon vary in the MIP form from 6.47×10^3 for Ni to 2.80×10^5 for Fe (30). Note that the newer commercial MIP system claims a general improvement in selectivities "by more than an order of magnitude (through) the use of appropriate reagent gases, the water-cooled thin-walled discharge tube and, most importantly, real-time multipoint background correction..." (31). While the experiments of that particular study are restricted to main-group elements, the quoted conclusion may as well be valid for transition metals. In the FPD, single-channel selectivity ratios against carbon (as in dodecane) vary from 4×10^4 for Mn and Fe to 7×10^5 for Ru in non-dispersive, and from 5×10^4 for Cr to 4×10^6 for Ru in dispersive (interference filter) mode (10). *Dual*-channel FPD modes generally increase these selectivity ratios further by one to two orders of magnitude (10). Hence, for those metals to which it responds well, the FPD appears superior in selectivity to the plasma detectors.

Yet, this statement requires the addition of an important caveat. "Selectivity" in hyphenated GC detector systems is traditionally understood to mean the selectivity of a hetero-

Can. J. Chem. Downloaded from www.nrcresearchpress.com by 92.62.229.171 on 09/08/12
For personal use only.

element versus *carbon*; this is the only specification generally accepted and commonly determined for the GC–MIP, GC–ICP, etc. (refs. 30, 31, etc.). However, selectivity in the FPD arises from different causes than in the MIP, ICP, DCP, etc. Selectivity in the FPD is primarily a function of relative photon yields from different elements, while in the MIP *et al.* it is primarily a function of spectral resolution and background correction. Hence, metal/carbon selectivity ratios are very high in the FPD simply because its response to a typical hydrocarbonaceous test compound such as dodecane happens to be very low. However, metal/metal selectivities could be a different matter altogether because plasma instruments (*a*) monitor line emission exclusively and with superior spectral resolution, and (*b*) use sources in which most elements radiate well and with comparable intensity. Some metal/metal selectivities in the FPD are given in the companion paper (10): many of these fall between one and two orders of magnitude in single-channel mode, with another one to three orders added by dual-channel operation. In our opinion (and we know of no relevant experiments concerning this point) the high-energy, high-resolution sources should be able to do better.

A further detector criterion is the linear range. Typical values in the MIP are three orders of magnitude (30), while in the FPD they span four orders or more (see refs. 7 and 9, and Fig. 1). Although the FPD's performance is clearly better here, we do not consider linear range an overly important criterion.

On still other analytical criteria, little information exists about transition metals in the two types of detectors. We are therefore forced to speculate on the basis of general principles.

The detector speed (resistance to peak broadening) should be somewhat better in the FPD than in the MIP or ICP due to the short residence time (less than 1 ms) in the very small FPD flame. However, capillary peaks of very low chromatographic dispersion have been reported from the two high-power sources. The quartz tube used in the MIP may lead to some sample hold-up (plus other problems), but this can usually be ameliorated by changing the chemical composition of the plasma. Thus speed is not likely to become a decisive criterion for choosing one or the other type of instrument.

A similar statement can be made about quantitation and long-term reproducibility. These are better in the FPD as judged by its much better track record over many years. However, the high-power sources should still be capable of adequate performance, particularly when used with internal standards.

As already mentioned, the range of applicability to different elements must be far wider in the high-energy sources. The FPD is valuable for some metals and worthless for others. The ICP (sans GC) can be easily used for aqueous samples; this is not practicable with commercial MIP or FPD models. If equipped with polychromatic readouts, both the ICP and the MIP are capable of producing several selective chromatograms from one separation. A dual-channel FPD with data acquisition by computer is capable of similar results (though by electronic, not spectral, means — and with a certain time delay for each chromatogram (10, 32)).

The FPD is, in the best sense of the word, a workhorse. In regard to the important analytical criteria of simplicity and ruggedness, it is patently preferable to the plasma systems. Its "prestige" is lower but so is its price: a simple, single-channel GC–FPD model can be had for under $10K, and it can be operated much more cheaply than the plasma systems, particularly the ICP.

In summary then, and with the understanding that all scores on this issue are by no means in, the FPD is cheaper, simpler, faster, and more reliable than the plasma sources. For a selected, small number of transition elements (Ru, Ni, Cr, Mn) it is of comparable or better sensitivity, selectivity (against carbon), and linear range. It may be marginally suited for a few more metals (Fe, Os, Re), but it is unsuited for several other transition elements for which the high-energy sources should provide good response.

(b) Noise and signal/noise

In accordance with its chromatographic origin, "noise" is defined in this manuscript as the short-term peak-to-peak fluctuation of the baseline. The critical problem here is whether ostensible outliers (signal spikes that are considered non-random, as caused for instance by a diatomaceous particle entering the flame) are to be included; and how short "short-term" should be (note that the result of peak-to-peak measurements of white noise increases with the time period covered). Most chromatographers will liberally exclude outliers; and they will measure over a time/distance that, to them, would include "flicker" but exclude "drift." Usually, that will involve one to ten base widths of an analyte peak. This graphic assessment is simpler to learn and use than to describe; but it is second nature to every chromatographer. It is also surprisingly reproducible in intra- (and, we presume, inter-) laboratory practice, despite being an overtly "subjective" measurement.

Various presumedly "objective" measurements have been described in the literature. They usually consider noise to be random and hence employ the normal (Gaussian) distribution to quantify it. Since the standard deviation (sigma, σ) can be easily and precisely calculated, once data points are stored in a computer and agreement exists on how many and (or) which ones to use, this approach seems preferable. If computer storage (or a suitable RMS meter) is not available, statistical methods based on recorder traces can be used (33). IUPAC recommends a detection limit of $S/\sigma = 3$ (ref. 34, cf. ref. 35), and nowadays its use is often requested by reviewers and editors.

In anticipation of such requests, our in-house computer program CHROM (10) offers a routine called SIGMA. It calculates the standard deviation, σ, of the baseline noise within user-defined time limits (and after removing drift from the baseline, if necessary). It is also capable, though with less accuracy, to calculate σ for fast noise superimposed on a considerably slower peak. We will be using it here to address the important points made by the reviewer.

Since the value of σ appears almost instantaneously on the CRT, it was easy for us to compare many baseline segments of varying duration. They were taken from several isothermal chromatograms (typical length: 20–25 min) that display from 10 to 20 peaks each or, as especially produced for the occasion, show only noise of different intensity. In the CHROM program, data points are taken every tenth of a second. For this additional study, the SIGMA routine was used on baseline segments 10–200 s long (i.e., 100–2000 data points were considered per calculation). Each original chromatogram was sent to a strip-chart recorder (with

Can. J. Chem. Downloaded from www.nrcresearchpress.com by 92.62.229.171 on 09/08/12
For personal use only.

damping off) and the peak-to-peak noise (with disregard for outliers) was graphically determined for the same time segments as examined by the computer.

Isothermal chromatograms are assumed to display constant noise levels throughout. Hence, in an ideal case, the σ values should remain constant while the peak-to-peak distances should increase slightly with the length of the chosen time span. In the experiments, six measurements of 10–60 s duration were taken of the peak-containing chromatograms and seven measurements of 10–200 s duration were taken of the noise-only chromatograms. The objective was to determine the variability of (*a*) the σ values and (*b*) the peak-to-peak noise values; to compare these variabilities; and then to determine the mutual conversion factor, and its variability, within and among the chromatograms. It should be noted that neither the computer-derived σ value nor the graphically determined peak-to-peak noise is a wholly objective measurement, but the latter does admittedly contain more subjective components than the former.

The experiment brought very clear results. The variability of the σ data within each chromatogram was somewhat less than that of the peak-to-peak data; the former ranging from 7 to 14% and the latter from 13 to 16% relative standard deviation. This means that the FPD's short-term noise was fairly constant and that the measurements were well reproducible. The conversion factor, i.e., the ratio of the graphically derived peak-to-peak distance to the computer-determined standard deviation, was calculated for each pair of measurements. It showed similar variability within and among chromatograms: the latter number, based on 27 data pairs, was 5.5 ± 0.4. This variability of only 7% RSD means that the two types of noise measurement can be reliably correlated (though formally only for *our* particular measurement techniques and circumstances).

If "our" noise did indeed conform to a normal distribution, a range of 5.5 standard deviations would include 99.4% of all data points. (If presumed outliers had been included, the number would have been somewhat higher and more dependent on the chosen time span.) This is close to the estimate, commonly employed in spectrophotometry, that σ (the root-mean-square noise) equals one-fifth of the peak-to-peak noise (ref. 36, cf. refs. 37, 38).

In this manuscript we used the ASTM definition commonly agreed upon in chromatography, namely that the minimum detectable amount has a signal/noise ratio of 2, with noise being defined as the short-term peak-to-peak fluctuation of the baseline (outliers disregarded). If we followed IUPAC (ref. 34, cf. ref. 35) recommendations, the limit of detection would be defined as three times the standard deviation of the blank. (Note, however, that IUPAC's LOD concept was developed based on spectroscopic, as opposed to chromatographic, precepts; and that it was designed to evaluate whole analytical procedures, not mere detector performance.) Its use for chromatographic measurements is not a trivial matter and has therefore been questioned (39). If our $N_{p\text{-}t\text{-}p}/\sigma$ ratio equals 5.5, then our minimum detectable amount determined at $S/N_{p\text{-}t\text{-}p} = 2$ involves 11 σ units and is therefore 3.7 times higher than the IUPAC $S/\sigma = 3$ limit of detection. In other words, the IUPAC recommended LOD values could be read from the (linearly extrapolated) calibration curves of Fig. 1 at an ordinate value of $S/N = 0.54$. While this number applies rigorously only to our own particular instruments and procedures, it should not be far from typical.

Thus we could reliably convert the $S/N_{p\text{-}t\text{-}p} = 2$ minimum detectable amounts determined in this paper to the IUPAC $S/\sigma = 3$ limits of detection based on random noise. (That this noise was truly random has not, however, been established!) For practical purposes, though, it still seems reasonable to stick with the initial data. First, the $S/N_{p\text{-}t\text{-}p} = 2$ definition is almost universally accepted among chromatographers, and its use therefore allows the widest comparison with literature data. Second, it is easily carried out on a recorder chart and does not require the services of an appropriately programmed computer. Third, its reproducibility, at least in our experience, is very good, close to that of the computer calculation. This is as far as this manuscript can go: for a more general comparison, such aspects as noise distributions resulting from different types of detectors, effects of ancillary electronic instruments (electrometer, recorder), effects of chromatographic parameters, etc., would all have to be considered.

Figure 1 uses the unconventional ordinate unit "signal/noise." Our reviewer pointed out, and correctly so, that plain "signal" is the *y*-axis most frequently used in spectrophotometry, and that confusion should be avoided between the true S/N ratio of, say, an atomic absorption signal, where N refers to noise measured on the *signal*, and the S/N ratio conventionally given for gas chromatographic peaks, where N refers to noise measured (usually of necessity) on the *baseline*.

First, where is noise best measured? Chromatographic peaks, in contrast to AA signals, do not lend themselves well to the measurement of superimposed noise. The SIGMA routine mentioned above was used to estimate noise on peaks that were close to the $S/N_{p\text{-}t\text{-}p} = 2$ detectability limit. Although the results were approximate, it was obvious that little difference existed between noise measured on the baseline and noise measured on the peak. This is as expected. (Note that FPD noise appearing on a *tall* peak should be larger than the noise appearing on the baseline, but that is of no consequence to a problem involving the detection limit.)

Second, why was "signal/noise," rather than "signal," used for the ordinate of Fig. 1? The experiments that produced these curves were each carried out under *individually S/N-optimized* conditions. If "signal" only had been used for the plot, and the reader were to compare one calibration curve to another in an effort to assess relative signal intensities or comparative detectabilities in planning an analysis, the results could be gravely in error. "Signal/noise", besides alerting the analyst to the potential problem, tends to reduce that error.

Also, just about every element reacts differently to the variation of H_2 and air supply rates in the FPD: some increase with increasing air flow, some decrease, some stay about constant, some show maxima. If, tempted by the signal-only ordinate, we had maximized the signal intensity, the resulting curves would have turned out very different from those produced by maximizing the signal/noise ratio. While signal-only curves have definite value for spectral assignments, and while they make general sense in the context of typical high-energy AES sources, they would have little analytical relevance for the FPD. The "signal-noise" ordinate allows the reader an immediate grasp of the important de-

tection limits. It seems far better suited to comparing a greater number of elements, each of which was determined under its own optimized set of conditions. (These sets also include individually optimized photomultiplier tube voltages that, in turn, introduce further large variations of *absolute* signal strength among the different elements.) Signal/noise measurements are also, of course, recommended for general analytical purposes (38).

Acknowledgements

This research was supported by the Natural Sciences and Engineering Research Council of Canada through operating grant A-9604. We thank Prof. G. Horlick for his most helpful comments.

1. M. Dressler. Selective gas chromatographic detectors. J. Chromatogr. Libr. **36** (1986).
2. P. T. Gilbert. Non-metals. *In* Analytical flame spectroscopy. *Edited by* R. Mavrodineanu. MacMillan, London. 1970. pp. 181–377.
3. S. S. Brody and J. E. Chaney. J. Gas Chromatogr. **4**, 42 (1966).
4. R. Ross and T. Shafik. J. Chromatogr. Sci. **11**, 46 (1973).
5. C. A. Burgett and L. E. Green. Spectrochim. Acta, **30B**, 55 (1975).
6. X.-Y. Sun and W. A. Aue. J. Chromatogr. **467**, 75 (1989).
7. X.-Y. Sun and W. A. Aue. Can. J. Chem. **67**, 897 (1989).
8. X.-Y. Sun and W. A. Aue. Mikrochim. Acta, **I**, 1 (1990).
9. W. A. Aue, B. Millier, and X.-Y. Sun. Anal. Chem. **62**, 2453 (1990).
10. W. A. Aue, B. Millier, and X.-Y. Sun. Can. J. Chem. **70**, 1143 (1992).
11. D. S. Lee. Anal. Chem. **54**, 1182 (1982).
12. D. H. Stedman, D. A. Tammaro, and D. K. Branch. 1976 Pittsburgh Conference Abstract No. 189. Anal. Lett. **9**, 81 (1976).
13. W. F. Meggers, C. H. Corliss, and B. F. Scribner. Tables of spectral line intensities. Part I. National Bureau of Standards Monograph 145. U.S. Government Printing Office, Washington, D.C. 1975.
14. M. L. Parsons and P. M. McElfresh. Flame spectroscopy: atlas of spectral lines. IFI Plenum, New York. 1971.
15. R. W. P. Pearse and A. G. Gaydon. The identification of molecular spectra. 4th ed. Chapman and Hall, London. 1976.
16. R. E. Smith. Proc. R. Soc. Lond. A: **332**, 113 (1973).
17. R. S. Juvet, Jr. and R. P. Durbin. Anal. Chem. **38**, 565 (1966)
18. R. M. Dagnall, B. Fleet, T. H. Risby, and D. R. Deans. Talanta, **18**, 155 (1971).
19. M. B. Kondratenko and V. A. Sokolov. Opt. Spectrosc. **20**, 94 (1966).
20. P. F. McCrea and T. S. Light. Anal. Chem. **39**, 1731 (1967).
21. J. W. Robinson and V. Smith. Anal. Chim. Acta, **36**, 489 (1966).
22. R. S. Braman. Anal. Chem. **38**, 734 (1966).
23. J. J. Kroeten, H. W. Moody, and M. L. Parsons. Anal. Chim. Acta, **52**, 101 (1970).
24. R. M. Dagnall, D. J. Smith, K. C. Thompson, and T. S. West. Analyst, **94**, 871 (1969).
25. F. M. Zado and R. S. Juvet, Jr. Anal. Chem. **38**, 571 (1966).
26. W. A. Aue and C. R. Hastings. J. Chromatogr. **87**, 232 (1973)
27. A. G. Gaydon. The spectroscopy of flames. 2nd ed. Chapman and Hall, London. 1974. pp. 317–319.
28. L. Ebdon, S. Hill, and R. W. Ward. Analyst, **111**, 1113 (1986).
29. P. W. J. M. Boumans and J. J. A. M. Vrakking. Spectrochim. Acta, **42B**, 553 (1987).
30. S. A. Estes, P. C. Uden, and R. M. Barnes. Anal. Chem. **53**, 1829 (1981).
31. B. D. Quimby and J. J. Sullivan. Anal. Chem. **62**, 1027 (1990).
32. W. A. Aue, B. Millier, and X.-Y. Sun. Abstract No. 36, 73rd CIC Conference, Halifax, N.S. July, 1990.
33. J. E. Knoll. J. Chromatogr. Sci. **23**, 422 (1985).
34. Analytical Methods Committee. Analyst, **112**, 199 (1987).
35. G. L. Long and J. D. Winefordner. Anal. Chem. **55**, 713 A (1983).
36. J. D. Ingle, Jr. and S. R. Crouch. Spectrochemical analysis. Prentice-Hall, Englewood Cliffs, N.J. 1988. p. 136.
37. V. D. Landon. Proc. I.R.E. **29**, 50 (1941).
38. T. C. O'Haver. *In* Trace analysis chemical analysis. Vol. 46. *Edited by* J. D. Winefordner. Wiley–Interscience, Toronto. 1976. pp. 28, 29.
39. J. P. Foley and J. G. Dorsey. Chromatographia, **18**, 503 (1984).

Can. J. Chem. Downloaded from www.nrcresearchpress.com by 92.62.229.171 on 09/08/12
For personal use only.

Flame photometric detection of some transition metals. II. Enhancement of selectivity[1]

WALTER A. AUE,[2] BRIAN MILLIER, AND XUN-YUN SUN
Department of Chemistry, Dalhousie University, Halifax, N.S., Canada B3H 4J3

Received May 10, 1991[3]

WALTER A. AUE, BRIAN MILLIER, and XUN-YUN SUN. Can. J. Chem. **70**, 1143 (1992).

A flame photometric detector was used in single-channel and in differential dual-channel modes to characterize and control its selectivity for various transition elements against a hydrocarbon background. The experiments included gas-chromatographable compounds of Cr, Mn, Fe, Co, Ni, Ru, Re, and Os. Single-channel dispersive modes brought only modest gains in selectivity vis-a-vis the non-dispersive (no optical filter) mode. In dual-channel differential modes, however, metal–carbon selectivities could be improved by factors of one to two orders of magnitude. The highest still measurable selectivity ratios are now in excess of 10^7. The differential dual-channel operation of the detector also made it possible to increase the selectivity of one hetero-element vis-a-vis another; and to distinguish between two hetero-elements, by oppositely directed peaks, in a (spectrally suppressed) matrix of carbon compounds. Metal–metal selectivities could be improved by factors of one to three orders of magnitude over the best dispersive single-channel modes.

WALTER A. AUE, BRIAN MILLIER et XUN-YUN SUN. Can. J. Chem. **70**, 1143 (1992).

On a utilisé un détecteur photométrique à flamme opérant dans un mode à canal unique ou dans un mode différentiel à double canal pour caractériser et pour contrôler sa sélectivité vis-à-vis de divers éléments de transition comportant un fond hydrocarboné. Les expériences comportaient des composés du Cr, du Mn, du Fe, du Co, du Ni, du Ru, du Re et du Os pouvant être chromatographiés en phase gazeuse. Par rapport au mode sans dispersion (sans filtre optique), les modes de dispersion à canal unique n'ont apporté qu'une modeste amélioration à la sélectivité. Toutefois, dans les modes différentiels à double-canaux, on a pu améliorer les sélectivités métal–carbone par des facteurs de un à deux ordres de grandeur. Les rapports les plus élevés de sélectivité encore mesurables sont maintenant plus grands que 10^7. L'opération du détecteur dans le mode différentiel à double canal a permis d'augmenter la sélectivité d'un hétéro-élément par rapport à un autre et de distinguer entre deux hétéro-éléments; pour ce faire, on fait appel à des raies directement opposées dans une matrice (supprimée d'une point de vue spectral) de composés carbonés. Par rapport aux meilleurs modes de dispersion en canal unique, on peut améliorer les sélectivités métal–métal par des facteurs de un à trois ordres de grandeur.

[Traduit par la rédaction]

Introduction

Selectivity in the flame photometric detector (FPD) is usually understood to mean the ratio of response from a particular hetero-atom vs. the response from carbon. This is in accordance with the most common use of the FPD: to determine gas-chromatographic analytes containing one particular hetero-element, e.g., sulfur or phosphorus or tin, in sample matrices of a mostly hydrocarbonaceous nature.

As the knowledge of further FPD-active elements has increased, so has the awareness that one element could possibly be mistaken for another. The danger is particularly acute in highly complex, environmental samples of largely unknown composition. This is but one of several reasons why improved understanding and control of selectivity ratios is needed, not just for each element against carbon, but for each element against all the others.

While the conventional interference filter – photomultiplier tube combination makes the FPD a very sensitive device (for elements that do produce strong chemiluminescence), its inherently low spectral resolution and the fact that it often monitors broad molecular bands raise the question of selectivity. Indeed, one of the FPD's teething problems happened to be the spectral interference of the S_2 bands of sulfur with the HPO signal of phosphorus at 526 nm (1). Furthermore, the highest sensitivity is often obtained by operating the FPD in the absence of optical dispersion (i.e., without interference filter). This "open" mode is particularly suited for monitoring *all* kinds of FPD-active elements, and for detecting analytes that produce expansive band systems. But it is also the one mode where selectivities are, in general, at their lowest.

While transition metals are most often determined by those methodologies that employ high-energy, high-resolution atomic spectrometry, several elements have shown analytically useful responses in the low-energy, low-resolution FPD (2). And although the vast majority of the industrially, environmentally, and biochemically important transition metal compounds are not volatile enough to make it through a *gas* chromatograph, they can be processed by capillary liquid chromatography and (or) supercritical fluid chromatography, two techniques that make increasing use of typical GC detectors (including the FPD).

Hence it would appear timely to explore the selectivity of various transition metals against each other. And it would appear challenging to improve such selectivities in the low-resolution FPD to the point where they could compete with those obtained in the high-resolution instruments of atomic spectroscopy.

Selectivity ratios in the FPD vary in accordance with the geometric, chemical, and spectral conditions of the detector. In this study we shall vary only spectral conditions, while imposing the same detector geometry and chemistry on all

[1]Excerpts from this study were presented at the 72nd CIC Conference (Victoria, B.C., June 1989), the 20th Ohio Valley Chromatography Symposium (Hueston Woods, Ohio, June 1989), and a session in honor of Prof. B. Kratochvil at the 73rd CIC Conference (Halifax, N.S., July 1990). This material forms part of the doctoral thesis requirements of X.Y.S.

[2]Author to whom correspondence may be addressed.

[3]Revision received November 29, 1991.

Can. J. Chem. Downloaded from www.nrcresearchpress.com by 92.62.229.171 on 09/08/12
For personal use only.

Can. J. Chem. Downloaded from www.nrcresearchpress.com by 92.62.229.171 on 09/08/12
For personal use only.

analytes. The latter is reasonable because the optimum detector gas flows do not change much from one transition element to the other. In return for this possible minor decrease in sensitivity, the results acquire both general applicability and comparability. The obvious starting point is to define selectivity ratios in the non-dispersive (open) mode. At the next stage, interference filters are chosen for each element, and the measurements are repeated. While this approach defines neither the best possible sensitivity for each element, nor its best possible selectivity against others, it does provide the most general and useful way of dealing with the multitude of potential analytes and chromatographic conditions.

How can selectivity against carbon/hydrogen — or, for that matter, against other transition metals — be further improved? Conventionally, single chromatograms are produced by only one optical channel. Yet, many FPD's have available two channels (a design intended to allow the simultaneous detection of phosphorus and sulfur), and one channel can be subtracted from the other with relative ease to produce a *differential* single output. We have used such an approach recently in the determination of methylcyclopentadienylmanganesetricarbonyl (MMT) in gasolines (3). Briefly: one channel monitored the wavelength at which the metal responded best but at which some response from carbon compounds was also seen; the other monitored a wavelength where carbon responded well but response from the metal was weak (or, preferably, absent). One of the amplified outputs was then attenuated such that the carbon responses in the two channels became equal, and hence vanished when one channel was subtracted from the other.

For this approach to be successful, the relevant emission spectra have to be known *at the analytical operating conditions* of the detector. For some FPD-active transition elements, as well as for different types of carbon compounds, such spectra have recently been determined (2).

The simple subtraction circuit we described earlier (3) would be too cumbersome and time-consuming to use for the measurement and manipulation of a larger number of transition-element selectivities. It requires multiple runs for establishing an acceptably precise intensity ratio of the two channels, or for subjecting the same sample to different modes of discrimination. On the other hand, such a circuit accepts a wide range of signal levels and, because of its simplicity and on-line operation, does appear preferable for routine analyses.

Two types of signal-processing devices were therefore developed. The first device is a more sophisticated version of the earlier circuit (3). This "Analog Interface" is designed to serve in simple tasks where the signals from the two electrometers, after scaling by a given factor, are used to produce a subtraction chromatogram on the recorder chart.

The second device is a computer-based system capable of performing a much wider variety of measurements and manipulations. This "Computer System" can store high-quality two-channel detector signals, filter digital data, correct baselines, scale channels with high precision, measure basic selectivity ratios and minimum detectable quantities, establish best analytical conditions, and subject single data sets to sequential algorithms that represent disparate selectivity regimes.

Such data-processing capabilities should be of interest beyond the confines of this study. For instance, they lend themselves to conventional analytical development and are helpful in the analysis of those environmental samples that are severely limited in supply and highly complex in composition: data from a single injection can generate several chromatograms of different selectivity and information content.

What effects can prevent the differential FPD mode from reaching infinite selectivity (= specificity) for the chosen metal vis-a-vis carbon? First, very large amounts of *any* compound disturb the extremely weak flame and lead to the kind of baseline fluctuation (involving, one assumes, changes in flame chemistry and hence both background and analyte spectra) that even the best differential circuitry cannot cancel. Second, it is well known that the FPD signal for carbon compounds depends to some degree on their structure: for instance, aliphatics respond more weakly than aromatics. The spectral profiles, while similar in one wavelength region, differ strongly in another (2). Consequently, the choice of a carbon standard with which to match the two channels can be crucial. Third, the position (retention) of a particular compound in a complex, temperature-programmed chromatogram can influence its response. The gas flow, the temperature, the column bleed, and the detector memory (e.g., from contamination by residual and (or) decomposed analyte) are all subject to change during the run. Fourth, there always exists the possibility that a co-eluting species may influence the response of the analyte, or that it may, by itself, produce response on one or both of the two channels. Fifth, the luminescence phenomena may not be of perfect spatial symmetry in regard to the two observation channels. Sixth, conventional GC electrometers are unlikely to meet the unusual, severe linearity requirements posed by the differential mode when it attempts to cancel a peak that is orders of magnitude larger than the operating scale. Peak distortions induced by two different R-C output circuits, for instance, are unlikely to match one another within the precision required for complete peak cancellation under overload conditions.

A truly comprehensive survey of *inter-metal* selectivity would be a time-consuming task. More to the point, its practical value could be questioned in light of disparate commercial FPD designs and the myriad of possible analytical circumstances under which these are used. We shall therefore rely on typical chromatograms as opposed to numerical tables to characterize the situation. In several simplified examples we shall illustrate what selectivity can be expected from a typical FPD, and how it can be manipulated.

The conventional way to improve FPD selectivity is to use a single channel with the best overall choice of interference filter for one element against another. A second way is to use a differential mode in which two channels are deducted from each other such that response from one element is maintained and response from the other element cancelled. Yet a third way is to use a differential mode in which the two channels are deducted such that both elements produce strong responses, but in opposite directions. (This "qualitative" form of selectivity makes sense only when compounds containing the two elements are chromatographically resolved, and when a multicomponent sample is to be scanned for the presence of particular elements.) A variant of the latter mode matches channels with the additional purpose of annulling carbon response. We shall examine all these types of selec-

tivity adjustments, while keeping in mind the continued integrity of calibration curves and other analytical performance criteria.

A word should be added here about the method used to measure various selectivity ratios. Selectivity ratios, to restate the conventional definition, are the ratios of response produced by equal amounts of analytes or, alternatively, the ratios of analyte amounts that produce the same response. These alternative definitions represent the horizontal (amount) and vertical (response) distances between conventional calibration curves.

Thus, a complete picture of selectivity among two or more compounds can be given only by a comparison of their fully extended calibration curves. If a *single number* is to suffice for describing a two-compound (and, by inference, a two-element) selectivity, it needs to be determined with *both* compounds well within their respective linear ranges. For a metal/carbon ratio, for instance, much higher "selectivity ratios" can be recorded if the interferent hydrocarbon is used in amounts beyond its linear range. In this study, all calibration curves are linear at low concentrations, and the choice was therefore made to determine the selectivity ratios from minimum detectable analyte flow rates. This approach, while somewhat more time-consuming, assures the applicability of results within respective linear ranges, and carries with it the additional benefit of defining the analytically important detection limits under a variety of optical (but a common set of chromatographic) conditions.

Experimental

A short description of the conventional gas chromatographic system and simple spectroscopic accessories can be found in the companion manuscript (2). The only major difference is that, in this study, the flame gas supplies were kept constant throughout at 300 mL/min hydrogen and 60 mL/min air.

The potentiometer, which regulates the photomultiplier tube voltage and is normally located inside the Shimadzu electrometer, was replaced by an external one for optimizing the dynode voltage to give a close-to-maximum S/N ratio (re the definition of N see the Note added in Revision to the companion manuscript (2)). A typical setting for our R-268 tube in open-mode runs was 550 V. Prior to data processing, large-step signal attenuations were carried out as usual at the electrometer level.

The analog interface

The interface was set up not only to display on-line differential (subtraction) chromatograms on a strip-chart recorder, but also to transmit unmodified signals to the data acquisition system of the computer. This circuit, a "2-channel low-pass filter," is shown in Fig. 1. It consists of an input attenuator (a ten-turn potentiometer with vernier dial) and a three-pole active filter. This circuit is duplicated for the second channel, and a simple switch selects either the intact two channels or their difference for output to the recorder. The potentiometers offer calibrated attenuation for each channel, and a choice of nominal cut-off frequencies is available via independent switches.

An advantage of this analog approach over the computer acquisition method is its dynamic range. Signals entering this circuit are typically on the order of 10 mV for a full-scale recorder output. Yet, large signals approaching 10 V can be accommodated, since the circuit is built for *passively* subtracting one signal from the other (see S4 in Fig. 1) before any filter action or amplification takes place. The CMRR (common mode rejection ratio) in this passive circuit is, in theory, infinite. When operated in the independent two-channel mode, signal overloads will make the two recorder pens go off scale. But, in the differential mode, the circuit has the ability to subtract signals much greater in amplitude than the chosen recorder scale. This contrasts with the developed computer acquisition system, which offers signal extension (data storage capacity) to two full scales, but which cannot approach the wide dynamic range of the analog interface. (A wider-ranging computer system, should it be needed for a particular purpose, appears entirely feasible.)

The computer system

For digital data processing, the "integrator" outputs of the two Shimadzu electrometers are connected to the computer through an interface. This interface is built around an IBM PC Prototype card, the schematic for which is available in the IBM PC Technical Reference Manual, publication 6025005. The schematic for the custom part of the circuit ("2-channel chromatographic interface") is given in Fig. 2.

The circuit consists of two identical channels. A simple R–C filter at the input blocks high-frequency noise. This is necessary as any noise with frequencies above 1/2 the sampling rate (10 Hz) must be removed prior to sampling and converting the analog detector output signal to a digital value; otherwise aliasing noise will be present in the digital data. A voltage-to-frequency converter is used to transform the signal to a digital pulse train, and a counter accumulates these pulses over 0.1 s intervals. A full-scale input signal will produce a digital count value of 16 000, providing resolution about equal to that of a 14-bit analog-to-digital converter. The input voltage to this circuit, required to produce the full-scale digital output, is about 200 mV. The Shimadzu electrometers' "integrator" outputs are slightly modified to provide the computer with a signal 10 times the amplitude of that sent to the recorder. Therefore the computer offers a 2:1 over-ranging capability compared to the recorder, assuming the latter is operated on its 10 mV scale.

An Analog Devices AD567 digital-to-analog converter generates an analog signal that is fed to a dedicated strip chart recorder for hard-copy output of computer-processed chromatograms. Since the DAC output is 0–10 V, that strip-chart recorder operates on its 10-V range.

To provide for a data display of satisfactory appearance and reasonable operating speed, the hardware configuration includes a 12 MHz AT-compatible computer with one megabyte memory, 40 meg hard disk, 80287 math coprocessor, VGA display adapter, and Multi-Sync monitor.

The program, named "CHROM," is written in compiled Quick Basic, which generates reasonably fast code. All data acquisition is performed by assembly language routines using interrupts for timing accuracy. However, due to the large amounts of data collected per run, a math coprocessor is needed to allow data manipulation such as filtering and scaling at a speed acceptable to the user.

The program samples the two channels every 0.1 s and provides up to 1600 seconds (26′40″) readout on the screen. The sample injection is marked and two horizontal and two vertical cursors appear for manipulation of the two chromatograms. The vertical cursors define the time section to be worked on; the horizontal cursors set the baselines and allow the approximate measurement of peak heights in subsequent routines.

In typical operation, a time window is selected and the peak(s) it contains are horizontally expanded to fill the screen. At this, as well as at later stages, several routines are available that offer convenient data processing such as cubic-spline baseline correction, digital filtering, and numerical definition of the baseline noise in Gaussian parameters. One peak is selected as a tuning standard for cancellation of its cogeners; e.g., dodecane may be selected for cancelling aliphatics. In both channels, the height of this standard peak is vertically defined by two horizontal cursors for a rough first measurement. The algorithm then scale-expands one of the channels in order to equalize the two peak heights, deduct one channel from the other, and display the result. It also lists on the screen the "magnification factor" (scaling factor) of one channel over the other, and keeps track of any changes in that number during further manipulations. For fine-tuning, the program then proceeds through

Can. J. Chem. Downloaded from www.nrcresearchpress.com by 92.62.229.171 on 09/08/12
For personal use only.

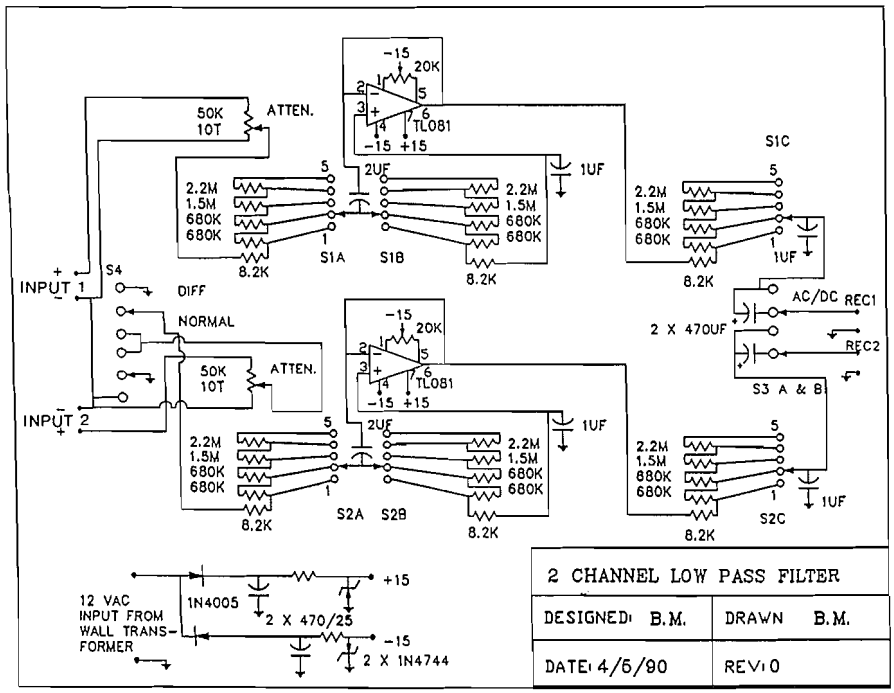

FIG. 1. Analog Interface for manipulation and recording of independent or dual-channel differential chromatograms.

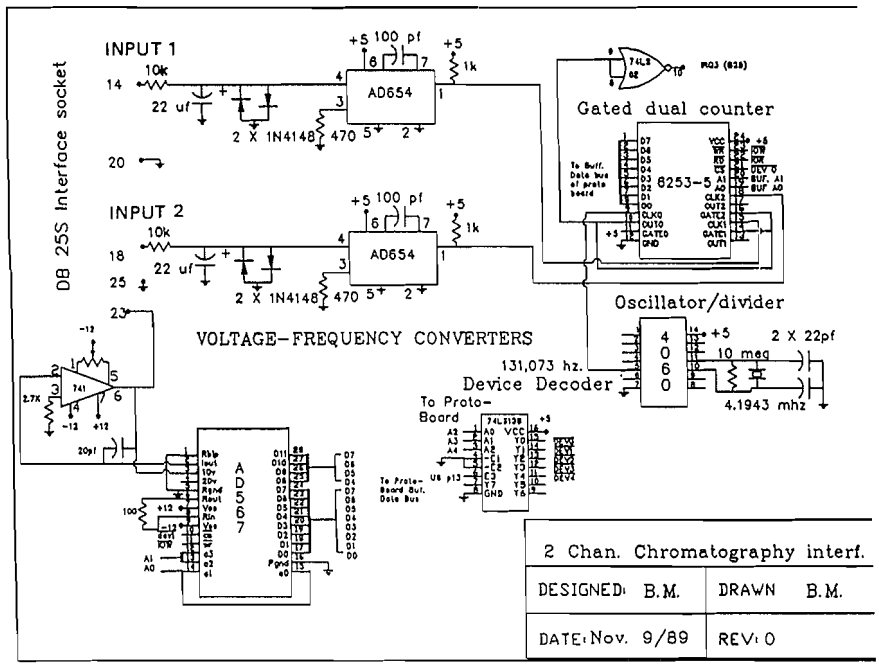

FIG. 2. Computer System interface for computer input and output of dual-channel chromatograms.

several user-prompted iterations in which the two-channel intensity ratio is changed by small increments. The visually "best" iteration is selected by the user to scale *all* of the data. This final magnification factor can be employed directly in further computer runs and (or) it can be manually transferred to the "Analog Interface." For analytes contained in complex matrices, this routine works well for obtaining the best overall discrimination against the background. The resulting differential chromatogram (plus magnification factor) can be stored on hard disc like any conventional chromatogram. It can also be processed using the routines described above (digital filtering, etc.) and can be sent, with or without time indicators, to its dedicated strip-chart recorder.

Results and discussion

The molar detection limits of metals (in organometallics), as well as carbon (in three selectivity probes) and nitrogen (in indole), are listed in Table 1 for the same, standard conditions in non-dispersive, single-channel FPD mode. These numbers can be used to calculate "innate" molar se-

Can. J. Chem. Downloaded from www.nrcresearchpress.com by 92.62.229.171 on 09/08/12
For personal use only.

TABLE 1. Molar detection limits of organometallics and standard carbon compounds in single-channel open mode with R-268 and R-1104 PMT's

Element	Compound	MDL[a]		Selectivity[b]	
		R-268	R-1104	R-268	R-1104
Ru	$Ru(C_5H_5)_2$	4×10^{-15}	5×10^{-15}	5×10^5	7×10^5
Ni	$Ni(C_5H_5)_2$[c]	2×10^{-14}	1×10^{-14}	1×10^5	4×10^5
Cr	$Cr(CO)_6$	6×10^{-14}	5×10^{-14}	4×10^4	7×10^4
Os	$Os(C_5H_5)_2$	9×10^{-14}	8×10^{-14}	2×10^4	5×10^4
Fe	$Fe(C_5H_5)_2$	1×10^{-13}	9×10^{-14}	2×10^4	4×10^4
Mn	$C_5H_4CH_3Mn(CO)_3$	1×10^{-13}	1×10^{-13}	2×10^4	4×10^4
Re	$Re_2(CO)_{10}$	5×10^{-13}	2×10^{-13}	4×10^3	2×10^4
Co	$Co(C_5H_5)_2$	2×10^{-12}	2×10^{-12}	1×10^3	2×10^3
C	Dodecane	2×10^{-9}	4×10^{-9}[d]		
C	Naphthalene	2×10^{-9}	2×10^{-9}		
C	Di-*n*-hexyl ether	3×10^{-9}	7×10^{-9}		
N	Indole	2×10^{-11}	2×10^{-11}		

[a]Molar detection limit, in mol of designated metal per second, measured at signal/noise = 2, with noise defined as the peak-to-peak short-term baseline fluctuation. Divide numerical value by 3.7 to obtain approximate detection limit according to the $S/\sigma = 3$ IUPAC definition (cf. Note Added in Revision in ref. 2).

[b]Minimum detectable mole of carbon in dodecane/minimum detectable mol of metal; (mol C/s)/(mol Me/s).

[c]A 0.5 m 5% Carbowax 20M column was used.

[d]Negative (inverted) analyte peak.

lectivities for atoms of one element against atoms of another. Such selectivities are listed in Table 1 for transition elements versus carbon. Inter-metal selectivities can be calculated in the same manner.

The response of a standard compound containing one metal atom (the usual case) could serve to construct a molar calibration curve valid for all analytes containing one atom of that metal. Or, nearer the current context, the selectivity of a particular metal vis-a-vis others could be used to define the molar selectivity behavior for all compounds containing these metals. However, that approach requires caution. It cannot be automatically assumed that every response observed is a strictly linear function of the amount of hetero-atom injected (although most of the time this is likely to be the case). For one, different compounds containing the same hetero-atom may be subject to different degrees of on-column decomposition. Also, response may to some extent depend on compound structure.

In those cases where a few compounds of the same metal have actually been tested, i.e., in the studies of iron (4) and manganese (3), response was roughly proportional to metal content. Other transition elements were not examined in that context (owing mainly to the limited commercial availability of suitable test compounds) but they should prove equally well behaved.

In the case of different types of carbon compounds, however, response is not proportional to carbon content. For instance, aromatics respond more strongly than aliphatics. There also exists considerable literature on the response of sulfur compounds depending — or, for other authors, not depending — on the type of functional sulfur group present. And, when a particular hetero-element responds but weakly in the FPD, special caution is called for. In the case of the nitrogen compound indole, for instance, the response will obviously contain some contribution from indole's aromatic carbons. Since this contribution is relatively small compared to that of nitrogen, it is disregarded in our calculation. The only reason why we have included indole here at all is to draw attention to the fact that nitrogen compounds, which often occur in complex sample matrices, do respond more strongly than carbon compounds and that they, because of their different spectrum, demand a different magnification ratio prior to subtraction. Having duly mentioned these caveats, we feel that FPD sensitivities and selectivities, which are reported in a general manner based on moles of atoms, are of wider analytical significance than those which are based on grams of compounds actually measured; hence the former are used in the tables. In any case, such data can be easily reconverted, i.e., recalculated to give the weights of the initial test compounds, within the precision allowed by one significant digit.

The reason that data in Table 1 (as in all other tables) are reported in this manner is that they are derived from minimum detectable amounts (which, to the purist, admit to only one significant figure). Also, one-digit data are used in awareness of the changes in detector sensitivity that occur with the passage of time, the variation of temperature, the severity of contamination, and the switching of individual photomultiplier tubes. Still, measurements were always taken, and calculations always carried out, on the basis of two or more significant digits.

Minimum detectable amounts and selectivity ratios are recorded here for the two most common types of photomultiplier tubes used with the FPD. These are, in Hamamatsu codes, the R-268 (bialkali, 300–650 nm) and the red-extended R-1104 (multi-alkali, 180–850 nm). Differences between the two sets of results conform to expectations based on analyte spectra. The important fact, however, is that these differences are comparatively small: they do not exceed a factor of five.

Can. J. Chem. Downloaded from www.nrcresearchpress.com by 92.62.229.171 on 09/08/12
For personal use only.

TABLE 2. Molar detection limits and selectivities of transition metals against carbon in single-channel dispersive mode, R-268 PMT

Metal	Compound	Max. (nm)	Filter (nm)	MDL[a] (mol/s)	Selectivity[b] against C_{RH}	C_{ArH}	C_{R_2O}	N_{ArN}
Ru	$Ru(C_5H_5)_2$	484	480	8×10^{-15}	1×10^6	6×10^5	2×10^6	3×10^3
		528	530	4×10^{-15}	4×10^6	5×10^5	5×10^6	6×10^3
Ni	$Ni(C_5H_5)_2$	508	510	1×10^{-14}	3×10^6	3×10^5	3×10^6	2×10^3
		542	540	1×10^{-14}	1×10^6	2×10^5	2×10^6	2×10^3
		572	570	7×10^{-15}	3×10^6	1×10^6	6×10^6	1×10^4
Cr	$Cr(CO)_6$	428	430	9×10^{-14}	3×10^4	1×10^4	7×10^4	5×10^2
		478	480	2×10^{-13}	5×10^4	3×10^4	6×10^4	1×10^2
Os	$Os(C_5H_5)_2$		720 cut-on			Not applicable		
Fe	$Fe(C_5H_5)_2$	345	340	8×10^{-13}	2×10^5	2×10^5	$>4 \times 10^5$	7×10^2
Mn	$C_5H_4CH_3Mn(CO)_3$	403	405	2×10^{-14}	1×10^5	9×10^4	2×10^4	1×10^3
		540	540	2×10^{-13}	6×10^4	1×10^4	1×10^5	1×10^2
Re	$Re_2(CO)_{10}$		553	1×10^{-12}	9×10^3	2×10^4	3×10^4	5×10^1
			500 wide-band	1×10^{-12}	4×10^3	2×10^3	1×10^4	1×10^1

[a]Molar detection limit, mol metal per second, at S/N = 2.
[b]Minimum detectable mole carbon per second in dodecane (RH), naphthalene (ArH), or di-*n*-hexyl ether (R_2O); or mol nitrogen per second in indole (ArN); divided by minimum detectable mol metal per second.

TABLE 3. Molar detection limits and selectivities of transition metals against carbon in single-channel dispersive mode, R-1104 PMT

Metal	Compound	Max. (nm)	Filter (nm)	MDL[a] (mol/s)	Selectivity[b] against C_{RH}	C_{ArH}	C_{R_2O}	N_{ArN}
Ru	$Ru(C_5H_5)_2$	484	480	8×10^{-15}	1×10^6	5×10^5	7×10^5	2×10^3
		528	530	4×10^{-15}	2×10^6	6×10^5	4×10^6	9×10^3
Ni	$Ni(C_5H_5)_2$	508	510	6×10^{-15}	9×10^5	5×10^5	3×10^6	5×10^3
		542	540	1×10^{-14}	9×10^5	2×10^5	1×10^6	3×10^3
		574	570	9×10^{-15}	2×10^6	8×10^5	1×10^7	6×10^3
Cr	$Cr(CO)_6$	428	430	1×10^{-13}	2×10^4	2×10^4	2×10^4	2×10^2
		478	480	2×10^{-13}	4×10^4	2×10^4	3×10^4	2×10^2
Os	$Os(C_5H_5)_2$		720 cut-on	9×10^{-14}	1×10^4	7×10^3	2×10^4	1×10^3
Fe	$Fe(C_5H_5)_2$	345	340	2×10^{-12}	5×10^4	5×10^4	1×10^5	2×10^2
Mn	$C_5H_4CH_3Mn(CO)_3$	403	405	3×10^{-14}	9×10^4	3×10^4	1×10^5	2×10^3
		540	540	4×10^{-13}	2×10^4	4×10^3	3×10^4	7×10^1
Re	$Re_2(CO)_{10}$		553	1×10^{-12}	1×10^4	1×10^4	4×10^4	5×10^1
			500 wide-band	1×10^{-12}	8×10^3	2×10^3	3×10^4	1×10^1

[a]Molar detection limit, mol metal per second, at S/N = 2.
[b]Minimum detectable mol carbon per second in dodecane (RH), naphthalene (ArH), or di-*n*-hexyl ether (R_2O); or mol nitrogen per second in indole (ArN); divided by minimum detectable mol metal per second.

The "innate" metal–carbon (carbon as in dodecane) selectivities for the clearly responding metals Ru, Ni, Cr, Os, Fe, Mn, and Re fall between 7×10^5 and 4×10^3 in non-dispersive mode, i.e., roughly between three and six orders of magnitude. These numbers could be expected to rise in the dispersive mode.

Results from dispersive, single-channel detection using a variety of filters are listed in Table 2 for the R-268 tube, and in Table 3 for the R-1104 tube. "Best" selectivities for each metal against carbon (again as in dodecane) now range from 4×10^6 to 1×10^4. This very small extent of improvement may come as a surprise to the reader who is accustomed to responses in the FPD being called "specific" and that behaviour being attributed to the choice of a particular interference filter. However, the numbers listed in Tables 2 and 3 for various transition metals are consistent with their respective spectra, i.e., with the location of the chosen metal wavelength in relation to the broad emissions of carbon

Can. J. Chem. Downloaded from www.nrcresearchpress.com by 92.62.229.171 on 09/08/12
For personal use only.

TABLE 4. Selected inter-metal selectivities, Me vs. X[a] at various wavelengths in single-channel mode

Metal	Filter (nm)	X							
		Ru	Ni	Cr	Fe	Mn	Os	Re	Co
Ru	480	(1)	1×10^1	2×10^1		$>1 \times 10^2$			
	530	(1)		1×10^1	4×10^1	9×10^1	1×10^1	8×10^1	3×10^3
Ni	510	2	(1)			9×10^1			
Cr	430	2×10^{-1}		(1)	4	6	8	6×10^1	8
Fe	340	2×10^{-2}		5×10^{-1}	(1)	$>1 \times 10^2$	$>1 \times 10^2$	$>1 \times 10^2$	$>1 \times 10^2$
Mn	405	3×10^{-1}		7	9	(1)	4×10^1	3×10^2	3×10^2

[a]Minimum detectable mol X per second divided by minimum detectable mol Me per second; R-1104 PMT. Note: selectivity values given as ">" are derived from chromatograms where the peak height of X was smaller than, and was therefore replaced by, the noise level.

Can. J. Chem. Downloaded from www.nrcresearchpress.com by 92.62.229.171 on 09/08/12
For personal use only.

compounds (2), as well as with the extent to which the metal spectra are dominated by lines or sharp bands as opposed to broad bands and continua. The factors that describe the improvement (or, occasionally, impairment) in selectivity, from the better suited of the two photomultipliers in the open mode, to the best filter/photomultiplier tube combination in the dispersive mode, never exceed one order of magnitude. Atomic selectivities vis-a-vis carbon (carbon as in dodecane) are thus bettered by a factor of 6 for Ru, 8 for Ni, 5 for Fe, and 3 for Mn, and worsened by a factor of 0.7 for Cr, 0.2 for Os, and 0.5 for Re.

Similarly, enhancement of selectivities among the various transition metals themselves depends on their spectra: how far and in what complexity they cover, in relation to each other, the accessed wavelength range. Some selectivity ratios are listed in Table 4; they were chosen for general importance as well as for later reference. These results suggest that the improvement in inter-metal selectivity from non-dispersive to single-channel dispersive mode, i.e., the improvement obtained from the judicious choice of an interference filter, is rather limited. If the numbers in Table 4 are compared with the open-mode metal–metal selectivities easily extracted from Table 1, most improvements of selectivity amount to no more than one order of magnitude. For instance, the improvement in selectivity from the best non-dispersive to the best dispersive mode involves a factor of 2 for Ru/Ni, Ru/Cr, Ru/Fe, Cr/Ru, Cr/Fe, and Cr/Re; a factor of 3 for Cr/Mn; and a factor of 4 for Cr/Fe, Cr/Os, and Ru/Mn (in these analyte/interferent pairs, the first-named element is considered the analyte and hence determines the choice of the interference filter). There are other cases where no improvement, or even some impairment, is noticed in progressing from a non-dispersive to a dispersive mode: this happens in the pairs Ru/Os, Ru/Re, Fe/Ru, and Fe/Cr. The *significant* improvements occur mainly in cases involving iron, Fe/Mn, Fe/Os, Fe/Re, where factors can exceed two orders of magnitude. This is due to the fact that Fe is monitored at 340 nm, where only a few of the other metals luminesce.

As mentioned earlier, a frequently held perception equates the use of an interference filter in the FPD with "specific" response for the monitored element. Within the confines of this study, such was definitely not the case. In fact, we doubt that true specificity (= infinite selectivity) can ever be associated with the use of a particular wavelength. To obtain more significant improvements than single-channel dispersive operation can offer, *dual*-channel differential modes must be used.

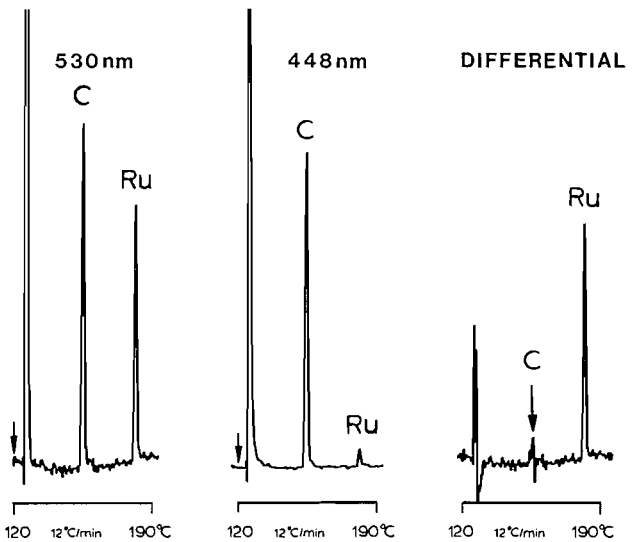

FIG. 3. Single-channel and dual-channel differential chromatograms of a sample containing 30 μg dodecane (C) and 300 pg $Ru(C_5H_5)_2$ (Ru) in acetone. Analog Interface.

A simple example is presented in Figure 3, which shows the separation of 30 μg of dodecane and 0.3 ng of ruthenocene. The chromatogram on the left was acquired from a single channel at 530 nm. This monitors a major wavelength of Ru that yields the best discrimination against carbon. The peaks are almost of the same height, suggesting a compound-to-compound selectivity of 7.4×10^4 (corresponding to an atomic Ru/C selectivity of 1.2×10^6). The chromatogram shown in the middle was taken from a single channel at 448 nm, where the ruthenium emission is fairly weak. The chromatogram captioned "Differential" was obtained from the 530/448 nm dual-channel differential mode tuned for quantitative discrimination against carbon. The amount of dodecane had been deliberately chosen from the upper end of its linear range, where its concentration just becomes large enough to start distorting the Gaussian peak shape. A vacillating, clearly non-Gaussian, signal appears in place of the dodecane peak. Even counting the full vertical pen displacement caused by this perturbation, the compound-to-compound selectivity is now in excess of 10^6, the atomic ruthenium-to-carbon selectivity in excess of 10^7.

Can. J. Chem. Downloaded from www.nrcresearchpress.com by 92.62.229.171 on 09/08/12
For personal use only.

For any reasonable analytical purpose, this seems more than adequate.

If still larger amounts of dodecane are injected, the peak distortion in single-channel mode becomes clearly visible and the characteristic flip-flop pattern of the differential mode intensifies. But does this flip-flop arise from the peak asymmetry (which, after all, is seen by both photomultipliers)?

As will be demonstrated later, purely electronic distortion is likely present in such peak remnants. But limitations of an other than electronic nature can contribute as well. This is not surprising, taking into account the puny and feeble FPD flame. Note for instance that, at the apex of the carbon peak shown in Fig. 3, the combustion of dodecane already requires more than 3% of the detector's oxygen supply, and significant changes in flame size, temperature, chemistry, and flicker behaviour could be expected under such severe overload.

Beyond electronic artifacts and flame perturbations, carbon compounds pose special difficulties that stem from the infinite variety of their structures. In particular, the spectra of aromatics are more intense than those of aliphatics in the 480–660 nm region (2). This is chromatographically illustrated in Fig. 4 with a mixture of three carbon compounds. The differential mode, when using two channels at 448 and 530 nm via the computer system, can cancel either the aromatic or the two aliphatics, but it cannot cancel all three at the same time. For producing the right-hand chromatogram in Fig. 4, the two channels are so tuned that the result distinguishes between aromatics and aliphatics in a qualitative sense, i.e., by the direction of response. While this would seem interesting in a general analytical context, it should be noted that the FPD's sensitivity to carbon is very low, and that ambiguous results can be expected from molecules combining different sites/degrees of saturation.

Still, it is possible to cancel all three carbon compound types if other wavelengths are used. The relevant spectra (2) suggest that wavelengths up to about 440 nm should be suitable. A chromatogram of the same three carbon compounds shown in Fig. 4, together with compounds of chromium and nitrogen (plus an impurity of unknown composition), is shown in Fig. 5. The differential mode, tuned to forestall the appearance of carbon compounds, achieves that objective quite well, despite the fact that the latter are of very different structure and overall spectrum. Thus, if no other circumstances militate against it, 430 nm (or a wavelength close to it) is the preferred choice for the channel used to neutralize the response of carbon compounds. (Obviously, the analyte channel wavelength also has to be lower than 440 nm.)

The eradication of carbon response can also be achieved while, at the same time, the two metals are being qualitatively differentiated by the direction of their peaks. This is shown for manganese and chromium in Fig. 6. Clearly, this detector mode can be easily extended to most if not all FPD-active elements, and should be of particular help in screening-type analyses.

Note that in Fig. 6 the solvent peak is not completely cancelled in the differential mode. This particular tuning and subtraction process, similar to the one whose results are shown in Fig. 5, was carried out by the Computer System. In contrast to the Analog Interface, the Computer System is not capable of subtracting a very large peak from its second-channel counterpart. What is shown in Fig. 6 as a clipped solvent peak merely represents the ratio of the upper limits of the two channels. Similarly, this ratio just happened to coincide with the baseline in Fig. 5, perhaps falsely suggesting there that the solvent acetone had been entirely suppressed. Obviously, this limitation in range of the Computer System does not affect peaks that are smaller than two full scales.

The next series of simplified chromatograms is designed to explore and illustrate the degree of control and the improvement of measured selectivity ratios that can be typi-

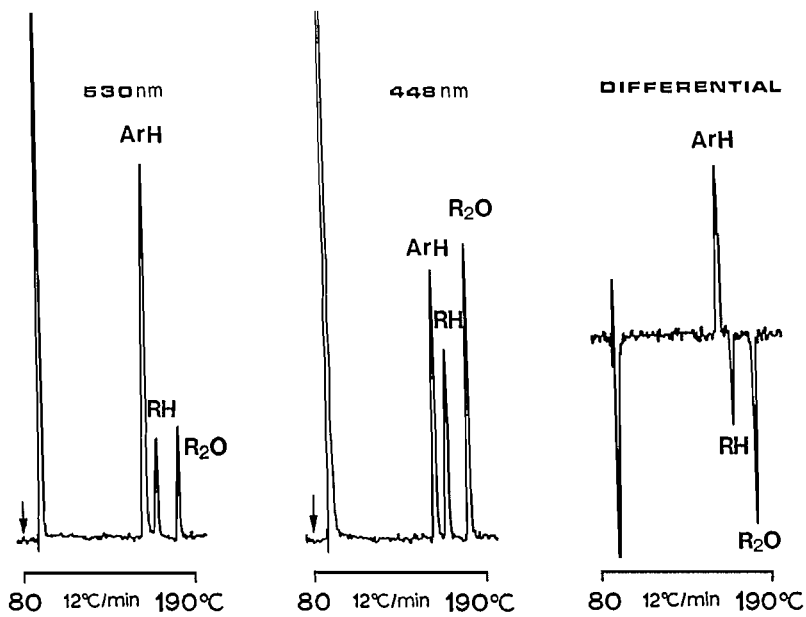

FIG. 4. Single-channel and dual-channel differential chromatograms of a sample containing 10 μg naphthalene (ArH), 10 μg dodecane (RH), and 15 μg di-*n*-hexyl ether (R_2O) in acetone. Computer System.

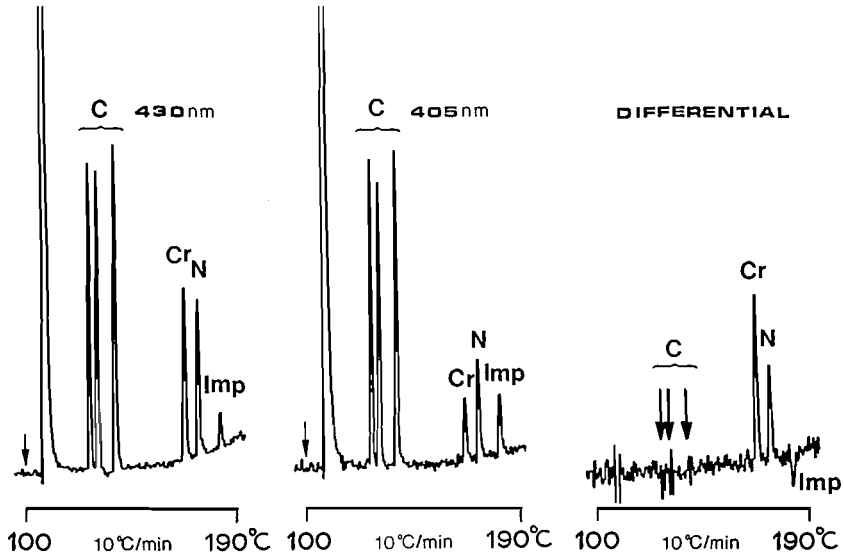

FIG. 5. Single-channel and dual-channel differential chromatograms of a sample containing 8 μg naphthalene, 8 μg dodecane, and 12 μg di-*n*-hexyl ether (C), together with 4 ng $C_6H_6Cr(CO)_3$ (Cr) and 600 ng indole (N) in acetone. Imp = impurity of unknown composition. Computer System.

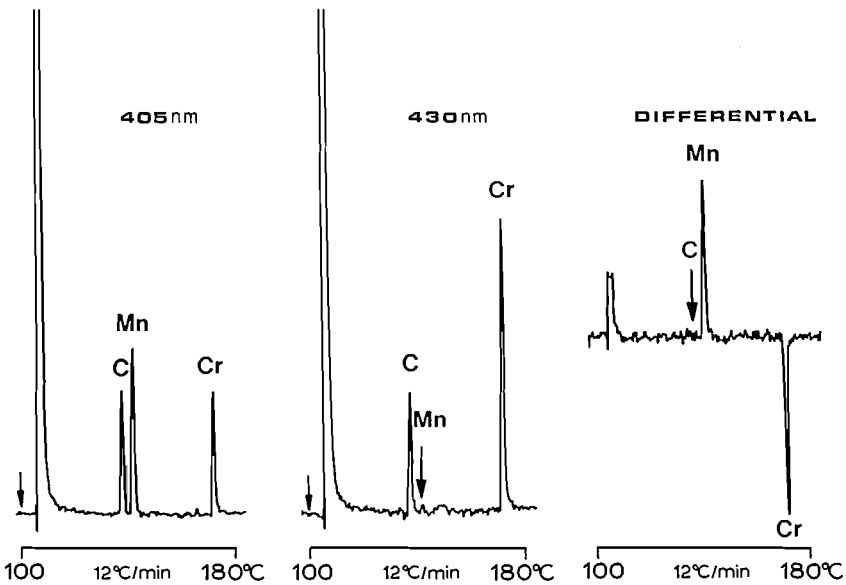

FIG. 6. Single-channel and dual-channel (carbon-suppressed) differential chromatograms of a sample containing 5 μg dodecane (C), 500 pg $C_5H_4CH_3Mn(CO)_3$ (Mn), and 4 ng $C_6H_6Cr(CO)_3$ (Cr) in acetone. Computer System.

cally expected for two transition metals. This example uses ruthenium and chromium. To set the scene, the series starts with single-channel chromatograms. The left side and the middle of Fig. 7 show these channels, at preferred wavelengths for the analysis of Ru (480 nm) and Cr (430 nm). Note that the single-channel operation provides only a modest enhancement of selectivity vis-a-vis the open mode and that, in a complex "real-life" situation, it might even fail to distinguish between the two metals. The *dual*-channel operation, in its qualitative mode, achieves that distinction quite readily (right side of Fig. 7). For the more important quantitative mode, the same channels are tuned (scaled) to different ratios, with the result that either Ru or Cr are annulled (Fig. 8). This absence of any visible trace of interferent begs the question: how large an amount of either of these two species can the system cancel? In other words, how large an improvement in selectivity can the differential modes provide?

The original demonstration sample for Figs. 7 and 8 had been mixed so that it would furnish comparably sized peaks in non-dispersive mode, and thence easily observable peaks for both species in the two single-channel modes. Both of these peaks, by having been obliterated in the differential mode, established lower limits to the respective selectivity ratios. For extending the measurement further, however, *two* mixtures must be made in which either one or the other compound is heavily fortified. But how heavy?

As pointed out earlier, amounts of interferents from be-

Can. J. Chem. Downloaded from www.nrcresearchpress.com by 92.62.229.171 on 09/08/12
For personal use only.

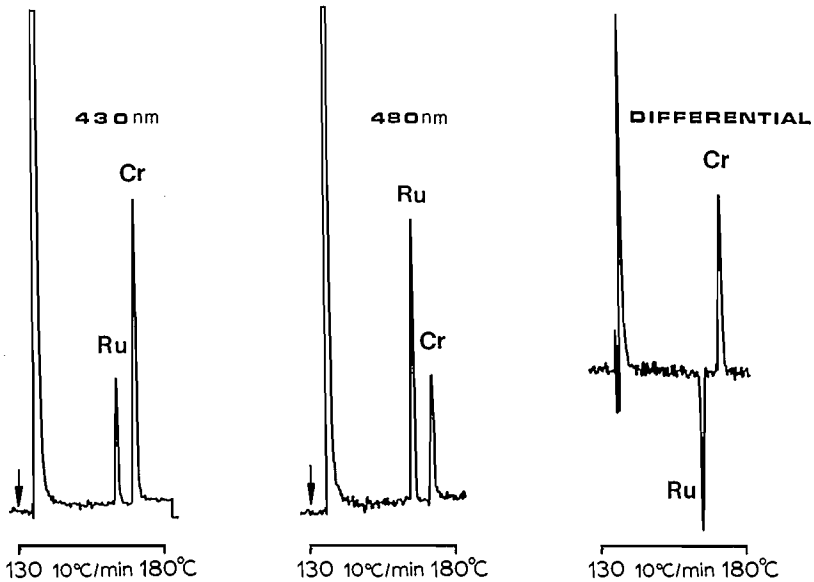

FIG. 7. Single-channel and dual-channel differential chromatography of a sample containing 500 pg $Ru(C_5H_5)_2$ (Ru) and 4 ng $C_6H_6Cr(CO)_3$ (Cr) in acetone. Computer System.

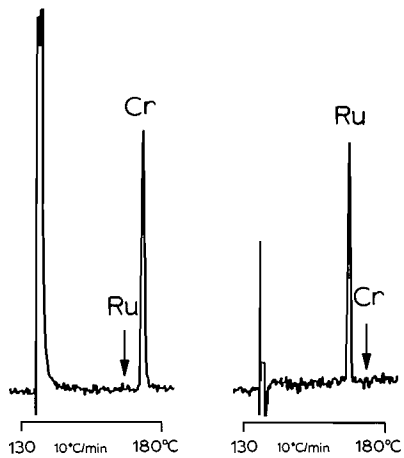

FIG. 8. Suppression of ruthenium and chromium by dual-channel differential chromatography in the same sample as shown in Fig. 7. Computer System.

yond their linear range are inappropriate candidates for determining selectivity ratios (even though they can produce much larger numbers). The amounts chosen for cancellation in this experiment were therefore taken from the upper ends of the single-channel linear calibration of the designated interferents (as seen by the channel chosen to elicit the best response of the *analyte*).

To put the results of this experiment in their proper perspective, it is reasonable to speculate first on the theoretically largest improvement in analyte/interferent selectivity that could be measured in moving from single-channel to dual-channel differential operation. Ideal circumstances imply that the analyte does not respond at all, while the interferent responds very strongly, on the particular channel that is used to cancel the interferent. Further, it is implied that the noise of the interferent channel would be significantly smaller than the noise of the analyte channel: only then could the analyte peak rise to full height above a baseline free of additional noise. And, of course, that there should be no perturbations present of an electronic, chemical, or physical nature. If we assume that the interferent (taken from the upper end of its linear range) fails to respond (more precisely: that it fails to respond above the S/N = 2 limit), then the largest improvement in selectivity ratio obtainable by switching from single to dual-channel differential operation *cannot exceed the linear range of the interferent*.

Note that this implies formal dependency, though to a numerically minor degree, on where the linear range is defined to start and to end. Note further that it is experimentally feasible to measure selectivity ratios that are larger than the "true" ones (by working outside the linear range of the interferent). And, when working inside the linear range but with the interferent peak completely cancelled (i.e., submerged in the baseline noise), only a lower limit to the true selectivity can be given. (A "true" selectivity ratio, following the conventional definition, is represented by the vertical (response) or the horizontal (amount) difference between two linear, or linearly extrapolated, calibration curves.)

To summarize: at ideal conditions and within respective linear ranges, the maximum observable improvement for dual-channel differential as opposed to single-channel operation is given by the linear range of the interferent (on the analyte channel). Thus, no greater a selectivity improvement than two to four orders of magnitude (with the number depending on the elemental nature of the interferent) can be measured by experiments in which the peak resulting from an amount of interferent close to its upper limit of linearity is successfully diminished to an amplitude smaller than the baseline noise of the differential chromatogram.

This theoretical extent of improvement could not be reached here. The reason is twofold: some of the "ideal" conditions mentioned above could not be realizd and, as is obvious from the fairly typical chromatograms of Figs. 9 and 10, very small remnants of the initially very large interferent peaks tended to persist as non-Gaussian artifacts. Still, in these figures the gain in selectivity is quite impressive. For a visual comparison, the respective mixtures are also portrayed in their best *single*-channel appearance on the left side of Figs. 9 and 10. The numerical improvement of selectiv-

Can. J. Chem. Downloaded from www.nrcresearchpress.com by 92.62.229.171 on 09/08/12
For personal use only.

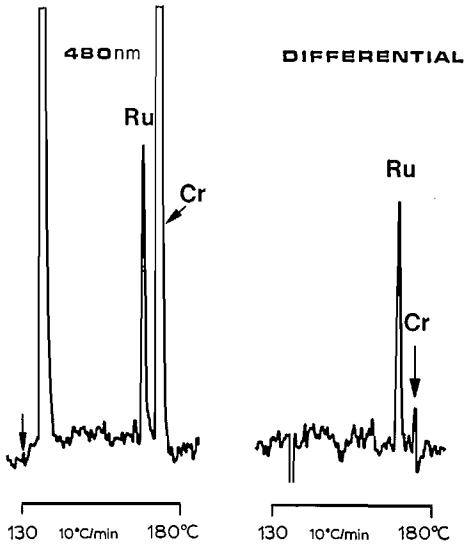

FIG. 9. Suppression of large amounts of chromium in a sample containing 250 ng $C_6H_6Cr(CO)_3$ and 200 pg Ru $(C_5H_5)_2$ in acetone. Other conditions as in Fig. 8. Analog Interface.

ity from single- to dual-channel differential operation is 3×10^2 for Ru/Cr and 2×10^1 for Cr/Ru (these numbers are based on peak heights; if peak areas are used they become much larger).

Figure 10 also contains, on the right-hand side and marked "Differential B," a chromatogram taken under the same chromatographic conditions and overall electronic amplification as the one marked "Differential A." (Note that the Cr peak remains at the same height.) However, different settings were used for the combination of input amplification and output attenuation of the two electrometers (which perform rough scaling on the signals before they reach the Analog Interface). The comparison of the two chromatograms demonstrates that the vacillating signal, which represents the difference between two very large off-scale peaks, is likely to contain electronic perturbations (in addition to other types of perturbations as have been discussed earlier). The chromatogram labelled "Differential A" is the best, the chromatogram labelled "Differential B" the worse, of a series of matches with the same overall electronic simplification. It is reasonable to expect that more attention to this problem (which, of course, never arises in "regular" chromatography) could reduce the size of the artifacts.

Improvements in selectivity similar to those shown in Figs. 7–10 can be realized for other pairs of transition elements as well. How large a number is obtained in each case depends strongly on the relative nature of the two spectra (and on the corresponding wavelengths chosen for the two channels), on the extent of the linear ranges, and on other considerations as discussed above. In our opinion, a visual record of performance, such as given in Figs. 7 through 10 for the fairly typical behaviour of ruthenium and chromium, is often preferable to a tabular one.

The dual-channel differential modes described in this manuscript work well on systems of two and possibly three different elements, particularly if the latter need to be differentiated with a very high degree of reliability. However, the methodology obviously runs into difficulties if more than two or three luminescing elements participate in the chromatogram. Although real-life samples of this type may be rare, it should be instructive to cast at least a cursory look at a mixture made up of several transition metals, in amounts that produce comparable peak heights in the open mode. The particular standard mixture shown here was also given a compound of sulfur, in recognition of the role that this main-group element plays in many natural samples.

Chromatograms of the mixture are shown in Fig. 11, first in single-channel, then in dual-channel differential mode. The first channel is open (no interference filter). The second channel at 530 nm was originally chosen for ruthenium. However, it also shows all the other peaks (though with different intensities). This reinforces the point made earlier that spectral discrimination in a single channel, as compared with the open mode, rarely affords the analyst the desired big increase in selectivity.

The differential-mode chromatogram shown on the right side of Fig. 11 is obtained by tuning the two channels such that the ruthenium responses cancel. This purpose is well

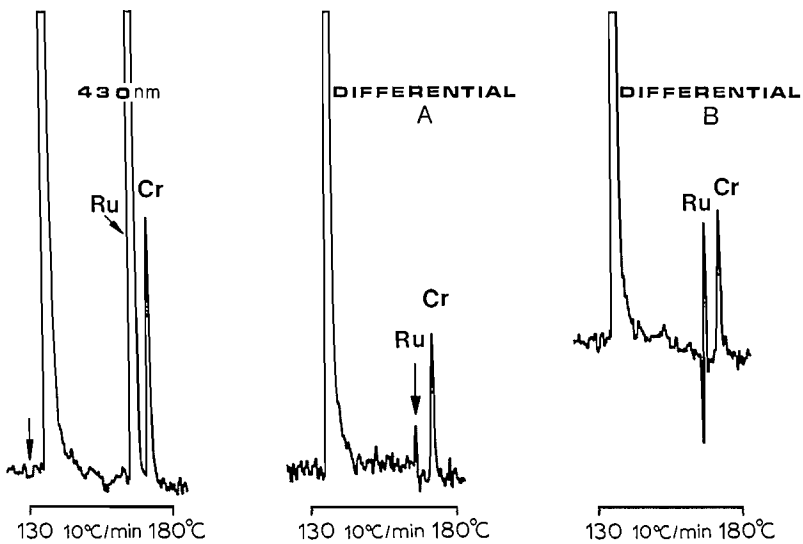

FIG. 10. Suppression of large amounts of ruthenium in a sample containing 10 ng $Ru(C_5H_5)_2$ (Ru) and 4 ng $C_6H_6Cr(CO)_3$ (Cr) in acetone. Other conditions as in Fig. 8. Analog Interface.

Can. J. Chem. Downloaded from www.nrcresearchpress.com by 92.62.229.171 on 09/08/12
For personal use only.

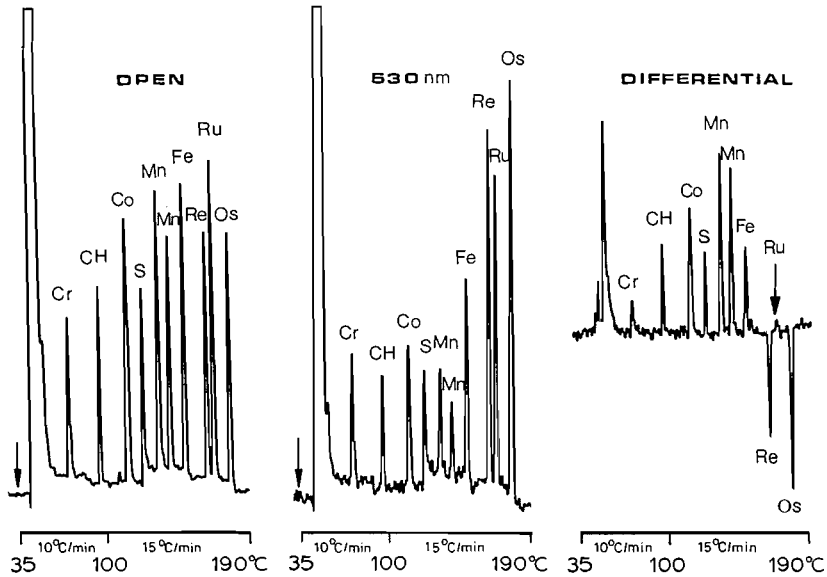

FIG. 11. Single-channel and dual-channel differential (ruthenium-suppressed) chromatograms of a mixture containing 1.3 ng $Cr(CO)_6$, 1.6 μg nonane (CH), 200 ng $Co(C_5H_5)_2$ (Co), 17 ng $[(CH_3)_3CS]_2$ (S), 3.2 ng $C_5H_5Mn(CO)_3$ and 4 ng $C_5H_4CH_3Mn(CO)_3$ (both Mn), 3.2 ng $Fe(C_5H_5)_2$ (Fe), 24 ng $Re_2(CO)_{10}$ (Re), 0.16 ng $Ru(C_5H_5)_2$ (Ru), and 4 ng $Os(C_5H_5)_2$ (Os) in acetone. Computer System.

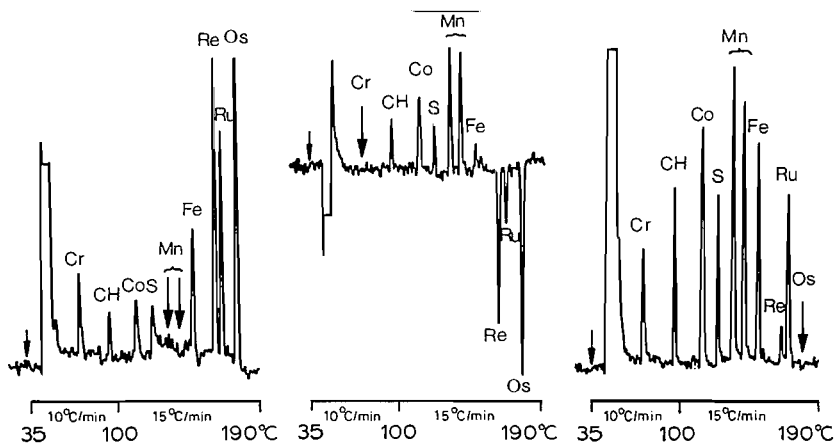

FIG. 12. Dual-channel differential chromatograms of the same mixture (and the same chromatographic run) as shown in Fig. 11, with suppression of, from left to right, manganese, chromium, and osmium. Computer System.

achieved. Thus, a peak vanishing from the chromatogram under this particular selectivity regime would alert the analyst to the possible presence of a ruthenium compound. And, other channel combinations (wavelengths) could be used to confirm that finding. In addition, clear *qualitative* discrimination is obtained between Cr, C, Co, S, Mn, and Fe on one hand, and Re and Os on the other.

Still, the situation is less than totally satisfying. What if the analyst wants to see *only* peaks of ruthenium, with compounds of all other elements vanishing from the chromatogram? While this is possible to achieve, the necessary algorithms are substantially different from the ones covered here and do display limitations of their own (6). They will be the subject of a separate manuscript. Within the present context, however, two further comments are relevant for the analysis of a multicomponent mixture as shown in Fig. 11.

First, different wavelength combinations could be used to achieve the disappearance of *any* element. At the same time, the choice of particular wavelengths can easily take into consideration the qualitative discrimination resulting among the other elements, and how it can best suit particular analytical needs. For instance, carbon compounds could have been eliminated in a manner similar to the process illustrated earlier in Fig. 6, with wavelengths particularly suited to the detection and qualitative distinction of interesting organometallic analytes.

Second, the two single channels of data stored in the computer could be used to impose, sequentially, a series of different selectivity regimes on the same chromatographic run. This makes little sense for a routine sample of qualitatively known composition, but it can be quite helpful for a complex sample that contains many components of a chemically disparate nature. For instance, the hypothetical question could be posed whether there were present in our test mixture any manganese compounds beyond the one "known" to contain Mn. To find the answer, the channels can be tuned

Can. J. Chem. Downloaded from www.nrcresearchpress.com by 92.62.229.171 on 09/08/12
For personal use only.

for the disappearance of the "known" manganese peak (or of a separately injected manganese standard if the contents of the mixture are *truly* unknown). If this is carried out, the second, pretendedly "unknown" manganese peak vanishes as well. A demonstration of this is shown on the left-hand side of Fig. 12.

The middle and right-hand sides of Fig. 12 display two further chromatograms in which the selfsame computer-stored data are used to cancel peaks of chromium and osmium, respectively, while leaving other peaks largely intact. Further elements can be so tested. This is interesting because it demonstrates that several new selectivity criteria can be meaningfully imposed on already existing data. The inter-metal differences in dual-channel response ratios are obviously large enough to allow such approaches, even though the original choice of wavelength had not been made with these additional combinations in mind.

In the high-resolution chromatography of complex samples that include a larger number of compounds containing the *same* hetero-element, procedures like the one mentioned above can lead to fast and facile early indications of which peaks are likely to represent the hetero-element of interest, which represent other hetero-elements, etc. Clearly, the underlying assumption, that the spectral response of the metal is independent of analyte amount and organic structure, may need to be ascertained for particular combinations of element and wavelength(s). Where such an assumption could be checked in our study of transition elements, as in the case of the two manganese compounds discussed above, it did indeed hold true.

NOTE ADDED IN PROOF: For lack of a better expression, this manuscript and its companion (2) use the term "dispersive" in its derivative meaning of "wavelength-selective". Thus, a "dispersive" FPD channel uses an interference (or other type of) filter, while a "non-dispersive" channel is doing without. It goes without saying, however, that filters "disperse" light neither in the etymological nor the original spectroscopic sense of the word (with the possible exception of the tilting effect in interference filters).

Acknowledgement

This research was supported by the Natural Sciences and Engineering Research Council of Canada through operating grant A-9604. We appreciate the valuable electronic assistance by Chris Wright.

1. V. A. Joonson and E. P. Loog. J. Chromatogr. **120**, 285 (1976).
2. X.-Y. Sun, B. Millier, and W. A. Aue. Can. J. Chem. **70**, 1129 (1992).
3. W. A. Aue, B. Millier, and X.-Y. Sun. Anal. Chem. **62**, 2453 (1990).
4. X.-Y. Sun and W. A. Aue. J. Chromatogr. **467**, 75 (1989).
5. X.-Y. Sun and W. A. Aue. Can. J. Chem. **67**, 897 (1988).
6. W. A. Aue, B. Millier, and X.-Y. Sun. Abstract No. 36. 73rd CIC Conference, Halifax, N.S. July, 1990.

Can. J. Chem. Downloaded from www.nrcresearchpress.com by 92.62.229.171 on 09/08/12
For personal use only.

NMR study of the protonation of domoic acid[1]

JOHN A. WALTER, DONALD M. LEEK, AND MICHAEL FALK[2]

Institute for Marine Biosciences, National Research Council of Canada, 1411 Oxford Street, Halifax, N.S., Canada B3H 3Z1

Received November 4, 1991

JOHN A. WALTER, DONALD M. LEEK, and MICHAEL FALK. Can. J. Chem. **70**, 1156 (1992).

The ^1H and ^{13}C NMR spectra of the amnesic shellfish poison, domoic acid, in H_2O and D_2O solutions have been studied as a function of pH or pD. The results yielded the NMR spectral parameters for each of the five protonation stages of domoic acid, provided accurate pK_a values, and enabled each pK_a to be associated with a particular protonation site.

JOHN A. WALTER, DONALD M. LEEK et MICHAEL FALK. Can. J. Chem. **70**, 1156 (1992).

On a étudié les changements observés dans les spectres RMN ^1H et ^{13}C de solutions d'acide domoïque, une toxine amnésique, dans H_2O et D_2O en fonction du pH ou du pD. Les résultats nous ont permis de calculer les paramètres spectraux pour les cinq étapes de la protonation de l'acide domoïque, d'obtenir des valeurs de pK_a plus précises et d'associer chaque pK_a avec un site de protonation particulier.

Can. J. Chem. Downloaded from www.nrcresearchpress.com by 79.173.37.17 on 09/08/12
For personal use only.

Introduction

Domoic acid (DA, Fig. 1) was recently identified as the toxin responsible for an episode of shellfish poisoning involving mussels from an area of eastern Canada (1). This compound had been known for some 30 years to have anthelmintic properties in humans, as well as to act as an insecticide (2, 3). Subsequently, it was found to have profound neurological effects when ingested by humans, and to be the agent binding most strongly to the kainate receptors of the central nervous system (4–6). This has prompted renewed interest in the spectroscopy of this compound both as a means of its identification and as a source of information regarding its physical properties, particularly those that may have some bearing on the physiological and neurological characteristics.

DA possesses one imino group, >NH, and three carboxylate groups, $-COO^-$ (Fig. 1), all capable of protonation. Therefore, DA molecules in solution are a mixture of five distinct protonation states (Table 1), their proportions in solution being determined by the four pK_a values, and varying with pH (7). A different NMR, IR, UV, etc. spectrum will correspond to each protonation state, and the solution spectra will therefore be pH dependent. We have recently reported the results of our studies of the UV spectrum (7) and solubility (8) of DA, and now present our investigation of ^1H NMR and ^{13}C NMR spectra as a function of pH and pD. The NMR spectra have the advantage of yielding more precise pK_a values and permitting the identification of the sites of protonation corresponding to each pK_a (9–12).

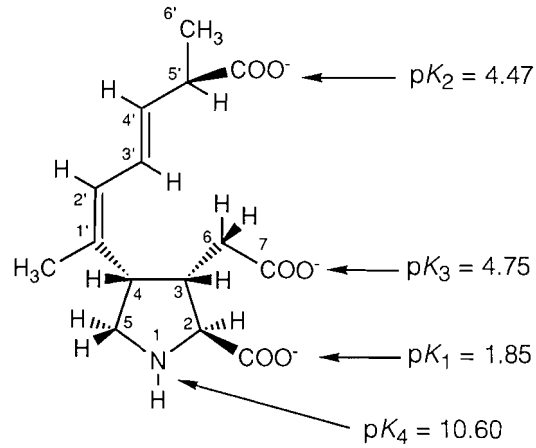

FIG. 1. Molecular structure of domoic acid in its fully deprotonated form.

Experimental

All NMR spectra were recorded using a Bruker MSL300 spectrometer at 300 MHz (^1H) or 75.5 MHz (^{13}C), at 20°C. DA from the stock used in previous studies (7, 8) was dissolved in H_2O or D_2O and placed in 5-mm sample tubes with a concentric 2-mm tube (Wilmad 520-1) containing TSP in D_2O for a reference. Acquisition times were 3.4 s (^1H) or 0.49 s (^{13}C), and chemical shifts were measurable to a precision of ca. 0.003 ppm or 0.02 ppm respectively, except where precluded by strong coupling, linewidth, or overlap. Adjustment of pH was by addition of minute amounts of 1 N NaOH (NaOD for solutions in D_2O) or 1 N HCl (DCl), starting with pH 3.4, which corresponds to the isoelectric point. Back titration was avoided to minimize the formation of salt. The concentration of DA was low enough (20 mM) to avoid precipitation at any pH (8), and dilution of the solution due to the addition of acid or base was negligible. All pH and pD measurements were made within the NMR tubes using a Fisher Accumet model 610A pH meter and an Ingold 6030 combination electrode calibrated for each measurement with Anachemia standard buffer solutions. Values of pD reported here are direct pH meter readings without correction for changes in electrode characteristics in D_2O (13), unless otherwise stated. Chemical shifts of strongly coupled protons were determined where necessary by simulation, using the Bruker PANIC program.

Titration curves for each ^1H and ^{13}C resonance were fitted to eq. [1], which is analogous to eq. [1] in ref. 11:

$$[1] \quad \delta = \delta_L + \Sigma\{\Delta_i.10^x/(10^x + 1)\}$$

where $x = pH - pK_{ai}$, Δ_i is the chemical shift variation at a given nucleus corresponding to a change from complete protonation to deprotonation at the ith site, δ_L is the shift for complete protonation, and $i = 1$–4 corresponding to each of the protonation sites. Equation [1] is based on the assumption that the different protonation states have equal activity coefficients, and that the proton

[1]NRCC No. 33781. Preliminary accounts of this work were presented at the Second Canadian Workshop on Harmful Marine Algae, Bedford Institute of Oceanography, Dartmouth, N.S., 2–4 October, 1990, and at the 4th European Conference on the Spectroscopy of Biological Molecules, York, U.K., September 1991.

[2]Author to whom correspondence may be addressed.

TABLE 1. Protonation states of domoic acid

	Imino	C-2	C-5′	C-7	
A:	$>NH_2^+$	-COOH	-COOH	-COOH	Cation
B:	$>NH_2^+$	$-COO^-$	-COOH	-COOH	Zwitterion
C:	$>NH_2^+$	$-COO^-$	$-COO^-$	-COOH	Singly charged anion
D:	$>NH_2^+$	$-COO^-$	$-COO^-$	$-COO^-$	Doubly charged anion
E:	>NH	$-COO^-$	$-COO^-$	$-COO^-$	Triply charged anion

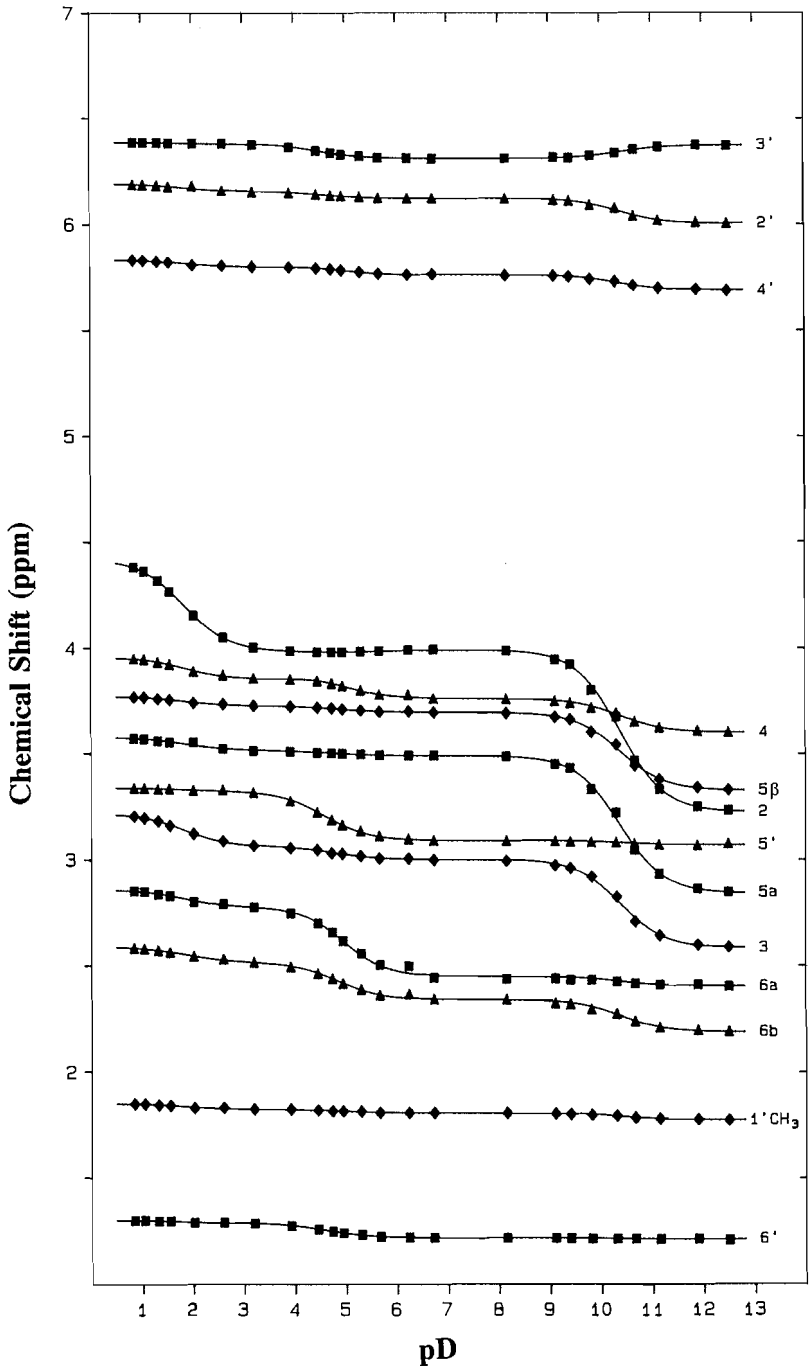

FIG. 2. Plot of chemical shift vs. pD for the ^1H signals of domoic acid in D_2O. The pD in this plot is the direct pH meter reading without correction for changes in glass electrode characteristics in D_2O solution (13).

Can. J. Chem. Downloaded from www.nrcresearchpress.com by 79.173.37.17 on 09/08/12
For personal use only.

Can. J. Chem. Downloaded from www.nrcresearchpress.com by 79.173.37.17 on 09/08/12
For personal use only.

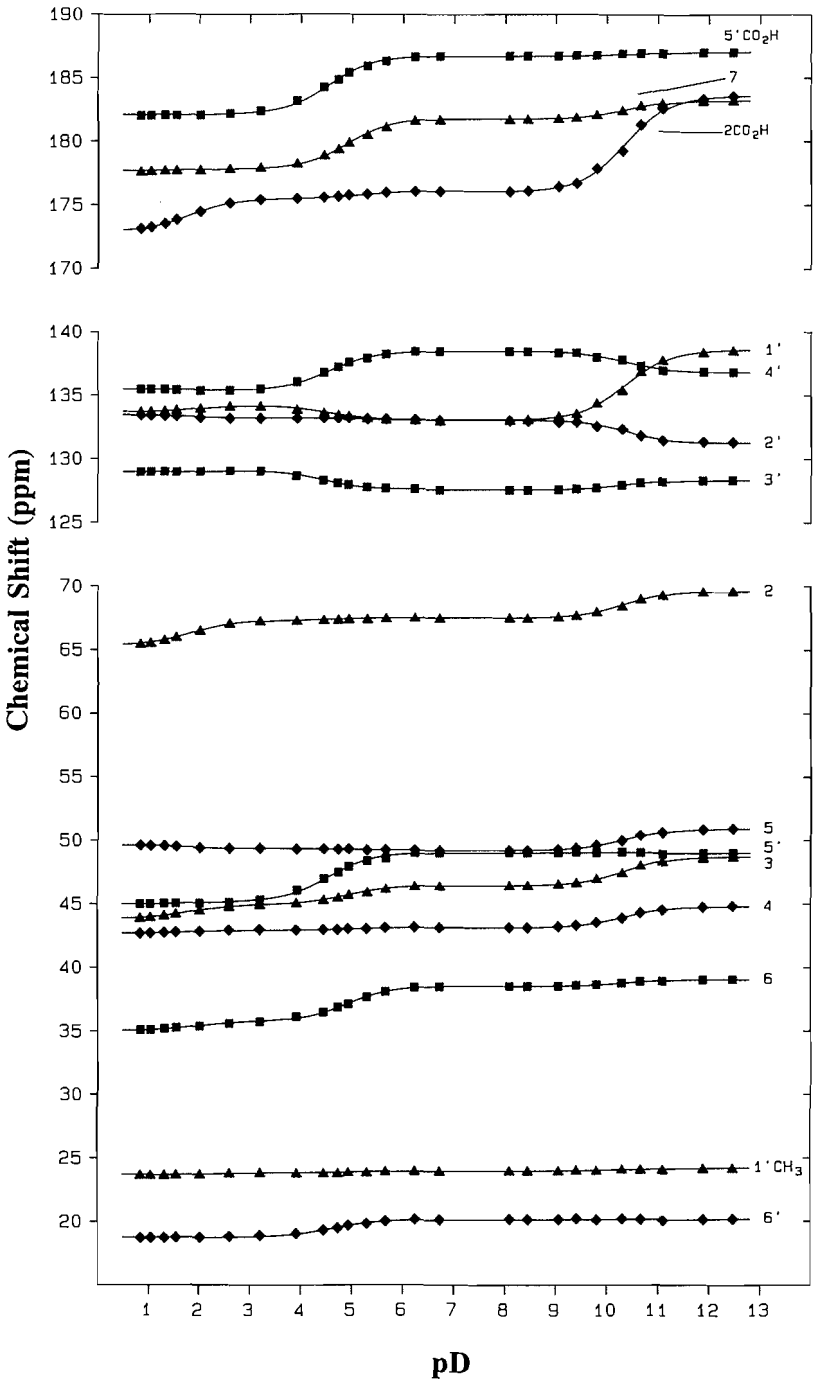

FIG. 3. Plot of chemical shift vs. pD for the ^{13}C signals of domoic acid in D_2O. The pD in this plot is the direct pH meter reading without correction for changes in glass electrode characteristics in D_2O solution (13).

exchange proceeds quickly compared to the time scale of the NMR experiment. Optimization to minimize the sum of squares of the residuals was performed with a SIMPLEX routine (14) written in Pascal for use with up to nine variable parameters and run on a PC/AT-compatible computer, which also generated the plots shown (Figs. 2–5).[3] Initial values of pK_a were estimated from logarithmic plots of the chemical shift titration curves of nuclei close to each of the four protonation sites. Resonance assignments were known previously (1). Thus, at pH < 6, the shifts of resonances of C-2, C-2 carboxyl, and H-2 were principally affected by protonation at the C-2 carboxylate; those of C-6, C-7, and H-6 by protonation at carboxylate C-7; and those of C-5′, C-5′ carboxyl, C-6′, H-5′, and H_3-6′ by protonation at the C-5′ carboxylate. Pronounced effects due to protonation of NH at pH > 7 occurred at C-1′, C-2 carboxyl, H-2, H-3, H-5α, and H-5β; lesser effects occurred at other nuclei. Within each of the above groups of nuclei, separate values of pK_a obtained by curve fitting agreed closely, confirming the dominant effect of the nearby protonation site and permitting each

[3]Figures 4 and 5, and complete tables of original ^1H and ^{13}C chemical shifts vs. pH, have been deposited, and may be purchased from: The Depository of Unpublished Data, Document Delivery, CISTI, National Research Council Canada, Ottawa, Canada K1A 0S2.

TABLE 2. Parameters[a] for least-squares fits of eq. [1] to titration curves for ^1H and ^{13}C resonances of domoic acid solutions in H_2O and D_2O[b] at 20°C and at 20 mM concentration. Tables of the original measurements have been deposited

(*a*) ^1H spectra: H_2O, $pK_{a1} = 1.84$, $pK_{a2} = 4.46$, $pK_{a3} = 4.73$, $pK_{a4} = 10.60$

Position	δ_L	Δ_1	Δ_2	Δ_3	Δ_4
2	4.388	−0.414	0.013	−0.009	−0.750
3	3.181	−0.130	0.018	−0.080	−0.415
4	3.930	−0.080	0.008	−0.111	−0.156
5α	3.563	−0.054	−0.020	−0.005	−0.640
5β	3.761	−0.038	0.003	−0.036	−0.360
6a	2.839	−0.061	0.026	−0.361	−0.042
6b	2.574	−0.066	0.003	−0.181	−0.147
2′	6.178	−0.034	−0.015	−0.016	−0.114
3′	6.375	−0.003	−0.083	0.013	0.067
4′	5.820	−0.023	−0.028	−0.012	−0.073
5′	3.331	−0.015	−0.231	0.002	−0.022
6′	1.296	−0.008	−0.080	0.012	−0.007
1′-CH_3	1.842	−0.016	−0.013	−0.013	−0.028

(*b*) ^1H spectra: D_2O*, $pK_{a1} = 1.84$, $pK_{a2} = 4.51$, $pK_{a3} = 4.87$, $pK_{a4} = 10.37$

Position	δ_L	Δ_1	Δ_2	Δ_3	Δ_4
2	4.422	−0.436	−0.031	0.036	−0.764
3	3.221	−0.154	−0.014	−0.050	−0.419
4	3.959	−0.106	0.096	−0.188	−0.161
5α	3.581	−0.061	−0.014	−0.014	−0.648
5β	3.773	−0.044	0.004	−0.037	−0.368
6a	2.863	−0.084	−0.085	−0.413	−0.047
6b	2.595	−0.074	−0.010	−0.167	−0.153
2′	6.194	−0.038	−0.028	−0.005	−0.119
3′	6.389	−0.008	−0.073	0.003	0.065
4′	5.835	−0.036	0.027	−0.064	−0.073
5′	3.342	−0.013	−0.188	−0.049	−0.021
6′	1.307	−0.013	−0.052	−0.020	−0.006
1′-CH_3	1.854	−0.024	−0.001	−0.020	−0.032

(*c*) ^{13}C spectra: H_2O, $pK_{a1} = 1.86$, $pK_{a2} = 4.47$, $pK_{a3} = 4.77$, $pK_{a4} = 10.60$

Position	δ_L	Δ_1	Δ_2	Δ_3	Δ_4
2	65.60	1.90	−0.02	0.25	2.04
2-CO_2H	173.12	2.36	−0.28	0.84	7.43
3	43.94	1.04	−0.04	1.54	2.22
4	42.76	0.27	−0.11	0.36	1.68
5	49.84	−0.34	0.45	−0.53	1.58
6	35.21	0.59	0.01	2.81	0.59
7	177.62	0.32	0.33	3.43	1.53
1′	133.87	0.33	−0.35	−0.67	5.46
1′-CH_3	23.78	0.14	−0.07	0.31	0.23
2′	133.37	−0.31	0.49	−0.54	−1.74
3′	128.92	0.10	−1.86	0.46	0.77
4′	135.56	−0.15	3.23	−0.01	−1.62
5′	45.02	0.20	3.71	0.12	−0.03
5′-CO_2H	181.92	0.29	4.53	−0.17	0.29
6′	18.85	0.11	0.69	0.69	−0.01

(*d*) ^{13}C spectra: D_2O*, $pK_{a1} = 1.86$, $pK_{a2} = 4.56$, $pK_{a3} = 4.91$, $pK_{a4} = 10.36$

Position	δ_L	Δ_1	Δ_2	Δ_3	Δ_4
2	65.31	2.06	−0.03	0.18	2.15
2-CO_2H	172.89	2.58	−0.02	0.57	7.64
3	43.86	1.17	−0.24	1.69	2.28
4	42.70	0.30	−0.18	0.35	1.68
5	49.65	−0.28	−0.04	−0.10	1.71
6	35.06	0.73	0.08	2.69	0.54
7	177.59	0.30	−0.05	3.91	1.52
1′	133.72	0.46	−1.12	0.00	5.55
1′-CH_3	23.73	0.18	−0.17	0.33	0.20
2′	133.46	−0.25	0.14	−0.31	−1.77
3′	128.99	0.04	−1.51	0.06	0.80
4′	135.47	−0.02	2.70	0.35	−1.70
5′	44.96	0.29	3.76	0.04	−0.03
5′-CO_2H	181.93	0.32	4.23	0.22	0.32
6′	18.77	0.17	0.66	0.65	−0.02

[a]Typical errors in δ_L resulting from independent fits to the same data are 0.005 ppm (^1H) or 0.03 ppm (^{13}C).

[b]pH and pK_a measurements used in generating Table 2 are **uncorrected** for changes in glass electrode characteristics when obtained in D_2O solution. Corrected values may be obtained by adding 0.40 to pH meter readings in D_2O and to the corresponding pK_a values derived from curve fitting (13) (see Table 3).

of the four pK_a's to be assigned to specific groups. Where nuclei were influenced by two or more protonation sites at pH < 6, fitted curves were generated by varying Δ_i's only, the pK_a's being held to the above values obtained from resonances of nuclei near protonation sites. It should be emphasized that, although the pK_a determinations are highly accurate, the values of the Δ_i parameters in Table 2 should be regarded as no more than indicators of the amount of influence that protonation at a particular site has on a given nucleus. When a nucleus is remote from the protonation site and Δ_i is small, and the site is one of the two with closely similar pK_a's, the quality of the curve fitting is insensitive to Δ_i and it is difficult to distinguish the contribution of a particular protonation site. Nevertheless, the parameters in Table 2 should yield predicted shifts for any pH with an accuracy close to that of the measurement.

Results and discussion

Titration curves for ^1H and ^{13}C resonances of DA at constant concentration in D_2O are shown in Figs. 2 and 3, together with curves generated by least-squares fitting of eq. [1], which yielded the parameters in Table 2. Similar plots for DA at the same concentration in H_2O (Figs. 4 and 5) are available in the depository, as are tables of the original chemical shift data on which these figures are based.[3] Comparison with preliminary results in H_2O, where the concentration was varied, showed slight concentration dependence of both ^1H and ^{13}C shifts: at 70 mM concentration, pH 7.1, ^1H resonances shifted upfield by 0.005–0.020 ppm, whereas ^{13}C peaks moved downfield by 0.04–0.24 ppm (excepting the C-4′ resonance, which moved upfield), relative to those observed at a concentration of 20 mM.

The results show that the pK_a's in ascending order are associated with deprotonation of carboxylate groups at positions 2 and 5′, carboxylate C-7, and the NH group at position 1, respectively. The pK_a values obtained are gathered in Table 3; we have adopted the mean H_2O values (underlined). The previously reported pK_a's (2) were obtained by an unstated

Can. J. Chem. Downloaded from www.nrcresearchpress.com by 79.173.37.17 on 09/08/12
For personal use only.

TABLE 3. Value of pK for each protonation site

Site	H_2O			D_2O[a]		
	^1H	^{13}C	Ave.	^1H	^{13}C	Ave.
C2-CO_2^-	1.84	1.86	1.85	2.24	2.26	2.25
C5′-CO_2^-	4.46	4.47	4.47	4.91	4.96	4.94
Carboxylate						
C-7	4.73	4.77	4.75	5.27	5.31	5.29
NH	10.60	10.60	10.60	10.77	10.76	10.77

Error: ca. ±0.05 pH units.
[a]Corrected by adding 0.40 pH units to pH meter readings in D_2O solution (13).

TABLE 4. The ^{13}C titration shifts for the corresponding carbon atoms in domoic acid and glutamic acid.

	Domoic acid (DA)				Glutamic acid (GA)		
	a	b	c		a	b	c
C-2							
CO_2H	2.4	0.8	7.4	C_o	2.6	0.5	9.0
C-2	1.9	0.3	2.0	C_α	2.0	0.5	1.3
C-3	1.0	1.5	2.2	C_β	0.7	1.3	5.2
C-6	0.6	2.8	0.6	C_γ	0.7	3.3	0.9
C-7	0.3	3.4	1.5	C_δ	0.7	3.3	1.7

Abbreviations: a = carboxyl titration (pK_a = 1.85 for DA and 2.23 for GA); b = side-chain titration (pK_a = 4.75 for DA and 4.37 for GA); c = amino titration (pK_a = 10.60 for DA and 9.53 for GA).

TABLE 5. Variation of coupling constants J(H,H) with pH. Domoic acid in H_2O

pH:	0.82	3.20	5.57	7.28	12.60
Proton pair	J(H,H), Hz[a]				
2,3	8.7	8.1	7.0	6.5	8.7
3,4	8.2[b]	8.4	8.2	8.2[b]	8.2
4,5α	7.9	7.3	7.9	7.9[b]	7.8
4,5β	8.1	7.9	8.1	8.1[b]	5.3
5α,5β	−12.3	−12.2	−12.2	−12.3	−11.5
3,6a	6.0	5.8	6.8	6.8	5.1
3,6b	8.4	9.1	8.2	8.2	10.0
6a,6b	−17.0	−16.7	−15.7	−15.7	−15.7
2′,3′	10.9	11.1	11.1	10.9	10.9
3′,4′	15.1	14.9	14.9	14.7	14.9
4′,5′	8.2	7.8	8.2	8.4	8.3
5′,6′	7.0	7.1	7.0	7.0	7.1

[a]Error ±0.3 Hz unless otherwise indicated.
[b]Error ±0.5 Hz.

method and are of unknown accuracy; our own UV study (7) could only confirm the pK_a values roughly and without assigning them to specific protonation sites. These rough pK_a values were used to calculate the proportions of the five protonation states of DA as a function of pH (7). The pH variation of the proportions determined from the NMR-derived pK_a's is similar, and is readily visualized with the aid of Fig. 5 of ref. 7.

In a strongly acid environment, at pH below 1, DA molecules exist largely as the fully protonated cations A (Table 1). As pH increases towards pK_{a1} = 1.85, the nominally neutral DA molecules B appear, in which the C-2 carboxyl group is deprotonated and negatively charged. The C-2 carboxyl group is nearest to the positively charged imino group, and the proximity of the two oppositely charged groups apparently makes this form of the zwitterion more stable than the ones involving the more remote C-5′ carboxyl group or carboxyl C-7. As pH increases further towards pK_{a2} = 4.47, the C-5′ carboxyl also becomes deprotonated, giving rise to the singly charged anion, C. The relative stability of the isomer with positive charge on the imino group and negative charges on C-5′ and C-2 carboxyls appears to be due to the large separation between the two negatively charged groups. As pH increases further towards pK_{a3} = 4.75, the carboxyl C-7 also becomes deprotonated, giving rise to the doubly charged anion D. At still higher pH values, approaching pK_{a4} = 10.60, the imino group loses its extra proton to yield the triply charged anion E.

It has been reported (12) that protonation of either a carboxylate or an amino group leads to upfield shifts of ^{13}C resonances and downfield shifts of ^1H resonances, the observed shifts decreasing monotonically with the number of bonds separating the nucleus from the field source. However, upon the titration of the amino group of an amino acid, larger ^{13}C shifts are observed (12) for the C_β and the carboxyl carbons than for C_α. This pattern is exactly what is observed in the case of DA. Table 4 shows the general similarity of the ^{13}C titration shifts for the corresponding carbon atoms in DA and glutamic acid (GA).

Proton coupling constants of DA (Table 5) are relatively little affected by protonation. The largest changes (up to 2.8 Hz) occur with protonation of the imino group, to J(2,3), J(4,5β), J(5α,5β), J(3,6a), and J(3,6b). Lesser changes to J(2,3), J(4,5α), J(3,6a), J(3,6b), and J(6a,6b) are associated with protonation at other sites.

Acknowledgements

Many of the NMR measurements were undertaken by P. W. Wiseman, summer assistant at this Institute, 1988 and 1989, and by P. F. Seto. We are grateful to Drs. J. L. C. Wright and A. G. McInnes for the provision of crystalline DA.

1. J. L. C. Wright, R. K. Boyd, A. S. W. de Freitas, M. Falk, R. A. Foxall, W. D. Jamieson, M. V. Laycock, A. W. McCulloch, A. G. McInnes, P. Odense, V. P. Pathak, M. A. Quilliam, M. A. Ragan, P. G. Sim, P. Thibault, J. A. Walter, M. Gilgan, D. J. A. Richard, and D. Dewar. Can. J. Chem. **67**, 481 (1989).
2. T. Takemoto and K. Daigo. Chem. Pharm. Bull. (Tokyo), **6**, 578 (1958).
3. T. Takemoto and K. Daigo. Archiv. Pharm. **293**, 627 (1960).
4. T. M. Perl, L. Bedard, T. Kosatsky, J. C. Hockin, E. C. D. Todd, and R. S. Remis. N. Engl. J. Med. **322**, 1775 (1990).
5. J. S. Teitelbaum, R. J. Zatorre, S. Carpenter, D. Gendron, A. C. Evans, A. Gjedde, and N. R. Cashman. N. Engl. J. Med. **322**, 1781 (1990).
6. G. Debonnel, L. Beauchesne, and C. de Montigny. Can. J. Physiol. Pharmacol. **67**, 29 (1989).
7. M. Falk, J. A. Walter, and P. W. Wiseman. Can. J. Chem. **67**, 1421 (1989).
8. M. Falk, P. F. Seto, and J. A. Walter. Can. J. Chem. **69**, 1740 (1991).

Can. J. Chem. Downloaded from www.nrcresearchpress.com by 79.173.37.17 on 09/08/12
For personal use only.

9. R. E. London, T. E. Walker, V. K. Kollman, and N. A. Matwiyoff. J. Am. Chem. Soc. **100**, 3723 (1978).
10. J. G. Batchelor, J. Feeney, and G. C. K. Roberts. J. Magn. Reson. **20**, 19 (1975).
11. M. H. Freedman, J. R. Lyerla, Jr., I. M. Chaiken, and J. S. Cohen. Eur. J. Biochem. **32**, 215 (1973).
12. A. R. Quirt, J. R. Lyerla, Jr., I. R. Peat, J. S. Cohen, W. F. Reynolds, and M. H. Freedman. J. Am. Chem. Soc. **96**, 570 (1974).
13. P. K. Glasoe and F. A. Long. J. Phys. Chem. **64**, 188 (1960).
14. J. W. Cooper. Introduction to Pascal for scientists. Wiley–Interscience, New York. 1981. p. 186.

Can. J. Chem. Downloaded from www.nrcresearchpress.com by 79.173.37.17 on 09/08/12
For personal use only.

Synthesis of cyclopentane analogs of 5-fluorouracil nucleosides

LUCJAN J. J. HRONOWSKI AND WALTER A. SZAREK[1]
Department of Chemistry, Queen's University, Kingston, Ont., Canada K7L 3N6

Received August 29, 1990[2]

LUCJAN J. J. HRONOWSKI and WALTER A. SZAREK. Can. J. Chem. **70**, 1162 (1992).

New carbocyclic analogs (**12**, **14**, and **15**) of 5-fluorouracil nucleosides have been prepared by fluorination, using elemental fluorine, of the acetylated analogs (**8**, **10**, and **11**, respectively) of 1-(2′,3′-dideoxy-*glycero*-pentofuranosyl)- and 1-(2′- and 3′-deoxy-β-*threo*-pentofuranosyl)-uracil nucleosides. The carbocyclic analog (**14**) of 1-(2′-deoxy-β-*threo*-pentofuranosyl)-5-fluorouracil was then utilized for the preparation of various new carbocyclic analogs of 1-(3′-substituted-2′,3′-dideoxy-β-*erythro*-pentofuranosyl)-5-fluorouracil nucleosides by S_N2 displacement of the 3′-mesyloxy group in the protected derivative **17**. In this way analogs having the chloro (see **23**), bromo (see **24**), and azido (see **25**) groups at the 3′-position were obtained; the analog **29** having a 3′-amino group was obtained by reduction of the azido group. In addition (±)-5-fluoro-1-{3-(hydroxymethyl)-3-cyclopenten-1-yl}-2,4(1*H*,3*H*)-pyrimidinedione (**26**) was obtained as an elimination side-reaction product in the preparation of the 3′-chloro and 3′-bromo analogs. Compounds **8**, **9**, **12**, **14**, **15**, **25**, and **29** were tested against the herpes simplex viruses and were found to be inactive. Compound **26** inhibited the growth of K-562 cells with an ID_{50} (10^{-4}–10^{-3}), which was about 100-fold greater than that of 5-fluorouracil in this test system. Analogs **12**, **25**, and **29** were slightly cytotoxic.

LUCJAN J. J. HRONOWSKI et WALTER A. SZAREK. Can. J. Chem. **70**, 1162 (1992).

On a préparé de nouveaux analogues carbocycliques (**12**, **14** et **15**) de nucléosides du 5-fluoro-uracile en effectuant la fluoration, à l'aide de fluor élémentaire, des analogues acétylés (respectivement **8**, **10** et **11**) des nucléosides des 1-(2′,3′-didésoxy-*glycéro*-pentofuranosyl)- et 1-(2′- et 3′-désoxy-β-*thréo*-pentofuranosyl)-uraciles. Faisant appel à une réaction de substitution S_N2 du groupe 3′-mésyloxy du dérivé protégé **17**, on a alors utilisé l'analogue carbocyclique (**14**) du 1-(2′-désoxy-β-*thréo*-pentofuranosyl)-5-fluoro-uracile pour préparer divers nouveaux analogues des nucléosides du 1-(2′,3′-didésoxy-β-*érythro*-pentofuranosyl)-5-fluoro-uracile substitués en position 3′. De cette façon, on a obtenu des analogues portant des groupes chloro (*voir* **23**), bromo (*voir* **24**) et azido (*voir* **25**) en position 3′; on a obtenu l'analogue **29** portant un groupe amino en position 3′ par réduction du groupe azido. De plus, on a obtenue la (±)-5-fluoro-1-[3-(hydroxyméthyl)-cyclopent-3-en-1-yl]-2,4-(1*H*,3*H*)-pyrimidinedione (**26**) comme sous-produit de la réaction d'élimination dans la préparation des analogues 3′-chloro et 3′-bromo. On a évalué l'activité des composés **8**, **9**, **12**, **14**, **15**, **25** et **29** contre les virus de l'herpes simplex et on a trouvé qu'ils sont inactifs. Le composé **26** inhibe la croissance des cellules du K-562 avec un ID_{50} de (10^{-4}–10^{-3}) qui, dans le système d'évaluation, est environ 100 fois plus grand que celui du 5-fluoro-uracile. Les analogues **12**, **25** et **29** sont légèrement cytotoxiques.

[*Traduit par la rédaction*]

Introduction

5-Fluorouracil (5-FUra) and its deoxynucleoside, 5-fluoro-2′-deoxyuridine (5-FdUrd), are widely used as anticancer drugs (1, 2). Both of these drugs are extensively metabolized in vivo such that the 5-fluorouracil base becomes incorporated into the ribo- and 2′-deoxyribo-nucleosides and nucleotides as well as the nucleic acids (1–5). In the case of 5-FdUrd, it may be converted first by the pyrimidine nucleoside phosphorylases into 5-FUra, which then is utilized for the synthesis of ribo- and 2′-deoxyribo-nucleotides (3). However, there is considerable evidence that the therapeutic effects of these compounds are due to the metabolite, 5-fluoro-2′-deoxyuridine 5′-phosphate, which is a potent inhibitor of thymidylate synthetase, an essential enzyme for DNA synthesis (6–9). As a result of these observations, there has been an interest in recent years in the development of 5-fluorouracil-containing nucleosides that are resistant to the pyrimidine nucleoside phosphorylases, in order to maximize the amount of the therapeutically active metabolite within the tumor cells.

Two approaches have provided 5-fluorouracil-containing nucleosides that did not function as substrates for the pyrimidine nucleoside phosphorylases. In the first approach fluorine was introduced into the sugar ring to provide 1-(2′-deoxy-2′-fluoro-β-D-arabinofuranosyl)-5-fluorouracil (10) and 5-fluoro-2′,3′-dideoxy-3′-fluorouridine (11). The 5′-monophosphates of these nucleosides were shown to be noncompetitive inhibitors of the thymidylate synthetase enzyme. In the second approach, described by Shealy *et al.* (12), the furanose-ring oxygen was replaced by a methylene group to provide carbocyclic analogs of 5-fluorouracil nucleosides. As expected, the carbocyclic analog of 5-fluoro-2′-deoxyuridine did not undergo phosphorolysis to 5-fluorouracil but was phosphorylated enzymatically to the analog of 5-FdUrd 5′-phosphate (12). The carbocyclic analog of 5-FdUrd was cytotoxic to L1210 cells in culture and showed slight activity against leukemia P-388 in vivo.

In the present work, elemental fluorine was used for the synthesis of carbocyclic analogs of 1-(2′- and 3′-deoxy-β-*threo*-pentofuranosyl)-5-fluorouracil nucleosides, and a series of carbocyclic analogs of 1-(3′-substituted-2′,3′-dideoxy-β-*erythro*-pentofuranosyl)-5-fluorouracil nucleosides. In addition, preliminary results of tests on these compounds for the inhibition of the growth of K-562 cells are discussed.

Results and discussion

The synthesis of the carbocyclic analogs (**4**–**7**)[3] that were utilized for the preparation of 5-fluorouracil analogs was described previously (13, 14). Briefly, the syntheses

[1]Author to whom correspondence may be addressed.
[2]Revision received October 9, 1991.

[3]All of the carbocyclic nucleoside analogs are racemic mixtures, although only one enantiomer is shown in Schemes 2–4.

Can. J. Chem. Downloaded from www.nrcresearchpress.com by 92.62.229.171 on 09/08/12
For personal use only.

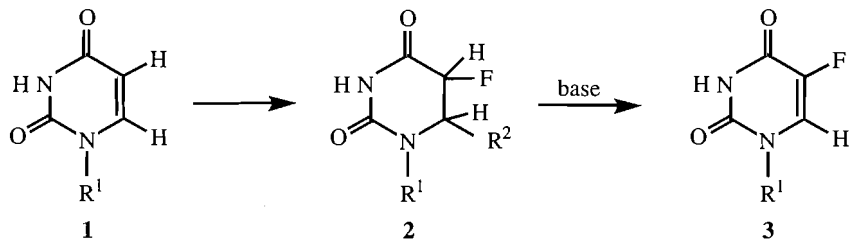

1 2 3

SCHEME 1

involved the coupling of an appropriate *cis*-3-aminocyclopentanemethanol with 3-ethoxypropenoyl isocyanate or 3-ethoxypropenoyl isothiocyanate to give the corresponding propenoylureas or propenoylthiourea. The propenoylureas were cyclized in 2 N H_2SO_4 and the propenoylthiourea was cyclized in 15 N aqueous ammonia to give the required carbocyclic nucleoside analogs.

Fluorination of the uracil and 2-thiouracil nucleoside analogs using elemental fluorine

Fluorination of carbocyclic analogs of uracil nucleosides using elemental fluorine was performed previously by Shealy *et al.* (12) using the unprotected nucleoside analogs. However, the yields reported by this approach were generally below 50%. The fluorination of the uracil base was also accomplished using a variety of other fluorinating reagents (15), including trifluoromethyl hypofluorite (16), xenon difluoride (17), cesium fluoroxysulfate (18), and acetyl hypofluorite (19). Moderate to high yields of fluorinated compounds were obtained using all except the xenon difluoride reagent (10% yield of 5-fluorouracil). The fluorination, using trifluoromethyl hypofluorite, elemental fluorine, or cesium fluoroxysulfate, was shown to proceed by way of an addition–elimination mechanism (see Scheme 1). Thus, treatment of uracil derivatives (**1**) dissolved in methanol with a solution of trifluoromethyl hypofluorite in fluorotrichloromethane gave adducts **2** having a methoxyl group at the 6-position (R^2 = OMe). In addition, ^1H and ^{19}F nmr spectroscopy and a single-crystal X-ray analysis of compound **2** (R^1 = Me, R^2 = OMe) established conclusively a *cis* stereochemistry of the adducts (16*f*). Barton *et al.* (16*b*) fluorinated uracil (**1**, R^1 = H) using the trifluoromethyl hypofluorite reagent in an aqueous solvent and obtained adduct **2** (R^1 = H, R^2 = OH) having a hydroxyl at the 6-position. The desired 5-fluorouracil (**3**) was obtained by heating, or by treatment of the adduct **2** with a base such as triethylamine or ammonium hydroxide. Similar adducts were obtained in fluorinations using elemental fluorine (12, 20) or cesium fluoroxysulfate (18); however, fluorinations using the latter reagent in methanol gave a mixture of *cis*- and *trans*-5-fluoro-6-methoxy adducts. However, all of the above fluorinations are regiospecific, so that only the 5-position of the uracil ring becomes fluorinated. There seems to be no advantage in using one of the three reagents in preference over the other two, since all were shown to give moderate to high yields of the fluorinated products. The elemental fluorine reagent has been shown to give higher yields and fewer decomposition products if the acetic acid solvent is saturated first with fluorine, and this solution is used then for fluorination, rather than if there is direct addition of fluorine to a solution of the uracil derivative in acetic acid (20).

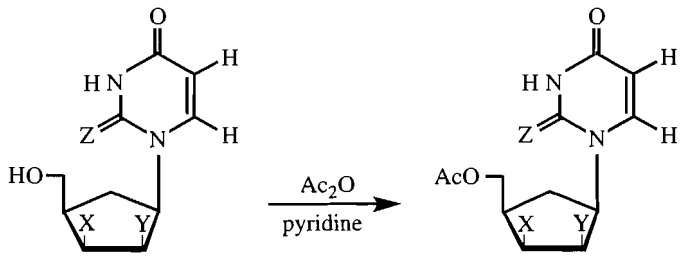

4 X = Y = H, Z = O
5 X = Y = H, Z = S
6 X = OH, Y = H, Z = O
7 X = H, Y = OH, Z = O

8 X = Y = H, Z = O
9 X = Y = H, Z = S
10 X = OAc, Y = H, Z = O
11 X = H, Y = OAc, Z = O

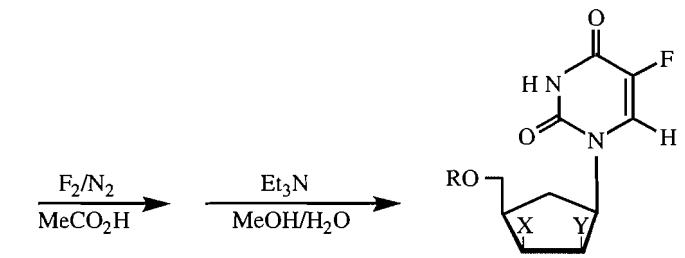

12 X = Y = R = H
13 X = Y = H, R = Ac
14 X = OH, Y = R = H
15 X = R = H, Y = OH

SCHEME 2

Also, both elemental fluorine and trifluoromethyl hypofluorite are extremely toxic, and violent decompositions have been observed (21) in the case of the cesium fluoroxysulfate reagent.

In fluorinations of unprotected 2′-deoxyuridine nucleosides using elemental fluorine, Cech and Holý (20*b*) had obtained low yields (~50%), similar to those obtained by Shealy *et al.* (12) with the carbocyclic analogs; however, considerably higher yields (69–82%) were obtained when the sugar hydroxyl groups were protected with benzoyl groups. Protection of the hydroxyl groups with acetyl groups also improved considerably the yields in this type of fluorination (20*a*). Thus, in the present work, as shown in Scheme 2, the carbocyclic analogs (**4**–**7**) of uracil and 2-thiouracil nucleosides were acetylated using acetic anhydride in pyridine to give compounds **8**–**11**, respectively. The protected nucleoside analogs were fluorinated then by passing a fluorine–nitrogen mixture (5:95) through solutions of the analogs in acetic acid. Treatment of the products with a solution of

Can. J. Chem. Downloaded from www.nrcresearchpress.com by 92.62.229.171 on 09/08/12
For personal use only.

Can. J. Chem. Downloaded from www.nrcresearchpress.com by 92.62.229.171 on 09/08/12
For personal use only.

triethylamine–methanol–water {2:9:9 (v/v/v)} gave the corresponding, unprotected 5-fluorouracil derivatives (**12**, **14**, and **15**); in the case of the 2-thiouracil derivative (**9**), only the 5-fluorouracil analogs **12** (40%) and **13** (10%) were obtained. The yields of the deprotected 5-fluorouracil derivatives (**12**, **14**, and **15**) from the protected uracil derivatives (**8**, **10**, and **11**, respectively) were 60–80%.

The ^{1}H nmr spectra of the protons in the cyclopentyl moieties of the 5-fluorouracil derivatives (**12**, **14**, and **15**) are nearly identical with those for the corresponding uracil derivatives (**4**, **6**, and **7**, respectively) (13, 14). However, the protons on the pyrimidine ring resonate 0.3–0.6 ppm further downfield in the case of the 5-fluorouracil derivatives than the corresponding protons in the case of the uracil derivatives.

Synthesis of cyclopentane analogs of 3′-substituted-2′,3′-dideoxy-5-fluorouridines

As shown in Scheme 3, the carbocyclic analog (**14**) of 1-(2′-deoxy-β-*threo*-pentofuranosyl)-5-fluorouracil was utilized for the synthesis of a variety of 3′-substituted-2′,3′-dideoxy-5-fluorouridine analogs. The primary hydroxyl group of compound **14** was protected by a trityl group using trityl chloride in pyridine at 100°C (22) to give **16**. Treatment of compound **16** with methanesulfonyl chloride in pyridine at room temperature afforded the 3′-mesylate (**17**) in 75% yield from **14**. Nucleophilic displacement of the 3′-mesyloxy group using tetra-*n*-butylammonium chloride (TBACl) in *N*,*N*-dimethylformamide gave the 3′-chloro derivative (**18**). The 3′-bromo derivative (**19**) was prepared analogously using tetra-*n*-butylammonium bromide (TBABr). The 3′-azido derivative (**20**) was prepared by displacement of the 3′-mesyloxy group using sodium azide in *N*,*N*-dimethylformamide. The elimination products, compounds **21** and **22**, were obtained also in the reactions with TBACl (in 29% yield) and TBABr (in 33% yield); the structures of these compounds were assigned on the basis of ^{1}H nmr spectral data. In the reaction with TBACl, **21** and **22** were obtained in a 3:1 ratio, respectively, whereas, with TBABr, compound **21** was formed preponderantly and only a trace of **22** was produced. Detritylation of compounds **18–22** in methylene chloride using diethylaluminum chloride at room temperature (23) afforded compounds **23–27**, respectively; in the cases of compounds **23–25**, the yields were 84–93%. The azido group in compound **25** was converted into the amino group as shown in Scheme 4. Treatment of the azide **25** with triphenylphosphine in pyridine (24) gave the triphenylphosphinimine intermediate (**28**), which, on hydrolysis using concentrated ammonium hydroxide (25), afforded the amino derivative **29** in 90% yield.

The assignments of the chemical shifts of the resonances of the protons in the compounds shown in Schemes 3 and 4 were made with the aid of spin–spin decoupling experiments. In the cases of compounds **18–20** and **23–25**, the signals of the 2′, 2″, 4′, and 5″ protons consist of complex overlapping multiplets (at 200 MHz) such that, in most instances, only a range of chemical shifts is given for these signals. The ^{1}H nmr spectra (at 200 MHz) of compounds **18** and **19** show similar multiplet patterns, and the chemical shifts of the resonances of corresponding protons in the two compounds are nearly identical, with the largest difference occurring for the resonance of the proton at C-3′. In the case of the bromine-containing analog (**19**), this proton resonates 0.05 ppm further downfield than does the proton in the chlorine-containing analog (**18**). The chemical shifts of the resonances of corresponding protons in the deprotected compounds **23** and **24** are also similar, and a similar trend was observed for the resonance of the proton at C-3′ in these compounds as was seen for the tritylated compounds. Also, the chemical shifts of the H-3′ signal are almost identical in the corresponding cases of the protected (**18**, **19**, and **20**) and deprotected (**23**, **24**, and **25**, respectively) compounds. Finally, the chemical shifts of the resonances of H-3 and H-6 on the pyrimidine base are almost identical in compounds **18–20** and **23–25**.

Ultraviolet spectra of the nucleoside analogs

The ultraviolet spectra of the acetylated, uracil- (**8**, **10**, and **11**) and 2-thiouracil- (**9**) nucleoside analogs resemble very closely those of the corresponding unprotected nucleoside analogs (**4–7**) (13, 14) and the spectra of 1-methyluracil and 1-methyl-2-thiouracil (26), respectively, at the corresponding pH's. However, in the cases of the acetylated, uracil-nucleoside analogs (**8**, **10**, and **11**), the absorption maxima are shifted slightly (1–3 nm) to shorter wavelengths compared to the cases of the corresponding unprotected compounds. In the case of the acetylated, 2-thiouracil-nucleoside analog (**9**), the absorption maxima occur at the same wavelengths as in the case of the unprotected analog (**5**). The absorption spectra of the 5-fluorouracil analogs (**12–15**, **25**, **26**, and **29**) have maxima at 208–210 nm and 273–275 nm in both neutral and acidic solvents, and at 218–221 nm and 272–274 nm in basic solvent. The positions of the absorption maxima at the short wavelengths (208–210 and 218–221 nm) differ little between the spectra of the uracil and 5-fluorouracil analogs; however, the long-wavelength maxima occur at significantly shorter wavelengths (265–268 nm) in the spectra of the uracil analogs (**4**, **6**, and **7**). Similar patterns have been observed for the cases of uracil and 5-fluorouracil (27), and their 1-methyl and 1-glycosyl derivatives (26–28).

Biological evaluation

Compounds **12**, **14**, **15**, **23–26**, and **29** were tested for cell-growth inhibition using cultured K-562 cells by methods described previously (29). Compounds **12**, **14**, **15**, **23**, **24**, and **29** showed no cell-growth inhibition at concentrations as high as 10^{-3} M. Compound **25** showed some cell-growth inhibition at 10^{-3} M, and compound **26** had an ID_{50} (dose which inhibits cell-number increase to 50% of the control) in the range 10^{-4}–10^{-3} M and was about 100-fold less active than 5-fluorouracil in this test system. Compounds **12**, **14**, **15**, and **29** were evaluated also for inhibition of leukemia L1210 cell growth in vitro. The ID_{50}'s of compounds **14** and **15** were greater than 10^{-4}, and those of **12** and **29** were 6.4×10^{-4} M and 7.3×10^{-4} M, respectively. In this test system the ID_{50} of 5-fluorouracil was $\sim 10^{-6}$ M. Compound **29** was evaluated also for cytotoxicity using B16-F10-murine melanoma, C26-murine colon, HCT-116-human colon, KB-human nasopharyngyl, Moser-human colon, and M109-murine lung cell lines, and showed no activity at 160 μg/mL. Compounds **8**, **9**, **12**, **14**, **15**, **25**, and **29** were tested also for antiviral activity against herpes simplex viruses 1 and 2, and were found to be inactive.

Conclusions

Three new carbocyclic analogs of 5-fluorouracil nucleosides have been synthesized by fluorination using elemental fluorine of acetylated uracil analogs that were synthesized

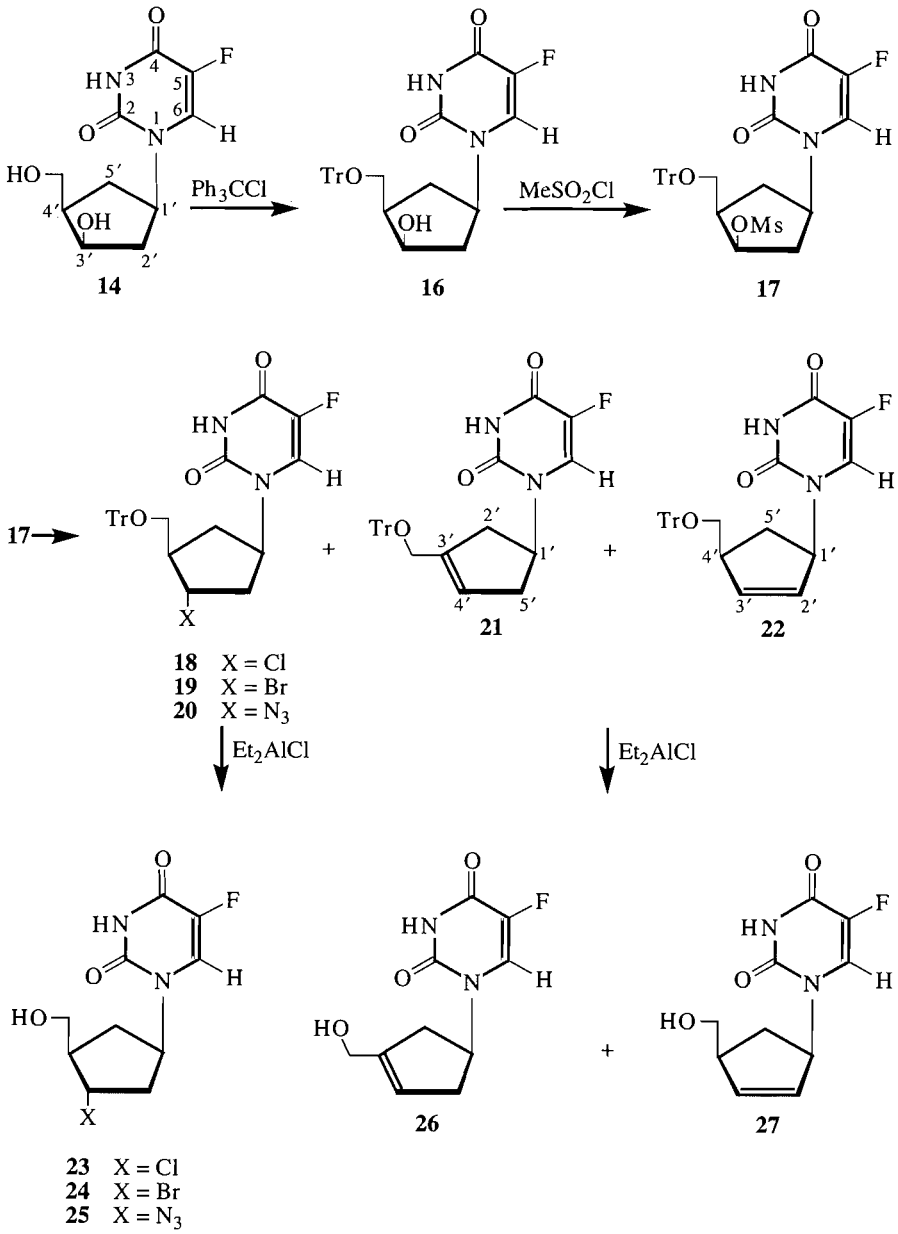

SCHEME 3

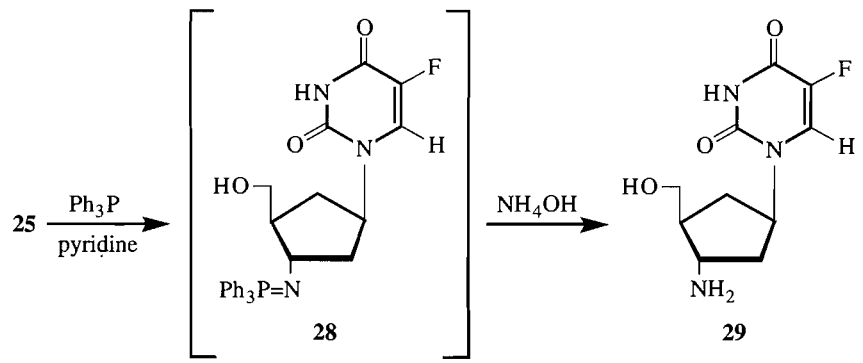

SCHEME 4

Can. J. Chem. Downloaded from www.nrcresearchpress.com by 92.62.229.171 on 09/08/12
For personal use only.

Can. J. Chem. Downloaded from www.nrcresearchpress.com by 92.62.229.171 on 09/08/12
For personal use only.

as described previously (13, 14). The carbocyclic analog (**14**) of 1-(2′-deoxy-β-*threo*-pentofuranosyl)-5-fluorouracil was utilized for the synthesis of novel carbocyclic analogs of 1-(3′-substituted-2′,3′-dideoxy-β-*erythro*-pentofuranosyl)-5-fluorouracil nucleosides by S_N2 displacement of the 3′-mesyloxy group in the protected derivative **17**. The novel nucleoside analogs produced in this way contained a chloro, bromo, or an azido group at the 3′-position; reduction of the azido group gave the 3′-amino analog. The ^{1}H nmr spectra (at 200 MHz) of all of the new analogs of nucleosides have been determined and discussed. In addition, the new analogs were evaluated for tumor-cell growth inhibition, and for antiviral activity against the herpes simplex viruses.

Experimental

Melting points were determined on a Fisher–Johns apparatus and are uncorrected. Infrared spectra were determined in potassium bromide on a Perkin–Elmer 598 spectrophotometer. The ^{1}H nmr spectra were recorded on a Bruker CXP-200 spectrometer at 200 MHz. The proton chemical shifts (δ) are given relative to Me_4Si (δ = 0). Assignments of chemical shifts and coupling constants were made with the aid of spin-decoupling experiments. The following abbreviations are used in describing ^{1}H nmr signals: singlet (s), doublet (d), triplet (t), quartet (q), quintuplet (qu), multiplet (m), and broadened (br). Ultraviolet spectra were recorded on a Perkin–Elmer 552 spectrophotometer without any precautions having been taken to exclude oxygen. Thin-layer chromatography (tlc) was performed using silica gel 60 F-254 plates and column chromatography on silica gel 60. The plates and silica gel 60 were purchased from BDH Chemicals. The developed plates were dried and sprayed with a solution of ceric sulfate (1%) and molybdic acid (1.5%) in 10% aqueous sulfuric acid, and heated at ~150°C. Unless otherwise indicated, the same solvent was used for both tlc and column chromatography.

*(±)-1-{*cis*-3-(Acetoxymethyl)cyclopentyl}-2,4(1*H*,3*H*)-pyrimidinedione (**8**)*

A solution of **4** (0.685 g, 3.26 mmol) and acetic anhydride (2.0 mL, 21.2 mmol) in pyridine (20 mL) was kept at room temperature for 13 h. The reaction solution was treated with ethanol (5 mL) and the solvent was evaporated under vacuum. The residue was evaporated then with ethanol–water {2 × 10 mL, 1:1 (v/v)} to give a crystalline solid, which was purified further by silica gel column chromatography to give **8** (0.641 g, 78%) as a white solid, R_f 0.45 {4:4:1 (v/v/v) ethyl acetate – toluene–2-propanol}. An analytical sample was prepared by recrystallization from ethyl acetate – hexanes, mp 140–141°C; uv λ_{max} (C_2H_5OH): 209 (ε 9000), 267 (10 200) nm; λ_{max} (0.01 M HCl in C_2H_5OH): 209 (ε 9100), 267 (10 200) nm; λ_{max} (0.01 M NaOH in C_2H_5OH): 219 (ε 9300), 266 (7400) nm; ^{1}H nmr (200 MHz, Me_2SO-d_6) δ: 1.33–2.34 (7H, m, H-2′, H-2″, H-3′, H-4′, H-4″, H-5′, and H-5″), 2.01 (3H, s, OAc), 3.98 (2H, m, AcOCH_2), 4.74 (1H, m, H-1′), 5.58 (1H, d of d, $^2J_{5,6}$ = 8.2, $^4J_{5,3}$ = 1.8 Hz, H-5), 7.74 (1H, d, $^3J_{6,5}$ = 8.2 Hz, H-6), 11.24 (1H, br s, H-3). Anal. calcd. for $C_{12}H_{16}O_4N_2$: C 57.13, H 6.39, N 11.10; found: C 57.07, H 6.03, N 11.10.

*(±)-2,3-Dihydro-1-{*cis*-3-(acetoxymethyl)cyclopentyl}-2-thioxo-4(1*H*)-pyrimidinone (**9**)*

A solution of **5** (0.492 g, 2.17 mmol) and acetic anhydride (2.0 mL, 21.2 mmol) in pyridine (20 mL) was kept at room temperature for 19 h. The reaction solution was treated then as described for the preparation of **8**, and, after fractionation by silica gel chromatography, compound **9** (0.466 g, 80%) was obtained as a white solid, mp 152–155°C; R_f 0.50 {8:8:1 (v/v/v) ethyl acetate – toluene–2-propanol}. Recrystallization from ethyl acetate – hexanes gave material having mp 152–154°C; uv λ_{max} (C_2H_5OH): 219 (ε 17 600), 273 (13 700) nm; λ_{max} (0.01 M HCl in C_2H_5OH): 219 (ε 17 700), 273 (13 600) nm; λ_{max} (0.01 M NaOH in C_2H_5OH): 240 (ε 19 700), 257 (14 600), 273 (16 300) nm; ^{1}H nmr (200 MHz, Me_2SO-d_6) δ: 1.29–2.37 (7H, m, H-2′, H-2″, H-3′, H-4′, H-4″, H-5′, and H-5″), 2.02 (3H, s, OAc), 4.02 (2H, m, AcOCH_2), 5.76 (1H, m, H-1′), 6.00 (1H, br d, $^3J_{5,6}$ = 8.2 Hz, H-5), 7.91 (1H, d, $^3J_{6,5}$ = 8.2 Hz, H-6), 12.61 (1H, br s, H-3). Anal. calcd. for $C_{12}H_{16}O_3N_2S$: C 53.71, H 6.01, N 10.44, S 11.95; found: C 53.96, H 6.04, N 10.39, S 12.45.

*(±)-1-{(1*β*,3*β*,4*β*)-3-Acetoxy-4-(acetoxymethyl)cyclopentyl}-2,4(1*H*,3*H*)-pyrimidinedione (**10**)*

A solution of **6** (0.500 g, 2.21 mmol) and acetic anhydride (2.0 mL, 21.2 mmol) in pyridine (20 mL) was kept at room temperature for 18 h. It was treated then as described for the preparation of **8**, and, after fractionation by silica gel column chromatography, **10** (0.525 g, 77%) was obtained as a solid, R_f 0.45 {3:3:1 (v/v/v) ethyl acetate – toluene–2-propanol}. An analytical sample was prepared by recrystallization from ethanol to give **10** as a white crystalline solid, mp 157–158°C; uv λ_{max} (C_2H_5OH): 208 (ε 10 100), 267 (10 600) nm; λ_{max} (0.01 M HCl in C_2H_5OH): 208 (ε 10 200), 267 (10 600) nm; λ_{max} (0.01 M NaOH in C_2H_5OH): 218 (ε 9800), 265 (7900) nm; ^{1}H nmr (200 MHz, Me_2SO-d_6) δ: 1.63 (1H, m, J_{gem} = 12.2, ^3J = 10.6 Hz, H-5′), 1.71 (1H, m, J_{gem} = 15.1, $^3J_{2',1'}$ = 6.6, $^3J_{2',3'}$ = 2.5 Hz, H-2′), 1.99 (3H, s, OAc), 2.05 (3H, s, OAc), 2.14 (1H, m, J_{gem} = 12.2, ^3J = 7.2 Hz, H-5″), 2.27–2.57 (2H, m, H-2″ and H-4′), 4.02 (1H, d of d, J_{gem} = 11.0, $^3J_{toH\text{-}4'}$ = 6.5 Hz, OCH_2), 4.12 (1H, d of d, J_{gem} = 11.0, $^3J_{toH\text{-}4'}$ = 8.2 Hz, OCH_2), 4.98 (1H, m, H-1′), 5.15 (1H, t of d, ^3J = 5.2, $^3J_{3',2'}$ = 2.2 Hz, H-3′), 5.66 (1H, d, $^3J_{5,6}$ = 8.1 Hz, H-5), 7.59 (1H, d, $^3J_{6,5}$ = 8.1 Hz, H-6), 11.27 (1H, br s, H-3). Spin–spin decoupling was performed at δ 2.14, 4.98, and 5.15. Anal. calcd. for $C_{14}H_{18}O_6N_2$: C 54.19, H 5.85, N 9.03; found: C 53.88, H 5.88, N 9.03.

*(±)-1-{(1*β*,2*β*,4*β*)-2-Acetoxy-4-(acetoxymethyl)cyclopentyl}-2,4(1*H*,3*H*)-pyrimidinedione (**11**)*

A solution containing **7** (0.705 g, 3.12 mmol) and acetic anhydride (2.5 mL, 26.5 mmol) in pyridine (25 mL) was kept at room temperature for 25 h. It was treated then as described for the preparation of **8**, and, after fractionation by silica gel column chromatography, **11** (0.83 g, 86%) was obtained as a solid, R_f 0.41 {4:4:1 (v/v/v) ethyl acetate – toluene–2-propanol}. An analytical sample was obtained by recrystallization from ethyl acetate – hexanes to give **11** as a white crystalline solid, mp 126–127°C; uv λ_{max} (C_2H_5OH): 208 (ε 9700), 265 (10 900) nm; λ_{max} (0.01 M HCl in C_2H_5OH): 208 (ε 9900), 265 (11 000) nm; λ_{max} (0.01 M NaOH in C_2H_5OH): 219 (ε 9500), 265 (8300) nm; ^{1}H nmr (200 MHz, Me_2SO-d_6) δ: 1.46 (1H, m, J_{gem} = 13.8, $^3J_{3',4'}$ = 5.9, $^3J_{3',2'}$ = 2.0 Hz, H-3′), 1.82–2.46 (4H, m, H-3″, H-4′, H-5′, and H-5″), 1.92 (3H, s, OAc), 2.03 (3H, s, OAc), 4.02 (2H, m, OCH_2), 4.78 (1H, m, $^3J_{1',5'}$ = 12.4, $^3J_{1',5''}$ = 7.4, $^3J_{1',2'}$ = 5.2 Hz, H-1′), 5.14 (1H, m, $^3J_{2',1'}$ = 5.2, $^3J_{2',3''}$ = 4.8, $^3J_{2',3'}$ = 2.0 Hz, H-2′), 5.51 (1H, d, $^3J_{5,6}$ = 8.1 Hz, H-5), 7.71 (1H, d, $^3J_{6,5}$ = 8.1 Hz, H-6), 11.28 (1H, br s, H-3). Spin–spin decoupling was performed at δ 1.46, 4.02, 4.78, and 5.14. Anal. calcd. for $C_{14}H_{18}O_6N_2$: C 54.19, H 5.85, N 9.03; found: C 53.92, H 5.98, N 9.03.

*(±)-5-Fluoro-1-{*cis*-3-(hydroxymethyl)cyclopentyl}-2,4(1*H*,3*H*)-pyrimidinedione (**12**)*

A fluorine–nitrogen mixture containing 5.1% fluorine was bubbled through a solution of acetic acid (150 mL) and compound **8** (0.505 g, 2.00 mmol) for 30 min. The reaction solution was flushed with N_2 for 10 min and the solvent was evaporated. The residue was dissolved in a solution of triethylamine–methanol–water {50 mL, 2:9:9 (v/v/v)}, and the solution was kept at room temperature for 15 h. The solvent was evaporated with 10 mL of ethanol. The residue was diluted with methanol and fractionated by silica gel column chromatography to give **12** (0.308 g, 67%) as a white solid, R_f 0.67 {1:1:1 (v/v/v) toluene – ethyl acetate – 2-propanol}. An analytical sample was prepared by recrystallization from ethanol–hexanes, mp 152–153°C; uv λ_{max} (C_2H_5OH): 209 (ε 9700), 275 (9100) nm; λ_{max} (0.01 M HCl in C_2H_5OH): 209 (ε 9500), 275 (9100) nm; λ_{max} (0.01 M NaOH in C_2H_5OH): 218 (ε 8700), 273

Can. J. Chem. Downloaded from www.nrcresearchpress.com by 92.62.229.171 on 09/08/12
For personal use only.

(6900) nm; ^{1}H nmr (200 MHz, Me_2SO-d_6) δ: 1.28–2.13 (7H, m, H-2′, H-2″, H-3′, H-4′, H-4″, H-5′, and H-5″), 3.38 (2H, t, ^3J = 5.4 Hz, OCH_2), 4.58 (1H, t, ^3J = 5.2 Hz, OH), 4.72 (1H, m, H-1′), 8.11 (1H, d, ^3J = 7.3 Hz, H-6), 11.74 (1H, br d, J = 4.7 Hz, H-3). Anal. calcd. for $C_{10}H_{13}O_3N_2F$: C 52.63, H 5.74, N 12.27, F 8.32; found: C 52.57, H 5.82, N 12.36, F 8.49.

Fluorination of compound ***9***

Compound **9** (0.361 g, 1.34 mmol) was treated as described for the preparation of compound **12**. After fractionation by silica gel column chromatography two components were isolated having R_f's 0.82 and 0.67 {1:1:1 (v/v/v) toluene – ethyl acetate – 2-propanol}. The component having R_f 0.67 (0.123 g, 40%) was shown by its mp, ^{1}H nmr and uv spectra, and elemental analysis to be identical with compound **12**. The component having R_f 0.82 (0.035 g, 10%) was compound **13**. An analytical sample of compound **13** was prepared by recrystallization from ethyl acetate – hexanes, mp 136–137°C; uv λ_{max} (C_2H_5OH): 208 (ε 10 400), 275 (9000) nm; λ_{max} (0.01 M HCl in C_2H_5OH): 209 (ε 10 000), 275 (9000) nm; λ_{max} (0.01 M NaOH in C_2H_5OH): 218 (ε 10 000), 273 (6900) nm; ^{1}H nmr (200 MHz, Me_2SO-d_6) δ: 1.34–2.08 (6H, m, H-2′, H-2″, H-4′, H-4″, H-5′, and H-5″), 2.01 (3H, s, OAc), 2.25 (1H, m, H-3′), 3.99 (2H, m, OCH_2), 4.75 (1H, m, H-1′), 8.15 (1H, d, ^3J = 7.7 Hz, H-6), 11.76 (1H, br d, J = 4.7 Hz, H-3). Spin–spin decoupling was performed at δ 2.25 and 4.75. Anal. calcd. for $C_{12}H_{15}O_4N_2F$: C 53.33, H 5.59, N 10.37, F 7.03; found: C 53.02, H 5.70, N 9.94, F 7.00.

*(±)-5-Fluoro-1-{(1β,3β,4β)-3-hydroxy-4-(hydroxymethyl) cyclopentyl}-2,4(1H,3H)-pyrimidinedione (**14**)*

An acetic acid solution (400 mL) of compound **10** (1.467 g, 4.72 mmol) was treated as described for the preparation of compound **12**. After fractionation by silica gel chromatography, **14** (0.698 g, 60%) was obtained as a solid, R_f 0.55 {1:1:1 (v/v/v) toluene – ethyl acetate – 2-propanol}. An analytical sample was prepared by recrystallization from ethanol, mp 213°C; uv λ_{max} (C_2H_5OH): 208 (ε 9900), 275 (9000) nm; λ_{max} (0.01 M HCl in C_2H_5OH): 209 (ε 9600), 275 (9000) nm; λ_{max} (0.01 M NaOH in C_2H_5OH): 221 (ε 7400), 273 (6900) nm; ^{1}H nmr (200 MHz, Me_2SO-d_6) δ: 1.37 (1H, t of d, J_{gem} = 12.1, ^3J = 8.6 Hz, H-5′), 1.56 (1H, br d of d, J_{gem} = 15.1, $^3J_{2',1'}$ = 3.4 Hz, H-2′), 1.88 (1H, m, H-4′), 2.08 (1H, m, H-5″), 2.27 (1H, m, J_{gem} = 15.1, $^3J_{2'',1'}$ = 11.0, $J_{2'',3'}$ = 4.5 Hz, H-2″), 3.42 (1H, m, J_{gem} = 10.6, ^3J = 5.3 Hz, OCH_2), 3.59 (1H, m, J_{gem} = 10.6, $^3J_{to\,OH}$ = 5.3, $^3J_{to\,H\text{-}4'}$ = 7.7 Hz, OCH_2), 4.11 (1H, m, H-3′), 4.39 (1H, t, ^3J = 5.3 Hz, $HOCH_2$), 5.04 (1H, m, H-1′), 5.12 (1H, d, $^3J_{to\,H\text{-}3'}$ = 3.6 Hz, OH), 8.19 (1H, d, ^3J = 7.3 Hz, H-6), 11.72 (1H, br d, J = 5.2 Hz, H-3). Spin–spin decoupling was performed at δ 4.11 and 5.04. Anal. calcd. for $C_{10}H_{13}O_4N_2F$: C 49.18, H 5.37, N 11.47, F 7.78; found: C 49.18, H 5.03, N 11.05, F 7.45.

*(±)-5-Fluoro-1-{(1β,2β,4β)-2-hydroxy-4-(hydroxymethyl) cyclopentyl}-2,4(1H,3H)-pyrimidinedione (**15**)*

An acetic acid solution (200 mL) of compound **11** (0.715 g, 2.30 mmol) was treated as described for the preparation of compound **12**. After fractionation by silica gel column chromatography, **15** (0.451 g, 80%) was obtained as a white solid, R_f 0.57 {1:1:1 (v/v/v) toluene – ethyl acetate – 2-propanol}. An analytical sample was obtained by recrystallization from ethanol–hexanes, mp 160–161°C; uv λ_{max} (C_2H_5OH): 208 (ε 10 000), 275 (9800) nm; λ_{max} (0.01 M HCl in C_2H_5OH): 209 (ε 9800), 275 (9800) nm; λ_{max} (0.01 M NaOH in C_2H_5OH): 219 (ε 9100), 273 (7500) nm; ^{1}H nmr (200 MHz, Me_2SO-d_6) δ: 1.30 (1H, m, H-3′), 1.66–2.15 (4H, m, H-3″, H-4′, H-5′, and H-5″), 3.39 (2H, m, OCH_2), 4.04 (1H, m, H-2′), 4.48 (1H, m, $^3J_{1',5'}$ = 11.6, $^3J_{1',5''}$ = 7.2 Hz, H-1′), 4.62 (1H, t, ^3J = 5.0 Hz, $HOCH_2$), 4.93 (1H, d, ^3J = 4.5 Hz, OH at 2′), 7.92 (1H, d, ^3J = 7.7 Hz, H-6), 11.74 (1H, br s, H-3). Spin–spin decoupling was performed at δ 4.04 and 4.48. Anal. calcd. for $C_{10}H_{13}O_4N_2F$: C 49.18, H 5.37, N 11.47, F 7.78; found: C 49.31, H 5.10, N 11.30, F 7.69.

*(±)-5-Fluoro-1-{(1β,3β,4β)-3-hydroxy-4-(triphenylmethoxy-methyl)cyclopentyl}-2,4(1H,3H)-pyrimidinedione (**16**)*

A solution of **14** (0.698 g, 2.86 mmol) and chlorotriphenylmethane (1.252 g, 4.49 mmol) in pyridine (30 mL) was heated at 100°C in an oil bath for 1 h. Additional chlorotriphenylmethane (0.292 g, 1.05 mmol) was added and the heating was continued for 0.5 h. The reaction solution was cooled to room temperature and poured into ice–water (150 mL), and the mixture was stirred until a solid was obtained. The solid was collected by filtration, washed with water (50 mL), dried, dissolved in methylene chloride – ethanol, and fractionated by silica gel column chromatography to give **16** (1.255 g, 90%) as a white solid, mp 223–224°C, R_f 0.59 {10:10:1 (v/v/v) toluene – ethyl acetate – 2-propanol}. A second purification by silica gel column chromatography gave a white powdery solid after dilution of the concentrated eluate with toluene, mp 226–228°C; ^{1}H nmr (200 MHz, Me_2SO-d_6) δ: 1.39 (1H, m, J_{gem} = 12.0 Hz, H-5′), 1.55 (1H, d of d, J_{gem} = 15.4 ^3J = 3.3 Hz, H-2′), 1.9–2.3 (2H, m, H-4′ and H-5″), 2.32 (1H, m, J_{gem} = 15.4, ^3J = 11.0, $^3J_{2'',3'}$ = 4.4 Hz, H-2″), 2.99 (1H, m, OCH_2), 3.24 (1H, d of d, J_{gem} = 8.3, ^3J = 6.8 Hz, OCH_2), 4.16 (1H, m, H-3′), 5.07 (1H, m, H-1′), 5.18 (1H, d, $^3J_{to\,H\text{-}3'}$ = 3.7 Hz, OH), 7.15–7.42 (15H, m, Ph), 8.08 (1H, d, ^3J = 7.3 Hz, H-6), 11.73 (1H, br d, J = 5.2 Hz, H-3). Spin–spin decoupling was performed at δ 4.16.

*(±)-5-Fluoro-1-{(1β,3β,4β)-3-(methylsulfonyloxy)-4-(triphenylmethoxymethyl)cyclopentyl}-2,4(1H,3H)-pyrimidinedione (**17**)*

A solution of **16** (1.184 g, 2.43 mmol) in pyridine (20 mL) was cooled in an ice bath and methanesulfonyl chloride (1.0 mL, 12.9 mmol) was added. The reaction solution was then stirred at room temperature for 16 h. The reaction solution was poured into ice–water (150 mL) and the mixture was stirred until the ice melted. The solid was collected by filtration, washed with water (100 mL), dried, dissolved in pyridine, and fractionated by silica gel column chromatography to give **17** (1.142 g, 83%) as a faintly yellow solid, mp 160–165°C (dec.), R_f 0.54 {12:12:1 (v/v/v) toluene – ethyl acetate – 2-propanol}; ^{1}H nmr (200 MHz, Me_2SO-d_6) δ: 1.56 (1H, m, H-5′), 1.98 (1H, br d of d, J_{gem} = 15.6, $^3J_{2',1}$ = 5.5 Hz, H-2′), 2.18 (1H, m, J_{gem} = 12.4, ^3J = 7.1 Hz, H-5″), 2.4–2.6 (1H, m, H-4′), 2.63 (1H, m, J_{gem} = 15.6, $^3J_{2'',1'}$ = 10.1, $^3J_{2'',3'}$ = 5.2 Hz, H-2″), 2.98 (3H, s, Me), 3.02–3.22 (2H, m, OCH_2), 5.03 (1H, m, H-1′), 5.21 (1H, m, H-3′), 7.14–7.43 (15H, m, Ph), 7.73 (1H, d, ^3J = 7.1 Hz, H-6), 11.81 (1H, br d, J = 5.2 Hz, H-3). Spin–spin decoupling was performed at δ 1.56 and 5.21.

*(±)-5-Fluoro-1-{(1β,3α,4β)-3-chloro-4-(triphenylmethoxy-methyl)cyclopentyl}-2,4(1H,3H)-pyrimidinedione (**18**),(±)-5-fluoro-1-{3-(triphenylmethoxymethyl)-3-cyclo-penten-1-yl}-2,4(1H,3H)-pyrimidinedione (**21**), and (±)-5-fluoro-1-{cis-4-(triphenylmethoxymethyl)-2-cyclopenten-1-yl}-2,4(1H,3H)-pyrimidinedione (**22**)*

A solution of **17** (0.191 g, 0.338 mmol) and tetra-*n*-butylammonium chloride (0.47 g, 1.70 mmol) (dried over 4 Å sieves) in *N*,*N*-dimethylformamide (10 mL) was heated in an oil bath at 85°C for 1 h and then kept at room temperature overnight. The volume of the solution was reduced by evaporation under reduced pressure and the residue was fractionated by silica gel column chromatography. Two components were isolated having R_f's 0.41 (**18**) and 0.29 (**21** and **22**) {3:1 (v/v) toluene – ethyl acetate}. Compound **18** (0.106 g, 62%) was recrystallized from ethanol–water to give a white crystalline solid (0.082 g), mp 231–233°C; ^{1}H nmr (200 MHz, Me_2SO-d_6) δ: 1.65 (1H, m, H-5′), 2.09–2.49 (4H, m, H-2′, H-2″, H-4′, and H-5″), 3.07 (1H, d of d, J_{gem} = 9.0, ^3J = 6.1 Hz, OCH_2), 3.18 (1H, d of d, J_{gem} = 9.0, ^3J = 5.2 Hz, OCH_2), 4.44 (1H, q, ^3J = 7.2 Hz, H-3′), 4.96 (1H, m, H-1′), 7.22–7.43 (15H, m, Ph), 8.09 (1H, d, ^3J = 7.3 Hz, H-6), 11.79 (1H, br d, J = 5.2 Hz, H-3). Spin–spin decoupling was performed at δ 4.44 and 4.96. The component having R_f 0.29 (0.046 g, 29%) was a colorless glassy solid and consisted of a mixture of compounds **21**

Can. J. Chem. Downloaded from www.nrcresearchpress.com by 92.62.229.171 on 09/08/12
For personal use only.

and **22** in a 3:1 ratio, respectively. This ratio was calculated from the integrals of the ^{1}H nmr signals of the 1′, 2′, 3′, and 4′ protons. Compound **22**: ^{1}H nmr (400 MHz, Me_2SO-d_6) δ: 1.29 (1H, m, H-5′), 2.41–2.50 (1H, m, H-5″), 2.94 (1H, m, H-4′), 3.05–3.07 (2H, m, OCH_2), 5.41 (1H, m, H-1′), 5.75 (1H, m, H-2′ or H-3′), 6.17 (1H, m, H-2′ or H-3′), 7.1–7.4 (15H, m, Ph), 7.44 (1H, d, ^3J = 6.8 Hz, H-6), 11.77 (1H, d, J = 5.3 Hz, H-3). The remaining signals in the ^{1}H nmr spectrum correspond to those in the spectrum of the compound, assigned the structure of **21**, obtained in the following experiment.

*(±)-5-Fluoro-1-{(1β,3α,4β)-3-bromo-4-(triphenylmethoxymethyl)cyclopentyl}-2,4(1H,3H)-pyrimidinedione (**19**), **21**, and **22***

A solution of **17** (0.160 g, 0.283 mmol) and tetra-*n*-butylammonium bromide (0.517 g, 1.60 mmol) (dried over 4 Å sieves) in *N*,*N*-dimethylformamide (10 mL) was heated in an oil bath at 85°C for 1 h and then kept at room temperature overnight. The volume of the solution was reduced by evaporation under reduced pressure and the residue was fractionated by silica gel column chromatography. Two components were isolated having R_f's 0.41 (**19**) and 0.29 (**21** and a trace of **22**) {3:1 (v/v) toluene – ethyl acetate}. Compound **19** (0.065 g, 42%) was recrystallized from ethanol–water to give a white crystalline solid (0.054 g), mp 205–208°C (dec.); ^{1}H nmr (200 MHz, Me_2SO-d_6) δ: 1.66 (1H, m, H-5′), 2.13–2.60 (4H, m, H-2′, H-2″, H-4′, and H-5″), 3.06 (1H, d of d, J_{gem} = 9.2, ^3J = 6.2 Hz, OCH_2), 3.19 (1H, d of d, J_{gem} = 9.2, ^3J = 5.2 Hz, OCH_2), 4.49 (1H, q, ^3J = 7.8 Hz, H-3′), 4.97 (1H, m, H-1′), 7.22–7.44 (15H, m, Ph), 8.10 (1H, d, ^3J = 7.5 Hz, H-6), 11.79 (1 H, br d, J = 5.2 Hz, H-3). Compound **21** (0.043 g, 33%) was obtained as a solid after drying under vacuum; ^{1}H nmr (200 MHz, Me_2SO-d_6) δ: 2.38–2.87 (4H, m, H-2′, H-2″, H-5′, and H-5″), 3.58 (2H, m, OCH_2), 5.12 (1H, m, H-1′), 5.78 (1H, m, H-4′), 7.14–7.46 (15H, m, Ph), 7.77 (1H, d, ^3J = 7.2 Hz, H-6), 11.78 (1H, br d, J = 5.2 Hz, H-3).

*(±)-5-Fluoro-1-{(1β,3α,4β)-3-azido-4-(triphenylmethoxymethyl)cyclopentyl}-2,4(1H,3H)-pyrimidinedione (**20**)*

A mixture of **17** (0.50 g, 0.88 mmol) and sodium azide (0.291 g, 4.48 mmol) in *N*,*N*-dimethylformamide (11 mL) was stirred in an oil bath at 85°C for 30 min. The reaction mixture was cooled and poured into ice–water (80 mL). The white solid was collected by filtration, washed with water (40 mL), and dried, to afford **20** (0.418 g, 93%) as a solid, R_f 0.34 {3:1 (v/v) toluene – ethyl acetate}; ir ν_{max}(KBr): 2110 (azide) cm^{-1}; ^{1}H nmr (200 MHz, Me_2SO-d_6) δ: 1.56 (1H, m, H-5′), 1.95 (1H, m, J_{gem} = 14.1, $^3J_{2',1'}$ = 8.8, $^3J_{2',3'}$ = 5.6 Hz, H-2′), 2.1–2.3 (3H, m, H-2″, H-4′, and H-5″), 3.03–3.19 (2H, m, OCH_2), 4.04 (1H, m, H-3′), 4.84 (1H, m, H-1′), 7.23–7.44 (15H, m, Ph), 8.12 (1H, d, ^3J = 7.4 Hz, H-6), 11.8 (1H, br s, H-3). Spin–spin decoupling was performed at δ 4.04 and 4.84.

*(±)-5-Fluoro-1-{(1β,3α,4β)-3-chloro-4-(hydroxymethyl)cyclopentyl}-2,4(1H,3H)-pyrimidinedione (**23**)*

To a solution of compound **18** (65.5 mg, 0.130 mmol) in dry methylene chloride (20 mL) was added diethylaluminum chloride (1.08 mmol) in toluene (0.6 mL) and the reaction solution was stirred at room temperature for 45 min. The solution was then treated with a saturated aqueous solution of sodium hydrogen carbonate (6 mL). The mixture was extracted with methylene chloride – acetonitrile solution {6 × 30 mL, 2:1 (v/v)}, the solvent was evaporated, and the residue was fractionated by silica gel column chromatography to give **23** (30.5 mg, 90%); R_f 0.46 {5:5:1 (v/v/v) toluene – ethyl acetate – 2-propanol}. An analytical sample was prepared by recrystallization from ethanol–hexanes, mp 150–152°C; ^{1}H nmr (200 MHz, Me_2SO-d_6) δ: 1.54 (1H, m, H-5′), 2.08–2.49 (4H, m, H-2′, H-2″, H-4′, and H-5″), 3.40–3.58 (2H, m, OCH_2), 4.43 (1H, d of t, ^3J = 6.8, ^3J = 5.1 Hz, H-3′), 4.90 (1H, t, ^3J = 5.3 Hz, OH), 5.02 (1H, qu, ^3J = 8.7 Hz, H-1′), 8.11 (1H, d, ^3J = 7.3 Hz, H-6), 11.80 (1H, br d, J = 5.2 Hz, H-3). Anal. calcd. for $C_{10}H_{12}N_2O_3ClF$: C 45.73, H 4.60, N 10.66, Cl 13.50, F 7.23; found: C 45.80, H 4.66, N 10.62, Cl 13.50, F 6.99.

*(±)-5-Fluoro-1-{(1β,3α,4β)-3-bromo-4-(hydroxymethyl)cyclopentyl}-2,4(1H,3H)-pyrimidinedione (**24**)*

Compound **19** (45.5 mg, 0.083 mmol) was treated with a solution of diethylaluminum chloride (0.54 mmol) in toluene (0.3 mL) as described for the preparation of compound **23**. After fractionation of the reaction product by silica gel column chromatography, **24** (21.5 mg, 84%) was obtained as a solid, R_f 0.47 {5:5:1 (v/v/v) toluene – ethyl acetate – 2-propanol}. An analytical sample of **24** was obtained by recrystallization from ethanol–hexanes, mp 162–165°C (dec.); ^{1}H nmr (200 MHz, Me_2SO-d_6) δ: 1.54 (1H, d, of t, J_{gem} = 12.7, ^3J = 9.4 Hz, H-5′), 2.10–2.64 (4H, m, H-2′, H-2″, H-4′, and H-5″), 3.3–3.8 (2H, m, OCH_2), 4.49 (1H, m, H-3′), 5.05 (1H, qu, ^3J = 8.6 Hz, H-1′), 8.12 (1H, d, ^3J = 7.1 Hz, H-6), 11.8 (1H, br d, J = 5.3 Hz, H-3). Anal. calcd. for $C_{10}H_{12}N_2O_3BrF$: C 39.11, H 3.94, N 9.12, Br 26.02, F 6.19; found: C 38.98, H 3.96, N 8.91, Br 26.32, F 5.96.

*(±)-5-Fluoro-1-{(1β,3α,4β)-3-azido-4-(hydroxymethyl)cyclopentyl}-2,4(1H,3H)-pyrimidinedione (**25**)*

Compound **20** (0.362 g, 0.71 mmol) was treated with a solution of diethylaluminum chloride (3.6 mmol) in toluene (2.0 mL) as described for the preparation of compound **23**. After fractionation of the reaction product by silica gel column chromatography, **25** (0.177 g, 93%) was obtained as a colorless oil, R_f 0.48 {4:4:1 (v/v/v) toluene – ethyl acetate – 2-propanol}; ir ν_{max} (KBr): 3480 (hydroxyl), 2120 (azide) cm^{-1}; uv λ_{max} (C_2H_5OH): 210 (ε 8600), 274 (8900) nm; λ_{max} (0.01 M HCl in C_2H_5OH): 211 (ε 8200), 274 (8900) nm; λ_{max} (0.01 M NaOH in C_2H_5OH): 220 (ε 8100), 272 (6800) nm; ^{1}H nmr (200 MHz, Me_2SO-d_6) δ: 1.49 (1H, m, H-5′), 1.91 (1H, m, J_{gem} = 13.3, $^3J_{2',1'}$ = 8.5, $^3J_{2',3'}$ = 4.6 Hz, H-2′), 1.97–2.23 (3H, m, H-2″, H-4′, and H-5″), 3.42–3.53 (2H, m, OCH_2), 4.04 (1H, d of t, ^3J = 7.8, ^3J = 4.7 Hz, H-3′), 4.83 (1H, m, H-1′), 4.89 (1H, t, ^3J = 5.0 Hz, OH), 8.12 (1H, d, ^3J = 7.3 Hz, H-6), 11.79 (1H, br d, J = 3.9 Hz, H-3).

*(±)-5-Fluoro-1-{3-(hydroxymethyl)-3-cyclopenten-1-yl}-2,4(1H,3H)-pyrimidinedione (**26**) and (±)-5-fluoro-1-{cis-4-(hydroxymethyl)-2-cyclopenten-1-yl}-2,4(1H,3H)-pyrimidinedione (**27**)*

A sample of compounds **21** and **22** (56.5 mg, 0.120 mmol), which were obtained as side-products in the preparation of compounds **18** and **19**, was treated with a solution of diethylaluminum chloride (0.72 mmol) in toluene (0.4 mL) as described for the preparation of compound **23**. After fractionation of the reaction product by silica gel column chromatography, a product (15 mg, 56%) was obtained as a white solid, R_f 0.29 {4:4:1 (v/v/v) toluene – ethyl acetate – 2-propanol}. The ^{1}H nmr spectrum showed that this material consisted of compound **26** and a small amount of compound **27**; the latter was identified by the chemical shifts for the signals of H-2′ and H-3′, namely, δ 5.68 and 6.09. The uv (of the mixture) λ_{max} (C_2H_5OH): 209 (ε 8500), 274 (8200) nm; λ_{max} (0.01 M HCl in C_2H_5OH): 210 (ε 7900), 275 (8200) nm; λ_{max} (0.01 M NaOH in C_2H_5OH): 219 (ε 8200), 274 (6300) nm. Compound **26**: ^{1}H nmr (200 MHz, Me_2SO-d_6) δ: 2.31–2.87 (4H, m, H-2′, H-2″, H-5′, and H-5″), 4.0 (2H, m, OCH_2), 5.10 (1H, m, H-1′), 5.55 (1H, m, H-4′), 7.71 (1H, d, ^3J = 7.3 Hz, H-6), 11.78 (1H, br d, J = 5.2 Hz, H;-3).

*(±)-5-Fluoro-1-{(1β,3α,4β)-3-amino-4-(hydroxymethyl)cyclopentyl}-2,4(1H,3H)-pyrimidinedione (**29**)*

A solution of **25** (0.132 g, 0.49 mmol) and triphenylphosphine (0.265 g, 1.01 mmol) in pyridine (15 mL) was kept at room temperature for 6 h; 15 M ammonia in water (2.0 mL) was added and the reaction solution was kept at room temperature for an additional 3 h. The volume of the solution was reduced to 2.0 mL and the residue was fractionated by silica gel column chromatography {3:3:1 (v/v/v) acetonitrile–2-propanol – 15 M ammonia in water} to give **29** (0.107 g, 90%) as a white solid. An analytical sample

was prepared by recrystallization from water–ethanol, mp 176–178°C (dec.); uv λ_{max} (C_2H_5OH): 210 (ε 7800), 275 (8500) nm; λ_{max} (0.01 M HCl in C_2H_5OH): 210 (ε 7700), 273 (8500) nm; λ_{max} (0.01 M NaOH in C_2H_5OH): 219 (ε 7600), 273 (6500) nm; ^1H nmr (200 MHz, Me_2SO-d_6) δ: 1.41 (1H, m, H-5′), 1.58–1.76 (2H, m, H-2′ and H-4′), 1.92 (1H, d of t, J_{gem} = 13.2, ^3J = 7.9 Hz, H-2″), 2.04 (1H, d of t, J_{gem} = 12.6, ^3J = 7.2 Hz, H-5″), 3.17 (1H, m, H-3′), 3.39–3.55 (2H, m, OCH_2), 4.94 (1H, m, H-1′), 8.06 (1H, d, ^3J = 7.3 Hz, H-6). Spin–spin decoupling was performed at δ 3.17 and 4.94. Anal. calcd. for $C_{10}H_{14}N_3O_3F \cdot H_2O$: C 45.98, H 6.17, N 16.08, F 7.27; found: C 46.26, H 5.90, N 16.14, F 7.11.

Acknowledgements

The authors are grateful to the Natural Sciences and Engineering Research Council of Canada for its support of this work in the form of a grant (to W. A. S.). They also thank Dr. K. Rosenthal of McMaster University for permitting the cell-growth inhibition studies using K-562 cells to be performed in his laboratory. Testing for cytotoxicity and antiviral activities was performed by the Bristol–Myers Company. The authors also thank D. R. J. Bernacki of the Grace Cancer Drug Center in Buffalo, New York, for cytotoxicity testing.

1. C. Heidelberger, P. V. Danenberg, and R. G. Moran. Adv. Enzymol. **54**, 57 (1983).
2. H. M. Pinedo and G. F. J. Peters. J. Clin. Oncol. **6**, 1653 (1988).
3. C. E. Myers. Pharmacol. Rev. **33**, 1 (1981).
4. P. V. Danenberg, C. Heidelberger, M. A. Mulkins, and A. R. Peterson. Biochem. Biophys. Res. Commun. **102**, 654 (1981).
5. G. W. M. Visser, G. C. M. Gorree, B. J. M. Braakhuis, and J. D. M. Herscheid. Eur. J. Nucl. Med. **15**, 225 (1989).
6. C. Heidelberger. Cancer Treat. Rep. **65** (Suppl. 3), 3 (1981).
7. E. De Clercq, J. Balzarini, P. F. Torrence, M. P. Mertes, C. L. Schmidt, D. Shugar, P. J. Barr, A. S. Jones, G. Verhelst, and R. T. Walker. Mol. Pharmacol. **19**, 321 (1981).
8. D. Farquhar, N. J. Kuttesch, M. G. Wilkerson, and T. Winkler. J. Med. Chem. **26**, 1153 (1983), and references therein.
9. J. J. Freed, D. Farquhar, and A. Hampton. Biochem. Pharmacol. **38**, 3193 (1989).
10. (*a*) K. A. Watanabe, U. Reichman, K. Hirota, C. Lopez, and J. J. Fox. J. Med. Chem. **22**, 21 (1979); (*b*) J. A. Coderre, D. V. Santi, A. Matsuda, K. A. Watanabe, and J. J. Fox. J. Med. Chem. **26**, 1149 (1983).
11. S. Ajmera, A. R. Bapat, K. Danenberg, and P. V. Danenberg. J. Med. Chem. **27**, 11 (1984).
12. Y. F. Shealy, J. L. Frye, N. F. Dubois, S. C. Shaddix, and R. W. Brockman. J. Med. Chem. **24**, 1083 (1981).
13. L. J. J. Hronowski and W. A. Szarek. Can. J. Chem. **63**, 2787 (1985).
14. L. J. J. Hronowski and W. A. Szarek. Can. J. Chem. **66**, 61 (1988).
15. M. R. C. Gerstenberger and A. Haas. Angew. Chem. Int. Ed. Engl. **20**, 647 (1981).
16. (*a*) M. J. Robins and S. R. Naik. J. Am. Chem. Soc. **93**, 5277 (1971); (*b*) D. H. R. Barton, R. H. Hesse, H. T. Toh, and M. M. Pechet. J. Org. Chem. **37**, 329 (1972); (*c*) R. A. Earl and L. B. Townsend. J. Heterocycl. Chem. **9**, 1141 (1972); (*d*) R. A. Sharma, M. Bobek, and A. Bloch. J. Med. Chem. **17**, 466 (1974); (*e*) M. J. Robins, G. Ramani, and M. Maccoss. Can. J. Chem. **53**, 1302 (1975); (*f*) M. J. Robins, M. Maccoss, S. R. Naik, and G. Ramani. J. Am. Chem. Soc. **98**, 7381 (1976), and references therein; (*g*) M. J. Robins, M. Maccoss, and S. R. Naik. *In* Nucleic acid chemistry. Part 2. *Edited by* L. B. Townsend and R. S. Tipson. John Wiley and Sons, Inc., New York. 1978. pp. 895–900; (*h*) T.-S. Lin, Y.-S. Gao, and W. R. Mancini. J. Med. Chem. **26**, 1691 (1983).
17. T. I. Yurasova. Zh. Obschch. Khim. **44**, 956 (1974).
18. S. Stavber and M. Zupan. J. Chem. Soc. Chem. Commun. 563 (1983).
19. G. W. M. Visser, S. Boele, B. W. v. Halteren, G. H. J. N. Knops, J. D. M. Herscheid, G. A. Brinkman, and A. Hoekstra. J. Org. Chem. **51**, 1466 (1986), and references therein.
20. (*a*) D. Cech, H. Meinert, G. Etzold, and P. Langen. J. Prakt. Chem. **315**, 149 (1973); (*b*) D. Cech and A. Holý. Collect. Czech. Chem. Commun. **41**, 3335 (1976).
21. E. H. Appelman, L. J. Basile, and R. C. Thompson. J. Am. Chem. Soc. **101**, 3384 (1979).
22. H. R. Munson, Jr. *In* Synthetic procedures in nucleic acid chemistry. Vol. 1. *Edited by* W. W. Zorbach and R. S. Tipson. John Wiley and Sons, Inc., New York. 1968. pp. 321–322.
23. H. Köster and N. D. Sinha. Tetrahedron Lett. **23**, 2641 (1982).
24. (*a*) H. Straudinger and E. Hauser. Helv. Chim. Acta, **4**, 21 (1921); (*b*) W. S. Mungall, G. L. Greene, G. A. Heavner, and R. L. Letsinger. J. Org. Chem. **40**, 1659 (1975).
25. T.-S. Lin, W. H. Prusoff, and D. C. Ward. *In* Nucleic acid chemistry. Part 1. *Edited by* L. B. Townsend and R. S. Tipson. John Wiley and Sons, Inc., New York. 1978. pp. 339–342.
26. M. Sano. Chem. Pharm. Bull. **10**, 320 (1962).
27. K. Berens and D. Shugar. Acta Biochim. Polon. **10**, 25 (1963).
28. K. L. Wierzchowski, E. Litońska, and D. Shugar. J. Am. Chem. Soc. **87**, 4621 (1965).
29. L. J. J. Hronowski and W. A. Szarek. J. Med. Chem. **25**, 522 (1982).

Can. J. Chem. Downloaded from www.nrcresearchpress.com by 92.62.229.171 on 09/08/12
For personal use only.

Isolation and structure of cribrostatins 1 and 2 from the blue marine sponge *Cribrochalina sp.*[1]

GEORGE R. PETTIT,[2] JEREMIAH C. COLLINS, DELBERT L. HERALD, DENNIS L. DOUBEK, MICHAEL R. BOYD,[3] JEAN M. SCHMIDT, JOHN N. A. HOOPER,[4] AND LARRY P. TACKETT

Cancer Research Institute and Department of Chemistry, Arizona State University, Tempe, AZ 85287-1604, U.S.A.

Received July 26, 1991

This paper is dedicated to the memory of Dr. Julius A. Rippel, 1901–1990

GEORGE R. PETTIT, JEREMIAH C. COLLINS, DELBERT L. HERALD, DENNIS L. DOUBEK, MICHAEL R. BOYD, JEAN M. SCHMIDT, JOHN N. A. HOOPER, and LARRY P. TACKETT. Can. J. Chem. **70**, 1170 (1992).

The blue marine sponge cribrostatins 1 (**1**, 8.8×10^{-6}% yield) and 2 (**2**, 3.1×10^{-6}% yield) active against the P388 lymphocytic leukemia cell line (ED_{50} 1.58 and 2.73 μg/mL respectively) have been isolated. The previously known isoquinolinequinones mimosamycin (**3**), renierone (**4**), and *O*-demethylrenierone (**5**) were also isolated and shown to display activity against the P388 cell line (ED_{50} 0.73, 2.75, and 8.36 μg/mL, respectively). Importantly, both cribrostatin 1 and mimosamycin showed selective activity against all of the nine human melanoma cell lines employed by the U.S. National Cancer Institute. Structural determinations were accomplished utilizing high field nuclear magnetic resonance (400 MHz) and mass spectral studies. Confirmation of the cribrostatin 1 structure was achieved by X-ray crystallographic techniques.

GEORGE R. PETTIT, JEREMIAH C. COLLINS, DELBERT L. HERALD, DENNIS L. DOUBEK, MICHAEL R. BOYD, JEAN M. SCHMIDT, JOHN N. A. HOOPER et LARRY P. TACKETT. Can. J. Chem. **70**, 1170 (1992).

On a isolé les cribrostatines 1 (**1**, rendement de $8{,}8 \times 10^{-6}$%) et 2 (**2**, rendement de $3{,}1 \times 10^{-1}$%) de l'éponge marine bleue; elles sont actives contre la lignée de cellules P388 de la leucémie lymphocytaire (ED_{50} respectives de 1,58 et 2,73 μg/mL). On a aussi isolé les isoquinoléinequinones suivantes qui sont déjà connues, mimosamycine (**3**), réniérone (**4**) et *O*-déméthylréniérone (**5**), et qui ont montré une activité contre la lignée de cellules P388 (ED_{50} respectives de 0,73, 2,75 et 8,36 μg/mL). Plus important encore, la cribrostatine 1 ainsi que la mimosamycine ont démontré une activité sélective contre les neuf lignées de cellules mélanomes humaines employées par l'Institut National du Cancer des États Unis. On a déterminé les structures à l'aide des spectres en résonance magnétique nucléaire à 400 MHz et par spectrométrie de masse. On a confirmé la structure de la cribrostatine 1 par les techniques de la diffraction des rayons X.
[Traduit par la rédaction]

Introduction

The phylum Porifera rapidly became of increasing importance in our early research devoted to the first systematic investigation of marine animals as new sources of potential anticancer drugs (2). Subsequent detection of antineoplastic activity in some of these sponge species led us to the isolation of such cell growth inhibitory compounds as macrocyclic lactones (3), pyrroles (4), peptides (5), and proteins (6). Meanwhile the isolation of heterocyclic marine sponge constituents such as pyrroles (7), imidazoles (8), oxazoles (9), indoles (10), pyridines (11), quinolizidines (12), pteridines (13), acridines (14), other nitrogen systems (15), and quinones (16) has been rapidly accelerating. So far ten isoquinolinequinones have been isolated from blue species of the sponge genera *Reniera* and *Xestospongia* (17).

In 1986 we conducted an exploratory survey of marine Porifera off remote islands in the Republic of the Maldives and located a deep-blue colored specimen of *Cribrochalina sp.* (Haplosclerida order) that afforded an orange ethanol extract. The encrusting sponge was found in areas of strong (and dangerous) currents to −45 m in the south side of east reef passages and yielded an ethanol extract that provided 40% life extension (at 50 mg/kg) against the U.S. National Cancer Institute's in vivo murine P388 lymphocytic leukemia (PS system). Bioassay-directed isolation using the in vitro PS leukemia led to the discovery of new cytostatic isoquinolinequinones designated cribrostatin 1 (**1**) and cribrostatin 2 (**2**), as well as several previously known pigments that were also found to possess PS cell growth inhibitory activity. Only one other species of the genus, *Cribrochalina dura* (from the Bahamas), appears to have received prior chemical study, and a cytotoxic acetylenic carbinol (duryne) was isolated (18).

A 1989 recollection (about 350 kg wet weight) of the Maldive *Cribrochalina sp.* was subjected to successive ethanol and 1:1 methanol – methylene chloride extractions, and an array of solvent partition separations, to provide a PS active methylene chloride extract, which upon evaporation yielded a black semisolid (PS ED_{50} 6.7 μg/mL). The PS active fraction was further separated by a series of size exclusion and partition chromatographic steps utilizing Sephadex LH-20 (Scheme 1) to afford the new isoquinolinequinones, cribrostatin 1 (**1**) as red-orange crystals (31 mg, 8.8×10^{-6}% yield) and the golden-yellow cribrostatin 2 (**2**, 11 mg, 3.1×10^{-6}% yield). The structure of the cytostatic metabolite cribrostatin 1 (**1**) was determined by hreims, a variety of high-field nmr techniques, and confirmed by single-crystal X-ray diffraction analysis. We also report here isolation of the previously known mimosamycin (**3**, 124 mg, ref. 21), renierone (**4**, 174 mg, ref. 19), and *O*-demethylrenierone (**5**, 94 mg, ref. 20), identical with authentic samples.[5]

[1]Part 228 of the series *Antineoplastic agents*. For Part 227 see ref. 1.

[2]Author to whom correspondence may be addressed.

[3]National Cancer Institute, Frederick Cancer Research and Development Center, Frederick, Maryland.

[4]Northern Territory Museum, Darwin, Australia.

[5]Authentic samples of renierone (**4**) and mimosamycin (**3**) were provided by Dr. D. J. Faulkner, Scripps Institution of Oceanography, California.

Printed in Canada

Can. J. Chem. Downloaded from www.nrcresearchpress.com by 92.62.229.171 on 09/08/12
For personal use only.

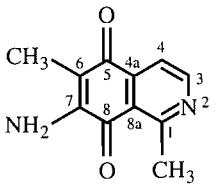

1

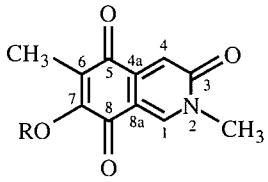

2, R = C_2H_5
3, R = CH_3

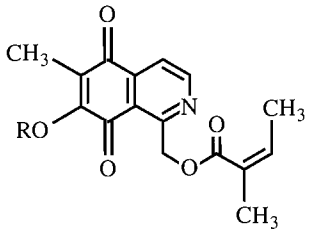

4, R = CH_3
5, R = H

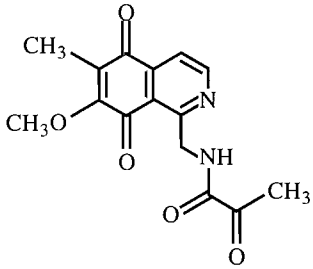

6

Mass spectral (by hreims) analysis of cribrostatin 1 revealed the molecular formula $C_{11}H_{10}N_2O_2$. The mass spectral fragmentation pattern of cribrostatin 1 exhibited the loss of HCN (27) and CO (28), indicating the possibility of a nitrogen-containing quinone. The results of uv/vis (232, 265, and 272 nm) and infrared spectra (1681 and 1635 cm^{-1}) suggested a quinone while further infrared absorptions (3405 and 3300 cm^{-1}) hinted at the presence of a primary amine. The 400 MHz ^1H nmr spectrum (Table 1) of cribrostatin 1 displayed a set of doublets at δ 7.86 and 8.83 (J = 4.9 Hz). The downfield signal at δ 8.83 suggested a proton adjacent to nitrogen in a heteroaromatic system. The spectrum also exhibited two methyl group resonances at δ 2.01 and 2.98 and a broad two-proton singlet at δ 5.20. The latter signal disappeared on deuterium exchange, again suggesting a primary amino group. The ^{13}C nmr spectrum of cribrostatin 1 revealed two carbonyl carbon signals at δ 180.9 and 181.85 suggestive of a quinone. Five other quaternary aromatic carbons were evident as well as two aromatic methine carbons and two methyl carbons. The substitution pattern was established by application of a heteronuclear multiple bond correlation (hmbc) (22) nmr experiment in conjunction with ^1H–^{13}C couplings (23). Most of the two- and three-bond ^1H–^{13}C coupling signals were evident and supported structure **1** for cribrostatin 1. An X-ray crystallographic analysis (cf. Fig. 1) was used to confirm the structure (**1**) of cribrostatin 1.

Mimosamycin (**3**), renierone (**4**), and *O*-demethylrenierone (**5**) were isolated employing chromatographic techniques on Sephadex LH-20 as summarized in Scheme 1. Mimosamycin was identified by hreims and ^{13}C and ^1H nmr techniques and was identical with an authentic sample isolated from the marine sponge *Reniera sp.* (20; see also footnote 5). The quinone was first isolated from *Streptomyces lavendulae* No. 314 (21) and subsequently from the sponge *Xestospongia caycedoi* (24). The first fully assigned ^{13}C nmr signals for mimosamycin are recorded in Table 2. Unambiguous assignment was made possible by employing hmbc nmr experiments. The long-range two- and three-bond ^1H–^{13}C coupling confirmed the structure of mimosamycin and provided a means for differentiating between the quinone carbonyl carbon signals and identifying the remaining carbon signals. Mimosamycin was earlier evaluated against the L1210 murine lymphocytic leukemia cell line (21) and found inactive. However, we found significant activity against the P388 leukemia cell line (ED_{50} 0.73 μg/mL) and this potentially important observation was pursued as noted in the sequel.

Cribrostatin 2 (**2**) was isolated (Scheme 1) from the same parent fraction as mimosamycin. The structure of this quinone (mp 194–195°C, 11 mg) was identified by analyzing the ^{13}C and ^1H nmr spectra. The ethoxy group was evident from the presence of a quartet and a triplet at δ 4.48 and 1.39 (J = 7.0 Hz) respectively, with the corresponding carbon signals at δ 69.78 and 16.07. The remaining proton and carbon nmr data were very similar to those of mimosamycin except for the distinct lack of any signals due to a methoxy group (Table 2). Further structural support for cribrostatin 2 was obtained from the mass spectral fragmentation pattern. Losses of HCN (27), CH_3 (15), and CO (28) were consistent with the structure. A fragmentation ion at m/z 218 was indicative of ethyl group removal from the molecular ion.

Renierone (**4**) and its *O*-demethyl derivative (**5**) were isolated from *Cribrochalina sp.* as outlined in Scheme 1. The sponge *Reniera sp.* (19) earlier yielded renierone (**4**), *O*-demethylrenierone (**5**) (20), and mimocin (**6**) (also isolated from *Streptomyces lavendulae* No. 314, ref. 25) and these represented the first examples of isoquinolinequinones found in nature. Cribrostatins 1 (**1**) and 2 (**2**) herewith join this relatively rare group of sponge and microorganism biosynthetic products. Indeed the sponge isoquinolinequinones may in turn be derived from commensal marine microorganisms.

Presently the *Cribrochalina sp.* constituents are undergoing detailed antineoplastic evaluation. Initial investigations of cribrostatin 1 (**1**) and mimosamycin (**3**) in the U.S. National Cancer Institute's new in vitro disease-oriented antitumor screen (26) revealed melanoma cell line subpanel specificity; the statistical criteria currently used to define subpanel specificity are defined elsewhere (27). The human tumor cell line panel currently used for these studies consists of a diverse array of 60 different cell lines representing eight major cancer subtypes (26). All nine of the melanoma cancer lines (LOX-1MVI; MALME-3M; M14: M19-MEL; SK-MEL-2; SK-MEL-28; SK-MEL-5; UACC-257; UACC-62) currently included in the panel showed sensitivity greater than the panel mean; LC_{50} values (27) ranged between 10^{-5} and 10^{-6} molar, with the greatest sensitivity shown by the M19-MEL and the SK-MEL-5 lines. Further biological studies are underway.

Experimental

General methods

Solvents used for chromatographic procedures were redistilled. The Sephadex LH-20 (25–100 μm) employed for gel permeation and partition chromatography was obtained from Pharmacia Fine Chemicals AB, Uppsala, Sweden. Gilson FC-220 and FC-202 fraction collectors were used for chromatographic fractionation experiments. Silica gel GF Uniplates for tlc and silica gel Si 60 Lobar columns were used for chromatographic separation. All tlc plates were viewed with uv light and (or) developed with a ceric sulfate – sulfuric acid spray (heating to approximately 150°C for 10 min).

The uncorrected melting points were observed with a Reichert type 7905 melting point apparatus. The ir spectral data were obtained using a Nicolet MX-1 FTIR spectrophotometer. Mass spectra were obtained using a Kratos MS-50 spectrometer (70 eV). The

Can. J. Chem. Downloaded from www.nrcresearchpress.com by 92.62.229.171 on 09/08/12
For personal use only.

Can. J. Chem. Downloaded from www.nrcresearchpress.com by 92.62.229.171 on 09/08/12
For personal use only.

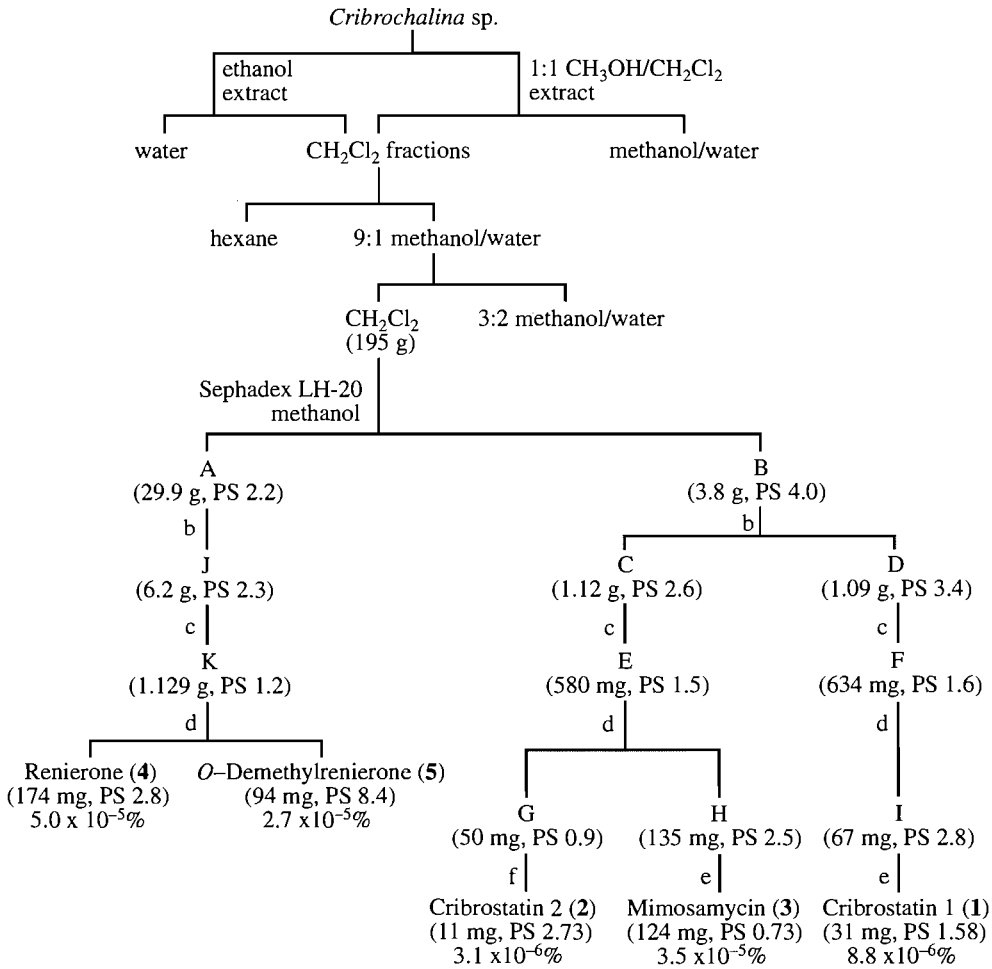

a: PS values determined in the P388 murine lymphocytic leukemia cell line are expressed as the ED_{50} in μg/mL
b: Sephadex LH-20, 3:2 CH_2Cl_2/methanol
c: Sephadex LH-20, 3:1:1 hexane/toluene/methanol
d: Sephadex LH-20, 8:1:1 hexane/2-propanol/methanol
e: Fractional crystallization
f: Lobar column (silica gel), 10–30% ethyl acetate/CH_2Cl_2

SCHEME 1. Isolation of cribrostatins **1** and **2**

TABLE 1. The ^1H and ^{13}C nmr spectra of cribrostatin 1 (**1**) with assignments relative to tetramethylsilane in deuteriochloroform

Position no.	^1H (400 MHz)	^{13}C (100 MHz)[a]
1		159.58
2		
3	8.83 d, J = 4.9 Hz	154.14
4	7.86 d, J = 4.9 Hz	117.70
4a		140.77
5		180.90
6		111.80
7		146.94
8		181.85
8a		122.38
1-CH_3	2.98 s	25.69
6-CH_3	2.01 s	9.23
7-NH_2	5.20 brs	

[a]Two drops of DMSO-d_6 were used to aid dissolution.

nmr experiments were conducted with Bruker WH-400 and Varian VXR-500 instruments using deuteriochloroform as solvent (TMS internal standard). The X-ray crystallographic experiments were conducted with an Enraf–Nonius CAD-4 diffractometer. Elemental analyses were performed by Spang Microanalytical Laboratories. Authentic samples of previously known compounds were compared with the isolated products by means of tlc, ir (KBr), and nmr techniques to establish mutual identities.

Animal collection and preliminary experiments

In June 1986, approximately 2 kg (wet wt.) of the sponge *Cribrochalina sp.* (Niphatidae family, Haplosclerida order, Demospongiae class) was collected by SCUBA in the channel between Guradu and Madu Islands of South Malé Atoll, Republic of the Maldives, at depths of −15 to −33 m and then preserved in ethanol. The combined ethanol and subsequent 2:1 methanol – methylene chloride extracts gave a confirmed level of activity against the murine P388 lymphocytic leukemia (PS system) with 40% life extension at 50 mg/kg.

Animal extraction and solvent partitioning

In 1988–1989 some 350 kg (wet wt.) of *Cribrochalina sp.* was collected at various locations on North and South Malé Atolls (on

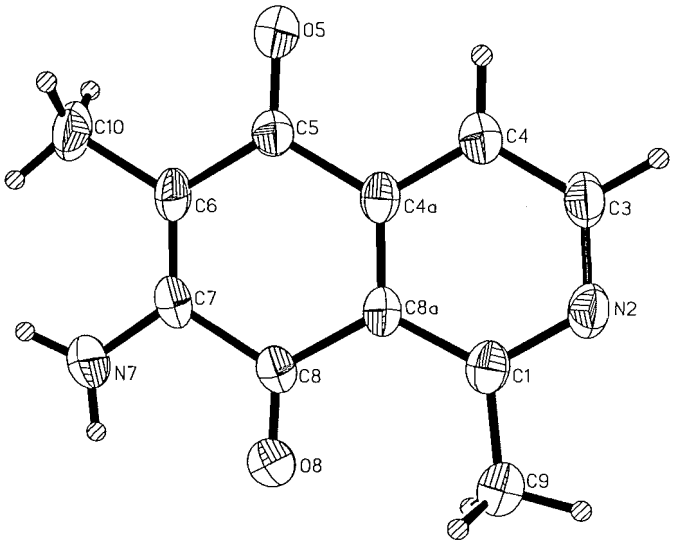

FIG. 1. The crystal structure of cribrostatin 1 (**1**) illustrated by a computer representation.

TABLE 2. The ^{1}H and ^{13}C nmr spectra of cribrostatin 2 (**2**) and mimosamycin (**3**). Each assignment is relative to tetramethylsilane in deuteriochloroform

	^{1}H (400 MHz)		^{13}C (100 MHz)	
Position no.	**2**	**3**	**2**	**3**
1	8.25	8.27	142.02	142.05
2				
3			162.79	162.77
4	7.10	7.11	116.67	116.70
4a			138.95	138.86
5			183.52	183.48
6			133.71	133.13
7			159.14	159.47
8			177.37	177.29
8a			111.29	111.25
2-CH_3	3.66	3.67	38.37	38.40
6-CH_3	2.07	2.07	9.66	9.53
7-OCH_3		4.17		61.27
7-OCH_2CH_3	1.39 t,	J = 7.0 H_2	16.07	
	4.48 q,	J = 7.0 H_2	69.78	

the south side of east coast passes), Republic of the Maldives, at depths of −5 to −45 m and were preserved in ethanol. The ethanol solution was decanted and the sponge reextracted twice with 1:1 methanol – methylene chloride over a period of 5–19 days. The ethanol solution was partitioned with methylene chloride in a counter-current manner, with each portion being partitioned five times. The methylene chloride was removed (evaporation *in vacuo*) to provide a 1.3 kg residue (PS ED_{50} 1.25 μg/mL). The chlorocarbon residue was partitioned between hexane and 9:1 methanol–water; the methanol–water phase was diluted to 3:2 methanol–water and partitioned against methylene chloride (the active fraction 127 g, PS ED_{50} 2.6 μg/mL). Meanwhile the two methanol – methylene chloride extracts of the sponge were processed by adding water (15%) to separate a methylene chloride phase, which was evaporated (*in vacuo*) to dryness (521 g, 323 g; PS ED_{50} 12.5, 0.2 μg/mL). These fractions were combined and partitioned as just summarized for the ethanol extract, yielding an additional active methylene chloride fraction (68 g, PS ED_{50} 6.7 μg/mL).

Isolation of cribrostatin 1 (1)

A 195 g sample of the PS active methylene chloride fraction was chromatographed on a column of Sephadex LH-20 (15 × 150 cm) in methanol, employing the same solvent as eluent. Twelve distinct fractions were separated; two fractions were combined and designated B (elution volume 3.0 L, 3.8 g, PS ED_{50} 4.0 μg/mL). Fraction B was separated by partition chromatography on a Sephadex LH-20 column (5 × 105 cm) with 3:2 methylene chloride – methanol as eluent to furnish active fraction D (elution volume 300 mL, 1.091 g, PS ED_{50} 3.4 μg/mL). Further partition chromatography on Sephadex LH-20 (3 × 90 cm column) and elution with 3:1:1 hexane–toluene–methanol gave active fraction F (elution volume 300 mL, 634 mg, PS ED_{50} 1.6 μg/mL). Final partition chromatography on a Sephadex LH-20 column (3 × 90 cm) employing 8:1:1 hexane–2-propanol–methanol as eluent resulted in six distinct composite fractions, of which the fraction labeled I (67 mg, PS ED_{50} 2.8 μg/mL) at elution volume 100 mL gave, on fractional recrystallization from methylene chloride – methanol, cribrostatin 1 as red-orange crystals (31 mg, 8.8×10^{-6}% yield): mp 220–235°C (dec.); tlc (on silica gel) R_f 0.48 (20:1 methylene chloride – methanol); uv/vis (CH_3OH) λ_{max}: 207 (ε 8730), 232(4700), 265(4170), 272(4160), 324(537) nm; ir ν_{max} (NaCl): 3405, 3300, 1681, 1635, 1602, 1558 cm^{-1}; ^{1}H nmr and ^{13}C nmr (see Table 1); hreims (*m/z*): 202.0737 (M^+ calcd. for $C_{11}H_{10}N_2O_2$ 202.0742). Anal. calcd. for $C_{11}H_{10}N_2O_2$: C 65.33, H 4.98, N 13.77; found: C 65.09, H 5.22, N 13.77.

Crystal structure of cribrostatin (1)

Dark-red crystals of cribrostatin 1 separated from a deuteriochloroform – dimethyl sulfoxide solution (in an nmr tube) of the quinone upon standing. A crystal of dimension ≈ 0.04 × 0.40 × 0.18 mm was obtained by cleavage from a larger crystal. Data were collected (Enraf–Nonius CAD-4 diffractometer) to a maximum of 2Θ = 140° at 26 ± 1°C. A quadrant of data was collected for the orthorhombic crystal, space group $Pna2_1$, with a = 16.792(3), b = 14.124(1), c = 3.912(1) Å, α = β = γ = 90°, V = 927.8 Å^3, ρ_0 = 1.431 g cm^{-3}, ρ_c = 1.447 g cm^{-3} for Z = 4. The ω/2Θ scan technique was used with graphite monochromated Cu Kα radiation (λ 1.54178 Å). After Lorentz and polarization corrections, merging of equivalent reflections, and rejection of systematic absences, a total of 720 reflections ($I > 3\sigma(I)$) were used in the structure determination. No absorption correction was made. Direct methods were used in the structure determination. All non-hydrogen atom coordinates were revealed in the initial run of SHELXS-86 (28). Refinement was performed with MOLEN (29). A non-Poisson contribution weighting scheme (scheme number 1 in MOLEN) was used with Dunitz–Seiler modified weight (30). The hydrogen atom coordinates were calculated at optimum positions and were included in a subsequent final stage of refinement, but were restrained to ride on the atom to which they were bonded. Full-matrix least-squares anisotropic refinement on all non-hydrogen atoms, and isotropic temperature factors for hydrogens, yielded standard crystallographic residuals of R = 0.084, Rw = 0.051. A computer-generated perspective view of cribrostatin 1, showing 50% probability ellipsoids, is shown in Fig. 1.

Isolation of cribrostatin 2 (2)

Separation of the active methylene chloride extract (195 g) on a Sephadex LH-20 column (15 × 150 cm) in methanol yielded 12 fractions of which the fraction designated B was further separated on a Sephadex LH-20 column (5 × 105 cm) in 3:2 methylene chloride – methanol to yield active fraction C (elution volume 300 mL, 1.12 g, PS ED_{50} 2.6 μg/mL). Additional chromatographic separations on Sephadex LH-20 employing the solvents recorded in Scheme 1 resulted in active fraction G (50 mg, PS ED_{50} 0.9 μg/mL). Final separation was performed on a Lobar column (silica gel) employing a gradient eluent (1:9 → 3:7 ethyl acetate – methylene chloride) with a flow rate of 1.5 mL/min to furnish the title compound as a golden-yellow solid (11 mg, 3.1×10^{-6}% yield): mp 194–195°C; tlc (on silica gel) R_f 0.58 (20:1 methylene chloride – methanol); uv/vis (CH_3OH) λ_{max}: 209 (ε 5829), 328 (4126) nm; ir ν_{max} (KBr): 2953, 2854, 1682, 1643, 1609, 1548 cm^{-1}; ^{1}H nmr and ^{11}C nmr (see Table 2); eims *m/z*: 247, 232, 218, 203, 191, 175, 163, 149, 135.

Can. J. Chem. Downloaded from www.nrcresearchpress.com by 92.62.229.171 on 09/08/12
For personal use only.

Can. J. Chem. Downloaded from www.nrcresearchpress.com by 92.62.229.171 on 09/08/12
For personal use only.

Isolation of mimosamycin (3)

Fraction B (3.8 g, PS ED_{50} μg/mL, see Scheme 1) derived from the 195 g active methylene chloride fraction was chromatographed on Sephadex LH-20 employing the three successive solvents as displayed in Scheme 1 to provide fraction H (135 mg, PS ED_{50} 2.5 μg/mL). Subsequent fractional recrystallization from methylene chloride – methanol furnished mimosamycin (**3**) as golden-yellow crystals (124 mg, 3.5×10^{-5}% yield): mp 223–227°C; tlc (on silica gel) R_f 0.51 (20:1 methylene chloride – methanol); ir ν_{max} (KBr): 1678, 1644, 1633, 1582 cm^{-1}; ^1H nmr and ^{13}C nmr (see Table 2); hreims (*m/z*): 233.0680 (M^+ calcd. for $C_{12}H_{11}NO_4$ 233.0688). Anal. calcd. for $C_{12}H_{11}NO_4$: C 61.80, H 4.75, N 6.01; found: C 61.74, H 4.89, N 5.71.

Isolation of renierone (4)

Scheme 1, fraction A (29.9 g, PS ED_{50} 2.2 μg/mL) was further separated by chromatography on a Sephadex LH-20 column (10 × 135 cm) with 3:2 methylene chloride – methanol as eluent to give fraction J (elution volume 640 mL, 6.2 g, PS ED_{50} 2.3 μg/mL). Further chromatographic separation of fraction I on a Sephadex LH-20 column (5 × 105 cm) with 3:1:1 hexane–toluene–methanol as solvent furnished fraction K (elution volume 900 mL, 1.13 g, PS ED_{50} 1.2 μg/mL). Final chromatography on Sephadex LH-20 with 8:1:1 hexane–isopropanol–methanol resulted in the isolation of renierone (**4**, 174 mg, 5.0×10^{-5}% yield, PS ED_{50} 2.8 μg/mL), which recrystallized from methylene chloride – methanol as amber colored crystals: mp 92.5–93.5°C; tlc (on silica gel) R_f 0.74 (20:1 methylene chloride – methanol); ir ν_{max} (KBr): 2957, 2924, 1718, 1669, 1653, 1570, cm^{-1}; ^1H nmr (400 MHz) δ: 1.97 (3H, dq, J = 1.5, 1.5 Hz) 2.01 (3H, dq, J = 7.2, 1.5 Hz), 2.08 (3H, s), 4.14 (3H, s), 5.77 (2H, s), 6.10 (1H, qq, J = 7.2, 1.5 Hz), 7.86 (1H, d, J = 4.9 Hz), 8.90 (1H, d, J = 4.9 Hz); ^{13}C nmr (100 MHz) δ: 9.07, 15.75, 20.62, 61.23, 65.34, 118.34, 122.66, 127.84, 130.49, 138.00, 138.87, 153.99, 156.88, 158.49, 167.93, 181.75, 184.56; eims *m/z*: 315, 216, 83, 82, 55.

Isolation of O-demethylrenierone (5)

The title compound was isolated from the same fraction K that furnished renierone by employing chromatography on Sephadex LH-20 with 8:1:1 hexane–isopropanol–methanol as eluent. *O*-Demethylrenierone crystallized from methylene chloride – hexane as yellow-lime micro-needles (94 mg, 2.7×10^{-5} yield, PS ED_{50} 8.4 μg/mL): mp 137–138°C; ir ν_{max} (KBr): 3280, 2950, 2920, 1700, 1660, 1650, 1640, 1570 cm^{-1}; ^1H nmr (400 MHz) δ: 1.97 (3H, dd, J = 1.5, 1.5 Hz), 2.01 (3H, dq, J = 7.1, 1.5 Hz), 2.11 (3H, s), 5.79 (2H, s), 6.11 (1H, qq, J = 7.1, 1.5 Hz), 7.51 (1H, br s), 7.94 (1H, d, J = 5.0 Hz), 8.96 (1H, d, J = 5.0 Hz); ^{13}C nmr (100 MHz) δ: 8.56, 15.76, 20.60, 65.18, 119.05, 120.36, 120.59, 127.69, 138.31, 139.96, 153.72, 155.29, 157.09, 167.84, 181.26, 183.57; eims *m/z*: 301, 273, 244, 202, 162, 146, 117, 83, 82, 55.

Acknowledgments

With appreciation we acknowledge the very necessary financial assistance provided by Outstanding Investigator Grant CA 44344-01A1 and PHS Grants CA-16049-07-12 awarded by the Division of Cancer Treatment, NCI, DHHS, the Fannie E. Rippel Foundation, the Arizona Disease Control Research Commission, the Robert B. Dalton Endowment Fund, Virginia Piper Ladies' Auxiliary, V. F. W., Dept. of Arizona, and the Eagles Art Ehrmann Cancer Fund.

For other very useful assistance we are pleased to thank the Government of the Republic of the Maldives (Maizan H. Maniku, A. Naseer, and M. Shiham), Drs. Ronald A. Nieman and Michael D. Williams, and Mrs. Denise K. Tackett, Mr. Lee Williams, Mr. Willie G. Schulz, and Mrs. Laura E. Galbreath, the U.S. National Science Foundation (Grant CHE-8409644), and the NSF Regional Instrumentation Facility in Nebraska (Grant CHE-8620177).

1. H. Quentmeier, S. Brauer, G. R. Pettit, and H. G. Drexler. Leukemia. Submitted.
2. G. R. Pettit, J. F. Day, J. L. Hartwell, and H. B. Wood. Nature, **227**, 962 (1970).
3. G. R. Pettit, Y. Kamano, C. L. Herald, J. M. Schmidt, and C. G. Zubrod. Pure Appl. Chem. **58**, 415 (1986).
4. G. R. Pettit, C. L. Herald, J. L. Leet, R. Gupta, D. E. Schaufelberger, R. B. Bates, P. J. Clewlow, D. L. Doubek, K. P. Manfredi, K. Rutzler, J. M. Schmidt, L. P. Tackett, F. B. Ward, M. Bruck, and F. Camou. Can. J. Chem. **68**, 1621 (1990).
5. G. R. Pettit, P. J. Clewlow, C. Dufresne, D. L. Doubek, R. Cerny, and K. Rutzler. Can. J. Chem. **68**, 708 (1990).
6. G. R. Pettit, J. A. Rideout, and J. A. Hasler. J. Nat. Prod. **44**. 588 (1981).
7. (*a*) W. D. Inman, M. O'Neill-Johnson, and P. Crews. J. Am. Chem. Soc. **112**, 1 (1990); (*b*) M. Aknin, J. Miralles, J. M. Kornprobst, R. Faure, E. M. Gaydou, N. Boury-Esnault, Y. Kato, and J. Clardy. Tetrahedron Lett. **31**, 2979 (1990); (*c*) J. Kobayashi and M. Tsuda. Tetrahedron, **46**, 5579 (1990); (*d*) R. West, C. L. Mayne, C. M. Ireland, L. S. Brinen, and J. Clardy. Tetrahedron Lett. **31**, 3271 (1990); (*e*) H. Hirota, S. Matsunaga, and N. Fusetani. Tetrahedron Lett. **31**, 4163 (1990).
8. (*a*) P. Ciminiello, E. Fattorusso, A. Mangoni, B. Di Blasio, and V. Pavone. Tetrahedron, **46**, 4387 (1990); (*b*) R. K. Akee, T. R. Carroll, W. Y. Yoshida, and P. J. Scheuer. J. Org. Chem. **55**, 1944 (1990).
9. E. O. Pordesimo and F. J. Schmitz. J. Org. Chem. **55**, 4704 (1990).
10. (*a*) S. A. Morris and R. J. Anderson. Tetrahedron, **46**, 715 (1990); (*b*) Can. J. Chem. **67**, 677 (1989).
11. J. Kobayashi, T. Murayama, Y. Ohizumi, T. Sasaki, T. Ohta, and S. Nozoe. Tetrahedron Lett. **30**, 4833 (1989).
12. (*a*) G. Cimino, A. Spinella, and E. Trivellone. Tetrahedron Lett. **30**, 133 (1989); (*b*) M. Kobayashi, K. Kawazoe, and I. Kitagawa. Tetrahedron Lett. **30**, 4149 (1989); (*c*) M. Kobayashi, K. Kawazoe, and I. Kitagawa. Chem. Pharm. Bull. **37**, 1676 (1989).
13. C. Debitus, M. Cesario, J. Guilhem, C. Pascard, and M. Pais. Tetrahedron Lett. **30**, 1535 (1989).
14. N. S. Burres, S. Sazesh, G. P. Gunawardana, and J. J. Clement. Cancer Res. **49**, 5267 (1989).
15. (*a*) M. Adamczeski, E. Quinoa, and P. Crews. J. Org. Chem. **55**, 240 (1990); (*b*) N. Fusetani, K. Yasumuro, S. Matsunaga, and K. Hashimoto. Tetrahedron Lett. **30**, 2809 (1989); (*c*) G. Cimino, C. A. Mattia, L. Mazzarella, R. Puliti, G. Scognamiglio, A. Spinella, and E. Trivellone. Tetrahedron **45**, 3863 (1989).
16. (*a*) H. H. Sun, S. Sakemi, N. Burres, and P. McCarthy. J. Org. Chem. **55**, 4964 (1990); (*b*) K. Iguchi, A. Sahashi, J. Kohno, and Y. Yamada. Chem. Pharm. Bull. **38**, 1121 (1990).
17. (*a*) A. Kubo, Y. Kitahara, and S. Nakahara. Chem. Pharm. Bull. **37**, 1384 (1989); (*b*) H. He and D. J. Faulkner. J. Org. Chem. **54**, 5822 (1989); (*c*) M. Tisler. *In* Adv. Heterocycl. Chem. Vol. 45. Academic Press, New York. 1989. p. 37.
18. A. E. Wright, O. J. McConnell, S. Kohmoto, M. S. Lui, W. Thompson, and K. M. Snader. Tetrahedron Lett. **28**, 137 (1987).
19. D. E. McIntyre, D. J. Faulkner, D. Van Engen, and J. Clardy. Tetrahedron Lett. 4163 (1979).
20. J. M. Frincke and D. J. Faulkner. J. Am. Chem. Soc. **104**. 265 (1982).
21. (*a*) T. Arai, K. Yazawa, and Y. Mikami. J. Antibiot. **29**, 39 (1976); (*b*) H. Fukumi, H. Kurihara, T. Hata, C. Tamura, and H. Mishima. Tetrahedron Lett. 3825 (1977).
22. (*a*) A. Bax and M. F. Summers. J. Am. Chem. Soc. **108**, 209 (1986); (*b*) A. Bax, A. Aszalos, Z. Dinya, and K. Sudo. J. Am. Chem. Soc. **108**, 8056 (1986).

23. (*a*) A. Bax and G. A. Morris. J. Magn. Reson. **42**, 501 (1981); (*b*) G. Bodenhausen and R. Freeman. J. Magn. Reson. **28**, 471 (1971).
24. T. C. McKee and C. M. Ireland. J. Nat. Prod. **50**, 754 (1987).
25. A. Kubo, S. Nakahara, R. Iwata, K. Takahashi, and T. Arai. Tetrahedron Lett. **21**, 3207 (1980).
26. M. R. Boyd. *In* Principles and practice of oncology. *Edited by* V. T. DeVita, Jr., S. Hellman, and S. A. Rosenberg. Lippincott, Philadelphia. 1989. pp. 1–12.
27. M. R. Boyd, K. D. Paull, and L. R. Rubinstein. *In* Antitumor drug discovery and development. *Edited by* F. A. Valeriote, T. Corbett, and L. Baker. Kluwer Academic Press, Amsterdam. 1990. In press.
28. G. M. Sheldrick. Institute für Anorganische Chemie der Universität Göttingen. Tammanstr, 4, D-3400 Göttingen, Germany.
29. MOLEN. An interactive structure solution procedure. Enraf–Nonius, Delft, The Netherlands. 1990.
30. J. D. Dunitz and P. Seiler. Acta Crystallogr. Sect. B: Struct. Crystallogr. Cryst. Chem. **B29**, 589 (1973).

Can. J. Chem. Downloaded from www.nrcresearchpress.com by 92.62.229.171 on 09/08/12
For personal use only.

Structural studies of organoboron compounds L.[1] 4-(2-Hydroxy-2,2-diphenylacetyl)-6,6-pentamethylene-2-phenyl-1,3-dioxa-4-aza-2-boracyclohexane and 4-[2,2-difluoro-5,5-bis(4-methoxyphenyl)-1,3-dioxa-2-borata-4-cyclopentylidene]-6,6-pentamethylene-2-phenyl-1,3-dioxa-4-azonia-2-boracyclohexane

WOLFGANG KLIEGEL, LUTZ PREU, AND UTE SCHUMACHER

Institut für Pharmazeutische Chemie der Technischen Universität Braunschweig, Beethovenstrasse 55, 3300 Braunschweig, Germany

AND

STEVEN J. RETTIG AND JAMES TROTTER

Department of Chemistry, University of British Columbia, 2036 Main Mall, Vancouver, B.C., Canada V6T 1Z1

Received December 6, 1990[2]

Can. J. Chem. Downloaded from www.nrcresearchpress.com by 92.62.229.171 on 09/08/12
For personal use only.

WOLFGANG KLIEGEL, LUTZ PREU, UTE SCHUMACHER, STEVEN J. RETTIG, and JAMES TROTTER. Can. J. Chem. **70,** 1176 (1992).

The preparation of the organoboron compounds 4-(2-hydroxy-2,2-diphenylacetyl)-6,6-pentamethylene-2-phenyl-1,3-dioxa-4-aza-2-boracyclohexane, **6**, 4-(2,2-difluoro-5,5-diphenyl-1,3-dioxa-2-borata-4-cyclopentylidene)-6,6-pentamethylene-2-phenyl-1,3-dioxa-4-azonia-2-boracyclohexane, **14***a*, and 4-[2,2-difluoro-5,5-bis(4-methoxyphenyl)-1,3-dioxa-2-borata-4-cyclopentylidene]-6,6-pentamethylene-2-phenyl-1,3-dioxa-4-azonia-2-boracyclohexane, **14***b*, are reported. Crystals of **6** are triclinic, $P\bar{1}$, a = 8.7348(5), b = 11.0529(6), c = 14.104(1) Å, α = 65.781(5)°, β = 72.147(6)°, γ = 79.928(6)°, Z = 2, ρ_c = 1.130 g cm^{-3}, and crystals of **14***b* · 1/2 CH_2Cl_2 are also triclinic, $P\bar{1}$, a = 11.799(1), b = 13.464(2), c = 10.047(2) Å, α = 103.28(2)°, β = 92.60(2)°, γ = 79.752(8)°, Z = 2, ρ_c = 1.285 g cm^{-3}. The structures were solved by direct methods and were refined by full-matrix least-squares procedures to final R values of 0.040 and 0.060 for 3881 and 3221 reflections with $I \geq 3\sigma(I)$, respectively. Compound **6** has a six-membered cycloboronate structure, bond distances involving the trigonal planar boron atom being (N)O—B = 1.390(2), (C)O—B = 1.345(2), and B—C(phenyl) = 1.557(2) Å. Compound **14***b* represents a derivative of **6** in which an intramolecularly hydrogen-bonded hydrogen atom has been replaced by a difluoroboron moiety and represents the first structurally characterized compound containing both a phenylboronate and a difluoroboron chelate ring within the same molecule. Bond lengths in **14***b* involving the trigonal planar boron atom are (N)O—B = 1.403(5), (C)O—B = 1.326(5), and B—C(phenyl) = 1.550(5) Å and those involving the tetrahedral boron atom are O—B = 1.427(5) and 1.547(5), F—B = 1.353(5) and 1.382(5) Å.

WOLFGANG KLIEGEL, LUTZ PREU, UTE SCHUMACHER, STEVEN J. RETTIG et JAMES TROTTER. Can. J. Chem. **70,** 1176 (1992).

On rapporte la préparation des composés organiques du bore suivants : 4-(2-hydroxy-2,2-diphénylacétyl)-6,6-pentaméthylène-2-phényl-1,3-dioxa-4-aza-2-boracyclohexane, **6**, 4-(2,2-difluoro-5,5-diphényl-1,3-dioxa-2-borata-4-cyclopentylidène)-6,6-pentaméthylène-2-phényl-1,3-dioxa-4-azonia-2-boracyclohexane, **14***a*, et 4-[2,2-difluoro-5,5-bis(4-méthoxyphényl)-1,3-dioxa-2-borata-4-cyclopentylidène]-6,6-pentaméthylène-2-phényl-1,3-dioxa-4-azonia-2-boracyclohexane, **14***b*. Les cristaux du produit **6** sont tricliniques, $P\bar{1}$, a = 8,7348(5), b = 11,0529(6), c = 14,104(1) Å, α = 65,781(5)°, β = 72,147(6)° et γ = 79,928(6)°, Z = 2, ρ_c = 1,130 g cm^{-3} alors que les cristaux du composé **14***b* · 1/2 CH_2Cl_2 sont tricliniques, $P\bar{1}$, a = 11,799(1), b = 13,464(2), c = 10,047(2) Å, α = 103,28(2)°, β = 92,60(2)° et γ = 79,752(8)°, Z = 2, ρ_c = 1,285 g cm^{-3}. On a résolu les structures par des méthodes directes et on les a affinées par la méthode des moindres carrés jusqu'à des valeurs de R de 0,040 et 0,060 respectivement pour 3881 et 3221 réflexions avec $I \geq 3\sigma(I)$. Le composé **6** comprend une structure cycloboronate à six chaînons dans laquelle les distances impliquant l'atome de bore plan trigonal sont (N)O—B = 1,390(2), (C)O—B = 1,345(2) et B—C(phényle) = 1,557(2) Å. Le composé **14***b* représente un dérivé du composé **6** dans lequel on a remplacé un atome d'hydrogène impliqué dans une liaison intramoléculaire par une entité difluorobore et il représente la premier composé de structure caractérisée comportant dans la même molécule un phénylboronate ainsi qu'un cycle chélate difluorobore. Les longeurs de liaisons du composé **14***b* impliquant l'atome de bore plan trigonal sont (N)O—B = 1,403(4), (C)O—B = 1,326(5) et B—C(phényle) = 1,550(5) Å alors que celle impliquant l'atome de bore tétraédrique sont O—B = 1.427(5) et 1,547(5) et F—B = 1,353(5) et 1,382(5) Å.

[Traduit par la rédaction]

Introduction

Hydroxamic acids have long been known to be important biologically active compounds (1), possessing numerous pharmacological, toxicological, and pathological properties in addition to potential therapeutic applications (2). In medicinal chemistry these compounds are of special interest in their capacity as sequestering agents (3). Thus the physical characteristics of the hydroxamate function, the changes therein upon complexation, and especially the site of chelation in polyfunctional hydroxamic acids are of great significance with respect to the biological and medicinal chemistry of these compounds. General data on the reactivity and structure of open-chain or cyclic hydroxamic acids and their chelating properties, particularly information on electron delocalization and (or) tautomeric phenomena, can be obtained by the synthesis and structure analysis of the

[1]Previous paper in this series: ref. 24.

[2]Revision received October 12, 1991.

Can. J. Chem. Downloaded from www.nrcresearchpress.com by 92.62.229.171 on 09/08/12
For personal use only.

boron derivatives that form part of this series (4). In these compounds a borenium cation (R_2B^+) functions as a "pseudometal" cation (5) and replaces a hydrogen-bonded proton of the hydroxamic acid group. Borate complexes of this kind also play a role in drug synthesis via hydroxamates or in the blocking of hydroxamic enzyme inhibitors (6). Structures deviating from the "normal" type of hydroxamate complexes have been established for the reaction products of some polyfunctional hydroxamic acids with boron compounds (7, 8).

The reaction of the bis(hydroxyalkyl)-substituted hydroxamic acid **1** with BF_3 leads to the formation of the difluoroboron chelate **2** via intramolecular ring closure to an oxazoline-*N*-oxide and the subsequent[3] formation of the BF_2 chelate. The structure of **2** has been established by an X-ray crystallographic analysis (8). To assess the capability of the polyfunctional ligand **1** for similar reactions with organoboron compounds we reacted it with phenylboronic acid, which, like BF_3, is both a Lewis acid and bears suitable leaving groups (the hydroxyl residues). The crystalline substance that was isolated after the reaction of **1** with phenylboronic acid in ethanol had the elemental composition expected for the *B*-hydroxy-*B*-phenylboron chelate **3**, analogous to **2**. The infrared spectrum of the product displayed a sharp O—H absorption band at 3390 cm^{-1}, and the ^1H nmr spectrum showed two exchangeable signals with a total peak area consistent with one OH proton. These data could support the desired product **3** or an isomeric chelate **4** with the "normal" boron hydroxamate moiety that has been established for several diphenyl- and difluoroboron chelates (4) and postulated for boron chelates derived from phenylboronic acid and various aryl-substituted hydroxamic acids (9). The ^{11}B nmr spectrum, however, displays a broad resonance at $\delta(Et_2OBF_3) = 33.4$ ppm, which usually indicates the presence of a trivalent (sp^2)-boron atom (10). Considering this information, the structures **3** and **4** seemed less probable than the alternative isomeric structures like **5–9**, which all contain sp^2-hybridized boron atoms incorporated into boronate ester functions. Compounds of type **5** having simple *N*-alkyl or -aryl residues (**10**, R = alkyl, aryl) are easily available by cyclocondensation of *N*-substituted glycolohydroxamic acids with arylboronic acids.[4] Six-membered cycloboronates like **6** can be obtained from *N*-(2-hydroxyalkyl) hydroxamic acids (eliminating the α-hydroxyl function of the carbonic acid moiety) and phenylboronic acid,[5] like compound **11** described in this work. The seven-membered cyclic *N*-oxide **7** could be the result of a cyclic anhydride formation between phenylboronic acid and a hydrogen-bond stabilized hydroximate form of **1** involving the carbonyl oxygen atom and the *N*-(2-hydroxyalkyl) substituent. Another case involving incorporation of the carbonyl function is exemplified by the isomeric five-membered phenylboronate **8** having the hydroximic *N*-oxide function in an exocyclic position. However, the fact that the carbonyl oxygen atom of hydroxamic acids generally is not the preferred site of attack for acylating agents (11) disclaims both of the *N*-oxide structures, **7** and **8**. The eight-membered isomer **9**, resulting from cycloboronate formation via esterification of both alcohol functions, also does not seem very likely, even though cyclic aryl- and alkylboronates of this ring size are reported to be quite stable compounds (12). In hypothetical compounds like **7–9** strong intramolecular hydrogen bonds should be present and result in broadened O—H stretching bands at lower wavenumbers in the infrared spectra. For the same reason the ^1H nmr signals of the OH protons should appear at lower fields in the spectra of these compounds. Thus, the spectroscopic data tend to support the six-membered cycloboronate structures **5** and **6**. Nevertheless the structural assignment remains uncertain, especially in view of the two separate signals observed for the OH proton as well as for some CH protons in the ^1H nmr spectra and double signals in the ^{13}C nmr spectrum that could indicate the presence of two isomers, at least in solution.

An X-ray crystallographic analysis (see below) confirms the structure **6** possessing an (*E*)-configuration about the hydroxamic C⋯N moiety and an intramolecular hydrogen bridge from the α-hydroxy group to the hydroxamic carbonyl oxygen atom (cf. **6*B***). The splitting of the OH signal in the ^1H nmr spectra of **6** into two differently shaped part signals (each about 50% of the total peak area) indicates the presence of nearly equimolar amounts of two different molecular species in solution. The upfield signal (between δ = 2.83 and 2.90 ppm in $CDCl_3$, or at 2.91 ppm in C_6D_6) could be assigned to the free cyclohexanol moiety of compound **5** by analogy to similar compounds containing the same alkanol moiety, like **12** which shows a signal at 2.68 ppm in $CDCl_3$ (4*e*) or 2.37 ppm in C_6D_6 (this work). The downfield signal (between 5.33 and 5.41 ppm in $CDCl_3$, or at 5.86 ppm in C_6D_6) should arise from the α-hydroxycarbonyl function of **6**; the corresponding OH signal for the model compound **13** (ref. 13 and footnote 4) appears at δ = 6.12 ppm in $CDCl_3$ solution. In full agreement with the splitting of the OH signal is the doubling of the NCH_2 singlet in the ^1H nmr spectra of **6**. Two separate peaks[6] indicate nearly equimolar amounts of two different species like **5** and **6**. Additional evidence is found in the region of aromatic proton resonance: the doublet arising from the *ortho* protons of the *B*-phenyl group of **5/6** is split into two different doublets (each about 50% of the total peak area). These findings from the ^1H nmr data are consistent with the ^{13}C nmr spectra, which show all of the carbons signals doubled, with varying differences in shift between the corresponding pairs of peaks. The ^{13}C signal of the NCH_2 group appears at δ = 52.51 and 59.36 ppm and can be assigned to the species **6** and **5**, respectively, by comparison with the corresponding NCH_2 signals for the reference compounds **11** and **12** (51.26 and 59.57 ppm, respectively).

In addition to the assignments made on the basis of the ^1H and ^{13}C nmr spectra of **6/5**, and the comparisons with the spectra of the reference compounds, a 2D heteronuclear nmr experiment yielded a $^{13}C,^1H$-COSY spectrum of **6** (in C_6D_6

[3]The mechanism of this reaction is not fully understood, and simultaneous or preliminary chelation of BF_2 is also possible.

[4]W. Kliegel and U. Schumacher. Unpublished results.

[5]W. Kliegel, U. Schumacher, and M. Tajerbashi. Unpublished results.

[6]The small difference between the δ values of the two NCH_2 singlets for **6** in $CDCl_3$ solution (Δ = 0.01 ppm, detectable at 400 MHz, but not at 90 MHz) is somewhat more distinct in aromatic solvents such as chlorobenzene or hexadeuterobenzene (Δ = 0.05 and 0.16 ppm, respectively). The signal at 3.56 ppm (in C_6D_6) is the same as that observed for the NCH_2 grouping within the six-membered ring of the cycloboronate **11**, indicating a comparable ring system for **6**.

Can. J. Chem. Downloaded from www.nrcresearchpress.com by 92.62.229.171 on 09/08/12
For personal use only.

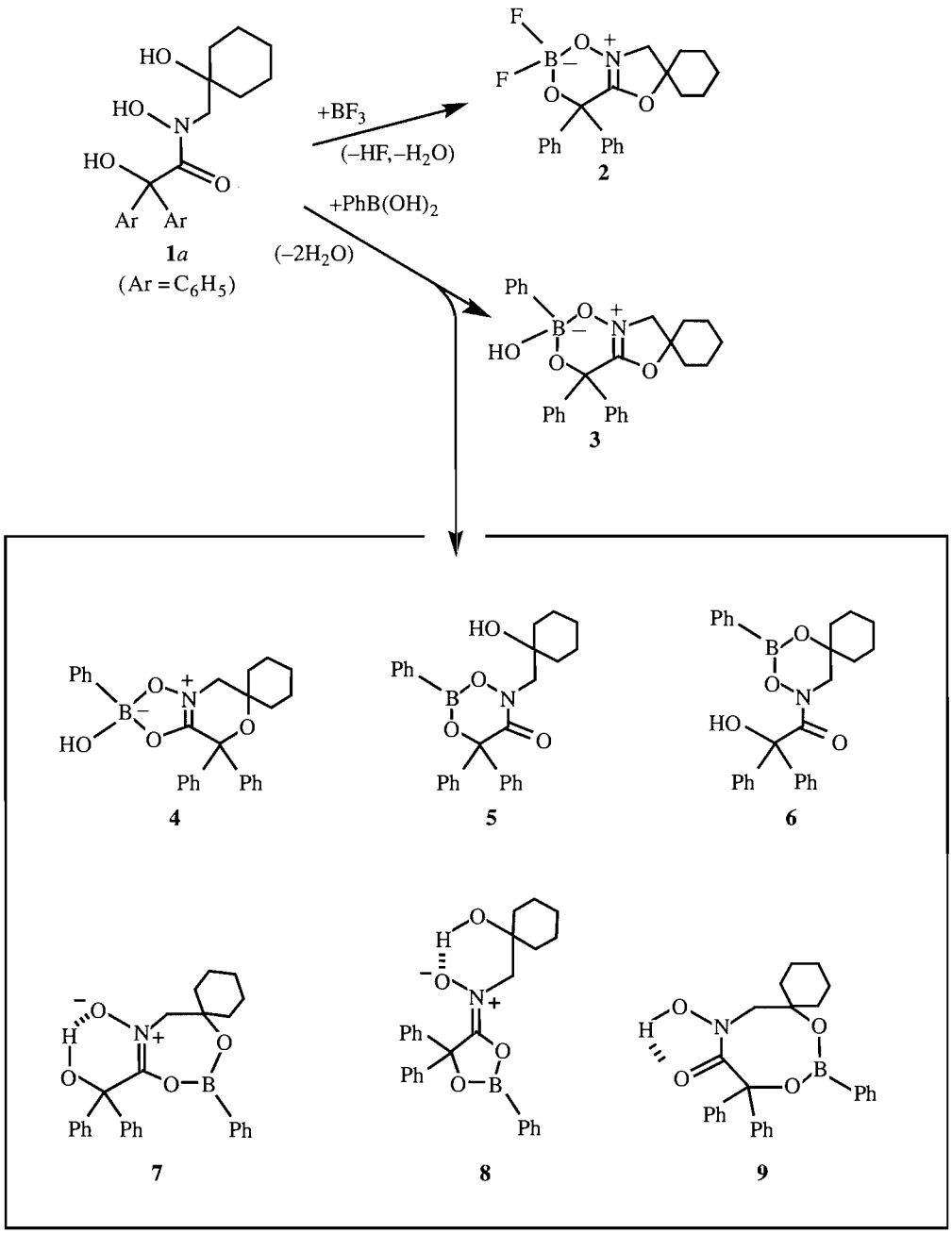

solution) that links the ^1H resonances at δ = 3.56 and 3.72 ppm to the ^{13}C resonances at δ = 52.51 and 59.36 ppm, respectively.

The presence of two different structural species in the solutions of **6** suggests an equilibrium reaction, obviously an intra- (or perhaps inter-) molecular reesterification process, running from the cycloboronate **5** through a (hypothetical) primary reesterification product to the isomeric cycloboronate **6A**, which could turn (by a 180° rotation about the (HO)C-C(=O) bond, C(8)—C(9) in Fig. 1) into the conformer **6B**, and vice versa. This chemical exchange process between **5** and **6** is further evidenced by a ^1H nmr saturation transfer experiment (14). Saturation of the NCH_2 signal at δ = 3.56 ppm (assigned to **6**) causes a distinct reduction of the intensity of the signal at 3.72 ppm (assigned to **5**), and vice versa. Likewise, an irradiation at the resonance frequency

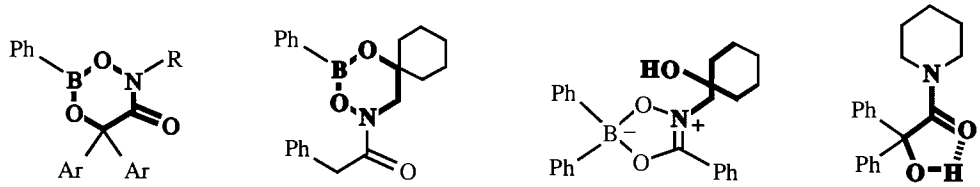

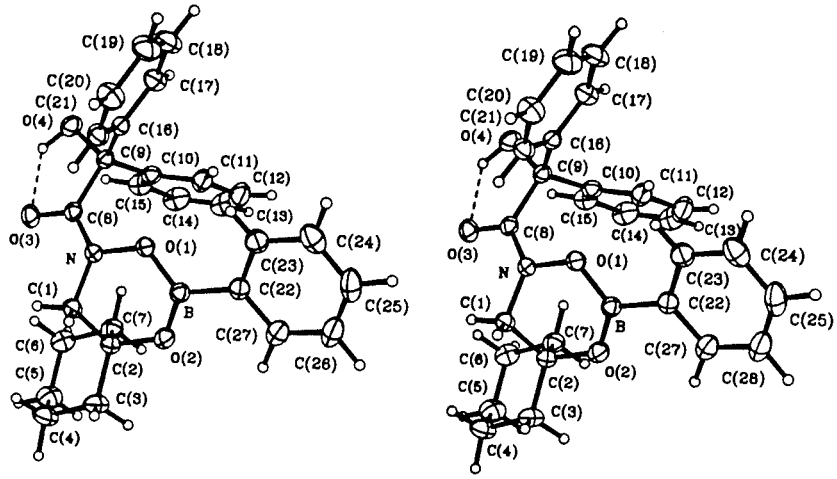

FIG. 1. Stereoview of **6**; 33% probability thermal ellipsoids are shown for the non-hydrogen atoms.

of the *ortho* protons of the *B*-phenyl group at $\delta = 7.42$ ppm leads to a marked decrease in the intensity of the corresponding signal at 7.96 ppm, and vice versa.

Preliminary variable-temperature ^{1}H nmr experiments between −35° and +100°C indicate a temperature dependence of the equilibrium between **5** and **6**. At 313 K (40°C) the spectrum of **6** (in chlorobenzene) reveals two singlets of nearly equal intensity at $\delta = 3.78$ and 3.83 ppm, indicating the NCH_2 groups of **5** and **6** in a 1:1 ratio. Lowering the temperature leads to a decrease in the intensity of the singlet at 3.83 ppm, whereas raising the temperature causes a reduction in the intensity of the singlet at 3.78 ppm. In addition, the chemical shifts of the two signals are temperature dependent. With increasing temperature the two singlets are both shifted downfield, to different extents, and form a virtual singlet at 3.87 ppm at a temperature of 373 K (100°C). Lowering the temperature results in an upfield shift of both signals, again differing in magnitude for the two components, which form a broad singlet at 3.67 ppm at a temperature of 238 K (−35°C).

It appears that **6** is the kinetically favored product predominating at lower temperatures and that **5** (which could not be isolated) is the thermodynamically favored product predominating at higher temperatures in the equilibrium in solution. Thus only **6** could be crystallized by cooling the solution.

Evidence for the intramolecular hydrogen bridge found in the solid state structure of **6** and depicted in formula **6B** is given by the reaction of compound **6** with BF_3 yielding nearly 70% of a difluoroboron chelate with the postulated structure

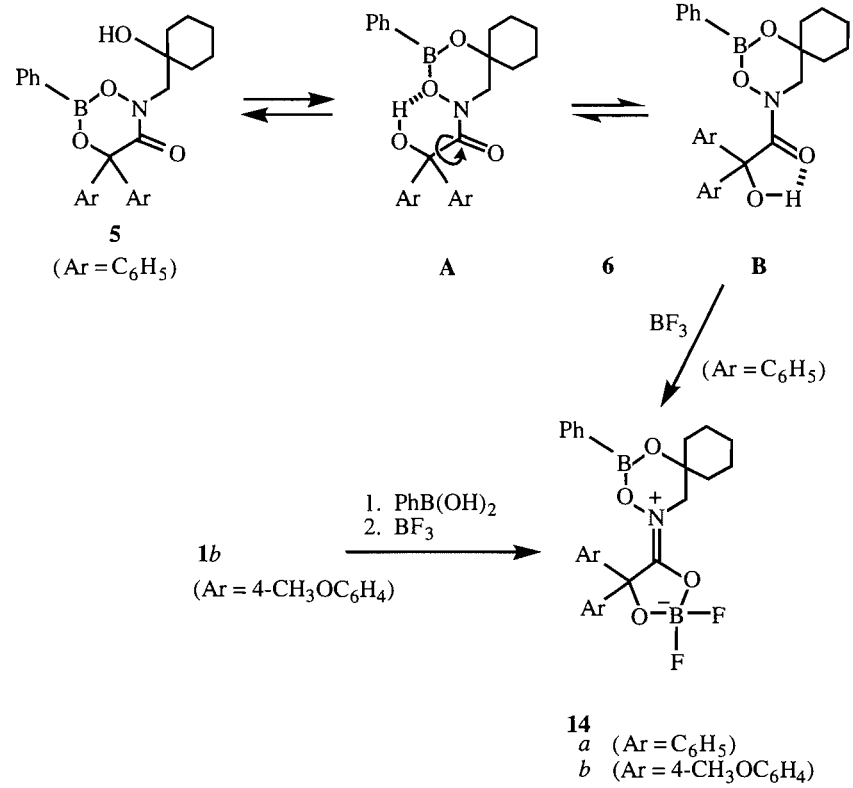

Can. J. Chem. Downloaded from www.nrcresearchpress.com by 92.62.229.171 on 09/08/12
For personal use only.

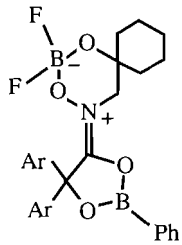

15

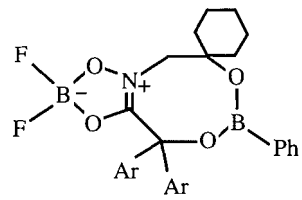

16

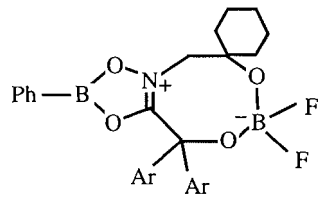

17

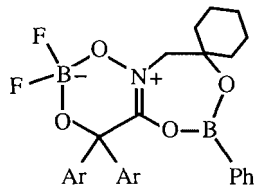

18

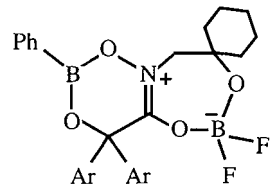

19

Can. J. Chem. Downloaded from www.nrcresearchpress.com by 92.62.229.171 on 09/08/12
For personal use only.

14*a*. Unfortunately we could not produce single crystals suitable for an X-ray analysis to establish this structure.[7] To this end we prepared the hydroxamic acid **1***b*, another example of a type **1** compound having a dianisyl instead of a diphenyl substitution at the α-carbon atom. The condensation of **1***b* with phenylboronic acid gave an oily product that could not be recrystallized and was reacted, without further purification, with BF_3. The resulting crystalline, high-melting product indeed showed the analytical data expected for **14***b*. Infrared and ^{1}H nmr spectra, however, were not sufficient to exclude the isomeric structures **15–19**. Two signals in the ^{11}B nmr spectrum at $\delta(Et_2OBF_3)$ = 12.2 and 32.5 ppm demonstrate the presence of two types of boron, presumably in tetracoordinate (sp^3) and tricoordinate (sp^2) environments (10). Formula **15** represents the BF_2 chelate of the ligand **8**. The "normal" difluoroboron hydroxamate **16** would require the formation of an eight-membered, probably less favorable, boronate ring **9**. Similarly the eight-membered BF_2 chelate **17** does not seem to be a very likely structure, even though the fused five-membered boronate ring is a stable moiety observed with *N*-unsubstituted hydroxamic acids.[8] The six-membered BF_2 chelate ring, as in **18**, is already well known.[9] The corresponding ligand for the chelate **18** would have the structure **7** (see above). Compound **19** would represent the BF_2 chelate of the ligand **5** and contains a six-membered phenylboronate ring system (c.f. **10**) that could be synthesized as such from *N*-substituted glycolohydroxamic acids.[4] Single crystals were available in this case, thus an X-ray crystallographic analysis was carried out.

Experimental

*4-(2-Hydroxy-2,2-diphenylacetyl)-6,6-pentamethylene-2-phenyl-1,3-dioxa-4-aza-2-boracyclohexane, **6***

N,2-Dihydroxy-*N*-(1-hydroxycyclohexyl)methyl-2,2-diphenylacetamide (8) (0.71 g, 2 mmol) and phenylboronic acid (0.24 g, 2 mmol) are dissolved under slight heating in a small amount of absolute ethanol. After partial evaporation a small amount of petroleum ether is added and crystallization starts upon cooling. Yield: 0.86 g (98%) colorless crystals, mp 136–138°C (from toluene/petroleum ether). Infrared (KBr): 3390 (O—H), 1635 (C=O) cm^{-1}; ^{1}H nmr (90 MHz, $CDCl_3$/TMS), δ (ppm): 1.17–1.95 (m, $(CH_2)_5$), 2.83 (s, 1/2 OH, exchangeable), 3.98 (s, NCH_2), 5.33 (s, 1/2 OH, exchangeable), 7.07–7.60 (m, 13 aromatic H), 7.75–7.95 (m, 2 aromatic H); ^{11}B nmr (64 MHz, $CDCl_3/Et_2OBF_3$); δ (ppm): 33.4 (broad); ^{1}H nmr (400 MHz, $CDCl_3$/TMS), δ (ppm): 1.33–1.68 (m, $(CH_2)_5$), 2.90 (s, 1/2 OH, exchangeable), 4.00 (s, 1/2 NCH_2), 4.01 (s, 1/2 NCH_2), 5.41 (s, 1/2 OH, exchangeable), 7.17–7.54 (m, 14 aromatic H), 7.89 (d, 1 aromatic H). ^{1}H nmr (400 MHz, C_6D_6/TMS), δ (ppm): 0.93–1.72 (m, $(CH_2)_5$), 2.91 (s, 1/2 OH), 3.56 (s, 1/2 NCH_2), 3.72 (s, 1/2 NCH_2), 5.86 (s, 1/2 OH), 7.01–7.27 (m, 9 aromatic H), 7.42 (d, 1 aromatic H), 7.74 (d, 4 aromatic H), 7.96 (d, 1 aromatic H); ^{13}C nmr (100.6 MHz, C_6D_6/TMS), δ (ppm): 21.72 (t, C(4) and C(6)[10]), 22.23 (t, C(4) and C(6)), 25.52 (t, C(5)), 26.08 (t, C(5)), 35.32 (t, C(3) and C(7)), 36.11 (t, C(3) and C(7)), 52.51 (t, C(1)), 59.36 (t, C(1)), 72.18 (s, C(2)), 74.27 (s, C(2)), 82.02 (s, C(9)), 83.04 (s, C(9)), 127.95 (d, aromatic C), 131.79 (d, aromatic C), 141.74 (s, aromatic C), 142.72 (s, aromatic C), 165.86 (s, C(8)), 171.37 (s, C(8)); ^{13}C,^{1}H nmr COSY spectrum (400 MHz/100.6 MHz, C_6D_6/TMS): cross peaks at $\delta(^1H)$ = 3.56/$\delta(^{13}C)$ = 52.51 ppm, and $\delta(^1H)$ = 3.72/$\delta(^{13}C)$ = 59.36 ppm; ^{1}H nmr (60 MHz, C_6H_5Cl/TMS, variable temperature): 313 K (40°C), δ (ppm): 3.78 (s, 1/2 NCH_2), 3.83 (s, 1/2 NCH_2); 238 K (−35°C), δ (ppm): 3.67 (s, broad, NCH_2); 373 K (100°C), δ (ppm): 3.87 (s, NCH_2). Anal. calcd. for $C_{27}H_{28}BNO_4$: C 73.48, H 6.40, B 2.45, N 3.17; found: C 73.48, H 6.51, B 2.43, N 3.15. Crystals suitable for X-ray analysis were obtained by recrystallization from benzene/petroleum ether.

*6,6-Pentamethylene-2-phenyl-4-phenylacetyl-1,3-dioxa-4-aza-2-boracyclohexane, **11***

N-Hydroxy-*N*-[(1-hydroxycyclohexyl)methyl]phenylacetamide[11] (0.26 g, 1 mmol) and phenylboronic acid (0.12 g, 1 mmol) are dissolved in 30 mL of benzene and refluxed for 30 min using a Dean–Stark trap for continuous removal of water. The solution is evaporated *in vacuo* to a volume of 1–2 mL. After addition of

[7]Analysis of a data set collected using a twinned crystal did not produce a publishable crystal structure but did confirm the proposed structure **14***a* (R = 0.12) (W. Kliegel, U. Schumacher, S. J. Rettig, and J. Trotter, unpublished results.

[8]W. Kliegel, D. Nanninga, and M. Tajerbashi. Unpublished results.

[9]Compound **2** (8), for example.

[10]Numbering scheme of Fig. 1.

[11]Prepared from phenylacetyl chloride and 1-(hydroxyaminomethyl)cyclohexanol as described for the analogous benzohydroxamic acid (4*e*). Melting point 121–123°C (from CH_2Cl_2/ether). Analytical and spectroscopic data will be published elsewhere.[4]

TABLE 1. Crystallographic data.[a]

Parameter	Values	
Compound	**6**[b]	**14***b* · 1/2 CH_2Cl_2[c]
Formula	$C_{27}H_{28}BNO_4$	$C_{29.5}H_{32}B_2ClF_2NO_6$
fw	441.33	591.65
Crystal system	Triclinic	Triclinic
Space group	$P\bar{1}$	$P\bar{1}$
a, Å	8.7348(5)	11.799(1)
b, Å	11.0529(6)	13.464(2)
c, Å	14.104(1)	10.047(2)
α°	65.781(5)	103.28(2)
β°	72.147(6)	92.60(2)
γ°	79.928(6)	79.752(8)
V, Å^3	1180.1(1)	1528.6(4)
Z	2	2
ρ_{calc}, g/cm^3	1.130	1.285
F(000)	468	618
μ, cm^{-1}	0.77	15.62
Crystal size, mm	0.17 × 0.23 × 0.24	0.05 × 0.25 × 0.45
Transmission factors	—	0.82–1.00
Scan type	ω–2θ	ω–2θ
Scan range, deg in ω	0.70 + 0.35 tan θ	1.05 + 0.20 tan θ
Scan speed, deg/min	1.2–10.0	16
Data collected[d]	$+h, \pm k, \pm l$	$+h, \pm k, \pm l$
$2\theta_{max}$, deg	55	155
Crystal decay	Negligible	6.5%
Total reflections	5403	6612
Total unique reflections	5403	6229
R_{merge}	—	0.022
No. of reflections with $I \geq 3\sigma(I)$	3881	3221
No. of variables	410	398
R	0.040	0.060
R_w	0.052	0.074
gof	2.36	2.24
Max Δ/σ (final cycle)	0.12	0.21
Residual density e/Å^3	−0.20 to +0.16	−0.24 to +0.35

[a]For both compounds: temperature 294 K, function minimized $\Sigma w(|F_o| - |F_c|)^2$ where $w = 4F_o^2/\sigma^2(F_o^2)$, $R = \Sigma||F_o| - |F_c||/\Sigma|F_o|$, $R_w = (\Sigma w(|F_o| - |F_c|)^2/\Sigma w|F_o|^2)^{1/2}$, and gof = $[\Sigma(|F_o| - |F_c|)^2/(m - n)]^{1/2}$. Values given for R, R_w, and gof are based on those reflections with $I \geq 3\sigma(I)$.

[b]Enraf-Nonius CAD4-F diffractometer, Mo-K_α radiation ($\lambda K_{\alpha 1}$ = 0.70930, $\lambda K_{\alpha 2}$ = 0.71359 Å), graphite monochromator, takeoff angle 2.7°, aperture (2.0 + tan θ) × 4.0 mm at a distance of 173 mm from the crystal, scan range extended by 25% on both sides for background measurement, $\sigma^2(F^2) = [C + 2B + (0.04(C - B))^2]/(Lp)^2$ (C = scan count, B = normalized background count).

[c]Rigaku AFC6S diffractometer, Cu-K_α radiation (λ = 1.54178 Å), graphite monochromator, takeoff angle 6.0°, aperture 6.0 × 6.0 mm at a distance of 285 mm from the crystal, stationary background counts at each end of the scan (scan/background time ratio 2:1, up to 8 rescans), $\sigma^2(F^2) = [S^2(C + 4B) + (0.04F^2)^2]/(Lp)^2$ (S = scan speed, C = scan count, B = background count).

[d]All 0, $\pm k$, $\pm l$ reflections collected and averaged for **14***b*, only unique data collected for **6**.

petroleum ether and cooling, colorless crystals begin to form. Yield: 0.32 g (91%); mp 97–99°C (from benzene/petroleum ether). Infrared (KBR): 1670 (C=O) cm^{-1}; ^{1}H nmr (90 MHz, $CDCl_3$/TMS), δ (ppm) = 1.15–2.00 (m, $(CH_2)_5$), 3.88 (s, NCH_2), 3.93 (s, $CH_2C{=}O$), 7.12–7.55 (m, 8 aromatic H), 7.67–7.88 (m, 2 aromatic H). Anal. calcd. for $C_{21}H_{24}BNO_3$: C 72.22, H 6.93, B 3.10, N 4.01; found: C 72.35, H 7.01, B 3.18, N 3.92.

4-[(1-Hydroxycyclohexyl)methyl]-2,2,5-triphenyl-1,3-dioxa-4-azonia-2-borata-4-cyclopentene, ***12*** (ref. 4e): ^{1}H nmr (400 MHz, C_6D_6/TMS), δ (ppm): 0.83–1.49 (m, $(CH_2)_5$), 2.37 (s, OH, exchangeable), 3.30 (s, NCH_2), 6.90–7.01 (m, 3 aromatic H), 7.26–7.30 (m, 2 aromatic H), 7.39–7.43 (m, 4 aromatic H), 7.56–7.58 (m, 2 aromatic H), 7.95–7.97 (m, 4 aromatic H); ^{13}C nmr (100.6 MHz, C_6D_6/TMS), δ (ppm): 21.55 (t, C(5) and C(7)[12]), 25.42 (t, C(6)), 35.68 (t, C(4) and C(8)), 59.57 (t, C(2)), 70.87 (s, C(3)), 124.39 (s, aromatic C), 127.16 (d, aromatic C), 128.91 (d, aromatic C), 129.22 (d, aromatic C), 132.36 (d, aromatic C), 132.77 (d, aromatic C), 163.90 (s, C(1)).

4-(2,2-Difluoro-5,5-diphenyl-1,3-dioxa-2-borata-4-cyclopentylidene)-6,6-pentamethylene-2-phenyl-1,3-dioxa-4-azonia-2-boracyclohexane, ***14***a

6 (0.88 g, 2 mmol) is dissolved in a small amount of toluene and mixed with dimethyl ether – boron trifluoride (0.23 g, 2 mmol).

[12]Atom numbering of Fig. 1 in ref. 4e.

Can. J. Chem. Downloaded from www.nrcresearchpress.com by 92.62.229.171 on 09/08/12
For personal use only.

Can. J. Chem. Downloaded from www.nrcresearchpress.com by 92.62.229.171 on 09/08/12
For personal use only.

TABLE 2. Final positional (fractional) and equivalent isotropic thermal parameters with estimated standard deviations in parentheses

Atom	x	y	z	B_{eq}[a]
		6		
O(1)	0.3085(1)	0.15374(8)	0.67624(6)	3.2
O(2)	0.2491(1)	0.38331(9)	0.57361(7)	3.9
O(3)	0.3083(1)	0.00161(9)	0.50274(7)	3.7
O(4)	0.1554(1)	−0.18033(9)	0.66804(8)	3.8
N	0.3378(1)	0.1316(1)	0.58109(8)	3.0
C(1)	0.4077(2)	0.2415(1)	0.4843(1)	3.1
C(2)	0.2889(2)	0.3630(1)	0.4728(1)	3.2
C(3)	0.3673(2)	0.4873(1)	0.3843(1)	4.2
C(4)	0.3955(2)	0.4855(2)	0.2729(1)	4.7
C(5)	0.2418(3)	0.4649(2)	0.2544(1)	5.1
C(6)	0.1630(2)	0.3406(2)	0.3424(1)	4.3
C(7)	0.1343(2)	0.3432(1)	0.4540(1)	3.8
C(8)	0.2839(1)	0.0235(1)	0.58505(9)	2.8
C(9)	0.1817(2)	−0.0737(1)	0.69279(9)	2.8
C(10)	0.0193(2)	0.0005(1)	0.7212(1)	3.2
C(11)	−0.0187(2)	0.0538(1)	0.7991(1)	4.0
C(12)	−0.1683(2)	0.1229(2)	0.8191(2)	5.5
C(13)	−0.2755(2)	0.1392(2)	0.7602(2)	5.9
C(14)	−0.2374(2)	0.0874(2)	0.6824(2)	5.3
C(15)	−0.0918(2)	0.0180(2)	0.6626(1)	4.2
C(16)	0.2668(2)	−0.1376(1)	0.78306(9)	2.8
C(17)	0.1774(2)	−0.2155(1)	0.8842(1)	3.8
C(18)	0.2502(2)	−0.2859(2)	0.9670(1)	4.7
C(19)	0.4133(2)	−0.2800(2)	0.9497(1)	4.9
C(20)	0.5027(2)	−0.2025(2)	0.8501(1)	4.4
C(21)	0.4302(2)	−0.1320(1)	0.7664(1)	3.4
C(22)	0.2375(2)	0.3123(1)	0.7703(1)	3.2
C(23)	0.2648(2)	0.2140(2)	0.8651(1)	3.9
C(24)	0.2464(2)	0.2435(2)	0.9548(1)	4.9
C(25)	0.2001(2)	0.3706(2)	0.9506(2)	5.4
C(26)	0.1718(2)	0.4690(2)	0.8581(2)	5.2
C(27)	0.1905(2)	0.4403(2)	0.7686(1)	4.2
B	0.2632(2)	0.2844(1)	0.6667(1)	3.1
		14*b* · 1/2 CH_2Cl_2		
Cl(1)	0.4390(6)	0.6415(5)	0.4146(7)	18.0
Cl(2)	0.4227(9)	0.4320(5)	0.2984(8)	16.1
Cl(2A)	0.510(1)	0.412(2)	0.413(2)	16
F(1)	0.3049(2)	−0.1230(2)	0.6477(3)	6.8
F(2)	0.1164(2)	−0.1282(2)	0.6532(2)	6.5
O(1)	0.0908(2)	0.2554(2)	0.5708(2)	4.3
O(2)	0.2257(2)	0.2885(2)	0.4223(3)	5.0
O(3)	0.1758(2)	−0.0095(2)	0.5430(2)	4.4
O(4)	0.1861(2)	0.0188(2)	0.7802(2)	4.4
O(5)	0.3842(3)	0.4328(2)	0.9645(4)	8.4
O(6)	−0.3327(2)	0.2104(2)	0.9385(3)	5.8
N(1)	0.1273(2)	0.1502(2)	0.5115(3)	3.7
C(1)	0.2558(3)	0.1804(2)	0.3496(4)	4.0
C(2)	0.2714(3)	0.1795(3)	0.2019(4)	4.7
C(3)	0.3222(3)	0.0721(3)	0.1187(4)	4.8
C(4)	0.4330(3)	0.0294(3)	0.1808(4)	5.3
C(5)	0.4185(3)	0.0279(3)	0.3275(4)	5.1
C(6)	0.3674(3)	0.1351(3)	0.4108(4)	4.8
C(7)	0.1554(3)	0.1271(2)	0.3684(4)	3.8
C(8)	0.1413(3)	0.0879(2)	0.5946(4)	3.5
C(9)	0.1280(3)	0.1126(2)	0.7489(3)	3.6
C(10)	0.1941(3)	0.1997(2)	0.8166(3)	3.6
C(11)	0.3123(3)	0.1845(3)	0.8026(4)	4.4
C(12)	0.3734(3)	0.2626(3)	0.8532(4)	5.4
C(13)	0.3163(3)	0.3591(3)	0.9193(4)	5.4
C(14)	0.2002(3)	0.3757(3)	0.9373(4)	5.1
C(15)	0.1383(3)	0.2955(3)	0.8852(4)	4.3
C(16)	0.0028(3)	0.1341(2)	0.7931(4)	3.6
C(17)	−0.0880(3)	0.1732(3)	0.7184(4)	4.4
C(18)	−0.1998(3)	0.1975(3)	0.7696(4)	4.8
C(19)	−0.2202(3)	0.1821(3)	0.8961(4)	4.4
C(20)	−0.1317(3)	0.1414(3)	0.9720(4)	4.6
C(21)	−0.0204(3)	0.1173(3)	0.9192(4)	4.3
C(22)	0.1188(3)	0.4380(3)	0.5955(4)	4.8
C(23)	0.1827(4)	0.5087(3)	0.5675(5)	6.2
C(24)	0.1591(5)	0.6125(3)	0.6335(6)	7.5
C(25)	0.0717(5)	0.6475(3)	0.7252(6)	7.3
C(26)	0.0077(5)	0.5808(4)	0.7534(5)	7.1
C(27)	0.0304(4)	0.4758(3)	0.6883(4)	5.8
C(28)	0.3245(6)	0.5369(4)	1.020(1)	13.5
C(29)	−0.3558(4)	0.2074(4)	1.0756(5)	6.9
C(30)	0.502(1)	0.511(2)	0.326(2)	15
B(1)	0.1485(4)	0.3221(3)	0.5216(5)	4.1
B(2)	0.1981(4)	−0.0651(3)	0.6628(5)	4.3

[a] $B_{eq} = (8\pi^2/3)\Sigma\Sigma U_{ij} a_i^* a_j^* (\mathbf{a}_i \cdot \mathbf{a}_j)$. Site occupancy factors for the solvent molecule in **14***b* are Cl(1) 0.5, Cl(2) 0.36, Cl(2A) 0.14, and C(30) 0.5.

After partial evaporation of the solvent *in vacuo* the remaining solution (2–3 mL) is cooled until colorless crystals begin to form. Yield: 0.74 g (76%); mp 196–197°C (dec.) (from dichloromethane/petroleum ether). Infrared (KBr): 1665 (C=O/C=N$^+$) cm^{-1}; ^{1}H nmr (90 MHz, $CDCl_3$/TMS), δ (ppm): 1.15–1.77 (m, $(CH_2)_5$), 4.10 (s, N-CH_2), 7.07–7.62 (m, 15 aromatic H). Anal. calcd. for $C_{27}H_{27}B_2F_2NO_4$: C 66.30, H 5.56, N 2.86; found: C 65.87, H 5.50, N 2.78. The crystals obtained by recrystallization from dichloromethane/petroleum ether were found to be twinned, and did not allow for a satisfactory crystal structure analysis.[7]

N,2-Dihydroxy-N-(1-hydroxycyclohexyl)methyl-2,2-bis(4-methoxyphenyl)acetamide, ***1***b

1-(Hydroxyaminomethyl)cyclohexanol (15) (30 mmol) is reacted with ethyl oxalyl chloride (30 mmol) and 4-methoxyphenylmagnesium bromide (225 mmol) according to literature methods (16). The product crystallizes from tetrachloromethane. Yield: 7.15 g (57%) of a colorless powdery material; mp 115–117°C (from CCl_4). Infrared (KBr): 3570, 3350, 3130 (O—H), 1640 (C=O) cm^{-1}; ^{1}H nmr (90 MHz, $CDCl_3$/TMS), δ (ppm): 1.40 (s, $(CH_2)_5$), 3.55 (s, N-CH_2), 3.70 (s, 2 OCH_3), 4.17 (s, broad, exchangeable, C-OH), 5.85 (s, broad, exchangeable, C-OH), 6.67–6.92 (m, 4 aromatic H), 7.03–7.27 (m, 4 aromatic H), 9.18 (s, broad, exchangeable, N-OH). Anal. calcd. for $C_{23}H_{29}NO_6$: C 66.49, H 7.04, N 3.37; found: C 66.82, H 6.96, N 3.38.

4-[2,2-Difluoro-5,5-bis(4-methoxyphenyl)-1,3-dioxa-2-borata-4-cyclopentylidene]-6,6-pentamethylene-2-phenyl-1,3-dioxa-4-azonia-2-boracyclohexane, ***14***b

1*b* (1.25 g, 3 mmol) and phenylboronic acid (0.37 g, 3 mmol) are dissolved in 30 mL of toluene and refluxed for 30 min using a Dean–Stark trap for the continuous removal of water. The solvent is distilled off *in vacuo*, and the oily residue dissolved in 10 mL of dichloromethane. After addition of dimethyl ether – boron trifluoride (0.34 g, 3 mmol) and freshly regenerated molecular sieve (type 4 Å, 2 g) the solution is kept at room temperature for 12 h. The molecular sieve is then filtered off, and the solution evaporated to a volume of 2 mL. Addition of petroleum ether initiates crystallization. Yield: 1.05 g (64%) colorless crystals; mp 159–161°C (dec.) (from CH_2Cl_2/petroleum ether). Infrared (KBr): 1655 (C=O/C=N$^+$) cm^{-1}; ^{1}H nmr (90 MHz, $CDCl_3$/TMS), δ (ppm): 1.20–1.80 (m, $(CH_2)_5$), 3.71 (s, 2 OCH_3), 4.10 (s, N-CH_2), 6.62–6.92 (m, 4 aromatic H), 7.17–7.55 (m, 9 aromatic H); ^{11}B nmr (64 MHz, $CDCl_3/Et_2OBF_3$), δ (ppm): 12.2 (broad), 32.5 (very

broad). Anal. calcd. for $C_{29}H_{31}B_2F_2NO_6$: C 63.42, H 5.69, B 3.93, N 2.55; found: C 63.41, H 5.70, B 3.78, N 2.38. Crystals suitable for X-ray analysis were obtained by recrystallization from dichloromethane and contain 1/2 mol CH_2Cl_2 as solvate; mp 154°C (dec.).

X-ray crystallographic analyses of ***6*** *and* ***14****b* · *1/2* CH_2Cl_2

Crystallographic data for the two complexes appear in Table 1. The final unit-cell parameters were obtained by least squares on the setting angles for 25 reflections with 2θ = 40.0–48.4° for **6** and 50.8–85.2° for **14***b* · 1/2 CH_2Cl_2. The intensities of three standard reflections, measured every hour of X-ray exposure time for **6** and every 250 reflections for **14***b* · 1/2 CH_2Cl_2 throughout the data collections, remained essentially constant for the former and showed a linear decay of 6.5% for the latter. The data were processed[13] and corrected for Lorentz and polarization effects. Decay and absorption (empirical, based on azimuthal scans for four reflections) corrections were applied for **14***b* · 1/2 CH_2Cl_2.

Both structure analyses were initiated in the centrosymmetric space group $P\bar{1}$ on the basis of *E*-statistics, these choices being confirmed by subsequent calculations. The structures were solved by direct methods, the coordinates of the non-hydrogen atoms being determined from *E*-maps or from subsequent difference Fourier syntheses. The non-hydrogen atoms were refined with anisotropic thermal parameters and hydrogen atoms were refined with isotropic thermal parameters for **6** and were fixed in idealized positions (C—H = 0.98 Å, B_H = 1.2 $B_{bonded\ atom}$) for **14***b* · 1/2 CH_2Cl_2. The dichloromethane solvate molecule in the structure of **14***b* · 1/2 CH_2Cl_2 was found to be disordered about a centre of symmetry and, in addition, was orientationally disordered (via a rotation about the C(30)—Cl(1) bond). Site occupancy factors for the two components of the disordered Cl atom were initially estimated from relative Fourier peak heights and were subsequently adjusted to yield approximately equal thermal parameters. Neutral atom scattering factors and anomalous dispersion corrections for the non-hydrogen atoms were taken from the *International tables for X-ray crystallography* (17). Final atomic coordinates and equivalent isotropic thermal parameters, bond lengths, bond angles, and intra-annular torsion angles appear in Tables 2–5, respectively. Hydrogen atom parameters, anisotropic thermal parameters, general torsion angles, intermolecular contacts, and least-squares planes (for **14***b* · 1/2 CH_2Cl_2 only), and measured and calculated structure factor amplitudes for the both structures are included as supplementary material.[14]

Results and discussion

As mentioned in the introduction, the reaction of **1** with phenylboronic acid results in a product (Fig. 1) having the structure **6** which features a six-membered cycloboronate ring derived from the *N*-(2-hydroxyalkyl)hydroxylamine residue. At least in the solid state, the compound has an (*E*)-configuration about the hydroxamic C=N grouping, formulated by **6A**. The relatively short C(8)—N, 1.333(2) Å, and long C(8)—O(3) bonds, 1.229(1) Å, are typical for acyclic amide groups (18). From plots of π-bond order vs. bond length (19), the C(8)—N bond has about 50–60% double bond character and the C(8)—O(3) bond retains about 80% of its double bond character. The O(1)—N-C(8)—O(3) torsion angle of −179.8(1)° attests to the planarity of the amide function. There is an intramolecular O—H···O hydrogen bond between the α-hydroxyl group and the carboxamide carbonyl oxygen atom (O(4)—H(O4)···O(3), O—H = 0.95(2), O···H = 1.85(2), O···O = 2.539(1) Å,

TABLE 3. Bond lengths (Å) with estimated standard deviations in parentheses

Bond	Length (Å)	Bond	Length (Å)
	6		
O(1)—N	1.401(1)	C(10)—C(15)	1.399(2)
O(1)—B	1.390(2)	C(11)—C(12)	1.404(2)
O(2)—C(2)	1.458(2)	C(12)—C(13)	1.377(3)
O(2)—B	1.345(2)	C(13)—C(14)	1.366(3)
O(3)—C(8)	1.229(1)	C(14)—C(15)	1.379(2)
O(4)—C(9)	1.430(1)	C(16)—C(17)	1.389(2)
N—C(1)	1.449(2)	C(16)—C(21)	1.381(2)
N—C(8)	1.333(2)	C(17)—C(18)	1.383(2)
C(1)—C(2)	1.530(2)	C(18)—C(19)	1.378(3)
C(2)—C(3)	1.521(2)	C(19)—C(20)	1.375(2)
C(2)—C(7)	1.521(2)	C(20)—C(21)	1.390(2)
C(3)—C(4)	1.521(2)	C(22)—C(23)	1.393(2)
C(4)—C(5)	1.514(3)	C(22)—C(27)	1.395(2)
C(5)—C(6)	1.520(2)	C(22)—B	1.557(2)
C(6)—C(7)	1.528(2)	C(23)—C(24)	1.389(2)
C(8)—C(9)	1.557(2)	C(24)—C(25)	1.374(3)
C(9)—C(10)	1.536(2)	C(25)—C(26)	1.374(3)
C(9)—C(16)	1.527(2)	C(26)—C(27)	1.380(2)
C(10)—C(11)	1.380(2)		
	14*b* · 1/2 CH_2Cl_2		
Cl(1)—C(30)	1.82(2)	C(4)—C(5)	1.497(6)
Cl(2)—C(30)	1.51(3)	C(5)—C(6)	1.526(5)
Cl(2A)—C(30)	1.74(3)	C(8)—C(9)	1.517(5)
F(1)—B(2)	1.353(5)	C(9)—C(10)	1.536(4)
F(2)—B(2)	1.382(5)	C(9)—C(16)	1.521(4)
O(1)—N(1)	1.402(3)	C(10)—C(11)	1.381(4)
O(1)—B(1)	1.403(5)	C(10)—C(15)	1.380(4)
O(2)—C(1)	1.459(4)	C(11)—C(12)	1.369(5)
O(2)—B(1)	1.326(5)	C(12)—C(13)	1.384(5)
O(3)—C(8)	1.293(4)	C(13)—C(14)	1.362(5)
O(3)—B(2)	1.547(5)	C(14)—C(15)	1.399(5)
O(4)—C(9)	1.420(4)	C(16)—C(17)	1.377(5)
O(4)—B(2)	1.427(5)	C(16)—C(21)	1.385(5)
O(5)—C(13)	1.370(4)	C(17)—C(18)	1.393(5)
O(5)—C(28)	1.447(6)	C(18)—C(19)	1.373(5)
O(6)—C(19)	1.374(4)	C(19)—C(20)	1.374(5)
O(6)—C(29)	1.428(5)	C(20)—C(21)	1.394(5)
N(1)—C(7)	1.440(4)	C(22)—C(23)	1.396(5)
N(1)—C(8)	1.300(4)	C(22)—C(27)	1.378(5)
C(1)—C(2)	1.501(5)	C(22)—B(1)	1.550(5)
C(1)—C(6)	1.516(5)	C(23)—C(24)	1.387(6)
C(1)—C(7)	1.529(5)	C(24)—C(25)	1.360(7)
C(2)—C(3)	1.527(5)	C(25)—C(26)	1.354(7)
C(3)—C(4)	1.500(6)	C(26)—C(27)	1.399(6)

[13]TEXSAN/TEXRAY structure analysis package or locally modified versions of the following: DIRDIF, direct methods for difference structures, by P. T. Beurskens; ORFLS, full-matrix least squares, and ORFFE, function and errors, by W. R. Busing, K. O. Martin, and H. A. Levy; ORTEP II, illustrations, by C. K. Johnson.

[14]Supplementary material mentioned in the text may be purchased from The Depository of Unpublished Data, Document Delivery, CISTI, National Research Council Canada, Ottawa, Canada K1A 0R6.

Tables of hydrogen atom coordinates, and bond lengths and angles involving hydrogen atoms, for **6**, and tables of hydrogen-atom coordinates, intramolecular distances and bond angles, and intermolecular distances for **14***b* · 1/2 CH_2Cl_2 have also been deposited with the Cambridge Crystallographic Data Centre and can be obtained on request from The Director, Cambridge Crystallographic Data Centre, University Chemical Laboratory, Lensfield Road, Cambridge CB2 1EW, U.K.

Can. J. Chem. Downloaded from www.nrcresearchpress.com by 92.62.229.171 on 09/08/12
For personal use only.

Can. J. Chem. Downloaded from www.nrcresearchpress.com by 92.62.229.171 on 09/08/12
For personal use only.

TABLE 4. Bond angles (deg) with estimated standard deviations in parentheses

Bonds	Angle (deg)	Bonds	Angle (deg)
	6		
N—O(1)—B	114.98(9)	C(9)—C(10)—C(15)	118.1(1)
C(2)—O(2)—B	122.3(1)	C(11)—C(10)—C(15)	119.1(1)
O(1)—N—C(1)	114.0(1)	C(10)—C(11)—C(12)	119.6(2)
O(1)—N—C(8)	119.3(1)	C(11)—C(12)—C(13)	120.3(2)
C(1)—N—C(8)	126.1(1)	C(12)—C(13)—C(14)	120.2(2)
N—C(1)—C(2)	108.8(1)	C(13)—C(14)—C(15)	120.3(2)
O(2)—C(2)—C(1)	106.7(1)	C(10)—C(15)—C(14)	120.5(2)
O(2)—C(2)—C(3)	106.8(1)	C(9)—C(16)—C(17)	117.7(1)
O(2)—C(2)—C(7)	108.6(1)	C(9)—C(16)—C(21)	123.2(1)
C(1)—C(2)—C(3)	111.0(1)	C(17)—C(16)—C(21)	118.9(1)
C(1)—C(2)—C(7)	112.6(1)	C(16)—C(17)—C(18)	120.7(1)
C(3)—C(2)—C(7)	110.8(1)	C(17)—C(18)—C(19)	120.1(1)
C(2)—C(3)—C(4)	111.8(1)	C(18)—C(19)—C(20)	119.7(1)
C(3)—C(4)—C(5)	111.8(1)	C(19)—C(20)—C(21)	120.5(2)
C(4)—C(5)—C(6)	111.3(1)	C(16)—C(21)—C(20)	120.2(1)
C(5)—C(6)—C(7)	111.3(1)	C(23)—C(22)—C(27)	118.1(1)
C(2)—C(7)—C(6)	111.7(1)	C(23)—C(22)—B	122.1(1)
O(3)—C(8)—N	120.5(1)	C(27)—C(22)—B	119.8(1)
O(3)—C(8)—C(9)	118.7(1)	C(22)—C(23)—C(24)	120.6(1)
N—C(8)—C(9)	120.7(1)	C(23)—C(24)—C(25)	120.0(2)
O(4)—C(9)—C(8)	104.99(9)	C(24)—C(25)—C(26)	120.4(1)
O(4)—C(9)—C(10)	108.8(1)	C(25)—C(26)—C(27)	119.9(2)
O(4)—C(9)—C(16)	105.76(9)	C(22)—C(27)—C(26)	121.1(2)
C(8)—C(9)—C(10)	106.93(9)	O(1)—B—O(2)	123.2(1)
C(8)—C(9)—C(16)	114.8(1)	O(1)—B—C(22)	115.8(1)
C(10)—C(9)—C(16)	115.0(1)	O(2)—B—C(22)	121.0(1)
C(9)—C(10)—C(11)	122.8(1)		
	14*b* · 1/2 CH_2Cl_2		
N(1)—O(1)—B(1)	113.9(2)	O(5)—C(13)—C(12)	115.7(4)
C(1)—O(2)—B(1)	124.1(3)	O(5)—C(13)—C(14)	124.1(4)
C(8)—O(3)—B(2)	107.7(3)	C(12)—C(13)—C(14)	120.2(3)
C(9)—O(4)—B(2)	111.9(3)	C(13)—C(14)—C(15)	119.7(3)
C(13)—O(5)—C(28)	116.2(4)	C(10)—C(15)—C(14)	120.5(3)
C(19)—O(6)—C(29)	117.1(3)	C(9)—C(16)—C(17)	124.2(3)
O(1)—N(1)—C(7)	115.2(3)	C(9)—C(16)—C(21)	117.6(3)
O(1)—N(1)—C(8)	116.1(3)	C(17)—C(16)—C(21)	118.1(3)
C(7)—N(1)—C(8)	128.4(3)	C(16)—C(17)—C(18)	121.0(4)
O(2)—C(1)—C(2)	107.3(3)	C(17)—C(18)—C(19)	119.7(4)
O(2)—C(1)—C(6)	107.5(3)	O(6)—C(19)—C(18)	115.2(4)
O(2)—C(1)—C(7)	106.9(3)	O(6)—C(19)—C(20)	124.1(4)
C(2)—C(1)—C(6)	110.8(3)	C(18)—C(19)—C(20)	120.6(3)
C(2)—C(1)—C(7)	111.4(3)	C(19)—C(20)—C(21)	118.9(4)
C(6)—C(1)—C(7)	112.8(3)	C(16)—C(21)—C(20)	121.5(4)
C(1)—C(2)—C(3)	112.3(3)	C(23)—C(22)—C(27)	117.5(4)
C(2)—C(3)—C(4)	111.1(3)	C(23)—C(22)—B(1)	119.7(4)
C(3)—C(4)—C(5)	111.8(3)	C(27)—C(22)—B(1)	122.8(4)
C(4)—C(5)—C(6)	111.2(3)	C(22)—C(23)—C(24)	120.9(4)
C(1)—C(6)—C(5)	112.3(3)	C(23)—C(24)—C(25)	120.3(5)
N(1)—C(7)—C(1)	109.1(3)	C(24)—C(25)—C(26)	120.1(4)
O(3)—C(8)—N(1)	117.5(3)	C(25)—C(26)—C(27)	120.5(4)
O(3)—C(8)—C(9)	113.1(3)	C(22)—C(27)—C(26)	120.7(4)
N(1)—C(8)—C(9)	129.4(3)	Cl(1)—C(30)—Cl(2)	116.2(9)
O(4)—C(9)—C(8)	101.1(2)	Cl(1)—C(30)—Cl(2A)	118(1)
O(4)—C(9)—C(10)	108.3(3)	O(1)—B(1)—O(2)	122.6(3)
O(4)—C(9)—C(16)	110.5(3)	O(1)—B(1)—C(22)	115.1(3)
C(8)—C(9)—C(10)	110.5(3)	O(2)—B(1)—C(22)	122.3(3)
C(8)—C(9)—C(16)	112.7(3)	F(1)—B(2)—F(2)	110.2(3)
C(10)—C(9)—C(16)	113.0(3)	F(1)—B(2)—O(3)	108.1(3)
C(9)—C(10)—C(11)	119.5(3)	F(1)—B(2)—O(4)	113.9(3)
C(9)—C(10)—C(15)	121.9(3)	F(2)—B(2)—O(3)	107.1(3)
C(11)—C(10)—C(15)	118.5(3)	F(2)—B(2)—O(4)	114.0(3)
C(10)—C(11)—C(12)	121.3(3)	O(3)—B(2)—O(4)	102.9(3)
C(11)—C(12)—C(13)	119.7(3)		

Can. J. Chem. Downloaded from www.nrcresearchpress.com by 92.62.229.171 on 09/08/12
For personal use only.

TABLE 5. Intra-annular torsion angles (deg) standard deviations in parentheses

Atoms	Value (deg)
6	
B—O(1)—N—C(1)	34.2(1)
O(1)—N—C(1)—C(2)	−62.3(1)
N—C(1)—C(2)—O(2)	53.8(1)
B—O(2)—C(2)—C(1)	−23.7(2)
C(2)—O(2)—B—O(1)	−3.5(2)
N—O(1)—B—O(2)	−0.4(2)
C(7)—C(2)—C(3)—C(4)	−54.6(2)
C(2)—C(3)—C(4)—C(5)	54.8(2)
C(3)—C(4)—C(5)—C(6)	−54.5(2)
C(4)—C(5)—C(6)—C(7)	54.6(2)
C(5)—C(6)—C(7)—C(2)	−55.2(2)
C(3)—C(2)—C(7)—C(6)	54.9(2)
14*b* · 1/2 CH_2Cl_2	
B—O(1)—N(1)—C(7)	−37.1(4)
O(1)—N(1)—C(7)—C(1)	61.9(3)
N(1)—C(7)—C(1)—O(2)	−50.2(4)
B(1)—O(2)—C(1)—C(7)	21.2(5)
C(1)—O(2)—B(1)—O(1)	2.7(6)
N(1)—O(1)—B(1)—O(2)	3.7(5)
C(6)—C(1)—C(2)—C(3)	53.7(4)
C(1)—C(2)—C(3)—C(4)	−54.9(4)
C(2)—C(3)—C(4)—C(5)	55.3(4)
C(3)—C(4)—C(5)—C(6)	−55.1(4)
C(4)—C(5)—C(6)—C(1)	54.2(4)
C(5)—C(6)—C(1)—C(2)	−53.4(4)
B(2)—O(3)—C(8)—C(9)	−3.3(4)
O(3)—C(8)—C(9)—O(4)	13.2(3)
C(8)—C(9)—O(4)—B(2)	−18.5(3)
C(9)—O(4)—B(2)—O(3)	17.0(4)
O(4)—B(2)—O(3)—C(8)	−7.9(4)

O—H···O = 127(2)°). The ring formed by the intramolecular hydrogen bond (O(3)—C(8)—C(9)—O(4)—H(O4)) is planar to within 0.04(2) Å, and is oriented approximately coplanar with the amide group (torsion angles O(4)—C(9)—C(8)—N = −176.3(1)° and O(1)—N-C(8)—C(9) = 3.2(2)°).

The six-membered BONCCO phenylboronate ring in **6** has a "semi-planar" C(1)-sofa conformation (see Table 5) similar to those observed for other six-membered cycloboronates (ref. 20 and references therein). As noted for other boronic acid esters, O—B *pp*(π) back-donation results in partial double bond character for the O—B bonds and is responsible for the near planarity (to within ~0.1 Å) of the N-O(1)-B-O(2)-C(2) portion of the phenylboronate ring. The two O—B bonds differ in length by 0.045(3) Å, that involving the alcoholate oxygen atom O(2) being shorter (1.345(2) Å), presumably as a result of the better *p*(π) donor ability of this oxygen atom relative to that of the hydroxamate oxygen atom O(1) (O(1)—B = 1.390(2) Å). The B—C(aryl) bond between the phenyl ring and the cycloboronate ring, 1.557(2) Å, is similar to those reported for other cyclic phenylboronates (ref. 20 and references therein). The *B*-phenyl ring and the boron coordination group are approximately coplanar, the dihedral angle between normals to the respective mean planes being 4.1°. The cyclohexane ring, spiro-fused to the cycloboronate ring at C(2), has a nearly ideal chair conformation (see Table 5) with the substituents C(1) and O(1) occupying axial and equatorial positions respectively.

The X-ray analysis establishes structure **14***b* (Fig. 2) for the compound obtained from the consecutive reaction of the hydroxamic acid **1***b* with phenylboronic acid and boron trifluoride and provides indirect evidence that compound **14***a* results from the same reaction sequence starting with the hydroxamic acid **1**. This demonstrates the replacement of the "chelated proton", as observed in the structure of **6** (see above), by a difluoroborenium ion (F_2B^+) to give **14***a* and the analogous derivative **14***b*. The structure is consistent with the fact that no exchange reactions take place between the difluoroboron and phenylboron moieties at the polyfunctional ligand that could lead to one of the alternative constitutions **15**–**19**. To the best of our knowledge this is the first structurally characterized compound containing both a phenylboronate and a difluoroboron chelate ring within the same molecule.

The general ring assembly of **14***b* is very similar to that of **6** and has an (*E*)-configuration about the hydroxamate

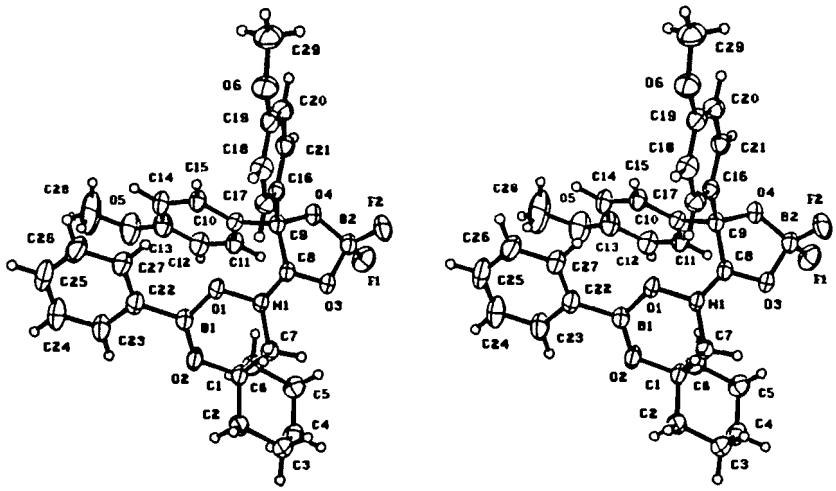

FIG. 2. Stereoview of **14***b*; 33% probability thermal ellipsoids are shown for the non-hydrogen atoms.

C⋯N bond that connects the six-membered cycloboronate ring to the five-membered difluoroboron chelate ring. Compared to **6** the double bond character of the hydroxamic C⋯N bond in **14***b* is enhanced: C(8)—N(1) = 1.300(4) Å is consistent with an estimated bond order of 1.75 from a plot of π-bond order vs. bond length (19). Correspondingly, the C(8)—O(3) bond is longer (1.293(4) Å) than the comparable C=O bond in **6** (1.229(1) Å), indicating a decreased double bond character for the carbonyl function in **14***b*. A 50% double-bond character for the carbonyl C—O bond in **14***b* is estimated from a plot of C—O bond length vs. π-bond order (19). The electron delocalization leads to a distinct iminium salt character (with the intramolecular borate counteranion) for **14***b*, which represents a new type of *B*,*N*-betaine (21). The torsion angles O(1)—N(1)—C(8)—O(3) = −179.5(3)°, O(1)—N(1)—C(8)—C(9) = −2.5(5)°, and O(3)—C(8)—N(1)—C(7) = −6.3(5)° show an approximately planar arrangement of the substituents about the hydroxamate C⋯N group, confirming the distinct double bond character and justifying the nomenclature employed that describes this compound as a zwitterionic species.

The are no dramatic changes in the other geometric parameters of **14***b* compared to those of **6**. The cyclohexane moiety of **14***b* has a chair conformation (see Table 5) and bears the oxygen atom O(2) of the spiro-connected boronate ring in an equatorial position and C(7) in an axial position, exactly as observed for **6**. The cycloboronate ring of **14***b* has a distorted C(7)-envelope (sofa) conformation and, like **6**, has significantly different O—B bond lengths. The difference between the two O—B bond lengths, 0.077(7) Å, is significantly larger than the value of 0.045(3) Å observed for **6**. This could be a consequence of an electron-withdrawing effect of the difluoroboron chelate formation, further reducing the already weaker donor properties of the hydroxamate oxygen atom O(1) (a Lewis acid effect on this atom).

The five-membered BOCCO chelate ring in **14***b* has a flattened B-envelope conformation (see Table 5), the ring being planar to within 0.129(4) Å. The B—F bond lengths in **14***b* (mean 1.368 Å) are in the range normally observed for B—F bonds in five-membered difluoroboron chelates: mean B—F = 1.358 (4*f*), 1.378 (4*a*), 1.404 (22), 1.405 Å (23). In contrast to other five-membered difluoroboron chelates (4*a*, 4*f*, 22, 23), the O—B bonds of the chelate moiety show a considerable (0.120(7) Å) difference in length: O(3)—B(2) = 1.547(5) and O(4)—B(2) = 1.427(5) Å. Once again, the alcoholate ligand C(9)—O(4) is the stronger donor compared to the hydroxamate ligand C(8)—O(3), analogous to the situation at the cycloboronate site in the same molecule where the difference in donor strength between the two oxygen atoms is very similar. The mean B—F/mean B—O bond length ratio of 0.920 lies in the range of 0.900–0.962 reported for other five-membered difluoroboron chelates (4*a*, 4*f*, 22, 23), consistent with intermediate overall binding strength of the *O*,*O*-chelating ligand with respect to the F_2B^+ moiety. The O(3)—B(2)—O(4) angle of 102.9(3)° is similar to those in other five-membered difluoroboron chelates that range from 101.8° to 108° with an average value of 104.4° (4*a*, 4*f*, 22, 23). Bond angles at B(2) range from 102.9(3)° to 114.0(3)°, corresponding to an irregular tetrahedral coordination geometry. The relatively small O—B—O angle in **14***b* is associated with an O(3)⋯O(4) "bite" of 2.326(4) Å.

Can. J. Chem. Downloaded from www.nrcresearchpress.com by 92.62.229.171 on 09/08/12
For personal use only.

Acknowledgements

We thank the Natural Sciences and Engineering Research Council of Canada and the Fonds der Chemischen Industrie, Frankfurt am Main, for financial support.

1. (*a*) F. Mathis. Bull. Soc. Chim. Fr. D. 9 (1953); (*b*) R. T. Coutts. Can. J. Pharm. Sci. **2**, 1 (1967); **2**, 27 (1967); (*c*) H. Maehr. Pure appl. Chem. **28**, 603 (1971); (*d*) T. Emery. Adv. Enzymol. **35**, 135 (1971); (*e*) G. L. Eichhorn. (*Editor*). Inorganic biochemistry. Vols. 1 and 2. Elsevier, Amsterdam. 1973; (*f*) J. S. Wald. *In* Soil biochemistry. Vol. 4. *Edited by* E. A. Paul and A. D. McLaren. Dekker. New York. 1965. p. 65; (*g*) H.-J. Michel. Pharmazie, **35**, 63 (1980); (*h*) G. R. Gale. Drugs Future, **5**, 599 (1980); (*i*) H. Kehl (*Editor*). Chemistry and biology of hydroxamic acids. Karger, Basel. 1982.
2. (*a*) N. P. Buu-Hoi, G. Lambelin, and C. Gillet. *In* Research progress in organic, biological and medicinal chemistry. Vol 2. *Edited by* U. Gallo and L. Santamaria. North Holland, Amsterdam. 1970. p. 1; (*b*) J. H. Weisburger and E. K. Weisburger. Pharmacol. Rev. **25**, 1 (1973); (*c*) M. J. Miller. Chem. Rev. **89**, 1563 (1989).
3. (*a*) M. B. Chenoweth. Pharmacol. Rev. **8**, 57 (1956); (*b*) M. J. Seven and L. A. Johnson (*Editors*). Metal-binding in medicine. Lippincott, Philadelphia. 1960; (*c*) W. O. Foye. J. Pharm. Sci. **50**, 93 (1961); (*d*) H. G. Brugsch. J. Occup. Med. **7**, 394 (1965); (*e*) M. B. Chenoweth. Clin. Pharmacol. Ther. **9**, 365 (1968); (*f*) D. D. Perrin. Masking and demasking of chemical reactions. Chem. Anal. (NY), **33**, 183 (1970); (*g*) M. N. Hughes. The inorganic chemistry of biological processes. Wiley, London. 1972. p. 283; (*h*) F. B. Williamson. Spore Res. **1**, 55 (1976); (*i*) D. D. Perrin. Top. Curr. Chem. **64**, 181 (1976); (*j*) R. A. Bulman. Structure Bonding, **67**, 91 (1987).
4. (*a*) S. J. Rettig, J. Trotter, W. Kliegel, and D. Nanninga. Can. J. Chem. **55**, 1 (1977); (*b*) Can. J. Chem. **56**, 1676 (1978); (*c*) W. Kliegel, D. Nanninga, S. J. Rettig, and J. Trotter. Can. J. Chem. **61**, 2493 (1983); (*d*) W. Kliegel, M. Tajerbashi, S. J. Rettig, and J. Trotter. Can. J. Chem. **68**, 69 (1990); (*e*) W. Kliegel, U. Schumacher, M. Tajerbashi, S. J. Rettig, and J. Trotter. Can. J. Chem. **69**, 545 (1991); (*f*) W. Kliegel, M. Tajerbashi, S. J. Rettig, and J. Trotter. Can. J. Chem. **69**, 673 (1991).
5. L. H. Toporcer, R. E. Dessy, and S. I. E. Green. Inorg. Chem. **4**, 1649 (1965).
6. W. Kliegel. Bor in biologie, medizin und pharmazie. Springer. Berlin. 1980.
7. (*a*) W. Kliegel, M. Tajerbashi, S. J. Rettig, and J. Trotter. Can. J. Chem. **66**, 2621 (1988); (*b*) W. Kliegel, M. Tajerbashi, S. J. Rettig, and J. Trotter. Can. J. Chem. **67**, 1644 (1989); (*c*) W. Kliegel, U. Schumacher, S. J. Rettig, and J. Trotter. Can. J. Chem. **69**, 1212 (1991).
8. W. Kliegel, U. Schumacher, S. J. Rettig, and J. Trotter. Can. J. Chem. **69**, 681 (1991).
9. M. K. Das, B. Biswas, and S. Chakraborty. Synth. React. Inorg. Met.-Org. Chem. **16**, 77 (1986).
10. H. Nöth and B. Wrackmeyer. Nuclear magnetic resonance spectroscopy of boron compounds. Springer-Verlag, Berlin. 1978.
11. L. Bauer and O. Exner. Angew. Chem. Int. Ed. Engl. **13**, 376 (1974).
12. (*a*) U. W. Gerwarth and W. Weber. Synth. React. Inorg. Met.-Org. Chem. **5**, 175 (1975); (*b*) W. Maringgele and A. Meller. J. Organomet. Chem. **188**, 401 (1980).
13. V. S. Shklyaev and Z. G. Kalugina. Nauch. Tr.–Permsk. Gos. Farm. Inst. **3**, 3 (1969); Chem. Abstr. **75**, 63562 d (1971).
14. D. Neuhaus and M. Williamson. The nuclear Overhauser ef-

fect in structural and conformational analysis. VCH Publishers. Weinheim. 1989. Chap. 5, p. 141.
15. W. Kliegel and H. Becker. Chem. Ber. **110**, 2067 (1977).
16. D. Geffken and T. Lauterbach. Chem.-Ztg. **109**, 192 (1985).
17. International tables for X-ray crystallography. Vol. IV. Kynoch Press, Birmingham, U.K. Present distributor: Kluwer Academic Publishers; Dordrecht, The Netherlands. 1974. pp. 99–102 and 149.
18. F. H. Allen, O. Kennard, D. G. Watson, L. Brammer, A. G. Orpen, and R. Taylor. J. Chem. Soc. Chem. Perkin Trans. 2, S1 (1987).
19. G. Häfelinger. Chem. Ber. **103**, 2941 (1970).
20. W. Kliegel, G. Lubkowitz, S. J. Rettig, and J. Trotter. Can. J. Chem. **69**, 234 (1991).
21. W. Kliegel. Organomet. Chem. Rev. Sect. A: **8**, 153 (1972).
22. C. M. Lukehart and K. Srinivasan. J. Am. Chem. Soc. **103**, 4166 (1981).
23. P. G. Lenhert, C, M. Lukehart, and K. Srinivasan. J. Am. Chem. Soc. **106**, 124 (1984).
24. W. Kliegel, G. Lubkowitz, S. J. Rettig, and J. Trotter. Can. J. Chem. **69,** 1227 (1991).

Can. J. Chem. Downloaded from www.nrcresearchpress.com by 92.62.229.171 on 09/08/12
For personal use only.

Structural studies of organoboron compounds LI.[1] *N*-Methylhydroxylamine(*O-B*)2,5-diphenyl-1,3,2-dioxaborolan-4-one[2]

WOLFGANG KLIEGEL AND UTE SCHUMACHER
Institut für Pharmazeutische Chemie der Technischen Universität Braunschweig, Beethovenstrasse 55, 3300 Braunschweig, Germany

AND

STEVEN J. RETTIG AND JAMES TROTTER
Department of Chemistry, University of British Columbia, 2036 Main Mall, Vancouver, B.C., Canada V6T 1Z1

Received January 21, 1991[3]

WOLFGANG KLIEGEL, UTE SCHUMACHER, STEVEN J. RETTIG, and JAMES TROTTER. Can. J. Chem. **70,** 1188 (1992).

Three synthetic methods for the preparation of *N*-methylhydroxylamine(*O-B*)2,5-diphenyl-1,3,2-dioxaborolan-4-one (2-(1-oxa-2-azoniapropyl)-2,5-diphenyl-1,3-dioxa-2-boratacyclopentan-4-one), **9**, in good yield are described. Crystals of this material are triclinic, a = 10.1073(7), b = 12.159(2), c = 14.116(2) Å, α = 65.079(8)°, β = 99.255(9)°, γ = 92.69(1)°, Z = 4, space group $P\bar{1}$. The structure was solved by direct methods and was refined by full-matrix least-squares procedures to R = 0.039 and R_w = 0.045 for 2603 reflections with $I \geq 3\sigma(I)$. Compound **9** is the first structurally characterized example of an *N*-alkylhydroxylamine(*O-B*)boron complex having an open-chain *B,N*-betaine structure. Average bond lengths involving the tetrahedrally coordinated boron atoms in the two crystallographically independent molecules (corrected for thermal libration) are (N)O—B = 1.494, (carboxylate)O—B = 1.524, (alcoholic)O—B = 1.486, and (aryl)C—B = 1.594 Å.

WOLFGANG KLIEGEL, UTE SCHUMACHER, STEVEN J. RETTIG et JAMES TROTTER. Can. J. Chem. **70,** 1188 (1992).

On décrit trois méthodes de synthèse de la *N*-méthylhydroxylamine(*O-B*)2,5-diphényl-1,3,2-dioxaborolan-4-one (2-(1-oxa-2-azoniapropyl)-2,5-diphényl-1,3-dioxa-2-boratacyclopentan-4-one), **9**, avec un bon rendement. Les cristaux de cette substance sont tricliniques, groupe d'espace $P\bar{1}$, avec a = 10,1073(7), b = 12,159(2) et c = 14,116(2) Å, α = 65,079(8)°, β = 99,255(9)° et γ = 92,69(1)° et Z = 4. On a résolu la structure par des méthodes directes et on l'affinée par la méthode des moindres carrés jusqu'à des valeurs de R = 0,039 et R_w = 0,045 pour 2603 réflexions avec $I \geq 3\sigma(I)$. Le composé **9** correspond au premier exemple d'un complexe de *N*-alkylhydroxylamine(*O-B*)bore possédant une structure de bétaïne-*B,N* en chaîne ouverte. Les longeurs moyennes des liaisons impliquant les atomes de bore cordonnés d'une façon tétraédrique dans les deux molécules indépendantes d'un point de vue cristallographique (corrigées pour la libration thermique) sont : (N)O—B = 1,494, (carboxylate)O—B = 1,524, (alcoolique)O—B = 1,486 et (aryl)C—B = 1,594 Å.

[Traduit par la rédaction]

Introduction

N-Methylmandelohydroxamic acid **1** was reacted with phenylboronic acid in ethanolic solution in an attempt to synthesize the six-membered cyclic phenylboronate **2**. Similar condensations leading to cycloboronates of type **2** were successful with various *N*-alkyl- and *N*-aryl-substituted diarylglycolohydroxamic acids using absolute ethanol as solvent.[4] The use of the monoarylglycolohydroxamic acid **1** as an educt, however, resulted in a crystalline compound having the elemental composition of **2** containing one mole of water. In addition to the ordinary hydrate structure **2** · H_2O, an intermediate "half-condensate" structure **3** (which could be stabilized by intramolecular O→B coordination) had to be considered, but the C=O stretching frequency at 1710 cm^{-1} in the infrared spectrum seemed contradictory since cyclic boronates of type **2** typically absorb at frequencies between 1640 and 1670 cm^{-1}.[4] The ^1H nmr spectrum would also be consistent with the isomeric structure **4**, the hypothetical rearrangement product of an N→O acyl shift, also stabilized by intramolecular coordination (N→B in this case). N→O acylotropy has been observed in thermally induced rearrangements of *N*-methyl benzohydroxamic acids (1) as well as in pentanoylation reactions of *N*-methyl hydroxylamine (2), and N→O transacylation products of *N*-aryl

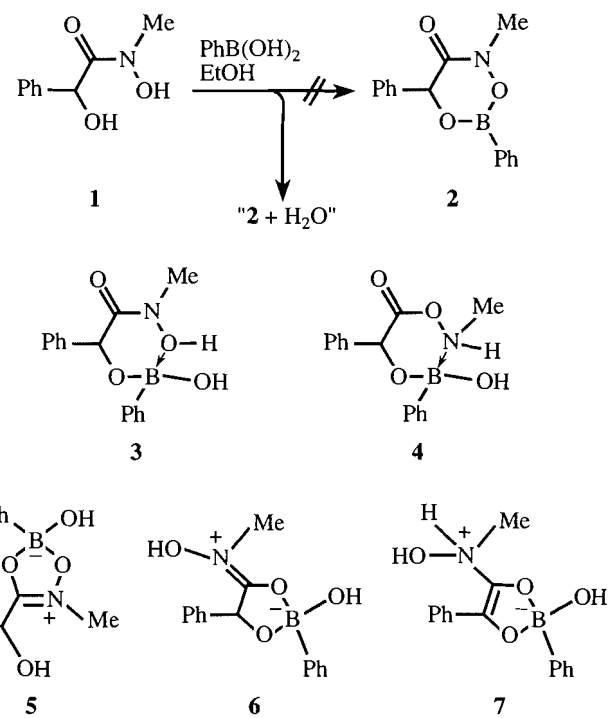

1 **2** **3** **4** **5** **6** **7**

[1]Previous paper in this series: ref. 28.

[2]2-(1-Oxa-2-azoniapropyl)-2,5-diphenyl-1,3-dioxa-2-boratacyclopentan-4-one.

[3]Revision received October 24, 1991.

[4]W. Kliegel and U. Schumacher. Unpublished results.

Can. J. Chem. Downloaded from www.nrcresearchpress.com by 92.62.229.171 on 09/08/12
For personal use only.

Can. J. Chem. Downloaded from www.nrcresearchpress.com by 92.62.229.171 on 09/08/12
For personal use only.

α-aminohydroxamic acids have been trapped *in situ* during amine-catalyzed N→O acyl transfer (3). *N*-Carbamoylated hydroxylamines are reported to undergo an N→O acyl migration if there is an *N-tert*-alkyl substituent (4).

The fact that certain hydroxamic acids can serve as ligands for phenylboronic acid (5) led to the consideration of the five-membered chelate structure **5**. Hydroxamate complexes of this type, however, show C=O/C=N$^+$ absorptions between 1610 and 1640 cm^{-1} in their infrared spectra (5). A similar C=O/C=N$^+$ stretching frequency can be expected for the isomeric five-membered chelate **6** having an exocyclic hydroxamic N-OH group. A comparable six-membered O—B—O chelate of *N*-methoxy-*N*-methylsalicylamide has a C=O/C=N$^+$ band at 1615 cm^{-1} (6). Thus the C=O/C=N$^+$ bands expected in the infrared spectra of **5** and **6** are quite different from the observed band at 1710 cm^{-1}. The tautomeric structure **7** can be ruled out by the ^{1}H nmr spectrum, which displays a one-proton singlet at 5.30 ppm, characteristic of a methine proton. In addition, the absence of a color reaction with $FeCl_3$ in ethanolic solution suggests that the molecule contains no hydroxamate moiety at all, these being detected by the formation of tris(hydroxamato)iron(III) complexes. An exchange (formal) of the *N*-methylhydroxylamino and *B*-hydroxy groups leads to the isomeric structures **8** or **9**, adducts of *N*-methylhydroxylamine and the phenylboronate **10** by N→B or O→B coordination, respectively. This is strongly supported by the synthesis via addition of *N*-methylhydroxylamine to the preformed[5] 1,3,2-dioxaborolan-4-one **10** or by the one-pot synthesis via three-component condensation of mandelic acid, *N*-methylhydroxylamine, and phenylboronic acid. Both of these procedures lead to products identical to that resulting from the reaction of **1** with phenylboronic acid. Yet, the C=O stretching frequency of 1710 cm^{-1} observed for "**2** + H_2O" is significantly different from the value of 1800 cm^{-1} reported for **10** (7).

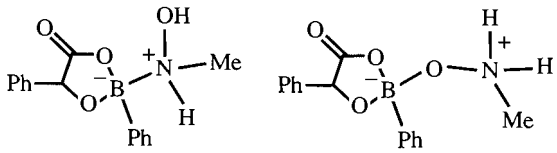

8 **9**

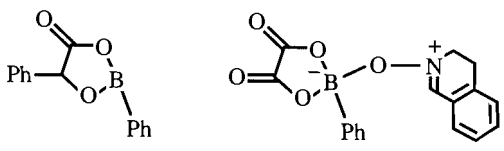

10 **11**

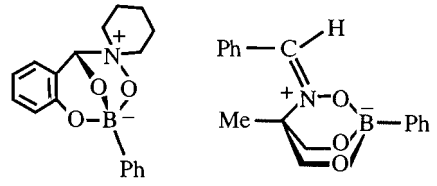

12 **13**

The formation of one of the isomers **3**–**6** could not be ruled out by the spectroscopic data nor by the independent synthetic routes studied. In addition, an unambiguous decision between the isomeric structures **8** and **9** could not be made on the basis of the infrared and ^{1}H nmr data. Complexes of hydroxylamine or *N*-monosubstituted derivatives thereof with Lewis acid boron compounds are traditionally formulated as N→B adducts (8), but there is also evidence for O→B coordination in BF_3 complexes of hydroxylamine (9). In the transition metal coordination chemistry of hydroxylamine (10) it is known that the neutral ligand can bind to the metal via nitrogen, as H_2N—OH, as well as via oxygen in the tautomeric aminoxide form H_3N^+—O^-. This has been established by X-ray and neutron diffraction studies, e.g., for Ni(II)—NH_2OH (11) and for U(VI)—ON^+H_3 (12). To resolve the ambiguities surrounding the structure of "**2** + H_2O" and the course of the reaction between **1** and phenylboronic acid, an X-ray crystallographic analysis has been carried out.

Experimental

N-*Methylhydroxylamine*(O-B)*2,5-diphenyl-1,3,2-dioxaborolan-4-one*, **9**

Method A

2-Hydroxy-*N*-methyl-2-phenylacetohydroxamic acid **1** (13) (0.18 g, 1 mmol) and phenylboronic acid (0.12 g, 1 mmol) are dissolved in a small amount of absolute ethanol with slight heating. Upon cooling and addition of petroleum ether colorless crystals of high purity are formed.

Method B

Mandelic acid (7.61 g, 50 mmol) and phenylboronic acid (6.10 g, 50 mmol) are suspended in 60 mL of benzene and refluxed for 1 h with continuous removal of water in a Dean–Stark trap. The hot solution is filtered and the solvent evaporated off *in vacuo* to a volume of 15 mL, at which time crystallization of **10** commences (yield: 10.85 g, 91%); mp 123°C (from benzene) (lit. (7) mp 124°C (from benzene/petroleum ether)). **10** (1.19 g, 5 mmol) is dissolved in 20 mL of dichloromethane and is mixed with a solution of *N*-methylhydroxylamine (5 mmol)[6] in absolute ethanol. Crystallization eventually starts at room temperature, after evaporation of the solvents.

Method C

Mandelic acid (1.52 g, 10 mmol), phenylboronic acid (1.22 g, 10 mmol), and *N*-methylhydroxylamine (10 mmol)[6] are each dissolved, separately, in the minimum amount of ethanol (necessary for solution). The three solutions are mixed and kept at room temperature. After partial evaporation of the solvent *in vacuo*, crystallization begins.

Yields: 0.20 g (70%, method A), 0.86 g (60%, method B), 2.37 g (83%, method C); mp 145–146°C (from ethanol/petroleum ether). Infrared (KBr): 3130, 2770, 2540 (N—H), 1710 (C=O) cm^{-1}. ^{1}H nmr (90 MHz, d_6-DMSO/TMS), δ (ppm): 2.78 (s, CH_3), 5.30 (s, O-CH), 6.97–7.63 (m, B-C_6H_5, C-C_6H_5), 9.45–10.75 (s, broad, exchangeable, NH_2). Anal. calcd. for $C_{15}H_{16}BNO_4$: C 63.19, H 5.66, N 4.91; found: C 63.24, H 5.68, N 4.90. Crystals suitable for X-ray analysis were obtained by recrystallization from absolute ethanol/petroleum ether.

X-ray crystallographic analysis of **9**

A crystal ca. 0.11 × 0.24 × 0.35 mm in size was mounted on a glass fiber. Unit-cell parameters were refined by least-squares on setting angles for 25 reflections (2θ = 24.0–35.2°) measured on a diffractometer with Mo-K_α radiation ($\lambda_{K\alpha1}$ = 0.70930, $\lambda_{K\alpha2}$ = 0.71359 Å). Crystal data at 21°C are:

$C_{15}H_{16}BNO_4$ fw = 285.11

[5]In a modification of the literature method (7), mandelic acid was condensed with phenylboronic acid.

[6]*N*-Methylhydroxylamine hydrochloride is added to the solution of an equimolar amount of KOH in absolute ethanol. After stirring for 10 min the precipitated KCl is filtered off, and the solution is used for the reaction.

Can. J. Chem. Downloaded from www.nrcresearchpress.com by 92.62.229.171 on 09/08/12
For personal use only.

Triclinic, a = 10.1073(7), b = 12.159(2), c = 14.116(2) Å, α = 65.079(8)°, β = 99.255(9)°, γ = 92.69(1)°, V = 1552.4(3) Å^3, Z = 4 (two molecules per asymmetric unit), ρ_c = 1.220 Mg m^{-3}, $F(000)$ = 600, μ(Mo-K_α) = 0.82 cm^{-1}. Absent reflections: none, space group $P\bar{1}$ (No. 2) from structure analysis.

Intensities were measured with graphite-monochromated Mo-K_α radiation on an Enraf–Nonius CAD4-F diffractometer. An ω-2θ scan at 1.0–10.0° min^{-1} over a range of (0.65 + 0.35 tan θ)° in ω (scan extended by 25% on each side for background measurement) was employed. Data were measured to 2θ = 55°. The intensities of three check reflections, measured every hour of X-ray exposure time throughout the data collection, showed only small random variations. The data were processed[7] and corrected for Lorentz and polarization effects. Of the 7089 independent reflections measured, 2603 (36.7%) had intensities greater than or equal to 3$\sigma(I)$ above background where $\sigma^2(I) = [C + 2B + (0.040(C-B))^2]$ with C = scan count, B = normalized total background count.

The structure analysis was initiated in the centrosymmetric space group $P\bar{1}$ on the basis of the E-statistics, this choice being confirmed by the subsequent successful solution and refinement of the structure. The structure was solved by direct methods, the coordinates of all non-hydrogen atoms of two crystallographically independent molecules being determined from an E-map. The non-hydrogen atoms were refined with anisotropic thermal parameters and the hydrogen atoms were fixed in idealized positions (N—H = 0.92, C(sp^2)—H = 0.97, C(sp^3)—H = 0.98 Å, U_H = 1.2 $U_{\text{bonded atom}}$). Scattering factors for all atoms and anomalous dispersion corrections for the non-hydrogen atoms were taken from ref. 14. The weighting scheme $w = 1/\sigma^2(F)$ gave uniform average values of $w(|F_o| - |F_c|)^2$ over ranges of both $|F_o|$ and sin θ/λ and was employed in the final stages of full-matrix least-squares refinement of 379 variables. Reflections with $I < 3\sigma(I)$ were not included in the refinement. Convergence was reached at R = 0.039 and R_w = 0.045 for 2603 reflections with $I \geq 3\sigma(I)$. The function minimized was $\Sigma w(|F_o| - |F_c|)^2$, $R = \Sigma||F_o| - |F_c||/\Sigma|F_o|$, $R_w = (\Sigma w(|F_o| - |F_c|)^2/\Sigma w|F_o|^2)^{1/2}$. On the final cycle of refinement the maximum parameter shift corresponded to 0.14σ. The mean error in an observation of unit weight was 1.36. The final difference map showed maximum fluctuations of ±0.16 e Å^{-3}.

The thermal motion has been analyzed in terms of the TLS model (15). The rms error in the temperature factors U_{ij} (derived from the least-squares analysis) is 0.0022 Å^2. Three structural subunits of each of the two independent molecules were separately analyzed (rms ΔU_{ij} = 0.0028–0.0045 Å^2). The bond lengths have been corrected for libration (15, 16) using shape parameters q^2 of 0.08 for all atoms. The final positional and (equivalent) isotropic thermal parameters for the non-hydrogen atoms appear in Table 1. Bond lengths (corrected and uncorrected) and angles are given in Tables 2 and 3 and intra-annular torsion angles in Table 4. Hydrogen atom parameters, anisotropic thermal parameters, general torsion angles, and structure factors have been deposited.[8]

TABLE 1. Final positional (fractional × 10^4) and isotropic thermal parameters (U × 10^3 Å^2) with estimated standard deviations in parentheses

Atom	x	y	z	U_{eq}
O(1)	8350(2)	4045(2)	8049(1)	54
O(2)	9059(2)	4106(2)	9687(1)	49
O(3)	6129(2)	4042(2)	8012(2)	68
O(4)	10374(2)	5185(2)	8259(2)	55
N	9834(2)	6258(2)	8221(2)	52
C(1)	7262(3)	4065(3)	8441(2)	52
C(2)	7628(3)	4156(3)	9489(2)	49
C(3)	7029(3)	3190(3)	10373(2)	46
C(4)	7294(3)	1990(3)	10662(2)	63
C(5)	6772(4)	1093(3)	11484(3)	84
C(6)	5974(4)	1393(5)	12019(3)	96
C(7)	5659(4)	2561(6)	11764(4)	103
C(8)	6201(3)	3480(4)	10919(3)	80
C(9)	10440(3)	7323(3)	7460(3)	71
C(10)	10615(3)	2972(3)	9073(2)	51
C(11)	10294(4)	2033(4)	8782(3)	87
C(12)	11167(5)	1082(4)	9049(4)	113
C(13)	12415(5)	1046(4)	9608(3)	89
C(14)	12772(4)	1948(4)	9896(3)	84
C(15)	11883(4)	2902(3)	9634(3)	72
B	9611(3)	4067(3)	8790(3)	48
O(1′)	5192(2)	6891(2)	6310(1)	50
O(2′)	5673(2)	6203(2)	5093(1)	42
O(3′)	7208(2)	6759(2)	7250(1)	52
O(4′)	3460(2)	5827(2)	5636(1)	48
N′	3926(2)	4640(2)	6369(2)	45
C(1′)	6474(3)	6630(2)	6530(2)	41
C(2′)	6882(2)	6164(2)	5783(2)	40
C(3′)	7974(3)	6880(3)	5195(2)	47
C(4′)	7773(3)	8087(3)	4541(3)	77
C(5′)	8807(4)	8744(4)	4017(3)	114
C(6′)	10006(4)	8189(5)	4154(4)	118
C(7′)	10208(3)	6994(5)	4800(4)	100
C(8′)	9199(3)	6328(3)	5335(3)	68
C(9′)	2871(3)	4020(3)	7007(2)	69
C(10′)	3873(2)	7936(3)	4416(2)	44
C(11′)	3683(3)	8958(3)	4572(3)	64
C(12′)	3138(4)	10030(3)	3750(4)	81
C(13′)	2775(3)	10095(4)	2767(3)	78
C(14′)	2945(3)	9105(4)	2578(3)	78
C(15′)	3486(3)	8035(3)	3396(3)	62
B′	4546(3)	6717(3)	5338(2)	42

Results and discussion

The X-ray analysis establishes the structure **9** for the reaction product. The two crystallographically independent molecules of **9** (Fig. 1) have bond lengths that agree to within experimental error, the most obvious difference between the two being in the orientation of the phenyl rings. There are two chiral centres in the molecule, at C(2) and B. The two independent molecules have the same relative configurations at the chiral centres (Fig. 1 shows the 2*S*,5*R* enantiomer (chemical numbering; B and C(2) in Fig. 1)) and equal numbers of both enantiomers are present in the centrosymmetric crystals. The crystal structure (Fig. 2) consists of infinite chains of molecules, double-linked by N—H···O hydrogen bonds. The asymmetric unit comprises two independent molecules that form a pseudo-centrosymmetric dimer linked by N—H···O hydrogen bonds involving the carbonyl oxygen atom (N—H(N1)···O(3′) and N′—H(N′2)···O(3), H···O = 1.86 and 1.96 Å, N···O =

[7]Computer programs used include locally written programs for data processing and locally modified versions of the following: MULTAN80, multisolution program by P. Main, S. J. Fiske, S. E. Hull, L. Lessinger, G. Germain, J. P. Declercq, and M. M. Woolfson; ORFLS, full-matrix least squares, and ORFFE, function and errors, by W. R. Busing, K. O. Martin, and H. A. Levy; FORDAP, Patterson and Fourier syntheses, by A. Zalkin; ORTEP II, illustrations, by C. K. Johnson.

[8] Supplementary material mentioned in the text may be purchased from the Depository of Unpublished Data, Document Delivery, CISTI, National Research Council Canada, Ottawa, Canada K1A 0R6.

The table of calculated hydrogen atom coordinates has also been deposited with the Cambridge Crystallographic Data Centre and can be obtained on request from The Director, Cambridge Crystallographic Data Centre, University Chemical Laboratory, Lensfield Road, Cambridge CB2 1EW U.K.

TABLE 2. Bond lengths (Å) with estimated standard deviations in parentheses

Bond	Uncorr.	Corr.	Bond	Uncorr.	Corr.
O(1)—C(1)	1.313(3)	1.318	O(1′)—C(1′)	1.306(3)	1.310
O(1)—B	1.520(3)	1.526	O(1′)—B′	1.516(3)	1.522
O(2)—C(2)	1.427(3)	1.432	O(2′)—C(2′)	1.423(3)	1.428
O(2)—B	1.482(4)	1.489	O(2′)—B′	1.478(4)	1.483
O(3)—C(1)	1.211(3)	1.214	O(3′)—C(1′)	1.220(3)	1.224
O(4)—N	1.415(3)	1.422	O(4′)—N′	1.422(3)	1.425
O(4)—B	1.494(4)	1.496	O(4′)—B′	1.486(3)	1.492
N—C(9)	1.473(4)	1.476	N′—C(9′)	1.476(3)	1.480
C(1)—C(2)	1.515(4)	1.522	C(1′)—C(2′)	1.507(4)	1.514
C(2)—C(3)	1.499(4)	1.506	C(2′)—C(3′)	1.503(4)	1.511
C(3)—C(4)	1.366(4)	1.382	C(3′)—C(4′)	1.369(4)	1.385
C(3)—C(8)	1.372(4)	1.389	C(3′)—C(8′)	1.383(4)	1.396
C(4)—C(5)	1.375(5)	1.383	C(4′)—C(5′)	1.396(5)	1.406
C(5)—C(6)	1.346(6)	1.361	C(5′)—C(6′)	1.361(6)	1.374
C(6)—C(7)	1.350(6)	1.365	C(6′)—C(7′)	1.355(6)	1.371
C(7)—C(8)	1.415(6)	1.423	C(7′)—C(8′)	1.386(5)	1.395
C(10)—C(11)	1.378(4)	1.402	C(10′)—C(11′)	1.376(4)	1.391
C(10)—C(15)	1.379(4)	1.393	C(10′)—C(15′)	1.385(4)	1.399
C(10)—B	1.584(5)	1.589	C(10′)—B′	1.593(4)	1.598
C(11)—C(12)	1.370(5)	1.375	C(11′)—C(12′)	1.392(5)	1.397
C(12)—C(13)	1.369(5)	1.381	C(12′)—C(13′)	1.347(5)	1.359
C(13)—C(14)	1.338(5)	1.364	C(13′)—C(14′)	1.362(5)	1.377
C(14)—C(15)	1.385(5)	1.390	C(14′)—C(15′)	1.386(4)	1.391

TABLE 3. Bond angles (deg) with estimated standard deviations in parentheses

Bonds	Angle (deg)	Bonds	Angle (deg)
C(1)—O(1)—B	111.6(2)	C(1′)—O(1′)—B′	111.6(2)
C(2)—O(2)—B	111.0(2)	C(2′)—O(2′)—B′	111.3(2)
N—O(4)—B	114.6(2)	N′—O(4′)—B′	113.8(2)
O(4)—N—C(9)	109.6(2)	O(4′)—N′—C(9′)	109.3(2)
O(1)—C(1)—O(3)	124.7(3)	O(1′)—C(1′)—O(3′)	122.9(3)
O(1)—C(1)—C(2)	110.3(2)	O(1′)—C(1′)—C(2′)	110.6(2)
O(3)—C(1)—C(2)	125.1(3)	O(3′)—C(1′)—C(2′)	126.5(2)
O(2)—C(2)—C(1)	104.7(2)	O(2′)—C(2′)—C(1′)	104.3(2)
O(2)—C(2)—C(3)	112.3(2)	O(2′)—C(2′)—C(3′)	112.4(2)
C(1)—C(2)—C(3)	113.7(2)	C(1′)—C(2′)—C(3′)	113.5(2)
C(2)—C(3)—C(4)	120.9(3)	C(2′)—C(3′)—C(4′)	120.3(3)
C(2)—C(3)—C(8)	121.3(3)	C(2′)—C(3′)—C(8′)	120.0(3)
C(4)—C(3)—C(8)	117.9(3)	C(4′)—C(3′)—C(8′)	119.6(3)
C(3)—C(4)—C(5)	121.6(3)	C(3′)—C(4′)—C(5′)	119.5(3)
C(4)—C(5)—C(6)	119.7(4)	C(4′)—C(5′)—C(6′)	120.3(4)
C(5)—C(6)—C(7)	121.6(4)	C(5′)—C(6′)—C(7′)	119.7(4)
C(6)—C(7)—C(8)	118.5(4)	C(6′)—C(7′)—C(8′)	120.3(4)
C(3)—C(8)—C(7)	120.7(4)	C(3′)—C(8′)—C(7′)	119.9(4)
C(11)—C(10)—C(15)	115.4(3)	C(11′)—C(10′)—C(15′)	116.2(3)
C(11)—C(10)—B	123.0(3)	C(11′)—C(10′)—B′	122.5(3)
C(15)—C(10)—B	121.6(3)	C(15′)—C(10′)—B′	121.2(3)
C(10)—C(11)—C(12)	122.2(3)	C(10′)—C(11′)—C(12′)	121.9(3)
C(11)—C(12)—C(13)	120.4(4)	C(11′)—C(12′)—C(13′)	120.3(4)
C(12)—C(13)—C(14)	119.2(4)	C(12′)—C(13′)—C(14′)	119.7(4)
C(13)—C(14)—C(15)	120.2(3)	C(13′)—C(14′)—C(15′)	120.1(3)
C(10)—C(15)—C(14)	122.5(3)	C(10′)—C(15′)—C(14′)	121.8(3)
O(1)—B—O(2)	102.3(2)	O(1′)—B′—O(2′)	101.9(2)
O(1)—B—O(4)	109.8(2)	O(1′)—B′—O(4′)	108.5(2)
O(1)—B—C(10)	112.5(3)	O(1′)—B′—C(10′)	112.5(2)
O(2)—B—O(4)	111.0(2)	O(2′)—B′—O(4′)	110.9(2)
O(2)—B—C(10)	116.1(2)	O(2′)—B′—C(10′)	115.8(2)
O(4)—B—C(10)	105.2(2)	O(4′)—B′—C(10′)	107.0(2)

Can. J. Chem. Downloaded from www.nrcresearchpress.com by 92.62.229.171 on 09/08/12
For personal use only.

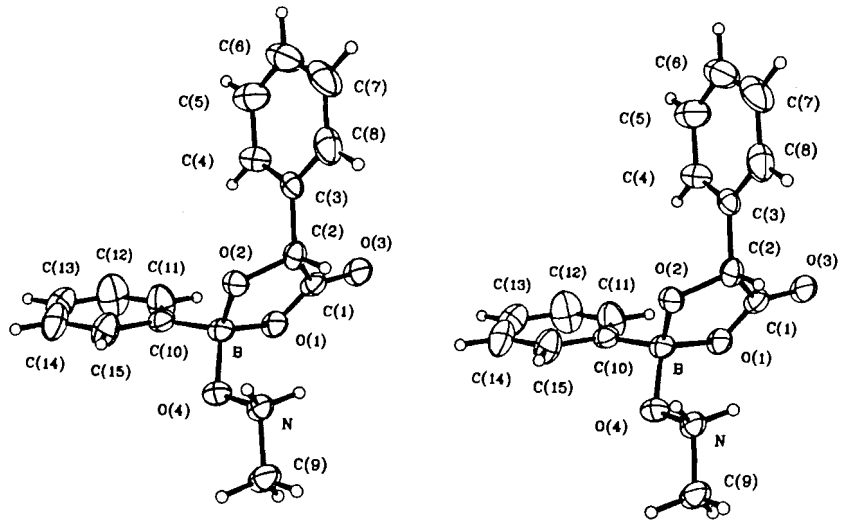

FIG. 1. Stereoview of one of the two crystallographically independent molecules of **9**; 33% probability thermal ellipsoids are shown for the non-hydrogen atoms. The 2*S*,5*R* enantiomer is shown. The primed molecule has a slightly different orientation of the *B*-phenyl group.

TABLE 4. Intra-annular torsion angles (deg) standard deviations in parentheses

Atoms	Value (deg)
B—O(1)—C(1)—C(2)	2.3(3)
O(1)—C(1)—C(2)—O(2)	−3.7(3)
B—O(2)—C(2)—C(1)	3.6(3)
C(2)—O(2)—B—O(1)	−2.4(3)
C(1)—O(1)—B—O(2)	−0.1(3)
B′—O(1′)—C(1′)—C(2′)	−3.5(3)
O(1′)—C(1′)—C(2′)—O(2′)	0.7(3)
B′—O(2′)—C(2′)—C(1′)	2.5(3)
C(2′)—O(2′)—B′—O(1′)	−4.2(3)
C(1′)—O(1′)—B′—O(2′)	4.7(3)

2.751(3) and 2.817(3) Å, N—H···O = 163° and 155°). Each of the two independent molecules is also hydrogen-bonded about a crystallographic centre of symmetry (at 1,1/2,1 and 1/2,1/2,1/2 for the unprimed and primed molecules, respectively) by interactions involving a ring oxygen atom (N—H(N2)···O(2)(2-*x*,1-*y*,2-*z*) and N′—H(N′1)···O(2′)(1-*x*,1-*y*,1-*z*), H···O = 1.96 and 1.86 Å, N···O = 2.838(3) and 2.751(3) Å, N—H···O = 159° and 161°), thus forming the infinite chain.

The reaction of **1** with phenylboronic acid in ethanol appears to involve a solvolytic scission of the hydroxamic acid releasing *N*-methylhydroxylamine which then adds to the Lewis acid cyclic phenylboronate **10**, a condensation product easily formed in ethanolic solution.[9] *N*-Methylhydroxylamine coordinates through the oxygen atom to the electron-deficient boron atom of the 1,3,2-dioxaborolan-4-one ring of **10**, resulting in the zwitterionic addition compound **9** having a (rehybridized) tetravalent borate anion and an ammonium cation. These findings confirm the assumption that *N*-methylhydroxylamine coordinates to Lewis acid boron compounds via the oxygen atom of the tautomeric *N*-oxide form rather than via the nitrogen atom of the hydroxylamine form, supporting the formulations postulated for boron complexes of unsubstituted hydroxylamine (9). To the best of our knowledge, compound **9** is the first structurally characterized example of an *N*-alkylhydroxylamine(*O*-*B*)boron complex having an open-chain *B*,*N*-betaine structure (17).

The geometry about the boron atom in **9** is very similar to that reported for compound **11**, an addition product between a 1,3,2-dioxaborolan-4,5-dione and a cyclic nitrone (7). The mean (N)O—B, (C)O—B, and B—C(phenyl) distances[10] of 1.494, 1.505, and 1.594 Å for **9** can be compared to corresponding values of 1.502, 1.503, and 1.576 Å for **11** (7). The mean bond angles about the distorted tetrahedral boron atom in **9**: O(1)—B—O(2) (within the five-membered chelate ring) = 102.1°, (phenyl)C—B—O(*N*-oxide) = 106.1°, O(1)—B—O(4) = 109.2°, O(2)—B—O(4) = 111.5°, C(10)—B—O(1) = 112.5°, and C(10)—B—O(2) = 116.0° are similar to the corresponding values of 102.9°, 105.6°, 109.5°, 109.5°, 113.7°, and 115.6° reported for **11**. The molecular structures of two other phenylboronate *N*-oxide complexes with Ph-B$^-$(O-C)$_2$(O-N)$^+$ 1,3-betaine moieties have been determined. Both of these compounds, **12** (18) and **13** (19), are cyclic *B*,*N*-betaines and represent examples of the intramolecular coordination of *N*-oxides to the phenylboronate function. The sums of bond lengths about the boron atom (one B—C(phenyl), one B—O(N), and two B—O(C)) are 6.099 (corrected) for **12**, 6.101 (corrected) for **13**, 6.100 for **9**, and 6.083 Å for **11**. The B—O(N) bonds in the acyclic compounds **9** and **11** (mean 1.494(2) and 1.502(8) Å, respectively) are distinctly shorter than the corresponding bonds in the cyclic derivatives **12** and **13** (1.539(2) and 1.604(7) Å, respectively),

[9]We have subsequently been able to obtain the six-membered cycloboronate **2** by carrying out the condensation reaction of **1** and phenylboronic acid in benzene solvent under water-eliminating conditions (see footnote 4).

[10]Libration-corrected bond lengths for **9** are employed throughout the discussion. Values reported for other compounds are uncorrected unless otherwise indicated.

Can. J. Chem. Downloaded from www.nrcresearchpress.com by 92.62.229.171 on 09/08/12
For personal use only.

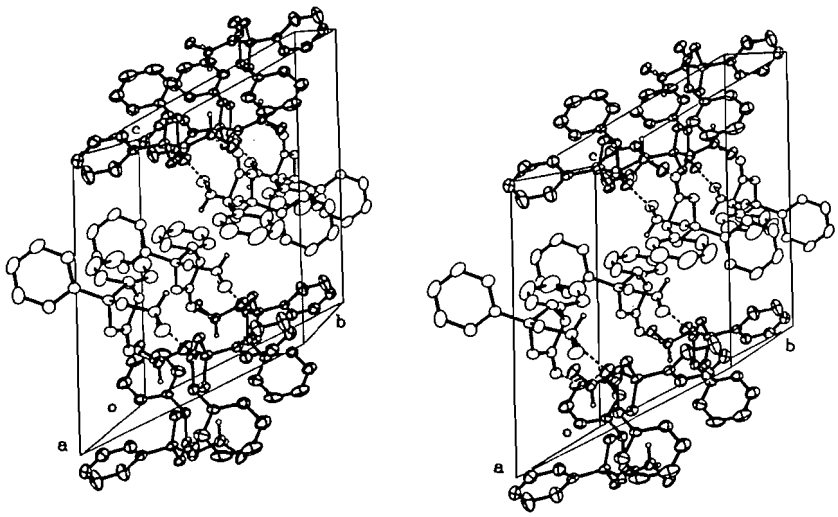

FIG. 2. Stereoview of the unit-cell of **9**; 50% probability thermal ellipsoids are shown for the non-hydrogen atoms. Hydrogen bonds are represented by dashed lines. Principal ellipses distinguish the unprimed molecule.

Can. J. Chem. Downloaded from www.nrcresearchpress.com by 92.62.229.171 on 09/08/12
For personal use only.

which are subject to some steric strain in the bicyclic ring systems formed by the intramolecular coordination.

The N—O bond length in the adduct **9** (mean 1.424(2) Å) is considerably shorter than the value of 1.477(2) Å reported for an electron diffraction study of free *N*-methylhydroxylamine (20) as a result of the influence of the Lewis acid. This effect appears to be more pronounced than that induced by protonation of *N*-methylhydroxylamine: N—O in $MeNH_2OH^+Cl^-$ = 1.447 Å (21), 1.45 Å (22). Similar differences have been reported for the N—O bonds of unsubstituted hydroxylamine where the N—O bond length in the free base is 1.476(30) Å in the solid state (23) and 1.453(2) Å in the vapor phase (by microwave spectroscopy) (24), while the N—O distance is 1.411(2) Å in the protonated form $NH_3OH^+Cl^-$ (25) and 1.42(1) Å in the H_3N^+–O–U(IV) moiety of a uranium complex (12). The N—C bond of *N*-methylhydroxylamine shows the opposite tendency, that in the free base (1.420(2) Å by electron diffraction) (20) being shorter than those in the protonated form $MeNH_2OH^+Cl^-$ (1.455 Å (21) and 1.46 Å (22)) and the Lewis acid adduct **9** (mean 1.478(2) Å). This shortening of the N—O bond and lengthening of the N—C bond may be indicative of a respective decrease/increase of repulsion between the nitrogen and the oxygen/methyl carbon atom as the electron-withdrawing proton or Lewis acid interacts with the free base. Steric crowding is not involved in this case.

The difference between the O(2)—B bond involving the alcoholate ligand in **9** (mean 1.486(3) Å) and the O(1)—B bond involving the carboxylate ligand (mean 1.524(2) Å) probably arises from the higher binding strength of the alcoholate oxygen atom O(2). The reduced donor quality of the carboxylate ligand through involvement of O(1) in the mesomeric carboxylate system is also obvious from the short O(1)—C(1) bond (mean 1.314(4) Å). In comparable γ-lactone ring systems the average (O=)C—O bond is known to be 1.350(12) Å in length (26). Correspondingly, the C=O bond in **9** (mean 1.219(5) Å) is slightly longer than those in the γ-lactones (mean 1.201(9) Å) (26). The enormous shift of the C=O frequency in the infrared spectrum going from **10** to **9** (1800 → 1710 cm^{-1}) can now be interpreted as a consequence of the rehybridization of the boron atom, which can interact with O(2) by pp(π) back-donation in **10**. This interaction is inhibited by tetracoordination of the boron atom in **9**. The high frequency of the C=O stretching vibration in **10** is similar to that reported for β,γ-unsaturated five-membered cyclic lactones, showing C=O absorptions around 1800 cm^{-1} that are shifted to lower frequencies if no π-bond is present in the β,γ-position of the lactone (27). The five-membered BOCCO chelate rings in **9** are planar to within 0.025(3) and 0.044(4) Å for the unprimed and primed molecules, respectively, and have flattened C(2)- and B′-envelope conformations (see Table 4).

Acknowledgements

We thank the Natural Sciences and Engineering Research Council of Canada and the Fonds der Chemischen Industrie, Frankfurt am Main, for financial support.

1. W. B. Ankers, D. B. Bigley, R. F. Hudson, and J. C. Thurman. Tetrahedron Lett. 4539 (1969).
2. G. I. Nikishin, E. I. Troyansky, I. V. Svitkano, and O. Chizhov. Tetrahedron Lett. **25**, 97 (1984).
3. C. Meier and G. Boche. Tetrahedron Lett. **31**, 1685 (1990); Tetrahedron Lett., **31**, 1693 (1990); Chem. Ber. **123**, 1691 (1990); Chem. Ber., **123**, 1699 (1990).
4. (*a*) H. G. Aurich, H. G. Scharpenberg, and K. Kabs. Tetrahedron Lett. 3559 (1970); (*b*) H. G. Aurich and H. G. Scharpenberg. Chem. Ber. **106**, 1881 (1973); (*c*) G. Zinner and B. Geister. Arch. Pharm. (Weinheim), **307**, 39 (1974); (*d*) G. Zinner, H. Grigat, and M. Psiorz. Arch. Pharm (Weinheim), **319**, 787 (1986).
5. M. K. Das, B. Biswas, and S. Chakraborty. Synth. React. Inorg. Met.-Org. Chem. **16**, 77 (1986).
6. W. Kliegel, M. Tajerbashi, S. J. Rettig, and J. Trotter. Can. J. Chem. **67**, 1636 (1989).
7. P. Paetzold, P. Bohm, A. Richter, and E. Scholl. Z. Naturforsch. B: Anorg. Chem. Org. Chem. **31***b*, 754 (1976).
8. (*a*) J. Goubeau. Angew. Chem. A, **58**, 78 (1945); (*b*) E. L. Muetterties. Z. Naturforsch. B: Anorg. Chem. Org. Chem. Biochem. Biophys. Biol. **12***b*, 265 (1957); (*c*) D. H. Campbell, T. C. Bissot, and R. W. Parry. J. Am. Chem. Soc. **80**, 1549 (1958); (*d*) F. Hodosan and V. Ciurdaru. Tetrahedron Lett.

1997 (1971); (*e*) I. I. Lapkin, G. A. Yuzhakova, S. E. Ukhanov, and R. N. Abramova. Zh. Obshch. Khim. **48**, 2215 (1978) (J. Gen. Chem., USSR, **48**, 2012 (1978)); (*f*) D. Armesto, J. C. Barnes, W. M. Horspool, and F. Langa. J. Chem. Soc. Chem. Commun. 123 (1990).
9. (*a*) K.-H. Günther. Dissertation, Göttingen. 1950; (*b*) U. Wannagat and R. Pfeiffenschneider. Z. Anorg. Allgem. Chem. **297**, 151 (1958); (*c*) L. G. Ryss and S. L. Idel's. Russ. J. Inorg. Chem. **10**, 383 (1965).
10. J. A. McCleverty. Transition Met. Chem. **12**, 282 (1987).
11. L. M. Engelhardt, P. W. G. Newman, C. L. Raston, and A. H. White. Aust. J. Chem. **27**, 503 (1974).
12. H. W. W. Adrian and A. Van Tets. Acta Crystallogr. Sect. B: Struct. Crystallogr. Cryst. Chem. **B35**, 153 (1979).
13. D. Geffken and H.-J. Kämpf. Chem.-Ztg. **103**, 19 (1979).
14. International tables for X-ray crystallography. Vol. IV. Kynoch Press, Birmingham, U.K. Present distributor: Kluwer Academic Publishers; Dordrecht, The Netherlands. 1974. pp. 99–102 and 149.
15. V. Schomaker and K. N. Trueblood. Acta Crystallogr. Sect. B: Struct. Crystallogr. Cryst. Chem. **B24**, 63 (1968).
16. D. W. J. Cruickshank. Acta Crystallogr. **9**, 747 (1956); **9**, 754 (1956); **14**, 896 (1961).
17. W. Kliegel. Organomet. Chem. Rev. Sect. A: **8**, 153 (1972).
18. W. Kliegel, H.-W. Motzkus, K. Drückler, S. J. Rettig, and J.Trotter. Can. J. Chem. **68**, 64 (1990).
19. W. Kliegel, L. Preu, S. J. Rettig, and J. Trotter. Can. J. Chem. **63**, 509 (1985).
20. D. W. H. Rankin, M. R. Todd, F. G. Riddell, and E. S. Turner. J. Mol. Struct. **71**, 171 (1981).
21. I. K. Larsen, L. Toft, and K. G. Jensen. Acta Crystallogr. **21**, A120 (1966).
22. L. Toft and B. Jerslev. Acta Chem. Scand. **21**, 1383 (1967).
23. E. A. Meyers and W. N. Lipscomb. Acta Crystallogr. **8**, 583 (1955).
24. S. Tsunekawa. J. Phys. Soc. Jpn. **33**, 167 (1972).
25. K.-L. Shi, R.-O. Wang, and T. C. W. Mak. J. Mol. Struct. **160**, 109 (1987).
26. F. H. Allen, O. Kennard, D. G. Watson, L. Brammer, A. G. Orpen, and R. Taylor. J. Chem. Soc. Perkin Trans. 2, S1 (1987).
27. D. H. Williams and I. Fleming. Spectroscopic methods in organic chemistry. London. 1973.
28. W. Kliegel, U. Schumacher, S. J. Rettig, and J. Trotter. Can. J. Chem. **70**, 1176 (1992).

Can. J. Chem. Downloaded from www.nrcresearchpress.com by 92.62.229.171 on 09/08/12
For personal use only.

Kinetics and mechanism of the formation of *N*-vinyl pyridinium cations in elimination reactions in aqueous base

JOHN W. BUNTING,[1] ANDREA TOTH, AND JAMES P. KANTER
Department of Chemistry, University of Toronto, Toronto, Ont., Canada M5S 1A1

Received June 28, 1991

JOHN W. BUNTING, ANDREA TOTH, and JAMES P. KANTER. Can. J. Chem. **70**, 1195 (1992).

The rates of the elimination reactions of *N*-(2-bromoethyl) pyridinium cations (**1**) and *N*,*N*′-ethylene bispyridinium dications (**3**) to give the corresponding *N*-vinyl pyridinium cations (**2**) have been measured spectrophotometrically in basic aqueous solutions (ionic strength 0.1, 25°C) for a variety of substituents in the pyridine rings of each of these classes of pyridinium cation. The reaction kinetics are first order in **1** or **3** and first order in hydroxide ion. Brønsted-type plots of the second-order rate constants (k_{OH}) as a function of the basicity (as pK_{BH}) of the corresponding substituted pyridine are nonlinear for each of **1** and **3** and can be interpreted in terms of E1cb reaction mechanisms. For **1**, the Brønsted-type plot displays two distinct "concave down" linear regions; rate-determining deprotonation for $pK_{BH} < 5.16$ (slope = −0.30), and a change in rate-determining step to bromide ion departure for $pK_{BH} > 5.16$ (slope −0.58). For **3**, the Brønsted-type plot appears to be smoothly curved for symmetrically disubstituted bispyridinium dications, as a consequence of the multiple substituent effects upon each step of the E1cb reactions of these dications. However, log k_{OH} for **3** is a smooth linear function of the previously reported log k_{OH} for the E1cb reactions of *N*-(2-cyanoethyl) pyridinium cations over a range in which a change in rate-determining step has been directly demonstrated for these latter cations. Thus a change in rate-determining step as a function of pyridine basicity is also required within the E1cb mechanism for **3**. The E1cb reactions of **1** are approximately 10^4-fold faster than the corresponding hydroxide ion catalyzed E2 eliminations from 2-phenylethyl bromides that are isoelectronic with **1**.

JOHN W. BUNTING, ANDREA TOTH et JAMES P. KANTER. Can. J. Chem. **70**, 1195 (1992).

Opérant en solutions aqueuses basiques (force ionique de 0,1, à 25°C) et faisant appel à des méthodes spectrophotométriques, on a mesuré les vitesses des réactions d'élimination des cations *N*-(2-bromoéthyl)pyridinium (**1**) et des dications *N*,*N*′-éthylène bispyridinium (**3**) qui portent une variété de substituants sur les pyridines de chacune des classes de cations pyridinium et qui conduisent à la formation des cations *N*-vinylpyridinium correspondants (**2**). Les cinétiques des réactions sont du premier ordre en composés **1** (ou **3**) et du premier ordre en ion hydroxyde. Pour chacun des produits **1** et **3**, les courbes de type Brønsted des constantes de vitesse du deuxième ordre (k_{OH}) en fonction de la basicité (exprimé en pK_{BH}) de la pyridine substituée correspondante ne sont pas linéaires; on peut interpréter ces résultats en fonction de mécanismes réactionnels E1cb. Pour les composés **1**, la courbe de type Brønsted présente deux régions linéaires «concaves vers le bas» distinctes; une déprotonation qui détermine la vitesse se produit à un $pK_{BH} < 5{,}15$ (pente = −0,30) et un changement dans l'étape qui détermine la vitesse de départ de l'ion bromure à un $pK_{BH} > 5{,}16$ (pente = −0,58). Pour les composés **3** impliquant des dications bispyridinium symétriquement disubstitués, la courbe de type Brønsted semble bien aplanie; cette situation résulte des multiples effets de substituants sur chacune des étapes des réactions E1bc de ces dications. Toutefois, dans les cas des composés **3**, le log k_{OH} est une fonction régulière de log k_{OH} rapportée antérieurement pour les réactions E1cb des cations *N*-(2-cyanoéthyl)pyridinium pour une plage de valeur impliquant, pour ces derniers cations, un changement dans l'étape qui détermine la vitesse. Pour le mécanisme E1cb des composés **3**, il est donc nécessaire de faire intervenir un changement, relié à la basicité de la pyridine, dans l'étape qui détermine la vitesse. Les réactions E1cb des composés **1** se font approximativement 10^4 fois plus rapidement que les réactions E2 correspondantes, catalysées par l'ion hydroxyde, réalisés sur le bromure de 2-phényléthle qui est isoélectronique avec les composés **1**.

[Traduit par la rédaction]

Katritzky and co-workers (1, 2) have reported synthetic procedures for the preparation of *N*-vinyl pyridinium cations (**2**) via base-catalyzed elimination reactions from the corresponding *N*-(2-bromoethyl) pyridinium cations (**1**) (eq. [1]). The *N*,*N*′-ethylene bispyridinium dications (**3**), which are usually obtained as by-products in the synthesis of **1** from the substituted pyridine and 1,2-dibromoethane, are also potential sources of **2** via elimination reactions (eq. [2]) although we can find no previous report of this reaction in the literature. In the current work we have found that both the elimination reactions of eqs. [1] and [2] proceed readily in dilute aqueous base at rates that are readily measured for most X-substituents.

The reactions of eqs. [1] and [2] would be expected to most probably proceed via either the E1cb or E2 mechanisms, although we have been unable to locate any mechanistic investigation of either of these two types of reaction. The elimination reactions of the *N*-(2-bromoethyl) pyridinium cations (**1**) are of particular mechanistic interest since they are clearly related to the analogous base-catalyzed eliminations from 2-phenylethyl bromides (**4**) (eq. [3]) (3–6). Base-catalyzed eliminations from **4** have been found to be E2 (6). However, for the related eliminations (eq. [4]) from *N*-(2-phenylethyl) quinuclidinium cations, changes between the E2 and E1cb reaction mechanisms, as well as changes in rate-determining step within the E1cb mechanism, can occur upon variation of the substituent X in the phenyl ring or upon variation of the reaction conditions (base concentration, solvent, etc.) (5–7).

In the current study, we have measured the rates of elimination from **1** and **3** for a variety of X-substituents over the range pH 11–13 in aqueous solution. Brønsted plots give nonlinear correlations between the second-order rate con-

[1]Author to whom correspondence may be addressed.

Can. J. Chem. Downloaded from www.nrcresearchpress.com by 92.62.229.171 on 09/08/12
For personal use only.

stants for the hydroxide ion catalyzed eliminations and the basicities of the corresponding substituted pyridines over the range pK_{BH} = 2–10. These data now allow detailed comparisons of the reactivities of **1**, **3**, and **4** in base-catalyzed eliminations in aqueous solution, and also demonstrate that the reactions of eqs. [1] and [2] are consistent with E1cb processes. Quantitative comparisons can also be made of the reactivities in these systems and in related elimination reactions in which substituted pyridines are the nucleofugic leaving groups (8, 9).

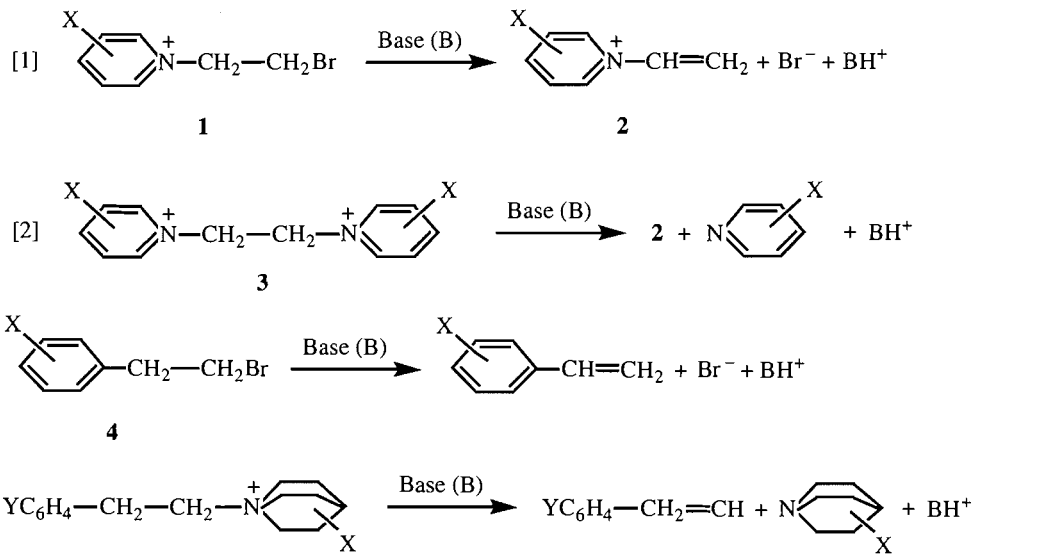

Experimental

Syntheses

A mixture of the bromide salts of **1** and **3** was usually obtained upon refluxing equimolar ethanolic solutions (≈ 0.04 M) of the substituted pyridine and 1,2-dibromoethane for periods ranging from 5 to 30 h. The bispyridinium dibromides (**3** · $(Br^-)_2$) precipitated from these solutions, and were recrystallized from ethanol. The filtrate contained predominantly the *N*-(2-bromoethyl) pyridinium bromide salt (**1** · Br^-), which was usually contaminated with a small amount of the corresponding **3** · $(Br^-)_2$. These crude **1** · Br^- salts were purified by several recrystallizations from appropriate solvent mixtures (usually 2-propanol–ethanol – ethyl acetate). Occasionally, a preparation using a threefold molar excess of either the substituted pyridine or 1,2-dibromoethane was used to maximize the yield of either **1** or **3** as desired.

The purified bromide salts were characterized by ^1H NMR spectroscopy (Table 1). The methylene signals at δ ≈ 5.5 in the spectra of **3** are useful indicators of the absence of **3** as a contaminant in purified samples of **1**. Vollhard titrations of the bromide ion content of purified samples of **1** · Br^- and **3** · $(Br^-)_2$ indicated purities of 100(±1)%.

Kinetic studies

All kinetic data were obtained spectrophotometrically in aqueous solutions of ionic strength 0.1 (KOH + KCl) at 25°C, on either a Durrum–Gibson stopped-flow spectrophotometer or a Cary 210 spectrophotometer. All data collection and analysis closely followed the methods that we have previously described (8). In most cases, analytical wavelengths were in the vicinity of 250 nm, although wavelengths in the vicinity of 300 nm were more appropriate for the 3- and 4-aminopyridinium cations. Substrate concentrations were in the range 0.05–0.1 mM.

Results

The time-dependence of the electronic absorption spectrum of **1***a* (X = H) in an aqueous solution of pH 11.9 is shown in Fig. 1. The spectrum of the product from **1***a* (λ_{max} = 253 nm, ε = 8100) is similar to that reported (2) for the unsubstituted *N*-vinyl pyridinium cation (**2**: X = H).[2] The time-dependence of the absorption spectrum of **1***m* (X = 4-$N(CH_3)_2$) at pH 13.0 is shown in Fig. 2. The spectrum of the product λ_{max} = 308 nm, ε = 27 300) is consistent with that reported (2) for **2**: X = 4-$N(CH_3)_2$. The tight isosbestic point that is indicated in Fig. 2 is consistent with the clean conversion of **1***m* to **2***m* without the formation of any significant concentration of intermediate species, and also indicates that there are no significant competing reactions of the *N*-vinyl pyridinium cation product on the time scale of the current elimination reaction.

Similar spectral observations, consistent with the formation of the various ring-substituted *N*-vinyl pyridinium cations (**2**), were made for the reactions of **1***a*–**1***m* and **3***a*–**3***k* in aqueous base. The spectral changes for the conversion of **3** to **2** were smaller than for the corresponding elimination reactions of **1** due to the presence of two pyridinium chromophores per dication in **3**. However, the products from **3** displayed spectra that were identical to those of 1:1 mole ratios of the appropriate X-substituted **2** and X-substituted pyridine. The 4,4′-diamino and 4,4′-bis-(dimethylamino) dications (**3***l* and **3***m*) appeared to be stable at pH 13 over several hours, so that we were unable to observe the elimination reactions for these two dications (see below).

We were unable to observe the elimination reaction from **1***d* (X = 3-CN), because of a competing reaction that generated a species having λ_{max} = 360 nm. We have not investigated this reaction in detail; similar reactions resulting from hydroxide ion addition to the pyridinium ring carbon atoms have been reported for the *N*-methyl 3-cyanopyridinium

[2]All absorption maxima in the current study are at 2–4 nm shorter wavelength than those previously reported (2). The wavelength scale of our instrument was recently calibrated against the absorption spectrum of benzene vapour.

Can. J. Chem. Downloaded from www.nrcresearchpress.com by 92.62.229.171 on 09/08/12
For personal use only.

TABLE 1. Characterization of the pyridinium bromide salts $\mathbf{1}\cdot Br^-$ and $\mathbf{3}\cdot(Br^-)_2$

Cation	X	Melting point (°C)	^{1}H NMR (δ)[a]
1*a*	H	106–108[b]	3.90 (t, 2H), 5.10 (t, 2H), 7.95–8.15 (m, 2H), 8.4–8.65 (m, 1H), 8.85 (d, 1H)
1*b*	3-Cl	114–115	3.98 (t, 2H), 5.18 (t, 2H), 8.3–8.8 (m, 1H), 8.6–9.1 (m, 3H)
1*c*	3-$CONH_2$	193–194	4.02 (t, 2H), 5.23 (t, 2H), 7.8 (br, 2H), 8.1–8.35 (m, 1H), 8.95–9.2 (m, 2H), 9.53 (s, 1H)
1*d*	3-CN	165–167	3.92 (t, 2H), 5.08 (t, 2H), 8.2 (m, 1H), 9.2 (d, 1H), 9.3 (d, 1H), 9.66 (s, 1H)
1*e*	3-CH_2CN	165–167	3.92 (t, 2H), 4.37 (s, 2H), 5.11 (t, 2H), 8.05–8.3 (m, 1H), 8.6–9.05 (m, 3H)
1*f*	3-C_6H_5	131–133	3.90 (t, 2H), 5.07 (t, 2H), 7.55 (s, 5H), 7.9–8.2 (m, 1H), 8.68 (d, 2H), 9.00 (s, 1H)
1*g*	3-CH_3	88–90[c]	2.63 (s, 3H), 3.90 (t, 2H), 5.02 (t, 2H), 7.8–8.7 (m, 4H)
1*h*	4-CH_3	[d]	2.77 (s, 3H), 3.90 (t, 2H), 5.00 (t, 2H), 7.87 (d, 2H), 8.64 (d, 2H)
1*k*	3,4-$(CH_3)_2$	133–135	2.60 (s, 3H), 2.72 (s, 3H), 3.92 (t, 2H), 5.00 (t, 2H), 7.92 (d, 1H), 8.67 (m, 2H)
1*l*	4-NH_2	177–179	3.70 (t, 2H), 4.55 (t, 2H), 6.92 (d, 2H), 7.88 (d, 2H)
1*m*	4-$N(CH_3)_2$	204–206[e]	3.33 (s, 6H), 3.75 (t, 2H), 4.57 (t, 2H), 6.92 (d, 2H), 8.00 (d, 2H)
3*a*	H	283(dec.)[f]	5.77 (s, 4H), 8.1–8.35 (m, 4H), 8.6–8.9 (m, 2H), 9.35 (d, 4H)
3*b*	3-Cl	285(dec.)	5.70 (s, 4H), 8.0–8.25 (m, 2H), 8.50 (d, 2H), 9.25 (d, 2H), 9.45 (s, 2H)
3*c*	3-$CONH_2$	275(dec.)	5.78 (s, 4H), 7.75 (br, 4H), 8.1–8.4 (m, 2H), 9.08 (d, 2H), 9.48 (d, 2H), 10.03 (s, 2H)
3*e*	3-CH_2CN	232(dec.)	4.42 (s, 4H), 5.68 (s, 4H), 8.05–8.25 (m, 2H), 8.64 (d, 2H), 9.22 (d, 2H), 9.42 (s, 2H)
3*f*	3-C_6H_5	301–303	5.50 (s, 4H), 7.35 (s, 10H), 7.8–8.0 (m, 2H), 8.47 (d, 2H), 8.93 (d, 2H), 9.30 (s, 2H)
3*g*	3-CH_3	258(dec.)[g]	2.70 (s, 6H), 5.53 (s, 4H), 7.85–8.1 (m, 2H), 8.4 (d, 2H), 9.03 (d, 2H), 9.08 (s, 2H)
3*h*	4-CH_3	274(dec.)[h]	2.75 (s, 6H), 5.45 (s, 4H), 7.88 (d, 4H), 8.95 (d, 4H)
3*i*	3-NH_2	235–237	5.42 (s, 4H), 7.65–8.1 (m, 4H), 8.41 (d, 2H), 8.79 (s, 2H)
3*j*	3,5-$(CH_3)_2$	282(dec.)	2.67 (s, 12H), 5.47 (s, 4H), 8.17 (s, 2H), 8.84 (s, 4H)
3*k*	3,4-$(CH_3)_2$	274(dec.)	2.57 (s, 6H), 2.67 (s, 6H), 5.40 (s, 4H), 7.82 (d, 2H), 8.82 (d, 2H), 8.90 (s, 2H)
3*l*	4-NH_2	264(dec.)	4.87 (s, 4H), 7.03 (d, 4H), 8.07 (d, 4H)
3*m*	4-$N(CH_3)_2$	301(dec.)[h]	3.30 (s, 12H), 4.77 (s, 4H), 6.87 (d, 4H), 8.05 (d, 4H)

[a]In CF_3CO_2H relative to tetramethylsilane.
[b]Reference 2 reports mp 95–102°C, but also quotes other literature data of 126–128°C and 100–103°C.
[c]Reference 2 reports this compound as a thick oil.
[d]Oil; could not be induced to crystallize. Reference 2 reports mp 145–147°C.
[e]Reference 2 reports mp 202–203°C.
[f]Reference 2 reports mp 280°C.
[g]Reference 2 reports mp 266–268°C.
[h]Reference 2 reports mp >300°C.

Can. J. Chem. Downloaded from www.nrcresearchpress.com by 92.62.229.171 on 09/08/12
For personal use only.

cation and related species (10–13). The 3-chloropyridinium cation, **1***b*, underwent a clean elimination to the *N*-vinyl cation; however, prolonged incubation in these basic solutions led to a subsequent unidentified slower reaction.

We have observed the elimination reaction of **1***m* (0.046 M) by ^{1}H NMR spectroscopy in basic D_2O (pD ≈ 12.5). The decrease in the intensity of the signals from **1***m* is concerted with the appearance of the spectrum of the corresponding *N*-vinyl pyridinium cation (**2***m*) (δ 3.32 (s, 6H), 5.36 (dd, 1H), 5.71 (dd, 1H), 7.00 (d, 2H), 7.06 (dd, 1H), 8.23 (d, 2H)). It should be noted that under these conditions the formation of **2***m* occurs without significant exchange of the vinylic proton (δ 7.06) adjacent to the ring-nitrogen atom. Consistent with this observation, there is no exchange of the corresponding methylene protons in unreacted **1***m* during the course of the elimination reaction.

The elimination reactions of both **1** and **3** proved to be strictly first order in pyridinium cation concentration for >95% of the reaction in all cases. Pseudo-first-order rate constants (k_{obs}) were evaluated as a function of pH, usually over the pH range 11–13. Some examples of the pH-dependences of k_{obs} are given in Figs. 3 and 4 for **1** and **3**, respectively. In most cases, log k_{obs} shows a linear dependence upon pH with unit slope (Table 2), although slight variations from unit slope were found in some cases. While the most reactive **1** and **3** cations in Table 2 appear to display accurate unit slopes within experimental error, there appears to be a trend towards increasing slope as the reactivity decreases. Similar deviations from unit slope in related elimination reactions from pyridinium and quinuclidinium cations have been attributed (5, 6, 9) to specific ion effects upon replacement of chloride ions by hydroxide ions in these constant ionic strength solutions. Second-order rate constants (k_{OH}) for the hydroxide ion catalyzed elimination reactions were evaluated by interpolation at pH 12 on the least-squares correlation lines, and are collected in Table 2.

In one case, **3***b* (X = 3-Cl), a nonlinear pH–rate profile is apparent in Fig. 4. In this case, k_{obs} was found to be consistent with eq. [5]. Fitting of the data to this equation gave: k_{OH} = 12 (±1) M^{-1} s^{-1} and pK_a = 12.77 (±0.07). We assume that pK_a = 12.77 for **3***b* represents pK_{R^+} for hydroxide ion addition to one of the ring-carbon atoms.

$$[5] \quad k_{obs} = k_{OH}[^-OH]/(1 + K_a/[H^+])$$

Discussion

The best available synthetic route to an *N*-vinyl pyridinium cation (**2**) involves the treatment of the corresponding *N*-(2-bromoethyl) pyridinium cation (**1**) with one equivalent of base in alcoholic solution at −10°C (1, 2). Higher temperatures lead to the loss of **2** to polymerization. In the current work, we found that the rates of elimination by **1** to give

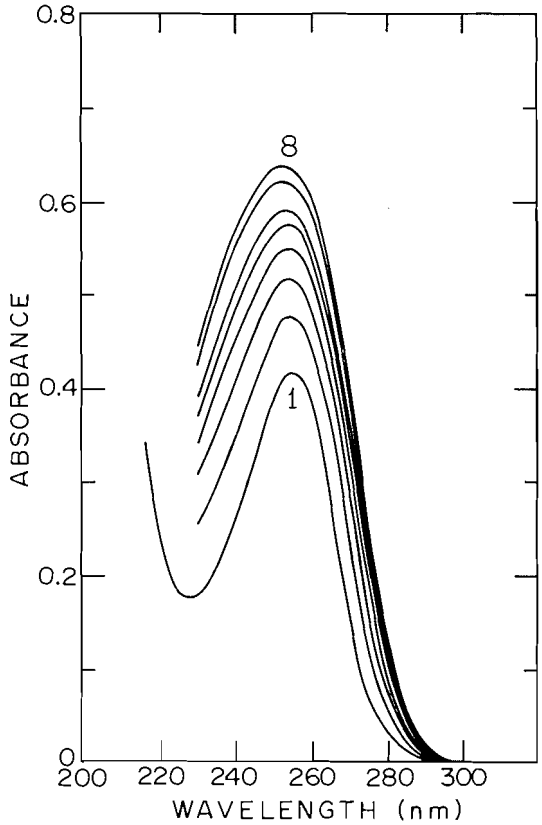

FIG. 1. Time dependence of the electronic absorption spectrum of the *N*-(2-bromoethyl) pyridinium cation (**1***a*) (0.08 mM) in aqueous solution of pH 11.9 at 25°C. Successive scans (1–8) are at 1, 4, 7, 9, 11, 14, 23, and 60 min, respectively.

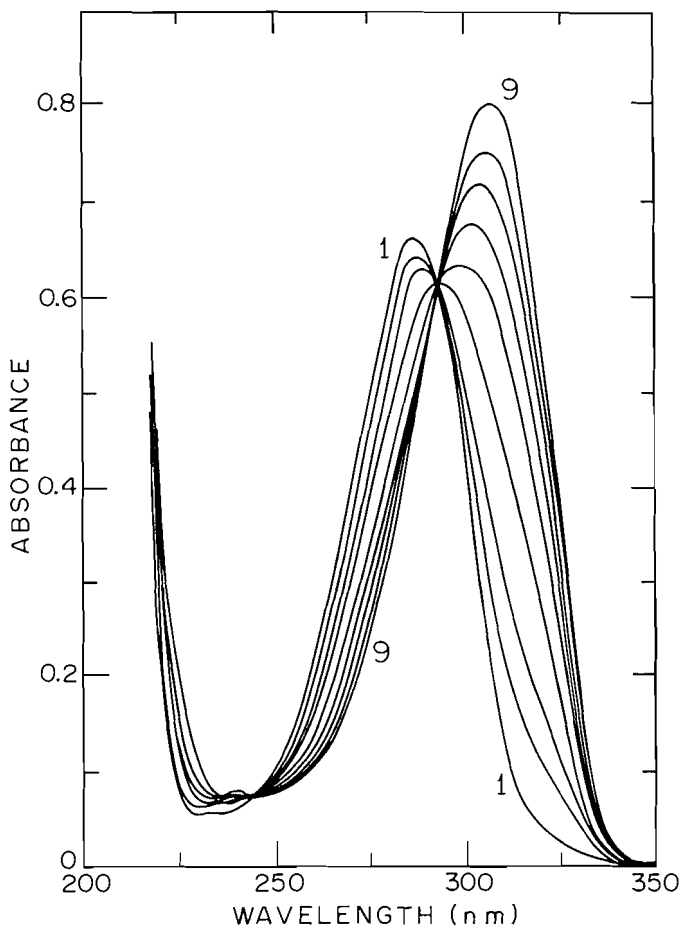

FIG. 2. Time dependence of the electronic absorption spectrum of the *N*-(2-bromoethyl) 4-dimethylaminopyridinium cation (**1***n*) (0.03 mM) in aqueous solution of pH 13.0 at 25°C. Successive scans (1–9) are at 0, 30, 60, 120, 180, 240, 300, 360, and 600 min, respectively.

2 can be studied spectrophotometrically in dilute aqueous base (pH 11–13) at 25°C. We did not observe any complications from polymerization processes at the low concentrations (0.05–0.1 mM) of *N*-vinyl pyridinium cations that are produced in these kinetic studies. We also found that the *N*,*N*′-ethylene bispyridinium dications (**3**) undergo a clean elimination reaction to give **2** in dilute aqueous base, although this reaction becomes extremely slow for the dications that are derived from the most basic pyridines.

The elimination reactions of eqs. [1] and [2] are kinetically first order in each of the pyridinium cation (**1** or **3**) and hydroxide ion. Although this observation is formally consistent with either an E2 or an E1cb reaction mechanism, we will argue below that all of the available data are only readily reconciled in terms of the E1cb mechanism for both **1** and **3**.

A Brønsted-type plot of k_{OH} for **1** as a function of the basicity of the corresponding substituted pyridine is shown in Fig. 5. This plot is nonlinear; the data can be represented by two distinct linear relationships (eqs. [6] and [7]) having Brønsted $\alpha = 0.30$ (for $pK_{BH} \leq 5.16$) and $\alpha = 0.58$ (for $pK_{BH} \geq 5.16$).

$$[6] \quad \log k_{OH} = -0.30(\pm 0.03)pK_{BH} + 1.13\ (\pm 0.05) \qquad (r = 0.991)$$

$$[7] \quad \log k_{OH} = -0.58(\pm 0.01)pK_{BH} + 2.54(\pm 0.05) \qquad (r = 0.999)$$

The data in Fig. 5 represent a classic case of a "concave-down" linear free energy relationship, which is only readily interpretable in terms of a change in rate-determining step. For base-catalyzed elimination reactions, this is an indication of an E1cb reaction mechanism (Scheme 1) rather than an E2 mechanism. We interpret eqs. [6] and [7] in terms of rate-determining deprotonation (k_1) for the more reactive **1** (eq. [6]), and rate-determining expulsion of the bromide ion from the zwitterionic conjugate base (k_2) for the less reactive **1** (eq. [7]).

For a steady-state zwitterionic intermediate (**5**), $k_{OH} = k_1$ and $\alpha = 0.30$ from eq. [6], and $k_{OH} = k_1k_2/k_{-1}$ and $\alpha = 0.58$ from eq. [7]. Irrespective of reaction mechanism, X-substituent effects upon the elimination reaction of **1** are predominantly expressed via their influence upon the acidity (kinetic or thermodynamic) of the methylene group adjacent to the ring-nitrogen atom. For the E1cb mechanism of Scheme 1, $\alpha = 0.30$ (eq. [6]) is a measure of the substituent effect upon the kinetic acidity of the methylene group adjacent to the ring-nitrogen atom. The broken line in Fig. 5 represents the extrapolation of eq. [6] to substituents for which k_1 is no longer rate determining. In eq. [7], $\alpha = 0.58$ is a combination of the equilibrium substituent effect upon the thermodynamic acidity of this methylene group ($k_1/k_{-1} = K_a/K_w$), and the

Can. J. Chem. Downloaded from www.nrcresearchpress.com by 92.62.229.171 on 09/08/12
For personal use only.

Can. J. Chem. Downloaded from www.nrcresearchpress.com by 92.62.229.171 on 09/08/12
For personal use only.

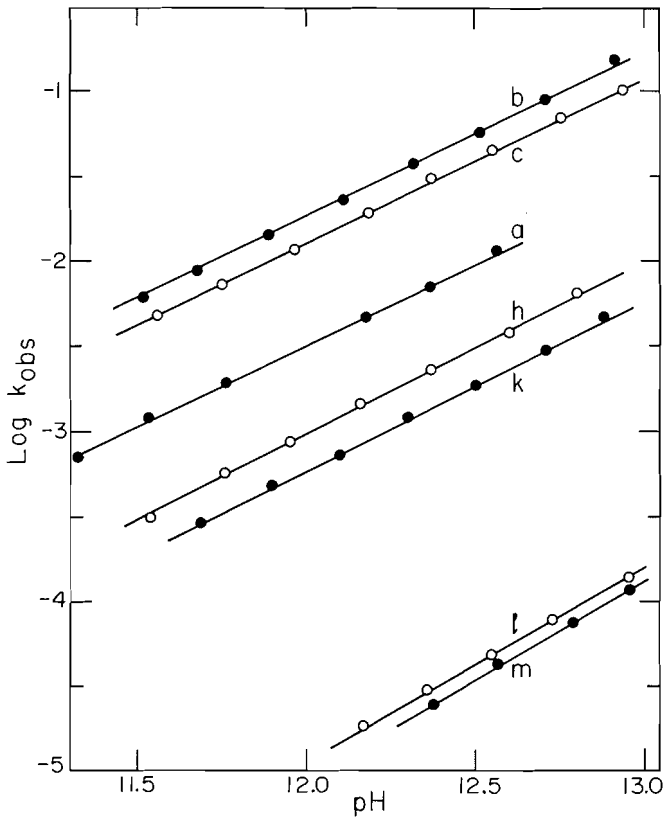

FIG. 3. The pH dependence of the pseudo-first-order rate constants (k_{obs}) for the elimination reactions of selected **1** in aqueous solution at ionic strength 0.1 and 25°C.

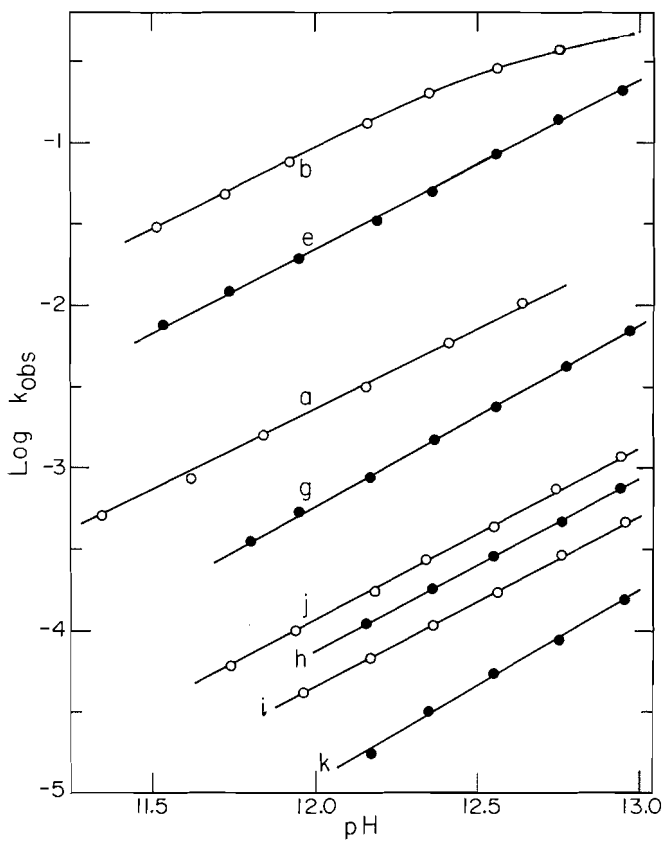

FIG 4. The pH dependence of the pseudo-first-order rate constants (k_{obs}) for the elimination reactions of selected **3** in aqueous solution at ionic strength 0.1 and 25°C.

substituent effect upon the k_2 step. Since substituent effects upon k_2 should oppose those upon K_a, the observed $\alpha = 0.58$ then represents a minimum value for the equilibrium substituent effect upon pK_a vs. pK_{BH}. This then sets a maximum value of $\alpha < (0.30/0.58 = 0.52)$ for substituent effects upon the kinetic acidity of **1** when this latter Brønsted α is defined in terms of log k_{OH} vs. pK_a for the deprotonation of **1**.

The equilibrium $\alpha > 0.58$ that is deduced above for the pK_a of **1** relative to pK_{BH} can be compared with the correspondingly defined[3] equilibrium $\alpha = 0.67$ for the deprotonation of *N*-hydroxy pyridinium cations (**6**) (eq. [8]) and $\alpha = 0.33$ for the deprotonation of *N*-di(ethoxycarbonyl)methyl pyridinium cations (**7**) (eq. [9]). These α values are consistent with the expectation that the delocalization of the negative charge in the conjugate base of **7** into the carbonyl substituents will result in the thermodynamic acidity of **7** being less sensitive to X-substituents than are the acidities of **1** (conjugate base = **5**) and **6**, for which the negative charge in each conjugate base is essentially localized on the atom adjacent to the ring nitrogen atom.

The observation that **1***m* undergoes elimination without exchange of the protons of the activated methylene group for deuterium in basic D_2O must be considered within the con-

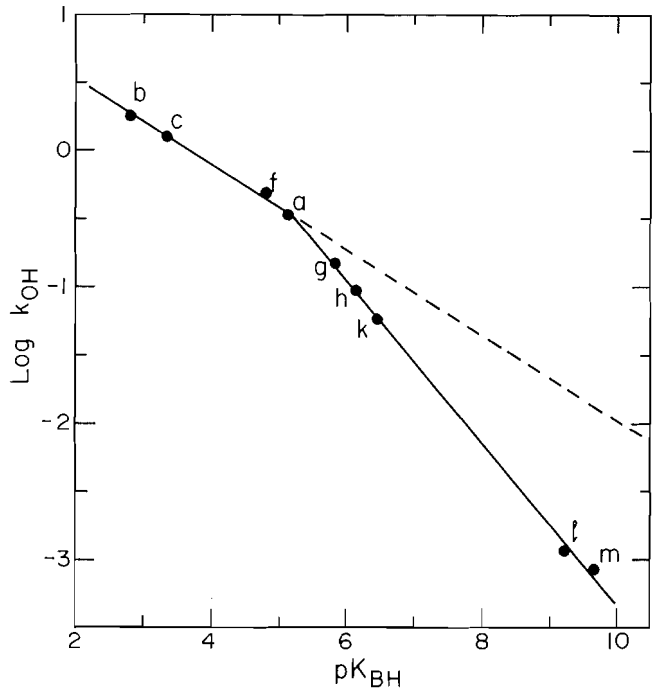

FIG. 5. Brønsted-type plot for k_{OH} as a function of pyridine basicity for the elimination reactions of **1**.

[3]Literature data (13, 14) for the pK_a values defined by eqs. [8] and [9] in aqueous solution are linearly correlated with pK_{BH} for the corresponding substituted pyridinium cations:

$pK_a(\mathbf{6}) = 0.67(\pm0.02)\ pK_{BH} + 2.6(\pm0.2)$ ($n = 11$; $r = 0.994$)

$pK_a(\mathbf{7}) = 0.33(\pm0.01)\ pK_{BH} + 3.41(\pm0.06)$ ($n = 7$; $r = 0.997$)

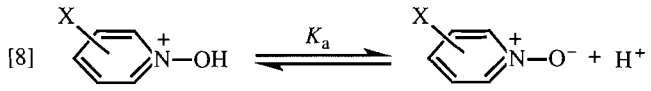

6

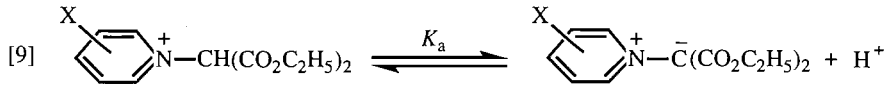

7

text of the rate-determining bromide ion departure from the carbanionic intermediate that is deduced above from the concave-down Brønsted plot. This result requires that elimination occurs within a solvated (hydrogen-bonded) intermediate in which bromide ion departure occurs more rapidly than exchange of the HOD molecule with bulk D_2O (i.e., $k_2 >> k_s$ in Scheme 2). A similar observation has been reported for rate-determining nucleofuge departure in the elimination reactions of **10**: X = 4-$N(CH_3)_2$ in aqueous base (9) and also for the analogous eliminations from 2-cyanoethyl sulfides (16). Such a process indicates that the elimination from **1***m* corresponds to an $(E1cb)_{ion\ pair}$ (i.e., $A_{xh}D_H{}^*D_N$) mechanism (17, 18).

The Brønsted plot for the elimination reactions of **3** (eq. [2]) is shown in Fig. 6. This plot appears to have pronounced curvature and cannot be as readily separated into two linear regions as can the plot in Fig. 5. The influence of X-substituents upon k_{OH} for **3** will be quite complex. In addition to the direct effect of X upon the acidity of the methylene group, analogous to that in **1** ⇌ **5**, there will also be a smaller indirect effect from the X-substituent in the other pyridinium ring upon this acidity. This latter effect cannot be ignored; a Brønsted $\alpha = 0.30$ has been found (8) upon the kinetic acidities for the analogous substituent effect in **8**. Another pronounced X-substituent effect will be derived from the pyridine leaving group when its departure is rate determining. Furthermore, superimposed upon all of these effects is the expected change in rate-determining step from deprotonation to nucleofuge departure, analogous to that which is observed for **1** and **8**.

The most reactive **3** (X = 3-Cl) undergoes hydroxide ion catalyzed elimination 3.3-fold faster (after allowing for the statistical factor in **3**) than the similarly substituted **1**. This result is only interpretable in terms of rate-determining deprotonation within an E1cb mechanism for both **1** (Scheme 1) and **3** (Scheme 4) since the 3-chloropyridine leaving group is a far poorer nucleofuge than is bromide ion. The best demonstration of this latter assertion is probably the fact that S_N2 reactions are essentially unknown for *N*-alkyl pyridinium cations under conditions in which such displacement reactions occur readily on simple alkyl bromides.

The limiting slopes are −0.5 at low pK_{BH} and −2.5 at high pK_{BH} for the curve that is sketched as a reasonable visual fit to the data in Fig. 6. The former value is about what is expected for the combined substituent effects from the two X-substituents upon the rate-determining deprotonation of **3** to give **9** in Scheme 4. The higher slope of approximately −2.5 must be interpreted in terms of rate-determining k_2 (i.e., k_{OH}

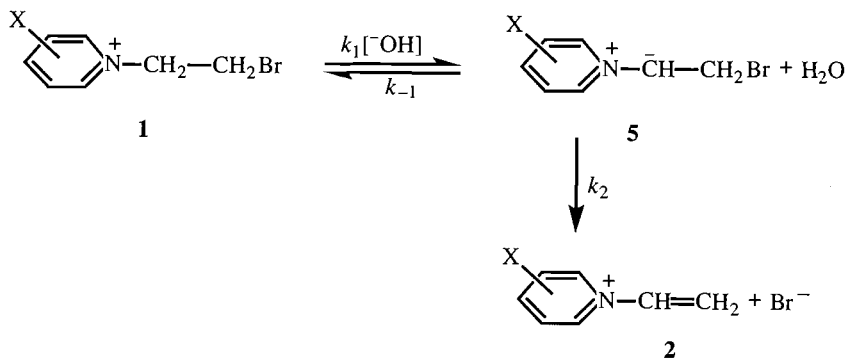

1 5 2

SCHEME 1

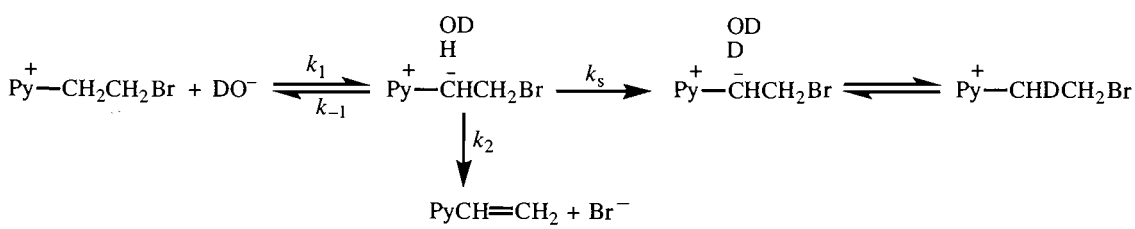

SCHEME 2

Can. J. Chem. Downloaded from www.nrcresearchpress.com by 92.62.229.171 on 09/08/12
For personal use only.

TABLE 2. Rate constants for the formation of **2** in the elimination reactions of **1** and **3**[a]

Cation	X	k_{OH} (M^{-1} s^{-1})	Slope[b]	pK_{BH}[c]
1*a*	H	0.32(±0.1)	0.98(±0.01)	5.16
1*b*	3-Cl	1.83(±0.06	1.03(±0.01)	2.84
1*c*	3-$CONH_2$	1.29(±0.02)	0.98(±0.02)	3.30
1*f*	3-C_6H_5	0.50(±0.01)	1.00(±0.01)	4.88
1*g*	3-CH_3	0.155(±0.010)	0.99(±0.03)	5.82
1*h*	4-CH_3	0.094(±0.001)	1.02(±0.01)	6.15
1*k*	3,4-$(CH_3)_2$	0.059(±0.002)	1.02(±0.02)	6.45
1*l*	4-NH_2	$1.31(\pm0.04) \times 10^{-3}$	1.06(±0.02	9.21
1*m*	4-$N(CH_3)_2$	$9.0(\pm0.5) \times 10^{-4}$	1.16(±0.03)	9.68
3*a*	H	0.23(±0.01)	0.98(±0.02)	5.16
3*b*	3-Cl	12(±1)	[d]	2.84
3*e*	3-CH_2CN	2.26(±0.03)	1.02(±0.01)	4.08
3*f*	3-C_6H_5	0.52(±0.01)	1.00(±0.01)	4.88
3*g*	3-CH_3	0.064(±0.002)	1.07(±0.01)	5.82
3*h*	4-CH_3	$8.1(\pm0.3) \times 10^{-3}$	1.06(±0.01)	6.15
3*i*	3-NH_2	$4.9(\pm0.3) \times 10^{-3}$	1.09(±0.01)	6.14
3*j*	3,5-$(CH_3)_2$	$1.22(\pm0.07) \times 10^{-2}$	1.08(±0.01)	6.14
3*k*	3,4-$(CH_3)_2$	$1.6(\pm0.1) \times 10^{-3}$	1.15(±0.02)	6.45

[a]In aqueous solution, at ionic strength 0.1, 25°C.
[b]log k_{obs} vs. pH.
[c]For deprotonation of the corresponding ring-substituted pyridinium cation (8).
[d]Nonlinear (eq. [4]: $pK_a = 12.77(\pm0.07)$).

$= k_1k_2/k_{-1}$); the reinforcing effects of both X-substituents are expressed upon $K_a/K_w = k_1/k_{-1}$, and are combined with a significant substituent effect upon k_2 from both X-substituents.

A simple linear extrapolation of log k_{OH} over the range pK_{BH} 5.82–6.45 to $pK_{BH} = 9.68$, allows an estimate of $k_{OH} \approx 8 \times 10^{-12}$ M^{-1} s^{-1} for **3***m* (X = 4-$N(CH_3)_2$). Alternatively, an estimate of the reactivity of **3***m* can be made from the observation that log k_{OH} for **3** is a simple linear function of log k_{OH} for **8** (Fig. 7; eq. [10]). Extrapolation of eq. [10] to $k_{OH} = 4.17 \times 10^{-3}$ M^{-1} s^{-1} for **8**: X = 4-$N(CH_3)_2$, gives $k_{OH} = 3 \times 10^{-11}$ M^{-1} s^{-1} for **3***m*, which is in reasonable

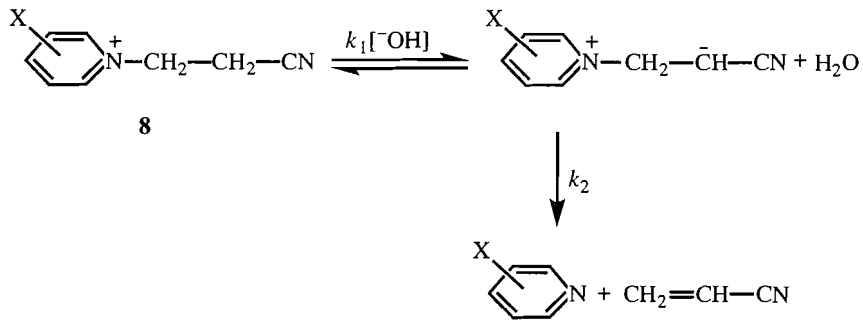

SCHEME 3

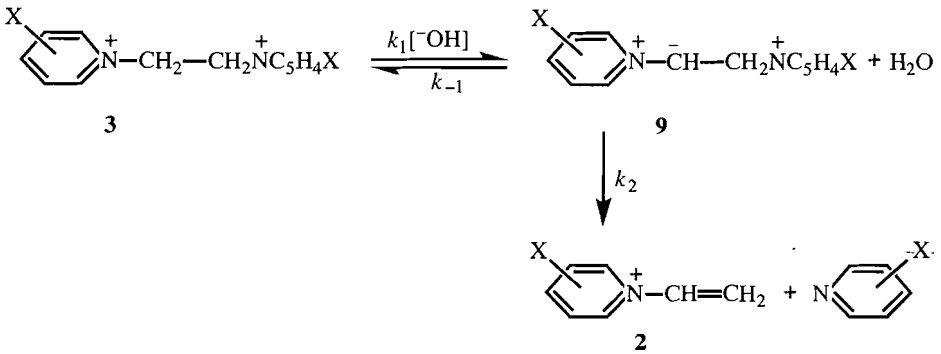

SCHEME 4

Can. J. Chem. Downloaded from www.nrcresearchpress.com by 92.62.229.171 on 09/08/12
For personal use only.

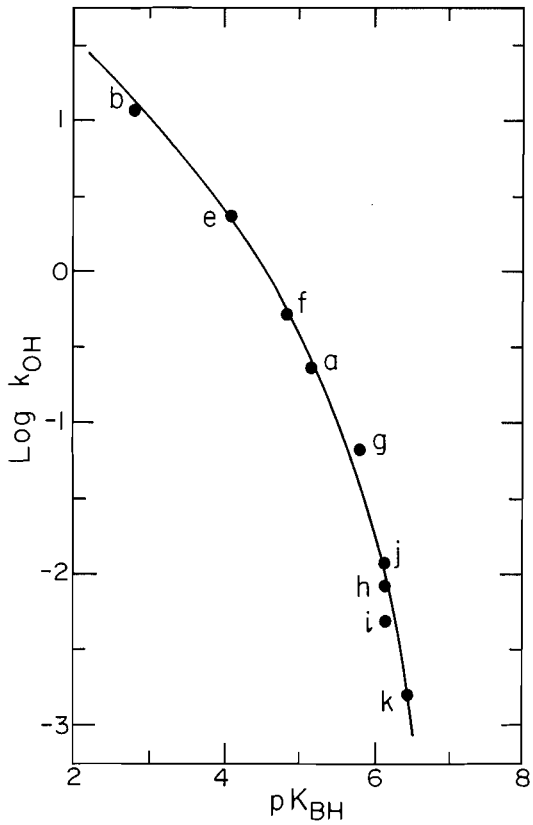

FIG. 6. Brønsted-type plot for k_{OH} as a function of pyridine basicity for the elimination reactions of **3**. The curve is sketched as a best visual fit to the data points.

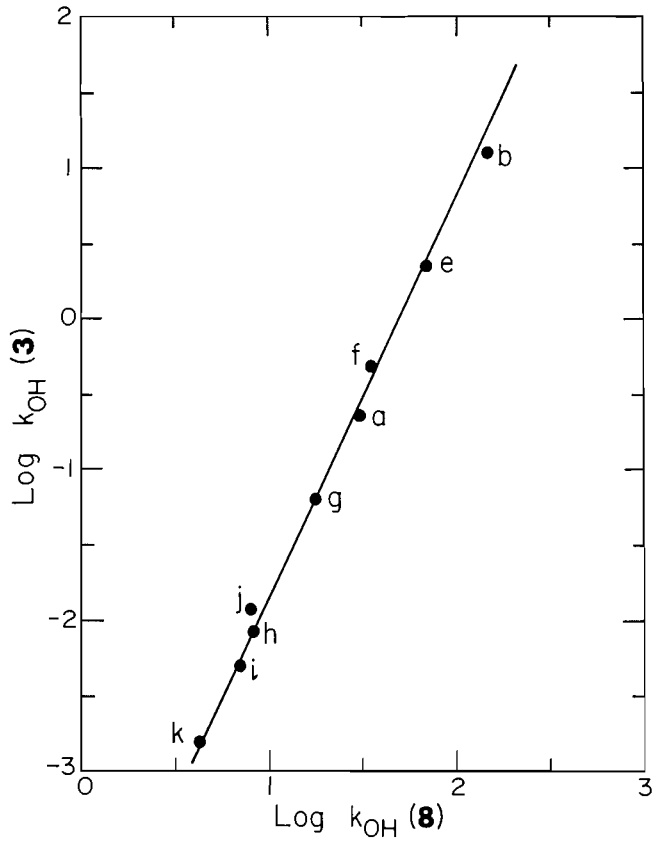

FIG. 7. The relationship between k_{OH} for the elimination reactions of **3** and **8**. The data for **8** are taken from ref. 8.

agreement with the estimate that is given above. This second-order rate constant ($k_{OH} \approx 10^{-11}$ M^{-1} s^{-1}) is 10^{12}-fold smaller than k_{OH} for the most reactive bispyridinium dication in Table 2 (**3***b*: X = 3-Cl), and corresponds to a reaction half-time of about 10^4 years for elimination from **3***m* at pH 13 and 25°C! This should be compared with a half-time of 0.6 s for **3***b* under the same reaction conditions, and a half-time of 2.2 h for **1***m* under these conditions.

[10] $\log k_{OH}(\mathbf{3}) = 2.55(\pm 0.07) \log k_{OH}(\mathbf{8}) - 4.4(\pm 0.1)$

$(r = 0.997)$

There is an additional implication in the linearity displayed in Fig. 7. The Brønsted plot for the hydroxide ion catalyzed elimination reaction of various ring-substituted **8** is concave-down, consistent with a change in rate-determining step from deprotonation (k_1) to nucleofuge departure (k_2) at pK_{BH} = 5.8 (8). The data in Fig. 7 cover a range pK_{BH} = 2.84–6.45, and can only display linearity over this range if the E1cb eliminations of **3** also undergo a similar change in rate-determining step near pK_{BH} = 5.8. We thus have direct evidence that the curvature in the Brønsted plot in Fig. 6 does combine dual substituent effects from the two X-substituents with a change in rate-determining step. The slope of 2.55 in Fig. 7 primarily reflects the difference in the influence of substituent effects upon carbanion stabilization from a pyridinium ring directly upon the carbanionic centre, with one that is a further methylene group removed. The magnitude of this slope is similar to that (1/0.36 = 2.8) associated with the transmission of polar effects through a saturated carbon atom (19).

The elimination reactions of 2-phenylethyl bromides (**4**) in aqueous base have been shown to occur via the concerted E2 reaction mechanism (6), whereas we have concluded above that the corresponding eliminations from **1** and **3** occur via the two-step E1cb mechanism. Table 3 summarizes the relative reactivities of **1**, **3**, **4**, and some related species in hydroxide ion catalyzed eliminations, and the mechanistic assignments (using Bordwell's convention (17)) that have been made for these reactions. Both **1***a* and **3***a* are clearly much more reactive than either 2-phenylethyl bromide (**4**: X = H) or even its 4-nitro derivative (**4**: X = 4-NO$_2$). However, the latter species is 3-fold more reactive than **1***m*, which is the least reactive *N*-(2-bromoethyl) pyridinium cation in the current study. The E1cb reaction of **1***a* (X = H) occurs over 10^4-fold faster than the E2 reaction of **4**: X = H. This comparison is of particular interest since these latter two species are isoelectronic.

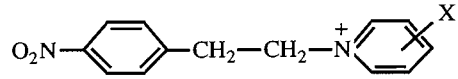

10

The reactants, **8** (X = H), **3***a*, and **10**, in Table 3, all have the same leaving group and have all been established as involving rate-determining deprotonation (i.e., (E1cb)$_{irrev}$), so that the relative reactivities of these species indicate the rel-

Can. J. Chem. Downloaded from www.nrcresearchpress.com by 92.62.229.171 on 09/08/12
For personal use only.

TABLE 3. Reactivity in hydroxide ion catalyzed elimination reactions[a]

$$Z—CH_2—CH_2—L \xrightarrow{k_{OH}[^-OH]} Z—CH=CH_2 + L^-$$

Reactant	Z	L	k_{OH} (M^{-1} s^{-1})	Mechanism	Ref.
1*a*	$C_5H_5\overset{+}{N}$	Br	0.32	$(E1cb)_{irrev}$	[b]
4(X = 4-NO_2)	4-$NO_2C_6H_4$	Br	2.82×10^{-3}	E2	6
1*m*	4-$(CH_3)_2NC_5H_4\overset{+}{N}$	Br	9.0×10^{-4}	$(E1cb)_{ion\ pair}$	[b]
4(X = H)	C_6H_5	Br	1.6×10^{-5}[c]	E2	6
8(X = H)	CN	$C_5H_5\overset{+}{N}$	29.6	$(E1cb)_{irrev}$	8
3*a*	$C_5H_5\overset{+}{N}$	$C_5H_5\overset{+}{N}$	0.115[d]	$(E1cb)_{irrev}$	[b]
10(X = H)	4-$NO_2C_6H_4$	$C_5H_5\overset{+}{N}$	5.13×10^{-4}	$(E1cb)_{irrev}$	9

[a]In aqueous solution, ionic strength 0.1, 25°C.
[b]Current work.
[c]Calculated from data in refs. 5 and 6, by assuming that the relative reactivities of **4**: X = H and **4**: X = 4-NO_2 are the same in aqueoous solution as they are in 40% dimethyl sulfoxide – 60% water.
[d]After correction by a statistical factor of 2.

ative influence of cyano, pyridinio, and 4-nitrophenyl substituents upon the kinetic acidities of adjacent methylene groups. If we tentatively assume that the 224-fold difference in the reactivities of **3***a* and **10** is also a reasonable estimate of the relative kinetic acidities of **1***a* and **4** (X = 4-NO_2), then a second-order rate constant, $k_{OH} = 1.4 \times 10^{-3}$ M^{-1} s^{-1}, is obtained for the deprotonation of this latter species. This value, which represents the upper limit to the second-order rate constant for an E1cb process for this molecule, is somewhat smaller than the experimentally observed k_{OH} for the hydroxide ion catalyzed elimination. This result is consistent with the mechanistic assignment of the hydroxide ion catalyzed elimination from 2-(4-nitrophenyl)ethyl bromide as an E2 process that does not involve an intermediate conjugate base species.

We previously demonstrated a change in rate-determining step within the E1cb reaction mechanism by variation of the substituents in the pyridine nucleofuge for two series of constant activating groups (cyano (**8**) (8) and 4-nitrophenyl (**10**) (9)). In the current work, we show a change in rate-determining step in an E1cb reaction for a constant leaving group (bromide ion) but with a systematic variation in reactivity via substitution in the pyridinio activating group (**1**). The *N*,*N*′-ethylene bispyridinium dications (**3**) combine these two effects via substitution in both the activating and leaving groups. Such double substitution results in an enormous range of reactivities in the elimination reactions from these dications.

Acknowledgement

We appreciate the support of this research by the Natural Sciences and Engineering Research Council of Canada.

1. A. R. Katritzky and O. Rubio. J. Org. Chem. **48**, 4017 (1983).
2. A. R. Katritzky and M. J. Mokrosz. Heterocycles, **22**, 505 (1984).
3. W. H. Saunders, Jr. Acc. Chem. Res. **9**, 19 (1976).
4. C. J. M. Stirling. Acc. Chem. Res. **12**, 198 (1979).
5. J. R. Gandler and W. P. Jencks. J. Am. Chem. Soc. **104**, 1937 (1982).
6. J. R. Keeffe and W. P. Jencks. J. Am. Chem. Soc. **105**, 265 (1983).
7. S. Alunni and W. P. Jencks. J. Am. Chem. Soc. **102**, 2052 (1980).
8. J. W. Bunting, A. Toth, C. K. M. Heo, and R. G. Moors. J. Am. Chem. Soc. **112**, 8878 (1990).
9. J. W. Bunting and J. P. Kanter. J. Am. Chem. Soc. **113**, 6950 (1991).
10. E. M. Kosower and J. W. Patton. Tetrahedron, **22**, 2081 (1966).
11. J. H. Blanch and K. Fretheim. J. Chem. Soc. (C), 1892 (1971).
12. F. M. Moracci, A. Casini, F. Liberatore, and V. Carelli. Tetrahedron Lett. 3723 (1976).
13. F. M. Moracci, S. Tortorella, B. Di Rienzo, and F. Liberatore. Tetrahedron, **35**, 2591 (1979).
14. J. H. Nelson, R. C. Garvey, and R. O. Ragsdale. J. Heterocycl. Chem. **4**, 591 (1967).
15. J. E. Douglass, M. W. Tabor, and J. E. Spradling III. J. Heterocycl. Chem. **9**, 53 (1972).
16. J. C. Fishbein and W. P. Jencks. J. Am. Chem. Soc. **110**, 5087 (1988).
17. F. G. Bordwell. Acc. Chem. Res. **5**, 374 (1972).
18. R. D. Guthrie. Pure Appl. Chem. **61**, 23 (1989).
19. R. W. Taft. *In* Steric effects in organic chemistry. *Edited by* M. S. Newman. John Wiley & Sons, Inc., New York. 1956. Chap. 13, pp. 607–610.

Can. J. Chem. Downloaded from www.nrcresearchpress.com by 92.62.229.171 on 09/08/12
For personal use only.

Annulations leading to diene systems. Total syntheses of the dolastane-type diterpenoids (±)-(5*S*,12*R*,14*S*)-dolasta-1(15),7,9-trien-14-ol and (±)-amijitrienol

EDWARD PIERS[1] AND RICHARD W. FRIESEN

Department of Chemistry, University of British Columbia, 2036 Main Mall, University Campus, Vancouver, B.C., Canada V6T 1Z1

Received October 15, 1991

EDWARD PIERS and RICHARD W. FRIESEN. Can. J. Chem. **70**, 1204 (1992).

Alkylation of the substituted cycloalkanones **14***a–d* and **30** with (*Z*)-1-bromo-4-methyl-3-trimethylstannyl-2-pentene (**13**) produced compounds **15***a–d* and **33**, which were readily converted into the corresponding enol trifluoromethanesulfonates (triflates) **16***a–d* and **34**. Intramolecular Pd(O)-catalyzed coupling of the vinylstannane and enol triflate functions in **16***a–d* and **34** provided the dienes **17***a–d* and **35**. The annulation product **35** served as a suitable starting material for the total syntheses of the dolastane diterpenoids (±)-(5*S*,12*R*,14*S*)-dolasta-1(15),7,9-trien-14-ol (**2**) and (±)-amijitrienol (**3**). The key steps of the synthesis of (±)-**2** involved the stereoselective methylation of the ketone **44** (readily derived from **35**) to provide **46** and the Barbier type ring closure of **47** to provide the target compound. For the synthesis of (±)-**3**, the notable conversions included the reductive transformation of the diene **35** into the alkene **53**, the aldol condensation of the ketone **54** with 4-trimethylstannyl-4-pentenal (**55**), the chemo- and stereoselective reduction of the dione **58**, and the one-pot conversion of the keto vinylstannane **63** into the triene **65**, via the intermediate **64**.

EDWARD PIERS et RICHARD W. FRIESEN. Can. J. Chem. **70**, 1204 (1992).

L'alkylation des cycloalcanones substituées **14***a–d* et **30** avec le (*Z*)-bromo-1-méthyl-4-triméthylstannyl-2-pentène (**13**) conduit aux composés **15***a–d* et **33** que l'on transforme facilement en les trifluorométhanesulfonates d'énol correspondants (triflates) **16***a–d* et **34**. Le couplage intramoléculaire, catalysé par le Pd(O), des fonctions stannane de vinyle et triflate d'énol des composés **16***a–d* et **34** donne les diènes **17***a–d* et **35**. Le produit d'annellation **35** sert parfaitement de produit de départ pour la synthèse totale des diterpènes dolastane (±)-(5*S*,12*R*,14*S*)-dolastatriène-1(15),7,9-ol-14 (**2**) et du (±)-amijitriénol (**3**). L'étape clé de la synthèse du composé (±)-**2** implique la méthylation stéréosélective de la cétone **44** (obtenue facilement à partir du composé **35**) qui conduit au composé **46** et la fermeture de cycle du type Barbier du composé **47** qui permet d'accéder au produit attendu. Dans le cas de la synthèse du composé (±)-**3** les transformations particulières comprennent la transformation réductrice du diène **35** en alcène **53**, la condensation aldolique de la cétone **54** sur le triméthylstannyl-4-pentenal-4 (**55**), la reduction chimique et stéréosélective de la dione **58** et la transformation *in situ* de la céto vinylstannane **63** en triène **65** par l'intermédiaire du composé **64**.

[Traduit par la rédaction]

Introduction

The dolastane family of diterpenoids share the structurally interesting carbon skeleton **1**.[2] Members of this class of natural products have been isolated from a variety of marine organisms (1–12). Collectively, they exhibit varying degrees of unsaturation and oxygen functionalization and their absolute configuration has been determined (8, 9). Furthermore, many of the dolastanes display useful and potentially important biological properties, including antimicrobial activity and cytotoxicity. A number of dolastanes contain, as part of their structures, conjugated diene units. For example, the structurally interesting trienol **2**,[3] which was isolated from an intertwined mixture of algae (*Dictyota linearis* (C. Ag.) and *D. divaricata* (lamour)) collected from the coral reefs of the Honduras Bay Islands, contains a heteroannular 1,3-butadiene moiety involving carbons 7–10. On the other hand, amijitrienol ((4*R*,5*S*,12*R*)-dolasta-1(15),8,13-trien-4-ol) (**3**), a dolastane derived from *D. linearis* collected in the

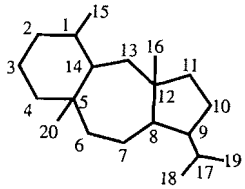

1

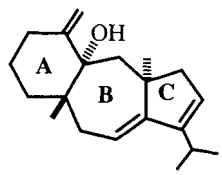

2

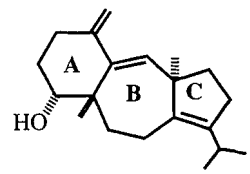

3

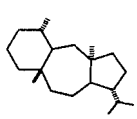

i

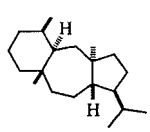

ii

[1]Author to whom correspondence may be addressed.

[2]In the two original reports (1, 2) regarding natural products possessing the carbon skeleton **1**, it was proposed that the names dolastane and clavularane be used to designate the carbon skeletons **i** and **ii**, respectively. Under these proposals, the dolastanes and clavularanes share a common skeletal framework and differ only in configuration at a number of stereogenic centers. In our opinion, this convention is unnecessarily complicated and confusing and its continuation should be discouraged. We propose that the name clavularane be dropped and that all diterpenoids that display the general skeleton **1**, devoid of configurational designations, be referred to as dolastanes.

[3]Substance **2** was originally named (14*S*)-14-hydroxydolasta-1(15),7,9-triene (7). However, on the basis of our proposal that the term dolastane should no longer include configurational implications (see footnote 2), we suggest that **2** should be designated (5*S*,12*R*,14*S*)-dolasta-1(15),7,9-trien-14-ol.

Can. J. Chem. Downloaded from www.nrcresearchpress.com by 92.62.229.171 on 09/08/12
For personal use only.

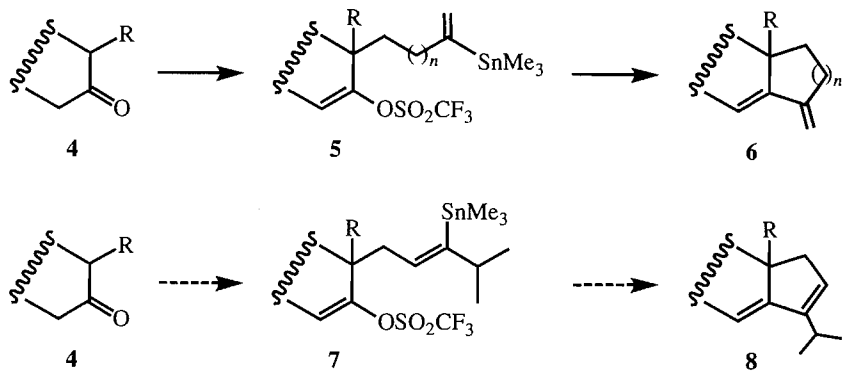

Can. J. Chem. Downloaded from www.nrcresearchpress.com by 92.62.229.171 on 09/08/12
For personal use only.

Bay of Tosa (11), embodies a conjugated diene system connecting carbons 13, 14, 1, and 15. The natural product **3** exhibits moderate antimicrobial activity against *Staphylococcus aureas* and *Mucor mucedo* (11).

Recent reports (13) from this laboratory have described a new annulation method represented in general terms by **4** → **5** → **6**. The key step of this sequence involved the intramolecular, palladium(O)-catalyzed coupling of the vinylstannane and enol trifluoromethanesulfonate (triflate) functions of the intermediate **5** to provide the annulation product **6**. If one compares the structure of **6** (n = 2) with that of amijitrienol (**3**), it is immediately evident that the AB ring portion of the natural product should be amenable to preparation via application of the new method. Furthermore, it was envisaged that an appropriate variant of the method, involving formation of products in which both double bonds of the diene unit are endocyclic (e.g., **4** → **7** → **8**) could serve effectively as a route for the synthesis of the BC ring segment of the dolastatrienol **2**. We report herein model studies that show that transformations represented in general terms by **4** → **7** → **8** are readily accomplished. Furthermore, we describe total syntheses of the dolastanes (±)-**2** and (±)-**3** via routes in which our new annulation methods play a key role.[4] It is important to note that other research groups have published work that culminated in the total syntheses of a number of dolastanes (16–18) or have described synthetic approaches to the preparation of members of this interesting family of diterpenoids (19–22).

Results and discussion

(a) Preparation of (Z)-1-bromo-4-methyl-3-trimethylstannyl-2-pentene (13) and its use in diene-producing annulation sequences

One of the bifunctional reagents required for this study, (*Z*)-1-bromo-4-methyl-3-trimethylstannyl-2-pentene (**13**), was prepared by use of (trimethylstannyl)cuprate chemistry developed earlier in our laboratory (see Scheme 1). Thus, treatment of methyl 4-methyl-2-pentynoate (**9**) with lithium (phenylthio)(trimethylstannyl)cuprate (**10**) (23) under appropriate reaction conditions (24) provided the *Z* enoate **11**. Reduction of this material with diisobutylaluminum hydride, followed by reaction of the resultant allylic alcohol **12** with triphenylphosphine dibromide in the presence of triethylamine, produced the required bromide **13** in 69% overall yield from **9**. Although it proved to be a viable reagent for our purposes (*vide infra*), compound **13** is quite unstable and could not be distilled without considerable decomposition. Even upon storage in the dark at −4°C, **13** slowly decomposed. Consequently, this substance was employed in subsequent reactions immediately after its preparation and was not distilled prior to use.

In spite of the "handling difficulties" associated with its instability and even though the CH_2Br function in **13** is *cis* to the sterically bulky Me_3Sn group, this substance served effectively as an alkylating agent. For example, reaction of the potassium enolate of 2-methoxycarbonylcyclopentanone (**14***a*) with the bromide **13** in refluxing tetrahydrofuran (THF) afforded the expected product **15***a* in 78% yield (Scheme 2). In similar fashion, the β-keto esters **14***b* and **14***c*

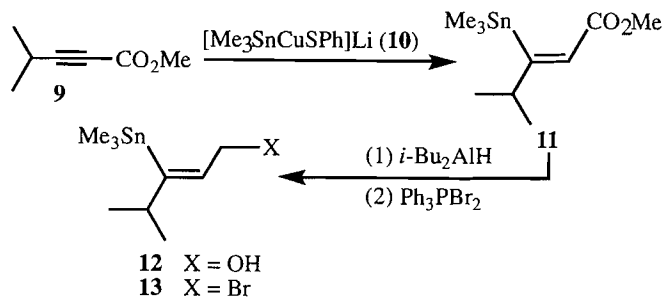

SCHEME 1

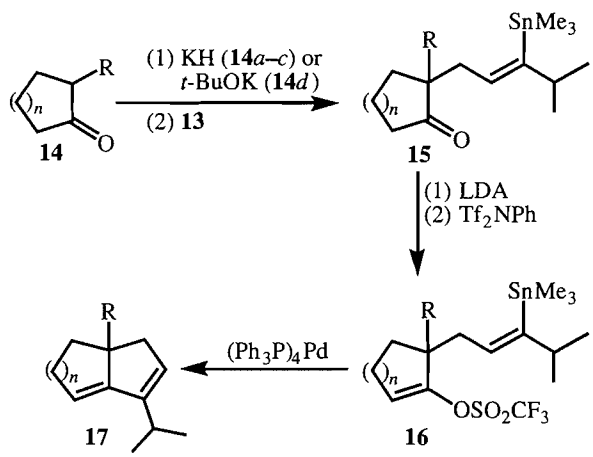

a n = 1, R = CO_2Me; *b* n = 2, R = CO_2Me
c n = 3, R = CO_2Me; *d* n = 3, R = Me

SCHEME 2

[4]For preliminary accounts, see refs. 14 and 15.

Can. J. Chem. Downloaded from www.nrcresearchpress.com by 92.62.229.171 on 09/08/12
For personal use only.

could be transformed cleanly and efficiently into the corresponding alkylation products **15***b* and **15***c*. Furthermore, alkylation of 2-methylcycloheptanone (**14***d*) (25) with **13** under conditions (*t*-BuOK, *t*-BuOH, THF) that would cause rapid enolate anion equilibration produced **15***d* as the major product, albeit in mediocre isolated yield (42%).

To determine whether or not **15***a–d* would serve as effective substrates for the synthesis of dienes of general structure **17** (Scheme 2), the former substances were allowed to react sequentially with lithium diisopropylamide (LDA) and *N*-phenyltrifluoromethanesulfonimide (Tf_2NPh) (26). The resultant enol trifluoromethanesulfonates (triflates) **16***a–d* were obtained in excellent yields (82–87%). Treatment of each of these intermediates with 0.05 equivalents of $(Ph_3P)_4Pd$ in THF or MeCN resulted in the smooth, efficient (>80%) formation of the dienes **17***a–d*.[5] Thus, this brief study showed clearly that the originally desired annulation sequence (**4** → **8**) is readily accomplished. The generality of the method was demonstrated to some degree by the formation of dienes possessing bicyclo[3.3.0]octane (**17***a*), bicyclo[4.3.0]nonane (**17***b*), and bicyclo[5.3.0]decane (**17***c*, *d*) carbon frameworks. It is highly likely that replacement of the isopropyl moiety in **13** by a different alkyl group or by a functionalized alkyl group would permit the extension of this chemistry to the facile preparation of a wide variety of bicyclic dienes represented in general terms by structural formula **18**. It should also be mentioned that the conversion of 2-methylcycloheptanone (**14***d*) into the diene **17***d* represented an excellent model for the preparation of the BC ring system present in the dolastatrienol **2**. The total synthesis of (±)-**2** via a route that utilizes this method is described in the next section of this paper.

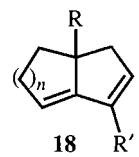

18 R′

An interesting observation was made in comparing the Pd(O)-catalyzed cyclizations of the vinylstannane-enol triflates **16***c* and **16***d*. These substrates, which differ only with respect to the nature of the substituent adjacent to the enol triflate moiety (CO_2Me vs. Me), undergo cyclization at significantly different rates. Thus, completion of the ring closure of **16***c* required ~30 min at 82°C (refluxing MeCN), while **16***d* was converted completely into **17***d* in 5 min at room temperature (THF solution).[6]

Presumably, the overall coupling processes involving **16***c* and **16***d* take place via a sequence of steps that, in broad terms, may be represented as shown in Scheme 3. In *inter*molecular reactions of this type, the rate-limiting step is proposed (27) to be the transmetalation reaction, corresponding to step B in Scheme 3. However, in *intra*molecular couplings, it is possible that the monomolecular transmetalation reaction (**19** → **20**, step B) is faster than the bimolecular oxidative addition (**16***c*, *d* → **19**, step A). In this case, the initial conversion in Scheme 3 would be rate limiting. It is likely that, in either case, the fact that **16***c* cyclizes at a rate significantly slower than **16***d* is due to the electron-withdrawing inductive effect of the CO_2Me function. Thus, if step A is rate determining, one would have to conclude that the adjacent CO_2Me group has a deleterious effect on the rate of oxidative addition of the Pd(O) catalyst to the C—O bond of the enol triflate moiety in **16***c*. On the other hand, if B is the slow step, one would postulate that intramolecular transmetalation of an "electron deficient" vinylpalladium(II) species (**19**, R = CO_2Me) is slower than the corresponding process involving an "electron rich" vinylpalladium(II) intermediate (**19**, R = Me).

(b) Total synthesis of (±)-(5S,12R,14S)-dolasta-1(15),7,9-trien-14-ol (2)

The starting material that was chosen for the total synthesis of the dolastatrienol (±)-**2** was the commercially available keto ketal **21** (see Scheme 4). Since the six-membered carbocyclic ring of this material was to become ring B of the target molecule **2**, it was necessary to convert **21** into the substituted cycloheptanone **30**. This overall transformation, requiring a methylation and a one-carbon ring expansion, was accomplished as summarized in Scheme 4.

Methylation of **21** was achieved by use of the method developed by Corey and Enders (29). Monoalkylation of the *N*,*N*-dimethylhydrazone **22** occurred cleanly and efficiently and, after cleavage of the hydrazone linkage in **23**, the keto ketal **24** was obtained in excellent yield. The required ring expansion of **24** was conveniently performed via the method reported by Saegusa *et al.* (30). Thus, cyclopropanation (31) of the enol silyl ether **25**, derived (32) from the ketone **24**, produced a mixture of the cyclopropanes **26** and **27**, in a ratio of approximately 2:1.[7] Treatment of this mixture with anhydrous ferric chloride in *N*,*N*-dimethylformamide containing one equivalent of pyridine (30) gave the rather unstable β-chloro ketone **28**. Dehydrochlorination (NaOAc in hot methanol) of this crude material produced, in 62% yield from the mixture of **26** and **27**, the enone ketal **29**. Hydrogenation (H_2, Pd–C) of **29** in hexane removed the unwanted carbon–carbon double bond and provided the required cycloheptanone **30**.

The stage was now set for subjection of the intermediate **30** to the diene-producing annulation sequence developed earlier (*vide supra*). To that end, the ketone **30** was alkylated with the allylic bromide **13** under reaction conditions (*t*-BuOK, *t*-BuOH, 1,2-dimethoxyethane (DME)) that would promote enolate anion equilibration (see Scheme 5). Analysis (tlc) of the crude product indicated the presence of a small amount of starting material, one major product, and two additional (minor) components. Column chromatogra-

[5]These Pd(O)-catalyzed cyclization reactions are intramolecular versions of the Stille coupling of vinylstannane and enol triflate functions. Stille and co-workers (27, 28) have studied in detail the intermolecular variants of this synthetically useful process.

[6]These reactions could be monitored conveniently by removal, work-up, and analysis (glc, tlc) of small aliquots of the reaction mixtures. In our studies, we have found that MeCN is generally a *better* solvent (faster reaction rates, higher product yields) than THF for cyclizations of this type. Therefore, the observations with respect to the rate of ring closures of **16***c* and **16***d* cannot be due to a solvent effect.

[7]Although no firm evidence was obtained for the configurations of **26** and **27**, it seems reasonable to propose that, for steric reasons, the major product should be **26**, resulting from preferential cyclopropanation of **25** from the side opposite the secondary methyl group. In any case, the fact that a mixture was obtained was of no consequence, since both **26** and **27** were subsequently converted into the same desired product **30**.

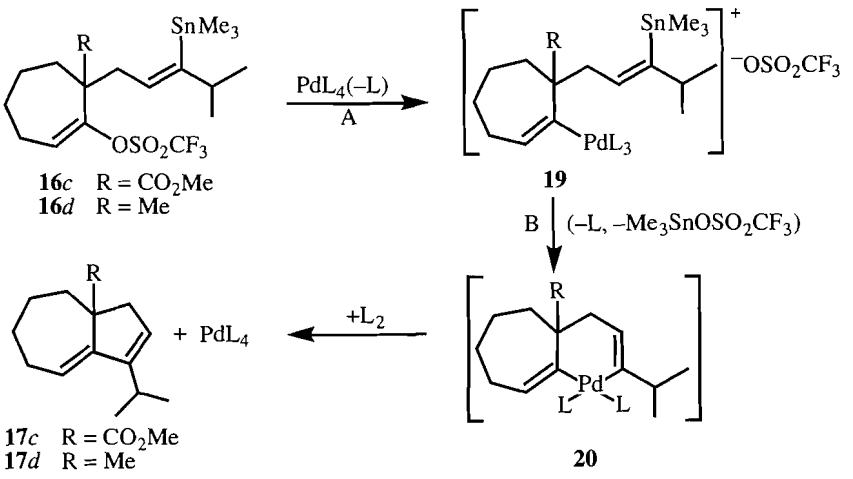

SCHEME 3

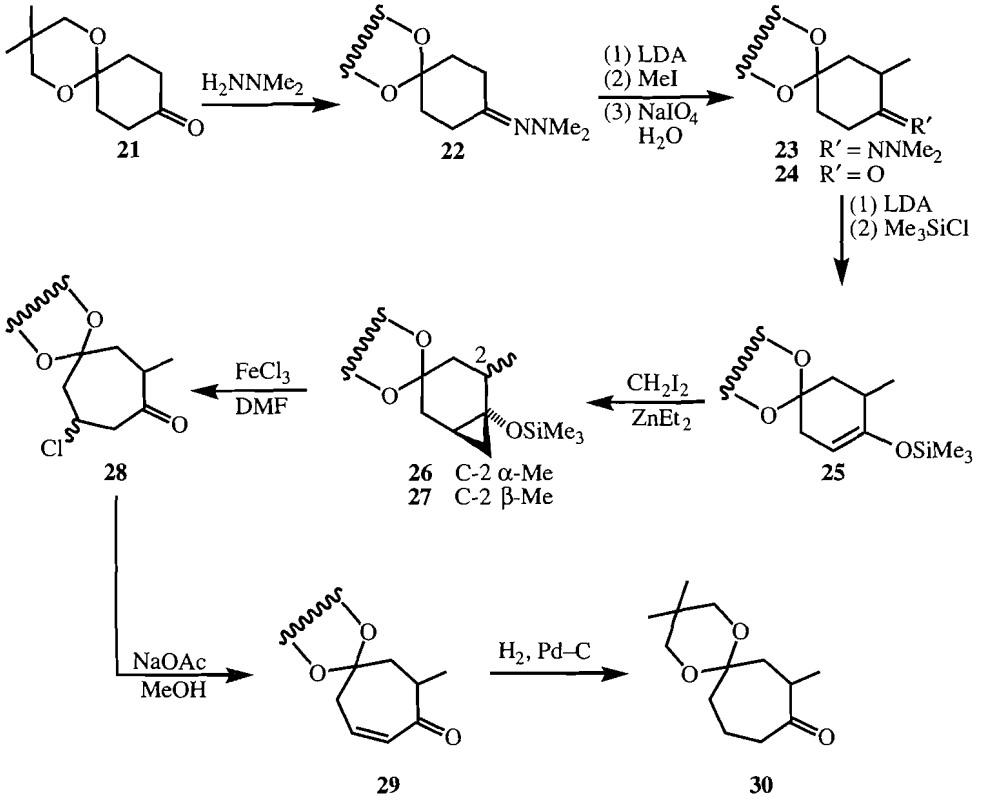

SCHEME 4

phy of this mixture on silica gel provided, in order of elution, the dialkylation product **31** (11%, a mixture of two diastereomers), the monoalkyl product **32** (2%, a single diastereomer of undetermined configuration), and the desired substance **33** (59%). The structural assignments were based on spectral data. Although the yield of **33** was not high, the procedure employed was straightforward and amenable to reasonably large scales. Furthermore, the overall process was faciliated by the fact that **33** was cleanly separated from the side products by chromatography.

Conversion of the ketone **33** into the corresponding enol triflate **34** was achieved in the normal manner (26) (Scheme 5). However, unlike the enol triflates **16***a–d* (*vide supra*), **34** was not isolated. Instead, a catalytic amount of $(Ph_3P)_4Pd$ was added directly to the reaction mixture derived from sequential treatment of **33** with LDA and Tf_2NPh in THF. Warming of the resultant solution to 30°C for 5 min, followed by work-up and product purification, provided the bicyclic ketal diene **35** in 81% yield.[8] Mild acid hydrolysis

[8]This one-pot procedure was significantly superior to that in which the enol triflate **34** was isolated and then cyclized in a separate operation. The two-pot process converted **33** into **35** in an overall yield of about 55%. The advantage of using a one-pot protocol for conversion of keto vinylstannanes into dienes has been noted previously (13).

Can. J. Chem. Downloaded from www.nrcresearchpress.com by 92.62.229.171 on 09/08/12
For personal use only.

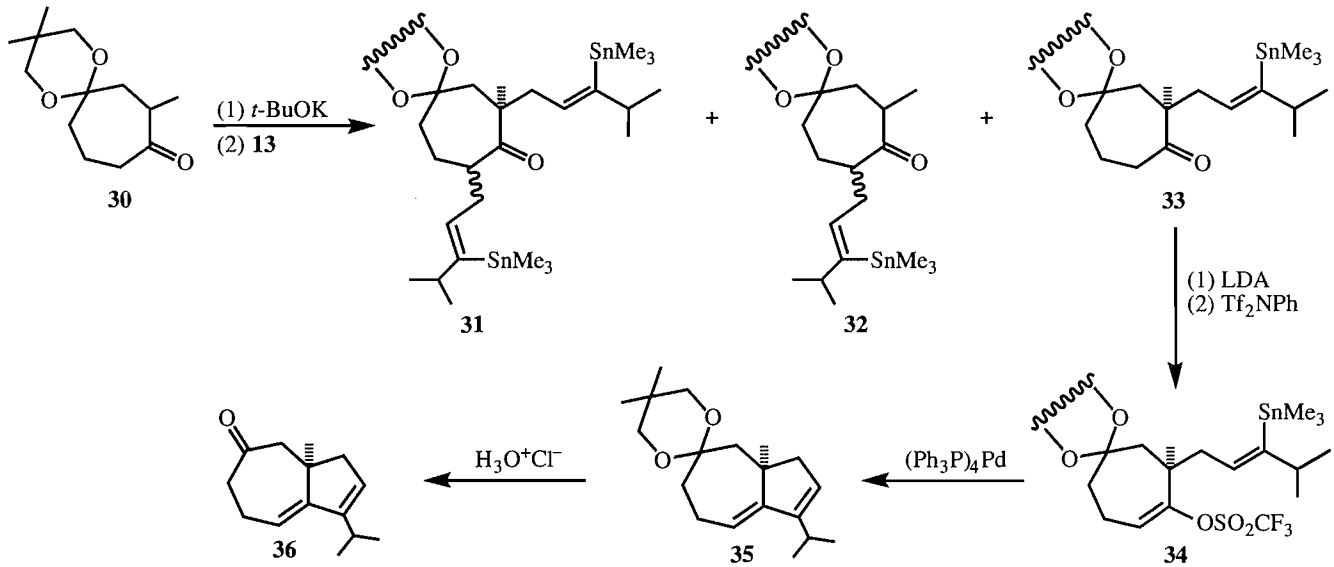

SCHEME 5

of **35** provided, in nearly quantitative yield, the keto diene **36**. Thus, the BC ring portion of the dolastatrienol (±)-**2** was in hand.

The final phase of the total synthesis of (±)-**2** required initially the stereocontrolled introduction of two substituents at C-4 of the ketone **36** (see Scheme 6). One of these appendages was a simple methyl group, while the other had to be a functionalized five-carbon unit that would permit a subsequent ring closure to give the allylic alcohol entity associated with ring A of the target compound.

With respect to stereochemistry, it was concluded that the order of introduction of the two substituents was crucial. It is obvious that, theoretically, alkylation of the enolate anion **37** (Scheme 7) with $R'CH_2I$ could provide one (or both) of the stereoisomeric products **40** or (and) **41**. However, if one assumes that, conformationally, the transition state(s) for alkylation has (have) product-like characteristics and that the reaction is subject to stereoelectronic control, then two possible transition states must be considered. These may be represented, in general terms, as shown in **38** and **39**. In transition state **38**, the stereoelectronic requirement is satisfied via a geometric arrangement in which the seven-membered ring is in a chair-like conformation. However, in transition state **39**, the stereoelectronically engendered axial attack of the alkylating agent requires that the (forming) cycloheptenone ring adopt a boat-like geometry. Clearly, one would reasonably conclude that, of these two possibilities, **38** should be energetically favored over **39**. Furthermore, molecular models show that, in **39**, there could well be some steric repulsion between the incoming alkylating agent and the angular methyl group. The fact that no comparable steric interaction destabilizes **38** provides additional weight to the proposal that the major product of alkylation of **37** should be **40**, formed via the lower energy transition state **38**.

If this reasoning has validity, the first alkylation at C-4 of **36** (see Scheme 6) would have to be done with a suitable five-carbon alkylating agent. A subsequent alkylation at C-4 with MeI would (presumably) provide a (major) product with the correct relative configuration at the newly introduced chiral center.

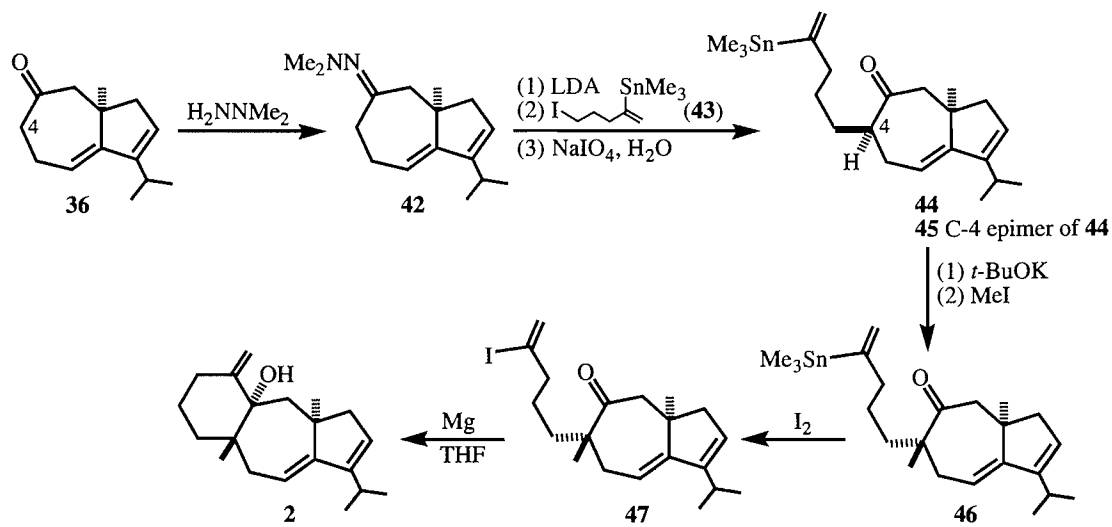

SCHEME 6

Can. J. Chem. Downloaded from www.nrcresearchpress.com by 92.62.229.171 on 09/08/12
For personal use only.

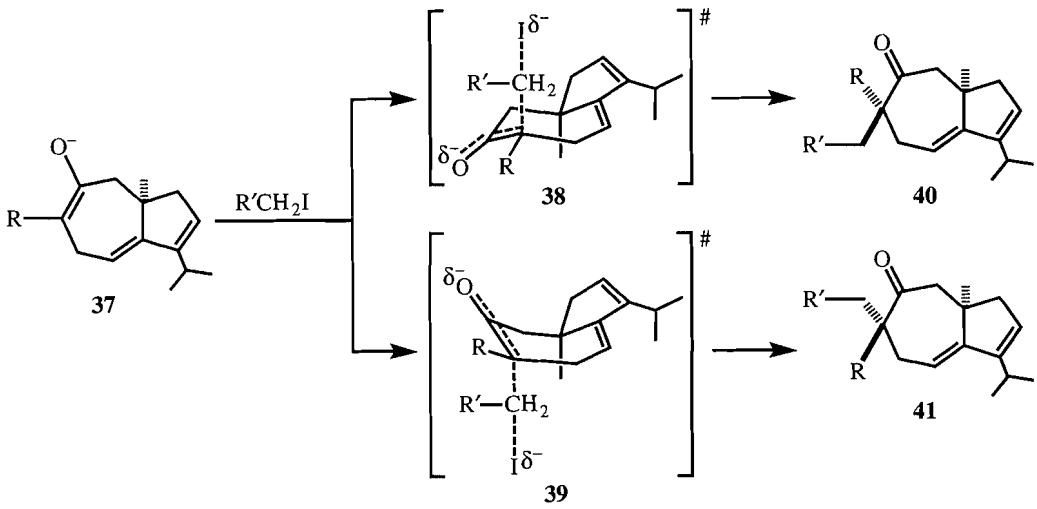

SCHEME 7

The bifunctional reagent 5-iodo-2-trimethylstannyl-1-pentene (**43**) (13) (Scheme 6) was chosen as the alkylating agent for incorporation of the necessary five-carbon side chain. Unfortunately, direct alkylation of **36** with **43**, employing a number of different bases (LDA, lithium 2,2,6,6-tetramethylpiperidide, *t*-BuOK) under a variety of experimental conditions, failed to produce the desired products **44** and (or) **45** cleanly. Although, in some of the reactions, **44** and **45** were formed as the major products, small amounts of other substances were also generated and these proved to be very difficult to separate from the desired material(s).

In view of these difficulties, the previously employed protocol of ketone alkylation via the corresponding dimethylhydrazone derivative (29) (see **21** → **24**, Scheme 4) was followed. Thus, conversion of **36** into **42**, followed by alkylation of the latter substance with **43** and subsequent hydrolysis of the hydrazone linkage, provided, in 68% overall yield, a single ketone. Anions of dimethylhydrazones of substituted cyclohexanones are known to show high preference for axial alkylation (29, 33, and references cited therein) and, therefore, on the basis of theoretical considerations similar to those presented earlier (*vide supra*, Scheme 7), the configuration of the alkylation product was assigned as shown in **44**. Unfortunately, the ^{1}H nmr spectrum of **44** failed to provide conclusive evidence to support this assignment.[9] However, during the next step of the synthesis, the chirality of C-4 in **44** would be destroyed (enolate anion formation) and, therefore, from a synthetic viewpoint, designation of the relative stereochemistry of this substance was not particularly important.

Methylation of the ketone **44** under conditions (*t*-BuOK, THF–HMPA) that would cause rapid enolate anion equilibration provided, in 63% yield, the keto triene **46**. The fact that alkylation had taken place at the desired site (C-4) was shown clearly by the ^{1}H nmr spectrum of the product **46**, which exhibited two three-proton singlets (δ 1.03, 1.11) due to the tertiary methyl groups. Since the spectral data derived from **46** did not provide unequivocal evidence for the stereochemistry of this substance, the assignment was based primarily on the previously discussed predictions regarding the (expected) preferred pathway for alkylation of the enolate anion **37** (Scheme 7).[10]

Reaction of the keto vinylstannane **46** with iodine in dichloromethane produced, cleanly and efficiently (84%), the keto vinyl iodide **47**.

On the basis of literature reports, it appeared that the required ring closure of **47** to the target compound (±)-**2** could be effected by use of a variety of synthetic methods. After a number of unsuccessful attempts, it was gratifying to find that the desired conversion could be achieved via a straightforward procedure that involved treatment of **47** with small pieces of freshly ground magnesium metal in refluxing THF. Chromatography of the crude product provided (±)-(5*S*,12*R*,14*S*)-dolasta-1(15),7,9-trien-14-ol (**2**) as the only tricyclic product (49% yield).[11] Recrystallization of this material from heptane gave material that exhibited mp 105–106°C and produced spectra in good agreement with those derived from the natural product.[12]

The stereochemical outcome of the transformation of **47** into **2** requires brief comment. Although the mechanistic details of this Barbier-type reaction are uncertain (34, 35), it is evident from an examination of molecular models that the conversion in question should occur in the desired stereochemical sense. Thus, the ring closure **47** to give **48**, the C-14 epimer of **2**, could take place via one (or both) of two transition states that may be represented, in somewhat simplistic terms, by **49** and **50**. In **49**, both the seven-membered ring and the forming six-membered ring are in chair-shaped conformations and the alkenyl moiety approaches the

[9]Treatment of **44** with NaOMe in MeOH provided a 1:1.4 mixture of the epimers **44** and **45**, from which a pure sample of **45** could be obtained by column chromatography. Again the ^{1}H nmr spectrum of **45** did not furnish unambiguous corroboration for the stereochemical assignment.

[10]It should be noted that, in their total synthesis of (±)-isoamijiol, Pattenden and co-workers carried out a comparable methylation on a substrate structurally similar to **44** (16).

[11]The crude product contained a small amount of a second component that, on the basis of its chromatographic and spectral properties, was considered to be the uncyclized keto triene (**47**, H in place of I). This material was not isolated or characterized further.

[12]We are grateful to Professor P. Crews for copies of the ^{1}H nmr, ^{13}C nmr, and mass spectra of natural **2**.

Can. J. Chem. Downloaded from www.nrcresearchpress.com by 92.62.229.171 on 09/08/12
For personal use only.

Can. J. Chem. Downloaded from www.nrcresearchpress.com by 92.62.229.171 on 09/08/12
For personal use only.

carbonyl group from an axial direction. However, this geometric arrangement is destabilized by steric interactions, the most notable of which is a severe repulsion between the angular methyl group (C-16, dolastane numbering) and the terminal methylene unit of the (approaching) vinyl group. This interaction is relieved in the alternative transition state **50**, in which the substituted alkenyl function approaches the carbonyl from an equatorial direction. However, this transition state is destabilized by a number of steric repulsions and by the torsional strain inherently present in the boat-like conformation of the cycloheptenone ring. On the other hand, the pathway leading from **47** to racemic **2** can proceed via a transition state (see **51**) that is devoid of serious steric interactions and in which both the seven-membered ring and the forming six-membered ring possess chairlike geometries.

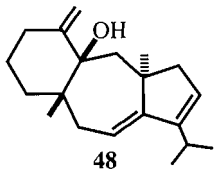

48

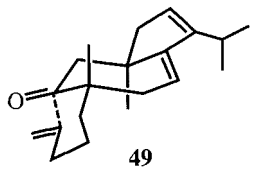

49

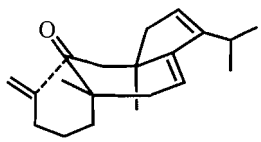

50

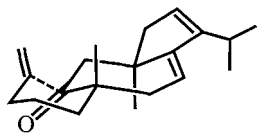

51

A few comments regarding the ^{1}H nmr spectrum of **2** are in order. The resonance at δ 2.60 (ddd, J = 6, 12.5, 12.5 Hz) was assigned by Crews *et al.* (7) to H_b. In a decoupling experiment, irradiation at δ 2.60 changed the broad doublet (J = 12.5 Hz) at 1.97 to a broad singlet, and therefore, the latter signal may be assigned to H_a. Crews *et al.* (7) had assigned the δ 1.97 resonance to one of the protons at C-13 (H_e or H_f). Actually, the signals due to H_e and H_f can be observed as a pair of doublets (J = 14.5 Hz) at δ 2.03 and 1.48. The doublet of doublets (J = 4.5, 15 Hz) at δ 3.22 had been ascribed by Crews *et al.* (7) to one of the C-6 protons (H_c or H_d). However, the other C-6 proton had not been assigned to a particular signal. Irradiation at δ 3.22 resulted in simplification of the doublet of doublets (J = 9.5, 15 Hz) at 1.51 and, consequently, the resonances at 1.51 and 3.22 may be assigned to protons H_c and H_d.

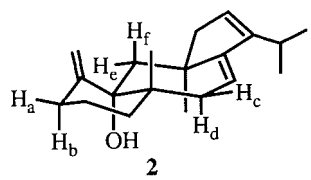

2

(c) Total synthesis of (±)-amijitrienol (3)

It was envisaged that the ketal diene **35** would serve as a suitable starting material for the synthesis of (±)-amijitrienol (**3**). The use of **35** in this context required, initially, the reductive conversion of this material into the ketal alkene **53** (see Scheme 8). To that end, **35** was treated with lithium in ammonia – diethyl ether. This reaction produced, in high yield, a mixture of two products in a ratio of ~4:1 (glc). Analysis of this mixture by glc – mass spectrometry and ^{1}H nmr spectroscopy showed that the two components were isomeric (M^+ = 292 for each substance) and that the major product was the desired alkene **53**. Furthermore, the ^{1}H nmr spectrum indicated that the minor product was the ketal alkene **52**.[13] Thus, the spectrum exhibited a single olefinic proton signal at δ 5.41, with a width at half-height of ~16 Hz. Had the minor product been the isomeric alkene **60**, one would probably have observed a signal in the alkene region of the spectrum with $w_{1/2} \approx$ 6 Hz. For example, in the ^{1}H nmr spectra of **35** and **36**, the signals due to the cyclopentene olefinic protons have $w_{1/2}$ = 6.5 Hz.

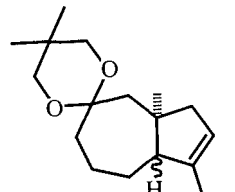

60

Unfortunately, compounds **52** and **53** proved to be very difficult to separate by chromatography on silica gel. However, it was gratifying to find that treatment of the mixture of these substances with a catalytic amount of iodine in refluxing hexane for 3 h caused quantitative isomerization of **52** into **53** (Scheme 8). Mild acid hydrolysis of the crude product[14] derived from this reaction provided the desired keto alkene **54** in 88% yield from the ketal diene **35**. Compound **54** had been prepared previously by Pattenden and co-workers (16), via a route very different from that described in this paper. The ^{1}H nmr spectra of the two synthetic samples were found to be identical.[15]

The final portion of the overall synthesis of (±)-amijitrienol (**3**) required two crucial operations, the stereoselective introduction of the secondary hydroxyl group at what would eventually become C-4 of **3**, and the construction, with concomitant ring closure, of the diene unit associated with carbons 13, 14, 1, and 15 of the target compound. The bifunctional reagent chosen for these purposes was 4-trimethylstannyl-4-pentenal (**55**). Clearly, condensation of this substance with the C-4 enolate anion of **54** (see Scheme 8) would place an oxygen function at the required position of the introduced side chain (see **56**). Furthermore, the vinylic trimethylstannyl function would, presumably, permit the subsequent desired ring closure via the method developed earlier in our laboratory (13) (see **4** → **6**).

The aldehyde **55** was produced conveniently by Swern oxidation (37) of the alcohol **61**, which, in turn, was prepared by reaction of 4-pentyn-1-ol with $Me_3SnCu \cdot SMe_2$ under conditions modified somewhat from those reported (38) earlier. The aldehyde **55** proved to be quite unstable and decomposed slowly even when stored under argon at low tem-

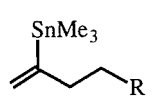

61 R = CH_2OH
55 R = CHO

[13]The stereochemical orientation of the isopropyl group in this substance was not determined.

[14]Distilled **53** exhibited spectra that agreed well with those reported (36) for this compound.

[15]We are very grateful to Professor Pattenden for a copy of the ^{1}H nmr spectrum of synthetic **54** prepared in his laboratory.

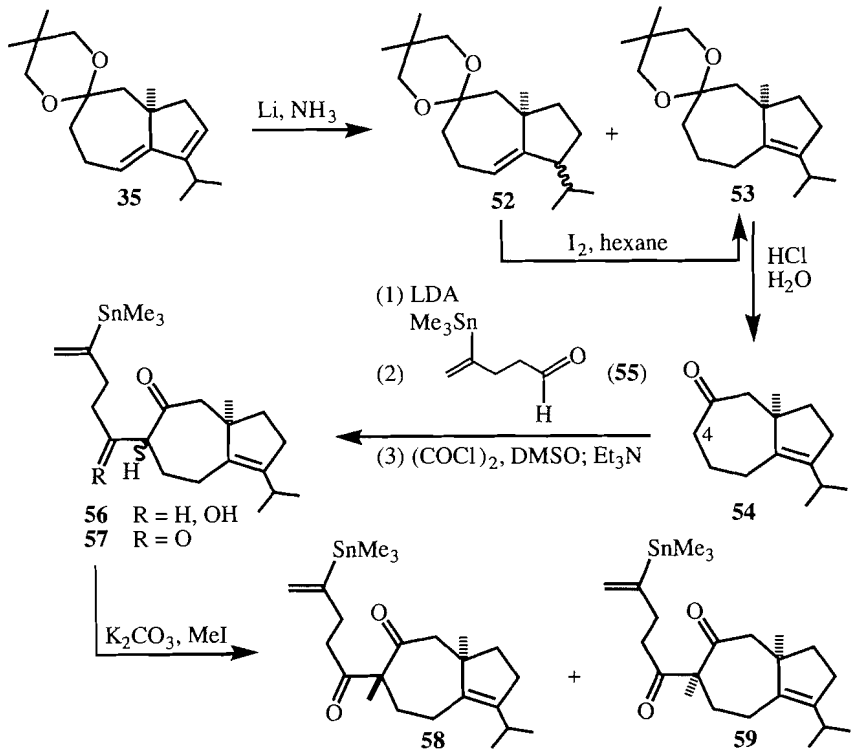

SCHEME 8

peratures (freezer). Consequently, it was generally used immediately after its preparation.

Deprotonation of **54** with LDA in THF at −78°C, followed by reaction of the resultant enolate anion with the aldehyde **55**, provided, in 62% yield, a mixture of three ketols of general structure **56**. Immediate subjection of this material to Swern oxidation (37) gave the diketone **57**, which, like the ketol mixture **56**, was quite unstable toward chromatography on silica gel. Therefore, **57** was directly methylated with K_2CO_3–MeI in acetone. This reaction gave a chromatographically separable mixture (~2:1 by ^1H nmr analysis) of the epimeric products **58** and **59**. The overall isolated yields of these two substances from the mixture of ketols **56** were 41 and 16%, respectively. Unambiguous spectroscopic evidence that would permit designation of the relative stereochemistry of **58** and **59** could not be obtained. Therefore, at this stage of the work, the configuration of the major alkylation product was assigned as shown in **58**. This assignment, which was made primarily on the basis of analogy with the stereochemical outcome of the methylation

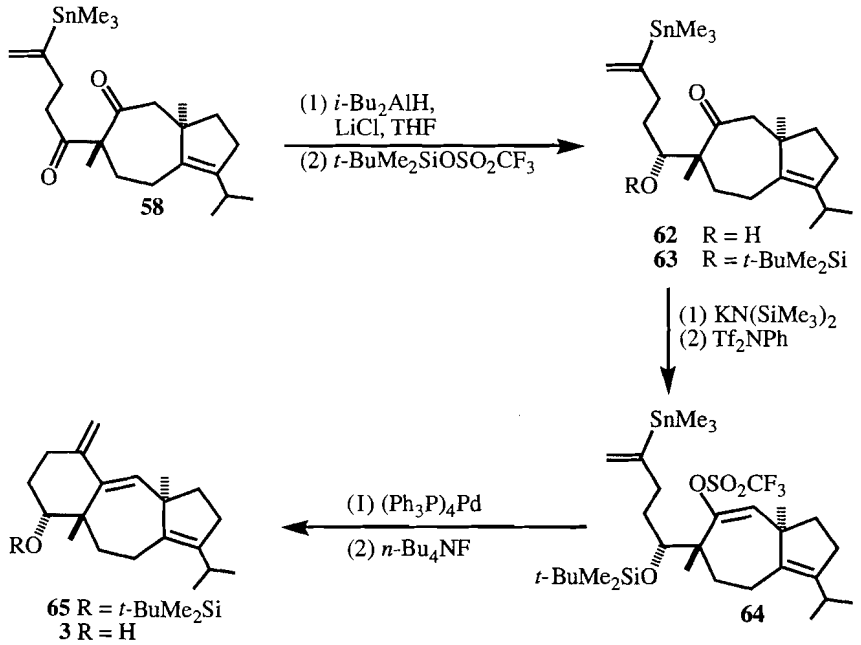

SCHEME 9

Can. J. Chem. Downloaded from www.nrcresearchpress.com by 92.62.229.171 on 09/08/12
For personal use only.

Can. J. Chem. Downloaded from www.nrcresearchpress.com by 92.62.229.171 on 09/08/12
For personal use only.

performed earlier (**44** → **46**, Scheme 6), was subsequently shown to be correct by acquisition of the target compound, (±)-**3**.

At this juncture of our synthesis, it was necessary to chemically differentiate between the two carbonyl groups of **58**. After a number of unsuccessful attempts to accomplish this objective, it was found that treatment of a THF solution of **58** with excess LiCl, followed by cooling of the mixture to −78°C and addition of excess *i*-Bu_2AlH, provided a *single* ketol **62** (see Scheme 9).[16] The latter material was immediately converted (*t*-$BuMe_2SiOTf$, 4-(*N*,*N*-dimethylamino)pyridine, Et_3N, CH_2Cl_2) into the corresponding silyl ether **63**, which was obtained in 79% yield from the diketone **58**.

Since compound **63** served as a precursor for the synthesis of (±)-**3** (*vide infra*) it was subsequently determined that the reduction of **58** with *i*-Bu_2AlH in the presence of LiCl had produced a product **62** with the correct relative configuration at the newly introduced chiral center. The chemo- and stereoselectivity of this interesting, synthetically pleasing reaction may be rationalized by proposing initially that coordination of the lithium cation with the 1,3-diketone system of **58** provides a "frozen" conformation as depicted in **66**. Approach of the reducing agent from the top face of either of the carbonyl groups in **66** would be hindered by adjacent, axially oriented methyl group. Furthermore, reduction of the ring carbonyl from the bottom face would involve steric repulsion between the approaching reagent and the axial, angular methyl group. Thus, the only mode of attack that is relatively free of steric repulsions is that involving delivery of hydride to the bottom face of the side-chain carbonyl function, as shown by the arrow in **66**. The result of such a chemo- and stereoselective pathway would be the production of the ketol **62**, the observed product.

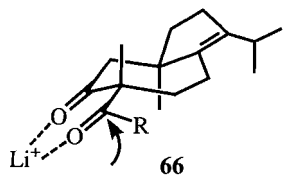

66

To complete the synthesis of (±)-amijitrienol (**3**), the keto vinylstannane **63** had to be subjected to the diene-producing annulation method developed earlier in our laboratory (13). This required, initially, the conversion of **63** into the corresponding enol triflate **64**. However, it was found that the lithium enolate of **63**, formed by treatment of **63** with LDA in THF, did not react with Tf_2NPh. Presumably, the failure of this (proposed) reaction was due primarily to the hindered nature of the enolate anion moiety. Fortunately, the use of the more reactive potassium enolate proved to be successful. Thus, sequential treatment of **63** with potassium hexamethyldisilazide and Tf_2NPh in THF provided the required enol triflate **64** (Scheme 9). Palladium(O)-catalyzed ring closure of this material in refluxing acetonitrile containing a small amount of triethylamine gave the tricyclic triene **65** in 74% yield from **63**. Cleavage of the silyl ether linkage with tetra-*n*-butylammonium fluoride provided, in 78% yield, crystalline (±)-amijitrienol (**3**), which exhibited mp 119–119.5°C (from hexane) and produced spectra identical with those of natural (+)-amijitrienol.[17]

One point regarding the cyclization reaction (**64** → **65**) deserves explicit mention. Triethylamine was added to the reaction mixture because it was found that the exocyclic double bond present in each of the substances **65** and **3** was quite prone to acid-catalyzed rearrangement. In fact, the $CDCl_3$ that was used to record the ^1H nmr spectra of **65** and **3** had to be shaken with solid Na_2CO_3–$MgSO_4$ and then filtered through basic alumina just prior to use. If "untreated" $CDCl_3$ was employed, the ^1H nmr spectra of (initially) pure samples of **65** and **3** showed that the major components present were the isomeric substances **67** and **68**, respectively. In these spectra, the H_a protons of **67** and **68** appear as multiplets at δ 5.26 and 5.37, while the vinyl methyl groups give rise to broad singlets at δ 1.80 and 1.84, respectively.

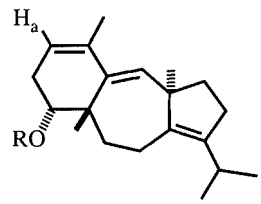

67 R = *t*-$BuMe_2Si$
68 R = H

Conclusion

The work reported in this paper includes (a) the development of a new annulation sequence that can be described in general terms by **4** → **7** → **8**, and (b) the application of this and a related, previously reported (13) annulation process to the total syntheses of the dolastane diterpenoids (±)-(5*S*,12*R*,14*S*)-dolasta-1(15),7,9-trien-14-ol (**2**) and (±)-amijitrienol (**3**). In this study, the bifunctional reagents **13**, **43**, and **55** served effectively as synthetic equivalents of the donor–acceptor synthons **69**–**71**, respectively. The fact that these reagents played such a central role in the work reported herein illustrates the value and versatility of organotin compounds in organic synthesis.

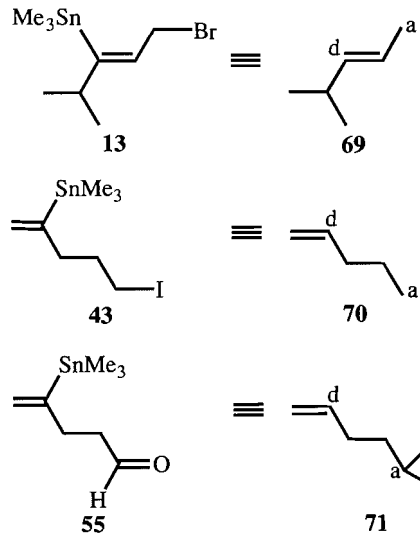

13 **69**
43 **70**
55 **71**

[16]Interestingly, reduction of **58** with *i*-Bu_2AlH (~1 equivalent) in various solvents (THF, Et_2O, PhMe) at −78°C in the *absence* of LiCl produced complex mixtures that contained **58**, ketols, and diols.

[17]We are indebted to Professor M. Ochi for copies of the ^1H nmr, ^{13}C nmr, and mass spectra of (+)-**3**.

Can. J. Chem. Downloaded from www.nrcresearchpress.com by 92.62.229.171 on 09/08/12
For personal use only.

Experimental

General information

Distillation temperatures, which refer to bulb-to-bulb (Kugelrohr) distillations, and melting points are uncorrected. Proton (^{1}H) and carbon (^{13}C) nuclear magnetic resonance (nmr) spectra were, unless otherwise noted, recorded on $CDCl_3$ solutions. Carbon chemical shifts are given relative to that of $CDCl_3$ (δ 77.0). Proton signal positions for compounds containing the Me_3Sn group are given relative to the signal for $CHCl_3$ (δ 7.25). Tin–proton coupling constants (J_{Sn-H}) are given as the average of the ^{117}Sn and ^{119}Sn values. For substances that contain the Me_3Sn function, high-resolution molecular mass determinations were determined on the (M^+ − Me) fragment (39) and are based on ^{120}Sn. Gas–liquid chromatography (glc) was performed using instruments equipped with 25 m × 0.21 mm fused silica columns coated with cross-linked SE-54. Thin-layer chromatography (tlc) was carried out with commercial aluminum-backed silica gel plates (E. Merck, Type 5554). Conventional (drip) column chromatography as well as medium pressure and flash chromatography (40) were performed with 230–400 mesh silica gel (E. Merck). Reagents and solvents were purified and dried using standard methods. Aqueous NH_4Cl–NH_4OH (pH 8) refers to a solution prepared by adding ~50 mL of aqueous ammonium hydroxide (58%) to ~1 L of saturated aqueous ammonium chloride.

NOTE: Unless otherwise noted, all reactions were carried out under an atmosphere of argon in flame- or oven-dried glassware.

NOTE: All compounds for which high resolution mass measurements are given exhibited, unless otherwise noted, clean ^{1}H nmr spectra and one spot on tlc analyses. Furthermore, the purity of these substances was judged to be ≥95% by glc analyses.

Methyl 4-methyl-2-pentynoate (9)

To a cold (−78°C), stirred solution of 3-methyl-1-butyne (3.4 g, 50 mmol) in 100 mL of dry THF was added a solution of MeLi in Et_2O (34 mL, 55 mmol). The solution was stirred at −78°C for 10 min and then at −20°C for 1 h. Methyl chloroformate (4.64 mL, 60 mmol) was added and the mixture was stirred at −20°C for 30 min and at room temperature for 30 min. Saturated aqueous $NaHCO_3$ (50 mL) and Et_2O (50 mL) were added. The organic phase was separated and the aqueous phase was extracted with 1:1 Et_2O–hexane. The combined organic extracts were washed with brine, dried ($MgSO_4$), and concentrated. Distillation (60–70°C/0.15 Torr (1 Torr = 133.3 Pa)) of the crude product gave 5.92 g (94%) of the ester **9**, a colorless oil that displayed ir (neat): 2220, 1715, 1390, 1370, 1260 cm^{-1}; ^{1}H nmr (80 MHz) δ: 1.18 (d, 6H, J = 7 Hz), 2.63 (septet, 1H, J = 7 Hz), 3.70 (s, 3H). Exact Mass calcd. for $C_7H_{10}O_2$: 126.0681; found: 126.0686.

Methyl (Z)-4-methyl-3-trimethylstannyl-2-pentenoate (11)

To a cold (−78°C), stirred solution of lithium (phenylthio)(trimethylstannyl)cuprate (**10**) (23) (45.4 mmol) in dry THF (400 mL) was added a solution of the acetylenic ester **9** (4.4 g, 34.9 mmol) in 50 mL of dry THF. The mixture was stirred at −78°C for 15 min and then at −48°C for 4 h. Methanol (50 mL) and petroleum ether (200 mL) were added and the vigorously stirred mixture was allowed to warm to room temperature. The yellow slurry was filtered through a plug of Celite and the collected material was washed thoroughly with petroleum ether (200 mL). The combined filtrate was concentrated and the residue was subjected to flash chromatography (240 g silica gel, 100:1 petroleum ether – Et_2O). Distillation (110–115°C/15 Torr) of the oil thus obtained afforded 8.43 g (83%) of the (*Z*)-2-pentenoate **11**, a colorless oil that exhibited ir (neat): 1700, 1599, 1210, 780 cm^{-1}; ^{1}H nmr (80 MHz) δ: 0.14 (s, 9H, $^2J_{Sn-H}$ = 54 Hz), 1.02 (d, 6H, J = 7 Hz), 2.71 (br septet, 1H, J = 7 Hz), 3.70 (s, 3H), 6.35 (d, 1H, J = 1 Hz, $^3J_{Sn-H}$ = 126 Hz). Exact Mass calcd. for $C_9H_{17}O_2Sn$ (M^+ − Me): 277.0250; found: 277.0252.

(Z)-4-Methyl-3-trimethylstannyl-2-penten-1-ol (12)

To a cold (−78°C), stirred solution of the α,β-unsaturated ester **11** (6.3 g, 21.7 mmol) in dry Et_2O (120 mL) was added slowly a solution of diisobutylaluminum hydride (54 mmol) in hexane. The mixture was stirred at −78°C for 1 h and then at 0°C for 2 h. Saturated aqueous NH_4Cl (20 mL) was added and the mixture was allowed to warm to room temperature. Anhydrous $MgSO_4$ was added to the slurry and the mixture was filtered through a plug of Celite. The collected material was washed thoroughly with Et_2O (150 mL). The combined filtrate was washed with brine, dried ($MgSO_4$), and concentrated. Distillation (110–115°C/15 Torr) of the residual material yielded 5.5 g (97%) of the allylic alcohol **12**, a colorless oil that showed ir (neat): 3300, 1380, 1360, 1025, 770 cm^{-1}; ^{1}H nmr (80 MHz) δ: 0.19 (s, 9H, $^2J_{Sn-H}$ = 52 Hz), 1.01 (d, 6H, J = 7 Hz), 1.30 (m, 1H, exchanges with D_2O), 2.46 (br septet, 1H, J = 7 Hz), 4.08 (br t, 2H, J = 6.5 Hz, $^4J_{Sn-H}$ = 110 Hz), 6.18 (dt, 1H, J = 1, 6.5 Hz, $^3J_{Sn-H}$ = 144 Hz). Exact Mass calcd. for $C_8H_{17}OSn$ (M^+ − Me): 249.0301; found: 249.0294.

(Z)-1-Bromo-4-methyl-3-trimethylstannyl-2-pentene (13)

To a cold (0°C), stirred solution of Ph_3P (7.07 g, 27.0 mmol) in dry CH_2Cl_2 (120 mL) was added, dropwise, Br_2 (1.38 mL, ~27 mmol) until the colorless solution became pale yellow. One crystal of solid Ph_3P was added, followed by Et_3N (3.76 mL, 27.0 mmol). The resulting white, cloudy mixture was cooled to −10°C and then a solution of the allylic alcohol **12** (5.90 g, 22.5 mmol) in 15 mL of dry CH_2Cl_2 was added dropwise. The mixture was stirred for 15 min and most of the solvent was removed under reduced pressure. The remaining slurry was diluted with petroleum ether (100 mL) and the mixture was filtered through a plug of Celite. The collected material was washed with petroleum ether (20 mL). The colorless solution was concentrated under reduced pressure and the petroleum ether washing–filtration procedure was repeated twice. The allylic bromide **13** (6.3 g, 86%) obtained after concentration of the final filtrate proved to be quite unstable, even when stored at −4°C in the dark, and, therefore, this material was used immediately in subsequent reactions. The bromide **13** was judged to be >90% pure (glc, ^{1}H nmr) and exhibited ir (neat): 1200, 775 cm^{-1}; ^{1}H nmr (80 MHz) δ: 0.25 (s, 9H, $^2J_{Sn-H}$ = 53 Hz), 1.01 (d, 6H, J = 7 Hz), 2.50 (septet, 1H, J = 7 Hz), 3.95 (d, 2H, J = 8 Hz), 6.23 (t, 1H, J = 8 Hz). Exact Mass calcd. for $C_8H_{16}{}^{79}BrSn$ (M^+ − Me): 310.9457; found: 310.9442.

2-Methoxycarbonyl-2-((Z)-4-methyl-3-trimethylstannyl-2-pentenyl)cyclopentanone (15a)

To a well-stirred suspension of KH (39 mg, 0.97 mmol) in dry THF (3 mL) at room temperature was added, dropwise, a solution of 2-methoxycarbonylcyclopentanone (**14***a*) (125 mg, 0.88 mmol) in 0.75 mL of dry THF. After the mixture had been stirred for 45 min, a solution of the allylic bromide **13** (316 mg, 0.97 mmol) in 1 mL of dry THF was added and the solution was heated under reflux for 1 h. The solution was cooled and most of the solvent was removed under reduced pressure. Column chromatography (27 g silica gel, 25:1 petroleum ether – ethyl acetate) of the residual oil–salt mixture, followed by distillation (145–149°C/0.6 Torr) of the oil thus obtained, provided 258 mg (78%) of the β-keto ester **15***a*, a colorless oil that displayed ir (neat): 1740, 1720, 1225, 773 cm^{-1}; ^{1}H nmr (400 MHz) δ: 0.19 (s, 9H, $^2J_{Sn-H}$ = 53 Hz), 0.97 (two d separated by 9 Hz, 3H each, J = 7 Hz in each case), 1.85–2.05 (m, 3H), 2.20 (m, 1H), 2.36–2.50 (m, 4H), 2.63 (dd, 1H, J = 8, 14.5 Hz), 3.69 (s, 3H), 5.75 (dt, 1H, J = 1, 8 Hz, $^3J_{Sn-H}$ = 144 Hz). In a decoupling experiment, irradiation at δ 5.75 simplified the signal at 2.63 to a d (J = 14.5 Hz) and sharpened the multiplet at 2.36–2.50. Exact Mass calcd. for $C_{15}H_{25}O_3Sn$ (M^+ − Me): 373.0825; found: 373.0821.

2-Methoxycarbonyl-2-((Z)-4-methyl-3-trimethylstannyl-2-pentenyl)cyclohexanone (15b)

Alkylation of 2-methoxycarbonylcyclohexanone (**14***b*) (140 mg, 0.90 mmol) with the allylic bromide **13** (321 mg, 0.99 mmol) was carried out via a procedure similar to that outlined above, except that the reaction was carried out at room temperature for 2 h. Column chromatography (30 g silica gel, 25:1 petroleum ether – ethyl acetate) of the crude product mixture and distillation (158–161°C/

Can. J. Chem. Downloaded from www.nrcresearchpress.com by 92.62.229.171 on 09/08/12
For personal use only.

0.6 Torr) of the resultant liquid produced 302 mg (85%) of the β-keto ester **15***b*, a colorless oil that showed ir (neat): 1710, 1203, 772 cm^{-1}; ^1H nmr (400 MHz) δ: 0.19 (s, 9H, $^2J_{Sn-H}$ = 53 Hz), 0.96 (d, 6H, *J* = 7 Hz), 1.33 (ddd, 1H, *J* = 4.5, 13, 14 Hz), 1.55–1.78 (m, 3H), 2.00 (m, 1H), 2.30 (dd, 1H, *J* = 7, 14 Hz), 2.35–2.53 (m, 4H), 2.63 (dd, 1H, *J* = 7, 14 Hz), 3.67 (s, 3H), 5.86 (dt, 1H, *J* = 1, 7 Hz, $^3J_{Sn-H}$ = 145 Hz); decoupling experiment: irradiation at δ 5.86 changed the signals at 2.30 and 2.63 to doublets (*J* = 14 Hz in each case). Exact Mass calcd. for $C_{16}H_{27}O_3Sn$ (M^+ − Me): 387.0982; found: 387.0983.

*2-Methoxycarbonyl-2-((Z)-4-methyl-3-trimethylstannyl-2-pentenyl)cycloheptanone (**15**c)*

Using a procedure similar to that outlined above, 190 mg (1.12 mmol) of 2-methoxycarbonylcycloheptanone (**14***c*) was alkylated with 400 mg (1.23 mmol) of the allylic bromide **13**. The reaction was carried out at room temperature for 1 h. Column chromatography (60 g silica gel, 25:1 petroleum ether – ethyl acetate) of the crude product, followed by distillation (160–163°C/0.6 Torr) of the liquid thus obtained, yielded 367 mg (80%) of the β-keto ester **15***c*, a colorless oil that displayed ir (neat): 1700, 1205, 770 cm^{-1}; ^1H nmr (400 MHz) δ: 0.19 (s, 9H, $^2J_{Sn-H}$ = 53 Hz), 0.96 (d, 6H, *J* = 7 Hz), 1.41 (m, 1H), 1.50–1.80 (m, 6H), 2.10 (dd, 1H, *J* = 9.5, 14 Hz), 2.33 (dd, 1H, *J* = 7, 14 Hz), 2.39–2.49 (m, 2H), 2.61 (m, 1H), 2.74 (dd, 1H, *J* = 7, 14 Hz), 3.68 (s, 3H), 5.81 (dt, 1H, *J* = 1, 7 Hz, $^3J_{Sn-H}$ = 145 Hz). In a decoupling experiment, irradiation at δ 5.81 simplified the signals at 2.33 and 2.74 to doublets (*J* = 14 Hz in each case). Exact Mass calcd. for $C_{17}H_{29}O_3Sn$ (M^+ − Me): 401.1139; found: 401.1139.

*2-Methyl-2-((Z)-4-methyl-3-trimethylstannyl-2-pentenyl)cycloheptanone (**15**d)*

To a well-stirred solution of *t*-BuOK (140 mg, 1.25 mmol) in a mixture of dry THF (4 mL) and dry *t*-BuOH (1 mL) at room temperature was added a solution of 2-methylcycloheptanone (**14***d*) (25) (166 mg, 1.32 mmol) in dry THF (2 mL). The mixture was stirred for 0.5 h and then a solution of the allylic bromide **13** (430 mg, 1.32 mmol) in dry THF (2 mL) was added. After the solution had been stirred at room temperature for 2 h, the mixture was concentrated under reduced pressure. Water (50 ml) was added to the residual material and the mixture was extracted with Et_2O (3 × 25 mL). The combined extracts were dried ($MgSO_4$) and concentrated. Column chromatography (120 g silica gel, 40:1 petroleum ether – Et_2O) of the remaining material, followed by distillation (116–119°C/0.1 Torr) of the acquired liquid, provided 205 mg (42%) of the ketone **15***d*, a colorless oil that displayed ir (neat): 1700, 760 cm^{-1}; ^1H nmr (400 MHz) δ: 0.20 (s, 9H, $^2J_{Sn-H}$ = 53 Hz), 0.99 (d, 6H, *J* = 7 Hz), 1.04 (s, 3H), 1.28–1.80 (m, 8H), 2.18 (dd, 1H, *J* = 7, 14 Hz), 2.22 (dd, 1H, *J* = 7, 14 Hz), 2.37–2.49 (m, 2H), 2.62 (dt, 1H, *J* = 2.5, 11.5 Hz), 5.89 (dt, 1H, *J* = 1, 7 Hz, $^3J_{Sn-H}$ = 147 Hz). In a decoupling experiment, irradiation at δ 5.89 simplified the signals at 2.18 and 2.22 to doublets (*J* = 14 Hz in each case). Exact Mass calcd. for $C_{16}H_{29}OSn$ (M^+ − Me): 357.1241; found: 357.1267.

*8-Isopropyl-5-methoxycarbonylbicyclo[3.3.0]octa-1,7-diene (**17**a)*

To a cold (−48°C), well-stirred solution of lithium diisopropylamide (LDA) (0.43 mmol) in dry THF (2.8 mL) was added, dropwise, a solution of the β-keto ester **15***a* (110 mg, 0.284 mmol) in 1.0 mL of dry THF. The solution was stirred at −48°C for 1 h. Finely ground, solid *N*-phenyltrifluoromethanesulfonimide (Tf_2NPh) (0.45 mmol) was added and the yellow solution was warmed to room temperature over a period of 30 min. Most of the solvent was removed under reduced pressure. Flash chromatography (18 g silica gel, 20:1 petroleum ether – ethyl acetate) of the residual material provided, upon concentration of the appropriate fractions and removal of last traces of solvent (vacuum pump), 117 mg (87%) of the enol triflate **16***a*, a colorless oil that showed ir (neat): 1732, 1422, 1207, 1142, 770 cm^{-1}; ^1H nmr (80 MHz) δ: 0.18 (s, 9H, $^2J_{Sn-H}$ = 52 Hz), 0.94 (d, 6H, *J* = 7 Hz), 1.75–2.75 (m, 7H), 3.71 (s, 3H), 5.65–5.85 (m, 2H). Exact Mass calcd. for $C_{16}H_{24}F_3O_5SSn$ (M^+ − Me): 505.0318; found: 505.0318.

To a stirred solution of the enol triflate **16***a* (90 mg, 0.174 mmol) in dry CH_3CN (8 mL) was added solid $(Ph_3P)_4Pd$ (0.009 mmol). The mixture was refluxed for 45 min, was cooled to room temperature, and then was concentrated under reduced pressure. Flash chromatography (15 g silica gel, 20:1 petroleum ether – ethyl acetate) of the remaining material, followed by distillation (52–55°C/0.1 Torr) of the acquired liquid, produced 30 mg (84%) of the diene **17***a*, a colorless oil that displayed ir (neat): 1735, 1390, 1370, 805 cm^{-1}; ^1H nmr (400 MHz) δ: 1.10 (d, 3H, *J* = 7 Hz), 1.14 (d, 3H, *J* = 7 Hz), 1.85 (ddd, 1H, *J* = 8.0, 10, 12.5 Hz), 2.19 (br d, 1H, *J* = 16 Hz), 2.39 (dd, 1H, *J* = 6, 12.5 Hz), 2.54 (m, 1H), 2.60 (ddd, 1H, *J* = 3.5, 8.0, 16 Hz), 2.83 (ddd, 1H, *J* = 1.0, 2.5, 16 Hz), 2.93 (m, 1H), 3.63 (s, 3H), 5.50 (br s, 1H, $w_{1/2}$ = 7 Hz), 5.76 (br s, 1H, $w_{1/2}$ = 6 Hz). The following decoupling experiments were carried out: irradiation at δ 1.85 simplified the signals at 2.39 and 2.60 to a d (*J* = 6 Hz) and a dd (*J* = 3.5, 16 Hz), respectively, and sharpened the m at 2.93; irradiation at δ 2.19 changed the m at 2.54 to a br septet (*J* = 7 Hz) and the ddd at 2.83 to a dd (*J* = 1.0, 2.5 Hz); irradiation at δ 2.39 simplified the signals at 1.85 and 2.93 to a dd (*J* = 8.0, 10 Hz), and a br dd (*J* = 10, 16 Hz); irradiation at δ 2.83 sharpened the resonances at 2.19 (to a br s) and 5.76; irradiation at δ 2.93 simplified the signals at 1.85, 2.39, 2.60, and 5.50 to a dd (*J* = 8.0, 12.5 Hz), a d (*J* = 12.5 Hz), a dd (*J* = 3.5, 8.0 Hz) and a br d (*J* = 3.5 Hz); irradiation at δ 5.50 changed the signals at 2.60 and 2.93 to a dd (*J* = 8.0, 16 Hz) and a br ddd (*J* = 6, 10, 16 Hz); irradiation at δ 5.76 sharpened the signal at 2.19 and changed the resonance at 2.83 to a br d (*J* = 16 Hz). Exact Mass calcd. for $C_{13}H_{18}O_2$: 206.1307; found: 206.1306.

*9-Isopropyl-6-methoxycarbonylbicyclo[4.3.0]nona-1,8-diene (**17**b)*

The β-keto ester **15***b* was transformed into the diene **17***b* via procedures similar to those outlined above. From 263 mg (0.656 mmol) of **15***b* there was obtained, after flash chromatography (40 g silica gel, 25:1 petroleum ether – ethyl acetate) of the crude product, 294 mg (84%) of the enol triflate **16***b*, a colorless oil that showed ir (neat): 1732, 1416, 1215, 1145, 733 cm^{-1}; ^1H nmr (80 MHz) δ: 0.20 (s, 9H, $^2J_{Sn-H}$ = 52 Hz), 0.95 (d, 6H, *J* = 7 Hz), 1.45–1.80 (m, 3H), 2.00–2.65 (m, 6H), 3.73 (s, 3H), 5.75–5.95 (m, 2H). Exact Mass calcd. for $C_{17}H_{26}F_3O_5SSn$ (M^+ − Me): 519.0475; found: 519.0475.

The reaction time for the Pd-catalyzed ring closure of the vinylstannane-enol triflate **16***b* was 3 h. Flash chromatography (30 g silica gel, 25:1 petroleum ether – ethyl acetate) of the crude product derived from 269 mg (0.504 mmol) of **16***b*, followed by distillation (69–73°C/0.6 Torr) of the resultant oil, provided 92 mg (83%) of the diene **17***b*, a colorless oil that exhibited ir (neat): 1722, 1385, 810 cm^{-1}; ^1H nmr (400 MHz) δ: 1.09 (d, 3H, *J* = 7 Hz), 1.14 (d, 3H, *J* = 7 Hz), 1.43–1.55 (m, 2H), 1.75 (m, 1H), 2.10 (m, 1H), 2.24 (m, 1H), 2.34 (br d, 1H, *J* = 16 Hz), 2.42 (m, 1H), 2.52 (br septet, 1H, *J* = 7 Hz), 2.73 (dd, 1H, *J* = 2.5, 16 Hz), 3.63 (s, 3H), 5.48 (br s, 1H, $w_{1/2}$ = 6 Hz), 5.56 (t, 1H, *J* = 4 Hz). Decoupling experiments: irradiation at δ 5.48 changed the signals at 2.34, 2.52, and 2.73 to a dd (*J* = 2, 16 Hz), a d of septets (*J* = 2, 7 Hz), and a d (*J* = 16 Hz); irradiation at δ 5.56 simplified the resonances at 2.10 and 2.24 to a br dt (*J* = 18 8 Hz) and a br dd (*J* = 5, 18 Hz). Exact Mass calcd. for $C_{14}H_{20}O_2$ 220.1464; found: 220.1456.

*10-Isopropyl-7-methoxycarbonylbicyclo[5.3.0]deca-1,9-diene (**17**c)*

Procedures similar to those described above were employed to convert the β-keto ester **15***c* into the bicyclic diene **17***c*. Flash chromatography (50 g silica gel, 25:1 petroleum ether – ethyl acetate) of the crude product obtained from 323 mg (0.779 mmol) of **15***c* provided 352 mg (82%) of the enol triflate **16***c*, a colorless oil that displayed ir (neat): 1735, 1418, 1220, 776 cm^{-1}; ^1H nmr

Can. J. Chem. Downloaded from www.nrcresearchpress.com by 92.62.229.171 on 09/08/12
For personal use only.

(80 MHz) δ: 0.21 (s, 9H, $^2J_{Sn-H}$ = 52 Hz), 0.96 (d, 6H, J = 7 Hz), 1.10–2.85 (m, 11H), 3.74 (s, 3H), 5.89 (br t, 1H, J = 7 Hz, $^3J_{Sn-H}$ = 132 Hz), 6.03 (t, 1H, J = 6 Hz). Exact Mass calcd. for $C_{18}H_{28}F_3O_5SSn$ (M^+ − Me): 533.0631; found: 533.0647.

From 243 mg (0.444 mmol) of the enol triflate **16***c* there was obtained, after flash chromatography (30 g silica gel, 25:1 petroleum ether – ethyl acetate) of the crude product and distillation (65–69°C/0.1 Torr) of the acquired liquid, 84 mg (81%) of the diene **17***c*. The reaction time for the cyclization reaction was 30 min. The product **17***c*, a colorless oil, displayed ir (neat): 1723, 1385, 832 cm^{-1}; ^{1}H nmr (400 MHz) δ: 1.08 (d, 3H, J = 7 Hz), 1.10 (d, 3H, J = 7 Hz), 1.34 (br q, 1H, J = 12 Hz), 1.54 (dt, 1H, J = 3, 13 Hz), 1.60–1.79 (m, 2H), 1.89 (m, 1H), 2.05–2.26 (m, 3H), 2.36–2.50 (m, 2H), 2.76 (dd, 1H, J = 2.5, 17.5 Hz), 3.69 (s, 3H), 5.53 (br s, 1H, $w_{1/2}$ = 6 Hz), 5.79 (dd, 1H, J = 5, 8.5 Hz). Decoupling experiments: irradiation at δ 2.76 simplified the m at 2.36–2.50; irradiation at δ 5.53 sharpened the m at 2.36–2.50 and changed the signal at 2.76 to a d (J = 17.5 Hz); irradiation at δ 5.79 simplified the m at 2.05–2.26. Exact Mass calcd. for $C_{15}H_{22}O_2$: 234.1621; found: 234.1617.

*10-Isopropyl-7-methylbicyclo[5.3.0]deca-1,9-diene (**17**d)*

The ketone **15***d* was converted into the diene **17***d* by means of procedures similar to those described above. Flash chromatography (15 g silica gel, 30:1 petroleum ether – Et_2O) of the crude product obtained from 50 mg (0.13 mmol) of the ketone **15***d*, followed by concentration of the appropriate fractions, gave 57 mg (84%) of the enol triflate **16***d*, a colorless oil that exhibited ir (neat): 1405, 1205, 1140, 768 cm^{-1}. Exact Mass calcd. for $C_{17}H_{28}F_3O_3SSn$ (M^+ − Me): 489.0733; found: 489.0720.

The palladium-catalyzed cyclization of the vinylstannane-enol triflate **16***d* was accomplished in THF at room temperature for 5 min. Flash chromatography (5 g silica gel, 30:1 petroleum ether – Et_2O) of the crude product obtained from 50 mg (0.10 mmol) of **16***d*, followed by distillation (142–144°C/30 Torr) of the acquired liquid, yielded 16 mg (85%) of the diene **17***d*, a colorless oil that showed ir (neat): 2890, 830 cm^{-1}; ^{1}H nmr (400 MHz) δ: 1.03 (d, 3H, J = 7 Hz), 1.10 (d, 3H, J = 7 Hz), 1.13 (s, 3H), 1.32 (br q, 1H, J = 12 Hz), 1.48–1.90 (m, 5H), 2.12 (dd, 1H, J = 2.5, 17 Hz), 2.15–2.42 (m, 4H), 5.54 (dd, 1H, J = 3.5, 8.5 Hz), 5.57 (d, 1H, J = 2.5 Hz). Exact Mass calcd. for $C_{14}H_{22}$: 190.1721; found: 190.1721.

Preparation of the N, N*-dimethylhydrazone **22***

A stirred solution of the commercially available ketone **21** (19.5 g, 98.3 mmol) and 1,1-dimethylhydrazine (9.0 mL, 117.6 mmol) in dry benzene (200 mL) was refluxed under a Dean–Stark water trap for 2 h. The solution was dried ($MgSO_4$) and concentrated. Distillation (105–120°C/0.03 Torr) of the residual oil gave 23.5 g (99%) of the hydrazone **22** as a white, crystalline material that exhibited mp 45–46°C; ir (KBr): 2773, 1640 cm^{-1}; ^{1}H nmr (80 MHz) δ: 0.99, 1.05 (s, s, 3H each), 1.83–2.15 (m, 4H), 2.20–2.75 (m, 4H), 2.49 (s, 6H), 3.56 (s, 4H). Exact Mass calcd. for $C_{13}H_{24}O_2N_2$: 240.1837; found: 240.1835.

*Preparation of the keto ketal **24***

To a cold (0°C), stirred solution of LDA (118 mmol) in dry THF (100 mL) was added a solution of the ketal *N*,*N*-dimethylhydrazone **22** (23.5 g, 97.8 mmol) in dry THF (50 mL) and the solution was stirred at 0°C for 1.5 h. Methyl iodide (12.2 mL, 196 mmol) was added; the mixture was allowed to warm to room temperature and then was stirred for 2 h. Water (100 mL) was added and most of the organic solvent was removed under reduced pressure. The residual mixture was extracted with ethyl acetate (3 × 250 mL) and with CH_2Cl_2 (3 × 100 mL). The combined organic extracts were washed with brine, dried ($MgSO_4$), and concentrated. A mixture of the remaining crude *N*,*N*-dimethylhydrazone **23**, sodium metaperiodate (46.0 g, 215 mmol), THF (350 mL), water (100 mL), and aqueous phosphate buffer (100 mL, pH 7) was stirred (mechanical stirrer) at room temperature for 24 h. The THF was removed under reduced pressure and the residual mixture was extracted with CH_2Cl_2 (6 × 150 mL). The combined organic extracts were dried ($MgSO_4$) and concentrated. Recrystallization of the remaining brownish solid from petroleum ether provided 20.5 g (99%) of the keto ketal **24** as colorless needles that displayed mp 66–66.5°C; ir ($CHCl_3$): 1711, 1115 cm^{-1}; ^{1}H nmr (80 MHz) δ: 1.01, 1.05 (s, s, 3H each), 1.06 (d, 3H, J = 7 Hz), 1.45–2.00 (m, 2H), 2.20–2.80 (m, 5H), 3.55, 3.58 (s, s, 2H each). Exact Mass calcd. for $C_{12}H_{20}O_3$: 212.1412; found: 212.1413.

*Preparation of the cyclopropane silyl ethers **26** and **27***

To a cold (0°C), stirred solution of LDA (222 mmol) in dry 1,2-dimethoxyethane (DME) (200 mL) was added, dropwise, a solution of the keto ketal **24** (31.4 g, 148 mmol) in dry DME (75 mL). The solution was stirred for 45 min and then Me_3SiCl (56.3 mL, 444 mmol) and Et_3N (68.1 mL, 444 mmol) were added sequentially. The mixture was stirred for 30 min at 0°C, was warmed to room temperature, and then was diluted with Et_2O (100 mL). The solution was washed with cold (0°C) aqueous $NaHCO_3$ (2%, 3 × 50 mL), dried ($MgSO_4$), and concentrated. The crude enol silyl ether **25** was dissolved in dry toluene (200 mL) and to the resultant stirred solution was added sequentially a solution of diethylzinc in toluene (166 mL, 15% solution, 200 mmol) and CH_2I_2 (16.2 mL, 200 mmol). The reaction mixture, under an air atmosphere and protected with a drying tube, was stirred at 55°C for 15 h. The mixture was cooled and Et_2O (100 mL) and saturated aqueous NH_4Cl (100 mL) were added. The phases were separated and the aqueous layer was extracted with Et_2O (3 × 150 mL). The combined organic extracts were washed with aqueous $NaHCO_3$ (2%, 100 mL), dried ($MgSO_4$), and concentrated. Distillation (110–115°C/0.1 Torr) of the residual liquid gave 37.9 g (86%) of a 2:1 mixture of the cyclopropane silyl ethers **26** and **27**, a colorless oil that showed ir (neat): 3073, 842, 765 cm^{-1}; ^{1}H nmr (400 MHz) δ: 0.09, 0.10 (s, s, ratio ~2:1, 9H), 0.22, 0.55 (t, dd, ratio ~1:2, 1H, J = 6 Hz, J = 5.0, 5.5 Hz), 0.70, 0.73 (t, dt, ratio ~2:1, 1H, J = 8 Hz, J = 1, 4.5 Hz), 0.88, 0.93, 0.935, 0.94 (s, s, s, s, ratio ~2:1:1:2, 6H), 1.04, 1.12 (d, d, ratio ~1:2, 3H, J = 6.5, 7 Hz), 1.10–2.68 (m, 6H), 3.34–3.52 (m, 4H). Exact Mass calcd. for $C_{16}H_{30}O_3Si$: 298.1965; found: 298.1963.

*Preparation of the enone ketal **29***

To a cold (0°C), stirred solution of dry ferric chloride (11.3 g, 69.6 mmol) in dry *N*,*N*-dimethylformamide (DMF) (75 mL) was added, over a period of 2 h (syringe pump), a solution of dry pyridine (1.87 mL, 23.2 mmol) and a 2:1 mixture of the silyl ethers **26** and **27** (6.89 g, 23.2 mmol) in dry DMF (30 mL). The cooling bath was removed and the mixture was stirred at room temperature for 2 h. Hydrochloric acid (2%, 100 mL) was added and the mixture was extracted with Et_2O (5 × 200 mL). The combined extracts were washed with brine (150 mL), dried ($MgSO_4$), and concentrated. The crude β-chloro ketone **28** was dissolved in MeOH (100 mL), NaOAc (13.3 g, 162 mmol) was added, and the resultant mixture was refluxed, with stirring, for 15 h. The cooled mixture was poured into water (50 mL) and the mixture was extracted with Et_2O (5 × 100 mL). The combined organic extracts were washed with saturated aqueous $NaHCO_3$ (100 mL), dried ($MgSO_4$), and concentrated. Flash chromatography (360 g silica gel, 4:1 to 1:1 petroleum ether – ethyl acetate) of the crude product, followed by distillation (126–130°C/0.1 Torr) of the acquired liquid, produced 3.22 g (62%) of the enone ketal **29**, a colorless oil that displayed ir (neat): 1672, 1109 cm^{-1}; ^{1}H nmr (400 MHz) δ: 0.93, 1.02 (s, s, 3H each), 1.17 (d, 3H, J = 7 Hz), 1.83 (dd, 1H, J = 11.5, 14.5 Hz), 2.33 (dd, 1H, J = 3.5, 14.5 Hz), 2.63–2.77 (m, 2H), 2.88 (dd, 1H, J = 7.5, 16.5 Hz), 3.40–3.56 (m, 4H), 6.08 (dd, 1H, J = 2.5, 12 Hz), 6.40 (ddd, 1H, J = 5, 7.5, 12 Hz). Decoupling experiments: irradiation at δ 2.33 collapsed the signal at 1.83 to a d (J = 14.5 Hz), and simplified the m at 2.63–2.77; irradiation at δ 2.88 simplified the m at 2.63–2.77 and changed the ddd at 6.40 to a dd (J = 5, 12 Hz); irradiation at δ 6.40 sharpened the m at 2.63–2.77 and changed the signals at 2.88 and 6.08 to a d (J = 16.5 Hz) and a br s. ^{13}C nmr

Can. J. Chem. Downloaded from www.nrcresearchpress.com by 92.62.229.171 on 09/08/12
For personal use only.

(75.3 MHz) δ: 16.7, 22.4 (two carbons), 29.9, 36.8, 38.4, 41.6, 70.1, 70.6, 100.2, 133.0, 138.4, 204.3. Exact Mass calcd. for $C_{13}H_{20}O_3$: 224.1412; found: 224.1410.

Preparation of the keto ketal ***30***

A solution-suspension of the enone ketal **29** (6.2 g, 27.7 mmol) and 10% palladium-on-carbon (200 mg) in dry hexane (100 mL) was stirred under an atmosphere of hydrogen (atmospheric pressure) for 2 h. The mixture was filtered through a plug of Celite and the collected material was washed with Et_2O (100 mL). Concentration of the filtrate, followed by distillation (110–114°C/0.1 Torr) of the residual liquid, afforded 6.2 g (99%) of the keto ketal **30**, a colorless oil that displayed ir (neat): 1703, 1104 cm^{-1}; ^1H nmr (400 MHz) δ: 0.99 (s, 6H), 1.10 (d, 3H, J = 7 Hz), 1.14 (ddd, 1H, J = 2.5, 12, 14.5 Hz), 1.56 (dd, 1H, J = 11.5, 15 Hz), 1.69–1.93 (m, 2H), 2.25 (dt, 1H, J = 15, 2.5 Hz), 2.42 (ddt, 1H, J = 14.5, 6, 2 Hz), 2.49 (dd, 2H, J = 4.5, 8 Hz), 2.78 (m, 1H), 3.40–3.57 (m, 4H); ^{13}C nmr (75.3 MHz) δ: 17.4, 17.9, 22.5, 22.6, 30.0, 35.6, 39.08, 39.14, 42.3, 69.9, 70.0, 98.3, 215.3. Exact Mass calcd. for $C_{13}H_{22}O_3$: 226.1570; found: 226.1565.

Preparation of the keto vinylstannane ***33***

To a stirred solution of *t*-BuOK (6.8 g, 60.4 mmol) in a mixture of dry *t*-BuOH (5 mL) and dry DME (150 mL) was added a solution of the keto ketal **30** (5.06 g, 22.36 mmol) in dry DME (50 mL). After the mixture had been stirred for 45 min at room temperature, a solution of the allylic bromide **13** (9.8 g, 29.1 mmol) in dry DME (50 mL) was added. The solution was stirred for 15 min and then water (100 mL) was added. The resultant mixture was extracted with ethyl acetate (3 × 150 mL). The combined extracts were washed with brine, dried ($MgSO_4$), and concentrated. Analysis (tlc) of the residual liquid indicated the presence of a small amount of the starting material **30** and three additional components. Medium pressure column chromatography (360 g silica gel, 6:1 petroleum ether – Et_2O) of this mixture provided three product fractions.

The first material to be eluted was a mixture of two diastereomeric, dialkylated ketones **31** (1.76 g, 11%). This colorless oil (not distilled) exhibited ir (neat): 1703, 1611, 770 cm^{-1}; ^1H nmr (270 MHz) δ: 0.164, 0.167, 0.179, 0.186, (s, s, s, s, 18H), 0.80–1.15 (21H), 1.15–2.55 (13H), 3.30–3.60 (4H), 5.75–5.95 (2H). Exact Mass calcd. for $C_{30}H_{55}O_3Sn_2$ (M^+ − Me): 703.2195; found: 703.2218.

The second fraction to be eluted consisted of a single monoalkylated ketone **32** of undetermined stereochemistry (210 mg, 2%). This colorless oil (not distilled) showed ir (neat): 1707, 1613, 1107, 770 cm^{-1}; ^1H nmr (270 MHz) δ: 0.16 (s, 9H, $^2J_{Sn-H}$ = 53 Hz), 0.90, 0.92 (s, s, 3H each), 0.94, 1.01 (d, d, 6H, 3H, J = 7 Hz in each case), 1.20–1.70 (m, 4H), 1.94–2.05 (m, 2H), 2.18–2.50 (m, 4H), 2.60–2.75 (m, 1H), 3.34–3.47 (m, 4H), 5.82 (t, 1H, J = 7 Hz, $^3J_{Sn-H}$ = 145 Hz). Exact Mass calcd. for $C_{21}H_{37}O_3Sn$ (M^+ − Me): 457.1765; found: 457.1769.

Distillation (188–193°C/0.1 Torr) of the liquid obtained from the third chromatography fraction yielded 6.17 g (59%) of the desired ketone **33**, a colorless oil that exhibited ir (neat): 1706, 1611, 1100, 770 cm^{-1}; ^1H nmr (400 MHz) δ: 0.20 (s, 9H, $^2J_{Sn-H}$ = 52 Hz), 0.99 (d, 6H, J = 7 Hz), 0.82, 1.05, 1.15 (s, s, s, 3H each), 1.58–1.84 (m, 3H), 2.06 (s, 2H), 2.13–2.27 (m, 3H), 2.38–2.50 (m, 2H), 2.65 (m, 1H), 3.32–3.58 (m, 4H), 5.92 (t, 1H, J = 7 Hz, $^3J_{Sn-H}$ = 146 Hz); ^{13}C nmr (75.3 MHz) δ: −6.9, 20.4, 22.3, 22.9, 22.95, 23.0, 23.1, 30.0, 31.8, 38.1, 39.5, 44.6, 46.0, 48.2, 69.8, 70.0, 100.0, 131.1, 154.5, 215.2. Exact Mass calcd. for $C_{21}H_{37}O_3Sn$ (M^+ − Me): 457.1765; found: 457.1772.

Preparation of the ketal diene ***35***

To a cold (−78°C), stirred solution of LDA (11.15 mmol) in dry THF (70 mL) was added dry $(Me_2N)_3PO$ (2.59 mL, 14.87 mmol) and the solution was stirred at −78°C for 10 min and at 0°C for 10 min. After the solution had been recooled to −78°C, a solution of the keto vinylstannane **33** (3.5 g, 7.436 mmol) in dry THF (30 mL) was added. After the mixture had been stirred at −78°C for 5 min and at 0°C for 1 h, Tf_2NPh (4.14 g, 11.67 mmol) was added as a powdery solid and the resultant mixture was stirred at room temperature for 2 h. Tetrakis(triphenylphosphine)palladium(0) (429 mg, 0.37 mmol) was added and the mixture was warmed to 30°C for 5 min. Most of the solvent was removed under reduced pressure and the residual material was subjected to flash chromatography (240 g silica gel, 20:1 petroleum ether – Et_2O). Distillation (142–146°C/0.1 Torr) of the acquired liquid gave 1.748 g (81%) of the ketal diene **35**, a colorless oil that displayed ir (neat): 1647, 1111, 832 cm^{-1}; ^1H nmr (400 MHz) δ: 0.93, 1.02, 1.20 (s, s, s, 3H each), 1.03, 1.10 (d, d, 3H each, J = 7 Hz in each case), 1.53 (d, 1H, J = 14 Hz), 1.59 (br d, 1H, J = 14 Hz), 2.03–2.48 (m, 6H), 2.51 (dd, 1H, J = 2.5, 14 Hz), 3.40–3.60 (m, 4H), 5.54 (br s, 1H, $w_{1/2}$ = 6.5 Hz), 5.60 (dd, 1H, J = 5, 8 Hz); ^{13}C nmr (75.3 MHz) δ: 20.7, 21.8, 22.2, 22.7, 22.9, 25.4, 25.6, 30.1, 36.5, 42.5, 43.7, 50.0, 69.8, 69.9, 100.4, 116.9, 124.6, 149.9, 154.9. Exact Mass calcd. for $C_{19}H_{30}O_2$: 290.2246; found: 290.2248.

Preparation of the keto diene ***36***

A solution of the ketal diene **35** (1.137 g, 3.915 mmol) and 5 drops of hydrochloric acid (1 N) in acetone (50 mL) was stirred at room temperature for 3 h. The solvent was removed under reduced pressure and the residual material was treated with 50 mL of water. The mixture was extracted with Et_2O (3 × 50 mL). The combined extracts were washed with brine, dried ($MgSO_4$), and concentrated. Flash chromatography (70 g silica gel, 7:1 petroleum ether – Et_2O) of the residual liquid and distillation (82–85°C/0.1 Torr) of the acquired material provided 796 mg (99%) of the keto diene **36**, a colorless oil that exhibited ir (neat): 1704, 1640, 831 cm^{-1}; ^1H nmr (400 MHz) δ: 1.10 (s, 3H), 1.07, 1.14 (d, d, 3H each, J = 7 Hz in each case), 2.22 (dd, 1H, J = 2.5, 17 Hz), 2.33–2.60 (m, 7H), 2.72 (d, 1H, J = 12 Hz), 5.64 (br s, 1H, $w_{1/2}$ = 6.5 Hz), 5.71 (t, 1H, J = 6 Hz). Decoupling experiments: irradiation at δ 2.22 sharpened the br s at 5.64 ($w_{1/2}$ = 4.5 Hz) and simplified the m at 2.33–2.60; irradiation at δ 5.64 changed the signal at 2.22 to a d (J = 17 Hz); irradiation at δ 5.71 simplified the m at 2.33–2.60. ^{13}C nmr (75.3 MHz) δ: 21.7, 22.0, 23.2, 25.4, 25.6, 43.3, 45.0, 48.1, 55.2, 115.5, 125.8, 149.8, 155.3, 211.8. Exact Mass calcd. for $C_{14}H_{20}O$: 204.1515; found: 204.1518.

Preparation of the N,N*-dimethylhydrazone* ***42***

A stirred solution of the keto diene **36** (200 mg, 0.98 mmol) and 1,1-dimethylhydrazine (0.74 mL, 9.8 mmol) in spectral grade MeOH (20 mL) was refluxed in the presence of 3 Å molecular sieves (~20 g) for 4.5 h. The mixture was cooled to room temperature and filtered. The collected material was washed with Et_2O (20 mL). Concentration of the filtrate, followed by distillation (95–105°C/0.1 Torr) of the remaining liquid, produced 238 mg (98%) of the hydrazone **42**, a colorless oil that consisted of a 2:1 mixture of geometric isomers. This material displayed ir (neat): 2769, 1626, 1447, 828 cm^{-1}; ^1H nmr (400 MHz) δ: 1.07 (s, 3H), 1.04, 1.11 (d, d, 3H each, J = 7 Hz in each case), 1.95–2.65 (m, 8H), 2.41, 2.49 (s, s, ratio ~1:2, 6H total), 3.31, 3.59 (m, dd, ratio ~2:1, 1H total, J = 2, 12.5 Hz), 5.58–5.67 (m, 2H). Exact Mass calcd. for $C_{16}H_{26}N_2$: 246.2096; found: 246.2095.

Preparation of the keto trienes ***44*** *and* ***45***

To a cold (0°C), stirred solution of LDA (1.68 mmol) in dry THF (10 mL) was added, dropwise, a solution of the *N*,*N*-dimethylhydrazone **42** (345 mg, 1.4 mmol) in dry THF (10 mL). The solution was stirred at −78°C for 1 h and at 0°C for 1 h. To the deep red solution was added a solution of 5-iodo-2-trimethylstannyl-1-pentene (**43**) (13) (502 mg, 1.68 mmol) in dry THF (6 mL). This mixture was warmed to room temperature and then was stirred for 1 h. Saturated aqueous ammonium chloride (25 mL) was added and the two phases were separated. The aqueous layer was extracted with Et_2O (3 × 100 mL). The combined organic extracts were washed with brine, dried ($MgSO_4$), and concentrated. The remaining oil was dissolved in THF (30 mL) and water (8 mL), aqueous phosphate buffer (pH 7, 9 mL), and sodium metaperiodate (1.2 g, 5.6 mmol) were added. The vigorously stirred mixture

Can. J. Chem. Downloaded from www.nrcresearchpress.com by 92.62.229.171 on 09/08/12
For personal use only.

was heated at 40°C for 48 h. Aqueous NH_4Cl–NH_4OH (pH 8) (10 mL) was added and the phases were separated. The aqueous layer was extracted with Et_2O (3 × 100 mL). The combined organic extracts were washed with brine, dried ($MgSO_4$), and concentrated. Flash chromatography (50 g silica gel, 10:1 petroleum ether – Et_2O) of the crude product and distillation (190–200°C/0.1 Torr) of the acquired liquid gave 420 mg (69%) of the keto triene **44**, a colorless oil that displayed ir (neat): 1699, 1641, 915, 841, 768 cm^{-1}; ^1H nmr (400 MHz) δ: 0.13 (s, 9H, $^2J_{Sn-H}$ = 52 Hz), 1.08 (s, 3H), 1.07, 1.13 (d, d, 3H each, J = 7 Hz in each case), 1.22–1.50 (m, 3H), 1.66 (m, 1H), 2.15–2.65 (m, 8H), 2.40 (br d, 1H, J = 12 Hz), 2.79 (d, 1H, J = 12 Hz), 5.13 (m, 1H, $^3J_{Sn-H}$ = 71 Hz), 5.22 (dd, 1H, J = 5, 8.5 Hz), 5.63 (m, 2H); ^{13}C nmr (75.3 MHz) δ: −9.5, 21.9, 22.0, 24.9, 25.5, 27.2, 27.7, 30.0, 40.5, 43.4, 48.4, 51.3, 54.6, 112.6, 124.8, 126.1, 149.6, 155.0, 155.2, 213.7. Exact Mass calcd. for $C_{21}H_{33}OSn$ (M^+ − Me): 421.1554; found: 421.1545.

A 10 mg sample of the ketone **44** was dissolved in dry MeOH (1 mL) and NaOMe (~1 mg) was added. The solution was stirred at room temperature for 22 h and the solvent was removed under reduced pressure. Water (2 mL) was added and the mixture was extracted with Et_2O (3 × 3 mL). The combined organic extracts were dried ($MgSO_4$) and concentrated. Analysis (glc) of the crude product indicated that it was composed of a 1:1.4 mixture of the ketones **44** and **45**. Column chromatography (5 g silica gel, 10:1 petroleum ether – Et_2O) of this material and distillation (190–200°C/0.1 Torr) of the acquired liquid provided a small sample of the keto triene **45**, a colorless oil that showed ir (neat): 1705, 1642, 914, 833, 768 cm^{-1}; ^1H nmr (400 MHz) δ: 0.13 (s, 9H, $^2J_{Sn-H}$ = 54 Hz), 1.04 (s, 3H), 1.05, 1.13, (d, d, 3H each, J = 7 Hz in each case), 1.19–1.43 (m, 3H), 1.77 (m, 1H), 2.05–2.52 (m, 8H), 2.55, 2.61 (d, d, 1H each, J = 11 Hz in each case), 5.13 (m, 1H, $^3J_{Sn-H}$ = 71 Hz), 5.63 (m, 2H), 5.67 (dd, 1H, J = 4.5, 9 Hz); ^{13}C nmr (75.3 MHz) δ: −10.0, 21.7, 22.0, 25.36, 25.38, 27.4, 30.5, 30.6, 40.8, 43.5, 48.0, 54.0, 55.1, 114.7, 124.5, 125.9, 149.7, 155.2, 155.4, 212.1. Exact Mass calcd. for $C_{21}H_{33}OSn$ (M^+ − Me): 421.1554; found: 421.1557.

*Preparation of the keto triene **46***

A stirred solution of the ketone **44** (150 mg, 0.345 mmol) and *t*-BuOK (155 mg, 1.725 mmol) in a mixture of dry THF (11 mL) and dry $(Me_2N)_3PO$ (3 mL) was heated at 60°C for 1 h. To the resultant dark red solution was added MeI (0.129 mL, 2.07 mmol) and the mixture was stirred at 60°C for 15 min. The solution was poured into cold water (25 mL). The mixture was extracted with Et_2O (3 × 50 mL). The combined extracts were washed with brine, dried ($MgSO_4$), and concentrated. Flash chromatography (40 g silica gel, 20:1 petroleum ether – Et_2O) of the crude product, followed by distillation (220–230°C/0.1 Torr)[18] of the acquired liquid, afforded 97 mg (63%) of the ketone **46**, a pale yellow oil that exhibited ir (neat): 1706, 1621, 915, 768 cm^{-1}; ^1H nmr (300 MHz) δ: 0.13 (s, 9H, $^2J_{Sn-H}$ = 54 Hz), 1.03, 1.11 (s, s, 3H each), 1.01, 1.08 (d, d, 3H each, J = 7 Hz in each case), 1.20–1.70 (m, 4H), 2.00 (dd, 1H, J = 8, 14 Hz), 2.10 (dd, 1H, J = 3, 16 Hz), 2.22 (br t, 2H, J = 7 Hz), 2.30–2.50 (m, 3H), 2.43 (d, 1H, J = 12 Hz), 2.83 (d, 1H, J = 12 Hz), 5.12 (m, 1H, $^2J_{Sn-H}$ = 72 Hz), 5.51–5.58 (m, 2H), 5.63 (m, 1H, $^3J_{Sn-H}$ = 154 Hz). Exact Mass calcd. for $C_{22}H_{35}OSn$ (M^+ − Me): 435.1710; found: 435.1704.

*Preparation of the keto vinyl iodide **47***

To a stirred solution of the vinylstannane ketone **46** (65 mg, 0.145 mmol) in dry CH_2Cl_2 (10 mL) was added, dropwise, a solution of iodine in dry CH_2Cl_2 (~3.6 mL of a 0.04 M solution, ~0.145 mmol) until the pale violet color of excess iodine persisted. The solution was stirred for a further 15 min and then water (10 mL) and Et_2O (100 mL) were added. The organic phase was separated and then was washed with saturated aqueous sodium thiosulfate until the organic solution was colorless. The solution was dried ($MgSO_4$) and concentrated. Flash chromatography (40 g silica gel, 20:1 petroleum ether – Et_2O) of the remaining material and distillation (210–220°C/0.1 Torr)[18] of the resultant liquid afforded 50 mg (84%) of the vinyl iodide **47**, a pale yellow oil that showed ir (neat): 1704, 1617, 893 cm^{-1}; ^1H nmr (400 MHz) δ: 1.09, 1.13 (s, s, 3H each), 1.03, 1.10 (d, d, 3H each, J = 7 Hz in each case), 1.25–1.65 (m, 4H), 2.04 (dd, 1H, J = 8.5, 15 Hz), 2.14 (dd, 1H, J = 2, 16 Hz), 2.33–2.44 (m, 3H), 2.44–2.52 (m, 2H), 2.54 (d, 1H, J = 12 Hz), 2.81 (d, 1H, J = 12 Hz), 5.55 (dd, 1H, J = 6, 8.5 Hz), 5.60 (br s, 1H, $w_{1/2}$ = 6 Hz), 5.71 (d, 1H, J = 1.5 Hz), 6.03 (m, 1H). Exact Mass calcd. for $C_{20}H_{29}IO$: 412.1265; found: 412.1261.

*(±)-(5S,12R,14S)-Dolasta-1(15),7,9-trien-14-ol (**2**)*

To a stirred solution of the vinyl iodide **47** (28 mg, 0.068 mmol) in dry THF (10 mL) was added metallic magnesium (small, finely ground pieces, ~20 mg, ~12 equiv.). The mixture was heated to reflux temperature and then one drop of 1,2-dibromoethane (passed through a plug of basic alumina immediately prior to use) was added. The mixture was refluxed for 2.5 h and then was cooled to room temperature. Saturated aqueous NH_4Cl (5 mL) was added and the phases were separated. The aqueous phase was extracted with Et_2O (3 × 10 mL). The combined organic extracts were washed with brine, dried ($MgSO_4$), and concentrated. Drip column chromatography (7 g silica gel, 20:1 petroleum ether – Et_2O) of the remaining material provided 9.5 mg (49%) of the dolastatrienol **2** as a white, crystalline solid. Recrystallization of this material from heptane produced needle-shaped crystals that exhibited mp 105–106°C; ir ($CHCl_3$): 3604, 3500, 1639, 1002, 906 cm^{-1}; ^1H nmr (400 MHz, C_6D_6) δ: 0.92 (s, 3H), 1.11, 1.14 (d, d, 3H each, J = 7 Hz in each case), 1.25–1.35 (m, 1H), 1.39 (s, 3H), 1.43–1.66 (m, 2H), 1.48 (d, 1H, J = 14.5 Hz), 1.51 (dd, 1H, J = 9.5, 15 Hz), 1.97 (br d, 1H, J = 12.5 Hz), 2.03 (d, 1H, J = 14.5 Hz), 2.05–2.15 (m, 2H), 2.22 (br d, 1H, J = 17 Hz), 2.42 (septet, 1H, J = 7 Hz), 2.60 (ddd, 1H, J = 6, 12.5, 12.5 Hz), 3.22 (dd, 1H, J = 4.5, 15 Hz), 4.61 (br s, 1H, $w_{1/2}$ = 4 Hz), 4.78 (br s, 1H, $w_{1/2}$ = 4 Hz), 5.46 (dd, 1H, J = 4.5, 9.5 Hz), 5.54 (br s, 1H, $w_{1/2}$ = 6.5 Hz). Decoupling experiments: irradiation at δ 2.60 sharpened the multiplet at 1.43–1.66 and collapsed the br d at 1.97 to a br s; irradiation at δ 3.22 changed the resonances at 1.51 and 5.46 to doublets (J = 9.5 Hz in each case); irradiation at δ 5.46 altered the signals at 1.51 and 3.22 to doublets (J = 15 Hz in each case). ^{13}C nmr (100.4 MHz) δ: 19.8, 22.1, 22.2, 23.2, 25.6, 27.4. 32.0, 35.1, 37.2, 41.5, 43.4, 45.4, 50.9, 79.5, 108.4, 114.4, 124.7, 149.8, 153.9, 154.1. Exact Mass calcd. for $C_{20}H_{30}O$: 286.2297; found: 286.2297.

*Preparation of the ketal alkene **53** and the keto alkene **54***

To cold (−48°C), stirred liquid ammonia (~100 mL) was added lithium metal (535 mg, 77.1 mmol) and the resultant mixture was stirred at −48°C for 30 min. A solution of the ketal diene **35** (2.239 g, 7.71 mmol) in 50 mL of dry Et_2O was added and the dark blue mixture was stirred at −48°C for 1.75 h. Saturated aqueous NH_4Cl (50 mL) was added carefully (vigorous stirring). The cooling bath was replaced with a warm water bath (~50°C) and the ammonia was allowed to evaporate over a period of a 2 h. The remaining mixture was extracted with Et_2O (3 × 200 mL). The combined extracts were washed with brine, dried ($MgSO_4$), and concentrated. Distillation (125–135°C/0.1 Torr) of the remaining liquid provided 2.15 g (95%) of a colorless oil that, on the basis of analysis by glc, consisted of a mixture of the ketal alkenes **52** and **53**, in a ratio of ~1:4, respectively. A glc – mass spectrometry experiment showed that both components of this mixture possessed a molecular mass of 292.

The 1:4 mixture of **52** and **53** (2.12 g, 7.25 mmol) was dissolved in spectral grade hexane (100 mL) and iodine (185 mg,

[18]Due to some decomposition at the elevated distillation temperatures, this material was generally not distilled.

Can. J. Chem. Downloaded from www.nrcresearchpress.com by 92.62.229.171 on 09/08/12
For personal use only.

0.72 mmol) was added. The stirred, pale red solution was refluxed for 3 h. Saturated aqueous sodium thiosulfate was added to the cooled solution until the organic phase became colorless. The phases were separated and the aqueous layer was extracted with Et_2O (2 × 25 mL). The combined organic extracts were washed with brine, dried ($MgSO_4$), and concentrated. Analysis (glc) of the residual material indicated that it consisted of a single component, the ketal alkene **53**. This liquid was dissolved in acetone (100 mL) and 1 mL of 1 N hydrochloric acid was added. The mixture was stirred at room temperature for 1 h and then saturated aqueous $NaHCO_3$ (50 mL) was added. The organic phase was separated and the aqueous phase was extracted with Et_2O (3 × 25 mL). The combined organic extracts were washed with brine, dried ($MgSO_4$), and concentrated. Distillation (80–85°C/0.1 Torr) of the crude product gave 1.39 g (93%) of the keto alkene **54** (16), a colorless oil that showed ir (neat): 1703, 1456, 1185 cm^{-1}; ^1H nmr (400 MHz) δ: 0.95, 0.98 (d, d, 3H each, J = 7 Hz in each case), 1.04 (s, 3H), 1.52–1.74 (m, 3H), 1.88–2.00 (m, 2H), 2.18–2.25 (m, 2H), 2.37–2.44 (m, 2H), 2.55 (s, 2H), 2.61–2.71 (m, 2H); ^{13}C nmr (75.3 MHz) δ: 21.0, 21.5, 24.0, 24.2, 24.8, 26.6, 27.3, 38.1, 43.9, 47.6, 54.9, 138.6, 141.9, 213.1. Exact Mass calcd. for $C_{14}H_{22}O$: 206.1671; found: 206.1671.

In another experiment, distillation (126–134°C/0.1 Torr) of a small sample of the liquid derived from the iodine-induced isomerization reaction (see above) provided the ketal alkene **53** (36) as a colorless oil that displayed ir (neat): 2954, 1110 cm^{-1}; ^1H nmr (400 MHz) δ: 0.92, 0.97, 1.04 (s, s, s, 3H each), 0.93, 0.94 (d, d, 3H each, J = 7 Hz in each case), 1.40–1.51 (m, 2H), 1.70–1.97 (m, 7H), 2.10–2.23 (m, 2H), 2.46 (dt, 1H, J = 7, 14 Hz), 2.63 (septet, 1H, J = 7 Hz), 3.39–3.54 (m, 4H); ^{13}C nmr (75.3 MHz) δ: 20.2, 21.2, 21.4, 22.76, 22.81, 23.6, 25.6, 26.7, 27.1, 30.0, 33.2, 39.5, 45.3, 47.7, 69.8, 69.9. 101.1, 139.2, 140.2. Exact Mass calcd. for $C_{19}H_{32}O_2$: 292.2404; found: 292.2402.

*4-Trimethylstannyl-4-penten-1-ol (**61**)*

To a cold (−78°C), stirred solution of $Me_3SnCu \cdot Me_2S$ (23) (43.8 mmol) in dry THF (300 mL) was added, dropwise, a solution of 4-pentyn-1-ol (2.45 g, 29.2 mmol) in dry THF (15 mL). Dry MeOH (59 mL) was added and the resulting solution was stirred at −78°C for 2 h and at 0°C for 1 h. Aqueous NH_4Cl–NH_4OH (pH 8) (150 mL) and petroleum ether (200 mL) was added. The resultant mixture was opened to the atmosphere and was stirred vigorously at room temperature until the aqueous phase was deep blue. The phases were separated and the aqueous layer was extracted with 4:1 pentane–Et_2O (200 mL). The combined organic extracts were washed with aqueous NH_4Cl–NH_4OH (pH 8) (3 × 100 mL), dried ($MgSO_4$), and concentrated. Flash chromatography (180 g silica gel, 2:1 petroleum ether – Et_2O) of the remaining liquid and distillation (95–100°C/20 Torr) of the acquired oil provided 3.9 g (54%) of the alcohol **61**, a colorless oil that exhibited spectra identical with those reported earlier (38).

*4-Trimethylstannyl-4-pentenal (**55**)*

To a cold (−78°C), stirred solution of oxalyl chloride (1.58 mL, 18.1 mmol) in dry CH_2Cl_2 (100 mL) was added dry Me_2SO (1.29 mL, 18.1 mmol). The solution was stirred for 5 min and then a solution of the alcohol **61** (3.47 g, 13.9 mmol) in dry CH_2Cl_2 (50 mL) was added. The mixture was stirred for 20 min and then dry Et_3N (7.78 mL, 55.6 mmol) was added. The mixture was stirred at −78°C for 5 min, was warmed to room temperature, and then was stirred for an additional 30 min. Water (100 mL) was added and the phases were separated. The aqueous phase was extracted with CH_2Cl_2 (3 × 50 mL) and the combined organic extracts were dried ($MgSO_4$) and concentrated. Distillation (80–90°C/15 Torr) of the crude product produced 2.20 g (64%) of the aldehyde **55**, a colorless oil. This material, which was somewhat unstable and slowly decomposed even when stored under argon in a freezer, exhibited ir (neat): 2719, 1728, 1601, 919, 770 cm^{-1}; ^1H nmr (80 MHz) δ: 0.18 (s, 9H, $^2J_{Sn-H}$ = 53 Hz), 2.29–2.68 (m, 4H), 5.21 (m, 1H, $^3J_{Sn-H}$ = 71 Hz), 5.68 (m, 1H, $^3J_{Sn-H}$ = 146 Hz), 9.78 (br s, 1H, $w_{1/2}$ = 3 Hz). Exact Mass calcd. for $C_7H_{13}OSn$ (M^+ − Me): 232.9988; found: 232.9987.

*Preparation of the diketones **58** and **59***

To a cold (−78°C), stirred solution of LDA (3.15 mmol) in dry THF (20 mL) was added, dropwise, a solution of the keto alkene **54** (500 mg, 2.42 mmol) in dry THF (6 mL). The solution was stirred at −78°C for 15 min and at 0°C for 15 min, and then was recooled to −78°C. A solution of the aldehyde **55** (717 mg, 2.90 mmol) in dry THF (5 mL) was added and the resultant mixture was stirred at −78°C for 15 min and at room temperature for 30 min. Water (50 mL) was added and the phases were separated. The aqueous layer was extracted with Et_2O (3 × 30 mL). The combined extracts were washed with brine, dried ($MgSO_4$), and concentrated. Flash chromatography (100 g silica gel, 10:1 to 5:1 petroleum ether – Et_2O) afforded 126 mg of the starting material **54** and 508 mg (62% based on recovered starting material) of a colorless oil that, based on ^1H nmr spectroscopy, consisted of a mixture of three keto alcohols of general structure **56**. This material was not characterized further.

To a cold (−78°C), stirred solution of oxalyl chloride (0.27 mL, 2.15 mmol) in dry CH_2Cl_2 (40 mL) was added dry Me_2SO (0.15 mL, 2.15 mmol). After the mixture had been stirred for 5 min, a solution of a mixture of the keto alcohols **56** (750 mg, 1.655 mmol) in dry CH_2Cl_2 (10 mL) was added. The mixture was stirred for 20 min and then dry Et_3N (0.92 mL, 6.6 mmol) was added. The solution was stirred at −78°C for 5 min, was warmed to room temperature, and then was stirred for an additional 30 min. Water (50 mL) was added, the phases were separated, and the aqueous phase was extracted with CH_2Cl_2 (3 × 75 mL). The combined organic extracts were dried ($MgSO_4$) and concentrated. The remaining oil was dissolved in spectral grade acetone (50 mL) and to the resulting stirred solution was added MeI (0.21 mL, 3.3 mmol) and dry K_2CO_3 (343 mg, 2.48 mmol). The mixture was refluxed for 15 h and then most of the solvent was removed under reduced pressure. Water (40 mL) was added and the mixture was extracted with Et_2O (3 × 50 mL). The combined organic extracts were dried ($MgSO_4$) and concentrated. Analysis (tlc, ^1H nmr) of the remaining liquid indicated that it consisted of two epimeric products in a ratio of ~2:1. Drip column chromatography (120 g silica gel, 30:1 petroleum ether – Et_2O) of this material provided three fractions. Distillation (180–190°C/0.1 Torr) of the initially eluted oil gave 315 mg (41%) of the diketone **58**, a colorless oil that displayed ir (neat): 1713, 1695, 1600, 918, 770 cm^{-1}; ^1H nmr (400 MHz) δ: 0.14 (s, 9H, $^2J_{Sn-H}$ = 54 Hz), 0.90, 0.94 (d, d, 3H each, J = 6 Hz in each case), 1.06, 1.23 (s, s, 3H each), 1.40 (ddd, 1H, J = 4, 7, 14 Hz), 1.60 (ddd, 1H, J = 3, 6.5, 9 Hz), 1.85 (dt, 1H, J = 12, 9 Hz), 2.06–2.23 (m, 3H), 2.32 (d, 1H, J = 11.5 Hz), 2.36–2.68 (m, 7H), 2.77 (d, 1H, J = 11.5 Hz), 5.16 (m, 1H, $^2J_{Sn-H}$ = 70 Hz), 5.63 (m, 1H, $^3J_{Sn-H}$ = 149 Hz); ^{13}C nmr (75.3 Hz) δ: −9.5, 19.7, 20.8, 21.1, 21.2, 25.7, 26.8, 27.7, 33.2, 33.9, 36.6, 38.2, 47.9, 52.4, 65.6, 125.0, 136.2, 143.4, 153.7, 208.8, 208.9. Exact Mass calcd. for $C_{22}H_{35}O_2Sn$ (M^+ − Me): 451.1659; found: 451.1652.

The second fraction to be eluted (76 mg, 10%) contained a mixture of the diketones **58** and **59**.

Distillation (180–190°C/0.1 Torr) of the liquid obtained from the third fraction produced 120 mg (16%) of the diketone **59**, a colorless oil that showed ir (neat): 1714, 1694, 917, 770 cm^{-1}; ^1H nmr (400 MHz) δ: 0.15 (s, 9H, $^2J_{Sn-H}$ = 53 Hz), 0.93, 1.00 (d, d, 3H each, J = 6.5 Hz in each case), 0.91, 1.37 (s, s, 3H each), 1.51–1.73 (m, 3H), 1.83 (ddd, 1H, J = 1.5, 8.5, 14 Hz), 2.13–2.28 (m, 3H), 2.40 (d, 1H, J = 11 Hz), 2.40–2.70 (m, 6H), 2.68 (d, 1H, J = 11 Hz), 5.15 (m, 1H, $^3J_{Sn-H}$ = 70 Hz), 5.62 (m, 1H, $^3J_{Sn-H}$ = 150 Hz); ^{13}C nmr (75.3 Hz) δ: −9.5, 19.7, 20.1, 21.1, 21.6, 23.3, 26.5, 27.7, 33.7, 33.8, 37.8, 38.7, 48.7, 53.8, 66.6, 124.9, 139.0, 140.7, 153.7, 208.6, 209.7. Exact Mass calcd. for $C_{22}H_{35}O_2Sn$ (M^+ − Me): 451.1659; found: 451.1656.

Can. J. Chem. Downloaded from www.nrcresearchpress.com by 92.62.229.171 on 09/08/12
For personal use only.

Preparation of the keto silyl ether ***63***

To a cold (−78°C), stirred solution of the diketone **58** (43.5 mg, 0.094 mmol) and LiCl (80 mg, 1.88 mmol) in dry THF (10 mL) was added, dropwise, a solution of diisobutylaluminum hydride in toluene (0.37 mL of a 1 M solution, 0.37 mmol). The mixture was stirred for 10 min and then saturated aqueous NH_4Cl (2 mL) was added. The cooling bath was removed and the mixture was stirred for 30 min as it was warmed to room temperature. Magnesium sulfate was added and the mixture was filtered. The collected material was washed with Et_2O (100 mL). The combined filtrate was concentrated. The residual material, which, on the basis of tlc analysis consisted of a single keto alcohol (**62**), was dissolved in dry CH_2Cl_2 (20 mL). To the resultant stirred solution at room temperature was added sequentially, 4-*N*,*N*-dimethylaminopyridine (2 mg), Et_3N (0.08 mL), and *t*-$BuMe_2SiOSO_2CF_3$ (0.11 mL, 0.47 mmol). The solution was stirred for 30 min and then water (20 mL) was added. The phases were separated and the aqueous phase was extracted with CH_2Cl_2 (3 × 20 mL). The combined organic solution was dried ($MgSO_4$) and concentrated. Flash chromatography (27 g silica gel, 60:1 petroleum ether – Et_2O) of the residual liquid gave 43 mg (79%) of the keto silyl ether **63**, a colorless oil that exhibited ir (neat): 1698, 915, 836, 774 cm^{-1}; ^1H nmr (400 MHz) δ: 0.08, 0.09, (s, s, 3H each), 0.13 (s, 9H, $^2J_{Sn-H}$ = 53 Hz), 0.89, 0.94 (d, d, 3H each, J = 7 Hz in each case), 0.91 (s, 9H), 0.94, 1.09 (s, s, 3H each), 1.35–1.60 (m, 4H), 1.82 (dt, 1H, J = 12.5, 10 Hz), 2.04–2.27 (m, 4H), 2.24 (d, 1H, J = 11.5 Hz), 2.38–2.58 (m, 3H), 2.60 (septet, 1H, J = 7 Hz), 3.07 (d, 1H, J = 11.5 Hz), 3.53 (dd, 1H, J = 3, 7.5 Hz), 5.11 (m, 1H, $^3J_{Sn-H}$ = 71 Hz), 5.62 (m, 1H, $^3J_{Sn-H}$ = 153 Hz). Exact Mass calcd. for $C_{29}H_{54}O_2SiSn$: 582.2916; found: 582.2917.

(±)-Amijitrienol (3)

To a cold (0°C), stirred solution of $(Me_3Si)_2NK$ (1.07 mL of a 0.5 M solution in toluene) in dry THF (15 mL) was added, dropwise, a solution of the ketone **63** (62 mg, 0.107 mmol) in dry THF (5 mL). The solution was stirred at room temperature for 30 min and then solid Tf_2NPh (190 mg, 0.54 mmol) was added. The pale yellow solution was stirred for 30 min and then the solvent was removed under reduced pressure. The residual material, containing the enol triflate **64**, was dissolved in dry acetonitrile (25 mL) containing 10 drops of dry Et_3N, and to the resulting stirred solution was added $(Ph_3P)_4Pd$ (7 mg, 0.006 mmol). The solution was refluxed for 30 min and then the solvent was removed under reduced pressure. Drip column chromatography (10 g silica gel, hexane) of the remaining material provided 32 mg (74%) of the silyl ether triene **65**, a colorless oil that was used directly for the next reaction.

A stirred solution of the ether **65** (12.5 mg, 0.031 mmol) and *n*-Bu_4NF (0.062 mL of a 1 M solution in THF) in dry THF (10 mL) was refluxed for 3.5 h. The reaction mixture was concentrated (reduced pressure) and the residual material was subjected to drip column chromatography (5 g silica gel, 3:1 hexane–Et_2O). Recrystallization (hexane) of the white solid thus obtained provided 7.0 mg (78%) of (±)-amijitrienol (**3**) as fine, white needles that exhibited mp 119–119.5°C; ir ($CHCl_3$): 3626, 1631, 1626, 1455, 900 cm^{-1}; ^1H nmr (400 MHz) δ: 0.87, 1.29 (s, s, 3H each), 0.92, 0.93 (d, d, 3H each, J = 7 Hz in each case), 1.34 (ddd, 1H, J = 5, 5, 12 Hz), 1.64 (ddd, 1H, J = 7, 8.5, 12 Hz), 1.72–1.83 (m, 2H), 1.94 (dddd, 1H, J = 2.5, 5, 14, 14 Hz), 2.08, (m, 2H), 2.16 (ddd, 1H, J = 2.5, 5, 13 Hz), 2.30 (m, 1H), 2.47 (ddddd, 1H, J = 2.3, 2.3, 5, 14, 14 Hz), 2.53–2.65 (m, 2H), 2.63 (septet, 1H, J = 7 Hz), 3.37 (br s, 1H, $w_{1/2}$ = 10 Hz), 4.63 (dd, 1H, J = 2.5, 2.5 Hz), 4.74 (dd, 1H, J = 2.5, 2.5 Hz), 5.81 (s, 1H). Decoupling experiments: irradiation at δ 3.37 simplified the m at 1.72–1.83 and changed the dddd at 1.94 to a ddd (J = 5, 14, 14 Hz). ^{13}C nmr (75.3 MHz) δ: 20.5, 20.8, 21.3, 21.9, 26.9, 27.1, 27.2, 28.5, 29.1, 33.3, 42.4, 44.7, 52.2, 78.2, 110.9, 136.6, 138.7, 139.5, 142.5, 150.3. The $CDCl_3$ used for the ^1H nmr and ^{13}C nmr measurements was shaken with Na_2CO_3–$MgSO_4$ and then was filtered through basic alumina immediately prior to use. Exact Mass calcd. for $C_{20}H_{30}O$: 286.2297; found: 286.2296.

Acknowledgements

We thank the Natural Sciences and Engineering Research Council of Canada for financial support and for a 1967 Centennial Science and Engineering Scholarship (to R.W.F.).

1. G. R. Pettit, R. H. Ode, C. L. Herald, R. B. Von Dreele, and C. Michel. J. Am. Chem. Soc. **98**, 4677 (1976).
2. J. C. Braekman, D. Daloze, R. Schubert, M. Albericci, B. Tursch, and R. Karlsson. Tetrahedron, **34**, 1551 (1978).
3. H. H. Sun, O. J. McConnell, W. Fenical, K. Hirotsu, and J. Clardy. Tetrahedron, **37**, 1237 (1981).
4. M. Ochi, M. Watanabe, I. Miura, M. Taniguchi, and T. Tokoroyama. Chem. Lett. 1229 (1980).
5. M. Ochi, M. Watanabe, M. Kido, Y. Ichikawa, I. Miura, and T. Tokoroyama. Chem. Lett. 1233 (1980).
6. M. Ochi, I. Miura, and T. Tokoroyama. J. Chem. Soc. Chem. Commun. 100 (1981).
7. P. Crews, T. E. Klein, E. R. Hogue, and B. L. Myers. J. Org. Chem. **47**, 811 (1982).
8. A. G. González, J. D. Martin, M. Norte, P. Rivera, A. Perales, and J. Fayos. Tetrahedron, **39**, 3355 (1983).
9. N. Harada, Y. Yokota, J. Iwabuchi, H. Uda, and M. Ochi. J. Chem. Soc. Chem. Commun. 1220 (1984).
10. V. L. Teixeira, T. Tomassini, B. G. Fleury, and A. Kelecom. J. Nat. Prod. **49**, 570 (1986).
11. M. Ochi, K. Asao, H. Kotsuki, I. Miura, and K. Shibata. Bull. Chem. Soc. Jpn. **59**, 661 (1986).
12. A. Kelecom and V. L. Teixeira. Phytochemistry, **27**, 2907 (1988).
13. E. Piers, R. W. Friesen, and B. A. Keay. J. Chem. Soc. Chem. Commun. 809 (1985); Tetrahedron, **47**, 4555 (1991).
14. E. Piers and R. W. Friesen. J. Org. Chem. **51**, 3405 (1986).
15. E. Piers and R. W. Friesen. J. Chem. Soc. Chem. Commun. 125 (1988).
16. G. Pattenden and G. M. Robertson. Tetrahedron Lett. **27**, 399 (1986); M. J. Begley, G. Pattenden, and G. M. Robertson. J. Chem. Soc. Perkin Trans. 1, 1085 (1988).
17. G. Mehta and N. Krishnamurthy. Tetrahedron Lett. **28**, 5945 (1987); G. Mehta, N. Krishnamurthy, and S. R. Karra. J. Am. Chem. Soc. **113**, 5765 (1991).
18. G. Majetich, J. S. Song, C. Ringold, and G. A. Nemeth. Tetrahedron Lett. **31**, 2239 (1990).
19. D. T. Belmont and L. A. Paquette. J. Org. Chem. **50**, 4102 (1985).
20. L. A. Paquette, H.-S. Lin, D. T. Belmont, and J. P. Springer. J. Org. Chem. **51**, 4807 (1986).
21. D. R. Williams, J. W. Benbon, and E. E. Allen. Tetrahedron Lett. **31**, 6769 (1990).
22. G. Saha, S. S. Roy, and S. Ghosh. Tetrahedron, **46**, 8229 (1990).
23. E. Piers, H. E. Morton, and J. M. Chong. Can. J. Chem. **65**, 78 (1987).
24. E. Piers, J. M. Chong, and H. E. Morton. Tetrahedron, **45**, 363 (1989).
25. H. Hart, B. Chen, and M. Jeffares. J. Org. Chem. **44**, 2722 (1979).
26. J. E. McMurry and W. J. Scott. Tetrahedron Lett. **24**, 979 (1983).
27. W. J. Scott, G. T. Crisp, and J. K. Stille. J. Am. Chem. Soc. **106**, 4630 (1984); W. J. Scott and J. K. Stille. J. Am. Chem. Soc. **108**, 3033 (1986).
28. J. K. Stille. Angew. Chem. Int. Ed. Engl. **25**, 508 (1986).
29. E. J. Corey and D. Enders. Chem. Ber. **111**, 1337 (1978).

30. T. Saegusa, Y. Ito, and S. Fujii. J. Org. Chem. **41**, 2073 (1976).
31. S. Furakawa, N. Kawabata, and J. Nishimura. Tetrahedron, **24**, 53 (1968); S. Miyano and H. Hashimoto. Chem. Commun. 1418 (1971).
32. H. O. House, L. J. Czuba, M. Gall, and H. D. Olmstead. J. Org. Chem. **34**, 2324 (1969).
33. R. A. Wanat and D. B. Collum. J. Am. Chem. Soc. **107**, 2078 (1985).
34. C. Blomberg and F. A. Hartog. Synthesis, 18 (1977).
35. G. Molle and P. Bauer. J. Am. Chem. Soc. **104**, 3481 (1982).
36. H. Wolf, M. Kolleck, and W. Rascher. Chem. Ber. **109**, 2805 (1976).
37. K. Omura and D. Swern. Tetrahedron, **34**, 1651 (1978).
38. E. Piers and J. M. Chong. Can. J. Chem. **66**, 1425 (1988).
39. J. L. Occolowitz. Tetrahedron Lett. 5291 (1966); H. G. Kuivila, K.-H. Tsai, and D. G. I. Kingston. J. Organomet. Chem. **23**, 129 (1970).
40. W. C. Still, M. Kahn, and A. Mitra. J. Org. Chem. **43**, 2923 (1978).

Can. J. Chem. Downloaded from www.nrcresearchpress.com by 92.62.229.171 on 09/08/12
For personal use only.

Synthesis and tritium-induced ^{19}F NMR shifts of 1,1,1,4,4,4-hexafluoro-2,3 ditritio-2-butene

G. ANGELINI,[1] G. LILLA, C. SPARAPANI, AND O. URSINI
Istituto di Chimica Nucleare del C.N.R. Area della Ricerca di Roma, C.P. 10, 00016 Monterotondo Stazione, Rome, Italy

E. ROSSI
Servizio N.M.R. Area della Ricerca di Roma, Monterotondo Stazione, Rome, Italy

A. L. SEGRE
Istituto Strutturistica Chimica "Giordano Giacomello" del C.N.R. Area della Ricerca di Roma, Monterotondo Stazione, Rome, Italy

AND

M. A. MCALLISTER AND T. T. TIDWELL
Department of Chemistry, Scarborough Campus, University of Toronto, Toronto, Ont., Canada M5S IA1

Received July 30, 1991

G. ANGELINI, G. LILLA, C. SPARAPANI, O. URSINI, E. ROSSI, A. L. SEGRE, M. A. MCALLISTER, and T. T. TIDWELL. Can. J. Chem. **70**, 1221 (1992).

The title compound **3** has been prepared by reaction of $CF_3C{\equiv}CCF_3$ with tritium gas on Lindlar catalyst poisoned with quinoline. The qualitative and quantitative analyses of the products ($CF_3CH{=}CHCF_3$, $CF_3CH{=}C^3HCF_3$, $CF_3C^3H{=}C^3HCF_3$) have been carried out using GC/MS and ^1H, ^3H, and ^{19}F NMR techniques. A strong isotope-induced shift has been detected in the ^{19}F spectra of **3**.

G. ANGELINI, G. LILLA, C. SPARAPANI, O. URSINI, E. ROSSI, A. L. SEGRE, M. A. MCALLISTER et T. T. TIDWELL. Can. J. Chem. **70**, 1221 (1992).

On a préparé le composé **3**, mentionné dans le titre, en faisant réagir du CF_3-C≡C-CF_3 avec du tritium gazeux sur un catalyseur de Lindlar empoisonné avec de la quinoléine. On a effectué les analyses qualitative et quantitative des produits (CF_3-CH=CH-CF_3, CF_3-CH=C^3H-CF_3 et CF_3-C_3H=C^3H-CF_3) à l'aide de techniques de CPG/SM et RMN du ^1H, du ^3H et du ^{19}F. Dans le spectre RMN du ^{19}F du produit **3**, on a détecté un déplacement chimique induit par l'isotope important.

[Traduit par la rédaction]

Introduction

The stability and reactivity of trifluoromethyl-substituted carbocations have recently received considerable attention (1). Theoretical studies have elucidated the potential energy surfaces for the $CF_3CH_2^+$(2*a*), $CH_3FCH_2^+$ (2*b*),[2] and $CF_3C{=}CH_2$ (3) ions and suggested that intramolecular fluoride transfers (eq. [1]) via bridged fluoronium ions may be viable processes for these ions. Several gas-phase investigations (4) have provided evidence for fluorine isomerization (eq. [1]), although some of these results have instead been interpreted (4*b*) by an elimination–readdition pathway

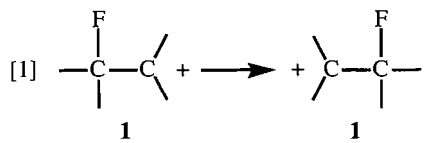

[1]

1 **1**

A further test of the occurrence of this process in both gas and liquid phases at atmospheric or higher pressure would be the "tritium nuclear decay technique." As described previously (5), tritium nuclear decay of a doubly tritiated molecule with the tritium atoms in chemically equivalent positions forms, at least initially, a well-characterized carbocation, whose stability and reactivity can be studied under different experimental conditions.

In this paper is reported the synthesis of no-carrier-added 1,1,1,4,4,4-hexafluoro-2,3-ditritio-2-butene **3** by partial tritium addition to hexafluoro-2-butyne **2** (eq. [2]). Compound **3** displays a strong isotope-induced shift in the ^{19}F NMR spectrum.

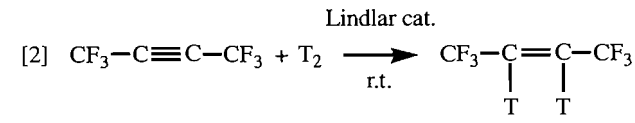

[2]

2 **3**

Experimental

Materials

Pure tritium gas was purchased from the Radiochemical Centre, Amersham, England and was used after a vacuum line distillation, trapping the impurities with a cold bath at −77 K.[3] Hexafluoro-2-butyne **2** was obtained from Strem Chemical Inc., analyzed by GC/MS, and used without further purification.

[1]Author to whom correspondence may be addressed.

[2]M. A. McAllister and T. T. Tidwell, unpublished results.

[3]To obtain the best radiochemical yield of product **3**, a tritium purification step was very important. One run using a directly purchased tritium sample without further purification produced a very low yield of **3** together with a considerable amount of oxygen containing compounds as indicated by ^3H NMR analysis.

Printed in Canada

Can. J. Chem. Downloaded from www.nrcresearchpress.com by 92.62.229.171 on 09/08/12
For personal use only.

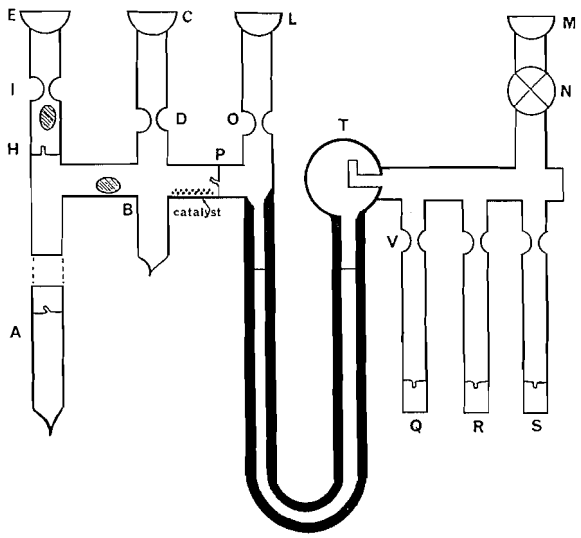

FIG. 1. Glass apparatus for the radiochemical synthesis.

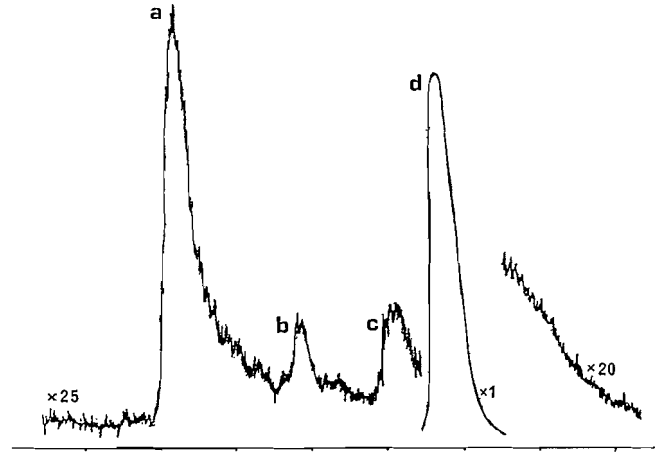

FIG. 2. Radio-gas chromatographic analysis of tritiated 1,1,1,4,4,4-hexafluoro-2 butenes **3** and **4** (peak d), decomposition products (peaks a,b), 1,1,1,4,4,4-hexafluorobutane (peak c).

Pure deuterium gas was obtained from Matheson and Lindlar catalyst from Aldrich.

Methods

Radio-gas chromatographic analyses of the radioactive products were performed using a Carlo Erba model 4200 instrument equipped with a 80/100 mesh Carbopack B with 1% SP-1000 column (2 m × 3 mm. stainless steel) and a TCD detector. A gaseous proportional counter (Berthold AG) was connected to the GC system, for radiochemical analyses.

Isotopic abundances (for deuteriated and tritiated products) were determined by capillary GC/MS analysis using a Hewlett Packard 5988A instrument equipped with a 50 m HP-FFAP quartz column (0.32 mm i.d.).

The isotopic distribution in the recovered tritiated products was also measured by ^{3}H and ^{19}F NMR analyses, in which about 0.55 GBq samples were examined on a Bruker AM 200 NMR spectrometer operating at 213.47 MHz according to spectroscopic procedures reported elsewhere (5).

Static determinations of the radioactivity during the steps of the synthetic procedure were obtained by liquid scintillation counting with a Packard Tri-Carb 2260 XL spectrometer. All the operations involving radioactive products were carried out using a greaseless high-vacuum line.

Preparation of 1,1,1,4,4,4-hexafluoro-2,3-ditritio-2-butene 3

The glass apparatus is shown in Fig. 1. The Pyrex vial A (7 mL), containing purified tritium gas (about 37 BqG at 46 Torr; 1 Torr = 133.3 Pa), was joined to the main part of the device and the central part of the apparatus was carefully outgassed under high vacuum for approximately 3 h at 150°C. Then 15 mg of fresh Lindlar catalyst was placed in B and carefully poisoned with 15 μL of quinoline. The apparatus was connected to the vacuum line with the ground joint C and outgassed. Then ca. 1.6×10^{-5} mol of **2** was transferred by the vacuum line into B, frozen in the cold finger, and the apparatus was sealed off at D. The break seal of ampoule A was broken with a magnetic hammer embedded in glass, and the tritium was allowed to react at room temperature for 4 h.

Unreacted tritium was then removed by connecting the apparatus through the ground joint E to the vacuum line. The cold finger was cooled in a liquid nitrogen bath and the system was carefully outgassed after breaking the seal H. Residual tritium gas (about 80 ± 10% of the starting amount) was recovered by cyclic Töpler pumpings, keeping the cold finger at −196°C.

The apparatus was sealed in I, and mercury (25 mL) was carefully put in the "U" shaped section of the system, which was then simultaneously connected by the ground joints L and M to the vacuum line. After short alternate pumpings through the ground joints L and M, the mercury balanced and the rest of the apparatus was completely outgassed. The stopcock N was closed and the system was sealed off at O.

The last break-seal P was broken using the corresponding magnetic hammer and the crude reaction product was allowed to expand in the "U" shaped section, unbalancing the mercury contained in it.

A slow polymerization process, probably induced by the ionic species formed by tritium nuclear decay, determined the minimum decrease of the pressure. Apart from this, the differential reading of the mercury levels substantially reflected the initial amount of the starting butyne **2**.

The apparatus permitted the consecutive sharing of the crude reaction products into the three collecting vials (Q, R, and S). By allowing the mercury to flow into the spherical head T, the gaseous mixture expanded throughout the apparatus. The return of the mercury into the "U" shaped section divided the gaseous mixture in a ratio that was approximately determined by the volume of the parts connected to the arms of the "U". The gas was condensed, with liquid nitrogen, in vial Q, which was then sealed off at V. The above operations were repeated exactly for the vial R.

The pressures of no-carrier-added products present in vials Q and R were 160 and 53 Torr respectively.

Then 1,1,1,4,4,4-hexafluoro-2,3-dideutero-2-butene was introduced from the stopcock M into the apparatus to wash out and recover any tritiated products absorbed on the walls or catalyst. This last fraction was collected in vial S, frozen at −196°C, keeping the mercury in the spherical head T.

Vial R was used to carry out the following radioanalytical and spectroscopic analyses. A measured sample was diluted in neopentane ($1:10^{4}$) and then a known volume was condensed in a vial containing scintillation liquid. This vial was sealed off and its radioactivity determined by a beta scintillation counter. This measurement permitted the evaluation of the activity of vial R (about 1.1 GBq) and of vials Q and S (about 3.7 and 0.6 GBq respectively) with a radiochemical total yield of 5.4 GBq (15%).

A second small sample (about 0.37 MBq) was analyzed by radio-GC to assay the purity of the product (Fig. 2). The results indicated that more than 94% of the total activity was localized in the ditritiated butene **3** and eventually in the 1,1,1,4,4,4-hexafluoro-2-tritio-2-butene **4**, as confirmed by the comparison of the retention time with an authentic inactive sample. Less than 5% was present in very volatile compounds (probably residual T_2 and HT) and only 1% as tritiated 1,1,1,4,4,4-hexafluorobutane.

Subsequently, a complete analysis of the mass region of interest was carried out using a GC/MS instrument HP 5988 A. This

Can. J. Chem. Downloaded from www.nrcresearchpress.com by 92.62.229.171 on 09/08/12
For personal use only.

TABLE 1. NMR parameters of $CF_3—C\equiv C—CF_3$ measured on ^{19}F NMR spectrum

$^{12}CF_3—^{12}C\equiv^{12}C—^{12}CF_3$	$\delta_{\nu^*_F}$ = 22.878 ppm
$^{13}CF_3\cdot—^{12}C\equiv^{12}C—^{12}CF_3$	$\Delta\delta_{\nu_F}$ = 0.280 ppm upfield from $\delta\nu^*_F$
$^{12}CF_3\cdot—^{13}C\equiv^{12}C—^{12}CF_3$	$\Delta\delta_{\nu_F}$ = 0.031 ppm from $\delta_{\nu^*_F}$

$J_{^{13}CF}$ geminal = |260.7| Hz
$J_{^{12}CF_3-^{13}C}$ vicinal = |56.2| Hz
$J_{CF_3\text{-}CF_3}$ = |2.6| Hz

analysis confirmed the tritiated butenes **3** and **4** as the only radioactive products, together with the inactive starting compound **2**.

The GC/MS analysis showed clearly fragments at *m/e* 149, 147, and 145, corresponding to the loss of one fluorine atom from butenes **3**, **4**, and 1,1,1,4,4,4-hexafluoro-2-butene **5**, in relative percentages of 20, 40, and 40, respectively, based on their corresponding ionic intensities.

Finally, about 0.55 GBq of crude products was transferred through the vacuum line into a 5-mm NMR tube containing 0.5 mL of acetone-d_6 (isotopic purity 99.996%). The tube, frozen at 77 K, was sealed, and gave ^3H and ^{19}F NMR data discussed below that fully agreed with the GC/MS product distribution.

Based on the above isotopic distribution, a very high specific activity (about 1000 TBq/mol) for butenes **3** and **4** is expected. Considering that the radioactive products are diluted by residual starting compound **2** at the end of the reaction, a significant amount (about 144 TBq/mol) of specific activity was obtained. To avoid collateral self-radiolytic decomposition, the contents of vial Q (about 3.7 GBq) were diluted with neopentane (1:200) in the presence of O_2 and trimethylamine as radical and ionic scavengers, respectively. The new specific activity was 0.72 TBq/mol. The radioactive mixture was then purified by several distillation and condensation processes through the vacuum line to eliminate any trace of radioactive impurities. The radioactive product was then stored in the dark prior to use in tritium nuclear decay experiments.

NMR analysis

The ^{19}F NMR spectrum of butyne **2** gave a chemical shift of 22.878 ppm (from 1% v/v of CF_3COOD in acetone-d_6); since **2** was not previously NMR characterized, its NMR parameters, measured on the ^{19}F NMR spectrum, are given in Table 1.

CF_3-CH=CH-CF_3 **5** (entry d of Table 2), was characterized in acetone-d_6 by ^1H NMR (Fig. 3). This spectrum shows the *cis/trans* isomers at 6.65 and 6.95 ppm, respectively, having an intensity ratio larger than 95:5. The only previous synthesis of **5** (6) reports the preparation of the *cis* isomer, with no acceptable proof of its structure, so complete analysis of ^1H and ^{19}F spectra of the major component was performed.

The spectrum of *cis* **5** is a strongly coupled $A_3A_3'XX'$ system with the following parameters: δ_{1_H} = 6.65 ppm; δ_{19_F} = 15.88 ppm; $J_{CF_3\text{-}CH}$ = 8.69 Hz; $J_{CF_3C=CH}$ = −0.4 Hz; J_{H-H} = 12.83 Hz; J_{CF_3,CF_3} = 9.96 Hz with a R.M.S.D. = 0.07 Hz.

The low value of J_{H-H} (7) supports the *cis* geometry, as does the high value of $J_{CF_3\text{-}CF_3}$ (8), especially if compared with the much lower value for butyne **2**, which has the two CF_3 groups nearly at the same distance as the *trans* isomer. A small amount of another compound (<1%) was also found, whose chemical shift suggests the presence of the $CF_3CH_2CH_2CF_3$ **6**.

Due to the strongly coupled $A_3A_3'XX'$ system the proton spectrum is extremely complex and a poor sensitivity in the corresponding ^3H spectrum is expected. The ^3H NMR spectrum of butenes **3** and **4** gave a broad main multiplet (see Fig. 4), and a barely observable ^3H multiplet attributable to the *trans* isomers. Since the ^3H NMR spectra were not useful as a measure of the ratio between mono- and ditritiated compounds, a ^{19}F NMR spectrum was measured (Fig. 5).

The ^{19}F singlet at 22.878 ppm is due to CF_3-C≡C-CF_3 and nearby there is a very small signal possibly due to a small amount (≈0.5%) of another perfluoroalkyne.

The main multiplet at about 15.8 ppm is shown enlarged in Fig. 6. This complex multiplet arises from the partial superimposition of the ^{19}F spectra due to CF_3-CH=CH-CF_3 **5**, CF_3-CH=C^3H-CF_3 **4**, and CF_3-C^3H=C^3H-CF_3 **3**. A strong isotope-induced shift must be invoked to rationalize the experimental spectra, which were simulated (see insert of Fig. 6) in order to perform a quantitative analysis. The following labelling:

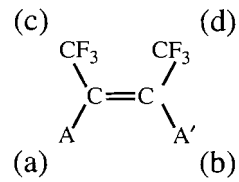

was used for compounds **5**, **4**, and **3**.

NMR data relative to light **5**, monotritiated **4**, and ditritiated 1,4-hexafluorobutenes **3** are summarized in Table 3.

As evinced by the values reported in Table 3, the ^3H induced shift on the ^{19}F NMR can be quantified as follows: $\Delta\delta_c$ = 0.06 ppm upfield and $\Delta\delta_d$ = 0.04 ppm upfield for monotritiated butene **4** with respect to the light one **5**; $\Delta\delta_c = \Delta\delta_d$ = 0.1 ppm upfield for bitritiated butene **3** with respect to light **5**.

TABLE 2. Relative distribution of the products in the deuterium addition to perfluoro-2-butyne **s**[a]

	Deuterium (mmol)	Perfluoro-2-butyne **2** (mmol)	Pressure (Torr)	Time (h)	Products (%)		
					2	**5**	**6**
(a)	0.18	0.16	300	1	95	5	—
(b)	0.017	0.016	50	4	85	15	—
(c)	0.18[b]	0.16	300	4	85	15	—
(d)	8.0	7.0	450	6	80	17	3
(e)	0.18	0.16	300	12	60	30	10
(f)	0.017	0.016	50	19	40	30	30
(g)	3.2	2.8	500	24	—	40	60

[a]All the experiments were carried out in the gas phase in the presence of Lindlar catalyst (0.5 mg for 1 Torr of starting compound **2**) poisoned with quinoline (1 μL/mg of catalyst). Different glass vessels with different internal volume were used for the reported blank runs.

[b]Similar conditions were used for radiochemical synthesis.

Can. J. Chem. Downloaded from www.nrcresearchpress.com by 92.62.229.171 on 09/08/12
For personal use only.

Can. J. Chem. Downloaded from www.nrcresearchpress.com by 92.62.229.171 on 09/08/12
For personal use only.

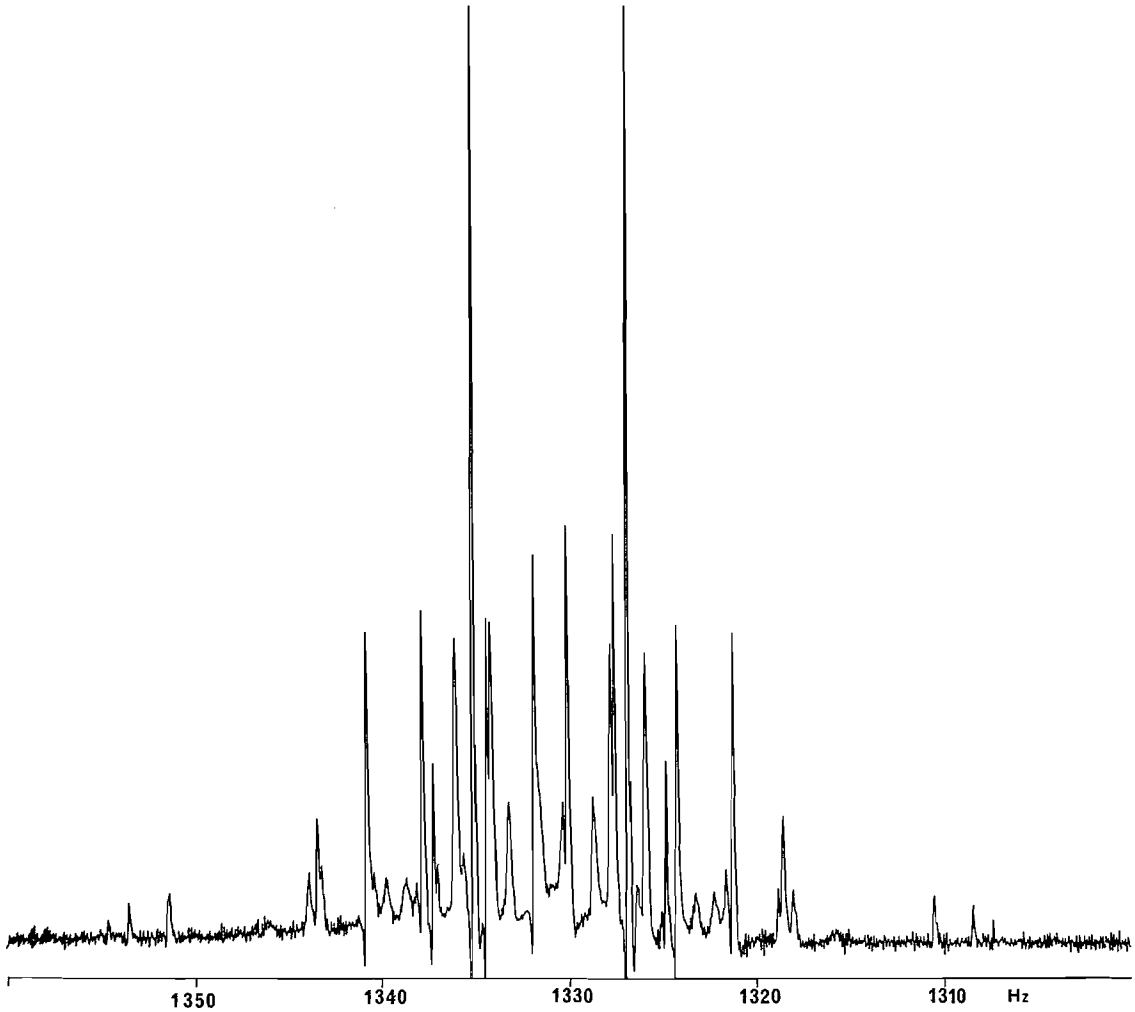

FIG. 3. ^{1}H NMR spectrum of CF_3-CH=CH-CF_3 **5**.

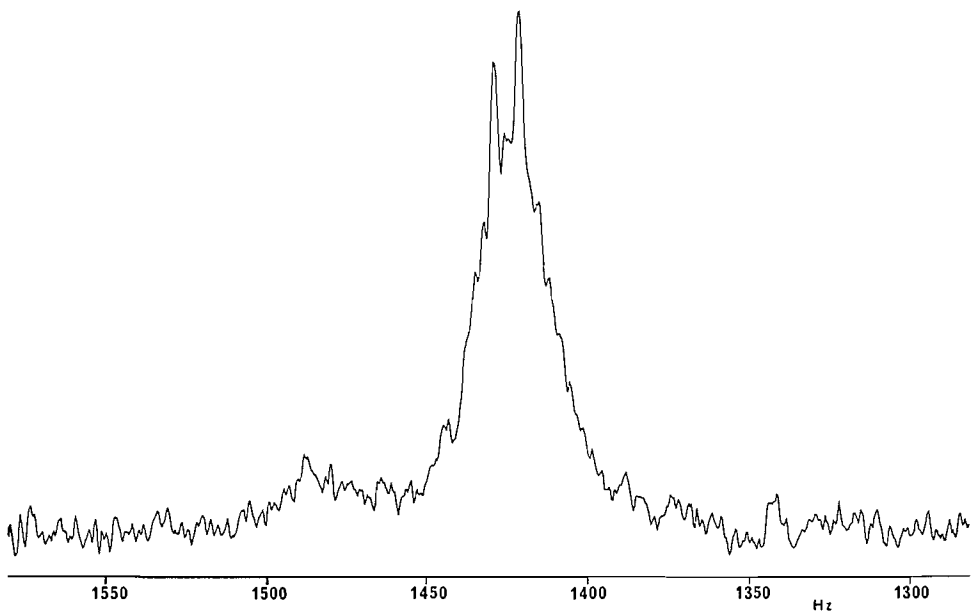

FIG. 4. ^{3}H NMR spectrum of tritiated 1,1,1,4,4,4-hexafluoro-2-butenes **3** and **4**.

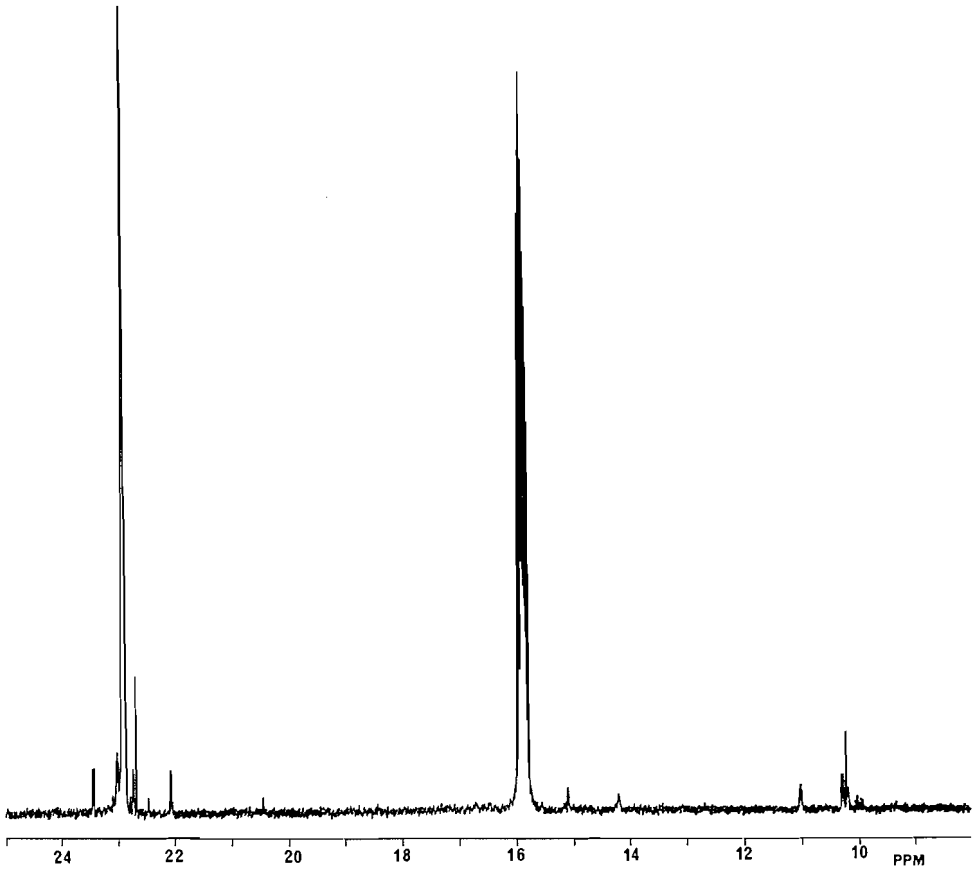

FIG. 5. ^{19}F NMR spectrum of butene mixture of **3**, **4**, and **5**.

To confirm the above interpretation an ^{1}H decoupled ^{19}F spectrum was run (Fig. 7). Here the spectrum of **5** becomes a singlet, the spectrum of **3** is unaffected (note the similarity of the dashed lines due to **3** with the calculated spectrum shown in the insert of Fig. 6), while the two CF_3 groups of the monotritiated moiety **4** are nonequivalent due to the different isotope chemical shifts induced by ^{3}H, respectively 3 of 5 bonds apart (note the different multiplicity of the two broad doublets at 15.83 and at 15.85 ppm, which confirms the previous assignment). However, due to the presence of the nuclear Overhauser effect (NOE), different in compounds **5** and **4** and absent in **3**, the quantitative analysis was performed on the undecoupled spectrum (Fig. 6); here the first peak on right is due only to the ditritiated moiety, the central broad resonance is due only to the monotritiated moiety, while the lowest field peak is due to the inactive butene; all these peaks have a known weight as shown by the simulated spectra. Quantitative analysis gave relative amounts of 40% **5**, 35% **4**, and 25% **3**.

Other extremely weak peaks in the ^{19}F spectrum are due to the *trans* impurity already detected in the ^{3}H spectrum and possibly to the saturated compound.

Results and discussion

The high-pressure hydrogenation of $CF_3C{\equiv}CCF_3$ butyne **2** is reported (6) to give 1,1,1,4,4,4-hexafluoro-2-butene **5** as the main product, plus hexafluorobutane **6** (eq. [3]).

$$[3]\quad \underset{\mathbf{2}}{CF_3C{\equiv}CCF_3} \xrightarrow{H_2} \underset{\mathbf{5}}{CF_3CH{=}CHCF_3} \xrightarrow{H_2} \underset{\mathbf{6}}{CF_3CH_2CH_2CF_3}$$

Three substantial changes were introduced to adapt this procedure to radiochemical requirements. First the synthesis was carried out in the gas phase in the presence of the catalyst with the initial total pressure in the range 150–500 Torr. These pressures were easily reached using standard glassware apparatus and reasonable amounts of radioactive tritium gas (37–110 GBq).

The second change was the use of poisoned Lindlar catalyst (9) instead of Raney nickel. The former catalyst was less reactive and so minimized further hydrogenation of the initial butene. However the ratio [quinoline]/[Lindlar catalyst] was important and numerous blank runs revealed that 1 μL/mg was best.

The last change was the use of a short reaction time (4 h or less) to limit formation of butane **6**.

Several blank runs were carried out using deuterium gas (>99 mol%) and perfluoro-2-butyne **2** at constant molar ratio ($[D_2]/[\mathbf{2}] = 1.15$) as reported in Table 2. The relative yields and isotopic distributions were determined by GC/MS. Whenever the reaction was stopped before 6 h no butane **6** was observed. For entries (a), (b), (c), and (d) of Table 2, the averaged relative abundances of d_2, d_1, and d_0 products were 60%, 30%, and 10% respectively. The butene **3** in the radiochemical synthesis was formed in smaller amount than butenes **4** and **5**. This different isotopic distribution is ascribed both to a low level of the radioisotopic purity of the tritium gas employed and some hydrogenated impurity present in the reaction medium during the radiochemical run.

The isotopic distribution values obtained for the radioactive butenes **3** and **4** by GC/MS analyses were quite reproducible, despite the limited amounts of the radioactive material employed in the investigation and the different iso-

Can. J. Chem. Downloaded from www.nrcresearchpress.com by 92.62.229.171 on 09/08/12
For personal use only.

Can. J. Chem. Downloaded from www.nrcresearchpress.com by 92.62.229.171 on 09/08/12
For personal use only.

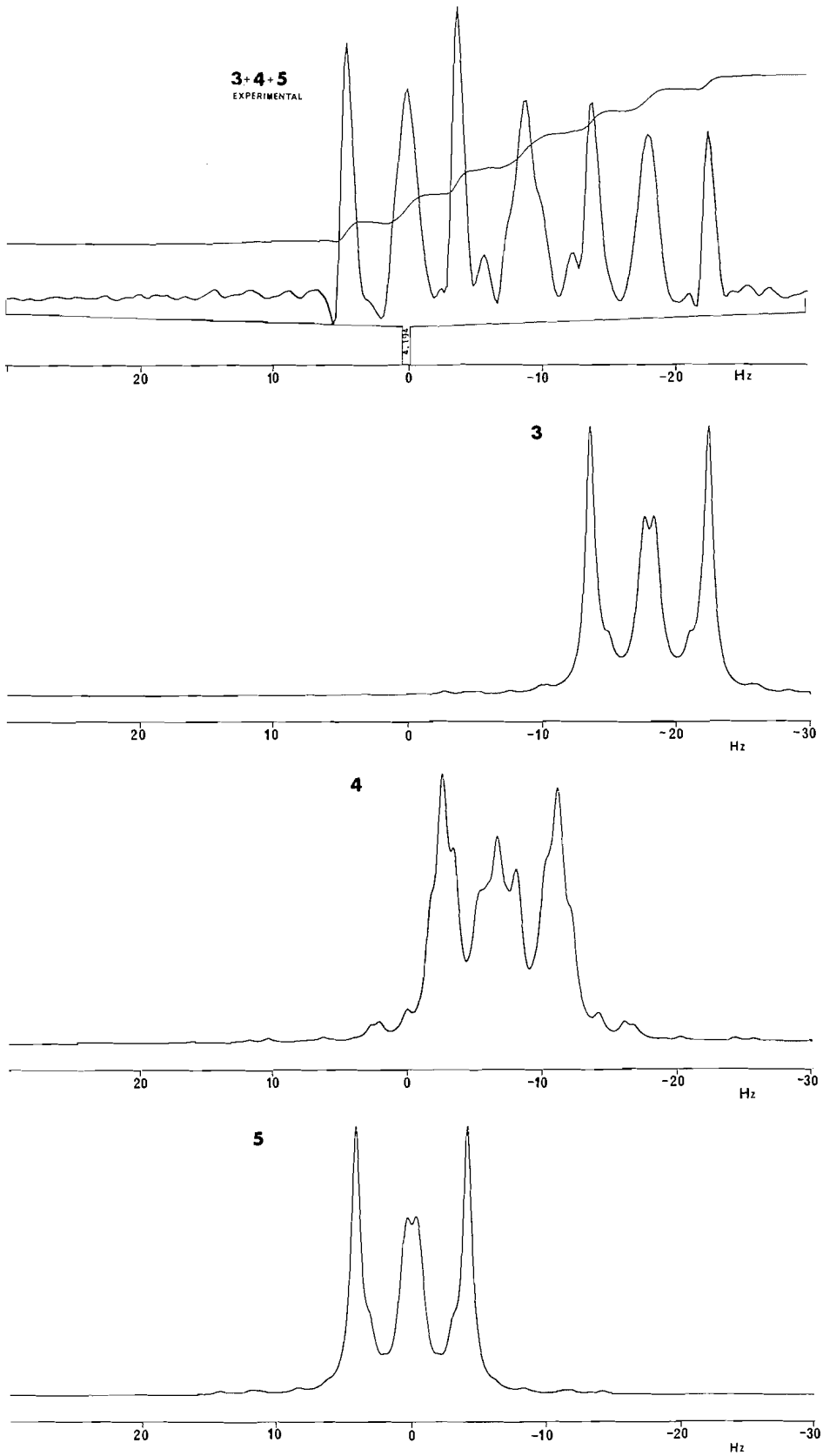

FIG. 6. Enlarged experimental ^{19}F NMR spectrum of the 15.8 ppm absorbance (Fig. 5) relative to **5** and tritiated butenes **3** and **4**. Simulated representations for the same products are reported (see the text) in the insert.

TABLE 3. NMR parameters of hexafluorobutenes **3**, **4**, and **5**

	δ_a	δ_b	δ_c	δ_d	$J_{a,b}$	$J_{a,c}$	$J_{a,d}$	$J_{b,c}$	$J_{b,d}$	$J_{c,d}$
	(ppm)				(Hz)					
5: A = A′ = ^{1}H	6.65	6.65	15.88	15.88	12.83	8.69	−0.4	−0.4	8.69	9.96
4: A = ^{3}H; A′ = ^{1}H	6.65	6.65	15.82	15.84	13.66[a]	9.25[a]	−0.4	−0.42	8.69	9.96
3: A = A′ = ^{3}H	6.65	6.65	15.78	15.78	14.50[a]	9.25[a]	−0.42[a]	−0.42[a]	9.25[a]	9.96

For compound **5**: $J_{^{13}C-F}$ geminal = |273.5| Hz and isotope-induced shift by geminal ^{13}C $\Delta\delta_{v}$ = 0.258 ppm upfield.
[a]Obtained by multiplying the values of **5** by γ^3H/γ^1H.

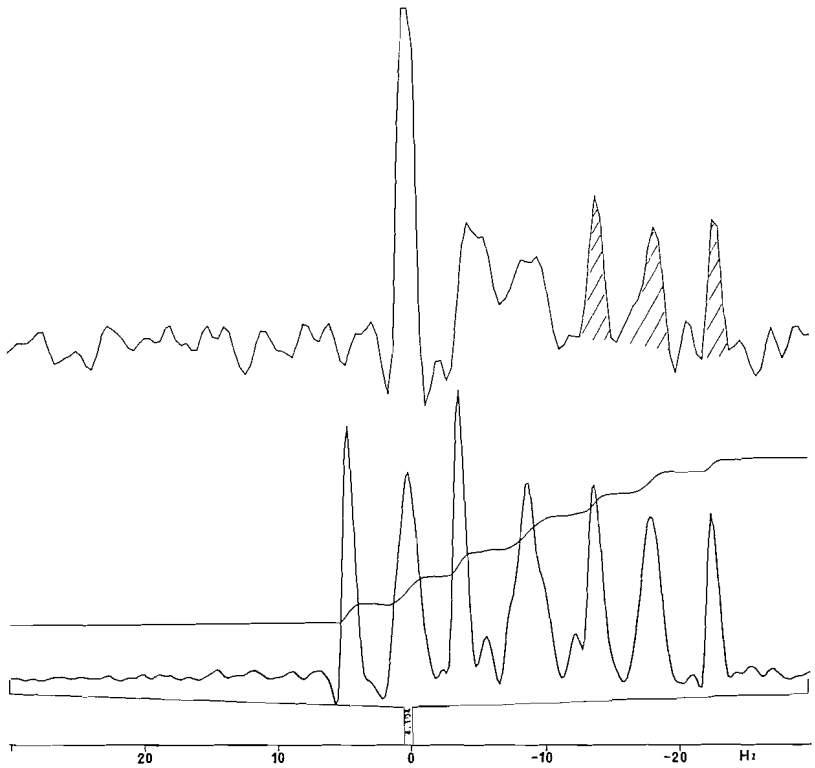

FIG. 7. Enlarged experimental ^{1}H decoupled ^{19}F spectrum (above) in comparison to the spectrum described in Fig. 6 (bottom) of the tritiated butenes **3** and **4** and the light **5**.

topic (tritium) contents present in the three butenes. The quantitative evaluation was done using the characteristic fragmentation peak, $[M^+ - F]$, for every butene of the mixture, avoiding in this way any possible uncertainties due to different isotopic fragmentation pathways, which a choice of other characteristic peaks could have induced.

Confirmation of the results came from the ^{3}H and ^{19}F NMR analyses of the butenes **3**, **4**, and **5**. Previously, ^{3}H NMR was shown (10) to be an important technique for the qualitative and quantitative analyses of products formed by radiochemical procedures. In the present study, this technique also provided some indications about the nature of the desired products and some other collateral substances (see footnote 2) formed during the synthesis.

However, due to the complex spectral multiplicity of the ^{3}H NMR signals for the butenes **3** and **4**, the quantitative evaluation of the isotopic (tritium) distribution between the two possible tritiated products was impossible. Fortunately, however, the tritium isotope-induced shift on the ^{19}F NMR spectra allowed the quantitative identification of the butenes **3**, **4**, and **5**, confirming the results obtained by the GC/MS technique.

While tritium isotope effects on ^{13}C spectra were reported previously (11), our results give the first evidence of a strong tritium isotope-induced shift shown in ^{19}F NMR (12), thus allowing a good quantitative analysis. This should be a generally useful way for the structural investigation of fluorinated molecules including those labeled also with stable isotopes, such as deuterium.

Acknowledgements

Financial support of this research by the donors of the Petroleum Research Fund, administered by the American Chemical Society, and by NATO is gratefully acknowledged.

1. (*a*) T. T. Tidwell. Adv. Carbocation Chem. **1**, 1 (1989); (*b*) G. A. Olah and Y. K. Mo. Adv. Fluorine Chem. **7**, 69 (1972); (*c*) T. T. Tidwell. Angew. Chem. Int. Ed. Engl. **23**, 29 (1984); (*d*) R. Filler. Adv. Fluorine Chem. **6**, 1 (1970).
2. (*a*) T. T. Tidwell, S. Wolfe, M. Charpentier, and J. Fossey.

Can. J. Chem. Downloaded from www.nrcresearchpress.com by 92.62.229.171 on 09/08/12
For personal use only.

Can. J. Chem. **65**, 473 (1987); (*b*) G. P. Ford and K. S. Raghuveer. Tetrahedron, **44**, 7489 (1988).
3. M. McAllister, T. T. Tidwell, M. R. Peterson, and I. G. Csizmadia. J. Org. Chem. **56**, 575 (1991).
4. (*a*) B. Ciommer and H. Schwarz. Z. Naturforsch. B: Anorg. Chem. Org. Chem. **38B**, 635 (1983); (*b*) T. A. Shaler and T. H. Morton. J. Am. Chem. Soc. **111**, 6868 (1989); (*c*) K. Stanney, J. M. Tedder and A. L. Mitchell. J. Chem. Soc. Perkin Trans. 2, 1383 (1986).
5. (*a*) F. Cacace and M. Speranza. *In* Techniques for the study of ion–molecule reactions, Vol. 20. *Edited by* F. M. Farrar and W. H. Saunders, Jr. Wiley, New York. 1988; (*b*) G. Angelini, A. L. Segre, M. Speranza and J. Altman. J. Org. Chem. **45**, 3291 (1980); (*c*) G. Angelini, S. Fornarini, and M. Speranza. J. Am. Chem. Soc. **104**, 4773 (1982); (*d*) M. Speranza, Y. Keheyan and G. Angelini. J. Am. Chem. Soc. **105**, 6377 (1983); (*e*) G. Angelini, Y. Keheyan, and M. Speranza. Helv. Chim. Acta, **71**, 107 (1988); (*f*) G. Angelini, C. Sparapani, P. Giacomello, and M. Speranza. J. Phys. Org. Chem. 467 (1989).
6. A. L. Henne and W. G. Finnegan. J. Am. Chem. Soc. **71**, 298 (1949).
7. Atta-ur-Rahman. Nuclear magnetic resonance. Springer Verlag, New York. 1986.
8. T. G. Appleton, H. C. Clark, R. C. Poller, and R. J. Puddephatt. J. Organomet. Chem. **39**, C13 (1972).
9. S. Fornarini and M. Speranza. Tetrahedron Lett. **25**, 869 (1984).
10. G. Angelini, Y. Keheyan, G. Lilla, and A. L. Segre. Gazz. Chim. Ital. **119**, 107 (1989).
11. C. H. Arrowsmith, L. Baltzer, A. J. Kresge, M. F. Powell, and Y. S. Tang. J. Am. Chem. Soc. **108**, 1356 (1986).
12. E. A. Evans, D. C. Warrel, J. A. Elvidge, and J. R. Jones. Handbook of tritium NMR spectroscopy and applications. J. Wiley & Sons, New York. 1986.

Can. J. Chem. Downloaded from www.nrcresearchpress.com by 92.62.229.171 on 09/08/12
For personal use only.

Phosphorus-31 chemical shieldings in a fused *cis*-1,2,3-benzothiadiphosphole: a dipolar NMR study

GANG WU, RODERICK E. WASYLISHEN,[1] AND WILLIAM P. POWER
Department of Chemistry, Dalhousie University, Halifax, N.S., Canada B3H 4J3

AND

GRAZIANO BACCOLINI
Dipartimento di Chimica Organicà, Universita, Viale Risorgimento 4, 40136 Bologna, Italy

Received June 17, 1991

GANG WU, RODERICK E. WASYLISHEN, WILLIAM P. POWER, and GRAZIANO BACCOLINI. Can. J. Chem. **70**, 1229 (1992).

Phosphorus-31 NMR static powder spectra and high-resolution magic angle spinning spectra have been obtained for a new heterocyclic compound, *cis*-2,10-dimethyl[1,2,3]benzothiadiphospholo[2,3*b*][1,2,3]benzothiadiphosphole (**1**), which contains a P(III)—P(III) single bond. The homonuclear $^{31}P-^{31}P$ dipolar interaction manifests itself in both the magic angle spinning spectra and the non-spinning line shape. Under the AX spin pair approximation, analysis of the spinning sidebands in the MAS experiment yields a full characterization of the two ^{31}P chemical shielding tensors. This approximation is confirmed by the exact powder line shape simulation for a homonuclear spin pair. Analysis of the dipolar subspectra also yields the absolute sign of $^1J(P,P)$, which is found to be negative.

Key words: phosphorus–phosphorus single bond, chemical shielding tensors, dipolar NMR, MAS, static line shape.

GANG WU, RODERICK E. WASYLISHEN, WILLIAM P. POWER et GRAZIANO BACCOLINI. Can. J. Chem. **70**, 1229 (1992).

On a déterminé le spectre RMN du ^{31}P, de la poudre statique ainsi qu'à l'aide de la technique de rotation à l'angle magique, d'un nouveau composé hétérocyclique, le *cis*-2-,10-diméthyl[1.2.3]benzothiadiphospholo[2,3*b*][1,2,3]benzothiadiphosphole (**1**), qui contient une liaison simple P(III)—P(III). L'interaction dipolarie $^{31}P-^{31}P$ homonucléaire se manifeste tant dans le spectre détermine à l'aide de la technique de rotation à l'angle magique que dans la forme de la raie du spectre statique. En utilisant l'approximation AX pour la paire de spin, l'analyse des bandes latérales de rotation obtenues lors des expériences réalisées à l'aide de la technique de rotation à l'angle magique, on obtient une caractérisation complète des deux tenseurs de blindage chimique du ^{31}P. Cette approximation est confirmée par la simulation exacte de la forme de la raie du spectre statique pour une paire de spin homonucléaires. L'analyse des sous-spectres dipolaires fournit aussi le signe absolu de la constante $^1J(P,P)$, qui est négative.

Mots clés : liaison simple phosphore–phosphore, tenseurs de blindage chimique, RMN dipolaire, technique de rotation à l'angle magique, forme de la raie du spectre statique.

[Traduit par la rédaction]

Introduction

A new heterocyclic system containing a P(III)—P(III) single bond, *cis*-2,10-dimethyl[1,2,3]benzothiadiphospholo[2,3*b*][1,2,3]benzothiadiphosphole (**1**), has recently been synthesized by the reaction of methyl *p*-tolyl sulphide with PCl_3 and $AlCl_3$ (1, 2). Based upon **1**, a highly stereospecific phosphorus–carbon exchange process has been developed (3, 4). The "butterfly" arrangement of **1** forces the phosphorus electron lone pairs to adopt an eclipsed

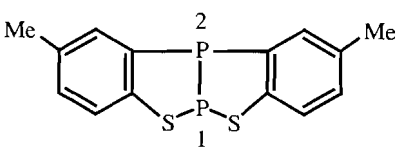

1

conformation. Because this conformation is unusual for a molecule containing a P(III)—P(III) single bond, we thought that it would be of interest to characterize the magnetic shielding tensor of each of the two phosphorus centres in **1**, where P6 and P12 (the IUPAC nomenclature) are renumbered as P1 and P2 for convenience. The technique used in this study is dipolar/chemical shift NMR spectroscopy and in the case of **1** it involves a study of the ^{31}P NMR spectrum of a solid powder sample with and without magic angle spinning (MAS). Although this technique has been widely used to study isolated spin pairs (5), there have been few reports dealing with $^{31}P-^{31}P$ spin pairs (6–9) and, to our knowledge, a full characterization of the ^{31}P chemical shielding (CS) tensor in a compound containing a P(III)—P(III) single bond has not appeared. In addition to obtaining information about the ^{31}P shielding tensors of **1**, we were interested in determining whether or not the solid-state ^{31}P NMR spectrum of **1** could be successfully analyzed as an AX spin system. Here we discuss the criterion that permits a homonuclear two-spin solid-state spectrum to be analyzed as an AX spectrum.

Theory

In the solid state the NMR spectrum of an isolated spin-$\frac{1}{2}$ nucleus is dominated by the orientation dependence of the chemical shift. The NMR spectrum of such a powder sample permits one to directly determine the three principal components of the shielding tensor. However, in general, information concerning the orientation of the shielding tensor is unavailable from the powder spectrum. If the isolated spin is adjacent to another spin-$\frac{1}{2}$ nucleus, then the spectrum is modified by the direct dipolar coupling and the indirect spin–spin "*J*" coupling interactions. The direct dipolar interaction is also dependent upon the orientation of the internuclear dipolar vector in the magnetic field and, in principle, provides a reference frame for fixing the orientation of the shielding tensor. Because the dipolar interaction is axially

[1]Author to whom correspondence may be addressed.

Can. J. Chem. Downloaded from www.nrcresearchpress.com by 92.62.229.171 on 09/08/12
For personal use only.

Can. J. Chem. Downloaded from www.nrcresearchpress.com by 92.62.229.171 on 09/08/12
For personal use only.

symmetric, the orientation of the shielding tensor cannot in general be completely determined from a dipolar/chemical shift NMR powder spectrum. In the discussion which follows we present a general discussion of the dipolar/chemical shift NMR spectrum of an isolated homonuclear spin pair. In particular, we will begin by describing the general NMR spectrum of a spin pair where the chemical shift difference between the two nuclei, A and X, is always much greater than both the J and the dipolar coupling between them at all orientations. In general, the static dipolar/chemical shift NMR spectrum of the homonuclear AX system consists of two dipolar subspectra for each nucleus. Each dipolar subspectrum has the same line shape as that well known for an isolated nucleus with anisotropic chemical shift, and can be characterized by three principal components of an effective dipolar/chemical shift tensor.

It is quite common that one principal axis of the chemical shift tensor is perpendicular to the dipolar vector (internuclear vector) in a dipolar coupled spin pair (10–16). If we assume that one principal component, ν_{ii}, of the CS tensor at one nucleus is perpendicular to the dipolar vector, matrix elements of the effective dipolar/chemical shift tensor **T** at this nucleus in the AX spin system are given by eq. [1] (10, 11):

$$[1a] \quad T_{ii} = \nu_{jj} + m\,(R_{\text{eff}} + J_{\text{iso}})$$

$$[1b] \quad T_{jj} = \nu_{jj} + m\,[R_{\text{eff}}(1 - 3\cos^2\theta) + J_{\text{iso}}]$$

$$[1c] \quad T_{kk} = \nu_{kk} + m\,[R_{\text{eff}}(1 - 3\sin^2\theta) + J_{\text{iso}}]$$

$$[1d] \quad T_{jk} = T_{kj} = -(3/2)m\,R_{\text{eff}}\sin 2\theta$$

$$[1e] \quad T_{ij} = T_{ji} = T_{ik} = T_{ki} = 0$$

where $i, j, k = 1, 2, 3$, and cyclic permutations, θ is the angle between ν_{jj} of the CS tensor and the dipolar vector, while $m = +\frac{1}{2}$ and $-\frac{1}{2}$ correspond to the two dipolar subspectra. R_{eff} is the effective dipolar coupling constant and J_{iso} is the isotropic indirect spin–spin coupling constant. The effective dipolar coupling constant can be written:

$$[2] \quad R_{\text{eff}} = \langle R_{\text{DD}}\rangle - \langle \Delta J\rangle/3$$

where $\langle R_{\text{DD}}\rangle = (\mu_0/4\pi)\gamma_{\text{P}}^2(\hbar/2\pi)\langle r_{\text{PP}}^{-3}\rangle$ is the dipolar coupling constant in frequency units, and $\Delta J = J_{\parallel} - J_{\perp}$ is the anisotropy in the indirect spin–spin interaction; $J_{\parallel}$ and $J_{\perp}$ refer to components parallel and perpendicular to the internuclear vector, respectively. Equation [2] is based upon the assumption that the indirect spin–spin interaction **J** tensor is axially symmetric with the unique axis along the internuclear dipolar vector. The angular brackets in eq. [2] indicate that both R_{DD} and ΔJ are subject to motional averaging (11, 17).

The matrix of eq. [1] can be diagonalized and the three principal values of each subspectra are given by eq. [3],

$$[3a] \quad T_i = \nu_{ii} + m\,(R_{\text{eff}} + J_{\text{iso}})$$

$$[3b] \quad T_j = \frac{1}{2}[\nu_{jj} + \nu_{kk} + m\,(2J_{\text{iso}} - R_{\text{eff}}) + \alpha]$$

$$[3c] \quad T_k = \frac{1}{2}[\nu_{jj} + \nu_{kk} + m\,(2J_{\text{iso}} - R_{\text{eff}}) - \alpha]$$

where

$$\alpha = [(\nu_{jj} - \nu_{kk})^2 - 6m(\nu_{jj} - \nu_{kk})R_{\text{eff}}\cos 2\theta + 9m^2R_{\text{eff}}^2]^{1/2}$$

When $|\nu_{jj} - \nu_{kk}| \gg R_{\text{eff}}$, one can neglect the off-diagonal elements in eq. [1] and obtain the three principal values of the effective dipolar/chemical shift tensor **T** to a zeroth order approximation

$$[4a] \quad T_i = \nu_{ii} + m\,(R_{\text{eff}} + J_{\text{iso}})$$

$$[4b] \quad T_j = \nu_{jj} + m\,[R_{\text{eff}}(1 - 3\cos^2\theta) + J_{\text{iso}}]$$

$$[4c] \quad T_k = \nu_{kk} + m\,[R_{\text{eff}}(1 - 3\sin^2\theta) + J_{\text{iso}}]$$

It is readily seen from eqs. [3] and [4] that the isotropic positions of the two effective dipolar/chemical shift tensors at each nucleus occur at $\nu_{\text{iso}} \pm \frac{1}{2}J_{\text{iso}}$, respectively. Therefore, two J-coupled doublets will be observed for a homonuclear AX spin pair under the MAS condition. From the intensity distribution of the spinning sidebands, effective dipolar/chemical shift tensors can be recovered (18, 19) and the effective dipolar coupling constant and the relative orientation of the chemical shift tensors in the molecular frame can be deduced. One important general feature of the dipolar subspectra is that the difference between effective tensor components at the direction perpendicular to the dipolar vector gives direct information on the effective dipolar coupling constant, since $\Delta T_i = T_i^+ - T_i^- = R_{\text{eff}} + J_{\text{iso}}$. The positive and negative superscripts refer to the sign of the spin quantum number m.

Experimental

Synthesis of the new heterocyclic compound **1** was reported previously (1, 2). Phosphorus-31 NMR spectra were obtained on a Bruker MSL-200 NMR spectrometer ($B_0 = 4.70$ T) operating at 81.033 MHz. A fine white powder sample of **1** was packed into a aluminum oxide rotor. All spectra were recorded at 21°C with high-power ^{1}H decoupling during data acquisition. Cross-polarization was fulfilled under the Hartmann–Hahn match. The 90° pulse width was 4.0 μs. Typical values of the contact time were 2–5 ms and the recycle time was 10 s. MAS spinning speeds ranged from 2 to 4 kHz. The magic angle was adjusted by examining the ^{79}Br NMR signal of a KBr sample (20).

All ^{31}P chemical shifts were referenced to 85% H_3PO_4(aq) by using solid $NH_4H_2PO_4$, which has a resonance at +0.81 ppm relative to 85% H_3PO_3(aq).

Spinning sideband analysis was performed using a simplex program based upon the method of Herzfeld and Berger (19). Typically, the relative intensities of six or seven spinning sidebands were used and three best-fit tensorial elements were obtained after a few iterations.

The static powder line shape for a homonuclear spin pair was simulated with a program written in FORTRAN-77 incorporated with the POWDER routine (21). The simulations were based upon the exact analytical expression for a homonuclear spin pair (10). Both the direct dipolar and indirect spin–spin interactions were taken into account. The calculated line shape was convoluted with a Gaussian line-broadening function.

Results and discussion

Analysis of MAS spectra

The slow MAS ^{31}P NMR spectrum of compound **1** with spinning speed 4.0 kHz is shown in Fig. 1. Two isotropic doublets were found centred at 75.8 and 52.0 ppm, and were assigned to P1 and P2, respectively. The assignment of the low-field doublet to P1, the phosphorus atom attached to two sulphur atoms, was based on the ^{1}H coupled solution ^{31}P

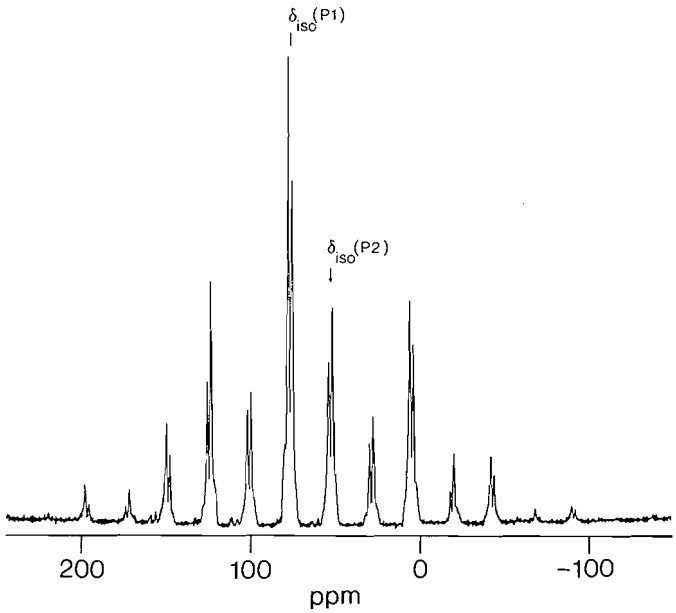

FIG. 1. ^{31}P CP/MAS NMR spectrum of **1**. The sample spinning rate is 4.0 kHz. Isotropic peaks are indicated by the arrows.

NMR spectrum, which shows a doublet for P1 arising from ^1J(P1,P2) = 211.5 Hz, and a doublet of triplets for P2 due to ^1J(P1,P2) and ^3J(P2, H) = 7.8 Hz, respectively. This assignment of P1 and P2 differs from that reported in ref. 1 and ref. 2. The observation of doublets arising from ^1J(P,P) coupling at each phosphorus site in the solid state ^{31}P NMR spectrum of **1** is consistent with the X-ray structure, which indicates that the triclinic unit cell contains two crystallographically equivalent molecules (1). Both of these isotropic chemical shifts are at low frequency (upfield shift) compared with those observed in solution state, i.e., 88.3 and 65.4 ppm for P1 and P2, respectively (1). The large number of spinning sidebands associated with each doublet in the MAS spectrum shown in Fig. 1 indicates that the chemical shift anisotropy at both phosphorus sites is large (*vide infra*).

The splitting of each doublet was 160 ± 5 Hz, arising from the homonuclear ^{31}P–^{31}P J interaction, and was confirmed by the MAS spectra at a higher field strength (B_0 = 7.04 T). This splitting was independent of spinning speed at 4.70 and 7.04 T. Although the homonuclear dipolar interaction between the two adjacent phosphorus nuclei is large in this compound (ca. R_{DD} = 1770 Hz based upon the P—P bond length, r_{PP} = 2.234 Å, determined by X-ray diffraction), we did not observe any spinning-frequency-dependent splitting as previously reported in the ^{31}P NMR spectra of dipolar coupled phosphorus spin pairs in some inorganic phosphates (9, 22) that contain ^{31}P nuclei with identical isotropic chemical shifts. It seems that such a spinning-rate-dependent splitting can only be observed easily in systems where the dipolar coupled spins have the same principal components of the chemical shielding tensor but different orientations with respect to the dipolar vector.

The magnitude of the one-bond J coupling constant in **1** was substantially smaller than the typical values reported for ^1J(P,P) in compounds containing two directly bonded tricoordinate phosphorus atoms, but significantly larger than those involving two five-coordinate phosphorus atoms (23, 24). Interestingly, the J coupling constant for **1** in the solid state was significantly smaller than the value observed in solution, 211.5 Hz (1). Since ^1J(P,P) is very dependent on the local geometry at the P—P unit (24), our observation of a smaller J in the solid state may indicate a slightly different geometric structure due to crystal packing effects. Such a change in conformation may also explain the rather large difference in solution and solid-state isotropic chemical shifts (≈12 ppm). It is worth noting that a correlation between the value of $|^1J$(P,P)| and the ^{31}P chemical shift was reported for various tetraalkyldiphosphanes, $(R_2P)_2$, with different substituents R in solution (25). Our observation on the changes of the ^1J(P,P) and $\delta(^{31}P)$ in compound **1** from solution state to solid state follows the same trend, which may indicate that crystal packing effects force the two "wings" of the butterfly molecule **1** to open slightly wider in the solid state.

TABLE 1. Principal values of the effective dipolar/chemical shift tensor in **1**[a]

Phosphorus[b]	T_1	T_2	T_3	ΔT_1	ΔT_2	ΔT_3
P1(+)	119	119	−7			
P1(−)	134	130	−40	−15	−11	+33
P2(+)	207	17	−66			
P2(−)	178	33	−58	+29	−16	−8

[a]The tensor components are in ppm and errors are estimated ±2 ppm.
[b]The plus and minus signs describe the high- and low-frequency peaks in each J-coupled doublet, respectively.

As stated in the theory section, the dipolar interaction manifests itself in the intensity distribution of each individual J-coupled sideband pattern. In Fig. 1 spinning sidebands associated with two isotropic doublets correspond to four different powder patterns, which are the four subspectra in the dipolar spectrum of a homonuclear spin pair. From the relative intensities of these spinning sidebands, all 12 principal components of the four effective dipolar/chemical shift tensors are readily calculated using the procedure of Herzfeld and Berger (19). Results are summarized in Table 1. Differences between corresponding principal components due to two relevant subspectra at each ^{31}P nucleus, $\Delta T_i = T_i^+ - T_i^-$ (i = 1,2,3), are also given in Table 1.

From the results shown in Table 1, the anisotropy of the dipolar subspectrum, defined as $|T_1 - T_3|$, is larger for the low-frequency peak of the P1 doublet than for the high-frequency one. This indicates that the absolute sign of the J coupling constant is negative (11). The anisotropies of the dipolar subspectra for the P2 doublet are in an opposite order, since the anisotropy is *negative* at P2, i.e., $|T_1 - T_{iso}| > |T_3 - T_{iso}|$, again confirming a negative ^1J(P,P). This is in agreement with the general observations and theoretical calculations of the sign of ^{31}P–^{31}P one-bond J couplings (23, 24).

The crystal structure of compound **1** indicates that, to a good approximation, the molecule has a mirror plane containing the P—P bond. As shown later, the excellent agreement between the observed powder line shape and the calculated spectrum supports this assumption. This element of molecular pseudo-symmetry requires that one of the principal axes for each of the ^{31}P shielding tensors be perpendicular to the mirror plane, and therefore perpendicular to the dipolar vector. In this case, only one angle is then required to specify the other two principal axes in the approximate mirror plane.

Given that the four subspectra contain a total of 12 effec-

Can. J. Chem. Downloaded from www.nrcresearchpress.com by 92.62.229.171 on 09/08/12
For personal use only.

TABLE 2. Principal components[a] and orientations of ^{31}P chemical shift tensors in **1**

Phosphorus	δ_{iso}	δ_{11}	δ_{22}	δ_{33}	$\Delta\delta$[b]	η[c]	θ[d]
P1	75.8	129	122	−25	154	0.07	10°
P2	52.0	190	25	−54	244	0.58	80°

[a] All principal components are in ppm and estimated errors are ±2 ppm.
[b] $\Delta\delta = |\delta_{11} - \delta_{33}|$.
[c] $\eta = (\delta_{11} - \delta_{22})/(\delta_{iso} - \delta_{33})$ for P1 and $\eta = (\delta_{22} - \delta_{33})/(\delta_{11} - \delta_{iso})$ for P2.
[d] θ is the angle between δ_{33} and the dipolar vector and the estimated error is less than ±5°.

tive principal components, we then have enough information to solve all ten remaining unknowns in this system: they are the six shielding tensorial elements for the two ^{31}P nuclei, one isotropic J coupling constant, one effective dipolar coupling constant, and two angles that specify the orientation of the dipolar vector in the principal axis system of the two ^{31}P shielding tensors.

We indicated in the theory section that the difference between effective tensor components of two subspectra along the principal direction perpendicular to the dipolar vector gives directly the sum of the effective dipolar coupling constant and the isotropic J coupling constant. From the data given in Table 1 we readily deduced that δ_{11} of P1 and δ_{22} of P2 are perpendicular to the molecular mirror plane respectively and that the effective dipolar coupling constant is $R_{eff} = 1459 \pm 162$ Hz. Substituting T_i ($i = 1,2,3$) listed in Table 1 and the above R_{eff} into eq. [3], the chemical shift tensor components and their orientations were obtained. Our calculations yield the following principal components for the chemical shift tensors: at P1, $\delta_{11} = 127$ ppm, $\delta_{22} = 124$ ppm, $\delta_{33} = -24$ ppm, and at P2, $\delta_{11} = 192$ ppm, $\delta_{22} = 25$ ppm, $\delta_{33} = -62$ ppm. The standard errors in these values were estimated to be ±2 ppm. Also, the calculations indicate that the angle between δ_{22} of P1 and the dipolar vector is 72° ± 10° while the angle between δ_{33} of P2 and the dipolar vector is 67° ± 10°. Equation [4] was also used for the above calculation and almost identical results were obtained within experimental error, indicating that the condition of $|\nu_{jj} - \nu_{kk}| \gg R_{eff}$ is valid in the present case where ν_{jj} and ν_{kk} describe the two principal components in the pseudo-mirror plane.

Analysis of the static spectrum

To examine the validity of the above calculations, i.e., to test the assumption that the ^{31}P spin pair in **1** can be treated as a homonuclear AX spin system, we performed computer simulation of the static powder line shape for a homonuclear AB spin pair, based upon the exact solution of four transitions in such a spin system (10). Although it is difficult to infer second-order (AB) character from magic angle spinning sidebands it should be readily apparent from static powder line shapes (10). Data calculated from the slow MAS spectrum were used as initial input for the simulation and they were further refined by comparing the observed powder line shape with the simulated spectrum. The final best-fit parameters for two ^{31}P chemical shift tensors are given in Table 2. The effective dipolar coupling constant was adjusted to be $R_{eff} = 1600 \pm 162$ Hz. This observed dipolar coupling constant is somewhat smaller than expected from the X-ray bond length considerations, $R_{DD} = 1770$ Hz. There are two possible reasons for such a decrease in the effective dipolar coupling constant. First, motional averaging may reduce the dipolar coupling constant. Second, there may be anisotropy in the indirect spin–spin interaction, ΔJ (see eq. [2]). If no motional correction is taken into account, the anisotropy in J is 510 ± 486 Hz assuming that R_{eff} is of the same sign as R_{DD}. Theoretical *ab initio* calculations of the $^1J(P,P)$ coupling constant in P_2H_4 indicated that the Fermi contact mechanism is dominant for the *cis* conformation (26, 27). Since the Fermi contact mechanism is isotropic, ΔJ is expected to be small in **1**. Therefore, the deviation of R_{eff} from R_{DD} is probably due to motional averaging.

It was found that the powder line-shape simulations were more sensitive to the orientation of the CS tensors than to the magnitude of the principal components. Therefore, in Table 2 all principal components are essentially the same as those obtained from the analysis of the slow MAS spectrum (except for δ_{33} of P2) while the orientations of the two CS tensors are modified by approximately 10°.

In a general heteronuclear AX spin system, any rotation of the CS tensor about the dipolar vector will give invariant powder line shapes in the static experiment, or intensity distribution of spinning sidebands in the slow MAS experiment. However, for a homonuclear spin pair, one has to be cautious about such a statement, since the relative orientation of the two CS tensors with respect to one another may become important. Obviously, two CS tensors are fixed in an AB spin pair to give a unique powder line shape. Even in the homonuclear AX approximation, it is still possible that changing the relative orientation between two CS tensors may break down the validity of the AX approximation, at least in some directions.

Within the constraints of the molecular symmetry, we have reduced the number of possible orientations to two for each ^{31}P CS tensor. Given that the angles between δ_{33} of the two CS tensors and the dipolar vector are known (θ in Table 2), there are still four possible ways to orient two CS tensors in the molecule, since both angles could be either positive or negative. All four possible orientations were put into our line-shape simulation program and a best fit is portrayed in Fig. 2. A schematic diagram illustrating the orientations of two ^{31}P CS tensors determined through this work is presented in Fig. 3. It places δ_{33} of P1 10° away from the internuclear vector towards the electron lone pair at P1, with δ_{22} lying almost in the S—P1—S plane. The determination of the CS tensor at P2 requires that δ_{11} lies in the mirror plane, being rotated by 10° from the P—P bond as indicated in Fig. 3. Similarly, δ_{33} of P2 is nearly in the plane containing the C—P2—C fragment. Simulated dipolar subspectra at each ^{31}P nucleus are also shown in Fig. 2 using the same parameters given in Table 2. The sum of the subspectra for P1 and P2 gives the powder line shape shown in Fig. 2(*b*). One does not observe any AB character in these calculated dipolar subspectra indicating that two ^{31}P nuclei in **1** could be treated as an AX system at $B_0 = 4.70$ T. One might at first expect some AB character for the homonuclear ^{31}P–^{31}P spin pair in **1**, since the difference between the isotropic chemical shifts of P1 and P2, $\Delta\delta_{iso} = 24$ ppm (ca. 1944 Hz at $B_0 = 4.70$ T), is comparable to the dipolar coupling constant between them, $R_{DD} = 1770$ Hz. However, one should realize that the ratio between $\Delta\delta_{iso}$ and R_{DD} is not the correct criterion for judg-

Can. J. Chem. Downloaded from www.nrcresearchpress.com by 92.62.229.171 on 09/08/12
For personal use only.

Can. J. Chem. Downloaded from www.nrcresearchpress.com by 92.62.229.171 on 09/08/12
For personal use only.

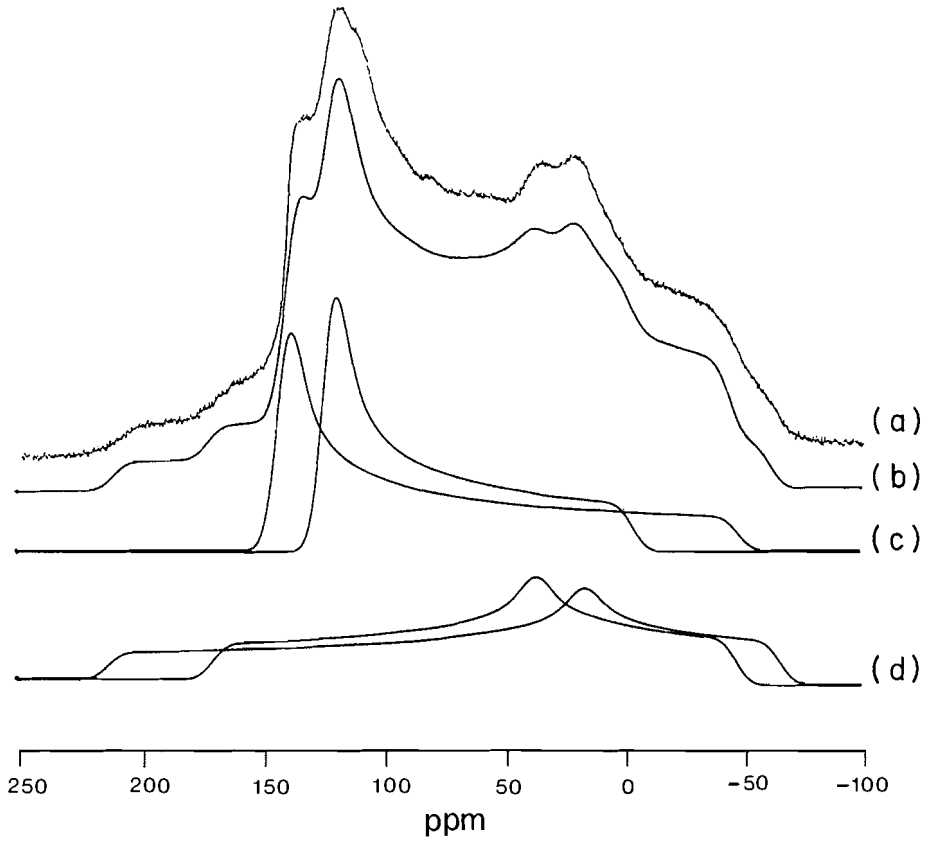

FIG. 2. (*a*) Experimental ^{31}P CP NMR spectrum of a static sample of **1**; (*b*) calculated ^{31}P NMR spectrum of **1** using the parameters in Table 2; (*c*) and (*d*) calculated dipolar subspectra for P1 and P2, respectively, using the same parameters as in (*b*).

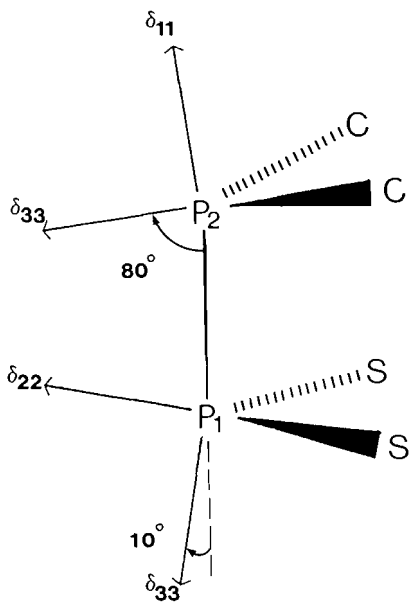

FIG. 3. A schematic diagram of the orientation of the two ^{31}P CS tensors in **1** obtained from an analysis of the ^{31}P NMR spectrum of a static powder sample. δ_{11}(P1) and δ_{22}(P2) are perpendicular to the approximate mirror plane of the molecule.

ing whether a dipolar coupled spin pair should be analyzed as an A_2, AB, or AX spin system. Because of the tensorial nature of chemical shifts in solids, one has to consider the relative orientation of the two CS tensors that make up the two-spin system. Although there is extensive overlap of the four dipolar subspectra in **1**, we found that at almost all orientations of $\boldsymbol{r}_{PP}$ in the applied magnetic field, $\boldsymbol{B}_0$, the AX approximation is valid. For example, if the magnetic field lies perpendicular to the molecular mirror plane, an orientation in which δ_{11} of P1 and δ_{22} of P2 are coincident, the chemical shift difference is about 100 ppm (ca. 8100 Hz at B_0 = 4.70 T). This is much greater than the dipolar coupling at this orientation, 800 Hz. A similar discussion also applies for the two orthogonal orientations. Extensive computer calculations of the ratio, $R/[\nu(P1) - \nu(P2)]$, as a function of orientation indicate that this ratio is less than 0.1 except when the polar angle is approximately 50° and the azimuthal angles are 50°–60° and 300°–310°. The actual contributions that these latter orientations make to the overall line shape are negligible.

We have ruled out the possible orientations of δ_{33} where two θ's have different signs, since it results in a similar, though inferior, fit. An alternative assignment occurs if both CS tensors are rotated simultaneously by 180° about the dipolar vector, giving two negative θ's. Although this gives an identical powder line shape, it will be argued below that the assignment shown in Fig. 3 is more reasonable.

The CS tensor of P1 shows near-axial symmetry ($\delta_{11} \approx \delta_{22}$), although there is no apparent local symmetry in the

Can. J. Chem. Downloaded from www.nrcresearchpress.com by 92.62.229.171 on 09/08/12
For personal use only.

molecular structure that would imply axial symmetry in the CS tensor. Since we have determined that δ_{11} of P1 is perpendicular to the molecular mirror plane, it is also perpendicular to the electron lone pair at P1. If we place δ_{33} of P1 10° away from the dipolar vector in the opposite direction to that shown in Fig. 3 (i.e., $\theta = -10°$), the direction of δ_{22} would lie nearly along the electron lone pair. Since it is unlikely that the chemical shielding would be the same along the lone pair (δ_{22} component) as in the direction perpendicular to the lone pair (δ_{11} component), this alternative assignment is discounted.

The results in Table 2 indicate that the ^{31}P shielding anisotropy of P2, $\Delta\delta = 244$ ppm, is much larger than the values reported in two related compounds containing a phosphorus–phosphorus single bond (8, 9) and by a theoretical calculation on P_2H_4 (28). The ^{31}P chemical shielding anisotropy in tetraphenyldiphosphine was also found to be relatively small ($\Delta\delta = 46$ ppm).[2] Another class of related compounds containing P(III) atoms are phosphines. Still, $\Delta\delta$ of P2 in **1** appears noticeably large compared with most of the reported values for the phosphines (ca. $\Delta\delta = 6$–85 ppm) (29). Additionally, the isotropic chemical shift of P2 in compound **1** is at a much lower field than the above-mentioned phospines and diphosphines. Although a large $\Delta\delta$ has been reported in a strained phosphirane (30), the shielding anisotropy at P2 shows an opposite trend and our data also deviate from the straight line in ref. 30. The large shielding anisotropy, $\Delta\delta$, and large isotropic shift at P2 in **1** result primarily from the significant deshielding in the δ_{11} direction, which is approximately perpendicular to the C—P—C plane. Probably, the unusual *cis* conformation of the adjacent electron lone pairs in **1** is responsible for the relatively large chemical shift anisotropy at P2. However, given the complicated nature of the anisotropic chemical shift and lack of reliable theoretical calculations, ^{31}P chemical shielding tensors are far from being fully understood.

The ^{31}P CS tensors of several inorganic phosphorus–sulphur systems were investigated recently by high-resolution solid state NMR (31–35). In these systems, $\Delta\delta$ of the $PS_{3/2}$ unit varies from 110 to 340 ppm. An attempt has been made to correlate the ^{31}P chemical shift anisotropy with the distortion from local C_{3v} symmetry (33). However, using additional data from a more recent study (34), the previous simple correlation was found to be invalid (35). With P1 bonded to two sulphur atoms and one phosphorus atom, its chemical shift anisotropy, $\Delta\delta = 154$ ppm, is smaller than the value, $\Delta\delta = 257$ ppm, found for the apical ^{31}P in P_4S_3, **2**; the two P—S bonds in **1** are much longer than the P—S bonds in P_4S_3.

It would be more informative if we were able to compare the orientation of the ^{31}P CS tensor in **1** with related compounds containing P—S single bonds. Unfortunately, only in P_4S_3 have the orientations of the CS tensor been determined by a single crystal study (36). In this case the least shielded component of the apical ^{31}P and the most shielded component of the basal ^{31}P are nearly parallel to the C_3 axis of the molecule. In the other systems, local symmetry was used to tentatively assign the unique axis in the CS tensors. Comparison of the principal values and their orientations of the ^{31}P CS tensor between the apical phosphorus atom in P_4S_3 and P1 in **1** reveals significant difference between these two ^{31}P CS tensors, although the difference in their isotropic chemical shift is relatively small. The unique component in the apical phosphorus atom in P_4S_3 corresponds to the least shielded direction while it is the most shielded in **1**. We are not in a position to give a complete explanation of the ^{31}P shielding anisotropies measured in this study, because of the limited data available and their complexity.

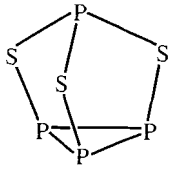

2

Conclusions

We have demonstrated that ^{31}P dipolar NMR spectroscopy is an invaluable alternative to single crystal NMR in providing a full characterization of the ^{31}P chemical shielding tensor in **1**. It is advantageous to combine the MAS experiment with the static (non-spinning) experiment in dealing with a dipolar coupled homonuclear ^{31}P spin pair, especially when there is *J* coupling between the two nuclei. This is because (*a*) resolved *J*-coupled sideband patterns in the MAS spectrum make it possible to separate different dipolar subspectra and to provide a good starting point for interpreting the static powder line shape, and (*b*) the static powder line shape contains all the information on the dipolar interaction and the shielding tensors, and thus serves as a test for the AX approximation that is usually used for analyzing the dipolar subspectra in the MAS experiment.

The CS tensor at P1 in **1** is nearly axially symmetric with the most shielded component δ_{33} as the unique direction. Significant deshielding is observed at P2 along the δ_{11} direction, which describes a direction perpendicular to the C—P—C plane. This deshielding effect results in a large anisotropy at P2, $\Delta\delta = 244$ ppm, compared with related compounds. The shielding anisotropy at P1 is 154 ppm and falls in the normal range reported for related compounds containing the P—S single bonds. Clearly, a complete understanding of the ^{31}P chemical shielding anisotropy still needs far more work from both experimentalists and theoreticians.

Acknowledgements

This research was supported by operating and equipment grants (R.E.W.) and a scholarship (W.P.P.) provided by the Natural Sciences and Engineering Research Council of Canada. We thank Dr. A. Berger and Dr. Kentgens for providing software to aid in the fitting of slow-spinning MAS spectra. Also, G.B. acknowledges financial support by the C.N.R. of Italy.

1. G. Baccolini, E. Mezzina, P. E. Todesco, and E. Foresti. J. Chem. Soc. Chem. Commun. 304 (1988).
2. G. Baccolini, E. Mezzina, and P. E. Todesco. J. Chem. Soc. Perkin Trans. 1, 3281 (1988).
3. G. Baccolini, E. Mezzina, P. E. Todesco, and E. Foresti. J. Chem. Soc. Chem. Commun. 122 (1989).
4. G. Baccolini and E. Mezzina. J. Chem. Soc. Perkin Trans. 1, 19 (1989).

[2]G. Wu, R. D. Curtis, and R. E. Wasylishen. Unpublished results.

5. W. P. Power and R. E. Wasylishen. Annu. Rep. NMR Spectrosc. **23**, 1 (1991).
6. A. R. Grimmer, P. Peter, and E. Fechner. Z. Chem. **18**, 109 (1978).
7. (*a*) P. N. Tutunjian and J. S. Waugh. J. Chem. Phys. **76**, 1223 (1982); (*b*) J. Magn. Reson. **49**, 155 (1982).
8. K. W. Zilm, G. G. Webb, A. H. Cowley, M. Pakulski, and A. Orendt. J. Am. Chem. Soc. **110**, 2032 (1988).
9. A. Kubo and C. A. McDowell. J. Chem. Phys. **92**, 7156 (1990).
10. K. W. Zilm and D. M. Grant. J. Am. Chem. Soc. **103**, 2913 (1981).
11. R. K. Harris, K. J. Packer, and A. M. Thayer. J. Magn. Reson. **62**, 284 (1985).
12. K. W. Zilm, A. J. Beeler, D. M. Grant, J. Michl, T. C. Chou, and E. L. Allred. J. Am. Chem. Soc. **103**, 2119 (1981).
13. R. E. Stark, L. W. Jelinski, D. J. Ruben, D. A. Torchia, and R. G. Griffin. J. Magn. Reson. **55**, 266 (1983).
14. G. S. Harbison, L. W. Jelinski, R. E. Stark, D. A. Torchia, J. Herzfeld, and R. G. Griffin. J. Magn. Reson. **60**, 79 (1984).
15. R. A. Santos, W. J. Chien, and G. S. Harbison. J. Magn. Reson. **84**, 357 (1989).
16. R. E. Wasylishen, W. P. Power, G. H. Penner, and R. D. Curtis. Can. J. Chem. **67**, 1219 (1989).
17. E. R. Henry and A. Szabo. J. Chem. Phys. **82**, 4753 (1985).
18. M. M. Maricq and J. S. Waugh. J. Chem. Phys. **70**, 3300 (1979).
19. J. Herzfeld and A. E. Berger. J. Chem. Phys. **73**, 6021 (1980).
20. J. S. Frye and G. E. Maciel. J. Magn. Reson. **48**, 125 (1982).
21. D. W. Alderman, M. S. Solum, and D. M. Grant. J. Chem. Phys. **84**, 3717 (1986).
22. S. Hayashi and K. Hayamizu. Chem. Phys. Lett. **161**, 158 (1989).
23. E. G. Finer and R. K. Harris. Prog. NMR Spectrosc. **6**, 61 (1971).
24. C. J. Jameson. *In* Phosphorus-31 NMR spectroscopy in stereochemical analysis. *Edited by* J. G. Verkade and L. D. Quin. VCH Publishers Inc., Deerfield Beach, Fla. 1987. pp. 205–230.
25. S. Aime, R. K. Harris, E. M. McVicker, and M. Fild. J. Chem. Soc. Dalton Trans. 2144 (1976).
26. J. P. Albrand, H. Faucher, D. Gagnaire, and J. B. Robert. Chem. Phys. Lett. **38**, 521 (1976).
27. V. Galasso. J. Magn. Reson. **36**, 181 (1979).
28. U. Fleischer, M. Schindler, and W. Kutzelnigg. J. Chem. Phys. **86**, 6337 (1987).
29. T. M. Duncan. A compilation of chemical shift anisotropies, The Farragut Press, Chicago. 1990.
30. A. L. Barra and J. B. Robert. Chem. Phys. Lett. **149**, 363 (1988).
31. R. K. Harris, P. J. Wilkes, P. T. Wood, and J. D. Woolins. J. Chem. Soc. Dalton Trans. 809 (1989).
32. T. Bjorholm and H. J. Jakobsen. J. Magn. Reson. **84**, 204 (1989).
33. H. Eckert, C. S. Liang, and G. D. Stucky. J. Phys. Chem. **93**, 452 (1989).
34. M. Tullius, D. Lathrop, and H. Eckert. J. Phys. Chem. **94**, 2145 (1990).
35. H. Eckert. J. Phys. Chem. **94**, 6515 (1990).
36. M. G. Gibby, A. Pines, W. K. Rhim, and J. S. Waugh. J. Chem. Phys. **56**, 991 (1972).

Can. J. Chem. Downloaded from www.nrcresearchpress.com by 92.62.229.171 on 09/08/12
For personal use only.

Natural products. Antitubulin effect of congeners of *N*-acetylcolchinyl methyl ether: synthesis of optically active 5-acetamidodeaminocolchinyl methyl ether and of demethoxy analogues of deaminocolchinyl methyl ether[1]

O. Boyé and A. Brossi[2]

Laboratory of Structural Biology, Natural Products Section, NIDDK, National Institutes of Health, Bethesda, MD 20892, U.S.A.

H. J. C. Yeh

Laboratory of Analytical Chemistry, NIDDK, National Institutes of Health, Bethesda, MD 20892 U.S.A.

E. Hamel

Laboratory of Molecular Pharmacology, DTP, DCT, NCI, National Institutes of Health, Bethesda, MD 20892, U.S.A.

and

B. Wegrzynski and V. Toome

Research Division, Hoffmann-La Roche Inc., Nutley, NJ 07110, U.S.A.

Received March 25, 1991

This paper is dedicated to Dr. Zdenek (Denny) Valenta on the occasion of his 65th birthday

O. Boyé, A. Brossi, H. J. C. Yeh, E. Hamel, B. Wegrzynski, and V. Toome. Can. J. Chem. **70**, 1237 (1992).

Trimethoxy-substituted dihydrodibenzocycloheptenes **4–7**, required for a structure–activity study measuring the inhibition of tubulin polymerization in vitro, were synthesized by four different routes: (1) Synthesis of **4** was achieved from 2,3-dimethoxybenzaldehyde via biphenyl aldehyde **17**, chain lengthening to propionic acid **20**, acid-catalyzed cyclization toward ketone **21**, and removal of the carbonyl group. (2) Compound **5** was obtained by eliminating the sterically most hindered methoxy group in **25** or **26** by metal reduction in alcohol. (3) Compound **6** was prepared from biphenyl aldehyde **34** obtained by Grignard reaction on oxazoline **32**. (4) Compound **7** was obtained by reductive deoxygenation of the tetrazolyl ether derivative of *N*-acetylcolchinol **41**. The key role of the aromatic oxygen atoms in colchicine and allo congeners as points of interaction with the colchicine binding site on tubulin was demonstrated by the lack of inhibitory activity of compounds **4–7**. Optically active 5-acetamide **8***a*,*b* isomers of *N*-acetylcolchinyl methyl ether **2** were obtained after chemical resolution of amine **47**. The absolute configuration of the optical isomers **47***a*,*b* and **8***a*,*b* was determined by ^{1}H NMR and CD measurements. These compounds were found inactive as inhibitors of tubulin polymerization.

O. Boyé, A. Brossi, H. J. C. Yeh, E. Hamel, B. Wegrzynski et V. Toome. Can. J. Chem. **70**, 1237 (1992).

Les triméthoxy-dihydrodibenzocycloheptènes **4–7** ont été synthetisés selon quatre voies différentes dans le cadre d'une étude de relation structure–activité concernant l'inhibition de polymérisation de la tubuline in vitro : (1) la synthèse du composé **4** a été effectuée à partir du 2,3-diméthoxybenzaldéhyde via l'intermédiaire aldéhydique **17** suivi d'une extension de chaîne vers l'acide propionique **20**, donnant, après cyclization, la cétone **21** dont la fonction carbonyle a finalement été réduite. (2) Le composé **5** a été obtenu par élimination du groupement méthoxy encombré de l'alcool **25** ou de l'oxime **26** par réduction métallique. (3) Le composé **6** a été synthétisé à partir de l'aldéhyde biphénylique **34**, obtenu par une réaction de Grignard sur l'oxazoline **32** selon la méthode de Meyer. (4) Le composé **7** provient de la déoxygénation réductive de l'éther de tétrazolyle du *N*-acétylcolchinol **41**. Le rôle clé des atomes d'oxygène aromatiques de la colchicine et des dérivés de type «allo», en tant que points d'interaction avec leur site de fixation sur la tubuline, a été demontré par l'absence de propriétés inhibitrices des composés **4–7**. Les acétamides **8***a*,*b* isomères en position 5 du *N*-acétylcolchinyl méthyl éther **2** ont été obtenues après résolution chimique de l'amine **47**. La configuration absolue des isomères optiques **47***a*,*b* et **8***a*,*b* a été determinée par des mesures de RMN et de dichroïsme circulaire. Ces composés se sont révélés inactifs en tant qu'inhibiteurs de polymérisation de la tubuline.

Mapping and full characterization of the colchicine binding site on tubulin remains a challenging and multifaceted research project (1, 2). Modification of natural (−)-(a*S*, 7*S*) colchicine **1** or the parent compound *N*-acetylcolchinol methyl ether **2** offers a possibility to gain valuable information on how these molecules bind to tubulin and inhibit its polymerization. Phenolic congeners of colchicine **1**, especially 1-demethylcolchicine, were found to be less potent than colchicine itself (1–4) as inhibitors of tubulin polymerization, with activity partially restored on esterification (5, 6). After the finding of the high potency of 6,7-dihydro-1,2,3,9-tetramethoxy-5*H*-dibenzo[*a*,*c*]cycloheptene (DBCH) **3** (7*a*), the systematic synthesis of its demethoxy derivatives **4–7** was undertaken in order to investigate the contribution of each aromatic oxygen atom in the binding process. The acetamido group in **1** and **2** is not required for binding to tubulin, as indicated by the high activity of compound **3** (7*a*). The investigation included a synthesis of the optically active amides **8***a*,*b*, with the acetamido group at C(5). Determination of their absolute configurations, a primary factor in tubulin binding ability, was made by ^{1}H NMR and CD.

[1]The results of this investigation were presented by O. Boyé at a poster session of the 200th meeting of the American Chemical Society in Washington, D.C., August 26–31, 1990 (Division of Medicinal Chemistry; Abstr. 68).

[2]Author to whom correspondence may be addressed.

Can. J. Chem. Downloaded from www.nrcresearchpress.com by 217.78.4.112 on 09/08/12
For personal use only.

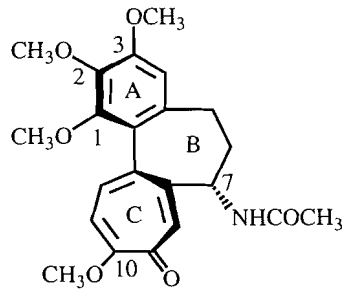

1 (a*S*, 7*S*)

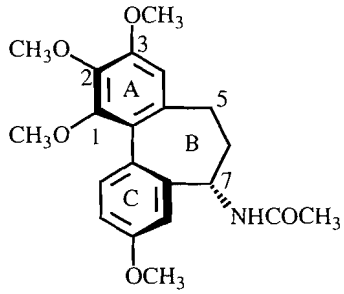

2 (a*S*, 7*S*)

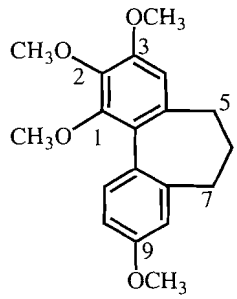

3

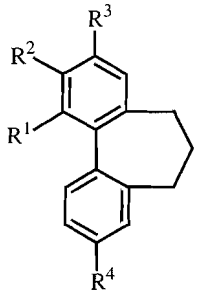

4 $R^1 = R^2 = R^4 = OCH_3$, $R^3 = H$
5 $R^1 = R^3 = R^4 = OCH_3$, $R^2 = H$
6 $R^2 = R^3 = R^4 = OCH_3$, $R^1 = H$
7 $R^1 = R^2 = R^3 = OCH_3$, $R^4 = H$

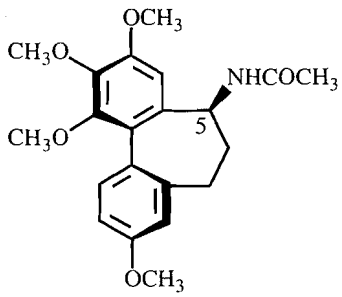

8A (a*R*, 5*S*)

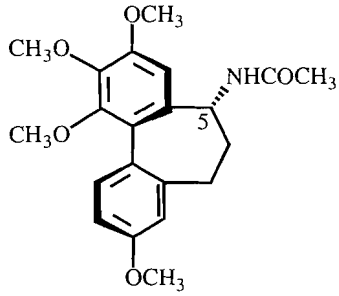

8B (a*S*, 5*R*)

Chemistry

DBCH 4 from 2,3-dimethoxybenzaldehyde (Scheme 1)

The synthesis of **4** followed a route used earlier in the synthesis of **3** (7*a*, *b*) which started from 2,3,4-trimethoxybenzaldehyde and gave ketone **24** as an intermediate. Azalactone **9**, prepared from 2,3-dimethoxybenzaldehyde and *N*-acetyl glycine, was hydrolyzed to give pyruvic acid **10***a* and acetylated enamine **10***b* as a by-product. The 16-step synthesis of **4** was handicapped by the relatively low yield encountered in the preparation of keto-ester **13** from pyruvic acid **10***a* via Robinson annelation with methyl vinyl ketone (8). The cyclization of acid **20** to ketone **21** in $(CF_3CO)_2O/CF_3COOH$ solution was greatly improved in comparison to previous work (7*a*) by conducting the reaction at low temperature.

DBCH 5 by sodium–isopropanol reduction (Scheme 2)

Reductive removal of the hindered methoxy group in alcohol **26**, obtained by reduction of ketone **24** (7*a*, *b*), was accomplished with sodium in refluxing isopropanol (12, 13) to afford DBCH **5**. This reaction is reminiscent of methoxy group eliminations observed in the aporphine alkaloid series with sodium in liquid ammonia (18, 19). DBCH **5** could also be obtained starting with oxime **25**, which, treated in the same manner as **26**, was demethoxylated and reduced in a one-pot procedure. Exhaustive methylation of amine **27** afforded quaternary salt **28***b*, which underwent Hofmann elimination to olefin **29**. Reduction of the latter afforded **5**. This material was identical with that directly obtained from **26** on treatment with sodium in isopropanol.

DBCH 6 by Meyers' biphenyl synthesis (Scheme 3)

The synthesis of **6** was tailored after Meyers' efficient synthesis of biphenyl aldehydes from phenyloxazolines with Grignard reagents (14–16).

Reaction of Grignard **31**, prepared from 5-bromoveratrole, with oxazoline **32** (obtained from 2,5-dimethoxybenzoic acid (14–16)) afforded oxazoline **33**. Deprotection of **33** was accomplished by quaternization with methyltriflate, reduction of the quaternary salt with sodium borohydride, and hydrolysis with oxalic acid to give aldehyde **34** (16). Conversion of aldlehyde **34** into ketone **38**, olefin **40**, and DBCH **6** followed the route used for the preparation of **3** and **4**.

Can. J. Chem. Downloaded from www.nrcresearchpress.com by 217.78.4.112 on 09/08/12
For personal use only.

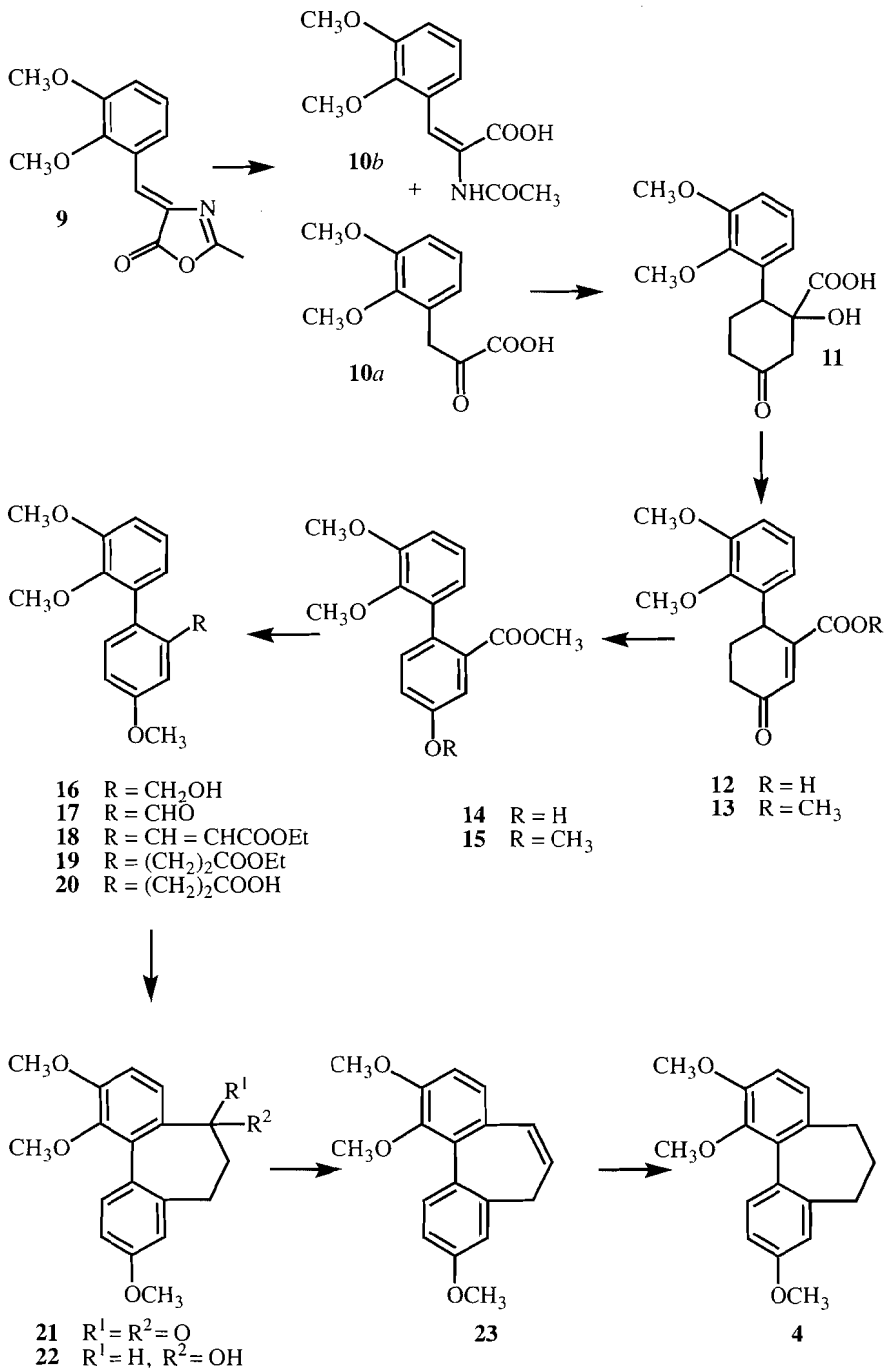

SCHEME 1

DBCH 7 from N-*acetylcolchinol* ***41*** *(Scheme 4)*

N-Acetylcolchinol, prepared from colchicine **1** by a published procedure (17), was deoxygenated by catalytic reduction of its phenyltetrazolyl ether **42** over Pd/C catalyst in acetic acid (20, 21), affording amide **43**. The latter on acid hydrolysis gave amine **44**, which after quarternization with methyl iodide and Hofmann degradation afforded olefin **46** and DBCH **7** on further reduction.

Synthesis of optically active 5-acetamidodeaminocolchinyl methyl ethers **8**a,b *(Scheme 5)*

Oxime **25** was also used to prepare the optically active isomers **8***a*,*b* (Scheme 5). Reduction of oxime **25** with hydrazine in the presence of Raney nickel catalyst afforded the racemic amine **47**, which was resolved with (+)- and (−)-dibenzoyltartaric acids in isopropanol to afford the optically active amines **47***a*,*b* after recrystallization from MeOH. Further acetylation gave the optically active amides **8***a*,*b*. The optical purity of the amines was measured by HPLC analysis of their urea derivatives **48***a*,*b*. The absolute configuration of compounds **47***a*,*b* and **8***a*,*b* was established by ^{1}H NMR spectroscopy and CD analysis. We have previously shown that natural (−)-7*S*-colchicine **1** and derived allo congeners exhibit negative Cotton effects at 260 nm (9, 10). This optical behavior results from the presence of the noncoplanar biaryl system. Ring C is twisted out of the plane

Can. J. Chem. Downloaded from www.nrcresearchpress.com by 217.78.4.112 on 09/08/12
For personal use only.

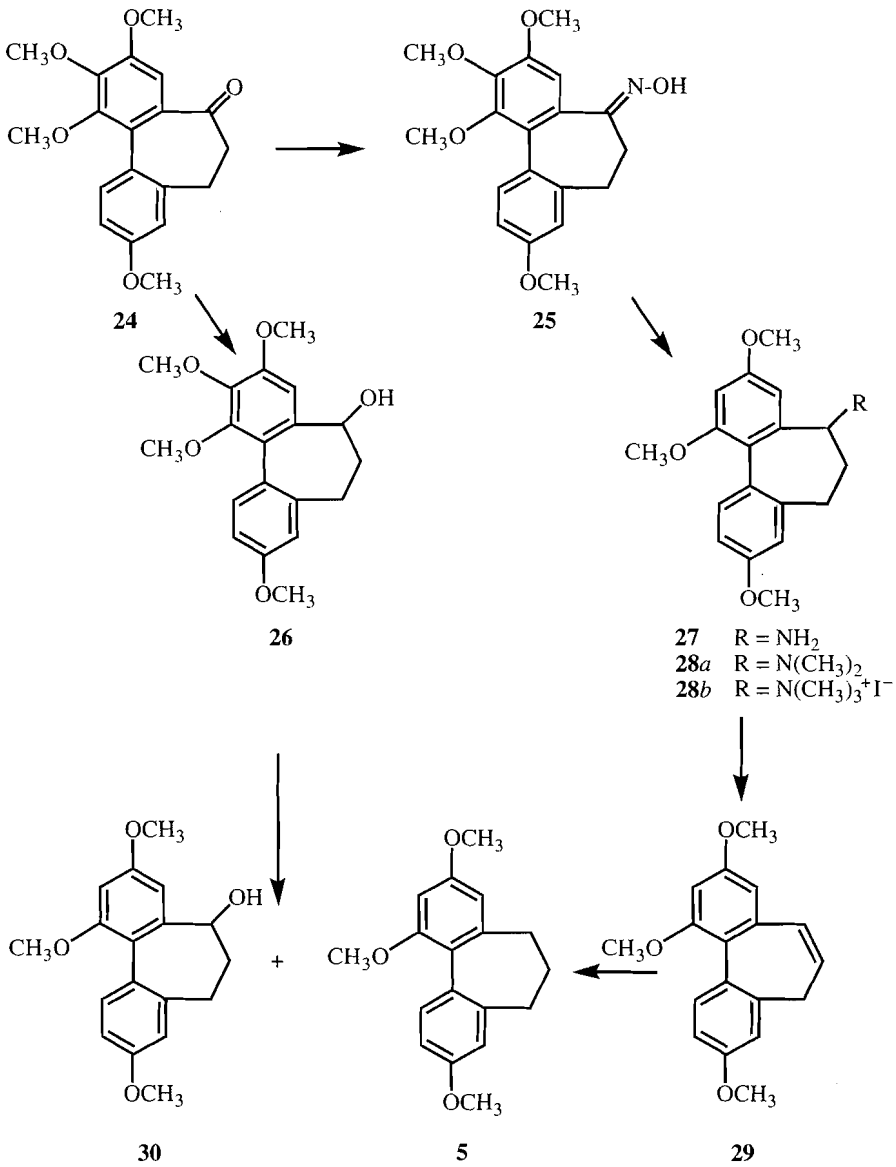

SCHEME 2

formed by ring A in a counterclockwise arrangement with a dihedral angle between the planes of ca. 53° (8). This gives an a*S* assignment to natural (−)-7*S*-colchicine, after consideration of the order of the *ortho–ortho'* substituents of the central bond, according to the chirality rules of Prelog and Helmchen (11). Counterclockwise arrangement of the biaryl systems is manifested by all the biologically active colchicinoids and their allo congeners and is considered to be an important molecular feature in their ability to bind to tubulin. Unnatural (+)-7*R*-colchicine, which has the biaryl system arranged in a clockwise fashion and has a positive Cotton effect at 260 nm, does not bind to tubulin.

Conformational equilibria and absolute configurations of 5-aminodeaminocolchinyl methyl ethers **47***a*,b *and derived acetamides* **8***a*,b

The optically active amines **47***a,b* and the derived acetamides **8***a,b* are in a solvent-dependent conformational equilibrium (Scheme 5). The absolute configurations of **47***a* and **8***a* were established as follows: the observed negative Cotton effect at 260 nm in ethanol (Fig. 1*a*) for **47***a* and **8***a* suggests that the phenyl rings in these compounds are arranged in a counterclockwise fashion, as in natural (−)-(a*S*,7*S*)-colchicine **1**. Despite the identical helicity of the biaryl system the configuration of **47***a* and **8***a* is a*R* due to the change occurring in the priority of the *ortho–ortho'* substituents as compared to (−)-colchicine (11). In conjunction with this finding, the 5*S* absolute configuration of these molecules was then derived by measuring vicinal proton coupling between H-C(5) and $H_{a,b}$-C(6) (Table 1). The dihedral angles between these protons were evaluated using the Karplus rule (23, 24). By examining the Dreiding model with the biphenyl system arranged in a counterclockwise configuration, one can conclude that H-C(5) in both compounds is axially oriented with the amino or acetamido groups in an equatorial position. This leads to a 5*S* absolute configuration for **47***a* and **8***a*. The solvent dependency of the conformational equilibrium is different for **47***a* and **8***a*. Whereas the ^{1}H NMR proton signal for H-(5) in amine **47***a* does not change significantly on switching solvents from CD_3OD to $CDCl_3$ and the negative Cotton effect at 260 nm is still sub-

Can. J. Chem. Downloaded from www.nrcresearchpress.com by 217.78.4.112 on 09/08/12
For personal use only.

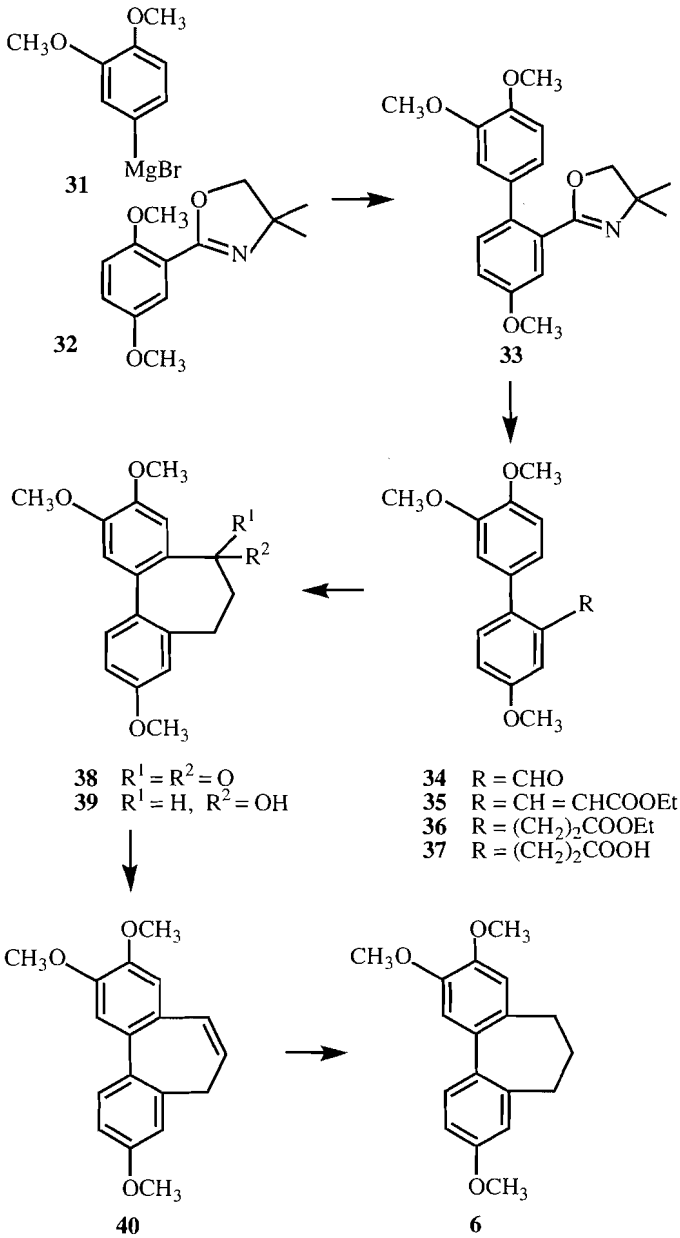

SCHEME 3

stantial, these situations are drastically different in the case of acetamide **8***a*. In $CDCl_3$, proton H-C(5) for **8***a* gives two ^1H NMR signals of nearly equivalent intensity, indicating a displacement of the conformational equilibrium toward the a*S* isomer, with the biphenyl system arranged in a clockwise fashion and with the acetamido group axially oriented. The existence of two isomers cannot be explained by a simple *cis–trans* rotameric arrangement of the amide group. This is shown by the optical behavior of **8***a*. The equilibration between a*R*- and a*S*-**8***a* conformers is demonstrated by the drastic decrease in the absorption at 260 nm in the CD spectra in $CHCl_3$ compared to the one displayed in ethanol (Fig. 1*a*, *b*). The specific optical rotation of **8***a* remains constant on standing in methanol and changes very little after several days in chloroform solution. This clearly indicates that the proportion of **8***a* (a*R*,5*S*) and (a*S*,5*S*) isomers present in solution is rapidly established and strongly influenced by the solvent. The optical isomer **8***b*, which was also analyzed, showed similar optical behavior.

Biological evaluation

Method (25)

The compounds were tested as potential inhibitors of the polymerization of purified bovine brain tubulin in vitro. Reaction components were 1.0 mg/mL (10 μM) tubulin, 1.0 M monosodium glutamate (inducer of polymerization), 1.0 mM $MgCl_2$, and 0.4 mM GTP (an essential cofactor for polymerization). All compounds were dissolved in dimethyl sulfoxide (with a final solvent concentration of 4%(v/v), which did not affect the polymerization reaction). All components except GTP were preincubated at 37°C for 15 min to permit the interaction of slow binding agents with tubulin. Reaction mixtures were chilled on ice and after addition of GTP were transferred to thermostated cuvettes held at 0°C in a recording spectrophotometer. Polymerization was initiated by a 75-s temperature jump to 37°C, and the reaction was followed turbidimetrically at 350 nm. For each compound an IC_{50} value was obtained in at least three independent experiments. The IC_{50} value was defined as the drug concentration that inhibits the extent of polymerization by 50% after a 20-min incubation. Values over 50 μM represent negligible activity in this assay, while the lowest IC_{50} value yet obtained has been 1.2 μM (i.e., 50% inhibition of polymerization when at most 12% of the tubulin in the reaction mixture has bound the inhibitor).

Results and discussion

Of the newly prepared compounds, only **5**, **29**, and **43** retained some activity as inhibitors of tubulin polymerization when compared with data obtained for colchicine **1** and *N*-acetylcolchinol methyl ether **2** (Table 2). *This marks dihydrodibenzo[*a,c*]cycloheptene **3** as the simplest tricyclic structure of this series that shows a high antitubulin activity.*

Any replacement of methoxy groups by hydrogen in **3** results in a substantial loss of activity, which is much greater than the loss observed in going from colchicine **1** to demethylated congeners (Table 2). This clearly demonstrates the importance of oxygen atoms at positions C(1), C(3), and C(9) (C(10) in colchicine) as major points of electrostatic interaction with the binding site while the oxygen in C(2) is slightly less important. The substituent at C(1) is also particularly critical because it affects the a*R*–a*S* equilibrium through steric hindrance with H-C(11). Switching the acetamido group from C(7) as in **2** to C(5), despite a proper counterclockwise absolute configuration for **8***a*, afforded inactive compounds **8***a*,*b*. Even an amino group at position C(5), as in **47***a*, resulted in complete loss of activity. This suggests that substitution at this position interferes with the tubulin binding process.

Experimental

General

TLC: silica gel GHLF plates from Analtech; visualization with UV light, I_2, Dragendorff's solution. Flash chromatography: silica gel 60 (Fluka), 230–400 mesh, 60 Å. Melting point (uncorrected): Fisher–Johns melting point apparatus. IR spectra: Beckman IR 4230. ^1H NMR spectra: Varian XL 300 (300 MHz). CIMS:

Can. J. Chem. Downloaded from www.nrcresearchpress.com by 217.78.4.112 on 09/08/12
For personal use only.

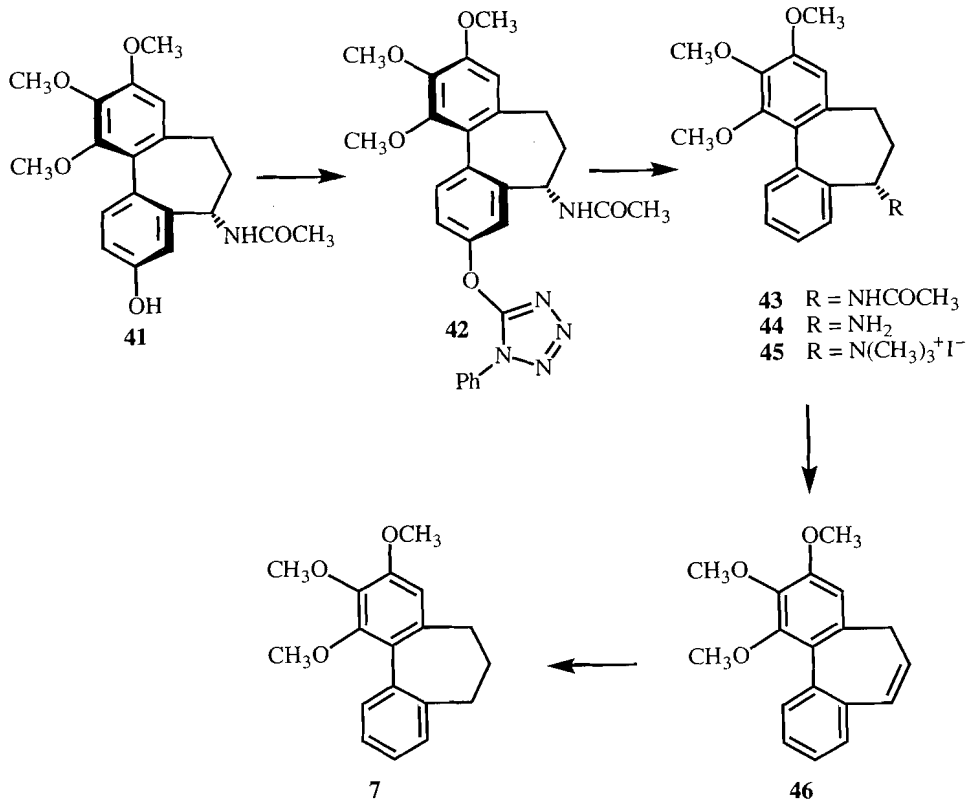

SCHEME 4

Can. J. Chem. Downloaded from www.nrcresearchpress.com by 217.78.4.112 on 09/08/12
For personal use only.

Finingan 1015 D; EIMS: VG 7070 F. GC: Hewlett Packard 5890A, column HP-1 (cross linked methyl silicone gum) 25 m × 0.32 mm. HPLC: Shimadzu LC-6A, column Alltech 250 mm, i.d. 4–6 mm fitting B. Optical rotation: Perkin–Elmer polarimeter 241MC.

Synthesis of DBCH ***4*** *(Scheme 1)*

*3-Methyl-4-[(2,3-dimethoxyphenyl)-methylidene]-5(4*H*)-oxazolone* ***9***

Oxazolone **9** was prepared according to published procedure (*7b*) and recrystallized from toluene as a bright yellow powder (39%): mp 130°C; IR ($CHCl_3$): 3020 (CH_3), 1810, 1770 (O-C=O), 1660 (C=NH), 1260 (Ph-O-CH_3) cm^{-1}; ^1H NMR ($CDCl_3$) δ: 2.40 (s, CH_3), 3.89 (s, CH_3O), 3.90 (s, CH_3), 7.00 (dd, J = 8.1 and 1.3 Hz, 1H, 4′-H), 7.14 (t, J = 8.1 Hz, 1H, 5′-H), 7.65 (s, 1H, Ph-CH=), 8.23 (dd, J = 8 and 1.4 Hz, 1H, 6′-H); CIMS (NH_3) m/z: 248 (MH^+). Anal. calcd. for $C_{13}H_{13}O_4N$ (247.25): C 63.15, H 5.30, N 5.66; found: C 63.06, H 5.33, N 5.60.

3-(2,3-Dimethoxyphenyl)pyruvic acid ***10***

A solution of **9** (50.0 g, 0.2 mol) in aqueous HCl (10%, 90 mL) and dioxane (180 mL) was refluxed for 3 h. After cooling, the solvents were evaporated to give a residue that was dissolved in ethyl acetate and washed with H_2O. The acid was extracted from the organic layer with concentrated ammonium hydroxide. The aqueous layer was washed with ethyl acetate, then acidified with concentrated HCl. The acid was then extracted with ethyl acetate. After washing with H_2O until neutral, and drying (Na_2SO_4), the solvent was evaporated to give 22 g of **10** (yield 49%), which was recrystallized from toluene to give a yellow powder: mp 123–124°C; IR ($CHCl_3$): 3460 (OH), 3000 (CH_3), 1690 (C=O), 1475, 1270 (CH_3O) cm^{-1}; ^1H NMR ($CDCl_3$) δ: 3.88 (s, CH_3O), 3.9 (s, CH_3O), 6.92 (d, J = 8.1 Hz, 1H, 4′-H), 6.94 (s, 1H, Ph-CH=), 7.12 (t, J = 8 Hz, 1H, 5′-H), 7.33 (d, J = 7.9 Hz, 1H, 6′-H); CIMS (NH_3) m/z: 242 ($MH^+ + NH_3$), 224 (M^+). Anal. calcd. for $C_{11}H_{12}O_5$(224.21): C 58.93, H 5.39; found: C 58.68, H 5.43.

1-Hydroxy-5-oxo-2-(2,3-dimethoxyphenyl)-1-cyclohexanecarboxylic acid ***11***

Acid **11** was prepared by published procedure (*7b*) as a crude mixture (57 g, 81%); a sample of the product (4 g) was flash chromatographed for analysis (SiO_2, $CHCl_3$–MeOH–CH_3COOH 9.25:0.5:0.25), giving **11** as a translucide oil (0.5 g, 10%): ^1H NMR ($CDCl_3$) δ: 1.45–2.26 (m, 4H, CH_2), 2.35 (d, J = 15 Hz, 1H, $CH_2C(OH)COOH$), 2.72 (d, J = 14.9 Hz, 1H, $CH_2C(OH)COOH$), 3.42 (dd, J = 12.9 and 3.7 Hz, 1H, CH), 3.58 (s, 3H, CH_3O), 3.62 (s, 3H, CH_3O), 5.68 (s, 1H, OH), 6.57 (d, J = 8.1 Hz, 1H, 4′-H), 6.63 (d, J = 8 Hz, 1H, 6′-H), 6.74 (t, J = 7.9 Hz, 1H, 5′-H). Recrystallization from ethyl acetate gave white crystals; mp 209–212°C (dec.); IR (film): 3460 (OH), 2930, 1720 (C=O), 1655–1620 (C=O), 1470 cm^{-1}; CIMS (NH_3) m/z: 329 ($MH^+ + 2NH_3$), 312 ($MH^+ + NH_3$), 295 (MH^+), 276 ($MH^+ - H_2O$).

3-Oxo-6-(2,3-dimethoxyphenyl)-1-cyclohexenecarboxylic acid ***12***

Acid **12** was prepared from crude compound **11** by published procedure (*7b*), obtained as a yellow oil (98%, crude), and used without further purification in the preparation of ester **13**; CIMS (NH_3) m/z: 294 ($MH^+ + NH_3$), 276 (M^+), 259 ($MH^+ - OH$).

Mixture of methyl 3-oxo-6(2,3-dimethoxyphenyl)-1-cyclohexene-1-carboxylate and methyl 5-oxo-2-(2,3-dimethoxyphenyl)-1-cyclohexene-1-carboxylate ***13***

K_2CO_3 (40.0 g, 0.29 mol) and MeI (25 mL, 0.4 mol) were added to a solution of acid **12** (44 g, crude, 0.15 mol) in anhydrous THF (250 mL). The mixture was refluxed for 4 h under N_2. After cooling, K_2CO_3 was removed by filtration and washed with Et_2O. The filtrate was evaporated to give a residue that was dissolved in ethyl acetate. The organic layer was washed with brine and dried (Na_2SO_4) to give, after evaporation, 42 g of a brown oil. The

Can. J. Chem. Downloaded from www.nrcresearchpress.com by 217.78.4.112 on 09/08/12
For personal use only.

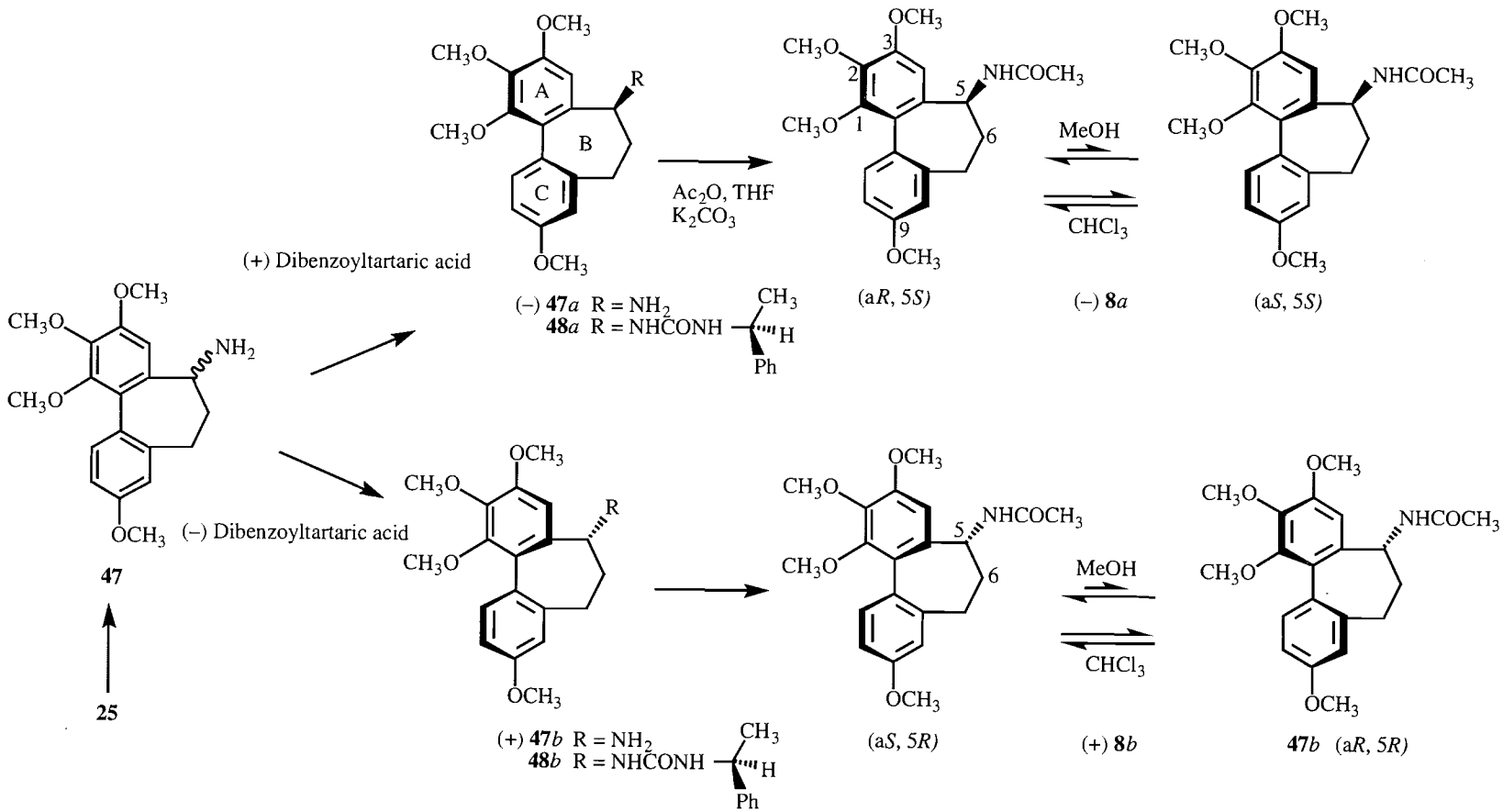

SCHEME 5

Can. J. Chem. Downloaded from www.nrcresearchpress.com by 217.78.4.112 on 09/08/12
For personal use only.

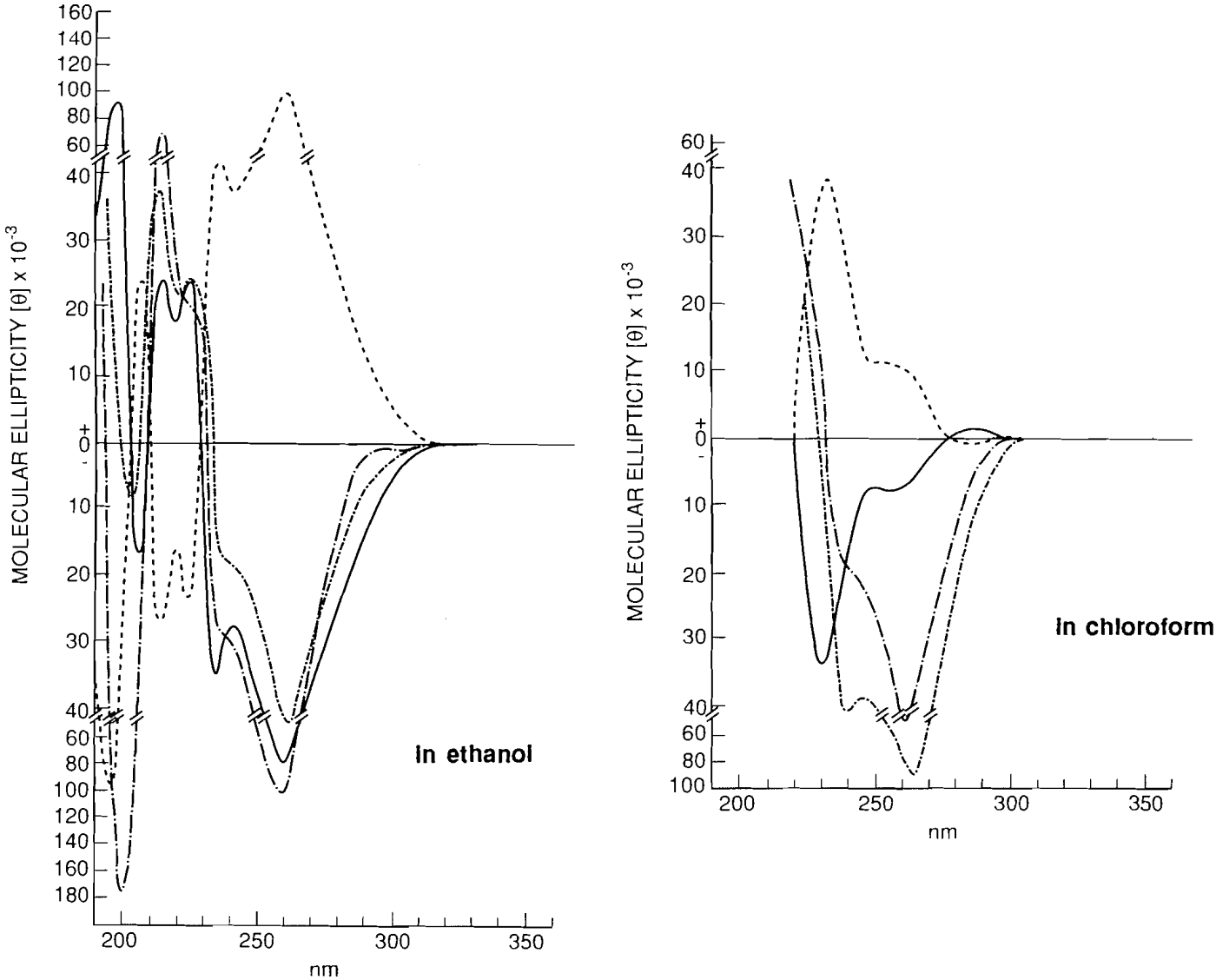

FIG. 1. CD spectra of *N*-acetylcolchinyl methyl ether **2** and its analogs **8***a*,*b* and **47***a*. (——) **8***a*; (- - - -) **8***b*; (—·—) *N*-acetylcolchinyl methyl ether **2**; (—·—·—·) **47***a*.

TABLE 1. Chemical shifts (ppm) of proton H(5) and its vicinal coupling constants (Hz), $J_{5,6a}$ and $J_{5,6b}$, in (*S*)-5-acetamidodeaminocolchinyl methyl ether **8***a* and (*S*)-5-aminodeaminocolchinyl methyl ether **47***a* in different solvents

	a*R* Conformation			a*S* Conformation			
	δH(5) ppm	$J_{5,6a}$ Hz	$J_{5,6b}$ Hz	δH(5) ppm	$J_{5,6a}$ Hz	$J_{5,6b}$ Hz	%a*R*
(*S*)-5-Acetamidodeaminocolchinyl methyl ether **8***a*							
Methanol-d_4	4.44	12.4	6.6	Not determined			~93
Acetone-d_6	4.62	12.2	6.1	Not determined			~92
Chloroform-*d*	4.59	12.2	6.2	5.00	~0	6.2	~46
(*S*)-5-Aminodeaminocolchinyl methyl ether, HCl salt **47***a*							
Methanol-d_4	3.90	11.8	6.3	Not determined			~95

product was chromatographed (SiO_2, eluent ethyl acetate – hexanes 1:4, then 3:7), giving a yellow oil that was crystallized from *i*PrOH – petroleum ether as pale yellow crystals (21%): mp 77–78°C; IR ($CHCl_3$): 3010, 2960 (CH_3), 1730 (C=O), 1685 (C=O), 1590 (Ph), 1480 (-CH_2-), 1290–1200 (Ph-O-CH_3) cm^{-1}; ^1H NMR ($CDCl_3$) δ: 1.63–2.04 (m, 2H, CH_2), 2.23–2.4 (m, 4H, CH_2), 3.62 (s, 3H, CH_3O), 3.8 (s, 3H, CH_3O), 3.87 (s, 3H, CH_3O), 4.52 (br t, *J* = 4.3 Hz, 1H, Ph-CH), 6.47 (dd, *J* = 7.6 and 1.4 Hz, 1H, 4′-H), 6.77 (dd, *J* = 8.2 and 1.4 Hz, 1H, 6′-H), 6.85 (s, 1H, COCH=), 6.88 (t, *J* = 8.0 Hz, 1H, 5′-H); CIMS (NH_3) *m*/*z*: 308($MH^+ + NH_3$), 291 (MH^+), 259 ($M^+ - OCH_3$). Anal. calcd. for $C_{16}H_{18}O_5$ (290.3): C 66.19, H 6.25; found: C 66.10, H 6.27.

Methyl 4-hydroxy-2′,3′-dimethoxy-1,1′-biphenyl-2-carboxylate ***14***

Ethyl ester **13** (2.0 g, 7.2 mmol) was pulverized and thoroughly mixed with Pd black (1.0 g, 9.4 mmol). This powder was heated to 200°C in a Kugelrohr apparatus under moderate vacuum (20 Torr; 1 Torr = 133.3 Pa). After 15 min, high vacuum (0.1 Torr) was applied and the product was distilled for 1 h to give a colorless oil (1.6 g). The residue remaining in the round-bottom flask was dissolved in EtO_2 and the Pd removed by filtration through

TABLE 2. Inhibitory effects of colchicine analogs on tubulin polymerization

Agent	IC_{50} (μM) (±S.D.)
Colchicine	2.4 ± 0.08
1-Demethylcolchicine	6.8 ± 0.5
2-Demethylcolchicine	3.7 ± 0.3
3-Demethylcolchicine	2.9 ± 0.5
Deacetylcolchicine	3.3 ± 0.4
Deacetamidocolchicine	2.6 ± 0.3
2	1.5 ± 0.2
3	1.9 ± 0.3
4	>50
5	23 ± 6
6	>50
7	>50
23	>50
29	9.4 ± 1
40	>50
43	15 ± 2
46	>50
8*a*	>50
8*b*	>50
47*a*	>50

Celite. The product was then chromatographed (SiO_2, ethyl acetate – hexanes 3:7) to give 200 mg more of oil. Total product 1.8 g (91%); IR ($CHCl_3$): 3600–3100 (OH), 2940 (CH_3), 1720 (C=O), 1600, 1570 (Ph), 1470, 1430, 900 cm^{-1}; CIMS (NH_3) *m/z*: 289 (MH^+), 288 (M^+), 257 ($M^+ - OCH_3$).

Methyl 2′,3′,4′-trimethoxy-1,1′-biphenyl-2-carboxylate ***15***

Carboxylate **15** was prepared by published procedure (7*b*) as a pale yellow oil (69%): IR: $CHCl_3$): 3000, 2940, 2815 (CH_3), 1720 (C=O), 1605, 1580 (Ph), 1465, 1300–1200 (CH_3-O-) cm^{-1}; ^1H NMR ($CDCl_3$) δ: 3.47 (s, 3H, CH_3O), 3.66 (s, 3H, CH_3O), 3.87 (s, 3H, CH_3O), 3.88 (s, 3H, CH_3O), 6.81 (dd, *J* = 1.5 and 7.7 Hz, 1H, 4′-H), 6.91 (dd, *J* 1.5 and 8.2 Hz, 1H, 6′-H), 7.07 (dd, *J* = 2.8 and 8.5 Hz, 1H, 5-H), 7.08 (t, *J* = 7.9 Hz, 1H, 5′-H), 7.27 (d, *J* = 8.4 Hz, 1H, 6-H), 7.43 (d, *J* = 2.8 Hz, 1H, 3-H); EIMS *m/z*: 302 (M^+), 271 ($M^+ - CH_3O$).

2′,3′,4′-Trimethoxy-1,1′-biphenyl-2-methanol ***16***

Prepared by published procedure (7*b*) as a colorless oil (82–88%); IR ($CHCl_3$): 3460 (OH), 3000, 2940, 2820 (CH_3), 1600, 1575 (Ph), 1460, 1250 (CH_3-O-) cm^{-1}; ^1H NMR ($CDCl_3$) δ: 3.47 (s, 3H, CH_3O), 3.85 (s, 3H, CH_3O), 3.89 (s,, 3H, CH_3O), 4.34 (br s, 1H, CH_2), 4.38 (br s, 1H, CH_2), 6.77 (d, *J* = 1.4 and 7.6 Hz, 1H, 4′-H), 6.89 (dd, *J* = 2.7 and 8.4 Hz, 1H, 5-H), 6.93 (dd, *J* = 1.4 and 8.2 Hz, 1H, 6′-H), 7.10 (t, *J* = 7.9 Hz, 1H, 5′-H), 7.11 (d, *J* = 2.7 Hz, 1H, 3-H), 7.15 (d, *J* = 8.4 Hz, 1H, 6-H); CIMS (NH_3) *m/z*: 274 (M^+), 257 ($M^+ - OH$).

2′,3′,4-Trimethoxy-1,1′-biphenyl-2-carbaldehyde ***17***

Aldehyde **17** was prepared by published procedure (7*b*) as pale yellow crystals (65%): mp 81–83°C; IR ($CHCl_3$): 3000, 2940, 2840 (CH_3), 1680 (C=O), 1610 (Ph), 1470, 1260 (CH_2-O-) cm^{-1}; ^1H NMR ($CDCl_3$) δ: 3.47 (s, 3H, CH_3O), 3.91 (s, 3H, CH_3O), 3.92 (s, 3H, CH_3O), 6.87 (dd, *J* = 1.4 and 7.6 Hz, 1H, 4′-H), 6.99 (dd, *J* = 1.3 and 8.3 Hz, 1H, 6′-H), 7.14 (t, *J* = 7.9 Hz, 1H, 5′-H), 7.19 (dd, *J* = 2.8 and 8.4 Hz, 1H, 5-H), 7.32 (d, *J* = 8.4 Hz, 1H, 6-H), 7.52 (d, *J* = 2.7 Hz, 1H, 3-H), 9.8 (s, 1H, CHO); CIMS (NH_3) *m/z*: 290 ($MH^+ + NH_3$), 273 (MH^+). Aldehyde **17** was also characterized as its 2,4-dinitrophenylhydrazone derivative, which crystallized in EtOH to give orange crystals; mp 233–234°C; CIMS (NH_3) *m/z*: 453 (MH^+), 270 ($M^+ - (NH - Ph(NO_2)_2)$).

Ethyl 3-(2′,3′,4-trimethoxy-1,1′-biphenyl-2-yl)prop-2-enoate ***18***

Ester **18** was prepared by published procedure (7*a*) (95%) and crystallized from iPr_2O as white crystals: mp 86–87°C; IR ($CHCl_3$): 3000 (CH_3), 1705 (C=O), 1635 (CH=CH), 1605 (Ph), 1470 cm^{-1}; ^1H NMR ($CDCl_3$) δ: 1.09 (t, *J* = 7.2 Hz, 3H, CH_3), 3.34 (s, 3H, CH_3O), 3.70 (s, 3H, CH_3O), 3.73 (s, 3H, CH_3O), 4.00 (q, *J* = 7.2 Hz, 2H, CH_2), 6.18 (d, *J* = 15.9 Hz, 1H, =CHCO), 6.55 (dd, *J* = 1.5 and 7.6 Hz, 4′-H), 6.77 (dd, *J* = 1.5 and 8.3 Hz, 1H, 6′-H), 6.8 (dd, *J* = 2.7 and 8.5 Hz, 1H, 5-H), 6.90 (t, *J* = 7.9 Hz, 1H, 5′-H), 7.04 (d, *J* = 2.6 Hz, 1H, 3-H), 7.08 (d, *J* = 8.5 Hz, 1H, 6-H), 7.38 (d, *J* = 15.9 Hz, 1H, Ph-CH=); CIMS (NH_3): 342 (M^+), 297 (M^+ – OEt). Anal. calcd. for $C_{20}H_{22}O_5$ (342.38): C 70.16, H 6.48; found: C 70.18, H 6.54.

Ethyl 2′,3′,4-trimethoxy-1,1′-biphenyl-2-propionate ***19***

Prepared by published procedure (7*a*) as a colorless oil (99%): IR ($CHCl_3$): 3000, 2940 (CH_3), 1730 (C=O), 1610, 1580, 1470, 1260, 1200 cm^{-1}; ^1H NMR ($CDCl_3$) δ: 1.01 (t, *J* = 7.2 Hz, 3H, CH_3), 2.27 (dt, *J* = 3 and 8.1 Hz, 2H, CH_2COO), 2.64 (t, *J* = 8 Hz, 2H, $PhCH_2$), 3.34 (s, 3H, CH_3O), 3.66 (s, 3H, CH_3O), 3.73 (s, 3H, CH_3O), 3.87 (q, *J* = 7.2 Hz, 2H, $COOCH_2$), 6.58 (dd, *J* = 1.5 and 7.6 Hz, 1H, 4′-H), 6.62 (dd, *J* = 2.7 and 8.3 Hz, 1H, 5-H), 6.67 (d, *J* = 2.7 Hz, 1H, 3-H), 6.75 (dd, *J* = 1.5 and 8.2 Hz, 1H, 6′-H), 6.90 (t, *J* = 7.8 Hz, 1H, 5′-H), 6.94 (d, *J* = 8.1 Hz, 1H, 6-H); CIMS (NH_3) *m/z*: 345 (MH^+), 344 (M^+), 316 (MH^+ – Et), 299 (M^+ – OEt).

2′,3′,4-Trimethoxy-1,1′-biphenyl-2-propionic acid ***20***

Acid **20** was prepared by published procedure (7*a*) as white crystals (100%): mp 147–148°C; IR ($CHCl_3$): 3000, 2940, 2840 (CH_3), 1705 (C=O), 1605, 1575 (Ph), 1500, 1465, 1260, 1200 (CH_3-O-); CIMS (NH_3): 316 (M^+), 299 (M^+ – OH), 271 (M^+ – COOH). Anal. calcd. for $C_{18}H_{20}O_5$ (316.36): C 68.34, H 6.37; found: C 68.16, H 6.39.

*6,7-Dihydro-1,2,9-trimethoxy-5*H*-dibenzo[*a,c*]cyclohepten-5-one* ***21***

Acid **20** (3.0 g, 9.5 mmol) was added to $(CF_3CO)_2O$ (30 mL) and the solution containing undissolved material was cooled to 0–5°C. CF_3COOH (25 mL) was added slowly under argon. The solution was stirred at low temperature and the reaction was followed by GC. After 2 h, additional $(CF_3CO)_2O$ (30 mL) was added. The reaction was stopped after 5 h. The solvent was evaporated, the residue diluted with EtOAc and washed with $NaHCO_3$ solution, brine, and dried (Na_2SO_4). Evaporation of solvent gave 2.7 g of yellow oil, which was chromatographed (SiO_2, ethyl acetate – hexanes 2:3). Ketone **21** was recrystallized from the same solvent system to give 2.62 g of white crystals (92%): mp 127–128°C; IR ($CHCl_3$): 3000, 2940 (CH_3), 1675 (C=O), 1620, 1590 (Ph), 1510, 1480, 1465, 1300–1200 cm^{-1}; ^1H NMR ($CDCl_3$) δ: 2.7–3.04 (br m, 3H, CH_2), 3.06–3.24 (m, 1H, CH_2), 3.49 (s, 3H, CH_3O), 3.84 (s, 3H, CH_3O), 3.94 (s, 3H, CH_3O), 6.81 (d, *J* = 2.4 Hz, 1H, 8-H), 6.84 (dd, *J* = 2.7 and 8.5 Hz, 1H, 10-H), 6.93 (d, *J* = 8.5 Hz, 1H, 3-H), 7.36 (d, *J* = 8.5 Hz, 1H, 4-H), 7.5 (d, *J* = 8.4 Hz, 11-H); CIMS (NH_3) *m/z*: 299 (MH^+). Anal. calcd. for $C_{18}H_{18}O_4$ (298.3): C 72.46, H 6.08; found: C 72.33, H 6.11.

*6,7-Dihydro-1,2,9-trimethoxy-5*H*-dibenzo[*a,c*]cyclohepten-5-ol* ***22***

Prepared by published procedure (7*a*) as a colorless oil (99%): IR ($CHCl_3$): 3600, 3480 (OH), 3020, 2940, 2850 (CH_3), 1610, 1580 (Ph), 1500, 1480, 1460, 1410 (CH_2), 1250–1200 (Ph-O-CH_3), 1100, 1020 cm^{-1}; ^1H NMR ($CDCl_3$) δ: 2.3–2.65 (m, 4H, CH_2), 3.5 (s, 3H, CH_3O), 3.85 (s, 3H, CH_3O), 3.91 (s, 3H, CH_3O), 4.44 (dd, *J* ~ 7 Hz, 1H, *CH*OH), 6.8 (d, *J* = 2.6 Hz, 8-H), 6.84 (dd, *J* = 2.7 and 8.4 Hz, 1H, 10-H), 6.95 (d, *J* = 8.4 Hz, 3-H), 7.34 (d, *J* = 8.4 Hz, 4-H), 7.45 (d, *J* = 8.4 Hz, 11-H); CIMS (NH_3) *m/z*: 283 (MH^+ – H_2O).

*1,2,9-Trimethoxy-7*H*-dibenzo[*a,c*]cycloheptene* ***23***

Alcohol **22** (140 mg, 0.5 mmol) was heated for 3 h at 190–200°C in a Kugelrohr apparatus *in vacuo*. The residue was dissolved in

Can. J. Chem. Downloaded from www.nrcresearchpress.com by 217.78.4.112 on 09/08/12
For personal use only.

Can. J. Chem. Downloaded from www.nrcresearchpress.com by 217.78.4.112 on 09/08/12
For personal use only.

Et_2O and filtered through celite filtration aid. Evaporation of the filtrate gave an oil, which was chromatographed on SiO_2. Elution with ethyl acetate – hexanes 3:7 gave 30 mg of the dehydrated product and 80 mg of starting material, which was reacted again. Total yield 42.6% of white crystals recrystallized from MeOH: mp 114–115°C, IR ($CHCl_3$): 3000, 2940, 2840 (CH_3), 1610 (Ph), 1500, 1480 (-CH_2-, -CH=CH_2), 1300–1200 (Ph-O-CH_3), 1100 cm^{-1}; ^1H NMR ($CDCl_3$) δ: 2.83 (ddd, J = 2.1, 5.4, and 12.6 Hz, 1H, 7-H), 3.11 (dd, J = 8.2 and 12.8 Hz, 1H, 7-H), 3.5 (s, 3H, CH_3O), 3.84 (s, 3H, CH_3O), 3.94 (s, 3H, CH_3O), 6.14 (m, 1H, 6-H), 6.49 (dd, J = 1.6 and 10.1 Hz, 5-H), 6.75 (d, J = 2.5 Hz, 1H, 8-H), 6.78 (dd, J = 2.7 and 8.5 Hz, 1H, 10-H), 6.93 (d, J = 8.5 Hz, 1H, 3-H), 7.04 (d, J = 8.5 Hz, 1H, 4-H), 7.65 (d, J = 8.4 Hz, 1H, 11-H); CIMS (NH_3) m/z: 283 (MH^+). Anal. calcd. for $C_{18}H_{18}O_3 \cdot H_2O$ (300.34): C 71.98, H 6.71; found: C 72.01, H 6.37.

*6,7-Dihydro-1,2,9-trimethoxy-5*H-*dibenzo*[a,c]*cycloheptene* ***4***

Prepared by published procedure (*7a*) (89%), giving white crystals after recrystallization from methanol: mp 80–81°C; IR ($CHCl_3$): 3020, 2940, 2840 (CH_3), 1610 (Ph), 1505–1450 (-CH_2-), 1300–1200 (Ph-O-CH_3), 1110, 1020, 800–700 cm^{-1}; ^1H NMR ($CDCl_3$) δ: 1.98–2.1 (m, 2H, CH_2), 2.15–2.32 (m, 1H, CH_2), 2.35–2.55 (m, 3H, CH_2), 3.49 (s, 3H, CH_3O), 3.85 (s, 3H, CH_3O), 3.89 (s, 3H, CH_3O), 6.80 (d, J = 2.7 Hz, 1H, 8-H), 6.82 (d, J = 8.3 Hz, 1H, 4-H), 6.85 (dd, J = 2.7 and 8.4 Hz, 1H, 10-H), 6.91 (d, J = 8.2 Hz, 1H, 3-H), 7.47 (d, J = 8.4 Hz, 1H, 11-H); CIMS (NH_3) m/z: 302 ($MH^+ + NH_3$), 285 (MH^+).

Synthesis of DBCH ***5*** *(Scheme 2)*

*6,7-Dihydro-1,2,3,9-tetramethoxy-5*H-*dibenzo*[a,c]*cyclohepten-5-oxime* ***25***

A solution of sodium acetate (150 mg, 1.8 mmol) and hydroxylamine hydrochloride (126 mg, 1.8 mmol) in EtOH (50 mL) was added to **24** (300 mg, 0.9 mmol) in EtOH (100 mL) and refluxed for 12 h. EtOH was evaporated, the residue dissolved in Et_2O and washed with NH_4Cl solution, brine, and dried (Na_2SO_4). Evaporation of the solvent gave a white foam that was recrystallized from ethyl acetate – hexanes 1:4 to give only one conformational isomer of the oxime as brilliant white crystals (96%): mp 176°C; IR ($CHCl_3$): 3600, 3300 (OH), 3000, 2945, (CH_3), 1615 (C=N), 1590 (Ph), 1400, 1360, 1330, 1310, 1250 (Ph-O-CH_3), 1120, 1090 cm^{-1}; ^1H NMR ($CDCl_3$) δ: 2.65–2.69 (m, 1H, CH_2), 2.82–2.92 (m, 2H, CH_2), 3.20–3.32 (m, 1H, CH_2), 3.57 (s, 3H, CH_3O), 3.85 (s, 3H, CH_3O), 3.94 (s, 3H, CH_3O), 3.97 (s, 3H, CH_3O), 6.80 (d, J = 2.7 Hz, 1H, 8-H), 6.82–6.87 (m, 2H, 4-H and 10-H), 7.41 (d, J = 8.6 Hz, 1H, 11-H); CIMS (NH_3) m/z: 361 ($MH^+ + NH_3$), 344 (MH^+), 328.

*5-Amino-6,7-Dihydro-1,3,9-trimethoxy-5*H-*dibenzo*[a,c]*cycloheptene* ***27***

Oxime **25** (100 mg, 0.3 mmol) was dissolved in absolute *i*PrOH (50 mL) at 90°C under N_2. Sodium (2 g, 86 mmol) was added in one portion and the mixture stirred at 90°C for 1 h. EtOH 95% (30 mL) was poured into the hot solution. The solvent was evaporated and H_2O was added. The aqueous layer was extracted with Et_2O (×3). The organic layer was extracted with HCl (5%). The acidic solution was made basic with NaOH (pellets) and the amine extracted with Et_2O. The organic layer was washed with H_2O and dried (Na_2CO_3). Evaporation gave the amine as a colorless oil, 90 mg (100%): IR ($CHCl_3$): 3700, 3500, 3400 (-NH_2), 1600 (CH-NH_2), 1460 (-CH_2-), 1340, 1290, 1260–1200 (Ph-O-CH_3), 1150, 1055 cm^{-1}; ^1H NMR ($CDCl_3$) δ: 1.9–2.04 (m, 1H, CH_2), 2.3–2.6 (m, 3H, CH_2), 3.69 (s, 3H, CH_3O), 3.71 (s, 3H, CH_3O), 3.76 (s, 3H, CH_3O), 3.81 (m, 1H, *CH*NH_2), 6.45 (d, J = 1.9 Hz, 1H, 2-H), 6.70 (dd, J = 2.6 Hz, 1H, 4-H), 6.76 (m, 1H, 8-H), 6.77 (dd, J = 2.7 and 8.4 Hz, 1H, 10-H), 7.31 (d, J = 8.4 Hz, 1H, 11-H); CIMS (NH_3) m/z: 300 (MH^+), 283 ($MH^+ - NH_3$).

*5-Dimethylamino-6,7-dihydro-1,3,9-trimethoxy-5*H-*dibenzo*[a,c]*cyclohepten* ***28****a*, *5-trimethylamino-6,7-dihydro-1,3,9-trimethoxy-5*H-*didenzo*[a,c]*cyclohepten iodide* ***28****b*, *and 1,3,9-trimethoxy-5*H-*dibenzo*[a,c]*cycloheptene* ***29***

MeI (6 mL) was added to a solution of **27** (190 mg, 0.63 mmol) and *t*BuOK (80 mg, 0.71 mmol) in THF (50 mL). The mixture was stirred at room temperature for 24 h and the insoluble material filtered. The quaternary ammonium salt ***28****b*, which is soluble in THF, was obtained after evaporation of the solution. Ethylene glycol (4 mL), H_2O (4 mL), and KOH (10 g) were added and the mixture was stirred at 190°C for 4 h. After cooling, the solution was diluted with H_2O and extracted with Et_2O; the organic layer was washed with H_2O until neutral and dried (K_2CO_3). Evaporation of the solvent gave an oil (200 mg), which was chromatographed (SiO_2, ethyl acetate – hexanes 1:4, 3:7, 1:1) to give olefin **29** (30 mg) and the dimethylamino compound ***28****a* (70 mg) as an oil. ***28****a* was reacted again with MeI (2 mL) in ethyl acetate at room temperature for 48 h and the mixture directly submitted to Hofmann elimination under the conditions described above to give 20 mg more of olefin **29** (total yield 28%). **29** was crystallized from $MeOH/H_2O$ as white crystals: mp 98–99°C. IR ($CHCl_3$): 3500, 3440, 3000, 2940, 2840 (CH_3), 1600, 1460 (-CH_2-), 1410, 1260, 1240–1200 (Ph-O-CH_3), 1160, 1090, 1060 cm^{-1}; ^1H NMR ($CDCl_3$) δ: 2.84 (ddd, J = 2.0, 5.5, and 12.7 Hz, 1H, 7-Ha), 3.1 (dd, J = 8.1 and 12.7 Hz, 1H, 7-Hb), 3.81 (s, 3H, CH_3O), 3.83 (s, 3H, CH_3O), 3.86 (s, 3H, CH_3O), 6.22 (ddd, J = 5.4, 8.1, and 13 Hz, 1H, 6-H), 6.44 (d, J = 2.6 Hz, 1H, 2-H), 6.47 (d, J = 13.3 Hz, 1H, 5-H), 6.52 (d, J = 2.5 Hz, 1H, 4-H), 6.75 (m, 1H, 8-H), 6.77 (dd, J = 2.8 and 8.6 Hz, 1H, 10-H), 7.56(d, J = 8.3 Hz, 1H, 11-H); CIMS (NH_3) m/z: 283 (MH^+). ***28****a*: IR ($CHCl_3$): 3000, 2940, 2840 (CH_3), 1600 (CH-N), 1450 (-CH_2-), 1420, 1320, 1240–1200 (Ph-O-CH_3), 1150 cm^{-1}; ^1H NMR ($CDCl_3$) δ: 2.04–2.1 (br m, 4H, CH_2), 3.75 (s, 6H, NCH_3), 3.84 (s, 6H, CH_3O), 3.92 (s, 3H, CH_3O), 3.99 (m, 1H, 5-H), 6.49 (d, J = 1.8 Hz, 1H, 2-H); MS (CI/NH_3) m/z: 328 (MH^+), 283 ($MH^+ - NH(CH_3)_2$).

*6,7-Dihydro-1,3,9-trimethoxy-5*H-*dibenzo*[a,c]*cycloheptene* ***5***

From ***26****:* alcohol **26** (80 mg, 0.24 mmol) was dissolved in absolute *i*PrOH (40 mL) and heated at 110°C under N_2, Sodium (3 g, 129 mmol) was added and the mixture stirred at 110°C for 4 h, then at room temperature for 12 h. The unreacted sodium was removed and the reaction was quenched with *i*PrOH/H_2O. Most of the *i*PrOH was evaporated. H_2O (30 mL) was added, and the products were extracted with Et_2O. The organic layer was dried (Na_2CO_3), filtered, and evaporated to give an oil, which was chromatographed (SiO_2, ethyl acetate – hexanes 1:9, 3:7). Compound **5** (10 mg, 15%) was crystallized from petroleum ether as white crystals. Alcohol **30** was obtained as a translucide oil (53 mg, 73%).

Compound ***5****:* mp 109–110°C; IR ($CHCl_3$): 3010, 2940, 2860, 2840 (CH_3), 1610, 1590, 1470 (-CH_2-), 1430, 1350, 1330, 1300, 1260, 1240–1200 (Ph-O-CH_3), 1160, 1090, 1070 cm^{-1}; ^1H NMR ($CDCl_3$) δ: 2.04–2.15 (m, 2H, CH_2), 2.25–2.51 (m, 4H, CH_2), 3.77 (s, 3H, CH_3O), 3.84 (s, 3H, CH_3O), 3.85 (s, 3H, CH_3O), 6.43 (d, J = 2.4 Hz, 1H, 2-H), 6.48 (d, J = 2.4 Hz, 1H, 4-H), 6.79 (d, J = 2.6 Hz, 1H, 8-H), 6.83 (dd, J = 2.8 and 8.4 Hz, 1H, 10-H), 7.41. (d, J = 8.4 Hz, 1H, 11-H); CIMS (NH_3) m/z: 285 (MH^+).

Compound ***30****:* IR ($CHCl_3$): 3620, 3020, 2940, 1610 (Ph), 1460, 1430, 1320, 1300, 1220 (br), 1160, 1050 cm^{-1}; ^1H NMR ($CDCl_3$) δ: 1.72 (br s, 1H, OH), 1.88–2.0 (m, 1H, CH_2), 2.4–2.6 (m, 3H, CH_2), 3.77 (s, 3H, CH_3O), 3.84 (s, 3H, CH_3O), 3.89 (s, 3H, CH_3O), 4.49 (dd, J = 6.3 and 11.1 Hz, 1H, 5-H), 6.52 (d, J = 2.4 Hz, 1H, 2-H), 6.80 (d, J = 2.5 Hz, 1H, 8-H), 6.82 (dd, J = 2.7 and 8.3 Hz, 1H, 10-H), 6.89 (d, J = 2.4 Hz, 1H, 4-H), 7.39 (d, J = 8.2 Hz, 1H, 11-H); CIMS (NH_3) m/z: 301 (MH^+), 2.83 ($MH^+ - H_2O$).

From ***29****:* olefin **29** (21 mg, 0.07 mmol) in acetic acid (4 mL)

Can. J. Chem. Downloaded from www.nrcresearchpress.com by 217.78.4.112 on 09/08/12
For personal use only.

was hydrogenated at 1 atm (101.3 kPa) for 3 h in the presence of Pd black (20 mg). After filtration of the catalyst on Celite and evaporation of the filtrate, the residue was dissolved in Et_2O, washed with brine, and dried (Na_2CO_3). Evaporation of the solvent gave an oil, which was crystallized from petroleum ether to give **5** as white crystals (20 mg, 95%).

*Synthesis of DBCH **6** (Scheme 3)*

*2-(2,5-Dimethoxyphenyl)-4,4-dimethyl-2-oxazoline **32***

Oxazoline **32** was prepared according to Meyers' procedure (16). The first acyl chloride intermediate (16), precursor of **32**, was distilled in a Kugelrohr apparatus at 105°C and 0.05 Torr. The oxazoline **32** was purified by distillation in the same manner at 120°C and 0.05 Torr and obtained as a translucent oil (93.4%, 100% pure by GC): IR ($CHCl_3$): 2960 (C-H), 1640 (C=N), 1490, 1460, 1420, 1200 (Ph-O-CH_3), 1140 (C-O) cm^{-1}; ^1H NMR ($CDCl_3$) δ: 1.39 (s, 6H, CH_3), 3.78 (s, 3H, CH_3O), 3.83 (s, 3H, CH_3O), 4.09 (s, 2H, CH_2), 6.88 (d, J = 9.1 Hz, 1H, 3'-H), 6.95 (dd, J = 3 and 9 Hz, 1H, 4'-H), 7.27 (d, J = 3 Hz, 1H, 6'-H); CIMS (NH_3) m/z: 236 (MH^+).

*4,3',4'-Trimethoxy-2-oxazolinyl-1,1'-biphenyl **33***

Magnesium (4.0 g, 0.17 mmol) and a few crystals of iodine were added to a three-neck, flame-dried, round-bottom flask under argon and heated at 40°C. 4-Bromoveratrole (26 g, 0.12 mol) dissolved in anhydrous THF (150 mL, distilled over $LiAlH_4$) was added dropwise while the temperature was raised to 80°C. The black mixture was stirred at 80°C for 2 h. **32** (7.0 g, 0.03 mol), dissolved in anhydrous THF (100 mL), was added slowly to the Grignard reagent and the mixture stirred under argon at room temperature for 30 h. An aqueous solution of NH_4Cl (100 mL) was added, followed by H_2O (150 mL), and the product was extracted with Et_2O. The organic layer was washed with brine and dried ($MgSO_4$). Evaporation of solvent gave a yellow oil, which was distilled in a Kugelrohr apparatus. Most of the impurities and nonreacted starting material distilled between 80°C and 120°C at 0.05 Torr while the crude product remained in the flask. Oxazoline **33** was purified by chromatography (SiO_2, ethyl acetate – hexanes 3:7, 1:1) to give 8.5 g of yellow oil, which crystallized after drying (84%, 100% pure by GC): mp 73–75°C; IR ($CHCl_3$): 3000, 2970 (C-H), 1640 (C=N), 1600, 1490, 1250–1200 (Ph-O-CH_3), 1040 cm^{-1}; ^1H NMR ($CDCl_3$) δ: 1.31 (s, 6H, CH_3), 3.82 (s, 2H, CH_2), 3.86 (s, 3H, CH_3O), 3.88 (s, 3H, CH_3O), 3.91 (s, 3H, CH_3O), 6.89 (m, 2H, 6-H, 2'-H), 6.92 (dd, J = 2 and 8.1 Hz, 1H, 5-H), 7.01 (dd, J = 2.8 and 8.5 Hz, 1H, 6'-H), 7.22 (d, J = 2.7 Hz, 1H, 3-H), 7.28 (d, J = 8.3 Hz, 1H, 5'-H); CIMS (NH_3) m/z: 342 (MH^+). Anal. calcd. for $C_{20}H_{23}O_4N$: C 70.36, H 6.79, N, 4.10; found: C 70.09, H 6.75, N 3.99.

*3',4',4-Trimethoxy-1,1'-biphenyl-2-carbaldehyde **34***

Aldehyde **34** was prepared according to Meyers' procedure (16), purified by column chromatography (SiO_2, ethyl acetate – hexanes 1:4), and obtained as white crystals (30%, 100% pure by GC): mp 98°C; IR ($CHCl_3$): 3000, 2950 (C-H), 1680 (C=O), 1600, 1480, 1460, 1250–1200 (Ph-O-CH_3), 1020, 900 cm^{-1}; ^1H NMR ($CDCl_3$) δ: 3.92 (s, 3H, CH_3O), 3.93 (s, 3H, CH_3O), 3.96 (s, 3H, CH_3O), 6.89 (m, 2H, 2'-H, 5-H), 6.97 (d, J = 8.7 Hz, 1H, 6-H), 7.21 (dd, J = 2.8 and 8.5 Hz, 1H, 6'-H), 7.40 (d, J = 8.6 Hz, 1H, 5'-H), 7.5 (d, J = 2.8 Hz, 1H, 3-H), 10.0 (s, 1H, CHO); CIMS (NH_3) m/z: 273 (MH^+), 255 ($MH^+ - H_2O$). Anal. calcd. for $C_{16}H_{16}O_4$: C 70.58, H 5.92; found: C 70.39, H 5.96.

*Ethyl 3-(3',4,4'-trimethoxy-1,1'-biphenyl-2-yl)prop-2-enoate **35***

Ester **35** was prepared by published procedure (7*a*) and obtained as white crystals after purification by column chromatography (SiO_2, ethyl acetate – hexanes 1:4) (79%): mp 74–75°C; IR ($CHCl_3$): 3020–2800 (CH_3), 1710 (C=O), 1640 (-CH=CH-), 1600 (Ph), 1500, 1470, 1440, 1340–1140, 1030 cm^{-1}; ^1H NMR ($CDCl_3$) δ: 1.29 (t, J = 7.1 Hz, 3H, CH_3), 3.88 (s, 6H, CH_3O), 3.93 (s, 3H, CH_3O), 4.22 (q, J = 7.1 Hz, 2H, CH_2), 6.37 (d, J = 15.9 Hz, 1H, =CH-CO), 6.81 (d, J = 1.9 Hz, 1H, 2'-H), 6.82 (dd, J = 1.9 and ~8 Hz, 1H, 5-H), 6.93 (d, J = 8 Hz, 1H, 6-H), 6.99 (dd, J = 2.5 and 8.5 Hz, 1H, 6'-H), 7.17 (d, J = 2.6 Hz, 1H, 3-H), 7.31 (d, J = 8.5 Hz, 1H, 5'-H), 7.76 (d, J = 16 Hz, 1H, PhCH=); CIMS (NH_3) m/z: 360 ($MH^+ + NH_3$), 343 (MH^+), 297 ($MH^+ -$ OEt). Anal. calcd. for $C_{20}H_{22}O_5$: C 70.16, H 6.48; found: C 70.11, H 6.53.

*Ethyl 3',4',4-trimethoxy-1,1'-biphenyl-2-propionate **36***

Ester **36** was prepared by published procedure (7*a*) (91%): IR ($CHCl_3$): 3010–2820 (CH_3), 1730 (C=O), 1600 (Ph), 1480, 1350–1120 cm^{-1}; ^1H NMR ($CDCl_3$) δ: 1.2 (t, J = 7.1 Hz, 3H, CH_3), 2.43 (t, J ~ 8 Hz, 2H, CH_2CO), 2.92 (t, J ~ 8 Hz, 2H, $PhCH_2$), 3.83 (s, 3H, CH_3O), 3.88 (s, 3H, CH_3O), 3.92 (s, 3H, CH_3O), 4.07 (q, J = 7.2 Hz, 2H, OCH_2), 6.78–6.84 (m, 4H, 2'-H, 6'-H, 3-H, 5-H), 6.9 (d, J = 8 Hz, 1H, 6-H), 7.14 (d, J = 8.2 Hz, 1H, 5'-H); CIMS (NH_3) m/z: 345 (MH^+) 300 ($MH^+ -$ OEt).

*3',4',4-Trimethoxy-1,1'-biphenyl-2-propionic acid **37***

Acid **37** was prepared by published procedure (7*a*) and obtained as a white powder (98.3%): mp 148–149°C: IR ($CHCl_3$): 3010, 2940 (CH_3), 1710 (C=O), 1610 (Ph), 1490, 1460, 1290–1190, 1170, 1130 cm^{-1}; ^1H NMR ($CDCl_3$) δ: 2.48 (t, J ~ 8 Hz, 2H, CH_2CO), 2.93 (t, J ~ 8 Hz, 2H, $PhCH_2$), 3.83 (s, 3H, CH_3O), 3.87 (s, 3H, CH_3O), 3.92 (s, 3H, CH_3O), 6.78–6.83 (m, 4H, 2'-H, 6'-H, 3-H, 5-H), 6.9 (d, J = 8.3 Hz, 1H, 6-H), 7.14 (d, J = 8.2 Hz, 1H, 5'-H); CIMS (NH_3) m/z: 334 ($MH^+ + NH_3$), 317 (MH^+), 299 ($MH^+ - H_2O$). Anal. calcd. for $C_{18}H_{20}O_5$: C 68.34, H 6.37; found: C 68.17, H 6.40.

*6,7-Dihydro-2,3,9-trimethoxy-5*H*-dibenzo[*a,c*]cyclohepten-5-one **38***

Acid **37** (510 mg, 1.61 mmol) was suspended in $(CF_3CO)_2O$ (20 mL) at low temperature (ice + NaCl). CF_3COOH (20 mL) was then added dropwise and the solution stirred for 2.5 h at 0°C. The reaction was followed by GC. The solvent was evaporated, the residue taken up in ethyl acetate, washed with $NaHCO_3$ solution, brine, and dried (Na_2SO_4). Evaporation of the solvent gave an oily yellow compound, which was crystallized from ethyl acetate – hexanes and obtained as a white powder (450 mg, 93%): mp 142–143°C; IR ($CHCl_3$): 3020, 2960, 2940 (C-H), 1660 (C=O), 1600 (Ph), 1500, 1460, 1440, 1350, 1290–1120 (Ph-O-CH_3), 1160 cm^{-1}; ^1H NMR ($CDCl_3$) δ: 2.94 (s, 4H, CH_2), 3.86 (s, 3H, CH_3O), 3.96 (s, 3H, CH_3O), 3.98 (s, 3H, CH_3O), 6.82 (d, J = 2.6 Hz, 1H, 8-H), 6.86 (s, 1H, 1-H), 6.89 (dd, J = 2.7 and 8.5 Hz, 1H, 10-H), 7.3 (s, 1H, 4-H), 7.35 (d, J = 8.5 Hz, 1H, 11-H); CIMS (NH_3) m/z: 299 (MH^+). Anal. calcd. for $C_{18}H_{18}O_4$: C 72.47, H 6.08; found: 72.26, H 6.12.

*6,7-Dihydro-2,3,9-trimethoxy-5*H*-dibenzo[*a,c*]cyclohepten-5-ol **39***

Alcohol **39** was prepared by published procedure (7*a*) and obtained as white crystals (92%): dec. >260°C; IR ($CHCl_3$): 3620 (OH), 3020, 2940 (CH_3), 1610 (Ph), 1490, 1460 (-CH_2-), 1290–1180 (Ph-O-CH_3), 1150, 1130, 1050 cm^{-1}; ^1H NMR ($CDCl_3$) δ: 2.48–2.62 (m, 4H, CH_2), 3.85 (s, 3H, CH_3O), 3.92 (s, 3H, CH_3O), 3.96 (s, 3H, CH_3O), 4.60 (dd, J = 6.9 and 9.8 Hz, 1H, 5-H), 6.82 (d, J = 2.6 Hz, 1H, 8-H), 6.87 (s, 1H, 1-H), 6.87 (dd, J = 2.7 and 8.3 Hz, 1H, 10-H), 7.2 (s, 1H, 4-H), 7.27 (d, J = 8.5 Hz, 1H, 11-H); CIMS (NH_3) m/z: 300 (M^+), 283 ($MH^+ - H_2O$).

*2,3,9-Trimethoxy-7*H*-dibenzo[*a,c*]cycloheptene **40***

Cycloheptene **40** was prepared by published procedure (7*a*) and obtained as white crystals after recrystallization from $MeOH/H_2O$ (92%): mp 115–116°C; IR ($CHCl_3$): 3020 (CH_3), 1610 (Ph), 1500, 1470 (-CH_2-), 1290–1180 (Ph-O-CH_3), 1140, 1050 cm^{-1}; ^1H NMR ($CDCl_3$) δ: 2.93 (br s, 2H, CH_2), 3.77 (s, 3H, CH_3O), 3.86 (s, 3H, CH_3O), 3.90 (s, 3H, CH_3O), 6.02 (dt, J = 6.8 and 10 Hz, 1H, 6-H), 6.43 (d, J = 10 Hz, 1H, 5-H), 6.70 (d, J = 2.7 Hz, 1H, 8-H), 6.72 (s, 1H, 1-H), 6.78 (dd, J = 2.7 and 8.6 Hz, 1H, 10-H), 7.04

Can. J. Chem. Downloaded from www.nrcresearchpress.com by 217.78.4.112 on 09/08/12
For personal use only.

(s, 1H, 4-H), 7.35 (d, J = 8.5 Hz, 1H, 11-H); MS (CI/NH_3) m/z: 283 (MH^+). Anal. calcd. for $C_{18}H_{18}O_3 \cdot 0.5\ H_2O$: C 74.34, H 6.41; found: C 74.34, H 6.26.

*6,7-Dihydro-2,3,9-trimethoxy-5*H-*dibenzo*[a,c]*cycloheptene* ***6***

Dihydrocycloheptene **6** was prepared by published procedure (*7a*) and crystallized as white crystals from MeOH–H_2O (72%): mp 75–76°C; IR ($CHCl_3$): 3010, 2940, 2860 (CH), 1600 (Ph), 1480, 1460 (-CH_2-), 1240, 1200 (Ph-O-CH_3), 1150, 1130, 1050, 1020 cm^{-1}; ^1H NMR ($CDCl_3$), δ: 2.07 (m, 2H, CH_2), 2.34–2.43 (m, 4H, CH_2), 3.77 (s, 3H, CH_3O), 3.84 (s, 3H, CH_3O), 3.85 (s, 3H, CH_3O), 6.69 (s, 1H, 1-H), 6.73 (d, J = 2.7 Hz, 1H, 8-H), 6.79 (dd, J = 2.7 and 8.3 Hz, 1H, 10-H), 6.81 (s, 1H, 4-H), 7.21 (d, J = 8.3 Hz, 1H, 11-H); CIMS (NH_3) m/z: 285 (MH^+).

Synthesis of DBCH 7 (Scheme 4)

*(S)-5-Acetamido-6,7-dihydro-9,10,11-trimethoxy-5*H-*dibenzo*[a,c]*cyclohepten-3-yl-1-phenyl-1*H-*5-tetrazolyl ether* ***42***

A mixture of *N*-acetylcolchinol (2.0 g, 5.6 mmol), 5-chloro-1-phenyl-1*H*-tetrazole (1.4 g, 7.7 mmol), and K_2CO_3 (1.9 g, 13.7 mmol) in DMF (50 mL, anhydrous, distilled over molecular sieves) was stirred under argon at 80°C for 6 h, then at room temperature for 3 days. H_2O was added and a white solid precipitated that was collected by filtration, dissolved in $CHCl_3$–*i*PrOH, and washed with brine. After drying ($MgSO_4$) and evaporation of solvent, a yellow oil was obtained that was crystallized from Et_2O to give a white powder (2.8 g, 99%): mp 192–193°C $[\alpha]_D^{25}$ −100.2 (c = 0.51, MeOH); IR ($CHCl_3$): 3500–3300 (-CO-NH-R), 3000, 2940 (CH_3), 1670 (C=O), 1600 (Ph), 1530, 1500, 1480, 1450, 1230–1200, 1150, 1100 cm^{-1}; ^1H NMR ($CDCl_3$) δ: 1.53 (s, $COCH_3$), 1.83–1.95 (m, 1H, CH_2), 2.05 (s, $COCH_3$), 2.32–2.55 (m, 3H, CH_2), 3.46 (s, 3H, OCH_3), 3.84 (s, 3H, OCH_3), 3.86 (s, 3H, OCH_3), 4.78–4.87 (m, 1H 82%, 7-H), 5.12 (m, 1H 18%, 7-H), 5.22 (br d, NH), 5.87 (d, J = 7.8 Hz, NH), 6.59 (s, 1H, 4-H), 7.30 (dd, J = 2.7 and 8.5 Hz, 1H, 10-H), 7.46 (d, J = 2.6 Hz, 1H, 8-H), 7.49–7.63 (m, 5H, Ph), 7.84 (d, J = 7.9 Hz, 1H, 11-H); CIMS (NH_3) m/z: 502 (MH^+).

*(S)-7-Acetamido-6,7-dihydro-1,2,3-trimethoxy-7*H-*dibenzo*[a,c]*cycloheptene* ***43***

A mixture of tetrazolyl ether **42** (2.8 g, 5.6 mmol) and 10%Pd/C (3 g) in AcOH (30 mL) was hydrogenated on a Parr apparatus at 50°C under 50 psi (1 psi = 6.89 kPa) of H_2 for 48 h. The catalyst was filtered and washed with AcOH. After evaporation of solvent the residue was dissolved in $CHCl_3$ and washed with NaOH (5%), H_2O, and dried (Na_2SO_4). Evaporation gave a white powder (1.87 g), which was recrystallized from ethyl acetate – hexanes (98%; 100% pure by GC): mp 189°C $[\alpha]_D^{25}$ −33.1 (c = 0.68, MeOH); IR ($CHCl_3$): 3440 (-CO-NH-R), 3000, 2940, (CH_3), 1670 (C=O), 1600, 1500, 1480, 1400, 1250–1200 (Ph-O-CH_3), 1140, 1100 cm^{-1}; ^1H NMR ($CDCl_3$) δ: 1.58 (s, $COCH_3$), 1.67–1.84 (m, 1H, CH_2), 2.06 (s, $COCH_3$), 2.3–2.49 (m, 3H, CH_2), 3.52 (s, CH_3O), 3.58 (s, CH_3O), 3.9 (s, 3H, CH_3O), 3.93 (s, 3H, CH_3O), 4.80–4.89 (m, 1H 78%, 7-H), 5.16–5.18 (m, 1H 22%, 7-H), 5.24 (m, NH), 5.75–5.78 (m, NH), 6.57 (s, 1H, 4-H), 7.25–7.4 (m, 3H, Ph), 7.5 (m, 1H, Ph); CIMS (NH_3) m/z: 359 ($MH^+ + NH_3$), 341 (MH^+).

*(S)-7-Amino-6,7-dihydro-1,2,3-trimethoxy-7*H-*dibenzo*[a,c]*cycloheptene* ***44***

Acetamide **43** (1.8 g, 5.3 mmol) in H_2SO_4 (20%, 100 mL) and MeOH (50 mL) was refluxed for 3 days, when the reaction was found to be complete by GC. After cooling, the solution was made basic with NaOH (5%), then NaOH pellets. The product was extracted with ethyl acetate, washed with H_2O until neutral, and dried (Na_2SO_4). Evaporation of solvent gave an oil, which was chromatographed (SiO_2, $CHCl_3$–MeOH 95:5) to give **44** as white crystals (1.5 g, 95%): mp 95–96°C; $[\alpha]_D^{25}$ −45 (c = 0.61, MeOH); IR ($CHCl_3$): 3000, 2940 (CH_3), 1600 (Ph), 1480, 1450, 1400, 1340, 1250–1180 (Ph-O-CH_3), 1140, 1090, 1000 cm^{-1}; ^1H NMR ($CDCl_3$) δ: 1.68–1.78 (m, 1H, CH_2), 2.28–2.5 (m, 3H, CH_2), 3.64 (s, 3H, CH_3O), 3.83–3.88 (m, 1H, 7-H), 3.92 (s, 6H, CH_3O), 6.60 (s, 1H, 4-H), 7.3–7.42 (m, 2H, 9-H, 10-H), 7.46 (d, J = 7.3 Hz, 1H, 8-H), 7.61 (d, J = 8.2 Hz, 1H, 11-H); CIMS (NH_3) m/z: 300 (MH^+), 283 ($MH^+ - NH_3$).

*1,2,3-Trimethoxy-5*H-*dibenzo*[a,c]*cycloheptene* ***46***

Amine **44** (250 mg, 0.84 mmol) was dissolved in a solution of anhydrous THF (10 mL) and MeI (10 mL). *t*BuOK (200 mg, 1.78 mmol) was added and the mixture stirred for 3 days at room temperature under argon. At this point the amount of ammonium salt **45** formed was very small and the mixture contained mainly the dimethyl amine derivative of **44**. The inorganic material was removed by filtration and the filtrate was evaporated to give a yellow oil that was stirred in MeI (10 mL) for 2 days. The yellow precipitate formed was collected (180 mg) and heated at 190°C for 3 h in a solution of ethylene glycol (4 mL), H_2O (4 mL), and KOH (10 g). After cooling, 20 mL of H_2O was added and the aqueous phase was extracted with Et_2O. The organic layer was washed with H_2O, dried ($MgSO_4$), and evaporated, leaving a yellow oil that was chromatographed (SiO_2, ethyl acetate – hexanes 1:4) to give 100 mg of pure cycloheptene **46**. Recrystallization from MeOH afforded white crystals (42%): mp 124–125°C; IR ($CHCl_3$): 3000, 2940 (CH_3), 1590 (Ph), 1480, 1400, 1330, 1250–1180 (Ph-O-CH_3), 1140, 1110, 1090, 1000 cm^{-1}; ^1H NMR ($CDCl_3$) δ: 2.78 (dd, J = 5.5 and 12.9 Hz, 1H, 5a-H), 3.05 (dd, J = 8.1 and 12.9 Hz, 1H, 5b-H), 3.45 (s, 3H, CH_3O), 3.90 (s, 3H, CH_3O), 3.91 (s, 3H, CH_3O), 6.24 (m, 1H, 6-H), 6.56–6.58 (m, 2H, 4-H, 7-H), 7.26–7.33 (m, 3H, 8-H, 9-H, 10-H), 7.81 (d, J = 7.5 Hz, 1H, 11-H); CIMS (NH_3) m/z: 300 ($MH^+ + NH_3$), 283 (MH^+). Anal. calcd. for $C_{18}H_{18}O_3 \cdot 1/2\ H_2O$: C 74.34, H 6.41; found: C74.70, H 6.28.

*6,7-Dihydro-1,2,3-tetramethoxy-5*H-*dibenzo*[a,c]*cycloheptene 7*

Cycloheptene **46** (70 mg, 0.25 mmol) in AcOH (10 mL) was hydrogenated at room temperature and 50 psi in a Parr hydrogenator for 3 h over Pd black catalyst (150 mg). Pd was removed by filtration through Celite and washed with AcOH. Evaporation of the filtrate gave **7** as an oil, which was purified by column chromatography (SiO_2, ethyl acetate – hexanes 1:4) (50 mg, 71%): IR ($CHCl_3$): 3020, 2940, 2860 (C-H), 1600 (Ph), 1490, 1460, 1410, 1350, 1320, 1280–1180 (Ph-O-CH_3), 1150, 1110, 1090, 1010 cm^{-1}; ^1H NMR ($CDCl_3$) δ: 2.08–2.13 (m, 2H, CH_2), 2.25–2.6 (m, 4H, CH_2), 3.6 (s, 3H, CH_3O), 3.92 (s, 3H, CH_3O), 3.93 (s, 3H, CH_3O), 6.6 (s, 1H, 4-H), 7.24–7.31 (m, 3H, 8-H, 9-H, 10-H), 7.48 (d, J = 7 Hz, 1H, 11-H); CIMS (NH_3) m/z: 302 ($MH^+ + NH_3$), 285 (MH^+).

Synthesis of 5-acetamidodeaminocolchinyl methyl ether (Scheme 5)

*5-Amino-6,7-dihydro-1,2,3,9-tetramethoxy-5*H-*dibenzo*[a,c]*cycloheptene* ***47***

Oxime **25** (250 mg, 0.73 mmol) was dissolved in EtOH (50 mL) and heated at 85–90°C. Raney nickel (3 g) and hydrazine hydrate (10 mL) were added and the mixture stirred at 85–90°C for 1 h. The catalyst was removed by filtration through Celite and the filtrate was evaporated. The residue was dissolved in HCl (5%) and washed with Et_2O. The aqueous layer was then basified with NaOH (30%) and the product extracted with Et_2O, washed with brine, and dried (Na_2CO_3). Evaporation of the solvent gave amine **47** as a colorless oil (230 mg, 95.8%, 98% pure by GC): IR ($CHCl_3$): 3010, 2945, 2845, (CH_3), 1610 (CH-NH_2), 1580, 1490, 1460 (-CH_2-), 1400, 1330, 1300, 1260–1200 (Ph-O-CH_3), 1160, 1135, 1080, 1000 cm^{-1}; ^1H NMR ($CDCl_3$) δ: 1.86 (m, 1H, CH_2), 2.4–2.6 (m, 3H, CH_2), 3.57 (s, 3H, CH_3O), 3.8 (m, 1H, *CH*NH_2), 3.85 (s, 3H, CH_3O), 3.88 (s, 3H, CH_3O), 3.92 (s, 3H, CH_3O), 6.78, (d, J = 2.6 Hz, 1H, 8-H), 6.85 (dd, J = 2.7 and 8.5 Hz, 1H, 10-H), 7.03 (s, 1H, 4-H), 7.38 (d, J = 8.5 Hz, 1H, 11-H); CIMS (NH_3) m/z: 330 (MH^+), 313 ($MH^+ - NH_3$).

*(−)-(a*R,5S*)-5-Amino-6,7-dihydro-1,2,3,9-tetramethoxy-5*H-*dibenzo[*a,c*]cycloheptene **47***a

Amine **47** (350 mg, 1.06 mmol) dissolved in *i*PrOH (5 mL) was resolved with (+)-dibenzoyl-D-tartaric acid in *i*PrOH (10%, 5 mL) and the salt was recrystallized twice from MeOH. Treatment of this salt with NH_4OH (30%) and extraction with ethyl acetate afforded amine **47***a* (120 mg, 68.7%): $[\alpha]_D^{25}$ −85 (*c* = 0.62, MeOH). Phenylethylurea **48***a* was prepared with *S*-(−)-1-phenylethyl isocyanate in CH_2Cl_2 (22): mp 90–93°C; $[\alpha]_D^{25}$ −55.3 (*c* = 0.93, MeOH); CIMS (NH_3) *m/z*: 477 (MH^+). HPLC purity 100%, retention time 12.6 min (ethyl acetate – hexanes 3:2, 1 mL min^{-1}).

*(+)-(a*S,5R*)-5-Amino-6,7-dihydro-1,2,3,9-tetramethoxy-5*H-*dibenzo[*a,c*]cycloheptene **47***b

The amine prepared from the mother liquor of the resolution of **47***a* afforded a salt on treatment with (−)-*o,o'*-dibenzoyl-L-tartaric acid in *i*PrOH. After recrystallization from methanol (×2) and basification with NH_4OH (30%), extraction with ethyl acetate gave the oily amine **47***b* (97 mg, 55.6%): $[\alpha]_D^{25}$ +85 (*c* = 0.59, MeOH). Phenylethylurea **48***b* prepared with *S*-(−)-1-phenylethyl isocyanate in CH_2Cl_2 (22): mp 242–243°C; $[\alpha]_D^{25}$ −58.9 (*c* = 0.19, MeOH); CIMS (NH_3) *m/z*: 477 (MH^+). HPLC purity 99.3%, retention time 10.6 min (ethyl acetate – hexanes 3:2, 1 mL min^{-1}).

*5-Acetamido-6,7-dihydro-1,2,3,9-tetramethoxy-5*H-*dibenzo[*a,c*]cyclohepten **8***a,b

Acetic anhydride (0.13 mL, 1.38 mmol) was added, after cooling, to a THF suspension (20 mL) of **47***a,b* (45 mg, 0.14 mmol) and K_2CO_3 (200 mg, 1.4 mmol), and the mixture was stirred at room temperature for 2 h. Saturated $NaHCO_3$ was added and the amide was extracted with Et_2O. The combined extracts were washed with saturated $NaHCO_3$, H_2O, and dried ($MgSO_4$). Evaporation of the solvent gave 66 mg of a colorless oil, which on addition of H_2O gave a white powder.

Compound **8***a*: 99%, mp 98–101°C; $[\alpha]_D^{25}$ −68.2 (*c* = 0.505, MeOH); IR ($CHCl_3$): 3440 (-CO-NH-), 3000, 2930, 2840 (CH_3), 1660 (C=O), 1600, 1570 (Ph), 1480, 1450 (-CH_2-), 1400, 1320, 1300, 1240–1200 (Ph-O-CH_3), 1085 cm^{-1}; ^1H NMR ($CDCl_3$) δ: 2.09 (s, 3H, $COCH_3$), 2.3–2.7 (m, 4H, CH_2), 3.56 (s, 3H 45%, CH_3O), 3.59 (s, 3H 55%, CH_3O), 3.84 (s, 3H 43%, CH_3O), 3.87 (s, 3H 57%, CH_3O), 3.89 (s, 3H, CH_3O), 3.90 (s, 3H 50%, CH_3O), 3.92 (s, 3H 50%, CH_3O), 4.64 (m, 1H 46%, 5-H), 5.06 (m, 1H 54%, 5-H), 5.18 (d, *J* = 8.8 Hz, NHCO), 6.16 (br s, NHCO), 6.61 (s, 1H 39%, 4-H), 6.67 (s, 1H 61%, 4-H), 6.76 (d, *J* = 2.6 Hz, 8-H), 6.82–6.94 (m, 1H, 10-H), 6.86 (d, *J* = 2.7 Hz, 8-H), 7.41 (d, *J* = 8.4 Hz, 1H 52%, 11-H), 7.42 (d, *J* = 8.3 Hz, 1H 48%, 11-H); EIMS *m/z*: 371 (M^+), 312 (M^+ − $NHCOCH_3$), 281.

Compound **8***b*: 99%, mp 94–95°C; $[\alpha]_D^{25}$ +71.8 (*c* = 0.545, MeOH).

Acknowledgment

The authors would like to thank Dr. N. A. Grayson-Boyé and Dr. J. T. M. Linders for much helpful advice and many suggestions.

1. H. G. Capraro and A. Brossi. Alkaloids (Academic Press), **23**, 1 (1984).
2. A. Brossi. J. Med. Chem. **33**, 2315 (1990).
3. A. Muzaffar, A. Brossi, C. M. Lin, and E. Hamel. J. Med. Chem. **33**, 567 (1990).
4. M. Rösner, H. G. Capraro, A. E. Jacobson, L. Atwell, A. Brossi, M. A. Iorio, T. H. Williams, R. H. Sik, and C. F. Chignell. J. Med. Chem. **24**, 257 (1981).
5. M. Cernoch, J. Malinsky, O. Telupilova, and F. Santavy. Arch. Int. Pharmacodyn. Ther. **99**, 141 (1954).
6. P. Kerekes, A. Brossi, J. L. Flippen-Anderson, and C. F. Chignell. Helv. Chim. Acta, **68**, 571 (1985).
7. (*a*) O. Boyé, Y. Itoh, E. Hamel, and A. Brossi. Helv. Chim. Acta, **72**, 1690 (1989); (*b*) Y. Itoh, C. M. Lin, E. Hamel, and A. Brossi. Helv. Chim. Acta, **71**, 1199 (1988).
8. B. Umezawa, O. Hoshino, S. Sawaki, H. Sashida, K. Mori, Y. Hamada, K. Kotera, and Y. Iitaka. Tetrahedron, **40**, 1783 (1984).
9. A. Brossi, H. J. C. Yeh, M. Chrzanowska, J. Wolff, E. Hamel, C. M. Lin, F. Quinn, M. Suffness, and J. V. Silverton. Med. Res. Rev. **8**, 77 (1988).
10. A. Brossi, O. Boyé, A. Muzaffar, H. J. C. Yeh, V. Toome, B. Wegrzynski, and C. George. FEBS Lett. **262**, 5 (1990).
11. V. Prelog and G. Helmchen. Angew. Chem. Int. Ed. Engl. **21**, 567 (1982).
12. H. House. Modern synthetic reactions. 2nd ed. W. A. Benjamin, Menlo Park, Calif. 1972. p. 201.
13. H. Zimmermann. Tetrahedron, **16**, 169 (1961).
14. A. I. Meyers, R. Gabel, and E. D. Michelich. J. Org. Chem. **43**, 1372 (1978).
15. A. I. Meyers, J. R. Flisak, and J. R. Aitken. J. Am. Chem. Soc. **109**, 5446 (1987).
16. A. I. Meyers and M. E. Flanagan. Org. Synth. **69**, 248 (1990).
17. J. W. Cook and J. D. Loudon. Alkaloids (Academic Press), **2**, 278 (1952); A. Windaus. Liebigs. Ann. Chem. **439**, 59 (1924).
18. M. Shamma. The isoquinoline alkaloids. Organic Chemistry Monographs. Vol. 25. Academic Press, San Diego, Calif. 1972. p. 208.
19. K. C. Rice and A. Brossi. Synth. Commun. **8**, 391 (1978).
20. W. J. Musliner and J. W. Gates. J. Am. Chem. Soc. **88**, 4271 (1966).
21. A. Brossi, M. F. Rahman, K. C. Rice, M. Gerecke, R. Borner, J. P. O'Brien, and S. Teitel. Heterocycles, **7**, 277 (1977).
22. B. DeCosta, C. George, R. B. Rothman, A. E. Jacobson, and K. C. Rice. FEBS Lett. **223**, 335 (1987).
23. L. M. Jackman and S. Sternhell. Applications of NMR spectroscopy in organic chemistry. 2nd ed. Pergamon Press, New York. 1969. p. 281.
24. C. A. G. Haasnoot, F. A. A. M. de Leeuw, and C. Altona. Tetrahedron, **36**, 2783 (1980).
25. J. K. Batra, G. J. Kang, L. Jurd, and E. Hamel. Biochem. Pharmacol. **37**, 2595 (1988).

Can. J. Chem. Downloaded from www.nrcresearchpress.com by 217.78.4.112 on 09/08/12
For personal use only.

Organometallic oxides and sulfides: preparation of $[(\eta\text{-}C_5H_5)Ti]_5(\mu_3\text{-}S)_6$, $[(\eta\text{-}C_5H_5)Ti]_5(\mu_3\text{-}S)_5(\mu_3\text{-}S_2)(\mu_4\text{-}O)$, and $(\eta\text{-}C_5H_5)_2Ti(SH)(\mu\text{-}O)Ti(\eta\text{-}C_5H_5)(\mu\text{-}S)_2\text{-}Ti(\eta\text{-}C_5H_5)_2$ by reductive aggregation of $(\eta\text{-}C_5H_5)_2Ti(SH)_2$ with zinc powder or by oxidation of $(\eta\text{-}C_5H_5)_2Ti(CO)_2$ with H_2S in the presence of water

FRANK BOTTOMLEY[1] AND ROBERT W. DAY

Department of Chemistry, University of New Brunswick, Fredericton, N.B., Canada E3B 5A3

Received April 2, 1991

This paper is dedicated to Professor Zdenek (Denny) Valenta on the occasion of his 65th birthday

FRANK BOTTOMLEY and ROBERT W. DAY. Can. J. Chem. **70**, 1250 (1992).

Reduction of $(\eta\text{-}C_5H_5)_2Ti(SH)_2$ with zinc powder gave a mixture of products, of which $[(\eta\text{-}C_5H_5)Ti]_5(\mu_3\text{-}S)_6$ (**1**), $[(\eta\text{-}C_5H_5)Ti]_5(\mu_3\text{-}S)_5(\mu_3\text{-}S_2)(\mu_4\text{-}O)$ (**2**), $(\eta\text{-}C_5H_5)_2Ti(SH)(\mu\text{-}O)Ti(\eta\text{-}C_5H_5)(\mu\text{-}S)_2Ti(\eta\text{-}C_5H_5)_2$ (**3**), $[(\eta\text{-}C_5H_5)Ti]_4(\mu_2\text{-}S_2)_4(\mu_2\text{-}O)(\mu_4\text{-}O)$ (**4**), and $[(\eta\text{-}C_5H_5)Ti(\mu_3\text{-}S)]_4$ (**5**) were identified by a combination of fractional crystallization and X-ray diffraction, electron spin resonance spectroscopy, or mass spectrometry. The source of the oxygen in **2**, **3**, and **4** is believed to be the zinc oxide coating on the zinc powder. A similar mixture of products was obtained from the reaction between $(\eta\text{-}C_5H_5)_2Ti(CO)_2$ and H_2S in the presence of small quantities of water. The structures of **2** and **3** are discussed in detail. **2** has a trigonal bipyramidal arrangement of Ti atoms (average Ti(ax)—Ti(eq) 3.22 Å, average Ti(eq)—Ti(eq) distance 3.24 Å) except for one long equatorial Ti—Ti edge of 3.60 Å, which is spanned by the $\mu_3\text{-}S_2$ unit. **2** is monoclinic, $P2_1/n$, a = 10.585(1), b = 28.133(4), c = 31.408(2) Å, β = 91.20(1)°, Z = 4 (for three independent molecules of **2** and one $C_6H_5CH_3$), R = 0.071 for 6911 observed reflections and 1141 refined parameters. **3** is triclinic, $P\bar{1}$, a = 9.146(1), b = 12.290(1), c = 13.027(1) Å, α = 100.72(1), β = 104.39(1), γ = 110.55(1)°, Z = 2, R = 0.037 for 3046 observed reflections and 304 parameters. The Ti—O—Ti unit in **3** has an angle of 175.6(2)°.

FRANK BOTTOMLEY et ROBERT W. DAY. Can. J. Chem. **70**, 1250 (1992).

La réduction du $(\eta\text{-}C_5H_5)_2Ti(SH)_2$ avec de la poudre de zinc conduit à un mélange dans lequel on a identifié le $[(\eta\text{-}C_5H_5)Ti]_5(\mu_3\text{-}S)_6$ (**1**), $[(\eta\text{-}C_5H_5)Ti]_5(\mu_3\text{-}S)_5(\mu_3\text{-}S_2)(\mu_4\text{-}O)$ (**2**), $(\eta\text{-}C_5H_5)_2Ti(SH)(\mu\text{-}O)Ti(\eta\text{-}C_5H_5)(\mu\text{-}S)_2Ti(\eta\text{-}C_5H_5)_2$ (**3**), $[(\eta\text{-}C_5H_5)Ti]_4(\mu_2\text{-}S_2)_4(\mu_2\text{-}O)(\mu_4\text{-}O)$ (**4**) et $[(\eta\text{-}C_5H_5)Ti(\mu_3\text{-}S)_4$ (**5**) par une combinaison de cristallisation fractionnée, de diffraction des rayons-X, de spectroscopie de résonance paramagnétique électronique et de spectrométrie de masse. On croit que la source de l'oxygène dans les composés **2**, **3** et **4** est l'oxyde de zinc recouvrant la poudre de zinc. On a obtenu un mélange semblable de produits lors de la réaction du $(\eta\text{-}C_5H_5)_2Ti(CO)_2$ et le H_2S, en présence de faibles quantités d'eau. On discute en détail des structures des composés **2** et **3**. Dans le composé **2**, les atomes de Ti possèdent un arrangement trigonal bipyramidal (Ti(ax)—Ti(éq) moyen = 3,22 Å; Ti(éq)—Ti(éq) moyen = 3,24 Å) à l'exception d'une liaison Ti—Ti équatoriale qui est particulièrement longue, à 3,60 Å, et qui est étendue par une unité de μ_3-S. Le composé **2** est monoclinique, $P2_1/n$, avec a = 10,585(1), b = 28,133(4) et c = 31,408(2) Å, β = 91,20°, Z = 4 (pour trois molécules indépendantes de **2** et une de $C_6H_5CH_3$) et R = 0,071 pour 6911 réflexions observées et 1141 paramètres affinés. Le composé **3** est triclinique, $P\bar{1}$, avec a = 9,146(1), b = 12,290(1) et c = 13,027(1) Å, α = 100,72(1), β = 104,39(1) et γ = 110,55(1)°, Z = 2 et R = 0,037 pour 3046 réflexions observées et 304 paramètres. L'angle de l'unité Ti—O—Ti dans le composé **3** est de 175,6(2)°.

[Traduit par la rédaction]

Introduction

We have shown previously that the organometallic oxide $[(\eta\text{-}C_5H_5)Ti]_6(\mu_3\text{-}O)_8$ and sulfide $[(\eta\text{-}C_5H_5)Ti]_5(\mu_3\text{-}S)_6$ can be obtained by oxidation of $(\eta\text{-}C_5H_5)_2Ti(CO)_2$ with H_2O or H_2S respectively (1–3). Floriani and co-workers obtained $[(\eta\text{-}C_5H_5)Ti]_6(\mu_3\text{-}Cl)_n(\mu_3\text{-}O)_{8-n}$ (n = 0, 2, 4) by reduction of the Ti(4+) complexes $[(\eta\text{-}C_5H_5)TiCl_2]_2(\mu\text{-}O)$ or $[(\eta\text{-}C_5H_5)\text{-}TiCl(\mu\text{-}O)]_4$ with aluminum or zinc powder (4). We wished to extend this preparation of (cyclopentadienyl)metal oxides by reductive aggregation of (cyclopentadienyl)metal oxo complexes to (cyclopentadienyl)metal sulfides and selenides. Therefore we investigated the reduction of $(\eta\text{-}C_5H_5)_2Ti(SH)_2$ (5) with zinc powder. We found previously that reductions with zinc powder introduce oxygen from the zinc oxide coating, which is invariably present on the metal surface, into the reactions (6–8). Because of this, reduction of $(\eta\text{-}C_5H_5)_2Ti(SH)_2$ with zinc powder produced not only the expected $[(\eta\text{-}C_5H_5)_2Ti]_5(\mu_3\text{-}S)_6$ but also several products containing oxygen, among which were $[(\eta\text{-}C_5H_5)Ti]_5(\mu_3\text{-}S)_5(\mu_3\text{-}S_2)(\mu_4\text{-}O)$ and $(\eta\text{-}C_5H_5)_2Ti(SH)(\mu\text{-}O)Ti(\eta\text{-}C_5H_5)(\mu\text{-}S)_2Ti(\eta\text{-}C_5H_5)_2$, which are new compounds. We also found that oxidation of $(\eta\text{-}C_5H_5)_2Ti(CO)_2$ with H_2S in the presence of trace amounts of H_2O gave a similar mixture to that obtained by the reduction of $(\eta\text{-}C_5H_5)_2Ti(SH)_2$. The reactions and characterization of many of the products are reported here in detail.

Results and discussion

Reduction of $(\eta\text{-}C_5H_5)_2Ti(SH)_2$ with zinc powder

Several products were formed when a toluene solution of $(\eta\text{-}C_5H_5)_2Ti(SH)_2$ was reduced with zinc powder. This was evident from the ESR spectra of the reaction solutions after removal of the excess zinc, zinc sulfide, and other insoluble materials. The spectra showed five major signals due to species containing titanium, as well as a number of minor features. The relative intensities varied with the conditions of the reaction, but all of the signals were consistently observed. A representative spectrum is shown in Fig. 1. The ESR signals have g values of 1.979, 1.992, 1.994, 2.004, and 2.010.

The signal with g = 1.994 was readily identified as being due to $[(\eta\text{-}C_5H_5)Ti]_5(\mu_3\text{-}S)_6$ (**1**) (literature value 1.993 (1)).

[1]Author to whom correspondence may be addressed.

Can. J. Chem. Downloaded from www.nrcresearchpress.com by 217.78.4.112 on 09/08/12
For personal use only.

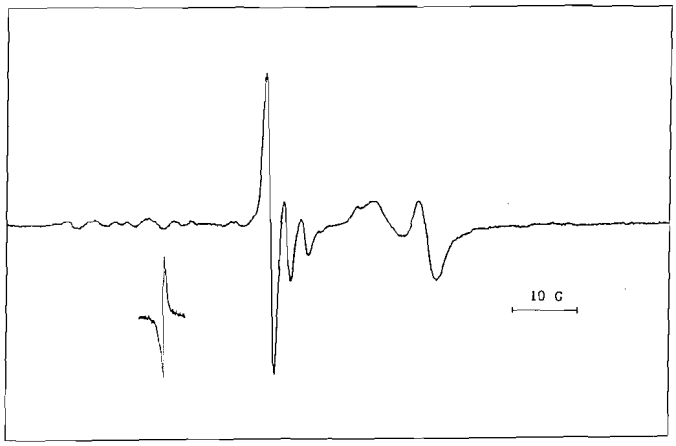

FIG. 1. The ESR spectrum of the product of the reduction of $(\eta\text{-}C_5H_5)_2Ti(SH)_2$ by zinc powder.

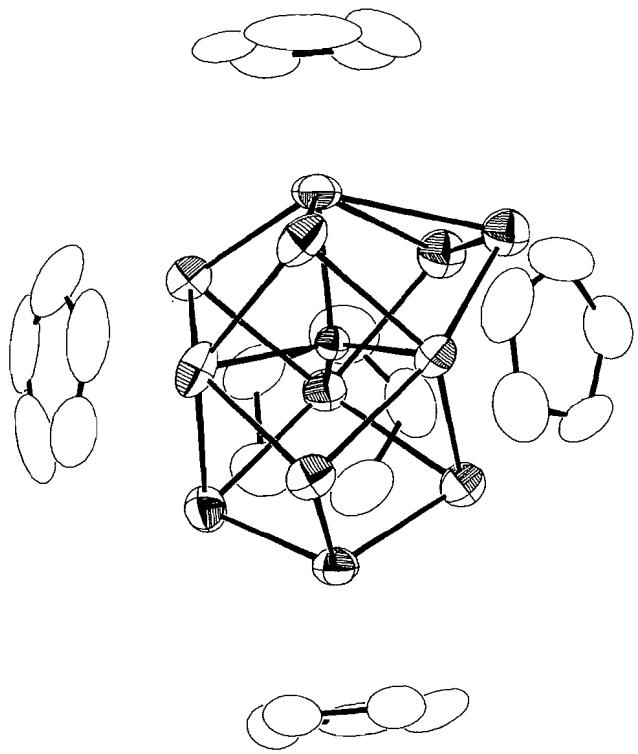

FIG. 2. ORTEP plot of one of the three independent molecules of $[(\eta\text{-}C_5H_5)Ti]_5(\mu_3\text{-}S)_5(\mu_3\text{-}S_2)(\mu_4\text{-}O)$ (**2**). Only a disordered molecule is shown.

The other signals must be due to species with one unpaired electron per molecule, or with unpaired electrons that do not interact with one another, since the signals are relatively sharp even at room temperature. Three methods were used to identify the compounds present: fractional crystallization from the toluene solution; mass spectrometry (performed on the solid obtained by removal of toluene under vacuum); and comparison of the ESR spectra of the mixture with those of known compounds or of compounds prepared as described below.

Fractional crystallization yielded **1**, $[(\eta\text{-}C_5H_5)Ti]_5(\mu_3\text{-}S)_5(\mu_3\text{-}S_2)(\mu_4\text{-}O)$ (**2**, Fig. 2), and $(\eta\text{-}C_5H_5)_2Ti(SH)(\mu\text{-}O)Ti(\eta\text{-}C_5H_5)(\mu\text{-}S)_2Ti(\eta\text{-}C_5H_5)_2$ (**3**, Fig. 3). Cluster **1** was identified by mass spectrometry, ESR spectroscopy, and by

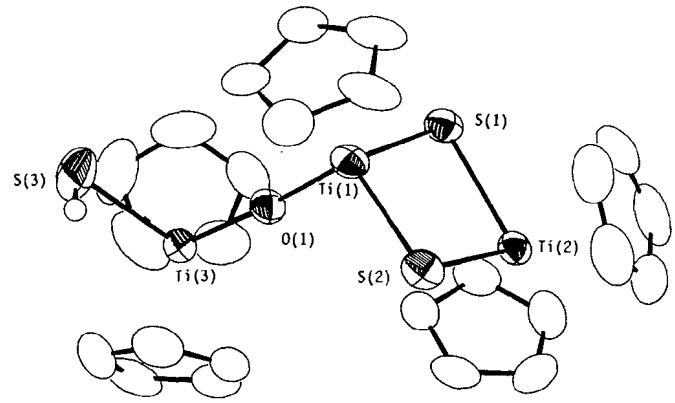

FIG. 3. ORTEP plot of $(\eta\text{-}C_5H_5)_2Ti(SH)(\mu\text{-}O)Ti(\eta\text{-}C_5H_5)(\mu\text{-}S)_2Ti(\eta\text{-}C_5H_5)_2$ (**3**).

comparison of the cell dimensions with the literature (1, 2). Compounds **2** and **3** were identified by X-ray diffraction (see Table 1). Their structures are discussed in detail below. We found previously that the zinc oxide coating present on the surface of zinc powder provided oxygen when oxochloro(cyclopentadienyl) derivatives of niobium and molybdenum were reduced (6–8). We believe that this zinc oxide is the source of the oxygen atoms in **2** and **3**, since normal precautions were taken to exclude oxygen and moisture from the solvents and reagents (9).

The mass spectrum of the reaction product showed a clear parent ion peak for $\mathbf{1}^+$ (*m/e* 757, relative intensity 17%) but not for **2** (M = 805). Peaks at *m/e* 739 (relative intensity 5%) and 580 (relative intensity 12%) were assigned to $\{[(C_5H_5)Ti]_4(S_2)_4(O)_2\}^+$ ($\mathbf{4}^+$) and $[(C_5H_5)TiS]_4^+$ ($\mathbf{5}^+$) respectively. The structure of **4** (see Fig. 4) is discussed below. The mass spectrum of the mixture also showed fragmentation of **1**, **4**, and **5** (principally by loss of C_5H_5), as well as peaks assignable to $[(C_5H_5)_2Ti(SH)_2]^+$ and $[(C_5H_5)_2TiS]^+$. The latter is probably derived from $[(\eta\text{-}C_5H_5)_2Ti(\mu\text{-}S)]_2$, which is, in turn, obtained from the starting material $(\eta\text{-}C_5H_5)_2Ti(SH)_2$ by the equilibrium [1] (2, 10).

[1] $2\,(\eta\text{-}C_5H_5)_2Ti(SH)_2 \rightleftharpoons [(\eta\text{-}C_5H_5)_2Ti(\mu\text{-}S)]_2 + H_2S$

The ESR spectrum of crystalline $[(\eta\text{-}C_5H_5)Ti]_5(\mu_3\text{-}S)_5(\mu_3\text{-}S_2)(\mu_4\text{-}O)$ (**2**) showed a single-line signal at g = 1.980, and we assign the signal at 1.979 in the mixture of products obtained by reducing $(\eta\text{-}C_5H_5)_2Ti(SH)_2$ with zinc powder to **2**. Since **2** formally contains Ti_5^{19+} it has only one cluster electron, and therefore it would show a single-line ESR spectrum regardless of its molecular structure. The compound $(\eta\text{-}C_5H_5)_2Ti(SH)(\mu\text{-}O)Ti(\eta\text{-}C_5H_5)(\mu\text{-}S)_2Ti(\eta\text{-}C_5H_5)_2$ (**3**) contains Ti_3^{12+}, and $[(\eta\text{-}C_5H_5)Ti]_4(\mu_2\text{-}S_2)_4(\mu_2\text{-}O)(\mu_4\text{-}O)$ (**4**) contains Ti_4^{16+}. Therefore neither **3** nor **4** can show any ESR signal. The cluster $[(\eta\text{-}C_5H_5)TiS]_4$ (**5**), which was observed by mass spectrometery, is known to be a diamagnetic cubane (11), as predicted by extended Hückel molecular orbital calculations (12). Therefore no ESR signal would be expected. However, independent experiments established that mixtures of $[(\eta\text{-}C_5H_5)Ti]_5(\mu_3\text{-}S)_6$ and $[(\eta\text{-}C_5H_5)Ti(\mu_3\text{-}S)]_4$ showed ESR signals at g = 1.994 and 1.987. These could arise from the equilibrium [2].

[2] $[(\eta\text{-}C_5H_5)Ti(\mu_3\text{-}S)]_4 + [(\eta\text{-}C_5H_5)Ti]_5(\mu_3\text{-}S)_6$
$\rightleftharpoons \{[(\eta\text{-}C_5H_5)Ti(\mu_3\text{-}S)]_4\}^+ + \{[(\eta\text{-}C_5H_5)Ti]_5(\mu_3\text{-}S)_6\}^-$

Can. J. Chem. Downloaded from www.nrcresearchpress.com by 217.78.4.112 on 09/08/12
For personal use only.

TABLE 1. Crystal and refinement data for $[(\eta\text{-}C_5H_5)Ti]_5(\mu_3\text{-}S)_5(\mu_3\text{-}S_2)(\mu_4\text{-}O)$ (**2**), $(\eta\text{-}C_5H_5)_2Ti(SH)(\mu\text{-}O)Ti(\eta\text{-}C_5H_5)(\mu\text{-}S)_2Ti(\eta\text{-}C_5H_5)_2$ (**3**), and $[(\eta\text{-}C_5H_5)Ti]_4(\mu_2\text{-}S_2)_4(\mu_2\text{-}O)(\mu_4\text{-}O)$ (**4**)

	2	**3**	**4**
Molecular formula	$C_{82}H_{83}O_3S_{21}Ti_{15}$[a]	$C_{25}H_{26}OS_3Ti_3$	$C_{23.5}H_{24}O_2S_8Ti_4$[b]
Formula weight, Da	2508.41	582.36	786.08
Crystal system	Monoclinic	Triclinic	Tetragonal
Space group	$P2_1/n$	$P\bar{1}$	$P4/ncc$
a, Å	10.585(1)	9.146(1)	17.759(1)
b, Å	28.133(4)	12.290(1)	17.759
c, Å	31.408(2)	13.027(1)	17.655(2)
α, deg	90	100.72(1)	90
β, deg	91.20(1)	104.39(1)	90
γ, deg	90	110.55(1)	90
V Å^3	9351(2)	1266.3(2)	5568.4(7)
Z	4	2	8
D (calcd.), Mg m^{-3}	1.78	1.53	1.88
μ (Mo Kα), cm^{-1}	16.3	11.7	17.0
Temperature, K	293	293	295
Crystal size, mm	0.25 × 0.35 × 0.35	0.10 × 0.25 × 0.50	0.35 × 0.35 × 0.25
2θ limits, deg	2–45	2–50	2–50
No. of reflns. for cell	25	24	25
2θ limits for cell, deg	40–50	40–50	30–40
Reflns. collected	15 655	8 873	10 615
Unique reflns.	12 105	4 439	2 471
Observed reflns.	6 911	3 046	1 714
Criteria for observation	$I > 2.5\ \sigma(I)$	$I > 2.5\ \sigma(I)$	$I > 2.0\ \sigma(I)$
R (F')	0.071	0.037	0.141
R_w (F')	0.059	0.047	0.138
GoF	1.980	1.144	2.67
No. of refined parameters	1141	304	185
Max Δ/σ	0.88	0.21	0.72
Max Δ, e Å^{-3}	0.75	0.36	1.06
N_o/N_v	6.06	10.0	6.35
K (weight modifier)	0.0001	0.001	0.001

[a]For $\{[(\eta\text{-}C_5H_5)Ti]_5(\mu_3\text{-}S)_5(\mu_3\text{-}S_2)(\mu_4\text{-}O)\}_3 \cdot C_6H_5CH_3$.
[b]For $[(\eta\text{-}C_5H_5)Ti]_4(\mu\text{-}S_2)_4(\mu_2\text{-}O)(\mu_4\text{-}O) \cdot 0.5C_6H_5CH_3$.

The alternative salt, $\{[(\eta\text{-}C_5H_5)Ti]_5(\mu_3\text{-}S)_6\}^+\{[(\eta\text{-}C_5H_5)Ti(\mu_3\text{-}S)]_4\}^-$, is highly unlikely because it would require one titanium to have a formal oxidation state of (2+). Cationic and anionic derivatives of $[(\eta\text{-}C_5H_5)V]_5(\mu_3\text{-}S)_6$ (13) and $[(\eta\text{-}C_5H_5)M(\mu_3\text{-}S)]_4$ (M = V, Fe, Co, Mo) (11, 14–17) were observed previously. We assign the ESR signal at $g = 1.987$ to $[(\eta\text{-}C_5H_5)Ti(\mu_3\text{-}S)]_4^+$.

The signals at $g = 2.004$ and 2.010 cannot be identified from the above experiments, nor can they be accounted for by the products obtained from the reaction between $(\eta\text{-}C_5H_5)_2Ti(CO)_2$ and H_2S in the presence of H_2O, which are described below. It is possible that they, like the signal at $g = 1.987$, are also due to equilibria that produce radicals, for example $\mathbf{4}^-$. However, if an anion of **4** was formed, it is not certain that the unpaired electron would be localized on titanium, since the S_2 unit could conceivably absorb an electron. In this respect the fact that the unassigned signals have g values greater than 2.002 may be significant.

Independent experiments established that **1** did not react with either H_2O or Ag_2O to form **2**, nor to form any characterizable cluster. The oxygen atoms present in **2**, **3**, and **4** must have been inserted during redox reactions between $(\eta\text{-}C_5H_5)_2Ti(SH)_2$ and the zinc/zinc oxide powder. The S_2^{2-} ligand present in **2** and **4** must also be a product of these redox reactions. Compounds **2**, **3**, and **4** all contain at least one titanium atom bearing only one $\eta\text{-}C_5H_5$ ring. Four of the five titanium atoms in **2**, and all of the titanium atoms in **3** and **4**, have the formal oxidation state of 4+. The substitution of an $\eta\text{-}C_5H_5$ ligand in the titanium(4+) compound $(\eta\text{-}C_5H_5)_2Ti(SH)_2$ by O^{2-} would be extremely slow, due to the very low concentration of O^{2-} in solution (18). The combination of Ti(4+) with a single $(\eta\text{-}C_5H_5)$ ligand is therefore further evidence that redox reactions are responsible for the insertion of O^{2-} in **2**, **3**, and **4**.

Oxidation of $(\eta\text{-}C_5H_5)_2Ti(CO)_2$ in the presence of traces of oxygen

Since the reduction of $(\eta\text{-}C_5H_5)_2Ti(SH)_2$ with zinc powder gave clusters containing oxygen as well as sulfur, we were interested in the effect of oxygen (either as O_2 or H_2O) on the oxidation of $(\eta\text{-}C_5H_5)_2Ti(CO)_2$ by H_2S. In the absence of oxygen this reaction gave $[(\eta\text{-}C_5H_5)Ti]_5(\mu_3\text{-}S)_6$ according to eq. [3] (1, 2). There was no evidence for other paramagnetic species in the ESR spectrum of the reaction

$$[3]\quad 10\,(\eta\text{-}C_5H_5)_2Ti(CO)_2 + 12\,H_2S \rightarrow 2\,[(\eta\text{-}C_5H_5)Ti]_5(\mu_3\text{-}S)_6 + 14\,H_2 + 20\,CO + 5\,(C_5H_6)_2$$

solutions. However, when the reaction was conducted in the presence of traces of oxygen, in the form of H_2O, the ESR spectra of the reaction solutions were similar to those of the

Can. J. Chem. Downloaded from www.nrcresearchpress.com by 217.78.4.112 on 09/08/12
For personal use only.

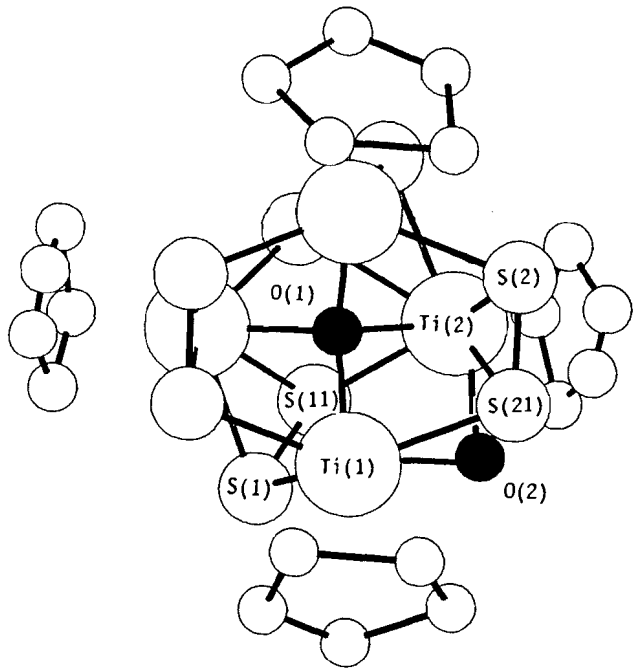

FIG. 4. The structure of $[(\eta\text{-}C_5H_5)Ti]_4(\mu_2\text{-}S_2)_4(\mu_2\text{-}O)(\mu_4\text{-}O)$ (**4**). Only one of the several disordered forms is shown.

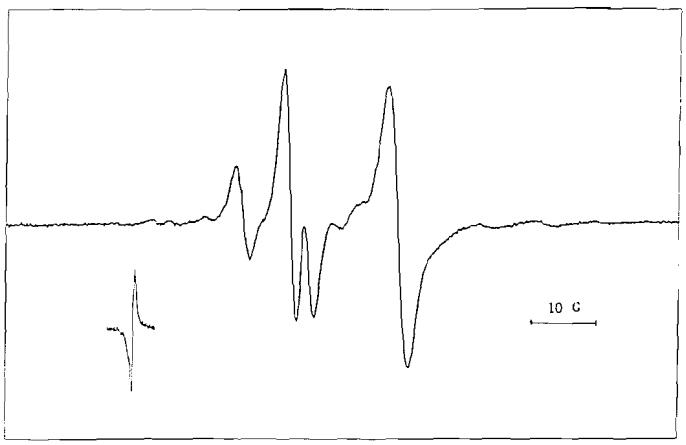

FIG. 5. The ESR spectrum of the product of the oxidation of $(\eta\text{-}C_5H_5)_2Ti(CO)_2$ by H_2S in the presence of water.

solutions obtained by reducing $(\eta\text{-}C_5H_5)_2Ti(SH)_2$ with zinc powder. A representative example is shown in Fig. 5; this may be compared with Fig. 1. In summary, signals were observed at g = 1.979, 1.987, 1.992, 1.994, and 2.007. The signals at 1.979, 1.987, and 1.994 were readily assigned to **2**, $\mathbf{5}^+$, and **1** respectively, as discussed above.

As with the reaction between $(\eta\text{-}C_5H_5)_2Ti(SH)_2$ and zinc powder, we attempted to identify the species responsible for the ESR signals at g = 1.992 and 2.007 by fractional crystallization of toluene solutions, produced by reacting $(\eta\text{-}C_5H_5)_2Ti(CO)_2$ with H_2S in the presence of H_2O. These attempts gave crystalline **1**, **2**, and **4**. Compound **4** (Fig. 4) had been observed in the mass spectrum of the reaction between $(\eta\text{-}C_5H_5)_2Ti(SH)_2$ and zinc powder, but not otherwise identified. The structure of the $\eta\text{-}C_5H_4Me$ derivative of **4** was completely determined by X-ray crystallography by Rauchfuss

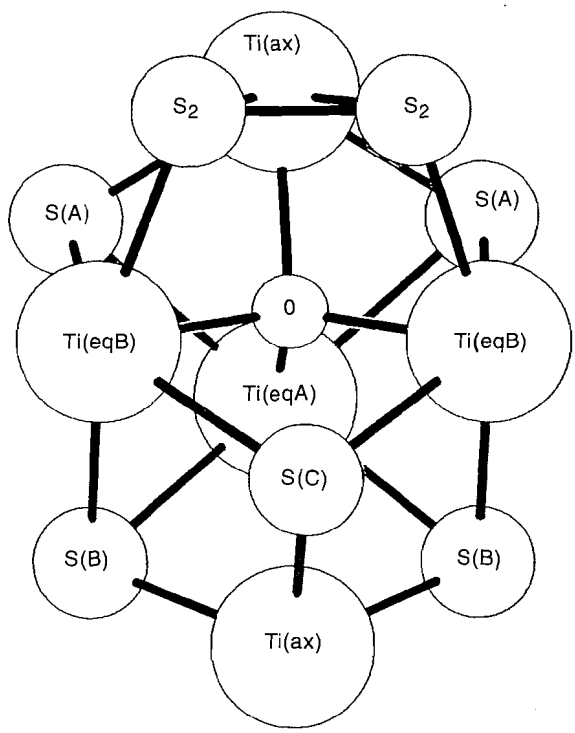

FIG. 6. Diagram of the $Ti_5(\mu_3\text{-}S)_5(\mu_3\text{-}S_2)(\mu_4\text{-}O)$ core of **2**, with numbering scheme.

and co-workers (19). The core of **4** also appears in $[TiCl]_4(\mu_2\text{-}S_2)_4(\mu_2\text{-}Cl)_2(\mu_4\text{-}O)$ (20), with chlorine replacing both $(\eta\text{-}C_5H_5)$ and the μ_2-oxygen, which is disordered over two positions in the structure of **4** (see Fig. 4). Because of serious disorder amongst the $\eta\text{-}C_5H_5$, S_2, and O ligands, and the presence of an ill-defined toluene molecule in the crystal lattice, the present analysis was only accurate enough to characterize the product unambiguously as $[(\eta\text{-}C_5H_5)Ti]_4(\mu_2\text{-}S_2)_4(\mu_2\text{-}O)(\mu_4\text{-}O)$.

The source of the oxygen atoms present in compounds **2** and **4**, obtained when $(\eta\text{-}C_5H_5)_2Ti(CO)_2$ was oxidized with H_2S, is believed with some certainty to be H_2O. There was no decrease in the amount of **2** when the H_2S was thoroughly degassed by freeze–thaw methods. This procedure would remove O_2 but not H_2O. However the amount of **2** increased markedly when small quantities of H_2O were deliberately added to the toluene solution of $(\eta\text{-}C_5H_5)_2Ti(CO)_2$ immediately prior to incubation with H_2S. The relative amount of **2** could be easily assessed from the ESR spectra, but there was no convenient method of detecting **3** or **4**. The introduction of oxygen by water is consistent with the preparation of $[(\eta\text{-}C_5H_5)Ti]_6(\mu_3\text{-}O)_8$ from $(\eta\text{-}C_5H_5)_2Ti(CO)_2$ and H_2O (2), but is in contrast to the preparation of $[(\eta\text{-}C_5H_4Me)Ti]_4(\mu_2\text{-}S_2)_4(\mu_2\text{-}O)(\mu_4\text{-}O)$ and $[(\eta\text{-}C_5H_4Me)Ti]_4S_8O$, where the source of oxygen was O_2 (19).

Structure of $[(\eta\text{-}C_5H_5)Ti]_5(\mu_3\text{-}S)_5(\mu_3\text{-}S_2)(\mu_4\text{-}O)$ (2)

The crystal of **2** contained four asymmetric units per cell, each unit consisting of three independent molecules of **2** and one of toluene. Including the disordered atoms there were 135 non-hydrogen and 88 hydrogen atoms to be refined, all in general positions, giving a total of 1141 parameters. Some of the available structure refinement programs do not ac-

Can. J. Chem. Downloaded from www.nrcresearchpress.com by 217.78.4.112 on 09/08/12
For personal use only.

Can. J. Chem. Downloaded from www.nrcresearchpress.com by 217.78.4.112 on 09/08/12
For personal use only.

TABLE 2. Important average distances (Å) in $[(\eta\text{-}C_5H_5)Ti]_5(\mu_3\text{-}S)_5(\mu_3\text{-}S_2)(\mu_4\text{-}O)$ (**2**)

Ti(ax)—Ti(eqA)[a]	3.207 (6, 3, 11)[b]
Ti(ax)—Ti(eqB)[a]	3.227 (12, 3, 109)
Ti(eqA)—Ti(eqB)[a]	3.236 (6, 3, 23)
Ti(eqB)—Ti(eqB)	3.597 (3, 3, 109)
Ti(ax)—S(A)[c]	2.384 (6, 4, 18)
Ti(ax)—S(B)[c]	2.306 (6, 4, 24)
Ti(eqA)—S(A)	2.529 (6, 6, 32)
Ti(eqB)—S(A)	2.488 (6, 4, 24)
Ti(eqA)—S(B)	2.552 (6, 4, 32)
Ti(eqB)—S(B)	2.516 (6, 4, 34)
Ti(ax)—S_2[d]	2.55 (10, 1, 11)
Ti(eqB)—S_2	2.53 (10, 1, 6)
Ti(ax)—S(C)[e]	2.25 (6, 1, 8)
Ti(eqB)—S(C)	2.62 (12, 1, 11)
Ti(ax)—O	2.03 (5, 2, 9)
Ti(eqA)—O	2.07 (5, 2, 11)
Ti(eqB)—O	2.01 (10, 2, 12)
Ti(ax)—Cp[f]	2.053 (6, 13, 18)
Ti(eqA)—Cp	2.060 (3, 14, 7)
Ti(eqA)—Cp	2.081 (6, 14, 25)
S—S	2.02 (5, 1, 2)

[a]Ti(ax) are the axial Ti atoms; Ti(eqA) is the unique equatorial Ti; Ti(eqB) are the equatorial Ti atoms which are bridged by the μ_3-S_2 unit (see Fig. 6).

[b]The first digit in parentheses is the number of parameters that have been averaged; the second digit is the average e.s.d.; the third digit is the maximum deviation from the mean.

[c]The S(A) and S(B) atoms are the μ_3-S that are attached to the unique equatorial Ti(eqA). The S(A) atoms are in the half of the trigonal bipyramid of titanium atoms that contains the μ_3-S_2 and μ_4-O units. The S(B) atoms are in the other half of the trigonal bipyramid (see text and Fig. 6).

[d]Distances are averaged to each sulfur of the S_2 moiety.

[e]The S(C) atoms are the μ_3-S that are attached to the Ti(eqB) atoms and are in the opposite half of the trigonal bipyramid to the μ_3-S_2 and μ_4-O units (see text and Fig. 6).

[f]Cp is the centroid of the C_5 ring of the C_5H_5 ligand.

commodate such a large number of atoms. The latest version of NRCVAX (21), which was used for the refinement, accommodated the atoms but only allowed a block refinement. In the final refinement the Ti, S, and all C atoms having unit occupancy were refined anisotropically. The solution of the structure was complicated by positional disorder involving the μ_3-S, μ_3-S_2, and μ_4-O ligands. The disorder is best described, with the aid of Fig. 6, by noting that **2** can be derived from **1** by replacing one μ_3-S by one μ_3-S_2 and at the same time placing a μ_4-O in that half of the trigonal bipyramid of titanium atoms that has the μ_3-S_2 ligand. In the crystal, the molecules were disordered so that the exchange of μ_3-S_2 for μ_3-S appeared to have taken place at two of the six possible sites, with a site occupancy for each position of less than unity. The site occupancies were different in each of the three independent molecules. The μ_4-O was disordered over two sites to follow the μ_3-S/μ_3-S_2 disorder. Figures 4 and 6 show only an undisordered molecule for clarity. Because of the disorder, the μ_3-S and μ_3-S_2 units were superimposed on one another in the observed structure. The site occupancies were determined by refinement, fixing the thermal parameters at the average isotropic value of the undisordered μ_3-S atoms. This refinement, in collaboration with the observed S—S and S—O distances, showed conclusively that the ligands in **2** were μ_3-S, μ_3-S_2, and μ_4-O, and that neither S_3^{2-} nor S_2O^{2-} was present. Because of the disorder, the S—S distance in the μ_3-S_2 unit was very poorly, and the Ti—μ_3-S_2, Ti—μ_4-O, and Ti—μ_3-S(C) distances were poorly, determined. The Ti—Ti, Ti—μ_3-S(A), Ti—μ_3-S(B), and Ti—C distances were well determined (see Fig. 6 for the definition of S(A), S(B), and S(C)). Table 2 lists the important distances, averaged over the three independent molecules. Surprisingly, only one of the 15 independent η-C_5H_5 rings showed evidence of disorder (that attached to Ti(34)), and this was treated as such.

As noted above, **2** is derived from **1** by replacement of one μ_3-S ligand by one μ_3-S_2 and one μ_4-O ligand. Both of the replacement ligands enter the same half of the trigonal bipyramid of titanium atoms. The axial Ti atoms are defined as those with the lower coordination numbers, and the two "halves" of the trigonal bipyramid are related by the twofold axis. The presence of the μ_3-S_2 ligand causes one equatorial Ti—Ti edge of the trigonal bipyramid to lengthen to 3.60 Å, compared to the other equatorial edges (3.24 Å), and to the axial–equatorial edges (3.22 Å) (see Fig. 6 and Table 2). In **1** the Ti(ax)—Ti(eq) distances average 3.18 Å (1). The Ti(ax)—μ_3-S distances in **2** average 2.38 Å for the S(A) atoms in the half of the trigonal bipyramid containing the μ_3-S_2 and μ_4-O ligands. This is much longer than the average Ti(ax)—S(B) distance of 2.31 Å; the latter can be compared to the Ti(ax)—μ_3-S distances in **1**, which average 2.28 Å, and to the Ti—μ_3-S distances in $[(\eta\text{-}C_5H_4Me)Ti(\mu_3\text{-}S)]_4$, 2.36 and 2.40 Å (11). The average Ti(eqA)—S(B) distance of 2.55 Å may also be compared to the Ti(eq)—μ_3-S distance of 2.47 Å in **1** (1). It is seen that **1** is more compact than **2**, probably because the μ_4-O must be accommodated in the core. The Ti—S_2 distances are the same for both the axial and equatorial titanium atoms within experimental error, averaging 2.54 Å. This is very similar to the average value of 2.55 Å in $[(\eta\text{-}C_5H_4Me)Ti]_4(\mu_2\text{-}S_2)_4(\mu_2\text{-}O)(\mu_4\text{-}O)$ (19). Because of the disorder it is unwise to attach much significance to the Ti—O distances in **2**, but the range, 2.01–2.07 Å, includes the values observed in $[(\eta\text{-}C_5H_4Me)Ti]_4(\mu_2\text{-}S_2)_4(\mu_2\text{-}O)(\mu_4\text{-}O)$ (2.06 Å (19)) and in $[(\eta\text{-}C_5H_5)Ti]_4(\mu_2\text{-}Se)(\mu_3\text{-}Se)_2(\mu_3\text{-}Se_2)_2(\mu_4\text{-}O)$ (1.95, 2.17 Å (22)). Cluster **2** appears to be the first example of a μ_4-oxygen enclosed in a trigonal bipyramidal arrangement of metal atoms.

The axial titanium attached to the S_2 unit is eight-coordinate, the other axial titanium is six-coordinate; Ti(eqA) is seven-coordinate, and Ti(eqB) is eight-coordinate. The different coordination numbers are the reason for the different Ti—Cp and Ti—S(C) distances, and contribute to the differences in the Ti—S and Ti—O distances discussed above.

Structure of

*$(\eta\text{-}C_5H_5)_2Ti(SH)(\mu\text{-}O)Ti(\eta\text{-}C_5H_5)(\mu\text{-}S)_2Ti(\eta\text{-}C_5H_5)_2$ (**3**)*

The structure of **3** is shown in Fig. 3 and a list of important distances and angles is given in Table 3. The asymmetry in the Ti(1)—(μ-O)—Ti(3) bridge (Ti—O—Ti 175.6(2)°, Ti(1)—O 1.807(2), Ti(3)—O 1.844(2) Å) and in the Ti(1)—(μ-$S)_2$—Ti(2) bridge (average Ti—S—Ti 88.06(4)°, average Ti(1)—S 2.288(1), average Ti(2)—S 2.416(1) Å) is caused by the different coordination numbers of the titanium atoms. The Ti(1) atom is six-coordinate, whereas Ti(2)

TABLE 3. Important distances (Å) and angles (°) in $(\eta\text{-}C_5H_5)_2Ti(SH)(\mu\text{-}O)Ti(\eta\text{-}C_5H_5)Ti(\mu\text{-}S)_2Ti(\eta\text{-}C_5H_5)_2$ (**3**)

Ti(1)—S(1)	2.289(1)[a]	S(1)—Ti(1)—S(2)	94.5 (1)
Ti(1)—S(2)	2.287(1)	S(1)—Ti(1)—O(1)	104.8 (1)
Ti(2)—S(1)	2.417(1)	S(2)—Ti(1)—O(1)	106.8 (1)
Ti(2)—S(2)	2.414(1)	S(1)—Ti(2)—S(2)	88.17(4)
Ti(1)—O(1)	1.807(2)	O(1)—Ti(3)—S(3)	97.93(9)
Ti(3)—O(1)	1.844(2)	Cp(1)—Ti(1)—S(1)	117.9
Ti(3)—S(3)	2.424(1)	Cp(1)—Ti(1)—S(2)	115.7
Ti(1)—Cp(1)[b,c]	2.07	Cp(11)—Ti(1)—O(1)	114.7
Ti(2)—Cp(21)[b,d]	2.076(5)	Cp(21)—Ti(2)—Cp(22)	131.3 (3)
Ti(2)—Cp(22)[b,d]	2.093(5)	Cp(31)—Ti(3)—Cp(32)	131.6 (3)
Ti(3)—Cp(31)[b,d]	2.087(5)	Ti(1)—S(1)—Ti(2)	88.00(4)
Ti(3)—Cp(32)[b,d]	2.081(4)	Ti(1)—S(2)—Ti(2)	88.12(4)
		Ti(1)—O(1)—Ti(3)	175.6 (2)

[a]Estimated standard deviations in brackets.
[b]Cp is the centroid of the C_5 ring of $\eta\text{-}C_5H_5$.
[c]Cp(1) is the average of the two disordered C_5 rings attached to Ti(1).
[d]Cp(21) is the centroid of C(21)—C(25), Cp(22) of C(26)—C(30), Cp(31) of C(32)—C(35), Cp(32) of C(36)—C(40) (see Table 4).

and Ti(3) are eight-coordinate. Otherwise the distances and angles are very similar to those in related compounds such as $(\eta\text{-}C_5H_5)_2Ti(SMe)_2$ (23), $(\eta\text{-}C_5H_5)_2Ti(SC_2H_5)_2$ (24), $(\eta\text{-}C_5Me_5)_2Ti(SH)_2$ (2), $[(\eta\text{-}C_5H_5)_2TiCl(\mu\text{-}O)]_2[(\eta\text{-}C_5H_5)TiCl]$ (25), and $[(\eta\text{-}C_5H_5)_2Ti(C_2H_5)]_2(\mu\text{-}O)$ (26).

Experimental

General techniques and reagents

All experiments were carried out under argon or vacuum using standard vacuum-line techniques (9). Volumes of H_2S were measured using a manometer and calibrated bulb. Solvents were predried by standard drying agents, stored over Bu^{n}Li, and distilled under vacuum. Literature methods were used to prepare $(\eta\text{-}C_5H_5)_2Ti(CO)_2$ (27) and $(\eta\text{-}C_5H_5)_2Ti(SH)_2$ (10); H_2S was purchased from Canadian Liquid Air, Montreal, and used as received. Zinc dust (<325 mesh, Aldrich) was evacuated prior to use and transferred to the reaction flask under argon. All other chemicals were reagent grade. Instruments used were a Varian XL-200 NMR spectrometer, a Kratos MS50 mass spectrometer, and a locally modified version of the Varian E-4 ESR spectrometer.

Reaction between $(\eta\text{-}C_5H_5)_2Ti(SH)_2$ and zinc powder

A solution of $(\eta\text{-}C_5H_5)_2Ti(SH)_2$ (1.022 g, 4.18 mmol) in toluene (150 cm^3) was stirred with zinc powder (0.269 g, 4.12 mmol) at room temperature for 3 days. The mixture was filtered, and the red filtrate was set aside. After 7 days the solution had deposited crystals of $(\eta\text{-}C_5H_5)_2Ti(SH)(\mu\text{-}O)Ti(\eta\text{-}C_5H_5)(\mu\text{-}S)_2Ti(\eta\text{-}C_5H_5)_2$ (**3**) (approx. 5%) and $[(\eta\text{-}C_5H_5)Ti]_5(\mu_3\text{-}S)_5(\mu_3\text{-}S_2)(\mu_4\text{-}O)$ (**2**) (approx. 10%). These were removed by filtration and structurally characterized by X-ray diffraction (see below). In addition **2** was characterized by the following data: ESR spectrum (toluene solution) g = 1.980; Anal. calcd. for $C_{82}H_{83}O_3S_{21}Ti_{15}$ ($\{[(C_5H_5)Ti]_5S_7O\}_3 \cdot C_6H_5CH_3$): C 39.3, H 3.4, S 26.8%; found: C 41.0, H 3.6, S 23.7%.

The volume of the filtrate was reduced to 100 cm^3 under vacuum, and the red solution layered with hexane (50 cm^3). This procedure gave $(\eta\text{-}C_5H_5)_2Ti(SH)_2$ (0.71 g, 2.9 mmol 70%), as determined by NMR spectroscopy (^{1}H, 200 MHz ($CDCl_3$ solution): 6.27 ppm (10 H), 3.36 ppm (2 H)) and mass spectrometry (EI, m/e 243 ($[(C_5H_5)_2Ti(SH)S]^+$); 210 ($[(C_5H_5)_2TiS]^+$)). Further reduction in volume to 50 cm^3 and further layering with hexane (50 cm^3) gave a red precipitate, which was a mixture of $(\eta\text{-}C_5H_5)_2Ti(SH)_2$ and $[(\eta\text{-}C_5H_5)Ti]_5(\mu_3\text{-}S)_6$ (approx. 10%), as determined by mass spectrometry (EI, m/e 757 ($[(C_5H_5)_5Ti_5S_6]^+$); 243 ($[(C_5H_5)_2Ti(SH)_2-H]^+$), 210 ($[(C_5H_5)_2TiS]^+$)) and NMR spectroscopy (^{1}H, 200 MHz, ($CDCl_3$ solution): 14.68 ppm (15 H, $(\eta\text{-}C_5H_5)_5Ti_5S_6$), 9.65 ppm (10 H, $(\eta\text{-}C_5H_5)_5Ti_5S_6$), 6.27 ppm (10 H, $(\eta\text{-}C_5\mathit{H}_5)_2Ti(SH)_2$), 3.36 ppm (2 H, $(\eta\text{-}C_5H_5)_2Ti(SH)_2$).

Reaction between $(\eta\text{-}C_5H_5)_2Ti(CO)_2$ and H_2S in the presence of water

To a solution of $(\eta\text{-}C_5H_5)_2Ti(CO)_2$ (1.532 g, 6.5 mmol) in toluene (100 cm^3) were added two drops of water. The solution was incubated with H_2S (7.8 mmol), with stirring, at 80°C for 72 h. Over this period the color of the solution changed from red to yellow-green and a dark brown precipitate of $[(\eta\text{-}C_5H_5)Ti(\mu_3\text{-}S)]_4$ (0.94 g, 1.10 mmol, 50%) deposited. The precipitate was removed by filtration, and the solution set aside. After 8 days, crystals of both $[(\eta\text{-}C_5H_5)Ti]_5(\mu_3\text{-}S)_6$ (**1**) (approx. 10%) (identified by comparison of cell dimensions with the literature (1)) and of $[(\eta\text{-}C_5H_5)Ti]_4(\mu_2\text{-}S_2)_4(\mu_2\text{-}O)(\mu_4\text{-}O)$ (**4**) (approx. 5%) were obtained. Compound **4** was characterized by X-ray crystallography as described below and by ^{1}H NMR (200 MHz, C_6D_6 solution): 6.21 (10 H), 5.65 (10 H), assigned to the two types of C_5H_5 ring. The crystals were removed by filtration and the filtrate was layered with hexane (50 cm^3), giving a dark-green powder. This was shown by a combination of NMR, ESR, and mass spectroscopies to be a mixture of $[(\eta\text{-}C_5H_5)Ti]_5(\mu_3\text{-}S)_6$ (**1**) (ESR: g = 1.993; MS, m/e 757, 692, 627 ($(C_5H_5)_nTi_5S_6^+$, n = 5, 4, 3)); $[(\eta\text{-}C_5H_5)Ti]_4(\mu_2\text{-}S_2)_4(\mu_2\text{-}O)(\mu_4\text{-}O)$ (**4**) (MS, m/e 740 ($(C_5H_5)_4Ti_4S_8O_2^+$), ^{1}H NMR (C_6D_6 solution): 6.21, 5.65 ppm, each 10 H); $[(\eta\text{-}C_5H_5)Ti]_5(\mu_3\text{-}S)_5(\mu_3\text{-}S_2)(\mu_4\text{-}O)$ (**2**) (ESR: g = 1.979); $[(\eta\text{-}C_5H_5)Ti(\mu_3\text{-}S)]_4$ (**5**) (MS, m/e 580, 515, 450 ($(C_5H_5)_nTi_4S_4^+$, n = 4, 3, 2), ^{1}H NMR (200 MHz, ^{2}H, $CHCl_3$ solution): 5.98 ppm); and $[(\eta\text{-}C_5H_5)TiS]_4^+$ (ESR: g = 1.988).

X-ray crystallography

X-ray diffraction experiments were carried out on an Enraf–Nonius CAD4 diffractometer operating under the control of the NRCCAD software (28). The radiation was Mo Kα, λ = 0.71073 Å. Data were collected using the θ/2θ scan method. Refinement used the NRCVAX suite of programs (21). The weighting scheme was of the form $w = 1/(\sigma(F)^2 + kF^2)$. Scattering factors were taken from ref. 29. Crystal and refinement data for **2**, **3**, and **4** are collected in Table 1. In the final refinements hydrogen atoms were included as fixed contributors (C—H = 0.96 Å, isotropic B equal to that of the carbon atom to which they were attached).

The structural analysis of **3** was uneventful. Atomic coordinates for **3** are given in Table 4 and important distances and an-

Can. J. Chem. Downloaded from www.nrcresearchpress.com by 217.78.4.112 on 09/08/12
For personal use only.

Can. J. Chem. Downloaded from www.nrcresearchpress.com by 217.78.4.112 on 09/08/12
For personal use only.

TABLE 4. Atomic coordinates and B_{iso} for $(\eta\text{-}C_5H_5)_2Ti(\mu\text{-}O)Ti(\eta\text{-}C_5H_5)(\mu\text{-}S)_2Ti(\eta\text{-}C_5H_5)_2$ (**3**)

Atom	*x*	*y*	*z*	B_{iso}[b]
Ti1	0.13910(8)[a]	0.03912(6)	0.26177(6)	2.85(4)
Ti2	0.18974(8)	0.78595(6)	0.23031(6)	2.75(3)
Ti3	0.51088(8)	0.28512(6)	0.26648(6)	2.76(3)
S1	0.06821(13)	−0.11933(10)	0.10811(8)	3.54(5)
S2	0.21930(13)	−0.05622(9)	0.38558(8)	3.18(5)
S3	0.39726(22)	0.43624(13)	0.27060(14)	6.46(10)
H3	0.303	0.402	0.176	6.3
O1	0.3266 (3)	0.15671(22)	0.26307(21)	3.02(14)
C11[c]	−0.14794	0.00048	0.21936	4.5 (8)
C12	−0.06918	0.13046	0.18734	4.9 (12)
C13	0.04937	0.19953	0.28883	4.8 (11)
C14	0.04004	0.14940	0.37920	4.9 (9)
C15	−0.08483	0.02862	0.33190	4.4 (9)
C11A[c]	−0.12105	0.04342	0.18562	7.6 (16)
C12A	−0.00451	0.16194	0.22635	4.6 (12)
C13A	0.06673	0.19503	0.34291	4.9 (9)
C14A	−0.01766	0.08838	0.37074	5.7 (16)
C15A	−0.12854	0.00215	0.27705	7.0 (16)
C21	0.4833 (5)	0.8652 (4)	0.3212 (3)	3.91(24)
C22	0.4291 (6)	0.7430 (4)	0.2685 (5)	4.8 (3)
C23	0.3705 (7)	0.7242 (4)	0.1550 (5)	5.4 (3)
C24	0.3878 (6)	0.8353 (5)	0.1366 (4)	4.3 (3)
C25	0.4562 (5)	0.9221 (4)	0.2395 (4)	3.65(23)
C26	−0.0944 (6)	0.6765 (5)	0.2185 (6)	6.1 (3)
C27	0.0071 (8)	0.6672 (5)	0.3113 (5)	6.3 (3)
C28	0.0904 (7)	0.6023 (5)	0.2778 (5)	5.8 (3)
C29	0.0400 (7)	0.5701 (4)	0.1641 (5)	5.6 (3)
C30	−0.0731 (7)	0.6160 (5)	0.1273 (4)	5.8 (3)
C31	0.6103 (6)	0.2459 (4)	0.4372 (4)	4.6 (3)
C32	0.5868 (7)	0.3511 (6)	0.4641 (4)	6.3 (4)
C33	0.7014 (10)	0.4403 (5)	0.4373 (5)	7.6 (4)
C34	0.7916 (7)	0.3889 (7)	0.3944 (5)	7.0 (3)
C35	0.7321 (6)	0.2692 (6)	0.3933 (4)	5.3 (3)
C36	0.4307 (6)	0.1469 (4)	0.0856 (3)	3.73(22)
C37	0.4005 (6)	0.2455 (5)	0.0695 (4)	4.6 (3)
C38	0.5528 (8)	0.3473 (4)	0.1072 (4)	5.5 (3)
C39	0.6725 (6)	0.3087 (5)	0.1476 (4)	5.5 (3)
C40	0.5988 (6)	0.1851 (5)	0.1374 (4)	4.4 (3)

[a]Estimated standard deviations, given in parentheses, refer to the last digit printed.
[b]B_{iso} is the mean of the principal axes of the thermal ellipsoid.
[c]C(11)—C(15) and C(11A)—C(15A) refer to a disordered C_5H_5 ring attached to Ti(1); each of these carbons was given an occupancy of 0.5.

gles in Table 3. Other data have been deposited.[2] Analysis of **4** was complicated by poor data and disorder in all atoms except Ti and μ_4-O. These are the reasons for the high *R* value. Brief attempts to refine the structure in space groups $P4_2/ncm$ or the cubic $P23$ showed that the disorder was not removed. In view of the previous determination of the structure of $[(\eta\text{-}C_5H_4Me)Ti]_4(\mu_2\text{-}S_2)_4(\mu_2\text{-}O)(\mu_4\text{-}O)$ (19), further investigation was deemed unnecessary. The experiments clearly characterized **4** as $[(\eta\text{-}C_5H_5)Ti]_4(\mu_2\text{-}S_2)_4(\mu_2\text{-}O)(\mu_4\text{-}O)$. All structural parameters for **4** have been deposited.[2] The structural analysis of **2** posed major problems of refinement, which are outlined in the Discussion above. The final atomic coordinates are given in Table 5 and the important averaged distances in Table 2. Other data, including a comprehensive table of distances and angles, and a listing of site occupancies, have been deposited.[2]

[2]Supplementary material available: Atom numbering scheme, tables of hydrogen atom positions, thermal parameters, site occupancies, distances and angles (33 pages), and a table of $|F_o|$ and $|F_c|$ (34 pages) for **2**. Atom numbering scheme, tables of hydrogen atom positions, thermal parameters, distances and angles (7 pages), and a table of $|F_o|$ and $|F_c|$ (15 pages) for **3**. Atom numbering scheme, atomic parameters for all atoms, thermal parameters, distances and angles (7 pages), and a table of $|F_o|$ and $|F_c|$ (7 pages) for **4**. This material may be purchased from: The Depository of Unpublished Data, Document Delivery, CISTI, National Research Council Canada, Ottawa, Canada K1A 0S2.

Atom numbering schemes, tables of hydrogen atom positions (for **2** and **3**) and atomic parameters (for **4**), distances and angles have also been deposited with the Cambridge Crystallographic Data Centre and can be obtained on request from The Director, Cambridge Crystallographic Data Centre, University Chemical Laboratory, Lensfield Road, Cambridge CB2 1EW, U.K.

Acknowledgements

We thank the Natural Sciences and Engineering Research Council of Canada, the Petroleum Research Fund (administered by the American Chemical Society), and the Imperial Oil University Research Fund for financial support. Dr.

TABLE 5. Atomic coordinates and B_{iso} for $[(\eta\text{-}C_5H_5)Ti]_5(\mu_3\text{-}S)_5(\mu_3\text{-}S_2)(\mu_4\text{-}O)$ (**2**)

	x	y	z	B_{iso}[a]
Ti11[b]	0.60618(23)	0.36365(8)	0.36935(7)	3.27(12)
Ti12	0.71931(24)	0.26657(9)	0.41067(7)	3.86(12)
Ti13	0.90827(22)	0.34817(8)	0.37666(7)	3.14(11)
Ti14	0.49670(22)	0.26066(8)	0.34259(8)	3.34(12)
Ti15	0.78230(23)	0.27347(8)	0.31049(7)	3.08(12)
S11	0.9305 (3)	0.26586(12)	0.37352(11)	3.36(17)
S12	0.6738 (4)	0.20854(13)	0.34986(12)	4.50(20)
S13	0.4942 (4)	0.29994(13)	0.40983(12)	4.47(20)
S14	0.7587 (3)	0.35242(13)	0.42962(11)	4.10(20)
S15	0.7985 (5)	0.36554(17)	0.31723(15)	3.4 (3)
S15A	0.5648 (9)	0.3187 (4)	0.2949 (3)	3.0 (5)
S16	0.5717 (5)	0.28866(19)	0.27212(16)	3.7 (3)
S16A	0.8807 (9)	0.3558 (3)	0.2942 (3)	3.1 (5)
S17	0.4757 (5)	0.33847(19)	0.30526(16)	4.0 (3)
S17A	0.7800 (10)	0.4058 (3)	0.3263 (3)	3.1 (3)
O11	0.6610 (11)	0.2960 (4)	0.3556 (4)	3.6 (3)
O11A	0.7430 (21)	0.3165 (8)	0.3582 (7)	3.1 (5)
C111	0.4436 (14)	0.4100 (5)	0.4004 (5)	6.7 (9)
C112	0.5578 (17)	0.4277 (5)	0.4169 (4)	7.2 (10)
C113	0.6158 (15)	0.4469 (5)	0.3798 (5)	6.7 (10)
C114	0.5371 (15)	0.4401 (5)	0.3463 (5)	6.2 (9)
C115	0.4321 (13)	0.4167 (5)	0.3584 (5)	6.0 (9)
C121	0.6400 (13)	0.2197 (6)	0.4665 (5)	7.0 (10)
C122	0.6986 (17)	0.2585 (5)	0.4842 (4)	7.4 (10)
C123	0.8279 (16)	0.2533 (6)	0.4770 (5)	8.0 (10)
C124	0.8405 (15)	0.2124 (6)	0.4538 (5)	8.8 (11)
C125	0.7279 (17)	0.1935 (5)	0.4466 (4)	7.3 (11)
C131	1.0112 (13)	0.4140 (5)	0.4079 (5)	5.3 (8)
C132	1.0571 (13)	0.3742 (5)	0.4279 (4)	5.0 (8)
C133	1.1225 (13)	0.3484 (5)	0.3996 (5)	5.6 (9)
C134	1.1177 (13)	0.3701 (6)	0.3612 (5)	6.6 (9)
C135	1.0483 (13)	0.4106 (5)	0.3665 (4)	5.2 (8)
C141	0.2763 (14)	0.2564 (6)	0.3247 (6)	8.2 (11)
C142	0.2903 (13)	0.2367 (5)	0.3637 (6)	8.4 (11)
C143	0.3628 (15)	0.1968 (6)	0.3605 (5)	7.7 (10)
C144	0.3945 (13)	0.1919 (5)	0.3175 (5)	5.9 (9)
C145	0.3411 (14)	0.2279 (6)	0.2957 (5)	7.8 (10)
C151	−0.2211 (12)	0.2295 (5)	0.2456 (4)	4.6 (7)
C152	−0.1413 (12)	0.2057 (4)	0.2726 (4)	4.2 (7)
C153	−0.0369 (12)	0.2335 (5)	0.2824 (4)	5.3 (8)
C154	−0.0534 (13)	0.2751 (5)	0.2602 (4)	5.9 (9)
C155	−0.1651 (15)	0.2749 (5)	0.2364 (4)	5.9 (9)
Ti21	0.37443(22)	0.07664(8)	0.08741(7)	2.88(11)
Ti22	0.67441(22)	0.10522(8)	0.08248(7)	2.98(11)
Ti23	0.27646(22)	0.11664(9)	0.17379(7)	3.33(12)
Ti24	0.56579(22)	0.08836(8)	0.17858(7)	3.20(12)
Ti25	0.46816(25)	0.17866(8)	0.12458(7)	3.65(13)
S21	0.4515 (3)	0.16023(12)	0.20213(11)	3.56(17)
S22	0.2491 (4)	0.14863(12)	0.10454(11)	3.90(18)
S23	0.6935 (3)	0.15127(12)	0.14218(10)	3.30(16)
S24	0.5029 (3)	0.14132(12)	0.05155(10)	3.39(17)
S25	0.5887 (3)	0.03779(12)	0.10989(11)	3.64(18)
S26	0.3601 (6)	0.04623(22)	0.16220(19)	2.9 (3)
S27	0.2739 (7)	0.02871(23)	0.14474(21)	3.4 (3)
S28	0.3839 (7)	0.03532(24)	0.19791(21)	3.7 (3)
O21	0.4380 (13)	0.1075 (5)	0.1392 (4)	1.8 (3)
C211	0.3338 (14)	0.0607 (5)	0.0144 (4)	5.7 (8)
C212	0.2193 (14)	0.0720 (5)	0.0327 (4)	5.6 (8)
C213	0.1898 (13)	0.0374 (6)	0.0602 (5)	6.7 (10)
C214	0.2833 (14)	0.0046 (5)	0.0615 (5)	6.2 (10)
C215	0.3701 (13)	0.0185 (5)	0.0341 (4)	5.3 (8)
C221	0.8148 (13)	0.0553 (5)	0.0444 (4)	5.2 (8)
C222	0.7690 (12)	0.0881 (5)	0.0158 (4)	4.4 (7)
C223	0.8097 (13)	0.1330 (5)	0.0286 (4)	4.8 (8)

Can. J. Chem. Downloaded from www.nrcresearchpress.com by 217.78.4.112 on 09/08/12
For personal use only.

TABLE 5 (*continued*)

C224	0.8846 (13)	0.1250 (5)	0.0661 (4)	5.6 (8)
C225	0.8826 (12)	0.0780 (6)	0.0752 (4)	6.2 (10)
C231	0.1813 (13)	0.1299 (6)	0.2395 (4)	5.8 (9)
C232	0.1353 (14)	0.1622 (5)	0.2126 (5)	7.4 (10)
C233	0.0636 (13)	0.1398 (7)	0.1805 (5)	9.2 (12)
C234	0.0701 (14)	0.0946 (7)	0.1905 (5)	8.4 (11)
C235	0.1407 (13)	0.0876 (5)	0.2258 (5)	6.0 (9)
C241	0.7525 (13)	0.0922 (5)	0.2227 (4)	5.2 (8)
C242	0.7436 (13)	0.0463 (5)	0.2050 (4)	5.3 (8)
C243	0.6401 (15)	0.0235 (5)	0.2205 (5)	6.0 (9)
C244	0.5840 (14)	0.0546 (5)	0.2476 (4)	6.1 (9)
C245	0.6508 (13)	0.0966 (5)	0.2495 (4)	4.8 (8)
C251	0.5781 (16)	0.2526 (5)	0.1226 (6)	8.8 (12)
C252	0.4896 (17)	0.2551 (4)	0.1554 (5)	7.0 (10)
C253	0.3739 (16)	0.2529 (5)	0.1367 (5)	7.1 (10)
C254	0.3852 (16)	0.2486 (5)	0.0934 (5)	6.9 (10)
C255	0.5099 (16)	0.2494 (5)	0.0851 (5)	6.9 (10)
Ti31	0.06759(22)	1.03682(8)	0.36760(7)	3.04(11)
Ti32	0.14495(23)	0.94127(8)	0.42053(7)	3.19(12)
Ti33	−0.04233(22)	0.93637(8)	0.34286(7)	2.98(12)
Ti34	0.24849(23)	0.93869(9)	0.32483(7)	3.66(12)
Ti35	0.36880(22)	1.01768(8)	0.39373 (7)	3.31(12)
S31	0.1959 (3)	1.02874(13)	0.43583(11)	3.94(18)
S32	−0.0672 (3)	0.98019(12)	0.40754(10)	3.43(17)
S33	0.3729 (3)	0.93539(13)	0.39396(11)	4.12(19)
S34	0.1184 (3)	0.88050(12)	0.36287(11)	3.80(18)
S35	0.2897 (4)	1.03435(15)	0.32693(13)	3.73(22)
S35A	0.0501 (10)	0.9854 (4)	0.3001 (3)	3.4 (5)
S36	−0.0287 (5)	1.01239(19)	0.29752(15)	4.0 (3)
S36A	0.2799 (15)	1.0662 (5)	0.3374 (5)	4.3 (7)
S37	0.0733 (5)	0.95883(18)	0.27293(15)	3.8 (3)
S37A	0.3796 (17)	1.0105 (6)	0.3169 (5)	6.2 (10)
O31	0.1247 (10)	0.9702 (4)	0.3604 (3)	3.9 (3)
O31A	0.207 (5)	0.9891 (17)	0.3786 (15)	10.0 (15)
C311	0.0787 (14)	1.1202 (5)	0.3670 (6)	7.7 (11)
C312	0.0161 (16)	1.1090 (5)	0.4037 (5)	6.9 (9)
C313	−0.0934 (14)	1.0895 (5)	0.3912 (5)	6.0 (9)
C314	−0.1050 (14)	1.0872 (5)	0.3497 (4)	5.8 (9)
C315	0.0002 (15)	1.1076 (5)	0.3316 (4)	6.1 (9)
C321	0.2428 (14)	0.9070 (5)	0.4809 (4)	6.1 (9)
C322	0.1649 (16)	0.9383 (5)	0.4958 (4)	7.1 (10)
C323	0.0426 (14)	0.9245 (6)	0.4854 (4)	7.1 (9)
C324	0.0517 (14)	0.8831 (6)	0.4628 (4)	6.8 (9)
C325	0.1750 (15)	0.8713 (5)	0.4611 (4)	5.8 (9)
C331	−0.1460 (13)	0.8686 (5)	0.3154 (5)	5.8 (9)
C332	−0.1881 (13)	0.8745 (5)	0.3552 (4)	5.1 (8)
C333	−0.2577 (12)	0.9174 (5)	0.3548 (4)	4.6 (8)
C334	−0.2490 (13)	0.9369 (5)	0.3151 (5)	5.3 (8)
C335	−0.1828 (13)	0.9053 (5)	0.2909 (4)	5.3 (8)
C341	0.4307 (25)	0.9189 (9)	0.2846 (8)	4.3 (7)
C342	0.413 (3)	0.8833 (11)	0.3044 (9)	6.4 (8)
C343	0.2989 (25)	0.8707 (9)	0.2851 (8)	4.3 (7)
C344	0.2818 (23)	0.9001 (8)	0.2576 (7)	3.2 (6)
C345	0.354 (3)	0.9250 (10)	0.2592 (8)	5.1 (7)
C341A	0.4432 (25)	0.8952 (9)	0.3089 (8)	4.0 (6)
C342A	0.3379 (22)	0.8608 (8)	0.3040 (7)	2.8 (5)
C343A	0.2451 (23)	0.8809 (8)	0.2693 (7)	3.2 (6)
C344A	0.296 (3)	0.9358 (10)	0.2498 (9)	5.2 (7)
C345A	0.4313 (24)	0.9412 (9)	0.2778 (8)	3.7 (6)
C351	0.5879 (13)	1.0319 (5)	0.3883 (5)	6.2 (9)
C352	0.5272 (14)	1.0760 (5)	0.3871 (5)	6.4 (9)
C353	0.4752 (13)	1.0820 (5)	0.4256 (4)	5.5 (8)
C354	0.4989 (14)	1.0441 (6)	0.4518 (4)	6.7 (9)
C355	0.5685 (13)	1.0131 (5)	0.4274 (5)	6.0 (9)

Can. J. Chem. Downloaded from www.nrcresearchpress.com by 217.78.4.112 on 09/08/12
For personal use only.

TABLE 5 (*concluded*)

C1T	0.9089 (17)	0.3043 (6)	0.0585 (5)	8.6 (11)
C2T	0.8875 (19)	0.3484 (7)	0.0465 (6)	11.4 (14)
C3T	0.8005 (18)	0.3528 (7)	0.0122 (6)	11.7 (15)
C4T	0.7438 (18)	0.3178 (7)	−0.0106 (6)	10.4 (13)
C5T	0.7711 (21)	0.2783 (7)	0.0041 (7)	13.2 (16)
C6T	0.8481 (18)	0.2706 (6)	0.0365 (6)	10.4 (13)
C7T	0.9874 (23)	0.2918 (10)	0.0936 (8)	18.3 (21)

[a] B_{iso} is the mean of the principal axes of the thermal ellipsoid.

[b] The Ti(ax) atoms are Ti(13), Ti(14); Ti(22), Ti(23); Ti(33), Ti(35). The Ti(eqA) atoms are Ti(12); Ti(25); Ti(32). The S(A) atoms are S(12), S(13); S(21), S(22); S(32), S(34). The S(B) atoms are S(11), S(14); S(23), S(24); S(31), S(33). The S(C) atoms are S(15), S(15A); S(25), S(26); S(35), S(35A). The site occupancies are given in the supplementary material.[2] C(1T)–C(7T) are the carbon atoms of the lattice toluene.

P. S. White collected the intensity data used for the structure determination of **2**.

1. F. Bottomley, G. O. Egharevba, and P. S. White. J. Am. Chem. Soc. **107**, 4353 (1985).
2. F. Bottomley, D. F. Drummond, G. O. Egharevba, and P. S. White. Organometallics, **5**, 1620 (1986).
3. F. Bottomley, T.-T. Chin, G. O. Egharevba, L. M. Kane, D. A. Pataki, and P. S. White. Organometallics, **7**, 1214 (1988).
4. A. Roth, C. Floriani, A. Chiesi-Villa, and C. Guastini. J. Am. Chem. Soc. **108**, 6823 (1986).
5. H. Köpf and M. Schmidt. Angew. Chem. **77**, 965 (1965).
6. F. Bottomley, P. N. Keizer, K. F. Preston, and P. S. White. Organometallics, **9**, 1916 (1990).
7. F. Bottomley, E. C. Ferris, and P. S. White. Organometallics, **9**, 1166 (1990).
8. F. Bottomley and S. Karslioglu. J. Chem. Soc. Chem. Commun. 222 (1991).
9. D. F. Shriver. The manipulation of air sensitive compounds. McGraw–Hill, New York. 1969.
10. A. Shaver and J. M. McCall. Organometallics, **3**, 1823 (1984).
11. J. Darkwa, J. R. Lockemeyer, P. D. W. Boyd, T. B. Rauchfuss, and A. L. Rheingold. J. Am. Chem. Soc. **110**, 141 (1988).
12. P. D. Williams and M. D. Curtis. Inorg. Chem. **25**, 4562 (1985).
13. C. M. Bolinger, J. Darkwa, G. Gammie, S. D. Gammon, J. W. Lyding, T. B. Rauchfuss, and S. R. Wilson. Organometallics, **5**, 2386 (1986).
14. Trinh-Toan, B. K. Teo, J. A. Ferguson, T. J. Meyer, and L. F. Dahl. J. Am. Chem. Soc. **99**, 408 (1977).
15. J. A. Bandy, C. E. Davies, J. C. Green, M. L. H. Green, K. Prout, and D. P. S. Rodgers. J. Chem. Soc. Chem. Commun. 1395 (1983).
16. M. L. H. Green, A. Hamnett, J. Qin, P. Baird, J. A. Bandy, K. Prout, E. Marseglia, and S. D. Obertelli. J. Chem. Soc. Chem. Commun. 1811 (1987).
17. G. L. Simon and L. F. Dahl. J. Am. Chem. Soc. **95**, 2164 (1973).
18. J. H. Toney and T. J. Marks. J. Am. Chem. Soc. **107**, 957 (1985).
19. G. A. Zank, C. A. Jones, T. B. Rauchfuss, and A. L. Rheingold. Inorg. Chem. **25**, 1886 (1986).
20. F. A. Cotton, X. Feng, P. A. Kilbala, and R. B. W. Sandor. J. Am. Chem. Soc. **111**, 2148 (1989).
21. E. J. Gabe, Y. LePage, J. P. Charland, F. L. Lee, and P. S. White. J. Appl. Crystallogr. **22**, 384 (1989).
22. P. G. Maué and D. Fenske. Z. Naturforsch. **43b**, 1213 (1988).
23. T. A. Wark and D. W. Stephan. Organometallics, **8**, 2836 (1989).
24. M. J. Calhorda, M. A. A. F. de C. T. Carrondo, A. R. Dias, C. F. Frazão, M. B. Hursthouse, J. A. M. Simões, and C. Teixeira. Inorg. Chem. **27**, 2513 (1988).
25. H.-P. Klein, U. Thewalt, K. Döppert, and R. Sanchez-Delgado. J. Organomet. Chem. **236**, 189 (1982).
26. H. G. Alt, K.-H. Schwind, M. D. Rausch, and U. Thewalt. J. Organomet. Chem. **349**, C7 (1988).
27. B. Demerseman, G. Bourquet, and M. Bignorgne. J. Organomet. Chem. **101**, C24 (1975).
28. Y. LePage, P. S. White, and E. J. Gabe. Annu. Meeting Am. Crystallogr. Assoc. Hamilton, Ontario. 1986.
29. International tables for X-ray crystallography. Vol. IV. Kynoch Press, Birmingham, U.K. 1974.

Can. J. Chem. Downloaded from www.nrcresearchpress.com by 217.78.4.112 on 09/08/12
For personal use only.

Ecuadorin, a novel tetranortriterpenoid of *Guarea kunthiana:* structure elucidation by 2-D NMR spectroscopy

BALDWIN S. MOOTOO
Department of Chemistry, University of the West Indies, St. Augustine, Trinidad

CUMANDÁ JÁTIVA
Department of Chemistry, Escuela Superior Politecnica de Chimborazo, Riobamba, Ecuador

AND

WINSTON F. TINTO, WILLIAM F. REYNOLDS, AND STEWART MCLEAN[1]
Department of Chemistry, University of Toronto, Toronto, Ont., Canada M5S 1A1

Received July 31, 1991

This paper is dedicated to Professor Zdenek (Denny) Valenta on the occasion of his 65th birthday

BALDWIN S. MOOTOO, CUMANDÁ JÁTIVA, WINSTON F. TINTO, WILLIAM F. REYNOLDS, and STEWART MCLEAN. Can J. Chem. **70**, 1260 (1992).

Ecuadorin (**1**), $C_{29}H_{34}O_{10}$, a novel tetranortriterpenoid, has been isolated from *Guarea kunthiana* (Meliaceae) collected in Ecuador. Its structure has been established by spectroscopic methods, mainly 2-D NMR spectroscopy; the value of the FLOCK pulse sequence in the determination of 2- and 3-bond $^{13}C-^{1}H$ connectivities is illustrated. Ecuadorin has been reduced to the dihydro and tetrahydro derivatives (**2** and **3**), and these have provided information regarding the stereochemistry of ecuadorin. Stereochemical arguments have been based on observed vicinal $^{1}H-^{1}H$ coupling constants and NOE measurements, as well as on biosynthetic hypothesis.

BALDWIN S. MOOTO, CUMANDÁ JÁTIVA, WINSTON F. TINTO, WILLIAM F. REYNOLDS et STEWART MCLEAN. Can. J. Chem. **70**, 1260 (1992).

On a isolé l'écuadorine (**1**), $C_{29}H_{34}O_{10}$, un nouveau tétranortriterpènoïde, à partir de *Guarea kunthiana* (Meliaceae) recueilli en Équateur. On a déterminé sa structure par des méthodes spectroscopiques, principalement par la RMN en 2-D; on illustre la valeur de la séquence de pulsation FLOCK dans la détermination des connectivités $^{13}C-^{1}H$ avec 2 et 3 liaisons. On a réduit l'écuadorine en dérivés dihydro et tétrahydro (**2** et **3**) et ces composés ont fournit de l'information concernant la stéréochimie de l'écuadorine. Les arguments stéréochimiques sont basés sur les constantes de couplages $^{1}H-^{1}H$ vicinales observées, sur des mesures d'EON ainsi que sur une hypothèse biosynthétique.

[Traduit par la rédaction]

The plant family Meliaceae has been a rich source of biosynthetically modified triterpenes that have useful biological activity; some are insect antifeedants, and some are cytotoxic and may be useful medicinally (*1*). Their structural complexity and diversity attracts the attention of the chemist. We have begun a study of the Meliaceae of Ecuador, and we report here on the elucidation of the structure of a new tetranortriterpenoid which we have isolated from *Guarea kunthiana* A. Juss, and to which we assign the name ecuadorin. The plant was collected in Pichincha province, and extraction of its aerial parts afforded ecuadorin.

Ecuadorin was obtained as colorless crystals, mp 237–238°C, $C_{29}H_{34}O_{10}$ (by HRMS); the IR spectrum included strong peaks at 1752, 1737, 1715, and 1660 cm^{-1}, and the UV spectrum showed peaks at 208 nm (ϵ, 11 000) and 236 nm (ϵ, 8 200). After the ^{1}H and ^{13}C NMR spectra has been obtained, a one-bond 2-D $^{13}C-^{2}H$ shift-correlation experiment was used to label carbons with their attached protons. Our FLOCK pulse sequence (*2*) was then used to determine *n*-bond ($n > 1$) $^{13}C-^{1}H$ connectivities; FLOCK provides excellent sensitivity while suppressing one-bond peaks, and can, in favorable cases, be used to distinguish between two-bond and three-bond connectivities. COSY-45 spectra were used to confirm $^{1}H-^{1}H$ connectivities. The data obtained from these NMR experiments are assembled in Table 1. The observed $^{13}C-^{1}H$ *n*-bond connectivities are sufficient to establish that ecuadorin has the molecular skeleton of **1** since all C–C connectivities are shown by them implicitly (often in several ways). The nonprotonated carbons C-8 and C-9 are exceptions since the three-bond connectivity between H-30 and C-9 was not observed, and the cross peak between H-11 and C-8 was extremely weak; in both cases it seems that $^{3}J_{CH}$ couplings are unusually small. However, it should be noted that, with all other C–C connectivities explicitly defined, only structure **1**, with C-8 and C-9 directly linked, can accommodate the molecular formula and the other spectroscopic data. To verify that C-8 and C-30 are part of an oxirane moiety, the $^{1}J_{CH}$ at C-30 was measured and found to be 179 Hz, a value that establishes that the carbon is in a three-membered ring (*3*). These NMR experiments were carried out with a solution of 20 mg of ecuadorin in benzene-d_6 since all significant signals were well resolved in this solvent, although the chemical shift between the C-11 methylene protons was effectively zero. As a result, these protons showed virtual coupling to the C-12 methylene protons, and only an average vicinal coupling (J = 6.7 Hz) was observed. In $CDCl_3$ solution, although some other signals were more poorly resolved, the C-11 methylene protons were observed at δ 2.18 and δ 2.35 with a geminal coupling of 15.6 Hz; in this solvent, the C-12 methylene protons appeared at δ 1.85 and δ 1.56, and all four vicinal couplings between the C-11 and C-12 protons were nonequivalent and observed.

Vicinal $^{1}H-^{1}H$ coupling constants were of limited value for making stereochemical assignments: the *trans*-diaxial relationship between the protons at C-5 and C-10 is clear from their 12.6 Hz coupling, but the 2.9 Hz coupling between the protons at C-5 and C-6 does not establish the relative con-

[1]Author to whom correspondence may be addressed.

Can. J. Chem. Downloaded from www.nrcresearchpress.com by 217.78.4.112 on 09/08/12
For personal use only.

TABLE 1. Assigned chemical shifts and connectivities for ecuadorin in benzene-d_6 solution [a]

Carbon	δ_C [b]	δ_H (J_{HH}) [c]	n-bond connectivities [d]
1	199.58	—	6.71, 1.09(w)
2	126.67	—	6.71, 3.67
3	160.96	6.71 (0.9)	0.88, 1.22, 3.67(w)
4	37.10	—	5.41(s), 1.22, 0.88, 6.71(vw)
5	50.30	2.16 (12.6, 2.9)	6.71, 5.41, 1.22, 0.88, 1.09(vw)
6	71.11	5.41 (2.9)	1.09 (vw, n = 4)
7	170.36	—	3.20, 5.41(s)
8	66.73	—	3.67, 2.31, 1.74, 2.22(w), 1.89(vw?)
9	201.30	—	1.89
10	40.16	2.34 (12.6, 6.7q)	1.09, 5.41(w)
11	36.27	⟨1.89⟩ (6.7t)	1.42(vw), 0.80(vw)
12	30.92	0.80 (6.7t, 14.6)	1.89, 0.63
		1.42 (6.7t, 14.6)	
13	38.08	—	1.89, 0.63, 1.42(vw)
14	41.08	1.74 (4.9, 8.0, 0.9)	0.63, 2.31(w), 2.22(w)
15	26.65	2.22 (4.9, 18.1)	1.74
		2.31 (8.0, 18.1)	
16	169.13	—	2.22, 2.31, 1.74(w)
17	76.55	6.10 (s)	0.63
18	20.45	0.63	6.10
19	12.60	1.09 (6.7)	2.34(vw)
20	121.30	—	7.61, 6.10, 7.06(vw)
21	141.90	7.61 (m)	7.06, 6.36, 6.10
22	110.63	6.36 (m)	7.06(w)
23	143.45	7.06 (m)	7.61, 6.36
28[e]	22.92	1.22	0.88, 2.16(w)
29[e]	28.11	0.88	1.22, 6.71
30	55.94	3.67 (0.9, 0.9)	6.71, 1.74
OCH_3	51.81	3.20	—
O_2CCH_3	169.54	—	1.66, 5.41
O_2CCH_3	20.10	1.66	—

[a] Spectral data were obtained on a Varian XL-400 spectrometer equipped with a 5-mm multinuclear probe with a solution of 20 mg ecuadorin in ca. 0.5 mL of benzene-d_6.

[b] ^{13}C chemical shifts in ppm from Me_4Si measured at 100.6 MHz.

[c] ^1H chemical shifts in ppm from Me_4Si measured at 400 MHz, and ^1H–^1H coupling constants (Hz) in parentheses; couplings are with single protons except where triplet (t) or quartet (q) splittings are indicated. The ⟨mean δ_H⟩ is shown for an incompletely resolved CH_2 multiplet.

[d] Hydrogens showing n-bond connectivities to the ^{13}C; n = 2 or 3 unless otherwise indicated. Strong (s), weak (w), or very weak (vw) cross peaks are indicated where appropriate.

[e] Assignment of methyl groups based on nOe experiment. Irradiation at δ 1.22 produces 4% nOe for H-10 and 4% for H-3; irradiation at δ 0.88 produces 5% nOe for H-5 and 9% for H-3. The weak cross peak between H-5 and C-28 in the n-bond connectivity experiment is consistent with their having *anti* orientation.

figuration at C-6. Other stereochemical relationships were determined from NOE difference spectra. In benzene-d_6 solution, irradiation of the C-30 proton produced a 10% NOE at the C-17 proton and a 7% NOE at the δ 2.22 proton of the C-15 methylene. The C-30 and C-17 protons can be brought closely enough together to produce the 10% NOE only when the two six-membered rings are *cis*-fused and the relative configuration at the five contiguous centres from C-30 to C-17 is as shown. Besides confirming this stereochemistry, the NOE at the δ 2.22 proton confirms the chemical shift assignments for the individual protons of the CH_2 group. It is apparent that these stereochemical features are divided into two sections by the C-2 to C-30 single bond and, while the stereochemical relationships *within* each section are secure as described above, the configurational relationship *between* the cyclohexenone ring and the polycylic part of the molecule is not established from the available data.

Further stereochemical information was obtained by treating ecuadorin with acidic sodium cyanoborohydride, which reduced first the C-9 carbonyl group to provide the dihydroecuadorin **2**, and then the α,β-unsaturated C-1 carbonyl, producing the tetrahydroecuadorin **3**. Structural and spectroscopic assignments based on one-bond ^{13}C–^1H connectivities were carried out on **2** and **3**, and the assignments are listed in Table 2. One feature that became immediately apparent was that reduction of the carbonyl groups significantly changed the conformational preference of the molecule. Both ^1H and ^{13}C spectra of dihydroecuadorin **2** showed significant peak broadening at room temperature, particularly for signals associated with the fused bicyclic portion of the molecule (C-8, C-9, and C-11 to C-18), and the spectra sharpened significantly when the sample was warmed to 50°C. The vicinal coupling constants from H-14 to the two protons at C-15 increase slightly from **1** (4.9, 8.0 Hz) to **2** (6.3, 8.1 Hz). These observations suggest that dihydroecuadorin is undergoing a slow chair-to-chair interconversion at room temperature. By constrast, tetrahydroecuadorin **3** gives sharp ^1H and ^{13}C spectra at room temperature; further-

Can. J. Chem. Downloaded from www.nrcresearchpress.com by 217.78.4.112 on 09/08/12
For personal use only.

TABLE 2. Assigned ^{13}C and ^{1}H chemical shifts for dihydro- and tetrahydroecuadorin (**2** and **3**)

Position	δ_C[a] for **2**	δ_H[b] (J_{HH})[c] for **2**	δ_C[a] for **3**	δ_H[b] (J_{HH})[c] for **3**)
1	200.62	—	73.96	4.03 (9.1)
2	130.20	—	128.17	—
3	157.26	6.49 (1.6)	139.20	5.33 (1.5)
4	37.34	—	36.44	—
5	50.23	2.43 (12.2, 2.8)	48.51	2.03 (11.7, 3.0)
6	70.93	5.39 (2.8)	70.88	5.32 (3.0)
7	170.34	—	170.77	—
8	64.14	—	62.69	—
9	68.81	3.52 (6.2, 3.8)	65.92	3.51 (m)
10	40.05	2.64 (12.2, 6.7q)	36.38	⟨1.83⟩
11	26.14	⟨1.83⟩	26.08	⟨1.39⟩
12	29.00	1.96 (13.5, 8.4, 4.4)	25.54	⟨1.91⟩
		1.40 (13.5, 7.5, 4.4)		
13	36.99	—	36.78	—
14	43.80	1.71 (8.1, 6.3)	42.69	1.57 (11.1, 6.9)
15	29.70	3.02 (17.9, 8.1)	31.32	3.38 (17.7, 11.1)
		2.76 (17.9, 6.3)		2.80 (17.7, 6.9)
16	169.96	—	170.02	—
17	79.80	5.74 (br)	82.71	5.08 (br)
18	21.94	1.05	22.03	1.02
19	12.74	1.23 (6.7)	15.52	1.05 (6.5)
20	120.88	—	121.27	—
21	140.96	7.53 (m)	140.30	7.41 (m)
22	109.67	6.42 (m)	109.38	6.36 (m)
23	143.23	7.42 (m)	143.39	7.43 (m)
28	22.34	1.24	24.63	1.14
29	28.69	1.16	29.39	0.97
30	57.32	3.39 (1.6)	60.06	3.20 (br)
OCH_3	52.40	3.76	52.21	3.74
$CH_3C{=}O$	171.67	—	173.03	—
$CH_3C{=}O$	20.65	2.16	20.86	2.16

[a] ^{13}C chemical shifts in ppm from Me_4Si measured at 100.6 MHz for solution in $CDCl_3$; assignments based on one-bond connectivities.

[b] ^{1}H chemical shifts in ppm from Me_4Si measured at 400 MHz for solution in $CDCl_3$. The δ_H for each identifiable proton (or methyl) is listed; the ⟨mean δ_H⟩ is reported for unresolved CH_2 multiplets.

[c] ^{1}H–^{1}H coupling constants (Hz) for couplings with single protons unless quartet (q) splitting is indicated. Complex or unresolved multiplets are designated (m).

more, H-14 now shows vicinal coupling constants of 6.9 and 11.1 Hz to the protons at C-15. In addition, a number of carbons well removed from C-1 (the point of difference between **2** and **3**) show surprisingly large chemical differences between the dihydro and tetrahydro derivatives; e.g., compare the ^{13}C chemical shifts at positions 8, 9, 12, 15, and 17 (Table 2). Similarly, there is a large difference between the H-17 chemical shifts of **2** and **3**. All of these observations suggest an inversion of the conformational preference of the *cis*-fused rings between ecuadorin and tetrahydroecuadorin. In **1** H-14 is equatorial to the lactonic ring and axial to the carbocyclic ring, while in **3**, with the alternative chair–chair conformation, H-14 is axial to the lactonic ring and equatorial to the carbocyclic ring. In the same way, H-17, which is axial in **1**, becomes equatorial in **3**, and the chemical shift also changes.

The vicinal coupling constants observed at H-9 in both **2** and **3** require this hydrogen to be equatorial, and the C-9 OH is, consequently, axial (and *trans* to H-14). In **3** the H-1 must be pseudoaxial and *trans* to H-10 (J = 9.1 Hz), and the C-1 OH is, therefore, pseudoequatorial; the *trans*-diaxial relationship between H-10 and H-5 is verified by the observed vicinal coupling (11.3 Hz). The OH peaks in the spectrum of **3** appear as a very broad signal centred near δ 4.25, even though the solution is quite dilute. The low-field shift and the broadness of the peak suggest that the OH groups are intramolecularly hydrogen-bonded to each other (with slow proton interchange). Rotation about the 2,30 single bond is consequently inhibited, the cyclohexene unit has a preferred orientation relative to the polycyclic part of the molecule, and NOE experiments can now give useful information about the stereochemical relationship *between* these two parts of the molecule. No measureable NOE was observed for H-9 on irradiation of H-1 (or vice versa) at room temperature. However, irradiation of H-9 produced a 4% enhancement of the H-3 signal, while irradiation of H-1 produced 2% enhancements of the H-30 and H-5 signals. These results show the preferred orientation of the cyclohexene ring relative to the polycylic part of the molecule is as shown in **3**; the conformational preference of the *cis*-fused rings has already been established, the C-1 and C-9 OH groups are hydrogen-bonded, and the configurational relationship between C-1 and the centres on the other side of the 2,30 bond can now be determined. Examination of molecular models shows that

Can. J. Chem. Downloaded from www.nrcresearchpress.com by 217.78.4.112 on 09/08/12
For personal use only.

Can. J. Chem. Downloaded from www.nrcresearchpress.com by 217.78.4.112 on 09/08/12
For personal use only.

only a molecule with the configuration shown can be placed in a conformation that is compatible with all of the data assembled. Experiments with a sample of **3** at 55°C gave results that differed in an interesting and informative way from those carried out at room temperature: the OH signal sharpened and moved to higher field (ca. δ 3.95), and positive NOE enhancements were observed at both H-1 and H-3 on irradiation of H-9. It follows that at the higher temperature two conformations, corresponding to a rotation about the 2,30 bond, must be populated to a significant extent.

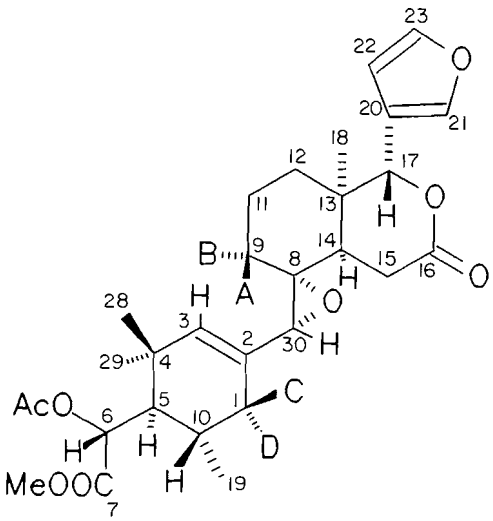

1 A + B = C + D = O

2 A = OH; B = H; C + D = O

3 A = OH; B = H; C = OH; D = H

The arguments for the configurational relationship between the two parts of the molecule are less securely based than those for the relative configuration within each part, but they gain additional support from a reasonable hypothesis concerning the biosynthetic origin of ecuadorin. Although its structural type is new, the relationship of ecuadorin to limonoids with the swietenine skeleton is easily seen; the structure and absolute configuration of swietenine (**4**) have been established unequivocally by an X-ray crystal structure analysis (4). The hypothetical biosynthetic precursor to ecuadorin has the 8,30 double bond of swietenine epoxidized, and C-9 is hydroxlyated; a retro-aldol reaction can then disconnect C-9 from C-10 and produce the ecuadorin skeleton, and a simple elimination introduces the 2,3 double bond. A swietenine derivative incorporating the 8,30 epoxide with the correct configuration but lacking the C-9 OH has been isolated from *Swietenia macrophylla* (5). The simplicity of the biosynthetic hypothesis and the existence of a limonoid incorporating all but one of the required features in the hypothetical precursor provide strong support for the biosynthetic proposal and collateral support for our stereochemical assignments. The configuration shown at C-6 is that expected on biosynthetic grounds. We would like to have used X-ray crystallography to provide unequivocal confirmation for all of our structural and stereochemical assignments, but no derivative of ecuadorin has yet provided crystals suitable for this purpose.

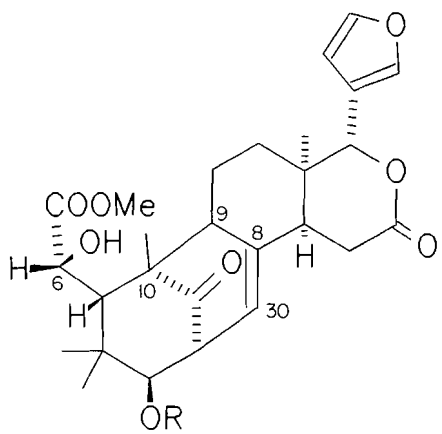

4 R = Tigloyl

Experimental

Guarea kunthiana was collected in Pichincha Province, Ecuador, in October 1986. A voucher specimen (QCA No. 1124) is lodged in the Herbarium of the Catholic University of Ecuador, Quito. Air-dried aerial parts of the plant (2.3 kg) were ground and extracted with cold dichloromethane. The extract afforded a dark green gum (17.9 g), which was partitioned into hexane-soluble (5.7 g) and hexane-insoluble (10.5 g) fractions. A portion (930 mg) of the latter fraction was treated with decolorizing charcoal in refluxing ethyl acetate, and then chromatographed on silica gel. Elution with hexane containing increasing amounts of ethyl acetate led, when the solvent contained 90% or more ethyl acetate, to the isolation of *ecuadorin* (**1**) (61 mg) as colorless needles, mp 237–328°C (recrystallized from methanol), $[\alpha]_D$ + 4.2 (*c* 0.7, $CHCl_3$); IR (Nujol): 1752, 1737, 1715, 1600 cm^{-1}; UV (EtOH) λ_{max}: 208 nm (ε, 11 000), 236 nm (ε, 8 200); HREIMS *m/z*: 542.2122; calcd. for $C_{29}H_{34}O_{10}$: 542.2152.

Dihydroecuadorin 2 and tetrahydroecuadorin 3

A solution of **1** (73 mg) in 5 mL of tetrahydrofuran was brought to approximately pH 1 by addition of 1 N hydrochloric acid, and sodium cyanoborohydride (84 mg) was then added in small portions; the pH was kept constant by the addition of acid when required. After 0.5 h, solvent was removed under reduced pressure, 5 mL of water was added, and the mixture was thoroughly extracted with dichloromethane. The extract afforded a residue (70 mg) that was subjected to preparative layer chromatography on silica gel with elution by 5:1 chloroform–acetate. Less polar fractions afforded *dihydroecuadorin 2* (16 mg), mp 248–249°C (recrystallized from $CHCl_3$–MeOH) $[\alpha]_D$ −16.4 (*c* 0.25, $CHCl_3$); UV (EtOH) λ_{max}: 221 nm (ε, 7 800), 238 nm (ε, 7 600); HREIMS *m/z*: 544.2292; calcd. for $C_{29}H_{36}O_{10}$: 544.2309. The more polar fractions afforded *tetrahydroecuadorin 3* (15 mg), mp 241–242°C (recrystallized from MeOH–$CHCl_3$), $[\alpha]_D$ −13.9 (*c* 0.6, $CHCl_3$); HREIMS *m/z*: 546.2449; calcd. for $C_{29}H_{38}O_{10}$: 546.2465.

Acknowledgements

We thank Mr. Vlastimil Zak and Dr. Jaime Jaramillo of the Herbarium of the Catholic University, Quito, Ecuador for help in plant collection, and Ms Isabel Guerra for technical assistance. One of us (B.S.M.) is grateful for a travel grant from the UNESCO Regional Office for Science and Technology for Latin America, Montevideo, Uruguay. Research in the Toronto laboratory is supported by grants from the Natural Sciences and Engineering Research Council of

Canada. A CIDA/NSERC Research Associateship (to W.F.T.) is gratefully acknowledged.

1. D. A. H. Taylor. Prog. Chem. Org. Nat. Prod. **45**, 1 (1984).
2. W. F. Reynolds, S. McLean, M. Perpick-Dumont, and R. G. Enriquez. Magn. Reson. Chem. **27**, 162 (1989).
3. P. E. Hansen. Prog. NMR Spectrosc. **14**, 175 (1981).
4. (*a*) J. D. Connolly, R. Henderson, R. McCrindle, K. H. Overton, and N. S. Bhacca. J. Chem. Soc. 6935 (1965); (*b*) A. T. McPhail and G. A. Sim. Tetrahedron Lett. 2599 (1964).
5. A. R. H. Taylor and D. A. H. Taylor. Phytochemistry, **22**, 2870 (1983).

Can. J. Chem. Downloaded from www.nrcresearchpress.com by 217.78.4.112 on 09/08/12
For personal use only.

Formation of 14-membered carbocycles by intramolecular Michael addition on ynones and enones

SUZANNE GIRARD[1] AND PIERRE DESLONGCHAMPS[2]

Laboratoire de synthèse organique, Département de Chimie, Faculté des Sciences, Université de Sherbrooke, Sherbrooke (Qué.), Canada J1K 2R1

Received March 27, 1991

This paper is dedicated to Professor Zdenek (Denny) Valenta on the occasion of his 65th birthday

SUZANNE GIRARD and PIERRE DESLONGCHAMPS. Can. J. Chem. **70**, 1265 (1992).

The base-catalyzed intramolecular Michael addition of substituted malonates on ynones or enones proceeds efficiently to give the 14-membered carbocycles.

SUZANNE GIRARD et PIERRE DESLONGCHAMPS. Can. J. Chem. **70**, 1265 (1992).

On rapporte la formation de carbocycles à 14 membres par l'addition de Michael intramoléculaire de malonates substitués sur des ynones et des énones.

Can. J. Chem. Downloaded from www.nrcresearchpress.com by 217.78.4.112 on 09/08/12
For personal use only.

Introduction

Previous studies in our laboratory, on the intramolecular Michael addition of cyclic β-ketoesters onto conjugated olefinic ketones, showed that it was possible to form 5- to 8-membered rings with fairly good yields (1). In addition it was shown that the analogous addition onto conjugated acetylenic ketones produced 5- to 7-membered rings (2). In yet another study, it was demonstrated that it was possible to use the intramolecular Michael reaction to close 9- and 10-membered rings, but the yields were moderate compared with the cyclization of smaller rings (3). At that time it was predicted that this synthetic strategy could lead to excellent yields (≥80%) in macrocyclization, provided that transannular steric interactions and conformational mobility could be decreased.

In this paper we wish to report the results of the study of the formation of 14-membered carbocycles by the intramolecular Michael addition of substituted malonates onto conjugated acetylenic and olefinic ketones. We describe first the preparation of several cyclization precursors (ynones **14**, **28**, and **34** and enones **30** and **36**), and then the macrocyclization of each of these compounds.

Results and discussion

Synthesis of the cyclization precursors

Our study began with ynone **14**, which was prepared from 3-butyn-1-ol **1** as shown in Scheme 1. **1** was protected as its tetrahydropyranyl ether **2** (74%), which was then treated with *n*-butyllithium in a mixture of tetrahydrofuran–hexamethylphosphoramide (HMPA) (3:2), followed by oxirane to give alcohol **3** (90%). It should be noted that replacing HMPA by other polar solvents such as HMPT (hexamethylphosphorous triamide) or DMPU (1,3-dimethyl-3,4,5,6-tetrahydro-2(1*H*)pyrimidinone) gave unsatisfactory yields of alcohol **3**.

Alcohol **3** was transformed into the mesylate **4** (95%), which was displaced by dimethylmalonate to form diester **5** (78%). The alkylation of diester **5** with iodide **6** (73%), available in two steps from tetrahydrofuran (4), followed by hydrolysis of the acetal with magnesium bromide etherate (5) gave alcohol **8** (82%).

The second malonate group was introduced as before, via mesylate **9** (99%), to obtain compound **10** in 87% yield. Hydrolysis of the silyl ether gave alcohol **11** (62%), which was in turn oxidized to aldehyde **12** (96%) using the Swern reaction conditions (6). The acetylenic group was introduced by the addition of acetylene anion to aldehyde **12** (74%). The resulting propargylic alcohol **13** was then oxidized with Jones' reagent (7) to give ynone **14** (88%).

The synthesis of compounds **28**, **30**, **34**, and **36** starts with 4-pentyn-1-ol protected as tetrahydropyranyl ether **16** (96%) (see Scheme 2). The sequence of reactions to malonate **19** was the same as previously described for compound **5**. Malonate **19** was then alkylated with iodide **20** to give diester **21** (74%). The iodide **20** was itself synthesized in two standard steps from 3-chloro-1-propanol. The rest of the synthesis of ynone **28** was done as described for compound **14** (Schemes 2 and 3).

To form enone **30**, aldehyde **26** was condensed with vinylmagnesium bromide to give allylic alcohol **29** (52%), which was then oxidized to **30** with Jones' reagent (72%).

To make compounds **34** and **36**, alkyne **25** was hydrogenated to the *cis* alkene **31** with hydrogen and Lindlar's catalyst (98%) (Scheme 4). Oxidation of the resulting alcohol **31**, using the Swern reaction conditions, gave aldehyde **32** (64%). The rest of the synthesis of ynone **34** was accomplished following the procedure previously described for ynone **14**. The last macrocyclization precursor, enone **36**, was synthesized from aldehyde **32** using the same reaction sequence as for enone **30**.

Macrocyclization

All the macrocyclizations were performed using the same reaction conditions. The ynone or enone, dissolved in acetonitrile, was added slowly over ca. 2.5 h to a solution of cesium carbonate in acetonitrile. The final concentration of the reaction mixture was 2×10^{-3} M. This pseudo high-dilution technique was used to minimize polymerization or dimerization.

Cyclization of ynone **14** (Scheme 5) gave macrocycle **37** in 90% yield as a mixture of *cis* and *trans* isomers (12:88). Ynone **28** gave macrocycle **38** as an 87:13 *cis–trans* mixture of isomers in 48% yield, while ynone **34** gave macrocycle **40** with a 20:80 ratio of *cis* and *trans* in 45% yield. The macrocyclizations of enones **30** and **36** afforded macrocycles **39** and **41** with 82% and 76% yields, respectively.

The configurations and ratios of *cis* and *trans* conjugated

[1]FCAR predoctoral fellowship, 1988–1990.

[2]Author to whom correspondence may be addressed.

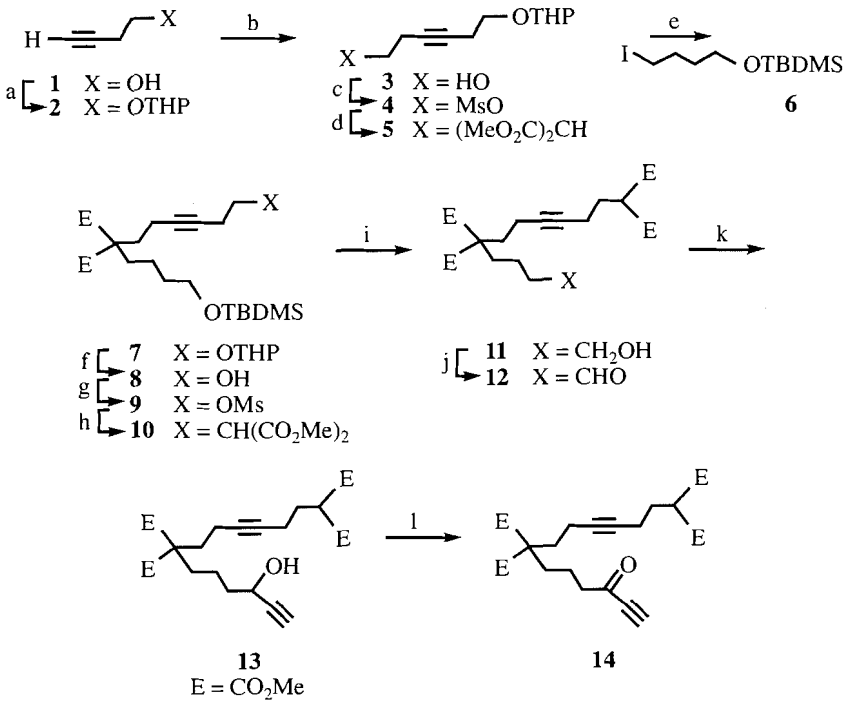

(a) DHP, *p*-TsOH, THF, r.t., 2 h (74%). (b) *n*-BuLi, THF, HMPA, oxirane −78°C to r.t., 22 h (90%). (c) CH_3SO_2Cl, Et_3N, CH_2Cl_2, 0°C to r.t., 3 h (95%). (d) $CH_2(CO_2Me)_2$, NaH, THF, DMF, reflux, 18 h (78%). (e) NaH, THF, DMF, r.t., 20 h (73%). (f) Et_2O, $MgBr_2 \cdot Et_2O$, 0°C to r.t., 16 h (82%). (g) CH_3SO_2Cl, Et_3N, CH_2Cl_2, 0°C to r.t. 3 h (99%). (h) $CH_2(CO_2Me)_2$, NaH, THF, DMF, reflux, 15 h (87%). (i) *n*-Bu_4NF, THF, 0°C to r.t., 18 h (62%). (j) $(ClC(O))_2$, Me_2SO, CH_2Cl_2, Et_3N, −78°C (96%). (k) *n*-BuLi, acetylene, THF, −78°C (74%). (l) H_2CrO_4/acetone (Jones') (88%).

SCHEME 1

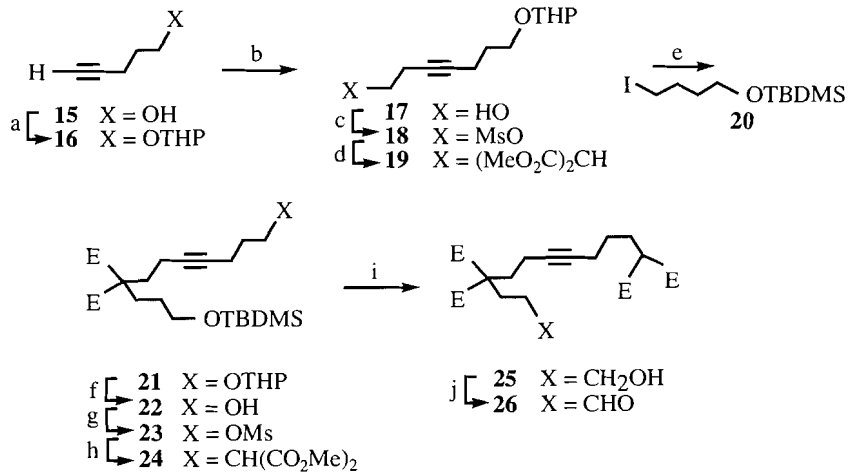

(a) DHP, *p*-TsOH, THF, r.t., 2 h (96%). (b) *n*-BuLi, THF, HMPA, oxirane −78°C to r.t., 22 h (82%). (c) CH_3SO_2Cl, Et_3N, CH_2Cl_2, 0°C to r.t., 3 h (92%). (d) $CH_2(CO_2Me)_2$, NaH, THF, DMF, reflux, 18 h (75%). (e) NaH, THF, DMF, r.t., 20 h (74%). (f) Et_2O, $MgBr_2 \cdot Et_2O$, 0°C to r.t., 16 h (78%). (g) CH_3SO_2Cl, Et_3N, CH_2Cl_2, 0°C to r.t. 3 h (94%). (h) $CH_2(CO_2Me)_2$, NaH, THF, DMF, reflux, 15 h (77%). (i) *n*-Bu_4NF, *p*-TsOH, THF, 0°C to r.t., 6 h (83%). (j) $(ClC(O))_2$, Me_2SO, CH_2Cl_2, Et_3N, −78°C (91%).

SCHEME 2

enones obtained from the macrocyclizations of the ynones were determined by proton nmr. These assignments were based on the coupling constants ($J_{H,H}$ (*cis*) ≈ 12.3 Hz and $J_{H,H}$ (*trans*) ≈ 16.9 Hz) observed for the olefinic hydrogens.

The modest yields obtained for the ynones macrocyclizations might be attributable to the fact that polymerization may occur. This fact was previously observed (8). To improve the yields of the macrocyclizations of the ynones, we tried several reaction conditions (Table 1) using the same pseudo high-dilution technique. However none of these conditions improved the initial results.

In summary, we have shown that the intramolecular Michael reaction can indeed be used to form carbocycles

Can. J. Chem. Downloaded from www.nrcresearchpress.com by 217.78.4.112 on 09/08/12
For personal use only.

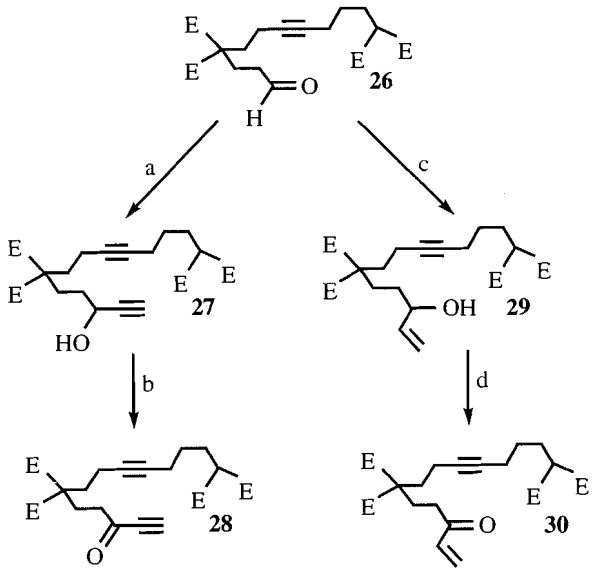

(a) *n*-BuLi, acetylene, THF, 15 min −78°C (54%). (b) H_2CrO_4/acetone (Jones') (88%). (c) Vinylmagnesium bromide, Et_2O, 15 min, −78°C (52%). (d) H_2CrO_4/acetone (Jones') (72%).

SCHEME 3

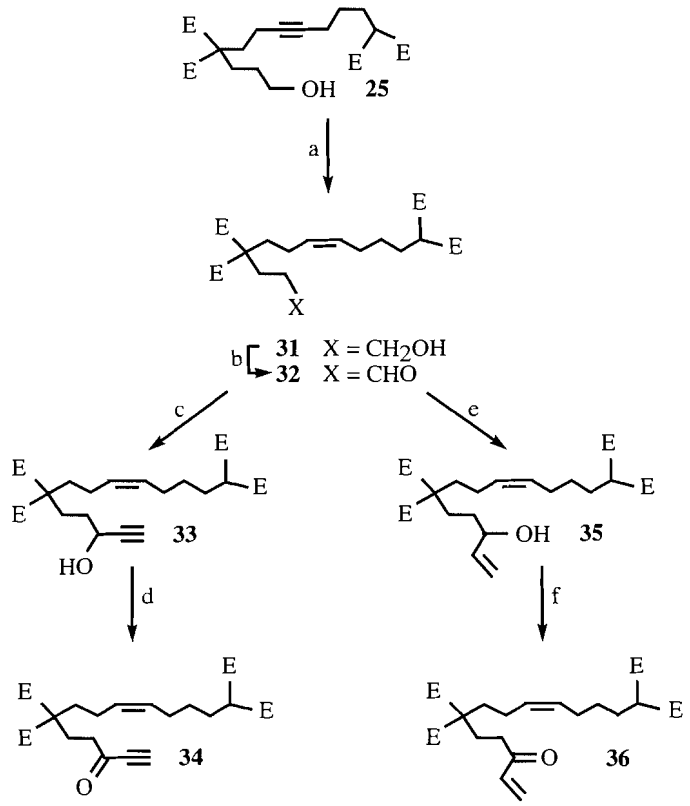

(a) H_2, $Pd/CaCO_3/Pb$ poisoned, EtOAc, 2h, r.t. (98%). (b) $(Cl(CO))_2$, Me_2SO, CH_2Cl_2, Et_3N, −78°C (64%). (c) *n*-BuLi, acetylene THF, −78°C, 20 min (92%). (d) Jones (76%). (e) Vinylmagnesium bromide, Et_2O, 20 min, −78°C (59%). (f) H_2CrO_4/acetone (Jones') (72%).

SCHEME 4

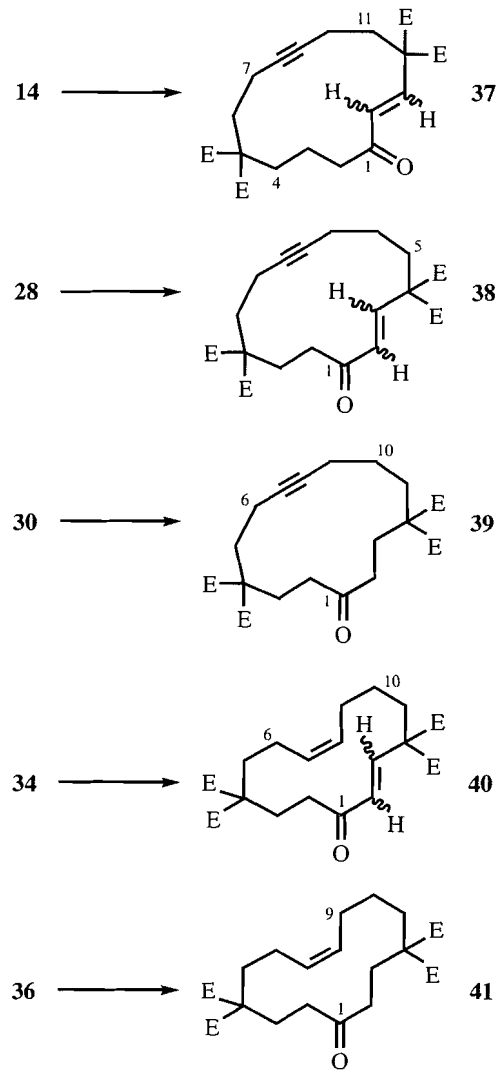

SCHEME 5

when the conditions of reduced transannular steric interactions and restricted mobility are met. The reaction is particularly efficient when an enone is used as the Michael acceptor. The yields for the preparation of macrocyclic enones might be improved by cyclizing an enone substituted with a labile group in the β position, which could then be used to introduce the desired α, β unsaturation.

The highly functionalized macrocycles described herewith are excellent substrates for further transformations. Thus, we obtained some promising preliminary results when we carried out the intramolecular Diels–Alder reaction on the silylated enol ether of macrocycle **40**. Subsequent hydrolysis of the silyl enol ether afforded a tricyclo-[8.4.0.$0^{2,7}$]tetradecan-8-one. Application of this strategy to the synthesis of steroids is under way in our laboratories.

Experimental

The infrared spectra (ir) were taken on a Perkin–Elmer 681 spectrophotometer. Protons nmr spectra were recorded on a Bruker WM-250 spectrometer. Chemical shifts are reported in δ relative to deuterated chloroform as the internal standard. Abbrevations used are m: multiplet, s: singlet, d: doublet, t: triplet, q: quartet. Mass spectral assays (ms *m/e*) and exact masses were obtained using a

Can. J. Chem. Downloaded from www.nrcresearchpress.com by 217.78.4.112 on 09/08/12
For personal use only.

TABLE 1. Reaction conditions for macrocylization of ynone **14**

Base	Solvent	T(°C)	Results
Cs_2CO_3	CH_3CN	0	46% macrocyclization
Cs_2CO_3	CH_3OH	r.t.	38% of starting material (and polymerization)
$Et_3N/Et_3N \cdot HCl$	CH_3CN	r.t.	Starting material
$Et_3N/MgBr_2 \cdot Et_2O$	CH_2Cl_2, THF	r.t.	Starting material

VG Micromass ZAB-1F spectrometer. Reactions were carried out under an argon atmosphere, except for hydrogenations. Chromatographic separations were done using Merck silica gel 230–400 mesh ASTM.

Acetylene 2

To a solution of alcohol **1** (10.8 mL, 0.143 mol) and *p*-toluenesulfonic acid (1.4 g, 0.007 mol) in tetrahydrofuran (60 mL) at room temperature was added 3,4-dihydropyran (30 mL, 0.329 mol). After stirring for 2 h, a saturated solution of sodium bicarbonate was added. The aqueous phase was extracted three times with diethyl ether. The combined organic layers were washed with brine, dried over magnesium sulfate, filtered, and evaporated. The residue was purified by distillation (90°C, 12 Torr; 1 Torr = 133.3 Pa) affording **2** (16.3 g, 74%); ir (neat): 3330, 2940–2870, 1440, 1355, 1200, 1130, 1035 cm^{-1}; ^1H nmr ($CDCl_3$) δ: 4.64 (1H, m, OC*H*O), 3.93–3.79 (2H, m, CH_2O), 3.61–3.47 (2H, m, CH_2O), 2.48 (2H, td, J = 7.0, 2.7 Hz, $CH_2C{\equiv}C$), 1.97 (1H, t, J = 2.7 Hz, $C{\equiv}CH$), 1.90–1.45 (6H, m, $(CH_2)_3$).

Alcohol 3

To a solution of **2** (5.00 g, 32.43 mmol) in tetrahydrofuran (45 mL) and HMPA (30 mL) at −78°C was added *n*-butyllithium (1.6 M in hexane, 21 mL, 34.05 mmol). The mixture was stirred for 5 min at −78°C. Liquid oxirane (25 mL, 486 mmol) was then added, and the reaction was allowed to warm gradually to room temperature (the oxirane was condensed in a bottle and was kept in the freezer prior to the reaction; it was syringed into the reaction using a cold syringe). After 22 h, a saturated solution of ammonium chloride was added and the aqueous phase was extracted three times with diethyl ether. The combined organic layers were washed twice with a 10% copper sulfate solution, then with brine, dried over magnesium sulfate, filtered and evaporated. The crude material was purified by column chromatography (30% increasing to 50% ethyl acetate in hexane) affording alcohol **3** (5.83 g, 90%). This alcohol can be distilled under reduced pressure (250 mTorr, 110°C); ir (neat): 3600–3200, 2980–2820, 1440, 1350, 1200–1020 cm^{-1}; ^1H nmr ($CDCl_3$) δ: 4.64 (1H, m, OC*H*O), 3.92–3.76 (2H, m, CH_2O), 3.67 (2H, q, J = 6.2 Hz, CH_2OH), 3.60–3.48 (2H, m, CH_2O), 2.51–2.39 (4H, m, $CH_2C{\equiv}CCH_2$), 1.96 (1H, t, J = 6.2 Hz, CH_2OH), 1.82–1.49 (6H, m, $(CH_2)_3$).

Mesylate 4

To a solution of alcohol **3** (14.6 g, 73.63 mmol) and triethylamine (14.4 mL, 103 mmol) in dichloromethane (245 mL) at 0°C, methanesulfonyl chloride (6.8 mL, 88.36 mmol) was added. The mixture was stirred for 3 h, letting the temperature rise to room temperature. Water was then added and the aqueous phase was extracted three times with dichloromethane. The combined organic layers were washed with brine, dried over magnesium sulfate, filtered, and concentrated. The crude material was purified by column chromatography (30% ethyl acetate in hexane) affording mesylate **4** (19.34 g, 95%); ir (neat): 2980–2840, 1440, 1355, 1175, 1070, 1035, 100–800 cm^{-1}; ^1H nmr ($CDCl_3$) δ: 4.62 (1H, m, OC*H*O), 4.26 (2H, t, J = 6.9 Hz, CH_2OMs), 3.87–3.74 (2H, m, CH_2O), 3.54–3.47 (2H, m, CH_2O), 3.04 (3H, s, OSO_2CH_3), 2.62 (2H, tt, J = 6.9, 2.4 Hz, $C{\equiv}CCH_2CH_2OMs$), 2.46 (2H, tt, J = 7.0, 2.4 Hz, $C{\equiv}CCH_2CH_2OTHP$), 1.80–1.51 (6H, m, $(CH_2)_3$).

Malonate 5

To a suspension of sodium hydride (60% in oil, 650 mg, 16.25 mmol) in *N*,*N*-dimethylformamide (65 mL), dimethylmalonate (1.93 mL, 16.93 mmol) was added slowly. The mixture was heated at ≈50°C, using a water bath, to help solubilize the formed anion. The reaction mixture was then added using a cannula to a solution of mesylate **4** (1.83 g, 6.62 mmol) and potassium iodide (1.1 g, 6.62 mmol) in tetrahydrofuran (60 mL). The mixture was refluxed for 18 h and then cooled to room temperature. A saturated solution of ammonium chloride was added and the aqueous phase was extracted three times with a mixture of diethyl ether and hexane (1:1). The combined organic layers were washed with brine, dried over magnesium sulfate, filtered, and concentrated. The crude product was purified by column chromatography (5% increasing to 50% ethyl acetate in hexane) affording ester **5** (1.61 g, 78%); ir (neat): 2980–2840, 1770–1720, 1440, 1370–1120, 1090–1010 cm^{-1}; ^1H nmr ($CDCl_3$) δ: 4.63 (1H, m, OC*H*O), 3.87–3.75 (2H, m, CH_2O), 3.74 (6H, s, CO_2CH_3), 3.61 (1H, t, J = 7.3 Hz, $CH(E)_2$), 3.56–3.39 (2H, m, CH_2O), 2.44 (2H, tt, J = 7.1, 2.3 Hz, CH_2CH_2OTHP), 2.27–2.20 (2H, m, $CH_2CH_2CH(E)_2$), 2.10–2.05 (2H, m, $CH_2CH(E)_2$), 1.75–1.49 (6H, m, $(CH_2)_3$).

Iodide 6

To a solution of tetrabutylammonium iodide (45.0 g, 0.122 mol) and tetrahydrofuran (11.4 mL, 0.122 mol) in chloroform (140 mL), at room temperature, boron trifluoride etherate (15.0 mL, 0.122 mol) was aded. The mixture was refluxed for 24 h, cooled, and a saturated solution of sodium bicarbonate was added. The aqueous phase was extracted three times with dichloromethane. The combined organic layers were washed with a 10% solution of sodium thiosulfate, then brine, dried over magnesium sulfate, filtered, and evaporated. The crude material was then triturated with diethyl ether affording crude 4-iodobutanol (16.9 g), which was used without further purification owing to fast decomposition by light.

To a solution of the crude iodobutanol (16.9 g, 0.085 mol) and imidazole (14.5 g, 0.20 mol) in dichloromethane (60 mL) at room temperature, *tert*-butyldimethylchlorosilane (15.3 g, 0.1 mol) was added. After stirring for 2 h, water was added and the aqueous phase was extracted three times with dichloromethane. The combined organic layers were washed with brine, dried over magnesium sulfate, filtered, and evaporated. The crude product was purified by column chromatography (5% increasing to 50% ethyl acetate in hexane) affording iodide **6** (24.26 g, 66%); ir (neat): 2980–2820, 1470, 1205, 1105 cm^{-1}; ^1H nmr ($CDCl_3$) δ: 3.63 (2H, t, J = 6.1 Hz, CH_2OSi), 3.22 (2H, t, J = 7.0 Hz, CH_2I), 1.90 (2H, m, CH_2CH_2OSi). 1.60 (2H, m, CH_2CH_2I), 0.89 (9H, s, *t*-Bu), 0.05 (6H, s, $(CH_3)_2Si$).

Alkyne 7

To a suspension of sodium hydride (134 mg, 3.36 mmol) in *N*,*N*-dimethylformamide (32 mL) and tetrahydrofuran (18 mL), malonate **5** (1.0 g, 3.2 mmol) dissolved in tetrahydrofuran (10 mL) was added. The mixture was stirred for 2–3 min at ≈50°C using a water bath, to help solubilize the anion formed. Iodide **6** (1.1 g, 3.52 mmol) was added at 50°C and then the bath was removed. After stirring for 20 h at room temperature, a saturated solution of ammonium chloride was added and the aqueous phase was ex-

Can. J. Chem. Downloaded from www.nrcresearchpress.com by 217.78.4.112 on 09/08/12
For personal use only.

Can. J. Chem. Downloaded from www.nrcresearchpress.com by 217.78.4.112 on 09/08/12
For personal use only.

tracted three times with a mixture of hexane and diethyl ether (1:1). The combined organic layers were washed with a 10% solution of sodium thiosulfate, then brine, dried over magnesium sulfate, filtered, and evaporated. The crude product was purified by column chromatography (5% increasing to 30% ethyl acetate in hexane) affording alkyne **7** (684.3 mg, 73%); ir (neat): 2980–2840, 1735, 1460, 1440, 1260–1030 cm^{-1}; ^1H nmr ($CDCl_3$) δ: 4.63 (1H, m, OC*H*O), 3.87–3.69 (2H, m, CH_2O), 3.70 (6H, s, CO_2CH_3), 3.58 (2H, t, J = 6.3 Hz, CH_2OSi), 3.55–3.45 (2H, m, CH_2O), 2.47–2.41 (2H, m, CH_2CH_2OTHP), 2.12–2.06 (4H, m, $CH_2C{\equiv}CCH_2$), 1.92–1.45 (10H, m, $CH_2C(E)_2$ CH_2CH_2OSi, $(CH_2)_3$), 1.26–1.16 (2H, m, $CH_2CH_2CH_2OSi$), 0.88 (9H, s, *t*-Bu), 0.08 (6H, s, $(CH_3)_2Si$).

Alcohol 8

To a solution of alkyne **7** (2.138 g, 4.29 mmol) in anhydrous diethyl ether (66 mL) at 0°C, magnesium bromide etherate (3.7 g, 12.87 mmol) was added. The reaction was stirred for 16 h, while allowing the mixture to warm gradually to room temperature, then water was added and the aqueous phase was extracted three times with diethyl ether. The combined organic layers were washed with brine, dried over magnesium sulfate, filtered, and evaporated. The crude product was purified by column chromatography (20–30% ethyl acetate in hexane) affording alcohol **8** (1.455 g, 82%); ir (neat): 3600–3200, 2980–2840, 1735, 1460–1430, 1260, 1100, 1050 cm^{-1}; ^1H nmr ($CDCl_3$) δ: 3.72 (6H, s, CO_2CH_3), 3.67 (2H, q, J = 6.2 Hz, CH_2OH), 3.59 (2H, t, J = 6.3 Hz, CH_2OSi), 2.40 (2H, t, J = 6.2 Hz, CH_2CH_2OH), 2.14 (4H, s, $C{\equiv}CCH_2$ $CH_2C(E)_2$), 1.99 (1H, t, J = 6.2 Hz, O*H*), 1.94–1.87 (2H, m, $CH_2(CH_2)_3OSi$), 1.57–1.46 (2H, m, CH_2CH_2OSi), 1.26–1.16 (2H, m, $CH_2CH_2CH_2OSi$), 0.88 (9H, s, *t*-Bu), 0.03 (6H, s, $(CH_3)_2Si$).

Mesylate 9

Mesylate **9** was synthesized using the same procedure as that for the preparation of mesylate **4**, from alcohol **8** (1.45 g, 5.0 mmol), dichloromethane (12 mL), triethylamine (0.7 mL, 5.0 mmol), and methanesulfonyl chloride (325 μL, 4.2 mmol). The crude product was purified by column chromatography (20–40% ethyl acetate in hexane) affording mesylate **9** (1.63 g, 99%); ir (neat): 3000–2860, 1480–1440, 1360, 1175, 1255, 1100, 1000–780 cm^{-1}; ^1H nmr ($CDCl_3$) δ: 4.25 (2H, t, J = 7.0 Hz, CH_2OMs), 3.71 (6H, s, CO_2CH_3), 3.59 (2H, t, J = 6.3 Hz, CH_2OSi), 3.04 (3H, s, $S(O)_2CH_3$), 2.60 (2H, t, J = 7.0 Hz, CH_2CH_2OMs), 2.10 (4H, s, $C{\equiv}CCH_2CH_2C(E)_2$), 1.92–1.85 (2H, m, $CH_2(CH_2)_3OSi$), 1.56–1.45 (2H, m, CH_2CH_2OSi), 1.27–1.17 (2H, m, $CH_2(CH_2)_2OSi$), 0.88 (9H, s, *t*-Bu), 0.03 (6H, s, $(CH_3)_2Si$).

Ester 10

Ester **10** was synthesized using the same procedure as for the preparation of ester **5**, from sodium hydride (60% in oil, 336 mg, 8.4 mmol), *N*,*N*-dimethylformamide (44 mL), dimethyl malonate (1 mL, 8.75 mmol), mesylate **9** (1.634 g, 3.5 mmol), potassium iodide (581 mg, 3.5 mmol), and tetrahydrofuran (20 mL). The crude product was purified by column chromatography (5–40% ethyl acetate in hexane) affording ester **10** (1.607 g, 87%); ir (neat): 3000–2840, 1770–1720, 1450, 1370–1090 cm^{-1}; ^1H nmr ($CDCl_3$) δ: 3.75 (6H, s, $CH(CO_2CH_3)_2$), 3.71 (6H, s, $R_2C(CO_2CH_3)_2$), 3.62–3.55 (3H, m, $CH(E)_2$, CH_2OSi), 2.26–2.20 (2H, m, $C{\equiv}CCH_2CH_2CH(E)_2$), 2.12–2.02 (6H, m, $CH_2CH_2C(E)_2$, $CH_2CH(E)_2$), 1.92–1.85 (2H, m, $CH_2(CH_2)_3OSi$), 1.55–1.48 (2H, m, CH_2CH_2OSi), 1.26–1.16 (2H, m, $CH_2CH_2CH_2OSi$), 0.88 (9H, s, *t*-Bu), 0.03 (6H, s, $(CH_3)_2Si$).

Alcohol 11

To a solution of ester **10** (1.607 g, 3.04 mmol) in tetrahydrofuran (15 mL), at 0°C, a solution of tetrabutylammonium fluoride (1M, 3.65 mL, 3.65 mmol) was added. The mixture was stirred for 18 h, while allowing the reaction to warm gradually to room temperature. A saturated solution of ammonium chloride was then added, and the aqueous phase was extracted three times with diethyl ether. The combined organic layers were washed with brine, dried over magnesium sulfate, filtered, and evaporated. The crude product was purified by column chromatography (50–100% ethyl acetate in hexane) affording alcohol **11** (756 mg, 62%); ir (neat): 3600–3200, 2980–2840, 1770–1700, 1450, 1370–1150, 1050 cm^{-1}; ^1H nmr ($CDCl_3$) δ: 3.75 (6H, s, $CH(CO_2CH_3)_2$), 3.72 (6H, s, $R_2C(CO_2CH_3)_2$), 3.65 (2H, t, J = 6.4 Hz, CH_2OH), 3.55 (1H, t, J = 7.3 Hz, $CH(E)_2$), 2.25–2.20 (2H, m, $CH_2CH_2CH(E)_2$), 2.15–2.02 (7H, m, O*H*, $CH_2CH_2C(E)_2$, $CH_2CH(E)_2$), 1.95–1.88 (2H, m, $CH_2(CH_2)_3OH$), 1.63–1.54 (2H, m, CH_2CH_2OH), 1.32–1.18 (2H, m, $CH_2CH_2CH_2OH$).

Aldehyde 12

To a solution of oxalyl chloride (182 μL, 2.09 mmol) in dichloromethane (2 mL) at −78°C, dimethyl sulfoxide (0.3-mL, 4.18 mmol) was added. The reaction was stirred for 5 min. Alcohol **11** (786 mg, 1.9 mmol) dissolved in dichloromethane was then added. After stirring for 15 min, triethylamine (1.3 mL, 9.5 mol) was added and the mixture stirred for another 5 min, allowing the reaction to warm slowly to room temperature. Water was then added and the aqueous phase was extracted three times with dichloromethane. The combined organic layers were washed with brine, dried over magnesium sulfate, filtered, and evaporated. The crude product was purified by column chromatography (30% ethyl acetate in hexane) affording aldehyde **12** (751 mg, 96%); ir (neat): 3000–2820, 2750, 1770–1700, 1450, 1370–1140, 1100, 1050 cm^{-1}; ^1H nmr ($CDCl_3$) δ: 9.75 (1H, t, J = 1.3 Hz, C(O)*H*), 3.75 (6H, s, $CH(CO_2CH_3)_2$), 3.73 (bH, s, $R_2C(CO_2CH_3)_2$), 3.57 (1H, t, J = 7.3 Hz, $CH(E)_2$), 2.47 (2H, td, J = 7.1, 1.3 Hz, $CH_2C(O)H$), 2.25–2.20 (2H, m, $CH_2CH_2CH(E)_2$), 2.19–2.04 (6H, m, $CH_2CH_2C(E)_2$), $CH_2CH(E)_2$), 1.93–1.86 (2H, m, $CH_2(CH_2)_2$-C(O)H), 1.58–1.48 (2H, m, $CH_2CH_2C(O)H$).

Alcohol 13

To *n*-butyllithium (1.6 M, 4.5 mL, 7.24 mmol) in tetrahydrofuran (3 mL) at −78°C, was added acetylene (14.48 mmol). The mixture was stirred for 5 min at −78°C and aldehyde **12** (748 mg, 1.81 mmol) dissolved in tetrahydrofuran (7 mL) was added. The reaction was stirred for another 15 min at −78°C, after which time a saturated solution of ammonium chloride was added and the aqueous phase was extracted three times with diethyl ether. The combined organic layers were washed with brine, dried over magnesium sulfate, filtered, and evaporated. The crude product was purified by column chromatography (30% increasing to 50% ethyl acetate in hexane) affording alcohol **13** (586 mg, 74%); ir (neat): 3600–3340, 3290, 3000–2840, 1770–1700, 1440, 1350–1150, 1110, 1050 cm^{-1}; ^1H nmr ($CDCl_3$) δ: 4.08 (1H, dq, J = 5.5, 2.1 Hz, $HC{\equiv}CCH(R)OH$), 3.75 (6H, s, $CH(CO_2CH_3)_2$) 3.72 (6H, s, $R_2C(CO_2CH_3)_2$), 3.57 (1H, t, J = 7.3 Hz, $CH(E)_2$), 2.47 (1H, t, J = 2.1 Hz, $C{\equiv}CH$), 2.26–2.20 (2H, m, $CH_2CH_2CH(E)_2$), 2.13–2.02 (6H, m, $CH_2CH(E)_2$), $CH_2CH_2C(E)_2$), 1.96–1.90 (3H, m, $CH_2(CH_2)_2CH(R)OH$), 1.77–1.68 (2H, m, $CH_2CH(R)OH$), 1.43–1.36 (2H, m, $CH_2CH_2CH(R)OH$).

Ynone 14

To a solution of alcohol **13** (583 mg, 1.33 mmol) in acetone (4 mL) at 0°C, Jones' reagent was added until a red color persisted for 15 min. Isopropanol was then added until a green color appeared. Water was then added and the aqueous phase was extracted three times with dichloromethane. The combined organic layers were washed with brine, dried over magnesium sulfate, filtered, and evaporated. The crude product was purified by column chromatography (30% ethyl acetate in hexane) affording alkyne **14** (512 mg, 88%); ir (neat): 3250, 3000–2840, 2100, 1770–1700, 1700–1670, 1450, 1350–1050 cm^{-1}; ^1H nmr ($CDCl_3$) δ: 3.75 (6H, s, $CH(CO_2CH_3)_2$), 3.72 (6H, s, $R_2C(CO_2CH_3)_2$), 3.58 (1H, t, J = 7.3 Hz, $CH(CO_2CH_3)_2$), 3.24 (1H, s, $C{\equiv}CH$), 2.61 (2H, t, J = 7.0 Hz, $CH_2C(O)C{\equiv}CH$), 2.22–2.19 (2H, m, CH_2CH_2CH-$(CO_2CH_3)_2$), 2.13–2.02 (6H, m, $CH_2CH(CO_2CH_3)_2$, $C{\equiv}CCH_2$-$CH_2C(CO_2CH_3)_2$), 1.92–1.85 (2H, m, $CH_2(CH_2)_2C(O)C{\equiv}CH$), 1.59–1.52 (2H, m, $CH_2CH_2C(O)C{\equiv}CH$); ms *m/e* (70 eV): 436 (M^+).

Can. J. Chem. Downloaded from www.nrcresearchpress.com by 217.78.4.112 on 09/08/12
For personal use only.

Acetylene ***16***

Acetylene **16** was synthesized using the same procedure as for the preparation of acetylene **2**, from 4-pentyn-1-ol (1.65 mL, 17.83 mmol), *p*-toluenesulfonic acid (0.03 g, 1.17 mmol), tetrahydrofuran (10 mL), and dihydropyran (3.8 mL, 41 mmol). The crude product was purified by column chromatography (10% ethyl acetate in hexane) affording **16** (2.89 g, 96%); ir (neat): 3300, 2980–2850, 1450, 1350, 1300–1000 cm^{-1}; ^1H nmr ($CDCl_3$) δ: 4.60 (1H, m, OC*H*O), 3.91–3.81 (2H, m, CH_2O), 3.54–3.43 (2H, m, CH_2O), 2.30 (2H, td, J = 7.3, 2.6 Hz CH_2C≡CH), 1.94 (1H, t, J = 2.6 Hz, C≡C*H*), 1.87–1.48 (8H, m, THPOCH$_2$CH_2, (CH_2)$_3$; ms m/e (70 eV): 176 (M^+).

Alcohol ***17***

Alcohol **17** was synthesized using the same procedure as for the preparation of alcohol **3**, from alkyne **16** (2.0 g, 11.89 mmol), tetrahydrofuran (30 mL), hexamethylphosphoramide (HMPA) (10 mL), *n*-butyllithium (1.6 M in hexane, 8.2 mL, 13.1 mmol), and oxirane (9 mL, 178.4 mmol). The crude product was purified by column chromatography (30–50% ethyl acetate in hexane) affording alcohol **17** (2.07 g, 82%); ir (neat): 3600–3200, 2980–2840, 1450, 1350, 1300–1000 cm^{-1}; ^1H nmr ($CDCl_3$) δ: 4.59 (1H, m, OC*H*O), 3.92–3.81 (2H, m, CH_2O), 3.67 (2H, q, J = 6.2 Hz, CH_2OH), 3.54–3.43 (2H, m, CH_2O), 2.42 (2H, tt, J = 6.2, 2.3 Hz, C≡CCH_2CH$_2$OH), 2.29 (2H, tt, J = 7.0, 2.3 Hz, CH_2C≡CCH$_2$CH$_2$OH), 1.98 (1H, t, J = 6.2 Hz, O*H*), 1.84–1.48 (8H, m, (CH_2)$_3$, THPOCH$_2$CH_2); ms m/e (70 eV): 211 (M^+ – H), 181 (M^+ – CH$_2$OH).

Mesylate ***18***

Mesylate **18** was synthesized using the same procedure as for the preparation of mesylate **4**, from alcohol **17** (2.05 g, 9.64 mmol), triethylamine (2 mL, 13.5 mmol), dichloromethane (32 mL), and methanesulfonyl chloride (0.9 mL, 11.6 mmol). The crude product was purified by column chromatography (30% ethyl acetate in hexane) affording mesylate **18** (2.55 g, 92%); ir (neat): 2980–2850, 1450, 1350, 1180, 1250–1000, 1000–750 cm^{-1}; ^1H nmr ($CDCl_3$) δ: 4.58 (1H, m, OC*H*O), 4.25 (2H, t, J = 6.9 Hz, CH_2OMs), 3.90–3.76 (2H, m, CH_2O), 3.54–3.41 (2H, m, CH_2O), 3.04 (3H, s, OSO$_2$CH_3), 2.61 (2H, tt, J = 6.9, 2.4 Hz, CH_2CH$_2$OMs), 2.26 (2H, tt, J = 7.1, 2.4 Hz, CH_2(CH$_2$)$_2$OTHP), 1.82–1.40 (8H, m, THPOCH$_2$CH_2), (CH_2)$_3$).

Malonate ***19***

Malonate **19** was synthesized using the same procedure as for the preparation of malonate **5**, from sodium hydride (50% in oil, 2.0 g, 42.33 mmol), *N*,*N*-dimethylformamide (172 mL), dimethyl malonate (5.0 mL, 43.05 mmol), mesylate **18** (5.0 g, 17.22 mmol), potassium iodide (2.9 g, 17.22 mmol), and tetrahydrofuran (172 mL). The crude product was purified by column chromatography (30% ethyl acetate in hexane) affording **19** (4.22 g, 75%); ir (neat): 2980–2850, 1750, 1450, 1350, 1300–1000 cm^{-1}; ^1H nmr ($CDCl_3$) δ: 4.58 (1H, m, OC*H*O), 3.86–3.71 (2H, m, CH_2O), 3.74 (6H, s, (CO$_2$CH_3)$_2$), 3.61 (1H, t, J = 7.3 Hz, C*H*(CO$_2$CH$_3$)$_2$), 3.52–3.40 (2H, m, CH_2O), 2.28–2.19 (4H, m, THPO(CH$_2$)$_2$CH_2C≡CCH_2), 2.10–2.05 (2H, m, CH_2CH(E)$_2$), 1.81–1.51 (8H, m, CH_2CH$_2$OTHP, (CH_2)$_3$); ms m/e (70 eV): 326 (M^+).

Iodide ***20***

A solution of chloropropanol (8.8 mL, 106 mmol) and sodium iodide (17 g, 117 mmol) in acetone (100 mL) was refluxed for 24 h. The mixture was cooled to room temperature and sodium thiosulfate was added to discolour the solution. Most of the solvent was evaporated and hexane was then added to precipitate the sodium chloride. The mixture was filtered on Celite. Hexane was added and the mixture was filtered and evaporated a second time. The resulting crude iodopropanol was then dissolved in dichloromethane (400 mL) and imidazole (18 g, 265 mL) was added followed by *t*-butyldimethylchlorosilane (19 g, 127 mmol). The reaction was stirred at room temperature for 2 h. Water was then added and the aqueous phase was extracted three times with dichloromethane. The combined organic layers were washed with brine, dried over magnesium sulfate, filtered, and evaporated. The crude product was purified by column chromatography (5–40% ethyl acetate in hexane) affording iodide **20** (26.96 g, 85%); ir (neat): 2980–2840, 1470, 1360, 1200–1000 cm^{-1}; ^1H nmr ($CDCl_3$) δ: 3.67 (2H, t, J = 5.7 Hz, CH_2OSi), 3.28 (2H, t, J = 6.7 Hz, CH_2I), 2.03–1.94 (2H, m, CH$_2$CH_2CH$_2$), 0.89 (9H, s, *t*-Bu), 0.07 (6H, s, (CH$_3$)$_2$Si); ms m/e (70 eV): 243 (M^+ – *t*-Bu).

Alkyne ***21***

To a suspension of sodium hydride (492 mg, 1.05 mmol) in *N*,*N*-dimethylformamide (9.75–mL), malonate **19** (3.18 g, 9.75 mmol) dissolved in tetrahydrofuran (15 mL) was added. The reaction mixture was heated at ≈50°C in a water bath to dissolve the anion formed. Iodide **20** (3.2 g, 10.7 mmol) was added at 50°C, and then the bath was removed. The mixture was stirred at room temperature for 20 h, and a saturated solution of ammonium chloride was then added. The aqueous phase was extracted three times with a mixture of diethyl ether and hexane (1:1). The combined organic layers were washed with brine, dried over magnesium sulfate, filtered, and evaporated. The crude product was purified by column chromatography (30% ethyl acetate in hexane) affording alkyne **21** (3.60 g, 74%); ir (neat): 2980–2840, 1740, 1450, 1350, 1300–1000 cm^{-1}; ^1H nmr ($CDCl_3$) δ: 4.59 (1H, m, OC*H*O), 3.87–3.70 (2H, m, CH_2O), 3.71 (6H, s, 2x CO$_2$CH_3), 3.58 (2H, t, J = 6.3 Hz, CH_2OSi), 3.49–3.43 (2H, m, CH_2O), 2.27–2.21 (2H, m, CH_2(CH$_2$)$_2$OTHP), 2.11–2.08 (4H, m, C≡CCH_2CH_2C(E)$_2$), 1.96–1.81 (2H, m, C≡CCH$_2$CH$_2$C(E)$_2$CH_2), 1.78–1.51 (8H, m, CH_2-CH$_2$OTHP, (CH_2)$_3$), 1.41–1.34 (2H, m, CH_2CH$_2$OSi), 0.88 (9H, s, *t*-Bu), 0.03 (6H, s, (CH$_3$)$_2$Si); ms m/e (70 eV): 498 (M^+), 441 (M^+ – *t*-Bu).

Alcohol ***22***

Alcohol **22** was synthesized using the same procedure as for the preparation of alcohol **8** from alkyne **21** (1.04 g, 1.98 mmol), anhydrous diethyl ether (100 mL), and magnesium bromide etherate (6.18 g, 21.66 mmol). The crude product was purified by column chromatography (30% ethyl acetate in hexane) affording alcohol **22** (1.33 g, 78%); ir (neat): 3600–3200, 2980–2850, 1450, 1350, 1300–1000 cm^{-1}; ^1H nmr ($CDCl_3$) δ: 3.75–3.70 (2H, m, CH_2OH), 3.71 (6H, s, 2× CO$_2$CH_3), 3.59 (2H, t, J = 6.2 Hz, CH_2OSi), 2.28–2.22 (2H, m, CH_2(CH$_2$)$_2$OH), 2.13–2.09 (4H, m, C≡CCH_2CH_2C(E)$_2$), 1.96–1.90 (2H, m, CH_2(CH$_2$)$_2$OSi), 1.73–1.67 (3H, m, CH_2CH$_2$O*H*), 1.40–1.34 (2H, m, CH_2CH$_2$OSi), 0.88 (9H, s, *t*-Bu), 0.03 (6H, s, (CH$_3$)$_2$Si); ms m/e (70 eV): 415 (M^+), 399 (M^+ – CH$_3$), 383 (M^+ – CH$_3$O), 357 (M^+ – *t*-Bu).

Mesylate ***23***

Mesylate **23** was synthesized using the same procedure as for the preparation of mesylate **9**, from alcohol **22** (1.38 g, 3.33 mmol), dichloromethane (20 mL), triethylamine (0.6 mL), and methanesulfonyl chloride (2.28 mL, 4.2 mmol). The crude product was purified by column chromatography (25% ethyl acetate in hexane) affording mesylate **23** (1.44 g, 94%); ir (neat): 2980–2850, 1450, 1350, 1180, 1300–1000, 1000–750 cm^{-1}; ^1H nmr ($CDCl_3$) δ: 4.33 (2H, t, J = 6.1 Hz, CH_2OMs), 3.71 (6H, s, 2× CO$_2$CH_3), 3.59 (2H, t, J = 6.2 Hz, CH_2OSi), 3.03 (3H, s, OSO$_2$CH_3), 2.35–2.27 (2H, m, CH_2(CH$_2$)$_2$OMs), 2.10 (4H, m, C≡CCH_2CH_2C(E)$_2$), 1.96–1.87 (4H, m, CH_2CH$_2$OMs, CH_2(CH$_2$)$_2$OSi), 1.45–1.30 (2H, m, CH_2CH$_2$OSi), 0.88 (9H, s, *t*-Bu), 0.04 (6H, s, (CH$_3$)$_2$Si).

Ester ***24***

Ester **24** was synthesized using the same procedure as for the preparation of ester **10**, from sodium hydride (60% in oil, 356 mg, 7.42 mmol), *N*,*N*-dimethylformamide (40 mL), dimethylmalonate (0.9 mL, 7.73 mmol), mesylate **23** (1.42 g, 3.09 mmol), potassium iodide (512 mg, 3.09 mmol), and tetrahydrofuran (40 mL). The crude product was purified by column chromatography (20% ethyl acetate in hexane) affording ester **24** (1.23 g, 77%); ir (neat): 2980–2850, 1740, 1450, 1350, 1300–

Can. J. Chem. Downloaded from www.nrcresearchpress.com by 217.78.4.112 on 09/08/12
For personal use only.

1000 cm^{-1}; ^1H nmr ($CDCl_3$) δ: 3.73 (6H, s, $CH(CO_2CH_3)_2$), 3.70 (6H, s, $R_2C(CO_2CH_3)_2$) 3.57 (2H, t, J = 6.2 Hz, CH_2OSi), 3.38 (1H, m, $CH(E)_2$), 2.18–2.02 (6H, m, $CH_2C{\equiv}CCH_2CH_2C(E)_2R$), 1.99–1.61 (4H, m, $CH_2CH(E)_2$, $CH_2(CH_2)_2OSi$), 1.60–1.33 (4H, m, CH_2CH_2OSi, $CH_2CH_2CH(E)_2$), 0.87 (9H, s, *t*-Bu), 0.03 (6H, s, $(CH_3)_2Si$).

Alcohol 25

To a solution of ester **24** (2.38 g, 4.77 mmol) and *p*-toluenesulfonic acid (1.36 g, 7.16 mmol) in tetrahydrofuran (16 mL) at 0°C, a solution of tetrabutylammonium fluoride (1 M, 3.65 mL, 3.65 mmol) was added. The mixture was stirred for 6 h, allowing the reaction to warm gradually to room temperature. A saturated solution of ammonium chloride was then added and the aqueous phase was extracted three times with diethyl ether. The combined organic layers were washed with brine, dried over magnesium sulfate, filtered, and evaporated. The crude product was purified by column chromatography (50% ethyl acetate in hexane) affording alcohol **25** (1.65 g, 83%); ir (neat): 3600–3200, 3010–2840, 1770–1700, 1450, 1350, 1300–1000 cm^{-1}; ^1H nmr ($CDCl_3$) δ: 3.74 (6H, s, $CH(CO_2CH_3)_2$), 3.72 (6H, s, $R_2C(CO_2CH_3)_2$) 3.67–3.60 (2H, m, CH_2OH), 3.38 (1H, t, J = 7.5 Hz, $CH(E)_2$), 2.18–2.11 (6H, m, $CH_2C{\equiv}CCH_2CH_2C(E)_2R$), 2.01–1.93 (4H, m, $CH_2CH(E)_2$, $CH_2(CH_2)_2OH$), 1.62–1.24 (5H, m, CH_2CH_2OH, $CH_2CH_2CH(E)_2$); ms m/e (70 eV): 397 (M^+ – OH), 383 (M^+ – OCH_3).

Aldehyde 26

Aldehyde **26** was synthesized using the same procedure as for the preparation of aldehyde **12**, from oxalyl chloride (0.12 mL, 1.33 mmol), dichloromethane (3 mL), dimethyl sulfoxide (0.19 mL, 2.66 mmol), alcohol **25** (500 mg, 1.21 mmol), dichloromethane (7 mL), and triethylamine (0.85 mL, 6.05 mmol). The crude product was purified by column chromatography (30% ethyl acetate in hexane) affording aldehyde **26** (456 mg, 91%); ir (neat): 3000–2880, 2840, 2740, 1760–1700, 1450, 1350, 1300–1000 cm^{-1}; ^1H nmr ($CDCl_3$) δ: 9.74 (1H, s, C(O)*H*), 3.74 (6H, s, $CH(CO_2CH_3)_2$), 3.72 (6H, s, $R_2C(CO_2CH_3)_2$), 3.38 (1H, t, J = 7.5 Hz, $CH(E)_2$), 2.48 (2H, t, J = 7.6 Hz, $CH_2C(O)H$), 2.25–2.11 (8H, m, $CH_2C{\equiv}CCH_2CH_2C(E)_2CH_2$), 2.02–1.93 (2H, m, $CH_2CH(E)_2$), 1.52–1.46 (2H, m, $CH_2CH_2CH(E)_2$); ms m/e (70 eV): 412 (M^+).

Alcohol 27

Alcohol **27** was synthesized using the same procedure as for the preparation of alcohol **13**, from tetrahydrofuran (3 mL), *n*-butyllithium (1.6 M in hexane, 2.75 mL, 4.4 mmol), acetylene (24.5 mL/mmol, 215 mL, 8.8 mmol), aldehyde **26** (454 mg, 1.1 mmol), and tetrahydrofuran (5 mL). The crude product was purified by column chromatography (40% ethyl acetate in hexane) affording alcohol **27** (262 mg, 54%); ir (neat): 3600–3340, 3300, 3000–2840, 1770–1700, 1450, 1350, 1300–1000 cm^{-1}; ^1H nmr ($CDCl_3$) δ: 4.42–4.31 (1H, m, C*H*-OH), 3.74 (6H, s, $CH(CO_2CH_3)_2$), 3.72 (6H, s, $R_2C(CO_2CH_3)_2$), 3.39 (1H, t, J = 7.6 Hz, $CH(E)_2$), 2.48 (1H, d, J = 2.0 Hz, C≡C*H*), 2.18–2.10 (8H, m, $CH_2C{\equiv}CCH_2(CH_2C(E)_2CH_2)$, 2.09–1.93 (3H, m, $CH_2CH(E)_2$, O*H*), 1.66–1.45 (4H, m, $CH_2CH_2CH(E)_2CH_2CH(OH)C{\equiv}CH$); ms m/e (70 eV): 439 (MH^+), 421 (M^+ – OH), 402 (M^+ – OCH_3).

Ynone 28

Ynone **28** was synthesized using the same procedure as for the preparation of ynone **14**, from alcohol **27** (252 mg, 0.574 mmol), Jones' reagent, and acetone (5 mL). The crude product was purified by column chromatography (30% ethyl acetate in hexane) affording alkyne **28** (220 mg, 88%); ir (neat): 3265, 3000–2840, 2100, 1770–1710, 1700–1680, 1450, 1350, 1300–1000 cm^{-1}; ^1H nmr ($CDCl_3$) δ: 3.74 (6H, s, $CH(CO_2CH_3)_2$), 3.73 (6H, s, $R_2C(CO_2CH_3)_2$), 3.38 (1H, t, J = 7.6 Hz, $CH(E)_2$), 3.24 (1H, s, C≡C*H*), 2.66–2.61 (2H, m, $CH_2C(O)$), 2.28–2.11 (8H, m, $CH_2C{\equiv}CCH_2CH_2C(E)_2CH_2$), 2.02–1.93 (2H, m, $CH_2CH(E)_2$), 1.52–1.46 (2H, m, $CH_2CH_2CH(E)_2$); ms m/e (70 eV): 436 (M^+), 304 (M^+ – OCH_3).

Alcohol 29

To a solution of aldehyde **26** (338 mg, 0.82 mmol) in anhydrous diethyl ether (20 mL) at −78°C, vinylmagnesium bromide (1 M in THF, 4.1 mL, 4.1 mmol) was added. The mixture was stirred for 15 min, and a saturated solution of sodium bicarbonate was added. The aqueous phase was extracted three times with diethyl ether. The combined organic layers were washed with brine, dried over magnesium sulfate, filtered, and evaporated. The crude product was purified by column chromatography (40% ethyl acetate in hexane) affording alcohol **29** (188 mg, 52%); ir (neat): 3600–3200, 3000–2840, 1760–1700, 1450, 1350 cm^{-1}; ^1H nmr ($CDCl_3$) δ: 5.84 (1H, ddd, J = 17.2, 10.4, 6.1 Hz, CH(OH)C*H*=CH_2), 5.24 (1H, d, J = 17.2 Hz, CH(OH)CH=C*H* (*cis* to alkyl group)), 5.13 (1H, d, J = 10.4 Hz, CH(OH)CH=C*H* (*trans* to alkyl group)), 4.18–4.00 (1H, m, C*H*(OH)), 3.74 (6H, s, $CH(CO_2CH_3)_2$), 3.72 (6H, s, $R_2C(CO_2CH_3)_2$), 3.39 (1H, t, J = 7.5 Hz, $CH(E)_2$), 2.19–2.09 (6H, m, $CH_2C{\equiv}CCH_2CH_2C(E)_2CH_3$), 2.09–1.90 (4H, m, $CH_2CH(E)_2$, $CH_2CH_2CH(OH)$), 1.67–1.64 (1H, O*H*), 1.58–1.38 (4H, m, $CH_2CH_2CH(E)_2$, $CH_2CH_2CH(OH)$); ms m/e (70 eV): 440 (M^+).

Enone 30

Enone **30** was synthesized using the same procedure as for the preparation of ynone **14**, from alcohol **29** (183 mg, 0.415 mmol), Jones' reagent, and acetone (5 mL). The crude product was purified by column chromatography (30% ethyl acetate in hexane) affording alkene **30** (131 mg, 72%); ir (neat): 300–2840, 1770–1700, 1700–1680, 1450, 1350, 1300–1000 cm^{-1}; ^1H nmr ($CDCl_3$) δ: 6.32 (1H, dd, J = 17.7, 10.1 Hz, C(O)-C*H*=CH_2), 6.24 (1H, dd, J = 17.7, 1.8 Hz, C(O)CH=C*H* *cis* to the ketone), 5.83 (1H, dd, J = 10.1, 1.8 Hz, C(O)CH=C*H* *trans* to the ketone), 3.74 (6H, s, $CH(CO_2CH_3)_2$), 3.72 (6H, s, $R_2C(CO_2CH_3)_2$), 3.38 (1H, t, J = 7.5 Hz, C*H*$(CO_2CH_3)_2$), 2.62–2.56 (2H, m, $CH_2(C(O))$, 2.24–2.11 (8H, m, $CH_2C{\equiv}CCH_2CH_2C(E)_2CH_2$), 2.04–1.92 (2H, m, $CH_2CH(E)_2$), 1.51–1.45 (2H, m, $CH_2CH_2CH(E)_2$); ms m/e (70 eV): 423 (M^+ – OH), 409 (M^+ – OCH_3).

Alcohol 31

Hydrogen was bubbled for 15 min in a solution of alkyne **25** (292 mg, 0.70 mmol) in ethyl acetate (10 mL) containing Lindlar's catalyst (30 mg). The mixture was stirred for 5.5 h under an hydrogen atmosphere. The mixture was then filtered on Celite and concentrated affording alkene **31** (286 mg, 98%); ir (neat): 3600–3200, 3010, 3000–2840, 1780–1680, 1450, 1350 cm^{-1}; ^1H nmr ($CDCl_3$) δ: 5.36–5.32 (2H, t, J = 4.7 Hz, C*H*=C*H*), 3.73 (6H, s, $CH(CO_2CH_3)_2$), 3.72 (6H, s, $R_2C(CO_2CH_3)_2$), 3.68–3.61 (2H, m, CH_2OH), 3.35 (1H, t, J = 7.5 Hz, C*H*$(CO_2CH_3)_2$), 2.04–1.84 (10H, m, $CH_2C(E)_2CH_2CH_2CH{=}CHCH_2CH_2CH_2CH(E)_2$), 1.71–1.65 (1H, m, O*H*), 1.48–1.25 (4H, m, CH_2CH_2OH, $CH_2CH_2CH(E)_2$); ms m/e (70 eV): 417 (MH^+).

Aldehyde 32

Aldehyde **32** was synthesized using the same procedure as for the preparation of aldehyde **12**, from oxalyl chloride (0.18 mL, 2.08 mmol), dichloromethane (5 mL), dimethyl sulfoxide (0.30 mL, 4.16 mmol), alcohol **31** (0.785 mg, 1.89 mmol), dichloromethane (11 mL), and triethylamine (1.3 mL, 9.5 mmol). The crude product was purified by column chromatography (30% ethyl acetate in hexane) affording aldehyde **32** (504 mg, 64%); ir (neat): 3010, 3000–1840, 1770–1700, 1450, 1350, 1300–1000 cm^{-1}; ^1H nmr ($CDCl_3$) δ: 9.75 (1H, s, C(O)*H*), 5.36–5.32 (2H, m, C*H*=C*H*), 3.74 (6H, s, $CH(CO_2CH_3)_2$), 3.71 (6H, s, $R_2C(CO_2CH_3)_2$), 3.35 (1H, t, J = 7.5 Hz, C*H*$(CO_2CH_3)_2$), 2.51–2.44 (2H, t, J = 7.5 Hz, $CH_2C(O)H$), 2.25–2.18 (2H, m, $CH_2CH_2C(O)H$), 2.06–1.98 (2H, m, $CH_2CH(E)_2$), 1.93–1.84 (6H, m, $RC(E)_2CH_2CH_2$-CH=CHCH_2), 1.58–1.33 (2H, m, $CH_2CH_2CH(E)_2$); ms m/e (70 eV): 415 (MH^+).

Can. J. Chem. Downloaded from www.nrcresearchpress.com by 217.78.4.112 on 09/08/12
For personal use only.

Alcohol 33

Alcohol **33** was synthesized using the same procedure as for the preparation of alcohol **13**, from tetrahydrofuran (3 mL), *n*-butyllithium (1.6 M in hexane, 1.8 mL, 2.9 mmol), acetylene (24.5 mL/mmol, 150 mL, 6.12 mmol), aldehyde **32** (301 mg, 0.726 mmol), and tetrahydrofuran (7 mL). The crude product was purified by column chromatography (40% ethyl acetate in hexane) affording alcohol **33** (294 mg, 92%); ir (neat): 3600–3200, 3300, 3010, 3000–2840, 1770–1700, 1450, 1350, 1300–1000 cm^{-1}; ^1H nmr ($CDCl_3$) δ: 5.36–5.32 (2H, m, C*H*=C*H*), 4.38 (1H, qd, *J* = 6.0, 2.1 Hz, C*H*(OH)), 3.74 (6H, s, $CH(CO_2CH_3)_2$), 3.73 (6H, s, $R_2C(CO_2CH_3)_2$), 3.35 (1H, t, *J* = 7.5 Hz, C*H*($CO_2CH_3)_2$), 2.5 (1H, d, *J* = 2.1 Hz, C≡C*H*), 2.30 (1H, d, *J* = 6.0 Hz, O*H*), 2.13–1.97 (4H, m, $CH_2CH_2CH(OH)$, $CH_2CH(E)_2$), 1.93–1.84 (6H, m, $(E)_2CCH_2CH_2CH$=CHCH_2), 1.66–1.57 (2H, $CH_2(CH(OH))$, 1.42–1.32 (2H, m, $CH_2CH_2CH(E)_2$); ms *m/e* (70 eV): 441 (MH^+).

Ynone 34

Ynone **34** was synthesized using the same procedure as for the preparation of ynone **14**, from alcohol **33** (288 mg, 0.654 mmol), Jones' reagent, and acetone (10 mL). The crude product was purified by column chromatography (30% ethyl acetate in hexane) affording alkyne **34** (219 mg, 76%); ir (neat): 3280, 3010, 3000–2840, 2100, 1770–1700, 1680, 1450, 1350, 1300–1000 cm^{-1}; ^1H nmr ($CDCl_3$) δ: 5.34–5.30 (2H, m, C*H*=C*H*), 3.73 (12H, s, 2× $(CO_2CH_3)_2$), 3.35 (1H, t, *J* = 7.5 Hz, C*H*($CO_2CH_3)_2$), 3.25 (1H, s, C≡C*H*), 2.66–2.59 (2H, m, $CH_2C(O)C$≡CH), 2.28–2.21 (2H, m, $CH_2CH_2C(O)C$≡CH), 2.03–1.90 (2H, m, $CH_2CH(CO_2CH_3)_2$), 1.98–1.84 (6H, m, $(E)_2CH_2CH_2CH$=CHCH_2), 1.56–1.32 (2H, m, $CH_2CH_2CH(CO_2CH_3)_2$); ms *m/e* (70 eV): 439 (MH^+).

Alcohol 35

To a solution of aldehyde **32** (190 mg, 0.458 mmol) in anhydrous diethyl ether (2 mL) at −78°C, was added vinylmagnesium bromide (1 M in THF, 4.6 mL, 4.6 mmol). The mixture was stirred for 20 min, and a saturated solution of ammonium chloride was added. The aqueous phase was extracted three times with diethyl ether. The combined organic layers were washed with brine, dried over magnesium sulfate, filtered, and evaporated. The crude product was purified by column chromatography (40% ethyl acetate in hexane) affording alcohol **35** (120 mg, 59%); ir (neat): 3600–3200, 3010, 3000–2840, 1770–1700, 1450, 1350, 1300–1000 cm^{-1}; ^1H nmr ($CDCl_3$) δ: 5.85 (1H, ddd, *J* = 17.2 10.4, 6.1 Hz, CH_2=C*H*CH(OH)), 5.36–5.32 (2H, m, C*H*=C*H*), 5.25 (1H, dt, *J* = 17.2, 1.4 Hz, C*H*=CHCH(OH) *cis* to alkyl group), 5.13 (1H, dt, *J* = 10.4, 1.3 Hz, C*H*=CHCH(OH) *trans* to alkyl group), 4.15–4.05 (1H, m, CH_2=CH-C*H*(OH)), 3.73 (6H, s, $CH(CO_2CH_3)_2$), 3.72 (6H, s, $R_2C(CO_2CH_3)_2$), 3.38 (1H, t, *J* = 7.6 Hz, C*H*($E)_2$), 2.08–2.02 (4H, m, $CH_2CH_2CH(OH)$, $CH_2CH(E)_2$), 1.99–1.79 (6H, m, $(E)_2CH_2CH_2CH$=CHCH_2), 1.47–1.32 (5H, m, $CH_2CH_2CH(E)_2$, $CH_2CH(OH)$).

Enone 36

Enone **36** was synthesized using the same procedure as for the preparation of ynone **14**, from alcohol **35** (116 mg, 0.262 mmol), Jones' reagent, and acetone (10 mL). The crude product was purified by column chromatography (30% ethyl acetate in hexane) affording alkene **36** (83 mg, 72%); ir (neat): 3110, 3000–2840, 1770–1700, 1690, 1620, 1450, 1350, 1300–1000, 900 cm^{-1}; ^1H nmr ($CDCl_3$) δ: 6.35 (1H, dd, *J* = 17.7, 9.8 Hz, C(O)C*H*=CH_2), 6.22 (1H, dd, *J* = 17.7, 1.8 Hz, C(O)CH=C*H* *cis* to the ketone), 5.84 (1H, dd, *J* = 9.8, 1.8 Hz, C(O)CH=C*H* *trans* to the ketone), 5.36–5.30 (2H, m, RC*H*=C*H*R), 3.73 (6H, s, $CH(CO_2CH_3)_2$), 3.72 (6H, s, $R_2CO_2CH_3)_2$), 3.35 (1H, t, *J* = 7.5 Hz, C*H*($CO_2CH_3)_2$), 2.63–2.56 (2H, m, $CH_2C(O)$). 2.24–2.19 (2H, m, $CH_2CHC(O)$), 2.06–2.00 (2H, m, $CH_2CH(CO_2CH_3)_2$), 1.98–1.84 (6H, m, CH_2CH_2CH=CHC$H_2CH_2CH_2CH(CO_2CH_3)_2$), 1.57–1.32 (2H, m, $CH_2CH_2CH(CO_2CH_3)_2$); ms *m/e* (70 eV): 441 (MH^+).

Macrocycle 37 (General procedure)

Ynone **14** (203 mg, 0.466 mmol) dissolved in acetonitrile (30 mL) was added slowly over 2.5 h, using a syringe pump, to a suspension of cesium carbonate (151 mg, 0.466 mmol) in acetonitrile (200 mL). When the addition was completed, the mixture was stirred for another 30 min. The mixture was then filtered on Celite and evaporated. The crude product was purified by column chromatography (30% ethyl acetate in hexane) affording macrocycle **37** as a mixture of *cis* and *trans* olefin isomers (88:12) (184 mg, 90%); ir ($CHCl_3$): 3010, 2900, 1770–1700, 1690, 1620, 1450, 1300–150 cm^{-1}; ^1H nmr ($CDCl_3$) δ: (for numbering see Scheme 5) *cis*: 6.74 (1H, d, *J* = 12.3 Hz, 3) 6.46 (1H, d, 12.3 Hz, 2), 3.77 (6H, s, 2× CO_2CH_3), 3.70 (6H, s, 2× CO_2CH_3), *trans*: 7.32 (1H, d, *J* = 16.9 Hz, 3), 6.00 (1H, d, *J* = 16.9 Hz, 2) 3.74 (6H, s, 2× CO_2CH_3), 3.71 (6H, s, 2× CO_2CH_3), *cis* and *trans*: 2.50 (2H, t, *J* = 2.5 Hz, $CH_2C(O)C$=C), 2.43 (2H, t, *J* = 6.7 Hz, $CH_2CH_2C(O)CH$=CH)), 2.19–2.02 (8H, m, CH_2-CH_2C≡CC H_2CH_2), 1.64–1.21 (2H, m, $CH_2CH_2C(O)CH$=CH); ^{13}C nmr ($CDCl_3$) δ: 201.9 (enone C=O, 1), 171.0 and 169.8 (esters C=O, 15, 17, 19, 21), 140.4 (*C*H=CH, 13), 128.7 (*C*H=CH, 14), 80.6 and 79.9 (*C*≡*C*, 8 and 9), 58.7 and 58.4 (5 and 12), 53.0 and 52.4 (16, 18, 20, 22), 43.6 (CH_2C=O, 2), 31.7 and 31.6 (6 and 11), 29.6 (4), 20.2 (3), 14.4 and 14.2 (7 and 10). Exact Mass (M^+) calcd.: 436.1733; found: 436.1728.

Macrocycle 38

Macrocycle **38** was synthesized using the general procedure for macrocyclization from ynone **28** (216 mg, 0.495 mmol) in acetonitrile (30 mL), cesium carbonate (161 mg, 0.495 mmol), and acetonitrile (220 mL). The crude product was purified by column chromatography (30% ethyl acetate in hexane) affording macrocycle **38** as a mixture (87:13) of isomers *cis* and *trans* (104 mg, 48%); ir ($CHCl_3$): 3010, 1740, 1700, 1450, 1300–1180 cm^{-1}; ^1H nmr ($CDCl_3$) δ: 7.38 (1H, d, *J* = 16.9 Hz, 3 *trans*), 6.50 (1H, d, *J* = 16.9 Hz, 2 *trans*), 6.74 (1H, d, *J* = 12.3 Hz, 3 *cis*), 6.36 (1H, d, *J* = 12.3 Hz, 2 *cis*), 3.76(6H, s, $(CO_2CH_3)_2C(R)CH$=CH, 15), (6H, s, $R_2C(CO_2CH_3)_2$, 16), 2.53–2.49 (2H, m, 10), 2.43–2.39 (2H, m, 7), 2.27–2.09 (8H, m, 5, 11, 13, 14), 1.30–1.20 (2H, m, 6); ^1H nmr (C_6D_6) δ: 7.87 (1H, d, *J* = 16.9 Hz, 3 *trans*), 6.87 (1H, d, *J* = 12.3 Hz, 3 *cis*), 6.70 (1H, d, *J* = 16.9 Hz, 2 *trans*), 5.80 (1H, d, 12.3 Hz, 2 *cis*), 3.42 (6H, s, $(CO_2CH_3)_2$ *cis*), 3.24 (6H, s, $(CO_2CH_3)_2$ *trans*), 3.21 (6H, s, $(CO_2CH_3)_2$ *cis*), 3.20 (6H, s, $(CO_2CH_3)_2$ *trans*), 2.72–1.80 (12H, m, not interpretable), 1.20–1.06 (2H, m, methylene 6). Exact Mass (M^+) calcd.: 436.1730; found: 436.1733.

Macrocycle 39

Macrocycle **39** was synthesized using the general procedure for macrocyclization, from enone **30** (126 mg, 0.287 mmol) in acetonitrile (30 mL), cesium carbonate (94 mg, 0.287 mmol), and acetonitrile (113 mL). The crude product was purified by column chromatography (30% ethyl acetate in hexane) affording macrocycle **39** (104 mg, 82%); ir ($CHCl_3$): 3010, 2880, 1750–1710, 1450, 1300–1000 cm^{-1}; ^1H nmr ($CDCl_3$) δ: 3.71 (12H, s, esters), 2.46 (4H, s, 5, 6), 2.45–2.30 (4H, m, 2, 14), 1.84–1.78 (2H, m, 9), 1.60–1.17 (2H, m, 10); ^1H nmr (C_6D_6) δ: 3.39 (6H, s, $(CO_2CH_3)_2$), 3.33 (6H, s, $CO_2CH_3)_2$), 3.00–2.17 (14H, m, not interpretable), 2.03–1.98 (2H, m, 9), 1.33–1.30 (2H, m, 10). Exact Mass (M^+) calcd.: 438.1890; found: 438.1886.

Macrocycle 40

Macrocycle **40** was synthesized using the general procedure for macrocyclization, from ynone **34** (216 mg, 0.493 mmol) in acetonitrile (30 mL), cesium carbonate (161 mg, 0.493 mmol), and acetonitrile (215 mL). The crude product was purified by column chromatography (30% ethyl acetate in hexane) affording macrocycle **40** as a mixture (20:80) of *cis* and *trans* isomers (98 mg, 45%); ir ($CHCl_3$): 3010, 2860, 1700–1680, 1655, 1450, 1300–1000 cm^{-1}; ^1H nmr ($CDCl_3$) δ: *cis*: 6.62 (1H, d, *J* = 12.8 Hz, C*H*=CHC(O)), 6.39 (1H, d, *J* = 12.8 Hz, CH=C*HC*(O)), 3.74 (6H, s, CH=CHC($CO_2CH_3)_2$), 3.72 (6H, s, $CH_2C(CO_2CH_3)_2CH_2$),

trans: 7.33 (1H, d, J = 17.0 Hz, CH=CHC(O)), 5.99 (1H, d, J = 17.0 Hz, CH=CH_2C(O)), 3.78 (6H, CH=CHC(CO_2CH_3)$_2$), 3.73 (6H, CH_2C(CO_2CH_3)$_2$$CH_2$), *cis* and *trans*: 2.55–2.41 (2H, m, CH_2C(O)CH=CH), 2.20–1.87 (6H, m, C(E)$_2$$CH_2$$CH_2$CH=CH-$CH_2$), 1.44–1.35 (2H, m, $CH_2$$CH_2$C(E)$_2$CH=CHC(O)); ^{1}H nmr ($C_6D_6$) δ: 7.62 (1H, d, J = 16.4 Hz, 13 *trans*), 6.68 (1H, d, J = 12.6 Hz, 13 *cis*), 6.25 (1H, d, J = 12.6 Hz, 14 *cis*), 5.74 (1H, d, J = 16.4 Hz, 14 *trans*), 5.35–5.25 (2H, m, 7 and 8), 3.25 (6H, s, esters), 3.24 (6H, s, esters), 2.50–2.40 (2H, m, 2), 2.32–2.20 (4H, m, 3 and 11), 2.12–2.01 (2H, m, 5), 1.94–1.82 (2H, m, 6), 1.82–1.72 (2H, m, 9), 1.43–1.30 (2H, m, 10). Exact Mass (M^+) calcd.: 438.1890; found: 438.1886.

Macrocycle ***41***

Macrocycle **41** was synthesized using the general procedure for macrocyclization, from enone **36** (80 mg, 0.181 mmol) in acetonitrile (30 mL), cesium carbonate (59 mg, 0.181 mmol), and acetonitrile (60 mL). The crude product was purified by column chromatography (30% ethyl acetate in hexane) affording macrocycle **41** (61 mg, 76%); ir ($CHCl_3$): 3010, 2880, 1730, 1450, 1270–1170 cm^{-1}; ^{1}H nmr ($CDCl_3$) δ: 5.47–5.40 (2H, m, CH=CH), 3.73 (6H, s, (CO_2CH_3)$_2$), 3.72 (6H, s, (CO_2CH_3)$_2$), 2.30 (8H, s, $CH_2$$CH_2$C(O)$CH_2$$CH_2$), 2.05–1.78 (8H, m, R(E)$_2$C$CH_2$$CH_2$CH=CH$CH_2$$CH_2$$CH_2$C(E)$_2$R), 1.29–1.15 (2H, CH=CHCH$_2$$CH_2$$CH_2$-C(E)$_2$R); ^{1}H nmr ($C_6D_6$) δ: 5.36–5.30 (2H, m, 7 and 8), 3.28 (6H, s, esters), 3.27 (6H, esters), 2.55–2.48 (2H, m, 14), 2.48–2.40 (2H, m, 2), 2.16–2.10 (2H, m, 13), 2.10–2.02 (4H, m, 3 and 5), 1.98–1.80 (4H, m, 6 and 11), 1.80–1.71 (2H, m, 9), 1.30–1.14 (2H, m, 10). Exact Mass (M^+) calcd.: 440.2046; found: 440.2043.

1. G. Berthiaume, J.-F. Lavallée, and P. Deslongchamps. Tetrahedron Lett. **27**, 5451 (1986).
2. J.-F. Lavallée, G. Berthiaume, P. Deslongchamps, and F. Grein. Tetrahedron Lett. **27**, 5455 (1986).
3. P. Deslongchamps and B. L. Roy. Can. J. Chem. **64**, 2068 (1986).
4. A. K. Mandal, N. R. Soni, and K. R. Ratman. Synthesis, **3**, 274 (1985).
5. S. Kim and J. H. Park. Tetrahedron Lett. **28**, 439 (1987).
6. A. J. Mancuso, S.-L. Huang, and D. Swern. J. Org. Chem. **43**, 2480 (1978).
7. K. E. Harding, L. M. May, and K. F. Dick. J. Org. Chem. **40**, 1664 (1975).
8. J.-F. Lavallée. Ph.D. Thesis, Université de Sherbrooke. August 1988.

Can. J. Chem. Downloaded from www.nrcresearchpress.com by 217.78.4.112 on 09/08/12
For personal use only.

β-Enolization in α-phenyl-α,α′,α′-trimethylcycloalkanones[1]

WENDY SIFTON, J. B. STOTHERS, AND SHIRLEY E. THOMAS
Department of Chemistry, University of Western Ontario, London, Ont., Canada N6A 5B7

Received August 16, 1991

This paper is dedicated to Professor Zdenek (Denny) Valenta on the occasion of his 65th birthday

WENDY SIFTON, J. B. STOTHERS, and SHIRLEY E. THOMAS. Can. J. Chem. **70**, 1274 (1992).

Ring expansion through β-proton abstraction from α-methyl groups has been observed for the α-phenyl-α,α′,α′-trimethyl derivatives of cyclopentanone and cyclohexanone upon treatment with *t*-BuO⁻/*t*-BuOH/185°C. This contrasts with the lack of rearrangement found for the α,α,α′,α′-tetramethyl derivatives but is analogous to the behavior of some α-phenyl acyclic ketones. However, this process is reversible in the cyclic systems, but irreversible in the acyclic cases. For all of these α-phenyl substituted ketones, rearrangement is in competition with Haller–Bauer type cleavage. In the cyclic systems, a minor process was observed whereby some of the ring-expanded product is reduced to the corresponding secondary alcohol but there was no evidence of rearrangement through γ-enolate formation involving phenyl proton abstraction, which is a minor process in the α-phenyl acyclic systems.

WENDY SIFTON, J. B. STOTHERS et SHIRLEY E. THOMAS. Can. J. Chem. **70**, 1274 (1992).

Lors du traitement des dérivés α-phényl-α,α′,α′-triméthylés de la cyclopentanone et de la cyclohexanone par du *t*-BuO⁻/*t*-BuOH/185°C, on a observé une extension de cycle qui a été initiée par l'abstraction d'un proton-β des groupes méthyles-α. Ce comportement diffère de celui observé avec les dérivés α,α,α′,α′-tétraméthylés qui ne donnent pas de transpositions; il est toutefois analogue à celui observé avec quelques cétones acycliques portant un groupe α-phényle. Ce processus est toutefois réversible en série cyclique et irréversible dans les composés acycliques. Pour toutes ces cétones substituées par un groupe phényle, la transposition est en compétition avec un clivage du type de Haller–Bauer. Dans les systèmes cycliques, on a observé un processus mineur par lequel une partie du produit résultant de l'extension de cycle est réduit en alcool correspondant; on n'a toutefois pas de données suggérant qu'une transposition s'effectue par le biais de la formation d'un γ-énolate impliquant l'abstraction d'un proton d'un phényle; cette réaction est un processus mineur dans les systèmes acycliques portant un phényle en α.

[Traduit par la rédaction]

Can. J. Chem. Downloaded from www.nrcresearchpress.com by 217.78.4.112 on 09/08/12
For personal use only.

Introduction

Rearrangements of several acyclic and polycyclic monoketones occur by homoenolization through proton abstraction from centres other than the α-carbons, generally from β-carbons via β-enolates (1). Competition with α-enolization has been blocked, in most cases, through α-methyl substitution and (or) structurally, such that only anti-Bredt enolates could form. In several polycyclic examples, rearrangement via β-enolization at the α-methyl carbons was not observed, although, in many cases, it was shown that these sites undergo H/D exchange. In contrast, chain extension occurred in acyclic monoketones through β-enolization at the α-methyl carbons (2).Furthermore, this rearrangement is accelerated by the presence of α-phenyl groups, presumably because of the stability of the benzylic carbanion generated from the putative β-enolate **1** formed via methyl proton abstraction, i.e., cleavage *b* leading to the chain-extended isomer. Evidence supporting cyclopropoxide species as intermediates in the α-methyl exchange process for cyclic systems has been presented (3).

While the only process observed for the aliphatic examples was slow conversion to the chain-extended ketones, the rearrangement of the α-phenyl systems was accompanied by Haller-Bauer type cleavage and, as a minor process, a 1,3-acyl shift from alkyl to aryl carbon. Examination of α,α,α′,α′-tetramethylcycloalkanones had shown earlier that the ketones with 5- to 8-membered rings are stable under typical homoenolization conditions, exhibiting H/D exchange at the methyl carbons with no evidence of isomerization (4). It became of interest, therefore, to examine derivatives in which one methyl is replaced with a phenyl group. The behavior of two examples contrasted sharply with that found for the tetramethyl analogs and differed significantly from that for acyclic α-phenyl ketones; the results of this study are described in this paper.

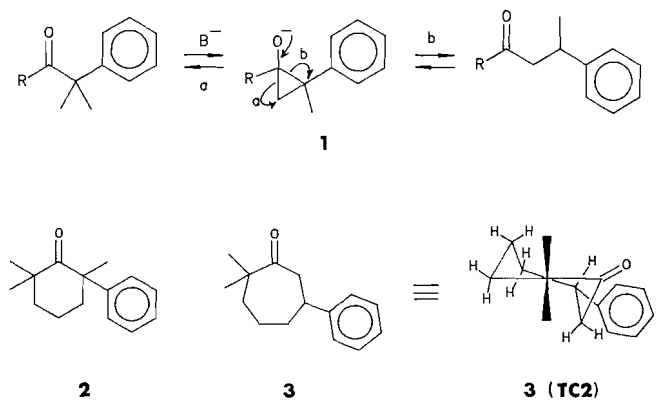

Results and discussion

Homoenolization experiments

The initial ketone selected for examination was 2-phenyl-2,6,6-trimethylcyclohexanone (**2**), which was readily prepared from commercially available 2-phenylcyclohexanone. Following our usual procedures (5), **2** was dissolved in anhydrous *t*-BuO⁻/*t*-BuOH to give a solution 0.25 M in ketone and 1.0 M in base. Aliquots of this solution were placed in dry Pyrex tubes under nitrogen, degassed, and sealed un-

[1]Part 143 in ^{13}Cmr studies. For Part 142 see ref. 2.

TABLE 1. Composition[a] of the product mixtures from **2**

Time (h)	Neutral fraction[b]			Acid fraction
	2	**3**	**8**	**12**
24	47	15	<2	30
48	31	16	<4	46
96	22	18	5	52

[a]Given as the proportion, on a % molar basis, of the isolated material.

[b]Estimated by GLC analysis on a SE-30 column, estimated precision ±2%.

der vacuum before heating at 185°C in an oil bath for various times. After cooling, the tube contents were diluted with brine and the neutral product isolated by ether extraction. The aqueous phase was acidified and extracted with ether to obtain any acidic product. Analysis by gas–liquid chromatography (GLC) showed that the neutral extract contained one new major component **3**, in addition to the initial ketone, together with small amounts of other material. The proportion of **3** in the neutral fraction slowly increased with reaction time: 24%, 24 h; 32%, 48 h; 40%, 96 h; but larger quantities of an acidic product were formed, exceeding 50% of the total product after 96 h (Table 1). The latter was found to be a single acid by NMR examination.

Flash chromatography of the neutral fraction furnished pure samples of component **3**. Strong carbonyl absorption at 1701 cm^{-1} and δ_C 216.6 indicated that it was a ketone, which was shown to be isomeric with **2** by precise mass measurement. NMR data, from ^1H, ^{13}C, and $^{13}C\{^1H\}$ COSY spectra, readily revealed its structure. Most notably, there were only two methyl absorptions and one quaternary carbon; a methyl and a quaternary carbon had been converted to methylene and methine carbons, consistent with ring expansion of **2** to a cycloheptanone system. Furthermore, the 2-methyl carbon of **2** must be involved in the generation of the new ketone because the *gem*-dimethyl unit was retained in the new ketone. The proton spectrum contained two sharp 3-proton singlets (δ_H 1.12, 1.13) and the long-range $^{13}C\{^1H\}$ COSY spectrum revealed that these methyl groups are bonded to the quaternary carbon, δ_C 47.8. It follows that the new ketone has structure **3**.

The ^1H spectrum of **3** clearly shows that it strongly favors a single conformation with the 3-phenyl group presumably serving as an effective "anchor." Conformational analysis of some dimethylated cycloheptanones through low-temperature ^1H studies and theoretical calculations led St-Jacqueus *et al.* (6) to deduce that these ketones exhibit a strong preference for twist-chair conformations with the carbonyl group at the "TC-2" position. The ^1HMR data for **3** are entirely consistent with this conclusion, indicating that **3(TC-2)** is the favored form.

The lowest field methylene protons at δ 2.43 (ddd, J = 10.5, 2.0, 1.5 Hz) and 3.20 (dd, J = 10.5, 12.1 Hz) exhibit geminal coupling comparable to that found for the α-methylene protons of 2,2-dimethylcycycloheptanone at low temperature, J = 10.4 Hz (6). This is clearly indicative of the orientation of the 2-methylene protons relative to the carbonyl group in **3(TC-2)**. The less shielded of these protons is strongly coupled (J = 12.1 Hz) with the 3-methinyl proton at δ 2.73 to which its partner is only weakly coupled (J = 2.0 Hz). The remaining coupling for the 2-proton at δ 2.43 arises from long-range interaction with the 4-methylene proton at δ 2.01; 1.5 Hz is a typical value for a four-bond coupling through a planar W pathway. The H-3 pattern contains another 12-Hz coupling to the other 4-methylene proton, δ 1.60. The latter multiplet has two more 12-Hz couplings: one with its 4-methylene partner (δ 2.01) and the second with one of the 5-protons, δ 1.37. Each of the protons at δ 3.20 (H-2), 2.73 (H-3), 1.60 (H-4), and 1.37 (H-5) exhibits vicinal antiperiplanar couplings of 12 Hz and, thus, is "axial." Their "equatorial" counterparts appear at δ 2.43 (H-2), 2.01 (H-4), and 1.8_5 (H-5), with the latter partially obscured by the 6-methylene pattern centred near δ 1.8 that could not be analyzed. These data neatly fit the **3(TC-2)** conformer; the NMR data are collected in Table 2.

The isomerization of **2** → **3** must involve proton abstraction leading to the intermediate β-enolate **4**, or its equivalent, which can suffer cleavage in two ways: path *a*, to regenerate **2**, or path *b*, to form a benzylic carbanion, protonation of which furnishes **3** (see Scheme 1). There was no evidence of products arising from proton abstraction from either of the 6-methyl sites that would give rise to **5** and lead to the isomeric cycyloheptanones **6**.

Proton abstraction from C-3 in **2** could produce β-enolate **7** whose cleavage to the benzylic anion would generate **8**. Analysis of neutral fractions from the longer reaction times by GLC revealed a small peak with a retention time slightly longer than that of **2**, but we were unable to isolate pure samples of this component free from **2**. The ^{13}CMR spectra of mixtures with **2**, however contained two new carbonyl signals at δ 223.3 and 223.1; these are indicative of a cyclopentanone derivative, present as a pair of diastereomers. There were two sets of eight sp^3 carbon signals, each arising from one quaternary, two methine, two methylene, and three methyl sites, as well as signals for two slightly different phenyl groups. The relative intensities of these two sets of signals were found to be 60:40. These data constituted strong evidence for the formation of **8**, as a diastereomeric mixture, though β-enolate **7** (Scheme 1).

The diastereomeric mixture **8** was prepared from 2,2-dimethylcyclopentanone by α-alkylation with 1-phenylethyl bromide and gave rise to the same two sets of ^{13}C signals in the same ratio as that found for the homoenolization product. GLC analysis of this sample showed two closely spaced peaks, one having the same retention time as **2**. Small samples of each of the two diastereomers were obtained by preparative GLC, with each containing ca. 20% of the other form.

From these results it is evident that the α-phenyl group in **2** biases cleavage of β-enolates **4** and **7** to generate the benzylic anions that lead to skeletal rearrangement. This is in sharp contrast to the behavior of 2,2,6,6-tetramethylcyclohexanone, which is virtually unchanged after treatment under the same conditions for 375 h (4).

At the outset, we recognized that the α-phenyl group in **2** could render cleavage of the Haller–Bauer type through **9** to be a major competitive process. It had been found that ketones **10** and **11** (R = ethyl, dimethylallyl, benzyl) undergo Haller–Bauer cleavage exclusively upon treatment with *t*-BuO^-/*t*-BuOH (7, 8). However, the more hindered carbonyl group in **2** could reduce its susceptibility to attack by

Can. J. Chem. Downloaded from www.nrcresearchpress.com by 217.78.4.112 on 09/08/12
For personal use only.

TABLE 2. NMR data for **3**[a]

Position	δ_H [J, Hz]	δ_C	Position	δ_H	δ_C
1	—	216.6	6	1.8	39.3
2	3.20 (dd, 10.5, 12.1)	46.5	7	—	47.8
	2.43 (ddd, 1.5, 2, 10.5)		CH_3	1.12	23.3
3	2.73 (dddd, 2, 4, 12, 12)	44.8		1.13	27.8
4	1.60 (dddd, 2, 13, 13, 13)	39.9	C_6H_5	7.15–7.35	126.3
	2.01 ("bd", 13)				126.5 (2)
5	1.37 (m, $\nu_{1/2}$ 42 Hz)	24.1			128.5 (2)
	1.8_5 (m)				146.6

[a]In ppm from TMS in $CDCl_3$ solution.

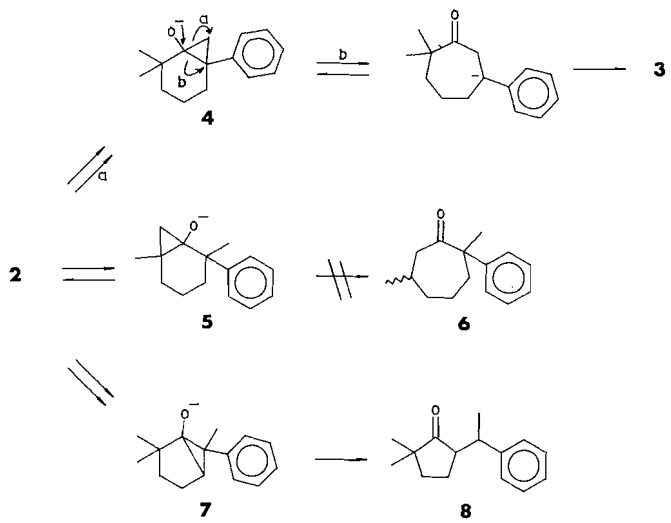

SCHEME 1

base because "ideally, the site of Haller–Bauer cleavage should not be subjected to any element of serious steric compression" (8) and this was found to be the case. Earlier studies have shown that the *tert*-butyl esters formed in Haller–Bauer cleavage of species such as **9** do not survive under the reaction conditions and the corresponding carboxylic acids are generated. Thus, the acidic product must be examined.

The acidic fraction contained one component, $C_{15}H_{22}O_2$, by precise mass measurement, having structure **12** according to its NMR spectra. The ^{1}HMR spectrum contained two methyl signals, δ 1.15 (s, 6H) and 1.24 (d, J = 6.9 Hz), with the latter coupled to one proton at δ 2.72 (m, 1H), methylene patterns at δ 1.2–1.3 (2H) and 1.5–1.7 (4H), and aryl absorption at δ 7.15–7.35 (5H). The ^{13}C spectrum contained 13 signals: CH_3, 22.3, 24.8, 25.0; CH_2, 22.9, 38.7, 40.4; CH, 39.6; C, 42.1; aryl CH, 125.9, 126.9 (2), 128.3 (2); aryl C, 147.7; C=O, 185.1.

From the results of these experiments with **2**, it became clear that its isomerization to **3** by β-enolization is significantly slower than Haller–Bauer cleavage whereas these two processes exhibit comparable rates in acyclic α-phenyl systems (2).

In a second series of experiments, the behavior of the 5-ring analog, 2-phenyl-2,5,5-trimethylcyclopentanone (**13**), was examined under the same conditions. Reaction of phenyl magnesium bromide with 2-chlorocyclopentanone gave 2-phenylcyclopentanone, which was methylated with MeI/$NaNH_2$ to furnish **13** in 86% yield.

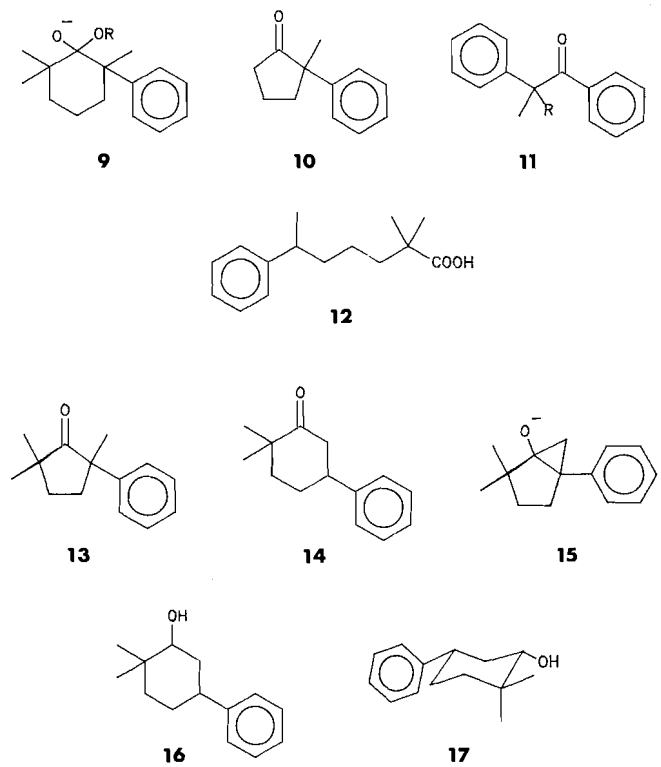

Upon treatment with t-BuO^-/t-BuOH in sealed tubes at 185°C, ketone **13** was found to be much more reactive than **2**. After 3 h, more than 50% of the starting material had reacted to afford a neutral fraction containing two new components, in addition to **13**, and a one-component acidic fraction.

The major new neutral compound, $C_{14}H_{18}O$ by precise mass measurement, exhibited strong carbonyl absorption at 1709 cm^{-1} and δ_C 215.2, indicative of a cyclohexanone derivative. The ^{13}CMR spectrum contained signals for two methyl (δ_C 25.2_0, 25.1_8), three methylene (29.3, 39.9, 45.3), one methine (45.4), a quaternary (44.6), and the carbons of a phenyl group (126.6 (2), 126.7, 128.7 (2), 144.4). Clearly, a methyl/quaternary pair of carbons has become a methylene/methine pair. The two methyl groups gave singlets in the ^{1}HMR spectrum (δ 1.05, 1.19) and, from the ^{13}C{^{1}H} COSY spectrum, are bonded to the quaternary carbon. Thus,

Can. J. Chem. Downloaded from www.nrcresearchpress.com by 217.78.4.112 on 09/08/12
For personal use only.

TABLE 3. Composition[a] of the product mixtures from **13**

Time (h)	Neutral fraction[b] 13	14	16	Acid fraction 18
3	45	9	7	27
6	33	20	9	33
9	17	27	10	38
12	11	34	10	39
24	6	27	10	48

[a]Given as the proportion, on a % molar basis, of the isolated material.
[b]Estimated by GLC analysis on a SE-30 column, estimated precision ±2%.

the new ketone is **14**, formed through β-enolate **15**, or an equivalent species, by proton abstraction from the 2-methyl group of **13**.

The second neutral compound was found to have the molecular formula $C_{14}H_{20}O$ by precise mass measurement and exhibited strong, broad hydroxyl absorption at 3420 cm^{-1}. In addition to a carbinyl signal at δ_C 77.7, the ^{13}C spectrum contained quaternary (35.1), methine (43.5), methylene (29.6, 38.0, 39.2), methyl (17.6, 29.0), and phenyl signals (126.2, 126.8 (2), 128.4 (2), 146.1). These data indicate that **14** is reduced to the corresponding alcohol **16**. The major features of the ^1H spectrum included two methyl singlets (δ 0.89, 0.98), a 4-line pattern at δ 3.45 (1H, J = 4.3, 11.4 Hz), and a 1-proton multiplet centred at δ 2.6 with a half-width of ca. 30 Hz. These two multiplets are readily assigned to axial protons on C-1 and -3, respectively, thus, the hydroxyl and phenyl groups are equatorial as in **17**.

The sole component in the acid fraction was readily shown to be **18** from its NMR spectra. The ^1HMR spectrum contained two methyl singlets (δ 1.13, 1.15) and a methyl doublet (δ 1.23, J = 6.9 Hz), with the latter coupled to a 1-proton multiplet at δ 2.60, as well as methylene (δ 1.30–1.65, m, 4H) and phenyl absorption (δ 7.14–7.34, 5H). Its ^{13}C spectrum exhibited signals for three methyl (δ 22.6, 24.7, 25.2), two methylene (33.2, 38.6), one methine (40.4), a quaternary (42.0), and six phenyl carbons (126.0, 127.0 (2), 128.4 (2), 147.3) as well as a carboxyl signal (184.5).

The distribution of the components in the product mixtures from **13** as a function of time is given in Table 3, from which it is apparent that the proportion of **14** passes through a maximum around 12 h and then diminishes. This finding indicated that the stability of **3** and **14** under homoenolization conditions should also be studied. To this end, the rearranged ketones were treated with t-BuO^-/t-BuOH in sealed tubes at 185°C for various times and the product mixtures analyzed.

The results of these two series of experiments are summarized in Table 4 from which it is clear that **3** and **14** are not stable under the reaction conditions. Within 24 h, almost 50% of **3** had been consumed primarily through isomerization to **2** and its cleavage to acid **12**; traces of **8** were also present. In addition, small amounts of a fourth neutral component were detected by GLC in each of the neutral products and the ^{13}C spectra contained a set of weak peaks, one of which appeared at δ_c 79.9, indicative of the presence of an alcohol. The retention time of this component coincided with that of a small signal in the gas chromatograms

TABLE 4. Composition[a] of the product mixtures from **3** and **14**

(*a*) From **3**:

Time (h)	3	2	8	19	12
3	86	6	—	4	Trace
6	67	8	—	6	14
24	52	18	Trace	7	19
48	31	27	<2	4	28

(*b*) From **14**:

Time (h)	14	16	18	Other[b]
3	88	7	2	<2
6	66	9	13	3
24	48	15	26	7
48	24	18	49	10

[a]Given as the proportion, on a % molar basis, of the isolated material with the relative amounts of the neutral products determined by GLC analysis on a SE-30 column, estimated precision ±2%.
[b]Unidentified neutral components.

of the neutral fractions obtained by homoenolization of **2**, indicating that trace amounts were present therein. To confirm this point, the neutral product mixtures from several experiments with **2** were combined and the components separated by column chromatography on alumina. This procedure provided a sample of the desired material as well as a clean sample of **8**, establishing the formation of both products in the homoenolization of **2**. The ^{13}C spectrum of the new component, however, revealed it to be a 2:1 mixture of isomeric alcohols; the formula was found to be $C_{15}H_{22}O$ by precise mass measurement. Thus, these were tentatively identified as **19**.

Ketone **14** was found to react at a rate comparable to that of **3**. The product mixtures contained **14**, alcohol **16**, acid **18**, and small amounts of unidentified material, but none of the isomeric ketone **13** was detected. Clearly, the cleavage of **13** to **18** is sufficiently rapid to destroy **13** as it is formed from **14**.

The reversible formation of **3** and **14** contrasts sharply with the findings for the acyclic cases. For example, **20** is isomerized unidirectionally to **21**, which, in turn, is converted to **22** under the same reaction conditions (2). These results showed that cleavage of **1** (R = $-C(CH_3)_2C_6H_5$ and $-CH_2CH(CH_3)C_6H_5$) proceeded irreversibly through path *b*. In the cyclic systems, however, the corresponding intermediates **4** and **15** are generated readily from the isomeric pairs **2**/**3** and **13**/**14**, respectively, presumably because the ring systems impose conformational constraints that favor formation of these intermediates.

To confirm the structures of **16** and **19**, ketones **3** and **14** were reduced with sodium borohydride. A 2:1 mixture of two alcohols was obtained from **3** and, interestingly, the minor alcohol was found to be identical to the major alcohol isolated from homoenolizations of **2** and **3**. Definitive stereochemical assignments for these isomeric cycloheptanols, however, cannot be made. From **14**, a 9:1 mixture of isomeric alcohols was obtained in which the major component was identical to **16**; the ^{13}CMR data for the minor alcohol were those expected for the *trans* isomer bearing an axial hydroxyl.

Can. J. Chem. Downloaded from www.nrcresearchpress.com by 217.78.4.112 on 09/08/12
For personal use only.

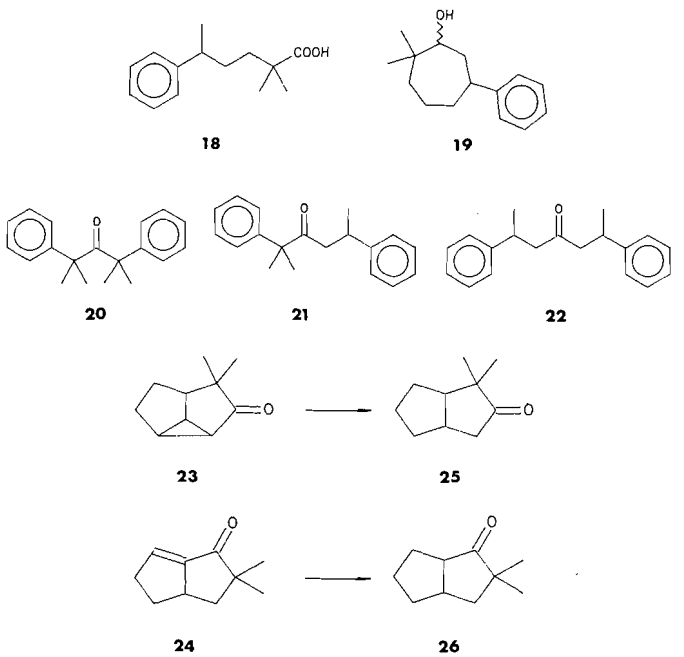

The reduction of **3** and **14** to the corresponding alcohols **19** and **16**, respectively, is puzzling and we were unable to isolate any oxidized products that could shed light on the process involved. We are aware of two other systems in which reduction occurs under homoenolization conditions and in each case an unsaturated grouping was affected, leading to a saturated ketone, not an alcohol; the isomeric ketones **23** and **24** were reduced to the [3.3.0] ketones **25** and **26**, respectively (9, 10). It was suggested that these processes involve single electron transfer from the *tert*-butoxide anion. Interestingly, there was no reduction in the homoenolizations of the α-phenyl acyclic ketones examined in our earlier study (2). However, in the cyclic systems the intermediates, depicted as **4** and **15**, are formed readily and reversibly. It is conceivable that these species undergo reduction, possibly initiated by homolysis of the more substituted bond in the cyclopropoxide ring to produce a diradical, e.g., **27**, which could then gain hydrogen from solvent molecules to produce the small amounts of alcohols observed. A precedent for the formation of such intermediates is provided by the observation that 1,4-diphenylbicyclo-[2.1.0]pentane (**28**) is in rapid equilibrium with 1,3-cyclopentanediyl **29**, through homolysis of the very weak 1,4-bond (11), and it has been shown that an oxy anion substituent has a sizable bond-weakening effect on adjacent bonds (12). Thus, it seems reasonable to suggest that **27** may be generated in these systems. It may be noted that **29** slowly undergoes a 1,2-hydrogen shift to give 1,3-diphenylcyclopentene at temperatures above 100°C; an analogous shift in **27** would regenerate **3** or **14** as their α-enolates.

A minor process detected in the homoenolization of the acyclic α-phenyl ketones involved an acyl shift from alkyl to aryl carbon through a cyclobutoxide intermediate **30** opening unidirectionally to **31**. The analogous reaction for **2** would lead to the tricyclic species **32**, which, in principle, could return to **2** or cleave to a 2,3-benzocyclooctanone. In fact, the benzocyclobutenol formed by protonation of **32** has been shown to cleave entirely to **2** and the amide of **12** upon treatment with $NaNH_2$/glyme (13). Thus, the formation of **32** would be undetectable in our experiments. It may be noted, however, that preliminary examination of the reaction of **2** with lithium 2,2,6,6-tetramethylpiperide has revealed the formation of **32** as well as rearrangement to **3**. Interestingly, photolysis of the benzocyclobutenol from **32** provides a synthetic route to **33** (14). The behavior of **2**, **13**, and related ketones upon treatment with nitrogen bases is now under investigation.

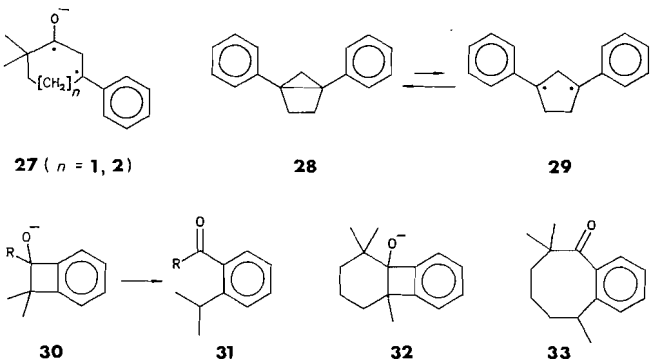

Summary

From the foregoing data, it is apparent that isomerization through proton abstraction from the 2-methyl group in **13** is approximately an order of magnitude faster than that for **2**. This is in agreement with the earlier finding that β-proton abstraction from the methyl sites in 2,2,5,5-tetramethylcyclopentanone is ten times faster than that in 2,2,6,6-tetramethylcyclohexanone (4). Both **2** and **13** are consumed more rapidly than the α-phenyl acyclic ketones examined previously under the same reaction conditions (2), but the present results also reveal other major differences in behavior between the cyclic and acyclic systems. The ready reversibility of β-enolate formation in these cyclic ketones stands in striking contrast to the results for the acyclic ketones and renders the ring expansion of little preparative utility because of the competitive Haller–Bauer cleavage; the latter process is also faster in the cyclic systems. The unusual minor process through which **3** and **14** undergo reduction was not observed for the α-phenyl acyclic systems perhaps owing to constraints imposed by the ring system that are lacking in the acyclic cases. The preliminary results obtained upon changing the base to lithium 2,2,6,6-tetramethylpiperide seem to indicate one way to minimize Haller–Bauer cleavage and the reduction process.

Experimental

Gas–liquid chromatography was carried out on a Varian 3300 instrument using a column of 5% SE-30 on Chromosorb W 80–100. Ether was dried over sodium and freshly distilled before use. Technical grade 2-phenylcyclohexanone and 2-chlorocyclopentanone are commercially available.

Infrared spectra were recorded using a Bruker/IBM FTIR 32 spectrometer. Mass spectral data were obtained with a Finnigan MAT 8230 instrument at 70 eV for routine spectra and at 20 eV for exact mass measurements.

Proton and carbon NMR spectra of each compound were recorded with Varian XL-200 (^{1}H) and XL-300 (^{13}C) spectrometers. The protonation level for each carbon signal was found by recording the APT spectrum. Specific assignments for the sp^3-carbon signals of **3** were obtained by heteronuclear correlation with its ^{1}H spectrum. The one-bond interactions were revealed with the HETRES sequence (15*a*), utilizing a 2048 × 144 data point matrix, with a 6 kHz spectral width for ^{13}C and 1 kHz for ^{1}H, and transforming 2048 and 512 points, respectively. A 0.90 s relaxa-

Can. J. Chem. Downloaded from www.nrcresearchpress.com by 217.78.4.112 on 09/08/12
For personal use only.

Can. J. Chem. Downloaded from www.nrcresearchpress.com by 217.78.4.112 on 09/08/12
For personal use only.

tion delay and a fixed time of 0.037 s were employed. Two- and three-bond correlations for the methyl protons were identified with the FLOCK sequence (15*b*). This spectrum was obtained using a 2048 × 120 data point matrix, with 6 kHz (^{13}C) and 1 kHz (^{1}H) spectral widths, and transforming 2048 and 512 points, respectively; a relaxation delay of 0.83 s, with Δ_1 = 0.090 s and Δ_2 = 0.024 s, was employed.

2-Phenylcyclopentanone

To a cold, stirred solution of phenylmagnesium bromide, from bromobenzene (9.3 mL) and magnesium (2.2 g) in 50 mL of dry ether, was added a solution of 2-chlorocyclopentanone (8.4 mL) in dry ether (30 mL) over 30 min. This mixture was heated under gentle reflux for 2 h before cooling to room temperature. The cooled mixture was treated with ice and dilute hydrochloric acid before extraction with benzene. The organic layer was washed with dilute sodium hydroxide and then with water before drying over anhydrous sodium sulfate. Evaporation of the benzene left a darkly colored residue, which was distilled to yield a light yellow oil (6 g), bp 112–116°/2 Torr (1 Torr = 133.3 Pa). Flash chromatography (hexane:ether; 19:1) gave 2-phenylcyclopentanone as a colorless oil (5.5 g, 41% yield) that slowly crystallized on standing to afford white crystals, mp 35–36°C (lit. (16) mp 36–37°C); IR($CHCl_3$): 1740 cm^{-1}; ^{13}CMR($CDCl_3$) δ: CH_2, 20.6, 31.5, 38.2; CH, 55.0; aryl CH, 127.9 (2), 128.3 (2), 126.6; aryl C, 138.3; C=O, 217.7. Exact Mass calcd. for $C_{11}H_{12}O$: 160.0888; found: 160.0894.

Preparation of the α-phenyl-α,α′,α′-trimethylcycloalkanones

To a stirred suspension of freshly powdered anhydrous sodium amide (0.12 mol) in dry ether (20 mL) was added a solution of the ketone (0.01 mol) in dry ether (10 mL) and the mixture heated under reflux for 2 h with vigorous stirring. The mixture was cooled and methyl iodide (0.05 mol) added slowly before refluxing for 2 h. Equivalent quantities of methyl iodide were added at intervals of 2, 2, and 15 h before a final reflux period of 2 h. After cooling, water (60 mL) was added. The ether layer was separated and the aqueous phase extracted with ether (3 × 20 mL). The combined extracts were washed with water and saturated NaCl solution before drying over anhydrous Na_2SO_4. Removal of the solvent afforded an oily residue, which was examined by GLC to check that the major product was fully methylated. In each case, the crude product was purified by flash chromatography (petroleum ether:ether, 19:1).

2-Phenyl-2,6,6-trimethylcyclohexanone (2): 85% yield: IR (liquid film): 1698 cm^{-1}; ^{1}HMR ($CDCl_3$) δ: 0.61 (s, 3H, Me), 1.06 (s, 3H, Me), 1.26 (s, 3H, Me), 1.50–2.10 (m, 5H), 2.65 (m, 1H), 7.15–7.30 (m, 5H, aryl H's); ^{13}CMR ($CDCl_3$) δ: CH_3, 27.2, 27.4, 30.6; CH_2, 18.2 (C-4), 36.1 (C-5), 40.4 (C-3), C, 45.7 (C-6), 52.4 (C-2); aryl CH, 125.6 (*ortho*), 128.6 (*meta*), 126.4 (*para*); aryl C, 142.8; C=O, 217.1. Exact Mass calcd. for $C_{15}H_{20}O$: 216.1514; found: 216.1511.

2-Phenyl-2,6,6-trimethylcyclopentanone (13): 86% yield; IR (liquid film): 1734 cm^{-1}; ^{1}HMR ($CDCl_3$) δ: 0.90 (s, 3H, Me), 1.04 (s, 3H, Me), 1.28 (s, 3H, Me), 1.67 (m, 2H), 1.90 (m, 1H), 2.36 (m, 1H), 7.05–7.30 (m, 5H); ^{13}CMR ($CDCl_3$) δ: CH_3, 24.9, 25.3, 26.3; CH_2, 34.5, 34.7; C, 45.3, 53.4; aryl CH, 126.1 (2), 126.4, 128.4 (2); aryl C, 143.3; C=O, 224.0. Exact Mass calcd. for $C_{14}H_{18}O$: 202.1358; found: 202.1368.

Homoenolization experiments

The general procedure for these experiments has been described previously (5). A solution of the desired ketone in *t*-BuO^-/*t*-BuOH, prepared from potassium metal and *t*-BuOH (H_2O content <200 μg/mL), was made up under nitrogen in a mole ratio: ketone/*t*-BuO^-/*t*-BuOH, 1:4:40. Aliquots were then transferred to predried, thick-walled glass tubes quickly and the solutions degassed before sealing under vacuum. The tubes were heated in an oil bath at 185°C for varying periods of time. After cooling, the reaction mixture was washed from the tube with water and saturated NaCl solution. The product was extracted with ether and the combined extracts washed with water before drying over anhydrous Na_2SO_4. Evaporation of the solvent gave the crude neutral fraction, which was initially examined by GLC. The individual components in each of the mixtures were identified from their NMR spectra and analytical samples were characterized after isolation by preparative GLC or column chromatography (see text).

3-Phenyl-7,7-dimethylcycloheptanone (3): IR (liquid film): 1701 cm^{-1}; ^{1}H and ^{13}CMR data: see text. Exact Mass calcd. for $C_{15}H_{20}O$: 216.1514; found: 216.1513.

3-Phenyl-6,6-dimethylcyclohexanone (14): IR (liquid film): 1709 cm^{-1}; NMR data: see text. Exact Mass calcd. for $C_{14}H_{18}O$: 202.1358; found: 202.1362.

cis-*3-Phenyl-6,6-dimethylcyclohexanol (16):* IR (liquid film): 3420 cm^{-1}; NMR data: see text. Exact Mass calcd. for $C_{14}H_{20}O$: 204.1514; found: 204.1509.

The aqueous phase was acidified with 5% HCl solution before the acidic fraction was isolated by ether extraction and the product identified by ^{1}HMR, ^{13}CMR, and precise mass measurement.

The experiments with **2** and **3** gave one acid having the formula $C_{15}H_{22}O_2$. Exact Mass calcd. for $C_{15}H_{22}O_2$: 234.1620; found: 234.1625. This was identified as **12** by the NMR spectra described in the text.

The reactions of **13** and **14** with strong base also gave a single acid. Exact Mass calcd. for $C_{14}H_{29}O_2$: 220.1463; found: 220.1459. This compound was shown to be **18** from its NMR spectra (see text).

Sodium borohydride reduction of 3 and 14

Sodium borohydride (18 mg, 0.5 mmol) was mixed with methanol (5 mL) before the addition of an ethereal solution of the ketone (1 mL) and the mixture was stirred. After 1 h, GLC analysis showed that the ketone had reacted completely and the product was isolated by ether extraction after dilution with water. The ether extracts were dried over anhydrous $MgSO_4$ before the solvent was evaporated to obtain the product.

Ketone **14** (20 mg) gave a colorless liquid (19.5 mg, >95% yield), which was found to be a 9:1 mixture of alcohols by ^{13}CMR. The major component was identical to alcohol **16**, described above, which was isolated from the reaction of **13** with *t*-BuO^-/*t*-BuOH. The ^{13}CMR spectrum of the minor alcohol contained signals for two methyl (δ_C 24.9, 27.6), three methylene (29.4, 33.4, 36.7), two methine (37.1, 75.2), one quaternary (34.0), and phenyl carbons (126.0, 127.0 (2), 128.4 (2), 146.7). These data are consistent with those expected for the *trans* isomer of **16** bearing an axial hydroxyl group.

Ketone **3** (7 mg) gave a colorless oil (6.8 mg, >95% yield), which was a 2:1 mixture of the 3-phenyl-7,7-dimethylcycloheptanols (**19**) from its ^{13}C spectrum; IR (liquid film): 3400 cm^{-1}. Exact Mass calcd. for $C_{15}H_{22}O$: 218.1671; found: 218.1670. The minor alcohol was identical to that isolated from the homoenolization experiments with **2**; ^{13}CMR ($CDCl_3$) δ_C: 21.8, 28.6 (CH_3's), 21.4, 38.7, 40.7, 41.2 (CH_2's), 44.8, 79.9 (CH's), 37.4 (quat C), 125.9, 126.7(2), 128.4(2) (aryl CH's), and 148.5 (aryl C); ^{1}HMR ($CDCl_3$) δ: 0.87 (s, 3H, CH_3), 1.00 (s, 3H, CH_3), 1.05–2.05 (m, CH_2), 2.70 (m, 1H), 3.4 (dd, 1H), and 7.05–7.20 (m, aryl H's). The major alcohol gave the following NMR spectra: ^{13}CMR ($CDCl_3$) δ_C: 26.1, 27.5 (CH_3's), 22.0, 36.2, 37.7, 39.4 (CH_2's), 38.1, 76.8 (CH's), 38.3 (quat C), 125.7, 126.9(2), 128.4(2) (aryl CH's), and 149.4 (aryl C); ^{1}HMR ($CDCl_3$) δ: 0.93 (s, 3H, CH_3), 0.95 (s, 3H, CH_3), 1.05–2.05 (m, CH_2), 3.08 (m, 1H), 3.55 (dd, 1H), and 7.05–7.20 (m, aryl H's).

2-(1-Phenylethyl)-5,5-dimethylcyclopentanone (8)

To a stirred solution of LDA, prepared from diisopropylamine (1.5 mL), *n*-BuLi (4 mL, 2.5 M in hexane), and THF (10 mL), at −78°C was added 2-methylcyclopentanone (1.16 g) dropwise. After stirring at −78°C for 0.5 h, the mixture was warmed to 0°C and left for 3 h before methyl iodide (1 mL) was added slowly. Stirring was continued for 3 h after which time GLC analysis of the reaction mixture indicated the absence of the monomethyl ketone. The re-

action mixture was quenched with water and the product isolated by ether extraction to yield 2,2-dimethylcyclopentanone (0.67 g, 68% yield), which was used without further purification.

To a solution of LDA (diisopropylamine (1.1 mL) and *n*-BuLi (2.8 mL, 2.5 M in hexane) in 10 mL of THF) at 0°C was added a solution of 2,2-dimethylcyclopentanone (150 mg) in THF (5 mL) dropwise. This mixture was stirred at 0°C for 0.3 h before 1-phenylethyl bromide (1.36 g) in THF (5 mL) was added slowly. After 5 h at 0°C, an identical addition of the bromide was made and the reaction mixture was left stirring overnight. Water was added and the product extracted with ether. Evaporation of the ether after drying the combined extracts over anhydrous $MgSO_4$ gave an oil (2.26 g) that was mainly the alkyl bromide. Most of the bromide was removed by chromatography on silica gel to yield a crude product (280 mg), which by GLC analysis contained ca. 75% of the diastereomeric mixture **8** in a 60:40 ratio, virtually the same as that found for the sample isolated from the homoenolization experiments with **2**. Small samples of each diastereomer, each of which contained about 20% of the other, were obtained by preparative GLC. Precise mass data for each diastereomer were obtained by GC/MS. The major diastereomer had the following properties: IR (liquid film): 1730 cm^{-1}; ^{13}CMR ($CDCl_3$) δ_c: 15.5, 23.1, 24.7 (CH_3's), 20.8, 36.3 (CH_2's), 38.0, 55.8 (CH's), 45.5 (quat C), 126.2, 127.4 (2), 128.4 (2) (aryl CH's), 145.4 (aryl C), and 223.1 (C—O). Exact Mass calcd. for $C_{15}H_{20}O$: 216.1514; found: 216.1512. The minor diastereomer exhibited the following data: IR (liquid film): 1730 cm^{-1}; ^{13}CMR ($CDCl_3$) δ_c: 19.6, 22.7, 24.5 (CH_3's), 21.9, 36.2 (CH_2's), 39.2, 55.3 (CH's), 45.4 (quat C), 126.4, 128.1 (2), 128.3 (2), (aryl CH's), 144.2 (aryl C), and 223.3 (C=O). Exact Mass calcd. for $C_{15}H_{20}O$: 216.1514; found: 216.1510.

Acknowledgements

We are grateful for the continued financial support of the Natural Sciences and Engineering Research Council of Canada and to Dr. B. Rangaswamy for some preliminary experiments. The assistance of Professor Wm. F. Reynolds through provision of the HETRES and FLOCK pulse sequences as well as his helpful comments on the proper choice of operating parameters are gratefully acknowledged. We wish to thank Professors R. R. Fraser and E. W. Warnhoff for valuable discussions concerning possible modes for the reduction process. This paper was taken in part from the honors B.Sc. thesis of W.S.

1. N. H. Werstiuk. Tetrahedron, **39**, 205 (1983).
2. R. A. Dyllick-Brenzinger, V. Patel, M. B. Rampersad, J. B. Stothers, and Shirley E. Thomas. Can. J. Chem. **68**, 1106 (1990).
3. V. Patel and J. B. Stothers. Can. J. Chem. **58**, 2728 (1980).
4. A. K. Cheng, J. B. Stothers, and C. T. Tan. Can. J. Chem. **55**, 447 (1977).
5. A. L. Johnson, J. B. Stothers, and C. T. Tan. Can. J. Chem. **53**, 212 (1975).
6. M. St-Jacques, C. Vaziri, D. A. Frenette, A. Goursot, and S. Fliszar. J. Am. Chem. Soc. **98**, 5759 (1976).
7. T. D. Hoffman and D. J. Cram. J. Am. Chem. Soc. **91**, 1000 (1972).
8. L. A. Paquette, J. P. Gilday, and C. S. Ra. J. Am. Chem. Soc. **109**, 6858 (1987).
9. A. K. Cheng, A. K. Ghosh, and J. B. Stothers. Can. J. Chem. **62**, 1385 (1984).
10. G. A. Antoniadis, M. T. M. Clements, S. Peiris, and J. B. Stothers. Can. J. Chem. **65**, 1557 (1987).
11. F. D. Coms and D. A. Dougherty. J. Am. Chem. Soc. **111**, 6894 (1989); W. Adams, H. Platsch, and J. Wirz. J. Am. Chem. Soc. **111**, 6896 (1989).
12. M. L. Steigerwald, W. A. Goddard III, and D. A. Evans. J. Am. Chem. Soc. **101**, 1994 (1979).
13. P. Caubere, M. S. Mourad, and G. Guillaumet. Tetrahedron, **29**, 1851 (1973).
14. M.-L. Virot-Villaume, C. Carre, and P. Caubere. J. Chem. Soc. Perkin Trans **1**, 1395 (1979).
15. (*a*) W. F. Reynolds, S. McLean, M. Perpick-Dumont, and R. A. Enriquez. Magn. Reson. Chem. **26**, 1068 (1988); (*b*) Magn. Reson. Chem. **27**, 162 (1989).
16. K. Mislow and C. L. Hamermesh. J. Am. Chem. Soc. **77**, 1590 (1950).

Can. J. Chem. Downloaded from www.nrcresearchpress.com by 217.78.4.112 on 09/08/12
For personal use only.

Isolation and characterization of enniatins from *Fusarium avenaceum* DAOM 196490[1]

L. A. BLAIS AND J. W. APSIMON
Ottawa–Carleton Chemistry Institute, Carleton University, Ottawa, Ont. Canada K1S 5B6

AND

B. A. BLACKWELL,[2] R. GREENHALGH, AND J. D. MILLER[2]
Plant Research Centre, Agriculture Canada, Central Experimental Farm, Ottawa, Ont., Canada K1A 0C6

Received July 9, 1991

This paper is dedicated to Professor Zdenek (Denny) Valenta on the occasion of his 65th birthday

L. A. BLAIS, J. W. APSIMON, B. A. BLACKWELL, R. GREENHALGH, and J. D. MILLER. Can. J. Chem. **70**, 1281 (1992).

Dried mycelia from a 15 L stirred-jar fermentation culture of *Fusarium avenaceum* (DAOM 196490) were extracted with dichloromethane and partitioned between hexane and methanol/water. Recrystallization of the hexane fraction yielded 6.750 g of a crude mixture of enniatins. Fast atom bombardment mass spectrometry showed, in accord with previous studies, that enniatin A was the predominant enniatin present, with smaller amounts of enniatins A1 and B1. HPLC purification of 500 mg of the enniatin mixture resulted in the isolation of 300 mg of enniatin A, 114 mg of enniatin A1, 9 mg of enniatin B1, and 46 mg of a new, *N*-methylleucine-containing enniatin (A2). This is the first reported isolation of a pure *N*-methylleucine-containing enniatin from *Fusarium*, though the existence of such compounds had previously been inferred from hydrolysis and NMR data. The purification and complete characterization of enniatins A1, B1, and A2 are reported.

L. A. BLAIS, J. W. APSIMON, B. A. BLACKWELL, R. GREENHALGH et J. D. MILLER. Can. J. Chem. **70**, 1281 (1992).

Utilisant du dichlorométhane, on a extrait des mycéliums séchés d'une culture effectuée dans un récipient de 15 L agité de *Fusarium avenaceum* (DAOM 196490) et on a fait la partition entre de l'hexane et un mélange de méthanol/eau. La recristallisation de la fraction hexanique fournit 6,750 g d'un mélange brut d'enniatines. La spectrométrie de masse par bombardement avec des atomes rapides a montré, en accord avec des études antérieures, que l'enniatine A est l'enniatine prédominante aux côtes de quantités plus faibles d'enniatines A1 et B1. Une purification par CLHP de 500 mg du mélange d'enniatine permet d'isoler 300 mg d'enniatine A, 114 mg d'enniatine A1, 9 mg d'enniatine B1 et 46 mg d'une nouvelle enniatine (A2) contenant de la *N*-méthylleucine. Même si l'existence de tels composés avait été suggérée antérieurement sur la base d'une hydrolyse et de données de RMN, il s'agit de la première enniatine contenant de la *N*-méthylleucine à être isolée à l'état pur à partir du *Fusarium*. On rapporte la purification et la caractérisation complète des enniatines A1, B1 et B2.

[Traduit par la rédaction]

Introduction

Fusarium avenaceum (Fr.) Sacc. (section *Roseum*) is chiefly a fungus of temperate zones and is a common pathogen of overwintering cereals. It is responsible for root-rot in both seedlings and mature plants of these cereals as well as of legumes and conifers. It has been associated with damping-off disease of nursery seedlings and is also involved in "spring yellows." *Fusarium avenaceum* has also been linked to wilt in a variety of plants (1).

Fusarium avenaceum (DAOM 196490) has been isolated from the phylloplane of needles from balsam fir infested with spruce budworm (*Choristoneura fumiferana* Clem.) by Miller *et al.* (2). This fungus was found by Strongman *et al.* to produce a group of cyclohexadepsipeptides, the enniatins, in liquid culture (3). Purification of crude extracts of the mycelia resulted in the isolation of a mixture of the enniatins A, A1, and B1, which was found to be toxic to spruce budworm larvae at concentrations of 400 ppm (3). In addition, the enniatins have been reported to be toxic to wheat seedlings (4), to have moderate insecticidal activity against blowfly and mosquito larvae (5), to show moderate antibiotic activity against some gram positive bacteria (6), and to be implicated in *Fusarium* wilt of tomato plants (7).

The enniatins were first isolated in 1947, by Gaumann *et al.* (8), and have been characterized as cyclodepsipeptides containing alternating D-2-hydroxyisovaleric acid (HyIv) and L-amino acid residues to form an 18-membered cyclic backbone. The amino acid residues can be either *N*-methylisoleucine (NMeIle) (enniatin A) (**1**), *N*-methylvaline (NMeVal) (enniatin B) (**2**), or mixtures of the two (enniatins A1 (**3**) and B1 (**4**)) (Fig. 1). Of these, only enniatins A and B have been obtained in the pure form and fully characterized (3, 9, 13). The presence of *N*-methylleucine (NMeLeu)-containing enniatins has been inferred from amino acid analysis of enniatin mixtures (10, 13), and although enniatin C (**5**) (containing only NMeLeu and HyIv) has been synthesized (12), no NMeLeu-containing enniatins have been purified and characterized previous to this work.

This work details the isolation and complete characterization of enniatins A1 and B1 in addition to a new, NMeLeu-containing enniatin, A2 (**6**). This is the first reported isolation and characterization of an *N*-methylleucine-containing enniatin from a *Fusarium* species.

Results and discussion

Strongman *et al.* (3) have shown that the major enniatin produced by *Fusarium avenaceum* DAOM 196490 is enniatin A.

HPLC purification of 500 mg of crude enniatins yielded five fractions. The largest fraction, peak 5, contained 300 mg of pure enniatin A. The identity of this compound

[1]PRC contribution No. 1345.
[2]Authors to whom correspondence may be addressed.

Can. J. Chem. Downloaded from www.nrcresearchpress.com by 217.78.4.112 on 09/08/12
For personal use only.

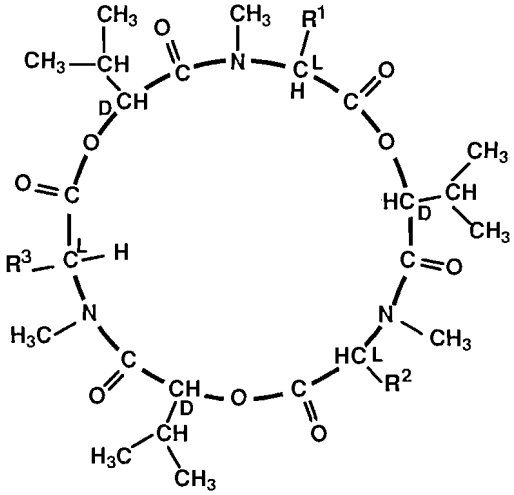

ENNIATIN

1	A	$R^1=R^2=R^3=$ $-CH(CH_3)CH_2CH_3$
2	B	$R^1=R^2=R^3=$ $-CH(CH_3)_2$
3	A_1	$R^1=R^2=$ $-CH(CH_3)CH_2CH_3$, $R^3=-CH(CH_3)_2$
4	B_1	$R^1=R^2=$ $-CH(CH_3)_2$, $R^3=-CH(CH_3)CH_2CH_3$
5	C	$R^1=R^2=R^3=$ $-CH_2CH(CH_3)_2$
6	A_2	$R^1=R^2=$ $-CH(CH_3)CH_2CH_3$, $R^3=-CH_2CH(CH_3)_2$

FIG. 1. Structures of the enniatins.

was confirmed by comparison to published melting point, mass spectral, and NMR data (3). The ^1H NMR chemical shifts and coupling constants and ^{13}C NMR chemical shifts for enniatin A are listed in Tables 1 and 2.

The structures of enniatins A1 and B1 have been determined from amino acid analysis and mass spectral data (10, 12). However, they have never been purified and fully characterized.

Peak 3 from the HPLC separation of the enniatin mixture yielded 114 mg of pure enniatin A1. The colourless, needle-shaped crystals melted at 66–67°C and exhibited an optical rotation of −62.8 (*c* 2.3 in chloroform at 25°C). The FAB mass spectrum showed a molecular ion at *m/z* 668.5 (M^+ + H), indicating a molecular weight of 667. This was confirmed by solid probe EI/MS, which also showed a molecular ion at *m/z* 667. Previous amino acid analyses of mixtures of enniatins containing enniatin A1 suggested a structure for this enniatin in which there are two *N*-methylisoleucine residues and one *N*-methylvaline residue alternating with D-2-hydroxyisovaleric acid residues to form the cyclohexadepsipeptide. The 500 MHz ^1H NMR spectrum of enniatin A1 is shown in Fig. 2(*a*). Comparison of these data with those obtained for enniatin A (see Table 1) indicates the presence of *N*-methylisoleucine, shown by a pair of doublets at 4.62 and 4.66 ppm (J = 9.2 Hz), which integrate for two protons. The multiplet resonances at 2.01 ppm (βCH), 1.04 and 1.42 ppm (γCH_2 AB), and overlapping triplets at 0.83 and 0.85 (δCH_3) are also due to NMeIle. The doublet at 4.42 ppm, with a coupling constant of 10.3 Hz, is assigned as the αCH of NMeVal by comparison to published ^1H NMR data for enniatin B (12). In addition, the multiplet at 2.28 ppm and the doublets at 1.03 and 0.87 ppm correspond to the βCH and γCH_3 resonances for this amino acid. There are two *N*-methyl singlets in this spectrum at 3.10 ppm (3 protons) and 3.08 (6 protons), which are assigned to NMeVal and the two NMeIle residues respectively. Finally, the αCH HyIv resonances have been assigned to the three overlapping doublets at 5.11 ppm. The βCH resonances and γCH_3 resonances for the HyIv residues are given in Table 1.

The 62.5 MHz ^{13}C NMR spectrum of enniatin A1 confirms the presence of two NMeIle residues and one NMeVal residue. The αCH region for the amino acids shows resonances at 63.4 ppm and 61.4 ppm, corresponding to the αCH groups of NMeVal and NMeIle respectively. Although integration of ^{13}C spectra is usually not accurate, in this case the peak at 61.4 ppm is approximately twice the height of the peak at 63.4 ppm, which would indicate the presence of two NMeIle residues. There are three resonances in the *N*-methyl region at 33.4, 32.8, and 32.7 ppm. Comparison to the spectra of enniatins A and B shows that the downfield resonance is due to NMeVal and the two upfield resonances to NMeIle. Finally, resonances that correspond to the γCH_3 groups of NMeVal occur at 19.5 and 20.5 ppm; the δCH_3 resonance of NMeIle occurs at 10.9 ppm and the γ-methyl resonance for this amino acid residue occurs at 16.2 ppm. The electron-impact mass spectrum shows fragment ions characteristic of the loss of alternating HyIv and amino acid moieties from the parent compound. The ion at *m/z* 423 accounts for a loss of 244 mass units from the parent enniatin A1, which corresponds to a dimer of HyIv–NMeIle. Loss of NMeVal from the remaining tetramer results in the ion at *m/z* 296, and loss of another HyIv residue yields the ion at *m/z* 196. Thus the GC/MS and ^1H and ^{13}C NMR data for enniatin A1 agree with the assigned structure of cyclo-[(NMeIle-HyIv)$_2$-NMeVal-HyIv].

The first peak from the HPLC separation of the enniatin mixture yielded 9 mg of enniatin B1. FAB mass spectra of this compound showed a molecular ion at *m/z* 654.5 (M^+ + H), indicating a molecular weight of 653. Solid probe EI/MS confirmed this molecular weight. Comparison with the literature indicated that this compound was enniatin B1. The structure of this compound was proposed to be a homologue of enniatin A1, in which one of the NMeIle residues is replaced by a second NMeVal residue.

The 500 MHz ^1H NMR spectrum of enniatin B1 is shown in Fig. 2(*b*). This spectrum is similar to the ^1H NMR spectrum of enniatin A1, except that the number of doublets and integration values representing the αCH of NMeIle and NMeVal are reversed. In addition, the singlets at 3.08 and 3.10 ppm, representing the methyl groups on the nitrogens of NMeIle and NMeVal respectively, show reversed intensities to those in the spectrum of enniatin A1. There is also a difference in the intensities for the βCH protons. In the spectrum of enniatin A1, the resonance for the βCH of NMeVal is a shoulder on that of HyIv (2.26 ppm). The observed intensity is only slightly greater for these overlapped βCH multiplets (integrating for four protons) than for the multiplet at 2.01 ppm corresponding to the βCH of NMeIle, which integrates for two protons. In the spectrum of enniatin B1, the overlapping of the βCH multiplets at 2.24 ppm (integrating for five protons) results in an observed intensity of at least four times that of the multiplet at 2.04 ppm (in-

Can. J. Chem. Downloaded from www.nrcresearchpress.com by 217.78.4.112 on 09/08/12
For personal use only.

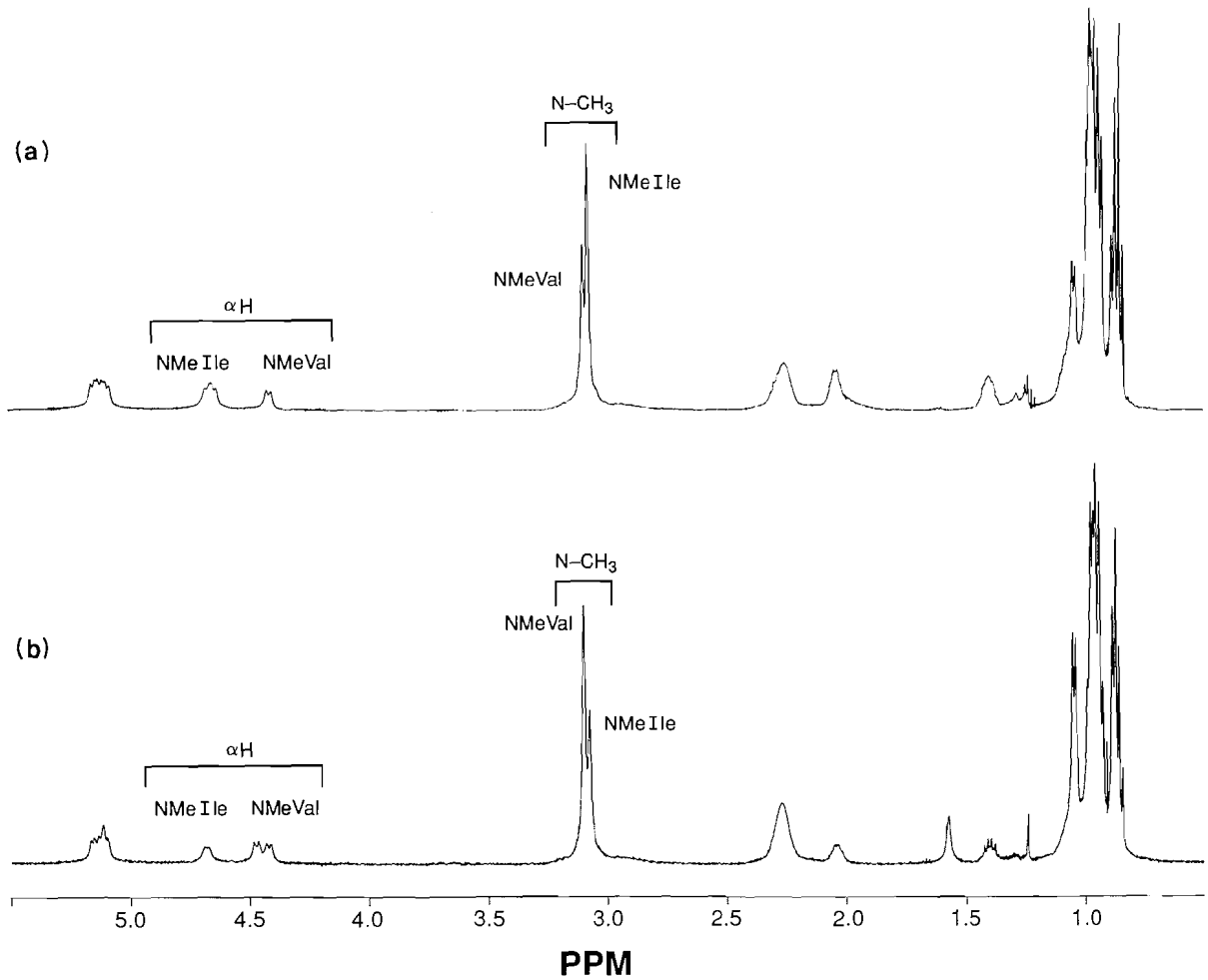

FIG. 2. 500 MHz ^{1}H NMR spectra of enniatin A1 (*a*) and enniatin B1 (*b*). Spectra were referenced to deuterochloroform at 7.24 ppm and reported relative to tetramethylsilane (Me_4Si).

tegrating for one proton). Finally, differences in intensity of the individual resonances can also be seen in the aliphatic methyl region.

The ^{13}C NMR spectrum of enniatin B1 also shows strong similarities to that of enniatin A1. There are two resonances, at 63.4 and 63.5 ppm, corresponding to the αCH of the two NMeVal residues, and one resonance at 61.5 ppm for the αCH of NMeIle, as well as two downfield resonances at 33.3 and 33.4 ppm corresponding the *N*-methyl groups of the NMeVal residues, and one resonance at 32.7 ppm for the *N*-methyl group of NMeIle. The aliphatic region of the spectrum is virtually identical to that of enniatin A1. Thus, the NMR data confirm the structure of enniatin B1 to be cyclo-[(NMeVal-HyIv)$_2$-NMeIle-HyIv].

In addition to the three known enniatins, a fourth enniatin, designated enniatin A2, was isolated as a shoulder on the HPLC peak corresponding to enniatin A1. This compound was recrystallized to give 46 mg of colourless needle-shaped crystals with a melting point of 123–125°C. The FAB mass spectrum showed a molecular ion at *m/z* 682.5, identical to that of enniatin A, indicating a molecular weight of 681. This was confirmed by solid probe EI/MS. Although this compound shows an identical molecular weight to enniatin A, its retention time on HPLC is 2 min less than that for enniatin A. The only structure that would correspond to this molecular weight involves the replacement of one or more of the NMeIle residues with NMeLeu residues. Although the presence of NMeLeu-containing enniatins has been suggested by amino acid analysis (10) and ^{13}C NMR spectra (3) of enniatin mixtures, and enniatin C (cyclo-[NMeLeu-HyIv]$_3$, MW 681) has been synthesized (12), no NMeLeu-containing enniatins have ever been purified from natural sources and characterized.

The 500 MHz ^{1}H NMR chemical shifts for enniatin A2 show that this compound is definitely an enniatin, but it is not enniatin A (Fig. 3). The presence of one NMeIle residue was determined by comparison to the spectrum of enniatin A, and was assigned to the resonances at 4.60 (αCH), 2.00 (βCH), 1.40 and 1.07 (γCH_2), 0.92 (γCH_3), 0.84 (δCH_3), and 3.09 ppm (N-CH_3). Integration of the resonance at 2.00 ppm accounted for two protons, indicating the presence of two NMeIle residues. By using ^{1}H/^{1}H correlation spectroscopy (COSY), another set of resonances were assigned to the second NMeIle residue. A triplet at 0.83 ppm, showing a coupling constant of 7.4 Hz, was assigned as the δCH_3 group. A second AB system at 1.06 and 1.33 ppm was attributed to the γCH_2 group, and the second multiplet at 2.00 ppm to the βCH. The doublet at 4.60 ppm was broadened in the ^{1}H NMR spectrum and integrated for two protons. However, a ^{1}H/^{13}C heteronuclear correlation

Can. J. Chem. Downloaded from www.nrcresearchpress.com by 217.78.4.112 on 09/08/12
For personal use only.

TABLE 1. 500 MHz ^{1}H NMR chemical shift assignments for enniatins A, A1, B1, and A2

	Proton	Chemical shift (ppm); J (Hz) A	A1	B1	A2
NMeIle[a]	αH	4.65($J_{\alpha,\beta}$ = 9.2)	4.62($J_{\alpha,\beta}$ = 9.2) 4.66($J_{\alpha,\beta}$ = 9.2)	4.65($J_{\alpha,\beta}$ = 9.0)	4.60($J_{\alpha,\beta}$ = 9.6) 5.02($J_{\alpha,\beta}$ = 9.6)
	βH	2.04($J_{\beta,\alpha}$ = 9.2; $J_{\beta,\gamma}$ = 3.2)	2.01	2.04	2.00($J_{\beta,\alpha}$ = 9.6); $J_{\beta,\gamma}$ = 3.1; J_{β,γ_2} = 7.7)
	$\gamma_1(CH_2)$	1.04(J_{AB} = 13.2; $J_{\gamma_1,\delta}$ = 7.5)	1.04	1.04	1.07(J_{AB} = 13.6; $J_{\gamma_1,\delta}$ = 7.5; $J_{\gamma_1,\beta}$ = 3.3)
		1.42($J_{\gamma_1,\delta}$ = 7.4; $J_{\gamma_1,\beta}$ = 3.2)	1.42($J_{\gamma_1,\delta}$ = 7.2)	1.42(J_{AB} = 13.8)	1.40($J_{\gamma_1,\delta}$ = 7.5) 1.02(J_{AB} = 13.6; $J_{\gamma_1,\delta}$ = 7.5; $J_{\gamma_1,\beta}$ = 3.2)
	$\gamma_2(CH_3)$	1.00($J_{\gamma_2,\beta}$ = 8.3)	0.98	0.98	1.34 0.94–0.96
	δH_3	0.84(J_{δ,γ_1} = 7.4)	0.83(J_{δ,γ_1} = 7.5)	0.82(J_{δ,γ_1} = 7.3)	0.83(J_{δ,γ_1} = 7.4) 0.84(J_{δ,γ_1} = 7.4)
	N-CH_3	3.09	3.08	3.08	3.09 3.14
NMeVal	αH		4.42($J_{\alpha,\beta}$ = 10.3)	4.42($J_{\alpha,\beta}$ = 8.6) 4.46($J_{\alpha,\beta}$ = 9.1)	
	βH		2.28	2.27	
	γH_3		1.03($J_{\gamma,\beta}$ = 6.2) 0.87	1.02($J_{\gamma,\beta}$ = 6.3) 0.87($J_{\gamma,\beta}$ = 6.5)	
	N-CH_3		3.10	3.10	
NMeLeu	αH				4.59(J = 9.6)
	βH_2				1.72(J_{AB} = 14.2; $J_{\beta,\gamma}$ = 4.9; $J_{\beta,\alpha}$ = 9.6)
	γH				1.81 1.52
	δH				0.90($J_{\delta,\gamma}$ = 7.1) 0.92($J_{\delta,\gamma}$ = 7.1)
	N-CH_3				3.05
HyIv	αH	5.10($J_{\alpha,\beta}$ = 7.8)	5.10($J_{\alpha,\beta}$ = 8.8, 9.1, 7.0)	5.11($J_{\alpha,\beta}$ = 7.3, 9.1, 7.9)	5.05($J_{\alpha,\beta}$ = 8.2) 4.92($J_{\alpha,\beta}$ = 8.9) 5.18($J_{\alpha,\beta}$ = 8.2)
	βH	2.25($J_{\beta,\gamma}$ = 6.8)	2.26	2.24	2.21 2.21 2.28
	δH_3	0.92($J_{\gamma,\beta}$ = 6.8) 0.98($J_{\gamma,\beta}$ = 7.2)	0.92–0.99	0.92–0.98	0.89–0.97

[a]NMeIle: *N*-methylisoleucine; NMeVal: *N*-methylvaline; NMeLeu: *N*-methylleucine; HyIv: D-2-hydroxyisovaleric acid.

spectrum (HETCOR) showed that this second αCH resonance did not correspond to NMeIle; rather, the correct αCH resonance had shifted downfield to 5.02 ppm. This assignment was confirmed from the COSY spectrum, which showed coupling between the resonance at 5.02 ppm and the resonance at 2.00 ppm. The *N*-methyl group was assigned to the resonance at 3.14 ppm, based on the downfield shift of the αCH proton. Comparison of the chemical shifts of the remaining resonances with those of enniatin C and a standard of *N*-methylleucine showed that the third amino acid in the molecule must be NMeLeu. The αCH of NMeLeu was assigned to the second broadened doublet at 4.59 ppm. This signal would be expected to appear as a double doublet due to coupling to the nonequivalent protons of the neighbouring CH_2 group. However, overlapping of these signals with the αCH resonance of NMeIle results in a broadened, poorly resolved pair of doublets. This resonance showed coupling in the COSY spectrum to an AB system at 1.81 and 1.72 ppm, which were assigned to the βCH_2 group. These latter multiplets showed coupling to a multiplet at 1.52 ppm, corresponding to the γCH group of NMeLeu, which in turn coupled to doublets at 0.90 and 0.92 ppm (δCH_3 groups). The *N*-methyl group of NMeLeu was assigned to the remaining singlet at 3.05 ppm. The downfield resonance at 5.18 ppm was assigned to the αCH of HyIv next to an NMeLeu residue by comparison to the data for enniatin C; the βCH resonance at 2.28 ppm was also attributed to this hydroxy acid. The upfield doublet at 4.92 ppm was assigned to the αCH of HyIv next to the second NMeIle, and the resonance at 5.05 ppm to the αCH of HyIv next to the other NMeIle. The βCH resonances for both of these hydroxy acid residues were assigned to the overlapped multiplets at 2.21 ppm.

The ^{13}C NMR spectrum of this compound was assigned

Can. J. Chem. Downloaded from www.nrcresearchpress.com by 217.78.4.112 on 09/08/12
For personal use only.

Can. J. Chem. Downloaded from www.nrcresearchpress.com by 217.78.4.112 on 09/08/12
For personal use only.

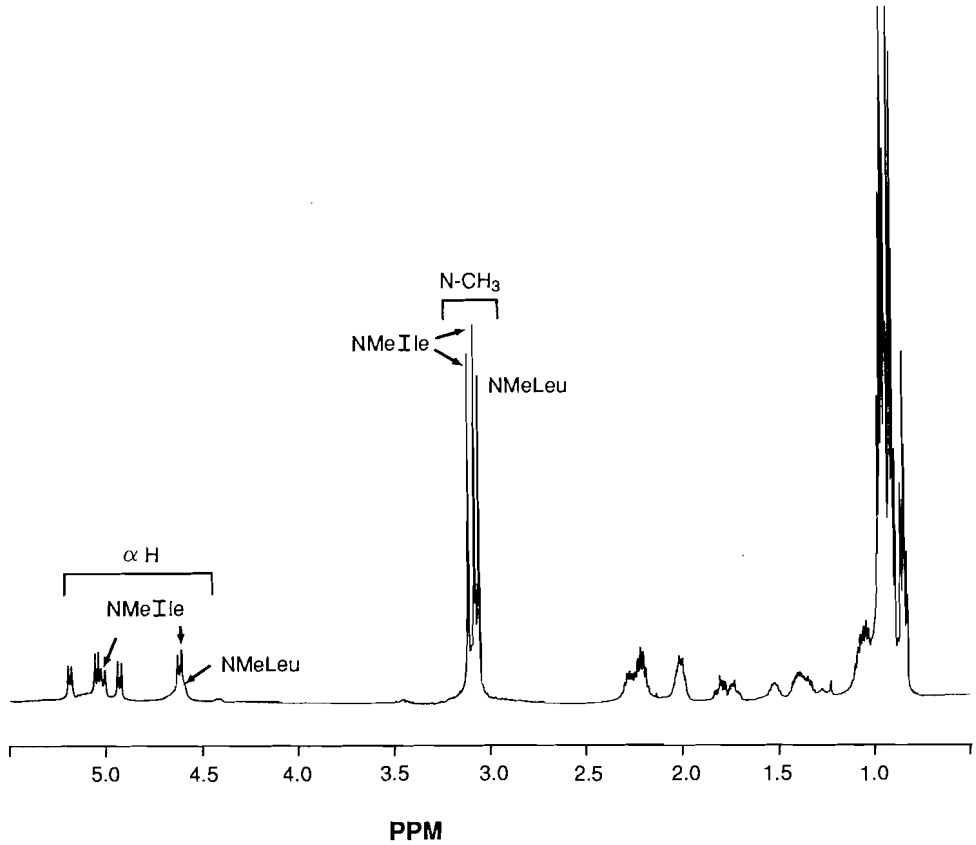

FIG. 3. 500 MHz ^{1}H NMR spectrum of enniatin A2. Spectrum was referenced to deuterochloroform at 7.24 ppm and reported relative to tetramethylsilane (Me_4Si).

by comparison to the spectrum of enniatin A and from the HETCOR. There are six carbonyl resonances for this compound. The resonances at 170.8 and 169.7 ppm correspond to the ester and amide carbonyl for HyIv next to NMeLeu; the other resonances at 170.5 and 169.4 ppm are the ester and amide carbonyls of NMeIle-HyIv. The resonances at 77.2 and 75.0 ppm represent the αCH carbons of HyIv next to the NMeIle residues, and the resonance at 75.2 ppm corresponds to the αCH of HyIv next to NMeLeu. The two downfield resonances at 61.4 and 60.0 ppm are the αCH carbons of the two NMeIle residues. The resonance at 57.4 ppm is that of the αCH of NMeLeu; the reduced intensity of the signal is presumably due to C–N coupling. The resonance at 37.9 ppm corresponds to the βCH_2 of NMeLeu. Resonances at 25.3 ppm (γCH), and 23.2 and 21.5 ppm (δCH_3) complete the NMeLeu residue. The *N*-methyl shifts have been assigned to 33.9 and 32.5 ppm (NMeIle) and 31.6 ppm (NMeLeu). The rest of the ^{13}C NMR chemical shift assignments for enniatin A2 are given in Table 2.

The presence of an NMeLeu residue in enniatin A2 was confirmed by amino acid analysis of the acid hydrolysate. A standard of *N*-methylleucine derivatized with MTBSTFA showed a retention time on GC/MS of 11.24 min, and a molecular ion at *m/z* 360. The standard of *N*-methylvaline had a retention time of 6.61 min and showed a molecular ion at *m/z* 346. GC/MS of the derivatized hydrolysate showed a peak at 8.83 min with a molecular ion at *m/z* 347; however, the intensity pattern of the fragment ions and the retention time did not match those of NMeVal. This peak could possibly have been due to HyIv present in the sample, as the structure of this acid is similar to that of valine. There were two peaks at 11.23 and 11.37 min with molecular ions at *m/z* 360. Comparison of the mass spectra with those of the standard of NMeLeu resulted in the assignment of the peak at 11.23 minutes to NMeLeu. The other peak, with an identical molecular ion and a similar mass spectrum, was assigned as NMeIle.

From the above data, the structure of enniatin A2 is assigned as cyclo-[(NMeIle-HyIv)$_2$-NMeLeu-HyIv]. This is the first reported *N*-methylleucine-containing enniatin to be isolated and characterized in the pure form from *Fusarium*.

A fifth fraction (7 mg) was obtained by separation of the crude mixture using HPLC. ^{1}H NMR of this fraction showed the presence of two enniatin-like compounds, with five singlets in the *N*-methyl region. The small amount of material did not permit separation of these compounds. However, as these compounds chromatograph as a shoulder following peak 1 (enniatin B1), two possible structures could be suggested: an enniatin containing two *N*-methylvaline residues and one *N*-methylleucine residue, or an enniatin containing one each of *N*-methylvaline, *N*-methylisoleucine, and *N*-methylleucine.

Previous reports in the literature have indicated the relatively nonspecific nature of the enzyme enniatin synthetase towards the branched-chain amino acids valine, isoleucine, and leucine. The isolation of the mixed enniatins A1, B1, and A2 agrees with these findings. The presence of large amounts of *N*-methylisoleucine-containing enniatins from extracts of *Fusarium avenaceum* DAOM 196490 would seem to indicate either a preference by the enzyme for isoleucine, or an

TABLE 2. 62.5 MHz ^{13}C NMR chemical shift assignments for enniatins A, A1, B1, and A2

	Carbon	^{13}C NMR (ppm) A	A1	B1	A2
NMeIle[a]	αC	61.8	61.4,61.4	61.5	60.4,61.4
	βC	34.0	33.9,34.0	33.8	33.7,33.8
	γCH_2	25.4	25.5	25.3	25.1,25.5
	γCH_3	16.2	16.2	16.1	15.9,16.1
	δCH_3	10.9	10.9	10.9	10.7,10.8
	$N\text{-}CH_3$	33.0	32.7,32.8	32.7	32.5,33.9
	C=O(ester)	170.4	170.5	170.4	170.5,170.5
	C=O(amide)	169.3	169.5	169.3	169.4,169.4
NMeVal	αC		63.4	63.5,63.4	
	βC		28.1	27.9	
	γC		19.5,20.5	19.4,20.5	
	$N\text{-}CH_3$		33.4	33.4	
	C=O(ester)		170.4	170.4	
	C=O(amide)		169.5	169.3	
NMeLeu	αC				57.4
	βC				37.9
	γC				25.3
	δC				21.5,23.2
	$N\text{-}CH_3$				31.6
	C=O(ester)				170.8
	C=O(amide)				169.7
HyIv	αC	75.6	75.4,75.2,76.0	75.7,75.4	77.2,75.0,75.2
	βC	29.8	29.8	29.8–30.2	29.7,29.8,30.3
	γC	18.3,18.4	18.4–18.7	18.4–18.7	18.2–18.9

[a]Abbreviations: see Table 1.

accumulation of the isoleucine pools relative to those of valine and leucine.

Experimental

Infrared spectra were obtained on either a Bomem Michealson 100 FT-IR or a Perkin Elmer 1600 series FT-IR. All compounds were run as films on NaCl plates.

Solid probe electron impact (EI) spectra were obtained on a Finnegan MAT 4500 GC/MS system with an INCOS data system. Probe temperature was programmed from 40 to 350°C, ion source temperature was 140°C, electron energy 70 eV, multiplier 1200 V. Fast atom bombardment spectra (FAB) were recorded on a high-resolution, double-focussing, reversed geometry Finnegan MAT-312 mass spectrometer equipped with an Ion Tech saddle-field atom gun and an INCOS data station. No heating was applied to the ion source. The acceleration potential was kept at 3 kV and the electron multiplier at 2 kV whereas the atom gun was operated with Xenon gas (99.9995%, Matheson) at 8 kV. The matrix used was diethanolamine (Aldrich Chemical Co., cat. no. D8, 330-3).

^1H and ^{13}C NMR spectra were run on Bruker AM 250 and AM 500 NMR spectrometers equipped with ASPECT 3000 data systems. Chemical shifts were referenced to deuterochloroform at 7.24 and 77.0 ppm for ^1H and ^{13}C, respectively, and reported relative to tetramethylsilane (Me_4Si). ^{13}C chemical shift assignments were made by using DEPT pulse sequence, $^1H/^{13}C$ heteronuclear correlation spectroscopy (HETCOR), and by comparison with known enniatins. Confirmation of ^1H chemical shift assignments was made by the use of $^1H/^1H$ homonuclear correlation spectra (COSY). The ^1H and ^{13}C NMR data for enniatins A, A1, B1, and A2 are given in Tables 1 and 2.

Preparative HPLC was conducted on a Varian Vista 5500 series chromatograph equipped with a Varian 2550 UV detector operating at 245 nm. A 10 μm Whatman Magnum 9 Partisil ODS-3 semi-preparative reverse-phase column (9.4 mm i.d. × 25 cm) was used with a solvent system of 80% acetonitrile/20% water for initial separation, and 70% acetonitrile/30% water for final purification, at a flow rate of 4 mL min^{-1}.

Amino acid analysis of enniatin A2

Ten milligrams of enniatin A2 was refluxed under nitrogen in 6 M HCl (2 mL) for 20 h. The pH of the hydrolysate was adjusted to 7 using triethylamine, followed by dilution with water until a concentration of 250 nM in each amino acid was obtained.

Standards of *N*-methyl-L-leucine and *N*-methyl-L-valine were dissolved in water to a concentration of 2.5 mM each. Twenty-five microlitres of each standard and the hydrolysate were transferred to 1-mL Reactivials, followed by removal of the water using an air stream. To each sample was added 0.2 μL of dichloromethane, and the samples were redried under nitrogen. The samples were then derivatized by addition of 15 μL of MTBSTFA (Pierce) and 16 μL of pyridine and triethylamine solution (100:7, v/v). The vials were capped, shaken, and heated at 90°C for 20 min, then cooled and analyzed by GC/MS. Samples were run on an HP-5 column with a 1/20 inlet split using two different temperature programs: (1) 110°C, then 12°/min to 194°C; 16°/min to 265°C, followed by an 8-min hold (ALLBSC); (2) 170°C, then 10°/min to 290°C; hold 1 min (MTXBSC).

Chemicals

Standards of *N*-methylleucine and *N*-methylvaline were obtained from the Sigma Chemical Company. A standard mixture of enniatins A, A1, and B1 was kindly provided by Dr. D. Strongman, Canadian Forestry Service–Maritimes, Fredericton, N.B., Canada.

Can. J. Chem. Downloaded from www.nrcresearchpress.com by 217.78.4.112 on 09/08/12
For personal use only.

Can. J. Chem. Downloaded from www.nrcresearchpress.com by 217.78.4.112 on 09/08/12
For personal use only.

All solvents used for isolation and purification were HPLC grade glass distilled purchased from Caledon or Anachemia.

Merck TLC grade silica gel G was used for vacuum liquid chromatography.

Fermentation of Fusarium avenaceum *(DAOM 196490)*

To obtain sufficient amounts of enniatins for isolation and characterization, *Fusarium avenaceum* DAOM 196490 was grown in a 15-L stirred-jar fermentor using the method of Miller and Blackwell (11), except that the production medium used was identical to that used for the seed culture (glucose (20 g), malt extract (2 g), yeast extract (2 g), peptone (2 g), KH_2PO_4 (2 g), $MgSO_4.7H_2O$ (2 g), $FeSO_4.7H_2O$ (0.2 g), and ammonium chloride (3 g); amounts given per litre water; distilled water put through a Barnstead Nanopure II system; 18.3 MΩ cm^{-1}). After 1 week, the culture was filtered through Whatman No. 1 filter paper and the mycelia were dried at 40°C under vacuum.

Extraction and purification of enniatins

Dried mycelia (71.540 g) were ground in a mortar, then extracted using the method of Strongman *et al.* (3). Partitioning of the dichloromethane extract of the mycelia (18.243 g) between hexane and methanol/water (1:1, v/v) yielded 12.751 g of hexane soluble material and 5.095 g of water soluble material.

FAB-MS of the hexane extract showed the presence of enniatins B1, A1, and A by molecular ions at *m/z* 654.5, 668.5, and 682.5 ($M^+ + H$). In addition, ions corresponding to the K^+ adducts at *m/z* 692.5, 706.5, and 720.5 were also present in the spectrum, as were ions corresponding to the addition of the diethanolamine matrix (*m/z* 759.5, 773.5, and 787.5 respectively).

TLC of the extract using a solvent system of CCl_4/diethyl ether (1:1, v/v) and visualization by iodine vapour showed the presence of three spots corresponding to fatty-acid type compounds (R_f 0.95), enniatins (R_f 0.44), and ergosterol (R_f 0.16), by comparison to standards of oleic acid and ergosterol.

The enniatins were purified from the crude extract using vacuum liquid chromatography with CCl_4/diethyl ether (3:2, v/v) as the eluting solvent. Twenty-four fractions (150 mL each) were collected and monitored by TLC as previously described. Fractions 7–24 (7.436 g) contained mainly enniatins. This fraction was recrystallized from ethanol–water at −20°C to give 6.750 g of colourless needles.

A 500 mg sample of the crystals dissolved in 5 mL of acetonitrile and chromatographed by HPLC showed the presence of five separate peaks. Peak 1 (enniatin B1) (**4**) ($C_{34}H_{59}N_3O_9$) was isolated as a pale yellow oil (9 mg): $[\alpha]_D$ +173.8 (*c* 0.6, $CHCl_3$, 25°C); IR ν_{max} (NaCl): 2966 (C-H, alkane), 1744 (C=O, ester), 1654 (C=O, amide); *m/z*: 653.4250 (calcd. 653.4254); solid probe MS EI *m/z*: 42(base), 55(26), 69(56), 86(89), 100(48), 112(8), 126(12), 142(20), 154(21), 169(42), 182(32), 196(72), 210(38), 228(6), 282(15), 296(19), 310(18), 423(6), 552(5), 571(4), 653(M^+).

Peak 3 (enniatin A1) (**3**) ($C_{35}H_{61}N_3O_9$) was isolated as a pale yellow oil. Recrystallization from ethanol/water yielded 114 mg of colourless needle crystals: mp 66–67°C; $[\alpha]_D$ −62.8 (*c* 2.3, $CHCl_3$, 25°C); IR ν_{max} (NaCl): 2965 (C-H, alkane), 1740 (C=O, ester), 1662 (C=O, amide); *m/z*: 667.4404 (calcd. 667.4410); solid probe MS EI *m/z*: 42(base), 55(20), 69(59), 86(51), 100(86), 112(8), 126(12), 142(18), 153(20), 169(29), 183(48), 196(52), 210(68), 228(11), 282(11), 296(18), 310(19), 324(10), 397(4), 423(7), 667(M^+).

Peak 4 (enniatin A2) (**6**) ($C_{36}H_{63}N_3O_9$) was isolated as a yellow oil, which was recrystallized from ethanol/water to give 46 mg of colourless needle crystals: mp 123–125°C; $[\alpha]_D$ −34.4 (*c* 4.1, $CHCl_3$, 25°C); IR ν_{max} (NaCl): 2965 (C-H, alkane), 1744 (C=O, ester), 1661 (C=O, amide); *m/z*: 681.4612 (calcd. 681.4567); solid probe MS EI *m/z*: 71(28), 83(20), 100(base), 112(9), 128(9), 143(12), 155(20), 169(15), 183(43), 196(19), 210(60), 228(8), 296(14), 310(8), 324(12), 681(M^+).

Peak 5, isolated as a yellow oil, was recrystallized, yielding 301 mg of colourless needle crystals, which were identified as enniatin A by comparison to published mass spectral and ^1H NMR data, melting points, and optical rotation.

The ^1H NMR of peak 2 showed the presence of two compounds. All attempts to separate these compounds were unsuccessful, and because of the small amount of material (7 mg), no further work was done on this fraction.

Acknowledgements

The authors would like to thank Dr. Peter Summers of the Department of Biology at Carleton University for the amino acid analysis of enniatin A2, and Mr. Pierre Lafontaine and Mr. Garry Montgomery for the solid probe EI mass spectra. In addition, we thank Mr. John Nikiforuk for the NMR spectra. This work was supported by a Natural Sciences and Engineering Research Council of Canada (NSERC) post graduate scholarship (L.B.) and by an NSERC strategic grant.

1. W. F. O. Marasas, P. E. Nelson, and T. A. Toussoun. *In* Toxigenic *Fusarium* Species: Identity and mycotoxicology. The Pennsylvania State University Press, University Park, Pa. 1984.
2. J. D. Miller, D. Strongman, and N. J. Whitney. Can. J. For. Res. **15**, 896 (1985).
3. Douglas B. Strongman, George M. Strunz, Pierre Giguere, Chao-Mei Yu, and Larry Calhoun. J. Chem. Ecol. **14**, 753 (1988).
4. H. Burmeister and R. D. Plattner. Phytopathology, **77**, 1483 (1987).
5. J. F. Grove and M. Pople. Mycopathologia, **70**, 103 (1980).
6. M. O. Tirunarayanan and M. Sirsi. J. Indian Inst. Sci. **39**, 185 (1957).
7. E. Gaumann, St. Naef-Roth, and H. Kern. Phytopathol. Z. **40**, 45 (1960).
8. E. Gaumann, S. Roth, L. Ettlinger, P. A. Plattner, and U. Nager. Experientia, **3**, 202 (1947).
9. Yu. A. Ovchinnikov, V. T. Ivanov, A. V. Evstratov, I. I. Mikhaleva, V. F. Bystrov, S. L. Portnova, T. A. Balashova, E. N. Meshcheryakova, and V. M. Tulchinsky. Int. J. Peptide Protein Res. **6**, 465 (1974).
10. T. K. Audhya and D. W. Russell. Can. J. Microbiol. **19**, 1051 (1973).
11. J. D. Miller and B. A. Blackwell. Can. J. Bot. **64**, 1 (1986).
12. Yu. A. Ovchinnikov, V. T. Ivanov, I. I. Mikhaleva, and M. M. Shemyakin. Izv. Akad. Nauk S.S.S.R., Ser. Khim. 1823 (1964).
13. P. A. Plattner and U. Nager. Helv. Chim. Acta, **31**, 665 (1948); **31**, 2192 (1948); **31**, 2203 (1948).

A general synthesis of 5,7-diaminoimidazo[4,5-*b*]pyridine ribosides ("2-amino-1-deazaadenosines") from 5-amino-4-imidazolecarboxamide riboside (AICA riboside)

JOHN E. FRANCIS[1] AND MICHAEL A. MOSKAL

Research Department, Pharmaceuticals Division, CIBA–GEIGY Corporation, Summit, NJ 07901, U.S.A.

Received July 31, 1991

This paper is dedicated to Professor Zdenek (Denny) Valenta on the occasion of his 65th birthday

JOHN E. FRANCIS and MICHAEL A. MOSKAL. Can. J. Chem. **70**, 1288 (1992).

A short general synthesis of 5-substituted 5,7-diaminoimidazo[4,5-*b*]pyridines from 5-amino-4-imidazolecarboxamide riboside (AICA riboside) was designed to prepare isosteres of substituted 2-aminoadenosines that are selective adenosine A_2 receptor agonists. AICA riboside was converted to a hydroxyl-protected 5-amino-4-imidazolecarbonitrile riboside and reacted with an *N*,*N*-disubstituted acetamide in the presence of phosphoryl chloride. Sodium hydride treatment completed the ring closure and introduced the 7-amino group. The hydroxyl protecting groups were removed under standard conditions. *N*-Substitution of the acetamide by one benzyl moiety led to a 5-*N*-substituted derivative through hydrogenolysis whereas *N*,*N*-dibenzylacetamide led to the 5,7-diamino compound. A 6-methyl analog was obtained from an *N*,*N*-disubstituted propionamide. This synthesis may be adapted to other heterocyclic systems, as illustrated by the preparation of an example of the imidazo[4,5-*b*]pyrrolo[3,2-*e*]pyridine ring system.

JOHN E. FRANCIS et MICHAEL A. MOSKAL. Can. J. Chem. **70**, 1288 (1992).

Dans le but de préparer des isostères des 2-aminoadénosines substituées qui sont des agonistes sélectifs du récepteur A_2 de l'adénosine, on a développé une courte méthode générale de synthèse des 5,7-diamino-imidazo[4,5-*b*]pyridines substituées en position 5 utilisant le riboside du 5-amino-4-imidazolecarboxamide (riboside du AICA) somme produit de départ. On a transformé le riboside du AICA en un riboside du 5-amino-4-imidazolecarbonitrile dont l'hydroxyle était protégé et on a fait réagir ce dernier avec un acétamide *N*,*N*-disubstitué, en présence de chlorure de phosphoryle. Un traitement avec de l'hydrure de sodium a permis de compléter la fermeture du cycle et l'introduction du groupe 7-amino. Utilisant des conditions standard, on a alors enlevé les groups protégeant les hydroxyles. La *N*-substitution de l'acétamide par une portion benzylique a conduit par hydrogénolyse à la formation d'un dérivé 5,*N*-substitué; dans les mêmes conditions, un *N*,*N*-dibenzylacétamide conduit au composé 5,7-diamino. À partir d'une propanamide *N*,*N*-disubstituée, on a obtenu un analogue portant un groupement méthyle en position 6. On peut adapter cette synthèse à d'autres systèmes hétérocycliques et on l'a illustré avec la préparation d'un exemple du système cyclique imidazo[4,5-*b*]pyrrolo[3,2-*e*]-pyridine.

[Traduit par la rédaction]

Can. J. Chem. Downloaded from www.nrcresearchpress.com by 217.78.4.112 on 09/08/12
For personal use only.

Adenosine (**1***a*), an endogenous purine nucleoside, was reported by Drury and Szent-Gyorgyi to have potent hypotensive and bradycardic activity in 1929 (*1*). In 1963, Berne (2) spurred additional interest when he proposed that adenosine plays an important role as the mediator of metabolically regulated coronary flow. Based on subsequent investigations (3), the role of adenosine as a local regulator of blood flow in other tissues was postulated. Although this short-acting compound seems an excellent lead structure for the design of novel cardiovascular drugs through molecular modification, research has not yet produced such a drug, except for the natural product itself, which was recently marketed[2] for the intravenous treatment of supraventricular tachycardia (4).

A recent rebirth of interest in modification of the adenosine structure (5) followed the recognition and characterization of purinergic receptors in peripheral cell membranes (6), particularly the A_1 and A_2 receptors (7, 8). The negative dromo-, chrono-, and inotropic effects of adenosine are thought to be A_1 mediated (9) whereas the vasodilatory effects are A_2 mediated (10).

Our interest in vasodilators led to a search for selective A_2 receptor agonists. A lead compound was the moderately A_2 selective agonist 2-anilinoadenosine (**1***b*) (11), which had been characterized as a coronary dilator in anaesthetized dogs (12) at the time we began our research. Subsequent modification of **1***b* led us to a series of 2-substituted aminoadenosines which were highly selective A_2 receptor agonists that lowered blood pressure effectively in spontaneously hypertensive rats (13).

Since 7-amino-3-(β-D-ribofuranosyl)imidazo[4,5-*b*]pyridine (1-deazaadenosine, **2***a*) showed adenosine-like activity (14), it seemed worthwhile to prepare 1-deaza analogs structurally related to **1***b* and our active 2-aminoadenosines, i.e., 5,7-diaminoimidazo[4,5-*b*]pyridine ribosides of the general structure **2***b*. Ethyl *N*-(7-chloro-3*H*-imidazo[4,5-*b*]pyridin-5-yl)carbamate (**3**), prepared in nine steps from chelidamic acid (**4**) (15), was converted in nine further steps to structures of type **2***b* in which the R′ group is hydrogen and the *R*″ group is hydrogen, alkyl, or substituted alkyl (16).

Herein we report a much shorter and more general synthesis starting from 5-amino-1-(β-D-ribofuranosyl)imidazole-4-carboxamide (AICA riboside, **5**), accessible chemically from inosine (17) or by fermentation (18). This had been used as a building block for **1***b* and many related 2-aminoadenosines (19) and contains all of the chiral centres and most of the atoms present in the compounds we planned to synthesize.

A route similar to the preparation of 2-alkylaminoadenosines from 2-chloroadenosine (**1***c*) (13) was not feasible in the 7-aminoimidazo[4,5-*b*]pyridine series because a halide at position 5 is not easily displaced. The report of a convenient synthesis of 2,4-diaminoquinoline derivatives (20) from anthranilonitriles suggested a viable route to our target compounds. We studied some variations of the published

[1]Author to whom correspondence may be addressed.

[2]Adenocard® (Fujisawa Pharmaceutical Company).

methodology through model reactions. We found that 5-chloroanthranilonitrile (**6**) reacted with dimethylacetamide dimethyl acetal in refluxing cyclohexane to form the intermediate **7***a* in 79% yield and this could be converted conveniently with sodium hydride in refluxing dioxane to **8***a* in 80% yield. Similarly, the aminocyanopyrazole **9** was converted via intermediate **10** (in this case prepared in refluxing acetonitrile) to the pyrazolo[3,4-*b*]pyridine **11** in 50% overall yield.

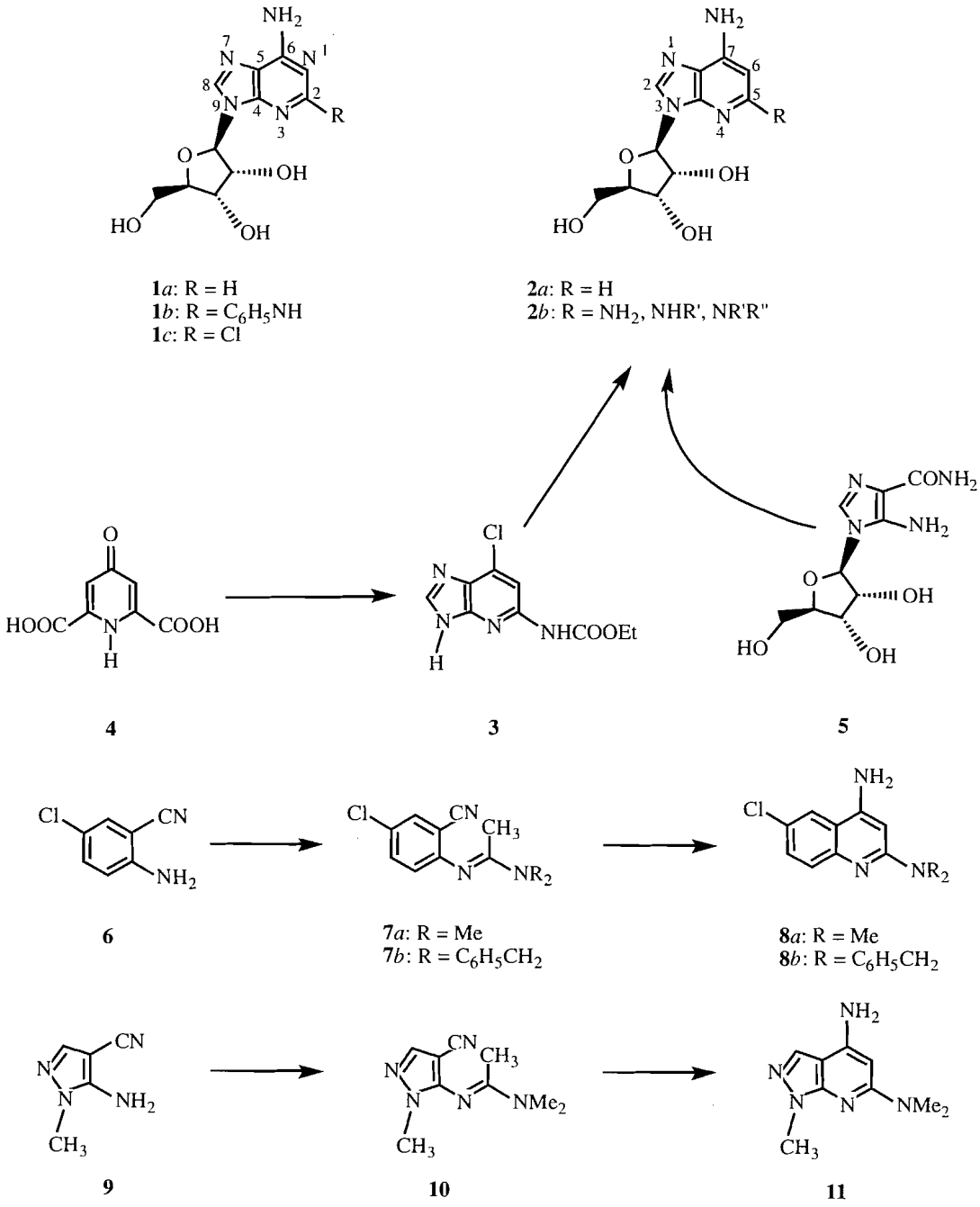

AICA riboside (**5**) was converted to the 2′,3′-protected aminonitrile **12** by a six-step literature route (21) in 25% yield. Reaction of this intermediate with commercial dimethylacetamide dimethyl acetal gave the expected product **13** under the mild conditions of overnight treatment at room temperature. The same result was obtained by the use of dimethylacetamide treated with dimethyl sulphate and neutralized with sodium methoxide. Cyclization with sodium hydride/dioxane at 110°C over 1 h followed by deprotection with 90% trifluoroacetic acid at 0°C in 0.5 h gave **2***c* (R = NMe_2) in 83% yield. Attempted removal of the isopropylidene protecting group with dilute hydrochloric acid, 80% acetic acid, or 50% formic acid resulted in some loss of the ribosyl moiety.

The paucity of commercially available orthoamides limits the general utility of this approach. Since condensation of an orthoester with the aminonitrile followed by displacement of the alkoxide group by a secondary amine was shown

Can. J. Chem. Downloaded from www.nrcresearchpress.com by 217.78.4.112 on 09/08/12
For personal use only.

Can. J. Chem. Downloaded from www.nrcresearchpress.com by 217.78.4.112 on 09/08/12
For personal use only.

to involve temperatures of 150°C in each step (20), we did not pursue this alternate two-step approach. Replacement of dimethylacetamide with other tertiary amides revealed a further disadvantage of the orthoamide approach. Reaction of **12** with *N*-methylacetanilide/dimethyl sulphate/sodium methoxide gave none of the desired compound **2***d* (R = $N(Me)C_6H_5$). *N*-Methylaniline was detected as a product of the reaction, indicative of preferential C—N bond cleavage rather than C—O cleavage with alkoxide elimination. The result is not surprising since the ready displacement of *N*-methylaniline anion rather than alkoxide from an amide acetal at basic pH has been observed previously (22).

We turned to the method of activating the tertiary amide through conversion to its imidinium chloride. Treatment of *N*,*N*-dibenzylacetamide with phosphoryl chloride in acetonitrile at room temperature followed by addition of **6** gave the desired intermediate **7***b* in 67% yield, which was converted to **8***b* with sodium hydride. By the same route, 5-amino-(1*H*)imidazole-4-carbonitrile (**14**) was converted to **15***a* and cyclized to **16***a*, a potential building block for a wide variety of 5,7-diaminoimidazo[4,5-*b*]pyridines. Substitution of *N*-methylacetanilide as the tertiary amide led to **15***b* and **16***b*. The synthesis of **10** from **9** with dimethylacetamide and phosphoryl chloride was achieved in 97% yield.

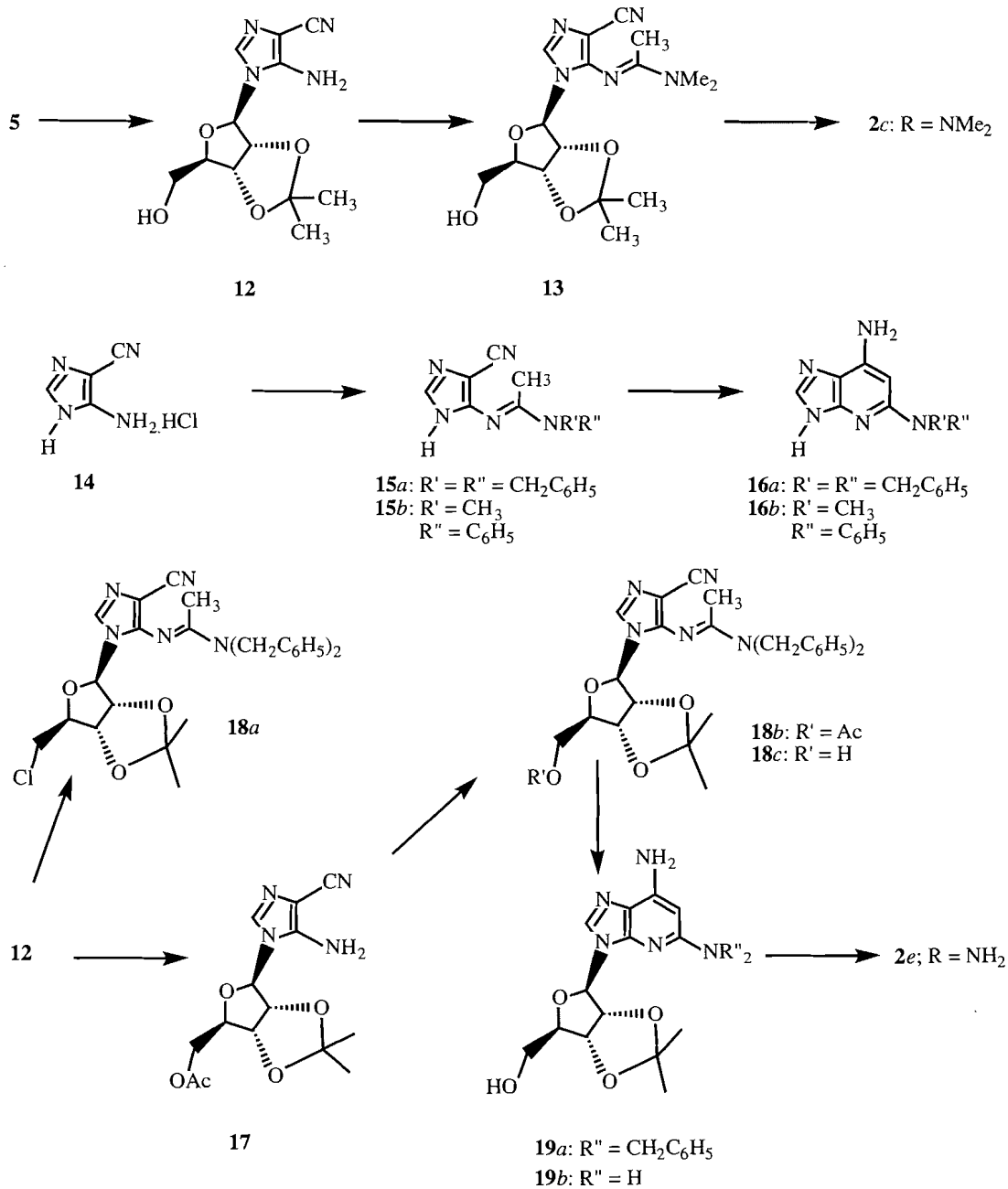

The remaining target compounds were then prepared in the following manner. Intermediate **12** was protected at the 5′-position as the acetate (**17**) before condensation with an imidinium chloride. Omission of this step in the reaction with dibenzylacetamide led to a significant amount of the 5′-chloro derivative **18***a*. Condensation of **17** with *N*,*N*-dibenzylacet-

Can. J. Chem. Downloaded from www.nrcresearchpress.com by 217.78.4.112 on 09/08/12
For personal use only.

amide/phosphoryl chloride in acetonitrile at room temperature over 16 h gave the desired intermediate **18***b* as an oil that was hydrolysed with methanolic ammonia to afford **18***c* in 90% overall yield. Cyclization with sodium hydride in dioxane produced crude **19***a* as a foam. Removal of both benzyl groups was achieved with hydrogen over palladium hydroxide in ethanol at 50°C and 45 psi (1 psi = 6.89 kPa) to afford **19***b* in nearly quantitative yield. Removal of the remaining protecting group with 90% trifluoroacetic acid gave **2***e* (R = NH_2), characterized as both the trifluoroacetate and dihydrochloride. When *N*-benzylacetanilide was substituted for *N*,*N*-dibenzylacetamide in the sequence, the target compound **2***f* (R = NHC_6H_5) was obtained. Targets **2***g* (R = $NHCH_2CH_2C_6H_4$-*p*-$CH_2CH_2C_6H_5$) and **2***h* (R = $NHCH_2CH_2$-C_6H_4-*p*-CH_2CH_2COOH) were also prepared. For **2***h*, the *p*-substituent was introduced conveniently by Heck reaction conditions (23) from the N^5-*p*-bromophenethyl intermediate with the 2′ and 3′ hydroxyls protected.

Substitution in the 6-position by methyl was achieved through the use of an *N*-substituted *N*-benzylpropionamide, as illustrated by the synthesis of **20**. Finally, annelation of the imidazopyridine ring system at the 5- and 6-positions was accomplished through the use of an *N*-benzylated lactam. Specifically, *N*-benzylbutyrolactam was converted through the usual steps to the tricyclic compound **21**, an example of the previously unreported imidazo[4,5-*b*]pyrrolo[3,2-*e*]pyridine ring system.

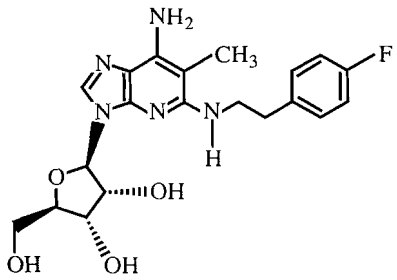

20

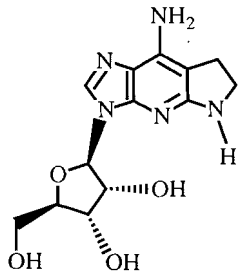

21

Some biochemical and pharmacological results on this series will be reported separately. Since these 1-deazaadenosine derivatives cannot be metabolized to intermediates that can form Watson–Crick base pairs (24), we hope that these compounds will show fewer side effects than their purine riboside isosteres.

Experimental

All reactions were carried out under nitrogen. Melting points (uncorrected) were determined on a Thomas–Hoover capillary apparatus. Proton NMR were determined on a Varian XL-300, Varian XL-400, Bruker AC-300, or Bruker AC-250 instrument with tetramethylsilane as internal standard in deuterated dimethyl sulphoxide unless otherwise stated. Spectral shifts are reported as δ (ppm) values. Solvents used were spectral or HPLC grade. Chromatography was done under nitrogen pressure with silica gel 60 (230–400 mesh) from E. Merck. Where noted, compounds analysed for C, H, and N within ±0.4 units unless otherwise stated. IR spectra, taken in Nujol mulls, were recorded on a Perkin–Elmer model 457 spectrometer and peaks are expressed in reciprocal centimeters. Mass spectra were taken with a Hewlett–Packard 5985B mass spectrometer in the Cl mode. Silica gel 60 TLC plates were obtained from EM Science.

*5-Chloro-2-[1-dimethylamino)ethylideneamino]benzonitrile (7*a*)*

A mixture of 5-chloroanthranilonitrile (9.5 g, 62 mM), dimethylacetamide dimethylacetal (ca. 90%, containing methanol, 9.7 mL), and cyclohexane (70 mL) was heated in a Dean–Stark apparatus at reflux until 40 mL of liquid were collected (ca. 4.5 h). The red solution was concentrated to dryness at 70°C under water pump vacuum, taken up in hot cyclohexane (100 mL), and filtered. The filtrate was treated with hexane (50 mL) as it cooled and crystals began to form. The mixture was refrigerated overnight and the off-white needles were collected and air dried to afford 10.47 g (79%), mp 84–87°C. A sample was sublimed for analysis at 60°/0.1 Torr (1 Torr = 133.3 Pa) to a pure white solid, mp 85–87°C; IR: 2222, 1602, 1586, 1300, 1191, 841; ^{1}HMR: 1.9 (s, 2 CH_3), 3.0 (s, CH_3), 6.8 (d, H at 3), 7.5 (dd, H at 4), 7.73 (d, H at 6); MS: 222 (M + 1). Anal. $C_{11}H_{12}ClN_3$: C, H, N.

*4-Amino-6-chloro-2-dimethylaminoquinoline (8*a*)*

A mixture of **7***a* (1.11 g, 5 nM), 50% sodium hydride in oil (0.5 g), and dioxane (15 mL) was heated under reflux for 5.5 h during which time a yellow solid began to form. The mixture was cooled and the product was collected, washed with a little dioxane, and suspended in ether (30 mL) in a separatory funnel to which water (20 mL) was cautiously added. The clear ether layer was collected and the aqueous layer extracted twice with ether (2 × 10 mL). The ether extract was dried (Mg_2SO_4) and concentrated to dryness at reduced pressure. The residue was triturated with hexane and collected as an off-white solid, pure by TLC (R_f = 0.1 with 3:1 toluene – ethyl acetate vs. starting material, R_f = 0.7) (0.89 g, 80%, mp 155–160°C). Recrystallization from toluene gave pure white crystals, mp 165–167°C; IR: 3341, 3188, 1643, 1591, 1503, 825; ^{1}HMR: 3.05 (s, 2 CH_3), 6.1 (s, H at 3), 6.4 (s, NH_2, exchangeable with D_2O), 7.35 (m, H, s at 3 and 4), 8.0 (s, H at 6). Anal. $C_{11}H_{12}ClN_3$: C, H, N.

*5-[1-(Dimethylamino)ethylideneamino]-1-methylpyrazole-4-carbonitrile (**10**)*

A mixture of 5-amino-1-methylpyrazole-4-carbonitrile (**9**) prepared by the literature method (25) (0.61 g, 5 nM), dimethylacetamide dimethyl acetal (1 mL), and acetonitrile (21 mL) was stirred at 90°C for 4 h. It was concentrated to dryness at 70°C under water vacuum to a dark oil and triturated with hexane to yellow-orange solid **10** (0.74 g, 77%, mp 45–50°C), pure by TLC (R_f = 0.5, 4:1 CH_2Cl_2–EtOAc vs. starting material, R_f = 0.33), and used directly to prepare **11**.

A mixture of **9** (0.8 g, 6.5 mM), dimethylacetamide (2.35 g), and acetonitrile (10 mL) was treated dropwise at room temperature with phosphoryl chloride. After 5 min, TLC (1:1 CH_2Cl_2–EtOAc) indicated complete reaction. The mixture was poured into ice-cold ammonium hydroxide and extracted with ethyl acetate (2 × 40 mL). The organic extract was washed with brine, dried (Na_2SO_4), and concentrated to dryness at reduced pressure. Treatment of the oily residue with hexane with seed crystals yielded **10** as a yellow solid (1.12 g, 90%, mp 59–61°C); IR: 2215, 1597, 1511, 1029; ^{1}HMR: 2.0 (s, N-CH_3), 3.1 (d, 2 CH_3), 3.5 (s, C-CH_3), 7.7 (s, H at 3). Anal. calcd. for $C_9H_{13}N_5$: C 56.53, H, N; found: C 57.08.

*4,6-Diamino-1,N^6,N^6-trimethylpyrazolo[3,4-b]pyridine (**11**)*

A mixture of **10** (0.74 g, 3.9 mM), 50% sodium hydride in oil (0.39 g), and dioxane (10 mL) was stirred at reflux for 1.5 h. It was cooled and filtered free of white solid (**caution ! nasal irritant !**) and concentrated at reduced pressure to a semisolid. This was triturated with ether, and water was then added to form a yellow solid, insoluble in both solvents. The material was collected, washed with water (3 × 10 mL), then with hexane (2 × 10 mL), and vacuum oven dried at 80°C/10 Torr) to afford **11** (0.47 g, 64%), mp 174–177°C. It was recrystallized from toluene to form the pure product as yellow crystals, mp 178–181°C; IR: 3352, 3210, 1606, 1592, 1165, 985; ^{1}HMR: 3.0 (s, 2 CH_3), 3.75 (s, N-CH_3), 5.55 (s, H at 5), 6.3 (s, NH_2, exchangeable with D_2O), 7.75 (H at 3); MS: 192 (M + 1). Anal. $C_9H_{13}N_5$: C, H, N.

Can. J. Chem. Downloaded from www.nrcresearchpress.com by 217.78.4.112 on 09/08/12
For personal use only.

*5-[1-(Dimethylamino)ethylideneamino]-1-[2′,3′-O-(1-methylethylidene)-β-D-ribofuranosyl]-1H-imidazole-4-carbonitrile (**13**)*

To a suspension of 5-amino-1-[2′,3′-*O*-)1-methylethyidene)-β-D-ribofuranosyl)]imidazole-4-carbonitrile (**12**), prepared as described in the literature (21), (0.56 g, 2 mM) in acetonitrile (10 mL) was added dimethylacetamide dimethylacetal (1.0 mL) and the mixture stirred at room temperature overnight. It was concentrated under high vacuum (0.1 Torr) and the residue was redissolved in ether–acetonitrile (1:1), treated with charcoal, filtered, and the filtrate was concentrated to dryness at reduced pressure and triturated with ether to afford **13** (0.45 g, 64%), mp 122–125°C. It was recrystallized from ethyl acetate to give the pure material, mp 127–129°C; IR: 2210, 1609; ^{1}HMR ($CDCl_3$): 1.35 (s, CH_3), 1.58 (s, CH_3), 2.13 (s, CH_3), 3.1 (s, 2 CH_3), 3.85 (m, 5′-CH_2), 4.1 (br s, OH), 4.33 (m, 4′-H), 4.95 (m, 3′ + 2′-H), 5.75 (d, H at 1′), 7.8 (s, H at 8); MS: 350 (M + 1). Anal. $C_{16}H_{23}N_5O_4$: C, H, N.

*5,7-Diamino-3-[β-D-ribofuranosyl]-N^5,N^5-dimethyl-3H-imidazo[4,5-b]pyridine(**2**c)*

Sodium hydride (60% in oil, 1.2 g) was prewashed with hexane, suspended in dioxane (60 mL), then treated with **13** (2.6 g, 7.4 mM), and the mixture was stirred at 110°C for 1 h. It was poured into ice-water (200 mL) and extracted with ethyl acetate (3 × 100 mL). The organic layer was washed with brine, dried (Na_2SO_4), decolorized with charcoal, filtered, and evaporated at reduced pressure to a semisolid. This was triturated with ether and collected as a white solid (1.95 g, 75%), which was pure *5,7-diamino-3-[2′,3′-O-(1-methylethylidene)-β-D-ribofuranosyl]-N^5,N^5-dimethyl-3H-imidazo[4,5-b]pyridine*, mp 176–178°C; $[\alpha]_D^{25}$ −8.15 (*c* = 1.36, DMSO); IR: 3437, 3361, 3248, 3098, 1637, 1598, 1510; ^{1}HMR ($CDCl_3$): 1.4 (s, CH_3), 1.65 (s, CH_3), 3.1 (s, 2 CH_3), 3.85 (m, 5′-CH_2), 4.4 (m, 4′-H), 4.9 (br s, NH_2), 5.15 (m, 3′-H), 5.6 (m, 2′-H), 5.75 (s, H at 6), 5.9 (d, 1′-H), 7.8 (s, H at 2); MS: 350 (M + 1), 178 (aglycone). Anal. $C_{16}H_{23}N_5O_4$: C, H, N. This intermediate (0.70 g, 2 mM) was stirred in an ice-cold 9:1 mixture of trifluoroacetic acid and water (5 mL) at 0–5°C for 1 h. Ether (75 mL) was added and after 10 min the trifluoroacetic acid salt of **2***c* was collected as a while solid (0.81 g, 95%). It was added to 8% aqueous sodium bicarbonate solution and, after several minutes, the free base crystallized. This was washed with water and dried under vacuum to afford white crystals (0.52 g, 85%, mp 219–222°C); $[\alpha]_D^{25}$ −36.87 (*c* = 1.55, DMSO); IR: 3408, 3312, 3218, 3125, 1634, 1602, 1522, 1078, 1032; ^{1}HMR: 2.9 (s, 2 CH_3), 3.6 (m, 5′-CH_2), 3.75 (m, 4′-H), 4.15 (dd, 3′-H), 4.65 (dd, 2′-H), 4.85 (br s, OH), 5.1 (br s, OH), 5.3 (br s, OH), 5.7 (s, H at 6), 5.8 (d, 1′-H), 5.95 (s, NH_2), 7.9 (s, H at 2); MS: 310 (M + 1), 178 (aglycone). Anal. $C_{13}H_{19}N_5O_4$: C, H, N.

*2-[1-(Dibenzylamino)ethylideneamino]-5-chlorobenzonitrile (**7**b)*

A stirring mixture of 5-chloroanthranilonitrile (1.52 g, 10 mM) and *N,N*-dibenzylacetamide (9.56 g, 40 mM) in acetonitrile (25 mL) was treated dropwise with phosphoryl chloride (3.06 g, 20 mM) and stirred 3 h at room temperature. The mixture was poured into ice-cold ammonium hydroxide and extracted with ethyl acetate (2 × 100 mL). The organic layer was washed with brine, dried (Na_2SO_4), and concentrated to dryness at reduced pressure to a red oil. The oil was triturated several times with hexane and the hexane wash discarded. The residue was triturated with isopropanol and the product obtained as a white solid after vacuum oven drying (2.48 g, 67%), mp 101–110°C; IR: 2220, 1592, 698; ^{1}HMR: 2.0 (s, CH_3), 4.7 (s, 2 CH_2), 6.9 (d, 3-H), 7.3 (m, 10 aromatic H), 7.57 (dd, 4-H), 7.8 (d, 6-H). Anal. $C_{23}H_{20}ClN_3$: C, H, N. By the same procedure, 5-aminoimidazole-4-carbonitrile hydrochloride (**14**) (26) was converted to **15***a*, a foam, mp 144–148°C, in 42% yield. Anal. $C_{20}H_{19}N_5$: C, H, N. Similarly, **17**, prepared as described by Suzuki and Kumashiro (27), was converted to **18***b*, an oil, in 88% yield; MS: 544 (M + 1). *N*-Methylacetanilide, combined with **14** and phosphoryl chloride by the same procedure, led to **15***b*, mp 222–225°C, in 67% yield. Anal. $C_{13}H_{13}N_5 \cdot 0.25H_2O$: C, H, N.

*2,4-Diamino-N^2,N^2-dibenzyl-6-chloroquinoline (**8**b)*

A mixture of **7***b* (0.37 g, 1 mM) and sodium hydride (60% in oil, 0.16 g) in dioxane (5 mL) was heated 3 h at reflux. It was poured into ice-water, extracted with ethyl acetate, and the organic layer was washed with brine, dried (Na_2SO_4), treated with charcoal, filtered, and concentrated to dryness at reduced pressure to a reddish-brown solid (0.28 g, 76%). This residue was triturated with hexane–ether to afford the pure material (0.21 g), mp 217–220°C; IR: 3490, 3305, 3175, 1638, 1592, 1497, 1215, 736; ^{1}HMR: 4.8 (2 CH_2), 6.1 (H at 3), 6.4 (NH_2, exchangeable with D_2O), 7.2–7.4 (m, 12 H), 8.0 (s, H at 5). Anal. $C_{23}H_{20}ClN_3$: C, H, N. By the same procedure, **15***a* was converted to **16***a*, mp 196–198°C, in 69% yield. Anal. $C_{20}H_{19}N_5$: C, H, N. Similarly, **15***b* was converted to **16***b*, mp 214–216°C, in 71% yield. Anal. $C_{13}H_{13}N_5$: C, H, N.

*5,7-Diamino-3-(β-D-ribofuranosyl)imidazo[4,5-b]pyridine (**2**e)*

A mixture of **18***b* (7.0 g, 13 mM) and methanol saturated with ammonia (250 mL) was stirred overnight at room temperature. The mixture was concentrated to dryness at room temperature and the residue was taken up in ethyl acetate (300 mL), washed with water (3 × 100 mL), then with brine (100 mL), dried (Na_2SO_4), and concentrated to dryness at reduced pressure to afford crude **18***c* as a foam. This was chromatographed on a 220 × 50 mm column with 2:1 methylene chloride – ethyl acetate as eluent (4 × 600 mL fractions) followed by ethyl acetate alone (30 mL) fractions. The product was collected in ethyl acetate fractions 19–60 and concentrated at reduced pressure to afford chromatographically pure **18***c* as a foam (5.9 g, 91%). The foam (5.8 g, 11.5 mM) was added in dioxane (50 mL) to sodium hydride (60% in oil, 1.85 g, prewashed with hexane) in dioxane (100 mL) and the mixture was heated at 100°C for 1 h. The reaction mixture was poured into ice-water, extracted with ethyl acetate (3 × 100 mL), and the extract washed with brine (50 mL), dried (Na_2SO_4), and concentrated to dryness to afford **19***a* as a foam (5.7 g, 98%). The cyclized intermediate **19***a* (5.6 g) was hydrogenated in the presence of palladium hydroxide (5.6 g) in 95% ethanol (200 mL) in a Parr apparatus at 45 psi and 50°C for 4.5 h. The mixture was filtered and the filtrate concentrated to dryness at reduced pressure to give **19***b*, the 2′,3′-*O*-(1-methylethylidene) derivative of **2***e*, as a colorless foam (3.3 g, 94%). This acetonide (2.65 g, 8.2 mM) was stirred in an ice-cold solution of 90% aqueous trifluoroacetic acid until TLC (9:1 CH_2Cl_2–NH_3-saturated methanol) showed complete loss of starting material, R_f = 0.5, with product R_f = 0.0. The solution was diluted with ether (375 mL), stirred 15 min, and the precipitated crude trifluoroacetate salt of **2***e* collected and air dried (3.2 g, 100%), mp 124–127°C. A portion (0.5 g) was dissolved in acetonitrile (50 mL), filtered, and the filtrate saturated with dry HCl under ice cooling. A turbid mixture formed that during 18 h at room temperture became a white solid. The product (0.35 g), mp 105°C (dec.), was the dihydrochloride of **2***e*; $[\alpha]_D^{25}$ −67.4 (*c* = 1, H_2O); ^{1}HMR (CD_3OD): 3.9 (m, 5′-CH_2), 4.3 (m, 4′-H + 3′-H), 4.45 (dd, 2′-H), 5.9 (s, H at 6), 5.95 (d, 1′-H), 8.55 (s, H at 2); MS: 150 (aglycone, M + 1). Anal. calcd. for $C_{11}H_{17}Cl_2N_5O_4$: C, H, N, Cl 20.01; found: Cl 19.57.

*7-Amino-5-anilino-3-(β-D-ribofuranosyl)imidazo[4,5-b]pyridine (**2**f)*

N-Benzylacetanilide, bp 135–150°C at 3 Torr, prepared by reacting *N*-benzylaniline with a 50% excess of triethylamine and a 40% excess of acetyl chloride at room temperature over 42 h (6.4 g, 28.8 mM), and **17** (2.3 g, 7.2 mM) in acetonitrile (25 mL) were treated dropwise under stirring with phosphoryl chloride (2.2 g, 14.4 mM). After 48 h, the mixture was quenched in ice-cold sodium bicarbonate solution, extracted with ethyl acetate, and the extract washed several times with dilute bicarbonate, then with water and brine, dried (Na_2SO_4), and concentrated to dryness at reduced pressure to an oily residue (3.8 g). The oil was flash

Can. J. Chem. Downloaded from www.nrcresearchpress.com by 217.78.4.112 on 09/08/12
For personal use only.

chromatographed with methylene chloride – ethyl acetate (5:1) and 60 35-mL fractions were collected. A 1:1 solvent mixture was used for the next 20 35-mL fractions. Combined fractions 41–80, one spot by TLC, were concentrated to dryness to afford the pure material (1.1 g, 29%) as an oil. This intermediate was stirred overnight in ammonia-saturated methanol (50 mL) and concentrated to dryness at reduced pressure. The residue was taken up in ethyl acetate (25 mL), washed with water (4 × 10 mL), then with brine, dried (Na_2SO_4), and concentrated to dryness to an off-white foam. This was combined with material from a similar run and flash chromatographed with 1:1 methylene chloride ethyl acetate (100 mL × 12 fractions) followed by ethyl acetate alone (100 mL × 4 fractions). Fractions 4–14 were combined and concentrated to a white foam, mp 68–78°C (1.85 g, 94%). This 5′-alcohol (1.8 g, 3.7 mM) in dioxane (15 mL) was added dropwise to a suspension of sodium hydride (60% in oil, 0.6 g, 14.8 mM, washed 3 times with hexane) in dioxane (30 mL) and heated at reflux for 1.5 h. The mixture was quenched in ice-water and extracted with ethyl acetate (3 × 70 mL). The extract was washed with water, then with brine, dried (Na_2SO_4), and concentrated at reduced pressure to a foam (1.8 g), which contained a trace of impurity (TLC). It was flash chromatographed with 3:1 methylene chloride – ethyl acetate, followed by a 1:1 mixture, then by ethyl acetate alone. The pure product was found in the ethyl acetate eluent. Evaporation of the combined fractions yielded the 2′,3′-*O*-(1-methylethylidene) derivative of N^5-benzyl **2***f* as a foam, mp 93–99°C (1.63 g, 90%). Anal. $C_{27}H_{29}N_5O_4$: C, H, N. The *N*-benzyl compound (1.5 g) was hydrogenolized in 95% ethanol (150 mL) with palladium hydroxide (1.5 g) at 50°C and 50 psi for 6 h, then with fresh catalyst for another 6 h. The mixture was filtered and the solvent removed at reduced pressure to afford the crude 2′,3′-*O*-(1-methylethylidene) derivative of **2***f* (1.0 g, 83%). Recrystallization from ethyl acetate gave pure material, mp 225–228°C; $[\alpha]_D^{25}$ 9.68 (c = 0.91, DMSO); ^{1}HMR: (CD_3OD): 1.4 (s, CH_3), 1.6 (s, CH_3), 3.65 (m, 5′-CH_2), 4.3 (m, 4′-H), 4.95 (dd, 3′-H), 5.45 (dd, 2′-H), 6.0 (s, H at 6), 6.1 (d, 1′-H), 6.9 (dd, *p*-H), 7.25 (dd, 2 *m*-H), 7.5 (d, 2 *o*-H), 8.0 (s, H at 2); MS: 398 (M + 1). Anal. $C_{20}H_{23}N_5O_4$: C, H, N. The acetonide (0.6 g) was stirred at 0–5°C in 90% aqueous trifluoroacetic acid (4 mL) for 1 h. It was diluted with ether (20 mL) and, after 20 min, the trifluoroacetate salt (320 mg) was collected, suspended in dilute sodium bicarbonate solution, extracted with ethyl acetate, and the organic extract washed with brine, dried (Na_2SO_4), and concentrated to dryness to an off-white solid (220 mg) containing trace impurities. The material was chromatographed with mixtures of methylene chloride and ammonia-saturated methanol, 15:1 for the first 44 × 25-mL fractions, followed by 5:1 for the next 8 × 25-mL fractions. Fractions 21–48 were combined and concentrated to pure **2***f* obtained as a foamy solid (160 mg, 30%). The analytical sample was recrystallized from water, mp 192–195°C; $[\alpha]_D^{25}$ −19.33 (c = 1.29, DMSO); ^{1}HMR: 3.8 (m, 5′-CH_2), 4.1 (dt, 4′-CH_2), 4.3 (dd, 3′-H), 4.75 (dd, 2′-H), 5.95 (d, 1′-H), 6.1 (s, H at 6), 6.9 (m, *p*-H), 7.25 (m, 2 *m*-H), 7.4 (m, 2 *o*-H), 8.05 (s, H at 2); MS: 358 (M + 1). Anal. $C_{17}H_{19}N_5O_4 \cdot 0.25H_2O$: C, H, N.

5,7-Diamino-N^5*-[2-[4-(2-phenylethyl)phenyl]ethyl]-3-(*β-D-*ribofuranosyl)imidazo[4,5-*b*]pyridine (***2***g)*

A mixture of 2-(4-bromophenyl)ethylamine (Aldrich, 50 g, 0.25 M), and benzaldehyde (26.5 g, 0.25 M) in petroleum ether (700 mL) and acetic acid (200 mL) was treated dropwise under stirring at room temperature with borane–pyridine complex (Fluka, 23 g, 0.25 M) and, after 2 h, 5 N hydrochloric acid (150 mL) was added slowly to give a white precipitate. The precipitated salt was collected and the filtrate was extracted with ether and the ether layer discarded. The solid was added to the aqueous acidic layer, made basic with ice-cold sodium hydroxide solution, and extracted with ether. The ether layer was washed with brine, dried (Na_2SO_4), and concentrated at reduced pressure to an oil (63.7 g), which was chromatographed with 5:1 methylene chloride – ethyl acetate. Fractions containing the desired product were combined and concentrated to afford N-*benzyl-2-(4-bromophenyl)ethylamine* as an oil (42.7 g, 59%; ^{1}HMR ($CDCl_3$): 1.65 (NH), 2.8 (m, 2 CH_2), 3.8 (s, CH_2), 7.05–7.45 (m, 9 aryl H)) used directly in the next step. A mixture of the amine (42.6 g, 147 mM) and triethylamine (22.3 g, 220 mM) in cold methylene chloride (400 mL) was treated dropwise under stirring with an ice-cold solution of acetyl chloride (12.6 g, 162 mM) and stirred for 18 h at ambient temperature. The solution was extracted with 1 N hydrochloric acid (4 × 100 mL), water (100 mL), dilute aqueous sodium bicarbonate (2 × 100 mL), and water (100 mL), then dried (Na_2SO_4) and concentrated to dryness at reduced pressure. The oily product (48.3 g) was distilled to give 42.5 g (87%) of N-*acetyl*-N-*benzyl-2-(4-bromophenyl)ethylamine*, bp 216–218°C at 0.5 Torr; IR (neat): 3028, 1646, 1489, 1419, 1011. Anal. $C_{17}H_{18}BrNO$: C, H, N. A mixture of this amide (20 g, 60 mM), styrene (8.1 g, 78 mM), palladium acetate (0.14 g, 0.6 mM), tri-*o*-tolylphosphine (0.73 g, 2.4 mM), and triethylamine (39.4 g, 0.39 M) was heated at reflux for 18 h. The residue was treated with ice-cold 2 N hydrochloric acid (300 mL) and extracted with methylene chloride (3 × 400 mL). The organic layer was washed with water, dried (Na_2SO_4), and concentrated to dryness at reduced pressure. The residue was recrystallized from ethanol to afford pure N-*acetyl*-N-*benzyl-2-[4-(2-phenylethenyl)phenyl]ethylamine* (14.3 g, 67%), mp 136–138°C: Anal. $C_{25}H_{25}NO$: C, H. N. This material (14.2 g, 40 mM) was reacted with **17** (3.22 g, 10 mM) and phosphoryl chloride (3.06 g, 20 mM) and worked up as described in **2***f* to afford the desired adduct as a foam (4.1 g, 62%). This was saponified with methanolic ammonia as described and obtained as one-spot material by TLC in quantitative yield. Cyclization with sodium hydride in dioxane (reflux, 2 h) and subsequent work-up gave *5,7-diamino-*N^5*-benzyl-*N^5*-[2-[4-(2-phenylethenyl)phenyl]ethyl]-3-[2′,3′-*O*-(1-methylethylidene)-*β-D-*ribofuranosyl]imidazo[4,5-b]pyridine*, mp 174–177°C; MS: 618 (M + 1). Anal. $C_{37}H_{39}N_5O_4$: C, H, N. This intermediate (2.6 g, 4.2 mM) was hydrogenated in 95% ethanol (200 mL) containing 1 N hydrochloric acid (10 mL) in the presence of palladium hydroxide (5.2 g) at 50 psi at room temperature over 6 h. The mixture was filtered and the filtrate was stirred with propylene oxide (10 mL) for 30 min. Removal of the solvent gave a crystalline mass, which was triturated with ether to afford the 2′,3′-*O*-(1-methylethylidene) derivative of **2***g* (1.7 g, 77%) as a foam; IR: 3327, 3221, 3135, 1655, 1625, 1605, 1514; MS: 530 (M + 1). The acetonide (1.6 g, 3 mM) was stirred in 90% trifluoroacetic acid (10 mL) at 0–5°C for 1 h. Ether (15 mL) was added and after 15 min the salt was collected (1.6 g). It was dissolved in methanol (75 mL), filtered, and the filtrate treated with 6.5 N HCl in methanol (0.5 mL). The dihydrochloride salt of **2***g* crystallized as a white solid (1.1 g, 65%), mp 150–156°C; $[\alpha]_D^{25}$ −14.9 (c = 1.01, DMSO); IR: 3455, 3403, 3321, 3294, 3234, 2720 (br), 1678, 1659, 1574, 1513, 1093; ^{1}HMR: 2.8 (m, 3 CH_2), 3.4 (dd, CH_2-N), 3.65 (m, 5′-CH_2), 4.05 (dt, 4′-H), 4.15 (dd, 3′-H), 4.4 (dd, 2′-CH_2), 5.75 (s, H at 6), 5.9 (d, 1′-H), 7.2-7.3 (m, 9 aryl H), 8.7 (br s, H at 2); MS: 490 (M + 1 of base, weak), 358 (M + 1, aglycone). Anal. $C_{27}H_{31}N_5O_4 \cdot 2HCl$: C, H, N.

5,7-Diamino-N^5*-[2-[4-(2-carboxyethyl)phenyl]ethyl]-3-(*β-D-*ribofuranosyl)imidazo[4,5-*b*]pyridine (***2***h)*

N-Acetyl-*N*-benzyl-2-(4-bromophenyl)ethylamine (25.6 g, 80 mM) was reacted with **17** (6.44 g, 20 mM) and phosphoryl chloride (6.12 g, 40 mM) in acetonitrile and worked up as described for **2***f* to afford the crude adduct containing residual amide. This material was saponified with methanolic ammonia as described previously and chromatographed with 2:1 methylene chloride – ethyl acetate followed by ethyl acetate to afford 8.8 g (75%) of foamy solid. This material was reacted with a fourfold excess of sodium hydride as described for **2***f* to afford *5,7-diamino-*N^5*-benzyl-*N^5*-[2-(4-bromophenyl)ethyl]-3-[2′,3′-*O*-(1-methylethylidene)-*β-D-*ribofuranosyl]imidazo[4,5-b]pyridine* in 80% yield; MS: 594/596 (M + 1); Anal. $C_{29}H_{32}BrN_5O_4 \cdot H_2O$: C, H, N. This interme-

Can. J. Chem. Downloaded from www.nrcresearchpress.com by 217.78.4.112 on 09/08/12
For personal use only.

diate (1.78 g, 3 mM) was mixed with benzyl acrylate (0.64 g, 3.9 mM), palladium acetate (7 mg, 0.03 mM), tri-*o*-tolylphosphine (36 mg, 12 mM), and triethylamine (1.97 g, 19.5 mM) and the whole refluxed over 18 h. The mixture was treated with dilute sodium bicarbonate solution, extracted with methylene chloride, and the organic extract dried (Na_2SO_4) and concentrated to dryness under vacuum (0.1 Torr). The crude product (1.7 g, 85%) was chromatographed with 20:1 methylene chloride – methanol and the product collected as a foam. It was triturated with methanol to produce crystals (0.57 g, 28%), mp 152–155°C; MS: 676 (M + 1). Anal. $C_{39}H_{41}N_5O_6 \cdot 0.5H_2O$: C, H, N. This product (0.54 g, 0.8 mM) was hydrogenated in 95% ethanol (100 mL) with palladium hydroxide (1.0 g) at 60°C and 45 psi for 5 h. The mixture was filtered and filtrate concentrated to an oil (0.35 g). The product crystallized on addition of a little methanol (0.32 g, 80%), mp 107–117°C. This intermediate (0.30 g, 0.6 mM) was treated with 90% trifluoroacetic acid over 1 h. Ether was added and HCl gas was bubbled through the mixture for ca. 5 min to afford **2***h* as a dihydrochloride dihydrate (210 mg, 62%), mp 63–78°C (dec.); $[\alpha]_D^{25}$ −38.36 (*c* = 2, MeOH); IR: 3400–3200 (br), 2760–2670 (br), 1742, 1679, 1081, 1019; MS: 458 (M + 1, free base, weak), 326 (M + 1, aglycone). Anal. $C_{22}H_{27}N_5O_6 \cdot 2HCl \cdot 2H_2O$: C, H, N.

*5,7-Diamino-*N^5*-[2-(4-fluorophenyl)ethyl]-6-methyl-3-(*β-D-*ribofuranosyl)imidazo[4,5-*b*]pyridine (**20**)*

Benzaldehyde was condensed with 2-(4-fluorophenyl)ethylamine in the presence of borane – pyridine as described previously to afford *N*-benzyl-2-(4-fluorophenyl)ethylamine in 44% yield as an oil; ^{1}HMR ($CDCl_3$): 1.35 (s, NH), 2.8 (m, 2 CH_2), 3.8 (s, CH_2), 6.9–7.4 (m, 9 aryl H). An ice-cold mixture of this amine (10.5 g, 46 mM) and triethylamine (7.0 g, 69 mM) in methylene chloride (150 mL) was treated dropwise with propionyl chloride (4.7 g, 51 mM) in methylene chloride (50 mL) and stirred overnight at ambient temperature. The mixture was worked up as described for previous amides and the crude material was distilled to afford pure N-*benzyl*-N-*propionyl-2-(4-fluorophenyl)ethylamine* (10.9 g, 83%), bp 162–163°C at 0.9 Torr; IR (neat): 1648, 1510, 1221, 1158, 827, 733. Anal. $C_{18}H_{20}FNO$: C, H, N. The amide was reacted with **17** and phosphoryl chloride as described previously and the amidine isolated after chromatography with 5:1 methylene chloride – ethyl acetate as an oil in 41% yield. Saponification of the 5′-ester with methanolic ammonia gave the 5′-alcohol as an oil in 85% crude yield. Cyclization of the amidine alcohol with sodium hydride in dioxane was achieved after 2 h reflux to afford crude product as an oil. Trituration with ether gave *5,7-diamino-*N^5*-benzyl-*N^5*-[2-[4- fluorophenyl]ethyl]- 6-methyl- 3-[2′,3′-*O*-(1-methylethylidene)-*β-D-*ribofuranosyl]imidazo[4,5-*b*]pyridine* as a white solid (0.7 g, 42%), mp 146–147°C; IR: 3470, 3377, 3127, 1626, 1603, 1227, 1066; ^{1}HMR: (CD_3OD): 1.35 (s, CH_3), 1.6 (s, CH_3), 2.15 (s, CH_3), 2.75 (m, CH_2), 3.3 (m, CH_2 + MeOH), 3.65 (m, 5′-CH_2), 4.25 (m, CH_2 + 4′-H), 5.05 (m, 3′-H), 5.45 (m, 2′-H), 6.1 (d, 1′-H), 6.85–7.1 (m, 9 aryl H), 8.1 (s, H at 2). Anal. $C_{30}H_{34}FN_5O_4$: C, H, N. Additional material from the mother liquor was combined in the following step. The intermediate (1.65 g, 3 mM) was hydrogenated in 95% ethanol (200 mL) containing 1 N hydrochloric acid (5 mL) with palladium hydroxide (3.3 g) at 50 psi for 6 h at room temperature. The catalyst was filtered off and the filtrate treated with propylene oxide (5 mL) for 30 min. Evaporation of the solvent and trituration with ether gave the 2′,3′-*O*-(1-methylethylidene) derivative of **20** as a solid (0.83 g, 56%), mp 199–205°C (dec); MS: 458 (M + 1). Anal. $C_{23}H_{28}FN_5O_4 \cdot 1.5\ H_2O$: C, H, N. This acetonide (0.8 g, 1.8 mM) was stirred in ice-cold 90% trifluoroacetic acid for 1 h. TLC indicated a single new product. Addition of ether formed a hygroscopic solid. This material was dissolved in a little isopropanol and treated with HCl in ethanol but no crystals formed. Propylene oxide was added and, after 30 min, the mixture was concentrated to dryness at reduced pressure. The residue was dissolved in ethyl acetate and washed with bicarbonate solution, then with brine, dried (Na_2SO_4), and concentrated to dryness to a foam. TLC indicated two products. The material was flash chromatographed with 15:1 methylene chloride – methanol followed by a 10:1 mixture. The first product isolated (foam, 110 mg) was shown to be the aglycone of **20**; ^{1}HMR (CD_3OD): 1.9 (s, CH_3), 2.9 (t, CH_2), 3.6 (t, CH_2), 7.0 (m, 2 aryl H), 7.2 (m, 2 aryl H), 7.7 (H at 2). The second product (foam, 270 mg, 36%) was **20**. This second product was triturated with ether to form a white solid (240 mg), mp 157–160°C; $[\alpha]_D^{25}$ +7.2 (*c* = 1, EtOH); ^{1}HMR: (CD_3OD): 1.9 (s, CH_3), 2.9 (t, CH_2), 3.55–3.85 (m, CH_2 + 5′-CH_2 + 4′-H), 4.1 (dd, 3′-H), 4.4 (dd, 2′-H), 5.95 (d, 1′-H), 7.0 (m, 2 aryl H), 7.25 (m, 2 aryl H), 7.95 (s, H at 2); MS: 418 (M + 1), 286 (aglycone). Anal. $C_{20}H_{24}FN_5O_4$: C, H, N.

*8-Amino-6,7-dihydro-3-(*β-D-*ribofuranosyl)imidazo[4,5-b]pyrrolo[2,3-*e*]pyridine (**21**)*

A solution of *N*-benzyl-2-pyrrolidinone (Aldrich, 4.9 g, 28 mM), **17** (2.25 g, 7 mM), and acetonitrile (30 mL) was treated dropwise with phosphoryl chloride (2.14 g, 14 mM) and stirred at room temperature overnight. After the usual work-up, the oily product was chromatographed with 1:1 methylene chloride – ethyl acetate to give the desired intermediate as an oil (2.75 g, 82%); IR (neat): 2885, 2217, 1746, 1616, 1299; MS 480 (M + 1). Saponification of 2.7 g (5.6 mM) with methanolic ammonia gave the 5′-alcohol as a foam in 95% yield; IR (KBr): 3280 (br), 2936, 2215, 1618, 1081; MS: 438 (M + 1), 266 (aglycone). Reaction of 2.2 g (5 mM) of this product with sodium hydride in dioxane (reflux, 2 h) followed by the standard work-up gave the cyclized product as a solid in 95% yield. It was recrystallized from methanol to afford pure *8-amino-5-benzyl-3-[2′,3′-*O*-(1-methylethylidene)-*β-D-*ribofuranosyl]imidazo[4,5-b]pyrrolo[2,3-*e*]pyridine* (1.2 g, 55%), mp 184–185°C; ^{1}HMR: 1.25 (s, CH_3), 1.5 (s, CH_3), 2.75 (dd, CH_2), 3.3 (dd, CH_2), 3.5 (m, 5′-CH_2), 4.1 (ddd, 4′-H), 4.45 (q, CH_2), 4.9 (dd, 3′-H), 5.05 (t, OH), 5.35 (dd, 2′-H), 5.9 (s, NH_2), 6.05 (d, 1′-H) 7.25 (m, 5 aryl H), 7.85 (H at 2); MS: 438 (M + 1), 266 (aglycone). Anal. $C_{23}H_{27}N_5O_4$: C, H, N. This material (2.0 g, 4.5 mM) was dissolved in 95% ethanol (200 mL) containing 1 N hydrochloric acid (10 mL) and hydrogenolysed with palladium hydroxide (4.0 g) at room temperature and 50 psi over 6 h. The catalyst was filtered off and propylene oxide (10 mL) added to the filtrate. After 30 min the solution was concentrated to dryness at reduced pressure to an oil (1.6 g) that contained two products (TLC). This was taken up in methanol and reevaporated under high vacuum to a mixture of oil and hard foam. The foam (0.65 g, still a mixture) was separated mechanically from the oil, which was a single component. The oil was dissolved in methanol (90 mL) and treated at 0°C with 90% trifluoroacetic acid, whereupon a solid began to form. It was diluted with ether to produce the debenzylated acetonide as a tan solid (0.24 g, 15%); MS: 348 (M + 1), 176 (agylcone). Treatment of the foam with 90% trifluoroacetic acid at 0°C produced an intractable mixture. The desired intermediate was deprotected cleanly with 90% trifluoroacetic acid (2.5 mL) at 0°C in 1 h and, on dilution with ether, a tan solid salt of **21** was obtained (0.16 g, 47%), mp 120–124°C (dec.); $[\alpha]_D^{25}$ −31.95 (*c* = 1.13, DMSO); IR: 3359, 3185, 3152, 2800–2500 (br), 1677, 1659, 1198, 723; ^{1}HMR: 3.0 (dd, CH_2), 3.75 (dd, CH_2), 3.8 (m, 5′-CH_2), 4.25 (m, 4′-H + 3′-H), 4.4 (m, 2′-H), 5.85 (d, 1′-H), 8.1 (s, H at 2); MS: 308 (M + 1, weak), 176 (aglycone). Anal. $C_{13}H_{17}N_5O_4 \cdot 2CF_3COOH$: C, H, N.

Acknowledgments

The authors are grateful to Mr. Michael Hatolski and Ms. Natalie Cahoon for recording the infrared spectra and the rotations, to Mrs. Magda Brzechffa for mass spectra, and to Mrs. Lia Raabis and Mr. Karl Gunderson for recording the ^{1}HMR spectra. Microanalyses were performed by Robertson Laboratory Inc., Madison, N.J.

1. A. N. Drury and A. Szent-Gyorgyi. J. Physiol. (London), **68**, 214 (1929).
2. R. M. Berne. Am. J. Physiol. **204**, 317 (1963).
3. M. G. Collis. Pharmacol. Ther. **41**, 143 (1989).
4. A. Munoz, A. Leenhardt, A. Sassine, P. Galley, and P. Puech. Eur. Heart J. **5**, 735 (1984).
5. J. W. Daly. J. Med. Chem. **25**, 197 (1982).
6. G. Burnstock. *In* Cell membrane receptors for drugs and hormones. A multidisciplinary approach. *Edited by* L. Bolis and R. W. Straub. Raven Press, New York. 1978, pp 107–118.
7. D. Van Calker, M. Mueller, and B. Hamprecht. Nature, **276**, 839 (1978).
8. C. Londos, D. M. F. Cooper, and J. Wolff. Proc. Natl. Acad. Sci. U.S.A. **77**, 2551 (1980).
9. L. Belardinelli, J. Linden, and R. M. Berne. Prog. Cardiovasc. Dis. **32**, 73 (1989).
10. (*a*) S. Kusachi, R. D. Thompson, and R. A. Olsson. J. Pharmacol. Exp. Ther. **227**, 316 (1983); (*b*) J. W. Daly, W. Padgett, R. D. Thompson, S. Kusachi, W. J. Bugni, and R. A. Olsson. Biochem. Pharmacol. **35**, 2467 (1986).
11. M. F. Jarvis, R. Schulz, A. J. Hutchison, U. H. Do, M. A. Sills, and M. Williams. J. Pharmacol. Exp. Ther. **251**, 888 (1989).
12. K. Kawazoe, N. Matsumoto, M. Tanabe, S. Fujiwara, M. Yanagimoto, M. Hirata, and K. Kikuchi. Arzneim.-Forsch. **30**, 1083 (1980).
13. J. E. Francis, R. L. Webb, G. R. Ghai, A. J. Hutchison, M. A. Moskal, R. deJesus, R. Yokoyama, S. L. Rovinski, N. Contardo, R. Dotson, B. Barclay, G. A. Stone, and M. F. Jarvis. J. Med. Chem. **34**, 2570 (1991).
14. G. Cristalli, M. Grifantini, S. Vittori, W. Balduini, and F. Cattabeni. Nucleosides Nucleotides, **4**, 237 (1985).
15. (*a*) J. E. Schelling and C. A. Salemink. Recl. Trav. Chim. Pays-Bas, **93**, 160 (1974); (*b*) R. D. Elliott, C. Temple, Jr., and J. A. Montgomery. J. Org. Chem. **31**, 1890 (1966); (*c*) J. A. Montgomery and N. F. Wood. J. Org. Chem. **29**, 734 (1964); (*d*) D. G. Markees and G. W. Kidder. J. Am. Chem. Soc. **78**, 4130 (1956).
16. R. A. Fujimoto, A. J. Hutchison, and J. E. Francis. U.S. Patent 4,977,144 (Dec. 11, 1990).
17. E. Shaw. J. Am. Chem. Soc. **81**, 6021 (1959).
18. T. Shiro, A. Yamanoi, S. Konishi, S. Okumura, and M. Takahashi. Agric. Biol. Chem. **26**, 785 (1962).
19. (*a*) R. Marumoto, Y. Yoshioka, O. Miyashita, S. Shima, K. Imai, K. Kawazoe, and M. Honjo. Chem. Pharm. Bull. **23**, 759 (1975); (*b*) K. Omura, R. Marumoto, and Y. Furukawa. Chem. Pharm. Bull. **29**, 1870 (1981); (*c*) R. Marumoto, S. Shima, K. Omura, M. Tanabe, S. Fujiwara, and Y. Furukawa. J. Takeda Res. Lab. **44**, 220 (1985).
20. S. F. Campbell, J. D. Hardstone, and M. J. Palmer. Tetrahedron Lett. **25**, 4813 (1984).
21. C. B. Reese, Y. S. Sanghvi, and R. Kuroda. J. Chem. Soc. Perkin Trans. **1**, 1527 (1987).
22. R. A. McClelland and R. Somani. J. Chem. Soc. Chem. Commun. 407 (1979).
23. N. A. Cortese, C. B. Ziegler, B. J. Hrnjez, and R. F. Heck. J. Org. Chem. **43**, 2952 (1978).
24. D. Voet and J. G. Voet. *In* Biochemistry. John Wiley & Sons, New York. 1990. Chap. 28.
25. K. Tagaki, K. Nagahara, and T. Ueda. Chem. Pharm. Bull. **18**, 2353 (1970).
26. (*a*) K. Suzuki, T. Saito, T. Meguro, I. Kumashiro, and T. Takenishi. Jpn. Patent No. 6910 (1967); Chem. Abstr. **68**, 68995n (1968); (*b*) Y. F. Shealy and C. A. O'Dell. J. Pharm. Sci. **64**, 934 (1975).
27. K. Suzuki and I. Kumashiro. U.S. Patent 3,450,693 (June 17, 1969); Chem. Abstr. **71**, 81698z (1969).

Can. J. Chem. Downloaded from www.nrcresearchpress.com by 217.78.4.112 on 09/08/12
For personal use only.

π-Facial diastereoselectivity in the Diels–Alder reactions of *cis*-cyclohexa-3,5-diene-1,2-diol and derivatives with *N*-phenylmaleimide

JAMES R. GILLARD AND D. JEAN BURNELL[1]

Department of Chemistry, Memorial University of Newfoundland, St. John's, Nfld., Canada A1B 3X7

Received August 8, 1991

This paper is dedicated to Professor Zdenek (Denny) Valenta on the occasion of his 65th birthday

JAMES R. GILLARD and D. JEAN BURNELL. Can. J. Chem. **70**, 1296 (1992).

N-Phenylmaleimide undergoes Diels–Alder cycloaddition predominantly to the face of *cis*-cyclohexa-3,5-diene-1,2-diol (**3**) *syn* to the oxygen functions. Derivatization can be used to alter the π-facial diastereoselectivity in a synthetically useful manner. The best cases are the exclusive, high yield, production of the *syn*-addition product with the trimethylsilyl ether derivative (**8**), and the *exo*-benzylidine derivative (**26**) gave a 96:4 *anti/syn* ratio of adducts.

JAMES R. GILLARD et D. JEAN BURNELL. Can. J. Chem. **70**, 1296 (1992).

La *N*-phénylmaléimide subit une cycloaddition de Diels–Alder qui se produit principalement par la face du *cis*-cyclohexa-3,5-diène-1,2-diol (**3**) qui est *syn* par rapport aux fonctions oxygénées. On peut faire appel à des dérivés pour altérer la diastéréosélectivité π-faciale d'une manière qui soit utile d'un point de vue synthétique. Les meilleurs cas sont ceux de la production exclusive, avec un excellent rendement, du produit d'addition *syn* avec l'éther triméthylsilyle **8** alors que le dérivé *exo*-benzylidine (**26**) conduit à un rapport 96 : 4 des adduits *anti/syn*.

[Traduit par la rédaction]

Introduction

1,3-Cyclopentadiene substituted at C-5 with an oxygen or a nitrogen function undergoes Diels–Alder cycloadditions by attachment of the dienophile to the face of the diene *syn*[2] to the heteroatom (1, 2). Many hypotheses have been forwarded to explain this π-facial diastereoselectivity (2–7), which does not seem to be controlled by steric factors. On the other hand, substitution at C-5 by some larger heteroatoms (sulfur, selenium, chlorine, bromine, and iodine) leads to Diels–Alder adducts mainly by *anti* addition (2, 7–9).

Plane-nonsymmetric 1,3-cyclohexadiene systems have received less attention, even though their synthetic utility must be similar to that of the cyclopentadienes. Auksi and Yates (10) reported that Diels–Alder adducts derived from diene **1** arise exclusively by addition to the face of the diene *syn* to the oxygen. This could be explained in terms of steric interactions, and steric effects were deemed important, but not the only significant effect, in Diels–Alder reactions involving some dienes in which the plane-nonsymmetric moieties were alkyl and acyl (11). Recently, we demonstrated that the addition of carbon dienophiles to benzene oxide and some of its derivatives (**2**) is exclusively *anti*, and we suggested that steric factors are important with these systems, too (12). In the early 1970's there were reports of the production of *cis*-cyclohexa-3,5-diene-1,2-diol (**3**) directly from benzene by the action of *Pseudomonas putida* (13, 14). In the last five years this type of diene has emerged as a very useful synthetic building block and of considerable interest in mechanistic studies (15). Diels–Alder reactions of some simple derivatives of **3** were carried out with maleic anhydride (13), 4-(4-bromophenyl)-1,2,4-triazoline-3,5-dione (16), and some acyclic dienophiles (17). While our work was in progress, Werbitzky *et al.* reported a reaction with a chiral nitroso dienophile (18), and Pittol *et al.* (19) disclosed the results of a study of the Diels–Alder reactions of the acetonide derivative of a trifluoromethyl analog of **3**. In all of these reports, the adducts were shown as arising by reaction exclusively, or in just one case preferentially (19), on the face of the diene *anti* to the oxygens, i.e., the π-facial selectivity of these reactions appeared consistent with steric control. However, the theories regarding π-facial selectivity, by and large based on the cyclopentadiene results, would predict that plane-nonsymmetric oxygen substituents on a 1,3-cyclohexadiene system should direct addition predominantly *syn*, just like with the 1,3-cyclopentadienes. Thus, we undertook a systematic and rigorous examination of the Diels–Alder reactions of *cis*-cyclohexa-3,5-diene-1,2-diol (**3**) and some of its derivatives. We chose *N*-phenylmaleimide as the dienophile for all the reactions because it is relatively reactive in thermal reactions giving *endo*-addition products that are often stable and crystalline, and its symmetry would not introduce unnecessary complications in the interpretation of the nmr spectra of its adducts.[3]

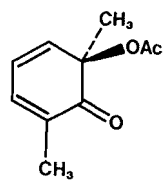

1

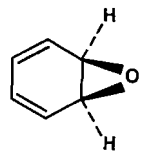

2

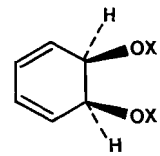

3 X = H
6 X = $COCH_3$
7 X = CH_3
8 X = $Si(CH_3)_3$

Results and discussion

The Diels–Alder reaction of **3** with *N*-phenylmaleimide was a simple matter of stirring the addends together in boiling chloroform solution. The adducts were not very soluble in the chloroform, and they precipitated during the reaction. The 300-MHz ^1H nmr spectrum of the crude reaction mixture showed signals for two adducts, which, by careful integration, were calculated to be in a ratio of 95:5. Each

[1]Author to whom correspondence may be addressed.

[2]In this paper "*syn* addition" means addition of a dienophile to the face of the diene that bears the plane-nonsymmetric heteroatom substituent(s); "*anti* addition" is addition to the opposite face.

[3]A preliminary account of this work appears in ref. 20.

Can. J. Chem. Downloaded from www.nrcresearchpress.com by 217.78.4.112 on 09/08/12
For personal use only.

TABLE 1. Relative amounts of *syn*- and *anti*-addition products from the Diels–Alder reaction of **3** with *N*-phenylmaleimide in different solvents

Solvent	% of adduct *syn*	% of adduct *anti*	% Yield of reaction[a]
Pyridine[b]	95	5	90
Acetone[c]	95	5	93
Chloroform[c]	95	5	93
Methanol[c]	93	7	80
Benzene[c]	92	8	91
Dimethyl sulfoxide[b]	92	8	87
Acetonitrile[c]	88	12	94

[a]Diene **3** was stirred with one molar equivalent of *N*-phenylmaleimide. Solvents were removed under vacuum, and the yields were calculated from the mass recovery and the adduct sample purity as determined by ^{1}H nmr.
[b]Heated at 80°C in an oil bath.
[c]Heated under reflux.

TABLE 2. Relative amounts of *syn*- and *anti*-addition products of **3** and its derivatives, and their relative rates of Diels–Alder reaction, with *N*-phenylmaleimide in $CHCl_3$

Diene	% of adduct *syn*	% of adduct *anti*	Rate of reaction (relative to 1,3-cyclohexadiene = 1)
3[a]	95	5	0.1
6[a]	88	12	0.002
7[b]	99	1	0.2
8[b]	100	0	0.03
9[b]	60	40	>100
10[b]	60	40	2.7
22[b]	45	55	[c]

[a]Heated under reflux.
[b]Room temperature reaction.
[c]Not measured.

pure adduct was heated in chloroform solution for 36 h after which time we could find no evidence of equilibration. The assignment of structure **4** to the major adduct and structure **5** to the minor adduct was made initially by chemical correlation with the adducts of some derivatives (see below). These structures have since been corroborated in an X-ray crystallographic study.[4]

The synthetic utility of dienes such as **3** would be enhanced if one could manipulate the diene so that the *anti*-addition product could be obtained, too. Hydrogen bonding between the diol diene **3** and the dienophile cannot be discounted as an important contributor to the π-facial selectivity of **3**. Therefore, a survey of the influence of different solvents on the π-facial selectivity was made. The results are summarized in Table 1. Variations were small, and there was no obvious correlation with the polarity of the solvent.

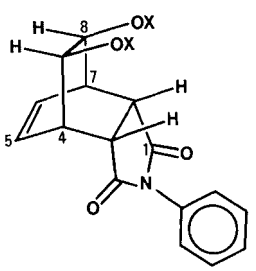

4 X = H
11 X = $COCH_3$
13 X = CH_3
15 X = $Si(CH_3)_3$

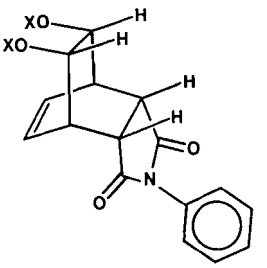

5 X = H
12 X = $COCH_3$
14 X = CH_3
16 X = $Si(CH_3)_3$

Many of the theories regarding π-facial selectivity would explain the π-facial selectivity of **3** in terms of some form of donation of electron density from the oxygens of **3**. Thus, our first three derivatives **6**, **7**, and **8**, were chosen to modulate the electron-donating ability of the oxygens. Furthermore, the derivatives could not hydrogen bond, and they would present more steric hindrance on the *syn* face than does diol **3**. Dienes **6** and **8** were obtained from **3** in a straightforward manner. The dimethoxy diene **7** was prepared in a phase-transfer reaction of **3** with dimethyl sulfate using the procedure of Merz (21). Two more derivatives, **9** and **10**, which might loosely be considered as cyclic analogues of **7** and **8**, respectively, were chosen because there would be less ambiguity regarding the conformations of these derivatives during reactions. The acetonide **9** was prepared by exchange with 2,2-dimethoxypropane. For the rather moisture-sensitive diene **10** we followed a procedure by Orr and Monder (22), and its Diels–Alder reaction was effected immediately in its original solution.

All of these dienes reacted smoothly with *N*-phenylmaleimide in chloroform solution to give Diels–Alder adducts in very high yield. The relative amounts of the adducts from these reactions were determined by integration of ^{1}H nmr spectra of the crude reaction products, and the results are given in Table 2. The rates of reaction of these dienes were determined in an approximate manner relative to 1,3-cyclohexadiene by means of competitive reactions with mixtures of two dienes and *N*-phenylmaleimide. This information appears in Table 2, also. The diacetate diene **6** was the least reactive, and, as expected, it showed less π-facial selectivity than did **3**, but the difference was small. Dienes **7** and **8** were also less reactive than 1,3-cyclohexadiene, but steric hindrance by the plane-nonsymmetric heteroatom substituents was clearly not a factor influencing π-facial selectivity in their reactions. Their adducts were overwhelmingly the results of *syn* addition. Indeed, we were unable to find any evidence of a minor adduct (**16**) in the product of the reaction of **8**, even though this diene bears the groups that are potentially the most sterically hindering. Thus, derivatization of **3** by these simple groups had little effect on the π-facial selectivity, i.e., they all direct *syn*. These findings are consistent with the cyclopentadiene results (1) and with the observation of Deslongchamps *et al.* (23) of a complete lack of π-facial selectivity in the Diels–Alder reaction of diene **21** with butenone.

The two dienes with cyclic derivatives **9** and **10**, were more reactive than **3**, but their π-facial selectivity was much lower than that of **3**. This was consistent with a result in work by Pittol *et al.* (19), who reported two adducts from the Diels–Alder reaction of the trifluoromethyl analogue of **9** with *N*-ethylmaleimide.

The two adducts obtained from the reaction of our acetonide diene **9** were stable and readily separable by flash

[4]A manuscript is in preparation for submission to this journal.

Can. J. Chem. Downloaded from www.nrcresearchpress.com by 217.78.4.112 on 09/08/12
For personal use only.

column chromatography. Measurement of nOe enhancements in the ^1H nmr spectrum of the major adduct established the proximity of the hydrogens on C-4a and C-7a with one of the acetonide's methyl groups (the "*syn*" methyl), as well as the proximity of the alkenic hydrogens with the hydrogens on C-3a and C-8a. Therefore, the major adduct had structure **17**, the result of *endo* addition *syn* to the oxygen functions of **9**. Conversely, nOe measurements in the ^1H nmr spectrum of the minor isomer showed that one acetonide methyl was near the alkenic hydrogens, and the hydrogens on C-3a and C-8a were in the proximity of the hydrogens on C-4a and C-7a. Thus, the minor isomer was **18**, also the result of an *endo* addition, but in this instance *anti* to the oxygen functions of **9**. (Measurements of nOe enhancements confirmed the structures of **19** and **20** in the same way.)

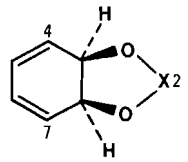

9 X = $C(CH_3)_2$
10 X = $Si(CH_3)_2$
22 X = B-CH_2-CH_3
34 X = CH_2

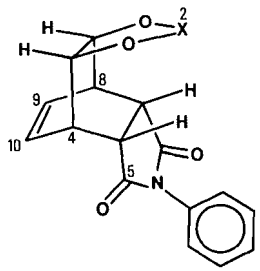

17 X = $C(CH_3)_2$
19 X = $Si(CH_3)_3$
23 X = B-CH_2-CH_3

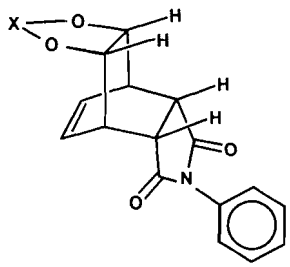

18 X = $C(CH_3)_2$
20 X = $Si(CH_3)_2$
24 X = B-CH_2-CH_3

With the structures for the major and minor acetonide adducts clearly established, we could confirm the structures of the other adducts. The two acetonide adducts, **17** and **18**, were hydrolysed separately under vigorous acidic conditions to give **4** and **5**, respectively, the products of the Diels–Alder reaction of **3**. The major adducts **11**, **13**, **15**, and **19** were made from **4**, and the minor adducts **12**, **14**, and **20** were made from **5**. In addition, the putative minor isomer **16** was produced from **5**, and it was confirmed that signals arising from **16** would not have been hidden by other signals in the ^1H nmr spectrum of the crude product of the Diels–Alder reaction of **8**.

The greater reaction rate (on both faces of the diene) of each cyclic derivative of **3** relative to its acyclic counterpart was attributable simply to the fact that the derivative ring would force the cyclohexadiene ring into a more planar, therefore more reactive, conformation. However, the lower π-facial selectivities suggested that the increase in reactivity was offset on the *syn* face by an unfavorable interaction. It seems likely that this was a steric interaction, although one cannot discount some subtle stereoelectronic effect at work. Thus, one might expect a significant amount of conformer **A** (X = Y = CH_3) as well as conformer **B** in solution, and clearly in **A** the *syn* face would be very hindered.

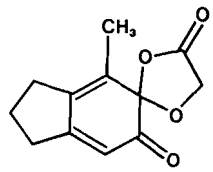

21

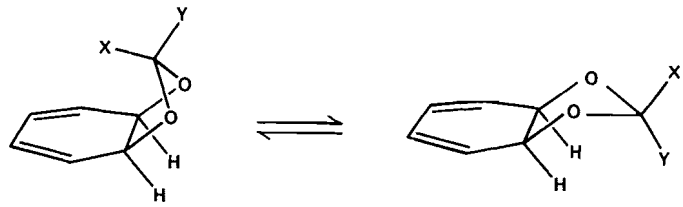

A **B**

It is opportune at this juncture to make some comment about the relationship between the relative rates shown in Table 2 and two of the theories that have been forwarded to explain how π-facial selectivity is governed by allylic heteroatoms. Anh (3) and later Kahn and Hehre (4) proposed what is in essence a nucleophilic role for the oxygen vis-à-vis the incoming dienophile. A logical extension of this to our dienes would be that the *syn* faces, which would be more nucleophilic, should be more reactive than the faces of 1,3-cyclohexadiene. This was not the case. In fact, one of the least reactive dienes (**8**) reacted exclusively by *syn* addition. Work by le Noble and co-workers (5) and by Macaulay and Fallis (2) supported the notion that π-facial selectivity in some Diels–Alder reactions is controlled by the σ-donor ability of the *anti* substituent (24). Whereas it might be argued that our derivatives must have had C—O bonds of varying σ-donor ability, the *anti* substituents were always hydrogens. Thus, it is difficult to reconcile the widely differing rates of *syn* addition of our substituted cyclohexadiene systems with this hypothesis.

Although we had conditions that gave a very high degree of selectivity for *syn* addition with dienes such as **3**, these first derivatization experiments had not managed to tip the selectivity in favor of the *anti* addition. π-Facial selectivity was very modestly affected by derivatization by the electron-withdrawing acetyls of diene **6**, and the cyclic derivatives suggested that steric interactions could be made important if the populations of the two major conformers could be controlled. These two options for increasing the proportion of the *anti*-addition product were explored further.

Firstly, we attempted to modify more drastically the electron-donating ability of the oxygens of **3** by using a boron derivative. A carefully measured amount of lithium triethylborohydride (25) was added to **3** to give the cyclic derivative **22**. This was not purified; *N*-phenylmaleimide was added immediately. The ^1H nmr of the reaction mixture showed two adducts, in a ratio of 55:45. The nmr data collected directly on this mixture of adducts included for the major adduct a 12% nOe enhancement of the signals due to the hydrogens on carbons 3a and 8a on saturation of the signals due to the hydrogens on carbons 4a and 7a. Thus, the major adduct was assigned structure **24**, the adduct result-

Can. J. Chem. Downloaded from www.nrcresearchpress.com by 217.78.4.112 on 09/08/12
For personal use only.

Can. J. Chem. Downloaded from www.nrcresearchpress.com by 217.78.4.112 on 09/08/12
For personal use only.

ing from *anti* addition. Given the planar geometry about boron, this result can be interpreted as a stereoelectronically derived modification of π-facial selectivity.

Whereas the result with **22** was interesting as a phenomenon, the proportion of *anti*-addition product was still not synthetically useful. We sought to increase steric interactions on the *syn* face by using a benzylidine derivative of **3**. The acid-catalysed reaction of **3** with benzaldehyde dimethyl acetal gave exclusively one of the two possible derivatives. The nOe data for this derivative showed that it had the "*endo*" relative stereochemistry **25**. To obtain both **25** and the "exo" isomer **26** it was necessary to proceed via the (racemic) dibromo-diol **27** by double derivatization followed by double dehydrobromination. We prepared this precurusor from 1,4-cyclohexadiene by literature methods (26, 27). The isomeric (racemic) dibromides **28** and **29** were readily separated by crystallization and chromatography as described by Yang *et al.* (27), then double dehydrobromination provided the dienes.

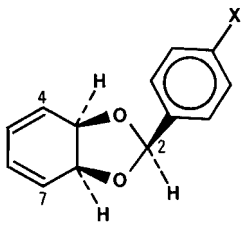

25 X = H
35 X = NO_2

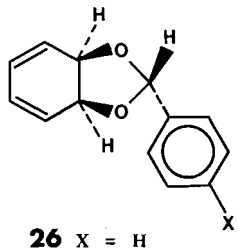

26 X = H
36 X = NO_2

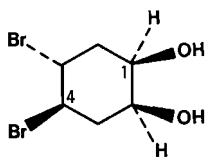

27

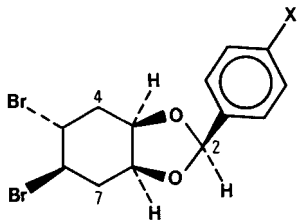

28 X = H
37 X = NO_2

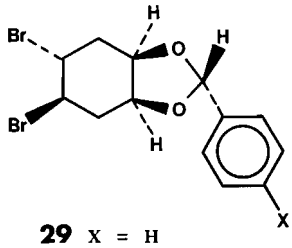

29 X = H
38 X = NO_2

Diene **25** reacted with *N*-phenylmaleimide at about one third the rate of diene **9**, and two adducts were evident, in a ratio of 72:28, in the ^{1}H nmr spectrum of the crude product. The two adducts were separable by flash chromatography. The nmr data for the major product included the following key observation: saturation of the signal due to the hydrogens on C-3a and C-8a led to an nOe enhancement of the acetal hydrogen signal (18%) and of the signal due to the hydrogens on C-4a and C-7a (16%). This established that the major product had arisen by *endo* addition to the face of **25** *anti* to the oxygen functions, i.e., it was **31**. In the ^{1}H nmr data for the minor adduct was evidence by nOe of the proximity of the hydrogens on C-3a and C-8a to the acetal hydrogen (12%) and to the alkenic hydrogens (2%). Furthermore, significant nOe enhancements confirmed that the hydrogens on C-4a and C-7a were located near the benzylidine aromatic ring. Thus, the minor adduct was **30**, the *syn-endo*-addition product. Neither product was the result of epimerization at the acetal center. It is worthy of note that the formation of the benzylidine derivative from **4** by a method that should give the thermodynamically preferred product gave only **30**, and from **5** only **31** was obtained.

The isomeric benzylidine diene **26** was prone to dimerize on standing, and it showed greater π-facial selectivity than did **25** in its Diels–Alder reaction with *N*-phenylmaleimide: the ratio of adducts, produced essentially quantitatively, was 96:4. It was gratifying that saturation of the signal due to the hydrogens on C-3a and C-8a in the ^{1}H nmr spectrum of the pure major adduct led to an nOe enhancement of the signal due to the hydrogens on C-4a and C-7a (14%), and saturation of the alkenyl proton signals gave a 4% nOe enhancement to the acetal hydrogen signal. Clearly, the very predominant adduct from this diene was the *anti-endo*-addition product **33**. The ^{1}H nmr data of the minor adduct showed an important nOe enhancement (9%) of the acetal hydrogen's signal on saturation of the signal due to the hydrogens on C-4a and C-7a. Thus, the minor adduct was the *syn-endo*-adduct **32**. In spite of the demonstrated thermodynamic preference for **30** over **32**, and **31** over **33**, we saw no evidence for epimerization at the acetal center during the reaction of **26**.

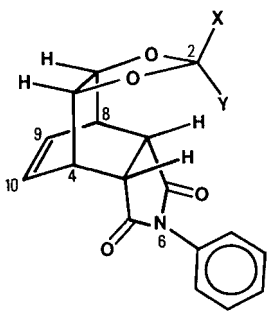

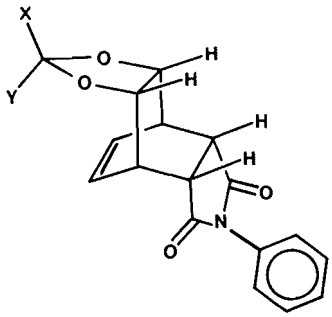

30 X = H, Y = C_6H_5
32 X = C_6H_5, Y = H
39 X = H, Y = $C_6H_4NO_2$
41 X = $C_6H_4NO_2$, Y = H

31 X = H, Y = C_6H_5
33 X = C_6H_5, Y = H
40 X = H, Y = $C_6H_4NO_2$
42 X = $C_6H_4NO_2$, Y = H

The reason for greater π-facial diastereoselectivity in the reaction of **26** over that of **25** may be related to their conformations. Both molecules might assume conformations with the phenyl group pseudoequatorial or pseudoaxial with respect to the 1,3-dioxolane moiety. Diene **26** should have a preference for conformer **A** (X = H, Y = C_6H_5), in which the phenyl is pseudoequatorial. In conformer **B** (X = H, Y = C_6H_5) of **26** there would be an unfavorable interaction between the phenyl group and the hydrogens on C-3a and C-7a. The acetal hydrogen of the preferred conformer **A** of **26** would be well positioned to hinder attack by the dienophile

Can. J. Chem. Downloaded from www.nrcresearchpress.com by 217.78.4.112 on 09/08/12
For personal use only.

on the *syn* face. By the same token, conformation **A** of **25** (X = C_6H_5, Y = H) should completely block *syn* addition, but **25** is likely to have a preference for the pseudoequatorial phenyl in conformation **B** (X = C_6H_5, Y = H), in which the *syn* face of the diene is relatively unencumbered. A rationalization of the selectivities of **26** (likely mainly **A**) and **25** (probably mainly **B**) based on a large stereoelectronic component would not be supported by *ab initio* calculations on **34**, which revealed that the differences in the π-orbitals in conformers **A** and **B** (X = Y = H) are very small indeed.[5]

Further support for steric rather than stereoelectronic control came from the reactions of the *para*-nitro analogues **35** and **36**, which were prepared via **27** and the dibromides **37** and **38**. The nmr spectra of the adducts derived from **35**, **39**, and **40** were similar to those from **25**, and their relative amounts (27:73, respectively) were not significantly different, either.[6] In the same way, **36** reacted in a manner reminiscent of **26**, producing adducts **41** and **42** (5:95, respectively). The lack of sensitivity with regard to the addition of the electron-withdrawing group is certainly consistent with steric interactions rather than stereoelectronic ones being of primary importance in the control of π-facial selectivity with the benzylidine dienes.

The *exo*-benzylidine dienes, **26** and **36**, dimerized readily by a Diels–Alder reaction. The structures of the dimers, **43** and **44**, were evident from measurements of nOe enhancements in their ^{1}H nmr spectra. Each arose by a process in which both the diene and dienophile partners underwent addition to their *anti* faces, the result that would be expected in a sterically controlled reaction.

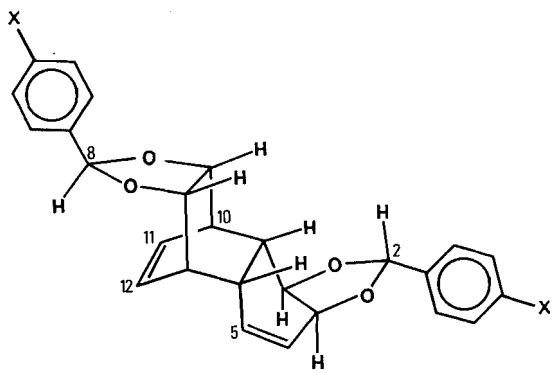

43 X = H
44 X = NO_2

Finally, as we had done with our first adducts from **3**, it was important to address the possibility that we had produced the thermodynamically preferred, rather than kinetically preferred, adducts from the derivatives. We tested a cross section of pure adducts for equilibration. Chloroform solutions of some major (**11**, **15**, **17**, **31**, **33**, **40**, and **42**) and some minor adducts (**12**, **14**, **18**, **30**, **32**, and **39**) were heated under reflux for 36 h. In no instance was there any evidence for the production of an isomeric adduct.

[5]A manuscript describing the results of our parallel computational study of π-facial diastereoselectivity is in preparation.

[6]The facial selectivity of **35** leads one to assume that it, like **25**, must also exist to a significant degree in its less favourable conformation, **A**. Whether this conformer might be stabilized by a "π-stacking" arrangement in chloroform was examined in a cursory manner. Running the Diels–Alder reaction of **35** in benzene led to an adduct mixture of 24:76 (**39** to **40**, respectively), which was not significantly different from the ratio in chloroform. Also, an nOe study failed to reveal proximity between the nitrophenyl moiety and the hydrogens on the diene portion of **35**.

Experimental

Melting points (mp) were determined on a Fisher–Johns apparatus and are uncorrected. Ultraviolet (uv) spectra were run on a Perkin–Elmer 202 instrument. Infrared (ir) spectra were recorded on a Mattson Polaris FT instrument; these abbreviations apply: s = strong; m = medium; w = weak; br = broad. Mass spectral data were from a V.G. Micromass 7070HS instrument, or from the model 5970 mass selective detector that is part of a Hewlett–Packard gas chromatograph – mass spectrometer (gc–ms) system. The ms data have this format: *m/z* (% of base peak). Nuclear magnetic resonance (nmr) spectra were obtained on a General Electric GE 300-NB instrument, except in a few instances in which a (60 MHz) Varian EM-360 instrument was employed. The ^{1}H shifts of $CDCl_3$ solutions were measured relative to internal tetramethylsilane, but in other solvents shifts were calibrated to a solvent resonance. Standard abbreviations apply, as well as br = broad and nar = narrow. All ^{13}C shifts were calibrated to a solvent resonance. For some carbon resonances for which rigorous assignments are not provided the number of attached protons (APT) may be indicated in parentheses after the chemical shift. Assignments were aided by COSY and heteronuclear 2-D spectra and by nuclear Overhauser effect (nOe) enhancement measurements, which also led to the assignment of stereochemistry. The nOe measurements were made from sets of interleaved ^{1}H experiments (16K) of 8 transients cycled 12 to 16 times through the list of frequencies to be saturated. The decoupler was gated on in CW mode for 6 s with sufficient attenuation to give a 70–90% reduction in intensity of the irradiated peak. Frequency changes were preceded by a 60-s delay. Four scans were used to equilibrate spins before data acquisition, but a relaxation delay was not applied between scans at the same frequency. The nOe difference spectra (28) were obtained from zero-filled 32K data tables to which a 1–2 Hz exponential line-broadening function had been applied. The nOe data are reported in this format: irradiated signal (enhanced signal, enhancement). Reactions were run under an atmosphere of dry nitrogen. Dry benzene was distilled from CaH_2 and stored over sodium wire; pyridine was distilled from, and stored over, KOH; tetrahydrofuran (THF) was freshly distilled from sodium/benzophenone. Routine solvents were distilled, and aqueous solutions are implied for saturated NaCl, etc. Flash column chromatography used 230–400 mesh silica gel, and elution was with hexane containing an increasing proportion of ethyl acetate.

Diels–Alder reaction of ***3****: (3aα,4α,7α,7aα,8S*,9R*)- (****4****) and (3aα,4α,7α,7aα,8R*,9S*)-3a,4,7,7a-tetrahydro-8,9-dihydroxy-2-phenyl-4,7-ethano-1H-isoindole-1,3(2H)-dione (****5****)*

A solution of diene **3** (Aldrich; 48 mg, 0.43 mmol) and *N*-phenylmaleimide (75 mg, 0.43 mmol) in $CHCl_3$ (5 mL) was heated under reflux for 16 h. During this time a precipitate formed that was composed of the adduct mixture. Evaporation of the solvent under vacuum left 115 mg (93%) of a colorless solid. This was dissolved completely in C_5D_5N, and the ^{1}H nmr spectrum of this mixture revealed signals for **4** and **5** in a ratio of 95:5, respectively, by integration. Repeated crystallization of the mixture from 25% methanol in ethyl acetate provided a pure sample (30 mg) of **4**: mp 218.5–220°C; ir (KBr) ν_{max}: 3423 (br), 2960, 1768 (w), 1693 (s), 1502, 1392, 1184, 689 cm^{-1}; ^{1}H nmr ($CDCl_3$) δ: 7.36–7.48 (3H, m), 7.18 (2H, br d, *J* = 7.3 Hz), 6.22 (2H, apparent dd, *J* = 3.3, 4.3 Hz), 3.84 (2H, br s), 3.50 (2H, br s), 3.42 (2H, br s), 2.97 (2H, br s); ^{1}H nmr (C_5D_5N) δ: 7.30–7.52 (3H, m), 6.26 (2H, dd, *J* = 3.2, 4.4 Hz), 5.14 (2H, OH's), 3.98 (2H, s, C-8H and C-9H), 3.88 (2H, s, C-3aH and C-7aH), 3.61 (2H, br s, C-4H and C-7H); ^{13}C nmr (C_5D_5N) δ: 179.5, 133.6, 132.2 (C-5 and C-6), 129.3, 128.6, 127.5, 63.7 (C-8 and C-9), 40.3 (C-4 and C-7), 38.6

Can. J. Chem. Downloaded from www.nrcresearchpress.com by 217.78.4.112 on 09/08/12
For personal use only.

(C-3a and C-7a); ms: 285 (M^+, 26), 256 (4), 226 (89), 120 (28), 119 (83), 105 (17), 91 (25), 79 (100), 78 (53). Exact Mass calcd. for $C_{16}H_{15}NO_4$: 285.1000; found: 285.0996.

A sample of **5** was obtained by hydrolysis of **18** (see below). The ^1H and ^{13}C nmr spectra were entirely in accord with the data for the minor component of the adduct mixture. For **5**: mp (after recrystallization from ethyl acetate/CH_3OH) 260–261°C; ir (KBr) ν_{max}: 3450, 3383 (br), 2901, 1775 (w), 1705, 1393, 1200, 734 cm^{-1}; ^1H nmr (C_5D_5N) δ: 7.28–7.55 (5H), 6.47 (2H, apparent t, $J \approx 3.7$ Hz), 5.04 (OH's), 4.32 (2H, s), 3.74 (2H, m), 3.33 (2H, s); ^{13}C nmr (C_5D_5N) δ: 177.6, 133.4, 131.3, 129.3, 128.7, 127.4, 69.2, 42.0, 40.9; ms: 285 (M^+, 18), 267 (4), 226 (95), 120 (23), 119 (100), 105 (11), 91 (24), 79 (67), 78 (60), 77 (24). Exact Mass calcd. for $C_{16}H_{15}NO_4$: 285.1000; found: 285.0993.

cis-*5,6-Diacetyloxy-1,3-cyclohexadiene (6)*

Acetic anhydride (1.0 mL) was added to a solution of **3** (0.240 g, 2.14 mmol) in pyridine (1.0 mL). After stirring at room temperature for 2 h, tlc indicated completion of the reaction. The volatiles were removed under vacuum, and flash chromatography of the residue gave **6** as a colorless oil (0.368 g, 88%): uv (CH_3OH) λ_{max}: 256 nm (ε = 3900); ir (film) ν_{max}: 1740 (s), 1371 (s), 1241 (s), 1064 (s) cm^{-1}; ^1H nmr ($CDCl_3$) δ: 6.15 (2H, m), 5.90 (2H, m), 5.54 (2H, nar m), 2.07 (6H, s); ^{13}C nmr ($CDCl_3$) δ: 170.1 (0), 126.1 (1), 125.1 (1), 66.8 (1), 20.7 (3); ms: 196 (M^+, 0.9), 154 (3), 136 (13), 112 (60), 95 (98), 94 (100), 83 (19), 78 (33), 77 (24), 66 (66), 43 (100). Exact Mass calcd. for $C_{10}H_{12}O_4$: 196.0735; found: 196.0725.

cis-*5,6-Dimethoxy-1,3-cyclohexadiene (7)*

The diol **3** (0.311 g, 2.77 mmol), dimethyl sulfate (2.10 g, 16.6 mmol), and tetra-*n*-butylammonium hydroxide (1.0 g, 40% w/w in H_2O) were added to a two-phase system of CH_2Cl_2 (100 mL) and 50% NaOH in H_2O. This was stirred vigorously for 3 days at room temperature. More H_2O (100 mL) was added. The organic layer was washed with H_2O (100 mL), saturated $NaHCO_3$ (100 mL), and saturated NaCl (100 mL), then it was dried ($MgSO_4$) and concentrated under vacuum. Flash chromatography provided **7** as a colorless liquid (0.296 g, 76%): uv (CH_3OH) λ_{max}: 262 nm (ε = 2500); ir (film) ν_{max}: 2929 (s), 1464, 1122 cm^{-1}; ^1H nmr ($CDCl_3$) δ: 5.99–6.08 (4H, m), 3.81 (2H, nar m), 3.44 (6H, s); ^{13}C nmr ($CDCl_3$) δ: 126.9 (1), 124.8 (1), 73.9 (1), 56.2 (3); ms (from gc–ms): 140 (M^+, 18), 125 (7), 109 (14), 97 (23), 82 (21), 78 (28), 77 (25), 75 (100), 65 (50). Exact Mass calcd. for $C_8H_{12}O_2$: 140.0837; found: 140.0834.

cis-*5,6-Bis(trimethylsilyloxy)-1,3-cyclohexadiene (8)*

Chlorotrimethylsilane (600 μL, 4.73 mmol) was added to a solution of **3** (0.232 g, 2.07 mmol) in pyridine (2 mL) at 0°C. The mixture was stirred for 1 h while it attained room temperature. After addition of CCl_4 (10 mL) the resulting precipitate was removed by filtration. The filtrate, after evaporation of most of the solvent under vacuum, was purified by flash chromatography to provide **8** as a colorless oil (0.456 g, 86%): uv (CH_3OH) λ_{max}: 259 nm (ε = 4000); ir (film) ν_{max}: 3043 (m), 2958 (s), 2898 (m), 2796 (w), 1412 (m), 1252 (s), 1119 (s), 840 (s) cm^{-1}; ^1H nmr ($CDCl_3$) δ: 5.97 (2H, m), 5.87 (2H, m), 4.14 (2H, nar m), 0.15 (18H, s); ^{13}C nmr ($CDCl_3$) δ: 130.4 (1), 124.0 (1), 68.9 (1), 0.2 (3); ms: 256 (M^+, 21), 191 (10), 151 (17), 147 (36), 75 (23), 73 (100). Exact Mass calcd. for $C_{12}H_{24}O_2Si_2$: 256.1314; found: 256.1314.

cis-*3a,7a,Dihydro-2,2-dimethyl-1,3-benzodioxole (9)*

A solution of **3** (0.200 g, 1.78 mmol) and *p*-toluenesulfonic acid (*p*TsOH) (10 mg) in 2,2-dimethoxypropane (15 mL) was stirred at room temperature for 1 h. After addition of CH_2Cl_2 (50 mL) the mixture was washed with 0.1 M NaOH (50 mL), saturated $NaHCO_3$ (50 mL), and saturated NaCl (50 mL). The organic solution was dried ($MgSO_4$) and concentrated under vacuum. Flash chromatography of the residue gave **9** as a colorless liquid (0.226 g, 83%): uv (CH_3OH) λ_{max}: 257 nm (ε = 3500); ir (film) ν_{max}: 3045 (m), 2987 (s), 2935 (m), 2888 (m), 1379 (s), 1209 (s), 1032 (s) cm^{-1}; ^1H nmr ($CDCl_3$) δ: 6.00 (2H, m), 5.89 (2H, m), 4.66 (2H, apparent t, J = 1.7 Hz), 1.43 (3H, s), 1.40 (3H, s); ^{13}C nmr ($CDCl_3$) δ: 125.2, 123.6, 104.4, 70.2, 26.6, 24.6; ms: 152 (M^+, 1.4), 137 (42), 95 (100), 94 (96), 78 (32), 77 (53), 68 (24), 66 (94), 65 (50), 43 (87). Exact Mass calcd. for $C_8H_9O_2$ ($M^+ - CH_3$): 137.0602; found: 137.0599.

cis-*3a,7a-Dihydro-2,2-dimethyl-1,3,2-benzodioxasilole (10)*

This reaction was best followed by nmr. Diacetoxydimethylsilane (222 μL, 1.26 mmol) was added to a solution of **3** (0.141 g, 1.26 mmol) in $CDCl_3$ (approx. 0.5 mL) and pyridine (10 μL) in an nmr tube. The tube was spun in the probe of a 60-MHz nmr instrument for 10 min after which time the spectrum indicated quantitative conversion to **10**. The solvent could be removed under vacuum: uv (CH_3OH) λ_{max}: 260 (ε = 3500); ir (film) ν_{max}: 3044, 2962, 2902, 1413, 1258 cm^{-1}; ^1H nmr ($CDCl_3$) δ: 5.94 (2H, m), 5.84 (2H, m), 4.70 (2H, nar m), 0.27 (3H, s), 0.23 (3H, s); ^{13}C nmr ($CDCl_3$) δ: 126.3, 123.2, 69.1, −1.3, −1.9; ms: 168 (M^+, 90), 167 (100), 153 (99), 151 (16), 135 (20), 133 (17), 94 (45), 91 (40), 77 (36), 75 (64), 66 (24), 65 (20), 45 (34). Exact Mass calcd. for $C_8H_{12}O_2Si$: 168.0606; found: 168.0587; calcd. for $C_8H_{11}O_2Si$ ($M^+ - H$): 167.0528; found: 167.0522.

Diels–Alder reaction of 6: (3aα,4α,7α,7aα,8S,9R*)- (11) and (3aα,4α,7α,7aα,8R*,9S*)-8,9-bis(acetyloxy)-3a,4,7,7a-tetrahydro-2-phenyl-4,7-ethano-1H-isoindole-1,3(2H)-dione (12)*

A solution of the diacetate diene **6** (0.214 g, 1.09 mmol) and *N*-phenylmaleimide (0.190 g, 1.10 mmol) in $CHCl_3$ (30 mL) was heated under reflux for 2 days. Evaporation of the solvent under vacuum provided a colorless mixture (0.402 g) that ^1H nmr showed was composed very predominantly of the *syn* (**11**) and the *anti* (**12**) adducts in a ratio of 88:12, respectively, along with only a trace of unreacted dienophile and residual solvent. The nmr signals of the adducts correlated exactly with authentic materials produced as follows. A solution of the *syn* diol adduct **4** (70.6 mg, 0.247 mmol) and acetic anhydride (1 mL) in pyridine (2 mL) was stirred overnight at room temperature. Evaporation of the volatiles under vacuum gave a colorless powder (94.6 mg), which was crystallized from ethyl acetate to provide **11**: mp 235–237°C; ir (film) ν_{max}: 1755, 1712, 1377, 1247 cm^{-1}; ^1H nmr ($CDCl_3$) δ: 7.35–7.49 (3H, m), 7.17 (2H, d, J = 7.1 Hz), 6.30 (2H, apparent dd, J = 3.0, 4.4 Hz), 4.90 (2H, br s, C-8H and C-9H), 3.48 (4H, br s), 2.10 (6H, s); ^{13}C nmr ($CDCl_3$) δ: 177.4, 169.4, 131.5 (C-1'), 131.3 (C-5 and C-6), 129.1, 128.7, 126.3, 64.7, 38.0, 36.5, 20.5; ms: 369 (M^+, 10), 327 (24), 310 (1), 285 (5), 226 (29), 119 (15), 91 (13), 79 (18), 43 (100). Exact Mass calcd. for $C_{18}H_{17}NO_5$ ($M^+ - C_2H_2O$): 327.1106; found: 327.1107.

Similarly, the *anti* diol **5** (43.0 mg, 0.151 mmol) and acetic anhydride (1 mL) in pyridine (5 mL) were stirred overnight, and evaporation of the volatiles under vacuum gave a colorless powder (55.8 mg), which was crystallized from 3:2 ethyl acetate/hexane to provide **12** (20.8 mg, 37%): mp 235.5–237°C; ir (film) ν_{max}: 1738, 1711, 1376, 1254, 1191 cm^{-1}; ^1H nmr ($CDCl_3$) δ: 7.35–7.49 (3H, m), 7.17 (2H, br d, $J \approx 7.0$ Hz), 6.35 (2H, apparent dd, J = 3.2, 4.2 Hz), 5.15 (2H, nar m, C-8H and C-9H), 3.52 (2H, m, C-4H and C-7H), 3.12 (2H, nar m, C-3aH and C-7aH), 2.04 (6H, s); ^{13}C nmr ($CDCl_3$) δ: 175.7, 169.9, 131.5 (C-1'), 130.4 (C-5 and C-6), 129.2, 128.9, 126.3, 69.8, 40.6 (C-3a and C-7a), 36.6 (C-4 and C-7), 20.5; ms: 369 (M^+, 10), 327 (40), 285 (7), 226 (43), 143 (10), 119 (22), 91 (14), 79 (25), 43 (100). Exact Mass calcd. for $C_{20}H_{19}NO_6$: 369.1211; found: 369.1216.

Diels–Alder reaction of 7: (3aα,4α,7α,7aα,8S,9R*)- (13) and (3aα,4α,7α,7aα,8R*,9S*)-3a,4,7,7a-tetrahydro-8,9-dimethoxy-2-phenyl-4,7-ethano-1H-isoindole-1,3(2H)-dione (14)*

A solution of **7** (67 mg, 0.48 mmol) and *N*-phenylmaleimide (59 mg, 0.34 mmol) in $CHCl_3$ (5 mL) was stirred at room temperature for 16 h. The solvent was evaporated under vacuum to provide an orange solid (113 mg). The ^1H nmr spectrum of this material in-

Can. J. Chem. Downloaded from www.nrcresearchpress.com by 217.78.4.112 on 09/08/12
For personal use only.

dicated some unreacted **7**, a small amount of unreacted *N*-phenylmaleimide, and the remainder was almost exclusively **13** (ratio of **13**/**14** estimated conservatively at 99:1). Recrystallization of this crude product from benzene afforded some **13**: mp 195–196°C; ir (KBr) ν_{max}: 2966, 2891, 1767 (w), 1709 (s), 1497, 1371, 1177, 730 cm^{-1}; ^1H nmr ($CDCl_3$) δ: 7.36–7.44 (3H, m), 7.19 (2H, d, J = 7.1 Hz), 6.22 (2H, dd, J = 3.1, 4.5 Hz), 3.51 (8H, br s), 3.43 (4H, br s); ^1H nmr (C_5D_5N) δ: 7.40–7.43 (4H, m), 7.31 (1H, br m), 6.20 (2H, dd, J = 3.2, 4.6 Hz), 3.62 (2H, t, J = 1.6 Hz, C-3aH and C-7aH), 3.51 (2H, br m, C-4H and C-7H), 3.34 (6H, s), 3.27 (2H, t, J = 1.5 Hz, C-8H and C-9H); nOe data (C_5D_5N): 6.20 (3.51, 16%; 3.27, 1%); 3.62 (3.34, 1%), 3.51 (6.20, 9%; 3.62, 6%; 3.34, 1%; 3.27, 6%), 3.34 (3.62, 2.5%; 3.51, 6%; 3.27, 3%), 3.27 (6.20, 2.5%; 3.51, 11%; 3.34, 2%); ^{13}C nmr (C_5D_5N) δ: 179.0, 133.4, 131.9 (C-5 and C-6), 129.3, 128.6, 127.4, 73.9 (C-8 and C-9), 58.0 (2 × CH_3), 38.7 (C-3a and C-7a), 37.4 (C-4 and C-7); ms: 314 (M^+ + 1, 0.7), 313 (M^+, 0.4), 282 (0.5), 173 (1), 134 (3), 126 (1), 119 (15), 91 (19), 88 (100), 78 (18), 77 (17), 73 (31), 45 (25). Exact Mass calcd. for $C_{18}H_{19}NO_4$: 313.1313; found: 313.1322. The nmr spectra of this adduct were identical with the spectra of material prepared as follows: 2.5 mol equivalents of KH, then 2.5 mol equivalents of iodomethane were added to a THF (30 mL) solution of **4** (55 mg, 0.19 mmol). This was heated under reflux for 18 h to effect complete reaction. After cooling, CH_2Cl_2 (150 mL) was added, and the solution was washed with H_2O (2 × 100 mL) and saturated NaCl (100 mL), then dried ($MgSO_4$) and concentrated under vacuum. Flash chromatography of the residue provided **13** (51 mg, 85%).

Signals for the minor adduct in the ^1H nmr spectrum correlated with the spectrum of **14**, which was made from **5** as above, except the reaction was over in 2 h at room temperature. Crystallization of the residue from $CHCl_3/CCl_4$ provided **14** (94%): mp 220–223°C; ir (KBr) ν_{max}: 2956, 2876, 1777 (w), 1708, 1498, 1385, 1180, 723 cm^{-1}; ^1H nmr ($CDCl_3$) δ: 7.37–7.48 (3H, m), 7.17 (2H, d, J = 7.0 Hz), 6.32 (2H, dd, J = 3.1, 4.4 Hz), 3.69 (2H, br s), 3.60 (2H, br m, C-4H and C-7H), 3.47 (6H, 2 × CH_3), 2.94 (2H, t, J = 1.4 Hz); ^{13}C nmr ($CDCl_3$) δ: 176.6, 131.6, 130.2, 129.1, 128.8, 126.3, 79.2 (C-8 and C-9), 58.5 (2 × CH_3), 40.9, 36.1; ms: 314 (M^+ + 1, 0.2), 313 (M^+, 0.05), 299 (0.6), 281 (0.6), 226 (11), 173 (1), 134 (4), 119 (22), 91 (26), 88 (100), 78 (27), 77 (24), 45 (34). Exact Mass calcd. for $C_{14}H_{12}NO_2$ (M^+ − $C_4H_7O_2$ = loss of the C-8 and C-9 bridge with H transfer): 226.0867; found: 226.0862.

Diels–Alder reaction of ***8****: (3aα,4α,7α,7aα,8S*,9R*)-3a,4,7,7a-tetrahydro-2-phenyl-8,9-bis[(trimethylsilyl)oxy]-4,7-ethano-1H-isoindole-1,3(2H)-dione (****15****)*

A solution of diene **8** (92 mg, 0.36 mmol) and *N*-phenylmaleimide (62 mg, 0.36 mmol) in $CHCl_3$ (6 mL) was stirred at room temperature for 20 h. Evaporation of the solvent under vacuum gave a pale yellow solid (120 mg). The ^1H nmr spectrum of this material showed major signals for **15** and minor signals for unreacted addends; no signals attributable to **16** were detected. The signals of this adduct were identical with the signals of the only product obtained as follows. Adduct **4** (60 mg, 0.21 mmol) and chlorotrimethylsilane (1.0 mL) in dry pyridine (2.0 mL) were stirred at room temperature for 24 h. Addition of CCl_4 gave a precipitate, which was removed by filtration. Evaporation of the filtrate gave a colorless solid that was crystallized from 25% hexane in CCl_4: mp 143–144°C; ir (KBr) ν_{max}: 3047, 2955, 2898, 1773 (w), 1710, 1391, 1183, 898, 753 cm^{-1}; ^1H nmr ($CDCl_3$) δ: 7.35–7.46 (3H, m), 7.17 (2H, br d, J = 7.1 Hz), 6.17 (2H, apparent dd, J = 3.3, 4.5 Hz), 3.72 (2H, nar m, C-8H and C-9H), 3.54 (2H, nar m, C-3aH and C-7aH), 3.18 (2H, m, C-4H and C-7H), 0.17 (18H, s); ^{13}C nmr ($CDCl_3$) δ: 179.1, 132.0 (C-1′), 131.5 (C-5 and C-6), 129.0, 128.4, 126.5, 65.3 (C-8 and C-9), 40.6 (C-4 and C-7), 37.9 (C-3a and C-7a), 0.3; ms: no M^+, 414 (1), 324 (3), 204 (100), 147 (10), 73 (51). Exact Mass calcd. for $C_{21}H_{28}NO_4Si_2$ (M^+ − CH_3): 414.1555; found: 414.1588; calcd. for $C_{18}H_{18}NO_3Si$ (M^+ − $C_4H_{13}OSi$): 324.1055; found: 324.1046.

(3aα,4α,7α,7aα,8R,9S*)-3a,4,7,7a-Tetrahydro-2-phenyl-8,9-bis[(trimethylsilyl)oxy]-4,7-ethano-1H-isoindole-1,3(2H)-dione (****16****)*

Addition of chlorotrimethylsilane (1.0 mL) to a solution of (mainly) adduct **5** (33.1 mg, 0.116 mmol) in dry pyridine (5.0 mL) immediately gave a white precipitate. Nevertheless, this was stirred at room temperature for a further 16 h before CCl_4 (10 mL) was added. The precipitate was removed by filtration, and evaporation of the filtrate under vacuum left **16** as a colorless solid (40.6 mg, 82%): mp 166–171°C; ir (KBr) ν_{max}: 3055, 2962, 1778 (w), 1718, 1499, 1385, 1109, 909, 843 cm^{-1}; ^1H nmr ($CDCl_3$) δ: 7.32–7.47 (3H, m), 7.16 (2H, br d, $J \approx 7.1$ Hz), 6.32 (2H, apparent dd, J = 3.1, 4.4 Hz), 3.95 (2H, br s, C-8H and C-9H), 3.26 (2H, m, C-4H and C-7H), 2.93 (2H, nar m, C-3aH and C-7aH), 0.16 (18H, s); ^{13}C nmr ($CDCl_3$) δ: 176.7, 131.6 (C-1′), 130.3 (C-5 and C-6), 129.0, 128.6, 126.3, 70.9 (C-8 and C-9), 41.2 (C-3a and C-7a), 40.3 (C-4 and C-7), 0.2; ms: no M^+, 414 (1), 324 (5), 204 (100), 147 (14), 132 (24), 116 (39), 73 (90). Exact Mass calcd. for $C_{18}H_{18}NO_3Si$ (M^+ − $C_4H_{13}OSi$): 324.1055; found: 324.1078.

Diels–Alder reaction of ***9****: (3aα,4α,4aβ,7aβ,8α,8aα)- (****17****) and (3aα,4β,4aα,7aα,8β,8aα)-4a,7a,8,8a-tetrahydro-2,2-dimethyl-6-phenyl-4,8-etheno-4H-1,3-dioxolo[4,5-f]isoindole-5,7(3aH,6H)-dione (****18****)*

A solution of diene **9** (66 mg, 0.41 mmol) and *N*-phenylmaleimide (77 mg, 0.44 mmol) in $CHCl_3$ (6 mL) was stirred at room temperature for 24 h. Evaporation of the solvent under vacuum gave a mixture of adducts, the ^1H nmr spectrum of which revealed a mixture of **17** and **18** in a ratio of 60:40, respectively. Preparative tlc (SiO_2; 2:1 hexane/EtOAc)) afforded samples of these adducts. For **17**: mp 189–190.5°C; ir (KBr) ν_{max}: 2981, 2913, 1773 (w), 1711, 1501, 1397, 1187, 1047 cm^{-1}; ^1H nmr ($CDCl_3$) δ: 7.32–7.45 (3H, m), 7.16 (2H, br d, J = 7.1 Hz), 6.21 (2H, apparent dd, J = 2.8, 4.3 Hz), 4.16 (2H, nar m), 3.48 (4H, s), 1.50 (3H, s), 1.35 (3H, s); ^1H nmr (C_6D_6) δ: 7.41 (2H, br d, J = 7.3 Hz), 7.18 (2H, m), 7.04 (1H, br t, J = 7.4 Hz), 5.68 (2H, dd, J = 3.0, 4.4 Hz), 3.60 (2H, nar m), 3.29 (2H, m), 3.19 (2H, nar m), 1.35 (3H, s), 1.10 (3H, s); nOe data (C_6D_6): 5.68 (3.60, 1.5%; 3.29, 4.5%), 3.60 (5.68, 1.5%; 3.29, 7%; 1.10, 1.5%), 3.29 (5.68, 5%; 3.60, 5.5%; 3.19, 4%), 3.19 (3.29, 5.5%; 1.35, 1%), 1.35 (3.19, 4%; 1.10, 1%), 1.10 (3.60, 7%; 1.35, 2%); ^{13}C nmr ($CDCl_3/C_6D_6$) δ: 178.3/177.7, 131.7/133.1 (C-1′), 131.4/131.6 (C-9 and C-10), 128.8/128.9, 128.3/128.1 (C-4′), 126.2/126.6, 112.2/112.2 (C-2), 73.7/74.0 (C-3a and C-8a), 37.5/37.9 (C-4a and C-7a), 36.8/37.3 (C-4 and C-8), 26.1/26.4 (*syn* CH_3), 24.0/24.1 (*anti* CH_3); ms: 325 (M^+, 8), 310 (17), 296 (7), 268 (20), 267 (22), 239 (17), 222 (31), 120 (39), 119 (55), 100 (47), 93 (47), 92 (54), 91 (100), 43 (45). Exact Mass calcd. for $C_{19}H_{19}NO_4$: 325.1313; found: 325.1308.

For **18**: mp 263–265°C; ir (KBr) ν_{max}: 2988, 2889, 1796 (w), 1711, 1500, 1391, 1188 cm^{-1}; ^1H nmr ($CDCl_3$) δ: 7.35–7.48 (3H, m), 7.18 (2H, br d, $J \approx 7.0$ Hz), 6.17 (2H, apparent dd, J = 3.2, 4.3 Hz), 4.32 (2H, br s, C-3aH and C-8aH), 3.53 (2H, m, C-4H and C-8H), 2.88 (2H, nar m, C-4aH and C-7aH), 1.35 (3H, s), 1.30 (3H, s); nOe data: 6.17 (3.53, 10%), 4.32 (3.53, 15%; 2.88, 13%; 1.30, 3%), 3.53 (6.17, 10%; 4.32, 2%; 2.88, 5%), 2.88 (4.32, 11%; 3.53, 7%), 1.35 (6.17, 2.5%), 1.30 (4.32, 6%); ^{13}C nmr ($CDCl_3$) δ: 176.3, 131.6 (C-1′), 129.6 (C-9 and C-10), 129.0, 128.6 (C-4′), 126.3, 109.6 (C-2), 77.1 (C-3a and C-8a), 40.3 (C-4a and C-7a), 36.9 (C-4 and C-8), 25.2 (*syn* CH_3), 24.8 (*anti* CH_3); ms: 325 (M^+, 2), 310 (18), 268 (15), 267 (14), 239 (12), 222 (21), 162 (100), 120 (31), 119 (42), 100 (35), 93 (36), 92 (39), 91 (79), 45 (91), 43 (46). Exact Mass. calcd. for $C_{19}H_{19}NO_4$: 325.1313; found: 325.1302.

Hydrolysis of ***17***

Adduct **17** (93 mg, 0.33 mmol) in 4 M HCl (15 mL) was heated under reflux for 1 h. After cooling, CH_2Cl_2 (15 mL) was added, and the organic layer was washed with saturated $NaHCO_3$ (100 mL) and saturated NaCl (100 mL), then dried ($MgSO_4$). Evaporation of the solvent under vacuum provided **4** (47 mg, 58%).

Can. J. Chem. Downloaded from www.nrcresearchpress.com by 217.78.4.112 on 09/08/12
For personal use only.

Hydrolysis of ***18***

Adduct **18** (80 mg, 0.28 mmol) was treated similarly to the above to provide **5** (37 mg, 53%).

Diels–Alder reaction of ***10****: (3aα,4α,4aβ,7aβ,8α,8aα)-* ***(19)*** *and (3aα,4β,4aα,7aα,8β,8aα)-4a,7a 8,8a-tetrahydro-2,2-dimethyl-6-phenyl-4,8-etheno-4H-1,3,2-dioxasilolo[4,5-f]isoindole-5,7(3aH,6H)-dione* ***(20)***

To the solution of **10**, prepared in an nmr tube exactly as described above, was added *N*-phenylmaleimide (0.217 g, 1.25 mmol) in $CDCl_3$ (0.5 ml). The reaction was followed at room temperature. After 3 h no **10** remained, and the formation of the adducts appeared to be quantitative. The ^1H nmr spectrum of the solution revealed signals for **19** and **20** in a ratio of 60:40, respectively.[7] The nmr signals matched exactly the signals of the individual adducts, prepared as follows. Diacetyloxydimethylsilane (32 μL, 0.18 mmol) was added to a solution of **4** (51.8 mg, 0.182 mmol) in C_5D_5N (approx. 0.5 mL). The reaction was complete within 15 min (by nmr), and the volatiles were evaporated under vacuum to leave **19** as a white powder (62.6 mg, 100%): mp 200–205°C; ^1H nmr ($CDCl_3$) δ: 7.36–7.47 (3H, m), 7.17–7.21 (2H, m), 6.22 (2H, apparent dd, J = 3.1, 4.5 Hz), 4.17 (2H, apparent t, J = 1.8 Hz, C-3aH and C-8aH), 3.49 (2H, m, C-4H and C-8H), 3.37 (2H, apparent t, J = 1.6 Hz, C-4aH and C-7aH), 0.37 (3H, s), 0.26 (3H, s); ^1H nmr (C_5D_5N) δ: 7.28–7.42 (5H, m), 6.22 (2H, apparent dd, J = 3.1, 4.4 Hz), 4.21 (2H, nar m, C-3aH and C-8aH), 3.65 (2H, nar m, C-4aH and C-7aH), 3.59 (2H, m, C-4H and C-8H), 0.32 (3H, s), 0.22 (3H, s); nOe data ($CDCl_3$): 6.22 (3.49, 3.5%), 4.17 (6.21, 3%; 3.49, 11%), 3.49 (6.22, 7%; 4.17, 6%; 3.37, 3%), 3.37 (3.49, 6%; 0.37, 2.5%), 0.37, (3.37, 6%); ^{13}C nmr (C_5D_5N) δ: 178.9, 133.5 (C-1′), 132.2 (C-9 and C-10), 129.4, 128.8, 127.5, 71.8 (C-3a and C-8a), 39.7 (C-4 and C-8), 38.5 (C-4a and C-7a), −0.1, −1.0; ms: 341 (M^+, 5), 285 (7), 226 (32), 119 (39), 116 (100), 79 (40), 78 (33). Exact Mass calcd. for $C_{18}H_{19}NO_4Si$: 341.1082; found: 341.1071.

Diacetyloxydimethylsilane (15 μL, 0.085 mmol) was added to a solution of **5** (23.0 mg, 0.081 mmol) in C_5D_5N (approx. 0.5 mL). The solution was warmed for 25 min to effect complete reaction (by nmr). Evaporation of all volatiles under vacuum left **20** as a white powder (28.0 mg, 100%): mp 220–225°C; ^1H nmr ($CDCl_3$) δ: 7.35–7.48 (3H, m), 7.15–7.19 (2H, m), 6.25 (2H, apparent dd, J = 3.2, 4.3 Hz), 4.36 (2H, br s, C-3aH and C-8aH), 3.54 (2H, m, C-4H and C-8H), 2.95 (2H, apparent t, J = 1.3 Hz, C-4aH and C-7aH), 0.19 (6H, s); ^1H nmr (C_5D_5N) δ: 7.28–7.41 (5H, m), 6.32 (2H, m), 4.46 (2H, s, C-3aH and C-8aH), 3.67 (2H, m, C-4H and C-8H), 3.22 (2H, s, C-4aH and C-7aH), 0.165 (3H, s), 0.158 (3H, s); nOe data ($CDCl_3$): 6.25 (3.54, 3%), 4.36 (3.54, 14%; 2.95, 12%), 3.54 (6.25, 1.5%; 4.36, 2.5%; 2.95, 2.5%), 2.95 (4.36, 12%; 3.54, 14%), 0.19 (6.25, 3%; 4.36, 1.5%); ^{13}C nmr (C_5D_5N) δ: 177.2, 133.3 (C-1′), 131.5 (C-9 and C-10), 129.3, 128.8, 127.4, 76.3 (C-3a and C-8a), 41.3 (C-4a and C-7a), 39.9 (C-4 and C-8), −0.1, −0.6; ms: 341 (M^+, 2), 326 (1), 193 (2), 179 (1), 116 (100), 101 (8), 78 (4), 77 (2), 75 (3). Exact Mass calcd. for $C_{18}H_{19}NO_4Si$: 341.1082; found: 341.1087.

cis*-2-Ethyl-3a,7a-dihydro-2,1,3-benzoboradioxole* ***(22)*** *and its Diels–Alder reaction: (3aα,4α,4aβ,7aβ,8α,8aα)-* ***(23)*** *and (3aα,4β,4aα,7aα,8β,8aα)-2-ethyl-4a,7a,8,8a-tetrahydro-4,8-etheno-4H-2,1,3-boradioxolo[4,5-f]isoindole-5,7(3aH,6H)-dione* ***(24)***

Diol **3** (60 mg, 0.54 mmol) in dry THF (5 mL) was added to solution of lithium triethylborohydride (Aldrich; 0.6 mL of 1 M in THF diluted with a further 2 mL of THF) at 0°C. After stirring for 1 h, a small amount of H_2O was added, and the mixture was evaporated on a vacuum line to leave a very viscous oil. To this was added CH_2Cl_2 (10 mL), and the insoluble material was removed by filtration. Evaporation of the solvent left the very moisture-sensitive **22** (24 mg, 30%), which was immediately taken up in $CDCl_3$ (0.5 mL): ^1H nmr (60 MHz) δ: 5.8 (4H, m), 4.9 (2H, s), 1.0 (5H, m). *N*-Phenylmaleimide (34.5 mg, 0.20 mmol) in $CDCl_3$ (0.5 mL) was added to this solution. The mixture was stirred at room temperature overnight, after which time ^1H nmr indicated clean conversion to **23** and **24** in a ratio of 45:55, respectively. Data were taken from this mixture of moisture-sensitive adducts: ^1H nmr ($CDCl_3$) δ: 7.1–7.6 (aromatics), 6.22 (C-9H and C-10H for **23** and **24**), 4.54 (s, C-3aH and C-8aH for **24**), 4.42 (nar m, C-3aH and C-8aH for **23**), 3.57 (m, C-4H and C-8H for **23** and **24**), 3.32 (nar m, C-4aH and C-7aH for **23**), 2.92 (nar m, C-4aH and C-7aH for **24**), 0.7–1.1 (multiplets); nOe data: 6.22 (4.42, 1%; 3.57, 5%), 4.54 (3.57, 4%; 2.92, 12%), 4.42 (6.22, 1%; 3.57, 4%), 3.57 (6.22, 7%; 4.54, 5%; 4.42, 8%; 3.32, 6%; 2.92, 5%), 3.32 (3.57, 3%), 2.92 (4.54, 12%; 3.57, 4%); ^{13}C nmr ($CDCl_3$) δ: 177.7, 176.1, 131.6 (C-9 and C-10 for **23**), 130.0 (C-9 and C-10 for **24**), 77.7 (C-3a and C-8a for **24**), 75.0 (C-3a and C-8 for **23**), 40.1 (C-4a and C-7a for **23**), 37.3 (C-4a and C-7a for **24**), 37.1, 37.0, 7.6, 7.5, 3.3 (broad), 2.2 (broad); ms of mixture of **23** and **24**: 323 (M^+, 10), 294 (3), 225 (12), 173 (90), 129 (19), 119 (100), 91 (23), 78 (38), 54 (36). Exact Mass calcd. for $C_{18}H_{18}BNO_4$: 323.1328; found: 323.1310; calcd. for $C_{16}H_{13}BNO_4$ ($M^+ - C_2H_5$): 294.0938; found: 294.0938.

(1R,2S*,4R*,5R*)-4,5-Dibromocyclohexane-1,2-diol* ***(27)***

Following literature procedures (26, 27) **27** was prepared from 1,4-cyclohexadiene via *trans*-4,5-dibromocyclohexene. For **27** (an off-white powder): mp 103–105°C (lit. (27) mp 103–105°C); ir (KBr) ν_{max}: 3380 (br s), 2910, 1445 (w), 1295 (m), 1060 (s), 990 (m) cm^{-1}; ^1H nmr (C_5D_5N) δ: 6.60 (2H, br s, OH's), 4.84 (1H, ddd, J = 4.5, 10.7, 12.0 Hz, C-4H), 4.39 (1H, ddd, J = 4.5, 10.7, 12.0 Hz, C-5H), 4.26 (1H, m, $W_{1/2}$ = 8 Hz, C-1H), 3.98 (1H, ddd, J = 2.8, 4.2, 11.3 Hz, C-2H), 2.92 (1H, ddd, J = 11.3, 12.0, 12.5 Hz, C-3H$_\alpha$), 2.82 (1H, ddd, J = 2.9, 4.5, 13.8 Hz, C-6H$_\alpha$), 2.70 (1H, ddd, J = 4.2, 4.5, 12.5 Hz, C-3H$_\beta$), 2.16 (1H, ddd, J = 2.2, 12.0, 13.8 Hz, C-6H$_\beta$); ^{13}C nmr (C_5D_5N) δ: 70.7 (C-2), 70.2 (C-1), 55.6 (C-5), 54.8 (C-4), 42.9 (C-6), 41.2 (C-3); ms: no M^+, 195 (14), 193 (14), 177 (20), 175 (21), 113 (13), 95 (67), 67 (100), 55 (79). Exact Mass calcd. for $C_6H_8{}^{81}BrO$ (M^+ − Br − H_2O): 176.9734; found: 176.9728.

(2α,3aβ,5β,6α,7aβ)- ***(28)*** *and (2α,3aα,5α,6β,7aα)-5,6-Dibromohexahydro-2-phenyl-1,3-benzodioxole* ***(29)***

A solution of **27** (5.88 g, 21.5 mmol), benzaldehyde dimethyl acetal (16.3 g, 107 mmol), and *p*TsOH (1.03 g) in dry CH_2Cl_2 (160 mL) was stirred at room temperature for 2 days. The solution was washed with 20% $NaHSO_3$ (50 mL), 1 M NaOH (100 mL), saturated $NaHCO_3$ (100 mL), and saturated NaCl. The solution was dried ($MgSO_4$), then concentrated under vacuum. Hexane (50 mL) was added, the solution was refrigerated (approx. −5°C) for 2 days. The crystals that formed were washed with cold hexane to provide **29** (1.77 g). The mother liquor and the hexane washings were combined and concentrated under vacuum. Flash chromatography of the residue gave an additional crop of **29** (0.88 g after recrystallization from hexane, for a total yield of 2.66 g, 34%) and **28** as a waxy solid (2.61 g, 34%): mp 63–65°C; ir (KBr) ν_{max}: 1412 (m), 1173 (m), 1069 (m), 1011 (s) cm^{-1}; ^1H nmr ($CDCl_3$) δ: 7.37–7.56 (5H, m), 5.85 (1H, C-2H), 4.45 (1H, ddd, J = 3.8, 6.7, 8.0 Hz, C-5H), 4.37 (1H, ddd, J = 5.2, 5.3, 5.7 Hz, C-3aH), 4.28 (1H, ddd, J = 5.3, 5.4, 6.0 Hz, C-7aH), 4.24 (1H, ddd, J = 4.8, 6.7, 6.7 Hz, C-6H), 2.84 (1H, ddd, J = 4.8, 5.4, 15.5 Hz, C-7H$_\beta$), 2.79 (1H, ddd, J = 3.8, 5.7, 15.0 Hz, C-4H$_\alpha$), 2.49 (1H, ddd, J = 6.0, 6.7, 15.5 Hz, C-7H$_\alpha$), 2.28 (1H, ddd, J = 5.2, 8.0, 15.0 Hz, C-4H$_\beta$); ^{13}C nmr ($CDCl_3$) δ: 137.1 (C-1′), 129.3, 128.4, 126.4, 103.8 (C-2), 73.3 (C-3a), 73.0 (C-7a), 50.8 (C-5), 48.3 (C-6), 35.5 (C-7), 34.4 (C-4); ms (from gc–ms): 364 (3), 362 (6), and 360 (3) (all M^+), 363 (11), 361 (22), and 359 (12) (all M^+ − H), 159 (10), 157 (8), 105 (100), 79 (96), 78 (48), 77 (76), 67 (67), 51 (39). Exact Mass calcd. for $C_{13}H_{13}{}^{79}Br_2O_2$ (M^+ − H): 358.9283; found: 358.9293.

For **29**: mp 125–127.5°C; ir (KBr) ν_{max}: 2903, 1459, 1362, 1219 (m), 1107, 1069, 976 cm^{-1}; ^1H nmr ($CDCl_3$) δ: 7.34–7.51 (5H, m),

[7]Attempts to separate these adducts by chromatography gave only hydrolysed materials: **4** (major) and **5** (minor).

Can. J. Chem. Downloaded from www.nrcresearchpress.com by 217.78.4.112 on 09/08/12
For personal use only.

6.17 (1H, s, C-2H), 4.47 (1H, ddd, J = 3.9, 7.4, 8.2 Hz, C-5H), 4.39 (1H, m, C-3aH), 4.33 (1H, m, C-7aH), 4.19 (1H, ddd, J = 4.5, 7.4, 7.8 Hz, C-6H), 2.84 (1H, ddd, J = 3.9, 5.5, 15.1 Hz, C-4H), 2.78 (1H, ddd, J = 4.5, 5.0, 15.2 Hz, C-7H$_\beta$), 2.46 (1H, ddd, J = 6.2, 7.8, 15.2 Hz, C-7H$_\alpha$), 2.25 (1H, ddd, J = 4.7, 8.2, 15.1 Hz, C-4H$_\beta$); ^{13}C nmr ($CDCl_3$) δ: 138.9 (C-1′), 129.0, 128.3, 125.9, 102.2 (C-2), 72.9 (C-3a), 72.6 (C-7a), 50.8 (C-5), 48.5 (C-6), 34.5 (C-7), 33.3 (C-4); ms (from gc–ms): 364 (3), 362 (6), and 360 (3) (all M^+), 363 (11), 361 (22), and 359 (11) (all $M^+ - H$), 159 (12), 157 (10), 105 (100), 79 (96), 78 (49), 77 (71), 67 (59), 51 (35). Exact Mass calcd. for $C_{13}H_{13}{}^{81}Br_2O_2$ ($M^+ - H$): 362.9241; found: 362.9231.

(2α,3aβ,7aβ)-3a,7a-Dihydro-2-phenyl-1,3-benzodioxole (25)

From 3

A solution of **3** (77 mg, 0.67 mmol), benzaldehyde dimethyl acetal (100 μL, 0.67 mmol), and *p*TsOH (1.4 mg) in $CDCl_3$ (approximately 1 mL) was stirred overnight. The analysis of the ^{1}H nmr spectrum revealed mainly signals for **25** (but no other derivative) and benzaldehyde along with some phenol. Diene **25** made in this way was purified by rotary thin-layer chromatography (SiO_2; 20% CH_2Cl_2 in hexane) in a yield of only 15%.

From 28

Based on a procedure by Yang *et al.* (27), a solution of **28** (0.356 g, 0.983 mmol) and 1,8-diazabicyclo[5.4.0]undec-7-ene (DBU; 0.60 g, 3.9 mmol) in dry benzene (50 mL) was heated under reflux for 16 h. After cooling, the solution was decanted from a white precipitate. The precipitate was extracted with more benzene (50 mL), and the combined benzene solutions were washed with saturated $NaHCO_3$ (3 × 100 mL), H_2O (100 mL), and saturated NaCl (100 mL), then dried ($MgSO_4$) and concentrated under vacuum. Flash chromatography afforded **25** (0.114 g, 58%): ir (film) ν_{max}: 3044, 2883, 1459, 1401, 1217, 1061 cm^{-1}; ^{1}H nmr ($CDCl_3$) δ: 7.46–7.50 (2H, m), 7.32–7.36 (3H, m), 6.01–6.08 (2H, m, C-5H and C-6H), 5.94–6.00 (2H, m, C-4H and C-7H), 5.64 (1H, s), 4.66 (2H, apparent t, J = 1.6 Hz); nOe data: 5.64 (7.46–7.50, 3.5%; 4.66, 4%), 4.66 (5.94–6.00, 4%; 5.64, 8.5%); ^{13}C nmr ($CDCl_3$) δ: 136.5 (C-1′), 129.4 (C-4′), 128.2 (C-3′ and C-5′), 126.8 (C-2′ and C-6′), 124.1 (C-4 and C-7), 123.8 (C-5 and C-6), 98.2 (C-2), 71.0 (C-3a and C-7a); ms: 200 (M^+, 4), 199 (3), 172 (6), 154 (39), 106 (35), 105 (90), 94 (100), 78 (64), 77 (86), 66 (100), 51 (50). Exact Mass calcd. for $C_{13}H_{12}O_2$: 200.0837; found: 200.0836.

(2α,3aα,7aα)-3a,7a-Dihydro-2-phenyl-1,3-benzodioxole (26)

By a procedure very similar to that for **25**, **29** (1.23 g, 3.34 mmol) and DBU (2.07 g, 13.4 mmol) gave **26** without chromatography as a yellow oil (0.490 g, 72%): ir (film) ν_{max}: 3043, 2927, 1641 (m), 1217, 1068 cm^{-1}; ^{1}H nmr ($CDCl_3$) δ: 7.47–7.55 (2H, m), 7.32–7.40 (3H, m), 6.05 (2H, m), 5.91 (2H, m), 5.83 (1H, s), 4.86 (2H, nar m); ^{13}C nmr ($CDCl_3$) δ: 137.4 (C-1′), 129.0 (C-4′), 128.2 (C-3′ and C-5′), 126.3 (C-2′ and C-6′), 124.9 (C-5 and C-6), 124.6 (C-4 and C-7), 100.7 (C-2), 70.6 (C-3a and C-7a); ms (from gc–ms): 199 ($M^+ - H$, 0.4), 153 (0.5), 128 (3), 122 (4), 105 (46), 94 (59), 78 (100), 77 (46), 66 (54), 51 (28). Exact Mass calcd. for $C_{13}H_{12}O_2$: 200.0837; found: 200.0828. Note that neat **26** will dimerize to **43** readily at room temperature (see below), but it can be stored in solution over moderate periods of time if kept refrigerated.

Diels–Alder reaction of 25: (2α,3aβ,4β,4aα,7aα,8β,8aβ)- (30) and (2α,3aβ,4α,4aβ,7aβ,8α,8aβ)-4a,7a,8,8a-tetrahydro-2,6-diphenyl-4,8-etheno-4H-1,3-dioxolo[4,5-f]isoindole-5,7-3aH,6H)-dione (31)

A solution of diene **25** (81.8 mg, 0.409 mmol) and *N*-phenylmaleimide (71.4 mg, 0.357 mmol) in $CHCl_3$ (2.0 mL) was stirred at room temperature for 16 h. Evaporation of the solvent under vacuum gave a mixture that ^{1}H nmr showed was a 28:72 mixture of **30** and **31**, respectively, along with some unreacted dienophile. Flash chromatography provided **31** (61.6 mg, 62%), but **30** co-eluted with *N*-phenylmaleimide (total fraction: 58.1 mg, which, by ^{1}H nmr integration, was 33% **30**). Careful crystallization of the mixture of **30** and *N*-phenylmaleimide from 1:1:1 $CHCl_3$/ethyl acetate/hexane gave a sample of **30**: mp 210–211.5°C; ir (film) ν_{max}: 2922, 1774 (w), 1712 (s), 1500, 1384, 1182, 1053, 710 cm^{-1}; ^{1}H nmr ($CDCl_3$) δ: 7.34–7.51 (8H, m), 7.18 (2H, d, J = 7.1 Hz), 6.31 (2H, dd, J = 3.1, 4.1 Hz), 5.94 (1H, s, C-2H), 4.26 (2H, s, C-3aH and C-8aH), 3.66 (2H, br s, C-4H and C-8H), 3.59 (2H, s, C-4aH and C-7aH); ^{1}H nmr (C_6D_6) δ: 7.52 (2H, d, J = 6.5 Hz), 7.35 (2H, d, J = 7.3 Hz), 7.12–7.24 (5H, m), 7.02 (1H, d, J = 7.4 Hz), 5.67 (2H, dd, J = 3.0, 4.5 Hz), 5.61 (1H, s, C-2H), 3.60 (2H, t, J = 2.0 Hz, C-3aH and C-8aH), 3.37 (2H, br m, C-4H and C-8H), 3.24 (2H, t, J = 1.6 Hz, C-4aH and C-7aH); nOe data (C_6D_6): 5.67 (3.60, 1%; 3.37, 6.5%), 5.61 (7.52, 1.5%; 3.60, 4.5%), 3.60 (5.67, 2%; 5.61, 12%; 3.37, 6%), 3.37 (5.67, 4.5%; 3.60, 4%; 3.24, 4%), 3.24 (7.52, 3%; 3.37, 5.5%); ^{13}C nmr ($CDCl_3$) δ: 178.1, 135.9, 131.8 (C-9 and C-10), 129.6, 129.1, 128.6, 126.4, 126.3, 105.8 (C-2), 74.8 (C-3a and C-8a), 37.9 (C-4a and C-7a), 36.8 (C-4 and C-8); ms: 373 (M^+, 10), 372 (12), 344 (43), 326 (11), 298 (2), 267 (9), 239 (15), 222 (25), 211 (8), 194 (4), 147 (14), 119 (47), 105 (40), 91 (100), 77 (29). Exact Mass calcd. for $C_{23}H_{19}NO_4$: 373.1313; found: 373.1312. The nmr data were identical with the product of this procedure: a solution of **4** (64 mg, 0.22 mmol), benzaldehyde dimethyl acetal (34 μL), and a catalytic amount of *p*TsOH in CH_2Cl_2 (15 mL) was stirred at room temperature for 14 h. The solution was washed with 10% NaOH and saturated NaCl, dried ($MgSO_4$), and evaporated under vacuum to provide **30** (78 mg, 93%).

For **31**: mp 231–234.5°C; ir (film) ν_{max}: 2896, 1778 (w), 1711 (s), 1498, 1395, 1186, 1065, 745 cm^{-1}; ^{1}H nmr ($CDCl_3$) δ: 7.35–7.48 (8H, m), 7.20 (2H, d, J = 7.0 Hz), 6.30 (2H, dd, J = 3.3, 4.1 Hz), 5.66 (1H, s, C-2H), 4.37 (2H, s, C-3aH and C-8aH), 3.70 (2H, s, C-4H and C-8H), 2.95 (2H, s, C-4aH and C-7aH); nOe data: 6.30 (3.70, 12%), 5.66 (4.37, 2%), 4.37 (5.66, 18%; 3.70, 13%; 2.95, 16%), 3.70 (6.30, 11%; 4.37, 6%; 2.95, 11%), 2.95 (4.37, 15%; 3.70, 12%); ^{13}C nmr ($CDCl_3$) δ: 176.1, 135.4, 131.6, 130.1 (C-9 and C-10), 129.9, 129.1, 128.8, 128.3, 127.2, 126.3, 103.8 (C-2), 77.8 (C-3a and C-8a), 40.5 (C-4a and C-7a), 36.6 (C-4 and C-8); ms: 373 (M^+, 7), 372 (11), 344 (5), 267 (15), 239 (21), 222 (25), 211 (8), 194 (3), 147 (15), 119 (50), 105 (76), 91 (100), 77 (29). Exact Mass calcd. for $C_{23}H_{19}NO_4$: 373.1313; found 373.1281; calcd. for $C_{22}H_{18}NO_3$ ($M^+ - H - CO$): 344.1287; found 344.1301. The nmr data were identical with the product of this procedure: **5** (51 mg, 0.18 mmol) was suspended in a solution of CH_2Cl_2, and benzaldehyde dimethyl acetal (30 μL) and catalytic *p*TsOH were added. After stirring overnight, the clear solution was worked up as above to afford **31** (66 mg, 99%).

Diels–Alder reaction of 26: (2α,3aα,4α,4aβ,7aβ,8α,8aα)- (32) and (2α,,3aα,4β,4aα,7aα,8β,8aα)-4a,7a,8,8a-tetrahydro-2,6-diphenyl-4,8-etheno-4H-1,3-dioxolo[4,5-f]isoindole-5,7-3aH,6H)-dione (33)

A solution of **26** (0.393 g, 1.96 mmol) and *N*-phenylmaleimide (0.337 g, 1.95 mmol) in $CHCl_3$ (10 mL) was stirred at room temperature overnight. The solvent was evaporated under vacuum, and the ^{1}H nmr spectrum of the residue revealed **32** and **33** in a ratio of 4:96, respectively. Flash chromatography of the residue provided some unreacted *N*-phenylmaleimide (60 mg), **32** (26 mg, 4%), **33** (0.520 g, 87%), and 31 mg of dimer **43**. For **32**: mp 232–234°C; ir (KBr) ν_{max}: 3056, 2926, 1772 (w), 1710 (s), 1598, 1502, 1397, 1191, 1086, 745 cm^{-1}; ^{1}H nmr ($CDCl_3$) δ: 7.35–7.47 (8H, m), 7.19 (2H, d, J = 7.2 Hz), 6.47 (1H, s, C-2H), 6.24 (2H, dd, J = 2.9, 3.9 Hz), 4.15 (2H, s, C-3aH and C-8aH), 3.62 (4H, br s); ^{1}H nmr (10% $CDCl_3$ in CCl_4) δ: 7.24–7.42 (8H, m), 7.16 (2H, d, J = 7.2 Hz), 6.40 (1H, s, C-2H), 6.21 (2H, dd, J = 3.1, 4.1 Hz), 4.08 (2H, s, C-3aH and C-8aH), 3.57 (2H, br m, C-4H and C-8H), 3.54 (2H, s, C-4aH and C-7aH); nOe data (10% $CDCl_3$ in CCl_4): 6.40 (3.54, 3%), 6.21 (4.08, 2%; 3.58, 7%), 4.08 (6.40, 2%; 6.21, 2.5%; 3.57, 11%); 3.57 (6.21, 6.5%; 4.08, 8%), 3.54

Can. J. Chem. Downloaded from www.nrcresearchpress.com by 217.78.4.112 on 09/08/12
For personal use only.

(6.40, 9%); ^{13}C nmr ($CDCl_3$) δ: 178.2, 139.2, 134.2, 131.7 (C-9 and C-10), 129.1, 128.7, 128.6, 128.4, 126.4, 125.5, 106.8 (C-2), 74.2 (C-3a and C-8a), 38.0, 37.1; ms: 373 (M^+, 4), 372 (3), 344 (24), 326 (4), 267 (6), 239 (8), 222 (17), 147 (11), 119 (38), 105 (29), 91 (100), 77 (33). Exact Mass calcd. for $C_{22}H_{18}NO_3$ (M^+ − H − CO): 344.1286; found: 344.1280.

For **33**: mp 269–270.5°C; ir (KBr) ν_{max}: 3056, 2926, 1772 (w), 1710 (s), 1598, 1502, 1397, 1191, 1086, 745 cm^{-1}; ^{1}H nmr ($CDCl_3$) δ: 7.31–7.47 (8H, m), 7.17 (2H, d, J = 7.0 Hz), 6.33 (2H, dd, J = 3.2, 4.3 Hz), 6.10 (1H, s, C-2H), 4.41 (2H, s, C-3aH and C-8aH), 3.68 (2H, br s, C-4H and C-8H), 2.87 (2H, t, J = 1.2 Hz, C-4aH and C-7aH); nOe data: 6.33 (6.10, 4%; 3.68, 8%), 6.10 (6.33, 1%), 4.41 (6.10, 2%; 3.64, 8%; 2.87, 14%), 3.68 (6.33, 8%; 4.41, 6%; 2.87, 5%), 2.87 (4.41, 14%; 3.68, 7%); ^{13}C nmr ($CDCl_3$) δ: 176.1, 138.7, 131.5, 130.6 (C-9 and C-10), 129.1, 128.9, 128.7, 128.4, 126.3, 125.8, 105.4 (C-2), 77.9 (C-3a and C-8a), 40.3 (C-4a and C-7a), 37.1 (C-4 and C-8); ms: 373 (M^+, 4), 372 (2), 344 (2), 266 (4), 239 (7), 222 (17), 200 (11), 175 (19), 147 (11), 119 (39), 105 (91), 91 (100), 77 (39).

*(2α,3aβ,5β,6α,7aβ)- (**37**) and (2α,3aα,5α,6β,7aα)-5,6-Dibromohexahydro-2-(4-nitrophenyl)-1,3-benzodioxole (**38**)*

A solution of **27** (5.01 g, 18.3 mmol), 4-nitrobenzaldehyde dimethyl acetal (3.51 g, 17.8 mmol), and dried *p*TsOH (250 mg) in dry benzene (160 mL) was heated under reflux for 16 h. After the solution cooled it was washed with 0.1 M NaOH (100 mL), saturated $NaHCO_3$ (100 mL), and saturated NaCl. The solution was dried ($MgSO_4$) and concentrated under vacuum. The resulting solid residue was purified by flash chromatography to give **37** as lustrous plates (2.39 g, 32%) and **38** as cubes (2.10 g, 28%). For **37**: mp 152–154°C; ir (KBr) ν_{max}: 3074, 2967, 1611, 1518 (s), 1345 (s), 1084 (s) cm^{-1}; ^{1}H nmr ($CDCl_3$) δ: 8.27 (2H, br d, J = 8.8 Hz), 7.74 (2H, br d, J = 8.8 Hz), 5.95 (1H, s, C-2H), 4.50 (1H, m, C-3aH), 4.45 (1H, m, C-5H), 4.38 (1H, m, C-7aH), 4.33 (1H, m, C-6H), 2.92 (1H, ddd, $J \approx$ 5.0, 5.0, 15.9 Hz, C-7H$_\beta$), 2.66 (1H, ddd, $J \approx$ 3.5, 6.7, 15.0 Hz, C-4H$_\alpha$), 2.53 (1H, ddd, $J \approx$ 5.3, 5.3, 15.9 Hz, C-7H$_\alpha$), 2.31 (1H, ddd, $J \approx$ 6.2, 6.2, 15.0 Hz, C-4H$_\beta$); ^{1}H nmr (C_5D_5N) δ: 8.23 (2H, br d, J = 8.7 Hz), 7.80 (2H, br d, J = 8.7 Hz), 5.98 (1H, s, C-2H), 4.65 (1H, ddd, J = 3.9, 7.7, 8.7 Hz, C-5H), 4.46 (1H, ddd, J = 4.6, 7.7, 7.8 Hz, C-6H), 4.35–4.43 (2H, m, C-3aH and C-7aH), 2.79–2.92 (2H, m, C-4H$_\alpha$ and C-7H$_\beta$), 2.43 (1H, ddd, J = 5.9, 7.8, 15.0 Hz, C-7H$_\alpha$), 2.35 (1H, ddd, J = 4.6, 8.7, 15.0 Hz, C-4H$_\beta$); nOe data ($CDCl_3$): 5.95 (7.74, 3%; 4.50, 6%; 4.38, 7%), 4.38 (5.95, 12%; 2.92, 6%); ^{13}C nmr (C_5D_5N) δ: 148.6, 145.3, 127.9 (C-2′ and C-6′), 124.0 (C-3′ and C-5′), 102.4 (C-2), 74.8 and 73.7 (C-3a and C-7a), 52.0 (C-5), 50.0 (C-6), 36.9 (C-7), 35.2 (C-4); ms: 408 (15), 406 (29), and 404 (16) (all M^+ − H), 392 (3), 390 (7), 388 (3), 246 (10), 218 (29), 150 (59), 107 (31), 95 (43), 80 (38), 79 (65), 77 (39), 67 (100). Exact Mass calcd. for $C_{13}H_{12}{}^{79}Br^{81}BrNO_4$ (M^+ − H): 405.9112; found 405.9119.

For **38**: mp 132–134°C; ir (KBr) ν_{max}: 3106, 2904, 1610 (m), 1520 (s), 1351 (s), 1080 (s) cm^{-1}; ^{1}H nmr ($CDCl_3$) δ: 8.22 (2H, br d, J = 8.7 Hz), 7.62 (2H, br d, J = 8.7 Hz), 6.24 (1H, s, C-2H), 4.51 (1H, ddd, J = 3.7, 6.9, 7.6 Hz, C-5H), 4.44 (1H, ddd, J = 5.0, 5.0, 5.8 Hz, C-3aH), 4.35 (1H, ddd, J = 5.0, 5.1, 6.0 Hz, C-7aH), 4.27 (1H, ddd, J = 4.7, 6.8, 6.9 Hz, C-6H), 2.85 (2H, m, C-4H$_\alpha$ and C-7H$_\beta$), 2.52 (1H, ddd, J = 6.0, 6.8, 15.5 Hz, C-7H$_\alpha$), 2.32 (1H, ddd, J = 5.0, 7.6, 15.1 Hz, C-4H$_\beta$); ^{1}H nmr (C_5D_5N) δ: 8.26 (2H, br d, J = 8.7 Hz), 7.69 (2H, br d, J = 8.7 Hz), 6.35 (1H, s, C-2H), 4.63 (1H, ddd, J = 4.2, 8.3, 9.3 Hz, C-5H), 4.48 (1H, ddd, J = 4.8, 5.8, 7.3 Hz, C-7aH), 4.43 (1H, ddd, J = 4.5, 8.3, 9.2 Hz, C-6H), 4.36 (1H, ddd, J = 4.4, 4.4, 4.8 Hz, C-3aH), 2.92 (1H, ddd, J = 4.2, 4.4, 15.1 Hz, C-4H$_\alpha$), 2.81 (1H, ddd, J = 4.5, 5.8, 14.6 Hz, C-7H$_\beta$), 2.47 (1H, ddd, J = 7.3, 9.2, 14.6 Hz, C-7H$_\alpha$), 2.35 (1H, ddd, J = 4.4, 9.3, 15.1 Hz, C-4H$_\beta$); nOe data ($CDCl_3$): 7.62 (8.22, 19%; 6.24, 4%), 6.24 (7.62, 3%; 2.85 [ddd, J = 3.7, 5.8, 15.1 Hz, therefore C-4H$_\alpha$], 2%; 2.52, 5%), 4.51 (2.85 [C-4H$_\alpha$], 5%; 2.52, 1%; 2.32, 1%), 4.44 (7.62, 1%; 2.85 [C-4H$_\alpha$], 2%; 2.32, 5%), 4.35 (7.62, 1%; 2.85 [ddd, J = 4.7, 5.1, 15.5 Hz, therefore C-7H$_\beta$], 6%; 2.52, 1%), 4.27 (2.85 [C-7H$_\beta$], 5%; 2.52, 2%; 2.32, 1%); ^{13}C nmr ($CDCl_3$/C_5D_5N) δ: 148.1/147.8, 145.8/146.0, 126.9/126.9 (C-2′ and C-6′), 123.5/123.1 (C-3′ and C-5′), 100.7/100.5 (C-2), 73.1/73.4 (C-3a), 72.7/73.0 (C-7a), 50.3/51.3 (C-5), 47.7/49.9 (C-6), 33.9/35.3 (C-7), 32.6/34.0 (C-4); ms: 408 (13), 406 (24), and 404 (13) (all M^+ − H), 392 (2), 390 (6), 388 (2), 285 (5), 246 (5), 218 (11), 150 (83), 107 (29), 95 (41), 80 (82), 79 (73), 77 (40), 67 (100).

*(2α,3aβ,7aβ)-3a,7a,Dihydro-2-(4-nitrophenyl)-1,3-benzodioxole (**35**)*

By a procedure very similar to that for **25**, **37** (0.524 g, 1.29 mmol) and DBU (0.78 g, 5.1 mmol), after flash chromatography gave **35** (0.161 g, 51%) as light green plates: mp 141–142°C; uv (CH_3OH) λ_{max}: 265 nm (ε = 15 000); ir (KBr) ν_{max}: 3047, 2914, 1611 (m), 1519 (s), 1349 (s) cm^{-1}; ^{1}H nmr ($CDCl_3$) δ: 8.19 (2H, br d, J = 8.7 Hz), 7.64 (2H, br d, J = 8.7 Hz), 6.07 (2H, m), 5.97 (2H, m), 5.74 (1H, s), 4.73 (2H, nar m); nOe data: 5.74 (7.64, 3%; 4.73, 4%), 4.73 (5.97, 5%; 5.74, 9%); ^{13}C nmr ($CDCl_3$) δ: 148.4, 143.8, 127.8 (C-2′ and C-6′), 124.2 (alkenic), 123.9 (alkenic), 123.4 (C-3′ and C-5′), 96.8 (C-2), 71.3 (C-3a and C-7a); ms: 245 (M^+, 0.4), 244 (1.5), 150 (15), 120 (3), 104 (7), 94 (98), 78 (21), 77 (24), 66 (100), 65 (21), 51 (19), 50 (10). Exact Mass calcd. for $C_{13}H_{10}NO_4$ (M^+ − H): 244.0609; found: 244.0601.

*(2α,3aα,7aα)-3a,7a-Dihydro-2-(4-nitrophenyl)-1,3-benzodioxole (**36**)*

By a procedure very similar to that for **25**, **38** (2.08 g, 5.11 mmol) and DBU (3.11 g, 20.4 mmol), after flash chromatography, gave **36** as colorless crystals (0.526 g, 42%): mp 128–131°C (melted and resolidified within a few seconds as the dimer **44**); uv (CH_3OH) λ_{max}: 264 nm (ε = 13 300); ir (KBr) ν_{max}: 3046, 2881, 1640 (m), 1525 (s), 1355 cm^{-1}; ^{1}H nmr ($CDCl_3$) δ: 8.58 (2H, br d, J = 8.7 Hz), 8.04 (2H, br d, J = 8.7 Hz), 6.47 (2H, m), 6.29 (2H, m), 6.23 (1H, s), 5.23 (2H, nar m); ^{13}C nmr ($CDCl_3$) δ: 148.2, 144.6, 127.4 (C-2′ and C-6′), 125.2 (alkenic), 124.2 (alkenic), 123.4 (C-3′ and C-5′), 99.2 (C-2), 70.9 (C-3a and C-7a); ms: no M^+, 244 (1), 150 (24), 121 (3), 120 (4), 104 (10), 94 (88), 78 (100), 77 (33), 66 (93), 65 (29), 51 (27), 50 (15). Exact Mass calcd. for $C_{13}H_{10}NO_4$ (M^+ − H): 244.0609; found: 244.0589.

*Diels–Alder reaction of **35**: (2α,3aβ,4β,4aα,7aα,8β,8aβ)- (**39**) and (2α,3aβ,4α,4aβ,7aβ,8α,8aβ)-4a,7a,8,8a-tetrahydro-2-(4-nitrophenyl)-6-phenyl-4,8-etheno-4H-1,3-dioxolo[4,5f]isoindole-5,7-(3aH,6H)-dione (**40**)*

A solution of **35** (0.610 g, 2.49 mmol) and *N*-phenylmaleimide (0.432 g, 2.49 mmol) in $CHCl_3$ (25 mL) was stirred at room temperature for 16 h. The solvent was evaporated under vacuum, and the ^{1}H nmr spectrum of the residue revealed signals for **39** and **40** in a ratio of 27:73, respectively. Flash chromatography provided **39** (0.242 g, 23%) and **40** (0.666 g, 64%). (Similarly, a solution of **35** (24 mg, 0.098 mmol) and *N*-phenylmaleimide (17 mg, 0.098 mmol) in benzene (1 mL) was stirred at room temperature for 2 days, during which time a colorless precipitate of the adducts formed. Evaporation of the benzene left 41 mg of solid, the ^{1}H nmr spectrum of which displayed signals for **39** and **40** in a ratio of 24:76, respectively.) For **39**: mp 254–255.5°C; ir (KBr) ν_{max}: 3069, 2949, 1772 (w), 1714 (s), 1527 cm^{-1}; ^{1}H nmr ($CDCl_3$) δ: 8.26 (2H, br d, J = 8.7 Hz), 7.69 (2H, br d, J = 8.7 Hz), 7.35–7.46 (3H, m), 7.16 (2H, br d, $J \approx$ 7.0 Hz), 6.31 (2H, apparent dd, J = 3.0, 4.5 Hz), 6.00 (1H, s, C-2H), 4.31 (2H, nar m, C-3aH and C-8aH), 3.67 (2H, m, C-4H and C-8H), 3.46 (2H, nar m, C-4aH and C-7aH); nOe data: 7.69 (8.26, 16%; 6.00, 4%; 3.46, 2%), 6.31 (4.31, 1.5%; 3.67, 11%), 6.00 (7.69, 2%; 4.31, 5%), 4.31 (6.31, 2%; 6.00, 24%; 3.67, 11%), 3.67 (6.31, 13%; 4.31, 8%; 3.46, 9%), 3.46 (7.69, 5%; 3.67, 10%); ^{13}C nmr ($CDCl_3$) δ: 177.8, 148.4, 142.6, 131.6 (C-9 and C-10 [& C-1″?]), 129.0, 128.6, 127.1, 126.3, 123.6, 104.1 (C-2), 75.0 (C-3a and C-8a), 37.7 (C-4a and C-7a), 36.6 (C-4 and C-8); ms: 418 (M^+, 19), 417 (3), 389 (77),

Can. J. Chem. Downloaded from www.nrcresearchpress.com by 217.78.4.112 on 09/08/12
For personal use only.

266 (9), 239 (11), 222 (31), 193 (19), 150 (17), 147 (15), 119 (52), 91 (100), 77 (20). Exact Mass calcd. for $C_{23}H_{18}N_2O_6$: 418.1164; found: 418.1182; calcd. for $C_{22}H_{17}N_2O_5$ ($M^+ - H - CO$): 389.1136; found: 389.1134.

For **40**: mp 237–239°C; ir (KBr) ν_{max}: 3067, 2901, 1776 (w), 1712 (s), 1519 cm^{-1}; ^1H nmr ($CDCl_3$) δ: 8.21 (2H, br d, $J \approx 8.8$ Hz), 7.61 (2H, br d, $J \approx 8.8$ Hz), 7.35–7.50 (3H, m), 7.19 (2H, m), 6.26 (2H, apparent dd, $J = 3.1$, 4.3 Hz), 5.74 (1H, s, C-2H), 4.44 (2H, br s, C-3aH and C-8aH), 3.72 (2H, m, C-4H and C-8H), 2.99 (2H, nar m, C-4aH and C-7aH); nOe data: 6.26 (7.61, 3%; 3.72, 9%), 5.74 (7.61, 6%; 4.44, 4%), 4.44 (5.74, 21%; 3.72, 8%; 2.99, 14%), 3.72 (6.26, 9%; 4.44, 4%; 2.99, 6%), 2.99 (4.44, 12%; 3.72, 10%); ^{13}C nmr ($CDCl_3$) δ: 175.9, 148.6, 142.3, 131.5 (C-1″), 130.1 (C-9 and C-10), 129.1, 128.8, 128.2, 126.3, 123.5, 102.1 (C-2), 78.1 (C-3a and C-8a), 40.3 (C-4a and C-7a), 36.5 (C-4 and C-8); ms: 418 (M^+, 4), 417 (2), 402 (3), 390 (5), 389 (9), 267 (3), 266 (5), 239 (11), 222 (21), 193 (11), 150 (14), 147 (10), 121 (12), 120 (42), 119 (47), 93 (35), 92 (42), 91 (100), 77 (28). Exact Mass. calcd. for $C_{23}H_{18}N_2O_6$: 418.1164; found: 418.1188; calcd. for $C_{22}H_{17}N_2O_5$ ($M^+ - H - CO$): 389.1136; found: 389.1136.

Diels–Alder reaction of ***36****: (2α,3aα,4α,4aβ,7aβ,8α,8aα)- (**41**) and (2α,3aα,4β,4aα,7aα,8β,8aα)-4a,7a,8,8a-tetrahydro-2-(4-nitrophenyl)-6-phenyl-4,8-etheno-4H-1,3-dioxolo[4,5-f]-isoindole-5,7-(3aH,6H)-dione (**42**)*

A solution of diene **36** (0.510 g, 2.08 mmol) and *N*-phenylmaleimide (0.358 g, 2.07 mmol) in $CHCl_3$ (25 mL) was stirred for 24 h at room temperature. The solvent was evaporated under vacuum, and the ^1H nmr spectrum of the residue revealed signals for adducts **41** and **42** in a ratio of 5:95, respectively. Flash chromatography provided **42** (0.784 g, 95%), but **41** co-eluted with some residual *N*-phenylmaleimide (total fraction: 50 mg). A small amount of **41** was obtained by recrystallization of this mixture from $CHCl_3$/CCl_4: mp 253–254.5°C; ir (KBr) ν_{max}: 3068, 2921, 1776 (w), 1713, 1517, 1347, 1196, 1085, 745 cm^{-1}; ^1H nmr ($CDCL_3$) δ: 8.24 (2H, d, $J = 8.6$ Hz), 7.63 (2H, d, $J = 8.6$ Hz), 7.27–7.53 (3H, m), 7.19 (2H, br d, $J \approx 7.1$ Hz), 6.50 (1H, s, C-2H), 6.25 (2H, apparent dd, $J = 3.0$, 4.2 Hz), 4.12 (2H, s, C-3aH and C-8aH), 3.66 (2H, nar m, C-4H and C-8H), 3.61 (2H, br s, C-4aH and C-7aH); nOe data: 7.63 (8.24, 19%; 6.50, 6%; 4.12, 2%), 6.50 (7.63, 2%; 3.61, 3%), 6.25 (4.12, 2%; 3.66, 10%), 4.12 (7.63, 6%; 6.50, 2.5%; 6.25, 4%; 3.66, 20%), 3.66 (6.25, 11%; 4.12, 13%), 3.61 (6.50, 20%); ^{13}C nmr ($CDCl_3$) δ: 177.9, 148.2, 146.0, 131.6 (C-9, C-10, and C-1″), 129.1, 128.7, 126.7, 126.4, 123.7, 105.5 (C-2), 74.4 (C-3a and C-8a), 37.8 (C-4a and C-7a), 36.9 (C-4 and C-8); ms: 418 (M^+, 10), 389 (65), 266 (7), 239 (8), 222 (25), 211 (6), 193 (15), 147 (12), 136 (10), 119 (52), 91 (100), 77 (20). Exact Mass calcd. for $C_{23}H_{18}N_2O_6$: 418.1164; found: 418.1166; calcd. for $C_{22}H_{17}N_2O_5$ ($M^+ - H - CO$): 389.1136; found: 389.1135.

For **42**: mp 273–274°C; ir (KBr) ν_{max}: 3070, 2972, 1776 (w), 1706, 1520, 1390 cm^{-1}; ^1H nmr ($CDCl_3$) δ: 8.23 (2H, br d, $J \approx 8.6$ Hz), 7.60 (2H, br d, $J \approx 8.6$ Hz), 7.36–7.50 (3H, m), 7.19 (2H, m), 6.36 (2H, m, C-9H and C-10H), 6.14 (1H, s, C-2H), 4.45 (2H, s, C-3aH and C-8aH), 3.75 (2H, m, C-4H and C-8H), 2.96 (2H, nar m, C-4aH and C-7aH); ^1H nmr (CD_3SOCD_3) δ: 8.23 (2H, d, $J = 8.6$ Hz), 7.63 (2H, d, $J = 8.6$ Hz), 7.37–7.49 (3H, m), 7.13 (2H, d, $J = 7.2$ Hz), 6.28 (2H, m, C-9H and C-10H), 6.13 (1H, s, C-2H), 4.56 (2H, s, C-3aH and C-8aH), 3.46 (2H, nar m, C-4H and C-8H), 3.12 (2H, s, C-4aH and C-7aH); nOe data ($CDCl_3$): 7.60 (8.23, 20%; 6.14, 7%; 4.45, 1%), 6.36 (7.19, 1.5%; 6.14, 9%; 3.75, 9%), 6.14 (7.60, 2%; 6.36, 1.5%), 4.45 (7.60, 4%; 6.14, 4%; 3.75, 12%; 2.96, 17%), 3.75 (6.36, 11%; 6.14, 1.5%; 4.45, 6%; 2.96, 5%), 2.96 (4.45, 16%; 3.75, 9%); ^{13}C nmr (CD_3SOCD_3) δ: 176.7, 147.7, 146.4, 132.2 (C-1″), 130.5, 128.9, 128.5, 127.4, 126.9, 123.6, 103.2 (C-2), 77.6 (C-3a and C-8a), 40.0 (C-4a and C-7a), 36.9 (C-4 and C-8); ms: 418 (M^+, 4), 402 (3), 390 (3), 389 (7), 388 (7), 387 (6), 268 (8), 222 (18), 175 (20), 174 (24), 173 (17), 150 (23), 121 (40), 120 (99), 119 (48), 93 (37), 92 (44), 91 (100), 78 (28), 77 (29). Exact Mass calcd. for $C_{23}H_{18}N_2O_6$: 418.1164; found: 418.1166; calcd. for $C_{22}H_{17}N_2O_5$ ($M^+ - H - CO$): 389.1136; found: 389.1141.

*(2α,3aα,5aβ,6α,6aβ,8β,9aβ,10α,10aβ,10bα)-3a,5a,6,6a,9a,10,10a,10b-Octahydro-2,8-diphenyl-6,10-ethenonaphtho[1,2-d:6,7-d′]bis[1,3]dioxole (**43**)*

A crude sample of **26** (98 mg, 0.49 mmol) was left neat at room temperature overnight. The resulting solid was flash chromatographed to give, as the sole product, **43** (83 mg, 85%): mp 176–179°C; ir (KBr) ν_{max}: 3034, 2943, 1457, 1368, 1224, 1097 (s), 1066 (2), 751, 696 cm^{-1}; ^1H nmr ($CDCl_3$) δ: 7.30–7.45 (10H, m), 6.17 (2H, t, $J = 3.2$ Hz, C-11H and C-12H), 6.04 (1H, s, C-8H), 5.83 (1H, s, C-2H), 5.80 (1H, ddd, $J = 1.5$, 3.9, 10.3 Hz, C-5H), 5.60 (1H, d, $J = 10.1$ Hz, C-4H), 4.50 (1H, dd, $J = 1.7$, 4.7 Hz, C-3aH), 4.41 (2H, s, C-6aH and C-9aH), 4.25 (1H, d, $J = 4.8$ Hz, C-10bH), 3.04 (2H, br s , C-6H and C-10H), 2.43 (1H, ddd, $J = 1.8$, 3.6, 9.0 Hz, C-5aH), 2.35 (1H, d, $J = 9.0$ Hz, C-10aH); ^1H nmr (C_5D_5N) δ: 7.70 (2H, d, $J = 7.5$ Hz), 7.60 (2H, d, $J = 7.6$ Hz), 7.37–7.48 (6H, m), 6.30 (1H, s, C-8H), 6.19 (2H, apparent t, $J \approx 3.8$ Hz, C-11H and C-12H), 6.11 (1H, s, C-2H), 5.80 (1H, dd, $J = 2.7$, 10.4 Hz, C-5H), 5.66 (1H, dd, $J = 0.6$, 10.4 Hz, C-4H), 4.59 (1H, d, $J = 4.2$ Hz, C-3aH), 4.50 (2H, symmetrical m, C-6aH and C-9aH), 4.34 (1H, d, $J = 4.7$ Hz, C-10bH), 3.03 (2H, m, C-6H and C-10H), 2.48 (2H, br s, C-5aH and C-10aH); nOe data (C_5D_5N): 5.80 (5.66, 4%; 3.03, 1.5%; 2.48, 1%), 5.66 (6.11, 2%; 5.80, 4%; 4.59, 4%), 4.59 (5.66, 1%); 4.50 (7.60, 2%; 6.30, 2%; 3.03, 2%; 2.48, 6%), 4.34 (7.70, 1.5%; 4.59, 8%; 3.03, 4%; 2.48, 1.5%), 2.48 (6.11, 3%; 5.80, 5%; 4.50, 13%; 4.34, 3.5%; 3.03, 2.5%); ^{13}C nmr ($CDCl_3$) δ: 139.2, 138.7, 133.2 (C-11 or C-12), 132.5 (C-5), 129.7 (C-11 or C-12), 129.0, 128.7, 128.3, 126.2, 125.8, 124.1 (C-4), 104.8 (C-8), 101.0 (C-2), 79.3 and 79.1 (C-6a and C-9a), 77.2 (C-10b), 71.7 (C-3a), 41.3 and 40.9 (C-6 and C-10), 34.3 (C-10a), 33.0 (C-5a); ms: 400 (M^+, 1), 399 (3), 323 (2), 294 (12), 279 (2), 200 (1), 188 (18), 172 (17), 159 (16), 144 (13), 129 (16), 105 (100), 94 (27), 91 (36), 77 (34), 66 (12). Exact Mass calcd. for $C_{19}H_{18}O_3$ ($M^+ - C_7H_6O$): 294.1255; found: 294.1250.

*(2α,3aα,5aβ,6α,6aβ,8β,9aβ,10α,10aβ,10bα)-3a,5a,6,6a,9a,10,10a,10b-Octahydro-2,8-bis(4-nitrophenyl)-6,10-ethenonaphtho[1,2-d:6,7-d′]bis[1,3]dioxole (**44**)*

Under N_2 a sample of diene **36** (60 mg, 0.12 mmol) was heated from room temperature up to approx. 250°C over a period of 10 min. On cooling, 53 mg of crude **44** was obtained as the only dimer detected. The brown solid was purified by several suspensions in 50% $CHCl_3$ in CCl_4 (**44** is only sparingly soluble in most common solvents) to yield 31 mg (52%) of **44**: mp 246–247°C; ir (KBr) ν_{max}: 3046, 2952, 1622, 1517, 1349, 1079, 739 cm^{-1}; ^1H nmr ($CDCl_3$) δ: 8.23 (2H, d, $J = 8.7$ Hz), 8.21 (2H, d, $J = 8.7$ Hz), 7.61 (2H, d, $J = 8.7$ Hz), 7.56 (2H, d, $J = 8.7$ Hz), 6.20 (2H, br m, C-11H and C-12H), 6.06 (1H, s, C-8H), 5.90 (1H, s, C-2H), 5.86 (1H, ddd, $J = 1.4$, 4.0, 10.4 Hz, C-5H), 5.63 (1H, d, $J = 10.1$ Hz, C-4H), 4.53 (1H, dd, $J = 1.6$, 4.5 Hz, C-3aH), 4.45 (2H, nar m, C-6aH and C-9aH), 4.22 (1H, d, $J = 4.8$ Hz, C-10bH), 3.06–3.12 (2H, br m, C-6H and C-10H), 2.47 (1H, br m, C-5aH), 2.38 (1H, d, $J = 8.9$ Hz, C-10aH); ^1H nmr (CD_3SOCD_3) δ: 8.23 (2H, d, $J = 8.8$ Hz), 8.21 (2H, d, $J = 8.7$ Hz), 7.69 (2H, d, $J = 8.8$ Hz), 7.60 (2H, d, $J = 8.7$ Hz), 6.11 (2H, m), 6.03 (1H, s), 5.86 (1H, s), 5.84 (1H, ddd, $J = 1.2$, 3.9, 10.0 Hz), 5.52 (1H, d, $J = 10.5$ Hz), 4.52 (3H, br m), 4.25 (1H, d, $J = 4.8$ Hz), 3.04 (2H, m), 2.44 (1H, m), 2.34 (1H, d, $J = 8.9$ Hz); nOe data ($CDCl_3$): 7.61 and 7.56 (8.23 and 8.21, 6%; 6.06, 1.5%; 5.90, 2%), 6.06 (7.56, 2.5%), 5.63 (5.90 and 5.86, 13%; 4.53, 4%), 4.53 (6.20, 1.5%; 5.63, 6%; 4.22, 5%), 4.45 (7.56, 3%; 6.06, 2%; 3.06–3.12, 6%; 2.47, 13%; 2.38, 16%), 4.22 (7.61, 1.5%; 4.53, 10%; 3.06–3.12, 6%; 2.38, 4%), 2.47 (5.86, 5%; 4.45, 4%; 3.06–3.12, 2.5%), 2.38 (4.47, 6%; 2.47, 2%); ^{13}C nmr (CD_3SOCD_3) δ: (4 quaternary aromatic signals too weak to be resolved) 132.9, 132.6, 130.0, 127.8, 127.4, 123.5 (3C), 102.7, 99.1, 78.9, 78.8, 77.0, 71.4, 40.7, 40.3, 33.2, 32.3; ms: 489 ($M^+ - H$, 2), 459 (1),

368 (2), 339 (5), 260 (3), 188 (26), 172 (23), 150 (92), 120 (47), 94 (90), 78 (100), 66 (65). Exact Mass calcd. for $C_{19}H_{17}NO_5$ ($M^+ - C_7H_5NO_3$): 339.1106; found: 339.1096.

Acknowledgements

We thank Dr. C. R. Jablonski, Ms. N. Brunet, Ms. J. Jacob, and Mr. R. Sammynaiken for nmr spectra, and Dr. B. Gregory and Miss M. Baggs for ms spectra. Dr. P. M. Giles, Manager, Authority Database Operations at Chemical Abstracts, kindly helped with the naming of the adducts. We are grateful to the Natural Sciences and Engineering Research Council of Canada for financial support.

1. S. Winstein, M. Shatavsky, C. Norton, and R. B. Woodward. J. Am. Chem. Soc. **77**, 4183 (1955); V. A. Mironov, M. E. Dolgaya, V. T. Lukyanov, and S. A. Yankovskii. Zh. Org. Khim. **12**, 1436 (1976); D. W. Jones. J. Chem. Soc. Chem. Commun. 739 (1980).
2. J. B. Macaulay and A. G. Fallis. J. Am. Chem. Soc. **112**, 1136 (1990).
3. N. T. Anh. Tetrahedron, **29**, 3227 (1973).
4. S. D. Kahn and W. J. Hehre. J. Am. Chem. Soc. **109**, 663 (1987).
5. W.-S. Chung, N. J. Turro, S. Srivastava, H. Li, and W. J. le Noble. J. Am. Chem. Soc. **110**, 7882 (1988).
6. S. Inagaki, H. Fujimoto, and K. Fukui. J. Am. Chem. Soc. **98**, 4054 (1976).
7. M. Ishida, Y. Beniya, S. Inagaki, and S. Kato. J. Am. Chem. Soc. **112**, 8980 (1990).
8. M. Ishida, T. Aoyama, and S. Kato. Chemistry Lett. 663 (1989); A. M. Naperstkow, J. B. Macaulay, M. J. Newlands, and A. G. Fallis. Tetrahedron Lett. **30**, 5077 (1989); S. B. King and B. Ganem. J. Am. Chem. Soc. **113**, 5089 (1991).
9. R. Breslow, J. M. Hoffman, Jr., and C. Perchonock. Tetrahedron Lett. 3723 (1973).
10. H. Auksi and P. Yates. Can. J. Chem. **59**, 2510 (1981).
11. A. G. Schultz, J. P. Dittami, F. P. Lavieri, C. Salowey, P. Sundararaman, and M. B. Szymula. J. Org. Chem. **49**, 4429 (1984); P. Yates, A. Gomes, D. J. Burnell, D. D. Cong, and J. F. Sawyer. Can. J. Chem. **67**, 37 (1989).
12. J. R. Gillard, M. J. Newlands, J. N. Bridson, and D. J. Burnell. Can. J. Chem. **69**, 1337 (1991).
13. D. T. Gibson, M. Hensley, H. Yoshioka, and T. J. Mabry. Biochemistry, **9**, 1626 (1970); D. T. Gibson, B. Gschwendt, W. K. Yeh, and V. M. Kobal. Biochemistry, **12**, 1520 (1973).
14. D. T. Gibson, M. Cardini, F. C. Maseles, and R. E. Kalio. Biochemistry, **9**, 1631 (1970); D. G. H. Ballard, A. Courtis, I. M. Shirley, and S. C. Taylor. J. Chem. Soc. Chem. Commun. 954 (1983).
15. N. C. Yang and M. G. Horner. Tetrahedron Lett. **27**, 543 (1986); S. V. Ley, F. Sternfeld, and S. Taylor. Tetrahedron Lett. **28**, 225 (1987); N. C. Yang and X. Yang. J. Am. Chem. Soc. **109**, 3804 (1987); T. Hudlicky, H. Luna, G. Barbieri, and L. D. Kwart. J. Am. Chem. Soc. **110**, 4735 (1988); N. C. Yang, T. Noh, H. Gan, S. Halfon, and B. J. Hrnjez. J. Am. Chem. Soc. **110**, 5919 (1988); S. V. Ley and F. Sternfeld. Tetrahedron Lett. **29**, 5305 (1988); H. A. J. Carless and O. Z. Oak. Tetrahedron Lett. **30**, 1719 (1989); H. A. J. Carless, J. R. Billinge, and O. Z. Oak. Tetrahedron Lett. **23**, 3113 (1989); T. Hudlicky, G. Seoane, and T. Pettus. J. Org. Chem. **54**, 4239 (1989); S. V. Ley and F. Sternfeld. Tetrahedron, **45**, 3463 (1989); T. Hudlicky, J. D. Price, H. Luna, and C. M. Andersen. Synlett, 309 (1990); H. A. J. Carless and K. Busia. Tetrahedron Lett. **31**, 1617 (1990).
16. V. M. Kobal, D. T. Gibson, R. E. Davis, and A. Garza. J. Am. Chem. Soc. **95**, 4420 (1973).
17. I. C. Cotterill, S. M. Roberts, and J. O. Williams. J. Chem. Soc. Chem. Commun. 1628 (1988).
18. O. Werbitzky, K. Klier, and H. Felber. Liebigs Ann. Chem. 267 (1990).
19. C. A. Pittol, R. J. Pryce, S. M. Roberts, G. Ryback, V. Sik, and J. O. Williams. J. Chem. Soc. Perkin Trans. I, 1160 (1989).
20. J. R. Gillard and D. J. Burnell. J. Chem. Soc. Chem. Commun. 1439 (1989).
21. A. Merz. Angew. Chem. Int. Ed. Engl. **12**, 846 (1973).
22. J. C. Orr and C. Monder. J. Biol. Chem. **250**, 7547 (1975).
23. P. Deslongchamps, A. Bélanger, D. J. F. Berney, H.-J. Borschberg, R. Brousseau, A. Doutheau, R. Durand, H. Katayama, R. Lapalme, D. M. Leturc, C.-C. Liao, F. N. MacLachlan, J.-P. Maffrand, F. Marazza, R. Martino, C. Moreau, L. Ruest, L. Saint-Laurent, R. Saintonge, and P. Soucy. Can. J. Chem. **68**, 115 (1990).
24. A. S. Cieplak. J. Am. Chem. Soc. **103**, 4540 (1981); A. S. Cieplak, B. D. Tait, and C. R. Johnson. J. Am. Chem. Soc. **111**, 8447 (1989).
25. L. Garbaschelli, G. Mellerio, and G. Vidari. Tetrahedron Lett. **30**, 597 (1989).
26. J. P. Wibaut and F. A. Hauk. Recl. Trav. Chim. Pays-Bas, **67**, 91 (1948).
27. N. C. Yang, M.-J. Chen, and P. Chen. J. Am. Chem. Soc. **106**, 7310 (1984).
28. J. K. M. Saunders and J. D. Mersh. Prog. Nucl. Magn. Reson. Spectrosc. **15**, 353 (1983).

Can. J. Chem. Downloaded from www.nrcresearchpress.com by 217.78.4.112 on 09/08/12
For personal use only.

Isolation and characterization of culmorin derivatives produced by *Fusarium culmorum* CMI 14764[1]

GERTRUDE C. KASITU AND JOHN W. APSIMON
Ottawa–Carleton Chemical Institute, Carleton University, Ottawa, Ont., Canada K1S 5B6

AND

BARBARA A. BLACKWELL,[2] DAVID A. FIELDER, ROY GREENHALGH, AND J. DAVID MILLER
Plant Research Centre, Agriculture Canada, Ottawa, Ont., Canada K1A 0C6

Received May 8, 1991

This paper is dedicated to Professor Zdenek (Denny) Valenta on the occasion of his 65th birthday

GERTRUDE C. KASITU, JOHN W. APSIMON, BARBARA A. BLACKWELL, DAVID A. FIELDER, ROY GREENHALGH, and J. DAVID MILLER. Can. J. Chem. **70**, 1308 (1992).

Liquid culture fermentations of *Fusarium culmorum* yield a wide variety of secondary metabolites. In addition to known isoprenoids, such as the trichothecenes and modified trichothecenes, four new derivatives of culmorin have been isolated and characterized by spectral analysis. These compounds are 15-hydroxyculmorone (**7**), and 5-hydroxy- (**8**), 12-hydroxy- (**10**), and 15-hydroxyculmorin (**9**). The structure of culmorone is confirmed. The biosynthesis of culmorin from farnesyl pyrophosphate is substantiated through the use of ^{13}C-acetate and the oxidation of these derivatives is discussed.

GERTRUDE C. KASITU, JOHN W. APSIMON, BARBARA A. BLACKWELL, DAVID A. FIELDER, ROY GREENHALGH et J. DAVID MILLER. Can. J. Chem. **70**, 1308 (1992).

Des fermentations liquides de cultures du *Fusarium culmorum* fournissent une grande variété de métabolites secondaires. En plus des isoprénoïdes connus, comme les trichothécènes et les trichothécènes modifiés, quatre nouveaux dérivés de la culmorine ont été isolés et caractérisés par analyse spectrale. Ces composés sont la 15-hydroxyculmorone (**7**) et les 5-hydroxy- (**8**), 12-hydroxy- (**10**) et 15-hydroxyculmorine (**9**). On a confirmé la structure de la culmorone. Utilisant un ^{13}C-acétate, on a ajouté des indices suggérant que la biosynthèse de la culmorine peut se faire à partir du pyrophosphate de farnésyle et on discute de l'oxydation de ces dérivés.

[Traduit par la rédaction]

Introduction

There are 24 toxigenic species of *Fusarium* and these are distributed worldwide. In North America, species such as *F. graminearum, F. culmorum,* and *F. crookwellense* infect cereals of economical importance including wheat, corn, and barley. These *Fusarium* species are closely related and are known to produce a wide variety of secondary metabolites including the trichothecene mycotoxins. Infected grains primarily contain 4-deoxynivalenol (vomitoxin, DON), 15- or 3-acetyldeoxynivalenol, and zearalenone (1). Trichothecenes are phytotoxic to the host species as well as toxic to both animals and humans upon consumption of contaminated grain (2). Animal studies with naturally infected feed containing known amounts of DON showed greater toxicity than feed fortified with the same level of DON (3). Efforts to study this difference in toxicity have included the isolation and characterization of minor metabolites present in both the mycelia and the fermentation broth, as well as testing component metabolites for synergism.

Previous studies showed that in addition to the major metabolite 3-acetyldeoxynivalenol (3-ADON) (**1**) *Fusarium culmorum* CMI 14764 (HLX1503) produces other secondary metabolites of various types such as butenolide (4-acetamido-4-hydroxy-2-butenoic acid γ lactone, $C_6H_7O_3N$) (4, 5), additional trichothecenes including calonectrin and isotrichodermin and their acylated and deacylated derivatives (5), as well as some modified trichothecenes such as sambucinol, sambucoin, 3α- and 3β-hydroxy-11-epiapotrichothecene (**2**) (6), 9α-hydroxytrichotriol (**3**) (7), and other isoprenoids including cyclonerodiol (8), cyclonerotriol (**4**) (9), culmorin (**5**), and culmorone (**6**) (see Fig. 1). A typical gas chromatogram of a crude extract of the fermentation broth of *F. culmorum* is presented in Fig. 2. This figure shows the variety of secondary metabolites produced in a typical culture as well as the relative retention times of several of the compounds described here. Since this extract was collected after 85 hours fermentation, culmorin and other metabolites are found in greater abundance than 3-ADON. Later during the fermentation 3-ADON predominates (10).

The present study reports the isolation and characterization of the derivatives of culmorin and culmorone. The parent sesquiterpene culmorin was first isolated in 1937 from *Fusarium culmorum* by Ashley *et al.* (11). Its structure was established by Barton and Werstiuk (12) and independently by Shilling (13) in 1967. Culmorin has since been detected and isolated from two other *Fusarium* species, namely, *F. graminearum* (*F. roseum* "graminearum") (14*a*) and *F. crookwellense* (15). Additional reports on culmorin include its synthesis (16), biosynthesis (17*a*,*b*), and toxicity (18).

The production of culmorin and culmorone by *F. roseum* was reported earlier, but these compounds were not fully characterized (14). Here we reexamine the structure of culmorone and the assignments of culmorin using ^{1}H, ^{13}C, and 2D techniques. These data facilitate characterization of the four new hydroxy derivatives. This is the first report of the isolation of trichotriol from *F. culmorum*. Revised NMR assignments for cyclonerotriol based on 2D NMR data are also reported.

[1]PRC Contribution No. 1343.
[2]Author to whom correspondence may be addressed.

Can. J. Chem. Downloaded from www.nrcresearchpress.com by 217.78.4.112 on 09/08/12
For personal use only.

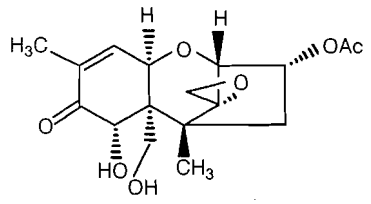

1

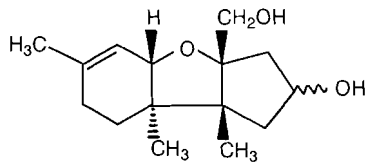

2

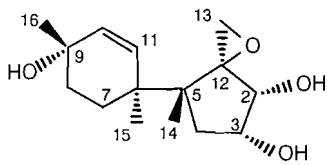

3

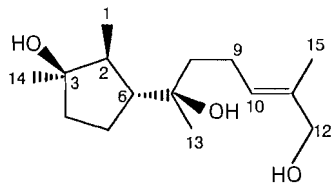

4

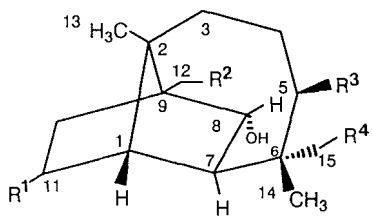

	R^1	R^2	R^3	R^4
5	α-OH	H	H	H
6	=O	H	H	H
7	=O	H	H	OH
8	α-OH	H	OH	H
9	α-OH	H	H	OH
10	α-OH	OH	H	H

FIG. 1. Structures of secondary metabolites isolated from *F. culmorum*.

Results and discussion

The extraction, separation, and isolation of the secondary metabolites from a large-scale liquid fermentation of *Fusarium culmorum* CMI 14764 was carried out as described in the experimental section.

Culmorin, culmorone, and hydroxyculmorone

Barton and Werstiuk (12) used extensive chemical degradation and ^{1}H NMR spectra to determine the structure and absolute stereochemistry of culmorin ($C_{15}H_{26}O_2$, MW 238) (**5**). The ^{1}H NMR spectrum of culmorin shows two resonances at 3.80 and 4.33 ppm, which integrate for one hydrogen each, consistent with a hydrogen geminal to a hydroxyl group. Four quaternary methyl groups (0.81, 0.91, 0.94, and 1.02 ppm) are also present. The latter two exhibit geminal coupling as indicated by their reduced intensity and the presence of a cross peak in the ^{1}H/^{1}H correlation (COSY) spectrum. This spectrum, obtained in deuteromethanol, also shows the presence of "W"-coupling between the carbinyl hydrogen H-8 (3.81 ppm) and the H-10β (1.59 ppm), which is further coupled to H-11 (4.30 ppm). In methanol, the H-10 methylenic hydrogens are nonequivalent and H-8 shows "W"-coupling to H-10β, whereas in chloroform the H-10 hydrogens are coincidental and the coupling to H-8 is minimized. This effect is observed in all the hydroxyl derivatives as well. The difference between the spectra in these two solvents is attributed to the different conformation of the molecule induced by hydrogen bonding in methanol. The hydrogen bonding present in methanol provides additional rigidity, which facilitates "W"-coupling, whereas greater molecular flexibility in chloroform reduces this effect through motional averaging. The methyl groups were assigned unambiguously by nOe difference spectra. Irradiation of the H-12 resonance enhances those of H-13, H-8β, and H-10β. Irradiation of H-13 enhances H-12, H-11, H-10, and H-1 resonances. Irradiation of the CH_3-14β resonance produces enhancements of CH_3-15α, H-1, and H-7, while irradiation of the CH_3-15α group enhances CH_3-14, H-7, and H-8. The proton assignments thus determined are reported in Table 1, and improve those of Barton and Werstiuk (12). The ^{13}C NMR spectrum is also consistent with the structure and was assigned with the aid of Distortionless Enhancement by Polarization Transfer (DEPT) and ^{1}H/^{13}C heteronuclear correlation (HETCOR) spectra (Table 2).

The oxidation of culmorin with chromic acid has been reported to produce two hydroxy mono keto isomers, namely 8- and 11-keto culmorin (12). In 1985, we isolated a minor metabolite from a liquid culture of *Fusarium roseum* ATCC

Can. J. Chem. Downloaded from www.nrcresearchpress.com by 217.78.4.112 on 09/08/12
For personal use only.

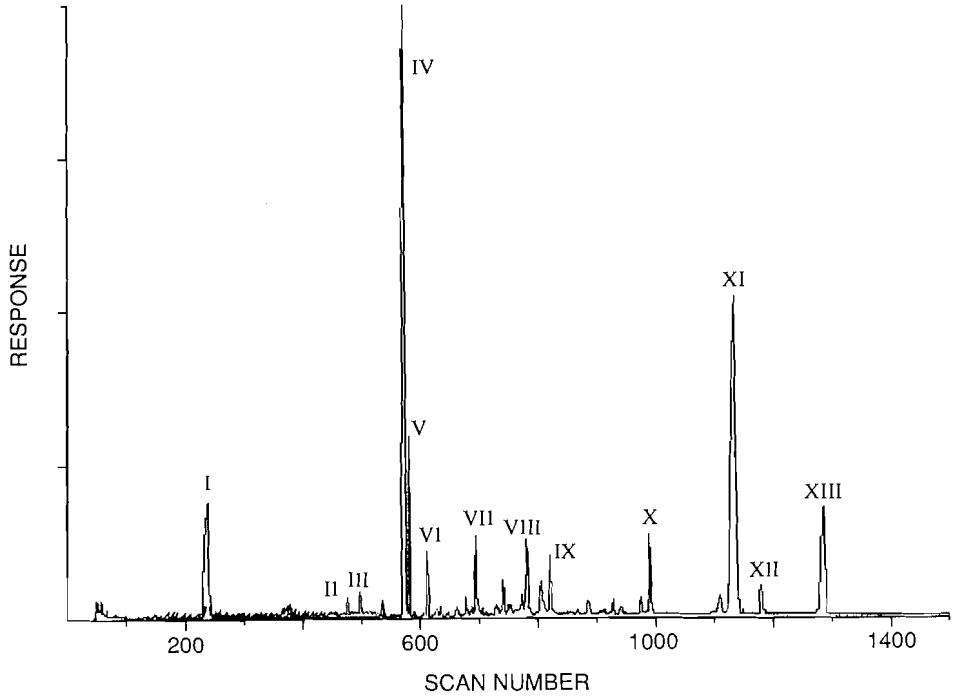

FIG. 2. GC profile of a crude extract of the medium from a *F. culmorum* fermentation 85 h after innoculation. I = butenolide; II = cyclonerodiol; III = cyclonerotriol (**4**); IV = culmorin (**5**); V = culmorone (**6**); VI = 3,11-epoxyepiapotrichothecene; VII = isotrichodermol; VIII = 3-hydroxyepiapotrichothecene (**2**); IX = sambucinol; X = calonectrin; XI = 3-acetyldeoxynivalenol (**1**); XII = 8-hydroxycalonectrin; XIII = 7,8-dihydroxycalonectrin.

TABLE 1. ^{1}H NMR assignments of culmorin and its derivatives (500 MHz, $CDCl_3$)

C	Culmorin[a] (**5**)	Culmorone[a] (**6**)	15-OH Culmorone (**7**)	5-OH Culmorin (**8**)	15-OH Culmorin (**9**)	12-OH Culmorin (**10**)
1	1.91 (d, 4.5)	2.34 (s)	2.30 (s)	1.94 (d, 4.5)	1.89 (d, 4.4)	1.92 (d, 4.4)
3 α	1.51–1.47 (m)	1.62–1.42 (m)	1.59 (m)	1.51 (m)	1.53–1.43 (m)	1.54–1.18 (m)
β			1.27 (brdd, 14.2, 6.5)	1.31 (ddd, 15.8, 6.9, 2.2)		
4	1.51–1.47 (m)	1.62–1.42 (m)	1.51 (m)	1.70–1.65 (m) 1.54 (dddd, 13.9, 7.0, 2.0, 2.0)	1.53–1.43 (m)	1.54–1.18 (m)
5	1.51–1.47 (m)	1.62–1.42 (m)	1.55 (m) 1.43 (m)	3.43 (ddd, 11.4, 5.7, 2.2)		
7	1.86 (d, 5.2)	1.20 (d, 4.9)	1.43 (d, 3.5)	1.89 (d, 5.2)	2.03 (d, 5.2)	1.77 (d, 4.9)
8	3.81 (dd, 5.2, 2.0)	4.01 (dd, 4.9, 2.0)	4.10 (d, 3.5)	3.75 (ddd, 5.2, 4.5, 1.3)	3.93 (dd, 5.2, 1.5)	4.30 (brdd, 4.9, 1.0)
10 α	1.71 (dd, 13.7, 4.2)	2.59 (d, 18.6)	2.58 (d, 18.5)	1.62 (dd, 13.7, 4.6)	1.63 (dd, 13.9, 4.8)	1.94 (dd, 14.0, 4.2)
β	1.59 (ddd, 13.7, 10.0, 2.0)	1.83 (ddd, 18.6, 1.9, 1.2)	1.82 (d, 18.5)	1.67 (ddd, 13.7, 9.2, 1.3)	1.67 (ddd, 13.9, 9.3, 1.7)	1.87 (ddd, 14.0, 9.6, 1.4)
11	4.30 (ddd, 10.0, 4.3, 4.3)	—	—	4.37 (ddd, 9.2, 4.6, 4.5)	4.38 (ddd, 9.2, 4.6, 4.6)	4.42 (ddd, 9.7, 4.8, 4.8)
12	0.91 (s)	1.02 (s)	0.99 (s)	0.79 (s)	0.80 (s)	3.81 (d, 10.4) 3.57 (d, 10.4)
13	0.81 (s)	0.89 (s)	0.87 (s)	0.90 (s)	0.89 (s)	0.90 (s)
14	0.94 (s)	1.00 (s)	0.87 (s)	0.86 (s)	0.86 (s)	0.90 (s)
15	1.02 (s)	0.97 (s)	3.46 (d, 11.1) 3.30 (d, 11.1)	1.15 (s)	3.53 (d, 11.2) 3.34 (d, 11.2)	1.01 (s)
			3.07 (s, OH)	1.36 (dd, 4.5, OH-11, OH-8) 1.22 (d, 5.7, OH-5)		

[a]Spectra obtained in CD_3OD.

Can. J. Chem. Downloaded from www.nrcresearchpress.com by 217.78.4.112 on 09/08/12
For personal use only.

TABLE 2. 125 MHz ^{13}C NMR assignments of culmorin and its derivatives ($CDCl_3$, ppm from TMS)

C	Culmorin (**5**)	Culmorone[a] (**6**)	15-OH Culmorone (**7**)	5-OH Culmorin[a] (**8**)	15-OH Culmorin (**9**)	12-OH Culmorin (**10**)
1	49.5	60.0	59.5	49.3	49.4	50.3
2	51.1	51.7	51.5	51.3	51.5	51.2
3	36.0	34.8	35.5	31.6	35.8	36.6
4	22.6	21.9	21.5	31.4	22.2	22.5
5	41.3	41.4	34.5	79.8	35.6	41.2
6	32.9	33.9	38.2	37.8	37.3	32.8
7	52.2	57.8	53.9	52.3	47.4	51.9
8	79.5	78.0	77.4	78.0	79.2	79.0
9	52.2	50.0	50.2	53.2	52.0	55.6
10	36.0	41.2	41.1	36.4	36.1	33.5
11	71.0	216.5	216.2	70.8	71.3	70.8
12	13.1	12.4	12.5	13.1	13.1	65.7
13	22.0	22.4	22.3	21.8	22.0	22.4
14	28.8	28.4	23.6	21.0	23.7	28.9
15	29.2	29.6	72.2	26.9	72.0	29.0

[a]Spectrum obtained in CD_3OD.

28114 (*F. graminearum*), which was identical to one of these compounds and was named culmorone (**6**) (14*b*).

The molecular formula of culmorone ($C_{15}H_{24}O_2$, *m/z* 236) was derived from its high-resolution and chemical ionization mass spectra. Absorptions in the infrared spectrum at 3420 and 1725 cm^{-1} are indicative of hydroxyl and carbonyl moieties, respectively. The presence of these functional groups is confirmed by resonances at 78.0 ppm (hydroxyl) and 216.5 ppm (carbonyl) in the ^{13}C NMR spectrum. The resonances of the remaining 13 carbon atoms are compatible with the oxidized form of culmorin (Table 2). The location of the keto group was assigned from the ^1H spectrum of culmorone. The signal at 4.01 ppm is assigned to H-8. It is coupled to H-7 (1.20 ppm, doublet) and to the hydroxyl hydrogen at 1.77 ppm (doublet), which disappears upon exchange with deuterium oxide. Furthermore, H-8 shows "W" coupling to H-10β of the methylene AB system at 1.83 and 2.59 ppm (both doublets, J = 18.6 Hz). The H-10α (2.59 ppm) is coupled to CH_3-12. The large geminal coupling constant ($J_{10\alpha,10\beta}$ = 18.6 Hz) is consistent with an sp^2 center, i.e., a keto group adjacent to the methylene group (19). If the keto group was located at C-8 there would be no methylene group adjacent. The presence of a cross peak between H-10β and H-7 in a Relayed Coherence (RELAY) spectrum (resulting from the coupling pattern H-7 to H-8 and H-8 to H-10β) confirms the above assignment, placing the keto group at C-11. Thus the structure of the culmorone isomer isolated as a natural product is identical to 8-hydroxyculmor-11-one (**6**), prepared by Barton and Werstiuk.

The distribution of secondary metabolites isolated during this study is shown in Table 3. Fraction 14, containing mainly culmorin, also afforded a compound (**7**) with molecular weight 252, indicative of a molecular formula $C_{15}H_{24}O_3$ (HRMS). Both the ^1H and ^{13}C NMR spectra are similar to those of culmorone (Tables 1 and 2). However, the ^1H spectrum shows that one of the four methyl groups of culmorone has been replaced by a methylenic AB system at 3.30 and 3.46 ppm, and in the ^{13}C spectrum a new hydroxy methylene appears at 72.2 ppm. Comparison of the ^{13}C chemical shifts with those of culmorone suggests that one of the *gem*-dimethyl groups is oxidized. The ^1H NMR spectrum indicates that the CH_3-15 group is hydroxylated, since the H-7 resonance shifts downfield by 0.23 ppm from that of culmorone, due to the deshielding effect of the C—OH bond. This is corroborated by the nOe effect observed between irradiated H-1 and H-7, H-14, while irradiation of H-8 enhances H-12 and H-15. The above data are consistent with the structure 15,8-dihydroxyculmor-11-one (**7**).

Hydroxy culmorins

Three isomeric hydroxy culmorins (**8**, **9**, and **10**) were isolated from the more polar fractions obtained upon column chromatography of the dichloromethane extract (see Table 3). Their mass spectra showed the same molecular ion, *m/z* 254, indicating a molecular formula $C_{15}H_{26}O_3$, which differs from that of culmorin by a single oxygen atom. The ^1H spectra show that this additional oxygen is present as a hydroxyl group in each case.

For isomer **8**, the hydroxyl group is assigned to C-5 in the eight-membered ring of culmorin. The COSY spectrum (Fig. 3) shows that the carbinyl hydrogens at 4.37 ppm (H-11), 3.75 ppm (H-8), and 3.43 ppm (H-5) are coupled to their respective hydroxyl hydrogens at 1.36 ppm (overlapping doublets, OH-8 and OH-11) and 1.22 ppm (doublet, OH-5). In addition, the OH-5 at 1.22 ppm shows long-range coupling to the CH_3-15 group at 1.15 ppm, which is further coupled to the geminal CH_3-14 at 0.86 ppm. The ^{13}C NMR data (Table 2) show that the resonances assigned to C-4 and C-6 are shifted downfield by 8.8 and 4.9 ppm, respectively, compared to culmorin. This is consistent with carbon atoms situated β to a hydroxyl group (20), thus confirming the location of the hydroxyl group at C-5. The HETCOR spectrum of this compound in CD_3OD (Fig. 4) allows determination of the ^{13}C assignments of the four methyl groups and the three hydroxyl-bearing carbons. Note that the most deshielded hydroxyl hydrogen (H-11) corresponds to the most shielded carbon C-11, and the reverse is true for H-5/C-5. Furthermore, the ambiguity between C-10 and C-4 is resolved. The resonance at 36.4 ppm is assigned to C-10, since this signal couples to H-10 at 1.67 ppm in the ^1H spectrum, assigned from the $^1H/^1H$ coupling to H-8 and

Can. J. Chem. Downloaded from www.nrcresearchpress.com by 217.78.4.112 on 09/08/12
For personal use only.

TABLE 3. Fractionation of crude dichloromethane extract of *Fusarium culmorum*[a]

Solvent (% $MeOH/CH_2Cl_2$)	Volume (L)	Fraction no.	Quantity (g)	Major components[b]
0	8	1		Phthalates
0.5	12	2–4	59.56	Phthalates
1	12	2–4		Phthalates
2.5	8	5–8		Phthalates
5	8	9		Phthalates
		10	0.15	ADON, phthalate
		11	0.27	ADON, SAM
		12	0.62	ADON, SAM
10	8	13	6.08	CUL, DHCAL, SAM, ADON, COL
		14	12.23	CUL, DHCAL, SAM, ADON, 15-OH-COL
		15	10.42	CUL
		16	6.58	CUL, DHCAL, APO
20	8	17	3.04	APO
		18	8.54	APO
		19	4.53	APO, 12-/15-OH-CUL, TCT
		20	5.03	12-/15-OH-CUL, TCT, CNT
100	8	21	1.28	TCT, 5-/12-OH-CUL
		22	0.62	5-OH-CUL
		23	0.17	Very polar material

[a]Methylene dichloride mother liquors after ppt of ADON.
[b]ADON = 3-acetyldeoxynivalenol; SAM = sambucinol; COL = culmorone; CUL = culmorin; DHCAL = 7,8-dihydroxy-calonectrin; APO = 3α/3β-hydroxyepiapotrichothecene; OH-CUL = 5-/12-/15-hydroxyculmorin; TCT = trichotriol; CNT = cyclonerotriol.

H-11. The hydroxyl group is shown to have a β configuration by nOe difference spectra. Positive nOe enhancements were observed between CH_3-15 and the hydrogens H-5α, H-8, and H-7, which are in the plane of the molecule, while irradiation of the CH_3-14 resonance enhances those of H-1 and H-7.

Based on the ^1H NMR spectra of isomers **9** and **10**, the hydroxyl groups of these compounds are associated with the quaternary methyl groups of the parent molecule culmorin. In compound **9**, it is one of the *gem*-dimethyl groups that is hydroxylated. As in 15-OH culmorone (**7**), in isomer **9**, H-7 is shifted downfield to 2.03 ppm from 1.72 ppm in culmorin, suggesting that the hydroxyl group is at C-15. The nOe difference experiments confirm this since H-1 and H-7 are enhanced upon irradiation of CH_3-14, while H-7 and CH_3-15 are enhanced upon irradiation of H-8. Comparison of the ^{13}C NMR spectrum with that of compound **7** confirms the position of hydroxylation. These data are consistent with a structure of 15-hydroxyculmorin for compound **9**.

In compound **10** the downfield shift of the H-8 resonance (from 3.81 to 4.30 ppm) relative to culmorin is indicative of a hydroxyl group at C-12. This is supported by ^{13}C NMR data in which the resonance at 13.1 ppm in culmorin is replaced by one at 65.8 ppm, associated with a hydroxylated methylene, and C-9 at 52.2 ppm shifts to 55.6 ppm (β shift from hydroxylated carbon) (Table 2). In addition, the irradiation of the CH_3-15 resonance in the nOe experiment enhances H-8 and H-7, while irradiation of H-8 resonance enhances those of H-12 and H-15, thus providing further proof for the structure of compound **10** as 12-hydroxyculmorin.

The NMR spectra of ^{13}C-enriched culmorin isolated from fermentor growths of *Fusarium culmorum* to which either ^{13}C-1 and ^{13}C-2 acetate have been added are shown in Fig. 5. Previous studies (10) have shown that culmorin is produced early in the fermentation and competes more successfully for the pool of enriched acetate than the other major metabolite 3-ADON. After biosynthesis of culmorin ceases (~60 h of fermentation), enrichment in ADON increases. ^{13}C-1 acetate (carbonyl group) results in enrichment of positions C-11, C-7, C-9, C-2, C-6, and C-4, while ^{13}C-2 acetate (methyl group) enriches positions C-1, C-8, C-3, C-5, C-10, C-12, C-13, C-14, and C-15. Signal enhancement of all positions occurs with approximately a factor of four. Carbon–carbon coupling resulting from enrichment at adjacent locations is seen at C-6/C-7 and C-2/C-9. This enrichment pattern is consistent with the proposal that culmorin is derived from one molecule of farnesyl pyrophosphate, which has folded in such a manner that the C-1 of farnesyl pryophosphate, which becomes C-7 of culmorin, has linked to the terminal *gem* dimethyl of farnesyl, which results in C-14 and C-15 of culmorin, as first proposed by Hanson and Nyfeler (17).

The isolation of an array of oxygenated culmorin derivatives is reminiscent of the variety of oxygenated trichothecenes and modified trichothecenes produced by the various *Fusaria*. The great variety of oxygenation patterns in these isolated metabolites has suggested the operation of a metabolic grid rather than a unique oxidative pathway (21), and indicates oxidative enzyme systems that are very flexible in substrate selection. However, a striking similarity exists between the general locus of oxygenation in both the trichothecenes (and related trichodienoids) and the culmorin derivatives described herein, once more suggesting the operation of a metabolic grid rather than a unique oxygenation pathway. Hanson and Nyfeler (17*b*) proposed that C-8 is the site of primary oxidation. The compounds isolated in this study support this hypothesis since all possess an oxygen atom at C-8 and imply that C-11 is the site of secondary oxidation, followed by less specific oxidation at postitions C-5, C-12, and C-15. To date, the C-8 monohydroxy intermediate has not been isolated.

Can. J. Chem. Downloaded from www.nrcresearchpress.com by 217.78.4.112 on 09/08/12
For personal use only.

Can. J. Chem. Downloaded from www.nrcresearchpress.com by 217.78.4.112 on 09/08/12
For personal use only.

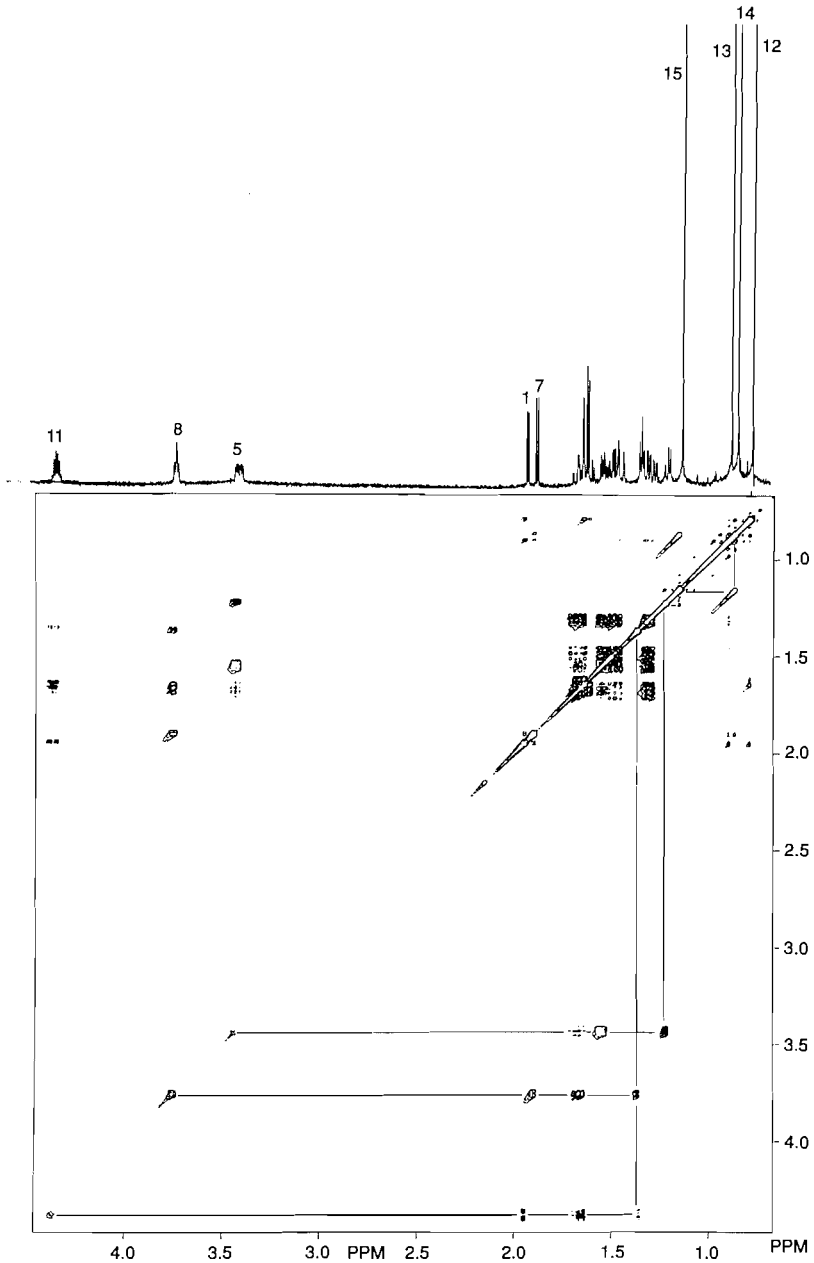

FIG. 3. $^1H/^1H$ correlation (COSY-45) spectrum of 5-OH culmorin (**8**) obtained in $CDCl_3$. A single pulse spectrum is shown as the projection.

Recent toxicological studies have shown that culmorin enhances the toxicity of DON in bioessays with caterpillars (18), and is currently under investigation with animal species. The synergistic effects of the hydroxyculmorin derivatives are also under investigation.

Experimental

Instrumentation

Gas chromatography (GC) was performed on a Varian Vista 5500 gas chromatograph coupled to a Finnigan ion trap (GC/ITD) operating with a split injector (10:1). Underivatized crude extracts were chromatographed on a DB-5 fused silica capillary column (20 m × 0.32 mm i.d., 0.25 μm film). The column temperature was programmed from 120 to 280°C at 20°C/min, holding for 12 min at the end of each run. Helium (10 psi; 1 psi = 6.89 kPa) was used as the carrier gas. The temperature of the detector was set at 300°C and that of the injector at 230°C. All data were acquired by an IBM PC using an Ion Trap Detection System (ITDS) software program. Gas chromatography – mass spectrometry (GC/MS) was performed on a Finnigan GC/MS system, model 4500, with a DS400 data system. High-resolution electron impact (HREI), fast atom bombardment (FAB), and chemical ionization (CI) mass spectrometry were performed on a Finnigan MAT 312 mass spectrometer. Mass spectra were calibrated against perfluorokerosene; the relative peak intensity (%) is indicated in parentheses.

Silica gel (Kieselgel 60, Merck) 70–230 and 230–400 mesh was used for normal and flash column chromatography, respectively. High-performance liquid chromatography (HPLC) was carried out on a Varian model 5500 equipped with a UV-200 variable wavelength detector set at 205 nm. Semi-preparative scale separations were done isocratically with CSC-S nitrile or silica columns using mixtures of isopropyl alcohol and hexane as mobile phases.

Can. J. Chem. Downloaded from www.nrcresearchpress.com by 217.78.4.112 on 09/08/12
For personal use only.

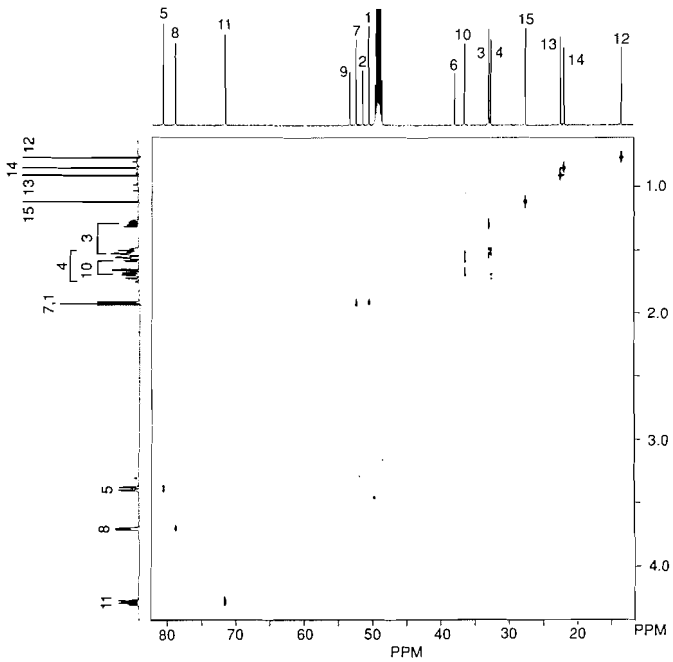

FIG. 4. $^1H/^{13}C$ correlation spectrum of 5-OH culmorin (**8**) obtained in CD_3OD. The projections constitute the single pulse spectra.

Melting points were obtained on a Fisher Johns melting point apparatus and are uncorrected. Optical rotations were determined on a Perkin–Elmer 241 polarimeter.

^1H and ^{13}C nuclear magnetic resonance (NMR) spectra were obtained on Bruker WM250 or AM500 NMR spectrometers in deuterochloroform ($CDCl_3$) or deuteromethanol (CD_3OD) using 5-mm dual probes. Chemical shifts were referenced to $CDCl_3$ at 7.24 ppm (^1H) and 77.00 ppm (^{13}C) or CD_3OD at 3.30 and 49.0 ppm relative to tetramethylsilane (TMS).

Typical spectra used a 32K data point set, 60° pulse, and 3–6 s recycle time. ^1H spectra were resolution enhanced. COSY spectra were run at 500 MHz and employed 512 FID's of 2K data points each, using a 90° pulse of 12 μs. The data matrix was processed using sine-bell squared functions shifted $\Pi/2$ in $F1$ and zero-filled for a final data resolution of 3 Hz per point. RELAY spectra were acquired similarly. $^1H/^{13}C$ HETCOR spectra and DEPT spectra were used to make unambiguous spectral assignments.

Fermentation, extraction, and isolation

Large-scale liquid fermentation of *Fusarium culmorum* CMI 14764 (HLX 1503) was carried out according to Greenhalgh *et al.* (14). The mycelia were separated from the broth by filtration and the broth was extracted successively with hexane and dichloromethane. The dichloromethane extract afforded the major trichothecene 3-ADON (**1**) by precipitation with ethanol. The mother liquors remaining after precipitation of 3-ADON were chromatographed on a silica gel column (75 × 12 cm, Kieselgel 60, Merck, 70–230 mesh, 3 kg). A sample (100 g) in dichloromethane (250 mL) was applied to the column, together with the dichloromethane rinses (2 × 50 mL). The column was eluted with dichloromethane, dichloromethane–methanol mixtures, and pure methanol to afford 23 fractions (Table 3). The fractions 1–9 contained phthalates as determined by GC/MS.

*Isolation of culmorin (**5**) and culmorone (**6**)*

These compounds were found in fractions 13–16. Fractions 15 and 16 (total 16 g) afforded pure culmorin (4 g) upon repeated crystallization from ethyl acetate. The physical (mp and $[\alpha]_D$) and spectral (MS and NMR) data of the sample were identical to those previously reported (14). The isolation of culmorone from *Fusarium roseum* (ATCC 28114) by us is reported elsewhere (14*b*). ^{13}C-enriched culmorin was prepared from a stirred-jar fermentor culture (10 L) of *F. culmorum* CMI 14764 according to Miller and Blackwell (10) and isolated as above.

*Isolation of 15-hydroxyculmorone (**7**)*

Fraction 14 (12 g, heavy oil) contained ADON, culmorin, 7,8-dihydrocalonectrin, and sambucinol, in addition to an unknown compound (**7**). This fraction was subjected to column chromatography on silica gel (4 × 35 cm) and eluted with chloroform (2 L) and methanol/chloroform mixtures, 2% (0.5 L), 5% (0.2 L), and 10% (0.5 L). The first two fractions (total 5 g) were combined and rechromatographed on a similar column, which was eluted isocratically with 40% ethyl acetate in hexane. Twenty-four fractions (100 mL) were collected. Recrystallization of the combined fractions 13–20 from ethyl acetate gave sambucinol (310 mg). The mother liquors were again chromatographed on silica gel (150 g, 3 cm i.d. column) and eluted with ethyl acetate in hexane (50%, 2 L) and (60%, 0.5 L), ethyl acetate (0.5 L), and methanol (0.5 L). The combined ethyl acetate and methanol fractions were evaporated to dryness and gave a white solid (718 mg), which crystallized from ethyl acetate as a white amorphous powder, mp 135–136°C; R_f 0.33 (10% hexane in ethyl acetate); $[\alpha]_D^{26}$ −4.2 (*c* 0.004 g/mL, $CHCl_3$); ^1H and ^{13}C NMR spectra, see Tables 1 and 2; HRMS, calcd. for $C_{15}H_{24}O_3$: 252.1726; found: *m/z* 252.1711 (19), 234 (100), 219 (47).

*Isolation of 5-hydroxyculmorin (**8**)*

Fraction 22 (620 mg, oil) was crystallized repeatedly from acetone to give compound **8** (450 mg) as colourless prisms; mp 210°C; R_f 0.22 (10% hexane in ethyl acetate); $[\alpha]_D^{26}$ +3.1 (*c* 0.01, MeOH); ^1H and ^{13}C NMR spectra, see Tables 1 and 2; HRMS, calcd. for $C_{15}H_{26}O_3$: 254.1883; found: *m/z* 254.1871 (3), 236 (100), 221 (47), 218 (78).

*Isolation of 15-hydroxyculmorin (**9**), cyclonerotriol (**4**), 9α-hydroxytrichotriol (**3**), and 12-hydroxyculmorin (**10**)*

Fraction 20 (5 g, yellowish oil) was crystallized from ethyl acetate – hexane and gave 15-hydroxyculmorin (**9**) (2 g); mp 161–163°C; R_f 0.10 (10% hexane in ethyl acetate) or 0.23 (10% methanol in chloroform); $[\alpha]_D^{26}$ −2.1 (*c* 0.01 g/mL, MeOH); ^1H and ^{13}C NMR spectra, see Tables 1 and 2; HRMS, calcd. for $C_{15}H_{26}O_3$: 254.1883; found: *m/z* 254.1898 (4), 236 (16), 218 (10), 206 (100).

The mother liquors from Fraction 20 (2 g) were fractionated by flash column chromatography (5 × 20 cm) and eluted with ethyl acetate. Eight fractions (A–H, 100 mL each) were collected.

Fraction D (174 mg) was rechromatographed on a silica gel column (2 × 25 cm) and eluted successively with 10% and 20% isopropyl alcohol in hexane (each 100 mL). The latter eluent gave a colourless oil (93 mg) that, after successive semipreparative HPLC separations on silica and CSC-S nitrile columns with 8% and 10% isopropyl alcohol/hexane, respectively, at 2 mL/min, gave cyclonerotriol (**4**) as a colourless solid (20 mg). This solid crystallized from chloroform as colourless prisms, mp 111.5–112.5°C; R_f 0.31 (10% hexane/ethyl acetate); $[\alpha]_D^{26}$ −20.0 (*c* 0.001 g/mL, MeOH); IR ν_{max}: 3381 cm^{-1} (hydroxyl); ^1H NMR ($CDCl_3$, 500 MHz) δ: 5.40 (t, 7.22, H-10), 3.98 (s, 2H-12), 2.10 (m, 2H-9), 1.85 (m, H-6 and H-5), 1.66 (m, H-4), 1.66 (s, 3H-15), 1.60–1.53 (m, H-2, H-4, H-5), 1.50 (t, 8.33, 2H-8), 1.24 (s, 3H-14), 1.16 (s, 3H-13), 1.03 (d, 6.78, 3H-1); ^{13}C NMR ($CDCl_3$, 125 MHz) δ: 134.9 (C-11), 126.1 (C-10), 81.3 (C-3), 74.8 (C-7), 68.7 (C-12), 54.3 (C-6), 44.3 (C-2), 40.3 (C-4), 40.1 (C-8), 26.0 (C-13), 25.3 (C-14), 25.0 (C-5), 24.3 (C-9), 14.5 (C-1), 13.6 (C-15). The ^1H and ^{13}C NMR assignments are based on COSY and HETCOR spectra and are similar to those reported by Hanson *et al.* (9). We have, however, revised the assignments for C-5, C-13, and C-14. HRMS, calcd. for $C_{15}H_{26}O_2$: 238.1934 (M − H_2O); found: 238.1945 (3), 223 (15), 220 (6), 205 (23), 139 (22), 125 (50), 107 (17), 95 (17), 81 (28).

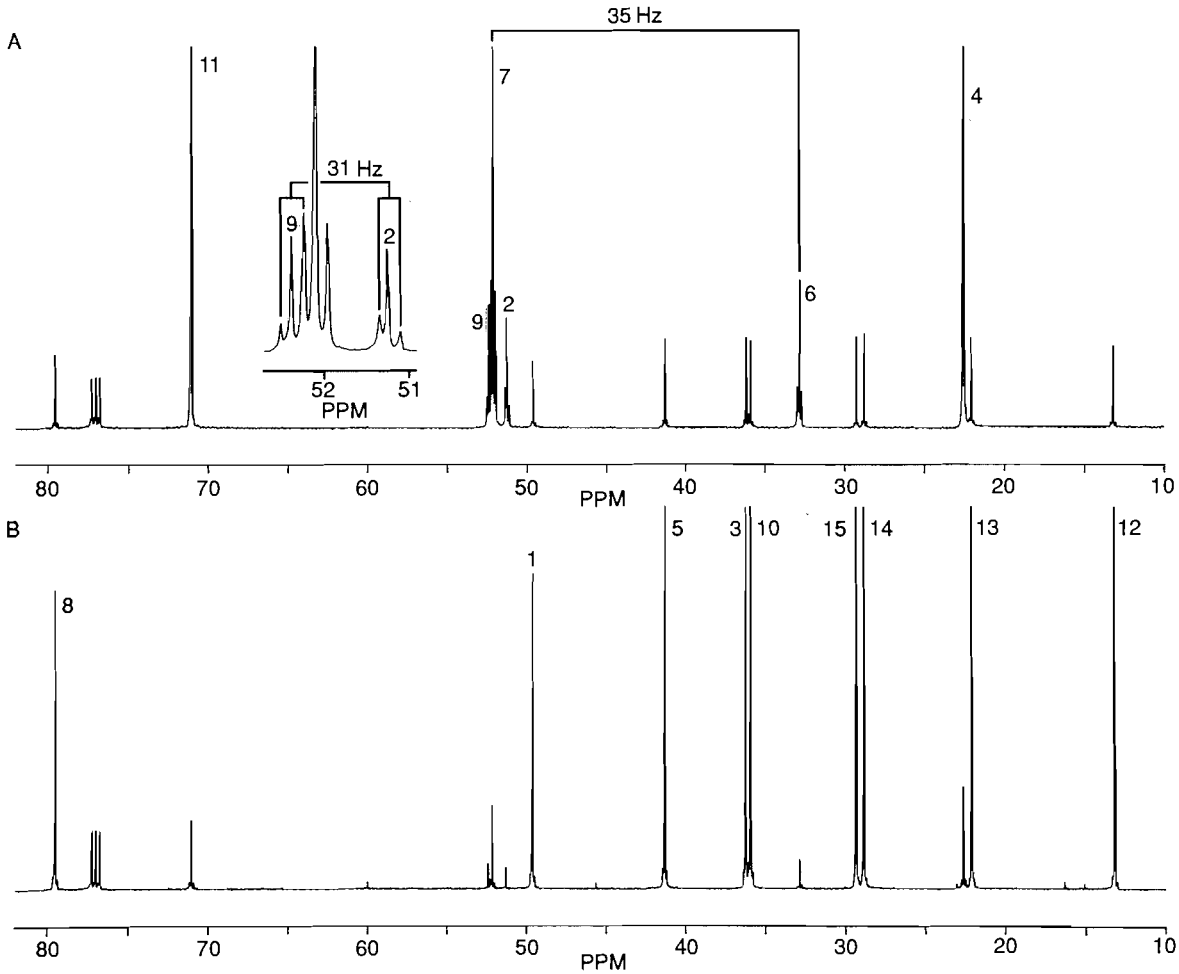

FIG. 5. 125 MHz ^{13}C NMR spectra of culmorin derived from (A) [^{13}C-1]-acetate, and (B) [^{13}C-2)]-acetate. The resonances that are enriched are assigned in each spectrum. The inset of spectrum (A) shows the ^{13}C–^{13}C coupling that occurs between C-2/C-9 and C-6/C-7 as a result of the folding pattern of farnesyl pyrophosphate.

A portion of Fraction F (54 mg) was rechromatographed by semi-preparative HPLC on CSC-S nitrile column using 15% isopropyl alcohol/hexane as eluent at flow rate of 2 mL/min. A colourless solid (26 mg, r.t. 20 min) which had the same MS and NMR spectra as an authentic sample of 9α-hydroxytrichotriol, was obtained. R_f 0.17 (10% hexane/ethyl acetate); ^1H NMR ($CDCl_3$, 500 MHz) δ: 5.69 (brd, 10.11, H-10), 5.51 (d, 10.11, H-11), 4.21 (App.q, 5.53, H-3), 3.64 (d, 4.47, H-2), 3.50 (d, 3.95, H-13), 2.97 (d, 3.95, H-13), 2.08 (dd, 13.3, 8.04, H-4), 1.79 (m, H-7), 1.71 (dd, 13.3, 6.35, H-4), 1.65 (m, H-7 and H-8), 1.30 (brd, 13.72, H-8), 1.24 (s, 3H-16), 1.05 (s, 3H-14), 0.87 (s, 3H-15); ^{13}C NMR ($CDCl_3$, 125 MHz) δ: 136.2 (C-10), 131.3 (C-11), 77.5 (C-2), 69.3 (C-12), 69.0 (C-3), 65.5 (C-9), 50.0 (C-13), 43.7 (C-5), 41.8 (C-4), 39.4 (C-6), 33.8 (C-8), 30.7 (C-16), 25.8 (C-7), 21.2 (C-15), 20.4 (C-14).

HPLC chromatography of a larger sample of Fraction F (428 mg) gave 8 fractions (F1–F8). Fraction F2 (101 mg), eluting 13–15 min before trichotriol, was rechromatographed using 5% isopropyl alcohol/hexane as mobile phase at a flow rate of 4 mL/min, and it gave 5 fractions (F2a–F2f). Fraction F2d (21 mg) containing 15-hydroxyculmorin (**9**) and 12-hydroxyculmorin (**10**) was subjected to preparative thin-layer chromatography (silica gel 150Å PLK5, Whatman) and developed three times in 10% methanol/chloroform. The higher R_f band was extracted with methanol–chloroform and gave 12-hydroxyculmorin (**10**) (7 mg, colourless solid), R_f 0.10 (10% hexane/ethyl acetate) or 0.38 (10% methanol in chloroform); ^1H and ^{13}C NMR spectra, see Tables 1 and 2; HRMS, calcd. for $C_{15}H_{26}O_3$: 254.1883; found: 254.1877 (0.15), 236 (6), 218 (100).

Acknowledgements

The authors wish to thank Mr. G. Montgomery, Mr. J. Nikiforuk, and Mr. P. Lafontaine for their technical assistance. We are grateful to Mr. R. D. Plattner for a sample of 9α-hydroxytrichotriol.

1. (*a*) J. D. Miller and J. C. Young. Can. J. Plant Pathol. **7**, 132 (1985); (*b*) J. D. Miller, J. C. Young, and H. L. Trenholm. Can. J. Bot. **61**, 3080 (1983); (*c*) J. D. Miller, R. Greenhalgh, Y. Z. Wang, and M. Lu. Mycologia, **83**, 121 (1991).
2. J. D. Miller. *In* Phytotoxins and plant pathogenesis. *Edited by* A. Graniti, R. Durbin, and A. Ballio. NATO ASI Ser. H:27, 449 (1989).
3. B. C. Foster, H. L. Trenholm, D. W. Friend, B. K. Thompson, and K. E. Harting. Can. J. Anim. Sci. **66**, 1149 (1986).
4. J. D. Miller, A. Taylor, and R. Greenhalgh. Can. J. Microbiol. **29**, 1171 (1983).
5. R. Greenhalgh, D. Levandier, W. Adams, J. D. Miller, B. A. Blackwell, A. J. McAlees, and A. Taylor. J. Agric. Food Chem. **34**, 98 (1986).

Can. J. Chem. Downloaded from www.nrcresearchpress.com by 217.78.4.112 on 09/08/12
For personal use only.

6. R. Greenhalgh, D. A. Fielder, L. A. Morrison, J. P. Charland, B. A. Blackwell, J. D. Miller, M. E. Savard, and J. W. ApSimon. Proc. – IUPAC 7th Int. Symp. Mycotoxins and Phycotoxins. *Edited by* K. Aibara. 1988. pp. 223–232.
7. D. G. Corley, G. E. Rottinghaus, and M. S. Tempesta. J. Org. Chem. **52**, 4405 (1987).
8. D. E. Cane, R. Iyengal, and M.-S. Shrao. J. Am. Chem. Soc. **103**, 914 (1981).
9. J. R. Hanson, P. B. Hitchcock, and R. Nyfeler. J. Chem. Soc. Perkin Trans. 1, 1586 (1975).
10. J. D. Miller and B. A. Blackwell. Can. J. Bot. **64**, 1 (1986).
11. J. N. Ashley, B. C. Hobbs, and H. Raistrick. Biochem. J. **31**, 385 (1937).
12. (*a*) D. H. R. Barton and N. H. Werstiuk. Chem. Commun. 30 (1967); (*b*) J. Chem. Soc. (C), 149 (1968).
13. K. J. Schilling. Ph.D. Thesis, University of California, Davis. 1967.
14. (*a*) R. Greenhalgh, R. Meier, B. A. Blackwell, J. D. Miller, A. Taylor, and J. W. ApSimon. J. Agric. Food Chem. **32**, 1261 (1984); (*b*) J. Agric. Food Chem. **34**, 115 (1986).
15. D. R. Lauren, A. Ashley, B. A. Blackwell, R. Greenhalgh, J. D. Miller, and G. A. Neish. J. Agric. Food Chem. **35**, 884 (1987).
16. (*a*) S. C. Welch, Ph.D. Thesis. University of Southern California. 1968; (*b*) B. W. Roberts, M. A. Pioonian, and S. C. Welch. J. Am. Chem. Soc. **91**, 3400 (1969); (*c*) S. J. Isser. Diss. Abstr. Int. B. **34**, 137 (1973); (*d*) R. Thimma and U. R. Nayak. Synth. Commun. **15**, 543 (1985); (*e*) R. T. Reddy and U. R. Nayak. Indian J. Chem. **25B**, 457 (1986).
17. (*a*) J. R. Hanson and R. Nyfeler. J. Chem. Soc. Chem. Commun. 824 (1975); (*b*) J. Chem. Soc. Perkin Trans. 1, 2471 (1976).
18. P. F. Dowd, J. D. Miller, and R. Greenhalgh. Mycologia, **81**, 646 (1989).
19. D. E. Leydon and R. H. Cox. Analytical applications of NMR. Vol. 48. John Wiley and Sons, New York. 1977. p. 177.
20. J. B. Stothers. Organic chemistry. Vol. 24. Carbon-13 NMR spectroscopy. Academic Press, New York. 1972. p. 139.
21. A. R. Hesketh, L. Gledhill, D. C. Marsh, B. W. Bycroft, P. M. Dewick, and J. Gilbert. J. Chem. Soc. Chem. Commun. 1184 (1990).

Can. J. Chem. Downloaded from www.nrcresearchpress.com by 217.78.4.112 on 09/08/12
For personal use only.

2,2-Dimethylsuccinic acid derivatives in isoprenoid synthesis: a 2,2-dimethylvinyl anion equivalent in the synthesis of *ar*-atlantone, *ar*-turmerone, and prenylated aromatic compounds

GEORGE M. STRUNZ[1] AND LI YA

Forestry Canada – Maritimes Region, P.O. Box 4000, Fredericton, N.B., Canada E3B 5P7

Received July 29, 1991

This paper is dedicated to Professor Zdenek (Denny) Valenta on the occasion of his 65th birthday

GEORGE M. STRUNZ and LI YA. Can. J. Chem. **70**, 1317 (1992).

The anion of methyl 2,2-dimethylsuccinate was alkylated with benzylic bromides to give the corresponding 3-substituted-2,2-dimethylsuccinates. Hydrolysis to the dicarboxylic acids, followed by bisdecarboxylation with lead tetraacetate, afforded 1-aryl-3-methyl-2-butenes, which are model prenylated aromatic compounds. Acylation of methyl 2,2-dimethylsuccinate with *E*-3-(4′-methylphenyl) crotonyl chloride gave the substituted succinate **9**. Hydrolysis of the ester groups and acid-catalyzed decarboxylation of the resulting β-ketoacid produced the keto acid **10**, which was decarboxylated by the Kochi method, furnishing *ar*-atlantone. Hydrogenation of **10** yielded **12**, which on similar decarboxylation afforded *ar*-turmerone.

GEORGE M. STRUNZ et LI YA. Can. J. Chem. **70**, 1317 (1992).

On a procédé à l'alkylation de l'anion du 2,2-diméthylsuccinate de méthyle par des bromures benzyliques pour obtenir les 2,2-diméthylsuccinates correspondants, substitués en position 3. Leur hydrolyse en acides dicarboxyliques, suivie d'une bisdécarboxylation à l'aide du tétraacétate de plomb, conduit aux 1-aryl-3-méthylbut-2-ènes qui sont des modèles de composés aromatiques prénylés. L'acylation du 2,2-diméthylsuccinate de méthyle par le chlorure de *E*-3-(4′-méthylphényl) crotonyle conduit au succinate substitué **9**. L'hydrolyse des groupes esters et la décarboxylation acido-catalysée du β-céto-acide qui en résulte fournit l'acide cétonique **10** qui, par décarboxylation par la méthode de Kochi, mène à la *ar*-atlantone. L'hydrogénation du produit **10** fournit le produit **12** qui, par une décarboxylation semblable, livre la *ar*-turmérone.

[Traduit par la rédaction]

Can. J. Chem. Downloaded from www.nrcresearchpress.com by 217.78.4.112 on 09/08/12
For personal use only.

Derivatives of 2,2-dimethylsuccinic acid have the potential for the synthesis of certain isoprenoids that has not, to our knowledge, been exploited hitherto. Thus, anions of 2,2-dimethylsuccinate esters can be alkylated or acylated to give products that, upon hydrolysis, afford 3-substituted-2,2-dimethylsuccinic acids. The latter can be decarboxylated to produce compounds having the dimethylvinyl group characteristic of many isoprenoid natural products (Scheme 1). Used in this manner, a 2,2-dimethylsuccinate ester is a masked 2,2-dimethylvinyl anion equivalent that may, in some situations, prove a useful alternative to 2-methyl-1-propenyl Grignard or cuprate reagents (1) (cf. the methallyl dithiocarbamate of Nakai *et al.* (2)). Whereas a 3-halo derivative of the same ester, **2** (R′ = hal), possesses the reverse polarity at C-3 and might, in principle, constitute a masked *electrophilic* 2,2-dimethylvinyl equivalent, steric hindrance prevents such halo-esters from being useful general alkylating agents. (The anhydride of 2,2-dimethylsuccinic acid may, however, be considered as a possible masked senecioyl (3-methyl-2-butenoyl) equivalent.)

In this paper we report some examples of syntheses using the methodology summarized in Scheme 1. Alkylation and acylation of dimethyl 2,2-dimethylsuccinate were employed in the synthesis, respectively, of the model prenylated aromatic compounds, 1-phenyl-3-methyl-2-butene, **3** (R′ = $PhCH_2$) (2, 3) and 1-(2′-methoxyphenyl)-3-methyl-2-butene, **3** (R′ = *o*-$MeOPhCH_2$) (4), and the isoprenoids *ar*-atlantone, **11** (5), and racemic *ar*-turmerone, **13** (6). The latter, with *S*-configuration, is found in the essential oil from rhizomes of turmeric, *Curcuma longa* Linn. (6); the former, though not yet reported as a natural product, is an aromatic derivative of *E*-α-atlantone, a constituent of *Cedrus deodara* (7).

The enone carboxylic acid, **10**, serves as a common intermediate for the synthesis of both isoprenoids. In the synthesis of *ar*-turmerone, the presence of the carboxyl group allows the ready introduction of a new double bond in the desired position after hydrogenation of **10**.

1-Phenyl-3-methyl-2-butene, **3** *(R′ = $PhCH_2$): (Scheme 1)*

The anion of dimethyl 2,2-dimethylsuccinate, prepared by treatment of the ester with a slight excess of lithium diisopropylamide (LDA), was alkylated with benzyl bromide to produce **2** (R = CH_3, R′ = $PhCH_2$) in 89% yield. Alkaline hydrolysis afforded an 87% yield of the trisubstituted succinic acid **2** (R = H, R′ = $PhCH_2$) and the latter was bisdecarboxylated by treatment with lead tetraacetate (8), affording the target prenylated benzene **3** (R′ = $PhCH_2$) (3) in 68% yield.

1-(2′-Methoxyphenyl)-3-methyl-2-butene,
3 *(R′ = o-$MeOPhCH_2$) (Scheme 1)*

The anion of dimethyl 2,2-dimethylsuccinate was alkylated as above using 2-methoxybenzyl bromide, prepared by bromination of 2-methylanisole with *N*-bromosuccinimide. The product **2** (R = CH_3, R′ = *o*-$MeOPhCH_2$), obtained in 81% yield, was hydrolyzed, then bisdecarboxylated with lead tetraacetate (8), furnishing **3** (R′ = *o*-$MeOPhCH_2$)(4) in an overall yield of 40% from the halide.

ar-Atlantone, **11** *(Scheme 2)*

3-(4′-Methylphenyl) crotonic acid ethyl ester, **7** (R = C_2H_5) was prepared as a mixture of *E* and *Z* isomers (9:1) from 4-methylacetophenone and triethyl phosphonoacetate according to Wadsworth and Emmons (9). The predominant *E* isomer, **7** (R = C_2H_5), could be separated by chro-

[1]Author to whom correspondence may be addressed.

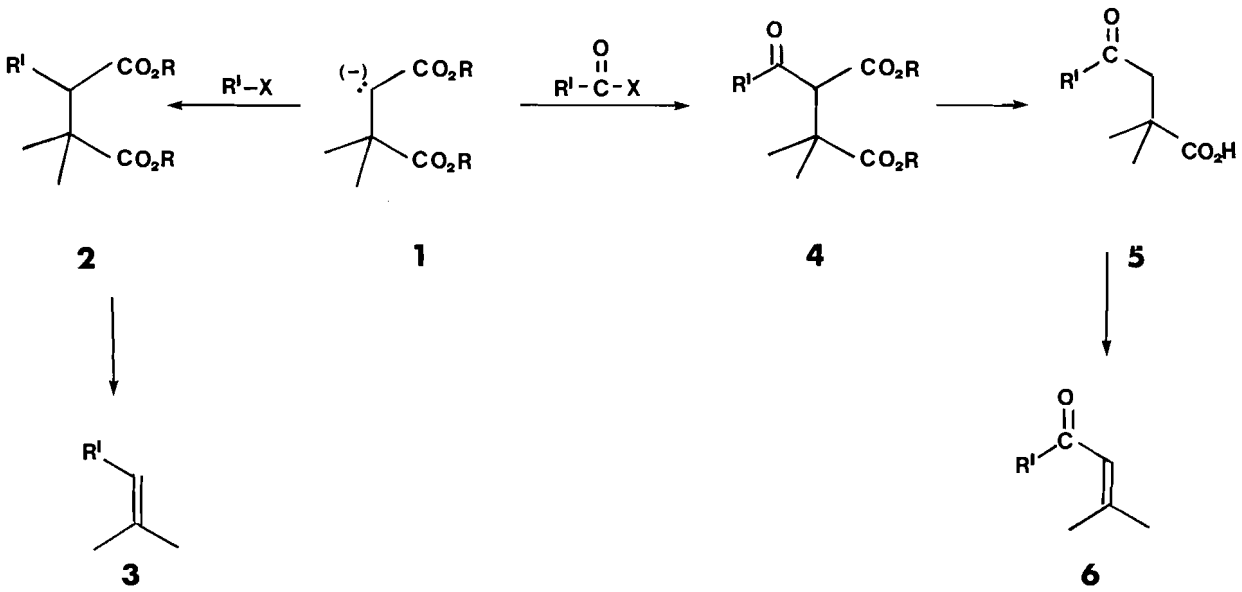

SCHEME 1

matography, and the corresponding acid **7** (R = H) was transformed into the acid chloride **8**. Acylation of the anion of dimethyl 2,2-dimethylsuccinate with this acid chloride afforded **9** in 44% yield. A by-product, isolated in yields of around 41%, was the amide derived from reaction of **8** with diisopropylamine. The amine, produced during proton abstraction from 2,2-dimethylsuccinate by LDA, evidently competes significantly as a nucleophile with the sterically encumbered anion **1** (R = CH_3). Attempts to avoid or suppress this competitive reaction, using as base potassium hydride or the lithium amide from 2,2,6,6-tetramethylpiperidine (which releases a more hindered amine) were not fruitful. As the amide by-product may be hydrolyzed back to **7** (R = H) and thus recycled, this side reaction, although undesirable, is not a major obstacle. (The yield for the conversion of **8** to **9**, based on consumed acid chloride not converted to amide, was 74%.)

Base-catalyzed hydrolysis of **9** and subsequent decarboxylation of the resulting β-keto acid under acidic conditions produced an 86% yield of **10**, which was decarboxylated by the Kochi method (10), furnishing *ar*-atlantone, **11**, with spectroscopic properties in accord with literature data (5). The yield for the transformation of **10** to **11** was 58%.

ar-Turmerone, **13** *(Scheme 2)*

Compound **10**, possessing a latent dimethylvinyl group, can serve as a common intermediate for the synthesis of both *ar*-atlantone, **11**, and *ar*-turmerone, **13**. Thus, hydrogenation of **10** produced **12** quantitatively, and decarboxylation with lead tetraacetate (10) afforded a 68% yield of enone isomers, convertible in quantitative yield under acid catalysis to racemic *ar*-turmerone, **13**, whose spectroscopic characteristics were in accord with published data (6).

Further studies illustrating the utility of 2,2-dimethylsuccinate as a dimethylvinyl synthon in isoprenoid synthesis are in progress and will be reported in the future.

Experimental

Melting points were determined on a hot-stage apparatus and are uncorrected. Infrared spectra were recorded on a Philips Pye Unicam PU 9516 infrared spectrophotometer, and ultraviolet spectra on a Philips PU 8800 uv/vis spectrophotometer. Proton and carbon magnetic resonance spectra were run on a Varian XL-200 instrument, operating at frequencies of 200.068 and 50.308 MHz, respectively. Accurate mass measurements were made on a Kratos MS-50 instrument. Microanalyses were performed by Spang Microanalytical Laboratory, Eagle Harbor, Michigan.

Dimethyl 2,2-dimethylsuccinate

A solution of 2,2-dimethylsuccinic acid (4.0 g; 27.4 mmol) in dry methanol (50 mL) containing concentrated sulfuric acid (15 drops) was heated at reflux under anhydrous conditions. After 5 h, the solution was concentrated to near dryness on a rotary vacuum evaporator. The oily residue was redissolved in ethyl acetate and the solution was washed successively with saturated $NaHCO_3$ and brine before being dried over anhydrous $MgSO_4$. The solvent was removed under reduced pressure, affording a quantitative yield of dimethyl 2,2-dimethylsuccinate as a colorless oil that was sufficiently pure to be used directly in subsequent operations without further purification; ir ($CHCl_3$) (inter alia): 2960, 1735, 1180, 1150, and 1140 cm^{-1}, ^1H nmr ($CDCl_3$, 200 MHz) δ: 1.27 (6H, s) 2.60 (2H, s), 3.66 (3H, s), 3.70 (3H, s); mass spectrum (inter alia), *m/e* (relative intensity) (ion): 174 (1.5) ($C_8H_{14}O_4$; M^+), 143 (37) $(M - OCH_3)^+$, 115 (51) $(M - CO_2CH_3)^+$, 101 (22) $(M - CH_2CO_2CH_3)^+$, 73 (100) $(CH_2CO_2CH_3)^+$.

Dimethyl 2,2-dimethyl-3-benzylsuccinate, **2** *(R = CH_3, R′ = Ph CH_2)*

To a solution of dry diisopropylamine (1.11 g; 11 mmol) in anhydrous THF (10 mL) at −78°C under argon was added *n*-butyllithium (4.4 mL of 2.5 M solution; 11 mmol) dropwise. The resulting yellow solution was stirred at −78°C for 30 min. A solution of dimethyl 2,2-dimethylsuccinate (1.74 g: 10 mmol) in anhydrous THF (ca. 3 mL) was added slowly with stirring to the lithium diisopropylamide (LDA) solution, and the reaction mixture was stirred at −78°C under argon for 1 h. (At this stage virtually complete conversion to the anion was demonstrated by removal of a small aliquot, which was quenched with D_2O.) To the anion solution was added a solution of benzyl bromide (1.71 g; 10 mmol) in dry THF (2.0 mL). The reaction mixture was allowed to attain ambient temperature during 2 h with stirring. A 10% aqueous HCl solution (10 mL) was then added, and the mixture was extracted with ether (15 mL). The aqueous phase was re-extracted with 2 × 20 mL ether, and the combined extracts were washed

Can. J. Chem. Downloaded from www.nrcresearchpress.com by 217.78.4.112 on 09/08/12
For personal use only.

Can. J. Chem. Downloaded from www.nrcresearchpress.com by 217.78.4.112 on 09/08/12
For personal use only.

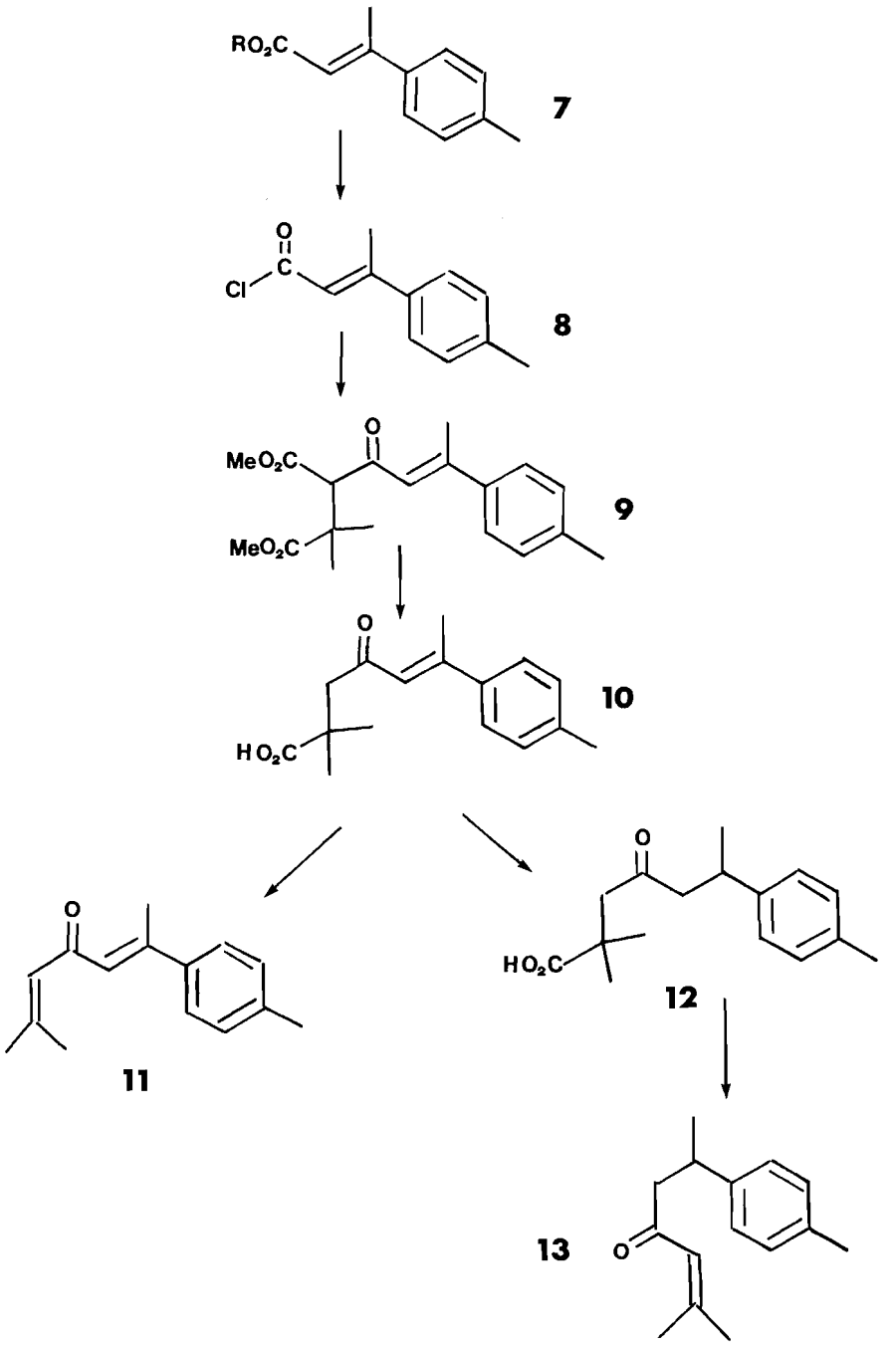

SCHEME 2

successively with saturated solutions of $NaHCO_3$ and brine. After drying over anhydrous $MgSO_4$, the solution was evaporated on a rotary vacuum evaporator. The crude product (3.07 g) was purified by flash chromatography (11) on a silica gel column, using hexane – ethyl acetate (1:0, 4:1) as eluent. The desired product **2** (R = CH_3, R′ = $PhCH_2$) (2.36 g; 89.4%) was an almost colorless oil; ir ($CHCl_3$) (inter alia): 2960, 1730 cm^{-1}, ^1H nmr ($CDCl_3$, 200 MHz) δ: 1.26 (3H, s), 1.34 (3H, s), 2.63–3.17 (3H, m), 3.51 (3H, s), 3.71 (3 H, s), 7.12–7.26 (5H, m); hrms (inter alia), *m/e* (relative intensity) (ion): 264.1340 (6.3) ($M^{\ddagger}$) (calcd. for $C_{15}H_{20}O_4$: 264.1362), 163.0754 (100) ($M - (CH_3)_2CCO_2CH_3)^+$ (calcd. for $C_{10}H_{11}O_2$: 163.0759), 91.0547 (74) $(C_7H_7)^+$ (calcd. for C_7H_7: 91.0548). Anal. calcd. for $C_{15}H_{20}O_4$: C 68.16, H 7.63%; found: C 68.18, H7.77%.

2,2-Dimethyl-3-benzylsuccinic acid: **2** *(R = H, R′ = $PhCH_2$)*

The ester (2.36 g; 8.9 mmol) was hydrolyzed by refluxing for 20 h in aqueous methanol (60 mL) (H_2O:MeOH, 2:1) containing sodium hydroxide (2 g). Most of the methanol was removed under reduced pressure, and addition of 20% aqueous HCl solution to the residue resulted in the separation of a white precipitate. The mixture was extracted with 4 × 50 mL ether and the combined extracts were washed with brine, dried over Na_2SO_4, and evaporated to dryness to yield 1.84 g (87%) of crystalline **2** (R = H, R′ = $PhCH_2$). A sample, recrystallized from aqueous methanol, melted at 140–143°C; ir ($CHCl_3$) (inter alia); 3680–2400, 1710, and 1600 cm^{-1}; ^1H nmr ($CDCl_3$, 200 MHz) δ: 1.35 (6H, s), 2.82–3.17 (3H, m), 7.17–7.30 (5H, m); hrms (inter alia), *m/e* (relative intensity) (ion): 236.1028 (2.7) ($M^{\ddagger}$) (calcd. for $C_{13}H_{16}O_4$: 236.1049),

Can. J. Chem. Downloaded from www.nrcresearchpress.com by 217.78.4.112 on 09/08/12
For personal use only.

218.0934 (45) $(M - H_2O)^+$ (calcd. for $C_{13}H_{14}O_3$: 218.0943), 149.0611 (23) $(M - (CH_3)_2CCO_2H)^+$ (calcd. for $C_9H_9O_2$: 149.0603) 91.0541 (100) $(C_7H_7)^+$ (calcd. for C_7H_7: 91.0548).

1-Phenyl-3-methyl-2-butene **3** *(R′ = $PhCH_2$)*

A stream of oxygen was passed through dry pyridine (7.0 mL) for 15 min. The trisubstituted succinic acid, **2** (R = H, R′ = $PhCH_2$) (0.5 g, 2.1 mmol), and lead tetraacetate (1.86 g, 4.2 mmol) were added with stirring and the flask was immersed in an oil bath at 75°C. When evolution of carbon dioxide ceased, the mixture was cooled, poured into excess dilute nitric acid, and extracted with 4 × 30 mL ether. The extracts were washed successively with saturated $NaHCO_3$ solution and brine. After drying over $MgSO_4$, removal of solvent *in vacuo* afforded an oily product (0.316 g). Flash chromatography on a column of silica gel with hexane – ethyl acetate (1:0, 9.5:0.5, 9:1) as eluent, yielded the pure olefin **3** (R′ = $PhCH_2$) as an almost colorless oil (0.21 g; 68%); ir ($CHCl_3$) (inter alia): 2925, 1603, 1500, 1455, and 1380 cm^{-1}; ^1H nmr ($CDCl_3$, 200 MHz) δ: 1.72 (3H, s), 1.75 (3H, d, $J \sim 1.3$ Hz), 3.34 (2H, br d, $J \sim 7.4$ Hz), 5.29–5.37 (1H, m), 7.13–7.33 (5H, m); mass spectrum, *m/e*: 146 $(M)^+$ $(C_{11}H_{14})$.

Dimethyl 2,2-dimethyl-3-(o-methoxybenzyl) succinate, **2** *(R = CH_3, R′ = o MeOPhCH$_2$)*

The ester **1** (R = CH_3) was alkylated with 2-methoxybenzyl bromide, essentially as described above, to give **2** (R = CH_3, R′ = *o*-MeOPhCH_2) in 81% yield: ir ($CHCl_3$) (inter alia): 2960, 1730, 1603, and 1590 cm^{-1}; ^1H nmr ($CDCl_3$, 200 MHz) δ: 1.27(3H, s), 1.35 (3H, s), 2.81–3.16 (3H, m), 3.50 (3H, s), 3.69 (3H, s), 3.81 (3H, s), 6.79–7.22 (4H, m); hrms (inter alia) *m/e* (relative intensity) (ion): 294.1428 (9.4) (M^+) (calcd. for $C_{16}H_{22}O_5$: 294.1467), 263.1308 (77) $(M - OCH_3)^+$ (calcd. for $C_{15}H_{19}O_4$: 263.1283), 193.0854 (76) $(M - C_5H_9O_2)^+$ (calcd. for $C_{11}H_{13}O_3$: 193.0865), 161.0602 (100) $(o\text{-MeOPh-CH=CH-C}{\equiv}O)^+$ (calcd. for $C_{10}H_9O_2$ 161.0603), 121.0655 (51) $(C_8H_9O)^+$ (calcd. 121.0653), 102.0672 (22) $(C_5H_9O_2H)^+$ (calcd. 102.0681), 91,0553 (42) $(C_7H_7)^+$ (calcd. for C_7H_7: 91.0568). Anal. calcd. for $C_{16}H_{22}O_5$: C 65.29, H 7.54%; found: C 65.32, H 7.59%.

2,2-Dimethyl-3-(o-methoxybenzyl) succinic acid, **2** *(R = H R′ = o MeOPhCH$_2$)*

Hydrolysis of dimethyl 2,2-dimethyl-3-(*o*-methoxybenzyl) succinate, **2** (R = CH_3, R′ = *o*-MeOPhCH_2), as described above, afforded the corresponding trisubstituted succinic acid in 80% yield: ir ($CHCl_3$) (inter alia): ~3000 (br), 1720, and 1600 cm^{-1}; ^1H nmr ($CDCl_3$, 200 MHz) δ: 1.20 (3H, s), 1.21 (3H, s), 2.69–2.99 (3H, m), 3.72 (3H, s), 6.67–7.07 (4H, m); hrms (inter alia), *m/e* (relative intensity) (ion): 266.1101 (3.9) (M^+) (calcd. for $C_{14}H_{18}O_5$ 266.1154), 248.1044 (49) $(M - H_2O)^+$ (calcd. for $C_{14}H_{16}O_4$: 248.1049), 178.0629 (22) $(o\text{-MeOPh-CH=CHCO}_2H)^+$ (calcd. for $C_{10}H_{10}O_3$ = 178.0630), 161.0738 (69) $(o\text{-MeOPh-CH=CH-C}{\equiv}O)^+$ (calcd. for $C_{10}H_9O_2$ 161.0603), 121.0656 (100) $(C_8H_9O)^+$ (calcd. 121.0653).

1-(o-Methoxyphenyl)-3-methyl-2-butene, **3** *(R′ = o-MeOPhCH$_2$)*

The trisubstituted succinic acid (0.50 g; 1.88 mmol) in dry oxygenated pyridine (8.0 mL) was decarboxylated through the agency of lead tetraacetate (1.75 g; 3.95 mmol) as described above. The yield of pure olefin, **3**(R′ = *o*-MeOPhCH_2), after chromatography was 61%; ir ($CHCl_3$), (inter alia): 2925, 1600, 1590, and 1495 cm^{-1}; ^1H nmr ($CDCl_3$, 200 Mz) δ: 1.71 (3H, s), 1.73 (3H, d, $J \sim 1$ Hz), 3.32 (2H, br d, $J \sim 7.4$ Hz), 3.83 (3H, s), 5.26–5.35 (1H, m), 6.82–7.21 (4H, m); mass spectrum (inter alia), *m/e* (relative intensity) (ion): 176 (75) (M^+) $(C_{12}H_{16}O)^+$, 161 (100) $(M - CH_3)^+$ $(C_{11}H_{13}O)^+$, 121 (30) $(C_8H_9O)^+$.

Ethyl E-3-(4′-methylphenyl) crotonate, **7** *(R = C_2H_5)*

Sodium hydride (2.0 g, 60% suspension in mineral oil; 1.2 g; 0.05 mol) was washed free of oil with 3 × 5 mL pentane. After addition of dry dimethoxyethane (100 mL), triethyl phosphonoacetate (11.21 g; 0.05 mol) was introduced dropwise with stirring. The mixture was stirred for 1 h, when evolution of hydrogen ceased. The temperature was maintained below 25°C while 4-methylacetophenone (6.71 g; 0.05 mol) was added dropwise to the yellow solution. The mixture was set aside with stirring at ambient temperature for ca. 8 h, when a gummy precipitate was observed to have separated. Water (300 mL) was added and the mixture was extracted with 4 × 50 mL ether. The combined extracts were dried over anhydrous $MgSO_4$, and removal of solvent *in vacuo* afforded an oily residue (10.31 g). The nmr spectrum of the crude product revealed the presence of two isomers (*vide infra*) in the approximate ratio 9:1. These were separated by flash chromatography on a column of silica gel, using hexane – ethyl acetate (10:0, 9.5:0.5, 9:1) as eluent. The total yield of combined *E* and *Z* isomers was 67%. The major, *E*, isomer, **7** (R = C_2H_5) was an almost colorless oil, ir ($CHCl_3$) (inter alia): 1708, 1630, and 1170 cm^{-1}; uv λ_{max} (EtOH): 273 nm (ε 16 700); ^1H nmr ($CDCl_3$, 200 MHz) δ: 1.32 (3H, t, $J = 7.2$ Hz), 2.37 (3H, s), 2.56 (3H, s), 4.21 (2H, q, $J = 7.2$ Hz), 6.13 (1H, s), 7.28 (4H, approx. ABq, $J_{AB} = 8.2$ Hz, $\Delta\nu_{AB} = 42.4$ Hz); ^{13}C nmr ($CDCl_3$) δ: 14.3 (q), 17.8 (q), 21.2 (q), 59.8 (t), 116.3 (d), 126.2 (d), 129.2 (d), 139.1 (s), 139.2 (s), 155.4 (s), 167.0 (s); hrms (inter alia), *m/e* (relative intensity) (ion): 204.1159 (82) (M^+) (calcd. for $C_{13}H_{16}O_2$: 204.1150), 159.0811 (100) $(M - OC_2H_5)^+$ (calcd. for $C_{11}H_{11}O$): 159.0810), 91.0546 (22) $(C_7H_7)^+$ (calcd. 91.0548).

The presence of the minor, *Z*, isomer in the crude reaction product was manifested in the ^1H nmr spectrum by the following signals: δ 1.12 (t), 2.16 (d, $J \sim 1.4$ Hz), 2.35 (s), 4.02 (q, $J \sim 7.1$ Hz), 5.88 (d, $J \sim 1.4$ Hz). A pure sample of the *Z* isomer showed uv λ_{max} (EtOH): 253 (ε 6420).

E-3-(4′-Methylphenyl) crotonyl chloride, **8**

The ester, **7** (R = C_2H_5) (2.9 g, 0.014 mol) was hydrolyzed by refluxing for ca. 8 h in a water–methanol mixture (2:1) (45 mL) containing sodium hydroxide (2 g). After most of the methanol was removed *in vacuo*, the mixture was made acidic by addition of concentrated HCl solution. The resulting mixture was extracted with 4 × 50 mL ether, and the extracts washed with brine, dried over anhydrous Na_2SO_4, and evaporated to yield 2.45 g (98%) of crystalline acid, **7** (R = H), mp 113–125°C; ir ($CHCl_3$) (inter alia): 3525–2400, 1690, and 1625 cm^{-1}; ^1H nmr ($CDCl_3$, 200 MHz) δ: 2.38 (3H, s), 2.59 (3H, d, $J = 1.2$ Hz), 6.17 (1H, apparent d, $J = 1.3$ Hz), 7.33 (4H, approx. ABq, $J_{AB} = 8.3$ Hz, $\Delta\nu_{AB}$ 34.8 Hz).

The acid, **7** (R = H) was dissolved in 95% ethanol (30 mL) and converted to its sodium salt by addition of an equimolar quantity of aqueous sodium hydroxide solution. The solvent was removed *in vacuo*, and the solid residue was powdered and dried to constant weight (2.69 g) under high vacuum. The powdered sodium salt (2.61 g, 13.2 mmol) was suspended in dry benzene (10.0 mL) containing five drops of dry pyridine. Oxalyl chloride (3.0 mL, 4.37 g, 34.4 mmol) was introduced gradually with stirring and ice-cooling. After the vigorous reaction had subsided, the mixture was allowed to attain ambient temperature and was stirred for an additional 3 h. Solid salt(s) were removed by filtration, and evaporation of the filtrate afforded 2.38 g (93%) of yellow oily product: ir ($CHCl_3$) (inter alia): 1798, 1770 cm^{-1}; ^1H nmr ($CDCl_3$, 200 MHz) δ: 2.39 (3H, s), 2.54 (3H, d, $J = 1.1$ Hz), 6.46 (1H, apparent d, $J = 1.1$ Hz), 7.33 (4H, approx. ABq, $J_{AB} = 8.2$ Hz, $\Delta\nu_{AB} = 42$ Hz).

Dimethyl 2,2-dimethyl-3-acylsuccinate, **9**

Dimethyl 2,2-dimethyl succinate (1.62 g, 9.3 mmol) in anhydrous THF (15 mL) was converted to its anion by treatment with LDA (9.2 mmol) as described above. The anion solution was introduced slowly with stirring at −78°C under argon to a solution of the acid chloride (1.8 g; 9.2 mmol) in dry THF (5.0 mL). The reaction mixture was set aside with stirring at −78°C for 4 h. Dilute HCl solution was then added and the mixture was extracted with ether (20 mL), and then with 3 × 50 mL ether. The combined extracts were washed successively with saturated $NaHCO_3$ and brine,

Can. J. Chem. Downloaded from www.nrcresearchpress.com by 217.78.4.112 on 09/08/12
For personal use only.

dried over $MgSO_4$, and evaporated *in vacuo* to yield 3.56 g of yellow amorphous residue. Flash chromatography on a silica gel column afforded the dimethyl 2,2-dimethyl-3-acylsuccinate, **9** (1.34 g; 44%); ir ($CHCl_3$) (inter alia): 2960, 1732, 1682, 1595, 1560, 1510, and 1437 cm^{-1}; ^1H nmr ($CDCl_3$, 200 MHz) δ: 1.37 (3H, s), 1.38 (3H, s), 2.38 (3H, s), 2.53 (3H, d, J = 1.2 Hz), 4.14 (1H, s), 6.47 (1H, apparent d, J = 1.2 Hz), 3.70 (3H, s), 3.73 (3H, s), 7.29 (4H, approx. ABq, J_{AB} = 8.3 Hz, $\Delta\nu_{AB}$ = 37.8 Hz); hrms (inter alia), *m/e* (relative intensity) (ion): 332.1600 (2.1) (M^+) (calcd. for $C_{19}H_{24}O_5$: 323.1624), 159.0793 (100) (*p*-MePhC(CH_3)CHC≡O^+) (calcd. for $C_{11}H_{11}O$: 159.0810). Anal. calcd. for $C_{19}H_{24}O_5$: C 68.65, H, 7.28%; found: C 68.75, H 7.14%.

A by-product (980 mg: 41%), the amide resulting from reaction of the acid chloride, **8**, with diisopropylamine, was also obtained from the chromatographic fractionation: ^1H nmr ($CDCl_3$, 200 MHz) δ: 1.18 (6H, d, J = 6.7 Hz), 1.47 (6H, d, J = 6.7 Hz), 2.20 (3H, s), 2.36 (3H, s), 3.5–3.75 (1H, m), 4.05–4.2 (1H, m), 6.24 (1H, s), 7.26 (4H, approx. ABq, J_{AB} = 8.0 Hz, $\Delta\nu_{AB}$ = 39.8 Hz).

Ketoacid **10**

A solution of acylated succinic ester, **9** (1.0 g; 3.01 mmol) in methanol–water (1:2) (30 mL) containing sodium hydroxide (2.0 g) was heated under reflux for 3 h. Most of the methanol was removed *in vacuo*, and the aqueous phase was made acidic by addition of 20% HCl, resulting in separation of a white precipitate. The suspension was warmed on a water bath at 40°C. When evolution of carbon dioxide ceased, the mixture was extracted with 4 × 30 mL ether. The combined extracts were washed with brine, dried over anhydrous Na_2SO_4, and evaporated *in vacuo*, yielding 670 mg (86%) of crystalline product: ir ($CHCl_3$) (inter alia): 3525–2400, 1710, 1600, 1565, 1510, 1095, and 915 cm^{-1}; ^1H nmr ($CDCl_3$, 200 MHz) δ: 1.29 (3H, s), 1.31 (3H, s), 2.38 (3H, s), 2.54 (3H, s), 2.90 (2H, s), 6.43 (1H, s), 7.29 (4H, approx. ABq, J_{AB} = 7.9 Hz, $\Delta\nu_{AB}$ = 40 Hz); hrms (inter alia), *m/e* (relative intensity) (ion): 260.1406 (14.2) (M^+) (calcd. for $C_{16}H_{20}O_3$: 260.1412), 245.1192 (11) ($M - CH_3$)$^+$ (calcd. for $C_{15}H_{17}O_3$: 245.1178), 159.0805 (*p*-MePhC(CH_3)CHC ≡ O^+) (calcd. for $C_{11}H_{11}O$: 159.0810).

ar-*Atlantone*, **11**

To the green solution that resulted from dissolving the keto acid **10** (380 mg; 1.46 mmol) and cupric acetate (100 mg) in dry pyridine (0.5 mL) and benzene (15 mL) was added lead tetraacetate (2.19 g; 4.94 mmol). The reaction mixture was set aside with stirring under an argon atmosphere at ambient temperature in the dark for 2 h.

The mixture was then heated at 80°C for 1 h, during which vigorous evolution of carbon dioxide occurred. When the reaction was complete, inorganic material was removed by filtration, and the filtrate was washed with water, 10% HCl solution, and saturated $NaHCO_3$. The organic phase was dried over $MgSO_4$, and removal of solvent on a rotary vacuum evaporator afforded a yellow oil (270 mg). The crude product was subjected to flash chromatography on a column of silica gel, with hexane – ethyl acetate (10:0, 9:1, 8:2) as eluent, to furnish pure *ar*-atlantone (180 mg; 58%) as an almost colorless oil: ir ($CHCl_3$) (inter alia): 2960, 2930, 2870, 1664, 1618, 1592, 1570, 1510, 1445, 1380, and 1120 cm^{-1}; uv λ_{max} (EtOH): 232 nm (ε 10 800), 305 nm (ε 23 600); ^1H nmr ($CDCl_3$, 200 MHz) δ: 1.92 (3H, s), 2.21 (3H, s), 2.37 (3H, s), 2.56 (3H, s), 6.18 (1H, apparent d, J = 1.2 Hz), 6.48 (1H, apparent d, J = 1.1 Hz), 7.29 (4H, approx. ABq, J_{AB} = 8.0 Hz, $\Delta\nu_{AB}$ = 44.5 Hz); ^{13}C nmr ($CDCl_3$) δ: 18.1 (q), 20.7 (q), 21.2 (q), 27.8 (q), 126.2 (d), 126.3 (d), 127.7 (d), 129.2 (d), 139.0 (s), 140.0 (s), 151.1 (s), 154.8 (s), 191.7 (s); hrms (inter alia), *m/e* (relative intensity) (ion): 214.1332 (31.5) (M^+) (calcd. for $C_{15}H_{18}O$: 214.1358), 199.1113 (100) ($M - CH_3$)$^+$ (calcd. for $C_{14}H_{15}O$: 199.1123), 159.0795 (45) ($M - C_4H_7$)$^+$ (calcd. for $C_{11}H_{11}O$: 159.0810), 148.0854 (41) ($C_{10}H_{12}O$)$^+$ (calcd. 148.0889), 119.0862 (42) (C_9H_{11})$^+$ (calcd. 119.0861).

Keto-acid **12**

The enone-acid **10**, (67 mg 0.257 mmol) in ethyl acetate (25 mL) was stirred under a hydrogen atmosphere with a prehydrogenated 10% palladium-on-charcoal catalyst (20 mg) for 30 min, when the theoretical volume of hydrogen had been taken up. The catalyst was removed by filtration, and evaporation of solvent *in vacuo* furnished a quantitative yield (100%) of crystalline keto-acid, **12**: mp 108–112°C, ir ($CHCl_3$) (inter alia): 3525–2400, 1710, 1515, and 915 cm^{-1}, ^1H nmr ($CDCl_3$, 200 MHz) δ: 1.17 (3H, s), 1.20 (3H, s), 1.23 (3H, d, J = 7.0 Hz), 2.31 (3H, s), 2.59–2.65 (4H, m), 3.2–3.35 (1H, m), 7.09 (4H, s); hrms (inter alia), m/e (relative intensity) (ion): 262.1577 (3.5) (M^+) (calcd. for $C_{16}H_{22}O_3$: 262.1569), 244.1471 (5) ($M - H_2O$)$^+$ (calcd. for $C_{16}H_{20}O_2$: 244.1463), 229.1221 (25) ($M-H_2O-CH_3$)$^+$ (calcd. for $C_{15}H_{17}O_2$: 229.1228), 161.0977 (15) (*p*-MePhCH(CH_3)CH_2-C≡O^+) (calcd. for $C_{11}H_{13}O$: 161.0966), 119.0858 (100) (C_9H_{11})$^+$ (calcd. 119.0861). Anal. calcd. for $C_{16}H_{22}O_3$: C 73.25, H 8.45%; found: C 73.39, H 8.29%.

ar-*Turmerone*, **13**

Keto-acid **12** (340 mg. 1.30 mmol) in benzene (15 mL) and pyridine (0.4 mL) was decarboxylated through the agency of lead tetraacetate (2.0 g, 4.50 mmol) and cupric acetate (100 mg) as described above. The crude yellow oily product (300 mg) was subjected to flash chromatography as described above for *ar*-atlantone, furnishing 191 mg (68%) of oily product, apparently homogeneous on tlc. The ^1H nmr spectrum, however, indicated that the product contained a mixture of conjugated and non-conjugated enones. (The diagnostic peaks for the latter were signals at δ 4.75 and 4.91 for a pair of terminal olefinic protons, and a signal at 1.65 for the protons of a vinylic methyl group.) The mixture (130 mg, 0.601 mmol) was heated under reflux for 3 h in benzene containing a catalytic quantity of *p*-toluenesulfonic acid. The solution was washed successively with saturated $NaHCO_3$ and brine solutions, and dried over $MgSO_4$. Removal of solvent under reduced pressure afforded *ar*-turmerone **13** (130 mg, 100%) as an oil: ir ($CHCl_3$) (inter alia): 2975, 2930, 1685, 1620, and 1515 cm^{-1}; uv λ_{max} (EtOH): 236 nm (ε 12 600); ^1H nmr ($CDCl_3$, 200 MHz) δ: 1.24 (3H, d, J = 6.9 Hz), 1.85 (3H, s), 2.10 (3H, s), 2.31 (3H, s), 2.5–2.8 (2H, m), 3.2–3.35 (1H, m), 6.03 (1H, s), 7.10 (4H, s); ^{13}C nmr ($CDCl_3$) δ: 20.7 (q), 20.9 (q), 22.0 (q), 27.6 (q), 35.2 (d), 52.6 (t), 124.0 (d), 126.6 (d), 129.1 (d), 135.5 (s), 143.6 (s), 155.1 (s), 199.8 (s), hrms (inter alia), *m/e* (relative intensity) (ion): 216.1509 (44) (M^+) (calcd. for $C_{15}H_{20}O$: 216.1514), 201.1269 (21) ($M - CH_3$)$^+$ (calcd. for $C_{14}H_{17}O$: 201.1279), 132.0935 (21) ($C_{10}H_{12}$)$^+$ (calcd. 132.0939), 119.0857 (85) (C_9H_{11})$^+$ (calcd. 119.0861), 83.0493 (100) (C_5H_7O)$^+$ (calcd. 83.0497).

Acknowledgments

This investigation was supported in part by the Natural Sciences and Engineering Research Council of Canada (NSERC). The authors thank Mr. Dan Drummond, University of New Brunswick, for the accurate mass measurements, and Mr. Art Spang for accurate and rapid microanalyses.

1. N. Jabri, A. Alexakis, and J. F. Normant. Bull. Soc. Chim. Fr. 321 (1983); G. H. Posner. Org. React. **22**, 253 (1975).
2. T. Nakai, H. Shiono, and M. Okawara. Chem. Lett. 249 (1975).
3. R. C. Haley, J. A. Miller, and H. C. S. Wood. J. Chem. Soc. (C), 264 (1969).
4. S. Araki, S. Manabe, and Y. Butsugan. Chem. Lett. 797 (1982).
5. J. Alexander and G. S. Krishna Rao. Indian J. Chem. **10**, 789 (1972).
6. H. Rupe and A. Gassmann. Helv. Chim. Acta, **19**, 569 (1936); V. K. Honwad and A. S. Rao. Tetrahedron, **20**, 2921 (1964);

A. I. Meyers and R. K. Smith. Tetrahedron Lett. 2749 (1979), and references cited therein.
7. A. S. Pfau and P. Plattner. Helv. Chim. Acta, **17**, 129 (1934); B. S. Pande, S. Krishnappa, S. C. Bisarya, and Sukh Dev. Tetrahedron, **27**, 841 (1971).
8. C. A. Grob, M. Ohta, and A. Weiss. Angew. Chem. **70**, 343 (1958); C. M. Cimarusti and J. Wolinsky. J. Chem. Soc. **90**, 113 (1968).
9. W. S. Wadsworth and W. D. Emmons. J. Am. Chem. Soc. **83**, 1733 (1961).
10. J. D. Bacha and J. K. Kochi. Tetrahedron, **24**, 2215 (1968); J. E. McMurry and L. C. Blaszczak. J. Org. Chem. **39**, 2217 (1974).
11. W. C. Still, M. Kahn, and A. Mitra. J. Org. Chem. **43**, 2923 (1978).

Can. J. Chem. Downloaded from www.nrcresearchpress.com by 217.78.4.112 on 09/08/12
For personal use only.

An alternative synthesis of temafloxacin, a potent antibacterial agent

DANIEL T. W. CHU,[1] ISABELLA M. LICO, AKIYO K. CLAIBORNE, AND HERMANN FAUBL
Anti-infective Research Division, Abbott Laboratories, One Abbott Park Road, Abbott Park, IL 60064-3500 U.S.A.

Received July 3, 1991

This paper is dedicated to Professor Zdenek (Denny) Valenta on the occasion of his 65th birthday

DANIEL T. W. CHU, ISABELLA M. LICO, AKIYO K. CLAIBORNE, and HERMANN FAUBL. Can. J. Chem. **70**, 1323 (1992).

An alternative synthesis of (±)-7-(3-methylpiperazin-1-yl)-6-fluoro-1-(2,4-difluorophenyl)-1,4-dihydro-4-oxoquinoline-3-carboxylic acid hydrochloride **4**, a potent antibacterial agent, was developed. The method was characterized by regiospecific displacement of the 4-fluoro of the 2,4,5-trifluoroacetophenone by 2-methylpiperazine to produce the key intermediate, 2,5-difluoro-4-(3-methylpiperazin-1-yl)acetophenone **12**, which was subsequently converted to **4** via an intramolecular nucleophilic displacement cyclization reaction.

DANIEL T. W. CHU, ISABELLA M. LICO, AKIYO K. CLAIBORNE et HERMANN FAUBL. Can. J. Chem. **70**, 1323 (1992).

On a mis au point une nouvelle méthode de synthèse du chlorhydrate de l'acide (±)-7-(3-méthylpipérazin-1-yl)-6-fluoro-1-(2,4-difluorophényl)-1,4-dihydro-4-oxoquinoléine-3-carboxylique (**4**), un agent antibactérien très puissant. La méthode est caractérisée par une substitution régiospécifique du fluor en position 4 de la 2,4,5-trifluoroacétophénone par une 2-méthylpipérazine pour préparer l'intermédiaire clé, la 2,5-difluoro-4-(3-méthylpipérazin-1-yl)acétophénone (**12**), que l'on peut transformer subséquemment en **4** par le biais d'une réaction de cyclisation impliquant un substitution nucléophilique intramoléculaire.

[Traduit par la rédaction]

Can. J. Chem. Downloaded from www.nrcresearchpress.com by 217.78.4.112 on 09/08/12
For personal use only.

Introduction

Recently many potent clinically important antibacterial agents having the 1,4-dihydro-4-oxoquinoline-3-carboxylic acid moiety, collectively known as quinolones, have been discovered. Representative examples of these are norfloxacin **1** (1), ciprofloxacin **2** (2), and enoxacin **3** (3). An excellent and comprehensive review of the synthetic chemistry associated with these antibacterial agents has been published (4). The most common synthetic methodology used to prepare ethyl 1-alkyl-1,4-dihydro-4-oxoquinoline-3-carboxylate is the reaction of an arylamine with diethyl ethoxymethylene malonate to yield an anilinomethylene malonate that may be cyclized by heating (the Gould–Jacobs reaction) or by the use of a Friedel–Crafts catalyst to yield the 4-hydroxyquinoline-3-carboxylate. Alkylation of this derivative with an alkyl halide followed by hydrolysis yields the desired quinolone. Another approach requires the reaction of an isatoic anhydride with sodio ethyl formylacetate, leading efficiently to the quinolone ester (5).

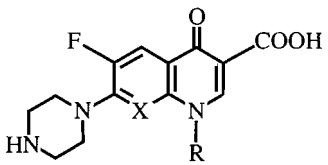

1 $R = C_2H_5$ $X = CH$
2 $R = c\text{-}C_3H_5$ $X = CH$
3 $R = C_2H_5$ $X = N$

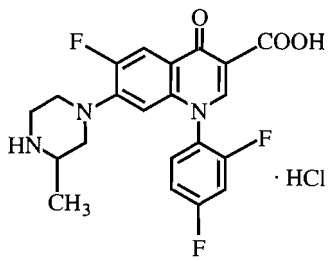

4

Temafloxacin hydrochloride **4** ((±)-7-(3-methylpiperazin-1-yl) - 6-fluoro-1-(2,4 - difluorophenyl)-1,4 - dihydro-4-oxoquinoline-3-carboxylic acid hydrochloride) is a potent quinolone antibacterial agent. It is currently under clinical development and an NDA has been filed in the United States. An approval for clinical use has been obtained in Italy and it will be in market shortly. It possesses excellent activity against both Gram-positive and Gram-negative bacteria (6). The general synthetic methods for the introduction of an N-1 substituent require the alkylation of 1,4-dihydro-4-oxoquinoline-3-carboxylic ester with a reactive alkyl halide. This process, however, makes the introduction of a 2,4-difluorophenyl group at the N-1 position difficult. Temafloxacin was synthesized via an intramolecular nucleophilic displacement cyclization reaction as illustrated in Scheme 1 (7–9).

Although this reported synthesis of temafloxacin hydrochloride is fairly efficient, it provides some problems during commercial production. Our manufacturing facility is not well equipped for the low-temperature reaction required in the preparation of the β-ketoester **8**. The oxidation of 2,4,5-trifluoroacetophene **6** to the 2,4,5-trifluorobenzoic acid **7** by the use of commercial bleach offers a physical problem since the reaction conditions required high dilution with vigorous agitation. The reaction time may not be constant due to the variations in agitation. While the above problems may be solved by engineering and modification of reaction conditions, the low yield (between 42 and 49%) of the displacement of **11** with 2-methylpiperazine to afford the desired product prompted us to investigate an alternative synthesis. This paper deals with a new and efficient route for the synthesis of temafloxacin hydrochloride.

Results and discussion

Our previous reported synthetic pathway to temafloxacin was designed to generate a common intermediate having the basic ring skeleton with a leaving group at the 7-position, such as **11**. Displacement at the 7-position with different amines would generate many derivatives for biological testing. A fluorine atom was chosen as the leaving group since aromatic fluorine groups are very susceptible to nucleophilic displacement. Unfortunately, the displacements of the fluorine atom with 2-methylpiperazine did not give a high-

[1]Author to whom correspondence may be addressed.

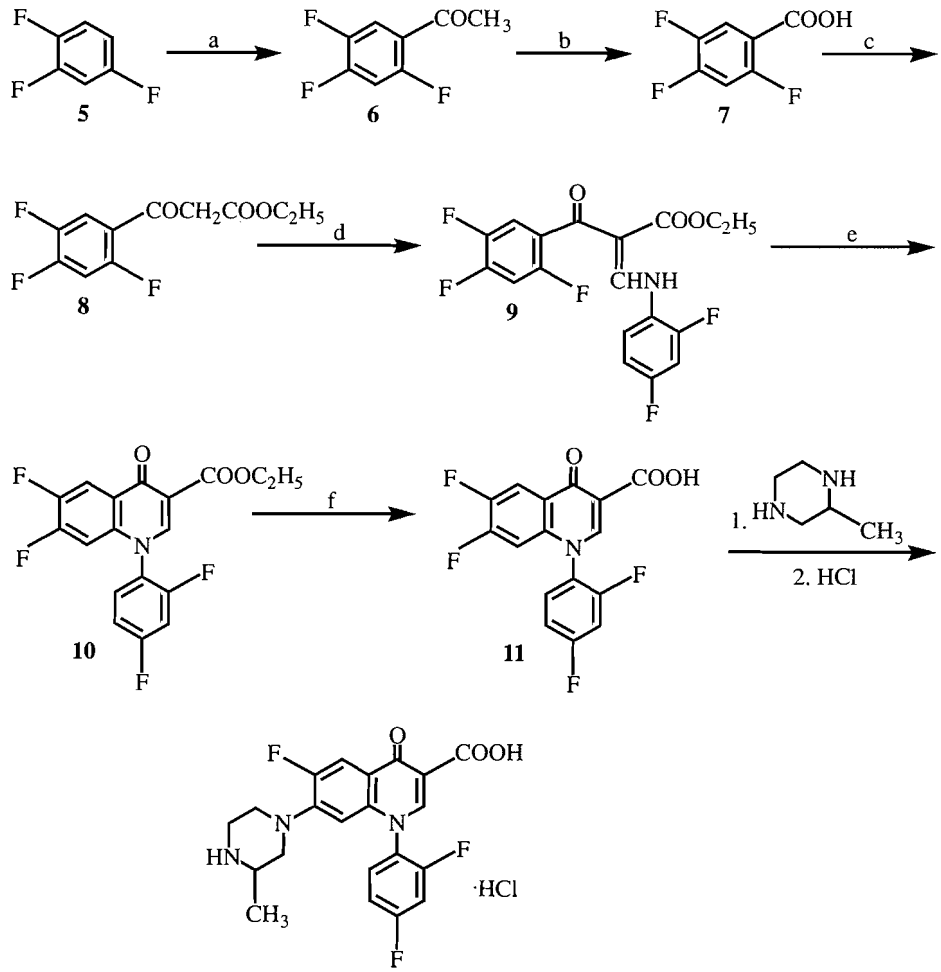

(a) $CH_3COCl/AlCl_3$; (b) NaOCl/NaOH; HCl; (c) $SOCl_2$; $CH_2(COOC_2H_5)COOH/n$-BuLi; HCl; (d) $CH(OC_2H_5)_3/Ac_2O$; *o,p*-difluoroaniline; (e) NaH/THF; (f) H^+

SCHEME 1

yield reaction. To avoid this low-yield reaction, as well as the other manufacturing problems mentioned above, we investigated a synthetic route that required an intermediate which could allow for addition of the C-7 amino group prior to the formation of the bicyclic nucleus. The 2,4,5-trifluoroacetophenone **6** was chosen as the appropriate intermediate since it is readily available.

Displacement of the C-4 fluoro moiety of **6** with 2-methylpiperazine in pyridine in the presence of excess triethylamine followed by precipitation with hydrochloric acid yielded the 2,5-difluoro-4-(3-methylpiperazin-1-yl)acetophenone hydrochloride (**12**) in 92% yield. The fluoro groups at C-2 or C-4 of **6** are both activated by the electron-withdrawing character of the carbonyl group and could be replaced by an appropriate amine. However, the displacement reaction proceeded regioselectively to give the desired key intermediate **12** as a single product. The signal of the critical acetyl proton in the ^1H NMR of **12** in DMSO-d_6 was obscured by the solvent peak. Since **12** is not soluble in $CDCl_3$, a small amount was converted to the free base by neutralization for detailed NMR analysis. The ^1H NMR spectrum of 2,5-difluoro-4-(3-methylpiperazin-1-yl)acetophenone in $CDCl_3$ shows a doublet at δ 2.57 (J_{H-F} = 5 Hz) (corresponding to the acetyl group), due to the long-range coupling[2] with the *ortho* fluorine atom on the benzene ring. Hence, the site of the displacement was assigned as position 4. Additional confirmation of this assignment was provided by the conversion of **12** to temafloxacin hydrochloride by the synthetic route outlined in Scheme 2.

Protection of the secondary amino group as a *tert*-butoxycarbonyl group was achieved by reaction of **12** with di-*tert*-butyl dicarbonate in methylene dichloride in the presence of triethylamine, yielding **13** (mp 100–102°C, 87%). Condensation of 2,5-difluoro-4-(3-methyl-4-*tert*-butoxycarbonylpiperazin-1-yl)acetophenone (**13**) with two molar equivalents of sodium hydride in diethylcarbonate in the presence of a catalytic amount of ethanol yielded the ethyl 2,5-difluoro- 4 -(3-methyl- 4 -*tert*-butoxycarbonylpiperazin-1-yl)benzoylacetate (**14**) (mp 105–108°C, 63%), which existed in both keto and enol forms in approximately 2:1 ratio. Its ^1H NMR spectrum showed the presence of a doublet at δ 2.91 (J_{H-F} = 4 Hz) corresponding to the two keto methylene protons and a singlet at δ 5.81 corresponding to the enol

[2]Long-range coupling was observed with 2,4,6-trifluoroacetophenone (9).

Can. J. Chem. Downloaded from www.nrcresearchpress.com by 217.78.4.112 on 09/08/12
For personal use only.

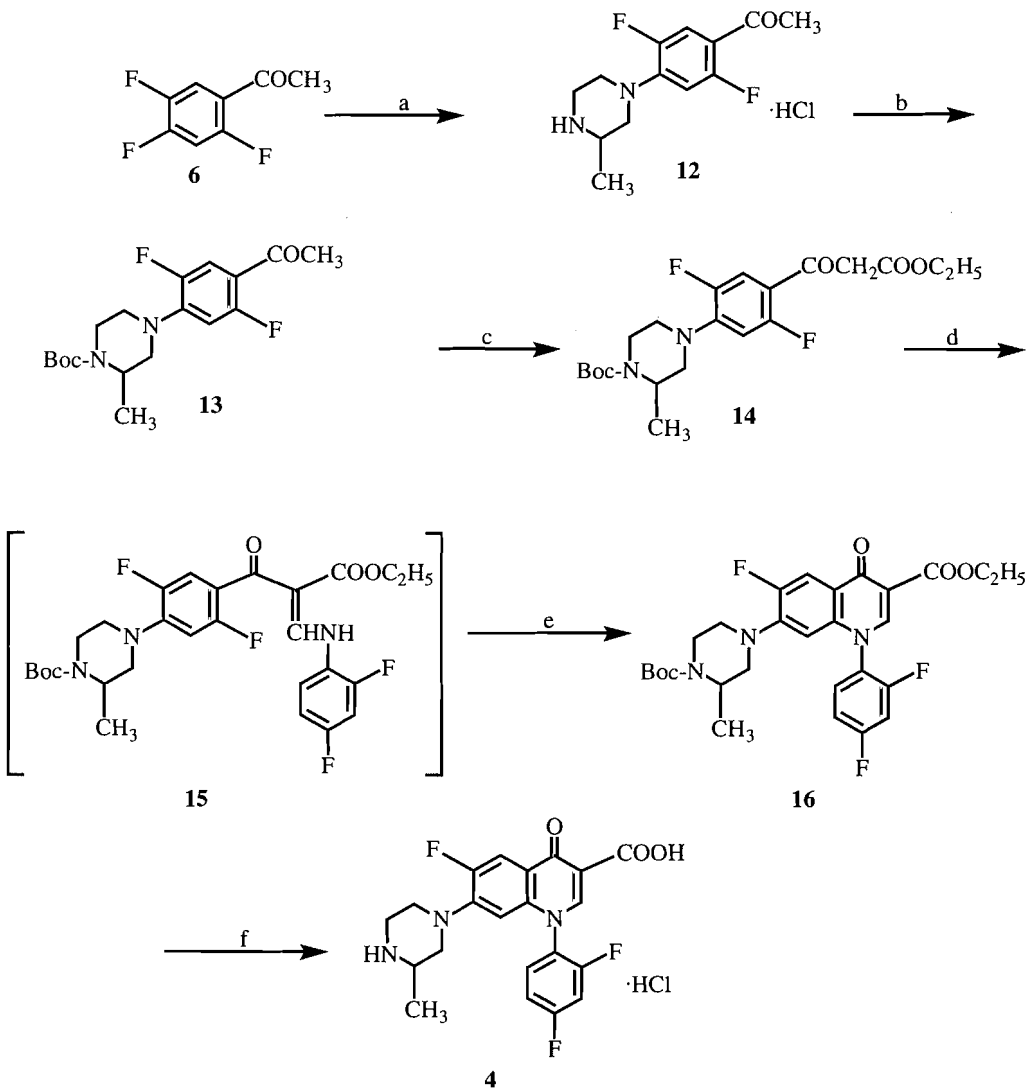

(a) 2-Methylpiperazine/pyridine/TEA; (b) Di-*tert*-butyl dicarbonate/TEA/CH_2Cl_2; (c) NaH/$CO(OC_2H_5)_2$/cat. C_2H_5OH; (d) 1. $CH(OC_2H_5)_3$/Ac_2O; 2. *o*,*p*-difluoroaniline/CH_2Cl_2; (e) NaH/THF; (f) 6 N HCl

SCHEME 2

olefinic proton. The ratio of intensities of these two signals was about 4:1. The long-range coupling with the *ortho* fluorine atom on the benzene ring observed for the methylene protons of the ketoester moiety[3] further confirmed our assignment of the substitution at position 4. Reaction of the ketoester (**14**) with triethylorthoformate in acetic anhydride gave the one-carbon homolog enol ether intermediate, which, upon evaporation of solvent, was allowed to react with a slight excess of 2,4-difluoroaniline in methylene chloride at room temperature to give ethyl 3-(2,4-difluoroanilino)-2-[2,5-difluoro- 4 -(3-methyl- 4 -*tert* - butoxycarbonylpiperazin-1-yl)]benzoylacrylate (**15**). Without purification, **15** was converted to ethyl 7-(3-methyl-4-*tert*-butoxycarbonylpiperazin-1-yl)-6-fluoro-1-(2,4-difluorophenyl)-1,4-dihydro-4-oxoquinoline-3-carboxylate (**16**) (mp 120–123°C, 72%) upon treatment with 1 molar equivalent of sodium hydride in refluxing tetrahydrofuran. Hydrolysis of **16** with 6 N hydrochloric acid yielded temafloxacin hydrochloride (**4**) in 98% yield. The structure of **4** was confirmed by direct comparison with authentic samples prepared by reported methods (9, 11).

In summary, we have developed an alternative synthesis of temafloxacin hydrochloride with an overall yield of 35.6% compared to 20.8% with the reported synthesis. The requirement for low-temperature reactions was also avoided. The key features for this synthesis are the use of easily accessible 2,4,5-trifluoroacetophenone as starting material and the regiospecific displacement of the 4-fluoro of the above acetophenone with 2-methylpiperazine to produce key intermediate **12** in high yield.

Experimental

Unless otherwise noted, materials were obtained from commercial suppliers and used without further purification. Melting points were taken in a Thomas–Hoover capillary apparatus and was uncorrected. NMR spectra were determined on a General Electric

[3]Similar long-range couplings were reported for ethyl 2,3,4,5,6-pentafluorobenzoylacetate (10*a*) and for ethyl 2,3,5-trifluoro-4-(4-methyl-1-piperazinyl)benzoylacetate (10*b*).

Can. J. Chem. Downloaded from www.nrcresearchpress.com by 217.78.4.112 on 09/08/12
For personal use only.

Can. J. Chem. Downloaded from www.nrcresearchpress.com by 217.78.4.112 on 09/08/12
For personal use only.

GN-300 spectrometer operating at 300.1 MHz. Chemical shifts are expressed in ppm downfield from internal tetramethylsilane. Significant ^{1}H NMR data are tabulated in the order: multiplicity (s, singlet; d, doublet; t, triplet; q, quartet; m, multiplet; b, broad; dd, double doublet), coupling constants, number of protons, and designation. The IR spectra were recorded on a Perkin–Elmer model 710A infrared spectrometer. Mass spectra were obtained with a Hewlett–Packard 5985A mass spectrometer or a Kratos MS-50 instrument with EI source (70 eV). The IR, NMR, and mass spectral data of all compounds were consistent with the assigned structures. Solutions were dried over magnesium sulfate. E. Merck silica (230–400 mesh) obtained from VWR Scientific was used for column chromatography, and yields of the reactions were not optimized. Elemental analyses were performed by the Abbott analytical department and IR, NMR, and mass spectra were recorded by the Abbott structural chemistry department.

2,5-Difluoro-4-(3-methylpiperazin-1-yl)acetophenone hydrochloride (**12**)

To a stirring solution of 2,4,5-trifluoroacetophenone (**6**) (8.7 g, 50 mmol) in pyridine (25 mL) and triethylamine (21 mL) was added 2-methylpiperazine (5.5 g, 55 mmol). After 2 days, the mixture was concentrated to an orange solid, which was dissolved in water (150 mL). Concentrated hydrochloric acid was added until the mixture became acidic, yielding a precipitate. The solid was collected by filtration and washed with small amounts of water, ethanol, and ether. The filtrate was basified with dilute sodium hydroxide solution and extracted with ethyl acetate, and dried and concentrated to give a red oil. 1 N Hydrochloric acid was added and the solid was collected as above. The combined solid was dried to yield **12** (mp >250°C, 13.4 g, 92%). IR (KBr): 1660 cm^{-1} (CO). ^{1}H NMR (DMSO-d_6)δ: 1.39 (d, J = 6.5 Hz, 3H, CH_3), 2.53 (d, J_{H-F} = 4.8 Hz, 3H, $COCH_3$: this signal is partly covered by solvent peak), 3.14 (m, 4H, NCH_2) 3.40 (m, 1H, NCH), 3.68 (m, 2H, NCH_2), 7.08 (dd, 1H, aromatic H), 7.54 (dd, 1H, aromatic H), 9.45 (bs, 1H, NH). Anal. calcd. for $C_{13}H_{17}ClF_2N_2O$: C 53.71, H 5.89, N 9.64; found: C 53.48, H 5.77, N 9.50.

A small amount of **12** was shaken with dilute sodium hydroxide solution and extracted with methylene chloride to yield the free amine of **12**. mp 86–89°C. ^{1}H NMR ($CDCl_3$) δ: 1.12 (d, J = 6.5 Hz, 3H, CH_3), 1.74 (bs, 1H, NH), 2.47 (m, 1H, NCH_2), 2.57 (d, J_{H-F} = 5 Hz, 3H, $COCH_3$), 2.83 (m, 1H, NCH_2), 3.04 (m, 3H, NCH_2 and NCH), 6.56 (dd, 1H, aromatic H), 7.55 (dd, 1H, aromatic H). Anal. calcd. for $C_{13}H_{16}F_2N_2O \cdot 1/5\ H_2O$: C 60.56, H 6.29, N 10.87; found: C 60.76, H 6.29, N 10.76.

*2,5-Difluoro-4-(3-methyl-4-*tert*-butoxycarbonylpiperazin-1-yl)acetophenone* (**13**)

To a suspension of **12** (12.45 g, 42.9 mmol) in methylene chloride (100 mL) in an ice bath was added triethylamine (18 mL, 129 mmol). After the addition of di-*tert*-butyl dicarbonate, the ice bath was removed and the reaction was allowed to warm up slowly to room temperature. After 3 h, the mixture was washed with 1 M H_3PO_4, saturated $NaHCO_3$, and brine solution in sequence. The organic solvent was dried and concentrated. The residue was crystallized from hexane, yielding **13** (13.18 g, 87%), mp 100–102°C. IR ($CDCl_3$): 1620, 1680 cm^{-1} (CO). ^{1}H NMR ($CDCl_3$) δ: 1.31 (d, J = 6.5 Hz, 3H, CH_3), 1.50 (s, 9H, $C(CH_3)_3$), 2.58 (d, J_{H-F} = 4.8 Hz, 3H, $COCH_3$), 2.55 (m, 1H, NCH_2), 2.99 (m, 1H, NCH_2), 3.27 (m, 1H, NCH_2), 3.45 (m, 2H, NCH_2), 3.96 (m, 2H, NCH_2), 4.34 (m, 1H, NCH), 6.53 (dd, 1H, aromatic H), 7.57 (dd, 1H, aromatic H). Anal. calcd. for $C_{18}H_{24}F_2N_2O_3$: C 61.00, H 6.83, N 7.90; found: C 60.97, H 6.82, N 7.87.

*2,5-Difluoro-4-(3-methyl-4-*tert*-butoxycarbonylpiperazin-1-yl)benzoylacetate* (**14**)

To a solution of **13** (3.6 g, 10.17 mmol) in diethyl carbonate (50 mL) was added sodium hydride (60% in oil suspension) (0.853 g, 21.3 mmol) at room temperature under nitrogen atmosphere. The temperature was raised to 80°C and 1 drop of ethanol was added. After 1 h, the mixture was cooled and acetic acid (2 mL) was added. It was concentrated to a red oily residue, which was partitioned between ether and water. The organic layer was separated and dried and concentrated. Flash chromatography of the residue (200 g silica, 1:7 ethyl acetate/hexane as eluent) yielded **14** (2.72 g, 63%). This oil solidified after standing a few days, mp 105–108°C. IR (thin film): 1620, 1695, 1740 cm^{-1} (CO). ^{1}H NMR ($CDCl_3$) δ: 1.27 and 1.33 (each t, J = 7 Hz, 3H, ethyl CH_3), 1.30 (d, J = 6.5 Hz, CH_3), 1.48 (s, 9H, $C(CH_3)_3$), 2.91 (m, 2H, NCH_2), 3.26 (m, 1H, NCH_2), 3.42 (m, 2H, NCH_2), 3.91 (d, J_{H-F} = 4 Hz, 2H × 2/3, $COCH_2COO$), 3.96 (m, 1H, NCH_2), 4.21 (q, J = 7 Hz, 2H × 2/3, ethyl CH_2), 4.21 (q, J = 7 Hz, 2H × 1/3, ethyl CH_2), 4.33 (m, 1H, NCH), 5.81 (s, 1H × 1/3, vinyl H), 6.51 (dd, 1H × 2/3, aromatic H), 6.57 (dd, 1H × 1/3, aromatic H), 7.54 (dd, 1H × 1/3, aromatic H), 7.61 (dd, 1H × 2/3, aromatic H), 12.72 (s, 1H × 1/3, enol OH). Anal. calcd. for $C_{21}H_{28}F_2N_2O_5$: C 59.14, H 6.62, N 6.57; found: C 59.43, H 6.69, N 6.55.

*Ethyl 7-(3-methyl-4-*tert*-butoxycarbonylpiperazin-1-yl)-6-fluoro-1-(2,4-difluorophenyl)-1,4-dihydro-4-oxoquinoline-3-carboxylate* (**16**)

A mixture of **14** (1 g, 2.3 mmol), acetic anhydride (0.96 g, 9.4 mmol), and triethylorthoformate (0.7 g, 4.7 mmol) was heated at 110°C for 2 h with the removal of the ethyl acetate formed during the reaction. The mixture was evaporated under reduced pressure to an oil, which was then dissolved in methylene chloride (25 mL). 2,4-Difluoroaniline (0.33 g, 2.6 mmol) in methylene chloride (5 mL) was then added to the solution. After 1.5 h, the solution was evaporated to dryness. The residue was dissolved in ether and washed with 1 N acetic acid to remove excess difluoroaniline and then water. The organic layer was dried and concentrated. A small amount of this residue was purified by flash chromatography on silica (using 5% ethyl acetate in methylene chloride as eluent) to yield pure **15**. The remaining residue was dissolved in tetrahydrofuran. To this cold solution was slowly added a 60% sodium hydride-in-oil suspension (0.105 g, 2.6 mmol). The mixture was heated at reflux for 2 h under nitrogen atmosphere and was cooled. A few drops of acetic acid were added. The mixture was concentrated. The residue was dissolved in methylene chloride and washed with water and dried. Upon evaporation of the solvent to dryness, the residue was purified by column chromatography on silica using 3% methanol in methylene chloride as eluent, yielding **16** (0.92 g, 72% from **14**), mp 120–123°C. IR (KBr): 1625, 1725 cm^{-1} (CO). ^{1}H NMR ($CDCl_3$) δ: 1.29 (d, J = 6.5 Hz, 3H, CH_3), 1.39 (t, J = 7 Hz, 3H, ethyl CH_3), 1.45 (s, 9H, $C(CH_3)_3$), 2.63 (m, 1H, NCH_2), 2.81 (m, 1H, NCH_2), 3.24 (m, 3H, NCH_2), 3.91 (m, 1H, NCH_2), 4.30 (m, 1H, NCH), 4.38 (q, J = 7 Hz, 2H, ethyl CH_2), 4.30 (m, 1H, NCH), 4.38 (q, J = 7 Hz, 2H, ethyl CH_2), 6.11 (d, J_{H-F} = 7 Hz, 1H, C_8-H), 7.17 (m, 2H, aromatic H), 7.51 (m, 1H, aromatic H), 8.08 (d, J_{H-F} = 13 Hz, 1H, C_5-H), 8.31 (s, 1H, olefinic H). Anal. calcd. for $C_{28}H_{30}F_3N_3O_5$: C 61.64, H 5.54, N 7.70; found: C 61.48, H 5.52, N 7.62.

Difluoroanilinobenzoylacrylate (**15**): IR ($CDCl_3$): 1625, 1675, 1685 cm^{-1} (CO). ^{1}H NMR ($CDCl_3$), 2 sets of signals, δ: 1.04, 1.15 (each t, J = 7 Hz, 3H, ethyl CH_3), 1.33, 1.34 (each d, J = 6.5 Hz, 3H, CH_3), 1.49 (s, 9H, $C(CH_3)_3$), 2.80 (m, 1H, NCH_2), 2.92 (m, 1H, NCH_2), 3.25 (m, 1H, NCH_2), 3.38 (m, 2H, NCH_2), 3.96 (m, 1H, NCH_2), 4.14, 4.15 (each q, J = 7 Hz, 2H, ethyl CH_2), 4.84 (m, 1H, NCH), 6.49 (m, 1H, aromatic H), 6.96 (m, 2H, aromatic H), 7.34 (m, 1H, aromatic H), 8.25, 8.43 (each d, J_{H-J} = 13 Hz, 1H, aromatic H), 10.90, 12.30 (each bd, J = 13 Hz, 1H, NH). Anal. calcd. for $C_{28}H_{31}F_4N_3O_5$: C 59.46, H 5.52, N 7.43; found: C 59.28, H 5.79, N 7.24.

Temafloxacin hydrochloride (**4**)

To a solution of **16** (0.26 g, 0.47 mmol) in acetic acid (1 mL) at 100°C under nitrogen atmosphere added 6 N HCl (10 mL). The mixture was heated at 100°C for 2.5 h. It was concentrated. The residue was crystallized from ethanol–water to yield temafloxacin hydrochloride (**4**) (0.212 g, 98%), mp > 300°C. IR (KBr): 1625, 1725 cm^{-1} (CO). ^{1}H NMR (DMSO-d_6) δ: 1.26 (d, J = 7 Hz, 3H,

CH_3), 2.95 (m, 1H, NCH), 3.11 (m, 2H, NCH_2), 3.48 (m, 2H, 2 NCH_2), 6.41 (d, J_{H-F} = 7 Hz, 1 H, C_8-H), 7.46 (m, 1H, aromatic H), 7.75 (m, 1H, aromatic H), 7.95 (m, 1H, aromatic H), 8.04 (d, J_{H-F} = 12 Hz, 1H, C_5-H), 9.52 (bs, 1H, NH), 14.87 (bs, 1H, OH). Anal. calcd. for $C_{21}H_{19}ClF_3N_3O_3 \cdot 1/2\ H_2O$: C 54.49, H 4.36, N, 9.08; found: C 54.64, H 4.25, N 9.03. **4** is identical in TLC and HPLC to the authentic samples prepared by the reported method.

Acknowledgements

We wish to thank the analytical research and structural chemistry departments of Abbott Laboratories for elemental analysis and spectral measurements, respectively, and Ms. Cynthia Shepherd for typing the manuscript.

1. H. Koga, A. Itoh, S. Murayama, S. Suzue, and T. Irikura. J. Med. Chem. **23**, 1358 (1980).
2. R. Wise, J. M. Andrews, and L. J. Edward. Antimicrob. Agents Chemother. **23**, 559 (1983).
3. J. Matsumoto, T. Miyamoto, A. Minamida, Y. Nishimura, H. Egawa, and H. Nishimura. J. Med. Chem. **27**, 292 (1984).
4. R. Albrecht. Prog. Drug Res. **21**, 9 (1977).
5. L. A. Mitscher, H. E. Gracey, G. W. Clark, and T. Suzuki. J. Med. Chem. **21**, 485 (1978).
6. D. J. Hardy, R. N. Swanson, D. N. Hensey, N. R. Ramer, R. R. Bower, C. W. Hanson, D. T. W. Chu, and P. B. Fernandes. Antimicrob. Agents Chemother. **31**, 1768 (1987).
7. D. T. W. Chu. J. Heterocycl. Chem. **22**, 1033 (1985).
8. D. T. W. Chu, P. B. Fernandes, A. K. Claiborne, E. Pihuleac, C. W. Nordeen, R. E. Maleczka, Jr., and A. G. Pernet. J. Med. Chem. **28**, 1558 (1985).
9. D. T. W. Chu, C. W. Nordeen, D. J. Hardy, R. N. Swanson, W. J. Giardina, A. G. Pernet, and J. J. Plattner. J. Med. Chem. **34**, 168 (1991).
10. (*a*) R. Filler, Y. S. Rao, A. Biezais, F. N. Miller, and V. D. Beaucaire. J. Org. Chem. **35**, 930 (1970); (*b*) H. Egawa, T. Miyamoto, and J. Matsumoto. Chem. Pharm. Bull. **34**, 4098 (1986).
11. D. T. W. Chu, P. B. Fernandes, A. K. Claiborne, R. E. Maleczka, P. Klock, L. Shen, J. Patel, and A. Pernet. 26th Interscience Conference on Antimicrobial Agents and Chemotherapy, Sept. 28, 1986. New Orleans. Abstr. no. 428.

Can. J. Chem. Downloaded from www.nrcresearchpress.com by 217.78.4.112 on 09/08/12
For personal use only.

Syntheses and antibacterial activity of novel 6-fluoro-7-(*gem*-disubstituted piperazin-1-yl)-quinolines[1]

DANIEL T. W. CHU,[2] AKIYO K. CLAIBORNE, JACOB J. CLEMENT AND JACOB J. PLATTNER
Anti-infective Research Division, Abbott Laboratories, One Abbott Park Road, Abbott Park, IL 60064-3500, U.S.A.

Received July 3, 1991

This paper is dedicated to Professor Zdenek (Denny) Valenta on the occasion of his 65th birthday

DANIEL T. W. CHU, AKIYO K. CLAIBORNE, JACOB J. CLEMENT, and JACOB J. PLATTNER. Can. J. Chem. **70**, 1328 (1992).

A series of quinoline and naphthyridine antibacterial agents possessing an acyclic or cyclic *gem*-disubstituted piperazine substituent at the C-7 position have been prepared and evaluated in vitro and in vivo for antibacterial activity against a variety of Gram-positive and Gram-negative organisms. They are, however, not as active as quinolones or naphthyridines with a monosubstituted piperazine substituent at C-7. The chemical synthesis of these derivatives is also described.

DANIEL T. W. CHU, AKIYO K. CLAIBORNE, JACOB J. CLEMENT et JACOB J. PLATTNER. Can. J. Chem. **70**, 1328 (1992).

On a préparé un série d'agents antibactériens dérivés de quinoléines et de naphtyridines portant comme substituant en position C-7 une pipérazine *gem*-disubstituée sur la portion aliphatique ou cyclique; on a évalué leur activité antibactérienne in vitro et in vivo contre une variété d'organismes Gram-positifs et Gram-négatifs. Ils ne sont toutefois pas aussi actifs que les quinolones ou les naphtyridines portant une pipérazine monosubstituée en position C-7. On décrit aussi la synthèse chimique de ces dérivés.

[Traduit par la rédaction]

Introduction

Since the introduction of nalidixic acid **1** (1) into clinical practice in 1963, a large number of related analogs have been synthesized. Recently, several highly potent broad-spectrum antibacterial agents of this class have been made. All of them possess a 1-substituted-1,4-dihydro-4-oxo-pyridine-3-carboxylic acid moiety and a fluorine atom at the C-6 position and are collectively known as quinolones. These agents include norfloxacin **2** (2), temafloxacin **3** (3), ciprofloxacin **4** (4), lomefloxacin **5** (5), fleroxacin **6** (6), ofloxacin **7** (7), and tosufloxacin **8** (8). They have been shown to inhibit DNA gyrase (9, 10). Chirality in the quinolone molecule may have a great impact on the biological activity. The *S* enantiomer of ofloxacin **9** (11, 12) and *S*-25930 **10** (13) were recently reported to possess greater biological activities (10- to 100-fold) than their antipodes. The enantiomers of the 3-ethylaminomethylpyrrolidin-1-yl derivative **11**, however, were reported to have similar biological activity (14).

Recently, it has been shown that coadministration of enoxacin and theophylline to rats causes an increase of elimination half-life of theophylline, leading to an increase in its plasma concentration (15). This results in increased theophylline-related adverse reactions such as headache, nausea, and tachycardia. It is suggested that enoxacin competitively inhibits the binding of theophylline to cytochrome P-448 (15). The coplanarity between the C-7 piperazinyl group and the naphthyridine nucleus of enoxacin may be a possible explanation for this interaction. To avoid this undesirable interaction with theophylline, it is highly desirable to produce a potent quinoline with a bulky substituent on the piperazine of the C-7 substituent so that the coplanarity between the C-7 substituent and the quinolone nucleus can be avoided by steric interaction.

We have synthesized both enantiomers of temafloxacin. They were found to possess identical antibacterial activities (16), suggesting that there may be a large pocket at the enzymatic site that allows a substituent at both the α and β position of the C-3 of the piperazin-1-yl group. As a continuation of our search for a potent quinolone without interaction with theophylline, we synthesized a series of 1-substituted-6-fluoro-1-(3-*gem*-disubstituted-piperazin-1-yl)-1,4-dihydro-4-oxoquinoline-3-carboxylic acids (or naphthyridine analogs) **12** for biological evaluation. In addition to *gem*-dimethyl substitution, these derivatives also included a 3-spirocyclopropane ring since substitution at N-1 of the quinoline ring with cyclopropyl group has been shown to dramatically increase in in vitro potency (17).

Chemistry

The synthesis of the desired 1-substituted-6-fluoro-7-(3-*gem*-disubstituted-piperazin-1-yl)-1,4-dihydro-4-oxoquinoline-3-carboxylic acids and their corresponding naphthyridine derivatives **12** (*a–j*) (Tables 1–3) is outlined in Scheme 1. They were prepared by displacement of the 7-halo of the known ethyl 1-substituted 6,7,8-trifluoro-1,4-dihydro-4-oxoquinoline-3-carboxylate, ethyl 1-substituted-6,7-difluoro-1,4-dihydro-4-oxoquinoline-3-carboxylate, or ethyl 1-substituted-6-fluoro-7-chloro-1,4-dihydro-4-oxo-1,8-naphthyridine-3-carboxylate (**14**) with the appropriate 2-spiro-substituted piperazine (**13***a*,*b*) followed by acid hydrolysis. The *gem*-dimethyl derivatives were prepared by direct displacement of the 7-halo of the quinoline or naphthyridine-3-carboxylic acid derivatives (**16**) with 2,2-dimethylpiperazine (**13***c*).

The requisite 6,9-diazaspiro[4,5]decane (**13***a*) was prepared by the reaction sequence outlined in Scheme 2. Esterification of 1-amino-1-cyclopentanecarboxylic acid (**17**) with thionyl chloride in ethanol yielded the α amino acid ethyl ester hydrochloride (**18**). Condensation of **18** with carbobenzyloxyglycyl-*O*-succinimide in the presence of sodium bicarbonate gave the protected dipeptide (**19**). Removal of the protecting group by hydrogenolysis provided the free amino derivative, which cyclized to yield the diketopiper-

[1]A preliminary account of this work was presented at the 30th Interscience Conference on Antimicrobial Agents and Chemotherapy, October, 1990, Atlanta; Abstr. No. 394.

[2]Author to whom correspondence may be addressed.

Can. J. Chem. Downloaded from www.nrcresearchpress.com by 217.78.4.112 on 09/08/12
For personal use only.

azine derivative (**20**). Borane–THF reduction of **20** gave the desired 6,9-diazaspiro[4,5]decane (**13***a*).

The above synthetic methodology was not regioselective for the synthesis of the 4,7-diazaspiro[2,5]octane (**13***b*). The key intermediate (**23**) not only provided the desired diketopiperazine **24** but also gave a substantial amount of the homoketopiperazine by-product **25** as illustrated in Scheme 3. It could be reasonable that displacement of the ethoxy group by the free amino group in **23** provided **24**. However, because of the presence of the ester function attached to the cyclopropane ring, the free amino group could also attack the carbon atom on the cyclopropane, generating a ring-opened product. To avoid this undesired ring opening, the previous reaction sequence was reversed. The desired 4,7-diazaspiro[2,5]octane (**13***b*) was prepared by a route shown in Scheme 4.

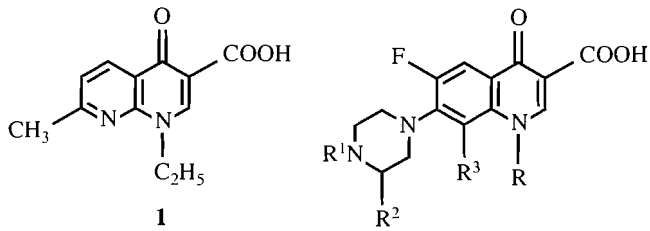

1

2 R = C_2H_5, $R^1 = R^2 = R^3 = H$

3 R = *o*,*p*-$C_6H_3F_2$, $R^1 = R^3 = H$, $R^2 = CH_3$

4 R = *c*-C_3H_5, $R^1 = R^2 = R^3 = H$

5 R = C_2H_5, $R^1 = H$, $R^2 = CH_3$, $R^3 = F$

6 R = C_2H_4F, $R^1 = CH_3$, $R^2 = H$, $R^3 = F$.

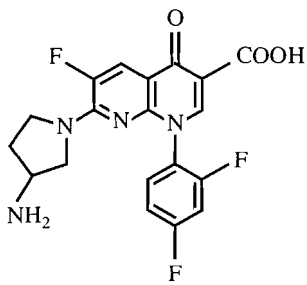

8

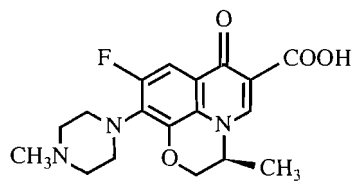

9

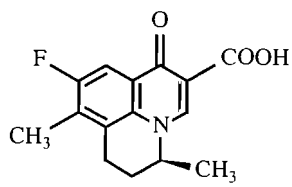

10

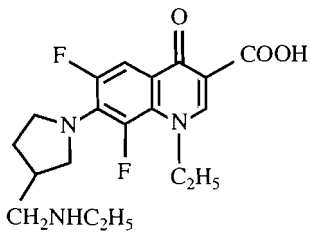

11

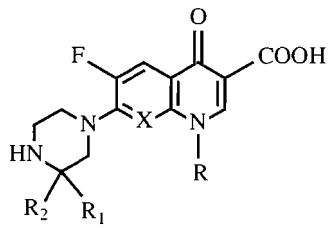

12

N-Protection of the 1-amino-1-cyclopropane carboxylic acid **21** with carbobenzyloxy-*O*-succinimide in the presence of sodium bicarbonate in THF gave the protected acid **26**. Activation of the carboxylic acid function of **26** with dicyclohexylcarbodiimide and *N*-hydroxyl-*O*-succinimide gave the *O*-succinimide derivative **27**. Treatment of **27** with ethyl glycine yielded the protected dipeptide **28**. Removal of the *N*-protecting group by hydrogenolysis yielded the free amino derivative **29**. Cyclization of **29** with DBU in refluxing toluene gave the desired diketopiperazine **24**. No ring opening by product was isolated. Borane–THF reduction of **24** provided the desired 4,7-diazaspiro[2,5]octane (**13***b*).

The 2,2-dimethylpiperazine (**13***c*) was prepared by the same reaction sequence as the preparation of 6,9-diazaspiro[4,5]decane (**13***a*) but using 2-amino-2-methylpropanoic acid instead of 1-amino-1-cyclopentanecarboxylic acid.

Results and discussion

Tables 4–6 summarize the in vitro antibacterial activity activity of the 7-*gem*-disubstituted piperazinyl quinolone derivatives (**12***a–j*) against ten Gram-positive bacteria (*Staphylococcus aureus* ATCC6538P, *Staphylococcus aureus* A5177, *Staphylococcus aureus* 642A, *Staphylococcus aureus* NCTC10649, *Staphylococcus aureus* CMX553, *Staphylococcus epidermidis* 3519, *Enterococcus faecium* ATCC 8043, *Streptococcus bovis* A5169, *Streptococcus agalactiae* CMX508, *Streptococcus pyogenes* EES61), and seven Gram-negative organisms (*Escherichia coli* Juhl, *Enterobacter aerogenes* ATCC13048, *Klebsiella pneumoniae* ATCC8045, *Pseudomonas aeruginosa* BMH10, *Pseudomonas aeruginosa* A5007, *Pseudomonas aeruginosa* K799/61, *Acinetobacter sp.* CMX669). The in vitro antibacterial activities are reported as minimum inhibitory concentration (MIC) in μg/mL determined by conventional agar dilution procedure. The data for ciprofloxacin (Cipro), a clinically useful antibacterial agent, are included for comparison.

The antibacterial activity for these compounds indicated that the 7-(4,7-diazaspiro[2,5]octan-7-yl)-quinolones and naphthyridines were more active than 7-(3,3-dimethylpiperazin-1-yl)-quinolones and naphthyridine derivatives, which were more active than 7-(6,9-diazaspiro[4,5]decan-9-

Can. J. Chem. Downloaded from www.nrcresearchpress.com by 217.78.4.112 on 09/08/12
For personal use only.

TABLE 1. Chemical structures for compound **12** (*a–d*)

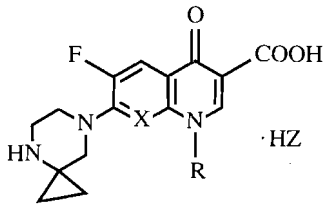

Compound	X	R	HZ
a	CH		HCl
b	CF		HCl
c	N		HCl
d	N	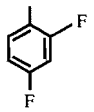	CF_3COOH

TABLE 2. Chemical structures for compound **12** (*e–g*)

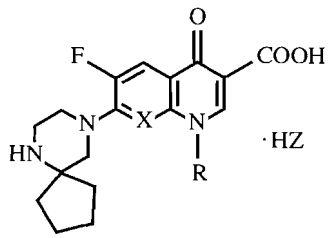

Compound	X	R	HZ
e	CH		HCl
f	CH	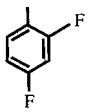	HCl
g	N	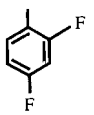	CF_3COOH

TABLE 3. Chemical structures for compound **12** (*h–j*)

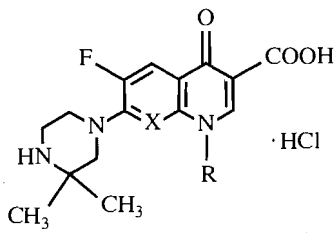

Compound	X	R
h	CH	
i	CH	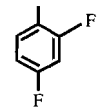
j	N	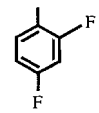

yl)-quinolones and naphthyridine derivatives. Although both enantiomers of temafloxacin were reported to possess identical antibacterial activity, the presence of two bulky substituents at C-3 of the piperazin-1-yl group reduced the antibacterial activity as did the 6,9-diazaspiro[4,5]decan-9-yl substituent. In general, the 1-substituted-6-fluoro-7-(4,7-diazaspiro[2,5]octan-7-yl)-1,4 - dihydro-4-oxoquinoline - 3-carboxylic acids and naphthyridine derivatives were more active against Gram-positive organisms than Gram-negative organisms. This is in contrast to traditional quinolones, which are more active against Gram-negative organisms. The 4,7-diazaspiro[2,5]octan-7-yl derivative **12***b* was the most active compound in this series and was found to be more active than ciprofloxacin against Gram-positive bacteria and slightly less active against Gram-negative bacteria.

To determine in vivo efficacy, several of these compounds were evaluated in mouse protection tests. Ciprofloxacin (Cipro) was used as a standard. The compounds were administered either orally (po) or subcutaneously (sc) with a specific amount of the test compound divided equally, to be administered 1 and 5 h after the injection. The potency is given in ED_{50} values, which are expressed as a total dose of the compound in mg/kg required to protect 50% of mice challenged intraperitoneally with the organism indicated. The results against *Staphylococcus aureus* and *E. coli* systemic infections are shown in Table 7. With the exception of **12***b*, all the compounds tested were inferior to ciprofloxacin. **12***b* possessed potency similar to ciprofloxacin against *S. aureus* infection in the mouse protection test.

In summary, we have synthesized a series of *gem*-disubstituted piperazin-1-yl quinolone derivatives with good antibacterial activity. However, they were found to be somewhat inferior to ciprofloxacin, which is currently used clinically as a broad spectrum antibacterial agent. This new series provided better anti-Gram-positive activity than anti-Gram-negative activity, an observation contrary to classical quinolone SAR.

Experimental

Unless otherwise noted, materials were obtained from commercial suppliers and used without further purification. Melting points were taken in a Thomas–Hoover capillary apparatus and were uncorrected. NMR spectra were determined on a General Electric GN-300 spectrometer operating at 300.1 MHz. Chemical shifts are expressed in ppm downfield from internal tetramethylsilane. Significant ^1H NMR data are tabulated in the order: multiplicity (s, singlet; d, doublet; t, triplet; q, quartet; m, multiplet; dd, double doublet; b, broad), coupling constants(s), number of protons, and designation. The IR spectra were recorded on a Perkin–Elmer model 710A infrared spectrometer. Mass spectra were obtained with a Hewlett–Packard 5985A mass spectrometer or a Kratos MS-50 instrument with EI source (70 eV). The IR, NMR, and mass spectral data of all compounds were consistent with the assigned structures. Solutions were dried over magnesium sulfate. E. Merck silica

Can. J. Chem. Downloaded from www.nrcresearchpress.com by 217.78.4.112 on 09/08/12
For personal use only.

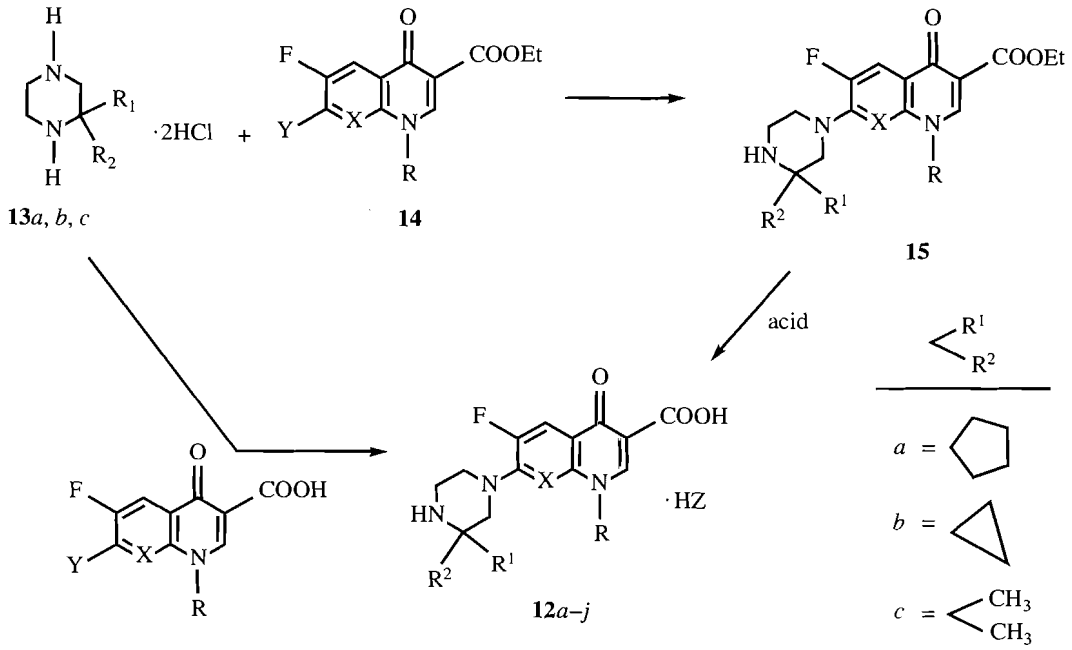

SCHEME 1

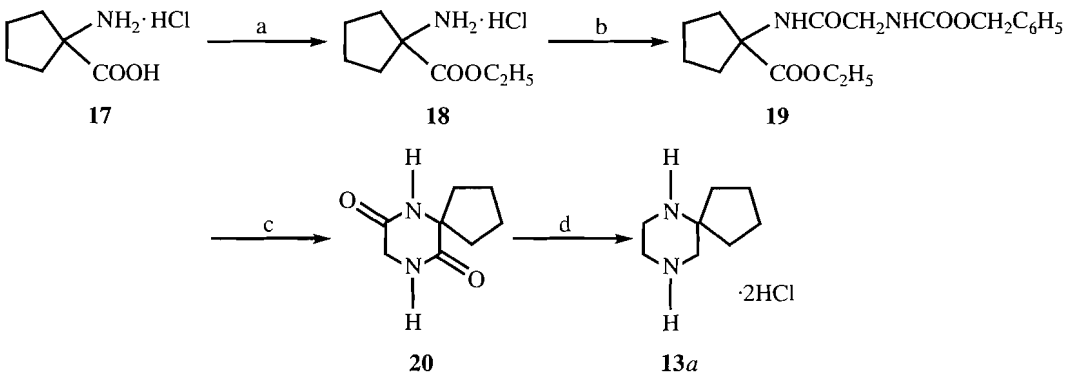

(a) $C_2H_5OH/SOCl_2$; (b) Cbz-glycyl-*O*-succinimide/$NaHCO_3$; (c) H_2; 10%Pd/C; (d) borane–THF/HCl

SCHEME 2

gel (230–400 mesh) obtained from VWR Scientific was used for column chromatography, and yields of the reactions were not optimized. Elemental analyses were performed by the Abbott analytical department and IR, NMR, and mass spectra were recorded by the Abbott structural chemistry department.

In vitro antibacterial activity

The in vitro antibacterial activity of the test compounds was tested in a side-by-side comparison with temafloxacin and determined by conventional agar dilution procedures. The organisms were grown overnight in brain–heart infusion (BHI) broth (Difco 0037-01-6) at 36°C. Twofold dilutions of the stock solution (2000 μg/mL) of the test compound were made in BHI agar to obtain test concentrations ranging from 200 to 0.005 μg/mL. They were then incubated at 36°C for 18 h. The minimal inhibitory concentration (MIC) was the lowest concentration of the test compund that yielded no visible growth on the plate.

In vivo antibacterial activity

The in vivo antibacterial activity of the test compounds was determined in CF-1 female mice weighing approximately 20 g. Aqueous solutions of the test compounds were made by dissolving the hydrochloride salt in distilled water and diluting it with distilled water to the desired volume. The median lethal dose of the test organisms was determined as follows.

After 18 h of incubation, the cultures of test organism in BHI broth were serially diluted by using 10-fold dilutions in 5% (w/v) hog gastric mucin. Cultures (0.5 mL), dilution from 10^{-1} to 10^{-8}, were injected intraperitoneally into mice. The LD_{50} for the test organism was calculated from cumulative mortalities on the sixth day by using the Reed and Muench procedure (18).

After 18 h, cultures of the above were diluted in 5% (w/v) hog gastric mucin to obtain 100 times the LD_{50}, and 0.5 mL was injected intraperitoneally into mice. The mice were treated subcutaneously (sc) or orally (po) with a specific amount of the test compound divided equally to be administered 1 and 5 h after injection. A group of 10 animals each for at least three dose levels was thus treated, and the deaths were recorded daily for 6 days. Ten mice were left untreated as infection control. ED_{50} values were calculated from the cumulative mortalities on the sixth day after infection by using the trimmed version of the logit method (19).

1-Amino-1-ethoxycarbonylcyclopentane hydrochloride (18)

To a stirred mixture of 1-amino-1-cyclopentanecarboxylic acid (50 g, 387 mmol) in absolute ethanol (600 mL) at 0°C was added,

Can. J. Chem. Downloaded from www.nrcresearchpress.com by 217.78.4.112 on 09/08/12
For personal use only.

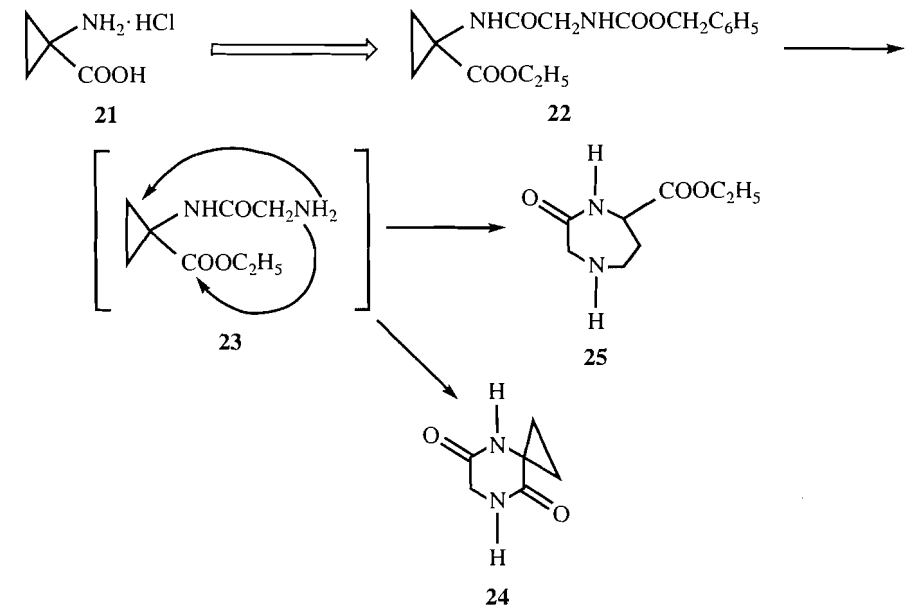

SCHEME 3

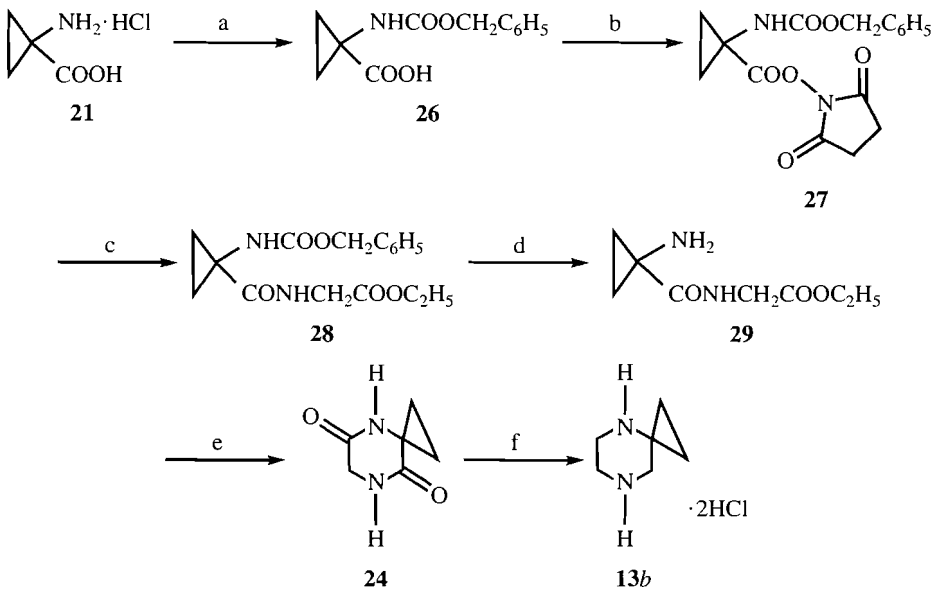

(a) Cbz-*O*-succinimide/$NaHCO_3$; THF; (b) *N*-hydroxysuccinimide/DCC; THF; (c) ethyl glycine hydrochloride/$NaHCO_3$; THF–H_2O; (d) H_2; 10%Pd/C; EtOAc; (e) DBU/toluene, heat; (f) borane–THF/HCl

SCHEME 4

dropwise, thionyl chloride (85 mL, 1.16 mol). The ice bath was removed, and the mixture was heated at reflux for 4 h and concentrated *in vacuo* to give a white solid, which was crystallized from ether–ethanol yielding **18** (62.4 g, 83%), mp 232°C. IR (KBr): 1740 (CO) cm^{-1}. ^1H NMR (DMSO-d_6) δ: 1.24 (t, J = 7 Hz, 3H, ethyl CH_3), 1.72 (m, 2H, CH_2), 1.88 (m, 2H, CH_2), 1.97 (m, 2H, CH_2), 2.10 (m, 2H, CH_2), 4.21 (q, J = 7 Hz, 2H, ethyl CH_2), 8.80 (bs, 3H, NH_3Cl). Anal. calcd. for $C_8H_{16}ClNO_2$: C 49.61, H 8.33, N 7.23; found: C 49.75, H 8.49, N 7.22.

By use of this procedure, 2-amino-2-methylpropanoic acid gave ethyl 2-amino-2-methylpropanoate hydrochloride in 97% yield, mp 159°C. IR (KBr): 1742 (CO) cm^{-1}. ^1H NMR (DMSO-d_6) δ: 1.24 (t, J = 7 Hz, 3H, ethyl CH_3), 1.47 (s, 6H, CH_3×2), 4.21 (q, J = 7 Hz, 2H, ethyl CH_2), 8.70 (bs, 3H, $NH_2 \cdot HCl$). Anal. calcd. for $C_6H_{14}ClNO_2$: C 42.99, H 8.36, N 8.36; found: C 42.92, H 8.61, N 8.31.

1-N-Carbobenzyloxyglycylamino-1-ethoxycarbonyylcyclopentane (19)

A solution of carbobenzyloxyglycine succinimido ester (19.4 g, 63 mmol) in THF (150 mL) was added dropwise to a solution of 1-amino-1-ethoxycarbonylcyclopentane hydrochloride (**18**) (11.6 h, 60 mmol) and sodium bicarbonate (15.1 g, 180 mmol) in water (200 mL) at 0°C. After the addition, the reaction was allowed to warm up to room temperature and was stirred for 16 h. The solvent was removed under reduced pressure and the residue was taken up in methylene chloride (350 mL) and washed twice with water. The organic portion was separated and dried. Removal of the solvent yielded 17.6 g (88%) of **19**, mp 99°C. IR

Can. J. Chem. Downloaded from www.nrcresearchpress.com by 217.78.4.112 on 09/08/12
For personal use only.

TABLE 4. In vitro activity of quinolones **12** (*a–d*)

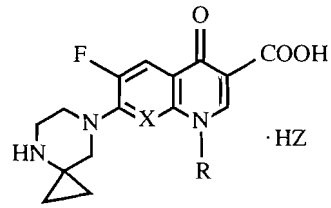

Organism	MIC (μg/mL)				
	a	*b*	*c*	*d*	Cipro
Staph. aureus ATCC6538P	0.2	0.1	0.39	0.39	0.2
Staph. aureus A5177	0.39	0.2	0.78	0.78	0.39
Staph. aureus 642A	0.39	0.2	0.78	0.78	0.39
Staph. aureus NCTC10649	0.12	0.1	0.78	0.39	0.39
Staph. aureus CMX553	0.78	0.2	0.78	0.78	0.78
Staph. epidermidis 3519	0.39	0.2	0.78	0.78	0.39
Enter. faecium ATCC 8043	1.56	0.78	0.2	3.1	0.39
Strep. bovis A5169	6.2	3.1	2.5	6.2	1.56
Strep. agalactiae CMX508	1.56	0.78	3.1	3.1	0.78
Strep. pyogenes EES61	0.78	1.56	3.1	3.1	0.78
Escherichia coli Juhl	0.1	0.05	0.2	3.1	0.01
Enter. aerogenes ATCC13048	0.2	0.1	0.2	6.2	0.05
Kleb. pneumoniae ATCC8045	0.05	0.02	0.05	1.56	0.02
Pseudo. aeruginosa BMH10	1.56	0.78	3.1	25	0.1
Pseudo. aeruginosa A5007	1.56	1.56	3.1	50	0.1
Pseudo. aeruginosa K799/61	0.2	0.1	0.2	3.1	0.02
Acinetobacter sp. CMX669	0.39	0.1	0.39	3.1	0.39

TABLE 5. In vitro activity of quinolones **12** (*e–g*)

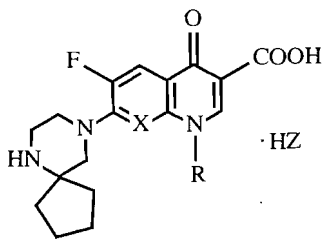

Organism	MIC (μg/mL)			
	e	*f*	*g*	Cipro
Staph. aureus ATCC6538P	0.39	0.39	0.39	0.2
Staph. aureus A5177	0.78	0.78	0.39	0.39
Staph. aureus 642A	0.78	0.78	0.39	0.39
Staph. aureus NCTC10649	0.39	0.39	0.39	0.39
Staph. aureus CMX553	1.56	0.78	0.78	0.78
Staph. epidermidis 3519	0.39	0.78	0.39	0.39
Enter. faecium ATCC8043	3.1	0.78	3.1	0.39
Strep. bovis A5169	6.2	3.1	12.5	1.56
Strep. agalactiae CMX508	1.56	12.5	3.1	0.78
Strep. pyogenes EES61	1.56	3.1	3.1	0.78
Escherichia coli Juhl	0.78	3.1	0.78	0.01
Enter. aerogenes ATCC13048	1.56	3.1	1.56	0.05
Kleb. pneumoniae ATCC8045	0.78	1.56	0.39	0.02
Pseudo. aeruginosa BMH10	6.2	25	12.5	0.1
Pseudo. aeruginosa A5007	12.5	25	12.5	0.1
Pseudo. aeruginosa K799/61	1.56	3.1	0.78	0.02
Acinetobacter sp. CMX669	3.1	3.1	1.59	0.39

Can. J. Chem. Downloaded from www.nrcresearchpress.com by 217.78.4.112 on 09/08/12
For personal use only.

TABLE 6. In vitro activity of quinolones **12** (*h–j*)

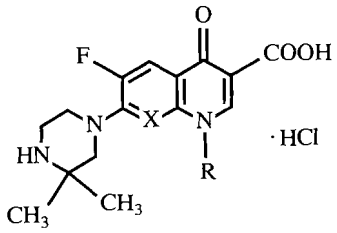

Organism	MIC (μg/mL)			
	h	*i*	*j*	Cipro
Staph. aureus ATCC6538P	0.39	0.2	0.39	0.2
Staph. aureus A5177	0.78	0.39	0.78	0.39
Staph. aureus 642A	0.78	0.39	0.78	0.39
Staph. aureus NCTC10639	0.39	0.2	0.39	0.39
Staph. aureus CMX553	1.56	0.78	0.78	0.78
Staph. epidermidis 3519	0.78	0.78	0.78	0.39
Enter. faecium ATCC8043	1.56	1.56	3.1	0.39
Strep. bovis A5169	6.2	6.2	6.2	1.56
Strep. agalactiae CMX508	1.56	1.56	3.1	0.78
Strep. pyogenes EES61	1.56	1.56	1.56	0.78
Escherichia coli Juhl	0.2	0.78	0.78	0.01
Enter. aerogenes ATCC13048	0.39	0.78	0.78	0.05
Kleb. pneumoniae ATCC8045	0.2	0.39	0.39	0.02
Pseudo. aeruginosa BMH10	1.56	3.1	6.2	0.1
Pseudo. aeruginosa A5007	3.1	6.2	6.2	0.1
Pseudo. aeruginosa K799/61	0.39	0.39	0.78	0.02
Acinetobacter sp. CMX669	1.56	0.78	1.56	0.39

TABLE 7. Mouse protection test of selected quinolones

Test organism (Dose)	Compound	Route	ED_{50} (95% confidence limits) mg/kg
S. aureus NCTC10649 (100 × LD_{50})	**12***b*	SC	6.2 (3.7–10.3)
		PO	13.1 (9.7–17.6)
	12*c*	SC	80.7 (8.6–760.5)
		PO	>100
	12*g*	SC	16.2 (10.1–25.3)
		PO	24.0 (15.2–38.0)
	Cipro	SC	1.6 (1.0–3.5)
		PO	15.5 (9.9–24.1)
E. coli Juhl (100 × LD_{50})	**12***b*	SC	2.0 (1.3–3.2)
		PO	5.0 (3.2–7.9)
	12*c*	SC	8.0 (5.1–12.7)
		PO	19.7 (8.5–45.9)

($CDCl_3$): 1682, 1727 (CO) cm^{-1}. ^1H NMR ($CDCl_3$) δ: 1.23 (t, J = 7 Hz, 3H, ethyl CH_3), 1.76 (m, 4H, CH_2×2), 1.95 (m, 2H, CH_2), 2.21 (m, 2H, CH_2), 3.86 (d, J = 5 Hz, 2H, NCH_2), 4.13 (q, J = 7 Hz, 2H, ethyl CH_2), 5.13 (s, 2H, OCH_2), 5.49 (bs, 1H, NH), 6.54 (bs, 1H, NH), 7.34 (m, 5H, aromatic H). Anal. calcd. for $C_{18}H_{24}N_2O_5$: C 62.05, H 6.94, N 8.04; found: C 62.04, H 7.05, N 8.12.

By use of this procedure, reacting ethyl 2-amino-2-methylpropionate hydrochloride instead of 1-amino-1-ethoxycarbonyl-cyclopentane hydrochloride (**18**) with carbobenzyloxyglycine succinimido ester, ethyl 2-*N*-carbobenzyloxyglycylamino-2-methylpropionate was obtained in 89% yield, mp 85°C. IR ($CDCl_3$): 1682, 1727 (CO) cm^{-1}. ^1H NMR ($CDCl_3$) δ: 1.27 (t, J = 7 Hz, 3H, ethyl CH_3), 1.56 (s, 6H, CH_3×2), 3.85 (d, J = 6Hz, 2H, CH_2), 4.20 (q, J = 7 Hz, 2H, ethyl CH_2), 5.14 (s, 2H, benzyl CH_2), 5.37 (bs, 1H, NH), 6.54 (bs, 1H, NH), 7.36 (m, 5H, aromatic H). Anal. calcd. for $C_{16}H_{22}N_2O_5$: C 59.63, H 6.83, N 8.70; found: C 59.72, H 6.92, N 8.67.

By use of the above procedure, ethyl 1-amino-1-cyclopropanecarboxylate (20) yielded ethyl 1-*N*-carbobenzyloxyglycylamino-1-cyclopropanecarboxylate (**22**) in 86% yield, mp 90–91°C. IR ($CDCl_3$): 1700, 1730 (CO) cm^{-1}. ^1H NMR ($CDCl_3$) δ: 1.14 (m, 2H, CH_2), 1.21 (t, J = 7 Hz, 3H, ethyl CH_3), 1.56 (m, 2H, CH_2), 3.87 (d, J = 6 Hz, 2H, NCH_2), 4.11 (q, J = 7 Hz, 2H, ethyl CH_2), 5.12

Can. J. Chem. Downloaded from www.nrcresearchpress.com by 217.78.4.112 on 09/08/12
For personal use only.

Can. J. Chem. Downloaded from www.nrcresearchpress.com by 217.78.4.112 on 09/08/12
For personal use only.

(s, 2H, OCH_2), 5.58 (bs, 1H, NH), 6.73 (bs, 1H, NH), 7.34 (m, 5H, aromatic H). Anal. calcd. for $C_{16}H_{20}N_2O_5$: C 59.99, H 6.29, N 8.75; found: C 60.06, H 6.28, N 8.74.

*6,9-Diaza-7,10-dioxospiro[4,5]decane (**20**)*

A solution of **19** (17.6 g, 53 mmol) in ethanol (250 mL) was hydrogenated at 4 atmospheres (1 atm = 101.3 kPa) of hydrogen with 10% palladium on carbon for 18 h. The solution was then filtered and the residue was washed with ethanol. The combined solution was filtered through a 0.45 μm Nylon filter to remove the residual catalyst. Concentration of the filtrate to dryness yielded a solid, which was crystallized in acetonitrile yielding 6.35 g (71.4%) of **20**, mp >255°C. IR (KBr): 1675 (CO) cm^{-1}. ^1H NMR (DMSO-d_6) δ: 1.66 (m, 6H, $CH_3\times2$), 2.06 (m, 2H, CH_2), 3.74 (d, J = 3 Hz, 2H, NCH_2), 7.93 (bs, 1H, NH), 8.35 (bs, 1H, NH). Anal. calcd. for $C_8H_{12}N_2O_2$: C 57.13, H 7.19, N 16.66; found C 57.33, H 7.36, H 16.78.

Using similar reaction conditions as above, ethyl 2-*N*-carbobenzyloxyglycylamino-2-methylpropionate produced 2,2-dimethyl-3,6-dioxopiperazine in 98% yield, mp 258–261°C. IR (KBr): 1680 (CO) cm^{-1}. ^1H NMR (DMSO-d_6) δ: 1.29 (s, 6H, $CH_3\times2$), 3.78 (d, J = 2.5 Hz, 2H, CH_2), 7.91 (bs, 1H, NH), 8.23 (bs, 1H, NH). Anal. calcd. for $C_6H_{10}N_2O_2$: C 50.70, H 7.04, N 19.72; found: C 50.55, H 7.14, N 19.79.

*2,2-Dimethylpiperazine dihydrochloride (**13**c)*

2,2-Dimethyl-3,6-dioxopiperazine (15 g, 106 mmol), was suspended in THF (650 mL). A 433 mL sample of 1 M borane–tetrahydrofuran complex (433 mmol) was then added dropwise to the above stirring suspension over 1 h. Gas evolution occurred and the mixture became nearly homogeneous at the end of the addition. The mixture was heated at 60°C for 20 h. It was cooled to room temperature and 200 mL of methanol was added over a 1 h period. Gas evolution occurred and the reaction mixture was concentrated to dryness. The residue was redissolved in methanol (150 mL), excess methanolic HCl solution (500 mL) was added, and the solution was refluxed for 2 h. It was cooled and allowed to stand at room temperature overnight. The reaction was evaporated to dryness. The mixture and added acetonitrile were boiled with stirring for 0.5 h, then cooled, and the acetonitrile was decanted off. The residue was dissolved in a small amount of hot methanol. Upon cooling, crystals appeared. After addition of ether, they were filtered inside a dry-box and the residue was dried under vacuum yielding 16.5 g (84%) 2,2-dimethylpiperazine dihydrochloride (**13***c*). This solid was very hygroscopic. Upon exposure to air, it turned watery within several seconds. The IR spectrum showed no carbonyl absorption signal. ^1H NMR (D_2O) δ: 1.54 (s, 6H, $CH_3\times2$), 3.42 (s, 2H, CH_2), 3.52 (m, 2H, CH_2), 3.60 (m, 2H, CH_2). Exact Mass calcd. for $C_6H_{15}N_2$: 115.1235; measured: 115.1235.

By use of this procedure, borane–THF reduction of 6,9-diaza-7,10-dioxospiro[4,5]decane (**20**) yielded 6,9-diazaspiro[4,5]decane dihydrochloride (**13***a*) in 99% yield. This compound behaved as **13***c* and was very hygroscopic. The IR spectrum showed no carbonyl absorption signal. ^1H NMR (DMSO-d_6) δ: 1.62 (m, 2H, CH_2), 1.75 (m, 2H, CH_2), 1.90 (m, 2H, CH_2), 1.99 (m, 2H, CH_2), 3.28 (bs, 4H, $NCH_2\times2$), 3.48 (m, 2H, NCH_2), 9.98 (bs, 2H, $NH\times2$). Exact Mass calcd. for $C_8H_{17}N_2$: 141.1392; measured: 141.1392.

By use of the above procedure, borane–THF reduction of 4,7-diaza-5,8-dioxospiro[2,5]octane (**24**) yielded 4,7-diazaspiro[2,5]-octane dihydrochloride (**13***b*) in 98% yield. This compound was very hygroscopic. The IR spectrum showed no absorption signal for carbonyl group. ^1H NMR (DMSO-d_6) δ: 0.99 (m, 2H, CH_2), 1.21 (m, 2H, CH_2), 3.48 (m, 6H, $NCH_2\times3$), 9.85 (bs, 2H, NH_2Cl), 10.29 (bs, 2H, NH_2Cl). Exact Mass calcd. for $C_{16}H_{13}N_2$: 113.1079; measured: 113.1079.

Hydrogenolysis of 22

A solution of **22** (18.5 g, 58 mmol) in ethanol (250 mL) was hydrogenated at 4 atmospheres of hydrogen with 10% palladium on carbon for 18 h. The solution was then filtered and the residue was washed with ethanol. The combined solution was filtered through a 0.45 μm Nylon filter to remove the residual catalyst. Concentration of the filtrate to dryness yielded a residue, which was suspended in acetonitrile and boiled for 10 min. It was cooled and filtered, yielding 3.17 g of two products in about 1:1 ratio by TLC. ^1H NMR showed the presence of two compounds; one corresponding to **24** that had an identical spectrum to an authentic samples prepared by another route. The remaining signals in this spectrum indicated the presence of **25**. Repeated purification through several chromatographies yielded a small amount of **25** for ^1H NMR analysis. ^1H NMR ($CDCl_3$) δ: 1.22 (m, 5H, CH_2 and ethyl CH_3), 1.58 (m, 2H, NCH_2), 1.89 (bs, 1H, NH), 3.32 (bs, 2H, NCH_2CO), 3.72 (m, 1H, NCH), 4.14 (q, J = 7 Hz, 2H, ethyl CH_2), 7.70 (bs, 1H, CONH). The mass spectrum showed a m/z (M + 1) at 187 consistent with the structure assigned.

*1-N-Carbobenzyloxyamino-1-cyclopropanecarbonylic acid (**26**)*

A solution of *N*-benzyloxycarbonyloxy succinimide (60.7 g, 24 mmol) in THF (300 mL) was added to a solution of 1-amino-1-cyclopropanecarboxylic acid hydrochloride (24.5 g, 17.8 mmol) in water (45 mL). At ice temperature, a solution of sodium bicarbonate (82 g, 96 mmol) in water (500 mL) was poured into the mixture. After the addition, the reaction was allowed to warm up to room temperature and was stirred for 16 h. The solvent was removed under reduced pressure. The residue was suspended in 200 mL of methylene chloride and extracted with water (500 mL). The water solution was acidified with acetic acid and the precipitate was filtered yielding **26** (18 g, 43%), mp 157°C. IR (KBr): 1690, 1710 (CO) cm^{-1}. ^1H NMR (DMSO-d_6) δ: 1.01 (m, 2H, CH_2), 1.31 (m, 2H, CH_2), 5.02 (s, 2H, OCH_2), 7.34 (m, 5H, aromatic H), 7.88 (s, 1H, NH), 12.42 (bs, 1H, OH). Anal. calcd. for $C_{12}H_{13}NO_4$: C 61.27, H 5.51, N 5.95; found: C 61.33, H 5.60, N 5.96.

*Preparation of active ester (**27**)*

Dicyclohexylcarbodiimide (7.74 g, 37.6 mmol) in THF (15 mL) was added dropwise to a mixture of **26** (8.83 g, 37.5 mmol) and *N*-hydroxysuccinimide (4.53 g, 39.4 mmol) in THF (60 mL). The mixture was allowed to stir at room temperature for 18 h. The precipitate was removed by filtration. The filtrate was concentrated to a residue, which was dissolved in ethyl acetate (300 mL). The organic solvent was washed with sodium bicarbonate solution. The organic layer was dried and concentrated to yield **27** (9.87 g, 79.2%), mp 119–120°C. IR (KBr): 1745, 1785, 1810 cm^{-1}. ^1H NMR ($CDCl_3$) δ: 1.46 (bs, 2H, CH_2), 1.86 (bs, 2H, CH_2), 5.15 (bs, 2H, OCH_2), 5.47 (bd, 1H, NH), 7.35 (m, 5H, aromatic H). Anal. calcd. for $C_{16}H_{16}N_2O_6$: C 57.83, H 4.85, N 8.43; found: C 57.84, H 4.88, N 8.38.

*Preparation of dipeptide (**28**)*

The active ester (**27**) (2 g, 6 mmol) in THF (15 mL) was added to a chilled solution of glycine ethyl ester hydrochloride (0.8 g, 5.1 mmol) in water (5 mL). Sodium bicarbonate solution (1.4 g in 20 mL of water) was then added to the reaction mixture. After the addition, the reaction was allowed to warm up to room temperature and was stirred for 18 h. The solvent was removed under reduced pressure and the residue was washed with water and extracted with methylene chloride. The organic layer was dried and concentrated to a solid under reduced pressure, yielding a solid **28** (1.88 g, 97.5%), mp 97–98°C. IR (KBr): 1675, 1740 (CO) cm^{-1}. ^1H NMR ($CDCl_3$) δ: 1.07 (bs, 2H, CH_2), 1.27 (q, J = 7 Hz, 3H, ethyl CH_3), 1.59 (m, 2H, CH_2), 3.99 (d, J = 5 Hz, 2H, NCH_2), 4.19 (q, J = 7 Hz, 2H, ethyl CH_2), 5.43 (s, 2H, OCH_2), 5.58 (s, 1H, NH), 6.98 (bs, 1H, NH), 7.34 (s, 5H, aromatic H). Anal. calcd. for $C_{16}H_{20}N_2O_5$: C 59.99, H 6.29, N 8.74; found: C 60.06, H 6.27, N 8.74.

*4,7-Diaza-5,8-dioxospiro[2,5]octane (**24**)*

A solution of the dipeptide (**28**) (8.63 g, 27 mmol) in ethyl acetate (250 mL) was hydrogenated under a hydrogen atmosphere at 4 atmospheres pressure with 10% palladium on carbon for 18 h. The

Can. J. Chem. Downloaded from www.nrcresearchpress.com by 217.78.4.112 on 09/08/12
For personal use only.

solution was filtered and the filtrate was concentrated under reduced pressure to a residue, **29**. ^{1}H NMR (DMSO-d_6) δ: 0.77 (dd, J = 4.5 Hz, 2H, CH_2), 1.05 (dd, J = 4.5 Hz, 2H, CH_2), 1.19 (t, J = 7 Hz, 3H, ethyl CH_3), 2.31 (bs, 2H, NH×2), 3.84 (d, J = 6.5 Hz, 2H, NCH_2), 4.09 (q, J = 7 Hz, 2H, ethyl CH_2), 8.43 (t, J = 6.5 Hz, 1H, CONH). The residual liquid **29** was dissolved in toluene (200 mL). To this solution was added DBU (2 mL). After heating at 115°C for 22 h, the mixture was cooled to room temperature to yield **24** (3.2 g, 89%), mp >260°C. IR (KBr): 1685, 1695 (CO) cm^{-1}. ^{1}H NMR (DMSO-d_6) δ: 0.94 (dd, J = 4.5 Hz, 2H, CH_2), 1.16 (dd, J = 4.5 Hz, 2H, CH_2), 3.85 (d, J = 2.5 Hz, 2H, NCH_2), 8.02 (bs, 1H, NH), 8.27 (bs, 1H, NH). Anal. calcd. for $C_6H_8N_2O_2$: C 51.42, H 5.75, N 20.00; found: C 51.10, H 5.66, N 19.80.

*1-Cyclopropyl-6-fluoro-7-(3,3-dimethylpiperazin-1-yl)-1,4-dihydro-4-oxoquinoline-3-carboxylic acid hydrochloride (**12**h)*

2,2-Dimethylpiperazine dihydrochloride (**13***c*) (423 mg, 2.3 mmol) was added to a mixture of 1-cyclopropyl-6,7-difluoro-1,4-dihydro-4-oxoquinoline-3-carboxylic acid (21) (500 mg, 1.9 mmol) and triethylamine (10 mL) in *N*-methyl pyrrolidinone (20 mL). The reaction mixture was heated at 50°C for 18 h. The reaction was cooled to room temperature and concentrated under reduced pressure to dryness. Ethanol was added and digested under reflux for 30 min. The mixture was cooled and filtered, yielding **12***h* (525 mg, 70%), mp >260°C. IR (KBr): 1730 (CO) cm^{-1}. ^{1}H NMR (D_2O) δ: 1.22 (m, 2H, CH_2), 1.44 (m, 2H, CH_2), 1.58 (s, 6H, CH_3×2), 3.43 (s, 2H, NCH_2), 3.58 (m, 4H, NCH_2×2), 3.73 (m, 1H, CH), 7.52 (d, J_{H-F} = 6.5 Hz, 1H, C8-H), 7.54 (d, J_{H-F} = 13 Hz, 1H, C5-H), 8.67 (s, 1H, C2-H). Anal. calcd. for $C_{19}H_{23}ClFN_3O_3$: C 57.65, H 5.82, N 10.62; found: C 57.73, H 6.02, N 10.42.

By use of this procedure, 1-(2,4-difluorophenyl)-6-fluoro-7-(3,3-dimethylpiperazin-1-yl)-1,4-dihydro-4-oxoquinoline-3-carboxylic acid hydrochloride **12***i* was prepared by reaction of **13***c* with 1-(2,4-difluorophenyl)-6,7-difluoro-1,4-dihydro-4-oxoquinoline-3-carboxylic acid (16) in 77% yield, mp >260°C. IR (KBr): 1730 (CO) cm^{-1}. ^{1}H NMR (D_2O) δ: 1.48 (s, 6H, CH_3×2), 3.25 (s, 2H, NCH_2), 3.36 (m, 2H, NCH_2), 3.42 (m, 2H, NCH_2), 6.47 (d, J_{H-F} = 6 Hz, 1H, C8-H), 7.37 (m, 2H, aromatic H), 7.72 (m, 1H, aromatic H), 7.92 (d, J_{H-F} = 12 Hz, 1H, C5-H), 8.82 (s, 1H, C2-H). Anal. calcd. for $C_{22}H_{21}ClF_3N_3O_3 \cdot 1/4\ H_2O$: C 55.93, H 4.56, N 8.90; found: C 55.85, H 4.68, N 8.90.

By use of this procedure, 1-(2,4-difluorophenyl)-6-fluoro-7-(3,3-dimethylpiperazin-1-yl)-1,4-dihydro-4-oxo[1,8]naphthyridine-3-carboxylic acid hydrochloride (**12***j*) was prepared by reaction of **13***c* with 1-(2,4-difluorophenyl)-6-fluoro-7-chloro-1,4-dihydro-4-oxo[1,8]-naphthyridine-3-carboxylic acid (22) in 94% yield, mp >260°C. IR (KBr): 1730 (CP) cm^{-1}. ^{1}H NMR (CF_3COOH) δ: 1.43 (s, 3H, CH_3), 1.47 (s, 3H, CH_3), 3.56 (m, 2H, NCH_2), 4.03 (bs, 2H, NCH_2), 4.26 (m, 2H, NCH_2), 7.28 (m, 2H, aromatic H), 7.75 (m, 1H, aromatic H), 8.33 (d, J_{H-F} = 13 Hz, 1H, C5-H), 9.26 (s, 1H, C2-H). Anal. calcd. for $C_{21}H_{20}ClF_3N_4O_3$: C 53.79, H 4.27, N 11.95; found: C 53.58, H 4.28, N 11.73.

*Ethyl 1-cyclopropyl-6-fluoro-7-(4,7-diazaspiro[2,5]octan-7-yl)-1,4-dihydro-4-oxoquinoline-3-carboxylate (**15**a)*

4,7-Diazaspiro[2,5]octane dihydrochloride (**13***b*) (1.5 g, 8 mmol) was added to a solution of ethyl 1-cyclopropyl-6,7-difluoro-1,4-dihydro-4-oxoquinoline-3-carboxylate (**14***a*) (750 mg, 2.6 mmol) in 1-methyl-2-pyrrolidione (30 mL) at 75°C. 1,8-Diazabicyclo[5.4.0]undec-7-ene (DBU) (1.2 g, 10.2 mmol) was then added to the reaction mixture. The mixture was heated at 100°C for 16 h. The solvent was removed by vacuum distillation. Column chromatography of the residue on silica gel using 5% methanol in methylene chloride as eluent yielded **15***a* (0.4 g, 40%), mp 223–225°C. IR ($CDCl_3$): 1680, 1720 (CO) cm^{-1}. ^{1}H NMR ($CDCl_3$) δ: 0.68 (m, 2H, CH_2), 0.72 (m, 2H, CH_2), 1.14 (m, 2H, CH_2), 1.21 (m, 2H, CH_2), 1.49 (t, J = 7 Hz, 3H, ethyl CH_3), 3.10 (s, 2H, NCH_2), 3.21 (m, 4H, NCH_2×2), 3.43 (m, 1H, CH), 4.48 (q, J = 7 Hz, 2H, ethyl CH_2), 7.22 (d, J_{H-F} = 7 Hz, 1H, C8-H), 8.04 (d, J_{H-F} = 13 Hz, 1H, C5-H), 8.53 (s, 1H, C2-H). Anal. calcd. for $C_{21}H_{24}FN_3O_3 \cdot 1/2\ H_2O$: C 63.94, H 6.39, N 10.65; found: C 64.09, H 6.23, N 11.04.

By use of this procedure, reaction of **13***b* with ethyl 1-cyclopropyl-6,7,8-trifluoro-1,4-dihydro-4-oxoquinoline-3-carboxylate (**14***b*) gave ethyl 1-cyclopropyl-6,8-difluoro-7-(4,7-diazaspiro[2,5]octan-7-yl)-1,4-dihydro-4-oxoquinoline-3-carboxylate (**15***b*) in 42% yield. IR ($CDCl_3$): 1685, 1725 (CO) cm^{-1}. ^{1}H NMR ($CDCl_3$) δ: 0.62 (m, 2H, CH_2), 0.69 (m, 2H, CH_2), 1.09 (m, 2H, CH_2), 1.23 (m, 2H, CH_2), 1.40 (t, J = 7 Hz, 3H, ethyl CH_3), 3.11 (m, 2H, NCH_2), 3.16 (s, 2H, NCH_2), 3.33 (m, 2H, NCH_2), 3.87 (m, 1H, CH), 4.38 (q, J = 7 Hz, 2H, ethyl CH_2), 7.90 (dd, J_{H-F} = 13 Hz, 1H, C5-H), 8.54 (s, 1H, C2-H). Anal. calcd. for $C_{21}H_{23}F_2N_3O_3 \cdot 1/4\ H_2O$: C 61.38, H 5.81, N 10.30; found: C 62.06, H 5.81, N 10.43.

Using a similar procedure, reaction of **13***b* with 1-cyclopropyl-6-fluoro-7-chloro-1,4-dihydro-4-oxo[1,8]naphthyridine-3-carboxylate (**14***c*) gave ethyl 1-cyclopropyl-6-fluoro-7-(4,7-diazaspiro-[2,5]octan-7-yl)-1,4 -dihydro- 4 -oxo[1,8]naphthyridine-3-carboxylate (**15***c*) in 46% yield, mp 174–175°C. IR ($CDCl_3$): 1685, 1725 (CO) cm^{-1}. ^{1}H NMR ($CDCl_3$) δ: 0.62 (m, 2H, CH_2), 0.66 (m, 2H, CH_2), 1.02 (m, 2H, CH_2), 1.18 (m, 2H, CH_2), 1.41 (t, J = 7 Hz, 3H, ethyl CH_3), 3.11 (m, 2H, NCH_2), 3.47 (m, 1H, CH), 3.70 (s, 2H, NCH_2), 3.83 (m, 2H, NCH_2), 4.39 (q, J = 7 Hz, 2H, ethyl CH_2), 8.09 (d, J_{H-F} = 13 Hz, 1H, C5-H), 8.50 (s, 1H, C2-H). Anal. calcd. for $C_{20}H_{23}FN_4O_3$: C 62.16, H 6.00, N 14.50; found: C 62.31, H 5.94, N 14.93.

By use of this procedure, reacting **13***b* with ethyl 1-(2,4-difluorophenyl)-6-fluoro-7-chloro-1,4-dihydro-oxo[1,8]naphthyridine-3-carboxylate (**14***d*) gave ethyl 1-(2,4-difluorophenyl)-6-fluoro-7-(4,7-diazaspiro[2,5]octan-7-yl)-1,4-dihydro-4-oxo[1,8]naphthyridine-3-carboxylate (**15***d*) in 53% yield, mp 172–174°C. IR ($CDCl_3$): 1685, 1725 (CO) cm^{-1}. ^{1}H NMR ($CDCl_3$) δ: 0.34 (m, 2H, CH_2), 0.54 (m, 2H, CH_2), 1.41 (t, J = 7 Hz, 3H, ethyl CH_3), 2.91 (t, J = 4 Hz, 2H, NCH_2), 3.42 (s, 2H, NCH_2), 3.56 (m, 2H, NCH_2), 3.39 (q, J = 7 Hz, 2H, ethyl CH_2), 7.06 (m, 2H, aromatic H), 7.49 (m, 1H, aromatic H), 8.11 (d, J_{H-F} = 13 Hz, 1H, C5-H), 8.39 (s, 1H, C2-H). Anal. calcd. for $C_{23}H_{21}F_3N_4O_3 \cdot 1/4\ H_2O$: C 59.67, H 4.68, N 12.10; found: C 59.57, H 4.72, N 12.06.

By a similar procedure, reaction of 6,9-diazaspiro[4,5]decane dihydrochloride (**13***a*) with quinolone ester (**14***a*) gave ethyl 1-cyclopropyl- 6-fluoro-7-(6,9 -diazaspiro[4,5]decan-9-yl)-1, 4 -dihydro-4-oxoquinoline-3-carboxylate (**15***e*) in 48% yield, mp >255°C. IR ($CDCl_3$): 1685, 1720 (CO) cm^{-1}. ^{1}H NMR ($CDCl_3$) δ: 1.13 (m, 2H, CH_2), 1.34 (m, 2H, CH_2), 1.41 (t, J = 7 Hz, 3H, ethyl CH_3), 1.77 (m, 2H, CH_2), 2.04 (m, 2H, CH_2), 2.17 (m, 4H, CH_2×2), 3.35 (s, 2H, NCH_2), 3.43 (m, 2H, NCH_2), 3.57 (m, 2H, NCH_2), 4.40 (q, J = 7 Hz, 2H, ethyl CH_2), 7.31 (d, J_{H-F} = 6 Hz, 1H, C8-H), 8.10 (d, J_{H-F} = 13 Hz, 1H, C5-H), 8.55 (s, 1H, C2-H). Exact Mass calcd. for $C_{23}H_{28}FN_3O_3$: 413.2115; measured: 413.2113.

By use of the above procedure, reaction of **13***a* with ethyl 1-(2,4-difluorophenyl)-6,7-difluoro-1,4 -dihydro- 4 -oxoquinoline-3 -carboxylate (**14***e*) gave ethyl 1-(2,4-difluorophenyl)-6-fluoro-7-(6,9-diazaspiro[4,5]decan-9-yl)-1,4-dihydro-4-oxoquinoline-3-carboxylate (**15***f*) in 39% yield, mp 216–218°C. IR ($CDCl_3$): 1690, 1725 (CO) cm^{-1}. ^{1}H NMR ($CDCl_3$) δ: 1.49 (t, J = 7 Hz, 3H, ethyl CH_3), 1.59 (m, 4H, CH_2×2), 1.79 (m, 4H, CH_2×2), 2.89 (m, 4H, NCH_2×2), 3.01 (m, 2H, NCH_2), 4.39 (q, J = 7 Hz, 2H, ethyl CH_2), 6.12 (d, J_{H-F} = 6.5 Hz, 1H, C8-H), 7.15 (m, 2H, aromatic H), 7.50 (m, 1H, aromatic H), 8.06 (d, J_{H-F} = 13 Hz, 1H, C5-H), 8.31 (s, 1H, C2-H). Anal. calcd. for $C_{26}H_{26}F_3N_3O_3 \cdot 1/2\ H_2O$: C 63.15, H 5.50, N 8.50; found: C 63.25, H 5.32, N 8.53.

Using a similar procedure, reaction of **13***a* with quinoline ester (**14***d*) gave ethyl 1-(2,4-difluorophenyl)-6-fluoro-7(6,9-diazaspiro[4,5]decan-9-yl)-1,4 -dihydro-4-oxo[1,8]naphthyridine-3-carboxylate (**15***g*) in 81% yield, mp 120–122°C. IR ($CDCl_3$): 1690, 1725 (CO) cm^{-1}. ^{1}H NMR ($CDCl_3$) δ: 1.40 (t, J = 7 Hz, 3H, ethyl CH_3), 1.46 (m, 4H, CH_2×2), 1.56 (m, 2H, CH_2), 1.68 (m, 2H, CH_2), 2.90 (t, J = 5 Hz, 2H, NCH_2), 3.42 (m, 2H, NCH_2), 3.53 (m, 2H, NCH_2), 4.49 (q, J = 7 Hz, 2H, ethyl CH_2), 7.06 (m, 2H,

aromatic H), 7.39 (m, 1H, aromatic H), 8.11 (d, J_{H-F} = 13 Hz, 1H, C5-H), 8.38 (s, 1H, C2-H). Anal. calcd. for $C_{25}H_{25}F_3N_4O_3 \cdot 1/4\ H_2O$: C 61.15, H 5.23, N 11.41; found: C 61.13, H 5.26, N 11.20.

*1-Cyclopropyl-6-fluoro-7-(4,7-diazaspiro[2,5]octan-7-yl)-1,4-dihydro-4-oxoquinoline-3-carboxylic acid hydrochloride (**12**a)*

A suspension of **15***a* (80 mg, 0.2 mmol) in 6 N HCl (3 mL) was refluxed for 48 h. The solvent was then concentrated to dryness under reduced pressure. Ethanol (5 mL) was added to digest the residue for 15 min under reflux. It was cooled, filtered, and dried to give 35 mg **12***a* (43%), mp 247–255°C (dec.). IR (KBr): 1720 (CO) cm^{-1}. ^1H NMR (DMSO-d_6) δ: 0.95 (m, 2H, CH_2), 1.05 (t, J = 7 Hz, 3H, ethyl CH_3), 1.15 (m, 2H, CH_2), 1.19 (m, 2H, CH_2), 1.32 (m, 2H, CH_2), 3.42 (m, 2H, NCH_2), 3.45 (s, 2H, NCH_2), 3.62 (m, 2H, NCH_2), 3.84 (m, 1H, CH), 7.59 (d, J_{H-F} = 7 Hz, 1H, C8-H), 7.96 (d, J_{H-F} = 13 Hz, 1H, C5-H), 8.68 (s, 1H, C2-H), 9.72 (bs, 2H, NH_2Cl), 15.13 (s, 1H, OH). Anal. calcd. for $C_{19}H_{21}ClFN_3O_3 \cdot 1/2\ H_2O$: C 56.64, H 5.50, N 10.43; found: C 56.60, H 5.50, N 10.15.

By use of a similar procedure, hydrolysis of **15***b* with 6 N HCl gave 1-cyclopropyl-6,8-difluoro-7-(4,7-diazaspiro[2,5]octan-7-yl)-1,4-dihydro-4-oxoquinoline-3-carboxylic acid hydrochloride (**12***b*) in 81% yield, mp >250°C. IR (KBr): 1725 (CO) cm^{-1}. ^1H NMR (DMSO-d_6) δ: 0.93 (m, 2H, CH_2), 1.14 (m, 2H, CH_2), 1.20 (m, 4H, CH_2×2), 3.35 (m, 2H, NCH_2), 3.47 (s, 2H, NCH_2), 3.65 (m, 2H, NCH_2), 4.12 (m, 1H, CH), 7.88 (dd, J_{H-F} = 12 Hz, 1H, C5-H), 8.71 (s, 1H, C2-H), 9.74 (bs, 2H, NH_2Cl), 14.66 (bs, 1H, OH). Anal. calcd. for $C_{19}H_{20}ClF_2N_3O_3 \cdot 1/2\ H_2O$: C 54.22, H 4.99, N 9.99; found: C 54.12, H 4.82, N 9.92.

Under similar conditions, hydrolysis of **15***c* with 6 N HCl gave 1-cyclopropyl-6-fluoro-7-(4,7-diazaspiro[2,5]octan-7-yl)-1,4-dihydro-4-oxo[1,8]naphthyridine-3-carboxylic acid hydrochloride (**12***c*) in 77% yield, mp >250°C. IR (KBr): 1720 (CO) cm^{-1}. ^1H NMR (DMSO-d_6) δ: 0.97 (m, 2H, CH_2), 1.12 (m, 4H, CH_2×2), 1.20 (m, 2H, CH_2), 3.40 (m, 2H, NCH_2), 3.72 (m, 1H, CH), 4.02 (s, 2H, NCH_2), 4.18 (m, 2H, NCH_2), 8.17 (d, J_{H-F} = 13 Hz, 1H, C5-H), 8.64 (s, 1H, C2-H), 9.92 (bs, 2H, NH_2Cl), 15.07 (bs, 1H, OH). Anal. calcd. for $C_{18}H_{20}ClFN_4O_3 \cdot 1/2\ H_2O$: C 53.53, H 5.20, N 13.88; found: C 53.25, H 5.31, N 13.74.

Hydrolysis of **15***d* in trifluoroacetic acid and 6 N HCl mixture yielded 1-(2,4-difluorophenyl)-6-fluoro-7-(4,7-diazaspiro[2,5]octan-7-yl)-1,4-dihydro-4-oxo[1,8]naphthyridine-3-carboxylic acid trifluoroacetic acid salt **12***d*, mp 229–230°C. IR (KBr): 1675, 1730 (CO) cm^{-1}. ^1H NMR (DMSO-d_6) δ: 0.53 (m, 2H, CH_2), 0.93 (m, 2H, CH_2), 3.24 (m, 2H, NCH_2), 3.66 (m, 2H, NCH_2), 3.88 (m, 2H, NCH_2), 7.37 (m, 1H, aromatic H), 7.64 (m, 1H, aromatic H), 7.83 (m, 1H, aromatic H), 8.25 (d, J_{H-F} = 13 Hz, 1H, C5-H), 8.93 (s, 1H, C2-H), 9.39 (bs, 2H, CF_3COONH_2), 14.86 (bs, 1H, OH). Anal. calcd. for $C_{23}H_{18}F_6N_4O_5$: C 50.74, H 3.33, N 10.29; found: C 50.83, H 3.53, N 10.20.

Hydrolysis of **15***e* with 6 N HCl gave 17-cyclopropyl-6-fluoro-7-(6,9-diazaspiro[4,5]decan-9-yl)-1,4-dihydro-4-oxoquinoline-3-carboxylic acid hydrochloride (**12***e*), mp >250°C. IR (KBr): 1720 (CO) cm^{-1}. ^1H NMR (DMSO-d_6) δ: 1.18 (m, 2H, CH_2), 1.33 (m, 2H, CH_2), 1.69 (m, 2H, CH_2), 1.82 (m, 4H, CH_2×2), 1.98 (m, 2H, CH_2), 3.36 (m, 4H, NCH_2×2), 3.50 (m, 2H, CH_2), 3.83 (m, 1H, CH), 7.03 (d, J_{H-F} = 7 Hz, 1H, C8-H), 7.98 (d, J_{H-F} = 13 Hz, 1H, C5-H), 8.70 (s, 1H, C2-H), 9.30 (bs, 2H, NH_2Cl), 15.12 (bs, 1H, OH). Exact Mass calcd. for $C_{21}H_{24}FN_3O_3$: 385.1802; measured: 385.1803.

Hydrolysis of **15***f* with 6 N HCl yielded 1-(2,4-difluorophenyl)-6-fluoro-7-(6,9-diazaspiro[4,5]decan-9-yl)-1,4-dihydro-4-oxoquinoline-3-carboxylic acid hydrochloride (**12***f*), mp >250°C. IR (KBr): 1730 (CO) cm^{-1}. ^1H NMR (DMSO-d_6) δ: 1.62 (m, 2H, CH_2), 1.82 (m, 6H, CH_2×3), 3.20 (m, 6H, NCH_2×3), 6.41 (d, J_{H-F} = 7 Hz, 1H, C8-H), 7.45 (m, 1H, aromatic H), 7.75 (m, 1H, aromatic H), 7.94 (m, 1H, aromatic H), 8.05 (d, J_{H-F} = 13 Hz, 1H, C5-H), 8.88 (s, 1H, C2-H), 9.52 (bs, 2H, NH_2Cl), 14.84 (bs, 1H, OH). Anal. calcd. for $C_{24}H_{23}ClF_3N_3O_3 \cdot 1/4\ H_2O$: C 57.83, H 4.75, N 8.43; found: C 57.66, H 4.70, N 8.41.

Hydrolysis of **15***g* in a mixture of trifluoroacetic acid and 6 N HCl yielded 1-(2,4-difluorophenyl)-6-fluoro-7-(6,9-diazaspiro[4,5]decan-9-yl)-1,4-dihydro-4-oxo[1,8]naphthyridine-3-carboxylic acid trifluoroacetic acid salt (**12***g*), mp 255°C. IR (KBr): 1680, 1735 (CO) cm^{-1}. ^1H NMR (DMSO-d_6) δ: 1.28 (m, 2H, CH_2), 1.64 (m, 6H, CH_2×3), 3.23 (m, 2H, NCH_2), 3.59 (m, 2H, NCH_2), 3.85 (m, 2H, NCH_2), 7.38 (m, 1H, aromatic H), 7.66 (m, 1H, aromatic H), 7.84 (m, 1H, aromatic H), 8.26 (d, J_{H-F} = 13 Hz, 1H, C5-H), 8.90 (s, 1H, C2-H), 9.19 (bs, 2H, CF_3COONH_2), 14.87 (bs, 1H, OH). Anal. calcd. for $C_{25}H_{22}F_6N_4O_5 \cdot 1/4\ H_2O$: C 52.04, H 3.90, N 9.71; found: C 51.82, H 3.85, H 9.60.

Acknowledgements

We wish to thank the analytical research and structural chemistry departments of Abbott Laboratories for elemental analysis and spectral measurements respectively, and Ms. Cynthia Shepherd for typing the manuscript.

1. G. Y. Lesher, E. J. Froelich, M. D. Gruett, J. H. Bailey, and P. R. Brundage. J. Med. Chem. **5**, 1063 (1962).
2. H. Koga, A. Itoh, S. Murayama, S. Suzue, and T. Irikura. J. Med. Chem. **23**, 1358 (1980).
3. D. J. Hardy, R. N. Swanson, D. N. Hensey, N. R. Ramer, R. R. Bower, C. W. Hanson, D. T. W. Chu, and P. B. Fernandes. Antimicrob. Agents Chemother. **31**, 1768 (1987).
4. R. Wise, J. M. Andrews, and L. J. Andrews. Antimicrob. Agents Chemother. **23**, 559 (1983).
5. Hokuriku Pharmaceutical Co. Ltd. (Japan). NY-198. Drugs Future, **11**, 578 (1986).
6. G. Shantz. Drug, News Perspectives, **1**, 297 (1988).
7. K. Sata, Y. Matsuura, M. Inoue, T. Une, Y. Osada, H. Ogawa, and S. Mitsuhashi. Antimicrob. Agents Chemother. **22**, 548 (1982).
8. D. T. W. Chu, P. B. Fernandes, A. K. Claiborne, E. H. Gracey, and A. G. Pernet. J. Med. Chem. **29**, 2363 (1986).
9. J. B. Cornett and M. P. Wentland. Annu. Rep. Med. Chem. **21**, 139 (1986), and references therein.
10. (*a*) P. B. Fernandes and D. T. W. Chu. Annu. Rep. Med. Chem. **22**, 117 (1987), and references therein; (*b*) Annu. Rep. Med. Chem. **23**, 133 (1988), and references therein.
11. M. Imamura, S. Shibamura, I. Hayakawa, and Y. Osada. Antimicrob. Agents Chemother. **29**, 163 (1986).
12. L. A. Mitscher, P. N. Sharma, L. L. Shen, and D. T. W. Chu. J. Med. Chem. **30**, 2283 (1987).
13. J. F. Gerster, S. R. Rohlfing, S. E. Pecore, R. M. Winandy, R. M. Stern, J. E. Landmesser, R. A. Olsen, and W. G. Gleason. J. Med. Chem. **30**, 839 (1987).
14. T. P. Culberton, J. M. Domagala, J. B. Nicholas, S. Priebe, and R. W. Skeean. J. Med. Chem. **31**, 503 (1988).
15. Y. Mizuki, M. Kamaura, T. Yamaguchi, Y. Sekine, and M. Hashimoto. Arzneim.-Forsch. **39**, 593 (1989).
16. D. T. W. Chu, C. W. Nordeen, D. J. Hardy, R. N. Swanson, W. J. Giardina, A. G. Pernet, and J. J. Plattner. J. Med. Chem. **34**, 168 (1991).
17. J. M. Domagala, C. L. Heifetz, M. P. Hutt, T. F. Mich, J. B. Nichols, M. Solomon, and D. F. Worth. J. Med. Chem. **31**, 991 (1988).
18. L. J. Reed and H. Muench. Am. J. Hyg. **27**, 493 (1938).
19. M. A. Hamilton, R. C. Russo, and R. V. Thurston. Environ. Sci. Technol. **11**, 714 (1977).
20. W. P. Wentland, R. B. Perni, P. H. Dorff, and J. B. Rake. J: Med. Chem. **31**, 1694 (1988).
21. J. P. Sanchez, M. J. Domagala, S. E. Hagen, C. L. Heifetz, M. P. Hutt, J. B. Nichols, and A. K. Trehan. J. Med. Chem. **31**, 983 (1988).
22. D. T. W. Chu, P. B. Fernandes, A. K. Claiborne, E. H. Gracey, and A. G. Pernet. J. Med. Chem. **29**, 2363 (1986).

Can. J. Chem. Downloaded from www.nrcresearchpress.com by 217.78.4.112 on 09/08/12
For personal use only.

Metabolites of the fungus *Arthropsis truncata*

WILLIAM A. AYER,[1] PETER A. CRAW, AND JOHN NEARY
Department of Chemistry, University of Alberta, Edmonton, Alta., Canada T6G 2G2

Received July 9, 1991

This paper is dedicated to Professor Zdenek (Denny) Valenta on the occasion of his 65th birthday

WILLIAM A. AYER, PETER A. CRAW, and JOHN NEARY. Can. J. Chem. **70**, 1338 (1992).

The structures of 12 new polyketide metabolites produced in liquid cultures of the fungus *Arthropsis truncata* have been determined by a combination of chemical and spectroscopic methods. Four of these metabolites possess an unusual 2-oxaspiro[4.5]decane skeleton, and the structure assigned to one of these metabolites **20** has been confirmed by an X-ray crystallographic study of the dibenzoyl derivative **21**. The absolute stereochemistry of these compounds has been predicted by application of the Harada–Nakanishi dibenzoate rule to arthropsolide D tribenzoate (**32**).

WILLIAM A. AYER, PETER A. CRAW et JOHN NEARY. Can. J. Chem. **70**, 1338 (1992).

Faisant appel à une combinaison de méthodes chimiques et spectroscopiques, on a déterminé les structures de 12 nouveaux polycétides obtenus à partir de cultures liquides du champignon *Arthropsis truncata*. Quatre de ces métabolites possèdent le squelette inhabituel du 2-oxaspiro[4.5]décane et la structure attribuée au métabolite **20** a été confirmée par une étude de diffraction des rayons X réalisée sur le dérivé dibenzoylé **21**. On a prédit la stéréochimie absolue de ces composés en appliquant la règle du dibenzoate de Harada–Nakanishi au tribenzoate **32** de l'arthropsolide D.
[Traduit par la rédaction]

Can. J. Chem. Downloaded from www.nrcresearchpress.com by 217.78.4.112 on 09/08/12
For personal use only.

Introduction

As part of our investigations of the chemistry of fungi associated with the economically important blue-stain disease of lodgepole pine (*Pinus contorta* Dougl. var *latifolia* Engelm.), we described the isolation of (−)arthrographol, which is produced in liquid cultures of the fungus *Arthrographis pinicola* Sigler and Yamaoka (1), and the total synthesis of (+/−)arthrographol from vanillin (2). We believe that arthrographol may be responsible for the antagonism observed between *Arthrographis pinicola* and *Ophiostoma clavigerum* (Robins.-Jeff. & Davids.) Harrington, a fungus strongly associated with tree mortality caused by the blue-stain fungi (3).

Recently we examined a number of species of fungi, thought to be morphologically related to *Arthrographis pinicola,* to see whether they might produce metabolites similar to those produced in our liquid cultures of *A. pinicola,* thereby providing chemotaxonomic evidence to support the classification of these new species of fungi in the same genus as *A. pinicola*. One of these species, *Arthropsis truncata* Sigler, Dunn & Carmichael, which was isolated from primary forest leaf litter near Puca Urquillo, Peru (4), produces a series of previously unreported polyketide metabolites when grown in liquid culture. Subsequently we observed *Arthropsis truncata* to be antagonistic to the growth of the blue-stain fungus *Ophiostoma clavigerum*. The structures of the metabolites produced by *Arthropsis truncata* are the subject of this report. Biosynthetic studies dealing with these compounds will be the subject of a subsequent paper.

Results and discussion

Arthropsis truncata was grown in shake culture on a modified malt extract medium for 4 weeks. The filtered culture broth was extracted with ethyl acetate and the metabolites were isolated by extensive chromatography and fractional crystallizations.

[1]Author to whom correspondence may be addressed.

Arthropsadiol A (1)

Arthropsadiol A (**1**) was obtained as needles, mp 78–79°C, $[\alpha]_D$ −245.7. High-resolution electron impact mass spectrometry (hreims) and chemical ionization mass spectrometry (cims) indicated a molecular formula of $C_{12}H_{16}O_4$. The presence of an α,β-unsaturated ketone was apparent from a maximum at 229 nm in the ultraviolet (uv) spectrum, a strong carbonyl absorption at 1689 cm^{-1} in the Fourier transform infrared (Ftir) spectrum, and signals at δ 6.68 (H5) and δ 6.08 (H6) in the ^1H nmr spectrum and δ 199.51 (C7), δ 154.65 (C5), and δ 125.02 (C6) in the ^{13}C nmr spectrum (see Table 1). The presence of an (*E*)-propenyl unit was suggested by signals at δ 5.53 (H2), δ 5.09 (H3), and δ 1.61 (H1) in the ^1H nmr spectrum, and signals at δ 129.03 (C3), δ 132.21 (C2), and δ 17.55 (C1) in the ^{13}C nmr spectrum. The coupling constants between the signals for H2 and H3 (J = 15.2–15.5 Hz) in the ^1H nmr spectrum and the position of the vinyl methyl signal in the ^{13}C nmr spectrum are consistent with an (*E*)-propenyl unit. Finally, the presence of a methyl ketone was indicated by a 3H singlet at δ 2.13 in the ^1H nmr spectrum and signals at δ 209.74 (C11) and δ 25.59 (C12) in the ^{13}C nmr spectrum. As the molecular formula requires the presence of five units of unsaturation, four of which have been accounted for by the two carbonyl and four alkene sp^2 carbon signals in the ^{13}C nmr spectrum, arthropsadiol A (**1**) must be monocyclic. The remaining two oxygen atoms in the molecular formula can be accounted for by two hydroxyl groups as the Ftir spectrum displays a broad OH absorption at 3450 cm^{-1}, the ^1H nmr spectrum contains D_2O exchangeable signals at δ 3.87 and δ 3.89, and the ^{13}C nmr contains carbinol signals at δ 75.27 (C10) and δ 72.12 (C8).

The presence of two hydroxyl groups is also confirmed by formation of diacetate **2** upon acetylation of arthropsadiol A (**1**). The structure of arthropsadiol A (**1**) was readily apparent from analyses of ^1H–^1H and ^1H–^{13}C COSY spectra of the diacetate **2**. The large coupling constants between the signals of H4 and H9 (J = 9.5–10.3 Hz) and the signals of H8 and H9 (J = 10.8–13.1 Hz) in the ^1H nmr spectra of both arthropsadiol A (**1**) and the diacetate (**2**) suggest *trans,trans*-stereochemistry of the cyclohexenone substituents at C4, C8,

TABLE 1. Nuclear magnetic resonance spectral parameters for arthropsadiol A (**1**) and arthropsolide A (**20**)[a]

Atom	1	20	Atom	1	20
C1	17.55	17.88	H1	1.61 (dd (6.7, 1.8)	1.63 dd (6.5, 1.5)
C2	132.21	132.75	H2	5.53 dq (15.2, 6.7)	5.69 dq (15.5, 6.5)
C3	129.03	126.20	H3	5.09 ddq (15.5, 9.5, 1.8)	5.46 ddq (15.5, 8.5, 1.5)
C4	39.74	40.85	H4	3.49 dddd (9.5, 9.5, 2.5, 2.5)	3.94 ddd (8.5, 2.5, 2.5)
C5	154.65	149.68	H5	6.68 dd (10.2, 2.5)	6.65 dd (10.5, 2.5)
C6	125.02	126.09	H6	6.08 dd (10.5, 3.0)	6.19 dd (10.5, 3.5)
C7	199.51	197.54	H8	4.32 dd (10.8, 1.5)	4.69 br d (1.5)
C8	72.12	71.91*	H9	2.39 ddd (10.8, 10.3, 1.6)	
C9	51.92	61.71	H10	4.54 br d (2.3)	5.30 br d (6.0)
C10	75.27	69.18*	H12	2.13 s	A 4.75 dd (3.0, 3.0)
C11	209.74	156.88			B 4.62 dd (2.8, 2.8)
C12	25.59	88.60	OH	3.89 d (3.9)	4.45 br s
C13		172.33	OH	3.87 d (1.8)	3.79 br d (7.2)

[a]Determined in $CDCl_3$; *interchangeable.

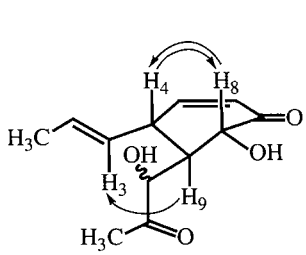

1

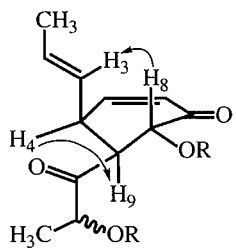

3 R = H
4 R = Ac

FIG. 1. Significant nOe's observed in the ^1H NMR spectra of arthropsadiol A (**1**), and arthropsadiol B (**3**) and diacetate (**4**).

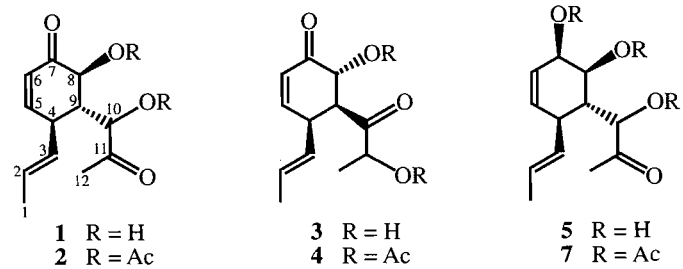

1 R = H
2 R = Ac

3 R = H
4 R = Ac

5 R = H
7 R = Ac

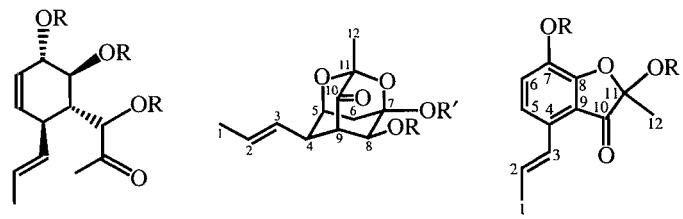

6 R = H
8 R = Ac

9 R = R′ = H
10 R = R′ = Ac
11 R = Ac, R′ = H

12 R = H
15 R = Ac

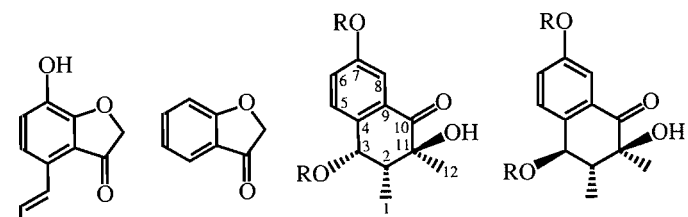

13

14

16 R = H
18 R = Ac

17 R = H
19 R = Ac

and C9. This is supported by nuclear Overhauser enhancements (nOe) observed in the ^1H nmr spectrum of arthropsadiol A (**1**) from the signals of H4–H8 (7.2%), H8–H4 (3.4%), and H9–H3 (4.4%) (Fig. 1). We are unable to assign the relative configuration at C10 due to the failure of attempts to prepare either the acetonide or carbonate derivatives of arthropsadiol A (**1**). We were hopeful that the size of the H9–H10 coupling constant in either of these derivatives would have allowed us to assign the stereochemistry at C10, provided no epimerization occurred at C10 during preparation of the acetonide or carbonate.

Arthropsadiol B (3)

Arthropsadiol B (**3**) was obtained as an oil that resisted attempts at crystallization. The hreims, uv, Ftir, and ^{13}C nmr spectra of this material indicated a close structural similarity to arthropsadiol A (**1**). The signals of an α,β-unsaturated ketone and an (*E*)-propenyl unit in the ^1H nmr spectrum of arthropsadiol B (**3**) are very similar to those in the spectrum of arthropsadiol A (**1**). However, a 3H doublet at δ 1.39 (J = 7.5 Hz) and a broad quartet of doublets at δ 4.36 (J = 7.0, 4.0 Hz) suggested the presence of a 2-hydroxy-1-propanone substituent at C9 in arthropsadiol B (**3**) rather than a 1-hydroxy-2-propanone unit as in arthropsadiol A (**1**). This was confirmed by a ^1H–^1H COSY spectrum of arthropsadiol B (**3**). The relative stereochemistry of arthropsadiol B (**3**) also differs from that of arthropsadiol A (**1**), but this difference is not readily discernable from the ^1H nmr spectra of either arthropsadiol B (**3**) or the corresponding diacetate **4** determined in $CDCl_3$ due to overlapping of the signals of H4 and H9. However, the signals of H4 and H9 are well separated in the ^1H nmr spectrum of the diacetate **4** determined in benzene-d_6. Thus, the H8–H9 coupling constant (J = 12.7 Hz) in the latter spectrum is consistent with a *trans* relationship of the C8 and C9 substituents (Fig. 1). The signal of H9 also shows coupling to an apparent quartet (J = 6.0 Hz) at δ 3.14 due to H4. A nOe is observed from H8 to H3 (6.1%) in the ^1H nmr spectrum of arthropsadiol B (**3**) determined in $CDCl_3$, and between H8 and H3 (7.3%, 4.3%) in the spectrum of the diacetate **4** also determined in $CDCl_3$. Furthermore, a nOe is observed from H4 to H9 (14.4%) in the ^1H nmr spectrum of the diacetate **4** determined in ben-

Can. J. Chem. Downloaded from www.nrcresearchpress.com by 217.78.4.112 on 09/08/12
For personal use only.

Can. J. Chem. Downloaded from www.nrcresearchpress.com by 217.78.4.112 on 09/08/12
For personal use only.

zene-d_6. Thus, we conclude that the C4 and C8 substituents are *trans* in arthropsadiol B (**3**) and the C4 and C9 substituents are *cis*. The relative configuration at C11 remains unassigned.

Arthropsatriols A (5) and B (6)

Two triols were isolated from the broth extract that did not give M^+ ions in their respective hreims. However, weak ions were observed in both spectra at m/z 208 ($M^+ - H_2O$) suggesting a molecular formula of $C_{12}H_{18}O_4$ for each triol, which was supported in each case by ions at m/z 244 ($M^+ + NH_4^+$) in the cims. The ^{13}C nmr spectra of each triol displayed signals for one non-conjugated ketone carbon, 4 non-conjugated alkene sp^2 carbons, and 3 carbinol carbons. Thus we concluded that arthropsatriols A (**5**) and B (**6**) are the epimeric triols derived from reduction of the C7 carbonyl group of arthropsadiol A (**1**), and this was supported by an examination of the ^1H nmr spectra of the triols and their respective triacetate derivatives **7** and **8**.

The relative stereochemistry of each of the triols was more readily assigned by examination of the ^1H nmr spectra of the triacetates of arthropsatriols A (**5**) and B (**6**) as the hydrogen signals are better dispersed in these spectra and allow more conclusive nOe experiments. In the spectra of both triacetates determined in $CDCl_3$ the large coupling constants between H4 and H9 (J = 9.5–10.5 Hz) and between H8 and H9 (J = 12.0–12.5 Hz) support a *trans,trans* relative stereochemistry of H4, H8, and H9 as in arthropsadiol A (**1**). The H7–H8 coupling constant (J = 8.5 Hz) in the spectrum of arthropsatriol B triacetate (**8**) is considerably larger than that (J = 3.8 Hz) in arthropsatriol A triacetate (**7**) and supports the relative stereochemistry assigned to each epimer at C7. The C7 stereochemistry assigned to arthropsatriol A triacetate (**7**) is also supported by a nOe from H7 to H8 (13.0%) and from H8 to H7 (16.5%) in the ^1H nmr spectrum determined in $CDCl_3$. Furthermore, nOe's from H4 to H8 (10.7%) and H8 to H4 (7.6%) support the *cis* relationship of H4 and H8 in arthropsatriol A triacetate (**7**). In the ^1H nmr spectrum of arthropsatriol B triacetate (**8**) determined in $CDCl_3$ the signal for H7 was obscured in a multiplet also containing the signals for H2, H5 and H6. However, in the spectrum of **8** determined in benzene-d_6 the signals for H2, H5, H6, and H7 are well resolved. The C4, C7, C8, and C9 relative stereochemistry assigned to arthropsatriol B triacetate (**8**) is supported by nOe's from H7 to H9 (6.5%), H9 to H7 (9.5%), and H4 to H8 (8.2%). As is the case for arthropsadiol A (**1**) the relative configuration at C10 of arthropsatriols A (**5**) and B (**6**) remains unassigned.

Cycloarthropsadiol C (9)

This compound was obtained as an oil and has a molecular formula of $C_{12}H_{16}O_5$ as determined by hreims. The Ftir spectrum shows absorptions characteristic of hydroxyl (3434 cm^{-1}) and C—O groups (1144–1091 cm^{-1}) as well as a strong ketone carbonyl absorption at 1743 cm^{-1}. The presence of a ketone group is also supported by a signal at δ 202.3 (C10) in the ^{13}C nmr spectrum. As 6-membered cyclic ketones usually have absorption near 1715 cm^{-1} in the infrared, the position of the ketone absorption in the Ftir of cycloarthropsadiol C (**9**) may reflect the effect of the two electronegative α-oxygen substituents on the ketone stretching absorption (5). These two α-oxygen substituents may also account for the upfield position of the ketone signal in the ^{13}C nmr spectrum. The presence of an (*E*)-propenyl unit was readily apparent from signals at δ 5.64 (H2), δ 5.46 (H3), and δ 1.67 (H1) in the ^1H nmr spectrum as well as signals at δ 129.1, δ 127.6 (C3, C2), and δ 18.0 (C1) in the ^{13}C nmr spectrum. The remaining signals in the ^{13}C nmr spectrum may be assigned to an acetal (C11, δ 100.1), a hemiacetal (C7, δ 94.1), two sp^3 mono-oxygenated carbons (C8, δ 78.4 and C5, δ 73.5), a CH_2 group (C6, δ 56.1) with 3 oxygen groups attached to the adjacent carbon atoms, a CH group (C9, δ 51.3) located α to the C10 ketone, a CH group (C4, δ 37.2) attached to the (*E*)-propenyl unit, and a methyl carbon (C12, δ 19.5).

The ^1H nmr spectrum of **9** is consistent with the structure assigned to cycloarthropsadiol C but unfortunately the signals for H5 and H8 overlap as an unresolved broad doublet at δ 4.24. To separate the signals due to H5 and H8 in the ^1H nmr, and to confirm the hydrogen connectivities in cycloarthropsadiol C (**9**) by ^1H–^1H COSY and nOe experiments, the compound was acetylated to give mainly the corresponding diacetate **10** and a trace of the monoacetate **11**. The ^1H nmr spectrum of the diacetate **10** was readily assigned with the aid of a ^1H–^1H COSY spectrum. In the COSY spectrum a weak cross peak exists between the signals for H5 (δ 4.25) and H9 (δ 2.99) due to W-coupling (J = 1.7–2.0 Hz). The position of the signal due to H5 is largely unchanged from that in cycloarthropsadiol C (**9**), but the signal for H8 is shifted significantly downfield to δ 5.27 in the monoacetate **11** and to δ 6.09 in the diacetate **10**. The signal for H8 in the spectrum of the diacetate **10** is a doublet (J = 4.0 Hz) and significant nOe's are observed to the signals of H4, H6α, and H9, thereby supporting the relative stereochemistry assigned to C8, as well as that of C4. Irradiation of the C12 methyl singlet at δ 1.44 in the spectrum of the diacetate **10** results in only a small nOe to the acetate singlets at δ 2.094 and δ 2.085 (1.2% combined) but nevertheless is consistent with the structure assigned to cycloarthropsadiol C (**9**).

Cycloarthropsone (12)

Cycloarthropsone (**12**) was obtained as an optically inactive yellow solid that gave an ion at m/z 220 in the hreims with a molecular formula of $C_{12}H_{12}O_4$, and an ion at m/z 238 ($M^+ + NH_4^+$) in the cims. The Ftir spectrum contains intense hydroxyl (3450, 3170 cm^{-1}) and conjugated ketone carbonyl (1685 cm^{-1}) absorptions, and the uv spectrum shows maxima at 236, 286, and 387 nm, which undergo a bathochromic shift in the presence of dilute sodium hydroxide. The ^1H nmr spectrum is relatively simple and displays signals for two *ortho*-coupled aromatic hydrogens (δ 6.99, δ 6.93, J = 8.8 Hz), an (*E*)-propenyl chain (δ 7.08, 6.27, 1.78), and a methyl singlet (δ 1.43). The aromatic carbon signals in the ^{13}C mr spectrum of cycloarthropsone (**12**) were assigned by comparison with the calculated chemical shifts of the aromatic carbons in 7-hydroxy-4(*E*)-propenyl-3(2*H*)-benzofuranone (**13**), which in turn were obtained by addition of the substituent effects for introduction of a 7-hydroxyl group and a 4(*E*)-propenyl group to the reported spectrum of 3(2*H*)-benzofuranone (**14**) (6) (see Table 2). The hydroxy and (*E*)-propenyl substituent effects were determined by comparison of the spectra of phenol and (*E*)-propenylbenzene with that of benzene (7). The positions of the signals for C4, C6, C7, and C8 are in good agreement with the calculated positions, but those of C5 and C9 differ significantly from the calculated positions. The additional

TABLE 2. Partial ^{13}C nmr data for cycloarthropsone (**12**) and related compounds

Atom	**14**[6]	Δ 7-OH	Δ 4-Propenyl	**13** calcd.	**12**
C4	124.3	−7.1	+9.5	126.7	130.0
C5	122.1	+2.6	−1.7	126.4	117.6
C6	138.1	−12.8	0.0	125.3	124.1
C7	113.8	+26.6	−2.6	137.8	141.1
C8	173.9	−12.8	0.0	161.1	158.2
C9	121.3	+2.6	−1.7	122.2	115.0

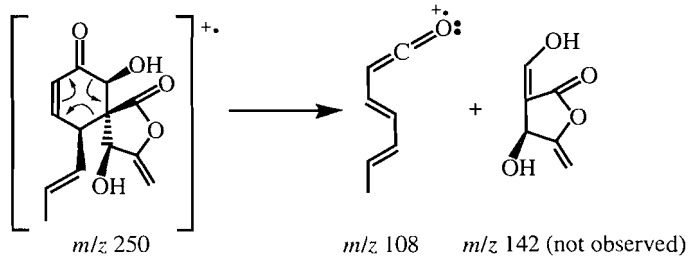

FIG. 2. Possible mass spectral fragmentation of arthropsolide A (**20**).

shielding of C5 and C9 is probably the result of conjugation between the C10 ketone and the (*E*)-propenyl group. This conjugation would also account for the shielding of C3 and the deshielding of C2 relative to the positions of the corresponding propenyl sp^2 carbon signals in the spectrum of (*E*)-propenylbenzene.

Acetylation of cycloarthropsone (**12**) gave the corresponding diacetate **15** as a clear oil. In the ^{13}C nmr spectrum of diacetate **15** the signals of C4 and C6 are shifted downfield by ca. 6 ppm and the signal of C7 is shifted upfield by 7.5 ppm relative to the positions of the corresponding signals in cycloarthropsone (**12**). These shifts are in accordance with those expected from a comparison of the spectra of phenol and phenyl acetate (7).

*Arthropsatriols C (**16**) and D (**17**)*

An inseparable mixture of arthropsatriol C (**16**) and D (**17**) was obtained by fractional crystallization of one of the combined fractions from flash chromatography of the crude broth extract. A molecular formula of $C_{12}H_{14}O_4$ was established for the mixture by hreims, and an ion at *m/z* 240 in the cims ($M^+ + NH_4^+$) is consistent with this formula. The Ftir spectrum displayed strong absorptions at 3406 and 1678 cm^{-1}, confirming the presence of hydroxyl and conjugated carbonyl groups, as well as a strong absorption at 1603 cm^{-1} due to C=C stretching. Maxima in the uv spectrum at 229, 255, and 321 nm are consistent with a tetralone, and the position of the $\pi \rightarrow \pi^*$ absorption at 255 nm is in agreement with the calculated position of 256 nm for 7-hydroxytetralone (8). The mixture was acetylated to give a mixture of the two diacetates **18** and **19**, which were separable by flash chromatography. Both diacetates gave ions at *m/z* 306 (M^+) in their hreims, confirming molecular formulae of $C_{16}H_{18}O_6$. The Ftir of each diacetate displayed absorptions for aliphatic and aromatic acetate groups, a conjugated ketone, and also a hydroxyl absorption at 3492 cm^{-1} indicating the presence of a tertiary hydroxyl group in each parent triol. The ^1H nmr spectra of the diacetates are very similar and in each case the coupling of the aromatic hydrogen signals indicates the presence of a 1,2,4-trisubstituted aromatic ring. The most noticeable difference between the ^1H nmr spectra of the two diacetates is the size of the H2–H3 coupling constants. In the spectrum of arthropsatriol D diacetate (**19**) this coupling is 10.6 Hz and supports a *trans* relationship of H2 and H3, whereas in the spectrum of arthropsatriol C diacetate (**18**) the H2–H3 coupling constant is 4.3 Hz. The structures assigned to the diacetates were confirmed by nOe experiments. Significant nOe's are observed between the signals of H3 and H5, and between the *ortho*-aromatic hydrogens (H5, H6) in the spectra of each diacetate, and therefore the aromatic acetate group must be located at C7. The stereochemistry assigned to arthropsatriol C diacetate (**18**) at C2, C3, and C11 is supported by nOe's from H12 to H1 (1.5%), H1 to H3 (6.1%), and between H2 and H3 (11.8%, 13.9%). For arthropsatriol D diacetate (**19**) a nOe from H12 to H3 (14.0%) confirms the relative configuration at C11 and C3 and a large nOe from H1 to H3 (10.2%) supports the *trans* relationship of C2 and C3 substituents. Accordingly arthropsatriols C (**16**) and D (**17**) differ only in their stereochemistry at C3.

*Arthropsolide A (**20**)*

This compound was obtained as needles, mp 142–145°C, $[\alpha]_D$ −302.4, which had a molecular formula of $C_{13}H_{14}O_5$ (*m/z* 250) as suggested by hreims, and confirmed by an ion at *m/z* 268 ($M^+ + NH_4^+$) in the cims. The base peak in the hreims at *m/z* 108 may arise via retro Diels–Alder fragmentation to give the ketene-heptadiene fragment shown in Fig. 2. The Ftir spectrum shows absorptions attributable to hydroxyl (3400 cm^{-1}), conjugated ketone (1685 cm^{-1}), and γ-lactone (1798 cm^{-1}) groups. The presence of the exocyclic methylene group is probably responsible for the shift of the lactone absorption from that of butyrolactone at 1770 cm^{-1} (cf. 2(3*H*)-furanone absorbs at 1790 cm^{-1} (5)). The ^1H nmr spectrum (Table 1) contains a number of features in common with that of arthropsadiol A (**1**), especially with regard to the α,β-unsaturated ketone and the (*E*)-propenyl group. A ^1H–^1H COSY spectrum of arthropsolide A (**20**) displays cross peaks between the vinyl hydrogen signals of both of these groups and a signal at δ 3.94 (H4), but in the absence of a hydrogen at C9 in arthropsolide A (**20**) the signal for H10 shows no further coupling (cf. in the spectrum of arthropsadiol A (**1**) the signal of H4 is coupled to H9, which in turn is coupled to the signals of H8 and H10). Two additional isolated spin systems are observed in the ^1H–^1H COSY spectrum of arthropsolide A (**20**), between H8 (δ 4.69) and 8-OH (δ 4.45), and between the methylene hydrogens (H12, δ 4.75, 4.62), H10 (δ 5.30), and 10-OH (δ 3.79).

The ^{13}C nmr spectrum of arthropsolide A (**20**) displays 13 signals (Table 1) and is fully consistent with the structure proposed for this compound. To establish the relative stereochemistry at the four asymmetric carbons, arthropsolide A (**20**) was converted into the corresponding dibenzoate **21** since the proximity of the signals of H12A, H12B, and H8 in the ^1H nmr spectrum of **20** complicated selective irradiation of these hydrogens during nOe experiments. The signals due to these hydrogens are well separated in the spectrum of the dibenzoate **21** as are those of the remaining hydrogens, with the exception of H10 (δ 6.31), which nearly overlaps with the H6 signal (δ 6.26). Irradiation of the H8

Can. J. Chem. Downloaded from www.nrcresearchpress.com by 217.78.4.112 on 09/08/12
For personal use only.

signal (δ 6.10) results in nOe's to the signals of H10 (4.9%) and H4 (10.7%), thereby establishing the relative stereochemistry at C4, C8, C9, and C10 in a single experiment. This is supported by a large nOe from H4 to H8 (16.0%). The signals due to H12A and H12B were also differentiated with the help of nOe experiments. Thus, the H12B signal (δ 4.62) shows nOe's to both the H10 (3.7%) and H12A (δ 4.96, 41.3%) signals, while the H12A signal shows a nOe only to the H12B signal (42.6%).

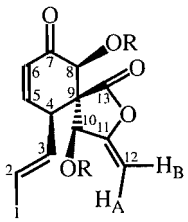

20 R = H
21 R = C_6H_5CO

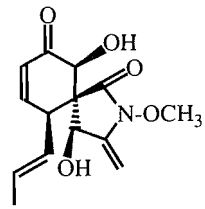

22

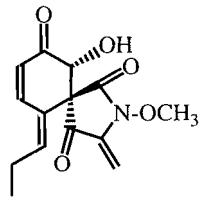

23

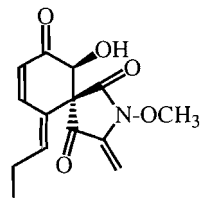

24

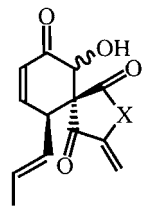

25 X = O, 6β-OH
26 X = O, 6α-OH
27 X = $NOCH_3$, 6α-OH
28 X = $NOCH_3$, 6β-OH

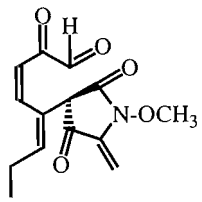

29

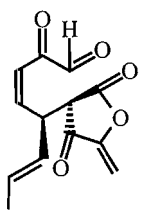

30

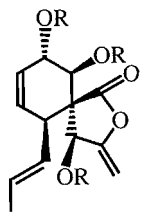

31 R = H
32 R = C_6H_5CO

The structure derived for arthropsolide A (**20**) on the basis of the spectroscopic data was unequivocally confirmed by an X-ray crystal structure determination carried out on the dibenzoate **21** (Fig. 3).[2] After determining the structure of **21** we became aware of a very similar series of fungal metabolites containing a 2-azaspiro[4.5]decane skeleton (e.g., spirostaphylotrichin K (**22**)) that were recently isolated from liquid cultures of *Staphylotrichum coccosporum* and mutant strains of this fungus (9–11). Two other 2-azaspiro[4.5]-decane fungal metabolites, triticone A (**23**) and triticone B (**24**) (= spirostaphylotrichin D and C respectively) have been isolated from *Drechslera tritici-repentis* (12).

[2]The X-ray crystallographic study was carried out by Dr. B. Santasiero, Structure Determination Laboratory, Chemistry Department, University of Alberta, Edmonton, Alberta T6G 2G2. Inquiries regarding the crystallographic results should be directed to Dr. Santasiero at the above address quoting report number SDL:WAA9002.

Arthropsolides B (25) and C (26)

These two compounds were obtained as an inseparable (tlc, hplc) mixture that decomposed slowly on standing. The hreims spectrum gave a weak ion at *m/z* 248, which suggested a molecular formula of $C_{13}H_{12}O_5$, and this is consistent with an ion at *m/z* 266 ($M^+ + NH_4^+$, 100%) in the cims. The base peak at *m/z* 108 in the hreims corresponds to a heptadiene-ketene fragment as in the spectrum of arthropsolide A (**20**). The ^1H nmr spectrum of arthropsolide B (**25**) and C (**26**) displays two sets of signals which are each very similar to the spectrum of arthropsolide A (**20**). However, the spectrum differs from that of arthropsolide A (**20**) by the absence of signals attributable to a hydrogen at C10, and by the downfield shift of the signals due to the exocyclic methylene group (H12) due to conjugation with the C10 ketone. Furthermore, in the absence of a hydrogen at C10 the signals of the exocyclic methylene hydrogens are simplified from a doublet of doublets in the spectrum of arthropsolide A (**20**) (δ 4.75, 4.62) to doublets in the spectrum of arthropsolides B (**25**) and C (**26**) (δ 5.15, 5.10, 4.63, 4.57). The ^{13}C nmr spectrum of arthropsolides B (**25**) and C (**26**) also reflects the effects of oxidation of only the C10 alcohol of arthropsolide A (**20**). Thus, the signal for C11 shifts upfield to δ 150.29 (cf. δ 156.88 for arthropsolide A (**20**)) and the signals for C12 are shifted downfield to δ 96.47, 95.90 (cf. δ 88.60 for arthropsolide A (**20**)) due to conjugation between the exocyclic double bond and the C10 ketone. Oxidation of arthropsolide A (**20**) with pyridinium chlorochromate gave a mixture of arthropsolides B (**25**) and C (**26**) as the only isolable product.

Arthropsolide B (**25**) and C (**26**) are very similar in terms of structure and instability to the inseparable mixtures of spirostaphylotrichin G (**27**) and H (**28**) from *Staphylotrichum coccosporum* (10), and triticone A (**23**) and B (**24**) from *Staphylotichum coccosporum* (9) and *Drechslera tritici-repentis* (12). *Drechslera tritici-repentis* is a major pathogen of wheat and it has been suggested that the retro-aldol intermediate **29** by which triticone A and B readily interconvert may be responsible for the lesions produced on wheat plants by this fungus (12). In an analogous fashion arthropsolide B (**25**) and C (**26**) may interconvert via the retroaldol intermediate **30** and these compounds may be responsible for inhibiting the growth of the blue-stain fungus *Ophiostoma clavigerum*.

Arthropsolide D (31)

The final compound from chromatography of the crude broth extract of our liquid culture of *A. truncata* was an oily solid that gave a weak ion at *m/z* 252 in the hreims and an ion at *m/z* 270 ($M^+ + NH_4^+$, 100) in the cims, thereby confirming a molecular formula of $C_{13}H_{16}O_5$. Several features in the ^1H and ^{13}C nmr spectra of this compound indicate that it is derived from reduction of the C7 ketone of arthropsolide A (**20**) to the corresponding allylic alcohol. Thus, in the absence of conjugation the signals for H6 and H5 in the ^1H nmr spectrum occur at δ 5.49 and δ 5.69, respectively (cf. δ 6.19, 6.65 for arthropsolide A (**20**)), while the signal of H8 (δ 3.69) shows coupling (^1H–^1H COSY) to the signal for H7 (δ 4.80) as well as to a hydroxyl signal at δ 5.60. The ^{13}C nmr spectrum of arthropsolide D (**31**) is also consistent with reduction of the C7 ketone of arthropsolide A (**20**). Thus, only one carbonyl signal (C13) and an extra carbinol signal (C7) are observed and the signals for C5 and C6 occur between δ 127 and 130.

Can. J. Chem. Downloaded from www.nrcresearchpress.com by 217.78.4.112 on 09/08/12
For personal use only.

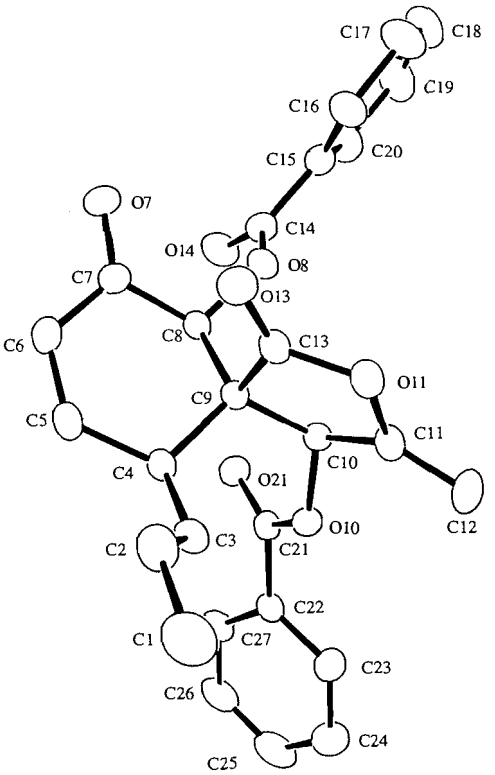

FIG. 3. A computer-generated perspective drawing of the final X-ray model of arthropsolide A dibenzoate (**21**) (hydrogen atoms have been omitted for clarity).

The relative configuration of arthropsolide D (**31**) was not readily apparent from an examination of the coupling constants of the signals due to H7 and H8 in the ^{1}H nmr spectrum, as both these signals appear as broad singlets. Furthermore, the proximity of these signals to other hydrogen signals made it difficult to do selective irradiations during nOe experiments. Since the dibenzoate of arthropsolide A had proven useful in this regard, the tribenzoate **32** of arthropsolide D was prepared. In the ^{1}H spectrum of the tribenzoate **32** the 8.5 Hz coupling between the signals due to H8 (δ 6.09, d, J = 8.5 Hz) and H7 (δ 6.42, dddd, J = 8.5, 3.0, 2.0, 2.0 Hz) suggested an antiperiplanar relationship of these hydrogens. Significant nOe's are observed from H8 to H10 (7.8%) and H4 (9.0%), and from H4 to H8 (11.1%) and H10 (1.4%), and allow the relative configuration of arthropsolide D (**31**) and the tribenzoate **32** at C4, C7, C8, C9 and C10 to be assigned as shown.

The CD spectrum of tribenzoate **32** shows a strong positive Cotton effect at 236 nm. Application of the Harada–Nakanishi dibenzoate rule (13) thus indicates a positive chirality between the benzoate at C8 and that at C7, indicating that the absolute configuration of **32** and, by inference, the other new metabolites discussed, is as indicated in the structural drawings.

Experimental

For general experimental details see publication 14 from these laboratories. For ease of spectral comparisons (^{1}H, ^{13}C nmr) the numbering of each compound is in accordance with that indicated diagrammatically for each carbon skeleton, and not the IUPAC nomenclature for each compound. The IUPAC name is provided with the experimental description of the compound. The numbering system used in the text is based on biosynthetic considerations which will be discussed in a subsequent paper. Signals indicated (*) or (**) in the ^{13}C nmr may be interchanged. Hexanes refers to Stanchem Ltd. (Edmonton) light petroleum, bp 62–70°C. Unless otherwise indicated, the following procedure was used for acetylations. The alcohol was stirred with acetic anhydride (10–20 equiv.), pyridine (10–20 equiv.), and a crystal of 4-dimethylaminopyridine (DMAP) in dichloromethane (5 mL) until tlc indicated complete reaction. The reaction mixture was then evaporated using benzene to assist with the azeotropic removal of pyridine, and the product was purified by flash chromatography eluting with ethyl acetate – Skellysolve B (1:3) to give the acetylated derivative.

Growth of Arthropsis truncata *and isolation of metabolites*

Freeze-dried cultures of *Arthropsis truncata* Sigler, Dunn & Carmichael (UAMH 4430) were obtained from Mrs. L. Sigler, University of Alberta Microfungus Herbarium, Edmonton. Lyophilized cultures were inoculated onto, and maintained on, plates of malt extract agar. After 6 weeks growth one plate was blended with water (100 mL) and used to inoculate five 2-L Erlenmeyer flasks each containing 1 L of modified malt extract medium (20 g malt extract (Difco), 20 g D-glucose, 1.0 g bacto-peptone (Difco), 1 L water). The cultures were grown on a rotary shaker (at 150 rpm) at room temperature for 4 weeks, then the black arthroconidia and mycelial fragments were separated by filtration through cheesecloth. The filtered culture broth was concentrated at reduced pressure to approximately 500 mL and then extracted with ethyl acetate (4 × 500 mL). The combined extracts were dried over magnesium sulfate and evaporated to give a brown oil (2.35 g).

A portion of the extract (1.20 g) was dissolved in ethyl acetate – methanol, adsorbed onto silica gel (5 g), and dried in air with gentle warming. The dried extract – silica gel mixture was poured onto the top of a column of silica gel (150 g) packed with ethyl acetate – hexanes (1:2), and 25-mL fractions were eluted successively with ethyl acetate – hexanes (1:2, fractions 1–36), ethyl acetate – hexanes (2:3, fractions 37–55), ethyl acetate – hexanes (1:1, fractions 56–72), ethyl acetate (fractions 73–112), and ethyl

Can. J. Chem. Downloaded from www.nrcresearchpress.com by 217.78.4.112 on 09/08/12
For personal use only.

Can. J. Chem. Downloaded from www.nrcresearchpress.com by 217.78.4.112 on 09/08/12
For personal use only.

acetate – methanol (20:1, fractions 113–130). Fractions containing similar components (tlc) were combined and further purified by fractional crystallization or additional chromatography.

Fractions 4–7 (7 mg) contained a mixture of triglycerides (^{1}H nmr). Fractions 12–17 (20 mg) were chromatographed, eluting with ethyl acetate – hexanes (1:3), to give an inseparable mixture of arthropsolides B (**25**) and C (**26**) (14 mg). Fractions 20–26 (22 mg) contained a mixture of diglycerides (^{1}H nmr). Fractions 27–32 (29 mg) crystallized from dichloromethane to give cycloarthropsone (**12**) (14 mg). Fractions 37–53 (164 mg) were crystallized from ethyl acetate – hexanes to give arthropsolide A (**20**) (55 mg). Column chromatography of the crystallization mother liquours from fractions 37–53, eluting with dichloromethane–methanol (20:1), gave arthropsadiol A (**1**) (28 mg) followed by further arthropsolide A (**20**) (31 mg). Fractions 63–71 (44 mg) were crystallized from dichloromethane to give an inseparable mixture of an arthropsatriols C (**16**) and D (**17**) (21 mg). Fractions 72–86 (59 mg) were chromatographed, eluting with dichloromethane–methanol (20:1), to give arthropsadiol B (**3**) (8 mg) followed by cycloarthropsadiol C (**9**) (12 mg). Fractions 87–112 (30 mg) were chromatographed, eluting with dichloromethane–methanol (20:1 then 10:1), to give arthropsolide D (**31**) (16 mg). Fractions 113–130 (48 mg) were chromatographed to give a mixture of arthropsatriols A (**5**) and B (**6**) (22 mg), which was separated by preparative tlc after developing several times with dichloromethane–methanol (15:1) to afford arthropsatriol A (**5**) (8 mg) and arthropsatriol B (**6**) (6 mg).

*Arthropsadiol A (**1**)* ((4*S**,5*S**6*S**)-6-hydroxy-5-(1-hydroxy-2-oxopropyl)-4-[(*E*)-prop-1-enyl[-2-cyclohexen-1-one) crystallized on standing, as thin needles, mp 78–79°C, $[\alpha]_D^{25}$ −245.7 (*c* 1.05, CH_3OH); cd (*c* 0.39 mM, CH_3OH): $[\theta]_{244}$ -5.14×10^6, $[\theta]_{328}$ -5.08×10^5; uv (CH_3OH) λ_{max} (log ϵ): 229 nm (3.88); Ftir ($CHCl_3$ cast): 3450, 1689, 1108, 1052, 1044 cm^{-1}; ^{1}H nmr ($CDCl_3$): see Table 1; nOe ($CDCl_3$): irradiate δ 4.32 (H8): 3.49 (H4, 3.4%); irradiate δ 3.49 (H4): 6.68 (H5, 3.9%), 5.53 (H2, 9.0%), 5.09 (H3, 3.4%), 4.54 (H10, 2.5%), 4.32 (H6, 7.2%); irradiate δ 2.39 (H5): 5.09 (H7, 4.4%), 4.54 (H10, 6.0%), 2.16 (H12, 2.7%); ^{13}C nmr ($CDCl_3$): see Table 1; hreims (probe 100°C), *m/z* calcd. for $C_{12}H_{16}O_4$ (M^+): 224.1049; found: 224.1050 (1.9), 181 (M^+ − CH_3CO, 100), 151 (20), 150 (26), 135 (38), 107 (28), 80 (21), 79 (27), 43 (30); cims: 242 ($M^+ + NH_4^+$, 100), 225 ($M^+ + NH_4^+$, 29).

Acetylation of arthropsadiol A (**1**) gave the diacetate **2** as a clear oil; uv (CH_3OH) λ_{max} (log ϵ): 225 nm (4.06); Ftir ($CHCl_3$ cast): 1752, 1729, 1701, 1372, 1232 cm^{-1}; ^{1}H nmr ($CDCl_3$) δ: 6.64 (1H, dd, *J* = 10.0, 2.2 Hz, H5), 6.05 (1H, dd, *J* = 10.2, 3.0 Hz, H6), 5.67 (1H, dq, *J* = 15.5, 7.0 Hz, H2), 5.34 (1H, d, *J* = 1.9 Hz, H10), 5.27 (1H, d, *J* = 13.1 Hz, H8), 5.13 (1H, ddq, *J* = 15.0, 9.5, 1.5 Hz, H3), 3.45 (1H, dddd, *J* = 10.0 ,10.0, 2.7, 2.7 Hz, H4), 3.02 (1H, ddd, *J* = 12.7, 10.0, 2.0 Hz, H9), 2.20, 2.18, (3H each, 2 s, 8-OAc, 10-OAc), 2.08 (3H, s, H12), 1.65 (3H, dd, *J* = 7.0, 1.5 Hz, H1); ^{13}C nmr ($CDCl_3$) δ: 204.44 (C11), 192.29 (C7), 169.87 (OAc), 169.81 (OAc), 152.52 (C5), 131.50 (C2), 129.76 (C3), 126.76 (C6), 75.37 (C10), 72.28 (C8), 46.98 (C9), 41.91 (C4), 26.74 (C12), 20.52 (OAc), 20.45 (OAc), 17.45 (C1); hreims (probe 150°C), *m/z* calcd. for $C_{16}H_{22}O_6$ (M^+): 308.1260; found: 308.1269 (0.1), 248 (M^+ − HOAc, 6), 188 (M^+ − 2HOAc, 6), 135 (33), 43 (100); cims: 326 ($M^+ + NH_4^+$, 100).

*Arthropsadiol B (**3**)* ((4*S**,5*S**,6*R**)- 6-hydroxy- 5-(2- hydroxy-1-oxopropyl)-4-[(*E*)]-prop-1-enyl]-2-cyclohexen-1-one) was obtained as a clear oil; $[\alpha]_D^{25}$ −389 (*c* 0.32, CH_3OH); uv (CH_3OH) λ_{max} (log ϵ): 235 nm (3.65); Ftir ($CHCl_3$ cast): 3448, 3426, 1716, 1687, 1096 cm^{-1}; ^{1}H nmr ($CDCl_3$) δ: 6.80 (1H, dd, *J* = 10.0, 5.5 Hz, H5), 6.13 (1H, dd, *J* = 10.0, 1.0 Hz, H6), 5.59 (1H, dq, *J* = 15.5, 6.5 Hz, H2), 5.29 (ddq, *J* = 15.0, 8.2, 1.5 Hz, H3), 4.71 (1H, d, *J* = 12.0 Hz, H8), 4.36 (1H, br qd, *J* = 7.0, 4.0 Hz, H11), 3.52 (1H, d, *J* = 5.7 Hz), 3.48 (1H, m), 3.40 (1H, br d, *J* = 4.5 Hz), 1.68 (3H, dd, *J* = 6.5, 1.5 Hz, H1), 1.39 (3H, d, *J* = 7.5 Hz, H12); nOe ($CDCl_3$): irradiate δ 4.71 (H8): 5.29 (H3, 6.1%); irradiate δ 4.36 (H11): 3.52 (8.1%), 1.39 (H12, 2.0%); irradiate δ 1.39 (H12): 5.29 (H3, 1.0%), 4.71 (H8, 3.3%), 4.36 (H11, 10.8%); ^{13}C nmr ($CDCl_3$) δ: 208.78 (C10), 198.77 (C7), 150.60 (C5), 131.58 (C2), 125.57 (C3), 124.09 (C6), 71.94 (C8), 68.93 (C11), 52.27 (C9), 42.06 (C4), 19.68 (C12), 17.98 (C1); hreims (probe 120°C), *m/z* calcd. for $C_{12}H_{16}O_4$ (M^+): 224.1049; found: 224.1045 (1.5), 206 (M^+ − H_2O, 1.1), 180 (26), 152 (100), 134 (20), 123 (24), 108 (22), 105 (20), 91 (25), 84 (23), 80 (34), 79 (34), 77 (24), 71 (44), 45 (23), 43 (24).

Acetylation of arthropsadiol B (**3**) gave the diacetate **4** as a clear oil; ^{1}H nmr ($CDCl_3$) δ: 6.82 (1H, dd, *J* = 10.0, 5.5 Hz, H5), 6.08 (1H, d, *J* = 10.5 Hz, H6), 5.74 (1H, d, *J* = 12.5 Hz, H8), 5.58 (1H, dqd, *J* = 15.5, 6.5, 1.0 Hz, H2), 5.35 (1H, ddq, *J* = 15.5, 7.5, 1.5 Hz, H3), 5.20 (1H, q, *J* = 7.5 Hz, H11), 3.71 (2H, m, H4, H9), 2.15 (3H, s, OAc), 2.08 (3H, s, OAc), 1.69 (3H, dd, *J* = 6.5, 1.0 Hz, H1), 1.41 (3H, d, *J* = 7.5 Hz, H12); ^{1}H nmr (C_6D_6) δ: 6.03 (1H, d, *J* = 12.8 Hz, H8), 5.99 (1H, dd, *J* = 10.0, 6.0 Hz, H5), 5.79 (1H, d, *J* = 9.8 Hz, H6), 5.35 (1H, ddq, *J* = 15.5, 7.5, 1.5 Hz, H3), 5.23 (1H, dqd, *J* = 15.5, 6.5, 1.0 Hz, H2), 4.77 (1H, q, *J* = 7.2 Hz, H11), 3.24 (1H, dd, *J* = 12.7, 5.5 Hz, H9), 3.14 (1H, br ddd, *J* = 6.0, 6.0, 6.0 Hz, H4), 1.69 (3H, s, OAc), 1.65 (3H, s, OAc), 1.43 (3H, br d, *J* = 6.5 Hz, H1), 1.05 (3H, d, *J* = 7.2 Hz, H12); nOe ($CDCl_3$): irradiate δ 6.82 (H5): 6.08 (H6, 18.7%), 3.71 (H4, H9, 5.2%); irradiate δ 5.74 (H8): 5.35 (H3, 7.3%); irradiate δ 5.35 (H3): 5.74 (H8, 4.3%), 3.71 (H4, H9, 2.7%); nOe (C_6D_6): irradiate δ 3.14 (H4): 3.24 (H9, 14.4%).

*Cycloarthropsone (**12**)* (2,7-dihydroxy-2-methyl-4-[(*E*)-prop-1-enyl[-3(2*H*)-benzofuranone) was obtained as a yellow solid, mp 168–172°C; $[\alpha]_D^{25}$ 0.0 (*c* 1.06, CH_3OH); uv (CH_3OH) λ_{max} (log ϵ): 236 (4.12), 286 (3.94), 387 (3.68), 650 nm (2.18); uv (CH_3OH + NaOH) λ_{max} (log ϵ): 214 (4.14), 258 (4.04), 300 (3.90), 422 (3.68), 650 nm (2.18); Ftir (KBr): 3450, 3170, 1684, 1652, 1627, 1588, 1516, 1288, 1201, 1182, 1084, 968, 908 cm^{-1}; ^{1}H nmr (CD_3OD) δ: 7.08 (1H, dq, *J* = 16.2, 1.7 Hz, H3), 6.99 (1H, d, *J* = 8.8 Hz, H5), 6.93 (1H, d, *J* = 8.8 Hz, H6), 6.27 (1H, dq, *J* = 16.2, 6.8 Hz, H2), 1.78 (3H, dd, *J* = 6.8, 1.5 Hz, H1), 1.43 (3H, s, H12); nOe (CD_3OD): irradiate δ 6.27 (H2): 6.99 (H5, 13.6%), 1.78 (H1, 4.7%); irradiate δ 1.78 (H1): 7.08 (H3, 13.8%), 6.27 (H2, 13.8%); ^{13}C nmr ($CDCl_3/CD_3OD$) δ: 200.67 (C10), 158.20 (8), 141.11 (C7), 130.03 (C4), 128.17 (C2), 125.04 (C3), 124.13 (C6), 117.57 (C5), 114.99 (C9), 103.29 (C11), 21.46 (C12), 18.17 (C1); hreims (probe 100°C), *m/z* calcd. for $C_{12}H_{12}O_4$ (M^+): 220.0735; found: 220.0733 (25), 178 (22), 177 (100), 43 (24); cims: 238 ($M^+ + NH_4^+$, 76), 221 ($M^+ + H^+$, 100).

Acetylation of cycloarthropsone (**12**) gave the diacetate **15** as a clear oil; uv (CH_3OH) λ_{max} (log ϵ): 233 (4.27), 279 (4.06), 287 (4.03), 352 nm (3.79); Ftir ($CHCl_3$ cast): 1768, 1731, 1592, 1507, 1371, 1191, 926 cm^{-1}; ^{1}H nmr ($CDCl_3$) δ: 7.27 (1H, dq, *J* = 16.0, 1.8 Hz, H3), 7.24 (1H, d, *J* = 8.1 Hz, H5 or H6), 7.19 (1H, d, *J* = 8.1 Hz, H5 or H6), 6.49 (1H, dq, *J* = 16.0, 6.9 Hz, H2), 2.33 (3H, s, 7-OAc), 2.09 (3H, s, 11-OAc), 1.94 (3H, dd, *J* = 7.0, 2.0 Hz, H1), 1.61 (3H, s, H12); ^{13}C nmr ($CDCl_3$) δ: 196.02 (C10), 168.11 (OAc), 168.03 (OAc), 159.16 (C8), 136.35 (C4), 133.62 (C7), 131.75 (C2), 130.34 (C6), 124.96 (C3), 118.11 (C5), 117.21 (C9), 102.32 (C11), 20.95 (C1), 20.62 (OAc), 20.25 (OAc), 18.81 (C12); hreims (probe 120°C), *m/z* calcd. for $C_{16}H_{16}O_6$ (M^+): 304.0947; found 304.0949 (4.3), 244 (17), 202 (38), 177 (100), 43 (58); cims: 322 ($M^+ + NH_4^+$, 100).

*Cycloarthropsadiol C (**9**)* ((5*R**,6*S**,8*R**)- 5,6- dihydroxy- 3-methyl- 8-[(*E*)-prop-1-enyl]- 2,4 -dioxatricyclo[3.3.1.1^{3,7}]decan-10-one) was obtained as a clear oil; $[\alpha]_D^{25}$ −38.7 (*c* 0.91, CH_3OH); Ftir ($CHCl_3$ cast)): 3434, 1743, 1440, 1385, 1333, 1235, 1199, 1144, 1129, 1091, 1076, 1048, 1020, 965, 930, 900, 861, 755 cm^{-1}; ^{1}H nmr ($CDCl_3$) δ: 5.64 (1H, dqd, *J* = 15.5, 6.5, 0.8 Hz, H2), 5.46 (1H, ddq, *J* = 15.4, 7.5, 1.5 Hz, H3), 4.24 (2H, br d, *J* = 3.8 Hz, H5, H8), 2.98 (1H, br d, *J* = 7.5 Hz, H4), 2.92 (1H, dd, *J* = 3.8, 3.8 Hz, H9), 2.45 (1H, dd, *J* = 13.4, 4.4 Hz, H6α), 1.94 (1H, dd, *J* = 13.1, 1.8 Hz, H6β), 1.67 (3H, br d, *J* = 6.5 Hz, H1), 1.36 (3H, s, H12); ^{13}C nmr ($CDCl_3$) δ: 202.3 (C10), 129.1 (C2)*, 127.6 (C3)*, 100.1 (C11), 94.1 (C7), 78.4 (C8), 73.5 (C5), 56.1 (C9), 51.3 (C6), 37.2 (C4), 19.5 (C12), 18.0 (C1); hreims (probe 140°C),

Can. J. Chem. Downloaded from www.nrcresearchpress.com by 217.78.4.112 on 09/08/12
For personal use only.

m/z calcd. for $C_{12}H_{16}O_5$ (M^+): 240.0997; found: 240.0993 (1.1), 212 (M^+ − CO, 18), 152 (49), 134 (20), 109 (22), 108 (63), 81 (23), 80 (22), 71 (22), 43 (100).

Acetylation of cycloarthropsadiol C

A solution of cycloarthropsadiol C (**9**) (4.8 mg), acetic anhydride (60 μL), pyridine (40 μL), and a crystal of DMAP in dichloromethane (1 mL) was stirred at room temperature for 3 h, then evaporated to dryness. The resulting oil was chromatographed, eluting with ethyl acetate – hexanes (1:3) to give cycloarthropsadiol C diacetate (**10**) (4.3 mg, 66%) which crystallized on standing; ^{1}H nmr ($CDCl_3$) δ: 6.09 (1H, d, *J* = 4.0 Hz, H8), 5.66 (1H, dqd, *J* = 15.0, 6.5, 1.0 Hz, H2), 5.42 (ddq, *J* = 15.5, 7.8, 1.5 Hz, H3), 4.25 (1H, br dddd, *J* = 3.8, 2.0, 2.0, 2.0 Hz, H5), 3.14 (1H, br d, *J* = 7.8 Hz, H4), 2.99 (1H, ddd, *J* = 4.0, 3.0, 1.7 Hz, H9), 2.79 (1H, dd, *J* = 13.0, 2.0 Hz, H6α), 2.60 (1H, dd, *J* = 13.0, 4.3 Hz, H6β), 2.094 (3H, s, OAc), 2.085 (3H, s, OAc), 1.67 (3H, dd, *J* = 6.5, 1.0 Hz, H1), 1.44 (3H, s, H12); nOe ($CDCl_3$): irradiate δ 6.09 (H8): 3.14 (H4, 6.9%), 2.99 (H9, 10.4%), 2.79 (H6α, 2.3%); irradiate δ 4.25 (H5): 5.42 (H3, 3.1%), 3.14 (H4, 5.2%), 2.79 (H6α, 2.4%), 2.60 (H6β, 5.2%); irradiate δ 3.14 (H4): 6.09 (H8, 10.7%), 5.66 (H2, 8.4%), 5.42 (H3, 4.7%), 4.25 (H5, 8.4%), 2.99 (H9, 7.7%), 2.79 (H6α, 4.7%), 2.60 (H6β, −1.4%); irradiate δ 2.99 (H9): 6.09 (H8, 9.8%), 5.66 (H2, 1.9%), 5.42 (H3, 3.5%), 3.14 (H4, 2.7%); irradiate δ 2.79 (H6α): 6.09 (H8, 8.3%), 4.25 (H5, 7.8%), 3.14 (H4, 5.3%), 2.60 (H6β, 29.6%); irradiate δ 2.60 (H6β): 4.25 (H5, 11.4%), 2.79 (H6α, 20.2%); hreims (probe 120°C), *m/z* calcd. for $C_{15}H_{20}O_6$ (M^+ − CO); 296.1260; found: 290.1260 (13), 152 (30), 134 (29), 108 (64), 43 (100); cims: 342 ($M^+ + NH_4^+$, 51), 325 ($M^+ + H^+$, 20), 282 (80), 265 (100).

Further elution of the column with ethyl acetate – hexanes (1:2) gave cycloarthropsadiol C-8-acetate (**11**) (1.5 mg, 27%); ^{1}H nmr ($CDCl_3$) δ: 5.66 (1H, dqd, *J* = 15.5, 6.5, 1.0 Hz, H2), 5.43 (1H, ddq, *J* = 15.5, 7.5, 1.5 Hz, H3), 5.27 (1H, d, *J* = 2.7 Hz, H8), 4.27 (1H, br dddd, *J* = 3.8, 2.0, 2.0, 2.0 Hz, H5), 3.07 (1H, br d, *J* = 7.5 Hz, H4), 2.98 (1H, ddd, *J* = 3.5, 3.5, 1.8 Hz, H9), 2.46 (1H, dd, *J* = 13.1, 4.0 Hz, H6), 2.14 (3H, s, OAc), 2.03 (1H, dd, *J* = 13.1, 1.8 Hz, H6), 1.67 (3H, dd, *J* = 6.5, 1.0 Hz, H1), 1.39 (3H, s, H12).

Arthropsatriol A (**5**) ((1*R**,4*S**,5*S**,6*S**)-5-(1-hydroxy-2-oxopropyl)-4-[(*E*)-prop-1-enyl]-2-cyclohexene-1,6-diol) was obtained as a clear oil; Ftir ($CHCl_3$ cast): 3400, 1708, 1357, 1234, 1110, 1074, 1031, 973 cm^{-1}; ^{1}H nmr ($CDCl_3$) δ: 5.82 (1H, ddd, *J* = 9.5, 5.5, 2.5 Hz, H6), 5.59 (1H, dd, *J* = 10.0, 2.5 Hz, H5), 5.37 (1H, dq, *J* = 15.2, 6.5 Hz, H2), 5.02 (1H, ddq, *J* = 15.5, 9.5, 1.5 Hz, H3), 4.60 (1H, br s, OH), 4.19 (1H, br dd, *J* = 4.5, 4.5 Hz, H7), 3.94 (1H, br s, H10), 3.81 (1H, dd, *J* = 10.5, 4.3 Hz, H8), 3.15 (1H, br s, OH), 2.97 (1H, br dddd, *J* = 9.5, 9.5, 2.5, 2.5 Hz, H4), 2.60 (1H, v br s, OH), 2.21 (1H, ddd, *J* = 10.5, 9.5, 1.5 Hz, H9), 2.17 (3H, s, H12), 1.57 (3H, dd, *J* = 6.5, 1.5 Hz, H1); ^{13}C nmr ($CDCl_3$) δ: 210.71 (C11), 135.98 (C5), 131.32 (C3), 129.92 (C2), 124.86 (C6), 75.16 (C10), 69.05 (C8), 65.86 (C7), 43.75 (C9), 39.67 (C4), 25.70 (C12), 17.49 (C1); hreims (probe 100°C), *m/z* calcd. for $C_{12}H_{16}O_3$ ($M^+ - H_2O$): 208.1099; found: 208.1103 (0.7), 190 ($M^+ - 2H_2O$, 1.3), 183 ($M^+ - CH_3CO$, 29), 165 (50), 147 (25), 135 (71), 134 (31), 119 (48), 110 (25), 107 (51), 95 (38), 95 (56), 93 (20), 91 (100), 81 (34), 79 (50), 77 (37), 74 (44), 73 (41), 71 (38), 67 (35), 57 (22), 55 (25), 53 (26); cims: 244 ($M^+ + NH_4^+$, 71), 226 (53), 209 (100).

Acetylation of arthropsatriol A (**5**) gave the corresponding triacetate **7** as a clear oil; Ftir ($CHCl_3$ cast): 1746, 1710, 1371, 1241, 1230, 1060, 1028, 1016 cm^{-1}; ^{1}H nmr ($CDCl_3$) δ: 5.72 (1H, ddd, *J* = 10.5, 5.5, 2.3 Hz, H6), 5.67 (1H, dd, *J* = 9.5, 2.1 Hz, H5), 5.53 (1H, dq, *J* = 15.0, 6.5 Hz, H2), 5.45 (1H, ddd, *J* = 5.0, 3.8, 1.0 Hz, H7), 5.34 (1H, d, *J* = 1.8 Hz, H10), 5.07 (1H, ddq, *J* = 15.2, 9.5, 1.6 Hz, H3), 4.94 (1H, dd, *J* = 12.2, 3.8 Hz, H8), 3.10 (1H, br dddd, *J* = 9.5, 9.5, 2.0, 2.0 Hz, H4), 2.80 (1H, ddd, *J* = 12.2, 10.5, 2.0 Hz, H9), 2.16, 2.12, 2.09, 2.01 (3H each, 4 s, 3 × OAc, H12), 1.61 (3H, dd, *J* = 6.5, 1.5 Hz, H1); nOe ($CDCl_3$): irradiate δ 5.45 (H7): 5.72 (H6, 9.0%), 4.94 (H8, 13.0%); irradiate δ 5.34 (H10): 4.94 (H8, 2.8%), 2.80 (H9, 10.8%); irradiate δ 4.94 (H8): 5.45 (H7, 16.5%), 3.10 (H4, 7.6%); irradiate δ 3.10 (H4): 5.67 (H5, 14.7%), 5.53 (H2, 10.7%), 5.07 (H3, 6.6%), 4.94 (H8, 10.7%); irradiate δ 2.80 (H9): 5.34 (H10, 16.6%), 5.07 (H3, 10.8%); hreims (probe 150°C), *m/z* calcd. for $C_{14}H_{18}O_4$ (M^+ −HOAc − CH_2CO): 250.1205; found: 250.1208 (0.6), 232 (M^+ −2HOAc, 0.6), 147 (27), 135 (28), 134 (27), 129 (28), 116 (25), 91 (27), 43 (100); cims: 370 ($M^+ + NH_4^+$, 100).

Arthropsatriol B (**6**) ((1*S**,4*S**,5*S**,6*S**)-5-(1-hydroxy-2-oxopropyl)-4-[(*E*)-prop-1-enyl]-2-cyclohexene-1,6-diol) was obtained as a clear oil; $[\alpha]_D^{25}$ − 216 (*c* 1.00, CH_3OH); ^{1}H nmr ($CDCl_3$) δ: 5.53 (1H, br ddd, *J* = 10.0, 2.0, 2.0 Hz, H6), 5.38–5.26 (2H, m, H5, H2), 4.95 (1H, ddq, *J* = 15.5, 9.5, 1.5 Hz, H3), 4.62 (1H, br s, OH), 4.25 (1H, br s, H10), 4.19 (1H, br d, *J* = 7.5 Hz, H7), 3.64 (1H, dd, *J* = 10.6, 8.0 Hz, H8), 2.99 (1H, br dddd, *J* = 9.5, 9.5, 5.5, 2.5 Hz, H4), 2.14 (3H, s, H12), 2.07 (1H, br dd, *J* = 10.2, 10.2 Hz, H9), 1.55 (3H, dd, *J* = 6.5, 1.5 Hz, H1); ^{13}C nmr ($CDCl_3$) δ: 210.65 (C11), 131.66 (C5), 131.53 (C3), 129.80 (C2), 127.67 (C6), 74.85 (C10), 72.98 (C7), 72.74 (C8), 47.53 (C9), 39.74 (C4), 25.78 (C12), 17.52 (C1); hreims (probe 120°C), *m/z* calcd. for $C_{12}H_{16}O_3$ ($M^+ - H_2O$): 208.1099; found: 208.1099 (0.9), 165 (37), 147 (30), 135 (100), 134 (43), 119 (40), 110 (43), 107 (52), 95 (61), 91 (74), 81 (29), 79 (35), 77 (26), 74 (56), 73 (24), 71 (22), 67 (28), 57 (25), 56 (23), 55 (21), 53 (20); cims: 244 ($M^+ + NH_4^+$, 100).

Acetylation of arthropsatriol B (**6**) gave the triacetate **8** as a clear oil; ^{1}H nmr ($CDCl_3$) δ: 5.56–5.45 (4H, m, H2, H5, H6, H7), 5.21 (1H, d, *J* = 2.0 Hz, H10), 5.12 (1H, dd, *J* = 12.0, 8.5 Hz, H8), 4.99 (1H, ddq, *J* = 15.5, 9.8, 1.5 Hz, H3), 3.18 (1H, br dd, *J* = 10.0, 10.0 Hz, H4), 2.63 (1H, ddd, *J* = 12.5, 10.5, 2.0 Hz, H9), 2.17 (3H, s, OAc), 2.05 (3H, s, OAc), 2.03 (6H, s, OAc, H12), 1.59 (3H, dd, *J* = 6.5, 1.5 Hz, H1); ^{1}H nmr (C_6D_6) δ: 5.73 (1H, dddd, *J* = 8.5, 3.0, 2.0, 2.0 Hz, H7), 5.42 (1H, d, *J* = 2.3 Hz, H10), 5.41 (1H, dd, *J* = 11.6, 8.2 Hz, H8), 5.38 (1H, ddd, *J* = 9.8, 2.2, 2.2 Hz, H6), 5.24 (1H, ddd, *J* = 10.0, 2.2, 2.2 Hz, H5), 5.20 (1H, dq, *J* = 15.5, 6.5 Hz, H2), 4.78 (1H, ddq, *J* = 15.0, 9.6, 1.5 Hz, H3), 3.09 (1H, br dddd, *J* = 9.6, 9.6, 5.6, 2.6 Hz, H4), 2.51 (1H, ddd, *J* = 12.5, 10.3, 2.0 Hz, H9), 1.840, 1.792, 1.690, 1.687 (3H each, 4s, 3 OAc, H12), 1.34 (3H, dd, *J* = 6.5, 1.8 Hz, H1); nOe (C_6D_6): irradiate δ 5.73 (H7): 5.38 (H6, 8.3%), 2.51 (H9, 6.5%); irradiate δ 4.78 (H3): 3.09 (H4, 1.9%), 2.51 (H9, 4.9%); irradiate δ 3.09 (H4): 5.41 (H8, 8.2%), 5.24–5.20 (H5, H2, 9.1%), 4.78 (H3, 3.0%); irradiate δ 2.51 (H9): 5.73 (H7, 9.5%), 5.42 (H10, 10.3%), 4.78 (H3, 7.8%).

Arthropsatriol C (**16**) and *arthropsatriol D* (**17**) ((2*S**, 3*R**,4*S**)- and (2*S**,3*R**,4*R**)-3,4-dihydro-2,3-dimethyl-2,4,6-trihydroxy-1(2*H*)-naphthalenone) were obtained as a white solid; uv (CH_3OH) λ_{max} (log ε): 229 (4.00), 255 (3.91), 321 nm (3.43); Ftir (KBr): 3406, 1678, 1603, 1445, 1390, 1315, 1223, 1166, 1154, 1135, 1011, 968, 834 cm^{-1}; ^{1}H nmr (CD_3OD) δ: (major epimer, arthropsatriol C): 7.32 (1H, d, *J* = 8.5 Hz, H5), 7.22 (1H, d *J* = 2.5 Hz, H8), 6.98 (1H, dd, *J* = 8.2, 2.5 Hz, H6), 4.96 (1H, d, *J* = 4.5 Hz, H3), 2.29 (1H, qd, *J* = 7.0, 4.6 Hz, H2), 1.29 (3H, s, H12), 0.94 (3H, d, *J* = 7.0 Hz, H1); δ (minor epimer, arthropsatriol D): 7.47 (1H, dd, *J* = 8.5, 1.0 Hz, H5), 7.21 (1H, d, *J* = 2.5 Hz, H8), 7.01 (1H, dd, *J* = 8.5, 2.6 Hz, H6), 4.33 (1H, d, *J* = 9.8 Hz, H3), 2.00 (1H, dq, *J* = 9.5, 6.8 Hz, H2), 1.19 (3H, d, *J* = 6.9 Hz, H1), 1.08 (3H, s, H12); hreims (probe 150°C), *m/z* calcd. for $C_{12}H_{14}O_4$ (M^+): 222.0892; found: 222.0888 (4.6), 204 (38), 162 (34), 161 (90), 150 (23), 122 (53), 121 (100), 65 (23), 43 (46), 39 (20); cims: 240 ($M^+ + NH_4^+$, 100).

Acetylation of the mixture of arthropsatriols C and D

A solution of the mixture of arthropsatriols C and D (20 mg), acetic anhydride (0.25 mL), pyridine (0.25 mL), and a crystal of DMAP in dichloromethane (5.5 mL) was stirred at room temperature for 4 h, then diluted with ethyl acetate and washed successively with 1 M hydrochloric acid, water, and saturated sodium hydrogen carbonate. Evaporation of the dried solution gave an oil that was subjected to preparative tlc. Several developments with dichloromethane – methanol (100:1) gave 3 bands, which were

Can. J. Chem. Downloaded from www.nrcresearchpress.com by 217.78.4.112 on 09/08/12
For personal use only.

eluted with ethyl acetate to give, in order of decreasing R_f: a mixture of 2 triacetates (2.0 mg, 6%); arthropsatriol D diacetate (**19**) (7.4 mg, 27%), and arthropsatriol C diacetate (**18**) (10.3 mg, 37%).

Arthropsatriol D diacetate (**19**) was obtained as a clear oil; uv (CH_3OH) λ_{max} (log ϵ): 218 (4.09), 243 (4.05), 292 nm (3.36); Ftir ($CHCl_3$ cast): 3492, 1765, 1749, 1693, 1609, 1371, 1230, 1206, 1190, 759 cm^{-1}; ^1H nmr ($CDCl_3$) δ: 7.76 (1H, d, J = 2.5 Hz, H8), 7.35 (1H, dd, J = 8.5, 2.5 Hz, H6), 7.27 (1H, d, J = 8.5 Hz, H5), 6.03 (1H, d, J = 10.6 Hz, H3), 3.87 (1H, s, OH), 2.38 (1H, dq, J = 10.6, 6.8 Hz, H2), 2.33 (3H, s, 7-OAc), 2.25 (3H, s, 3-OAc), 1.28 (3H, s, H12), 1.22 (3H, d, J = 6.5 Hz, H1); nOe ($CDCl_3$): irradiate δ 7.27 (H5): 7.35 (H6, 3.8%), 6.03 (H3, 2.4%); irradiate δ 6.03 (H3): 7.27 (H5, 4.0%); irradiate δ 2.38 (H2): 1.22 (H1, 1.7%); irradiate δ 1.28 H12): 6.03 (H3, 14.0%); irradiate δ 1.22 (H1): 6.03 (H3, 10.2%); ^{13}C nmr ($CDCl_3$) δ: 200.15 (C10), 171.07 (OAc), 169.01 (OAc), 150.76 (C7), 138.97 (C4), 130.11 (C9), 128.29 (C6), 128.14 (C8), 120.14 (C5), 75.96 (C11), 72.29 (C3), 45.39 (C2), 21.01 (OAc), 20.92 (OAc), 19.58 (C12), 10.61 (C1); hreims (probe 140°C), m/z calcd. for $C_{16}H_{18}O_6$ (M^+): 306.1103; found: 306.1100 (1.1), 246 (18), 204 (77), 203 (21), 192 (24), 162 (57), 161 (100), 150 (45), 149 (25).

Arthropsatriol C diacetate (**18**) was obtained as a clear oil; uv (CH_3OH) λ_{max} (log ϵ): 212 (4.21), 246 (4.01), 294 nm (3.23); Ftir ($CHCl_3$ cast): 3492, 1767, 1740, 1694, 1608, 1371, 1234, 1205, 1191, 757 cm^{-1}; ^1H nmr ($CDCl_3$) δ: 7.75 (1H, d, J = 2.5 Hz, H8), 7.53 (1H, d, J = 8.5 Hz, H5), 7.33 (1H, dd, J = 8.5, 2.5 Hz, H6), 6.27 (1H, d, J = 4.3 Hz, H3), 3.57 (1H, br s, OH), 2.58 (1H, qd, J = 7.0, 4.5 Hz, H2), 2.33 (3H, s, 7-OAc), 2.12 (3H, s, 3-OAc), 1.42 (3H, s, H12), 1.21 (3H, d, J = 7.0 Hz, H1); nOe ($CDCl_3$): irradiate δ 7.53 (H5): 7.33 (H6, 13.6%), 6.27 (H3, 9.1%); irradiate δ 7.33 (H6): 7.53 (H5, 11.1%); irradiate δ 6.27 (H3): 7.53 (H5, 10.7%), 2.58 (H2, 13.9%); irradiate δ 2.58 (H2): 6.27 (H3, 11.8%); irradiate δ 1.42 (H12): 1.21 (H1, 1.5%); irradiate δ 1.21 (H1): 6.27 (H3, 6.1%), 2.58 (H2, 15.3%); ^{13}C nmr ($CDCl_3$) δ: 200.86 (C10), 170.62 (OAc), 169.06 (OAc), 151.28 (C7), 137.59 (C4), 131.49 (C8)*, 130.69 (C9), 128.28 (C6)*, 120.57 (C5), 75.26 (C11), 69.89 (C3), 41.12 (C2), 22.44 (C12), 20.99 (OAc), 10.20 (C1), one signal obscured; hreims (probe 110°C), m/z calcd. for $C_{16}H_{18}O_6$ (M^+): 306.1103; found: 306.1102 (1.8), 246 (37), 204 (100), 192 (21), 162 (49), 161 (78), 150 (41), 149 (22), 43 (57).

Arthropsolide A (**20**) ((4*S**,5*R**,6*S**,10*S**)-4,6-dihydroxy-3-methylidene-10-[(*E*)-prop-1-enyl]- 2- oxospiro[4.5]dec- 8-en-1,7-dione) crystallized from dichloromethane as fine needles, mp 142–145°C, $[\alpha]_D^{25}$ −302 (*c* 1.00, CH_3OH); cd (*c* 0.40 mM, CH_3OH): $[\theta]_{241}$ -4.85×10^6, $[\theta]_{332}$ -4.49×10^5; uv (CH_3OH) λ_{max} (log ϵ): 204 (4.39), 236 nm (4.07); Ftir ($CHCl_3$ cast): 3400, 1798, 1685, 1164, 1143, 1117, 1080 cm^{-1}; ^1H nmr ($CDCl_3$): see Table 1; ^{13}C nmr ($CDCl_3$): see Table 1; hreims (probe 120–180°C), m/z calcd. for $C_{13}H_{14}O_5$ (M^+): 250.0841; found: 250.0838 (1.1), 232 ($M^+ - H_2O$, 3.3), 214 ($M^+ - 2H_2O$, 1.3), 108 (100), 100 (20), 80 (93), 79 (46), 77 (24), 39 (23); cims: 268 ($M^+ + NH_4^+$, 100).

Benzoylation of arthropsolide A

A solution of arthropsolide A (**20**) (9.0 mg), benzoyl chloride (40 μL), pyridine (50 μL), and a crystal of DMAP in dichloromethane (2 mL) was stirred at room temperature for 3 days under argon. The mixture was diluted with ethyl acetate and washed successively with 1 M hydrochloric acid, water, and saturated sodium hydrogen carbonate. Evaporation of the dried solution and flash chromatography of the product, eluting with ethyl acetate – hexanes (1:3), gave successively arthropsolide A dibenzoate (**21**) (12.3 mg, 74%), and a monobenzoate of arthropsolide A (3.5 mg, 25%). Arthropsolide A dibenzoate (**21**) crystallized from acetone–dichloromethane–hexanes as prisms, mp 182–184°C; Ftir ($CHCl_3$ cast): 1809, 1737, 1709, 1682, 1600, 1583, 1452, 1250, 1111, 1071, 1061, 1022, 972, 755, 708 cm^{-1}; ^1H nmr ($CDCl_3$) δ: 8.15–8.04 (4H, m, ArH), 7.73–7.42 (6H, m, ArH), 6.58 (1H, dd, J = 10.1, 2.5 Hz, H5), 6.31 (1H, dd, J = 2.2, 2.2 Hz, H10), 6.26 (1H, dd, J = 10.1, 3.0 Hz, H6), 6.10 (1H, s, H8), 5.82 (1H, dq, J = 15.2, 6.5 Hz, H2), 5.62 (1H, ddq, J = 15.2, 8.0, 1.5 Hz, H3), 4.96 (1H, dd, J = 3.0, 3.0 Hz, H12A), 4.62 (1H, dd, J = 2.5, 2.5 Hz, H12B), 3.71 (1H, br ddd, J = 8.0, 2.5, 2.5 Hz, H4), 1.76 (3H, dd, J = 6.3, 1.5 Hz, H1); nOe ($CDCl_3$): irradiate δ 6.10 (H8): 6.31 (H10, 4.9%), 3.71 (H4, 10.7%); irradiate δ 4.96 (H12A): 4.62 (H12B, 42.6%); irradiate δ 4.62 (H12B): 6.31 (H10, 3.7%), 4.96 (H12A, 41.3%); irradiate δ 3.71 (H4): 6.58 (H5, 10.6%), 6.31 (H10, 1.0%), 6.26 (H6, −1.0%), 6.10 (H8, 16.0%), 5.82 (H2, 6.9%), 5.62 (H3, 8.8%); hreims (probe 200°C), m/z calcd. for $C_{27}H_{22}O_7$ (M^+): 458.1365; found: 458.1370 (1.3), 336 $M^+ - C_6H_5CO_2H$, 3.7), 105 (100), 77 (23).

Arthropsolide B (**25**) and *arthropsolide C* (**26**) ((5*R**,6*S**,10*S**)- and (5*R**,6*R**,10*S**)-6-hydroxy-3-methylidene-10-[(*E*)-prop-1-enyl]-2-oxaspiro[4.5]dec-8-en-1,4,7-trione respectively) were obtained as an unstable pink oil; uv (CH_3OH) λ_{max} (log ϵ): 213 (3.93), 242 nm (3.93); Ftir ($CHCl_3$ cast): 3480, 1814, 1753, 1698, 1649, 1260, 1116 cm^{-1}; ^1H nmr ($CDCl_3$) δ (major epimer): 6.67 (1H, dd, J = 10.0, 2.3 Hz, H5), 6.30 (1H, dd, J = 10.5, 3.3 Hz, H6), 5.70 (1H, dq, J = 15.0, 6.8 Hz, H2), 5.49 (1H, d, J = 3.4 Hz, H8), 5.29 (1H, ddq, J = 14.9, 8.8, 1.5 Hz, H3), 5.15 (1H, d, J = 2.8 Hz, H12), 4.57 (1H, d, J = 2.0 Hz, H12), 3.80 (1H, d, J = 2.3 Hz, OH), 3.76 (1H, ddd, J = 9.2, 2.5, 2.5 Hz, H4), 1.66 (3H, dd, J = 6.6, 2.0 Hz, H1); (minor epimer): 6.68 (1H, dd, J = 10.0, 2.3 Hz, H5), 6.30 (1H, dd, J = 10.5, 3.3 Hz, H6), 5.80 (1H, dq, J = 15.0, 6.8 Hz, H2), 5.39 (1H, d, J = 2.7 Hz, H8), 5.23 (1H, ddq, J = 15.2, 9.5, 2.0 Hz, H3), 5.10 (1H, d, J = 3.3 Hz, H12), 4.63 (1H, d, J = 2.2 Hz, H12), 3.86 (1H, ddd, J = 9.5, 2.5, 2.5 Hz, H4), 3.70 (1H, d, J = 1.9 Hz, OH), 1.67 (3H, dd, J = 6.6, 2.0 Hz, H1); ^{13}C nmr ($CDCl_3$) δ: 194.41 (C10), 193.52/193.36 (C7), 169.83/168.55 (C13), 150.29 (C11), 148.38/148.04 (C5), 134.44/134.38 (C6), 126.42/126.38 (C3), 123.91/123.63 (C2), 96.47/95.90 (C12), 73.21/72.78 (C8), 61.41 (C9), 45.26/44.56 (C4), 17.84 (C1); hreims (probe 80–150°C), m/z calcd. for $C_{13}H_{12}O_5$ (M^+): 248.0685; found: 248.0688 (0.5), 219 ($M^+ - CHO$, 0.5), 191 ($M^+ - C_2HO_2$, 0.5), 191 ($M^+ - C_3H_5O$, 0.3), 165 ($M^+ - C_4H_3O_2$, 2.8), 108 ($M^+ - C_6H_4O_4$, 100), 80 (75), 79 (40); cims: 266 ($M^+ + NH_4^+$, 100).

Arthropsolide D (**31**) ((4*S**,5*R**,6*S**,7*S**,10*S**)-3-methylidene- 10-[(*E*)-prop-1-enyl]-4,6,7-trihydroxy- 2-oxaspiro[4.5]dec-8-en-1-one was obtained as an oily solid; $[\alpha]_D^{25}$ −239 (*c* 1.09, CH_3OH); Ftir ($CHCl_3$ cast): 3400, 1784, 1679, 1099, 1063 cm^{-1}; ^1H nmr ($CDCl_3$) δ: 5.69 (1H, br d, J = 9.5 Hz, H5), 5.63 (1H, dq, J = 15.0, 7.0 Hz, H2), 5.60 (1H, br d, J = 6.0 Hz, OH), 5.49 (1H, br dd, J = 10.0, 1.5 Hz, H6), 5.28 (1H, ddq, J = 15.5, 8.5, 1.8 Hz, H3), 5.19 (1H, br ddd, J = 6.5, 2.0, 2.0 Hz, H10), 4.80 (1H, br s, H7), 4.75 (1H, dd, J = 2.2, 2.2 Hz, H12), 4.65 (1H, dd, J = 2.2, 2.2 Hz, H12), 4.24 (1H, br s, OH), 3.69 (1H, br s, H8), 3.60 (1H, br d, J = 8.5 Hz, H4), 2.48 (1H, br s, OH), 1.60 (3H, dd, J = 6.5, 1.5 Hz, H1); ^{13}C nmr ($CDCl_3$) δ: 174.49 (C13), 157.02 (C11), 131.07 (C2)*, 129.78 (C6)*, 127.28 (C5)*, 127.20 (C3)*, 88.67 (C12), 72.22 (C10)**, 69.70 (C8)**, 69.14 (C7)**, 57.72 (C9), 39.40 (C4), 17.81 (C1); hreims (probe 150°C), m/z calcd. for $C_{13}H_{16}O_5$ (M^+): 252.0997; found: 252.0980 (1.0), 234 ($M^+ - H_2O$, 38), 162 (62), 161 (100), 147 (37), 134 (41), 133 (29), 125 (20), 121 (25), 110 (38), 107 (32), 105 (24), 95 (79), 91 (55), 88 (36), 81 (43), 79 (40), 77 (46), 73 (48), 72 (43), 71 (34), 70 (51), 43 (20); cims: 270 ($M^+ + NH_4^+$, 100).

Benzoylation of arthropsolide D

A solution of arthropsolide D (**31**) (8.0 mg), benzoyl chloride (110 μL), pyridine (100 μL), and a crystal of DMAP in dichloromethane (2 mL) was stirred at room temperature for 24 h under argon. The mixture was diluted with ethyl acetate and washed successively with 1 M hydrochloric acid, water, and saturated sodium hydrogen carbonate. Evaporation of the dried solution and flash chromatography of the product, eluting with ethyl acetate – hexanes (1:5), gave arthropsolide D tribenzoate (**32**) as an oil (7.3 mg, 41%); cd (*c* 0.135, CH_3OH) 25°C: $[\theta]_{236}$ $+4.65 \times 10^4$; ^1H nmr ($CDCl_3$) δ: 8.14–7.33 (15H, m, ArH), 6.42 (1H, dddd,

J = 8.5, 3.0, 2.0, 2.0 Hz, H7), 6.25 (1H, dd, J = 2.2, 2.2 Hz, H10), 6.09 (1H, d, J = 8.5 Hz, H8), 5.91 (1H, ddd, J = 10.5, 2.6, 2.6 Hz, H6), 5.78 (1H, dqd, J = 15.5, 6.5, 1.0 Hz, H2), 5.62 (1H, ddd, J = 10.5, 2.2, 2.2 Hz, H5), 5.54 (1H, ddq, J = 15.5, 8.2, 1.5 Hz, H3), 4.86 (1H, dd, J = 2.6, 2.6 Hz, H12A), 4.48 (1H, dd, J = 3.2, 2.6 Hz, H12B), 3.57 (1H, br dddd, J = 8.0, 2.5, 2.0, 2.0 Hz, H4), 1.71 (3H, dd, J = 6.5, 1.0 Hz, H1); nOe ($CDCl_3$): irradiate δ 6.42 (H7): 5.91 (H5, 9.8%); irradiate δ 6.25 (H10): 6.09 (H8, 9.3%), 4.48 (H12B, 1.6%); irradiate δ 6.09 (H8): 6.25 (H10, 7.8%), 3.57 (H4, 9.0%); irradiate δ 5.91 (H6): 6.42 (H7, 12.4%), 5.62 (H5, 12.9%); irradiate δ 5.62 (H5): 5.91 (H6, 14.2%), 3.57 (H4, 8.1%); irradiate δ 4.86 (H12A): 4.48 (H12B, 39.5%); irradiate δ 4.48 (H12B): 6.25 (H10, 4.1%), 4.86 (H12A, 37.0%); irradiate δ 3.57 (H4): 6.25 (H10, 1.4%), 6.09 (H8, 11.1%), 5.78 (H2, 7.2%), 5.62 (H5, 8.3%), 5.54 (H3, 9.4%).

Oxidation of arthropsolide A

Pyridinium chlorochromate (20 mg) was added to a stirred solution of arthropsolide A (**20**) (5.0 mg) in dichloromethane (1 mL) and the mixture was stirred at room temperature for 30 min. Further pyridinium chlorochromate (30 mg) was added and stirring continued for an additional 2 h. The mixture was poured onto a pad of silica gel and eluted with ethyl acetate – hexanes (1:1). Evaporation of the filtrate and flash chromatography of the product, eluting with ethyl acetate – hexanes (1:2), gave a mixture of arthropsolides B (**25**) and C (**26**) as a clear oil (1.4 mg); ^{1}H nmr identical with that of the mixture of arthropsolides B and C isolated from the culture broth.

Acknowledgements

The financial support of the Natural Sciences and Engineering Research Council of Canada is gratefully acknowledged. The authors wish to thank Dr. B. Santasiero of the Chemistry Department of the University of Alberta for the X-ray structure determination of arthropsolide A dibenzoate, and Lynne Sigler, University of Alberta Microfungus Herbarium, for cultures of *A. truncata* and for valuable discussion. We would like to wish Denny Valenta continued good health and good chemistry in the years ahead, and thank him for friendship and inspiration over the years.

1. W. A. Ayer and K. Nozawa. Can. J. Microbiol. **36**, 83 (1990).
2. W. A. Ayer and P. A. Craw. Can. J. Chem. Accepted for publication.
3. L. Sigler, Y. Yamaoka, and Y. Hiratsuka. Can. J. Microbiol. **36**, 77 (1990).
4. L. Sigler, M. T. Dunn, and J. W. Carmichael. Mycotaxon, **15**, 409 (1982).
5. K. Nakanishi and P. H. Solomon. Infrared absorption spectroscopy. Holden–Day, Inc., Oakland, Calif. 1977. pp. 38–41. 2nd ed.
6. M. Baiwir, G. Llabres, L. Christiaens, A. Luxen, and J.-L. Piette. Spectrochim. Acta, **39A**, 693 (1983).
7. E. Breitmaier and W. Voelter. Carbon-13 NMR spectroscopy. 3rd ed. VCH Publishers, Weinheim. 1987. pp. 256–257.
8. R. M. Silverstein, C. G. Bassler, and T. C. Morrill. Spectrometric identification of organic compounds. 3rd ed. John Wiley & Sons, New York. 1974. pp. 249–251.
9. P. Sandmeier and C. Tamm. Helv. Chim. Acta, **72**, 784 (1989).
10. P. Sandmeier and C. Tamm. Helv. Chim. Acta, **72**, 1107 (1989).
11. P. Sandmeier and C. Tamm. Helv. Chim. Acta, **73**, 975 (1990).
12. F. Sugawara, N. Takahashi, G. A. Strobel, S. A. Strobel, H. S. M. Lu, and J. Clardy. J. Am. Chem. Soc. **110**, 4086 (1988).
13. N. Harada and K. Nakanishi. J. Am. Chem. Soc. **91**, 3989 (1969).
14. W. A. Ayer, P. A. Craw, T. J. Stout, and J. Clardy. Can. J. Chem. **67**, 773 (1989).

Can. J. Chem. Downloaded from www.nrcresearchpress.com by 217.78.4.112 on 09/08/12
For personal use only.

Biosynthesis and biogenetic interrelationships of metabolites of the fungus *Arthropsis truncata*

WILLIAM A. AYER[1] AND PETER A. CRAW
Department of Chemistry, University of Alberta, Edmonton, Alta., Canada T6G 2G2

Received November 11, 1991

This paper is dedicated to Professor Zdenek (Denny) Valenta on the occasion of his 65th birthday

WILLIAM A. AYER and PETER A. CRAW. Can. J. Chem. **70**, 1348 (1992).

The incorporation of sodium [1-^{13}C]acetate and sodium [1,2-$^{13}C_2$]acetate into a number of polyketide metabolites produced by the fungus *Arthropsis truncata* has been examined. The location of sodium [1-^{13}C]acetate incorporation into arthropsadiol A (**1**), cycloarthropsone (**2**), and arthropsatriol C (**3**) has been determined by ^{13}C nuclear magnetic resonance spectra of the corresponding diacetate derivatives, and a biosynthetic pathway is proposed to account for the formation of **1–3**. Multiple incorporation of sodium [1,2-$^{13}C_2$]acetate into arthropsadiol A (**1**) leads to a complicated pattern of satellite multiplets in the ^{13}C nmr spectrum of the corresponding diacetate **6** that are interpreted with the aid of 2D-INADEQUATE spectra. A biosynthesis of arthropsolide A (**5**) is proposed and the absence of **5** and related metabolites in cultures of the *Arthropsis truncata* fed with ^{13}C-labelled sodium acetate is discussed.

WILLIAM A. AYER et PETER A. CRAW. Can. J. Chem. **70**, 1348 (1992).

On a étudié l'incorporation du [1-^{13}C] acétate de sodium et du [1,2-$^{13}C_2$]acétate de sodium dans un certain nombre de métabolites polycétides produits par le champignon *Arthropsis truncata*. En se basant sur le spectre RMN du ^{13}C des diacétates correspondants, on a déterminé la position d'incorporation du [1-^{13}C] acétate de sodium dans l'arthropsadiol A (**1**), la cycloarthropsone (**2**) et l'arthropsatriol C (**3**) et on propose une voie de biosynthèse qui tient compte de la formation des produits **1–3**. L'incorporation multiple du [1,2-^{13}C] acétate de sodium dans l'arthropsadiol A (**1**) conduit à un patron compliqué de multiplets satellites dans le spectre RMN du ^{13}C du diacétate correspondant **6** que l'on a pu interpréter à l'aide de spectres 2D-INADEQUATE. On propose une voie de biosynthèse de l'arthropsolide A (**5**) et on discute de l'absence de **5** et des métabolites apparentés dans les cultures de l'*Arthropsis truncata* dans lesquelles on a ajouté de l'acétate de sodium marqué au ^{13}C.

[Traduit par la rédaction]

Introduction

In the preceding paper we described the isolation and structure determination of 12 new polyketide metabolites produced in liquid cultures of the fungus *Arthropsis truncata* (1). As a continuation of our investigations of the chemistry of this fungus we have examined the incorporation of sodium [1-^{13}C]acetate and sodium [1,2-$^{13}C_2$]acetate by the fungus with the aim of elucidating the biosynthesis and biogenetic interrelationship of these interesting polyketide metabolites.

Discussion

Incorporation of sodium [1-^{13}C]acetate

Arthropsis truncata was grown as before (1) in liquid shake culture on a modified malt extract medium and was periodically supplemented with injections of a sterile solution of sodium [1-^{13}C]acetate. Chromatography of the ethyl acetate extract of the culture broth gave mainly arthropsadiol A (**1**) and lesser amounts of cycloarthropsone (**2**), and arthropsatriols C (**3**) and D (**4**). Surprisingly, none of the 2-oxaspiro[4.5]dec-8-ene metabolites (e.g., arthropsolide A (**5**)) isolated from our previous cultures of *Arthropsis truncata* were isolated from several cultures of the fungus that were fed sodium [1-^{13}C]acetate (arthropsolide A (**5**) was the major metabolite (35 mg/L) isolated previously).

Arthropsadiol A (**1**) isolated from cultures of *Arthropsis truncata* that had been injected with sodium [1-^{13}C]acetate was acetylated so that the intensities of each of the signals in the ^{13}C nmr spectrum could be normalized (2) to those of the introduced acetate carbonyl and methyl signals. This allows for direct comparison with the corresponding normalized signal intensities in the spectrum of natural ^{13}C abundance arthropsadiol A diacetate (**6**). The two spectra were recorded successively using identical nmr instrument parameters and similar concentrations of arthropsadiol A diacetate (**6**). Enhancements of the signals due to C2, C4, C6, C8, and C10 were observed (Table 1), and a starter effect (3) was apparent from the slightly greater enhancement

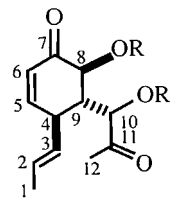

1 R = H
6 R = Ac

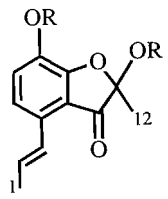

2 R = H
12 R = Ac

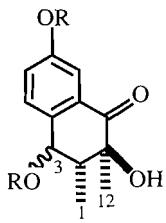

3 3β-H, R = H
4 3α-H, R = H
13 3β-H, R = Ac

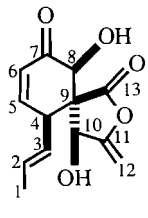

5

[1]Author to whom correspondence may be addressed.

Can. J. Chem. Downloaded from www.nrcresearchpress.com by 217.78.4.112 on 09/08/12
For personal use only.

TABLE 1. The ^{13}C nmr spectra of arthropsadiol A diacetate (**6**), cycloarthropsone diacetate (**12**), and arthropsatriol C diacetate (**13**) incorporating sodium [1-^{13}C]acetate

	6		**12**		**13**	
Atom	δ	Atom % enrichment[a]	δ	Atom % enrichment[a]	δ	Atom % enrichment[a]
C1	17.5	—	18.8	—	10.2	–
C2	131.5	1.9	131.7	1.6	41.1	2.5
C3	129.8	–	124.9	—	69.9	—
C4	41.9	1.2	136.4	1.0	137.6	0.3
C5	152.5	—	118.1	—	131.6	—
C6	126.8*	0.9	130.3	0.6	120.6	1.3
C7	204.4	—	133.6	—	151.3	—
C8	72.3*	0.6	159.2	0.9	128.3	0.8
C9	47.0	—	117.2	—	130.7	—
C10	75.4	0.9	196.0	0.3	200.9	1.1
C11	192.3	—	102.3	—	75.3	—
C12	26.7	—	20.9	—	22.4	—

[a]Atom % enrichment $= \frac{\text{sodium [1-}^{13}\text{C]acetate intensity}}{\text{natural intensity}} - 1.1$

*Satellite doublet ($^2J_{6,8}$ 15 Hz) due to multiple incorporation of sodium [1-^{13}C]acetate.

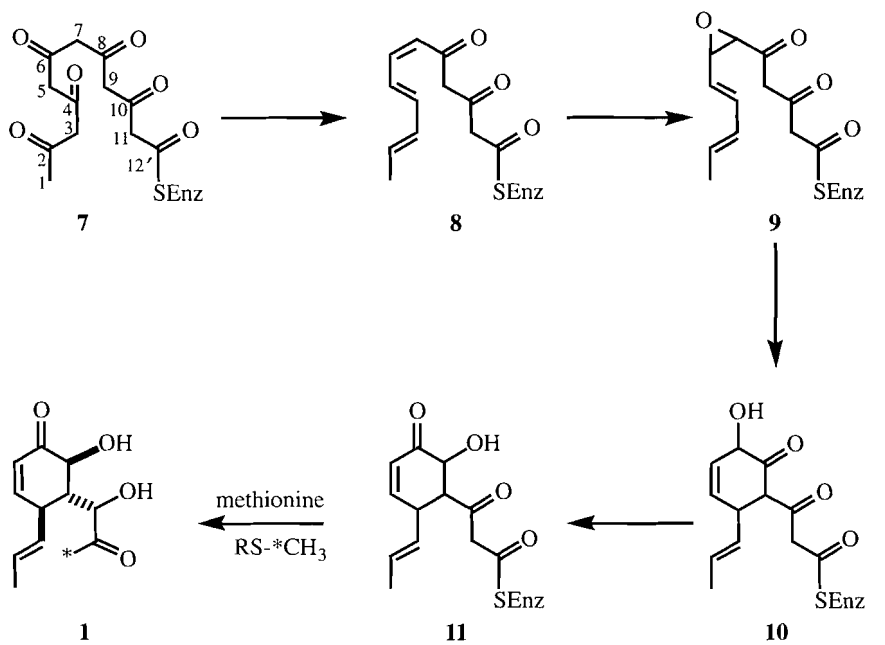

7 8 9 10 11 1 12′

SCHEME 1. Possible biosynthesis of arthropsadiol A (**1**) from a hexaketide precursor.

of the signal for C2. The signal of the terminal methyl group (C12) showed no enhancement.

The ^{13}C labelling of arthropsadiol A diacetate (**6**) suggests that the carbon skeleton of this metabolite is derived from a polyketide such as **7** assembled from six acetate units (Scheme 1).[2] Reduction of the C2, C4, and C6 ketone groups of **7** followed by elimination of three equivalents of water would give the triene **8**. Epoxidation of **8** to give the C6–C7 epoxide **9** and ensuing S_N2'-like reaction with a C9 anion might then give the cyclohexenone intermediate **10**. Isomerization of the α-hydroxy ketone moiety in **10** to the conjugated α′-hydroxy enone would give intermediate **11**, which possesses the cyclohexenone unit of arthropsadiol A (**1**). Methylation of the terminal acetate unit at C11 by methionine, followed by oxidative decarboxylation of the enzyme-bound carboxyl group (C12′), would form the three-carbon chain (C10–C12), and account for the lack of enhancement of the signal for C12 in the ^{13}C nmr spectrum of arthropsadiol A diacetate (**6**).

In the ^{13}C nmr spectrum of the arthropsadiol A diacetate (**6**) incorporating sodium [1-^{13}C]acetate the signals due to C6 (δ 126.8) and C8 (δ 72.3) display satellite peaks ($^2J_{CC}$ = 15.0) resulting from multiple incorporation of sodium [1-^{13}C]acetate

[2]The numbering of the biosynthetic intermediates corresponds to that used previously for the metabolites (1).

Can. J. Chem. Downloaded from www.nrcresearchpress.com by 217.78.4.112 on 09/08/12
For personal use only.

Can. J. Chem. Downloaded from www.nrcresearchpress.com by 217.78.4.112 on 09/08/12
For personal use only.

into some molecules of arthropsadiol A (**1**). This $^2J_{CC}$ is comparable to the 15.2 Hz coupling reported between C1 and C3 of 2-butanone (4). Excessive incorporation of ^{13}C-labelled precursors leading to multiple ^{13}C labels within a single molecule is often encountered during pulse feeding of ^{13}C-labelled biosynthetic precursors (5).

The ^{13}C nmr spectra of two further metabolites incorporating sodium [1-^{13}C]acetate were also obtained after conversion into their corresponding diacetate derivatives (Table 1). In the ^{13}C nmr spectra of both cycloarthropsone diacetate (**12**) and arthropsatriol C diacetate (**13**) the signals of C2, C4, C6, C8, and C10 are enhanced, but again there is no apparent enhancement of the signals due to C12. These results lead us to propose that cycloarthropsone (**2**) and arthropsatriols C (**3**) and D (**4**) are formed from arthropsadiol A (**1**) as outlined in Scheme 2. Thus oxidation of arthropsadiol A (**1**) at C8 (path a) gives the α-diketone **14**, which upon aromatization would give the catechol **15**. Oxidation at C10 and cyclization between the C8 phenolic oxygen and C11 then leads to formation of cycloarthropsone (**2**). Alternatively, dehydration of arthropsadiol A (**1**) (path b) would give the phenol **16**. Epoxidation of the C2–C3 olefin and enolization of the C11 carbonyl group gives intermediate **17**, which may cyclize in the indicated fashion to give arthropsatriols C (**3**) and D (**4**).

Incorporation of sodium [1,2-$^{13}C_2$]acetate

In Scheme 1 it was postulated that the terminal acetate of a polyketide precursor of arthropsadiol A (**1**) is methylated by methionine and the enzyme-bound carboxyl group is removed, possibly by an oxidative decarboxylation process. Accordingly, if sodium [1,2-$^{13}C_2$]acetate is incorporated by *Arthropsis truncata* into arthropsadiol A (**1**), the signals for C11 and C12 in the ^{13}C nmr spectrum of labelled **1** should appear as singlets whereas the signals for C1–C10 might be expected to display satellite peaks due to $^1J_{CC}$ from incorporation of intact acetate units. Chromatography of the ethyl acetate extract of the broth from a culture of *Arthropsis truncata* that had periodically been supplemented with a solution of sodium [1,2-$^{13}C_2$]acetate gave arthropsadiol A (**1**) as the major isolable metabolite along with lesser amounts of arthropsatriols C (**3**) and D (**4**). No arthropsolide A (**5**) or related 2-oxaspiro[4.5]dec-8-ene metabolites were isolated.

In the ^{13}C nmr spectrum of the diacetate (**6**) from sodium [1,2-$^{13}C_2$]acetate labelled arthropsadiol A the signal for C12 occurs as a singlet, confirming that C11 and C12 of arthropsadiol A (**1**) are not derived from incorporation of a single acetate unit. However, the signal for C11 is not a singlet due to multiple incorporation of labelled acetate in some molecules of **1**. The signal for C11 displays satellite peaks with $J_{C10-C11}$ 43 Hz as a result of successive incorporation of two labelled acetate units at C9–C10 and C11–C12′. Similar multiple incorporation of labelled acetate into other molecules of arthropsadiol A (**1**) results in complex multiplets for the signals of C2–C10. The signal of C1, being the methyl terminus of the postulated polyketide intermediates (Scheme 1), displays only a single intense pair of satellites (J_{C1-C2} 42 Hz). The signals of C2 and C3 display asymmetric satellites (Fig. 1). The signal for C2 (δ 131.4) shows the expected satellite peaks *a* (J_{C1-C2} 43 Hz) due to molecules that have incorporated sodium [1,2-$^{13}C_2$]acetate at C1–C2 but not C3–C4 (Table 2). Molecules that have incorporated sodium [1,2-$^{13}C_2$]acetate at both C1–C2 and C3–C4 display a C2 signal having the appearance of a doublet of doublets *b* (J_{C2-C3} 72 Hz, J_{C2-C1} 43 Hz), the centre of which occurs slightly downfield from δ 131.4 due to an isotope shift. The signal for C3 at δ 129.8 displays a satellite doublet *c* (J_{C3-C4} 44 Hz) due to molecules that contain sodium [1,2-$^{13}C_2$]acetate at C3–C4, and an isotope-shifted doublet of doublets *d* (J_{C3-C2} 68 Hz, J_{C3-C4} 44 Hz) due to molecules that contain sodium [1,2-$^{13}C_2$]acetate at C3–C4 and C1–C2.

The additional satellite multiplets for the signals of C4–C10 in the ^{13}C nmr spectrum of **6**, which arise from multiple incorporation of sodium [1,2-$^{13}C_2$]acetate into some molecules of arthropsadiol A (**1**), have been assigned in Table 2. The assignments are consistent with correlations observed in 2D-INADEQUATE (6) spectra of **6** that were optimized for J_{CC} 20 Hz (Fig. 2) and J_{CC} 40 Hz (Fig. 3). As in the ^{13}C nmr spectrum of **6** incorporating sodium [1-^{13}C]acetate (see Table 1), a $^2J_{CC}$ is observed between C6 and C8 (15 Hz) in the ^{13}C nmr spectrum of **6** incorporating sodium [1,2-

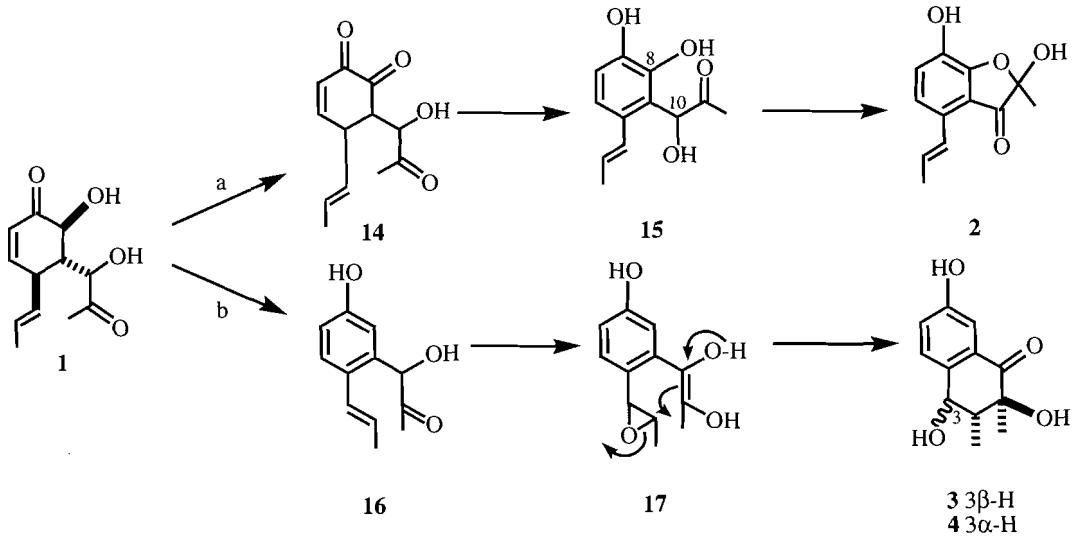

SCHEME 2. Possible biogenesis of metabolites from arthropsadiol A (**1**).

Can. J. Chem. Downloaded from www.nrcresearchpress.com by 217.78.4.112 on 09/08/12
For personal use only.

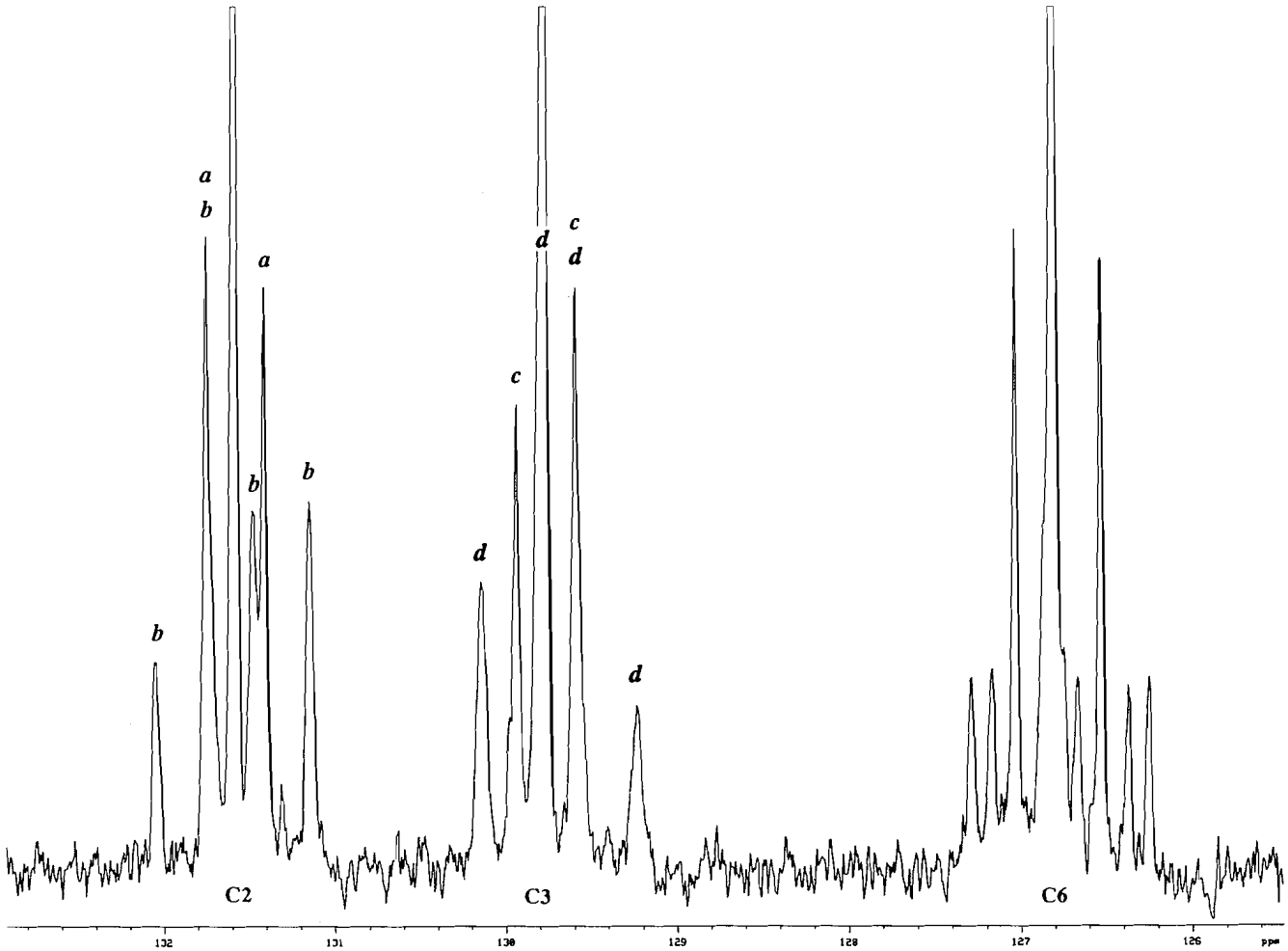

FIG. 1. Expansion showing the signals of C2, C3, and C6 in the ^{1}H-decoupled ^{13}C nmr spectrum of arthropsadiol A diacetate (**6**) incorporating sodium [1,2-$^{13}C_2$]acetate.

TABLE 2. The ^{13}C nmr spectrum of arthropsadiol A diacetate (**6**) incorporating sodium [1,2-$^{13}C_2$]acetate

		Satellite multiplicities	
Atom	δ	1 × Na [1,2-$^{13}C_2$]acetate incorporated	Multiple Na [1,2-$^{13}C_2$]acetate incorporation
C1	17.5	d, $J_{1,2}$ 42 Hz	—
C2	131.5	d, $J_{2,1}$ 41 Hz	dd, $J_{2,3}$ 72, $J_{2,1}$ 42 Hz
C3	129.8	d, $J_{3,4}$ 44 Hz	dd, $J_{3,2}$ 68, $J_{3,4}$ 44 Hz
C4	41.9	d, $J_{4,3}$ 43 Hz	ddd, $J_{4,3}$ 45, $J_{4,5}$ 38, $J_{4,9}$ 35–40 Hz
C5	152.5	d, $J_{5,6}$ 62 Hz	dd, $J_{5,6}$ 62, $J_{5,4}$ 38 Hz
C6	126.8	d, $J_{6,5}$ 62 Hz	dd, $J_{6,5}$ 62, $J_{6,7}$ 53, $J_{6,8}$ 15 Hz
C7	192.3	d, $J_{7,8}$ 43 Hz	dd, $J_{7,6}$ 62, $J_{7,8}$ 38 Hz
C8	72.3	d, $J_{8,7}$ 43 Hz	m
C9	47.0	d, $J_{9,10}$ 35 Hz	dd, $J_{9,10}$ 35, $J_{9,8}$ 35 Hz dd, $J_{9,10}$ 35, $J_{9,4}$ 35–40 Hz
C10	75.4	d, $J_{10,9}$ 35 Hz	dd, $J_{10,11}$ 43, $J_{10,9}$ 35 Hz
C11	204.4	s	d, $J_{11,10}$ 43 Hz
C12	26.7	s	—

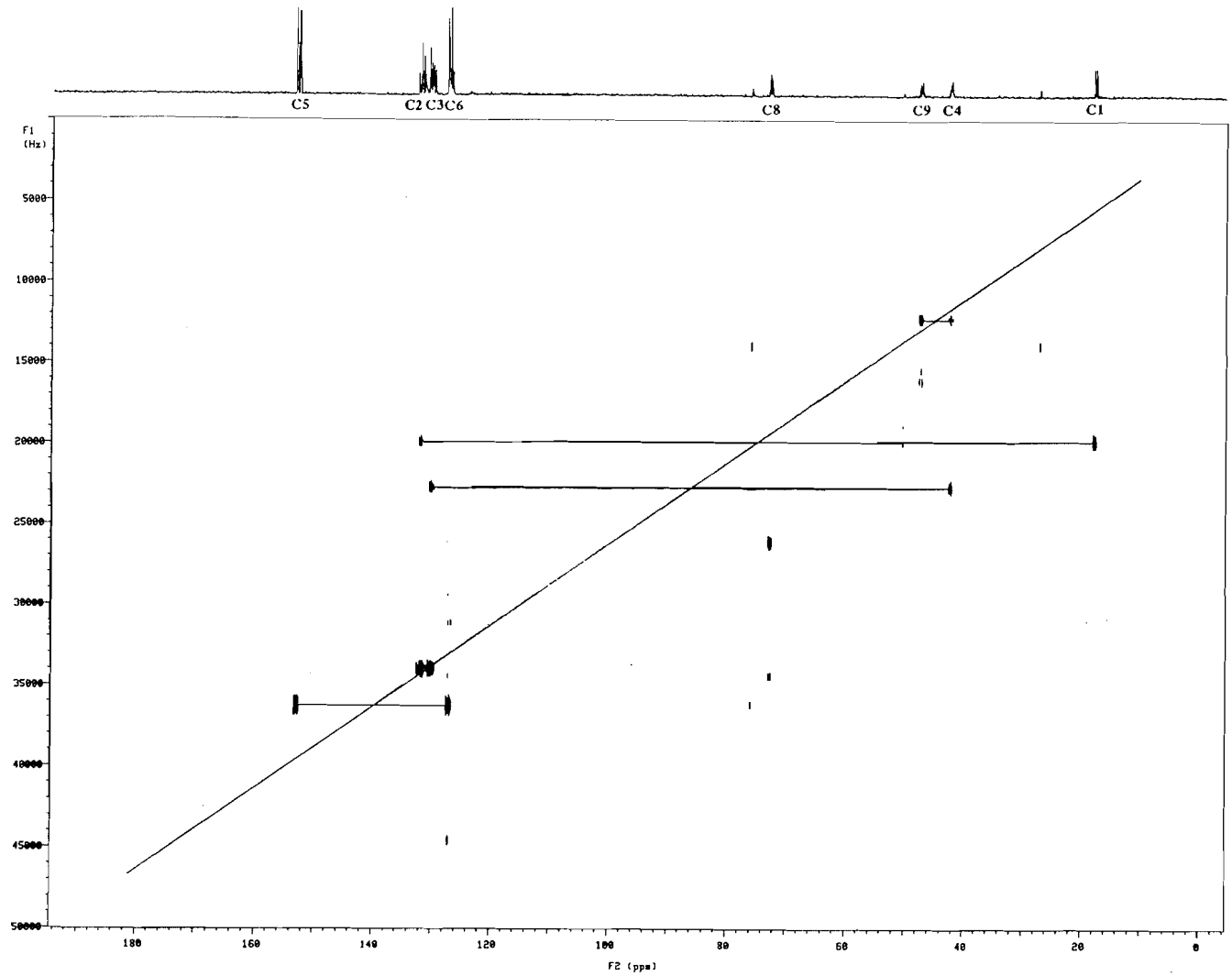

FIG. 2. 2D-INADEQUATE spectrum (optimized for J_{CC} 20 Hz) of arthropsadiol A diacetate (**6**) incorporating sodium [1,2-$^{13}C_2$]acetate.

$^{13}C_2$]acetate (Fig. 1). The signal for C4 displays a strong satellite doublet (J_{C4-C3} 43 Hz) due to incorporation of an intact [1,2-$^{13}C_2$]acetate unit at C3–C4. In the 2D-INADEQUATE spectra of **6** the signal of C4 is correlated not only to the signal of C3 but also to C5 and C9. This suggests that a significant number of molecules of arthropsadiol A (**1**) have multiple incorporation of sodium [1,2-$^{13}C_2$]acetate at C3–C4, C5–C6, and C9–C10. Assuming that J_{CC} between C4 and C9 is approximately 35–40 Hz, then incorporation of sodium [1,2-$^{13}C_2$]acetate at C3–C4, C5–C6, and C9–C10 would result in a ddd of satellite peaks due to coupling of C4 to C3, C5, and C9. If the ddd overlaps both the C4 singlet due to natural abundance ^{13}C, and the dd due to incorporation of sodium [1,2-$^{13}C_2$]acetate at C3–C4, then a pattern of satellites similar to that observed for the signal of C4 (Fig. 4) might be expected. The C4–C9 coupling of 35–40 Hz is not immediately apparent from examination of the signal due to C9 because the dd of satellites (J_{C9-10} 35 Hz, J_{C9-C8} 35 Hz) due to multiple sodium [1,2-$^{13}C_2$]acetate incorporation at C7–C8 and C9–C10 is coincident with the dd of satellites (J_{C9-C4} 35–40 Hz, J_{C9-C10} 35 Hz) due to sodium [1,2-$^{13}C_2$]acetate incorporation at C3–C4 and C9–C10.

The fact that C11 is derived from acetate in the sodium [1,2-$^{13}C_2$]acetate feeding experiment suggests that C12 is derived from the one carbon pool, not from the incorporation of propionate (or lactate) during the assembly of the polyketide chain.

*Possible biosynthesis of arthropsolide A (**5**) and related metabolites*

Arthropsolide A (**5**) and the related 2-oxaspiro[4.5]dec-8-ene metabolites isolated from *Arthropsis truncata* (1) are structurally very similar to a number of metabolites (spirostaphylotrichins A–T) isolated recently from the fungus *Staphylotrichum coccosporum* (7–9). The biosynthesis of a number of the compounds produced by *Staphylotrichum coccosporum* has been investigated, and it has been proposed that a pentaketide precursor and aspartic acid combine to give an amide that undergoes ring formation to generate the 2-azaspiro[4.5]dec-8-ene skeleton common to spirostaphyotrichins A–T (10). In an analogous fashion (Scheme 3) we propose that the 2-oxaspiro[4.5]dec-8-ene skeleton of arthropsolide A (**5**) might be formed by the condensation of a pentaketide precursor and malic acid to give the ester **18**. The γ-lactone intermediate **19** could then arise from C9–C10 bond formation and subsequent ketone re-

Can. J. Chem. Downloaded from www.nrcresearchpress.com by 217.78.4.112 on 09/08/12
For personal use only.

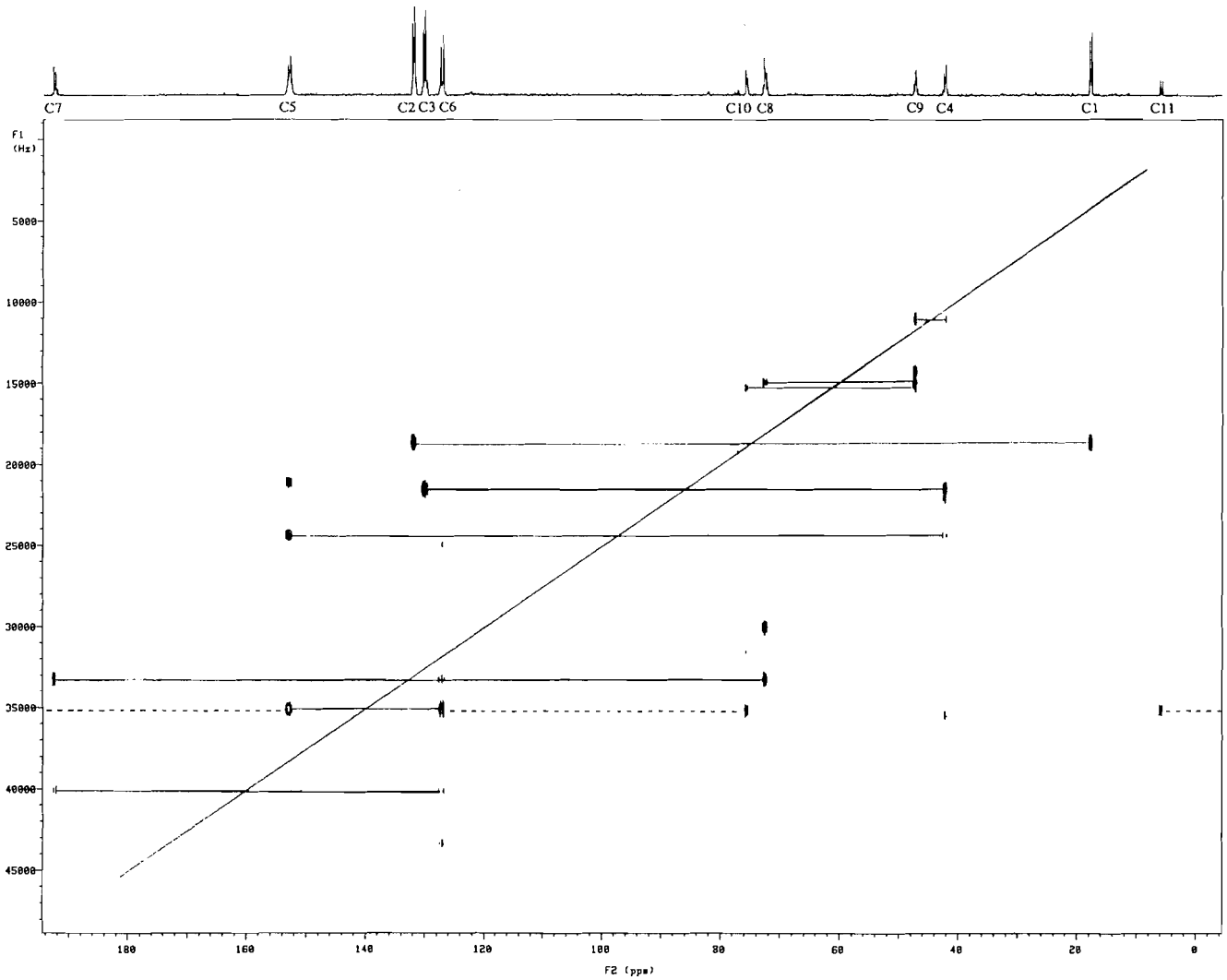

FIG. 3. 2D-INADEQUATE spectrum (optimized for J_{CC} 40 Hz) of arthropsadiol A diacetate (**6**) incorporating sodium [1,2-$^{13}C_2$]acetate. Note the folded signal of C11.

ductions and elimination of water to give triene intermediate **20**. Epoxidation of **20** to give the C6–C7 epoxide **21** and ensuing S_N2'-like reaction with a C9 anion would form the 2-oxaspiro[4.5]dec-8-ene precursor **22** of arthropsolides A–D.

Unfortunately we were unable to isolate arthropsolides A–D from three successive liquid cultures of *Arthropsis truncata* that were periodically fed sodium [1-^{13}C]acetate. In one culture the production of arthropsolide A (**5**) was detected by hplc of an aliquot of the culture medium at day 9 following inoculation (sodium [1-^{13}C]acetate was added at day 5), and in another culture arthropsolide A (**5**) was detected at day 11 (sodium [1-^{13}C]acetate added at days 3 and 6). However, in each case, when the cultures were harvested several days later arthropsolide A (**5**) was not detected in the ethyl acetate extract of the culture broth. We must at this stage postulate that the addition of sodium acetate to the culture broth of *Arthropsis truncata* alters the balance between biosynthesis of C_{12} metabolites such as arthropsadiol A (**1**), and the biosynthesis of C_{13} metabolites such as arthropsolide A (**5**) to favor the predominant formation of C_{12} metabolites.

The possibility that arthropsolide A (**5**) is converted into arthropsadiol A (**1**) via hydrolysis of the γ-lactone moiety and subsequent decarboxylation (Scheme 4) can be discounted on the basis of the results from incorporation of sodium [1,2-$^{13}C_2$]acetate into arthropsadiol A (**1**). Thus if arthropsadiol A (**1**) were formed from arthropsolide A (**5**), then C9 and C10 in **1** would not be derived from a single acetate unit and accordingly these two carbon atoms should not display coupling in the ^{13}C nmr spectrum of arthropsadiol A diacetate (**6**). However, as can be seen in the ^{13}C nmr data for arthropsadiol A diacetate (**6**) labelled with sodium [1,2-$^{13}C_2$]acetate (Table 2), C9 and C10 display a J_{CC} of 35 Hz. The coupling between C9 and C10 was confirmed by the 2D-INADEQUATE spectrum optimized for J_{CC} 40 Hz. Hence we believe that the conversion of arthropsolide A (**5**) into arthropsadiol A (**1**) as in Scheme 4 does not account for the absence of **5** among the metabolites isolated from cultures of *Arthropsis truncata* that have been fed ^{13}C labelled sodium acetate.

Experimental

For general experimental details see ref. 1. High-performance liquid chromatography (hplc) was performed with a Waters model

Can. J. Chem. Downloaded from www.nrcresearchpress.com by 217.78.4.112 on 09/08/12
For personal use only.

Can. J. Chem. Downloaded from www.nrcresearchpress.com by 217.78.4.112 on 09/08/12
For personal use only.

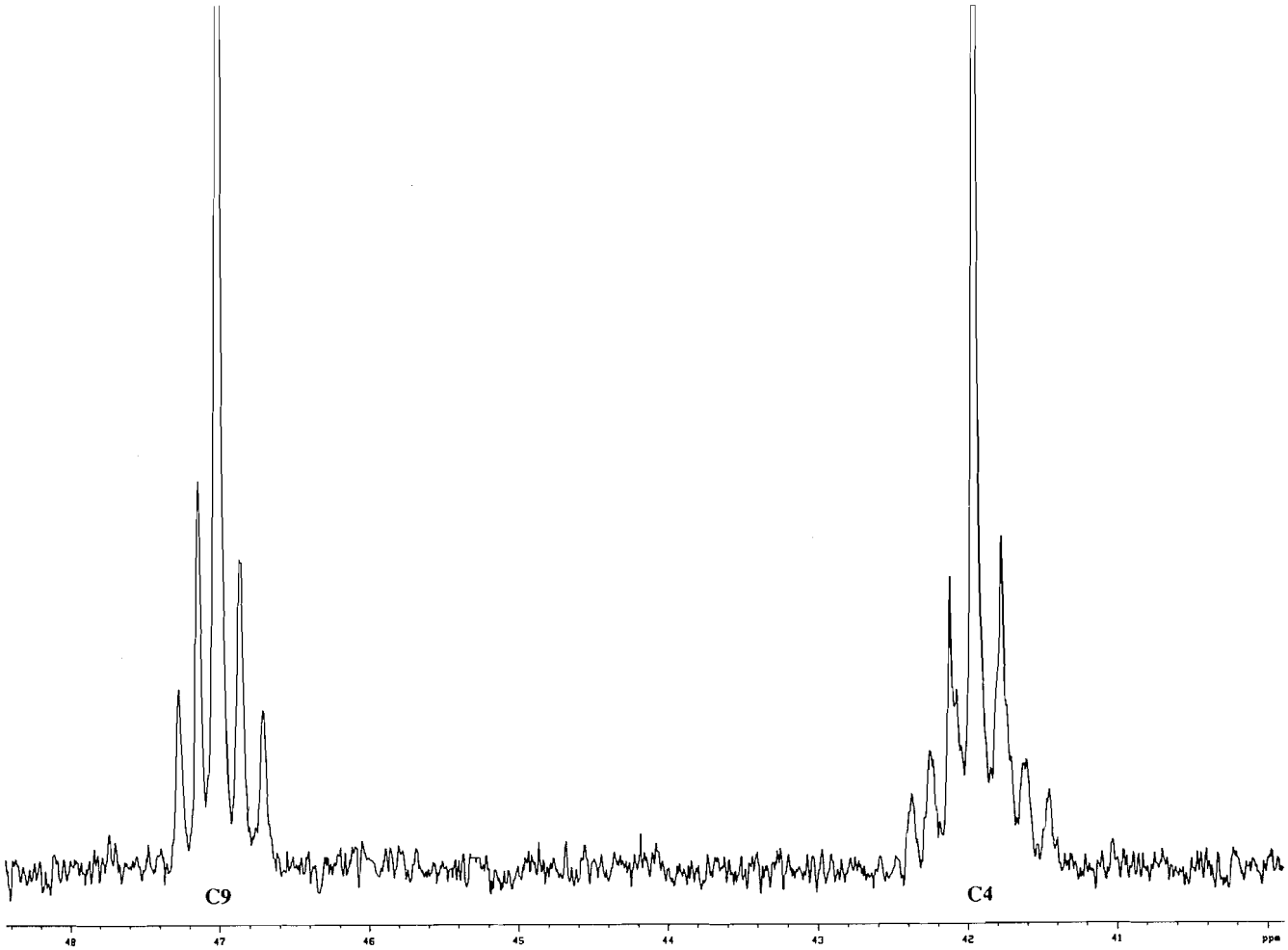

FIG. 4. Expansion showing the signals of C4 and C9 in the ^{1}H-decoupled ^{13}C nmr spectrum of arthropsadiol A diacetate (**6**) incorporating sodium [1,2-$^{13}C_2$]acetate.

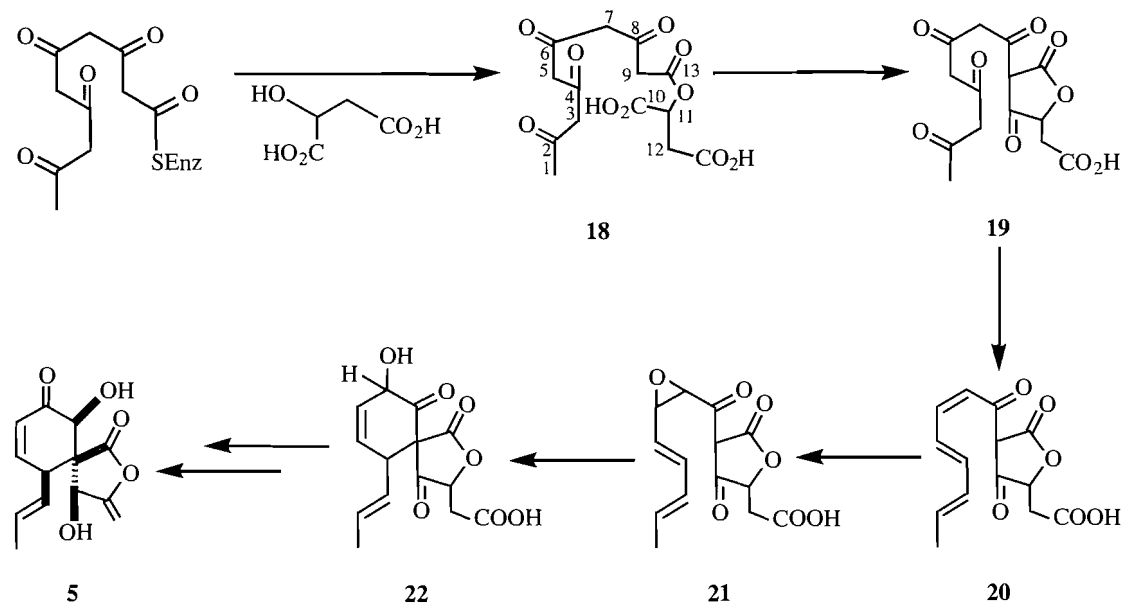

SCHEME 3. Possible biosynthesis of arthropsolide A (**5**).

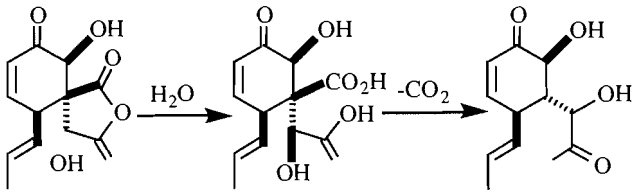

5 1

SCHEME 4. Possible biogenesis of arthropsadiol A (**1**) from arthropsolide A (**5**).

6000A solvent delivery system and a Waters model 480 LC spectrophotometer set at 254 nm. Analytical hplc was carried out using a Waters Radial Compression Z module fitted with a Waters 8MBC1810μ Radial Pak liquid chromatography cartridge (8 mm i.d.), and semi-preparative scale hplc was carried out on a Waters μ-Bondapak C18 column (7.8 × 300 mm). Sodium [1-^{13}C]acetate (99 at.% ^{13}C) and sodium [1,2-$^{13}C_2$]acetate (99 at.% ^{13}C) were purchased from MSD Isotopes (Montreal). Acetylations were performed as described previously (1). 2D-INADEQUATE and ^{1}H-decoupled ^{13}C nmr spectra of sodium [1,2-$^{13}C_2$]acetate labelled arthropsadiol A diacetate (**6**) were recorded in $CDCl_3$ solution at 125 MHz using a Varian Unity 500 spectrometer.

Biosynthetic studies of Arthropsis truncata *metabolites*

Incorporation of sodium [1-^{13}C]acetate

Arthropsis truncata was grown in liquid shake culture on a sterile modified malt extract medium (4 × 1 L) as described in the experimental section of the previous paper (1). After 3 days' growth a sterile solution of sodium [1-^{13}C]acetate (5 mL, 0.2 mol L^{-1}) was injected into each of the flasks, then further sodium [1-^{13}C]acetate (5 mL, 0.2 mol L^{-1}) was added to each of the flasks at day 6 and day 9 following inoculation of the liquid culture. At day 12 the culture was filtered through cotton wool and the culture broth extracted with ethyl acetate (1.5 L) for 24 h. The ethyl acetate extract was dried over magnesium sulfate and evaporated to give a yellow-brown foam (0.56 g).

The extract was adsorbed onto a small amount of silica gel using ethyl acetate, then dried in air with gentle warming and poured onto a column of silica gel slurry packed using dichloromethane–methanol (10:1). Fractions of 7 mL were eluted from the column using dichloromethane–methanol (10:1) to give fractions containing arthropsadiol A (**1**) (fractions 8–11, 35 mg), cycloarthropsone (**2**) (fractions 12–21, 52 mg), and mixtures of arthropsatriol C (**3**) and arthropsatriol D (**4**) (fractions 22–33, 27 mg).

The crude arthropsadiol A (**1**) was purified by hplc (methanol–water (50:50), 2 mL min^{-1}) to give arthropsadiol A (19 mg), which crystallized on standing; ^{1}H nmr identical with that reported previously (1). Acetylation gave arthropsadiol A diacetate (**6**); ^{1}H nmr identical with that reported previously (1).

The impure cycloarthropsone (**2**) was chromatographed, eluting with ethyl acetate – hexanes (1:2) to give cycloarthropsone (3.1 mg), which crystallized as a yellow solid; ^{1}H nmr identical with that reported previously (1). Acetylation of this material gave cycloarthropsone diacetate (**12**); ^{1}H nmr identical with that reported previously (1).

The mixture containing arthropsatriol C (**3**) and arthropsatriol D (**4**) was acetylated and the product mixture separated by preparative tlc on silica gel. After two developments with dichloromethane–methanol (100:1) two main bands were observed which were then separately eluted from the silica gel using ethyl acetate, and further purified by hplc (methanol–water (60:40)) to give arthropsatriol D diacetate (3.6 mg) and arthropsatriol C diacetate (**13**) (5.1 mg). The ^{1}H nmr spectra of each of these diacetates were identical with those reported previously (1).

Incorporation of sodium [1,2-$^{13}C_2$]acetate

Arthropsis truncata was grown in liquid shake culture on a sterile modified malt extract medium (4 × 1 L) as described in the experimental section of the previous paper (1). After 3 days' growth a sterile solution of sodium [1,2-$^{13}C_2$]acetate (5 mL, 0.1 mol L^{-1}) was injected into each of the flasks, then further sodium [1,2-$^{13}C_2$]acetate (5 mL, 0.1 mol L^{-1}) was added to each of the flasks at day 6, day 9, and day 12. At day 17 the culture was filtered and the culture broth extracted with ethyl acetate (2 L) for 24 h. The ethyl acetate extract was dried over magnesium sulfate and evaporated to give an orange-brown foam (1.10 g).

Chromatography of the ethyl acetate extract as above using dichloromethane–methanol (20:1, fractions 1–50; then 10:1, fractions 51–78) successively gave fractions containing arthropsadiol A (**1**) (fractions 14–18, 30 mg), and arthropsatriol C (**3**) and arthropsatriol D (**4**) (fractions 51–63, 26 mg).

The fractions containing arthropsadiol A (**1**) were subjected to hplc as above to give arthropsadiol A (18 mg), which crystallized on standing; ^{1}H nmr identical with that reported previously (1). Acetylation gave arthropsadiol A diacetate (**6**); ^{1}H nmr identical with that reported previously (1).

The fractions containing arthropsatriol C (**3**) and arthropsatriol D (**4**) were acetylated and the product mixture was separated as above to give arthropsatriol D diacetate (3.2 mg) and arthropsatriol C diacetate (**4**) (5.7 mg). The ^{1}H nmr spectra of each of these diacetates were identical with those reported previously (1).

Acknowledgements

The financial support of the Natural Sciences and Engineering Research Council of Canada is gratefully acknowledged. The authors wish to thank Dr. T. Nakashima for obtaining 2D-INADEQUATE spectra and for helpful discussions, and L. Sigler, University of Alberta Microfungus Herbarium, for cultures of *Arthropsis truncata*.

1. W. A. Ayer, P. A. Craw, and J. Neary. Can. J. Chem. **70**, 1338 (1992).
2. T. J. Simpson. Chem. Soc. Rev. **4**, 497 (1975).
3. P. W. Jeffs and D. McWilliams. J. Am. Chem. Soc. **103**, 6185 (1981).
4. F. J. Weigert and J. D. Roberts. J. Am. Chem. Soc. **94**, 6021 (1972).
5. M. P. Lane, T. T. Nakashima, and J. C. Vederas. J. Am. Chem. Soc. **104**, 913 (1984).
6. A. Bax, R. Freeman, T. A. Frenkiel, and M. H. Levitt. J. Magn. Reson. **43**, 478 (1981); T. H. Mareci and R. Freeman. J. Magn. Reson. **48**, 158 (1982).
7. P. Sandmeier and C. Tamm. Helv. Chim. Acta. **72**, 784 (1989).
8. P. Sandmeier and C. Tamm. Helv. Chim. Acta, **72**, 1107 (1989).
9. P. Sandmeier and C. Tamm. Helv. Chim. Acta, **73**, 975 (1990).
10. P. Sandmeier and C. Tamm. Helv. Chim. Acta, **72**, 774 (1989).

Can. J. Chem. Downloaded from www.nrcresearchpress.com by 217.78.4.112 on 09/08/12
For personal use only.

Ring expansion by tandem double Tebbe–Claisen technology

LEO A. PAQUETTE,[1] CHRISTOPHE M. G. PHILIPPO, AND NHA HUU VO
Evans Chemical Laboratories, The Ohio State University, Columbus, OH 43210 U.S.A.

Received May 24, 1991

This paper is dedicated to Professor Zdenek (Denny) Valenta on the occasion of his 65th birthday

LEO A. PAQUETTE, CHRISTOPHE M. G. PHILIPPO, and NHA HUU VO. Can. J. Chem. **70**, 1356 (1992).

2-Cyclohexenone rings that form part of a larger structural assembly are amenable to peracid oxidation with formation of an epoxy lactone. These intermediates are readily transformed under acidic, basic, or neutral conditions to ring-contracted aldehydo lactones, which are then subjected to condensation with a slight excess of Tebbe reagent. These conditions result in methylenation of carbonyl groups and set the stage for operation of a Claisen rearrangement. When the latter is catalyzed by Tribal, the sigmatropic process occurs at room temperature. With systems typified by **17** and **24**, the isomerization is complete within 15 min. The presence of a proximate angular methyl group as in **9***b*, **29**, and **37** exerts a retarding kinetic effect. In such examples, a period of 6 h is required to achieve completion. Swern oxidation completes the conversion to the 4-cyclooctenones, where the two carbons stemming from the Tebbe reagent are inserted between the original carbonyl and α-olefinic carbons. The overall process is tolerant of ether functionality and additional sites of unsaturation.

LEO A. PAQUETTE, CHRISTOPHE M. G. PHILIPPO et NHA HUU VO. Can. J. Chem. **70**, 1356 (1992).

Il est possible de soumettre des cyclohexèn-2-ones faisant partie de l'assemblage de grandes structures à des oxydations par les peracides avec formation d'une époxy-lactone. On peut facilement transformer ces intermédiaires, dans des conditions acidique, basique ou neutre, en aldéhydo-lactones ayant subi une contraction de cycle; ces dernières sont alors soumises à une condensation avec un léger excès de réactif de Tebbe. Ces conditions permettent d'effectuer la méthylénation des deux groupes carbonyles permettant de procéder à une transposition de Claisen. Quand on effectue celle-ci à l'aide de Tribal comme catalyseur, le processus sigmatropique que se produit à la température ambiante. Avec des systèmes comme **17** et **24**, l'isomérisation est complète en 15 min. La présence d'un groupe méthyle angulaire à proximité comme il en existe dans les composés **9***b*, **29** et **37**, exerce un effet cinétique qui ralentit la réaction. Dans ces exemples, il faut 6 h pour arriver à une réaction complète. Une oxydation de Swern complète la conversion en cyclo-octèn-4-ones dans lesquelles les deux carbones provenant du réaction de Tebbe sont insérés entre les carbones du carbonyle original et celui du carbone α-oléfinique. On peut effectuer l'ensemble des ces opérations en présence d'une fonction éther et d'autres sites d'insaturation.

[Traduit par la rédaction]

Can. J. Chem. Downloaded from www.nrcresearchpress.com by 217.78.4.112 on 09/08/12
For personal use only.

Previous accounts from this laboratory (1) dealt with development of the alicyclic Claisen rearrangement (2) for accessing eight-membered-ring natural products by ring expansion. These studies established the feasibility of incorporating, in stepwise fashion, all of the essential features of 4-cyclooctenones into their 2-methylene-6-vinyltetrahydrofuran precursors. The latter were produced by Tebbe olefination (3) of the related lactones obtained, in turn, by means of various highly stereoselective pathways. The fundamental issue of stereochemical transmission during the [3,3] sigmatropic event in these systems is customarily controlled by thermodynamic factors, chair–chair transition states related to **1** being adopted to the exclusion of boat–chair options (e.g., **2**) to skirt production of unstable *trans*-4-cyclooctenone products (1, 4).

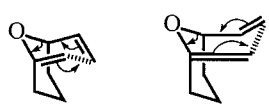

1 **2**

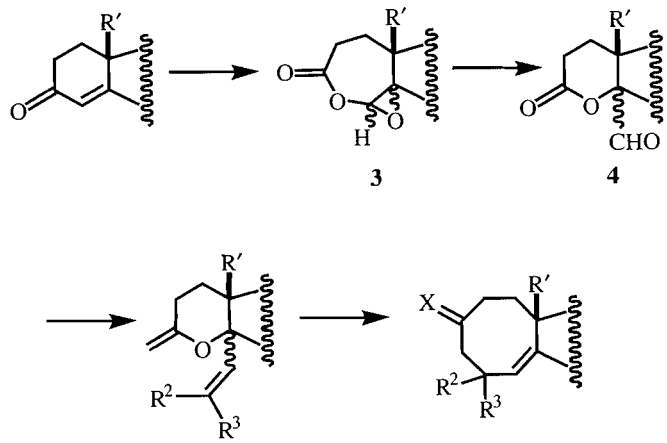

3 **4** **5** **6**

SCHEME 1

The present study demonstrates the workability of a new variant of this ring expansion strategy within the context of a synthetically useful two-carbon insertion (5, preliminary communication). We envisioned that a short three-stage sequence could be implemented to considerable advantage. The first step necessitates exhaustive peracid oxidation of a 2-cyclohexenone to give epoxy lactone **3**, with ensuing isomerization to aldehydo lactone **4** (Scheme 1). Conversions of this type are, in fact, known (6) and have been effected in a single reaction vessel. As will be discussed, efficiency is improved if **3** is first isolated. Subsequent condensation of **4** with [bis(cyclopentadienyl)titanium]-(μ-chloro)(μ-methylidene)dimethylaluminum (3*a*, 3*b*) was viewed as a ready means of performing dual olefination at both car-

[1]Author to whom correspondence may be addressed.

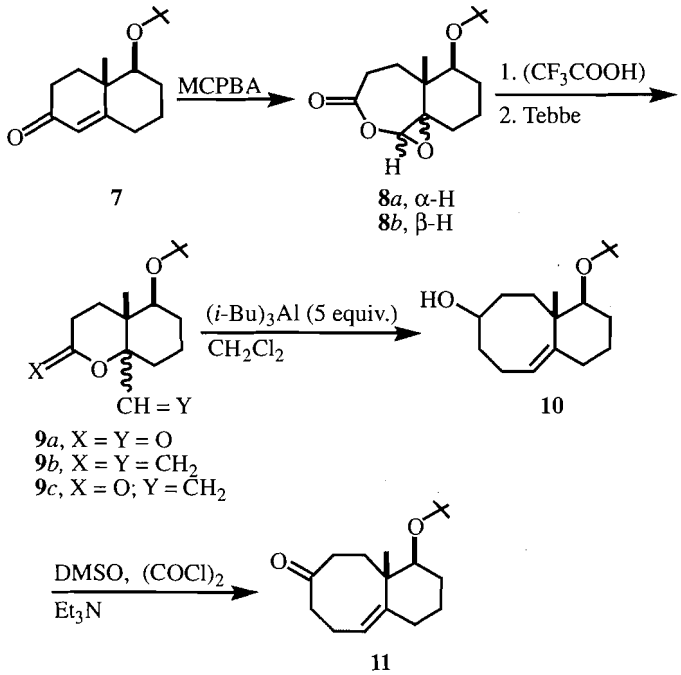

SCHEME 2

bonyl sites with formation of **5**. In light of the widely differing reactivities of aldehyde and lactone carbonyl groups, added scope could be potentially infused into the protocol by performing a chemoselective Wittig reaction[2] on **4** prior to condensation with the Tebbe reagent. In this way, R^2 and R^3 in **6** could be extended beyond the level of hydrogen as desired or needed.

Finally, catalysis of the Claisen rearrangement of **5** with triisobutylaluminum (Tribal) (1*e*, 8) should permit operation of the targeted ring expansion at room temperature, if necessary to safeguard thermally sensitive functional groups. Otherwise, recourse could be made to conventional thermal conditions.

Results and discussion

The readily availability of enantiomerically homogeneous ketone **7** from the regioselective sodium borohydride reduction (9) and *tert*-butylation of optically active Wieland–Mischer ketone (10) prompted its initial utilization. Oxidation with 3 equivalents of MCPBA gave rise to **8** as a 1:3 mixture of α- and β-oxido isomers (Scheme 2). The stereochemical assignments to these epoxy lactones follow convincingly from their ^{1}H nmr spectra. Thus, while the oxiranyl proton in **8***a* appears as a singlet at δ 4.75 that in **8***b* experiences greater magnetic shielding and appears at somewhat higher field (δ 4.67). These characteristics extend as well to the aldehydic protons of the ring-contracted isomers **9***a*. The thermodynamically more stable *trans* isomer (6*c*) exhibits an absorption at δ 9.87 (in $CDCl_3$), in excess of 0.2 ppm downfield from the signal observed for its *cis* counterpart (δ 9.63). The conversion to **9** was found to proceed efficiently under catalysis by trifluoroacetic acid. Equal success was realized under neutral (165°C for 15 min) or basic conditions (aqueous methanolic NaOH at 0°C).

[2]Lactone carbonyls are commonly, but not always, unreactive toward Wittig reagents (7).

An important aspect of the twofold Tebbe reaction is proper control of the stoichiometry in order to avoid internal isomerization of the exocyclic vinyl ether double bond in the product. The latter process is thermodynamically driven and known to occur with ease (1). This prototypic isomerization came to be recognized as a reaction equally prone to catalysis by the aluminum coreagent. It is therefore crucial that only a modest excess (2.5 equiv.) of the Tebbe reagent be employed and that the quenched reaction mixture be purified as rapidly as possible. The use of freshly prepared Tebbe reagent was found to be especially advantageous. Finally, all glassware must be base washed, a consideration that extends to the nmr tubes used for spectral analysis. Failure to exercise this precaution results in isomerization of the *cis* and *trans* allyl vinyl ethers while in C_6D_6 solution, albeit at somewhat different rates (Table 1).

The Tribal-promoted Claisen rearrangement of **9***b* required an unexpectedly long time (6 h at 25°C) to proceed to completion. Attempts to perform this isomerization at lower temperatures (−20 and −78°C) resulted only in the formation of **12**. The [3,3] sigmatropic product **10** constitutes a diastereomeric mixture, oxidation of which under Swern conditions provided **11** exclusively (62%). The direct conversion of **9***b* to **1** could be accomplished thermally in base-coated soft-glass tubes (**1***a*) at 190°C for 48 h. In Pyrex tubes, the starting material was diverted to **12** prior to ultimate conversion to **13**. In a similar vein, the prototropic isomerization to give **12** (and subsequently **13**) became the dominant thermal pathway if organometallic residues from the Tebbe reaction were not completely removed during the chromatographic purification of **9***b*.

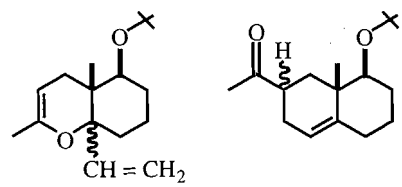

12 **13**

Evidence suggesting that the angular methyl group in **9** is responsible for sterically imposed kinetic retardation of the Al(III)-catalyzed Claisen process was gained from an in-depth examination of the less substituted octalone **14**. Oxidation of **14** according to DeBoer and Ellwanger (6*e*) cleanly produced **15**, the acid-catalyzed isomerization of which provided the *trans*-fused aldehydo lactone **16** (Scheme 3). Once **17** became available, its exposure to an excess of Tribal, as before, was met with substantial acceleration of the Claisen process. The conversion to a stereochemically pure isomer of cyclooctenol **18** (86%) was complete within 15 min at room temperature. Ensuing oxidation furnished ketone **19** in 86% yield. The direct conversion of **17** to **19** could be accomplished at 180°C, but the product was invariably contaminated with a minimum 13% of the acetyl derivative **20**.

The favorable accelerating influence of an angular C—H substituent was tested further by making recourse to manool (**21**) as starting material. Following Grant's procedure (6*f*), this terpenic alcohol was transformed into epoxy lactone **22** (Scheme 4), thereby setting the stage for quantitative base-catalyzed isomerization to **23** and twofold methylenation to give **24**. Like **17**, **24** isomerized approximately 20 times faster than **9***b* when admixed with Tribal in CH_2Cl_2 solution at

Can. J. Chem. Downloaded from www.nrcresearchpress.com by 217.78.4.112 on 09/08/12
For personal use only.

TABLE 1. Rearrangement behavior of **9*b*** in C_6D_6 solution (nonbase-washed tubes, 25°C)

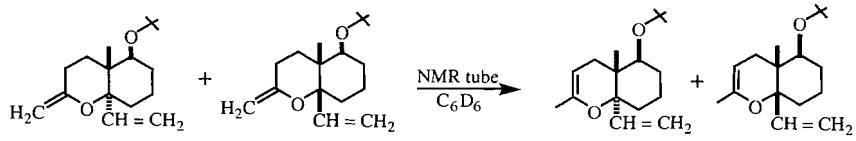

t	(%)	(%)	(%)	(%)
0	30	70	0	0
36 h	15	50	15	20
5 days	0	25	30	45
15 days	0	6	30	64

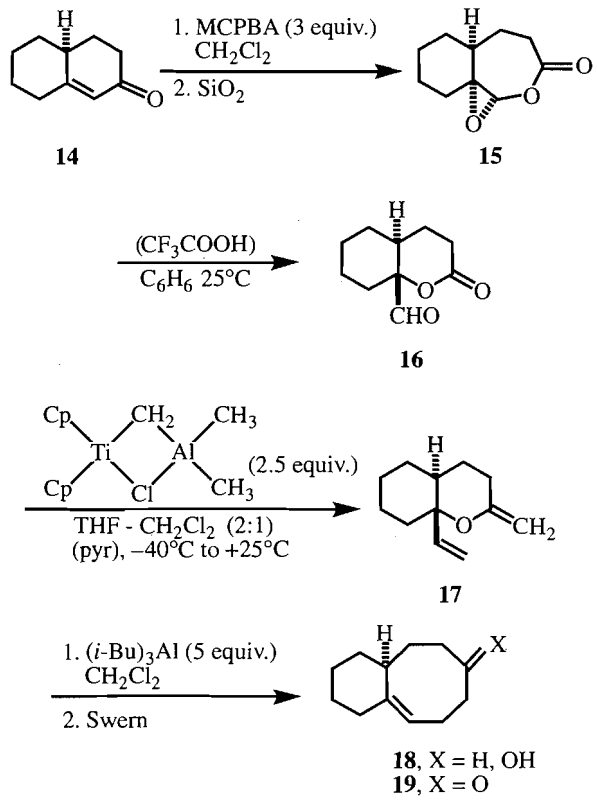

SCHEME 3

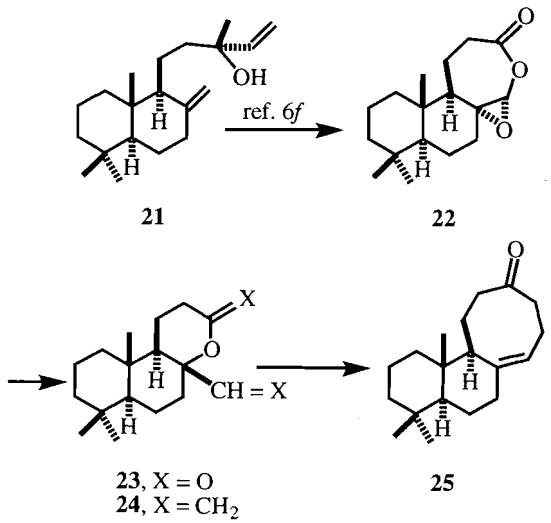

SCHEME 4

25°C. Again, in contrast to the thermal Claisen rearrangement, the Lewis-acid-accelerated alternative appears insensitive to the presence of metal impurities carried over from the Tebbe homologation reaction.

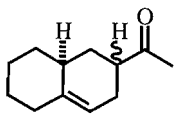

20

The synthetic versatility of this two-carbon insertion process is further demonstrated by the ease with which it can be successfully applied to steroidal systems. As summarized in Scheme 5, silylation of the secondary hydroxyl group of testosterone (**26*a***) followed by enone oxidation with 3 equivalents of MPCBA in refluxing CH_2Cl_2 furnished the epoxylactones **27**. The latter were cleanly transformed into aldehydo lactones **28** following admixture with a catalytic quantity of *d*-camphor-10-sulfonic acid in benzene solution. At this stage, it proved an easy matter to effect homologation to **29**. In agreement with our earlier observations involving **9*b***, the Tribal-promoted Claisen rearrangement of **29** required 6 h to achieve complete conversion to the cyclooctenol (64% after chromatographic purification). In this instance, different aluminum catalysts (e.g., diethylaluminum chloride in combination with triphenylphosphine (11) and methylaluminum bis(4-bromo-2,6-di-*tert*-butylphenoxide (12)) were briefly examined, but these proved ineffective. Ketone **30** was arrived at by oxidation of the cyclooctenol as well as by heating **29**. The latter reaction also produces isomerized vinyl ether **31** and acetyl cyclohexene **32** in relative amounts sufficient to permit their independent characterization.

17β-Methyltestosterone (**33**) underwent the oxidation reaction without prior need for hydroxyl-group protection (Scheme 6). Upon treatment with a catalytic amount of *d*-camphor-10-sulfonic acid, **34** was isomerized to **35**. Recourse to anhydrous perchloric acid in CH_2Cl_2 for the same purpose led instead to **36**. Evidently, this reagent system is more conducive to generation of the tertiary carbocation. A Wagner–Meerwein shift of the C-18 methyl group ensues with net overall dehydration (13). The resulting aldehydo lactone **36** reacts very efficiently with the Tebbe reagent to provide **37** (91%). Since this vinyl ether has no additional oxygen substituents, its relatively slow (6 h, 25°C) rate of [3,3] sigmatropic rearrangement in the presence of excess

Can. J. Chem. Downloaded from www.nrcresearchpress.com by 217.78.4.112 on 09/08/12
For personal use only.

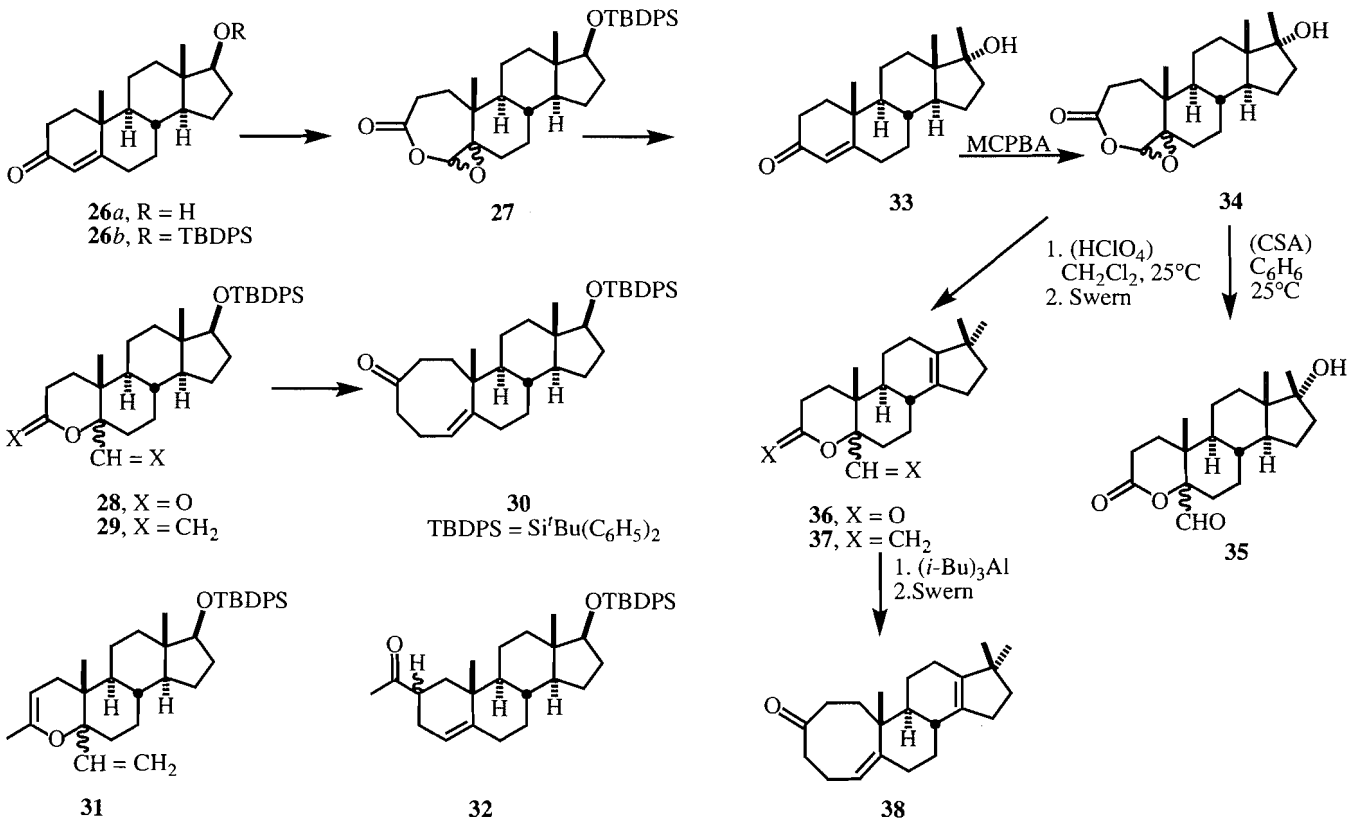

SCHEME 5

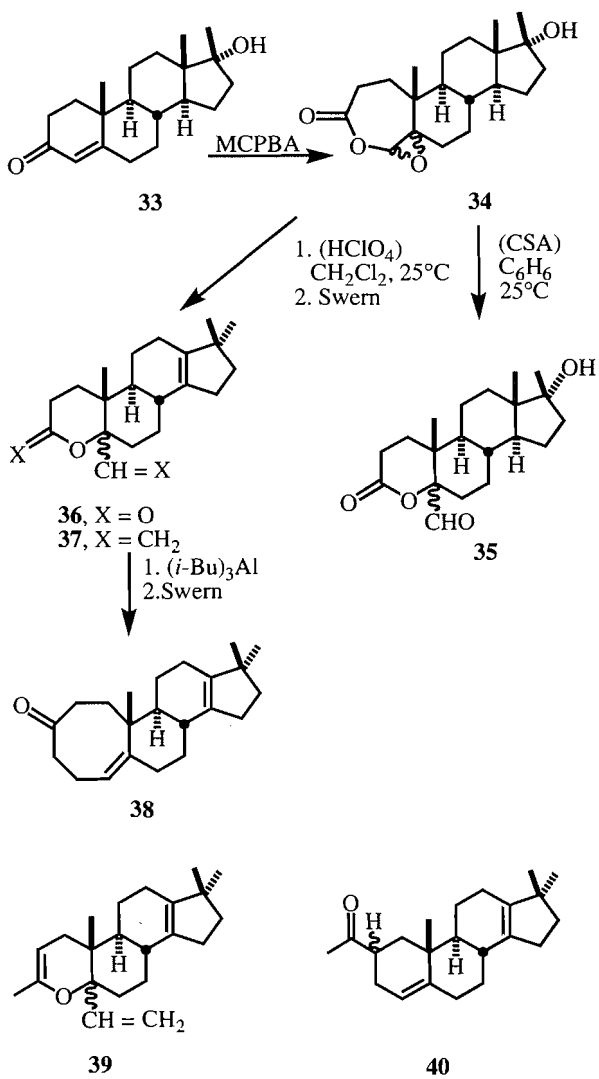

SCHEME 6

Tribal can be attributed with confidence to steric hindrance imposed by the C-19 methyl substituent. Heating **37** at 190°C for 46 h in base-coated soft-glass tubes served as an alternative means of securing **38** (40%), but with concomitant production of **39** (18%) and its Claisen product **40** (30%).

Within the context of a ready means for the ring expansion of 2-cyclohexenones to 4-cyclooctenones, the transformations documented above serve as an ample illustrative precedent. The two carbon atoms that become inserted are introduced simultaneously by Tebbe olefination of both carbonyl groups in an aldehydo lactone and ultimately connected during Claisen rearrangement. The ring juncture stereochemistry in the allyl vinyl ether is not of consequence since [3,3] sigmatropy in either isomer necessarily proceeds via that transition state guaranteed to generate a *cis* double bond within the medium-sized ring. The less sterically hindered examples undergo the Claisen rearrangement efficiently when thermally activated. The presence of a quaternary carbon in close proximity to the reaction site is the source of significant kinetic retardation and side reactions operate competitively. In these instances, Tribal catalysis plays a particularly attractive and serviceable role. This modification, which allows Claisen rearrangements to be conducted routinely at room temperature and gives rise cleanly to 4-cyclooctenols, merits increased use as an effective cationic counterpart of the more established anionic oxy-Cope process (14).

Experimental

Melting points are uncorrected. Infrared spectra were recorded on a Perkin–Elmer model 1320 spectrometer. The ^{1}H nmr spectra were recorded at 300 MHz and the ^{13}C nmr data obtained at either 75 or 20 MHz as indicated. Mass spectra were measured on a Kratos MS-30 instrument by Mr. Dick Weisenberger at The Ohio State University Chemical Instrumentation Center. Elemental analyses were performed at the Scandinavian Microanalytical Laboratory, Herlev, Denmark. All flash chromatographic separations were carried out on Merck silica gel 60 (60–200 mesh) and reactions were routinely performed under an inert atmosphere (nitrogen or argon) unless otherwise indicated. Solvents were reagent grade and dried prior to use.

(4aS,5S)-4,4a,5,6,7,8-Hexahydro-5-hydroxy-4a-methyl-2(3H)-naphthalenone 7

To a solution of Wieland–Miescher ketone (1.0 g, 5.6 mmol) exhibiting $[\alpha]_D^{25}$ +100 (*c* 1.0, toluene) in methanol (30 mL) at 0°C was added, dropwise, a solution of $NaBH_4$ (0.14 g, 3.7 mmol) in methanol (20 mL). The solution was stirred at 0°C for 30 min and several drops of acetic acid were added. The mixture was concentrated under vacuum, water was added, and the product was extracted into ether (3 × 20 mL), dried, concentrated, and purified by flash chromatography (elution with 30% ethyl acetate in petroleum ether) to give 0.980 g (97%) of the 2β-ol-5-one as a colorless oil; $[\alpha]_D^{25}$ +183 (*c* 1.7, $CHCl_3$); ir ($CHCl_3$): 3600, 3450, 1665, and 1620 cm^{-1}; ^{1}H nmr (300 MHz, $CDCl_3$) δ; 5.73 (s, 1H), 3.37 (dd, *J* = 11.5, 4.4 Hz, 1H), 2.66 (br s, 1H), 2.45–2.10 (series of m, 6H), 1.82 (m, 2H), 1.64 (m, 1H), 1.45 (m, 1H), 1.15 (s, 3H); ^{13}C nmr (75 MHz, $CDCl_3$): 199.84, 169.04, 125.17, 77.95, 41.58, 34.10, 33.59, 31.96, 30.09, 23.08, 15.19 ppm; ms *m/z* (M^+) calcd.: 180.1150; found: 180.1167.

Can. J. Chem. Downloaded from www.nrcresearchpress.com by 217.78.4.112 on 09/08/12
For personal use only.

Can. J. Chem. Downloaded from www.nrcresearchpress.com by 217.78.4.112 on 09/08/12
For personal use only.

To a cold (−78°C) solution of the keto alcohol (0.90 g, 5.42 mmol) in CH_2Cl_2 (20 mL) was added liquified isobutylene (40 mL). The mixture was stirred for 16 h at room temperature, then cooled to −10°C and poured into dilute KOH solution. The mixture was extracted with ether (3 × 40 mL), the combined organic phases were dried and concentrated, and the residue was purified by flash chromatography on silica gel (elution with 60% ether in petroleum ether) to give 0.914 g (76%) of **7** as a viscous, colorless oil; $[\alpha]_D^{25}$ +108 (*c* 4.1, $CHCl_3$); ir ($CHCl_3$): 1660 and 1620 cm^{-1}; ^1H nmr (300 MHz, $CDCl_3$) δ: 5.69 (s, 1H), 3.15 (dd, *J* = 11.2, 4.1 Hz, 1H), 2.30 (m, 2H), 2.15 (m, 1H), 2.05 (m, 1H), 1.75 (m, 5H), 1.31 (m, 1H), 1.13 (s, 9H), 1.11 (s, 3H); ^{13}C nmr (75 MHz, $CDCl_3$): 199.60, 169.40, 124.82, 77.36, 73.32, 41.54, 34.69, 33.87, 32.23, 30.22, 29.00 (3C), 22.99, 16.18 ppm; ms/fab *m/z* (M^+ + 1) calcd.: 237.36; found: 237.26.

Peracid oxidation of ***7*** *to epoxylactone* ***8***

To a solution of **7** (0.120 g, 0.51 mmol) in CH_2Cl_2 (30 mL) was added $NaHCO_3$ (0.40 g) and MCPBA (0.26 g, 1.5 mmol). The mixture was refluxed for 1 day, quenched with water, and extracted with ether (3 × 60 mL). The combined ethereal layers were dried and concentrated, and the residue was purified by flash chromatography on silica gel (elution with 40% ether in petroleum ether) to give 0.086 g (63%) of **8**; ir ($CHCl_3$): 1750 cm^{-1}; ^1H nmr (300 MHz, $CDCl_3$) δ: 4.75 (s, 1H, ***8a***), 4.67 (s, 1H, ***8b***), 3.42 (dd, *J* = 10.6, 4.2 Hz, 1H), 2.54 (m, 2H), 1.97–1.03 (series of m, 8H), 1.16 (s, 9H), 1.14 (s, 3H, ***8a***), 1.12 (s, 3H, ***8b***); ^{13}C nmr (75 MHz, $CDCl_3$): 171.68, 171.55, 87.48, 84.81, 74.22, 73.91, 73.67, 73.57, 72.33, 69.63, 41.41, 41.00, 31.29, 31.08, 30.75, 29.62, 29.47, 29.24, 29.19 (6C), 28.99, 27.45, 19.84, 19.02, 17.54, 16.39 ppm; ms *m/z* ($M^+ - [C_4H_8]$) calcd.: 212.1048; found: 212.1081.

*(4aR,5S)-5-*tert*-Butoxy-8a-formylhexahydro-4a-methyl-hydrocoumarin* ***9a***

To a solution of ***9a*** (80 mg, 0.299 mmol) in CH_2Cl_2 (10 mL), trifluoroacetic acid (10 drops) was added. The mixture was stirred for 24 h at room temperature and diluted with ether. The ethereal phase was washed with saturated $NaHCO_3$ solution, dried, and concentrated. The residue was purified by flash chromatography on silica gel (elution with 15% ethyl acetate in petroleum ether) to give 70.5 mg (88%) of ***9a*** as a white solid, mp 132–135°C; ir ($CHCl_3$): 1735 cm^{-1}; ^1H nmr (300 MHz, $CDCl_3$) (major isomer) δ: 9.87 (s, 1H), 3.77 (dd, *J* = 10.6, 4.4 Hz, 1H), 2.60 (m, 2H), 2.20–1.08 (series of m, 8H), 1.14 (s, 9H), 1.04 (s, 3H); ^{13}C nmr (75 MHz, $CDCl_3$): 200.06, 199.05, 171.23, 171.05, 90.96, 88.99, 73.71, 73.58, 71.92, 67.61, 41.25, 38.39, 29.31, 29.19, 29.07 (3C), 28.85 (3C), 28.17, 27.21, 26.66, 26.58, 26.15, 18.52, 18.36, 16.61, 13.16 (1C not observed) ppm; ms *m/z* ($M^+ - [C_4H_8]$) calcd.: 212.1049; found: 212.1031. Anal. calcd. for $C_{15}H_{24}O_4$: C 67.14; H 9.01; found: C 66.96; H 9.01.

*(4aR,5S)-5-*tert*-Butoxyhexahydro-4a-methyl-2-methylene-8a-vinylchroman* **9**b

A solution of ***9a*** (53 mg, 0.20 mmol), pyridine (3 drops), THF (2 mL), and CH_2Cl_2 (1 mL) was prepared under argon. The mixture was cooled to −40°C and 0.5 M Tebbe reagent (1.0 mL, 0.5 mmol) in toluene was added dropwise. The solution was kept at this temperature for 15 min, then warmed to 25°C and stirred at this temperature for 90 min before being returned to −40°C and quenched with 10% KOH solution (1 mL). A 0.5% triethylamine solution in ether was added and the mixture was filtered through a pad of basic alumina (act. III). Most of the solvent was evaporated and the residue was purified by chromatography on basic alumina (act. III) (elution with pentane) to provide 43.3 mg (63%) of ***9b*** as a light yellow oil; ir (neat): 1670, 1260, 1190, and 1060 cm^{-1}; ^1H nmr (300 MHz, C_6D_6) δ: 6.10 (dd, *J* = 17.1, 11.0 Hz, 1H), 5.63 (dd, *J* = 17.1, 1.9 Hz, 1H), 5.23 (dd, *J* = 11.0, 1.2 Hz, 1H), 4.52 (*d*, *J* = 1.8 Hz, 1H), 4.11 (d, *J* = 1.7 Hz, 1H), 3.29 (m, 1H), 2.50 (m, 1H), 2.41 (m, 1H), 1.90 (m, 2H), 1.59–0.92 (series of m, 6H), 1.24 (s, 9H), 1.02 (s, 3H); ^{13}C nmr (75 MHz, C_6D_6): 157.68, 140.16, 117.74, 89.69, 81.55, 73.34, 72.78, 34.78, 31.34, 30.25, 29.14, 29.03 (3C), 24.56, 19.81, 13.74 ppm; ms *m/z* ($M^+ - [C_4H_8]$) calcd.: 208.1463; found: 208.1445.

*(4aR,5S)-5-*tert*-Butoxyhexahydro-4a-methyl-8a-vinylhydrocoumarin* **9**c

To a solution of methyltriphenylphosphonium bromide (357 mg, 1 mmol) in THF (3 mL) at −10°C was added KHMDS (1.90 mL, 0.95 mmol). The mixture was stirred for 30 min and a solution of ***9a*** (0.15 g, 0.71 mmol) in THF (1 mL) was introduced. The reaction mixture was stirred for 1 h at room temperature and quenched with water. After the usual extractive work-up with ether and purification by flash chromatography (silica gel, elution with 5% ether in petroleum ether) 138 mg (93%) of ***9c*** was obtained as a white solid, mp 110°C; ir ($CHCl_3$): 1720 cm^{-1}; ^1H nmr (300 MHz, $CHCl_3$) (major isomer) δ: 6.40 (dd, *J* = 17.0, 11.1 Hz, 1H), 5.38 (dd, *J* = 17.0, 1.1 Hz, 1H), 5.32 (dd, *J* = 11.1, 1.1 Hz, 1H), 3.48 (m, 1H), 2.54 (m, 2H), 2.00–1.06 (series of m, 8H), 1.16 (s, 9H), 1.03 (s, 3H); ^{13}C nmr (75 MHz, $CHCl_3$): 172.85, 172.63, 138.79, 138.64, 116.16, 115.07, 89.31, 86.18, 73.48, 73.33, 72.84, 68.03, 41.28, 39.77, 33.40, 32.61, 29.81, 29.58, 29.22 (3H), 28.95 (3C), 28.19, 27.16, 26.37, 25.60, 19.44, 19.19, 17.24, 12.60 ppm; ms *m/z* ($M^+ - [C_4H_8]$) calcd.: 210.1256; found: 210.1242.

*(4S,4aS)-4-*tert*-Butoxy-1,2,3,4,4a,5,6,7,8,9-decahydro-4a-methyl-7-benzo-cyclooctenol* ***10***

To a solution of ***9b*** (42 mg, 0.16 mmol) in CH_2Cl_2 (2 mL) was added, at room temperature and under argon, a solution of Tribal in toluene (0.8 mL, 0.8 mmol). The mixture was stirred for 6 h. Ether was then added followed by water. After the usual extractive work-up with ether and purification by flash chromatography (silica gel, elution with 30% ether in petroleum ether) 26.2 mg (62%) of **10** was obtained as a viscous oil; ir ($CHCl_3$): 3600 cm^{-1}; ^1H nmr (300 MHz, $CDCl_3$) (major isomer) δ: 5.34 (m, 1H), 4.07 (m, 1H), 3.39 (dd, *J* = 10.9, 4.5 Hz, 1H), 2.68 (br s, 1H), 2.49 (br s, 1H), 2.36–0.87 (series of m, 14H), 1.19 (s, 9H), 1.05 (s, 3H); ^{13}C nmr (62.5 MHz, $CDCl_3$) (major isomer) 145.32, 121.85, 73.08, 72.75, 65.30, 46.71, 36.14, 35.96, 35.89, 32.33, 30.82, 30.66, 29.52 (3C), 23.00, 22.21 ppm; ms *m/z* ($M^+ - [C_4H_8]$) calcd.: 210.1620; found: 210.1628.

*(4S,4aS)-4-*tert*-Butoxy-1,2,3,4,4a,5,6,7,8,9-decahydro-4a-methyl-7-benzocyclooctenone* ***11***

To a solution of DMSO (200 μL) in CH_2Cl_2 (2 mL) was treated at −78°C and under argon with oxalyl chloride (100 μL). The mixture was stirred for 15 min and a solution of **10** (25 mg, 0.094 mmol) in CH_2Cl_2 (2 mL) was introduced. The mixture was warmed to −45°C, stirred for 20 min, cooled to −78°C, and quenched by addition of triethylamine (400 μL). The mixture was then allowed to warm to room temmperature and water was added. After the usual extractive work-up with ether and purification by flash chromatography (silica gel, elution with 5% ether in petroleum ether) 20.8 mg (84%) of **11** was obtained as a viscous oil; $[\alpha]_D^{25}$ +46 (*c* 0.6, $CHCl_3$); ir ($CHCl_3$, cm^{-1}): 1695 cm^{-1}; ^1H nmr (300 MHz, $CDCl_3$) δ: 5.39 (t, *J* = 8.2 Hz, 1H), 3.31 (dd, *J* = 10.8, 4.6 Hz, 1H), 2.53 (m, 4H), 2.26 (m, 4H), 1.86 (m, 2H), 1.69–1.10 (series of m, 4H), 1.17 (s, 9H), 1.08 (s, 3H); ^{13}C nmr (75 MHz, $CDCl_3$): 213.65, 145.95, 121.36, 74.26, 73.09, 46.73, 43.72, 40.70, 35.56, 32.27, 30.21, 29.35 (3C), 24.52, 22.85, 19.71 ppm; ms *m/z* ($M^+ - [C_4H_8]$) calcd.: 208.1463; found: 208.1441. Anal. calcd. for $C_{17}H_{28}O_2$: C 77.22, H 10.67; found: C 77.33, H 10.68.

Thermal Claisen rearrangement of **9**b

A solution of ***9b*** (78 mg, 0.295 mmol) in toluene (1 mL) was sealed under vacuum in a potassium hydroxide-coated soft glass tube (8 mm o.d.) and heated at 190°C for 48 h. The tube was opened and rinsed three times with ether. After evaporation of the solvent, the residue was purified by flash chromatography on silica

Can. J. Chem. Downloaded from www.nrcresearchpress.com by 217.78.4.112 on 09/08/12
For personal use only.

gel (elution with 5% ether in petroleum ether). There was isolated 10.3 mg (13%) of **12**, 21.0 mg (27%) of **13**, and 38.5 mg (49%) of cyclooctenone **11**.

For **12**: ir ($CHCl_3$): 1680, 1465, 1195, and 1060 cm^{-1}; ^1H nmr (300 MHz, $CHCl_3$) (major isomer) δ: 6.16 (dd, J = 17.0, 10.9 Hz, 1H), 5.28 (dd, J = 17.0, 1.8 Hz, 1H), 5.22 (dd, J = 10.9, 1.8 Hz, 1H), 4.41 (m, 1H), 3.47 (dd, J = 10.5, 5.1 Hz, 1H), 1.88–0.88 (series of m, 8H), 1.74 (s, 3H), 1.16 (s, 9H), 0.95 (s, 3H); ^{13}C nmr (75 MHz, $CHCl_3$) (major isomer): 147.51, 138.03, 114.23, 95.84, 80.99, 73.07, 72.84, 39.50, 33.36, 31.73, 30.25, 29.06 (3C), 19.84, 19.64, 13.28 ppm; ms m/z ($M^+ - [C_4H_8]$) calcd.: 208.1463; found: 208.1448.

For **13**: ir ($CHCl_3$): 1705 cm^{-1}; ^1H nmr (300 MHz, $CDCl_3$) (major isomer) δ: 5.35 (m, 1H), 3.07 (dd, J = 10.5, 4.1 Hz, 1H), 2.61 (m, 1H), 2.32–0.81 (series of m, 10 H), 2.17 (s, 3H), 1.17 (s, 9H), 1.06 (s, 3H); ^{13}C nmr (75 MHz, $CDCl_3$): 212.19, 211.98, 144.34, 142.96, 119.14, 118.47, 78.91, 73.35, 72.02, 44.75, 44.53, 41.58, 41.17, 39.80, 34.88, 31.70, 31.47, 31.07, 29.69, 29.29, (3C), 29.20 (3C), 28.28, 28.09, 27.89, 27.52, 26.10, 24.58, 20.89, 18.28 (1C not observed) ppm; ms m/z ($M^+ - [C_4H_8]$) calcd.: 208.1463; found: 208.1451.

(4aS,8aS)-Hexahydro-2-methylene-8a-vinylchroman ***17***

A solution of aldehydo lactone **16** (6*e*) (68.0 mg, 0.37 mmol), pyridine (3 drops), THF (2 mL), and CH_2Cl_2 (1 mL) was prepared under argon. The mixture was cooled to −40°C and 0.5 M Tebbe reagent (1.9 mL, 0.95 mmol) in toluene was added dropwise. The solution was kept for 15 min at this temperature, then warmed to 25°C, and stirred for 90 min at this temperature before being re-cooled to −40°C and quenched with 10% KOH solution (1 mL). A 0.5% triethylamine solution in ether was added and the mixture was filtered through a pad of basic alumina (act. III). Most of the solvent was evaporated and the residue was purified by chromatography on basic alumina (act. III) (elution with pentane) to provide 45.9 mg (69%) of **17** as a light yellow oil; ir (neat): 1640, 1460, 1260, 1140, and 1020 cm^{-1}; ^1H nmr (300 MHz, C_6D_6) δ: 5.87 (dd, J = 17.4, 11.0 Hz, 1H), 5.61 (dd, J = 17.4, 2.1 Hz, 1H), 5.27 (dd, J = 11.0, 2.1 Hz, 1H), 4.50 (s, 1H), 4.12 (t, J = 2.3 Hz, 1H), 2.20 (m, 2H), 1.97 (m, 1H), 1.64 (m, 1H), 1.47 (m, 3H), 1.33–0.92 (series of m, 6H); ^{13}C nmr (75 MHz, C_6D_6): 157.68, 137.09, 117.74, 91.52, 79.53, 43.42, 40.65, 29.29, 29.07, 25.83, 25.08, 22.98 ppm; ms m/z (M^+) calcd.: 178.1358; found: 178.1346.

(4aS)-1,2,3,4,4a,5,6,7,8,9-Decahydro-7-benzocyclooctenol ***18***

To a solution of **17** (74 mg, 0.42 mmol) in CH_2Cl_2 (2 mL) was added, at room temperature and under argon, a solution of Tribal in toluene (2 mL, 2 mmol). The mixture was stirred for 15 min, diluted with ether, and treated with water. After the usual extractive work-up with ether and purification by flash chromatography (silica gel, elution with 30% ether in petroleum ether) 64.4 mg (86%) of **18** was obtained; ir ($CHCl_3$): 3600 cm^{-1}; ^1H nmr (300 MHz, $CDCl_3$) δ: 5.35 (t, J = 8.0 Hz, 1H), 3.93 (m, 1H), 2.76 (m, 1H), 2.50 (m, 1H), 2.14–1.79 (series of m, 16H); ^{13}C nmr (75 MHz, $CDCl_3$): 141.85, 122.11, 71.27, 38.86, 36.40, 35.19, 32.49, 32.18, 30.20, 26.70, 22.17, 21.42 ppm; ms m/z (M^+) calcd.: 180.1514; found: 180.1551.

(4aS)-2,3,4,4a,5,6,7,8,9-Octahydro-7-benzocyclooctenone ***19***

A solution of DMSO (200 μL) in CH_2Cl_2 (2 mL) was prepared at −78°C under argon and treated with oxalyl chloride (100 μL). The mixture was stirred for 15 min and a solution of **18** (30 mg, 0.17 mmol) in CH_2Cl_2 (2 mL) was added. The mixture was warmed to −45°C, stirred for 20 min, cooled back to −78°C, and quenched with triethylamine (400 μL). The mixture was allowed to warm to room temperature and water was added. After the usual extractive work-up with ether and purification by flash chromatography (silica gel, elution with 5% ether in petroleum ether), 25.5 mg (86%) of **19** was obtained; ir ($CHCl_3$): 1695 cm^{-1}; ^1H nmr (300 MHz, $CDCl_3$) δ: 5.52 (t, J = 6.4 Hz, 1H), 2.57–0.77 (series of m, 17 H); ^{13}C nmr (75 MHz, $CDCl_3$): 215.74, 142.46, 121.56, 48.22, 39.82, 34.57, 31.84, 31.07, 26.66, 26.53, 22.50, 21.51 ppm; ms m/z (M^+) calcd.: 178.1358; found 178.1358. Anal. calcd. for $C_{12}H_{18}O$: C 80.85, H 10.18; found: C 80.63, H 10.12.

Thermal Claisen rearrangement of ***17***

A solution of **17** (63 mg, 0.354 mmol) in toluene (1 mL) was sealed under vacuum in a KOH-coated soft-glass tube (8 mm o.d.) and heated at 180°C for 24 h. The tube was opened and rinsed three times with ether. After evaporation of solvent, the residue was purified by flash chromatography on silica gel (elution with 5% ether in petroleum ether). There was isolated 8.1 mg (13%) of **20** and 46.2 mg (73%) of cyclooctenone **19**.

For **20**: ir ($CHCl_3$): 1705 cm^{-1}; ^1H nmr (300 MHz, $CDCl_3$) δ: 5.31 (m, 1H), 2.51 (m, 1H), 2.12 (s, 3H), 2.21–0.81 (series of m, 13H); ^{13}C nmr (75 MHz, $CDCl_3$): 211.60, 211.51, 141.39, 140.46, 117.49, 116.24, 47.55, 44.70, 37.55, 36.39, 35.63, 35.07, 35.04, 34.73, 33.42, 31.61, 28.36, 27.89, 27.70, 27.46, 27.33, 26.87, 26.55, 25.99 ppm; ms m/z (M^+) calcd.: 178.1358; found: 178.1376.

Isomerization of ***17***

Allyl vinyl ether **17** was isomerized to the internal olefinic isomer in an nmr tube with $CHCl_3$ as solvent; ir ($CHCl_3$): 1680, 1465, 1195, and 1060 cm^{-1}; ^1H nmr (300 MHz, $CHCl_3$) δ: 5.87 (dd, J = 17.4, 11.0, Hz, 1H), 5.61 (dd, J = 17.4, 2.1 Hz, 1H), 5.27 (dd, J = 11.0, 2.1 Hz, 1H), 4.50 (s, 1H), 4.12 (t, J = 2.3 Hz, 1H), 2.20 (m, 2H), 1.97 (m, 1H), 1.64 (m, 1H), 1.47 (m, 3H), 1.33–0.92 (series of m, 6 H); ^{13}C nmr (75 MHz, $CHCl_3$): 142.49, 135.51, 114.80, 111.99, 93.06, 37.45, 35.28, 27.60, 26.02, 25.64, 21.41, 20.09 ppm; ms m/z (M^+) calcd.: 178.1358; found: 178.1346.

Base-catalyzed isomerization of ***22***

Sodium hydroxide solution (8.2 mL of 2 M) was added dropwise to a stirred solution of **22** (413 mg, 1.48 mmol) in cold (−10°C) methanol (40 mL). The reaction mixture was stirred at this temperature for 1 h before being neutralized with 5% HCl, diluted with water, and extracted with CH_2Cl_2. The combined organic phases were dried and evaporated, and the residual viscous oil was treated with a few drops of ethyl acetate, then pentane, until cloudy. Crystallization at room temperature afforded 378 mg (92%) of **23** as colorless crystals, mp 143–145°C, whose ir and ^1H nmr spectra were identical to those previously reported (6*f*); ^{13}C nmr (75 MHz, $CDCl_3$): 198.23, 170.26, 85.73, 54.84, 54.31, 41.49, 38.21, 37.03, 33.84, 33.20, 33.09, 29.32, 21.36, 19.25, 18.32, 16.17, 16.01 ppm.

Tebbe olefination of ***23***

A solution of **23** (145 mg, 5.22×10^{-4} mol), THF (1.5 mL), CH_2Cl_2 (1.5 mL), and pyridine (10 drops) was cooled to −45°C and treated dropwise with a solution of the Tebbe reagent in toluene (2.60 mL of 0.5 M, 1.30×10^{-3} mol). The reaction mixture was stirred for 30 min at −45°C and for 90 min at room temperature, then returned to −45°C and quenched with 10% NaOH solution (0.40 mL). The resulting mixture was worked up in the described manner to give 92 mg of colorless crystals (64%) of **24**, mp 72–73°C (from pentane at −78°C); $[\alpha]_D^{25}$ −38.3 (*c*0.6, cyclohexane); ir (CCl_4): 1675, 1630, and 1460 cm^{-1}; ^1H nmr (300 MHz, C_6D_6) δ: 6.13 (dd, J = 17.4, 11.1 Hz, 1H), 5.51 (dd, J = 17.4, 1.7 Hz, 1H), 5.17 (dd, J = 11.1, 1.7 Hz, 1H), 4.53 (d, J = 1.8 Hz, 1H), 4.13 (d, J = 1.8 Hz, 1H), 2.34–2.13 (m, 2H), 1.73–0.82 (series of m, 14H), 0.79 (s, 3H), 0.72 (s, 3H), 0.66 (s, 3H); ^{13}C nmr (75 MHz, C_6D_6): 158.09, 139.84, 115.64, 91.34, 79.24, 56.49, 56.22, 42.28, 39.84, 39.05, 37.39, 33.51, 33.28, 30.03, 21.58, 20.08, 18.80, 17.97, 15.73 ppm; ms m/z (M^+) calcd.: 274.2296; found: 274.2320. Anal. calcd. for $C_{19}H_{30}O$: C 83.15, H 11.02; found: C 83.15, H 11.05.

Internalization of the exocyclic double bond in **24** was most conveniently accomplished by allowing a sample to stand in chloroform at room temperature for 2 days. The yield of **41** was quantitative; ir (CCl_4): 1680, 1460, 1445, 1390, 1380, and 1350 cm^{-1}; ^1H nmr (300 MHz, $CDCl_3$) δ: 6.12 (dd, J = 17.3, 11.0 Hz, 1H),

5.24 (dd, J = 17.3, 1.5 Hz, 1H), 5.10 (dd, J = 11.0, 1.3 Hz, 1H), 4.44 (d, J = 4.8 Hz, 1H), 2.18 (td, J = 12.4, 1.5 Hz, 1H), 1.89–0.91 (series of m, 13H), 1.70 (s, 3H), 0.83 (s, 3H), 0.81 (s, 3H); ^{13}C nmr (75 MHz, $CDCl_3$): 147.98, 137.68, 113.66, 94.98, 77.57, 56.03, 52.84, 41.79, 39.19, 38.78, 36.79, 33.36, 33.04, 21.45, 19.93, 19.65, 18.42, 17.90, 15.44 ppm; ms m/z (M^+) calcd.: 274.2297; found: 274.22.79. Anal. calcd. for $C_{19}H_{30}O$: C 83.15, H 11.02; found: C 83.24, H 11.04.

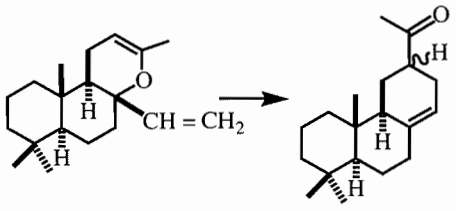

41 **42**

Ring expansion of ***24***

A solution of **24** (36 mg, 0.13 mmol) in CH_2Cl_2 (1 mL) was treated with Tribal (1 mL of 1 M in hexanes). Although the rearrangement was essentially complete within 15 min, stirring was maintained for 1 h. The reaction mixture was diluted with ether and transferred slowly to a separatory funnel containing a slurry of ice and 5% HCl. The organic layer was washed with saturated $NaHCO_3$ and brine solutions, then dried and evaporated. Chromatography on silica gel (elution with 10% ethyl acetate in hexane) gave a 3:7 epimeric mixture of cyclooctenols (25 mg, 69%); ir ($CHCl_3$): 3600 cm^{-1}; ^{1}H nmr (300 MHz, $CDCl_3$) δ: 5.47–5.36 (m, 1H), 4.08–4.04 (m, 0.3H), 3.74–3.66 (m, 0.7H), 2.70–0.88 (series of m, 21H), 0.85 (s, 3H), 0.84 (s, 3H), 0.83 (s, 3H); ^{13}C nmr (75 MHz, $CDCl_3$): 142.29, 140.18, 121.86, 120.77, 73.67, 68.92, 58.09, 57.78, 55.57, 54.75, 42.33, 42.19, 40.08, 40.05, 39.66, 39.42, 39.02, 37.07, 36.61, 35.91, 35.78, 33.57, 33.45, 24.78, 24.71, 21.90, 21.76, 21.48, 20.13, 19.47, 19.31, 14.79 ppm; ms m/z (M^+) calcd.: 276.2453; found: 276.2476.

A 46 mg sample of this cyclooctenol mixture (0.167 mmol) was added to a cold (−78°C) solution consisting of DMSO (142 μL, 2 mmol), oxalyl chloride (87 μL, 1 mmol), and CH_2Cl_2 (1 mL). The mixture was stirred at −78°C for 30 min and at −45°C for 30 min before being recooled to −78°C and treated with triethylamine (348 μL, 2.5 mmol). After 15 min, the reaction mixture was quenched with water and worked up as described above to give, after SiO_2 chromatography, 38.5 mg (84%) of **25** as a colorless solid, mp 87–88°C (after sublimation); $[\alpha]_D^{25}$ −60.5 (c 0.9, CCl_4); ir (CCl_4): 1710 cm^{-1}; ^{1}H nmr (300 MHz, $CDCl_3$) δ: 5.36 (m, 1H), 2.57–2.35 (m, 6H), 2.27–2.17 (m, 1H), 2.06–1.36 (series of m, 10H), 1.19–0.96 (m, 3H), 0.90 (s, 3H), 0.85 (s, 3H), 0.83 (s, 3H); ^{13}C nmr (75 MHz, $CDCl_3$): 214.00, 143.30, 121.24, 55.79, 51.43, 45.10, 42.40, 42.36, 41.41, 38.89, 34.25, 33.40, 33.18, 23.52, 23.25, 22.02, 21.80, 19.03, 15.50 ppm; ms m/z (M^+) calcd.: 274.2296; found: 274.2296. Anal. calcd. for $C_{19}H_{30}O$: C 83.15, H 11.02; found: C 83.01, H 11.11.

Thermal Claisen rearrangement of ***24***

Freshly prepared **24** (42.3 mg) was dissolved in toluene (1 mL), transferred to a soft-glass tube coated with KOH, and sealed under vacuum. The tube was heated at 190°C for 20 h, the solvent evaporated, and the residue chromatographed on silica gel (elution with 6% ethyl acetate hexane). There was isolated 1.4 mg (3%) of **42** and 34 mg (80%) of **25**.

For **42**: colorless oil; ir (CCl_4): 1710 cm^{-1}; ^{1}H nmr (300 MHz, $CDCl_3$) δ: 5.44 (br s, 1H), 2.60–0.9 (series of m), and methyl singlets at 2.13, 0.88, 0.87, 0.84, 0.83, 0.80, 0.75; ^{13}C nmr (75 MHz, $CDCl_3$): 215.35, 211.36, 138.70, 138.56, 119.27, 118.68, 54.94, 54.70, 51.64, 48.31, 48.19, 45.90, 41.12, 39.30, 39.22, 38.92, 38.45, 35.88, 35.33, 33.72, 33.69, 33.36, 33.33, 28.22, 27.63, 27.35, 26.16, 25.51, 24.04, 22.89, 22.47, 22.09, 22.02, 19.02, 18.92, 15.21, 14.39 ppm; ms m/z (M^+) calcd.: 274.22.97: found: 274.2322. Anal. calcd. for $C_{19}H_{30}O$: C 83.15, H 11.02; found: C 83.15, H 11.06.

Thermal Claisen rearrangement of ***41***

A solution of **41** (29 mg) in toluene (1 mL) was sealed into a KOH-coated soft glass tube under vacuum and heated at 180°C for 20 h. The predescribed work-up afforded 25 mg (86%) of **42** as an inseparable mixture of two isomers.

*17β-(*tert*-Butyldiphenylsiloxy)androst-4-en-3-one* ***26***b

To a solution of testosterone (***26****a*) (0.288 g, 1 mmol) in DMF (1 mL) was added *tert*-butyldiphenylchlorosilane (0.33 g, 1.2 mmol), imidazole (150 mg), and DMAP (15 mg). The mixture was stirred at room temperature for 16 h. Water was added and the mixture was extracted with ether (3 × 10 ml). The combined organic layers were dried and concentrated, and the residue purified by flash chromatography (silica gel, elution with 10% ethyl acetate in petroleum ether) to give 0.500 g (95%) of ***26****b* as a white solid, mp 138°C; $[\alpha]_D^{25}$ +12.7 (c 0.6, $CHCl_3$); ir ($CHCl_3$): 1660 and 1615 cm^{-1}; ^{1}H nmr (300 MHz, $CDCl_3$) δ: 7.69 (m, 4H), 7.38 (m, 6H), 5.72 (s, 1H), 3.68 (t, J = 8.2 Hz, 1H), 2.35 (m, 4H), 2.00 (m, 1H), 1.82–0.79 (series of m, 14H), 1.18 (s, 3H), 1.12 (s, 9H), 0.95 (s, 3H); ^{13}C nmr (75 MHz, $CDCl_3$): 199.22, 171.10, 135.81 (2C), 135.78 (2C), 134.72, 129.40, 129.34, 127.41, 127.30 (2C), 127.25 (2C), 123.64, 82.13, 53.74, 49.62, 43.42, 38.47, 36.56, 35.56, 33.78, 32.64, 31.39, 30.63, 26.98 (3C), 26.51, 23.35, 20.58, 19.19, 17.26, 11.57 ppm; ms fab m/z (M^++1) calcd.: 527.33; found: 527.32.

*17β-(*tert*-Butyldiphenylsiloxy)-4α,5-epoxy-A-homo-4-oxaandrostan-3-one* ***27***

To a solution of ***26****b* (1.052 g, 2 mmol) in CH_2Cl_2 (40 mL) was added Na_2CO_3 (3.00 g) and MCPBA (2.16 g, 6 mmol). The mixture was refluxed for 14 h, quenched with water, and extracted with ether (3 × 60 ml). The combined organic layers were dried and concentrated, and the residue was purified by flash chromatography (silica gel, elution with 5% ethyl acetate in petroleum ether) to give 0.715 g (64%) of **27** as a 4:1 mixture of isomers; white solid, mp 52°C; ir ($CHCl_3$): 1750 cm^{-1}; ^{1}H nmr (300 MHz, $CDCl_3$) (major isomer) δ: 7.67 (m, 4H), 7.36 (m, 6H), 4.73 (s, 1H), 3.64 (t, J = 8.2 Hz, 1H), 2.69 (m, 1H), 2.51 (m, 1H), 1.94 (td, J = 14.1, 4.4 Hz, 1H), 1.81–0.89 (series of m, 16H), 1.18 (s, 3H), 1.08 (s, 9H), 0.89 (s, 3H); ^{13}C nmr (75 MHz, $CDCl_3$) (major isomer) 171.51, 135.93 (2C), 135.91 (2C), 134.27, 133.73, 129.52, 129.46, 127.41 (2C), 127.37 (2C), 87.45, 82.18, 71.11, 49.73, 48.90, 43.54, 38.54, 36.55, 34.83, 31.24, 30.66, 29.48, 29.28, 27.04 (3C), 23.44, 20.90, 19.30, 18.84, 11.58 (1C not observed) ppm; ms/fab m/z (M^++1) calcd.: 559.32; found: 559.34.

*17β-(*tert*-Butyldiphenylsiloxy)-3-oxo-4-oxaandrostane-5-carboxaldehyde* ***28***

To a solution of **27** (342 mg, 0.613 mmol) in benzene (10 mL) was added 10-camphor-*d*-sulphonic acid (50 mg). The mixture was stirred at room temperature for 24 h, then poured into a saturated $NaHCO_3$ solution. After the usual extractive work-up with ether and purification by flash chromatography on silica gel (elution with 15% ether in petroleum ether) 321.5 mg (94%) of **28** was obtained as a 1:4 mixture of isomers; white solid, mp 90–92°C; ir ($CHCl_3$): 1740 cm^{-1}; ^{1}H nmr (300 MHz, $CDCl_3$) (major isomer) δ: 9.95 (s, 1H), 7.66 (m, 4H), 7.38 (m, 6H), 3.64 (t, J = 8.2 Hz, 1H), 2.58 (m, 2H), 1.96–0.86 (series of m, 17H), 1.08 (s, 9H), 1.07 (s, 3H), 0.89 (s, 3H); ^{13}C nmr (75 MHz, $CDCl_3$) (major isomer): 200.29, 170.79, 135.87 (4C), 134.65, 134.21, 129.49, 129.44, 127.38 (2C), 127.34 (2C), 88.24, 82.07, 49.66, 47.90, 43.81, 38.96, 36.40, 34.45, 30.60, 29.04, 27.29, 27.02 (3C), 26.32, 23.38, 20.97, 19.27, 14.44, 11.74 (1C not observed) ppm; ms/fab m/z (M^++1) calcd.: 559.32; found: 559.35.

This substance is subject to slow air oxidation. For the corresponding acid: Anal. calcd. for $C_{35}H_{46}O_5Si$: C 73.13, H 8.07; found: C 73.30, H 8.22.

Can. J. Chem. Downloaded from www.nrcresearchpress.com by 217.78.4.112 on 09/08/12
For personal use only.

Can. J. Chem. Downloaded from www.nrcresearchpress.com by 217.78.4.112 on 09/08/12
For personal use only.

tert-*Butyl[(3-methylene-5-vinyl-4-oxaandrostan-17β-yl)oxy]diphenylsilane* ***29***

A solution of **28** (132 mg, 0.237 mmol), pyridine (3 drops), THF (2 mL), and CH_2Cl_2 (2 mL) was prepared under argon. The mixture was cooled to −40°C and 0.5 M Tebbe reagent (1.2 mL, 0.60 mmol) in toluene was added dropwise. The solution was kept for 15 min at this temperature, then warmed to 25°C and stirred for 90 min before being cooled to −40°C and quenched with 10% KOH solution (1 mL). A 0.5% triethylamine solution in ether was added and the mixture was filtered through a pad of basic alumina (act. III). Most of the solvent was evaporated and the residue was purified by chromatography on basic alumina (act. III) (elution with pentane) to provide 120.6 mg (92%) of **29** as a light yellow oil; ir (neat): 1675, 1460, 1260, 1115, and 1090 cm^{-1}; ^1H nmr (300 MHz, C_6D_6) (major isomer) δ: 7.82 (m, 4H), 7.26 (m, 6), 6.13 (dd, J = 17.2, 11.1 Hz, 1H), 5.62 (dd, J = 17.2, 1.9 Hz, 1H), 5.23 (dd, J = 11.0, 1.9 Hz, 1H), 4.52 (s, 1H), 4.08 (s, 1H), 3.66 (t, J = 8.3 Hz, 1H), 2.29 (m, 2H), 1.90–0.93 (series of m, 17 H), 1.23 (s, 9H), 1.02 (s, 3H), 0.92 (3 H); ^{13}C nmr (75 MHz, C_6D_6): 158.18, 157.79, 140.88, 140.73, 136.45 (4C), 136.39 (4C), 135.21 (2C), 134.80 (2C), 129.98 (2C), 129.92 (2C), 129.27 (4C), 128.49 (4C), 127.85, 127.63, 117.02, 113.21, 91.64, 88.74, 82.80, 81.38, 49.93, 49.71, 48.46, 44.25, 43.72, 40.92, 38.72, 37.32, 36.96, 35.45, 35.07, 34.63, 33.00, 31.32, 31.18, 30.16, 29.48, 29.00, 27.37 (6C), 27.01, 26.17, 24.49, 23.66, 23.48, 21.37, 21.10, 20.63, 19.62, 18.58, 15.40, 12.18 (2C not observed) ppm; ms/fab m/z (M^++1) calcd. 555.36; found: 555.46.

Tribal-promoted Claisen rearrangement of ***29***

To a solution of **29** (177.3 mg, 0.32 mmol) in CH_2Cl_2 (2 mL) was added, at room temperature and under argon, a solution of Tribal in toluene (2 mL, 2 mmol). The mixture was stirred for 6 h at room temperature, then ether and water were added. After the usual extractive work-up with ether and purification by flash chromatography (silica gel, elution with 25% ether in petroleum ether) 50 mg (64%) of the cyclooctenol was obtained as a viscous oil; ir ($CHCl_3$): 3600 cm^{-1}; ^1H nmr (300 MHz, $CDCl_3$) (major isomer) δ: 7.61 (m, 4H), 7.31 (m, 6H), 5.32 (t, J = 9.1 Hz, 1H), 3.81 (m, 1H), 3.62 (t, J = 8.3 Hz, 1H), 2.38 (br s, 1H), 2.29–0.83 (series of m, 23 H), 1.07 (s, 9H), 1.03 (s, 3H) 0.86 (s, 3H); ^{13}C nmr (75 MHz, $CDCl_3$) (major isomer): 147.67, 135.92 (2C), 134.93, 134.37, 129.44, 129.36, 128.48, 127.55, 127.36 (2C), 127.32 (2C), 126.92, 82.44, 65.20, 50.28, 43.65, 43.53, 37.07, 37.01, 36.54, 36.28, 35.94, 35.82, 32.33, 31.67, 30.88, 29.65, 29.31, 27.05 (3C), 23.49, 23.20, 19.32, 11.64 ppm; ms/fab m/z (M^++1) calcd.: 557.37; found: 557.42.

17β-(tert-Butyldiphenylsiloxy)-A-dihomoandrost-4b-3n-3-one ***30***

A solution of DMSO (300 mL) in CH_2Cl_2 (2 mL) was prepared at −78°C under argon was treated with oxalyl chloride (150 μL). The mixture was stirred for 15 min and a solution of the above alcohol (83.4 mg, 0.15 mmol) in CH_2Cl_2 (2 mL) was introduced. The mixture was warmed to −45°C, stirred for 20 min, cooled to −78°C, and quenched by addition of triethylamine (700 μL). The mixture was allowed to warm to room temperature and water was added. After the usual extractive work-up with ether and purification by flash chromatography (silica gel, elution with 5% ether in petroleum ether), 68 mg (86%) of **30** was obtained as a viscous oil; $[\alpha]_D^{25}$ +16.3 (c 1.19, $CHCl_3$); ir ($CHCl_3$): 1695 cm^{-1}; ^1H nmr (300 MHz, $CDCl_3$) δ: 7.65 (m, 4H), 7.36 (m, 6H), 5.29 (t, J = 9.1 Hz, 1H), 3.65 (t, J = 8.2 Hz, 1H), 2.70–0.81 (series of m, 23H), 1.07 (s, 12H), 0.86 (s, 3H); ^{13}C nmr (75 MHz, $CDCl_3$): 212.96, 147.00, 135.92 (4C), 134.96, 134.42, 129.47, 129.29, 127.41 (2C), 127.35 (2C), 119.35, 82.41, 49.98, 47.87, 43.92, 43.81, 43.59, 41.07, 36.86, 36.45, 35.80, 33.31, 32.40, 30.87, 27.08 (3C), 23.46, 23.04, 22.94, 20.61, 19.37, 11.68 ppm; ms/fab m/z (M^++1) calcd.: 555.36; found: 555.43. Anal. calcd. for $C_{37}H_{50}O_2Si$: C 80.09, H 9.08; found: C 79.69, H 9.35.

Thermal Claisen rearrangement of ***29***

A solution of **29** (56 mg, 0.10 mmol) in toluene (1 mL) was sealed under vacuum in a potassium hydroxide-coated soft-glass tube (8 mm o.d.) and heated at 190°C for 48 h. The tube was opened and rinsed three times with ether. After evaporation of the solvent, the residue was purified by flash chromatography on silica gel (elution with 5% ether in petroleum ether). There was isolated 10 mg of (18%) of **31**, 16 mg (29%) of **32**, and 21.5 mg (39%) of **30**.

For **31**: ir ($CHCl_3$): 1680, 1460, 1370, 1265, 1115, and 840 cm^{-1}; ^1H nmr (300 MHz, $CDCl_3$) δ: 7.58 (m, 4H), 7.32 (m, 6H), 6.09 (dd, J = 17.1, 10.9 Hz, 1H), 5.17 (dd, J = 17.1, 1.8 Hz, 1H), 4.98 (dd, J = 10.9, 1.8 Hz, 1H), 4.29 (t, J = 3.2 Hz, 1H), 3.55 (t, J = 8.3 Hz, 1H), 1.76–0.83 (series of m, 17 H), 1.75 (s, 3H), 1.09 (s, 9H), 0.94 (s, 3H), 0.89 (s, 3H); ^{13}C nmr (75 MHz, $CDCl_3$): 147.86, 138.51, 136.01 (2C), 135.97 (2C), 134.94, 134.46, 129.47, 129.41, 127.40 (2C), 127.35 (2C), 114.17, 95.58, 82.44, 80.74, 50.12, 48.02, 44.00, 37.00, 36.58, 35.17, 33.78, 32.22, 30.76, 27.10 (3C), 23.40, 21.07, 19.94, 19.35, 14.76, 11.88 (1 C not observed) ppm; ms/fab m/z (M^++1) calcd.: 555.36; found: 555.47.

For **32**: ir (neat); 1705 cm^{-1}; ^1H nmr (300 MHz, $CDCl_3$) (major isomer) δ: 7.65 (m, 4H), 7.36 (m, 6H), 5.26 (m, 1H), 3.62 (t, J = 8.3 Hz, 1H), 2.60 (m, 1H), 2.16 (2, 3H), 2.10–0.67 (series of m, 19H), 1.07 (s, 9H), 1.04 (s, 3H), 0.88 (s, 3 H); ^{13}C nmr (75 MHz, $CDCl_3$): 212.18, 211.99, 146.55, 144.77, 135.99 (4C), 135.96 (4C), 134.94 (2C), 134.42 (2C), 129.49, (2C), 129.39 (2C), 127.38 (4C), 127.33 (4C), 116.90, 116.08, 82.44, 82.39, 54.61, 50.88, 50.22, 49.99, 44.66, 44.54, 43.96, 43.62, 39.87, 38.55, 36.99, 36.87, 36.34, 36.30, 35.99, 33.80, 32.51, 32.03, 31.95, 30.85, 30.96, 29.68, 28.07, 27.97, 27.62, 27.55, 27.07 (6C), 23.55, 22.60, 21.90, 21.34, 21.12, 19.60, 19.42, 19.32, 11.82, 11.68 ppm; ms/fab m/z (M^++1) calcd.: 555.36; found: 555.41.

4α,5-Epoxy-17α-hydroxy-17-methyl-A-homo-4-oxaandrostan-3-one ***34***

To a solution of **33** (0.302 g, 1 mmol) in CH_2Cl_2 (30 mL) was added Na_2CO_3 (0.80 g) and MCPBA (0.52 g, 3 mmol). The mixture was refluxed for 1 day, quenched with water, and extracted with ether (3 × 50 mL). The combined organic layers were dried and concentrated, and the residue was purified by flash chromatography (silica gel, elution with 35% ethyl acetate in petroleum ether) to give 0.274 g (82%) of **34** as an 8:1 *cis*:*trans* mixture; white solid, mp 74–76°C; ir ($CHCl_3$): 1750 cm^{-1}; ^1H nmr (300 MHz, $CDCl_3$) (major isomer) δ: 4.76 (s, 1H), 2.78–0.96 (series of m, 19H), 1.21 (s, 3H), 1.18 (s, 3H), 0.87 (s, 3H) (hydroxyl signal not observed); ^{13}C nmr (75 MHz, $CDCl_3$) (major isomer): 171.42, 87.41, 81.39, 71.07, 50.12, 48.79, 45.33, 38.76, 38.57, 35.61, 31.31, 31.26, 30.13, 29.44, 25.74, 23.16, 20.87, 18.84, 13.77 (1C not observed) ppm; ms m/z (M^+) calcd.: 334.2142; found; 334.2105.

17α-Hydroxy-17-methyl-3-oxo-4-oxaandrostane-5-carboxaldehyde ***35***

To a solution of **34** (43.2 mg, 0.129 mmol) in benzene (3 mL) was added 10-camphor-*d*-sulfonic acid (10 mg). The mixture was stirred for 24 h at room temperature and diluted with ether. The organic layer was washed with saturated $NaHCO_3$ solution, dried, and concentrated. The residue was purified by flash chromatography (silica gel, elution with 30% ethyl acetate in petroleum ether) to give 40.6 mg (94%) of **35** as a white solid, mp 74–76°C; ir ($CHCl_3$): 1740 cm^{-1}; ^1H nmr (300 MHz, $CDCl_3$) (major isomer) δ 9.95 (s, 1H), 2.53 (m, 2H), 2.03–0.78 (series of m, 17H), 1.16 (s, 3H), 1.04 (s, 3H), 0.83 (s, 3H) (hydroxyl signal not observed); ^{13}C nmr (75 MHz, $CDCl_3$): 200.30, 170.80, 88.24, 81.34, 50.07, 47.81, 45.65, 38.99, 38.76, 35.26, 31.22, 29.04, 27.32, 27.08, 26.50, 25.81, 23.04, 20.95, 14.53, 13.96 ppm; ms m/z (M^+-H_2O) calcd.: 316.2038; found: 316.2105.

17,17-Dimethyl-3-oxo-18-nor-4-oxaandrost-13-ene-5-carboxaldehyde ***36***

To a solution of **34** (120 mg, 0.359 mmol) in CH_2Cl_2 (10 mL) was added an anhydrous CH_2Cl_2 solution of perchloric acid (5 mL). The mixture was stirred for 24 h at room temperature and diluted with ether. The solution was washed with a saturated $NaHCO_3$ so-

Can. J. Chem. Downloaded from www.nrcresearchpress.com by 217.78.4.112 on 09/08/12
For personal use only.

lution, dried, and concentrated. The residue was purified by flash chromatography (silica gel, elution with 5% ethyl acetate in petroleum ether) to give 99.9 mg (88%) of **36** as a white solid, mp 94°C; ir ($CHCl_3$): 1740 cm^{-1}; ^1H nmr (300 MHz, $CDCl_3$) (major isomer) δ: 10.04 (s, 1H), 2.33–0.87 (series of m, 18H), 1.04 (s, 3H), 0.96 (s, 3H), 0.95 (s, 3H); ^{13}C nmr (75 MHz, $CDCl_3$): 200.30, 170.91, 142.15, 134.06, 88.17, 45.60, 45.43, 39.39, 39.10, 35.43, 29.63, 28.93, 27.82, 27.04, 26.66, 26.29, 22.80, 21.90, 14.31 (1C not observed) ppm; ms *m/z* (M^+) calcd.: 316.2038; found: 316.2076. Anal. calcd. for $C_{20}H_{28}O_3$: C 75.91, H 8.92; found: C 75.89, H 8.88.

17,17-Dimethyl-3-methylene-5-vinyl-18-nor-4-oxaandrost-13-ene **37**

Aldehydo lactone **36** (126.4 mg, 0.40 mmol) was dissolved in pyridine (6 drops), THF (3 mL), and CH_2Cl_2 (2 mL), cooled to −45°C, and treated with the Tebbe reagent (2 mL, 0.5 mmol). The reaction mixture was warmed to room temperature and stirred for 1 h. The solution was cooled to −40°C and a 5% solution of KOH was carefully added. The reaction mixture was passed through a pad of basic alumina (act. III), concentrated under vacuum, and purified by flash chromatography on basic alumina (act. III) (elution with pentane) to give 113.6 mg (91%) of **37** as a light yellow oil; ir (neat): 1680, 1460, 1260, 1100, and 1020 cm^{-1}; ^1H nmr (300 MHz, C_6D_6) δ: 6.15 (dd, *J* = 17.0, 11.0 Hz, 1H), 5.60 (dd, *J* = 17.0, 2.0 Hz, 1H), 5.13 (dd, *J* = 11.0, 2.0 Hz, 1H), 4.52 (d, *J* = 1.1 Hz, 1H), 4.07 (d, *J* = 1.4 Hz, 1H), 2.40–0.93 (series of m, 18 H), 1.05 (s, 3H), 1.03 (s, 3H), 1.00 (s, 3H); ^{13}C nmr (75 MHz, C_6D_6): 157.91, 140.82, 136.06, 128.05, 116.87, 88.09, 45.88, 39.95, 36.34, 36.12, 34.81, 32.40, 29.99, 29.24, 27.14, 27.01 (2C), 26.59, 24.36, 22.95, 22.60, 15.27 ppm; ms *m/z* (M^+) calcd.: 312.2453; found: 312.2450.

Tribal-promoted Claisen rearrangement of **37**

To a solution of **37** (104 mg, 0.33 mmol) in CH_2Cl_2 (2 mL) was added, at room temperature and under argon, a solution of Tribal in toluene (2 mL, 2 mmol). The mixture was stirred for 15 min, then treated with ether and water. After the usual extractive work-up with ether and purification by flash chromatography (silica gel, elution with 20% ether in petroleum ether) 90 mg (63%) of the cyclooctenol was obtained as a 3:1 mixture of isomers; viscous oil; ir ($CHCl_3$): 3600 cm^{-1}; ^1H nmr (300 MHz, $CDCl_3$) (major isomer) δ: 5.38 (t, *J* = 9.1 Hz, 1H), 3.82 (m, 1H), 2.55–0.88 (series of m, 22 H), 1.00 (s, 3H), 0.96 (s, 3H), 0.94 (s, 3H) (hydroxyl signal not observed); ^{13}C nmr (75 MHz, $CDCl_3$): 147.36, 141.49, 136.19, 121.33, 119.16, 72.06, 68.49, 45.35, 45.29, 43.47, 43.09, 40.07, 39.66, 37.16, 37.07, 36.90, 35.90, 35.57, 33.31, 32.57, 32.41, 32.30, 32.20, 31.91, 31.46, 29.75, 29.67, 29.33, 27.28, 26.84, 26.74, 26.70, 26.50, 23.56, 23.40, 23.34, 23.14, 23.09, 22.94, 22.63, 22.50, 22.34, 21.53, 21.24 ppm; ms *m/z* (M^+) calcd.: 314.2210; found: 314.2190.

*17,17-Dimethyl-*A*-dihomo-18-norandrosta-4b,13-dien-3-one* **38**

Oxalyl chloride (66 μL) was added to a solution of DMSO (140 μL) in CH_2Cl_2 (2 mL) at −78°C and under argon. The mixture was stirred for 15 min and a solution of the above cyclooctenol (21 mg, 0.067 mmol) in CH_2Cl_2 (2 mL) was added. The mixture was warmed to −45°C, stirred for 20 min, cooled back to −78°C, and quenched by the addition of triethylamine (300 μL). The mixture was allowed to warm to room temperature and water was added. After the usual extractive work-up with ether and purification by flash chromatography on silica gel (elution with 5% ether in petroleum ether) 16.1 mg (86%) of **38** was obtained as a viscous oil; $[\alpha]_D^{25}$ +31.4 (*c* 1.12, $CHCl_3$); ir ($CHCl_3$): 1695 cm^{-1}; ^1H nmr (300 MHz, $CDCl_3$) δ: 5.36 (t, *J* = 9.0 Hz, 1 H), 3.10 (m, 1H), 2.68 (m, 2H), 2.52–0.84 (series of m, 18H), 1.05 (s, 3H), 0.96 (s, 3H), 0.95 (s, 3 H); ^{13}C nmr (75 MHz, C_6D_6): 211.82, 146.52, 141.38, 135.90, 120.20, 45.46, 45.31, 43.65, 43.57, 40.85, 39.62, 36.92, 36.74, 32.88, 31.84, 29.74, 26.68, 26.5, 23.14, 22.68, 22.29 (1C not observed) ppm; ms *m/z* (M^+) calcd.: 312.2453; found: 312.2450. Anal. calcd. for $C_{22}H_{32}O$: C 84.56, H 10.32; found: C 84.35, H 10.37.

Thermal Claisen rearrangement of **37**

A solution of **37** (50 mg, 0.16 mmol) in toluene (1 mL) was sealed under vacuum in a potassium hydroxide-coated soft-glass tube (8 mm o.d.) and heated at 190°C for 46 h. The tube was opened and rinsed three times with ether. After evaporation of solvent, the residue was purified by flash chromatography on silica gel (elution with 5% ether in petroleum ether) to give 9 mg (18%) of isomerized vinyl ether **37**, 15 mg (30%) of **40**, and 20 mg (40%) of cyclooctenone **38**.

For **39**: ir ($CHCl_3$): 1680 cm^{-1}; ^1H nmr (300 MHz, $CDCl_3$) δ: 6.29 (dd, *J* = 17.0, 10.9 Hz, 1H), 5.29 (dd, *J* = 17.0, 1.7 Hz, 1H), 5.10 (dd, *J* = 10.0, 1.7 Hz, 1H), 4.41 (t, *J* = 1.3 Hz, 1H), 2.20–1.00 (series of m, 16H), 1.80 (s, 3H), 0.97 (s, 3H), 0.96 (s, 3H), 0.91 (s, 3 H); ^{13}C nmr (62.5 MHz, $CDCl_3$): 147.93, 141.27, 138.72, 135.47, 114.04, 95.65, 80.88, 45.38, 45.20, 39.54, 36.57, 36.16, 34.45, 32.00, 29.66, 26.97, 26.76, 26.40, 22.94, 22.27, 19.95, 14.37 ppm; ms *m/z* (M^+) calcd.: 312.2453; found: 312.2458.

For **40**: ir ($CHCl_3$): 1700 cm^{-1}; ^1H nmr (300 MHz, $CDCl_3$) (major isomer) δ: 5.32 (m, 1H), 2.60 (m, 1H), 2.24–0.86 (series of m, 18H), 2.18 (s, 3H), 1.03 (s, 3H), 0.96 (s, 3H), 0.94 (s, 3 H); ^{13}C nmr (75 MHz, $CDCl_3$): 211.98, 211.80, 145.97, 144.31, 135.85, 135.30 (2C), 117.38 (2C), 116.75, 52.19, 48.33, 45.22, 45.15, 44.67, 44.51, 39.39, 38.26, 37.72, 37.41, 36.83, 36.23, 33.30, 32.54, 32.36, 32.07, 29.68, 29.60, 27.93, 27.61, 27.53, 26.59, 26.51, 26.33, 26.30, 23.30, 22.93, 22.25, 22.04, 21.36, 19.05 (3C not observed) ppm; ms *m/z* (M^+) calcd.: 312.2453; found: 312.2460.

Acknowledgments

The financial support of this work by the National Institutes of Health (Grant GM-30827) is gratefully acknowledged. We also thank the Upjohn Company for providing us with **26***a* and **33**, and especially Dr. Peter K. Grant (University of Otago) for a generous supply of manool together with revised instructions for its conversion to **22**.

1. (*a*) W. A. Kinney, M. J. Coghlan, and L. A. Paquette. J. Am. Chem. Soc. **106**, 6868 (1984); **107**, 7352 (1985); (*b*) H.-J. Kang and L. A. Paquette. J. Am. Chem. Soc. **112**, 3253 (1990); **113** (1991). In press; (*c*) L. A. Paquette and T. J. Sweeney. J. Org. Chem. **55**, 1703 (1990); Tetrahedron, **46**, 4487 (1990); (*d*) D. Friedrich and L. A. Paquette. J. Org. Chem. **56**, 3831 (1991); (*e*) D. Friedrich, L. A. Paquette, and R. D. Rogers. J. Org. Chem. **56**, 3841 (1991).
2. (*a*) F. E. Ziegler. Chem. Rev. **88**, 1423 (1988); (*b*) S. J. Rhoads and N. R. Raulins. Org. React. (N.Y.), **22**, 1 (1975); (*c*) F. E. Ziegler. Accounts Chem. Res. **10**, 227 (1977).
3. (*a*) F. N. Tebbe, G. W. Parshall, and G. S. Reddy. J. Am. Chem. Soc. **100**, 3611 (1978); (*b*) S. H. Pine, R. Zaler, D. A. Evans, and R. H. Grubbs. J. Am. Chem. Soc. **102**, 3270 (1980); (*c*) N. A. Petasis and E. I. Bzowej. J. Am. Chem. Soc. **112**, 6392 (1990).
4. N. A. Petasis and M. A. Patane. Tetrahedron Lett. **31**, 6799 (1990).
5. C. M. G. Philippo, N. H. Vo, and L. A. Paquette. J. Am. Chem. Soc. **113**, 2762 (1991).
6. (*a*) J. T. Pinhey and K. Schaffner. Tetrahedron Lett. *b*, 601 (1965); Aust. J. Chem. **21**, 1873 (1968); (*b*) C. W. J. Chang and S. W. Pelletier. Tetrahedron Lett. **7**, 5483 (1966); (*c*) M. Gorodetsky, N. Danieli, and Y. Mazur. J. Org. Chem. **32**, 760 (1967); (*d*) S. W. Pelletier, C. W. J. Chang, and K. N. Iyer. J. Org. Chem. **34**, 3477 (1969); (*e*) A. DeBoer and R. E. Elhwanger. J. Org. Chem. **39**, 77 (1974); (*f*) P. K. Grant, H. T. L. Liau, and W. A. Temple. Aust. J. Chem. **32**, 1353 (1979) and private communication.
7. P. J. Murphy and J. Brennan. Chem. Soc. Rev. **17**, 1 (1988).
8. T. Mori, K. Takai, K. Oshima, and H. Nozaki. Tetrahedron, **40**, 4013 (1984).

9. (*a*) C. B. C. Boyce and J. S. Whitehurst. J. Chem. Soc. 2680 (1960); (*b*) J. S. Dutcher, J. G. Macmillan, and C. H. Heathcock. J. Org. Chem. **41**, 2663.
10. (*a*) P. Buchshacher and A. Fürst. Org. Synth. **63**, 37 (1985); (*b*) J. Gutzwiller, P. Buchshacher, and A. Fürst. Synthesis, 167 (1977).
11. I. Mori, K. Takai, K. Ishima, and H. Nozaki. Tetrahedron Lett. **22**, 3985 (1981); Tetrahedron, **40**, 4013 (1984); Bull. Chem. Soc. Jpn. **57**, 446 (1984).
12. K. Maruoka, K. Nonoshita, H. Banno, and H. Yamamoto. J. Am. Chem. Soc. **110**, 7922 (1988).
13. D. C. Ayres and D. P. Levy. Tetrahedron, **42**, 4259 (1986).
14. L. A. Paquette. Synlett. **2**, 67 (1990); Angew. Chem. Int. Ed. Engl. **29**, 609 (1990).

Can. J. Chem. Downloaded from www.nrcresearchpress.com by 217.78.4.112 on 09/08/12
For personal use only.

Synthesis and characterization of derivatized capped porphyrins

HANG TANG, TILAK P. WIJESEKERA, AND DAVID DOLPHIN[1]

Department of Chemistry, University of British Columbia, 2036 Main Mall, Vancouver, B.C., Canada V6T 1Z1

Received August 8, 1991

This paper is dedicated to Professor Zdenek (Denny) Valenta on the occasion of his 65th birthday

HANG TANG, TILAK P. WIJESEKERA, and DAVID DOLPHIN. Can. J. Chem. **70**, 1366 (1992).

The syntheses of porphyrins carrying either a fully hydrophobic cavity with a benzene moiety (**32***a*,*b*) or a polar cavity with an amidobenzene (**32***c*–*d*) are described. Terephthaldehyde (**1**) was converted to benzene-bisalkanoic acids (**8**, **10**) and nitrobenzene-bisalkanoic acids (**13** and **16**) by using standard methods. The corresponding diacid chlorides **17***a*–**d** were used to acylate two equivalents of a β-unsubstituted pyrrole, and the ketonic groups were reduced by diborane. Following the transformation of the nitro function to the acetamide, appropriate modifications of the ethyl ester functions afforded the key bisformylpyrroles **25***a*–*d*. The cyanoacrylate-protected formyl pyrrole derivatives were monochlorinated at the α-methyl groups and condensed with two equivalents of an α-unsubstitutued pyrrole to give the dipyrromethane dimers. Strong aqueous alkali caused saponification of the two ester groups and deprotection of the formyl functions to produce the dipyrromethane dimer **30**, which, after thermal decarboxylation, was cyclized intramolecularly in acidic medium to give the porphyrins **32** (n = 4 or 5, X = H or $NHCOCH_3$).

HANG TANG, TILAK P. WIJESEKERA et DAVID DOLPHIN. Can. J. Chem. **70**, 1366 (1992).

On décrit la synthèse de porphyrines portant soit une cavité complètement hydrophobe avec une portion benzénique (**32***a*,*b*) soit une cavité polaire avec un amidobenzène (**32***c*–*d*). Utilisant des méthodes courantes, on a transformé le téréphtaldéhyde (**1**) en acides benzène-bisalcanoïques (**8**, **10**) et en acides nitrobenzène-bisalcanoïques (**13** et **16**). On a utilisé les chlorures d'acides correspondants (**17***a*–*d*) pour acyler deux équivalents d'un pyrrole non substitué en position β, puis on a réduit les groupes cétoniques avec du diborane. Après avoir transformé les fonctions nitro en acétamide, des modifications appropriées des fonctions esters éthyliques ont fourni les bis-formyl pyrroles **25***a*–*d* clés. On a effectué une monochloration des dérivés du formyl pyrrole protégés par le cyanoacrylate sur les groupes méthyles en α et on a condensé les produits avec deux équivalents d'un pyrrole non substitué en α afin d'obtenir des dimères dipyrrométhanes. Sous l'influence de solutions alcalines aqueuses concentrées, il se produit une saponification des deux groupes esters et une déprotection des fonctions formyles pour conduire au dimère dipyrrométhane **30** qui, après décarboxylation thermique et sous l'influence d'un acide, se cyclise d'une façon intramoléculaire pour donner les porphyrines **32** (n = 4 ou 5; X = H ou $NHCOCH_3$)

[Traduit par la rédaction]

Introduction

Dioxygen and carbon monoxide binding propertites of hemoglobin and myoglobin are largely controlled by steric and electrostatic effects provided by the protein. Hemoglobin has a lower affinity for carbon monoxide relative to dioxygen (1, 2), when compared with simple iron-porphyrin systems, due to the steric hindrance on the distal side of the heme (2, 3–6) and the porphyrin skeletal deformations (7, 8). Hydrogen bonding between the bound dioxygen and the histidine E7 residue (9) increases the stability of the dioxygen complex, and therefore leads to a higher O_2 affinity. The H-bonding was demonstrated by a neutron diffraction study of oxymyoglobin (10) and X-ray analysis of oxyhemoglobin (11).

To evaluate the influence of the immediate protein environment on the ligand binding, it is necessary to construct models with the minimum of added molecular structure essential to mimic the active site behaviour of a hemoprotein. By designing different model compounds with different structural features, it is possible to investigate separately the effects of the heme environment on its reactivity. Continued efforts to overcome the problems associated with synthetic dioxygen carriers have led to the development of several model hemes, the syntheses and structural features of which have been surveyed in a recent review (12). Simple ferrous porphyrins undergo rapid and irreversible oxidation in the absence of a large excess of base to yield μ-oxo Fe(III) species (13, 14), while in the presence of excess base a six-coordinate ferrous porphyrin is formed that is incapable of binding dioxygen (15). Synthetic model compounds have been prepared to sterically retard the formation of both the hexacoordinated system and the μ-oxo dimer.

Non-functionalized hydyrocarbon strapped porphyrins (16) were prepared by us for distorting the porphyrin plane and the methodology developed was later extended to prepare durene-capped porphyrins (17), a myoglobin model with a fully hydrophobic cavity. With the latter, the influence of distal steric effects on CO and O_2 binding were examined in the absence of stabilizing electrostatic interaction, and the relative contribution of steric effects, both proximal and distal, for R- and T-state heme systems were revealed (18). Introduction of a polar function to such heme model systems was expected to help clarify the contribution of electrostatic effects to the discriminatory binding of CO and O_2 in hemoglobin and myoglobin. For this purpose, an amide-substituted benzene-capped porphyrin model system has been designed and synthesized to mimic the hydrogen bonding between bound dioxygen and histidine E7 in hemoglobin and myoglobin. The corresponding unsubstituted benzene-capped porphyrins were also synthesized for comparison.

Results and discussion

The synthetic strategy involved the transformation of terephthaldehyde (**1**) into benzene-bisalkanoic acids (Scheme 1; **8** and **10**) and nitrobenzene-bisalkanoic acids (**13** and **16**),

[1]Author to whom correspondence may be addressed.

Can. J. Chem. Downloaded from www.nrcresearchpress.com by 217.78.4.112 on 09/08/12
For personal use only.

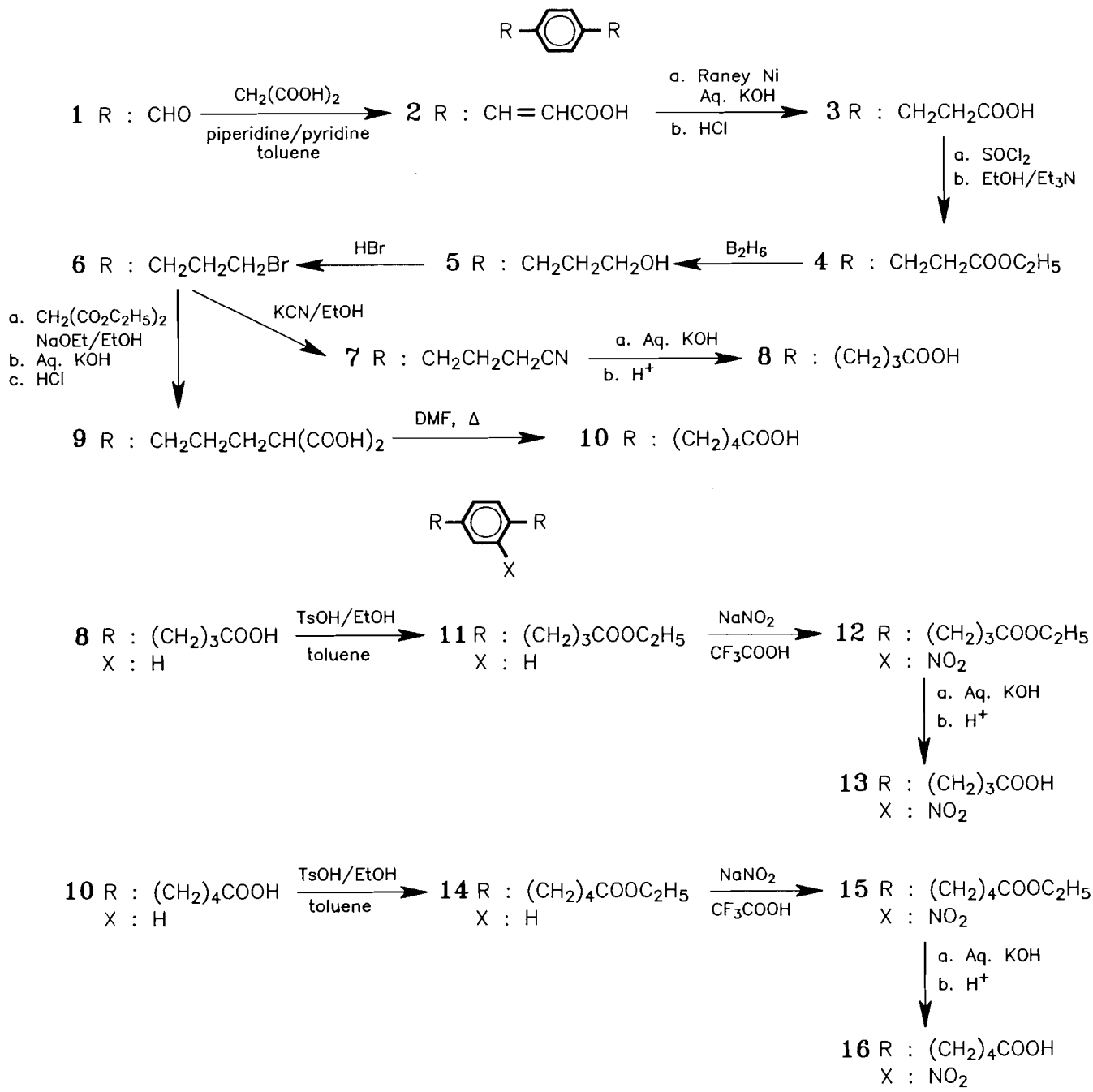

SCHEME 1

the latter to be modified to give the anilide cap. These bis-alkanoic acids could then be transformed into the capped porphyrins using the chemistry developed for the synthesis of the deformed porphyrins (16) and the durene-capped porphyrins (17).

Terephthaldehyde (**1**) was reacted with malonic acid in the presence of piperidine and pyridine to produce the diacid **2**, which was catalytically hydrogenated to give the dicarboxylic acid **3**. The transformation of **3** to the diol **5** (in order to carry out further chain extension) was effected via the more soluble diester **4** using diborane and was subsequently converted to the more reactive bisbromopropyl derivative **6**. The diacid **8**, which required the extension of the methylene side chain by one carbon, was readily prepared via the nitrile **7** using KCN in ethanol, followed by hydrolysis in aqueous alkali. To generate the bispentanoic acid **10**, a malonate synthesis was employed on the dibromide **6**. The tetraester was not isolated, but saponified *in situ* to give the tetracid **9**. The benzene-bispentanoic acid **10** was obtained by decarboxylation of **9** in boiling DMF.

The synthetic strategy for the porphyrins involved the transformation of the diacids to chain-linked bispyrroles and dipyrromethane dimers followed by an intramolecular cyclization. Since the pyrrole nucleus is sensitive to strong

Can. J. Chem. Downloaded from www.nrcresearchpress.com by 217.78.4.112 on 09/08/12
For personal use only.

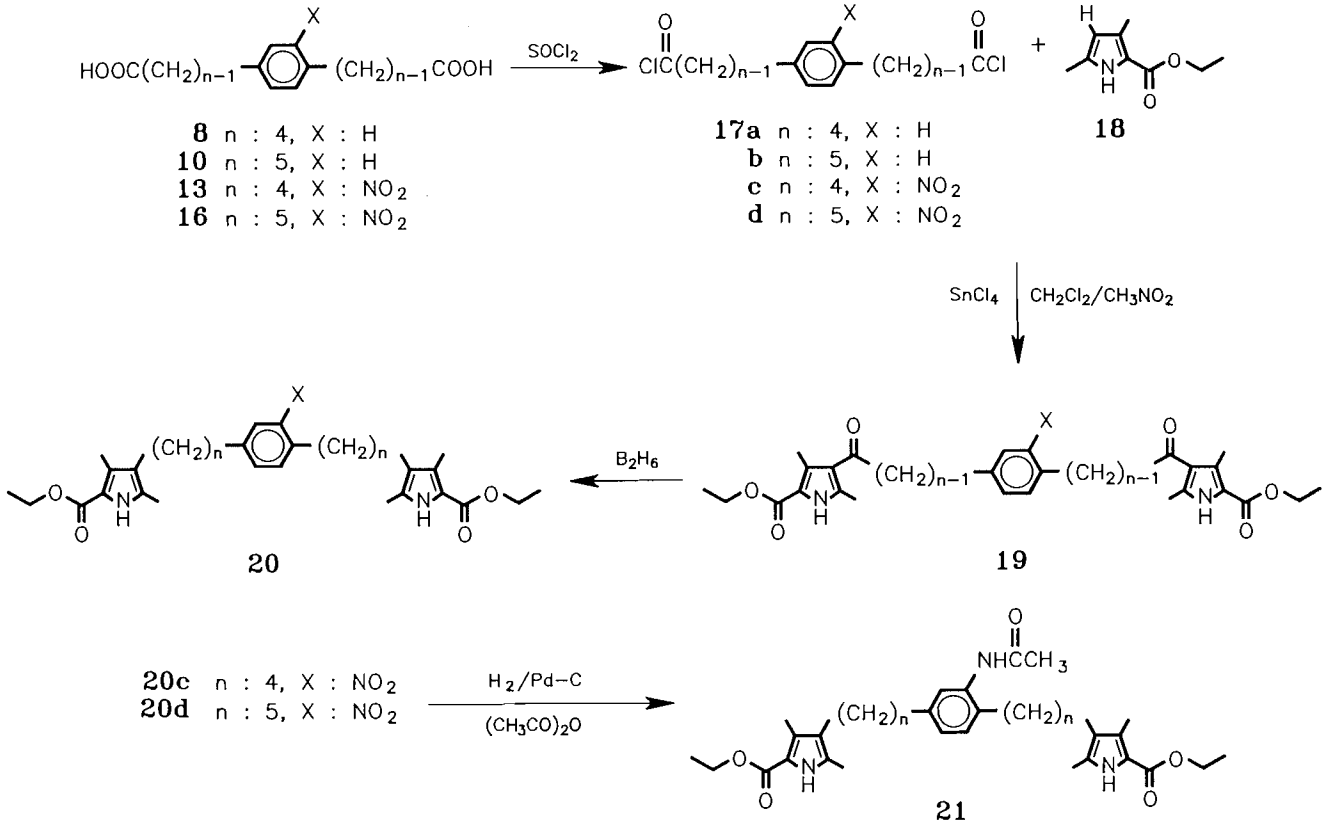

SCHEME 2

oxidizing agents, all efforts to nitrate the chain-linked bispyrrolic derivatives led to decomposition. Therefore, the nitro functionality had to be introduced before the coupling of pyrroles. Nitration of diacids **8** and **10** were found not to be practical due to the insolubility of the starting materials and the products. Therefore, nitration of the diester analogues was preferred. A sodium nitrite-trifluoroacetic acid (19) mixture was found to nitrate the diesters **11** and **14** successfully in reasonable yields (65–73%). The nitrobenzene-bisalkanoic acids **13** and **16** were obtained by hydrolysis with aqueous alkali.

The first step towards the strapped porphyrin was to link the dicarboxylic acids to two β-unsubstituted pyrroles **18** (20, 21) via Friedel–Crafts alkylation reactions. The pyrroles were acylated with the corresponding bisacid chloride **17** in a mixture of methylene chloride and nitromethane using anhydrous stannic chloride as the catalyst. The ketonic carbonyls of the resulting bispyrrole diketones **19** were reduced by diborane in yields >80% (Scheme 2).

With the chain in place, the next step was transformation of the α-ethyl ester into the synthetically useful α-formyl group. This included the removal of the ethyl ester, thermal decarboxylation of the resulting diacid, and formylation of the unsubstituted α-position by the Vilsmeier reaction (20–22). Since the direct saponification of the ethyl ester **20** led to extensive decomposition, the acids could only be obtained via a transbenzylation–debenzylation route. For the two bispyrrolic ethyl esters without the nitro function (**20***a* and **20***b*), the transesterification was effected in refluxing benzyl alcohol by using a solution of sodium in benzyl alcohol as the catalyst (Scheme 3). After quenching the reaction mixture with a mixture of acetic acid and methanol, the product was crystallized out by diluting with water. However, the two nitro-substituted bisethyl esters **20***c* and **20***d* were sensitive to the strongly basic conditions of transbenzylation at high temperature. Therefore, the nitro function was converted to the acetamide at this stage by catalytic hydrogenation in the presence of acetic anhydride (Scheme 2). Transbenzylation of the amide derivatives **21***c* and **21***d* was carried out at a lower temperature (100°C) and 12 Torr (1 Torr = 133.3 Pa) pressure to give a 60–70% yield of the bisbenzyl ester **22**.

The bisbenzyl ester **22** was cleaved by catalytic hydrogenolysis in THF and the resulting diacid **23** was decarboxylated in refluxing DMF. The formyl function was introduced by using phosphorus oxychloride – DMF (for **24***a* and **24***b*) or benzoyl chloride – DMF (for **24***c* and **24***d*) as the Vilsmeier reagent (22). The resulting iminium salt was hydrolyzed by using aqueous sodium bicarbonate, to give the chain-linked bis-α-formylpyrrole **25**. The formyl groups were protected by a Knoevenagel condensation with methyl cyanoacetate under basic conditions (23), in preparation for the subsequent oxidation of the α-methyl groups. This also helps in purifying the formylpyrrole **25** by chromatography.

The synthesis of the dipyrromethane dimer was carried out in two stages. In the first stage, the α-methyl groups of the protected bispyrroles (**26**) were monochlorinated and the resulting monochloro derivatives reacted with two equivalents of the α-unsubstituted pyrrole **28** (20, 21) in warm glacial acetic acid (Scheme 4). Deprotection of the formyl groups and

Can. J. Chem. Downloaded from www.nrcresearchpress.com by 217.78.4.112 on 09/08/12
For personal use only.

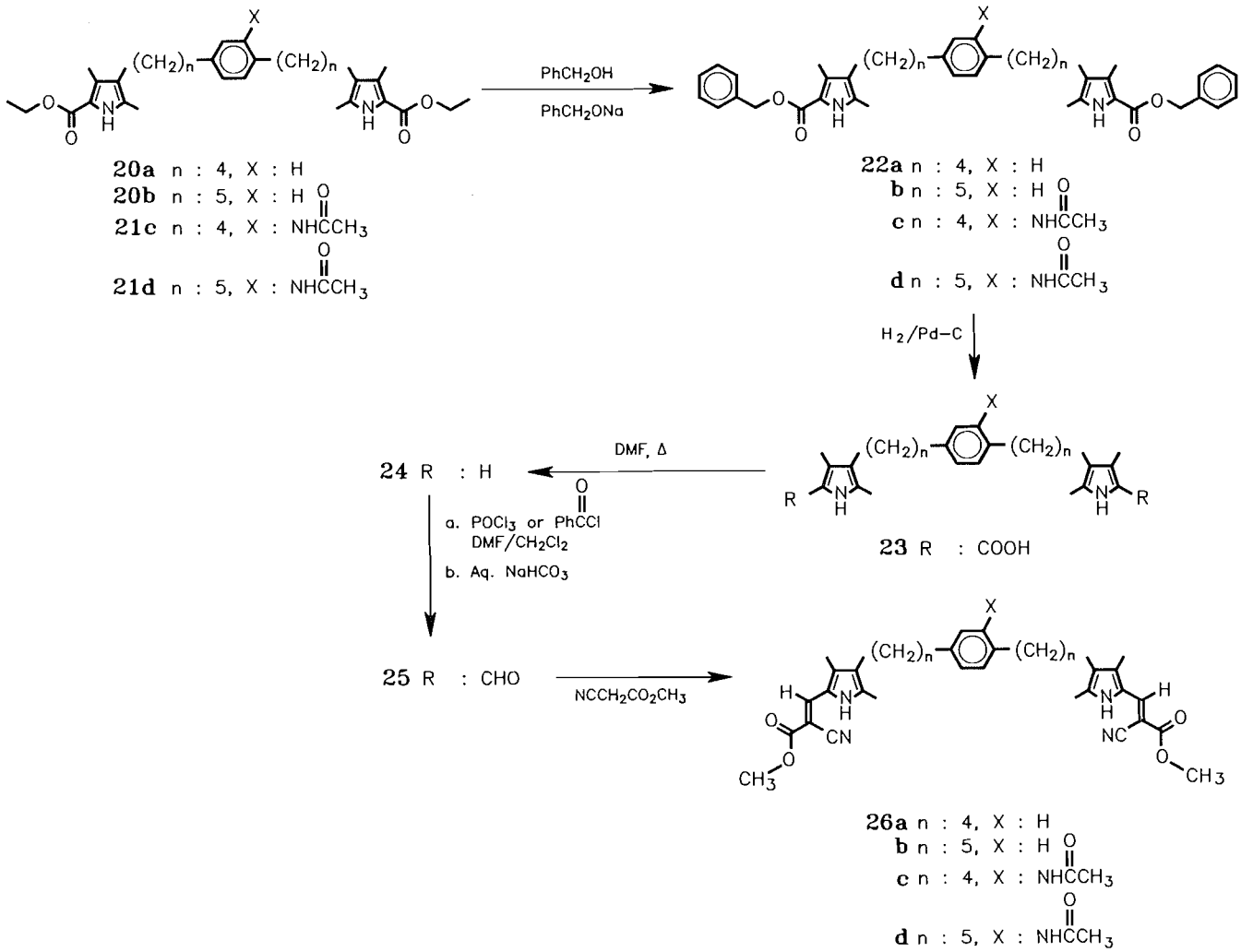

SCHEME 3

saponification of the esters of **29** were effected in one step using aqueous alkali. Because of the sensitivity of the acetamide substituents of **29***c* and **29***d* towards alkali, the reaction had to be performed under controlled conditions. A 30:1 molar ratio of base to starting material with a base concentration of 1.5 M in water and a mixed solvent system of water:*n*-propanol of ratio 2:1 were found to be optimal.

Decarboxylations of compounds **30** were carried out in refluxing DMF under nitrogen and the reaction was monitored by uv/visible spectroscopy. The absorption maximum at 280 nm (due to the carboxypyrrole group) was observed to be reduced to a shoulder within 2 h. The solution was concentrated *in vacuo*, diluted with methylene chloride, and the remaining DMF removed by extraction with water. To improve the solubility of the product **31**, the methylene chloride solution was concentrated to a small volume and diluted with THF. The cyclization to the porphyrin was accomplished by adding the THF solution of the 5-unsubstituted-5-formyldipyrromethane dimer **31** to a solution of *p*-toluenesulfonic acid in methanol/methylene chloride by means of a syringe pump. The high dilution conditions were required during cyclization in order to effect an *intra* molecular reaction leading to the desired product. The monomeric capped porphyrins **32** were isolated and purified by chromatography. The yields, dependent on the purity of the starting material, varied between 19 and 45%.

The proton nmr spectra of **32***a–d* exhibit significant upfield shifts for some of the methylene strap proton resonances and the benzene protons, resulting from the shielding effect of the porphyrin diamagnetic ring current. The signals due to the porphyrin methyl and methine protons split to two singlets, because of the asymmetry resulting from the strap.

Work describing the formation of Fe(III) and Fe(II) derivatives of these capped porphyrins and thermodynamic data on the binding of CO and O_2 to the latter (26) will be published elsewhere.

Experimental

Melting points were obtained using a Thomas model 49 Micro Hot Stage apparatus equipped with a Bristoline 6548-J17 microscope and are uncorrected. Elemental analysis was performed by Mr. P. Borda of the Microanalytical Laboratory, U.B.C. The proton nmr spectra were obtained in the indicated solvents, using a Varian XL-300 Fourier-transform spectrometer or a Bruker WH-400 spectrometer. Experimental details and analytical data for compounds **2–16** and selected examples of chain-linked mono- and

Can. J. Chem. Downloaded from www.nrcresearchpress.com by 217.78.4.112 on 09/08/12
For personal use only.

Can. J. Chem. Downloaded from www.nrcresearchpress.com by 217.78.4.112 on 09/08/12
For personal use only.

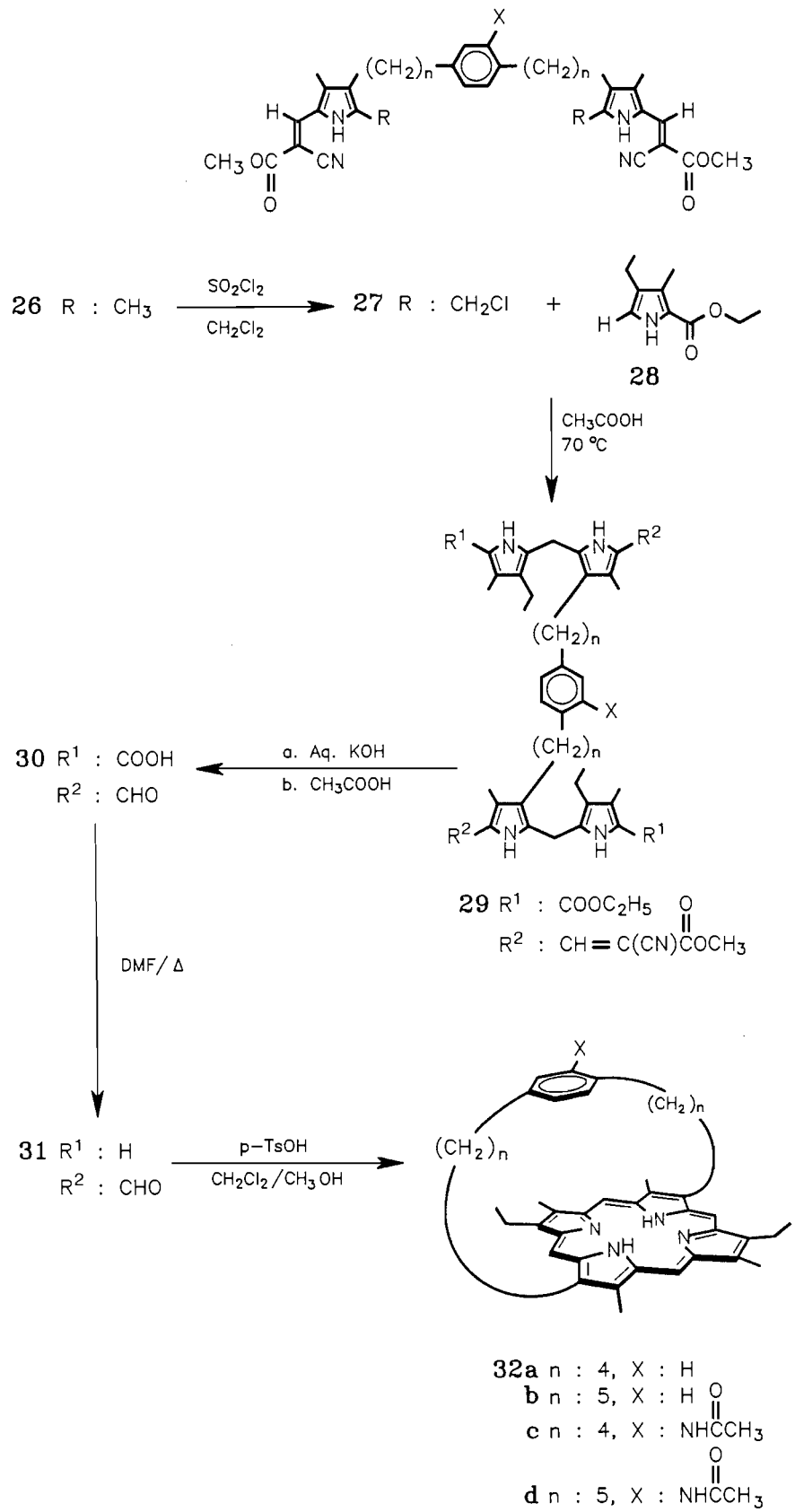

SCHEME 4

Can. J. Chem. Downloaded from www.nrcresearchpress.com by 217.78.4.112 on 09/08/12
For personal use only.

dipyrrolic precursors to the porphyrins are available as supplementary material.[2]

*1,4-Bis[4-(5-ethoxycarbonyl-2,4-dimethylpyrrol-3-yl)-4-oxobutyl]benzene (**19**a)*

1,4-Bis(3-carboxylpropyl)benzene (**8**) (10 g, 0.04 mol) and thionyl chloride (19 g, 0.16 mol) were refluxed on a steam bath for 30 min and the excess thionyl chloride removed by evaporation under reduced pressure. After repeated evaporations with CCl_4 (4 × 25 mL) the dark red residue of the bis-acid chloride was taken into distilled CH_2Cl_2 (30 mL), transferred into a flask containing 2-ethoxy-3,5-dimethylpyrrole (**18**) (16.7 g, 0.1 mol), distilled CH_2Cl_2 (140 mL), and nitromethane (150 mL) under nitrogen, and treated rapidly with anhydrous stannic chloride (41.7 g, 0.16 mol). The reaction mixture was stirred overnight at room temperature and the dark brown solution was poured into 0.1 M aqueous hydrochloric acid (100 mL) and stirred for 15 min. The precipitated yellow solid was filtered, washed with water, CH_2Cl_2, and methanol, and a second crop was collected from the combined filtrate. Overall yield was 12.5 g (57%).

An analytical sample was recrystallized by adding methanol to a concentrated solution of **19***a* in CH_2Cl_2 and minimum trifluoroacetic acid; mp 185.0–186.5°C; ^{1}H nmr (300 MHz, δ, 10% TFA/$CDCl_3$): 1.48 (t, 6H, J = 6 Hz), 1.99–2.09 (m, 4H), 2.53 (s, 6H), 2.57 (s, 6H), 2.74 (t, 4H, J = 6 Hz), 2.90 (t, 4H, J = 6 Hz), 4.45 (q, 4H, J = 6.2 Hz), 7.15 (s, 4H), 10.25 (bs, 2H); mass spectrum (*m/e* (relative intensity)): 548 (M^+, 4), 340 (17), 209 (100), 194 (66), 148 (74). Mol. wt. calcd. for $C_{32}H_{40}N_2O_6$: 548.2886; found by high resolution mass spectrometry: 548.2894. Anal. calcd. for $C_{32}H_{40}N_2O_6$: C 70.05, H 7.35, N 5.11; found: C 70.00, H 7.35, N 5.24.

*1,4-Bis[4-(5-ethoxycarbonyl-2,4-dimethylpyrrol-3-yl)butyl]-benzene (**20**a)*

The diketone **19***a* (14 g, 0.0255 mol) was suspended in anhydrous THF (150 mL) (N_2 atmosphere) and treated with a 1 M borane–THF solution (10 mL). The resulting mixture was stirred for 1 h, during which time the starting material went into solution. Following tlc analysis of an aliquot, a further 10 mL of BH_3–THF solution was added and the mixture was stirred for another hour, when the reaction was found to be complete.

The excess BH_3 was destroyed with methanol (20 mL), the solution concentrated under reduced pressure, and methanol added to crystallize the white product, yield 10.6 g (80%); mp 162–163°C; ^{1}H nmr (300 MHz, δ, $CDCl_3$): 1.35 (t, 6H, J = 7.5 Hz), 1.44–1.51 (m, 4H), 1.58–1.68 (m, 4H), 2.18 (s, 6H), 2.26 (s, 6H), 2.38 (t, 4H, J = 7.5 Hz), 2.59 (t, 4H, J = 9.4 Hz), 4.30 (q, 4H, J = 7.5 Hz), 7.08 (s, 4H), 8.70 (bs, 2H); mass spectrum (*m/e* (relative intensity)): 520 (M^+, 19), 474 (23), 428 (13), 206 (100), 180 (71), 134 (94). Mol. wt. calcd. for $C_{32}H_{44}N_2O_4$: 520.3301; found by high resolution mass spectrometry: 520.3307. Anal. calcd. for $C_{32}H_{44}N_2O_4$: C 73.81, H 8.52, N 5.38; found: C 73.69, H 8.52, N 5.45.

*1,4-Bis[4-(5-ethoxycarbonyl-2,4-dimethylpyrrol-3-yl)butyl]-2-acetamidobenzene (**21**c)*

1,4-Bis[4-(5-ethoxycarbonyl-2,4-dimethylpyrrol-3-yl)butyl]-2-nitrobenzene (**20***c*) (7.3 g, 12.9 mmol) was dissolved in THF (200 mL), treated with 10% Pd/C (0.7 g), acetic anhydride (10 mL), and sodium acetate (0.5 g), and the solution stirred under a hydrogen atmosphere (1 atm (101.3 kPa)) overnight. The solution had to be retreated with fresh catalyst and hydrogenated again for complete reaction.

The catalyst was filtered off and the product was crystallized out by concentrating the solution, in the presence of hexane, yield 90% (6.7 g); mp 215.5–216.5°C; ^{1}H nmr (400 MHz, δ, $CDCl_3$): 1.27 (t, 6H, J = 8 Hz), 1.35–1.58 (m, 8H), 2.10 (s, 9H), 2.18 (s, 6H), 2.28–2.34 (m, 4H), 2.44–2.54 (m, 4H), 4.22 (q, 4H, J = 6.7 Hz), 6.83–6.87 (s, d, 2H), 7.00 (d, 1H, J = 8 Hz), 7.48 (s, 1H), 8.49 (b, 2H); mass spectrum (*m/e* (relative intensity)): 577 (M^+, 15), 531 (18), 485 (14), 206 (16), 180 (46), 134 (100). Mol. wt. calcd. for $C_{34}H_{47}N_3O_5$: 577.3516; found by high resolution mass spectrometry: 577.3514. Anal. calcd. for $C_{34}H_{47}N_3O_5$: C 70.68, H 8.20, N 7.27; found: C 70.44, H 8.39, N 7.07.

*1,4-Bis[4-(5-benzyloxycarbonyl-2,4-dimethylpyrrol-3-yl)-butyl]benzene (**22**a)*

1,4-Bis[4-(5-ethoxycarbonyl-2,4-dimethylpyrrol-3-yl)butyl]-benzene (**20***a*) (7.8 g, 15 mmol) and distilled benzyl alcohol (100 mL) were heated to reflux under nitrogen and treated (in 1-mL portions) with a concentrated solution of sodium in benzyl alcohol. After addition of 3 mL of the catalyst, no further effervescence (corresponding to ethanol) could be observed and the hot solution was carefully poured into methanol (150 mL) with sufficient acetic acid (10 mL) to quench the catalyst. Water was added slowly to precipitate the product, which was filtered and washed with 50% MeOH/water. The dibenzylester was obtained in 86% yield (8.3 g); mp 147–149°C; ^{1}H nmr (400 MHz, δ, $CDCl_3$): 1.42–1.49 (m, 4H), 1.57–1.66 (m, 4H), 2.16 (s, 6H), 2.27 (s, 6H), 2.37 (t, 4H, J = 8 Hz), 2.58 (t, 4H, J = 8 Hz), 5.29 (s, 4H), 7.07 (s, 4H), 7.31–7.43 (m, 10H), 8.54 (bs, 2H); mass spectrum (*m/e* (relative intensity)): 644 (M^+, 8), 536 (4), 509 (7), 401 (10), 268 (23), 108 (31), 91 (100). Mol. wt. calcd. for $C_{42}H_{48}N_2O_4$: 644.3614; found by high resolution mass spectrometry: 644.3610. Anal. calcd. for $C_{42}H_{48}N_2O_4$: C 78.23, H 7.50, N 4.34; found: C 78.04, H 7.59, N 4.38.

*1,4-Bis[4-(5-benzyloxycarbonyl-2,4-dimethylpyrrol-3-yl)butyl]-2-acetamidobenzene (**22**c)*

1,4-Bis[4-(5-ethoxycarbonyl-2,4-dimethylpyrrol-3-yl)butyl]-2-acetamidobenzene (**21***c*) (1 g, 1.73 mmol) was placed in distilled benzyl alcohol (10 mL) and treated with metallic sodium (0.05 g). The resulting mixture was heated at 100°C under 12 Torr pressure for 30 min when all of the starting material dissolved, resulting in a brownish yellow solution. The solution was cooled to room temperature (still under vacuum) and neutralized with acetic acid.

Benzyl alcohol was distilled off under vacuum (0.1 Torr), and the pink residue taken into methylene chloride (30 mL) and washed with water (3 × 30 mL) to remove salts. After evaporating the methylene chloride, the solid was dissolved in ethyl acetate (10 mL), and cooled in a refrigerator at 4°C.

The white solid was filtered off and washed with cold ethyl acetate to give 0.91 g product (75%); mp 187–189°C; ^{1}H nmr (400 MHz, δ, $CDCl_3$): 1.42–1.65 (m, 8H), 2.16 (s, 9H), 2.27 (s, 6H), 2.35–2.41 (m, 4H), 2.52–2.61 (m, 4H), 5.29 (s, 4H), 6.86 (b, 1H), 6.92 (bd, 1H), 7.06 (bd, 1H), 7.32–7.45 (m, 10H), 7.56 (b, 1H), 8.53 (b, 2H); mass spectrum (*m/e* (relative intensity)): 701 (M^+, 3), 593 (3), 458 (9), 108 (69), 91 (100). Mol. wt. calcd. for $C_{44}H_{51}N_3O_5$: 701.3829; found by high resolution mass spectromemtry: 701.3834. Anal. calcd. for $C_{44}H_{15}N_3O_5$: C 75.29, H 7.32, N 5.99; found: C 75.13, H 7.50, N 5.78.

*1,4-Bis[4-(5-formyl-2,4-dimethylpyrrol-3-yl)butyl]benzene (**25**a)*

*(i) Debenzylation of **22**a*

The dibenzylester **22***a* (5 g, 9.62 mmol) and 10% Pd/C (0.5 g) in THF (150 mL) were stirred under hydrogen (1 atm) overnight. When the uptake of hydrogen ceased, the catalyst was filtered and the solution checked by tlc for any unconverted starting material. The solvents were evaporated *in vacuo*, and the bis(carboxy)pyrrole **23***a* was used in the next step without purification.

*(ii) Decarboxylation of **23**a*

The crude bis(carboxy)pyrrole **23***a* was refluxed in DMF (100 mL) under nitrogen. The uv absorption spectrum showed a

[2]Experimental details and analytical data for compounds **2**–**16**, **19***b*–*d*, **20***b*–*d*, **21***d*, **22***b*,*d*, **23***b*,*d*, **23***b*–*d*, **24***b*–*d*, **25***b*–*d*, **26***b*–*d*, **29***b*–*d*, and **30***b*–*d* are available as supplementary material and may be purchased from: The Depository of Unpublished Data, Document Delivery, CISTI, National Research Council Canada, Ottawa, Canada K1A 0S2.

Can. J. Chem. Downloaded from www.nrcresearchpress.com by 217.78.4.112 on 09/08/12
For personal use only.

reduction of the band at 282 nm to just a shoulder, within 2 h. The solution containing the bis α-free pyrrole **24***a* was cooled to room temperature and used directly in the next reaction.

(iii) Vilsmeier formylation of ***24***a

To an ice-cooled solution of DMF (11 mL) in dry CH_2Cl_2 (40 mL), phosphorus oxychloride (9.8 mL) was added dropwise and the Vilsmeier reagent thus prepared was added rapidly to the chilled DMF solution of the bis α-free pyrrole **24***a* prepared earlier. The solution was stirred for a further 30 min and poured onto crushed ice (100 g). Solid sodium bicarbonate was added carefully until the solution became basic, and CH_2Cl_2 was boiled off. Water (300 mL) was added and the mixture was heated at 75°C for 1 h. The grey-colored solid that crystallized out was filtered and washed with water. An overall yield of 85% of crude **25***a* was obtained from the dibenzylester **22***a*. An analytically pure sample of the bisformylpyrrole was prepared by deprotecting the cyanoacrylate derivative **26***a* with aqueous potassium hydroxide in *n*-propanol; mp 217–219°C; ^{1}H nmr (300 MHz, δ, $CDCl_3$): 1.40–1.51 (m, 4H), 1.58–1.68 (m, 4H), 2.21 (s, 6H), 2.25 (s, 6H), 2.38 (t, 4H, J = 7.5 Hz), 2.60 (t, 4H, J = 7.5 Hz), 7.07 (s, 4H), 9.47 (s, 4H); mass spectrum (*m/e* (relative intensity)): 432 (M^+, 44), 404 (34), 389 (18), 296 (10), 136 (100), 108 (58). Mol. wt. calcd. for $C_{28}H_{36}N_2O_2$: 432.2777; found by high resolution mass spectrometry: 432.2783. Anal. calcd. for $C_{28}H_{36}N_2O_2$: C, 77.74; H, 8.39; N, 6.48; found: C 77.57, H 8.28, N 6.32.

*1,4-Bis{4-[5-(2-cyano-2-methoxycarbonylvinyl)-2,4-dimethylpyrrol-3-yl]butyl}benzene (****26****a)*

The crude 1,4-bis[4-(5-formyl-2,4-dimethylpyrrol-3-yl)butyl]-benzene (**25***a*) (1 g, 2.31 mmol) was taken up in toluene (50 mL) with methyl cyanoacetate (0.56 g, 5.65 mmol) and cyclohexylamine (0.5 mL). The mixture was heated at reflux under nitrogen. The reaction was monitored by tlc and was found to be complete in 2 h. The solvent was evaporated, *in vacuo*, and the residue was taken to dryness on a vacuum line.

The crude product was dissolved in CH_2Cl_2 and chromatographed on silica gel (50 g). The solvent polarity was gradually increased, 0.5% ethyl acetate/CH_2Cl_2 and then 1% ethyl acetate/CH_2Cl_2, to facilitate elution without causing the impurities to move. The bright yellow product was crystallized from the eluates by concentrating, in the presence of methanol, to yield 1.06 g (76.9%). The solid thus obtained was analytically pure; mp 198.3–200.3°C; ^{1}H nmr (400 MHz, δ, $CDCl_3$); 1.43–1.50 (m, 4H), 1.58–1.66 (m, 4H), 2.15 (s, 6H), 2.28, 2.29 (s, s, 6H), 2.38–2.43 (m, 4H), 2.60 (t, 4H, J = 8 Hz), 3.86 (s, 6H), 7.07 (s, 4H), 7.20, 7.91 (s, s, 2H), 9.48 (bs, 2H); mass spectrum (*m/e* (relative intensity)): 594 (M^+, 49), 562 (14), 530 (26), 217 (68), 185 (100). Mol. wt. calcd. for $C_{36}H_{42}N_4O_4$: 594.3206; found by high resolution mass spectrometry: 594.3207. Anal. calcd. for $C_{36}H_{42}N_4O_4$: C 72.70, H 7.12, N 9.42; found: C 72.87, H 7.27, N 9.32.

*1,4-Bis{4-[2-((5-ethoxycarbonyl-3-ethyl-4-methylpyrrol-2-yl)methyl)-5-(2-cyano-2-methoxycarbonylvinyl)-4-methylpyrrol-3-yl]butyl}benzene (****29****a)*

(i) Monochlorination of the α-methyl group of ***26***a

1,4-Bis(4-[5-(2-cyano-2-methoxycarbonylvinyl)-2,4-dimethylpyrrol-3-yl]butyl)benzene (**26***a*) (0.44 g, 0.74 mmol) in dry methylene chloride (50 mL) was treated, dropwise, with a solution of sulfuryl chloride (0.22 g, 1.63 mmol) in methylene chloride (10 mL) over a period of 10 min at room temperature. The pale yellow solution, which turned orange during addition, was stirred for a further 0.5 h. The solvent was removed *in vacuo*, and the yellow residue of the corresponding α-chloromethyl derivative **27***a* was used directly in the next reaction without purification.

(ii) Condensation of ***27***a *with* ***28***

The α-chloromethyl derivative **27***a*, prepared above, was suspended in glacial acetic acid (50 mL) together with 2-ethoxycarbonyl-4-ethyl-3-methylpyrrole **28** (0.35 g, 1.9 mmol) and heated under nitrogen. When the temperature reached 70°C, all of the starting material went into solution, resulting in a clear dark-red solution. After the reaction mixture was heated for a further 30 min, tlc analysis of the reaction mixture indicated a single product (colored violet by bromine vapor). The mixture was evaporated to dryness *in vacuo*, the residue taken up in methylene chloride (50 mL), and the remaining acid removed by extraction with saturated aqueous sodium bicarbonate (3 × 50 mL) and water (3 × 50 mL). The dried methylene chloride solution was then chromatographed on silica gel (50 g). The excess α-free pyrrole starting material **28** was eluted with methylene chloride and the product was eluted with 5–10% ethyl acetate/methylene chloride. Since attempted crystallization of the product failed, it was isolated as a non-crystallizable glass, by evaporating the solvents, yield 0.65 g (92%). An analytically pure sample was obtained using a chromatotron (silica gel, 1-mm plate, 0.5% methanol/methylene chloride as the eluent); mp 244°C (dec.); ^{1}H nmr (400 MHz, δ, $CDCl_3$): 1.01 (t, 6H, J = 8 Hz), 1.31, 1.29–1.40 (t, m, 10H), 1.55–1.64 (m, 4H), 2.10, 2.11, 2.12 (s, s, s, 6H), 2.29 (s, 6H), 2.33–2.43 (m, 8H), 2.53–2.61 (m, 4H), 3.78, 3.83 (s, s, 6H), 3.87–4.20 (m, 4H), 4.24 (q, 4H, J = 8 Hz), 7.06 (s, 4H), 7.20, 7.84, 7.85 (s, s, s, 2H), 9.00 (b, 2H), 9.37 (b, 2H); mass spectrum (*m/e* (relative intensity)): 952 (M^+, 3), 906 (15), 860 (20), 698 (29), 666 (20). Mol. wt. calcd. for $C_{56}H_{68}N_6O_8$: 952.5099; found by high resolution mass spectrometry: 952.5090. Anal. calcd. for $C_{56}H_{68}N_6O_8$: C 70.56, H 7.19, N 8.82; found: C 69.83, H 7.36, N 8.36.

*1,4-Bis{4-[2-((5-carboxy-3-ethyl-4-methylpyrrol-2-yl)methyl)-5-formyl-4-methylpyrrol-3-yl]butyl}benzene (****30****a)*

In a 25-mL round-bottom flask fitted with a Claisen adaptor, a nitrogen inlet, and a reflux condenser was placed a stirred suspension of 1,4-bis{4-[2-((5-ethoxycarbonyl-3-ethyl-4-methylpyrrol-2-yl)methyl)-5(2-cyano-2-methoxycarbonylvinyl)-4-methylpyrrol-3-yl]butyl}benzene (**30***a*) (0.46 g, 0.48 mmol), KOH (0.81 g, 14.5 mmol), and water (9.6 mL). The magnetically stirred suspension was heated to reflux and treated with *n*-propanol (4.8 mL) when the yellow starting material went into solution immediately, resulting in a pale brown solution. Refluxing was continued and the reaction was monitored using uv/visible spectroscopy. During the reaction, the absorption band at 388 nm (corresponding to the starting material) diminished in intensity with a simultaneous increase in the intensity of the peak at 280 nm and the appearance of a new peak at 324 nm. In 3 h, the peak at 388 nm had disappeared completely, indicating the complete removal of the cyanoacrylate protecting groups. The lower wavelength bands (now at 268 nm and 322 nm) were very intense.

n-Propanol was evaporated off until the reflux temperature reached 100°C, and the solution was cooled to room temperature, while under nitrogen, when the product partially separated out as a brown slimy material. The solution was filtered under suction and the brown material was dissolved in more water. The clear aqueous solution was cooled in ice and acidified with glacial acetic acid. The brown powder was collected by filtration and washed with water. The final product was dried in a vacuum desiccator over KOH for 2 days, yield 0.33 g (93%); mp 179–181°C; ^{1}H nmr (300 MHz, δ, DMSO-d_6): 0.90 (m, 6H), 1.04–1.60 (b, 8H), 2.12 (s, 12H), 2.20–2.36 (m, 8H), 2.40–2.56 (m, 4H), 3.80 (s, 4H), 7.00 (s, 4H), 9.44 (s, 2H), 11.06–11.48 (m, 4H); mass spectrum (*m/e* (relative intensity)): 734 (M^+, from FAB), 646 [$(M - 2COO)^+$, 3], 617 (3), 508 (5), 169 (11), 122 (42), 109 (58), 94 (100).

*7,17-Diethyl-2,8,12,18-tetramethyl-3,13-[phenylene-1,4-bis(tetramethylene)]-porphyrin (****32****a)*

(i) Decarboxylation of ***30***a

The magnetically stirred solution of the dipyrromethane derivative **30***a* (0.31 g, 0.42 mmol) in DMF (100 mL) was heated at its reflux under nitrogen and the decarboxylation monitored by uv-visible spectroscopy. The intensity of the 280 nm band decreased considerably relative to that of the 318 nm band, which was an indication of the extent of decarboxylation. In 2 h, the 280 nm band was reduced to a shoulder.

The solution was cooled to room temperature under nitrogen, concentrated to 10 mL, methylene chloride (100 mL) added, and

Can. J. Chem. Downloaded from www.nrcresearchpress.com by 217.78.4.112 on 09/08/12
For personal use only.

the solution extracted with water (3 × 50 mL). The dried organic phase was evaporated to 10 mL and diluted to 200 mL with distilled THF to be used in the subsequent cyclization reaction.

(ii) Intramolecular 2+2 coupling

The cyclization was carried out in two 2-L Erlenmeyer flasks, covered with aluminum foil; each flask contained toluene-*p*-sulphonic acid (4.0 g) dissolved in methanol (25 mL) and diluted with distilled methylene chloride (600 mL). The dipyrromethane derivative prepared above was added to the magnetically stirred acid catalyst solution by means of a syringe pump. The syringe pump, operating at its slowest speed, took approximately 9 h to empty one 50-mL syringe.

Once the addition was complete (20 h), the reddish-violet solution was concentrated down to 10 mL and taken into methylene chloride (100 mL) and extracted with saturated aqueous sodium bicarbonate (3 × 50 mL). It was then taken to dryness *in vacuo* and the residue was purified by chromatography.

The crude porphyrin was first chromatographed on silica gel (120 g, activity I) using methylene chloride as the solvent. Some pink materials that eluted first were discarded. The solvent was then changed to 1% MeOH/CH_2Cl_2 and the porphyrin eluted with some brown impurities.

The partially purified porphyrin was chromatographed again on alumina (30 g, 4% water added) with methylene chloride as the eluting solvent. Some brown, fast moving impurities initially eluted out, and then the porphyrin eluted cleanly, leaving all other impurities adsorbed at the origin. Crystallization from a solution of MeOH/CH_2Cl_2 afforded 89.2 mg (34.8%) of the purple porphyrin; mp > 300°C; visible spectrum (CH_2Cl_2), λ_{max} (nm) (log ε): 404 (5.26), 506 (4.08), 542 (4.10), 572 (3.91), 626 (3.60); ^{1}H nmr (400 MHz, δ, CD_2Cl_2): 9.98 (s, 2H, methine protons 10-H and 20-H), 9.77 (s, 2H, methine protons 5-H and 15-H), 4.08 (q, 4H, J = 6.7 Hz, -CH_2CH_3), 3.96–4.05 (m, 2H, one proton each at chain termini), 3.63–3.70 (m, 2H, one proton each at chain termini), 3.63 (s, 6H, $2CH_3$), 3.44 (s, 6H, $2CH_3$), 2.38 (s, 4H, benzene-H), 1.87 (t, 6H, J = 8 Hz, -CH_2CH_3), 1.36–1.50 (m, 2H, chain protons), 1.18–1.27 (m, 2H, chain protons), 0.83–0.91 (m, 2H, chain protons), 0.07–0.18 (m, 4H, chain protons), −0.08–0.02 (m, 2H, chain protons), −3.26 (bs, 2H, nH). Mol. wt. calcd. for $C_{42}H_{48}N_4$: 608.3879; found by high resolution mass spectrometry: 608.3883. Anal. calcd. for $C_{42}H_{48}N_4$: C 82.85, H 7.95, N, 9.20; found: C 82.40, H 7.87, N 8.95.

*7,17-Diethyl-2,8,12,18-tetramethyl-3,13-[phenylene-1,4-bis(pentamethylene)]porphyrin (***32***b)*

This porphyrin was prepared and purified in the same way as described for porphyrin **32***a*. The yield was 19.1%; mp > 300°C; visible spectrum (CH_2Cl_2), λ_{max} (nm) (log ε): 400 (5.10), 498 (3.90), 543 (3.77), 568 (3.46), 622 (3.13). ^{1}H nmr (400 MHz, δ, CD_2Cl_2): 10.19 (s, 2H, methine protons 10-H and 20-H), 10.09 (s, 2H, methine protons 5-H and 15-H), 4.34–4.41 (m, 2H, one proton each at chain termini), 4.22–4.32 (m, 2H, -CH_2CH_3), 4.06–4.15 (m, 2H, -CH_2CH_3), 3.95–4.05 (m, 2H, one proton each at chain termini), 3.67 (s, 6H, $2CH_3$), 3.54 (s, 6H, $2CH_3$), 2.68 (s, 4H, benzene-H), 2.17–2.27 (m, 2H, chain protons), 1.91, 1.87–1.91 (t, m, 8H, -CH_2CH_3, chain protons), 0.86–0.97 (m, 6H, chain protons), 0.28–0.35 (m, 2H, chain termini), −0.13 to −0.24 (m, 2H, chain protons), −1.13 (m, 2H, chain protons), −3.58 (bs, 2H, NH). Mol. wt. calcd. for $C_{44}H_{52}N_4$: 636.4192: found by high resolution mass spectrometry: 636.4189. Anal. calcd. for $C_{44}H_{52}N_4$: C 82.97, H 8.23, N 8.80; found: C 80.72, H 8.62, N 8.57.

*7,17-Diethyl-2,8,12,18-tetramethyl-3,13-[2-acetamido-phenylene-1,4-bis(tetramethylene)]porphyrin (***32***c)*

The procedure used in preparation of this porphyrin was the same as that employed in the preparation of porphyrin **32***a*.

This porphyrin was found to be adsorbed onto silica gel more strongly than **32***a* and **32***b*. Activity I silica gel, 2% MeOH/CH_2Cl_2, was necessary to move the porphyrin. The porphyrin eluate, which contained some impurities, was purified again using a chromatotron with a 1-mm Al_2O_3 plate and a gradient of 1:1 decreasing to 1:3 hexane/CH_2Cl_2. The porphyrin product was obtained by evaporating the solvents. The residue was dried under vacuum for 3 days to give a 44.8% yield. Crystallization was achieved by evaporating a hexane/CH_2Cl_2 solution of the porphyrin; mp > 300°C; visible spectrum (CH_2Cl_2), λ_{max} (nm) (log ε): 404 (5.23), 506 (4.07), 542 (4.09), 572 (3.89), 624 (3.60); ^{1}H nmr (400 MHz, δ, CD_2Cl_2): 9.94 (d, 2H, J = 16 Hz, methine protons 10-H and 20-H), 9.77 (d, 2H, J = 16 Hz, methine protons 5-H and 15-H), 5.54, 5.36 (s, s, 2H, benzene-H), 3.94–4.14 (m, 6H, -CH_2CH_3, one proton each at chain termini), 3.60–3.78 (m, d, 9H, one proton each at chain termini, two CH_3, one benzene-H), 3.41 (d, 6H, two CH_3), 1.86–1.92 (m, 6H, -CH_2CH_3), 1.59 (s, 3H, NHCOCH_3), 1.31–1.59 (m, 2H, chain protons), 0.70–0.95 (m, 2H, chain protons), 0.01–0.20 (b, 4H, chain protons), −0.10 to −0.35 (b, 4H, chain protons), −3.30 (b, 2H, NH). Mol. wt. calcd. for $C_{44}H_{51}N_5O$: 665.4095; found by high resolution mass spectrometry: 665.4093.

*7,17-Diethyl-2,8,12,18-tetramethyl-3,13-[2-acetamido-phenylene-1,4-bis(pentamethylene)] porphyrin (***32***d)*

This compound was obtained by the same method described for **32***c*. The yield was 28.6%; mp > 300°C; visible spectrum (CH_2Cl_2), λ_{max} (nm) (log δ): 400 (5.26), 500 (4.20), 536 (4.13), 568 (3.96), 622 (3.82); ^{1}H nmr (400 MHz, δ, CD_2Cl_2): 10.17 (d, 2H, methine protons 10-H and 20-H), 10.07 (d, 2H, methine protons 5-H and 15-H), 5.62 (m, 2H, benzene-H), 4.32–4.42 (m, 2H, one proton each at chain termini), 4.21–4.32 (m, 2H, -CH_2CH_3), 4.05–4.16 (m, 2H, -CH_2CH_3), 3.95–4.05 (m, 2H, two proton each at chain termini), 3.68 (s, 6H, $2CH_3$), 3.54 (s, 8H, $2CH_3$, two benzene-H), 2.22 (b, 2H, chain protons), 1.86, 1.91 (m, t, 8H, -CH_2CH_3 and chain protons), 1.55 (s, 3H, NHCOCH_3), 0.83–1.03 (m, 6H, chain protons), 0.10–0.24 (m, 2H, chain protons), −0.23 (m, 2H, chain protons), −1.23, −1.38 (b, b, 2H, chain protons), −3.82 (b, 2H, NH). Mol. wt. calcd. for $C_{46}H_{55}N_5O$: 693.4407; found by high resolution mass spectrometry: 693.4423. Anal. calcd. for $C_{46}H_{55}N_5O$: C 79.61, H 7.99, N 10.09; found: c 79.44, H 8.09, N 9.86.

Acknowledgements

This work was supported by the U.S. National Institutes of Health (DK 17989) and the Natural Sciences and Engineering Research Council of Canada.

1. J. P. Collman, J. I. Brauman, T. R. Halbert, and K. S. Suslick. Proc. Natl. Acad. Sci. U.S.A. **73**, 3333 (1976).
2. E. J. Heidner, R. C. Ladner, and M. F. Perutz. J. Mol. Biol. **104**, 707 (1976).
3. J. M. Baldwin. J. Mol. Biol. **136**, 103 (1980).
4. J. Kuigan, S. Wilz, M. Karplus, and G. A. Petsko. J. Mol. Biol. **192**, 133 (1986).
5. J. C. Norvell, A. C. Nunes, and B. P. Schoenborn, Science, **190**, 568 (1975).
6. S.-M. Peng and J. A. Ibers. J. Am. Chem. Soc. **98**, 8032 (1976).
7. Z. Derewenda, G. Dodson, P. Emsley, D. Harris, K. Nagai, M. F. Perutz, and J.-P. Renaud. J. Mol. Biol. **211**, 515 (1990).
8. K. Kim, J. Fettinger, J. L. Sessler, M. Cyr, J. Hugdahl, J. P. Collman, and J. A. Ibers. J. Am. Chem. Soc. **111**, 403 (1989).
9. L. Pauling. Nature, **203**, 182 (1964).
10. S. E. V. Phillips and B. P. Schoenborn. Nature, **292**, 81 (1981).
11. (*a*) B. Shaanan, Nature **296**, 683 (1982); (*b*) J. Mol. Biol. **171**, 31 (1983).
12. B. Morgan and D. Dolphin. Structure Bonding (Berlin), **64**, 115 (1987).
13. B. R. James. *In* The porphyrins. Vol. V. *Edited by* D. Dolphin. Academic Press, New York. 1978. p. 205.
14. R. D. Jones, D. A. Summerville, and F. Basolo. Chem. Rev. **79**, 139 (1979).
15. D. Brault and M. Rougee. Biochemistry, **13**, 4591 (1974).
16. (*a*) T. P. Wijesekera, J. B. Paine III, D. Dolphin, F. W. B.

Einstein, and T. Jones. J. Am. Chem. Soc. **105**, 6747 (1983); (*b*) T. P. Wijesekera, J. B. Paine III, and D. Dolphin. J. Org. Chem. **53**, 1345 (1988).
17. (*a*) S. David, D. Dolphin, B. R. James, J. B. Paine III, T. P. Wijesekera, F. W. B. Einstein, and T. Jones. Can. J. Chem. **64**, 208 (1986); (*b*) T. P. Wijesekera, S. David, J. B. Paine III, B. R. James, and D. Dolphin. Can. J. Chem. **66**, 2063 (1988).
18. (*a*) S. David, D. Dolphin, and B. R. James. *In* Frontiers of bioinorganic chemistry. Edited by A. V. Xavier. VCH Verlagsgesellschaft, Weinheim, Germany. 1985. p. 163; (*b*) S. David, B. R. James, and D. Dolphin. J. Inorg. Biochem. **28**, 125 (1986); (*c*) Can. J. Chem. **65**, 1098 (1987).
19. S. Uemura, A. Toshimitsu, and M. Okano. J. Chem. Soc. Perkin Trans. 1, 1076 (1978).
20. G. G. Kleinspehn. J. Am. Chem. Soc. **77**, 1546 (1955).
21. T. P. Wijesekera, J. P. Paine III, and D. Dolphin. J. Org. Chem. **50**, 3832 (1985).
22. J. B. Paine III. *In* The porphyrins. Vol. 1. *Edited by* D. Dolphin. Academic Press, New York. 1978. p. 101.
23. E. J.-H. Chu and T. C. Chu. J. Org. Chem. **19**, 266 (1954).
24. R. Chong, P. S. Clezy, A. J. Liepa, and A. W. Nichol. Aust. J. Chem. **22**, 229 (1969).
25. J. B. Paine III, R. B. Woodward, and D. Dolphin. J. Org. Chem. **41**, 2826 (1976).
26. H. Tang. Ph.D. Thesis, University of British Columbia (1990).

Can. J. Chem. Downloaded from www.nrcresearchpress.com by 217.78.4.112 on 09/08/12
For personal use only.

Diels–Alder approach to (±)-longifolene: A formal synthesis

TSE-LOK HO
Department of Chemistry, National Taiwan University, Taipei, Taiwan

AND

WEN-LUNG YEH, JOHN YULE, AND HSING-JANG LIU[1]
Department of Chemistry, University of Alberta, Edmonton, Alta., Canada T6G 2G2

Received September 6, 1991

This paper is dedicated to Professor Zdenek (Denny) Valenta on the occasion of his 65th birthday

TSE-LOK HO, WEN-LUNG YEH, JOHN YULE, and HSING-JANG LIU. Can. J. Chem. **70**, 1375 (1992).

A formal synthesis of longifolene in racemic form is concluded starting from the Diels–Alder reaction of 6,6-dimethylfulvene and maleic anhydride. Key steps are cyclodehydration, conjugate methylation, and ring expansion.

TSE-LOK HO, WEN-LUNG YEH, JOHN YULE et HSING-JANG LIU. Can. J. Chem. **70**, 1375 (1992).

On a réalisé une synthèse formelle du longifolène racémique par le biais d'une réaction de Diels–Alder entre le 6,6-diméthylfulvène et l'anhydride maléique. Les étapes clés sont une cyclodéshydratation, un méthylation conjuguée et une extension de cycle.

[Traduit par la rédaction]

Introduction

Longifolene (**1**), a tricyclic sesquiterpene isolated from *Pinus longifolia* occupies a significant position in natural products chemistry (1). Its structural elucidation marked the transition from the classical degradation period to routine application of X-ray crystallographic diffraction techniques. The full report of the first total synthesis of longifolene (2) also promulgated the retrosynthetic analysis that revolutionized, systematized, and elevated carbogenic synthesis to a level of sophistication and efficiency unmatched by other scientific disciplines.

Corey's inspiring approach was based on an intramolecular Michael reaction of a homodecalin system for constructing the tricyclic framework. Later, McMurry and Isser (3) modified this route to achieve the cyclization by an alkylation step, with the necessary ring expansion maneuver at a later stage. Johnson's synthesis (4) was an extension of a serendipitous discovery of bisannelation during solvolysis of a cyclopentenol by participation of an alkynyl sidechain. Oppolzer and Godel (5) exploited an intramolecular de Mayo reaction with great effectiveness in the assemblage of the bridged ring skeleton. The key step of the synthesis by Schultz and Puig (6) was a vinylcyclopropane to cyclopentene rearrangement that transformed a fused tricyclic system to the bridged ring isomer. Kuo and Money's route (7), predicated on the known Wagner–Meerwein rearrangement of isolongiborneol, relied on an intramolecular aldol condensation and construction of the required intermediate from 8-bromocamphor. Finally, an intramolecular Diels–Alder method described by Lei and Fallis (8) concluded a long search for a proper cyclopentadiene that would undergo the cycloaddition without yielding to the facile [1,5]-sigmatropic rearrangement.

In our investigation directed towards the synthesis of longifolene the merits of an intermolecular Diels–Alder reaction were considered. Specifically, we sought a norbornane derivative bearing functionalized carbon chains that are suitable to be elaborated into the seven-membered ring.

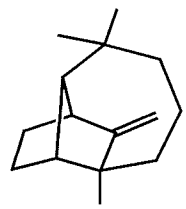

1

Results and discussion

In longifolene the presence of a *gem*-dimethyl group in the four-carbon bridge spanning C-2 and C-7 of a norbornane skeleton is a structural feature that attracted our attention. It led us to recognize a correlation between a potential *seco*-longifolene precursor and the *exo*-adduct **2***a* of 6,6-dimethylfulvene and maleic anhydride (Scheme 1). This adduct, possessing readily differentiated double bonds, was identified as a useful synthetic intermediate based on the speculation that bond formation between one of the carbonyl groups and the dimethylated carbon atom is feasible, since they project into the same space and are four bonds apart. Upon bridging, ring expansion can be effected. The other carbonyl group of the anhydride unit represents a latent exocyclic methylene pendant.

We became aware of the work by Alder and Ruhlmann (9) who reported the formation of a dihydrolactone acid (the saturated version of **3**) from the cycloadduct of 6,6-dimethylfulvene and maleic anhydride. Such a compound fits our purpose well, as we expected a ready transformation of the corresponding ester into a 3-methyl-2-cyclohexenone derivative on reaction with polyphosphoric acid. Sacrifice of one methyl group in the process would not be detractive, because restoring the substitution pattern of the bridging ring by conjugate methylation (10) should be rather straightforward. Ring expansion, removal of the ketone group, and degradation of the carboxylic residue would culminate in Johnson's norketone. On the other hand, a strained α,β-unsaturated ester may be created for the introduction of the angular methyl group.

As will be mentioned later, the idea of using citraconic anhydride as a dienophile in the initial Diels–Alder reaction

[1]Author to whom correspondence may be addressed.

Can. J. Chem. Downloaded from www.nrcresearchpress.com by 217.78.4.112 on 09/08/12
For personal use only.

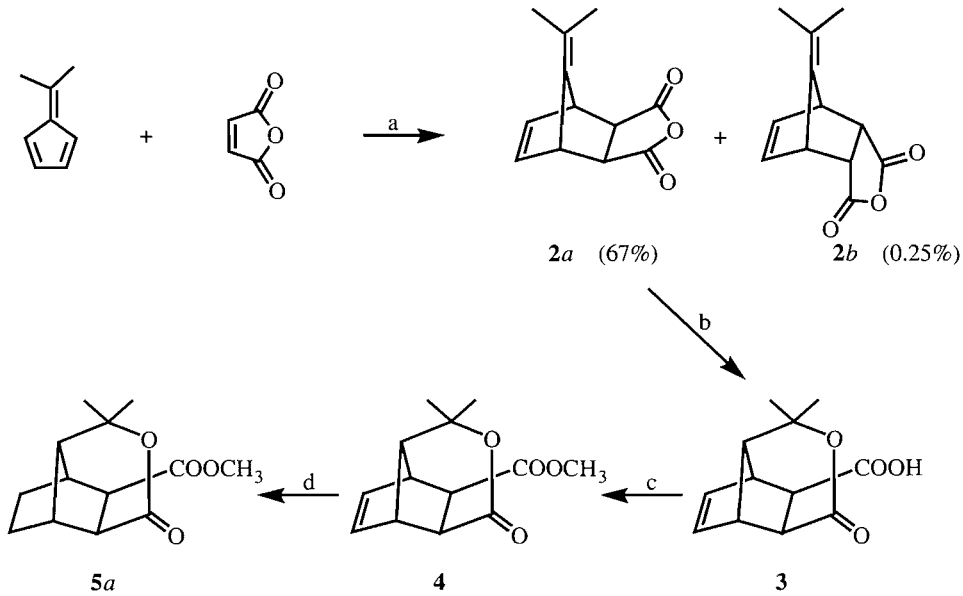

(a) PhH, reflux, 48 h; (b) 50% H_2SO_4, 20°C, 48 h, 53%; (c) H_2SO_4, MeOH, 20°C, 16 h, 100%; (d) H_2, 5% Pd–C, EtOAc, 20°C, 6 h, 98%

SCHEME 1

was also entertained. This modification represents a more direct pathway as all the carbon atoms present in the initial adduct would be preserved in the target molecule. The dissymmetry conferred to the adduct was deemed inconsequential; in fact it was anticipated that the carboxyl group attached to the quaternary carbon atom would tilt slightly toward the tetrasubstituted double bond, rendering its bond formation with that moiety more favorable.

Owing to the literature precedence and the lower cost of maleic anhydride our initial studies were devoted to the route traversing the simpler intermediates. Scheme 1 summarizes the preparation of dihydrolactone *exo*-ester **5***a* from 6,6-dimethylfulvene over four synthetic steps in an overall yield of 35%. The Diels–Alder addition of maleic anhydride to 6,6-dimethylfulvene, performed in refluxing benzene, gave almost exclusively the desired *exo* adduct **2***a*. Treatment of this compound with 50% sulfuric acid followed by esterification of the resulting lactone acid **3** gave rise to lactone ester **4**. Subsequent hydrogenation using 5% palladium on carbon as a catalyst furnished the dihydro-derivative **5***a*.

When compound **5***a* was subjected to treatment with phosphorus pentoxide and methanesulfonic acid (11) at 65°C, it underwent cyclodehydration to give the epimeric enones **6***a* and **6***b* in a 3:1 ratio and a combined yield of 37% (Scheme 2). Gratifyingly, much improved results emerged when the cyclodehydration was carried out with *endo*-ester **5***b*, readily obtained by epimerization of **5***a* using sodium methoxide in methanol. In this case, a high yield (82%) of enone **6***b* was produced along with a minute amount (1%) of the epimer **6***a*.

The reaction of enone **6***b* with lithium dimethylcuprate occurred readily to give keto ester **7** in nearly quantitative yield (Scheme 3). This set the stage for the construction of the ring skeleton of longifolene via ring expansion. Towards this end, keto ester **7** was treated with ethyl diazoacetate in the presence of boron trifluoride etherate (12). The reaction proceeded smoothly to give, in quantitative yield, an isomeric (regio-, stereo-, and enolic) mixture of the desired homologation products. While we expected the ring expansion to show a better regioselectivity (12, 13), the generation of two regioisomers **8***a* and **8***b* in a ratio of ca. 2.5:1[2] was not detrimental. Functionalities in the seven-membered ring were to be deleted immediately afterwards. In the event, decarbethoxylation of the ring expansion products with moist lithium iodide in refluxing collidine afforded a mixture of regioisomeric keto acids **9***a* and **9***b* as a result of concomitant demethylation of the methyl ester. This ester group was subsequently restored using methyl iodide and potassium carbonate in refluxing acetone. Keto esters **10***a* and **10***b*[3] thus obtained in a combined yield of 86% over two steps could not be separated. The ^1H nmr spectrum of the mixture displayed a ratio of 2.5:1 for **10***a* and **10***b*, respectively.

Much effort was directed towards the supposedly trivial deoxygenation of the ketone carbonyl. A number of experiments carried out to effect Wolff–Kishner reduction led invariably to extensive decomposition. Attempted thioacetalization using 1,2-ethanedithiol and boron trifluoride etherate in methylene chloride at 0°C resulted in the formation of several products whose spectral data were inconsistent with those expected. Consequently, a less direct approach was explored. Sodium borohydride reduction of keto esters **10***a* and **10***b* furnished a 85% yield of alcohols **11***a* and **11***b*, each as an approximately 1:1 mixture of epimers (Scheme 4). These alcohols were readily converted to the corresponding xanthates **12***a* and **12***b*, chlorides **13***a* and **13***b*, and mesylates **14***a* and **14***b* under usual conditions. The attempted re-

[2]The ratio of **8***a* and **8***b* follows from subsequent transformations.

[3]These compounds were also obtained in pure form and characterized as such by oxidation of each of the corresponding alcohols **11***a* and **11***b* with pyridinium chlorochromate on alumina (14) (see Experimental).

Can. J. Chem. Downloaded from www.nrcresearchpress.com by 217.78.4.112 on 09/08/12
For personal use only.

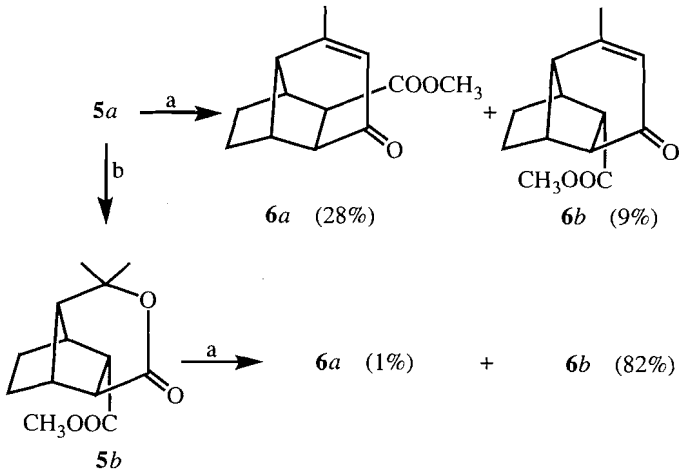

(a) P_2O_5, $MeSO_3H$, CH_2Cl_2, 65°C, 40 h; (b) NaOMe, MeOH, reflux, 8 h, 93%

SCHEME 2

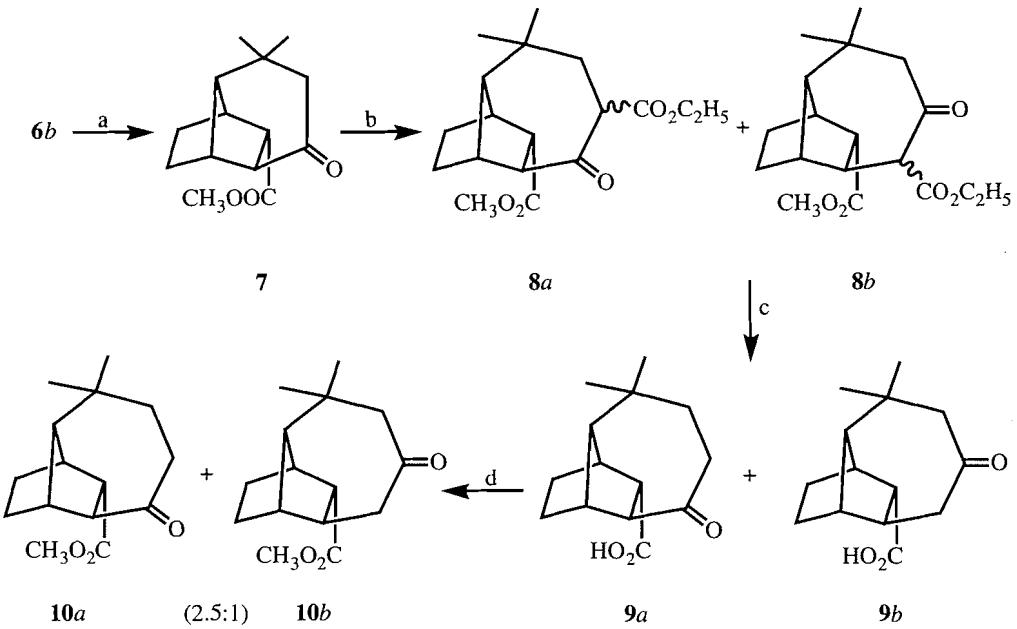

(a) Me_2CuLi, ether, 0°C, 2 h, 96%; (b) N_2CHCO_2Et, BF_3·OEt, 20°C, 17 h, ether, 100%; (c) LiI, H_2O, collidine, reflux, 3 h, 90%; (d) K_2CO_3, acetone, 20°C, 2.5 h; then MeI, reflux, 12 h, 95%

SCHEME 3

duction of the xanthates and chlorides using tri-*n*-butyltin hydride and a catalytic amount of azobisisobutyronitrile in refluxing toluene failed to give any of the desired product **15**. Mesylates **14***a* and **14***b*, on the other hand, gave rise to a mixture of **15** and olefins **16** upon heating with sodium iodide and zinc dust (15) in tetrahydrofuran at reflux temperature. Subsequent hydrogenation of this inseparable mixture using Adams catalyst furnished ester **15** in 75% overall yield from the mixture of alcohols **11***a* and **11***b*.

With ester **15** in hand, the introduction of a double bond conjugated to the ester group via selenation-oxidative elimination (16) was attempted in light of the prospect that it would permit conjugate addition of the required methyl group. The maneuver proved unfruitful. Under no conditions examined could a phenylselenenyl group be incorporated. In fact we were unable to deuterate ester **15** by consecutive treatment with lithium diisopropylamide and deuterium oxide. At this stage, the conversion of **15** into Johnson's norketone **24** was initiated. Accordingly, the ester group was reduced with lithium aluminium hydride (**15** → **17**) (Scheme 5), but since conversion of the primary alcohol to the corresponding selenide using known procedures (**17**, **18**) failed, the formation of an exocyclic methylene group via selenoxide pyrolysis could not be executed. Problems were also encountered during a Barbier–Wieland degradation. Although the addition of phenyllithium and the dehydration of the resulting alcohol **18** to olefin **19** with copper(II) sulfate on silica gel (19) could be easily carried out, the ensuing ozonolysis did not give any detectable amount of norketone **24**.

Can. J. Chem. Downloaded from www.nrcresearchpress.com by 217.78.4.112 on 09/08/12
For personal use only.

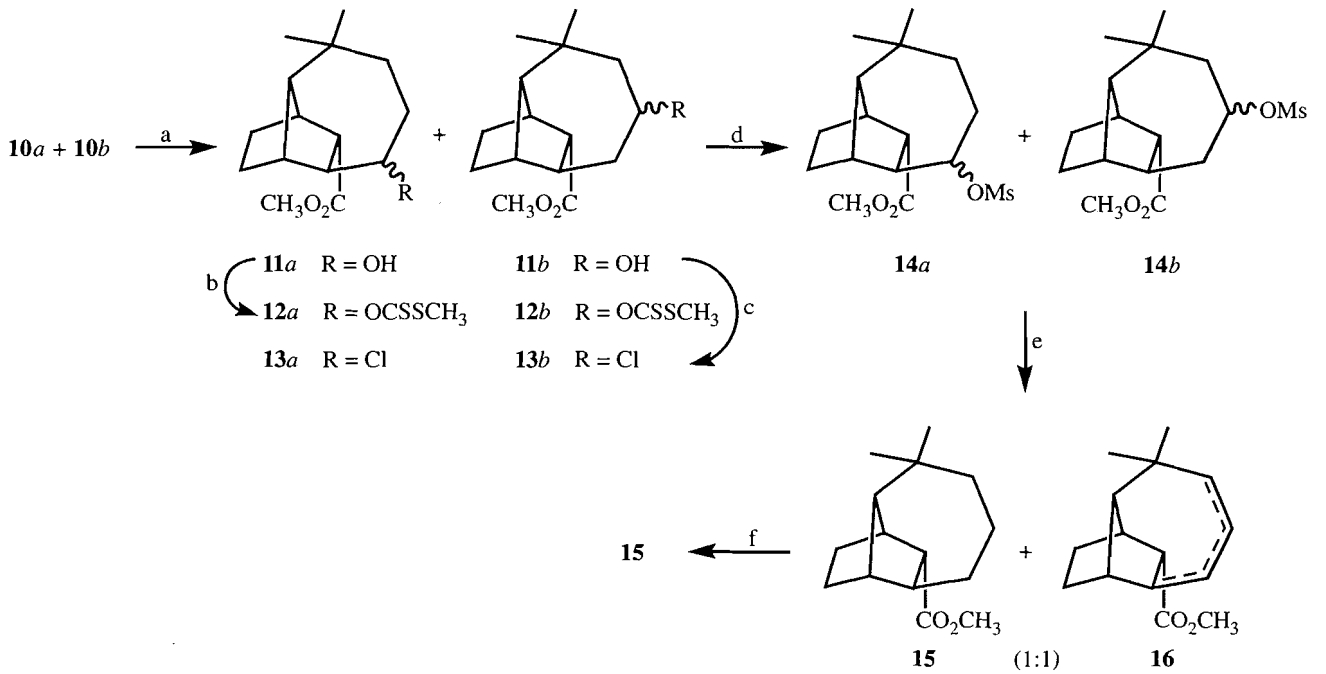

(a) $NaBH_4$, MeOH, 0°C, 1 h, 82%; (b) NaH, THF, 0°C, 0.5 h; then CS_2, 0°C; then MeI, 20°C, 4.5 h, 95%; (c) $SOCl_2$, Py, CH_2Cl_2, reflux, 13 h, 64%; (d) MsCl, Et_3N, Py, CH_2Cl_2, 0°C, 0.5 h, 85%; (e) NaI, Zn, THF, reflux, 15 h, 90%; (f) H_2, PtO_2, MeOH, 20°C, 24 h, 98%

SCHEME 4

The conversion of ester **15** into **24** was finally accomplished via the following synthetic sequence. Saponification of **15** with aqueous potassium hydroxide followed by treatment of the resulting acid **20** with methyllithium gave rise to an 87% yield of ketone **21**, which was subjected to Baeyer–Villiger oxidation using trifluoroperacetic acid in the presence of disodium hydrogen phosphate as a buffer (20). Acetate **22** thus formed, in 48% yield, was hydrolyzed with alkali and the resulting alcohol **23** oxidized with pyridinium chlorochromate on alumina to generate an 80% yield of norketone **24**, which was identified by spectroscopic comparison (ir, ^{1}H nmr, ^{13}C nmr, and ms) with an authentic sample. Accordingly, a formal synthesis of (±)-longifolene is complete.

Regarding the route involving citraconic anhydride it turned out to be a disappointment. Firstly, an *endo*-selectivity of the Diels–Alder reaction was observed; at best the desired *exo* adduct **25** was obtained in a 30% yield when the reaction was carried out in refluxing benzene. All attempts at ameliorating the situation by changing solvents, reaction temperatures, and the addition of Lewis acid catalysts seemed to elicit a counter effect. Secondly, the desired δ-lactone **26** was produced in poor yield (18%), in the subsequent step, along with a small amount (8%) of γ-lactone **27**. The tedious separation and low yields in these steps forced us to abandon the alternative synthesis.

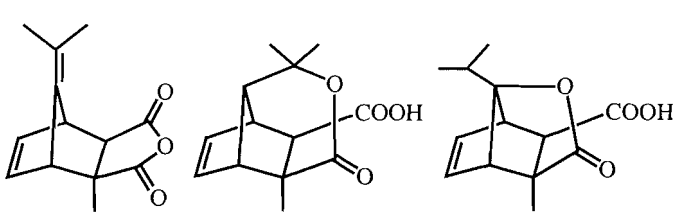

25 **26** **27**

Experimental

General

Melting points were recorded on a Köfler hot stage apparatus and are uncorrected. Infrared spectra (ir) were recorded using Nicolet 7199 FTIR or Nicolet MX-1 FTIR spectrometers. High-resolution mass spectra (ms) were obtained using a Kratos AEI MS50 high-resolution mass spectrometer. Elemental analyses were carried out by the microanalytical laboratory of this department. Proton nuclear magnetic resonance spectra (^{1}H nmr) were obtained using the following spectrometers: Bruker WH-200 (200 MHz), Bruker WH-400 (400 MHz), and Bruker AM-300 (300 MHz). Coupling constants are reported to within ±0.5 Hz. Carbon-13 nuclear magnetic spectra (^{13}C nmr) were recorded on a Bruker AM-300 (75.47 MHz) spectrometer. Carbon-13 mutiplicities were derived from off-resonance decoupling or Carr–Purcel–Meiboom–Gill spin echo *J*-modulated experiments (APT or Attached Proton Test). Methylene groups and quaternary carbons appear as signals in phase (p) with respect to the deuteriochloroform signal while the signals having an antiphase (a) to that of deuteriochloroform are for the methyl and methine groups. The following abbreviations were used: s = singlet, d = doublet, t = triplet, q = quartet, m = multiplet, and br = broad.

Materials

Other then hydrogenation, all reactions were carried out under a positive pressure of argon gas. Anhydrous magnesium sulfate was used for drying organic solutions. Still's procedure (21) for flash chromatography using silica gel of mesh 230–400 was routinely used for separations. Thin-layer chromatography was performed on aluminum-backed plates precoated with silica gel 60 F_{254} as supplied by E. Merck, Darmstadt. Skellysolve B was distilled prior to use. Other solvents were purified as follows: benzene by distillation from lithium aluminum hydride; diethyl ether and tetrahydrofuran by distillation from a blue or purple solution of sodium

Can. J. Chem. Downloaded from www.nrcresearchpress.com by 217.78.4.112 on 09/08/12
For personal use only.

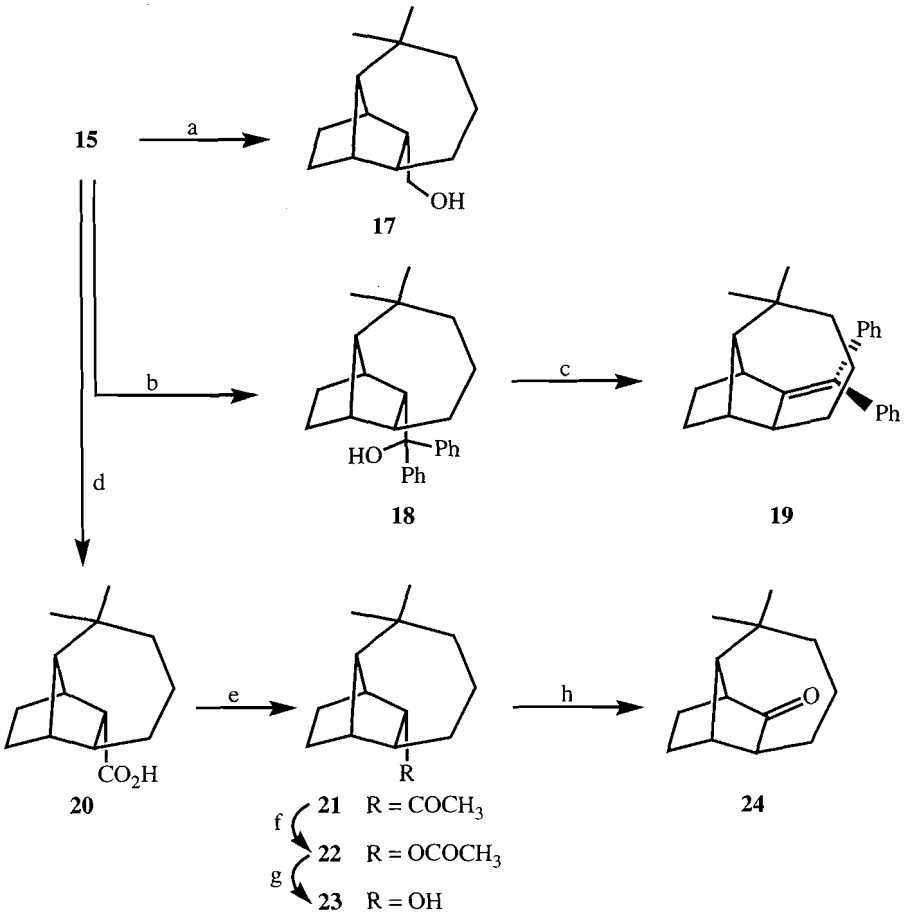

(a) $LiAlH_4$, THF, 20°C, 20 min, 100%; (b) PhLi, THF, 20°C→reflux, 4.5 h, 100%; (c) $CuSO_4$–SiO_2, CCl_4, reflux, 0.5 h, 92%; (d) 20% KOH, THF, reflux, 39 h, 100%; (e) MeLi, THF, 20°C, 16 h, 87%; (f) CF_3CO_3H, Na_2HPO_4, CH_2Cl_2, reflux, 5 h, 48%; (g) 1 N NaOH, MeOH, 20°C, 5 h, 93%; (h) PCC–Al_2O_3, CH_2Cl_2, 20°C, 1.5 h, 86%

SCHEME 5

benzophenone ketyl under argon; dichloromethane by distillation from calcium hydride; acetone by distillation first over potassium permanganate and then magnesium and iodine; and methanol by distillation from magnesium and a trace amount of carbon tetrachloride. Pyridine and trimethylsilyl chloride were distilled prior to use. Copper(I) iodine was purified according to the procedure described by Dieter *et al* (22).

(1R,2R,6S,7S)-10-Isopropylidene-4-oxatricyclo[5.2.1.$0^{2,6}$]non-8-ene-3,5-dione (2a) and (1R,2S,6R,7S)-10-isopropylidene-4-oxatricyclo[5.2.1.$0^{2,6}$]non-8-ene-3,5-dione (2b)

A solution of 6,6-dimethylfulvene (8.82 g, 0.083 mol) and maleic anhydride (10.58 g, 0.108 mol) in benzene (76 mL) was heated under reflux for 48 h. Cooling this solution produced a large amount of yellow-white solid that was filtered and recrystallized from pet. ether – ether to furnish the white crystalline anhydride **2***a*. The filtrate and mother liquor were combined, concentrated, and recrystallized to give more of **2***a*. The remaining filtrate and mother liquor were then combined, concentrated, and subjected to flash chromatography (5–33% ether in pet. ether) to give starting fulvene (1.1 g, 12% recovery), followed by *endo*-isomer **2***b* (37 mg, 0.25% based on consumed fulvene): ir ($CHCl_3$ cast): 1783 cm^{-1} (C=O); ^1H nmr (200 MHz, $CDCl_3$) δ: 6.46 (m, 2H), 3.94 (m, 2H), 3.40 (m, 2H), and 1.61 (s, 6H); ms: M^+ 204.0788 (calcd. for $C_{12}H_{12}O_3$: 204.0787). Continued elution gave *exo* isomer **2***a*: mp 138–140°C; ir ($CHCl_3$ cast): 1771 cm^{-1} (C=O); ^1H nmr (300 MHz, $CDCl_3$) δ: 6.45 (dd, J = 2, 2 Hz, 2H), 3.87 (dd, J = 2, 2 Hz, 2H), 3.04 (s, 2H), and 1.60 (s, 6H); ms: M^+ 204.0779 (calcd. for $C_{12}H_{12}O_3$: 204.0787). The *exo* product **2***a* obtained by recrystallization and chromatography gave a combined yield of 10 g (67% based on consumed fulvene).

(1S,5S*,6S*,9R*,10R*)-10-Carboxy-4,4-dimethyl-3-oxatricyclo[4.3.1.$0^{5,9}$]dec-7-en-2-one (3)*

The Diels–Alder adduct **2***a* (9.25 g, 45.3 mmol) was dissolved in 50% sulfuric acid (45 mL). The solution was stirred at room temperature for 48 h. The resulting dark red-brown solution was then diluted with water (50 mL) and filtered through Celite. The filtrate was then extracted with ethyl acetate (4 × 20 mL). The combined extracts were dried, concentrated, and recrystallized from ethyl acetate to give acid **3** (5.3 g, 53% yield) as a white crystalline solid: mp 174–176°C; ir ($CHCl_3$ cast): 3440 (br, COOH) and 1721 cm^{-1} (C=O); ^1H nmr (400 MHz, $CDCl_3$) δ: 6.63 (ddd, J = 6, 3, 1 Hz, 1H), 6.15 (ddd, J = 6, 3, 1 Hz, 1H), 3.41 (m, 1H), 3.26 (m, 1H), 2.87 (ddd, J = 8, 1.5, 1.5 Hz, 1H), 2.49 (dd, J = 8, 1.5 Hz, 1H), 1.98 (m, 1H), 1.40 (s, 3H), and 1.35 (s, 3H); ms: M^+ 222.0877 (calcd. for $C_{12}H_{14}O_4$: 222.0892).

(1S,5S*,6S*,9R*,10R*)-10-Carbomethoxy-4,4-dimethyl-3-oxatricyclo[4.3.1.$0^{5,9}$]dec-7-en-2-one (4)*

Acid **3** (4.4 g, 19.7 mmol) was dissolved in methanol (25 mL). Concentrated sulfuric acid (ca, 20 mg) was added. The resulting solution was stirred at room temperature for 16 h. At the end of this time, the reaction flask was filled with a white solid. Filtration gave white crystalline ester **4** (2.5 g). The filtrate was concentrated and then dissolved in chloroform. The chloroform solution was washed

Can. J. Chem. Downloaded from www.nrcresearchpress.com by 217.78.4.112 on 09/08/12
For personal use only.

Can. J. Chem. Downloaded from www.nrcresearchpress.com by 217.78.4.112 on 09/08/12
For personal use only.

with water, 5% aqueous sodium bicarbonate, and saturated aqueous sodium chloride. The organic solution was then dried and concentrated to give more of ester **4** (2.1 g). The combined yield of ester **4** was 4.6 g (100% yield). This material was used in the following step without further purification: mp 159–160°C; ir ($CHCl_3$ cast): 1748 (C=O) and 1731 cm^{-1} (C=O); ^1H nmr (300 MHz, $CDCl_3$) δ: 6.61 (ddd, J = 6, 3, 1 Hz, 1H), 6.14 (ddd, J = 6, 3, 1 Hz, 1H), 3.70 (s, 3H), 3.45 (m, 1H), 3.24 (m, 1H), 2.85 (ddd, J = 8, 1.5, 1.5 Hz, 1H), 2.43 (d, J = 8 Hz, 1H), 1.97 (dd, J = 1.5, 1.5 Hz, 1H), 1.39 (s, 3H), and 1.34 (s, 3H); ms: M^+ 236.1047 (calcd. for $C_{13}H_{16}O_4$: 236.1049). Anal. calcd. for $C_{13}H_{16}O_4$: C 66.08, H 6.83; found: C 65.87, H 6.76.

(1S,5S*,6S*,9R*,10R*)-10-Carbomethoxy-4,4-dimethyl-3-oxatricyclo[4.3.1.0^{5,9}]dec-2-one (**5**a)*

Ester **4** (5.53 g, 23.4 mmol) was dissolved in ethyl acetate (50 mL). 5% Palladium on carbon (100 mg) was added. The mixture was hydrogenated under 20 psi (1 psi = 6.9 kPa) of hydrogen for 6 h using a Parr hydrogenation apparatus. The mixture was then filtered and concentrated to give *exo*-ester **5***a* (5.47 g, 98% yield) as a white solid: mp 118–120°C; ir ($CHCl_3$ cast): 1736 cm^{-1} (br, C=O); ^1H nmr (300 MHz, $CDCl_3$) δ: 3.68 (s, 3H), 2.97 (m, 2H), 2.63 (br d, J = 5.5 Hz, 1H), 2.58 (d, J = 7.5 Hz, 1H), 1.87 (m, 2H), 1.68 (m, 1H), 1.50–1.42 (m, 2H), 1.46 (s, 3H), and 1.39 (s, 3H); ^{13}C nmr (75 MHz, $CDCl_3$) δ: 171.97 (p), 171.77 (p), 82.60 (p), 54.33 (a), 52.10 (a), 49.07 (a), 48.60 (a), 39.96 (a), 38.87 (a), 31.96 (p), 31.14 (a), 26.36 (a), and 25.33 (p); ms: M^+ 238.1209 (calcd. for $C_{13}H_{18}O_4$: 238.1205). Anal. calcd. for $C_{13}H_{18}O_4$: C 65.53, H 7.61; found: C 65.19, H 7.55.

(1S,5S*,6S*,9R*,10S*)-10-Carbomethoxy-4,4-dimethyl-3-oxatricyclo[4.3.1.0^{5,9}]dec-2-one (**5**b)*

A solution of sodium methoxide in methanol was prepared by dissolving sodium metal (0.49 g, 21.3 g-atom) in methanol (25 mL). *Exo*-ester **5***a* (4.59 g, 19.3 mmol) was added and the resulting solution was heated under reflux for 8 h. The solution was then acidified with 1 N hydrochloric acid and extracted with chloroform (3 × 30 mL). The combined extracts were dried and concentrated to give the *endo*-ester **5***b* (4.28 g, 93% yield) as a white solid: mp 91–93°C; ir ($CHCl_3$ cast): 1737 cm^{-1} (C=O); ^1H nmr (200 MHz, $CDCl_3$) δ: 3.74 (s, 3H), 3.10 (m, 1H), 2.88 (m, 1H), 2.73 (m, 1H), 2.50 (d, J = 5 Hz, 1H), 2.06 (dd, J = 3, 1.5 Hz, 1H), 1.78 (m, 1H), 1.62–1.47 (m, 3H), 1.48 (s, 3H), and 1.44 (s, 3H); ms: M^+ 238.1193 (calcd. for $C_{13}H_{18}O_4$: 238.1205). Anal. calcd. for $C_{13}H_{18}O_4$: C 65.53, H 7.61; found: C 65.39, H 7.77.

(1S,5R*,6S*,9R*,10R*)-10-Carbomethoxy-4-methyltricyclo[4.3.1.0^{5,9}]dec-3-en-2-one (**6**a) and (1S*,5R*,6S*,9R*,10S*)-10-carbomethoxy-4-methyltricyclo[4.3.1.0^{5,9}]dec-3-en-2-one (**6**b)*

Preparation of P_2O_5–$MeSO_3H$ reagent

Phosphorus pentoxide (9 g) was added to freshly distilled methanesulfonic acid (95 g). The mixture was stirred at room temperature overnight. The resulting clear solution was stored at room temperature.

From exo-*ester* **5**a

A solution of *exo*-ester **5***a* (0.20 g, 0.84 mmol) in dichloromethane (1 mL) was added to the P_2O_5–$MeSO_3H$ reagent (2.01 g) and the resulting solution was then stirred at 65°C for 40 h. At the end of this time the dark brown solution was diluted with dichloromethane and poured into water (10 mL). The organic layer was then removed and washed with water, 5% aqueous sodium bicarbonate, and water. The organic solution was dried and concentrated to give a brown oil. Flash chromatography (50% ether in Skelly B) gave enone **6***b* (16 mg, 9% yield) as a white solid: mp 39–40°C; ir ($CHCl_3$ cast): 1739 (C=O ester), 1676 (C=O ketone), and 1623 cm^{-1} (C=C); ^1H nmr (300 MHz, $CDCl_3$) δ: 5.75 (m, 1H), 3.71 (s, 3H), 3.02 (m, 1H), 2.78 (m, 1H), 2.70 (m, 1H), 2.61 (m, 1H), 2.51 (m, 1H), 2.03 (d, J = 1.5 Hz, 3H), 1.73–1.54 (m, 3H), and 1.39 (m, 1H); ^{13}C nmr (75 MHz, $CDCl_3$) δ: 202.07 (p), 173.21 (p), 161.79 (p), 124.30 (a), 54.76 (a), 54.10 (a), 51.88 (a), 50.43 (a), 47.07 (a), 42.28 (a), 28.18 (p), 24.89 (p), and 23.73 (a); ms: M^+ 220.1098 (calcd. for $C_{13}H_{16}O_3$: 220.1100). Anal. calcd. for $C_{13}H_{16}O_3$: C 70.89, H 7.32; found: C 70.98, H 7.37. Continued elution gave enone **6***a* (52 mg, 28% yield) as a yellow oil: ir ($CHCl_3$ cast): 1733 (C=O ester), 1681 (C=O ketone), and 1623 cm^{-1} (C=C); ^1H nmr (300 MHz, $CDCl_3$) δ: 5.64 (m, 1H), 3.54 (s, 3H), 2.98 (m, 1H), 2.93 (br d, J = 8.5 Hz, 1H), 2.89 (d, J = 8.5 Hz, 1H), 2.65 (m, 1H), 2.33 (s, 1H), 1.99 (d, J = 2 Hz, 3H), 1.88–1.63 (m, 3H), and 1.27 (m, 1H); ^{13}C nmr (75 MHz, $CDCl_3$) δ: 201.00 (p), 176 (p), 163.44 (p), 124.65 (a), 57.51 (a), 53.49 (a), 51.72 (a), 51.51 (a), 49.15 (a), 42.16 (a), 32.12 (p), 25.78 (p), and 23.58 (a); ms: M^+ 220.1098 (calcd. for $C_{13}H_{16}O_3$: 220.1100).

From endo-*ester* **5**b

A solution of *endo*-ester **5***b* (4.23 g, 17.8 mmol) in dichloromethane (20 mL) was added to the P_2O_5–$MeSO_3H$ reagent (43 g) and the resulting solution was stirred at 65°C for 40 H. At the end of this time the dark brown solution was diluted with dichloromethane and poured into water (100 mL). The organic layer was then removed and washed with water, 5% aqueous sodium bicarbonate, and water. The organic solution was dried and concentrated to give a brown oil. Flash chromatography (50% ether in Skelly B) gave enones **6***b* (3.21 g, 82% yield) and **6***a* (12 mg, 1% yield).

(1S,5R*,6S*,9R*,10S*)-10-Carbomethoxy-4,4-dimethyltricyclo[4.3.1.0^{5,9}]decan-2-one (**7**)*

Purified copper(I) iodide (5.20 g, 27.3 mmol) was added to ether (160 mL) at 0°C. Methyllithium (1.6 M in ether, 34.1 mL, 54.6 mmol) was added dropwise to this stirred suspension and the mixture was stirred at 0°C until all the yellow-brown solid had dissolved (ca. 1 h). A solution of **6***b* (2.00 g, 9.07 mmol) in ether (10 mL) was added dropwise to the lithium dimethylcopper reagent and the resulting solution stirred at 0°C for 2 h. The reaction was then quenched by addition of 1 N hydrochloric acid. Chloroform was added and the mixture filtered through Celite. The organic layer was removed and the aqueous layer extracted with chloroform (2 × 50 mL). The combined organic extracts were then washed with water, dried, concentrated, and purified by flash chromatography (50% ether in Skelly B) to give keto ester **7** (2.07 g, 96% yield) as a white solid: mp 93–93.5°C; ir ($CHCl_3$ cast): 1736 (C=O ester) and 1714 cm^{-1} (C=O ketone); ^1H nmr (400 MHz, $CDCl_3$) δ: 3.68 (s, 3H), 2.91 (s, 1H), 2.89 (m, 1H), 2.72 (m, 1H), 2.35 (d, J = 18 Hz, 1H), 2.31 (d, J = 5 Hz, 1H), 2.23 (d, J = 18 Hz, 1H), 1.71 (m, 2H), 1.48 (m, 2H), 1.27 (m, 1H), 1.13 (s, 3H), and 1.02 (s, 3H); ^{13}C nmr (75 MHz, $CDCl_3$) δ: 212.22 (p), 173.09 (p), 59.50 (a), 55.86 (a), 51.86 (a), 49.50 (p), 45.37 (a), 43.61 (a), 42.03 (a), 34.04 (p), 32.37 (a), 29.64(a), 27.21 (p), and 25.82 (p); ms: M^+ 236.1413 (calcd. for $C_{14}H_{20}O_3$: 236.1413). Anal. calcd. for $C_{14}H_{20}O_3$: C 71.16, H 8.53; found: C 70.85, H 8.64.

(1S,6R*,7S*,10R*,11S*)-3-Carbethoxy-11-carbomethoxy-5,5-dimethyltricyclo[5.3.1.0^{6,10}]undecan-2-one (**8**a) and (1S*,6R*,7S*,10R*,11S*)-2-carbethoxy-11-carbomethoxy-5,5-dimethyltricyclo[5.3.1.0^{6,10}]undecan-3-one (**8**b)*

Boron trifluoride etherate (1.60 mL, 12.95 mmol) was added to a solution of keto ester **7** (2.00 g, 8.47 mmol) in ether (50 mL) at 0°C. Ethyl diazoacetate (1.36 mL, 12.95 mmol) was then added to this solution. The reaction mixture was allowed to warm up to room temperature and left to stir in the dark for 17 h. At the end of this time, the solution was neutralized with saturated aqueous sodium bicarbonate and then extracted with chloroform (3 × 50 mL). The combined extracts were washed with water, dried, concentrated, and purified by flash chromatography (50% ether in Skelly B) to give a mixture of the desired ring expansion products (2.73 g, 100% yield) as a yellow oil. The ^1H nmr spectrum (300 MHz, $CDCl_3$) of this mixture was very complex due to the likely presence of all six possible isomers (regioisomers **8***a* and **8***b*

Can. J. Chem. Downloaded from www.nrcresearchpress.com by 217.78.4.112 on 09/08/12
For personal use only.

and their respective stereoisomers and enols). Only the following few isolated signals could be clearly identified δ: 13.10, 12.95 (-C(COOEt)=C(O*H*)-), 4.05–4.25 (-COO*CH*$_2$CH$_3$), 3.70 (-COO-C*H*$_3$). During the flash chromatography, a small amount of regioisomer **8***a* was isolated. This material was shown by the following spectral data to exist as a pair of epimers (10% each) and in the corresponding enol form (80%): ir ($CHCl_3$ cast): 1739 (C=O, ester), 1704 (C=O, ketone), 1636 (C=O, enol ester), and 1608 cm^{-1} (C=C, enol); ^1H nmr (300 MHz, $CDCl_3$) δ: 13.1 (s, 0.8H), 4.20 (q, *J* = 6.5 Hz, 2H), 3.70 (s, 3H), 3.47 (m, 1H), 3.12 (m, 0.1H), 3.19 (m, 0.1H), 2.93 (d, *J* = 3.5 Hz, 1H), 2.65 (m, 1H), 2.44 (d, *J* = 18.5 Hz, 1H), 2.32 (d, *J* = 18.5 Hz, 1H), 2.32 (d, *J* = 5 Hz, 1H), 1.60 (m, 2H), 1.46 (m, 1H), 1.29 (t, *J* = 6.5 Hz, 3H), 1.24–1.13 (m, 2H), 1.06 (s, 3H), and 0.92 (s, 3H); ms: M^+ 322.1779 (calcd. for $C_{18}H_{26}O_5$: 322.1781).

*(1*S*,*6*R*,*7*S*,*10*R*,*11*S*)-11-Carbomethoxy-5,5-dimethyltricyclo[5.3.1.0^{6,10}]undecan-2-one (**10***a*) and (1S*,6R*,7S*,10R*,11S*)-11-carbomethoxy-5,5-dimethyltricyclo[5.3.1.0^{6,10}]undecan-3-one (**10**b)*

*From carboxylic acids **9**a and **9**b*

A mixture of **8***a* and **8***b* (2.93 g, 9.10 mmol) was dissolved in collidine (40 mL) in a flask wrapped in aluminum foil. Lithium iodide (9.77 g, 73.0 mmol) and water (1.3 ml, 73.0 mmol) were added. The mixture was heated under reflux for 3 h. The resulting solution was cooled and poured into ice-cold 10% hydrochloric acid (100 mL). Ether (100 mL) was then added. The ether layer was removed, washed with 10% hydrochloric acid (2 × 100 mL) and water. The ether solution was then dried and concentrated to give a mixture of carboxylic acids **9***a* and **9***b* (1.94 g, 90% yield) as a brown oil. This mixture (1.94 g, 8.23 mmol) was then dissolved in acetone (45 mL) and potassium carbonate (2.85 g, 20.64 mmol) was introduced. After stirring at room temperature for 2.5 h, methyl iodide (2.6 ml, 41.29 mmol) was added and the resulting mixture heated to reflux for 12 h. The reaction mixture was then acidified with 1 N hydrochloric acid and extracted with chloroform (3 × 50 mL). The combined extracts were washed with saturated aqueous sodium bisulfide and water, dried, and concentrated to give a yellow oil that was purified by flash chromatography (50% ether in Skelly B) to give an inseparable mixture of **10***a* and **10***b* (1.96 g, 95% yield) in a ratio of 2.5:1 on the basis of 300 MHz ^1H nmr integration.

*Keto ester **10**a from alcohol **11**a*

To a solution of alcohol **11***a* (37 mg, 0.15 mmol) in dichloromethane (1 mL), pyridinium chlorochromate on alumina (0.93 mmol/g, 246 mg, 0.22 mmol) was added. The resulting mixture was stirred at room temperature for 17 h and then filtered through Celite. The filtrate was concentrated and purified by flash chromatography (30% ether in Skelly B) to give keto ester **10***a* (35 mg, 95% yield) as a white crystalline solid: mp 97–99°C; ir ($CHCl_3$ cast): 1738 (C=O, ester) and 1697 cm^{-1} (C=O, ketone); ^1H nmr (300 MHz, $CDCl_3$) δ: 3.68 (s, 3H), 3.13 (ddd, *J* = 5, 5, 2.5 Hz, 1H), 2.93 (d, *J* = 5 Hz, 1H), 2.61 (m, 2H), 2.39 (d, *J* = 5 Hz, 1H), 2.32 (ddq, *J* = 16, 5, 1 Hz, 1H), 1.81 (dd, *J* = 14, 14 Hz, 1H), 1.70–1.57 (m, 2H), 1.51–1.12 (m, 4H), and 1.06 (s, 6H); ^{13}C nmr (75 MHz, $CDCl_3$) δ: 212.50 (p), 173.25 (p), 63.65 (a), 58,32 (a), 52.02 (a), 48.43 (a), 41.41 (a), 40.00 (a), 38.56 (p), 35.58 (p), 33.60 (p), 31.01 (a), 29.63 (a), 29.12 (p), and 25.97 (p); ms: M^+ 250.1564 (calcd. for $C_{15}C_{22}O_3$: 250.1570). Anal. calcd. for $C_{15}H_{22}O_3$: C 71.97, H 8.86; found: C 71.64, H 8.96.

*Keto ester **10**b from alcohol **11**b*

To a solution of alcohol **11***b* (29 mg, 0.12 mmol) in dichloromethane (1 mL) was added pyridinium chlorochromate on alumina (0.93 mmol/g, 249 mg, 0.23 mmol). After stirring at room temperature for 11 h, the reaction mixture was filtered through Celite, concentrated, and purified by flash chromatography (30% ether in Skelly B) to give keto ester **10***b* (26 mg, 90% yield) as a white solid: mp 101–103°C; ir ($CHCl_3$ cast): 1726 (C=O, ester) and 1687 cm^{-1} (C=O, ketone); ^1H nmr (300 MHz, $CDCl_3$) δ: 3.70 (s, 3H), 3.18 (ddd, *J* = 5, 5, 2.5 Hz, 1H), 2.76 (d, *J* = 12 Hz, 1H), 2.65 (m, 2H), 2.42 (m, 1H), 2.31 (dd, *J* = 16, 3 Hz, 1H), 2.18 (br d, *J* = 12 Hz, 1H), 2.02 (d, *J* = 4.5 Hz, 1H), 1.70–1.56 (m, 2H), 1.46 (m, 1H), 1.37–1.15 (m, 2H), 1.11 (s, 3H), and 1.00 (s, 3H); ^{13}C nmr (75 MHz, $CDCl_3$) δ: 210.61 (p), 174.58 (p), 62.68 (a), 55.29 (p), 51.78 (a), 51.59 (a), 49.37 (p), 41.81 (a), 41.69 (a), 39.50 (a), 33.71 (p), 30.88 (a), 30.60 (a), 29.78 (p), and 25.62 (p); ms: M^+ 250.1565 (calcd. for $C_{15}H_{22}O_3$: 250.1570). Anal. calcd. for $C_{15}H_{22}O_3$: C 71.97, H 8.86; found: C 71.99, H 8.76.

(1S,6R*,7S*,10R*,11S*)-11-Carbomethoxy-5,5-dimethyltricyclo[5.3.1.0^{6,10}]undecan-2-ol (**11**a) and (1S*,6R*,7S*,10R*,11S*)-11-carbomethoxy-5,5-dimethyltricyclo[5.3.1.0^{6,10}] undecan-3-ol (**11**b)*

The 2.5:1 mixture of **10***a* and **10***b* (33 mg, 0.13 mmol) was dissolved in methanol (1 mL). Sodium borohydride (10 mg, 0.26 mmol) was then added to this solution at 0°C. The resulting mixture was stirred at 0°C for 1 h. It was then acidified with 1 N hydrochloric acid and extracted with ether (3 × 2 mL). The combined extracts were washed with water, dried, concentrated, and subjected to flash chromatography (70% ether in Skelly B) to give a 1:1 mixture of epimeric alcohols **11***a* (4 mg, 12% yield): ir ($CHCl_3$ cast): 3450 (br, OH) and 1736 cm^{-1} (C=O); ^1H nmr (400 MHz, $CDCl_3$) δ: 4.12 (br dd, *J* = 11, 4 Hz, 0.5H), 3.71 (s, 1.5H), 3.68 (s, 1.5H), 3.63 (br t, *J* = 8 Hz, 0.5H), 3.32 (m, 0.5H), 2.78 (td, *J* = 5, 2.5 Hz, 0.5H), 2.52 (t, *J* = 4.5 Hz, 0.5H), 2.46 (t, *J* = 4.5 Hz, 0.5H), 2.38 (d, *J* = 4.5 Hz, 0.5H), 2.35 (d, *J* = 6.5 Hz, 0.5H), 2.25 (br d, *J* = 6.5 Hz, 0.5H), 2.07 (d, *J* = 4.5 Hz, 0.5H), 1.94–1.70 (m, 2H), 1.67–1.51 (m, 3H), 1.49–1.39 (m, 2H), 1.35–1.07 (m, 3H), 1.02 (s, 1.5H), 1.01 (s, 1.5H), 0.98 (s, 1.5H), and 0.97 (s, 1.5H); ms: M^+ 252.1719 (calcd. for $C_{15}H_{24}O_3$: 252.1726). Continued elution gave a mixture of **11***a* and **11***b* (19 mg, 58% yield) and then **11***b* (4 mg, 12% yield) in a ratio of 3:2: ir ($CHCl_3$, cast): 3370 (br, OH) and 1735 cm^{-1} (C=O); ^1H nmr (400 MHz, $CDCl_3$)[4] δ: 3.94 (m, 0.4H), 3.81 (m, 0.6H), 3.67 (s, 3H), 2.87 (td, *J* = 5.5, 2.5 Hz, 0.4H), 2.64 (td, *J* = 5.5, 3 Hz, 0.6H), 1.06, 1.08 (both s, total 3H), 0.99, and 1.00 (both s, total 3H); ms: M^+ 252.1727 (calcd. for $C_{15}H_{24}O_3$: 252.1726). The epimeric mixture of alcohols **11***b* was subjected to flash chromatography again to give the major epimer as a solid: mp 83–85°C; ^1H nmr (300 MHz, $CDCl_3$) δ: 3.81 (tdd, *J* = 11, 5, 2.5 Hz, 1H), 3.66 (s, 3H), 2.64 (td, *J* = 5, 2.5 Hz, 1H), 2.38 (t, *J* = 4 Hz, 1H), 2.30 (m, 1H), 2.07–1.98 (m, 2H), 1.65 (m, 2H), 1.59–1.30 (m, 4H), 1.28–1.09 (m, 3H), 1.07 (s, 3H), 1.01 (s, 3H). Anal. calcd. for $C_{15}H_{24}O_3$: C 71.39, H 9.59; found: C 71.39, H 9,84. The combined yield of **11***a* and **11***b* was 27 mg (82% yield).

(1S,2R*,7S*,8R*,11S*)-11-Carbomethoxy-3,3-dimethyl-6-(methylmercaptothiocarbonyloxy)tricyclo[5.3.1.0^{2,8}]-undecane (**12**a) and (1S*,2R*,7S*,8R*,11S*)-11-carbomethoxy-3,3-dimethyl-5-(methylmercaptothio-carbonyloxy)tricyclo[5.3.1.0^{2,8}]undecane (**12**b)*

Sodium hydride (80% dispersion in mineral oil, 38 mg, 1.27 mmol) was added to a solution of alcohols **11***a* and **11***b* (44 mg, 0.17 mmol) in tetrahydrofuran (1 mL) at 0°C and the resulting solution was stirred at 0°C for 30 min. At the end of this time, the solution was treated with carbon disulfide (136 μL, 2.26 mmol), followed by methyl iodide (70 μL, 1.13 mmol). After stirring at room temperature for 4.5 h, the solution was poured into ice-water (10 mL) and extracted with ether. The organic layer was washed with water, dried, and concentrated. Flash chromatography (5% ether in Skelly B) of the residue gave an inseparable mixture of xanthates **12***a* and **12***b* (57 mg, 95% yield) as a yellow oil: ir ($CHCl_3$ cast): 1738 (C=O) and 1048 cm^{-1} (C=S); ^1H nmr (300 MHz, $CDCl_3$) (see, footnote 4) δ: 5.92, 5.80, 5.46, 5.02 (all m, total 1H), 3.60 (s, 3H), 2.53 (s, 1.5H), 2.52 (s, 1.5H), 1.17

[4]This ^1H nmr spectrum is too complex to be fully analyzed. Only characteristic signals are cited.

Can. J. Chem. Downloaded from www.nrcresearchpress.com by 217.78.4.112 on 09/08/12
For personal use only.

(s, 3H), and 1.07 (s, 3H); ms: M^+ 342.1328 (calcd. for $C_{17}H_{26}O_3S_2$: 342.1325).

(1S,2R*,7S*,8R*,11S*)-11-Carbomethoxy-6-chloro-3,3-dimethyltricyclo[5.3.1.0^{2,8}]undecane (**13**a) and (1S*,2R*,7S*,8R*,11S*)-11-carbomethoxy-5-chloro-3,3-dimethyltricyclo[5.3.1.0^{2,8}]undecane (**13**b)*

Pyridine (1 mL) was added to a solution of alcohols **11***a* and **11***b* (19 mg, 0.08 mmol) in dichloromethane (0.5 mL) and the solution was kept at 0°C. To this solution thionyl chloride (55 μL, 0.75 mmol) was added and the resulting solution heated to reflux for 13 h. At the end of this time, the dark mixture was diluted with ether (1 mL) and water (1 mL). The organic layer was removed and the aqueous layer extacted with ether (3 × 1 mL). The combined organic solutions were washed with 1 N hydrochloric acid and water, dried, concentrated, and purified by flash chromatography (Skelly B) to give an inseparable mixture of **13***a* and **13***b* (13 mg, 64% yield) as a yellow solid: ir ($CHCl_3$ cast): 1736 cm^{-1} (C=O); ^1H nmr (300 MHz, $CDCl_3$) (see, footnote 4) δ: 4.39 (m, 0.5H), 4.16 (m, 0.5H), 3.63 (s, 1.5H), 3.62 (s, 1.5H), 3.21 (m, 0.5H), 2.83 (td, J = 5.5, 2.5 Hz, 0.5H), 1.03 (s, 1.5H), 0.98 (s, 3H), and 0.91 (s, 1.5H); ms: M^+ 270.1379 (calcd. for $C_{15}H_{23}O_2Cl$: 270.1388).

(1S,2R*,7S*,8R*,11S*)-11-Carbomethoxy-3,3-dimethyl-6-methanesulfonyloxytricyclo[5.3.1.0^{2,8}]undecane (**14**a) and (1S*,2R*,7S*,8R*,11S*)-11-carbomethoxy-3,3-dimethyl-5-methanesulfonyloxytricyclo[5.3.1.0^{2,8}]undecane (**14**b)*

Pyridine (1.30 mL, 16.30 mmol), methanesulfonyl chloride (1.3 mL, 16.30 mmol) and triethylamine (2.3 mL, 16.30 mmol) were added sequentially to a solution of alcohols **11***a* and **11***b* (0.82 g, 3.26 mmol) in dichloromethane (30 mL) at 0°C. The resulting mixture was stirred at 0°C for 30 min. Water was added and the resulting solution diluted with ether (20 mL) and acidified with 1 N hydrochloric acid. The organic layer was removed and the aqueous layer extracted with ether (2 × 30 mL). The combined organic solutions were washed with 1 N hydrochloric acid and water, dried, and concentrated. The residue was subjected to flash chromatography (30–50% ether in Skelly B) to give an inseparable mixture of mesylates **14***a* and **14***b* (0.92 g, 85% yield) as a yellow oil: ^1H nmr (300 MHz, $CDCl_3$) (see, footnote 4) δ: 5.01, 4.90, 4.79, 4.48 (all m, total 1H), 3.69, 3.67 (both s, total 3H), 3.04, 2.56, 2.54 (all s, total 3H), 1.09, 1.07, 1.02, and 0.98 (all s, total 6H); ms: *m/z* 299.1314 ($M^+ - CH_3$, calcd. for $C_{15}H_{23}O_4S$: 299.1318).

(1S,2R*,7S*,8R*,11S*)-11-Carbomethoxy-3,3-dimethyltricyclo[5.3.1.0^{2,8}]undecane (**15**)*

Sodium iodide (2.07 g, 13.8 mmol) and zinc dust (30-mesh granular, 1.82 g, 27.8 g-atom) were added to a solution of **14***a* and **14***b* (0.92 g, 2.77 mmol) in tetrahydrofuran (25 mL). The resulting mixture was heated under reflux for 15 h. The mixture was then cooled and filtered through Celite. The filtrate was washed with water and saturated aqueous sodium chloride, dried, concentrated, and applied to flash chromatography (5–50% ether in Skelly B) to give a mixture of compounds **15** and **16** (0.50 g, 90% yield based on consumed starting mesylates) in a ratio of 1:1 as determined by ^1H nmr analysis. Continued elution gave the starting mesylates (0.13 g, 15% recovery). The mixture of **15** and **16** (0.50 g, 2.12 mmol) was dissolved in methanol (50 mL). Platinum(IV) oxide (44 mg) was added. The mixture was hydrogenated at room temperature under 30 psi (1 psi = 6.9 kPa) of hydrogen for 24 h using a Parr apparatus. It was then filtered, concentrated, and purified by flash chromatography (2% ether in Skelly B) to give ester **15** (0.49 g, 98% yield) as a white solid: mp 59–61°C; ir ($CHCl_3$ cast): 1736 cm^{-1} (C=O); ^1H nmr (300 MHz, $CDCl_3$) δ: 3.67 (s, 3H), 2.76 (ddd, J = 5, 4, 2 Hz, 1H), 2.39 (dd, J = 4, 4 Hz, 1H), 2.18 (dd, J = 6, 5 Hz, 1H), 2.03 (d, J = 4.5 Hz, 1H), 1.75 (m, 1H), 1.55–1.01 (m, 10H), and 0.92 (s, 6H); ^{13}C nmr (75 MHz, $CDCl_3$) δ: 175.83 (p), 62.86 (a), 53.32 (a), 51.44 (a), 43.42 (a), 41.71 (a), 40.27 (a), 40.07 (p), 33.22 (p), 32.66 (p), 32.08 (a), 30.16 (p), 29.91 (a), 25.55 (p), and 21.29 (p); ms: M^+ 236.1777 (calcd. for $C_{15}H_{24}O_2$: 236.1777). Anal. calcd. for $C_{15}H_{24}O_2$: C 76.23, H 10.24; found: C 76.29, H 10.33.

(1S,2R*,7S*,8R*,11S*)-3,3-Dimethyl-11-(hydroxymethyl)-tricyclo[5.3.1.0^{2,8}]undecane (**17**)*

To a solution of ester **15** (22 mg, 0.09 mmol) in tetrahydrofuran (1 mL), lithium aluminum hydride (13 mg, 0.34 mmol) was added. The resulting mixture was stirred at room temperature for 20 min, poured slowly into water (10 mL), and extracted with ether (3 × 10 mL). The extracts were combined and washed with 1 N hydrochloric acid and water. The organic solution was dried and concentrated to give alcohol **17** (19 mg, 100% yield) as a white solid: ir ($CHCl_3$ cast): 3310 cm^{-1} (br, OH); ^1H nmr (300 MHz, $CDCl_3$) δ: 3.65 (m, 1H), 3.51 (m, 1H), 2.23 (t, J = 4 Hz, 1H), 2.12 (m, 1H), 2.04 (d, J = 4.5 Hz, 1H), 1.79 (m, 1H), 1.70–1.00 (m, 12H), 0.98 (s, 3H), and 0.97 (s, 3H); ms: M^+ 208.1826 (calcd. for $C_{14}H_{24}O$: 208.1828).

(1S,2R*,7S*,8R*,11S*)-3,3-Dimethyl-11-(diphenylhydroxymethyl)-tricyclo[5.3.1.0^{2,8}]undecane (**18**)*

To a solution of phenyllithium (2.0 M in ether, 64 μL, 0.13 mmol) in tetrahydrofuran (1 mL) at 0°C, was added dropwise a solution of ester **15** (10 mg, 0.04 mmol) in tetrahydrofuran (0.5 mL). The resulting solution was stirred at room temperature for 1.5 h and then heated to reflux for 3 h. At the end of this time the reaction was quenched with ice. The resulting mixture was extracted with ether (2 mL). The extract was washed with saturated aqueous sodium chloride, dried, and concentrated. Purification of the residue by flash chromatography (5% ether in Skelly B) gave alcohol **18** (15 mg, 100% yield) as a colorless oil: ir ($CHCl_3$ cast): 3600 (OH) and 1600 cm^{-1} (Ph); ^1H nmr (300 MHz, $CDCl_3$) δ: 7.63 (m, 2H), 7.52 (m, 2H), 7.36 (m, 2H), 7.23 (m, 3H), 7.13 (m, 1H), 3.15 (m, 1H), 2.44 (br s, 1H), 2.34 (br t, J = 4 Hz, 1H), 2.11 (d, J = 5 Hz, 1H), 1.94–1.82 (m, 2H), 1.68–1.27 (m, 10H), 1.08 (s, 3H), and 0.99 (s, 3H); ms: M^+ 360.2451 (calcd. for $C_{26}H_{32}O$: 360.2455).

(1S,2R*,7S*,8R*)-3,3-Dimethyl-11-(diphenylmethylidene)-tricyclo[5.3.1.0^{2,8}]undecane (**19**)*

A mixture of alcohol **18** (14 mg, 0.04 mmol) and copper(II) sulfate on silica gel (1 mmol/g, 38 mg, 0.04 mmol) in carbon tetrachloride (1 mL) was heated under reflux for 30 min. The resulting solution was diluted with Skelly B (2 mL), filtered, concentrated, and purified by flash chromatography (Skelly B) to give olefin **19** (12 mg, 92% yield): ir (CH_2Cl_2 cast): 1600 cm^{-1} (Ph); ^1H nmr (300 MHz, $CDCl_3$) δ: 7.35–7.11 (m, 10H), 2.88 (d, J = 6 Hz, 1H), 2.82 (d, J = 3.5 Hz, 1H), 2.24 (d, J = 4 Hz, 1H), 1.78 (br t, J = 12.5 Hz, 1H), 1.70–1.15 (m, 10H), 1.01 (s, 3H), and 0.97 (s, 3H); ms: M^+ 342.2345 (calcd. for $C_{26}H_{30}$: 342.2349).

(1S,2R*,7S*,8R*,11S*)-11-Carboxy-3,3-dimethyltricyclo-[5.3.1.0^{2,8}]undecane (**20**)*

A 20% aqueous potassium hydroxide solution (15 mL) was added to a solution of ester **15** (76 mg, 0.32 mmol) in tetrahydrofuran (2 mL). The reaction mixture was heated to reflux for 39 h. It was then poured into 1 N hydrochloric acid (100 mL) and extracted with ether (3 × 100 mL). The combined extracts were washed with water, dried, and concentrated to give acid **20** (73 mg, 100% yield) as a white solid: mp 156–157°C, ir ($CHCl_3$ cast): 3030 (br COOH) and 1698 cm^{-1} (C=O); ^1H nmr (300 MHz, $CDCl_3$) δ: 2.90 (ddd, J = 5, 4, 2 Hz, 1H), 2.51 (t, J = 4 Hz, 1H), 2.22 (br t, J = 5 Hz, 1H), 2.13 (d, J = 4.5 Hz, 1H), 1.84 (m, 1H), 1.76–1.21 (m, 10H), and 1.00 (s, 6H); ^{13}C nmr (75 MHz, $CDCl_3$) δ: 181.15 (p), 62.86 (a), 53.20 (a), 43.31 (a), 41.66 (a), 40.31 (a), 40.03 (p), 33.23 (p), 32.59 (p), 32.09 (a), 30.16 (p), 29.90 (a), 25.49 (p), and 21.26 (p); ms: M^+ 222.1619 (calcd. for $C_{14}H_{22}O_2$: 222.1621). Anal. calcd. for $C_{14}H_{22}O_2$: C 75.63, H 9.97; found: C 75.93, H 10.08.

Can. J. Chem. Downloaded from www.nrcresearchpress.com by 217.78.4.112 on 09/08/12
For personal use only.

(1S,2R*,7S*,8R*,11S*)-11-Acetyl-3,3-dimethyltricyclo-[5.3.1.0^{2,8}]undecane (21)*

Methyllithium (0.9 M in ether, 1.3 mL, 1.12 mmol) was added to a solution of acid **20** (62 mg, 0.28 mmol) in tetrahydrofuran (10 mL) at 0°C and the resulting solution was stirred at room temperature for 16 h. At the end of this time the reaction mixture was cooled to 0°C and trimethylsilyl chloride (0.7 mL, 5.58 mmol) was added rapidly. The reaction mixture was then warmed up to room temperature and 1 N hydrochloric acid (20 mL) was added. The resulting mixture was stirred for 30 min. The ether layer was removed and the aqueous layer extracted with ether (3 × 20 mL). The combined organic solutions were washed with water, dried, concentrated, and purified by flash chromatography (10% ether in Skelly B) to give ketone **21** (53 mg, 87% yield) as a colorless oil: ir ($CHCl_3$ cast): 1708 cm^{-1} (C=O); ^{1}H nmr (300 MHz, $CDCl_3$) δ: 2.84 (td, J = 5, 2 Hz, 1H), 2.53 (t, J = 4.5 Hz, 1H), 2.32 (dd, J = 7, 5 Hz, 1H), 2.10 (s, 3H), 2.09 (m, 1H), 1.80 (m, 1H), 1.66–1.07 (m, 10H), 1.01 (s, 3H), and 0.98 (s, 3H); ^{13}C nmr (75 MHz, $CDCl_3$) δ: 210.00 (p), 63.16 (a), 62.47 (a), 41.60 (a), 40.59 (a), 40.38 (a), 40.18 (p), 33.23 (p), 32.81 (p), 32.04 (a), 30.14 (p), 30.01 (a), 29.66 (a), 25.11 (p), and 21.35 (p); ms: M$^+$ 220.1825 (calcd. for $C_{15}H_{24}O$: 220.1828).

(1S,2R*,7S*,8R*,11S*)-11-Acetoxy-3,3-dimethyltricyclo-[5.3.1.0^{2,8}]-undecane (22)*

Trifluoroacetic anhydride (0.4 mL, 2.93 mmol) was added dropwise to a solution of 90% hydrogen peroxide (64 μL, 2.34 mmol) in dichloromethane (0.5 mL) at 0°C. After stirring at 0°C for 15 min the solution was warmed up to room temperature and added to a mixture of ketone **21** (43 mg, 0.20 mmol) and disodium hydrogen phosphate (555 mg, 3.90 mmol) in dichloromethane (0.5 mL). The resulting mixture was heated under reflux for 5 h. At the end of this time, the mixture was filtered through Celite and the filtate washed with 10% aqueous sodium sulfite, saturated aqueous sodium bicarbonate, and water. The organic layer was dried, concentrated, and purified by flash chromatography (5% ether in Skelly B) to give acetate **22** (22 mg, 48% yield) as a yellow oil: ir (CH_2Cl_2 cast): 1737 cm^{-1} (C=O); ^{1}H nmr (300 MHz, $CDCl_3$) δ: 5.09 (br t, J = 4 Hz, 1H), 2.41 (m, 1H), 2.07 (br d, J = 4 Hz, 1H), 2.03 (s, 3H), 1.82–1.15 (m, 12H), and 0.98 (s, 6H); ^{13}C nmr (75 MHz, $CDCl_3$) δ: 171.38 (p), 83.14 (a), 62.56 (a), 48.62 (a), 41.94 (a), 40.19 (p), 39.57 (a), 33.19 (p), 31.30 (p), 31.20 (a), 30.54 (p), 30.47 (a), 21.36 (a), 21.30 (p), and 20.99 (p); ms: M$^+$ 236.1763 (calcd. for $C_{15}H_{24}O_2$: 236.1777). Anal. calcd. for $C_{15}H_{24}O_2$: C 76.23, H 10.24; found: C 75.94, H 10.15.

(1S,2R*,7S*,8R*,11S*)-3,3-Dimethyltricyclo[5.3.1.0^{2,8}]-undecan-11-ol (23)*

A 1 N aqueous sodium hydroxide solution (0.5 mL) was added to a solution of ester **22** (13 mg, 0.05 mmol) in methanol (0.5 mL) and the resulting solution was stirred at room temperature for 5 h. The solution was then acidified with 1 N hydrochloric acid and extracted with ether (3 × 2 mL). The combined extracts were washed with water, dried, concentrated, and purified by flash chromatography (30% ether in Skelly B) to give alcohol **23** (10 mg, 93% yield) as a white solid: mp 68–70°C; ir ($CHCl_3$ cast): 3320 cm^{-1} (br, OH); ^{1}H nmr (300 MHz, $CDCl_3$) δ: 4.23 (br t, J = 4.5 Hz, 1H), 2.17 (dd, J = 4.5, 3 Hz, 1H), 1.98 (d, J = 4.5 Hz, 1H), 1.77 (m, 2H), 1.61–1.15 (m, 11H), 0.91 (s, 3H), and 0.88 (s, 3H); ms: M$^+$ 194.1672 (calcd. for $C_{13}H_{22}O$: 194.1672).

(1S,2R*,7S*,8R*)-3,3-Dimethyltricyclo[5.3.1.0^{2,8}]undecan-11-one (24)*

Pyridinium chlorochromate on alumina (0.9 mmol/g, 176 mg, 0.16 mmol) was added to a solution of alcohol **23** (10 mg, 0.045 mmol) in dichloromethane (1 mL) and the mixture was stirred at room temperature for 1.5 h. The mixture was then filtered through Florisil, concentrated, and purified by flash chromatography (10% ether in Skelly B) to give **24** (8 mg, 86% yield) as a colorless oil: ir ($CHCl_3$ cast): 1739 cm^{-1} (C=O); ^{1}H nmr (300 MHz, $CDCl_3$) δ: 2.57 (br d, J = 4 Hz, 1H), 2.49 (m, 1H), 2.02–1.05 (m, 12H), 1.01 (s, 3H), and 0.91 (s, 3H); ^{13}C nmr (75 MHz, $CDCl_3$) δ: 223.80 (p), 60.90 (a), 51.33 (a), 50.47 (a), 38.75 (a), 37.17 (p), 33.56 (p), 30.94 (a), 29.67 (p), 29.30 (p), 28.89 (a), 24.28 (p), and 20.32 (p); ms: M$^+$ 192.1516 (calcd. for $C_{13}H_{20}O$: 192.1515).

(1S,2S*,6R*,7R*)-10-Isopropylidene-2-methyl-4-oxatricyclo-[5.2.1.0^{2,6}]non-8-ene-3,5-dione (25)*

Citraconic anhydride (9.7 mL, 0.11 mol) and 6,6-dimethylfulvene (8.81 g, 0.08 mol) were dissolved in benzene (75 mL). The solution was heated under reflux for 14–16 h. The reaction was monitored closely by tlc after about 14 h for the buildup of a second spot on the tlc attributed to the undesired *endo* adduct. Once this began, the reaction was cooled to room temperature and concentrated. At this point a solid appeared coated with a yellow oil of the unreacted fulvene. This mixture was filtered and washed with pet. ether to remove most of the yellow oil. The residue was purified by flash chromatography (5% ether in pet. ether) to remove any remaining fulvene (1.1 g, 17% recovery). Continued elution with a solution of pet. ether, ether, and ethyl acetate (3:4:1) gave the desired anhydride **25** (4.7 g, 30% yield based on consumed fulvene) as a white solid: mp 107–109°C; ir ($CHCl_3$ cast): 1850 and 1768 cm^{-1} (C=O); ^{1}H nmr (300 MHz, $CDCl_3$) δ: 6.49 (m, 2H), 3.83 (m, 1H), 3.58 (m, 1H), 2.47 (d, J = 1 Hz, 1H), 1.57 (s, 6H), and 1.32 (s, 3H); ms: M$^+$ 218.0943 (calcd. for $C_{13}H_{14}O_3$: 218.0943).

(1S,5S*,6S*,9R*,10R*)-10-Carboxy-1,4,4-trimethyl-3-oxatricyclo[4.3.1.0^{5,9}]dec-7-en-2-one (26) and (1S*,4S*,5R*,8S*,9R*)-9-carboxy-4-isopropyl-1-methyl-3-oxatricyclo[3.3.1.0^{4,8}]non-6-en-2-one (27)*

Anhydride **25** (4.0 g, 0.02 mol) was dissolved in 50% sulfuric acid (20 mL). The reaction mixture was stirred at room temperature for 48 h. At the end of this time, the solution was diluted with water and filtered through Celite leaving a large amount of a brown solid residue on the Celite. The filtrate was extracted with ethyl acetate (3 × 20 mL), dried, concentrated, and recrystallized from ethyl acetate to give acid **26** (0.79 g, 18% yield): mp 214–217°C; ir ($CHCl_3$ cast): 1737 (C=O, lactone) and 1705 cm^{-1} (C=O, acid); ^{1}H nmr (200 MHz, $CDCl_3$) δ: 6.59 (m, 1H), 6.19 (m, 1H), 5.44 (br s, 1H), 3.40 (s, 1H), 3.01 (s, 1H), 2.12 (d, J = 1.5 Hz, 1H), 2.00 (d, J = 1.5 Hz, 1H), 1.41 (s, 3H), and 1.33 (s, 6H); ms: M$^+$ 236.1036 (calcd. for $C_{13}H_{16}O_4$: 236.1049). Anal. calcd. for $C_{13}H_{16}O_4$: C 66.08, H 6.83; found: C 65.70, H 6.69. The solid residue from the filter was recovered and extracted with chloroform. The extract was then concentrated and recrystallized from ethyl acetate to give acid **27** (0.21 g, 5% yield): mp 208–210°C; ir ($CHCl_3$ cast): 1784 (C=O, lactone) and 1706 cm^{-1} (C=O, acid); ^{1}H nmr (400 MHz, $CDCl_3$) δ: 6.58 (m, 1H), 5.83 (m, 1H), 3.18 (dd, J = 2, 2 Hz, 1H), 3.01 (dd, J = 2, 2 Hz, 1H), 2.19 (s, 1H), 2.17 (septet, J = 7 Hz, 1H), 1.40 (s, 3H), 1.00 (d, J = 7 Hz, 3H), and 0.91 (d, J = 7 Hz, 3H); ms: M$^+$ 236.1045 (calcd. for $C_{13}H_{16}O_4$: 236.1049).

Acknowledgements

We are grateful to the Natural Sciences and Engineering Research Council of Canada for financial support and to Professor W. Oppolzer for the spectra of the relay compound.

1. S. Dev. Fortschr. Chem. Org. Naturst. **40**, 50 (1981).
2. E. J. Corey, M. Ohno, R. B. Mitra, and P. A. Vatachencherry. J. Am. Chem. Soc. **86**, 478 (1964).
3. J. E. McMurry and S. J. Isser. J. Am. Chem. Soc. **94**, 7132 (1972).

4. R. A. Volkmann, G. C. Andrews, and W. S. Johnson. J. Am. Chem. Soc. **97**, 4777 (1972).
5. W. Oppolzer and T. Godel. J. Am. Chem. Soc. **100**, 2583 (1978).
6. A. G. Schultz and S. Puig. J. Org. Chem. **50**, 915 (1985).
7. D. L. Kuo and T. Money. Can. J. Chem. **66**, 1794 (1988).
8. B. Lei and A. G. Fallis. J. Am. Chem. Soc. **112**, 4609 (1990).
9. K. Alder and R. Ruhlmann. Ann. **566**, 1 (1950).
10. H. O. House, W. L. Repess, and G. M. Whitesides. J. Org. Chem. **31**, 3128 (1966).
11. P. E. Eaton, G. R. Carlson, and J. T. Lee. J. Org. Chem. **35**, 4071 (1973).
12. H. J. Liu and T. Ogino. Tetrahedron Lett. 4937 (1973).
13. H. J. Liu and S. P. Majumdar. Synth. Commun. **5**, 125 (1975).
14. Y. S. Cheng, W. L. Liu, and S. H. Chen. Synthesis, 223 (1980).
15. Y. Fujimoto and T. Tatsuno. Tetrahedron Lett. 3325 (1976).
16. K. B. Sharpless, R. F. Lauer, and P. Y. Teranishi. J. Am. Chem. Soc. **95**, 6137 (1973).
17. P. A. Grieco, S. Gilman, and M. Nishizawa. J. Org. Chem. **41**, 1485 (1976).
18. P. A. Grieco, J. Y. Jaw, D. A. Claremon, and K. C. Nicolaou. J. Org. Chem. **46**, 1215 (1981).
19. T. Nishiguchi, N. Machida, and E. Yamamoto. Tetrahedron Lett. **28**, 4565 (1987).
20. W. D. Emmons and G. B. Lucas. J. Am. Chem. Soc. **77**, 2287 (1955).
21. W. C. Still, M. Kahn, and A. Mitra. J. Org. Chem. **43**, 2923 (1978).
22. R. K. Dieter, L. A. Silks III, J. R. Fishpaugh, and M. E. Kastner. J. Am. Chem. Soc. **107**, 4679 (1985).

Can. J. Chem. Downloaded from www.nrcresearchpress.com by 217.78.4.112 on 09/08/12
For personal use only.

Annulation sequences employing methyl (*E*)- and (*Z*)-6-iodo-3-trimethylstannyl-2-hexenoates and related bifunctional reagents. Preparation of *cisoid cis* and *cisoid trans* bicyclic dienes

EDWARD PIERS,[1] RICHARD W. FRIESEN, AND STEVEN J. RETTIG

Department of Chemistry, University of British Columbia, 2036 Main Mall, University Campus, Vancouver, B.C., Canada V6T 1Z1

Received July 15, 1991

This paper is dedicated to Professor Zdenek (Denny) Valenta on the occasion of his 65th birthday

EDWARD PIERS, RICHARD W. FRIESEN, and STEVEN J. RETTIG. Can. J. Chem. **70**, 1385 (1992).

A useful annulation method leading to the stereospecific synthesis of structurally novel, functionalized bicyclic dienes is described. Alkylation of 2-(methoxycarbonyl)cyclopentanone (**34**) and 2-(methoxycarbonyl)cyclohexanone (**35**) with methyl (*E*)- and (*Z*)-6-iodo-3-trimethylstannyl-2-hexenoates (**27**, **28**) provided the keto diesters **36–39**. Conversion of these substances into the corresponding enol triflates **47–50**, followed by palladium(0)-catalyzed ring closure of the latter compounds, afforded the bicyclic dienes **55–58**. In similar fashion, the keto esters **34** or **35** were transformed into the dienes **59–65**. An X-ray crystallographic analysis of the *p*-nitrobenzoate **69**, which was derived from the *cisoid cis* diene **64**, showed that, in **69**, the dihedral angle between the two carbon–carbon double bonds is −54.0(5)°.

EDWARD PIERS, RICHARD W. FRIESEN et STEVEN J. RETTIG. Can. J. Chem. **70**, 1385 (1992).

On décrit un méthode d'annellation utile pour la synthèse stéréospécifique de dienes bicycliques fonctionnalisés et nouveaux de par leur structure. L'alkylation de la 2-(méthoxycarbonyl)cyclopentanone (**34**) et de la 2-(méthoxycarbonyl)cyclohexanone (**35**) avec les (*E*)- et (*Z*)-6-iodo-3-triméthylstannylhexèn-2-oates de méthyle (**26**, **28**) conduit aux céto diesters **36–39**. La conversion de ces substances en triflates énoliques correspondants (**47–50**), suivie d'une cyclisation de ces derniers composés catalysée par le palladium(0), fournit les dienes bicycliques **59–65**. Une étude du *p*-nitrobenzoate **69**, obtenu à partir du diène *cisoïde cis* **64**, a été réalisée par diffraction des rayons X; elle montre que, dans cet ester, l'angle dièdre entre les deux doubles liaisons carbone–carbone est égal à −54,0(5)°.

[Traduit par la rédaction]

Introduction

It has been shown (1) that geometrically isomeric alkyl (*E*)- and (*Z*)-3-trimethylstannyl-2-alkenoates (**4** and **5**, respectively) can be prepared readily by reaction of α,β-acetylenic esters **1** with a suitable (trimethylstannyl)copper(I) reagent. Thus, under appropriate experimental conditions (1), reaction of **1** with $Me_3SnCu \cdot Me_2S$ (**2**) (2, 3), provides, highly stereoselectively, the *E* isomers **4**, while stereoselective conversion of **1** into the *Z* isomers **5** can be accomplished conveniently by use of the cuprate reagent $(Me_3SnCuSPh)Li$ (**3**) (2).

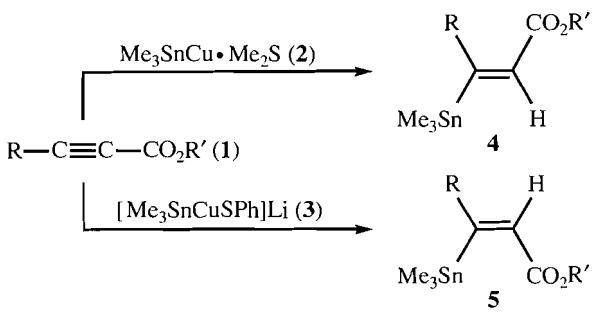

Other recent work has shown that substances containing vinylstannane and alkyl halide functions are, or can be converted into, very useful bifunctional reagents. For example, compounds **6** (4), **7** (5), and **8** (6) can readily be transformed into novel reagents that can be employed to carry out synthetically valuable methylenecyclopentane, methylenecyclohexane, and (*Z*)-ethylidenecyclopentane annulation sequences, respectively. Furthermore, the vinylstannane iodides **9** have been used effectively to develop a new type of annulation method that culminates in the formation of conjugated bicyclic dienes (7). This method can be represented in general terms by the conversion of **12** into **13** (*n* = 1, 2, or 3). We wished to extend this work, with the aims of preparing dienes more highly functionalized than **13**, of studying the chemistry of these structurally novel systems, and of using (some of) these substances for natural product synthesis. More explicitly, we wanted to determine whether the new annulation method (**12** → **13**) would be amenable to the synthesis of dienes of general structures **14** and **15** (*n* = 2, *W* = CO_2Me, CH_2OR, or Et). To achieve these goals, alkylating agents **10** and **11** (W = CO_2Me, CH_2OR, or Et) would have to be prepared. Presumably, the previously described methods (**1** → **4** or **5**) would serve well in this regard. We report in this paper the details of our studies[2] that have led to the stereospecific preparation of a variety of structurally unique bicyclic dienes of general structures **14** and **15** (*n* = 2, W = CO_2Me, CH_2OR, or Et).

Results and discussion

Preparation of methyl (E)- and (Z)-6-iodo-3-trimethylstannyl-2-hexenoates 27 and 28 and the related alkylating agents 29–33

Commercially available 5-chloro-1-pentyne was readily transformed into methyl 6-chloro-2-hexynoate (**16**). By use of the methods developed earlier (1), along with standard functional group manipulations, compound **16** served as a suitable synthetic precursor for all the alkylating agents **27–33** (Chart 1) that were employed in this study.

[1]Author to whom correspondence may be addressed.

[2]For a preliminary report regarding a portion of this work, see ref. 8.

Can. J. Chem. Downloaded from www.nrcresearchpress.com by 217.78.4.112 on 09/08/12
For personal use only.

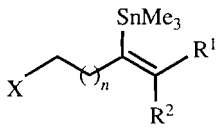

W = CO_2Me, CH_2OCH_2OMe, $CH_2OSi(t\text{-}Bu)Me_2$, or Et

6 $R^1 = R^2 = H$, X = Cl, $n = 1$
7 $R^1 = R^2 = H$, X = Cl, $n = 2$
8 $R^1 = Me$, $R^2 = H$, X = Cl, $n = 1$
9 $R^1 = R^2 = H$, X = I, $n = 1$, 2, or 3
10 $R^1 = H$, $R^2 = W$, X = I, $n = 2$
11 $R^1 = W$, $R^2 = H$, X = I, $n = 2$

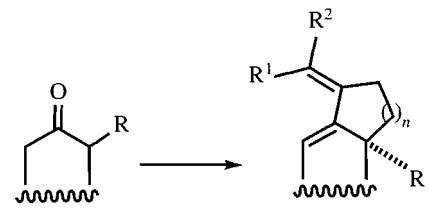

12

13 $R^1 = R^2 = H$
14 $R^1 = H$, $R^2 = W$
15 $R^1 = W$, $R^2 = H$

Treatment (THF, −78°C, 3 h) of **16** with $Me_3SnCu \cdot Me_2S$ (**2**) provided methyl (*E*)-6-chloro-3-trimethylstannyl-2-hexynoate (**17**) in 79% yield (Chart 1). On the other hand, reaction (THF, −48°C, 4 h) of **16** with $(Me_3SnCuSPh)Li$ (**3**) gave the *Z* isomer **18** in 87% yield. Reduction (*i*-Bu_2AlH, Et_2O) of the esters **17** and **18** produced the corresponding alcohols **19** and **20**, which could readily be converted by standard methods into the methoxymethyl (MOM) ethers **21** and **22** or the *tert*-butyldimethylsilyl (TBDMS) ethers **23** and **24**.

$ClCH_2CH_2CH_2C{\equiv}CCO_2Me$

16

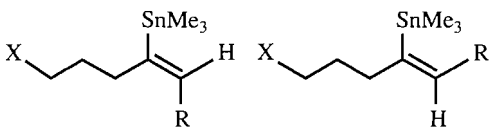

17	X = Cl, R = CO_2Me	**18**	
19	X = Cl, R = CH_2OH	**20**	
21	X = Cl, R = CH_2OMOM	**22**	
23	X = Cl, R = $CH_2OTBDMS$	**24**	
25	X = Cl, R = CH_2OAc		
26	X = Cl, R = CH_2CH_3		
27	X = I, R = CO_2Me	**28**	
29	X = I, R = CH_2OMOM	**30**	
31	X = I, R = $CH_2OTBDMS$	**32**	
33	X = I, R = CH_2CH_3		

CHART 1

Conversion of the alcohol **19** into the acetate **25**, followed by reaction (9) of the latter substance with Me_2CuLi in Et_2O afforded (*E*)-7-chloro-3-trimethylstannyl-3-heptene (**26**) in excellent yield.

Reaction of each of the primary chlorides **17**, **18**, **21**–**24**, and **26** with NaI in refluxing acetone gave excellent yields of the corresponding iodides **27**–**33**. These substances were quite stable when stored at −20°C under an argon atmosphere and, generally, were not distilled prior to use.

*Alkylation of the β-keto esters **34** and **35** with the iodides **27**–**33** (see Table 1)*

Treatment of 2-(methoxycarbonyl)cyclopentanone (**34**) with KH in THF, followed by reaction of the resultant enolate anion with each of the iodides **27**–**30**, provided the corresponding alkylation products **36**, **38**, **40**, and **42**, respectively. In similar fashion, employing 2-(methoxycarbonyl)cyclohexanone (**35**) (10) and the iodides **27**–**33** as starting materials, the keto esters **37**, **39**, **41**, and **43**–**46** were prepared. The results of these alkylation reactions are summarized in Table 1. The yields of the purified products, which ranged from 57 to 88%, were generally quite good, and, in each case, analysis (glc, ^1H nmr) of the crude product showed that it contained none of the *O*-alkylated product. The alkylation reactions proceeded smoothly with primary alkyl iodides containing an α,β-unsaturated ester function (**27**, **28**) or allylic CH_3OCH_2O (**29**, **30**) or *t*-$BuMe_2SiO$ (**31**, **32**) moieties.

The alkylation products **36**–**46** displayed spectra in full accord with structural assignments. With respect to the configuration of the carbon–carbon double bond in each of these substances, the ^1H nmr spectra were particularly instructive. For example, the ^1H nmr spectra of the geometrically isomeric diesters **37** and **39** displayed signals due to the olefinic protons at δ 5.96 (*t*, J = 1.3 Hz, $^3J_{Sn-H}$ = 72 Hz) and 6.34 (*t*, J = 1 Hz, $^3J_{Sn-H}$ = 118 Hz). It is well known (11) that when an R_3Sn group and a proton are vicinal on a carbon–carbon double bond, the $^3J_{Sn-H}$ value is much larger when these moieties are *trans* than when they are *cis*.

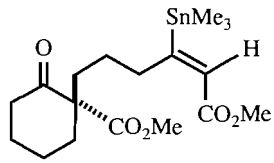

37

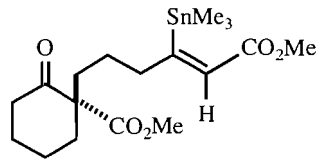

39

*Preparation of the dienes **55**–**65** (see Table 2)*

Preparation of the enol trifluoromethanesulfonates (triflates) **47**–**54** was carried out via a method developed by McMurry and Scott (12). Thus, deprotonation (*i*-Pr_2NLi, THF, −48°C) of the keto esters **36**–**43**, followed by trapping of the resultant enolate anions with *N*-phenyltrifluoromethanesulfonimide (Tf_2NPh) (THF, −48°C to room temperature) provided the desired products **47**–**54** (Table 2, entries 1–5, 7, 8, 10) in good to excellent yields. In a similar manner, the keto esters **44**–**46** were transformed into the corresponding enol triflates. However, in these cases, the latter substances were not isolated (Table 2, entries 11–13).

Synthesis of the bicyclic dienes **55**–**65** (Table 2) was conveniently achieved by use of intramolecular versions of the synthetically valuable coupling method developed by Stille *et al.* (13, 14).[3] Thus, treatment of the vinylstannane-enol triflates **47**–**54** with 0.05 equivalents of tetrakis(triphenylphosphine)palladium(0) in a suitable solvent (THF, **47**–**51**, **53**, **54**; MeCN, **52**) provided the corresponding dienes **55**–**62** in very good to excellent yields (Table 2, entries 1–5, 7, 8, 10). Alternatively, the overall conversion of the keto esters **40**, **42**, and **44**–**46** into the dienes **59**, **61**, and **63**–**65**, respectively, was accomplished conveniently via a "one-pot" protocol in which the intermediate enol triflates were not isolated. In each of these cases, addition of 0.05 equivalents of $(Ph_3P)_4Pd$ to the reaction mixture derived from formation of the enol triflate, followed by refluxing of the

[3]Stille and his group studied in detail the Pd(0)-catalyzed intermolecular coupling of vinylstannanes with enol triflates (13, 14). Prior to our investigations (7, 8), the intramolecular version of this versatile coupling process had not been described or utilized.

Can. J. Chem. Downloaded from www.nrcresearchpress.com by 217.78.4.112 on 09/08/12
For personal use only.

TABLE 1. Alkylation of the β-keto esters **34** and **35** with the iodides **27–33**[a]

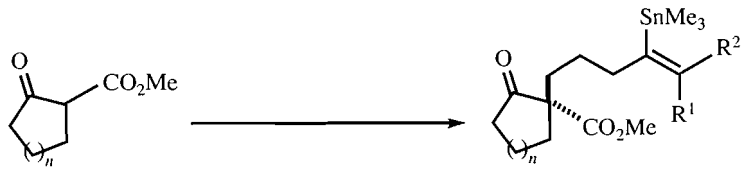

34, 35 **36–46**

Entry	Keto ester	*n*	Iodide	R^1	R^2	Reaction time (h)	Product (yield, %)[b]
1	**34**	1	**27**	CO_2Me	H	18	**36** (78)
2	**35**	2	**27**	CO_2Me	H	9	**37** (57)
3	**34**	1	**28**	H	CO_2Me	18	**38** (63)
4	**35**	2	**28**	H	CO_2Me	18	**39** (71)
5	**34**	1	**29**	CH_2OMOM[c]	H	13	**40** (67)
6	**35**	2	**29**	CH_2OMOM[c]	H	6	**41** (74)
7	**34**	1	**30**	H	CH_2OMOM[c]	14	**42** (68)
8	**35**	2	**30**	H	CH_2OMOM[c]	19	**43** (70)
9	**35**	2	**31**	$CH_2OTBDMS$[d]	H	24	**44** (88)
10	**35**	2	**32**	H	$CH_2OTBDMS$[d]	24	**45** (69)
11	**35**	2	**33**	CH_2CH_3	H	20	**46** (75)

[a]Reaction conditions: KH (1.1 equiv.), THF, room temperature, 30–45 min; add iodide, reflux.
[b]Yields refer to purified, distilled product.
[c]MOM = CH_2OCH_3.
[d]TBDMS = *t*-$BuMe_2Si$.

TABLE 2. Preparation of the dienes **55–65**

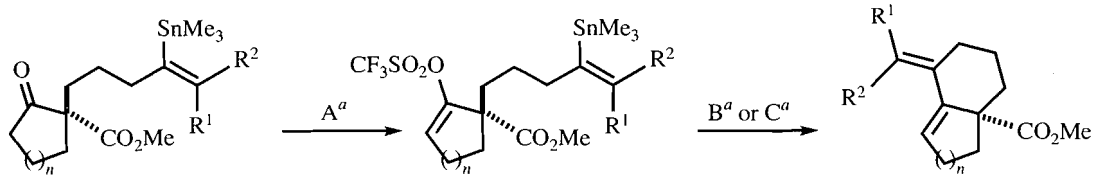

36–46 **47–54** **55–65**

Entry	Keto ester	*n*	R^1	R^2	Enol triflate (yield, %)[b]	Diene (yield, %)[c]
1	**36**	1	CO_2Me	H	**47** (57)	**55** (89)
2	**37**	2	CO_2Me	H	**48** (62)	**56** (90)
3	**38**	1	H	CO_2Me	**49** (64)	**57** (75)
4	**39**	2	H	CO_2Me	**50** (64)	**58** (75)
5	**40**	1	CH_2OMOM[d]	H	**51** (88)	**59** (83)
6	**40**	1	CH_2OMOM[d]	H	— (—)	**59** (84)[e]
7	**41**	2	CH_2OMOM[d]	H	**52** (92)	**60** (84)[f]
8	**42**	1	H	CH_2OMOM[d]	**53** (84)	**61** (86)
9	**42**	1	H	CH_2OMOM[d]	— (—)	**61** (73)[e]
10	**43**	2	H	CH_2OMOM[d]	**54** (90)	**62** (87)
11	**44**	2	$CH_2OTBDMS$[g]	H	— (—)	**63** (61)[e](50)[e,h]
12	**45**	2	H	$CH_2OTBDMS$[g]	— (—)	**64** (65)[e](61)[e,h]
13	**46**	2	CH_2CH_3	H	— (—)	**65** (61)[e]

[a]A: (*i*-$Pr)_2NLi$ (1.1–1.5 equiv.), THF, −48°C, 1 h; $PhN(SO_2CF_3)_2$ (1.17–1.57 equiv.), −48°C → room temperature, 30 min. B: $(Ph_3P)_4Pd$ (5 mol%), THF, reflux. C: As in B, but without isolation of enol triflate ("one-pot procedure").
[b]Yield of chromatographically purified product.
[c]Yield of purified, distilled product.
[d]MOM = CH_2OCH_3.
[e]These dienes were prepared using reaction conditions A and C; all others were prepared using A and B.
[f]CH_3CN was used as solvent in B, instead of THF.
[g]TBDMS = *t*-$BuMe_2Si$.
[h]$Pd(OAc)_2$ was used instead of $(Ph_3P)_4Pd$.

Can. J. Chem. Downloaded from www.nrcresearchpress.com by 217.78.4.112 on 09/08/12
For personal use only.

Can. J. Chem. Downloaded from www.nrcresearchpress.com by 217.78.4.112 on 09/08/12
For personal use only.

resultant solution, afforded the corresponding diene directly (Table 2, entries 6, 9, 11–13).

Several points should be made regarding the data given in Table 2.

The preparation of the dienes **55–65** constitutes a significant extension to the annulation method reported previously (7). Each of the intramolecular coupling processes cataloged in Table 2 was clean and the desired diene could easily be obtained in pure form by subjection of the crude product to flash chromatography (15) and distillation. Even the sterically encumbered *cisoid cis* dienes **57**, **58**, **61**, **62**, and **64** (Table 2, entries 3, 4, 8–10, 12) were obtained cleanly and efficiently.

The overall conversion of keto vinylstannanes (e.g., **40**, **42**, **44–46**) into the corresponding dienes (e.g., **59**, **61**, **63–65**, entries 6, 9, 11–13) via a "one-pot" procedure is particularly attractive. This protocol precludes the necessity of isolating and purifying the intermediate enol triflates, which are rather unstable and tend to decompose when subjected to column chromatography in silica gel. Furthermore, use of the "one-pot" method usually provides yields of dienes better than those derived from a two-step procedure (compare entries 5 and 6, Table 2).

Two of the intramolecular coupling processes were carried out with both $(Ph_3P)_4Pd$ and $Pd(OAc)_2$ (Table 2, entries 11 and 12). The yields of the dienes derived from the two procedures, although similar, were slightly lower when $Pd(OAc)_2$ was employed. Presumably, in these latter cases, the active catalyst is produced by *in situ* reduction of palladium(II) to palladium(0).

It should be noted explicitly that the Pd(0)-catalyzed ring closure reactions are completely stereospecific. Although this finding was not unexpected (13, 14), it is, from a synthetic viewpoint, of some importance. Thus, the reactions summarized in Table 2 have led to the smooth production of five pairs of structurally novel, geometrically isomeric, dienes. Of particular note is the clean, efficient synthesis of the *cisoid cis* dienes **57**, **58**, **61**, **62**, and **64**.

Proton nmr spectroscopy was especially useful in corroborating the stereochemical assignments with respect to the dienes **55–65**. In the ^1H nmr spectra of each pair of diastereomers of general structure **66** and **67**, the proton H_a of the *trans* isomer resonated at lower field than the corresponding proton H_b of the *cis* isomer ($\Delta\delta$ = 0.18–0.30 ppm). These observations may be rationalized by noting that H_a in **66** is influenced by the deshielding cone of the nearby endocyclic carbon–carbon double bond. In appropriate cases, nuclear Overhauser enhancement (nOe) difference experiments provided clear-cut evidence for the stereochemical assignments. For example, in the ^1H nmr spectrum of the diene **60**, irradiation at δ 5.82 (H_a signal) caused enhancement of the resonance due to H_b (δ 5.57). On the other hand, irradiation at δ 5.59 (H_c) in the spectrum of the isomeric diene **62** increased the intensity of the signals (δ 4.19–4.21) due to the allylic CH_2OMOM protons.

X-ray crystal structure of the p*-nitrobenzoate* ***69***

Molecular models show that, for substances **55–65**, conformations in which the conjugated diene units are planar would be destabilized by angle and torsional strain, particularly with respect to the six-membered ring bearing the exocyclic double bonds. Furthermore, the planar conformations of the *cisoid cis* dienes of general structure **67** would be additionally destabilized by steric strain between the R group and H_c. Clearly, the chemical reactivity of these substances in, for example, Diels–Alder reactions would be significantly influenced by the actual conformation of the conjugated diene system. Therefore, it was of interest to determine the extent to which the diene unit of a particular *cisoid cis* diene deviated from planarity. For this purpose, it was decided to convert the silyl ether **64** into a crystalline derivative that would be suitable for a single crystal X-ray structure determination.

Treatment of **64** with tetra-*n*-butylammonium fluoride in THF, followed by reaction of the resultant alcohol **68** with *p*-nitrobenzoyl chloride (CH_2Cl_2, Et_3N, 4-(*N*,*N*-dimethylamino)pyridine), provided the benzoate **69**. Recrystallization of this material from hexane provided crystals (mp 131–132°C) suitable for an X-ray study.

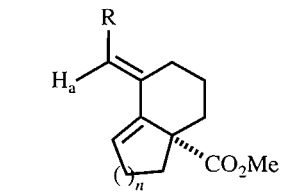

66

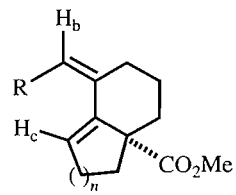

67

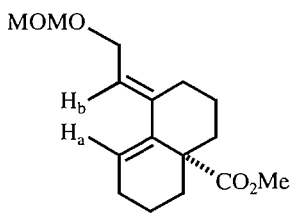

60

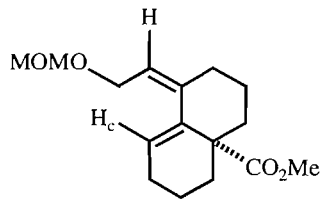

62

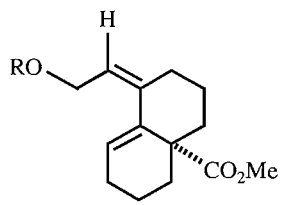

64 R = Me_2(*t*-Bu)Si
68 R = H
69 R = *p*-nitrobenzoyl

The stereoview of **69** is shown in Fig. 1. In the solid state, molecules are linked along the *b* axis by C—H···O hydrogen bonds (C(18)—H(18)···O(4), (*x*, *y* − 1, *z*), H···O = 2.38 Å, C···O = 3.321(4) Å, C—H···O = 163°). The chains are reinforced by possible weak C—H···O interactions (C(21)—H(21)···O(5) (*x*, *y* + 1, *z*), H···O = 2.50 Å, C···O = 3.431(5) Å, C—H···O = 160°). The significance of the latter interaction is evidenced by the fact that the nitro group N—O bond involved (N—O(5) = 1.216(4) Å) is longer than the otherwise chemically equivalent N—O bond (N—O(6) = 1.197(4) Å).

The aromatic ring, the nitro group, and the two ester functions are all planar to within experimental error. The *p*-nitrobenzoate moiety as a whole is nearly planar, the angles between normals to the mean plane of the aromatic ring and those of the nitro and ester groups being 1.3° and 3.7°, respectively. The effects of ring strain and steric interactions

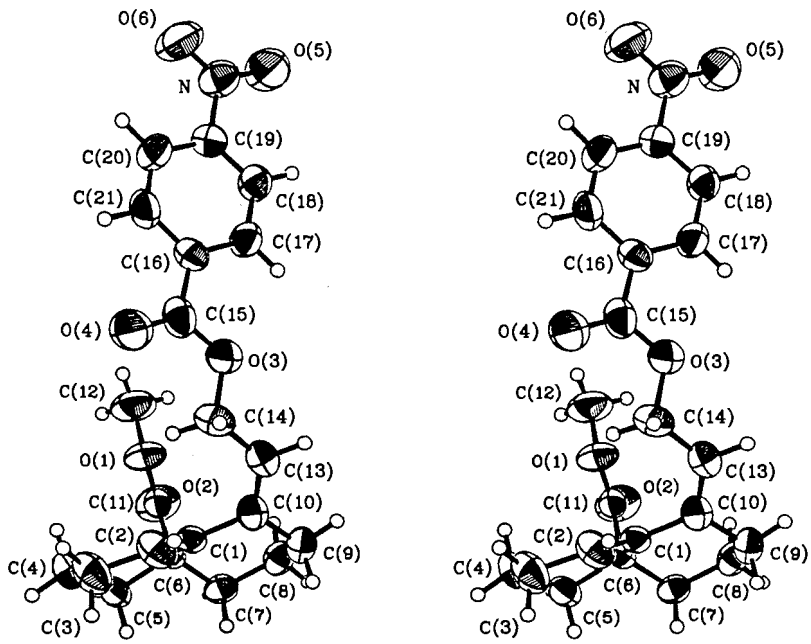

FIG. 1. Stereoview of the *p*-nitrobenzoate **69**; 50% probability thermal ellipsoids are shown for the non-hydrogen atoms.

are evidenced by non-planarity about both of the carbon–carbon double bonds (e.g., torsion angles C(6)—C(1)=C(2)—C(3) = −5.5(5)° and C(1)—C(10)=C(13)—C(14) = 2.0(5)°. Within the fused-ring system, the six-membered ring containing the exocyclic double bonds has a chair conformation that is slightly flattened about the sp^2-hybridized atoms C(1) and C(10). On the other hand, the cyclohexene ring (C(1)–C(6)) has a twisted C(4)-sofa conformation. Bond lengths and angles (Tables 5 and 6, experimental section) are normal.

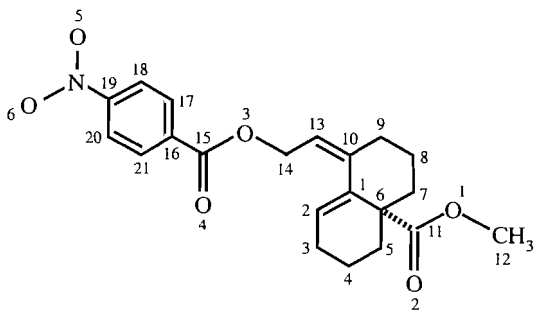

69

The C(2)—C(1)—C(10)—C(13) torsion angle, which defines the angle between the C(1)=C(2) and C(10)=C(13) double bonds, is −54.0(5)°. The C(2)···C(14) and C(2)···H(14a) distances are 3.111(5) and 2.57 Å, respectively. Thus, it is evident that the diene unit in **69** is far from being planar and, if the crystal structure data accurately reflect the ground state conformation of the molecule in solution, it is not surprising that the *cisoid cis* diene **64** (from which **69** was derived) undergoes Diels–Alder reactions very sluggishly (8).

Conclusion

The work described in this paper demonstrates the effectiveness and versatility of a new annulation sequence leading to the stereospecific synthesis of functionalized bicyclic dienes. The two key steps of the sequence involve (a) the alkylation of 2-(methoxycarbonyl)cycloalkanones with a variety of bifunctional reagents derived from methyl (*E*)- and (*Z*)-6-chloro-3-trimethylstannyl-2-hexenoates and (b) the palladium(0)-catalyzed ring closure of the vinylstannane-enol triflates obtained from the alkylation products. The application of this and other similar annulation methods to the total synthesis of natural products will be the subject of future reports.[4]

Experimental

General information

Distillation temperatures, which refer to short-path (Kugelrohr) distillations, are uncorrected. Proton nuclear magnetic resonance (^{1}H nmr) spectra were taken on $CDCl_3$ solutions. Signal positions (δ values) for compounds containing the Me_3Sn group were measured relative to the $CHCl_3$ signal (δ 7.25). The tin–proton coupling constants (J_{Sn-H}) are given as an average of the ^{117}Sn and ^{119}Sn values. Carbon nuclear magnetic resonance (^{13}C nmr) spectra were recorded at 75.3 MHz and signal positions are given relative to the signal for $CDCl_3$ (δ 77.0). For compounds containing the Me_3Sn moiety, high-resolution mass spectrometric measurements are based on ^{120}Sn (unless otherwise noted) and were made on the (M^+ − Me) peak. Flash chromatography (15) was carried out with 230–400 mesh silica gel (E. Merck). Gas–liquid chromatography (glc) was carried out on instruments equipped with 25 m × 0.21 mm fused silica columns coated with cross-linked SE-54. Thin-layer chromatography (tlc) was carried out with commercial silica gel plates. Reagents and solvents were purified and dried using standard methods. Aqueous NH_4Cl–NH_4OH (pH 8) refers to a solution prepared by addition of ~50 mL of aqueous NH_4OH (58%) to ~1 L of saturated aqueous NH_4Cl.

Note: Unless otherwise noted, all reactions were carried out under an atmosphere of argon in flame- or oven-dried glassware.

Note: All compounds for which high resolution mass measurements are given exhibited one spot on the tlc analysis and, for those

[4]For preliminary accounts, see ref. 16.

Can. J. Chem. Downloaded from www.nrcresearchpress.com by 217.78.4.112 on 09/08/12
For personal use only.

Can. J. Chem. Downloaded from www.nrcresearchpress.com by 217.78.4.112 on 09/08/12
For personal use only.

substances that could be distilled, essentially one peak by glc analysis.

*Methyl 6-chloro-2-hexynoate (**16**)*

To a cold (−78°C), stirred solution of 5-chloro-1-hexyne (5.13 g, 50.0 mmol) in dry THF (100 mL) was added a solution of methyllithium in Et_2O (46.0 mL, 55.0 mmol) and the resultant solution was stirred at −78°C for 10 min, warmed to −20°C, and then stirred for a further 1 h. Methyl chloroformate (4.64 mL, 60.0 mmol) was added and the mixture was stirred at −20°C for 30 min and at room temperature for 30 min. Saturated aqueous $NaHCO_3$ (50 mL) and Et_2O (50 mL) were added. The organic phase was separated, dried ($MgSO_4$), and concentrated. Distillation (65–75°C/0.1 Torr (1 Torr = 133.3 Pa)) of the residual oil afforded 7.50 g (93%) of **16** as a colorless oil that displayed ir (neat): 2228, 1712, 1433, 1259, 1080, 755 cm^{-1}; ^1H nmr (80 MHz) δ: 2.08 (m, 2H), 2.61 (br t, 2H, J = 6.5 Hz), 3.66 (t, 2H, J = 6 Hz), 3.78 (s, 3H). Exact Mass calcd. for $C_7H_9{}^{35}ClO_2$: 160.0292; found: 160.0290.

*Methyl (E)-6-chloro-3-trimethylstannyl-2-hexenoate (**17**)*

To a cold (−78°C), stirred solution of $Me_3SnCu \cdot Me_2S$ (**2**) (2, 3) (24.3 mmol) in dry THF (180 mL) was added, dropwise, a solution of the α,β-acetylenic ester **16** (3.0 g, 18.7 mmol) in dry THF (40 mL). After the mixture had been stirred at −78°C for 3 h, it was treated sequentially with aqueous NH_4Cl–NH_4OH (pH 8) (100 mL) and Et_2O (60 mL). The mixture was opened to the atmosphere, allowed to warm to room temperature, and was stirred vigorously until the aqueous phase was deep blue. The layers were separated and the aqueous phase was extracted with Et_2O (2 × 60 mL). The combined organic extracts were washed with aqueous NH_4Cl–NH_4OH (pH 8) until the washings were colorless, and then were dried ($MgSO_4$) and concentrated. Flash chromatography (240 g silica gel, 20:1 petroleum ether – Et_2O) of the remaining material, followed by distillation (115–120°C/0.6 Torr), yielded 4.79 g (79%) of **17**, a colorless oil that showed ir (neat): 1710, 1595, 1195, 1175, 777 cm^{-1}; ^1H nmr (80 MHz) δ: 0.21 (s, 9H, $^2J_{Sn-H}$ = 53 Hz), 1.60–2.10 (m, 2H), 3.00 (br t, 2H, J = 7 Hz), 3.53 (t, 2H, J = 6.5 Hz), 3.65 (s, 3H), 5.99 (t, 1H, J = 1 Hz, $^3J_{Sn-H}$ = 71 Hz). Exact Mass calcd. for $C_9H_{16}{}^{35}ClOSn$ (M^+ − Me): 310.9861; found: 310.9853.

*Methyl (Z)-6-chloro-3-trimethylstannyl-2-hexenoate (**18**)*

To a cold (−78°C), stirred solution of $(Me_3SnCuSPh)Li$ (**3**) (2) (24.3 mmol) in dry THF (180 mL) was added, dropwise, a solution of the α,β-acetylenic ester **16** (3.0 g, 18.7 mmol) in dry THF (40 mL). The mixture was stirred at −78°C for 15 min, warmed to −48°C, and then stirred for 4 h. After sequential addition of MeOH (40 mL) and petroleum ether (100 mL), the vigorously stirred mixture was allowed to warm to room temperature. The resulting yellow slurry was filtered through a plug of Celite and the collected material was washed with petroleum ether (100 mL). The filtrate was concentrated and the residual material was subjected to flash chromatography (240 g silica gel, 20:1 petroleum ether – Et_2O). Distillation (106–116°C/0.6 Torr) of the liquid thus obtained afforded 5.3 g (87%) of **18**, a colorless oil that exhibited ir (neat): 1701, 1600, 1210, 778 cm^{-1}; ^1H nmr (80 MHz) δ: 0.21 (s, 9H, $^2J_{Sn-H}$ = 54 Hz), 1.60–2.10 (m, 2H), 2.59 (br t, 2H, J = 7 Hz, $^3J_{Sn-H}$ = 46 Hz), 3.51 (t, 2H, J = 6.5 Hz), 3.73 (s, 3H), 6.40 (t, 1H, J = 1.5 Hz, $^3J_{Sn-H}$ = 117 Hz). Exact Mass calcd. for $C_9H_{16}{}^{35}ClO_2Sn$ (M^+ − Me): 310.9861; found: 310.9862.

*(E)-6-Chloro-3-trimethylstannyl-2-hexen-1-ol (**19**)*

To a cold (−78°C), stirred solution of the ester **17** (3.1 g, 9.5 mmol) in dry Et_2O (70 mL) was added slowly a solution of diisobutylaluminum hydride (23.8 mmol) in hexane. The mixture was stirred at −78°C for 1 h, warmed to 0°C, and then stirred for 2 h. Saturated aqueous NH_4Cl (10 mL) was added and the mixture was warmed to room temperature. Anhydrous $MgSO_4$ was added to the resultant slurry and the mixture was filtered through a plug of Celite. The collected material was washed with Et_2O (70 mL). Concentration of the filtrate and distillation (100–110°C/0.03 Torr) of the remaining liquid provided 2.52 g (89%) of **19**, a colorless oil that displayed ir (neat): 3300, 1020, 770 cm^{-1}; ^1H nmr (80 MHz) δ: 0.15 (s, 9H, $^2J_{Sn-H}$ = 53 Hz), 1.65 (br s, 1H, exchanges with D_2O), 1.60–2.00 (m, 2H), 2.45 (br t, 2H, J = 7 Hz, $^3J_{Sn-H}$ = 67 Hz), 3.50 (t, 2H, J = 6 Hz), 4.25 (m, 2H, d after D_2O addition, J = 6 Hz), 5.82 (tt, 1H, J = 0.5, 6 Hz, $^3J_{Sn-H}$ = 75 Hz). Exact Mass calcd. for $C_8H_{16}{}^{35}ClOSn$ (M^+ − Me): 282.9912; found: 282.9919.

*(Z)-6-Chloro-3-trimethylstannyl-2-hexen-1-ol (**20**)*

Following a procedure identical with that described above, 3.44 g (10.6 mmol) of the ester **18** was converted into 3.03 g (97%, distillation temperature 100–110°C/0.03 Torr) of the alcohol **20**, a colorless oil that showed ir (neat): 3350, 1010, 777 cm^{-1}; ^1H nmr (80 MHz) δ: 0.19 (s, 9H, $^2J_{Sn-H}$ = 53 Hz), 1.41 (t, 1H, exchanges with D_2O, J = 5.5 Hz), 1.60–2.00 (m, 2H), 2.40 (br t, 2H, J = 7 Hz, $^3J_{Sn-H}$ = 49 Hz), 3.48 (t, 2H, J = 6 Hz), 4.08 (m, 2H, d after D_2O addition, J = 6 Hz), 6.24 (tt, 1H, J = 1.5, 6 Hz, $^3J_{Sn-H}$ = 134 Hz). Exact Mass calcd. for $C_8H_{16}{}^{35}ClOSn$ (M^+ − Me): 282.9912; found: 282.9917.

*(E)-6-Chloro-1-(methoxymethoxy)-3-trimethylstannyl-2-hexene (**21**)*

To a cold (0°C), stirred solution of the alcohol **19** (740 mg, 2.49 mmol) in dry CH_2Cl_2 (5 mL) was added sequentially ethyldiisopropylamine (0.65 mL, 3.74 mmol) and chloromethyl methyl ether (0.28 mL, 3.74 mmol). The mixture was allowed to warm to room temperature and was stirred for 15 h. Removal of the solvent, followed by distillation (95–105°C/0.6 Torr) of the crude liquid, gave 802 mg (94%) of **21**, a colorless oil that exhibited ir (neat): 1152, 1104, 1042, 772 cm^{-1}; ^1H nmr (80 MHz) δ: 0.14 (s, 9H, $^2J_{Sn-H}$ = 53 Hz), 1.60–2.00 (m, 2H), 2.47 (br t, 2H, J = 7 Hz, $^3J_{Sn-H}$ = 62 Hz), 3.36 (s, 3H), 3.48 (t, 2H, J = 7 Hz), 4.15 (br d, 2H, J = 6 Hz), 4.63 (s, 2H), 5.78 (tt, 1H, J = 1.3, 6 Hz, $^3J_{Sn-H}$ = 75 Hz). Exact Mass calcd. for $C_{10}H_{20}{}^{35}ClO_2Sn$ (M^+ − Me): 327.0174; found: 327.0163.

*(Z)-6-Chloro-1-methoxymethoxy)-3-trimethylstannyl-2-hexene (**22**)*

Following a procedure identical with that described above, 1.9 g (6.39 mmol) of the alcohol **20** was transformed into 1.90 g (87%, distillation temperature 100–105°C/0.6 Torr) of the ether **22**, a colorless oil that displayed ir (neat): 1156, 1110, 1040, 778 cm^{-1}; ^1H nmr (80 MHz) δ: 0.20 (s, 9H, $^2J_{Sn-H}$ = 53 Hz), 1.60–2.00 (m, 2H), 2.38 (br t, 2H, J = 7 Hz, $^3J_{Sn-H}$ = 48 Hz), 3.35 (s, 3H), 3.49 (t, 2H, J = 6.5 Hz), 4.00 (br d, 2H, J = 6 Hz), 4.62 (s, 2H), 6.38 (tt, 1H, J = 1.3, 6 Hz, $^3J_{Sn-H}$ = 134 Hz). Exact Mass calcd. for $C_{10}H_{20}{}^{35}ClO_2Sn$ (M^+ − Me): 327.0174; found: 327.0172.

*(E)-1-*tert*-Butyldimethylsiloxy-6-chloro-3-trimethylstannyl-2-hexene (**23**)*

To a solution of the alcohol **19** (4.1 g, 13.8 mmol) in dry *N*,*N*-dimethylformamide (40 mL) at room temperature was added *t*-$BuMe_2SiCl$ (2.5 g, 16.6 mmol) and imidazole (2.35 g, 34.5 mmol) and the mixture was stirred for 15 h. After Et_2O (100 mL) had been added, the solution was washed with saturated aqueous $NaHCO_3$ (3 × 75 mL) and then was dried ($MgSO_4$) and concentrated. Distillation (155–170°C/11 Torr) of the remaining oil gave 4.75 g (84%) of **23**, a colorless oil that showed ir (neat): 1256, 1088, 1006, 839, 775 cm^{-1}; ^1H nmr (80 MHz) δ: 0.08 (s, 6H), 0.13 (s, 9H, $^2J_{Sn-H}$ = 53 Hz), 0.91 (s, 9H), 1.65–2.00 (m, 2H), 2.43 (br t, 2H, J = 7 Hz), 3.49 (t, 2H, J = 6 Hz), 4.21, 4.36 (d, d, 1H each, J = 6 Hz in each case), 5.74 (br t, 1H, J = 6 Hz, $^3J_{Sn-H}$ = 76 Hz). Exact Mass calcd. for $C_{14}H_{30}{}^{35}ClOSiSn$ (M^+ − Me): 397.0777; found: 397.0782.

*(Z)-1-*tert*-Butyldimethylsiloxy-6-chloro-3-trimethylstannyl-2-hexene (**24**)*

Following a procedure identical with that described above, 3.9 g (13.1 mmol) of the alcohol **20** was converted into 5.4 g (89%, distillation temperature 155–170°C/11 Torr) of the silyl ether **24**, a colorless oil that exhibited ir (neat): 1256, 1093, 1061, 1006, 838,

Can. J. Chem. Downloaded from www.nrcresearchpress.com by 217.78.4.112 on 09/08/12
For personal use only.

776 cm^{-1}; ^1H nmr (80 MHz) δ: 0.06 (s, 6H), 0.19 (s, 9H, $^2J_{Sn-H}$ = 52 Hz), 0.90 (s, 9H), 1.63–2.00 (m, 2H), 2.35 (br t, 2H, J = 6 Hz), 3.50 (t, 2H, J = 6 Hz), 4.02, 4.18 (d, d, 1H each, J = 6 Hz in each case), 6.16 (br t, 1H, J = 6 Hz, $^3J_{Sn-H}$ = 138 Hz). Exact Mass calcd. for $C_{14}H_{30}{}^{35}ClOSiSn$ (M^+ − Me): 397.0777; found: 397.0780.

(E)-7-Chloro-4-trimethylstannyl-3-heptene (26)

To a stirred solution of the alcohol **19** (1.0 g, 3.36 mmol), 4-*N*,*N*-dimethylaminopyridine (41 mg, 0.34 mmol) and Et_3N (0.7 mL, 5.0 mmol) in dry CH_2Cl_2 (20 mL) at room temperature was added, dropwise, Ac_2O (0.48 mL, 5.0 mmol). The mixture was stirred for 15 h and then was poured into brine (50 mL). The phases were separated and the aqueous layer was extracted with CH_2Cl_2 (2 × 30 mL). The combined organic phases were dried ($MgSO_4$) and concentrated and the remaining liquid was distilled (90–100°C/0.03 Torr) to give 1.11 g (97%) of the acetate **25**, a colorless oil that showed ir (neat): 1741, 1230, 1028, 769 cm^{-1}; ^1H nmr (400 MHz) δ: 0.16 (s, 9H, $^2J_{Sn-H}$ = 52 Hz), 1.81 (quintet, 2H, J = 7 Hz), 2.07 (s, 3H), 2.48 (br t, 2H, J = 7 Hz, $^3J_{Sn-H}$ = 60 Hz), 3.49 (t, 2H, J = 7 Hz), 4.64–4.70 (m, 2H), 5.74 (br t, 1H, J = 6 Hz, $^3J_{Sn-H}$ = 68 Hz). Exact Mass calcd. for $C_{10}H_{18}{}^{35}ClO_2Sn$ (M^+ − Me): 325.0018; found: 325.0021.

To a cold (0°C), stirred suspension of $CuBr \cdot Me_2S$ (1.21 g, 5.9 mmol) in dry Et_2O (80 mL) was added a solution of MeLi (11.8 mmol) in Et_2O (9 mL) and the solution was stirred for 5 min. A solution of the acetate **25** (1.0 g, 2.95 mmol) in dry Et_2O (20 mL) was added and the mixture was stirred for 15 min. Saturated aqueous NH_4Cl (100 mL) was added slowly; the mixture was opened to the air and was stirred vigorously at room temperature until the aqueous phase became deep blue. The phases were separated and the aqueous layer was extracted with Et_2O (2 × 50 mL). The combined organic phases were dried ($MgSO_4$) and concentrated. Distillation (85–95°C/15 Torr) of the residual liquid afforded 757 mg (87%) of the alkene **26**, a colorless oil that displayed ir (neat): 1609, 776 cm^{-1}; ^1H nmr (400 MHz) δ: 0.12 (s, 9H, $^2J_{Sn-H}$ = 52 Hz), 0.98 (t, 3H, J = 7 Hz), 1.80 (quintet, 2H, J = 7 Hz), 2.14 (quintet, 2H, J = 7 Hz, $^4J_{Sn-H}$ = 58 Hz), 2.42 (br t, 2H, J = 7 Hz, $^3J_{Sn-H}$ = 61 Hz), 3.50 (t, 2H, J = 7 Hz), 5.60 (t, 1H, J = 7 Hz, $^3J_{Sn-H}$ = 72 Hz). Exact Mass calcd. for $C_9H_{18}{}^{35}ClSn$ (M^+ − Me): 281.0119; found: 281.0114.

General procedure for the conversion of primary chlorides into the corresponding iodides

A stirred solution of the primary chloride (1 equiv.) and NaI (5–10 equiv.) in dry acetone (~4 mL per mmol of the chloride) was refluxed until analysis (glc) showed the absence of the starting material (24–48 h). The mixture was concentrated and the residual material was partitioned between Et_2O and water. The aqueous phase was separated and extracted three times with Et_2O. The combined organic phases were dried ($MgSO_4$) and concentrated and the remaining liquid was distilled to produce the iodide.

Methyl (E)-6-iodo-3-trimethylstannyl-2-hexenoate (27)

Following the general procedure, 1.0 g (3.07 mmol) of the chloride **17** was converted into 1.2 g (94%, distillation temperature 125–135°C/0.6 Torr) of the iodide **27**, a colorless oil that displayed ir (neat): 1712, 1559, 1195, 1175, 772 cm^{-1}; ^1H nmr (80 MHz) δ: 0.22 (s, 9H, $^2J_{Sn-H}$ = 53 Hz), 1.70–2.20 (m, 2H), 2 .95 (br t, 2H, J = 7.5 Hz), 3.17 (t, 2H, J = 7 Hz), 3.66 (s, 3H), 5.99 (t, 1H, J = 1 Hz, $^3J_{Sn-H}$ = 71 Hz). Exact Mass calcd. for $C_9H_{16}IO_2Sn$ (M^+ − Me): 402.9217; found: 402.9212.

Methyl (Z)-6-iodo-3-trimethylstannyl-2-hexenoate (28)

By means of the general procedure, 1.8 g (5.54 mmol) of the chloride **18** was converted into 2.26 g (98%, distillation temperature 110–116°C/0.6 Torr) of **28**, a colorless oil that showed ir (neat): 1706, 1601, 1225, 1210, 780 cm^{-1}; ^1H nmr (80 MHz) δ: 0.21 (s, 9H, $^2J_{Sn-H}$ = 54 Hz), 1.70–2.10 (m, 2H), 2.55 (br t, 2H, J = 7 Hz, $^3J_{Sn-H}$ = 46 Hz), 3.15 (t, 2H, J = 7 Hz), 3.73 (s, 3H), 6.40 (t, 1H, J = 1.5 Hz, $^3J_{Sn-H}$ = 117 Hz). Exact Mass calcd. for $C_9H_{16}IO_2Sn$ (M^+ − Me): 402.9219; found: 402.9231.

(E)-6-Iodo-1-(methoxymethoxy)-3-trimethylstannyl-2-hexene (29)

Following the general procedure, 1.69 g (4.95 mmol) of the chloride **21** was transformed into 2.03 g (95%, distillation temperature 110–115°C/0.6 Torr) of **29**, a colorless oil that showed ir (neat): 1156, 1108, 1042, 774 cm^{-1}; ^1H nmr (80 MHz) δ: 0.15 (s, 9H, $^2J_{Sn-H}$ = 53 Hz), 1.60–2.10 (m, 2H), 2.42 (br t, 2H, J = 7 Hz), 3.14 (t, 2H, J = 7 Hz), 3.37 (s, 3H), 4.16 (br d, 2H, J = 6 Hz), 4.64 (s, 2H), 5.78 (tt, 1H, J = 1.2, 6 Hz, $^3J_{Sn-H}$ = 75 Hz). Exact Mass calcd. for $C_{10}H_{20}IO_2{}^{116}Sn$ (M^+ − Me): 414.9527; found: 414.9532.

(Z)-6-Iodo-1-(methoxymethoxy)-3-trimethylstannyl-2-hexene (30)

Using the general procedure, 1.9 g (5.57 mmol) of the chloride **22** was converted into 2.26 g (94%, distillation temperature 110–115°C/0.6 Torr) of the iodide **30**, a colorless oil that displayed ir (neat): 1156, 1105, 1035, 779 cm^{-1}; ^1H nmr (80 MHz) δ: 0.20 (s, 9H, $^2J_{Sn-H}$ = 53 Hz), 1.70–2.10 (m, 2H), 2.34 (br t, 2H, J = 7 Hz, $^3J_{Sn-H}$ = 48 Hz), 3.14 (t, 2H J = 7 Hz), 3.36 (s, 3H), 4.00 (m, 2H), 4.62 (s, 2H), 6 .21 (tt, 1H, J = 1.2, 6 Hz, $^3J_{Sn-H}$ = 134 Hz). Exact Mass calcd. for $C_{10}H_{20}IO_2Sn$ (M^+ − Me): 418.9530; found: 418.9530.

*(E)-1-*tert*-Butyldimethylsiloxy-6-iodo-3-trimethylstannyl-2-hexene (31)*

Following the general procedure, 5.27 g (12.8 mmol) of the chloride **23** was transformed into 5.97 g (93%, distillation temperature 175–185°C/11 Torr) of **31**, a colorless oil that exhibited ir (neat): 1256, 1099, 837, 775 cm^{-1}; ^1H nmr (80 MHz) δ: 0.08 (s, 6H), 0.13 (s, 9H, $^2J_{Sn-H}$ = 53 Hz), 0.91 (s, 9H), 1.63–2.03 (m, 2H), 2.25–2.50 (m, 2H), 3.13 (t, 2H, J = 7 Hz), 4.23, 4.38 (d, d, 1H each, J = 6 Hz in each case), 5.71 (tm, 1H, J = 6 Hz, $^3J_{Sn-H}$ = 76 Hz). Exact Mass calcd. for $C_{14}H_{30}IOSiSn$ (M^+ − Me): 489.0133; found 489.0126.

*(Z)-1-*tert*-Butyldimethylsiloxy-6-iodo-3-trimethylstannyl-2-hexene (32)*

By means of the general procedure, 5.4 g (13.1 mmol) of the chloride **24** was converted into 5.65 g (86%, distillation temperature 175–185°C/11 Torr) of **32**, a colorless oil that displayed ir (neat): 1256, 1099, 837, 776 cm^{-1}; ^1H nmr (80 MHz) δ: 0.08 (s, 6H), 0.19 (s, 9H, $^2J_{Sn-H}$ = 52 Hz), 0.90 (s, 9H), 1.63–2.05 (m, 2H), 2.20–2.45 (m, 2H), 3.15 (t, 2H, J = 7 Hz), 4.03, 4.08 (d, d, 1H, J = 6 Hz in each case), 6.18 (br t, 1H, J = 6 Hz, $^3J_{Sn-H}$ = 138 Hz). Exact Mass calcd. for $C_{14}H_{30}IOSiSn$ (M^+ − Me): 489.0133; found: 489.0130.

(E)-7-Iodo-4-trimethylstannyl-3-heptene (33)

By means of the general procedure, 1.45 g (4.91 mmol) of the chloride **26** was converted into 1.78 g (94%, distillation temperature 95–105°C/15 Torr) of the iodide **33**, a colorless oil that showed ir (neat): 1609, 1220, 776 cm^{-1}; ^1H nmr (400 MHz) δ: 0.12 (s, 9H, $^2J_{Sn-H}$ = 52 Hz), 0.99 (t, 3H, J = 7 Hz), 1.85 (quintet, 2H, J = 7 Hz), 2.16 (quintet, 2H, J = 7 Hz), 2.38 (br t, 2H, J = 7 Hz, $^3J_{Sn-H}$ = 53 Hz), 3.16 (t, 2H, J = 7 Hz), 5.59 (br t, 1H, J = 7 Hz, $^3J_{Sn-H}$ = 78 Hz). Exact Mass calcd. for $C_9H_{18}ISn$ (M^+ − Me): 372.9477; found: 372.9475.

*General procedure for alkylation of the β-keto esters **34** and **35** with the iodides **27–33***

To a well-stirred suspension of KH (1.1 equiv.) in dry THF (3 mL per mmol of β-keto ester) at room temperature was added, dropwise, a solution of the β-keto ester (1 equiv.) in dry THF (1 mL per mmol of ester). The mixture was stirred for 30–45 min and then a solution of the iodide (1.1 equiv.) in dry THF (1 mL per mmol of iodide) was added. The reaction mixture was refluxed and, after the reaction was determined to have reached completion (analysis by glc and (or) tlc), the mixture was cooled and concentrated. Direct flash chromatography of the remaining oil–salt mixtures, followed by distillation of the liquid thus obtained, provided the desired alkylation product. The following compounds were prepared by use of this procedure.

Can. J. Chem. Downloaded from www.nrcresearchpress.com by 217.78.4.112 on 09/08/12
For personal use only.

Keto diester ***36***

Alkylation of 2-(methoxycarbonyl)cyclopentanone (**34**) (155 mg, 1.09 mmol) with the iodide **27** (500 mg, 1.2 mmol, reaction time 18 h), followed by flash chromatography (27 g silica gel, 10:1 petroleum ether – EtOAc) of the crude product and distillation (169–173°C/0.6 Torr) of the acquired liquid, provided 366 mg (78%) of **36**, a colorless oil that showed ir (neat): 1750, 1720, 1170, 775 cm^{-1}; ^1H nmr (400 MHz) δ: 0.20 (s, 9H, $^2J_{Sn-H}$ = 53 Hz), 1.30–1.50 (m, 2H), 1.62 (ddd, 1H, J = 4.5, 11.5, 13.5 Hz), 1.80–2.05 (m, 4H), 2.25 (m, 1H), 2.39 (m, 1H), 2.54 (m, 1H), 2.80–3.00 (m, 2H), 3.68 (s, 3H), 3.69 (s, 3H), 5.96 (br s, 1H, $^3J_{Sn-H}$ = 72 Hz). Exact Mass calcd. for $C_{16}H_{25}O_5Sn$ (M^+ – Me): 417.0723; found: 417.0710.

Keto diester ***37***

Flash chromatography (35 g silica gel, 14:1 petroleum ether – EtOAc) of the crude product derived from alkylation of 2 -(methoxycarbonyl)cyclohexanone (**35**) (200 mg, 1.28 mmol) with the iodide **27** (588 mg, 1.41 mmol, reaction time 9 h), followed by distillation (176–181°C/0.6 Torr) of the resultant liquid, gave 322 mg (57%) of **37**, a colorless oil that displayed ir (neat): 1710, 1195, 1170, 775 cm^{-1}; ^1H nmr (400 MHz) δ: 0.19 (s, 9H, $^2J_{Sn-H}$ = 53 Hz), 1.20–1.50 (m, 3H), 1.55–1.80 (m, 4H), 1.85–2.05 (m, 2H), 2.20–2.55 (m, 3H), 2.75–3.00 (m, 2H), 3.68 (s, 3H), 3.72 (s, 3H), 5.96 (t, 1H, J = 1.3 Hz, $^3J_{Sn-H}$ = 72 Hz). Exact Mass calcd. for $C_{17}H_{27}O_5Sn$ (M^+ – Me): 431.0880; found: 431.0873.

Keto diester ***38***

The keto ester **34** (300 mg, 2.11 mmol) was alkylated with the iodide **28** (967 mg, 2.32 mmol, reaction time 18 h). Flash chromatography (50 g silica gel, 10:1 petroleum ether – EtOAc) of the crude product and distillation (185–189°C/0.6 Torr) of the liquid thus obtained afforded 564 mg (63%) of **38**, a colorless oil that exhibited ir (neat): 1750, 1720, 1705, 1210, 780 cm^{-1}; ^1H nmr (400 MHz) δ: 0.15 (s, 9H, J_{Sn-H} = 53 Hz), 1.23–1.50 (m, 2H), 1.52 (dt, 1H, J = 4.5, 13 Hz), 1.80–2.05 (m, 4H), 2.25 (dt, 1H, J = 19, 8 Hz), 2.34–2.48 (m, 3H), 2.53 (m, 1H), 3.69 (s, 3H), 3.71 (s, 3H), 6.31 (t, 1H, J = 1 Hz, $^3J_{Sn-H}$ = 119 Hz). Exact Mass calcd. for $C_{16}H_{25}O_5Sn$ (M^+ – Me): 417.0723; found: 417.0718.

Keto diester ***39***

Alkylation of the keto ester **35** (300 mg, 1.92 mmol) with the iodide **28** (881 mg, 2.1 mmol, reaction time 18 h), followed by flash chromatography (50 g silica gel, 10:1 petroleum ether – EtOAc) of the crude product and distillation (201–204°C/0.6 Torr) of the acquired liquid, produced 610 mg (71%) of **39**, a colorless oil that displayed ir (neat): 1710, 1210, 780 cm^{-1}; ^1H nmr (400 MHz) δ: 0.16 (s, 9H, $^2J_{Sn-H}$ = 53 Hz), 1.20–1.80 (m, 7H), 1.86 (dt, 1H, J = 4.5, 13 Hz), 2.00 (m, 1H), 2.35–2.60 (m, 5H), 3.72 (s, 3H), 3.73 (s, 3H), 6.34 (t, 1H, J = 1 Hz, $^3J_{Sn-H}$ = 118 Hz). Exact Mass calcd. for $C_{17}H_{27}O_5Sn$ (M^+ – Me): 431.0880; found: 431.0881.

Keto ester ***40***

Flash chromatography (18 g silica gel, 8:1 petroleum ether – EtOAc) of the crude product obtained from alkylation of the keto ester **34** (100 mg, 0.70 mmol) with the iodide **29** (335 mg, 0.77 mmol, reaction time 13 h), followed by distillation (159–164°C/0.6 Torr) of the liquid thus obtained provided 210 mg (67%) of **40**, a colorless oil that showed ir (neat): 1750, 1725, 1155, 1050, 775 cm^{-1}; ^1H nmr (400 MHz) δ: 0.11 (s, 9H, $^2J_{Sn-H}$ = 53 Hz), 1.15–1.44 (m, 2H), 1.53 (ddd, 1H, J = 4.5, 12, 13.5 Hz), 1.78–2.04 (m, 4H), 2.17–2.33 (m, 3H), 2.37 (m, 1H), 2.52 (m, 1H), 3.35 (s, 3H), 3.67 (s, 3H), 4.11 (d, 2H, J = 6 Hz), 4.62 (s, 2H), 5.72 (t, 1H, J = 6 Hz, $^3J_{Sn-H}$ = 77 Hz). Exact Mass calcd. for $C_{17}H_{29}O_5Sn$ (M^+ – Me): 433.1037; found: 433.1038.

Keto ester ***41***

Alkylation of the keto ester **35** (670 mg, 4.29 mmol) with the iodide **29** (2.04 g, 4.72 mmol, reaction time 6 h), followed by flash chromatography (100 g silica gel, 5:1 petroleum ether – EtOAc) of the crude product and distillation (164–167°C/0.6 Torr) of the acquired liquid, provided 1.46 g (74%) of **41**, a colorless oil that showed ir (neat): 1710, 1055, 772 cm^{-1}; ^1H nmr (400 MHz) δ: 0.11 (s, 9H, $^2J_{Sn-H}$ = 53 Hz), 1.12–1.35 (m, 2H), 1.42 (m, 1H), 1.52 (dt, 1H, J = 4.5, 13 Hz), 1.58–1.80 (m, 3H), 1.86 (ddd, 1H, J = 4.5, 13, 13.5 Hz), 1.99 (m, 1H), 2.29 (br t, 2H, J = 7.5 Hz, $^3J_{Sn-H}$ = 53 Hz), 2.40–2.45 (m, 2H), 2.49 (m, 1H), 3.37 (s, 3H), 3.71 (s, 3H), 4.14 (d, 2H, J = 6 Hz), 4.63 (s, 2H), 5.72 (br t, 1H, J = 6 Hz, $^3J_{Sn-H}$ = 77 Hz). Exact Mass calcd. for $C_{18}H_{31}O_5Sn$ (M^+ – Me): 447.1193; found: 447.1196.

Keto ester ***42***

The keto ester **34** (670 mg, 4.71 mmol) was alkylated with the iodide **30** (2.24 g, 5.18 mmol, reaction time 14 h). Flash chromatography (100 g silica gel, 7:1 petroleum ether – EtOAc) of the crude product and distillation 170–175°C/0.6 Torr) of the oil thus obtained provided 1.43 g (68%) of **42**, a colorless oil that displayed ir (neat): 1747, 1720, 1155, 1040, 780 cm^{-1}; ^1H nmr (400 MHz) δ: 0.18 (s, 9H, $^2J_{Sn-H}$ = 54 Hz), 1.20–1.42 (m, 2H), 1.53 (dt, 1H, J = 4.5, 13 Hz), 1.80–2.05 (m, 4H), 2.20–2.32 (m, 3H), 2.39 (m, 1H), 2.54 (m, 1H), 3.35 (s, 3H), 3.69 (s, 3H), 4.01 (d, 2H, J = 6 Hz), 4.61 (s, 2H), 6.12 (t, 1H, J = 6 Hz, $^3J_{Sn-H}$ = 136 Hz). Exact Mass calcd. for $C_{17}H_{29}O_5Sn$ (M^+ – Me): 433.1037; found: 433.1035.

Keto ester ***43***

Alkylation of the keto ester **35** (740 mg, 4.74 mmol) with the iodide **30** (2.25 g, 5.2 mmol, reaction time 19 h), followed by flash chromatography (120 g silica gel, 7:1 petroleum ether – EtOAc) of the crude product and distillation (174–177°C/0.6 Torr) of the acquired liquid, gave 1.53 g (70%) of **43**, a colorless oil that displayed ir (neat): 1715, 1040, 779 cm^{-1}; ^1H nmr (400 MHz) δ: 0.15 (s, 9H, $^2J_{Sn-H}$ = 53 Hz), 1.13–1.33 (m, 2H), 1.37–1.77 (m, 5H), 1.84 (dt, 1H, J = 4.5, 13.5 Hz), 1.97 (m, 1H), 2.10–2.30 (m, 2H), 2.37–2.44 (m, 2H), 2.48 (m, 1H), 3.35 (s, 3H), 3.70 (s, 3H), 3.99 (d, 2H, J = 6.3 Hz), 4.60 (s, 2H), 6.12 (t, 1H, J = 6.3 Hz, $^3J_{Sn-H}$ = 131 Hz). Exact Mass calcd. for $C_{18}H_{31}O_5Sn$ (M^+ – Me): 447.1193; found: 447.1195.

Keto ester ***44***

The keto ester **35** (400 mg, 2.56 mmol) was alkylated with the iodide **31** (1.42 g, 2.82 mmol, reaction time 24 h). Flash chromatography (50 g silica gel, 10:1 petroleum ether – EtOAc), followed by distillation (200–210°C/0.03 Torr) of the oil thus obtained, produced 1.21 g (81%) of **44**, a colorless oil that exhibited ir (neat): 1741, 1718, 1254, 1093, 837, 776 cm^{-1}; ^1H nmr (400 MHz) δ: 0.07 (s, 6H), 0.11 (s, 9H, $^2J_{Sn-H}$ = 52 Hz), 0.90 (s, 9H), 1.12–1.34 (m, 2H), 1.37–1.57 (m, 2H), 1.60–1.88 (m, 3H), 1.85 (dt, 1H, J = 4.5, 13 Hz), 1.99 (m, 1H), 2.23 (br t, 2H, J = 8 Hz, $^3J_{Sn-H}$ = 61 Hz), 2.36–2.45 (m, 2H), 2.49 (m, 1H), 3.71 (s, 3H), 4.26 (d, 2H, J = 5.5 Hz), 5.66 (br t, 1H, J = 5.5 Hz, $^3J_{Sn-H}$ = 79 Hz). Exact Mass calcd. for $C_{22}H_{41}O_4SiSn$ (M^+ – Me): 517.1796; found: 517.1792.

Keto ester ***45***

The keto ester **35** (400 mg, 2.56 mmol) was alkylated with the iodide **32** (1.42 g, 2.82 mmol, reaction time 24 h). Distillation (200–210°C/0.03 Torr) of the liquid derived by flash chromatography (50 g silica gel, 10:1 petroleum ether – EtOAc) of the crude product afforded 940 mg (69%) of **45**, a colorless oil that showed ir (neat): 1741, 1718, 1255, 1095, 837, 776 cm^{-1}; ^1H nmr 400 MHz) δ: 0.07 (s, 6H), 0.17 (s, 9H, $^2J_{Sn-H}$ = 52 Hz), 0.90 (s, 9H), 1.15–1.34 (m, 2H), 1.39–1.58 (m, 2H), 1.62–1.79 (m, 3H), 1.85 (ddd, 1H, J = 4.5, 13, 13.5 Hz), 2.00 (m, 1H), 2.20 (br t, 2H, J = 7 Hz), 2.40–2.54 (m, 3H), 3.72 (s, 3H), 4.10 (d, 2H, J = 6 Hz), 6.10 (t, 1H, J = 6 Hz, $^3J_{Sn-H}$ = 140 Hz). Exact Mass calcd. for $C_{22}H_{41}O_4SiSn$ (M^+ – Me): 517.1796; found: 517.1790.

Keto ester ***46***

Alkylation of the keto ester **35** (1.12 g, 7.18 mmol) with the iodide **33** (2.94 g, 7.90 mmol), reaction time 20 h), followed by flash chromatography (180 g silica gel, 15:1 petroleum ether – EtOAc) of the crude product and distillation (140–150°C/0.3 Torr) of the

Can. J. Chem. Downloaded from www.nrcresearchpress.com by 217.78.4.112 on 09/08/12
For personal use only.

liquid thus obtained, provided 2.23 g (75%) of **46**, a colorless oil that displayed ir (neat): 1740, 1716, 1211, 767 cm^{-1}; ^1H nmr (400 MHz) δ: 0.09 (s, 9H, $^2J_{Sn-H}$ = 52 Hz), 0.97 (t, 3H, J = 7 Hz), 1.12–1.33 (m, 2H), 1.39–1.80 (m, 5H), 1.88 (dt, 1H, J = 4, 13 Hz), 2.00 (m, 1H), 2.11 (quintet, 2H, J = 7 Hz), 2.25 (br t, 2H, J = 8 Hz), 2.40–2.55 (m, 3H), 3.72 (s, 3H), 5.53 (br t, 1H, J = 7 Hz, $^3J_{Sn-H}$ = 73 Hz). Exact Mass calcd. for $C_{17}H_{29}O_3Sn$ (M^+ − Me): 401.1138; found: 401.1131.

General procedures for the synthesis of bicyclic dienes via the corresponding (isolated) enol trifluoromethanesulfonate intermediates (Table 2, Entries 1–5, 7, 8, 10)

To a cold (−48°C), stirred solution of lithium diisopropylamide (LDA, 1.1–1.5 equiv.) in dry THF (~10 mL per mmol of β-keto ester) was added, dropwise, a solution of the β-keto ester (1 equiv.) in dry THF (~5 mL per mmol of β-keto ester) and the resultant mixture was stirred at −48°C for 1 h. Solid finely ground $PhN(SO_2CF_3)_2$ ($PhNTf_2$) (1.17–1.57 equiv.) was added and the solution was warmed to room temperature over a period of 30 min. Concentration of the reaction mixture under reduced pressure was followed by flash chromatography of the residual oil on silica gel. The enol triflate thus obtained was characterized and then was used as soon as possible in the subsequent reaction.

To a stirred solution of the enol triflate (1 equiv.) in dry THF or MeCN (5 mL per 0.1 mmol of substrate) at room temperature was added $Pd(PPh_3)_4$ (0.05 equiv.) as a solid and the resulting solution was refluxed. When the reaction was determined to have reached completion (by glc and (or) tlc analyses), the mixture was cooled to room temperature and concentrated. The residual oil was purified by flash chromatography and the liquid thus obtained was distilled to provide the expected diene.

The following compounds were prepared via these procedures.

Diene 55

The keto ester **36** (190 mg, 0.44 mmol) was converted into the enol triflate **47** (141 mg, 57%, flash chromatography on 40 g of silica gel, 10:1 petroleum ether – EtOAc), using 0.48 mmol of LDA and 0.52 mmol of $PhNTf_2$. Compound **47** displayed ir (neat): 1734, 1719, 1642, 1599, 1423, 1210, 1143, 772 cm^{-1}; ^1H nmr (80 MHz) δ: 0.22 (s, 9H, $^2J_{Sn-H}$ = 53 Hz), 1.20–3.20 (m, 10H), 3.69 (s, 3H), 3.72 (s, 3H), 5.76 (br s, 1H), 5.98 (t, 1H, J = 1 Hz, $^3J_{Sn-H}$ = 72 Hz). Exact Mass calcd. for $C_{17}H_{24}F_3O_7SSn$ (M^+ − Me): 549.0216; found: 549.0212.

Compound **47** (100 mg, 0.178 mmol) was converted (THF, reflux, 3.5 h) into 39 mg (89%) of **55** (flash chromatography on 20 g of silica gel, 10:1 petroleum ether – EtOAc; distillation temperature 117–121°C/0.6 Torr), a colorless oil that exhibited ir (neat): 1710, 1620 cm^{-1}; ^1H nmr (400 MHz) δ: 1.43 (dt, 1H, J = 3.5, 13 Hz), 1.51 (ddq, 1H, J = 3, 4.5, 13 Hz), 1.78–1.88 (m, 2H), 2.06 (m, 1H), 2.35–2.50 (m, 4H), 3.65 (s, 3H), 3.67 (m, 1H), 3.69 (s, 3H), 5.97 (d, 1H, J = 2.5 Hz), 6.01 (br s, 1H). Exact Mass calcd. for $C_{14}H_{18}O_4$: 250.1205; found: 250.1206.

Diene 56

Flash chromatography (40 g silica gel, 10:1 petroleum ether – EtOAc) of the crude product derived from sequential treatment of the keto ester **37** (200 mg, 0.45 mmol) with LDA (0.50 mmol) and $PhNTf_2$ (0.53 mmol) gave 160 mg (62%) of the enol triflate **48**, a colorless oil that showed ir (neat): 1732, 1712, 1594, 1415, 1210, 772 cm^{-1}; ^1H nmr (80 MHz) δ: 0.20 (s, 9H, $^2J_{Sn-H}$ = 53 Hz), 1.20–2.40 (m, 10H), 2.85 (m, 2H), 3.68 (s, 3H), 3.72 (s, 3H), 5.87 (t, 1H, J = 4 Hz), 5.97 (t, 1H, J = 1.1 Hz). Exact Mass calcd. for $C_{18}H_{26}F_3O_7SSn$ (M^+ − Me): 563.0373; found: 563.0383.

Cyclization of **48** (110 mg, 0.19 mmol) was carried out in THF (reflux, 3.5 h). Flash chromatography (18 g silica gel, 10:1 petroleum ether – EtOAc) of the crude product and distillation (118–122°C/0.6 Torr) of the acquired liquid produced 45 mg (90%) of **56**, a colorless oil that showed ir (neat): 1710, 1615 cm^{-1}; ^1H nmr (400 MHz) δ: 1.35–1.50 (m, 4H), 1.66 (m, 1H), 1.77 (m, 1H), 2.01 (dddt, 1H, J = 2.5, 2.5, 5.5, 13.5 Hz), 2.14 (m, 2H), 2.20 (dd, 1H, J = 5, 11 Hz), 2.30 (m, 1H), 3.65 (s, 3H), 3.69 (s, 3H), 3.82 (br d, 1H, J = 4 Hz), 5.85 (d, 1H, J = 2 Hz), 5.96 (t, 1H, J = 4 Hz). Exact Mass calcd. for $C_{15}H_{20}O_4$: 264.1362; found: 264.1362.

Diene 57

Treatment of the keto ester **38** (300 mg, 0.70 mmol) with LDA (0.77 mmol) and $PhNTf_2$ (0.82 mmol), followed by flash chromatography (40 g silica gel, 10:1 petroleum ether – EtOAc) of the crude product, furnished 250 mg (64%) of the enol triflate **49**, a colorless oil that exhibited ir (neat): 1739, 1703, 1645, 1600, 1422, 1215, 770 cm^{-1}; ^1H nmr (80 MHz) δ: 0.20 (s, 9H, $^2J_{Sn-H}$ = 55 Hz), 1.20–2.75 (m, 10H), 3.74 (s, 6H), 5.76 (m, 1H), 6.35 (t, 1H, J = 1 Hz, $^3J_{Sn-H}$ = 118 Hz). Exact Mass calcd. for $C_{17}H_{24}F_3O_7SSn$ (M^+ − Me): 549.0216; found: 549.0215.

Compound **49** (125 mg, 0.222 mmol) was converted (THF, reflux 19 h) into 42 mg (75%) of **57** (flash chromatography on 27 g of silica gel, 10:1 petroleum ether – EtOAc; distillation temperature 114–117°C/0.6 Torr), a colorless oil that showed ir (neat): 1725, 1630 cm^{-1}; ^1H nmr (400 MHz) δ: 1.45 (dt, 1H, J = 4, 13.5 Hz), 1.69 (tq, 1H, J = 4, 13.5 Hz), 1.77–1.90 (m, 2H), 2.19 (ddt, 1H, J = 2, 5, 13.5 Hz), 2.33 (br d, 1H, J = 13.5 Hz), 2.38–2.49 (m, 3H), 2.63 (dddd, 1H, J = 2.5, 8.5, 8.5, 17.5 Hz), 3.63 (s, 3H), 3.66 (s, 3H), 5.68 (d, 1H, J = 2 Hz), 6.10 (t, 1H, J = 2.5 Hz). Exact Mass calcd. for $C_{14}H_{18}O_4$: 250.1205; found: 250.1206.

Diene 58

The keto ester **39** (220 mg, 0.495 mmol) was converted into the enol triflate **50** (194 mg, 64%; flash chromatography on 50 g of silica gel, 10:1 petroleum ether – EtOAc), using 0.54 mmol of LDA and 0.58 mmol of $PhNTf_2$. Compound **50** exhibited ir (neat): 1738, 1707, 1601, 1415, 1220, 1150, 779 cm^{-1}; ^1H nmr (80 MHz) δ: 0.19 (s, 9H, $^2J_{Sn-H}$ = 54 Hz), 1.20–2.55 (m, 12H), 3.73 (s, 3H), 3.74 (s, 3H), 5.87 (t, 1H, J = 4 Hz), 6.34 (t, 1H, J = 1 Hz, $^3J_{Sn-H}$ = 117 Hz). Exact Mass calcd. for $C_{18}H_{26}F_3O_7SSn$ (M^+ − Me): 563.0373; found: 563.0374.

Compound **50** (150 mg, 0.26 mmol) was converted (THF, reflux, 16 h) into 52 mg (75%) of the diene **58** (flash chromatography on 27 g of silica gel, 10:1 petroleum ether – EtOAc; distillation temperature 116–118°C/0.6 Torr), a colorless oil that displayed ir (neat): 1728, 1633; ^1H nmr (400 MHz) δ: 1.40–1.68 (m, 5H), 1.79 (m, 1H), 2.10 (dddd, 1H, J = 3, 6, 9.5, 18.5 Hz), 2.15–2.26 (m, 3H), 2.30 (m, 1H), 3.63 (s, 3H), 3.66 (s, 3H), 5.60 (d, 1H, J = 2 Hz), 5.99 (dd, 1H, J = 3, 4 Hz). Exact Mass calcd. for $C_{15}H_{20}O_4$: 264.1362; found: 264.1364.

Diene 59

Sequential treatment of the keto ester **40** (700 mg, 1.57 mmol) with LDA (2.35 mmol) and $PhNTf_2$ (2.46 mmol), followed by flash chromatography (120 g silica gel, 8:1 petroleum ether – EtOAc) of the crude product, gave 798 mg (88%) of the enol triflate **51**, a colorless oil that showed ir (neat): 1732, 1643, 1420, 1210, 770 cm^{-1}; ^1H nmr (80 MHz) δ: 0.10 (s, 9H, $^2J_{Sn-H}$ = 52 Hz), 1.20–2.70 (m, 10H), 3.35 (s, 3H), 3.68 (s, 3H), 4.10 (d, 2H, J = 6 Hz), 4.61 (s, 2H), 5.73 (m, 2H). Exact Mass calcd. for $C_{18}H_{28}F_3O_7SSn$ (M^+ − Me): 565.0529; found: 565.0520.

Cyclization of **51** (87 mg, 0.15 mmol) was carried out in THF (reflux, 6 h). Flash chromatography (18 g silica gel, 10:1 petroleum ether – EtOAc) of the crude product and distillation (105–110°C/0.6 Torr) of the acquired liquid provided 33 mg (83%) of the diene **59**, a colorless oil that displayed ir (neat): 1720, 1640 cm^{-1}; ^1H nmr (400 MHz) δ: 1.35 (dt, 1H, J = 3.5, 13 Hz), 1.48 (ddq, 1H, J = 3, 3.5, 13 Hz), 1.72–1.93 (m, 3H), 2.30–2.45 (m, 3H), 2.49 (br d, 1H, J = 13 Hz), 2.62 (br d, 1H, J = 13 Hz), 3.38 (s, 3H), 3.65 (s, 3H), 4.13 (m, 2H), 4.62, 4.65 (d, d, 1H each, J = 6 Hz in each case), 5.73 (dt, 1H, J = 2.5, 7 Hz), 5.84 (t, 1H, J = 2.5 Hz). Exact Mass calcd. for $C_{15}H_{22}O_4$: 266.1519; found: 266.1524.

Diene 60

Treatment of the keto ester **41** (1.01 g, 2.19 mmol) with LDA (3.28 mmol) and $PhNTf_2$ (3.44 mmol), followed by flash chro-

Can. J. Chem. Downloaded from www.nrcresearchpress.com by 217.78.4.112 on 09/08/12
For personal use only.

matography (180 g silica gel, 10:1 petroleum ether – EtOAc) of the crude product, afforded 1.19 g (92%) of the enol triflate **52**, a colorless oil that exhibited ir (neat): 1732, 1420, 1210, 770 cm^{-1}; ^1H nmr (80 MHz) δ: 0.14 (s, 9H, $^2J_{Sn-H}$ = 53 Hz), 1.20–2.45 (m, 12H), 3.38 (s, 3H), 3.73 (s, 3H), 4.13 (d, 2H, J = 6 Hz), 4.64 (s, 2H), 5.74 (br t, 1H, J = 6 Hz, $^3J_{Sn-H}$ = 76 Hz), 5.87 (t, 1H, J = 4 Hz). *Exact Mass* calcd. for $C_{19}H_{30}F_3O_7SSn$ (M^+ − Me): 579.0686; found: 579.0670.

Cyclization of **52** (660 mg, 1.11 mmol) was carried out in MeCN (reflux, 15 h). Flash chromatography (120 g silica gel, 12:1 petroleum ether – EtOAc) of the crude product and distillation (120–124°C/0.6 Torr) of the liquid thus obtained gave 262 mg (84%) of **60**, a colorless oil that exhibited ir (neat): 1721, 1640 cm^{-1}; ^1H nmr (400 MHz) δ: 1.30–1.50 (m, 4H), 1.62 (m, 1H), 1.73 (m, 1H), 1.86 (br t, 1H, J = 12 Hz), 2.11 (m, 3H), 2.33 (br d, 1H, J = 12 Hz), 2.65 (br d, 1H, J = 14 Hz), 3.37 (s, 3H), 3.65 (s, 3H), 4.09 (dd, 1H, J = 7, 12 Hz), 4.14 (dd, 1H, J = 7, 12 Hz), 4.61, 4.64 (d, d, 1H each, J = 6 Hz in each case), 5.57 (dt, 1H, J = 2.4, 7 Hz), 5.82 (t, 1H, J = 4 Hz). In a nOe difference experiment, irradiation at δ 5.82 caused enhancement of the signal at δ 5.57. Exact Mass calcd. for $C_{16}H_{24}O_4$: 280.1675; found: 280.1679.

*Diene **61***

The keto ester **42** (700 mg, 1.57 mmol) was converted into 766 mg (84%) of the enol triflate **53** (flash chromatography on 90 g of silica gel, 8:1 petroleum ether – EtOAc), using 2.35 mmol of LDA and 2.46 mmol of $PhNTf_2$. Compound **53** exhibited ir (neat): 1739, 1650, 1422, 1218, 1147, 778 cm^{-1}; ^1H nmr (80 MHz) δ: 0.18 (s, 9H, $^2J_{Sn-H}$ = 53 Hz), 1.10–2.70 (m, 10H), 3.36 (s, 3H), 3.71 (s, 3H), 4.00 (d, 2H, J = 6 Hz), 4.62 (s, 2H), 5.75 (br s, 1H), 6.13 (br t, 1H, J = 6 Hz, $^3J_{Sn-H}$ = 132 Hz). Exact Mass calcd. for $C_{18}H_{28}F_3O_7SSn$ (M^+ − Me): 265.0529; found: 265.0527.

The enol triflate **53** (230 mg, 0.397 mmol) was transformed (THF, reflux, 2 h) into 91 mg (86%) of the diene **61** (flash chromatography on 40 g of silica gel, 7:1 petroleum ether – EtOAc; distillation temperature 99–105°C/0.6 Torr), a colorless oil that showed ir (neat): 1724, 1640 cm^{-1}; ^1H nmr (400 MHz) δ: 1.32 (dt, 1H, J = 3.5, 13 Hz), 1.46 (ddq, 1H, J = 3, 4, 13 Hz), 1.68 (m, 1H), 1.77 (dt, 1H, J = 13.5, 9.5 Hz), 2.04 (br t, 1H, J = 13 Hz), 2.19–2.28 (m, 2H), 2.33 (ddt, 1H, J = 9.5, 16.5, 2.5 Hz), 2.40–2.53 (m, 2H), 3.31 (s, 3H), 3.57 (s, 3H), 4.10 (ddd, 1H, J = 2.5, 6, 12 Hz), 4.17 (ddd, 1H, J = 1, 7.5, 12 Hz), 4.58, 4.60 (d, d, 1H each, J = 7 Hz in each case), 5.43 (ddd, 1H, J = 2, 6, 7.5 Hz), 5.60 (t, 1H, J = 2.5 Hz). In a nOe difference experiment, irradiation at δ 5.60 caused enhancement of the signals at δ 4.10 and 4.17. Exact Mass calcd. for $C_{15}H_{22}O_4$: 266.1519; found: 266.1517.

*Diene **62***

Sequential treatment of the keto ester **43** (820 mg, 1.78 mmol) with LDA (2.7 mmol) and $PhNTf_2$ (2.8 mmol), followed by flash chromatography (100 g silica gel, 8:1 petroleum ether – EtOAc) of the crude product, furnished 950 mg (90%) of the enol triflate **54**, a colorless oil that displayed ir (neat): 1736, 1675, 1418, 1219, 776 cm^{-1}; ^1H nmr (80 MHz) δ: 0.17 (s, 9H, $^2J_{Sn-H}$ = 53 Hz), 1.10–2.50 (m, 2H), 3.36 (s, 3H), 3.71 (s, 3H), 3.98 (d, 2H, J = 6 Hz), 4.60 (s, 2H), 5.85 (t, 1H, J = 4 Hz), 6.13 (br t, 1 H, J = 6 Hz, $^3J_{Sn-H}$ = 132 Hz). Exact Mass calcd. for $C_{19}H_{30}F_3O_7SSn$ (M^+ − Me): 579.0686; found: 579.0678.

Cyclization (THF, reflux, 2h) of **54** (190 mg, 0.32 mmol) provided 78 mg (87%) of the diene **62** (flash chromatography on 40 g of silica gel, 7:1 petroleum ether – EtOAc; distillation temperature 108–111°C/0.6 Torr), a colorless oil that showed ir (neat): 1726, 1645 cm^{-1}; ^1H nmr (400 MHz) δ: 1.36–1.59 (m, 4H), 1.61 (m, 1H), 1.72 (m, 1H), 2.00–2.20 (m, 4H), 2.26 (m, 1H), 2.35 (m, 1H), 3.39 (s, 3H), 3.63 (s, 3H), 4.19 (ddd, 1H, J = 2.3, 6, 12 Hz), 4.21 (ddd, 1H, J = 1.2, 7.3, 12 Hz), 4.65, 4.68 (d, d, 1H each, J = 6.5 Hz in each case), 5.39 (ddd, 1H, J = 2, 6, 7.3 Hz), 5.59 (dd, 1H, J = 3, 4.6 Hz). In a nOe difference experiment, irradiation at δ 5.59 caused enhancement of the resonances at δ 4.19 and 4.21. Exact Mass calcd. for $C_{16}H_{24}O_4$: 280.1675; found: 280.1666.

General procedure for the preparation of bicyclic dienes in a "one-pot" process from keto vinylstannanes (Table 2, Entries 6, 9, 11–13)

To a cold (−78°C), stirred solution of LDA (1.5 equiv.) in dry THF (~10 mL per mmol of β-keto ester) was added dry HMPA (2 equiv.) and the resultant solution was stirred at −78°C for 10 min and then at 0°C for 10 min. The mixture was recooled to −78°C and a solution of the β-keto ester (1 equiv.) in dry THF (~5 mL per mmol of substrate) was added dropwise. The mixture was stirred at −78°C for 10 min and at 0°C for 1 h. Solid, finely ground $PhNTf_2$ (1.57 equiv.) was added and the solution was stirred at room temperature for 30 min. Solid $Pd(PPh_3)_4$ (0.03 equiv.) or $Pd(OAc)_2$ (0.03 equiv.) was added and the solution was heated under reflux. When the reaction was determined to have reached completion (analyses by glc and (or) tlc), the solution was cooled to room temperature and then was concentrated. Flash chromatography of the remaining material on silica gel, followed by distillation of the liquid thus obtained, provided the desired diene.

The following compounds were prepared by means of this procedure. Unless otherwise noted, $Pd(PPh_3)_4$ was employed as the catalyst in the cyclization step.

*Diene **59***

The keto ester **40** (300 mg, 0.672 mmol) was converted into the diene **59** (151 mg, 84%; cyclization reaction time 30 min; flash chromatography on 50 g of silica gel, 8:1 petroleum ether –EtOAc; distillation temperature 100–108°C/0.5 Torr). The spectral data for the product were identical with those summarized above.

*Diene **61***

The keto ester **41** (300 mg, 0.672 mmol) was transformed into the diene **61** (131 mg, 73%; cyclization reaction time 30 min; flash chromatography on 50 g of silica gel, 8:1 petroleum ether – EtOAc; distillation temperature 100–105°C/0.6 Torr). This product exhibited spectra identical with those summarized above.

*Diene **63***

The keto ester **44** (500 mg, 0.94 mmol) was converted into 200 mg (61%) of the diene **63** (flash chromatography on 90 g of silica gel, 15:1 petroleum ether – EtOAc; distillation temperature 135–145°C/0.03 Torr). The cyclization reaction time was 3 h. The diene **63**, a colorless oil, displayed ir (neat): 1729, 1650, 835, 776 cm^{-1}; ^1H nmr (400 MHz) δ: 0.06 (s, 6H), 0.90 (s, 9H), 1.29–1.48 (m, 4H), 1.58–1.87 (m, 3H), 2.05–2.14 (m, 3H), 2.32 (m, 1H), 2.55 (br d, 1H, J = 13 Hz), 3.63 (s, 3H), 4.18 (ddd, 1H, J = 1, 6.5, 13 Hz), 4.26 (ddd, 1H, J = 1, 6.5, 13 Hz), 5.53 (dt, 1H, J = 2, 6.5 Hz), 5.78 (t, 1H, J = 3.8 Hz). Exact Mass calcd. for $C_{20}H_{34}O_3Si$: 350.2278; found: 350.2274.

In a separate, identical experiment, but using $Pd(OAc)_2$ in place of $Pd(PPh_3)_4$, 1.15 g (2.17 mmol) of **44** was transformed into 381 mg (50%) of **63**.

*Diene **64***

The keto ester **45** (500 mg, 0.94 mmol) was converted into the diene **64** (215 mg, 65%; cyclization reaction time 14 h; flash chromatography on 90 g of silica gel, 20:1 petroleum ether – Et_2O; distillation temperature 140–150°C/0.03 Torr). The product, a colorless oil, exhibited ir (neat): 1731, 1650, 837, 776 cm^{-1}; ^1H nmr (400 MHz) δ: 0.07, 0.08 (s, s, 3H each), 0.92 (s, 9H), 1.31–1.76 (m, 6H), 2.01–2.38 (m, 6H), 3.63 (s, 3H), 4.26, 4.27 (d, d, 1H each, J = 6.5 Hz in each case), 5.35 (dt, 1H, J = 2.0, 6.5 Hz), 5.60 (br t, 1H, J = 4.0 Hz). Exact Mass calcd. for $C_{20}H_{34}O_3Si$: 350.2278; found: 350.2276.

In an identical experiment, but using $Pd(OAc)_2$ in place of $Pd(PPh_3)_4$, 2.04 g (3.84 mmol) of **45** was converted into 820 mg (61%) of **64**.

*Diene **65***

The keto ester **46** (2.232 g, 5.38 mmol) was converted into the diene **65** (764 mg, 61%; cyclization reaction time 3.5 h; flash

Can. J. Chem. Downloaded from www.nrcresearchpress.com by 217.78.4.112 on 09/08/12
For personal use only.

TABLE 3. Crystallographic data[a] for compound **69**

Parameter	Value
Formula	$C_{21}H_{23}NO_6$
fw	385.42
Crystal system	Triclinic
Space group	$P\bar{1}$[b]
a (Å)	7.4619(9)
b (Å)	7.6458 (7)
c (Å)	19.027(1)
α (deg)	94.547(8)
β (deg)	96.718(9)
γ (deg)	113.290(6)
V (Å^3)	980.8(2)
Z	2
D_c (g/cm^3)	1.305
F(000)	408
μ(Mo-K$_\alpha$) (cm^{-1})	0.90
Crystal dimensions (mm)	0.063 × 0.275 × 0.450
Scan type	ω − 2θ
Scan range (deg in ω)	0.85 + 0.35 tan θ
Scan speed (deg/min)	1.3–10.0
Data collected	$\pm h$, $-k$, $\pm l$
$2\theta_{max}$ (deg)	55
Crystal decay	Negligible
Unique reflections	4471
Reflections with $I \geq 3\sigma(I)$	1758
Number of variables	253
R	0.049
R_w	0.055
S	2.198
Mean Δ/σ (final cycle)	0.001
Max Δ/σ (final cycle)	0.005
Residual density (e/Å^3)	−0.17 to +0.27

[a]Temperature 294 K, Enraf–Nonius CAD4-F diffractometer, Mo-K$_\alpha$ radiation ($\lambda_{K\alpha_1}$ = 0.70930, $\lambda_{K\alpha_2}$ = 0.71359 Å), graphite monochromator, takeoff angle 2.7°, aperture (2.0 + tan θ) × 4.0 mm at a distance of 173 mm from the crystal, scan range extended by 25% on both sides for background measurement, $\sigma^2(I) = C + 2B + [0.04(C - B)]^2$ (C = scan count, B = normalized background count), function minimized: $\Sigma w(|F_o| - |F_c|)^2$ where $w = 1/\sigma^2(F)$, $R = \Sigma||F_o| - |F_c||/\Sigma|F_o|$, $R_w = (\Sigma w(|F_o| - |F_c|)^2/\Sigma w|F_o|^2)^{1/2}$, $S = (\Sigma w(|F_o| - |F_c|)^2/(m - n))^{1/2}$. Values given for R, R_w, and S are based on those reflections with $I \geq 3\sigma(I)$.

[b]Reduced cell.

TABLE 4. Final positional (fractional × 10^4) and isotropic thermal parameters ($U \times 10^3$ Å^2) with estimated standard deviations in parentheses

Atom	x	y	z	U_{eq}
O(1)	103(3)	6184(3)	2770(1)	69
O(2)	−1615(4)	5029(4)	3619(1)	82
O(3)	4186(3)	6023(3)	1822(1)	68
O(4)	3264(5)	7518(4)	1008(1)	116
O(5)	2197(5)	−1628(4)	−726(2)	114
O(6)	1079(5)	−290(4)	−1500(2)	107
N	1798(5)	−316(5)	−907(2)	74
C(1)	3216(4)	8857(4)	3629(1)	43
C(2)	3794(5)	10542(5)	3380(2)	66
C(3)	2615(6)	11707(5)	3298(2)	82
C(4)	488(6)	10592(5)	3376(2)	71
C(5)	383(5)	9506(5)	4003(2)	58
C(6)	1286(4)	8024(4)	3922(1)	43
C(7)	1686(5)	7407(4)	4657(2)	53
C(8)	2765(5)	6088(5)	4635(2)	57
C(9)	4699(5)	7012(5)	4359(2)	60
C(10)	4381(4)	7699(4)	3654(2)	52
C(11)	−231(5)	6259(5)	3436(2)	49
C(12)	−1238(6)	4535(6)	2276(2)	94
C(13)	5018(5)	7179(5)	3074(2)	60
C(14)	4700(5)	7735(5)	2352(2)	64
C(15)	3490(5)	6132(6)	1181(2)	69
C(16)	3022(5)	4383(5)	657(2)	55
C(17)	3395(5)	2832(5)	835(2)	61
C(18)	2994(5)	1294(5)	330(2)	63
C(19)	2212(5)	1332(5)	−351(2)	57
C(20)	1797(5)	2822(6)	−543(2)	69
C(21)	2206(5)	4354(5)	−42(2)	68

TABLE 5. Bond lengths (Å) with estimated standard deviations in parentheses

Bond	Length (Å)	Bond	Length (Å)
O(1)—C(11)	1.321(4)	C(5)—C(6)	1.537(4)
O(1)—C(12)	1.439(4)	C(6)—C(7)	1.543(4)
O(2)—C(11)	1.201(4)	C(6)—C(11)	1.519(4)
O(3)—C(14)	1.477(4)	C(7)—C(8)	1.520(4)
O(3)—C(15)	1.292(4)	C(8)—C(9)	1.512(4)
O(4)—C(15)	1.201(4)	C(9)—C(10)	1.505(4)
O(5)—N	1.216(4)	C(10)—C(13)	1.344(4)
O(6)—N	1.197(4)	C(13)—C(14)	1.488(5)
N—C(19)	1.485(4)	C(15)—C(16)	1.497(5)
C(1)—C(2)	1.332(4)	C(16)—C(17)	1.379(4)
C(1)—C(6)	1.521(4)	C(16)—C(21)	1.391(5)
C(1)—C(10)	1.466(4)	C(17)—C(18)	1.368(4)
C(2)—C(3)	1.483(5)	C(18)—C(19)	1.365(4)
C(3)—C(4)	1.508(5)	C(19)—C(20)	1.359(5)
C(4)—C(5)	1.499(5)	C(20)—C(21)	1.359(5)

chromatography on 240 g of silica gel, 15:1 petroleum ether – Et_2O; distillation temperature 70–80°C/0.03 Torr). The diene **65**, a colorless oil, exhibited ir (neat): 1726, 1649, 813 cm^{-1}; ^{1}H nmr (400 MHz) δ: 0.96 (t, 3H, J = 7 Hz), 1.24–1.83 (m, 7H), 1.94–2.13 (m, 5H), 2.31 (br d, 1H, J = 12 Hz), 2.59 (br d, 1H, J = 12 Hz), 3.64 (s, 3H), 5.41 (dt, 1H, J = 2, 7 Hz), 5.73 (t, 1H, J = 4 Hz). Exact Mass calcd. for $C_{15}H_{22}O_2$: 234.1620; found: 234.1618.

Preparation of the p*-nitrobenzoate* ***69***

To a solution of the diene **64** (215 mg, 0.613 mmol) in dry THF (10 mL) was added a solution of n-Bu_4NF in THF (1.23 mL of a 1 M solution, 2 equiv.). The resulting mixture was stirred at room temperature for 3 h and then was poured into water (25 mL). The organic phase was removed and the aqueous phase was extracted with Et_2O (2 × 25 mL). The combined organic phases were dried ($MgSO_4$) and concentrated. The residual oil was dissolved in dry CH_2Cl_2 (20 mL). To the resulting solution of the alcohol **68** was added, sequentially, Et_3N (1.53 mL, 1.23 mmol), 4-*N*,*N*-(dimethylamino)pyridine (7 mg, 0.06 mmol), and *p*-nitrobenzoyl chloride (153 mg, 0.41 mmol). The mixture was stirred for 15 min and then was poured into water (25 mL). The layers were separated and the aqueous phase was extracted with CH_2Cl_2 (2 × 25 mL). The combined organic phases were dried ($MgSO_4$) and concentrated. Flash chromatography (27 g of silica gel, 8:1 petroleum ether – Et_2O) provided 94 mg (45%) of the diester **69**, which exhibited mp 131–132°C (from hexane); ir ($CHCl_3$): 1719, 1609, 1530, 1347 cm^{-1}; ^{1}H nmr (400 MHz) δ: 1.40–2.40 (m, 12H), 3.62 (s, 3H), 5.00 (ddd, 1H, J = 2, 6, 12 Hz), 5.07 (dd, 1H, J = 7.5, 12 Hz), 5.50 (ddd, 1H, J = 1.5, 6, 7.5 Hz), 5.66 (dd, 1H, J = 3, 4 Hz), 8.24 (d, 2H, J = 9 Hz), 8.29 (d, 2H, J = 9 Hz); ^{13}C nmr (75.3 MHz) δ: 18.9, 24.3, 25.6, 35.7, 36.9, 38.1, 49.4, 51.8, 63.9, 118.1, 123.4, 127.5, 130.6, 135.7, 135.9, 146.6, 150.4, 164.6, 176.4. Exact Mass calcd. for $C_{21}H_{23}NO_6$: 385.1525; found: 385.1531. Anal. calcd. C 65.44, H 6.02, N 3.63; found: C 65.36, H 5.94, N 3.48.

TABLE 6. Bond angles (deg) with estimated standard deviations in parentheses

Bonds	Angle (deg)	Bonds	Angle (deg)
(C11)—O(1)—C(12)	117.0(3)	C(1)—C(10)—C(9)	115.8(3)
C(14)—O(3)—C(15)	115.8(3)	C(1)—C(10)—C(13)	122.1(3)
O(5)—N—O(6)	124.0(4)	C(9)—C(10)—C(13)	122.0(3)
O(5)—N—C(19)	117.5(4)	O(1)—C(11)—O(2)	121.7(3)
O(6)—N—C(19)	118.6(4)	O(1)—C(11)—C(6)	113.3(3)
C(2)—C(1)—C(6)	121.3(3)	O(2)—C(11)—C(6)	125.0(3)
C(2)—C(1)—C(10)	123.4(3)	C(10)—C(13)—C(14)	125.3(3)
C(6)—C(1)—C(10)	115.3(3)	O(3)—C(14)—C(13)	107.6(3)
C(1)—C(2)—C(3)	125.5(3)	O(3)—C(15)—O(4)	123.7(4)
C(2)—C(3)—C(4)	112.1(3)	O(3)—C(15)—C(16)	114.1(3)
C(3)—C(4)—C(5)	110.0(3)	O(4)—C(15)—C(16)	122.2(4)
C(4)—C(5)—C(6)	112.8(3)	C(15)—C(16)—C(17)	122.9(4)
C(1)—C(6)—C(5)	111.0(2)	C(15)—C(16)—C(21)	117.9(3)
C(1)—C(6)—C(7)	109.0(2)	C(17)—C(16)—C(21)	119.2(3)
C(1)—C(6)—C(11)	111.6(2)	C(16)—C(17)—C(18)	120.5(3)
C(5)—C(6)—C(7)	109.6(2)	C(17)—C(18)—C(19)	118.4(3)
C(5)—C(6)—C(11)	107.8(2)	N—C(19)—C(18)	118.9(3)
C(7)—C(6)—C(11)	107.8(2)	N—C(19)—C(20)	118.4(3)
C(6)—C(7)—C(8)	112.7(3)	C(18)—C(19)—C(20)	122.6(3)
C(7)—C(8)—C(9)	111.4(3)	C(19)—C(20)—C(21)	118.9(3)
C(8)—C(9)—C(10)	110.8(3)	C(16)—C(21)—C(20)	120.3(3)

X-ray crystallographic analysis of the p-*nitrobenzoate* ***69***

Crystallographic data appear in Table 3. Final unit-cell parameters were obtained by least squares on 2 sin θ/λ values for 25 reflections with 2θ = 30–40°. The intensities of three standard reflections, measured each 4000 s of X-ray exposure time throughout the data collection, showed only small random fluctuations. The data were corrected for Lorentz and polarization effects but, in view of the low value of μ, not for absorption.[5]

The structure analysis was initiated in the centrosymmetric space group $P\bar{1}$, this choice being verified by subsequent calculations. The structure was solved by direct methods, the coordinates of all non-hydrogen atoms being determined from an *E*-map. In the final stages of full-matrix least-squares refinement the non-hydrogen atoms were refined with anisotropic thermal parameters. Hydrogen atoms were fixed in idealized positions (methyl orientation based on observed positions, C(sp^2)—H = 0.97 Å, C(sp^3)—H = 0.98 Å, $U_H \propto U_{\text{bonded atom}}$). Neutral atom scattering factors were taken from ref. 17. Final positional and equivalent isotropic thermal parameters ($U_{eq} = \frac{1}{3}$ trace of diagonalized U) for the non-hydrogen atoms are listed in Table 4. Bond lengths and angles are given in Tables 5 and 6, respectively. Hydrogen atom parameters, anisotropic thermal parameters, intra-annular torsional angles, a complete listing of torsion angles, and measured and calculated structure factors (Tables S1–S5) have been supplied as supplementary material.[6]

[5]The computer programs used include locally written programs for data processing and locally modified versions of the following: ORFLS, full-matrix least squares, and ORFFE, function and errors, by W. R. Busing, K. O. Martin, and H. A. Levy; FORDAP, Patterson and Fourier syntheses, by A. Zalkin; ORTEP II, illustrations, by C. K. Johnson; AGNOST, absorption corrections, by J. A. Ibers; MULTAN 80, multisolution program by P. Main, S. J. Fiske, S. E. Hull, L. Lessinger, G. Germain, J. P. Declercq, and M. M. Woolfson.

[6]These data may be purchased from: The Depository of Unpublished Data, Document Delivery, CISTI, National Research Council Canada, Ottawa, Canada K1A 0S2.

Table S1 (hydrogen atom parameters) has also been deposited with the Cambridge Crystallographic Data Centre and can be obtained on request from the Director, Cambridge Crystallographic Data Centre, University Chemical Laboratory, Lensfield Road, Cambridge, CB2 1EW, U.K.

Acknowledgements

We are grateful to the Natural Sciences and Engineering Research Council of Canada for financial support and for a 1967 Centennial Science and Engineering Scholarship to (R.W.F.). We thank Professor J. Trotter for the use of X-ray equipment and computer programs.

1. E. Piers, J. M. Chong, and H. E. Morton. Tetrahedron, **45**, 363 (1989).
2. E. Piers, H. E. Morton, and J. M. Chong. Can. J. Chem. **65**, 78 (1987).
3. E. Piers and J. M. Chong. Can. J. Chem. **66**, 1425 (1988).
4. E. Piers and V. Karunaratne. Tetrahedron, **45**, 1089 (1989); Can. J. Chem. **67**, 160 (1989).
5. E. Piers and B. W. A. Yeung. J. Org. Chem. **49**, 4567 (1989); E. Piers, B. W. A. Yeung, and S. J. Rettig. Tetrahedron, **43**, 5521 (1987).
6. E. Piers and A. V. Gavai. J. Org. Chem. **55**, 2380 (1990).
7. E. Piers, R. W. Friesen, and B. A. Keay. J. Chem. Soc. Chem. Commun. 809 (1985); Tetrahedron, **47**, 4555 (1991).
8. E. Piers and R. W. Friesen. Can. J. Chem. **65**, 1681 (1987).
9. P. A. Grieco, R. Lis, R. F. Zelle, and J. Finn. J. Am. Chem. Soc. **108**, 5908 (1986).
10. L. Ruest, G. Blouin, and P. Deslongchamps. Synth. Commun. **6**, 169 (1976).
11. A. J. Leusink, H. A. Budding, and J. W. Marsman. J. Organometal. Chem. **9**, 285 (1967).
12. J. E. McMurry and W. J. Scott. Tetrahedron Lett. **24**, 979 (1983).
13. W. J. Scott, G. T. Crisp, and J. K. Stille. J. Am. Chem. Soc. **106**, 4630 (1984); W. J. Scott and J. K. Stille. J. Am. Chem. Soc. **108**, 3033 (1986).
14. J. K. Stille. Angew. Chem. Int. Ed. Engl. **25**, 508 (1986).
15. W. C. Still, M. Kahn, and A. Mitra. J. Org. Chem. **43**, 2923 (1978).
16. E. Piers and R. W. Friesen. J. Org. Chem. **51**, 3405 (1986); J. Chem. Soc. Chem. Commun. 125 (1988); E. Piers and M. Llinas-Brunet. J. Org. Chem. **54**, 1483 (1989).
17. International tables for X-ray crystallography. Vol. IV. Kynoch Press, Birmingham. 1974. pp. 99–102. (Present distributor D. Reidel, Dordrecht.)

Can. J. Chem. Downloaded from www.nrcresearchpress.com by 217.78.4.112 on 09/08/12
For personal use only.

Formation, reactions, and NMR spectra of 1,20-cycloatidanes

OLIVER E. EDWARDS,[1] DUSAN DVORNIK, AND RALPH J. KOLT
Division of Chemistry, National Research Council of Canada, Ottawa, Ont., Canada K1A 0R6

AND

BARBARA A. BLACKWELL[2]
Plant Research Centre, Agriculture Canada, Central Experimental Farm, Ottawa, Ont., Canada K1A 0C6

Received August 8, 1991

This paper is dedicated to Professor Zdenek (Denny) Valenta on the occasion of his 65th birthday

OLIVER E. EDWARDS, DUSAN DVORNIK, RALPH J. KOLT, and BARBARA A. BLACKWELL. Can. J. Chem. **70**, 1397 (1992).

Imines derived from the alkaloid atisine gave *N*-acetyl 1,20-cycloatidane derivatives when heated with acetic anhydride. Vigorous alkaline hydrolysis cleaved the cyclopropane ring, regenerating the parent imine. The ^1H and ^{13}C NMR spectra of several 1,20-cyclo derivatives have been assigned and compared to those of the parent imines **2**. All of the *N*-acetyl compounds showed doubling of the majority of the NMR resonances, due to amide rotamers. The effects of the cyclopropane ring current are noted.

OLIVER E. EDWARDS, DUSAN DVORNIK, RALPH J. KOLT et BARBARA A. BLACKWELL. Can. J. Chem. **70**, 1397 (1992).

Par chauffage avec l'anhydride acétique, des imines provenant de l'alcaloïde atisine conduisent à des dérivés du *N*-acétyl 1,20-cycloatidane. Une hydrolyse alcaline vigoreuse coupe le cyclopropane en régénérant l'imine de départ. On a attribué les spectres RMN du ^1H et du ^{13}C de plusieurs dérivés 1,20-cyclo et on les a comparés à ceux des imines parentes **2**. Dans les spectres RMN des composés *N*-acétylés, on observe pratiquement toujours un dédoublement des résonances; ce résultat est attribuable à la présence des rotamères de l'amide. On a noté les effets du courant de cycle du cyclopropane.

[Traduit par la rédaction].

Can. J. Chem. Downloaded from www.nrcresearchpress.com by 217.78.4.112 on 09/08/12
For personal use only.

During the course of our early work on the structure of atisine **1** and related diterpenoid alkaloids, attempts were made to use the readily available (1) imine (azomethine) **2** to obtain the nitrogen-free skeleton. One of these approaches succeeded (2), but another, based on a hoped-for

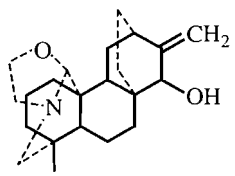

1

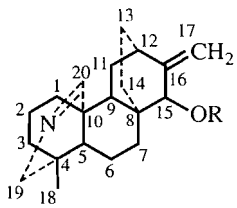

2

sequence shown in eq. [1], was abortive (3). This paper deals with the structure of the major product formed in the reac-

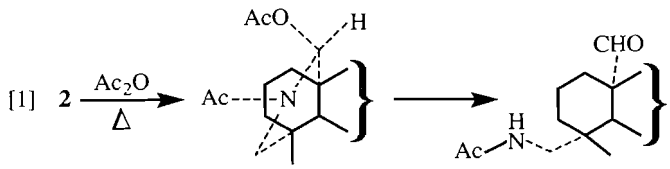

tion with acetic anhydride, and its anomalous alkaline cleavage to parent imino alcohol **2** (R=H).

Results

The main product formed when **2** was heated in refluxing acetic anhydride for 20 h was an *O*,*N*-diacetyl compound (neutral, ν_{max} 1725 and 1630 cm^{-1}) analysing for $C_{24}H_{33}NO_3$. This result was confirmed by Pelletier and Parthasarathy (4). Thus it did not have the new *O*-acetyl group expected from eq. [1]. The formula required that a new double bond or ring had been formed, since the infrared spectrum showed the exocyclic methylene to be unchanged. Oxidation of the product with potassium permanganate gave a hydroxy acid analyzing for $C_{24}H_{33}NO_6$. This, and the analyses and IR spectra of its methyl ester and the dihydroxy acid produced by gentle alkaline hydrolysis, indicated that only the allyl acetate group had been oxidized as in eq. [2], and hence confirmed this function was intact in the unknown product.

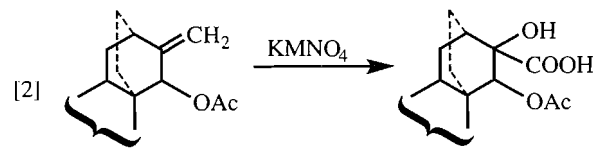

Finally, a 60 MHz ^1H NMR spectrum indicated the absence of any new vinyl hydrogen. Thus it appeared that a new ring had been formed. It was suggested that this was an aziridine ring and that the product from **2** had structure **3** (3).

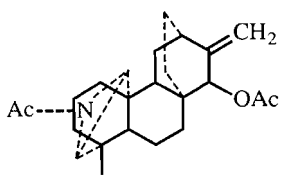

3

The formation of **3** and its hydrolysis under vigorous alkaline conditions back to **2** (R=H) could be rationalized (3).

[1]Author to whom correspondence should be addressed at Department of Chemistry, Carleton University, Ottawa, Ont., Canada K1S 5B6.

[2]This represents publication no. 1344 from the Plant Research Center.

Can. J. Chem. Downloaded from www.nrcresearchpress.com by 217.78.4.112 on 09/08/12
For personal use only.

However, reinvestigation of the problem using more sophisticated NMR equipment and techniques showed clearly that three hydrogens were present on carbons attached to nitrogen (δ 2.6–3.9) instead of the two required for **3**. It was thus clear that a new carbocyclic ring was present instead of the aziridine ring. Mechanistic considerations (see discussion) and the spectra (^{13}C NMR showed the sequence -CH_2-NAc-CH-) suggested structures **4** (R=Ac) or **5** for the product, with **4** strongly favoured. Finally an X-ray crystallographic analysis confirmed that structure **4** (*N*-acetyl

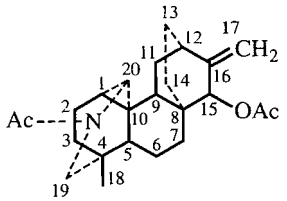

4

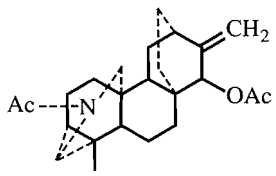

5

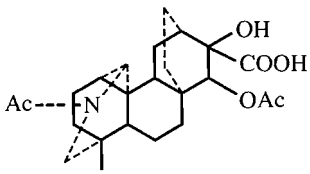

6

15-acetoxy-1,20-cyclo-16,17-didehydro-4-methylatidane) was correct (5). The hydroxy acid derived from **4** thus had structure **6**. Simplified analogues of **4**, compounds **7**, **8**, and **9**, were prepared in early studies of the reaction.

The slow hydrolysis of **4** in triethylene glycol containing potassium hydroxide at 150°C to give imino alcohol **2** (R=H) was confirmed repeatedly.

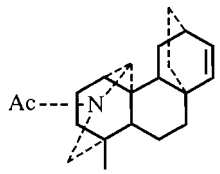

7

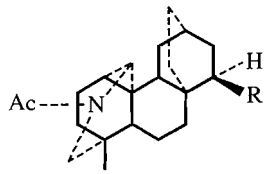

8 R = H
9 R = OAc

Discussion

The first reactive intermediate in the formation of **4** was undoubtedly the *N*-acetyl cation **10** (some charge delocalization onto nitrogen). The formation of a cyclopropane ring

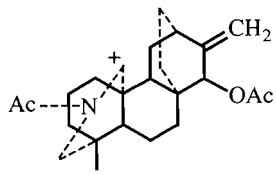

10

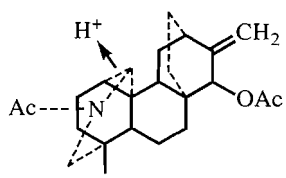

11

from such a cation has parallels in the chemistry of monoterpenes and the behaviour of α-acyl carbocations (6, 7). The biochemical formation of cyclopropane rings is a vital part of the squalene-to-steroid pathway in plants. However, attempts to duplicate this in the laboratory have so far failed (8). Thus a delicate balance seems to exist between an initial cation **A**, corner-protonated cyclopropane **B**, edge-protonated cyclopropane **C**, and rearranged (Wagner–Meerwein) cation **D** as illustrated in eq. [3]. The counterion or sol-

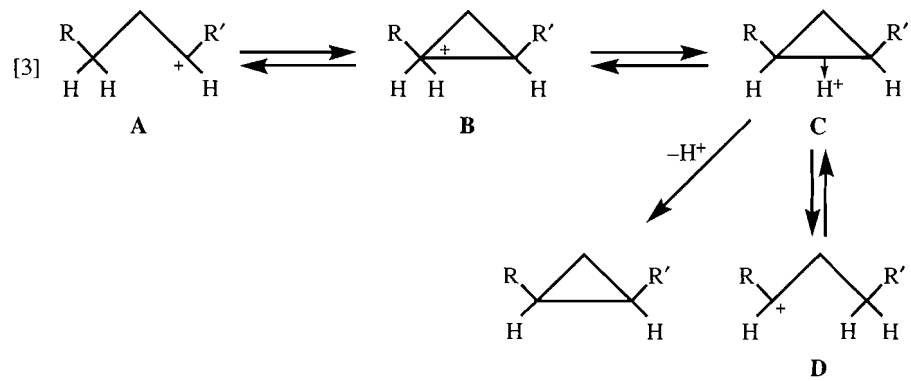

[3]

A **B** **C** **D**

vent can capture ions **A** and **D** or remove a proton from **C** to give the cyclopropane (6). The edge-protonated cyclopropane precursor to **4** would be cation **11**.

The alkaline hydrolysis of **4** to give **2** (R=H) was surprising. It was first discovered when **4** was subjected to Wolff–Kischner reduction conditions in the hope that the compound had the amido aldehyde structure shown in eq. [1]. We view the cleavage as an analogue of the Haller–Bauer fission of non-enolizable ketones (9). The ready base-initiated cleavage of cyclopropanes with heavy electronegative loading is a well-known phenomenon (10).

Thus the process can be visualized as attack of hydroxide ion on **4** to give anion **12**, followed by cleavage to anion **13**. Then proton abstraction from solvent would give **2** (R=H) (eq. [4]). The overall conversion to **4** and reversion to **2** is efficient enough (30%) that the reaction could be used as a method of masking the reactive imine function while other transformations were carried out on the molecule.

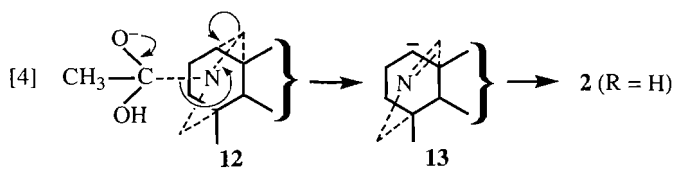

[4]

12 **13**

NMR spectra

The ^{13}C and ^{1}H NMR spectral assignments for the parent azomethine **2**, the 1,20-cyclo amides **4**, **7**, **8**, and **9**, and the

Can. J. Chem. Downloaded from www.nrcresearchpress.com by 217.78.4.112 on 09/08/12
For personal use only.

reference *N*-acetyl compound **16** determined by a variety of 2D NMR experiments are given in Tables 1 and 2. The spectra of the *N*-acetyl 1,20-cyclo derivatives are noteworthy because of the long-range effects of the *N*-acetyl group, the anisotropic shielding due to this group, and a marked shielding by the cyclopropane ring. Molecular models suggested that **16** had a normal chair conformation for ring A in contrast to the 1,20-cyclo cases in which ring A is considerably flattened (5). This probably results in moving the *N*-acetyl group closer to ring B, with some effect on chemical shifts.

The NMR spectra of the starting material (**2**) showed the presence of only one form in solution ($CDCl_3$) and therefore was the simplest to assign. The ^{13}C assignments afforded by $^1H/^1H$ and $^1H/^{13}C$ correlation spectra agreed for the most part with those previously reported by Mody and Pelletier (11). The only exception was a reversal of the assignments to C-1 and C-3. The $^1H/^1H$ correlation spectrum discriminates between the spin systems on carbons 1, 2, and 3 and those on 5, 6, and 7. This enabled assignment of resonances at 1.3 and 1.44 ppm to H-2 and at 1.05 and 1.55 ppm to C-6. These resonances correlate in the HETCOR spectrum with methylenic resonances at 20.1 and 19.5 ppm respectively. The assignment of H-5 to 0.99 ppm is confirmed by the presence of W-coupling to H-20. C-1 and C-3 are distinguished by the presence of W-coupling of the protons of position 3 to those on C-19. These H-3 signals at 1.2 and 1.4 ppm correlate to the carbon resonance at 42.4 ppm. The anisotropy of the C=N group seems responsible for the rather large chemical shift difference between the α and β hydrogens[3] on C-6 (0.5 ppm) and C-7 (0.65 ppm). The assignment of the quaternary positions C-4, C-8, and C-10 was confirmed by heteronuclear correlation optimized for long-range coupling. The resonance at 42.5 ppm showed correlation to proton resonances assigned to H-1, H-9, and CH_3-18, while the resonance at 37.9 ppm showed correlation to proton resonances assigned to H-15, H-14, H-11, and H-6, thus enabling assignment of these resonances to C-10 and C-8, respectively. The assignment of C-4 to the quaternary resonance at 32.3 ppm is confirmed by correlation to the protons on C-5 and C-18.

A major feature of the NMR spectra of the *N*-acetyl derivatives near room temperature is the doubling of most signals due to the presence of two rotamers about the CO-N bonds (Tables 1 and 2). The effect is most marked for those resonances in close proximity to the nitrogen, i.e., positions 19 and 20, as well as 18, 4, and 10, but extends even to position 17. The extent of doubling is more easily seen in the ^{13}C spectra, since the ^1H spectra are complicated by homonuclear coupling and extensive overlap in the methylene region. The effect of the cyclopropane ring is seen by comparing the chemical shift assignments of compounds **2** and **16** with **4**.

The NMR spectra of **4** were assigned by a combination of techniques. The combined information from DEPT and $^1H/^{13}C$ correlation spectra permitted the assignment of the methylene protons in the highly overlapped region (0.5–2.5 ppm) in the ^1H spectrum. $^1H/^1H$ correlation and RELAY spectra distinguished between the coupled systems H-1, H-2, and H-3; H-5, H-6, and H-7; and H-12, H-13, H-14, which are the three similar $CH\text{-}CH_2\text{-}CH_2$ systems in the molecule. Finally, a long-range heteronuclear correlation spectrum confirmed the assignment of the quaternary carbons. The $^1H/^{13}C$ correlation spectrum of **4** (Fig. 1) illustrates these points. The projections of the spectrum are the single pulse $^1H/^{13}C$ spectra that show the effect of the amide anisotropy. Every ^{13}C resonance is doubled, with the exception of the methyl resonance of the OAc group, the effect varying from 3 ppm at C-19 to 0.1–0.2 ppm at C-8 and C-9. In general, the effect decreases with distance from the amide bond. However, some unusually long-range effects occur at C-7 (0.7 ppm), C-13 (0.6 ppm), and C-17 (0.5 ppm). The population of the rotamers in deuterochloroform is approximately 2:1. The ^1H spectra of the *N*-acetyl compounds were also doubled where the signals were simple enough to permit analysis (Table 1). Again the most dramatic shifts were for hydrogens close to the amide function, but the effects were noted as distant as C-17.

A parallel observation was made earlier on the long-range effect of remote polar substituents in rigid molecules on the pK_a of a basic nitrogen (3, 13). Three possible causes of these effects could exist: through bond effects, *trans* spatial effects through the centre of the molecule, or solvent shell reorganization. In view of the long-range effects observed, and the fact that these effects vary with solvent, we now favour the latter possibility. Figure 2 shows the effect of temperature on the rotamer population of **4** in dimethylformamide (DMF). The ^1H and ^{13}C spectra at room temperature (30°C, A and B) again show doubling, although the rotamer population in this solvent is now 1:1, and the magnitude of the effect as seen on the resonances due to H-15 and H-17 is different. At 125°C (C and D), the doubling collapses reversibly and there are some temperature-induced chemical shifts. Thus the barrier to rotation in the amide is large. However an X-ray crystallographic study of compound **4** showed that it crystallizes as one amide rotamer (5). The

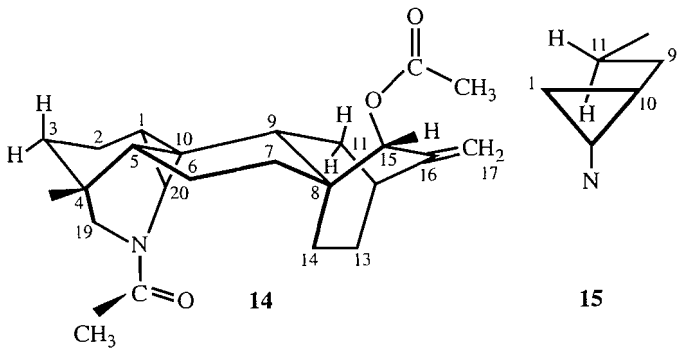

14 **15**

^1H NMR data for **4** show that H-20 of the major isomer in solution resonates at higher field than the minor isomer (3.8 ppm). In addition, the chemical shift difference for the two hydrogens on C-19 is much larger (0.7 ppm) for the major isomer than for the minor one (0.2 ppm). This would be expected if the dominant isomer was one in which the carbonyl of the *N*-acetyl group was oriented towards C-19. Thus the dominant rotamer in deuterochloroform is the opposite to the one observed for the crystals (5) (see **14**).

The cyclopropane ring of the 1,20-cyclo compounds had two important effects on the ^1H NMR spectra. The well-known effect on protons attached to the ring resulted in upfield shifts of H-1 to near 0.9 ppm and of H-20 to near

[3]Although atisine belongs to the *ent* series, we have used α and β in the original steroid sense, i.e., below and above the main plane of the molecule.

Can. J. Chem. Downloaded from www.nrcresearchpress.com by 217.78.4.112 on 09/08/12
For personal use only.

TABLE 1. 500 MHz ^{1}H NMR chemical shift assignments (ppm from TMS, δ of minor rotamer in parentheses)

Proton no.	**2**	**4**
1	1.03 (m) 1.65 (m)	0.92 (0.90) (t, $J_{1,20} = J_{1,2} = 7.4$)
2	1.28 ($J_{AB} = 13.3$) 1.45 ($J_{2,3} = 4.3$; $J_{3,19} = 2.5$)	1.89 ($J_{AB} = 14.5$; $J_{1,2} = 7.4$) 1.47 ($J_{2,3} = 1.2$; 9.5)
3	1.19 ($J_{AB} = 13.9$) 1.41 $J_{3,2} = 12.3$; 4.5)	1.25 1.39
5	0.99 (m)	1.25 (m)
6α	1.07	1.30
β	1.59	1.57
7	1.09 ($J_{AB} = 14.2$; $J_{7,6} = 10.0$) 1.78 ($J_{7,6} = 7.1$)	1.22 1.27
9	1.79 ($J_{9,14} = 2.2$; $J_{9,11} = 10.0$)	2.27 (2.20) ($J_{9,11} = 5.8$, 11.7; $J_{9,14} = 1.9$)
11α	1.70–1.74 (m)	0.70 (0.84) ($J_{11\alpha,12} = 2.6$; $J_{11\alpha,9} = = 5.8$)
β		1.42 ($J_{AB} = 13.5$)
12	2.35 ($J_{12,13} = J_{12,11} = 3.0$)	2.23 (2.20) ($J_{12,11\alpha} = 2.6$; $J_{12,13} = 3.0$)
13	1.53–1.57 (m)	1.54 1.42
14α	0.85 ($J_{AB} = 15.1$; $J_{14,9} = 2.2$)	0.98 ($J_{9,14\alpha} = 1.9$; $J_{AB} = 12.1$)
β	1.88 ($J_{14,13} = 11.0$, 4.5)	1.99 ($J_{14\beta,13} = 4.5$)
15	3.65 ($J_{15,17} = 1.5$)	5.18 (5.17) ($J_{15,17} = 2.0$)
16	—	—
17	5.00 5.06 ($J_{17,15} = 1.5$)	4.84 (4.80) ($J_{17,15} = 2.0$)
18	0.80 (s)	0.79 (0.81) (s)
19	3.38 (d, $J_{19,3} = 2.5$)	2.83 (2.99) ($J_{19,3} = 1.7$) 3.47 (3.12) ($J_{AB} = 13.6$ (11.8))
20	7.9 (brs)	2.87 (3.78) ($J_{20,1} = 7.4$ (8.1))
NAc	—	2.11 (2.10)
OAc	—	2.08

Proton no.	**7**	**8**
1	0.89 (t, $J_{1,20} = J_{1,2} = 7.3$)	0.95 (t, $J_{1,20} = J_{1,2} = 7.4$)
2	1.81 (m) 1.50–1.57 (m)	1.90 (m) 1.50–1.57 (m)
3	1.17–1.38 (m) 1.50–1.57	1.15–1.25 (m) 1.29–1.38 (m)
5	1.17–1.38	1.29
6α	1.17–1.38	1.15–1.25
β	1.50–1.57	1.50–1.57
7	1.17–1.38	1.29–1.38
9	1.16	1.82 (1.75) ($J_{9,11}$ 6.0, 1.2; $J_{9,14} = 2.1$)
11α	0.49 (ddd)	0.62 (0.78) ($J_{AB} = 13.6$; $J_{11,12} = J_{11,13} = 3.1$)
β	1.60 (m)	1.29–1.38
12	2.40 (2.38) (m)	1.50–1.57
13	1.50–1.57 1.17–1.38	1.50–1.57 1.29–1.38
14α	0.77 (m)	0.87 (m)
β	1.91 (m)	1.91 (m)
15	5.96 (d, $J_{15,16} = 8.1$)	1.29–1.38 1.15–1.25
16	6.21 (dd, $J_{16,15} = 8.1$; $J_{16,12} = 6.5$)	1.50–1.57 1.29–1.38
17	—	—
18	0.83 (0.85) (s)	0.81 (0.83) (s)
19	2.88 (3.00) ($J_{AB} = 13.6$ (11.7)) 3.50 (3.17)	2.86 (2.99) ($J_{19,3} = 2.0$) 3.48 (3.13) ($J_{AB} = 13.6$ (11.7))
20	2.90 (3.78) ($J_{20,1} = 7.3$ (8.0))	2.89 (3.78) ($J_{20,1} = 7.4$(8.1))
NAc	2.15 (2.14)	2.14 (2.13)
OAc	—	—

TABLE 1 (*concluded*)

Proton no.	**9**	**16**
1	0.99 (0.98) (t, $J_{1,20} = J_{1,2} = 7.2$)	1.00–1.07 (1.13) (m) 1.87 (dt, $J_{AB} = J_{1,2} = 12.7$; $J_{1,2} = 5.5$)
2	1.92–2.04 (m) 1.55–1.65 (m)	1.39–1.43 (m) 1.64–1.75 (m)
3	1.20 (m) 1.55–1.65	1.39–1.43 1.57–1.63
5	1.32–1.35 (m)	0.94
6α	1.32–1.35	1.35
β	1.55–1.65	1.47–1.55 (m)
7	1.28 (m) 1.36 (m)	1.19–1.28
9	2.34 (2.28) (dddd, $J_{9,14} = 2.3$; $J_{9,11} = 5.7, 11.8$)	1.57–1.63
11α	0.65 (0.82) ($J_{AB} = 13.5$; $J_{11\alpha,12} = 2.6$; $J_{11\alpha,9} = 5.7$)	1.47–1.55
β	1.42 (m)	1.64–1.75
12	1.69 (1.64) (m)	2.31 (2.33) (t, $J_{12,13} = J_{12,16} = 2.6$)
13	1.32–1.35 1.50 (m)	1.47–1.55
14α	0.94 (0.88) (m)	1.00–1.07 (m)
β	1.92–2.04 (m)	2.00 (dd; $J_{AB} = 14.8$, $J_{14,13} = 7.5$)
15	4.58 (dd, $J_{15,16} = 3.5, 9.9$)	5.04 ($J_{15,17} = 2.0$)
16	1.32–1.35 2.15–2.20	—
17	—	4.83 (4.88) 4.95 (4.97)
18	0.85 (0.87) (s)	0.82 (0.80) (s)
19	2.89 (3.04) ($J_{AB} = 13.5$ (11.6)) 3.52 (3.17) ($J_{19,3} = 2.1$)	3.08 (3.50) (12.9 ($J_{AB} = 13.2$)) 3.26 (3.55) ($J_{19,3} = 2.0$ (2.4))
20	2.91 (3.82) (d, $J_{20,1} = 7.5$ (8.2))	4.40 (4.10) 2.99 (2.59) ($J_{AB} = 13.8$(13.6); $J_{20,1} = 2.2$(2.0))
NAc	2.17 (2.16)	2.03 (2.06
OAc	2.08 (2.07)	2.08 (2.09)

2.9 ppm in the major rotamer. The second major effect was on the 11α hydrogen. As illustrated in **15** this hydrogen is close to and orthogonal to the plane of the cyclopropane ring. As was observed earlier (12), the cyclopropane "ring current" shields this zone. As a consequence the 11α hydrogens resonate between 0.5 and 0.75 ppm in the major rotamers (Table 1). The magnitude and sign of the smaller effect on the other hydrogens is made uncertain by changing proximity of these to the amide group in the 1,20-cyclo compounds compared to the reference amide **16**.

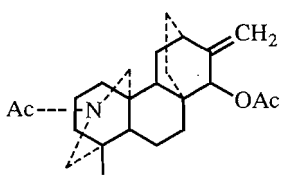

16

The H-5 resonance shifts from 0.95 in **16** to near 1.4 in the 1,20-cyclo examples. Since not much effect from the ring current is expected, it appears that a change in relation to the anisotropic amide function as ring A flattens in the 1,20-cyclo compounds is responsible for this (see above).

In all the compounds studied there was a large geminal shift difference (ca. 1 ppm) between the 14-hydrogens. This is a consequence of the proximity of the 14α hydrogen to the C=N or amide functions, resulting in marked shielding (see ref. 5). Similar proximity between hydrogens on 14 and 20 has been invoked to account for the abnormal basic strength of atisine-type oxazolidines (3, 13) (note the numbering change).

Comparison of the ^{13}C NMR spectra of the 1,20-cyclo amides with **16** reveals the expected large upfield shift for C-1 (to ca. 13 ppm), C-10 (to 23 ppm), and C-20 (to 35 ppm). The C-2 and C-5 resonances are affected to a lesser extent (ca. 4 ppm upfield shift) while C-9 is more influenced by substituents in ring D. Both C-2 and C-6 resonances are at high field, probably as a result of shielding by either the C=N or *N*-acetyl groups. The reversal of assignment for these carbons for **16** needs justification. The homo- and heteronuclear correlation spectra of **16** showed clearly that the resonances at 17.4 ppm correlated with proton resonances at 1.4 and 1.5 ppm. Since these were coupled to H-5 at 0.95 ppm, this confirms the assignment of this signal to C-6, hence the signal at 20.9 to C-2. Again we suggest that **16** has ring A in a chair conformation with the *N*-acetyl group closer to ring A than in the 1,20-cyclo analogues, resulting in the changed shielding.

Experimental

Infrared spectra were obtained on a Perkin–Elmer model 683 grating spectrophotometer in dichloromethane solutions, unless

Can. J. Chem. Downloaded from www.nrcresearchpress.com by 217.78.4.112 on 09/08/12
For personal use only.

TABLE 2. 125 MHz ^{13}C NMR chemical shift assignments (ppm from TMS, chemical shifts of minor rotamer in parentheses)

Carbon no.	2	4	7	8	9	16
1	34.2	13.7(13.3)	15.2(14.8)	13.6(13.2)	13.6(13.1)	39.9(40.0)
2	20.1	16.1(16.4)	16.4(16.7)	16.3(16.6)	16.2(16.5)	20.9(—)
3	42.4	31.4(31.6)	36.2(36.3)	36.1(36.3)	31.8(31.9)	41.1(40.8)
4	32.9	33.4(33.9)	33.6(34.1)	33.5(34.0)	33.4(34.0)	33.2(32.5)
5	47.0	41.8(42.2)	42.2(42.6)	42.3(42.7)	41.8(42.3)	49.5(49.4)
6	19.5	20.3(20.5)	20.9(21.0)	21.0(21.2)	20.4(20.6)	17.4(17.3)
7	31.0	36.0(36.7)	35.1(35.3)	36.4(36.9)	36.1(36.8)	31.8(31.6)
8	37.3	37.1(37.2)		30.4(30.6)	34.2(34.4)	36.9(36.8)
9	38.1	35.4(35.5)	42.7(43.1)	41.7(41.8)	33.7(33.8)	40.4(40.1)
10	42.5	23.1(22.6)	23.4(23.0)	23.7(23.3)	23.2(22.7)	37.0(37.5)
11	28.1	26.7(26.6)	26.6(—)	26.1(26.0)	25.7(25.6)	27.9(28.2)
12	36.0	34.1(34.2)	29.7(29.8)	24.7(–)	24.8(24.7)	36.1(—)
13	26.0	26.1(25.5)	25.7(—)	26.3(26.2)	25.5(25.4)	25.9(26.3)
14	25.2	23.7(23.9)	24.4(24.5)	25.7(25.9)	23.8(24.1)	27.2(27.3)
15	75.7	75.8(76.0)	141.3(141.0)	38.3(38.6)	75.8(76.0)	151.1(150.6)
16	156.6	150.8(151.3)	133.5(133.9)	26.6(—)	35.8(35.9)	151.1(150.6)
17	109.0	110.3(109.7)	—	—	—	110.7(111.3)
18	25.9	25.3(25.6)	25.4(25.7)	25.4(25.6)	25.4(24.3)	25.9(—)
19	60.6	47.0(51.0)	47.1(51.0)	47.2(51.1)	47.1(51.0)	52.6(47.0)
20	165.9	36.4(34.0)	36.8(34.5)	36.7(34.5)	36.4(36.1)	42.1(47.5)
OAc		21.2			21.2	21.3
		171.1(171.0)			170.7(170.8)	169.4
NAc		22.2(22.3)	22.3(22.4)	22.3(22.4)	22.3(22.4)	22.4(—)
		171.5(171.4)	171.7(171.4)	171.7(171.4)	171.6(171.5)	171.2(171.1)

otherwise indicated. Initial NMR spectra were obtained on Varian EM360 and Bruker WP80 spectrometers. For assignment purposes, ^1H and ^{13}C NMR spectra were obtained at 500.13 and 125.77 MHz, respectively, on a Bruker AM 500 spectrometer. Samples of 10–20 mg were dissolved in deuterochloroform and chemical shifts are referenced to $CDCl_3$ at 7.24 ppm and 77.0 ppm for ^1H and ^{13}C, respectively, and are reported relative to tetramethylsilane (TMS). ^1H NMR assignments were made using $^1H/^1H$ homonuclear shift correlation (COSY-45) and, occasionally, relayed coherence transfer (RELAY). In all cases, the data matrix was acquired as 512W by 2KW data set and zero-filled in $F1$ to give a final digital resolution of 1.8 Hz/pt. ^{13}C NMR spectra were assigned with the aid of DEPT and $^1H/^{13}C$ correlation spectra (HETCOR). HETCOR spectra were acquired as 256 FID's of 4K each. Sine-bell squared functions shifted $\pi/4$ in $F1$ and $\pi/2$ in $F2$ were used for processing. The matrix was zero-filled in $F1$ and spectra were plotted as power spectra. The resolution was sufficient to assign the rotamer pairs belonging to each position in compounds **4**, **8**, and **16**. The assignments of the quaternary carbons 4, 8, and 10 in compounds **2** and **4** were confirmed using heteronuclear correlation optimized for long-range coupling acquired in inverse mode. Over a narrow ^{13}C sweep width (15–50 ppm), 128 FID's of 2K each were obtained, using a 0.7 s delay optimizing for J_{CH} = 7 Hz. ^1H NMR spectra in the text were observed at 60 MHz unless otherwise indicated.

Azomethine acetate 2 (R=Ac)

This was prepared as described earlier (1). An 80% yield was obtained after purification. It had mp 151–153°C and gave ^1H NMR signals at 7.85 (1H, brs), 5.13 (1H, brs), 4.97 (1H, brs), 3.37 (2H, brs), 2.13 (3H, s), and 0.80 (3H, s). A modified version of this internal Hoffman reaction was reported by Mody and Pelletier (11) to give a 91% yield.

Azomethine alcohol 2 (R=H)

Hydrolysis of **2** (R=Ac) using KOH in refluxing methanol gave the alcohol. It formed shimmering plates from acetone, mp 179–180°C, and gave ^1H NMR signals (250 MHz, C_6D_6) at 7.91 (1H, q, J_1 = 4, J_2 = 2 Hz), 5.12 (1H, t, J = 1.7 Hz), 4.98 (1H, t, J = 1.9 Hz), 3.63 (1H, brs, OH), 3.48 (2H, d, J = 2.6 Hz), 2.58 (1H, brs), 2.15 (1H, t, J = 2.9 Hz), and 0.64 (3H, s). Its ^{13}C spectrum is given in Table 2.

N-Acetyl 15-acetoxy-1,20-cyclo-16,17-didehydro-4-methylatidane (4, R=Ac)

The initial experiments leading to **4** involved heating **2** in 17% (v/v) acetic acid in acetic anhydride containing 4% by weight of sodium acetate at 145°C for 24 h. When the sodium acetate, then the acetic acid, were eliminated the yield increased moderately.

Azomethine acetate **2** (R=Ac) (519 mg) in 8 mL of acetic acid was kept in a bath at 145–150°C for 27.5 hr. The mixture was then evaporated to a thick syrup at 60°C under 0.5 Torr (1 Torr = 133.3 Pa). The residue was heated for 15 min in methanol, then the solvent removed *in vacuo*. The product was dissolved in 15 mL of dichloromethane. Two extractions with 5-mL portions of 6 N sulfuric acid were followed by a sodium carbonate wash (emulsion, centrifuged). The aqueous layers were reextracted with 10 mL of dichloromethane. The combined dichloromethane solutions yielded 685 mg of gum. This crystallized from acetone–hexane solution giving 445 mg of crude **4** (R=Ac). After recrystallization, and recovery of more material from mother liquors by separation on silica gel plates using 20% hexane in ethyl acetate, 299 mg (51%) of nearly pure *N*-acetyl cyclopropane acetate was obtained (mp 195–198°C). No other neutral product was characterized.

Further recrystallization from acetone – ethyl acetate gave **4** (R=Ac) as laths with mp 196–199°C. It had $[\alpha]_D$ +80 (*c* 1.0 in ethanol) and ν_{max} ($CHCl_3$): 1725, 1630, and 905 cm^{-1}. Its ^1H NMR spectrum had signals at δ: 5.25 (1H, brs), 5.07–4.83 (2H, m), 3.9–3.35 (1H, m), 3.2–2.6 (2H, m), 2.16 (6H, s), and 0.87 (3H, s). Its ^{13}C NMR spectrum (125 MHz) is reported in Table 2. Anal. calcd. for $C_{24}H_{33}NO_3$: C 75.16, H 8.67, N 3.65; found: C 75.07, H 8.73, N 3.58.

N-Acetyl 1,20-cyclo-15-hydroxy-16,17-didehydro-4-methylatidane (4, R=H)

Hydrolysis of acetate **4** (R=Ac) using a refluxing solution of KOH in 90% methanol – 10% water, then chromatography on a 20-fold ratio of neutral alumina (act. 2–3) gave a 61% yield of nearly pure alcohol, mp 188°C. Recrystallization from methanol–

Can. J. Chem. Downloaded from www.nrcresearchpress.com by 217.78.4.112 on 09/08/12
For personal use only.

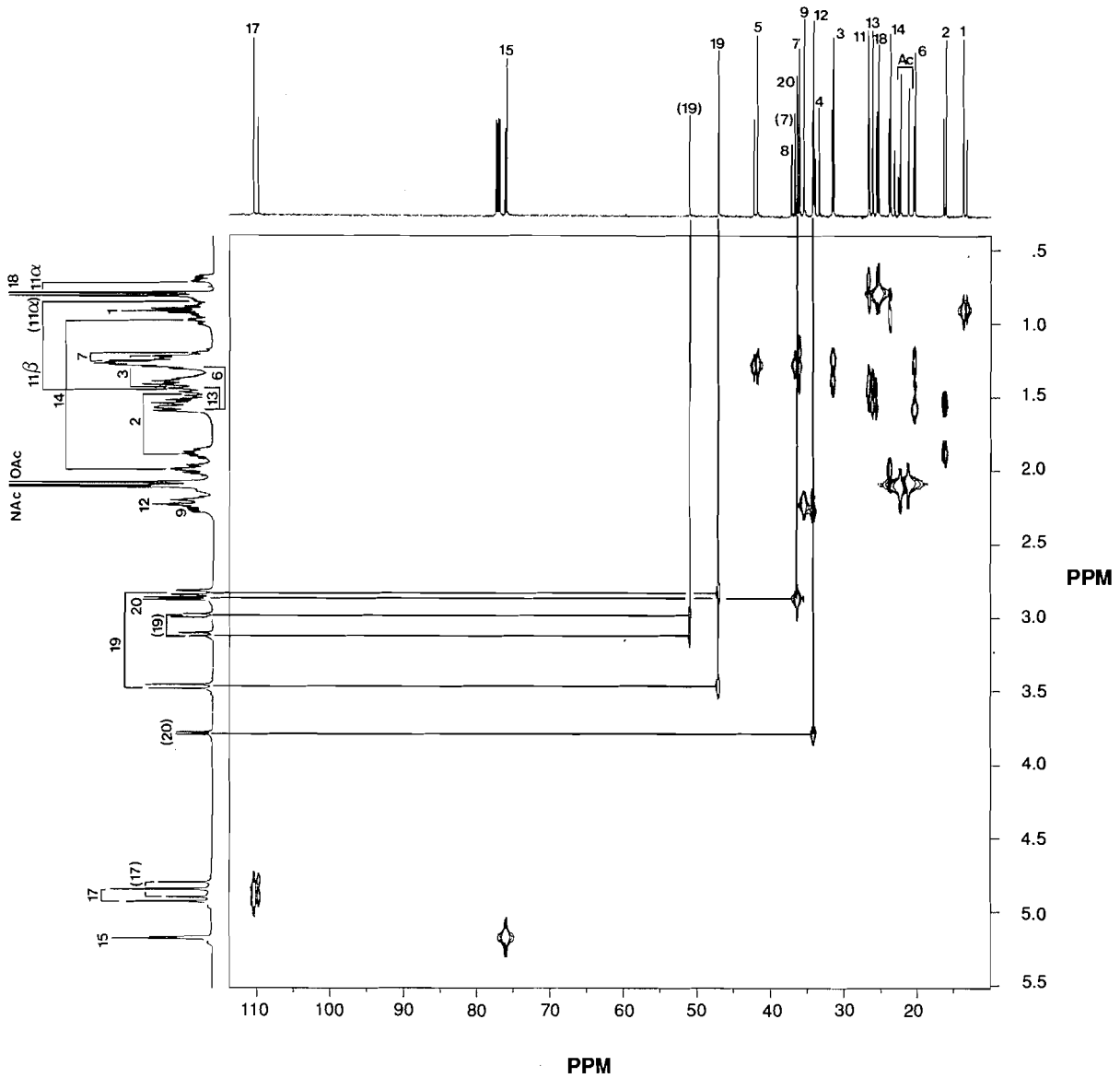

FIG. 1. $^{13}C/^{1}H$ correlation spectrum of **4** acquired in $CDCl_3$. The projections are shown as the single pulse spectra. The presence of the two rotamers can be seen in both spectra, and the assignment of resonances of the minor component are shown in parentheses, for those resonances close to the amide bond. The correlation spectrum resolves the highly overlapped methylene protons in the 0.5–2.5 ppm range of the ^{1}H spectrum.

ether gave pure material with mp 193–194°C (lit. (4) mp 191–192°C). This had ν_{max} (CH_2Cl_2): 3590, 3410, and 1630 cm^{-1}; and ^{1}H NMR signals at δ: 4.9–5.2 (2H, m), 3.6–4.0 (1H, m), 2.6–3.2 (2H, m), 2.16 (3H, s), and 0.87 (3H, s).

Carboxylic acid **6**

A mixture of 18 mL of acetone, 2 mL of water, and 0.5 mL of acetic acid was prepared. The *N*-acetylcyclopropane acetate **4** (R=Ac) (185 mg) was dissolved in 5 mL of this mixture. A solution of 400 mg of potassium permanganate in 10 mL of the above solvent mixture was prepared. Five milliliters of the permanganate solution was added to the solution of **4**. After 3 h, 2 mL of permanganate solution was added. An excess oxidant was still present after a further 5.5 h. This was reduced using aqueous sodium hydrogen sulfite, then the manganese dioxide removed by filtration. The filtrate and acetone washings were evaporated under reduced pressure, then the residue was taken up in dichloromethane. Acids were extracted into dilute aqueous sodium carbonate solution. The residual neutral material weighed 66 mg (some unchanged **4**). The carbonate solutions yielded 122 mg of acids that crystallized readily from acetone. The crystalline acid (79 mg) had mp 238–247°C. Recrystallization from methanol gave a product with mp 246–247°C (dec.) and ν_{max} (Nujol): 3460, 1742, 1719, 1620, and 1238 cm^{-1}. Anal. (dried 25 h at 100°C, 10^{-3} Torr) calcd. for $C_{24}H_{33}NO_6$: C 66.80, H 7.71; found: C 67.22, H 7.74.

Its methyl ester (CH_2N_2) crystallized from methanol–ether mixtures with mp 210°C. It had ν_{max} (Nujol): 3230, 1750 (sh), 1735, and 1647 cm^{-1}. Anal. calcd. for $C_{25}H_{35}NO_6$: 1-OCH_3 6.95; found: OCH_3 7.02.

Dihydroxy acid **6** *(15-hydroxyl)*

Hydrolysis of acetoxy acid **6** (R^1=H, R^2=Ac) for 1 h in refluxing methanol containing potassium hydroxide gave the dihydroxy acid. After recrystallization from acetone this had mp 222–227°C and ν_{max} (Nujol): 3060 (br) 1743, 1632, and 1248 cm^{-1}. Anal. calcd. for $C_{22}H_{31}NO_5$: C 67.84, H 8.02; found: C 67.90, H 8.01.

Vigorous alkaline treatment of **4** *(R=Ac)*

Crushed potassium hydroxide pellets (749 mg) were added to a solution of 124 mg of **4** (R=Ac) (mp 195°C) in 4 mL of triethy-

Can. J. Chem. Downloaded from www.nrcresearchpress.com by 217.78.4.112 on 09/08/12
For personal use only.

Can. J. Chem. Downloaded from www.nrcresearchpress.com by 217.78.4.112 on 09/08/12
For personal use only.

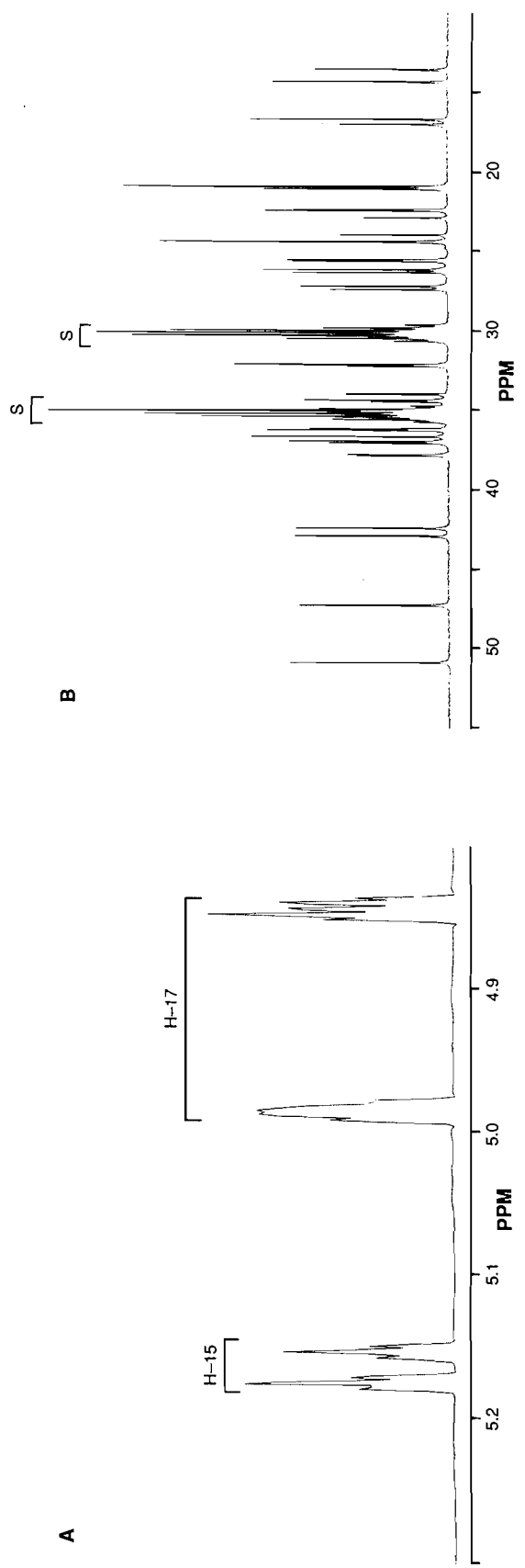

FIG. 2. The effect of temperature on the rotamer population in dimethylformamide (DMF) solution of compound **4**. A and B represent portions of the ^{1}H and ^{13}C spectra acquired at 30°C while C and D show the same spectral regions at 125°C. Collapse of the doubled resonances occurs at the higher temperature.

Can. J. Chem. Downloaded from www.nrcresearchpress.com by 217.78.4.112 on 09/08/12
For personal use only.

lene glycol. The mixture was heated under argon in a bath at 174°C for 23 h. The dark solution was cooled, diluted with 10 mL of water, then the products extracted into benzene (3 × 5 mL). The combined benzene layers were extracted twice with 5-mL portions of 3 N sulfuric acid. The aqueous layers were made basic using sodium carbonate, then the bases were extracted into dichloromethane. The 87 mg of base so obtained crystallized from hexane containing a few percent of acetone, yielding 38 mg of **2** (R=H), mp 167–169°C. Separation of the mother liquors on a 500 μm SiO_2 plate using 5% pyridine and 2.5% methanol in dichloromethane gave 6 mg (R_f 0.7) rich in **2**. The yield of moderately pure **2** (R=H) was thus 54%. In comparable runs the yield never exceeded 64% based on unrecovered neutral products. However, one of the contaminants of the crude bases was shown to be **4** (R=H), making the true yield higher.

Further plate purification as above, and recrystallization from acetone–hexane, gave crystals of base (shimmering plates) with mp 176–177°C. It showed no mixture mp depression with authentic **2** (R=H), had $[\alpha]_D$ −13 (*c* 1.1 in absolute ethanol), and gave identical IR spectrum and ^1H and ^{13}C NMR spectra in benzene-d_6.

N-*Acetyl 1,20-cyclo-15,16-didehydro-17-nor-4-methylatidane 7*

The azomethine *N*,20,15,16-tetradehydro-17-nor-4-methylatidane (1) (151 mg) in 4.5 mL of 15% acetic acid in acetic anhydride (v/v) was held at 140°C for 24 h in a sealed tube under nitrogen. Work-up as for **4** gave 138 mg of neutral product, which crystallized. After three recrystallizations from aqueous acetone, **7** (41 mg) had mp 152–153°C and ν_{max} (Nujol): 1649 cm^{-1}. Its ^1H NMR spectrum gave signals at δ: 6.45–5.7 (2H, m), 3.9–2.6 (3H, m), 2.17 (3H, s), 0.84 (3H, s). Its ^{13}C nmr spectrum is given in Table 2. Anal. calcd. for $C_{21}H_{29}NO$: C 80.98, H 9.39; found: C 80.77, H 9.28.

N-*Acetyl 1,20-cyclo-17-nor-4-methylatidane 8*

The azomethine *N*,20-didehydro-17-nor-4-methylatidane (126 mg) (1) was heated under reflux for 23 h in 17% acetic acid in acetic anhydride (v/v). Work-up as for **4** gave a 94% yield of neutral product. This was purified by chromatography on a 20-fold ratio of neutral alumina activity III. The hexane and 1:1 benzene–hexane eluates (80 mg) crystallized from aqueous acetone, giving **8** with mp 152–154°C and ν_{max} (Nujol): 1645 cm^{-1}. It gave ^1H NMR signals at δ: 3.9–3.35 (1H, m), 3.2–2.6 (2H, m), 2.16 (3H, s), and 0.84 (3H, s). Anal. calcd. for $C_{21}H_{31}NO$: C 80.46, H 9.97; found: C 80.36, H 9.88.

N-*Acetyl 15-acetoxy-1,20-cyclo-17-nor-4-methylatidane 9*

The azomethine *N*,20-didehydro-15-hydroxy-17-nor-4-methyl atidane (1) (185 mg) in 2 mL of acetic anhydride was heated in a bath at 150°C for 24 h under argon. The brown solution was worked up as for **4**, giving 8 mg of base and 200 mg of neutral product. The latter was purified on two 20 cm × 20 cm 1000 μm silica gel plates using 5% methanol in chloroform. The main zone (R_f 0.75) gave 155 mg of nearly pure **9**. The preceding zone (30 mg) contained around 20% of **9** and two faster-moving products. The estimated yield of **9** was 71% based on unrecovered base. It could be distilled over a short path at 170°C, 0.1 Torr, or freed from a trace of colour by passage of a dichloromethane solution through a short bed of Act. II neutral alumina. After long standing it crystallized, forming prisms from ethyl acetate – heptane, mp 156–159°C. It gave ^1H NMR signals at δ: 4.60 (1H, q, J_1 = 10, J_2 = 3 Hz) 3.9–2.8 (3H, m), 2.19, 2.18, 2.09, 2.10, 2.19, 2.18 (6H), 0.89, 0.87 (3H singlets), 0.69–0.61. Its EI mass spectrum gave peaks at 371.2504 ($C_{23}H_{33}NO_3$ requires 371.2462), 329.236 [M − CH_2CO]$^+$, and 311.2277 [M − CH_3COOH]$^+$.

N-*Acetyl 15-acetoxy-16,17-didehydro-4-methylatidane 16*

Excess sodium borohydride reduced imine **2** in methanol to give the corresponding secondary amine (partial hydrolysis of the ester). The product was acetylated at room temperature, using acetic anhydride in pyridine, during 22 h. The reagents were removed under reduced pressure, traces of anhydride destroyed using methanol, then a dichloromethane solution of the product was washed with dilute sulfuric acid, followed by sodium bicarbonate solution. The product **16** crystallized as rectangular plates from ethyl acetate, mp 165–167°C. Its ^1H NMR spectrum had signals at δ: 5.05 (1H, s), 5.0–4.8 (2H, m), 4.45–2.55 (3H, m), 2.4–2.3 (1H, m), 2.1, 2.06, 2.04 (6H), and 0.802, 0.805 (3H). Its ^{13}C NMR spectrum is given in Table 2. Its EI mass spectrum had a peak at *m/z* 385.26192. Exact Mass calcd. for $C_{24}H_{35}NO_3$: 385.26168.

Acknowledgement

We thank H. Sequin for the microanalyses and K. Bourque, D. Fielder, and J. Nikiforuk for NMR spectral analysis. One of us (O.E.E.) is grateful to Prof. J. W. ApSimon for the opportunity to finish this work at Carleton University. D. Dvornik was an NRCC Postdoctorate Fellow (1956–1959).

1. D. Dvornik and O. E. Edwards. Can. J. Chem. **35**, 860 (1957).
2. J. W. ApSimon, O. E. Edwards, and R. Howe. Can. J. Chem. **40**, 630 (1962).
3. O. E. Edwards. Chem. Can. 40 (1961).
4. S. W. Pelletier and P. C. Parthasarathy. J. Am. Chem. Soc. **87**, 777 (1965).
5. M. Przybrylska and F. R. Ahmed. Acta Crystallogr. Sect. C: Cryst. Struct. Commun. **C46**, 2405 (1990).
6. O. E. Edwards, J. Dixon, J. W. Elder, R. J. Kolt, and M. Lesage. Can. J. Chem. **59**, 2096 (1981).
7. O. E. Edwards and T. Sano. Can. J. Chem. **47**, 3489 (1969).
8. (*a*) O. E. Edwards and Z. Paryzek. Can. J. Chem. **61**, 1973 (1983); (*b*) O. E. Edwards and R. J. Kolt. Can. J. Chem. **65**, 595 (1987).
9. K. E. Hamlin and A. W. Weston. Org. React. (NY), **9**, 1 (1957).
10. S. Danishevsky. Acc. Chem. Res. **12**, 66 (1979).
11. N. V. Mody and S. W. Pelletier. Tetrahedron Lett. 3313 (1978).
12. C. E. Poulter, R. S. Boikess, J. I. Brauman, and S. Winstein. J. Am. Chem. Soc. **94**, 2291 (1972).
13. D. Dvornik and O. E. Edwards. Can. J. Chem. **42**, 137 (1964); Tetrahedron, **14**, 54 (1961).

Stereoselective synthesis of *cis*-decalins via Diels–Alder and double Michael addition of substituted Nazarov reagents

JEAN-FRANÇOIS LAVALLÉE, CLAUDE SPINO,[1] RÉJEAN RUEL, KEITH T. HOGAN, AND PIERRE DESLONGCHAMPS[2]

Laboratoire de synthèse organique, Département de chimie, Faculté des sciences, Université de Sherbrooke, Sherbrooke (Québec), Canada J1K 2R1

Received May 10, 1991

This paper is dedicated to Professor Zdenek (Denny) Valenta on the occasion of his 65th birthday

JEAN-FRANÇOIS LAVALLÉE, CLAUDE SPINO, RÉJEAN RUEL, KEITH T. HOGAN, and PIERRE DESLONGCHAMPS. Can. J. Chem. **70**, 1406 (1992).

The base-catalyzed cycloaddition and double Michael cyclization of substituted Nazarov reagents and of 1-phenylsulfinyl analogs, with 2-carbomethoxy-2-cyclohexen-1-one **1** yielding *cis*-decalins is reported. The reaction is highly stereoselective affording *cis,cis*- or *cis,trans*-decalins. Mechanistic aspects are briefly discussed.

JEAN-FRANÇOIS LAVALLÉE, CLAUDE SPINO, RÉJEAN RUEL, KEITH T. HOGAN et PIERRE DESLONGCHAMPS. Can. J. Chem. **70**, 1406 (1992).

On décrit la cycloaddition catalysée par des bases des réactifs de Nazarov substitués, ainsi que d'un analogue 1-phénylsulfinylé, avec la 2-carbométhoxy-2-cyclohexénone **1** produisant des *cis*-décalines. La réaction est hautement stéréosélective générant des *cis,cis*- ou *cis,trans*-décalines. Les mécanismes de ces réactions sont brièvement discutés.

Can. J. Chem. Downloaded from www.nrcresearchpress.com by 217.78.4.112 on 09/08/12
For personal use only.

Introduction

Substituted decalins have been prepared in a number of ways, among which the Robinson annelation and the Diels–Alder cycloaddition occupy a prominent place (1). Whereas the Robinson annelation usually gives rise to dehydrodecalins with one new asymmetric center, the Diels–Alder cycloaddition can produce *cis*-decalin systems with the introduction of up to four asymmetric centers. Decalins have been used extensively as intermediates in the synthesis of numerous natural products, in particular terpenoids and steroids (1). Thus, the stereocontrolled synthesis of substituted decalins is highly desired. Decalins with a β-alkyl substituent at C8 (*cis,cis*-decalins) have been prepared via a Lewis acid-catalyzed Diels–Alder cycloaddition of 2-carbomethoxy-2-cyclohexenone **1** (2) and various substituted 1,3-dienes (3). The stereocontrol at the C8-substituent was in the order of 7:1 in favor of the more desirable β isomer.

In a preliminary communication we reported the highly stereoselective synthesis of *cis,cis*-decalins via a base-catalyzed [2+4] cycloaddition of substituted Nazarov reagents like **2** with 2-carbomethoxy-2-cyclohexenone **1** (4) (Scheme 1). We now wish to report a full account of this work, which includes cycloadditions between Nazarov reagents substituted at positions 4 and 5 and various substituted 2-cyclohexenones. Their use in the construction of polycyclic compounds as well as a novel synthesis of substituted Nazarov reagents (5) is also disclosed. In addition, the mechanistic aspect of the reaction is discussed briefly.

Results and discussion

Synthesis of Nazarov reagents

There are many ways to prepare substituted Nazarov reagents (6, 7). Bodalski and co-workers (7*a*) as well as Van Den Goorbergh and Van Der Gen (7*b*) report that substituted Nazarov reagents like **7** can be obtained in one step from the condensation of the phosphonate dianion derived from **6** and aldehydes or ketones (Scheme 2). We prepared the previously unknown *tert*-butyl γ-diethoxyphosphono β-keto esters **9***a* and **9***b* in 67 and 45% yields by *C*-phosphorylation of the dianion of β-keto esters **8***a* and **8***b*, respectively (8). The dianion of **9***a* (7*c*) was condensed with the known aldehyde **10***a* (9), to obtain the substituted Nazarov reagent **11***a* in 35% yield (Scheme 2). Also, substituted Nazarov reagents **11***b* and **11***c* were obtained in 76 and 33% yields, respectively, from the condensation of the dianion of **9***a* with aldehydes **10***b* and **10***c*. The latter were prepared in two standard steps from the corresponding diols. The dianions of phosphonate **9***a* and the methyl-substituted phosphonate **9***b* were condensed with aldehyde **12** to give, respectively, a 77 and 44% yield of the *trans* olefinic products **13***a* and **13***b* as the only detectable isomers. Aldehyde **12** was prepared in a 72% yield via the alkylation of the lithium salt of 1-trimethylsilylpropyne **14** with protected 3-bromo-1-tetrahydropyranyloxy-propane **15** followed by deprotection and oxidation of the resulting product. The cleavage of the silyl groups, in **13***a* and **13***b*, was effected in 90 and 86% yields, respectively, with tetrabutylammonium fluoride in tetrahydrofuran (THF) (10). Treating the resulting products with sodium hydride followed by butyllithium generated their dianion whose acylation with methyl chloroformate gave, respectively, 93 and 51% yields of the Nazarov reagents **16***a* and **16***b*. Selective catalytic hydrogenation of **16***a* gave **17**.

While this method proved to be highly selective and very expedient for the construction of Nazarov reagents with an *E*-double bond, the reaction proved sensitive to the presence of functional groups on the aldehyde, as well as substitution on the phosphonate reagent, giving somewhat lower yields (cf. **11***a*, **11***c*, and **13***b*). Another, more general, method for the preparation of Nazarov reagents is depicted in Scheme 3. For example, α,β-unsaturated aldehyde **18***a* was treated with the zinc enolate of *tert*-butyl bromoacetate **19** to produce the corresponding β-hydroxy ester, which was oxidized to the desired substituted Nazarov reagent **20***a* in a 61% overall yield by treatment with manganese dioxide in ethyl acetate. Nazarov reagents **20***b*–**20***d* were prepared by the same method from the known aldehydes **18***b*–**18***d* (for

[1]Present address: University of Victoria, Department of Chemistry, P.O. Box 3055, Victoria, B.C., Canada V8W 3P6.

[2]Author to whom correspondence may be addressed.

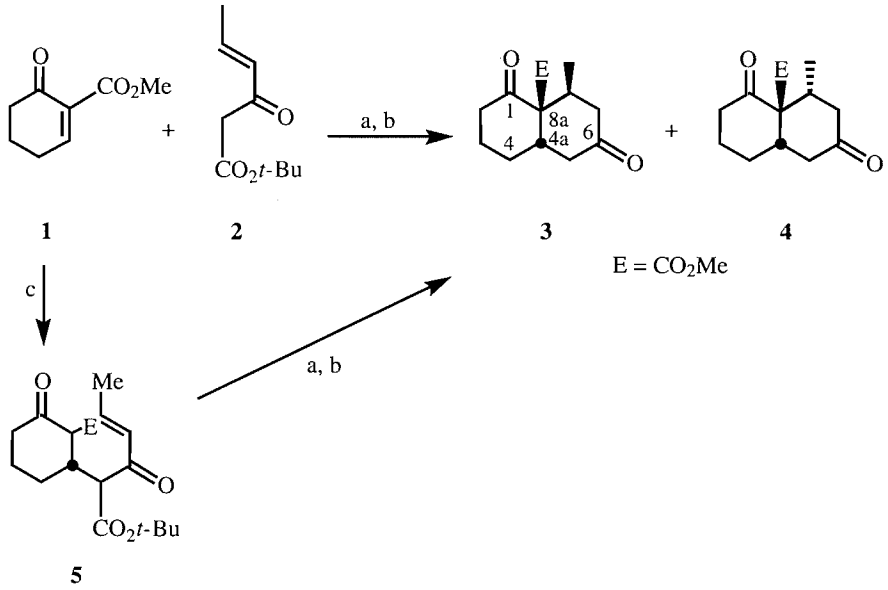

(a) Cs_2CO_3 in solvent, 25°C, 3.5 h; (b) *p*-TsOH in benzene at reflux, 1.5 h; (c) Cs_2CO_3 in acetonitrile, −15°C, 0.5 h

SCHEME 1

18*c* see ref. 11) in 49, 45, and 57% overall yields, respectively. Aldehyde **18***e* was synthesized in a 68% overall yield by the reduction and protection of 2-bromocyclohexenone following lithiation and formylation, according to the method reported by Smith *et al.* (12). The reaction of **18***e* with the zinc enolate of **19**, followed by oxidation of the resulting β-hydroxy ester, gave β-keto ester **20***e* in a 62% yield for the two steps. Lastly, the aldehyde **18***f* was treated in the same manner to afford the Nazarov reagent **20***f* in a 41% overall yield. The aldehyde **18***f* was synthesized in six steps from methyl acetoacetate, as depicted in Scheme 4, in an overall yield of 30%.

The β-keto sulfoxide **26** could be prepared directly by the condensation of the anion of methylphenylsulfoxide **25** (13) with methyl crotonate in a 56% yield (Scheme 4). Oxidation of **26** with *m*-chloroperbenzoic acid in dichloromethane gave a 67% yield of β-keto sulfone **27**.

Cycloadditions with substituted Nazarov reagents

β-Keto esters

The base-catalyzed [2+4] cycloaddition of substituted Nazarov reagent **2** with 2-carbomethoxy-2-cyclohexenone **1** afforded, after decarboxylation with *p*-toluenesulfonic acid in refluxing benzene, the known (3) *cis,cis* and *cis,trans* bicyclic diketones **3** and **4** with a very high degree of stereoselectivity (4*a*, 8) (Scheme 1). The ratios were determined by gas chromatographic analysis and the results are summarized in Table 1. The selectivity of the reaction was found to be highly dependent on the solvent used (4*a*). The use of more polar solvents (entries 1, 2, and 3) led to mixtures of isomers **3** and **4**, whereas the use of less polar solvents (entries 5 and 6) gave almost exclusively the *cis,cis* isomers **3**. The best results were obtained using chloroform (entry 6), where the selectivity was greater than 99.5% with an overall yield of 69%. The counterion also had some effect on the selectivity, as can be seen from entry 2 vs. entry 3.

Adding a substituent on the diene at the 4-position had no effect on the selectivity of the reaction. The cycloaddition–decarboxylation sequence between β-keto ester **20***b* and dienophile **1** gave stereoselectivity, in 65% yield, the *cis*-decalins **28** and **29** in a 7:3 ratio (Scheme 5). In the case of **20***c* the two isomers **30** and **31** were isolated in 66% yield in a 1:1 ratio. Each of those four isomers could be isolated in pure form by flash chromatography. The ratios obtained are a reflection of the equilibrium mixture, since the same ratios of isomers **28** and **29**, as well as **30** and **31**, were recovered when each of these compounds was separately resubmitted to the acidic decarboxylation conditions. The structure and stereochemistry of **30** and **31** were assigned based on a single crystal X-ray crystallographic analysis of **30** (14) and ^1H nmr data. The structures of **28** and **29** were based on the following ^1H nmr experiments: irradiation of one of the methyls on the major isomer **28** revealed a doublet at 3.07 ppm of $J = 5$ Hz. This coupling constant must be that of H_b and H_c (Fig. 1), thereby establishing the *cis* relationship of the two methyl groups. The same experiment with **29** clearly showed the *trans* arrangement of the two methyls by virtue of a 13 Hz coupling between protons H_b and H_c.

The fact that **28** was formed in preference to **29** in equilibrating acidic media tends to show that C8-substituted *cis*-decalins like **3** adopt conformation **A** rather than conformation **B** (R^2 = H, Fig. 1). This was supported by MM2 calculations, which indicated that **28** in conformation **A** is more stable than **29** in conformation **B** by a value of 1.8 kcal/mol. It was also possible to correlate the ^1H nmr chemical shifts of H_b and the C8-methyl group in the different adducts to those of compounds **28** and **29**. Table 2 lists the chemical shifts of these protons for the different adducts. The C8-methyl resonates below 1.0 ppm in compounds thought to have the stereochemistry shown in **A** and above 1.0 ppm in those having the stereochemistry shown in **B**. Proton H_b in compounds of conformation **A** resonances at a higher field than expected for a proton in such a chemical environment (above 2.5 ppm), probably due to the deshielding anisotropic effect of the C1-carbonyl. The same proton is found below 2.5 ppm in compounds thought to have conformation

Can. J. Chem. Downloaded from www.nrcresearchpress.com by 217.78.4.112 on 09/08/12
For personal use only.

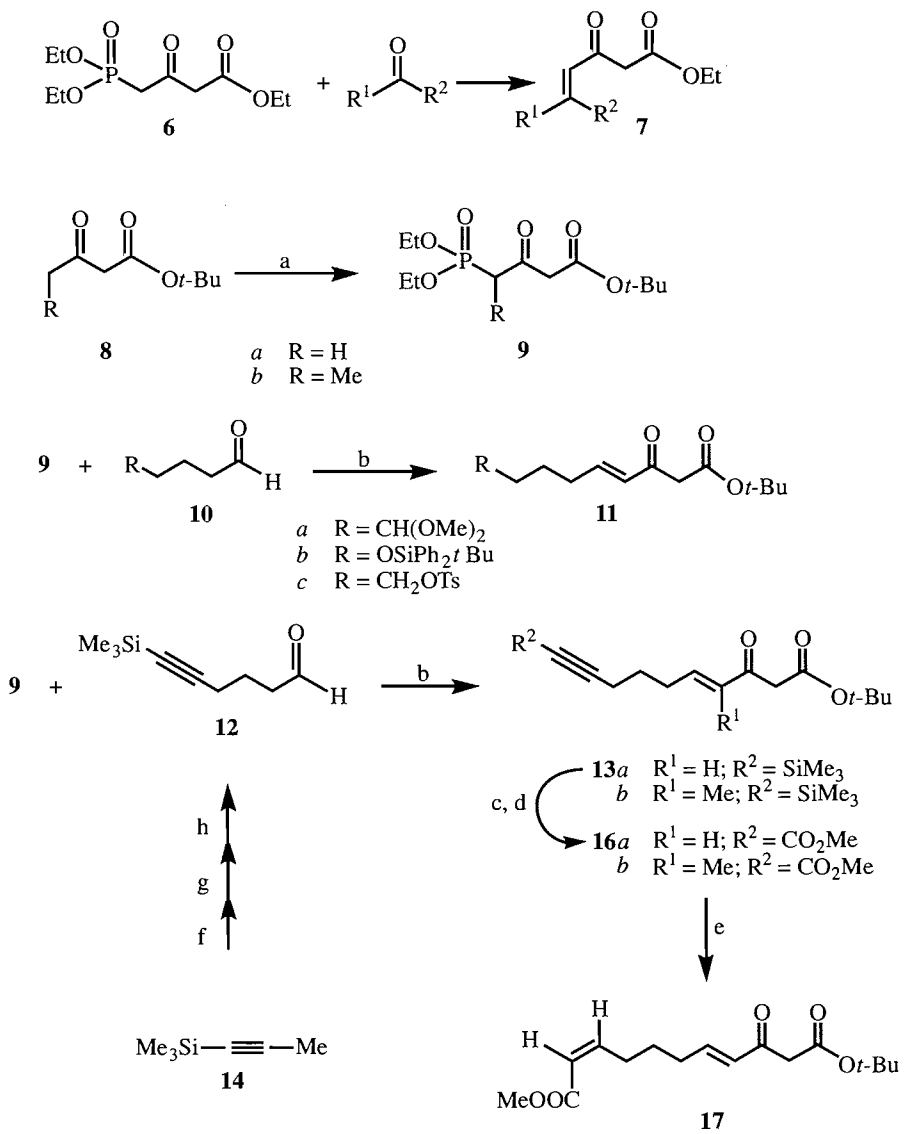

(a) NaH, *n*-BuLi, THF, 0°C, then $(EtO)_2P(O)Cl$; (b) NaH, *n*-BuLi, THF, −30°C, then warm to r.t.; (c) *n*-Bu_4NF, THF, 0°C, 1 h; (d) NaH, *n*-BuLi, THF, −78°C, $ClCO_2Me$, then warm to r.t.; (e) Lindlar, H_2, EtOAc, r.t.; (f) *n*-BuLi, TMEDA, ether, −15°C then $Br(CH_2)_3OTHP$ (**15**); (g) MeOH, PPTS, 0°C; (h) DMSO, $(COCl)_2$, CH_2Cl_2, −78°C, then Et_3N and warm to r.t.

SCHEME 2

B. The coupling pattern of H_a and H_c with adjacent protons were also characteristic for the two conformations. It should therefore be possible to assign the stereochemistry of future Diels–Alder adducts, with a good degree of confidence, by inspection of their ^1H nmr spectra. In addition, knowing the preferred conformation of those adducts might help in understanding the stereochemical outcome of reactions in their elaboration into synthetic intermediates.

When a methyl group was present at position 5 of the starting β-keto ester, *cis* to the keto ester moiety, as in **20***d*, the reaction stopped at the single Michael adduct stage to give **32** (Scheme 5). It is interesting to note that this single adduct was formed in 57% yield in acetonitrile, and 29% yield in chloroform.

If the chain at position 5 of the Nazarov reagent contains an appropriately located functional group, interesting polycyclic compounds can, in principle, be prepared. For example, when tosylate **39**, prepared in four steps from the cycloaddition of Nazarov reagent **11***b* (Scheme 6), was treated with potassium *tert*-butoxide in a mixture of tetrahydrofuran–*tert*-butanol, an 86% yield of the known tricyclic compound **40** was isolated (15). However, the corresponding higher homolog **35** obtained from **11***c* via **33** gave none of the tricyclic adducts **36**. Also, **34** was not obtained from the corresponding **33**, which was formed *in situ* from **11***c*. The formation of the 5-membered ring to give **40** is possible since the proper geometry for backside attack of the ketone enolate on the carbon bearing the tosylate can be achieved. A similar cyclization might be prevented by steric interactions and angle strain in the formation of a 6-membered ring as indicated in Fig. 2. The cyclization of bicyclic ketones, by intramolecular Michael addition to an α,β-unsaturated ester, to form tricyclic compounds having an additional 6-membered ring was also unsuccessful as shown in

Can. J. Chem. Downloaded from www.nrcresearchpress.com by 217.78.4.112 on 09/08/12
For personal use only.

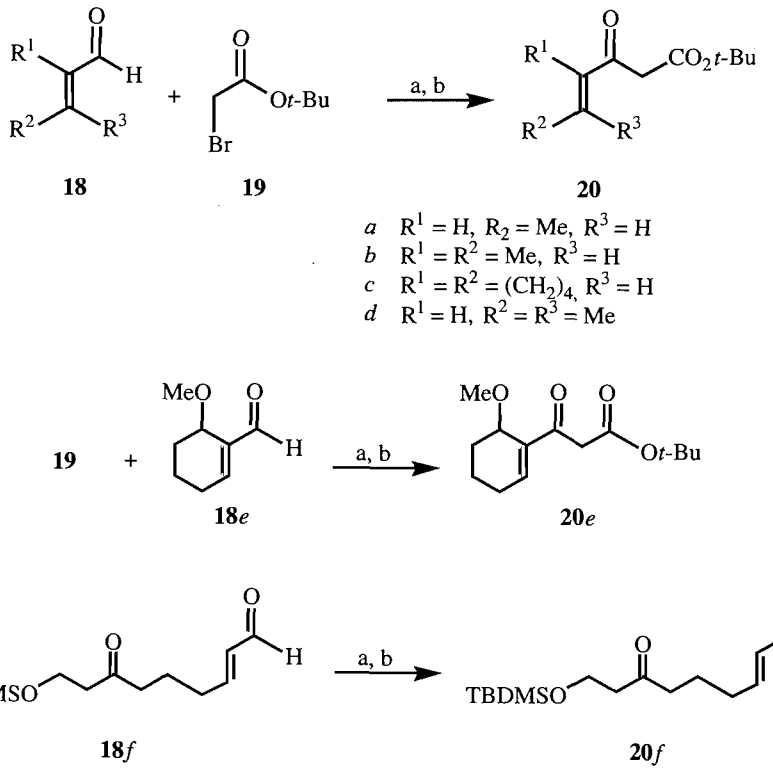

(a) Zn, THF, reflux, then **18**, ether, 0°C to r.t.; (b) MnO_2, EtOAc, r.t., 15–48 h

SCHEME 3

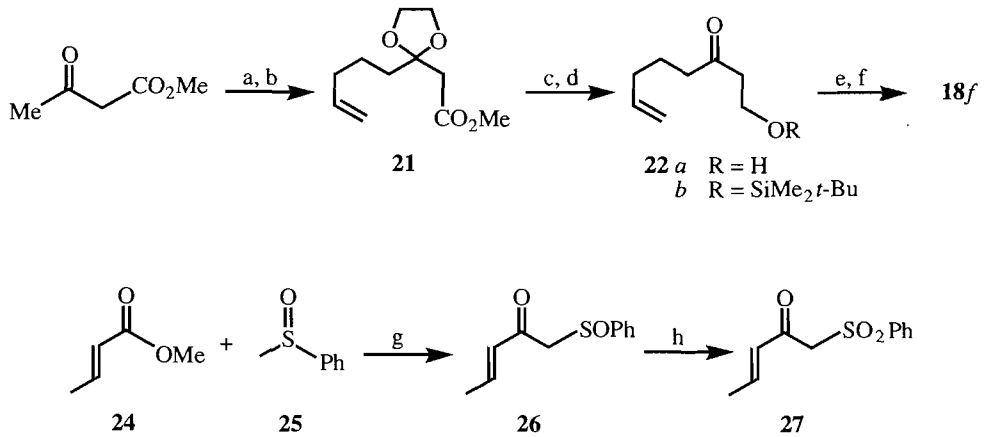

(a) NaH, *n*-BuLi, THF, 0°C, then 4-bromo-1-butene, r.t.; (b) *p*-TsOH, $(HOCH_2)_2$, benzene, reflux, 24 h; (c) $LiAlH_4$, THF, 0°C, 1 h, then HCl 1 N; (d) TBDMSOTf, Et_3N, CH_2Cl_2, 0°C, 1 h; (e) O_3, CH_2Cl_2, −78°C, then Ph_3P; (f) Ph_3P=CHCHO (**23**), benzene, reflux, 18 h; (g) **25**, LDA, THF, −78°C, then **24**, 0.5 h; (h) *m*-CPBA, CH_2Cl_2, 0°C

SCHEME 4

Scheme 7. No trace of the desired tricyclic compounds **43** or **44** was formed when the bicyclic intermediates were treated under a variety of basic conditions, such as sodium methoxide in methanol, potassium *tert*-butoxide in *tert*-butanol, etc.

Bicyclic acetal **45**, made by the cycloaddition between **1** and **11***a*, gave tricyclic aldehyde **46** upon treatment with *p*-toluenesulfonic acid (Scheme 7). The desired aldol condensation product **48** could not be detected. Compound **48** could be prepared, however, in a 52% yield from the cycloaddition–decarboxylation of **1** and β-keto ester **20***e*. The structure of **48** was secured by a single crystal X-ray crystallographic analysis.[3] The tetracyclic compound **51** analogous to **46** was also formed when bicyclic compound **50** was treated with *p*-toluenesulfonic acid (Scheme 7). The propensity of the C13-methylene to undergo aldol condensation with the C1-carbonyl, in preference to the desired aldol reaction between the C8-methylene and the C14-carbonyl,

[3]M. Drouin, A. G. Michel, and C. Spino. Unpublished results.

Can. J. Chem. Downloaded from www.nrcresearchpress.com by 217.78.4.112 on 09/08/12
For personal use only.

TABLE 1. Stereoselectivities of the cyclizations to **3** and **4**

Entry	Cyclization	Conditions	Ratio **3**:**4**
1	**1** and **2**	DMF, Cs_2CO_3	54:46
2	**1** and **2**	CH_3CN, KH	50:50
3	**1** and **2**	CH_3CN, Cs_2CO_3	75:25
4	**1** and **2**	Benzene, *p*-TSOH, 80°C	83:17
5	**1** and **2**	Benzene, Cs_2CO_3	95:5
6	**1** and **2**	$CHCl_3$, Cs_2CO_3	≥99:1
7	**1** and **26**	DMF, Cs_2CO_3	≥1:99*
8	**1** and **26**	CH_2Cl_2, Cs_2CO_3	≥1:99*
9	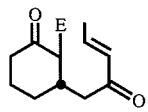 **67** (E=CO_2Me)	DMF, Cs_2CO_3	25:75
10	**5**	CH_3CN, Cs_2CO_3	70:30
11	**68**	CH_3CN, Cs_2CO_3	≥1:99*
12	**68**	CH_2Cl_2, Cs_2CO_3	≥1:99*

*After reduction.

Can. J. Chem. Downloaded from www.nrcresearchpress.com by 217.78.4.112 on 09/08/12
For personal use only.

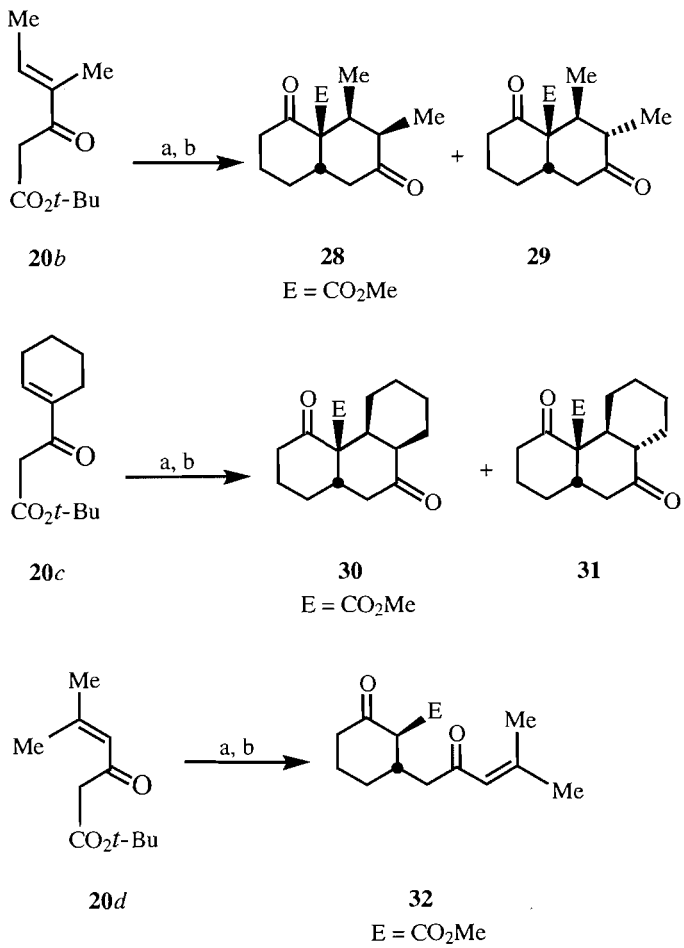

(a) Cs_2CO_3, $CHCl_3$, then **1**, r.t.; (b) CF_3CO_2H, then benzene, reflux

SCHEME 5

TABLE 2. Cycloadditions of Nazarov reagents and decalin conformations

Entry	Decalin	Equilibrium ratio	Conformation	Proton nmr shifts (δ) at C8	
				H_b	Me
1	**3**	—	**A**	2.90	0.88
2	**28**	(**28**:**29**) 7:3	**A**	2.91	0.65
	29		**B**	2.35	1.09
3	**30**	(**30**:**31**) 1:1	**A**	2.85	—
	31		**B**	<2.00	—
4	**42***a*	—	**A**	2.65	—
5	**42***b*	(**A**:**B**) 9:1	**A**	2.67	—
			B	<2.50	—
6	**55**	—	**B**	2.70	1.04
7	**57**	—	**A**	2.95	0.84
8	**61**	—	**B**	1.99	1.04

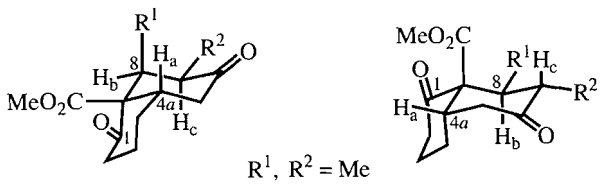

A B

FIG. 1

is quite clear form the above results. However, it is possible to effect the desired C8–C14 aldol reaction when the alternative is not possible (4, 16).

Double Michael addition of the β-keto sulfoxide and sulfone analogues of the methyl substituted Nazarov reagent

Diketone **4** can be prepared stereoselectively by the use of 1-phenylsulfoxide or 1-phenylsulfonyl analogues of the Nazarov reagents (17) (Scheme 8). When compound **26** was treated with cesium carbonate and **1** under the same reaction conditions as for the corresponding β-keto ester **2**, dehydrodecalin **52** was isolated in 70% yield after column chromatography. It was found that the elimination of the phenylsulfoxide moiety took place on the silica gel during chromatography. Catalytic hydrogenation of bicyclic compound **52** furnished a 13:1 ratio of the decalinedione **4** and a second bicyclic product in a combined chemical yield of 60%. This demonstrated that the dehydrodecalin adduct **52** from the cycloaddition had in fact α stereochemistry at C8. The minor isomer in the catalytic reduction had spectral data different from those of compound **3** and is thought to be the *trans*-decalin resulting from the α attack of the hydrogen molecule.

This complete reversal of stereoselectivity observed with the sulfoxide analog of the Nazarov reagent is somewhat surprising and its cause remains unclear at present. In addition, the stereoselectivity was shown to be independent of the solvent used for the reaction. For example, similar results were obtained in acetonitrile or dimethylformamide as solvents.

The double Michael addition of β-ketosulfone **27** on **1** afforded bicyclic adduct **53** (50%), which was reduced with aluminium amalgam (18) to give **4** as the sole product in 48% yield (79% based on recovered starting material) (Scheme 8). However, the reaction between **27** and **1** was slower than that with **26**. The cycloaddition using β-keto sulfoxides and sulfones appears to be complementary to the one using β-keto esters. Applications of this reaction to the synthesis of natural products are underway in our laboratory.

Cycloadditions with substituted-2-cyclohexenones

Substituents around the cyclohexenone ring in **1** can be used to direct the approach of the incoming diene, while retaining the same relative stereochemistry of the newly formed asymmetric centers in the Diels–Alder adducts. Results are summarized in Table 3. Cycloaddition of Nazarov reagent **2** with racemic 4-methyl-2-carbomethoxy-2-cyclohexenone **54** (entry 1) gave adduct **55** in 73% yield, where the diene added *anti* to the methyl group. *Anti* addition is also predominant in the alkylcuprate 1,4-addition to 4-methyl cyclohexenones (19). When (−)-2-carbomethoxy-5-methylethenyl-2-cyclohexen-1-one **56** ($[\alpha]_D$-18.6, c = 2, $CHCl_3$, 25°C), derived from (−)-carvone, was allowed to react with **2** (entry 2), three compounds were formed in a 85:11:4 ratio. The major compound could be purified and was assigned structure *57* ($[\alpha]_D$ + 117.3, c = 1, $CHCl_3$, 25°C) based on a correlation of its ^1H nmr spectrum with a related steroidal compound of known structure (16). Again addition *anti* to the isopropenyl group was expected by analogy to the 1,4-additions of alkyl cuprates on similar systems (1, 19). The other two isomeric compounds could not be obtained in pure form and therefore their structures could not be secured. The use of compound **56** allows the synthesis of optically pure bicyclic adducts in which the isopropenyl might serve as a handle for further elaboration of the A ring of these adducts. The synthesis of **56** was carried out starting from the known epoxide **63** (20) (Scheme 9) derived from (−)-carvone. Opening of the epoxide in **63** occurred with sulfuric acid in tetrahydrofuran to give a 1:1 mixture of *cis*-diol **64** and its corresponding *trans* isomer. Only the desired *cis*-diol underwent cleavage with sodium periodate and after treat-

Can. J. Chem. Downloaded from www.nrcresearchpress.com by 217.78.4.112 on 09/08/12
For personal use only.

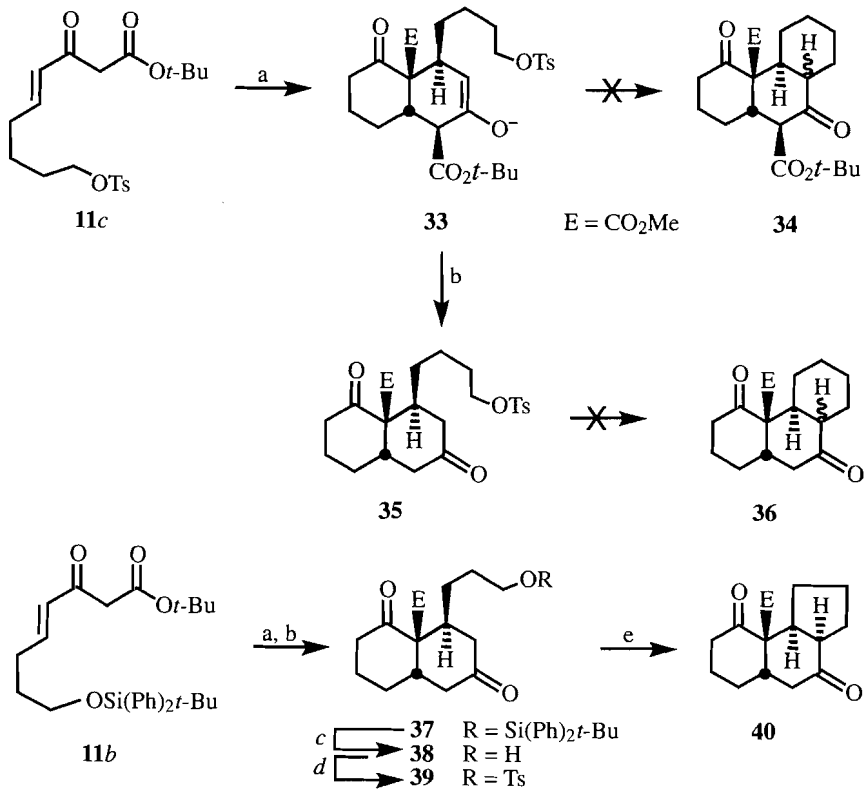

(a) $CsCO_3$, $CHCl_3$, then **1**, 25°C, 3.5 h; (b) *p*-TsOH, benzene, reflux, 1.5 h; (c) $(Bu)_4N^+F^-$, THF, 25°C, 0.5 h; (d) *p*-TsCl, $(Et)_3N$, CH_2Cl_2, 0°C, 2 h; (e) *t*-BuO^-K^+, *t*-BuOH/THF, 25°C, 20 min

SCHEME 6

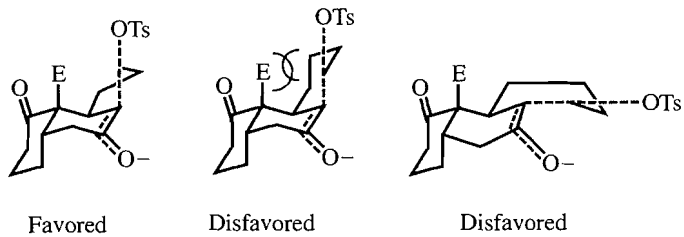

FIG. 2

ment with ethylene glycol and acid the resulting acetal-glycidyl ester was transesterified with sodium methoxide in methanol to give compound **65** (21). Then, in two steps, the methyl ester was transformed into β-keto ester **66** (22), which was then treated with aqueous acetic acid to give the desired compound **56** (23).

The cycloaddition can also be carried out on 4,4-disubstituted cyclohexenones. Reaction of substituted Nazarov reagent **2** with 4,4-dimethyl-2,5-cyclohexadienone derivative **58** (entry 3) gave the expected adduct **59** in 60% yield. The reaction of **58** with Nazarov reagents produces compounds that have the advantage of having an additional olefin functionality for further elaboration. However, its cycloaddition is slower and a large excess of the diene is needed. The stereochemistry in **59** was deduced by its transformation to a known structure (compound **33** in ref. 27*b*), using a sequence of reactions involving reduction of the ketone in the 6-position, tosylation, and elimination. Reaction using the 4-ketal derivative **60** gave, after decarboxylation, a 93% isolated yield of the expected adduct **61**. This dienophile has the marked advantage of being more reactive and more stable than **1** to the basic reaction conditions used in the Diels–Alder cycloaddition. Thus no excess of this reagent was needed to achieve completion of the cycloaddition reaction with **2** in higher yield. The protected ketone at the 4 position might then be used to epimerize the proton at C4a and thus give *trans*-decalins.

Mechanistic aspects of the reaction

Diels–Alder vs. double Michael

The reaction of a dienolate with a conjugated ketone can in principle follow a sequential double Michael addition or a Diels–Alder cycloaddition pathway (24). Determining which of these two processes is operative in any particular case can be very difficult. In such a reaction, the asynchronicity of the Diels–Alders (25) might be large enough so that differentiation between the two mechanisms becomes almost redundant. In addition, we cannot exclude the possibility that both mechanisms may be involved at the same time. The cycloaddition reaction might be favored by the fact that the diene is really an enolate ion. By analogy with the anionic oxy-Cope rearrangement (26), the negative charge on the oxygen enriches the diene in electron density and thus activates it. Note that the *silyl enol ether* of the β-keto ester **2** and of the β-keto sulfoxide **26** did not yield any trace of the Diels–Alder adducts when heated in toluene in the presence of dienophile **1** or when catalyzed by tin tetrachloride at low temperature. In both cases, only decomposition products were isolated.

Can. J. Chem. Downloaded from www.nrcresearchpress.com by 217.78.4.112 on 09/08/12
For personal use only.

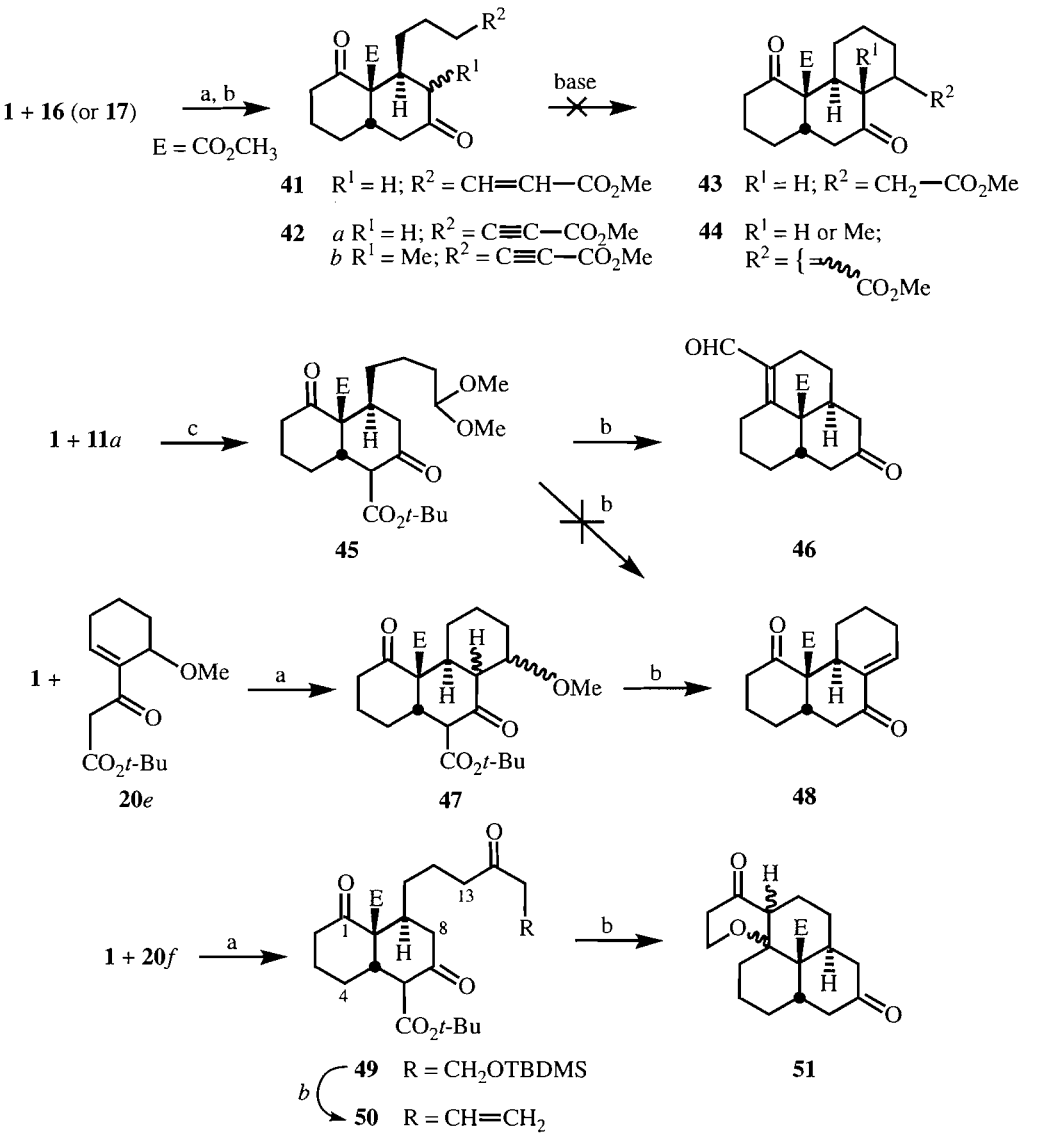

(a) Cs_2CO_3 in CH_2Cl_2, r.t.; (b) *p*-TsOH, benzene, reflux; (c) Cs_2CO_3 in $CHCl_3$, r.t.

SCHEME 7

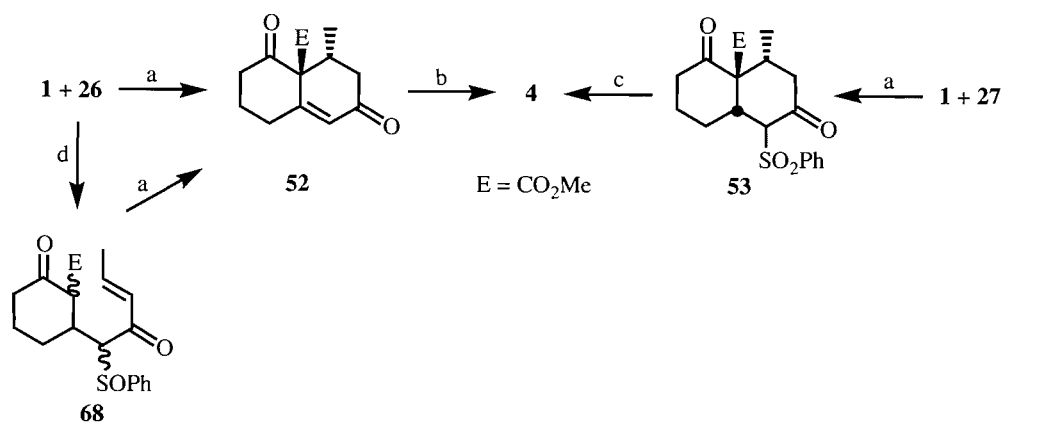

(a) Cs_2CO_3, CH_2Cl_2, 25°C, 2 h; (b) H_2, Pd/C, 72 h; (c) Al/Hg, THF–H_2O, 25°C, 4.5 h; (d) Cs_2CO_3, CH_2Cl_2, 0°C, 1 h

SCHEME 8

Can. J. Chem. Downloaded from www.nrcresearchpress.com by 217.78.4.112 on 09/08/12
For personal use only.

TABLE 3. Cycloadditions of diene **2** with substituted cyclohexenones

Entry	Dienophile	Diketone product	Yield (%)
		E=CO_2Me	
1	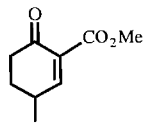 **54**	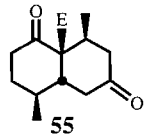 **55**	73
2	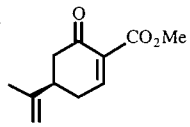 **56**	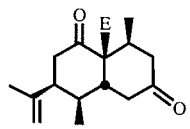 **57**	64
3	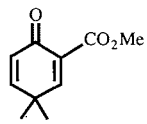 **58**	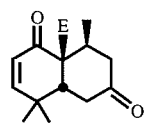 **59**	60
4	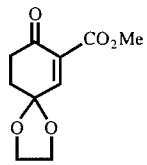 **60**	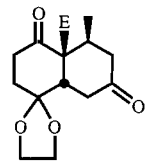 **61**	93

The results presented below indicate that the solvent greatly influences the pathway that the reaction will take. The solvent also affects the stereoselectivity of the reaction when β-keto esters are used as the diene. However, it would be wrong to assume that the degree of selectivity can be an indication of the mechanism involved. In other words, it is possible that the selectivity can be affected by the properties of the solvent for a given mechanism. We also observed differences in reactivity and rates of reaction in the different solvents.

The single Michael adduct **5** was isolated in 53% yield from the cesium carbonate catalyzed reaction of **1** and **2** in acetonitrile at −15°C (Scheme 1). But when the same reaction was carried out in chloroform at −15°C, only starting material was recovered, even after several hours. In addition, the mono-adduct **5** could not be cyclized in chloroform at 25°C. However, resubmitting **5** to the same reaction conditions at 25°C in acetonitrile afforded a 55% yield of a 7:3 mixture of decalin products **3** and **4**, after the usual decarboxylation reaction. These results indicate that the double Michael addition pathway is the preferred one in polar solvents such as acetonitrile and that the cycloaddition mechanism would be operative in less polar solvents such as chloroform.

In the case of the reaction of β-keto sulfoxide **26** with **1**, at −5°C in acetonitrile or at 0°C in dichloromethane, the single Michael adduct **68** was isolated along with starting material (Scheme 8). This adduct could be cyclized to the *cis*-decalin product **52** when resubmitted to the same reaction conditions at 25°C in either solvent. Here, the double Michael mechanism seems to be the preferred pathway no matter what solvent is used. Note, however, that in acetonitrile, at −5°C, the dehydrodecalin **52** was also isolated. This result likely reflects a faster rate of ring closure of the mono-adduct **68** in acetonitrile than in dichloromethane, although we cannot rule out the Diels–Alder mechanism in this case.

Mechanism and stereochemistry of the decalin products

Table 1 gives a summary of the different ratios of decalin products **3** and **4** obtained via the double Michael addition of Diels–Alder cycloaddition of dienolates to dienophile **1**, as well as via the Michael addition of single-Michael adducts. In cases where a Diels–Alder mechanism is thought to operate (entries 5 and 6), the preferred formation of the *cis,cis*-decalin **3** probably results from a most sterically favored approach of the diene and the dienophile as well as secondary orbital interaction between the ester function and the diene (*endo* rule due to the ester function) (27). Liu and

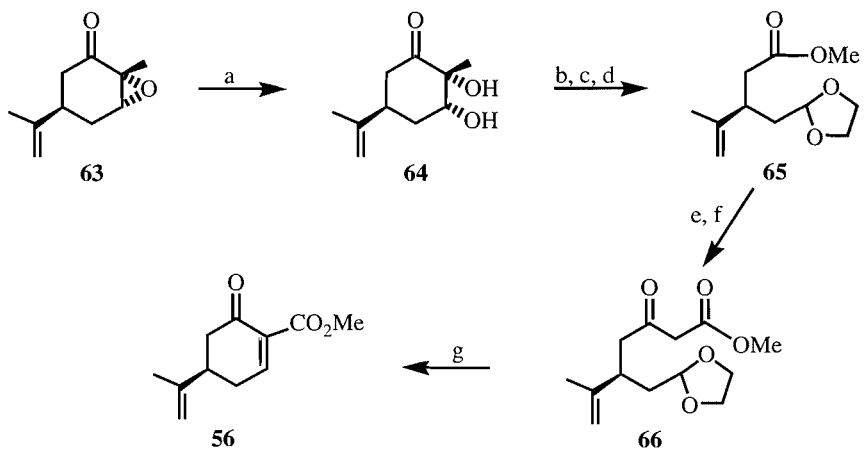

(a) THF, H_2SO_4–water 1:3, reflux, 24 h; (b) 2.2 equiv. $NaIO_4$, MeOH, 25°C; (c) Ethylene glycol, *p*-toluenesulfonic acid, benzene, reflux. 6 h; (d) NaOMe, MeOH, 12 h; (e) KOH, EtOH, reflux, 1.5 h; (f) Im_2CO, THF, 50°C, 1.5 h then *i*PrMgCl/$HO_2CCH_2CO_2CH_3$, (**62**), THF, then 0.5 N HCl; (g) 50% aqueous acetic acid, 25°C, 20 h

SCHEME 9

Can. J. Chem. Downloaded from www.nrcresearchpress.com by 217.78.4.112 on 09/08/12
For personal use only.

Can. J. Chem. Downloaded from www.nrcresearchpress.com by 217.78.4.112 on 09/08/12
For personal use only.

Ngooi also explained, in this way, the selectivity observed in the tin tetrachloride catalyzed [2+4] cycloadditions of dienes to dienophile **1** (3).

The selectivity observed in those cases where the double Michael addition is thought to be the preferred pathway is not easily explained. The exclusive formation of the *cis*-fused decalin is explained on the basis of stereoelectronic control (28) at the stage of the second Michael reaction. The formation of *cis*-fused decalin by an intramolecular Michael reaction has been previously demonstrated (4*a*,4*c*). As for the stereochemistry of the C8-alkyl substituent, it is thought to be thermodynamically controlled because of the fact that the monoadduct **5** gave, upon cyclization in base, the same product ratio as for the reaction of **1** with the corresponding dienolate **2** (Table 1, entry 10 vs. entry 3). (On the other hand, compound **67** lacking the additional ester function gave after basic cyclization a reverse ratio of **3** and **4**, Table 1, entry 9.) Correspondingly, the single Michael adduct **68** gave only the dehydrodecalin **52** when cyclized, as was found for the reaction of **1** and the diene-sulfoxide **26** (entries 8 and 12, respectively). One likely explanation is that the formation of the second bond is reversible and that the relative stabilities of the intermediates determine the final stereochemical outcome of the reaction.

Conclusion

The cycloaddition or double Michael addition of substituted Nazarov reagents with 2-carbomethoxy-2-cyclohexenones gives stereoselectively *cis,cis*-decalins or *cis, trans*-decalins. The reaction is quite general and proceeds with various substituted Nazarov reagents containing different functional groups. We wish to emphasize that these results are important with respect to natural products synthesis. Indeed, this type of stereochemistry is found at the A, B, and C ring junctions in several steroids and terpenoids. Work to further develop this approach for various natural products, including quassinoids, is presently being pursued in our laboratory.

Experimental

Unless otherwise stated, all reagents were used as received from the supplier. Tetrahydrofuran and diethyl ether were distilled over sodium and benzophenone. Dimethylformamide, chloroform, dichloromethane, and diisopropylamine were distilled over calcium hydride. Methylphenylsulfoxide and methyl iodide were distilled prior to use. Sodium hydride suspension in oil was washed with hexane prior to use except in reactions using less than 0.1 mmol where it was used as received. Potassium *tert*-butoxide was prepared freshly prior to use. *tert*-Butyldimethylsilyltriflate was prepared and distilled before us. *p*-Toluenesulfonyl chloride was recrystallized from benzene. Zinc granules were washed with 1 N hydrochloric acid, water, and acetone and dried prior to use. Pure aluminium foil was obtained from BDH.

Reactions were carried out under argon unless specified otherwise. Anhydrous magnesium sulfate was used as drying agent in the work-up of reactions. Flash chromatography was performed using Kieselgel 60 (230–400 mesh ASTM) silica gel from Merck. Infrared (ir) spectra were registered in chloroform solution (unless stated otherwise) on a Perkin–Elmer 681 spectrophotometer; the following abbreviations were used in ir: w = weak, m = medium, s = strong, b = broad. Proton or ^{13}C nuclear magnetic resonance (nmr) spectra were recorded on a Bruker WP-80, or WM-250 instrument; the following abbreviations were used in nmr: s = singlet, d = doublet, t = triplet; q = quartet, qi = quintet, m = multiplet, b = broad. Deuterated chloroform was used as solvent and internal standard. Mass spectra (ms) were recorded on a VG Micromass ZAB-1F mass spectrometer. All new compounds have been proven homogeneous by tlc and gc where possible prior to taking their H 250 MHz nmr and mass spectra.

IUPAC numbering was used for all compound names.

Preparation of substituted Nazarov reagents

tert-*Butyl 3-oxo-4-diethylphosphonyl-butanoate (**9**a)*

tert-Butyl acetoacetate (10 g, 0.063 mol) was slowly added to a suspension of NaH (2.78 g, 0.069 mol) in 500 mL of anhydrous THF at 0°C. After all evolution of H_2 had ceased, the reaction was stirred for 0.5 h at 0°C and *n*-BuLi (39.5 mL, 0.063 mol) was added over a period of 1 h. The resulting mixture was stirred at 0°C for an extra 30 min and diethylchlorophosphate (5.45 g, 0.032 mol) was slowly added. After the reaction mixture was stirred for 1 h at room temperature, an additional 19.75 mL of *n*-BuLi (0.031 mol) was slowly added. Then it was stirred for 30 min and diethylchlorophosphate (5.45 g, 0.032 mol) was slowly added. After it was stirred for 1 h at 0°C, the reaction mixture was poured into 500 mL of saturated aqueous ammonium chloride and 200 mL of ice cold 1 N HCl. The aqueous phase was extracted several times with diethyl ether, the combined organic layers were washed with brine, dried, and evaporated *in vacuo* to give an orange oil. Chromatography with hexane – ethyl acetate 1:3 afforded 12.6 g (67%) of a slightly yellow oil; ir (cm^{-1}): 1740, 1720, 1040; ^1H nmr (δ): 4.10 (4H, dq, J = 7.1, 8.3 Hz, -(OCH_2CH$_3$)$_2$), 3.51 (2H, s, -CO-CH_2-CO$_2$-), 3.20 (2H, d, J = 22.7 Hz, -PO-CH_2-CO-), 1.40 (9H, s, -CO$_2$C(CH_3)$_3$), 1.28 (6H, t, J = 7.1 Hz, -(OCH$_2$(CH_3)$_2$); ms (m/e): 294 (M^+), 239 (M^+ + 2 − C(CH$_3$)$_3$), 221 (M^+ − OC(CH$_3$)$_3$). Exact Mass calculated for $C_{12}H_{23}O_6P$: 294.1232; found: 294.1230.

tert-*Butyl 3-oxopentanoate (**8**b)*

tert-Butyl acetoacetate (10 g, 0.063 mol) was slowly added to a suspension of NaH (2.78 g, 0.069 mol) in 500 mL of anhydrous THF at 0°C. After all evolution of H_2 had ceased, the reaction was stirred for 30 min at 0°C and *n*-BuLi (39.5 mL, 0.063 mol) was added over a period of 1 h. The resulting mixture was stirred at 0°C for an extra 30 min and methyl iodide (9.35 g, 0.066 mol) was slowly added. After the reaction mixture was stirred for 1 h at room temperature, it was poured into 750 mL of ice cold 1 N HCl, the aqueous phase was extracted several times with diethyl ether, the combined organic phase was washed with brine, dried, and evaporated *in vacuo* to give an orange oil. Distillation (100°C/0.25 Torr (1 Torr = 133.3 Pa)) afforded 7.35 g (68%) of *tert*-butyl 3-oxopentanoate as a pale yellow oil; ir (cm^{-1}): 3000–2800, 1730 (bs); ^1H nmr (δ): 3.35 (s, 2H, O=C-CH_2-CO$_2$R), 2.55 (q, 2H, J = 7.0 Hz, CH$_3$-CH_2-C=O), 1.45 (s, 9H, OC(CH_3)$_3$), 1.08 (t, 3H, J = 7.0 Hz, CH_3-CH$_2$-C=O); ms (*m/e*): 115 (M^+ − *t*-Bu), 100, 57.

tert-*Butyl 3-oxo-4-diethylphosphonyl-pentanoate (**9**b)*

tert-Butyl 3-oxopentanoate (10.0 g, 0.058 mol) was treated in the same way as for the preparation of *tert*-butyl 3-oxo-4-diethoxyphosphonyl-butanoate **9***a*. This time 2.6 g (0.064 mol) of NaH, 36.2 and 18.1 mL (0.058 and 0.029 mol) of *n*-BuLi, and 2 × 5.01 g (0.029 mol) of diethylchlorophosphate were used in the reaction. After column chromatography (hexane – ethyl acetate 1:5), 8.05 g (45%) of the desired product **9***b* was isolated as a pale yellow oil; ir (cm^{-1}): 1740, 1720, 1040; ^1H nmr (δ): 4.15 (dq, 4H, J_{HH} = 8.5 and J_{PH} = 7.0 Hz, 2 × CH$_3$-CH_2-OP), 3.79 (d, 1H, J = 15.5 Hz, O=C-CH_2-CO$_2$R), 3.50 (m, 1H, O=P-(CH$_3$)C*H*-C=O), 3.54 (d, 1H, J = 15.5 Hz, O=C-CH_2-CO$_2$R), 1.7–1.2 (m, 9H, 2 × CH_3-CH$_2$-OP and O=P-(CH_3)CH-C=O), 1.46 (s, 9H, OC(CH_3)$_3$).

tert-*Butyl 9,9-dimethoxy-3-oxo-4-nonenoate (**11**a)*

To a stirred solution of phosphonate **9***a* (65 mg, 0.220 mmol) in THF (3 mL) was added sodium hydride (10 mg, 60% in oil, 0.250 mmol). After 15 min at room temperature, the solution was cooled to −30°C and a solution of *n*-BuLi (138 μL, 1.6 M in hex-

Can. J. Chem. Downloaded from www.nrcresearchpress.com by 217.78.4.112 on 09/08/12
For personal use only.

ane, 0.22 mmol) was added. After 10 min, a solution of the known aldehyde **10***a* (29 mg, 0.198 mmol) in THF (1 mL) was added and, after 5 min, the solution was warmed to room temperature for a period of 30 min. The mixture was then poured into a saturated solution of ammonium chloride (10 mL) at 0°C. The aqueous layer was extracted with diethyl ether (4 × 10 mL). The combined organic layers were washed with brine (1 × 10 mL), dried, filtered and the solvents were removed under reduced pressure. The residue was purified by flash chromatography with hexane – ethyl acetate (3:1) to afford substituted Nazarov reagent **11***a* (22 mg, 35%); ir (cm^{-1}): 1725, 1690, 1670, 1630, 1600, 1150; ^1H nmr (δ): 11.50 (<1H, d, J = 1.5 Hz, enol form), 7.10–6.30 (1H, 2 dt, J = 6.8, 16.1 Hz, =C*H*-CH_2-), 6.30–5.60 (1H, dt and dq, J = 1.5, 16.1 Hz, -CO-C*H*=), 4.89 (<1H, s, =C*H*-CO_2- enol form), 4.36 (1H, t, J = 5.4 Hz, -O-C*H*-O-), 3.47 (<2H, s, -CO-CH_2-CO_2-), 3.32, (6H, s, -C(OCH_3)$_2$), 2.25 (2H, m, =CH-CH_2-), 1.75–1.50 (4H, m), 1.49 (<9H, s, -CO_2(CH_3)$_3$), 1.46 (<9H, s, -CO_2(CH_3)$_3$).

tert-*Butyl 8*-tert-*butyldiphenylsilyloxy-3-oxo-4-octenoate (**11**b)*

The substituted Nazarov reagent **11***b* was prepared in the same manner as **11***a* except that the saturated solution of ammonium chloride was replaced by a solution of hydrochloric acid (1 N). The aldehyde **10***b* (102 mg, 0.312 mmol) gave, after purification, substituted Nazarov reagent **11***b* (110 mg, 76%); ir (cm^{-1}): 1730, 1690, 1670, 1630, 1600, 1150; ^1H nmr (δ): 11.48 (<1H, d, J = 3.9 Hz, enol form), 7.80–7.30 (10H, m, aromatic protons), 7.00–6.40 (1H, 2, dt, J = 6.8, 15.6 Hz, -CH_2-C*H*=), 6.30–5.60 (1H, dt and dq, J = 1.7, 15.6 Hz, -CO-C*H*=), 4.89 (<1H, s, =CH-CO_2- enol form), 3.70 (2H, t, J = 5.9 Hz, -CH_2-O-), 3.47 (<2H, s, -CO-CH_2-CO_2-), 2.30 (2H, m, =CH-CH_2-), 1.70 (2H, m, -CH_2-CH_2-O-), 1.50 (9H, s, -CO_2C(CH_3)$_3$), 1.10 (9H, s, -SiC(CH_3)$_3$), 0.03 (6H, s, -Si-(CH_3)$_2$-C(CH_3)$_3$).

tert-*Butyl 9*-p-*toluenesulfonyloxy-3-oxo-4-nonenoate (**11**c)*

The substituted Nazarov reagent **11***c* was prepared in the same manner as **11***b*. The aldehyde **10***c* (44 mg, 0.172 mmol) gave, after purification, substituted Nazarov reagent **11***c* (22 mg, 33%); ir (cm^{-1}): 1730, 1690–1660, 1630, 1600, 1365, 1175; ^1H nmr (δ): 11.51 (<1H, d, J = 1.5 Hz, enol form), 7.90–7.20 (4H, 2d, J = 8.5 Hz, aromatic protons), 7.00–6.25 (1H, 2 dt, J = 6.8, 15.6 Hz, =C*H*-CH_2-), 6.20–5.50 (1H, dt and dq, J = 1.5, 15.6 Hz, -CO-C*H*=), 4.88 (<1H, s, -C*H*=C-O- enol form), 4.04 (2H, t, J = 5.9 Hz, -CH_2-OSO_2-), 3.46 (<2H, s, -CO-CH_2-CO_2-), 2.45 (3H, s, =C-CH_3), 2.20 (2H, m, =CH-CH_2-), 1.70–1.30 (4H, m, -(CH_2)$_2$-CH_2-OSO_2-), 1.49 (<9H, s, -CO_2C(CH_3)$_3$), 1.45 (<9H, s, -CO_2C(CH_3)$_3$).

*3-Bromo-1-tetrahydropyranyloxy-propane (**15**)*

To a solution of 3-bromopropanol (10.0 g, 0.072 mol) in 500 mL of anhydrous THF at 0°C were added 7.84 g of dihydropyran (0.093 mol) and 1.3 g of *p*-toluenesulfonic acid (0.007 mol). The resulting mixture was stirred at 0°C for 1 h and at room temperature for 12 h, then it was poured into 750 mL of saturated sodium bicarbonate. The aqueous phase was extracted several times with diethyl ether, the combined organic phase was washed with brine, dried, and evaporated *in vacuo* to give an yellow oil. Distillation (95°C/3.5 Torr) afforded 14.70 g (92%) of 1-bromo-3-tetrahydropyranyloxy-propane as a colorless oil; ir (cm^{-1}): 3000–2800, 1475, 1370, 1150(s); ^1H nmr (δ): 4.56 (m, 1H, O-C*H*-O), 4.0–3.3 (m, 6H, 2 × RCH_2-O and Br-CH_2), 2.10 (qi, 2H, J = 7.0 Hz, CH_2-CH_2-CH_2), 1.9–1.2 (m, 6H, O-CH_2-(CH_2)$_3$-CH-O); ms (*m/e*): 224 (M^+), 223, 222 (M^+), 142, 140.

*6-Trimethylsilyl-5-hexynal (**12**)*

A solution of *n*-BuLi in hexanes (1.6 M, 8.4 mL, 13.5 mmol) was placed in a 100 mL round bottom flask. The solvent was removed under vacuum at 20°C and 60 mL of anhydrous diethyl ether was added. After cooling the mixture to −15°C, tetramethylethylenediamine (1.57 g, 13.5 mmol) was added followed by 1-trimethylsilyl-1-propyne (1.51 g, 13.5 mmol) and the resulting mixture was stirred at −10°C for 3 h. Then 1-bromo-3-tetrahydropyranyloxy-propane (1.50 g, 6.7 mmol) was added and the resulting reaction mixture was stirred overnight at a temperature between −10 and −3°C. After 12 h, a yellow precipitate formed. The reaction mixture was poured into 100 mL of ice cold 1 N hydrochloric acid, the aqueous phase was extracted several times with diethyl ether, the combined organic layers were washed with saturated sodium bicarbonate, then with brine, dried, and evaporated *in vacuo* to give an orange oil. Distillation (110–115°C/0.25 Torr) afforded 1.79 g (99%) of 6-tetrahydropyranyloxy-1-trimethylsilyl-1-hexyne as a colorless oil; ir (cm^{-1}): 3000–280, 2170, 1455, 1445, 1250, 1140, 1120, 1075, 1035(s), 850 (s); ^1H nmr (δ): 4.55 (m, 1H, O-C*H*-O), 3.2–4.0 (m, 4H, 2 × RCH_2-O-R), 2.26 (t, 2H, J = 6.5 Hz, CH_2-CH_2-C≡CTMS), 1.7–1.4 (m, 10H), 0.15 (s, 9H, Si(CH_3)$_3$); ms (m/e): 254 (M^+), 239, 225, 211, 209.

A solution of 6-tetrahydropyranyloxy-1-trimethylsilyl-1-hexyne (4.79 g, 18.8 mmol) in 60 mL of anhydrous methanol was cooled to 0°C and 459 mg (1.83 mmol) of pyridinium *p*-toluenesulfonate acid was added. The mixture was stirred at room temperature for 24 h. Then solid potassium bicarbonate (700 mg, 7.0 mmol) was added and the solvent was removed *in vacuo*. The residue was taken up in diethyl ether and was washed with 2 × 25 mL of water, dried, and evaporated *in vacuo* to give a yellow oil. Chromatography with hexane – ethyl acetate 5:1, then 3:1, afforded 2.61 g (82%) of 6-trimethylsilyl-5-hexyn-1-ol as a colorless oil; ir (cm^{-1}): 3600, 3000–2800, 2175, 1250, 1230–1200(s), 1045, 850(s); ^1H nmr (δ): 3.72 (bt, 2H, J = 5.5 Hz, HO-CH_2-), 2.28 (t, 2H, J = 6.5 Hz, CH_2-CH_2-C≡CTMS), 1.85–1.45 (m, 4H), 1.30 (bs, 1H, *H*O-CH_2-), 0.18 (s, 9H, Si(CH_3)$_3$); ms (*m/e*): 169 (M^+ − 1), 155, 153, 139, 137, 127, 126.

Dimethyl sulfoxide (2.31 g, 0.027 mol) was slowly added to a solution of oxalyl chloride (1.89 g, 0.015 mol) in 130 mL of anhydrous dichloromethane at −78°C. After 15 min., 6-trimethylsilyl-5-hexyn-1-ol (2.61 g, 0.027 mol), was added and the mixture was stirred for 15 min. Triethylamine (6.5 g, 0.064 mol) was added and the reaction was allowed to warm to room temperature. The solvent was then removed *in vacuo* and the residue was taken up in hexane, washed with water (2 × 50 mL), dried, and evaporated under reduced pressure to give 1.70 g (78%) of 6-trimethylsilyl-5-hexynal **12** as a yellow oil that was used directly in the next reaction.

tert-*Butyl (4E)-3-oxo-10-trimethylsilyl-4-decen-9-ynoate (**13**a)*

Sodium hydride (60% in oil, 430 mg, 10.8 mmol) was washed twice with 5 mL of hexane; 100 mL of anhydrous THF was added and the suspension was cooled down to 0°C. *tert*-Butyl 3-oxo-4-diethylphosphonylbutanoate **9***a* (3.1 g, 10.4 mmol) was added slowly and the mixture was stirred for 15 min, then it was cooled to −30°C and *n*-BuLi (1.6 M in hexanes, 6.5 mL, 10.4 mmol) was added. After stirring for 10 min, 6-trimethylsilyl-5-hexynal (1.70 g, 10.1 mmol) in 10 mL of THF was added and the resulting mixture was stirred for 5 min, then it was allowed to warm to room temperature and stirred for another 30 min. The reaction mixture was poured into 100 mL of ice cold 1 N hydrochloric acid, the aqueous phase was extracted several times with diethyl ether, the combined organic layers were washed with brine, dried, and evaporated *in vacuo* to give an orange oil. Chromatography with hexane – ethyl acetate 8:1 afforded 2.41 g (77%) of *tert*-butyl (3*E*)-3-oxo-10-trimethylsilyl-4-decen-9-ynoate (**13***a*) as a colorless oil; ir (cm^{-1}): 3100–3000, 3000–2800, 2180, 1725, 1675, 1625, 1600, 1370, 1250, 1215(s), 1150, 850(s); ^1H nmr (δ): 12.35 (s, <1H, *H*O-C=CH-CO_2R), 6.85 (dt, <1H, J = 15.5, 6.5 Hz, O=C-CH=C*H*-), 6.36 (dt, <1H, J = 15.5, 6.5 Hz, HO-C=CH=C*H*-), 6.15 (dt, <1H, J = 15.5, 1.5 Hz, O=C-C*H*=CH-), 5.77 (dt, <1H, J = 15.5, 1.5 Hz, HO-C=C*H*=CH-), 4.87 (s, <1H, HO-C=C*H*=CO_2R), 3.44 (s, <2H, O=C-CH_2-CO_2R), 2.5–2.1 (m, 4H), 1.9–1.1 (m, 3H), 1.45 (s, <9H, OC(CH_3)$_3$, enol), 1.41 (s, <9H, OC(CH_3)$_3$), 0.12 (s, 9H, Si(CH_3)$_3$); ms (*m/e*): 251 (M^+ − *t*-Bu), 237, 235, 219, 107. Exact Mass calculated for $C_{13}H_{19}O_3Si$: 251.1103; found: 251.1107.

Can. J. Chem. Downloaded from www.nrcresearchpress.com by 217.78.4.112 on 09/08/12
For personal use only.

tert-*Butyl (4*E*)-4-methyl-3-oxo-10-trimethylsilyl-4-decen-9-ynoate (**13***b*)

This procedure was identical to that used in the preparation of *tert*-butyl (3*E*)-3-oxo-10-trimethylsilyl-4-decen-9-ynoate **13***a*. *tert*-Butyl 3-oxo-4-diethylphosphonylpentanoate **9***b* (2.74 g, 8.91 mmol), sodium hydride (374 mg, 9.35–mmol), *n*-BuLi (5.56 mL, 8.91 mmol), 6-trimethylsilyl-5-hexynal **12** (1.50 g, 8.91 mmol) in 10 mL of THF gave 1.12 g (44%) of the desired β-keto ester **13***b*; ir (cm^{-1}): 3100–3000, 3000–2800, 2180, 1730, 1675, 1630, 1380, 1250(s), 1150, 850(s); ^1H nmr (δ): 6.57 (bt, 1H, J = 5.5 Hz, O=C-C(CH_3)=C*H*-), 3.60 (s, 2H, O=C-CH_2-CO_2R), 2.39 (q, 2H, J = 5.5 Hz, C(CH_3)=CH-CH_2), 2.26 (t, 2H, J = 5.5 Hz, CH_2-CH_2-CH_2-C≡CTMS), 1.83 (d, 3H, J = 1.0 Hz, O=C-C(CH_3)=CH-), 1.68 (qi, 2H, J = 5.5 Hz, CH_2-CH_2-CH_2-C≡CTMS), 1.46 (s, 9H, OC(CH_3)$_3$), 0.15 (s, 9H, Si(CH_3)$_3$); ms (*m/e*): 265 (M^+ − *t*-Bu), 251, 249, 233. Exact Mass calculated for $C_{14}H_{21}O_3Si$: 265.1260; found: 265.1260.

tert-*Butyl (4*E*)-3-oxo-10-carbomethoxy-4-decen-9-ynoate (**16***a*)

Tetrabutylammonium fluoride (1 M in THF, 2.78 mL, 2.78 mmol) was added to a solution of *tert*-butyl (4*E*)-3-oxo-10-trimethylsilyl-4-decen-9-ynoate **13***a* (715 mg, 2.32 mmol) in 10 mL of anhydrous THF at 0°C. The reaction mixture was stirred at 0°C for 1 h. Then it was poured into 50 mL of brine, the aqueous phase was extracted several times with diethyl ether, the combined organic layers were dried and evaporated *in vacuo* to give an orange oil. Chromatography with hexane – ethyl acetate 15:1 afforded 468 mg (90%) of a colorless oil; ir (cm^{-1}): 3100–3000, 3000–2800, 2180, 1725, 1675, 1625, 1600, 1370, 1250, 1215(s), 1150, 850(s); ^1H nmr (δ): 12.31 (s, <1H, *H*O-C=CH-CO_2R), 6.83 (dt, <1H, J = 15.5, 6.5 Hz, O=C-CH=C*H*-), 6.36 (dt, <1H, J = 15.5, 6.5 Hz, HO-CH=C*H*-), 6.10 (dt, <1H, J = 15.5, 1.5 Hz, O=C-C*H*=CH-), 5.69 (dt, <1H, J = 15.5, 1.5 Hz, HC=C(OH)-CH=CH), 4.78 (s, <1H, HO-C=C*H*-CO_2R), 3.34 (s, <2H, O=C-CH_2-CO_2R), 2.4–0.9 (m, 7H), 1.36 (s, <9H, OC(CH_3)$_3$, enol), 1.33 (s, <9H, OC (CH_3)$_3$); ms (*m/e*): 179 (M^+ − *t*-Bu), 163, 153, 136, 134, 122. Exact Mass calculated for $C_{10}H_{11}O_3$: 179.0708; found: 179.0711.

Sodium hydride (66 mg, 1.66 mmol) was added to a solution of *tert*-butyl (4*E*)-3-oxo-4-decen-9-ynoate (208 mg, 0.83 mmol) in 10 mL of anhydrous THF at 0°C. After 30 min, the mixture was cooled to −78°C and *n*-BuLi (0.52 mL, 0.83 mmol) was slowly added. The resulting mixture was stirred for 10 min at −78°C and then warmed slowly to 0°C and stirred at that temperature for 15 min. Then it was cooled again to −78°C and methyl chloroformate (78 mg, 0.83 mmol) was added. The reaction mixture was stirred while warming slowly to room temperature. Then it was poured into 20 mL of saturated aqueous ammonium chloride, the aqueous phase was extracted several times with diethyl ether, the combined organic layers were washed with brine, dried, and evaporated *in vacuo* to give an orange oil. Chromatography with hexane – ethyl acetate 8:1 afforded 226 mg (93%) of **16***a* as a colorless oil; ir (cm^{-1}): 3100–3000, 3000–2800, 2180, 1725, 1675, 1625, 1600, 1370, 1250, 1215(s), 1150, 850(s); ^1H nmr (δ): 12.01 (s, <1H, *H*O-C=CH-CO_2R), 6.83 (dt, <1H, J = 15.9, 6.9 Hz, O=C-CH=C*H*-), 6.55 (dt, <1H, J = 15.9, 6.9 Hz, HO-C-CH=C*H*-), 6.20 (dt, <1H, J = 15.9, 1.5 Hz, O=C-C*H*=CH-), 5.78 (dt, <1H, J = 15.9, 1.5 Hz, HC=C(OH)-C*H*=CH-), 4.90 (s, <1H, OH-C=C*H*-CO_2R), 3.76 (s, 3H, O=C-OCH_3), 3.48 (s, <2H, O=C-CH_2-CO_2R), 2.45–2.25 (m, 4H, -CH_2CH_2CH_2-), 1.76 (qi, 2H, J = 7.5 Hz, -CH_2C$H_2$$CH_2$-), 1.49 (m, <9H, OC(C$H_3$)$_3$, enol), 1.45 (m, <9H, OC(CH_3)$_3$); ms (*m/e*): 239 (M^+ − *t*-Bu), 189, 179, 162, 160, 138. Exact Mass calculated for $C_{12}H_{13}O_5$: 237.0763; found: 237.0759.

tert-*Butyl (4*E*)-4-methyl-3-oxo-10-carbomethoxy-4-decen-9-ynoate (**16***b*)

The title compound was prepared as described in the preparation of *tert*-butyl (3*E*)-3-oxo-10-carbomethoxy-4-decen-9-ynoate **16***a*. The removal of the trimethylsilyl group was achieved using 1.12 g of *tert*-butyl (4*E*)-4-methyl-3-oxo-10-trimethylsilyl-4-decen-9-ynoate **13***b* (3.60 mmol) and 4.36 mL of tetrabutylammonium fluoride (4.36 mmol). Chromatography using hexane – ethyl acetate 15:1 gave 786 mg (86%) of *tert*-butyl (4*E*)-4-methyl-3-oxo-4-decen-9-ynoate as a colorless liquid; ir (cm^{-1}): 3100–3000, 3000–2800, 2180, 1725, 1675, 1625, 1600, 1370, 1250, 1215(s), 1150, 850(s); ^1H nmr (δ): 6.57 (dt, 1H, J = 5.0, 1.0 Hz, O=C-C(CH_3)=C*H*-), 3.59 (s, 2H, O=C-CH_2-CO_2R), 2.39 (q, 2H, J = 5.5 Hz, C(CH_3)=CH-CH_2), 2.24 (dt, 2H, J = 5.5, 1.8 Hz, CH_2-CH_2-CH_2-C≡CH), 1.98 (t, 1H, J = 1.8 Hz, CH_2-CH_2-CH_2-C≡C*H*), 1.81 (d, 3H, J = 1.0 Hz, O=C-C(CH_3)=CH-), 1.70 (qi, 2H, J = 5.5 Hz, CH_2-CH_2-CH_2-C≡CH), 1.43 (s, 9H, OC(CH_3)$_3$); ms (*m/e*): 193 (M^+ − *t*-Bu), 177, 167, 150, 148, 136. Exact Mass calculated for $C_{11}H_{13}O_3$: 193.0865; found: 193.0866.

Then 160 mg of *tert*-butyl (4*E*)-4-methyl-3-oxo-4-decen-9-ynoate (0.64 mmol), 51 mg of sodium hydride (1.30 mmol), 0.42 mL of *n*-BuLi (0.64 mmol), and 60 mg of methyl chloroformate (0.64 mmol) were used for the reaction. Chromatography using hexanes – ethyl acetate 8:1 gave 101 mg (51%) of **16***b* as a colorless liquid; ir (cm^{-1}): 3100–3000, 3000–2800, 2180, 1725, 1675, 1625, 1600, 1370, 1250, 1215(s), 1150, 850(s); ^1H nmr (δ): 6.54 (dt, 1H, J = 6.0, 1.0 Hz, O=C-C(CH_3)=C*H*-) , 3.76 (s, 3H, O=COCH_3), 3.60 (s, 2H, 2H, O=C-CH_2-CO_2R), 2.39 (t, 2H, J = 7.0 Hz, CH_2-CH_2-CH_2-C≡C-), 2.38 (q, 2H, J = 7.0 Hz, C(CH_3)=CH-CH_2), 1.81 (d, 3H, J = 1.0 Hz, O=C-C(CH_3)=CH-), 1.76 (qi, 2H, J = 7.0 Hz, CH_2-CH_2-CH_2-C≡C-), 1.44 (s, 9H, OC(CH_3)$_3$); ms (*m/e*): 251 (M^+ − *t*-Bu), 203, 193, 162, 160, 138. Exact Mass calculated for $C_{13}H_{15}O_5$: 251.0919; found: 251.0916.

tert-*Butyl (4*E*,9*Z*)-3-oxo-10-carbomethoxy-4,9-decadienoate (**17**)*

tert-Butyl (4*E*)-3-oxo-10-carbomethoxy-4-decen-9-ynoate **16***a* (50 mg, 0.17 mmol) was dissolved in 2.5 mL of ethyl acetate. Then 2.5 mg of Lindlar's catalyst (5% w/w) was added and hydrogen was bubbled through the solution while the reaction was monitored by tlc. When all the starting material had gone, the mixture was filtered on Celite and the solvent evaporated *in vacuo* to give a yellow oil. Chromatography on silica gel using hexane – ethyl acetate 6:1 gave 30 mg (59%) of the desired *cis* olefin; ir (cm^{-1}): 3100–3000, 3000–2800, 2180, 1725, 1675, 1625, 1600, 1370, 1250, 1215(s), 1150, 850(s); ^1H nmr (250 MHz δ): 12.02 (s, <1H, *H*O-C=CH-CO_2R), 6.87 (dt, <1H, J = 15.9, 6.8 Hz, O=C-CH=C*H*-), 6.61 (dt, <1H, J = 15.9, 6.8 Hz, HO-CH=C*H*-), 6.28–6.12 (m, 2H, -C*H*=C*H*-CO_2CH_3), 5.85–5.74 (m, 1H, O=C-C*H*=CH- and enol), 4.88 (s, <1H, HO-C=CH_2-CO_2R), 3.71 (s, 3H, O=C-OCH_3), 3.48 (s, <2H, O=C-CH_2-CO_2R), 2.70 (m, 2H, CH_2-CH_2-CH_2-), 2.26 (m, 2H, CH_2-CH_2-CH_2-), 1.63 (m, 2H, CH_2-CH_2-CH_2-), 1.49 (m, <9H, OC(CH_3)$_3$), enol), 1.46 (m, <9H, OC(CH_3)$_3$); ms (*m/e*): 241 (M^+ − *t*-Bu), 191, 181, 166, 164, 162, 140. Exact Mass calculated for $C_{12}H_{15}O_5$: 239.0919; found: 239.0915.

tert-*Butyl (4*E*)-3-oxo-4-hexanoate (**2**)*

To zinc granules (3.92 g, 60.0 mmol) in THF (6 mL) was added *tert*-butyl bromoacetate (0.6 mL, 3.7 mmol) and one crystal of iodine. This mixture was refluxed under argon for 5 min and when the reaction had started, *tert*-butyl bromoacetate (7.4 mL, 45.6 mmol) in THF (25 mL) was added dropwise in order to maintain a gentle reflux. Reflux was continued for 1 h after the addition, then the mixture was cooled to room temperature and transferred, via a cannula, into a stirred solution of crotonaldehyde (2.71 g, 38.5 mmol) in diethyl ether (50 mL) at 0°C. After 30 min, a saturated ammonium chloride solution was added and the aqueous layer was extracted with diethyl ether (3 × 30 mL). The combined organic layers were dried, filtered, and the solvents were evaporated. The oily residue was chromatographed on silica gel (hexane:ethyl acetate, 2:1) to give *tert*-butyl (4*E*)-3-hydroxy-4-hexenoate (6.0 g, 83%); ir (cm^{-1}): 3600–3300, 171; ^1H nmr (δ):

Can. J. Chem. Downloaded from www.nrcresearchpress.com by 217.78.4.112 on 09/08/12
For personal use only.

5.90–5.30 (2H, m, olefinic), 4.42 (1H, m, -C*H*-OH), 2.97 (1H, d, J = 4.0 Hz, -CHO*H*), 2.44 (2H, d, J = 5.8 Hz, -CH_2-), 1.68 (3H, dd, J = 1.0, 4.9 Hz, CH_3-CH), 1.45 (9H, s, -C(CH_3)$_3$).

To a stirred solution of *tert*-butyl (4*E*)-3-hydroxy-4-hexenoate (1.34 g, 7.21 mmol) in ethyl acetate (105 mL) was added, at 25°C, manganese dioxide (12.6 g, 144.9 mmol). After stirring 5 h under argon, the mixture was filtered through silica gel and the solvent was evaporated and the residue purified by flash chromatography (dichloromethane – diethyl ether, 95:5) to give *tert*-butyl (4*E*)-3-oxo-4-hexenoate (967 mg, 73%); ir (cm^{-1}): 1730, 1690, 1670 (enol), 1630, 1600; ^{1}H nmr (δ): 7.10–6.30 (1H, dq, J = 6.8, 17.0 Hz, =C*H*-CH$_3$), 6.30–5.65 (1H, 2 dq, J = 1.5, 17.0 Hz, CO-C*H*=CH), 4.86 (<1H, s, C=C*H*-CO$_2$, of enol form), 3.46 (<2H, s, -CH$_2$-), 1.92 (3H, 2 dd, J = 1.5, 6.8 Hz, =CH-C*H*$_3$), 1.45 (9H, 2s, -CO$_2$C(C*H*$_3$)$_3$).

tert-*Butyl 4-methyl-3-oxo-4-hexenoate (**20**b)*

To a stirred suspension of granular zinc (412 mg, 6.3 mmol) in THF (15 mL) at room temperature and under an argon atmosphere, were added *tert*-butyl bromoacetate (0.68 mL, 4.2 mmol) and a crystal of iodine. The mixture was heated to reflux for 1 h and then cooled to 0°C. A solution of commerically available *trans*-2-methyl-2-butenal (234 mg, 2.5 mmol) in ether (5 mL) was then added via a cannula to the Reformatsky reagent. After stirring for 1 h, a saturated ammonium chloride solution (10 mL) was added, and the salts formed were dissolved in water (40 mL). The separated aqueous layer was extracted with diethyl ether (4 × 25 mL). The combined organic layers were washed with brine (25 mL), dried, and the solvents evaporated under reduced pressure. Flash chromatography (hexane – ethyl acetate 4:1) yielded 389 mg (70%) of the corresponding allylic alcohol; ir (neat, cm^{-1}): 3440 (OH), 1740–1710 (C=O ester); ^{1}H nmr (δ): 5.55 (1H, m, CH$_3$C*H*=C(CH$_3$)-), 4.37 (1H, m, -C*H*OH), 2.92 (1H, d, J = 3.4 Hz, -O*H*, exchanges with D$_2$O), 2.50 (1H, dd, J = 15.8, 8.5 Hz, -CH(OH)C*H*$_2$CO$_2$-), 2.40 (1H, dd, J = 15.8, 4.3 Hz, -CH(OH)C*H*$_2$CO$_2$-), 1.61 (3H, s, CH$_3$CH=C-C*H*$_3$-), 1.60 (3H, dd, J = 8.3, 0.8 Hz, C*H*$_3$CH=C-CH$_3$-), 1.45 (9H, s, -CO$_2$(C*H*$_3$)$_3$).

To a stirred solution of *trans-tert*-butyl-3-hydroxy-4-methyl-4-hexenoate (127 mg, 0.6 mmol) in ethyl acetate (15 mL) was added manganese dioxide (825 mg, 9.5 mmol). After stirring for 15 h at room temp., the mixture was filtered through silica gel and the solvent was evaporated under reduced pressure. Flash chromatography (hexane – ethyl acetate (3:17)) yielded 88 mg (70%) of β-keto ester **21**; ir (neat, cm^{-1}): 1735 (C=O ester), 1690 (C=O conjugated ketone); ^{1}H nmr (δ): 12.35 (<1H, s, -CH=C-O*H*), 6.65 (>1H, m, CH$_3$C*H*=C(CH$_3$)-), 5.07 (<1H, s, -C*H*=C-OH), 3.60 (2H, s, -COC*H*$_2$CO$_2$-), 1.88 (3H, dd, J = 6.9, 1.0 Hz, C*H*$_3$CH=C(CH$_3$)-), 1.80 (>3H, m, CH$_3$CH=C-C*H*$_3$, enol form and β-keto ester, and C*H*$_3$CH=C-CH$_3$, enol form), 1.50 (<9H, s, -CO$_2$C(C*H*$_3$)$_3$), 1.45 (9H, s, -CO$_2$(C*H*$_3$)$_3$).

tert-*Butyl 3-(1-cyclohexen-1-yl)-3-oxopropanoate (**20**c)*

The procedure described for the synthesis of substituted Nazarov reagent **2** was performed using 1-formyl-1-cyclohexene (100 mg, 0.9 mmol), granular zinc (119 mg, 1.8 mmol), *tert*-butyl bromoacetate (0.22 mL, 1.4 mmol). Flash chromatography yielded 142 mg (69%) of a β-hydroxy-ester; ir (neat, cm^{-1}): 3440 (OH), 1750–1700 (C=O ester); ^{1}H nmr (δ): 5.73 (1H, m, -C*H*=C), 4.33 (1H, ddd, J = 7.5, 5.0, 3.8 Hz, -C*H*OH, becomes dd, J = 7.5, 5.0 Hz upon treatment with D$_2$O), 2.93 (1H, d, J = 3.8 Hz, -CHO*H*, exchanges with D$_2$O), 2.80–1.45 (10H, m), 1.45 (9H, s, -CO$_2$C(C*H*$_3$)$_3$); ms (*m/e*): 170 (MH$^+$ – C$_4$H$_9$), 152 (MH$^+$ – C$_4$H$_9$-H$_2$O). Exact Mass calculated for C$_9$H$_{14}$O$_3$ (MH$^+$ – C$_4$H$_9$): 170.0943; found: 170.0940.

This β-hydroxy ester (140 mg, 0.6 mmol) was dissolved in ethyl acetate (10 mL) and the procedure described for allylic oxidation leading to **2** was followed using manganese dioxide (808 mg, 9.3 mmol). The *tert*-butyl β-keto ester **20***c* was purified by flash chromatography (hexane – ethyl acetate 4:1), which yielded 90 mg (65%); ir (neat, cm^{-1}): 3440 (OH), 1750–1700 (C=O ester); ^{1}H nmr (δ): 12.27 (<1H, s, -CH=C-O*H*), 6.87 (>1H, m, -C*H*=C-), 5.02 (<1H, s, -C*H*=C-OH), 3.58 (2H, s, -COC*H*$_2$CO$_2$-), 2.81–1.52 (>8H, m), 1.46 (<9H, s, -CO$_2$C(C*H*$_3$)$_3$), 1.45 (9H, s, -CO$_2$C(C*H*$_3$)$_3$); ms (*m/e*): 168 (MH$^+$ – C$_4$H$_9$), 150 (MH$^+$ – C$_4$H$_9$ – H$_2$O). Exact Mass calculated for C$_9$H$_{12}$O$_3$ (MH$^+$ – C$_4$H$_9$): 168.0787; found: 168.0781.

tert-*Butyl 5-methyl-3-oxo-4-hexenoate (**20**d)*

The procedure described for the preparation of Nazarov reagent **2** was performed using 3-methyl-2-butenal (230 mg, 2.5 mmol), granular zinc (412 mg, 6.3 mmol), *tert*-butyl bromoacetate (0.68 mL, 4.2 mmol) in THF (20 mL) and ether (5 mL). The corresponding β-hydroxy ester was purified by flash chromatography (hexane – ethyl acetate (3:1) to yield 416 mg (74%); ir (neat, cm^{-1}): 3440 (OH), 1740–1720 (C=O ester); ^{1}H nmr (δ): 5.17 (1H, dt, J = 8.7, 1.3 Hz, (CH$_3$)$_2$C=C*H*-), 4.71 (1H, m, -C*H*OH), 2.91 (1H, d, J = 3.3 Hz, -CHO*H*), 2.45 (1H, dd, J = 16.3, 8.1 Hz, -C*H*$_2$CO$_2$-), 2.35 (1H, dd, J = 16.3, 4.6 Hz, -C*H*$_2$CO$_2$-), 1.71 (3H, d, J = 1.1 Hz, -C=C(C*H*$_3$)$_2$), 1.69 (3H, d, J = 1.3 Hz, -C=C(C*H*$_3$)$_2$), 1.45 (9H, s, -CO$_2$(C*H*$_3$)$_3$); ms (*m/e*): 144 (MH$^+$ – C$_4$H$_9$), 129 (MH$^+$ – C$_4$H$_9$ – CH$_3$), 111 (MH$^+$ – OC$_4$H$_9$ – OH). Exact Mass calculated for C$_7$H$_{12}$O$_3$ (MH$^+$ – C$_4$H$_9$): 144.0786; found: 144.0789.

The β-hydroxy ketone (400 mg, 2.0 mmol) was dissolved in ethyl acetate (30 mL) and the procedure described for the preparation of **2** was performed using manganese dioxide (3.5 g, 40.0 mmol). Flash chromatography (hexane – ethyl acetate 17:3) of the crude product yielded 305 mg (77%) of β-keto ester **20***d*; ir (neat, cm^{-1}): 1735 (C=O ester), 1690 (C=O conjugated ketone); ^{1}H nmr (δ): 6.11 (1H, t, J = 1.3 Hz, (CH$_3$)$_2$C=C*H*-), 3.34 (2H, s, -COC*H*$_2$CO$_2$-), 2.15 (3H, d, J = 0.9 Hz, -C=C(C*H*$_3$)$_2$), 1.90 (3H, d, J = 1.3 Hz, -C=C(C*H*$_3$)$_2$), 1.46 (9H, s, -CO$_2$C(C*H*$_3$)$_3$); ms (*m/e*): 198 (M$^+$), 183 (M$^+$ – CH$_3$), 142 (MH$^+$ – C$_4$H$_9$). Exact Mass calculated for C$_{11}$H$_{18}$O$_3$: 198.1256; found: 198.1259.

*2-Formyl-1-methoxy-2-cyclohexene (**18**e)*

2-Bromo-2-cyclohexenone (10.0 g, 57.0 mmol) was dissolved in 500 mL of ethanol and the solution was cooled to 0°C. Cerium chloride heptahydrate (23.31 g, 63.0 mmol) was then added followed by sodium borohydride (2.15 g, 57.0 mmol) and the reaction mixture was stirred for 1 h. It was then poured into 500 mL of ice cold 1 N hydrochloric acid, the aqueous phase was extracted several times with dichloromethane, the combined organic layers were washed with brine, dried, and evaporated *in vacuo* to give an orange oil. Distillation at 100–105°C (400 mTorr) afforded 9.71 g (96%) of 2-bromo-2-cyclohexen-1-ol as a white solid; mp: 39–41°C; ir (cm^{-1}): 3600(s, free OH), 3700–3400(bs), 3100–3000, 3000–2800, 2180, 1650, 1445, 1385, 1335, 1220(bs), 1050, 995, 980(s); ^{1}H nmr (δ): 6.20 (t, 1H, J = 4.0 Hz, Br-C=C*H*-CH$_2$-), 4.20 (bt, 1H, J = 4.5 Hz, HO-C*H*-CBr=CH-), 2.23 (bd, 1H, J = 4.5 Hz, O*H*), 2.2–1.55 (m, 6H, -C*H*$_2$-C*H*$_2$-C*H*$_2$-); ms (*m/e*): 178 (M$^+$), 176 (M$^+$), 160, 158, 150, 148. Exact Mass calculated for C$_6$H$_9$O^{79}Br: 175.9837; found: 175.9824.

Potassium hexamethyldisilazide (56.9 mL, 56.0 mmol), 1 M solution in toluene) was added to a −78°C solution of 2-bromo-2-cyclohexen-1-ol (9.2 g, 52.0 mmol) in 250 mL of dry THF and the reaction mixture was stirred for 1 h at −78°C. Then methyl iodide (14.68 g, 0.104 mol) was added and the solution stirred for 1 h. It was then poured into 250 mL of saturated aqueous ammonium chloride, the aqueous phase was extracted several times with diethyl ether, the combined organic layers were washed with brine, dried, and evaporated *in vacuo* to give an orange oil. Distillation (90°C at 0.3 Torr) afforded 9.02 g (95%) of 1-bromo-5-methoxy-1-cyclohexene as a pale yellow oil; ir (cm^{-1}): 3100–3000, 3000–2800, 1645, 1455, 1370, 1195, 1095(s), 1070, 955, 945; ^{1}H nmr (δ): 6.24 (dd, 1H, J = 5.0, 3.5 Hz, Br-C=C*H*-CH$_2$-), 3.75 (m, 1H, CH$_3$-O-C*H*-C=CH-), 3.45 (s, 3H, C*H*$_3$-O-), 2.20–1.95–1.55 (m, 6H, -C*H*$_2$-C*H*$_2$-C*H*$_2$-); ms (*m/e*): 192 (M$^+$), 190 (M$^+$), 164, 162, 160, 158, 121, 119. Exact Mass calculated for C$_7$H$_{11}$O^{79}Br: 189.9994; found: 189.9989.

Can. J. Chem. Downloaded from www.nrcresearchpress.com by 217.78.4.112 on 09/08/12
For personal use only.

1-Bromo-5-methoxy-1-cyclohexene (132 mg, 0.30 mmol) was dissolved in 5 mL of dry THF and the solution was cooled to −78°C. *n*-BuLi (132 mg, 0.30 mmol) was then added slowly and the reaction mixture was stirred for 1 h at −78°C. Then *N*,*N*-dimethylformamide (132 mg, 0.30 mmol) was added and the mixture was stirred at this temperature for another 2 h, after which it was poured into 100 mL of ice cold 1 N hydrochloric acid. The aqueous phase was extracted several times with diethyl ether, the combined organic layers were washed with brine, dried, and evaporated *in vacuo* to give an orange oil. Chromatography on silica gel with hexane – ethyl acetate 4:1 gave 4.93 g (75%) of the desired aldehyde **18***e*; ir (cm^{-1}): 3110, 2950, 2815, 1690(s), 1650, 1215(bs), 1170, 1095, 1070; ^1H nmr (δ): 9.46 (s, 1H, O=C*H*-C=CH-), 6.94 (dd, 1H, J = 5.0, 2.8 Hz, -C=C*H*-CH_2-), 4.13 (t, 1H, J = 3.5 Hz, CH_3-O-C*H*-C=CH-), 3.41 (s, 3H, CH_3-O-), 2.47 (ddt, 1H, J = 20.6, 5.0, 1.0 Hz, -C=CH-CH_2-, β), 2.24 (ddddd, 1H, J = 20.6, 10.5, 7.0, 2.8, 0.5 Hz, -C=CH-CH_2-, α), 2.10 (dq, 1H, J = 14.0, 3.5 Hz, RO-CH-CH_2-CH_2-CH_2-, α), 1.82 (dddt, 1H, J = 14.0, 10.5, 5.0, 3.5 Hz, CH_2-CH_2-CH_2-CH=C-, β), 1.72 (m, 1H, CH_2-CH_2-CH_2-CH=C-, α), 1.34 (tt, 1H, J = 14.0, 3.5 Hz, RO-CH-CH_2-CH_2-CH_2-, β); ms (*m*/*e*): 140 (M^+), 125, 122, 111, 108.

2-{1-Carbo-tert-*butoxyacetyl}-1-methoxy-2-cyclohexene (**20***e*)

The procedure was identical to that described for the preparation of **18***a*. The aldehyde **18***e* (4.0 g, 28.0 mmol) was added to the zinc enolate prepared from *tert*-butyl bromoacetate (10.02 g, 51.0 mmol) and zinc powder (3.91 g, 59.0 mmol). Isolation of the product and chromatography on silica gel with hexane – ethyl acetate 5:1 gave 5.1 g (71%) of the desired β-hydroxy ester 2-{1-carbo-*tert*-butoxy-2-hydroxyethan-2-yl}-1-methoxy-2-cyclohexene as a 1:1 mixture of diastereomers; ir (cm^{-1}): 3700–3400(b), 3100–3000, 3000–2800, 1720(s), 1455, 1370, 1215, 1155(bs), 1095, 1070; ^1H nmr (δ): 5.90 and 5.89 (m, 1H, -C*H*=C-CHOH), 4.55 and 4.45 (m, 1H, -CH=C-C*H*OH), 3.96 and 3.80 (bt, 1H, -CH=C-C*H*OCH_3), 3.47 and 3.45 (s, 3H, -CH=C-CHOCH_3), 2.66–2.46 (m, 2H, HOCH-CH_2-CO_2-), 2.2–1.4 (m, 12H), 1.44 and 1.42 (s, 9H, -$CO_2C(CH_3)_3$); ms (*m*/*e*): 256 (w, M^+), 238, 200, 199, 183, 182, 168. Exact Mass calculated for $C_{14}H_{24}O_4$: 256.1674; found: 256.1674.

This β-hydroxy ester (500 mg, 1.96 mmol) and a large excess of manganese dioxide (4.0 g, 53.0 mmol) were then used to afford 440 mg (88%) of **20***e* after chromatography on silica gel using hexane – ethyl acetate 5:1; ir (cm^{-1}): 3100–3000, 3000–2800, 1730(bs), 1675, 1370, 1325, 1150(bs), 1095, 1070; ^1H nmr (δ): 6.99 (dd, 1H, J = 5.0, 2.5 Hz, -C*H*=C-C=O), 4.21 (t, 1H, J = 3.0 Hz, -CH=C-C*H*OCH_3), 3.58 (ABq, 2H, O=C-CH_2-CO_2-), 3.38 (s, 3H, -OCH_3), 2.38 (ddt, 1H, J = 20.6, 5.0, 1.0 Hz, -C=CH-CH_2-, β), 2.24 (ddddd, 1H, J = 20.6, 10.5, 7.0, 2.8, 0.5 Hz, -C=CH-CH_2-, α), 2.07 (dq, 1H, J = 13.0, 3.0 Hz, RO-CH-CH_2-CH_2-CH_2-, α), 1.82 (dddt, 1H, J = 13.0, 10.5, 5.0 3.0 Hz, CH_2-CH_2-CH_2-CH=C-, β), 1.72 (m, 1H, CH_2-CH_2-CH_2-CH=C-, α), 1.35 (tt, 1H, J = 13.0, 3.0 Hz, RO-CH-CH_2-CH_2-CH_2-, β), 1.46 (s, 9H, -$CO_2C(CH_3)_3$); ms (*m*/*e*): 255 (M^+ + 1), 231, 213, 200, 199, 198. Exact Mass calculated for $C_{14}H_{23}O_4$: 255.1596; found: 255.1598.

*2-(Methyl 2-ethanoyl)-2-(4-penten-1-yl)-1,3-dioxolane (**21**)*

Methyl 3-oxo-7-octenoate (5.0 g, 29.4 mmol), ethylene glycol (4.56 g, 73.4 mmol), and *p*-toluenesulfonic acid monohydrate (56 mg, 0.29 mmol) were added to 300 mL of benzene in a 500 mL round bottom flask equipped with a Dean–Stark apparatus. The solution was heated to reflux for 24 h. Then it was cooled and 5 g of K_2CO_3 were added. The suspension was filtered through silica gel topped with a layer of $MgSO_4$, and washed with dichloromethane. Evaporation of the solvents and distillation (110–110°C at 0.2 Torr) gave **21** as a colorless oil (5.19 g, 82%); ^1H nmr (δ): 6.0–5.5 (m, 1H, CH_2=C*H*-), 5.15–4.8 (m, 2H, CH_2=CH-), 3.97 (s, 4H, -O(CH_2)$_2$-O-), 3.67 (s, 3H, O=COCH_3), 2.65 (s, 2H, O=C-CH_2-CO_2CH_3), 2.2–1.2 (m, 6H, CH_2=CH-(CH_2)$_3$).

*3-Oxo-7-octen-1-ol (**22**a)*

The ester **21** (6.56 g, 0.031 mol) was dissolved in 300 mL of anhydrous THF and the solution was cooled to 0°C. Lithium aluminium hydride (871 mg, 0.23 mol) was then slowly added and the resulting suspension was stirred at 0°C for 1 h. Then, ice cold 1 N HCl was added to destroy the excess hydride and the reaction mixture was poured into 300 mL of ice cold 1 N HCl and stirred at room temperature for 4 h. The aqueous phase was extracted several times with diethyl ether, the combined organic layers were washed with brine, dried, and evaporated *in vacuo* to give 3-oxo-7-octen-1-ol **22** as a colorless oil (4.22 g, 73% crude). The crude product was used without purification in the next reaction. A small sample was purified for characterization; ^1H nmr (δ): 6.0–5.5 (m, 1H, CH_2=C*H*-), 5.2–4.8 (m, 2H, CH_2=CH-), 3.83 (t, 2H, J = 5.6 Hz, O=C-CH_2-CH_2-OH), 2.63 (t, 2H, J = 5.6 Hz, O=C-CH_2-CH_2-OH), 2.44 (t, 2H, J = 7.0 Hz, CH_2=CH-CH_2-(CH_2)$_2$-), 2.2–1.4 (m, 4H, CH_2=CH-CH_2-(CH_2)$_2$-).

*(2E)-7-Oxo-9-*tert-*Butyldimethylsilyloxy-2-nonenal (**18***f*)*

3-Oxo-7-octen-1-ol (4.22 g, 1.19 mmol) was dissolved in 200 mL of anhydrous dichloromethane and cooled to 0°C. Diisopropylethylamine (0.50 mL, 2.82 mmol) followed by *tert*-butyldimethylsilyl triflate (0.30 mL, 1.30 mmol) were added and the reaction mixture was stirred 1 h at 0°C, after which it was poured into 200 mL of saturated aqueous $NaHCO_3$. The aqueous layer was extracted with dichloromethane and the combined organic layers were dried and the solvent evaporated *in vacuo* to give a yellow oil. Chromatography on silica gel eluting with hexane – ethyl acetate 10:1 afforded 7.21 g (90%) of 3-oxo-1-*tert*-butyldimethylsilyloxy-7-octene a colorless oil; ir (cm^{-1}): 3100–3000, 3000–2800, 1710, 1640, 1470, 1465, 1370, 1260, 1210(s), 1090(bs), 915, 850(s); ^1H nmr (δ): 6.0–5.5 (m, 1H, CH_2=C*H*-), 5.15–4.8 (m, 2H, CH_2=CH-), 3.89 (t, 2H, J = 6.5 Hz, O=C-CH_2-CH_2-OR), 2.58 (t, 2H, J = 6.5 Hz, O=C-CH_2-CH_2-OR), 2.47 (t, 2H, J = 7.0 Hz, CH_2=CH-CH_2-(CH_2)$_2$-), 2.2–1.5 (m, 4H, CH_2=CH-CH_2-(CH_2)$_2$-), 0.86 (s, 9H, $OSi(CH_3)_2C(CH_3)_3$), 0.03 (s, 6H, $OSi(CH_3)_2C(CH_3)_3$).

Ozone was bubbled through a −78°C solution of 3-oxo-1-*tert*-butyldimethylsilyloxy-7-octene (1.0 g, 3.90 mmol) in 50 mL of anhydrous dichloromethane until a blue color developed in the solution. Excess triphenylphosphine was then added at this temperature and the solution was left to warm to room temperature and stirred for 2 h. Then, 350 mL of hexane were added to precipitate the triphenylphosphine oxide and the suspension was filtered through Celite. The solvent was evaporated *in vacuo* and the residue was taken up in hexane. Filtration through Celite and evaporation of the solvent afforded the expected aldehyde essentially free of triphenylphosphine oxide. Chromatography on silica gel eluting with hexane – ethyl acetate 7:1 gave 870 mg (83%) of pure 7-*tert*-butyldimethylsilyloxy-5-oxoheptanal; ir (cm^{-1}): 3100–3000, 3000–2800, 1720, 1640, 1470, 1465, 1260, 1215(bs), 1100(bs), 840(s); ^1H nmr (δ): 9.85 (t, 1H, J = 1.5 Hz, O=C*H*-(CH_2)$_3$-), 3.88 (t, 2H, J = 6.5 Hz, O=C-CH_2-CH_2-OR), 2.55 (t, 2H, J = 6.5 Hz, O=C-CH_2-CH_2-OR), 2.45 (t, 2H, J = 7.0 Hz, O=CH-CH_2-(CH_2)$_2$-), 2.0–1.3 (m, 4H, O=CH-CH_2-(CH_2)$_2$-), 0.89 (s, 9H, $OSi(CH_3)_2C(CH_3)_3$), 0.02 (s, 6H, $OSi(CH_3)_2C(CH_3)_3$).

A solution of 7-*tert*-butyldimethylsilyloxy-5-oxo-heptanal (870 mg, 3.4 mmol) and phosphorane **23** (1.126 g, 3.7 mmol) in 50 mL of benzene were heated to reflux for 18 h. After cooling to room temperature the mixture was diluted with 100 mL of diethyl ether and filtered through silica gel, washing several times with diethyl ether. Evaporation of the solvents under reduced pressure gave an orange oil that was chromatographed on silica gel eluting with hexane – ethyl acetate 4:1. Evaporation of the solvents gave 814 mg (84%) of **18***f*; ^1H nmr (δ): 9.5 (d, 1H, J = 7.5 Hz, O=C*H*-CH=CH-(CH_2)$_3$-), 6.82 (dt, 1H, J = 15.0, 6.5 Hz, O=CH-CH=C*H*-(CH_2)$_3$-), 6.10 (ddt, 1H, J = 15.0, 7.5, 1.0 Hz, O=CH-C*H*=CH-(CH_2)$_3$-), 3.85 (t, 2H, J = 6.5 Hz, O=C-CH_2-CH_2-OR), 2.7–1.5 (m, 8H), 0.90 (s, 9H, $OSi(CH_3)_2C(CH_3)_3$), 0.02 (s, 6H, $OSi(CH_3)_2C(CH_3)_3$).

Can. J. Chem. Downloaded from www.nrcresearchpress.com by 217.78.4.112 on 09/08/12
For personal use only.

*tert-Butyl (4E)-3,9-dioxo-11-tert-butyldimethylsilyloxy-4-undecenoate (**20**f)*

Zinc powder (466 mg, 7.12 mmol) was activated by stirring for 1 h in 1 N HCl, following washing several times with distilled water, acetone, and diethyl ether, successively. After drying under vacuum overnight, it was charged in a 100 mL round bottom flask and flushed with argon. Anhydrous THF (50 mL) was added followed by ~10% of the *tert*-butyl bromoacetate (0.98 mL, 6.01 mmol) and one small crystal of iodine. The solution was heated to reflux for 10 min. Then the rest of the bromoacetate was slowly syringed in over 1 h. After completing the addition, the solution was further refluxed for 1 h and then cooled to room temperature. Then **18***f* (248 mg, 1.47 mmol) was added while cooling the solution to 0°C (prior cooling to 0°C may result in the precipitation of the magnesium enolate). The solution was then warmed to room temperature and stirred overnight, after which it was poured into 100 mL of ice cold saturated aqueous ammonium chloride. The aqueous phase was extracted several times with diethyl ether, the combined organic layers were washed with brine, dried, and evaporated *in vacuo* to give an orange oil. Chromatography with hexane – ethyl acetate 3:1 afforded 289 mg (70%) of *tert*-butyl (4*E*)-3-hydroxy-9-oxo-11-*tert*-butyldimethylsilyloxy-4-undecenoate as a colorless oil: ^{1}H nmr (δ): 5.55 (m, 2H, HO-CH-CH=C*H*-), 4.42 (m, 1H, HO-C*H*-CH=CH-), 3.87 (t, 2H, J = 6.5 Hz, O=C-CH$_2$-C*H*$_2$-OR), 2.7–1.1 (m, 10H), 1.45 (s, 9H, -CO$_2$C-(C*H*$_3$)$_3$), 0.88 (s, 9H, OSi(CH$_3$)$_2$(C*H*$_3$)$_3$), 0.03 (s, 6H, OSi(C*H*$_3$)$_2$-C(CH$_3$)$_3$).

The *tert*-butyl (4*E*)-3-hydroxy-9-oxo-11-*tert*-butyldimethylsilyloxy-4-undecenoate (651 mg, 1.62 mmol) was dissolved in 50 mL of ethyl acetate and 2.82 g (32.4 mmol) of manganese dioxide were added. The suspension was stirred at room temperature for 24 h (more manganese dioxide was added if needed). The suspension was then filtered through Celite and the solvent removed *in vacuo* to yield a yellow oil. Chromatography on silica gel eluting with hexane – ethyl acetate 5:1 gave 375 mg (58%) of the desired β-keto ester **20***f*; ^{1}H nmr (δ): 6.83 (dt, 1H, J = 16.0, 7.0 Hz, O=C-CH=C*H*-(CH$_2$)$_3$-), 6.15 (dt, 1H, J = 16.0, 0.5 Hz, O=C-C*H*=CH-(CH$_2$)$_3$-), 3.87 (t, 2H, J = 6.2 Hz, O=C-CH$_2$-C*H*$_2$-OR), 3.47 (s, 2H, RO$_2$C-C*H*$_2$-C=O), 2.57 (t, 2H, J = 6.2 Hz, O=C-C*H*$_2$-CH$_2$-OR), 2.49 (t, 2H, J = 7.0 Hz, CH=CH-CH$_2$-CH$_2$-C*H*$_2$-), 2.22 (dt, 2H, J = 7.0 Hz, CH=CH-C*H*$_2$-CH$_2$-Ch$_2$-), 1.75 (qi, 2H, J = 7.0 Hz, CH=CH-CH$_2$-C*H*$_2$-CH$_2$-), 1.45 (s, 9H, -CO$_2$C(C*H*$_3$)$_3$), 0.86 (s, 9H, OSi(CH$_3$)$_2$C(C*H*$_3$)$_3$), 0.03 (s, 6H, OSi(C*H*$_3$)$_2$C(CH$_3$)$_3$).

Preparation of 1-phenylsulfinyl analogs of Nazarov reagents

*(3E)-1-Phenylsulfinyl-2-oxo-3-pentene (**26**)*

A 500 mL, one-neck round bottom flask, oven dried and flushed with argon, was charged with 5.82 mL (41.5 mmol) of dry diisopropylamine and 500 mL of anhydrous THF. After cooling the solution to −78°C, 25.3 mL of *n*-BuLi (1.6 M in hexanes, 40.5 mmol) was slowly added and the reaction mixture was stirred 30 min at 0°C. Then it was cooled to −78°C again and methylphenylsulfoxide (5.55 g, 39.6 mmol) was slowly added via a syringe. After stirring at that temperature for 5 min methyl crotonate (2.1 mL, 19.8 mmol) was added. The reaction mixture was stirred at −78°C for 30 min after which time it was poured into 500 mL of saturated aqueous ammonium chloride. The aqueous phase was extracted with diethyl ether (3 × 100 mL) and the combined organic layers were washed with brine, dried, and evaporated under reduced pressure to give a pale yellow oil. Multiple chromatography on silica gel with hexane – ethyl acetate 1:1 furnished 2.3 g of pure keto sulfoxide **26** (56%) along with 110 mg of a side product (3%) resulting from a Michael addition of methylphenylsulfoxide as a 1:1 mixture of diastereomers. Data for β-keto sulfoxide **26**; ir (cm^{-1}): 3100–3000, 3000–2800, 1735, 1700–1650, 1630; ^{1}H nmr (δ): 7.7–7.4 (m, 5H, C$_6$*H*$_5$-SO-), 6.86 (dq, 1H, J = 15.8, 6.9 Hz, O=C-CH=C*H*-CH$_3$), 6.15 (dq, 1H, J = 15.8, 1.6 Hz, O=C-C*H*-CH-CH$_3$), 4.09 (d, 1H, J = 13.5 Hz, O=C-C*H*$_2$-SOPh), 3.88, (d, 1H, J = 13.5 Hz, O=C-C*H*$_2$-SOPh), 1.90 (dd, 3H, J = 6.9, 1.7 Hz, O=C-CH=CH-C*H*$_3$); ms (*m/e*): 208 (M$^+$), 193, 160, 145, 136, 132, 127, 124, 119. Exact Mass calculated for C$_{11}$H$_{12}$O$_2$S: 208.0558; found: 208.0553. Data for Michael addition products; ir (cm^{-1}): 3100–3000(s), 3000–2800, 1735, 1445, 1305, 1230–1200, 1035. ^{1}H nmr (δ): 7.7–7.5 (m, 10H, C$_6$*H*$_5$-SO-), 3.68 (s, 3H, -CO$_2$C*H*$_3$) and 3.67 (s, 3H, -CO$_2$C*H*$_3$), 3.0–2.3 (m, 10H), 1.24 (d, 3H, J = 6.0 Hz, PhSO-CH$_2$-CH-C*H*$_3$) and 1.16 (d, 3H, J = 6.3 Hz, PhSO-CH$_2$-CH-C*H*$_3$); ms (*m/e*): 241 (M$^+$), 215, 211, 209.

*(3E)-1-Phenylsulfonyl-2-oxo-3-pentene (**27**)*

(3*E*)-1-Phenylsulfinyl-2-oxo-3-pentene **26** (247 mg, 1.19 mmol) was dissolved in 8 mL of dichloromethane and cooled to 0°C. *m*-Chloroperbenzoic acid (80% purity, 306 mg, 1.42 mmol) was added quickly and the reaction mixture was stirred at 0°C for 30 min. Then it was poured into 50 mL of saturated sodium bicarbonate and the aqueous phase was extracted with dichloromethane. The combined organic layers were washed with brine, dried, and evaporated under reduced pressure. Chromatography of the resulting yellow oil eluting with hexane – ethyl acetate gave 166 mg (67%) of **27** as a colorless oil; mp: 68–70°C; ir (cm^{-1}): 3100–3000, 3000–2800, 1695 (s), 1675 (s), 1630 (vs), 1510, 1450, 1325 (vs), 1160 (vs), 975; ^{1}H nmr (δ): 8.0–7.5 (m, 5H, C$_6$*H*$_5$-SO$_2$-), 6.99 (dq, 1H, J = 15.5, 6.8 Hz, O=C-CH=C*H*-CH$_3$), 6.30 (dq, 1H, J = 15.5, 1.5 Hz, O=C-C*H*=CH-CH$_3$), 4.27 (s, 2H, O=C-C*H*$_2$-SO$_2$Ph), 1.95 (dd, 3H, J = 6.8, 1.5 Hz, O=C-CH=CH-C*H*$_3$); ms (*m/e*): 224 (M$^+$), 161, 160, 159, 145. Exact Mass calculated for C$_{11}$H$_{12}$O$_2$S: 208.0507; found: 208.0501.

Preparation of substituted cyclohexenones (dienophiles)

*2,3-Dihydroxy-5β-methylethenyl-2-methylcyclohexanone (**64**)*

A solution of the known epoxide **63** (37.95 g, 0.228 mol) and concentrated sulfuric acid (5 mL) in 300 mL of dry THF and 15 mL of water was heated to reflux for 3 h. Then, dichloromethane was added and the organic extracts were washed with saturated sodium bicarbonate, dried, and the solvents were evaporated *in vacuo*. Flash chromatography of the residue using hexane – ethyl acetate 3:1 afforded the desired *cis* diol **64** (21.1 g, 50%) and a 1:1 mixture of *cis* and *trans* diols (17.3 g, 41%). Data for *cis* diol **64** [α]$_D$ +57.36 (*c* = 4.13, CHCl$_3$); ir (cm^{-1}): 3460, 2960, 1720, 1650, 1380, 1170, 1135, 1055; ^{1}H nmr (δ): 4.82 (bs, 1H, -C=C*H*$_2$), 4.78 (bs, 1H, -C=C*H*$_2$), 4.26 (bs, 1H, -O*H*), 4.07 (t, 1H, J = 2.9 Hz, C*H*-OH), 2.97 (bs, 1H, -O*H*), 2.89 (m, 1H, CH$_2$=C-C*H*-CH$_2$), 2.18 (m, 2H, -CH-C*H*$_2$-C=O), 1.89 (m, 2H, -CH-C*H*$_2$-CH-OH), 1.76 (s, 3H, CH$_2$=C-C*H*$_3$), 1.40 (s, 3H, HO-C-C*H*$_3$). ^{13}C nmr (δ): 212.8 (s, *C*=O), 146.4 (s, CH$_3$-*C*=CH$_2$), 110.2 (t, CH$_3$-C=*C*H$_2$), 78.2 (s, CH$_3$-*C*-OH), 75.8 (d, -*C*H(OH)-), 41.5 (t, -CH-*C*H$_2$-C=O), 39.7 (d, CH$_2$=C-*C*H-CH$_2$), 33.0 (t, -CH-*C*H$_2$-CH-OH), 23.2 (q, *C*H$_3$-C=CH$_2$), 20.4 (q, *C*H$_3$-C-OH).

*Ketal ester **65***

A solution of sodium metaperiodate (6.23 g, 29.3 mmol) in 30 mL of water was added slowly to a vigorously stirred (overhead stirrer) solution of *cis* diol **64** (2.38 g, 12.9 mmol) in 20 mL of methanol, while maintaining the temperature below 20°C. The reaction mixture was stirred vigorously for 1 h and then filtered through Celite, washing with excess ethyl acetate. The organic layer was washed several times with brine, dried, and concentrated under reduced pressure to give the crude aldehyde-acid. This product was dissolved in 30 mL of benzene and ethylene glycol (3 mL, 48.0 mmol) was added followed by *p*-toluenesulfonic acid (33 mg, 0.17 mmol). The reaction flask was equipped with a Dean–Stark apparatus and the mixture was heated to reflux for 6 h. The organic layer was washed with aqueous sodium bicarbonate, water, brine, dried, and the solvents were removed under reduced pressure. The resulting crude ketal-ester, dissolved in 25 mL of methanol, was transesterified with 28% sodium methoxide in methanol (2 mL). After stirring the reaction overnight, the solution was neutralized with acetic acid to pH 7.5 and the solvent was removed under reduced pressure. The residue was extracted with diethyl ether, the organic layer was washed with water, then brine,

dried, and concentrated *in vacuo*. Flash chromatography eluting with hexane – ethyl acetate 3:1 afforded 2.03 g (73%) of **65** as a clear liquid. $[\alpha]_D$ + 12.56 (c = 3.24, $CHCl_3$); ir (cm^{-1}): 3080, 2960, 2885, 1740, 1650, 1440, 1140; ^1H nmr (δ): 4.80 (dd, 1H, J = 9.6, 3.8 Hz, -CH_2CH-($O(CH_2)_2O$)), 4.79 (s, 2H, -C=CH_2), 3.95 (m, 2H, -O-CH_2-CH_2-O-), 3.81 (m, 2H, -O-CH_2-CH_2-O-), 3.63 (s, 3H, -CO_2CH_3), 2.83 (m, 1H, CH_2=C-CH-CH_2), 2.50 (dd, 1H, J = 14.9, 6.4 Hz, -CH-CH_2-C=O), 2.39 (dd, 1H, J = 14.9, 8.8 Hz, -CH-CH_2-C=O), 1.80 (m, 1H, -CH_2-CH-C($O(CH_2)_2O$), 1.69 (s, 3H, CH_2=C-CH_3), 1.66 (m, 1H, -CH_2-CH-C($O(CH_2)_2O$). ^{13}C nmr (δ): 172.3 (s, C=O), 145.9 (s, CH_3-C=CH_2), 111.7 (t, CH_3-C=CH_2), 103.0 (d, -CH_2-CH-($O(CH_2)_2O$)), 64.5 (2t, -O-(CH_2)$_2$O-), 51.1 (q, -CO_2CH_3), 39.3 (d, CH_2=C-CH-CH_2), 38.7 (t, -CH_2-CH-C($O(CH_2)_2O$)), 37.0 (t, -CH-CH_2-C=O), 18.9 (q, CH_3-C=CH_2). Exact Mass calculated for $C_{10}H_{15}O_3$: 183.1021; found: 183.1018.

β-Keto ester ***66***

A mixture of ketal ester **65** (12.5 g, 58.43 mmol) and potassium hydroxide (4.9 g, 87.33 mmol) in 60 mL of ethanol was heated to reflux for 1.5 h. Water (60 mL) was added and the reaction mixture was washed with diethyl ether. The aqueous layer was acidified with 1 N hydrochloric acid to pH 4–5 and 60 mL of brine were added following extraction with diethyl ether. The combined organic extracts were dried and concentrated under reduced pressure. Toluene was added and evaporated until the residue was free of excess water. The crude ketal-acid and carbonyl diimidazole (10.4 g, 64.38 mmol) in 125 mL of dry THF were heated to 50°C for 1 h. The reaction mixture was then cooled to 0°C and added to a previously prepared solution of monomethyl malonate (17.28 g, 0.146 mol) and isopropyl magnesium chloride (2 M in THF, 146 mL, 0.293 mol) in 100 mL of dichloromethane cooled to 0°C. The resulting solution was allowed to warm to room temp. and stirred for 12 h. The hetereogeneous solution was then cooled to 0°C and 0.5 N HCl was added with continuous stirring for 15 min. Diethyl ether was added and the organic layer was washed with saturated sodium bicarbonate, then brine, dried, and concentrated under reduced pressure. Flash chromatography eluting with hexane – ethyl acetate 3:1 afforded 14.4 g (96%) of the desired β-keto ester **66** as a clear liquid. $[\alpha]_D$ + 11.54 (c = 3.38, $CHCl_3$); ir (cm^{-1}): 2960, 2895, 1755, 1720, 1650, 1440, 1320, 1145; ^1H nmr (δ): 4.78 (t, 1H, J = 4.9 Hz, -CH_2-CH-($O(CH_2)_2O$)), 4.77 (s, 2H, -C=CH_2), 3.93 (m, 2H, -O-CH_2-CH_2-O-), 3.79 (m, 2H, -O-CH_2-CH_2-O-), 3.71 (s, 3H, -CO_2CH_3), 3.43 (s, 2H, -CO$CH_2CO_2CH_3$), 2.88 (qi, 1H, J = 7.1 Hz, CH_2=C-CH-CH_2-), 2.72 (dd, 1H, J = 16.6, 9.6 Hz, -CH-CH_2-C=O), 2.62 (dd, 1H, J = 16.6, 11.0 Hz, -CH-CH_2-C=O), 1.81 (ddd, 1H, J = 14.0, 7.5, 3.6 Hz, -CH_2-CH-C($O(CH_2)_2O$), 1.70 (s, 3H, CH_2=C-CH_3), 1.65 (m, 1H, -CH_2-CH-C($O(CH_2)_2O$); ^{13}C nmr (δ): 200.7 (s, C=O), 167.0 (s, CO_2CH_3), 146.1 (s, CH_3-C=CH_2), 111.1 (t, CH_3-C=CH_2), 102.6 (d, -CH_2-CH-($O(CH_2)_2O$)), 64.2 (t, -O-(CH_2)$_2$O-), 64.1 (t, -O-(CH_2)$_2$O-), 51.5 (q, CO_2CH_3), 48.6 (t, -CO$CH_2CO_2CH_3$), 46.6 (t, -CH_2-CH-C($O(CH_2)_2O$)), 37.3 (d, CH_2=C-CH-CH_2), 36.8 (t, -CH-CH_2-C=O), 19.2 (q, CH_3-C=CH_2). Exact Mass calculated for $C_{13}H_{20}O_5$: 256.1311; found: 256.1308.

2-Carbomethoxy-5β-methylethenyl-2-cyclohexen-1-one ***(56)***

A solution of β-keto ester **66** (512 mg, 2.00 mmol) in 50% aqueous acetic acid (25 mL) was stirred under argon for 24 h. Then water (25 mL) and brine (25 mL) were added and the solution was extracted with diethyl ether. The combined organic extracts were washed with water, saturated sodium bicarbonate, water, and brine. After drying the solvent was removed under reduced pressure. The crude product was filtered through a small plug of Florisil eluting with diethyl ether. The solvent was removed under reduced pressure to give the desired cyclohexenone **56** as a pale yellow oil (398 mg, 100%); $[\alpha]_D$ −18.6 (c = 2.38, $CHCl_3$); ir (cm^{-1}): 3080, 2960, 1750, 1720, 1650, 1440, 1380, 1275, 1082, 900; ^1H nmr (δ): 7.74 (dd, 1H, J = 5.9, 2.9 Hz, -C=CH-), 4.84 (bs, 1H, -C=CH_2), 4.78 (s, 1H, -C=CH_2), 3.81 (s, 3H, -CO_2CH_3), 2.67 (m, 3H), 2.44 (m, 2H), 1.75 (s, 3H, CH_2=C-CH_3). Exact Mass calculated for $C_{11}H_{14}O_3$: 194.0943; found: 194.0935.

2-Carbomethoxy-4,4-ethylenedioxy-2-cyclohexenone ***(60)***

A solution of 1,4-cyclohexanedione, mono-ethylene ketal (1.0 g, 6.4 mmol), in 5 mL of dry THF, was added via an addition funnel to a suspension of sodium hydride (793 mg, 19.8 mmol) and dimethyl carbonate (1.44 g, 16.0 mml) in 10 mL of THF at reflux. After 2 min of addition, KH (24 mg, 0.6 mmol) was added and the addition of 1,4-cyclohexanedione, monoethylene ketal, was continued over 1 h. The reaction mixture was heated under reflux for 0.5 h and cooled to 0°C. Acetic acid (10 mL, 3 M in water) was slowly added and the resulting solution was added to 50 mL of brine. The aqueous layer was separated and extracted with dichloromethane. The combined organic layers were washed with brine, dried, and evaporated under reduced pressure to give a white solid. The product was chromatographed on silica gel with hexane – ethyl acetate 5:1 to give 1.21 g (88%) of 2-carbomethoxy-4,4-ethylenedioxy-1-cyclohexanone; mp: 60–61°C; ir (cm^{-1}): 3100–3000, 3000–2800, 1745, 1720, 1660, 1620, 1440, 1350, 1290, 1230, 1215, 1195, 1060; ^1H nmr (δ): 12.80 (s, 1H, HOC=C-CO_2CH_3), 4.00 (m, 4H, -O(CH_2)$_2$O-), 3.75 (s, 3H, -CO_2CH_3), 2.52 (t, 2H, J 6.5 Hz, O=C-CH_2-CH_2-), 2.48 (s, 2H, $(RO)_2$-CH_2-C=C-), 1.86 (t, 2H, J = 6.5 Hz, O=C-CH_2-CH_2-); ms (m/e): 214 (M^+), 183, 182, 157.

This product was then treated according to the procedure described by Liotta *et al.* (2). 2-Carbomethoxy-4,4-ethylenedioxy-1-cyclohexanone (250 mg, 1.17 mmol), phenylselenyl chloride (234 mg, 1.23 mmol), pyridine (102 mg, 1.28 mmol), and hydrogen peroxide (0.1 mL, 1.20 mmol) were used as the reagents. The product **60** (237 mg, 96%) was used without further purification in the next step; ir (cm^{-1}): 3100–3000, 3000–2800, 1745, 1720, 1690, 1440, 1355, 1290, 1230, 1215, 1135, 1055; ^1H nmr (δ): 7.14 (s, 1H, -CH=C-CO_2CH_3), 4.06 (m, 4H, -O(CH_2)$_2$O-), 3.80 (s, 3H, -CO_2CH_3), 2.70 (t, 2H, J = 6.5 Hz, O=C-CH_2-CH_2-), 2.22 (t, 2H, J = 6.5 Hz, O=C-CH_2-CH_2-); ms (m/e): 212 (M^+), 184, 181, 170, 169.

Base-catalyzed cycloaddition or double Michael cyclization of substituted Nazarov reagents

General procedure

2-Carbomethoxy-2-cyclohexenone **1** was slowly added over the indicated period of time to a suspension of cesium carbonate and the substituted Nazarov reagent in a dry solvent at room temperature using a syringe pump. After the required period of time, the reaction mixture was filtered through a pad of Celite or silica gel rinsing first with dichloromethane and then with plenty of ethyl acetate. The solvents were then removed under reduced pressure. Single Michael adducts were prepared in the same way at the indicated temperatures.

Decarboxylations

Method A. The crude product from the cycloaddition was treated directly with *p*-toluenesulfonic acid (0.1 equiv.) in refluxing benzene for the required period of time. Excess solid sodium bicarbonate or pyridine was added to neutralize the mixture and the suspension was stirred for 5 min, then filtered and the solvents evaporated *in vacuo*.

Method B. The crude product from the cycloaddition was dissolved in trifluoroacetic acid (usually 10 mL per mmol) and the solution was stirred at room temperature for 2 h. The excess acid was removed *in vacuo* and the product was found from all acid traces by dissolving it in benzene and evaporating *in vacuo* several times. The remaining product was dissolved in benzene and refluxed for the required period of time. The solvent was then evaporated under reduced pressure.

8aβ-Carbomethoxy-8β-methyl-2,3,4,4a,5,7,8,8a-octahydronaphthalene-1,6-dione ***(3)***

A solution of 2-carbomethoxy-2-cyclohexenone **1** (89 mg, 0.577 mmol) in chloroform (4 mL) was added over a period of

Can. J. Chem. Downloaded from www.nrcresearchpress.com by 217.78.4.112 on 09/08/12
For personal use only.

Can. J. Chem. Downloaded from www.nrcresearchpress.com by 217.78.4.112 on 09/08/12
For personal use only.

25 min to cesium carbonate (89 mg, 0.273 mmol) and *tert*-butyl (4*E*)-3-oxo-4-hexenoate **2** (149 mg, 0.808 mmol) in chloroform (10 mL) according to the general procedure. The mixture was stirred for 3 h after the end of the addition. The crude product was decarboxylated according to method A for 1.5 h and neutralized with pyridine (20 μL, 0.24 mmol). Flash chromatography on silica gel (hexane – ethyl acetate 2:1) gave 1-carbomethoxy-10-methyl-bicyclo[4.4.0]decane-2,8-dione **3** (95 mg, 69%); mp: 71–72°C; ir (cm^{-1}): 1740, 1715; ^1H nmr (δ): 3.72 (3H, s, $-CO_2CH_3$), 3.18 (1H, m, CH_2-*H*C-CH_2), 2.95 (1H, m, *H*C-CH_3), 2.80 (1H, dd, J = 5.0, 14.0 Hz, CH(CH_3)-C*H*$_2$-C=O), 2.55–2.00 (6H, m), 2.00–1.90 (2H), 1.56 (1H), 0.88 (3H); ^{13}C nmr (δ): 209.5, 206.2, 170.5, 63.7, 52.5, 45.2, 42.6, 40.2, 39.1, 33.4, 27.0, 22.5, 16.2. Exact Mass calculated for $C_{13}H_{18}O_4$: 238.1205; found: 238.1203.

Single Michael adduct ***5***

To a stirred solution of 2-carbomethoxy-2-cyclohexenone **1** (43 mg, 0.279 mmol) and *tert*-butyl (4*E*)-3-oxo-4-hexenoate **2** (62 mg, 0.337 mmol) in acetonitrile (6 mL) at −15°C was added cesium carbonate (45 mg, 0.138 mmol) and the reaction mixture was stirred for 30 min. The crude product was purified by flash chromatography with hexane – ethyl acetate 4:1 to afford single Michael adduct **5** as a colorless oil (50 mg, 53%); ir (cm^{-1}): 1735, 1710, 1690, 1650, 1630; ^1H nmr (δ): 7.20–6.60 (1H, m, -CH=C*H*-CH_3), 6.60–6.00 (1H, m, -CO-C*H*=CH-), 3.90–3.60 (5H, m, $-CO_2CH_3$, 2 × -CO-C*H*-CO_2-), 2.60–1.60 (7H), 2.00–1.80 (3H, m, =CH-CH_3), 1.55–1.40 (9H, m, $-CO_2$-C(CH_3)$_3$).

Cyclization of single Michael adduct ***5***

Single Michael adduct **5** (8 mg, 0.023 mmol) in acetonitrile (4 mL) and cesium carbonate (6 mg, 0.018 mmol) were stirred for 1 h at room temperature. The crude product was decarboxylated according to method A and neutralized with pyridine (2 μL, 0.025 mmol). The solution was then filtered through silica gel, washing with ethyl acetate, and the solvents evaporated to afford a mixture of *cis*-decalin **3** and **4** (3 mg, 55%), in a 68:32 ratio, as determined by gas chromatography. For spectroscopic data of isomer **4** see ref. 2.

*8aβ-Carbomethoxy-7β,8β-dimethyl-2,3,4,4a,5,7,8,8a-octahydronaphthalene-1,6-dione (**28**) and its 7α isomer (**29**)*

A solution of *tert*-butyl β-keto ester **20***b* (84 mg, 0.4 mmol), 2-carbomethoxy-2-cyclohexen-1-one **1** (47 mg, 0.31 mol), and cesium carbonate (44 mg, 0.13 mmol) in chloroform (7.5 mL) were stirred for 3 h. The crude product was then decarboxylated using method B. Flash chromatography (hexane – ethyl acetate 7:3 yielded 50 mg (65%) of a mixture of epimeric compounds **28**:**29** (7:3). Data for compound **28**: mp: 91–92°C (heptane); R_f 0.29 (hexene – ethyl acetate (4:1); ^1H nmr (δ): 3.74 (3H, s, -COOC*H*$_3$), 3.20 (1H, m, -CH_2C*H*CH_2-), 3.05 (1H, qd, J = 6.6, 5.1 Hz, -(CH_3)C*H*CO-), 2.89 (1H, qd, J = 7.3, 5.1 Hz, -(CH_3)C*H*-CH(CH_3)CO-), 2.55–1.49 (8H, m), 1.00 (3H, d, J = 6.6 Hz, -(C*H*$_3$)CHCO-), 0.64 (3H, d, J = 7.3 Hz, -(C*H*$_3$)CHCH(CH_3)CO-; irradiation of this doublet transforms the signal (qd) at d 2.89 ppm in a doublet, J = 5.1 Hz). Data for compound **29**: mp: 84–86°C (heptane); R_f 0.26 (hexane – ethyl acetate 4:1); ^1H nmr (δ): 3.80 (3H, s, -COOC*H*$_3$), 3.09 (1H, dq, J = 11.2, 5.0 Hz, -CH_2-C*H*CH_2-), 2.72 (1H, dq, J = 12.1, 6.5 Hz, -(CH_3)C*H*CO-), 2.44–1.50 (9H, m), 1.12 (3H, d, J = 6.9 Hz, -(C*H*$_3$)CHCO-), 1.08 (3H, d, J = 6.5 Hz, -(C*H*$_3$)CHCH(CH_3)C -); simultaneous irradiation of the doublets at d 1.12 and 1.08 ppm transformed the signal (dq) at d 2.72 ppm in a doublet, J = 12.1 Hz).

Compounds ***30*** *and* ***31***

A solution of *tert*-butyl β-keto ester **20***c* (173 mg, 0.77 mmol), 2-carbomethoxy-2-cyclohexen-1-one **1** (166 mg, 1.1 mmol), and cesium carbonate (113 mg, 0.34 mmol) in chloroform (19 mL) was stirred for 3 h. The crude product was then decarboxylated using method B. Flash chromatography (hexane – ethyl acetate 4:1) yielded 142 mg (66%) of a 1:1 mixture of epimeric compounds **30** and **31**. Data for mixture: ir (cm^{-1}): 1740–1710 (C=O ester and ketone); ms (*m/e*): 278 (M^+), 246 ($M^+ - CH_3OH$), 197 ($MH^+ - C_6H_{10}$). Exact Mass calculated for $C_{16}H_{22}O_4$ (M^+): 278.1518; found: 278.1514. Data for compound **30**: mp 175–177°C (heptane); R_f 0.41 (hexane – ethyl acetate (1:1)); ^1H nmr (δ): 3.74 (3H, s, -COOC*H*$_3$), 3.20 (1H, m, -CH_2C*H*CH_2-), 2.98 (1H, m, -CHC*H*CO-), 2.84 (1H, dt, J = 12.0, 5.0 Hz, -C*H*CHCO-), 2.58–0.97 (16H, m). Data for compound **31**: mp: 116–118°C (heptane); R_f 0.37 (hexane – ethyl acetate 1:1); ^1H nmr (δ): 3.80 (3H, s, -COOC*H*$_3$), 3.09 (1H, dq, J = 11.0, 5.0 Hz, -CH_2C*H*CH_2-), 2.65 (1H, td, J = 11.3, 5.0 Hz, -CHC*H*CO-), 2.50–1.05 (17H, m).

*2-Carbomethoxy-3-{2-oxo-3-penten-1-yl}-1-cyclohexanone (**32**)*

A solution of *tert*-butyl β-keto ester **20***d* (76 mg, 0.38 mmol), 2-carbomethoxy-2-cyclohexen-1-one **1** (59 mg, 0.38 mmol), and cesium carbonate (56 mg, 0.17 mmol) in chloroform (9 mL) was stirred for 3 h. Flash chromatography (hexane – ethyl acetate 4:1) yielded 21 mg (33%, the yield was 64% when this reaction was run in acetonitrile as solvent) of the bis-β-keto ester intermediate, which was decarboxylated according to method B. Data for the bis-β-keto ester intermediate: ^1H nmr (δ): 12.52, 12.48 (<2H, 2s, -(O*H*)C=C(COOCH_3)- and -(O*H*)C=COOC(CH_3)$_3$-), 6.05 (>1H, m, $(CH_3)_2$C=C*H*-), 3.77 (3H, s, -COOC*H*$_3$ bis-β-keto ester form), 3.76 (<3H, s, -COOC*H*$_3$ enol forms), 3.75–1.50 >9H, m), 2.16 (3H, s, -C=C(CH_3)CH_3'), 2.13 (<3H, s, -C=C(C*H*$_3$)CH_3, enol forms), 1.91 (>3H, m, -C=C(CH_3)C*H*$_3$, enol forms and bis-β-keto ester), 1.43 (9H, s, -COOC(C*H*$_3$)$_3$ bis-β-keto ester form), 1.46 (<9H, s, $-CO_2$C(C*H*$_3$)$_3$), 1.39 (<9H, s, $-CO_2$C(C*H*$_3$)$_3$); ms (*m/e*): 352 (weak, M^+), 296 ($MH^+ - C_4H_9$), 279 ($M^+ - OC_4H_9$), 265 ($MH^+ - C_4H_9 - CH_3$). Exact Mass calculated for $C_{15}H_{20}O_6$ ($MH^+ - C_4H_9$): 296.1260; found: 296.1257.

Decarboxylation (method B): bis-β-keto ester (25 mg, 0.07 mmol), trifluoroacetic acid (5 mL), benzene (10 mL). Flash chromatography (hexane – ethyl acetate 7:3) yielded 16 mg (89%) of **32**: ir (cm^{-1}): 1740 (C=O ester), 1710 (C=O ketone), 1680 (C=O conjugated ketone), 1620 (conjugated C=C); ^1H nmr (δ): 12.37 (1H, s, -C=C-O*H*), 6.05 (>1H, m, $(CH_3)_2$C=C*H*-), 3.76 (<3H, s, -(HO)C=C(COOC*H*$_3$)-), 3.75 (3H, s, -COCH(COOC*H*$_3$)-), 3.29 (<1H, dd, J = 11.1, 0.8 Hz, -COC*H*(COOCH$_3$)-), 3.20–1.30 (>9H, m), 2.16 (3H, d, J = 1.1 Hz, -C=C(CH_3)CH_3'), 2.14 (<3H, d, J = 1.1 Hz, -C=C(CH_3)C*H*$_3$, enol form), 1.90 (3H, s, -C=C(C*H*$_3$)CH_3), 1.89 (<3H, s, -C=C(C*H*$_3$)CH_3, enol form); ms (*m/e*): 252 (M^+), 220 (M^+ − CH3OH), 205 ($M^+ - CH_3OH$-CH_3). Exact Mass calculated for $C_{14}H_{20}O_4$ (M^+): 252.1361; found: 252.1356.

*8aβ-Carbomethoxy-8β-{p-toluenesulfonyloxybutan-1-yl}-2,3,4,4a,5,7,8,8a-octahydronaphthalene-1,6-dione (**35**)*

A solution of substituted Nazarov reagent **11***c* (41 mg, 0.103 mmol), 2-carbomethoxy-2-cyclohexenone **1** (24 mg, 0.154 mmol), and cesium carbonate (25 mg, 0.069 mmol) was stirred for 3.5 h. Decarboxylation of the crude product using method A for 1.5 h afforded bicyclic tosylate **35** (27 mg, 58%); ir (cm^{-1}): 1740, 1715, 1600, 1365, 1180; ^1H nmr (δ): 7.90–7.20 (4H, 2d, J = 8.3 Hz, -CH_2-OSO_2-), 3.76 (3H, s, $-CO_2CH_3$), 3.09 (1H, ddd, J = 5.0, 10.0, 10.0 Hz, HβC5), 2.70 (2H, m), 2.45 (3H, s, =C-CH_3), 2.50–2.00 (6H, m), 2.00–1.90 (2H, m), 1.60–1.10 (7H, m); ms (*m/e*): 450 (M^+), 419 ($M^+ - OCH_3$), 391 ($M^+ - CO_2CH_3$). Exact Mass calculated for $C_{23}H_{30}O_7S$: 450.1712; found: 450.1709.

*18aβ-Carbomethoxy-8β-{tert-butyldiphenylsilyloxypropan-1-yl}-2,3,4,4a,5,7,8,8a-octahydronaphthalene-1,6-dione (**37**)*

A solution of substituted Nazarov reagent **11***b* (183 mg, 0.392 mmol), 2-carbomethoxy-2-cyclohexenone **1** (50 mg, 0.327 mmol), and cesium carbonate (53 mg, 0.147 mmol) was stirred for 3.5 h. Decarboxylation of the crude product using method A for 1.5 h afforded bicyclic compound **37** (103 mg, 60%); ir ($CHCl_3$): 1740, 1715, 1110; ^1H nmr ($CDCl_3$, δ): 7.60 and 7.40 (10H, 2m, aromatic protons), 3.71 (3H, s, $-CO_2CH_3$), 3.60 (2H, m, -CH_2-O-), 3.15 (1H, m, *H*βC5), 2.80–2.00 (7H, m), 2.00–1.90 (2H, m), 1.80–1.20 (6H, m), 1.03 (9H, s, Si-C(C*H*$_3$)$_3$).

Can. J. Chem. Downloaded from www.nrcresearchpress.com by 217.78.4.112 on 09/08/12
For personal use only.

*8aβ-Carbomethoxy-8β-{hydroxypropan-1-yl}-2,3,4,4a,5,7,8,8a-octahydronaphthalene-1,6-dione (**38**)*

To a stirred solution of bicyclic compound **37** (101 mg, 0.194 mmol) in THF (4 mL) at room temperature was added a solution of tetrabutylammonium fluoride (213 μL, 1 M in THF, 0.213 mmol). After 30 min, the solution was filtered through silica gel with ethyl acetate as eluent and the solvents were evaporated under reduced pressure. The residue was purified by flash chromatography with hexane – ethyl acetate (1:1) to afford bicyclic alcohol **38** (39.5 mg, 73%); ir ($CHCl_3$): 3620, 1740, 1715, 1220; ^{1}H nmr ($CDCl_3$, δ): 3.76 (3H, s, -CO_2CH_3), 3.58 (2H, t, J = 6.2 Hz, -CH_2-O-), 3.13 (1H, ddd, J = 5.5, 5.6, 10.1 Hz, HβC5), 2.70 (2H, m), 2.60–2.00 (6H, m), 2.00–1.90 (2H, m), 1.80–1.20 (6H, m).

*8aβ-Carbomethoxy-8β-{p-toluenesulfonyloxypropan-1-yl}-2,3,4,4a,5,7,8,8a-octahydronaphthalene-1,6-dione (**39**)*

To a stirred solution of bicyclic alcohol **38** (7.4 mg, 0.026 mmol) in methylene chloride (0.4 mL) at 0°C were added tosyl chloride (19 mg, 0.10 mmol) and triethylamine (20 μL, 0.14 mmol). Then the solution was slowly warmed to room temperature. After 2 h, the mixture was filtered through silica gel washing with ethyl acetate and the solvents were evaporated under reduced pressure. The residue was purified by flash chromatography with hexane – ethyl acetate (1:1) to afford bicyclic tosylate **39** (9.5 mg, 84%); mp: 128–130°C; ir ($CHCl_3$): 1740, 1715, 1600, 1365, 1175. ^{1}H nmr ($CDCl_3$, δ): 7.90–7.20 (4H, 2d, J = 8.3 Hz, aromatic protons), 3.94 (2H, m, -CH_2-OSO_2-), 3.76 (3H, s, -CO_2CH_3), 3.07 (1H, ddd, J = 5.5, 10.0, 10.0 Hz, HβC5), 2.70 (2H, m), 2.45 (3H, s, =C-CH_3), 2.50–2.00 (6H, m), 2.00–1.90 (2H, m), 1.85–1.20 (5H, m); ms (*m/e*): 436 (M^+), 404 (M^+ – CH_3OH), 3.77 (M^+ – CO_2CH_3). Exact Mass calculated for $C_{22}H_{28}O_7S$: 436.1556; found: 436.1550.

*Tricyclic compound **40***

To a stirred solution of bicyclic tosylate **39** (12.5 mg, 0.029 mmol) in THF (10 mL) and *tert*-butanol (10 mL) at room temperature was added a solution of potassium *tert*-butoxide (140 μL, 0.286 M in *tert*-butanol, 0.043 mmol). After 20 min, pyridinium *p*-toluenesulfonate (5 mg, 0.020 mmol) was added and the solvents were evaporated under reduced pressure. Methylene chloride was added and the mixture was filtered through silica gel, washing with ethyl acetate, the solvents were evaporated, and the residue was purified by flash chromatography with hexane – ethyl acetate to afford pure tricyclic compound **40** (6.5 mg, 86%); mp: 117.5–118°C; ir ($CHCl_3$): 1740 and 1710; ^{1}H nmr ($CDCl_3$, δ): 3.74 (3H, s, -CO_2CH_3), 3.12 (1H, m, HβC5), 2.97 (2H, m, HαC8, HαC9), 2.60–2.10 (5H, m), 2.09 (1H, dd, J = 4.1, 13.5 Hz, HβC6), 2.00–1.80 (2H, m), 1.70–1.10 (6H, m); ms (*m/e*): 264 (M^+), 232 (M^+ – CH_3OH), 205 (M^+ – CO_2CH_3). Exact Mass calculated for $C_{15}H_{20}O_4$: 264.1361; found: 264.1353.

*8aβ-Carbomethoxy-8aβ-{(2Z)-1-Carbomethoxy-1-penten-5-yl}-2,3,4,4a,5,7,8,8a-octahydronaphthalene-1,6-dione (**41**)*

Compound **41** was prepared according to the general procedure for 2 h and decarboxylated using method A for 2 h. Dichloromethane (5 mL), *tert*-butyl (3*E*,9*Z*)-3-oxo-10-carbomethoxy-4.9-decadienoate **17** (150 mg, 0.49 mmol), 2-carbomethoxy-2-cyclohexenone **1** (114 mg, 0.68 mmol), and cesium carbonate (71 mg, 0.22 mmol) afforded, after chromatography on silica gel and eluting with hexane – ethyl acetate 3:1, 20 mg (69%) of the decalin product; ir (cm^{-1}): 3020, 3000–2800, 1700, 1690, 1435, 1260(bs), 1215(bs), 1080; ^{1}H nmr (δ): 6.14 (dt, 1H, J = 11.5, 7.5 Hz, CH_3O_2C-CH=CH-CH_2-), 5.76 (dt, 1H, J = 11.5, 1.6 Hz, CH_3O_2C-CH=CH-CH_2-), 3.75 (s, 3H, -CO_2CH_3), 3.69 (s, 3H, CO_2CH_3), 3.13 (m, 1H, O=C-CH_2-CH-$(CH_2)_3$-C=O), 2.8–1.03 (m, 17H), ms (*m/e*): 350 (M^+), 251, 237, 223. Exact Mass calculated for $C_{19}H_{26}O_6$: 350.1729; found: 350.1732.

*8aβ-Carbomethoxy-8β-{1-carbomethoxy-1-pentyn-5-yl}-2,3,4,4a,5,7,8,8a-octahydronaphthalene-1,6-dione (**42**a)*

Compound **42***a* was prepared according to the general procedure (2 h) and decarboxylated using method A for 2 h. Dichloromethane (5 mL), β-keto ester **16***a* (150 mg, 0.51 mmol), 2-carbomethoxy-2-cyclohexenone (119 mg, 0.71 mmol), and cesium carbonate (75 mg, 0.23 mmol) afforded, after chromatography on silica gel and eluting with hexane – ethyl acetate 3:1, 71 mg (40%) of product **42***a*; ir (cm^{-1}): 3020, 3000–2800, 2240, 1710, 1435, 1260(bs), 1215(bs), 1080; ^{1}H nmr (δ): 3.76 (s, 3H, -CO_2CH_3), 3.72 (s, 3H, -CO_2CH_3), 3.10 (m, 1H, O=C-CH_2-CH-$(CH_2)_3$-C=O), 2.78–2.65 (m, 2H, -CH-$(CH_2)_3$-C≡C- and O=C-CH_2-CH-$(CH_2)_3$-C≡C-, β), 2.55–2.10 (m, 8H), 2.00–1.88 (m, 2H), 1.80–1.50 (m, 5H); ^{13}C nmr (62.5 MHz, δ), 209.7 (s, *C*=O), 206.3 (s, *C*=O), 170.4 (s, -*C*O_2CH_3), 168.9 (s, -*C*O_2CH_3), 64.3 (s, CH_3O_2C-*C*-C=O), 52.7 (q, -CO_2CH_3), 52.5 (q, -CO_2CH_3), 42.8 (t), 41.4 (t), 40.1 (t), 39.9 (d, O=C-CH_2-*C*H-$(CH_2)_3$-C=O), 38.0 (d, -*C*H-$(CH_2)_3$-C≡C-), 28.4 (t), 27.0 (t), 25.2 (t), 22.7 (t), 18.3 (t); ms (*m/e*): 348 (M^+), 251, 237, 223. Exact Mass calculated for $C_{19}H_{24}O_6$: 348.1572; found: 348.1569.

*8aβ-Carbomethoxy-8β-{1-carbomethoxy-1-pentyn-5-yl}-7-methyl-2,3,4,4a,5,7,8,8a-octahydronapthalene-1,6-dione (**42**b)*

Compound **42***b* was prepared according to the general procedure (2 h) and decarboxylated using method A for 2 h. Dichloromethane (5 mL), β-keto ester **16***b* (150 mg, 0.49 mmol), 2-carbomethoxy-2-cyclohexenone (114 mg, 0.68 mmol), and cesium carbonate (71 mg, 0.22 mmol) afforded, after chromatography on silica gel, eluting with hexane – ethyl acetate 3:1, 89 mg (52%) of product **42***b* as a mixture of α- and β-methyl isomers in a 5:2 ratio; ir (cm^{-1}): 3020, 3000–2800, 2240, 1710, 1435, 1260(bs), 1215(bs), 1080. ^{1}H nmr (δ): 3.75 (s, 6H, 2 × -CO_2CH_3), 3.16 (m, 1H, O=C-CH_2-CH-$(CH_2)_3$-C=O), 3.03 (m, 1H, O=C-C$H$$CH_3$), 2.67 (q, 1H, J = 4.8 Hz, -CH-$(CH_2)_3$-C≡C-), 2.6–1.0 (m, 14H), 1.03 (d, 3H, J = 6.5 Hz, O=C-CHCH_3). Signals distinguishable for the other isomers: 3.81 (s, <3H, -CO_2CH_3), 2.79 (m, <1H, O=C-C$H$$CH_3$), 1.14 (s, <3H, O=C-CHC$H_3$). ms (*m/e*): 362 ($M^+$), 265, 251, 237. Exact Mass calculated for $C_{20}H_{26}O_6$: 362.1728; found: 362.1727.

*Tricyclic aldehyde **46***

The tricyclic aldehyde **46** was obtained according to the general procedure (1 h) and decarboxylated using method A for 45 min. Substituted Nazarov reagent **11***a* (28.5 mg, 0.100 mmol) and 2-carbomethoxy-2-cyclohexenone **1** (19 mg, 0.123 mmol) gave, after purification, tricyclic aldehyde **46** (9 mg, 32%); mp: 134–137°C; ir (cm^{-1}): 1720, 1710, 1665, 1635; ^{1}H nmr (δ): 10.14 (1H, s, -CHO), 3.71 (3H, s, -CO_2CH_3), 3.35 (1H, dd, J = 8.3, 13.9 Hz, HβC12), 2.80 (2H, m), 2.50–1.20 (13H, m); ms (*m/e*): 276 (M^+), 217 (M^+ – CO_2CH_3). Exact Mass calculated for $C_{16}H_{20}O_4$: 276.1361; found: 276.1361.

*Compound **48***

Compound **48** was prepared according to the general procedure (5 h) and decarboxylated using method A for 3 h. Dichloromethane (50 mL), β-keto ester **20***e* (684 mg, 2.69 mmol), 2-carbomethoxy-2-cyclohexenone (584 mg, 3.76 mmol), and cesium carbonate (350 mg, 1.07 mmol) afforded, after chromatography on silica gel and eluting with hexane – ethyl acetate, 3:1, 386 mg (52%) of product **48**, which can be recrystallized from hexane – ethyl acetate 3:1; mp: 137–138°C. ir (cm^{-1}); 3010, 3000–2800, 1740, 1715, 1685, 1620, 1215(vs); ^{1}H nmr (δ): 6.99 (q, 1H, J = 4.0 Hz, CH_2-CH=C-C=O), 3.74 (s, 3H, -CO_2CH_3), 3.30 (m, 1H, CH_2-CH-C=CH-), 2.97 (m, 1H, -CH-CH_2-C=O), 2.48 (m, 2H), 2.34 (dd, 2H, J = 8.1, 6.2 Hz), 2.24 (m, 2H), 2.1–1.4 (m, 8H); ms (*m/e*): 277 (M^+ + 1), 276 (M^+), 258, 245, 244, 218, 217, 216. Exact Mass calculated for $C_{16}H_{20}O_4$: 276.1358; found: 276.1361. X-ray analysis (see footnote 3).

*8aβ-Carbomethoxy-5-carbo-*tert*-butoxy-8β-{1-tert-butyldimethylsilyloxy-3-oxo-hexan-6-yl}-2,3,4,4a,5,7,8,8a-octahydronaphthalene-1,6-dione (**49**)*

Compound **49** was prepared according to the general procedure (2 h). Dichloromethane (5 mL), β-keto ester **20***f* (100 mg, 0.25 mmol), 2-carbomethoxy-2-cyclohexenone (54 mg, 0.35 mmol),

Can. J. Chem. Downloaded from www.nrcresearchpress.com by 217.78.4.112 on 09/08/12
For personal use only.

and cesium carbonate (33 mg, 0.10 mmol) afforded, after chromatography on silica gel and eluting with hexane – ethyl acetate 6:1, 85 mg (75%) of the product **49**; ir (cm^{-1}); 3000–2800, 1735, 1710, 1685, 1620, 1470, 1465, 1260, 1215(bs), 1100(bs), 840(s); ^1H nmr (δ): 12.44 (s, 1H, RO_2C-C=CO*H*), 3.85 (t, 2H, J = 6.3 Hz, O=C-CH_2-CH_2-OR), 3.67 (s, 3H, -CO_2CH_3), 3.41 (dd, 1H, J = 12.0, 4.5 Hz, -CH-$CH(CO_2C(CH_3)_3)_3$), 2.56 (t, 2H, J = 6.3 Hz, O=C-CH_2-CH_2-OR), 2.5–2.3 (m, 6H), 2.15–1.1 (m, 9H), 1.49 (s, 9H, -$CO_2C(CH_3)_3$), 0.86 (s, 9H, $OSi(CH_3)_2C(CH_3)$), 0.03 (s, 6H, $OSi(CH_3)_2C(CH_3)_3$). ms (*m/e*): 550 (w, M^+), 493, 436, 418. Exact Mass calculated for $C_{29}H_{46}O_8Si$: 550.2962; found: 550.2966.

*Tetracyclic compound **51***

Compound **49** (74 mg, 0.13 mmol) was decarboxylated using method A. The product was chromatographed on silica gel eluting with hexane – ethyl acetate 5:1, to afford 18 mg (32%) of the decarboxylated decalin **50** and 6 mg (14%) of the nondecarboxylated decalin. The silyloxy group had been eliminated in both compounds. Compound **50**: ^1H nmr (δ): 6.33 (dd, 1H, J = 17.7, 10.0 Hz, -C*H*=CH_2), 6.18 (dd, 1H, J = 17.7, 1.6 Hz, -CH=C*H*$_2$, *trans*), 5.82 (dd, 1H, J = 10.0, 1.6 Hz, -CH=C*H*$_2$, *cis*), 3.67 (s, 3H, -CO_2CH_3), 3.42 (dd, 1H, J = 11.6, 4.0 Hz, -CH-C*H*$CO_2C(CH_3)_3)_3$), 2.6–1.1 (m, 16H), 1.50 (s, 9H, -$CO_2C(CH_3)_3$). Minor compound: ^1H nmr (δ): 6.30 (dd, 1H, J = 17.5, 10.0 Hz, -C*H*=CH_2), 6.15 (dd, 1H, J = 17.5, 1.5 Hz, -CH=C*H*$_2$, *trans*), 5.79 (dd, 1H, J = 10.0, 1.5 Hz, -CH=C*H*$_2$, *cis*), 3.72 (s, 3H, -CO_2CH_3), 3.13 (m, 1H, O=C-CH_2-C*H*-$(CH_2)_3$-C=O), 2.9–1.1 (m, 17H).

The major compound **50** (18 mg, 0.043 mmol) was resubmitted to the same conditions and 17 mg (94%) of tetracyclic compound **51** as a 2:2:1 mixture of three isomers were isolated after column chromatography with hexane – ethyl acetate 1:1. One isomer (eluting first) could be purified and was characterized; ir (cm^{-1}): 3000–2800, 1735–1710(bs), 1470, 1450, 1435, 1260, 1215(bs), 1160, 1105; ^1H nmr (δ): 4.1–3.9 (m, 2H, -O-C*H*$_2$-CH_2-C=O), 3.72 (s, 3H, -CO_2CH_3), 3.52 (ddt, 1H, J = 14.0, 6.25, 2.0 Hz, O=C-CH_2-C*H*-$(CH_2)_3$-C=O), 2.88 (m, 1H), 2.7–1.1 (m, 17H). ms (*m/e*): 320 (M^+), 302, 288, 277, 261, 260, 243. Exact Mass calculated for $C_{18}H_{24}O_5$: 320.1624; found: 320.1624.

*8aβ-Carbomethoxy-7α-methyl-2,3,4,4a,5,7,8,8a-octahydronaphthalene-1,6-dione (**52**)*

To a solution of 100 mg (0.5 mmol) of (3*E*)-1-phenylsulfinyl-2-oxo-3-pentene **26** in 5 mL of anhydrous dichloromethane, was added 63 mg of cesium carbonate (0.19 mmol). Then, 2-carbomethoxy-2-cyclohexenone **1** (104 mg, 0.67 mmol) was added over a period of 1 h and the resulting suspension was stirred 1 h at room temperature, after which it was filtered through a pad of silica gel and washed with ethyl acetate. The crude product was chromatographed on silica gel (10 g, at least 100:1 w/w of silica gel to product) eluting with hexane – ethyl acetate 3:1, to yield 79 mg (70%) of pure **52** as a white crystalline compound; mp: 80–82°C; ir (cm^{-1}): 3010 (s), 3000–2800 (m), 1750, 1735, 1720, 1675(s), 1440, 1235; ^1H nmr (δ): 5.99 (bd, 1H, J = 2.0 Hz, O=C-C*H*-C-), 3.75 (s, 3H, -CO_2CH_3), 3.23 (ddq, 1H, J = 6.9, 4.8, 3.2 Hz, H_3C-C*H*-CH_2-), 2.90 (dddd, 1H, J = 14.9, 12.5, 4.9, 2.0 Hz, O=C-CH_2-CH_2-C*H*$_2$-C=CH-C=O), β), 2.75 (dd, 1H, J = 17.8, 4.8 Hz, O=C-C*H*$_2$-CH_2-CH_2-C=CH-C=O), 2.7–2.5 (m, 3H, O=C-CH_2-CH_2-C*H*$_2$-C=CH-C=O, α and H_3C-CH-C*H*$_2$-), 2.30 (ddd, 1H, J = 17.8, 3.2, 0.9 Hz, O=C-C*H*$_2$-CH_2-CH_2-C=CH-C=O), 2.12 (m, 1H, O=C-CH_2-C*H*$_2$-CH_2-C=CH-C=O), 1.7 (m, 1H, O=C-CH_2-C*H*$_2$-CH_2-C=CH-C=O), 0.95 (d, 3H, J = 6.9 Hz, *H*$_3$C-CH-). ^{13}C nmr (δ): 203.5 (s, *C*=O), 197.4 (s, *C*=O), 156.3 (s, -*C*O_2CH_3), 127.0 (d, -C=*C*H), 126.1 (s, -*C*=CH), 66.4 (s, CH_3O_2C-*C*-C=CH), 53.5 (q, CO_2CH_3), 42.6 (t, -*C*H_2C=O), 40.1 (t, -CH_2C=O), 34.5 (d, -*C*H-CH_3), 33.0 (t, -*C*H_2-C=CH-), 20.7 (t, -CH_2-*C*H_2-CH_2-), 16.0 (q, -CH-*C*H_3). ms (*m/e*): 236 (M^+), 208, 194, 179, 177, 176, 163, 162, 135, 134. Exact Mass calculated for $C_{13}H_{16}O_4$: 236.1049; found: 236.1046.

*Monoaddition product **68***

To a solution of 100 mg (0.5 mmol) of (3*E*)-1-phenylsulfinyl-2-oxo-3-pentene **26** and 2-carbomethoxy-2-cyclohexenone **1** (104 mg, 0.67 mmol) in 5 mL of anhydrous dichloromethane at 0°C (or −5°C in acetonitrile) was added 63 mg of cesium carbonate (0.19 mmol). The resulting suspension was stirred at that temperature for 1 h. Then it was filtered through a pad of silica gel and washed with ethyl acetate. The crude product was chromatographed on silica gel, eluting with hexane – ethyl acetate 3:1 (200 mL) and then 1:1, to yield 81 mg (46%, 68% based on recovered starting material of pure **68** as a mixture of diastereomers along with 33 mg of the starting sulfoxide **26**. Both diastereomers of adduct **68** exist as a mixture of keto and enol forms; ir (cm^{-1}): 3010 (s), 3000–2800 (m), 1740, 1715, 1655, 1620, 1445, 1225, 1205, 1045; ^1H nmr (δ): 12.67 and 12.60 (s, C=C-O*H*), 7.7–7.4 (m), 6.83 (dq, J = 15.7, 6.9 Hz), 6.7;–6.3 (m), 5.77 and 5.66 (dq, J = 6.9, 1.6 Hz), 4.47 (d, J = 12.0 Hz, (C=O)C*H*-SOPh), 4.29 (d, J = 7.1 Hz, (C=O)C*H*-SOPh), 4.2–4.0 (m), 3.87 (s, -$COCH_3$), 3.84 (s, -$COCH_3$), 2.9–1.5 (m), 1.76 and 1.66 (dd, J = 6.9, 1.6 Hz, -CH-CH_3). ms (*m/e*): 362 (M^+), 346, 345, 344, 314, 313, 312. Exact Mass calculated for $C_{19}H_{22}O_5S$: 362.1195; found: 362.1188.

*Cyclization of adduct **68***

To a solution of 29 mg (0.08 mmol) of adduct **68** in 0.5 mL of anhydrous dichloromethane was added 10 mg of cesium carbonate (0.032 mmol) and the resulting suspension was stirred for 1 h at room temperature. Then it was filtered through a pad of silica gel, washing with ethyl acetate. The crude product was chromatographed on silica gel (2.9 g, at least 100:1 w/w of silica gel/product), eluting with hexane – ethyl acetate 3:1 (100 mL) and then 1:1, to yield 11 mg (58%) of a compound whose spectral data were identical with those of compound **52**.

*Catalytic hydrogenation of compound **52***

Palladium on charcoal (3 mg, 10% w/w) was added to a solution of 30 mg (0.13 mmol) of **52** in 1 mL of ethyl acetate. The flask was then flushed with hydrogen several times and the solution was stirred under a positive pressure of hydrogen for 72 h. The reaction mixture was then filtered through a pad of Celite and the solvent was evaporated under reduced pressure yielding a colorless oil. Chromatography on silica gel eluting with hexane – ethyl acetate 3:1 furnished 19 mg (60%) of the known compound **4** (2); ir (cm^{-1}): 3100–3000, 3000–2800, 1735, 1730–1700; ^1H nmr (δ): 3.81 (s, 3H, -CO_2CH_3), 3.0-2.7 (m, 3H), 2.5–1.5 (m, 9H), 1.15 (d, 3H, J = 6.9 Hz, CH-CH_3).

*8aβ-Carbomethoxy-7-methyl-5-phenylsulfonyl-2,3,4,4a,5,7,8,8a-octahydronaphthalene-1,6-dione (**53**)*

A solution of 60 mg (0.5 mmol) of (3*E*)-1-phenylsulfonyl-2-oxo-3-pentene **27** in 2 mL of anhydrous dichloromethane was treated with cesium carbonate (35 mg, 0.11 mmol) and 2-carbomethoxy-2-cyclohexenone **1** (58 mg 0.37 mmol) in the same way as for (3*E*)-1-phenylsulfinyl-2-oxo-3-pentene **26**. Chromatography on silica gel, eluting with hexane – ethyl acetate 3:1, yielded 46 mg (45%) of pure **53**; ir (cm^{-1}): 3120, 3000–2800, 1720(s), 1450, 1435, 1320, 1310, 1250, 1215, 1150, 1080; ^1H nmr (δ): 7.8–7.5 (m, 5H, C_6H_5-SO_2-), 4.00 (m, 1H), 3.86 (s, 3H, -CO_2CH_3), 3.58 (d, 1H, J = 6.6 Hz), 2.8–2.5 (m, 4H), 2.4–1.5 (m, 5H), 1.09 (d, 3H, J = 6.1, CH-CH_3). ms (*m/e*): 378 (M^+), 363, 347, 319, 292, 265, 237, 236, 233. Exact Mass calculated for $C_{19}H_{22}O_6S$: 378.1137; found: 378.1144.

*Reduction of sulfone **53***

The sulfone **53** (20 mg, 0.53 mmol) was dissolved in 1 mL of a mixture of THF and water (9:1). Aluminium foil (BDH, 23 mg, 0.84 mmol) was cut in small chunks, soaked in an aqueous mercuric chloride solution (2%) for 15 s, and rinsed with absolute ethyl alcohol and diethyl ether. The chunks were then dropped in the reactant solution and the mixture was stirred at room temperature for 4.5 h. The aluminium foil had completely dissolved after 2 h and the solution then took on a grayish color. The solution was then

Can. J. Chem. Downloaded from www.nrcresearchpress.com by 217.78.4.112 on 09/08/12
For personal use only.

filtered through a pad of Celite and the solvents were evaporated under reduced pressure. The residue was taken up in ether, washed with saturated sodium bicarbonate and then with brine, dried and the solvents evaporated under reduced pressure. Chromatography on silica gel, eluting with hexane – ethyl acetate 3:1, furnished 6 mg (48%, 79% based on recovered starting material of **4** and 8 mg of starting sulfone **53**.

*8aβ-Carbomethoxy-4β,8β-dimethyl-2,3,4,4a,5,7,8,8a-octahydronaphthalene-1,6-dione (**55**)*

A solution of *tert*-butyl (4*E*)-3-oxo-4-hexenoate **2** (459 mg, 2.5 mmol), 2-carbomethoxy-4-methyl-2-cyclohexenone **54** (344 mg, 2.0 mmol), and cesium carbonate (365 mg, 1.12 mmol) in chloroform (60 mL) was stirred for 3 h. The crude product was then decarboxylated using method B. Data for the bis-β-keto ester (before decarboxylation): ^{1}H nmr (δ): 12.67 (1H, s, -C=O*H*), 3.65 (3H, s, -COC*H*$_3$), 3.26 (1H, d, *J* = 12.5 Hz, -(CH$_3$)$_2$CC*H*C=C-OH), 2.80–1.52 (8H, m), 1.48 (9H, s, -C(C*H*$_3$)$_3$), 1.14 (3H, d, *J* = 7.1 Hz, -CH(C*H*$_3$), 0.97 (3H, d, *J* = 7.3 Hz, -CH$_2$C(C*H*$_3$)CH-); ms, (*m/e*): 334 (M$^+$ – H$_2$O), 295 (M$^+$ – C$_4$H$_9$).

β-Keto ester **55** (73% yield): mp: 86–88°C; ir (cm^{-1}): 1735–1720 (C=O ester and ketones); ^{1}H nmr (δ): 3.79 (3H, s, -COOC*H*$_3$), 2.75–1.43 (11H, m), 1.08 (3H, d, *J* = 6.5 Hz, -CH(C*H*$_3$), 1.04 (3H, d, *J* = 6.3 Hz, -CH$_2$CH(C*H*$_3$)CH-); ^{13}C nmr (δ): 208.9, 207.8 (2s, -*C*=O), 171.4 (s, -*C*O$_2$CH$_3$), 64.7 (s, O=C-*C*(CO$_2$CH$_3$)-C-), 52.1 (q, -CO$_2$*C*H$_3$), 48.0 (d, -CH$_2$CH(CH$_3$)*C*HCH$_2$-), 45.5, 41.9, 38.2, 32.8 (4t, -*C*H$_2$), 33.3 (d, -*C*H(CH$_3$), 31.1 (d, -CH$_2$*C*H(CH$_3$)-CH-), 19.4 (q, -CH$_2$CH(*C*H$_3$)CH-), 16.3 (q, -CH(*C*H$_3$)).

*8aβ-Carbomethoxy-8β-methyl-3β-methylethenyl-2,3,4,4a,5,7,8,8a-octahydronaphthalene-1,6-dione (**57**)*

A solution of *tert*-butyl (4*E*)-3-oxo-4-hexenoate **2** (285 mg, 1.5 mmol), 2-carbomethoxy-5β-methylethenyl-2-cyclohexenone **56** (600 mg, 3.1 mmol), cesium carbonate (250 mg, 0.8 mol) in CHCl$_3$ (38 mL) was stirred for 3 h. The crude product was then decarboxylated using method B to afford ester **57** as the major compound of a (85:11:4) mixture of three compounds (75% total yield). Compound **57** was isolated pure by means of flash chromatography (hexane – ethyl acetate 7:3) while the two diastereomeric side products could not be separated from each other: R_f for **57** and its isomers were 0.30 and 0.25, respectively, in hexane – ethyl acetate 7:3). **57** was recrystallized in a 20:1 mixture of heptane and dichloromethane: mp: 97–98°C; $[\alpha]_D$ + 117.3 (*c* = 1.3, CHCl$_3$); ir (CH$_2$Cl$_2$, cm^{-1}): 1740–1710 (C—O ester and ketones); ^{1}H nmr (δ): 4.81, 4.74, (2H, 2s, -C=C*H*$_2$), 3.76 (3H, s, -CO$_2$C*H*$_3$), 3.22–1.55 (11H, m), 1.72 (3H, s, -(C*H*$_3$)C=CH$_2$), 0.84 (3H, d, *J* = 7.4 Hz, -CHC*H*$_3$); ^{13}C nmr (δ): 209.7, 205.5 (2s, -*C*=O), 170.5 (s, -*C*O$_2$CH$_3$), 146.3 (s, -(CH$_3$)*C*=CH$_2$), 110.7 (t, -(CH$_3$)C=*C*H$_2$), 62.7 (s, O=C-*C*(CO$_2$CH$_3$)-C-), 52.8 (q, -CO$_2$*C*H$_3$), 45.8, 45.1, 52.7, 32.5, (4t, -*C*H$_2$), 40.8, 37.2 (2d, -*C*H), 33.5 (d, -*C*HCH$_3$), 20.5 (q, -C(*C*H$_3$)=CH$_2$), 16.5 (q, -CH*C*H$_3$); unseparated mixture of minor compounds: ^{1}H nmr (δ): 4.82–4.74 (>2H, m, -C=C*H*$_2$), 3.82 (<3H, s, -CO$_2$C*H*$_3$), 3.81 (3H, s, -CO$_2$C*H*$_3$), 3.20–1.45 (11H, m), 1.73 (>3H, s, -(C*H*$_3$)C=CH$_2$), 1.16 (<3H, d, *J* = 6.9 Hz, -CH-C*H*$_3$), 1.14 (3H, d, *J* = 6.6 Hz, -CH-C*H*$_3$).

*8aβ-Carbomethoxy-4,4,8β-trimethyl-4,4a,5,7,8,8a-hexahydronaphthalene-1,6-dione (**59**)*

To a stirred solution of *tert*-butyl (4*E*)-3-oxo-4-hexenoate **2** (77 mg, 0.42 mmol) and 2-carbomethoxy-4,4,dimethylcyclohexadienone **58** (603 mg, 3.3 mmol) in acetonitrile (10 mL) was added cesium carbonate (60 mg, 0.19 mmol). After 3 h, the cesium carbonate was filtered through silica gel and the solvent was evaporated under reduced pressure. Flash chromatography (hexane – ethyl acetate 4:1) yielded 106 mg (70%) of bis-β-keto ester; ^{1}H nmr (δ): 12.79 (1H, s, -C=C-O*H*), 6.61 (1H, d, *J* = 10.2 Hz, -C*H*=CH-CO-), 5.89 (1H, d, *J* = 10.2 Hz, -CH=C*H*-CO-), 3.77 (1H, s, -(CH$_3$)$_2$CC*H*C=C-OH), 3.63 (3H, s, -CO$_2$C*H*$_3$), 2.55–2.40 (3H, m), 1.48 (9H, s, -CO$_2$(C*H*$_3$)$_3$), 1.20, 1.06 (6H, 2s, -C(C*H*$_3$)$_2$), 1.10 (3H, d, *J* = 6.2 Hz, -CHC*H*$_3$); ms (*m/e*): 364 (M$^+$), 333 (M$^+$ – OCH$_3$), 307 (M$^+$ – C$_4$H$_9$).

This crude product was then decarboxylated using method B. Flash chromatography (hexane – ethyl acetate 3:2) of the residue yielded 66 mg (86%) of **59** as a solid. The product could be recrystallized in heptane; mp: 88–89°C; ir (CH$_2$Cl$_2$, cm^{-1}): 1740–1710 (C=O ester and ketone), 1680 (C=O conjugated ketone); ^{1}H nmr (δ): 6.54 (1H, d, *J* = 10.3 Hz, -C*H*=CH-CO-), 5.96 (1H, d, *J* = 10.3 Hz, -CH=C*H*-CO-), 3.75 (3H, s, -CO$_2$C*H*$_3$), 3.04 (1H, t, *J* = 6.0 Hz, -(CH$_3$)$_2$CC*H*CH$_2$-), 2.75–2.20 (5H, m), 1.20 (3H, s, -C(C*H*$_3$)$_2$), 1.12 (3H, s, -C(C*H*$_3$)$_2$), 1.09 (3H, d, *J* = 6.4 Hz, -CHC*H*$_3$); ^{13} C nmr (δ): 209.5 (s, *C*=O), 196.0 (s, -C=C-*C*=O), 171.4 (s, -*C*O$_2$CH$_3$), 156.8 (d, -*C*H=CH-CO-), 124.6 (d, -CH—*C*H-CO-), 60.0 (s, O=C-*C*(CO$_2$CH$_3$)-C-), 52.3 (q, -CO$_2$*C*H$_3$), 45.2 (t and d, -*C*H$_2$ and -(CH$_3$)$_2$*C*CHCH$_2$-), 40.0 (t, -*C*H$_2$), 36.3 (s, -*C*(CH$_3$)$_2$), 33.3 (d, -*C*H-CH$_3$), 30.8, 25.6 (2q, -C(*C*H$_3$)$_2$), 16.6 (q, -CH-*C*H$_3$); ms (*m/e*): 264 (M$^+$), 249 (M$^+$ – CH$_3$), 232 (M$^+$ – CH$_3$OH); Exact Mass calculated for C$_{15}$H$_{20}$O$_4$ (M$^+$): 264.1361; found: 264.1363.

*8aβ-Carbomethoxy-4,4-ethylenedioxy-8β-methyl-2,3,4,4a,5,7,8,8a-octahydronaphthalene-1,6-dione (**61**)*

Dichloromethane (5 mL), β-keto ester **2** (288 mg, 1.67 mmol), 4,4-ethylenedioxy-2-carbomethoxy-2-cyclohexenone **60** (237 mg, 1.12 mmol), and cesium carbonate (146 mg, 0.45 mmol) were stirred for 2 h. Chromatography on silica gel with hexane – ethyl acetate 5:1 afforded 441 mg (98%) of a colorless oil; ir (cm^{-1}); 3000–2800, 1740, 1710, 1645, 1395, 1295, 1225, 1210(s), 1155; ^{1}H nmr (δ): 12.4 (s, <1H, -C=CO*H*), 4.0–3.7 (m, 4H, -O(C*H*$_2$)$_2$O-), 3.66 (s, <3H, -CO$_2$C*H*$_3$), 3.65 (s, <3H, -CO$_2$C*H*$_3$), 3.20 (m, 1H), 2.74 (m, 2H), 2.45–2.35 (m, 3H), 2.1–1.95 (m, 2H), 1.46 (s, 9H, -CO$_2$C(C*H*$_3$)$_3$), 1.06 (d, <3H, *J* = 7.0 Hz, -CH-C*H*$_3$), 1.05 (d, <3H, *J* = 7.0 Hz, -CH-C*H*$_3$). ms (*m/e*): 396 (M$^+$), 340, 323, 322, 309, 296, 295, 294. Exact Mass calculated for C$_{20}$H$_{28}$O$_8$: 396.1780; found: 396.1784.

This product (220 mg, 0.55 mmol) was then decarboxylated according to method A to afford, after chromatography on silica gel eluting with hexane – ethyl acetate 3:1, 151 mg (93%) of decalin **61**; ir (cm^{-1}): 3000–2800, 1715(s), 1225(s), 1125, 1090, 1045; ^{1}H nmr (δ): 4.05–3.95 (m, 4H, -O(C*H*$_2$)$_2$O-), 3.78 (s, 3H, -CO$_2$C*H*$_3$), 3.22 (t, 1H, *J* = 5.8 Hz, (RO)$_2$C-C*H*-CH$_2$-C=O), 3.0 (m, 1H, H$_3$C-C*H*-CH$_2$-), 2.8–2.55 (m, 3H), 2.5–2.3 (m, 2H), 2.1–1.9 (m, 3H), 1.05 (d, 3H, *J* = 7.0 Hz, -CH-C*H*$_3$); ms (*m/e*): 296 (M$^+$), 281, 237, 195. Exact Mass calculated for C$_{15}$H$_{20}$O$_6$: 296.1265; found: 296.1260.

Acknowledgements

Support for this work by the Natural Sciences and Engineering Research Council of Canada (NSERCC) and by the Fonds pour la formation de chercheurs et l'aide à la recherche (FCAR du Québec) is gratefully acknowledged. This paper was taken in part from the Ph.D. theses of J.-F. Lavallée and R. Ruel. C. Spino was the recipient of an NSERCC Postdoctorate Fellowship in 1988–1990.

1. T. L. Ho. Carbocycle construction in terpene synthesis. VCH Publishers, Inc., New York, N.Y. 1988.
2. D. Liotta, C. Barnum, R. Puleo, G. Zima, C. Bayer, and H. S. Kezar, III. J. Org. Chem. **46**, 2920 (1981).
3. H.-J. Liu and T. K. Ngooi. Can. J. Chem. **62**, 2676 (1984).
4. (*a*) J.-F. Lavallee and P. Deslongchamps. Tetrahedron Lett. **29**, 5117 (1988); (*b*) J.-F. Lavallee and P. Deslongchamps. Tetrahedron Lett. **29**, 6033 (1988); (*c*) G. Berthiaume, J.-F. Lavallee, and P. Deslongchamps. Tetrahedron Lett. **27**, 5451 (1986); (*d*) R. Ruel, K. T. Hogan, and P. Deslongchamps. SynLett. 516 (1990).
5. R. Zibuck and J. M. Streiber. J. Org. Chem. **54**, 4717 (1989).
6. (*a*) I. N. Nazarov and S. I. Zavyalov. Zh. Obshch. Khim **23**, 1703 (1953); (*b*) G. Stork and R. N. Ghikonda. Tetrahedron

Lett. **13**, 2755 (1972); (*c*) B. M. Trost and R. A. Kunz. J. Am. Chem. Soc. **97**, 7152 (1975); (*d*) B. M. Trost and R. A. Kunz. J. Org. Chem. **39**, 2648 (1974); (*e*) S. Ohta, A. Shimbayashi, S. Hatano, and M. Okamoto. Synthesis, 715 (1983).
7. (*a*) R. Bodalski, K. M. Pietrusiewicz, J. Monkiewicz, and J. Koszuk. Tetrahedron Lett. **21**, 2287 (1980); (*b*) J. A. M. Van Den Goorbergh, and A. Van Der Gen. Tetrahedron Lett. **21**, 3621 (1980); (*c*) C. M. Moorhoff and D. F. Schneider. Tetrahedron Lett. **28**, 559 (1987).
8. J.-F. Lavallee. Ph.D. thesis, Université de Sherbrooke. 1988.
9. S. L. Schreiber, R. E. Claus, and J. Reagan. Tetrahedron Lett. **23**, 3867 (1982).
10. E. J. Corey and W. L. Seibel. Tetrahedron Lett. **27**, 905 (1986).
11. H. J. Reich, J. M. Renga, and I. L. Reich. J. Am. Chem. Soc. **97**, 5434 (1975).
12. A. B. Smith, III, S. J. Branca, N. N. Pilla, and M. A. Guaciaro. J. Org. Chem. **47**, 1855 (1982).
13. S. Goldmann. Synthesis, 640 (1980).
14. A. G. Michel, R. Ruel, and N. Michel-Dewez. Acta Crystallogr. Sect. C: Cryst. Struct. Commun. **C46**, 291 (1990).
15. R. B. Boeckman Jr., J. J. Napier, E. W. Thomas, and R. I. Sato. J. Org. Chem. **48**, 4152 (1983).
16. R. Ruel and P. Deslongchamps. Tetrahedron Lett. **31**, 3961 (1990).
17. C. Spino and P. Deslongchamps. Tetrahedron Lett. **31**, 3969 (1990).
18. H. O. House and J. K. Larson. J. Org. Chem. **33**, 61 (1968).
19. G. H. Posner. Org. React. (N.Y.), **19**, 1 (1972).
20. E. Klein and G. Ohloff. Tetrahedron, **19**, 1091 (1963).
21. T. Kitahara, H. Kutara, T. Matsuoka, and K. Mori. Tetrahedron, **41**, 5475 (1985).
22. D. W. Brooks, L. D.-L. Lu, and S. Masamune. Angew. Chem. Int. Ed. Engl. 72 (1979).
23. M. Kato, V. P. Kamat, and A. Yoshikoshi. Synthesis, 699 (1988).
24. (*a*) R. A. Lee. Tetrahedron Lett. **14**, 3333 (1973); (*b*) K. B. White and W. Reusch. Tetrahedron, **34**, 2439 (1978).
25. K. N. Houk, R. J. Loncharich, J. F. Blake, and W. L. Jorgensen. J. Am. Chem. Soc. **111**, 9172 (1989) and references cited therein.
26. D. A. Evans and A. M. Golob. J. Am. Chem. Soc. **97**, 4765 (1975).
27. (*a*) D. Caine, C. R. Harrison, and D. G. Vanderveer. Tetrahedron Lett. **24**, 1353 (1983); (*b*) H.-J. Liu and E. N. C. Browne. Can. J. Chem. **65**, 1262 (1987).
28. P. Deslongchamps. Stereoelectronic effects in organic chemistry. Organic Chemistry Series Vol. 1. *Edited by* J. E. Baldwin. Pergamon Press, Oxford, England. 1983. p. 275.

Can. J. Chem. Downloaded from www.nrcresearchpress.com by 217.78.4.112 on 09/08/12
For personal use only.

The synthesis of β-keto lactones via cyclization of β-keto ester dianions or the cyclization of Meldrum's acid derivatives

LEONARD LERMER, EDWARD G. NEELAND, JAMES P. OUNSWORTH, RUSSELL J. SIMS, SAMUEL A. TISCHLER, AND LARRY WEILER[1]

Department of Chemistry, University of British Columbia, 2036 Main Mall, Vancouver, B.C., Canada V6T 1Z1

Received August 8, 1991

This paper is dedicated to Professor Zdenek (Denny) Valenta on the occasion of his 65th birthday

LEONARD LERMER, EDWARD G. NEELAND, JAMES P. OUNSWORTH, RUSSELL J. SIMS, SAMUEL A. TISCHLER, and LARRY WEILER. Can. J. Chem. **70**, 1427 (1992).

Two new methods to synthesize macrocyclic β-keto lactones have been developed. The first involves the synthesis of ω-halo-β-keto esters and an intramolecular alkylation of the dianions to these compounds. The reaction is complicated by elimination in the small and medium ring systems and by difficulties in purifying the final products. However, it is possible to obtain modest yields of the desired β-keto lactones. This procedure was used to synthesize the 25- and 27-membered ring β-hydroxy lactones that are the constituents of termite defense compounds. The second method involves the thermolysis of acylated Meldrum's acid derivatives, which leads directly to β-keto lactones. This process gives modest yields of macrocyclic systems and good yield of the unsubstituted 3-oxopentan-5-olide (**25**). The 14-membered macrocyclic β-keto lactone **9*j*** has a complex ^{1}H NMR spectrum, which has been interpreted in terms of multiple conformations. The temperature dependence of the NMR spectrum of **9*j*** is consistent with entropic, rather than enthalpic, control of the equilibrium. Quasiharmonic entropy calculations are consistent with this model.

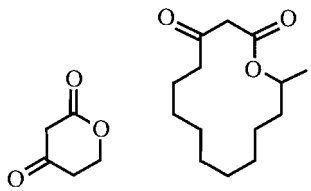

25 **9*j***

LEONARD LERMER, EDWARD G. NEELAND, JAMES P. OUNSWORTH, RUSSELL J. SIMS, SAMUEL A. TISCHLER et LARRY WEILER. Can. J. Chem. **70**, 1427 (1992).

On a mis au point deux nouvelles méthodes de synthèse de β-céto lactones macrocycliques. La première implique la synthèse des β-cétoesters ω-halogénés et une alkylation intramoléculaire des dianions de ces composés. La réaction est compliquée par une réaction d'élimination dans les systèmes comportant des petits cycles et des cycles moyens et par des difficultés à purifier les produits finals. Toutefois, il est possible d'obtenir des rendements modestes des β-céto lactones désirées. On a utilisé cette procédure pour synthétiser les β-hydroxy lactones à 25 et à 27 chainons qui font partie des produits de défense des termites. La seconde méthode implique la thermolyse de dérivés acylés de l'acide de Meldrum et elle conduit directement aux β-céto lactones. Cette méthode donne des rendements modestes des systèmes macrocycliques et un bon rendement du 3-oxopentan-5-olide (**25**). Le spectre RMN du ^{1}H de la β-céto lactone macrocyclique à 14 chainons (**9*j***) est complexe et on l'a interprété en fonction de conformations multiples. La relation entre le spectre RMN du composé **9*j*** et la température est en accord avec un contrôle entropique, plutôt qu'enthalpique, de l'équilibre. Des calculs d'entropie quasiharmonique sont en accord avec ce modèle.

[Traduit par la rédaction]

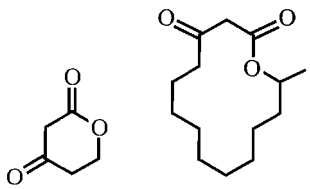

25 **9*j***

Introduction

β-Keto lactones have been found in a number of macrocyclic natural products. Picromycin (**1**) (ref. 1*a*, structure; 1*b*, synthesis), narbomycin (**2**) (ref. 2*a*, structure; 2*b*, synthesis), and kromycin (**3**) (see ref. 1*a* for structure; for synthesis, ref. 3) are 14-membered β-keto lactone antibiotics that have attracted interest as synthetic targets. The β-keto lactone moiety led to confusion in the initial structural work on these compounds (4). This particular array of functional groups also generated one of the most challenging aspects of the synthesis of these compounds. Indeed, in three of the syntheses of these compounds, a β-hydroxy lactone was

[1]Author to whom correspondence may be addressed.

Can. J. Chem. Downloaded from www.nrcresearchpress.com by 217.78.4.112 on 09/08/12
For personal use only.

synthesized and subsequently oxidized to the β-keto lactone at a very late stage in the synthesis.

Boeckman and Pruitt used an ingenious cyclization of a hydroxy ketene to give the β-keto lactone directly (eq. [1]) (3). In model studies directed towards the synthesis of simple β-keto lactones, Ireland and Brown provided a direct route to such systems through a sulfide contraction of the product from an intramolecular reaction of an α-halo ester and a thioamide (eq. [2]) (5) and Booth *et al.* found that ω-hydroxy-β-keto thioesters can be cyclized to macrocyclic β-keto lactones (eq. [3]) (6).

For several years we have been interested in the synthesis and reactivity of β-keto ester derivatives. The mono anions of ω-halo-β-keto esters cyclize rather slowly. As a result, we were able to generate the dianions of these compounds and cyclize the resulting intermediate to the β-keto esters shown in eq. [4] (7). This suggested a possible route to β-keto lactones via the intramolecular alkylation of the dianions of ω-halo-β-keto esters **4**.[2]

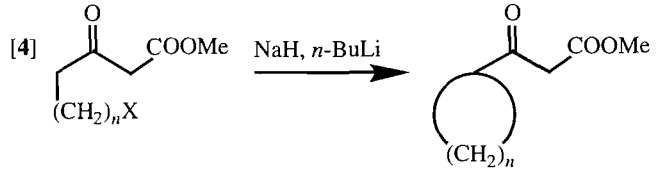

β-Keto esters substituted on the alcohol fragment are readily obtained from alcoholysis of the acyl Meldrum's acid derivative **5** (9). Thus, alcoholysis of **5** with the halo alcohols **6** gave the desired ω-halo-β-keto esters **4** in good to excellent yields (eq. [5] and Table 1). The ω-halo alcohols **6** were prepared according to literature procedures (see Experimental).

[2] A preliminary account of a portion of this work has appeared (8).

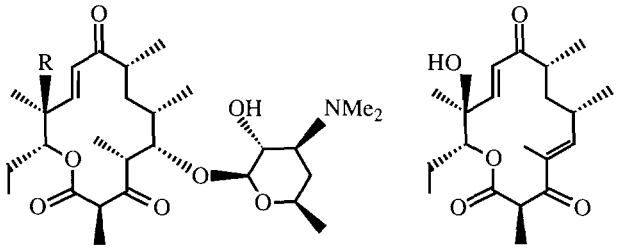

1 R = OH
2 R = H

3

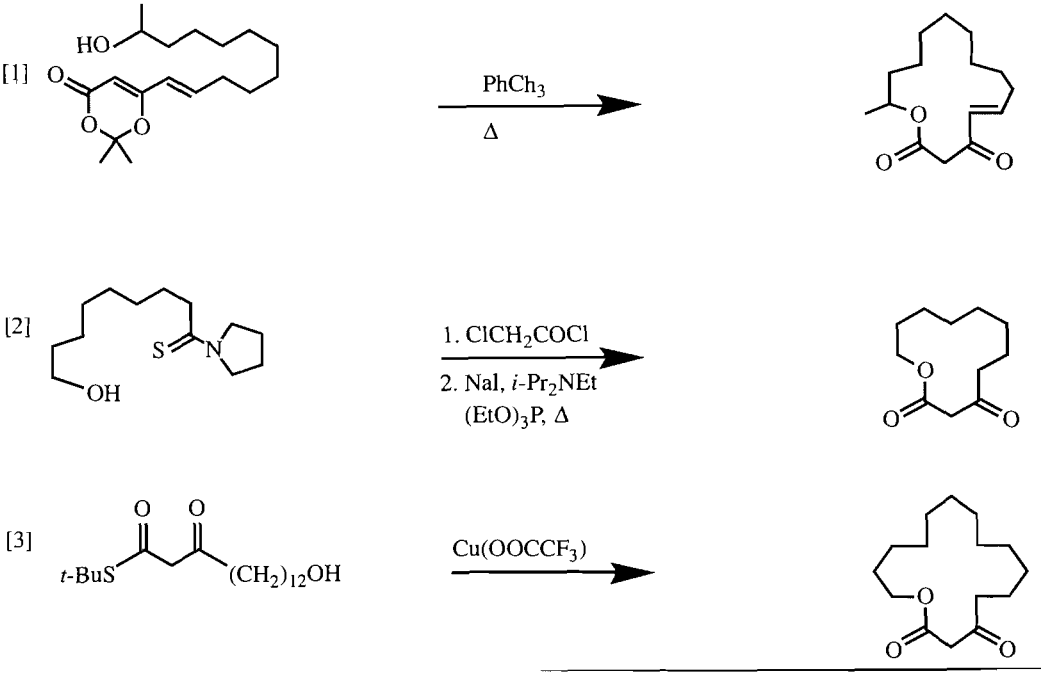

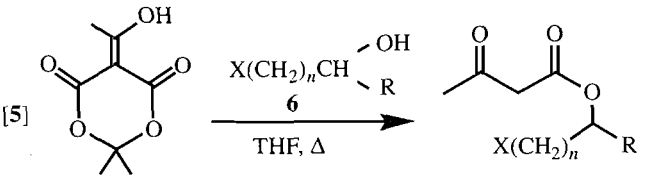

5 **4**

We then undertook an extensive study of the cyclization of the β-keto esters **4** via their dianions. Treatment of **4***a* with two equivalents of lithium diisopropylamide (LDA) gave a complex mixture of products from which we were unable to isolate any cyclic β-keto lactone or other identifiable product. Lowering the reaction temperature did not lead to any improvement in the reaction. The addition of β-keto ester **4***b* to a solution of two equivalents of LDA in THF gave a single product by TLC that was isolated in 58% yield. The NMR and IR spectra of the product clearly showed that it was an olefinic β-keto ester and the spectral data were consistent with the structure of the product being **7**. This was confirmed by an independent synthesis of **7** from acetyl Meldrum's acid **5** and 2-propen-1-ol.

Can. J. Chem. Downloaded from www.nrcresearchpress.com by 217.78.4.112 on 09/08/12
For personal use only.

Can. J. Chem. Downloaded from www.nrcresearchpress.com by 217.78.4.112 on 09/08/12
For personal use only.

TABLE 1. Yields of ω-halo-β-keto esters **4** by alcoholysis of acetyl Meldrum's acid **5**

Entry	R	X	*n*	Yield (%)
a	H	Br	1	67
b	H	Br	2	80
c	H	Cl	3	79
d	H	Br	4	74
e	H	Br	5	86
f	Me	Cl	5	85
g	H	Br	6	84
h	H	Br	7	86
i	H	Br	8	88
j	Me	Br	8	98
k	H	Br	9	92
l	H	Br	10	85

TABLE 2. Cyclization of ω-halo-β-keto esters **4** using LDA in THF (eq. [6])

Entry **4**	R	X	*n*	Yield (%) **9**	**10**
b	H	Br	2	0	58
d	H	Br	4	0	41
e	H	Br	5	0	45
g	H	Br	6	0	57
h	H	Br	7	0	41
i	H	Br	8	43	3
j	Me	Br	8	47	0
k	H	Br	9	45	2
l	H	Br	10	49	4

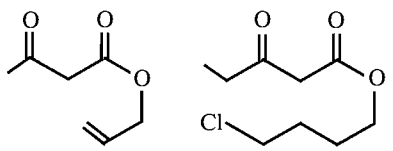

7 **8**

Treatment of **4***c* and **4***d* with two equivalents of LDA in THF gave only unreacted starting material even on prolonged reaction conditions. Verification of dianion formation was obtained by the addition of one equivalent of methyl iodide to the solution of **4***c* in base. This reaction gave the γ-alkylated product **8** in 75% yield. The fact that exclusive γ-alkylation had occurred was readily shown from the NMR data. With the question of dianion formation no longer in doubt, it appeared that the failure of the cyclization was linked either to the poor leaving group ability of the chloride or to the geometric requirements of the cyclization. The chloride in **4***c* was replaced with iodide. Attempted cyclization of this iodide gave only the elimination product.

From a study of molecular models, we concluded that the formation of 8- to 11-membered β-keto lactones via the intramolecular alkylation would be difficult because of the need for the halide chain to span four contiguous planar sp^2 carbons. This analysis suggested that the first ring that we might expect to form under these conditions would be the 12-membered system. To test this hypothesis and to determine the chain length at which cyclization becomes competitive with other side reactions, we prepared the series of β-keto esters **4***e*–**4***l*. An extensive study of cyclization of **4***l* to give the 16-membered lactone was carried out.

When the β-keto ester **4***l* was added to a solution of two equivalents of LDA in THF, two new products were formed in addition to some unreacted starting material. The major product was shown to be the desired 3-oxopentadecanolide (**9***l*) from its spectroscopic data and the minor product was the alkene (**10***l*) formed in an elimination reaction. Increasing the amount of LDA in the reaction mixture to three equivalents led to complete reaction of the starting material. The ^{1}H NMR of the crude product indicated that it contained mainly the desired β-keto lactone along with a small amount of the elimination product. Careful chromatographic purification of the product gave approximately a 50% yield of the desired lactone. Other methods of purification were not successful. Subsequently we found that these β-keto lactones are relatively unstable to chromatography and distillation.

Adding HMPA to the solvent led to increased yields of the alkene **10***l*. Reaction in less polar solvents, such as hexane, gave lower yields of lactone and increased recovery of starting material. The reaction was sensitive to temperature and maximum yields were obtained when the addition of **4** to the base was carried out at either −78°C or 0°C and the reaction mixture allowed to warm to room temperature. No cyclization could be detected at temperatures below −10°C. Yet at 0°C, the proportion of β-keto lactone began to diminish prior to complete consumption of starting material. At lower temperatures increased recovery of starting material occurred. We were unable to improve the yield of product using other metal counterions or leaving groups. Thus we returned to the original conditions of LDA in THF to study the cyclization of the ω-bromo-β-keto esters shown in Table 2.

The cyclization for 14-membered and larger rings proceeded in reasonable yield. However, we obtained only elimination products and no cyclization in those reactions directed towards generating smaller β-keto lactones. These cyclizations are not run under dilute conditions and they are not complicated by formation of dimers and trimers (see for example refs. 5, 6, and 10). No doubt the formation of the

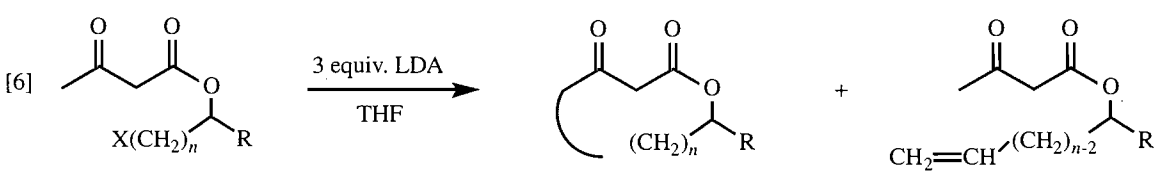

4 **9** **10**

Can. J. Chem. Downloaded from www.nrcresearchpress.com by 217.78.4.112 on 09/08/12
For personal use only.

dianionic intermediates suppresses bimolecular reactions that complicate many macrocyclization reactions (11). We did find that the resulting β-keto lactones slowly decompose in the strongly basic reaction mixture. This, along with their instability to chromatography and distillation, is the major reason for the modest yields of the macrocyclic β-keto lactones.

In a detailed study of the rates of cyclization versus elimination of bromo phenoxides, Cort *et al.* suggested that elimination is favoured over substitution for medium sized rings, and even for larger rings the transition state for elimination is less strained than that for intramolecular substitution (12). Pross and Shaik concluded that the geometric requirements for substitution are more stringent than those for elimination in bimolecular reactions (13). If the transition state for an intramolecular substitution is tighter than that for elimination, this could be the origin of the marked change in reactivity in going from the 13-membered (entry *h*) to the 14-membered ring (entry *i*) in Table 2.

Prestwich and Collins found that β-hydroxy lactones **11***a* and **11***b* containing 25- and 27-membered rings are major components of the cephalic secretions of soldier termites (14). It has been suggested that the wounds on ants and other insects bitten by the termite mandibles receive a coating of these anithealant compounds leading to their death. These β-hydroxy lactones are a key element in the termite's defense mechanism. We have synthesized **11***a* and **11***b* as shown in Scheme I. Alcoholysis of acetyl Meldrum's acid with **15***a* or **15***b* gave the complex β-keto esters **16***a* and **16***b* in excellent yield. The cyclization reactions were not as high yielding as above. We had hoped that the *cis* double bond might facilitate the formation of the large ring. The final products **11***a* and **11***b* are crystalline solids with spectral data fully consistent with their structures. The natural product was an inseparable mixture of the two isomers **11***a* and **11***b*, which prevented a direct comparison of their spectral data with that of the pure synthetic compounds.

The ^{1}H NMR spectra of **11***a* and **11***b* did show some interesting differences, which we attribute to differences between their conformations. The C-24 methylene group of **11***a* is a complex multiplet at δ 4.15, which collapses to an AB quartet (J = 12 Hz) on irradiation of the C-23 methylene protons at δ 1.64. Thus **11***a* must exist in conformation(s) in which the asymmetry due to C-3 renders the two protons on C-24 chemically nonequivalent. On the other hand, the C-26 methylene protons in **11***b* are a triplet (J = 6 Hz) at δ 4.19, which collapses to a singlet when the C-25 protons at δ 1.66 are irradiated. Thus **11***b* exists in conformation(s) in which the coupling constants of the protons on C-26 with those on C-25 are averaged to give an apparent triplet, and the two protons on C-25 are chemically equivalent.

An alternate strategy for the preparation of β-keto lactones using Meldrum's acid derivatives was also briefly examined. In this approach, the key cyclization step involves lactonization through intramolecular alcoholysis of an acyl Meldrum's acid derivative as shown in Scheme 2 for the synthesis of 3-oxo-13-tridecanolide (**9***i*). To minimize intermolecular reactions the alcohol **21** was slowly added to a refluxing THF solution to give the desired lactone **9***i* in 25% overall yield from 11-hydroxyundecanoic acid.

The generality of this methodology in modified form was explored as outlined below. The ω-benzyloxy carboxylic acids **22** (n = 2–10) were converted into their acid chlorides and condensed with Meldrum's acid to give **23** (n = 2–10). The benzyl protecting group was removed to give **24** (n = 2–10). In this reaction a catalytic amount of acid greatly accelerated the reaction (15). The cyclizations were attempted by slowly adding a dilute THF solution of **24** to refluxing THF. The 6-membered ring compound, 3-oxo-5-pentanolide (**25**), was obtained in 87% in this way. However, we could not detect any monomeric lactone with any of the other systems except for n = 2 or 10. When **23** (n = 3) was hydrogenolyzed, the enol ether **26** was obtained directly in 80% yield (Scheme 3), demonstrating the strong kinetic preference for formation of 5-membered rings over 7-membered rings (16).

It is interesting to note that although many 3-oxo-5-pentanolide derivatives have been synthesized (17), the unsubstituted parent **25** has only been reported recently (18). Fetizon *et al.* have prepared the corresponding ketal (17*c*). The β-keto lactone **25**, although a solid, is unusually labile. Hydrolysis occurs readily on standing unless moisture is carefully excluded. The high reactivity of this lactone is due to the significant dipole–dipole interactions of the *s-cis* ester moiety and the additional carbonyl in this system (19). The solution infrared spectrum of **25** has carbonyl stretching bands at 1745 and 1780 cm^{-1} with the lower frequency band notably stronger, which is consistent with a significant degree of strain in the molecule. The larger ring β-keto lactones have two carbonyl stretches of equal intensity at approximately 1710 and 1735 cm^{-1}. It is unclear why the C-5 substituted derivatives of **25** (17) are so much more stable than **25**. Compound **25** has no significant enol content in chloroform solution from its NMR or IR spectrum, which is unusual for these β-keto δ-lactones (for example, see ref. 20). The NMR spectrum of an acetone solution of **25** and its solid state infrared spectrum indicate substantial amounts of enol (18).

The conformation of these macrocyclic β-keto lactones both in solution and the solid state is of interest. X-ray studies of the highly substituted macrolide antibiotics **1–3** illustrate that the substituents on these molecules significantly influence their solid state conformation. All have the expected (21) *s-trans* conformation about the C—O—CO—C bond of the lactone. More recently Booth *et al.* provided X-ray data on a number of simpler β-keto lactones and this same restriction is seen even more clearly (6). These researchers also found that the two carbonyl groups often have their dipoles in a nonplanar arrangement. In addition, the two carbonyl groups are oriented so as to minimize their dipolar repulsions.[3] The solution conformation of these β-keto lactones is not well understood. However, based on solution NMR and CD data, it has been suggested that pikromycin and narbomycin adopt a different conformation in solution than in the solid state (22).

We have used NMR, IR, and molecular mechanics calculations to probe the conformation of the above lactones in solution. The IR spectra of **9***i*–**9***l* had one carbonyl band at 1705–1715 cm^{-1} and a second band at 1730–1740 cm^{-1}. This is consistent with the carbonyl groups adopting a strain-free conformation in which the CO dipoles are not aligned in the

[3]Recently the X-ray structure of (−)-menthyl 2-oxocyclopentanecarboxylate was solved and found to have the two carbonyl groups in approximately a *trans* coplanar arrangement: C. P. Decicco and J. N. Bridson, Memorial University of Newfoundland, personal communication, 1991.

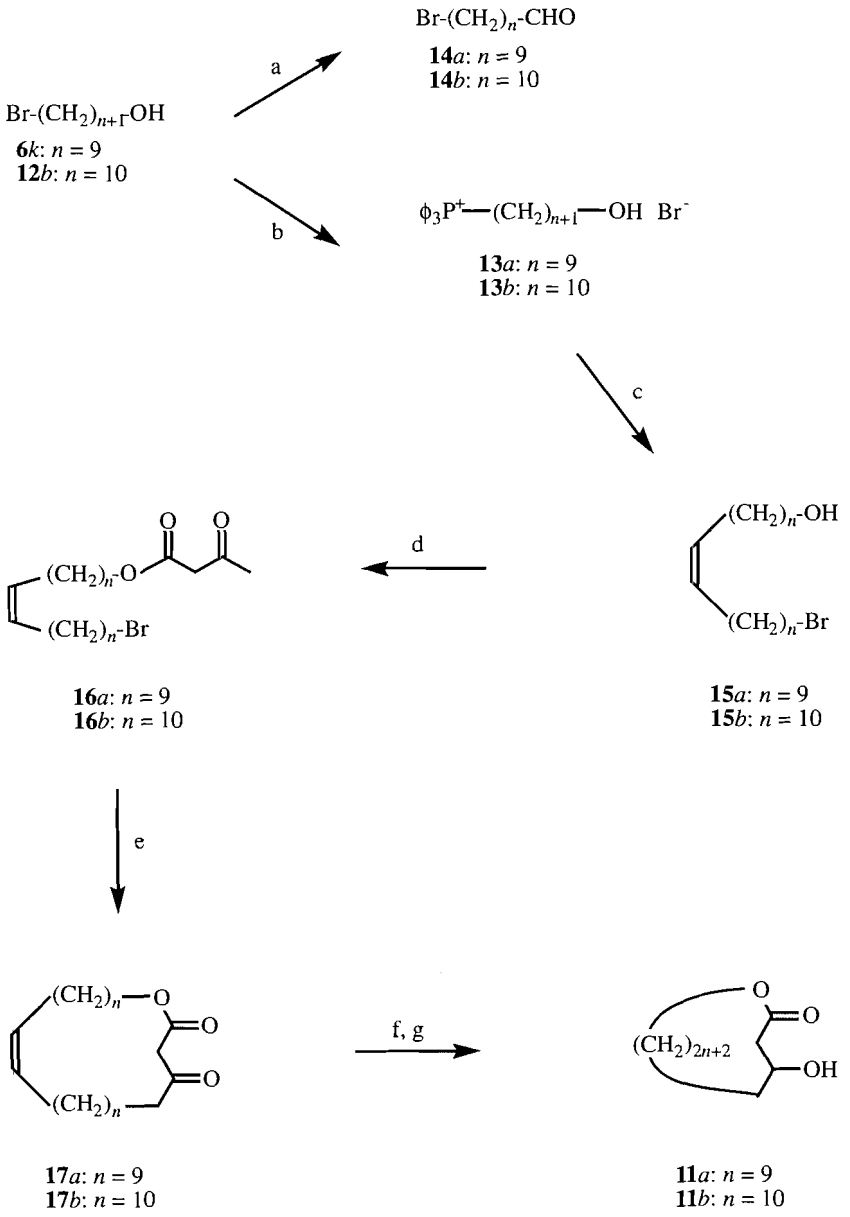

(a) PCC, CH_2Cl_2, 80–95%; (b) ϕ_3P, MeCN, Δ, 60–95%; (c) *n*-BuLi, THF, −78°C, then add **14**, −20°C, 47–55%; (d) acetyl Meldrum's acid (**5**), THF, Δ, 95–97%; (e) 3 equiv. LDA, THF, 0°C to 25°C, 37–39%; (f) H_2, PtO_2, EtOAc, 75–98%; (g) $Zn(BH_4)_2$, Et_2O, 48–96%

SCHEME 1

same plane. The ^1H NMR spectra of the unsubstituted β-keto lactones consisted of a triplet (J = 6–8 Hz) at δ 4.2 ppm for the ω-methylene, a singlet at δ 3.45 ppm for the C-2 methylene, and a triplet (J = 6–8 Hz) at δ 2.6 ppm for the C-4 methylene. For the 14-membered ring compound **9*i***, these signals did not change on cooling to −100°C. Similarly the ^{13}C NMR spectra of these compounds contained the expected number of signals and we could not detect any conformational equilibria in the case of **9*i*** on cooling to −100°C. From this we conclude that these β-keto lactones either are a single conformation at room temperature or, more likely, they are a mixture of rapidly interconverting conformations that could not be frozen out on cooling to −100°C. To provide some insight into which of these two possibilities might be occurring we carried out molecular mechanics calculations on the 14-membered β-keto lactone.

A search for the possible conformations of **9*i*** using MACROMODEL's internal coordinate Monte Carlo methodology (23) and the MM2 force field (24) gave the global minimum conformation as **27**. However, there are 55 or so conformations within 2 kcal/mol of the global minimum. Thus we conclude that in fact **9*i*** is a mixture of conformational isomers at room temperature. The next lowest three conformations, **28**–**30**, are shown below with their relative energies in parentheses. Note that conformations **27** and **28** are [3434][4] conformations, **29** is an irregular conformation with the two carbonyl groups *syn* coplanar, and **30** is a [3344] conformation. In the conformations **27**, **28**, and **30** the car-

[4]We have used the conformational descriptors for large rings proposed by Dale (26*b*).

Can. J. Chem. Downloaded from www.nrcresearchpress.com by 217.78.4.112 on 09/08/12
For personal use only.

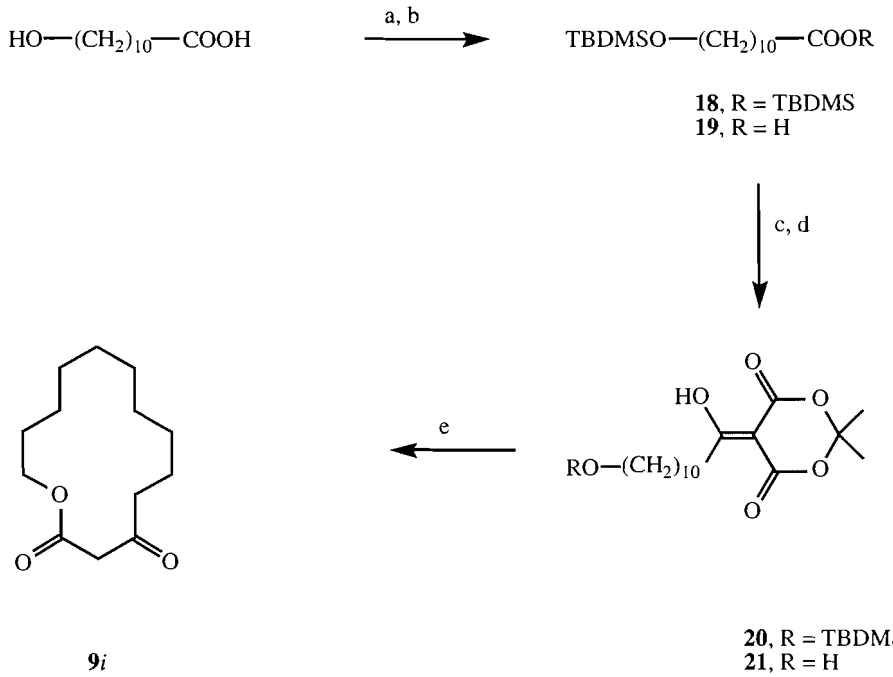

(a) TBDMSCl, ImH, DMF, 95%; (b) NaOH, H_2O, 97%; (c) $(Im)_2CO$, Meldrum's acid, py, CH_2Cl_2, 78%; (d) Bu_4NF, THF, 98%; (e) THF, Δ, 35%

SCHEME 2

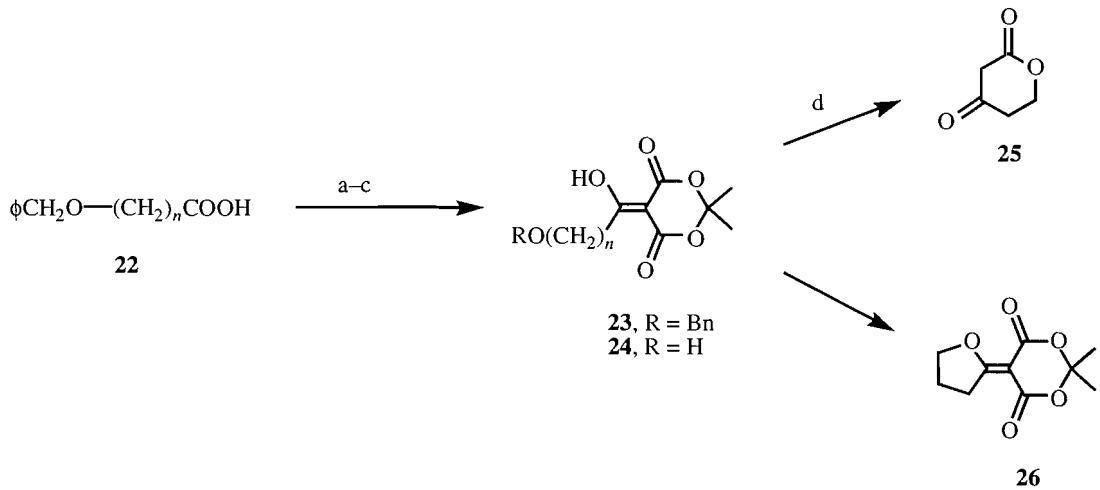

(a) $COCl_2$, py, CH_2Cl_2, 0°C; (b) Meldrum's acid, py, CH_2Cl_2; (c) H_2, Pd–C, EtOH; (d) THF, Δ

SCHEME 3

bonyl groups point in opposite directions and the geometries of the ketone and lactone moieties are very similar.

The infrared spectrum of the methyl substituted lactone **9*j*** also indicated that the carbonyls were unstrained in either the *trans* coplanar or nonplanar conformation(s). The ^1H NMR spectrum of **9*j*** was much more complex than that of **9*i*** as a result of the diastereomeric methylene protons. For example, in $CDCl_3$ the C-2 methylene group is an AB quartet at δ 3.35 and 3.46 with J = 13.5 Hz. The C-4 methylene protons are a multiplet at δ 5.0, which depends on temperature and solvent. In fact the entire NMR spectrum shows significant changes with solvent and temperature. For example, the C-2 methylene protons at room temperature consist of an AB quartet *plus* a *singlet* (Fig. 1). These signals are assigned to two sets of conformations that are not rapidly interconverting on the NMR time scale. It is not entirely clear why one of the barriers to conformational change in the methyl-substituted lactone **9*j*** is so much higher than that in **9*i***. Cooling a CD_3OD solution of **9*j*** produced the changes shown in Fig. 2. From these data we see that the AB quartet diminishes in intensity relative to solvent on cooling, while the lower-field singlet increases. We interpet this data as follows. The singlet in this case overlaps with the second lowest field line of the AB quartet and is due to conforma-

Can. J. Chem. Downloaded from www.nrcresearchpress.com by 217.78.4.112 on 09/08/12
For personal use only.

Can. J. Chem. Downloaded from www.nrcresearchpress.com by 217.78.4.112 on 09/08/12
For personal use only.

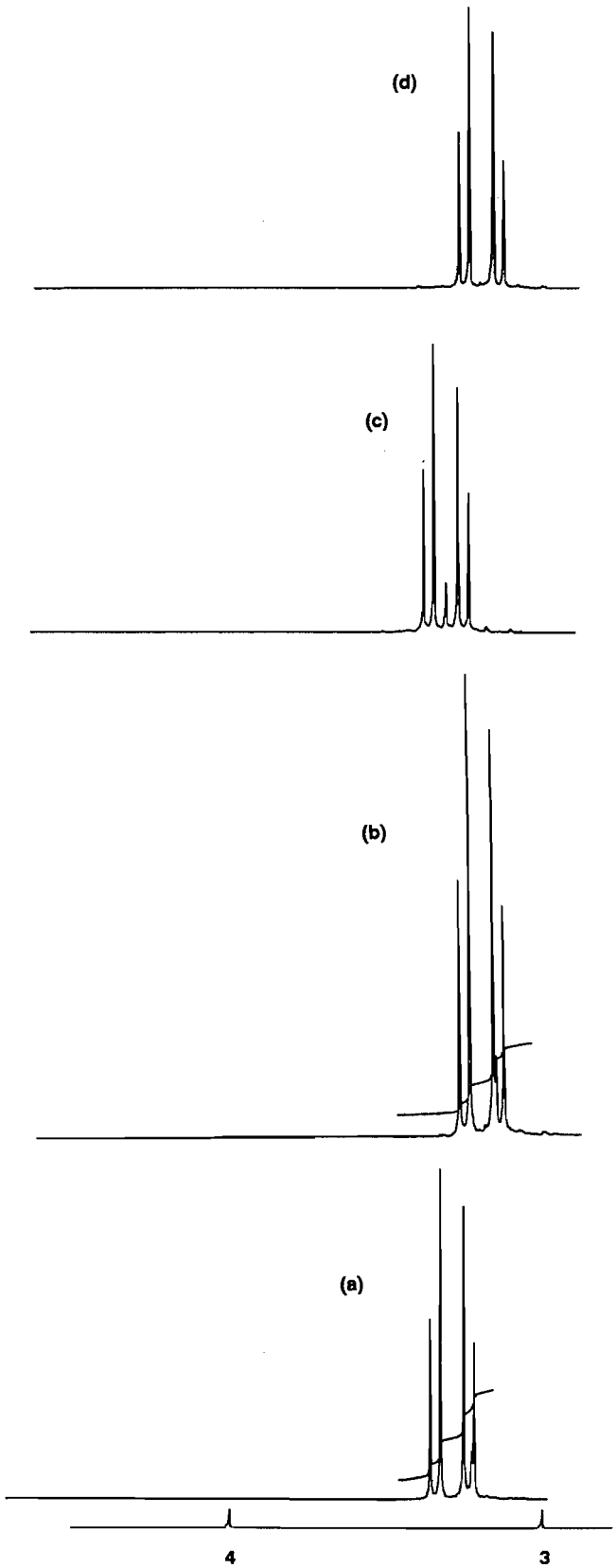

FIG. 1. ^{1}H NMR spectrum of the C-2 methylene protons of **9*i*** in various solvents; (*a*) C_6D_6; (*b*) C_6D_6–$CDCl_3$ (4:1); (*c*) C_6D_6–$CDCl_3$ (1:4); (*d*) $CDCl_3$. Note the small peak that is a shoulder on the high-field line of the AB quartet in (*a*) and moves to lower field as more chloroform is added, until (*d*) in which this signal overlaps with the second lowest field line of the AB quartet.

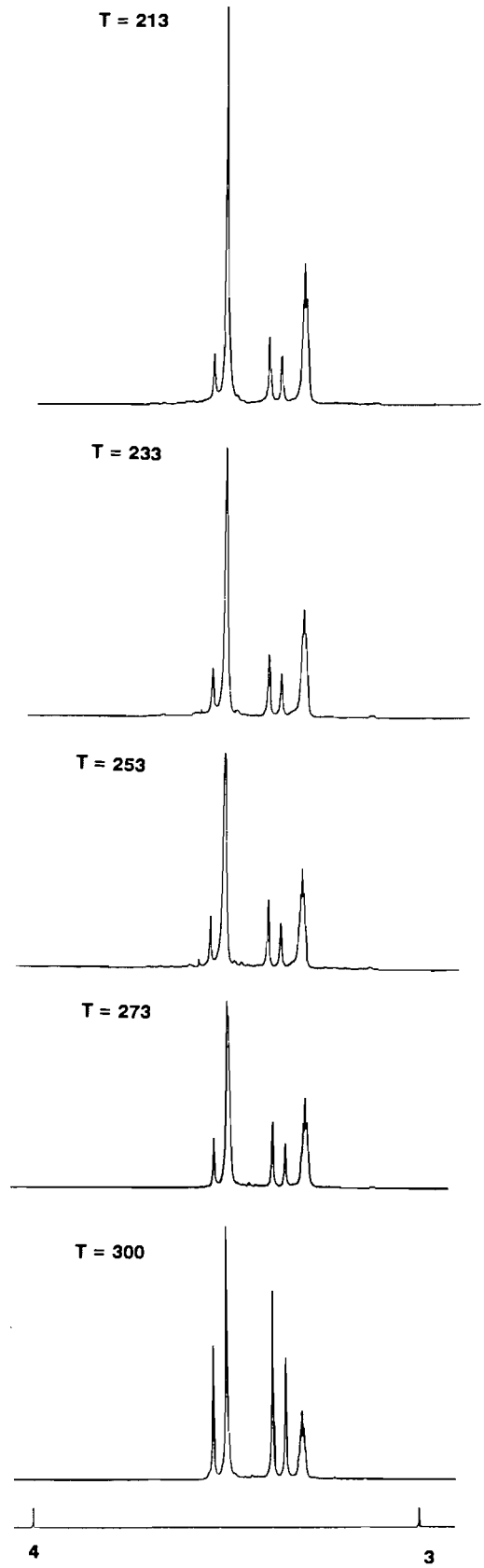

FIG. 2. ^{1}H NMR spectrum of the C-2 methylene protons of **9*i*** at various temperatures in CD_3OD (the peak at δ 3.3 is due to solvent).

tion **34**, which is a minor component of the room temperature ensemble but, on cooling, becomes the major component at the expense of the conformations **31** and **32**, which are responsible for the AB quartet and are the major conformers at room temperature.

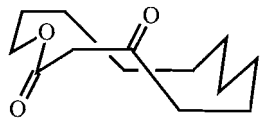

27 (0.0 kcal/mol)

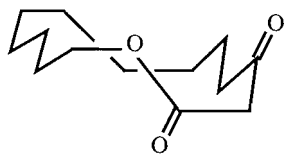

28 (0.15 kcal/mol)

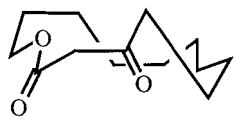

29 (0.60 kcal/mol)

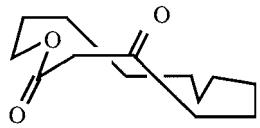

30 (0.60 kcal/mol)

The barrier to interconversion of conformations **31** ⇆ **32** involves the change of three torsional angles in the hydrocarbon chain remote from the functional groups. The barrier to this equilibrium should be comparable to that found in cyclotetradecane for the barrier conformational interconversion, which is in the range 5–7 kcal/mol (25). The interconversion of **31** and (or) **32** with **34** involves torsional changes about six bonds, one of which involves the ketone carbon. The mechanism for the interconversion of two [3434] conformations in cyclotetradecane is suggested to involve a pseudorotation process (25, 26*a*); such a process in the interconversion of **31** ⇆ **34** would force the two carbonyl groups out of their *trans* coplanar geometry and add to the barrier to such a process. In addition, in **34** the methyl group on C-13 is brought into a 1,3 diaxial relation with a hydrogen on C-11 that is also expected to affect the barrier to the interconversion of **31** ⇆ **34**.

We carried out MACROMODEL calculations to determine the feasibility of such a model. A search of conformational space showed that there were about 30 conformations within 2 kcal/mol of the global minimum. The four lowest three conformations, **31**–**34**, are shown below with their relative energies in parentheses. Note that conformations **31**, **33**, and **34** are all [3434] conformations and **32** is a [3344] conformation. There is no low-energy conformation comparable to **30** for **9***j*. In these four conformations the carbonyl groups point in opposite directions and geometries of the ketone and lactone moieties are very similar. This may be important in rationalizing the chemical reactivity of this compound.

The coupling constant $J_{H_{4,4'}}$ in **9***j* is 18.5 Hz, which is very large for a geminal coupling constant. Barfield and Grant found that geminal coupling constants for methylenes adjacent to π systems are at a maximum when the π bond bisects the H—C—H angle of the adjacent methylene group (27). This is the geometry of the ketone carbonyl and the C-4 methylene group in conformations **31**–**34**. The coupling constant $J_{H_{2,2'}}$ is 13.5 Hz, which is low for a geminal coupling constant with adjacent π systems. Barfield and Grant state that this will occur when the π bond is aligned with one of the C═H bonds of the adjacent methylene group (27). This is the geometry in conformations **31** and **34** and very close to the geometry in **32** and is consistent with our suggestion that these conformations are the major ones to consider in analyzing the conformation of **9**j.

TABLE 3. Quasiharmonic entropy calculations of conformations **31**–**34** in cal deg^{-1} mol^{-1}

Temperature (K)	**31**	**32**	**33**	**34**
300	230	236	232	232
273	227	233	234	238
253	223	228	228	246
213	219	221	221	226

Next we applied temperature-dependent molecular dynamics calculations to the four lowest energy conformations to compute the quasiharmonic entropies of these conformations. A summary of the results of these conformations for the conformations **31**–**34** is given in Table 3. The calculated entropy difference between **31** and **34** at 300 K gives a $T\Delta S$ term of 0.6 kcal/mol, which is comparable to the enthalpy difference from the strain energy calculations. However, at 253 K the $T\Delta S$ value for **31** ⇄ **34** is 5.8 kcal/mol, which is significantly larger than the ΔH difference between these conformations. This highlights a difficulty in analyzing the conformations of large rings. Exclusive use of enthalpy (strain) energy differences may be misleading in these systems with large numbers of conformations close to the global minimum. Entropy differences may be required to correctly rationalize the physical and chemical properties of these compounds.

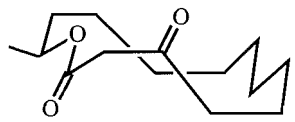

31 (0.0 kcal/mol)

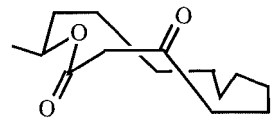

32 (0.53 kcal/mol)

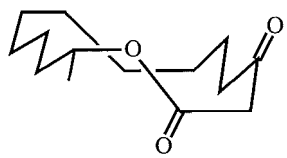

33 (0.62 kcal/mol)

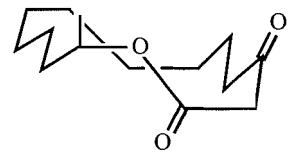

34 (0.74 kcal/mol)

In conformation **33** the torsional angle between the lactone carbonyl and the C-13 methine hydrogen is close to 180°. Schweizer and Dunitz (21) observed a preference for esters of secondary esters to exist in a conformation in which the C—O—C—H torsional angle is within the range 0–40°. We have shown that this rule also applies to 14-membered lactones of secondary alcohols (28). Thus we have neglected conformation **33** in our analysis of the conformation of **9***j*. The origins of the torsional angle preference for secondary esters and lactones may well be electronic and hence not handled properly by the current molecular mechanics force fields.

Can. J. Chem. Downloaded from www.nrcresearchpress.com by 217.78.4.112 on 09/08/12
For personal use only.

Can. J. Chem. Downloaded from www.nrcresearchpress.com by 217.78.4.112 on 09/08/12
For personal use only.

The C-13 methine proton of **9***j* has couplings of 5.1 and 6.6 Hz with the C-12 methylene protons in CD_3OD and C_6D_6, while in CD_3Cl these couplings are 3.4 and 8.0 Hz. Again we attribute these differences to a solvent-dependent distribution of conformations. A similar solvent effect was observed for the coupling of the C-4 and C-5 protons. A solution to the coupling constants in CD_3Cl is that the conformational equilibrium is 13% **31**, 49% **32**, and 38% **34**, which is in reasonable agreement with the values calculated above from the molecular mechanics data. We have been unable to develop a model with a small number of conformations that is consistent with the observed values for these coupling constants in CD_3OD or C_6D_6. However, we believe that the bulk of the data is consistent with a fast, on the NMR time scale, equilibrium between **31** $\rightleftarrows$ **32**, which are the predominant conformations at room temperature and these conformations are in a slow, on the NMR time scale, equilibrium with **34**, which is the predominant conformation at lower temperatures.

In conclusion we have generated two new methods to synthesize macrocyclic β-keto lactones. The spectral and physical properties of these lactones are consistent with each being a mixture of conformations, which will no doubt complicate their chemistry.

Experimental section

General procedures

Melting points were determined on a Kofler hot stage microscope and are uncorrected. Kugelrohr distillations were performed by means of a Büchi Kugelrohr thermostat. Infrared spectra were recorded in chloroform solution on Perkin–Elmer model 700 or 710B spectrophotometers, and were calibrated with the 1601 cm^{-1} band of polystyrene. Proton nuclear magnetic resonance spectra were recorded on a Varian T-60 (60 MHz), a Bruker WP-80 (80 MHz), or a Bruker WH–400 (400 MHz) spectrometer. Chemical shifts are reported on the δ scale, with deuterochloroform as solvent and tetramethylsilane as an internal standard. The multiplicity, coupling constants (if observable), and integrated peak area are indicated in parentheses after each signal. Low-resolution mass spectra were recorded on an Atlas CH-4B or a Kratos-AEI MS-50 mass spectrometer, and high-resolution mass measurements were obtained using a Kratos-AEI MS-9 or MS-50 mass spectrometer. All instruments were operated at an ionizing potential of 70 eV. Elemental analyses were performed by Mr. Peter Borda, Microanalysis Laboratory, University of British Columbia, Vancouver, B.C.

Silica gel $PF_{254+366}$ supplied by E. Merck was used for both analytical and preparative thin-layer chromatography, while 100–200 mesh ASTM was employed for column chromatography. Flash chromatography (29) was performed using Silica Gel 60, 230–400 mesh ASTM, supplied by E. Merck. All solvent systems are expressed in ratios by volume (v/v).

Materials

The petroleum ether used was of boiling range 30–60°C. Dry solvents and reagents were prepared as follows: diethyl ether and tetrahydrofuran by distillation from lithium aluminum hydride or sodium–benzophenone; dichloromethane by distillation from phosphorus pentoxide; *N*,*N*-dimethylformamide and hexamethyl phosphoramide by distillation from calcium hydride at reduced pressure; benzene, 1,2-dichloroethane, diisopropylamine, pyridine, triethylamine, and toluene by distillation from calcium hydride; and ethanol and methanol by distillation from magnesium. Methyllithium (in ether) *n*-butyllithium (in hexane), and methylmagnesium chloride (in THF) were obtained from Aldrich Chemical Company. The alkyllithium solutions were standardized either by titration against 0.1 M *tert*-butanol in benzene using 1,10-phenanthroline as indicator (30*a*) or by titration against 1,3-diphenyl-2-propanone tosylhydrazone in THF (30*b*). Sodium hydride (Aldrich Chemical Company) was weighed as a 60% dispersion in mineral oil and was washed with dry ether to remove the oil prior to use. All other reagents and solvents were either of reagent grade and used directly, or purified according to literature procedures (31). All reactions were run under a dry nitrogen or argon atmosphere. Organic extracts were dried over anhydrous magnesium sulphate.

2,2-Dimethyl-1,3-dioxan-4,6-dione (Meldrum's acid)

A 250-mL Erlenmeyer containing a large magnetic stirring bar was charged with malonic acid (52 g, 0.50 mol) and acetic anhydride (60 mL, 0.60 mol). To the resulting suspension was added concentrated sulfuric acid (1.5 mL) with constant stirring. Most of the malonic acid dissolved with spontaneous cooling. Acetone (40 mL, 0.55 mol) was introduced slowly while cooling to 20–25°C and the reaction mixture was allowed to stand in the fridge overnight. The resultant crystals were filtered by suction, washed with ice water (3 × 75 mL), and allowed to air dry. The resulting white solid was dissolved in acetone (110 mL), filtered to remove any undissolved material, and diluted with water (220 mL). Filtration gave a flocculent white solid, which was dried in a vacuum desiccator over phosphorus pentoxide to yield 35 g (49%) of product, mp 93–94°C (lit. (32) mp 94–95°C); IR ν_{max}: 1755 cm^{-1}; ^1H NMR (60 MHz) δ: 1.78 (s, 6H), 3.57 (s, 2H); MS *m*/*z* (relative intensity): 144 (M^+, 1), 129 (100), 100 (88), 72 (20), 69 (72), 61 (40), 59 (35), and 58 (34).

*5-(1'-Hydroxyethylidene)-2,2-dimethyl-1,3-dioxan-4,6-dione (**5**)*

A 250-mL, two-necked round bottom flask was charged with Meldrum's acid (10.0 g, 69.4 mmol) and 150 mL of dry dichloromethane. The solution was cooled to 0°C in an ice-water bath and dry pyridine (10.99 g, 139 mmol) was added. After stirring for 10 min, acetyl chloride (6.0 g, 76 mmol) was introduced dropwise and the reaction mixture was allowed to stand at 0°C for 1 h, then at room temperature for 1 h. The dichloromethane solution was washed with 5% hydrochloric acid (2 × 25 mL) and water (2 × 50 mL), then dried. Removal of the solvent under reduced pressure followed by recrystallization from ethyl ether gave 10.5 g (81%) of **5** as a pale yellow solid. An analytical sample was prepared by sublimation (60°C/0.35 Torr; 1 Torr = 133.3 Pa) and had the following properties: mp 83.5–84.5°C; IR ν_{max}: 3600–3300, 1740, 1665, and 1580 cm^{-1}; ^1H NMR (60 MHz) δ: 1.75 (s, 6H), 2.67 (s, 3H), and 15.0 (bs, 1H); MS *m*/*z* (relative intensity): 186 (M^+, 47), 171 (17), 128 (100), 111 (16), 85 (36), 84 (55), and 69 (36). Anal. calcd. for $C_8H_{10}O_5$: C 51.61, H 5.41; found: C 51.82, H 5.22.

*4-Chloro-1-butanol (**6***c*)

A 250-mL, three-necked round bottom flask was charged with 1,4-butanediol (20 g, 0.22 mol) and dry pyridine (17.6 g, 0.22 mmol). The flask was placed in a water bath maintained at 55°C and thionyl chloride (26.4 g, 0.22 mol) was added dropwise over 1 h. The temperature of the water bath was then raised to 80°C for 1 h as sulfur dioxide was vented off. The reaction mixture was cooled and extracted with ether (3 × 100 mL). The ethereal extracts were washed with 5% hydrochloric acid (50 mL), water (50 mL), brine (50 mL), then dried. The solvent was removed under reduced pressure and the residue fractionally distilled to give 8.7 g (36%) of **6***c* as a colourless liquid; bp 67–69°C/5.0 Torr (lit. (33) bp 84–85°C/16 Torr); IR ν_{max}: 3620, 3450, and 2950 cm^{-1}; ^1H NMR (60 MHz) δ: 1.70–2.00 (m, 4H), 2.65 (s, 1H), and 3.43–3.72 (m, 4H); MS *m*/*z* (relative intensity): 108 (M^+ ^{35}Cl, 1), 92 (14), 90 (59), 71 (100), 62 (23), 57 (13), and 55 (78).

5-Acetoxy-1-bromopentane

This compound was prepared according to the literature procedure (34) from anhydrous zinc chloride (ca. 20 mg), tetrahydropyran (8.61 g, 0.10 mol), and acetyl bromide (7.99 g, 0.065 mol) in 88% (11.0 g) distilled yield: bp 89–91°C/4.5 Torr (lit. (34) bp

Can. J. Chem. Downloaded from www.nrcresearchpress.com by 217.78.4.112 on 09/08/12
For personal use only.

106–107°C/12 Torr); IR ν_{max}: 1720 cm^{-1}; ^1H NMR (60 MHz) δ: 1.53–2.10 (m, 6H), 2.03 (s, 3H), 3.37 (t, J = 7 Hz, 2H), and 4.03 (t, J = 6 Hz, 2H); MS m/z (relative intensity): 210 (M^+ ^{81}Br, 0.5), 208 (M^+ ^{79}Br, 0.5), 150 (35), 148 (35), 73 (18), 69 (100), 68 (28), and 61 (45).

*5-Bromo-1-pentanol (**6**d)*

A solution of the above acetate (10.8 g, 0.052 mol) in dry methanol (150 mL) was prepared in a 250-mL round bottom flask. Anhydrous potassium carbonate (16 g, 0.12 mol) was then added in portions and the resulting suspension was stirred vigorously for 4 h at room temperature. Dilute hydrochloric acid was added until the mixture became acidic and the solution was extracted with ethyl acetate (3 × 100 mL). The combined organic extracts were washed with water (50 mL) and brine (50 mL), then dried. Removal of the solvent under reduced pressure, followed by vacuum distillation of the crude material, gave 5.71 g (66%) of **6***d* as a colourless liquid: bp 53–56°C/0.20 Torr (lit. (35) bp 75–76°C/0.5 Torr); IR ν_{max}: 3620 and 3400 cm^{-1}; ^1H NMR (60 MHz) δ: 1.30–2.03 (m, 6H), 2.50 (s, 1H, exchangeable with D_2O), 3.40 (t, J = 6 Hz, 2H), and 3.60 (t, J = 6 Hz, 2H); MS m/z (relative intensity): 168 (M^+ ^{81}Br, 0.1), 166 (M^+ ^{79}Br, 0.1), 1.50 (4), 148 (4), 137 (5), 135 (5), 122 (1), 120 (1), 109 (2), 107 (2), 70 (9), 69 (100), 68 (16), 57 (10), 56 (13), and 55 (26).

6-Chloro-2-hexanone

A 1-L, two-necked round bottom flask equipped with a large magnetic stirring bar and an addition funnel was charged with a solution of sodium hypochlorite in water (400 mL of a 5% solution). The flask was cooled to 0°C and 1-methylcyclopentanol (10 g, 0.10 mol) in carbon tetrachloride (2.0 mL) was added dropwise. A solution of glacial acetic acid (40 mL) in carbon tetrachloride (5 mL) was introduced and the reaction mixture was vigorously stirred for 5.5 h. The greenish-yellow carbon tetrachloride layer was combined with carbon tetrachloride extracts of the aqueous phase (3 × 10 mL), washed with a saturated sodium carbonate solution (2 × 10 mL), and dried. Filtration of the drying agent left 1-methylcyclopentyl hypochlorite in carbon tetrachloride solution, ready for the rearrangement step. The carbon tetrachloride solution was refluxed for 1.5 h, then the solvent was removed under reduced pressure. Excess saturated aqueous sodium bisulfite was added and the resulting addition compound was washed with ether (25 mL), then decomposed with warm aqueous sodium carbonate solution. The aqueous layer was extracted with ether (2 × 50 mL) and the ethereal solution dried. Removal of the solvent under reduced pressure followed by vacuum distillation gave 4.0 g (30%) of 6-chloro-2-hexanone as a colourless liquid: bp 64–66°C/3.8 Torr lit. (36*a*) bp 52.5–54°C/2.3 Torr); IR ν_{max}: 1710 cm^{-1}; ^1H NMR (60 MHz) δ: 1.60–1.90 (m, 4H), 2.16 (s, 3H), 2.48 (t, J = 7 Hz, 2H), and 3.52 (t, J = 7 Hz, 2H); MS m/z (relative intensity): 136 (M^+ ^{37}Cl, 0.25), 134 (M^+ ^{35}Cl, 0.75), 118 (6), 99 (13), 98 (46), 71 (21), 58 (100), and 55 (58).

*6-Chloro-2-hexanol (**6**f)*

A 50-mL, two-necked round bottom flask was charged with 6-chloro-2-hexanone (4.0 g, 30 mmol) and ethanol (25 mL). The flask was cooled to 0°C and sodium borohydride (1.13 g, 30 mmol) was added slowly in portions. The reaction mixture was allowed to warm to room temperature and stand for 4.5 h. The ethanol was removed under reduced pressure and 5% hydrochloric acid solution was added cautiously to the residue. The aqueous solution was then extracted with ether (4 × 25 mL) and the combined organic extracts were washed with water (20 mL), and brine (20 mL). The ethereal solution was dried and the solvent was removed under reduced pressure, leaving the desired alcohol as a yellow liquid. Vacuum distillation of the crude material gave 2.8 g (70%) of **6***f* as a colourless liquid: bp 78–79°C/2.3 Torr (lit. (36*b*) bp (58°C/1.1 Torr); IR ν_{max}: 3620 and 3470 cm^{-1}; ^1H NMR (60 MHz) δ: 1.17 (d, J = 6 Hz, 3H), 1.30–1.90 (m, 6H), 2.07 (s, exchanged with D_2O, 1H), 3.50 (t, J = 7 Hz, 2H), and 3.50–3.90 (m, 1H); MS m/z (relative intensity): 138 (M^+ ^{37}Cl, 0.4), 136 (M^+ ^{35}Cl, 1), 123 (28), 121 (100), 102 (17), 85 (56), 67 (53), 57 (48), 56 (46), and 55 (100).

*General procedure for the preparation of (1,*n*) bromo alcohols from (1,*n*)-diols*

A solution of the diol in 48% HBr was placed in a 100-mL liquid–liquid extractor. The solution was heated in an oil bath while being continuously extracted with an appropriate solvent. The solution was cooled and the organic layer separated, washed with saturated sodium bicarbonate solution, water, then dried. Removal of the solvent under reduced pressure gave the crude bromo alcohol, which was further purified by vacuum distillation.

*6-Bromo-1-hexanol (**6**e)*

This compound was prepared according to the general procedure for bromo alcohol formation using 1,6-hexanediol (6.00 g, 50.9 mmol) and 48% hydrochloric acid (12 mL). The solution was heated to 75–80°C and the extraction was continued for 39 h using toluene (50 mL) as solvent. Distillation of the crude product gave 5.16 g (56%) of **6***e* as a colourless liquid: bp 59–62°C/0.10 Torr (lit. (37) bp 105–106°C/5.0 Torr); IR ν_{max}: 3620 and 3450 cm^{-1}; ^1H NMR (60 MHz) δ: 1.30–2.00 (m, 8H), 2.27 (s, exchangeable with D_2O, 1H), 3.43 (t, J = 7 Hz, 2H), and 3.63 (t, J = 6Hz, 2H); MS m/z (relative intensity): 164 (M^+ −16, 6), 162 (6), 136 (14), 134 (14), 83 (63), 32 (16), and 55 (100).

*7-Bromo-1-heptanol (**6**g)*

This compound was prepared according to the general procedure for bromo alcohol formation using 1,7-heptanediol (7.00 g, 53.0 mmol) and 48% HBr (36 mL). The solution was heated to 75–80°C and the extraction was continued for 16 h using toluene (100 mL) as solvent. Distillation of the crude product gave 4.85 g (47%) of **6***g* as a colourless liquid: bp 107–108°C/4.0 Torr (lit. (38) bp 111–112°C/4 Torr); IR ν_{max}: 3640 and 3450 cm^{-1}; ^1H NMR (60 MHz) δ: 1.30–2.00 (m, 10H), 3.02 (s, exchangeable with D_2O, 1H), 3.37 (t, J = 6 Hz, 2H), and 3.60 (t, J = 7 Hz, 2H); MS m/z (relative intensity): 195 (M^+ −1, 1), 193 (1), 150 (24), 148 (24), 97 (22), 69 (48), 68 (20), and 55 (100).

*8-Bromo-1-octanol (**6**h)*

This compound was prepared according to the general procedure for bromo alcohol formation using 1,8-octanediol (6.00 g, 41.2 mmol) and 48% HBr (6 mL). The solution was heated to 90°C and the extraction was continued for 72 h using toluene (100 mL) as solvent. The crude material was distilled to give 3.86 g (45%) of **6***h* as colourless liquid: bp 95–100°C/0.27 Torr (lit. (39) bp 77–78°C/0.01 Torr); IR ν_{max}: 3620 and 3450 cm^{-1}; ^1H NMR (60 MHz) δ: 1.10–2.00 (m, 12H), 2.08 (s, exchangeable with D_2O, 1H), 3.40 (t, J = 7 Hz, 2H), and 3.58 (t, J = 6 Hz, 2H); MS m/z (relative intensity): 192 (M^+ −18, 3), 190 (3), 164 (14), 162 (14), 150 (14), 148 (14), 111 (11), 82 (38), 69 (80), 68 (34), 67 (14), 56 (20), and 55 (100).

*9-Bromo-1-nonanol (**6**i)*

This compound was prepared according to the general procedure for bromo alcohol formation using 1,9-nonanediol (6.00 g, 37.4 mmol) and 48% HBr (8 mL). The solution was heated to 90°C and the extraction was continued for 72 h using toluene (100 mL) as solvent. The crude material was distilled to give 3.19 g (38%) of **6***i* as a colourless liquid: bp 92–94°C/0.06 Torr (lit. (40) bp 97–000°C/0.06 Torr); IR ν_{max}: 3630 and 3450 cm^{-1}; ^1H NMR (60 MHz) δ: 1.27–2.00 (m, 14H), 2.00 (s, exchangeable with D_2O, 1H), 3.35 (t, J = 7 Hz, 2H), and 3.57 (t, J = 6 Hz, 2H); MS m/z (relative intensity): 206 (M^+ −18, 1), 204 (1), 169 (3), 167 (3), 150 (11), 148 (11), 137 (35), 135 (35), 97 (43), 69 (80), 68 (20), 57 (13), 56 (16), and 55 (100).

*10-Bromo-1-decanol (**6**k)*

This compound was prepared according to the general procedure for bromo alcohol formation using 1,10-decanediol (6.00 g, 34.4 mmol) and 48% HBr (27 mL). The solution was heated to 90–95°C and the extraction was continued for 65 h using petroleum ether, bp 100–115°C (100 mL) as solvent. Vacuum distillation gave

Can. J. Chem. Downloaded from www.nrcresearchpress.com by 217.78.4.112 on 09/08/12
For personal use only.

5.33 g (65%) of **6***k* as a colourless liquid: bp 115–117°C/0.30 Torr (lit. (41) bp 166–169°C/10 Torr); IR ν_{max}: 3625 and 3445 cm^{-1}; ^1H NMR (60 MHz) δ: 1.33–2.00 (m, 16H), 3.10 (s, exchangeable with D_2O, 1H), 3.37 (t, J = 7 Hz, 2H), and 3.58 (t, J = 7 Hz, 2H); MS m/z (relative intensity): 220 (M^+ −18, 1) 218 (1), 192 (3), 190 (3), 164 (6), 162 (6), 150 (28), 148 (28), 137 (16), 135 (16), 97 (26), 69 (90), 68 (25), 57 (20), 56 (20), and 55 (100).

10-Oxoundecanoic acid

A mixture of 36.8 g (0.20 mol) of 10-undecenoic acid, 12.6 g (40 mmol) of mercuric acetate, 5 mL of water, and 400 mL of acetone was stirred at room temperature. To this mixture was added 150 mL of Jones reagent over a period of 3.5 h while the temperature of the reaction mixture was maintained at 25 ± 5°C by means of an ice-water bath. The resulting mixture was stirred at room temperature for an additional 20 h, then the acetone layer was decanted, concentrated under reduced pressure, and diluted with ether. The residue was dissolved in water and the resulting aqueous layer was extracted three times with ether. The combined ether layers were washed twice with brine, dried, and concentrated under reduced pressure to give 54.8 g of crude product as a pale yellow solid. Two recrystallizations from petroleum ether – ether (5:1) afforded 37.2 g (93%) of the desired keto acid as a white solid; mp 55–57°C (lit. (42) mp 56–57°C); IR ν_{max}: 2950 and 1715 cm^{-1}; ^1H NMR (80 MHz) δ: 1.10–1.93 (m, 12H), 2.13 (s, 3H), 2.20–2.57 (m, 4H), and 10.87 (s, 1H, exchangeable with D_2O); MS m/z (relative intensity): 200 (M^+, 1), 182 (2), 152 (2), 142 (2), 125 (15), 124 (4), 97 (10), 96 (5), 84 (9), 83 (10), 81 (5), 73 (6), 71 (12), 69 (13), 60 (7), 59 (14), 58 (71), 55 (35), 45 (7), and 43 (100).

10-Bromo-2-decanone

This compound was prepared by means of a modified Hunsdiecker reaction (43). A 500-mL three-necked round bottom flask equipped with a pressure-equalizing dropping funnel, a heavier-than-water, liquid–liquid extractor and condenser, and a stopper was charged with 5.0 g (25 mmol) of the above carboxylic acid and 3.4 g (7.8 mmol) of red mercuric oxide. A total of 200 mL of carbon tetrachloride was added to the liquid–liquid extractor and reaction flask. The mixture was heated at rapid reflux for 20 min and a solution of 5.0 g (32 mmol) of bromine in 5 mL of carbon tetrachloride was added over a period of 40 min while heating was maintained. After heating at reflux for an additional 1 h, the mixture was cooled and filtered. The filtrate was washed three times with 10% aqueous sodium hydroxide and twice with brine, dried, and concentrated under reduced pressure to give 5.85 g (100%) of the crude bromo ketone as a yellow oil. This crude product, containing a small amount of 1,8-dibromooctane, was used without further purification in the preparation of the bromo alcohol **6***j*, Kugelrohr distillation of a small amount of this material afforded pure bromo ketone as a colourless oil; bp (Kugelrohr distillation) 100°C/0.15 Torr; IR ν_{max}: 1715 cm^{-1}; ^1H NMR (60 MHz) δ: 1.00–2.20 (m, 12H), 2.12 (s, 3H), 2.20–2.62 (m, 2H), and 3.38 (t, J = 6 Hz, 2H); MS m/z (relative intensity): 236 (M^+ ^{81}Br, 7), 234 (M^+ ^{79}Br, 7), 221 (5), 219 (6), 178 (16), 176 (21), 155 (16), 97 (31), 82 (21), 81 (20), 80 (22), 71 (98), 69 (68), 67 (27), 59 (87), 58 (99), 57 (29), 55 (92), 44 (60), and 43 (100). Exact Mass calcd. for $C_{10}H_{19}BrO$: 236.0600, 234.0619; found: 236.0617, 234.0625.

*10-Bromo-2-decanol (**6**j)*

To a solution of 8.83 g (37.6 mmol) of the above bromo ketone in 75 mL of ethanol at room temperature was added 1.42 g (37.6 mmol) of sodium borohydride. After stirring for 30 min, the reaction was quenched with 1 M HCl, concentrated under reduced pressure, and diluted with ether. The organic phase was washed twice with 1 M HCl, twice with saturated aqueous sodium bicarbonate, and once with brine, dried, and concentrated under reduced pressure to give 7.71 g of crude bromo alcohol as a yellow oil. Purification by flash chromatography using petroleum ether – ethyl acetate (4:1) as eluant gave 5.60 g (63% from carboxylic acid) of alcohol **6***j* as a pale yellow oil. Distillation of a portion of this material afforded pure **6***m* as a colourless oil; bp 98–100°C/0.15 Torr; IR ν_{max}: 3630 and 3480 cm^{-1}; ^1H NMR (60 MHz) δ: 1.13–2.22 (m, 14H), 1.17 (d, J = 6 Hz, 3H), 1.58 (s, 1H, exchangeable with D_2O), 3.38 (t, J = 6 Hz, 2H), and 3.57–3.98 (m, 1H); MS m/z (relative intensity): 237 (M^+ ^{81}Br, 0.3), 235 (M^+ ^{79}Br, 0.3), 223 (2), 221 (2), 220 (2), 218 (2), 192 (3), 190 (2), 137 (3), 135 (3), 123 (4), 97 (6), 95 (2), 83 (5), 81 (4), 71 (3), 69 (9), 67 (3), 57 (5), 56 (4), 55 (16), 46 (3), and 45 (100). Anal. calcd. for $C_{10}H_{21}BrO$: C 50.64, H 8.92, Br 33.69; found: C 50.88, H 9.00, Br 33.55.

*General procedure for the alcoholysis of the acyl Meldrum's acid **5***

A 50-mL, single-necked round bottom flask equipped with a reflux condenser fitted with a nitrogen inlet was charged with **5** (1.2 equiv.), the appropriate alcohol (1.0 equiv.), and dry tetrahydrofuran (25 mL). The reaction mixture was heated to reflux for 4 h, cooled to room temperature, and transferred to a separatory funnel containing 50 mL of ether. The solution was washed with saturated sodium bicarbonate solution (1 × 15 mL), water (1 × 15 mL), and brine (1 × 10 mL), then dried. Removal of the solvent under reduced pressure gave the crude β-keto ester.

*(2′-Bromo-1′-ethyl)-3-oxobutanoate (**4**a)*

This compound was prepared according to the general procedure using **5** (3.60 g, 19.4 mmol) and 2-bromoethanol (Aldrich Chemical, 1.99 g, 16.0 mmol). Distillation of the crude material gave 2.27 g (67%) of **4***a* as a colourless liquid: bp 62–64°C/0.18 Torr; IR ν_{max}: 1755 and 1725 cm^{-1}; ^1H NMR (60 MHz) δ: 2.27 (s, 3H), 3.46 (s, 2H), 3.48 (t, J = 6 Hz, 2H), and 4.40 (t, J = 6 Hz, 2H); MS m/z (relative intensity): 210 M^+ ^{81}Br, 19), 208 (M^+ ^{79}Br, 19), 168 (30), 166 (29), 129 (52), 109 (100), 107 (100), and 102 (59). Anal. calcd. for $C_6H_9BrO_3$: C 34.47, H 4.34; found: C 34.66, H 4.29.

*(3′-Bromo-1′-3-propyl)-oxobutanoate (**4**b)*

This compound was prepared according to the general procedure using **5** (1.20 g, 6.45 mmol) and 3-bromo-1-propanol (Aldrich Chemical, 742 mg, 5.34 mmol). Vacuum distillation of the crude material gave 953 mg (80%) of **4***b* as a colourless liquid: bp 80–82°C/0.40 Torr; IR ν_{max}: 1745, 1720, and 1663 cm^{-1}; ^1H NMR (60 MHz) δ: 2.27 (s, 3H), 1.93–2.36 (m, 2H), 3.43 (t, J = 6 Hz, 2H), 3.43 (s, 2H), and 4.25 (t, J = 6 Hz, 2H); MS m/z (relative intensity): 224 (M^+ ^{81}Br, 32), 222 (M^+ ^{79}Br, 32), 206 (24), 204 (24), 182 (78), 180 (78), 143 (100), 123 (48), 122 (77), 121 (48), 120 (78), 103 (73), 102 (53), and 101 (35). Anal. calcd. for $C_7H_{11}BrO_3$: C 37.69, H 4.97; found: C 37.65, H 5.10.

*(4′-Chloro-1′-butyl)-3-oxobutanoate (**4**c)*

This compound was prepared according to the general procedure for alcoholysis using **5** (3.60 g, 19.2 mmol) and **6***c* (1.72 g, 16.0 mmol). Vacuum distillation of the crude material gave 2.44 g (79%) of **4***c* as a colourless liquid: bp 87–88°C/0.18 Torr; IR ν_{max}: 1745 and 1720 cm^{-1}; ^1H NMR (60 MHz) δ: 1.70–1.90 (m, 4H), 2.26 (s, 3H), 3.43 (s, 2H), 3.50 (t, J = 5.5 Hz, 2H), and 4.13 (t, J = 6 Hz, 2H); MS m/z (relative intensity): 194 (M^+ ^{37}Cl, 9), 192 (M^+ ^{35}Cl, 18), 157 (12), 152 (11), 150 (33), 116 (17), 115 (23), 103 (100), and 102 (53). Anal. calcd. for $C_8H_{13}ClO_3$: C 49.88, H 6.80; found: C 49.82, H 6.91.

*(5′-Bromo-1′-pentyl)-3-oxobutanoate (**4**d)*

This compound was prepared according to the general procedure for alcoholysis using **5** (2.23 g, 12.0 mmol) and **6***d* (1.67 g, 10.0 mmol). Vacuum distillation of the crude material gave 1.87 g, (74%) of **4***d* as a colourless liquid: bp 98–99°C/0.2 Torr; IR ν_{max}: 1740, 1720, and 1660 cm^{-1}; ^1H NMR (60 MHz) δ: 1.50–2.00 (m, 6H), 2.27 (s, 3H), 3.40 (t, J = 7 Hz, 2H), 3.45 (s, 2H), and 4.13 (t, J = 6 Hz, 2H); MS m/z (relative intensity): 252 (M^+ ^{81}Br, 0.6), 250 (M^+ ^{79}Br, 0.6), 210 (0.3), 208 (0.3), 171 (1), 150 (7), 148 (10), 103 (38), 85 (33), and 69 (100). Exact Mass calcd. for $C_9H_{15}BrO_3$: 252.0184, 250.0205; found: 252.0175, 250.0205.

Can. J. Chem. Downloaded from www.nrcresearchpress.com by 217.78.4.112 on 09/08/12
For personal use only.

*(6'-Bromo-1'-hexyl)-3-oxobutanoate (**4**e)*

This compound was prepared according to the general procedure for alcoholysis using **5** (2.47 g, 13.3 mmol) and **6***e* (2.00 g, 11.1 mmol). Solvent removal gave 2.53 g (86%) of crude **4***e* as a yellow liquid, which was homogeneous by TLC analysis. A small sample was purified by preparative TLC on silica gel using 3:1 ether – petroleum ether and gave **4***e* as a colourless liquid: R_f 0.75; bp (Kugelrohr distillation) 97–100°C/0.12 Torr; IR ν_{max}: 1740 and 1718 cm^{-1}; ^1H NMR (60 MHz) δ: 1.30–1.96 (m, 8H), 2.28 (s, 3H), 3.44 (t, J = 7 Hz, 2H), 3.48 (s, 2H), and 4.18 (t, J = 6.5 Hz, 2H); MS m/z (relative intensity): 266 (M^+ ^{81}Br, 0.1), 264 (M^+ ^{79}Br, 0.1), 164 (3), 162 (3), 103 (100), 85 (44), 83 (81), and 55 (73). Exact Mass calcd. for $C_{10}H_{17}BrO_3$: 266.0341; found: 266.0346. Anal. calcd. for $C_{10}H_{17}BrO_3$: C 45.30, H 6.46; found: C 45.82, H 6.70.

*(6'-Chloro-2'-hexyl-3-oxobutanoate (**4**f)*

This compound was prepared according to the general procedure for alcoholysis using **6***f* (4.62 g, 2.48 mmol) and **5** (2.80 g, 2.06 mmol). Vacuum distillation of the crude material gave 3.82 g (85%) of **4***f* as a colourless liquid: bp 96–98°C/0.20 Torr; ν_{max}: 1740 and 1715 cm^{-1}; ^1H NMR (60 MHz) δ: 1.27 (d, J = 6 Hz, 3H), 1.40–2.00 (m, 6H), 2.23 (s, 3H), 3.41 (s, 2H), 3.48 (t, J = 6 Hz, 2H), and 4.77–5.07 (m, 1H); MS m/z (relative intensity): 222 (M^+ ^{37}Cl, 0.70), 220 (M^+ ^{35}Cl, 2), 118 (58), 103 (74), and 85 (100). Anal. calcd. for $C_{10}H_{17}ClO_3$: C 54.42, H 7.76; found: C 54.44, H 7.79.

*(7'-Bromo-1'-heptyl)-3-oxobutanoate (**4**g)*

This compound was prepared according to the general procedure for alcoholysis using **5** (1.92 g, 10.3 mmol) and **6***g* (1.67 g, 8.56 mmol). Solvent removal gave 2.02 g (84%) of crude **4***g* as a pale yellow liquid, which was homogeneous by TLC analysis. A small sample was purified by preparative TLC on silica gel using ether as solvent to give **4***g* as a colourless liquid: R_f 0.81; bp (Kugelrohr distillation) 120–125°C/0.50 Torr; IR ν_{max}: 1735 and 1710 cm^{-1}; ^1H NMR (60 MHz) δ: 1.30–1.98 (m, 10H), 2.30 (s, 3H), 3.44 (t, J = 7 Hz, 2H), 3.49 (s, 2H), and 4.18 (t, J = 7 Hz, 2H); MS m/z (relative intensity): 280 (M^+ ^{81}Br, 0.1), 278 (M^+ ^{79}Br, 0.1), 188 (2), 186 (2), 150 (4), 148 (4), 103 (100), 97 (42), 85 (30), 69 (20), and 55 (70). Anal. calcd. for $C_{11}H_{19}BrO_3$: C 47.32, H 6.86; found: C 47.42, H 6.77.

*(8'-Bromo-1'-octyl)-3-oxobutanoate (**4**h)*

This compound was prepared according to the general procedure for alcoholysis using **5** (1.07 g, 5.74 mmol) and **6***h* (1.00 g, 4.78 mmol). Evaporation of the solvent gave 1.20 g (86%) of crude **4***h* as a yellow liquid, which was homogeneous by TLC analysis. A small sample was purified by preparative TLC on silica gel using 3:1 ether – petroleum ether and gave **4***h* as a colourless liquid: R_f 0.77; bp (Kugelrohr distillation) 115–118°C/0.40 Torr; IR ν_{max}: 1740 and 1713 cm^{-1}; ^1H NMR (60 MHz) δ: 1.14–1.97 (m, 12H), 2.28 (s, 3H), 3.43 (t, J = 7 Hz, 2H), 3.47 (s, 2H), and 4.17 (t, J ≈ 7 Hz, 2H); MS m/z (relative intensity): 294 (M^+ ^{81}Br, 0.2), 292 (M^+ ^{79}Br, 0.2), 2.13 (3), 192 (4), 190 (4), 164 (4), 162 (4), 150 (7), 148 (7), 137 (4), 135 (4), 111 (18), 103 (100), 85 (19), 69 (35), and 55 (21). Anal. calcd. for $C_{12}H_{21}BrO_3$: C 49.07, H 7.38; found: C 49.29, H 7.35.

*(9'-Bromo-1'-nonyl)-3-oxobutanoate (**4**i)*

This compound was prepared according to the general procedure for alcoholysis using **5** (1.00 g, 5.38 mmol) and **6***i* (1.00 g, 4.48 mmol). Evaporation of the solvent gave 1.21 g (88%) of crude **4***i* as a yellow liquid, which was homogeneous by TLC analysis. A small sample was purified by preparative TLC on silica gel using 3:1 ether – petroleum ether and gave **4***i* as a colourless liquid: R_f 0.78; bp (Kugelrohr distillation) 110–113°C/0.12 Torr; IR ν_{max}: 1735 and 1710 cm^{-1}; ^1H NMR (60 MHz) δ: 1.30–1.96 (m, 14H), 2.27 (s, 3H), 3.42 (t, J = 7 Hz, 2H), 3.46 (s, 2H), and 4.16 (t, J ≈ 7 Hz, 2H); MS m/z (relative intensity): 308 (M^+ ^{81}Br, 0.1), 306 (M^+ ^{79}Br, 0.1), 150 (1), 148 (1), 137 (1), 135 (1), 103 (100), 85 (18), 83 (9), 69 (21), and 55 (19). Exact Mass calcd. for $C_{13}H_{23}BrO_3$: 308.0812, 306.0830; found: 308.0814, 306.0832.

*(10'-Bromo-2'-decyl)-3-oxobutanoate (**4**j)*

This compound was prepared according to the general procedure for alcoholysis using **5** (9.17 g, 49.0 mmol) and alcohol **6***j* (9.75 g, 41.0 mmol) in 50 mL of THF. Work-up as usual gave 14.0 g (85%) of crude **4***j* as a red oil. Filtration, with suction, of this oil through a short column of silica using petroleum ether – ethyl acetate (9:1) as eluant, followed by removal of solvent, yielded 13.3 g (98%) of **4***j* as a pale yellow oil. Distillation of a small amount of this material gave pure **4***j* as a colourless oil: bp (Kugelrohr distillation) 130°C/0.2 Torr; IR ν_{max}: 1745 and 1720 cm^{-1}; ^1H NMR (60 MHz) δ: 1.07–2.03 (m, 17H), 2.25 (s, 3H), 3.40 (t, J = 7 Hz, 2H), 3.40 (s, 2H), and 4.77–5.17 (m, 1H); MS m/z (relative intensity): 322 (M^+ ^{81}Br, 1), 320 (M^+ ^{79}Br, 1), 220 (15), 218 (16), 150 (6), 148 (7), 104 (5), 103 (100), 102 (13), 97 (17), 87 (7), 85 (56), 83 (22), 71 (10), 69 (26), 67(5), 58 (7), 57 (17), 56 (10), 55 (39), 45 (13), and 43 (88). Anal. calcd. for $C_{14}H_{25}BrO_3$: C 52.34, H 7.84, Br 24.87; found: C 52.59, H 8.00, Br 24.61.

*(10'-Bromo-1'-decyl)-3-oxobutanoate (**4**k)*

This compound was prepared according to the general procedure for alcoholysis using **5** (2.00 g, 11.1 mmol) and **6***k* (2.00 g, 9.00 mmol). Removal of the solvent gave 2.49 g (92%) of crude **4***k* as a yellow oil, which was homogeneous by TLC analysis. A small sample was purified by preparative TLC using 3:1 ether – petroleum ether and gave **4***k* as a colourless liquid: R_f 0.79; bp (Kugelrohr distillation) 120–125°C/0.12 Torr; IR ν_{max}: 1740 and 1715 cm^{-1}; ^1H NMR (60 MHz) δ: 1.30–1.96 (m, 16H), 2.29 (s, 3H), 3.46 (t, J = 7 Hz, 2H), 3.48 (s, 2H), and 4.17 (t, J = 7 Hz, 2H); MS m/z (relative intensity): 322 (M^+ ^{81}Br, 0.1), 320 (M^+ ^{79}Br, 0.1), 192 (13), 190 (14), 164 (36), 162 (34), 150 (67), 148 (68), 137 (44), 135 (46), 103 (100), 85 (88), 69 (99), 57 (72), 56 (82), 55 (100), and 54 (65). Anal. calcd. for $C_{14}H_{25}BrO_3$: C 52.34, H 7.84; found: C 52.75, H 8.09.

*(11'-Bromo-1'-undecyl)-3-oxobutanoate (**4**l)*

This compound was prepared according to the general procedure for alcoholysis using **5** (1.78 g, 9.57 mmol) and 11-bromo-1-undecanol (Aldrich Chemical, 2.00 g, 7.97 mmol). Work-up as usual gave 2.26 g (85%) of crude **4***l* as a yellow liquid, which was homogeneous by TLC analysis. A small sample was purified by preparative TLC using chloroform as solvent and gave **4***l* as a colourless liquid: R_f 0.40; bp (Kugelrohr distillation) 135–140°C/0.13 Torr; IR ν_{max}: 1740 and 1715 cm^{-1}; ^1H NMR (60 MHz) δ: 1.25–1.95 (m, 18H), 2.28 (s, 3H), 3.43 (t, J = 7 Hz, 2H), 3.45 (s, 2H), and 4.15 (t, J = 6.5 Hz, 2H); MS m/z (relative intensity): 336 (M^+ ^{81}Br, 2), 334 (M^+ ^{79}Br, 2), 318 (3), 316 (3), 255 (14), 164 (26), 162 (26), 150 (40), 148 (40), 85 (100), and 69 (100). Anal. calcd. for $C_{15}H_{27}BrO_3$: C 53.73, H 8.12; found: C 53.92, H 8.08.

*(2'-Propen-1'-yl)-3-oxobutanoate (**7**)*

This compound was prepared according to the general procedure for alcoholysis using **5** (2.40 g, 12.9 mmol) and 2-propene-1-ol (624 mg, 10.8 mmol). Vacuum distillation of the crude material gave 1.37 g (90%) of **7** as a colourless liquid: bp 71–72°C/25 Torr; IR ν_{max}: 1742, 1715, and 1650 cm^{-1}; ^1H NMR (60 MHz) δ: 2.24 (s, 3H), 3.45 (s, 2H), 4.57 (d, J = 5 Hz, 2H), and 5.00–6.17 (m, 3H); MS m/z (relative intensity): 142 (M^+, 9), 100 (15), 84 (100), and 58 (100). Anal. calcd. for $C_7H_{10}O_3$: C. 59.14, H 7.09; found: C 59.24, H 7.16.

*General procedure for the attempted cyclization of β-keto esters **4**a–l*

A solution of diisopropylamine (3 equiv.) in dry THF was prepared in a 200-mL, two-necked round bottom flask equipped with a pressure-equalizing dropping funnel and a nitrogen inlet. The flask was cooled to 0°C in an ice-water bath and three equivalents of *n*-butyllithium as a 1.6 M solution in hexane was added dropwise. The colourless to pale yellow solution was stirred for 10 min and a solution of one equivalent of the halo β-keto ester in THF was added dropwise. The reaction mixture was then stirred for 5 h and

Can. J. Chem. Downloaded from www.nrcresearchpress.com by 217.78.4.112 on 09/08/12
For personal use only.

the solution was slowly allowed to warm to room temperature over this period. On work-up, water and ether were added, and the organic phase was separated. The organic extract was washed with water and brine, then dried. Removal of the solvents under reduced pressure gave the crude products.

(2'-Propen-1'-yl)-3-oxobutanoate (7) from the attempted cyclization of **4**b

Following the above general procedure, diisopropylamine (222 mg, 2.20 mmol) in 12 mL of THF, 1.55 mL of *n*-butyllithium (1.43 M, 2.20 mmol), and 223 mg of **4***b* (1.00 mmol) in 3 mL of THF were stirred at 0°C for 30 min. Work-up followed by purification gave 82.5 mg (58%) of a pale yellow oil, which exhibited identical spectral properties to those reported above for compound **7**.

(4'-Chloro-1'-butyl)-3-oxopentanoate (8)

Following the above general procedure for cyclization, 223 mg of diisopropylamine (2.20 mmol) in 12 mL of THF, 1.38 mL of *n*-butyllithium (1.6 M, 2.20 mmol), and 193 mg of a solution of **4***c* (1.00 mmol) in 3 mL of THF was stirred at 0°C for 30 min, then the reaction mixture was quenched with methyl iodide (143 mg, 1.00 mmol). On work-up, the solution was treated with 5% HCl solution until acidic, then diluted with ether (25 mL). The ethereal layer was separated, washed with water (10 mL), then dried. Removal of the solvent under reduced pressure gave **8** as a yellow oil. Preparative TLC of this crude material on silica gel using chloroform gave 155 mg (75%) of **5** as a colourless liquid: R_f 0.41; bp (Kugelrohr distillation) 70–72°C/0.13 Torr; IR ν_{max}: 1745 and 1718 cm^{-1}; ^1H NMR (60 MHz) δ: 1.09 (t, J = 7 Hz, 3H), 1.85 (m, 4H), 2.56 (q, J = 7 Hz, 2H), 3.46 (s, 2H), 3.58 (t, J = 6 Hz, 2H), and 4.20 (t, J = 6 Hz, 2H); MS m/z (relative intensity): 208 (M^+ ^{37}Cl, 3), 206 (M^+ ^{35}Cl, 7), 171 (5), 116 (8), 98 (15), 93 (37), and 91 (100). Anal. calcd. for $C_9H_{15}ClO_3$: C 52.30, H 7.32; found: C 52.30, H 7.39.

*(4'-Penten-1'-yl)-3-oxobutanoate (**10**d)*

This compound was generated in the general procedure for cyclization using diisopropylamine (1.52 g, 15.0 mmol), *n*-butyllithium as a 1.6 M solution in hexane (9.38 mL, 15.0 mmol), and **6***d* (1.27 g, 5.00 mmol). Flash chromatography of the crude material using chloroform as eluant gave 353 mg (41%) of **10***d* as a colourless liquid: bp (Kugelrohr distillation) 40–42°C/0.20 Torr; IR ν_{max}: 1742, 1720, and 1645 cm^{-1}; ^1H NMR (60 MHz) δ: 1.63–2.19 (m, 4H), 2.28 (s, 3H), 3.46 (s, 2H), 4.19 (t, J = 7 Hz, 2H), 4.97–5.16 (m, 2H), and 5.64–7.03 (m, 1H); MS m/z (relative intensity): 170 (M^+, 6), 103 (5), 85 (30), 69 (21), 68 (100), and 67 (35). Anal. calcd. for $C_9H_{14}O_3$: C 63.51, H 8.29; found: C 63.65, H 8.30.

*(7'-Hexen-1'-yl)-3-oxobutanoate (**10**e)*

This compound was generated in the general procedure for cyclization using diisopropylamine (1.21 g, 12.0 mmol), *n*-butyllithium as a 1.6 M solution in hexane (7.50 mL, 12.0 mmol), and **6***e* (1.06 g, 4.00 mmol). Flash chromatography of the crude material using petroleum ether – ethyl acetate (9:1) as eluant gave 331 mg (45%) of **10***e* as a colourless liquid: bp 30–45°C/0.20 Torr; IR ν_{max}: 1735, 1718, and 1645 cm^{-1}; ^1H NMR (60 MHz) δ: 1.26–1.80 (m, 4H), 1.92–2.20 (m, 2H), 2.28 (s, 3H), 3.46 (s, 2H), 4.18 (t, J = 6 Hz, 2H), 4.93–5.12 (m, 2H), and 5.64–7.04 (m, 1H); MS m/z (relative intensity): 184 (M^+, 0.3), 137 (8), 103 (10), 85 (43), 82 (100), 67 (59), 56 (44), and 55 (85). Anal. calcd. for $C_{10}H_{16}O_3$: C 65.19, H 8.75; found: C 65.36, H 8.90.

*(6'-Hepten-1'-yl)-3-oxobutanoate (**10**g)*

This compound was generated in the general procedure for cyclization using diisopropylamine (1.21 g, 12.0 mmol), *n*-butyllithium as a 1.6 M solution in hexane (7.50 mL, 12.0 mmol), and **6***g* (1.12 g, 4.00 mmol). Flash chromatography of the crude material using petroleum ether – ethyl acetate (9:1) as eluant gave 457 mg (57%) of **10***g* as a colourless liquid: bp (Kugelrohr distillation) 45–48°C/0.23 Torr; IR ν_{max}: 1735, 1718, and 1635 cm^{-1}; ^1H NMR (60 MHz) δ: 1.26–1.80 (m, 6H), 1.94–2.12 (m, 2H), 2.28 (s, 3H), 3.45 (s, 2H), 4.16 (t, J = 6 Hz, 2H), 4.92–5.09 (m, 2H), and 5.63–7.03 (m, 1H); MS m/z (relative intensity): 198 (M^+, 0.1), 102 (72), 96 (63), 85 (67), 81 (41), 69 (25), 68 (59), 67 (69), 56 (28), 55 (100), and 54 (74). Anal. calcd. for $C_{11}H_{18}O_3$: C 66.64, H 9.15; found: 66.71, H 9.25.

*(7'-Octen-1'-yl)-3-oxobutanoate (**10**h)*

This compound was generated in the general procedure for cyclization using diisopropylamine (1.21 g, 12.0 mmol), *n*-butyllithium as a 1.6 M solution in hexane (7.50 mL, 12.0 mmol), and **6***h* (1.17 g, 4.00 mmol). Flash chromatography of the crude material using petroleum ether – ethyl acetate (9:1) as eluant gave 348 mg (41%) of **10***h* as a colourless liquid: bp (Kugelrohr distillation) 60–63°C/0.4 Torr; IR ν_{max}: 1740, 1718, and 1650 cm^{-1}; ^1H NMR (60 MHz) δ: 1.26–1.85 (m, 8H), 1.93–2.10 (m, 2H), 2.28 (s, 3H), 3.46 (s, 2H), 4.17 (t, J = 6 Hz, 2H), 4.93–5.10 (m, 2H), and 5.66–7.04 (m, 1H); MS m/z (relative intensity): 212 (M^+, 0.1), 103 (87), 95 (20), 85 (87), 82 (50), 81 (58), 69 (100), 68 (84), 67 (80), 66 (11), 56 (79), and 55 (100). Anal. calcd. for $C_{12}H_{20}O_3$: C 67.89, H 9.50; found: C 67.94, H 9.55.

*3-Oxotridecan-13-olide (**9**i)*

This compound was prepared according to the general procedure for cyclization using diisopropylamine (1.21 g, 12.0 mmol), *n*-butyllithium as a 1.6 M solution in hexane (7.50 mL, 12.0 mmol), and **6***i* (1.23 g, 4.00 mmol). Purification by flash chromatography using petroleum ether – ethyl acetate (9:1) as eluant gave 389 mg (43%) of **9***i* as a colourless semi-solid: sublimation temperature 103–105°C/0.18 Torr; IR ν_{max}: 1750 and 1725 cm^{-1}; ^1H NMR (60 MHz) δ: 1.25–1.81 (m, 16H), 2.61 (t, J = 7 Hz, 2H), 3.44 (s, 2H), and 4.24 (t, J = 5 Hz, 2H); MS m/z (relative intensity): 226 (M^+, 8), 208 (6), 124 (23), 103 (25), 82 (36), 69 (46), 67 (29), 56 (23), and 55 (100). Anal. calcd. for $C_{13}H_{22}O_3$: C 68.99, H 9.80; found: C 68.78, H 9.84.

*3-Oxotetradecan-13-olide (**9**j)*

This compound was prepared according to the general procedure for cyclization using diisopropylamine (1.90 mL, 13.6 mmol), *n*-butyllithium as a 1.0 M solution in hexane (13.6 mL, 13.6 mmol), and **6***j* (2.00 g, 6.20 mmol). Flash chromatography using petroleum ether – ethyl acetate (9:1) as eluant yielded 694 mg (47%) of **9***j* as a very pale yellow oil. Preparative TLC of a small amount of this material using petroleum ether – ethyl acetate as solvent gave a pure sample of **9***j* as a colourless oil; bp (Kugelrohr distillation) 80°C/0.01 Torr; IR ν_{max}: 1740 and 1715 cm^{-1}; ^1H NMR (400 MHz) δ: 1.17–1.81 (m, 16H), 1.26, (d, J = 7 Hz, 3H), 2.51 (dt, $J_{4a,4b}$ = 18.5 Hz, $J_{4a,5a}$ = $J_{4a,5b}$ = 7 Hz, 1H), 2.70 (dt, $J_{4a,4b}$ = 18 Hz, $J_{4b,5a}$ = $J_{4b,5b}$ = 7 Hz, 1H), 3.35 (d, $J_{2a,2b}$ = 14 Hz, 1H), 3.46 (d, $J_{2a,2b}$ = 13.5 Hz, 1H), and 4.98–5.06 (m, 1H); ^{13}C NMR (100 MHz) δ: 20.29, 21.00, 22.91, 24.66, 25.17, 26.03, 26.11, 26.27, 35.15, 40.57, 50.83, 71.95, 166.71, and 202.10; MS m/z (relative intensity): 240 (M^+, 6), 222 (8), 181 (80), 180 (8), 138 (22), 103 (56), 102 (33), 97 (28), 96 (39), 85 (34), 83 (36), 82 (30), 81 (30), 69 (45), 68 (34), 67 (30), 56 (22), and 55 (100). Anal. calcd. for $C_{14}H_{24}O_3$: C 69.96, H 10.07; found: C 69.77, H 10.20.

*3-Oxotetradecan-14-olide (**9**k)*

This compound was prepared according to the general procedure for cyclization using diisopropylamine (1.21 g, 12.0 mmol), *n*-butyllithium as a 1.6 M solution in hexane (7.50 mL, 12.0 mmol), and **6***k* (1.28 g, 4.00 mmol). Purification by flash chromatography using petroleum ether – ethyl acetate (9:1) as eluant gave 432 mg (45%) of **9***k* as a colourless semi-solid: bp (Kugelrohr distillation) 85-88°C/0.10 Torr; IR ν_{max}: 1742 and 1718 cm^{-1}; ^1H NMR (60 MHz) δ: 1.20–1.82 (m, 18H), 2.57 (t, J = 7 Hz, 2H), 3.46 (s, 2H), and 4.22 (t, J = 6 Hz, 2H); MS m/z (relative intensity): 240 (M^+, 1), 148 (17), 103 (19), 96 (24), 83 (19), 82 (31), 81 (20), 69 (33), 68 (28), 67 (27), 56 (14), 55 (100), and 54 (17). Anal. calcd. for $C_{14}H_{24}O_3$: C 69.96, H 10.07; found: C 70.00, H 10.14.

Can. J. Chem. Downloaded from www.nrcresearchpress.com by 217.78.4.112 on 09/08/12
For personal use only.

*3-Oxopentadecan-15-olide (**9l**)*

This compound was prepared according to the general procedure for cyclization using diisopropylamine (1.21 g, 12.0 mmol), *n*-butyllithium as a 1.6 M solution in hexane (7.50 mL, 12.0 mmol), and **6*l*** (1.34 g, 4.00 mmol). Flash chromatography of the crude product using petroleum ether – ethyl acetate (7:1) as eluant gave 498 mg (49%) of **9*l*** as a colourless semi-solid: sublimation temperature 110–113°C/0.25 Torr; IR ν_{max}: 1735 and 1710 cm^{-1}; ^1H NMR (60 MHz) δ: 1.20–1.80 (m, 20H), 2.56 (t, J = 6.5 Hz, 2H), 3.46 (s, 2H), and 4.22 (t, J = 5 Hz, 2H); MS m/z (relative intensity): 254 (M^+, 26), 236 (22), 152, (55), 103 (100), 95 (68), and 55 (91). Anal. calcd. for $C_{15}H_{26}O_3$: C 70.83, H 10.30; found: C 70.65, H 10.17.

*(10-Hydroxydecyl)triphenylphosphonium bromide (**13**a)*

A solution of bromo alcohol **6*k*** (11.85 g, 50 mmol) and 13.1 g of triphenylphosphine (50 mmol) in 50 mL of dry acetonitrile was heated to reflux for 16 h. The solvent was removed *in vacuo* to give a yellow glass, which was extracted with 60 mL of hot ether to dissolve any unreacted starting materials. The final residue crystalized under vacuum to give 24.0 g (96%) of a crude product, which was used directly in the next step; mp 75–78°C (lit. (44) mp 82–84°C).

*(11-Hydroxyundecyl)triphenylphosphonium bromide (**13**b)*

Using the same procedure as above, a solution of bromo alcohol **12*b*** (10.04 g, 40 mmol) and 10.5 g of triphenylphosphine (40 mmol) in 80 mL of dry acetonitrile was heated to reflux for 16 h. The solvent was removed *in vacuo* to give a yellow glass, which was extracted with 60 mL of hot ether to dissolve any unreacted starting materials. The final residue crystalized under vacuum to give 12.4 g (60%) of a crude product, which was used directly in the next step; mp 85–87°C (lit. (44) mp 85–86°C).

*10-Bromodecanal (**14**a)*

A mixture of alcohol **6*k*** (17.7 g, 75 mmol) and pyridium chlorochromate (PCC, 16.1 g, 75 mmol) was stirred in 200 mL of dichloromethane at room temperature. After 4 h, the mixture was poured into ether and the residue was washed with 3 × 75 mL of ether. The combined organic extracts were dried and evaporated. The residue was dissolved in ether and passed through a Florisil column. Evaporation of the solvents gave 16.7 g (95%) of a crude product, which was used directly in the next step; IR ν_{max}: 2750 and 1735 cm^{-1}; ^1H NMR (60 MHz) δ: 1.1–1.8 (m, 14H), 2.4 (m, 2H), 3.37 (t, J = 7 Hz, 2H), and 9.77 (t, J = 2 Hz, 1H).

*11-Bromoundecanal (**14**b)*

A mixture of alcohol **12*b*** (Aldrich Chemical, 7.0 g, 28 mmol) and PCC (6.0 g, 28 mmol) was stirred in 100 mL of dichloromethane at room temperature. After 4 h, the mixture was poured into ether and the residue was washed with 3 × 75 mL of ether. The combined organic extracts were dried and evaporated. The residue was dissolved in ether an passed through a Florisil column. Evaporation of the solvents gave 6.7 g (96%) of a crude product, which was used directly in the next step; IR ν_{max}: 2750 and 1725 cm^{-1}; ^1H NMR (60 MHz) δ: 1.1–1.85 (m, 16H), 2.4 (m, 2H), 3.38 (t, J = 7 Hz, 2H), and 9.72 (t, J = 1.5 Hz, 1H).

*20-Bromo-(10Z)-eicosen-1-ol (**15**a)*

A suspension of the phosphonium salt **13*a*** (23.2 g, 46.5 mmol) in 300 mL of dry THF was cooled to −30°C and treated with 54.7 mL of 1.7 M *n*-butyllithium (93 mmol). The resulting red solution was stirred at −30°C for 2 h. Some salt remained undissolved. The solution was cooled to −78°C and treated with a solution of aldehyde **14*a*** (10.9 g, 46.5 mmol) in 30 mL of THF. This mixture was stirred at −78°C for 2 h and allowed to warm to room temperature over 16 h. The reaction was quenched with 100 mL of a saturated aqueous solution of NH_4Cl. The aqueous layer was extracted with 2 × 75 mL of ether. The organic extracts were combined, washed with 50 mL of 1 M HCl, then saturated brine (2 × 50 mL), and dried. Evaporation of the solvents gave 22.3 g of a light yellow solid, which was purified by flash chromatography using petroleum ether – ethyl acetate (4:1) to give 8.1 g (47%) of **15*a***; mp 30–32°C; IR ν_{max}: 3460, 3450, 2940, and 2870 cm^{-1}; ^1H NMR (80 MHz) δ: 1.2–1.6 (m, 29H), 1.8–2.1 (m, 4H), 3.43 (t, J = 8 Hz, 2H), 3.65 (t, J = 8 Hz, 2H), and 5.38 (t, J = 4 Hz, 2H); MS m/z (relative intensity): 376 (M^+ ^{81}Br, 0.2). 374 (M^+ ^{79}Br, 0.2), 358 (12), 356 (12), 294 (8), 138 (12), 137 (12), 124 (18), 123 (19), 110 (29), 109 (29), 96 (77), 83 (52), 82 (100), 81 (55), 69 (67), 68 (47), 67 (59), 55 (98), and 54 (90). Exact Mass calcd. for $C_{20}H_{39}BrO$: 376.2163, 374.2184; found: 376.2142, 374.2155.

*22-Bromo-(11Z)-docosen-1-ol (**15**b)*

A suspension of the phosphonium salt **13*b*** (12.4 g, 24 mmol) in 250 mL of dry THF was treated with 28 mL of 1.7 M *n*-butyllithium (48 mmol) and a solution of aldehyde **14*b*** (6.7 g, 24 mmol) in 20 mL of the THF as above. Work-up gave 22.3 g of a light yellow gum, which was purified by flash chromatography using petroleum ether – ethyl acetate (4:1) to give 5.4 g (56%) of **15*b***; mp 30–31°C; IR ν_{max}: 3600, 3430, 3010, 2940, and 2860 cm^{-1}; ^1H NMR (80 MHz) δ: 1.1-1.6 (m, 32H), 1.8–2.1 (m, 5H), 3.45 (t, J = 8 Hz, 2H), 3.65 (t, J = 8 Hz, 2H), and 5.38 (t, J = 6 Hz, 2H); MS m/z (relative intensity): 404 (M^+ ^{81}Br, 0.5), 402 (M^+ ^{79}Br, 0.5), 386 (3), 384 (3), 322 (7), 278 (7), 152 (10), 138 (10), 137 (10), 124 (14), 123 (14), 110 (23), 109 (23), 96 (65), 95 (40), 83 (51), 82 (84), 81 (48), 69 (59), 68 (37), 67 (48), 55 (100), and 54 (35). Exact Mass calcd. for $C_{22}H_{43}BrO$: 404.2476, 402.2445; found: 404.2492, 402.2471.

*(20′-Bromo-(10′Z)-1′-eicosenyl)-3-oxobutanoate (**16**a)*

This compound was prepared according to the general procedure for alcoholysis using **5** (4.2 g, 19 mmol) and bromo alcohol **15*a*** (8.1 g, 19 mmol) in 50 mL of THF. Work-up gave 9.62 g (97%) of crude **16*a*** as a light yellow oil, which was homogeneous by TLC and GC analysis. IR ν_{max}: 1750 and 1725 cm^{-1}; ^1H NMR (400 MHz) δ: 1.2–1.5 (m, 24H), 1.64 (m, 2H), 1.85 (q, J = 7 Hz, 2H), 2.0 (m, 4H), 2.27 (s, 3H), 3.40 (t, J = 6 Hz, 2H), 3.43 (s, 2H), 4.13 (t, J = 8 Hz, 2H), and 5.35 (t, J = 4 Hz, 2H); MS m/z (relative intensity): 460 (M^+ ^{81}Br, 2), 458 (M^+ ^{79}Br, 2), 358 (12), 356 (14), 124 (12), 110 (16), 109 (16), 103 (100), 97 (17), 96 (38), 95 (28), 85 (30), 69 (37), and 55 (56). Exact Mass calcd. for $C_{24}H_{43}BrO_3$: 460.2375, 458.2395; found: 460.2382, 458.2397.

*(22′-Bromo-(11′Z)-docosen-1′-yl)-3-oxobutanoate (**16**b)*

This compound was prepared according to the general procedure for alcoholysis using **5** (1.2 g, 6.2 mmol) and bromo alcohol **15*b*** (2.5 g, 6.2 mmol) in 100 mL of THF. Work-up and flash chromatography using petroleum ether – ethyl acetate 9:1 gave 2.78 g (95%) of **16*b*** as a light yellow oil, which crystallized below room temperature. IR ν_{max}: 1745 and 1720 cm^{-1}; ^1H NMR (270 MHz) δ: 1.1–1.4 (m, 28H), 1.63 (m, 2H), 1.76 (m, 2H), 2.0 (m, 4H), 2.27 (s, 3H), 3.45 (s, 2H), 3.51 (t, J = 6 Hz, 2H), 4.12 (t, J = 8 Hz, 2H), and 5.47 (t, J = 4 Hz, 2H); MS m/z (relative intensity): 488 (M^+ ^{81}Br, 3), 486 (M^+ ^{79}Br, 3), 386 (9), 384 (10), 124 (10), 110 (14), 109 (14), 103 (100), 97 (19), 96 (35), 95 (26), 85 (30), 69 (37), and 55 (58). Exact Mass calcd. for $C_{26}H_{47}BrO_3$: 488.2688, 486.2734; found: 488.2678, 486.2721.

*14Z-3-Oxotetracosen-24-olide (**17**a)*

This compound was prepared according to the general procedure for cyclization of **4** using diisopropylamine (1.26 mL, 9.0 mmol), *n*-butyllithium as a 1.6 M solution in hexane (5.62 mL, 9.0 mmol), and **16*a*** (1.38 g, 3.0 mmol). Purification by flash chromatography using petroleum ether – ethyl acetate (95:5) as eluant gave 440 mg (39%) of **17*a*** as white crystals: mp 55–57°C; IR ν_{max}: 1750 and 1725 cm^{-1}; ^1H NMR (400 MHz) δ: 1.2–1.41 (m, 28H), 1.62 (m, 4H), 2.04 (m, 2H), 2.53 (t, J = 8 Hz, 2H), 3.41 (s, 2H), 4.15 (t, J = 6Hz, 2H), and 5.35 (t, J = 4 Hz, 2H); MS m/z (relative intensity): 378 (M^+, 23), 360 (20), 110 (21), 103 (48), 97 (26), 96 (51), 95 (42), 82 (56), 81 (53), 69

Can. J. Chem. Downloaded from www.nrcresearchpress.com by 217.78.4.112 on 09/08/12
For personal use only.

(65), 67 (29), 57 (23), and 55 (100). Exact Mass calcd. for $C_{24}H_{42}O_3$: 378.3133; found: 378.3119.

*15Z-3-Oxohexacosen-26-olide (**17**b)*

This compound was prepared according to the general procedure for cyclization using diisopropylamine (1.26 mL, 9.0 mmol), *n*-butyllithium as a 1.6 M solution in hexane (5.62 mL, 9.0 mmol), and **16***b* (1.46 g, 3.0 mmol). Purification by flash chromatography using petroleum ether – ethyl acetate (95:5) as eluant gave 447 mg (37%) of **17***b* as white crystals: mp 68–70°C; IR ν_{max}: 1750 and 1720 cm^{-1}; ^1H NMR (270 MHz) δ: 1.15–1.5 (m, 32H), 1.6 (m, 4H), 2.04 (m, 2H), 2.51 (t, J = 8 Hz, 2H), 3.40 (s, 2H), 4.13 (t, J = 6 Hz, 2H), and 5.36 (t, J = 4 Hz, 2H); MS m/z (relative intensity): 406 (M^+, 22), 389 (21), 388 (35), 135 (14), 124 (15), 123 (18), 121 (18), 110 (28), 109 (32), 103 (14), 97 (25), 96 (68), 95 (59), 82 (65), 81 (63), 69 (52), 67 (60), and 55 (100). Exact Mass calcd. for $C_{26}H_{46}O_3$: 406.3446; found: 406.3450.

3-Oxotetracosan-24-olide

A suspension of 20 mg of PtO_2 in 5 mL of ethyl acetate was hydrogenated at atmospheric pressure overnight. A solution of alkene **17***a* (592 mg, 1.51 mmol) in 5 mL of ethyl acetate was added to the activated catalyst mixture and this was hydrogenated at atmospheric pressure for 2 days. The catalyst was filtered off and the solvents evaporated to give 584 mg (98%) of a crystalline solid: mp 50–52°C; IR ν_{max}: 1745 and 1720 cm^{-1}; ^1H NMR (400 MHz) δ: 1.25–1.4 (m, 34H), 1.63 (m, 4H), 2.53 (t, J = 8 Hz, 2H), 3.41 (s, 2H), and 4.15 (t, J = 6 Hz, 2H); MS m/z (relative intensity): 380 (M^+, 35), 362 (22), 115 (12), 111 (14), 107 (16), 102 (17), 97 (29), 96 (23), 91 (21), 85 (23), 83 (34), 82 (26), 81 (20), 69 (45), 57 (41), and 55 (100). Exact Mass calcd. for $C_{24}H_{44}O_3$: 380.3291; found: 380.3301.

3-Oxohexacosan-26-olide

The alkene **17***b* (53 mg, 0.13 mmol) was hydrogenated as above to yield 40 mg (75%) of saturated β-keto lactone: mp 53–54°C; IR ν_{max}: 1745 and 1725 cm^{-1}; ^1H NMR (400 MHz) δ: 1.22–1.4 (m, 38H), 1.62 (m, 4H), 2.53 (t, J = 8 Hz, 2H), 3.42 (s, 2H), and 4.14 (t, J = 8 Hz, 2H); MS m/z (relative intensity): 408 (M^+, 41), 390 (24), 306 (8), 115 (14), 111 (15), 110 (14), 103 (86), 102 (16), 98 (17), 97 (37), 96 (27), 95 (19), 83 (39), 82 (27), 81 (27), 69 (57), 57 (43), and 55 (100). Exact Mass calcd. for $C_{26}H_{48}O_3$: 408.3603; found: 406.3607.

*3-Hydroxytetracosan-24-olide (**11**a)*

A solution of the above 25-membered ring β-keto lactone (127 mg, 0.33 mmol) in 10 mL of ether was treated with 1.2 mL of a 0.14 M solution of $Zn(BH_4)_2$ in ether (0.16 mmol) and the resulting solution was stirred at 0°C for 3 h, then at room temperature for 24 h. The reaction mixture was diluted with 30 mL of ether and washed with 2% aqueous HCl (2 × 10 mL) and saturated brine (20 mL). The extracts were dried and the solvents removed to give 101 mg of a colourless gum, which was purified by flash chromatography using petroleum ether – ethyl acetate (5:1) to give 60.4 mg (48%) of **11***a*: mp 36–38°C; IR ν_{max}: 3550 and 1725 cm^{-1}; ^1H NMR (400 MHz) δ: 1.2–1.4 (m, 38H), 1.64 (m, 2H), 2.45 (AB q, J = 8 and 16 Hz, 1H), 2.54 (AB q, J = 4 and 16 Hz, 1H), 4.0 (m, 1H), and 4.15 (m, 2H); MS m/z (relative intensity): 382 (M^+, 15), 364 (51), 346 (12), 292 (15), 111 (22), 105 (32), 97 (44), 96 (39), 95 (27), 89 (34), 83 (54), 82 (44), 81 (32), 71 (41), 69 (66), 57 (61), and 55 (100). Exact Mass calcd. for $C_{24}H_{46}O_3$: 382.3444; found: 382.3446.

*3-Hydroxyhexacosan-26-olide (**11**b)*

The 27-membered ring β-keto lactone (41.5 mg, 0.10 mmol) was reduced with $Zn(BH_4)_2$ (0.14 mmol) as above to give 96% yield of **11***b*: mp 71–74°C; IR ν_{max}: 3525 and 1730 cm^{-1}; ^1H NMR (400 MHz) δ: 1.2–1.4 (m, 43H), 1.64 (m, 2H), 2.53 (AB q, J = 8 and 16 Hz, 1H), 2.67 (AB q, J = 4 and 16 Hz, 1H), 4.12 (m, 1H), and 4.19 (t, J = 6 Hz, 2H); MS m/z (relative intensity): 410 (M^+, 1), 392 (43), 374 (10), 332 (6), 326 (7), 97 (38), 96 (39), 95 (29), 89 (20), 83 (46), 82 (46), 81 (32), 69 (60), 57 (47), and 55 (100). Exact Mass calcd. for $C_{26}H_{50}O_3$: 410.3760; found: 410.3773.

tert-*Butyldimethylsilyl 11*-tert-*butyldimethylsiloxyundecanoate (**18**)*

A 50-mL, single-necked round bottom flask was charged with 11-hydroxyundecanoic acid (1.52 g, 7.50 mmol), *tert*-butyldimethylchlorosilane (2.70 g, 18.0 mmol), imidazole (2.55 g, 37.5 mmol), and dimethylformamide (15 mL). The resulting solution was stirred for 72 h, then water (15 mL) and ether (15 mL) were added. The organic layer was separated, and the aqueous layer was further extracted with ether (2 × 20 mL). The combined organic extracts were washed with water (15 mL), brine (15 mL), then dried. Removal of the solvent, followed by vacuum distillation, gave 3.06 g (95%) of **18** as a colourless liquid: bp 154–156°C/0.20 Torr; IR ν_{max}: 1710 and 835 cm^{-1}; ^1H NMR (60 MHz) δ: 0.00 (s, 6H), 0.20 (s, 6H), 0.86 (s, 9H), 0.90 (s, 9H), 1.10–1.69 (m, 16H), 2.28 (t, J = 7 Hz, 2H), and 3.54 (t, J = 6Hz, 2H); MS m/z (relative intensity): 430 (M^+, 1), 415 (10), 373 (100), 357 (49), 241 (35), 149 (36), 147 (32), 83 (20), 81 (13), 75 (97), 73 (94), and 55 (23). Anal. calcd. for $C_{23}H_{50}O_3Si_2$: C 64.12, H 11.70; found: C 64.34, H 11.60.

11-tert-*Butyldimethylsiloxyundecanoic acid (**19**)*

A 50-mL, single-necked round bottom flask was charged with the silyl ester **18** (3.13 g, 7.28 mmol) and 25 mL of 10% sodium hydroxide solution. The resulting solution was stirred for 4 h, then it was acidified with dilute HCl. The aqueous layer was extracted with ethyl acetate (3 × 20 mL) and the organic extracts were washed with water (15 mL), brine (15 mL), and dried. Removal of the solvent followed by vacuum distillation gave 2.23 g (97%) of **19** as a thick, colourless oil: bp 148–150°C/0.10 Torr; IR ν_{max}: 3550–2550, 1718, and 845 cm^{-1}; ^1H NMR (60 MHz) δ: 0.00 (s, 6H), 0.86 (s, 9H), 1.20–172 (m, 16H), 2.34 (t, J = 7 Hz, 2H), 3.58 (t, J = 6 Hz, 2H), and 10.13 (bs, 1H); MS m/z (relative intensity): 316 (M^+, 1), 283 (8), 259 (20), 241 (100), 149 (6), 83 (14), 81 (11), 75 (29), 73 (25), and 55 (20). Anal. calcd. for $C_{17}H_{36}O_3Si$: C 64.50, H 11.46; found: C 64.57, H 11.35.

*5-(11'-*tert-*Butyldimethylsiloxy-1'-hydroxyundecylidene)-2,2-dimethyl-1,3-dioxane-4,6-dione (**20**)*

A 50-mL, single-necked round bottom flask was charged with **19** (1.74 g, 4.18 mmol) and 30 mL of dichloromethane. *N,N*-Carbonyldiimidazole (981 mg, 6.05 mmol) was added in portions and the reaction mixture was stirred until gas evolution ceased. A 100-mL, single-necked round bottom flask was charged with Meldrum's acid (1.13 g, 6.07 mmol) and 40 mL of dichloromethane. Pyridine (1.07 g, 13.5 mmol) was introduced in a single portion and the reaction mixture was stirred for 1 h. The contents of the first flask were syringed into the second flask and the combined reaction mixture stirred for an additional 14 h. On work-up, the dichloromethane solution was washed with dilute hydrochloric acid, water, brine, then dried. Removal of the solvent gave 1.45 g (78%) of **20** as a yellow semi-solid: IR ν_{max}: 1730, 1635, and 835 cm^{-1}; ^1H NMR (60 MHz), δ: 0.10 (s, 6H), 0.97 (s, 9H), 1.27–1.83 (m, 16H), 1.81 (s, 6H), 2.90 (t, J = 7 Hz, 2H), and 3.47 (t, J = 6 Hz, 2H).

*5-(11'-Hydroxy-1'-hydroxyundecylidene)-2,2-dimethyl-1,3-dioxane-4,6-dione (**21**)*

A 100-mL, single-necked round bottom flask was charged with **20** (1.25 g, 2.83 mmol), tetra-*n*-butylammonium fluoride (1.85 g, 7.07 mmol), and 50 mL of THF. The resulting solution was stirred for 3.5 h, then 5% HCl (15 mL) and ether (25 mL) were added. The organic layer was separated, washed with water and brine, then dried. Removal of the solvent gave 866 mg (98%) of **21** as a yellow oil: IR ν_{max}: 3400, 1735, and 1635 cm^{-1}; ^1H NMR (60 MHz)

δ: 1.20–1.65 (m, 16H), 1.73 (s, 6H), 2.90 (t, J = 7 Hz, 2H), 3.53 (t, J = 6 Hz, 2H), and 3.56 (bs, 2H, exchangeable with D_2O); MS m/z (relative intensity): 311 (M^+ − OH, 0.1), 269 (6), 211 (12), 126 (12), 100 (14), 98 (15), 86 (31), 84 (48), 77 (40), 75 (100), 72 (43), 71 (40), 67 (30), 61 (59), and 58 (82). Exact Mass calcd. for $C_{17}H_{27}O_5$ (M^+ − OH): 311.1858; found: 311.1858.

*3-Oxotridecan-13-olide (**9**i) from thermolysis of the acyl Meldrum's acid derivative **21***

To a 200-mL, two-necked round bottom flask equipped with a pressure-equalizing dropping funnel was added 100 mL of THF. The solvent was heated to reflux and a solution of **21** (850 mg, 2.73 mmol) in 20 mL of THF was added dropwise over 5 h. The reaction mixture was allowed to cool and ether (75 mL) was introduced. The organic phase was washed with saturated sodium bicarbonate (2 × 25 mL), water (2 × 25 mL), brine (25 mL), then dried. Removal of the solvent, followed by purification via flash chromatography using petroleum ether – ethyl acetate (9:1), gave 213 mg (35%) of **9***i* as a pale yellow semi-solid with identical spectral properties to **9***i* prepared above.

*3-Benzyloxypropanoic acid (**22**, n = 2)*

This compound was prepared from 10 mL (0.16 mol) of β-propiolactone and 100 mL of benzyl alcohol according to the procedure of Bloomfield (45). Distillation afforded 21.6 g (76%) of **22** (n = 2) as a colourless oil, which crystallized on standing to give an amorphous white solid; mp 30–32°C (lit. (45) mp 31.5–33.5°C); bp 130–132°C/0.05 Torr (lit. (45) bp 124–130°C/0.01 Torr); IR ν_{max}: 3550–2820 and 1720 cm^{-1}; ^1H NMR (60 MHz) δ: 2.63 (t, J = 6 Hz, 2H), 3.73 (t, J = 6 Hz, 2H), 4.53 (s, 2H), 7.35 (s, 5H), and 11.48 (s, 1H, exchangeable with D_2O); MS m/z (relative intensity): 180 (M^+, 20), 108 (11), 107 (100), 106 (8), 105 (8), 92 (13), 91 (63), 90 (6), 89 (7), 79 (35), 77 (16), 73 (6), 65 (15), 51 (9), 45 (7), and 39 (9).

General procedure for the preparation of benzyloxycarboxylic acids from lactones (ref. 46)

A mixture of the lactone, potassium hydroxide, freshly distilled benzyl chloride, and dry toluene was heated at reflux for 14–16 h. The cooled mixture was diluted with water and the aqueous phase was washed once with ether, acidified with concentrated HCl, and extracted three times with ether. The combined ether extracts were washed with brine, dried, and concentrated under reduced pressure.

*4-Benzyloxybutanoic acid (**22**, n = 3)*

This compound was prepared according to general procedure using 8.9 mL (0.12 mol) of γ-butyrolactone, 32.5 g (0.58 mol) of potassium hydroxide, 40 mL (0.35 mol) of benzyl chloride, and 200 mL of toluene. Work-up of the reaction mixture yielded 19.1 g of crude product as a yellow oil. Distillation gave 16.5 g (73%) of desired acid as a colourless oil; bp 133–134°C/0.05 Torr (lit. (47) bp 133–134°C/0.5 Torr); IR ν_{max}: 3540–2850 and 1715 cm^{-1}; ^1H NMR (60 MHz) δ: 1.63–2.30 (m, 2H), 2.30–2.62 (m, 2H), 3.50 (t, J = 6 Hz, 2H), 4.48 (s, 2H), 7.33 (s, 5H), and 11.02 (s, 1H, exchangeable with D_2O); MS m/z (relative intensity): 194 (M^+, 14), 108 (18), 107 (83), 105 (7), 92 (21), 91 (100), 90 (5), 89 (7), 87 (10), 85 (28), 79 (21), 77 (12), 70 (5), and 65 (19).

*5-Benzyloxypentanoic acid (**22**, n = 4)*

This compound was prepared according to general procedure using 5.0 mL (54 mmol) of δ-valerolactone, 15.1 g (0.27 mol) of potassium hydroxide, 20 mL (0.16 mol) of benzyl chloride, and 125 mL of toluene. Work-up of the reaction mixture yielded 11.3 g of crude product as a yellow oil. Distillation gave 8.5 g (75%) of protected acid as a colourless oil; bp 140–144°C/0.1 Torr; IR ν_{max}: 3550–2850 and 1715 cm^{-1}; ^1H NMR (60 MHz) δ: 1.40–1.80 (m, 4H), 2.07–2.42 (m, 2H), 3.18–3.57 (m, 2H), 4.37 (s, 2H), 7.20 (s, 5H), and 10.82 (s, 1H, exchangeable with D_2O); MS m/z (relative intensity): 208 (M^+, 12), 108 (17), 107 (68), 101 (12), 99 (16), 92 (22), 91 (100), 90 (5), 89 (5), 83 (5), 79 (14), 77 (8), 73 (6), 71 (6), and 65 (15). Anal. calcd. for $C_{12}H_{16}O_3$: C 69.21, H 7.74; found: C 68.76, H 7.58.

*6-Benzyloxyhexanoic acid (**22**, n = 5)*

This compound was prepared according to general procedure using 10.0 mL (90 mmol) of ϵ-caprolactone, 25 g (0.45 mol) of potassium hydroxide, 30 mL (0.27 mol) of benzyl chloride, and 200 mL of toluene. Work-up of the reaction mixture yielded 19.2 g of crude product as a yellow oil and distillation gave 17.0 g (85%) of the desired protected acid as a colourless oil; bp 148–150°C/0.07 Torr; IR ν_{max}: 3550;–2850 and 1715 cm^{-1}; ^1H NMR (60 MHz) δ-: 1.23–1.80 (m, 6H), 2.12–2.47 (m, 2H), 3.25–3.60 (m, 2H), 4.43 (s, 2H), 7.25 (s, 5H), and 11.57 (s, 1H, exchangeable with D_2O); MS m/z (relative intensity): 222 (M^+, 12), 113 (12), 108 (13), 107 (59), 105 (5), 98 (5), 97 (5), 92 (25), 91 (100), 89 (5), 79 (12), 77 (6), 73 (8), 69 (8), 67 (6), and 65 (15). Exact Mass calcd. for $C_{13}H_{18}O_3$: 222.1255; found: 222.1255.

6-Benzyloxy-1-chlorohexane

This compound was prepared by treating 1.64 g (41 mmol) of sodium hydride dispersion in 60 mL of THF, with 4.00 g (29 mmol) of 6-chloro-1-hexanol (48), 5.2 mL (44 mmol) of benzyl bromide, and 60 mL of THF. The reaction was refluxed for 16 h and worked up to give 8.4 g of crude product as a yellow oil. Distillation yielded 5.99 g (90%) of pure benzyl ether as a colourless oil: bp 112–114°C/0.2 Torr; IR ν_{max}: 1100 cm^{-1}; ^1H NMR (60 MHz) δ: 1.13–1.97 (m, 8H), 3.30–3.67 (m, 4H), 4.50 (s, 2H), and 7.37 (s, 5H); MS m/z (relative intensity): 228 (M^+ ^{37}Cl, 0.8), 226 (M^+ ^{35}Cl, 2), 208 (1), 182 (2), 135 (1), 130 (1), 119 (2), 117 (5), 108 (10), 107 (7), 105 (4), 93 (8), 92 (71), 91 (100), 81 (6), 79 (10), 77 (8), 65 (16), and 55 (10). Exact Mass. calcd. for $C_{13}H_{19}OCl$: 228.1095, 226.1124; found: 228.1011, 226.1130.

8-Benzyloxy-1-chlorooctane

This compound was prepared as above using 1.70 g (43 mmol) of sodium hydride dispersion, 5.00 g (30 mmol) of 8-chloro-1-octanol (48), 5.4 mL (46 mmol) of benzyl bromide, and 60 mL of THF. Work-up of the reaction mixture gave 9.7 g of crude product as a yellow oil. Distillation yielded 7.48 g (97%) of pure chloro ether as a colourless oil; bp 133–135°C/0.2 Torr; IR ν_{max}: 1100 cm^{-1}; ^1H NMR (60 MHz) δ: 1.13–1.97 (m, 12H), 3.27–3.63 (m, 4H), 4.47 (s, 2H), and 7.32 (s, 5H); MS m/z (relative intensity): 256 (M^+ ^{37}Cl, 0.4), 254 (M^+ ^{35}Cl, 1), 236 (0.3), 208 (0.7), 182 (0.7), 165 (1), 163 (2), 145 (2), 144 (2), 124 (2), 123 (2), 110 (2), 109 (18), 108 (9), 107 (7), 93 (8), 92 (84), 91 (100), 79 (8), 77 (6), 69 (7), 65 (12), and 55 (15). Exact Mass calcd. for $C_{15}H_{23}OCl$: 256.1408, 254.1438; found: 256.1411, 254.1434.

*9-Benzyloxynonanoic acid (**22**, n = 8)*

A Grignard reagent was prepared from a mixture of magnesium turnings (664 mg, 26.5 mmol) and 4.00 g of 6-benzyloxy-1-chlorohexane (17.7 mmol) in dry THF under a nitrogen atmosphere. One drop of 1,2-dibromoethane was added to initiate the reaction. The mixture was heated to reflux for 2.5 h and was cooled to room temperature, resulting in a grey suspension of the Grignard reagent. In a second flask, 1.34 mL of β-propiolactone (21.2 mmol) in 20 mL of THF was added to 8.9 mL of a 0.1 M solution of lithium tetrachlorocuprate (0.89 mmol) in THF. This solution was cooled to −10°C and the solution of the Grignard reagent was added via cannulation at such a rate that the internal temperature of the reaction mixture remained below 0°C. The reaction mixture was stirred at −10°C for 1 h, then was quenched with 1 M HCl and diluted with ether. The organic phase was extracted repeatedly with 5% aqueous potassium hydroxide. The combined aqueous extracts were acidified with concentrated HCl and extracted three times with ether. The combined ether layers were washed twice with brine, dried, and concentrated under reduced pressure to give 4.47 g of crude acid product as well as 1.2 g (34%) of quenched Grignard reagent. Distillation afforded a small forerun of 3-chloropropanoic acid (bp 54°C/0.2 Torr) followed by 2.77 g (59%) of **22** (n = 8) as a colourless oil; bp 176–178°C/0.3 Torr; IR ν_{max}: 3640–2850 and 1715 cm^{-1}; ^1H NMR (60 MHz) δ: 1.10–1.90 (m,

Can. J. Chem. Downloaded from www.nrcresearchpress.com by 217.78.4.112 on 09/08/12
For personal use only.

Can. J. Chem. Downloaded from www.nrcresearchpress.com by 217.78.4.112 on 09/08/12
For personal use only.

12H), 2.33 (t, J = 6 Hz, 2H), 3.47 (t, J = 6 Hz, 2H), 4.50 (s, 2H), 7.35 (s, 5H), and 11.10 (br s, 1H, exchangeable with D_2O); MS m/z (relative intensity): 264 (M^+, 13), 246 (2), 218 (2), 155 (6), 144 (5), 138 (5), 123 (6), 108 (17), 107 (77), 106 (9), 105 (19), 97 (10), 92 (33), 91 (100), 84 (9), 83 (7), 79 (11), 73 (15), 69 (15), 68 (9), 65 (9), 60 (18), and 55 (39). Exact Mass calcd. for $C_{16}H_{24}O_3$: 264.1724; found: 264.1724.

*11-Benzyloxyundecanoic acid (**22**, n = 10)*

This compound was prepared according to the above procedure, using 860 mg (35.4 mmol) of magnesium turnings, 6.00 g (23.6 mmol) of 8-benzyloxy-1-chlorooctane, and 20 mL of THF to generate the Grignard reagent. The second solution was prepared from 11.8 mL (1.18 mmol) of a 0.1 M solution of lithium tetrachlorocuprate in THF, 3.0 mL (47 mmol) of β-propiolactone, and 20 mL of THF. Work-up of the reaction mixture gave 5.95 g of crude acid as well as 1.77 g (34%) of quenched Grignard reagent. Distillation afforded a forerun of 3-chloropropanoic acid (0.90 g; bp 54°C/0.2 Torr), followed by 3.89 g (56%) of **22** (n = 10) as a colourless oil, which solidified on standing to give a white amorphous solid; mp 30–32°C; bp 188°C/0.05 Torr; IR ν_{max}: 3620–2820 and 1715 cm^{-1}; ^1H NMR (60 MHz) δ: 1.08–1.90 (m, 16H), 2.33 (t, J = 7 Hz, 2H), 3.45 (t, J = 6 Hz, 2H), 4.50 (s, 2H), 7.33 (s, 5H), and 11.50 (s, 1H, exchangeable); MS m/z (relative intensity): 292 (M^+, 12), 109 (11), 108 (14), 107 (50), 100 (10), 92 (49), 91 (100), 79 (9), 77 (8), 73 (17), 71 (9), 69 (16), 65 (9), 60 (13), and 55 (32). Exact Mass calcd. for $C_{18}H_{28}O_3$: 292.2038; found: 292.2038.

5-(3'-Benzyloxy-1'-hydroxypropylidene)-2,2-dimethyl-1,3-dioxan-4,6-dione

To 5.12 g (28.4 mmol) of carboxylic acid **22** (n = 2) was added 5.0 mL (57 mmol) oxalyl chloride and the resulting solution was stirred for 2.5 h at room temperature. The excess oxalyl chloride was then removed under reduced pressure and the residual acid chloride was dissolved in 30 mL of dry dichloromethane. This acid chloride solution was added to a solution of 3.72 g (25.8 mmol) of Meldrum's acid and 6.3 mL (77 mmol) of pyridine in 50 mL of dichloromethane at 0°C. The reaction was stirred at 0°C for 1 h and allowed to warm to room temperature for 1 h. Work-up of the reaction mixture gave 7.72 g of crude product as a red syrup. Purification by flash chromatography using petroleum ether – ethyl acetate (4:1) as eluant afforded 5.99 g (76%) of acylated Meldrum's acid as a yellow oil; IR ν_{max}: 3600–3300, 1740, 1680, and 1580 cm^{-1}; ^1H NMR (60 MHz) δ: 1.70 (s, 6H), 2.68–2.92 and 3.36–3.62 (2 multiplets, 2H; enol and keto forms), 3.68–3.97 (m, 2H), 4.57 (s, 2H), 7.35 (s, 5H), and 15.35 (br s, 1H, exchangeable with D_2O); MS m/z (relative intensity): 306 (M^+, 5), 248 (9), 144 (5), 143 (40), 142 (8), 125 (22), 124 (21), 114 (5), 113 (5), 108 (7), 107 (31), 106 (5), 105 (6), 98 (26), 96 (8), 91 (100), 89 (6), 79 (10), 77 (8), 65 (17), 59 (15), and 58 (12). Exact Mass calcd. for $C_{16}H_{18}O_6$: 306.1104; found: 306.1116.

*5-(4'-Benzyloxy-1'-hydroxybutylidene-2,2-dimethyl-1,3-dioxan-4,6-dione (**23**, n = 3)*

The acid chloride of carboxylic acid **22** (n = 3) was prepared as above, using 5.0 g (26 mmol) of **22** (n = 3), 2.25 mL (25.8 mmol) of oxalyl chloride, 2.1 mL (26 mmol) of pyridine, and 30 mL of dichloromethane. This acid chloride was treated with 3.38 g (24 mmol) of Meldrum's acid, and 5.7 mL (71 mmol) of pyridine in 30 mL of dichloromethane as above. Work-up of the reaction mixture gave 7.25 g of crude product as a red syrup. Purification by flash chromatography using petroleum ether – ethyl acetate (2:1) as eluant afforded 6.34 g (84%) of **23** (n = 3) as a yellow oil; IR ν_{max}: 3640–3300, 1740, 1670, and 1580 cm^{-1}; ^1H NMR (60 MHz) δ: 1.70 (s, 6H), 1.73–2.27 (m, 2H), 2.30–2.70 and 3.03–3.33 (2 multiplets, 2H; enol and keto forms), 3.37–3.70 (m, 2H), 4.47 (6, 2H), 7.33 (s, 5H), and 15.20–15.53 (br s, 1H, exchangeable with D_2O); MS m/z (relative intensity): 320 (M^+, 0.8), 262 (7), 157 (6), 155 (8), 139 (5), 128 (14), 112 (13), 111 (5), 108 (6), 107 (29), 105 (8), 92 (14), 91 (100), 87 (6), 85 (18), 84 (16), 79 (9), 77 (9), 69 (12), 65 (14), and 57 (10). Exact Mass calcd. for $C_{17}H_{20}O_6$: 320.1260; found: 320.1278.

*5-(5'-Benzyloxy-1'-hydroxypentylidene)-2,2-dimethyl-1,3-dioxan-4,6-dione (**23**, n = 4)*

The acid chloride of **22** (n = 4) was prepared from 1.00 g (4.8 mmol) of acid, 0.41 mL (4.8 mmol) of oxalyl chloride, 0.39 mL (4.8 mmol) of pyridine, and 15 mL of dichloromethane. This acid chloride was treated with 0.63 g (4.4 mmol) of Meldrum's acid, and 1.1 mL (13 mmol) of pyridine in 10 mL of dichloromethane. Work-up of the reaction mixture gave 1.53 g of crude product as a red syrup. Purification by flash chromatography using petroleum ether – ethyl acetate (4:1) as eluant afforded 1.16 g (80%) of **23** (n = 4) as a yellow oil; IR ν_{max}: 3650–3400, 1740, 1670, and 1580 cm^{-1}; ^1H NMR (60 MHz) δ: 1.50–1.93 (m, 4H), 1.73 (s, 6H), 2.27–2.57 and 2.90–3.25 (2 multiplets, 2H; enol and keto forms), 3.37–3.63 (m, 2H), 4.48 (s, 2H), 7.33 (s, 5H), and 15.20–15.53 (br s, 1H, exchangeable with D_2O); MS m/z (relative intensity): 334 (M^+, 3), 276 (7), 258 (3), 208 (6), 185 (5), 176 (4), 170 (6), 169 (6), 167 (5), 152 (8), 141 (8), 124 (5), 108 (8), 107 (32), 101 (13), 99 (15), 92 (18), 91 (100), 83 (5), 79 (9), 77 (6), 71 (8), 69 (7), 65 (13), and 58 (14). Exact Mass calcd. for $C_{18}H_{22}O_6$: 334.1416; found: 334.1428.

*5-(6'-Benzyloxy-1'-hydroxyhexylidene)-2,2-dimethyl-1,3-dioxan-4,6-dione (**23**, n = 5)*

The acid chloride of **22** (n = 5) was prepared from 2.14 g (9.6 mmol) of acid, 0.84 mL (9.6 mmol) of oxalyl chloride, 0.78 mL (9.6 mmol) of pyridine, and 20 mL of dichloromethane. This acid chloride was treated with 1.26 g (8.7 mmol) of Meldrum's acid, 2.2 mL (26 mmol) of pyridine, and 20 mL of dichloromethane. Work-up of the reaction mixture gave 3.22 g of crude product as a red syrup. Purification by flash chromatography using petroleum ether – ethyl acetate (4:1) as eluant afforded 2.53 g (83%) of **23** (n = 5) as a yellow oil; IR ν_{max}: 3620–3420, 1740, 1670, and 1575 cm^{-1}; ^1H NMR (60 MHz) δ: 1.40–1.90 (m, 6H), 1.72 (s, 6H), 2.13–2.50 and 2.90–3.27 (2 multiplets, 2H; enol and keto forms), 3.33–3.63 (m, 2H), 4.48 (s, 2H), 7.32 (s, 5H), and 15.13–15.50 (br s, 1H, exchangeable with D_2O); MS m/z (relative intensity): 348 (M^+, 0.2), 290 (3), 272 (0.5), 222 (3), 199 (3), 141 (3), 115 (4), 113 (4), 108 (4), 107 (17), 97 (4), 92 (10), 91 (55), 79 (7), 77 (5), 73 (4), 69 (7), 65 (9), 59 (7), 58 (28), 44 (34), and 43 (100). Exact Mass calcd. for $C_{19}H_{24}O_6$: 348.1572; found: 348.1571.

*5-(9'-Benzyloxy-1'-hydroxynonylidene)-2,2-dimethyl-1,3-dioxan-4,6-dione (**23**, n = 8)*

The acid chloride of **22** (n = 8) was prepared from 2.0 g (7.6 mmol) of acid, 0.66 mL (7.6 mmol) of oxalyl chloride, 0.61 mL (9.6 mmol) of pyridine, and 15 mL of dichloromethane. This acid chloride was treated with 0.99 g (6.9 mmol) of Meldrum's acid, and 1.7 mL (21 mmol) of pyridine in 15 mL of dichloromethane. Work-up of the reaction mixture gave 2.49 g of crude product as a red syrup. Purification by flash chromatography using petroleum ether – ethyl acetate (4:1) as eluant afforded 1.69 g (63%) of **23** (n = 8) as a yellow oil; IR ν_{max}: 3620–3400, 1740, 1670, and 1575 cm^{-1}; ^1H NMR (60 MHz) δ: 1.15–1.87 (m, 12H), 1.73 (s, 6H), 2.13–2.50 and 2.92–3.27 (m, 12H), 1.73 (s, 6H), 2.13–2.50 and 2.92–3.27 (2 multiplets, 2H; enol and keto forms), 3.47 (t, J = 6 Hz, 2H), 4.50 (s, 2H), 7.35 (s, 5H), and 15.17–15.50 (br s, 1H, exchangeable with D_2O); MS m/z (relative intensity): 390 (M^+, 0.3), 375 (0.3), 332 (4), 265 (8), 155 (5), 108 (13), 107 (50), 97 (5), 95 (5), 92 (24), 265 (8), 155 (5), 108 (13), 107 (50), 97 (5), 95 (5), 92 (24), 91 (89), 79 (7), 77 (5), 71 (9), 69 (6), 65 (9), 59 (6), 58 (33), 57 (5), 55 (15), 44 (57), and 43 (100). Exact Mass calcd. for $C_{19}H_{24}O_5$ (M^+ − acetone): 332.1623; found: 332.1616.

*5-(11'-Benzyloxy-1'-hydroxyundecylidene)-2,2-dimethyl-1,3-dioxan-4,6-dione (**23**, n = 10)*

The acid chloride of **22** (n = 10) was prepared from 1.46 g (5.0 mmol) of acid, 0.41 mL (5.0 mmol) of oxalyl chloride,

Can. J. Chem. Downloaded from www.nrcresearchpress.com by 217.78.4.112 on 09/08/12
For personal use only.

0.40 mL (5.0 mmol) of pyridine, and 15 mL of dichloromethane. This acid chloride was treated with 0.79 g (5.5 mmol) of Meldrum's acid, and 1.3 mL (17 mmol) of pyridine in 15 mL of dichloromethane. Work-up of the reaction mixture gave 1.87 g of crude product as a red syrup. Purification by flash chromatography using petroleum ether – ethyl acetate (4:1) as eluant afforded 1.05 g (50%) of pure **23** (n = 10) as a yellow oil; IR ν_{max}: 3620–3400, 1740, 1670, and 1575 cm^{-1}; ^1H NMR (60 MHz) δ: 1.03–1.92 (m, 16H), 1.73 (s, 6H), 2.08–2.58 and 2.90–3.27 (2 multiplets, 2H; enol and keto forms), 3.47 (t, J = 6 Hz, 2H), 4.50 (s, 2H), 7.35 (s, 5H), and 15.17–15.50 (br s, 1H, exchangeable with D_2O); MS m/z (relative intensity): 418 (M^+, 1), 403 (1), 401 (1), 360 (4), 342 (1), 312 (1), 293 (3), 292 (14), 183 (3), 123 (3), 108 (14), 107 (64), 92 (28), 91 (10), 85 (7), 83 (7), 81 (8), 79 (8), 77 (7), 71 (15), 69 (11), 67 (7), 65 (10), 60 (7), 59 (8), and 58 (21). Exact Mass calcd. for $C_{21}H_{28}O_5$ (M^+ − acetone): 360.1937; found: 360.1954.

*5-(1',3'-Dihydroxypropylidene)-2,3-dimethyl-1,3-dioxan-4,6-dione (**24**, n = 2)*

A mixture of 710 mg (2.32 mmol) of the above acetylated Meldrum's acid and 70 mg of 10% palladium-on-charcoal in 10 mL of ethanol – ethyl acetate (1:1) was stirred under a hydrogen atmosphere (1 atm = 101.3 kPa) at room temperature. After 57 mL (1 equiv.) of hydrogen had been absorbed during a period of 2 h, the uptake of hydrogen ceased. The catalyst was removed by filtration and was washed with ethyl acetate. The filtrate was concentrated under reduced pressure to give 448 mg (89%) of **24** (n = 2) as a pale yellow oil; IR ν_{max}: 3640–3350, 1740, 1680, and 1580 cm^{-1}; ^1H NMR (60 MHz) δ: 1.70 (s, 6H), 2.56–2.83 and 3.13–3.53 (2 multiplets, 2H; enol and keto forms), and 3.67–4.07 (m, 2H); MS m/z (relative intensity); 216 (M^+, 1), 159 (15), 158 (32), 141 (14), 140 (13), 114 (27), 105 (13), 91 (12), 73 (57), 69 (19), 59 (79), and 58 (14). Exact Mass calcd. for $C_9H_{12}O_6$: 216.0634; found: 216.0634.

*3-Oxopentan-5-olide (**25**)*

To 25 mL of dry THF heated at reflux under a nitrogen atmosphere was added a solution of 302 mg (1.40 mmol) of alcohol **24** (n = 2) in 15 mL of THF over a period of 4 h, using a constant-rate addition funnel. The solution was heated at reflux for an additional 30 min. Removal of solvent gave 235 mg of a yellow oil. Distillation, in glassware that had been treated with trimethylsilyl chloride and pyridine, then rinsed with water, and dried, gave 139 mg (87%) of **25** as a colourless oil, which slowly crystallized to give an amorphous white solid. ^1H NMR analysis indicated that the product was ca. 95% pure; mp 61–64°C; bp (Kugelrohr distillation) 130°C/0.1 Torr; IR ν_{max}: 1780 and 1745 cm^{-1}; ^1H NMR (60 MHz) δ: 2.72 (t, J = 6 Hz, 2H), 3.60 (s, 2H), and 4.63 (t, J = 6 Hz, 2H); MS m/z (relative intensity): 114 (M^+, 8), 105 (3), 104 (3), 91 (3), 85 (5), 77 (4), 73 (3), 72 (5), 71 (5), 70 (3), 69 (5), 60 (4), 58 (3), 56 (7), 55 (51), 45 (4), 44 (7), 43 (25), and 42 (100). Exact Mass calcd. for $C_5H_6O_3$: 114.0317; found: 114.0319.

*5-(Tetrahydro-2'-furylidene)-2,2-dimethyl-1,3-dioxan-4,6-dione (**26**)*

A mixture of 1.93 g (6.0 mmol) of **23** (n = 3) and 0.19 g of 5% palladium-on-charcoal in 15 mL of ethyl acetate was stirred under a hydrogen atmosphere (1 atm) at room temperature. After 208 mL (141% of 1 molar equivalent) of hydrogen had been absorbed during a period of 19 h, the uptake of hydrogen ceased. The catalyst was removed by filtration and was washed with dichloromethane. The filtrate was concentrated under reduced pressure to give 1.03 g crude **26** as pale yellow crystals. Recrystallization from petroleum ether – ethyl acetate gave 0.89 g (70%) of **26** as a white solid; mp 145.0–146.5°C; IR ν_{max}: 1755 and 1715 cm^{-1}; ^1H NMR (60 MHz) δ: 1.73 (s, 6H), 1.93–2.53 (m, 2H), 3.50 (t, J = 8 Hz, 2H), and 4.73 (t, J = 7 Hz, 2H); MS m/z (relative intensity): 212 (M^+, 13), 197 (13), 156 (6), 155 (55), 154 (29), 113 (8), 111 (20), 110 (100), 69 (28), 53 (11), 52 (8), 44 (7), 43 (47), and 42 (78). Exact Mass calcd. for $C_{10}H_{12}O_5$: 212.0685; found: 212.0685.

Acknowledgements

We are grateful to the Natural Sciences and Engineering Research Council of Canada for financial support, to Professor W. C. Still for copies of MACROMODEL and assistance in implementing this program on our systems, and to Professor G. N. Patey for assistance with the quasiharmonic entropy calculations.

1. (*a*) C. Tsai, J. J. Stezowski, and R. E. Hughes. J. Am. Chem. Soc. **93**, 7286 (1971); (*b*) S. Masamune. Aldrichimica Acta, **11**, 23 (1978); (*c*) N. Nakajima, T. Hamada, T. Tanaka, Y. Oikawa, and O. Yonemitsu. J. Am. Chem. Soc. **108**, 4645 (1986).
2. (*a*) V. Prelog, A. M. Gold, G. Talbot, and Z. Zamojski. Helv. Chim. Acta, **45** 4 (1962); (*b*) T. Kaiho, S. Masamune, and T. Toyoda. J. Org. Chem. **47**, 1612 (1982).
3. R. K. Boeckman, Jr. and J. R. Pruitt. J. Am. Chem. Soc. **111**, 8286 (1989).
4. H. Brockmann and R. Oster. Chem. Ber. **90**, 605 (1957).
5. R. E. Ireland and F. R. Brown, Jr. J. Org. Chem. **45**, 1868 (1980).
6. P. M. Booth, H. B. Broughton, M. J. Ford, C. M. J. Fox, S. V. Ley, A. M. Z. Slawin, D. J. Williams, and P. R. Woodward. Tetrahedron, **45**, 7565 (1989).
7. P. E. Sum and L. Weiler. Can. J. Chem. **55**, 996 (1977).
8. R. J. Sims, S. A. Tischler, and L. Weiler. Tetrahedron Lett. **24**, 253 (1983).
9. Y. Oikawa, K. Sugano, and O. Yonemitsu. J. Org. Chem. **43**, 2087 (1978).
10. W. H. Kruizinga and R. M. Kellogg. J. Am. Chem. Soc. **103**, 5183 (1981).
11. T. Takahashi, T. Nagashima, H. Ikeda, and J. Tsuji. Tetrahedron Lett. **23**, 4361 (1982).
12. A. D. Cort, L. Mandolini, and B. Masci. J. Org. Chem. **48**, 3979 (1983).
13. A. Pross and S. S. Shaik. J. Am. Chem. Soc. **104**, 187 (1982).
14. (*a*) G. D. Prestwich and M. S. Collins. Tetrahedron Lett. **22**, 4587 (1981); (*b*) G. D. Prestwich. Tetrahedron, **38**, 1911 (1982).
15. F. C. Uhle, J. E. Krueger, and A. E. Rogers. J. Am. Chem. Soc. **78**, 1932 (1956).
16. J. P. Célérier, E. Deloisy, P. Kapron, G. Lhommet, and P. Maitte. Synthesis, 130 (1981).
17. (*a*) D. Seebach and H. Meyer. Angew. Chem. Intt. Ed. Engl. **13**, 77 (1974); (*b*) D. Seebach and H. Meyer. Liebigs Ann. Chem. 2261 (1975); (*c*) M. Fetizon, M. Golfier, and J. M. Louis. Tetrahedron, **31**, 171 (1975); (*d*) R. W. Drugger and C. H. Heathcock. J. Org. Chem. **45**, 1181 (1980); (*e*) S. Castellino and J. J. Sims. Tetrahedron Lett. **25**, 2307 (1984); (*f*) S. Brandange, L. Flodman, and A. Norberg. J. Org. Chem. **49**, 927 (1984).
18. J. d'Angelo and D. Gomez-Pardo. Tetrahedron Lett. **32**, 3063 (1991).
19. (*a*) X. Wang and K. N. Houk. J. Am. Chem. Soc. **110**, 1870 (1988); (*b*) K. B. Wiberg and K. E. Laidig. J. Am. Chem. Soc. **110**, 1872 (1988).
20. H. Achenbach and J. Witzke. Liebigs Ann. Chem. 2384 (1981).
21. W. B. Schweizer and J. D. Dunitz. Helv. Chim. Acta, **65**, 1547 (1982).
22. H. Ogura, K. Furuhata, H. Kuwano, and M. Suzuki. Tetrahedron, **37**, Supplement 1, 165 (1981).
23. G. Chang, W. C. Guida, and W. C. Still. J. Am. Chem. Soc. **111**, 4379 (1989).
24. U. Burkert and N. L. Allinger. *In* Molecular mechanics; ACS Monograph 177, American Chemical Society, Washington, D.C. 1982.
25. (*a*) F. A. L. Anet, A. K. Cheng, and J. Krane. J. Am. Chem.

Soc. **95**, 7877 (1973); (*b*) H. Drotloff, H. Rotter, D. Emeis, and M. Möller. J. Am. Chem. Soc. **109**, 7797 (1987).
26. J. Dale. Acta Chem. Scand. (*a*) **27**, 1130 (1973); (*b*) **27**, 1115 (1973).
27. M. Barfield and D. M. Grant. J. Am. Chem. Soc. **85**, 1899 (1963).
28. T. H. Keller, E. G. Neeland, S. Rettig, J. Trotter, and L. Weiler. J. Am. Chem. Soc. **110**, 7858 (1988).
29. W. C. Still, M. Kahn, and A. Mitra. J. Org. Chem. **43**, 2923 (1978).
30. (*a*) S. C. Watson and J. F. Eastham. J. Organomet. Chem. **9**, 165 (1967); (*b*) M. F. Lipton, C. M. Sorensen, A. C. Sadler, and R. H. Shapiro. J. Organomet. Chem. **186**, 155 (1980).
31. D. D. Perrin, W. L. F. Armarego, and D. R. Perrin. *In* Purification of laboratory chemicals. Pergamon Press, Oxford. 1966.
32. A. N. Meldrum. J. Chem. Soc. **93**, 598 (1908).
33. W. R. Kirner and G. H. Holmes. J. Am. Chem. Soc. **51**, 2503 (1929).
34. I. J. Borowitz, V. Bandurco, M. Heyman, R. D. G. Rigby, and S. N. Ueng. J. Org. Chem. **38**, 1234 (1973).
35. D. E. Ames and P. J. Islip. J. Chem. Soc. 4363 (1963).
36. (*a*) J. W. Wilt and J. W. Hill. J. Org. Chem. **26**, 3523 (1961); (*b*) P. E. Peterson, R. J. Bopp, D. M. Chevli, E. L. Curran, D. E. Dillard, and R. J. Kamat. J. Am. Chem. Soc. **89**, 5902 (1967).
37. E. F. Degering and L. G. Boatright. J. Am. Chem. Soc. **72**, 5137 (1950).
38. K. Mori. Tetrahedron, **30**, 3807 (1974).
39. B. Maurer and A. Grieder. Helv. Chim. Acta, **60**, 1155 (1977).
40. A. Butenandt, E. Hecker, M. Hopp, and W. Koch. Liebigs Ann. Chem. **658**, 39 (1962).
41. F. L. M. Pattison, J. B. Stothers, and R. G. Woolford. J. Am. Chem. Soc. **78**, 2255 (1956).
42. R. Toubiana and J. Asselineau. Ann. Chim. **7**, 9 (1962).
43. S. J. Cristol and W. C. Firth, Jr. J. Org. Chem. **26**, 280 (1961).
44. M. Horiike, M. Tanouchi, and C. Hirano. Agric. Biol. Chem. **44**, 257 (1980).
45. J. J. Bloomfield. J. Org. Chem. **27**, 2742 (1962).
46. M. Sheehan, R. J. Spangler, and C. Djerassi. J. Org. Chem. **36**, 3526 (1971).
47. (*a*) T. Fujisawa, T. Mori, T. Kawara, and T. Sato. Chem. Lett. 569 (1982); (*b*) T. Sato, T. Kawara, M. Kawashima, and T. Fujisawa. Chem. Lett 571 (1980).
48. T. R. Hoye, M. J. Kurth, and V. Lo. Tetrahedron Lett. **22**, 815 (1981).

Can. J. Chem. Downloaded from www.nrcresearchpress.com by 217.78.4.112 on 09/08/12
For personal use only.

Approach to the synthesis of candelabrone and synthesis of 3,7-diketo-12-hydroxyabieta-8,11,13-triene

ROBERT H. BURNELL[1] AND STÉPHANE CARON
Chemistry Department, Université Laval, Québec, Que., Canada G1K 7P4

Received July 30, 1991

This paper is dedicated to Professor Zdenek (Denny) Valenta on the occasion of his 65th birthday

ROBERT H. BURNELL and STÉPHANE CARON. Can. J. Chem. **70**, 1446 (1992).

An approach to the synthesis of aromatic diterpenes was tested for its generality. Phenylacetonitriles with increasing substitution on the aromatic ring were prepared and alkylated with geranyl bromide and the resulting dienes subjected to cationic cyclization. The less-substituted examples afforded tricyclic products of the required stereochemistry while the more highly substituted compounds cyclized with reduced yields or not at all. One of the intermediates was used to synthesize nimosone (3,7-diketo-12-methoxyabieta-8,11,13-triene), a natural diterpene isolated originally from *Chamaecyparis formosensis* and recently from *Azadirachta indica*.

ROBERT H. BURNELL et STÉPHANE CARON. Can. J. Chem. **70**, 1446 (1992).

Une serie de phénylacétonitriles substitués par une chaîne géranyle et un nombre croissant de groupements méthoxyles a été soumise à des conditions de cyclisation cationique pour déterminer la généralité de la réaction. Seulement les substrats les moins encombrés ont réagis efficacement donnant les produits tricycliques de la stéréochimie requise et un de ces derniers a servi comme intermédiaire clé pour la synthèse de la nimosone, une dicétone diterpènique isolée de *Chamaecyparis formosensis* et plus récemment de *Azadirachta indica*.

Can. J. Chem. Downloaded from www.nrcresearchpress.com by 217.78.4.112 on 09/08/12
For personal use only.

In recent years more examples of aromatic diterpenes with oxygen functions in the A ring have appeared in the literature. Hypagenins A, D, and E (1), candelabrone (2) and several coleons (3) fall in this category and the neem tree, *Azadirachta indica*, is a rich source of these new compounds (4). Few syntheses are reported for these products since many of the schemes that start with simpler naturally occuring chiral terpenes, such as podocarpic and dehydroabietic acids (5), do not lend themselves readily to the introduction of functions into the A ring past the quaternary centres at C4 and C10. A more total approach could be advantageous but, unlike those derived from chiral precursers, the final products from most sequences would be racemic.

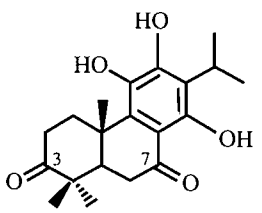

1

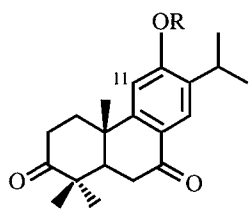

2*a* R = H
2*b* R = Me

After first probing the application of radical cyclizations of the type described by Snider *et al.* (6) it was decided to test the generality of the cationic equivalent as championed by Livinghouse and co-workers (7). Ultimately we hope to apply the scheme to the synthesis of candelabrone **1** but the first objective was the simpler 3,7-diketo-12-hydroxyabieta-8,11,13-triene **2***a* originally isolated from *Chamaecyparis formosensis* (8) and more recently from *Azadirachita indica* when it was given the name nimosone (4*a*).

This synthetic approach involves the cyclization of nonconjugated dienes such as **5***a* in which half the molecule comes from the naturally derived geranyl bromide **3** and the other 10 skeletal carbon atoms are provided by substituted phenylacetonitriles, such as **4**. Specifically the latter has been prepared from *o*-isopropylanisole **6***a* in an overall yield of close to 65%. Bromination of **6***a* by potassium bromide and *m*-CPBA in the presence of 18-crown-6 afforded 84% of the bromo derivative **6***b* and the yields were as good or better in the followingGrignard reaction (with DMF, 98% **6***c*), hydride reduction (97% **6***d*), and the two substitutions (first with PBr_3, pyridine 98% **6***e* and then KCN, 18-crown-6, 80% **4**).

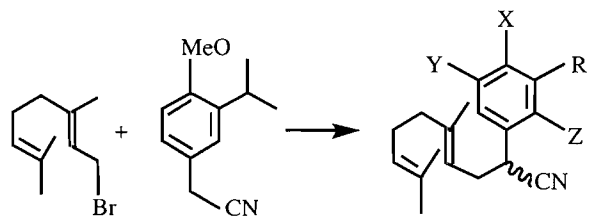

3 **4**

5*a* X = OMe R = isoPr Y = Z = H
5*b* X = Y = Z = R = H
5*c* X = Y = Z = OMe R = isoPr
5*d* X = Z = OMe R = isoPr Y = H

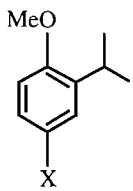

6*a* X = H
6*b* X = Br
6*c* X = CHO
6*d* X = CH_2OH
6*e* X = CH_2Br → **4**

The anion of nitrile **4** coupled with the reactive geranyl bromide **3** at room temperature to afford the diene **5***a* (85%). Attempts to cyclize the latter using published procedures (9) were disappointing so, for experimentation, a simpler model **5***b* was prepared (in 92% yield) by alkylating phenylaceto-

[1]Author to whom correspondence may be addressed.

nitrile with geranyl bromide. Finally, using methyl benzenesulfenate with boron trifluoride in nitromethane (*7b*),[2] this model diene gave the cyclized product **7***b* in reasonable yield (63%). In the same manner, the methoxy isopropyl analog **5***a* afforded the tricyclic **7***a* with slightly better results (76%). The ring closures produced specifically the AB *trans* geometry, the relative configuration at C3 was mostly β, while the two epimers at C7 were roughly equally represented. No particular effort was made to separate these diasteromers since their stereochemical peculiarities would disappear in subsequent steps as the carbonyl groups were established at these positions. Both the simple models **7***b* and **7***a* were subjected to the following reactions, the former serving as an expendable forerunner to determine the most rewarding experimental conditions.

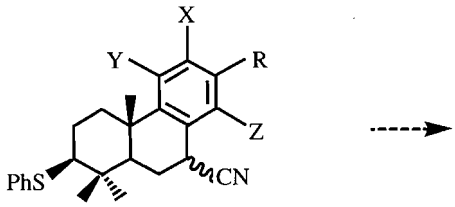

7*a* R = isoPr X = OMe Y = Z = H
7*b* R = X = Y = Z = H
7*c* R = isoPr X = Y = Z = OMe
7*d* R = isoPr X = Z = OMe Y = H

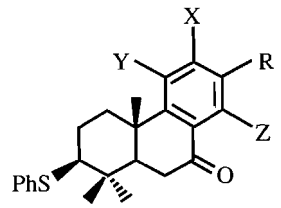

8*a* R = isoPr X = OMe Y = Z = H
8*b* R = X = Y = Z = H

8*d* R = isoPr X = Z = OMe Y = H

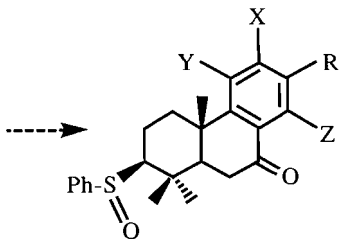

9*a* R = isoPr X = OMe Y = Z = H
9*b* R = X = Y = Z = H

9*d* R = isoPr X = Z = OMe Y = H

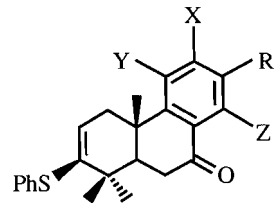

10*a* R = isoPr X = OMe Y = Z = H
10*b* R = X = Y = Z = H

Bubbling oxygen into solutions containing the anions of **7***a* and **7***b* and reduction of the hydroperoxy intermediates gave the C7 ketones **8***a* and **8***b* (55% and 50%, respectively). The phenylthio residues were smoothly oxidized to the sulfoxides (**9***a* and **9***b*) but when the latter were treated with trifluoroacetic anhydride, Pummerer rearrangement led to the enolthio-ethers **10***a* and **10***b*. Hydrolysis of these vinyl ethers under the influence of titanium tetrachloride gave the diketones **11***a* and **11***b*. The phenol **2***a* arising from the demethylation of **11***a* (**2***b*) gave spectra identical in all respects with those of the natural product, 3,7-diketo-12-hydroxyabieta-8,11,13-triene (now named nimosone (*4a*) provided by Dr. Yu-Shia Cheng (8). The synthetic product was racemic of course.

To continue towards candelabrone **1***a* it had been hoped that **2***a* could be oxidized to the *o*-quinone but neither Fremy's salt, salcomine, nor phenylselenenic anhydride afforded any recognisable products. This suggested that the only route to candelabrone would be to place the aromatic substituents from the outset. The necessary trimethoxy-isopropylphenylacetonitrile **15***a* was prepared from methyl 2,6-dimethoxybenzoate **12***a* via di-*O*-methyl-2-isopropylresorcinol **12***d* (Grignard, dehydration, and hydrogenation). After methylation of the phenol **13***a* obtained by *m*-CPBA oxidation of **12***d*, the product **13***b* was brominated exclusively to the 1,2,4-trimethoxy-5-bromo derivative **13***c* and then the same steps used to prepare **4** were followed (Grignard → **13***d*, reduction → **13***e*, substitutions → **13***f*, and then **15***a*). The nitrile **15***a* was readily alkylated with geranyl bromide **3** to form the diene **5***c* (yield 97%).

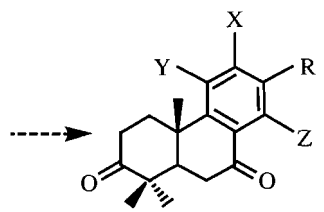

11*a* R = isoPr X = OMe Y = Z = H
11*b* R = X = Y = Z = H

11*d* R = isoPr X = OMe Z = OH Y = H

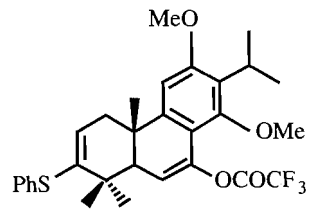

17

When subjected to the cyclization reaction none of the tricyclic product **7***c* was obtained, not even when the more efficient Ph-S-O-CH_2-CH_2-O-CH_3 was used in conjunction with BF_3/CH_3NO_2 (see footnote 2). The activation afforded by a methoxyl group *ortho* to the site of ring closure is apparently offset by the two *meta* effects and the steric crowding on the aromatic ring.

Some indication of the relative importance of the elec-

[2]T. Livinghouse. Private communication.

Can. J. Chem. Downloaded from www.nrcresearchpress.com by 217.78.4.112 on 09/08/12
For personal use only.

tronic and steric factors that prevented the cyclization could be inferred from the reaction of the dimethoxy analog **5***d*. It is well known that the 11-position in tricyclic compounds such as **2***b* is resistant to Friedel–Crafts acylation and forcing such reactions leads to C13 *ipso* substitution and the replacement of the isopropyl by the acyl moiety (10). The diene **5***c* must be unable to assume the appropriate geometry for synchronous cyclization as shown in **16***c* whereas the absence of the methoxyl in **5***d* could allow such a pretransition regrouping (**16***d*).

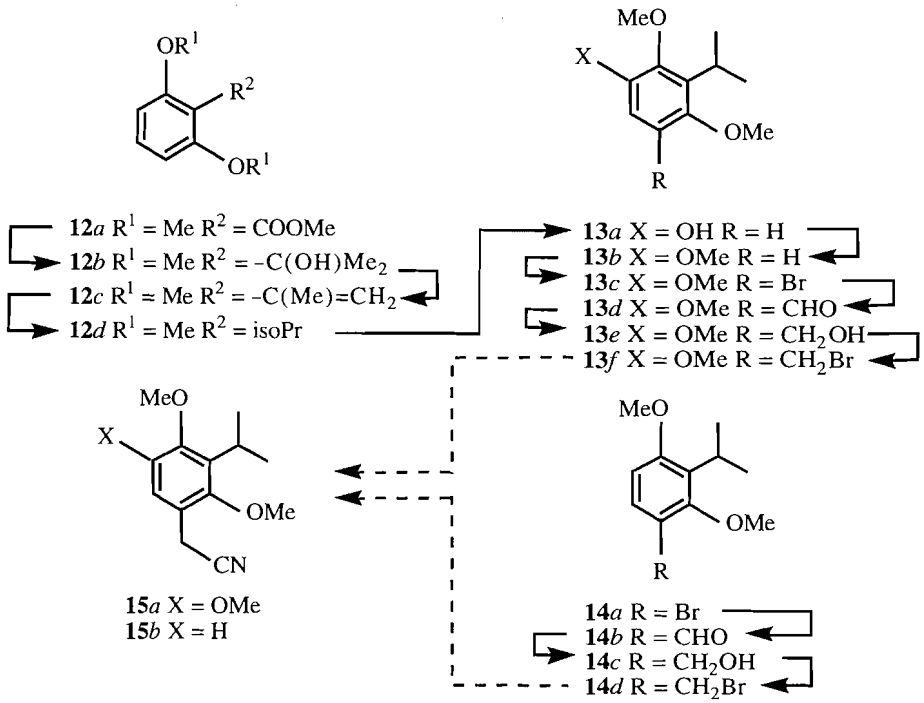

The diene **5***d* was prepared from the dimethoxyisopropylbenzene **12***d* using the same sequence as in the synthesis of **4**(**14***a* → **14***b* → **14***c* → **14***d* → **15***b*) and finally **15***b* was coupled with geranyl bromide **3**. After methyl benzenesulfenate provoked cyclization several products were present and spectral evidence suggested some structures in which only the A ring had closed during the reaction. The product from double annelation **7***d* was isolated in 41% yield and despite numerous attempts this could never be improved. The subsequent reactions proceeded almost normally. The carbonyl at C7 was introduced using the same conditions that had lead to **8***a* and **8***b* and high yields were obtained of the sulfoxide **9***d*. The product isolated after treating the latter with trifluoroacetic anhydride was actually the enol trifluoracetate **17**. As expected, the final reaction (hydrolysis with $TiCl_4$) not only established the C3 carbonyl but also hydrolysed the methoxyl *peri* to the conjugated ketone to give the chelated **11***d*.

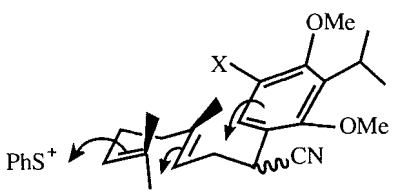

16*c* X = OMe
16*d* X = H

In conclusion one can say that, not surprisingly, this type of cyclization is seriously hampered by increasing substitution on the aromatic ring. As demonstrated by the synthesis of the natural product **2***a*, the approach is excellent for less-substituted members of this class of terpenes.

Experimental

Unless otherwise stated, the conditions used to characterize the products were as follows: melting points, Electrothermal, uncorrected; ultraviolet spectra, λ_{max} ethanol solutions (ϵ in parentheses), Perkin–Elmer Lambda 5; infrared spectra, carbon tetrachloride solutions, Mattson Sirius 100 FTIR; 200 MHz proton and 50 MHz carbon-13 magnetic resonance spectra, deuteriochloroform solutions (multiplicity, integrated peak areas, coupling constants in hertz and where necessary, assignments in parentheses), "dis. D_2O" signifies that the peak in question disappeared on shaking the solution with a small volume of D_2O, Varian XL-200 (300 MHz spectra courtesy of Prof. D. J. Burnell, Memorial University, Newfoundland; 400 MHz spectra were performed at the Laboratoire régional de RMN à haut champ, Université de Montréal); mass spectra, Hewlett Packard 5992 and Exact Mass measurements at the Centre régional de spectrométrie de masse, Université de Montréal. Chromatography implies the use of Terochem silica gel (for flash chromatography) with the solvents determined by prior thin-layer chromatography using DC-Alufolien Kieselgel 60 F_{254} precoated aluminium sheets. Reactions were normally carried out under nitrogen or argon. Elemental analyses were by Galbraith Laboratories, Knoxville, Tenn.

Simple products are numbered according to normal rules but for easier comparison, the dienes **5***a–d* and all subsequent compounds are numbered as tricyclic diterpenes. For ^{13}C figures, all skeletal carbons are listed first and after "and" all the peripheral groups are given (Me-O, Ph-S, CN, etc.). The assignments result

Can. J. Chem. Downloaded from www.nrcresearchpress.com by 217.78.4.112 on 09/08/12
For personal use only.

Can. J. Chem. Downloaded from www.nrcresearchpress.com by 217.78.4.112 on 09/08/12
For personal use only.

from COSY, HETCOR, and APT experiments, which are not described in the text.

Preparation of nitrile ***4***

Bromination of o-*isopropylanisole* ***6***a

Following the procedure of Srebnik *et al.* (11), KBr (82.01 g; 0.69 mmol), 18-crown-6 (4.29 g), and the isopropylanisole ***6a*** (21.45 g; 0.143 mmol) were suspended in vigorously stirred CH_2Cl_2(300 mL) under argon and cooled to 0°C. *m*-CPBA (58.82 g of 80%; 0.272 mmol) in CH_2Cl_2(160 mL) was slowly added and stirring continued for 30 min. The mixture was poured into ether (800 mL) and washed with 10% aqueous sodium bisulfite (400 mL), saturated $NaHCO_3$, saturated NaCl, and dried. After concentration, the residue was chromatographed (pet. ether) to give *4-bromo-2-isopropylanisole* ***6b*** (27.57 g; 84%): ^{1}Hmr δ: 1.21 (d, 6H, J = 7.0 Hz), 3.29 (q, 1H, J = 7.0 Hz), 3.81 (s, 3H), 6.71 (d, J = 8.6 Hz), 7.25 (dd, J = 8.6 and 2.3 Hz), and 7.29 (d, J = 2.3 Hz); ^{13}Cmr δ: 155.7, 139.2, 129.0, 112.9, 129.0, 111.9, 26.8, 22.5, and 55.5; mass *m/z*: 230 (9), 228(8), 215(17), 213(18), 104(12), 91(38), 83(100), and 77(35).

Grignard reaction to give aldehyde ***6***c

The Grignard reagent was prepared from the bromo derivative ***6b*** (5.01 g; 21.9 mmol) and magnesium (0.817 g) in anhydrous THF (30 mL) in the usual manner. To the cooled mixture was added dropwise anhydrous DMF (8.50 mL; 115 mmol) and after the vigorous reaction had subsided the solution was refluxed for 5 min, cooled, and then treated with saturated NH_4Cl (50 mL). The oil obtained by ether extraction was chromatographed (pet. ether/ether 7:1) to give the *4-methoxy-3-isopropylbenzaldehyde* ***6c*** (3.80 g; 98%): ir: 1690 cm^{-1}; ^{1}Hmr δ: 1.20 (d, 6H, J = 7.0 Hz), 3.29 (q, 1H, J = 7.0 Hz), 3.86 (s, 3H), 6.90 (d, J = 8.6 Hz), 7.66 (dd, J = 8.6 and 2.3 Hz), 7.72 (d, J = 2.3 Hz), and 9.83 (s, 1H); ^{13}Cmr δ: 161.7, 137.7, 130.3, 129.5, 126.8, 109.9, 190.9, 26.5, 22.3, 22.3, and 55.5; mass *m/z*: 178(47), 163(100), 147(18), 135(20), 120(11), 105(35), 103(18), 91(25), and 77(36). Exact Mass (showed that the aldehyde had oxidized to the acid during transport) calcd. for $C_{11}H_{14}O_3$: 194.0919; found: 194.0931.

Reduction of the aldehyde ***6***c

Excess $NaBH_4$ 2.05 g; 54 mmol) was added to the aldehyde ***6c*** (8.68 g; 48.8 mmol) in MeOH (125 mL) at 0°C. After stirring 12 min, water was added and the product extracted into ether, *2-isopropyl-4-hydroxymethylanisole* ***6d*** (8.53 g; 97%) sufficiently pure for the next step: ir: 3550–3100 (br OH) cm^{-1}; ^{1}Hmr δ: 1.21 (d, 6H, J = 6.6 Hz), 2.05 (br s, dis. D_2O), 3.33 (q, J = 6.6 Hz), 3.83 (s, 3H), 4.59 (s, 2H, 2H-C7), 6.83 (d, J = 8.2 Hz), 7.15 (dd, J = 8.2 and 2.3 Hz), and 7.22 (d, J = 2.3 Hz); ^{13}Cmr δ: 156.2, 137.0, 125.2, 132.8, 125.5, 110.2, 65.2, 26.7, 22.7, 22.7, and 55.4.

Formation of the benzyl bromide ***6***e

Based on the procedure of Hess and co-workers (12) the alcohol ***6d*** (4.88 g; 27.1 mmol) was dissolved in benzene (180 mL) under argon. Pyridine (1.25 mL; 15.5 mmol) was added followed by PBr_3 (2.60 mL; 14.3 mmol) dropwise, which resulted in the appearance of a white precipitate. The mixture was stirred for 3 h and then water (50 mL) was added and the product obtained by extraction, *2-isopropyl-4-bromomethylanisole* ***6e*** (6.47 g; 98%), which was used without further purification in the next step: ^{1}Hmr δ: 1.28 (d, 6H, J = 7.0 Hz), 3.36 (q, 1H, J = 7.0 Hz), 3.86 (s, 3H), 4.56 (s, 2H, 2H-C7), 6.84 (d, J = 8.1 Hz), 7.25 (dd, J = 8.1 and 2.2 Hz), and 7.29 (d, J = 2.2 Hz); ^{13}Cmr δ: 156.7, 137.2, 126.9, 127.3, 110.2, 34.6, 26.8, 22.5, and 55.3; mass *m/z*: 244(2) and 242(2), 163(100), 148(10), 133(23), 91(8), and 77(10). Exact Mass calcd. for $C_{11}H_{15}O^{79}Br$: 242.0344; found: 242.0325.

Substitution to give nitrile ***4***

As suggested by Liotta and co-workers (13) the bromide ***6e*** (3.16 g; 13.01 mmol) and 18-crown-6 (0.586 g) were dissolved in CH_3CN (12 mL). After adding KCN (4.76 g; 73.5 mmol) the suspension was heated at 60°C for 1 h and the product extracted into ether and chromatographed (pet. ether/ether 6:1) giving *4-methoxy-3-isopropylphenylacetonitrile* ***4*** (2.83 g: 80%): ir: 2250 cm^{-1}; ^{1}Hmr δ: 1.22 (d, 6H, J = 7.0 Hz), 3.33 (q, 1H, J = 7.0 Hz), 3.67 (s, 2H, CH_2CN), 3.82 (s, 3H), 6.83 (J = 9.0 Hz), 7.10 (dd, J = 9.0 and 2.5 Hz), and 7.14 (d, J = 2.5 Hz); ^{13}Cmr δ: 137.6, 125.5, 130.3, 156.2, 110.5, 125.8, 22.8, 121.4, 26.7, 22.4, 22.4, and 55.3; mass *m/z*: 189(18), 174(100), 159(10), 147(12), 134(24), 131(12), 130(11), 117(38), 115(32), 104(28), 103(32), 91(52), and 77(63). Exact Mass calcd. for $C_{12}H_{15}NO$: 189.1154; found: 189.1185.

In the absence of the crown ether (KCN, DMSO, 85°C) the yield was only 67%.

Alkylation of nitrile ***4*** *with geranyl bromide* ***3***

Under argon, THF (40 mL) containing diisopropylamine (2.00 mL; 14.3 mmol) was cooled to −78°C and *n*-butyllithium (5.21 mL of 2.5 M in hexane; 13.0 mmol) was introduced dropwise. The mixture was allowed to warm to 0°C for 15 min and then recooled to −78°C before adding the nitrile ***4*** (2.487 g; 13.2 mmol) in THF (30 mL). After stirring for 5 min, geranyl bromide (2.65 mL; 13.4 mmol) was added and the temperature allowed to rise to ambient as stirring was continued for 3 h. The mixture was poured onto ice and extracted with ether. The liquid left after concentration was chromatographed (pet. ether) to afford the *2-geranyl-2-(3-isopropyl-4-methoxyphenyl)acetonitrile* ***5a*** (3.635 g; 85%) as a colorless oil: ir: 2240 cm^{-1}; ^{1}Hmr (400 MHz) δ: 1.21 (d, 6H, J = 6.9 Hz, iso-Pr methyls), 1.55 (s, 3H, Me_{trans}-C4), 1.61 (s, 3H, C10-Me), 1.69 (s, 3H, Me_{cis}-C4), 2.05 (m, 4H, H-C1 and C2), 2.57 (m, 2H, H-C6), 3.31 (t, 1H, J = 6.9 Hz, iso-Pr CH), 3.72 (t, 1H, J = 7.0 Hz, CH-CN), 3.83 (s, 3H, Me-O), 5.08 (t, 1H, J = 6.6 Hz, H-C3), 5.20 (t, 1H, J = 7.2 Hz, H-C5), 6.82 (d, 1H, J = 7.9 Hz, H-C11), 7.11 (d, 1H, J = 2.4 Hz, H-C14), and 7.13 (dd, 1H, J = 7.9 and 2.4 Hz, H-C9); ^{13}Cmr δ (carbons numbered as in the cyclized diterpene): 39.6, 26.5, 123.9, 131.5, 118.6, 34.4, 37.2, 127.9, 125.1, 139.8, 110.4, 156.4, 137.5, 125.4, 26.8, 22.5, 22.5, 17.6, 16.2, 25.6, and 55.4, and 121.2(CN); mass *m/z*: 325(M^+, 1.4), 190(12), 189(100), 156(23), 137(14), 91(5), 81(20), and 77(6). Exact Mass calcd. for $C_{22}H_{31}NO$: 325.2406; found: 325.2415.

Cyclization of diene ***5***a

Based on the Livinghouse conditions,[2] a solution of methyl benzenesulfenate (0.126 g; 0.875 mmol, prepared from diphenyldisulfide following the methods of Mueller and Butler (14) and Denny and co-workers (15), in $MeNO_2$ (11.9 mL) was cooled to −30°C under argon. Previously prepared $BF_3/MeNO_2$ (1.34 mL of 1.24 M) was added and after stirring 2.5 min the diene ***5a*** (0.207 g; 0.817 mmol) was added in $MeNO_2$ (2 mL) and stirring was continued for 2 h at −30°C. Saturated $NaHCO_3$ (20 mL) was introduced and once the mixture had warmed to room temperature, it was extracted with ether and washed with $NaHCO_3$, NaCl, water, and again with NaCl. The dried solution ($MgSO_4$) was concentrated and the residue chromatographed (pet.ether/ether 6:1) to give the cyclized product ***7a*** (0.224 g; 76%), mp 194–195°C, *7-cyano-3-phenylthio-12-methoxyabieta-8,11,13-triene*: ir: 2227 cm^{-1}; ^{1}Hmr (300 MHz) δ: 1.02 (s, 3H, Me_α-C4), 1.18 and 1.19 (2d, 6H, J = 6.9 Hz, iso-Pr methyls), 1.23 (s, 3H, Me_β-C4), 1.40 (s, 3H, Me-C10), 1.51 and 2.25 (2m, H-C1), 1.76 (dd, 1H, J = 11.9 and 1.2 Hz, H-C5), 2.04 (m, 2H, H-C6), 2.02 and 2.25 (2m, 2H, H-C2), 2.95 (dd, 1H, J = 9.1 and 7.7 Hz, H-C3), 3.21 (sept, 1H, J = 6.9 Hz, H-C15), 3.77 (s, 3H, Me-O), 4.06 (d, 1H, J = 5.2 Hz, H-C7), 6.65 (s, 1H, H-C11), 7.01 (s, 1H, H-C14), 7.25 (m, 3H, *meta* and *para* H of Ph-S), and 7.40 (m, 2H, *ortho* H of Ph-S); ^{13}Cmr (75 MHz) δ: 38.7, 23.9, 60.3, 38.1, 49.6, 24.5, 31.9, 122.4, 147.2, 37.9, 106.7, 156.8, 135.8, 126.7, 26.5, 22.5, 22.4, 29.5, 27.7, 17.9 and 55.3, 119.3(CN), 136.2, 131.4, 128.9, 126.5(*ipso*,*ortho*,*meta*, and *para* C of Ph-S); mass *m/z*: 433(M^+, 16), 309(12), 308(52), 255(37), 254(19), 241(19), 240(41), 229(35), 228(100), 227(31), 226(32), 185(25), 110(41), and 97(23). Exact Mass calcd. for $C_{28}H_{35}NOS$: 433.2269; found: 433.2354.

Can. J. Chem. Downloaded from www.nrcresearchpress.com by 217.78.4.112 on 09/08/12
For personal use only.

Preparation of model diene **5**b

Using exactly the same procedure as described for **5***a*, phenylacetonitrile (5.80 g) was alkylated with geranyl bromide (9.83 mL) to afford the diene **5***b*, *2-geranyl-2-phenylacetonitrile* (11.59 g; 92%); ir: 2242 cm^{-1}; ^{1}Hmr δ: 1.53 (s, 3H, Me_{trans}-C4), 1.61 (s, 3H, Me-C10), 1.70 (s, 3H, Me_{cis}-C4), 2.04 (m, 4H, H-C1 and C2), 2.61 (m, 2H, H-C6), 3.78 (t, 1H, J = 7.0 Hz, CH-CN), 5.09 (m, 1H, =C3-H), 5.20 (t, 1H, J = 7.3 Hz, =C5-H), and 7.35 (br s, 5H, arom. H); ^{13}Cmr δ: 39.6, 26.4, 123.8, 131.4, 118.2, 34.3, 37.7, 135.5, 127.2, 140.0, 128.7, 127.8, 127.2, 17.7, 16.1, 25.7, and 120.6(CN); mass *m/z*: 253(M^+, 8), 210(9), 138(9), 137(82), 124(14), 117(64), 116(100), 89(24), 81(42), and 77(10). Exact Mass calcd. for $C_{18}H_{23}N$: 253.1783; found: 253.1807.

Cyclization of **5**b *to* **7**b

As described for **9***a*, the diene **5***b* (5.06 g) reacted with Ph-SOMe to afford **7***b*, *9-cyano-2-phenylthio-1,1,4a-trimethyl-1,2,3,4,4a,9,10,10a-octahydrophenanthrene* (4.475 g; 62%) as a white foam: ir: 2239 cm^{-1}; ^{1}Hmr (300 MHz) (numbered as a desisopropyl abietatriene) δ: 1.02 (s, Me_α-C4), 1.25 (s, Me_β-C4), 1.32 (s, Me-C10), 1.45 and 2.40 (2m, 2H, H-C1), 1.74 (dd, J = 12.0 and 1.7 Hz, H-C5), 2.01 (m, 2H, H-C6), 2.01 and 2.40 (2m, 2H, H-C2), 2.85 (t, J = 8.2 Hz, CH-SPh), 4.09 (m, 1H, CH-CN), 7.20 (m, 6H), and 7.38 (m, 3H, arom H); ^{13}Cmr δ: 38.5, 23.7, 60.3, 37.7, 49.3, 27.6, 32.7, 127.4, 148.4, 37.6, 125.4, 128.8, 126.5, 128.3, 29.8, 24.9, 17.6 and 121.9(CN), 121.9, 136.2, 131.4, 128.8, 126.4(-S-Ph); mass *m/z*: 361(M^+, 27), 252(34), 237(16), 236(76), 183(24), 182(32), 169(22), 168(53), 167(20), 157(20), 156(100), 142(36), 141(30), 129(30), 110(60), and 109(49). Exact Mass calcd. for $C_{24}H_{27}NS$: 361.1786; found: 361.1825.

Oxidation of **7**a *to the C7 ketone* **8**a

This procedure is based on that of Selikson and Watt (16). Diisopropylamine (0.27 mL; 1.9 mmol) and THF (10 mL) were cooled to −78°C under argon and *n*-butyllithium (0.75 mL of 2.5 M in hexane; 1.9 mmol) was added. The solution was allowed to warm to 0°C and then cooled to −78°C again before adding the nitrile **7***a* (0.526 g; 1.21 mmol) in THF (20 mL). After stirring for 5 min, a gentle stream of purified oxygen was passed through the solution for 1 h. The mixture was then warmed to 0°C and a solution of 1 M $SnCl_2$/2 M HCl (4 mL) was added and after stirring for 30 min the product was obtained by ether extraction. The ether was well washed with 1 M NaOH and saturated NaCl and dried, and the solid left on concentration was chromatographed (pet.ether/ether 6:1) to give the ketone **8***a* (0.276 g; 55%), *7-oxo-3-phenylthio-12-methoxyabieta-8,11,13-triene*, mp 130–132°C: uv: 205(28 900), 227(21 300), and 277(15 200) nm, ir: 1671 cm^{-1}; ^{1}Hmr δ: 1.09 (s, Me_α-C4), 1.19 and 1.21 (2d, 6H, J = 7.0 Hz, iso-Pr Me), 1.28 (s, 6H, Me_β-C4 and Me-C10), 1.65 (m, 1H, H_α-C1), 1.99 (dd, J = 11.7 and 5.9 Hz, H-C5), 2.07 (m, 2H, H-C2), 2.33 (dt, J = 12.8 and 3.3 Hz, H_β-C1), 2.71 (d, 1H, J = 11.7 Hz, H_β-C6), 2.73 (d, 1H, J = 5.9 Hz, H_α-C6), 2.89 (m, 1H, H-C3), 3.24 (sept, 1H, J = 7.0 Hz, iso-Pr CH), 3.85 (s, 3H, Me-O), 6.68 (s, 1H, H-C11), 7.27 (m, 3H) and 7.42 (m, 2H, S-Ph protons), and 7.89 (s, 1H, H-C14); ^{13}Cmr δ: 38.2, 27.4, 60.5, 38.4, 51.0, 36.4, 197.5, 123.6, 155.2, 38.1, 104.3, 161.5, 135.3, 125.3, 26.7, 22.3, 22.4, 29.3, 23.1, 17.4, and 55.3, 136.2, 131.4, 128.8, 126.4 (S-Ph carbons); mass *m/z*: 422(M^+, 11), 313(17), 297(29), 271(17), 245(34), 243(26), 217(100), 215(29), 203(25), 110(44), and 109(38). Exact Mass calcd. for $C_{27}H_{34}O_2S$: 422.2287; found: 422.2283.

NOTE: Using the MoOPh reagent (17) afforded the same product but in only 48% yield.

Oxidation to the model C7 ketone 8b

As described above, the model **7***b* (1.092 g) was treated with oxygen under basic conditions to afford the ketone **8***b* (0.529 g; 50%), amorphous solid, *9-keto-3-phenylthio-1,1,4a-trimethyl-1,2,3,4,4a,9,10,10a-octahydrophenanthrene*; uv: 205(40 400) and 253(19 400) nm; ir: 1682 cm^{-1}; ^{1}Hmr δ: 1.10 (s, 3H), 1.29 (s, 3H), 1.57 (m, 1H), 1.98 (dd, 1H, J = 11.7 and 5.9 Hz), 2.06 (m, 2H), 2.36 (dt, 1H, J = 12.9 and 3.5 Hz), 2.76 (d, 1H, J = 11.7 Hz), 2.78 (d, 1H, J = 5.9 Hz), 2.92 (m, 1H), 7.32 (m, 8H) 8.01 (dd, J = 7.4 and 1.6 Hz, arom H adjacent to ketone); ^{13}Cmr δ: 38.2, 27.5, 60.5, 38.4, 50.7, 36.6, 198.6, 130.4, 155.0, 38.1, 123.6, 134.0, 126.5, 127.2, 29.3, 23.3, 17.4 and 136.2, 131.5, 128.8, 126.2; mass *m/z*: 350(M^+, 29), 241(45), 226(17), 225(100), 199(21), 185(11), 181(12), 173(47), 171(69), 157(44), 145(99), and 109(38). Exact Mass calcd. for $C_{23}H_{26}OS$: 350.1690; found: 350.1697.

Oxidation of the thio-ether **8**a *to the sulfoxide* **9**a

To the thio-ether **8***a* (0.466 g; 1.10 mmol) in CH_2Cl_2 (10 mL) at −78°C under argon, was added *m*-CPBA (0.640 g; 2.97 mmol) as a suspension in CH_2Cl_2 (5 mL). After stirring for 1 h, saturated $NaHSO_3$ (10 mL) was added and the temperature allowed to rise to ambient. Ether extraction, washing with saturated $NaHSO_3$, saturated $NaHCO_3$, and saturated NaCl, drying, and concentrating gave a solid that was chromatographed (ether) to afford the sulfoxide **9***a* (0.443 g; 92%), *7-keto-3-phenylsulfinyl-12-methoxyabieta-8,11,13-triene*, mp 187–189°C: ir: 1672 cm^{-1}; ^{1}Hmr δ: 1.13 (2d, 6H, J = 6.6 Hz, iso-Pr Me), 1.24 (s, 3H, Me_α-C4), 1.31 (s, 3H, Me_β-C4), 1.37 (s, 3H, Me-C10), 1.50 (m, 2H, H_α-C1 and H-C2), 1.85 (dd, 1H, J = 11.0 and 6.6 Hz, H-C5), 2.15 (m, 2H, H-C2 and H-C3), 2.39 (m, 1H, H_β-C1), 2.67 (d, 1H, J = 11.0 Hz, H_β-C6), 2.68 (d, 1H, J = 6.6 Hz, H_α-C6), 3.17 (sept, 1H, J = 6.6 Hz, iso-Pr CH), 3.78 (s, 3H, O-Me), 6.60 (s, 1H, H-C11), 7.49 (m, 5H, S(O)-Ph protons), and 7.82 (s, 1H, H-C14); ^{13}Cmr δ: 36.9, 30.3, 75.2, 38.1, 51.0, 35.5, 197.0, 123.5, 154.7, 37.4, 104.3, 161.5, 135.5, 125.4, 26.4, 22.3, 22.4, 22.8, 18.3, 13.6 and 55.3, 143.5, 123.9, 128.8, 130.1(S(O)-Ph carbons); mass *m/z*: facile elimination of Ph-S(O) resulted in no molecular ion, 314(16), 313(70), 312(18), 297(36), 271(24), 245(48), 243(25), 231(31), 230(50), 229(56), 217(100), 215(98), 173(26), 128(38), 126(70), 109(36), and 78(70).

Model sulfoxide **9**b

Similar oxidation of **8***b* (0.911 g) with *m*-CPBA afforded the sulfoxide **9***b* (0.812 g: 85%): ir: 1677 cm^{-1}; ^{1}Hmr δ: 1.26 (s, 3H), 1.34 (s, 3H), 1.39 (s, 3H), 1.53 (m, 2H), 1.90 (dd, 1H, J = 11.0 and 6.6 Hz), 2.17 (m, 2H), 2.44 (dd, 1H, J = 9.9 and 3.2 Hz), 2.74 (d, 1H, J = 11.0 Hz), 2.76 (d, 1H, J = 6.6 Hz), 7.2 to 7.3 (m, 2H), 7.4 to 7.56 (m, 6H), and 7.97 (dd, 1H, J = 7.7 and 1.5 Hz); ^{13}Cmr δ: 36.7, 30.2, 75.1, 37.9, 50.6, 35.7, 198.1, 130.2, 154.4, 37.4, 123.6, 134.0, 126.3, 127.2, 23.0, 18.3, 13.6 and 143.5, 123.9, 128.8, 130.1; mass *m/z*: no molecular ion, 242(18), 240(100), 225(27), 223(11), 199(15), 185(16), 173(38), 172(11), 171(57), 159(33), 158(41), 157(47), 145(88), 128(50), and 115(35). Exact Mass calcd. for $C_{25}H_{26}O_2S$: 366.1532; found: 366.1593.

Formation of the enol thioether **10**a

Using the Matsumoto method (18), the sulfoxide **9***a* (0.251 g; 0.574 mmol) in CH_2Cl_2 (10 mL) at 0°C under argon was treated with trifluoroacetic anhydride (0.81 mL; 5.7 mmol) and pyridine (1.16 mL). After stirring at room temperature for 5 h, water (25 mL) was added slowly and the product, extracted and washed (H_2O, saturated $NaHCO_3$, H_2O, dilute HCl, saturated NaCl), was chromatographed (pet.ether/ether 10:1) to afford the enol ether **10***a* (0.174 g; 72%), white solid mp 183–184°C, *7-keto-3-phenylthio-12-methoxyabieta-2,8,11,13-tetraene*: ^{1}Hmr δ: 1.19 (s, 3H, Me_β-C4), 1.20 and 1.22 (2d, 6H, J = 7.0 Hz, iso-Pr Me), 1.22 (s, 3H, Me_α-C4), 1.39 (s, 3H, Me-C10), 2.30 (t, 1H, J = 8.8 Hz, H-C5), 2.42 (dd, 1H, J = 17.2 and 1.8 Hz, H_α-C1), 2.69 (d, 2H, J = 8.4 Hz, H-C6), 2.79 (dd, 1H, J = 17.2 and 6.6 Hz, H_β-C1), 3.25 (sept, 1H, J = 6.96 Hz, iso-Pr CH), 3.87 (s, 3H, O-Me), 5.92 (dd, 1H, J = 6.6 and 1.8 Hz, H-C2), 6.71 (s, 1H, H-C11), 7.24 (m, 3H) and 7.42 (m, 2H, S-Ph protons), and 7.91 (s, 1H, H-C14); ^{13}Cmr δ: 40.8, 130.2, 141.6, 40.0, 48.1, 36.8, 197.1, 123.6, 153.4, 37.1, 105.5, 161.8, 135.8, 124.9, 26.6, 22.5, 22.4, 29.6, 23.0, 21.2 and 55.4, 136.9, 130.2, 128.8, 126.3(S-Ph carbons); mass *m/z*: 420(M^+, 40), 257(16), 230(23), 229(17), 228(13), 227(17), 217(35), 216(28), 215(100), 203(20), 190(74), 175(63), 115(55),

Can. J. Chem. Downloaded from www.nrcresearchpress.com by 217.78.4.112 on 09/08/12
For personal use only.

108(70), and 86(83). Exact Mass calcd. for $C_{27}H_{32}O_2S$: 420.2163; found: 420.2143.

Transformation of model sulfoxide **9**b *to thio-enol-ether* **10**b

In the same manner, the sulfoxide **9***b* (19 mg) reacted with TFAA and pyridine to give the enol ether **10***b* (15 mg: 83%): ir: 1685 cm^{-1}; ^{1}Hmr δ: 1.20, 1.23 and 1.39 (3s, each 3H), 2.32 (t, 1H, J = 8.4 Hz), 2.39 (dd, 1H, J = 17.6 and 1.8 Hz), 2.75 (d, 2H, J = 8.4 Hz), 2.81 (dd, 1H, J = 17.6 and 6.6 Hz), 5.92 (dd, 1H, J = 6.6 and 2.2 Hz), 7.1–7.6 (m, 5H), 7.55 (ddd, 1H, J = 7.7, 7.7, and 1.5 Hz), and 8.06 (dd, 1H, J = 7.7 and 1.5 Hz); ^{13}Cmr δ: 40.7, 130.4, 141.4, 40.0, 47.8, 37.0, 198.1, 130.3, 153.2, 38.7, 125.3, 134.3, 126.4, 126.8, 29.5, 23.2, 21.1 and 138.6, 130.2, 128.8, 126.4; mass m/z: 348(M^+, 57), 209(10), 191(16), 190(58), 189(19), 179(23), 175(60), 165(36), 158(52), 145(31), 141(31), 129(56), 115(100), 109(59), and 79(59). Exact Mass calcd. for $C_{23}H_{24}OS$: 348.1474; found: 348.1511.

Formation of the 3,7-diketone **11**a

Based on the method of Trost *et al.* (19), $TiCl_4$ (0.78 mL; 7.3 mmol) was added to a suspension of the enol ether **10***a* (0.749 g; 1.78 mmol) in glacial HOAc (10 mL). The orange mixture was stirred for 20 min, then diluted with water (2.40 mL) and refluxed for 1 h. After cooling, the product was obtained by dilution with more water, extraction, washing, and chromatography (pet. ether/ether 1:1), white solid, mp 150–151°C, *3,7-diketo-12-methoxyabieta-8,11,13-triene* **11***a*: uv: 207(15 800), 230(16 200), and 280(13 200) nm; ir: 1710 and 1671 cm^{-1}; ^{1}Hmr δ: 1.12 (s, 3H, Me_α-C4), 1.18 (s and 2d, 9H, J = 7.0 Hz, Me_β-C4 and iso-Pr Me), 1.44 (s, 3H, Me-C10), 2.02 (dt, 1H, J = 13.2 and 5.1 Hz, H_β-C1), 2.30 (dd, 1H, J = 13.6 and 4.0 Hz, H-C5), 2.58 (dd, 1H, J = 17.6 and 4.0 Hz, H_β, H_β-C6), 2.75 (dd, 1H, J = 17.6 and 13.6 Hz, H_α-C6), 2.53 (ddd, 1H, J = 17.9, 5.1, and 2.9 Hz, H_β-C2), 2.81 (m, 1H, H_α-C2), 2.88 (m, 1H, H_α-C1), 3.23 (sept, 1H, J = 7.0 Hz, iso-Pr CH), 3.88 (s, 3H, O-Me), 6.69 (s, 1H, H-C11), and 7.89 (s, 1H, H-C14); ^{13}Cmr δ: 36.9, 34.5, 214.1, 47.3, 49.6, 36.1, 196.7, 123.6, 153.5, 37.8, 104.7, 161.7, 136.0, 125.6, 26.6, 22.5, 22.4, 25.0, 22.6, 21.5, and 55.5; mass m/z: 328(M^+, 69), 313(100), 271(13), 257(13), 243(28), 232(23) < 229(29), 217(21), 215(39), 201(20), 175(20), and 125(52, typical of C3 ketones with 4,4-dimethyl grouping). Exact Mass calcd. for $C_{21}H_{28}O_3$: 328.2011; found: 328.2025.

Model diketone **11**b

Prepared from **10***b* (150 mg) by the procedure described above. After chromatography the *3,9-diketo-1,14a-trimethyl-1,2,3,4,4a,9,10,10a-octahydrophenanthrene* **11***b* (84 mg; 77%) was obtained as a white solid, mp 113–114°C; uv: 206(21 900), 250(10 900), and 291(1800) nm; ^{1}Hmr δ: 1.11 and 1.18 (2s, each 3H), 1.43 (δ, 3H, J = 1.1 Hz), 2.01 (ddt, 1H, J = 13.2, 5.5, and 1.1 Hz), 2.31 (dd, 1H, J = 13.6 and 4.4 Hz), 2.37 (m, 5H), 7.30 (m, 2H), 7.53 (ddd, 1H, J = 8.1, 7.7, and 1.4 Hz), and 8.00 (dd, 1H, J = 7.7 and 1.4 Hz); ^{13}Cmr δ: 36.9, 34.5, 214.0, 47.3, 49.6, 36.3, 197.7, 130.4, 153.3, 37.6, 124.0, 134.2, 126.7, 127.4, 25.0, 22.8, 21.4; mass m/z: 256(M^+, 100), 223(19), 213(21), 200(50), 199(86), 185(22), 171(52), 159(58), 145(40), 128(49), 125(58), 115(69), and 91(53). Exact Mass calcd. for $C_{17}H_{20}O$: 256.1458; found: 256.1461.

Demethylation to the (±) natural product **2**a

At 0°C under argon, BBr_3 (0.21 mL; 2.2 mmol) was introduced to a solution of diketone **13***a* (0.156 g; 0.476 mmol) in CH_2Cl_2 (2.0 mL). The temperature was allowed to rise to ambient and stirring was continued overnight. The mixture was diluted with water and extracted with ether, which was washed (water, aqueous sodium thiosulfate, saturated NaCl) and concentrated. Chromatography of the residue (pet. ether/ether 1:1) gave the phenol **2***a* (0.136 g; 91%), mp 190–191°C, unchanged by sublimation (lit. (8) mp 213–215°C), *3,7-diketo-12-hydroxyabieta-8,11,13-triene*: uv: 207(15 800), 233(14 300), and 290(12 200) nm; ir: 3500–3050(br OH), 1707, and 1684 cm^{-1}; ^{1}Hmr (400 MHz) δ: 1.14 (s, 3H, Me_α-C4), 1.21 (s, 3H, Me_β-C4), 1.25 (t, 6H, J = 7.0 Hz, isp-Pr Me), 1.43 (s, 3H, Me-C10), 1.97 (dt, 1H, J = 13.7 and 5.2 Hz, H_β-C1), 2.30 (dd, 1H, J = 13.8 and 3.7 Hz, H-C5), 2.51 (dd, 1H, J = 19.6 and 3.4 Hz, H_β-C2), 2.64 (dd, 1H, J = 17.7 and 3.7 Hz, H_β-C6), 2.78 (dd, 1H, J = 17.7 and 13.8 Hz, H_α-C6), 2.80 (m, 1H, H_α-C2), 2.88 (m, 1H, H_α-C1), 3.18 (sept, 1H, J = 7.0 Hz, iso-Pr CH), 6.52 (br s, 1H, OH – dis. D_2O), 6.71 (s, 1H-C11), and 7.93 (s, 1H-C14); ^{13}Cmr δ: 36.7, 34.6, 214.5, 47.4, 49.6, 36.2, 197.1, 124.0, 153.6, 37.4, 110.3, 158.7, 133.6, 126.8, 26.8, 22.4, 22.3, 25.0, 22.7, 21.6; mass m/z: 314(M^+, 41), 299(30), 258(13), 257(16), 243(12), 229(41), 218(52), 217(24), 216(18), 215(36), 203(21), 201(36), 187(24), and 125(100). Exact Mass calcd. for $C_{20}H_{26}O_3$: 314.1888; found 314.1885.

Direct comparison of the ^{1}Hmr spectrum with that of the natural product kindly provided by Dr. Yu-Shia Cheng (National Taiwan University, Republic of China) showed the two to be identical.

Synthesis of the trimethoxy diene **5**c

Grignard reaction on methyl 2,6-dimethoxybenzoate **12**a

Excess Grignard reagent was prepared from Mg (1.104 g) and CH_3I (4.1 mL) in ether (100 mL) and cooled to 0°C. The ester **12***a* (1.636 g) in ether (40 mL) was added dropwise and the mixture then refluxed for 10 min. After cooling, saturated NH_4Cl (150 mL) was added and the product obtained by ether extraction. Concentration and chromatography gave the *1,3-dimethoxy-(2-hydroxyisopropyl)benzene* **12***b* (1.531 g; 94%): ^{1}Hmr δ: 1.65 (s, 6H), 3.81 (s, 6H), 5.0 (br s, 1H, dis. D_2O), 6.59 (d, 2H, J = 8.1 Hz), and 7.14 (t, 1H, J = 8.1 Hz); ^{13}Cmr δ: 157.5, 124.0, 157.5, 105.8, 127.4, 105.8, 74.0, 30.9, and 56.0; mass m/z: 196(3), 181(100), 163(46), 151(39), 148(23), 135(48), 107(24), 105(33), 91(22), and 77(28).

Dehydration of the alcohol to **12**c

The alcohol **12***b* (12.29 g) was refluxed in glacial HOAc (75 mL) for 2 h. The cooled mixture was diluted with water (250 mL) and the ether extract was well washed with 10% NaOH, water, and saturated NaCl. The olefin (10.94 g; 98%) was obtained by evaporation of the dried solution followed by chromatography (pet.ether/ether 6:1), *1,3-dimethoxy-2-isopropenylbenzene* **12***c*: ^{1}Hmr δ: 2.08 (d, 3H, J = 1.5 Hz), 3.83 (s, 6H), 4.93 and 5.38 (2q, each 1H, J = 1.5 Hz), 6.61 (d, 2H, J = 8.4 Hz), and 7.22 (t, 1H, J = 8.4 Hz); ^{13}Cmr δ: 157.0, 115.5, 157.0, 103.9, 127.7, 103.9, 121.2, 138.9, 23.4, and 55.8; mass m/z: 178(100), 164(86), 163(86), 148(72), 147(75), 136(57), 135(68), 133(55), 131(48), and 120(35). Exact Mass calcd. for $C_{11}H_{14}O_2$: 178.0997; found: 178.0958.

Hydrogenation to 1,3-dimethoxy-2-isopropylbenzene **12**d

The alkene (1.056 g) was shaken in a Parr apparatus with 5% Pd/C (40 mg) in ether (40 mL) under hydrogen at 40 psi (1 psi = 6.89 kPa) for 19 h. The catalyst was filtered (Celite) and the ether evaporated to give the isopropyl derivative (1.036 g; 97%) pure enough for the next step: ^{1}Hmr δ: 1.40 (d, 6H, J = 7.0 Hz), 3.73 (sept, 1H, J = 7.0 Hz), 3.88 (s, 6H), 6.63 (d, 2H, J = 8.1 Hz), and 7.19 (t, 1H, J = 8.1 Hz); ^{13}Cmr δ: 158.5, 124.3, 158.5, 104.4, 126.4, 104.5, 24.1, 20.7, and 55.6; mass m/z: 180(23), 166(11), 165(100), 135(7), 105(13), and 91(9).

Hydroxylation to the compound **13**a

According to the Srebnik and Mechoulam procedure (20) the product **12***d* (1.527 g; 8.48 mmol) in CH_2Cl_2 (20 mL) was added to a stirred solution of *m*-CPBA (2.851 g; 13.22 mmol) in CH_2Cl_2 (50 mL) at 0°C under argon. After 5 h at room temperature more *m*-CPBA (0.805 g; 3.73 mmol) was added and stirring was continued for 2 h. The mixture was poured into aqueous $NaHSO_3$ (100 mL of 5%) and the product was extracted into ether and well washed ($NaHSO_3$, saturated $NaHCO_3$, and saturated NaCl). Concentration and chromatography (pet.ether/ether 6:1) gave first some unreacted **12***d* (0.370 g) and then the phenol **13***a* (0.812 g; 64% adjusted for the recuperated starting material), *1-3-dimethoxy-4-hydroxy-2-isopropylbenzene*: ^{1}Hmr δ: 1.35 (d, 6H, J = 7.0 Hz), 3.40 (sept, 1H, J = 7.0 Hz), 3.78 (s, 6H), 5.47 (br s, 1H, dis.

Can. J. Chem. Downloaded from www.nrcresearchpress.com by 217.78.4.112 on 09/08/12
For personal use only.

D_2O), 6.56 (d, 1H, J = 8.8 Hz), and 6.76 (d, 1H, J = 8.8 Hz); ^{13}Cmr δ: 145.1, 129.8, 152.7, 108.0, 112.1, 142.9, 25.9, 21.1, and 55.8, 61.8; mass *m/z*: 196(87), 181(100), 166(40), 133(15), 125(27), 123(12), 91(11), and 77(13). Exact Mass calcd. for $C_{11}H_{16}O_3$: 196.1099; found: 196.1101.

O-Methylation of the phenol ***13****a*

Methyl iodide (5.0 mL) was added to a solution of the phenol **13***a* (1.629 g) in acetone (150 mL) containing anhydrous K_2CO_3 (5.0 g) and the mixture was refluxed for 5 days after which it was cooled, filtered, and concentrated. The residue was lixiviated with warm ether and the latter well washed (water, saturated NaCl) and concentrated. Chromatography of the residue (pet.ether/ether 10:1) gave the *1,2,4-trimethoxy-3-isopropylbenzene* **13***b* (1.538 g; 88%): ^{1}Hmr δ: 1.34 (d, 6H, J = 7.0 Hz), 3.57 (sept, 1H, J = 7.0 Hz), 3.77 (s, 3H), 3.82 (s, 6H), 6.56 (d, 1H, J = 8.8 Hz), and 6.70 (d, 1H, J = 8.8 Hz); ^{13}Cmr δ: 147.7, 130.6, 152.7, 106.1, 109.4, 147.2, 25.2, 21.2, 21.2 and 55.8, 56.0, 60.9; mass *m/z*: 210(82), 195(100), 180(69), 165(25), 152(16), 137(28), 135(17), 105(12), 91(15), and 77(15). Exact Mass calcd. for $C_{12}H_{18}O_3$: 210.1256; found: 210.1268.

Bromination leading to ***13****c*

Using exactly the same conditions for the preparation of **6***b*, the trimethoxy compound **13***b* (5.321 g) gave *5-bromo-1,2,4-trimethoxy-3-isopropylbenzene* **13***c* (6.308 g; 88%): ^{1}Hmr δ: 1.32 (d, 6H, J = 7.3 Hz), 3.45 (sept, 1H, J = 7.3 Hz), 3.76, 3.80, and 3.82 (3s, 9H), and 6.92 (s, 1H); ^{13}Cmr δ: 148.9, 129.6, 149.9, 110.8, 114.1, 136.6, 26.8, 21.9, 21.9 and 56.0, 60.8, 61.5. Exact Mass calcd. for $C_{12}H_{17}O_3{}^{79}Br$: 288.0361; found: 288.0359.

Grignard reaction to give the benzaldehyde ***13****d*

As described for the reaction with **6***b*, the bromo compound **13***c* (6.308 g) was converted to the Grignard reagent and reacted with DMF to give the aldehyde **13***d* (4.626 g; 89%), *2,4,5-trimethoxy-3-isopropylbenzaldehyde*: ir: 1682 cm^{-1}; ^{1}Hmr δ: 1.33 (d, 6H, J = 7.0 Hz), 3.42 (sept, 1H, J = 7.0 Hz), 3.81, 3.84, and 3.90 (3s, 9H), 7.22 (s, 1H), and 10.25 (s, 1H, CHO); ^{13}Cmr δ: 155.1, 135.5, 156.8, 124.4, 107.7, 150.0, 189.1, 25.4, 21.6, 21.6 and 55.8, 60.8, 65.3; mass *m/z*: 238(M$^+$, 100), 223(97), 208(16), 205(26), 193(22), 180(24), 177(21), 166(27), 165(25), 147(20), 135(30), 91(36), and 77(35).

Reduction of the aldehyde ***13****d*

Sodium borohydride reduced the aldehyde **13***d* (1.864 g) as described earlier for **6***d*. The product (1.875; 100%) was isolated after 15 min and was pure enough to continue without further purification, *2,4,5-trimethoxy-3-isopropylbenzyl alcohol* **13***e*: ^{1}Hmr δ: 1.33 (d, 6H, J = 7.0 Hz), 2.15 (br s, 1H, dis. D_2O), 3.38 (sept, 1H, J = 7.0 Hz), 3.70, 3.82, and 3.83 (3s, 9H), 4.66 (s, 2H), and 6.78 (s, 1H); ^{13}Cmr δ: 149.4, 135.0, 149.5, 128.6, 110.1, 148.1, 61.3, 25.9, 21.9, 21.9 and 55.8, 60.7, 62.4; mass *m/z*: 240(M$^+$, 100), 225(18), 206(52), 195(17), 192(18), 177(17), 155(36), 140(38), 91(38), and 77(41).

NOTE: longer periods of stirring resulted in increasing quantities of the corresponding dibenzyl ether.

Bromination of the benzyl alcohol ***13****e*

When treated as described earlier, the alcohol **13***e* (67 mg) afforded the pure bromide **13***f* (83 mg; 96%), *2,4,5-trimethoxy-3-isopropylbenzyl bromide*: ^{1}Hmr δ: 1.33 (d, 6H, J = 7.0 Hz), 3.38 (sept, 1H, J = 7.0 Hz), 3.80, 3.83, and 3.85 (3s, 9H), 4.57 (s, 2H), and 6.77 (s, 1H); ^{13}Cmr δ: 149.7, 135.3, 150.0, 125.5, 111.8, 149.5, 29.4, 26.4, 21.8, 21.8 and 55.8, 60.7, 62.3; mass *m/z*: 304(4) and 302(4), 223(100), 208(72), 193(28), 178(19), 161(31), 91(28), and 77(20).

NOTE: treating the dibenzyl ether from the previous reaction with 48% HBr in benzene gave this same bromide (88%).

Transformation of the bromide ***13****f to the nitrile* ***15****a*

In the presence of 18-crown-6, KCN replaced the bromine in **13***f* (2.82 g) to give after chromotography (pet.ether/ether 4:1) the *2,4,5-trimethoxy-3-isopropylphenylacetonitrile* **15***a* (2.098 g: 91%) as described for the substitution of **6***e*: ir: 2250 cm^{-1}; ^{1}Hmr δ: 1.32 (d, 6H, J = 7.0 Hz), 3.35 (sept, 1H, J = 7.0 Hz), 3.69 (s, 2H, CH_2CN), 3.67, 3.82, and 3.83 (3s, 9H), and 6.77 (s, 1H); ^{13}Cmr δ: 149.0, 135.3, 149.7, 117.9, 110.2, 148.7, 18.4, 26.0, 21.7, 21.7 and 55.8, 60.6, 61.9, 118.2(CN); mass *m/z*: 249(M$^+$, 100), 234(63), 207(57), 194(16), 177(10), 166(15), 164(11), 151(12), 149(10), 91(13), and 77(13). Exact Mass calcd. for $C_{14}H_{19}NO_3$: 249.1365; found: 249.1362.

Alkylation with geranyl bromide to give ***5****c*

In exactly the same manner as described for **5***a*, the nitrile **15***a* (1.242 g) was alkylated with geranyl bromide to afford the diene **5***c* (1.857 g; 97%) after chromatography (pet.ether/ether 6:1). *2-Geranyl-2-(2,4,5-trimethoxy-3-isopropylphenyl)acetonitrile*: ir: 2239 cm^{-1}; ^{1}Hmr δ: 1.32 and 1.35 (2d, 6H, J = 7.3 Hz, iso-Pr Me), 1.56 (d, 3H, J = 1.5 Hz, Me_{trans}-C4), 1.59 (s, 3H, Me-C10), 1.67 (s, 3H, Me_{cis}-C4), 2.02 (m, 2H, H-C1 and H-C2), 2.55 (t, 2H, J = 7.3 Hz, H-C6), 3.34 (sept, 1H, J = 7.3 Hz, iso-Pr CH), 3.69, 3.84, and 3.85 (3s, 9H, Me-O), 4.07 (t, 1H, J = 7.3 Hz, H-C7), 5.08 (m, 1H, H-C3), 5.24 (t, 1H, J = 7.3 Hz, H-C5), and 6.79 (s, 1H, H-C9); ^{13}Cmr δ: 39.7, 23.6, 123.8, 131.5, 118.7, 33.4, 31.9, 123.5, 109.3, 139.9, 148.2, 148.9, 135.2, 149.8, 26.6, 21.8, 17.7, 25.7, 16.2 and 55.0, 60.7, 62.6, 121.4; mass *m/z*: 385(M$^+$, 65), 251(11), 250(87), 249(100), 248(100), 235(17), 234(99), 233(30), 221(62), 218(48), 205(27), 191(29), 190(37), 186(48), and 179(54). Exact Mass calcd. for $C_{24}H_{35}NO_3$: 385.2612; found: 385.2597.

When subjected to the cyclization conditions described above for diene **5***a* (with Ph-S-OMe or with Ph-S-O-CH_2-CH_2-O-Me), the diene **5***c* gave a variety to products, none of which showed the properties expected for the tricyclic compound.

Preparation of the dimethoxy diene ***5****d*

Bromination of dimethoxyisopropylbenzene ***12****d*

The dimethoxy compound **12***d* (0.322 g) was brominated following the procedure described for **6***a* affording after chromatography (pet.ether) *1,3-dimethoxy-4-bromo-isopropylbenzene* **14***a*: ^{1}Hmr δ: 1.32 (d, 6H, J = 7.0 Hz), 3.50 (qt, 1H, J = 7.0 Hz), 3.78 (s, 6H), 6.54 (d, 1H, J = 8.8 Hz), and 7.30 (d, 1H, J = 8.8 Hz); ^{13}Cmr δ: 158.9, 131.5, 154.9, 108.5, 130.1, 108.7, 26.2, 20.9, 20.9 and 55.5, 61.4; mass *m/z*: 260(44) and 258(46), 245(97) and 243(100), 230(17) and 228(31), 164(11), 149(28), 134(50), 110(27), and 77(18).

Grignard reaction to give the aldehyde ***14****b*

Using the same conditions as for **6***c*, the Grignard reagent prepared from **14***a* (0.250 g) reacted with DMF to give the aldehyde **14***b* (0.170 g; 85%) after chromatography (pet.ether/ether 10:1), *2,4-dimethoxy-3-isopropylphenylacetaldehyde*: ir: 1685 cm^{-1}; ^{1}Hmr δ: 1.30 (d, 6H, J = 7.0 Hz), 3.49 (sept, 1H, J = 7.0 Hz), 3.82 and 3.85 (2s, 6H), 6.72 (d, 1H, J = 8.4 Hz), 7.70 (d, 1H, J = 8.4 Hz), and 10.17 (s, 1H); ^{13}Cmr δ: 164.6, 129.4, 161.8, 122.8, 128.3, 107.5, 189.0, 24.7, 20.7, 20.7 and 55.5, 64.5; mass *m/z*: 208(29), 194(13), 193(97), 163(15), 135(11), and 91(15).

Reduction of aldehyde ***14****b*

As detailed earlier, the aldehyde **14***b* (1.212 g) was reduced with $NaBH_4$ to the alcohol **14***c* (1.222 g; quant), *2,4-dimethoxy-3-isopropylbenzyl alcohol*: ^{1}Hmr δ: 1.33 (d, 6H, J = 7.0 Hz), 2.31 (br s, 1H, dis. D_2O), 3.45 (sept, 1H, J = 7.0 Hz), 3.76 and 3.80 (2s, 6H), 4.63 (s, 2H), 6.64 (d, 1H, J = 8.4 Hz), and 7.12 (d, 1H, J = 8.4 Hz); ^{13}Cmr δ: 159.5, 129.5, 156.4, 126.3, 126.3, 107.3, 61.5, 25.4, 20.9, 20.9 and 55.3, 62.2; mass *m/z*: 210(96), 195(98), 177(99), 165(100), 149(67), 119(64), 105(55), 91(49), and 77(40).

Preparation of the benzyl bromide ***14****d*

Treatment of the alcohol **14***c* (1.170 g) with PBr_3, as described earlier, gave the bromo derivative **14***d* (1.330 g; 87%), *2,4-dimethoxy-3-isopropylbenzyl bromide*, mp 49–50°C: ^{1}Hmr δ: 1.33 (d, 6H, J = 7.3 Hz), 3.46 (sept, 1H, J = 7.3 Hz), 3.81 and 3.86 (2s, 6H), 4.60 (s, 2H), 6.55 (d, 1H, J = 8.8 Hz), and 7.21 (d, 1H, J = 8.8 Hz); ^{13}Cmr δ: 160.3, 129.1, 156.5, 128.2, 128.2, 107.7,

29.9, 25.7, 20.9, 20.9 and 55.3, 62.3; mass *m/z*: 274(3) and 272(3), 193(100), 165(30), 153(24), 135(29), 91(25), and 77(14).

Formation of the nitrile ***15***b

Potassium cyanide in the presence of 18-crown-6 converted the bromide **14***d* (1.169 g) to the nitrile **15***b* (0.724 g; 77%) after chromatography (pet.ether/ether 4:1), *2,4-dimethoxyisopropylphenylacetonitrile*: ir: 2251 cm^{-1}; ^{1}Hmr δ: 1.33 (d, 6H, *J* = 7.0 Hz), 3.41 (sept, 1H, *J* = 7.0 Hz), 3.67 (s, 2H), 3.74 and 3.80 (2s, 6H), 6.66 (d, 1H, *J* = 8.4 Hz), and 7.14 (d, 1H, *J* = 8.4 Hz); ^{13}Cmr δ: 159.8, 129.9, 155.8, 115.7, 126.9, 107.7, 18.4, 25.7, 20.7, 20.8 and 55.4, 61.9; mass *m/z*: 219(24), 204(54), 175(100), 147(14), 134(14), 119(14), 117(17), 115(17), 91(21), and 77(14). Exact Mass calcd. for $C_{13}H_{17}NO_2$: 219.1259; found: 219.1260.

Alkylation with geranyl bromide

Catalysed by LDA prepared *in situ* as described previously (see **5***a*), the nitrile **15***b* (0.429 g) was alkylated with geranyl bromide to give, after chromatography (pet. ether/ether 10:1) the diene **5***d* (0.666 g; 96%), *2-geranyl-2-(2,4-dimethoxy-3-isopropylphenyl)-acetonitrile*: ^{1}Hmr δ: 1.31 and 1.34 (2d, 6H, *J* = 7.0 Hz, iso-Pr Me), 1.57 (s, 3H, Me_{trans}-C4), 1.60 (s, 3H, Me-C10), 1.68 (s, 3H, Me_{cis}-C4), 2.03 (m, 4H, H-C1 and C2), 2.54 (dd, 2H, *J* = 8.1 and 7.3 Hz, H-C6), 3.40 (sept, 1H, *J* = 7.0 Hz, iso-Pr CH), 3.74 and 3.80 (2s, 6H, Me-O), 4.02 (t, 1H, *J* = 8.1 Hz, H-C7), 5.08 (m, 1H, H-C3), 5.23 (t, 1H, *J* = 7.3 Hz, H-C5), 6.67 (d, 1H, *J* = 8.4 Hz), and 7.22 (d, 1H, *J* = 8.4 Hz); ^{13}Cmr δ: 39.7, 25.9, 129.3, 131.4, 118.9, 33.4, 31.8, 121.3, 126.0, 139.6, 1071.7, 159.6, 129.6, 155.3, 26.6, 20.8, 20.8, 17.7, 16.2, 25.7 and 55.3, 62.5, 121.5(CN); mass *m/z*: 355(M^+, 1), 220(14), 219(99), 218(37), 204(20), 191(13), 188(24), 137(12), and 91(10).

Cyclization of diene ***5***d

The diene **5***d* (1.006 g) was cyclized in the manner described previously (see **7***a*). Chromatography (pet.ether/ether 6:1) afforded many unidentifiable fractions and the product **7***d* (0.543 g; 41%), *7-cyano-3-phenylthio-12,14-dimethoxyabieta-8,11,13-triene*, mp 213–215°C (dec.): ir: 2250 cm^{-1}; ^{1}Hmr δ: 1.01 (s, 3H, Me_α-C4), 1.21 (s, 3H, Me_β-C4), 1.29 and 1.31 (2d, 6H, *J* = 7.0 Hz, iso-Pr Me), 1.40 (s, 3H, H-C10), 1.56 (m, 1H, H_α-C1), 1.74 (d, 1H, *J* = 11.7 Hz, H-C5), 2.00 (dd, 1H, *J* = 11.7 Hz, H_α-C6), 2.03 (m, 1H, H_β-C6), 2.22 (dd, 1H, *J* = 7.3 and 1.1 Hz, H_β-C1), 2.03 and 2.22 (2m, 2H, H-C2), 2.95 (m, 1H, H-C3), 3.33 (sept, 1H, *J* = 7.0 Hz, iso-Pr CH), 3.75 and 3.84 (2s, 6H, Me-O), 4.15 (dd, 1H, *J* = 5.9 and 1.8 Hz, H-C7), 6.49 (s, 1H, H-C11), 7.23 (m, 3H), and 7.45 (ddd, 2H, Ph-S arom H); ^{13}Cmr δ: 38.9, 24.1, 60.4, 38.3, 49.7, 24.8, 31.8, 114.5, 148.0, 38.2, 104.0, 159.9, 126.7, 156.0, 25.9, 20.9, 20.8, 29.6, 27.9, 18.2 and 55.2, 62.2, 122.6, 136.3, 131.4, 128.9, 126.5; mass *m/z*: 463(M^+, 11), 258(12), 224(11), 135(18), 123(16), 110(100), 109(76), 97(11), and 77(10). Exact Mass calcd. for $C_{29}H_{37}NO_2S$: 463.2545; found: 463.2545.

Oxidation to the ketone ***8***d

Oxygen bubbled into the basic solution of **7***d* (0.270 g) as described for the preparation of **8***a*, gave the ketone **8***d* (0.154 g; 58%) after chromatography (pet.ether/ether 4:1), *7-keto-3-phenylthio-12,14-dimethoxyabieta-8,11,13-triene*, mp 140–142°C; ^{1}Hmr δ: 1.08 (s, 3H, Me_α-C4), 1.24 and 1.25 (2d, 6H, *J* = 7.0 Hz, iso-Pr Me), 1.26 (s, 3H, Me_β-C4), 1.30 (s, 3H, Me-C10), 1.61 (m, 1H, H_β-C1), 1.91 (dd, 1H, *J* = 11.0 and 7.0 Hz, H-C5), 2.03 (t, 1H, *J* = 3.3 Hz, H_β-C2), 2.03 (dd, 1H, *J* = 12.8 and 4.8 Hz, H_α-C2), 2.26 (dt, 1H, *J* = 12.8 and 3.3 Hz, H_β-C1), 2.69 (d, 1H, *J* = 11.0 Hz, H_β-C6), 2.71 (d, 1H, *J* = 7.0 Hz, H_α-C6), 2.91 (m, 1H, H-C3), 3.54 (sept, 1H, *J* = 7.0 Hz, iso-Pr CH), 3.74 and 3.82 (2s, 6H, Me-O), 6.52 (s, 1H, H-C11), 7.25 (m, 3H), and 7.40 (dt, 2H, Ph-S arom H); ^{13}Cmr δ: 38.8, 23.1, 60.7, 49.7, 27.6, 196.4, 114.6, 147.1, 38.3, 101.6, 160.0, 129.0, 156.6, 24.5, 21.0, 38.1, 29.3, 17.4 and 55.2, 62.3, 136.4, 131.4, 128.8, 126.5; mass *m/z*: 452(M^+, 51), 438(30), 437(100), 343(21), 327(18), 275(25), 247(33), and 207(20). Exact Mass calcd. for $C_{28}H_{36}O_3S$: 452.2385; found: 452.2312.

Oxidation to the sulfoxide ***9***d

In the same manner as the preparation of **9***a*, the previous product **8***d* (0.069 g) was oxidized to the sulfoxide **9***d* (0.065 g; 91%) after chromatography (pet.ether/ether 1:3), *7-keto-3-phenylsulfinyl-12,14-dimethoxyabieta-8,11,13-triene*, mp 179–180°C: ^{1}Hmr δ: 1.22 (s, 3H) and 1.34 (s, 3H, Me-C4), 1.22 and 1.26 (2d, 6H, *J* = 7.0 Hz, iso-Pr Me), 1.38 (s, 3H, Me-C10), ca 1.5 (br m, 2H, H_α-C1 and H-C2), 1.84 (dd, 1H, *J* = 10.6 and 7.7 Hz, H-C5), 2.15 (m, 2H, H_β-C1 and H-C3), 2.70 (m, 2H, H-C6), 3.48 (sept, 1H, *J* = 7.0 Hz, iso-Pr CH), 3.73 and 3.78 (2s, 6H, Me-O), 6.47 (s, 1H, H-C11), and 7.51 (m, 5H, Ph-SO arom H); ^{13}Cmr δ: 37.5, 30.2, 75.5, 38.5, 49.7, 37.2, 195.9, 118.2, 156.0, 37.5, 101.6, 163.1, 128.5, 159.8, 24.5, 21.0, 20.8, 18.3, 13.9 and 55.2, 62.4, 143.8, 123.9, 128.9, 130.1; mass *m/z*: no molecular ion, 343(M − 125, 37), 342(22), 327(100), 275(11), 247(16), 203(10), 126(38), and 78(37).

Formation of the enol thioether enol trifluoroacetate ***17***

Employing the procedure described above (see preparation of **10***a*), the sulfoxide **9***d* (47 mg) was treated with TFAA and the product chromatographed (pet.ether/ether 10:1) to afford **17** (45 mg; 82%): ^{1}Hmr δ: 1.10 (s, 3H) and 1.25 (s, 3H, Me-C4), 1.30 and 1.31 (2d, 6H, *J* = 7.0 Hz, iso-Pr Me), 1.34 (s, 3H, Me-C10), 2.58 and 2.59 (2d, 2H, *J* = 3.3 Hz, H_α-C1 and H-C5), 2.63 (d, 1H, *J* = 5.9 Hz, H_β-C1), 3.45 (sept, 1H, *J* = 7.0 Hz, iso-Pr CH), 3.77 and 3.81 (2s, 6H, Me-O), 5.87 (dd, 1H, *J* = 5.5 and 2.9 Hz, H-C7), 6.49 (s, 1H, H-C11), 6.81 (d, 1H, *J* = 2.9 Hz, H-C6), and ca. 7.35 (br m, 5H, Ph-S arom H); ^{13}Cmr δ: 39.3, 129.5, 141.2, 36.8, 50.0, 144.6, 117.9, 113.9, 144.7, 39.8, 102.9, 160.8, 127.9, 158.0, 25.3, 20.9, 20.8, 30.0, 22.9, 22.0 and 55.3, 63.3, 154.5 and 110.4 (O-CO-CF_3, respectively), 136.3, 130.5, 129.0, 126.6; mass *m/z*: no molecular ion, 461(M − 85, 24), 460(33), 459(100), 350(55), 334(18), 308(60), 283(37), 282(72), 269(57), and 190(94).

Hydrolysis to the diketone ***11***d

The ether **17** (75 mg) was dissolved in HOAc and treated with $TiCl_4$ as described above. After chromatography (pet.ether/ether 1:1) the diketone **11***d* (44 mg: 93%) was obtained as a white solid, mp 150–152°C: ir: 1701 (br) cm^{-1}; ^{1}Hmr δ: 1.13 and 1.19 (2s, 6H, Me-C4), 1.26 (d, 6H, *J* = 7.0 Hz, iso-Pr Me), 1.42 (s, 3H, Me-C10), 2.03 (m, 1H, H_α-C1), 2.24 (dd, 1H, *J* = 13.6 and 4.0 Hz, H-C5), 2.53 (ddd, 1H, *J* = 9.5 and 3.3 Hz, H_β-C2), 2.59 (dd, 1H, *J* = 17.9 and 4.0 Hz, H_β-C6), 2.83 (t, 1H, *J* = 9.5 Hz, H_α-C2), 2.85 (dd, 1H, *J* = 17.9 and 13.6 Hz, H_α-C6), 2.88 (m, 1H, H_α-C1), 3.54 (sept, 1H, *J* = 7.0 Hz, iso-Pr CH), 3.86 (s, 3H, Me-O), 6.31 (s, 1H, H-C11), and 13.26 (s, 1H, OH – dis. D_2O); ^{13}Cmr δ: 36.8, 34.5, 213.9, 47.2, 49.1, 36.0, 202.3, 109.8, 143.4, 37.8, 98.1, 162.9, 120.8, 154.0, 23.5, 20.2, 20.2, 24.9, 22.6, 21.7 and 55.5; mass *m/z*: 344(M^+, 26), 330(26), 329(100), 283(13) and 282(33). Exact Mass calcd. for $C_{21}H_{28}O_4$: 344.1988; found: 344.1988.

Acknowledgments

We thank the Natural Sciences and Engineering Council of Canada for operating and equipment grants and we are grateful to the Ministère de l'éducation du Québec (F.C.A.R.) for their financial help and for a Graduate bursary (S.C.).

1. A. Ulubelen, N. Evren, E. Tuzlaci, and C. Johansson. J. Nat. Prod. **51**, 1178 (1988).
2. S. Canigueral, J. Iglesias, F. Sanchez-Ferrando, and A. Virgili. Phytochemistry, **27**, 221 (1988).
3. C. H. Eugster. Helv. Chim. Acta, **56**, 2534 (1973).
4. (*a*) I. Ara, B. S. Siddiqui, S. Faizi, and S. Siddiqui, J. Nat. Prod. **51**, 1054 (1988); (*b*) S. Siddiqui, I. Ara, S. Faizi, T. Mahmood, and B. S. Siddiqui. Phytochemistry, **27**, 3903

Can. J. Chem. Downloaded from www.nrcresearchpress.com by 217.78.4.112 on 09/08/12
For personal use only.

(1988); (*c*) I. Ara, B. S. Siddiqui, S. Faizi, and S. Siddiqui. J. Nat. Prod. **53**, 816 (1990).
5. R. H. Burnell, M. Jean, and D. Poirier. Can. J. Chem. **65**, 775 (1987), and references therein.
6. B. S. Snider, R. Mohan, and S. A. Yates. J. Org. Chem. **50**, 3659 (1985); R. H. Burnell and M. Girard. Synth. Commun. **20**, 2469 (1990).
7. (*a*) E. D. Edstrom and T. Livinghouse. J. Org. Chem. **52**, 949 (1987); (*b*) S. Harring and T. Livinghouse. Tetrahedron Lett. **30**, 1499 (1989).
8. J-M. Fang, C-M. Sheu, and Y-S. Cheng. J. Chin. Chem. Soc. **33**, 245 (1986).
9. E. D. Edstrom and T. Livinghouse. J. Am. Chem. Soc. **108**, 1334 (1986); M. Nishizawa, H. Takenaka, and Y. Hayashi. J. Org. Chem. **51**, 806 (1986).
10. R. H. Burnell and C. Cote. Synth. Commun. **18**, 1753 (1988).
11. M. Srebnik, R. Mechoulam, and I. Yona. J. Chem. Soc. Perkin Trans. 1, 1423 (1987).
12. M. Wilcox, R. W. Viola, K. W. Johnson, A. P. Billington, B. K. Carpenter, J. A. McCray, A. P. Guzikowski, and G. P. Hess. J. Org. Chem. **55**, 1585 (1990).
13. F. L. Cook, C. W. Bowers, and C. L. Liotta. J. Org. Chem. **39**, 3416 (1974).
14. W. H. Mueller and P. E. Butler. J. Am. Chem. Soc. **90**, 2075 (1968).
15. L. L. Chang, D. B. Denney, D. Z. Denney, and R. J. Kazior. J. Am. Chem. Soc. **99**, 2293 (1977).
16. S. J. Selikson and D. S. Watt. J. Org. Chem. **40**, 267 (1975).
17. E. Vedejs, D. A. Engler, and J. E. Telschow. J. Org. Chem. **43**, 188 (1978).
18. K. Konno, K. Hashimoto, H. Shirahama, and T. Matsumoto. Tetrahedron Lett. **27**, 3865 (1986).
19. B. M. Trost, K. Hiroi, and S. Kurozumi. J. Am. Chem. Soc. **97**, 438 (1975).
20. M. Srebnik and R. Mechoulam. Synthesis, 1046 (1983).

Can. J. Chem. Downloaded from www.nrcresearchpress.com by 217.78.4.112 on 09/08/12
For personal use only.

Studies with tissue cultures of the Chinese herbal plant, *Tripterygium wilfordii*. Isolation of metabolites of interest in rheumatoid arthritis, immunosuppression, and male contraceptive activity

JAMES P. KUTNEY,[1] GARY M. HEWITT, GIN LEE, KRYSTYNA PIOTROWSKA, MALCOLM ROBERTS, AND STEVEN J. RETTIG

Department of Chemistry, University of British Columbia, 2036 Main Mall, Vancouver, B.C., Canada V6T 1Y6

Received March 17, 1991

This paper is dedicated to Professor Zdenek (Denny) Valenta on the occasion of his 65th birthday

JAMES P. KUTNEY, GARY M. HEWITT, GIN LEE, KRYSTYNA PIOTROWSKA, MALCOLM ROBERTS, and STEVEN J. RETTIG. Can. J. Chem. **70**, 1455 (1992).

A detailed study of metabolites produced by the plant cell culture line of *Tripterygium wilfordii*, a Chinese herbal plant, is presented. Eighteen compounds within the diterpene and triterpene families have been isolated and fully characterized. Of these, five are novel compounds, and their structures were determined by a combination of spectral analysis, chemical correlation and single crystal X-ray diffraction. The interest of these compounds in the treatment of rheumatoid arthritis, skin allergies, and for male contraception is noted.

JAMES P. KUTNEY, GARY M. HEWITT, GIN LEE, KRYSTYNA PIOTROWSKA, MALCOLM ROBERTS et STEVEN J. RETTIG. Can. J. Chem. **70**, 1455 (1992),

On rapporte une étude détaillée des métabolites produits par une lignée de culture cellulaire du *Tripterygium wilfordii*, un plante galénique chinoise. On a isolé et caractérisé 18 composés des familles des di- et des triterpènes. Cinq de ces produits sont de nouveaux composés; on a déterminé leur structure par une combinaison d'analyses spectrales, de corrélations chimiques et de diffraction des rayons X par des cristaux uniques. On a noté l'intérêt de ces composés pour le traitement de l'arthrite rhumatismale, d'allergies de la peau et comme contraceptifs pour les males.

[Traduit par la rédaction]

Tripterygium wilfordii Hook f is a perennial twining vine of the family *Celastraceae*, which is cultivated in many parts of southern China such as Zhejiang, Anhui, Jiangxi, Fujian, and Guangdong provinces and also in Taiwan. The herb is commonly known in China as Lei Gong Teng (Thunder God vine) or Mang Cao (rank grass). Its use in Chinese traditional medicine dates back many centuries, and it is first mentioned in the Saint Peasant's Scripture of Materia Medica (1), written about two thousand years ago, as being used for the treatment of fever, chills, oedema, and carbuncle. Chinese gardeners used the powdered root to protect their crops from chewing insects. Most recently, crude extracts and refined extracts (a so-called multi-glycoside extract, or GTW) have been used increasingly to treat such disorders as rheumatoid arthritis, ankylosing spondilitis, and a variety of dermatological disorders (2–4).

In 1972, Morris Kupchan *et al.* first isolated the novel diterpenoid triepoxides, tripdiolide (**1**), triptolide (**2**), and triptonide (**2***a*) from the roots of *Tripterygium wilfordii* (5) and showed that **1** and **2** have significant antileukaemic activity. The biological properties of **1** and **2** stimulated studies in our laboratory directed at developing a plant cell culture line that would hopefully produce these compounds in higher yield and under laboratory controlled conditions. The earlier studies, with these objectives in mind, have been published (6, 7) and the stable cell line, coded as TRP4a, was shown to produce **1** in yields 40 times that of the living plant. As these studies were underway, we became aware of more recent research data from various laboratories in the People's Republic of China that revealed an increasing interest in the clinical use of extracts from *T. wilfordii* plants. Various disorders (rheumatoid arthritis, skin disorders) have been treated with hot water or alcohol extracts of the dried root xylem (8). Toxic side effects are minimal (9–12).

Observed effects of these extracts on the reproductive system have stimulated a great deal of research, particularly relating to the male reproductive system, and their possible use as a birth control agent. Studies in animals (13–15) and in humans (16–18) have provided considerable encouragement for the development of a novel non-steroidal male contraceptive agent.

In view of the increased current interest, the present investigation is aimed at a more comprehensive investigation of the metabolites present in the tissue culture cell line TRP4a than that published earlier (6, 7).

To isolate sufficient quantities of extracts (and later, metabolites) from the tissue culture cells (TRP4a cell line) for biological screening, it was necessary to produce large-scale quantities of the suspension culture. Batch fermentations were carried out on 10–17 L scale in glass or in steel air-lift fermentors. Suspension cultures were grown according to the procedure described earlier (6, 7). The cells were separated from the spent medium (that is, the supernatant liquid obtained after cells were removed by filtration).

A general extraction procedure was developed in which the cells and the spent medium were extracted separately (Figs. 1 and 2).

Samples of the extracts from an initial 15-L bioreactor experiment (TRP#221, Tables 1 and 2) were submitted for preliminary screening of biological activity to laboratories in Shanghai and Nanjing, People's Republic of China (see Acknowledgement). Assays for immunosuppressive activity and antifertility activity were carried out.

The results of the preliminary screening of the crude extracts showed that the ethyl acetate extracts had both immunosuppressive activities and antifertility activity while the methanol extracts were inactive in both cases.

[1]Author to whom correspondence may be addressed.

Can. J. Chem. Downloaded from www.nrcresearchpress.com by 217.78.4.112 on 09/08/12
For personal use only.

Three further batches of the TRP4a cell suspension cultures were grown and harvested in the same way (Table 1). Extraction of the cells and the spent medium was carried out as above to give ethyl acetate and methanol extracts (Table 2). These data illustrate the relative weights of the extracts (EtOAc and MeOH) obtained to illustrate the production capabilities of the stable TRP4a cell line.

The ethyl acetate extracts from batches TRP#222, TRP#224, and TRP#225 were combined to give 3.73 g of cell extract and 1.71 g of spent medium extract. The methanol extracts were not further investigated since no biological activity of interest was detected. The ethyl acetate extracts were subjected to partial separation in order to give crude fractions for further preliminary biological screening.

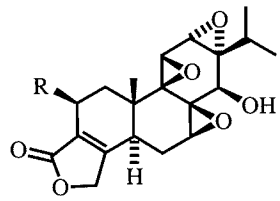

1, R = OH
2, R = H

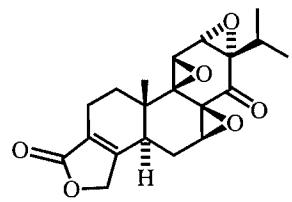

2*a*

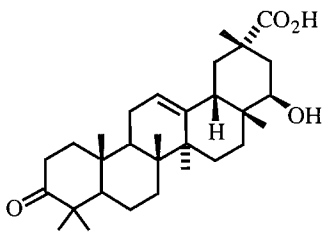

3

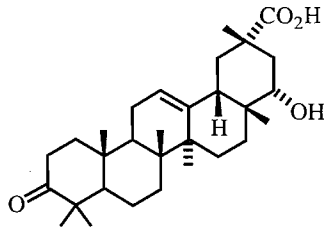

4

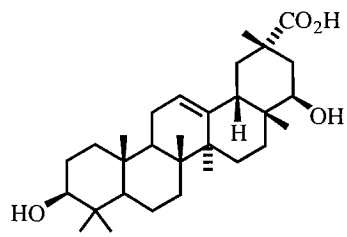

5

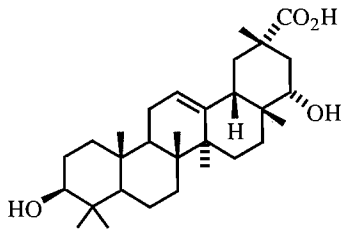

6

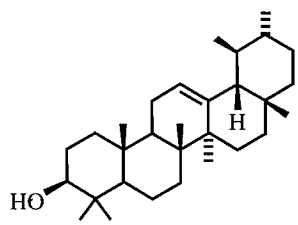

12

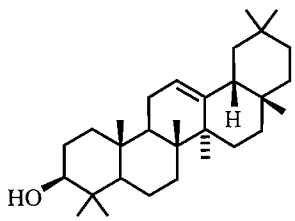

13

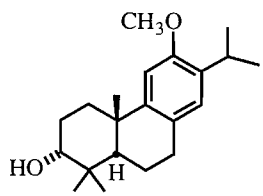

14

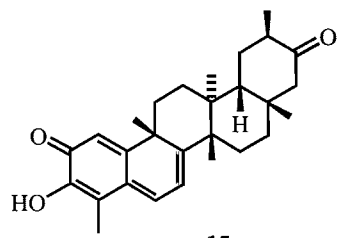

15

Partial separation of the cell extract was carried out by vacuum liquid chromatography (vlc) as described by Pelletier *et al.* (19) and Coll and Bowden (20) (see Experimental) to afford eight crude fractions containing complex mixtures of metabolites. Fractions 2–7 were yellow to orange-brown solids containing sterols, diterpenes, and triterpenes (0.39, 0.27, 0.27, 0.51, 0.29, and 0.18 g respectively). Fraction 8 was a dark brown solid (1.22 g) containing the polar material.

Biological screening of the fractions showed that fractions 6 and 7 were active in antifertility and in inhibition of lymphocyte proliferation (immunosuppressive activity). Further studies, as noted below, revealed that fractions 6 and 7 contained triterpenes as the major constituents.

Partial separation of the spent medium extract was similarly conducted by means of vlc to afford ten fractions containing complex mixtures of compounds. Fractions 1–5 consisted of complex mixtures of diterpenes, sterols, etc. (4, 24, 14, 61, and 129 mg respectively), and were all yellow-brown solids. Fraction 6 (ethyl acetate elution) consisted of triptolide (**2**) and a number of triterpenes as the major constituents (206 mg). Fraction 7 (ethyl acetate elution) consisted of tripdiolide (**1**) and triterpenes as the major con-

Can. J. Chem. Downloaded from www.nrcresearchpress.com by 217.78.4.112 on 09/08/12
For personal use only.

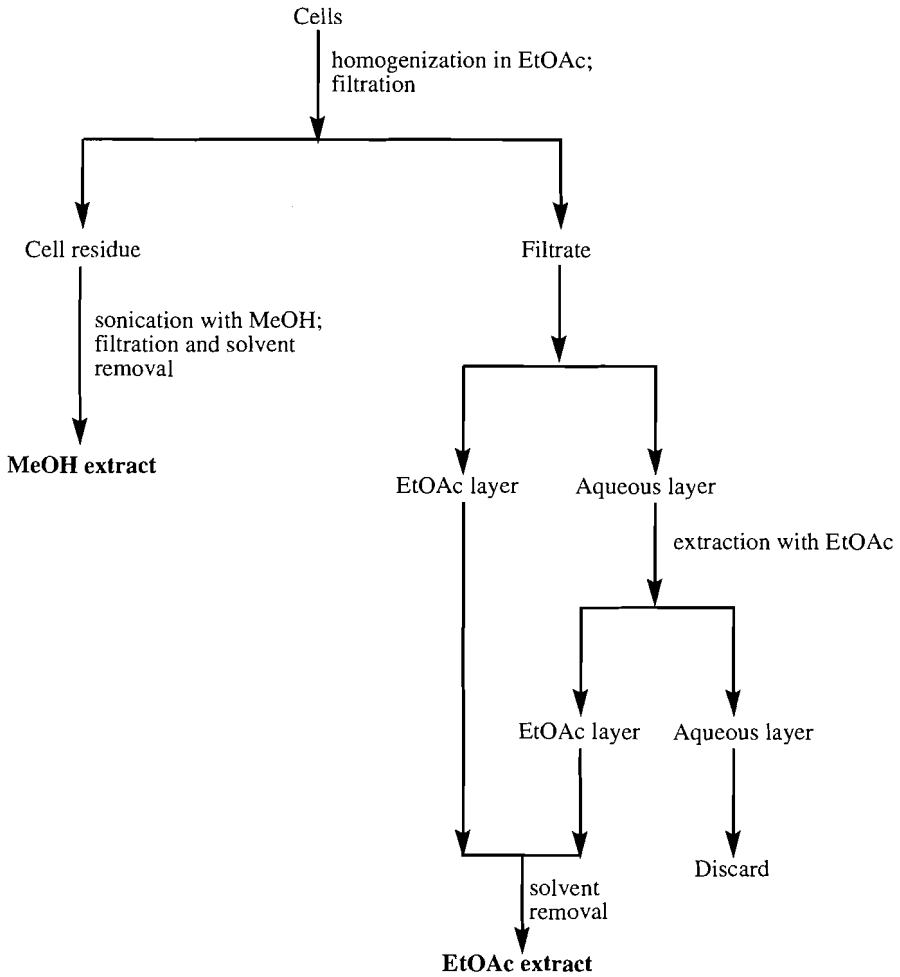

FIG. 1. Extraction procedure for the TRP4a cells.

Can. J. Chem. Downloaded from www.nrcresearchpress.com by 217.78.4.112 on 09/08/12
For personal use only.

stituents (205 mg). Elution with ethyl acetate – methanol (1:1) provided fractions 8, 9, and 10 (brown solids, 52, 304, and 77 mg respectively). Fraction 8 contained triterpenes as minor components and other polar material, while fractions 9 and 10 contained only polar material.

Biological screening of the spent medium fractions showed that fractions 6 and 7 possessed the highest antifertility activity while fraction 8 showed moderate activity. Fractions 6 and 7 also demonstrated inhibitory activity against lymphocyte proliferation.

In summary, the screening data on the above crude fractions suggested that interesting biological activity resides in both the "diterpene" and "triterpene" fractions, thus demanding a further study to complete structural elucidation of the "active" compounds. For this purpose, additional fermentations (total, 78 L of broth) were carried out to obtain sufficient quantities of cell and broth-derived extracts for proper chromatographic separation and purification. Figures 3 and 4 illustrate the overall separation and purification of the various metabolites isolated from the cells (Fig. 3) and broth (Fig. 4) of the fermentation experiments. Table 3 summarizes the yields of the various metabolites (structures **1–6**; **12–25**) isolated from the 78-L fermentation experiment. A total of 18 compounds (5 new and 13 known) were isolated and characterized. Tripdiolide (**1**), triptolide (**2**), oleanolic acid (**23**), β-sitosterol (**24**), pulpunonic acid (**25**), the diterpene **20**, dehydroabietic acid (**21**), and celastrol (**22**) were isolated in our previous study (6, 7) so it is now appropriate to discuss the additional and novel compounds obtained in the present study.

The triterpene **3** was isolated as optically active ($[\alpha]^{22}$ +92.9) colourless prisms (mp 268–270°C) with a molecular formula of $C_{30}H_{46}O_4$ (high-resolution mass spectrometry) and with characteristic ir adsorption bands for hydroxyl and carboxylic acid functions. Strong evidence for an oleanene-type triterpene skeleton is given in the fragmentation pattern of the mass spectrum of **3**. A retro Diels–Alder (RDA) fragmentation is characteristic of the oleanene skeleton where the DE ring fragment maintains the positive charge. The AB ring fragment also maintains the positive charge, but to a much lesser extent (21, 22). This fragmentation places the double bond at C12.

Nuclear magnetic resonance spectra (^{1}Hmr and ^{13}Cmr) revealed characteristic signals for an oleanene-type system (see Experimental) and final confirmation of structure was established through chemical correlation with triterpene **6** (Fig. 6), the latter having been subjected to X-ray analysis (see later).

The triterpene **4**, isomeric with **3**, was isolated as optically active ($[\alpha]^{22}$ +84.4) colourless prisms (mp 289–290°C). Its spectroscopic data revealed a close relationship to **3** and its structure was also correlated with that of **6** (Fig. 6).

The dihydroxy triterpene **5** was isolated as optically active ($[\alpha]^{22}$ +55.0) colourless prisms (mp 281–283°C) with a molecular formula of $C_{30}H_{48}O_4$. Again, nmr data (^1H and ^{13}C) supported the structure indicated but final confirmation was established via chemical correlation with **3** and **6** (Fig. 6).

The dihydroxy triterpene **6** was isolated as optically active ($[\alpha]^{22}$ +93.5) colourless prisms (mp 293–298°C) with a molecular formula of $C_{30}H_{48}O_4$. Spectroscopic data revealed an oleanene-type structure closely related to the above triterpenes.

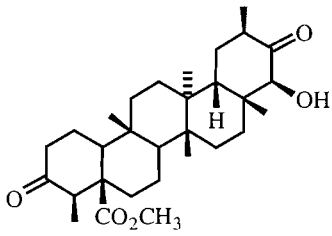

16

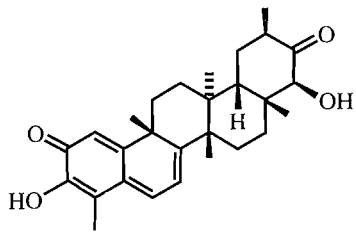

17

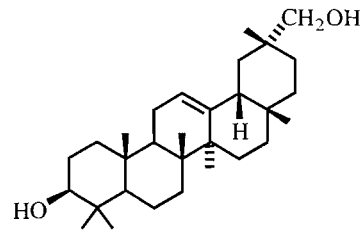

18

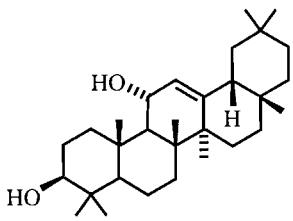

19

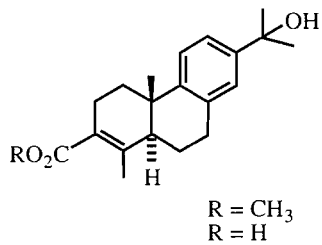

20

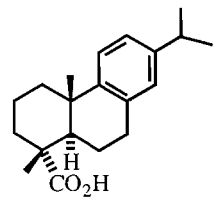

21

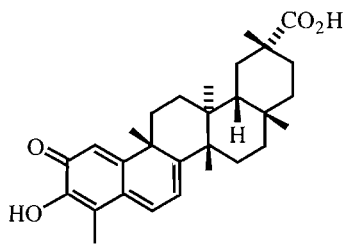

22

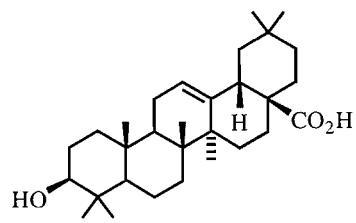

23

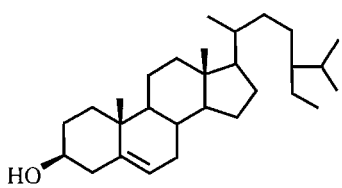

24

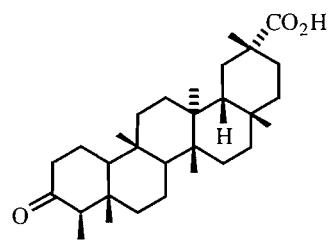

25

The structure and relative stereochemistry of **6** were confirmed by a single crystal X-ray analysis (Fig. 5). The computer-generated X-ray structure depicts ring E in a chair conformation placing the C20α carboxylic acid and the C22α hydroxyl group in equatorial orientations. The C3 hydroxyl group is also shown to be equatorial (C3β) as predicted from the ^1Hmr spectrum. The crystal exists as the 1:1 methanol solvate, with the methanol oxygen coordinating with the hydroxyl groups of the triterpene.

With the complete structure of **6** available from the above studies, the chemical correlations between **3–5** and **6** were now considered (Fig. 6).

The triterpenes **3** and **4** were both reduced with sodium borohydride to the corresponding alcohols. Triterpene **3** yielded a compound with identical tlc, mp, ir, ms, and ^1Hmr spectra to those of **5**, while **4** yielded a compound with identical tlc, mp, ir, ms, and ^1Hmr spectra to those of **6**. Esterification of **6–10** followed by oxidation with pyridinium

Can. J. Chem. Downloaded from www.nrcresearchpress.com by 217.78.4.112 on 09/08/12
For personal use only.

Can. J. Chem. Downloaded from www.nrcresearchpress.com by 217.78.4.112 on 09/08/12
For personal use only.

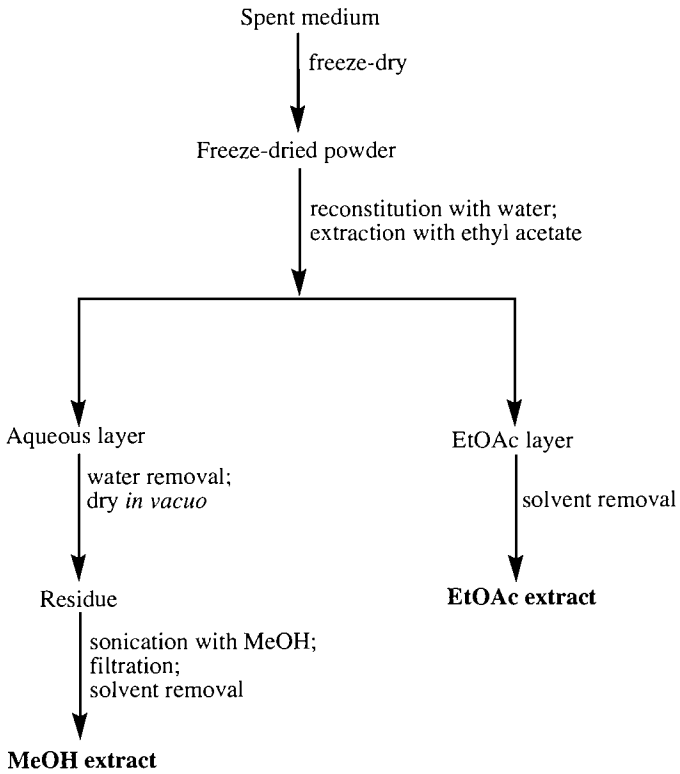

FIG. 2 Extraction procedure for the TRP4a spent medium.

TABLE 1. Volumes and growth times for initial batches of TRP4a suspension cultures for preliminary biological screening

Batch no.	Culture vol. (L)	Incubation time (days)	R.I. on harvesting
TRP#221	15.0	33	1.3345
TRP#222	10.0	48	1.3338
TRP#224	16.0	42	1.3345
TRP#225	10.5	30	1.3335

chlorochromate yielded the diketone, **11**, as an optically active ($[\alpha]^{22}$ +5.7) white solid (mp 180.5–182°C) with a molecular formula of $C_{31}H_{46}O_4$. Its ir spectrum shows carbonyls at 1721 and 1698 cm^{-1} and C-O absorption at 1218 cm^{-1}. The ^{1}Hmr spectrum shows four signals corresponding to protons adjacent to the carbonyl at δ 2.39 (1H, ddd, C2αH), 2.48 (1H, d, C21βH), 2.56 (1H, ddd, C2βH), and 2.99 (1H, d, C21αH).

Esterification and oxidation of **5** in the same manner yielded a compound with identical tlc, mp, ir, ms, and ^{1}Hmr spectra to those of **11**.

The spectral data and chemical interconversions establish that **3** is 22β-hydroxy-3-oxoolean-12-en-29-oic acid, **4** is 22α-hydroxy-3-oxoolean-12-en-29-oic acid, **5** is 3β,22β-dihydroxyolean-12-en-29-oic acid, and that **6** is 3β,22α-dihydroxyolean-12-en-29-oic acid.

The known triterpenes α-amyrin (**12**) and β-amyrin (**13**), isolated for the first time from the TRPa cell line, were established via spectral comparison with authentic samples.

The abietane-type diterpene, **14**, was isolated as optically active ($[\alpha]^{22}$ +44.4) colourless needles (mp 157–158°C) with a molecular formula of $C_{21}H_{32}O_2$. The mass spectrum of **14** has a molecular ion peak at *m/z* 316 and a base peak at *m/z* 283 corresponding to $M^+ - CH_3$, H_2O. The remaining peaks are of low intensity; however, diagnostic peaks are observed at *m/z* 215 and 189 (Fig. 7) (23). In the ^{1}Hmr spectrum, signals are present for 3 tertiary methyl groups (δ 0.96, 1.05, and 1.20), an isopropyl group (δ 1.20, d, CH_3; δ 1.21, d, CH_3 and δ 3.28, septet, benzylic methine), and a methoxyl group at δ 3.72. Also observed are signals at δ 2.76 (1H, ddd, H7α) and 3.02 (1H, br dd, H7β) indicating a benzylic methylene, δ 3.51 (1H, br t, $W_{1/2}$ = 7.0 Hz, C*H*OH) indicating an axially oriented hydroxyl functionality, and two aromatic signals at δ 7.04 (1H, s) and 7.05 (1H, s).

The characteristic signals in the ^{13}Cmr spectrum of **14** are seen at δ 60.2 (OCH_3), 75.5 (CHOH), and 6 aromatic signals at δ 120.4, 123.7, 128.5, 137.9, 148.9, and 154.8. The APT spectrum confirms the presence of 6 methyl groups (δ 22.1, C10-CH_3; 23.9, 24.0, isopropyl methyl groups; 24.7, 25.9, C4 methyl groups and 60.2, OCH_3), a secondary alcohol (δ 75.5), and a tetrasubstituted benzene ring (the signals at δ 120.4 and 123.7 are inverted).

A 2D ^{1}H–^{1}H COSY spectrum of **14** shows coupling of the downfield proton at δ 3.51 with 2 other protons (3β/2, 3β/2′) that show geminal coupling (2/2′) and show cross peaks to 2 other protons (2′/1, 2′/1′, 2/1, and 2/1′). The benzylic proton at C15 shows the expected coupling with a cross peak to the isopropyl methyl groups (15/16, 17) while the benzylic protons at C7 show cross peaks to the protons at C6 (7β/6, 7β/6′, 7α/6, and 7α/6′). Coupling of H5 with H6 and H6′ is obscured by diagonal crowding.

A SINEPT experiment was carried out on **14** to determine whether the methoxyl group is attached to C11 or C12. Irradiation of the signal at δ 3.28 (H15) in the ^{1}Hmr spectrum was expected to enhance carbons 12 and 14 in the ^{13}Cmr spectrum (enhancement of carbon through three bonds ($^3J_{C,H}$) via polarization transfer from hydrogen). Irradiation of the signal at δ 3.28 (H15), however, resulted in enhancement of signals in the ^{13}Cmr spectrum at δ 123.7, 128.5, 137.9,

TABLE 2. Weights of extracts from TRP4a suspension cultures

Batch no.	Wet wt. cells (kg)	Spent medium vol. (L)	EtOAc extract (g)		MeOH extract (g)	
			Cells	Spent medium	Cells	Spent medium
TRP#221	1.51	12.0	0.84	0.48	17.13	36.10
TRP#222	0.97	8.2	1.00	0.70	1.53	3.24
TRP#224	1.41	11.8	0.87	0.37	6.53	59.89
TRP#225	1.03	9.0	1.85	0.10	—[a]	—

[a]Extraction with methanol was not performed in this case.

Can. J. Chem. Downloaded from www.nrcresearchpress.com by 217.78.4.112 on 09/08/12
For personal use only.

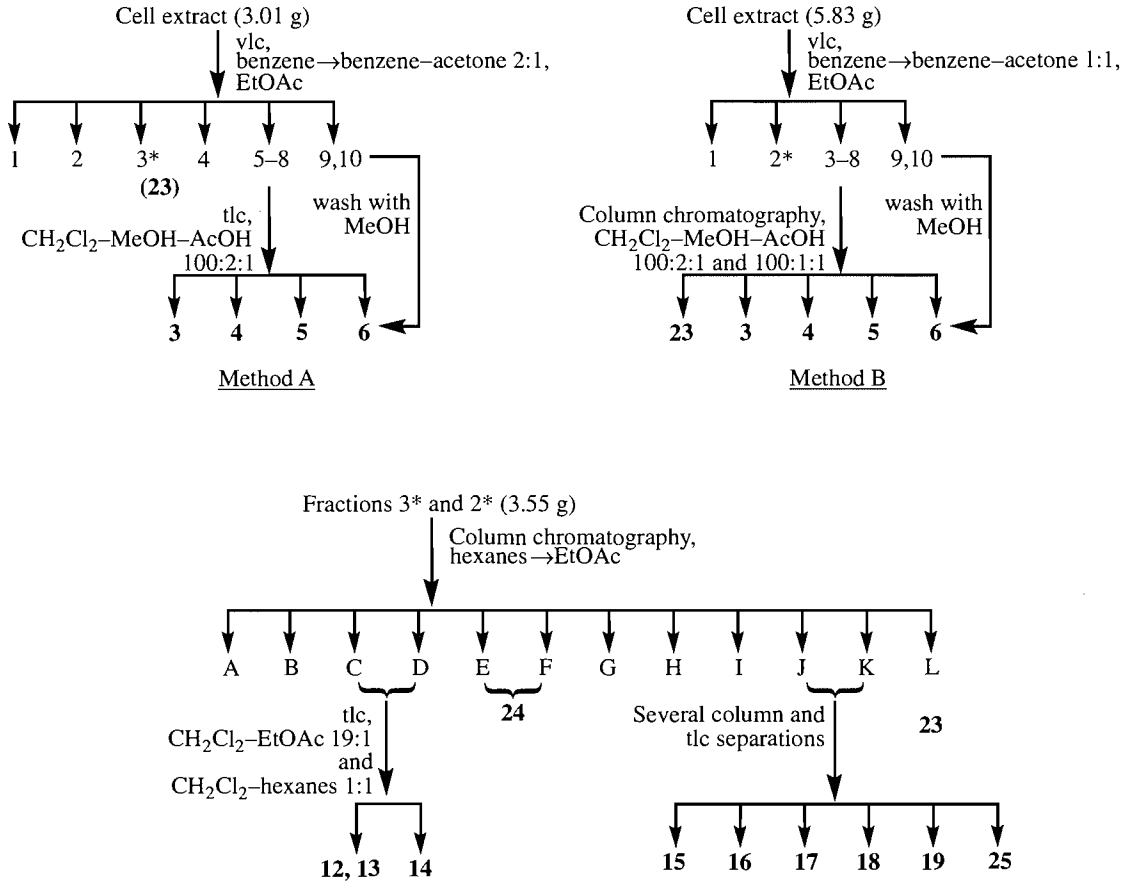

FIG. 3. Chromatographic separation of the cell extract.

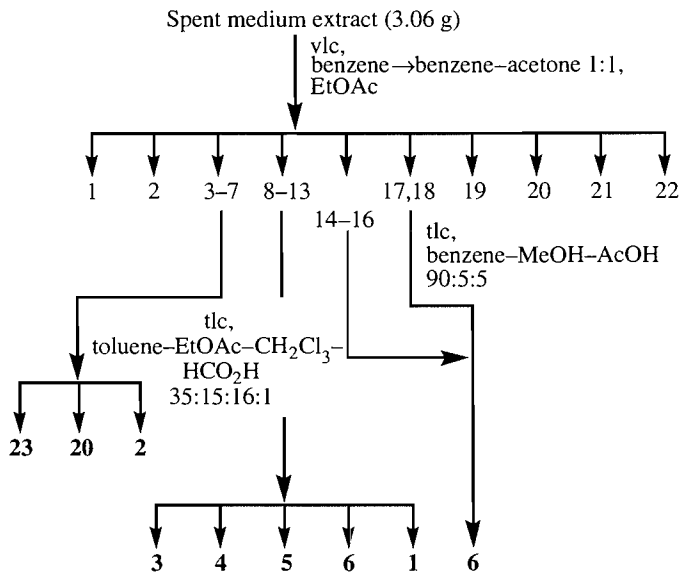

FIG. 4. Chromatographic separation of the spent medium extract.

TABLE 3. Yields of the metabolites isolated from 78 L of TRP4a suspension culture

Compound	Yield (mg)		
	Cells	Spent medium	Total
1		200	200
2		179	179
3	83	13	96
4	355	22	377
5	202	9	211
6	624	104	728
12, 13	122		122
14	50		50
15	29		29
16	14		14
17	29		29
18	51		51
19	28		28
20		135	135
23	1109	60	1169
24	553		553
25	247		247

148.9, and 154.8. Since the experiment was set up to enhance the $^3J_{C,H}$ coupled carbons (i.e., C12 and C14), the result was rather surprising. Nevertheless, the result indicates that attachment of the methoxyl group is at C12 since only one of the unsubstituted benzene carbons is enhanced (δ 123.7). Also, the quaternary carbon at δ 154.8 (the most deshielded carbon) is not observed in the ^{13}Cmr spectrum, but is quite strongly enhanced in the SINEPT spectrum, placing the methoxyl group at C12.

A series of nOe difference experiments were carried out

Can. J. Chem. Downloaded from www.nrcresearchpress.com by 217.78.4.112 on 09/08/12
For personal use only.

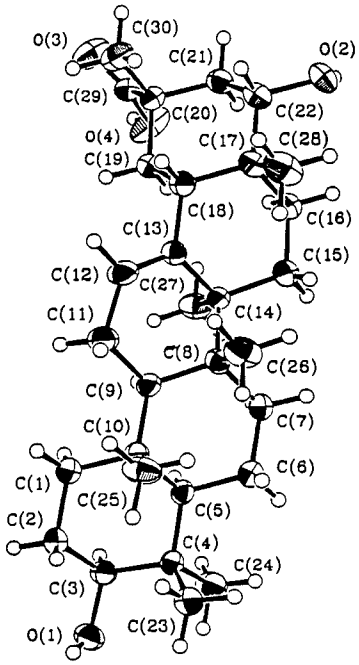

FIG. 5. Computer generated X-ray structure of triterpene **6**.

in order to confirm that the hydroxyl group is situated at C3 and to provide further evidence for the location of the methoxyl group at C12. Irradiation of OCH_3 at δ 3.72 shows enhancement of the isopropyl methine proton at δ 3.28 while irradiation of the latter produced enhancement of the OCH_3 signal. This evidence supports the assignment of the OCH_3 group to C12. Irradiation of the signal at δ 3.51 (C*H*OH) produced enhancements of both the C4 methyl groups at δ 0.96 and 1.05, confirming the location of the hydroxyl group at C3α (axial).

In summary, the spectral evidence confirms the structure of **14** as 12-methoxyabieta-8,11,13-trien-3α-ol, a novel diterpene isolated for the first time from the tissue cultures of *Tripterygium wilfordii*.

The quinone methide, **15**, was isolated as optically active ($[\alpha]^{22}$ −82.6) dark orange crystals (mp 140–142°C) with a molecular formula of $C_{28}H_{36}O_3$. The uv spectrum provided maxima typical of a quinone methide (λ_{max} 225 (ε 5.13 × 10^3), 256 (ε 8.20 × 10^3), and 424 nm (ε 8.72 × 10^3)). The mass spectrum of **15** shows a strong molecular ion peak at *m/z* 420, and principal fragment ions occurring at *m/z* 406, 405, 267, 253, 241, 227, 202, and 201, consistent with fragmentation at rings C and D of quinone methide triterpenes (23). The remaining spectral data (^{1}Hmr, COSY, see Experimental) were in support of structure **15** but a single crystal X-ray analysis established the structure and relative stereochemistry shown in **15** (Fig. 8). This compound is therefore identical to tingenone, and comparison with an authentic sample confirmed its identity.

The isolation of tingenone constitutes its first isolation from tissue cultures of *T. wilfordii*. Furthermore, the present X-ray study establishes, unambiguously, the relative stereochemistry of this quinone methide, a matter that was not entirely clear from the earlier isolations of this compound (24, 25). The X-ray structure shows rings C, D, and E in the chair conformation and the incorporation of ethyl acetate (crystallization solvent) in the crystal lattice.

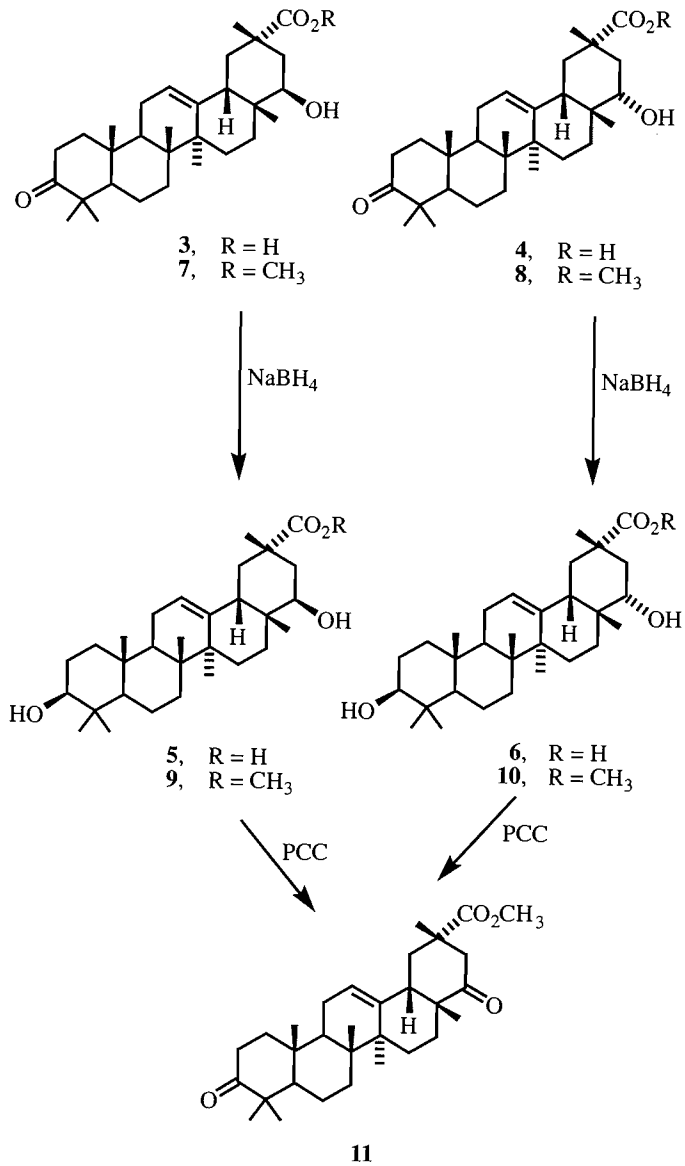

FIG. 6. Chemical correlation of the triterpenes **3**, **4**, **5**, and **6**.

The friedelane methyl ester, **16**, was isolated as optically active ($[\alpha]^{22}$ +101.4) yellow crystals (mp 150–151°C) with a molecular formula of $C_{30}H_{46}O_5$. Confirmation of the structure of **16** was achieved by a single crystal X-ray analysis. The absolute stereochemistry (by anomalous dispersion) is that shown in the computer-generated X-ray structure (Fig. 9). The methyl ester is established at C5 and all the rings are in the expected chair conformation. The friedelane methyl ester, **16**, is a novel triterpene exhibiting an unusual oxidation at C5.

The quinone methide, **17**, was isolated as optically active ($[\alpha]^{22}$ −484.6) dark orange crystals (mp 220–224°C) with a molecular formula of $C_{28}H_{36}O_4$. Its spectral data (see Experimental) revealed a close relationship to tingenone but the unambiguous assignment of an additional hydroxyl function, as suggested by the mass and ^{1}Hmr spectral data, was established by a single crystal X-ray analysis (Fig. 10) to be 22β-hydroxytingenone, the first isolation of this triterpene from the tissue cultures of *T. wilfordii*. Previous studies with several plants of the *Celastraceae* family, including

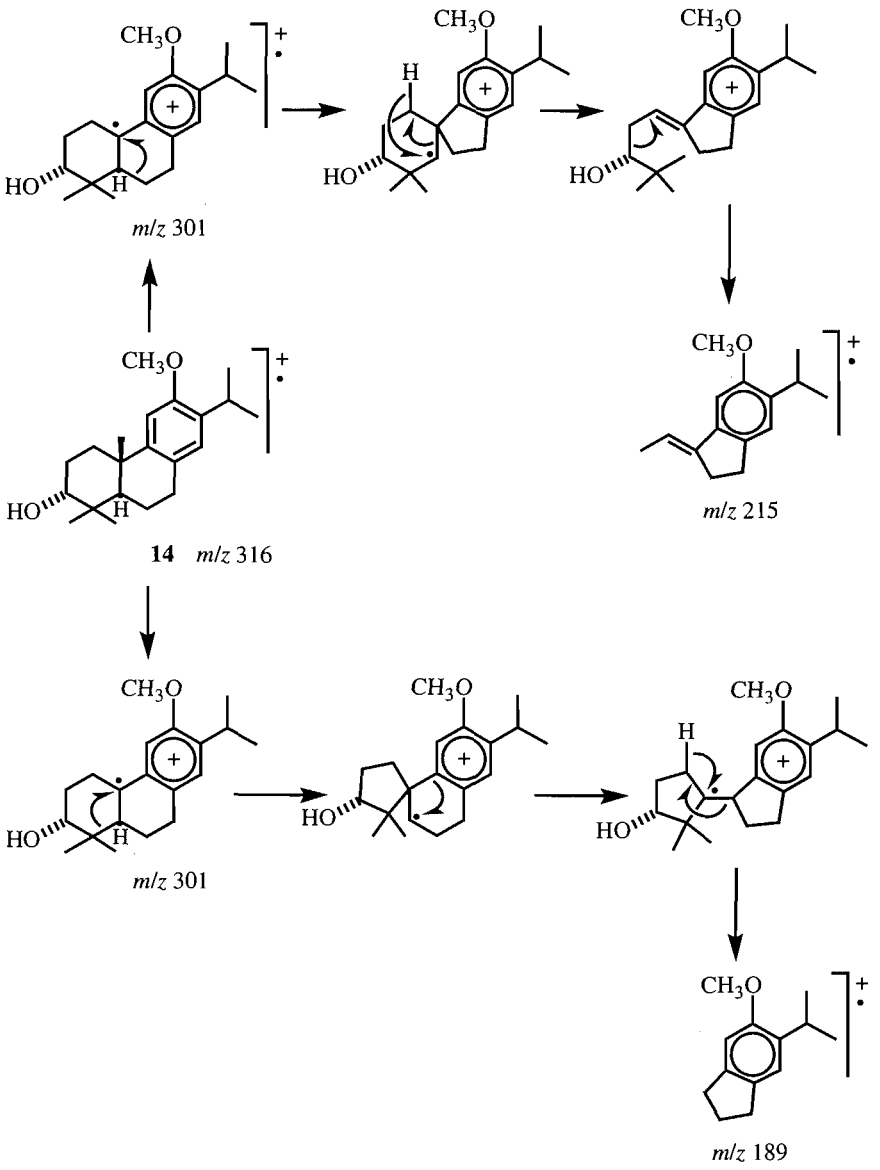

FIG. 7. Mass spectral fragmentation for diterpene **14**.

Euonymus tingens and various *Maytenus* species (24–30), have indicated the isolation of **17**, but an authentic sample could not be obtained.

The dihydroxyoleanene, **18**, was isolated as optically active ($[\alpha]^{22}$ +115.9) colourless prisms (mp 241–242°C) with a molecular formula of $C_{30}H_{50}O_2$. Although the extensive spectral data obtained for this compound (see Experimental) strongly suggested an oleanene-type structure, the conclusive location of the hydroxyl groups, particularly the hydroxymethyl group, was established via X-ray analysis (Fig. 11).

The isolation of **18** constitutes its first isolation from tissue cultures of *T. wilfordii*. A compound with a similar structure is reported to be isolated from *Celastrus paniculatus* and given the name paniculatadiol (31) but no spectral data are presented and an authentic sample could not be obtained for comparison.

Extensive studies into the pharmacological effects of oleanene-type compounds by Shibata and coworkers (32–36) have revealed the importance of a hydroxymethyl group in such compounds in terms of their ability to inhibit stress-induced peptic ulcer, activity against allergies, anti-tumour and analgesic activity, etc. As yet, no data are available with respect to **18**.

The dihydroxy triterpene, **19**, was isolated as optically active ($[\alpha]^{22}$ +55.3) colourless prisms (mp 230–234°C) with a molecular formula of $C_{30}H_{50}O_2$. Spectral data (see Experimental) suggested a β-amyrin type system. Final confirmation of structure and relative stereochemistry of **19** as 11α-hydroxy-β-amyrin was provided by a single crystal X-ray analysis (Fig. 12). A previous isolation of a compound corresponding to **19** has been reported in the gummy secretion of *Salvia glutinosa* (37) but again an authentic sample was unavailable.

In summary, the extraction of the TRP4a suspension cultures and separation of the extracts led to the isolation of 18 compounds, mainly triterpenes and also some diterpenes. Twelve of the compounds, of which five are new com-

Can. J. Chem. Downloaded from www.nrcresearchpress.com by 217.78.4.112 on 09/08/12
For personal use only.

Can. J. Chem. Downloaded from www.nrcresearchpress.com by 217.78.4.112 on 09/08/12
For personal use only.

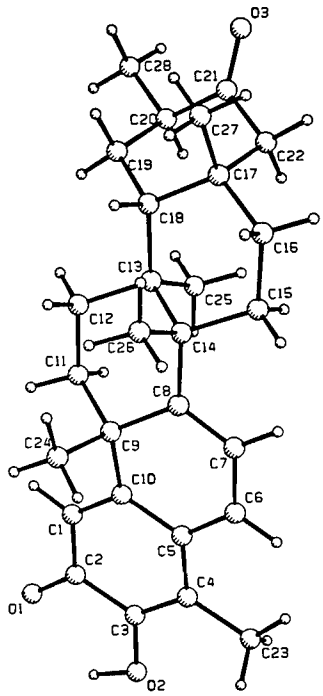

FIG. 8. Computer generated X-ray structure of **15**.

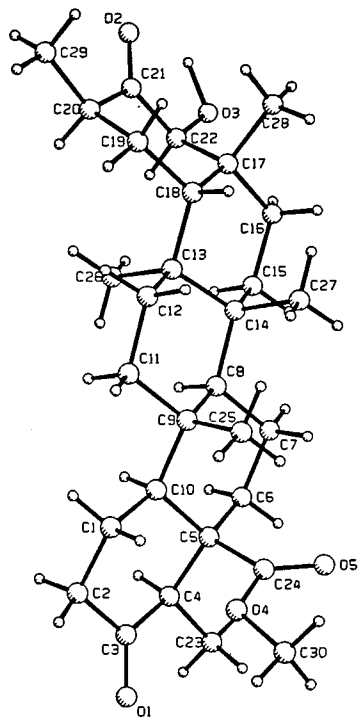

FIG. 9. Computer generated X-ray structure of **16** (the absolute stereochemistry is shown).

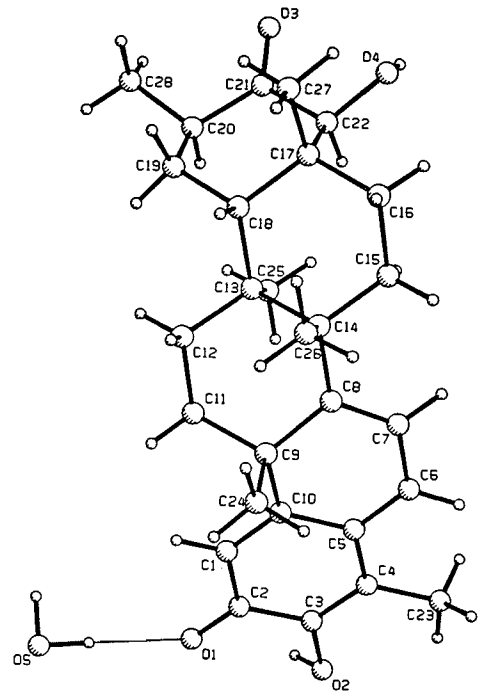

FIG. 10. Computer generated X-ray structure of **17**.

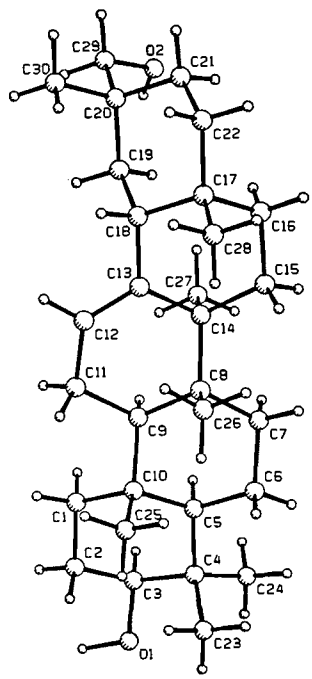

FIG. 11. Computer generated X-ray structure of **18**.

pounds (**3**, **4**, **5**, **14**, and 16), were not isolated previously from the TRP4a cultures. Pharmacological evaluation of some of these in terms of male contraceptive, immunosuppressive, and other activities is presently in progress and these results will be published elsewhere.

Experimental

TRP4a cell suspension cultures were grown in glass or in steel air-lift fermentors (Microferm, New Brunswick Scientific or an in-house fabricated fermentor, respectively). The spent medium was freeze-dried using a Dura-Dry freeze-dryer with a Dura-Top Bulk Tray Dryer (FTS Systems Inc.).

The ^{1}Hmr spectra were run at 300 and 400 MHz using Varian XL 300 and Bruker WH 400 spectrometers, respectively. Tetramethylsilane was used as the internal standard and all peaks are recorded in ppm (δ) relative to TMS (δ 0.00 ppm). The ^{13}Cmr spectra were run at 75.3 MHz using a Varian XL 300 spectrometer, using the ^{13}C signals of the deuterated solvents as the internal standards.

Low-resolution mass spectra were recorded using Kratos

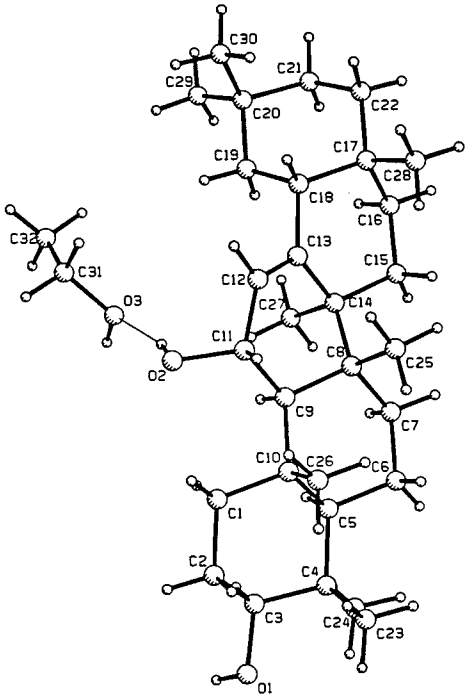

FIG. 12. Computer generated X-ray structure of **19**.

MS 50 and MS 80 mass spectrometers. High-resolution mass spectra were run on a Kratos MS 50 mass spectrometer. Chemical ionization mass spectra were recorded on a Delsi–Nermag R10-10C mass spectrometer using isobutane as the carrier gas.

The ir spectra were recorded on a Perkin Elmer 710B infrared spectrophotometer, and Fourier transform ir spectra were recorded on a Perkin Elmer 1710 infrared Fourier transform spectrophotometer. Optical rotations were recorded on a Perkin Elmer 141 polarimeter at the sodium D line. The uv spectra were recorded on a Unicam SP 800B ultraviolet spectrophotometer.

All melting points were recorded on a Reichert melting point apparatus or a Fisher–Johns melting point apparatus and are uncorrected.

Column chromatography was carried out using Merck silica gel 60, 230–400 mesh, while analytical and preparative tlc was performed using Merck precoated silica gel 60 F_{254} tlc plates. Vacuum liquid chromatography (vlc) was carried out using Merck silica gel 60G in sintered glass funnels with medium glass frits. Preparative hplc separations were performed on a Waters Associates Prep LC/System 500 installed with PrepPAK-500/silica cartridges and a refractive index detector. All solvents used for chromatography were BDH Omnisolv glass-distilled spectro-grade solvents.

Synthetic samples were visualized on analytical tlc plates (Merck) by uv and by spraying with a 5% solution of ammonium molybdate in 10% sulphuric acid, followed by heating at 125°C until blue spots developed. Tissue culture extracts were visualized on tlc spraying first with a 30% solution of concentrated sulphuric acid in glacial acetic acid, then with a 5% solution of anisaldehyde in isopropanol, followed by heating at 125°C for approximately 10 min.

Growth conditions for the TRP4a cell suspension cultures

The cultures were grown and maintained as discussed previously (6, 7) in PRD_2Co_{100} medium at 26°C for 22 days and then resuspended as a 10% inoculum in $MSNA_{0.5}K_{0.5}$ production medium. The cultures were incubated at 26°C in air-lift fermentors for 33–48 days before harvesting. The cells were harvested by filtration through Miracloth (Calbiochem) and were frozen until the time of extraction. The spent medium was freeze-dried and stored frozen until the time of extraction.

Extraction of the TRP4a cell suspension cultures

This is a typical procedure followed for the various bioreactor experiments, for example, TRP#221.

Cells (compare Fig. 1)

The cells were thawed and homogenized in a Waring blender with ethyl acetate (1 L). The cells were then filtered using Celite, and washed with ethyl acetate (300 mL). The filtrate was separated and the aqueous layer was extracted with ethyl acetate (3 × 200 mL) and discarded. The ethyl acetate layers were combined, dried over sodium sulphate (anhydrous), and the solvent was evaporated. The orange-brown extract was dried under vacuum and kept frozen until further use.

The filtered cell homogenate was suspended in methanol (500 mL) and sonicated for 2 h. Filtration and solvent evaporation gave a brown gummy extract which was dried under vacuum and kept frozen until further use.

Spent medium (compare Fig. 2)

The freeze-dried spent medium was reconstituted in water (300–500 mL) and extracted with ethyl acetate (3 × 200 mL). The organic layers were combined, dried over sodium sulphate (anhydrous), and the solvent was evaporated. The dark brown extract was dried under vacuum and frozen until further use. The aqueous layer was evaporated and the residue was sonicated with methanol (200 mL) and filtered. The filtrate was evaporated and the brown extract was dried under vacuum and frozen until further use.

Extraction of batches TRP#221, 222, 224, and 225, according to the above procedures, provides the weights of the extracts as given in Tables 1 and 2.

Preparation of crude samples for bioassay

Samples of the crude TRP#221 culture extracts were forwarded for immunological assay and for antifertility assay to the laboratories indicated in the Acknowledgement.

The solids obtained from the ethyl acetate extracts were prepared in a manner (see below) so as to generate emulsions in water (*vide infra*) while the solids obtained from the methanol extracts were forwarded without further preparation.

The ethyl acetate cell extract (0.84 g) from batch TRP#221 was dissolved in ethanol (15 mL) and polyvinylpyrrolidone (PVP, 4.20 g) was added. The solvent was evaporated and the residue was dried under vacuum to give 5.03 g of a water emulsifiable solid. The procedure was repeated with the ethyl acetate spent medium extract (0.44 g, with 2.19 g of PVP) to give 2.65 g of a water emulsifiable solid.

Partial separation of the ethyl acetate cell extracts for biological assay

The remaining ethyl acetate cell extracts (from batches TRP#222, 224, and 225) were combined (3.73 g) and separated into 8 partially purified fractions by vacuum liquid chromatography using Merck silica gel 60G (80 g) packed into a sintered glass funnel (150 mL, medium frit), attached to a bell jar with a sidearm, which was connected to a water aspirator. Fifty-milliliter fractions were collected and stepwise elution was carried out using: (*i*) hexanes – ethyl acetate 4:1 (6 × 50 mL); (*ii*) hexanes – ethyl acetate 3:1 (6 × 50 mL); (*iii*) hexanes – ethyl acetate 2:1 (6 × 50 mL); (*iv*) hexanes – ethyl acetate 1:1 (6 × 50 mL); and (*v*) ethyl acetate (6 × 50 mL). The column was flushed with ethyl acetate – methanol 1:1 (250 mL) to elute the polar material.

Elution with hexanes – ethyl acetate 4:1 yielded an oily fraction (378.76 mg) containing fatty acid-like compounds (fraction 1). Further elution with hexanes – ethyl acetate 4:1 and hexanes – ethyl acetate 3:1 yielded fraction 2 (389.66 mg), containing nonpolar diterpenes and sterols. Elution with hexanes – ethyl acetate 3:1 and 2:1 yielded fraction 3 (273.60 mg) as a brown solid containing several terpenoid components. Further elution with hexanes – ethyl acetate 2:1 gave fraction 4 (267.59 mg) while elution with hexanes – ethyl acetate 1:1 yielded fraction 5 (505.63 mg). Both fractions contained triterpenoid components. Elution with ethyl acetate gave fraction 6 (291.01 mg) as a light brown solid con-

Can. J. Chem. Downloaded from www.nrcresearchpress.com by 217.78.4.112 on 09/08/12
For personal use only.

Can. J. Chem. Downloaded from www.nrcresearchpress.com by 217.78.4.112 on 09/08/12
For personal use only.

taining polar triterpenes. Elution with ethyl acetate and ethyl acetate – methanol 1:1 gave fraction 7 (175.80 mg) as a light brown solid containing polar triterpenes. Fraction 8 (1.22 g) was eluted with ethyl acetate – methanol 1:1, yielding polar material as a dark brown solid.

Partial separation of the spent medium ethyl acetate extracts for biological assay

The remaining ethyl acetate spent medium extracts (from batches TRP#222, 224, and 225) were combined (1.17 g) and partially separated by vacuum liquid chromatography using a sintered glass funnel (60 mL, medium frit, Merck silica gel 60G, 30 g). Thirty-milliliter fractions were collected to give 10 partially purified fractions. Stepwise elution was carried out using: (*i*) hexanes (5 × 30 mL); (*ii*) hexanes – ethyl acetate 19:1 (5 × 30 mL); (*iii*) hexanes – ethyl acetate 9:1 (5 × 30 mL); (*iv*) hexanes – ethyl acetate 4:1 (5 × 30 mL); (*v*) hexanes – ethyl acetate 1:1 (5 × 30 mL); and (*vi*) ethyl acetate (5 × 30 mL). The polar material was eluted from the column using ethyl acetate – methanol 1:1 (150 mL).

Elution with hexanes and hexanes – ethyl acetate 19:1 gave fraction 1 (4.32 mg) as a yellow solid containing nonpolar terpenoid components. Elution with hexanes – ethyl acetate 19:1, 9:1, and 4:1 gave fraction 2 (23.89 mg) and elution with hexanes – ethyl acetate 4:1 gave fraction 3 (14.28 mg). Both fractions contained several terpenoid components. Further elution with hexanes – ethyl acetate 4:1 and 1:1 yielded fraction 4 (60.64 mg) as a light brown solid containing diterpenoid and triterpenoid metabolites. Elution with hexanes – ethyl acetate 1:1 and ethyl acetate yielded fraction 5 (128.52 mg) as a brown solid containing diterpenoids and triterpenoids. Elution with ethyl acetate gave fraction 6 (206.21 mg) as a yellow-brown solid containing triptolide (**2**) and several triterpenes. Further elution with ethyl acetate yielded fraction 7 (204.75 mg) as a yellow-brown solid containing tripdiolide (**1**) and several triterpenes. Elution with ethyl acetate and ethyl acetate – methanol 1:1 gave fraction 8 (52.43 mg) as a brown solid containing triterpenes and polar material. Elution with ethyl acetate – methanol 1:1 gave fraction 9 (303.69 mg) while further elution with ethyl acetate – methanol 1:1 yielded fraction 10 (76.54 mg) as polar material in the form of brown solids.

Preparation of the partially purified extracts for biological assay

All the fractions were treated as above with polyvinylpyrrolidone (5:1, PVP:fraction, w/w) in order to obtain samples capable of forming emulsions in water. The samples were then forwarded for immunological and antifertility assays.

Isolation of pure metabolites from the TRP4a cell suspension cultures

To obtain large quantities of cells and spent medium, 6 batches (10–17 L) were grown in bioreactors for 25–39 days to afford a total of 78 L (Table 3). The batches were combined on harvesting and filtered through Miracloth. The cells (wet weight 8.94 kg) were frozen and the spent media (60.6 L) were concentrated to 1.4 L by freeze-drying.

Extraction of the combined cells and the combined spent media was performed as described above, with the 5-fold increase of the extraction solvent and omission of a sonication with methanol. Cell extraction yielded 13.08 g of a dark orange extract. Spent media extraction gave 14.73 g of an orange-brown extract.

Chromatographic separation of the cell extract metabolites

Initial purification of the cell extract (13.08 g) was carried out by filtration through silica gel (Merck silica gel 230–400 mesh, 60 mL) using ethyl acetate, to remove the polar material. Evaporation of the solvent yielded 9.04 g of crude extract as an orange solid; 3.01 g of this extract was purified following the procedure described as Method A, 5.83 g was purified by Method B (compare Fig. 3).

Method A

The cell extract (3.01 g) was partially separated by vacuum liquid chromatography using a 150-mL sintered glass funnel (medium frit, Merck silica gel 60G, 90 g). Stepwise elution using (*i*) benzene (5 × 30 mL); (*ii*) benzene–acetone 4:1 (25 × 30 mL); (*iii*) benzene–acetone 3:1 (15 × 30 mL); (*iv*) benzene–acetone 2:1 (18 × 30 mL); and (*v*) ethyl acetate (300 mL) gave 10 fractions. Fractions 1 (349.11 mg) and 2 (45.70 mg) were colorless oily fractions consisting of fatty acid-like compounds. Fraction 3 (1.17 g), a dark orange fraction, contained diterpenes, sterols, triterpenes, and quinone methides (see below for the separation of this fraction). Fraction 4 yielded oleanolic acid (**23**, 432.26 mg). Fraction 5 (162.39 mg) consisted of triterpenes **3** and **4** and fraction 6 (147.96 mg) contained triterpenes **3**, **4**, **5**, and **6**. Fraction 7 (92.80 mg) contained triterpenes **4**, **5**, and **6**, while fraction 8 (75.03 mg) contained a small quantity of triterpenes **5** and **6**. Fractions 9 and 10 (347.58 and 52.42 mg respectively) consisted of triterpene **6** and some polar material.

Separation of fractions 5–8 was carried out by preparative tlc (Merck silica 60G, 6 × 0.5 mm silica gel plates) using methylene chloride – methanol–acetic acid 100:2:1 (the plates were eluted four times) to give triterpene **3** (27.25 mg), triterpene **4** (65.77 mg), triterpene **5** (20.85 mg), and triterpene **6** (21.80 mg). Fractions 9 and 10 were combined and washed with methanol to give a further quantity of **6** (157.13 mg).

In summary, chromatographic separation yielded oleanolic acid (**23**, 432.26 mg) and triterpenes **3** (27.25 mg), **4** (65.77 mg), **5** (20.85 mg), and **6** (157.13 mg).

Method B

The cell extract (5.83 g) was partially separated by vacuum liquid chromatography using a 150-mL sintered glass funnel (medium frit, Merck silica gel 60G, 90 g). Stepwise elution was carried out using: (*i*) benzene (5 × 30 mL); (*ii*) benzene–acetone 4:1 (15 × 30 mL); (*iii*) benzene–acetone 3:1 (10 × 30 mL); (*iv*) benzene–acetone 2:1 (30 mL); (*v*) benzene–acetone 1:1 (10 × 30 mL); and (*vi*) ethyl acetate (250 mL), yielded 10 crude fractions. Fraction 1 (756.14 mg) was an oily fraction consisting of fatty acid-like compounds. Fraction 2 (2.38 g) containing diterpenes, sterols, triterpenes, and quinone methides was subsequently combined with fraction 3 from Method A for further separation (*vide infra*). Fraction 3 (126.58 mg) was a mixture of oleanolic acid (**23**) and triterpene **3**, while fraction 4 (281.26 mg) contained triterpenes **3** and **4**. Fractions 5 and 6 (74.93 mg and 62.50 mg respectively) consisted of mainly triterpene **4** and a small quantity of triterpene **5**. Fraction 7 (219.67 mg) contained triterpenes **4** and **5**, while fraction 8 (106.61 mg) contained triterpenes **4**, **5**, and **6**. Fractions 9 and 10 (569.53 mg and 534.98 mg respectively) contained triterpene **6** and polar material.

Fractions 3–8 were combined and separated by column chromatography (Merck silica gel 230–400 mesh, methylene chloride – methanol acetic acid 100:2:1) to give oleanolic acid (**23**, 101.97 mg), a mixture of **3** and **4** (101.97 mg), triterpene **4** (167.69 mg), triterpene **5** (181.17 mg), and triterpene **6** (85.34 mg). The mixture of **3** and **4** was separated by further column chromatography (Merck silica gel 230–400 mesh, methylene chloride – methanol – acetic acid 100:1:1) to give **3** (55.80 mg) and a further quantity of **4** (121.74 mg). Fractions 9 and 10 were combined and washed with methanol to give **6** (359.65 mg).

In summary, chromatographic separation via Method B yielded oleanolic acid (**23**, 101.97 mg) and triterpenes **3** (55.80 mg), **4** (289.43 mg), **5** (181.17 mg), and **6** (444.99 mg).

*22β-Hydroxy-3-oxoolean-12-en-29-oic acid (**3**)*

Colourless prisms (ethyl acetate); mp 268–270°C; $[\alpha]^{22}$ +92.9 (*c* 0.70, MeOH); uv (MeOH) λ_{max} 217 (ϵ 726); ir ($CHCl_3$) cm^{-1}: 3618 (OH), 2938 (CH), 2640 (OH), 1698 (C=O); ^{1}Hmr ($CDCl_3$) δ: 0.91 (3H, s), 1.04 (3H, s), 1.07 (3H, s), 1.09 (3H, s), 1.11 (3H, s), 1.15 (3H, s), 1.41 (3H, s), 0.86–2.32 (2OH, m), 2.39 (1H, ddd, H2α, *J* = 4, 6, 16), 2.55 (1H, ddd, H2β, *J* = 4, 11, 16), 3.50 (1H, s, OH), 3.58 (1H, dd, H22α, *J* = 3.5, 7.0), 5.33 (1H, t, H12); ^{13}Cmr (C_5D_5N) δ: 15.4, 17.2, 19.9, 21.1, 21.8, 24.0, 25.3, 25.4, 26.4, 26.7, 29.1, 32.7, 34.5, 36.9, 38.0, 38.2, 39.4, 39.9, 41.7,

Can. J. Chem. Downloaded from www.nrcresearchpress.com by 217.78.4.112 on 09/08/12
For personal use only.

42.6, 44.9, 47.1, 47.5, 55.3, 75.4, 122.9, 144.2, 181.6, 217.8; ms *m/z* (rel. int., %): 470 (M^+, 3.8), 452 (7.0), 437 (2.7), 426 (4.4), 424 (5.5), 408 (15.7), 391 (3.2), 340 (11.1), 325 (4.1), 264 (43.7), 246 (67.8), 217 (79.9), 205 (57.3), 201 (38.3), 189 (46.0), 171 (44.5), 159 (42.7), 147 (55.9), 135 (82.3), 119 (95.1), 107 (90.5), 81 (89.8), 69 (71.4), 55 (100), 43 (53.4). High-resolution mass measurement: calcd. for $C_{30}H_{46}O_4$: 470.3398; found: 470.3414. Anal. calcd. for $C_{30}H_{46}O_4$: C 76.55, H 9.85; found: C 76.02, H 9.97.

*22α-Hydroxy-3-oxoolean-12-en-29-oic acid (**4**)*

Colourless prisms (meOH); mp 289–290°C; $[\alpha]^{22}$ + 84.4 (*c* 1.09, MeOH); uv (MeOH) λ_{max} 212 (ε 1938); ir ($CHCl_3$) cm^{-1}: 3615 (OH), 2976 (CH), 2630 (OH), 1698 (C=O), ^{1}Hmr ($CDCl_3$) δ: 1.02 (3H, s), 1.04 (3H, s), 1.07 (3H, s), 1.08 (3H, s), 1.10 (3H, s), 1.18 (3H, s), 1.29 (3H, s), 1.26–2.27 (21H, m), 2.38 (1H, ddd, H2α, *J* = 4, 6, 16), 2.55 (1H, ddd, H2β, *J* = 4, 11, 16), 3.60 (1H, dd, H22β, *J* = 4, 12), 5.29 (1H, t, H12); ^{13}Cmr ($CDCl_3$) δ: 15.3, 16.7, 19.2, 19.7, 20.4, 21.6, 23.7, 24.5, 25.5, 26.1, 26.5, 32.0, 34.2, 36.5, 36.6, 38.3, 39.3, 39.6, 39.9, 42.2, 42.7, 46.3, 46.8, 47.5, 55.2, 75.3, 123.1, 142.6, 183.3, 217.8; ms *m/z* (rel int., %): 470 (M^+, 0.6), 452 (11.8), 437 (2.0), 408 (1.5), 391 (1.3), 353 (0.6), 340 (0.5), 326 (1.7), 299 (1.2), 285 (2.2), 264 (3.7), 246 (100.0), 228 (12.2), 218 (25.1), 205 (35.8), 201 (20.0), 185 (20.9), 173 (14.2), 159 (16.9), 145 (23.6), 131 (31.0), 119 (38.0), 107 (29.3), 95 (34.3), 81 (22.1), 69 (14.4), 55 (24.6), 43 (21.7). High-resolution mass measurement: calcd. for $C_{30}H_{46}O_4$: 470.3398; found: 470.3417. Anal. calcd. for $C_{30}H_{46}O_4$: C 76.55, H 9.85; found: C 76.40, H 9.90.

*3β,22β-Dihydroxyolean-12-en-29-oic acid (**5**)*

Colorless prisms (MeOH–H_2O); mp 281–283°C; $[\alpha]^{22}$ +55.0 (*c* 0.60, MeOH); uv (MeOH) λ_{max} 216 (ε 835); ir (KBr) cm^{-1}: 3467 (OH), 3422 (OH), 2976 (CH), 2640 (OH), 1698 (C=O); ^{1}Hmr (C_5D_5N) δ: 0.76 (3H, s), 0.85 (6H, s), 1.02 (3H, s), 1.03 (3H, s), 1.08 (3H, s), 1.63 (3H, s), 0.62–2.63 (24H, m), 3.22 (1H, dd, $H_3\alpha$, *J* = 6, 9.5), 3.80 (1H, brd, H22α, *J* = 4.5), 5.21 (1H, t, H12); ^{13}Cmr (C_5D_5N) δ: 15.8, 16.6, 17.2, 18.7, 21.0, 23.8, 24.9, 25.5, 26.3, 28.0, 28.7, 28.8, 30.7, 33.2, 37.2, 37.7, 38.0, 39.1, 39.3, 39.9, 41.5, 42.4, 44.6, 48.0, 55.7, 75.3, 77.9, 123.1, 144.2, 181.0; ms *m/z* (rel. int., %): 472 (M^+, 6.1), 454 (5.0), 439 (2.6), 426 (2.0), 411 (2.1), 393 (1.5), 264 (99.7), 246 (53.0), 231 (15.4), 217 (100.0), 207 (59.9), 190 (45.2), 175 (39.3), 161 (22.7), 147 (37.9), 135 (74.1), 119 (49.9), 107 (48.2), 95 (52.4), 81 (49.9), 69 (48.6), 55 (48.7), 43 (30.7). High-resolution mass measurement: calcd. for $C_{30}H_{48}O_4$: 472.3554; found: 472.3567. Anal. calcd. for $C_{30}H_{48}O_4 \cdot H_2O$: C 73.43, H 10.27; found: C 73.53, H 10.40.

*3β-22α-Dihydroxyolean-12-en-29-oic acid (**6**)*

Colourless prisms (MeOH); mp 293–298°C (subl.); $[\alpha]^{22}$ +93.5 (*c* 0.46, MeOH); uv (MeOH) λ_{max} 212 (ε 1509); ir (KBr) cm^{-1}: 3475 (OH), 3387 (OH), 2946 (CH), 2550 (OH), 1698 (C=O); ^{1}Hmr (C_5D_5N) δ: 0.98 (3H, s), 1.03 (3H, s), 1.04 (3H, s), 1.23 (3H, s), 1.28 (3H, s), 1.37 (3H, s), 1.58 (3H, s), 0.82–2.74 (24H, m), 3.42 (1H, dd, H3α, *J* = 6, 10), 4.01 (1H, dd, H22β, *J* = 5.5, 13), 5.38 (1H, t, H12); ^{13}Cmr (C_5D_5N) δ: 15.8, 16.6, 17.0, 18.8, 19.9, 21.4, 23.9, 25.4, 26.1, 26.3, 28.0, 28.7, 32.9, 37.2, 38.6, 39.1, 39.4, 40.2, 41.2, 42.4, 47.2, 47.9, 55.6, 74.7, 78.0, 123.1, 144.2, 181.1; ms *m/z* (rel int., %): 472 (M^+, 0.2), 454 (2.6), 436 (1.7), 421 (1.3), 410 (0.6), 393 (1.2), 342 (1.1), 325 (0.6), 314 (0.9), 299 (2.0), 264 (2.7), 246 (100.0), 218 (21.6), 207 (18.1), 201 (15.5), 190 (35.6), 175 (20.3), 159 (14.8), 145 (20.1), 131 (22.5), 119 (32.2), 107 (23.2), 95 (25.9), 81 (17.7), 69 (12.2), 55 (14.7). High-resolution mass measurement: calcd. for $C_{30}H_{48}O_4$: 472.3554; found: 472.3540. Anal. calcd. for $C_{30}H_{48}O_4$:[2] C 76.23, H 10.23; found: C 76.10, H 10.33.

[2]All the data for this compound were obtained on a sample that was recrystallized from ethanol, except for the X-ray analysis. Recrystallization from methanol was shown by X-ray analysis to yield crystals as the 1:1 methanol solvate.

*Oleanolic acid (**7**)*

The isolated sample was compared (mp, identical ir, ^{1}Hmr, and ms spectra) with an authentic sample available in our sample collection.

*Reduction of 22α-hydroxy-3-oxoolean-12-en-29-oic acid (**4**)*

The acid **4** (11.24 mg, 0.02 mmol) was dissolved in ethanol (1 mL) and sodium borohydride (4.52 mg, 0.12 mmol) was added. The reaction mixture was stirred at room temperature for 30 min and ethyl acetate (30 mL) was added. The solution was washed with 10% HCl (2 × 5 mL) and water (2 × 10 mL) and the solvent was evaporated to give 8.63 mg (76.4%) of **6** as a white solid (tlc, mp, ^{1}Hmr, and ms were identical with those of isolated **6**).

*Reduction of 22β-hydroxy-3-oxoolean-12-en-29-oic acid (**3**)*

The acid **3** (6.18 mg, 0.01 mmol) was treated as above with sodium borohydride, which yielded, after work-up, 5.92 mg (95.3%) of **5** as a white solid (tlc, mp, ^{1}Hmr, and ms were identical with those of isolated **5**).

*Esterification of **3**, **4**, **5**, and **6***

Suspensions of the triterpenes **3**, **4**, **5**, and **6** in ether (3 mL) were treated with an ethereal solution of excess diazomethane at room temperature overnight. Evaporation of the solvent gave the methyl esters **7**, **8**, **9**, and **10** as white solids. They were then crystallized (MeOH as solvent) to provide the pure compounds with constant melting points.

*Methyl-22β-hydroxy-3-oxoolean-12-en-29-oate (**7**)*

White solid; mp 195–197°C; $[\alpha]^{22}$ +82.3 (*c* 1.15, $CHCl_3$); ir ($CHCl_{33}$) cm^{-1}: 3425 (OH), 2910 (CH), 1719 (C=0), 1698 (C=O); ^{1}Hmr ($CDCl_3$) δ: 0.90 (3H, s), 1.04 (3H, s), 1.06 (3H, s), 1.08 (3H, s), 1.10 (3H, s), 1.14 (3H, s), 1.36 (3H, s), 0.82–2.27 (20H, m), 2.38 (1H, ddd, H2α, *J* = 4, 6, 16), 2.55 (1H, ddd, H2β, *J* = 4, 11, 16), 3.55 (1H, dd, H22α, *J* = 3, 4), 3.69 (3H, s, OCH_3), 5.33 (1H, t, H12); ms *m/z* (rel. int., %): 484 (M^+, 42.5), 469 (4.6), 466 (7.9), 453 (10.4), 425 (16.9), 407 (4.7), 391 (3.5), 375 (6.3), 278 (100.0), 265 (57.1), 260 (25.7), 247 (43.3), 231 (83.2), 219 (35.5), 205 (40.5), 200 (41.7), 187 (27.9), 171 (58.1), 161 (16.9), 144 (40.7), 125 (60.7), 112 (37.7), 95 (26.7), 81 (20.1), 69 (16.7), 55 (15.7). High-resolution mass measurement: calcd. for $C_{31}H_{48}O_4$: 484.3552; found: 484.3554.

*Methyl-22α-hydroxy-3-oxoolean-12-en-29-oate (**8**)*

White solid; mp 149–151°C; $[\alpha]^{22}$ +92.9 (*c* 0.85, $CHCl_3$); ir ($CHCl_3$) cm^{-1}: 3600 (OH), 2930 (CH), 1718 (C=O), 1698 (C=O); ^{1}Hmr ($CDCl_3$) δ: 1.02 (3H, s), 1.04 (3H, s), 1.07 (3H, s), 1.08 (3H, s), 1.11 (3H, s), 1.18 (3H, s), 1.26 (3H, s), 1.35–2.23 (20H, m), 2.38 (1H, ddd, H2α, *J* = 4, 6, 16), 2.55 (1H, ddd, H2β, *J* = 4, 11, 16), 3.59 (1H, dd, H22β, *J* = 4, 12), 3.68 (3H, s, OCH_3), 5.28 (1H, t, H12); ms *m/z* (rel. int., %): 484 (M^+, 18.5), 466 (5.0), 452 (21.2); 437 (3.4), 406 (3.4), 391 (3.5), 340 (2.3), 326 (4.1), 299 (1.9), 278 (43.3), 265 (6.8), 260 (13.3), 246 (100.0), 231 (28.9), 218 (18.2), 205 (29.8), 185 (21.6), 171 (23.0), 159 (13.1), 147 (21.0), 131 (19.2), 120 (22.3), 107 (17.8), 95 (27.9), 81 (10.5), 69 (1.9), 55 (9.1). High-resolution mass measurement: calcd. for $C_{31}H_{48}O_4$: 484.3552; found: 484.3570.

*Methyl-3β,22β-dihydroxyolean-12-en-29-oate (**9**)*

White solid; mp 228–229°C; $[\alpha]^{22}$ +64.0 (*c* 0.88, $CHCl_3$); ir ($CHCl_3$) cm^{-1}: 3665 (OH), 3586 (OH), 2900 (CH), 1718 (C=O); ^{1}Hmr ($CDCl_3$) δ: 0.80 (3H, s), 0.90 (3H, s), 0.96 (3H, s), 0.99 (3H, s), 1.01 (3H, s), 1.13 (3H, s), 1.36 (3H, s), 0.73–2.27 (23H, m), 3.23 (1H, dd, H3α, *J* = 4, 10), 3.55 (1H, dd, H22α, *J* = 4, 8), 3.68 (3H, s, OCH_3), 5.30 (1H, t, H12); ms *m/z* (rel. int., %): 486 (M^+, 13.3), 471 (1.2), 468 (3.0), 455 (3.6), 427 (2.0), 409 (1.5), 354 (1.4), 330 (1.4), 304 (1.3), 292 (3.4), 278 (100.0), 260 (23.6), 246 (23.3), 231 (79.5), 219 (23.3), 207 (47.9), 200 (47.3), 189 (25.6), 171 (60.2), 144 (43.0), 135 (34.8), 119 (37.3), 112 (37.6), 107 (28.1), 95 (27.3), 81 (23.1), 69 (17.0), 55 (18.5). High-res-

olution mass measurement: calcd. for $C_{31}H_{50}O_4$: 486.3711; found: 486.3722.

*Methyl-3α-22α-dihydroxyolean-12-en-29-oate (**10**)*

White solid; mp 118–121°C; $[\alpha]^{22}$ +74.9 (*c* 0.90, $CHCl_3$); ir ($CHCl_3$) cm^{-1}: 3655 (OH), 3600 (OH), 2932 (CH), 1718 (C=O); ^{1}Hmr ($CDCl_3$) δ: 0.80 (3H, s), 0.94 (3H, s), 0.98 (3H, s), 1.00 (6H, s), 1.17 (3H, s), 1.26 (3H, s), 0.73–2.22 (23H, m), 3.23 (1H, dd, H3α, *J* = 4, 10), 3.58 (1H, dd, H22β, *J* = 4, 12), 3.67 (3H, s, OCH_3), 5.26 (1H, t, H12); ms *m/z* (rel. int., %): 486 (M^+, 3.1), 468 (1.1), 454 (4.7), 436 (1.9), 421 (1.2), 409 (0.7), 393 (1.0), 342 (0.8), 328 (1.1), 314 (0.9), 300 (1.7), 278 (16.9), 246 (100.0), 231 (14.9), 218 (17.6), 207 (24.1), 190 (35.0), 175 (15.6), 159 (11.9), 147 (15.8), 131 (16.1), 119 (20.6), 107 (14.5), 95 (22.5), 81 (9.3), 69 (7.5), 55 (7.7). High-resolution mass measurement: calcd. for $C_{31}H_{50}O_4$: 486.3711; found: 486.3695.

*Methyl-3,22-dioxoolean-12-en-29-oate (**11**)*

Excess pyridinium chlorochromate was added to a stirred solution of **9** (10.00 mg, 0.02 mmol) in methylene chloride (1.0 mL) and the reaction mixture was stirred at room temperature for 30 min. The reaction mixture was filtered through Florisil (30 mL) and the Florisil was washed with ether. The washing and the filtrate were combined and the solvent was evaporated to give 8.23 mg (83.0%) of **11** as a white solid, mp 180.5–182°C; $[\alpha]^{22}$ +5.7 (*c* 4.75, $CHCl_3$); ir ($CHCl_3$) cm^{-1}: 3000 (CH), 2940 (CH), 1721 (C=O), 1698 (C=O); ^{1}Hmr ($CDCl_3$) δ: 1.03 (3H, s), 1.04 (3H, s), 1.07 (3H, s), 1.09 (3H, s), 1.11 (3H, s), 1.16 (3H, s), 1.24 (3H, s), 1.21–2.11 (20H, m), 2.32 (1H, dd, H19β, *J* = 3.5, 15), 2.39 (1H, ddd, H2α, *J* = 4, 6, 16), 2.48 (1H, d, H21β, *J* = 14.5), 2.56 (1H, ddd, H2β, *J* = 4, 11, 16), 2.99 (1H, d, H21α, *J* = 14.5), 3.71 (3H, s, OCH_3), (1H, t, H12); ms *m/z* (rel. int., %): 482 (M^+, 18.4), 467 (2.3), 464 (2.7), 451 (1.8), 423 (2.0), 405 (1.6), 339 (1.7), 298 (0.8), 276 (100.0), 263 (11.1), 247 (16.4), 215 (17.6), 205 (13.5), 199 (16.7), 187 (13.8), 173 (9.8), 159 (9.9), 142 (25.5), 134 (24.3), 119 (20.5), 114 (68.7), 105 (13.2), 93 (9.4), 81 (8.8), 69 (4.9), 55 (10.3). High-resolution mass measurement: calcd. for $H_{31}H_{46}O_4$: 482.3398; found: 482.3405.

*Oxidation of **10***

Excess pyridinium chlorochromate was added to a stirred solution of **10** (5.03 mg, 0.01 mmol) in methylene chloride (1.0 mL) and the reaction mixture was stirred at room temperature for 30 min. The reaction mixture was filtered through Florisil (30 mL) and the Florisil was washed with water. The washings and the filtrate were combined and the solvent was evaporated to give 3.76 mg (75.4%) of **11** as a white solid.

Separation and identification of the metabolites from fraction 3 (from Method A) and fraction 2 (from Method B) (compare Fig. 3)

Fraction 3 (1.17 g) from Method A and fraction 2 (2.38 g) from Method B (*vide supra*) were combined (3.55 g) and partially separated by column chromatography (Merck silica gel 230–400, 350 g). Stepwise elution was carried out using: (*i*) hexanes (250 mL); (*ii*) hexanes – ethyl acetate 9:1 (500 mL); (*iii*) hexanes – ethyl acetate 4:1 (1500 mL); (*iv*) hexanes – ethyl acetate 3:1 (1000 mL); (*v*) hexanes – ethyl acetate 2:1 (1000 mL); and (*vi*) ethyl acetate (1000 mL) to give 12 crude fractions. Fractions A and B (126.30 and 178.25 mg respectively) were complex mixtures of minor components and were not further investigated, while fractions C and D (198.84 and 49.34 mg respectively) consisted of two major components (see below for the separation). Fractions E and F (489.19 and 64.06 mg respectively) yielded β-sitosterol (**24**), while fractions G, H, and I (69.81, 46.35, and 38.15 mg respectively) were complex mixtures and were not further investigated. Fractions J and K (815.16 and 195.71 mg respectively) contained orange-coloured quinone methides and polpunonic acid (**25**) (see below for the separation), and fraction L yielded oleanolic acid (**23**, 564.65 mg).

The identities of β-sitosterol, polpunonic acid, and oleanolic acid were confirmed by comparison with authentic samples.

Separation of fractions C and D

Fractions C and D were subjected to preparative tlc (Merck silica gel 60 F_{254}, 2 mm) using methylene chloride – ethyl acetate 19:1 (the plate was eluted twice) and a further separation using methylene chloride – hexanes 1:1 (the plate was eluted three times), to give an inseparable mixture (121.81 mg) of two compounds that spectral data suggests is a mixture of α-amyrin (**12**) and β-amyrin (**13**), and the diterpene **14** (49.68 mg).

*α-Amyrin (**12**) and β-amyrin (**13**)*

The identity of this mixture was confirmed by comparing a 1:1 mixture of authentic α- and β-amyrins by nmr spectroscopy (^{1}Hmr and ^{13}Cmr).

*12-Methoxyabieta-8,11,13-trien-3α-ol (**14**)*

Colourless needles (hexanes); mp 157–158°C; $[\alpha]^{22}$ +44 (*c* 0.72, $CHCl_3$); ir ($CHCl_3$) cm^{-1}: 3620 (OH), 2951 (CH); ^{1}Hmr ($CDCl_3$) δ: 0.96 (3H, s, C4-CH_3), 1.05 (3H, s, C4-CH_3), 1.20 (3H, s, C10-CH_3), 1.20 (3H, d, $CH(CH_3)_2$, *J* = 7), 1.21 (3H, d, $CH(CH_3)_2$, *J* = 7), 1.26–2.17 (11H, m), 2.76 (1H, ddd, H7α, *J* = 2, 7, 16), 3.02 (1H, dd, H7β, *J* = 7, 16), 3.28 (1H, septet, H15), 3.51 (1H, brt, H3β, $W_{1/2}$ = 7), 3.72 (3H, s, OCH_3), 7.04 (1H, s, H11), 7.05 (1H, s, H14); ^{13}Cmr ($CDCl_3$) δ: 18.2, 22.1, 23.9, 24.0, 24.7, 24.8, 25.9, 26.0, 28.1, 29.7, 31.7, 37.7, 43.3, 60.2, 75.5, 120.4, 123.7, 128.5, 137.9, 148.9, 154.8; ms *m/z* (rel. int., %): 316 (M^+, 20.9), 301 (4.7), 283 (100.0), 241 (4.6), 215 (5.1), 199 (3.6), 189 (6.9), 173 (5.7), 159 (4.1), 147 (4.8), 129 (4.5), 115 (3.9), 91 (4.1), 81 (2.0), 69 (3.4), 55 (5.6), 43 (9.8). High-resolution mass measurement: calcd. for $C_{21}H_{32}O_2$: 316.2404; found: 316.2411.

Separation of fractions J and K

Fractions J (815.16 mg) and K (195.71 mg) were combined (1.01 g) and partially separated by column chromatography (Merck silica gel 230–400 mesh, 100 g). Gradient elution was carried out using: (*i*) methylene chloride – ethyl acetate 19:1 (750 mL); (*ii*) methylene chloride – ethyl acetate 9:1 (700 mL); and (*iii*) ethyl acetate (200 mL) to give 9 fractions. Fractions 1 and 2 (13.18 and 36.17 mg respectively) contained a major orange-coloured compound and a minor compound, while fraction 3 (62.11 mg) consisted of two orange-coloured compounds. Fractions 4 and 5 (25.97 and 21.21 mg respectively) consisted of a major orange-coloured compound and a minor component. Fractions 6 and 7 (28.69 and 232.43 mg respectively) showed two compounds on tlc, while fractions 8 and 9 (411.67 and 40.97 mg respectively) consisted of one major compound and several minor compounds.

Separation of fractions 1 and 2 by preparative tlc (Merck silica F_{254}, 0.5 mm, chloroform–methanol 98.2), followed by a further separation using toluene – ethyl acetate – chloroform – formic acid 35:15:16:1 yielded tingenone (**15**, 15.30 mg) and the friedelane methyl ester (**16**, 13.62 mg). Separation of fraction 3 by preparative tlc (Merck silica F_{254}, 0.5 mm, toluene – ethyl acetate – chloroform – formic acid 35:15:16:1, plate eluted twice) gave tingenone (**15**, 14.00 mg) and 22β-hydroxytingenone (**17**, 13.04 mg). Fractions 4 and 5 were separated by preparative tlc (Merck silica F_{254}, 0.5 mm, chloroform–methanol 98:2) to yield 22β-hydroxytingenone (**17**, 15.55 mg) and an unidentified mixture (9.12 mg). Column chromatography of fraction 7 (Merck silica gel 230–400 mesh, 25 g, methylene chloride – ethyl acetate 5:1) gave the dihydroxy triterpene, **18** (50.75 mg), an unidentified mixture (27.27 mg), and the triterpene, **19** (28.48 mg). Column chromatography of fractions 8 and 9 (Merck silica gel 230–400 mesh,

Can. J. Chem. Downloaded from www.nrcresearchpress.com by 217.78.4.112 on 09/08/12
For personal use only.

50 g, methylene chloride – ethyl acetate 5:1) gave polpunonic acid (**25**, 247.13 mg).

In summary, chromatographic separation yielded tingenone (**15**, 29.30 mg), the friedelane methyl ester, **16** (13.62 mg), 22β-hydroxytingenone (**17**, 28.59 mg), the dihydroxy triterpenes, **18** (50.75 mg) and **19** (28.48 mg), and polpunonic acid (**25**, 247.13 mg).

*Tingenone (**15**)*

The identity of the isolated sample was confirmed by comparison of the physical and spectral data with those of the authentic sample.

*Methyl-22β-hydroxy-3,21-dioxo-D:A-friedo-29-noroleanan-24-oate (**16**)*

Yellow crystals (EtOH); mp 250–251°C; $[\alpha]^{22}$ +101.4 (*c* 0.22, MeOH); uv (meOH) λ_{max} 203 (ε 1810); ir ($CHCl_3$) cm^{-1}: 3460 (OH, br), 3010, 2950 (CH), 1725 (C=O, sh), 1710 (C=O), 1700 (C=O, sh); ^{1}Hmr ($CDCl_3$) δ: 0.80 (3H, s), 0.84 (3H, s), 0.91 (3H, d), 0.94 (3H, s), 1.07 (3H, d), 1.36 (3H, s), 3.64 (3H, s, OCH_3), 1.16–1.85 (14H, m), 2.02 (1H, m), 2.15–2.38 (5H, m), 2.60–2.65 (2H, m), 2.77 (1H, m, H20α), 3.66 (1H, s, OH), 4.61 (1H, brd, H22α); ms *m/z* (rel. int., %): 486 (M^+, 100.0), 471 (3.1), 468 (5.2), 426 (75.2), 411 (7.6), 399 (16.7), 398 (16.7), 385 (19.5), 357 (5.7), 340 (13.4), 317 (27.0), 257 (27.5), 231 (15.0), 217 (29.5), 203 (14.0), 189 (16.7), 177 (17.5), 163 (21.2), 149 (25.8), 135 (36.5), 121 (81.1), 109 (67.7), 95 (55.2), 81 (51.3), 67 (44.2), 55 (60.6). High-resolution mass measurement: calcd. for $C_{30}H_{46}O_5$: 486.3343; found: 486.3352.

*22β-Hydroxytingenone (**17**)*

All physical and spectral data of the isolated sample were identical with the data published earlier (26–30).

*3β,29-Dihydroxyolean-12-ene (**18**)*

Colourless prisms (EtOH); mp 241–242°C; $[\alpha]^{22}$ +115.9 (*c* 0.82, MeOH); ir (KBr) cm^{-1}: 3294 (OH), 2946 (CH); ^{1}Hmr ($CDCl_3$) δ: 0.80 (3H, s), 0.85 (3H, s), 0.91 (3H, s), 0.94 (3H, s), 0.97 (3H, s), 1.00 (3H, s), 1.14 (3H, s), 0.73–2.02 (25H, m), 3.22 (1H, dd, H3α, J = 3.5, 11), 3.27 (2H, d, H29, J = 5.5), 5.21 (1H, t, H12); ms *m/z* (rel. int., %): 442 (M^+, 6.1), 427 (1.8), 411 (9.6), 393 (0.5), 288 (0.7), 273 (1.0), 234 (100.0), 219 (8.7), 203 (21.1), 201 (21.3), 187 (21.6), 175 (13.1), 161 (8.1), 147 (14.3), 135 (18.5), 119 (19.1), 107 (19.8), 95 (28.0), 81 (22.9), 69 (18.0), 55 (21.9). High-resolution mass measurement: calcd. for $C_{30}H_{50}O_2$: 442.3813; found: 442.3805.

Chromatographic separation of the spent medium extract metabolites (compare Fig. 4)

The spent medium extract (3.06 g) was partially separated by vlc using a 150-mL sintered glass funnel (medium frit, Merck silica 60G, 90 g). Stepwise elution was carried out using: (*i*) benzene (5 × 30 mL); (*ii*) benzene–acetone 5:1 (19 × 30 mL); (*iii*) benzene–acetone 4:1 (19 × 30 mL); (*iv*) benzene–acetone 3:1 (12 × 30 mL); (*v*) benzene–acetone 2:1 (230 mL); (*vi*) benzene–acetone 1:1 (18 × 30 mL), and (*vii*) ethyl acetate (250 mL) to give 22 crude fractions. All the fractions were complex mixtures of metabolites. Fractions 3, 4, 5, 6, and 7 (204.68, 117.77, 158.08, 72.62, and 58.75 mg, respectively) were separated further by preparative tlc (Merck silica F_{254}, 4 × 2 mm plates, fractions 6 and 7 were combined) using toluene – ethyl acetate – chloroform-formic acid 35:15:161 (the plates were eluted three times) to give oleanolic acid (**23**, 59.66 mg), the hydroxy acid, **20** (134.63 mg), triptolide (**2**, 179.09 mg), and a complex mixture (168.31 mg) that was not further investigated. Fractions 8, 9, 10, 11, 12, and 13 (71.00, 113.66, 44.34, 84.0, 63.94, and 222.09 mg, respectively) were separated by preparative tlc (Merck silica F_{254}, 5 × 2 mm plates, 1 × 0.5 mm plate (fraction 10), toluene – ethyl acetate – chloroform – formic acid 35:15:16:1, the plates were eluted four times) to give **3** (13.22 mg), a mixture of **3** and **4** (10.30 mg), **4** (21.72 mg), a mixture of **4**, **5**, and **6** (42.48 mg), **5** (8.73 mg), **6** (25.53 mg), tripdiolide (**1**, 199.77), and a complex mixture (166.65 mg). Fractions 14, 15, and 16 (80.90, 38.65, and 10.96 mg, respectively) were separated by preparative tlc (Merck silica F_{254}, 1 × 2 mm plate (fraction 14), 1 × 0.5 mm plate (fractions 15 and 16), toluene – ethyl acetate – chloroform – formic acid 35:15:16:1, the plates were eluted three times) to give **6** (48.10 mg). Fractions 17 and 18 (56.27 and 151.71 mg, respectively) were separated by preparative tlc (1 × 0.5 mm plate and 1 × 2 mm plate, respectively, benzene–methanol – acetic acid 90:5:5, the plates were eluted three times) to give a further quantity of **6** (30.67 mg). Attempted separation of fractions 19–22 (174.08, 83.45, 39.59, and 49.50 mg, respectively) by preparative tlc (Merck silica F_{254}, 2 × 2 mm plates, benzene–methanol – acetic acid 90:5:5, the plates were eluted three times) was unsuccessful due to the complexity of the mixture of polar compounds.

The identity of all isolated compounds was confirmed by comparison of physical and spectral data with those of the original samples and (or) with data published earlier.

Acknowledgements

Financial aid from the Natural Sciences and Engineering Research Council of Canada is gratefully acknowledged. We are also grateful to Professor Xiao-Yu Li, Shanghai Institute of Materia Medica, Academia Sinica, Shanghai, China, and Professor Shao-Zhen Qian, Jiangsu Family Planning Institute, Nanjing, China, for performing pharmacological screening of our chromatographic fractions and purified compounds.

1. S. Huang (*Editor*). The Saint Peasant's Scripture of Materia Medica. Publishing House for Chinese Medical Classics, Beijing. 1982. p. 309.
2. D. Y. Yu. Gendai Toyo Igaku, **3**, 125 (1983).
3. J. Guo, S. Yuan, X. Wang, S. Xu, and D. Li. Chin. Med. J. (Beijing, Engl. Ed.) **7**, 405 (1981).
4. W. Xu, J. Zheng, and X. Lu. Int. J. Dermatol. **24**, 152 (1985).
5. S. M. Kupchan, W. A. Court, R. G. Dailey, C. J. Gilmore, and R. F. Bryan. J. Am. Chem. Soc. **94**, 7194 (1972).
6. J. P. Kutney, L. S. L. Choi, R. Duffin, G. Hewitt, N. Kawamura, T. Kurihara, P. Salisbury, R. Sindelar, K. L. Stuart, P. M. Townsley, W. T. Chalmers, F. Webster, and G. G. Jacoli. Planta Med. **48**, 158 (1983).
7. J. P. Kutney, G. M. Hewitt, T. Kurihara, P. J. Salisbury, R. D. Sindelar, K. L. Stuart, P. M. Townsley, W. T. Chalmers, and G. G. Jacoli. Can. J. Chem. **59**, 2677 (1981).
8. S. Z. Qian. Contraception, **36**, 335 (1987).
9. T. W. Yang. Chin. Med. J. (Peking, 1932–1966), **60**, 222 (1941).
10. W-L. Jian, Y-Z. Oyang, and S-Y. Cheng. J. Chin. Herbs, **3**, 27 (1981).
11. J. Zheng, L. Xu, L. Ma, D. Wang, and J. Gao. Zhongguo Yixue Kexueyuan Xuebao, **5**, 1 (1983).
12. Tripterygium Study Group, Institute of Dermatology, Chinese Academy of Medical Sciences. Chin. J. Dermatol. **15**, 199 (1982).
13. J. Zheng, J. Liu, L. Hsu, J. Gao, and B. Jiang. Zhongguo Yixue Kexueyuan Xuebao, **5**, 73 (1983).
14. J. Zheng, J. Fang, L. Xu, J. Gao, H. Guo, Z. Li and H. Sun. Zhongguo Yixue Kexueyuan Xuebao, **7**, 1 (1985).
15. S-Z. Qian, C-Q. Zhong, and X. Ye. Contraception, **33**, 105 (1986).
16. S-Z. Qian, C-Q. Zhong, Y. Xu, L-Q. Ni, and G-Z. Feng. Adv. Contracept. **2**, 253 (1986).

Can. J. Chem. Downloaded from www.nrcresearchpress.com by 217.78.4.112 on 09/08/12
For personal use only.

Can. J. Chem. Downloaded from www.nrcresearchpress.com by 217.78.4.112 on 09/08/12
For personal use only.

17. S-Z. Qian, C-Q. Zhong, and Y. Xu. Adv. Contracept. **2**, 298 (1986).
18. S-Z. Qian. *In* Fertility regulation today and tomorrow. *Edited by* E. Diczfalusy and M. Bygdeman. Raven Press, New York. 1987. p. 217.
19. S. W. Pelletier, H. P. Chokshi, and H. K. Desai. J. Nat. Prod. **49**, 892 (1986).
20. J. C. Coll and B. F. Bowden. J. Nat. Prod. **49**, 934 (1986).
21. K. Biemann. Mass spectrometry: organic chemical applications. McGraw–Hill, New York. 1962. p. 347.
22. H. Budziciewicz, C. Djerassi, and D. H. Williams. Structure elucidation of natural products by mass spectrometry. Vol. II. Holden Day, San Francisco. 1964.
23. G. R. Waller. Biochemical applications of mass spectrometry. Wiley Interscience, New York. 1972. p. 366.
24. P. M. Brown, M. Moir, R. H. Thomson, T. J. King, V. Krishnamoorthy, and J. R. Seshadri. J. Chem. Soc. Perkin Trans. 1, 2721 (1973).
25. F. Delle Monache, G. B. Marini-Bettolo, O. Goncalves deLima, I. Leoncio d'Albuquerque, and J. Sydney de Barros Coelho. J. Chem. Soc. Perkin Trans. 1, 2725 (1973).
26. A. G. Gonzalez, V. Darias, J. Boada, and G. Alonso. Planta Med. **32**, 282 (1977).
27. A. R. Campanelli, M. D'Alagni, and G. B. Marini-Bettolo. FEBS Lett. **122**, 256 (1980).
28. J. P. Kutney, M. H. Beale, P. J. Salisbury, K. L. Stuart, B. R. Worth, P. M. Townsley, W. T. Chalmers, K. Nilsson, and G. G. Jacoli. Phytochemistry, **20**, 653 (1981).
29. F. Delle Monache, G. B. Marini-Bettolo, O. Goncalves de Lima, and J. Sydney de Barros Coelho. Gazz. Chim. Ital. **102**, 317 (1972).
30. K. Nakanishi, V. P. Gullo, T. R. Govindachari, and N. Viswanathan. J. Am. Chem. Soc. **95**, 6473 (1973).
31. D. D. Nanavati. J. Oil Technol. Assoc. India (Kanpur, India), **7**, 51 (1975).
32. S. Shibata, K. Takahashi, S. Yano, M. Harada, H. Saito, Y. Tamura, A. Kumagai, K. Hirabayashi, M. Yamamoto, and N. Nagata. Chem. Pharm. Bull. **35**, 1910 (1987).
33. H. Inoue, T. Mori, S. Shibata, and H. Saito. Chem. Pharm. Bull. **35**, 3888 (1987).
34. H. Inoue, T. Mori, S. Shibata, and Y. Koshihara. J. Pharm. Pharmacol. **40**, 272 (1988).
35. H. Nishino, A. Nishino, J. Takayasu, T. Hasegawa, A. Iwashima, and K. Hirabayashi. Cancer Res. **48**, 5210 (1988).
36. H. Inoue, T. Mori, S. Shibata, and Y. Koshihara. Br. J. Pharmacol. **96**, 204 (1989).
37. D. A. H. Taylor. J. Chem. Soc. (c), 490 (1967).
38. International tables for X-ray crystallography. Vol. IV. Kynoch Press; Birmingham, U.K. Present distributor: Kluwer Academic Publishers: Dordrecht, The Netherlands. 1974. pp. 99–102 and 149.

Appendix A

X-ray crystallographic analyses of compounds 6, 15, 16, 17, 18, and 19.

Experimental

X-ray crystallographic analyses of ***6***·*MeOH,* ***15***·*1/2EtOAc,* ***16****,* ***17***·*1/2* H_2O*,* ***18****, and* ***19***·*EtOH*

Crystallographic data for the six compounds appear in Table A1. The final unit-cell parameters were obtained by least squares on the setting angles for 25 reflections with 2θ = 34.0–41.3, 40.1–56.5, 46.6–76.3, 20.0–35.8, 40.4–72.5, and 40.1–70.8° for **6**·MeOH, **15**·1/2EtOAc, **16**, **17**·1/2 H_2O, **18**, and **19**·EtOH, respectively. The intensities of three standard reflections, measured every hour of X-ray exposure time for **6**·MeOH and every 150 reflections for the remaining compounds throughout the data collections, remained essentially constant except for **15**·1/2 EtOAc and **19**·EtOH where 4.6% and 19.2% decay, respectively, were noted. The data were processed[3] and corrected for Lorentz and polarization effects, linear decay for **15**·1/2 EtOAc and **19**·EtOH, and absorption for **15**·1/2 EtOAc, **16**, **17**·1/2 H_2O, **18**, and **19**·EtOH (empirical, based on azimuthal scans for four reflections).

The structure analyses of **16** and **19**·EtOH were initiated in the noncentrosymmetric space group $P2_1$ on the basis of the known chirality of these compounds. The structures were solved by direct methods, the coordinates of the non-hydrogen atoms being determined from *E*-maps and subsequent difference Fourier syntheses. The asymmetric units of **15**, **16**, and **18** each contain two molecules and those of **6**, **15**, **17**, and **19** contain solvent molecules (methanol, ethyl acetate, water (1/2 molecule), and ethanol respectively). The solution of the structure of **16** by direct methods was not routine. The structure was eventually solved by excluding all *h*0*l* reflections from the phase determination. This led to the isolation of *one* correctly oriented, but incorrectly positioned, molecule. This oriented fragment was then positioned and the atoms of the second molecule in the asymmetric unit were located by direct methods for difference structures using the computer program DIRDIF.[3] The ethyl acetate solvate molecule in **15**·1/2 EtOAc was disordered. Site occupancy factors were initially estimated from relative Fourier map peak heights and were subsequently adjusted[4] to result in approximately equal equivalent isotropic thermal parameters for the eight positions included in the model. All non-hydrogen atoms were refined with anisotropic thermal parameters. Oxygen-bound hydrogen atoms were refined with isotropic thermal parameters (**6**·MeOH and **16**) or placed in difference map positions, and for all six structures the carbon-bound hydrogen atoms were fixed in idealized positions (C(sp^2)—H = 0.97, C(sp^3)—H = 0.98 Å, $U_H \propto U_{\text{bonded atom}}$ for **6**·MeOH and C—H = 0.98 Å, $B_H = 1.2\,B_{\text{bonded atom}}$ for the other five structures). Neutral atom scattering factors and anomalous dispersion corrections for the non-hydrogen atoms were taken from the *International tables for X-ray crystallography* (38). The absolute configurations of **6**, **15**, and **17**–**19** are based on known configurations for one or more of the chiral centres and that of **16** has been determined by anomalous scattering. Parallel refinements of the opposite enantiomers were carried out for the four structures determined with Cu radiation, resulting in marginally higher residuals in each case. For compound **16**, the R and R_w ratios are both 1.003, representing a confidence level of 99.5%. Final atomic coordinates and equivalent isotropic thermal parameters, bond lengths, bond angles, and intra-annular torsion angles appear in Tables A2–A5, respec-

[3]Computer programs used include locally written programs for data processing and locally modified versions of the following for the structure of **6**·MeOH: MULTAN80, multisolution program by P. Main, S. J. Fiske, S. E. Hull, L. Lessinger, G. Germain, J. P. Declercq, and M. M. Woolfson; ORFLS, full-matrix least squares, and ORFFE, function and errors, by W. R. Busing, K. O. Martin, and H. A. Levy; FORDAP, Patterson and Fourier syntheses, by A. Zalkin; ORTEP II, illustrations, by C. K. Johnson. The TEXSAN/TEXRAY structure analysis package, which includes versions of the following, was employed for the other five structures: MITHRIL, integrated direct methods, by C. J. Gilmore; DIRDIF, direct methods for difference structures, by P. T. Beurskens; ORFLS, full-matrix least squares, and ORFFE, function and errors, by W. R. Busing, K. O. Martin, and H. A. Levy; ORTEP II, illustrations, by C. K. Johnson.

[4]Attempts to refine even some of the population parameters led to nearly singular matrices due to high correlations with the thermal parameters.

TABLE A1. Crystallographic data[a]

Compound	**6**·MeOH	**15**·1/2 EtO/Ac	**16**	**17**·1/2 H_2O	**18**	**19**·EtOH
Formula	$C_{31}H_{52}O_5$	$C_{30}H_{40}O_4$	$C_{30}H_{46}O_5$	$C_{28}H_{37}O_{4.5}$	$C_{30}H_{50}O_2$	$C_{32}H_{56}O_3$
fw	504.75	464.64	486.69	445.60	442.74	488.79
Crystal system	Orthorhombic	Orthorhombic	Monoclinic	Orthorhombic	Orthorhombic	Monoclinic
Space group	$P2_12_12_1$	$P2_12_12_1$	$P2_1$	$P2_12_12$	$C222_1$	$P2_1$
a, Å	8.1397(5)	14.719(2)	7.282(2)	13.922(5)	19.872(5)	14.640(2)
b, Å	11.9965(8)	28.375(8)	28.742(2)	15.253(2)	19.946(2)	6.695(2)
c, Å	29.161(1)	12.221(2)	12.421(2)	11.067(2)	27.211(3)	15.618(2)
β, deg	–	–	97.23(2)	–	–	98.57(2)
V, Å^3	2847.5(3)	5104(2)	2579.0(7)	2350(1)	10786(3)	1513.6(9)
Z	4	8	4	4	16	2
ρ_{calc}, g/cm^3	1.18	1.21	1.25	1.26	1.09	1.07
$F(000)$	1112	2016	1064	964	3936	544
Radiation	Mo	Cu	Cu	Mo	Cu	Cu
μ, cm^{-1}	0.72	5.83	6.23	0.78	4.66	4.77
Crystal size, mm	0.20 × 0.40 × 0.45	0.05 × 0.10 × 0.25	0.10 × 0.30 × 0.35	0.10 × 0.35 × 0.35	0.15 × 0.25 × 0.35	0.04 × 0.30 × 0.35
Transmission factors	—	0.93–1.00	0.96–1.00	0.97–1.00	0.93–1.00	0.83–1.00
Scan type	ω–θ	ω–2θ	ω–2θ	ω–2θ	ω–2θ	ω–2θ
Scan range, deg in ω	0.85 + 0.35 tan θ	0.95 + 0.30 tan θ	0.95 + 0.30 tan θ	1.26 + 0.35 tan θ	1.00 + 0.30 tan θ	1.10 + 0.30 tan θ
Scan rate, deg/min	1.8–10.0	8	16	16	16	8
Data collected	$+h, +k, +l$	$+h, +k, +l$	$+h, +k, +l$	$+h, +k, +l$	$+h, +k, +l$	$+h, +k, +l$
$2\theta_{max}$, deg	55	150	155	55	150	125
Cryst. decay	Negligible	4.6%	Negligible	Negligible	Negligible	19.2%
Total reflections	3681	5416	5862	3034	5756	2862
Unique reflections	3681	5416	5425	3034	5756	2601
R_{merge}	–	–	0.032	–	–	0.029
R_{merge}	–	–	0.032	–	–	0.029
Reflections with $I \geq 3\sigma(I)$	2386	3120	3738	1939	3567	1605
Variables	341	632	639	295	587	316
R	0.047	0.054	0.044	0.046	0.045	0.045
R_w	0.057	0.071	0.056	0.059	0.057	0.059
gof	1.73	2.34	1.51	1.73	1.53	1.88
Max Δ/σ (final cycle)	0.13	0.08	0.06	0.14	0.004	0.01
Residual density e/Å^3	−0.18 to +0.27	−0.18 to +0.38	−0.20 to +0.21	−0.19 to +0.23	−0.24 to +0.21	−0.16 to +0.17

[a]Temperature 294 K, function minimized $\Sigma w(|F_o| - |F_c|)^2$ where $w = 4F_o^2/\sigma^2(F_o^2)$, $R = \Sigma||F_o| - |F_c||/\Sigma|F_o|$, $R_w = (\Sigma w(|F_o| - |F_c|)^2/\Sigma w|F_o|^2)^{1/2}$, and gof $[\Sigma(|F_o| - |F_c|)^2/(m - n)]^{1/2}$. Values given for R, R_w, and gof are based on those reflections with $I \geq 3\sigma(I)$.

[b]Enraf–Nonius CAD4-F diffractometer, Mo-K_α radiation ($\lambda K_{\alpha 1}$ = 0.70930, $\lambda K_{\alpha 2}$ = 0.71359 Å), graphite monochromator, takeoff angle 2.7°, apertu (2.0 + tan θ) × 4.0 mm at a distance of 173 mm from the crystal, scan range extended by 25% on both sides for background measurement, $\sigma^2(I) = C + 2B$ $[0.04(C - B)]^2$ (S = scan rate, C = scan count, B = normalized background count).

[c]Rigaku AFC6S diffractometer, Cu-K_α(λ = 1.54178 Å) or Mo-K_α(λ = 0.71069 Å) radiation, graphite monochromator, takeoff angle 6.0°, aperture 6.0 6.0 mm at a distance of 285 mm from the crystal, stationary background counts at each end of the scan (scan/background time ratio 2:1, up to 8 rescans $\sigma^2(F^2) = [S^2(C + 4B) + (0.04F^2)^2]/Lp^2$($S$ = scan rate, C = scan count, B = normalized background count).

tively. Hydrogen atom parameters, anisotropic thermal parameters, stereoviews of the molecules, packing diagrams (where relevant), and measured and calculated structure factor amplitudes for the six structures are included as supplementary material.[5]

Discussion of crystal structures

The crystal structure of **6**·MeOH features extensive hydrogen bonding, the methanol solvate molecule being involved in two hydrogen bonds: a very strong hydrogen bond to the carboxylic acid function and a strong hydrogen bond to a hydroxyl group (O(4)—H(O4)···O(5) and O(5)—H(O5)···O(1), O···H = 1.65(4) and 1.84(6) Å, O···O = 2.595(4) and 2.742(4) Å, O—H···O = 167(4) and 175(5)°). There are also two weaker hydrogen bonds directly linking each molecule of **6** to four others (O(1)—H(O1)···O(2) and O(2)—H(O2)···O(3), O···H = 2.07(5) and 2.00(6) Å, O···O = 2.813(4) and 2.848(4) Å, O—H···O = 176(5) and 168(4)°). All of the saturated six-membered rings have chair conformations and the unsaturated C ring has a sofa conformation. The saturated ring fusions A:B, B:C, and D:E are *trans*, *trans*, and *cis*, respectively.

The crystal structure of **15**·1/2 EtOAc consists of molecules of **15** and ethyl acetate, those of the triterpene being linked into infinite chains extending along the c axis by O—H···O hydrogen bonds between the O(2) hydroxyl group and the O(1) carbonyl oxygen atom (O(2)—H(36)···O(1′) and O(2′)—H(36′)···O(1), H···O = 1.83 and 1.83 Å, O···O = 2.726(6) and 2.659(7) Å, O—H···O = 153 and 136°,

[5]Supplementary material mentioned in the text may be purchased from: The Depository of Unpublished Data, Document Delivery, CISTI, National Research Council Canada, Ottawa, Canada K1A 0R6.

Tables of hydrogen atom parameters, stereoviews of the molecules, and relevant packing diagrams have also been deposited with the Cambridge Crystallographic Data Centre and can be obtained on request from The Director, Cambridge Crystallographic Data Centre, University Chemical Laboratory, Lensfield Road, Cambridge CB2 1EW, U.K.

Can. J. Chem. Downloaded from www.nrcresearchpress.com by 217.78.4.112 on 09/08/12
For personal use only.

TABLE A2. Final positional (fractional) and equivalent isotropic thermal parameters with estimated standard deviations in parentheses

Atom	x	y	z	U_{eq}/B_{eq}[a]
		6 · MeOH		
O(1)	−0.0691(4)	0.1512(2)	0.4351(1)	42
O(2)	0.4000(3)	−0.0417(2)	0.0062(1)	42
O(3)	0.6832(4)	0.3906(2)	0.0387(1)	62
O(4)	0.4208(4)	0.3679(3)	0.0514(1)	67
C(1)	0.2619(4)	0.1447(3)	0.3438(1)	42
C(2)	0.1850(4)	0.1450(3)	0.3916(1)	41
C(3)	−0.0005(4)	0.1464(3)	0.3898(1)	34
C(4)	−0.0731(4)	0.0496(3)	0.3618(1)	32
C(5)	0.0133(4)	0.0484(3)	0.3139(1)	30
C(6)	−0.0538(5)	−0.0394(3)	0.2808(1)	42
C(7)	−0.0020(4)	−0.0127(3)	0.2313(1)	40
C(8)	0.1848(4)	−0.0044(3)	0.2250(1)	32
C(9)	0.2595(4)	0.0694(3)	0.2635(1)	31
C(10)	0.2033(4)	0.0466(3)	0.3141(1)	30
C(11)	0.4474(5)	0.0758(4)	0.2582(1)	52
C(12)	0.5048(5)	0.0729(4)	0.2096(1)	46
C(13)	0.4135(4)	0.0619(3)	0.1727(1)	30
C(14)	0.2262(4)	0.0532(3)	0.1772(1)	29
C(15)	0.1489(5)	−0.0103(3)	0.1372(1)	41
C(16)	0.2263(5)	0.0153(3)	0.0900(1)	39
C(17)	0.4119(5)	−0.0059(3)	0.0896(1)	33
C(18)	0.4945(4)	0.0704(3)	0.1256(1)	33
C(19)	0.5042(5)	0.1923(3)	0.1111(1)	37
C(20)	0.5912(4)	0.2111(3)	0.0646(1)	34
C(21)	0.4981(4)	0.1395(3)	0.0287(1)	37
C(22)	0.4865(4)	0.0181(3)	0.0415(1)	35
C(23)	−0.0596(5)	−0.0592(3)	0.3888(1)	43
C(24)	−0.2559(5)	0.0743(4)	0.3548(1)	50
C(25)	0.2766(5)	−0.0627(4)	0.3339(1)	47
C(26)	0.2560(6)	−0.1232(3)	0.2260(1)	51
C(27)	0.1580(5)	0.1734(3)	0.1747(1)	42
C(28)	0.4463(6)	−0.1280(3)	0.1009(1)	55
C(29)	0.5728(5)	0.3315(3)	0.0504(1)	38
C(30)	0.7742(5)	0.1806(4)	0.0666(1)	48
O(5)	0.6454(4)	0.0713(. 3)	0.4726(1)	76
C(31)	0.5702(7)	0.1491(4)	0.5003(2)	75
		15 · 1/2 EtOAc		
O(1)	0.2579(3)	0.2773(2)	−0.1597(4)	7.0(3)
O(2)	0.4176(3)	0.2336(2)	−0.1834(3)	4.7(2)
O(3)	0.3572(5)	0.5847(2)	0.4929(5)	8.6(4)
C(1)	0.2891(4)	0.3029(2)	0.0195(5)	4.3(3)
C(2)	0.3119(4)	0.2793(2)	−0.0812(6)	4.4(3)
C(3)	0.3982(4)	0.2569(2)	−0.0893(5)	3.7(3)
C(4)	0.4589(4)	0.2577(2)	−0.0071(6)	3.8(3)
C(5)	0.4372(4)	0.2824(2)	0.0942(5)	3.4(3)
C(6)	0.4972(4)	0.2891(2)	0.1770(5)	4.1(3)
C(7)	0.4789(4)	0.3189(2)	0.2677(5)	4.2(3)
C(8)	0.3975(4)	0.3375(2)	0.2889(5)	3.6(3)
C(9)	0.3181(4)	0.3216(2)	0.2179(5)	3.5(3)
C(10)	0.3482(4)	0.3038(2)	0.1051(5)	3.4(3)
C(11)	0.2417(4)	0.3574(2)	0.2075(5)	4.5(3)
C(12)	0.2270(4)	0.3891(2)	0.3081(5)	4.4(3)
C(13)	0.3157(4)	0.4111(2)	0.3495(5)	3.7(3)
C(14)	0.3807(4)	0.3708(2)	0.3854(5)	4.0(3)
C(15)	0.4690(5)	0.3933(2)	0.4274(6)	5.2(4)
C(16)	0.4538(5)	0.4256(3)	0.5239(6)	6.2(4)
C(17)	0.3779(5)	0.4624(2)	0.5135(5)	4.5(3)
C(18)	0.2949(4)	0.4438(2)	0.4484(5)	4.3(3)
C(19)	0.2266(5)	0.4833(3)	0.4310(6)	5.4(4)

TABLE A2 (*continued*)

Atom	x	y	z	U_{eq}/B_{eq}[a]
C(20)	0.2624(5)	0.5316(3)	0.3926(6)	5.5(4)
C(21)	0.3458(6)	0.5443(3)	0.4542(6)	6.0(4)
C(22)	0.4167(5)	0.5071(3)	0.4630(6)	5.6(4)
C(23)	0.5509(5)	0.2330(3)	−0.0208(6)	5.6(4)
C(24)	0.2788(5)	0.2751(3)	0.2714(6)	5.8(4)
C(25)	0.3584(4)	0.4389(2)	0.2527(5)	4.2(3)
C(26)	0.3408(6)	0.3404(2)	0.4816(6)	6.2(4)
C(27)	0.3483(6)	0.4746(3)	0.6302(6)	6.3(4)
C(28)	0.1902(7)	0.5701(3)	0.4003(7)	8.7(5)
O(1′)	0.3208(3)	0.2163(2)	0.6307(4)	6.2(3)
O(2′)	0.1700(3)	0.2686(2)	0.6512(4)	6.0(3)
O(3′)	0.3235(4)	0.0991(2)	−0.3488(4)	8.1(3)
C(1′)	0.2707(4)	0.1789(2)	0.4699(5)	4.5(3)
C(2′)	0.2616(4)	0.2105(2)	0.5597(5)	4.3(3)
C(3′)	0.1779(5)	0.2384(2)	0.5653(5)	4.6(3)
C(4′)	0.1131(4)	0.2357(2)	0.4887(5)	4.1(3)
C(5′)	0.1235(4)	0.2016(2)	0.4020(5)	3.5(3)
C(6′)	0.0596(4)	0.1966(2)	0.3219(5)	4.1(3)
C(7′)	0.0706(4)	0.1662(2)	0.2310(5)	4.3(3)
C(8′)	0.1406(4)	0.1363(2)	0.2185(5)	3.5(3)
C(9′)	0.2107(4)	0.1327(2)	0.3122(5)	3.2(2)
C(10′)	0.2046(4)	0.1732(2)	0.3951(5)	3.6(3)
C(11′)	0.3074(4)	0.1296(2)	0.2641(5)	4.2(3)
C(12′)	0.3163(4)	0.0976(2)	0.1642(5)	4.4(3)
C(13′)	0.2501(4)	0.1112(2)	0.0715(5)	3.7(3)
C(14′)	0.1504(4)	0.1062(2)	0.1166(5)	3.7(3)
C(15′)	0.0858(4)	0.1213(2)	0.0239(6)	4.5(3)
C(16′)	0.0934(5)	0.0901(3)	−0.0783(6)	5.2(4)
C(17′)	0.1905(5)	0.0806(2)	−0.1231(5)	4.6(3)
C(18′)	0.2632(4)	0.0771(2)	−0.0300(5)	4.1(3)
C(19′)	0.3600(5)	0.0765(2)	−0.0789(5)	4.5(3)
C(20′)	0.3821(5)	0.1137(3)	−0.1684(6)	5.8(4)
C(21′)	0.3083(6)	0.1102(3)	−0.2537(7)	6.0(4)
C(22′)	0.2151(5)	0.1183(3)	−0.2099(6)	5.5(4)
C(23′)	0.0322(5)	0.2680(2)	0.4936(7)	5.8(4)
C(24′)	0.1917(5)	0.0884(2)	0.3824(6)	5.5(4)
C(25′)	0.2687(5)	0.1630(2)	0.0428(5)	4.6(3)
C(26′)	0.1243(5)	0.0545(2)	0.1460(6)	5.1(3)
C(27′)	0.1868(6)	0.0333(3)	−0.1825(7)	6.6(4)
C(28′)	0.4781(6)	0.1064(4)	−0.2146(7)	7.6(5)
O(4)	0.0678(7)	0.3510(4)	0.7843(8)	11.5(7)
O(5)	0.0341(9)	0.3814(3)	0.6176(9)	11.2(7)
C(29)	0.100(2)	0.3807(4)	0.698(1)	10(1)
C(30)	0.147(1)	0.4041(6)	0.676(1)	10(1)
C(31)	0.026(1)	0.4052(6)	0.513(1)	10(1)
C(32)	−0.0157(8)	0.4471(5)	0.515(1)	9.6(8)
C(33)	0.043(1)	0.4573(6)	0.679(2)	10(1)
C(34)	0.032(1)	0.433(1)	0.607(2)	10(2)
		16		
O(1)	0.5929(6)	0.5857	0.4792(3)	5.3(2)
O(2)	0.8356(5)	0.1300(1)	0.7155(3)	4.7(2)
O(3)	1.0781(5)	0.1725(2)	0.6100(3)	5.0(2)
O(4)	0.4766(5)	0.5088(2)	0.3115(2)	4.0(1)
O(5)	0.6799(6)	0.4726(2)	0.2215(3)	5.7(2)
C(1)	0.4326(6)	0.4702(2)	0.5187(3)	3.2(2)
C(2)	0.4802(7)	0.5191(2)	0.5624(4)	3.7(2)
C(3)	0.6114(7)	0.5448(2)	0.5010(3)	3.6(2)
C(4)	0.7786(7)	0.5175(2)	0.4748(4)	3.5(2)
C(5)	0.7229(6)	0.4702(2)	0.4181(3)	2.9(2)
C(6)	0.8961(6)	0.4416(2)	0.4067(4)	3.5(2)
C(7)	0.8621(6)	0.3912(2)	0.3749(4)	3.4(2)
C(8)	0.7478(5)	0.3665(2)	0.4530(3)	2.3(1)
C(9)	0.5581(5)	0.3915(2)	0.4539(3)	2.4(1)

Can. J. Chem. Downloaded from www.nrcresearchpress.com by 217.78.4.112 on 09/08/12
For personal use only.

Can. J. Chem. Downloaded from www.nrcresearchpress.com by 217.78.4.112 on 09/08/12
For personal use only.

TABLE A2 (*continued*)

Atom	*x*	*y*	*z*	U_{eq}/B_{eq}[a]
C(10)	0.6009(6)	0.4427(2)	0.4915(3)	2.5(1)
C(11)	0.4490(6)	0.3669(2)	0.5361(3)	2.8(2)
C(12)	0.4451(6)	0.3133(2)	0.5273(3)	2.7(2)
C(13)	0.6402(5)	0.2914(2)	0.5359(3)	2.4(1)
C(14)	0.7421(6)	0.3123(2)	0.4435(3)	2.5(1)
C(15)	0.9411(6)	0.2924(2)	0.4586(4)	3.2(2)
C(16)	0.9437(6)	0.2394(2)	0.4474(4)	3.4(2)
C(17)	0.8092(6)	0.2112(2)	0.5095(3)	2.8(2)
C(18)	0.6242(5)	0.2373(2)	0.5220(3)	2.5(1)
C(19)	0.5135(6)	0.2111(2)	0.5997(3)	2.8(2)
C(20)	0.6161(6)	0.1926(2)	0.7077(4)	3.2(2)
C(21)	0.7901(6)	0.1694(2)	0.6854(3)	3.1(2)
C(22)	0.9132(6)	0.1973(2)	0.6222(4)	3.4(2)
C(23)	0.9072(9)	0.5475(2)	0.4161(5)	5.5(3)
C(24)	0.6274(7)	0.4824(2)	0.3060(3)	3.4(2)
C(25)	0.4321(6)	0.3914(2)	0.3435(3)	3.2(2)
C(26)	0.7361(6)	0.3037(2)	0.6500(3)	3.0(2)
C(27)	0.6521(7)	0.2979(2)	0.3291(3)	3.3(2)
C(28)	0.7646(7)	0.1660(2)	0.4458(4)	3.9(2)
C(29)	0.4928(8)	0.1612(2)	0.7662(4)	4.1(2)
C(30)	0.382(1)	0.5273(2)	0.2123(4)	5.8(3)
O(6)	1.0397(7)	0.1783(2)	−0.0363(3)	6.5(2)
O(7)	0.5525(6)	−0.2632(2)	−0.1027(3)	5.4(2)
O(8)	0.3915(5)	−0.2133(2)	0.0351(4)	5.9(2)
O(9)	1.0302(6)	0.0818(2)	0.2989(3)	5.2(2)
O(10)	1.1816(5)	0.1191(2)	0.1805(3)	4.3(1)
C(31)	1.1868(7)	0.0582(2)	−0.0076(4)	3.6(2)
C(32)	1.1417(8)	0.1026(2)	−0.0727(4)	4.7(2)
C(33)	1.0223(8)	0.1369(2)	−0.0237(4)	4.2(2)
C(34)	0.8652(7)	0.1171(2)	0.0324(4)	4.0(2)
C(35)	0.9220(6)	0.0744(2)	0.1058(3)	3.1(2)
C(36)	0.7486(7)	0.0528(2)	0.1432(4)	3.6(2)
C(37)	0.7740(6)	0.0038(2)	0.1912(4)	3.3(2)
C(38)	0.8514(5)	−0.0285(2)	0.1107(3)	2.4(1)
C(39)	1.0451(5)	−0.0115(2)	0.0870(3)	2.6(1)
C(40)	1.0161(6)	0.0380(2)	0.0368(3)	2.7(2)
C(41)	1.1194(6)	−0.0439(2)	0.0039(3)	3.0(2)
C(42)	1.0964(6)	−0.0961(2)	0.0267(4)	2.9(2)
C(43)	0.8952(6)	−0.1099(2)	0.0367(3)	2.4(1)
C(44)	0.8331(6)	−0.0817(2)	0.1337(3)	2.4(1)
C(45)	0.6298(6)	−0.0944(2)	0.1411(4)	3.2(2)
C(46)	0.6063(6)	−0.1456(2)	0.1673(4)	3.3(2)
C(47)	0.6961(6)	−0.1809(2)	0.0975(3)	2.8(2)
C(48)	0.8826(5)	−0.1629(2)	0.0605(3)	2.5(1)
C(49)	0.9448(6)	−0.1958(2)	−0.0260(3)	3.1(2)
C(50)	0.8011(7)	−0.2102(2)	−0.1206(3)	3.4(2)
C(51)	0.6290(7)	−0.2260(2)	−0.0778(4)	3.6(2)
C(52)	0.5506(6)	−0.1939(2)	−0.0005(4)	3.6(2)
C(53)	0.763(1)	0.1547(2)	0.0864(6)	5.8(3)
C(54)	1.0465(6)	0.0910(2)	0.2054(4)	3.2(2)
C(55)	1.1937(6)	−0.0095(2)	0.1879(3)	3.2(2)
C(56)	0.7799(7)	−0.0978(2)	−0.0723(3)	3.3(2)
C(57)	0.9443(7)	−0.0936(2)	0.2439(3)	3.4(2)
C(58)	0.7374(7)	−0.2254(2)	0.1639(4)	4.0(2)
C(59)	0.8772(9)	−0.2460(2)	−0.1925(4)	4.9(2)
C(60)	1.3072(8)	0.1379(2)	0.2691(5)	5.2(2)
		17 · 1/2 H_2O		
O(1)	0.5163(2)	0.6371(2)	0.7708(3)	4.5(2)
O(2)	0.5471(2)	0.7922(2)	0.6600(3)	4.3(1)
O(3)	0.4017(2)	0.1890(2)	−0.0912(3)	3.9(1)
O(4)	0.2970(2)	0.3306(2)	−0.1439(2)	4.3(1)
O(5)	1/2	1/2	0.9525(6)	11.0(5)
C(1)	0.4121(3)	0.5851(2)	0.6185(4)	3.0(2)

TABLE A2 (*continued*)

Atom	*x*	*y*	*z*	U_{eq}/B_{eq}[a]
C(2)	0.4738(3)	0.6496(3)	0.6740(4)	3.1(2)
C(3)	0.4891(3)	0.7314(3)	0.6085(3)	2.9(2)
C(4)	0.4457(3)	0.7469(3)	0.5009(4)	2.9(2)
C(5)	0.3837(3)	0.6801(2)	0.4484(3)	2.5(2)
C(6)	0.3417(3)	0.6915(3)	0.3391(4)	3.1(2)
C(7)	0.2943(3)	0.6234(3)	0.2767(3)	3.2(2)
C(8)	0.2779(3)	0.5442(2)	0.3245(3)	2.6(2)
C(9)	0.2990(3)	0.5304(2)	0.4585(3)	2.5(2)
C(10)	0.3697(3)	0.5973(2)	0.5107(3)	2.5(2)
C(11)	0.3326(3)	0.4359(2)	0.4871(3)	2.9(2)
C(12)	0.2919(3)	0.3631(2)	0.4081(3)	2.7(2)
C(13)	0.2977(3)	0.3856(2)	0.2720(3)	2.2(1)
C(14)	0.2331(3)	0.4699(2)	0.2515(3)	2.5(2)
C(15)	0.2333(3)	0.4900(3)	0.1154(3)	3.3(2)
C(16)	0.1878(3)	0.4168(3)	0.0391(4)	3.6(2)
C(17)	0.2324(3)	0.3258(3)	0.0585(3)	2.8(2)
C(18)	0.2554(3)	0.3078(2)	0.1945(3)	2.5(1)
C(19)	0.3098(3)	0.2201(2)	0.2080(3)	2.9(2)
C(20)	0.3954(3)	0.2033(3)	0.1246(3)	2.9(2)
C(21)	0.3748(3)	0.2310(3)	−0.0045(3)	2.7(2)
C(22)	0.3235(3)	0.3183(2)	−0.0206(3)	2.7(2)
C(23)	0.4642(3)	0.8318(3)	0.4356(4)	3.5(2)
C(24)	0.2037(3)	0.5514(3)	0.5323(4)	3.6(2)
C(25)	0.4034(3)	0.4060(2)	0.2431(3)	2.7(2)
C(26)	0.1274(3)	0.4574(3)	0.2881(4)	3.5(2)
C(27)	0.1598(3)	0.2565(3)	0.0152(4)	3.5(2)
C(28)	0.4287(4)	0.1084(3)	0.1317(4)	4.0(2)
		18		
O(1)	0.5317(2)	−0.1026(1)	0.1684(1)	4.8(2)
O(2)	0.1550(2)	0.3796(2)	0.2088(1)	5.1(2)
C(1)	0.5012(2)	0.0822(2)	0.1800(2)	3.6(2)
C(2)	0.5366(2)	0.0142(2)	0.1838(2)	3.5(2)
C(3)	0.4939(2)	−0.0418(2)	0.1643(2)	3.6(2)
C(4)	0.4696(2)	−0.0313(2)	0.1108(2)	3.3(2)
C(5)	0.4373(2)	0.0399(2)	0.1080(1)	2.9(2)
C(6)	0.4073(2)	0.0570(2)	0.0579(2)	3.7(2)
C(7)	0.3597(2)	0.1164(2)	0.0614(2)	3.6(2)
C(8)	0.3918(2)	0.1804(2)	0.0830(1)	3.0(2)
C(9)	0.4318(2)	0.1614(2)	0.1300(1)	3.1(2)
C(10)	0.4800(2)	0.0989(2)	0.1278(1)	2.9(2)
C(11)	0.4666(2)	0.2234(2)	0.1524(2)	5.2(3)
C(12)	0.4267(2)	0.2863(2)	0.1466(2)	4.4(2)
C(13)	0.3696(2)	0.2936(2)	0.1219(2)	3.0(2)
C(14)	0.3359(2)	0.2331(2)	0.0982(1)	3.0(2)
C(15)	0.2931(2)	0.2538(2)	0.0532(2)	3.8(2)
C(16)	0.2553(2)	0.3203(2)	0.0593(2)	3.9(2)
C(17)	0.3015(2)	0.3787(2)	0.0724(2)	3.6(2)
C(18)	0.3363(2)	0.3626(2)	0.1219(2)	3.3(2)
C(19)	0.2894(2)	0.3691(2)	0.1661(2)	3.5(2)
C(20)	0.2525(2)	0.4362(2)	0.1706(2)	3.6(2)
C(21)	0.2158(2)	0.4491(2)	0.1224(2)	4.2(2)
C(22)	0.2619(2)	0.4452(2)	0.0780(2)	4.4(2)
C(23)	0.5268(3)	−0.0434(2)	0.0739(2)	4.7(2)
C(24)	0.4142(2)	−0.0835(2)	0.1010(2)	5.0(2)
C(25)	0.5441(2)	0.1124(2)	0.0972(2)	4.5(2)
C(26)	0.4388(3)	0.2110(3)	0.0440(2)	4.9(2)
C(27)	0.2862(2)	0.2040(2)	0.1368(2)	3.4(2)
C(28)	0.3539(3)	0.3896(2)	0.0325(2)	5.1(3)
C(29)	0.2026(2)	0.4327(2)	0.2131(2)	4.2(2)
C(30)	0.3016(2)	0.4930(2)	0.1836(2)	5.2(3)
O(1′)	−0.0308(2)	0.2757(1)	0.1675(1)	4.3(1)
O(2′)	0.3547(2)	−0.2191(2)	0.2240(1)	4.6(2)
C(1′)	−0.0007(2)	0.0913(2)	0.1879(1)	2.9(2)

TABLE A2 (*continued*)

Atom	*x*	*y*	*z*	U_{eq}/B_{eq}[a]
C(2′)	−0.0368(2)	0.1586(2)	0.1877(1)	3.1(2)
C(3′)	0.0064(2)	0.2136(2)	0.1666(2)	3.1(2)
C(4′)	0.0322(2)	0.1994(2)	0.1145(1)	3.0(2)
C(5′)	0.0660(2)	0.1285(2)	0.1155(1)	2.7(2)
C(6′)	0.0980(2)	0.1066(2)	0.0670(1)	3.3(2)
C(7′)	0.1458(2)	0.0481(2)	0.0743(1)	3.4(2)
C(8′)	0.1139(2)	−0.0134(2)	0.0993(1)	2.6(2)
C(9′)	0.0741(2)	0.0104(2)	0.1447(1)	2.4(2)
C(10′)	0.0240(2)	0.0701(2)	0.1372(1)	2.4(2)
C(11′)	0.0425(2)	−0.495(2)	0.1722(1)	3.3(2)
C(12′)	0.0801(2)	−0.1140(2)	0.1675(1)	2.9(2)
C(13′)	0.1359(2)	−0.1237(2)	0.1420(1)	2.6(2)
C(14′)	0.1703(2)	−0.0645(2)	0.1165(1)	2.6(2)
C(15′)	0.2139(2)	−0.0885(2)	0.0724(2)	3.3(2)
C(16′)	0.2493(2)	−0.1555(2)	0.0793(2)	3.3(2)
C(17′)	0.2007(2)	−0.2122(2)	0.0936(1)	3.0(2)
C(18′)	0.1679(2)	−0.1933(2)	0.1431(1)	2.8(2)
C(19′)	0.2163(2)	−0.2004(2)	0.1864(1)	3.1(2)
C(20′)	0.2506(2)	−0.2688(2)	0.1907(1)	3.1(2)
C(21′)	0.2845(2)	−0.2856(2)	0.1419(2)	3.6(2)
C(22′)	0.2378(2)	−0.2796(2)	0.0981(2)	3.5(2)
C(23′)	−0.0246(3)	0.2061(2)	0.0765(2)	4.5(2)
C(24′)	0.0861(3)	0.2518(2)	0.1027(2)	4.7(2)
C(25′)	−0.0373(2)	0.0519(2)	0.1063(2)	3.4(2)
C(26′)	0.0665(2)	−0.0485(2)	0.0621(1)	3.3(2)
C(27′)	0.2196(2)	−0.0337(2)	0.1540(2)	3.4(2)
C(28′)	0.1468(2)	−0.2207(2)	0.0538(2)	3.7(2)
C(29′)	0.3027(2)	−0.2670(2)	0.2317(2)	3.9(2)
C(30′)	0.1998(2)	−0.3231(2)	0.2050(2)	4.5(2)
		19 · EtOH		
O(1)	0.4637(2)	0.2874	0.2709(2)	4.2(1)
O(2)	0.4142(2)	0.4790(7)	0.6819(2)	3.8(1)
O(3)	0.4661(3)	0.1460(8)	0.7789(2)	7.2(2)
C(1)	0.4210(3)	0.430(1)	0.4955(3)	3.6(2)
C(2)	0.4612(3)	0.441(1)	0.4104(3)	4.0(2)
C(3)	0.4201(3)	0.282(1)	0.3487(3)	3.5(2)
C(4)	0.3159(3)	0.293(1)	0.3254(3)	3.3(2)
C(5)	0.2761(3)	0.2903(9)	0.4137(2)	3.1(2)
C(6)	0.1717(3)	0.280(1)	0.4039(3)	4.1(2)
C(7)	0.1415(3)	0.207(1)	0.4874(3)	4.3(2)
C(8)	0.1774(3)	0.3337(9)	0.5669(3)	3.0(2)
C(9)	0.2821(3)	0.3759(8)	0.5714(2)	2.7(2)
C(10)	0.3151(3)	0.4440(8)	0.4836(2)	2.9(2)
C(11)	0.3167(3)	0.5063(8)	0.6499(2)	3.1(2)
C(12)	0.2647(3)	0.4805(9)	0.7243(2)	3.3(2)
C(13)	0.1965(3)	0.3527(9)	0.7297(3)	2.9(2)
C(14)	0.1638(3)	0.2183(9)	0.6531(3)	3.3(2)
C(15)	0.0620(3)	0.154(1)	0.6499(3)	4.7(3)
C(16)	0.0344(4)	0.110(1)	0.7375(3)	5.6(3)
C(17)	0.0540(3)	0.286(1)	0.8017(3)	5.2(3)
C(18)	0.1584(3)	0.326(1)	0.8149(3)	4.2(2)
C(19)	0.2146(4)	0.171(1)	0.8714(3)	5.5(3)
C(20)	0.1836(5)	0.129(1)	0.9594(4)	7.0(4)
C(21)	0.0800(5)	0.081(2)	0.9415(4)	8.4(4)
C(22)	0.0238(4)	0.235(1)	0.8897(4)	7.1(4)
C(23)	0.2859(3)	0.473(1)	0.2678(3)	4.6(2)
C(24)	0.2832(4)	0.104(1)	0.2745(3)	4.8(3)
C(25)	0.1217(3)	0.529(1)	0.5598(3)	4.5(2)
C(26)	0.2882(4)	0.660(1)	0.4588(3)	4.1(2)
C(27)	0.2230(3)	0.0245(9)	0.6653(3)	4.1(2)
C(28)	0.0011(4)	0.467(2)	0.7657(4)	8.1(4)
C(29)	0.2365(7)	−0.047(2)	1.0028(5)	11.6(6)
C(30)	0.1987(6)	0.312(2)	1.0187(4)	10.0(5)

TABLE A2 (*concluded*)

Atom	*x*	*y*	*z*	U_{eq}/B_{eq}[a]
C(31)	0.5125(8)	0.202(2)	0.8604(5)	11.8(6)
C(32)	0.520(1)	0.055(4)	0.9199(8)	20(1)

[a]For compound **6** the thermal parameter given is $1000 \times U_{eq} = 1/3$ trace of diagonalized **U** tensor. For all of the other compounds, the parameter given is $B_{eq} = (8/3)_{\pi}{}^{2}\Sigma\Sigma U_{ij}a_i{}^{*}a_j{}^{*}(\mathbf{a}_i \cdot \mathbf{a}_j)$.

TABLE A3. Bond lengths (Å) with estimated standard deviations in parentheses

Bond	Length (Å)	Bond	Length (Å)
		6·MeOH	
O(1)—C(3)	1.435(4)	C(10)—C(25)	1.552(5)
O(2)—C(22)	1.439(4)	C(11)—C(12)	1.493(5)
O(3)—C(29)	1.195(4)	C(12)—C(13)	1.313(4)
O(4)—C(29)	1.313(5)	C(13)—C(14)	1.534(4)
C(1)—C(2)	1.527(5)	C(13)—C(18)	1.527(4)
C(1)—C(10)	1.538(5)	C(14)—C(15)	1.530(4)
C(2)—C(3)	1.510(5)	C(14)—C(27)	1.547(5)
C(3)—C(4)	1.538(5)	C(15)—C(16)	1.544(5)
C(4)—C(5)	1.565(4)	C(16)—C(17)	1.532(5)
C(4)—C(23)	1.528(5)	C(17)—C(18)	1.546(5)
C(4)—C(24)	1.531(5)	C(17)—C(22)	1.555(4)
C(5)—C(6)	1.530(5)	C(17)—C(28)	1.526(5)
C(5)—C(10)	1.546(5)	C(18)—C(19)	1.524(5)
C(6)—C(7)	1.536(5)	C(19)—C(20)	1.545(5)
C(7)—C(8)	1.535(5)	C(20)—C(21)	1.551(5)
C(8)—C(9)	1.553(4)	C(20)—C(29)	1.510(5)
C(8)—C(14)	1.592(4)	C(20)—C(30)	1.535(5)
C(8)—C(26)	1.538(5)	C(21)—C(22)	1.506(5)
C(9)—C(10)	1.569(4)	O(5)—C(31)	1.378(5)
C(9)—C(11)	1.540(5)		
O(1)—H(01)	0.75(5)	O(4)—H(04)	0.96(4)
O(2)—H(02)	0.86(4)	O(5)—H(05)	0.91(6)
		15·1/2 EtOAc	
O(1)—C(2)	1.247(7)	O(1′)—C(2′)	1.240(7)
O(2)—C(3)	1.357(7)	O(2′)—C(3′)	1.363(7)
O(3)—C(21)	1.252(8)	O(3′)—C(21′)	1.224(9)
C(1)—C(10)	1.362(8)	C(1′)—C(10′)	1.344(8)
C(1)—C(2)	1.441(8)	C(1′)—C(2′)	1.425(9)
C(2)—C(3)	1.423(8)	C(2′)—C(3′)	1.465(9)
C(3)—C(4)	1.345(9)	C(3′)—C(4′)	1.338(8)
C(4)—C(5)	1.459(8)	C(4′)—C(5′)	1.444(8)
C(4)—C(23)	1.534(9)	C(4′)—C(23′)	1.503(9)
C(5)—C(6)	1.357(8)	C(5′)—C(6′)	1.365(8)
C(5)—C(10)	1.449(8)	C(5′)—C(10′)	1.444(8)
C(6)—C(7)	1.421(9)	C(6′)—C(7′)	1.417(9)
C(7)—C(8)	1.335(8)	C(7′)—C(8′)	1.342(8)
C(8)—C(9)	1.524(8)	C(8′)—C(14′)	1.517(8)
C(8)—C(14)	1.531(8)	C(8′)—C(9′)	1.546(8)
C(9)—C(11)	1.521(8)	C(9′)—C(10′)	1.534(8)
C(9)—C(10)	1.533(8)	C(9′)—C(11′)	1.542(8)
C(9)—C(24)	1.582(8)	C(9′)—C(24′)	1.548(8)
C(11)—C(12)	1.539(9)	C(11′)—C(12′)	1.528(9)
C(12)—C(13)	1.534(8)	C(12′)—C(13′)	1.543(8)
C(13)—C(14)	1.554(8)	C(13′)—C(25′)	1.535(8)
C(13)—C(25)	1.555(8)	C(13′)—C(14′)	1.574(8)
C(13)—C(18)	1.556(8)	C(13′)—C(18′)	1.585(8)
C(14)—C(15)	1.537(9)	C(14′)—C(15′)	1.540(9)

Can. J. Chem. Downloaded from www.nrcresearchpress.com by 217.78.4.112 on 09/08/12
For personal use only.

Can. J. Chem. Downloaded from www.nrcresearchpress.com by 217.78.4.112 on 09/08/12
For personal use only.

TABLE A3 (*continued*)

Bond	Length (Å)	Bond	Length (Å)
C(14)—C(26)	1.572(9)	C(14′)—C(26′)	1.560(9)
C(15)—C(16)	1.51(1)	C(15′)—C(16′)	1.54(1)
C(16)—C(17)	1.54(1)	C(16′)—C(17′)	1.55(1)
C(17)—C(22)	1.52(1)	C(17′)—C(27′)	1.526(9)
C(17)—C(27)	1.53(1)	C(17′)—C(22′)	1.55(1)
C(17)—C(18)	1.550(9)	C(17′)—C(18′)	1.565(9)
C(18)—C(19)	1.52(1)	C(18′)—C(19′)	1.544(9)
C(19)—C(20)	1.54(1)	C(19′)—C(20′)	1.55(1)
C(20)—C(21)	1.48(1)	C(20′)—C(21′)	1.51(1)
C(20)—C(28)	1.53(1)	C(20′)—C(28′)	1.54(1)
C(21)—C(22)	1.49(1)	C(21′)—C(22′)	1.49(1)
		16	
O(1)—C(3)	1.210(5)	O(6)—C(33)	1.208(6)
O(2)—C(21)	1.226(5)	O(7)—C(51)	1.227(5)
O(3)—C(22)	1.421(5)	O(8)—(C52)	1.406(6)
O(4)—C(24)	1.343(5)	O(10)—C(54)	1.340(5)
O(4)—C(30)	1.436(6)	O(10)—C(60)	1.445(6)
O(5)—C(24)	1.195(5)	O(9)—C(54)	1.211(5)
C(1)—C(2)	1.529(6)	C(31)—C(32)	1.523(7)
C(1)—C(10)	1.531(6)	C(31)—C(40)	1.535(6)
C(2)—C(3)	1.491(7)	C(32)—C(33)	1.495(8)
C(3)—C(4)	1.518(7)	C(33)—C(34)	1.523(7)
C(4)—C(23)	1.525(7)	C(34)—C(53)	1.516(7)
C(4)—C(5)	1.561(6)	C(34)—C(35)	1.555(6)
C(5)—C(24)	1.517(6)	C(35)—C(54)	1.515(6)
C(5)—C(6)	1.527(6)	C(35)—C(36)	1.530(6)
C(5)—C(10)	1.564(6)	C(35)—C(40)	1.563(6)
C(6)—C(7)	1.512(6)	C(36)—C(37)	1.532(6)
C(7)—C(8)	1.531(6)	C(37)—C(38)	1.524(6)
C(8)—C(9)	1.558(5)	C(38)—C(39)	1.556(5)
C(8)—C(14)	1.562(5)	C(38)—C(44)	1.564(5)
C(9)—C(11)	1.542(5)	C(39)—C(41)	1.538(5)
C(9)—C(25)	1.551(6)	C(39)—C(55)	1.550(6)
C(9)—C(10)	1.563(5)	C(39)—C(40)	1.558(5)
C(11)—C(12)	1.544(5)	C(41)—C(42)	1.540(6)
C(12)—C(13)	1.546(5)	C(42)—C(43)	1.538(6)
C(13)—C(26)	1.540(5)	C(43)—C(56)	1.541(5)
C(13)—C(14)	1.563(5)	C(43)—C(48)	1.559(5)
C(13)—C(18)	1.569(5)	C(43)—C(44)	1.565(5)
C(14)—C(27)	1.544(6)	C(44)—C(45)	1.539(6)
C(14)—C(15)	1.547(6)	C(44)—C(57)	1.539(6)
C(15)—C(16)	1.532(6)	C(45)—C(46)	1.522(6)
C(16)—C(17)	1.549(6)	C(46)—C(47)	1.532(6)
C(17)—C(28)	1.533(6)	C(47)—C(58)	1.531(6)
C(17)—C(22)	1.557(6)	C(47)—C(52)	1.556(6)
C(17)—C(18)	1.567(6)	C(47)—C(48)	1.574(6)
C(18)—C(19)	1.530(5)	C(48)—C(49)	1.542(6)
C(19)—C(20)	1.545(6)	C(49)—C(50)	1.528(6)
C(20)—C(21)	1.489(6)	C(50)—C(51)	1.493(7)
C(20)—C(29)	1.521(6)	C(50)—C(59)	1.513(7)
C(21)—C(22)	1.497(6)	C(51)—C(52)	1.495(7)
		17·1/2 H_2O	
O(1)—C(2)	1.238(5)	C(9)—C(24)	1.590(5)
O(2)—C(3)	1.356(5)	C(11)—C(12)	1.523(5)
O(3)—C(21)	1.213(4)	C(12)—C(13)	1.548(5)
O(4)—C(22)	1.426(5)	C(13)—C(25)	1.537(5)
C(1)—C(10)	1.344(5)	C(13)—C(18)	1.578(5)
C(1)—C(2)	1.445(5)	C(13)—C(14)	1.585(5)
C(2)—C(3)	1.459(6)	C(14)—C(15)	1.538(5)
C(3)—C(4)	1.356(6)	C(14)—C(26)	1.538(6)
C(4)—C(5)	1.456(6)	C(15)—C(16)	1.536(6)
C(4)—C(23)	1.506(6)	C(16)—C(17)	1.536(6)
C(5)—C(6)	1.355(5)	C(17)—C(27)	1.538(6)
C(5)—C(10)	1.453(5)	C(17)—C(22)	1.546(5)

TABLE A3 (*concluded*)

Bond	Length (Å)	Bond	Length (Å)
C(6)—C(7)	1.411(6)	C(17)—C(18)	1.564(5)
C(7)—C(8)	1.339(5)	C(18)—C(19)	1.544(5)
C(8)—C(14)	1.526(5)	C(19)—C(20)	1.530(6)
C(8)—C(9)	1.527(5)	C(20)—C(21)	1.517(5)
C(9)—C(10)	1.532(5)	C(20)—C(28)	1.522(6)
C(9)—C(11)	1.549(5)	C(21)—C(22)	1.521(6)
		18	
O(1)—C(3)	1.431(5)	O(1′)—C(3′)	1.443(5)
O(2)—C(29)	1.424(5)	O(2′)—C(29′)	1.423(5)
C(1)—C(10)	1.517(6)	C(1′)—C(10′)	1.523(5)
C(1)—C(2)	1.531(6)	C(1′)—C(2′)	1.523(5)
C(2)—C(3)	1.499(6)	C(2′)—C(3′)	1.507(6)
C(3)—C(4)	1.550(6)	C(3′)—C(4′)	1.536(6)
C(4)—C(23)	1.536(6)	C(4′)—C(24′)	1.531(6)
C(4)—C(24)	1.538(6)	C(4′)—C(23′)	1.535(6)
C(4)—C(5)	1.559(5)	C(4′)—C(5′)	1.566(5)
C(5)—C(6)	1.527(6)	C(5′)—C(6′)	1.529(5)
C(5)—C(10)	1.549(5)	C(5′)—C(10′)	1.551(5)
C(6)—C(7)	1.518(6)	C(6′)—C(7′)	1.517(6)
C(7)—C(8)	1.545(6)	C(7′)—C(8′)	1.539(5)
C(8)—C(26)	1.538(6)	C(8′)—C(9′)	1.543(5)
C(8)—C(9)	1.554(5)	C(8′)—C(26′)	1.549(5)
C(8)—C(14)	1.585(5)	C(8′)—C(14′)	1.586(5)
C(9)—C(11)	1.544(6)	C(9′)—C(11′)	1.542(5)
C(9)—C(10)	1.574(5)	C(9′)—C(10′)	1.566(5)
C(10)—C(25)	1.546(6)	C(10′)—C(25′)	1.525(5)
C(11)—C(12)	1.492(6)	C(11′)—C(12′)	1.493(5)
C(12)—C(13)	1.327(6)	C(12′)—C(13′)	1.323(5)
C(13)—C(14)	1.524(5)	C)13′)—C(18′)	1.527(5)
C(13)—C(18)	1.528(5)	C(13′)—C(14′)	1.529(5)
C(14)—C(15)	1.547(6)	C(14′)—C(27′)	1.543(5)
C(14)—C(27)	1.554(6)	C(14′)—C(15′)	1.556(5)
C(15)—C(16)	1.533(6)	C(15′)—C(16′)	1.522(6)
C(16)—C(17)	1.526(6)	C(16′)—C(17′)	1.536(6)
C(17)—C(28)	1.520(6)	C(17′)—C(28′)	1.533(6)
C(17)—C(18)	1.549(6)	C(17′)—C(22′)	1.537(5)
C(17)—C(22)	1.549(6)	C(17′)—C(18′)	1.543(5)
C(18)—C(19)	1.524(6)	C(18′)—C(19′)	1.528(5)
C(19)—C(20)	1.532(6)	C(19′)—C(20′)	1.529(5)
C(20)—C(21)	1.523(6)	C(20′)—C(29′)	1.523(6)
C(20)—C(29)	1.525(6)	C(20′)—C(21′)	1.525(6)
C(20)—C(30)	1.538(6)	C(20′)—C(30′)	1.531(6)
C(21)—C(22)	1.518(6)	C(21′)—C(22′)	1.516(6)
		19·EtOH	
O(1)—C(3)	1.455(5)	C(10)—C(26)	1.535(7)
O(2)—C(11)	1.451(5)	C(11)—C(12)	1.492(6)
O(3)—C(31)	1.400(9)	C(12)—C(13)	1.327(6)
C(1)—C(2)	1.534(6)	C(13)—C(14)	1.516(6)
C(1)—C(10)	1.537(6)	C(13)—C(18)	1.529(6)
C(2)—C(3)	1.500(7)	C(14)—C(15)	1.546(7)
C(3)—C(4)	1.516(6)	C(14)—C(27)	1.556(7)
C(4)—C(23)	1.528(7)	C(15)—C(16)	1.514(7)
C(4)—C(24)	1.531(7)	C(16)—C(17)	1.547(9)
C(4)—C(5)	1.576(6)	C(17)—C(28)	1.51(1)
C(5)—C(6)	1.514(6)	C(17)—C(18)	1.535(7)
C(5)—C(10)	1.547(6)	C(17)—C(22)	1.545(8)
C(6)—C(7)	1.520(6)	C(18)—C(19)	1.520(8)
C(7)—C(8)	1.532(6)	C(19)—C(20)	1.537(7)
C(8)—C(25)	1.537(7)	C(20)—C(29)	1.51(1)
C(8)—C(9)	1.550(6)	C(20)—C(30)	1.53(1)
C(8)—C(14)	1.591(6)	C(20)—C(21)	1.535(9)
C(9)—C(11)	1.528(6)	C(21)—C(22)	1.48(1)
C(9)—C(10)	1.587(6)	C(31)—C(32)	1.35(2)

TABLE A4. Bond angles (deg) with estimated standard deviations in parentheses

Bonds	Angle (deg)	Bonds	Angle (deg)
		6·MeOH	
C(2)—C(1)—C(10)	112.9(3)	C(12)—C(13)—C(18)	119.0(3)
C(1)—C(2)—C(3)	112.3(3)	C(14)—C(13)—C(18)	120.7(3)
O(1)—C(3)—C(2)	111.0(3)	C(8)—C(14)—C(13)	108.4(3)
O(1)—C(3)—C(4)	111.7(3)	C(8)—C(14)—C(15)	111.4(3)
C(2)—C(3)—C(4)	113.2(3)	C(8)—C(14)—C(27)	111.8(3)
C(3)—C(4)—C(5)	108.0(3)	C(13)—C(14)—C(15)	112.2(3)
C(3)—C(4)—C(23)	110.2(3)	C(13)—C(14)—C(27)	106.8(3)
C(3)—C(4)—C(24)	107.4(3)	C(15)—C(14)—C(27)	106.3(3)
C(5)—C(4)—C(23)	114.8(3)	C(14)—C(15)—C(16)	114.4(3)
C(5)—C(4)—C(24)	108.6(3)	C(15)—C(16)—C(17)	112.1(3)
C(23)—C(4)—C(24)	107.7(3)	C(16)—C(17)—C(18)	109.0(3)
C(4)—C(5)—C(6)	114.2(3)	C(16)—C(17)—C(22)	111.1(3)
C(4)—C(5)—C(10)	116.6(3)	C(16)—C(17)—C(28)	109.8(3)
C(6)—C(5)—C(10)	110.4(3)	C(18)—C(17)—C(22)	109.4(3)
C(5)—C(6)—C(7)	110.6(3)	C(18)—C(17)—C(28)	110.0(3)
C(6)—C(7)—C(8)	113.5(3)	C(22)—C(17)—C(28)	107.5(3)
C(7)—C(8)—C(9)	109.7(3)	C(13)—C(18)—C(17)	112.5(3)
C(7)—C(8)—C(14)	110.1(3)	C(13)—C(18)—C(19)	109.7(3)
C(7)—C(8)—C(26)	108.1(3)	C(17)—C(18)—C(19)	113.7(3)
C(9)—C(8)—C(14)	107.6(3)	C(18)—C(19)—C(20)	114.0(3)
C(9)—C(8)—C(26)	111.6(3)	C(19)—C(20)—C(21)	106.7(3)
C(14)—C(8)—C(26)	109.8(3)	C(19)—C(20)—C(29)	109.5(3)
C(8)—C(9)—C(10)	117.7(3)	C(19)—C(20)—C(30)	112.1(3)
C(8)—C(9)—C(11)	110.2(3)	C(21)—C(20)—C(29)	107.2(3)
C(10)—C(9)—C(11)	113.1(3)	C(21)—C(20)—C(30)	111.6(3)
C(1)—C(10)—C(5)	107.5(3)	C(29)—C(20)—C(30)	109.5(3)
C(1)—C(10)—C(9)	107.8(3)	C(20)—C(21)—C(22)	113.5(3)
C(1)—C(10)—C(25)	108.5(3)	O(2)—C(22)—C(17)	111.2(3)
C(5)—C(10)—C(9)	106.7(2)	O(2)—C(22)—C(21)	109.6(3)
C(5)—C(10)—C(25)	113.4(3)	C(17)—C(22)—C(21)	115.3(3)
C(9)—C(10)—C(25)	112.7(3)	O(3)—C(29)—O(4)	121.2(4)
C(9)—C(11)—C(12)	113.9(3)	O(3)—C(29)—C(20)	124.9(4)
C(11)—C(12)—C(13)	127.1(3)	O(4)—C(29)—C(20)	113.9(3)
C(12)—C(13)—C(14)	119.9(3)		
C(3)—O(1)—H(O1)	116(4)	C(29)—O(4)—H(O4)	112(3)
C(22)—O(2)—H(O2)	116(3)	C(31)—O(5)—H(O5)	113(4)
		15·1/2 EtOAc	
C(10)—C(1)—C(2)	121.1(5)	C(10′)—C(1′)—C(2′)	122.2(6)
O(1)—C(2)—C(3)	119.7(6)	O(1′)—C(2′)—C(1′)	123.8(6)
O81)—C(2)—C(1)	122.0(6)	O(1′)—C(2′)—C(3′)	119.2(6)
C(3)—C(2)—C(1)	118.4(6)	C(1′)—C(2′)—C(3′)	117.0(6)
C(4)—C(3)—O(2)	120.1(6)	C(4′)—C(3′)—O(2′)	120.9(6)
C(4)—C(3)—C(2)	122.2(6)	C(4′)—C(3′)—C(2′)	122.5(6)
O(2)—C(3)—C(2)	117.7(6)	O(2′)—C(3′)—C(2′)	116.6(6)
C(3)—C(4)—C(5)	119.8(5)	C(3′)—C(4′)—C(5′)	118.4(6)
C(3)—C(4)—C(23)	119.8(6)	C(3′)—C(4′)—C(23′)	120.2(6)
C(5)—C(4)—C(23)	120.4(6)	C(5′)—C(4′)—C(23′)	121.4(6)
C(6)—C(5)—C(10)	117.5(6)	C(6′)—C(5′)—C(4′)	121.5(6)
C(6)—C(5)—C(4)	123.8(5)	C(6′)—C(5′)—C(10′)	118.0(5)
C(10)—C(5)—C(4)	118.5(5)	C(4′)—C(5′)—C(10′)	120.4(5)
C(5)—C(6)—C(7)	122.8(5)	C(5′)—C(6′)—C(7′)	123.1(5)
C(8)—C(7)—C(6)	123.8(6)	C(8′)—C(7′)—C(6′)	124.2(6)
C(7)—C(8)—C(9)	117.5(5)	C(7′)—C(8′)—C(14′)	121.5(5)
C(7)—C(8)—C(14)	122.5(6)	C(7′)—C(8′)—C(9′)	118.1(5)
C(9)—C(8)—C(14)	119.9(5)	C(14′)—C(8′)—C(9′)	120.5(5)
C(11)—C(9)—C(8)	114.7(5)	C(10′)—C(9′)—C(11′)	110.3(5)
C(11)—C(9)—C(10)	111.1(5)	C(10′)—C(9′)—C(8′)	113.6(4)
C(11)—C(9)—C(24)	108.7(5)	C(10′)—C(9′)—C(24′)	103.4(5)
C(8)—C(9)—C(10)	112.8(5)	C(11′)—C(9′)—C(8′)	109.7(5)
C(8)—C(9)—C(24)	106.9(5)	C(11′)—C(9′)—C(24′)	109.4(5)
C(10)—C(9)—C(24)	101.6(5)	C(8′)—C(9′)—C(24′)	110.1(5)

Can. J. Chem. Downloaded from www.nrcresearchpress.com by 217.78.4.112 on 09/08/12
For personal use only.

TABLE A4 (*continued*)

Bonds	Angle (deg)	Bonds	Angle (deg)
C(1)—C(10)—C(5)	120.0(5)	C(1′)—C(10′)—C(5′)	119.4(6)
C(1)—C(10)—C(9)	120.8(5)	C(1′)—C(10′)—C(9′)	119.8(5)
C(5)—C(10)—C(9)	118.8(5)	C(5′)—C(10′)—C(9′)	120.4(5)
C(9)—C(11)—C(12)	115.3(5)	C(12′)—C(11′)—C(9′)	114.7(5)
C(13)—C(12)—C(11)	112.4(4)	C(11′)—C(12′)—C(13′)	112.6(5)
C(12)—C(13)—C(14)	108.6(5)	C(25′)—C(13′)—C(12′)	107.1(5)
C(12)—C(13)—C(25)	107.4(5)	C(25′)—C(13′)—C(14′)	109.4(5)
C(12)—C(13)—C(18)	109.3(5)	C(25′)—C(13′)—C(18′)	112.6(5)
C(14)—C(13)—C(25)	109.9(5)	C(12′)—C(13′)—C(14′)	108.0(5)
C(14)—C(13)—C(18)	110.0(5)	C(12′)—C(13′)—C(18′)	110.2(5)
C(25)—C(13)—C(18)	111.5(5)	C(14′)—C(13′)—C(18′)	109.4(5)
C(8)—C(14)—C(15)	112.2(5)	C(8′)—C(14′)—C(15′)	112.9(5)
C(8)—C(14)—C(13)	109.6(5)	C(8′)—C(14′)—C(26′)	108.5(5)
C(8)—C(14)—C(26)	107.3(5)	C(8′)—C(14′)—C(13′)	109.1(5)
C(15)—C(14)—C(13)	108.0(5)	C(15′)—C(14′)—C(26′)	106.2(5)
C(15)—C(14)—C(26)	107.2(5)	C(15′)—C(14′)—C(13′)	107.1(5)
C(13)—C(14)—C(26)	112.7(5)	C(26′)—C(14′)—C(13′)	113.2(5)
C(16)—C(15)—C(14)	112.8(6)	C(16′)—C(15′)—C(14′)	113.2(5)
C(15)—C(16)—C(17)	117.1(6)	C(15′)—C(16′)—C(17′)	117.0(5)
C(22)—C(17)—C(27)	107.2(6)	C(27′)—C(17′)—C(22′)	106.8(6)
C(22)—C(17)—C(16)	109.1(6)	C(27′)—C(17′)—C(16′)	106.7(6)
C(22)—C(17)—C(18)	111.8(5)	C(27′)—C(17′)—C(18′)	108.3(6)
C(27)—C(17)—C(16)	106.4(6)	C(22′)—C(17′)—C(16′)	109.7(6)
C(27)—C(17)—C(18)	109.3(6)	C(22′)—C(17′)—C(18′)	112.5(6)
C(16)—C(17)—C(18)	112.6(5)	C(16′)—C(17′)—C(18′)	112.6(5)
C(19)—C(18)—C(17)	110.0(5)	C(19′)—C(18′)—C(17′)	110.5(5)
C(19)—C(18)—C(13)	117.5(5)	C(19′)—C(18′)—C(13′)	114.9(5)
C(17)—C(18)—C(13)	116.5(5)	C(17′)—C(18′)—C(13′)	116.5(5)
C(18)—C(19)—C(20)	118.2(6)	C(18′)—C(19′)—C(20′)	117.3(6)
C(21)—C(20)—C(28)	111.8(6)	C(21′)—C(20′)—C(28′)	113.5(7)
C(21)—C(20)—C(19)	110.0(6)	C(21′)—C(20′)—C(19′)	106.9(6)
C(28)—C(20)—C(19)	112.3(7)	C(28′)—C(20′)—C(19′)	111.1(6)
O(3)—C(21)—C(20)	121.5(8)	O(3′)—C(21′)—C(22′)	123.3(8)
O(3)—C(21)—C(22)	121.9(8)	O(3′)—C(21′)—C(20′)	122.8(8)
C(20)—C(21)—C(22)	116.5(6)	C(22′)—C(21′)—C(20′)	113.9(7)
C(21)—C(22)—C(17)	110.9(6)	C(21′)—C(22′)—C(17′)	110.7(6)
		16	
C(24)—O(4)—C(30)	118.1(4)	C(54)—O(10)—C(60)	117.6(4)
C(2)—C(1)—C(10)	113.6(4)	C(32)—C(31)—C(40)	112.1(4)
C(3)—C(2)—C(1)	113.8(4)	C(33)—C(32)—C(31)	115.8(4)
O(1)—C(3)—C(2)	122.4(5)	O(6)—C(33)—C(32)	121.5(5)
O(1)—C(3)—C(4)	121.6(5)	O(6)—C(33)—C(34)	121.6(5)
C(2)—C(3)—C(4)	115.9(4)	C(32)—C(33)—C(34)	116.6(4)
C(3)—C(4)—C(23)	111.6(4)	C(53)—C(34)—C(33)	112.0(4)
C(3)—C(4)—C(5)	112.1(4)	C(53)—C(34)—C(35)	114.4(4)
C(23)—C(4)—C(5)	114.6(4)	C(33)—C(34)—C(35)	113.8(4)
C(24)—C(5)—C(6)	109.2(4)	C(54)—C(35)—C(36)	108.1(4)
C(24)—C(5)—C(4)	106.0(3)	C(54)—C(35)—C(34)	108.6(4)
C(24)—C(5)—C(10)	115.1(3)	C(54)—C(35)—C(40)	113.5(4)
C(6)—C(5)—C(4)	109.9(4)	C(36)—C(35)—C(34)	109.2(4)
C(6)—C(5)—C(10)	108.6(3)	C(36)—C(35)—C(40)	109.4(3)
C(4)—C(5)—C(10)	108.1(3)	C(34)—C(35)—C(40)	108.0(3)
C(7)—C(6)—C(5)	115.4(4)	C(35)—C(36)—C(37)	115.3(4)
C(6)—C(7)—C(8)	111.3(4)	C(38)—C(37)—C(36)	110.0(4)
C(7)—C(8)—C(9)	110.1(3)	C(37)—C(38)—C(39)	110.6(3)
C(7)—C(8)—C(14)	115.2(3)	C(37)—C(38)—C(44)	115.4(3)
C(9)—C(8)—C(14)	116.5(3)	C(39)—C(38)—C(44)	116.2(3)
C(11)—C(9)—C(25)	106.7(3)	C(41)—C(39)—C(55)	107.2(3)
C(11)—C(9)—C(8)	108.9(3)	C(41)—C(39)—C(38)	109.9(3)
C(11)—C(9)—C(10)	109.5(3)	C(41)—C(39)—C(40)	109.1(3)
C(25)—C(9)—C(8)	114.8(3)	C(55)—C(39)—C(38)	114.6(3)
C(25)—C(9)—C(10)	109.9(3)	C(55)—C(39)—C(40)	109.6(3)
C(8)—C(9)—C(10)	107.0(3)	C(38)—C(39)—C(40)	106.4(3)

Can. J. Chem. Downloaded from www.nrcresearchpress.com by 217.78.4.112 on 09/08/12
For personal use only.

TABLE A4 (*continued*)

Bonds	Angle (deg)	Bonds	Angle (deg)
C(1)—C(10)—C(9)	114.6(3)	C(31)—C(40)—C(39)	114.4(3)
C(1)—C(10)—C(5)	113.4(3)	C(31)—C(40)—C(35)	112.1(3)
C(9)—C(10)—C(5)	114.0(3)	C(39)—C(40)—C(35)	116.0(3)
C(9)—C(11)—C(12)	114.7(3)	C(39)—C(41)—C(42)	114.3(3)
C(11)—C(12)—C(13)	113.1(3)	C(43)—C(42)—C(41)	113.1(3)
C(26)—C(13)—C(12)	106.1(3)	C(42)—C(43)—C(56)	106.9(3)
C(26)—C(13)—C(14)	112.7(3)	C(42)—C(43)—C(48)	110.3(3)
C(26)—C(13)—C(18)	110.3(3)	C(42)—C(43)—C(44)	107.4(3)
C(12)—C(13)—C(14)	108.0(3)	C(56)—C(43)—C(48)	110.4(3)
C(12)—C(13)—C(18)	110.0(3)	C(56)—C(43)—C(44)	112.5(3)
C(14)—C(13)—C(18)	109.6(3)	C(48)—C(43)—C(44)	109.4(3)
C(27)—C(14)—C(15)	107.2(3)	C(45)—C(44)—C(57)	107.2(3)
C(27)—C(14)—C(8)	109.9(3)	C(45)—C(44)—C(38)	110.4(3)
C(27)—C(14)—C(13)	112.8(3)	C(45)—C(44)—C(43)	107.2(3)
C(15)—C(14)—C(8)	110.1(3)	C(57)—C(44)—C(38)	109.5(3)
C(15)—C(14)—C(13)	107.0(3)	C(57)—C(44)—C(43)	113.5(3)
C(8)—C(14)—C(13)	109.8(3)	C(38)—C(44)—C(43)	109.0(3)
C(16)—C(15)—C(14)	112.3(4)	C(46)—C(45)—C(44)	112.2(3)
C(15)—C(16)—C(17)	117.4(4)	C(45)—C(46)—C(47)	116.8(3)
C(28)—C(17)—C(16)	107.0(4)	C(58)—C(47)—C(46)	108.4(3)
C(28)—C(17)—C(22)	107.1(4)	C(58)—C(47)—C(52)	106.8(4)
C(28)—C(17)—C(18)	109.1(3)	C(58)—C(47)—C(48)	108.2(3)
C(16)—C(17)—C(22)	108.4(3)	C(46)—C(47)—C(52)	107.8(3)
C(16)—C(17)—C(18)	113.9(3)	C(46)—C(47)—C(48)	113.2(3)
C(22)—C(17)—C(18)	111.1(3)	C(52)—C(47)—C(48)	112.2(3)
C(19)—C(18)—C(17)	110.8(3)	C(49)—C(48)—C(43)	116.0(3)
C(19)—C(18)—C(13)	117.1(3)	C(49)—C(48)—C(47)	110.1(3)
C(17)—C(18)—C(13)	115.7(3)	C(43)—C(48)—C(47)	116.7(3)
C(18)—C(19)—C(20)	118.7(3)	C(50)—C(49)—C(48)	117.9(4)
C(21)—C(20)—C(29)	112.9(4)	C(51)—C(50)—C(59)	112.9(4)
C(21)—C(20)—C(19)	108.9(3)	C(51)—C(50)—C(49)	109.4(3)
C(29)—C(20)—C(19)	111.7(4)	C(59)—C(50)—C(49)	111.8(4)
O(2)—C(21)—C(20)	124.2(4)	O(7)—C(51)—C(50)	123.4(4)
O(2)—C(21)—C(22)	119.9(4)	O(7)—C(51)—C(52)	120.1(5)
C(20)—C(21)—C(22)	115.9(4)	C(50)—C(51)—C(52)	116.5(4)
O(3)—C(22)—C(21)	110.9(4)	O(8)—C(52)—C(51)	110.7(4)
O(3)—C(22)—C(17)	110.8(4)	O(8)—C(52)—C(47)	110.9(4)
C(21)—C(22)—C(17)	110.7(3)	C(51)—C(52)—C(47)	111.9(4)
O(5)—C(24)—O(4)	122.1(4)	O(9)—C(54)—O(10)	121.1(4)
O(5)—C(24)—C(5)	126.2(5)	O(9)—C(54)—C(35)	126.4(4)
O(4)—C(24)—C(5)	111.5(3)	O(10)—C(54)—C(35)	112.5(4)
	17·1/2 H_2O		
C(10)—C(1)—C(2)	122.9(4)	C(25)—C(13)—C(14)	110.5(3)
O(1)—C(2)—C(1)	123.1(4)	C(12)—C(13)—C(18)	110.0(3)
O(1)—C(2)—C(3)	119.5(4)	C(12)—C(13)—C(14)	106.8(3)
C(1)—C(2)—C(3)	117.3(3)	C(18)—C(13)—C(14)	108.7(3)
O(2)—C(3)—C(4)	121.1(4)	C(8)—C(14)—C(15)	111.7(3)
O(2)—C(3)—C(2)	117.5(3)	C(8)—C(14)—C(26)	110.1(3)
C(4)—C(3)—C(2)	121.4(4)	C(8)—C(14)—C(13)	107.2(3)
C(3)—C(4)—C(5)	119.6(4)	C(15)—C(14)—C(26)	106.5(3)
C(3)—C(4)—C(23)	119.7(4)	C(15)—C(14)—C(13)	107.5(3)
C(5)—C(4)—C(23)	120.7(4)	C(26)—C(14)—C(13)	113.9(3)
C(6)—C(5)—C(10)	118.5(4)	C(16)—C(15)—C(14)	113.1(4)
C(6)—C(5)—C(4)	121.5(4)	C(17)—C(16)—C(15)	114.4(3)
C(10)—C(5)—C(4)	119.9(3)	C(16)—C(17)—C(27)	108.2(3)
C(5)—C(6)—C(7)	123.0(4)	C(16)—C(17)—C(22)	108.6(3)
C(8)—C(7)—C(6)	123.4(3)	C(16)—C(17)—C(18)	112.1(3)
C(7)—C(8)—C(14)	122.1(3)	C(27)—C(17)—C(22)	108.2(3)
C(7)—C(8)—C(9)	118.4(3)	C(27)—C(17)—C(18)	108.3(3)
C(14)—C(8)—C(9)	119.3(3)	C(22)—C(17)—C(18)	111.3(3)
C(8)—C(9)—C(10)	113.4(3)	C(19)—C(18)—C(17)	110.2(3)
C(8)—C(9)—C(11)	112.6(3)	C(19)—C(18)—C(13)	114.6(3)
C(8)—C(9)—C(24)	108.1(3)	C(17)—C(18)—C(13)	117.9(3)

Can. J. Chem. Downloaded from www.nrcresearchpress.com by 217.78.4.112 on 09/08/12
For personal use only.

TABLE A4 (*continued*)

Bonds	Angle (deg)	Bonds	Angle (deg)
C(10)—C(9)—C(11)	110.4(3)	C(20)—C(19)—C(18)	118.0(3)
C(10)—C(9)—C(24)	102.1(3)	C(21)—C(20)—C(28)	111.8(3)
C(11)—C(9)—C(24)	109.6(3)	C(21)—C(20)—C(19)	111.9(3)
C(1)—C(10)—C(5)	118.9(3)	C(28)—C(20)—C(19)	111.4(4)
C(1)—C(10)—C(9)	121.6(3)	O(3)—C(21)—C(20)	122.6(4)
C(5)—C(10)—C(9)	119.1(3)	O(3)—C(21)—C(22)	120.9(4)
C(12)—C(11)—C(9)	116.7(3)	C(20)—C(21)—C(22)	116.3(3)
C(11)—C(12)—C(13)	112.2(3)	O(4)—C(22)—C(21)	110.4(3)
C(25)—C(13)—C(12)	107.3(3)	O(4)—C(22)—C(17)	108.6(3)
C(25)—C(13)—C(18)	113.3(3)	C(21)—C(22)—C(17)	112.5(3)
		18	
C(10)—C(1)—C(2)	112.7(4)	C(10′)—C(1′)—C(2′)	113.2(3)
C(3)—C(2)—C(1)	112.0(3)	C(3′)—C(2′)—C(1′)	112.0(3)
O(1)—C(3)—C(2)	107.9(3)	O(1′)—C(3′)—C(2′)	109.9(3)
O(1)—C(3)—C(4)	110.5(4)	O(1′)—C(3′)—C(4′)	110.2(3)
C(2)—C(3)—C(4)	114.1(3)	C(2′)—C(3′)—C(4′)	114.1(3)
C(23)—C(4)—C(24)	108.1(4)	C(24′)—C(4′)—C(23′)	108.3(4)
C(23)—C(4)—C(3)	111.2(3)	C(24′)—C(4′)—C(3′)	107.5(3)
C(23)—C(4)—C(5)	114.6(4)	C(24′)—C(4′)—C(5′)	108.6(3)
C(24)—C(4)—C(3)	107.1(4)	C(23′)—C(4′)—C(3′)	111.2(3)
C(24)—C(4)—C(5)	108.3(3)	C(23′)—C(4′)—C(5′)	114.0(3)
C(3)—C(4)—C(5)	107.3(3)	C(3′)—C(4′)—C(5′)	107.0(3)
C(6)—C(5)—C(10)	110.8(3)	C(6′)—C(5′)—C(10′)	109.8(3)
C(6)—C(5)—C(4)	114.1(3)	C(6′)—C(5′)—C(4′)	115.0(3)
C(10)—C(5)—C(4)	116.7(3)	C(10′)—C(5′)—C(4′)	117.0(3)
C(7)—C(6)—C(5)	111.2(3)	C(7′)—C(6′)—C(5′)	111.6(3)
C(6)—C(7)—C(8)	114.3(3)	C(6′)—C(7′)—C(8′)	114.4(3)
C(26)—C(8)—C(7)	108.5(4)	C(7′)—C(8′)—C(9′)	108.7(3)
C(26)—C(8)—C(9)	110.8(3)	C(7′)—C(8′)—C(26′)	108.8(3)
C(26)—C(8)—C(14)	110.1(3)	C(7′)—C(8′)—C(14′)	110.6(3)
C(7)—C(8)—C(9)	108.8(3)	C(9′)—C(8′)—C(26′)	110.6(3)
C(7)—C(8)—C(14)	111.0(3)	C(9′)—C(8′)—C(14′)	108.8(3)
C(9)—C(8)—C(14)	107.8(3)	C(26′)—C(8′)—C(14′)	109.4(3)
C(11)—C(9)—C(8)	111.0(3)	C(11′)—C(9′)—C(8′)	111.0(3)
C(11)—C(9)—C(10)	112.1(3)	C(11′)—C(9′)—C(10′)	113.2(3)
C(8)—C(9)—C(10)	118.3(3)	C(8′)—C(9′)—C(10′)	117.1(3)
C(1)—C(10)—C(25)	108.3(3)	C(1′)—C(10′)—C(25′)	108.0(3)
C(1)—C(10)—C(5)	108.1(3)	C(1′)—C(10′)—C(5′)	108.0(3)
C(1)—C(10)—C(9)	107.9(3)	C(1′)—C(10′)—C(9′)	107.4(3)
C(25)—C(10)—C(5)	113.3(3)	C(25′)—C(10′)—C(5′)	113.5(3)
C(25)—C(10)—C(9)	112.6(3)	C(25′)—C(10′)—C(9′)	113.5(3)
C(5)—C(10)—C(9)	106.3(3)	C(5′)—C(10′)—C(9′)	106.2(3)
C(12)—C(11)—C(9)	113.2(4)	C(12′)—C(11′)—C(9′)	115.1(3)
C(13)—C(12)—C(11)	126.9(4)	C(13′)—C(12′)—C(11′)	126.1(4)
C(12)—C(13)—C(14)	120.3(4)	C(12′)—C(13′)—C(18′)	118.1(3)
C(12)—C(13)—C(18)	118.0(4)	C(12′)—C(13′)—C(14′)	120.0(3)
C(14)—C(13)—C(18)	121.6(3)	C(18′)—C(13′)—C(14′)	121.6(3)
C(13)—C(14)—C(15)	111.4(3)	C(13′)—C(14′)—C(27′)	106.9(3)
C(13)—C(14)—C(27)	106.8(3)	C(13′)—C(14′)—C(15′)	111.3(3)
C(13)—C(14)—C(8)	109.1(3)	C(13′)—C(14′)—C(8′)	108.4(3)
C(15)—C(14)—C(27)	106.6(3)	C(27′)—C(14′)—C(15′)	106.2(3)
C(15)—C(14)—C(8)	110.9(3)	C(27′)—C(14′)—C(8′)	112.8(3)
C(27)—C(14)—C(8)	112.0(3)	C(15′)—C(14′)—C(8′)	111.3(3)
C(16)—C(15)—C(14)	114.4(4)	C(16′)—C(15′)—C(14′)	115.6(3)
C(17)—C(16)—C(15)	113.0(4)	C(15′)—C(16′)—C(17′)	112.8(3)
C(28)—C(17)—C(16)	110.7(4)	C(28′)—C(17′)—C(16′)	110.0(3)
C(28)—C(17)—C(18)	110.3(4)	C(28′)—C(17′)—C(22′)	107.1(3)
C(28)—C(17)—C(22)	107.2(4)	C(28′)—C(17′)—C(18′)	110.4(3)
C(16)—C(17)—C(18)	108.2(3)	C(16′)—C(17′)—C(22′)	111.3(3)
C(16)—C(17)—C(22)	111.8(4)	C(16′)—C(17′)—C(18′)	107.9(3)
C(18)—C(17)—C(22)	108.6(4)	C(22′)—C(17′)—C(18′)	110.3(3)
C(19)—C(18)—C(13)	110.0(3)	C(13′)—C(18′)—C(19′)	111.2(3)
C(19)—C(18)—C(17)	113.3(3)	C(13′)—C(18′)—C(17′)	112.5(3)

Can. J. Chem. Downloaded from www.nrcresearchpress.com by 217.78.4.112 on 09/08/12
For personal use only.

TABLE A4 (*concluded*)

Bonds	Angle (deg)	Bonds	Angle (deg)
C(13)—C(18)—C(17)	112.3(4)	C(19′)—C(18′)—C(17′)	112.6(3)
C(18)—C(19)—C(20)	115.5(4)	C(18′)—C(19′)—C(20′)	115.0(3)
C(21)—C(20)—C(29)	110.5(4)	C(29′)—C(20′)—C(21′)	110.0(4)
C(21)—C(20)—C(19)	108.0(4)	C(29′)—C(20′)—C(19′)	109.7(3)
C(21)—C(20)—C(30)	112.1(4)	C(29′)—C(20′)—C(30′)	106.1(3)
C(29)—C(20)—C(19)	109.4(4)	C(21′)—C(20′)—C(19′)	109.1(3)
C(29)—C(20)—C(30)	105.8(4)	C(21′)—C(20′)—C(30′)	111.0(3)
C(19)—C(20)—C(30)	111.1(3)	C(19′)—C(20′)—C(30′)	110.9(3)
C(22)—C(21)—C(20)	112.9(4)	C(22′)—C(21′)—C(20′)	113.3(3)
C(21)—C(22)—C(17)	115.4(4)	C(21′)—C(22′)—C(17′)	115.2(3)
O(2)—C(29)—C(20)	113.9(4)	O(2′)—C(29′)—C(20′)	113.7(3)
		19·EtOH	
C(2)—C(1)—C(10)	113.8(3)	C(12)—C(11)—C(9)	114.4(4)
C(3)—C(2)—C(1)	110.6(4)	C(13)—C(12)—C(11)	126.9(4)
O(1)—C(3)—C(2)	109.6(4)	C(12)—C(13)—C(14)	119.0(4)
O(1)—C(3)—C(4)	110.4(3)	C(12)—C(13)—C(18)	120.5(4)
C(2)—C(3)—C(4)	114.5(4)	C(14)—C(13)—C(18)	120.2(4)
C(3)—C(4)—C(23)	111.6(4)	C(13)—C(14)—C(15)	112.4(4)
C(3)—C(4)—C(24)	108.3(4)	C(13)—C(14)—C(27)	107.1(3)
C(3)—C(4)—C(5)	106.3(3)	C(13)—C(14)—C(8)	108.4(3)
C(23)—C(4)—C(24)	107.7(3)	C(15)—C(14)—C(27)	106.8(4)
C(23)—C(4)—C(5)	114.2(4)	C(15)—C(14)—C(8)	110.4(4)
C(24)—C(4)—C(5)	108.6(4)	C(27)—C(14)—C(8)	111.8(3)
C(6)—C(5)—C(10)	111.2(4)	C(16)—C(15)—C(14)	114.3(4)
C(6)—C(5)—C(4)	114.4(3)	C(15)—C(16)—C(17)	112.7(5)
C(10)—C(5)—C(4)	117.8(4)	C(28)—C(17)—C(18)	110.9(6)
C(5)—C(6)—C(7)	110.3(4)	C(28)—C(17)—C(22)	108.2(5)
C(6)—C(7)—C(8)	114.0(4)	C(28)—C(17)—C(16)	109.8(5)
C(7)—C(8)—C(25)	107.5(3)	C(18)—C(17)—C(22)	109.3(4)
C(7)—C(8)—C(9)	110.9(3)	C(18)—C(17)—C(16)	107.7(4)
C(7)—C(8)—C(14)	110.2(4)	C(22)—C(17)—C(16)	110.9(5)
C(25)—C(8)—C(9)	111.0(4)	C(19)—C(18)—C(13)	110.5(4)
C(25)—C(8)—C(14)	110.0(3)	C(19)—C(18)—C(17)	113.7(5)
C(9)—C(8)—C(14)	107.3(3)	C(13)—C(18)—C(17)	112.9(4)
C(11)—C(9)—C(8)	110.3(3)	C(18)—C(19)—C(20)	115.9(5)
C(11)—C(9)—C(10)	115.0(4)	C(29)—C(20)—C(30)	109.4(6)
C(8)—C(9)—C(10)	116.0(3)	C(29)—C(20)—C(21)	110.1(7)
C(26)—C(10)—C(1)	107.7(4)	C(29)—C(20)—C(19)	110.1(6)
C(26)—C(10)—C(5)	113.3(3)	C(30)—C(20)—C(21)	109.2(7)
C(26)—C(10)—C(9)	113.0(4)	C(30)—C(20)—C(19)	111.1(6)
C(1)—C(10)—C(5)	107.7(3)	C(21)—C(20)—C(19)	106.9(5)
C(1)—C(10)—C(9)	108.1(3)	C(22)—C(21)—C(20)	113.9(6)
C(5)—C(10)—C(9)	106.9(3)	C(21)—C(22)—C(17)	115.5(5)
O(2)—C(11)—C(12)	107.9(3)	C(32)—C(31)—O(3)	114(1)
O(2)—C(11)—C(9)	113.3(3)		

Can. J. Chem. Downloaded from www.nrcresearchpress.com by 217.78.4.112 on 09/08/12
For personal use only.

respectively). The same atoms are also involved in intramolecular hydrogen bonds (O(2)—H(36)···O(1) and O(2′)—H(36′)···O(1′), H···O = 2.27 and 2.11 Å, O···O = 2.673(6) and 2.683(7) Å, O—H···O = 104 and 113°, respectively). The solvent molecules are not involved in any short intermolecular contacts. The saturated ring junctions C:D and D:E are *trans* and *cis*, respectively. The aromatic A ring deviates slightly from planarity while the B ring has an irregular C(9)-envelope conformation and the C, D, and E rings have chair conformations. The two independent molecules exhibit some structural differences, particularly in the torsion angles (see Table A5). These differences (also noted for the crystallographically independent molecules of **16** and **18**) are not chemically significant and most likely arise from asymmetry in the packing arrangement.

The structure of **16** consists of molecules separated by normal van der Waals distances; the most significant intermolecular contact is O(2)···H(51) = 2.55 Å. As for compound **15**, there is intramolecular hydrogen bonding between the O(3)/O(8) hydroxyl group and the adjacent O(2)/O(7) carbonyl function (O(3)—H(1)···O(2) and O(8)—H(47)···O(7), H···O = 1.91(8) and 2.09(8) Å, O···O = 2.628(5) and 2.621(6) Å, O—H···O = 117(6) and 116(6)°, respectively). The A:B, B:C, C:D, and D:E ring junctions are *trans*, *trans*, *trans*, and *cis*, respectively. All five rings of the triterpene skeleton have chair conformations. Only minor differences are noted for the two crystallographically independent molecules.

The lattice-held water molecule in **17**·1/2 H_2O lies on a crystallographic C_2 axis and is hydrogen-bonded to

TABLE A5. Intra-annular torsion angles (deg) with estimated standard deviations in parentheses

Atoms	**6**·MeOH	**15**·1/2EtOAc molecule 1	**15**·1/2ETOAc molecule 2	**16** molecule 1	**16** molecule 2	**17**·1/2 H_2O	**18** molecule 1	**18** molecule 2	**19**·EtOH
C(10)—C(1)—C(2)—C(3)	−56.7(4)	0(1)	−2(1)	44.2(5)	44.1(6)	0.4(8)	−56.7(5)	−56.2(5)	−56.2(5)
C(1)—C(2)—C(3)—C(4)	55.8(4)	−1(1)	−2(1)	−45.7(5)	−38.9(6)	1.2(6)	55.3(5)	56.3(5)	59.0(5)
C(2)—C(3)—C(4)—C(5)	−51.8(4)	0(1)	5(1)	52.1(5)	43.8(6)	−1.0(6)	−50.9(5)	−51.9(4)	−54.6(5)
C(3)—C(4)—C(5)—C(10)	52.9(4)	2.7(8)	−3.6(9)	−54.6(4)	−52.3(5)	−0.7(5)	51.6(4)	51.9(4)	52.0(5)
C(4)—C(5)—C(10)—C(1)	−53.6(4)	−3.9(8)	−0.3(8)	54.9(4)	58.8(5)	2.2(5)	−54.0(4)	−52.7(4)	−50.6(5)
C(5)—C(10)—C(1)—C(2)	53.3(4)	3(1)	3(1)	−50.5(5)	−55.2(5)	−2.1(6)	53.8(4)	52.5(4)	50.6(5)
C(10)—C(5)—C(6)—C(7)	−63.5(4)	−5(1)	−2(1)	49.8(5)	47.0(5)	−7.6(6)	−62.6(4)	−61.6(4)	−63.3(6)
C(5)—C(6)—C(7)—C(8)	57.6(4)	10(1)	6(1)	−54.8(5)	−55.2(5)	7.1(7)	56.9(5)	55.7(5)	56.9(6)
C(6)—C(7)—C(8)—C(9)	−47.2(4)	6(1)	4(1)	58.9(5)	61.9(4)	8.7(6)	−47.0(5)	−47.3(4)	−47.4(5)
C(7)—C(8)—C(9)—C(10)	46.8(4)	−24.6(7)	−15.1(8)	−59.8(4)	−60.9(4)	−21.4(5)	46.9(5)	49.5(4)	45.9(5)
C(8)—C(9)—C(10)—C(5)	−52.3(4)	29.3(7)	18.7(7)	58.3(4)	55.5(4)	20.7(5)	−52.5(4)	−56.0(4)	−51.1(5)
C(9)—C(10)—C(5)—C(6)	58.5(4)	−15.1(8)	−10.6(8)	−52.4(4)	−48.6(5)	−7.1(5)	57.5(4)	59.0(4)	58.6(5)
C(14)—C(8)—C(9)—C(11)	−61.7(4)	31.2(7)	41.9(7)	48.4(4)	47.0(4)	36.2(5)	−61.1(4)	−57.9(4)	−60.8(4)
C(8)—C(9)—C(11)—C(12)	33.4(5)	−31.7(7)	−42.0(7)	−46.9(4)	−45.3(5)	−31.7(5)	34.7(6)	28.8(5)	29.2(5)
C(9)—C(11)—C(12)—C(13)	−2.5(7)	48.8(7)	55.4(7)	55.2(4)	55.2(5)	47.5(5)	−5.3(8)	−0.9(6)	3.3(6)
C(11)—C(12)—C(13)—C(14)	1.4(6)	−61.9(7)	−61.0(7)	−58.3(4)	−60.5(4)	−62.7(4)	3.6(8)	3.9(6)	−1.6(7)
C(12)—C(13)—C(14)—C(8)	−30.2(5)	57.9(6)	56.0(6)	56.8(4)	58.8(4)	63.1(4)	−30.2(5)	−33.0(5)	−31.2(6)
C(13)—C(14)—C(8)—C(9)	59.4(3)	−44.6(7)	−50.1(7)	−55.2(4)	−55.2(4)	−52.7(4)	57.8(4)	59.4(4)	61.5(4)
C(18)—C(13)—C(14)—C(15)	32.9(4)	−60.0(6)	−61.6(6)	−63.9(4)	−62.1(4)	−58.1(4)	32.5(5)	30.1(5)	32.8(6)
C(13)—C(14)—C(15)—C(16)	−39.4(4)	60.1(7)	61.6(7)	62.1(4)	63.3(4)	63.3(4)	−38.1(5)	−35.5(5)	−38.7(6)
C(14)—C(15)—C(16)—C(17)	55.9(4)	−49(1)	−49.2(8)	−46.9(5)	−50.2(5)	−55.2(5)	55.6(5)	54.1(5)	55.4(7)
C(15)—C(16)—C(17)—C(18)	−60.5(4)	36(1)	34.4(8)	31.5(5)	33.9(5)	40.5(5)	−60.9(5)	−61.3(4)	−61.1(6)
C(16)—C(17)—C(18)—C(13)	51.3(4)	−37.3(8)	−36.5(8)	−34.2(5)	−34.4(5)	−39.8(5)	51.6(4)	53.0(4)	52.4(6)
C(17)—C(18)—C(13)—C(14)	−39.8(4)	50.8(7)	51.5(7)	51.5(4)	49.5(4)	49.3(4)	−40.6(5)	−40.7(5)	−41.5(7)
C(22)—C(17)—C(18)—C(19)	47.6(4)	−50.9(7)	−45.5(7)	−47.8(4)	−47.1(4)	−52.1(4)	47.7(5)	48.1(4)	46.2(7)
C(17)—C(18)—C(19)—C(20)	−55.5(4)	45.8(8)	46.6(7)	45.2(5)	47.9(5)	49.1(4)	−53.4(5)	−53.1(5)	−51.9(7)
C(18)—C(19)—C(20)—C(21)	56.3(4)	−43.4(8)	−51.6(8)	−45.6(5)	−48.6(5)	−42.9(5)	54.0(5)	53.4(5)	52.6(9)
C(19)—C(20)—C(21)—C(22)	−55.2(4)	47.7(9)	58.5(8)	51.9(5)	51.3(5)	43.1(4)	−53.8(5)	−52.1(5)	−53.6(9)
C(20)—C(21)—C(22)—C(17)	54.2(4)	−56(1)	−61.9(8)	−59.2(5)	−54.6(5)	−50.5(4)	55.6(5)	52.7(5)	55.7(8)
C(21)—C(22)—C(17)—C(18)	−47.7(4)	56.3(8)	53.5(8)	54.9(4)	51.1(5)	54.3(4)	−50.0(5)	−49.1(5)	−49.3(8)

the carbonyl oxygen atoms O(1) of two molecules of **17**(O(5)—H(37)···O(1), H···O = 1.96 Å, O···O = 2.910(6) Å, O—H···O = 176°). O(1) is also hydrogen-bonded to the O(4) hydroxyl group (at C(22)) of another molecule of **17** related by a screw axis, forming a one-dimensional H-bonded array of molecules of **17** and water (O(4)—H(36)···O(1), H···O = 1.91 Å, O···O = 2.809(5) Å, O—H···O = 165°). The saturated ring junctions C:D and D:E are *trans* and *cis*, respectively. The aromatic A ring deviates slightly from planarity; the B ring has a flattened C(9)-envelope conformation; and the C, D, and E rings have chair conformations.

The structure of **18** is dominated by O—H···O hydrogen bonding which is not the same for the two independent molecules. All of the hydroxyl groups are hydrogen bond donors, but the unprimed molecule O(1) accepts one strong H-bond and O(2) accepts two (one weak and one strong) while the primed molecule acts as an acceptor for only one hydrogen bond (via O(2′)) (O(1)—H(49)···O(2), O(2)—H(50)···O(1), O(1′)—H(49′)···O(2′), and O(2′)—H(50′)···O(2); H···O = 2.41, 1.64, 1.83, and 1.70 Å; O···O = 2.710(5), 2.710(5), 2.693(5), and 2.747(4) Å; O—H···O = 117, 160, 134, and 167°; respectively). The A:B and B:C ring junctions are *trans* and the D:E junction is *cis*. The unsaturated C ring has a C(8)-sofa conformation and the other four rings all have chair conformations.

In the solid state structure of **19**·EtOH, molecules of **19** are directly hydrogen-bonded to one another and to the ethanol solvate molecules, each of the three hydroxyl groups (two from **19** and that of the EtOH solvate) acting as both donor and acceptor (O(1)—H(54)···O(2), O(2)—H(55)···O(3), and O(3)—H(56)···O(1); H···O = 1.70, 1.66, and 1.80 Å; O···O = 2.758(4), 2.739(5), and 2.768(5) Å; O—H···O = 163, 153, and 169°; respectively). The ring junctions and ring conformations within the triterpene skeleton are as noted above for **18**.

Bond lengths and angles for all six structures are generally as expected (see Tables A3 and A4). There is some shortening of distances resulting from thermal motion, for example in the EtOH solvate molecule of **19**·EtOH, and some lengthening due to steric effects such as the long bond between fully substituted ring junction atoms in **6**(C(8)—C(14) = 1.592(4) Å).

Can. J. Chem. Downloaded from www.nrcresearchpress.com by 217.78.4.112 on 09/08/12
For personal use only.

Diels–Alder reactions of bicyclic, heteroannular dienones[1]

LUCIO MINUTI, ROBERTA SELVAGGI, AND ALDO TATICCHI[2]
Dipartimento di Chimica, Università di Perugia, 06100 Perugia, Italy

AND

MING GUO AND ERNEST WENKERT[2]
Department of Chemistry (0506), University of California – San Diego, La Jolla, CA 92093, U.S.A.

Received September 4, 1991

This paper is dedicated to Professor Zdenek (Denny) Valenta on the occasion of his 65th birthday

LUCIO MINUTI, ROBERTA SELVAGGI, ALDO TATICCHI, MING GUO, and ERNEST WENKERT. Can. J. Chem. **70**, 1481 (1992).

Aluminum chloride catalyzed Diels–Alder reactions of bicyclic dienones of the hexalone type with 1,3-butadiene, isoprene, (*E*)-piperylene, and (*E*)-1-methoxy-1,3-butadiene are described. Structure analysis of the adducts by NMR spectroscopy is presented. The site-, *endo–exo*-, and face-selectivity of the reactions are discussed.

LUCIO MINUTI, ROBERTA SELVAGGI, ALDO TATICCHI, MING GUO et ERNEST WENKERT. Can. J. Chem. **70**, 1481 (1992).

On décrit des réactions de Diels–Alder catalysées par le chlorure d'aluminium entre des diénones bicycliques du type de l'hexalone et le buta-1,3-diène, l'isoprène, le (*E*)-pipérylène et le (*E*)-1-méthoxybuta-1,3-diène. On présente une analyse structurale des adduits qui est basée sur la spectroscopie RMN. On discute des sélectivités entre les sites, *endo/exo* et entre les faces de ces réactions.

[Traduit par la rédaction]

Can. J. Chem. Downloaded from www.nrcresearchpress.com by 217.78.4.112 on 09/08/12
For personal use only.

Recently it was shown that hexalone **2***a* undergoes cycloaddition with (*E*)-1-methoxy-1,3-butadiene (**3***d*) and 2,3-dimethyl-1,3-butadiene at its least substituted (i.e., γ, δ) carbon–carbon double bond site, providing a facile route of synthesis of functionalized hydrophenanthrenones (2). To determine the generality of the process, reactions now have been carried out with 1,3-butadiene (**3***a*), isoprene (**3***b*), and (*E*)-piperylene (**3***c*). Furthermore, since the hydrophenanthrenones could be envisaged to serve as intermediates en route to steroids and (or) tricarbocyclic diterpenes, if the angular methyl group were located at the proper bridgehead, Diels–Alder reactions of hexalone **2***b* with dienes **3***a–d* were undertaken also.[3]

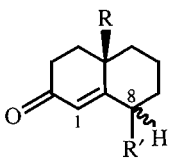

1

a, R = Me, R′ = H; *b*, R = H, R′ = Me

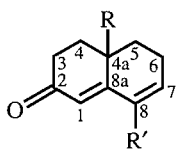

2

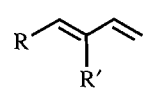

3*a*, R = R′ = H
b, R = H, R′ = Me
c, R = Me, R′ = H
d, R = OMe, R = H

The cycloadditions of hexalones **2***a* and **2***b*, prepared from octalone **1***b* (4) by dehydrogenation with chloranil (2, 5), were performed in dry toluene solution under aluminum chloride catalysis except for the reaction with dienol ether **3***d*, which was executed under non-catalytic, thermal conditions. Interactions of dienone **2***a* with 1,3-butadiene (**3***a*) and isoprene (**3***b*) afforded adducts **4***a* and **4***b* in 33 and 18% yield, respectively, and with (*E*)-piperylene (**3***c*) a 9:1 mixture of adducts **4***c* and **5** in 62% yield. All products were kinetically based Diels–Alder adducts, as shown by the constancy of the product ratio throughout the course of the last reaction, by the absence of appearance of other volatile products (monitored by gc analysis) during all reactions, and, finally, by the maintenance of product integrity on resubmission of pure adducts **4** and **5** to the reaction conditions.

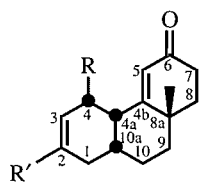

4*a*, R = R′ = H
b, R = H, R′ = Me
c, R = Me, R′ = H

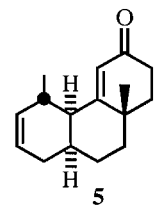

5

The Diels–Alder reaction of dienone **2***b* with 1,3-butadiene (**3***a*) furnished adducts **7***a* and **6***a* as a 2.3:1 mixture in 37% yield. Observation of the reaction progress by gc analysis revealed isomerization of adduct **6***a* into ketone **7***a*. Furthermore, exposure of pure tricycle **7***a* to the reaction conditions led to its nearly quantitative recovery, whereas the same treatment of adduct **6***a* yielded a **6***a*–**7***a* mixture enriched in the latter ketone. The cycloaddition of dienone **2***b* with isoprene (**3***b*) was so poor as to preclude isolation of any adduct.[4] On the other hand, interaction of hexalone **2***b* with (*E*)-piperylene (**3***c*) gave products **8**, **6***b*, and **7***b* as a 1.4:1.1:1 mixture in 45% yield. As in the aforementioned butadiene reaction, adduct **6***b* was transformed into ketone **7***b* throughout the course of the reaction (gc analytically monitored).

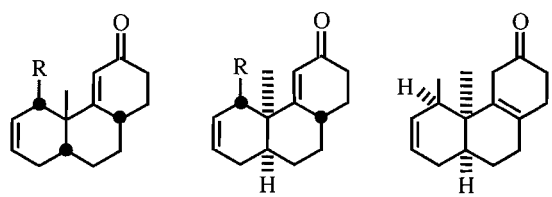

6 **7** **8**

a, R = H; *b*, R = Me; *c*, R = OMe

[1]Diels–Alder reactions of cycloalkenones. 23. For part 22 see ref. 1.

[2]Authors to whom correspondence may be addressed.

[3]For other, recent hydrophenanthrenone syntheses by the Diels–Alder reaction approach see, inter alia, ref. 3.

[4]This experiment was duplicated in a reaction with 2,3-dimethyl-1,3-butadiene.

TABLE 1. Carbon shifts of ketones **4** and **5**

Carbons	**4***a*	**4***b*	**4***c*	**5**
1	25.1	30.2	26.1	33.6[a]
2	126.1	132.8	125.5	125.8
3	123.5	117.5	130.2	134.1
4	27.1	27.2	38.6	37.5
4a	36.9	36.5	43.3	52.5
4b	169.6	169.8	166.9	170.8
5	123.1	123.2	124.7	128.1
6	199.6	199.8	199.6	199.1
7	33.6	33.7	33.4	33.8[a]
8	38.4	38.4	37.2[a]	38.2
8a	36.2	36.3	36.6	35.8
9	37.0	37.0	36.5[a]	39.6
10	26.2	26.1	26.4	27.7
10a	34.9	35.3	33.4	35.6
8a-Me	23.2	23.1	24.1	27.5
Me	—	23.4	17.1	20.6

[a]Signals in any vertical column may be interchanged.

Finally, cycloaddition of dienone 2b with (*E*)-1-methoxy-1,3-butadiene (**3***d*) at 170°C without catalyst led to ketones **6***c*, **9**, **10**, and **7***c* as a 6.3:4.6:2.4:1 mixture in 42% yield. Whereas samples of pure adducts **7***c* and **9** proved stable to the reaction conditions, adduct **10** was transformed into a **9**–**10** mixture and adduct **6***c* decomposed into intractable material.

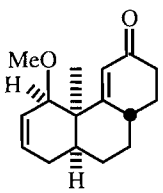

9

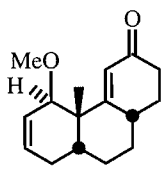

10

Product structures

The structure determination of all cycloaddition products rests mostly on their NMR analyses. Comparison of the carbon shifts of the **2***a*-based adducts (Table 1) and inspection of the $^1H-^1H$ and $^1H-^{13}C$ connectivities (COSY spectra) of the tricycles **4***b* and **4***c* reveals their regiochemistry. The all-*cis* arrangement of H(10a), H(4a), and the 8a-methyl group of compounds **4** emanates from the similarity of the chemical shifts of relevant carbons and the coupling characteristics of relevant hydrogens with those of Diels–Alder adducts of like stereochemistry and etablished configuration (2). Finally, the absence of a γ-effect on C(10a) and the observation of a strong *peri* interaction with H(5) (i.e., considerable deshielding of this hydrogen) shows the 4-methyl group of ketone **4***c* to be equatorial and hence a 4α substituent.

2D NMR analysis of adducts **5** and a strong β-effect exerted on C(4a) by the neighboring methyl group reveal the regiochemistry of ketone **5**. The ca. 3 ppm deshielding of its angular methyl group (vs. the methyl shift of ketone **1***a* and ketones **4**) indicates the removal of a γ-effect (i.e., the loss of the axial H(4aβ)) and thus an inversion of the C(4a) and C(10a) stereochemistry. The deshielding of C(1) and C(9), showing the disappearance of a reciprocal γ-effect, is in accord with the inverted configuration at the two cycloaddition centers. Finally, the absence of any H(3)–H(4) coupling, indicative of a ca. 90° H(3)—C(3)—C(4)—H(4) dihedral angle, limits the 4-methyl group to an equatorial (hence 4α) configuration.

NMR analysis of the **2***b*-based Diels–Alder adducts (Table 2) shows them to fit into two structure patterns, *a* (**6** and **10**) and *b* (**7** and **9**), leaving ketone **8** as a unique system. The latter's carbonyl infrared absorption band (1707 cm^{-1}) and carbonyl carbon shift (211.8 ppm) show tricycle **8**, in contrast to the other substances, to be a non-conjugated enone. Furthermore, the appearance of two strongly coupled (20 Hz) C(5) hydrogens (2.67 and 3.07 ppm) in the ^1H NMR spectrum and of non-protonated, olefinic carbon signals in the ^{13}C NMR spectrum is in accord with the β,γ-unsaturated ketone structure depicted in formula **8**. The simplest stereochemical differentiation of the adducts of structure type *a* from those of *b* is the strong, reciprocal γ-effect exhibited by C(1) and C(9) in *a*-like compounds (as earlier in ketones **4**), indicative of the axiality of C(1) toward the central ring and hence of a *cis*-β relationship of the 4a-methyl group with H(8a) and H(10a).

Examination of the hydrogen connectivities (by the COSY method) of all cyclohexene-substituted substances reveals the secondary methyl group or the methoxy function to be attached to C(4), thus settling the regiochemistry of ketones **6**–**10**. Shift comparison of *a*-like ethers **6***c* and **10** shows C(10a) of the latter strongly shielded, indicative of a γ-effect, of a 1,3-diaxial MeO–H(10a) relationship and of the presence of a β-methoxy group in ketone **10** and a 4α-ether in ketone **6***c*. Comparison of the angular methyl shifts of ethers **7***c* and **9** portrays the methyl group of the former to be strongly shielded (γ-effect), characteristic of a *cis* methoxy-methyl relationship in compound **7***c* and a *trans*-diaxial one in ether **9**. The H(3)–H(4) coupling behavior of the four ethers confirms their methoxy configurations. Thus 3–4 Hz coupling in ketones **9** and **10** is in agreement with the presence of an equatorial H(4α) substituent in these compounds. Nearly zero coupling in ketones **6***c* and **7***c*, indicative of a ca. 90° dihedral H(3)—C(3)—C(4)—H(4) bonding arrangement, points to an axial H(4β) for these ethers. The C(4) shift of the ethers is also diagnostic of their configurations. The strong C(4) shielding of ketone **10** (vs. **6***c*) shows a γ-effect from C(5), blocked by the methoxy group in ketone **6***c*, and the strong C(4) shielding of cycloadduct **7***c* (vs. **9**) due to γ-effects exerted by C(8a) and C(10) is precluded in adduct **9** by the 4β-methoxy group. Great similarity of carbon shifts of comparable sites of ketones **6***b* and **6***c* as well as of compounds **7***b* and **7***c* reveals that the secondary methyl compounds to possess stereochemistry identical to their ether counterparts. The shielding of the secondary methyl hydrogens of tricycle **7***b* (vs. **6***b*) reflects (as seen in models) the methyl function being more in the shielding zone of the C(4b)–C(5) double bond in this compound vs. its isomer **6***b*. The interconvertibility of ketones **6***b* and **7***b* and the lack of isomerization of either substance into a β,γ-unsaturated ketone (*vide supra*) suggests the immediate precursor of ketone **8** to be 4-epi-**6***b* or 4-epi-**7***b*. The ^1H NMR spectrum of the non-conjugated ketone reveals its secondary methyl hydrogens to be quite shielded (0.87 ppm), a fact accommodated most readily by a *trans*-diaxial relationship of the two methyl groups, placing, as a consequence, the secondary methyl group within the shielding cone of the C(4b)–C(8b) double bond.

Can. J. Chem. Downloaded from www.nrcresearchpress.com by 217.78.4.112 on 09/08/12
For personal use only.

TABLE 2. Carbon shifts of ketones **6–10**

Carbons	**6***a*	**6***b*	**6***c*	**7***a*	**7***b*	**7***c*	**8**	**9**	**10**
1	24.3	25.1	24.4	29.3[a]	29.4[a]	29.3[a]	29.6[a]	29.8	23.7
2	125.7	123.9	126.2	123.5[b]	124.3	125.8[b]	121.6	126.6	129.7
3	123.9	131.1	125.3	122.7	129.8	125.2	129.9	123.6	124.4[a]
4	35.9	40.5	84.8	34.1	31.8	77.7	36.9[b]	82.7	77.7
4a	40.0	41.0	45.5	36.0	42.9	44.6	29.4	43.2	43.7
4b	170.1	168.5	166.0	173.0	171.4	169.9	131.3	172.9	170.0
5	123.4	125.3	125.8	123.4[b]	123.3	125.2[b]	40.0	124.0	124.2[a]
6	200.3	199.9	200.3	200.8	200.5	200.2	211.8	200.8	200.1
7	36.1	34.3	35.4	39.7	35.7	35.7	38.0	37.1	36.4
8	29.8[a]	29.4	29.2[a]	29.5[a]	29.6[a]	29.6[a]	30.7[a]	30.8	30.1
8a	33.4	33.5	33.3	34.3	34.1	34.4	129.1	38.0	33.4
9	29.5	28.5	29.1[a]	33.6	34.3	34.1	30.2[a]	33.5	28.9
10	27.2	27.7	27.5	28.2	27.8	28.2	26.2	27.8	27.7
10a	39.3	40.5	39.6	39.2	42.2	43.2	37.1[b]	38.4	34.2
4a-Me	28.3	25.6	23.9	22.1	16.8	16.6	25.7	22.9	22.8
Me	—	15.9	58.0	—	14.4	58.4	19.7	57.9	57.6

[a,b]Signals in any vertical column may be interchanged.

Can. J. Chem. Downloaded from www.nrcresearchpress.com by 217.78.4.112 on 09/08/12
For personal use only.

Discussion

Several interesting facts emerge from the above cycloaddition processes. Firstly, as in the earlier two examples (2), the reactions are fully site-selective and regioselective. Secondly, reactions at γ, δ sites of dienones afford lower product yields than those at α, β sites of enones, especially with dienes, e.g., isoprene (**3***b*), which are sterically encumbering in the transition state. Thirdly, the reactions of dienone **2***a* are mostly *anti*-diastereoselective, in accord with expectations (6). Its interaction with (*E*)-piperylene (**3***c*) leads predominantly to *anti-endo* product accompanied by some *syn-exo* product, reflecting the interplay of stabilizing secondary orbital interactions with destabilizing nonbonded steric repulsions in the transition states resulting from diene attack on the two dienone faces in *endo* or *exo* mode (7). Fourthly, the major product of the **2***b*–**3***c* reaction (under either acid catalysis or thermal conditions) is a ketone (**8**) of anomalous structure, which could be shown experimentally not to be derived from its accompanying products **6***b* and **7***b*. It presumably represents a product of rapid double bond isomerization of an elusive 4-epi-**7**.

The most surprising result is the discovery of the Diels–Alder reactions of dienone **2***b* being strongly under thermodynamic control, permitting conversion of *anti* adducts into *syn* adducts. [4+2] Cycloreversions are rare among substances liberating acyclic dienes and the reason for the facile cycloreversion of ketones **6** and **10** in the face of the stability of ketones **4** remains an enigma.

Experimental section[5]

*4,4a,5,6-Tetrahydro-8-methyl-2(3*H*)-naphthalenone (***2***b)*, prepared according to a known procedure (2, 5) by oxidation of octalone **1***b* (4) (H-8β isomer: ^{1}H NMR δ: 0.95 (d, 3, J = 6 Hz, Me), 5.70 (s, 1, H-1); ^{13}C NMR δ: 17.1 (Me), 25.1 (C-6), 28.2 (C-4), 34.3 (C-5), 35.1 (C-7), 36.0 (C-3), 37.9 (C-4a, C-8), 120.6 (C-1), 170.8 (C-8a), 200.0 (C-2). H-8α isomer: ^{1}H NMR δ: 0.97 (d, 3, J = 6 Hz, Me), 5.67 (s, 1, H-1); ^{13}C NMR δ: 19.4 (C-6), 20.1 (Me), 28.9 (C-4), 31.9 (C-7), 33.4 (C-4a), 34.0 (C-5), 36.1 (C-3), 37.4 (C-8), 123.5 (C-1), 171.9 (C-8a), 199.9 (C-2)) with chloranil in *tert*-butanol: colorless liquid (52% yield); bp 87–88°/0.15 Torr (1 Torr = 133.3 Pa); IR: C=O 1648 (s), C=C 1624 (s), 1581 (m) cm^{-1}; ^{1}H NMR δ: 1.84 (br s, 3, Me), 5.92 (s, 1, H-1), 6.15 (br s, 1, H-7); ^{13}C NMR δ: 18.9 (Me), 25.9 (C-6), 29.5 (C-4), 30.2 (C-5), 35.7 (C-4a), 37.5 (C-3), 120.8 (C-1), 131.6 (C-8), 136.9 (C-7), 159.1 (C-8a), 200.4 (C-2); MS *m/e* (rel. intensity): 162 (M^+, 56), 134 (80), 119 (20), 105 (33), 91 (base), 77 (21). Anal. calcd. for $C_{11}H_{14}O$: C 81.44, H 8.70; found: C 81.40, H 8.70.

General procedure for the Diels–Alder reactions

The mixtures of the starting materials were prepared in a dry box and the cycloadditions were carried out in degassed solutions. Table 3 delineates the conditions of the Diels–Alder reactions, the following discussion describing the **2***a*–**3***a* reaction in greater detail.

A solution of 1.00 g (6.2 mmol) of ketone **2***a* in 6.5 mL of dry toluene was added slowly to 5.6 mL (5.6 mmol) of a stirring 1.0 M solution of $AlCl_3$ in nitrobenzene at room temperature and stirring was continued for 40 min. A 4.0 M toluene solution (18.5 mL, 74 mmol) of 1,3-butadiene (**3***a*) was added and the ampule was sealed under vacuum and heated at 55°C for 117 h. The ampule was cooled and opened and the contents poured into ice water. The mixture was extracted with ether and the extract was washed with 10% $NaHCO_3$ solution and saturated brine, dried (Na_2SO_4), and evaporated under vacuum. Nitrobenzene was removed by vacuum distillation and the residue purified by medium-pressure chromatography on a prepacked Merck Lichoprep Si 60 column and elution with 33:1 hexane – ethyl acetate, leading to 400 mg (30%) of ketone **4***a*.

*8aβ-Methyl-1,4,4aβ,8,8a,9,10,10aβ-octahydro-6(7*H*)-phenanthrenone (***4***a):* colorless, crystalline solid; mp 84–85°C (hexane); IR: C=O 1660 (s), C=C 1610 (w) cm^{-1}; ^{1}H NMR δ: 1.29 (s, 3, Me), 2.76 (br t, 1, J = 4 Hz, H-4a), 5.58 (s, 2, H-2, H-3), 5.75 (s, 1, H-5); MS *m/e* (rel. intensity): 216 (M^+, 60), 134 (73), 91 (base), 79 (56), 77 (55). Anal. calcd. for $C_{15}H_{20}O$: C 83.29, H 9.32; found: C 83.40, H 9.35.

*2,8aβ-Dimethyl-1,4,4aβ,8,8a,9,10,10aβ-octahydro-6(7*H*)-phenanthrenone (***4***b):* colorless, crystalline solid; mp 118–119°C (hexane): IR: C=O 1660 (s), C=C 1610 (w) cm^{-1}; ^{1}H NMR δ: 1.29 (s, 3, Me), 1.57 (br s, 3, 2-Me), 2.70 (br t, 1, J = 4 Hz, H-4a), 5.28 (br s, 1, H-3), 5.74 (s, 1, H-5); MS *m/e* (rel. intensity): 230 (M^+, 53), 163 (95), 134 (base), 105 (43), 91 (70). Anal. calcd. for $C_{16}H_{22}O$: C 83.43, H 9.63; found: C 84.00, H 9.60.

*4α,8aβ-Dimethyl-1,4,4aβ,8,8a,9,10,10aβ-octahydro-6(7*H*)-phenanthrenone (***4***c)*: colorless liquid (eluted with 8:1:1 hexane/EtOAc/MeOH); IR: C=O 1654 (s), C=C 1610 (w) cm^{-1}; ^{1}H

[5]For general experimental details, see ref. 7.

TABLE 3. Reaction conditions of the Diels–Alder reactions of dienones **2** with dienes **3**[a]

Reactants	$AlCl_3$/ketone[b]	Diene/ketone[b]	Reaction time (h)	Products yield (%)[c]
2*a*–**3***a*	0.9	12	117	33
2*a*–**3***b*	0.25	30	70	18
2*a*–**3***c*	0.5	15	64	62
2*b*–**3***a*	0.9	12	152	37
2*b*–**3***c*	0.5	15	24	51[e]
2*b*–**3***d*[d]	—	5	31	42

[a]Complexation time (ref. 8): 40 min; complexation temperature (8): 22°C; ketone concentration: 0.2 M; reaction temperature: 55–60°C.
[b]Ratio of equivalents.
[c]GC-based yields (those of isolated products being 3–10% lower).
[d]Thermal reaction at 170°C.
[e]Includes 6% yield of product of unknown constitution.

NMR δ: 1.13 (d, 3, J = 6 Hz, 4-Me), 1.26 (s, 3, Me), 2.6–2.8 (m, 1, H-4), 2.77 (br t, 1, J = 4 Hz, H-4a), 5.50 (s, 2, H-2, H-3), 5.93 (s, 1, H-5); MS *m/e* (rel. intensity): 230 (M^+, 67), 163 (72), 134 (72), 105 (63), 91 (base), 77 (56). Anal. calcd. for $C_{16}H_{22}O$: C 83.43, H 9.63; found: C 83.10; H 9.63.

*4*α,*8a*β*-Dimethyl-1,4,4a*α,*8,8a,9,10,10a*α*-octahydro-6(7*H*)-phenanthrenone (**5**):* colorless, crystalline solid (eluted with 8:1:1 hexane/EtOAc/MeOH); mp 63–64°C (hexane); IR: C=O 1654 (s), C=C 1617 (m) cm^{-1}; ^1H NMR δ: 1.03 (d, 3, J = 6 Hz, 4-Me), 1.26 (s, 3, Me), 2.47 (ddd, 1, J = 17, 11, 6 Hz, H-7), 5.50 (d, 1, J = 10 Hz, H-3), 5.56–5.72 (m, 1, H-2); MS *m/e* (rel. intensity): 230 (M^+, 30), 163 (base), 134 (70), 91 (48), 77 (29). Anal. calcd. for $C_{16}H_{22}O$: C 83.43, H 9.63; found: C 83.20, H 9.65.

*2*b–*3*a *reaction.*

Chromatography of the crude product and elution with 20:1 hexane – ethyl acetate furnished pure ketone **7***a* and fractions of **6***a*–**7***a* mixtures. The combined fractions were evaporated under vacuum. HPLC of the residue (C-18 column) and elution with 2:1 MeCN/H_2O yielded pure ketone **6***a*.

*4a*β*-Methyl-1,4,4a,8,8a*β*,9,10,10a*β*-octahydro-6(7*H*)-phenanthrenone (**6**a):* colorless, crystalline solid; mp 46–47°C (hexane); IR: C=O 1660 (s), C=C 1610 (w) cm^{-1}; ^1H NMR δ: 1.24 (s, 3, Me), 2.62–2.75 (m, 1, H-8a), 5.5–5.6 (m, 2, H-2, H-3), 5.88 (s, 1, H-5); MS *m/e* (rel. intensity): 216 (M^+, 51), 162 (71), 134 (base), 91 (95), 79 (41), 77 (47). Anal. calcd. for $C_{15}H_{20}O$: C 83.29, H 9.32; found: C 83.50, H 9.32.

*4a*α*-Methyl-1,4,4a,8,8a*β*,9,10,10a*α*-octahydro-6(7*H*)-phenanthrenone (**7**a):* colorless, crystalline solid; mp 58–59°C (hexane); IR: C=O 1660 (s), C=C 1608 (w) cm^{-1}; ^1H NMR δ: 1.16 (s, 3, Me), 2.55–2.68 (m, 1, H-8a), 5.5–5.6 (m, 2, H-2, H-3), 6.07 (s, 1, H-5); MS *m/e* (rel. intensity): 216 (M^+, 36), 162 (95), 134 (base), 91 (58), 77 (27). Anal. calcd. for $C_{15}H_{20}O$: C 83.29, H 9.32; found: C 83.30, H 9.34.

*2*b–*3*c *reaction*

Chromatography of the crude product and elution with 20:1 hexane – ethyl acetate led to ketones **6***b*, **7***b*, and **8**.

*4*α,*4a*β*-Dimethyl-1,4,4a,8,8a*β*,9,10,10a*β*-octahydro-6(7*H*)-phenanthrenone (**6**b):* colorless liquid; IR: C=O 1654 (s), C=C 1607 (w) cm^{-1}; ^1H NMR δ: 1.15 (d, 3, J = 7 Hz, 4-Me), 1.32 (s, 3, Me), 5.4–5.6 (m, 2, H-2, H-3), 6.01 (d, 1, J = 1 Hz, H-5); MS *m/e* (rel. intensity): 230 (M^+, 28), 163 (89), 134 (base), 105 (36), 91 (78). Anal. calcd. for $C_{16}H_{22}O$:C 83.43, H 9.63; found: C 83.40, H 9.62.

*4*α,*4a*α*-Dimethyl-1,4,4a,8,8a*β*,9,10,10a*α*-octahydro-6(7*H*)-phenanthrenone (**7**b):* colorless liquid; IR: C=O 1658 (s), C=C 1602 (w) cm^{-1}; ^1H NMR δ: 0.76 (d, 3, J = 7 Hz, 4-Me), 0.98 (s, 3, Me), 5.39 (dd, 1, J = 10, 2 Hz, H-3), 5.55–5.67 (m, 1, H-2), 6.03 (s, 1, H-5); MS *m/e* (rel. intensity); 230 (M^+, 1), 163 (base), 134 (66), 91 (47), 77 (18). Anal. calcd. for $C_{16}H_{22}O$: C 83.43, H 9.63; found: C 83.60, H 9.65.

*4*β,4aα*- Dimethyl -1,4,4a,7,8, 9,10,10a*α*- octahydro- 6(5*H*)-phenanthrenone (**8**):* colorless liquid; IR: C=O 1707 (s), C=C 1630 (w) cm^{-1}; ^1H NMR δ: 0.87 (d, 3, J = 7 Hz, 4-Me), 1.06 (s, 3, Me), 2.67 (d, 1, J = 20 Hz, H-5), 3.07 (d, 1, J = 20 Hz, H-5), 5.5–5.6 (m, 2, H-2, H-3); MS *m/e* (rel. intensity): 230 (M^+, 3), 162 (base), 120 (24), 105 (26). Anal. calcd. for $C_{16}H_{22}O$: C 83.43, H 9.63; found: C 83.40, H 9.62.

*2*b–*3*d *reaction*

Repetitive column chromatographies and gradient elution (30:1 to 10:1 hexane – ethyl acetate mixtures) led to ketones **6***c*, **7***c*, **9**, and **10**.

*4*α*-Methoxy-4a*β*-methyl-1,4,4a,8,8a*β*,9,10,10a*β*-octahydro-6(7*H*)-phenanthrenone (**6**c):* colorless, crystalline solid; mp 111–112°C (hexane); IR: C=O 1658 (s), C=C 1602 (w) cm^{-1}; ^1H NMR δ: 1.38 (s, 3, Me), 3.38 (s, 3, OMe), 3.60 (br s, 1, H-4), 5.59 (dd, 1, J = 10, 2 Hz, H-2), 5.85 (br d, 1, J = 10 Hz, H-3), 6.35 (s, 1, H-5); MS *m/e* (rel. intensity): 246 (M^+, 1), 134 (3), 91 (9), 84 (base). Anal. calcd. for $C_{16}H_{22}O_2$: C 78.01, H 9.00; found: C 78.00, H 9.00.

*4*α*-Methoxy-4a*α*-methyl-1,4,4a,8,8a*β*,9,10,10a*α*-octahydro-6(7*H*)-phenanthrenone (**7**c):* colorless, crystalline solid; mp 55–56°C (hexane); IR: C=O 1660 (s), C=C 1608 (w) cm^{-1}; ^1H NMR δ: 1.12 (s, 3, Me), 2.43 (ddd, 1, J = 16, 5, 5Hz, H-10a), 3.30 (s, 3, OMe), 4.10 (br s, 1, H-4), 5.68 (br s, 2, H-2, H-3), 6.13 (br s, 1 H-5); MS *m/e* (rel. intensity): 246 (M^+, 0.06), 91 (6), 84 (base), 69 (16). Anal. calcd. for $C_{16}H_{22}O_2$: C 78.01, H 9.00; found: C 78.20, H 9.03.

*4*β*-Methoxy-4a*α*-methyl-1,4,4a,8,8a*β*,9,10,10a*α*-octahydro-6(7*H*)-phenanthrenone (**9**):* colorless, crystalline solid; mp 65–66°C (hexane); IR: C=O 1660 (s), C=C 1604 (w) cm^{-1}; ^1H NMR δ: 1.09 (s, 3, Me), 1.5–1.6 (m, 1, H-10a), 2.88–2.92 (m, 1, H-8a), 3.00 (d, 1, J = 4 Hz, H-4), 3.19 (s, 3, OMe), 5.73 (ddd, 1, J = 10, 5, 2 Hz, H-2), 5.81 (dd, 1, J = 10, 4 Hz, H-3), 6.10 (d, 1, J = 2 Hz, H-5); MS *m/e* (rel. intensity): 246 (M^+, 0.1), 91 (11), 84 (base), 69 (18). Anal. calcd. for $C_{16}H_{22}O_2$: C 78.01, H. 9.00; found: C 78.09, H 9.05.

*4*β*-Methoxy-4a*β*-methyl-1,4,8,8a*β*,9,10,10a*β*-octahydro-6(7*H*)-phenanthrenone (**10**):* colorless liquid; IR: C=O 1656 (s), C=C 1610 (w) cm^{-1}; ^1H NMR δ: 1.29 (s, 3, Me), 2.1–2.2 (m, 1, H-10a), 2.6–2.8 (m, 1, H-8a), 3.40 (s, 3, OMe), 3.52 (d, 1, J = 3 Hz, H-4), 5.77 (dm, 1, J = 10 Hz, H-2), 5.89 (s, 3, H-5), 5.95 (dd, 1, J = 10, 3 Hz, H-3); MS *m/e* (rel. intensity): 246 (M^+, 3), 91 (8), 84 (base), 69 (16). Anal. calcd. for $C_{16}H_{22}O_2$: C 78.01, H 9.00; found: C 77.90, H 9.09.

Acknowledgments

L. M., R. S., and A. T. thank the Ministero della Università e della Ricerca Scientifica e Tecnologica and the Consiglio Nazionale delle Ricerche for financial support of

Can. J. Chem. Downloaded from www.nrcresearchpress.com by 217.78.4.112 on 09/08/12
For personal use only.

the work in Perugia. This paper is based in part on the doctoral dissertation of Enrico Minelli (Perugia).

1. R. W. Aben, L. Minuti, H. W. Scheeren, and A. Taticchi. Tetrahedron Lett. In press.
2. M. Guo, L. Minuti, and E. Wenkert. J. Org. Chem. **54**, 6138 (1989).
3. (*a*) F. Orsini, F. Pelizzoni, D. Pitea, E. Abbondanti, and A. Mugnoli. J. Org. Chem. **48**, 2866 (1983); (*b*) A. Sicherer-Roetman, B. J. M. Jansen, and A. de Groot. Recl. Trav. Chim. Pays-Bas, **104**, 193 (1985); (*c*) E. C. Angell, F. Fringuelli, F. Pizzo, A. Taticchi, and E. Wenkert. J. Org. Chem. **53**, 1424 (1988); (*d*) B. J. M. Jansen, G. C. Schepers, and A. de Groot. Tetrahedron, **45**, 2773 (1989); (*e*) F. Fringuelli, A. Taticchi, and E. Wenkert. Org. Prep. Proced. Int. **22**, 131 (1990); (*f*) M. Kim, K. Kawada, R. S. Gross, and D. S. Watt. J. Org. Chem. **55**, 504 (1990).
4. W. M. B. Konst, J. G. Witteveen, and H. Boelens. Tetrahedron, **32**, 1415 (1976).
5. E. J. Agnello and G. C. Laubach. J. Am. Chem. Soc. **82**, 4293 (1960).
6. (*a*) E. C. Angell, F. Fringuelli, F. Pizzo, B. Porter, A. Taticchi, and E. Wenkert. J. Org. Chem. **51**, 2642 (1986); (*b*) F. Fringuelli and A. Taticchi. Dienes in the Diels–Alder reaction. John Wiley and Sons, New York, N.Y. 1990.
7. S. Alunni, L. Minuti, P. Pasciuti, A. Taticchi, M. Guo, and E. Wenkert. J. Org. Chem. **56**, 5353 (1991).
8. F. Fringuelli, F. Pizzo, A. Taticchi, and E. Wenkert. J. Org. Chem. **48**, 2802 (1983).

Can. J. Chem. Downloaded from www.nrcresearchpress.com by 217.78.4.112 on 09/08/12
For personal use only.

Directed *ortho* metalation – radical-induced cyclization synthetic connections. A route to highly substituted benzofurans[1]

MASAO TSUKAZAKI AND VICTOR SNIECKUS
Guelph–Waterloo Centre for Graduate Work in Chemistry, University of Waterloo, Waterloo, Ont., Canada N2L 3G1

Received September 30, 1991

MASAO TSUKAZAKI and VICTOR SNIECKUS. Can. J. Chem. **70**, 1486 (1992).

The synthesis of benzofurans **20***a–c*, which constitute analogues of 5-lipoxygenase inhibitors **4**, is described. The route, representing a potential general method for benzofuran construction, proceeds from phenyl carbamate **11** and involves key directed *ortho* metalation (**11** → **12**), anionic *ortho*-Fries rearrangement (**12** → **13***a*), and radical-induced cyclization (**17***a–c* → **18***a–c*) steps.

MASAO TSUKAZAKI et VICTOR SNIECKUS. Can. J. Chem. **70**, 1486 (1992).

On décrit la synthèse des benzofuranes **20***a–c* qui constituent des analogues des produits **4**, des inhibiteurs de la 5-lipoxygénane. La voie, qui correspond à une méthode générale potentielle de synthèse des benzofuranes, utilise le carbamate de phényle **11** comme produit de départ et elle implique une métallation orientée en *ortho* (**11** → **12**), une transposition anionique *ortho*-Fries (**12** → **13***a*) et une cyclisation induite par des radicaux (**17***a–c* → **18***a–c*).

[Traduit par la rédaction]

Can. J. Chem. Downloaded from www.nrcresearchpress.com by 217.78.4.112 on 09/08/12
For personal use only.

Steeped in the fundamental studies of radical reactivity (1), the 5-*exo*-trig ring closure of aryl butenyl systems has emerged as a versatile and broadly useful synthetic reaction especially for heteroannelation routes to benzofuran (2) and indole (3) ring systems. As part of a dominant theme of linking the directed *ortho* metalation strategy (4) to other modern synthetic methods (5), we previously developed a radical-induced cyclization route to benzodihydrofurans, **2** → **3** (Scheme 1) (2*a*) whose regiochemistry is determined by regiospecific halogen introduction, **1** → **2**, courtesy of the synergistic effects of *meta*-related directed metalation groups (DMGs). The major consequence of this fact is the ability to derive, from rationally formulated aromatics (**1**), a variety of substituted benzofurans (**3**) whose construction normally involves difficult and prolonged classical sequences (6).

Since 2- and 3-substituents may be conveniently introduced into benzofurans by metalation (7) and electrophilic substitution (6), we focussed on demonstrating the value and efficacy of the combined metalation – radical cyclization chemistry by incorporating scope in the assemblage of **1**. Thus the recent reports by Merck Frosst chemists of a new benzofuran class (**4**) of 5-lipoxygenase inhibitors, of potential value in treatment of inflammatory and allergic diseases,[2] sparked our interest because of its display of a diverse array of benzene ring substituents. Herein we report a successful route to such systems (**19**, **20**) that not only constitutes a new and potentially general benzofuran assemblage but also complements the previous very comprehensive synthetic work (9) in that it delivers unavailable substitution patterns in **4**. The strategy is based on constructing pentasubstituted benzenes **5** as key intermediates for radical cyclization using *O*-aryl carbamate metalation chemistry (**6**). The envisaged retrosynthesis, in-between metalation (step 1) followed by anionic *ortho*-Fries rearrangement (10) (step 2) and *ipso* bromo desilylation (11) (step 3), has previously found utility for the preparation of polysubstituted aromatics (10) and elaboration of natural products (12, 13). The faster rate of metal–halogen exchange compared to DMG-induced deprotonation (4) precludes consideration of direct introduction of the bromo substituent (step 3).

In initial experiments, the synthesis of the differentially *O*-protected tetrasubstituted aromatic **10** (Scheme 2) was explored from the OMOM carbamate **7**. Metalation followed by silylation afforded the expected **8**, which upon a second metalation under standard −78°C conditions and chlorination led exclusively to the carbamoyl migration product **9**. Although synthetically befitting in other situations (12, 13) (see below), this result points to the facility of the anionic *ortho*-Fries rearrangement in sterically encumbered systems (14). The required product **10** was obtained by carrying out the metalation and chlorination at −100°C but in a yield (48%) that discouraged the continuation of this sequence.

In the ultimately successful sequence, bis-carbamate **11** (Scheme 3), prepared from commercial 4-chlororesorcinol, was subjected to metalation–silylation to give **12** with excellent regioselectivity and in high yield. A minor amount of bis-silylated by-product was easily separated (see experimental section). Anionic *ortho*-Fries rearrangement proceeded smoothly to give **13***a*, which, upon standard methylation, afforded **13***b*. The silylation – carbamate rearrangement was also carried out in a one-pot procedure to give a satisfactory yield (68%) of **13***a*. Although *ipso* bromodesilylation of **13***b* to give **16** occurred in high yield, the conversion of this product to the corresponding phenol was not achieved even under forcing conditions (20% NaOH/EtOH–H_2O/reflux), presumably owing to steric effects. Attempts to hydrolyze the carbamate **13***b* under mild basic conditions (3% LiOH/THF) furnished only the desilylated material **15***a*; only under more vigorous base treatment (10% NaOH/EtOH–H_2O) was decarbamoylation achieved but also with loss of the TMS group to give phenol **15***b*. With this material available and an eye on Occam's razor, classical electrophilic bromination was pursued and gave, pleasantly, the key bromophenol **14** in excellent yield.

To set the stage for radical-induced cyclization, com-

[1]Dedicated to Denny Valenta with appreciation and respect for his many imaginative leaps in synthetic organic chemistry.

[2]See ref. 8*a* for chemistry, ref. 8*b* for chemistry and biology, of these compounds.

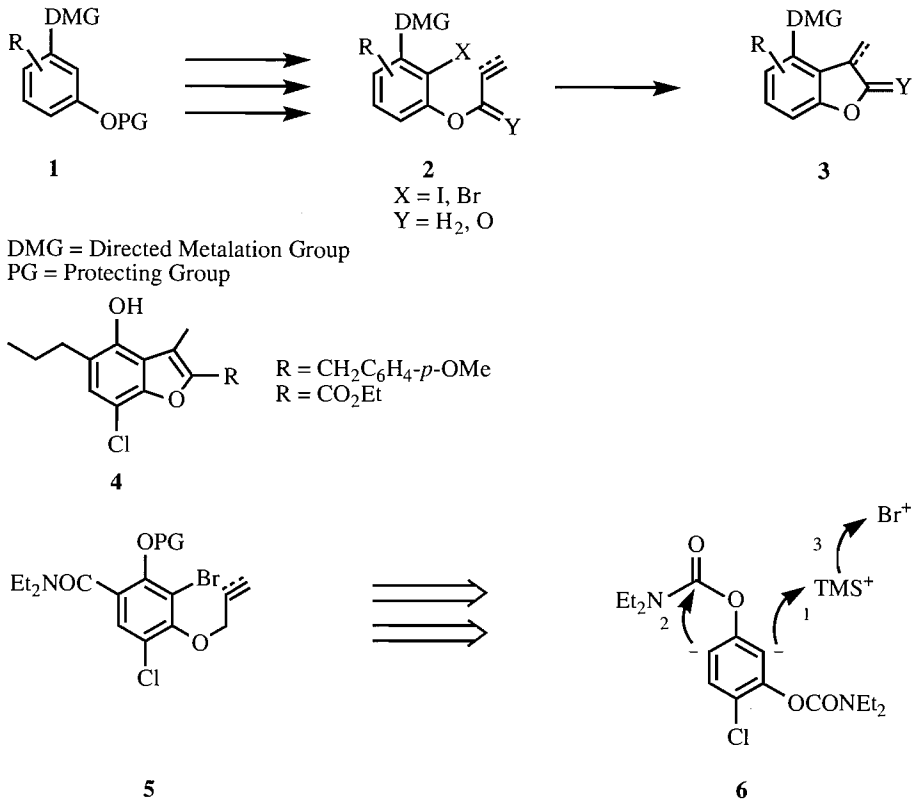

SCHEME 1

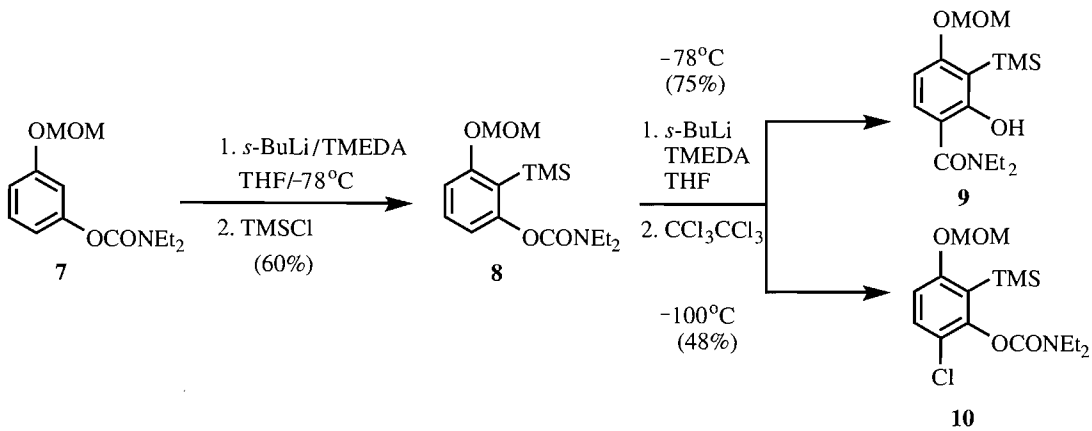

SCHEME 2

pound **14** (Scheme 4) was converted into the *O*-allyl (**17***a*), *O*-propargyl (**17***b*), and *O*-acryloyl (**17***c*) derivatives. Application of standard cyclization conditions (Bu_3SnH/AIBN/PhH/reflux) afforded benzofurans **18***a* (93%), **18***b* (39%), and **18***c* (35%). The unsatisfactory yields of functionalized products **18***b* and **18***c*, expected for **17***b* (2*a*) and due to partial reduction for **17***c*, necessitated the development of dehydrogenation conditions for conversion of **18***a* into benzofuran **19**. After numerous attempts with reagents known to effect this transformation (DDQ/PhH or dioxan/reflux/5–11 days (54–68%); NBS/CCl_4/room temp./12 h (35%); Pd–C/MeCN/reflux/24 h (0%), use of activated MnO_2 was found to give the desired **19** in reasonable yield and time frame.

pK_a considerations (4, 15) argue in favor of deprotonation of **19** at the 2- rather than at the 6-position. In the event, treatment with *n*-BuLi/THF/0°C and LDA/THF/0°C followed by TMSCl quench (−78°C) afforded the 2-silylated benzofurans **20***a* in 54% and 71% yield, respectively. Application of the more favorable conditions for benzoyl chloride and *p*-anisaldehyde electrophiles led to the corresponding products **20***b* and **20***c* in similar yields.

In summary, several new benzofuran analogues to the Merck Frosst 5-lipoxygenase inhibitors **4** have been synthesized.[3] The synthesis takes advantage of regiospecific di-

[3]Selected compounds prepared in this study were subjected to broad screening by Merck Frosst Canada and showed insignificant activity (Dr. R. N. Young, personal communication).

Can. J. Chem. Downloaded from www.nrcresearchpress.com by 217.78.4.112 on 09/08/12
For personal use only.

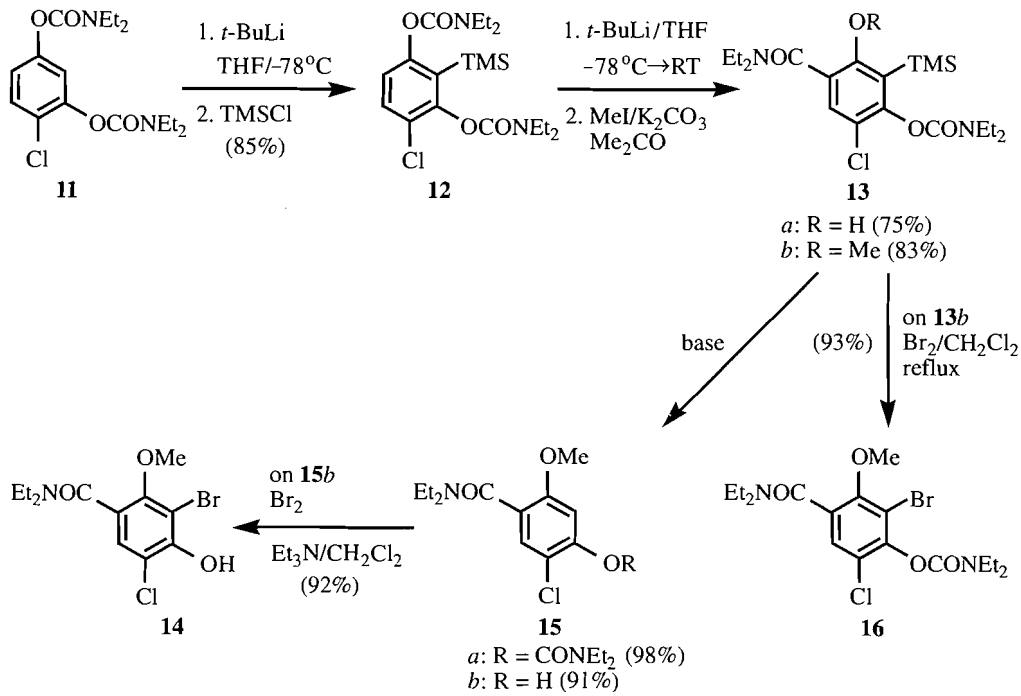

SCHEME 3

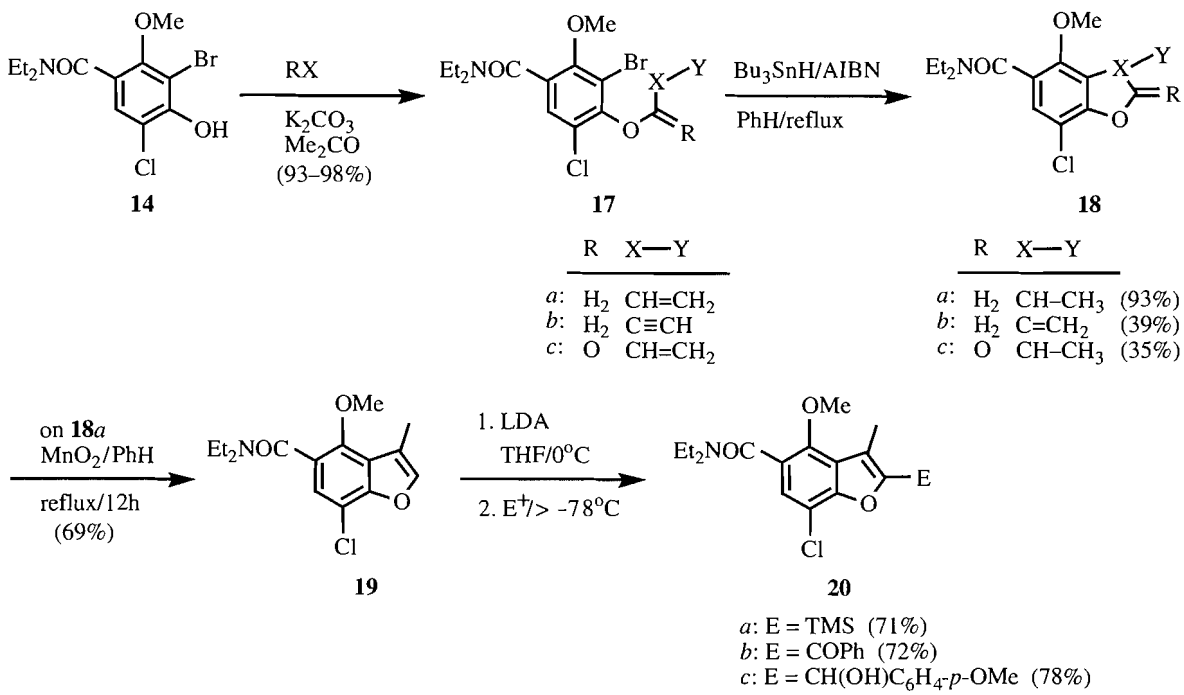

SCHEME 4

rected *ortho* metalation and anionic rearrangement of *O*-aryl carbamates (**11** → **12** → **13**) to construct key intermediates (**14**) for radical-induced cyclization (**17** → **18**). In view of the existing rich metalation chemistry (4), the use of this new strategy for the general construction of benzofurans with aromatic ring substitution patterns not readily achieved by other methods is anticipated. For the potential preparation of congeners to **4**, we note that reduction of 2-benzoyl derivatives analogous to **20***b* have previously been reported (9) and further directed metalation-mediated C-6 functionalization may be feasible.

Experimental section

General procedures

Melting points were recorded on a Buchi SMP-20 apparatus and are uncorrected. IR spectra were recorded on a Perkin–Elmer 983

Can. J. Chem. Downloaded from www.nrcresearchpress.com by 217.78.4.112 on 09/08/12
For personal use only.

Can. J. Chem. Downloaded from www.nrcresearchpress.com by 217.78.4.112 on 09/08/12
For personal use only.

spectrometer. ^{1}H NMR spectra were recorded on Bruker AM-250 and AC-200 instruments in $CDCl_3$ with tetramethylsilane as an internal standard. Microanalyses were performed by Oneida Research Services, Whitesboro, N.Y. Mass spectra were determined on a high-resolution Varian MAT-CH7 instrument.

n-BuLi, *s*-BuLi, *t*-BuLi, diisopropylamine (DIA), *N,N,N',N'*-tetramethylethylenediamine (TMEDA) and 4-chlororesorcinol were purchased from Aldrich Chemical Co. The titer of all alkyllithiums were determined prior to use with 2,5-dimethoxybenzylalcohol as a standard. DIA and TMEDA were dried and distilled from CaH_2 and stored under argon. THF was freshly distilled from sodium benzophenone ketyl prior to use. Metalation reactions were performed in oven- or flame-dried glassware under argon, using syringe – septum cap techniques. The phrase "standard work-up" is the equivalent of addition of saturated NH_4Cl solution, extraction with diethyl ether, washing the organic extract with brine, drying ($MgSO_4$), filtration, and evaporation to dryness *in vacuo*. TLC was performed on E-Merck silica gel 60 strips and medium pressure column chromatography was carried out on BDH silica gel 60 (0.04–0.063 and 0.063–0.20 mm with hexane/EtOAc (1:1 to 10:1) eluent unless otherwise indicated.

N,N-*Diethyl O-(3-methoxymethoxyphenyl) carbamate (7)*

To a solution of *N,N*-diethyl *O*-(3-methoxyphenyl) carbamate (17.8 g, 80.0 mmol) in CH_2Cl_2 (200 mL) was added BBr_3 (11.3 mL, 120 mmol) at −78°C. The mixture was warmed to room temperature and stirred overnight. After cooling to −78°C, the reaction was quenched with MeOH. Standard work-up followed by recrystallization gave *N,N*-diethyl *O*-(3-hydroxyphenyl) carbamate (15.4 g, 92%): mp 62–63°C (Et_2O–hexane) (lit. (16) mp 64–66°C); IR ($CHCl_3$) ν(max): 1695 cm^{-1}; ^{1}H NMR δ ($CDCl_3$): 1.23 (t, 6H, J = 7.1 Hz), 3.43 (q, 4H, J = 7.1 Hz), 6.52–6.74 (m, 3H), 7.08–7.29 (m, 2H); MS *m/e* (rel. intensity): 209 (M^+, 100). A solution of *N,N*-diethyl (3-hydroxyphenyl) carbamate (10.5 g, 50.0 mmol) in DMF was added to a suspension of NaH (60 mmol) in DMF at 0°C. After 1 h, chloromethyl methyl ether (4.56 mL, 60.0 mmol) was added and the mixture was warmed to room temperature and stirred overnight. Standard work-up followed by distillation afforded **7** (9.98 g, 79%): bp 138–140°C (1.2 Torr); IR (neat) ν(max): 1710 cm^{-1}; ^{1}H NMR δ ($CDCl_3$): 1.21 (t, 6H, J = 7.1 Hz), 3.42 (q, 4H, J = 7.1 Hz), 3.45 (s, 3H), 5.15 (s, 2H), 6.71–6.94 (m, 3H), 7.24 (dd, 1H, J = 7.3 and 8.8 Hz); MS *m/e* (rel. intensity): 253 (M^+, 100). Anal. calcd. for $C_{13}H_{19}NO_4$: C 61.64, H 7.56, N 5.52; found: C 61.65, H 7.76, N 5.26.

N,N-*Diethyl O-(3-methoxymethoxy-2-trimethylsilylphenyl) carbamate (8)*

A solution of **7** (5.06 g, 20.0 mmol) dissolved in dry THF (5 mL) was added dropwise to a stirred solution of 1:1 *s*-BuLi–TMEDA (24.0 mmol) mixture in dry THF (200 mL) at −78°C. After 1 h, TMSCl (3.81 mL, 30.0 mmol) was added slowly and the reaction mixture was allowed to warm to room temperature. Standard work-up afforded crude product, which was purified by column chromatography followed by distillation to give pure **8** (3.84 g, 60%); bp 160–162°C (1.5 Torr); IR (neat) ν(max): 1716 cm^{-1}; ^{1}H NMR δ ($CDCl_3$): 0.30 (s, 9H), 1.19 (t, 3H, J = 7.1 Hz), 1.24 (t, 3H, J = 7.1 Hz), 3.38 (q, 2H, J = 7.1 Hz), 3.44 (q, 2H, J = 7.1 Hz), 3.46 (s, 3H), 5.15 (s, 2H), 6.62 (dd, 1H, J = 8.1 and 0.6 Hz), 6.91 (dd, 1H, J = 8.3 and 0.6 Hz), 7.26 (dd, 1H, J = 8.1 and 8.3 Hz); MS *m/e* (rel. intensity): 325 (M^+, 1). HRMS calcd. for $C_{16}H_{27}No_4Si$: 325.1710; found: 325.1687.

N,N-*Diethyl 2-hydroxy-4-methoxymethoxy-3-trimethylsilylbenzamide (9)*

Using the above procedure, **8** (1.63 g, 5.00 mmol) was treated with *s*-BuLi–TMEDA (6.00 mmol) at −78°C. Standard work-up followed by column chromatography gave pure **9** (1.27 g, 78%); mp 49–50°C (Et_2O–hexane); IR (KBr) ν(max): 1615 cm^{-1}; ^{1}H NMR δ ($CDCl_3$): 0.34 (s, 9H), 1.26 (t, 6H, J = 7.1 Hz), 3.47 (s, 3H), 3.49 (q, 4H, J = 7.1 Hz), 5.16 (s, 2H), 6.54 (d, 1H, J = 8.7 Hz), 7.21 (d, 1H, J = 8.7 Hz), 10.53 (s, 1H); MS *m/e* (rel. intensity): 325 (M^+, 36). HRMS calcd. for $C_{16}H_{27}NO_4Si$: 325.1710; found: 325.1704.

N,N-*Diethyl O-(6-chloro-3-methoxymethoxy-2-trimethylsilyl) carbamate (10)*

The procedure for the preparation of **8** was followed except that the metalation was carried out at −100°C. From **8** (0.650 g, 2.00 mmol) and *s*-BuLi–TMEDA (2.40 mmol) in THF and hexachloroethane (0.615 g, 2.60 mmol) as the electrophile, there was obtained 0.345 g (48%) of **10** as an oil; IR (neat) ν(max): 1724 cm^{-1}; ^{1}H NMR δ ($CDCl_3$): 0.30 (s, 9H), 1.20 (t, 3H, J = 7.2 Hz), 1.29 (t, 3H, J = 7.2 Hz), 3.29–3.65 (m, 4H), 3.46 (s, 3H), 5.13 (d, 1H, J = 6.7 Hz), 5.15 (d, 1H, J = 6.7 Hz), 6.90 (d, 1H, J = 8.8 Hz), 7.30 (d, 1H, J = 8.8 Hz); MS *m/e* (rel. intensity): 359 (M^+, 1). HRMS calcd. for $C_{16}H_{27}NO_4SiCl$: 359.1321; found: 359.1310.

N,N-*Diethyl O-[4-chloro-3-(*N,N-*diethylcarbamoyloxy)phenyl] carbamate (11)*

A solution of 4-chlororesorcinol (7.23 g, 50.0 mmol) and *N,N*-diethyl carbamoyl chloride (15.2 mL, 120 mmol) in pyridine (50 mL) was refluxed for 12 h. The solvent was removed and the resulting residue was dissolved in ether (200 mL). The ether layer was washed successively with water, 2 N HCl, 2 N NaOH, and brine and dried ($MgSO_4$). Removal of ether *in vacuo* followed by distillation gave pure **11** (14.2 g, 83%, bp 178–180°C/0.1 Torr); IR (neat) ν(max): 1717 cm^{-1}; ^{1}H NMR δ ($CDCl_3$): 1.07–1.33 (m, 12H), 3.31–3.52 (m, 8H), 6.96 (dd, 1H, J = 2.7 and 8.8 Hz), 7.11 (d, 1H, J = 2.7 Hz), 7.37 (d, 1H, J = 8.8 Hz); MS *m/e* (rel. intensity): 342 (M^+, 2). Anal. calcd. for $C_{16}H_{23}N_2O_4Cl$: C 56.06, H 6.76, N 8.17; found: C 55.96, H 6.57, N 8.28.

N,N-*Diethyl O-[4-chloro-3-(*N,N-*diethylcarbamoyloxy)-2-trimethylsilylphenyl] carbamate (12)*

To a stirred solution of **11** (3.43 g, 10.0 mmol) in THF (150 mL) at −78°C was added a solution of *t*-BuLi (6.67 mL of 1.65 M solution, 11.0 mmol). After stirring for 30 min, the solution was treated with TMSCl (1.90 mL, 15.0 mmol) and then allowed to warm to room temperature. Standard work-up followed by column chromatography gave **12** (3.53 g, 85%): mp 58–59°C (hexane); IR (KBr) ν(max): 1717 cm^{-1}; ^{1}H NMR δ ($CDCl_3$): 0.30 (s, 9H), 1.19 (t, 3H, J = 7.1 Hz), 1.20 (t, 3H, J = 7.1 Hz), 1.23 (t, 3H, J = 6.8 Hz), 1.30 (t, 3H, J = 7.1 Hz), 3.26–3.66 (m, 8H), 6.83 (d, 1H, J = 8.7 Hz), 7.37 (d, 1H, J = 8.7 Hz); MS *m/e* (rel. intensity): 415 (M^+ +1, 92). Anal. calcd. for $C_{19}H_{31}N_2O_4SiCl$: C 54.99, H 7.53, N 6.75; found: C 54.96, H 7.53, N 6.71.

N,N-*Diethyl 5-chloro-4-(*N,N-*diethylcarbamoyloxy)-2-hydroxy-3-trimethylsilylbenzamide (13*a*)*

According to the procedure for the preparation of **9**, **12** (2.06 g, 4.97 mml) was treated with *s*-BuLi–TMEDA (5.56 mmol). Standard work-up followed by recrystallization gave **13***a* (1.64 g, 80%); mp 103–104°C (Et_2O–hexane); IR (KBr) ν(max): 1616, 1717 cm^{-1}; ^{1}H NMR δ ($CDCl_3$): 0.33 (s, 9H), 1.21 (t, 3H, J = 7.1 Hz), 1.27 (t, 6H, J = 7.0 Hz), 1.31 (t, 3H, J = 7.0 Hz), 3.29–3.64 (m, 8H), 7.29 (s, 1H), 10.37 (s, 1H); MS *m/e* (rel. intensity): 415 (M^+ +1, 1). Anal. calcd. for $C_{19}H_{31}N_2O_4SiCl$: C 54.99, H 7.53, N 6.75; found: C 54.91, H 7.48, N 6.69.

N,N-*Diethyl 5-chloro-4-(*N,N-*diethylcarbamoyloxy)-2-methoxy-3-trimethylsilylbenzamide (13*b*)*

A mixture of **13***a* (1.87 g, 4.52 mmol), methyl iodide (1.13 mL, 1.81 mmol), and K_2CO_3 (6.21 g, 45.2 mmol) in acetone was refluxed for 1 h. Standard work-up followed by column chromatography and recrystallization gave **13***b* (1.63 g, 84%); mp 85–86°C (Et_2O–hexane); IR (KBr) ν(max): 1627, 1721 cm^{-1}; ^{1}H NMR δ ($CDCl_3$): 0.31 (s, 9H), 1.07 (t, 3H, J = 7.0 Hz), 1.20 (t, 3H, J = 7.0 Hz), 1.25 (t, 3H, J = 7.1 Hz), 1.29 (t, 3H, J = 7.1 Hz), 3.18–3.71 (m, 8H), 3.76 (s, 1H), 7.29 s, 1H); MS *m/e*

Can. J. Chem. Downloaded from www.nrcresearchpress.com by 217.78.4.112 on 09/08/12
For personal use only.

(rel. intensity): 429 (M^+ +1, 1). Anal. calcd. for $C_{20}H_{33}N_2O_4SiCl$: C 55.99, H 7.75, N 6.53; found: C 55.99, H 7.82, N 6.56.

N,N-*Diethyl 2-bromo-5-chloro-4-hydroxy-2-methoxybenzamide (**14**)*

To a stirred solution of **15***b* (4.34 g, 16.8 mmol) and triethylamine (3.51 mL, 25.2 mmol) in $CHCl_3$ at 0°C was added dropwise Br_2 (1.07 mL, 20.2 mmol). After stirring for 30 min, the mixture was quenched with 5% $Na_2S_2O_3$ aqueous solution. Standard work-up followed by recrystallization gave **14** (5.21 g, 92%); mp 150–151°C (CH_2Cl_2–Et_2O); IR (KBr) ν(max): 1608 cm^{-1}; ^1H NMR δ ($CDCl_3$): 1.06 (t, 3H, *J* = 7.1 Hz), 1.25 (t, 3H, *J* = 7.1 Hz), 3.17 (q, 2H, *J* = 7.1 Hz), 3.37–3.82 (m, 2H), 3.87 (s, 3H), 6.47 (br s, 1H), 7.20 (s, 1H); MS *m/e* (rel. intensity): 336 (M^+ +1, 25). Anal. calcd. for $C_{12}H_{15}NO_3ClBr$: C 42.82, H 4.49, N 4.16; found: C 42.69, H 4.66, N 4.12.

N,N-*Diethyl 5-chloro-4-hydroxy-2-methoxybenzamide (**15**b)*

13*b* (5.15 g, 12.0 mmol) was dissolved into 10% NaOH/EtOH–H_2O solution (100 mL) and refluxed for 4 h. After removal of EtOH, the solution was acidified with concentrated HCl. The resulting white solid was collected and recrystallized to give **15***b* (2.78 g, 91%): mp 190–191°C (CH_2Cl_2–EtO_2); IR (KBr) ν(max): 1617 cm^{-1}; ^1H NMR δ ($CDCl_3$): 1.05 (t, 3H, *J* = 7.1 Hz), 1.23 (t, 3H, *J* = 7.1 Hz), 3.16 (q, 2H, *J* = 7.1 Hz), 3.54 (q, 3H, *J* = 7.1 Hz), 3.69 (s, 3H), 6.49 (s, 1H), 7.06 (br s, 1H), 7.09 (s, 1H); MS *m/e* (rel. intensity) 258 (M^+ +1, 31). Anal. calcd. for $C_{12}H_{16}NO_3Cl$: C 55.93, H 6.26, N 5.43; found: C 55.70, H 6.84, N 5.43.

N,N-*Diethyl 3-bromo-5-chloro-4-(*N,N-*diethylcarbamoyloxy)-2-methoxybenzamide (**16**)*

13*b* (0.429 g, 1.00 mmol) and Br_2 (0.11 mL, 2.0 mmol) were dissolved in CH_2Cl_2 (20 mL) and the solution was refluxed for 2 h. Standard work-up followed by column chromatography gave **16** (0.413 g, 95%) as an oil; IR (neat) ν(max): 1638, 1737 cm^{-1}; ^1H NMR δ ($CDCl_3$): 1.06 (t, 3H, *J* = 7.1 Hz), 1.23 (t, 3H, *J* = 7.1 Hz), 1.25 (t, 3H, *J* = 7.1 Hz), 1.35 (t, 3H, *J* = 7.1 Hz), 3.16 (q, 2H, *J* = 7.1 Hz), 3.36–3.57 (m, 5H), 3.67–3.80 (m, 1H), 3.87 (s, 2H), 7.27 (s, 1H); MS *m/e* (rel. intensity): 436 (M^+ +2, 8). HRMS calcd. for $C_{17}H_{24}N_2O_4ClBr$: 434.0609; found: 434.0598.

N,N-*Diethyl 3-bromo-5-chloro-2-methoxy-4-(2-propenyloxy)benzamide (**17**a)*

A mixture of **14** (0.522 g, 1.55 mmol), allyl bromide (0.27 mL, 3.1 mmol), and K_2CO_3 (1.07 g, 7.75 mmol) in acetone was heated at reflux for 2 h. Standard work-up followed by column chromatography gave **17***a* (0.574 g, 98%) as an oil; IR (neat) ν(max): 1635 cm^{-1}; ^1H NMR δ ($CDCl_3$): 1.07 (t, 3H, *J* = 7.1 Hz), 1.25 (t, 3H, *J* = 7.1 Hz), 3.16 (q, 2H, *J* = 7.1 Hz), 3.7 (m, 1H), 3.8 (m, 1H), 4.57 (ddd, 2H, *J* = 1.2, 1.3, and 5.9 Hz), 5.31 (dd, 1H, *J* = 1.2, 1.4, and 10.3 Hz), 5.46 (ddd, 1H, *J* = 1.5, 1.6, and 17.1 Hz), 6.17 (ddt, 1H, *J* = 10.3, 17.1, and 5.9 Hz), 7.23 (s, 1H); MS *m/e* (rel. intensity): 377 (M^+ +2, 10). Anal. calcd. for $C_{15}H_{19}NO_3ClBr$: C 47.83, H 5.08, N 3.72; found: 47.84, H 4.97, N 3.94.

N,N-*Diethyl 3-bromo-5-chloro-2-methoxy-4-(2-propynyloxy)benzamide (**17**b)*

The procedure for the preparation of **17***a* was followed. From **14** (0.337 g, 1.00 mmol), propargyl bromide (0.22 mL, 2.0 mmol), and K_2CO_3 (0.69 g, 5.0 mmol) there was obtained 0.367 g (98%) of **17***b* as an oil; IR (neat) ν(max): 1631 cm^{-1}; ^1H NMR δ ($CDCl_3$): 1.07 (t, 3H, *J* = 7.1 Hz), 1.25 (t, 3H, *J* = 7.1 Hz), 2.58 (t, 1H, *J* = 2.3 Hz), 3.15 (q, 2H, *J* = 7.1 Hz), 3.32–3.46 (m, 1H), 3.66–3.80 (m, 1H), 3.87 (s, 3H), 4.78 (d, 2H, *J* = 2.3 Hz), 7.24 (s, 1H); MS *m/e* (rel. intensity): 375 (M^+ +2, 31). HRMS calcd. for $C_{15}H_{17}NO_3ClBr$: 373.0081; found: 373.0083.

N,N-*Diethyl 4-acryloyloxy-3-bromo-5-chloro-2-methoxybenzamide (**17**c)*

To a solution of **14** (0.337 g, 1.00 mmol) in ether (20 mL) at 0°C were successively added triethylamine (0.28 mL, 2.0 mmol) and acryloyl chloride (0.12 mL, 1.5 mmol). The reaction mixture was stirred for 3 h at 0°C and warmed to room temperature. Standard work-up followed by column chromatography gave **17***c* (0.363 g, 93%) as an oil; IR (neat) ν(max): 1636, 1757 cm^{-1}; ^1H NMR δ ($CDCl_3$): 1.09 (t, 3H, *J* = 7.1 Hz), 1.26 (t, 3H, *J* = 7.1 Hz), 3.21 (q, 2H, *J* = 7.1 Hz), 3.32–3.50 (m, 1H), 3.66–3.82 (m, 1H), 3.88 (s, 3H), 6.14 (dd, 1H, *J* = 0.6 and 10.5 Hz), 6.39 (dd, 1H, *J* = 10.5 and 17.2 Hz), 6.72 (dd, 1H, *J* = 0.6 and 17.2 Hz), 7.30 (s, 1H); MS *m/e* (rel. intensity): 391 (M^++2, 17). HRMS calcd. for $C_{15}H_{17}NO_4ClBr$: 389.0030; found: 388.9992.

*7-Chloro-5-(*N,N-*diethylcarbamoyl)-4-methoxy-3-methyl-2,3-dihydrobenzofuran (**18**a)*

A solution of **17***a* (1.13 g, 3.00 mmol), Bu_3SnH (1.62 mL, 6.00 mmol), and AIBN (15 mg) in benzene (300 mL) was refluxed for 1 h. After removal of benzene, the residue was dissolved in CH_3CN (200 mL), washed with hexane (30 mL × 3), and evaporated. The product was purified by column chromatography to give **18***a* (0.830 g, 93%); mp 64–65°C (Et_2O–hexane); IR (KBr) ν(max): 1624 cm^{-1}; ^1H NMR δ ($CDCl_3$): 1.07 (t, 3H, *J* = 7.1 Hz), 1.24 (t, 3H, *J* = 7.1 Hz), 1.36 (d, 3H, *J* = 6.9 Hz), 3.20 (q, 2H, *J* = 7.1 Hz), 3.35–3.79 (m, 3H), 3.83 (s, 3H), 4.27 (dd, 1H, *J* = 5.5 and 8.9 Hz), 4.76 (t, 1H, *J* = 8.9 Hz), 7.01 (s, 1H); MS *m/e* (rel. intensity): 297 (M^+, 25). Anal. calcd. for $C_{15}H_{20}NO_3Cl$: C 60.50, H 6.77, N 4.70; found: 60.42, H 6.75, N 4.65.

*7-Chloro-5-(*N,N-*diethylcarbamoyl)-4-methoxy-3-methylene-2,3-dihydrobenzofuran (**18**b)*

The procedure for the preparation of **18***a* was followed. From **17***b* (0.356 g, 0.95 mmol), Bu_3SnH (0.51 mL, 1.90 mmol), and AIBN (10 mg) there was obtained 0.109 g (39%) of **18***a* as an oil; IR (neat) ν(max): 1620 cm^{-1}; ^1H NMR δ ($CDCl_3$): 1.07 (t, 3H, *J* = 7.1 Hz), 1.25 (t, 3H, *J* = 7.1 Hz), 3.14–3.78 (m, 4H), 3.85 (s, 3H), 5.16–5.21 (m, 3H), 5.72–5.76 (m, 1H), 7.07 (s, 1H); MS *m/e* (rel. intensity): 295 (M^+, 4).

*7-Chloro-5-(*N,N-*diethylcarbamoyl)-4-methoxy-3-methyl-2(3*H*)-benzofuranone (**18**c)*

The procedure for the preparation of **18***a* was followed. From **17***c* (0.365 g, 0.93 mmol), Bu_3SnH (0.50 mL, 1.07 mmol), and AIBN (10 mg) there was obtained 0.109 g (35%) of **18***c* as a oil; IR (neat) ν(max): 1624, 1820 cm^{-1}; ^1H NMR δ ($CDCl_3$): 1.09 (t, 3H, *J* = 7.1 Hz), 1.26 (t, 3H, *J* = 7.1 Hz), 1.64 (d, 3H, *J* = 7.6 Hz), 3.20 (q, 2H, *J* = 7.1 Hz), 3.34–3.77 (m, 3H), 3.87 (s, 3H), 7.17 (s, 1H); MS *m/e* (rel. intensity): 310 (M^+ −1, 66). HRMS calcd. for $C_{15}H_{18}NO_4Cl$: 311.0925; found: 311.0909.

*7-Chloro-5-(*N,N-*diethylcarbamoyl)-4-methoxy-3-methylbenzofuran (**19**)*

A mixture of **18***a* (0.100 g, 0.34 mmol) and MnO_2 (0.29 g) in benzene was heated under reflux for 12 h with azeotropic removal of water. The MnO_2 was removed by filtration and the filtrate was evaporated to dryness. The crude material was subjected to column chromatography to afford **19** (0.069 g, 69%); mp 90–91°C (Et_2O–hexane); IR (KBr) ν(max): 1624 cm^{-1}; ^1H NMR δ ($CDCl_3$): 1.06 (t, 3H, *J* = 7.1 Hz), 1.28 (t, 3H, *J* = 7.1 Hz), 2.36 (d, 3H, *J* = 1.3 Hz), 3.23–3.77 (m, 4H), 3.92 (s, 3H), 7.14 (s, 1H), 7.41 (q, 1H, *J* = 1.3 Hz); MS *m/e* (rel. intensity): 295 (M^+, 17). Anal. calcd. for $C_{15}H_{18}NO_3Cl$: C 60.91, H 6.13, N 4.74; found: C 60.96, H 6.17, N 4.70.

*7-Chloro-5-(*N,N-*diethylcarbamoyl)-4-methoxy-3-methyl-2-trimethylsilylbenzofuran (**20**a)*

To a solution of LDA (0.41 mmol, prepared *in situ* from *n*-BuLi and diisopropylamine) in THF (15 mL) was added a solution of **19** (0.100 g, 0.41 mmol) in THF at −78°C. The solution was warmed to 0°C and stirred for 30 min. After cooling to −78°C again, TMSCl (0.064 mL, 0.51 mmol) was added and the mixture was warmed to room temperature. Standard work-up followed by column chromatography gave **20***a* (0.090 g, 71%); mp 86–87°C (Et_2O–hexane); IR (KBr) ν(max): 1635 cm^{-1}; ^1H NMR δ ($CDCl_3$): 0.40 (s, 9H), 1.04 (t, 3H, *J* = 7.1 Hz), 1.27 (t, 3H, *J* = 7.1 Hz), 2.43 (s,

3H), 3.17–3.88 (m, 4H), 3.89 (s, 3H), 7.10 (s, 1H); MS *m/e* (rel. intensity): 367 (M^+, 33). HRMS calcd. for $C_{18}C_{26}NO_3SiCl$: 367.1372; found: 367.1356.

*2-Benzoyl-7-chloro-5-(*N,N*-diethylcarbamoyl)-4-methoxy-3-methylbenzofuran (**20**b)*

The procedure for the preparation of **20***a* was followed except that benzoyl chloride was added at −100°C. From **19** (0.178 g, 0.60 mmol), LDA (0.78 mmol), and benzoyl chloride (0.14 mL, 1.20 mmol) there was obtained 0.172 g (72%) of **20***b*; mp 89–90°C (Et_2O–hexane); IR (KBr) ν(max): 1624, 1646 cm^{-1}; ^1H NMR δ ($CDCl_3$): 1.08 (t, 3H, J = 7.1 Hz), 1.30 (t, 3H, J = 7.1 Hz), 2.80 (s, 3H), 3.2 (m, 2H), 3.4 (m, 1H), 3.8 (m, 1H), 3.97 (s, 3H), 7.32 (s, 1H), 7.49–7.67 (m, 3H), 8.12–8.16 (m, 2H); MS *m/e* (rel. intensity): 399 (M^+, 36). Anal. calcd. for $C_{22}H_{22}NO_4Cl$: C 66.08, H 5.55, N 3.50; found: C 66.05, H 5.45, N 3.48.

*7-Chloro-5-(*N,N*-diethylcarbamoyl)-4-methoxy-2-[(4-methoxyphenyl)hydroxymethyl]-3-methylbenzofuran (**20**c)*

The procedure for the preparation of **20***a* was followed. From **19** (0.296 g, 1.00 mmol) LDA (1.20 mmol), and *p*-anisaldehyde (0.164 mL, 1.20 mmol) there was obtained 0.328 g (76%) of **20***c*: mp 200–201°C (CH_2Cl_2–hexane); IR (KBr) ν(max): 3371, 1607 cm^{-1}; NMR δ ($CDCl_3$): 1.03 (t, 3H, J = 7.1 Hz), 1.27 (t, 3H, J = 7.1 Hz), 2.35 (s, 3H), 2.78 (br s, 1H), 3.2 (m, 2H), 3.4 (m, 1H), 3.7 (m, 1H), 3.81 (s, 3H), 3.88 (s, 3H), 5.96 (d, 1H, J = 5.6 Hz), 6.91 (d, 2H, J = 8.7 Hz), 7.09 (s, 1H), 7.42 (d, 2H, J = 8.7 Hz); MS *m/e* (rel. intensity): 431 (M^+, 51). Anal. calcd. for $C_{23}H_{26}NO_5Cl$: C 63.96, H 6.07, N 3.17; found: C 63.77, H 6.06, N 3.17.

Acknowledgements

We are grateful to NSERC and Merck Frosst Canada for support of this research via CRD No. 661-046/87 and Operating Grants. We thank Drs. R. N. Young and J. G. Atkinson for useful discussion and information.

1. D. P. Curran. Synthesis 417, 489 (1988); C. Chatgilialoglu, K. U. Ingold, and J. C. Scaiano. J. Am. Chem. Soc. **103**, 7739 (1981).
2. (*a*) K. Shankaran, C. P. Sloan, and V. Snieckus. Tetrahedron Lett. **26**, 6001 (1985); (*b*) A. J. Walkington and D. A. Whiting. Tetrahedron Lett. **30**, 4731 (1989); (*c*) K. Last and H. M. R. Hoffmann. Synthesis, 901 (1989); (*d*) D. P. Curran, T. L. Fevig, and M. J. Totleben. Synlett, 773 (1990).
3. W. R. Bowman, H. Heaney, and B. M. Jordan. Tetrahedron Lett. **29**, 6657 (1988); A. J. Clark and K. Jones. Tetrahedron Lett. **30**, 5485 (1989), and refs. cited therein; D. L. Boger and R. J. Wyscoki, Jr. J. Org. Chem. **54**, 1239 (1989); R. Grigg, V. Loganathan, S. Sukirthalingam, and V. Sridharan. Tetrahedron Lett. **31**, 6573 (1990); D. L. Boger, T. Ishizaki, P. A. Kitos, and O. Suntornwat. J. Org. Chem. **55**, 5823 (1990); D. L. Boger, R. J. Wysocki, Jr., and T. Ishizaki. J. Am. Chem. Soc. **112**, 5230 (1990).
4. V. Snieckus. Chem. Rev. **90**, 879 (1990).
5. B. I. Alo, A. Kandil, P. A. Patil, M. J. Sharp, M. A. Siddiqui, and V. Snieckus. J. Org. Chem. **56**, 3763 (1991), and refs. cited therein.
6. P. Cagnianti and D. Cagnianti. Adv. Heterocycl. Chem. **18**, 337 (1975); A. Mustafa. *In* Benzofurans. *Edited by* A. Weissberger and E. C. Taylor. Wiley, New York. 1974. Chap. 1. For newer methods, see R. C. Larock, N. Berrios-Pena, and K. Narayanan. J. Org. Chem. **55**, 3447 (1990); G. Pandey, A. Krishna, and U. T. Bhalerao. Tetrahedron Lett. **30**, 1867 (1989); R. C. Larock, and D. E. Stinn. Tetrahedron Lett. **29**, 4687 (1988); W. T. Brady and Y. F. Giang. J. Org. Chem. **51**, 2145 (1986), and refs. cited in each of these publications.
7. F. M. Dean. Adv. Heterocycl. Chem. **31**, 237 (1982).
8. (*a*) J. Rokach, Y. Guindon, and R. N. Young, *et al. In* The total synthesis of natural products. Vol. 7. *Edited by* J. ApSimon. Wiley, New York. 1988. p. 141; (*b*) L. W. Chakrin and D. M. Bailey (*Editors*) The leukotrienes. Academic Press, 1984; J. G. Atkinson, Y. Guindon, and C. K. Lau. U.S. Patent 4,663,347 (1987); J. Adams and Y. Guindon. U.S. Patent 4,800,228 (1989); P. C. Belanger, J. Scheigetz and J. Rokach. U.S. Patent 4,863,958 (1989).
9. C. K. Lau *et al.* J. Med. Chem. **32**, 1190 (1989).
10. M. P. Sibi and V. Snieckus. J. Org. Chem. **48**, 1935 (1983).
11. R. J. Mills, N. J. Taylor, and V. Snieckus. J. Org. Chem. **54**, 4372 (1989).
12. M. P. Sibi, S. Chattopadhyay, J. W. Dankwardt, and V. Snieckus. J. Am. Chem. Soc. **107**, 6312 (1985).
13. S. Danishefsky and J. Y. Lee. J. Am. Chem. Soc. **111**, 4829 (1989).
14. W. Wang and V. Snieckus. J. Org. Chem. **57**, 424 (1992).
15. O. A. Reutov, I. P. Beletskaya, and K. P. Butin. *In* CH acids. *Edited by* T. R. Crompton. Pergamon Press, London. 1978. p. 68.
16. E. Bartholomaus. U.S. Patent 2,209,245 (1941); Chem. Abstr. **35**, 282 (1941).

Can. J. Chem. Downloaded from www.nrcresearchpress.com by 217.78.4.112 on 09/08/12
For personal use only.

The synthesis of norbornanes with functionalized carbon substituents at a bridgehead. 1-(3-Oxonorborn-1-yl)ethanone and 1-(3-oxonorborn-1-yl)-2-propanone

PETER YATES AND MAGDY KALDAS
Lash Miller Chemical Laboratories, University of Toronto, Toronto, Ont., Canada M5S 1A1

Received August 16, 1991

Dedicated to Professor Zdenek (Denny) Valenta on the occasion of his 65th birthday

PETER YATES and MAGDY KALDAS. Can. J. Chem. **70**, 1492 (1992).

Treatment of 2-norobornene-1-carboxylic acid (**7**) with one equivalent of methyllithium in ether followed by a second molar equivalent after dilution with tetrahydrofuran gave 1-(norborn-2-en-lyl)ethanone (**10**) and only a trace of the tertiary alcohol **11**. Reaction of **7** with formic acid followed by hydrolysis gave a 4:3 mixture of *exo*-3- and *exo*-2-hydroxynorbornane-1-carboxylic acid (**16** and **17**), whereas oxymercuration–demercuration gave only the *exo*-3-hydroxy isomer **16**. Oxidation of **16** and **17** gave 3- and 2-oxonorbornane-1-carboxylic acid (**27** and **29**), respectively. Oxymercuration–demercuration of **10** gave exclusively 1-(*exo*-3-hydroxynorborn-1-yl)ethanone (**30**), which was also prepared by treatment of **16** with methyllithium in analogous fashion to that used for the conversion of **7** to **10**. Oxidation of **30** gave 1-(3-oxonorborn-1-yl)ethanone (**1**). Dehydrobromination of *exo*-2-bromonorbornane-1-acetic acid and dehydration of 2-hydroxy-norbornane-2-acetic acid derivatives gave 1-(norborn-2-ylidene)acetic acid derivatives to the exclusion of norborn-2-ene-1-acetic acid derivatives. Treatment of *exo*-5-acetyloxy-2-norobornanone (**52**) with ethyl bromoacetate and zinc gave ethyl *exo*-5-acetyloxy-2-hydroxynorbornane-*exo*- and *endo*-2-acetate (**53** and **54**). Reaction of **53** with hydrogen bromide gave initially ethyl *endo*-3-acetyloxy-*exo*-6-bromonorbornane-1-acetate (**59**), which was subsequently converted to a mixture of **59** and its *exo*-3-acetyloxy epimer **61**. Catalytic hydrogenation of this mixture gave a mixture of ethyl *endo*- and *exo*-3-acetyloxynorbornane-1-acetate (**62** and **63**). Basic hydrolysis of this gave a mixture of the corresponding hydroxy acids, **70** and **71**; the former was slowly converted to the latter at pH 5. Oxidation of the mixture of **70** and **71** gave 3-oxonorbornane-1-acetic acid (**72**). Treatment of the mixture with methyllithium as for **16** gave a mixture of 1-(*endo*- and *exo*-3-hydroxynorborn-1-yl)-2-propanone (**73** and **74**), which was oxidized to 1-(3-oxonorborn-1-yl)-2-propanone (**2**). Reaction of *exo*-2-hydroxynorbornane-1-acetic acid lactone (**75**) with methyllithium in ether gave (1-(*exo*-2-hydroxynorborn-1-yl)-2-propanone (**76**), which on oxidation gave the 2-oxo isomer **78** of **2**.

PETER YATES et MAGDY KALDAS. Can. J. Chem. **70**, 1492 (1992).

Le traitement de l'acide norborn-2-ène-1-carboxylique (**7**) par un équivalent de méthyllithium dans l'éther, suivi par un deuxième équivalent molaire après dilution avec du tétrahydrofurane, fournit de la 1-(norborn-2-èn-1-yl) éthanone (**10**) et que des traces de l'alcool tertiaire **11**. La réaction du produit **7** avec de l'acide formique, suivie d'une hydrolyse, fournit un mélange 4 : 3 des acides *exo*-3- et *exo*-2-hydroxynorbornane-1-carboxyliques (**16** et **17**) alors que l'oxymercuration suivie d'une démercuration ne donne que l'isomère *exo*-3-hydroxy **16**. Les oxydations des produits **16** et **17** conduisent respectivement aux acides 3- et 2-oxonorbornane-1-carboxyliques (**27** et **29**). L'oxymercuration–démercuration de **10** fournit exclusivement de la 1-(*exo*-3-hydroxynorborn-1-yl)éthanone (**30**) que l'on a aussi préparée par traitement du composé **16** avec du méthyllithium d'une façon analogue à celle utilisée pour transformer le composé **7** et **10**. L'oxydation de **30** fournit d la 1-(3-oxonorborn-1-yl)éthanone (**1**). L'enlèvement d'acide bromhydrique de l'acide *exo*-2-bromonorbornane-1-acétique et la déshydratation de dérivés de l'acide 2-hydroxy-norbornane-2-acétique fournit des dérivés de l'acide 1-(norborn-2-ylidène)acétique à l'exclusion de dérivés de l'acide norborn-2-ène-1-acétique. Le traitement de la *exo*-5-acétyloxy-norbornan-2-one (**52**) avec du bromoacétate d'éthyle et du zinc fournit des *exo*-5-acétyloxy-2-hydroxynorbornane-*exo*- et *endo*-2-acétates d'éthyle (**53** et **54**). La réaction du produit **53** avec du bromure d'hydrogène fournit initialement du *endo*-3-acyloxy-*exo*-6-bromonorbornane-1-acétate d'éthyle (**59**) qui se transforme subséquemment en un mélange du produit **59** et de son épimère *exo*-3-acétyloxy **61**. L'hydrogenation catalytique de ce mélange fournit un mélange des *endo*- et *exo*-3-acétyloxynorbornane-1-acétates d'éthyle (**62** et **63**). L'hydrolyse basique de ce mélange fournit un mélange des hydroxy-acides correspondants, **70** et **71**; à un pH de 5, le premier se transforme lentement vers le second. Une oxydation du mélange de **70** et de **71** fournit de l'acide 3-oxonorbornane-1-acétique (**72**). Le traitement du mélange avec un méthyllithium, suivant une procédure analogue à celle utilisée pour le composé **16**, fournit un mélange des 1-(*endo*- et *exo*-3-hydroxynorborn-1-yl) propan-2-ones (**73** et **74**) que l'on peut oxyder en 1-(3-oxonorbornyl-1-yl) propan-2-one (**2**). Le réaction de la lactone de l'acide *exo*-2-hydroxynorbornane-1-acétique (**75**) avec du méthyllithium dans l'éther donne de la 1-(*exo*-2-hydroxynorborn-1-yl) propan-2-one (**76**), qui par oxydation conduit à l'isomère 2-oxo **78** du produit **2**.

[Traduit par la rédaction]

In the course of our studies of the photochemistry of norbornanones (bicyclo[2.2.1]heptanones) (1), we undertook the synthesis of the diketones, 1-(3-oxonorborn-1-yl)ethanone (**1**) and 1-(3-oxonorborn-1-yl)-2-propanone (**2**). These relatively simple molecules turned out to be more difficult of access than we had anticipated. However, in the course of our synthetic investigations we made a number of observations of intrinsic interest, which we now report. The structures of compounds **1** and **2** and their precursors[1] follow from their elemental composition and methods of preparation, and from their spectra and the relationship of these to the spectra of related compounds (see Experimental).[2]

[1]All products are racemic and their structures are drawn without any implication of their absolute configurations.

[2]Their ^{13}C nmr spectra will be discussed elsewhere.

Can. J. Chem. Downloaded from www.nrcresearchpress.com by 217.78.4.112 on 09/08/12
For personal use only.

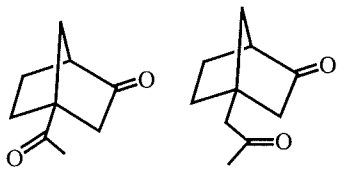

1 2

1-(3-Oxonorborn-1-yl)ethanone (1)

Of the relatively few known norbornane derivatives with a functionalized carbon substituent at a bridgehead, we chose 2-norbornene-1-carboxylic acid (**7**) as the starting material. This was prepared by the method of Wilt *et al.* (2) from *exo*-2-bromonorbornane-1-carboxylic acid (**5**), itself prepared from the diastereomeric mixture of norbornane-2-carboxylic acids (**4**) obtained on hydrogenation of the Diels–Alder adducts **3** of acrylic acid and cyclopentandiene (3) (Scheme 1). A key step in this sequence is the skeletal rearrangement in the bromination of **4** to give **5** (cf. ref. 4). The final dehydrobromination of the ester **6** followed by hydrolysis gives a mixture of the desired product **7** and the retro-rearrangement product **8** (cf. refs. 3 and 5). We found that the ratio of these products is critically dependent on the quality of the potassium *tert*-butoxide used in the dehydrobromination. When commerical potassium *tert*-butoxide was used, only compound **8** was isolated: when freshly prepared potassium *tert*-butoxide was used under scrupulously anhydrous conditions compound **7** was obtained to the virtual exclusion of **8**. We also found, as did Wilt *et al.* (2), that treatment of the bromo acid **5** with potassium *tert*-butoxide under anhydrous conditions gave predominantly the rearranged acid **8**, and thus it appears that the formation of **8** from **6** results from hydrolysis of the latter to **5** by potassium hydroxide in the commerical potassium *tert*-butoxide. Facilitation of rearrangement in the acid can be interpreted as resulting from stabilization of the transition state **9** by the carboxylate ion (Scheme 2).[3]

In our first route for the conversion of **7** to the target **1**, we investigated its conversion to 1-(norborn-2-en-1-yl)ethanone (**10**). Treatment with two molar equivalents of methyllithium in ether gave a 10:3 mixture of **10** and a tertiary alcohol that was not fully characterized, but which is considered to be **11** (Scheme 3). Although several of the modifications that are known to minimize the formation of the tertiary alcohol by-product (6) were exercised, formation of **11** could not be avoided. However, the use of tetrahydrofuran as solvent in the reaction with the second molar equivalent of methyllithium solved the problem. Our procedure involved addition of the first molar equivalent of methyllithium under minimun solvation conditions, i.e., with enough ether to dissolve **7** but not its lithium salt **12**, thus allowing the latter to precipitate, thereby rendering it relatively unreactive. After gas evolution had ceased, a second molar equivalent of ethereal methyllithium was added followed by tetrahydrofuran, which immediately dissolved **12**, and complete reaction was rapidly achieved to give what is presumed to be **13**. Aqueous acid work-up gave **10** containing only a trace of **11**; distillation provided pure **10** in 93% yield.

In a second route for the conversion of **7** to **1** we investigated the hydration of its ethylenic double bond. We considered that the use of methods involving cationic intermediates would favor the formation of the desired 3-hydroxy relative to the 2-hydroxy products because formation of an intermediate of type **14** rather than **15** would be preferred owing to the greater electrostatic destabilization by the carboxyl group in the latter. Treatment of **7** with formic acid gave a mixture of formates that, on basic hydrolysis, afforded a 4:3 mixture of *exo*-3-hydroxy-norbornane-1-carboxylic acid (**16**) and the known (5, 7) *exo*-2-hydroxy-norbornane-1-carboxylic acid (**17**) (Scheme 4). Although this reaction was highly stereoselective, its regioselectivity is poor, albeit qualitatively in accord with expectation. The reaction of **7** with mercuric acetate followed by sodium hydroxide and sodium borohydride was next examined. Oxymercuration–demercuration occurred very rapidly with both high stereoselectivity and high regioselectivity to give the *exo*-3-hydroxy compound **16** as the sole product (Scheme 4). The stereoselectivity is in accord with previous observations of *exo* nucleophilic attack on norbornyl cations (8). Brown *et al.* (9), for example, have previously observed high *exo* stereoselectivity in the addition of hydroxide ion to the intermediate **19**, formed on mercuration of 1-methyl-2-norbornene (**18**), to give **20** and **21** (Scheme 5). No significant regioselectivity was observed in this case. We consider that the high regioselectivity in the present case reflects both an electrostatic preference for **22** over **23** (cf. **14** vs. **15**) and interaction between the

[3]Alternatively, α- or β-lactonic intermediates may be involved (cf. ref. 2).

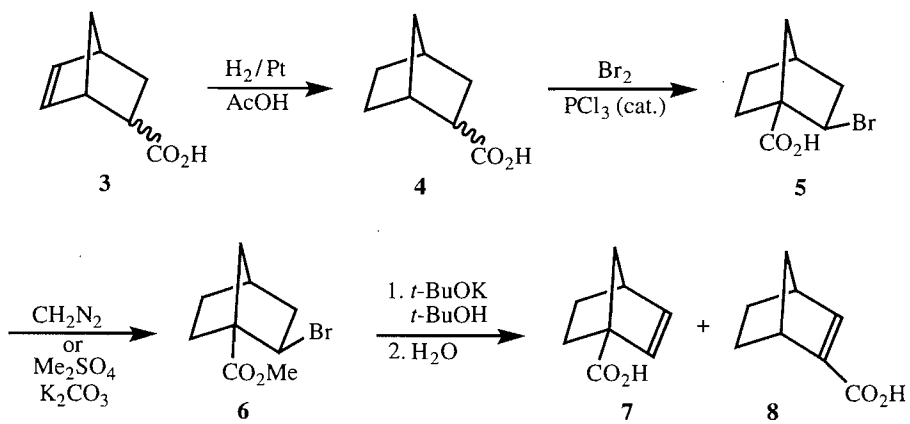

SCHEME 1

Can. J. Chem. Downloaded from www.nrcresearchpress.com by 217.78.4.112 on 09/08/12
For personal use only.

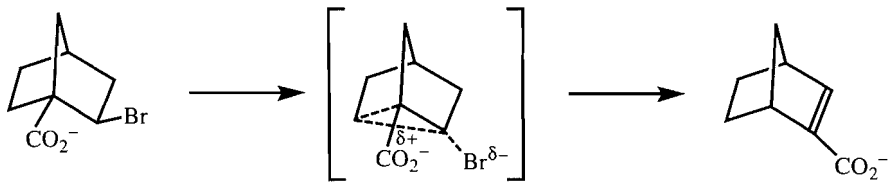

9

SCHEME 2

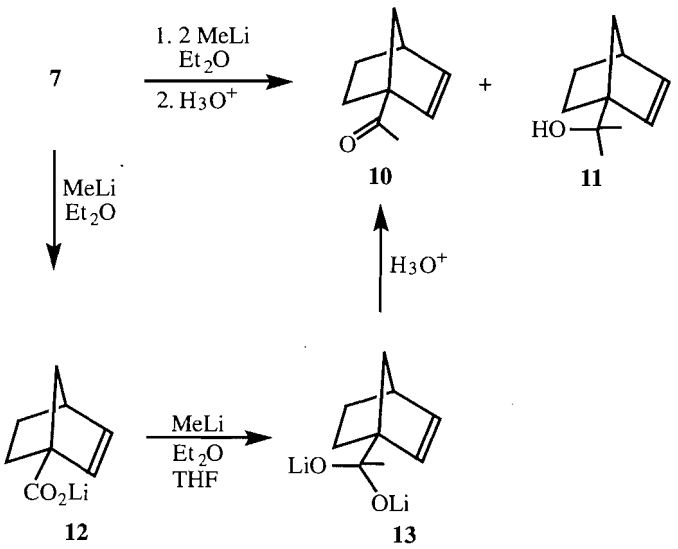

SCHEME 3

carbonyl group and mercury as in **24**.[4] That the hydroxyl group of the carboxylic acid **7** is not involved as such in this effect was established by the demonstration that **25**, the *tert*-butyl ester of **7**, prepared by treatment of the bromo methyl ester **6** with potassim *tert*-butoxide and *tert*-butyl alcohol (2), gave the *exo*-3-hydroxy ester **26** (Scheme 6) with high regioselectivity and stereoselectivity upon oxymercuration–demercuration.

Oxidation of *exo*-3-hydroxynorbornane-1-carboxylic acid (**16**) and its *tert*-butyl ester **26** with chromic acid and aqueous sulfuric acid in acetone (Jones reagent) gave 3-oxonorbornane-1-carboxylic acid (**27**) and its *tert*-butyl ester **28**, respectively. For comparison, the known 2-oxonorbornane-1-carboxylic acid **29** (5, 7) was prepared by Jones oxidation (11) of the 2-hydroxy acid **17**, itself prepared by treatment of the bromo acid **5** with aqueous acid (Scheme 6).

The two routes now converged on the target, 1-(3-oxonorborn-1-yl)ethanone (**1**). 1-(Norborn-2-en-1-yl)ethanone (**10**) on oxymercuration–demercuration gave exclusively 1-(*exo*-3-hydroxynorborn-1-yl)ethanone (**30**), which on oxidation with Jones reagent gave **1**. Compound **16** on treatment with two molar equivalents of methyllithium in ether followed by one equivalent in tetrahydrofuran in analogous fashion to the conversion of **7** to **10**, also gave **30** (Scheme 7).

[4]For a discussion of the effect of other C-1 substituents on the regioselectivity in the oxymercuration–demercuration and formylation of 2-norbornenes, see ref. 10.

1-(3-Oxonorborn-1-yl)-2-propanone (2)

In our initial approaches to the synthesis of the diketone **2** we sought to employ intermediates that we have utilized in the synthesis of **1**. The hydroxyl group of the hydroxy acid **16** was protected by conversion of the latter to *exo*-3-acetyloxynorbornane-1-carboxylic acid (**31**) by treatment with acetic anhydride, 4-(dimethylamino)pyridine, and triethylamine preparatory to attempting an Arndt–Esitert homologation to **32**. However, this sequence foundered when **31** could not be converted to its acid chloride **33** with oxalyl chloride, giving instead the acid anhydride **34**. An Arndt–Eistert homologation of *exo*-2-bromonorbornane-1-carboxylic acid (**5**) to **35** was also undertaken in the hope that the latter could be converted to 2-norbornene-1-acetic acid (**36**).[5] Here there was no problem in preparing the acid chloride **37**, which had been prepared previously (12), by treatment of **35** with oxalyl chloride, but attempted conversion of this with diazomethane to the α-diazo ketone **38** gave a mixture of products; this approach was discontinued owing to the difficulty of separating the components of this mixture.

We next investigated the utilization of ethyl *exo*-2-bromonorbornane-1-acetate (**39**), which is was planned to convert to the unsaturated ester **40**. The mixture of diastereomeric ethyl 2-hydroxynorbornane-2-carboxylates (**41**) prepared by the Reformatsky reaction of 2-norbornanone with ethyl bromoacetate and zinc (13), on treatment with hydrogen bromide in acetic acid gave **39** as the major product, accompanied by the corresponding bromo acid **35**, which is also obtained on hydrolysis of **39** with aqueous acid (Scheme 8). These reactions, which find analogy in the conversion of camphene-8-carboxylic acid (**42**) to the chloro acid **43** on treatment with hydrogen chloride (14) (cf. ref. 15), must proceed via Wagner–Meerwein rearrangement as in **44**. Treatment of **39** with potassium *tert*-butoxide in *tert*-butyl alcohol followed by hydrolysis gave a mixture of the rearranged dehydrobromination products (*E*)- and (*Z*)-(norborn-1-ylidene)acetic acid (**45** and **46**). These were formed in higher yield when **39** was treated with ethanolic sodium ethoxide followed by hydrolysis. In this case a third, unconjugated unsaturated acid was detected, which is considered to be **47**. Compounds **45** and **46** and their ethyl esters **48** and **49** are also formed on treatment of **35** and **41** with bases (Scheme 8). Compound **48** had been obtained previously in low yield by metalation of norcamphene (**50**) with amylsodium followed by carboxylation (16) (cf., also, ref. 17), and esters **48** and **49** by a Wittig reaction of 2-norbornanone (18).

[5]Wilt *et al.* (2) had previously prepared **36** by the Arndt–Eistert homologation of **7**; however, the modesty of the overall yield (15%) led us to seek other methods for its preparation.

Can. J. Chem. Downloaded from www.nrcresearchpress.com by 217.78.4.112 on 09/08/12
For personal use only.

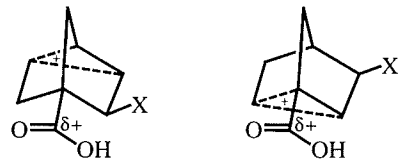

14 X = H
22 X = HgOAc

15 X = H
23 X = HgOAc

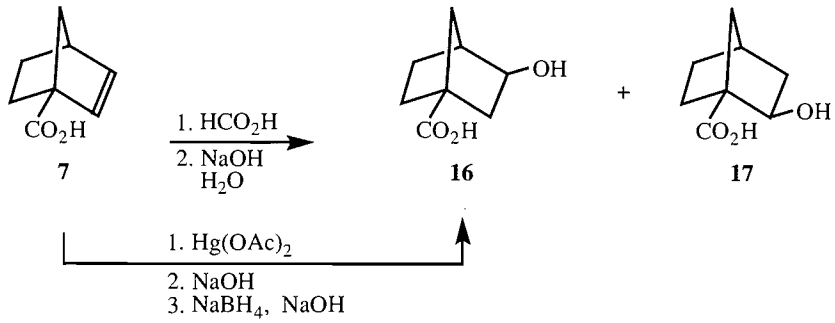

7 **16** **17**

SCHEME 4

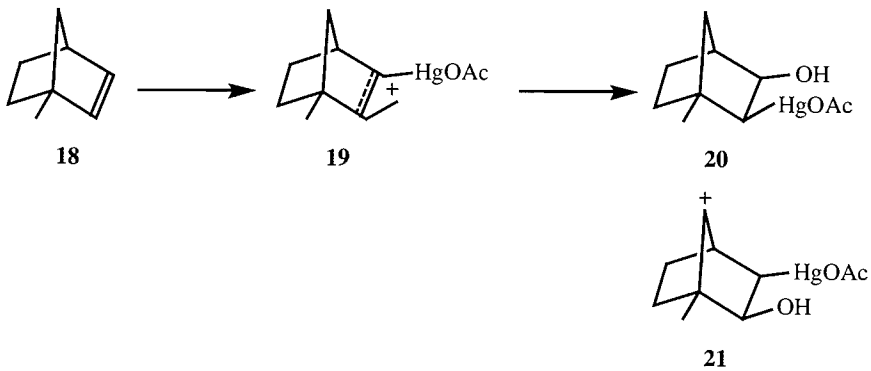

18 **19** **20** **21**

SCHEME 5

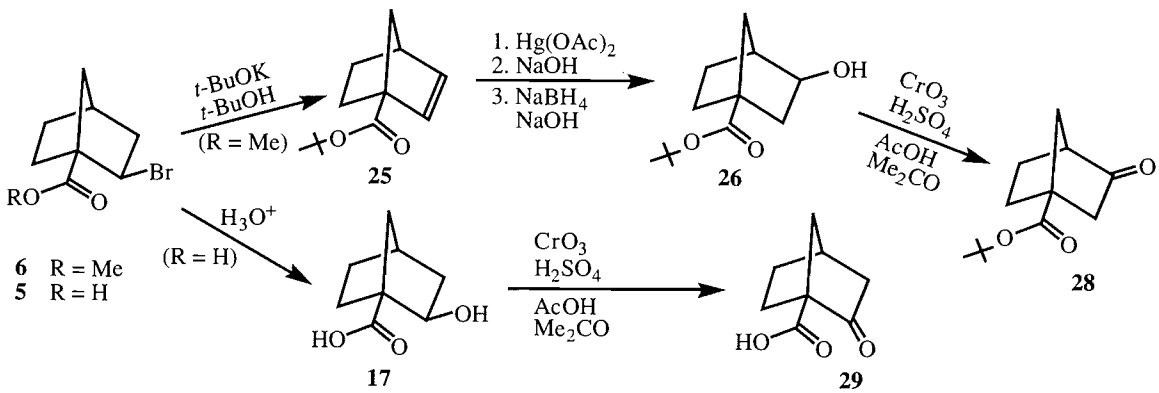

6 R = Me
5 R = H

25 **26** **28** **17** **29**

SCHEME 6

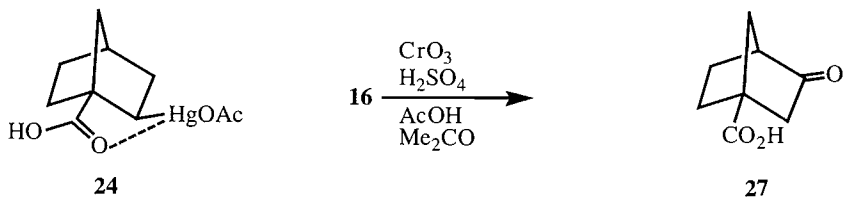

24 **27**

Can. J. Chem. Downloaded from www.nrcresearchpress.com by 217.78.4.112 on 09/08/12
For personal use only.

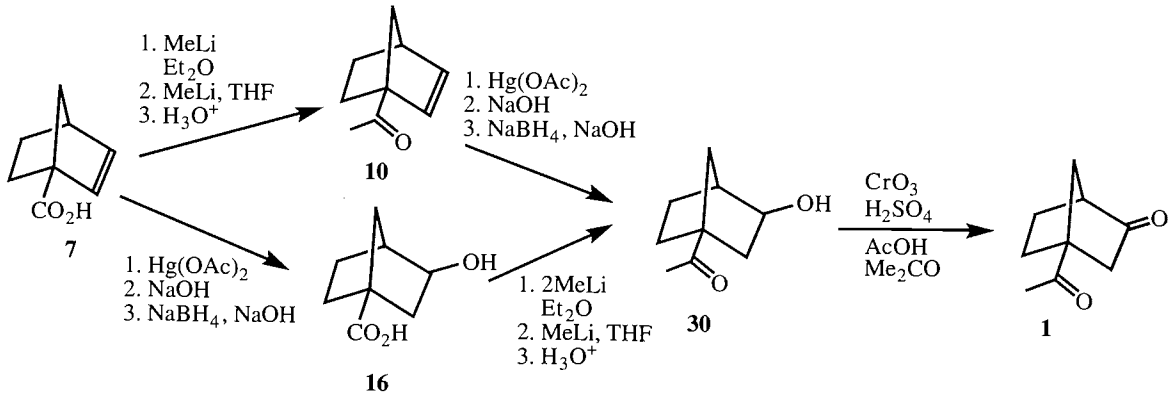

SCHEME 7

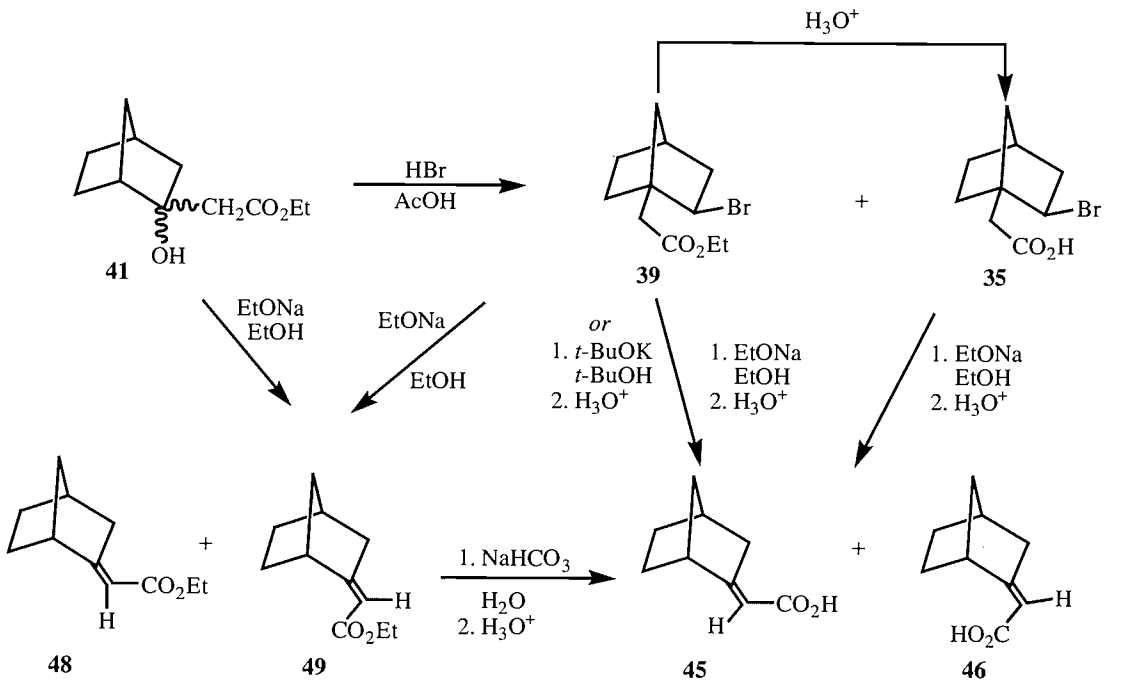

SCHEME 8

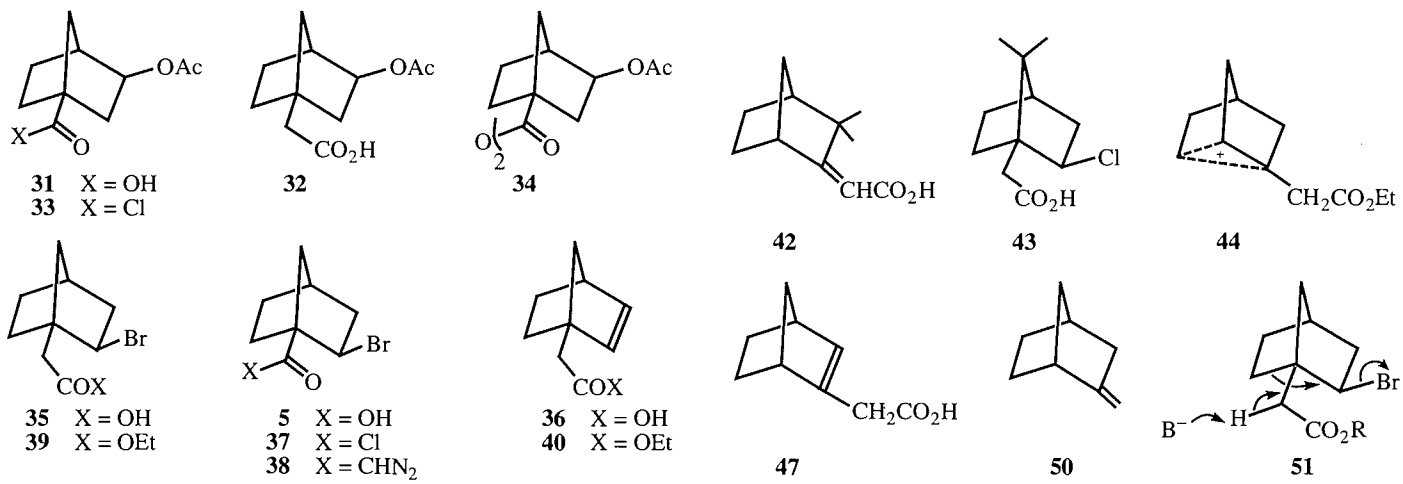

Can. J. Chem. Downloaded from www.nrcresearchpress.com by 217.78.4.112 on 09/08/12
For personal use only.

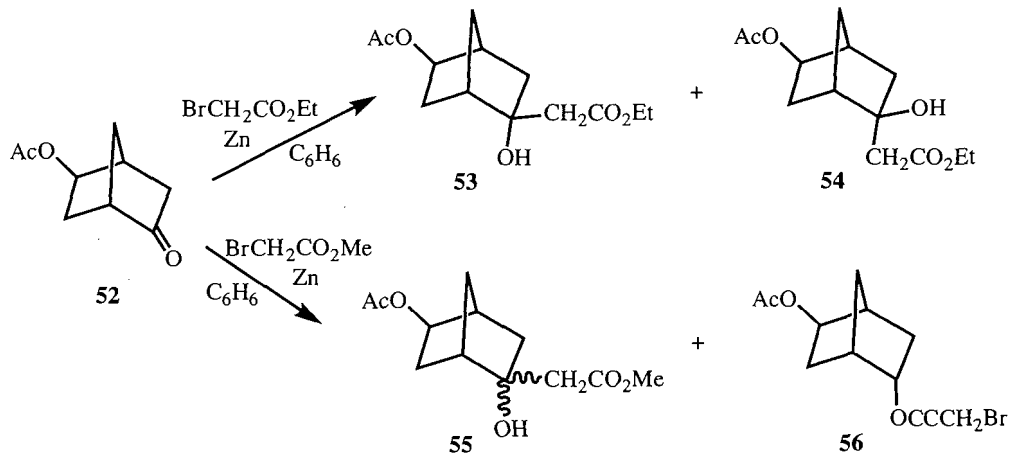

SCHEME 9

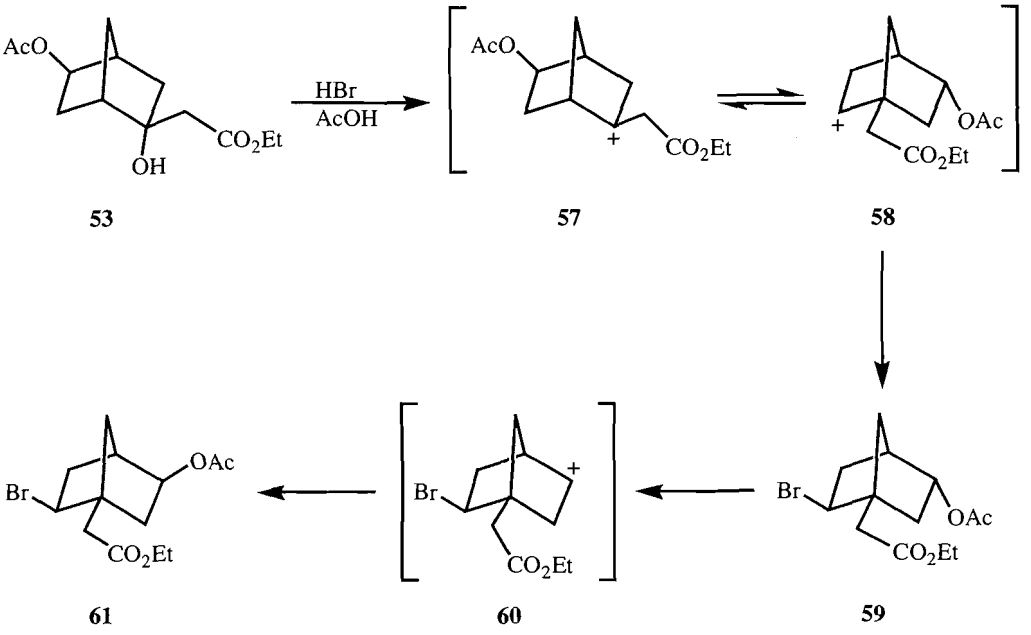

SCHEME 10

The rearrangement during dehydrobromination of halo acids and esters of these types to norborn-2-ylidene derivatives can be interpreted in terms of processes of the kind shown in **51**, facilitated by conjugation of the developing ethylenic double bond with the carbonyl group. The overall sequences **41** → **39** (**35**) → **48**, **49** (**45**, **46**) represent rearrangement – retro-rearrangement processes analogous to the sequence **4** → **5** → **8** and this type of route is not applicable to the synthesis of **2**.

In devising a different approach to **2** we sought a strategy that avoided dehydrobromination. This led us to investigate the Reformatsky reaction of *exo*-5-acetyloxy-2-norbornanone (**52**) (19). Reaction with ethyl bromoacetate and zinc gave a mixture of ethyl 2-hydroxynorbornane-*exo*- and *endo*-2-acetates (**53** and **54**), from which the major component could be isolated in 57% yield by fractional distillation (Scheme 9). This is considered to be **53** on the ground that attack of the Reformatsky reagent would occur preferentially on the less hindered, *exo* face of **52**. When methyl bromoacetate was used in the Reformatsky reaction a third product was obtained in addition to the hydroxy esters **55**. This is considered to be the bromo ester **56**, formed via reduction of **52** followed by transesterification by methyl bromoacetate. The introduction of the freshly activated zinc in small portions at a time and addition of a crystal of iodine increased the **55**:**56** product ratio.

Treatment of the acetyloxy ester **53** with hydrogen bromide gave initially ethyl *endo*-3-acetyloxy-*exo*-6-brononorbornane-1-acetate (**59**), which was partially converted to its *exo*-3-acetyloxy epimer **61** in the presence of hydrogen bromide. These products are considered to arise via Wagner–Meerwein rearrangement of cation **57** to **58** and by slower conversion of **59** to the cation **60** and reaction of this to give **61** (Scheme 10).

It was next necessary to remove reductively the bromine from compounds **59** and **61**. Since these are unstable and

Can. J. Chem. Downloaded from www.nrcresearchpress.com by 217.78.4.112 on 09/08/12
For personal use only.

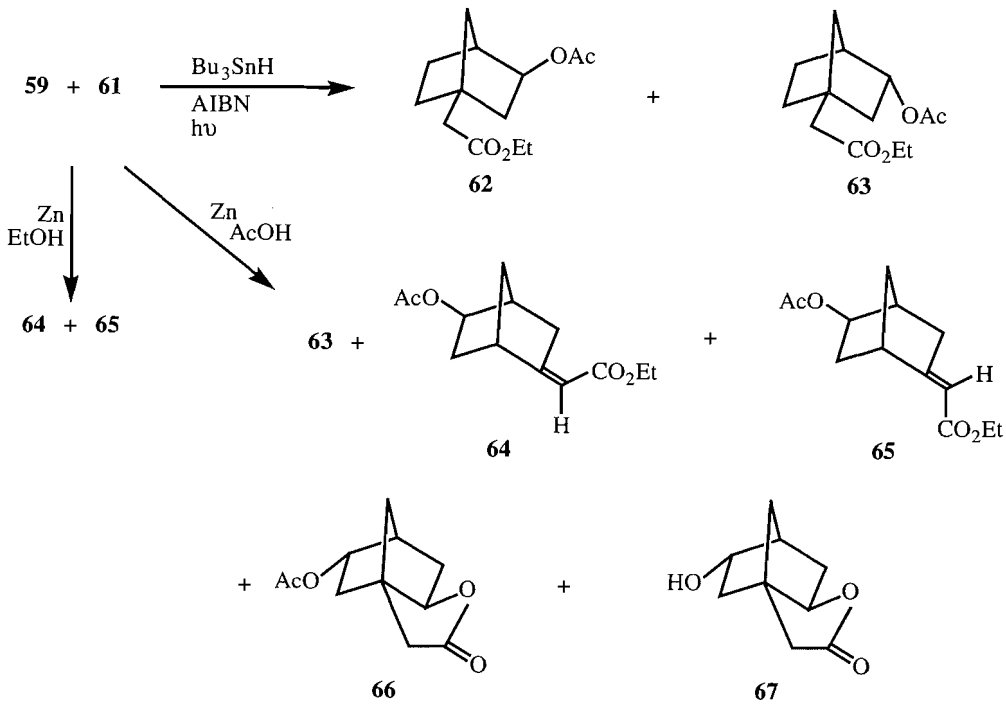

SCHEME 11

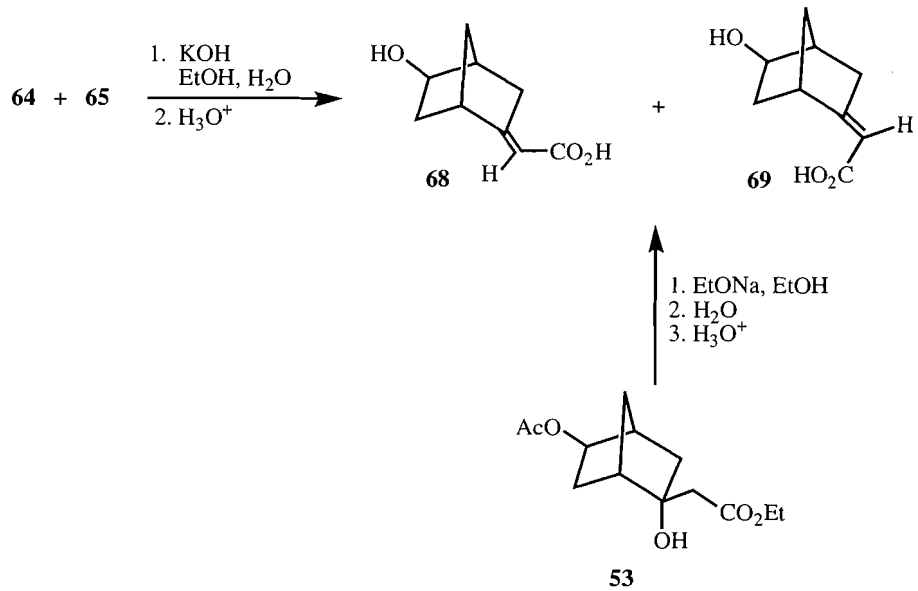

SCHEME 12

decompose on standing at room temperature their separation was not attempted; this did not present a problem, other than complicating spectroscopic interpretations, since the acetyloxy groups were eventually destined to be converted to a carbonyl group. Reduction of the mixture with tributyltin hydride initiated by photolysis of azobisisobutyronitrile (AIBN) (20) gave a mixture of the desired products, ethyl *exo*- and *endo*-3-hydroxynorbornane-1-acetate (**62** and **63**); however, these were accompanied by other products and were difficult to purify. Treatment of the mixture of **59** and **61** with freshly activated zinc and acetic acid gave **63**, together with ethyl (*E*)- and (*Z*)-2-(*exo*-5-acetyloxynorborn-2-ylidene)-acetate (**64** and **65**), and two lactones, which are tentatively assigned structures **66** and **67** (Scheme 11). Treatment of the mixture of **59** and **61** with zinc and ethanol gave only **64** and **65**. Hydrolysis of this mixture with aqueous ethanolic potassium hydroxide gave a mixture of the unsaturated hydroxy acids **68** and **69** whose spectra were identical with those of a mixture of **68** and **69** obtained by treatment of **53** with ethanolic sodium ethoxide followed by hydrolysis (Scheme 12).

The method of choice for the reduction of the mixture of **59** and **61** to the desired acetyloxy esters **62** and **63** was discovered to be catalytic hydrogenation (Scheme 13). The

Can. J. Chem. Downloaded from www.nrcresearchpress.com by 217.78.4.112 on 09/08/12
For personal use only.

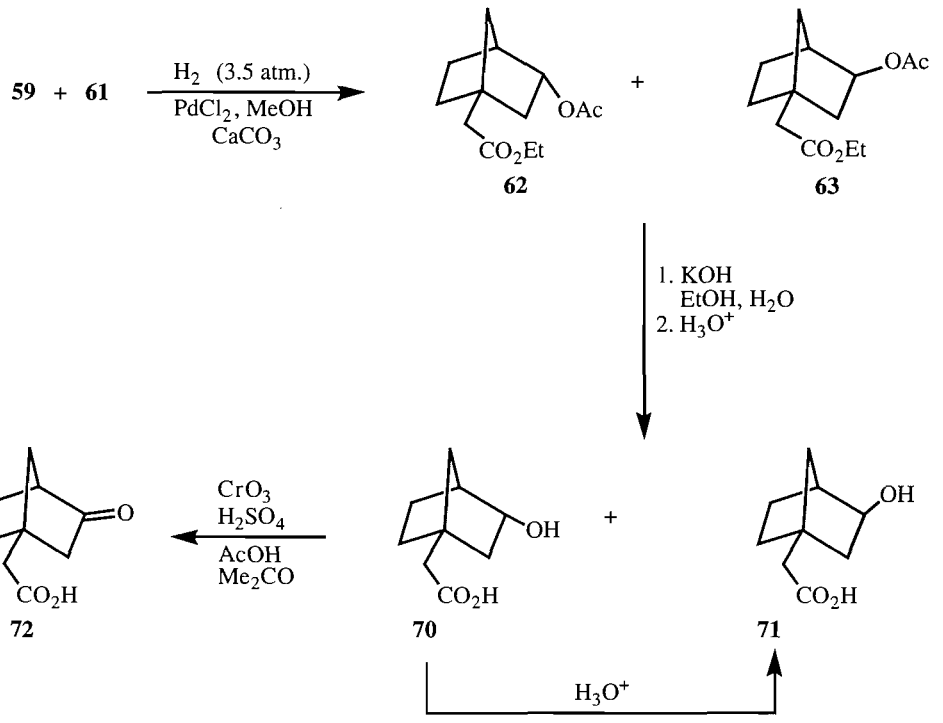

SCHEME 13

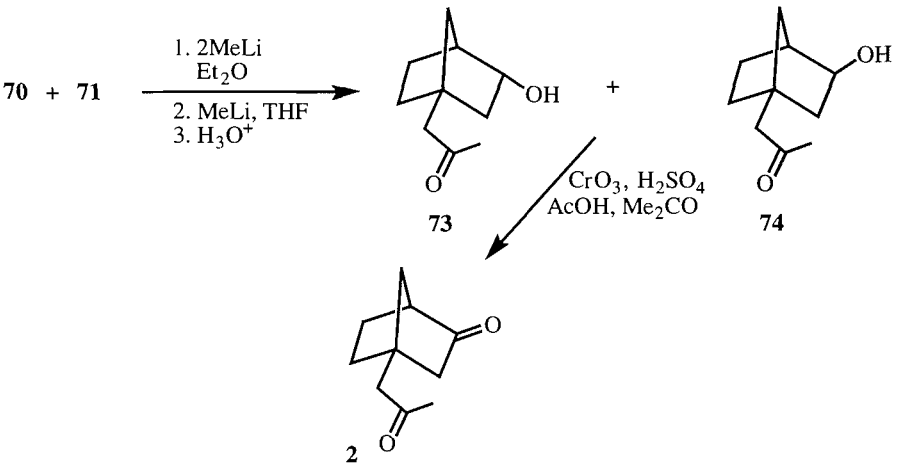

SCHEME 14

latter mixture was hydrolyzed by base to give a mixture of *endo*- and *exo*-3-hydroxynorbornane-1-acetic acids (**70** and **71**). Treatment of this mixture with dilute hydrochloric acid at pH 5 slowly converted the *endo* isomer **70** to the *exo* isomer **71**, presumably via carbonium ion formation (cf. **59** → **61** via **60**). This permitted the isolation of the pure *exo* isomer **17**; after treatment for 3 days at pH 5 crystallization gave **71** in 53% yield. Oxidation of the mixture of **70** and **71** with Jones reagent gave a single keto acid, 3-oxonorbornane-1-acetic acid (**72**).

The synthesis of 1-(3-oxonorborn-1-yl)-2-propanone (**2**) was now completed by reaction of the mixture of hydroxy acids **70** and **71** with three molar equivalents of methyllithium in ether and tetrahydrofuran as in the case of **16** to give a mixture of 1-(*endo*- and *exo*-3-hydroxynorborn-1-yl)-2-propanone (**73** and **74**), and oxidation of this with Jones reagent (Scheme 14; our overall synthetic route to **2** is summarized in Scheme 15).

For the purpose of spectroscopic comparison the 2-keto isomer of **7**, 1-(2-oxonorborn-1-yl-2-propanone (**78**), was prepared via treatment of the lactone **75** with methyllithium in ether to give a mixture of 1-(*exo*-2-hydroxy-norborn-1-yl)-2-propanone (**76**) and the diol **77**. These were separated and oxidized individually with Jones reagent to give **78** and the hydroxy ketone **79** (Scheme 16).

Experimental

Melting points were taken with a Fisher–Johns melting point apparatus and are uncorrected. The ir spectra were recorded in chloroform and the ^{1}H nmr spectra were recorded at 60 MHz in deuterochloroform. Low-resolution mass spectra were recorded with a Bell and Howell CEC 21-490 mass spectrometer and Exact Mass

Can. J. Chem. Downloaded from www.nrcresearchpress.com by 217.78.4.112 on 09/08/12
For personal use only.

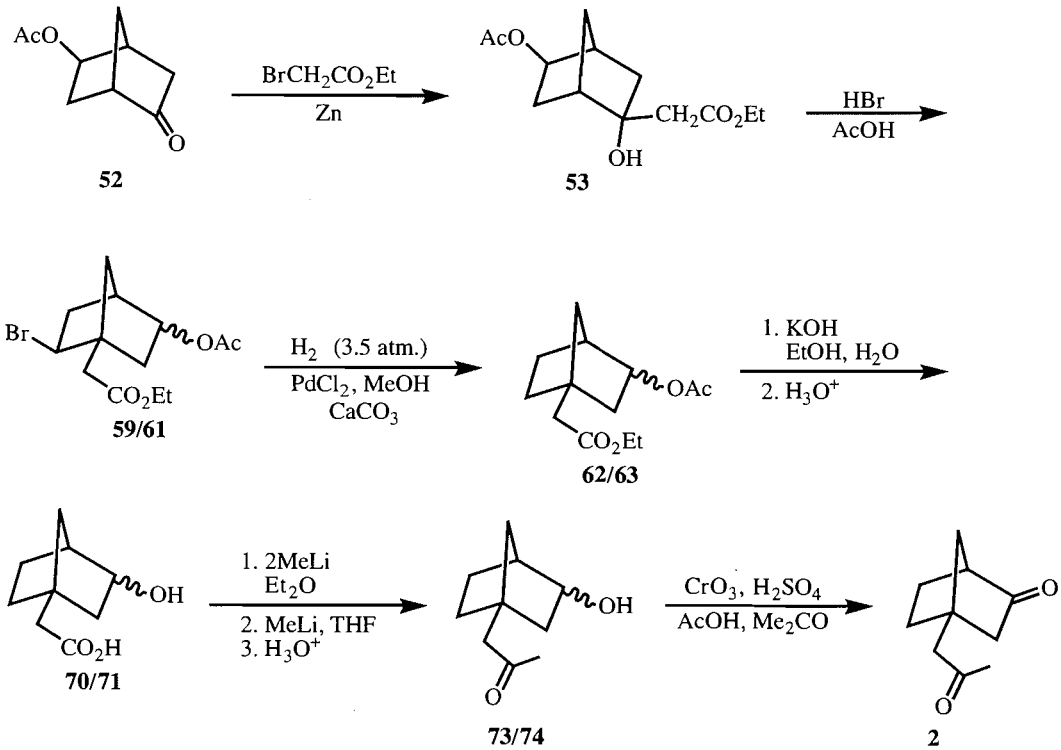

SCHEME 15

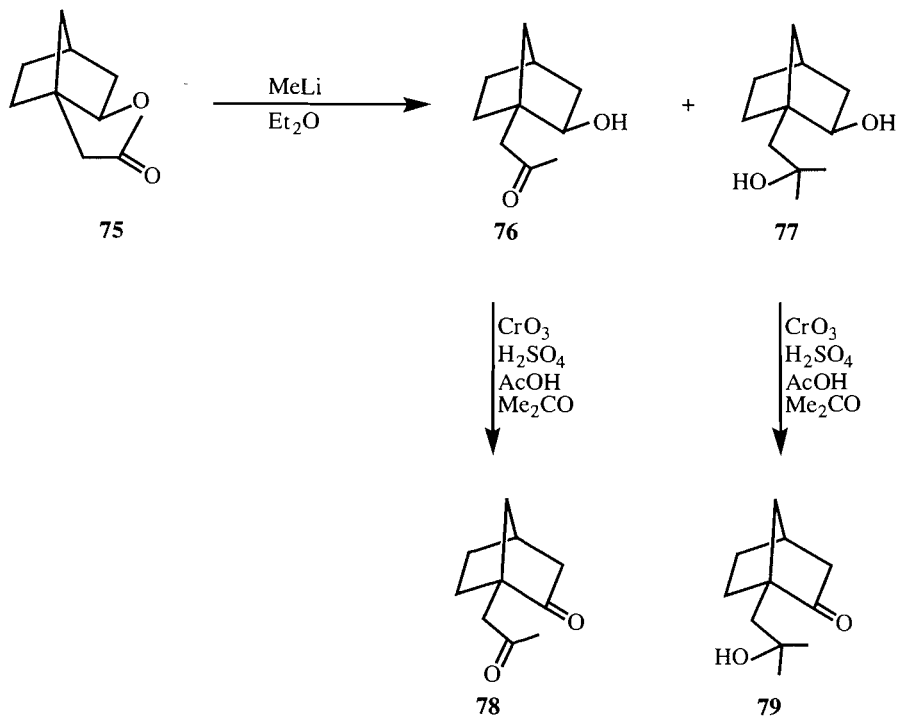

SCHEME 16

measurements were made with an AEI MS-902 spectrometer on samples whose homogeneity had been established by ^1H nmr spectroscopy and (or) thin-layer chromatography. Solutions in organic solvents were dried over anhydrous sodium sulfate and concentrated on a rotary evaporator under water-aspirator pressure.

Treatment of 2-norbornene-1-carboxylic acid (7) with methyllithium. Formation of 1-(norborn-2-en-1-yl)ethanone (10)

2-Norbornene-1-carboxylic acd (**7**) was prepared by treatment of methyl *exo*-2-bromonorbornane-1-carboxylate (**6**) with freshly

Can. J. Chem. Downloaded from www.nrcresearchpress.com by 217.78.4.112 on 09/08/12
For personal use only.

Can. J. Chem. Downloaded from www.nrcresearchpress.com by 217.78.4.112 on 09/08/12
For personal use only.

prepared potassium *tert*-butoxide in *tert*-butyl alcohol under scrupulously anhydrous conditions followed by basic hydrolysis (2).

(*i*) Under anhydrous conditions a solution of **7** (690 mg, 5.00 mmol) in ether (20 mL) was cooled in an ice bath and stirred as a solution of methyllithium (1.3 M in ether; 10 mmol) was added dropwise over ca. 90 min. The temperature was raised slowly to room temperature and the solution was stirred for 10 h. The reaction mixture was poured into cold 4 N hydrochloric acid (300 mL). Additional ether (300 mL) was added and the ether layer was washed with aqueous 5% sodium bicarbonate (100 mL) and water (3 × 50 mL), dried, and concentrated under reduced pressure to give a yellow oil (655 mg), which was found by ^{1}H nmr spectroscopy to be a 10:3 mixture of **10** and an alcohol considered to be 1-(2-norbornenyl)-1-methylethanol (**11**). The crude product was chromatographed on a column of Florisil that had been packed in chloroform–benzene (1:1). Elution with the same solvent afforded ketone **10** (354 mg, 52%) as a colorless oil. Molecular distillation (63–64°C, 0.025 Torr) (1 Torr = 133.3 Pa) gave an analytical sample; ir ν_{max}: 1700 (s) cm^{-1}; ^{1}H nmr δ: 0.80–2.15 (m, 6H), 2.24 (s, 3H), 2.9 (m, 1H), 6.15 (m, 2H); ms *m/z*: 136 (25) M$^+$). Anal. calcd. for $C_9H_{12}O$: C 79.37, H 8.83; found: C 79.05, H 9.10.

(*ii*) Under anhydrous conditions **7** (690 mg, 5.00 mmol) was stirred while a solution of methyllithium (1.38 M in ether; 5.00 mmol) was added dropwise at room temperature. The mixture was occasionally warmed in a water bath (40°C). After the evolution of gas had ceased, methyllithium (1.38 M in ether; 5 mmol) was added dropwise at room temperature and stirring was continued for 3 h. Tetrahydrofuran (20 mL) was added to the stirred solution via a syringe. After 1 h the reaction mixture was poured into well-stirred hydrochloric acid – ice–water (pH 2; 750 mL). The combined mixture was thoroughly extracted with ether (5 × 100 mL). The combined ether layers were washed with aqueous 5% sodium bicarbonate (100 mL) and water (2 × 50 mL), dried, and concentrated under reduced pressure to give a pale yellow oil that was molecularly distilled (60–65°C, 0.03 Torr) to give the ketone **10** (531 mg, 78%) as a colorless oil. Its spectral data were identical with those of **10** obtained by procedure (*i*) above.

Treatment of **7** *with formic acid followed by basic hydrolysis. Formation of* exo-*3-hydroxynorbornane-1-carboxylic acid* (**16**) *and* exo-*2-hydroxynorbornane-1-carboxylic acid* (**17**)

A solution of acid **7** (500 mg, 3.6 mmol) in 90% formic acid (15 mL) was boiled under reflux for 12 h. The solution was cooled, poured into water (15 mL), and distilled to remove formic acid and water. Distillation of the residue afforded a mixture (510 mg, 77%) of *exo*-3- and *exo*-2-formyloxynorbornane-1-carboxylic acid; ^{1}H nmr δ: 1.24–2.13 (m, 9H), 2.44 (m, 1H), 4.90 (m, 1H), 8.00 (s, 1H), 10.92 (s, 1H; absent after D_2O treatment); ms *m/z*: 184 (5), (M$^+$).

To a solution of the mixture (510 mg, 2.77 mmol) in ethanol (30 mL) and water (3 mL) potassium hydroxide (6 g) was added and the solution was heated on a steam bath for 3 h; it was then diluted with water (150 mL) and distilled until the temperature reached 98°C. The distillate was cooled in an ice bath and acidified with concentrated hydrochloric acid. The solution was extracted with ethyl acetate (2 × 100 mL), and the combined extracts were washed with water (2 × 100 mL), dried, and concentrated under reduced pressure to give a mixture of the hydroxy acids **16** and **17** as a viscous yellow oil that solidified on standing (294 mg, 68%); mp 105–112°C; ir ν_{max}: 3450–2380 (br, m), 1698 (s) cm^{-1}; ^{1}H nmr δ: 1.25–2.61 (m, 9H), 3.94 (m, 1H), 7.34 (br s,; absent after D_2O treatment; 2H); ms *m/z*: 156 (10) (M$^+$). Crystallization from ether gave **16** (134 mg, 31%), mp 118–119.5°C, whose ir, ^{1}H nmr, and mass spectra were identical with those of a sample of **16** prepared by oxymercuration–demercuration of **7** (*vide infra*).

Oxymercuration–demercuration of **7**. *Formation of* exo-*3-hydroxynorbornane-1-carboxylic acid* (**16**)

To a stirred mixture of mercuric acetate (3.19 g, 10.00 mmol) in water (10 mL) and tetrahydrofuran (10 mL) was added **7** (1.38 g, 10.00 mmol), and the mixture was stirred for 10 min at room temperature by which time the oxymercuration was complete. Aqueous sodium hydroxide (3 M, 10 mL) was added followed by a solution of sodium borohydride (0.5 M in 3 M aqueous NaOH, 10 mL). Reduction of the oxymercurial was almost instantaneous. The mercury was allowed to settle and was separated, and the aqueous layer was cooled, acidified with 6 N hydrochloric acid, saturated with sodium chloride, and extracted with ethyl acetate (3 × 25 mL). The ethyl acetate extracts were dried and concentrated under reduced pressure. The residue was crystallized from dichloromethane–ether to give **16** (889 mg, 57%) as colorless plates, mp 118–119.5°C; ir ν_{max}: 3450–2470 (m), 1700 (s) cm^{-1}; ^{1}H nmr δ: 1.00–2.09 (m, 9H), 2.26 (m, 1H), 3.90 (d of m, J_{app} 5 Hz, 1H, 7.43 (s, 2H; absent after D_2O treatment); ms *m/z*: 156 (12) (M$^+$). Anal. calcd. for $C_8H_{12}O_3$: C 61.52, H 7.74; found: C 61.21, H 7.73.

Oxymercuration–demercuration of tert-*butyl norborn-2-ene-1-carboxylate* (**25**). *Formation of* tert-*butyl* exo-*3-hydroxynorbornane-1-carboxylate* (**26**)

To a stirred mixture of mercuric acetate (3.19 g, 10.00 mmol), water (10 mL), and tetrahydrofuran (20 mL) ester **25** (2), (2.10 g, 10.00 mmol) was added and the mixture was stirred for 10 min at room temperature. Aqueous sodium hyroxide (3 M, 10 mL) was added followed by a solution of sodium borohydride (0.5 M in 3 M aqueous NaOH, 10 mL). Reduction of the oxymercurial was almost instantaneous. The mercury was allowed to settle and removed. Additional tetrahydrofuran (50 mL) was added and the tetrahydrofuran layer was separated and concentrated under reduced pressure. The residue was dissolved in dichloromethane, and the solution was dried and concentrated under reduced pressure to give **26** as a colorless oil (1.93 g, 91%); ir ν_{max}: 3510 (w), 3390 (w), 1720 (s), cm^{-1}; ^{1}H nmr δ: 0.92–2.03 (m, with prominent s at 1.50; 17H), 2.24 (m, 1H), 3.16 (s, 1H; absent after D_2O treatment), 3.86 (d of m, J_{app} = 5 Hz; 1H). This was used without further purification.

Oxidation of **16**. *Formation of 3-oxonorbornane-1-carboxylic acid* (**27**)

A solution of **16** (780 mg, 5.00 mmol) in acetone was cooled to 5–10°C, stirred, and titrated with a freshly prepared solution of Jones reagent (11) until the orange color persisted for 1 h. The excess oxidant was destroyed by dropwise addition of methanol. The acetone layer was concentrated under reduced pressure, and the residue was dissolved in dichloromethane. The solution was dried, and the solvent was removed. Crystallization of the residue from dichloromethane–ether afforded **27** (732 mg, 95%) as white plates, mp 96–97°C; ir ν_{max}: 3470–2450 (br m), 1751 (s), 1700 (s), cm^{-1}; ^{1}H nmr δ: 1.24–2.45 (m, with prominent s at 2.00; 8H), 2.75 (m, 1H), 10.00 (s, 1H; absent after D_2O treatment); ms *m/z*: 154 (50) (M$^+$). Anal. calcd. for $C_8H_{10}O_3$: C 62.32, H 6.54; found: C 62.43; H 6.57.

Oxidation of **26**. *Formation of* tert-*butyl 3-oxonorbornane-1-carboxylate* (**28**)

A solution of **26** (1.696 g, 8.00 mmol) in acetone (100 mL) was cooled to ca. 5°C, stirred, and titrated with Jones reagent (11) until the orange color persisted for 30 min. The excess oxidant was destroyed by dropwise addition of methanol. The solution was concentrated under reduced pressure and the residue was dissolved in dichloromethane. The solution was dried, and the solvent was removed under reduced pressure. Sublimation of the residue afforded **26** as white needles (1.646 g, 98%) mp 53–54°C; ir ν_{max}: 1740 (s), 1718 (s), cm^{-1}; ^{1}H nmr δ: 1.12–2.34 (m, with prominent s at 1.46; 17H), 2.67 (m, 1H). Exact Mass calcd. for $C_{12}H_{18}O_3$: 210.1252; found: 210.1252. Anal. calcd. for $C_{12}H_{18}O_3$: C 68.55, H 8.63; found: C 68.35, H 8.59.

Treatment of **16** *with methyllithium. Formation of 1-(*exo-*3-hydroxynorborn-1-yl)ethanone* (**30**)

Under anhydrous conditions a solution of methyllithium (1.38 M in ether, 15.00 mmol) was added dropwise to a stirred

Can. J. Chem. Downloaded from www.nrcresearchpress.com by 217.78.4.112 on 09/08/12
For personal use only.

solution of **16** (780 mg, 5.00 mmol) in dry ether (30 mL), which was cooled in an ice bath. The temperature was raised slowly to room temperature and the solution was stirred for 8 h. The reaction mixture was poured into saturated aqueous ammonium chloride (250 mL). Additional ether (250 mL) was added and the ether layer was washed with water (2 × 50 mL), dried, and concentrated under reduced pressure to give a pale yellow oil that was chromatographed on a column of silica gel that had been packed in dichloromethane–ether (9:1). Elution with the same solvent gave **30** (431 mg, 56%) as a colorless oil that was molecularly distilled (123–125°C, 0.025 Torr) to give an analytical sample of **30**; ir ν_{max}: 3610 (m), 3450 (m), 1695 (s), cm^{-1}; ^1H nmr δ: 1.10–2.24 (m, with prominent s at 2.15; 12H) 3.02 (br s, 1H; absent after D_2O treatment), 3.85 (d of m, J_{app} = 6 Hz; 1H). Exact Mass calcd. for $C_9H_{14}O_2$: 154.0992; found: 154.1000.

A further amount of **30** (218 mg, 28%) was obtained from the column by elution with ether.

*Oxymercuration–demercuration of **10**. Formation of **30***

To a stirred mixture of mercuric acetate (1.59 g, 5.00 mmol), water (5 mL), and tetrahydrofuran (5 mL) unsaturated ketone **10** (680 mg, 5.00 mmol) was added and the mixture was stirred for 10 min at room temperature by which time the oxymercuration was completed. Aqueous sodium hydroxide (3 M, 5 mL) was added followed by a solution of sodium borohydride (0.5 M in 3 M aqueous NaOH, 5 mL). The mercury was immediately separated by three successive suction filtrations. Ether (50 mL) was added to the filtrate, and this was saturated with sodium chloride. The ether layer was separated, washed with cold aqueous 5% sodium bicarbonate (10 mL), and water (2 × 10 mL), dried, and concentrated under reduced pressure. Molecular distillation of the residue gave **30** (547 mg, 71%) as a colorless oil. Its R_f value and spectra were identical with those of **30** obtained from the methyllithium treatment of **16** (*vide supra*).

*Oxidation of **30**. Formation of 1-(3-oxonorborn-1-yl)ethanone (**1**)*

A solution of **30** (616 mg, 4.00 mmol) in acetone (75 mL) was cooled in an ice bath, stirred, and titrated with Jones reagent (11) until the orange color persisted for 15 min. The excess oxidant was destroyed by dropwise addition of methanol until the solution was colorless. The solution was concentrated under reduced pressure, and the residue was dissolved in dichloromethane. The solution was dried, and concentrated under reduced pressure. Molecular distillation (153–156°C, 0.125 Torr) of the residue afforded **1** (547 mg, 90%) as a colorless oil. ir ν_{max}: 1754 (s), 1709 (s) cm^{-1}; ^1H nmr δ: 1.10–2.20 (m, 8H), 2.22 (s, 3H), 2.66 (m, 1H). Anal. calcd. for $C_9H_{12}O_2$: C 71.03, H 7.95; found: C 71.04, H 8.00.

*Acetylation of **16**. Formation of* exo*-3-acetyloxynorbornane-1-acetic acid (**31**)*

To a solution of **16** (1.56 g, 10.0 mmol) in triethylamine (10 mL) was added acetic anhydride (2 g) and a catalytic amount of 4-(dimethylamino)pyridine (100 mg). The mix was stirred at room temperature for 5 h. Water (100 mL) was added and the mixture was extracted with ethyl acetate (3 × 75 mL). The ethyl acetate extracts were combined, washed with water several times, and concentrated under reduced pressure. The residue was crystallized from ether – ethyl acetate and sublimed to give **31** (1.80 g, 91%) as needles, mp 86–88°C; ir ν_{max}: 3310–2880 (m), 1745 (s), 1704 (s), cm^{-1}; ^1H nmr δ: 1.17–2.00 (m, 8H), 2.03 (s, 3H), 2.41 (m, 1H), 4.68 (m, 1H), 10.90 (br s, 1H; absent after D_2O treatment). Anal. calcd. for $C_{10}H_{14}O_4$: C 60.59, H 7.12; found: C 60.47, H 7.13.

*Treatment of a mixture of ethyl 2-hydroxynorbornane-*exo*- and* endo*-2-acetate (**41**) with hydrogen bromide. Formation of* exo*-2-bromonorbornane-1-acetic acid (**35**) and its ethyl ester (**39**)*

A solution of a mixture of the epimeric esters **41**, prepared by treatment of 2-norbornanone with zinc and ethyl bromoacetate (13) (1.00 g, 5.00 mmol) in a 32% solution of hydrogen bromide in acetic acid (10 mL) was stirred at room temperature. After 20 h the brown reaction mixture was poured into stirred ice-water (75 g) and extracted with ether (5 × 50 mL). The combined ether extracts were washed with aqueous 5% sodium bicarbonate (50 mL) and water (4 × 50 mL), and dried. The solvent was removed to give a yellow oil, which was molecularly distilled (84–87°C, 0.125 Torr) to give the bromo ester **39** (970 mg, 72%) as a colorless oil; ir ν_{max}: 1730 (s) cm^{-1}; ^1H nmr δ: 1.14–2.02 (m, with prominent t at 1.25, J = 7 Hz; 10H), 2.15–2.33 (m, 2H), 2.76 (ABq, J = 17 Hz; 2H), 4.14 (q, J = 7 Hz; 2H), 4.23–4.47 (m, 1H); ms m/z: 260 (1), 262 (1), (M^+). Anal. calcd. for $C_{11}H_{17}BrO_2$: C 50.59, H 6.56, Br 30.60; found: C 50.91, H 6.46, Br 30.90).

The aqueous layer was cooled in an ice–salt bath, acidified (pH 2) by dropwise addition of concentrated hydrochloric acid, and extracted immediately with ether (3 × 50 mL). The combined ether extracts were washed with water (2 × 50 mL) and dried, and the solvent was removed to give a yellowish white solid, which was crystallized from chloroform to give the bromo acid **35** (160 mg, 14%) as needles. Sublimation (30°C, 0.125 Torr) gave long needles, mp 125–127°C; ir ν_{max}: 3510–2325 (m), 1706 (s) cm^{-1}; ^1H nmr δ: 1.14–2.00 (m, 6H), 2.20–2.36 (m, 3H), 2.86 (ABq, J_{AB} = 17 Hz; 2H), 4.28–4.50 (m, 1H), 11.42 (br s, 1H; absent after D_2O treatment); ms m/z: 232 (1), 234 (1) (M^+). Anal. calcd. for $C_9H_{13}BrO_2$: C 46.37, H 5.62; found: C 46.89, H 5.66.

Acid **35** could also be prepared by acidic hydrolysis of its ethyl ester **39**.

*Treatment of **39** with ethanolic sodium ethoxide. Formation of ethyl (*E*)- and (*Z*)-(norborn-2-ylidene)acetate (**48** and **49**)*

Under anhydrous conditions, a solution of **39** (530 mg, 2.00 mmol) in ethanol (25 mL) was added to a cold stirred solution of sodium ethoxide (6.10 mmol) prepared by addition of sodium (140 mg) to ethanol (100 mL), and the mixture was boiled under reflux with stirring. After 6 h the mixture was cooled, neutralized with 3 N hydrochloric acid, and extracted with ether. The extract was washed with water several times and dried. Removal of solvent and molecular distillation (76°C, 0.05 Torr) afforded a mixture of the known (16) **48** and **49** as a colorless oil (188 mg, 52%); ir ν_{max}: 1702 (s), 1658 (m) cm^{-1}; ^1H nmr δ: 1.12–2.34 (m, with prominent t at 1.29, J = 7 Hz; 10H), 2.49 (m, 2H), 2.82 (m, 1H), 4.13 (q, J = 7 Hz, 2H), 5.53 and 5.73 (2 m in a ratio of 1:4, 1H); ms m/z: 180 (33) (M^+).

*Dehydration of **41** with ethanolic sodium ethoxide. Formation of **48** and **49***

Under anhydrous conditions, a solution of **41** (198 mg, 1.00 mmol) in ethanol (20 mL) was added to a stirred solution of sodium ethoxide (1.20 mmol) prepared by addition of sodium (28 mg) to ethanol (20 mL), and the mixture was boiled under reflux for 9 h. The mixture was cooled, neutralized with concentrated hydrochloric acid, and extracted with ether. The extract was washed with water several times, and dried. The solvent was removed to give **48** and **49** (164 mg, 91%) as a yellow oil, which displayed ir and ^1H nmr spectra and tlc behavior identical with those of the mixture from the dehydrobromination of **39**.

*Hydrolysis of **48** and **49**. Formation of (*E*)- and (*Z*)-(norborn-2-ylidene)acetic acid (**45** and **46**)*

A mixture of **48** and **49** (360 mg, 2.00 mmol) and aqueous 5% sodium bicarbonate (300 mL) was stirred at room temperature. After 58 h the solution was washed with ether, cooled in an ice bath, stirred, and acidified to pH 2 by dropwise addition of concentrated hydrochloric acid. The acidic solution was extracted with dichloromethane (2 × 200 mL). The combined extracts were dried and the solvent was removed to give a viscous, colorless oil, which was sublimed to give a mixture of the known (14, 15) **45** and **46** (131 mg, 43%) as a waxy white solid, mp 24–61°C; ir ν_{max}: 3450–2325 (br m), 1681 (s), 1656 (s) cm^{-1}; ^1H nmr δ: 1.00–2.90 (m, 10H), 55.53 and 5.73 (2 m in a ratio of 1:3, 1H), 11.12 (br s, 1H; absent after D_2O treatment). Exact Mass calcd. for $C_9H_{12}O_2$: 152.0837; found: 152.0835.

Can. J. Chem. Downloaded from www.nrcresearchpress.com by 217.78.4.112 on 09/08/12
For personal use only.

*Treatment of **39** with ethanolic sodium ethoxide followed by hydrolysis. Formation of (E)- and (Z)-norborn-2-ylidene)acetic acid (**45** and **46**)*

Under anhydrous conditions a solution of **39** (520 mg, 2.00 mmol) in ethanol (30 mL) was added to a cold stirred solution of sodium ethoxide (8.70 mmol) prepared by addition of sodium (200 mg) to ethanol (100 mL), and the mixture was boiled under reflux with stirring. After 4 h, water (2 mL) was added and refluxing was continued for another 6 h. The reaction mixture was concentrated under reduced pressure, diluted with water (200 mL), and washed with ether (2 × 50 mL). The aqueous solution was cooled, acidified with 6 N hydrochloric acid, and extracted with chloroform (3 × 100 mL). The combined extracts were dried and the solvent was removed to give a 3:1 mixture of **45** and **46** accompanied by a small amount of a third product, considered to be **47** on the basis of ^{1}H nmr spectroscopy.

Treatment of **39** with potassium *tert*-butoxide in *tert*-butyl alcohol followed by hydrolysis in analogous fashion also gives **45** and **46**.

Reformatsky reaction of exo-*5-acetyloxy-2-norbornanone (**52**). Formation of ethyl* endo- *and* exo-*2-hydroxy*-exo-*5-acetyloxynorbornane-2-acetate (**53** and **54**)*

A mixture of **52** (19) (7.80 g) 46.40 mmol) and ethyl bromoacetate (7.80 g, 46.40 mmol) in benzene (30 mL) was added dropwise to freshly activated zinc (21) (3.10 g) suspended in boiling benzene (25 mL). The mixture was boiled under reflux for 28 h, cooled; and washed with 10% sulfuric acid, 5% sodium carbonate, and water. The mixture was dried and the solvent was removed to give **53** and **54** (11.18 g, 93%) as a yellow oil. Fractional distillation gave **53** as a colorless oil (8.89 g, 57%), bp 64°C, 0.025 Torr; ir ν_{max}: 3495 (m), 1721 (s), 1712 (s) cm^{-1}; ^{1}H nmr δ: 1.04–2.80 (m, with prominent t at 1.29, J = 7 Hz, and s's at 2.00 and 2.57; 16H), 3.51 (br s, 1H; absent after D_2O treatment), 4.16 (q, J = 7 Hz, 2H), 4.69 (d of d, J = 3 and 7 Hz; 1H). Exact Mass calcd. for $C_{13}H_{20}O_5$: 256.1309; found: 256.1320. Anal. calcd. for $C_{13}H_{20}O_5$: C 60.93, H 7.86; found: C 61.41, H 8.00.

*Treatment of **53** with hydrogen bromide. Formation of ethyl* exo-*2-bromo*-endo- *and* exo-*5-acetyloxynorbornane-1-acetate (**59** and **61**)*

A solution of **53** (5.00 g, 19.50 mmol) in a 32% solution of hydrogen bromide in acetic acid (50 mL) was stirred at room temperature. After 18 h the brown reaction mixture was poured into stirred ice-water (200 g) and the mixture was extracted with dichloromethane (3 × 100 mL). The combined extracts were washed with aqueous 5% sodium bicarbonate (100 mL) and water (2 × 100 mL), and dried. The solvent was removed to give a yellow oil, which was molecularly distilled (92–95°C, 0.025 Torr) to give a 1:1 mixture of **59** and **61** (5.85 g, 94%) as a colorless oil; ir ν_{max}: 1730 (s) cm^{-1}; ^{1}H nmr δ: 1.0–2.8 (m, with prominent s at 1.98, ABq at 2.66, J = 16.5 Hz; 15H), 4.07 (q, J = 7 Hz; 2H), 4.10 (m, 1H), 4.40 (m, 0.5H), 4.72 (m, 0.5H). Exact Mass calcd. for $C_{13}H_{19}BrO_4$: 318.0459, 320.0453; found: 318.0463, 320.0456.

After shorter reaction times the **59**:**61** ratio was greater.

*Hydrogenolysis of **59** and **61**. Formation of ethyl* endo- *and* exo-*3-acetyloxynorbornane-1-acetate (**62** and **63**)*

To a solution of 1:1 mixture of **59** and **61** (3.19 g, 10.00 mmol) in methanol (300 mL) was added palladium chloride (100 mg) and calcium carbonate (5.00 g), and the mixture was shaken under hydrogen (3.5 atm (1 atm = 101.325 kPa)) at ca. 50°C for 22 h. The reaction mixture was filtered and stripped of methanol under reduced pressure to give a yellow oil (2.41 g), which was molecularly distilled (88–91°C, 0.05 Torr) to give a 1:1 mixture of **62** and **63** (2.26 g, 94%) as a colorless oil; ir ν_{max}: 1721 (s) cm^{-1}; ^{1}H nmr δ: 1.10–3.00 (m, with prominent t at 1.24, J = 7.5 Hz and s at 2.02; 17H), 4.07 (q, J = 7.5 Hz; 2H), 4.52 (m, 0.5H), 4.92 (m, 0.5H); ms m/z: 240 (33) (M^+). Anal. calcd. for $C_{13}H_{20}O_4$: C 64.98, H 8.39; found: C 64.95, H 8.23.

Treatment of **59** and **61** with tributyltin hydride and azobisisobutyronitrile initiated by photolysis (20) also gave a mixture containing **62** and **63**, as shown by ^{1}H nmr spectroscopy, but these could not be purified.

*Treatment of **59** and **61** with zinc and ethanol. Formation of ethyl (E)- and (Z)-(*exo-*5-acetyloxynorborn-2-ylidene)acetates (**64** and **65**)*

To a solution of **59** and **61** (362 mg, 1.19 mmol) in ethanol (10 mL) was added freshly activated zinc dust (155.6 mg, 2.38 mmol) and water (1 mL). The mixture was boiled under reflux with stirring for 8 h, filtered to remove zinc, diluted with water (100 mL), and extracted with ether (3 × 100 mL). After the extracts had been dried, the ether was removed under reduced pressure to give a viscous, yellow oil (273 mg). Its ^{1}H nmr and ir spectra indicated that it was a mixture of **64** and **65**, which was confirmed by its hydrolysis to a mixture of the corresponding hydroxy acids, **68** and **69** (*vide infra*).

*Treatment of **59** and **61** with zinc and acetic acid. Formation of **63–65**,* endo-*5-acetyloxy*-exo-*2-hydroxynorbornane-1-acetic acid lactone (**66**) and* endo-2-exo-*5-dihydroxynorbornane-1-acetic acid γ-lactone (**67**)*

To a stirred solution of **59** and **61** (9.57 mg, 3.00 ml) in acetic acid (15 mL) was added freshly activated zinc dust (1.00 g). The mixture was heated at 90°C for 5 h, cooled to room temperature, and filtered. The filtrate was concentrated under reduced pressure, diluted with water, extracted with dichloromethane (33 × 100 mL), and the combined extracts were washed with water (4 × 100 mL) and dried. The solvent was removed to give a yellow oil (921 mg), which was chromatographed on a silica-gel column that had been packed in dichloromethane/benzene (1:1). Elution with dichloromethane–benzene (1:1) and concentration of the eluate (260 mL) afforded the lactone **66** (120 mg, 19%), mp 91–96°C.[6] Crystallization from ether gave **66** as plates, mp 65–66°C; ir ν_{max}: 1773 (s), 1764 (s) cm^{-1}; ^{1}H nmr δ: 1.0–2.7 (with prominent s's at 2.03 and 2.56, 12H); 4.27 (dd, J = 3 and 7 Hz, 1H)), 5.10 (m, 1H); ms m/z: 210 (7) (M^+). Anal. calcd. for $C_{11}H_{14}O_4$: C 62.84, H 6.71; found: C 62.21, H 6.73.

Further elution with dichloromethane–benzene – ethyl acetate (5:4:1) afforded a mixture of **63–65**, as shown by ^{1}H nmr spectroscopy.

*Treatment of **64** and **65** with base. Formation of (E)- and (Z)-(*exo-*5-hydroxynorborn-2-ylidene)acetic acid (**68** and **69**)*

The mixture of **64** and **65** formed from **59** and **61** was dissolved in ethanol (15 mL) and potassium hydroxide (1.00 g) was added with continuous swirling. The mixture was heated on a steam bath for 30 min followed by stirring without external heating for 3 h. Water (50 mL) was added, and the mixture was concentrated under reduced pressure to ca. 10 mL. The concentrate was cooled in ice-water and acidified to pH 5 with 6 N sulfuric acid. The solution was immediately extracted with ethyl acetate (5 × 10 mL) and dried. The solvent was removed and the residue was sublimed to give white plates (88.00 mg, 44%) of **68** and **69**, mp 179–183°C; shown by ir, ^{1}H nmr, and tlc comparison to be identical with the products obtained below from treatment of **53** with base.

*Treatment of **53** with base. Formation of **68** and **69***

Under anhydrous conditions a solution of **53** (768 mg, 3.00 mmol) in ethanol (20 mL) was added to a cold stirred solution of sodium ethoxide (10.00 mmol) prepared by addition of sodium (230 mg) to ethanol (10 mL), and the mixture was boiled under reflux with stirring. After 5 h, water (2 mL) was added, and boiling was continued for another 5 h. The reaction mixture was concentrated under reduced pressure, diluted with water (150 mL), and washed with ether (3 × 50 mL). The aqueous so-

[6]This material contained a small amount of the lactone **67**, as shown by ^{1}H nmr spectroscopy. Compounds **66** and **67** have been independently synthesized (P. Yates and M. Kaldas, to be submitted for publication).

Can. J. Chem. Downloaded from www.nrcresearchpress.com by 217.78.4.112 on 09/08/12
For personal use only.

lution was cooled, acidified with 6 N hydrochloric acid, and extracted with dichloromethane (4 × 50 mL). The extracts were dried and the solvent was removed to give the crude product (408 mg, 81%) as a yellowish white solid. This was chromatographed on a column of silica gel (5 g) that had been packed in dichloromethane; 100-mL fractions were collected. Elution with dichloromethane (8 fractions) gave a mixture (31 mg) that was not investigated further. Elution with ether–methanol (9:1) (2 fractions) gave **68** and **69** in a 4:3 ratio (228 mg, 45%) as a white solid; mp 191–196°C; ir ν_{max}: 3585 (w), 3510 (w), 1681 (s), 1667 (m), cm^{-1}; ^1H nmr (acetone-d_6) δ: 1.09–2.80 (m, 8H), 3.87 (m, 1H), 5.16 (br s; absent after D_2O treatment; 2H), 5.53 and 5.73 (2 m, 1H). Exact Mass calcd. for $C_9H_{12}O_3$: 168.0785; found: 168.0786. Anal. calcd. for $C_9H_{12}O_3$: 64.27, H 7.19; found: C 63.88, H 7.20.

*Hydrolysis of **62** and **63**. Formation of* endo- *and* exo-*3-hydroxynorbornane-1-acetic acids (**70** and **71**)*

To a stirred solution of **62** and **63** (2.40 g, 10.00 mmol) in 95% ethanol (50 mL) was added potassium hydroxide (5.60 g). The mixture was heated on a steam bath for 1 h, cooled to room temperature, and stirred for 5 h. The solution was diluted with water (200 mL) and distilled to remove ethanol. The aqueous solution was cooled in an ice bath and titrated by dropwise addition of concentrated hydrochloric acid with stirring to ca. pH 6. The solution was extracted with ethyl acetate (3 × 100 mL), the combined extracts were dried, and the solvent was removed to give a mixture of **70** and **71** as a white solid (1.30 g, 76%). This crude product was used for the preparation of **72** (*vide infra*).

In a further run the product mixture was crystallized from ethyl acetate – ether to give the *exo* epimer **71** (663 mg, 39%) as needles, mp 113–4°C; ir ν_{max}: 3625–2835 (br, m), 1709 (s) cm^{-1}; ^1H nmr (acetone-d_6) δ: 1.28–2.15 (m, 9H), 2.18 (ABq, J = 20 Hz; 2H), 3.62 (m, 1H), 5.87 (br s, 2H); absent after D_2O treatment); Exact Mass calcd. for $C_9H_{14}O_3$: 170.0941; found: 170.0941.

In another run, after hydrolysis the solution was acidified with hydrochloric acid to pH 5 and stirred at room temperature for 3 days. The solution was saturated with sodium chloride, and extracted with ethyl acetate; the extract was dried and concentrated under reduced pressure. The residue was crystallized from ethyl acetate – ether to give the *exo* epimer **71** (901 mg, 53%).

*Oxidation of **70** and **71**. Formation of 3-oxonorbornane-1-acetic acid (**72**)*

A solution of **70** and **71** (646 mg, 3.80 mmol) in acetone was cooled in an ice bath, stirred, and titrated with Jones reagent (11) until the orange color persisted for 20 min. The excess oxidant was destroyed by dropwise addition of methanol until the solution became colorless. The solution was concentrated under reduced pressure, and the residue was dissolved in dichloromethane. The solution was dried and the solvent was removed. Molecular distillation (103–105°C, 0.05 Torr) of the residue afforded **72** (530 mg, 83%) as a colorless oil that solidified on standing; mp 62–3°C; ir ν_{max}: 3570–2440 (m), 1736 (s), 1706 (s) cm^{-1}; ^1H nmr δ: 1.00–2.70 (m, with prominent s's at 2.44 and 2.66; 11H), 11.15 (br s, 1H; absent after D_2O treatment). Exact Mass calcd. for $C_9H_{12}O_3$: 168.0785; found: 168.0784.

*Treatment of **70** and **71** with methyllithium. Formation of 1-(*endo- *and* exo-*3-hydroxynorborn-1-yl)-2-propanone (**73** and **74**)*

Under anhydrous conditions a solution of methyllithium (1.48 M in ether, 6.00 mmol) was added dropwise to a stirred solution of a mixture of **70** and **71** (340 mg, 2.00 mmol) in dry ether (25 mL), and the mixture was stirred for 13 h. The reaction mixture was added dropwise to cold 3 N hydrochloric acid (200 mL) with stirring. Additional ether (100 mL) was added and the ether layer was washed with water (2 × 50 mL), dried, and concentrated under reduced pressure to give a yellow oil that was molecularly distilled (71–73°C, 0.105 Torr) to give a mixture of **73** and **74** as a colorless oil (205 mg, 61%); ir ν_{max}: 3510 (w), 3450 (w), 1715 (s), cm^{-1}; ^1H nmr δ: 1.00–2.00 (m, H), 2.12 (s, 3H), 2.46 (s, 2H), 2.53 (s, 1H; absent after D_2O treatment), 3.67 (m, 0.56H), 4.30 (m, 0.44H). Anal. calcd. for $C_{10}H_{16}O_2$: C 71.39, H 9.59; found: C 71.28, H 9.87.

*Oxidation of **73** and **74**. Formation of 1-(3-oxonorborn-1-yl)-2-propanone (**2**)*

A solution of **73** and **74** (168 mg, 1.00 mmol) in acetone (100 mL) was stirred and titrated with Jones reagent (11) until the orange color persisted for 20 min. The excess oxidant was destroyed by dropwise addition of methanol until the solution became colorless. The reaction mixture was concentrated under reduced pressure, and the residue was dissolved in dichloromethane. The solution was dried, and the solvent was removed. Molecular distillation (77–79°C, 0.025 Torr) of the residue gave **2** (165 mg, 99%) as a colorless oil; ir ν_{max}: 1751 (s), 1724 (s) cm^{-1}; ^1H nmr δ: 0.80–1.85 (m, 6H), 2.14 (s, 3H), 1.95–2.73 (m, 2H). Exact Mass calcd. for $C_{10}H_{14}H_2$: 166.0992; found: 166.0996. Anal. calcd. for $C_{10}H_{14}H_2$: C 72.26, H 8.49; found: C 72.37, H 8.53.

Treatment of exo-*2-hydroxynorbornane-1-acetic acid lactone (**75**) with methyllithium. Formation of 1-(*exo-*2-hydroxynorborn-1-yl)-2-propanone (**76**) and 1-(2-hydroxynorborn-1-yl)-2-methyl-2-propanol (**77**)*

Under anhydrous conditions a solution of methyllithium (1.3 M in ether, 5.00 mmol) was added dropwise to a stirred solution of **75**[7] (760 mg, 5.00 mmol) in dry ether (15 mL), and the mixture was stirred for 6 h and poured into ice-cold 3 N hydrochloric acid (300 mL). Additional ether (200 mL) was added and the ether layer was washed with water (3 × 25 mL), dried, and concentrated under reduced pressure to give a pale yellow (819 mg) that was chromatographed on a column of silica gel that had been packed in dichloromethane. Elution with dichloromethane gave unchanged starting material (153 mg, 20%), followed by **76** as an oil (267 mg, 32%); ir ν_{max} 3333 (m), 1710 (s) cm^{-1}. Anal. calcd. for $C_{10}H_{16}O_2$: C 71.39, H 9.59; found: C 71.36, H 9.63.

Further elution with ether afforded **77** (171 mg, 10%), which was crystallized from ether to give white needles, mp 90–92°C; ir ν_{max}: 3510 (w), 3335 (w), cm^{-1}; ^1H nmr δ: 0.87–2.32 (m, with prominent s's at 1.27 and 1.33, and ABq at 1.90, J = 15 Hz; 17H), 3.86 (d of m, 1H), 4.36 (br s, 2H; absent after D_2O treatment). Anal. calcd. for $C_{11}H_{20}O_2$: C 71.69, H 10.94; found: C 71.52, H 10.88.

*Oxidation of **76**. Formation of 1-(2-oxonorborn-1-yl)-2-propanone (**78**)*

A solution of **76** (260 mg, 1.60 mmol) in acetone was cooled in an ice bath, stirred, and titrated with a freshly prepared solution of Jones reagent until the orange color persisted for 10 min. The excess oxidant was destroyed by dropwise addition of methanol until the solution became colorless. The solution was concentrated under reduced pressure, and the residue was dissolved in dichloromethane. The solution was dried, and the solvent was removed. Molecular distillation (100–103°C, 0.125 Torr) of the residue afforded **78** (231 mg, 88%) as a colorless oil; ir ν_{max}: 1754 (s), 1724 (s), cm^{-1}; ^1H nmr δ: 0.80–2.64 (m, with prominent s at 2.16; 12H), 2.79 (ABq, J = 17 Hz; 2H). Exact Mass calcd. for $C_{10}H_{14}O_2$: 166.0992; found: 166.1000. Anal. calcd. for $C_{10}H_{14}O_2$: C 72.26, H 8.49; found: C 72.31, H 8.51.

*Oxidation of **77**. Formation of 1-(2-oxonorborn-1-yl)-2-methyl-2-propanol (**79**)*

A solution of **76** (162 mg, 0.90 mmol) in acetone as cooled in an ice bath, stirred, and titrated with a freshly prepared solution of Jones reagent (11) until the orange color persisted for 20 min. The excess oxidant was destroyed by dropwise addition of methanol until the solution became colorless. The solution was concentrated under reduced pressure, and the residue was dissolved in ether. The so-

[7]Lactone **75** was prepared by treatment of **41** with strong acids (P. Yates and M. Kaldas, accepted for publication).

lution was dried, and the solvent was removed. Molecular distillation (63–65°C, 0.025 Torr) of the residue afforded **79** (144 mg, 90%) as a colorless oil; ir ν_{max}: 3390 (w), 1727 (s), cm^{-1}; ^1H nmr δ: 1.24 (s, 6H), 1.24–2.40 (m, with an ABq at 2.09, J = 17 Hz; 10H), 2.60 (m, 1H), 2.98 (br s, 1H; absent after D_2O treatment).

Acknowledgement

We thank the Natural Sciences and Engineering Research Council of Canada for support of this work.

1. P. Yates and R. O. Loutfy. Acc. Chem. Res. **8**, 209 (1975); P. Yates. J. Photochem. **5**, 91 (1976).
2. J. W. Wilt, C. T. Parsons, C. A. Schneider, D. G. Schultenover, S. J. and W. J. Wagner. J. Org. Chem. **33**, 694 (1968).
3. W. R. Boehme. J. Am. Chem. Soc. **81**, 2762 (1959).
4. H. Kwart and G. Null. J. Am. Chem. Soc. **80**, 248 (1958).
5. W. R. Vaughan, R. Caple, J. Csapilla, and P. Scheiner. J. Am. Chem. Soc. **87**, 2204 (1965).
6. M. J. Jorgensen. Org. Reactions, **18**, 1 (1970); T. M. Bare and H. O. House. Org. Synth. Collect. **5**, 775 (1973); M. P. Cooke, Jr. J. Org. Chem. **51**, 951 (1986).
7. R. S. Abeywickrema and E. W. Della. Org. Prep. Proc. Int. **12**, 357 (1980).
8. G. D. Sargent. *In* Carbonium ions. Vol. 3. *Edited by* G. A. Olah and P. v. R. Schleyer. John Wiley & Sons, New York. 1972. Chap. 24.
9. H. C. Brown, J. H. Kawakami, and S. Ikegami. J. Am. Chem. Soc. **89**, 1525 (1967).
10. W. Luef, U.-C. Vogeli, and R. Keese. Helv. Chim. Acta, **66**, 2729 (1983).
11. L. F. Fieser and M. Fieser. Reagents for organic synthesis. Vol. 1. John Wiley & Sons, New York. 1967. p. 142.
12. E.-P. Krebs and R. Keese. Helv. Chim. Acta, **65**, 2029 (1982).
13. F. Lauria, V. Vecchietti, W. Logemann, G. Tosolini, and E. Dradi. Tetrahedron, **25**, 3989 (1969).
14. W. R. Vaughan, J. Wolinsky, R. R. Dueltgen, S. Grey, and F. S. Seichter. J. Org. Chem. **35**, 400 (1970).
15. N. A. Belikova, A. A. Bobyleva, A. N. Kalinichenko, A. F. Plate, T. I. Pekhk, and E. Lippmaa. J. Org. Chem. USSR, **10**, 241 (1974).
16. R. A. Finnegan and R. S. Mcnees. J. Org. Chem. **29**, 3241 (1964).
17. W. R. Vaughan, B. A. Gross, S. E. Burkle, M. A. Langell, R. Caple, and D. B. Oakes. J. Org. Chem. **48**, 4792 (1983).
18. G. A. Olah, A. Wu, O. Farooq, and G. K. S. Prakash. Synthesis, 537 (1988).
19. J. Meinwald, J. K. Crandall, and P. G. Gassman. Tetrahedron, **18**, 815 (1962).
20. F. D. Greene and N. N. Lowry. J. Org. Chem. **32**, 882 (1967; G. L. Grady and H. G. Kuivila. J. Org. Chem. **34**, 2014 (1969).
21. L. F. Fieser and M. Fieser. Reagents for organic synthesis. Vol. 1. John Wiley & Sons, New York. 1967. p. 1285.

Can. J. Chem. Downloaded from www.nrcresearchpress.com by 217.78.4.112 on 09/08/12
For personal use only.

Glaciasterols A and B, 9,11-secosteroids from the marine sponge *Aplysilla glacialis*

JANA PIKA, MARK TISCHLER, AND RAYMOND J. ANDERSEN[1]

Departments of Chemistry and Oceanography, University of British Columbia, Vancouver, B.C., Canada V6T 1Z4

Received August 7, 1991

This paper is dedicated to Professor Zdenek (Denny) Valenta on the occasion of his 65th birthday

JANA PIKA, MARK TISCHLER, and RAYMOND J. ANDERSEN. Can. J. Chem. **70**, 1506 (1992).

The glaciasterols, a family of cytotoxic 9,11-secosteroids, have been isolated from extracts of the northeastern Pacific sponge *Aplysilla glacialis*. The structures of glaciasterol A (**2**) and glaciasterol B (**3**) were elucidated by a combination of spectroscopic analysis and chemical interconversions on the native steroid **2** and the diacetate **5** of glaciasterol B (**3**).

JANA PIKA, MARK TISCHLER et RAYMOND J. ANDERSEN. Can. J. Chem. **70**, 1506 (1992).

On a isolé les glaciastérols, appartenant à la famille des seco-9,11 stéroides cytotoxiques, à partir des extraits de l'éponge du Pacifique Nord Est *Aplysilla glacialis*. On a élucidé la structure du glaciastérol A (**2**) et du glaciastérol B (**3**) en faisant appel à l'analyse spectroscopique et à des interconversions chimiques du stéroide naturel **2** et du diacétate **5** de glaciastérol B (**3**).

[Traduit par la rédaction]

Can. J. Chem. Downloaded from www.nrcresearchpress.com by 217.78.4.112 on 09/08/12
For personal use only.

Many highly oxygenated steroids (**1**), including a small number of 9,11-secosteroids (2–4), have been isolated from marine invertebrates in recent years. A representative example is herbasterol (**1**), which was isolated from Australian specimens of the sponge *Dysidea herbacea* (4). Herbasterol was found to have both icthyotoxic and antimicrobial properties. As part of our earlier investigations of the terpenoid metabolism of the Northeastern Pacific marine sponge *Aplysilla glacialis* (5), we discovered that the polar fractions from silica gel chromatography purification of the organic soluble *A. glacialis* metabolites exhibited moderate in vitro cytotoxicity. Further bioassay guided separation of the active fractions led to the isolation of the glaciasterols, a new family of cytotoxic 9,11-secosteroids. In this paper we describe the structural elucidation of glaciasterols A (**2**) and B (**3**).

Samples of *A. glacialis* were collected in Sydney Inlet and Barkley Sound, British Columbia. Freshly collected sponge specimens were extracted sequentially with methanol and 1:1 methanol/CH_2Cl_2 and the extracts were combined. Chromatographic fractionation of the combined extracts yielded pure glaciasterol A (**2**) and an inseparable mixture of related sterols. Acetylation of the inseparable mixture expedited the purification of one of the major components, glaciasterol B diacetate (**5**).

Glaciasterol A (**2**) was isolated as a white amorphous solid that gave a parent ion in the EIHRMS at m/z 416.2936 Da appropriate for a molecular formula of $C_{26}H_{40}O_4$ (ΔM +0.9 mmu). The ^{1}H NMR spectrum of glaciasterol A (Table 1) contained resonances that could be assigned to the two tertiary methyl groups (δ 0.68, s, 3H and 1.24, s, 3H) and three secondary methyl groups (δ 0.94, d, J = 6.7 Hz, 6H and 1.02, d, J = 6.8 Hz, 3H) that are typically present in steroids. Additional evidence in support of the steroidal nature of glaciasterol A came from the COSY data, which contained correlations that readily identified the truncated side chain **i** found in many C26 steroids (6) (Table 1: δ 1.02 (Me21), 2.13 (H20), 5.27 (H22), 5.29 (H23), 2.22 (H24), 0.94 (Me25 and Me26)). The ^{13}C NMR spectrum of glaciasterol A contained deshielded resonances that could be assigned to one disubstituted and one trisubstituted olefin (Table 1: δ 132.2(CH), 134.2(C), 136.0(CH), and 139.3(CH)) and to an α,β-unsaturated ketone (δ 201.8 (C)). Since there was no additional ^{13}C NMR evidence for unsaturated functional groups in glaciasterol A, the remaining four sites of unsaturation required by the molecular formula ($C_{26}H_{40}O_4$: requires 7 sites of unsaturation) were attributed to rings.

Correlations in the COSY and ^{1}H Detected Heteronuclear Multiple Quantum Coherence (HMQC) spectra of glaciasterol A (**2**) identified proton (Table 1: δ 3.69 and 3.81 (H11, H11′); 1.15 and 1.63 (H12, H12′)) and carbon resonances (Table 1: δ 59.1 (CH_2, C11) and 40.4 (CH_2, C12)) that could be assigned to an isolated ethyl fragment bearing an oxygen substituent at one terminus (i.e., C11). Acetylation of **2** with acetic anhydride and pyridine gave the diacetate **4**. The geminal methylene resonances found at δ 3.69 and 3.81 in **2** were shifted downfield to δ 4.10 and 4.19 in **4**, demonstrating that the oxygen substituent on the ethyl fragment in **2** was an alcohol functionality. Since the structure of the side chain in **2** had already been established as **i**, the spin-isolated ethyl fragment had to be present in the nucleus of glaciasterol A. This requirement demanded a ring-opened structure for the nucleus. The chemical shifts of the carbon atoms in the hydroxyethyl fragment in **2** were almost identical to the chemical shifts assigned to the C11 and C12 carbon atoms (δ 58.9 and 41.2) in herbasterol (**1**) (4), suggesting that glaciasterol was also a 9,11-secosteroid.

The formation of the diacetate **4** showed that two of the four oxygen atoms in glaciasterol A were part of alcohol functionalities and the ^{13}C NMR data for **2** (δ 201.8 (C)) showed that a third oxygen was part of an unsaturated ketone functionality. A pair of resonances at δ 63.3 (C) and 53.5 (CH) in the ^{13}C NMR spectrum of **2** were tentatively assigned to a trisubstituted epoxide functionality, which accounted for the final oxygen atom. Treatment of the diacetate **4** with perchloric acid in THF followed by acetylation of the resulting diol gave the triacetate **6**, confirming the presence of an epoxide in glaciasterol A. Subtracting the epoxide ring from the total of four rings earlier determined to be present in glaciasterol A revealed that three carbocyclic rings were present in the remainder of the nucleus, in agreement with a secosteroid structure.

COSY45, HMQC, and ^{1}H Detected Multiple Bond Het-

[1]Author to whom correspondence may be addressed.

eronuclear Multiple Quantum Coherence (HMBC) data for the diacetate **4** were used to establish the functionality on the A and B rings of glaciasterol A. Starting from a deshielded ^{1}H NMR resonance at δ 4.99 (HMQC correlation to δ 70.7), assigned to a methine proton attached to a carbon bearing an acetoxy group, COSY45 and HMQC correlations elaborated an isolated proton spin system consisting of -CH_2-CH_2-CHOAc-CH_2- (Table 2: C1 to C4, respectively). This four-carbon fragment could only be accommodated by the A ring of a steroid skeleton. An HMBC correlation between a carbon resonance at δ 27.6 (C1), assigned to the terminal methylene carbon furthest removed from the acetoxy functionality in the four-carbon fragment, and a proton resonance (δ 1.22, s, 3H) assigned to Me19 situated the fragment in a manner such that the acetoxy functionality was at the standard C3 position in the A ring. Additional HMBC correlations from the Me19 proton resonance at δ 1.22 to the ketone carbonyl resonance at δ 200.0 and to the quaternary epoxide carbon resonance at δ 63.0 located the carbonyl functionality at C9 and the trisubstituted epoxide functionality at C5, C6. The epoxide methine proton resonance at δ 3.37 (H6: HMQC correlation to δ 53.4 (C6)) showed a COSY45 correlation to an olefinic resonance at δ 6.76 (d, J = 4.5 Hz: HMQC correlation to δ 138.6) indicating that there was a $\Delta^{7,8}$ trisubstituted olefin in ring B. Conjugation between the $\Delta^{7,8}$ olefin and the C9 ketone accounted for the relatively shielded chemical shift of the ketone carbon resonance (δ 200.0) in **4**.

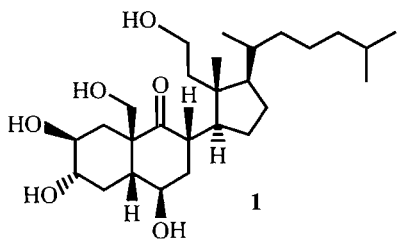

1

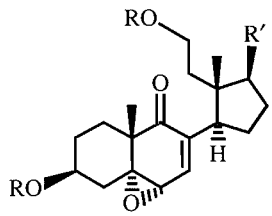

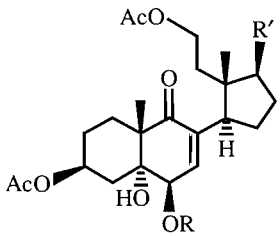

2 R = H R′ =

3 R = H R′ =

4 R = Ac R′ =

5 R = Ac R′ =

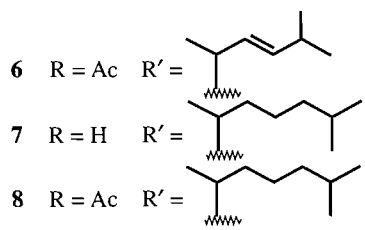

6 R = Ac R′ =

7 R = H R′ =

8 R = Ac R′ =

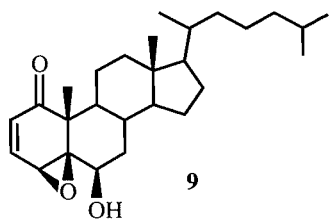

9

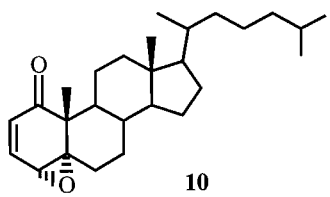

10

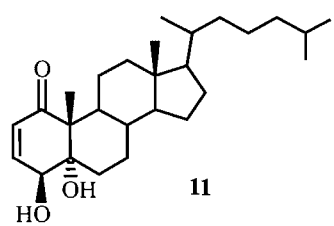

11

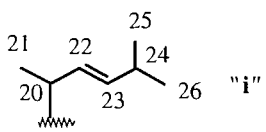

"i"

A second tertiary methyl resonance at δ 0.73 (s, 3H) in the ^{1}H NMR spectrum of the diacetate **4** was assigned to Me18. HMBC correlations were observed between this methyl resonance and carbon resonances at δ 36.7 (CH_2: HMQC cor-

Can. J. Chem. Downloaded from www.nrcresearchpress.com by 217.78.4.112 on 09/08/12
For personal use only.

TABLE 1. ^1H and ^{13}C NMR data for glaciasterol A (**1**) (recorded in $CDCl_3$)

Carbon no.	^1H (400 MHz)	COSY (400 MHz)	^{13}C (125 MHz)[a]
1	—	—	26.6[b]
2	1.68	H2′, H3	30.4[b]
2′	2.13	H2, H3	—
3	3.99, m	H2, H2′, H4, H4′	68.4
4	1.59	H3, H4′	37.4
4′	2.19, m	H3, H4	—
5	—	—	63.5
6	3.39, d, J = 4.6 Hz	H7	53.5
7	6.80, dd, J = 4.6, 0.9 Hz	H6	139.3
8	—	—	134.2
9	—	—	201.8
10	—	—	45.6
11	3.69, m	H11′, H12, H12′	59.1
11′	3.81, m	H11, H12, H12′	—
12	1.15	H11, H11′, H12	40.4
12′	1.63	H11, H11′, H12	—
13	—	—	46.1
14	3.39, ddd, J = 11.3, 8.1, 0.9 Hz	H15, H15′	43.9
15	1.62	H14, H15′	26.9[b]
15′	1.74	H14, H15	—
16	—	—	29.8[b]
17	—	—	49.6
18	0.68, s	—	17.8
19	1.24, s	—	21.5
20	2.13	H21, H22	38.5
21	1.02, d, J = 6.8 Hz	H20	21.3
22	5.27, dd, J = 15.3, 7.6 Hz	H20, H23	136.0
23	5.29, dd, J = 15.3, 6.1 Hz	H22, H24	132.2
24	2.22, m	H23, H25, H26	31.0
25	0.94, d, J = 6.7 Hz	H24	22.6[c]
26	0.94, d, J = 6.7 Hz	H24	22.7[c]

[a]Assigned from the HMQC spectrum.
[b,c]May be interchanged.

Can. J. Chem. Downloaded from www.nrcresearchpress.com by 217.78.4.112 on 09/08/12
For personal use only.

relation to δ1.64, 1.26) and 43.8 (CH: HMQC correlation to δ 3.22) assigned to C12 of the isolated acetoxyethyl fragment and C14 of the D ring, respectively. The deshielded chemical shift of the H14 resonance (δ 3.22), which indicated that it was an allylic proton, was consistent with linkage of the AB ring system to the D ring through a C8/C14 bond. HMBC correlations between H7 (δ 6.76) and C14 (δ 43.8) and between H14 (δ 3.22) and C7 (δ 138.6) and C8 (δ 141.2) confirmed the C8/C14 linkage. Diacetate **4** had a λ_{max} 254 nm in the UV spectrum, in close agreement with the reported λ_{max} 242 nm for the model steroid **9** (7), once the standard increment of 10 nm for the additional α-alkyl substituent in **4** was added (8). The NMR experiments described above established the constitution of glaciasterol A; however, the small amounts of pure glaciasterol A (**2**) and its diacetate **4** that were available were insufficient for complete elucidation of the stereochemical features of the molecule. Therefore, the stereochemical details of glaciasterol A and B were elucidated on the more accessible glaciasterol B diacetate **5**.

Glaciasterol B diacetate **5** was isolated as white needles (mp 55–57°C) that gave a parent ion in the EIHRMS at m/z 516.3451 Da appropriate for a molecular formula of $C_{31}H_{48}O_6$ (ΔM 0.0 mmu). The NMR data for glaciasterol B diacetate **5** (Table 2) showed that it had a nucleus identical with glaciasterol A diacetate **4** and a side chain identical with the side chain of cholesterol.

A number of spectroscopic and chemical experiments were used to unravel the stereochemistry of glaciasterols A (**2**) and B (**3**). Simultaneous irradiation of the H20 (δ 2.13) and H24 (δ 2.22) resonances in the ^1H NMR spectrum of **2** collapsed the H22/H23 multiplet at δ 5.27–5.28 to an AB doublet with a coupling constant of 15.3 Hz consistent with an *E* olefinic geometry. The observation of a *trans* diaxial coupling between $H4_{ax}$ (δ 2.24, dd, J = 12.5, 12.6 Hz) and H3, in conjunction with the observation of an NOE between the $H4_{ax}$ (δ 2.24) and Me19 (δ 1.23) proton resonances in glaciasterol B diacetate **5**, showed that the A ring of the glaciasterols was in a chair conformation and that the 3-acetoxy substituent had the β configuration. Irradiation of the H14 resonance (δ 3.22) in glaciasterol B diacetate **5** induced an NOE in one of the H11 resonances (δ 4.10) consistent with the expected *trans* relationship between H14 and Me18. C17 and C20 were assumed to have the standard steroidal configurations in the glaciasterols; however, these configurations were not verified experimentally.

Spectroscopic evidence failed to unambiguously establish the 5,6-epoxide stereochemistry. Therefore, the diacetate **5** was treated with aqueous perchloric acid in THF to give the *trans* diol **7**. It had previously been shown that the re-

TABLE 2. ^{1}H and ^{13}C NMR data for glaciasterol diacetate A (**4**) and glaciasterol B diacetate **5** (recorded in $CDCl_3$)

Carbon no.	Glaciasterol A diacetate (**4**)				Glaciasterol B diacetate (**5**)	
	^{1}H (400 MHz)	COSY (400 MHz)	^{13}C (125 MHz)[a]	HMBC (500 MHz)[c]	^{1}H (400 MHz)	^{13}C (75 MHz)
1	1.77	H1′, H2, H2′	27.6	—	1.77	27.6[b]
1′	2.10	H1, H2, H2′	—	—	2.10	—
2	1.70	H1, H1′, H2′, H3	26.6	—	1.72	26.6[b]
2′	2.17	H1, H2, H3	—	—	2.17	—
3	4.99, m	H2, H2′, H4, H4′	70.7	—	4.99, m	70.6
4_{ax}	2.26, dd, J = 12.6, 12.5 Hz	H3, H4′	34.0	C3	2.24, dd, J = 12.6, 12.5 Hz	33.9
$4'_{eq}$	1.65	H3, H4	—	—	1.64	—
5	—	—	63.0	—	—	63.0
6	3.37, d, J = 4.5 Hz	H7	53.4	C7, C8	3.36, d, J = 4.5 Hz	53.4
7	6.76, d, J = 4.5 Hz	H6	138.6	C5, C6, C9, C14	6.75, d, J = 4.5 Hz	138.6
8	—	—	141.2	—	—	141.3
9	—	—	200.0	—	—	200.0
10	—	—	45.3	—	—	45.3
11	4.10, m	H11′, H12, H12′	61.1	—	4.10	61.1
11′	4.19, m	H11, H12, H12′	—	—	4.19	—
12	1.26	H11, H11′, H12′	36.7	—	1.23	36.6
12′	1.64	H11, H11′, H12	—	—	1.69	—
13	—	—	46.1	—	—	46.0
14	3.23, dd, J = 10.7, 7.5 Hz	H15, H15′	43.8	C7, C8, C13, C15, C18	3.23, dd, J = 10.8, 7.5 Hz	43.5
15	1.57	H14	27.4	—	1.58	25.9[b]
15′	1.71	H14	—	—	1.68	—
16	—	—	25.1	—	—	27.4[b]
16′	—	—	—	—	—	—
17	—	—	50.4	—	1.83	49.8
18	0.73, s	—	17.6	C12, C13, C14, C17	0.73, s	17.2
19	1.23, s	—	21.1	C1, C5, C9, C10	1.23, s	21.1[c]
20	2.17	H21, H22	38.2	—	1.44	34.8[d]
21	0.97, d, J = 6.8 Hz	H20	21.5	—	0.97, d, J = 6.7 Hz	18.9[d]
22	5.27, dd, J = 15.3, 6.2 Hz	H21, H23	136.2	—	—	35.4[d]
23	5.28, dd, J = 15.3, 6.2 Hz	H22, H24	131.9	—	—	24.5[d]
24	2.21	H23, H25, H26	31.0	—	—	39.4[d]
25	0.87, d, J = 6.8 Hz	H24	22.6	—	1.54	28.0[d]
26	0.87, d, J = 6.8 Hz	H24	22.7	—	0.86, d, J = 6.6 Hz	22.6
27	—	—	—		0.86, d, J = 6.6 Hz	22.8
OAc	2.01, s; 2.04, s	—	21.2; 21.2; 170.1; 171.0	—	2.00, s; 2.04, s	21.1[c]; 21.3[c]; 170.1; 170.1

[a]Assigned from the HMQC spectrum.
[b,c]May be interchanged.
[d]Assignments based on APT data and a comparison with cholesterol.
[c]Carbons in HMBC column are correlated to protons in Carbon no. column.

Can. J. Chem. Downloaded from www.nrcresearchpress.com by 217.78.4.112 on 09/08/12
For personal use only.

lated steroidal epoxide **10** underwent reaction with aqueous perchloric acid in THF to give the *trans* diol **11**, resulting from backside nucleophilic attack of water at the allylic carbon rather than at the tertiary carbon of the epoxide (9). To confirm that water had attacked the diacetate **5** at C6, a separate ring opening experiment was carried out using perchloric acid in ≈1:1 $H_2{}^{16}O/H_2{}^{18}O$ and THF. The ^{13}C NMR resonance assigned by HMQC correlations to C6 (δ 72.4) in the resulting isotopically labelled diol **7** showed a 2.9 Hz splitting due to the $^{16}O/^{18}O$ isotope shift and none of the other resonances in the spectrum showed splitting. Diol **7** was acetylated with acetic anhydride in pyridine to give the triacetate **8**. Comparison of the ^{1}H NMR data for **8** recorded in $CDCl_3$ with the data recorded in pyridine-d_5 revealed a large Δδ for the H3α resonance (+0.58 ppm), consistent with an α configuration for the hydroxyl group at C5. The ring opening and pyridine shift experiments together demonstrated that the epoxide functionality in the glaciasterols had the 5α,6α configurations as shown.

Glaciasterol A (**2**) showed in vitro cytotoxicity in murine leukemia L1210 (ED_{50} ≈ 7 μg/mL) and human breast cancer (ED_{50} ≈ 20 μg/mL) cell line assays.[2]

Experimental

Isolation and purification of glaciasterol A (2) and glaciasterol B diacetate (5)

Samples of *A. glacialis* was collected by hand using SCUBA (−5 m) in Sydney Inlet and Barkley Sound, British Columbia.

[2]The murine leukemia L1210 assays were conducted by Dr. T. Allen, Department of Pharmacology, University of Alberta, and the breast cancer cell line assays were conducted by Dr. J. Emerman, Department of Anatomy, U.B.C. For bioassay details see ref. 10.

Can. J. Chem. Downloaded from www.nrcresearchpress.com by 217.78.4.112 on 09/08/12
For personal use only.

Freshly collected sponge specimens (160 g wet wt.) were extracted with methanol and 1:1 methanol/CH_2Cl_2. The extracts were combined and concentrated *in vacuo* to give an aqueous suspension that was partitioned between brine and ethyl acetate. Separation of the ethyl acetate soluble materials by gradient silica gel flash chromatography (hexanes/ethyl acetate/methanol) gave a fraction containing a complex mixture of glaciasterols (148 mg). The ^{1}H NMR spectrum of the mixture showed that the glaciasterols possessed a common nucleus attached to a variety of side chains. A small amount (≈1 mg) of pure glaciasterol A (**2**) was obtained from the mixture by sequential application of $AgNO_3$ – silica gel radial TLC (ethyl acetate/benzene 2:3) and reversed phase HPLC (H_2O/methanol 3:7). The remainder of the glaciasterols were not separable in their native forms so the mixture was acetylated. Pure glaciasterol B diacetate (**5**) was obtained from the acetylated steroid mixture by sequential application of silica gel flash chromatography (methanol/CH_2Cl_2 1:99), silica gel radial TLC (methanol/CH_2Cl_2 1:99), and reversed phase HPLC (H_2O/methanol 15:85).

Glaciasterol A (2): amorphous white solid; ^{1}H NMR (Table 1); ^{13}C NMR (Table 1); EILRMS *m/z*: 416, 400, 383, 365, 301, 239, 97; EIHRMS *m/z*: 416.2936 ($C_{26}H_{40}O_4$, ΔM + 0.9 mmu).

Acetylation of glaciasterol A (2)

Glaciasterol A (**2**) (1 mg) was stirred overnight with pyridine and acetic anhydride (0.5 mL each). Excess reagent was removed *in vacuo* to yield pure *glaciasterol A diacetate (4):* white solid; UV (CH_2Cl_2) λ_{max}: 254 nm (ε = 2850); IR (film): 1737, 1685, 1240 cm^{-1}; ^{1}H NMR (Table 2); ^{13}C NMR (Table 2); EILRMS *m/z*: 500, 440, 424, 364, 349, 327, 267, 97; EIHRMS *m/z*: 500.3139 ($C_{30}H_{44}O_6$, ΔM +0.1 mmu).

Acid-catalyzed ring opening of the 5,6-epoxide of glaciasterol A diacetate (4)

Glaciasterol A diacetate (**4**) was stirred for 2 h with THF (0.5 mL) and perchloric acid (20 μL, 69–72%). Excess acid was neutralized with 5% $NaHSO_3$(aq.) and the resulting aqueous solution was extracted with dichloromethane. The organic extracts were pooled, dried over Na_2SO_4, filtered, and evaporated *in vacuo*. The resulting diol was acetylated as previously described and purified by reversed phase HPLC (H_2O/methanol 1:4) to yield the triacetate **6**: white solid; IR (film): 3402, 1738, 1688 cm^{-1}. ^{1}H NMR (400 MHz, $CDCl_3$) δ: 0.68 (s, Me18), 0.95 (d, *J* = 6.7 Hz, Me25, Me26), 1.03 (d, *J* = 6.8 Hz, Me21), 1.35 (s, Me19), 2.01 (s, OAc), 2.04 (s, OAc), 2.13 (s, OAc), 3.29 (dd, *J* = 10.4, 7.6 Hz, H14), 4.17–4.28 (m, H11, H11′), 5.09 (m, H3), 5.19 (d, *J* = 5.1 Hz, H6), 6.34 (d, *J* = 5.1 Hz, H7); EIHRMS *m/z*: 560.3340 ($C_{32}H_{48}O_8$, ΔM −0.9 mmu).

Glaciasterol B diacetate (5): white needles (H_2O/methanol), mp 55–57°C; IR (film): 1735, 1684 cm^{-1}; CD (MeOH) Cotton effects: λ_{max} (molar elipticities) 335 nm (+8.0 × 10^3), 263 nm (−1.7 × 10^4), 201 nm (−2.6 × 10^4); ^{1}H NMR (Table 2); ^{13}C NMR (Table 2); EILRMS *m/z* (rel. intensity): 516(7), 456(34), 440(16), 343(7: M^+ − (HOAc + C_8H_{17})); EIHRMS *m/z*: 516.3451 ($C_{31}H_{48}O_6$, ΔM 0.0 mmu).

Acid-catalyzed ring opening of the 5,6-epoxide of glaciasterol B diacetate (5)

Glaciasterol B diacetate (**5**) (4 mg) was stirred for 4 h with THF (0.25 mL) and perchloric acid (25 μL). The reaction work-up was identical to that described above for the reaction of glaciasterol A diacetate (**4**). The resulting white solid was purified by reversed phase HPLC (H_2O/methanol 1:4) to yield 5α,6β-dihydroxy glaciasterol B diacetate (**7**). Acetylation of the diol, as described above, gave 5α-hydroxyglaciasterol B triacetate (**8**).

5α,6β-Dihydroxyglaciasterol B diacetate (7): white solid; IR (film): 1739, 1714, 1677 cm^{-1}; ^{1}H NMR (400 MHz, $CDCl_3$) δ: 0.76 (s, Me18), 0.87 (d, *J* = 6.6 Hz, Me26, Me27), 0.99 (d, *J* = 6.7 Hz, Me21), 1.38 (s, Me19), 2.00 (s, OAc), 2.04 (s, OAc), 3.29 (dd, *J* = 11.0, 8.6 Hz, H14), 4.03 (d, *J* = 5.1 Hz, H6), 4.12–4.25 (m, H11, H11′), 5.11 (m, H3), 6.42 (d, *J* = 4.9 Hz, H7); ^{13}C NMR (125 MHz, benzene-d_6, partial assignments from HMQC data) δ: 202.3(C9) 170.3(OAc), 170.1(OAc), 138.2(C7), 137.3(C8), 76.5(C5), 72.4(C6), 70.7(C3), 61.5(C11), 50.5, 48.2, 46.4, 43.2(C14), 39.9, 37.4, 35.9, 35.8, 35.1, 28.3, 27.8, 27.1, 26.8, 26.4, 25.0, 23.0(C27), 22.8(C26), 21.5(C19), 21.0, 20.7, 19.2, 17.4(C18); EIHRMS *m/z*: 534.3560 ($C_{31}H_{50}O_7$, ΔM +0.3 mmu).

5α-Hydroxyglaciasterol B triacetate (8): white solid; IR (film): 3448, 1739, 1683 cm^{-1}; ^{1}H NMR (400 MHz, benzene-d_6) δ: 0.66 (s, Me18), 0.90 (d, *J* = 6.6 Hz, Me26, Me27), 0.98 (d, *J* = 6.7 Hz, Me21), 1.27 (s, Me19), 1.70 (s, OAc), 1.72 (s, 6H, OAc), 3.40 (dd, *J* = 10.8, 8.9 Hz, H14), 4.44 (m, 2H, H11, H11′), 5.04 (d, *J* = 5.0 Hz, H6), 5.15 (m, H3), 6.27 (d, *J* = 5.1 Hz, H7); EIHRMS *m/z*: 576.3670 ($C_{33}H_{52}O_8$, ΔM +0.8 mmu).

Acid-catalyzed ring opening of the 5,6-epoxide of glaciasterol B diacetate (5) with $H_2{}^{18}O$

Glaciasterol B diacetate (**5**) (4 mg) was stirred for 4 h with THF (0.25 mL), H_2O (100 μL), $H_2{}^{18}O$ (97.5 at.% ^{18}O, 125 μL), and perchloric acid (25 μL). The reaction work-up was identical to that described above to yield ^{18}O-labelled 5α,6β-dihydroxyglaciasterol B diacetate (**7**).

Acknowledgement

Financial support was provided by grants to R.J.A. from the Natural Sciences and Engineering Research Council of Canada and the National Cancer Institute of Canada. J.P. was supported by a fellowship from the Fonds pour la formation de chercheurs et l'aide à la recherche (FCAR). The authors wish to thank Dr. W. Austin, M. LeBlanc, and the staff of the Bamfield Marine Station for assisting the collection of *A. glacialis* and Dr. Austin for identifying the sponge. We wish to thank Drs. Allen and Emerman for conducting the cytotoxicity assays.

1. (*a*) F. E. Koehn, M. Gunasekera, and S. S. Cross. J. Org. Chem. **56**, 1322 (1991); (*b*) A. Madaio, G. Notaro, V. Piccialli, and D. Sica. J. Nat. Prod. **53**, 565 (1990); (*c*) M. Tischler, S. W. Ayer, R. J. Andersen, J. F. Mitchell, and J. Clardy. Can. J. Chem. **66**, 1173 (1988); (*d*) R. R. West and J. H. Cardellina. J. Org. Chem. **53**, 2782 (1988).
2. (*a*) E. L. Enwall, D. Van Der Helm, I. Nan Hsu, T. Pattabkiraman, F. J. Schmitz, R. L. Spraggins, and A. J. Weinheimer. J. Chem. Soc. Chem. Commun. 215 (1972); (*b*) R. Kazlauskas, P. T. Murphy, B. N. Ravi, R. L. Sanders, and R. J. Wells. Aust. J. Chem. **35**, 69 (1982); (*c*) C. Bonini, C. B. Cooper, R. Kazlauskas, R. J. Wells, and C. Djerassi. J. Org. Chem. **48**, 2108 (1983).
3. A. Migiuolo, V. Piccialli, and D. Sica. Tetrahedron, **37**, 7937 (1991).
4. R. J. Capon and D. J. Faulkner. J. Org. Chem. **50**, 4771 (1985).
5. (*a*) M. Tischler, R. J. Andersen, I. Choudhary and J. Clardy. J. Org. Chem. **56**, 42 (1991); (*b*) M. Tischler and R. J. Andersen. Tetrahedron Lett. **30**, 5717 (1989).
6. R. J. Stonard, J. C. Petrovich, and R. J. Andersen. Steroids, **36**, 81 (1980).
7. M. Ishiguro, A. Kajikawa, T. Haruyama, Y. Ogura, M. Okabayashi, M. Morisaki, and N. Ikekawa. J. Chem. Soc. Perkin Trans. 1, 2296 (1975).
8. R. Silverstein, G. Bassler, and T. Morrill. Spectroscopic identification of organic compounds. 4th Ed. John Wiley and Sons, New York. 1981. p. 318.
9. M. Weissenberg, D. Lavie, and E. Glotter. J. Chem. Soc. Perkin Trans. 1, 795 (1977).
10. J. Stingl, R. J. Andersen, and J. T. Emerman. Cancer Chemother. Pharmacol. In press.

Molecular recognition XII. The binding of the H human blood group determinants and congeners by a lectin of *Galactia tenuiflora*[1]

RÉMY CROMER, ULRIKE SPOHR, DEVESHWARI P. KHARE, JACQUES LEPENDU,[2] AND RAYMOND U. LEMIEUX[3]

Department of Chemistry, University of Alberta, Edmonton, Alta., Canada T6G 2G2

Received December 6, 1991

This paper is dedicated to Professor Zdenek (Denny) Valenta on the occasion of his 65th birthday

RÉMY CROMER, ULRIKE SPOHR, DEVESHWARI P. KHARE, JACQUES LEPENDU, and RAYMOND U. LEMIEUX. Can. J. Chem. **70,** 1511 (1992).

The H-type 2 human blood group-related trisaccharide (α-L-Fuc-(1c→2b)-β-D-Gal-(1b→4a)-β-D-GlcNAc-OMe (**52**)) is bound by the anti-H lectin of *Galactia tenuiflora* very differently than by the lectin I of *Ulex europaeus*. The reason why the *Galactia* lectin binds the H-type 1 related trisaccharide (α-L-Fuc-(1c→2b)-β-D-Gal-(1b→3a)-β-D-GlcNAc-OMe (**5**)) more strongly and methyl α-L-fucopyranoside much more weakly than does the *Ulex* lectin is that, for the *Galactia* lectin, the hydroxyl groups at positions 3a, 3b, 4b, and 4c are indispensable to complex formation whereas it is the hydroxyl groups at positions 3b, 2c, 3c, and 4c which provide the key polar intractions in the case of the *Ulex* lectin. The H-type 2 (**52**) · *Galactia* lectin complex appears to have the hydroxyl groups at positions 6b, 2c, and 3c at or near the periphery of the combining site and the three key hydroxyl groups hydrogen bonded to the protein deep within the combining site and sheltered from water. The CH_3O-1a, NHAc-2a, and CH_2OH-6a groups likely remain in the aqueous phase remote from the surface of the protein.

RÉMY CROMER, ULRIKE SPOHR, DEVESHWARI P. KHARE, JAQUES LEPENDU et RAYMOND U. LEMIEUX. Can. J. Chem. **70,** 1511 (1992).

On observe que la liaison entre le trisaccharide du groupe sanguin H-de type 2 (α-L-Fuc-(1c→2b)-β-D-Gal-(1b→4a)-β-D-GlcNAc-OMe (**52**)) et la lectine anti-H de *Galactia tenuiflora* est très différente de celle qui le lie à la lectine I de l'*Ulex europaeus*. La raison de la liaison entre la lectine de *Galactia* et le trisaccharide relié groupe H de type 1 (α-L-Fuc-(1c→2b)-β-D-Gal-(1b→3a)-β-D-GlcNAc-OMe (**5**)) qui est plus forte — et la liaison avec l'α-L-fucopyranoside de méthyle qui est beaucoup plus faible — que celles avec la lectine d'*Ulex* est que, pour la lectine de *Galactia*, les groupes hydroxyles aux positions 3a, 3b, 4b et 4c sont indispensables pour la formation de complexe alors que ce sont les groupes hydroxyles en positions 3b, 2c, 3c et 4c qui fournissent les interactions polaires clés dans le cas de la lectine d'*Ulex*. Le complexe groupe H de type 2 (**52**) · la lectine de *Galactia* semble posséder des groupes hydroxyles dans les positions 6b, 2c et 3c au niveau de, ou à la proximité de, la périphérie du site de liaison alors que les trois groupes hydroxyles clés sont liés par des ponts hydrogènes avec la protéine qui se trouve à l'intérieur du site de liaison, protégé de l'eau. Les groupes CH_3O-en la, NHAc- en 2a et Ch_2OH- en 6a restent vraisemblablement dans la phase aqueuse qui se trouve éloignée de la surface de la protéine.

[Traduit par la rédaction]

Can. J. Chem. Downloaded from www.nrcresearchpress.com by 217.78.4.112 on 09/08/12
For personal use only.

Introduction

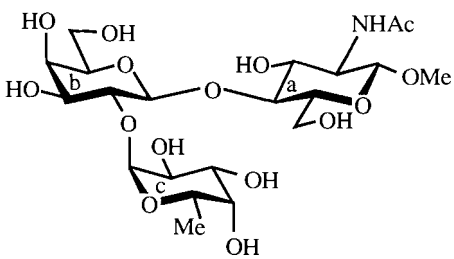

H-type 2 (**52**)

We recently reported detailed studies of the binding of the H-type 2 determinant (α-L-Fuc-(1→2)-β-D-Gal-(1→4)-β-D-GlcNAc-OMe (**52**)) both by the lectin I of *Ulex europaeus* (1, 2) and by a monoclonal anti-H-type 2 antibody (2). It was concluded that the interactions leading to complex formation are very similar in that the 3b, 2c, 3c, and 4c hydroxyl groups provide the key polar interactions for binding by the *Ulex* lectin whereas that by the antibody involves the 3b, 2c, and 3c hydroxyl groups. In each case, the remaining hydroxyl groups were found to reside either at the periphery of the combining site or remote from the protein and exposed to interaction with bulk water molecules. These similar interactions for a lectin and an antibody are in sharp contrast to the difference between how the Lewis-b human blood group determinant-related tetrasaccharide (α-L-Fuc-(1→2)-β-D-Gal-(1→3)-[α-L-Fuc-(1→4)]-β-D-GlcNAc-OMe) is bound by the lectin IV of *Griffonia simplicifolia* (3) and by a monoclonal anti-Lewis b antibody (4). In the case of the lectin, the key polar interactions are established by OH-3, OH-4 of the β-D-Gal unit and OH-4 of the α-L-Fuc-(1→4) unit, whereas for the antibody only the involvements of OH-3 of the β-D-Gal and OH-2 of the α-L-Fuc-(1→2) units are essential. We now report that the binding of the H-type 2 trisaccharide (**52**) by a recently reported lectin from the seeds of the plant *Galactia tenuiflora* (5) is much different from that previously reported (1) for the lectin I of *Ulex europaeus*.

Discussion

Synthesis

The starting material for the synthesis of the methyl glycoside of the H-type 1 trisaccharide **5** (Scheme 1) was the alcohol **2** obtained from the previously described disaccharide **1** (6). Compound **2** was reacted with tri-*O*-benzyl fucosyl bromide (**3**) (6, 7) under halide ion catalyzed conditions (8) to produce the trisaccharide **4** in 73% yield. Hydrogen-

[1]Part XI in this series is ref. 2.

[2]Université de Nantes, Institut National de la Santé et de la Recherche Médicale, 1, rue Gaston Veil, 44035 Nantes Cédex 01, France.

[3]Author to whom correspondence may be addressed.

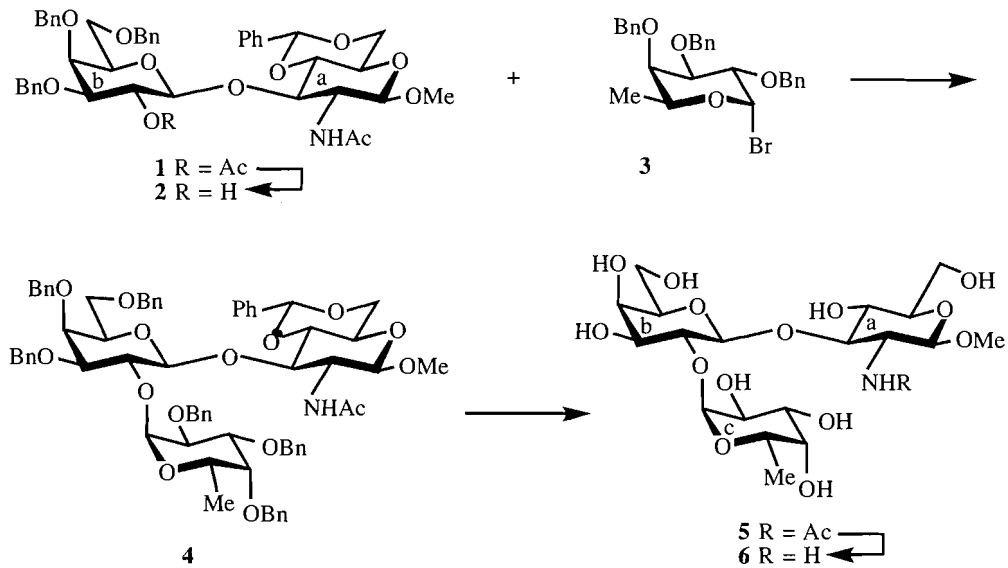

SCHEME 1

ation of **4** over 5% palladium-on-carbon provided **5** in 82% yield. Treatment of **5** with 85% hydrazine hydrate at 140°C for 12 days afforded the amine (**6**) in 66% yield. The ^{13}C nmr data presented in Table 1 and ^{1}H nmr parameters reported in the experimental section fully support the structural assignment.

The syntheses of the 4a- and 6a-deoxy derivatives of **5** are outlined in Scheme 2. Reductive cleavage of the benzylidene ring of **1** with sodium cyanoborohydride – hydrogen chloride (9) produced both the alcohols **7** (73%) (6) and **8** (17%). The Robins and Wilson modification (10) of the Barton–McCombie reaction (11) was used to prepare the deoxy derivative **10** by way of **9** in 50% overall yield. The de-*O*-acetylated derivative (**11**) was α-L-fucosylated to **12** in 57% yield and this product was de-*O*-benzylated in the usual fashion to provide 4a-deoxy-H-type 1-OMe (**13**) in 60% yield.

The **6a**-deoxy-H-type 1-OMe congener (**19**) was prepared first by tosylation of **8** to **14**, then replacement of the tosyloxy group by iodine to form **15** followed by reduction with tributyltin hydride. The overall yield from **8** was 51%. Deacetylation to **17** and subsequent α-L-fucosylation provided **18** in 90% yield which was de-*O*-benzylated in 98% yield to the desired compound **19**.

The 6b-deoxy-*nor*-compound **24** was prepared as outlined in Scheme 3. The known disaccharide **20** (12) was deacetylated to **21** and the 3b and 4b were positions protected by benzylidenation with α,α-dimethoxytoluene in the presence of *p*-toluenesulfonic acid to provide **22** in 90% yield. α-L-Fucosylation in the usual way gave **23** in 81% yield. Catalytic hydrogenolysis removed both the benzyl and benzylidene groups to afford **24** in 92% yield.

To synthesize 3a-deoxy H-type 2-OMe (**33**) (Scheme 4), the disaccharide **27** was prepared, in 53% yield, by reaction of the bromide **25** (13) with alcohol **26** (6) under Helferich conditions. Compound **27** was deallylated to the alcohol **28**, which was deoxygenated at the 3a position in the manner described above for the conversion of **7** to **10**. The origin of the 3-*O*-phenoxycarbonyl derivative of **28**, isolated as a by-product in 8.3% yield, was not determined. The structural assignments were confirmed by fab-mass and ^{1}H nmr spectroscopy. Deacetylation of **30** gave the alcohol **31** which was α-L-fucosylated in the usual way to provide **32** in 69% yield. Catalytic hydrogenolysis afforded the desired congener (**33**). The overall yield from **27** was 42%.

The coupling constants for H-1a and H-2a listed in Table 2 for compounds **27**, **30**–**32** in $CDCl_3$ are much smaller than the near 8 Hz expected should the substituted β-D-GlcNAc residue be in the $^{4}C_{1}$ conformation (**A**) that is normally observed for all-*trans gluco* compounds. Evidently, important contributions to these time-averaged coupling constants are made by these hydrogens in *syn*-clinal relationship. The presence of such conformers could arise from the formation, in an aprotic solvent, of an intramolecular hydrogen bond between the AcN-H group and O-4a in *syn*-axial relationship as shown in Table 2 for the β-D-GlcNAc residue in either the $^{1}C_{4}$ (**B**) or $^{3,0}B$ (**C**) conformations. This must be the case since, as seen in Table 2, the $^{4}C_{1}$ conformation becomes highly populated when the solvent is changed to CD_3OD. The actual ring conformational preferences are surely in between the extremes presented in Table 2, and, therefore, analyses of the coupling constants can only provide qualitative assessments of the conformational equilibria.

The influence of solvent on the equilibrium presented in Table 2 is reminiscent of the conformational preferences for 1,3-diols (14). The fact that the alcohol **28** (R=OH) retains the $^{4}C_{1}$ conformation for the β-D-GlcNAc residue in $CDCl_3$ can be attributed to the highly favorable O-5b→HO-3a intramolecular hydrogen bond (15). An importantly destabilizing nonbonded interaction is expected to occur in **27** between the allyloxy group and O-5b of the β-D-Gal unit. Therefore, the O-4a→HN-2a hydrogen-bonded conformer becomes more abundant, as reflected by the smaller value for $J_{1a,2a}$, when the allyloxy group is replaced by hydrogen. In an aprotic solvent, OH-2b of alcohol **31** (R=H) can be expected to tend to form a hydrogen bond with O-4a and, thereby, weaken the competing O-4a→H-N-2a bond. This would explain the larger value for $J_{1a,2a}$ of **31** as compared to that of **30** (see Table 2). The fact that the substitution of

Can. J. Chem. Downloaded from www.nrcresearchpress.com by 217.78.4.112 on 09/08/12
For personal use only.

TABLE 1. The ^{13}C nmr chemical shifts (ppm) for the H-type 1 blood group determinant (α-L-Fuc-(1→2)-β-D-Gal-(1→3)-β-D-GlcNAc-OMe (**5**)) and related structures[a]

		Derivatives of H-type 1-OMe (**5**)			
	H-type 1-OMe (**5**)	*N*-Deacetyl (**6**)	4a-Deoxy (**14**)	6a-Deoxy (**19**)	5b-Dehydroxymethylene (**24**)
β-D-GlcNAc a-unit					
C-1	103.47	103.94	104.09	103.43	103.35
C-2	55.58	57.16[b]	56.68	55.81	55.56
C-3	78.19	84.32	74.74[b]	77.77	78.74
C-4	69.63	69.27	35.42	74.94	69.46
C-5	76.32	76.57	73.23[b]	72.36	76.39
C-6	61.63[b]	61.60[c]	64.43	17.74	61.59
CH_3O	58.05	58.19[b]	58.01	58.13	58.04
CH_3CO	23.04	—	23.08	23.03	23.04
CO	174.57	—	174.72	174.57	174.66
β-D-Gal b-unit					
C-1	100.97	101.76	102.24	100.95	101.35
C-2	77.51	77.79	77.35	77.50	77.67
C-3	74.35	74.01	74.34	74.31	73.48
C-4	69.98	69.75	69.87	69.97	69.15
C-5	75.95	76.13	75.98	75.89	66.27
C-6	61.94[b]	61.77[c]	61.77	61.32	—
α-L-Fuc c-unit					
C-1	100.33	100.41	100.24	100.35	100.44
C-2	68.95	68.52	68.96	68.92	68.91
C-3	70.30	70.46	70.33	70.27	70.27
C-4	72.68	72.54	72.65	72.67	72.65
C-5	67.31	68.10	67.40	67.29	67.40
C-6	16.03	16.24	16.07	16.02	16.07

[a]0.05 M solutions in D_2O with dioxane as internal standard at 67.4 ppm were measured at 75 MHz at 295°. The assignments were made by inspection.

[b,c]The corresponding assignments of the chemical shifts are tentative and may be reversed.

Can. J. Chem. Downloaded from www.nrcresearchpress.com by 217.78.4.112 on 09/08/12
For personal use only.

the 2b-*O*-acetyl group of **30** by the much bulkier 2,3,4-tri-*O*-benzyl-α-L-fucopyranosyl group of **32** has little effect on the conformational equilibrium in $CDCl_3$ is in accord with expectation based on an important contribution to conformational preference by the *exo*-anomeric effect (16). Since this stereoelectronic effect stabilizes the *anti*-periplanar relationship for the C-4a and C-2b atoms, it will favor projection of the substituted β-D-GlcNAc unit away from the *O*-benzylated α-L-Fuc residue. It is noteworthy that the values of the coupling constants assigned to the β-D-GlcNAc unit of compounds **58** and **64** also indicate important contributions to the conformational equilibria in $CDCl_3$ by conformers that allow the intramolecular hydrogen bond depicted in Table 2.

The syntheses of H-type 2-OMe (**52**) (17), which served as the reference inhibitor, and its 3b-, 2c-, 3c-, and 4c-deoxy congeners (**53–56**) are outlined in Scheme 5. Reductive cleavage (9) of methyl 2-acetamido-3-*O*-benzyl-4,6-*O*-benzylidene-2-deoxy-β-D-glucopyranoside (18) provided **39**, which was condensed with bromide **40** (19) under Helferich conditions (66% yield). This product was deacetylated to produce **42**. Benzylidenation with α,α-dimethoxytoluene in the presence of *p*-toluenesulfonic acid then provided the diol **43** in 87% yield. Selective benzoylation of **43** with benzoyl chloride at −78°C provided **44**, which was α-L-fucosylated to the blocked trisaccharide **45** in 74% yield. Debenzoylation and hydrogenolysis of the product (**46**) then produced the H-type 2 trisaccharide as its methyl β-glycoside (**52**). The overall yield from the diol **43** was 41%.

The blocked trisaccharide **46** was also used for the preparation of blocked 3b-deoxy-H-type 2-OMe (**48**), in 52% overall yield, by way of the intermediate 3b-phenylthionocarbonate (**47**). Since partial decomposition occurred in the course of the catalytic hydrogenation to remove the benzyl groups of **48**, the product had to be processed by way of its acetate to obtain pure 3b-deoxy-H-type 2-OMe (**53**) and a meaningful yield cannot be provided.

To prepare 2c-deoxy-H-type 2-OMe **54** (Scheme 5), the disaccharide **44** was reacted with a tenfold excess of bromide **38** (20) under halide-ion-catalyzed conditions. After deacetylation, **49** was isolated in 44% yield and was deblocked by catalytic hydrogenolysis to provide **54** (79% yield).

The 3- and 4-deoxy-α-L-fucopyranosyl bromides (**36** and **37**) were prepared from **34** and **35**, which were obtained by hydrolyses of methyl 2,4-di-*O*-benzyl-3,6-dideoxy- (21) and methyl 2,3-di-*O*-benzyl-4,6-dideoxy-α-L-*xylo*-hexopyranosides.[4] Halide-ion-catalyzed reactions of the bromides **36** and **37** with **44** then produced the 3c- and 4c-deoxy blocked trisaccharides **50** and **51** in 86 and 91% yields. Debenzoyla-

[4]P. Bird and R. U. Lemieux, unpublished results.

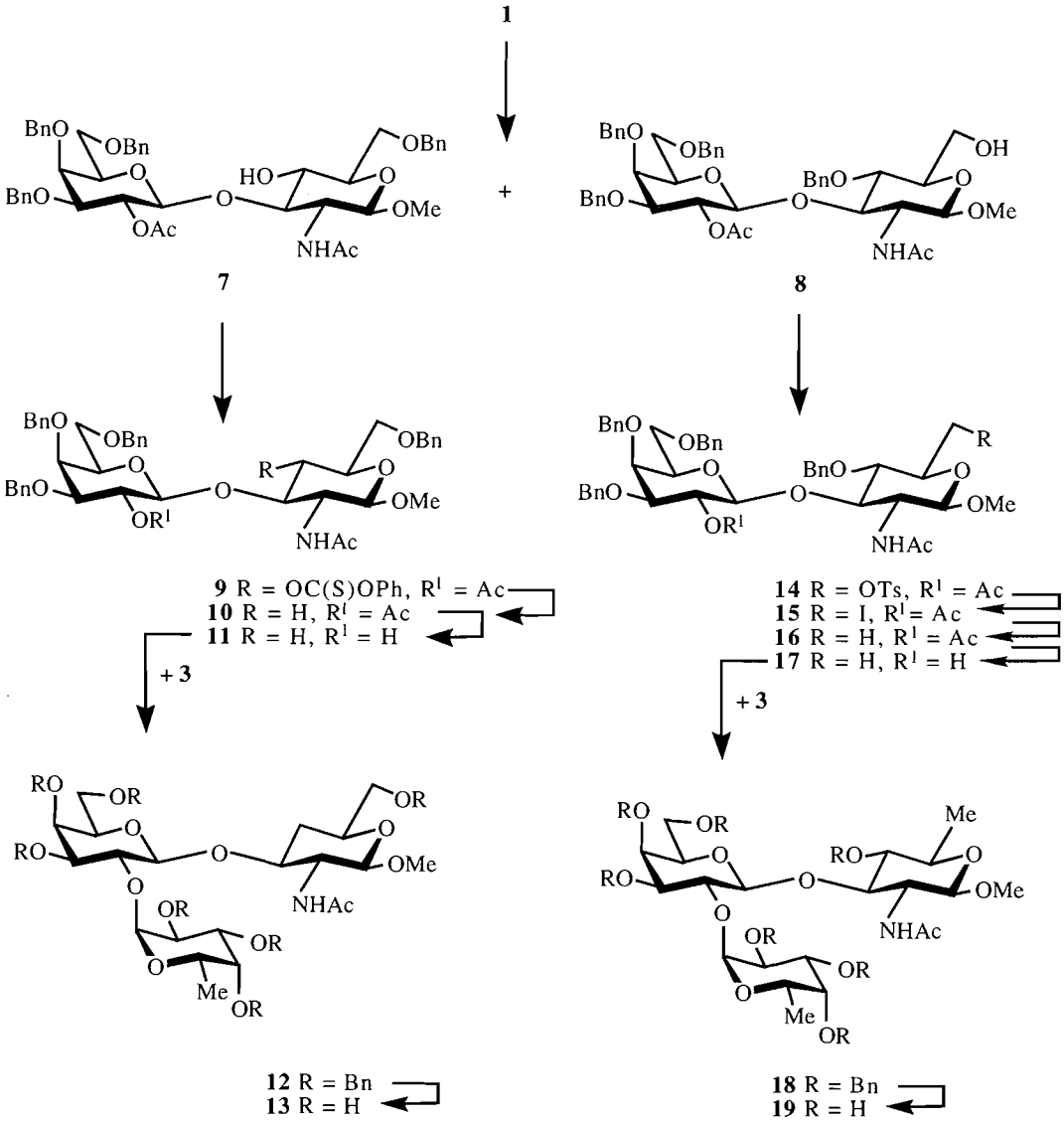

SCHEME 2

tion and subsequent catalytic hydrogenation led to the target molecules **55** (61% yield) and **56** (75% yield).

Scheme 6 outlines the synthesis leading to the 6b-deoxy-H-type 2 congener (**62**). Mercuric cyanide promoted glycosylation of **39** with 6-deoxy acetobromogalactose (**57**) (22) provided the blocked disaccharide **58** in 68% yield. Deacetylation to **59** followed by benzylidenation with α,α-dimethoxytoluene in the presence of *p*-toluenesulfonic acid afforded the alcohol **60** in near quantitative yield. α-L-Fucosylation of **60** provided **61** in 81% yield. The target compound **62** was then obtained in 78% yield by hydrogenolysis in the usual manner.

For the synthesis of 4b-deoxy-H-type 2-OMe congener (**66**) (Scheme 7), the alcohol **39** was glycosylated with the previously reported bromide **63** (12) under Helferich conditions. The disaccharide **64** was isolated in only 19% yield. Since sufficient material was obtained, no optimization was attempted. Deacetylation of **64** was followed by α-L-fucosylation with **3** to give **65** (62% yield). The benzyl groups of **65** were then removed by catalytic hydrogenation to provide the desired 4b-deoxy derivative (**66**) of **52** in 94% yield.

Structural and conformational assignments

The ^{13}C nmr data for H-type 2-OMe (**52**), H-type 1-OMe (**5**), and congeners are reported in Tables 2 and 3. These data together with the ^{1}H nmr parameters reported in the experimental section are in full agreement with the structural assignments. The characteristic interunit deshielding of H-1c for both **52** and **5** by 0.54 and 0.41 ppm, respectively, in comparison to H-1 of α-L-FucOMe, is interpreted as resulting from the proximity of H-1c to O-3b of the βDGal unit (23, 24). Similar specific interunit deshieldings of H-5c of **52** and **5** by 0.19 and 0.26 ppm, respectively, can be attributed to the proximity of H-5c to O-4a in **52**, and to O-3a in **5** (23). Except for 3b-deoxy-H-type 2-OMe (**53**), these deshieldings, relative to H-1 and H-5 of α-L-FucOMe and its monodeoxy derivatives, are observed for all the H-type 2 and H-type 1 congeners. However, whereas deoxygenation of H-type 2-OMe at the 3b position to produce **53** did not affect the chemical shift for H-5c, the signal for H-1c was shifted upfield by 0.33 ppm. A similar specific interunit effect of the chemical shift of H-1d was recently observed on deoxygenation of the 3b-position of the Lewis b tetrasac-

Can. J. Chem. Downloaded from www.nrcresearchpress.com by 217.78.4.112 on 09/08/12
For personal use only.

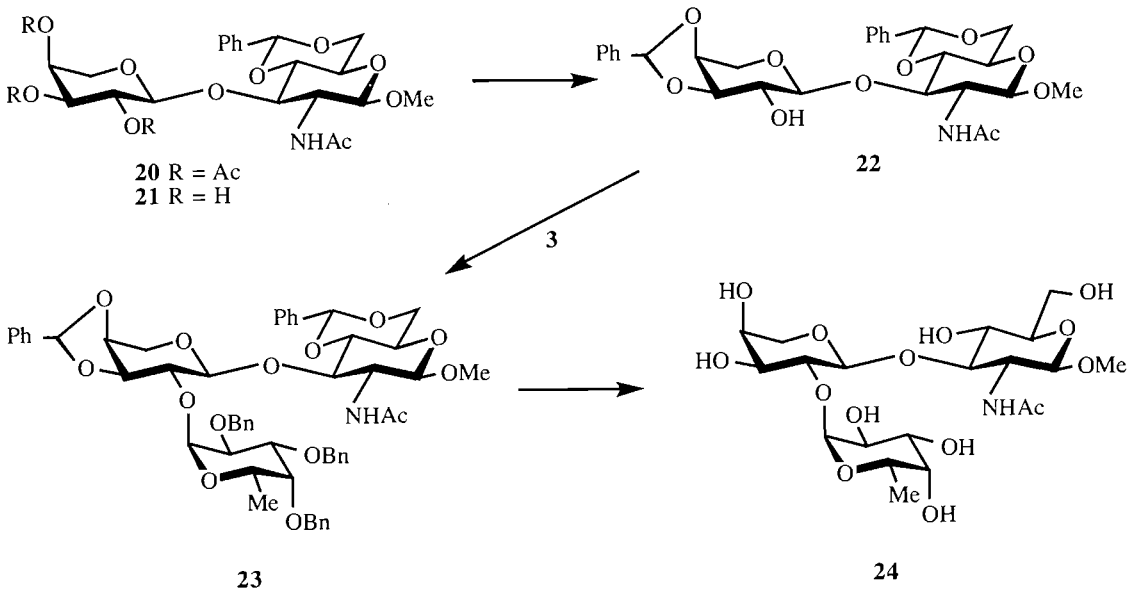

SCHEME 3

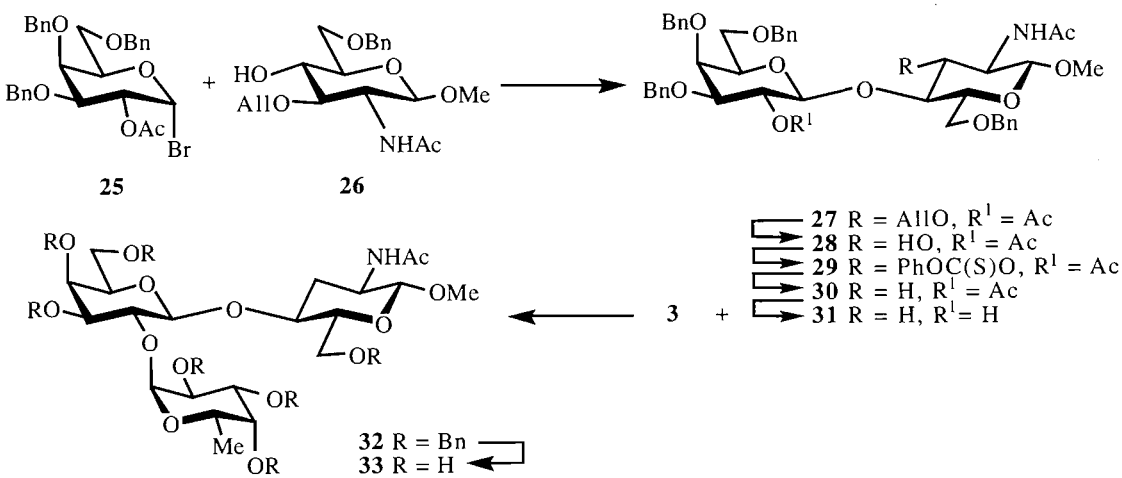

SCHEME 4

charide (12). Thus, the ^{1}H nmr data indicate that the conformational preferences for the interunit glycosidic bonds are not significantly changed by the structural modifications leading to the various H-type 1 and H-type 2 congeners. Consequently, the interpretations attached to the immunochemical data will be based on the HSEA conformers (23), which well accommodate the ^{1}H nmr data. In fact, as will be seen below, the interpretations are highly attractive.

Immunochemical studies

The immunochemical data are based on a previously reported solid-phase competitive radioimmunoassay (3) by which the amounts of haptens required for 50% inhibition of the binding of an ^{125}I-labelled H-type 2-BSA artificial antigen by the immobilized lectin are determined. The results are reported in Tables 4–6.

LePendu *et al.* (5) reported that the *Galactia* lectin has a specificity for the H-type 2 blood group determinant. However, the present investigation has revealed the lectin to also have an affinity for the H-type 1 trisaccharide (**5**) that is only 2–3 times less than that for H-type 2 trisaccharide (**52**). To ensure that the H-type 1 specificity is due to a cross-reaction and not to the presence of a second lectin with an H-type 1 affinity, the lectin preparations were affinity purified both on H-type 2- and H-type 1-Synsorb® columns and the products examined by SDS gel electrophoresis under non-reducing conditions (25). Both the preparations provided bands at 27 and 29 kDa of the same relative intensity of 3:1 as was found in previous preparations (5) and appeared identical. It is concluded, therefore, that the preparation is a single lectin that has an affinity for both the type 1 and type 2 structures (**5** and **52**, respectively) and that these epitopes share common structural features. This can be appreciated from the surfaces presented in Fig. 1 which conform with the following inhibition data.

As seen in Table 4, the H-type 2 related structure (**52**) is only three times more potent an inhibitor of the H-type 2 artificial antigen than is the diastereoisomeric H-type 1-OMe (**5**). That the β-D-GlcNAc unit is involved in the binding of **52** is surely indicated by the inactivity of its 3a-deoxy de-

Can. J. Chem. Downloaded from www.nrcresearchpress.com by 217.78.4.112 on 09/08/12
For personal use only.

TABLE 2. Effects of changes of substituents and solvent on the conformational equilibria of derivatives of lactosamine

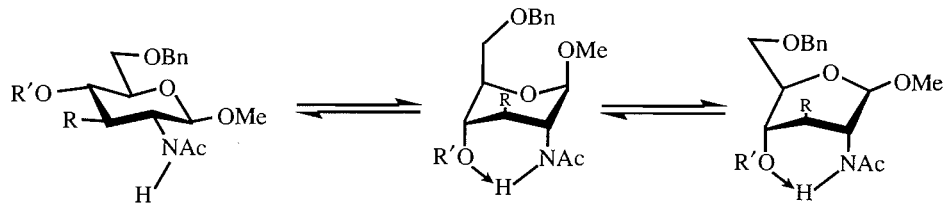

Compound	R[a]	$J_{1a,2a}$, Hz[b]	
		$CDCl_3$	CD_3OC
27	CH_2=CH-CH_2O	4.0	8.0
28	OH	8.0	8.0
30	H	2.0	7.2
31	H	4.0	7.5
32	H	2.5	8.0

[a]The structures for R′ are presented in Scheme 4.
[b]The coupling constants for the other ring protons of the β-D-GlcNAc residues are in accord with the changes listed for $J_{1a,2a}$ (see Experimental).

rivative (**33**). Since the 4a-hydroxyl group of **5** is expected, as seen in Fig. 1, to project toward the β-D-Gal unit in a very similar manner as does OH-3a in **52** (1), the inactivity of 4a-deoxy-H-type 1-OMe (**13**) was not surprising. The difucose derivatives **68** and **76** were also inactive. In view of the high activity retained by the variety of compounds (**69**–**75**) obtained by modifying the CH_2OH group of the GlcNAc unit of **52**, this hydroxyl group is surely not involved in the binding and remains in the aqueous phase. It would be expected, therefore, that *N*-deacetylation of **5** to produce **6** would not materially affect the binding, as was indeed the case. Clearly, however, in the complex, the CH_2OH-5a group of **52** and the NHAc-2a group of **5** must be at the periphery of the combining site (Table 4). This conclusion is in accord with the conformational preferences assigned to these compounds (Fig. 1), which infer that these groups are in close proximity to OH-4c, one of the four hydroxyl groups that, as will be seen below, provide key polar interactions. In view of these observations, the remote methyl aglycons of **52** and **5** were not expected to be directly involved in the complexation. This was confirmed by the high activity of **67**. It appears that the aglycon of **67** contributes a small hydrophobic stabilization of the complex.

Since OH-3a of **52** (or OH-4a of **5**) is essential to complex formation, it could be expected that an H-related disaccharide would be inactive. However, as seen in Table 4, **77** is only about 12 times less potent an inhibitor than is **52**. Evidently, the polar group of the lectin that forms a hydrogen bond with OH-3a of **52** (or OH-4a of **5**) can come into contact with the aqueous phase. Therefore, it is not the loss of the hydrogen bond with the GlcNAc unit that leads to the inactivities displayed by the deoxy compounds **33** and **13**. Instead, these inactivities must result from the resistance by the polar group of the protein to shed its water of hydration in order to form the complex when it is faced with the hydrophobic environment presented by the deoxy compounds. This observation provides experimental support for the postulation earlier made in this regard (26). The about 1.5 kcal/mol lower stability of the complex provided by the H-disaccharide must be related to the changes in protein structure required to accommodate the water molecules that remain attached to the polar group of the combining site.

The involvement of the β-D-Gal unit in the complex formed by the *Galactia* lectin with either H-type 2-OMe (**52**) or H-type 1-OMe (**5**) can be appreciated from the data presented in Table 5 with reference to Fig. 1. It is seen in Fig. 1 that the topography presented by this unit is the same for both the epitopes. Since the changes at the 3b or 4b positions resulted in inactive compounds, these hydroxyl groups provide key polar interactions deep in the combining site where the resulting hydrogen bonds are sheltered from exchange with water. The inactivity of the 6b-deoxy-*nor* derivative (**24**) of H-type 1-OMe (**5**) implies that the CH_2-5b group comes into contact with the combining site. That this nonpolar interaction is at the periphery is indicated by the high activity of the 6b-deoxy H-type 2 compound (**62**). It is to be recognized that, as recently demonstrated (27), the reduced activity does not necessarily mean that OH-6b becomes engaged in a hydrogen bond with the protein. Instead, small changes in the stability of a complex that result from a structural modification of the ligand may indicate that the modification occurred near the surface of the protein and thereby affected the energy of hydration (28).

The results presented in Table 6 require that both OH-4c and Me-5c of the fucose unit are involved in the complexation of **52** by the *Galactia* lectin. Although the replacement of either one of these groups by hydrogen resulted in important loss in activity, complex formation could be detected since the losses in stability were less than 2 kcal/mol. Whereas the removal of OH-4c leads to the loss of a polar interaction, the substitution of the methyl group by hydrogen leads to a loss of complementarity. The OH-2c and OH-3c groups clearly remain in contact with the aqueous phase. It is noteworthy that the methyl glycosides of α-L-fucose (**81**) and *N*-acetyl-β-lactosamine (**80**) are essentially inactive although both provide structural features essential to the epitope.

Can. J. Chem. Downloaded from www.nrcresearchpress.com by 217.78.4.112 on 09/08/12
For personal use only.

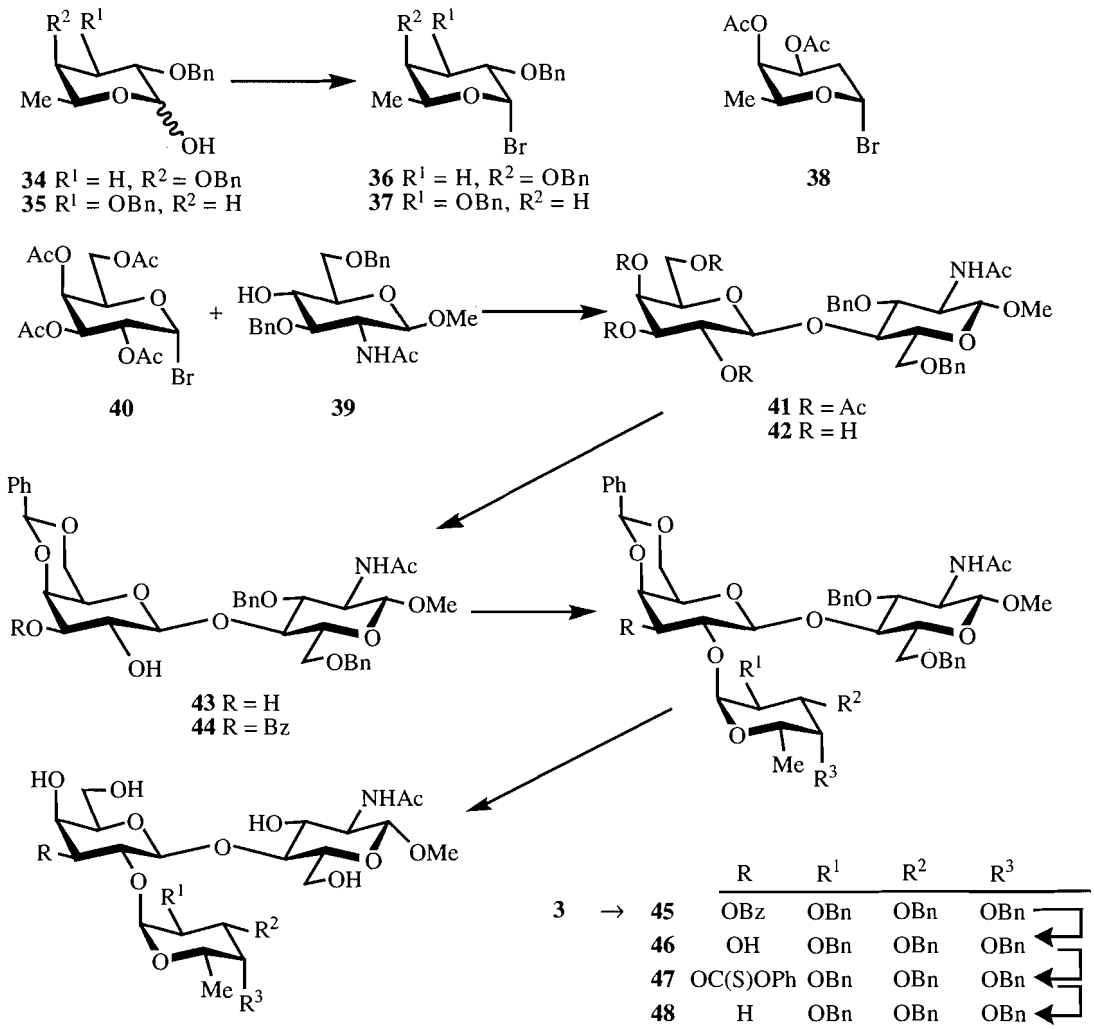

		R	R1	R2	R3
3	→ 45	OBz	OBn	OBn	OBn
	46	OH	OBn	OBn	OBn
	47	OC(S)OPh	OBn	OBn	OBn
	48	H	OBn	OBn	OBn
38	→→ 49	OH	H	OH	OH
36	→ 50	OBz	OBn	H	OBn
37	→ 51	OBz	OBn	OBn	H

	R	R1	R2	R3
52	OH	OH	OH	OH
53	H	OH	OH	OH
54	OH	H	OH	OH
55	OH	OH	H	OH
56	OH	OH	OH	H

SCHEME 5

According to the foregoing interpretations of the experimental data, the lower activity of H-type 1-OMe (**5**) as compared to that of H-type 2-OMe (**52**) is related to the difference in hydration about the acetamido group of **52** to that about the hydroxymethyl group of the β-D-GlcNAc unit of **5**. We have unequivocally established in the case of the binding of the Lewis b-OMe tetrasaccharide by the lectin IV of *Griffonia simplicifolia* (28) that decreases in the stability of a complex by as much as 0.7 kcal/mol can occur by substitutional changes in groups that are near the periphery of the combining site but remain in bulk water solution. These observations are of major significance to attempts at drawing conclusions as to the size of combining sites. Thus, for example, the binding of linear, regular oligosaccharides has been observed on several occasions to increase with increasing chain length (29). Normally, after the trisaccharide level, the increases are less than 0.5 kcal/mol. In view of the present findings (27), changes of this magnitude do not necessarily relate to the size of the combining site. Instead, these may be related to changes in the hydration of the complex that result from increasing the chain length by sugar units that are close to, but not in contact with, the protein.

In contrast to the *Galactia* lectin, which binds the H-type 2 trisaccharide (**52**) only three times more strongly than the H-type 1 isomer (**5**) (see Table 4), we have now determined that the lectin I of *Ulex europaeus* binds **52** 100 times more strongly than it does **5**. As previously reported (30), de-*N*-acetylation of **5** provides a much superior inhibitor. Indeed, we now find that the amine (**6**) is only four times less potent

Can. J. Chem. Downloaded from www.nrcresearchpress.com by 217.78.4.112 on 09/08/12
For personal use only.

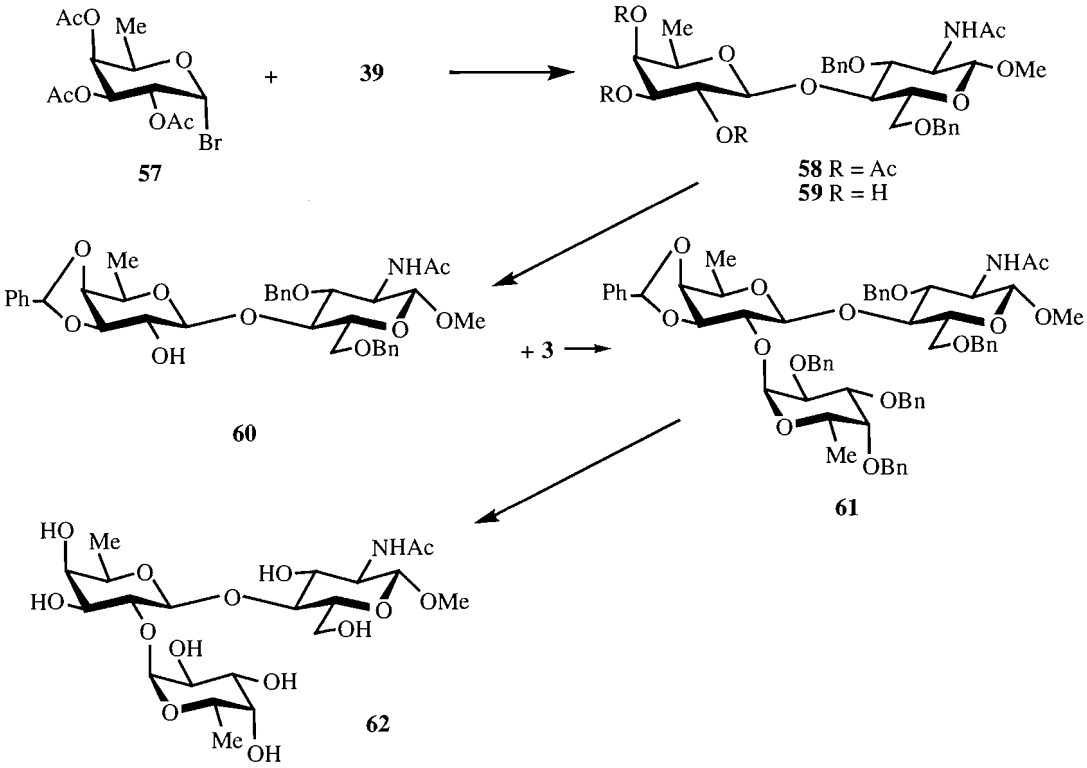

SCHEME 6

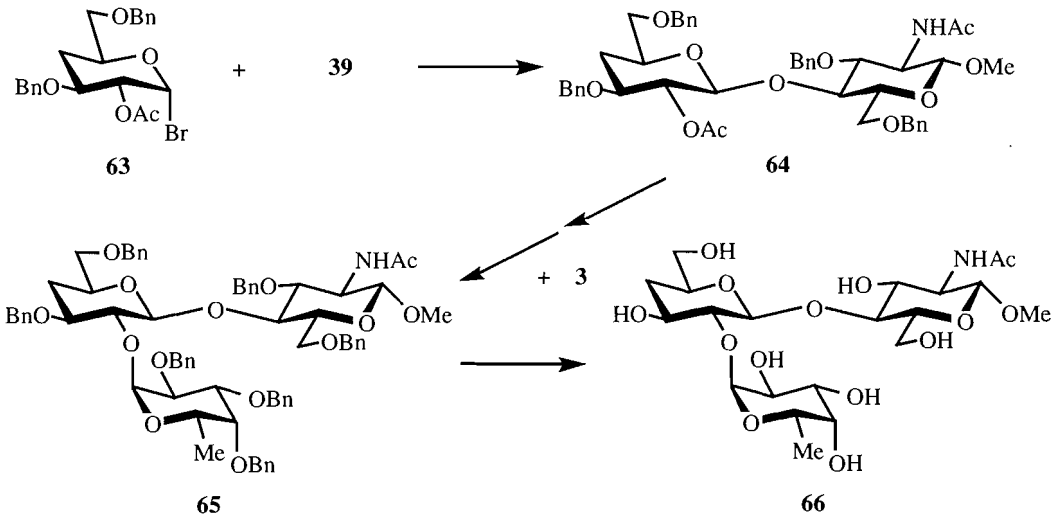

SCHEME 7

an inhibitor than is **52**. These results are readily appreciated from the structures presented in Fig. 2.

The probing of the combining site of the *Ulex* lectin has shown (2) that the binding of **52** involves the polyamphiphilic surface presented in Fig. 2 wherein the four hydroxyl groups known to provide key polar interactions are displayed. Much the same surface can be presented by the H-type 1 isomer (**5**). The main difference is that the acetamido group of **5** is projected to near the region that is bound. In view of the activity of **6**, the involvement of the acetamido group must be at the periphery of the combining site. Also the 6a-methylene group of the β-D-GlcNAc unit of **52** must be at, or close to, the periphery of the combining site since the 6a-hydroxyl group, in contrast to earlier indications (1), is not directly involved in the binding reaction (2). These data therefore allow the important conclusion that the surface recognized by the lectin is much smaller than that suggested on the basis of probing experiments (1). Indeed, the binding appears to be restricted to the rather small hydrophilic, but polyamphiphilic, surface presented in Fig. 2. The data also lend strong support to the conformational preferences assigned to the trisaccharides (**5** and **52**).

Can. J. Chem. Downloaded from www.nrcresearchpress.com by 217.78.4.112 on 09/08/12
For personal use only.

TABLE 3. The ^{13}C nmr chemical shifts (ppm) for the H-type 2 blood group determinant (α-L-Fuc-(1→2)-β-D-Gal-(1→4)-β-D-GlcNAc-OMe (**52**)) (17) and related structures[a]

		Derivatives of H-type 2-OMe (**52**)						
	H-type 2-OMe (**52**)	3a-Deoxy (**33**)	3b-Deoxy (**53**)	4b-Deoxy (**66**)	6b-Deoxy (**62**)	2c-Deoxy (**54**)	3c-Deoxy (**55**)	4c-Deoxy (**56**)
β-D-GlcNAc a-unit								
C-1	102.73	104.18	102.69	102.65	102.67	102.74	102.73	102.73
C-2	56.03	49.73	55.89	56.18	55.94	56.03	56.02	55.99
C-3	73.23	36.13	73.29	73.11	73.21	73.25	73.27	73.28
C-4	77.26[b]	72.95	78.65[b]	77.90	76.93	77.38	77.02[b]	77.41[b]
C-5	76.14[c]	79.57	76.14	76.16	76.01	76.13[b]	76.13[c]	76.06
C-6	61.10	61.68	61.17	61.15	61.19	61.10	61.06	61.01
CH_3O	57.90	57.61	57.91	57.87	57.92	57.91	57.89	57.91
CH_3CO	23.05	22.86	23.03	23.07	23.05	23.04	23.04	23.04
CO	175.41	174.61	175.44	175.39	175.41	175.41	175.41	175.42
β-D-Gal b-unit								
C-1	101.19	102.30	103.34	101.42	101.22	101.30	101.32	101.30
C-2	77.32[b]	77.10	70.49	81.06	78.03	76.31[b]	77.34[b]	77.31[b]
C-3	74.43	74.45	34.69	72.15	74.64	74.52	74.52	74.41
C-4	69.97	69.80	68.49[c]	35.36	72.58	70.08	69.98	69.93
C-5	76.09[c]	75.94	79.30[b]	73.61	71.72	76.13[b]	76.08[c]	76.06
C-6	61.87	61.68	62.10	64.36	16.05	61.86	61.88	61.88
α-L-Fuc c-unit								
C-1	100.26	100.15	95.98	100.32	100.19	99.39	99.53	100.73
C-2	69.13	69.08	66.27[c]	69.20	69.12	31.72	64.11	74.30
C-3	70.54	70.43	70.49	70.58	70.53	65.94	33.80	68.12
C-4	72.56	72.56	72.58	72.58	72.58	71.15	69.06	40.46
C-5	67.74	67.72	67.63	67.73	67.72	67.74	67.40	66.03
C-6	16.14	16.17	16.04	16.14	16.14	16.67	16.19	20.45

[a]0.05 M solutions in D_2O with dioxane as internal standard at 67.4 ppm were measured at 75 MHz at 295°. The assignments were made by inspection.
[b,c]The corresponding assignments of the chemical shifts are tentative and may be reversed.

Can. J. Chem. Downloaded from www.nrcresearchpress.com by 217.78.4.112 on 09/08/12
For personal use only.

Experimental

Methods

The isolation of the lectin of *Galactia tenuiflora* was carried out as described (5). Approximately 200 mg of the affinity-purified lectin were isolated from 50 g mature seeds. Stock solutions of the lectin in phosphate buffer solution (3) were of light brownish colour.

The radioimmunoassays were performed following the procedure recently described (3) using an ^{125}I-labelled [α-L-Fuc-(1→2)-β-D-Gal-(1→4)-β-D-GlcNAcO-$(CH_2)_8$CONH]$_{16}$–BSA antigen with an initial activity of 250 000 cpm/100 μL provided by Chembiomed Ltd., Edmonton, Canada. The coated polystyrene vials were prepared with the affinity-purified lectin at a concentration of 100 μg/mL in PBS buffer. In the absence of inhibitor, the coated tubes acquired about 120 000 cpm.

The ^1H nmr spectra were measured at 300, 360, and 400 MHz (Bruker AM 300, WM 360, and WH 400) with tetramethylsilane as internal standard for $CDCl_3$ solutions. Reference standard for D_2O solutions was acetone (2.225 ppm). The ^{13}C nmr spectra were recorded at 100 and 75 MHz (Bruker WH 400 and AM 300) using as a solvent either $CDCl_3$ (77.0 ppm) or D_2O with dioxane (67.4 ppm) as internal standard. Optical rotations were measured at room temperature (23 ± 1°C) in a 1-dm cell on a Perkin Elmer 241 polarimeter. Thin-layer chromatograms were performed on precoated plates of silica gel (60-F 254, E. Merck, Darmstadt) and visualized by spraying with 10% sulfuric acid in ethanol followed by heating. For column chromatography, silica gel 60 (230–240 mesh, E. Merck) and distilled solvents were used. Solvents and reagents were purified and dried according to standard procedures. Melting points are uncorrected.

Methyl 2-acetamido-4,6-O-benzylidene-2-deoxy-3-O-(3,4,6-tri-O-benzyl-β-D-galactopyranosyl)-β-D-glucopyranoside (2)

Compound **1** (5.0 g, 6.27 mmol) (6) was dissolved in a mixture of methanolic 0.05 N sodium methoxide (110 mL) and dichloromethane (50 mL) and left at room temperature for 1 day. Deionization with Amberlite IRC 50 H^+ followed by evaporation left a white solid that was recrystallized from chloroform – ethyl acetate to give pure **2** (4.12 g, 87%); mp 212–213°C; $[\alpha]_D$ −39 (*c* 0.5, dichloromethane); ^1H nmr ($CDCl_3$) δ: 7.5–7.2 (m, 20H, 4Ph), 6.07 (d, 1H, $J_{NH,2a}$ 7.0 Hz, NH), 5.52 (s, 1H, C*H*Ph), 4.91 and 4.60 (ABq, 2H, $J_{A,B}$ 12.0 Hz, CH_2Ph), 4.78 (d, 1H, $J_{1a,2a}$ 8.5 Hz, H-1a), 4.65 and 4.63 (ABq, 2H, $J_{A,B}$12.0 Hz, CH_2Ph), 4.42 and 4.39 (ABq, 2H, $J_{A,B}$ 12.0 Hz, CH_2Ph), 4.39 (d, overlapped by CH_2Ph, $J_{1b,2b}$ ~ 8.0 Hz, H-1b), 4.35 (dd, 1H, $J_{6a,6a'}$ 10.5 Hz, $J_{6a,5a}$ 5.0 Hz, H-6a), 4.30 (t, 1H, $J_{2a,3a}$ 9.0 Hz, $J_{3a,4a}$ 9.0 Hz, H-3a), 4.0 (dt, 1H, $J_{2b,3b}$ 9.5 Hz, $J_{2b,OH}$ 1.5 Hz, H-2b), 3.91 (d, 1H, $J_{4b,3b}$ 2.5 Hz, H-4b), 3.79 (t, 1H, $J_{5a,6a'}$ 10.0 Hz, H-6a'), 3.65 (t, 1H, $J_{4a,5a}$ 9.0 Hz, H-4a), 3.49 (s, overlapped, CH_3O), 3.34 (dd, 1H, H-3b), 2.9 (s, 1H, OH), 1.91 (s, 3H, CH_3CO). Anal. calcd. for $C_{43}H_{49}NO_{11}$: C 68.33, H 6.53, N 1.85; found: C 67.92, H 6.44, N 1.79.

2,3,4-Tri-O-benzyl-α-L-fucopyranosyl bromide (3) (7)

Bromide **3** was prepared just prior to use from 2,3,4-tri-*O*-benzyl-L-fucopyranose (7) as reported (6), which is according to the preparation of bromide **36**.

Methyl 2-acetamido-4,6-O-benzylidene-2-deoxy-3-O-[3,4,6-tri-O-benzyl-2-O-(2,3,4-tri-O-benzyl-α-L-fucopyranosyl)-β-D-galactopyranosyl]-β-D-glucopyranoside (4)

A solution of freshly prepared bromide **3** (8.51 mmol) in dichloromethane (10 mL) was added to a solution of **2** (3.0 g,

TABLE 4. Involvement of the β-D-GlcNAc a-unit in the binding by the lectin of *Galactia tenuiflora*

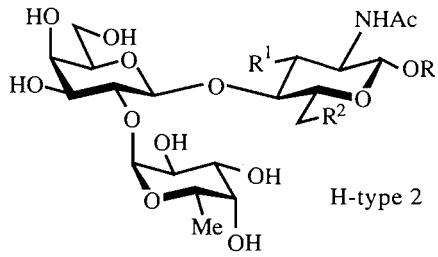

H-type 2

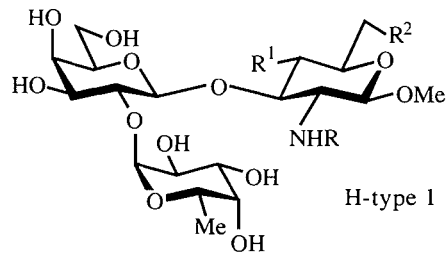

H-type 1

Compound	Substituent R	Substituent R^1	Substituent R^2	50% Inhibition, μmol/L	Relative potency	$\Delta\Delta G^0$, kcal/mol
H-type 2 related						
52 (H-type 2)	CH_3	OH	OH	290	100	0
67	$(CH_2)_8COOCH_3$	OH	OH	225	129	−0.15
33	CH_3	H	OH	30% at 5055	Inactive	—
68 (Y)	CH_3	OαLFuc	OH	5% at 1450	Inactive	—
69	CH_3	OH	H	210	138	−0.19
70	CH_3	OH	OCH_3	302	96	0.02
71	CH_3	OH	F	326	89	0.07
72	CH_3	OH	Cl	414	70	0.21
73	CH_3	OH	NH_2	254	114	−0.08
74	CH_3	OH	NHAc	318	91	0.05
75	CH_3	OH	NHPiv	349	83	0.11
H-type 1 related						
5 (H-type 1)	Ac	OH	OH	829	35	0.62
6	H	OH	OH	833	35	0.62
13	Ac	H	OH	23% at 3800	Inactive	
76 (Le^b)	Ac	OαLFuc	OH	6% at 2500	Inactive	
19	Ac	OH	H	381	76	0.16
H-related						
77 α-L-Fuc-(1→2)-β-D-Gal-OMe				3625	8	1.49

3.97 mmol) and tetraethylammonium bromide (840 mg, 4.00 mmol) in dichloromethane (15 mL) and *N,N*-dimethylformamide (4 mL) containing 4 Å molecular sieves (10 g). The mixture was stirred for 20 h, then methanol (2 mL) was added and stirring continued for two more hours. It was diluted with dichloromethane, filtered through a pad of Celite, washed with aqueous saturated sodium hydrogencarbonate and water, dried, and evaporated. The crude product was applied to a silica gel column (hexane – ethyl acetate, 2:1; dichloromethane – ethyl acetate, 2:1) to provide the title compound **4** (3.4 g, 73%) as a foam; $[\alpha]_D$ −83 (*c* 0.5, dichloromethane); ^{1}H nmr ($CDCl_3$) δ: 7.5–7.1 (m, 35H, 7Ph), 6.46 (d, 1H, $J_{NH,2a}$ 7.5 Hz, NH), 5.52 (d, 1H, $J_{1c,2c}$ 3.5 Hz, H-1c), 5.50 (s, 1H, C*H*Ph), 3.49 (s, CH_3O), 3.37 (m, 1H, H-2a), 1.82 (s, 3H, CH_3CO), 1.22 (d, 3H, $J_{5c,6c}$ 6.5 Hz, H_3-6c). Anal. calcd. for $C_{70}H_{77}NO_{15}$: C 71.72, H 6.62, N 1.19; found: C 71.83, H 6.58, N 0.91. Further development with ethyl acetate eluted the starting material **2** (680 mg, 23%).

*Methyl 2-acetamido-2-deoxy-3-*O*-[2-*O*-(α-L-fucopyranosyl)-β-D-galactopyranosyl]-β-D-glucopyranoside (5)*

Compound **4** (100 mg, 0.09 mmol) in 95% ethanol (7 mL) was hydrogenated for 2 days over 5% palladium-on-carbon (100 mg) at 110 psi (1 psi = 6.89 kPa). After filtration, evaporation of the solvent, and twofold precipitation of the product from methanol – ethyl acetate, compound **5** (38.0 mg, 82%) was obtained as a white powder; $[\alpha]_D$ −77.3 (*c* 0.62, water); ^{1}H nmr (D_2O) δ: 5.18 (d, 1H, $J_{1c,2c}$ 3.8 Hz, H-1c), 4.63(d, 1H, $J_{1b,2b}$ 7.5 Hz, H-1b), 4.34 (d, 1H, $J_{1a,2a}$ 8.5 Hz, H-1a), 4.30 (q, 1H, $J_{5c,6c}$ 6.5 Hz, $J_{4c,5c}$ < 1.0 Hz, H-5c), 3.98 (dd, 1H, $J_{2a,3a}$ 10.0 Hz, $J_{3a,4a}$ 8.5 Hz, H-3a), 3.94 (dd, 1H, $J_{6a,6a'}$ 12.0 Hz, $J_{5a,6a}$ 1.5 Hz, H-6a), 3.88 (dd, 1H, $J_{3b,4b}$ 3.3 Hz, H-4b), 3.83 (dd, 1H, $J_{2b,3b}$ 9.5 Hz, H-3b), 3.78 (H-2a), 3.76 (H-6a′), 3.76 (H-4c), 3.75 (H-2c), 3.68 (H-3c), 3.67 ± 0.02 (H-5b), 3.58 (dd, 1H, H-2b), 3.49 (H-4a), 3.48 (H-5a), 3.48 (CH_3O), 2.04 (s, 3H, CH_3CO), 1.22 (d, 3H, H_3-6c). The ^{13}C nmr data are reported in Table 1.

*Methyl 2-amino-2-deoxy-3-*O*-[2-*O*-(α-L-fucopyranosyl)-β-D-galactopyranosyl]-β-D-glucopyranoside (6)*

A solution of **5** (35 mg, 0.06 mmol) in hydrazine hydrate 85% (6 mL) was heated in a metal bomb at 140°C for 12 days. After evaporation and codistillation with water and methanol, the crude product was applied to a column of Sephadex LH 20 and eluted with ethanol–water 1:1. After another gel filtration, the product was precipitated from methanol – ethyl acetate to provide **6** (21.3 mg, 66%); $[\alpha]_D$ −69 (*c* 0.6 water); ^{1}H nmr (D_2O) δ: 5.30 (d, 1H, $J_{1c,2c}$ 2.5 Hz, H-1c), 4.72 (d, 1H, $J_{1b,2b}$ 7.8 Hz, H-1b), 4.37 (d, 1H, $J_{1a,2a}$ 8.0 Hz, H-1a), 4.32 (q, 1H, $J_{5c,6c}$ 6.5 Hz, H-5c), 3.94 (dd, overlapped, $J_{5a,6a}$ 1.9 Hz, H-6a), 3.92 (overlapped, H-4b), 3.90 (dd, overlapped, $J_{3b,4b}$ 3.3 Hz, H-3b), 3.81 (H-4c), 3.80 (H-2c), 3.74 (H-6a′), 3.71 (H-3a), 3.70 (H-2b), 3.55 (CH_3O), 3.48 (H-5a), 2.83 (dd, 1H, $J_{2a,3a}$ 10.0 Hz, H-2a), 1.22 (d, 3H, H_3-6c). The ^{13}C nmr data are reported in Table 1.

*Methyl 2-acetamido-3-*O*-(2-*O*-acetyl-3,4,6-tri-*O*-benzyl-β-D-galactopyranosyl)-4-*O*-benzyl-2-deoxy-β-D-glucopyranoside (8)*

Compound **8** was obtained as a minor compound (17%) besides the main product **7** (73%) when **1** was treated with sodium cyano-

Can. J. Chem. Downloaded from www.nrcresearchpress.com by 217.78.4.112 on 09/08/12
For personal use only.

TABLE 5. Involvement of the β-D-Gal b-unit in the binding by the lectin of *Galactia tenuiflora*

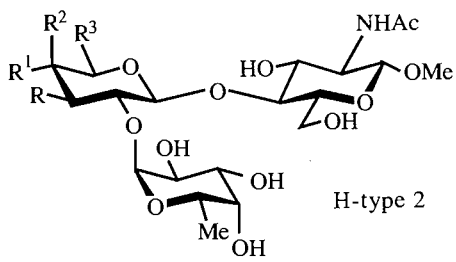

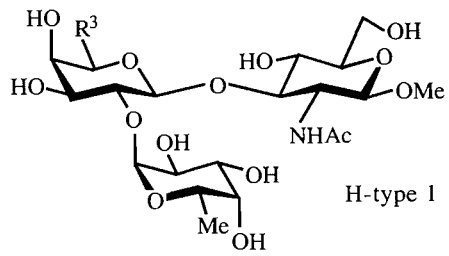

Compound	Substituent R	R¹	R²	R³	50% Inhibition, μmol/L	Relative potency	ΔΔG°, kcal/mol
H-type 2 related							
52 (H-type 2)	OH	H	OH	CH_2OH	290	100	0
53	H	H	OH	CH_2OH	25% at 3000	Inactive	—
66	OH	H	H	CH_2OH	6% at 2500	Inactive	—
78[a]	OH	OH	H	CH_2OH	10% at 2400	Inactive	—
62	OH	H	OH	CH_3	970	30	0.71
H-type 1 related							
24	—	—	—	H	31% at 5200	Inactive	—

[a]The $(CH_2)_8COOMe$ glycoside was used.

TABLE 6. Involvement of the α-L-Fuc c-unit in the binding by the lectin of *Galactia tenuiflora*

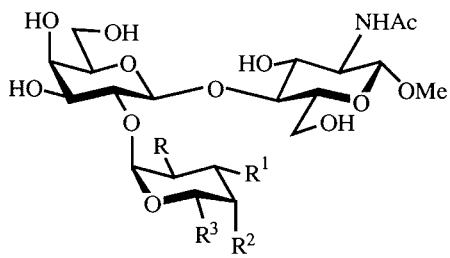

Compound	Substituent R	R¹	R²	R³	50% Inhibition, μmol/L	Relative potency	ΔΔG°, kcal/mol
52 (H-type 2)	OH	OH	OH	CH_3	290	100	0
54	H	OH	OH	CH_3	130	225	−0.47
55	OH	H	OH	CH_3	260	110	−0.06
56	OH	OH	H	CH_3	38% at 3160	~6[b]	~1.7
79[a]	OH	OH	OH	H	46% at 2900	~9[b]	~1.4
80 β-D-Gal-(1→4)-β-D-GlcNAc-OMe					8% at 7900	Inactive	—
81 α-L-Fuc-OMe					17% at 11200	Inactive	—

[a]The $(CH_2)_8COOMe$ glycoside was used.
[b]Estimated from extrapolation.

borohydride as reported (6). Chromatography of the mother liquor of **7** on a column of silica gel (ethyl acetate) provided **8** as a white powder; $[\alpha]_D$ −12.5 (*c* 1.0, chloroform); ^1H nmr ($CDCl_3$) δ: 7.40–7.20 (m, 20H, 4Ph), 6.03 (d, 1H, $J_{NH,2a}$ 8.0 Hz, NH), 5.28 (dd, 1H, $J_{2b,3b}$ 10.0 Hz, $J_{1b,2b}$ 8.0 Hz, H-1b), 4.60 (d, 1H, H-1b), 4.45 (d, 1H, $J_{1a,2a}$ 8.0 Hz, H-1a), 4.10 (t, 1H, $J_{3a,4a} \sim J_{2a,3a} \sim$ 8.0 Hz, H-3a), 3.93 (bd, 1H, $J_{3b,4b}$ 3.0 Hz, $J_{4b,5b} <$ 1 Hz, H-4b), 3.61 (t, 1H, $J_{4a,5a}$ 8.0 Hz, H-4a), 3.52 (dd, overlapped, H-3b), 3.42 (s, 3H, CH_3O), 2.05 and 1.92 (2s, each 3H, $2CH_3CO$). Anal. calcd. for $C_{45}H_{53}NO_{12}$: C 67.57, H 6.68, N 1.75; found: C 67.66, H 6.74, N 1.75. An analytical sample was acetylated conventionally (pyridine, acetic anhydride). The ^1H nmr spectrum of the resulting di-*O*-acetate showed a doublet (2H, $J_{5a,6a} \sim$ 4 Hz, H_2-6a) at 4.32 ppm.

Methyl 2-acetamido-3-O-(2-O-acetyl-3,4,6-tri-O-benzyl-β-D-galactopyranosyl)-6-O-benzyl-2-deoxy-4-O-phenoxythiocarbonyl-β-D-glucopyranoside (9)

A mixture of **7** (100 mg, 0.125 mmol), 4-dimethylaminopyridine (519 mg, 4.25 mmol), and phenyl chlorothionocarbonate (346 μL, 2.5 mmol) in dry acetonitrile (4 mL) was boiled under reflux for 20 h and then left at room temperature for 20 h. The mixture was diluted with dichloromethane and sequentially washed

Can. J. Chem. Downloaded from www.nrcresearchpress.com by 217.78.4.112 on 09/08/12
For personal use only.

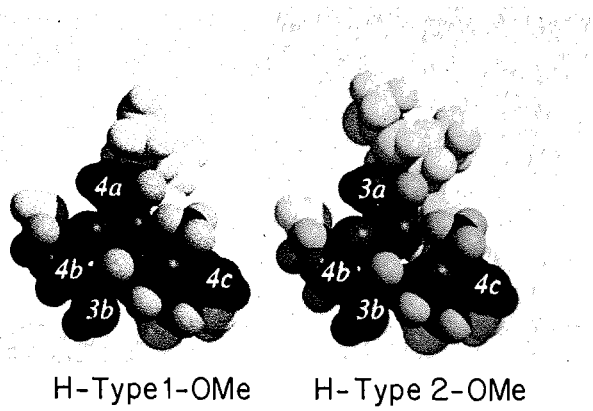

FIG. 1. The surface common to the H-type 1 (**5**) and H-type 2 (**52**) trisaccharides that is recognized by the lectin of *Galactia tenuiflora* is represented by the darkly colored atoms. The off-white groups are expected to remain solvated by water.

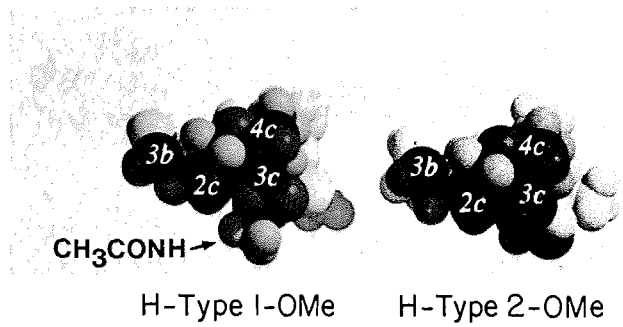

FIG. 2. The surface of the H-type 2 trisaccharide (**52**) that is recognized by the lectin I of *Ulex euroaeus* and the very similar surface present in the H-type 1 trisaccharide (**5**). It is seen that de-*N*-acetylation of the H-type 1 compound will improve the complementarity to the combining site of the lectin by rendering the surface more similar to that presented by the H-type 2 isomer.

with ice-cold 0.5 N hydrochloric acid, saturated aqueous sodium hydrogencarbonate, and water, followed by drying and evaporation. The resultant material was recrystallized from methanol–ether–hexane to provide **9** (76 mg, 65%); mp 173.5–174°C; $[\alpha]_D$ +17.5 (*c* 0.5, chloroform); ^{1}H nmr ($CDCl_3$) δ: 7.40–7.00 (m, 25H, 5Ph), 5.73 (d, 1H, $J_{NH,2a}$ 8.0 Hz, NH), 5.51 (t, 1H, $J_{3a,4a} \sim J_{4a,5a}$ 7.5 Hz, H-4a), 5.29 (dd, 1H, $J_{2b,3b}$ 10.0 Hz, $J_{1b,2b}$ 8.0 Hz, H-2b), 4.91 (d from ABq, 1H, $J_{A,B}$ 12.0 Hz, 1CH_2Ph), 4.78 (d, 1H, $J_{1a,2a}$ 7.0 Hz, H-1a), 4.47 (d, 1H, H-1b), 3.96 (bd, 1H, $J_{3b,4b}$ 2.5 Hz, $J_{4b,5b}$ < 1 Hz H-4b), 3.48 (s, 3H, CH_3O), 2.02 and 1.93 (2s, each 3H, 2CH_3CO). Anal. calcd. for $C_{52}H_{57}NO_{13}S$: C 66.72, H 6.14, N 1.50, S 3.42; found: C 66.77, H 6.23, N 1.34, S 3.23.

*Methyl 2-acetamido-3-*O*-(2-*O*-acetyl-3,4,6-tri-*O*-benzyl-*β*-D-*galactopyranosyl)-6-O-*benzyl-2,4-dideoxy-*β*-D-*xylo-*hexopyranoside (**10**)*

Argon was passed through a solution of **9** (290 mg, 0.31 mmol) in toluene (18 mL) for 50 min at 80°C. Then 2,2′-azobis(isobutyronitrile) (46 mg, 0.28 mmol) and tributyltin hydride (0.83 mL, 3.1 mmol) were added. After 2 h at 80°C, the mixture was allowed to reach room temperature and was washed with aqueous potassium fluoride solution and water, followed by drying and evaporation. The crude product was applied to a column of silica gel (dichloromethane–methanol, 98:2) and eluted in 77% yield (188 mg). The analytical sample was recrystallized from methanol–ether–hexane; mp 201–203°C; $[\alpha]_D$ +4.2 (*c* 0.8, chloroform); ^{1}H nmr ($CDCl_3$) δ: 7.40–7.20 (m, 20H, 4Ph), 5.66 (d, 1H, $J_{NH,2a}$ 7.5 Hz, NH), 5.28 (dd, 1H, $J_{1b,2b}$ 8.0 Hz, $J_{2b,3b}$ 10.0 Hz, H-2b), 4.90 (d, from ABq, 1H, $J_{A,B}$ 12.0 Hz, 1CH_2Ph), 4.80 (d, 1H, $J_{1a,2a}$ 8.0 Hz, H-1a), 4.65–4.30 (m, 7H, CH_2Ph), 4.44 (d, 1H, H-1b), 3.90 (bd, 1H, $J_{3b,4b}$ 3.0 Hz, $J_{4b,5b}$ < 1 Hz, H-4b), 3.66 (bm, 1H, H-5a), 3.47 (s, 3H, CH_3O), 2.94 (ddd, 1H, $J_{2a,3a} \sim$ 9.0 Hz, H-2a), 2.15 (bdd, 1H, $J_{4aeq,4aax}$ 13.0 Hz, $J_{3a,4aeq} \sim$ 6 Hz, $J_{4aeq,5a} \sim$ 2 Hz, H-4aeq), 2.01 and 1.92 (2s, each 3H, 2CH_3CO), 1.51 (q, 1H, $J_{4aax,5a} \sim J_{3a,4aax} \sim$ 11 Hz, H-4aax). Anal. calcd. for $C_{45}H_{53}NO_{11}$: C 68.88, H 6.81, N 1.79; found: C 68.66, H 6.93, N 1.75.

*Methyl 2-acetamido-6-*O*-benzyl-2,4-dideoxy-3-*O*-(3,4,6-tri-*O*-benzyl-*β*-D-*galactopyranosyl)-*β*-D-*xylo-*hexopyranoside (**11**)*

A solution of acetate **10** (180 mg, 0.23 mmol) in methanolic 0.05 N sodium methoxide (25 mL) was kept overnight at room temperature. The mixture was neutralized with Amberlite IRC 50 (H^+) resin and evaporated to leave **11** (150 mg, 88%) as a solid. An analytical sample was recrystallized from dichloromethane–hexane; mp 202–204°C; $[\alpha]_D$ −4.7 (*c* 1.4, chloroform); ^{1}H nmr ($CDCl_3$) δ: 7.40–7.20 (m, 20H, 4Ph), 6.19 (d, 1H, $J_{NH,2a}$ 7.0 Hz, NH), 4.85–4.37 (m, 8H, 4CH_2Ph), 4.77 (d, 1H, $J_{1a,2a}$ 8.0 Hz, H-1a), 4.28 (d, 1H, $J_{1b,2b}$ 8.0 Hz, H-1b), 3.90 (dd, 1H, $J_{2b,3b}$ 10.0 Hz, H-2b), 3.85 (bd, 1H, $J_{3b,4b}$ 3.0 Hz, $J_{4b,5b}$ < 1 Hz, H-4b), 3.70 (bm, 1H, H-5a), 3.48 (s, 3H, CH_3O), 3.34 (dd, 1H, H-3b), 3.11 (ddd, 1H, $J_{2a,3a}$ 10.0 Hz, H-2a), 3.09 (bs, 1H, OH), 2.17 (bddd, 1H, $J_{4aeq,4aax}$ 13.0 Hz, $J_{3a,4aeq}$ 5.5 Hz, $J_{4aeq,5a}$ 2.0 Hz, H-4aeq), 1.91 (s, 3H, CH_3CO), 1.51 (ddd, 1H, $J_{4aax,5a} \sim J_{3a,4aax}$ 11.0 Hz, H-4aax). Anal. calcd. for $C_{43}H_{51}NO_{10}$: C 69.62, H 6.93, N 1.89; found: C 69.73, H 6.89, N 1.83.

*Methyl 2-acetamido-6-*O*-benzyl- 2,4-dideoxy-3-*O*-[3,4,6-tri-*O*-benzyl-2-*O*-(2,3,4-tri-*O*-benzyl-*α*-L-*fucopyranosyl)-*β*-D-galactopyranosyl]-*β*-D-*xylo-*hexopyranoside (**12**)*

A solution of bromide **3** (0.62 mmol) in dichloromethane (0.7 mL) was transferred into a stirred mixture of alcohol **11** (150 mg, 0.202 mmol), tetraethylammonium bromide (63 mg, 0.30 mmol), 4 Å molecular sieves (powdered, 2g), and *N,N*-dimethylformamide (0.5 mL) in dichloromethane (3 mL). After stirring for 24 h, methanol (0.5 mL) was added and stirring continued for 1 h. Usual processing followed by column chromatography on silica gel (dichloromethane–methanol, 98.5:1.5) provided pure **12** (134 mg, 57%) after recrystallization from ether–hexane; mp 83–85°C; $[\alpha]_D$ −61.4 (*c* 0.8, chloroform); ^{1}H nmr ($CDCl_3$) δ: 7.40–7.10 (m, 35H, 7Ph), 5.95 (d, 1H, $J_{NH,2a}$ 7.5 Hz, NH), 5.60 (d, 1H, $J_{1c,2c}$ 3.5 Hz, H-1c), 4.95–4.42 (m, 14H, 7CH_2Ph), 4.46 (d, 1H, H-1b), 4.44 (d, 1H, $J_{1a,2a}$ 8.0 Hz, H-1a), 4.25 (q, 1H, $J_{5c,6c}$ 6.5 Hz, $J_{4c,5c}$ < 1 Hz, H-5c), 4.16 (dd, 1H, $J_{2b,3b}$ 9.5 Hz, $J_{1b,2b}$ 8.0 Hz, H-2b), ~4.04 (bm, 1H, H-5a), 4.01 (dd, 1H, $J_{2c,3c}$ 10.0 Hz, H-2c), ~3.88 (m, 2H, $J_{3c,4c} \sim$ 2.5 Hz, H-3c, H-4c), 3.77 (bd, 1H, $J_{3b,4b}$ 2.5 Hz, $J_{4b,5b}$ < 1 Hz, H-4b), 3.45 (s, 3H, CH_3O), 3.38 (H-2a), 2.17 (bdd, 1H, $J_{4aeq,4aax}$ 12.5 Hz, $J_{4aeq,3a}$ 4.5 Hz, $J_{4aeq,5a} \sim$ 1 Hz, H-4aeq), 1.86 (s, 3H, CH_3CO), 1.54 (bq, 1H, $J_{3a,4aax} = J_{4aax,5a}$ 12.0 Hz, H-4aax), 1.18 (d, 3H, H_3-6c). Anal. calcd. for $C_{70}H_{79}NO_{14} \cdot 1H_2O$: C 71.45, H 6.94, N 1.19; found: C 71.21, H 6.88, N 1.27.

*Methyl 2-acetamido-2,4-dideoxy-3-*O*-[2-*O*-(*α*-L-*fucopyranosyl)-*β*-D-galactopyranosyl]-*β*-D-*xylo-*hexopyranoside (**13**)*

A mixture of **12** (110 mg, 0.095 mmol) and 5% palladium-on-carbon (115 mg) in 95% ethanol (20 mL) was hydrogenated at atmospheric pressure for 16 h. Filtration and solvent evaporation left a residue that was passed through a column of Biogel P-2 (ethanol–water, 1:9). Freeze-drying an aqueous solution provided **13** (30 mg, 60%) as a light white powder; $[\alpha]_D$ −88 (*c* 0.3, water); ^{1}H nmr (D_2O) δ: 5.17 (d, 1H, $J_{1c,2c}$ 4.0 Hz, H-1c), 4.60 (d, 1H, $J_{1b,2b}$ 8.0 Hz, H-1b), 4.25 (q, 1H, $J_{5c,6c}$ 6.5 Hz, $J_{4c,5c}$ < 1 Hz, H-5c), 4.24 (d, 1H, $J_{1a,2a}$ 8.0 Hz, H-1a), 4.08 (ddd, 1H, $J_{3a,4aax} = J_{2a,3a}$ 11.0 Hz, $J_{3a,4aeq}$ 5.0 Hz, H-3a), 3.88 (bd, 1H, $J_{3b,4b}$ 3.3 Hz, $J_{4b,5b}$ < 1 Hz, H-4b), 3.80 (dd, H-3b), 3.53 (dd, 1H, $J_{2b,3b}$ 9.8 Hz, $J_{1b,2b}$ 8.0 Hz, H-2b), 3.46 (s, 3H, CH_3O), 2.14 (bdd, $J_{4aax,4aeq}$ 13.0 Hz, $J_{4aeq,5a}$ 1.3 Hz, H-4aeq), 2.03 (s, 3H, CH_3CO), 1.47 (ddd, 1H, $J_{4aax,5a}$

Can. J. Chem. Downloaded from www.nrcresearchpress.com by 217.78.4.112 on 09/08/12
For personal use only.

Can. J. Chem. Downloaded from www.nrcresearchpress.com by 217.78.4.112 on 09/08/12
For personal use only.

11.0 Hz, H-4aax), 1.19 (d, 3H, H_3-6c). The ^{13}C nmr data are reported in Table 1.

*Methyl 2-acetamido-3-*O*-(2-*O*-acetyl-3,4,6-tri-*O*-benzyl-β-D-galactopyranosyl)-4-*O*-benzyl-2-deoxy-6-*O*-p-toluenesulfonyl-β-D-glucopyranoside (**14**)*

A solution of *p*-toluenesulfonyl chloride (200 mg, 1.05 mmol) in dichloromethane (8 mL) was added to a solution of **8** (644 mg, 0.81 mmol) in pyridine (10 mL) at ice-bath temperature. After 2 h, another portion of *p*-toluenesulfonyl chloride (150 mg, 0.79 mmol) was added and the mixture was kept at room temperature for another two hours. It was poured into ice-water, extracted with dichloromethane, evaporated and codistilled with toluene. The resulting material was purified on a column of silica gel (dichloromethane – ethyl acetate, 1:2) to provide in the first main fraction compound **14** (565 mg, 74%) as a solid. The analytical sample was recrystallized from ethyl acetate – hexane; mp 146–147°C; $[\alpha]_D$ −1, $[\alpha]_{365}$ −4 (*c* 0.6, chloroform); ^1H nmr ($CDCl_3$) δ: 7.80 (d, 2H, J = 8.0 Hz, Ts), 7.40–7.20 (m, 22H, Ph), 5.80 (d, 1H, $J_{NH,2a}$ 8.5 Hz, NH), 5.30 (dd, 1H, $J_{1b,2b}$ 8.0 Hz, $J_{2b,3b}$ 10.0 Hz, H-2b), 4.52 (d, 1H, H-1b), 4.45 (d, 1H, $J_{1a,2a}$ 6.0 Hz, H-1a), 4.26 and 4.21 (ABq, 2H, $J_{6a,6a'}$ 10.0 Hz, $J_{5a,6a}$ 5.5 Hz, $J_{5a,6a'}$ 3.5 Hz, H-6a, H-6a′), 4.09 (t, 1H, $J_{2a,3a} \sim J_{3a,4a} \sim$ 6.5 Hz, H-3a), 3.93 (d, 1H, $J_{3b,4b}$ 3.0 Hz, $J_{4b,5b} <$ 1 Hz, H-4b), 3.75 (m, 1H, H-5a), 3.65 (ddd, 1H, H-2a), 3.52–3.42 (m, 5H, H-4a, H-3b, H-5b, 2H-6b), 3.32 (m, 3H, CH_3O), 2.40 (s, 3H, CH_3-Ts), 2.00 and 1.85 (2s, each 3H, CH_3CO). Anal. calcd. for $C_{52}H_{59}NO_{14}S$: C 65.46, H 6.23, N 1.47, S 3.35; found: C 65.35, H 6.14, N 1.63, S 3.57.

*Methyl 2-acetamido-3-*O*-(2-*O*-acetyl-3,4,6-tri-*O*-benzyl-β-D-galactopyranosyl)-4-*O*-benzyl-2,6-dideoxy-6-iodo-β-D-glucopyranoside (**15**)*

A mixture of **14** (1.09 g, 1.14 mmol) and potassium iodide (2.2 g, 13.3 mmol) in *N,N*-dimethylformamide (30 mL) was heated at 100°C for 5.5 h. It was diluted with dichloromethane, and washed successively with water, aqueous sodium thiosulfate solution, and water, followed by evaporation. The reaction product was purified on a column of silica gel (dichloromethane – ethyl acetate, 1:1) to provide solid **15** (817 mg, 83%); mp 75–76°C; $[\alpha]_D$ 0, $[\alpha]_{365}$ 0 (*c* 0.7, chloroform); ^1H nmr ($CDCl_3$) δ: 7.40–7.20 (m, 20H, 4Ph), 5.80 (d, 1H, $J_{NH,2a}$ 8.5 Hz, NH), 5.34 (dd, 1H, $J_{1b,2b}$ 8.0 Hz, $J_{2b,3b}$ 10.0 Hz, H-2b), 4.96, 4.93, 4.67 (3d from 3ABq, each 1H, $J_{A,B}$ 11.5, 10.5, 12.0 Hz, CH_2Ph), 4.60–4.46 (m, 5H, CH_2Ph, H-1a, H-1b), 4.38 and 4.30 (ABq, 2H, $J_{A,B}$ 12.0 Hz, CH_2Ph), 4.20 (t, 1H, $J_{3a,4a} \sim J_{2a,3a}$ 7.5 Hz, H-3a), 3.94 (d, 1H, $J_{3b,4b}$ 3.0 Hz, $J_{4b,5b} <$ 1 Hz, H-4b), 3.44 (s, 3H, CH_3O), 2.07 and 1.88 (2s, each 3H, $2CH_3CO$). Anal. calcd. for $C_{45}H_{52}INO_{11}$: C 59.41, H 5.76, I 13.95, N 1.54; found: C 59.26, H 5.61, I 13.79, N 1.57.

*Methyl 2-acetamido-3-*O*-(2-*O*-acetyl-3,4,6-tri-*O*-benzyl-β-D-galactopyranosyl)-4-*O*-benzyl-2,6-dideoxy-β-D-glucopyranoside (**16**)*

A mixture of **15** (775 mg, 0.85 mmol), 2,2′-azobis(isobutyronitrile) (35 mg, 0.21 mmol), and tributyltin hydride (1 mL, 3.72 mmol) in toluene (10 mL) was heated at 80°C for 25 min. The solvent was evaporated and the reaction product was purified on a column of silica gel (hexane – ethyl acetate, 3:1, dichloromethane – ethyl acetate, 2:1, 1:1) to afford **16** (555 mg, 83%); mp 58–60°C; $[\alpha]_D$ −5 (*c* 0.5, chloroform); ^1H nmr ($CDCl_3$) δ: 7.40–7.20 (m, 20H, 4Ph), 5.60 (d, 1H, $J_{NH,2a}$ 8.5 Hz, NH), 5.35 (dd, 1H, $J_{1b,2b}$ 8.0 Hz, $J_{2b,3b}$ 10.0 Hz, H-2b), 4.95 (d from 2ABq, 2H, $J_{A,B}$ 12.0 Hz, CH_2Ph), 4.68 (d from ABq, 1H, $J_{A,B}$ 12.0 Hz, CH_2Ph), 4.50 (d, 1H, $J_{1a,2a}$ 8.0 Hz, H-1a), 4.55 (d, 1H, H-1b), 4.36 and 4.28 (ABq, 2H, $J_{A,B}$ 12.0 Hz, CH_2Ph), 4.18 (t, 1H, $J_{2a,3a} \sim J_{3a,4a}$ 8.5 Hz, H-3a), 3.92 (d, 1H, $J_{3b,4b}$ 3.0 Hz, $J_{4b,5b} <$ 1 Hz, H-4b), 3.41 (s, 3H, CH_3O), 3.18 (t, 1H, $J_{4a,5a}$ 8.0 Hz, H-4a), 2.05 and 1.90 (2s, each 3H, $2CH_3CO$), 1.34 (d, 3H, $J_{5a,6a}$ 6.3 Hz, H_3-6a). Anal. calcd. for $C_{45}H_{53}NO_{11}$: C 68.88, H 6.81, N 1.79; found: C 68.53, H 6.62, N 1.65.

*Methyl 2-acetamido-4-*O*-benzyl-3-*O*-(3,4,6-tri-*O*-benzyl-β-D-galactopyranosyl)-2,6-dideoxy-β-D-glucopyranoside (**17**)*

Compound **16** (280 mg, 0.36 mmol) was treated with methanolic 0.05 N sodium methoxide (16 mL) for 1 day. The solution was made neutral with Amberlite IRC 50 (H^+), filtered, and evaporated to provide **17** (260 mg, 98%) as a solid. The analytical sample was purified by column chromatography on silica gel (dichloromethane – ethyl acetate, 1:1); mp 58–60°C; $[\alpha]_D$ −9 (*c* 0.2, chloroform); ^1H nmr ($CDCl_3$) δ: 7.40–7.20 (m, 20H, 4Ph), 6.20 (d, 1H, $J_{NH,2a}$ 7.5 Hz, NH), 4.90 (d from 2ABq, 2H, $J_{A,B}$ 12.0 Hz, CH_2Ph), 4.72 (d from ABq, 1H, $J_{A,B}$ 12.0 Hz, CH_2Ph), 4.71 (d, 1H, $J_{1a,2a}$ 7.0 Hz, H-1a), 4.64, 4.58, 4.54 (3d from 2ABq, $J_{A,B}$ 12.0 Hz, CH_2Ph), 4.36 and 4.30 (ABq, 2H, $J_{A,B}$ 11.5 Hz, CH_2Ph), 4.36 (d, overlapped, 1H, $J_{1b,2b}$ 8.5 Hz, H-1b), 3.91 (d, 1H, $J_{3b,4b}$ 3.0 Hz, H-4b), 3.46 (s, 3H, CH_3O), 3.28 (t, 1H, $J_{4a,5a}$ 8.0 Hz, H-4a), 3.31 (bs, 1H, OH), 1.85 (s, 3H, CH_3CO), 1.37 (d, 3H, $J_{5a,6a}$ 6.5 Hz, H_3-6a). Anal. calcd. for $C_{43}H_{51}NO_{10}$: C 69.62, H 6.93, N 1.89; found: C 69.42, H 7.11, N 1.75.

*Methyl 2-acetamido-4-*O*-benzyl-2,6-dideoxy-3-*O*-[3,4,6-tri-*O*-benzyl-2-*O*-(2,3,4-tri-*O*-benzyl-α-L-fucopyranosyl)-β-D-*galactopyranosyl]-β-D-glucopyranoside (**18**)*

A solution of bromide **3** (1.3 mmol) in dichloromethane (1.4 mL) was transferred into a stirred mixture of alcohol **17** (280 mg, 0.38 mmol), tetraethylammonium bromide (170 mg, 0.81 mmol), 4 Å molecular sieves (powdered, 4g), and *N,N*-dimethylformamide (1 mL) in dichloromethane (6 mL). After stirring for 30 h, methanol (0.5 mL) was added and stirring continued for 2 h. Usual work-up was followed by column chromatography on silica gel (hexane – ethyl acetate, 1:1 and dichloromethane – ethyl acetate, 3:1) to provide crystalline **18** (392 mg, 90%). The analytical sample was recrystallized from ether–hexane; mp 114–115°C; $[\alpha]_D$ −55.7 (*c* 0.7, chloroform); ^1H nmr ($CDCl_3$) δ: 7.40–7.08 (m, 35H, 7Ph), 5.71 (d, 1H, $J_{1c,2c}$ 4.0 Hz, H-1c), 5.68 (d, 1H, $J_{NH,2a}$ 8.0 Hz, NH), 4.55 (d, overlapped, 1H, $J_{1b,2b}$ 8.0 Hz, H-1b), 4.51 (d, overlapped, $J_{1a,2a}$ 8.5 Hz, H-1a), 4.37 (overlapped, H-5c), 4.24 (dd, 1H, $J_{2b,3b}$ 9.0 Hz, H-2b), 4.17 (dd, 1H, $J_{3a,4a}$ 8.0 Hz, $J_{2a,3a}$ 9.5 Hz, H-3a), 4.02 (dd, 1H, $J_{2c,3c}$ 10.0 Hz, H-2c), 3.97 (d, 1H, $J_{3b,4b}$ 2.5 Hz, $J_{4b,5b} <$ 1 Hz, H-4b), 3.92 (dd, 1H, $J_{3c,4c}$ 2.5 Hz, H-3c), 3.85 (bd, 1H, H-4c), 3.44 (s, 3H, CH_3O), 3.06 (t, 1H, $J_{4a,5a}$ 8.5 Hz, H-4a), 1.89 (s, 3H, CH_3CO), 1.34 (d, 3H, $J_{5a,6a}$ 6.0 Hz, H_3-6a), 1.20 (d, 3H, $J_{5c,6c}$ 6.5 Hz, H_3-6c). Anal. calcd. for $C_{70}H_{79}NO_{14}$: C 72.58, H 6.87, N 1.21; found: C 72.10, H 6.93, N 1.29.

*Methyl 2-acetamido-2,6-dideoxy-3-*O*-[2-*O*-(α-L-fucopyranosyl)-β-D-galactopyranosyl]-β-D-glucopyranoside (**19**)*

Compound **18** (150 mg, 0.13 mmol) and 5% palladium-on-carbon (150 mg) in 95% ethanol (30 mL) were hydrogenated at atmospheric pressure for 11 h. Work-up and gel filtration as described for **13** provided trisaccharide **19** (67 mg, 98%) as a light white powder after freeze-drying an aqueous solution. $[\alpha]_D$ −96.7 (*c* 0.3, water); ^1H nmr (D_2O) δ: 5.17 (d, 1H, $J_{1c,2c}$ 4.0 Hz, H-1c), 4.62 (d, 1H, $J_{1b,2b}$ 7.8 Hz, H-1b), 4.32 (d, 1H, $J_{1a,2a}$ 8.2 Hz, H-1a), 4.30 (q, 1H, $J_{5c,6c}$ 6.5 Hz, H-5c), 3.93 (dd, 1H, $J_{2a,3a}$ 10.2 Hz, $J_{3a,4a}$ 9.0 Hz, H-3a), 3.87 (d, 1H, $J_{3b,4b}$ 3.3 Hz, H-4b), 3.82 (dd, 1H, $J_{3b,2b}$ 9.8 Hz, H-3b), 3.57 (dd, 1H, H-2b), 3.54 (dq, 1H, overlapped by H-2b, $J_{4a,5a}$ 9.5 Hz, $J_{5a,6a}$ 6.0 Hz, H-5a), 3.22 (t, 1H, H-4a), 2.05 (s, 3H, CH_3CO), 1.33 (d, 3H, H_3-6a), 1.21 (d, 3H, H_3-6c). The ^{13}C nmr data are reported in Table 1.

*Methyl 2-acetamido-4,6-*O*-benzylidene-3-*O*-(3,4-*O*-benzylidene-α-L-arabinopyranosyl)-2-deoxy-β-D-*glucopyranoside (**22**)

A pure isomer **20** (12) (190 mg, 0.327 mmol) in 0.05 N methanolic sodium methoxide (15 mL) and dichloromethane (3 mL) was kept at room temperature for 5 h. After neutralization with Amberlite IRC 50 H^+, filtration, and evaporation to dryness, the resulting powder (**21**) was desolved in *N,N*-dimethylformamide (7 mL) and acetonitrile (15 mL) and then treated with α,α-dimethoxytoluene (0.24 mL, 1.5 mmol) and *p*-toluenesulfonic acid (25 mg) for 1 day. The mixture was neutralized with triethylamine and evaporated to dryness. Recrystallization from dichloro-

Can. J. Chem. Downloaded from www.nrcresearchpress.com by 217.78.4.112 on 09/08/12
For personal use only.

methane–ether gave the title compound **22** (160 mg, 90%); mp 255–257°C; $[\alpha]_D$ −36.8 (*c* 0.7, chloroform); ^{1}H nmr ($CDCl_3$) δ: 7.58–7.30 (m, 10H, 2Ph), 5.95 (s, 1H, C*H*Ph), 5.84 (d, 1H, $J_{NH,2a}$ 8.0 Hz, NH), 5.53 (s, 1H, C*H*Ph), 4.75, 4.45 (2d, each 1H, *J* = 8.5 Hz, *J* = 7.5 Hz, H-1a, H-1b), 3.53 (s, 3H, CH_3O), 3.12 (d, 1H, $J_{OH,2b}$ 3.0 Hz, OH), 2.03 (s, 3H, CH_3CO). Anal. calcd. for $C_{28}H_{33}NO_{10}$: C 61.87, H 6.12, N 2.58; found: C 61.80, H 5.97, N 2.59.

*Methyl 2-acetamido-4,6-*O*-benzylidene-3-*O*-[3,4-*O*-benzylidene-2-*O*-(2,3,4-tri-*O*-benzyl-α-L-fucopyranosyl)-α-L-arabinopyranosyl]-2-deoxy-β-D-glucopyranoside (23)*

Alcohol **22** (140 mg, 0.26 mmol) was reacted with bromide **3** (0.92 mmol) as described for the preparation of **4**. Usual work-up after 30 h, followed by chromatography on a column of silica gel (dichloromethane–methanol, 98.5:1.5) and crystallization from dichloromethane–ether–hexane provided **23** (200 mg, 81%); mp 187–188°C; $[\alpha]_D$ −67.1 (*c* 0.6, chloroform); ^{1}H nmr ($CDCl_3$) δ: 7.50–7.25 (m, 25H, 5Ph), 5.90 (d, 1H, $J_{NH,2a}$ 8.5 Hz, NH), 5.82 (s, 1H, C*H*Ph), 5.50 (s, 1H, C*H*Ph), 5.44 (d, 1H, $J_{1c,2c}$ 4.0 Hz, H-1c), 4.71 (d, 1H, $J_{1b,2b}$ 7.5 Hz, H-1b), 4.64 (d, 1H, $J_{1a,2a}$ 8.0 Hz, H-1a), 4.08 (q, 1H, $J_{5c,6c}$ 6.5 Hz, H-5c), 3.45 (s, 3H, CH_3O), 1.82 (s, 3H, CH_3CO), 1.18 (d, 3H, H_3-6c). Anal. calcd. for $C_{55}H_{61}NO_{14}$: C 68.81, H 6.40, N 1.46; found: 68.53, H 6.42, N 1.58.

*Methyl 2-acetamido-2-deoxy-3-*O*-[2-*O*-(α-L-fucopyranosyl)-α-L-arabinopyranosyl]-β-D-glucopyranoside (24)*

Compound **23** (150 mg, 0.16 mmol) in 95% ethanol (35 mL) was hydrogenated in the presence of 5% palladium-on-carbon (150 mg) at atmospheric pressure for 22 h. Work-up and gel filtration as described for **13** provided **24** (74 mg, 92%) as a light white powder after freeze-drying an aqueous solution; $[\alpha]_D$ −86 (*c* 0.4); ^{1}H nmr (D_2O) δ: 5.15 (d, 1H, $J_{1c,2c}$ 4.0 Hz, H-1c), 4.56 (d, 1H, $J_{1b,2b}$ 7.0 Hz, H-1b), 4.34 (d, 1H, $J_{1a,2a}$ 8.5 Hz, H-1a), 4.25 (q, 1H, $J_{5c,6c}$ 6.5 Hz, $J_{4c,5c}$ < 1 Hz, H-5c), 3.93 (m, H-6a, H-5beq), 3.92 (H-4b), 3.85 (dd, overlapped, $J_{2b,3b}$ 9.0 Hz, $J_{3b,4b}$ 3.3 Hz, H-3b), ~3.83 (H-3a, overlapped), 3.68 (dd, 1H, $J_{2c,3c}$ 10.0 Hz, $J_{3c,4c}$ 3.0 Hz, H-3c), 3.59 (H-5bax, overlapped by H-2b), 3.58 (H-2b), 3.48 (s, 3H, CH_3O), 2.04 (s, 3H, CH_3CO), 1.21 (d, 3H, H_3-6c). The ^{13}C nmr data are reported in Table 1.

*Methyl 2-acetamido-4-*O*-(2-*O*-acetyl-3,4,6-tri-*O*-benzyl-β-D-galactopyranosyl)-3-*O*-allyl-6-*O*-benzyl-2-deoxy-β-D-glucopyranoside (27)*

A solution of bromide **25** (13) (4.50 mmol) in toluene-nitromethane (1:1, 10 mL) was added to a stirred mixture of alcohol **26** (6) (1.2 g, 3.28 mmol), mercuric cyanide (1.6 g, 6.3 mmol), powdered calcium sulfate (1 g), and 4 Å molecular sieves (1 g) in toluene–nitromethane (1:1, 30 mL). After 3 h, the mixture was filtered through a pad of Celite and poured into a mixture of aqueous sodium hydrogencarbonate and dichloromethane. The organic solution was washed with water, dried, and evaporated. The reaction product was purified on a column of silica gel (hexane – ethyl acetate, 3:1 to 1:2) to provide **27** (1.47 g, 53%) as a white solid; mp 132–133°C; $[\alpha]_D$ −30.2 (*c* 0.6, chloroform); ^{1}H nmr ($CDCl_3$) δ: 7.40–7.20 (m, 20H, 4Ph), 6.28 (d, 1H, $J_{NH,2a}$ 9.5 Hz, NH), 5.80 (m, 1H, CH_2=C*H*), 5.28 (dd, 1H, $J_{1b,2b}$ 8.0 Hz, $J_{2b,3b}$ 10.0 Hz, H-2b), 5.18 and 5.07 (2 m, 2H, CH_2=CH), 4.92 (d from ABq, $J_{A,B}$ 12.0 Hz, 1CH_2Ph), 4.46 (d, 1H, $J_{1a,2a}$ 4.0 Hz, H-1a), 4.33 (d, 1H, H-1b), 4.08 (m, 2H, CH_2=CH-CH_2), 4.00 (ddd, 1H, $J_{2a,3a}$ = $J_{1a,2a}$ 4.0 Hz, H-2a), 3.96 (bd, 1H, $J_{3b,4b}$ ~ 2.5 Hz, $J_{4b,5b}$ < 1 Hz, H-4b), 3.92 (t, 1H, $J_{3a,4a}$ ~ $J_{4a,5a}$ ~ 4 Hz, H-4a), 3.69 (t, 1H, H-3a), 3.40 (s, 3H, CH_3O), 2.02 and 2.00 (2s, each 3H, CH_3CO). Anal. calcd. for $C_{48}H_{57}NO_{12}$: C 68.44, H 6.84, N 1.67; found: 68.56, H 6.83, N 1.87.

*Methyl 2-acetamido-4-*O*-(2-*O*-acetyl-3,4,6-tri-*O*-benzyl-β-D-galactopyranosyl)-6-*O*-benzyl-2-deoxy-β-D-glucopyranoside (28)*

A mixture of **27** (800 mg, 0.95 mmol), tris(triphenylphosphine)rhodium(I)chloride (75 mg, 0.08 mmol), and 1.4-diazabicyclo[2.2.2]octane (33 mg, 0.29 mmol) in 95% ethanol–toluene–water (7:3:1, 68 mL) was boiled under reflux for 19 h. The solvent was removed and the resulting material was taken up in acetone (60 mL) containing mercuric oxide (12 mg). A solution of mercuric chloride (1.87 g) in acetone–water (9:1, 30 mL) was added and the mixture stirred for 30 min. Then the solvent was evaporated and the remainder dissolved in dichloromethane. The solution was washed with aqueous saturated potassium bromide and water, followed by drying with sodium sulfate and evaporation. Two recrystallizations from ethyl acetate gave pure **28** (603 mg). Chromatography of the mother liquor on a column of silica gel (ethyl acetate) provided more product (70 mg, total yield 88%); mp 198–198.5; $[\alpha]_D$ +9.7 (*c* 0.4, chloroform); ^{1}H nmr ($CDCl_3$) δ: 7.40–7.20 (m, 20H, 4Ph), 5.52 (d, 1H, $J_{NH,2a}$ 8.0 Hz, NH), 5.33 (dd, 1H, $J_{1b,2b}$ 8.0 Hz, $J_{2b,3b}$ 10.0 Hz, H-2b), 4.91 (d, from ABq, 1H, $J_{A,B}$ 12.0 Hz, CH_2Ph), 4.59 (d, 1H, $J_{1a,2a}$ 8.0 Hz, H-1a), 4.34 (d, 1H, H-1b), 3.89 (d, overlapped, H-4b), 3.50 (s, 3H, CH_3O), 3.42 (dd, 1H, $J_{3b,4b}$ 3.0 Hz, H-3b), 1.98 and 1.97 (2s, each 3H, 2CH_3CO); ^{1}H nmr after addition of trichloroacetyl isocyanate ($CDCl_3$) δ: 7.40–7.20 (m, 20H, 4Ph), 6.17 (d, 1H, $J_{NH,2a}$ 9.5 Hz, NH), 5.20 (dd, 1H, $J_{2b,3b}$ 10.0 Hz, $J_{1b,2b}$ 8.0 Hz, H-2b), 5.07 (dd, 1H, $J_{2a,3a}$ 10.0 Hz, $J_{3a,4a}$ 9.0 Hz, H-3a), 4.37 and 4.32 (2d, 2H, *J* 8.0 Hz, H-1a, H-1b), 4.13 (ddd, 1H, $J_{2a,3a}$ 10.0 Hz, H-2a), 3.93 (t, 1H, $J_{4a,5a}$ 9.0 Hz, H-4a), 3.85 (d, 1H, $J_{3b,4b}$ 3.0 Hz, H-4b), 3.74 (d, 2H, $J_{5a,6a}$ 2.5 Hz, H_2-6a), 3.64 (dd, 1H, $J_{6b,6b'}$ 9.0 Hz, $J_{5b,6b}$ 6.5 Hz, H-6b), 3.53 (m, 2H, H-6b', H-5a), 3.44 (s, 3H, CH_3O), 3.40 (t, 1H, $J_{5b,6b'}$ 6.5 Hz, H-5b), 3.34 (dd, 1H, H-3b), 2.00, 1.89 (2s, each 3H, 2CH_3CO). Anal. calcd. for $C_{45}H_{53}NO_{12}$: C 67.57, H 6.68, N 1.75; found: C 67.37, H 6.72, N 1.55.

*Methyl 2-acetamido-4-*O*-(2-*O*-acetyl-3,4,6-tri-*O*-benzyl-β-D-galactopyranosyl)-6-*O*-benzyl-2-deoxy-3-*O*-phenoxythiocarbonyl-β-D-glucopyranoside (29)*

A mixture of **28** (230 mg, 0.29 mmol) 4-dimethylaminopyridine (160 mg, 1.43 mmol), and phenyl chlorothionocarbonate (0.2 mL, 1.45 mmol) in dry dichloromethane (10 mL) was stirred at room temperature under argon for 38 h. The yellowish mixture was then washed with water, dried, and evaporated to dryness. Flash chromatography on a column of silica gel (dichloromethane–methanol, 99.5:0.5) afforded **29** (208 mg, 77%) as a yellowish gum; $[\alpha]_D$ −16.5 (*c* 0.5, chloroform); ^{1}H nmr ($CDCl_3$) δ: 7.40–7.00 (m, 25H, 5Ph), 5.94 (d, 1H, $J_{NH,2a}$ 9.5 Hz, NH), 5.66 (t, 1H, $J_{2a,3a}$ = $J_{3a,4a}$ 7.5 Hz, H-3a), 5.28 (dd, 1H, $J_{1b,2b}$ 8.0 Hz, $J_{2b,3b}$ 10.0 Hz, H-2b), 4.89 (d from ABq, 1H, $J_{A,B}$ 12.0 Hz, 1CH_2Ph), 4.47 (overlapped, $J_{1a,2a}$ 7.0 Hz, H-1a), 4.37 (overlapped, H-1b), 4.23 (ddd, 1H, H-2a), 4.07 (t, 1H, $J_{4a,5a}$ 7.5 Hz, H-4a), 3.96 (bd, 1H, $J_{3b,4b}$ 3.0 Hz, $J_{4b,5b}$ < 1 Hz, H-4b), 3.75 (d, 2H, $J_{5a,6a}$ 4.0 Hz, H_2-6a), 3.68–3.47 (m, 4H, H-5a, H-5b, 2H-6b), 3.46 (s, 3H, CH_3O), 3.41 (dd, 1H, H-3b), 1.96 (s, 6H, 2CH_3CO); fab-ms, *m/z*: 958 (0.98, $[M + Na]^+$), 936.5 (1.86, $[M + H]^+$), 935.5 (0.35, M^+), 904 (3.37, $[M - OMe]^+$). Anal. calcd. for $C_{52}H_{57}NO_{13}S$: C 66.72, H 6.14, N 1.50; found: C 66.37, H 6.42, N 1.57.

A minor compound (22 mg, 8.3%) was isolated on further elution of the column and identified as *methyl 2-acetamido-4-*O*-(2-*O*-acetyl,3,4,6-tri-*O*-benzyl-β-D-galactopyranosyl)-6-*O*-benzyl-2-deoxy-3-*O*-phenoxycarbonyl-β-D-glucopyranoside;* mp 169–171°C (methanol–ether); $[\alpha]_D$ −10 (*c* 0.2, chloroform); ^{1}H nmr ($CDCl_3$) δ: 7.40;–6.95 (m, 25H, 5Ph), 5.81 (d, 1H, $J_{NH,2a}$ 9.0 Hz, NH), 5.19 (dd, 1H, $J_{1b,2b}$ 8.0 Hz, $J_{2b,3b}$ 10.0 Hz, H-2b), 4.90 (dd, 1H, $J_{3a,4a}$ 8.5 Hz, $J_{2a,3a}$ 10.0 Hz, H-3a), 4.31, 4.27 (2d, each 1H, *J* 8.0 Hz, H-1a, H-1b), 4.00 (ddd, 1H, H-2a), 3.88 (d, t, 2H, $J_{3b,4b}$ ~ 3 Hz, H-4b, and $J_{4a,5a}$ 8.5 Hz, H-4a), 3.36 (s, 3H, CH_3O), 3.30 (dd, 1H, H-3b), 1.85 and 1.65 (2s, each 3H, CH_3CO); fab-ms, *m/z*: 942 (0.24, $[M + Na]^+$), 920.5 (1.28, $[M + H]^+$), 919 (0.44, M^+), 888 (1.04, $[M - OMe]^+$). Anal. calcd. for $C_{52}H_{57}NO_{14}$: C 67.89, H 6.24, N 1.52; found: C 67.72, H 6.33, N 1.53.

*Methyl 2-acetamido-4-*O*-(2-*O*-acetyl-3,4,6-tri-*O*-benzyl-β-D-galactopyranosyl)-6-*O*-benzyl-2,3-dideoxy-β-D-*xylo*-hexopyranoside (30)*

Argon was passed through a solution of **29** (280 mg, 0.22 mmol) in toluene (15 mL) at 80°C for 1 h. Then tributyltin hydride

Can. J. Chem. Downloaded from www.nrcresearchpress.com by 217.78.4.112 on 09/08/12
For personal use only.

(0.63 mL, 2.34 mmol) and 2,2′-azabis(isobutyronitrile) (35 mg, 0.21 mmol) were added and heating was continued for 2 h. Evaporation and recrystallization from dichloromethane–hexane afforded **30** (161 mg, 92%); mp 161–163°C; $[\alpha]_D$ +40 (*c* 0.7, chloroform); ^{1}H nmr ($CDCl_3$) δ: 7.40–7.20 (m, 20H, 4Ph), 6.80 (d, 1H, $J_{NH,2a}$ 9.0 Hz, NH), 5.36 (dd, 1H, $J_{1b,2b}$ 8.0 Hz, $J_{2b,3b}$ 10.0 Hz, H-2b), 4.92 (d, from ABq, 1H, $J_{A,B}$ 12.0 Hz, 1CH_2Ph), 4.70–4.41 (m, 7H, CH_2Ph), 4.36 (d, 1H, $J_{1a,2a}$ 2.0 Hz, H-1a), 4.26 (d, 1H, H-1b), 4.01 (bm, 1H, H-2a), 3.96 (bd, 1H, $J_{3b,4b}$ 3.0 Hz, H-4b), 3.87 (m, overlapped, H-4a), 3.52 (overlapped, H-3b), 3.37 (s, 3H, CH_3O), 2.17 (td, 1H, $J_{3aeq,3aax}$ 15.0 Hz, $J_{3a,4a} \sim J_{3a,2a} \sim$ 4.5 Hz, H-3a), 2.04 and 2.03 (2s, each 3H, 2CH_3CO), 1.81 (btd, $J_{3a',4a} \sim J_{3a',2a} \sim$ 3 Hz, H-3a′); ^{13}C nmr ($CDCl_3$) δ: 100.70 ($J_{C,H}$ 169.0 Hz, C-1b), 99.94 ($J_{C,H}$ 158.0 Hz, C-1a). Anal. calcd. for $C_{45}H_{53}NO_{11}$: C 68.88, H 6.81, N 1.79; found: C 69.17, H 6.56, N 1.89.

*Methyl 2-acetamido-6-*O*-benzyl-2,3-dideoxy-4-*O*-(3,4,6-tri-*O*-benzyl-*β*-*D*-galactopyranosyl)-*β*-*D*-*xylo*-hexopyranoside (31)*

Compound **30** (140 mg, 0.18 mmol) was deacetylated in methanolic 0.05 N sodium methoxide (15 mL) for 1 day. Neutralization with Amberlite IRC 50 H^+, filtration, evaporation, and precipitation from dichloromethane–hexane afforded **31** (130 mg, 98%) as a powder; $[\alpha]_D$ −7.1 (*c* 1.0, chloroform); ^{1}H nmr ($CDCl_3$) δ: 7.40–7.20 (m, 20H, 4Ph), 6.44 (d, 1H, $J_{NH,2a}$ 8.0 Hz, NH), 4.90–4.41 (m, 8H, 4CH_2Ph), 4.39 (d, 1H, $J_{1a,2a}$ 4.0 Hz, H-1a), 4.33 (d, 1H, $J_{1b,2b}$ 7.5 Hz, H-1b), 3.94 (overlapped, H-4b), ~ 3.90 (m, 3H with H-2a and H-2b), 3.40 (s, 3H, CH_3O), 3.38 (dd, overlapped, $J_{3b,4b}$ 2.8 Hz, H-3b), 2.32 (ddd, $J_{3aeq,3aax}$ 14.0 Hz, $J_{3a,4a} \sim J_{3a,2a} \sim$ 4 Hz, H-3a), 1.85 (s, 3H, CH_3CO), 1.81 (td, 1H, $J_{3a',4a} \sim J_{2a,3a'} \sim$ 6.5 Hz, H-3a′); ^{1}H nmr (MeOD-d_4, Me signal set at 3.20 ppm) δ: 7.40–7.10 (m, 20H, 4Ph), 4.70–4.30 (m, 8H, 4CH_2Ph), 4.20 (d, 1H, $J_{1a,2a}$ 7.5 Hz, H-1a), 4.14 (d, 1H, $J_{1b,2b}$ 8.0 Hz, H-1b), 3.34 (s, 3H, CH_3O), 2.30 (td, 1H, $J_{3aeq,3aax}$ 13.0 Hz, $J_{2a,3aeq} = J_{3aeq,4a}$ 5.0 Hz, H-3aeq), 1.78 (s, 3H, CH_3O), 1.49 (td, 1H, $J_{2a,3aax} \sim J_{3aax,4a} \sim$ 11 Hz, H-3aax). Anal. calcd. for $C_{43}H_{51}NO_{10} \cdot 1H_2O$: C 68.14, H 7.04, N 1.85; found: 67.84, H 7.12, N 1.68.

*Methyl 2-acetamido-6-*O*-benzyl-2,3-dideoxy-4-*O*-[3,4,6-tri-*O*-benzyl-2-*O*-(2,3,4-tri-*O*-benzyl-*α*-*L*-fucopyranosyl)-*β*-*D*-galactopyranosyl]-*β*-*D*-*xylo*-hexopyranoside (32)*

Alcohol **31** (120 mg, 0.16 mmol) was reacted with bromide **3** (0.69 mmol) as described for the preparation of **4**. After 24 h, conventional work-up was followed by column chromatography on silica gel (dichloromethane–methanol, 98.5:1.5) to provide the title compound **32** (130 mg, 69%) as a gum; $[\alpha]_D$ −40.7 (*c* 0.5, chloroform); ^{1}H nmr ($CDCl_3$) δ: 7.35–7.05 (m, 35H, 7Ph), 6.76 (d, 1H, $J_{NH,2a}$ 8.0 Hz, NH), 5.73 (d, 1H, $J_{1c,2c} \sim$ 3.8 Hz, H-1c), 4.58 (overlapped, H-1b), 4.40 (H-5c), 4.39 (d, $J_{1a,2a}$ 2.5 Hz, H-1a), 4.18 (dd, 1H, $J_{2b,3b}$ 9.5 Hz, $J_{1b,2b}$ 8.0 Hz, H-2b), 4.03 (dd, 1H, $J_{2c,3c}$ 10.0 Hz, H-2c), 3.96 (bd, 1H, overlapped by H-3c, $J_{3b,4b}$ 2.5 Hz, $J_{4b,5b} < 1$ Hz, H-4b), 3.94 (dd, 1H, $J_{3c,4c}$ 2.5 Hz, H-3c), 3.90 (bm, 1H, H-2a), 3.81 (bm, 2H, with H-4a), 3.74 (dd, 1H, H-3b), 3.70 (bm, 2H, with H-4c), 3.47 (s, 3H, CH_3O), 2.17 (ddd, 1H, $J_{3aeq,3aax}$ 14.0 Hz, $J_{2a,3a} \sim J_{3a,4a}$ 3.5 Hz, H-3a), 1.94 (ddd, 1H, $J_{3a',4a} = J_{2a,3a'}$ 4.8 Hz, H-3a′), 1.74 (s, 3H, CH_3CO), 1.16 (d, 3H, $J_{5c,6c}$ 6.5 Hz, H_3-6c). Anal. calcd. for $C_{70}H_{79}NO_{14}$: C 72.58, H 6.87, N 1.21; found: C 72.53, H 7.15, N 1.10.

*Methyl 2-acetamido-2,3-dideoxy-4-*O*-[2-*O*-(α-*L*-fucopyranosyl)-β-*D*-galactopyranosyl]-β-*D*-xylo-hexopyranoside (33)*

Compound **32** (112 mg, 0.097 mmol) in 95% ethanol (20 mL) was hydrogenated in the presence of 5% palladium-on-carbon (115 mg) for 14 h. Processing and gel filtration as described for the preparation of **13** provided **33** (51 mg, 97%) as a light white powder after freeze-drying an aqueous solution; ^{1}H nmr (D_2O) δ: 5.30 (d, 1H, $J_{1c,2c}$ 2.5 Hz, H-1c), 4.52 (d, 1H, $J_{1b,2b}$ 7.8 Hz, H-1b), 4.42 (d, 1H, $J_{1a,2a}$ 8.5 Hz, H-1a), 4.22 (q, 1H, $J_{5c,6c}$ 6.5 Hz, H-5c) 3.94 (dd, 1H, $J_{5a,6a}$ 1.8 Hz, $J_{6a,6a'}$ 12.0 Hz, H-6a), 3.88 (bd, 1H, $J_{3b,4b}$ 3.0 Hz, $J_{4b,5b} < 1$ Hz, H-4b), 3.65 (dd, 1H, $J_{5b,6b}$ 4.5 Hz, $J_{5b,6b'}$ 7.5 Hz, H-5b), 3.60 (dd, 1H, $J_{2b,3b}$ 9.5 Hz, H-2b), 3.50 (s, 3H, CH_3O), 2.44 (td, 1H, $J_{3aeq,3aax}$ 13.0 Hz, $J_{3aeq,4a} = J_{3aeq,2a}$ 4.5 Hz, H-3aeq), 1.98 (s, 3H, CH_3CO), 1.64 (td, 1H, $J_{3aax,4a} = J_{2a,3aax}$ 11.5 Hz, H-3aax), 1.22 (d, 3H, H_3-6c). The ^{13}C nmr data are reported in Table 3.

*2,4-Di-*O*-benzyl-3,6-dideoxy-*L*-xylo-hexopyranose (34)*

Methyl 2,4-di-*O*-benzyl-3,6-dideoxy-α-L-*xylo*-hexopyranoside (21) (2.3 g, 6.72 mmol) was dissolved in 60 mL of 70% aqueous trifluoroacetic acid and kept at room temperature for 16 h. Solvent removal and codistillation with toluene left a syrupy residue that was applied to a column of silica gel using hexane – ethyl acetate (2:1) as eluent. Evaporation of the main fraction gave **34** (1.96 g, 89%) as a syrup. On storage in the fridge for several months, very slow crystallization occurred. The analytical sample was recrystallized from ether–hexane; mp 67–70°C; $[\alpha]_D$ −17.6 (*c* 0.8, methanol, no mutarotation after 24 h); ^{1}H nmr ($CDCl_3$, α:β = 5:3) δ: 7.43–7.2 (m, 10H, 2Ph), 5.29 (bs, H-1α), 4.80–4.39 (m, 2CH_2Ph and H-1β), 4.14 (dq, $J_{5,6}$ 6.5 Hz, $J_{4,5}$ 1.5 Hz, H-5α), 3.87 (ddd, $J_{1,2}$ 3.0 Hz, $J_{2,3eq}$ 5.0 Hz, $J_{2,3ax}$ 11.5 Hz, H-2α), 3.67 (dq, $J_{4,5}$ 1.0 Hz, $J_{5,6}$ 6.5 Hz, H-5β), 3.53 (ddd, $J_{1,2}$ 7.5 Hz, $J_{2,3eq}$ 5.0 Hz, $J_{2,3ax}$ 12.0 Hz, H-2β), 3.45 (bs, H-4α), 3.37 (bs, H-4β), 2.37 (ddd, $J_{3eq,3ax}$ 13.5 Hz, $J_{3eq,4}$ 3.0 Hz, H-3βeq), 2.16 (m, $J_{3eq,3ax}$ 13.0 Hz, $J_{3eq,4}$ 3.0 Hz, $J_{3eq,1}$ 1.0 Hz, H-3αeq), 1.84 (ddd, $J_{3ax,4}$ 2.5 Hz, H-3αax), 1.46 (ddd, $J_{3ax,4}$ 2.5 Hz, H-3βax), 1.26 (d, H_3-6β), 1.19 (d, H_3-6α). Anal. calcd. for $C_{20}H_{24}O_4$: C 73.15, H 7.37; found: C 72.99, H 7.32.

*2,3-Di-*O*-benzyl-4,6-dideoxy-*L*-xylo-hexopyranose (35)*

A solution of methyl 2,3-di-*O*-benzyl-4,6-dideoxy-α-L-*xylo*-hexopyranoside[4] (2.3 g, 6.72 mmol) in 70% aqueous trifluoroacetic acid (60 mL) was kept at room temperature for 13 h. Evaporation and codistillation with toluene left a syrupy residue that was purified by column chromatography (silica gel, hexane – ethyl acetate, 3:1) to provide **35** (2.03 g, 92%) as a syrup; $[\alpha]_D$ −47.7 (*c* 0.7, methanol, no mutarotation after 24 h); ^{1}H nmr ($CDCl_3$, α:β = 1:1) δ: 7.44–7.20 (m, 10H, 2Ph), 5.23 (t, $J_{1,2}$ 3.5 Hz, $J_{1,OH}$ 2.0 Hz, H-1α), 4.94–4.66 (m, 4H, 2CH_2Ph), 4.61 (dd, $J_{1,2}$ 7.5 Hz, $J_{1,OH}$ 5.5 Hz, H-1β), 4.13 (m, 1H, $J_{5,6}$ 6.5 Hz, $J_{4ax,5}$ 12.0 Hz, $J_{4eq,5}$ 2.0 Hz, H-5α), 3.90 (ddd, $J_{3,4eq}$ 5.0 Hz, $J_{3,4ax}$ 12.0 Hz, $J_{2,3}$ 9.0 Hz, H-3α), 3.59 (ddd, $J_{2,3}$ 9.0 Hz, $J_{3,4ax}$ 12.0 Hz, $J_{3,4eq}$ 5.0 Hz, H-3β), 3.56 (m, 1H, $J_{5,6}$ 6.0 Hz, $J_{4eq,5}$ 2.0 Hz, $J_{4ax,5}$ 12.0 Hz, H-5β), 3.48 (dd, H-2α), 3.34 (d, OH-β), 3.24 (dd, 1H, H-2β), 2.99 (d, 1H, OH-α), 2.09 (ddd, $J_{4eq,4ax}$ 13.0 Hz, H-4αeq), 2.06 (ddd, $J_{4eq,4ax}$ 13.0 Hz, H-4βeq), 1.44 (q, H-4βax), 1.36 (q, H-4αax), 1.27 (d, H_3-6β), 1.18 (d, 3H, H_3-6α). Anal. calcd. for $C_{20}H_{24}O_4$: C 73.15, H 7.37; found: C 73.46, H 7.46.

*2,4-Di-*O*-benzyl-3,6-dideoxy-α-*L*-xylo-hexopyranosyl bromide (36)*

A solution of oxalyl bromide (0.25 mL, 2.5 mmol) in dichloromethane (1.5 mL) was added in portions to a stirred solution of **34** (650 mg, 1.98 mmol) in dichloromethane (3 mL) and *N*,*N*-dimethylformamide (0.2 mL) under nitrogen. The mixture was stirred for 20 min, then diluted with dichloromethane and poured into ice-water. The organic layer was washed three times with ice-water, dried with sodium sulfate and 4 Å molecular sieves, and concentrated to a smaller volume, before being transferred into the glycosidation mixture. **36** was freshly prepared before use; ^{1}H nmr ($CDCl_3$) δ: 7.43–7.20 (m, 10H, 2Ph), 6.69 (bs, 1H, H-1), 4.7–4.37 (4H, CH_2Ph), 4.12 (dq, 1H, $J_{5,6}$ 6.5 Hz, $J_{4,5}$ 1.0 Hz, H-5), 3.78 (ddd, 1H, $J_{1,2}$ 3.0 Hz, $J_{2,3eq}$ 5.0 Hz, $J_{2,3ax}$ 10.0 Hz, H-2), 3.50 (bs, 1H, H-4), 2.17 (m, 1H, $J_{3eq,3ax}$ 13.0 Hz, $J_{3eq,4}$ 3.0 Hz, $J_{1,3eq} \sim$ 1 Hz, H-3eq), 1.99 (ddd, 1H, $J_{3ax,4}$ 2.5 Hz, H-3ax), 1.23 (d, 3H, H_3-6).

*2,3-Di-*O*-benzyl-4,6-dideoxy-α-*L*-xylo-hexopyranosyl bromide (37)*

Compound **35** (750 mg, 2.28 mmol) was reacted with oxalyl bromide (315 μL, 3.25 mmol) and *N*,*N*-dimethylformamide (0.2 mL) to form **37** as described for the preparation of **36**. It was prepared just prior to use. ^{1}H nmr ($CDCl_3$) δ: 7.4–7.2 (m, 10H, 2Ph), 6.45 (d, 1H, $J_{1,2}$ 3.5 Hz, H-1), 4.8–4.6 (4H, CH_2Ph), 4.19 (m, 1H,

$J_{5,6}$ 6.5 Hz, $J_{4ax,5}$ 12.0 Hz, $J_{4eq,5}$ 2.0 Hz, H-5), 3.98 (ddd, 1H, $J_{3,4eq}$ 5.0 Hz, $J_{3,4ax}$ 12.0 Hz, $J_{2,3}$ 9.0 Hz, H-3), 3.4 (dd, 1H, H-2), 2.13 (ddd, 1H, $J_{4ax,4eq}$ 13.0 Hz, H-4eq), 1.48 (q, 1H, H-4ax), 1.23 (d, 3H, H_3-6).

*Methyl 2-acetamido-3,6-di-*O*-benzyl-2-deoxy-*β*-*D*-glucopyranoside (**39**)*

Ether saturated with hydrogen chloride was added at 0°C to a stirred mixture of methyl 2-acetamido-3-*O*-benzyl-4,6-*O*-benzylidene-2-deoxy-β-D-glucopyranoside (**18**) (7.5 g, 18.1 mmol), sodium cyanoborohydride (12.5 g, 198.9 mmol), and a crystal of methyl orange in dry tetrahydrofuran (200 mL) until the colour of the indicator turned red and gas evolution occurred. When tlc indicated the reaction to be complete, the mixture was diluted with dichloromethane and poured into aqueous saturated sodium hydrogencarbonate. The organic solution was washed with water, dried, and evaporated. The reaction product was purified by column chromatography on silica gel (dichloromethane–methanol, 19:1) and crystallization from ethyl acetate to afford **39** (5.0 g, 66%); mp 169–170°C; $[\alpha]_D$ − 14.5 (*c* 1.0, dichloromethane); ^{1}H nmr ($CDCl_3$) δ: 7.40–7.20 (m, 10H, 2Ph), 5.54 (d, 1H, $J_{NH,2}$ 7.5 Hz, NH), 4.80 and 4.71 (ABq, 2H, $J_{A,B}$ 12.0 Hz, CH_2Ph), 4.76 (d, 1H, $J_{1,2}$ 7.5 Hz, H-1), 4.63 and 4.57 (ABq, 2H, $J_{A,B}$ 12.0 Hz, CH_2Ph), 3.99 (dd, 1H, $J_{2,3}$ 10.0 Hz, $J_{3,4}$ 8.5 Hz, H-3), 3.79 and 3.75 (ABq, 2H, $J_{5,6} \sim J_{5,6'} \sim 5$ Hz, $J_{6,6'}$ 11.0 Hz, H-6, H-6'), 3.69 (ddd, 1H, $J_{4,5}$ 9.5 Hz, $J_{3,4}$ 8.5 Hz, $J_{4,OH}$ 2.2 Hz, H-4), 3.54 (m, 1H, H-5), 3.31 (m, 1H, H-2), 2.81 (d, 1H, OH), 1.90 (s, 3H, CH_3CO). Addition of trichloroacetyl isocyanate into the nmr tube resulted in a new spectrum with δ H-4 at 5.09 ppm (t, $J_{3,4} = J_{4,5}$ 9.0 Hz); ^{13}C nmr ($CDCl_3$) δ: 170.55 (CO), 100.97 (C-1), 56.91, 56.67 (C-2, CH_3O), 23.66 (*C*H_3CO). Anal. calcd. for $C_{23}H_{29}NO_6$: C 66.49, H 7.04, N 3.37; found: C 65.77, H 6.99, N 3.32.

*Methyl 2-acetamido-3,6-di-*O*-benzyl-2-deoxy-4-*O*-(2,3,4,6-tetra-*O*-acetyl-*β*-*D*-galactopyranosyl)-*β*-*D*-glycopyranoside (**41**)*

A solution of 2,3,4,6-tetra-*O*-acetyl-α-D-galactopyranosyl bromide (**40**) (19) (5.34 g, 13.0 mmol) in benzene–nitromethane (1:1, 25 mL) was added to a stirred mixture of **39** (3.6 g, 8.67 mmol), mercuric cyanide (4.38 g, 17.3 mmol), and powdered calcium sulfate (10.0 g) in the same solvent (175 mL). After stirring for 6 h at 40°C, more bromide solution (5.34 g, 13.0 mmol in 25 mL) was added and heating continued for 20 h. Then the reaction mixture was cooled to room temperature, diluted with dichloromethane, and washed with aqueous saturated sodium hydrogen carbonate and water. The material obtained on evaporation was applied to a column of silica gel and eluted with dichloromethane–methanol (19:1). Evaporation of the major fraction provided **41** (4.24 g, 66%); mp 75–76°C; $[\alpha]_D$ −23 (*c* 1.1, dichloromethane); ^{1}H nmr ($CDCl_3$) δ: 7.45–7.25 (m, 10H, 2Ph), 5.93 (d, 1H, $J_{NH,2a}$ 8.5 Hz, NH), 5.32 (d, 1H, $J_{3b,4b}$ 3.5 Hz, H-4b), 5.12 (dd, 1H, $J_{2b,3b}$ 10.0 Hz, $J_{1b,2b}$ 8.0 Hz, H-2b), 4.91 (dd, 1H, H-3b), 4.76 and 4.65 (ABq, 2H, $J_{A,B}$ 12.0 Hz, CH_2Ph), 4.67 and 4.49 (ABq, 2H, $J_{A,B}$ 12.0 Hz, CH_2Ph), 4.65 (overlapped, H-1a), 4.49 (overlapped, H-1b), 3.71 (m, 1H, H-2), 3.46 (s, 3H, CH_3O), 2.15–1.93 (5s, each 3H, 5CH_3CO); ^{13}C nmr ($CDCl_3$) δ: 101.17, 99.83 (C-1 and C-1'). Anal. calcd. for $C_{37}H_{47}NO_{15}$: C 59.59, H 6.35, N 1.88; found: C 60.06, H 6.64, N 1.92.

*Methyl 2-acetamido-3,6-di-*O*-benzyl-2-deoxy-4-*O*-(β-*D*-galactopyranosyl)-β-*D*-glucopyranoside (**42**)*

Compound **41** (4.0 g, 5.37 mmol) was treated with methanolic 0.08 N sodium methoxide (80 mL) for 16 h. Neutralization with Amberlite IRC 50 H^+, evaporation, and column chromatography on silica gel (dichloromethane–methanol, 19:1) provided **42** (2.7 g, 87%), which was crystallized from methanol–ether; mp 105–106°C; $[\alpha]_D$ −6.3 (*c* 0.7, methanol).

*Methyl 2-acetamido-3,6-di-*O*-benzyl-4-*O*-(4,6-*O*-benzylidene-β-*D*-galactopyranosyl)-2-deoxy-β-*D*-glucopyranoside (**43**)*

A mixture of **42** (2.0 g, 3.46 mmol), α,α-dimethoxytoluene (1.02 mL, 6.80 mmol), and *p*-toluenesulfonic acid monohydrate (25 mg) in dry acetonitrile (35 mL) was stirred for 1 h at room temperature. Neutralization with triethylamine and solvent evaporation gave a residue that was dissolved in methanol and precipitated from ether as a white solid (2.0 g, 87%). An analytical sample was recrystallized from hot ethyl acetate; mp 204–205°C; $[\alpha]_D$ −51.5 (*c* 0.5, methanol); ^{1}H nmr ($CDCl_3$) δ: 7.50–7.20 (m, 15H, 3Ph), 5.63 (d, 1H, $J_{NH,2a}$ 7.5 Hz, NH), 5.48 (s, 1H, C*H*Ph), 4.75, 4.51 (2d, each 1H, *J* 7.5 Hz, *J* 8.0 Hz, H-1a, H-1b), 3.50 (s, 3H, CH_3O), 1.90 (s, 3H, CH_3CO). Anal. calcd. for $C_{36}H_{43}NO_{11}$: C 64.95, H 6.51, N 2.10; found: C 64.44, H 6.49, N 2.29.

*Methyl 2-acetamido-4-*O*-(3-*O*-benzoyl-4,6-*O*-benzylidene-β-*D*-galactopyranosyl)-3,6-di-*O*-benzyl-2-deoxy-β-*D*-glucopyranoside (**44**)*

Compound **43** (1.8 g, 2.70 mmol) and pyridine (1.4 mL, 17.3 mmol) were dissolved in dry dichloromethane (50 mL). Benzoyl chloride (0.47 mL, 4.05 mmol) was added within 30 min at −78°C. Examination by tlc then showed the completion of the reaction. The excess of reagent was destroyed by the addition of methanol (1.0 mL). The mixture was allowed to reach room temperature and poured into ice-water. Washing of the organic layer with water, followed by drying and evaporation, left a white residue that was recrystallized from hot ethyl acetate to provide **44** (1.44 g, 69%) as white needles; mp 207–208°C; $[\alpha]_D$ +51.7 (*c* 0.5, dichloromethane); ^{1}H nmr ($CDCl_3$) δ: 8.20, 7.60–7.20 (d, 2H, m, 18H, 4Ph), 5.64 (d, 1H, $J_{NH,2a}$ 7.5 Hz, NH), 5.44 (s, 1H, C*H*Ph), 4.98 (dd, 1H, $J_{2b,3b}$ 10.0 Hz, $J_{3b,4b}$ 3.5 Hz, H-3b), 4.78, 4.65 (2d, each 1H, *J* 7.5 Hz, *J* 8.0 Hz, H-1a, H-1b), 4.35 (d, 1H, H-4b), 3.48 (m, 3H, CH_3O), 3.40 (m, H-2a), 1.90 (s, 3H, CH_3CO); ^{13}C nmr ($CDCl_3$) δ: 103.47, 101.10, 100.76 (C-1a, C-1b, *C*HPh). Anal. calcd. for $C_{43}H_{47}NO_{12}$: C 67.09, H 6.15, N 1.82; found: C 66.69, H 6.16, N 1.92.

*Methyl 2-acetamido-4-*O*-[3-*O*-benzoyl-4,6-*O*-benzylidene-2-*O*-(2,3,4-tri-*O*-benzyl-α-*L*-fucopyranosyl)-β-*D*-galactopyranosyl]-3,6-di-*O*-benzyl-2-deoxy-β-*D*-glucopyranoside (**45**)*

Bromide **3** (1.62 mmol) was reacted with alcohol **44** (500 mg, 0.65 mmol) as described for the preparation of **4**. After 20 h, the mixture was processed in the normal way and purified by column chromatography on silica gel (dichloromethane–methanol, 98:2) to provide **45** (570 mg, 74%). The analytical sample was recrystallized from methanol as white needles; mp 124–125°C; $[\alpha]_D$ −23.6 (*c* 1.0, dichloromethane); ^{1}H nmr ($CDCl_3$) δ: 7.97, 7.50–7.05 (d, 2H, m, 33H, 7Ph), 5.69 (d, 1H, $J_{NH,2a}$ 7.5 Hz, NH), 5.45 (s, 1H, C*H*Ph), 5.43 (d, 1H, $J_{1c,2c}$ 3.8 Hz, H-1c), 5.13 (dd, 1H, $J_{2b,3b}$ 10.0 Hz, $J_{3b,4b}$ 3.5 Hz, H-3b), 4.78 (d, 1H, $J_{1a,2a}$ 7.0 Hz, H-1a), 4.54 (d, 1H, $J_{1b,2b}$ 8.0 Hz, H-1b), 4.40 (d, 1H, H-4b), 4.33 (t, overlapped, H-2b), 4.09 (t, 1H, $J_{3a,4a} \sim J_{4a,5a} \sim 7.5$ Hz, H-4a), 4.03 (dd, 1H, $J_{2a,3a}$ 9.0 Hz, H-3a), 3.84 (dd, 1H, $J_{2c,3c}$ 10.0 Hz, H-2c), 3.47 (s, 3H, CH_3O), 3.40 (m, 1H, H-2a), 1.87 (s, 3H, CH_3CO), 1.21 (d, 3H, $J_{5c,6c}$ 6.5 Hz, H_3-6c). ^{13}C nmr ($CDCl_3$) δ: 170.32, 165.85 (2CO), 101.19, 100.88, 100.75, 97.47 (C-1a, C-1b, C-1c, PhC*H*), 23.58 (*C*H_3CO), 16.79 (C-6c). Anal. calcd. for $C_{70}H_{75}NO_{16}$: C 70.87, H 6.37, N 1.18; found: C 70.68, H 6.30, N 1.18.

*Methyl 2-acetamido-3,6-di-*O*-benzyl-4-*O*-[4,6-*O*-benzylidene-2-*O*-(2,3,4-tri-*O*-benzyl-α-*L*-fucopyranosyl)-β-*D*-galactopyranosyl]-2-deoxy-β-*D*-glucopyranoside (**46**)*

Compound **45** (500 mg, 0.42 mmol) was treated with methanolic 0.07 N sodium methoxide (14 mL) for 5 days. After neutralization with Amberlite IRC 50 (H^+), filtration, and evaporation, the resulting product was chromatographed on a column of silica gel (dichloromethane–methanol, 19:1) to provide **46** (400 mg, 88%) as a white powder; $[\alpha]_D$ −65.8 (*c* 1.0, dichloromethane); ^{1}H nmr ($CDCl_3$) δ: 7.50–7.10 (m, 30H, 6Ph), 5.67 (d, 1H, $J_{NH,2a}$ 7.5 Hz, NH), 5.55 (s, 1H, C*H*Ph), 5.00 (overlapped by CH_2Ph, H-1c), 3.75 (dd, 1H, $J_{2b,3b}$ 9.5 Hz, H-2b), 3.45 (s, 3H, CH_3O), 1.12 (d, 3H, $J_{5c,6c}$ 6.5 Hz, H_3-6c).

Can. J. Chem. Downloaded from www.nrcresearchpress.com by 217.78.4.112 on 09/08/12
For personal use only.

Can. J. Chem. Downloaded from www.nrcresearchpress.com by 217.78.4.112 on 09/08/12
For personal use only.

*Methyl 2-acetamido-3,6-di-*O*-benzyl-4-*O*-[4,6-*O*-benzylidene-3-*O*-phenoxythiocarbonyl-2-*O*-(2,3,4-tri-*O*-benzyl-α-L-fucopyranosyl)-β-D-galactopyranosyl]-2-deoxy-β-D-glucopyranoside (**47**)*

A mixture of **46** (300 mg, 0.28 mmol), 4-dimethylaminopyridine (180 mg, 1.47 mmol), and phenyl chlorothionocarbonate (0.13 mL, 0.94 mmol) in dry acetonitrile (20 mL) was kept at 50°C for 24 h. The solvent was evaporated and the resulting material was applied to a column of silica gel (hexane – ethyl acetate, 7:3) to provide **47** (273 mg, 80%) as a pale yellow solid; mp 88–89°C; $[\alpha]_D$ −11.4 (*c* 0.9, dichloromethane); ^{1}H nmr ($CDCl_3$) δ: 7.50–6.85 (m, 35H, 7Ph), 5.68 (d, 1H, $J_{NH,2a}$ 7.0 Hz, NH), 5.52 (s, 1H, C*H*Ph), 5.35 (dd, 1H, $J_{2b,3b}$ 10.0 Hz, $J_{3b,4b}$ 3.5 Hz, H-3b), 5.33 (d, 1H, $J_{1c,2c}$ 3.5 Hz, H-1c), 4.52 (d, overlapped, H-1b), 4.28 (dd, 1H, $J_{1b,2b}$ 7.5 Hz, H-2b), 3.49 (s, 3H, CH_3O), 3.35 (m, 1H, H-2a), 1.86 (s, 3H, CH_3CO), 1.22 (d, 3H, $J_{5c,6c}$ 6.2 Hz, H_3-6c). Anal. calcd. for $C_{70}H_{75}NO_{17}S$: C 68.11, H 6.13, N 1.13; found: C 68.66, H 6.17, N 1.23.

*Methyl 2-acetamido-3,6-di-*O*-benzyl-4-*O*-[4,6-*O*-benzylidene-3-deoxy-2-*O*-(2,3,4-tri-*O*-benzyl-α-L-fucopyranosyl)-β-D-xylo-hexopyranosyl]-2-deoxy-β-D-glucopyranoside (**48**)*

A solution of **47** (250 mg, 0.20 mmol) in dry toluene (15 mL) was heated to 75°C under nitrogen for 30 min. Then 2,2′-azobis(isobutyronitrile) (45 mg, 0.27 mmol) and tributyltin hydride (0.8 mL, 2.97 mmol) were added. After 4 h at 75°C, the solvent was evaporated and the remainder purified on a column of silica gel (dichloromethane – ethyl acetate, 6:4) to provide **48** (140 mg, 65%) as a white solid; mp 74–75°C; $[\alpha]_D$ −71.1 (*c* 1.0, dichloromethane); ^{1}H nmr ($CDCl_3$) δ: 7.50–7.20 (m, 30H, 6Ph), 5.75 (d, 1H, $J_{NH,2a}$ 7.5 Hz, NH), 5.46 (s, 1H, C*H*Ph), 4.95 (d, 1H, $J_{1c,2c}$ 3.5 Hz, H-1c), 4.76 (d, 1H, $J_{1a,2a}$ 7.0 Hz, H-1a), 4.50 (d, 1H, $J_{1b,2b}$ 7.5 Hz, H-1b), 4.04 (dd, 1H, $J_{2c,3c}$ 10.0 Hz, H-1c), 3.48 (s, 3H, CH_3O), 3.46 (H-2a), 2.39 (m, 1H, $J_{3bax,3beq}$ 13.5 Hz, H-3beq), 1.88 (s, 3H, CH_3CO), 1.56 (m, 1H, H-3bax), 1.17 (d, 3H, $J_{5c,6c}$ 6.5 Hz, H_3-6c). ^{13}C nmr ($CDCl_3$) δ: 170.20 (CO), 103.14, 101.35, 101.06, 94.93 (C-1a, C-1b, C-1c, and PhCH), 33.53 (C-3b), 23.59 (CH_3CO), 16.78 (C-6c). Anal. calcd. for $C_{63}H_{71}NO_{14}$: C 70.97, H 6.71, N 1.31; found: C 70.08, H 6.60, N 1.56.

*Methyl 2-acetamido-3,6-di-*O*-benzyl-4-*O*-[4,6-*O*-benzylidene-2-*O*-(2,6-dideoxy-α-L-lyxo-hexopyranosyl)-β-D-galactopyranosyl]-2-deoxy-β-D-glucopyranoside (**49**)*

A solution of freshly prepared 3,4-di-*O*-acetyl-2,6-dideoxy-α-L-*lyxo*-hexopyranosyl bromide (**38**, 1.30 mmol) (20) in dichloromethane (3.0 mL) was added to a stirred mixture of **44** (100 mg, 0.13 mmol), tetraethylammonium bromide (37 mg, 0.18 mmol), 4 Å molecular sieves (powdered, 1.5 g), and *N*,*N*-dimethylformamide (0.30 mL) in dichloromethane (3.0 mL). After stirring for 2 h, the reaction was quenched by the addition of methanol (0.5 mL). Usual work-up was followed by column chromatography on silica gel (dichloromethane–methanol, 98:2). The resultant impure product was deacylated in methanolic 0.17 N sodium methoxide (3 mL) for 12 h. Neutralization with Amberlite IRC 50 H^+, filtration, and evaporation gave a residue that was chromatographed on a column of silica gel (dichloromethane–methanol, 19:1), to provide **49** (45 mg, 44%) as a white solid, mp 120–121°C; $[\alpha]_D$ −73 (*c* 0.6, dichloromethane); ^{1}H nmr ($CDCl_3$) δ: 7.40–7.20 (m, 15H, 3Ph), 5.65 (d, 1H, $J_{NH,2a}$ 7.5 Hz, NH), 5.50 (s, 1H, C*H*Ph), 5.44 (d, 1H, $J_{1c,2eax}$ 3.5 Hz, $J_{1c,2eeq}$ < 1 Hz, H-1c), 4.83 (d, 1H, $J_{1a,2a}$ 7.5 Hz, H-1a), 4.36 (d, 1H, $J_{1b,2b}$ 8.0 Hz, H-1b), 4.24 (q, overlapped, $J_{5c,6c}$ 6.5 Hz, H-5c), 3.49 (s, 3H, CH_3O), 3.30 (m, 1H, H-2a), 1.96 (bdd, $J_{2eax,2eeq}$ 13.0 Hz, $J_{2eeq,3c}$ 4.5 Hz, H-2ceq), 1.91 (s, 3H, CH_3CO), 1.74 (ddd, 1H, $J_{3c,2eax}$ 12.5 Hz, H-2cax), 1.29 (d, 3H, H_3-6c); ^{13}C nmr ($CDCl_3$) δ: 170.40 (CO), 101.57, 101.03 (2C), 97.63 (C-1a, C-1b, C-1c, PhCH), 32.74 (C-2c), 23.59 (CH_3CO), 16.78 (C-6c). Anal. calcd. for $C_{42}H_{53}NO_{14}$: C 63.38, H 6.71, N 1.76; found: C 62.49, H 6.68, N 1.82.

*Methyl 2-acetamido-4-*O*-[3-*O*-benzoyl-4,6-*O*-benzylidene-2-*O*-(2,4-di-*O*-benzyl-3,6-dideoxy-α-L-xylo-hexopyranosyl)-β-D-galactopyranosyl]-3,6-di-*O*-benzyl-2-deoxy-β-D-glucopyranoside (**50**)*

Freshly prepared bromide **36** (0.30 mmol) was reacted with alcohol **44** (100 mg, 0.13 mmol) as described for the preparation of **4**. After stirring for 20 h, methanol (0.5 mL) was added, followed by the usual processing and column chromatography of the resulting product on silica gel. Elution with dichloromethane–methanol (98:2) provided the title compound **50** (120 mg, 86%) as a white solid; mp 99–100°C; $[\alpha]_D$ −9.9 (*c* 1.0, dichloromethane); ^{1}H nmr ($CDCl_3$) δ: 8.02, 7.60–6.90 (d, 2H, m, 28H, 6Ph), 5.70 (d, 1H, $J_{NH,2a}$ 7.5 Hz, NH), 5.45 (s, 1H, PhC*H*), 5.38 (d, 1H, $J_{1c,2c}$ 3.2 Hz, H-1c), 5.19 (dd, 1H, $J_{2b,3b}$ 9.5 Hz, $J_{3b,4b}$ 3.5 Hz, H-3b), 4.78 (d, 1H, $J_{1a,2a}$ 7.5 Hz, H-1a), 4.62 (d, 1H, $J_{1b,2b}$ 8.0 Hz, H-1b), 4.42 (bd, 1H, H-4b), 4.39 (dd, 1H, H-2b), 4.09 and 4.05 (2t, AB, 2H, $J_{3a,4a} \sim J_{4a,5a} \sim$ 7.5 Hz, H-4a, $J_{2a,3a}$ 8.0 Hz, H-3a), 3.70 (td, 1H, $J_{2c,3cax}$ 11.5 Hz, $J_{2c,3ceq} \sim$ 4.5 Hz, H-2c), 3.47 (s, 3H, CH_3O), 3.41 (m, 1H, H-2a), 1.98 (dt, 1H, $J_{3cax,3ceq}$ 12.5 Hz, H-3ceq), 1.88 (s, 3H, CH_3CO), 1.71 (m, 1H, $J_{3cax,4c} \sim$ 2 Hz, H-3cax), 1.24 (d, 3H, $J_{5c,6c}$ 6.5 Hz, H_3-6c); ^{13}C nmr ($CDCl_3$) δ: 170.27 and 165.84 (2CO), 101.35, 100.99, 100.79, 96.76 (C-1a, C-1b, C-1c, PhCH), 27.84 (C-3c), 23.60 (CH_3CO), 16.61 (C-6c). Anal. calcd. for $C_{63}H_{69}NO_{15}$: C 70.05, H 6.44, N 1.29; found: C 69.92, H 6.39, N 1.55.

*Methyl 2-acetamido-4-*O*-[3-*O*-benzoyl-4,6-*O*-benzylidene-2-*O*-(2,3-di-*O*-benzyl-4,6-dideoxy-α-L-xylo-hexopyranosyl)-β-D-galactopyranosyl]-3,6-di-*O*-benzyl-2-deoxy-β-D-glucopyranoside (**51**)*

The disaccharide **44** (55 mg, 0.07 mmol) was glycosylated with bromide **37** (0.30 mmol) as described for the preparation of **4**. After stirring for 20 h, the mixture was processed in the usual way. The resultant product was purified by column chromatography (dichloromethane–methanol, 98:2) to provide the title compound **51** (70 mg, 91%). Compound **51** had mp 94–95°C; $[\alpha]_{365}$ + 21.9 (*c* 0.9, dichloromethane); ^{1}H nmr ($CDCl_3$) δ: 8.0, 7.5–7.05 (d, 2H, m, 28H, 6Ph), 5.72 (d, 1H, $J_{NH,2a}$ 7.5 Hz, NH), 5.45 (s, 1H, PhC*H*), 5.37 (d, 1H, $J_{1c,2c}$ 3.5 Hz, H-1c), 5.12 (dd, 1H, $J_{2b,3b}$ 9.5 Hz, $J_{3b,4b}$ 3.5 Hz, H-3b), 4.82 (d, 1H, $J_{1a,2a}$ 7.2 Hz, H-1a), 4.54 (d, 1H, $J_{1b,2b}$ 8.0 Hz, H-1b), 4.39 (d, 1H, H-4b), 4.33 (dd, 1H, H-2b), 4.10 and 4.07 (2t, AB, 2H, $J_{3a,4a} \sim J_{4a,5a}$ 7.5 Hz, H-4a, $J_{2a,3a} \sim$ 8.5 Hz, H-3a), 3.88 (dd, 1H, $J_{2c,3c}$ 10.0 Hz, H-2c), 3.50 (s, 3H, CH_3O), 3.38 (overlapped, H-2a), 2.03 (m, 1H, $J_{4cax,4ceq}$ 12.5 Hz, $J_{4ceq,5c} \sim$ 2 Hz, $J_{4ceq,3c}$ 5.0 Hz, H-4ceq), 1.88 (s, 3H, CH_3CO), 1.32 (m, 1H, $J_{4cax,3c} \sim J_{4cax,5c} \sim$ 12 Hz, H-4cax), 1.20 (d, 3H, $J_{5c,6c}$ 6.5 Hz, H_3-6c). Anal. calcd. for $C_{63}H_{69}NO_{15}$: C 70.05, H 6.44, N 1.29; found: C 69.64, H 6.49, N 1.47.

*Methyl 2-acetamido-2-deoxy-4-*O*-[2-*O*-(α-L-fucopyranosyl)-β-D-galactopyranosyl]-β-D-glucopyranoside (**52**)*

Compound **46** (0.09 mmol) and 5% palladium-on-carbon (100 mg) in 95% ethanol (4 mL) were hydrogenated at 120 psi for 18 h. Removal of the catalyst by filtration, evaporation, and gel filtration of the remainder through a column of Sephadex LH 20 (ethanol–water, 1:1) provided **52** (40 mg, 80%) as a white solid after lyophilization of an aqueous solution. Compound **52** had mp 215–216°C; $[\alpha]_D$ −94.3 (*c* 0.9, water) and ^{1}H and ^{13}C nmr data identical to those reported previously (14) (Table 3).

*Methyl 2-acetamido-2-deoxy-4-*O*-[3-deoxy-2-*O*-(α-L-fucopyranosyl)-β-D-xylo-hexopyranosyl]-β-D-glucopyranoside (**53**)*

Trisaccharide **48** (125 mg, 0.12 mmol) and 5% palladium-on-carbon (125 mg) in 95% ethanol (8 mL) were hydrogenated at 120 psi for 36 h. Examination by tlc (isopropanol–water, 4:1) indicated a mixture of three compounds. After removal of the catalyst and evaporation, the remainder was acetylated conventionally (pyridine – acetic anhydride, 2:1) overnight. The product obtained on evaporation and codistillation with toluene was applied to a column of silica gel (dichloromethane–methanol, 49:1). The major fraction was evaporated and the remainder was deacety-

Can. J. Chem. Downloaded from www.nrcresearchpress.com by 217.78.4.112 on 09/08/12
For personal use only.

lated conventionally in methanolic 0.1 N sodium methoxide, followed by neutralization with Amberlite IRC 50 H^+ and evaporation. Purification on a column of Sephadex LH-20 (ethanol–water, 1:1) then provided **53** (20 mg, 32.3%) as a white powder after freeze-drying an aqueous solution; mp 209–210°C; $[\alpha]_D$ − 125.5 (*c* 0.8, water); ^{1}H nmr (D_2O) δ: 4.98 (d, 1H, $J_{1c,2c}$ 3.5 Hz, H-1c), 4.63 (d, 1H, $J_{1b,2b}$ 7.8 Hz, H-1b), 4.46 (d, 1H, $J_{1a,2a}$ 8.0 Hz, H-1a), 4.17 (bq, 1H, $J_{5c,6c}$ 6.5 Hz, $J_{5c,4c}$ < 1 Hz, H-5c), 4.03 (H-4b), 4.01 (dd, overlapped, $J_{6a,6a'}$ 12.0 Hz, $J_{6a,5a}$ 1.8 Hz, H-6a), 3.51 (s, 3H, CH_3O), ~ 3.46 (overlapped, H-5a), 2.37 (ddd, 1H, $J_{3bax,3beq}$ 14.0 Hz, $J_{3beq,2b}$ 5.0 Hz, $J_{3beq,4b}$ 3.5 Hz, H-3beq), 2.04 (s, 3H, CH_3CO), 1.72 (ddd, 1H, $J_{3bax,2b}$ 11.0 Hz, $J_{3bax,4b}$ 2.8 Hz, H-3bax), 1.24 (d, 3H, H_3-6c). ^{13}C nmr data are reported in Table 3.

*Methyl 2-acetamido-2-deoxy-4-*O*-[2-*O*-(2,6-dideoxy-*α*-L-lyxo-hexopyranosyl)-*β*-D-galactopyranosyl]-*β*-D-glucopyranoside (**54**)*

Trisaccharide **49** (40 mg, 0.05 mmol) and 5% palladium-on-carbon (40 mg) were hydrogenated as described for the preparation of **52**. Usual work-up and gel filtration provided **54** (21 mg, 79%) as a white powder after freeze-drying an aqueous solution; mp 204–205°C; $[\alpha]_D$ −77.8 (*c* 0.4, water); ^{1}H nmr (D_2O) δ: 5.32 (dd, 1H, $J_{1c,2cax}$ 3.5 Hz, $J_{1c,2ceq}$ < 1 Hz, H-1c), 4.47 (d, 1H, $J_{1b,2b}$ 7.8 Hz, H-1b), 4.43 (dd, 1H, $J_{1a,2a}$ 8.2 Hz, H-1a), 4.12 (m, 1H, $J_{5c,6c}$ 6.5 Hz, $J_{5c,4c}$ < 1 Hz, H-5c), 3.97 (m, 2H, H-6a and H-3c), 3.90 (d, 1H, $J_{3c,4c}$ 3.5 Hz, H-4c), 3.49 (s, 3H, CH_3O), 3.46 (m, H-5a), 2.02 (s, 3H, CH_3CO), 1.96 (dd, 1H, $J_{2cax,2ceq}$ 13.2 Hz, $J_{2ceq,3c}$ 5.0 Hz, H-2ceq), 1.88 (dt, $J_{2cax,3c}$ 12.0 Hz, H-2cax), 1.22 (d, 3H, H_3-6c). The ^{13}C nmr data are reported in Table 3.

*Methyl 2-acetamido-2-deoxy-4-*O*-[2-*O*-(3,6-dideoxy-*α*-L-xylo-hexopyranosyl)-*β*-D-galactopyranosyl]-*β*-D-glucopyranoside (**55**)*

Compound **50** (100 mg, 0.09 mmol) was debenzoylated as described for the preparation of **46**, followed by chromatography on silica gel (dichloromethane–methanol, 19:1). The debenzoylated material (80 mg) and 5% palladium-on-carbon (80 mg) were hydrogenated in 95% ethanol (5 mL) at 120 psi for 20 h. Usual work-up and gel filtration as described for **52** provided **55** (30 mg, 61%) as a white solid after freeze-drying an aqueous solution; mp 194–195°C; $[\alpha]_D$ −78 (*c* 0.8, water); ^{1}H nmr (D_2O) δ: 5.25 (d, 1H, $J_{1c,2c}$ 3.5 Hz, H-1c), 4.56 (d, 1H, $J_{1b,2b}$ 7.8 Hz, H-1b), 4.45 (d, 1H, $J_{1a,2a}$ 8.2 Hz, H-1a), 4.18 (q, 1H, $J_{5c,6c}$ 6.5 Hz, $J_{4c,5c}$ < 1 Hz, H-5c), 4.04 (td, overlapped by H-6a, $J_{2c,3cax}$ 11.5 Hz, $J_{2c,3ceq}$ 5.0 Hz, H-2c), 4.03 (dd, $J_{6a,6a'}$ 12.0 Hz, $J_{5a,6a}$ 2.0 Hz, H-6a), 3.66 (dd, $J_{2b,3b}$ 10.0 Hz, H-2b), 3.51 (s, 3H, CH_3O), 3.47 (m, H-5a), 2.04 (s, 3H, CH_3CO), 2.01 (ddd, 1H, $J_{3cax,3ceq}$ 13.0 Hz, $J_{3ceq,4c}$ 3.0 Hz, H-3ceq), 1.92 (ddd, 1H, $J_{3cax,4c}$ 2.5 Hz, H-3cax), 1.12 (d, 3H, H_3-6c). The ^{13}C nmr data are reported in Table 3.

*Methyl 2-acetamido-2-deoxy-4-*O*-[2-*O*-(4,6-dideoxy-*α*-L-xylo-hexopyranosyl)-*β*-D-galactopyranosyl]-*β*-D-glucopyranoside (**56**)*

Trisaccharide **51** (60 mg, 0.06 mmol) was debenzoylated as described for the preparation of **46**, followed by chromatography on a column of silica gel (dichloromethane–methanol, 19:1) to provide a white solid (50 mg). This material and 5% palladium-on-carbon (50 mg) were hydrogenated with subsequent gel filtration of the hydrogenation product as described for **52**. After lyophilization of an aqueous solution, **56** (22 mg, 75%) was obtained as a light white solid; mp 168–170°C; $[\alpha]_D$ −82 (*c* 0.5, water); ^{1}H nmr (D_2O) δ: 5.32 (d, 1H, $J_{1c,2c}$ 3.5 Hz, H-1c), 4.54 (d, 1H, $J_{1b,2b}$ 7.8 Hz, H-1b), 4.45 (d, 1H, $J_{1a,2a}$ 8.2 Hz, H-1a), 4.22 (m, 1H, H-5c), 4.03 (dd, 1H, $J_{6a,6a'}$ 12.5 Hz, $J_{6a,5a}$ 1.8 Hz, H-6a), 3.65 (dd, overlapped, $J_{2b,3b}$ 10.0 Hz, H-2b), 3.51 (s, 3H, CH_3O), 3.49 (dd, overlapped, $J_{2c,3c}$ 10.0 Hz, H-2c and H-5a), 2.06 (ddd, $J_{4cax,4ceq}$ 12.0 Hz, $J_{4ceq,3c}$ 5.0 Hz, $J_{4ceq,5c}$ 2.0 Hz, H-4ceq), 2.04 (s, 3H, CH_3CO), 1.40 (ddd, 1H, $J_{4cax,3c}$ ~ $J_{4cax,5c}$ ~ 12.0 Hz, H-4cax), 1.22 (d, 3H, $J_{5c,6c}$ 6.5 Hz, H_3-6c). The ^{13}C nmr data are reported in Table 3.

*Methyl 2-acetamido-3,6-di-*O*-benzyl-2-deoxy-4-*O*-(2,3,4-tri-*O*-acetyl-6-deoxy-*β*-D-galactopyranosyl)-*β*-D-glucopyranoside (**58**)*

A solution of freshly prepared bromide **57** (22) (1.7 mmol) in benzene–nitromethane (1:1, 5.0 mL) was added to a stirred mixture of **39** (200 mg, 0.48 mmol), mercuric cyanide (243 mg, 0.96 mmol), and powdered calcium sulfate (1 g) in the same solvent (25 mL). After stirring for 48 h at 40°C, it was worked up in the usual way and the resulting material was applied to a column of silica gel (dichloromethane–methanol, 19:1). Evaporation of the major fraction gave a white foamy solid **58** (225 mg, 68%); mp 79–80°; $[\alpha]_D$ −15.4 (*c* 1.1, dichloromethane); ^{1}H nmr ($CDCl_3$) δ: 5.98 (d, 1H, $J_{NH,2a}$ 8.5 Hz, NH), 5.17 (bd, 1H, $J_{4b,5b}$ < 1 Hz, $J_{3b,4b}$ 3.5 Hz, H-4b), 5.11 (dd, 1H, $J_{2b,3b}$ 10.5 Hz, $J_{1b,2b}$ 8.0 Hz, H-2b), 4.92 (dd, 1H, H-3b), 4.76 and 4.68 (ABq, 2H, $J_{A,B}$ 12.0 Hz, CH_2Ph), 4.64 and 4.50 (ABq, 2H, $J_{A,B}$ 12.0 Hz, CH_2Ph), 4.62 (d, overlapped, $J_{1a,2a}$ 5.0 Hz, H-1a), 4.46 (d, 1H, H-1b), 4.00 (t, 1H, $J_{3a,4a}$ ~ $J_{4a,5a}$ ~ 5.5 Hz, H-4a), 3.91 (t, 1H, $J_{2a,3a}$ ~ 6 Hz, H-3a), 3.85 (dd, overlapped by H-2a, $J_{5a,6a}$ 5.5 Hz, $J_{6a,6a'}$ 10.0 Hz, H-6a), 3.79 (dd, $J_{5a,6a'}$ 4.5 Hz, H-6a'), 3.67 (q, 1H, H-5a), 3.55 (q, 1H, $J_{5b,6b}$ 6.5 Hz, H-5b), 3.44 (s, 3H, CH_3CO), 2.18, 2.04, 1.98, 1.95 (4s, each 3H, $4CH_3CO$). Anal. calcd. for $C_{35}H_{45}NO_{13}$: C 61.12, H 6.60, N 2.04; found: C 61.25, H 6.82, N 2.04.

*Methyl 2-acetamido-3,6-di-*O*-benzyl-2-deoxy-4-*O*-(6-deoxy-*β*-D-galactopyranosyl)-*β*-D-glucopyranoside (**59**)*

Compound **58** (200 mg, 0.29 mmol) was deacetylated in methanolic 0.08 N sodium methoxide (4 mL) for 16 h. The solution was made neutral with Amberlite IRC 50 H^+ and the solvent evaporated. The remainder was subjected to column chromatography on silica gel (dichloromethane–methanol, 9:1) to provide **59** (150 mg, 92%) as a white powder; mp 194–195°C; $[\alpha]_D$ + 0.8 (*c* 0.8, methanol). Anal. calcd. for $C_{27}H_{39}NO_{10}$: C 62.02, H 7.00, N 2.49; found: C 61.38, H 6.89, N 2.58.

*Methyl 2-acetamido-3,6-di-*O*-benzyl-4-*O*-(3,4-*O*-benzylidene-6-deoxy-*β*-D-galactopyranosyl)-2-deoxy-*β*-D-glucopyranoside (**60**)*

To a solution of **59** (140 mg, 0.25 mmol) in dry acetonitrile (5.0 mL) were added α,α-dimethoxytoluene (73 μL, 0.49 mmol) and *p*-toluenesulfonic acid monohydrate (3 mg). After 30 min, the reaction was neutralized and the solvent evaporated. The remainder was purified by column chromatography on silica gel (dichloromethane–methanol, 19:1) to provide **60** (160 mg, 99%) as a white powder. The ^{1}H nmr data showed it to be a 1:1 mixture of two isomers with *exo* and *endo* phenyl groups; mp 89–90°C; $[\alpha]_D$ +162.3 (*c* 1.2, dichloromethane); ^{1}H nmr ($CDCl_3$) δ: 7.50–7.20 (m, 15H, 3Ph), 6.12, 5.93 (2s, 1H, PhC*H*), 5.64 (d, 1H, $J_{NH,2a}$ 7.5 Hz, NH), 3.48, 3.47 (2s, 3H, CH_3O), 1.870, 1.865 (2s, 3H, CH_3CO), 1.34, 1.29 (d, 3H, $J_{5b,6b}$ 6.5 Hz, H_3-6b). Anal. calcd. for $C_{36}H_{43}NO_{10}$: C 66.55, H 6.67, N 2.16; found: C 65.75, H 6.51, N 2.22.

*Methyl 2-acetamido-3,6-di-*O*-benzyl-4-*O*-[3,4-*O*-benzylidene-6-deoxy-2-*O*-(2,3,4-tri-*O*-benzyl-α-L-fucopyranosyl)-*β*-D-galactopyranosyl]-2-deoxy-*β*-D-glucopyranoside (**61**)*

Disaccharide **60** (120 mg, 0.18 mmol) was fucosylated with bromide **3** (0.7 mmol) as described for the preparation of trisaccharide **4**. After stirring for 20 h, the mixture was processed in the usual way and the resulting product was purified by column chromatography on silica gel (dichloromethane–methanol, 98:2) to provide solid **61** (160 mg, 81%) as a 1:1 mixture of isomers with *exo* and *endo* phenyl groups; mp 78–79°C; $[\alpha]_D$ −41 (*c* 1.6, dichloromethane); ^{1}H nmr ($CDCl_3$) δ: 7.50–7.20 (m, 30H, 6Ph), 6.07, 5.89 (2s, 1H, PhC*H*), 5.69 (2d, 1H, NH), 5.58, 5.47 (d, 1H, $J_{1c,2c}$ 3.5 Hz, H-1c), 3.48, 3.47 (2s, 3H, CH_3O), 1.89, 1.84 (2s, 3H, CH_3CO), 1.34, 1.31 (2d, 3H, $J_{5b,6b}$ 6.5 Hz, H_3-6b), 1.19, 1.13, (2d, 3H, $J_{5c,6c}$ 6.5 Hz, H_3-6c). Anal. calcd. for $C_{63}H_{71}NO_{14}$: C 70.97, H 6.71, N 1.31; found: C 70.73, H 6.77, N 1.41.

Methyl 2-acetamido-2-deoxy-4-O-[6-deoxy-2-O-(α-L-fucopyranosyl)-β-D-galactopyranosyl]-β-D-glucopyranoside (62)

Compound **62** (120 mg, 0.11 mmol) was hydrogenated in the presence of 5% palladium-on-carbon (120 mg) as described for **52**. Gel filtration and freeze-drying of an aqueous solution provided **62** (46 mg, 78%) as a white powder; mp 178–179°C; $[\alpha]_D$ −107.8 (*c* 0.8, water); ^{1}H nmr (D_2O) δ: 5.34 (d, 1H, $J_{1c,2c}$ 3.2 Hz, H-1c), 4.51 (d, 1H, $J_{1b,2b}$ 7.8 Hz, H-1b), 4.46 (d, 1H, $J_{1a,2a}$ 8.0 Hz, H-1a), 4.24 (q, 1H, $J_{5c,6c}$ 6.5 Hz, $J_{4c,5c}$ < 1 Hz, H-5c), 3.99 (dd, 1H, $J_{6a,6a'}$ 12.0 Hz, $J_{5a,6a}$ 1.5 Hz, H-6a), 3.88 (dd, 1H, $J_{2b,3b}$ 10.0 Hz, $J_{3b,4b}$ ~ 3.5 Hz, H-3b), 3.74 (overlapped, H-2a), 3.64 (dd, 1H, H-2b), 3.52 (s, 3H, CH_3O), 3.49 (H-5a), 2.05 (s, 3H, CH_3CO), 1.25, 1.23 (2d, *J* 6.5 Hz, H_3-6c, H_3-6b). The ^{13}C nmr data are reported in Table 3.

Methyl 2-acetamido-4-O-(2-O-acetyl-3,6-di-O-benzyl-4-deoxy-β-D-xylo-hexopyranosyl)-3,6-di-O-benzyl-2-deoxy-β-D-glucopyranoside (64)

Alcohol **39** (320 mg, 0.77 mmol) was glycosylated with 2-*O*-acetyl-3,6-di-*O*-benzyl-4-deoxy-α-D-*xylo*-hexopyranosyl bromide (**53**, 1.46 mmol) (12) as described for the preparation of **27**. After 16 h, the mixture was worked up and the resulting product was purified by column chromatography on silica gel (dichloromethane–methanol, 98:2) to afford **64** (112 mg, 19%); mp 124–126°C; $[\alpha]_D$ −6 (*c* 0.1, chloroform); ^{1}H nmr ($CDCl_3$) δ: 7.40–7.20 (m, 20H, 4Ph), 6.07 (d, 1H, $J_{NH,2a}$ 9.0 Hz, NH), 4.84 (dd, $J_{1b,2b}$ 8.0 Hz, $J_{2b,3b}$ 10.0 Hz, H-2b), 4.72–4.45 (m, 9H, 4CH_2Ph, with H-1a, d, at 4.51), 4.33 (d, 1H, H-1b), 3.98 (m, overlapped, H-2a), 3.96 (t, overlapped, $J_{3a,4a}$ ~ $J_{4a,5a}$ 5.0 Hz, H-4a), 3.80 (d, 2H, $J_{5a,6a}$ 5.0 Hz, H_2-6a), 3.76 (t, 1H, $J_{2a,3a}$ 5.5 Hz, H-3a), 3.70 (m, 1H, H-5a), 3.42 (s, 3H, CH_3O), 2.20 (ddd, 1H, $J_{4beq,4bax}$ 12.0 Hz, $J_{4beq,5b}$ 2.0 Hz, $J_{4beq,3b}$ 5.0 Hz, H-4beq), 2.04 and 1.94 (2s, each 3H, 2CH_3CO), 1.50 (q, 1H, $J_{4bax,3b}$ = $J_{4bax,5b}$ 12.0 Hz, H-4bax); fab-ms, *m/z*: 807.76 (0.43, $[MH + Na]^+$), 806.74 (0.98, $[M + Na]^+$), 784.74 (1.04, MH^+), 783.67 (0.16, M^+), 753.52 (1.73, $[MH - OMe]^+$), 752.50 (3.91, $[M - OMe]^+$).

Methyl 2-acetamido-3,6-di-O-benzyl-2-deoxy-4-O-[3,6-di-O-benzyl-4-deoxy-2-O-(2,3,4-tri-O-benzyl-α-L-fucopyranosyl)-β-D-xylo-hexopyranosyl]-β-D-glucopyranoside (65)

Compound **64** (87 mg, 0.11 mmol) was treated with methanolic 0.05 N sodium methoxide (5 mL) for 18 h. The solution was neutralized with Amberlite IRC 50 H^+, evaporated to dryness, and the resulting alcohol crystallized from methanol–ether. This alcohol (85 mg, 0.11 mmol) was fucosylated with bromide **3** (0.77 mmol) as described for the preparation of **4**. Usual work-up after 18 h and subsequent column chromatography on silica gel (dichloromethane – ethyl acetate, 3:1) of the crude product provided, after precipitation from ether–hexane, trisaccharide **65** (80 mg, 62%) as a white powder; $[\alpha]_D$ −35 (*c* 0.1, chloroform); ^{1}H nmr ($CDCl_3$) δ: 7.40–7.10 (m, 35H, 7Ph), 5.73 (d, 1H, $J_{1c,2c}$ 4.0 Hz, H-1c), 5.64 (d, 1H, $J_{NH,2a}$ 8.0 Hz, NH), 4.89–4.35 (m, 16H, 7CH_2Ph, with H-1a, H-1b at 4.72 and 4.45), 4.31 (bq, 1H, $J_{5c,6c}$ 6.5 Hz, $J_{4c,5c}$ < 1H, H-5c), 4.03 (dd, 1H, $J_{2c,3c}$ 10.0 Hz, H-2c), 3.95 (overlapped, $J_{3c,4c}$ 2.5 Hz, H-4c), 3.83 (dd, 1H, H-3c), 3.47 (s, 3H, CH_3O), 2.22 (bdd, 1H, $J_{4beq,4bax}$ 12.0 Hz, $J_{4beq,5b}$ ~ 1 Hz, $J_{3b,4beq}$ ~ 4 Hz, H-4beq), 1.86 (s, 3H, CH_3CO), 1.38 (bq, $J_{4bax,5b}$ ~ $J_{3b,4bax}$ ~ 12 Hz, H-4bax), 1.21 (d, 3H, H_3-6c); fab-ms, *m/z*: 1181.57 (0.48, $[MH + Na]^+$), 1180.53 (0.61, $[M + Na]^+$), 1158.57 (0.34, MH^+), 1157.51 (0.06, M^+), 1127.43 (0.62 $[MH - OMe]^+$), 1126.45 (0.81 ($[M - OMe]^+$).

Methyl 2-acetamido-2-deoxy-4-O-[4-deoxy-2-O-(α-L-fucopyranosyl)-β-D-xylo-hexopyranosyl]-β-D-glucopyranoside (66)

Compound **66** (49 mg, 0.042 mmol) in 95% ethanol (5 mL) was hydrogenated over 10% palladium-on-carbon (22 mg) at 35 psi for 14 h. Usual work-up and gel filtration on Sephadex LH 20 (ethanol–water, 1:1) provided **66** (21 mg, 94%) as a white powder after lyophilization of an aqueous solution; $[\alpha]_D$ −136.5 (*c* 0.2, water); ^{1}H nmr (D_2O) δ: 5.35 (d, 1H, $J_{1c,2c}$ 3.0 Hz, H-1c), 4.50 (d, 1H, $J_{1b,2b}$ 8.0 Hz, H-1b), 4.44 (d, 1H, $J_{1a,2a}$ 8.5 Hz, H-1a), 4.24 (q, 1H, $J_{5c,6c}$ 6.5 Hz, H-5c), 4.01 (dd, overlapped, H-6a), 3.98 (ddd, $J_{2b,3b}$ 10.0 Hz, H-3b), ~3.80 (m, H-2c, H-3c, H-4c), 3.51 (s, 3H, CH_3O), 3.48 (H-5a), 3.39 (dd, 1H, H-2b), 2.07 (s, 3H, CH_3CO), 1.96 (ddd, 1H, $J_{4beq,4bax}$ 12.5 Hz, $J_{4beq,3b}$ 5.0 Hz, $J_{4beq,5b}$ 1.5 Hz, H-4beq), 1.48 (q, 1H, $J_{4bax,5b}$ ~ $J_{4bax,3b}$ ~ 12.5 Hz, H-4bax), 1.23 (d, 3H, H_3-6c). The ^{13}C nmr data are reported in Table 3.

Acknowledgements

This research was supported by the Natural Sciences and Engineering Research Council of Canada (Grant OPG-172 to R.U.L.) and the Alberta Heritage Foundation for Medical Research. The provision of the ^{125}I-labelled [α-L-Fuc-(1→2)β-D-Gal-(1→4)-β-D-GlcNAcO$(CH_2)_8$CONH]$_{16}$-BSA antigen by Chembiomed Ltd. is gratefully acknowledged. The authors are indebted to Dr. Helmut Beierbeck who prepared the computer graphics based on HSEA calculations. R.C. was a University of Alberta Postdoctoral Fellow, 1986–1988; U.S. was a Research Associate, 1984–1988 and 1991–present; and D.P.K. held a Postdoctoral Fellowship from the Alberta Heritage Foundation for Medical Research, 1982–1984.

1. O. Hindsgaul, D. P. Khare, M. Bach, and R. U. Lemieux. Can. J. Chem. **63**, 2653 (1985).
2. U. Spohr, E. Paszkiewicz-Hnatiw, N. Morishima, and R. U. Lemieux. Can. J. Chem. **70**, 254 (1992).
3. U. Spohr, O. Hindsgaul, and R. U. Lemieux. Can. J. Chem. **63**, 2644 (1985).
4. U. Spohr, N. Morishima, O. Hindsgaul, and R. U. Lemieux. Can. J. Chem. **63**, 2659 (1985).
5. J. LePendu, G. Gérard, F. Lambert, R. Mollicone, and R. Oriol. Glycoconjugate J. **3**, 203 (1986).
6. U. Spohr and R. U. Lemieux. Carbohydr. Res. **174**, 211 (1988).
7. M. Dejter-Juszynski and H. M. Flowers. Carbohydr. Res. **18**, 219 (1971).
8. R. U. Lemieux, K. B. Hendriks, R. V. Stick, and K. James. J. Am. Chem. Soc. **97**, 4056 (1975).
9. P. J. Garegg and H. Hultberg. Carbohydr. Res. **93**, c10–c11 (1981).
10. M. J. Robins and J. S. Wilson. J. Am. Chem. Soc. **103**, 932 (1981).
11. D. H. R. Barton and S. W. McCombie. J. Chem. Soc. Perkin Trans. 1, 1574 (1975).
12. R. U. Lemieux, R. Cromer, and U. Spohr. Can. J. Chem. **66**, 3083 (1988).
13. S. Hanessian, T. J. Liak, and D. M. Dixit. Carbohydr. Res. **88**, c14–c19 (1981).
14. R. U. Lemieux and A. A. Pavia. Can. J. Chem. **47**, 4441 (1969).
15. E. A. Kabat, J. Liao, M. H. Burzynska, T. C. Wong, H. Thøgersen, and R. U. Lemieux. Mol. Immunol. **18**, 873 (1981).
16. J. P. Praly and R. U. Lemieux. Can. J. Chem. **65**, 212 (1987).
17. E. Petrakova, U. Spohr, and R. U. Lemieux. Can. J. Chem. **70**, 233 (1992).
18. A. S. Shashkov, A. Y. Evstigneev, and V. A. Darevitskaya. Bioorg. Khim. **4**, 1495 (1978).
19. R. W. Jeanloz and P. J. Stoffyn. Methods Carbohydr. Chem. **1**, 221 (1962).
20. H. S. El Khadem, D. L. Swartz, J. K. Nelson, and L. A. Berry. Carbohydr. Res. **58**, 230 (1977).
21. T. Iversen and D. R. Bundle. Can. J. Chem. **60**, 299 (1982).
22. R. H. Shah and O. P. Bahl. Carbohydr. Res. **32**, 15 (1974).
23. H. Thøgersen, R. U. Lemieux, K. Bock, and B. Meyer. Can. J. Chem. **60**, 44 (1982).

Can. J. Chem. Downloaded from www.nrcresearchpress.com by 217.78.4.112 on 09/08/12
For personal use only.

24. R. U. Lemieux and K. Bock. Arch. Biochem. Biophys. **221**, 125 (1983).
25. U. K. Laemmli. Nature, **227**, 680 (1970).
26. R. U. Lemieux. Chem. Soc. Rev. **18**, 347 (1989).
27. P. V. Nikrad, H. Beierbeck, and R. U. Lemieux. Can. J. Chem. **70**, 241 (1992).
28. R. U. Lemieux, L. T. J. Delbaere, H. Beierbeck, and U. Spohr. Ciba Foundation Symposium 158. Host–guest molecular interactions: from chemistry to biology. London. July 3–5, 1990. John Wiley & Sons, Chichester, 1991. p. 231.
29. J. Sharon, E. A. Kabat, and S. L. Morrison. Mol. Immunol. **19**, 375 (1982).
30. O. Hindsgaul, T. Norberg, J. LePendu, and R. U. Lemieux. Carbohydr. Res. **109**, 109 (1982).

Can. J. Chem. Downloaded from www.nrcresearchpress.com by 217.78.4.112 on 09/08/12
For personal use only.

Syntheses of a potential fluorescence probe, (−)-(*R*)-7-azatryptophan, via alkylation of the (1*R*,4*R*)-camphor imine of *tert*-butylglycinate

RUBÉN SÁNCHEZ-OBREGÓN[1] AND ALEX G. FALLIS[2]

The Ottawa–Carleton Chemistry Institute, Department of Chemistry, University of Ottawa, Ottawa, Ont., Canada K1N 6N5

AND

ARTHUR G. SZABO

Molecular Biochemistry, Division of Biological Sciences, National Research Council of Canada, Ottawa, Ont. Canada K1A 0R6

Received August 13, 1991

This paper is dedicated to Professor Zdenek (Denny) Valenta on the occasion of his 65th birthday

RUBÉN SÁNCHEZ-OBREGÓN, ALEX G. FALLIS, and ARTHUR G. SZABO. Can. J. Chem. **70**, 1531 (1992).

The synthesis of (−)-(*R*)-7-azatryptophan (**2**) from commercially available 7-azaindole (**4**) is described. The key step involved the diastereoselective alkylation of *tert*-butyl [(1*R*,4*R*)-bornylideneamino]acetate (**3**) with 1-(*tert*-butyloxycarbonyl-3-(iodomethyl)-7-azaindole (**19**) derived from 3-formyl-7-azaindole (**14**). The alkylation, conducted at −100°C in a THF/HMPA solvent using potassium hexamethyldisilazide as the base, afforded **7** in greater than 98% diastereomeric excess. Hydrolysis and deprotection gave (−)-(*R*)-7-azatryptophan.

RUBÉN SÁNCHEZ-OBREGÓN, ALEX G. FALLIS et ARTHUR G. SZABO. Can J. Chem. **70**, 1531 (1992).

On décrit la synthèse du (−)-(*R*)-7-azatryptophane (**2**) réalisée à partir du 7-azaindole (**4**) disponible commercialement. L'étape clé implique une alkylation disastéréosélective du [(1*R*,4*R*)-bornylidènamino]acétate de *tert*-butyle (**3**) par du 1-(*tert*-butyloxycarbonyl-3-(iodométhyl)-7-azaindole (**19**) obtenu à partir du 3-formyl-7-azaindole (**14**). L'alkylation, réalisée à 100°C, dans un mélange de THF/HMPA et utilisant de l'hexaméthyldisilazure de potassium comme base, conduit au composé **7** avec un excès de diastéréo-isomère de plus de 98%. Son hydrolyse et sa déprotection fournissent le (−)-(*R*)-7-azatryptophane.

[Traduit par la rédaction]

Introduction

There is considerable current interest in the fluorescence decay of aromatic amino acids, such as tryptophan (**1**), as a vehicle for probing the structure and dynamics of proteins and peptides. The sensitivity of molecular excited state relaxation rates to the local microenvironment has prompted the development of numerous fluorescence methods (1) and intense study of the photophysics of tryptophan (2–4). In spite of these studies the relationship between tryptophan fluorescence decay and its ground state structure is not well understood. Consequently additional spectroscopic investigations continue to be reported on tryptophan derivatives using fluorescence (5) and related spectroscopic techniques (6).

A promising candidate for further study owing to its unique spectroscopic properties and the fact that it can be substituted for tryptophan in many biological systems is 7-azatryptophan (**2**). Unfortunately it is not available as a single enantiomer and efforts to resolve it have proved unrewarding.[3] 7-Azatryptophan is of additional interest owing to its effect on nitrogen fixation in certain algae (7). The racemate was synthesized several years ago from 7-azagramine (3-(dimethyaminomethyl)-7-azaindole) (8). We wish to report the first synthesis of (−)-(*R*)-7-azatryptophan (**2**) via the intermediacy of the (1*R*,4*R*)-camphor imine of *tert*-butyl glycinate **3**.

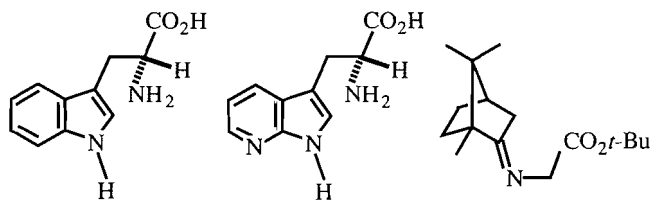

1 **2** **3**

Results and discussion

In view of the commercial availability of 7-azaindole the most straightforward strategy for the synthesis of **2** was to effect the selective functionalization of the intact indole system and thus avoid *de novo* construction of the heterocyclic nucleus. Provided a diastereoselective alkylation with a suitably functionalized indole species such as **5** was employed, rapid preparation of the amino acid should be possible. Asymmetric alkylation of glycine derivatives has received considerable attention with a variety of chiral auxiliaries to provide amino acids of known configuration in high optical purity (9–14). In their study of the alkylation of the enolate, obtained from the (1*R*,4*R*)-camphor imine of *tert*-butyl glycinate McIntosh *et al.* (13) determined that the π electron density and steric effects in the electrophile significantly influenced the diastereomeric excess. The best results (>98% diasteromeric excess (de)) were achieved with benzyl bromides. The presence of an aryl moiety was criti-

[1]Permanent address: Universidad Nacional Autonoma de Mexico, Instituto de Quimica, Circuito Exterior, Ciudad Universitaria, Coyoacan 04510, Mexico, D.F.

[2]Author to whom correspondence may be addressed.

[3]A. G. Szabo and A. G. Fallis, unpublished results.

Can. J. Chem. Downloaded from www.nrcresearchpress.com by 217.78.4.112 on 09/08/12
For personal use only.

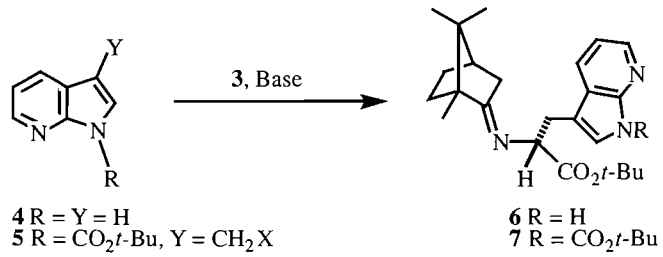

4 R = Y = H
5 R = CO_2t-Bu, Y = CH_2X

6 R = H
7 R = CO_2t-Bu

SCHEME 1

cal in order to obtain high selectivity. It therefore appeared reasonable to anticipate a similarly high level of induction with the aromatic azaindole system, which is also capable of π complexation with the lithium atom of the enolate derived from **3**. As illustrated in Scheme 1, alkylation of **3** should generate species of type **6** that could be transformed into the desired amino acid.

To investigate this possibility 7-azaindole (**4**) was treated under Mannich conditions to afford 7-azagramine (**8**) in 80% yield by analogy with previous studies with indole (15). Conversion of **8** into its ammonium salt **9** occurred readily with excess methyl iodide (Scheme 2). The (1*R*,4*R*)-camphor-imine **3** was prepared by $BF_3 \cdot Et_2O$ mediated condensation of natural (1*R*,4*R*)-camphor with *tert*-butyl glycinate (**10**) (15). The requisite amino ester **10** was synthesized following literature procedures (16) commencing with *tert*-butyl bromoacetate followed by azide displacement and reduction.

As will become apparent, a detailed study of the alkylation of **3** was necessary to achieve a respectable level of diastereomeric excess. The yield of **6** was 26% when the ammonium salt **9** was employed in tetrahydrofuran/dimethylformamide (THF/DMF) at −78°C using lithium diisopropylamide (LDA) as the base. This was disappointing, but of greater concern was the absence of any diastereoselectivity. This may be a consequence of the known tendency of these systems to undergo facile Hofmann elimination so that the product probably arose by an elimination–addition sequence involving the intermediacy of **11**. Substitution of the indole nitrogen will block, or at least retard, this pathway and thus 7-azagramine (**8**) was converted to its *tert*-butyloxycarbonyl derivative **12**. Excess methyl iodide afforded the blocked ammonium salt **13**. As summarized in Table 1 (entries 2, 3), the alkylation reaction with this material was unsuccessful, although at −10°C a 33% yield of the deprotected product was obtained. However, no diastereomeric excess was oberved, and thus it seems likely that deprotection preceded alkylation. To improve the reactivity better leaving groups were required.

The aldehyde **14** was prepared from **8** with hexamethylenetetramine and aqueous propionic acid following the method of Robison and Robison (17). The *tert*-butyloxycarbonyl derivative **15** was generated in a 96% yield and reduced to the primary alcohol **16** with $NaBH_4$ (Scheme 2). Treatment of this alcohol separately with triphenylphosphine/carbon tetrachloride and triphenylphosphine/carbon tetrabromide afforded the corresponding chloride **17** and bromide **18**, respectively. The iodide **19** was prepared by displacement of the chloride with sodium iodide in acetone at room temperature. However, even under these mild conditions it decomposed slowly and the bromide was also

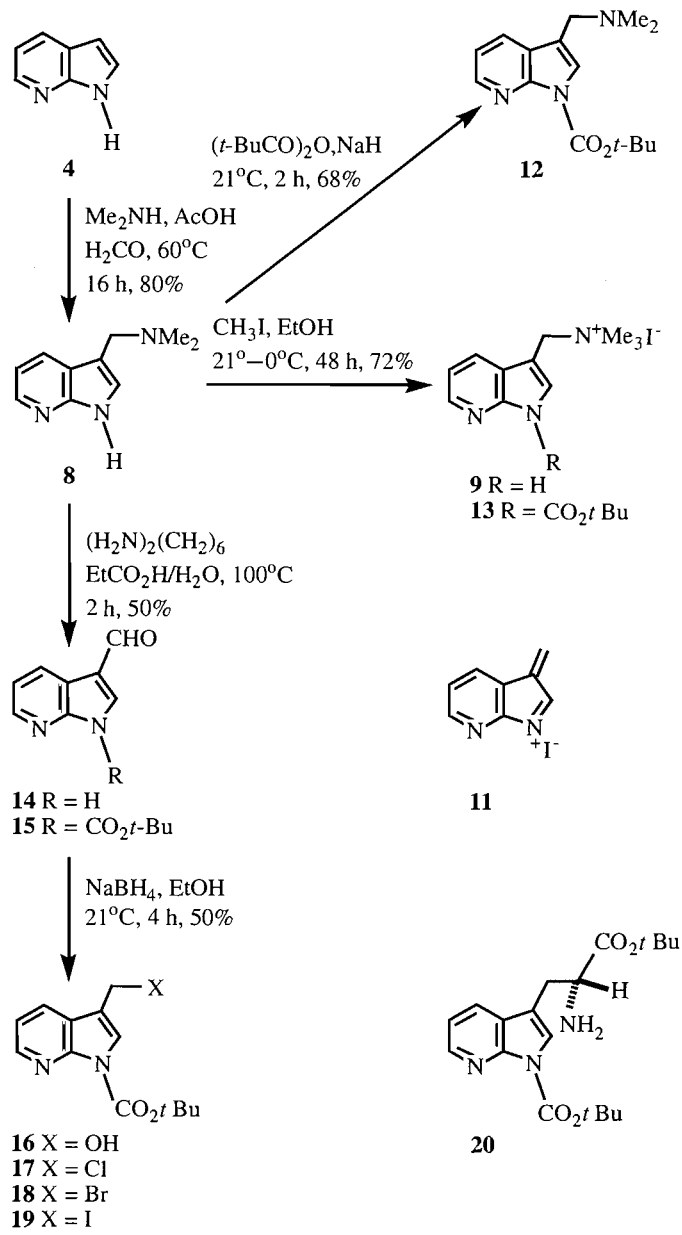

SCHEME 2

troublesome during chromatography on silica gel, so Florisil was utilized instead.

Guided by the earlier studies of McIntosh and co-workers (13, 15) plus related investigations of diastereoselective conjugate additions of lithiated camphor imines of glycine esters (18), the additional alkylations listed in Table 1 were examined. Unfortunately in all cases the chemical yields were very modest. A referee has suggested that these yields are not satisfactory and we agree they are disappointing. However, we have been unable to establish conditions that afford both a good chemical yield and retain a high level of diastereomeric excess in spite of considerable experimentation. Nevertheless, results such as these help drive organic chemistry and may stimulate novel synthetic improvements for these and related cases in the future. A reactive alkylating agent was required even for these allylic species since the chloride **17** was unreactive (entries 4–6) at the temperature

Can. J. Chem. Downloaded from www.nrcresearchpress.com by 217.78.4.112 on 09/08/12
For personal use only.

TABLE 1. Alkylation of the enolate of **3** with 7-azaindole derivatives

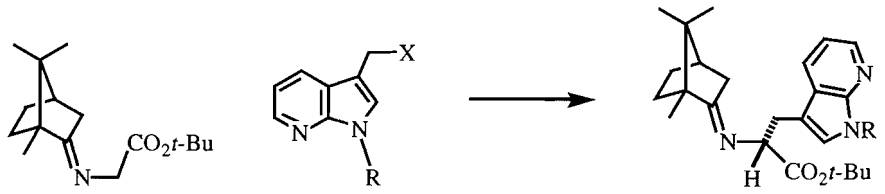

3 **7**

9 R = H, X = NMe_3I
13 R = *t* BOC, X = NMe_3I
17 R = *t* BOC, X = Cl
18 R = *t* BOC, X = Br
19 R = *t* BOC, X = I

Entry	Alkylating agent	Solvent	Base	*T*(°C)	*t* (h)	Yield[a] (%)	Diastereomeric excess (de)[b]
1	**9**	THF/DMF	LDA	−78	4	26	0
2	**13**	THF/DMF	LDA	−78	3.5	—	—
3	**13**	THF/DMF	LDA	−78	0.5	—	0
				−10	4.5	33	
4	**17**	THF	LDA	−100	2	—	—
5	**17**	THF/HMPA	LDA	−78	2	—	—
6	**17**	THF	LDA	−78	3	—	—
7	**18**	THF/DMF	LDA	−78	2.5	28	55
8	**18**	THF/DMF	LDA	−78	1	8.5	33
				−40	1		
9	**18**	THF	LDA	−100	2	32	60
10	**19**	THF	LDA	−78	2	—	—
11	**19**	THF	LDA	−100	2	—	—
12	**19**	THF/HMPA	LDA	−78	2.5	7.5	65
13	**19**	THF/HMPA	$KNSi_2Me_6$	−78	2.5	16	83
14	**19**	THF/HMPA	$KNSi_2Me_6$	−100	3	27	>98

[a]Isolated yields.
[b]Determined by integration of the diastereomeric methyl signals in the ^1H nmr spectra.

examined. Unfortunately, raising the temperature in the case of the bromide **18** (entries 8 and 9) did not improve the chemical yield and resulted in a decrease in diastereoselectivity. To achieve reasonable success it was necessary to counterbalance several interrelated factors. These included the instability of the iodide **19** coupled with the limited solubility of the reactants, including the enolate, at the low temperatures required. Previously McIntosh and Mishra (15*b*) had shown that one equivalent of hexamethylphosphoramide (HMPA) does not lower the selectivity but excess was deleterious. In spite of this potentially adverse effect, excess HMPA was essential and reasonable results were achieved (entry 14) by conducting the alkylation at −100°C in a THF/HMPA solvent using potassium hexamethyldisilazide as the base. These conditions afforded **7** in greater than 98% diastereomeric excess.

The camphor methyl groups displayed separate, readily integrated singlets for each diastereomer in the ^1H nmr spectrum, facilitating this analysis. In the case of entry 14 only a single diastereomer could be detected. It should be noted (entries 12 and 13) that for reactions conducted under the same conditions the potassium base afforded both higher yields and better diastereomeric excess (65 vs. 83% de) than did LDA. Possibly other counterions will also facilitate this alkylation, improve the enolate solubility, and consequently the chemical yield in spite of the limitation of the low temperatures required for high diastereoselectivity.

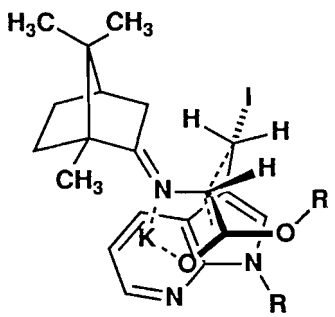

FIG. 1. π-Associated alkylation transition state.

Consistent with the McIntosh model, preferential attack occurred from the sterically less emcumbered bottom (re face) of the enolate to afford the *R* product. Benzylic halides have been shown to introduce a favourable π-π electrostatic interaction with the enolate π-system in related systems. This resulted in an enhanced steric bias and higher selectivity. These features are illustrated in Fig. 1, which represents a possible π-associated transition state for the alkylation.

To complete the synthesis a series of hydrolysis steps were required. The camphor auxiliary was removed in the presence of hydroxylamine hydrochloride and sodium acetate to provide the protected amino ester **20**. The optically active tris-[3-(heptafluoropropylhydroxymethylene)-(+)-camphor eu-

Can. J. Chem. Downloaded from www.nrcresearchpress.com by 217.78.4.112 on 09/08/12
For personal use only.

Can. J. Chem. Downloaded from www.nrcresearchpress.com by 217.78.4.112 on 09/08/12
For personal use only.

ropium(III) nmr shift reagent was added to a sample of **20** but there was no evidence of the presence of the other enantiomer. We were surprised to find that the optical rotation values were so small in these compounds in view of the fact that none of the minor diastereomer of **7** could be detected by ^{1}H nmr analysis. To be certain that the values were accurate the rotations were also determined independently on a second polarimeter in a different institution. In spite of the efforts of Brewester several years ago to establish a predictive set of rules they are not suffiently general to allow an estimate of the 7-azaindoyl substituent (19). Hydrolysis of the tertiary butyl esters was accomplished with trifluoroacetic acid at room temperature to afford (−)-(*R*)-7-azatryptophan (**2**) as a crystalline solid (from H_2O) 69% yield, mp 26–261°C(dec.) $[\alpha]_D^{22}$ −1.2 (c = 0.5, H_2O).

In summary, a direct synthesis of **2** has been achieved via the (1*R*,4*R*)-camphor imine ester **3** as a chiral template. It is known that with lithium enolates HMPA can alter the aggregation and chelation of the transition state complex owing to competition for lithium coordination (20). Further study is required, with potassium enolates in the presence of added salts and complexing agents, in order to increase our understanding of these transition state interactions. In due course this knowledge will lead to improved chemical yields and more sophisticated applications. The majority of natural amino acids possess the *S* (or L) configuration and thus to obtain material for incorporation into peptides it will be necessary to repeat the synthesis commencing with *tert*-butyl[(1*S*,4*S*)-bornylideneamino]acetate, the enantiomer of **3**. It was established earlier that the steady-state absorption and fluorescence properties of 7-azatryptophan may be distinguished from tryptophan so as to allow its use as a non-invasive *in situ* probe of protein structure and dynamics (22).[4] The spectroscopy of **2** will be described in due course.

Experimental

Melting points were determined in capillary tubes with a Thomas–Hoover Uni-Melt or a Fisher–Johes melting point apparatus, and are uncorrected. Infrared (ir) spectra were recorded on a Perkin–Elmer 783 spectrophotometer or a Bomem MB100 FTIR spectrometer. Proton magnetic resonance spectra (^{1}H nmr) were measured at 200 MHz with a Varian Gemini spectrometer or at 300 MHz with a Varian XL-300 spectrometer in deuterochloroform unless otherwise stated. Carbon magnetic resonance spectra (^{13}C nmr) were measured at 50 MHz (Varian Gemini) or at 75 MHz (Varian XL-300). The residual solvent signal ($CDCl_3$) was used as an internal lock; $CDCl_3$; ^{1}H: δ 7.262, ^{13}C: δ 77.0. Chemical shifts are reported in ppm downfield from tetramethylsilane (δ scale) as an internal standard. The multiplicity, number of protons, coupling constants, and proton assignments are indicated in parentheses. Mass spectra (ms) were determined on a V.G. micromass 7070 HS instrument using an ionization energy of 70 eV. Elemental analyses were conducted by M-H-W Laboratories, Phoenix, Ariz., U.S.A. Optical rotations were measured using a Perkin–Elmer 243 polarimeter (sodium light, cell length = 10 cm, c = g/100 mL). Analytical thin-layer chromatography (tlc) employed commercial aluminum sheets precoated (0.2 mm layer thickness) with silica gel 60 F_{254} (E. Merck). Flash column chromatography using E. Merck silica gel 60 (230–400 mesh) was employed for all column chromatography.

Petroleum (pet) ether refers to a fraction with boiling range 30–60°C. Anhydrous diethyl ether (ether) and diisopropylamine were obtained by distillation from $LiAlH_4$ and anhydrous tetrahydrofuran (THF) from potassium/benzophenone. Absolute ethanol was dried by distillation from magnesium. Dry benzene, dimethylformamide (DMF), and carbon tetrachloride (CCl_4) were prepared by distillation from phosphorus pentoxide. Anhydrous hexamethylphosphoramide (HMPA) was obtained by distillation from calcium hydride, and acetone was dried by distillation from anhydrous K_2CO_3. Solutions in organic solvents were dried over anhydrous magnesium sulfate and stripped of solvents with a Büchi rotatory evaporator connected to a water aspirator. Unless otherwise indicated, all the alkylation reactions were conducted under an atmosphere of dry nitrogen.

tert-*Butyl glycinate*

This ester was prepared by the method of Moore and Rydon (17) using *tert*-butylbromoacetate (Aldrich) and oxalic acid to isolate the glycine *tert*-butyl ester; bp 55–62°C, 18 Torr (1 Torr = 133.3 Pa); (lit. (21) bp 68°C, 21 Torr); ir (neat): 3395, 3330 (NH), 1740 (C=O) cm^{-1}; ^{1}H nmr δ: 3.28 (s, 2H, -CH_2-), 1.43 (s, 9H, $(CH_3)_3$C); ms m/z: 130 (M^+ −1).

tert-*Butyl [(1R,4R)-Bornylideneamino]acetate (3) (ref. 15)*

(1*R*,4*R*)-(+)-Camphor (1.52 g, 0.01 mol), *tert*-butyl glycinate (1.31 g, 0.01 mol), dry benzene (40 mL), and $BF_3 \cdot Et_2O$ (0.1 mL) were refluxed for 48 h in a Dean–Stark trap with azeotropic removal of water. The solution was cooled, washed with brine, dried, filtered, and concentrated. Chromatography (20% ethyl acetate/hexane) afforded the imine **3** (1.9 g, 72%): ir (neat): 1690 (C=N), 1745 (C=O) cm^{-1}; ^{1}H nmr δ: 3.94 (AB q 2H, J = 16 Hz, N-CH_2-CO), 2.35–2.20 (m, 1H), 1.95–1.35 (m, 5H), 1.43 (s, 9H, *t*-Bu), 1.25–1.06 (m, 1H), 0.95 (s, 3H, Me), 0.90 (s, 3H, Me), 0.75 (s, 3H, Me); ^{13}C nmr δ: 187.0, 169.3, 80.8, 54.5, 54.0, 47.2, 43.7, 35.6, 31.8, 28.0, 27.3, 19.5, 18.9, 11.2. Exact Mass calcd. for $C_{16}H_{27}NO_2$: 265.2041; found: 265.2024.

3-(N-*Dimethylaminomethyl)-7-azaindole (7-azagramine, 8) (ref. 17)*

Glacial acetic acid (7.2 g, 0.119 mol) was added to a stirred 40% aqueous dimethylamine solution (6 g, 0.054 mol) maintained at 5°C. Formalin (37%, 4.2 g, 0.051 mol) was added to this solution and the mixture was poured into the 7-azaindole (**4**) (6 g, 0.051 mol, Aldrich) and stirred until homogeneous. The reaction was heated at 60°C for 16 h and neutralized with aqueous NaOH (7.2 g in 50 mL). Cooling afforded pale yellow crystals of **8** (7.15 g, 80%): mp 160–162°C (lit.(17) mp 157–158.5°C); ir ($CHCl_3$): 3466, 3147 (N-H), 2819, 2776 (-CH-N<, -CH_2-N-) cm^{-1}; ^{1}H nmr δ: 11.74 (br, s, 1H, N-*H*); 8.33–8.22 (dd, 1H, J = 1.6, 4.8 Hz), 8.07–7.96 (dd, 1H, J = 1.6, 7.8 Hz), 7.23 (br s, 1H), 2.1–7.0 (dd, 1H, J = 4.8, 7.8 Hz), 3.58 (s, 2H), 2.24 (s, 6H); ^{13}C nmr δ: 148.8, 142.5, 127.3, 124.9, 119.8, 115.1, 110.7, 54.5, 44.9. Exact Mass calcd. for $C_{10}H_{13}N_3$: 175.1117; found: 175.1110.

1-tert-*Butyloxycarbonyl-3-(N-dimethylaminomethyl)-7-Azaindole (12)*

To a stirred suspension of sodium hydride (80% dispersion in mineral oil, 0.3 g, 0.01 mol, Aldrich) in HMPA (10 mL), was added 3-(*N*-Dimethylaminomethyl)-7-azaindole (**8**) (1.75 g, 0.01 mol) in HMPA (15 mL). After stirring for 0.5 h, di-*tert*-butyl carbonate (2.4 g, 0.011 mol, Aldrich) in HMPA (10 mL) was added and stirring continued at 21°C for 2 h. The reaction was quenched with water (40 mL), and extracted with ether (4 × 40 mL). The combined organic layers were washed with brine, water, dried, filtered, and concentrated. Chromatography (20% methanol/ethyl acetate) afforded **12** (1.87 g, 68%): mp 94–96°C (petroleum ether); ir ($CHCl_3$): 2820, 2790 (-CH-N<, -CH_2-N-), 1755 (C=O), 1425 (C-N) cm^{-1}; ^{1}H nmr δ: 8.42–8.35 (dd, 1H, J = 2.5, 5 Hz), 7.92–7.87 (dd, 1H, J = 2.5, 5 Hz), 7.42 (s, 1H), 7.11–7.01 (dd, 1H, J = 5.0, 5.0 Hz), 3.40 (s, 2H), 2.15 (s, 6H), 1.55 (s, 9H); ^{13}C nmr (DMSO-d_6) δ: 148.5, 147.2, 145.0, 128.2, 124.5, 123.1, 118.2, 115.6, 83.7, 54.6, 45.4, 28.0. Exact Mass calcd. for $C_{15}H_{21}N_3O$: 275.1634; found: 275.1622.

[4] A. G. Szabo, unpublished results.

Can. J. Chem. Downloaded from www.nrcresearchpress.com by 217.78.4.112 on 09/08/12
For personal use only.

3-(N-Dimethylaminomethyl)-7-azaindole ammonium iodide (9)

Methyl iodide (3 g, 0.02 mol) was added dropwise to a stirred solution of compound **8** (3 g, 0.02 mol) dissolved in anhydrous ethanol (60 mL). The mixture was allowed to stand at room temperature (21°C) for 24 h followed by a further 24 h at 0°C. The resulting salt **9** (4.8 g, 72%) was collected by filtration (water aspirator) and washed with anhydrous ethanol (3 × 10 mL) and anhydrous ether (3 × 30 mL); mp 205–207°C (dec.); ir (KBr): 3450 (NH) cm^{-1}; ^1H nmr (DMSO-d_6) δ: 8.40–8.22 (m, 2H), 7.92–7.81 (m, 1H), 7.30–7.17 (m, 1H), 4.84 (s, 1H), 4.72 (s, 1H); ms *m/z*: 317 (M^+).

*1-(*tert*-Butyloxycarbonyl)-3-(N-dimethylaminomethyl)-7-azaindole ammonium iodide (13)*

Methyl iodide (0.5 g, 3.5 mmol) was added dropwise to a stirred solution of **12** (0.83 g, 3 mmol) in anhydrous ethanol (10 mL) maintained at 0°C with an external ice bath. The mixture was allowed to stand at 0°C for 1 h and then at 5°C for 4 days. The product **13** (1.06 g, 84%) was collected by filtration, washed with anhydrous ether (3 × 3 mL), and dried under vacuum: mp 165–166°C (dec.); ir (KBr): 1750 (C=O) cm^{-1}; ^1H nmr δ: 8.64–8.52 (dd, 1H, *J* = 1.5, 8 Hz), 8.51–8.46 (dd, 1H, *J* = 1.5, 4.7 Hz), 8.14 (s, 1H), 7.29–7.19 (m, 1H), 5.26 (s, 2H), 3.45 (s, 9H), 1.61 (s, 9H); ms *m/z*: 275 ($M^+ - CH_3I$).

3-Formyl-7-azaindole (14)

This compound was prepared by the method of Robison and Robison (17) using a solution of 3-(*N*-dimethylaminomethyl)-7-azaindole (**8**) (15 g, 0.0857 mol) and hexamethylenetetramine (12 g, 0.0857 mol, Aldrich) in 66% aqueous propionic acid (65 mL). This was added to a second solution of hexamethylenetetramine in propionic acid (45 mL). After 1 h at 21°C the reaction was heated at 100°C for 2 h, cooled, water added, and the mixture cooled further (0°C) to afford white crystals of **14** (6.24 g, 50%): mp 221–223°C (water) (lit. (17) mp 214–215°C); ir (KBr): 2788 (C-H), 1658 (C=O) cm^{-1}; ^1H nmr (acetone-d_6) δ: 10.03 (s, 1H, H-C=O), 8.60–8.47 (dd, 1H, *J* = 1.3, 7.8 Hz, C(6)Ar-H), 8.39 (br s, 2H, N-CH=C, C(4)Ar-H), 7.39–7.25 (dd, 1H, *J* = 4.7, 7.8 Hz, C(5)Ar-H); ^{13}C nmr (DMSO-d_6) δ: 185.7, 149.5, 145.0, 138.9, 129.3, 118.5, 116.7, 116.6; ms *m/z*: 146 (M^+), 145 ($M^+ - 1$).

*1-(*tert*-Butyloxycarbonyl)-3-formyl-7-azaindole (15)*

3-Formyl-7-azaindole (**14**) (6 g, 0.041 mol) dissolved in dry HMPA (50 mL) was added dropwise to a stirred suspension of sodium hydride (1.23 g, 0.041 mol, 80% dispersion in mineral oil) in HMPA (40 mL) at 21°C. Stirring was continued until a transparent solution was obtained, a solution of di-*tert*-butyl dicarbonate (9.84 g, 0.045 mol, Aldrich) in HMPA (40 mL) added and the reaction stirred for a further 3 h. The reaction was quenched with water (200 mL), ether (200 mL) was added, and the organic layer separated. The aqueous layer was extracted with ether (2 × 200 mL) and the combined organic layers were washed with saturated aqueous $NaHCO_3$ solution (3 × 150 mL), brine, water dried, filtered, and concentrated. Recrystallization of the residue from hexane afforded compound **15** (9.9 g, 98%); mp 13–132°C (hexane); ir ($CHCl_3$): 1763 (N-COO-), 1678 (C=O) cm^{-1}; ^1H nmr δ: 10.04 (s, 1H, H-C=O), 8.64–848 (m, 2H, C(6)Ar-H, C(4)Ar-H), 8.24 (s, 1H, N-CH=C), 7.4–7.25 (m, 1H, C(5)Ar-H), 1.68 (s, 9H, *t*-Bu); ^{13}C nmr δ: 185.4, 148.5, 146.9, 146.8, 136.3, 130.8, 120.3, 119.0, 118.9, 85.9, 27.9. Exact Mass calcd. for $C_{13}H_{14}N_2O_3$: 246.1004; found: 246.1018.

*1-(*tert*-Butyloxycarbonyl)-3-(hydroxymethyl)-7-azaindole (16)*

1-(*tert*-Butyloxycarbonyl)-3-formyl-7-azaindole **15** (8 g, 32.5 mmol) and sodium borohydride (0.308 g, 8.14 mmol) in 95% ethanol (65 mL) were stirred at 21°C for 4 h. The reaction was concentrated and the residual oil triturated with 1.0 N NaOH (98 mL). The alkaline solution was extracted with ether (1 × 200 mL) and ethyl acetate (1 × 200 mL). The combined organic extracts were washed with brine, water, dried, filtered, and concentrated. Chromatography (50% ethyl acetate/hexane) yielded the alcohol **16** (4.85 g, 60%): mp 156–158°C (ethyl acetate); ir ($CHCl_3$): 3620 (-OH), 1752 (C=O) cm^{-1}; ^1H nmr δ: 8.52–8.47 (dd, 1H, *J* = 1.4, 4.8 Hz, C(6)Ar-H), 7.98–7.92 (dd, 1H, *J* = 1.4, 7.5 Hz, C(4)Ar-H), 7.59 (s, 1H, N-CH=C), 7.22–7.14 (dd, 1H, *J* = 4.8, 7.58 Hz, C(5)Ar-H), 4.80 (br s, 2H, CH_2-O), 1.64 (s, 9H, *t*-Bu); ^{13}C nmr δ: 148.3, 147.8, 145.1, 128.0, 123.7, 121.9, 118.3, 117.9, 84.0, 56.9, 28.0; ms *m/z*: 248 (M^+). Anal. calcd. for $C_{13}H_{16}N_2O$: C 62.89, H 6.50, N 11.28; found: C 63.00, H 6.56, N 11.40.

*1-(*tert*-Butyloxycarbonyl)-3-(chloromethyl)-7-azaindole (17)*

1-(*tert*-Butyloxycarbonyl)-3-(hydroxymethyl)-7-azaindole (**16**) (4.5 g, 0.018 mol), triphenylphosphine (4.8 g, 0.018 mol, Aldrich), dry CCl_4 (110 mL), and dry DMF (40 mL) were stirred at room temperature (21°C) for 4.5 days. The solvents were removed with the aid of a vacuum pump (0.5 Torr). Chromatography (50% ethyl acetate/hexane) of the residue afforded the chloride **17** (2.19 g, 45%): mp 87–89°C; ir ($CHCl_3$): 1755 (C=O), 765 (C-Cl) cm^{-1}; ^1H nmr δ: 8.57–8.47 (m, 1H, C(6)Ar-H), 8.02–7.92 (dd, 1H, *J* = 1.6, 7.9 Hz, C(4)Ar-H), 7.65 (s, 1H, N-CH=C), 7.26–7.17 (m, 1H, C(5)Ar-H), 4.71 (s, 2H, CH_2-Cl), 1.63 (s, 9H, *t*-Bu); ^{13}C nmr δ: 148.1, 145.8, 145.7, 127.8, 125.2, 121.4, 118.6, 114.5, 84.4, 37.6, 28.0; ms *m/z* = 266 (M^+), 268 ($M^+ + 2$). Anal. calcd. for $C_{13}H_{15}N_2O_2Cl$: C 58.54, H 5.64, N 10.50, Cl 13.29; found: C 5873, H 5.96, N 1046, Cl 13.46.

*1-(*tert*-Butyloxycarbonyl)-3-(bromomethyl)-7-azaindole (18)*

1-(*tert*-Butyloxycarbonyl)-3-(hydroxymethyl)-7-azaindole (**16**) (0.124 g, 0.5 mmol), triphenylphosphine (0.137 g, 0.52 mmol, Aldrich), and carbon tetrabromide (0.175 g, 0.53 mmol, Aldrich) in dry DMF (2 mL) were stirred at 21°C for 20 h. The solvent was removed with the aid of a vacuum pump (0.5 Torr) and the residue chromatographed on Florisil (methylene chloride/ether) to give the bromo derivative **18** (0.060 g, 39%); mp 79–82°C; ir ($CHCl_3$): 1738 (C=O), 774 (C-Br) cm^{-1}; ^1H nmr δ: 8.61–8.5 (dd, 1H, *J* = 1.6, 4.8 Hz, C(6)Ar-H), 8.10–7.98 (dd, 1H, *J* = 1.6, 7.9 Hz, C(4)Ar-H), 7.69 (s, 1H, N-CH=C), 7.34–7.22 (m, 1H, C(5)Ar-H), 4.61 (s, 2H, CH_2-Br), 1.63 (s, 9H, *t*-Bu); ms *m/z*: 313 ($M^+ + 2$).

*1-(*tert*-Butyloxycarbonyl)-3-(iodomethyl)-7-azaindole (19)*

The chloroderivative **17** (2.10 g, 7.8 mmol) was dissolved in dry acetone (15 mL) and added to a stirred acetone solution (15 mL) of anhydrous NaI (1.2 g, 8 mmol). The reaction was stirred at 21°C for 24 h, and filtered. Concentration of the filtrate yielded the iodo compound **19** (2.7 g, 96%): mp 102–104°C; ir ($CHCl_3$): 1748 (C=O), 760 C-I) cm^{-1}; ^1H nmr δ: 8.54–8.43 (dd, 1H, *J* = 1.5, 4.7 Hz, C(6)Ar-H), 7.99–7.88 (dd, 1H, *J* = 1.6, 7.9 Hz, C(4)Ar-H), 7.70 (s, 1H, N-CH=C), 7.18–7.27 (m, 1H, C(5)Ar-H), 4.48 (s, 2H, CH_2-I), 1.60 (s, 9H, *t*-Bu); ^{13}C nmr δ: 145.8, 128.0, 123.9, 121.6, 118.3, 115.7, 84.4, 83.9, 28.0, 18.5; ms *m/z*: 231 ($M^+ - I$).

General procedure for the alkylation of camphor imine 3

1. LDA alkylation

LDA (1.25 mmol) was prepared at 0°C in dry THF (5 mL) under nitrogen and then cooled to −78°C. Imine **3** (0.265 g, 1 mmol) in THF (2 mL) was added. The solution was stirred at −100° to −78°C for 30 min and then the desired alkylating agent (**9**, **13**, **17**, **18**, or **19**) dissolved in THF, or DMF, or HMPA was added (see Table 1). The reaction was stirred at −100° to −10°C for 2–5 h depending on the entry (Table 1). The reaction was quenched with water (5 mL) and allowed to warm to room temperature. Ether (10 mL) was added and the organic layer separated. The aqueous layer was extracted with ether (3 × 10 mL), the combined organic layers washed with brine, water, dried, filtered, concentrated, and chromatographed (50% ethyl acetate/hexane) to give the product **6** or **7**.

2. $KNSi_2Me_6$ alkylation

Potassium bis(trimethylsilyl)amide in toluene (7.5 mmol) was added to dry THF (15 mL) under nitrogen. The reaction was cooled to −100° to −78°C and the camphor imine **3** (2 g, 7.5 mmol) in

dry THF (40 mL) was added accompanied by HMPA (2–4 equiv.). Stirring was continued for 30 min, then the alkylating agent **19** (1 equiv.) dissolved in dry THF (40 mL) was added. The mixture was allowed to stir for 2.5–3 h (see Table 1), quenched with water (60 mL), allowed to warm to room temperature, and extracted with ether (3 × 80 mL). The combined organic extracts were washed with brine, water, dried, filtered, and concentrated. Chromatography (50% ethyl acetate/hexane) afforded the compound **7**.

Alkylation product ***6****:* mp 155–157°C (ethyl acetate/hexane); ir ($CHCl_3$): 3480 (N-H), 1735 (C=O) cm^{-1}; ^1H nmr δ: 8.9 (b, 1H), 8.28–8.19 (dd, 1H, J = 1.4, 4.7 Hz), 8.02–7.92 (bd, 1H, J = 7.8 Hz), 7.12 (b, s, 1H), 7.08–6.96 (m, 1H), 4.12–3.98 (m, 1H), 3.41–3.06 (m, 2H), 2.27–2.07 (m, 1H), 1.83–1.02 (m, 6H), 1.39 and 1.37 (2s, 9H each 2 isomers), 0.92–0.68 (5s, for camphor CH_3's); ^{13}C nmr δ: 184.9, 171.2, 170.9, 148.6, 142.3, 142.2, 127.7, 123.6, 123.5, 120.4, 115.1, 115.0, 111.4, 111.2, 80.8, 66.2, 65.9, 54.0, 53.8, 46.9, 46.4, 43.6, 43.4, 35.6, 31.9, 31.5, 28.4, 28.0, 27.3, 27.1, 19.4, 18.8, 18.7, 18.4, 11.5, 11.3; ms m/z 395 (M^+).

Alkylation product ***7****:* $[\alpha]_D^{22}$ −0.6 (c=1, $CHCl_3$); ir (neat): 1734 (C=O) cm^{-1}; ^1H nmr δ: 8.48–8.41 (dd, 1H, J = 1.5, 4.8 Hz, C(6)Ar-H), 7.96–7.82 (dd, 1H, J = 1.5, 7.8 Hz, C(4)Ar-H), 7.38 (s, 1H, N-CH=C), 7.19–7.09 (dd, 1H, J = 4.8, 7.8 Hz, C(5)Ar-H), 4.04–3.93 (dd, 1H, J = 4.2, 9.6 Hz, =N-CH-CO), 3.33–3.28 (dd, 1H, J = 4.2, 9.6 Hz, HC-Ar), 3.18–3.01 (dd, 1H, J = 9.6, 12 Hz, HC-Ar), 2.3–1.61 (m, 6H), 1.58 (s, 9H, *t*-BOC), 1.38 (s, 1H, *t*-Bu), 0.93 (s, 3H, Me), 0.80 (s, 3H, Me), 0.69 (s, 3H, Me); ^{13}C nmr δ: 185.5, 170.7, 148.0, 145.0, 127.7, 124.6, 123.3, 118.1, 114.7, 83.6, 81.1, 64.8, 53.9, 47.0, 43.4, 35.8, 31.8, 28.1, 28.0, 27.2, 19.4, 18.8, 11.5; ms m/z 495. Anal. calcd. for $C_{29}H_{41}N_3O_4$: C 70.27, H 8.33, N 8.47; found: C 70.14, H 8.23, N 8.27.

A typical diastereomeric mixture displayed camphor methyl signals major (minor) as follows: 0.95(0.92), 0.82(0.79), 0.71(shoulder). The chemical shifts varied slightly with the mixture due to the anisotropic nature of the heterocyclic ring system.

Hydrolysis of ***7*** *to give* tert*-butyl α-amino-β-(1-*tert*-butyloxycarbonyl-7-azaindolyl)propionate (****20****)*

Hydroxylamine hydrochloride (0.12 g, 1.72 mmol), sodium acetate (0.14 g, 1.7 mmol), and **7** (0.85 g, 1.7 mmol) were added to 95% ethanol (8 mL) and stirred for 3 days at 21°C. The solvent was evaporated with the aid of a vacuum pump (0.5 Torr) and the residue triturated with THF (25 mL) and filtered. The filtrate was concentrated and chromatographed (ethyl acetate) to give the α-amino-β-(1-*tert*-butyloxycarbonyl-7-azaindole)propionic acid *tert*-butylester (**20**) (0.423 g, 69%) as a yellow viscous oil: $[\alpha]_D^{22}$ −0.8 (c = 1.24, $CHCl_3$); ir (neat): 3392 (-NH), 1736 (C=O) cm^{-1}; ^1H nmr δ: 8.53–8.42 (dd, 1H, J = 1.6, 4.8 Hz, C(6)Ar-H), 7.92–7.84 (dd, 1H, J = 1.6, 7.8 Hz, C(4)Ar-H), 7.44 (s, 1H, N-CH=C), 7.20–7.10, (dd, 1H, J = 4.8, 7.8 Hz, C(5)Ar-H), 3.71–3.59 (m, 1H, HC-CO_2), 3.16–3.0 (dd, 1H, J = 6, 14 Hz, HC-Ar), 3.0–2.82 (dd, 1H, J = 8, 14 Hz, HC-Ar), 1.8–1.61 (br s, 2H, NH_2), 1.60 (s, 9H, *t*-BOC), 1.36 (s, 9H, CO_2*t*-Bu); ^{13}C nmr δ: 174.1, 148.4, 147.6, 145.2, 127.6, 124.4, 123.2, 118.2, 113.7, 83.9, 81.4, 55.1, 30.4, 28.0, 27.9; ms m/z: 361 (M^+). Anal. calcd. for $C_{19}H_{27}N_3O_4$: C 63.14, H 7.53, N 11.63; found: C 62.44, H 7.65, N 11.35.

Hydrolysis and deprotection of ***20*** *: (−)-(R)-7-azatryptophan (****2****)*

The amino ester **20** (0.210 g, 0.582 mmol) was dissolved in trifluoroacetic acid (1.33 g, 0.9 mL, 11.68 mmol) and allowed to stir at 21°C for 2 h. Evaporation of the mixture with the aid of a vacuum pump (0.5 Torr) and addition of ammonium hydroxide afforded, after cooling and recrystallization from water, (−)-(*R*)-7-azatryptophan (**2**) (0.082 g, 69%): mp 260-–261°C (dec.); $[\alpha]_D^{22}$ −1.2 (c = 0.5, H_2O); ir (KBr): 3427–2338 (superimposed -OH and NH_3^+ stretching bands), 1627, 1584, 1418 (-COO^--) cm^{-1}; ^1H nmr (DMSO-d_6:D_2O) δ: 8.2–8.0 (m, 2H), 7.28 (br s, 1H), 7.19–7.10 (m, 1H), 3.85–3.73 (m, 1H), 3.40–3.10 (m, 2H). Exact Mass calcd. for $C_{10}H_{11}N_3O_2$: 205.0855; found: 205.0865.

Acknowledgements

We are grateful to the Natural Sciences and Engineering Research Council of Canada for financial support of this research and to Drs. H. Baer and M. Perry for the use of their polarimeters.

1. J. R. Lakowicz. Principles of fluorescence spectroscopy. Plenum Publishing Corp., New York. 1983.
2. D. Creed, Photochem. Photobiol. **39**, 537 (1984).
3. J. M. Beechem and L. Brand. Annu. Rev. Biochem. **54**, 43 (1985).
4. A. G. Szabo and D. M. Rayner. J. Am. Chem. Soc. **102**, 554 (1980).
5. L. Tilstra, M. C. Sattler, W. R. Cherry, and M. D. Barkley. J. Am. Chem. Soc. **112**, 9176 (1990).
6. J. Teraoka, P. A. Harmon, and S. A. Asher. J. Am. Chem. Soc. **112**, 2892 (1990).
7. H. Bothe and G. Eisbrenner. Biochem. Physiol. Pflanz. **171**, 323 (1977).
8. M. M. Robison and B. L. Robison. J. Am. Chem. Soc. **78**, 1247 (1956).
9. D. Seebach and D. Wasmuth. Angew. Chem. Int. Ed. Engl. **21**, 654 (1981).
10. D. Seebach, D. D. Miller, S. Muller, and T. Weber. Helv. Chim. Acta, **68**, 949 (1985).
11. W. Oppolzer, R. Pedrosa, and R. Moretti. Tetrahedron Lett. **27**, 831 (1986).
12. S. Ikegami, T. Hayama, T. Katsuki, and M. Yamaguchi. Tetrahedron Lett. **27**, 3403 (1986).
13. J. M. McIntosh, R. K. Leavitt, P. Mishra, K. C. Cassidy, J. E. Drake, and R. Chadha. J. Org. Chem. **53**, 1947 (1988).
14. T. A. Geissman and A. Armen. J. Am. Chem. Soc. **74**, 3916 (1952).
15. (*a*) L. C. Matassa. Ph.D. thesis, University of Windsor, 1989; (*b*) J. M. McIntosh and P. Mishra. Can. J. Chem. **64**, 726 (1986).
16. A. T. Moore and H. N. Rydon. Org. Synth. Collect. Vol. **5**, 586 (1973).
17. M. M. Robison and B. L. Robison. J. Am. Chem. Soc. **77**, 457 (1955).
18. S. Kanemasa, A. Tatsukawa, and E. Wada. J. Org. Chem. **56**, 2875 (1991).
19. J. H. Brewester. J. Am. Chem. Soc. **81**, 5475 (1959).
20. G. J. McGarvey and J. M. Williams. J. Am. Chem. Soc. **107**, 1435 (1985).
21. A. Vollmar and M. S. Dunn. J. Org. Chem. **25**, 387 (1960).
22. M. Negreric, S. M. Bellefeuille, S. Whitham, J. W. Petrich, and R. W. Thornburg. J. Am. Chem. Soc. **112**, 7419 (1990).

Can. J. Chem. Downloaded from www.nrcresearchpress.com by 217.78.4.112 on 09/08/12
For personal use only.

An enantiospecific route to C,D ring synthons for steroid synthesis

J. Andrew Clase and Thomas Money[1]

Chemistry Department, University of British Columbia, Vancouver, B.C., Canada V6T 1Z1

Received July 9, 1991

This paper is dedicated to Professor Zdenek (Denny) Valenta on the occasion of his 65th birthday

J. Andrew Clase and Thomas Money. Can. J. Chem. **70**, 1537 (1992).

A simple enantiospecific route to a hydrindenone intermediate for steroid synthesis has been accomplished. The introduction of a wide variety of side-chain units is made possible by stereoselective alkylation of a bicyclic ester **13** derived from (+)-camphor **4**.

J. Andrew Clase et Thomas Money. Can. J. Chem. **70**, 1537 (1992).

On a réalisé une synthèse énantiospécifique simple d'un intermédiaire hydrindénone nécessaire dans la synthèse de stéroïdes. L'introduction d'une grande variété de chaines latérales est rendue possible par l'alkylation stéréosélective de l'ester bicyclique **13** obtenu à partir du (+)-camphre (**4**).

[Traduit par la rédaction]

Can. J. Chem. Downloaded from www.nrcresearchpress.com by 217.78.4.112 on 09/08/12
For personal use only.

The recent resurgence of interest in steroid synthesis (1) is due, in part, to the important role of 1α,25-dihydroxycholecalciferol **1** and other metabolites of vitamin D_3 in calcium homeostasis (2*a–e*) and in the regulation of cell differentiation and proliferation (2*f–k*). The important biological activity of a variety of steroids with structurally diverse side chains (insect moulting hormones, plant growth-promoting steroids, anti-tumor steroids, marine steroids, etc.) has also provided a stimulus for synthetic efforts in this area. Most of the published synthetic effort (3) has concentrated on the development of imaginative new ways of synthesizing hydrindanone and hydrindenone derivatives (cf. **2** and **3**) that may be regarded as synthetic precursors of the C,D ring system and side-chain unit in steroids.

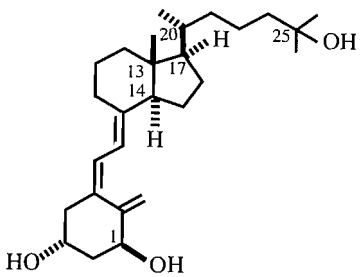

1

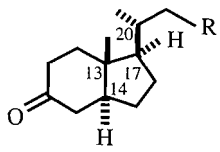

2

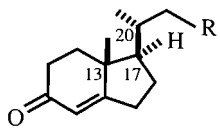

3

Our research objective was to develop a convenient, simple route from camphor to a suitably functionalized hydrindenone that could be used as an intermediate in the synthesis of steroids and triterpenoids. It is important to note that the late Professor R. V. Stevens and his co-workers previously established that the C,D ring system of steroids could be synthesized by ring cleavage of functionalized C(9) camphor derivatives (3*a*,*b*). The initial stages of our synthetic route (Scheme 1) are based on our previous investigations, which established that (+)-9,10-dibromocamphor **5**, readily derived (4, 5) from (+)-camphor **4**, undergoes efficient ring cleavage (5) with base to provide hydroxy-acid **6** in 88% yield. The potential of this compound as a ring D synthon in steroid synthesis is obvious and, indeed, hydroxy-acid **6** was used as an intermediate in a recent synthesis of estrone (6).

For the present purpose, hydroxy-acid **6** was converted to unsaturated diester **9**, which was then reduced with Mg/MeOH (7) to provide diester **10** in ~80% overall yield. Cyclization of the corresponding diacid **11** with trifluoroacetic anhydride (8) followed by methanol work-up produced hydrindenone ester **12** in ~80% yield. The chiral centres at C(13) and C(17) (steroid numbering) in ester **12** originate from the C(7) and C(4) positions in (+)-9,10-dibromocamphor **5** and have the same absolute configuration as the corresponding centres in the steroid target compounds. The remaining objective was the stereoselective introduction of a side-chain unit into the C(20) position (steroid numbering) of ester **12** and creation of the correct 20*R* stereochemistry. Literature reports have shown that acyclic (9), monocyclic (10), bicyclic (11), and steroidal esters (12) undergo stereoselective alkylation when the ester group is flanked by a chiral centre containing hydrogen and two groups with significantly different steric effects. In general, the diastereoselective alkylation of esters of this type has been explained by postulating approach of the electrophile from the less hindered face of the ester enolate ion (*anti* to largest

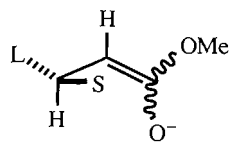

13*a*

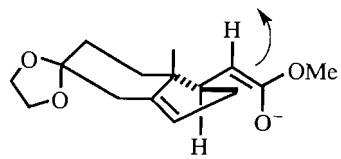

13*b*

group) in a conformation represented by **13***a* or, in the particular case of ketal-ester **13**, by conformation **13***b*. Evans described (13) this π-facial stereoselectivity as "stereorational extraannular chirality transfer" and theoretical explanations for this general phenomenon have been proposed (14–16). By analogy with the literature examples cited above, we expected that alkylation of ketal-ester **13** would be almost completely stereoselective (cf. **13***b*) and subsequent experiments confirmed this prediction. Thus alkylation of ketal-ester **13** with 5-iodo-2-methylpent-2-ene followed by reduction with $LiAlH_4$ provided hydroxy-ketal **15** in ~85% yield. The relative configuration of the C(20) position in hydroxy-ketal

[1]Author to whom correspondence may be addressed.

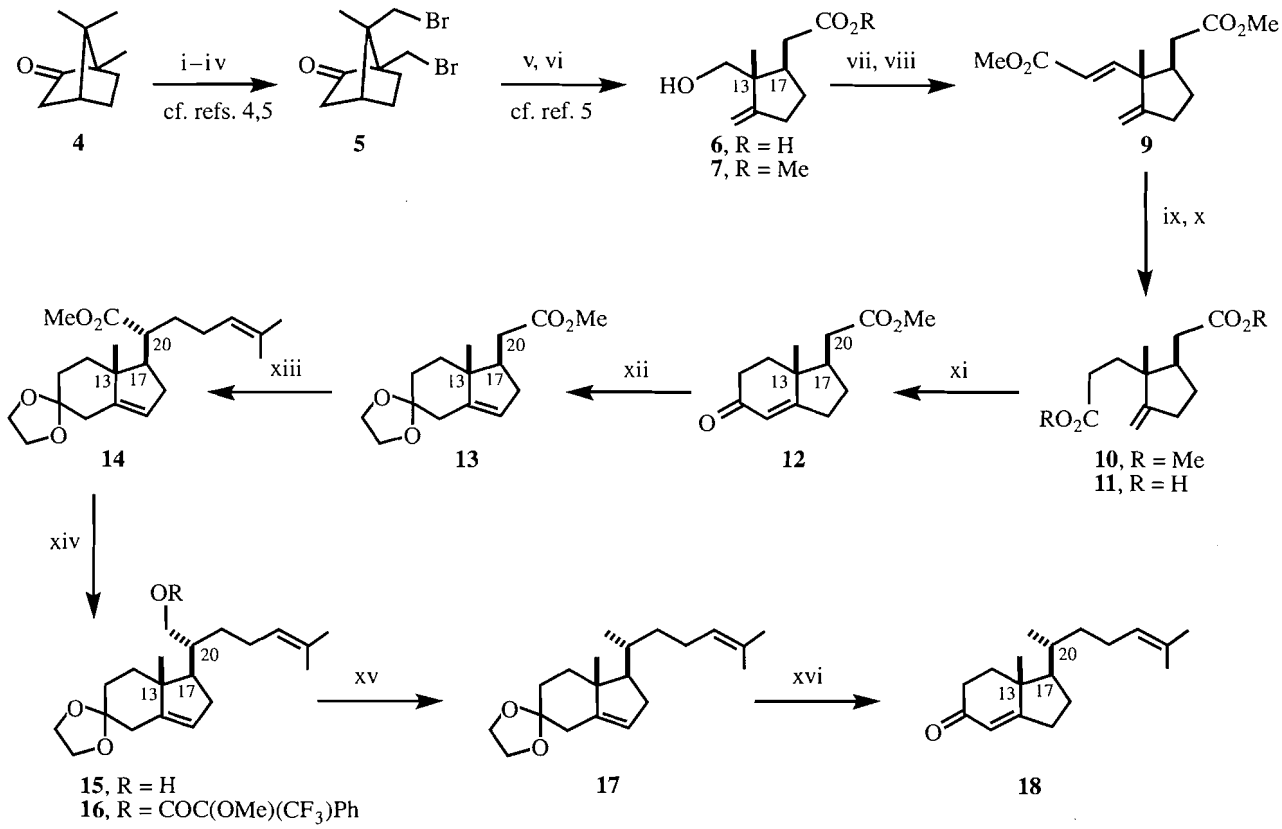

(i) Br_2, HOAc(75%); (ii) Br_2, $ClSO_3H$, 1 h (65%); (iii) Br_2, $ClSO_3H$, 5 days; (iv) Zn, HOAc, Et_2O, 0°C; (iii + iv, 40%); (v) KOH, DMSO:H_2O(9:1), 90°C, 24 h (88%); (vi) K_2CO_3, DMF, MeI, 4 h (96%); (vii) $(COCl)_2$, Me_2SO, CH_2Cl_2, -60°C; NEt_3, 24 h (95%); (viii) NaH, THF, $(MeO)_2P(O)CH_2CO_2Me$ (86%); (ix) Mg, MeOH, 4 h (98%); (x) KOH, MeOH, H_2O, 2 h (77%); (xi) $(CF_3CO)_2O$, CH_2Cl_2, 1.5 h; TsOH, MeOH, 24 h (82%); (xii) $(CH_2OH)_2$, PPTS, C_6H_6, reflux, 16 h (75%); (xiii) LDA, THF, −78°C; $Me_2CH{=}CHCH_2CH_2I$, THF, −78–25°C (95%); (xiv) $LiAlH_4$, THF (87%); (xv) $MeSO_2Cl$, DMAP, NEt_3, CH_2Cl_2; $LiBHEt_3$, THF (84%); (xvi) HCl, Me_2CO, H_2O, reflux, 1 h (91%).

SCHEME 1

15 was established by X-ray crystallographic analysis[2] and its diastereomeric purity was estimated to be ~100% by glc and by examination of the ^1H NMR (400 MHz) spectrum of the corresponding Mosher (17) ester **16**. However, the ^{19}F NMR (282 MHz) spectrum of **16** did exhibit a small peak at 4.896 ppm adjacent to the major signal at 4.936 ppm, suggesting that a small amount (~3–5%) of the 20*S* stereoisomer was formed during the alkylation of ketal-ester **13**. Finally, conversion of hydroxy-ketal **15** to the corresponding mesylate, followed by reduction with lithium triethylborohydride (18) and subsequent acid hydrolysis, provided the required hydrindenone **18** in 85% yield.

The synthetic route described above (Scheme 1) can provide intermediates (cf. **18**) with the correct absolute configuration at C(13), C(17), and C(20) (steroid numbering) and in which the nature of the steroidal side-chain unit is predetermined by the choice of an appropriate electrophilic reagent in the alkylation of ketal-ester **13**. The conversion of simple derivatives of **12** to steroids and triterpenoids may be possible by the application of literature methods (3*i*, 19–21) and this is the objective of current investigations in our laboratory.

[2]S. J. Rettig and J. Trotter, unpublished results.

Experimental

All reagents used were of commercial grade and were not purified unless otherwise specified. (+)-*endo*-3-Bromocamphor was purchased from Aldrich Chemical Co. Dry solvents and reagents were obtained as follows: diethyl ether (Et_2O) was distilled from lithium aluminum hydride ($LiAlH_4$); tetrahydrofuran(THF) was distilled from Na/benzophenone; benzene (C_6H_6), toluene, and dichloromethane (CH_2Cl_2) were distilled from calcium hydride; methanol (MeOH) was distilled from Mg turnings in the presence of I_2; triethylamine (Et_3N) and pyridine were distilled from KOH; and dimethyl sulphoxide (DMSO) and hexamethyl phosphoramide (HMPA) were stored over 4Å molecular sieves. Low-boiling petroleum ether (PE, bp 30–60°C) was distilled prior to use in chromatography.

All reactions involving air- or moisture-sensitive reagents were performed in flame- or oven-dried glassware under an atmosphere of argon. Where not specified, reactions were performed at room temperature (rt). Unless otherwise specified, all aqueous solutions of salts used in work-up were saturated.

Thin-layer chromatography (TLC) was performed on Merck 5735 Precoated Silica Gel 60, PF_{254} on plastic sheets, visualizing the plates with either I_2 (g) or an ammonium molybdate/H_2SO_4 spray. Gas–liquid chromatography (GC) was performed on a Hewlett–Packard HP5830A instrument, using a 0.2 mm × 11 m column of OV-101, with He as the carrier gas. Column chromatography was performed on Merck Silica Gel 60, of either 70–230 or 230–400 mesh, column dimensions are given as diameter × height. Radial

Can. J. Chem. Downloaded from www.nrcresearchpress.com by 217.78.4.112 on 09/08/12
For personal use only.

chromatography was performed under an atmosphere of argon on a Harrison Research Chromatotron® 7924T, using plates of Merck Silica Gel 60, PF_{254}, containing gypsum, of 1, 2, or 4 mm thickness and 4.0–11.25 cm radius.

Infrared (IR) spectra were recorded on a Perkin–Elmer 710B scanning spectrophotometer, either as neat films between NaCl plates or as solutions in NaCl cells of 0.1-mm path length. Proton nuclear magnetic resonance (^{1}H NMR) spectra were recorded at 300 MHz on a Varian XL-300 spectrometer, and at 400 MHz on a Bruker WH-400 spectrometer, with signal positions referenced to tetramethylsilane (TMS). ^{13}C NMR spectra were recorded at 75 MHz on a Varian XL-300 spectrometer, with signal positions referenced to TMS. ^{19}F NMR spectra were recorded at 282 MHz on a Varian XL-300 spectrometer, with signal positions referenced to trifluoroacetic acid. Low-resolution mass spectra (MS) were recorded on a Kratos MS-80 spectrometer and high-resolution mass spectra were recorded on a Kratos MS-50 spectrometer. Specific rotations ([α]) were recorded on a Perkin–Elmer 141 polarimeter, in a 1-dm cell at ambient temperature, using the sodium D line (589 nm); all compounds for which specific rotations were recorded were analytically pure and exhibited single spots on TLC and single peaks on GC. Melting points (mp) were measured on a Reichert heating stage, and are uncorrected. Boiling points (bp) were determined either as the temperature at the still head for those samples which were distilled in bulk, or as the temperature of the oil bath, when small-scale distillation was performed. Elemental analyses were performed by Mr. P. Borda, Microanalytical Laboratory, Department of Chemistry, U.B.C.; all compounds submitted for elemental analysis exhibited a single spot by TLC and a single peak by GC, with the exception of those consisting of diastereomeric mixtures. X-ray structural determinations were performed by Dr. S. Rettig, U.B.C.

(+)-9,10-Dibromocamphor (**5**)

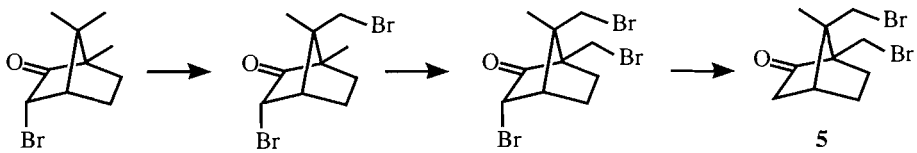

5

A solution of bromine (35 mL, 110 g, 0.68 mol) in chlorosulphonic acid (80 mL) was added cautiously to a cooled flask containing (+)-*endo*-3-bromocamphor (100 g, 0.43 mol) and after 5 min the ice bath was removed. The reaction was then stirred at room temperature for 1.5 h before being quenched by carefully pouring the solution into a slurry of $NaHSO_3$ (25 g) and ice (250 g). The mixture was allowed to stand with occasional stirring, until the orange colour of bromine had faded. The aqueous solution was decanted and the residual off-white solid triturated with water (5 × 250 mL), collected by suction filtration, and washed further with $NaHCO_3$ (aq) (2 × 50 mL) and water (50 mL). The wet solid was dissolved in CH_2Cl_2 (500 mL), the water separated, and the solution dried over $MgSO_4$. Methanol (75 mL) was added and the solvents removed by rotary evaporation until the first crystals appeared. The solution was then cooled and allowed to crystallize, affording (+)-*endo*-3,9-dibromocamphor as a white crystalline solid; yield: 80.0 g, 60%. The mother liquor was concentrated and a second crop of pale yellow crystals (21 g) was obtained; total yield: 101 g, 72%; mp 157–159°C (lit.(19) mp 157–159°C); [α]^{23} 91(*c* 0.43, $CHCl_3$) (lit.(22) [α]^{19} 100(*c* 1, $CHCl_3$)). IR ($CHCl_3$)*ν*: 2980, 2895 (C-H); 1755 (C=O) cm^{-1}. ^{1}H NMR ($CDCl_3$)δ: 1.02 (3H, s, C(10)H_3), 1.10 (3H, s, C(8)H_3), 1.48–1.57 (1H, ddd, *J* = 16, 7, 5 Hz, C(6) *endo* H), 1.73 (1H, ddd, *J* = 16, 12, 4 Hz, C(5) *endo* H), 1.84–1.94 (1H, m, C(5) *exo* H), 2.19 (1H, ddd, *J* = 16, 10, 4 Hz, C(6) *exo* H), 2.70 (1H, t, *J* = 4 Hz, C(4)H), 3.29, 3.65 (2H, q_{AB}, *J* = 11 Hz, C(9)H_2Br), 4.57 (1H, dd, *J* = 4, 1 Hz, C(3)H). MS (70 eV) *m/z* (%): 312, 310, 308 (M^+, 4.6, 9.5, 5.4); 231, 229 (25.9, 27.1); 203, 201 (29.6, 32.1); 81 (100). Mass calcd. for $C_{10}H_{14}Br_2O$: 311.9371, 309.9391, 307.9411; measured: 311.9381, 309.9387, 307.9433. (+)-3,9-Dibromocamphor (105 g, 0.34 mol) was placed in a 500 mL flask equipped with a stir bar, and cooled in an ice bath. A solution of bromine (26 mL, 81 g, 0.51 mol) in chlorosulphonic acid (100 mL) was added cautiously. After sitrring at 0°C for 15 min the ice bath was removed and stirring was continued with bromine (10 mL) and chlorosulphonic acid (10 mL) being added after 3 days and again after 6 days. After 8 days, the reaction was quenched by cautiously pouring into a slurry of $NaHSO_3$ (50 g) and ice (500 g). The mixture was extracted with $CHCl_3$ (2 × 250 mL), and the combined organic solvents were washed with water (100 mL) and $NaHCO_3$ (3 × 100 mL, until the washings were basic), and dried over $MgSO_4$. Evaporation of the solvents yielded crude (+)-3,9,10-tribromocamphor (124 g, 70% pure by GC) as an orange viscous oil, which was used without further purification.

A solution of crude 3,9,10-tribromocamphor in 1:1 Et_2O:AcOH (500 mL) was cooled in an ice bath and stirred with an overhead mechanical stirrer. Zinc (50 g, 0.76 mol) was added in portions over 90 min, maintaining the temperature below 20°C. Following the addition the mixture was stirred for a further 3 h, after which Celite (5 g) was added and the mixture filtered. The solution was washed with 50% brine (200 mL), water (2 × 100 mL), $NaHCO_3$ (6 × 100 mL, until the washings were basic), and brine (100 mL), and dried over $MgSO_4$. The solvent was evaporated to provide an orange solid, which was triturated with methanol to give yellow crystals. Recrystallization from methanol provided (+)-9,10-dibromocamphor (**5**) as a white crystalline solid; yield: 55 g, 52% over two steps; mp 97–8°C (lit.(4) mp 98–100°C); [α]^{22} 67(*c* 1.1, $CHCl_3$)(lit.(4)[α]^{20} 68(*c* = 2, MeOH))). IR($CHCl_3$)*ν*: 2975, 2900 (C-H); 1740 (C=O) cm^{-1}. ^{1}H NMR ($CDCl_3$)δ: 1.10(3H, s, C(8)H_3), 1.43–1.58(2H, m, C(5) and C(6) *endo* H), 1.98 (1H, d_{AB}, *J* = 18 Hz, C(3) *endo* H), 2.05(1H, ddd_{AB}, J_{AB} = 18 Hz, *J* = 5, 4 Hz, C(3) *exo* H), 2.25–2.35 (1H, m, C(6) *exo* H), 2.41(1H, dt, *J* = 19, 4 Hz, C(5) *exo* H), 2.60 (1H, t, *J* = 5 Hz, C(4)H), 3.48 and 3.59 (1H each), 3.70 (2H) ($3d_{AB}$, *J* = 12 Hz, C(9)H_2Br and C(10)H_2Br). MS (70 eV) *m/z* (%): 312, 310, 308 (M^+, 0.5, 0.9, 0.4); 231, 229 (33.1, 33.4); 203, 201 (1.5, 1.3); 107 (100). Mass calcd. for $C_{10}H_{14}Br_2O$: 311.9371, 309.9391, 307.9411; measured: 311.9377, 309.9396, 307.9449.

Hydroxy-ester **7**

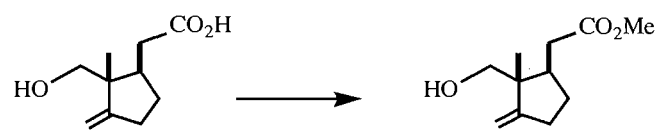

6 **7**

Hydroxy-acid **6** (5) (2.33 g, 12.6 mmol) was dissolved in dry DMF (35 mL) and anhydrous K_2CO_3 (3.50 g, 25.3 mmol) was added. The suspension was stirred under Ar for 1.5 h, after which CH_3I (1.6 mL, 3.6 g, 25 mmol) was added by syringe, and stirring continued in the dark for 3 h. The mixture was poured into brine (50 mL), extracted with Et_2O (3 × 30 mL), and the combined extracts were washed with brine (30 mL) and water (30 mL), and dried over $MgSO_4$. The solvents were evaporated to

Can. J. Chem. Downloaded from www.nrcresearchpress.com by 217.78.4.112 on 09/08/12
For personal use only.

provide a yellow oil, which was purified by column chromatography (15 × 3.5 cm, 230–400 mesh silica gel), eluting with 4:1 PE-Et_2O to provide hydroxy-ester **7** as a pale yellow oil; yield: 2.42 g, 96%; bp 102°C/0.05 Torr (1 Torr = 133.3 Pa); $[\alpha]^{24}$ −25.1 (*c* 1.66, $CHCl_3$). IR (neat)ν: 3450 (O-H); 3090 (vinyl C-H); 2950, 2880 (C-H); 1730 (C=O); 1655 (C=CH_2); 885 (vinyl C-H) cm^{-1}. ^1H NMR ($CDCl_3$)δ: 0.87 (3H, s, CH_3), 1.31–1.43 (1H, m), 1.79 (1H, br s, -OH), 1.90–1.99 (1H, m), 2.21 (1H, dd, J = 17, 11 Hz), 2.28–2.40 (1H, m), 2.42–2.55 (3H, m), 3.41, 3.54 (2H, br q_{AB}, J = 12 Hz, -CH_2O), 3.70 (3H, s, -CO_2CH_3), 4.83 and 5.02 (1H each, 2 t, J = 2 Hz, 2 Hz, =CH_2). MS (70 eV) *m/z* (%): 198 (M^+, 0.2), 180 (0.7), 168 (25.1), 167 (20.0), 135 (12.2), 107 (100), 94 (99.1). Anal. calcd. for $C_{11}H_{18}O_3$: C 66.64, H 9.15%; found: C 66.45, H 9.15%.

Aldehyde-ester **8**

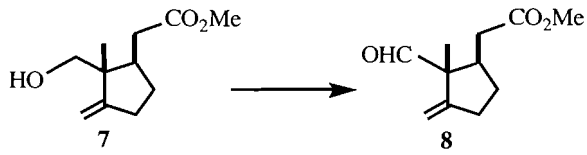

7 **8**

A solution of oxalyl chloride (2.64 mL, 3.85 g, 30.3 mmol) in dry CH_2Cl_2 was cooled under Ar to −78°C. A solution of DMSO (2.15 mL, 2.37 g, 30.3 mmol) in dry CH_2Cl_2(20 mL) was added dropwise over 20 min, keeping the temperature below −60°C. After stirring an additional 15 min, a solution of hydroxy-ester **7** (5.00 g, 25.2 mmol) in dry CH_2Cl_2(40 mL) was added over 20 min, again keeping the temperature below −60 °C. Following the addition, the solution was stirred for 1.5 h, after which triethylamine (10.5 mL, 7.65 g, 75.6 mmol) was added and the temperature was allowed to increase to rt overnight. Water (50 mL) was added, the layers were separated, and the aqueous phase was extracted with CH_2Cl_2(25 mL). The combined organics were washed with 1 N HCl (2 × 25 mL), $NaHCO_3$(25 mL), and brine (25 mL), and dried over $MgSO_4$. Evaporation of the solvent afforded a pale orange oil, which was purified by column chromatography (70–230 mesh SiO_2, 4.5 × 15 cm), eluting with 5:1 PE:Et_2O to provide the aldehyde-ester **8** as a pale yellow mobile liquid; yield: 4.68 g, 95%; bp 75°C (0.1 Torr); $[\alpha]^{24}$ −47.4 (*c* 2.07, $CHCl_3$). IR (neat)ν: 3090 (=C-H); 2960, 2895, 2850 (C-H); 2820, 2725 (-CO-H); 1740 (C=O, ester); 1710 (C=O, aldehyde); 1650 (C=C); 895 (=CH_2) cm^{-1}. ^1H NMR ($CDCl_3$)δ: 1.05 (3H, s, CH_3), 1.51 (1H, qd, J = 12, 8.5 Hz), 1.98–2.06 (1H, m), 2.34 (2H, dd, J = 7, 1.5 Hz, -CH_2CO_2Me), 2.38–2.47 (1H, m), 2.52 (1H, d_{AB}dq, J = 17, 8.5, 2 Hz), 2.77 (1H, dq, J = 12, 7 Hz), 3.67 (3H, s, -OCH_3), 4.78 and 5.12 (1H each, 2 t, J = 2 Hz, 2Hz, =CH_2), 9.30 (1H, s, -CHO). MS (70 eV) *m/z* (%): 182 (M^+, 10.5), 168 (12.6), 167 (24.5), 166 (11.8), 165 (17.4), 123 (19.9), 107 (100.0). Anal. calcd. for $C_{11}H_{16}O_3$: C 67.32, H 8.22%; found: C 67.21, H 8.36%.

Unsaturated diester **9**

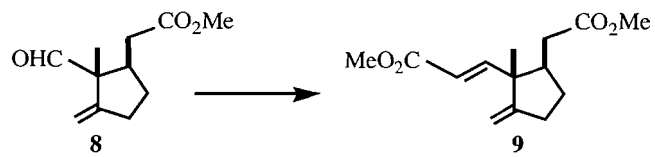

8 **9**

A suspension of NaH (1.35 g, 56.0 mmol) in dry THF (100 mL) was stirred under argon, and a solution of trimethyl phosphonoacetate (10.2 g, 56.0 mmol) in dry THF (50 mL) was added dropwise over 15 min, forming a thick white suspension. This was stirred an additional 1 h before a solution of the aldehyde-ester **9** (9.16 g, 46.7 mmol) in dry THF (100 mL) was added dropwise over 30 min. The mixture was stirred overnight, after which water (100 mL) and Et_2O (100 mL) were added. The layers were separated and the organic phase was washed with brine (2 × 50 mL). The combined aqueous phases were extracted with Et_2O (2 × 40 mL) and the combined organic solvents were dried over $MgSO_4$. Evaporation of the solvents produced a yellow oil, which was purified by column chromatography (70–230 mesh SiO_2, 6.5 × 12 cm), eluting with 5:1 PE:Et_2O, to afford unsaturated diester **9** as a pale yellow, mobile liquid; yield: 10.2 g, 86%. IR (neat)ν: 3090 (=C-H); 2960, 2925, 2855 (C-H); 1735 (C=O, saturated); 1720 (C=O, unsaturated); 1650 (C=C); 890 (=CH_2) cm^{-1}. ^1H NMR ($CDCl_3$)δ: 1.02 (3H, s, CH_3), 1.43–1.53 (1H, m), 1.97–2.05 (1H, m), 2.11–2.20 (1H, m), 2.28–2.39 (2H, m), 2.40–2.48 (1H, m), 2.50–2.58 (1H, m), 3.65 and 3.75 (3H each, 2 s, 2 × -OCH_3), 4.70 and 4.93 (1H each, 2 t, J = 2.5 Hz, 2.5 Hz, =CH_2), 5.85 (1H, d, J = 16 Hz, -C(O)C*H*=CH-), 6.88 (1H, d, J = 16 Hz, -C(O)CH=C*H*-). MS (70 eV) *m/z* (%): 252 (M^+, 10.6), 232 (1.7), 221 (23.6), 220 (72.6), 205 (8.4), 192 (26.8), 119 (100.0). Anal. calcd. for $C_{14}H_{20}O_4$: C 66.65, H 7.99%; found: C 66.76, H 7.90%.

Diester **10**

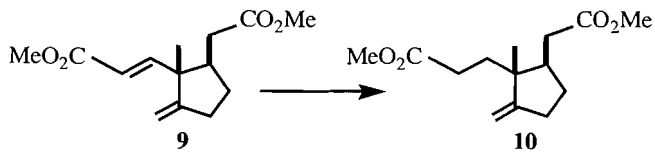

9 **10**

A solution of unsaturated ester **9** (10.2 g, 40.4 mmol) in dry MeOH (300 mL) was cooled to 0°C and Mg (2.95 g, 120 mmol) was added in one portion. The suspension was stirred at 0°C for 2 h and at rt for a further 2 h before water (100 mL) was added. Just enough 6 N HCl was added to dissolve the solids and the mixture was diluted further with water (300 mL), extracted with 1:1 PE:Et_2O (4 × 200 mL), and the combined extracts were washed with $NaHCO_3$ (50 mL) and brine (50 mL), and dried over $MgSO_4$. The solvents were evaporated to provide the saturated diester **10** as a pale yellow oil, which was used without further purification; yield: 10.1 g, 98%; bp 140°C (0.1 Torr); $[\alpha]^{21}$ −29.8 (*c* 0.752, $CHCl_3$). IR (neat)ν: 3090 (=C-H); 2955, 2880, 2850 (C-H); 1740 (C=O); 1650 (C=C); 885 (=CH_2) cm^{-1}. ^1H NMR ($CDCl_3$)δ: 0.89 (3H, s, CH_3), 1.27–1.37 (1H, m), 1.70–1.85 (2H, m), 1.86–1.94 (1H, m), 2.10–2.18 (2H, m), 2.22–2.34 (3H, m), 2.36–2.47 (2H, m), 3.66 and 3.68 (3H each, 2 s, 2 × -OCH_3), 4.73 and 4.93 (1H each, 2 t, J = 2 Hz, 2 Hz, =CH_2). MS (70 eV) *m/z* (%): 254 (M^+, 3.2), 224 (11.4), 223 (51.3), 222 (56.3), 220 (10.8), 207 (15.5), 180 (65.2), 107 (100.0). Anal. calcd. for $C_{14}H_{22}O_4$: C 66.12, H 8.72%; C 66.11, H 8.65%.

Diacid **11**

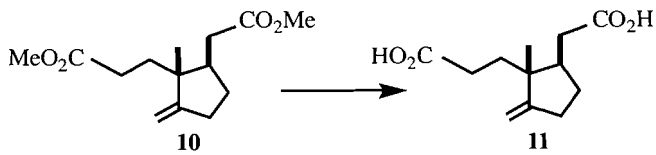

10 **11**

A solution of KOH (11.4 g, 0.20 mol) in water (200 mL) was added to a stirred solution of the diester **10** (10.1 g, 39.7 mmol) in MeOH (200 mL). After stirring for 2 h the solution was acidified to pH 2 with 6 N HCl and immediately extracted with EtOAc (4 × 100 mL). The combined extracts were washed with brine (2 × 50 mL) and dried over $MgSO_4$. Evaporation of the solvent provided an off-white solid, which was recrystallized from hexane/EtOAc to afford diacid **11** as white crystals; yield: 7.08 g, 77%; mp 90–91°C; $[\alpha]^{23}$ −58.7 (*c* 1.54, $CHCl_3$). IR ($CHCl_3$)ν: 3450–2300 (broad, -COOH); 2960, 2945 (C-H); 1710 (C=O); 1655 (C=C); 885 (=CH_2) cm^{-1}. ^1H NMR ($CDCl_3$)δ: 0.89 (3H, s, CH_3), 1.30–1.42 (1H, m), 1.85 and 1.91 (2H, q_{AB}t, J = 14, 7.5 Hz, -$CH_2CH_2CO_2H$), 2.00–2.10 (2H, m), 2.13–2.20 (1H, m), 2.24–2.38 (3H, m), 2.43–2.55 (2H, m), 4.72 and 4.93 (1H each, 2 t, J = 2.5 Hz, 2 Hz, =CH_2), 11.20–12.50 (2H, broad, 2 × -COOH). MS (70 eV) *m/z* (%): 208 ($M^+ - H_2O$, 23.0), 190 (6.7), 180 (5.7), 166 (50.7), 153 (100.0). Anal. calcd. for $C_{12}H_{18}O_4$: C 63.70, H

Can. J. Chem. Downloaded from www.nrcresearchpress.com by 217.78.4.112 on 09/08/12
For personal use only.

8.02%; found: C 63.66, H 7.89%. Mass calcd.: 226.1205; measured: 226.1205.

Bicyclic enone-ester **12***: Method A*

A solution of diacid **11** (285 mg, 1.26 mmol) in dry CH_2Cl_2 (25 mL) was stirred under Ar, and trifluoroacetic anhydride (0.54 mL, 790 mg, 3.8 mmol) was added by syringe. The solution was stirred for 1 h before the CH_2Cl_2 was removed and replaced with MeOH (20 mL). Saturated $NaHCO_3$ (5 mL) was added and the solution was stirred for 1 h, after which it was diluted with water (30 mL), and acidified to pH 2 with 6 N HCl. The mixture was extracted with EtOAc (3 × 20 mL) and the combined extracts were washed with water (20 mL) and brine (20 mL), and dried over $MgSO_4$. Evaporation of the solvent provided a viscous yellow oil, which was purified by column chromatography (60–100 mesh Florisil, 1 × 15 cm), eluting with 1:2 PE:Et_2O, to provide the bicyclic enone-acid **11***a* as a pale yellow oil; yield: 148 mg, 56%. IR (neat)ν: 3700–2300 (broad, -COOH); 2980, 2900 (C-H); 1720 (C=O, acid); 1660 (C=O, enone) cm^{-1}. ^1H NMR ($CDCl_3$)δ: 1.06 (3H, s, CH_3), 1.50–1.67 (1H, m), 1.83 (1H, d_{AB}dd, J = 15, 14, 5 Hz), 2.02 (1H, d_{AB}dd, J = 15, 6, 2 Hz), 2.07–2.20 (2H, m), 2.29–2.36 (1H, m), 2.37–2.44 (1H, m), 2.47–2.61 (3H, m), 2.71 (1H, d_{AB}dt, J = 20, 11, 2 Hz), 5.81 (1H, broad s, =C-H). MS (70 eV) m/z (%): 208 (M^+, 21.1), 190 (11.1), 180 (11.3), 166, (15.0), 149 (20.9), 148 (24.7), 121 (100.0). Mass calcd. for $C_{12}H_{16}O_3$: 208.1099; measured: 208.1100.

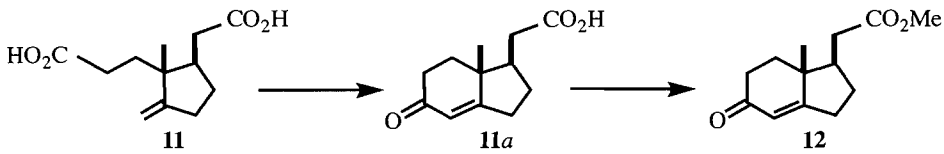

The bicyclic enone-acid **11***a* (203 mg, 0.97 mmol) was dissolved in dry DMF (5 mL) and K_2CO_3 (210 mg, 1.5 mmol) was added. The suspension was stirred vigorously for 1.5 h, after which CH_3I (0.093 mL, 210 mg, 1.5 mmol) was added by syringe, and stirring was continued overnight in the dark. The mixture was diluted with Et_2O (30 mL) and washed with water (3 × 5 mL). The washings were extracted with Et_2O (5 mL) and the combined Et_2O was washed with 10% $Na_2S_2O_3$ (5 mL) and dried over $MgSO_4$. Evaporation of the solvent provided an orange oil, which was purified by radial chromatography (1 mm plate), eluting with 1:1 PE:Et_2O, to afford the ester **12** as a pale yellow oil; yield: 144 mg, 66%; bp 110°C (0.1 Torr); $[\alpha]^{24}$ 85.7 (*c* 0.62, $CHCl_3$). IR (neat)ν: 2950 (C-H); 1740 (C=O, ester); 1660 (C=O, enone) cm^{-1}. ^1H NMR ($CDCl_3$)δ: 1.05 (3H, s, CH_3), 1.54–1.66 (1H, m), 1.80 (1H, d_{AB}dd, J = 15, 14, 5 Hz), 1.97 (1H, d_{AB}dd, J = 15, 6, 2 Hz), 2.05–2.14 (2H, m), 2.30 (1H, d_{AB}d, J = 15, 9 Hz), 2.39 (1H, d_{AB}dd, J = 18, 5, 2 Hz), 2.44–2.57 (3H, m), 2.68 (1H, d_{AB}dt, J = 20, 11, 2 Hz), 3.71 (3H, s, -OCH_3), 5.80 (1H, s, =C-H). MS (70 eV) m/z (%): 222 (M^+, 33.6), 207 (15.4), 194 (22.4), 191 (21.8), 180 (43.2), 121 (100.0). Anal. calcd. for $C_{13}H_{18}O_3$: C 70.24, H 8.16%; found: C 69.98, H 8.00%. Mass calcd.: 222.1256; measured: 222.1260.

Bicyclic enone-ester **12***: Method B*

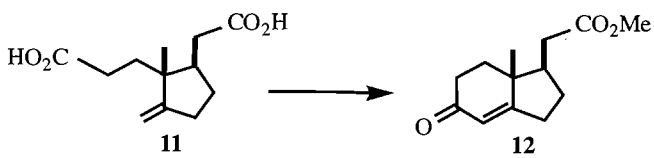

Trifluoroacetic anhydride (8.60 mL, 12.8 g, 60.8 mmol) was added by syringe to a solution of diacid **11** (5.50 g, 24.3 mmol) in dry CH_2Cl_2 (350 mL) and the solution was stirred under Ar for 1.25 h. The solvent was removed and replaced with dry MeOH (100 mL), and TsOH (460 mg, 2.4 mmol) was added. The solution was stirred overnight before the MeOH was evaporated and the orange-brown residue was partitioned between water (100 mL) and EtOAc (50 mL). The layers were separated and the aqueous phase was extracted with EtOAc (2 × 50 mL). The combined organic solvents were washed with brine (50 mL) and dried over $MgSO_4$. Evaporation of the solvents provided a viscous, orange oil, which was purified by column chromatography (70–230 mesh SiO_2, 4.5 × 16 cm), eluting with 2:3 PE:Et_2O to afford the bicyclic enone-ester **12** as a pale yellow mobile oil; yield: 4.42 g, 82%. The spectral characteristics of this compound were identical to those described above.

Further elution provided a small quantity (300 mg) of the corresponding bicyclic enone-acid **11***a* as a viscous, pale yellow oil.

Ketal-ester **13**

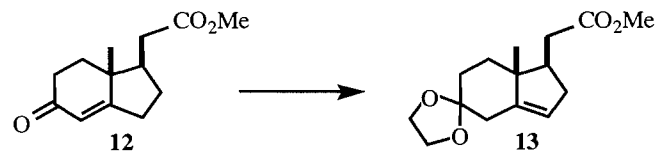

A solution of ethylene glycol (1.70 mL, 1.86 g, 30 mmol) and PPTS[79] (120 mg, 0.46 mmol) in dry C_6H_6 (50 mL) was refluxed in a Dean–Stark apparatus for 30 min. After cooling briefly, a solution of enone-ester **12** (684 mg, 3.08 mmol) in dry C_6H_6 (10 mL) was added and the mixture was heated again to reflux, overnight. The solution was cooled, poured into brine (100 mL), and the layers were separated. The aqueous phase was extracted with Et_2O (2 × 25 mL) and the combined organic solvents were dried over $MgSO_4$. After evaporation of the solvents, the resultant orange oil was purified by column chromatography (70–230 mesh SiO_2, 2 × 7 cm), eluting with 3:1 PE:Et_2O to afford ketal **13** as a pale yellow, mobile liquid; yield: 615 mg, 75%; $[\alpha]^{25}$ 16.6 (*c* 1.16, $CHCl_3$). IR (neat)ν: 3050 (=C-H); 2960, 2900, 2860 (C-H); 1740 (C=O) cm^{-1}. ^1H NMR ($CDCl_3$)δ: 0.92 (3H, s, CH_3), 1.51–1.59 (1H, m), 1.65–1.74 (2H, m), 1.79–1.88 (1H, m), 1.99–2.07 (1H, m), 2.32–2.52 (6H, m), 3.67 (3H, s, -OCH_3), 3.93–4.00 (4H, m, -$O(CH_2)_2O$-), 5.33 (1H, s, =C-H). MS (70 eV) m/z (%): 266 (M^+, 2.1), 235 (1.2), 99 (100.0). Anal. calcd. for $C_{15}H_{22}O_4$: C 67.65, H 8.33%; found: C 67.47, H 8.30%. Mass calcd.: 266.1518; measured: 266.1522.

Ketal-ester **14**

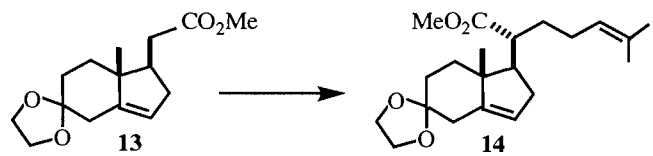

A solution of diisopropylamine (0.30 mL, 210 mg, 2.1 mmol) in dry THF (10 mL) was cooled under argon to 0°C and "BuLi (1.6 M/hexane, 1.2 mL, 2.0 mmol) was added by syringe. After stirring at 0°C for 30 min, the solution was cooled to −78°C and a solution of ketal-ester **13** (433 mg, 1.63 mmol) in dry THF (5 mL) was added by cannula. After a further 40 min, 5-iodo-2-methyl-2-pentene (526 mg, 2.50 mmol) was added by syringe and the solution was stirred at −78°C for 1.5 h; the temperature was then

Can. J. Chem. Downloaded from www.nrcresearchpress.com by 217.78.4.112 on 09/08/12
For personal use only.

allowed to increase to rt overnight. NH_4Cl (5 mL) and water (5 mL) were added, and the mixture was diluted with Et_2O (30 mL). The layers were separated and the organic phase was washed with water (10 mL), 10% $Na_2S_2O_3$ (10 mL), and brine (10 mL), and dried over $MgSO_4$. Evaporation of the solvents afforded an orange, mobile liquid, which was purified by radial chromatography (2-mm plate), eluting with 4:1 PE:Et_2O, to afford the ketal-ester **14** as a pale yellow, mobile liquid; yield: 541 mg, 95%; $[\alpha]^{25}$ 26.0 (*c* 0.534, $CHCl_3$). IR (neat)ν: 3050 (=C-H); 2945, 2900 (C-H); 1735 (C=O) cm^{-1}. ^1H NMR ($CDCl_3$)δ: 0.99 (3H, s, angular CH_3), 1.47–1.67 (5H, m), 1.58 and 1.69 (3H each, 2 s, 2 allylic CH_3's), 173–1.79 (1H, m), 1.89 and 1.93 (2H, q_{AB}, J = 8 Hz), 1.96–2.01 (1H, m), 2.17–2.24 (1H, m), 2.31–2.42 (3H, m), 2.52 (1H, td, J = 11.5, 4.5 Hz), 3.68 (3H, s, $-OCH_3$), 3.91–3.98 (4H, m, $-O(CH_2)_2O-$), 5.08 (1H, t, J = 7 Hz, $-CH_2CH{=}C(CH_3)_2$), 5.31 (1H, s, ring =C-H). MS (70 eV) m/z (%): 348 (M^+, 12.5), 317 (2.1), 267 (2.8), 266 (7.1), 99 (100.0). Anal. calcd. for $C_{21}H_{32}O_4$ (348.5): C 72.38, H 9.26%; found: C 72.51, H 9.19%. Mass calcd.: 348.2300; measured: 348.2306.

Hydroxyl-ketal **15**

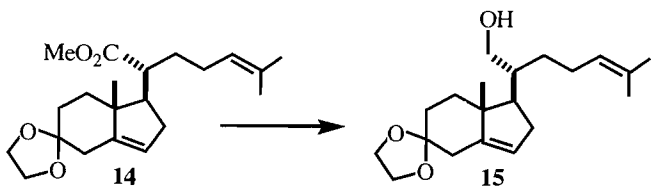

A suspension of $LiAlH_4$ (68 mg, 1.8 mmol) in dry THF (10 mL) was cooled under Ar to 0°C. A solution of ester **14** (514 mg, 1.47 mmol) in dry THF (5 mL) was added by cannula and the mixture was stirred at 0°C for 1 h and then at rt for 2 h, before $Na_2SO_4.10H_2O$ (100 mg) was added and the mixture was diluted with Et_2O (10 mL). After stirring vigorously overnight, $MgSO_4$ was added and the mixture was filtered. Evaporation of the solvents provided a viscous, colourless oil, which was purified by radial chromatography (2-mm plate), eluting with 1:1 PE:ET_2O, to afford hydroxy-ketal **15** as a viscous, colourless oil that solidified on standing; yield: 412 mg, 87%; mp 83–84°C; $[\alpha]^{25}$ 19.8 (*c* 0.656, $CHCl_3$). Recrystallization of a small amount of ketal **15** from Et_2O/PE afforded white needles (mp 72–73°C), which were submitted for X-ray structural determination. The X-ray structure indicated that the crystal contained 1/2 equivalent of water of crystallization. IR (neat)ν: 3425 (O-H); 3060, 3040 (=C-H); 2975, 2950, 2900 (C-H); 1190 (C-O) cm^{-1}. ^1H NMR ($CDCl_3$)δ: 0.97 (3H, s, angular CH_3), 1.09–1.21 (1H, m), 1.35–1.42 (1H, m), 1.48–1.58 (2H, m), 1.61 and 1.69 (3H each, 2 s, 2 × allylic CH_3), 1.63–1.69 (1H, m), 1.71 (1H, broad s, -OH), 1.80–2.08 (6H, m), 2.31–2.40 (3H, m), 3.62 (1H, d_{AB}d, J = 12, 6 Hz) and 3.76 (1H, d_{AB}d, J = 12, 3.5 Hz, $-CHCH_2OH$), 3.92–3.99 (4H, m, $-O(CH_2)_2O-$), 5.13 (1H, t, J = 8 Hz, $-CH_2CH{=}C(CH_3)_2$), 5.34 (1H, s, ring =C-H). MS (70 eV) m/z (%): 320 (M^+, 20.5), 302 (4.9), 292 (5.1), 291 (5.4), 290 (15.9), 289 (15.8), 99 (100.0). Anal. calcd. for $C_{20}H_{32}O_3$: C 72.91, H 10.10% (M + 1/2 H_2O); found: C 72.62, H 10.16%. Mass calcd.: 320.2351; measured: 320.2343.

Mosher ester **16**

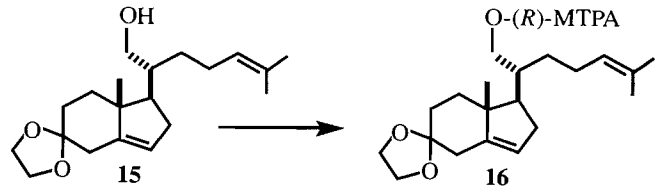

A solution of hydroxy-ketal **15** (301 mg, 0.94 mmol) in dry CH_2Cl_2 (10 mL) was stirred under argon, and pyridine (0.25 mL, 250 mg, 3.1 mmol) and a solution of MTPACl (475 mg, 2.0 mmol) in dry CH_2Cl_2 (2 mL) were added by syringe. The solution was stirred for 3 days, when TLC indicated that none of the alcohol remained. After adding Et_2O (20 mL), the solution was washed with water (2 × 5 mL), 1 N HCl (5 mL), $NaHCO_3$ (5 mL), and brine (5 mL), and dried over $MgSO_4$. Evaporation of the solvents provided a viscous, yellow oil, which was purified by radial chromatography (2-mm plate), eluting with 4:1 PE:Et_2O to afford ester **16** as a viscous, colourless oil; yield: 402 mg, 80%; $[\alpha]^{25}$ 29.1 (*c* 0.412, $CHCl_3$). IR (neat)ν: 3050 (=C-H); 2960, 2900 (C-H); 1755 (C=O); 1460 (C=C, aromatic), 800, 760, 715 (aromatic C-H bend cm^{-1}). ^1H NMR ($CDCl_3$)δ: 0.98 (3H, s, angular CH_3), 120–1.30 (1H, m), 1.36–1.45 (1H, m), 1.46–1.64 (2H, m), 1.56 and 1.67 (3H each, 2 s, 2 allylic CH_3's), 1.74 (1H, dt, J = 13, 3 Hz), 1.81 (1H, d_{AB}d, J = 14, 4 Hz), 1.84–2.05 (5H, m), 2.29–2.41 (3H, m), 3.54 (3H, s, $-OCH_3$), 4.15 (1H, d_{AB}d, J = 12, 6 Hz) and 4.56 (1H, d_{AB}d, J = 12, 4 Hz, $-CHCH_2O-$), 4.99 (1H, t, J = 8 Hz, $-CH_2CH{=}C(CH_3)_2$), 5.31 (1H, s, ring =C-H), 7.37–7.42 (3H, m) and 7.51–7.55 (2H, m). ^{19}F NMR ($CDCl_3$)δ: 4.936 (s, CF_3 of major diastereomer), 4.896 (s, CF_3 of minor diastereomer). MS (70 eV) m/z (%): 536 (M^+, 0.2), 450 (0.3), 302 (1.3), 189 (9.0), 99 (100.0). Anal. calcd. for $C_{30}H_{39}F_3O_5$: C 67.15, H 7.33%; found: C 67.36, H 7.51%. Mass calcd.: 536.2749; measured: 536.2751.

Ketal **17**

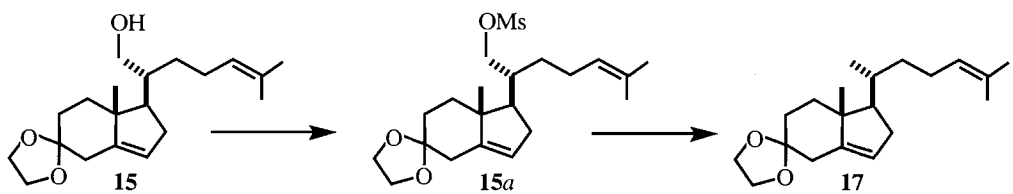

A solution of hydroxy-ketal **15** (88 mg, 0.27 mmol) and DMAP (cat.) in dry CH_2Cl_2 (2 mL) was stirred under argon and Et_3N (0.27 mL, 190 mg, 1.9 mmol) and methanesulphonyl chloride (0.075 mL, 110 mg, 0.97 mmol) were added by syringe. The solution was stirred for 1.5 h after which it was diluted with Et_2O (15 mL) and water (5 mL). The layers were separated and the Et_2O was washed with water (5 mL) and dried over $MgSO_4$. Evaporation of the solvents provided mesylate **15***a* as a pale yellow, viscous oil, which was used without further purification, yield: 120 mg.

A solution of crude mesylate **15***a* (120 mg, 0.27 mmol maximum) in dry THF (5 mL) was cooled to 0°C under argon and $LiEt_3BH$ (1 M/THF, 1.1 mL, 1.1 mmol) was added by syringe. The solution was stirred for 3 h, allowing the temperature to increase to room temperature. Et_2O (20 mL) was added and the solution was washed with 1 N HCl (2 × 5 mL) and brine (5 mL), and dried over $MgSO_4$. Evaporation of the solvents provided a pale yellow oil, which was purified by radial chromatography (1-mm plate), eluting with 19:1 PE:Et_2O, to afford bicyclic ketal **17** as a colourless mobile liquid; yield: 69.2 mg, 84% over two steps; $[\alpha]^{24}$

Can. J. Chem. Downloaded from www.nrcresearchpress.com by 217.78.4.112 on 09/08/12
For personal use only.

21 (*c* 0.17, $CHCl_3$). IR (neat)*v*: 3045 (=C-H); 2960, 2945, 2900 (C-H); 1120, 1090 (C-O) cm^{-1}. ^1H NMR ($CDCl_3$)δ: 0.95 (3H, d, J = 6 Hz, CH_3CHRR'), 0.97 (3H, s, angular CH_3), 1.05–1.15 (1H, m), 1.39–1.47 (1H, m), 1.57–1.67 (3H, m), 1.60 and 1.69 (3H each, 2 s, 2 allylic CH_3's), 1.81–2.09 (5H, m), 2.32–2.44 (4H, m), 3.91–3.99 (4H, m, $-O(CH_2)_2O-$), 5.10 (1H, broad t, J = 7.5 Hz, $-CH_2CH{=}C(CH_3)_2$), 5.30 (1H, broad s, ring =C-H). MS (70 eV) *m/z* (%): 304 (M^+, 1.5), 99 (100.0). Anal. calcd. for $C_{20}H_{32}O_2$: C 78.90, H 10.59%; found: C 79.12, H 10.50%. Mass calcd.: 304.2402; measured: 304.2398.

Bicyclic enone **18**

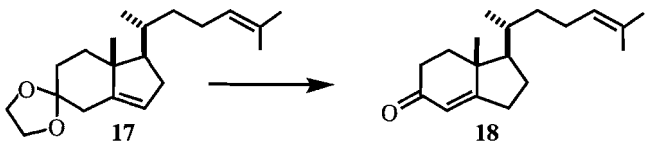

A solution of ketal **17** (44.6 mg, 0.146 mmol) in acetone (4 mL) and 1 N HCl (2 mL) was heated to reflux for 1 h. After diluting with water (5 mL), the solution was extracted with Et_2O (3 × 10 mL), and the combined extracts were washed with $NaHCO_3$ (5 mL) and dried over $MgSO_4$. Evaporation of the solvents provided a yellow oil, which was purified by radial chromatography (1-mm plate), eluting with 9:1 PE:Et_2O, to afford bicyclic enone **18** as a pale yellow oil; yield: 38.4 mg, 91%; $[\alpha]^{25}$ 73 (*c* 0.28, $CHCl_3$). IR (neat)*v*: 3035 (=C-H); 2960, 2885 (C-H); 1670 (C=O) cm^{-1}. ^1H NMR ($CDCl_3$)δ: 0.99 (3H, d, J = 3 Hz, CH_3CHRR'), 1.10 (3H, s, angular CH_3), 1.12–1.20 (1H, m), 1.39–1.60 (4H, m), 1.62 and 1.70 (3H each, 2 s, 2 allylic CH_3's), 1.81–1.97 (2H, m), 1.99–2.11 (2H, m), 2.25 (1H, ddd, J = 8, 3, 1 Hz), 2.29–2.37 (1H, m), 2.38–2.46 (1H, m), 2.48–2.58 (1H, m), 2.62 (1H, $d_{AB}dt$, J = 10, 5.5, 1 Hz), 5.10 (1H, tq, J = 3.5, 1 Hz, $-CH_2CH{=}CMe_2$), 5.74 (1H, broad s, -C(O)CH=). MS (70 eV) *m/z* (%): 260 (M^+, 71.6), 245 (29.6), 218 (31.0), 203 (5.6), 189 (10.7), 177 (30.7), 176 (27.2), 175 (61.4), 41 (100.0). Mass calcd. for $C_{18}H_{28}O$: 260.2140; measured: 260.2141.

Acknowledgement

We are grateful to the Natural Sciences and Engineering Research Council of Canada, Ottawa, for financial support of this research.

1. (*a*) A. B. Turner. Nat. Prod. Rep. **8**, 17 (1991), and references cited; (*b*) H. Jones and G. H. Rasmusson. Fortschr. Chem. Org. Naturst. **39**, 64 (1980); (*c*) R. Pardo and M. Santelli. Bull. Soc. Chim. Fr. II-98 (1985).
2. (*a*) P. E. Georghiou. Chem. Soc. Rev. **6**, 83 (1977); (*b*) A. W. Norman. Vitamin D, molecular biology and clinical nutrition. Marcel Dekker, New York, 1980; (*c*) H. F. DeLuca and H. K. Schnoes. Annu. Rev. Biochem. **52**, 411 (1983); (*d*) A. W. Norman. Vitamin D, the calcium homeostatic steroid hormone. Academic Press, New York. 1979; (*e*) A. W. Norman, K. Schaefer, and H.-G. Grigoleit, and D. v. Herrath (*Editors*). Vitamin D: chemical, biochemical, and clinical update. Walter de Gruyter and Co., Berlin and New York. 1985; (*f*) J. A. MacLaughlin, W. Gange, D. Taylor, F. Smith, and M. F. Holick. Proc. Natl. Acad. Sci. U.S.A. **82**, 5409 (1985); (*g*) C. D. Touskas, D. M. Provvedini, and S. C. Manolagas. Science, **224**, 1438 (1984), and references cited; (*h*) M. J. Calverly. Tetrahedron, **43**, 4609 (1987), and references cited; (*i*) N. Ikekawa, T. Eguchi, N. Hara, S. Takatsuto, A. Honda, Y. Mori, and S. Otomo. Chem. Pharm. Bull. **35**, 4362 (1987), and references cited; (*j*) V. K. Ostrem and H. F. DeLuca. Steroids, **49**, 73 (1987); (*k*) H. S. Gull, J. M. Londowski, R. A. Corradino, A. R. Zinsmeister, and R. Kumar. J. Med. Chem. **33**, 480 (1990).
3. (*a*) R. V. Stevens, F. C. A. Gaeta, and D. S. Lawrence. J. Am. Chem. Soc. **105**, 7713 (1983), and references cited; (*b*) R. V. Stevens and D. S. Lawrence. Tetrahedron, **41**, 101 (1985); (*c*) B. Lythgoe and I. Waterhouse. J. Chem. Soc. Perkin Trans. 1, 1405 (1980); (*d*) S.-J. Shiuey, J. J. Partridge, and M. R. Uskokovic. J. Org. Chem. **53**, 1040 (1988); (*e*) E. G. Baggiolini, J. A. Iacobelli, B. M. Hennessy, A. D. Batcho, J. F. Sereno, and M. R. Uskokovic. J. Org. Chem. **51**, 3098 (1986); (*f*) T. Suzuki, E. Sato, K. Unno, and T. Kametani. J. Chem. Soc. Chem. Commun. 724 (1988); (*g*) H. Nemoto, H. Kurobe, K. Fukumoto, and T. Kametani. Tetrahedron Lett. **25**, 4669 (1984); (*h*) H. Nemoto, H. Kurobe, K. Fukumoto, and T. Kametani. Chem. Lett. 259 (1985); (*i*) R. K. Haynes, S. C. Vonwiller, and T. W. Hambley. J. Org. Chem. **54**, 5162 (1989); (*j*) P. A. Grieco, T. Takigawa, and D. R. Moore. J. Am. Chem. Soc. **101**, 4380 (1979); (*k*) B. M. Trost, P. R. Bernstein, and P. C. Funfschilling. J. Am. Chem. Soc. **101**, 4378 (1979); (*l*) T. Takahishi, H. Yamada, and J. Tsuji. Tetrahedron Lett. **26**, 4463 (1985); (*m*) F. E. Ziegler and J. J. Mencel. Tetrahedron Lett. **24**, 1859 (1983); (*n*) D. Desmaele, J. Ficini, A. Guingant, and Ph. Khan. Tetrahedron Lett. **24**, 3079 (1983); (*o*) D. Desmaele, J. Ficini, A. Guingant, and A. M. Touzin. Tetrahedron Lett. **24**, 3083 (1983); (*p*) S. Hatakeyama, H. Numata, and S. Takano. Tetrahedron Lett. **25**, 3617 (1984); (*q*) W. S. Johnson, J. D. Elliott, and G. J. Hanson. J. Am. Chem. Soc. **106**, 1138 (1984); (*r*) S. Hatakeyama, H. Numata, K. Osanai, and S. Takano. J. Chem. Soc. Chem. Commun. 1893 (1989); (*s*) E. Brandes, P. A. Grieco, and P. Garner. J. Chem. Soc. Chem. Commun. 500 (1988); (*t*) K. A. Parker and T. Iqbal. J. Org. Chem. **47**, 337 (1982); (*u*) S. R. Wilson and M. S. Haque. Tetrahedron Lett. **25**, 3147 (1984); (*v*) Y. Horiguchi, E. Nakamura, and I. Kuwajima. J. Org. Chem. **51**, 4323 (1986), and references cited; (*w*) G. Stork and N. Saccomano. Tetrahedron Lett. **28**, 2087 (1987), and references cited.
4. W. M. Dadson, M. Lam, T. Money, and S. E. Piper. Can. J. Chem. **61**, 343 (1983).
5. J. H. Hutchinson, T. Money, and S. E. Piper. Can. J. Chem. **64**, 854 (1986).
6. J. H. Hutchinson and T. Money. Can. J. Chem. **65**, 1 (1987).
7. (*a*) I. K. Youn, G. H. Yon, and C. S. Pak. Tetrahedron Lett. **27**, 2409 (1987); (*b*) cf. J. A. Profitt, D. S. Watt, and E. J. Corey. J. Org. Chem. **40**, 127 (1975).
8. J. Blumbach, D. A. Hammond, and D. A. Whiting. J. Chem. Soc. Perkin Trans. 1, 261 (1986), and references cited.
9. (*a*) W. Bernhard, I. Fleming, and D. Waterson. J. Chem. Soc. Chem. Commun. 28 (1984); (*b*) Y. Yamamoto and K. Maruyama. J. Chem. Soc. Chem. Commun. 904 (1984); (*c*) I. Fleming and J. J. Lewis. J. Chem. Soc. Chem. Commun. 149 (1985); (*d*) H. F. Chow and I. Fleming. Tetrahedron Lett. **26**, 397 (1985); (*e*) I. Fleming, J. H. M. Hill, D. Parker, and D. Waterson. J. Chem. Soc. Chem. Commun. 318 (1985); (*f*) K. Tomioka, H. Kawasaki, and K. Koga. Tetrahedron Lett. **26**, 3027 (1985); (*g*) H. Kawasaki, K. Tomioka, and K. Koga. Tetrahedron Lett. **26**, 3031 (1985); (*h*) D. Kim, Y. M. Jang, I. O. Kim, and S. W. Park. J. Chem. Soc. Chem. Commun. 760 (1988).
10. (*a*) T. Dieck-Aularach. Ph.D. Thesis, University of Alberta, Edmonton, Alberta. 1984; (*b*) J. H. Hutchinson and T. Money. J. Chem. Soc. Chem. Commun. 288 (1986); (*c*) G. Stork and N. Sacccomano. Tetrahedron Lett. **28**, 2087 (1987).
11. S.-J. Shiuey, J. J. Partridge, and M. R. Uskokovic. J. Org. Chem. **53**, 1040 (1988).
12. (*a*) J. Wicha and K. Bal. J. Chem. Soc. Perkin Trans. 1, 1282 (1978); (*b*) J. J. Partridge, S.-J. Shiuey, N. K. Chadha, E. G. Baggiolini, B. M. Hennessy, M. R. Uskokovic, J. L. Napoli, T. A. Reinhardt, and R. L. Horst. Helv. Chim. Acta, **64**, 2138 (1981); (*c*) J. J. Partridge, S.-J. Shiuey, N. K. Chadha, E. G. Baggiolini, J. F. Blount, and M. R. Uskokovic. J. Am. Chem. Soc. **103**, 1253 (1981).

Can. J. Chem. Downloaded from www.nrcresearchpress.com by 217.78.4.112 on 09/08/12
For personal use only.

13. D. A. Evans. Asymmetric synthesis. Vol. 3. *Edited by* J. D. Morrison. Academic Press, New York. 1984.
14. M. N. Paddon-Row, N. G. Rondau, and K. N. Houk. J. Am. Chem. Soc. **104**, 7162 (1982), and references cited.
15. G. J. McGarvey and J. M. Williams. J. Am. Chem. Soc. **107**, 1435 (1985), and references cited.
16. I. Fleming and J. J. Lewis. J. Chem. Soc. Chem. Commun. 149 (1985), and references cited.
17. J. A. Dale, D. L. Dull, and H. S. Mosher. J. Org. Chem. **34**, 2543 (1969).
18. S. Krishnamurty and H. C. Brown. J. Org. Chem. **41**, 3064 (1976).
19. Z. G. Hajos, D. R. Parrish, and E. P. Oliveto. Tetrahedron, **24**, 2039 (1968).
20. W. Dai and W. Zhou. Tetrahedron, **41**, 4475 (1985).
21. (*a*) M. Ihara, Y. Tokunaga, and K. Fukumoto. J. Org. Chem. **55**, 4497 (1990); (*b*) M. Ihara, T. Takahashi, N. Shimizu, Y. Ishida, I. Sudow, K. Fukumoto, and T. Kametani. J. Chem. Soc. Chem. Commun. 1467 (1987); (*c*) M. Ihara, I. Sudow, and K. Fukumoto. J. Chem. Soc. Perkin Trans. 1, 117 (1986).
22. E. J. Corey, S. W. Chow, and R. A. Scherrer. J. Am. Chem. Soc. **79**, 5773 (1957).

Can. J. Chem. Downloaded from www.nrcresearchpress.com by 217.78.4.112 on 09/08/12
For personal use only.

Diels–Alder reactions of 2-carbomethoxy-4,4-dimethyl-2-cyclopenten-1-one

HSING-JANG LIU, GERARDO ULÍBARRI,[1] AND ERIC N. C. BROWNE[2]
Department of Chemistry, The University of Alberta, Edmonton, Alta., Canada T6G 2G2

Received July 16, 1991

This paper is dedicated to Professor Zdenek (Denny) Valenta on the occasion of his 65th birthday

HSING-JANG LIU, GERARDO ULÍBARRI, and ERIC N. C. BROWNE. Can J. Chem. **70**, 1545 (1992).

Diels–Alder additions to keto ester **2** proceed in moderate to high yields with a variety of dienes under selected Lewis acid and thermal conditions. Thermal conditions provide the highest total yields for non-functionalized dienes, but Lewis acid catalysts, particularly stannic chloride, provide highly selective additions in greater net yields. A study of several functionalized dienes shows that zinc chloride is particularly effective in catalyzing additions to **2**. No difference in stereoselectivity is observed between zinc chloride and thermal reactions for highly functionalized dienes. The significance of the regiochemical and stereochemical results of the Diels–Alder reactions is discussed.

HSING-JANG LIU, GERARDO ULÍBARRI et ERIC N. C. BROWNE. Can. J. Chem. **70**, 1545 (1992).

Les réactions d'addition de Diels–Alder sur le céto-ester **2** s'effectuent avec des rendements allant de modérés à très élevés avec un certain nombre de dièenes dans certaines conditions thermiques et avec certains acides de Lewis. Les conditions thermiques fournissent les rendements les plus élevés avec les dièenes non fonctionnalisés, mais les catalyseurs acides de Lewis, en particulier le chlorure stannique, conduisent à une addition hautement sélective avec un rendement net plus élevé. Une étude de plusieurs dièenes fonctionnalisés montre que le chlorure de zinc est particulièrement efficace comme catalyseur des additions sur le composé **2**. On n'observe aucune différence de stéréosélectivité entre le chlorure de zinc et les réactions thermiques impliquant les dièenes très fonctionnalisés. On discute de la signification des résultats régiochimiques et stéréochimiques des réactions de Diels–Alder.

[Traduit par la rédaction]

Introduction

In conjunction with synthetic studies on the marine sesquiterpene acetate spirodysin (**1**) (1) we have studied Diels–Alder reactions of the cyclopentenone ester **2**. Cycloaddition of **2** with a 1,3-difunctionalized Danishefsky-type diene would provide a key intermediate such as **3**, which is ideally suited for conversion to spirodysin. While this group made a large-scale investigation of larger ringed cross-conjugated dicarbonyl dienophiles (2–5) and Wenkert's group examined primarily cyclohexenones, in a series of papers,[3] relatively few examples (7–9) of Diels–Alder additions to cross-conjugated 5-membered ring unsaturated carbonyl compounds are known.

Cyclopentenones have generally performed poorly in Diels–Alder additions (10–12) and consequently have not been extensively studied. Wenkert and co-workers (13, 14) demonstrated the expected improvement in reactivity of simple cyclopentenones **4** with Lewis acid catalysis. Caine *et al.* (7) reported a very brief study of enone ester **2** using a rationale based in part on our work. In the same report he also noted the complete failure of the simpler enone **5** to produce adducts.

Detailed examination of the Diels–Alder reactivity of **2** will expand on our previous studies and offer further insight into the stereoelectronic effects relating to Diels–Alder reactions in general. Furthermore, this study should provide essential data required to select the specific diene best suited to use in the synthesis of spirodysin.

Results and discussion

The brief study of Caine *et al.* (7) used keto eter **2**, which they prepared essentially in six steps from ethyl acetoacetate via coupling of methyl 3-bromo-2-methoxycrotonate (15) and isobutyraldehyde in reportedly "low yield." For our Diels–Alder study and the planned synthesis of spirodysin we required a supply of **2** by a simpler route and in useful yield and so the efficient preparation of the reagent was examined first.

Several alternative approaches that might be applied to the formation of **2** are reported in the literature. One (16) employs a protected acyloin condensation of the ethyl diester of 3,3-dimethylglutaric acid obtained (16) in 92% yield from the inexpensive commercial diacid. The intermediate bis-silyl enol ether **6** is hydrolyzed to the unsaturated ketone **5** (63% overall yield in three steps). Another approach (17) to intermediate **5** in slightly lower yield uses vinylic oxidation of olefin aldehyde **7** obtained (18) in one step by coupling of isobutyraldehyde and allyl alcohol. The resulting keto aldehyde undergoes aldol condensation to give **5** in 49% overall yield (three steps) from isobutyraldehyde. Conversion of **5**[4] from either route to dienophile **2** would require reduction of the double bond, regioselective carbomethoxylation,[5] and oxidation to regenerate the double bond. Clearly, a simpler approach than either of these lengthy (six-step) procedures is desirable.

In a fundamentally different approach, keto ester **8** was prepared (20) in high yield from commercial 3,3-dimethyl glutaric acid by a modified Dieckmann condensation on the dimethyl ester (67% overall yield in two steps). A fourth approach (21) to enone ester **2** uses a Wolff rearrangement of the diazoketone **9**, which can be prepared (22) from dimedone, to give the keto ester **8** (72% overall yield in two steps). Oxidation of **8** at the α-position would provide dienophile **2**. This last approach would be preferable since it

[1]Taken in part from the Ph.D. thesis of Gerardo Ulíbarri, The University of Alberta, 1991.

[2]Present address: Wyeth–Ayerst Research Inc., 1025 Laurentian Blvd., St. Laurent, Que., H4R 1J6.

[3]For the most recent paper in the series see ref. 6.

[4]Ketone **5** is available at very high cost from Aldrich Chemical Co.

[5]This carbomethoxylation has already been reported in 60–63% yield by two other groups (19, 20).

Can. J. Chem. Downloaded from www.nrcresearchpress.com by 217.78.4.112 on 09/08/12
For personal use only.

Can. J. Chem. Downloaded from www.nrcresearchpress.com by 217.78.4.112 on 09/08/12
For personal use only.

would produce the β-keto ester directly in highest yield in only three or four steps from commercial materials.

Thus, photolysis of **9** by the established method (21) gave **8**, which was brominated with *N*-bromosuccinimide to give **10** (93% yield). Dehydrobromination of **10** with 1,8-diazabicyclo[5.4.0]undec-7-ene (DBU) was unsuccessful and the use of lithium chloride in dimethylformamide (23) gave the desired product **2** in only 20% yield. Considering the observed difficulty in achieving dehydrobromination, we examined the popular and reliable selenylation – oxidative elimination approach previously used successfully (24) to prepare **2** in unreported yield. Keto ester **8** was treated with phenylselenenyl chloride and pyridine (3, 25, 26). The intermediate selenide was oxidized with hydrogen peroxide to give dienophile **2** in 95% overall yield from **8**.

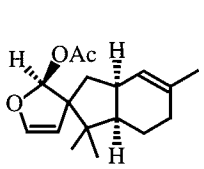

1

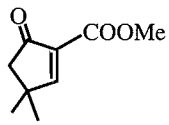

2

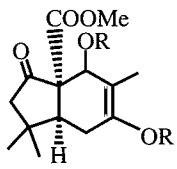

3

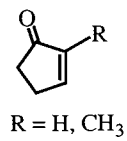

R = H, CH_3

4

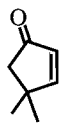

5

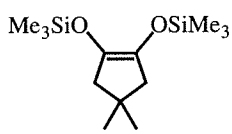

6

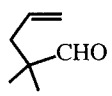

7

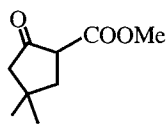

8

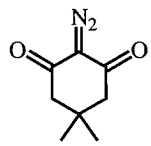

9

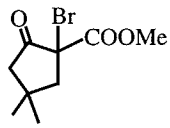

10

In general enone ester **2** was reacted with a selection of Lewis acids and dienes in ether solution at ambient or subambient temperatures with a stoichiometric excess of the diene and one equivalent or a slight excess of the Lewis acid. For comparison, a series of thermal Diels–Alder reactions was also run on a small scale (~50 mg). The reaction mixtures (ether solutions) of **2** developed colorful complexes with some Lewis acids; pink–red with stannic chloride, violet with ferric chloride, and green with aluminum chloride. However, these Lewis acids were accompanied by considerable polymerization of the diene. In contrast, the reactions with zinc chloride (27) and boron trifluoride etherate were colorless, less polymerization occurred, and the purification of the adducts was considerably easier to accomplish. The details of the reactions and structural assignments will be presented individually for each diene studied, followed by discussion of the stereoelectronic effects that control the product structure.

Reactions with isoprene

The reactions of **2** with isoprene are summarized in Table 1. In general, adducts are formed in moderate to high yields at routine temperatures. In each case a single adduct **11** was obtained, except with thermal and boron trifluoride etherate catalyzed conditions where an inseparable isomeric product **12** was coproduced. Gross examination of the analytical data of the pure major product **11** clearly confirmed that a normal Diels–Alder adduct had been formed and the regiochemistry was tentatively assigned on the basis of the ^{1}H nmr spectrum. The C-6 vinylic proton (δ 5.37) showed couplings to two *gem*-coupled (18 Hz) methylenic signals at δ 2.86 (4 Hz) and δ 2.03 (2.5 Hz). As established in structural analyses of similar adducts in these laboratories (2, 8), the downfield shift of the proton at δ 2.86 is characterisic of the *peri*-deshielding effect of the adjacent ketone carbonyl on the β-proton at C-7.

The regiochemistry of **11** was conclusively demonstrated by conversion to keto enone **13** in 41% yield by photooxygenation (28). The distinctive β-proton of the enone system at δ 6.58 appeared as a doublet of doublets with couplings to the ring junction (δ 3.31, 5 Hz) and allylic methyl (δ 1.85, 2 Hz) protons. If the major Diels–Alder product were the anti-*para* adduct **12**, the signal for the enone hydrogen in the photo-oxygenation derivative **14** would be a singlet.[6] Also, in the ^{1}H nmr spectrum of **13** the bridgehead hydrogen (δ 3.31) shows couplings to the vinylic proton (δ 6.58, 5 Hz) and to the allylic methyl (δ 1.85, 1.5 Hz). The isomeric derivative **14** would show no couplings between those protons but would show couplings between the bridgehead proton and the keto-methylene protons at C-4.[7]

The structure of the inseparable minor adduct **12** was assigned based on the ^{1}H nmr and ^{13}C nmr spectra of the 1:1 mixture originating from the thermal reaction, which showed closely corresponding sets of peaks not present in the spectra of pure **11**. Similar correspondence has been observed between isomeric adducts **15** and **16** obtained in a related study (2).

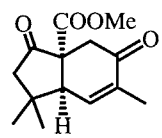

13

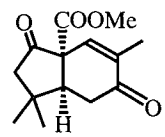

14

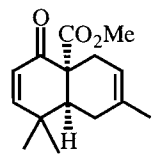

15

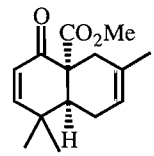

16

Reactions with trans*-piperylene*

Cycloadditions of **2** with *trans*-piperylene are summarized in Table 2. Adducts were easily obtained in moderate to high yields, giving almost invariably chromatographically separable mixtures of the two epimeric products **17** and **18** except in the case of boron trifluoride etherate where pure **17** was obtained.

[6]Indeed the ^{1}H nmr spectrum of **14** prepared by an unambiguous alternate route (*vide infra*) shows the β-proton as a very finely split doublet of quartets (δ 6.69, $J = J' = 1$ Hz) due to long-range couplings with the vinylic methyl (δ 1.83) and the C-3a hydrogen (δ 3.17).

[7]The proton of authentic **14** (*vide infra*) at δ 3.17 showed two identical couplings (5 Hz) to the C-4 methylenic protons (δ 2.67).

TABLE 1. Lewis acid catalyzed Diels–Alder addition of isoprene to enone ester **2**

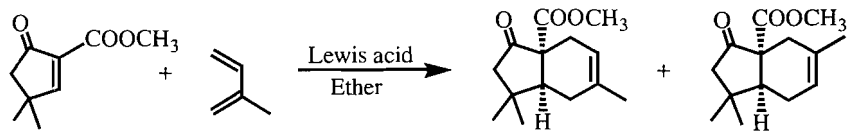

2 **11** **12**

Lewis acid (equiv.)	Isoprene (equiv.)	*t* (h)	*T* (°C)	Yield (%)	Adduct (ratio)
$SnCl_4$ (1)	10	10	0	86	**11**
$FeCl_3$ (1)	10	3	0	76	**11**
$AlCl_3$ (1)	10	5	0	64	**11**
$ZnCl_2$ (1.5)	10	168	0	20[a,b]	**11**
$ZnCl_2$ (1.3)	10	10	20	75	**11**
$BF_3 \cdot OEt_2$ (1)	20	150	20	89[a,c]	**11/12** (7:1)[d]
Thermal[e]	30	11	200	>95	**11/12** (1:1)[d]

[a]Based on consumed starting material.
[b]Starting material was recovered in 38%.
[c]Starting material was recovered in 8%.
[d]Ratio calculated by nmr integrals.
[e]Reaction was run with no solvent.

TABLE 2. Lewis acid catalyzed Diels–Alder addition of *trans*-piperyline to enone ester **2**

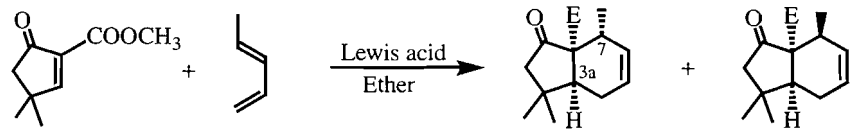

E = $COOCH_3$

2 **17** **18**

Lewis acid (equiv.)	*trans*-Pip. (equiv.)	*t* (h)	*T* (°C)	Yield (%)	Adduct (ratio)
$SnCl_4$ (1)	10	6	0	73	**17/18** (6:1)
$FeCl_3$ (1)	10	2.5	0	50	**17/18** (2:1)
$ZnCl_2$ (1.2)	10	5	20	47[a,b]	**17/18** (1.5:1)
$BF_3 \cdot OEt_2$ (1)	10	90	20	73	**17**
Thermal[c]	20	6	200	90	**17/18** (2:1)

[a]Starting material was recovered in 34%.
[b]Based on consumed starting material.
[c]Reaction was run with no solvent.

The gross structure of the pure major isomer **17** was evident from the analytical data. The bridgehead proton (δ 2.67) showed two couplings (7 and 2.5 Hz) to adjacent protons, one of which (δ 2.39) also showed a geminal coupling (15 Hz) thus confirming the regiochemistry of the addition. For the pure minor isomer **18** the ring junction proton was obscured by a complex signal (δ 2.35); however, the two adjacent *gem*-coupled (16 Hz) methylene protons were clearly identified (δ 2.38, δ 2.06). Neither showed the effect of downfield shifting by an adjacent ketone carbonyl, confirming the regiochemistry as shown and confirming that **18** is epimeric with the major isomer **17**. Preliminary indication of the stereochemistry was defined by the shift of the C-7 methine proton, which in **17** (δ 2.85) showed the expected downfield shift due to the *peri*-effect of the ketone carbonyl, while the same signal in **18** (part of the complex signal at δ 2.35) showed no such deshielding.

The stereochemistry of the methyl at C-7 was confirmed by nOe experiments on both epimers **17** and **18**. Compound **17** showed an enhancement of the ester methyl (δ 3.75, 4%) and C-3a proton (δ 2.67, 2%) signals upon irradiation of the C-7 methyl (δ 1.18). Irradiation of the C-3a proton (δ 2.67) enhanced the C-7 methyl (δ 1.18, 11%) and ester methyl (δ 3.75, 8%). Irradiation of the C-7 methyl of the minor isomer **18** (δ 1.21) gave no enhancement to either the ester methyl (δ 3.70) or the C-3a proton (δ 2.35). With these observations we concluded that the stereochemistry of **17** and **18** at C-7 is as shown.

Reactions of furan

Additions of furan to **2** (Table 3) gave modest to poor yield of the 1,4-addition product **19**[8] or decomposition products

[8]The stereochemistry of this compound could not be unambiguously assigned based on the available spectral data. The tentative assignment was made assuming that the facile epimerization of the β-keto ester system would allow for the exclusive formation of the more stable *trans* isomer.

Can. J. Chem. Downloaded from www.nrcresearchpress.com by 217.78.4.112 on 09/08/12
For personal use only.

TABLE 3. Lewis acid catalyzed addition of furan to enone ester **2**

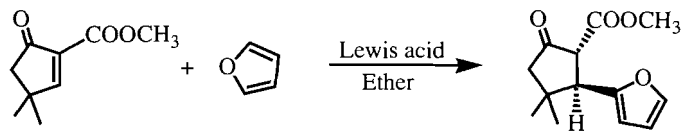

2 **19**

Lewis acid (equiv.)	Furan (equiv.)	*t* (h)	*T* (°C)	Yield (%)	Adduct (ratio)
$SnCl_4$ (1)	10	2.5	−10	—	[a]
$FeCl_3$ (1)	10	25	0	42	**19**
$ZnCl_2$ (1)	10	48	20	—	[b]
$BF_3 \cdot OEt_2$ (1)	10	28	20	54	**19**
Thermal[c]	20	7	150	7	**19**[a,d]

[a]Decomposition of starting material took place.
[b]Starting material was recovered in 100%.
[c]Reaction was run with no solvent.
[d]Starting material was recovered in 71%.

TABLE 4. Lewis acid catalyzed Diels–Alder addition of C-1 functionalized dienes **22***a* and **22***b* to enone ester **2**

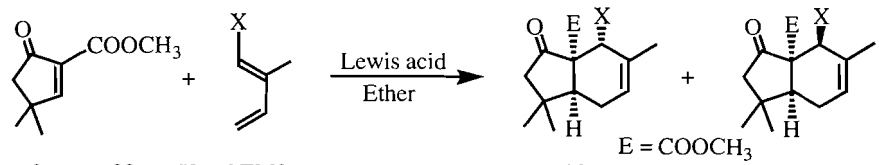

2 **22***a*: X = OTMS; **22***b*: X = OTBDMS **23***a*, **23***b* **24***a*, **24***b*

Lewis acid (equiv.)	Diene (equiv.)	*t* (h)	*T* (°C)	Yield (%)	Adduct (ratio)
$ZnCl_2$ (1)	**22***a* (10)	16	20	—	[a]
$FeCl_3$ (1)	**22***a* (10)	2	0	—	[a]
$SnCl_4$ (1)	**22***a* (10)	28	−25	—	[a]
Thermal[b]	**22***a* (15)	12	150	86	**23***a*/**24***a* (1:1)
$ZnCl_2$ (1)	**22***b* (2)	168	20	17	**23***b*/**24***b* (1:1)[c]
$SnCl_4$ (1)	**22***b* (2)	5	−10	—	[d]

[a]Decomposition took place.
[b]Reaction was run with no solvent.
[c]Starting material was recovered in 52%, ratio by nmr.
[d]Starting material was recovered in 48%.

rather than the expected Diels–Alder adduct **20**. Production of a similar 1,4-addition product was previously observed for addition of furan to the unsaturated γ-lactone dienophile **21** (8).

Reactions of C-1 functionalized dienes **22***a* *and* **22***b*

A study of the Diels–Alder cycloaddition of functionalized dienes to keto ester **2** was undertaken to determine which dienes would be suitable for the planned synthesis of spirodysin. The C-1 functionalized diene **22***a* (29) was prepared by condensation of *trans*-2-methyl-2-butenal (tiglic aldehyde) with trimethylsilyl chloride in the presence of zinc chloride and triethylamine. It was extremely sensitive to the acidity of the Lewis acid catalysts and could only be used successfully in the thermal Diels–Alder reaction (Table 4).

The thermal reaction of **22***a* gave a mixture of epimers, which was separated by flash chromatography on silica gel. The ^1H nmr spectrum of epimer **24***a*, which eluted first, displayed an allylic signal for the C-7 hydrogen at δ 4.72 as a singlet. The C-3a hydrogen was at δ 2.70 (dd, $J = J' =$ 8 Hz). The second epimer to be eluted was compound **23***a*. In its ^1H nmr spectrum the vinylic hydrogen appeared at δ 5.67 (dd, $J = 6$, $J' = 5$ Hz), the C-7 hydrogen at δ 4.40 (singlet), and the C-3a hydrogen at δ 2.83 (dd, $J = 7$, $J' =$ 4 Hz). The multiplicity of these sets of signals confirmed the regiochemistry of the two adducts.

The stereochemistry at the C-7 carbon of the two epimers was confirmed by a simple nOe experiment. Irradiation of compound **24***a* at the C-3a proton (δ 2.70) gave enhancement of the C-7 hydrogen signal (δ 4.72, 2%). Irradiation at δ 4.72 produced an enhancement of the ester methyl signal (δ 3.68, 4%) and the C-3a proton (δ 2.70, 2%). On the other hand, irradiation of the C-7 proton (δ 4.40) of compound **23***a* produced no enhancement at C-3a (δ 2.83). Based on these results, the stereochemistry at C-7 in epimers **23***a* and **24***a* was assigned as shown.

Can. J. Chem. Downloaded from www.nrcresearchpress.com by 217.78.4.112 on 09/08/12
For personal use only.

Can. J. Chem. Downloaded from www.nrcresearchpress.com by 217.78.4.112 on 09/08/12
For personal use only.

The regiochemistry of the Diels–Alder reaction was confirmed by independent decarbomethoxylations of the epimers **23***a* and **24***a* using lithium iodide dihydrate in refluxing collidine (30). The same aromatic compound **25** was obtained in 54% yield in each case, apparently by concurrent displacement of the trimethylsiloxy group and aromatization of the resulting diene. The ^{1}H nmr of **25** showed a *peri*-deshielded signal for the C-7 aromatic proton at δ 7.50 as a broadened singlet, conclusively proving the position of the methyl at C-6.

The *tert*-butyldimethylsilyloxy diene **22***b* was also studied to determine if it would be more stable in the presence of a Lewis acid during the reaction. This diene could not be prepared by the method used for **22***a*. Instead, tiglic aldehyde was deprotonated with lithium diisopropylamide and the resulting enolate was trapped with *tert*-butyldimethylsilyl chloride (31). The silyloxy diene **22***b*[9] was slightly more stable to the acidic conditions of the Diels–Alder cycloadditions and an adduct was obtained (Table 4) with zinc chloride as the catalyst. A poor yield (~17% after 168 h) of an inseparable 1:1 mixture of epimers **23***b* and **24***b* that could not be completely purified was obtained. When stannic chloride was used, complete decomposition of the diene took place. The ratio of the mixture of adducts **23***b* and **24***b* was obtained from the ^{1}H nmr spectrum of the crude mixture.

Reactions of C-2 functionalized diene ***26***

Diene **26** (31) was prepared from 3-methyl-3-buten-2-one by deprotonation with lithium diisopropylamide and trapping of the resulting enolate produced with *tert*-butyldimethylsilyl chloride. The diene was obtained in 80% yield after being distilled in a Kugelrohr apparatus at 90°C (15 Torr; 1 Torr = 133.3 Pa).

The Diels–Alder reaction of diene **26** with dienophile **2** gave only adduct **27** (Table 5). The reaction proceeded very cleanly when zinc chloride was used, giving a better yield than with the thermal reaction. When stannic chloride was used as the catalyst a messy reaction took place and none of the adduct **27** or the starting material was recovered. Instead only the difficult to purify hydrolyzed ketone **28** (3.8:1) was collected in low yield. Pure **28** was prepared directly from pure **27**. Hydrolysis of silyl enol ether **27** with dilute hydrochloric acid gave ketone **28** as a mixture (3.8:1) of epimers at C-6. The ^{1}H nmr spectrum of **28** displayed a complex set of doubled signals that did not allow confident assignment of stereochemistry at C-6 for each epimer.

Reactions of difunctionalized diene ***29***

Diene **29**[10] can be prepared (31) from 4-ethoxy-3-methyl-3-buten-2-one (32) and purified by bulb-to-bulb distillation (2.0 Torr, 60°C). Diels–Alder cycloaddition of dienophile **2** with diene **29** (Table 6) proceeded smoothly when zinc chloride or thermal conditions were used, but when stannic chloride, a stronger Lewis acid, was used as a catalyst no initial Diels–Alder adduct could be isolated from the messy reaction. Instead, only the hydrolysis product ketone **14** was recovered in 36% yield. This again showed the great acid sensitivity of this type of dienes, making the Diels–Alder reactions with them subject to some limitations. Nevertheless, use of the less acidic Lewis acid zinc chloride allowed cycloaddition to take place, giving a 1:1 mixture of epimeric silyl enol ethers **30** and **31** in good yield. The chromatographic separation of the epimers was accomplished with great difficulty and was done only for the purpose of identification since the C-7 chiral center would be destroyed upon hydrolysis of the enol ethers in any planned synthetic scheme. Compound **30** was the first epimer to be eluted. The ^{1}H nmr spectrum of compound **30** displayed the C-7 hydrogen (δ 4.49) as a broad singlet, thus confirming the orientation of the addition. Interestingly, the methylenic hydrogens at the ethoxyl chain appeared as two sets of peaks at δ 3.46 (q, J = 7 Hz), and at δ 3.35 (q, J = 7 Hz). The C-3a hydrogen (δ 2.91) appeared as a doublet of doublets ($J = J'$ = 8 Hz).

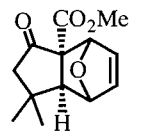

20

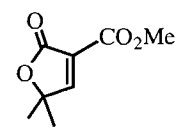

21

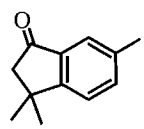

25

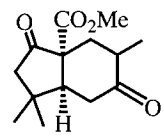

28

The ^{1}H nmr spectrum of compound **31**, the second epimer to be eluted, showed the C-7 hydrogen (δ 4.35) as a singlet and the C-3a hydrogen (δ 3.16) as a doublet of doublets (J = 7.5, J' = 1.5 Hz), again confirming the regiochemistry. The methylenic hydrogens of the ethoxyl group were displayed together at δ 3.42 (q, J = 7 Hz). Irradiation of the vinylic methyl signal at δ 1.63 (d, J = 2 Hz), to induce decoupling affected only the signal at δ 2.71 due to one of the C-4 methylenic protons, indicating a homo-allylic coupling with this particular hydrogen.

Although a confident assignment of the stereochemistry at C-7 for epimers **30** and **31** was not possible with the data obtained from the ^{1}H nmr spectrum, it was interesting to observe that the methylene hydrogens in the ethoxyl chain appeared as separate signals in the case of compound **30** at δ 3.46 and δ 3.35 and in one single signal in compound **31** at δ 3.42. If there were an interaction between the ethoxyl chain and the ester group causing the methylene hydrogens to appear as separate signals, then silyl enol ether **30** would be the epimer with the ethoxyl group *cis* to the ester moiety. Also the C-3a hydrogen in compound **30** is at higher field (δ 2.91) in the ^{1}H nmr spectrum than the same hydrogen of the epimer **31** (δ 3.16), indicating that the C-3a hydrogen in compound **30** could be within the shielding area of the ether oxygen. This is not the case for silyl enol ether **31**. Because the center at C-7 would be destroyed in a later stage in the

[9]This compound obtained in 40% yield showed the following spectral data: ^{1}H nmr (400 MHz, $CDCl_3$) δ: 6.40 (br s, 1H, -OC*H*=), 6.28 (dd, J = 16, J' = 12 Hz, 1H, -C*H*=), 4.97 (d, J = 16 Hz, 1H, *H*HC=), 4.82 (d, J = 12 Hz, 1H, H*H*C=), 1.70 (s, 3H, =C(CH_3)-), 0.93 (s, 9H, -SiC(CH_3)$_3$), and 0.15 (s, 6H, -Si(CH_3)$_2$); ir (neat): 1732 (C=C) and 1255 (Si-CH$_3$) cm^{-1}.

[10]This compound, obtained in 45% yield, showed the following spectral data: ^{1}H nmr (400 MHz, $CDCl_3$) δ: 6.67 (br s, 1H, -OC*H*=), 4.22 (d, J = 1 Hz, 1H, *H*HC=), 4.12 (d, J = 1 Hz, 1H, H*H*C=), 3.87 (q, J = 6 Hz, 2H, -CH_2CH$_3$), 1.72 (s, 3H, =C(CH_3)-), 1.28 (t, J = 6 Hz, 3H, -CH$_2$CH_3), 0.96 (s, 9H, -SiC(CH_3)$_3$), and 0.18 (s, 6H, -Si(CH_3)$_2$); ir (neat): 1641, 1657 (C=C), and 1253 (Si-CH$_3$) cm^{-1}.

TABLE 5. Lewis acid catalyzed Diels–Alder addition of C-2 functionalized diene **26** to enone ester **2**

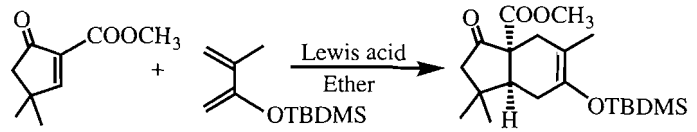

2 **26** **27**

Lewis acid (equiv.)	**26** (equiv.)	*t* (h)	*T* (°C)	Yield (%)	Adduct ratio
$ZnCl_2$ (1)	2.5	49	20	93	**27**
$SnCl_4$ (1)	1.1	9	−10	37	**27**[a]
Thermal[b]	7	12	150	77	**27**

[a]Recovered as the ketone **28**.
[b]Reaction was run with no solvent.

TABLE 6. Lewis acid catalyzed Diels–Alder addition of C-1 and C-3 difunctionalized diene **29** to enone ester **2**

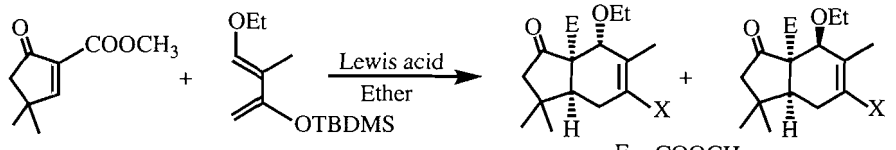

2 **29** **30** **31**

Lewis acid (equiv.)	**29** (equiv.)	*t* (h)	*T* (°C)	Yield (%)	Adduct (ratio)
$ZnCl_2$ (1)	2	2	20	90	**30/31** (1:1)[a]
$SnCl_4$ (1)	2	120	−10	—	**30/31**[b,c]
Thermal[d]	2	30	80	97	**30/31** (1:1)

[a]The hydrolysis product ketone **14** was also recovered in 9%.
[b]The hydrolysis product ketone **14** derived from **30/31** was the only product recovered in 36%.
[c]Starting material was also recovered in 15%.
[d]Benzene was used as solvent.

planned synthesis of spirodysin, the stereochemistry at this position was not essential to our study. As the ratio of stereoisomers obtained was always 1:1 there was no noteworthy stereoselectivity expressed in the Diels–Alder cycloaddition of **29**.

Degradation of the adduct mixture provided conclusive proof of the Diels–Alder orientation. Hydrolysis of the mixture of silyl enol ethers **30** and **31** with aqueous 0.1 N hydrochloric acid in tetrahydrofuran gave the α,β-unsaturated ketone **14** in 70% yield. The ^1H nmr spectrum of compound **14** displayed the C-7 hydrogen of the unsaturated ketone at δ 6.69 (dq, $J = J' = 1$ Hz), with a long-range W-coupling to the vinylic methyl and to the C-3a hydrogen. The C-3a hydrogen was displayed at δ 3.17 (ddd, $J = J' = 5$, $J'' = 1$ Hz) and the adjacent C-4 hydrogens appeared together at δ 2.67 (d, $J = 5$ Hz).

Orientation effects

As we demonstrated with related dienophiles (2–5, 8), additions to keto ester **2** showed stereochemical and electronic influences in the orientations of the additions which were reflected in the structures of the adducts. Additions of isoprene showed significant proportions of the *anti*-para adduct **12** in the thermal and boron trifluoride catalyzed cases. We interpreted this result as due to the steric interaction between diene and dienophile methyl groups in the keto-*endo* transition state **A** ($R^1 = R^2 = H$, $R^3 = CH_3$). Weaker Lewis acids capable of accepting bidentate ligand complexes showed complete predominance of the *para* product of addition by ester-*endo* transition state **B** ($R^1 = R^2 = H$, $R^3 = CH_3$). In that transition state steric interaction between the methyl groups would be absent.

Additions of *trans*-piperylene as well as functionalized dienes **22***a* and **22***b* proceeded exclusively according to the expected *ortho* rule and the complete regiospecificity observed in *para* addition of silyloxy diene **26** was in the direction predicted by normal empirical priority rules for predicting the controlling substituent. Similarly, additions of bifunctional diene **29** gave exclusively the *ortho*-rule products.

Dienophile **2** was somewhat unusual relative to the other systems we studied in that *exo-endo* selectivity of the addition was very low in most cases. High ratios of one epimer, in each case the product of ester-*endo* addition (transition state **B**, $R^1 = CH_3$; $R^2 = R^3 = H$), were only obtained for *trans*-piperylene additions under boron trifluoride and stannic

Can. J. Chem. Downloaded from www.nrcresearchpress.com by 217.78.4.112 on 09/08/12
For personal use only.

chloride catalysis. The other dienophiles each showed a clear preference for keto-*endo* addition (2) or ester-*endo* addition (3–5, 8) under the various preferred reaction conditions. In fact we regard the production of the keto-*endo* product **31**, which must be formed by addition of **29** through transition state **A** (R^1 = OEt, R^2 = CH_3, R^3 = OTBDMS), as quite remarkable. Steric interaction of the large silyloxy group with the *gem*-dimethyl of **2** should at first glance have a large destabilizing effect on the transition state and promote formation of the epimeric product **30**. The reasons for the absence of this expected steric effect and for the general *exo-endo* orientational ambivalence of additions to **2** are unclear. Further investigations into the effects influencing *exo-endo* selectivity in this and other cross conjugated dicarbonyl dienophiles is the subject of ongoing investigation in this laboratory.

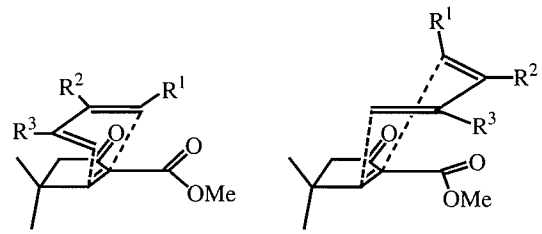

A **B**

Conclusions

Keto ester **2** is a general and potentially versatile intermediate for the assembly of indene ring synthons useful in the synthesis of natural products. As a dienophile, **2** shows the expected stereoelectronic influences on the regiochemistry of the adducts. With functionalized dienes zinc chloride is a particularly suitable choice as the catalyst.

Towards the synthesis of spirodysin (**1**), at this point it would only be necessary to modify an intermediate such as **14** or **28** into a system that would allow for dialkylation at the α-position of the ketone in the cyclopentanone ring. Further studies on both intermediate ring systems are under way in these laboratories.

Experimental

General

Melting points were measured on a Köfler hot stage apparatus and are uncorrected. Elemental analyses were carried out using a Perkin Elmer 240-B elemental analyzer for C, H, and N detection. Infrared spectra (ir) were obtained on a Nicolet 7199 FTIR spectrophotometer. Mass spectra (ms) were determined using a AEI Kratos MS-50 high-resolution mass spectrometer attached to a Data General Nova 2 with Kratos DS-55 software. Proton nuclear magnetic resonance spectra (^{1}H nmr) were obtained using one of the following spectrometers: Bruker WH-200 (200 MHz), Bruker AM-300 (300 MHz), or Bruker AM-400 (400 MHz). Coupling constants are recorded to within ±0.5 Hz. Carbon nuclear magnetic resonance spectra (^{13}C nmr) were run on a Bruker AM-300 (75 MHz), or a Bruker AM-400 (100.6 MHz). Two methods were used to determine the carbon-13 multiplicities: the distortionless enhancement by polarization transfer (DEPT) experiment with proton decoupling using a Bruker software microprogram (DETP.AUR) and the attached proton test (APT) (used for most compounds). Peaks in antiphase (a) with deuteriochloroform were assigned as methyls or methines, while peaks in phase (p) correspond to methylenes or quaternary carbons. Aldehydic carbonyls appear in antiphase with $CDCl_3$ and other carbonyls in phase with the deuteriochloroform signal. Nuclear Overhauser enhancement (nOe) experiments were obtained after computer subtraction of the uncoupled spectrum from the irradiated spectrum. Positive enhancements are defined as signals in antiphase with the enhanced irradiated signal. Immediately before the experiment each sample was deoxygenated by passing helium gas through the solution for 10 min. Reaction yields are quoted with a degree of purity better than 95% as determined by NMR spectroscopy.

Materials

Products were purified either by flash chromatography using silica gel 60 (230–400 mesh), distillation using a bulb-to-bulb Kugelrohr apparatus, or by fractional crystallization. Reactions were monitored by thin-layer chromatography using Merck aluminum-backed plates precoated with silica gel 60 GF_{254}. Solvents were dried and distilled prior to use as follows: ethyl ether from a blue–purple solution of sodium benzophenone ketyl under an argon atmosphere: benzene, pyridine, and dichloromethane from calcium hydride or lithium hydride. Dienes **22***a* (29) and **26** (31) were prepared according to the reported procedures. Dienes **22***b* and **29** were prepared from *trans*-2-methyl-2-butenal and 4-ethoxy-3-methyl-3-buten-2-one (32) respectively, using the same procedure as described for the preparation of diene **26** (31).

*1-Bromo-4,4-dimethyl-2-oxocyclopentane-1-carboxylic acid, methyl ester (**10**)*

2-Carboxymethoxy-4,4-dimethylcyclopentan-1-one (**8**) (0.70 g, 4.1 mmol) was dissolved in carbon tetrachloride (10 mL). *N*-Bromosuccinimide (890 mg, 5.0 mmol) was added and the solution was stirred at room temperature for 10 h. The solid formed during the reaction was filtered and the filtrate was concentrated to give a yellowish oil (950 mg, 3.8 mmol, 93%); ir ($CHCl_3$ cast): 1761 (ester) and 1723 (ketone) cm^{-1}; ^{1}H nmr (400 MHz, $CDCl_3$) δ: 3.80 (s, 3H, -OC*H*$_3$), 2.89 (d, *J* = 15 Hz, 1H, -C*H*HCOCBr-), 2.50 (d, *J* = 15 Hz, 1H, -CH*H*COCBr-), 2.41 (d, *J* = 10 Hz, 1H, -COCBrC*H*H-), 2.37 (d, *J* = 10 Hz, 1H, -COCBrCH*H*-), 1.28 (s, 3H, -C*H*$_3$), and 1.10 (s, 3H, -C*H*$_3$); ^{13}C nmr APT (100.6 MHz, $CDCl_3$) δ: 206.2 (a), 168.3 (a), 59.3 (a), 54.0 (p), 52.2 (a), 51.0 (a), 34.0 (a), 29.6 (p), and 29.4 (p); ms; M^+: 250.0026 (248.0027) (calcd. for $C_9H_{13}O_3Br$: 250.0027 (248.0048)).

*3,3-Dimethyl-5-oxo-1-cyclopentene-1-carboxylic acid, methyl ester (**2**)*

Phenylselenenyl chloride (7.5 g, 32 mmol) was dissolved in dichloromethane (200 mL) and the solution was cooled in an ice–water bath. Dry pyridine (3.20 mL, 40 mmol) was slowly added and the solution was stirred for 45 min. Then 2-carboxymethoxy-4,4-dimethylcyclopentan-1-one (**8**) (5.46 g, 32 mmol) dissolved in dichloromethane (30 mL) was added to the reaction mixture. The solution was stirred at 0°C for 45 min then poured into an ice – 5% hydrochloric acid mixture (200 mL). The organic layer was washed with aqueous 5% hydrochloric acid (3 × 10 mL) and dried ($MgSO_4$). Hydrogen peroxide (30%, 6 mL) was added to the dichloromethane solution at 0°C and allowed to react for 10 min. Additional hydrogen peroxide (30%, 6 mL) was then added. After another 10 min the reaction was quenched with water (20 mL). The aqueous layer was extracted with dichloromethane (3 × 5 mL). The organic extracts were combined, washed with water (2 × 5 mL), aqueous 5% sodium bicarbonate (1 × 5 mL) and brine (1 × 5 mL), dried ($MgSO_4$), filtered, and concentrated. Purification by flash chromatography on silica gel (0–20% ether in petroleum ether) gave a colorless oil (3.22 g, 20 mmol, 62%); ir ($CHCl_3$ cast): 1754 (ester), 1724 (ketone), and 1621 (olefin) cm^{-1}; ^{1}H nmr (400 MHz, $CDCl_3$) δ: 8.07 (s, 1H, -C(COOCH$_3$)=C*H*-), 3.74 (s, 3H, -OC*H*$_3$), 2.34 (s, 2H, -C*H*$_2$CO-), and 1.20 (s, 6H, 2 × -C*H*$_3$); ^{13}C nmr APT (100.6 MHz, $CDCl_3$) δ: 202.2 (p), 180.2 (a), 162.2 (p), 133.7 (p), 51.8 (a), 51.0 (p), 38.8 (p), and 27.3 (a); ms, M^+: 168.0987 (calcd. for $C_9H_{12}O_3$: 168.0987). Anal. calcd. for $C_9H_{12}O_3$: C 64.15, H 6.95%; found: C 64.26, H 7.19%.

*Diels–Alder reactions of keto ester **2***

The reactions were carried out using the general procedures illustrated below for isoprene. Temperature and time of reactions as

Can. J. Chem. Downloaded from www.nrcresearchpress.com by 217.78.4.112 on 09/08/12
For personal use only.

Can. J. Chem. Downloaded from www.nrcresearchpress.com by 217.78.4.112 on 09/08/12
For personal use only.

well as quantities of diene and Lewis acid relative to **2** are noted in Tables 1–6. Purification and separation of the adducts were carried out using 0–10% ether in petroleum ether as eluant. When separation occurred, the products are reported in order of elution.

*7aα-Carbomethoxy-2,3,3aα,4,7,7a-hexahydro-3,3,5-trimethylindene-1-one (**11**) and 7aα-carbomethoxy-2,3,3aα,4,7,7a-hexahydro-3,3,6-trimethylinden-1-one (**12**)*

Lewis acid catalyzed conditions (other than zinc chloride)

Keto ester **2** (25 mg, 0.15 mmol) was dissolved in dry ether (1 mL) and placed under an argon atmosphere. The reaction mixture was cooled with an ice-water bath. Tin(IV) chloride (18 μL, 0.15 mmol) was added and the resulting mixture stirred for 15 min. Isoprene (150 μL, 1.5 mmol) was introduced with a syringe. The reaction mixture was stirred for 10 h at 0°C, then quenched by the addition of saturated aqueous sodium bicarbonate (1 mL). The aqueous layer was extracted with ether (3 × 1 mL). The organic extracts were combined, washed with water (2 × 2 mL) and brine (1 × 1 mL), dried ($MgSO_4$), filtered, and concentrated. Purification by flash chromatography on silica gel (0–5% ether in petroleum ether) gave pure compound **11** (30 mg, 86%): ir ($CHCl_3$ cast): 1752 (ester) and 1731 (ketone) cm^{-1}; ^1H nmr (400 MHz, $CDCl_3$) δ: 5.37 (br dd, J = 4, J' = 2.5 Hz, 1H, -C(CH_3)=C*H*-), 3.71 (s, 3H, -OCH_3), 2.86 (ddd, J = 18, J' = 4, J'' = 2 Hz, 1H, -C*H*HCH=), 2.79 (br d, J = 8 Hz, 1H, -C(CH_3)$_2$C*H*CH_2-), 2.37 (s, 2H, -CH_2CO-), 2.17 (ddd, J = 18, J' = 8, J'' = 2 Hz, 1H, -CHC*H*HC(CH_3)=), 2.03 (ddd, J = 18, J' = 2.5, J'' = 2 Hz, -CH*H*CH=), 1.93 (br dd, J = 18, J' = 2 Hz, 1H, -CHCH*H*C(CH_3)=), 1.69 (s, 3H, -CH=C(CH_3)-), 1.20 (s, 3H, -CH_3), and 0.88 (s, 3H, -CH_3); ^{13}C nmr APT (100.6 MHz, $CDCl_3$) δ: 214.3 (p), 172.5 (p), 132.6 (p), 117.3 (a), 57.4 (p), 53.1 (p), 52.8 (a), 47.1 (a), 37.2 (p), 30.0 (a), 27.2 (p), 25.3 (p), 23.6 (a), and 23.5 (a); ms, M^+: 236.1413 (calcd. for $C_{14}H_{20}O_3$: 236.1413). Anal. calcd. for $C_{14}H_{20}O_3$: C 71.14, H 8.53%; found: C 71.21, H 8.49%.

Zinc chloride catalyzed Diels–Alder conditions

Zinc chloride (45 mg, 0.33 mmol) was added to dry ether (2 mL) and stirred at room temperature until all the solid had dissolved (~30 min). A solution of keto ester **2** (43 mg, 0.26 mmol) in dry ether (1 mL) was added to the cloudy solution of zinc chloride followed immediately by isoprene (260 μL, 2.6 mmol). The reaction mixture was stirred at room temperature for 10 h, then a saturated aqueous solution of sodium bicarbonate (1 mL) was added. The aqueous layer was extracted with ether (3 × 2 mL). The combined organic extracts were washed with water (2 × 2 mL) and brine (1 × 2 mL), dried ($MgSO_4$), filtered, and concentrated. Purification of the residual oil by flash chromatography on silica gel (0–5% ether in petroleum ether) gave adduct **11** (46 mg, 75%).

Thermal conditions

Keto ester **2** (50 mg, 0.30 mmol) was introduced into a small thick-walled glass container. Isoprene (0.90 mL, 9 mmol) was added with a syringe and argon was passed through the solution for 5 min. The glass container was cooled with liquid nitrogen until the solution had solidified. While the ampule was still in the nitrogen it was sealed and allowed to warm to room temperature over 20 min. The ampule was placed in a protected oven and heated to 200°C for 10 h. The oven was turned off and the temperature was allowed to cool to ambient temperature. Concentration, followed by flash chromatography of the residue on silica gel (0–5% ether in petroleum ether) gave an inseparable 1:1 mixture of compounds **11** and **12** (70 mg, 98%). This mixture showed the following signals, which were not present in the spectra of pure compound **11**: ^1H nmr (400 MHz, $CDCl_3$) δ: 5.41 (br s, 1H, -C(CH_3)=C*H*-), 3.68 (s, 3H, -OCH_3), 2.71 (br s, 2H, -CH_2C(CH_3)=), 2.67 (d, J = 6 Hz, 1H, -C*H*CH_2CH=), 2.37 (s, 2H, -CH_2CO-), 1.69 (s, 3H, -CH=C(CH_3)-), 1.18 (s, 3H, -CH_3), and 0.88 (s, 3H, -CH_3), other peaks were overlapped with those of isomer **11**; ^{13}C nmr APT (100.6 MHz, $CDCl_3$) δ: 214.0 (p), 172.2 (p), 130.4 (p), 119.5 (a), 58.9 (p), 53.2 (p), 52.6 (a), 46.1 (a), 37.1 (p), 31.1 (p), 30.0 (a), 23.5 (a), 23.4 (a), and 21.1 (p).

The other adducts showed the following spectral data.

*7aα-Carbomethoxy-2,3,3aα,4,7,7a-hexahydro-3,3,7α-trimethylinden-1-one (**17**) and 7aα-carbomethoxy-2,3,3aα,4,7,7a-hexahydro,3,3,7β-trimethylinden-1-one (**18**)*

Major isomer **17**: ir ($CHCl_3$ cast): 1742 (ester) and 1729 (ketone) cm^{-1}; ^1H nmr (400 MHz, $CDCl_3$) δ: 6.01 (ddd, J = 10, J' = 6.5, J'' = 2.5 Hz, 1H, -CH(CH_3)CH=C*H*-), 5.65 (ddd, J = 10, J' = 7, J'' = 3 Hz, 1H, -CH(CH_3)C*H*=CH-), 3.75 (s, 3H, -OCH_3), 2.85 (complex m, 1H, -C*H*(CH_3)CH=CH-), 2.67 (dd, J = 7, J' = 2.5 Hz, 1H, -C(CH_3)$_2$C*H*CH_2-), 2.39 (ddd, J = 15, J' = 7, J'' = 3 Hz, 1H, -CHC*H*HCH=CH-), 2.10 (complex m, 3H, -CHCH*H*CH=CH- and -CH_2CO-), 1.18 (d, J = 7 Hz, 3H, -CH(CH_3)CH=CH-), 1.09 (s, 3H, -CH_3), and 1.07 (s, 3H, -CH_3); ^{13}C nmr DEPT (100.6 MHz, $CDCl_3$) δ: 213.2 (s), 173.8 (s), 134.2 (d), 128.3 (d), 65.4 (s), 55.4 (t), 52.6 (d), 37.0 (s), 35.1 (q), 31.6 (d), 25.9 (q), 24.4 (t), 15.9 (q), and 5.8 (q); ms, M^+: 236.1413 (calcd. for $C_{14}H_{20}O_3$: 236.1413).

Minor isomer ***18***: ir ($CHCl_3$ cast): 1754 (ester) and 1732 (ketone) cm^{-1}; ^1H nmr (400 MHz, $CDCl_3$) δ: 5.80 (ddd, J = 10, J' = J'' = 2.5 Hz, 1H, -CH(CH_3)CH=C*H*-), 5.51 (ddd, J = 10, J' = 2.5, J'' = 2 Hz, 1H, -CH(CH_3)C*H*=CH-), 3.70 (s, 3H, -OCH_3), 2.38 (dd, J = 16, J' = 2 Hz, 1H, -CHC*H*HCH=CH-), 2.35 (complex, 4H, -C*H*(CH_3)CH=CH-, -C(CH_3)$_2$C*H*CH_2- and -CH_2CO-), 2.06 (ddd, J = 16, J' = J'' = 2.5 Hz, 1H, -CHCH*H*CH=CH-), 1.21 (d, J = 7 Hz, 3H, -CH(CH_3)CH=CH-), 1.15 (s, 3H, -CH_3), and 1.00 (s, 3H, -CH_3); ^{13}C nmr DEPT (100.6 MHz, $CDCl_3$) δ: 213.6 (s), 171.5 (s), 130.0 (d), 125.2 (d), 60.2 (s), 53.4 (t), 51.8 (d), 49.2 (q), 36.8 (s), 31.7 (d), 30.1 (q), 23.8 (q), 21.4 (t), and 16.5 (q).

*2-(1-Furanyl)-3,3-dimethyl-5-oxocyclopentanecarboxylic acid, methyl ester (**19**):* ir ($CHCl_3$ cast): 1758 (ester), 1730 (ketone), and 738 (furan) cm^{-1}; ^1H nmr (400 MHz, $CDCl_3$) δ: 7.36 (d, J = 2 Hz, 1H, -OC*H*=CHCH=C-), 6.32 (dd, J = 3, J' = 2 Hz, 1H, -OCH=C*H*CH=C-), 6.14 (d, J = 3 Hz, 1H, -OCH=CHC*H*=C-), 3.78 (d, J = 12 Hz, 1H, -COC*H*(COOCH_3)CH-), 3.73 (s, 3H, -OCH_3), 3.69 (d, J = 12 Hz, 1H, -COCH(COOCH_3)C*H*-), 2.40 (s, 2H, -CH_2COCH-), 1.30 (s, 3H, -CH_3), and 0.80 (s, 3H, -CH_3); ^{13}C nmr DEPT (100.6 MHz, $CDCl_3$) δ: 208.8 (s), 168.8 (s), 151.9 (s), 142.0 (d), 110.2 (d), 107.4 (d), 57.5 (d), 54.1 (t), 52.6 (q), 49.5 (d), 38.4 (s), 27.7 (q), and 23.4 (q); ms, M^+: 236.1044 (calcd. for $C_{13}H_{16}O_4$: 236.1049).

*7aα-Carbomethoxy-2,3,3aα,4,7,7a-hexahydro-3,3,6-trimethyl-7α-(trimethylsilyloxy)inden-1-one (**23**a) and 7aα-carbomethoxy-2,3,3aα,4,7,7a-hexahydro-3,3,6-trimethyl-7β-(trimethylsilyloxy)inden-1-one (**24**a)*

Compound ***23a****:* ir ($CHCl_3$ cast): 1757 (ester), 1734 (ketone), and 1250 (Si-CH_3) cm^{-1}; ^1H nmr (400 MHz, $CDCl_3$) δ: 5.67 (dd, J = 6, J' = 5 Hz, 1H, -CH(OTMS)C(CH_3)=C*H*-), 4.40 (s, 1H, -C*H*(OTMS)C(CH_3)=CH-), 3.68 (s, 3H, -OCH_3), 2.83 (dd, J = 7, J' = 4 Hz, 1H, -C(CH_3)$_2$C*H*CH_2-), 2.50 (ddd, J = 16.5, J' = 7, J'' = 5 Hz, 1H, -CHC*H*HCH=C(CH_3)-), 2.19 (d, J = 17 Hz, 1H, -C*H*HCO-), 2.08 (d, J = 17 Hz, 1H, -CH*H*CO-), 2.0 (ddd, J = 16.5, J' = 6, J'' = 4 Hz, 1H, -CHCH*H*CH=C(CH_3)-), 1.70 (br s, 3H, -CHCH_2CH=C(CH_3)-), 1.05 (s, 3H, -CH_3), 0.93 (s, 3H, -CH_3), and 0.08 (s, 9H, -OSi(CH_3)$_3$); ^{13}C nmr DEPT (100.6 MHz, $CDCl_3$) δ: 212.1 (s), 170.1 (s), 136.7 (s), 124.8 (d), 72.9 (d), 68.2 (s), 52.9 (t), 52.3 (q), 47.4 (d), 36.4 (s), 30.4 (q), 25.2 (q), 22.6 (t), 21.0 (q), and 0.25 (q); ms, M^+: 324.1753 (calcd. for $C_{17}H_{28}O_4Si$: 324.1757).

Compound ***24a****:* ir ($CHCl_3$ cast): 1753 (ester), 1726 (ketone), and 1251 (Si-CH_3) cm^{-1}; ^1H nmr (400 MHz, $CDCl_3$) δ: 5.66 (ddd, J = 6, J' = 5, J'' = 1.5 Hz, 1H, -CH(OTMS)C(CH_3)=C*H*-), 4.72 (s, 1H, -C*H*(OTMS)C(CH_3)=CH-), 3.68 (s, 3H, -OCH_3), 2.70 (dd, J = J' = 8 Hz, 1H, -C(CH_3)$_2$C*H*CH_2-), 2.30 (d, J = 16 Hz, 1H, -C*H*HCO-), 2.35–2.25 (complex, 1H, -CHC*H*HCH=C(CH_3)-), 2.14 (multiplet, 2H, -CH*H*CO-, -CHCH*H*CH=C(CH_3)-), 1.79 (d,

Can. J. Chem. Downloaded from www.nrcresearchpress.com by 217.78.4.112 on 09/08/12
For personal use only.

J = 1.5 Hz, 3H, -CHCH$_2$CH=C(CH_3)-), 1.39 (s, 3H, -CH_3), 1.20 (s, 3H, -CH_3), and 0.18 (s, 9H, -OSi(CH_3)$_3$); ^{13}C nmr APT (100.6 MHz, $CDCl_3$) δ: 211.9 (p), 171.7 (p), 136.7 (p), 125.4 (a), 70.3 (a), 67.7 (p), 54.6 (p), 52.5 (a), 47.9 (a), 35.7 (p), 31.5 (a), 24.1 (a), 22.4 (p), 21.5 (a), and 0.17 (a); ms, M^+: 324.1750 (calcd. for $C_{17}H_{28}O_4Si$: 324.1757).

*7-[*tert*-Butyldimethylsilyloxy] 7aα-carbomethoxy-2,2,3aα,4,7,7a-hexahydro-3,3,6-trimethylinden-1-ones (**23**b and **24**b):* ir ($CHCl_3$ cast): 1750 (ester), 1732 (ketone), and 1250 (Si-CH$_3$) cm^{-1}; ^{1}H nmr (400 MHz, $CDCl_3$) δ: 5.83 (br s, 1H, =C*H*), 4.78 (s, $\frac{1}{2}$ H, -C*H*O-), 4.68 (s, $\frac{1}{2}$ H, -C*H*O-), 3.82 (s, $\frac{3}{2}$ H, -OCH_3), 3.74 (s, $\frac{3}{2}$ H, -OCH_3), 3.25 (br d, J = 8 Hz, $\frac{1}{2}$ H, -C*H*CH$_2$-), 2.72 (dd, J = 8, J' = 3 Hz, $\frac{1}{2}$ H, -C*H*CH$_2$-), 2.65 (complex m, $\frac{1}{2}$ H), 2.50 (d, J = 16 Hz, $\frac{1}{2}$ H), 2.45 (complex m, $\frac{1}{2}$ H), 0.34 (d, J = 16 Hz, $\frac{1}{2}$ H), 2.30–2.05 (complex, 2H), 1.90 (s, $\frac{3}{2}$ H, -C(CH_3)=), 1.79 (s, $\frac{3}{2}$ H, -C(CH_3)=), 1.25 (s, $\frac{3}{2}$ H, -CH_3), 1.20 (s, $\frac{3}{2}$ H, -CH_3), 1.12 (s, $\frac{3}{2}$ H, -CH_3), 1.10 (s, $\frac{3}{2}$ H, -CH_3), 0.88 (s, $\frac{9}{2}$ H, -SiC(CH_3)$_3$), 0.86 (s, $\frac{9}{2}$ H, -SiC(CH_3)$_3$), 0.14 (s, $\frac{3}{2}$ H, -SiCH_3), 0.12 (s, $\frac{3}{2}$ H, -SiCH_3), 0.08 (s, $\frac{3}{2}$ H, -SiCH_3), and 0.05 (s, $\frac{3}{2}$ H, -SiCH_3); ms, M^+: 366.2223 (calcd. for $C_{20}H_{34}O_4Si$: 366.2226).

*5-[*tert*-Butyldimethylsilyloxyl]-7aα-carbomethoxy-2,3,3aα,4,7,7a-hexahydro-3,3,6-trimethylinden-1-one (**27**):* ir ($CHCl_3$ cast): 1753 (ester), 1732 (ketone), and 1190 (Si-CH$_3$) cm^{-1}; ^{1}H nmr (400 MHz, $CDCl_3$) δ: 3.70 (s, 3H, -OCH_3), 2.87 (d, J = 8.5 Hz, 1H, -C*H*CH$_2$C(OTBDMS)=), 2.76 (dd, J = 16.5, J' = 1.5 Hz, 1H, -C*H*HC(CH$_3$)=), 2.41 (d, J = 18 Hz, 1H, -C*H*HCO-), 2.34 (d, J = 18 Hz, 1H, -CH*H*CO-), 2.26 (ddd, J = 18, J' = 8.5, J'' = 1.5 Hz, 1H, -CHC*H*HC(OTBDMS)=), 2.11 (d, J = 16.5 Hz, 1H, -C*H*HC(CH$_3$)=), 2.03 (d, J = 18 Hz, 1H, -CHCH*H*C-(OTBDMS)=), 1.60 (s, 3H, -CH$_2$C(CH_3)=), 1.20 (s, 3H, -C(CH_3)$_2$), 0.90 (complex, 12H, -C(CH_3)$_2$, -SiC(CH_3)$_3$), 0.16 and 0.14 (both s, 3H each, -Si(CH_3)$_2$); ^{13}C nmr APT (100.6 MHz, $CDCl_3$) δ: 213.5 (p), 172.1 (p), 141.8 (p), 107.9 (p), 58.7 (p), 52.9 (p), 52.7 (a), 48.2 (a), 36.8 (p), 32.8 (p), 30.2 (a), 25.9 (p), 25.8 (a), 25.6 (a), 23.7 (p), 18.1 (a), 16.1 (p), −3.80 (a), and −4.00 (a); ms, M^+: 366.2227 (calcd. for $C_{20}H_{34}O_4Si$: 366.2227).

*5-[*tert*-Butyldimethylsilyloxy]-7aα-carbomethoxy-7α-ethoxy-2,3,3aα,4,7,7a-hexahydro-3,3,6-trimethylinden-1-one (**30**) and 5-[*tert*-butyldimethylsilyloxy]-7aα-carbomethoxy-7β-ethoxy-2,3,3aα,4,7,7a-hexahydro-3,3,6-trimethylinden-1-one (**31**)*

*Adduct **30**:* ir ($CHCl_3$ cast): 1753 (ester), 1728 (ketone), 1679 (C=C), and 1253 (Si-CH$_3$) cm^{-1}; ^{1}H nmr (400 MHz, $CDCl_3$) δ: 4.49 (br s, 1H, -C*H*(OEt)-), 3.65 (s, 3H, -OCH_3), 3.46 (q, J = 7 Hz, 1H, -OC*H*HCH$_3$), 3.35 (q, J = 7 Hz, 1H, -OCH*H*CH$_3$), 2.91 (dd, J = J' = 8 Hz, 1H, -C*H*CH$_2$C(OTBDMS)=), 2.46 (ddq, J = 15, J' = 8, J'' = 1.5 Hz, 1H, -CHC*H*HC(OTBDMS)=), 2.43 (d, J = 17 Hz, 1H, -C*H*HCO-), 2.25 (d, J = 17 Hz, 1H, -CH*H*CO-), 2.08 (dd, J = 15, J' = 8 Hz, 1H, -CHCH*H*C-(OTBDMS)=), 1.71 (d, J = 1.5 Hz, 3H, -CHC(CH_3)=), 1.05 (dd, J = J' = 7 Hz, 3H, -OCH$_2$CH_3), 0.96 (s, 9H, -OSiC(CH_3)$_3$), 0.90 (s, 3H, -CH_3), 0.86 (s, 3H, -CH_3), 0.12 (s, 3H, -Si(CH_3)$_2$), and 0.11 (s, 3H, -Si(CH_3)$_2$); ^{13}C nmr APT (100.6 MHz, $CDCl_3$) δ: 211.1 (p), 171.1 (p), 149.0 (p), 112.2 (p), 80.0 (a), 67.2 (p), 65.2 (p), 54.5 (p), 52.6 (a), 49.0 (a), 35.4 (p), 31.4 (a), 28.5 (p), 26.2 (a), 25.7 (a), 23.9 (a), 18.1 (p), 15.9 (a), 15.3 (a), −3.84 (a), and −3.95 (a); ms (CI), $(M + H)^+$: 411 (calcd. for $C_{22}H_{38}O_5Si$: 411). Anal. calcd. for $C_{22}H_{38}O_5Si$: C 64.35, H 9.33%; found: C 64.10, H 9.50%.

*Adduct **31**:* ir ($CHCl_3$ cast): 1755 (ester), 1732 (ketone), 1679 (C=C), and 1229 (Si–CH$_3$) cm^{-1}; ^{1}H nmr (400 MHz, $CDCl_3$) δ: 4.35 (s, 1H, -C*H*(OEt)-), 3.68 (s, 3H, -OCH_3), 3.42 (q, J = 7 Hz, 2H, -OCH_2CH$_3$), 3.16 (dd, J = 7.5, J' = 1.5 Hz, 1H, -C*H*CH$_2$C(OTBDMS)=), 2.71 (ddq, J = 16.5, J' = 7.5, J'' = 2 Hz, 1H, -CHC*H*HC(OTBDMS)=), 2.16 (d, J = 17 Hz, 1H, -C*H*HCO-), 2.07 (d, J = 17 Hz, 1H, -CH*H*CO-), 2.05 (dd, J = 16.5, J' = 1.5 Hz, 1H, -CHCH*H*C(OTBDMS)=), 1.63 (d, J = 2 Hz, 3H, -CH(OEt)C(CH_3)=), 1.09 (t, J = 7 Hz, 3H, -OCH$_2$CH_3), 0.98 (s, 3H, -CH_3), 0.95 (s, 12H, -OSiC(CH_3)$_3$, -CH_3), 0.14 (s, 3H, -Si(CH_3)$_2$), and 0.13 (s, 3H, -Si(CH_3)$_2$); ^{13}C nmr APT (100.6 MHz, $CDCl_3$) δ: 210.2 (p), 169.4 (p), 149.9 (p), 110.7 (p), 81.5 (a), 67.7 (p), 64.4 (p), 53.0 (p), 52.6 (a), 46.0 (a), 36.7(p), 30.5 (a), 29.0 (p), 25.6 (a), 24.7 (a), 18.0 (p), 16.2 (a), 15.3 (a), −3.7 (a), and −4.1 (a).

*7aα-Carbomethoxy-3,3aα,7,7a-tetrahydro-3,3,5-trimethyl-2*H*-indene-1,6-dione (**13**)*

Oxygen was passed for 10 min through a dichloromethane (0.5 mL) solution of keto ester **11** (25 mg, 0.10 mmol), dry pyridine (15 μl, 0.18 mmol), acetic anhydride (20 μL, 0.21 mmol), a catalytic quantity of 4-(dimethylamino)pyridine (~5 mg), and a catalytic quantity of 5,10,15,20-tetraphenyl-21*H*,23*H*-porphine (~5 mg). The solution was irradiated with a tungsten lamp (200 W) for 10 h while oxygen was continuously passed through the solution. The reaction was quenched with saturated aqueous sodium bicarbonate solution (1 mL) and the aqueous layer was extracted with dichloromethane (3 × 2 mL). The organic extracts were combined and washed with aqueous 10% hydrochloride acid (3 × 2 mL), saturated aqueous copper(II) sulfate (1 × 2 mL) and brine (1 × 2 mL), dried ($MgSO_4$), filtered, and concentrated. Purification by flash chromatography on silica gel eluting with 0–10% ether in petroleum ether gave recovered keto ester **11** (5 mg, 20%). Further elution gave diketone **13** as a colorless oil (9 mg, 0.036 mmol, 41% yield): ir ($CHCl_3$ cast): 1753 (ester), 1732 (ketone), and 1679 (enone) cm^{-1}; ^{1}H nmr (400 MHz, $CDCl_3$) δ: 6.58 (dq, J = 5, J' = 2 Hz, 1H, -CHC*H*=C(CH$_3$)CO-), 3.72 (s, 3H, -OCH_3), 3.31 (dq, J = 5, J' = 1.5 Hz, 1H, -C*H*CH=C(CH$_3$)CO-), 3.14 (d, J = 17 Hz, 1H, -C*H*HCOC(CH$_3$)=), 2.69 (d, J = 17 Hz, 1H, -CH*H*COC(CH$_3$)=), 2.46 (d, J = 11 Hz, 1H, -C*H*HCO-), 2.42 (d, J = 11 Hz, 1H, -CH*H*CO-), 1.85 (dd, J = 2, J' = 1.5 Hz, 3H, -CHCH=C(CH_3)CO-), 1.40 (s, 3H, -CH_3), and 1.05 (s, 3H, -CH_3); ^{13}C nmr APT (100.6 MHz, $CDCl_3$) δ: 211.0 (p), 194.4 (p), 171.8 (p), 139.1 (a), 136.3 (p), 63.7 (p), 55.1 (p), 53.3 (a), 51.4 (a), 38.5 (p), 38.4 (p), 28.6 (a), 25.2 (a), and 16.3 (a); ms, M^+: 250.1204 (calcd. for $C_{14}H_{18}O_4$: 250.1205).

*3,3,6-Trimethyl-2,3-dihydroinden-1-one (**25**)*

Compound **23***a* (24 mg, 0.074 mmol) was dissolved in 2,4,6-collidine under argon atmosphere. Anhydrous lithium iodide (40 mg, 5 equiv.) was added followed by water (14 μL, 10 equiv.). The mixture was refluxed for 4 h, cooled down, and poured into aqueous 5% hydrochloric acid (2 mL). The aqueous layer was extracted with ether (3 × 2 mL). The organic layer was washed with aqueous 5% hydrochloric acid (2 × 2 mL), water (1 × 2 mL), and brine (1 × 2 mL), dried ($MgSO_4$), filtered, and concentrated. Purification by flash chromatography on silica gel (0–3% ether in petroleum ether) gave pure compound **25** (7 mg, 54%): ir ($CHCl_3$ cast): 1736 (ketone) and 825 (aromatic) cm^{-1}; ^{1}H nmr (400 MHz, $CDCl_3$) δ: 7.50 (br s, 1H, C-7 H), 7.44 (dd, J = 8, J' = 1 Hz, 1H, C-5 H), 7.38 (d, J = 8 Hz, C-4 H), 2.60 (s, 2H, -CH_2CO-), 2.40 (s, 3H, C-6-CH_3), 1.40 (s, 6H, -C(CH_3)$_2$); ms, M^+: 174.1043 (calcd. for $C_{12}H_{14}O$: 174.1042).

*7aα-Carbomethoxy-2,3,3aα,4,7,7a-hexahydro-3,3,6-trimethylindene-1,5-diones (**28**)*

Silyl enol ether **27** (50 mg, 0.14 mmol) was hydrolyzed in tetrahydrofuran (2 mL) with aqueous 0.1 N hydrochloric acid (1 mL). The solution was stirred at room temperature for 24 h. Water (2 mL) was added and the aqueous layer was extracted with ether (3 × 2 mL). The combined organic extracts were washed with water (2 × 2 mL) and brine (1 × 1 mL), dried ($MgSO_4$), filtered, and concentrated. Purification of the resulting oil by flash chromatography on silica gel (0–5% ether in petroleum ether) gave the epimeric mixture **28** (3.8:1) as a colorless oil (29 mg, 0.11 mmol, 78%): ir ($CHCl_3$ cast): 1751 (ester), 1716 (ketone) cm^{-1}; ^{1}H nmr (400 MHz, $CDCl_3$), major isomer, δ: 3.77 (s, 3H, -OCH_3), 3.16 (ddd, J = 7.5, J' = 5, J'' = 1 Hz, 1H), 2.75–2.30 (complex, 4H), 1.61 (dd, J = J' = 9 Hz, 1H), 1.35 (dd, J = 6, J' = 1 Hz, 2H), 1.18 (s, 3H, -CH_3), 1.03 (d, J = 6 Hz, 3H, -CH_3), and 0.95 (s,

3H, -CH_3); minor isomer, δ: 3.72 (s, 3H, -OCH_3), 3.09 (dd, J = 7.5, J' = 5.5 Hz, 1H), 1.96 (dd, J = 12, J' = 9 Hz, 1H), 1.15 (s, 3H, -CH_3), 1.04 (d, J = 6 Hz, 3H, -CH_3), and 0.91 (s, 3H, -CH_3), other peaks were overlapped with those of the major isomer; ^{13}C nmr APT (100.6 MHz, $CDCl_3$), major isomer, δ: 211.9 (p), 211.5 (p), 171.5 (p), 59.1 (p), 53.3 (p), 53.1 (a), 50.7 (a), 40.6 (a), 37.2 (p), 37.0 (p), 34.8 (p), 29.3 (a), 24.5 (a), and 14.4 (a); minor isomer, δ: 212.8 (p), 211.2 (p), 172.2 (p), 63.7 (p), 59.9 (p), 51.9 (p), 48.9 (a), 40.2 (a), 38.5 (p), 36.2 (p), 30.2 (a), 24.9 (a), 17.7 (a), and 15.3 (a); ms, M^+: 252.1359 (calcd. for $C_{14}H_{20}O_4$: 252.1356).

*7aα-Carbomethoxy-3,3,aα,4,7a-tetrahydro-3,3,6-trimethyl-2*H-*indene-1,5-dione (**14**)*

A mixture of silyl enol ethers **30** and **31** (115 mg, 0.28 mmol) was hydrolyzed in tetrahydrofuran (THF, 2 mL) with aqueous 0.1 N hydrochloric acid (1 mL). The solution was stirred at room temperature for 24 h before water (2 mL) was added. The aqueous layer was extracted with ether (3 × 2 mL). The combined organic extracts were washed with water (2 × 2 mL) and brine (1 × 1 mL), dried ($MgSO_4$), filtered, and concentrated. Purification of the resulting oil by flash chromatography on silica gel (0–10% ether in petroleum ether) gave compound **14** as a colorless oil (50 mg, 0.20 mmol, 70%): ir ($CHCl_3$ cast): 1756 (ester), 1727 (ketone), and 1679 (enone) cm^{-1}; ^{1}H nmr (400 MHz, $CDCl_3$) δ: 6.69 (dq, J = J' = 1 Hz, 1H, -CH=C(CH_3)CO-), 3.77 (s, 3H, -OCH_3), 3.17 (ddd, J = J' = 5, J'' = 1 Hz, 1H, -CHCH_2CO-), 2.67 (d, J = 5 Hz, 2H, -CHCH_2CO-), 2.50 (d, J = 17 Hz, 1H, -CHHCO-), 2.29 (d, J = 17 Hz, 1H, -CHHCO-), 1.83 (s, J = 1 Hz, 3H, -CH=C(CH_3)CO-), 1.24 (s, 3H, -CH_3), and 0.79 (s, 3H, -CH_3); ^{13}C nmr DEPT (100.6 MHz, $CDCl_3$) δ: 209.0 (s), 196.3 (s), 169.5 (s), 138.8 (d), 136.9 (s), 60.7 (s), 53.7 (t), 53.4 (q), 48.2 (d), 37.6 (t), 33.9 (t), 27.6 (q), 23.5 (q), and 16.0 (q); ms, M^+: 250.1200 (calcd. for $C_{14}H_{18}O_4$: 250.1205). Anal. calcd. for $C_{14}H_{18}O_4$: C 67.17, H 7.25%; found: C 67.04, H 7.16%.

Acknowledgements

We are grateful to the Natural Sciences and Engineering Research Council of Canada and the University of Alberta for financial support.

1. R. Kazlauskas, P. T. Murphy, and R. J. Wells. Tetrahedron Lett. 4949 (1978).
2. H. J. Liu and E. N. C. Browne. Can. J. Chem. **65**, 1262 (1987).
3. H. J. Liu, E. N. C. Browne, and S. Y. Chew. Can. J. Chem. **66**, 2345 (1988).
4. H. J. Liu, T. K. Ngooi, and E. N. C. Browne. Can. J. Chem. **66**, 3143 (1988).
5. H. J. Liu, S. Y. Chew, and E. N. C. Browne. Tetrahedron Lett. **32**, 2005 (1991).
6. L. Minuti, L. Radics, A. Tatacchi, L. Venturini, and E. Wenkert. J. Org. Chem. **55**, 4261 (1990).
7. D. Caine, C. R. Harrison, and D. G. VanDerveer. Tetrahedron Lett. **24**, 1353 (1983).
8. H. J. Liu, E. N. C. Browne, and P. R. Pednekar. Can. J. Chem. **60**, 921 (1982).
9. T. R. Hoye, A. J. Caruso, and A. S. Magee. J. Org. Chem. **47**, 4152 (1982).
10. E. Dane and K. Elder. Ann. Chem. **539**, 207 (1939).
11. R. Granger, P. F. G. Nau, and C. Francois. Bull. Soc. Chim. Fr. 1902 (1962).
12. A. Ichihara, R. Kimura, K. Moriyasu, and S. Sakamura. Tetrahedron Lett. 4331 (1977).
13. F. Fringuelli, F. Pizzo, A. Taticchi, T. D. J. Halls, and E. Wenkert. J. Org. Chem. **47**, 5056 (1982).
14. F. Fringuelli, F. Pizzo, A. Taticchi, and E. Wenkert. J. Am. Chem. Soc. **48**, 2802 (1983).
15. S. M. Weinreb and J. Auerbach. J. Am. Chem. Soc. **97**, 2503 (1975).
16. R. W. Holder, J. P. Daub, W. E. Baker, R. H. Gilbert, and N. A. Graf. J. Org. Chem. **47**, 1445 (1982).
17. D. Pauley, F. Anderson, and T. Hudlicky. Org. Synth. **67**, 121 (1989).
18. R. G. Salomon and S. Ghosh. Org. Synth. **62**, 125 (1984).
19. W. F. Berkowitz and S. C. Grenetz. J. Org. Chem. **41**, 10 (1976).
20. K. Cooper and G. Pattenden. J. Chem. Soc. Perkin Trans. 1, 799 (1984).
21. J. Froborg and G. Magnusson. J. Am. Chem. Soc. **100**, 6728 (1978).
22. M. Rosenberger, P. Yates, J. B. Hendrickson, and W. Wolf. Tetrahedron Lett. 2285 (1964).
23. J. de P. Teresa, A. F. Mateos, and R. R. Gonzales. Tetrahedron Lett. **23**, 3405 (1982).
24. R. L. Funk and M. M. Abelman. J. Org. Chem. **51**, 3247 (1986).
25. D. Liotta, C. Barnum, R. Puleo, G. Zima, C. Bayer, and H. S. Kezar. J. Org. Soc. **46**, 2920 (1981).
26. K. B. Sharpless, R. F. Lauer, and P. Y. Teranishi. J. Am. Chem. Soc. **95**, 6137 (1973).
27. A. I. Meyers and C. A. Busacca. Tetrahedron Lett. **30**, 6977 (1989).
28. E. D. Mihelich and D. J. Eickhoff. J. Org. Chem. **48**, 4135 (1983).
29. K. Krohn, K. Tolkiehn, V. Lehne, H. W. Schmalle, and H. F. Grützmacher. Liebigs Ann. Chem. 1311 (1985).
30. F. Elsinger. Org. Synth. **45**, 7 (1965).
31. R. E. Ireland and W. J. Thompson. J. Org. Chem. **44**, 3041 (1979).
32. J. Lin, M. M. Nikaido, and G. Clark. J. Org. Chem. **52**, 3745 (1987).

Can. J. Chem. Downloaded from www.nrcresearchpress.com by 217.78.4.112 on 09/08/12
For personal use only.

Enantioselective synthesis of 1-substituted tetrahydroisoquinoline-1-carboxylic acids

ZBIGNIEW CZARNOCKI
Department of Chemistry, University of Warsaw, ul. L. Pasteura 1, 01-093 Warsaw, Poland

DENNIS SUH AND DAVID B. MACLEAN[1]
Department of Chemistry, McMaster University, Hamilton, Ont., Canada L8S 4M1

AND

PHILIP G. HULTIN AND WALTER A. SZAREK[1]
Department of Chemistry, Queen's University, Kingston, Ont., Canada K7L 3N6

Received September 11, 1991

This paper is dedicated to Professor Zdenek (Denny) Valenta on the occasion of his 65th birthday

ZBIGNIEW CZARNOCKI, DENNIS SUH, DAVID B. MACLEAN, PHILIP G. HULTIN, and WALTER A. SZAREK. Can. J. Chem. **70**, 1555 (1992).

The 3,4-dihydroisoquinolinium salt **1** and its enantiomer have been converted readily and stereoselectively into (+)- and (−)-1,2,3,4-tetrahydro-6,7-dimethoxy-1-methylisoquinoline-1-carboxylic acids. The synthetic route described should be applicable to the enantioselective synthesis of a variety of 1-alkyl- or 1-aryl-1,2,3,4-tetrahydroisoquinoline-1-carboxylic acids. The absolute configuration of the amino acid hydrochloride **11** was established to be as depicted in Scheme 2.

ZBIGNIEW CZARNOCKI, DENNIS SUH, DAVID B. MACLEAN, PHILIP G. HULTIN et WALTER A. SZAREK. Can. J. Chem. **70**, 1555 (1992).

Le sel de 3,4-dihydroisoquinoléinium (**1**) et son énantiomère ont pu facilement et stéréosélectivement être transformés en acides (+)- et (−)-1,2,3,4-tétrahydro-6,7-diméthoxy-1-méthylisoquinoléine-1-carboxyliques. La voie de synthèse décrite devrait être applicable à la synthèse énantiosélective d'une variété d'acides 1-alkyl- ou 1-aryl-1,2,3,4-tétrahydroisoquinoléine-1-carboxyliques. On a pu déterminé que la configuration absolue du chlorhydrate de l'acide aminé **11** est celle décrite dans le schéma 2.

[Traduit par la rédaction]

Can. J. Chem. Downloaded from www.nrcresearchpress.com by 217.78.4.112 on 09/08/12
For personal use only.

Tetrahydroisoquinolines in which C-1 is a quaternary centre have been found in nature, and include a number of cactus alkaloids (1), several mammalian alkaloids (2), and the spirobenzylisoquinoline alkaloids (3). Brossi and coworkers (4) have prepared enantiomeric 1-alkyltetrahydroisoquinoline-1-carboxylic acids by resolution of racemic mixtures. Here we describe an enantioselective synthesis of (+)- and (−)-tetrahydro-6,7-dimethoxy-1-methylisoquinoline-1-carboxylic acids; the work is to our knowledge the first report of the enantioselective synthesis of this class of compounds.

Dörnyei and Szántay (5) reported the preparation of **1** and showed that it undergoes stereoselective reduction with hydrides, or with hydrogen in the presence of a catalyst, to the corresponding tetrahydroisoquinoline **2**. We employed the enantiomer of **2** in the enantioselective synthesis of a number of tetrahydroisoquinoline alkaloids having the (*S*) configuration at C-1 of the tetrahydroisoquinoline system (6). Here we show that **1** and its enantiomer may be converted readily and stereoselectively into (+)- and (−)-tetrahydro-6,7-dimethoxy-1-methylisoquinoline-1-carboxylic acids.

The synthesis of the target amino acids from **1** or its enantiomer requires alkylation at C-1 followed by transformation of the three-carbon side chain at C-1 into a carboxylic acid group. In the first approach to the synthesis we proceeded through the nitrone **3** (Scheme 1). A variety of methods were investigated for the conversion of **1** into **3**. The most satisfactory method proved to be an oxidation using hydrogen peroxide in the presence of sodium tungstate. This procedure was originally used for epoxidation of α,β-unsaturated acids (7). Organic peroxy acids have been used also to convert imines into a mixture of nitrones and oxaziranes (8), and a mixture of hydrogen peroxide and sodium tungstate has been used to convert primary amines into oximes (9). In our case, the conversion of imine **1** into nitrone **3** proceeded in 87% yield. The nitrone was characterized through its spectroscopic properties.

Alkylation of **3** was accomplished by treatment with a large excess of methyllithium, a reaction that afforded hydroxylamine **4** in 40% yield. Addition of methyllithium to the carbon–nitrogen double bond was accompanied by alkylation at the ester function to afford a tertiary alcohol. The structure of **4** was deduced from its ^{1}H and ^{13}C nmr spectra. The ^{1}H nmr spectrum had three singlets corresponding to C-Me groups, two singlets attributed to OMe groups, two signals attributed to adjacent CHOH groups, two signals corresponding to aromatic protons, and signals corresponding to the four protons associated with C-3 and C-4 of the tetrahydroisoquinoline system. The signals were assigned through the use of nuclear Overhauser enhancement (nOe) difference spectra and through $^{1}H,^{13}C$ chemical-shift correlation experiments. The nOe experiments showed that irradiation of the C-Me signal at δ 1.59 enhanced the signals at 6.44 and 4.25, whereas irradiation of the C-Me signal at δ 1.13 enhanced the signals at 2.95 and 4.25. On this basis the signal at 1.59 was assigned to the methyl group at C-1 and that at 1.13 to one of the two methyl groups at C-3′. It follows that the signals at δ 2.95, 4.25, and 6.44 may be assigned to H-2′, H-1′, and H-8, respectively. Using these data and the information derived from the $^{1}H,^{13}C$ chemical-shift correlation experiments it was possible to assign virtually all signals in the ^{1}H and ^{13}C nmr spectra of **4**.

[1]Authors to whom correspondence may be addressed.

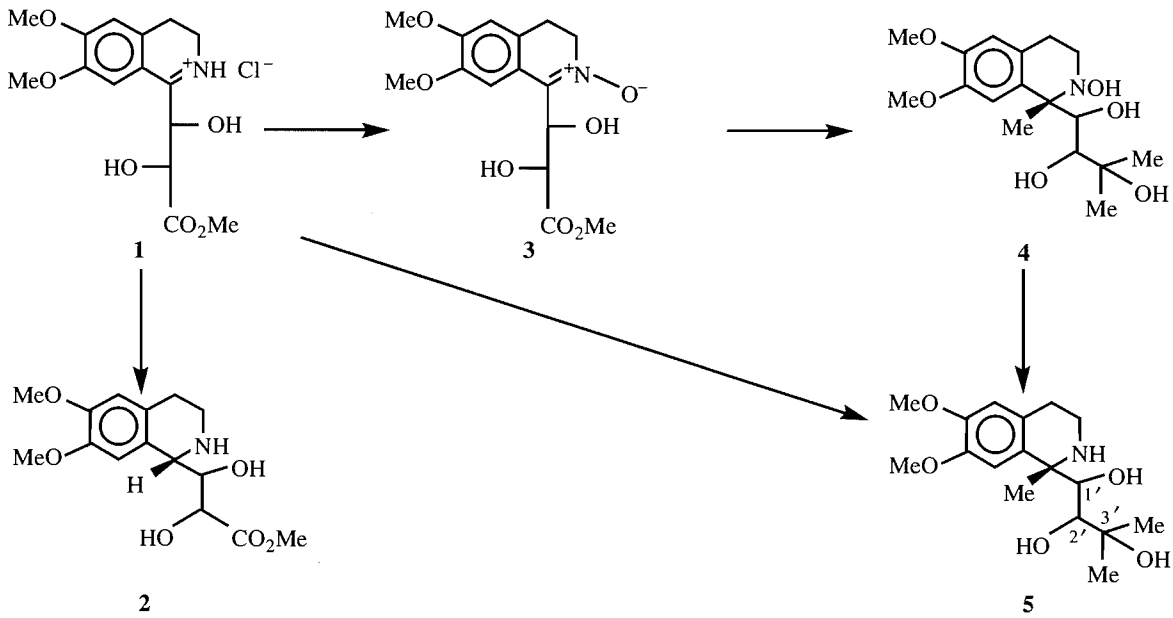

SCHEME 1

The oxidation of **4** with lead tetraacetate afforded an aldehyde in low yield (13%) as an unstable oil that decomposed rapidly at room temperature. Reduction of **4** with hydrogen over Adams' catalyst converted it in high yield into the secondary amine **5**, a stable compound, which appeared to be a suitable intermediate for elaboration to the target molecule. Thus, an alternative route to **5** was investigated in the hope that the compound might be obtained in higher overall yield.

It was found that **1** upon treatment with an excess of methyllithium afforded **5** in 80% yield. This procedure provided a convenient route to **5** and established that the addition of methyllithium to the nitrone and to the imine proceeded in the same stereochemical sense; however, it was not possible at this stage to establish the configuration at C-1 of **4** or **5**.

The signals of the ^{1}H and ^{13}C nmr spectra of **5** were assigned in a manner similar to that used for **4** through application of nOe difference spectra and $^{1}H,^{13}C$ chemical-shift correlation experiments. Irradiation of the C-Me signal at δ 1.55 enhanced the signals at δ 3.01, 4.07, and 6.45 whereas irradiation of the C-Me signal at δ 1.08 enhanced the signal at 2.98. Also, irradiation at δ 2.55 enhanced the signals at 6.57 and 3.01. Thus, the nOe experiments enabled the signals at δ 1.08, 1.55, 2.55, 2.98, 3.01, 4.07, 6.45, and 6.57 to be assigned, respectively, to a C-Me at C-3′, the C-Me at C-1, an H at C-4, H-2′, a hydrogen at C-3 or C-4, H-1′, H-8, and H-5. These data, together with $^{1}H,^{13}C$ chemical-shift correlation experiments, enabled us to assign the majority of signals in the ^{1}H and ^{13}C spectra of **5**. With the structure of **5** secure it now remained to oxidize the side chain at C-1 to a carboxylic acid (Scheme 2).

The oxidation of the side chain was effected with sodium periodate. When the starting material had been consumed a large excess of sodium borohydride was added to the reaction mixture in order to reduce the aldehyde formed in the oxidation step to a primary alcohol. Upon completion of the reduction reaction the alcohol **6** was isolated in 76% yield from the reaction mixture. Its spectroscopic properties were in agreement with the assigned structure.

The amino alcohol **6** was converted into its 2-ethoxycarbonyl derivative **7** by treatment of **6** with sodium hydroxide and ethyl chloroformate under carefully controlled conditions in a two-phase system. If the reaction time were extended beyond the optimum, compound **7** was slowly converted into the 3*H*-oxazolo[4,3-*a*]isoquinolin-3-one **8**; compound **8** was the major product when the reaction period was 2 h. Also, compound **8** was obtained when methyl chloroformate was substituted for ethyl chloroformate, under the conditions used to prepare **7**.

The oxidation of the primary alcohol group of **7** was now examined. Treatment of **7** with Jones' reagent or with a variety of other common oxidizing agents afforded the aldehyde **9**, which was seemingly impervious to further oxidation. Eventually it was found that oxidation to the carboxylic acid **10** could be effected by treatment of **7** with ruthenium dioxide and sodium periodate (10). Compound **7** was converted, first, into **9** and then much more slowly into **10**. The final step in the synthesis, the hydrolysis of the ethoxycarbonyl group, was effected with aqueous ethanolic hydrochloric acid. The overall yield in the five steps from **1** to **11** was 35%. The spectroscopic properties of compounds **6**–**11** were in accord with the assigned structures.

The absolute configuration of the amino acid **11** was established in the following manner. Brossi and co-workers (4) performed a resolution of racemic salsoline-1-carboxylic acid (**12**) in the form of its methyl ester **12***a* according to the sequence outlined in Scheme 3. The critical step, the separation of the diastereomers **13** and **14**, was accomplished by chromatography. The diastereomerically pure ureas, **13** and **14**, were converted into the hydantoins, **15** and **16**, respectively, and thence into the amino acid hydrochlorides, **17** and **18**. The (+)-enantiomer **17** as its hydrobromide salt was shown by X-ray diffraction to have the (*S*) configuration (4).

Can. J. Chem. Downloaded from www.nrcresearchpress.com by 217.78.4.112 on 09/08/12
For personal use only.

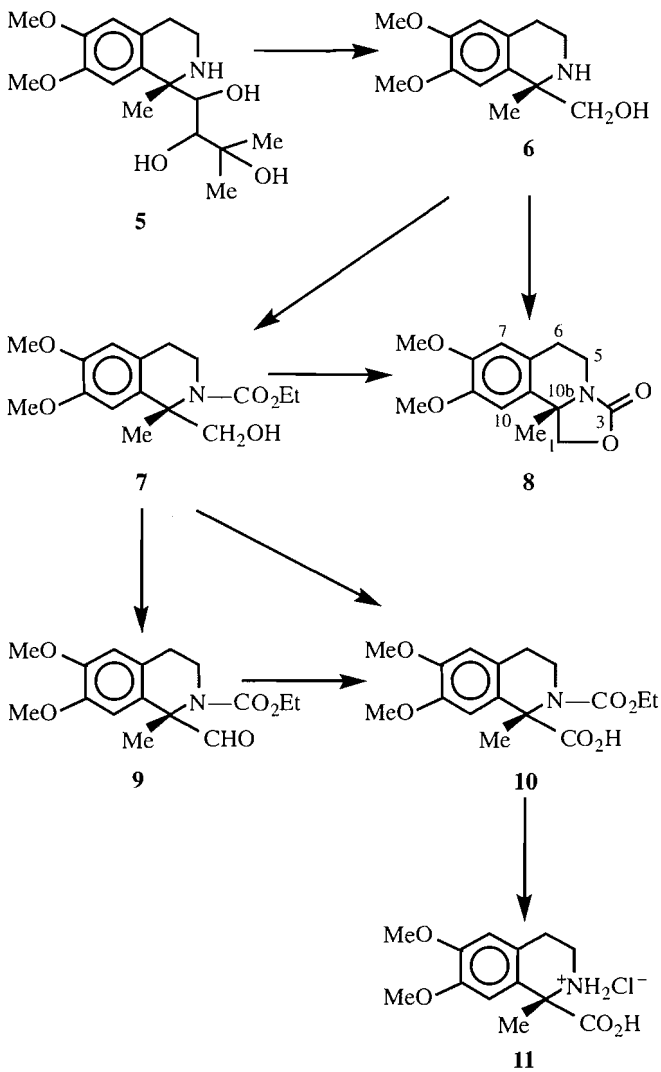

SCHEME 2

It follows, therefore, that the ureas, **13** and **14**, and hydantoins, **15** and **16**, must have the configurations depicted in Scheme 3.

We prepared **13** and **14** by the procedure of Brossi and coworkers (4). Treatment of each isomer with diazomethane afforded the hydantoins, **19** and **20**, respectively. In this reaction the phenolic hydroxyl group was *O*-methylated and, surprisingly, the urea underwent cyclization to the hydantoin. Vigorous hydrolysis of the (*R*,*R*) isomer **20** yielded **22**, the (*R*)-(−)-amino acid hydrochloride. By inference the (+)-enantiomer **21** must have the (*S*) configuration.

In our synthesis the (+)-enantiomer was derived from **1**, which owes its chirality to L-(+)-tartaric acid ((*R*,*R*)-tartaric acid). It is apparent that the methyl group is added from the top face of the molecule to the carbon–nitrogen double bond. The stereoselectivity of the addition reaction may be accounted for if one assumes that the C-1′ oxygen and the imine nitrogen are coordinated with lithium in a five-membered ring. Under these circumstances the bottom face of the molecule is effectively shielded, from attack, by C-2′ and C-3′ and their associated groups (see Fig. 1). The enantiomeric amino acid **22** was obtained through the same reaction sequence using D-(−)-tartaric acid ((*S*,*S*)-tartaric acid) as starting material.

The synthetic route described here should be applicable to the enantioselective synthesis of a variety of 1-alkyl- or 1-aryl-1,2,3,4-tetrahydroisoquinoline-1-carboxylic acids. Further application of the methodology will be reported.

Experimental

The ^{1}H nmr spectra were recorded on a Bruker AM400 or Bruker AM500 spectrometer at 400 or 500 MHz, or a Varian EM390 spectrometer at 90 MHz; $CDCl_3$ was the solvent and tetramethylsilane (TMS) was used as the internal standard, unless otherwise stated. Chemical shifts are reported in ppm (δ) downfield from the signal of TMS. The symbols, s (singlet), d (doublet), t (triplet), q (quartet), m (multiplet), and br (broadened), are used to report the multiplicity and shape of signals. The ^{13}C nmr spectra were recorded at 125.76 MHz on a Bruker AM500 FT spectrometer or at 100.6 MHz on a Bruker AM400 spectrometer at ambient temperature. Nuclear Overhauser enhancement (nOe) difference spectra were obtained by subtraction of the off-resonance control FID from the on-resonance FID. The signal of interest was selectively saturated for 5.0 s and the decoupler was gated off during acquisition. This saturation period also served as the relaxation delay. Either 8 or 16 scans were acquired for each irradiation with the cycle of irradiations repeated 4–10 times. Free induction decays were processed using exponential multiplication (line broadening: 4–5 Hz) before Fourier transformation. Samples were not degassed. EI mass spectra were recorded on a VG Micromass 7070F mass spectrometer at an ionizing voltage of 70 eV or on a VG Analytical ZAB-E mass spectrometer, and CI spectra were recorded using NH_3 at ~1 Torr (1 Torr = 133.3 Pa) as reagent gas; data are given as *m/z* (% relative intensity.) The exact masses were determined under EI conditions for those compounds which gave molecular ions in their EI spectra, and under CI conditions using methane as reagent gas for those compounds which did not have molecular ions in their EI spectra. The high-resolution measurements were performed by peak matching using perfluorokerosene as a reference standard and at a resolution of ~4000.

Melting points were determined using a Gallenkamp or a Fisher–Johns apparatus and are uncorrected. Optical rotations were measured using a Perkin–Elmer 247MC or 241 polarimeter in a 1-mL microcell that is 1 dm in length. Flash chromatography was performed on Kieselgel 60 (230–400 mesh). Preparative high-pressure liquid chromatography (HPLC) was performed using a Waters PrepLC System 500 instrument fitted with a PrepPAK 500 silica column.

The homogeneity of the products was established on the basis of chromatographic and spectroscopic (^{1}H nmr and mass spectral) examination.

Preparation of the nitrone 3

A stirred solution of **1** (5) (7.10 g) in water (25 mL) was cooled to 0°C in an ice–salt bath and treated first with sodium tungstate dihydrate (6.10 g) and then with a saturated aqueous solution of sodium hydrogencarbonate (50 mL). To the resulting mixture hydrogen peroxide (30%, 10 mL) was added over a period of 10 min and the solution stirred for an additional 30 min. The solution was then treated with sodium chloride (10 g) and extracted four times with chloroform. The extract was washed with a saturated aqueous solution of sodium chloride, dried over sodium sulfate, and taken to dryness. The crystalline residue was recrystallized from chloroform–ether to afford **2** (5.83 g, 87%) as colorless crystals; mp 178–180°C (dec.); $[\alpha]_D^{23}$ −150.24 (*c* 8.16, $CHCl_3$); ν_{max}(KBr): 1600, 1615, 1735, 1755 cm^{-1}; ^{1}H nmr (90 MHz) δ: 2.96–3.23 (2H, m, C-4 H's), 3.76 (3H, s, CO_2CH_3), 3.93 and 3.98 (3H each, s, 2 × $ArOCH_3$), 4.03–4.23 (2H, m, C-3 H's), 4.63 (1H, d, J = 3.6 Hz, H-2′), 5.27 (1H, d, J = 3.6 Hz, H-1′), 6.80 and 6.98 (1H each, s, H-5 and H-8), the OH protons appear as a broad signal in the

Can. J. Chem. Downloaded from www.nrcresearchpress.com by 217.78.4.112 on 09/08/12
For personal use only.

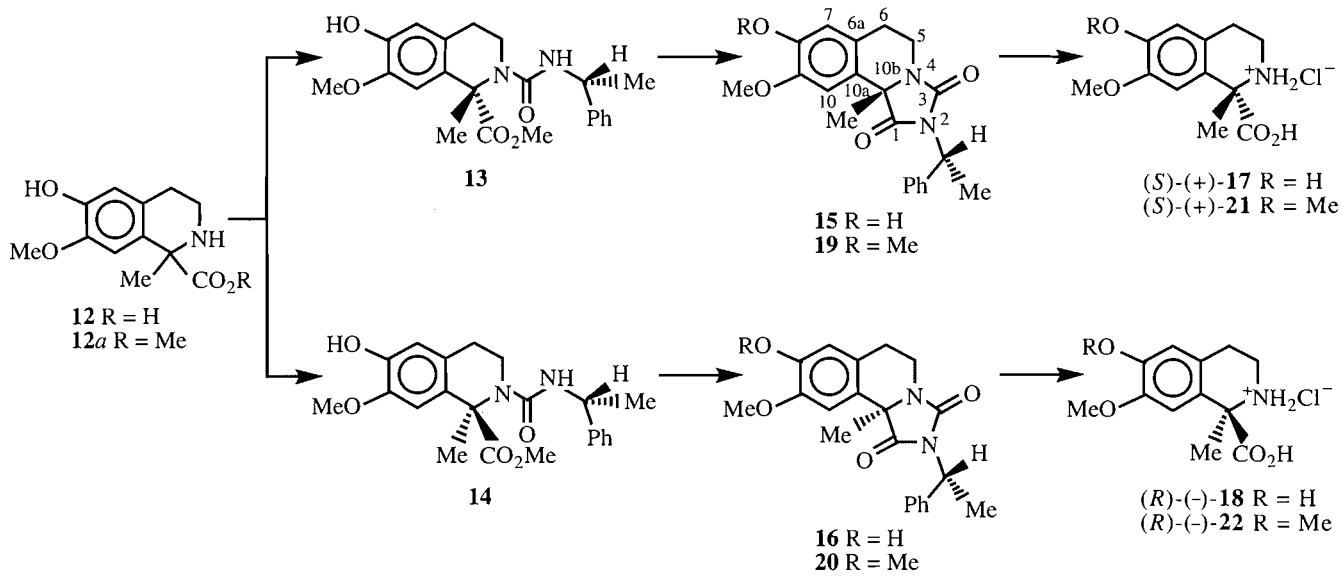

SCHEME 3

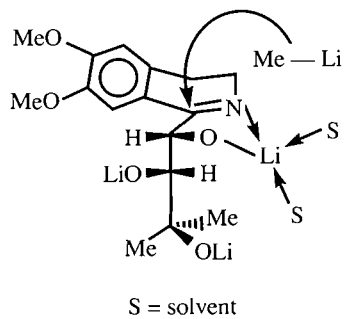

FIG. 1. Rationalization of the stereoselectivity of the addition of methyllithium to **1**.

region 3.5–4.5; ms (EI): 325 (M^+) (10), 308 (10), 248 (11), 236 (100), 219 (82), 204 (14); ms (CI, NH_3): 326 $(M + H)^+$ (95), 308 (37), 292 (10), 276 (15), 220 (100). Exact Mass calcd. for $C_{15}H_{19}NO_7$: 325.1161; found (hrms): 325.1159.

*Treatment of nitrone **3** with methyllithium*

A solution of methyllithium in diethyl ether (1.5 M, 55 mL) was added slowly over a period of 20 min to a stirred solution of **3** (3.00 g) in tetrahydrofuran (100 mL) at −70°C. The mixture was stirred at the same temperature for 40 min, the cooling bath removed, and first methanol (20 mL), and then acetic acid (5 mL), were added slowly. The resulting mixture was evaporated to dryness and a saturated aqueous solution of sodium chloride (30 mL) was added to the residue. The mixture was extracted three times with 30-mL portions of chloroform, and the extract was washed, dried, and evaporated to dryness. Chromatography of the residue on silica (Merck, 230–400 mesh) was effected with chloroform–methanol (98:2, v/v) to afford **4** as a brown oil that crystallized on standing. Recrystallization from a mixture of chloroform – diethyl ether – petroleum ether gave **4** as long needles (40%), mp 158–160°C (dec.); $[\alpha]_D^{25}$ +170.9 (*c* 1.5, $CHCl_3$); ^1H nmr (500 MHz) δ: 1.09 and 1.13 (3H each, s, CH_3's at C-3′), 1.59 (3H, s, CH_3 at C-1), 2.62 (1H, d, J = 15.0 Hz, H-4_{ax}), 2.95 (1H, s, H-2′), 3.08 and 3.12 (2H, m, H-3_{ax}, H-3_{eq}), 3.15 (1H, m, H-4_{eq}), 3.75 and 3.79 (3H each, s, 2 × ArOCH_3), 4.25 (1H, s, H-1′), 6.43 and 6.52 (1H, each, s's, H-8 and H-5, resp.), the OH protons appear as 3 broad signals centered at 3.51, 5.35, and 7.50; ^{13}C nmr ($CDCl_3$) δ: 17.5 (CH_3 at C-1), 24.9 and 27.4 (CH_3's at C-3′), 29.4 (C-4), 48.1 (C-3), 55.7 and 59.9 (OCH_3), 67.9 (C-1), 74.0 (C-3′), 74.2 (C-2′), 78.0 (C-1′), 108.6 (C-8), 111.2 (C-5), 126.3 (C-8a), 130.2 (C-4a), 147.6 and 147.9 (C-6 and C-7); ms (CI, NH_3): 342 $(M + H)^+$ (10), 326 (12), 222 (50), 206 (100), 190 (20). Exact Mass calcd. for $C_{17}H_{28}NO_6$ $(M + H)^+$: 342.1916; found (hrms): 342.1913.

*Reduction of hydroxylamine **4** to amine **5***

A sample of **4** (90 mg) was dissolved in methanol (30 mL) containing distilled water (10 mL) and acetic acid (4 drops), PtO_2 catalyst (20 mg) was added, and the stirred mixture was treated with hydrogen at atmospheric pressure for 4 h. The catalyst was removed, the volatile solvents evaporated, and the residual solution was made basic by addition of an aqueous solution of sodium carbonate (10%, 10 mL) and then extracted with chloroform (3 × 15 mL). The extract was washed, dried, and evaporated to afford a residue that was purified by chromatography on silica (230–400 mesh). Residual starting material was eluted using chloroform–methanol (98:2, v/v) and the product **5** using chloroform–methanol (4:1, v/v). Compound **5** was obtained as a colorless oil (71 mg, 83%); $[\alpha]_D^{25}$ +81.9 (*c* 2.83, $CHCl_3$). (See below for spectroscopic data.)

*Preparation of **5** by treatment of **1** with methyllithium*

A suspension of **1** (4.50 g) in dry 1,2-dimethoxyethane (150 mL) at −10 to −5°C was treated with methyllithium in diethyl ether (1.5 M, 90 mL) over a period of 30 min under a nitrogen atmosphere. The mixture was stirred at the same temperature for 3 h and then treated with methanol (30 mL) to destroy the excess of reagent. The volatile solvents were removed by evaporation, water (45 mL) was added to the residue, and the mixture was extracted with chloroform (5 × 30 mL). The extract was washed, dried, and evaporated to afford a residue that was chromatographed on silica (70–230 mesh) using chloroform–methanol (98:2, v/v) to remove nonpolar impurities. Further elution using chloroform–methanol (4:1, v/v) gave **5** as a brownish oil (3.37 g, 80%); $[\alpha]_D^{25}$ +80.5 ±2 (*c* 2.30, $CHCl_3$) (the rotation was difficult to measure because of the dark solution); ^1H nmr (500 MHz) δ: 1.08 and 1.18 (3H each, s's, C-CH_3's at C-3′), 1.55 (3H, s, CH_3 at C-1), 2.55 (1H, m, H-4_{ax}), 2.98 (1H, s, H-2′), 2.99 (1H, m, H-4_{eq}), 3.01 and 3.10 (2H, m, H-3's), 3.77 and 3.82 (3H each, s's, 2 × OCH_3), 4.07 (1H, s, H-1′), 6.45 and 6.57 (1H each, s's, H-8 and H-5, resp.), OH and NH signals appear as a broad singlet at 4.50; ^{13}C nmr ($CDCl_3$) δ: 24.1 and 27.6 (CH_3's at C-3′), 25.7 (CH_3 at C-1), 29.8 (C-4), 37.9 (C-3), 59.7 (C-1), 74.0 (C-3′), 74.6 (C-2′), 75.5

Can. J. Chem. Downloaded from www.nrcresearchpress.com by 217.78.4.112 on 09/08/12
For personal use only.

Can. J. Chem. Downloaded from www.nrcresearchpress.com by 217.78.4.112 on 09/08/12
For personal use only.

(C-1′), 108.5 (C-8), 112.1 (C-5), 127.7 (C-8a), 130.5 (C-4a), 147.5 (C-6 and C-7); ms(EI): 310 $(M - 15)^+$ (5), 266 (8), 206 (100), 190 (4); ms(CI, NH_3): 326 $(M + 1)^+$ (100), 206 (14); Exact Mass calcd. for $C_{17}H_{28}NO_5$ $(M + H)^+$: 326.1967; found (hrms): 326.1963.

*Preparation of 1,2,3,4-tetrahydro-1-hydroxymethyl-6,7-dimethoxy-1-methylisoquinoline (**6**)*

The amine **5** (608 mg) in methanol (100 mL) at −5°C was treated all at once with a solution of sodium periodate (1.0 g) in water (5 mL). The progress of the reaction was monitored by thin-layer chromatography (TLC) (chloroform–methanol (4:1, v/v), silica gel), and, when the starting material was consumed (~40 min), a large excess of sodium borohydride was added over a period of 15 min. The mixture was allowed to warm to room temperature, filtered to remove inorganic matter, and the filtrate evaporated to dryness. The residue was quenched with water (40 mL) and the mixture extracted with chloroform (4 × 25 mL). The extract was dried, evaporated, and the residue chromatographed on silica (230–400 mesh) using chloroform–methanol (19:1, v/v) to remove nonpolar impurities, and then chloroform–methanol (4:1, v/v) to elute **6**. Removal of solvent afforded **6** as a yellowish oil in 76% yield. A solution of **6** in chloroform decomposed rapidly; $[\alpha]_D^{25}$ −9.2 (*c* 3.09, $CHCl_3$); ^{1}H nmr (90 MHz) δ: 1.38 (3H, s, C-CH_3), 2.57 (2H, br s, NH, OH, disappeared on addition of D_2O), 2.66 (2H, m, H-4_{ax} and H-4_{eq}), 3.02 (2H, m, H-3_{ax} and H-3_{eq}), 3.43 and 3.85 (2H, AB q, J = 7.5 Hz, CH_2OH), 3.88 (6H, s, 2 × OCH_3), 6.58 and 6.65 (1H each, s's, H-5 and H-8); ms (CI, CH_4): 238 $(M + 1)^+$ (25), 220 (7), 206 (100), 192 (15); ms (CI, NH_3): 238 $(M + H)^+$ (100), 220 (15), 206 (85), 192 (8). Exact Mass calcd. for $C_{13}H_{20}NO_3$ $(M + H)^+$: 238.1443; found (hrms); 238.1453.

*2-Ethoxycarbonyl-1,2,3,4-tetrahydro-1-hydroxymethyl-6,7-dimethoxy-1-methylisoquinoline (**7**)*

A solution of **6** (602 mg) in chloroform (15 mL) and an aqueous solution composed of sodium hydroxide (4.5 g) and acetic acid (0.5 g) in water (15 mL) were mixed and vigorously stirred. To this two-phase system ethyl chloroformate (3 mL) was added in two portions at 5-min intervals and the stirring continued for 15 min. The temperature was kept below 20°C. The organic layer was separated, washed with an aqueous solution of sodium chloride, dried, and evaporated to afford **7** as a homogeneous oil (TLC, chloroform–methanol (19:1, v/v)). The compound crystallized slowly from petroleum ether containing a small amount of benzene, yield 89%; mp 106–108°C; $[\alpha]_D^{23}$ +137.3 (*c* 1.87, $CHCl_3$); ^{1}H nmr (500 MHz) δ: 1.31 (3H, t, J = 7.1 Hz, CH_2CH_3), 1.68 (3H, s, CH_3 at C-1), 2.62 (1H, distorted d, J = 15.5 Hz, H-4_{ax}), 2.84 (1H, m, H-4_{eq}), 3.28 (1H, m, H-3_{eq}), 3.79 (1H, d, J = 12.2 Hz, C*H*-OH), 3.86 (6H, s, 2 × OCH_3), 4.18 (2H, q, J = 7.1 Hz, CH_2CH$_3$) and (1H, m, H-3_{ax}), 4.25 (1H, d, J = 12.2 Hz, C*H*-OH), 4.80 (1H, br s, OH, disappears on addition of D_2O), 6.56 and 6.77 (1H each, s's, H-5 and H-8); ms(EI): 278 $(M - 31)^+$ (18), 263 (16), 248 (100), 205 (5), 190 (10); ms (CI, NH_3): 310 $(M + H)^+$ (7), 281 (100), 264 (55), 248 (10). Exact Mass calcd. for $C_{16}H_{24}NO_5$ $(M + H)^+$: 310.1654; found (hrms): 310.1653.

*1,5,6,10b-Tetrahydro-8,9-dimethoxy-10b-methyl-3H-oxazolo[4,3-a]isoquinolin-3-one (**8**)*

The title compound was isolated in 70% yield when methyl chloroformate was substituted for ethyl chloroformate under the conditions described above for the preparation of **7**. It was isolated also in reactions with ethyl chloroformate when the reactions were allowed to proceed for periods longer than 15–20 min, and is the preponderant product at reaction times greater than 2 h. Compound **8** was isolated as a colorless oil, $[\alpha]_D^{23}$ +213.9 (*c* 1.88, $CHCl_3$); ^{1}H nmr (90 MHz) δ: 1.63 (3H, s, CH_3 at C-1), 2.50–3.43 (3H, m, H-4_{ax}, H-4_{eq}, H-3_{ax}), 3.88 (6H, s, 2 × OCH_3), 3.95–4.17 (1H, m, H-3_{eq}), 4.38 (2H, AB q, J = 9.0 Hz, CH_2-OH), 6.57 and 6.65 (1H each, s's, H-5 and H-8); ms(EI): 263 $(M)^+$ (35), 248 (100); ms (CI, NH_3); 264 $(M + H)^+$ (30), 248 (100). Exact Mass calcd. for $C_{14}H_{18}NO_4(M + H)^+$: 264.1236; found (hrms): 264.1234.

*Preparation of 2-ethoxycarbonyl-1,2,3,4-tetrahydro-6,7-dimethoxy-1-methylisoquinoline-1-carboxaldehyde (**9**)*

A solution of **7** (164 mg) in acetone (distilled from $KMnO_4$, 10 mL) was treated dropwise with stirring at room temperature with Jones' reagent (0.23 mL). After 5 min the excess of oxidant was destroyed by addition of methanol (0.5 mL) and the resulting mixture evaporated to dryness. A saturated aqueous solution of sodium chloride (10 mL) was added to the residue and the mixture extracted with chloroform (3 × 5 mL). The extract was washed, dried, and evaporated to afford a residue that was chromatographed on silica gel using chloroform as eluant. Compound **9** was obtained as a colorless oil (61%), $[\alpha]_D^{23}$ −72.1 (*c* 2.32, $CHCl_3$); ^{1}H nmr (90 MHz) δ: 1.30 (3H, t, J = 7.0 Hz, CH_2CH_3), 1.73 (3H, s, CH_3 at C-1), 2.58–3.23 (3H, m, H-4_{ax}, H-4_{eq}, H-3_{ax}), 3.85 and 3.88 (3H each, s's, 2 × OCH_3), 4.25 (2H, q, J = 7.0 Hz, CH_2CH$_3$, and 1H, m, H-3_{eq}), 6.58 and 6.65 (1H each, s's, H-5 and H-8), 9.15 (1H, s, CH=O); ms (CI, NH_3): 308 $(M + H)^+$ (100), 278 (12), 206 (8). Exact Mass calcd. for $C_{16}H_{22}NO_5$ $(M + H)^+$: 308.1497; found (hrms): 308.1498.

*Preparation of 2-ethoxycarbonyl-1,2,3,4-tetrahydro-6,7-dimethoxy-1-methylisoquinoline-1-carboxylic acid (**10**)*

A solution of **7** (410 mg) in a mixture of acetone (35 mL) and water (7 mL) was treated with $RuO_2 \cdot xH_2O$ (13% water, Alfa Products) (10 mg) and sodium periodate (99.8%, Aldrich) (600 mg). The mixture was stirred for ~48 h at room temperature or until the reaction was complete as indicated by TLC (chloroform–methanol (19:1, v/v)). (It was established that the alcohol **7** was completely converted into aldehyde **9** after 2–3 h.) The reaction mixture was then treated with water (50 mL) and ethylene glycol (10 mL). The volatile solvent was removed, the residual liquid made basic with sodium hydroxide, and the basic solution extracted with chloroform (3 × 15 mL). The aqueous solution was acidified with hydrochloric acid and extracted with chloroform (3 × 20 mL). The latter extract was dried and evaporated to afford a residual oil that crystallized from water to afford compound **10** (274 mg, 64%), mp 191–193°C; $[\alpha]_D^{25}$ +65.6 (*c* 0.57, $CHCl_3$); ^{1}H nmr (90 MHz) δ: 1.24 (3H, t, J = 7.0 Hz, CH_2CH_3), 1.82 (3H, s, CH_3 at C-1), 2.50–3.40 (3H, m, H-4_{ax}, H-4_{eq}, H-3_{ax}), 3.80 and 3.85 (3H each, s's, 2 × OCH_3), 4.14 (2H, q, J = 7.0 Hz, CH_2CH$_3$, and 1H, m, H-3_{eq}), 6.62 and 6.82 (1H each, s's, H-5 and H-8), 8.70 (1H, br s, CO_2H, disappears on addition of D_2O); ms (CI, NH_3): 341 $(M + NH_4)^+$ (95), 324 $(M + H)^+$ (100), 278 (85), 264 (24), 206 (62); ms (EI): 278 (100), 264 (88), 250 (35), 206 (53), 190 (34). Exact Mass calcd. for $C_{16}H_{22}NO_6$ $(M + H)^+$: 324.1447; found (hrms): 324.1452.

*Preparation of 1,2,3,4-tetrahydro-6,7-dimethoxy-1-methylisoquinoline-1-carboxylic acid hydrochloride (**11**)*

Compound **10** (213 mg) was dissolved in a solution of water (4 mL), ethanol (2 mL), and concentrated hydrochloric acid (0.5 mL) and the solution heated gently at reflux temperature for 7 days; the progress of the reaction was monitored by TLC (methanol–chloroform (1:9, v/v)). The residue obtained on evaporation of the reaction mixture was dried overnight in a vacuum desiccator over P_2O_5. The residue was taken up in the minimum amount of isopropyl alcohol and then diisopropyl ether was added to afford a fine, hygroscopic powder (187 mg) in 98% yield (based on **10**), mp 210°C (dec.); $[\alpha]_D^{25}$ +44.6 (*c* 1.12, CH_3OH); ^{1}H nmr (400 MHz, D_2O, sodium 3-(trimethylsilyl)-1-propanesulfonate as internal standard) δ: 1.85 (3H, s, CH_3 at C-1), 3.01 (2H, m, H-4_{ax} and H-4_{eq}), 3.48 (2H, m, H-3_{ax} and H-3_{eq}), 3.83 (3H, s, OCH_3 at C-7), 3.87 (3H, s, OCH_3 at C-6), 6.85 (1H, s, H-5), 7.16 (1H, s, H-8); ms (CI, NH_3): 503 $(2M + H)^+$(6), 252 $(M + H)^+$ (15), 234 (12), 220 (10), 206 (100), 192 (26). Exact Mass calcd. for $C_{13}H_{18}NO_4$ $(M + H)^+$: 252.1236; found (hrms): 252.1232.

The enantiomer of **11** was prepared by the same sequence of reactions, starting with the enantiomer of **1**, and had mp 250–253°C (dec.); $[\alpha]_D$ −52.2 (*c* 0.58, H_2O).

Can. J. Chem. Downloaded from www.nrcresearchpress.com by 217.78.4.112 on 09/08/12
For personal use only.

*(±)-1,2,3,4-Tetrahydro-6-hydroxy-7-methoxy-1-methoxycarbonyl-1-methylisoquinoline (**12**a)*

(3-Hydroxy-4-methoxyphenyl)ethylamine hydrochloride (1.905 g, 9.35 mmol) was dissolved in aqueous ammonia (2.9 mL). Distilled pyruvic acid (1.24 g, 14 mmol) was added cautiously, with cooling to control the vigorous exothermic reaction. The pH of the solution was adjusted to 7 with concentrated hydrochloric acid, and the reaction mixture was stirred at 32°C for 18 h. The precipitated product was isolated by filtration, and was dried under vacuum at 50°C to afford the racemic amino acid **12** as pale yellow crystals (1.99 g, 89%). An analytical sample was obtained by recrystallization from water to afford white needles; mp 260°C (dec.) (lit. (11) mp 254°C (dec.)); ^{1}H nmr (400 MHz, D_2O, K_2CO_3, sodium 3-(trimethylsilyl)-1-propanesulfonate as internal standard) δ: 1.46 (3H, s, CH_3 at C-1), 2.51–2.68 (2H, m, H-4 and H-4′), 2.97 (2H, m, H-3 and H-3′), 3.65 (3H, s, OCH_3), 6.32 (1H, s, H-5), 6.80 (1H, s, H-8).

Acid **12** was immediately esterified (see ref. 4). A suspension of the acid (1.99 g, 8.39 mmol) in dry methanol (20 mL) was cooled in an ice bath while thionyl chloride (4 mL, 50 mmol) was slowly added. During the addition, the suspension cleared, and then became turbid again. The cooling was terminated, and the mixture was stirred at reflux temperature for 5 h and then at 20°C overnight. TLC (1-butanol–water – acetic acid (4:1:1, v/v)) indicated that the reaction was incomplete; accordingly, the reaction mixture was heated at reflux temperature for an additional 1.5 h. The mixture was cooled, quenched with a saturated aqueous solution of sodium hydrogen carbonate (20 mL), and extracted with chloroform. The extract was dried over anhydrous magnesium sulfate and concentrated to give a solid. Recrystallization from dichloromethane–hexanes gave the ester **12***a* (1.16 g, 55%); mp 154–156°C (lit. (4) mp 156–157°C); ^{1}H nmr (400 MHz) δ: 1.62 (3H, s, CH_3 at C-1), 2.50–2.61 (1H, m, H-4), 2.68–2.80 (1H, m, H-4′), 3.00–3.09 (2H, m, H-3 and H-3′), 3.70 (3H, s, ester OCH_3), 3.85 (3H, s, ether OCH_3), 6.60 (1H, s, H-5), 6.87 (1H, s, H-8).

Acidification of the aqueous layer, concentration to dryness, and extraction of the solid residue with methanol allowed recovery of racemic **12** as its hydrochloride salt (0.522 g, 1.9 mmol). Taking this into account, the yield of **12***a* was 71%.

*(1S)-1,2,3,4-Tetrahydro-6-hydroxy-7-methoxy-1-methoxycarbonyl-1-methyl-2-[{(R)-1-phenylethyl}carbamoyl]isoquinoline (**13**) and its (1R) diastereomer (**14**)*

The ester **12***a* (1.159 g, 4.61 mmol) was dissolved in dry chloroform (20 mL). The solution was cooled to 0°C, and (*R*)-(+)-α-methylbenzyl isocyanate (730 μL, 5.08 mmol) was added dropwise (see ref. 4). The reaction was allowed to proceed at 0°C for 2 h and then the mixture was warmed to 20°C. Removal of solvent afforded a residue that solidified on standing under vacuum. The crude mixture of diastereomers (2.13 g) was resolved by preparative HPLC on silica using hexanes – ethyl acetate (3:1, v/v) as eluant. The product fractions (500 mL) were identified by TLC; the plates were developed 6 times (hexanes – ethyl acetate (3:1, v/v)) in order to separate the two diastereomers. The less-polar diastereomer **13** (757 mg, 41%) was obtained as a glassy foam, and the more-polar isomer **14** (702 mg, 38%) as crystals. Compound **13**: $[\alpha]_D^{25}$ +61.9 (*c* 1.7, $CHCl_3$) (lit. (4) $[\alpha]_D^{25}$ +56.1 (*c* 1.5, $CHCl_3$)). According to ref. 4 compound **13** has the (*S*,*R*) configuration; ^{1}H nmr (400 MHz) δ: 1.46 (3H, d, J = 7.0 Hz, $CHCH_3$), 1.77 (3H, s, CH_3 at C-1), 2.75 (1H, ddd, $J_{3ax,4eq}$ = 5.0 Hz, $J_{3eq,4eq}$ = 6.0 Hz, J_{gem} = 15.0 Hz, H-4_{eq}), 2.90 (1H, ddd, $J_{3eq,4ax}$ = 4.5 Hz, $J_{3ax,4ax}$ = 8.0 Hz, J_{gem} = 15.0 Hz, H-4_{ax}), 3.39 (3H, s, ester OCH_3), 3.42–3.36 (1H, m, H-3_{ax}), 3.56 (1H, ddd, $J_{3eq,4ax}$ = 4.5 Hz, $J_{3eq,4eq}$ = 6.0 Hz, J_{gem} = 12.0 Hz, H-3_{eq}), 3.78 (3H, s, ether OCH_3), 4.73 (1H, d, J = 7.0 Hz, NH), 4.98 (1H, dq, $J_{to\ NH}$ = 7.0 Hz, $J_{to\ CH_3}$ = 7.0 Hz, benzylic H), 5.63 (1H, s, OH), 6.65 (1H, s, H-5 or H-8), 6.69 (1H, s, H-5 or H-8), 7.17–7.34 (5H, m, phenyl H's). Compound **14**: mp 138–140°C; $[\alpha]_D^{25}$ −36.5 (*c* 1.2, $CHCl_3$) (lit.(4) mp 139–140°C; $[\alpha]_D^{25}$ −34.3 (*c* 1.2, $CHCl_3$)). According to ref. 4 compound **14** has the (*R*,*R*) configuration; ^{1}H nmr (400 MHz) δ: 1.47 (3H, d, J = 7.0 Hz, $CHCH_3$), 1.74 (3H, s, CH_3 at C-1), 2.78 (1H, ddd, $J_{3ax,4eq}$ = 3.5 Hz, $J_{3eq,4eq}$ = 5.5 Hz, J_{gem} = 15.5 Hz, H-4_{eq}), 2.93 (1H, ddd, $J_{3eq,4ax}$ = 4.0 Hz, $J_{3ax,4ax}$ = 9.0 Hz, J_{gem} = 15.5 Hz, H-4_{ax}), 3.32 (1H, ddd, $J_{3ax,4eq}$ = 3.5 Hz, $J_{3ax,4ax}$ = 9.0 Hz, J_{gem} = 12.0 Hz, H-3_{ax}), 3.62 (3H, s, ester OCH_3), 3.66–3.53 (1H, m, H-3_{eq}), 3.80 (3H, s, ether OCH_3), 4.69 (1H, d, $J_{to\ benzylic\ H}$ = 7.2 Hz, NH), 5.03 (1H, dq, $J_{to\ NH}$ = 7.2 Hz, $J_{to\ CH_3}$ = 7.0 Hz, benzylic H), 5.60 (1H, s, OH), 6.66 (1H, s, H-5 or H-8), 6.72 (1H, s, H-5 or H-8), 7.20–7.40 (5H, m, phenyl H's).

*(10bS)-6,10b-Dihydro-8,9-dimethoxy-10b-methyl-2-[(R)-1-phenylethyl]-5H-imidazo[4,3-a]isoquinoline-1(2H),3(4H)-dione (**19**)*

The less-polar phenol **13** (620 mg, 1.56 mmol) was dissolved in methanol (5 mL), and the solution was cooled to 0°C. A solution of diazomethane in ether (~10 mmol) was added gradually. The cooling was terminated, and the reaction mixture was stirred for 16 h at 23°C. The excess of diazomethane was evaporated under a stream of nitrogen, and the remaining solvent was evaporated. The resulting semi-solid was triturated with ether to afford **19** as white crystals (518 mg, 87%); mp 127–130°C; $[\alpha]_D^{25}$ +112.9 (*c* 1.15, $CHCl_3$); ^{1}H nmr (400 MHz) δ: 1.61 (3H, s, CH_3 at C-10b), 1.77 (3H, d, $J_{to\ benzylic\ H}$ = 7.3 Hz, $CHCH_3$), 2.59 (1H, dd, $J_{5ax,6eq}$ = 4.0 Hz, J_{gem} = 16.3 Hz, H-6_{eq}), 2.95 (1H, ddd, $J_{5eq,6ax}$ = 6.0 Hz, $J_{5ax,6ax}$ = 12.7 Hz, J_{gem} = 16.3 Hz, H-6_{ax}), 3.17 (1H, ddd, $J_{5ax,6eq}$ = 4.0 Hz, $J_{5ax,6ax}$ = 12.7 Hz, J_{gem} = 13.3 Hz, H-5_{ax}), 3.85 (3H, s, OCH_3 at C-9), 3.90 (3H, s, OCH_3 at C-8), 4.31 (1H, dd, $J_{5eq,6eq}$ = 6.0 Hz, J_{gem} = 13.3 Hz, H-5_{eq}), 5.33 (1H, q, J = 7.3 Hz, $CHCH_3$), 6.56 (1H, s, H-10), 7.24 (1H, s, H-7), 7.22–7.46 (5H, *m*-phenyl H's); ^{13}C nmr (100.6 MHz, $CDCl_3$) δ: 17.2($CHCH_3$), 26.4 (CH_3 at C-10b), 27.5 (C-6), 35.4 (C-5), 50.5 ($CHCH_3$), 55.8 (OCH_3), 56.0 (OCH_3), 60.8 (C-10b), 108.6 (C-7), 111.3 (C-10), 124.8 (C-10a), 125.8 (C-6a), 127.0 (*o*-phenyl C's), 127.5 (*p*-phenyl C), 128.4 (*m*-phenyl C's), 140.1 (phenyl quaternary C), 147.9 (C-8 or C-9), 148.6 (C-8 or C-9), 155.6 (C-3), 175.0 (C-1). Exact Mass calcd. for $C_{22}H_{24}N_2O_4$: 380.1737; found (hrms): 380.1733.

*(10bR)-6,10b-Dihydro-8,9-dimethoxy-10b-methyl-2-[(R)-1-phenylethyl]-5H-imidazo[4,3-a]isoquinoline-1(2H),3(4H)-dione (**20**)*

The more-polar phenol **14** (640 mg, 1.61 mmol) was treated with diazomethane as described above. Trituration and filtration provided white crystals of **20** (612 mg, ~100%). A sample was recrystallized from diisopropyl ether to afford colorless needles; mp 132°C; $[\alpha]_D^{25}$ −72.9 (*c* 1.29, $CHCl_3$); ν_{max}(KBr): 1760 (m), 1700 (s), 1605, 1512, 1400, 1250 cm^{-1}; ^{1}H nmr (400 MHz) δ: 1.67 (3H, s, CH_3 at C-10b), 1.80 (3H, d, J = 7.3 Hz, $CHCH_3$), 2.61 (1H, dd, $J_{5ax,6eq}$ = 4.0 Hz, J_{gem} = 16.5 Hz, H-6_{eq}), 2.98 (1H, ddd, $J_{5eq,6ax}$ = 6.0 Hz, $J_{5ax,6ax}$ = 12.0 Hz, J_{gem} = 16.5 Hz, H-6_{ax}), 3.16 (1H, ddd, $J_{5ax,6eq}$ = 4.0 Hz, $J_{5ax,6ax}$ = 12.0 Hz, J_{gem} = 13.5 Hz, H-5_{ax}), 3.85 (3H, s, OCH_3 at C-9), 3.91 (3H, s, OCH_3 at C-8), 4.28 (1H, dd, $J_{5eq,6eq}$ = 6.0 Hz, J_{gem} = 13.5 Hz, H-5_{eq}), 5.36 (1H, q, J = 7.3 Hz, $CHCH_3$), 6.57 (1H, s, H-10), 7.25 (1H, s, H-7), 7.23–7.46 (5H, *m*-phenyl H's); ^{13}C nmr (100 MHz, $CDCl_3$) δ: 17.3 ($CHCH_3$), 26.4 (CH_3 at C-10b), 27.4 (C-6), 35.3 (C-5), 50.3, ($CHCH_3$), 55.8 (OCH_3), 56.0 (OCH_3), 61.1 (C-10b), 108.6 (C-7), 111.3 (C-10), 124.9 (C-10a), 125.8 (C-6a), 127.0 (*o*-phenyl C's), 127.6 (*p*-phenyl C), 128.4 (*m*-phenyl C's) 140.0 (phenyl quaternary C), 147.8 (C-8 or C-9), 148.6 (C-8 or C-9), 155.5 (C-3), 175.3 (C-1). Exact Mass calcd. for $C_{22}H_{24}N_2O_4$: 380.1737; found (hrms): 380.1744.

*(R)-1,2,3,4-Tetrahydro-6,7-dimethoxy-1-methylisoquinoline-1-carboxylic acid hydrochloride (**22**)*

The (*R*,*R*)-hydantoin **20** (350 mg, 0.92 mmol) was dissolved in methyl cellosolve (3.5 mL). An aqueous 20% sodium hydroxide solution (3 mL) was added, and the mixture was heated at reflux temperature for 3.5 h. The reaction mixture was cooled and acidified to pH 2 with concentrated hydrochloric acid. The mixture was filtered, the filtrate concentrated, and the residue taken up in 2-propanol. The mixture was filtered and the filtrate was concentrated to dryness. The residue was fractionated by column chro-

matography (1-butanol – acetic acid – methanol (5:1:1, v/v)). Compound **22** was obtained as white crystals (78 mg, 31%) that were recrystallized from methanol – isopropyl ether; mp 255–262°C (dec.); $[\alpha]_D^{25}$ −56.3 (*c* 1.2, H_2O). The ^1H nmr spectrum (400 MHz, D_2O) was identical with that obtained for compound **11**.

Acknowledgements

We thank the Natural Sciences and Engineering Research Council of Canada for financial support of this research in the form of grants to D.B.M. and W.A.S., and an International Scientific Exchange Award to Z.C. We thank also Dr. A. Brossi for reference samples.

1. J. Lundstrom. *In* The alkaloids. Vol. 21. *Edited by* A. Brossi. Academic Press, New York, N.Y. 1983. pp. 255–327.
2. M. A. Collins. *In* The alkaloids. Vol. 21. *Edited by* A. Brossi. Academic Press, New York, N.Y. 1983. pp. 329–335.
3. M. Shamma. The isoquinoline alkaloids. Academic Press, New York, N.Y. 1972. pp. 380–398.
4. M. Chrzanowska, B. Schönenberger, A. Brossi, and J. L. Flippen-Anderson. Helv. Chim. Acta, **70**, 1721 (1987); B. Schönenberger and A. Brossi. Helv. Chim. Acta, **69**, 1486 (1986); see also: Helv. Chim. Acta, **70**, 271 (1987).
5. G. Dörnyei and Cs. Szántay. Acta Chim. Acad. Sci. Hung. **89**, 161 (1976).
6. Z. Czarnocki, D. B. MacLean, and W. A. Szarek. J. Chem. Soc. Chem. Commun. 493 (1987); Can. J. Chem. **65**, 2356 (1987).
7. G. B. Payne and P. H. Williams. J. Org. Chem. **24**, 54 (1959).
8. Y. Ogata and Y. Sawaki. J. Am. Chem. Soc. **95**, 4692 (1973).
9. K. Kahr and C. Berther. Chem. Ber. **93**, 132 (1960).
10. D. G. Lee and M. Van Den Engh. *In* Oxidation in organic chemistry. Part B. *Edited by* W. S. Trahanovsky. Academic Press, New York, N.Y. 1973. p. 177.
11. G. Hahn and F. Rumpf. Chem. Ber. **71**, 2141 (1938).

Can. J. Chem. Downloaded from www.nrcresearchpress.com by 217.78.4.112 on 09/08/12
For personal use only.

The anomeric and reverse anomeric effect. A simple energy decomposition model for acetals and protonated acetals

F. GREIN

Department of Chemistry, University of New Brunswick, Fredericton, N.B., Canada E3B, 6E2

AND

P. DESLONGCHAMPS

Department of Chemistry, University of Sherbrooke, Sherbrooke, Que., Canada J1K 2R1

Received August 7, 1991

This paper is dedicated to Professor Zdenek (Denny) Valenta on the occasion of his 65th birthday

F. GREIN and P. DESLONGCHAMPS. Can. J. Chem. **70**, 1562 (1992).

Geometry optimizations at the 6-31G** level were performed on various conformers of $XH_mCH_2YH_n$ and $XH_mCH_2YH_{n+1}^+$ (protonated), with X, Y = N, O. The resulting anomeric stabilization energies were decomposed into steric, electrostatic (lone pair – lone pair, lone pair – hydrogen), and electronic contributions. Using approximate values for steric and electrostatic terms, the electronic energy was determined to be about −2 kcal/mol for the anomeric effect to arise from O, and −2.5 kcal/mol if it arises from N. For protonated systems, an additional energy term for the reverse anomeric effect had to be added, having a value of −4 kcal/mol for O in $OH\text{-}CH_2\text{-}NH_3^+$ and −5 kcal/mol for N in $NH_2\text{-}CH_2\text{-}NH_3^+$. The anomeric effect due to N drives $NH_2\text{-}CH_2\text{-}OH_2^+$ to a charge-dipole complex of the type $NH_2{=}CH_2^+ \ldots OH_2$. The energy parameters obtained have been applied to predict relative stabilities of various conformers of methanetriol, aminomethanediol, and protonated methanetriol, with good success.

F. GREIN et P. DESLONGCHAMPS. Can. J. Chem. **70**, 1562 (1992).

On a effectué des optimisations de géométries, au niveau 6-31G**, pour divers conformères de $XH_mCH_2YH_n$ et $XH_mCH_2YH_{n+1}^+$ (protonés) dans lesquels, X, Y = N, O. Les énergies de stabilisation anomériques qui en résultent ont été décomposées en contributions stériques, électrostatiques (paire libre/paire libre, paire libre/hydrogène) et électroniques. Utilisant des valeurs approximatives pour les termes stériques et électrostatiques, on a déterminé que l'énergie électronique de l'effet anomérique est d'environ −2,0 kcal/mol s'il est dû à l'oxygène et d'environ −2,5 kcal/mol s'il est dû à l'azote. Pour les systèmes protonés, on a dû ajouter un terme additionnel d'énergie pour l'effet anomérique inverse; sa valeur est de −4 kcal/mol pour O dans $HO\text{-}CH_2\text{-}NH_3^+$ et de −5 kcal/mol pour N dans $NH_2\text{-}CH_2\text{-}NH_3^+$. L'effet anomérique dû au N force le $NH_2\text{-}CH_2\text{-}OH_2^+$ vers un complexe de charge dipolaire du type $NH_2{=}CH_2^+ \ldots OH_2$. On a appliqué les paramètres d'énergie obtenus pour prédire avec succès les stabilités relatives de divers conformères du méthanetriol, de l'aminométhanediol et du méthanetriol protoné.

[Traduit par la rédaction]

Introduction

A vast amount of literature, both experimental and theoretical, has appeared on the anomeric effect. Suitable reviews can be found in the books by Deslongchamps (1) and Kirby (2), and in the review article by Gorenstein (3).

It has been known for a long time that quantum chemical calculations are quite capable of reproducing the experimental findings on stabilization energies and geometry changes (4). Many theoretical studies have been performed on large systems, of immediate interest to the organic chemist, as well as on small model systems such as simple acetals and simple esters. The ease and speed of computations on small systems allows for systematic investigations into the nature of the anomeric effect.

In this paper, a model will be presented for decomposing the anomeric stabilization energy as obtained from *ab initio* calculations into components based upon familiar terms like steric, electrostatic, and electronic energies.

In the literature, several energy decomposition schemes have appeared. Smits *et al.* (5) considered *anti* and *gauche* conformers of systems XH_mCH_2OH, with X = F, O, N, C. Using localized nonorthogonal molecular orbitals (MO), they write the one-electron density as a sum of quasi-classical, interference, and charge-transfer terms, and decompose the energy correspondingly. In this scheme, the anomeric effect is found to result mainly from XCH_2O interference interactions, in particular from a weakening of the destructive CX-CO interference as the electronegativity of X increases.

Reed and Schleyer (6, 7) used the concept of natural bond orbitals (NBO) for an analysis of the energy stabilization as well as geometry changes. By checking the occupancy of the n and σ^* localized orbitals, the significance of $n \rightarrow \sigma^*$ negative hyperconjugation to the anomeric stabilization can be checked. Furthermore, by deleting in the Fock matrix the matrix element corresponding to $n \rightarrow \sigma^*$, the calculated increase in energy can be taken as a measure of the energetic stabilization due to the $n \rightarrow \sigma^*$ interaction. A detailed study of $FSNH_2$ with NBO's shows that the $n_N \rightarrow \sigma_{SF}^*$ hyperconjugation can account for the very strong anomeric effect in this system, as well as in others.

Wiberg and Murcko (8) estimated for $OCH_3\text{-}CH_2\text{-}OCH_3$ (DMM) a quantity corresponding to the lone pair – lone pair (lp) repulsion (notation of this paper) to be 1.4 kcal/mol, by calculating energy differences between corresponding conformers of methyl propyl ether. From this, the anomeric stabilization energy of DMM, corrected for lp–lp repulsions, is calculated to be 4.7 kcal/mol.

Energy decomposition schemes can be developed in two ways. Either highly accurate energy terms (depending on the model) are obtained for one particular system, or average parameters are developed that fit a class of systems. In the

Can. J. Chem. Downloaded from www.nrcresearchpress.com by 217.78.4.112 on 09/08/12
For personal use only.

Can. J. Chem. Downloaded from www.nrcresearchpress.com by 217.78.4.112 on 09/08/12
For personal use only.

second case, the loss in accuracy for a specific system is compensated for by more general applicability, and by predictive capabilities. The latter approach is taken in this work.

In the following, anomeric stabilization energies, calculated by *ab initio* methods for simple hydroxyl and amino compounds and corresponding protonated species, will be decomposed into steric, electrostatic, and electronic components. Basically, steric and electrostatic energies will be subtracted from the total energy of anomeric stabilization, to arrive at the underlying electronic energy. The latter is considered to be a fundamental quantity, similar in many systems, whereas steric and electrostatic energies are incidental, depending on the particular conformation. The forthcoming analysis will confirm the fundamental nature of the electronic energy component involved in anomeric stabilization.

2. Methods and molecules studied

Geometry optimizations were performed at the SCF level using the 6-31G** basis set (unless noted otherwise). All calculations were carried out with the GAUSSIAN 86 computer programs (9).

For the systems XH_m-CH_2-YH_n, with X, Y, = N, O (neutral systems) and XH_m-CH_2-YH_{n+1}^+ (protonated systems, same X and Y), the dihedral angles of one XH_m and one YH_n hydrogen were fixed in order to define the desired conformation, whereas all other internal coordinates were optimized. For each system the energies relative to the most stable conformer will be listed. Since the emphasis will be placed upon an analysis of the energy differences, and not upon geometries, only CX and CY optimized bond distances will be given.

All of the neutral systems discussed in this paper have received theoretical treatment in the past. Only the most recent references will be cited. As mentioned earlier, systems XCH_2OH, with X = CH_3, NH_2, OH, and F, were studied by Smits *et al.* (5). Work on NH_2-CH_2-NH_2 was recently reported by Aped et al. (10). The system OCH_3-CH_2-OCH_3 was studied in detail by Wiberg and Murcko (8), as was mentioned above.

Only few calculations were reported on the protonated molecules of interest here. Wipff (11), Williams *et al.* (12), and Maggiora and Williams (13) considered OH-CH_2-OH_2^+, whereas Lehn and Wipff (14) described OH-CH_2-NH_3^+.

3. Model for energy decomposition

Due to the anomeric effect (ae), systems XH_m-CH_2-YH_n are stabilized when a hydrogen, say on Y, is moved from the *anti* to the *gauche* position (relative to CX). With X and Y being electronegative substituents (like O and N), the model system may have 0 ae when a hydrogen from both X and Y is *anti* relative to CY and CX, respectively, or 1 ae when a hydrogen from XH_m or YH_n is *anti* while the other hydrogens are *gauche*, or 2 ae when all hydrogens are *gauche*. This formulation is simplified by considering idealized sp^3 lone pairs on both X and Y. The anomeric effect (also called generalized ae) is active when one lone pair, or two lone pairs, one from X and one from Y, are antiperiplanar (app) to the other polar bond.

From *ab initio* calculations on systems XH_m-CH_2-YH_n, the energy differences between conformers with 0, 1, or 2 ae's can be calculated. It is desirable to subtract components corresponding to steric and electrostatic effects (e.g., lone pair repulsions) from the energy of stabilization, in order to be left with the electronic energy responsible for the energy lowering. It is assumed that the electronic energy causing the anomeric effect is a fundamental quantity, more so than observed or calculated total energies of stabilization, which are conditioned by various steric and electrostatic effects. It will be seen that for different systems the total energy lowerings upon anomeric stabilization may be large or small, but after correction for steric and electrostatic effects the underlying electronic energies of stabilization are the same or very similar.

In detail, the (*ab initio*) energy differences will be decomposed into a steric component for 1,3-diaxial H–H repulsion (denoted by parameter r, always positive), into electrostatic components for 1,3-diaxial lp–lp repulsion (parameter l, always positive), and for intramolecular "hydrogen bonding," meaning 1,3-diaxial H–lp interaction (parameter h, always negative or stabilizing), and finally into an electronic energy component, applicable when a lone pair is antiperiplanar to a polar bond (parameter e, always negative). In the above, lp stands for a sp^3 lone pair. The use of lone pairs can be avoided by considering the interaction of local dipole moments. If they are parallel (**1***a*), they destabilize the system; if antiparallel (**1***b*) they stabilize it.

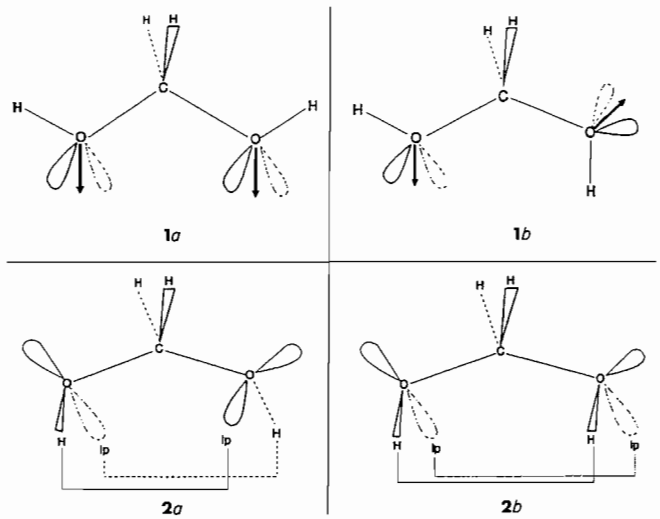

First, the quantities r, l, and h will be estimated, such that values for e can be obtained from the calculated energy differences. The 6-31G** energy difference between g,g-OH-CH_2-OH (**2***a*) and g,g^*-OH-CH_2-OH (**2***b*) is 3.57 kcal/mol. For NH_2-CH_2-OH in the 1 ae(O) conformation, the sterically favored form **3***a* is 4.37 kcal/mol (6-31G**) more stable than the less favored form **3***b*. Using the above energy decomposition scheme, $\Delta E = l + r - 2h$ for both systems. The methoxy systems, to be discussed later, will show that $h \cong -1$ kcal/mol; therefore, $l + r$ is chosen to be 2 kcal/mol. (In order to have a wide range of applicability, only integral or half integral numbers (in kcal/mol) will be used for the energy parameters.) The above data do not allow for a distinction between l and r. Using a 6-31G** basis set and optimized geometries, a Fourier analysis on OH-CH_2-OH performed by Grein and Deslongchamps (15) gave for the a-OH-CH_2-OH system $V_1 = -4.69$ kcal/mol. V_1 corresponds to the energy difference between structures **1***a* and

TABLE 1. Energy differences ΔE in kcal/mol for neutral systems, relative to most stable conformer, obtained by 6-31G** geometry optimizations

XH_m-CH_2-YH_n	OH-CH_2-OH	OH-CH_2-OCH_3	OCH_3-CH_2-OCH_3	NH_2-CH_2-NH_2	NH_2-CH_2-OH
0 ae	8.35	6.78	5.30	0.82	5.06
1 ae(X)	3.86	2.51	2.27	0.64	0.17
1 ae(Y)	3.86	3.79	2.27	0.64	0.95
2 ae	0.0	0.0	0.0	0.0	0.0

1*b* when only the 180° component of the energy is considered. (The 90° component V_2, corresponding to the electronic part of the anomeric energy, and the 60° component V_3, corresponding to the repulsion between the rotating H with the three bonds on C, have been separated out). For the *s*-OH-CH_2-OH system, V_1 = 3.82 kcal/mol (15). Starting from structure **1***b*, in the first case the 180° rotation results in two lp–lp repulsions (**1***a*), being 4.69 kcal/mol less stable than **1***b*, whereas in the second case the rotation results in in-plane H–H repulsion, being 3.82 kcal/mol less stable than **1***b*. These data show that the lp–lp and H–H repulsions are of similar magnitude. Therefore, the assumption $r \cong l \cong 1$ kcal/mol will be made, such that $l + r \cong 2$ kcal/mol as required.

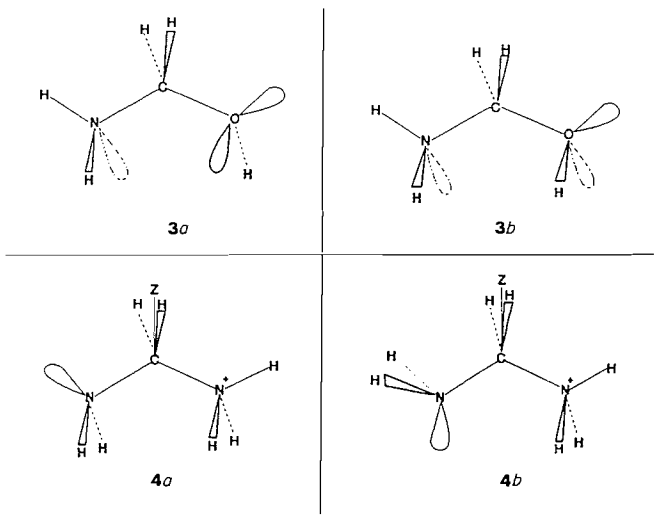

In the following, the electronic component of the anomeric stabilization energy will be deduced for the systems investigated. In all cases, the above values of the parameters for steric and electrostatic effects will be retained. It is not the purpose of this work to optimize the values of the energy parameters for each individual system, but to allow for enough flexibility such that the energy decomposition model has predictive qualities.

4. Results and energy analysis for neutral systems

In Table 1, the calculated (6-31G**) energy differences are given for the neutral systems XH_m-CH_2-YH_n, with X, Y = O, N. The various conformers, designated by the notation 0 ae, 1 ae, and 2 ae, are shown in Fig. 1. In Table 2, the optimized CO and CN distances are given. Using MP2/6-31G** geometry optimizations on OH-CH_2-OH, the ΔE values are (in kcal/mol) 9.19 for 0 ae, 4.48 for 1 ae, and 0 for 2 ae, while the CO distances are (in Å) 1.402 for 0 ae, 1.391 and 1.415 for 1 ae, and 1.406 for 2 ae. For the purpose of the general energy model to be applied here, the differences in ΔE between MP2 and RHF optimizations are of little significance. Bond distances generally increase when electron correlation is added to RHF wavefunctions that have polarization functions in the basis set.

Table 1 shows that for all neutral systems the most stable conformer is 2 ae (ΔE = 0), while 0 ae is the least stable, as one would expect. However, there are large differences in ΔE (0 ae). While ΔE(0 ae) is about 8, 7, and 5 kcal/mol, for systems with OH or OCH_3, it is only 0.82 kcal/mol for NH_2-CH_2-NH_2. It will be shown that such huge differences in the 0 ae energies can be explained by steric and electrostatic effects, while the electronic components for anomeric stabilization are virtually the same in all cases. In Table 3, the energy analysis for the neutral systems is presented. For OH-CH_2-OH, the 0 ae conformer has 2 lone pair repulsions ($2l$), whereas 2 ae has 2 hydrogen bonds ($2h$) in addition to $2e$ from the two anomeric effects. Using l = 1 and h = −1 kcal/mol, one obtains $e \cong -2$ kcal/mol. On the other hand, for NH_2-CH_2-NH_2, the 0 ae conformer has $2h$, whereas 2 ae has $2e_N + 2r$. Using $l = r = -h = 1$ kcal/mol leads to $e_N = -2.5$ kcal/mol. In the process of going to the favorable conformation 2 ae, the electrostatic effects destabilize whereas the electronic effects stabilize the molecule. In balance, there is only a small energy gain of 0.82 kcal/mol between 0 ae and 2 ae.

For the mixed system NH_2-CH_2-OH, the previously obtained energy parameters, with $e_O = -2$ and $e_N = -2.5$ kcal/mol, predict the calculated energy differences within 0.5 kcal/mol. This is the first successful test of the model.

Tables 1 and 3 also contain results for the methoxy compounds OH-CH_2-OCH_3 and OCH_3-CH_2-OCH_3. Whereas the 1,3-diaxial H–lp interaction was energy lowering (h = −1 kcal/mol), a corresponding CH_3–lp 1,3-diaxial interaction is not expected to be. Therefore, in comparison with the OH compounds, the parameter h is omitted from the energy formula for OCH_3. This explains nicely why the 0 ae energy drops from 8.35 to 6.78 to 5.30 kcal/mol as one moves across the top of Table 1 from the hydroxyl to the methoxy compounds. It also provides justification, as mentioned earlier, for the introduction of the energy parameter h, with an approximate value of −1 kcal/mol.

For neutral systems, the energy decomposition model gave values for the electronic parameter of −2 kcal/mol for oxygen, and −2.5 kcal/mol for nitrogen.

5. Results and energy analysis for protonated systems

In Tables 4 and 5, ΔE values and optimized bond distances are given for the various conformers of the protonated systems, as shown in Fig. 2. For the protonated systems XH_m-CH_2-YH_{n+1}^+, geometry optimizations often lead to unusual structures, mostly caused by the desire of the sys-

Can. J. Chem. Downloaded from www.nrcresearchpress.com by 217.78.4.112 on 09/08/12
For personal use only.

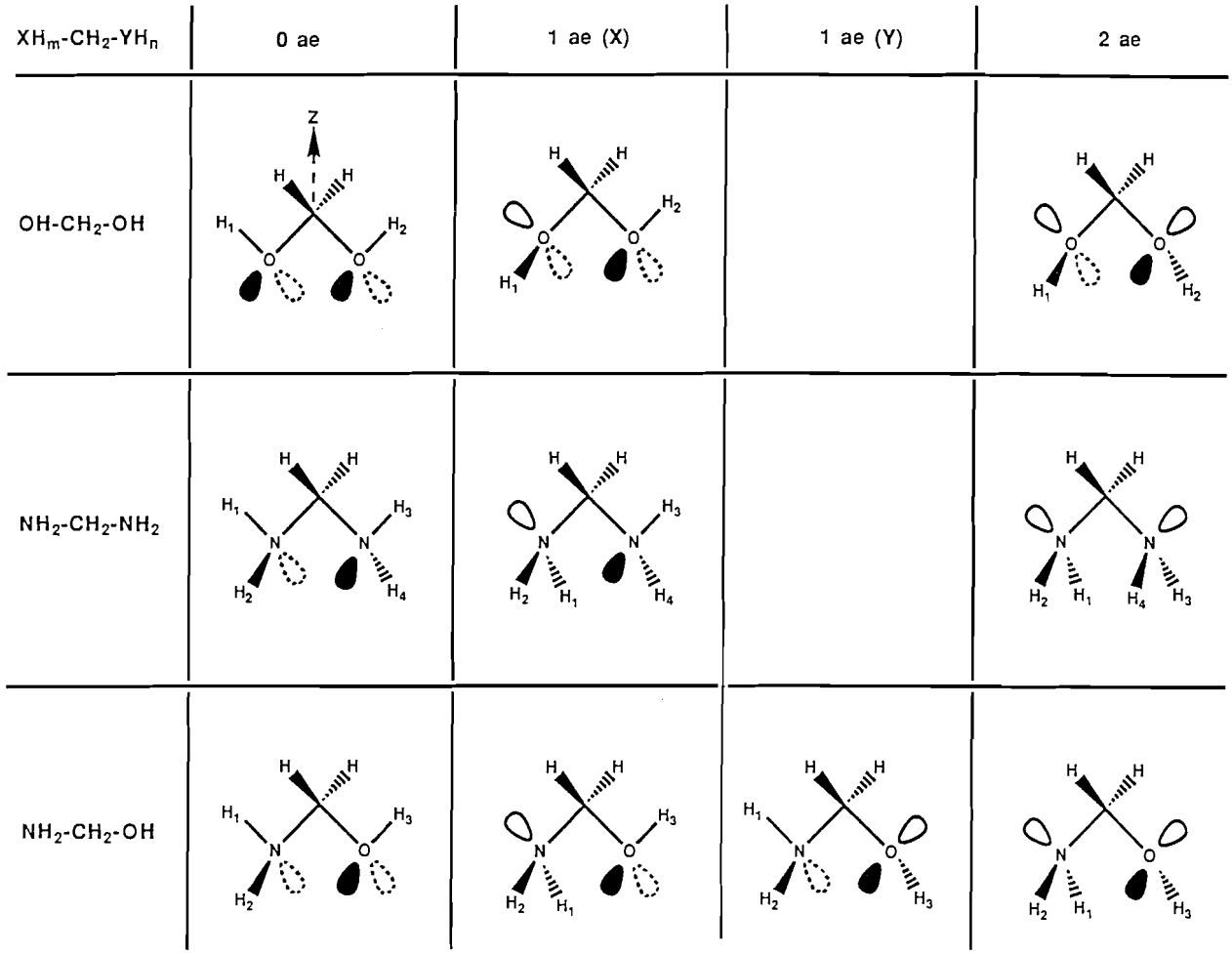

FIG. 1. Conformers of $OH\text{-}CH_2\text{-}OH$, $NH_2\text{-}CH_2\text{-}NH_2$, and $NH_2\text{-}CH_2\text{-}OH$, corresponding to 0, 1, and 2 anomeric effects. See text for details.

TABLE 2. Optimized C—X and C—Y (X, Y = N, O) bond distances in Å for neutral systems. Basis set 6-31G**

$XH_m\text{-}CH_2\text{-}YH_n$	$OH\text{-}CH_2\text{-}OH$	$OH\text{-}CH_2\text{-}OCH_3$	$OCH_3\text{-}CH_2\text{-}OCH_3$	$NH_2\text{-}CH_2\text{-}NH_2$	$NH_2\text{-}CH_2\text{-}OH$
0 ae	1.381/1.381	1.382/1.376	1.376/1.376	1.445/1.445	1.435/1.394
1 ae(X)	1.372/1.393	1.373/1.388	1.369/1.388	1.439/1.456	1.423/1.407
1 ae(Y)	1.393/1.372	1.396/1.369	1.388/1.369	1.456/1.439	1.443/1.388
2 ae	1.385/1.385	1.387/1.382	1.385/1.385	1.448/1.448	1.431/1.403

tem to move towards a charge-dipole complex, but unable to do so due to fixed dihedral angles for one XH_m and one YH_{n+1} hydrogen, as are required for defining the conformation. The resulting energies also reflect unusual stabilizations, and are not suitable for an energy analysis. Therefore, the results of Tables 4 and 5 were obtained for a "restricted series" of optimizations, where the dihedral angles of all XH_m and YH_{n+1} hydrogens have been frozen at 0 or $\pm 120°$, according to the diagrams in Fig. 2.

Table 4 shows that for the systems $OH\text{-}CH_2\text{-}OH_2^+$ and $NH_2\text{-}CH_2\text{-}OH_2^+$, the 2 ae conformer is no longer the most stable one. Similarly, for $NH_2\text{-}CH_2\text{-}NH_3^+$ and $OH\text{-}CH_2\text{-}NH_3^+$, unexpected situations occur. They will be discussed in the light of the energy decomposition scheme.

For the energy analysis of the protonated systems, the parameters r, l, and h will be used again. For a start, they are retained at the values 1 and -1 kcal/mol, as before. Also, the electronic energy component e will be given the same values as before, -2 kcal/mol for anomeric stabilization due to a lone pair on O, and -2.5 kcal/mol due to a lone pair on N, except in the case of complex stabilization. Lone pairs on O^+ (these are only formal charges, and do not imply actual positive partial charges on O) are expected to be weaker, and the electronic parameter e_{O^+} will be determined by comparison with the *ab initio* energies.

Table 5 shows that two conformers of $NH_2\text{-}CH_2\text{-}OH_2^+$, 1 ae(N) and 2 ae, optimized to charge-dipole complexes, with CO bonds of 2.381 Å, and associated large stabilization energies (13 to 15 kcal/mol relative to 0 ae).

The energy decomposition scheme is given in Table 6. A choice of 0 for e_{O^+} of $OH\text{-}CH_2\text{-}OH_2^+$ gives ΔE values close to the *ab initio* values for this system, with a maximum de-

Can. J. Chem. Downloaded from www.nrcresearchpress.com by 217.78.4.112 on 09/08/12
For personal use only.

TABLE 3. Energy decomposition for neutral systems. Energy parameters are r for H–H repulsion, l for lp–lp repulsion, h for internal hydrogen bonding, and e for electronic energy stabilization due to the anomeric effect. Given is the energy formula (first line), the values for the energy parameters (second line), and the relative energies ΔE according to this model, with the *ab initio* values of Table 1 in parentheses (third line). All energies in kcal/mol

	$OH\text{-}CH_2\text{-}OH$	$OH\text{-}CH_2\text{-}OCH_3$	$OCH_3\text{-}CH_2\text{-}OCH_3$	$NH_2\text{-}CH_2\text{-}NH_2$	$NH_2\text{-}CH_2\text{-}OH$
0 ae	$2l$ 2 8(8.35)	$2l$ 2 7(6.78)	$2l$ 2 6(5.30)	$2h$ −2 1(0.82)	$h + l$ −1 + 1 4.5(5.06)
1 ae(X)		$e_O + h + l$ −2 − 1 + 1			$e_N + 2h$ −2.5 − 2
	$e_O + h + l$ −2 −1 + 1	3(2.51)	$e_O + l$ −2 + 1	$e_N + h + r$ −2.5 − 1 + 1	0(0.17)
1 ae(Y)	4(3.86)	$e_O + l$ −2 + 1	3(2.27)	0.5(0.64)	
		4(3.79)			$e_O + 2h$ −2 −2
					0.5(0.95)
2 ae	$2e_O + 2h$ −4 − 2 0(0.0)	$2e_O + h$ −4 − 1 0(0.0)	$2e_O$ −4 0(0.0)	$2e_N + 2r$ −5 + 2 0(0.0)	$e_N + e_O + h + r$ −2.5 −2 −1 +1 0(0.0)

TABLE 4. Energy differences ΔE in kcal/mol for protonated systems, obtained by 6-31G** geometry optimizations. Restricted series (see text)

$XH_m\text{-}CH_2\text{-}YH_n^+$	$OH\text{-}CH_2\text{-}OH_2^+$	$NH_2\text{-}CH_2\text{-}OH_2^+$
0 ae	4.73	13.45
1 ae(X)	0	0
1 ae(Y)	1.18	15.04
2 ae	1.81	1.10
	$NH_2\text{-}CH_2\text{-}NH_3^+$	$OH\text{-}CH_2\text{-}NH_3^+$
0 ae	0.12	0
1 ae	0	3.80
Inverted	−5.62	

TABLE 5. CX and CY distances (in Å) for protonated systems. Basis set 6-31G**. Restricted series

$XH_m\text{-}CH_2\text{-}YH_n^+$	$OH\text{-}CH_2\text{-}OH_2^+$	$NH_2\text{-}CH_2\text{-}OH_2^+$
0 ae	1.341/1.521	1.401/1.546
1 ae(X)	1.303/1.656	1.289/2.381
1 ae(Y)	1.348/1.503	1.406/1.536
2 ae	1.311/1.630	1.290/2.381
	$NH_2\text{-}CH_2\text{-}NH_3^+$	$OH\text{-}CH_2\text{-}NH_3^+$
0 ae	1.424/1.513	1.365/1.501
1 ae	1.401/1.561	1.350/1.534
Inverted	1.427/1.513	

TABLE 6. Energy decomposition for protonated systems. Energy parameters and format of table same as in Table 3. Parameter v for reverse anomeric effect

$XH_m\text{-}CH_2\text{-}YH_n^+$	$OH\text{-}CH_2\text{-}OH_2^+$	$NH_2\text{-}CH_2\text{-}OH_2^+$
0 ae	$l + h$ 1 −1 4(4.73)	$2h$ −2 13(13.45)
1 ae(X)	$e_O + 2h$ −2 −2 0(0)	$e_N + h + r$ −15 −1 +1 0(0)
1 ae(Y)	$e_O + 2h$ 0 − 2 2(1.18)	$e_O + h + r$ 0 −1 + 1 15(15.04)
2 ae	$e_O + e_O^+ + r + h$ −2 + 0 + 1 − 1 2(1.81)	$e_N + e_O^+ + 2r$ −15 + 0 + 2 2(1.10)
	$NH_2\text{-}CH_2\text{-}NH_3^+$	$OH\text{-}CH_2\text{-}NH_3^+$
0 ae	$r + h$ 1 − 1 0.5(0.12)	$v_O + 2h$ −4 − 2 0(0)
1 ae	$e_N + 2r$ −2.5 +2 0(0)	$e_O + r + h$ −2 + 1 − 1 4(3.80)
Inverted	$v_N + h$ −5 −1 −5.5(−5.62)	

viation of 0.8 kcal/mol. For $NH_2\text{-}CH_2\text{-}OH_2^+$ a charge-dipole complex is obtained whenever the lone pair on N is app to CO. Therefore, the parameter e_N has to be reevaluated. Using $e_{O^+} = 0$, e_N is found to be −15 kcal/mol, reflecting the large complex destabilization. Omitting in the formula $h + r$ for 1 ae(X) and $2r$ for 2 ae, due to the large CO distance in $NH_2\text{-}CH_2\text{-}OH_2^+$, changes the prediction for 2 ae to 0 kcal/mol from 2.

A special situation is encountered for $NH_2\text{-}CH_2\text{-}NH_3^+$. When optimizing the 1 ae conformer, starting with dihedral angles of ±120° for the NH_2 hydrogens (relative to

Can. J. Chem. Downloaded from www.nrcresearchpress.com by 217.78.4.112 on 09/08/12
For personal use only.

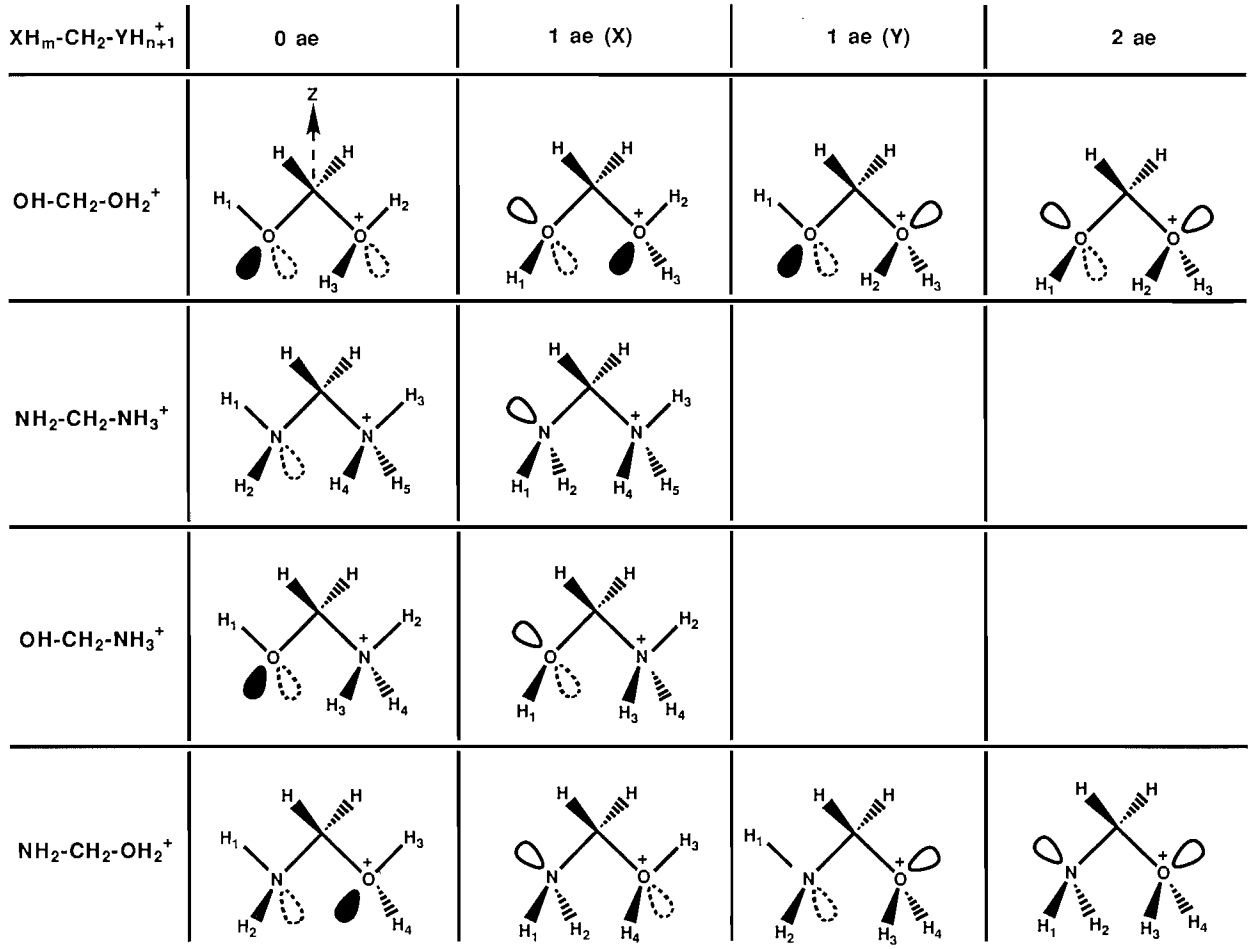

FIG. 2. Conformers of $OH\text{-}CH_2\text{-}OH_2^+$, $NH_2\text{-}CH_2\text{-}NH_3^+$, $OH\text{-}CH_2\text{-}NH_3^+$, and $NH_2\text{-}CH_2\text{-}OH_2^+$, corresponding to 0, 1, and 2 anomeric effects. See text for details.

Z—C—N, structure **4***a*), the NH_2 group inverts, leading to structure **4***b*, which is 5.62 kcal/mol more stable than **4***a*. Situations where the expected anomeric stabilization does not take place, and another conformer is more stable, have been referred to as the "reverse anomeric effect" (rae). Lemieux and Morgan (16) and Lemieux (17), who introduced the term reverse anomeric effect, discovered that in certain pyridinium glycosides the pyridinium group acquired equatorial rather than the expected axial position, contrary to the predictions for the anomeric effect. They attributed this exceptional behavior to destabilizing electrostatic effects arising from a positively charged atom (usually N) in axial orientation at the anomeric center. In the spirit of the present model, one may attribute the increased stability of **4***b* over **4***a* to the proximity of the lone pair on N to the positive charge on NH_3^+, which supersedes the stabilization due to the antiperiplanar lone pair. It is known that α-pyridinium glycosides prefer to exist in the twist-boat rather than the chair conformation. Using our model, this unexpected behavior, referred to as the reverse anomeric effect, is simply rationalized by the fact that there is maximum electrostatic attraction between the ring oxygen lone pairs and the equatorially oriented pyridinium group when the tetrahydropyranyl ring adopts the twist-boat conformation.

For the energy analysis, a new parameter v is required (v for reverse ae). For $NH_2\text{-}CH_2\text{-}NH_3^+$, ΔE betwen 0 ae and 1 ae is well explained with $e_N = -2.5$ kcal/mol. For the inverted structure, however, a value of $v_N = -5$ kcal/mol is needed to fit the *ab initio* energies.

The system $OH\text{-}CH_2\text{-}NH_3^+$ is clearly in favor of the reverse ae, having 0 ae more stable than 1 ae. Retaining e_O as −2 kcal/mol leads to $v_O = -4$ kcal/mol, again showing that the rae stabilization exceeds the ae stabilization by a significant amount.

Obviously, it will be interesting to investigate changes in bond distances and atomic charges due to the reverse anomeric effect. Such items, however, exceed the scope of the present paper, which deals exclusively with the energy model, and will be referred to future publications.

6. Application of energy decomposition model to methanetriol and aminomethanediol

Figure 3 shows optimized C—O distances for six of the seven conformers of methanetriol that can be formed by having a lone pair or hydrogen of one OH group antiperiplanar to one of the other C—O bonds. In the triangular diagrams (see structure **5** as example) a lobe on O_A, lined up with the line O_A–O_B, indicates that a lone pair on O_A is antiperiplanar to O_B. A short line on O_A, lined up with O_A–O_C, would indicate a hydrogen on O_A being antiperiplanar to C–O_C. The second lone pair on O_A is shown pointing to the inside of the triangle, towards C. For this lone pair, O–lp is

Can. J. Chem. Downloaded from www.nrcresearchpress.com by 217.78.4.112 on 09/08/12
For personal use only.

Can. J. Chem. Downloaded from www.nrcresearchpress.com by 217.78.4.112 on 09/08/12
For personal use only.

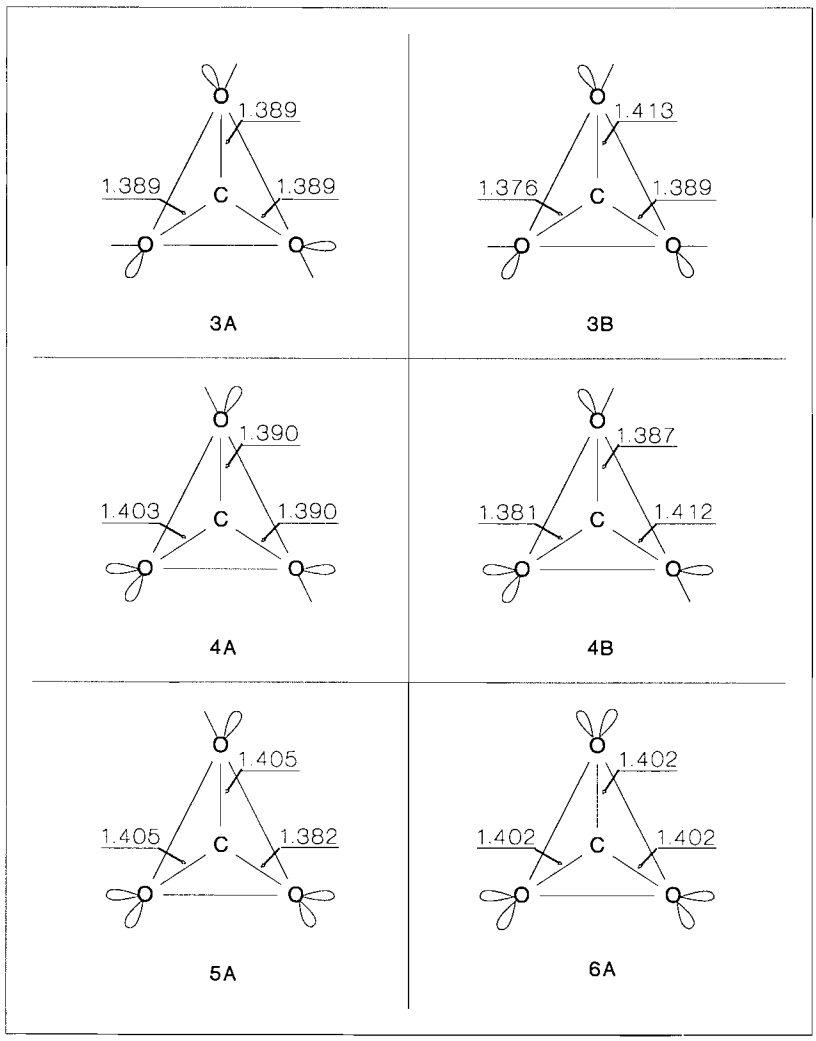

FIG. 3. Schematic diagrams of $CH(OH)_3$, showing 6 of the 7 conformers having a lone pair or hydrogen on O *anti* relative to the other CO bond. The conventions are explained in text and structure **5**.

TABLE 7. Energy decomposition for various conformers of methanetriol. Energy difference ΔE in kcal/mol, obtained from formula, and comparison with *ab initio* values ΔE_{abin} (4-31G)

Structure	Formula	ΔE	ΔE^*	ΔE_{abin}
3A	$3e + 3h + 3l$	4	4.5	4.01
3B	$3e + h + 4l + r$	8	9.5	9.93
4A	$4e + 4h + 2l$	0	0	1.85
4B	$4e + 4h + 2l$	0	0	0.00
4C	$4e + 2h + 3l + r$	4	5	4.66
5A	$5e + 3h + 2l + r$	0	0.5	1.10
6A	$6e + 0h + 3l + 3r$	4	6	7.27

anti to CH. In this way, the triangular diagrams uniquely define the conformations of $CH(OH)_3$ for the purpose of the present analysis.

The number labelling the diagrams in Fig. 3, e.g., 4 in 4A, gives the number of anomeric effects, whereas the letter corresponds to an (arbitrary) sequence of conformations. In the diagrams of Fig. 3 (and following figures) the three CO distances are shown. The lone pairs or hydrogens on the inside of the triangle have been omitted to allow for lines connecting O with C.

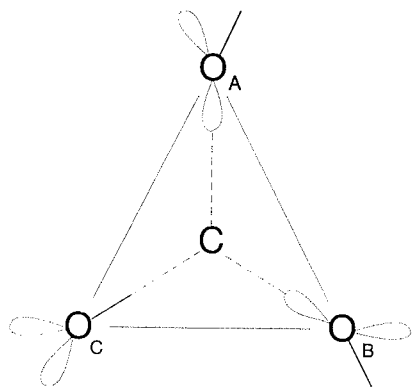

5

In Table 7, an energy analysis equivalent to the one performed on methanediol is applied. For example, for structure **5** (4B of Fig. 3) there are four ae's ($4e$), four internal hydrogen bonds ($4h$), and two lp–lp repulsions ($2l$). Using $e_O = -2$ kcal/mol, and $l = r = -h = 1$ kcal/mol, as before, leads to the prediction that structure 4A, 4B, or 5A should be the most stable one (column "ΔE"). In the last column of Table 7, the *ab initio* energy differences (4-31G basis set) are given. It is seen that 4B is most stable, and that

Can. J. Chem. Downloaded from www.nrcresearchpress.com by 217.78.4.112 on 09/08/12
For personal use only.

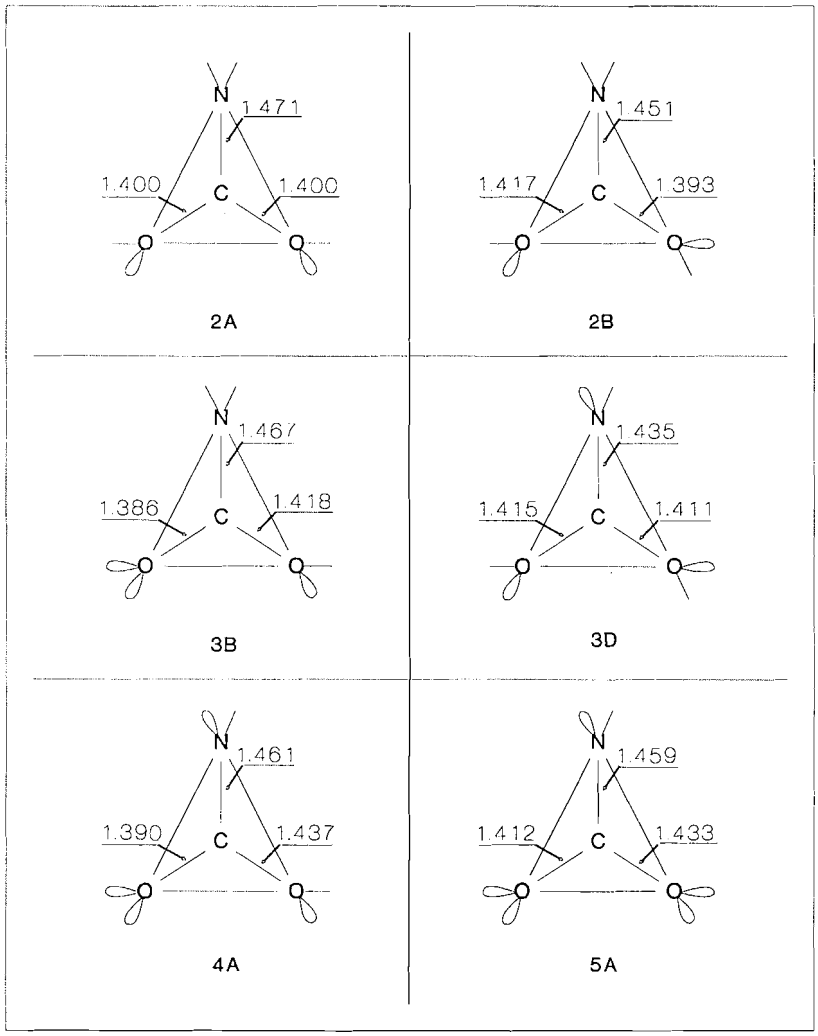

FIG. 4. Schematic diagrams of $CH(OH)_2NH_2$, showing 6 of the 15 conformers having a lone pair or hydrogen on O and N *anti* to other CO or CN bond. For conventions see text and structure **5**.

TABLE 8. Energy decomposition for various conformers of $CHNH_2(OH)_2$. Energy differences ΔE in kcal/mol, obtained from formula, and comparison with *ab initio* values ΔE_{abin} (3-21G)

Structure	Formula	ΔE	ΔE_{abin}
2A	$2e_O + 4l + 2r$	15	16.39
2B	$2e_O + 2h + 3l + r$	10	10.51
2C	$2e_O + 2h + 3l + r$	10	11.18
3A	$3e_O + 5h + l$	0.5	1.71
3B	$3e_O + 3h + 2l + r$	5.5	5.44
3C	$e_N + 2e_O + 3h + 2l + r$	5	7.56
3D	$e_N + 2e_O + 5h + l$	0	0
3E	$e_N + 2e_O + 3h + 2l + r$	5	4.84
3F	$e_N + 2e_O + 3h + 2l + r$	5	6.16
4A	$e_N + 3e_O + 2h + 2l + 2r$	5.5	6.40
4B	$e_N + 3e_O + 4h + l + r$	0.5	1.99
4C	$e_N + 3e_O + 4h + l + r$	0.5	0.98
4D	$e_N + 3e_O + 4h + l + r$	0.5	2.48
4E	$4e_O + 4h + l + r$	1	1.86
5A	$e_N + 4e_O + h + 2l + 3r$	6	6.93

4A and 5A differ by 1–2 kcal/mol from 4B. In general, ΔE_{abin} is larger than the formula value, the largest deviation (3.27 kcal/mol) occurring for structure 6A. In this case, the formula contains $3l + 3r$, the maximum number of repulsion terms. From this, an adjustment of the formula values of l and r, from 1 to 1.5 kcal/mol, is suggested, in order to achieve better agreement between ΔE and ΔE_{abin}. Adjusted formula values, ΔE^*, also given in Table 7, show a marked improvement. Now the largest deviation occurs for 4A, which has the same formula as the most stable structure 4B, and does therefore not benefit from a change of the repulsion parameters. Intuitively one expects repulsion on the more crowded methanetriols to be higher than in the corresponding methanediols. An adjustment of the repulsion parameters from 1 to 1.5 kcal/mol may not be necessary for 6-31G* energy differences (assuming 6-31G* geometry optimizations), since 6-31G* energy differences are usually smaller than corresponding 4-31G (or 3-21G) values. For lack of computer resources, only 4-31G optimizations were performed on methanetriol. Single point calculations in 6-31G**, using the 4-31G optimized geometries (6-31G**//4-31G), gave energies that were found less suitable for interpretation.

Many other adjustments and refinements to the parame-

Can. J. Chem. Downloaded from www.nrcresearchpress.com by 217.78.4.112 on 09/08/12
For personal use only.

TABLE 9. Energy decomposition for various conformers of protonated methanetriol. Energy differences ΔE in kcal/mol, obtained from formula, and comparison with *ab initio* values ΔE_{abin} (4-31G)

Structure	Formula	ΔE	ΔE_{abin}
2A	$2e + 0h + 4l + 2r$	14	11.96
2B	$2e + 2h + 3l + r$	9	9.93
2C	$2e + 2h + 3l + r$	9	13.30
3A	$2e + 3h + 2l + r$	6.5	5.60
3B	$2e + 5h + l$	1.5	0
3C	$2e + 3h + 2l + r$	6.5	7.77
3D	$3e + 5h + l$	1.5	3.26
3E	$2e + 3h + 2l + r$	6.5	7.36
3F	$3e + 3h + 2l + r$	4.5	2.48
4A	$4e + 4h + l + r$	0	1.72
4B	$3e + 2h + 2l + 2r$	7	5.45
4C	$3e + 4h + l + r$	2	3.72
4D	$3e + 4h + l + r$	2	0.81
4E	$3e + 4h + l + r$	2	5.75
5A	$4e + h + 2l + 3r$	7.5	8.47

ters, and to the formula, have been tried. For example, one might distinguish between "outer" and "inner" l, r, and h interactions, where "outer" and "inner" are most easily defined by inspecting structure **5**. However, it is important to retain the simplicity of the formula, and to have steric and electrostatic parameters as general and transferable as possible.

As another example, aminomethanediol may be investigated. There are 15 conformers having a lone pair or hydrogen antiperiplaner to another CX bond. Figure 4 shows six of them. A simple energy analysis, with $e_O = 2$, $e_N = -2.5$, $l = r = 1.5$, and $h = -1$ kcal/mol, predicts structure 3D to be most stable (Table 8). Indeed, this was found to be the case. Structure 2A is predicted to be least stable, again to be confirmed. Table 8 gives calculated ΔE values (3-21G basis set) and the formula for the energy analysis together with the predicted ΔE value. The agreement is quite satisfactory. Details for systems $CHNH_2(OH)_2$, as well as $CH(NH_2)_2OH$ and $CH(NH_2)_3$, will be published elsewhere.

7. Application of energy decomposition model to protonated methanetriol

In Fig. 5 six of the 15 conformers of $CH(OH)_2OH_2^+$ are shown, where again either a lone pair or a hydrogen is app to one of the other C—O bonds. The C—O bond distances, optimized with the 4-31G basis set, are given.

In Table 9 the energy formulae, as well as ΔE's obtained from the formula and ΔE_{abin} values (4-31G), are given. The standard parameters for triols, $e_O = -2$, $e_{O^+} = 0$, $h = -1$, and $l = r = 1.5$ kcal/mol have been used. While the largest deviation between ΔE and ΔE_{abin} is 4.3 kcal/mol (2C), most ΔE's agree within 1–2 kcal/mol. Structure 3B has the lowest *ab initio* energy, predicted at 1.5 kcal/mol by the formula, while 4A has the lowest predicted energy, at 1.72 kcal/mol by *ab initio* calculations. For a simple energy decomposition model as applied here, the predictive ability is judged to be quite satisfactory. As was noticed for protonated methanediols, energy predictions for protonated systems are much more difficult to perform than for neutral systems. Special situations would arise in cases of the reverse ae and of charge-dipole complexes. Details on protonated triols, and on other protonated systems of the type $CH(OH)_m(NH_2)_nH^+$, with $m + n = 3$, will be published elsewhere.

8. Discussion

In the energy decomposition scheme presented in this paper, approximate energy parameters have been used in order to decompose anomeric stabilization energies for compounds XH_m-CH_2-YH_n, with X, Y = N, O. After deducting steric (H–H interactions) and electrostatic (lp–lp and lp–H interactions) terms from the stabilization energies, electronic components are left, having values of 2 for O and 2.5 kcal/mol for N, and acting towards stabilization of the *gauche* over the *anti* conformer. The larger stabilization energy of N, compared with O, is explained by N being a better electron donor than O, and OH being a better leaving group than NH_2.

Frank (18) placed the experimental value of the anomeric stabilization energy (electronic part) for *O*-alkyl systems at a minimum of 2.1 kcal/mol, whereas a previous estimate by Deslongchamps *et al.* (19) gave a minimum of 1.4 kcal/mol. Wolfe *et al.* (20) found a theoretical value of 2.8 kcal/mol.

A new theoretical interpretation of the reverse anomeric effect is offered. For the first time, to the best of our knowledge, estimates have been obtained for the energy stabilization due to this effect. The systems OH-CH_2-NH_3^+ and NH_2-CH_2-NH_3^+ prefer comformations where the lone pair on O or N is not app to CN^+ but is located in the proximity of the (formal) positive charge on N. Apparently, the lp–N^+ electrostatic attraction exceeds the desire of lp delocalization, corresponding to the regular anomeric effect. The energy parameters v for the reverse anomeric effect are found to be -4 for the OH, and -5 kcal/mol for the NH_2 system, twice the amounts obtained for the respective anomeric stabilization energies.

In an investigation into the nature of the anomeric effect, Grein and Deslongchamps (15) studied the systems XH_m-CH_2-OH, with X = F, O, N, and C. For a given conformation of XH_m, the OH group was held at dihedral angles of 0°, 60°, 90°, 120°, and 180°. By Fourier analysis, and by comparison with properties of the $CH_2{=}OH^+$ cation, it could be shown that anomeric stabilization for X = F and O is π-driven, whereby the CH_2-OH portion of XH_m-CH_2-OH is trying to assume the optimal structure of $CH_2{=}OH^+$. For X = N and C, however, the OH *gauche* conformer is no longer the most stable one, and there is no anomeric stabilization due to the lone pair on oxygen. A similar analysis has been performed for systems XH_m-CH_2-NH_2 and for the corresponding protonated systems with OH or NH_2 rotation (to be published). The energy parameters obtained by Fourier analysis can be roughly classified as electronic, steric, and electrostatic, and therefore some relation can be obtained with the energy parameters of the present paper (the terms are not identical). It should be emphasized again that the energy parameters used in this work are approximate, designed to cover a wide range of compounds rather than one compound accurately. Applications to methanetriol and protonated methanetriol, as well as to aminomethanediol, allow for predicting the energies of all *anti* conformers (lp or H in *anti* position relative to other CO or CN) with reasonable accuracy. Adjustment of the repulsion parameters l and r from 1

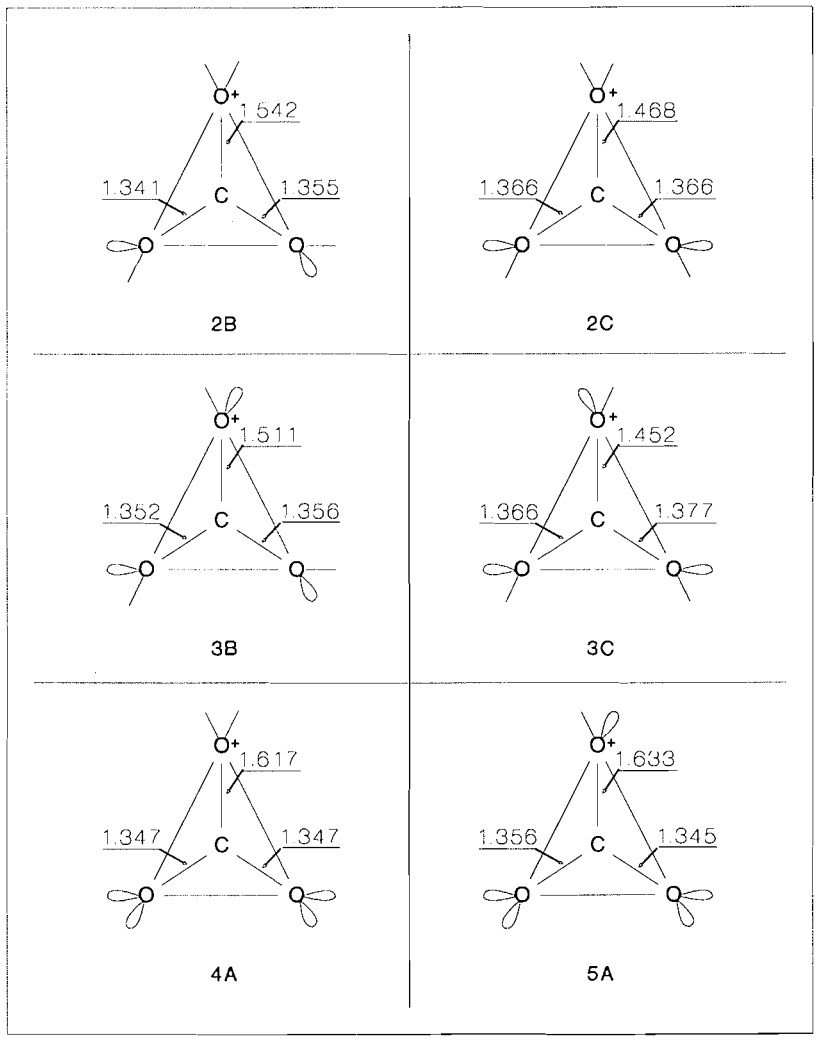

FIG. 5. Schematic diagrams of $CH(OH)_2OH_2^+$, showing 6 of the 15 conformers having a lone pair or hydrogen on O *anti* to other CO bond. For conventions see text and structure **5**.

to 1.5 kcal/mol improves the agreement. Such increase either reflects the increased repulsion in triols over diols, or is due to the lower level basis sets used for calculations on the triol systems (or both).

9. Summary and future work

A simple energy decomposition scheme, as proposed earlier by Grein and Deslongchamps (21), has been developed. In this scheme, the anomeric stabilization energies for acetal and protonated acetal-type systems XH_m-CH_2-YH_n and XH_m-CH_2-YH_{m+1}^+, with X, Y = N, O, are decomposed into steric (H–H), electrostatic (H–lp and lp–lp), and electronic terms. The validity of this model, which is easy to use, has been tested by application to methanetriol and protonated methanetriol, with good success. The important energy parameter is the electronic energy of anomeric stabilization, calculated by subtracting steric and electrostatic terms from the total energy of stabilization as obtained from *ab initio* calculations. The electronic energy is the basic underlying driving force in anomeric stabilizations, and has indeed been found to be very similar for all systems studied, even if the total energies of stabilization differ by large amounts.

For protonated systems, the anomeric effect may be so strong that the molecule separates to form a charge-dipole complex. In such cases, the (formal) electronic energy of stabilization is very large. For two of the protonated systems studied here, the conformation expected to be the most stable one was found to be less stable than a conformation allowing the lone pair(s) (on O or N) to be close to the (formal) positive charge (on N). A new parameter, for the reverse anomeric effect, has been introduced, with energies exceeding, as expected, the electronic energy for the regular anomeric effect.

A recent paper by Schleifer *et al.* (22) concludes that based on a systematic analysis of hundreds of carbohydrate structures "the structural parameters are the most characteristic manifestation of the anomeric effect rather than the energy (relative stability) factors". We believe that by accounting not only for steric but also for electrostatic effects, in the manner shown above, the remaining electronic energy can be a useful part of demonstrating the anomeric effect. However, it is readily admitted that estimating steric and electrostatic energies is not always easy, and that accurate values for such energy components are hard to come by. We hope that the present paper opens the way for more work in this field.

In future work, the energy decomposition scheme presented here will be extended to anionic acetal systems as well

Can. J. Chem. Downloaded from www.nrcresearchpress.com by 217.78.4.112 on 09/08/12
For personal use only.

as to esters and protonated esters. A rationalization of the energy parameters on the basis of energy components obtained by Fourier analysis will be attempted. More detailed studies of the geometry changes occurring for systems that are governed by the reverse anomeric effect will be of interest.

Acknowledgement

Computational help by several undergraduate students, in particular Michelle Carnell and Amy Wortman, as well as the grant of operating funds by the Natural Sciences and Engineering Research Council of Canada and the allocation of computer time by the University of New Brunswick are gratefully acknowledged. We would also like to thank Robert Mawhinney for preparing most of the figures. Special thanks go to Dr. Z. Valenta for his interest in this project and for helpful discussions.

1. P. Deslongchamps. Stereoelectronic effects in organic chemistry. Pergamon Press, Oxford. 1983.
2. A. J. Kirby. The anomeric effect and related stereoelectronic effects at oxygen. Springer Verlag, Berlin. 1983.
3. D. G. Gorenstein. Chem. Rev. **87**, 1047 (1987).
4. S. Wolfe, A. Rauk, L. M. Tel, and I. G. Csizmadia. J. Chem. Soc. B, 136 (1971).
5. G. F. Smits, M. C. Krol, and C. Altona. Mol. Phys. **65**, 513 (1988).
6. A. E. Reed and P. v. R. Schleyer. Inorg. Chem. **27**, 3969 (1988).
7. A. E. Reed and P. v. R. Schleyer. J. Am. Chem. Soc. **109**, 7362 (1987).
8. K. B. Wiberg and M. A. Murcko. J. Am. Chem. Soc. **111**, 4821 (1989).
9. M. J. Frisch, J. S. Binkley, H. B. Schlegel, *et al.* GAUSSIAN 86, Carnegie–Mellon Quantum Chemistry Publishing Unit, Pittsburgh, Pa. 1984.
10. P. Aped, L. Schleifer, B. Fuchs, and S. Wolfe. J. Comput. Chem. **10**, 265 (1989).
11. G. Wipff. Tetrahedron Lett. **35**, 3269 (1978).
12. I. H. Williams, G. M. Maggiora, and R. L. Schowen. J. Am. Chem. Soc. **102**, 7831 (1980).
13. G. M. Maggiora and I. H. William. Theochem, **88**, 23 (1982).
14. J. M. Lehn and G. J. Wipff. J. Am. Chem. Soc. **102**, 1347 (1980).
15. F. Grein and P. Deslongchamps. Can. J. Chem. **70**, 000 (1992).
16. R. U. Lemieux and A. R. Morgan. Can. J. Chem. **43**, 2205 (1965).
17. R. U. Lemieux. Pure Appl. Chem. **25**, 527 (1971).
18. R. W. Frank. Tetrahedron, **39**, 3251 (1983).
19. P. Deslongchamps, D. P. Rowan, N. Pothier, T. Sauve, and J. K. Saunders. Can. J. Chem. **59**, 1105 (1981).
20. S. Wolfe, M. H. Whangbo, and D. J. Mitchell. Carbohydr. Res. **69**, 1 (1979).
21. F. Grein and P. Deslongchamps. Second World Congress of Theoretical Organic Chemists, Toronto. July 1990.
22. L. Schleifer, H. Senderowitz, P. Aped, E. Tartakovsky, and B. Fuchs. Carbohydr. Res. **206**, 21 (1990).

Can. J. Chem. Downloaded from www.nrcresearchpress.com by 217.78.4.112 on 09/08/12
For personal use only.

Synthesis of the thymidine building blocks for a nonhydrolyzable DNA analogue

STEPHEN H. KAWAI, DAGUANG WANG, AND GEORGE JUST[1]
Department of Chemistry, McGill University, Montréal, Que., Canada H3A 2K6

Received July 11, 1991

This paper is dedicated to Dr. Zdenek (Denny) Valenta on the occasion of his 65th birthday

STEPHEN H. KAWAI, DAGUANG WANG, and GEORGE JUST. Can. J. Chem. **70**, 1573 (1992).

The 3′-deoxy-3′-*C*-(2″-hydroxyethyl)thymidine derivatives **4** and **13** were efficiently synthesized from either thymidine via a known 3′-radical allylation, or from the branched-chain furanose **5** involving the removal of the 2′-hydroxyl after stereospecific nucleosidation. The 5′-deoxy-5′-thiothymidine **20** was prepared via a regiospecific Mitsunobu coupling, providing the third unit required for the synthesis of sulfide-linked DNA analogues.

STEPHEN H. KAWAI, DAGUANG WANG et GEORGE JUST. Can. J. Chem. **70**, 1573 (1992).

On peut synthétiser les dérivés **4** et **13** de la 3′-désoxy-3′-*C*-(2″-hydroxyéthyl)thymidine d'une façon efficace soit à partir de la thymine par le biais d'une allylation du radical-3′ soit à partir du furanose **5** à chaine ramifiée en enlevant la fonction 2′-hydroxyle après une nucléosidation stéréospécifique. On a préparé la 5′-désoxy-5′-thiothymidine **20** par le biais d'un couplage régiospécifique de Mitsunobu et l'on a ainsi obtenu la troisième unité nécessaire pour la synthèse d'analogues de l'ADN liés par un pont sulfure.

[Traduit par la rédaction]

Can. J. Chem. Downloaded from www.nrcresearchpress.com by 217.78.4.112 on 09/08/12
For personal use only.

Introduction

Since the discovery, a decade ago, that bacterial gene expression is naturally regulated by the binding of specific messenger RNA species by complementary RNA strands, the antisense strategy has developed into a major field of investigation (1). Much work has been devoted to both natural and modified oligonucleotides that are capable of forming stable double-helices with complementary mRNA, thus blocking translation to the protein product. Many of these systems bear uncharged phosphodiester group analogues that facilitate the uptake of the oligonucleotide strands into cells and confer increased stability towards degradation by celular nucleases.

A factor that makes these systems attractive is the fact that they can be prepared in a relatively straightforward manner by small modifications to existing automated DNA synthetic techniques. However, such phosphate-modified systems, which include methylphosphonate (2), phosphoramidate (3, 4), and phosphorothioate-linked (5) oligodeoxynucleotide analogues, possess some inherent drawbacks. Modification or replacement of one of the phosphoryl oxygens (or both by different groups) gives rise to a chiral phosphorus center that results in a mixture of diastereomeric oligonucleotide products. In addition, the removal of the negative charge on the internucleoside linkage results in the loss of the high chemical stability associated with phosphodiesters. The absence of the charged phosphodiester group has also been implicated in the reduced stability exhibited by hybrid (P-modified/natural) helices (6).

As an alternative to phosphate-modified systems, a few examples of DNA analogues in which the nucleoside units are altered and joined by the natural phosphodiester linkages have been studied. These include both mixed and homogeneous oligomers bearing α-anomeric (7, 8) and L-2′-deoxynucleosides (9, 10). There have also been a number of examples of DNA analogues in which the phosphodiester groups have been replaced altogether with hydrolytically stable, nonchiral linkages. Notable examples of such "dephospho" analogues are those containing sulphur atoms. Benner and co-workers have reported the details of the syntheses of 3′,5′-bis-homo-thionucleosides (11), whose short polysulfone-oligomers were found to bind to complementary RNA. A dinucleoside analogue in which the phosphodiester is replaced with a sulfonyl ester and which exhibits surprising chemical stability was recently described (12).

In tandem with our work with sulfide-linked oligoribonucleotide analogues (13), we are presently involved in the synthesis of nonhydrolyzable oligodeoxyribonucleotide strands of type **A**. In addition to the poly-sulfide (or sulfone) homopolymers, systems in which short modified regions are incorporated into natural DNA are being prepared. Such mixed molecules are of interest since it has been shown that the addition of backbone-modified units to the 3′ and 5′ ends of otherwise unaltered DNA greatly increases the strands' stability towards nuclease degradation (2, 14, 15). We believe that proper protection or activation of the sulphur-containing fragments (as in **B**) will allow for straightforward incorporation of the pieces into DNA by standard automated techniques.

In the present work, we describe the preparation of the three thymidine nucleoside units required for the construction of systems such as **A** and **B**. The syntheses are also important in that they represent an efficient and general route to 2′,3′-dideoxy-3′-*C*-substituted nucleosides, which are presently receiving much attention for their potential as antiviral agents (16).

Results and discussion

Key intermediates in the preparation of the target sulfide-linked DNA analogues are the 3′-deoxy-3′-*C*-(2″-hydroxyethyl)thymidine "5′-end" and "middle" units shown in Scheme 1. Two basic approaches exist for the synthesis of these molecules: the direct two-carbon homologation of nucleosides, or the preparation of the branched-chain sugar followed by the attachment of the nitrogenous base. The recent report (17) that the tributyltin-mediated radical allylation using 3′-thiocarbonate derivatives of thymidine occurs with high stereoselectivity provided us with a rapid entry to the branched-chain system. The oxidative cleavage of the olefinic bond of the 3′-*C*-allyl nucleoside **1** to the aldehyde

[1]Author to whom correspondence may be addressed.

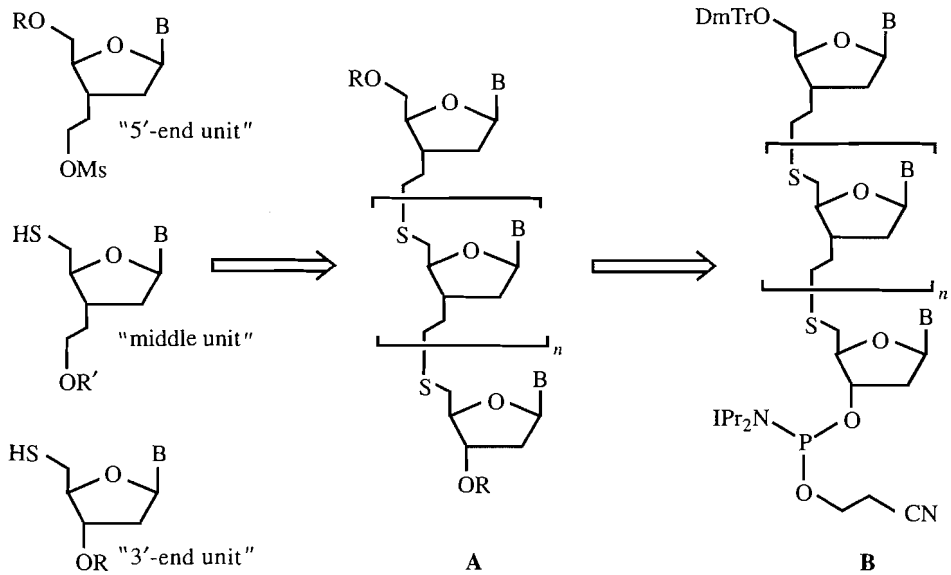

SCHEME I

has also been reported (18) but no experimental details were given. We found that treatment of **1** with osmium tetroxide and sodium periodate (Scheme 2) following the two-phase "ether–water method" (19) gave best results, the aldehyde **2** being obtained in 74% yield. Subsequent reduction with sodium borohydride in methanol cleanly provided, in 85% yield, the 3′-*C*-(2″-hydroxyethyl) nucleoside **3**. Mesylation afforded the thymidine "5′-unit" **4** in 90% yield.

The principal drawback of this approach is that the radical allylation is not generally applicable to all the purines and pyrimidines that will eventually be required. Attempts to allylate 2′-deoxy-3′-*O*-phenoxythiocarbonyl cytidine derivatives resulted in complex mixtures. In addition, 2′-deoxynucleosides other than thymidine are very expensive starting materials. We therefore developed a route to the branched-chain nucleosides following the second approach, namely, attachment of the hydroxyethyl group prior to base attachment.

This scheme proceeds from 3′-deoxy-3-*C*-(2′-hydroxyethyl)-1,2-*O*-isopropylidene-5-*O*-trityl-D-ribofuranose **5**, which is efficiently prepared in large scale from monoacetone xylofuranose in four steps and in 61% overall yield (20). The 2′-hydroxyl group of the sugar was protected as the *p*-methoxyphenyl ether, formed under Mitsunobu conditions using diethyl azodicarboxylate and triphenylphosphine in THF, to give **6** in 91% yield. The acetolysis of this sugar in a mixture of acetic acid and acetic anhydride containing camphorsulfonic acid heated to 70°C resulted in simultaneous cleavage of both the trityl and isopropylidene groups, affording the β-triacetate **7** in 69% yield, accompanied by a small amount of the expected acetylated *aldehydrol* derivatives (20). The Vorbrüggen coupling (21) of **7** and bis-(trimethylsilyl)thymine (22) in refluxing dichloroethane, using trimethylsilyl triflate as catalyst, proceeded smoothly to give nucleoside **8** in 91% yield. Subsequent deacetylation using methanolic ammonia afforded diol **9** in a quantitative manner that was selectively monosilylated to give the 5′-TBDMSi ether **10** in 86% yield. Having served its function (when acetylated) of directing the stereochemistry of the nucleosidation reaction, the 2′-OH was removed by forming the 2′-*O*-phenoxythiocarbonate **11** followed by treatment with tributyltin hydride (AIBN initiation) in hot toluene (23). The 2′-deoxy compound **12** was thus obtained in 81% yield for the two steps. The stereo- and regioselectivity of nucleoside formation was conclusively verified by comparing this product with the *p*-methoxyphenyl ether prepared from alcohol **3** obtained via the 3′-radical allylation route. The two samples of nucleoside **12** were identical in all respects. The product was also identical to material prepared by a completely different asymmetric synthesis (24) commencing from 4-*O*-benzyl-3,4-dihydroxybutyne.

The thymidine "middle unit" **13** was prepared from either compounds **9** or **12**. The Mitsunobu coupling (25) of alcohol **9** and thiolacetic acid employing diisopropyl azodicarboxylate and triphenylphosphine proceeded regioselectively to afford thiolester **14** in 85% yield. However, the subsequent removal of the remaining 2′-hydroxyl, again via the tributyltin hydride reduction of the phenoxythiocarbonate **15**, gave only fair yields of **16**, presumably due to interference with the radical reaction by the 5′-thiolester functionality. The target nucleoside was much more efficiently obtained by the desilylation, using tetra-*n*-butylammonium fluoride in THF, of the 2′-deoxynucleoside **12** to give alcohol **17**, followed by Mitsunobu coupling with thiolacetic acid, which afforded the thiolester **16** in 87% yield for the two steps. The deprotection of the *S*-acetate was carried out in methanolic sodium hydroxide followed by neutralization with acidic resin. Careful deoxygenation of all of the solutions proved necessary to prevent the rapid oxidation of the resultant thiolate to the symmetrical disulfide. The reaction could also be performed using methanolic ammonia, again carefully removing and excluding any oxygen. The thiol **13** was thus obtained in 98% yield.

The thymidine "3-end unit" was prepared in three steps from thymidine (Scheme 3). The Mitsunobu coupling of the free nucleoside and thiolacetic acid in a mixture of THF and DMF gave the 5′-monothiolester **18** in 52% yield that was converted to the 3′-silyl ether **19** in 92% yield. The deacetylation was again performed using methanolic hydroxide, being careful to exclude oxygen from the reaction, which

Can. J. Chem. Downloaded from www.nrcresearchpress.com by 217.78.4.112 on 09/08/12
For personal use only.

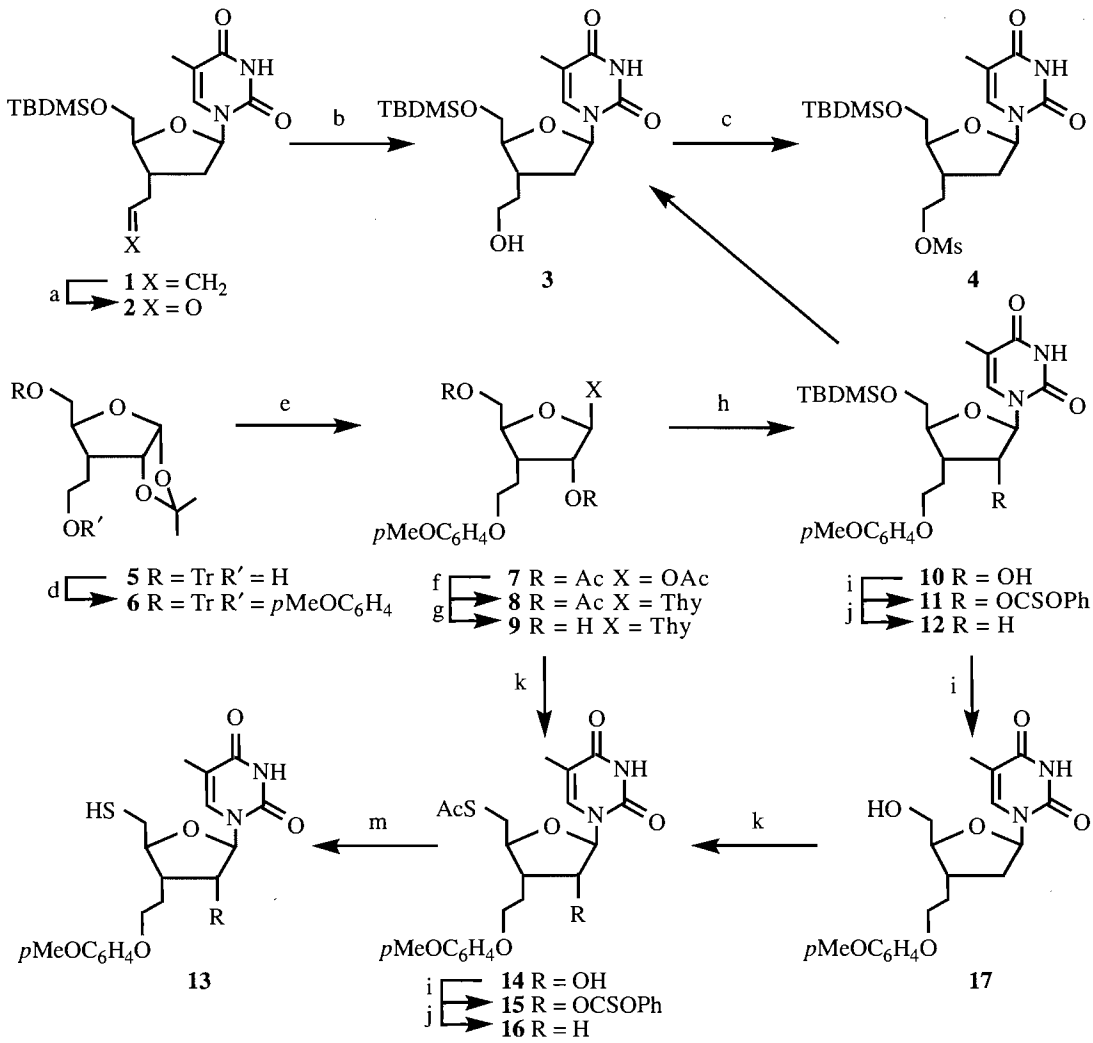

(a) $OsO_4/NaIO_4/Et_2O/H_2O$; (b) $NaBH_4$/MeOH; (c) MsCl/pyridine/CH_2Cl_2; (d) *p*-$MeOC_6H_4OH$/DEAD/PPh_3/THF; (e) AcOH/Ac_2O/camphorsulfonic acid/70°C; (f) $(TMSi)_2$Thy/TMSiOTf/$ClCH_2CH_2Cl$/reflux; (g) $NH_{3(g)}$/MeOH; (h) TBDMSiCl/imidazole/DMF; (i) PhOSCCl/pyridine/CH_2Cl_2; (j) *n*-Bu_3SnH/toluene/75°C; (k) AcSH/DIAD/PPh_3/THF; (l) *n*-Bu_4NF/THF; (m) conditions (g) or NaOH/MeOH

SCHEME 2

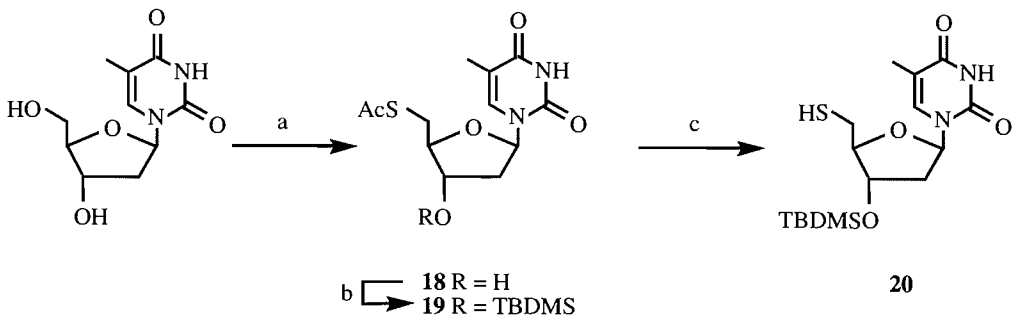

(a) AcSH/DIAD/PPh_3/DMF/THF; (b) TBDMSiCl/imidazole/DMF; (c) NaOH/MeOH

SCHEME 3

gave the thiol **20** in quantitative yield. It should be pointed out that, unlike 5′-deoxy-5′-thiouridine derivatives that exist as Michael adducts with the pyrimidine base (26), the analogous derivatives of thymidine are stable as the free thiol.

In summary, the thiothymidine and 3′-deoxy-3′-*C*-(2″-hydroxyethyl)thymidine derivatives **4**, **13**, and **20** required for the preparation of a sulfide-linked DNA analogue have been efficiently synthesized by two routes. One of these ap-

Can. J. Chem. Downloaded from www.nrcresearchpress.com by 217.78.4.112 on 09/08/12
For personal use only.

proaches is applicable to all four bases and work in this regard is ongoing. The coupling of the units has been successfully carried out and, in the case of the dimer, the molecule has been deprotected and activated for incorporation into DNA. The details of this work will be described shortly.

Experimental

General methods

Melting points (mp) were determined using an Electrothermal MP apparatus and are uncorrected. Low-resolution chemical ionization mass spectra (CI) were obtained on an HP 5980A quadrapole mass spectrometer in the direct-inlet mode. High-resolution CI and fast-atom bombardment (FAB) mass spectra (HRMS) were obtained on a VG ZAB-HS sector mass spectrometer, again, in the direct-inlet mode. The measurements were carried out at a resolving power of 10 000. Elemental analyses were performed by Guelph Chemical Laboratories Ltd., Guelph, Ontario. All compounds were shown to be homogeneous by thin-layer chromatography (tlc) and high-field NMR and (or) to have a purity of >95% by elemental analysis.

^{1}H NMR spectra were recorded on either Varian XL200 or Varian XL300 spectrometers and the assignments are based on homonuclear decoupling and (or) COSY experiments. When deuteriochloroform was employed as solvent, internal tetramethylsilane (TMS) was used as the reference. The residual proton signal or methanol, assigned a value of 3.30 ppm, was used as the reference in this case. The multiplicities are recorded using the following abbreviations: s, singlet; d, doublet; t, triplet; q, quartet; h[7], heptet; m, multiplet; m″, symmetical signal of *n* lines; br, broad. ^{13}C NMR spectra were all obtained at 75.4 MHz using a Varian XL300 spectrometer. The $^{13}CDCl_3$ and $^{13}CD_3OD$ signals, assigned values of 77.00 and 49.00 ppm, respectively, were used as references in these solvents. Peak assignments were, in some cases, made with the aid of APT or HETCOR experiments.

Tetrahydrofuran was distilled from sodium benzophenone ketyl. Dichloromethane and 1,2-dichloroethane were distilled from P_2O_5. Toluene was dried over sodium wire. Pyridine was distilled from calcium hydride. *N,N*-Dimethylformamide was dried by shaking with KOH followed by distillation, at reduced pressure, from BaO. Thin-layer chromatography (tlc) was performed using Kieselgel 60 F_{254} aluminium-backed plates (0.2 mm thickness) and visualized by UV and (or) dipping in a solution of ammonium molybdate (2.5 g) and ceric sulfate (1 g) in 10% v/v aqueous sulphuric acid (100 mL), followed by heating. Kieselgel 60 (Merck 230–400 mesh) silica gel was employed for column chromatography.

*Aldehyde (**2**)*

Osmium tetroxide (100 mg, 0.393 mmol) was added to a two-phase system comprising ethyl ether (8 mL) and water (8 mL) containing nucleoside **1** (1.00 g, 2.63 mmol). To the resulting brown mixture was then added sodium metaperiodate (1.24 g, 5.80 mmol) in small portions over 0.5 h. The reaction was stirred at ambient temperature under nitrogen in the dark. After an additional 1 h the mixture was extracted with dichloromethane (2 × 200 mL) and washed with aqueous sodium bicarbonate (5% w/v, 300 mL) and water (300 mL). The combined organic phases were then dried (Na_2SO_4), filtered, and the solvent removed *in vacuo* yielding a colorless glass. Chromatography over silica gel (2:1 to 4:1 ethyl acetate/hexanes, v/v) afforded aldehyde **2** as a white solid (740 mg, 74% yield); ^{1}H NMR ($CDCl_3$, 200 MHz) δ: 0.120 and 0.122 (two s, 6H, Si*Me*$_2$), 0.93 (s, 9H, *t*-Bu), 1.94 (fine d, 3H, J = 1.2 Hz, 5-Me), 2.08 (A of ABXY, 1H, H2′$_A$), 2.32 (B of ABXY, 1H, H2′$_B$), 2.50–2.84 (m, 3H, H1″$_{AB}$ and H3′), 3.73–3.84 (m, 2H, H5′$_A$, and H4′), 3.97 (dd, 1H, H5′$_B$), 6.14 (dd, 1H, H1′), 7.54 (fine q, 1H, J = 1.2 Hz, H6), 8.72 (br s, 1H, NH), 9.80 (s, 1H, C*H*O), $J_{H1'-H2'A}$ = 6.7 Hz, $J_{H1'-H2'B}$ = 5.2, $^2J_{H2'A-H2'B}$ = −13.5, $J_{H2'A-H3'}$ = 6.8, $J_{H2'B-H3'}$ = 7.8; ^{13}C NMR ($CDCl_3$): 12.58 ppm (5-Me), 18.40 (*C*Me$_3$), 25.90 (C*Me*$_3$ and Si*Me*$_2$), 32.24 (C3′), 38.57 (C2′), 46.72 (C1″), 63.25 (C5′), 84.65 and 85.36 (C1′ and C4′), 110.58 (C5), 135.40 (C6), 150.50 (C2), 164.04 (C4), 199.80 (*C*HO); MS (CI–NH_3) *m/e*: 383 ([MH^+], 100%), 274 ([M + NH_4^+ − ThyH], 17), 257 ([MH^+ − ThyH], 68), 127 ([ThyH + H^+], 10); HRMS (CI–NH_3) *m/e* calcd. for $C_{18}H_{31}N_2O_5Si$: 383.20022; found: 383.220018.

*5′-O-tert-Butyldimethylsilyl-3′-deoxy-3′-C-(2″-hydroxyethyl)thymidine (**3**)*

Sodium borohydride (34 mg, 0.90 mmol) was added to a stirred solution of aldehyde **2** (690 mg, 1.80 mmol) in methanol (16 mL) and the reaction was stirred at ambient temperature. After 1.5 h glacial acetic acid (200 mL) was added to the solution and the solvent evaporated *in vacuo* affording a colorless syrup that was extracted with dichloromethane (150 + 100 mL) and washed with aqueous sodium bicarbonate (saturated, 300 mL) and brine (300 mL). The combined organic phases were then dried (Na_2SO_4), filtered, and the solvent removed *in vacuo* affording essentially pure alcohol **3** as a colorless glass (593 mg, 85% yield), which was used in the next step without further purification: ^{1}H NMR ($CDCl_3$, 300 MHz) δ: 0.12 and 0.13 (two s, 6H, Si*Me*$_2$), 0.94 (s, 9H, *t*-Bu), 1.51–1.62 (m, 1H, H1″$_A$), 1.74–1.85 (m, 1H, H1″$_B$), 1.92 (fine d, 3H, J = 1.3 Hz, 5-Me), 2.14 (A of ABXY, 1H, H2″$_A$), 2.25 (B of ABXY, 1H, H2″$_B$), 2.37–2.49 (m, 1H, H3′), 3.65–3.81 (m, 5H, H5′$_A$; H4′; H2″$_{AB}$ and -O*H*), 4.01 (dd, 1H, H5′$_B$), 6.08 (dd, 1H, H1′), 7.57 (fine q, 1H, J = 1.3 Hz, H6), 8.34 (br s, 1H, N*H*), $J_{H1'-H2'A}$ = 6.8 Hz, $J_{H1'-H2'B}$ = 3.9, $^2J_{H2'A-H2'B}$ = −13.5, $J_{H2'A-H3'}$ = 9.2, $J_{H2'B-H3'}$ = 7.6; ^{13}C NMR ($CDCl_3$): 12.84 (5-Me), 1942 (Si*C*Me$_3$), 26.53 (SiC*Me*$_3$ and Si*Me*$_2$), 35.57 (C3′), 35.88 (C1″), 39.76 (C2′), 61.31 (C5′), 64.02 (C2″), 86.32 and 87.94 (C1′ and C4′), 110.78 (C5), 137.80 (C6), 152.29 (C2), 166.42 (C4); MS (CI–NH_3), *m/e*: 385 ([MH^+], 17%), 276 ([M + NH_4^+ − ThyH], 21), 259 ([MH^+ − ThyH], 100), 127 ([ThyH + H^+], 10); HRMS (CI–NH_3) *m/e* calcd. for $C_{18}H_{33}N_2O_5Si$: 385.21588; found: 385.21593.

*5′-O-tert-Butyldimethylsilyl-3′-deoxy-3′-C-(2″-hydroxyethyl)-2″-O-(methanesulfonyl)thymidine (**4**)*

Methanesulfonyl chloride (201 μL, 2.60 mmol) was added dropwise to a stirred solution of alcohol **3** (500 mg, 1.30 mmol) in dry dichloromethane (5 mL) containing pyridine (946 μL, 11.7 mmol) and the resulting solution was stirred at room temperature under a nitrogen atmosphere. After 5 h the reaction was extracted with dichloromethane (2 × 100 mL) and washed with dilute sulphuric acid (2.5% w/v, 200 mL), aqueous sodium bicarbonate (saturated, 200 mL) and water (200 mL). The combined organic phases were then dried (Na_2SO_4), filtered, and the solvent removed *in vacuo*. The resulting syrup was chromatographed over silica gel (8:1 ethyl acetate/hexanes, v/v) to afford mesylate **4** as a crystalline solid (556 mg, 92% yield): mp 72–76°C (dec.); ^{1}H NMR ($CDCl_3$, 300 MHz) δ: 0.12 (s, 6H, Si*Me*$_2$), 0.93 (s, 9H, *t*-Bu), 1.74 (m[10], 1H, H1″$_A$), 1.93 (fine d, 3H, J = 1.2 Hz, 5-Me), 1.97–2.06 (m, 1H, H1″$_B$), 2.16 (A of ABXY, 1H, H2′$_A$). 2.27 (B of ABXY, 1H, H2′$_B$), 2.40–2.52 (m, 1H, H3′), 3.03 (s, 3H, OMs), 3.74–3.81 (m, 2H, H4′ and H5′$_A$), 4.00 (dd, 1H, H5′$_B$), 4.23–4.35 (m, 2H, H2″AB), 6.12 (dd, 1H, H1′), 7.53 (fine q, 1H, J = 1.2 Hz, H6), 8.73 (br s, 1H, N*H*), $J_{H1'-H2'A}$ = 6.8 Hz, $J_{H1'-H2'B}$ = 4.4, $^2J_{H2'A-H2'B}$ = −13.5, $J_{H2'A-H3'}$ = 8.3, $J_{H2'B-H3'}$ = 8.0; ^{13}C NMR ($CDCl_3$): 12.54 ppm (5-Me), 18.36 (Si*C*Me$_3$), 25.86 (SiC*Me*$_3$ and Si*Me*$_2$), 31.72 (C1″), 34.39 (C3′), 37.42 (O*Ms*), 38.46 (C2′), 62.81 (C5′), 67.67 (C2″), 84.70 and 85.60 (C1′ and C4′), 110.40 (C5), 135.40 (C6), 150.51 (C2), 164.04 (C4); MS (CI–NH_3) *m/e*: 480 ([M + NH_4^+], 2.3%), 463 ([MH^+], 87%), 354 ([M + NH_4^+ − ThyH], 51), 337 ([MH^+ − ThyH], 100); HRMS (CI–NH_3) *m/e* calcd. for $C_{19}H_{35}N_2O_7SSi$: 463.19342; found: 463.19343.

*3-Deoxy-3-C-(2′-hydroxyethyl)-1,2-O-isopropylidene-2′-O-para-methoxyphenyl-5-trityl-α-D-ribofuranose (**6**)*

A solution of alcohol **5** (2.96 g, 6.43 mmol), *para*-methoxyphenol (2.39 g, 19.29 mmol), triphenylphosphine (2.19 g, 8.36 mmol), and diethyl azodicarboxylate (1.32 mL, 8.36 mmol)

Can. J. Chem. Downloaded from www.nrcresearchpress.com by 217.78.4.112 on 09/08/12
For personal use only.

Can. J. Chem. Downloaded from www.nrcresearchpress.com by 217.78.4.112 on 09/08/12
For personal use only.

in dry tetrahydrofuran was refluxed for 20 min. The solvent was then removed *in vacuo* yielding a violet syrup. Chromatography over silica gel (3:1 hexanes/ethyl acetate, v/v) afforded ether **6** as a white solid (3.30 g, 91% yield). Recrystallization from dichloromethane gave white crystals: mp 117–118°C; ^{1}H NMR (300 MHz, $CDCl_3$) δ: 1.34 and 1.51 (two s, 6H, C*Me*$_2$), 1.69–1.95 (m, 2H, H1′$_{AB}$), 2.39 (h^7, 1H, H3), 3.10 (A of ABX, 1H, H5$_A$), 3.40 (B of ABX, 1H, H5$_B$), 3.76 (s, 3H, O*Me*), 3.91–3.98 (m, 3H, H4 and H2′$_{AB}$), 4.70 (t, 1H, H2), 5.90 (d, 1H, H1), 6.76 (apparent d, 4H, MeO*Ph*O-), 7.21–7.47 (two m, 15H, C*Ph*$_3$), J_{H1-H2} = 3.8, J_{H2-H3} = 4.2, J_{H4-H5A} = 3.9, J_{H4-H5B} = 3.0, $^2J_{H5A-H5B}$ = −10.6; ^{13}C NMR ($CDCl_3$): 24.64 ppm (C1′), 26.42 and 26.76 (C*Me*$_2$), 41.87 (C3), 55.69 (O*Me*), 63.15 (C5), 66.34 (C2′), 80.90 and 81.03 (C2 and C4), 86.45 (*C*Ph$_3$), 104.99 (C1), 111.42 (*C*Me$_2$), 114.55 and 115.27 (*C*H of MeO*Ph*O-), 126.90; 127.76; 128.70 (*C*H of Tr), 143.92 (4° of Tr), 152.83 and 153.69 (4° of MeO*Ph*O-), MS (CI–NH$_3$), *m/e*: 567 ([MH$^+$], 4.9%), 243 ([CPh$_3^+$], 100), HRMS (CI–NH$_3$) *m/e* calcd. for $C_{36}H_{39}O_6$: 567.27466; found: 567.27489; Anal. calcd. for $C_{36}H_{38}O_6$: C 76.30, H 6.76; found: C 76.04, H 7.14.

1,2,5-Tri-O-*acetyl-3-deoxy-3*-C-*(2′-hydroxyethyl)-2′*-O-para-*methoxyphenyl-α-D-ribofuranose (7)*

Acetonide **6** (576 mg, 1.00 mmol) was dissolved in glacial acetic acid (15 mL) containing acetic anhydride (2.37 mL, 25.0 mmol) and the solution was heated to 70°C and stirred for 15 min. Camphorsulfonic acid (464 mg, 2.00 mmol) was then added and the resulting solution was stirred under nitrogen for 12 min. The solution was then cooled to 0°C and carefully poured into a solution of sodium carbonate (27.2 g) in water (170 mL) and the resulting suspension swirled occasionally over 30 min. The product was extracted with ethyl ether (2 × 200 mL) and washed with aqueous sodium bicarbonate (saturated, 200 mL) and water 200 mL). The combined ether extracts were then dried ($MgSO_4$), filtered, and the solvent evaporated *in vacuo* affording a colorless syrup that was chromatographed over silica gel (3:1 hexanes/ethyl acetate, v/v) to give triacetate **7** as a colorless syrup (282 mg, 69% yield): ^{1}H NMR (300 MHz, $CDCl_3$) δ: 1.72–2.16 (m, 2H, H1′$_{AB}$), 2.06; 2.07, and 2.09 (three s, 9H, OAc), 2.49 (h^7, 1H, H3), 3.76 (s, 3H, O*Me*), 3.86–4.05 (m, 2H, H2′$_{AB}$), 4.05–4.34 (m, 3H, H4, and H5$_{AB}$), 5.30 (d, 1H, H2), 6.09 (s, 1H, H1), 6.81 (s, 4H, MeO*Ph*O-), J_{H1-H2} ~ 0, J_{H2-H3} = 4.8; ^{13}C NMR ($CDCl_3$): 20.16; 20.26, and 20.64 ppm (OC*OMe*), 24.46 (C1′), 38.98 (C3), 55.15 (O*Me*), 64.98 (C5), 66.13 (C2′), 76.68 (C2), 82.36 (C4), 98.42 (C1), 114.22 and 114.76 (*C*H of MeO*Ph*O-), 152.14 and 153.52 (4° of MeO*Ph*O-), 168.62; 169.42, and 170.17 (*C*OMe); MS (CI–NH$_3$) *m/e*: 428 ([M + NH$_4^+$], 16%), 411 ([MH$_4^+$], 1.2), 351 ([MH$^+$ − AcOH], 100); HRMS (CI–NH$_3$) *m/e* calcd. for $C_{20}H_{27}O_9$: 411.1655; found: 411.1657.

2′,5′-Di-O-*acetyl-3′-deoxy-3′*-C-*(2″-hydroxyethyl)-2″*-O-para-*methoxyphenyl-(β-D-ribofuranosyl)thymine (8)*

Trimethylsilyl trifluoromethanesulfonate (0.75 mL, 1.56 mmol) was added dropwise to a stirred solution of triacetate **7** (6.41 g, 15.64 mmol) and bis-(trimethylsilyl)thymine (4.10 g, 17.20 mmol) in dry 1,2-dichloroethane (120 mL) and the resulting solution was heated to reflux under a nitrogen atmosphere. After 6 h the solution was cooled in an ice bath and poured into ice-cold aqueous sodium bicarbonate (5% w/v, 500 mL) and extracted with dichloromethane (500 mL). The organic phase was dried (Na_2SO_4), filtered, and the solvent removed *in vacuo* yielding a brown foam that was chromatographed over silica gel (2:1 ethyl acetate/hexanes, v/v) to give **8** as a white foam (6.78 g, 91% yield): ^{1}H NMR (300 MHz, $CDCl_3$) δ: 1.93 (fine d, 3H, 5-Me, J = 0.7), 2.11 and 2.13 (two s, 6H, OAc), 2.55 (h^7, 1H, H3′), 3.76 (s, 3H, O*Me*), 3.89–4.00 (m, 2H, H2″$_{AB}$), 4.20 (ddd, 1H, H4′), 4.38 (A of ABX, 1H, H5′$_A$), 4.45 (B of ABX, 1H, H5′$_B$), 5.51 (dd, 1H, H2′), 5.72 (d, 1H, H1′), 6.80 (s, 4H, MeO*Ph*O-), 7.26 (fine q, 1H, J = 0.8 Hz, H6), 8.74 (br s, 1H, NH), $J_{H1'-H2'}$ = 1.3, $J_{H2'-H3'}$ = 6.1, $J_{H3'-H4'}$ = 10.2, $J_{H4'-H5'A}$ = 4.8, $J_{H4'-H5'B}$ = 2.2, $^2J_{H5'A-H5'B}$ = −12.6; ^{13}C NMR ($CDCl_3$): 12.48 ppm (5-Me), 20.57 and 20.64 (CO*Me*), 24.48 (C1″), 39.00 (C3′), 55.53 (O*Me*), 63.20 (C5′), 66.06 (C2″), 77.31 (C2′), 82.00 (C4′), 91.23 (C1′), 110.63 (C5), 114.52 and 115.08 (*C*H of MeO*Ph*O-), 135.64 (C6), 149.95; 152.35 and 153.80 (C2 and 4° of MeO*Ph*O-), 163.85 (C4), 169.50 and 170.30 (*C*OMe); MS (CI–NH$_3$), *m/e*: 477 ([MH$^+$], 100%), 417 ([MH$^+$ − AcOH], 4.6), 351 ([MH$^+$ − ThyH], 86); HRMS (CI–NH$_3$) *m/e* calcd. for $C_{23}H_{29}N_2O_9$: 477.18730; found: 477.18742. Anal. calcd. for $C_{23}H_{28}N_2O_9$: C 57.98, H 5.92, H 5.88; found: C 57.99, H 6.27, N 5.75.

3′-Deoxy-3′-C-*(2″-hydroxyethyl)-2″*-O-para-*methoxyphenyl-(β-D-ribofuranosyl)thymine (9)*

Nucleoside **8** (107 mg, 0.20 mmol) was dissolved in methanol (1.00 mL), cooled to 0°C, and a steady stream of NH_3 gas bubbled through the solution for 10 min. The solution was then allowed to warm to ambient temperature and was stirred for 10 h. The solvent was removed *in vacuo* and the residue was chromatographed over silica gel (20:1 dichloromethane/methanol, v/v) yielding the diol **9** as a white foam (92 mg, 100% yield): ^{1}H NMR (300 MHz, $CDCl_3$) δ: 1.88 (s, 3H, 5-Me), 1.76–1.92 (m, 1H, H1″$_A$), 2.08–2.23 (m, 1H, H1″$_B$), 2.33–2.41 (m, 1H, H3′), 3.75 (s, 3H, O*Me*), 3.82 (br d, 1H, H4′), 4.04 (br t, 2H, H2″$_{AB}$), 4.16 (br t, 2H, H5′$_{AB}$), 4.39 (d, 1H, H2′), 5.55 (br s, 2H, -O*H*), 5.77 (s, 1H, H1′), 6.81 (s, 4H, MeO*Ph*O-), 7.89 (s, 1H, H6), 10.03 (s, 1H, N*H*), $J_{H1'-H2'}$ ~ 0, $J_{H2'-H3'}$ = 4.16; ^{13}C NMR ($CDCl_3$): 12.38 ppm (5-Me), 24.01 (C1″), 37.73 (C3′), 55.60 (O*Me*), 60.74 (C5′), 67.05 (C2″), 76.85 (C2′), 85.41 (C4′), 92.59 (C1′), 109.85 (C5), 114.58 and 115.32 (*C*H of MeO*Ph*O-), 136.50 (C6), 150.88; 152.49 and 153.85 (C2 and 4° of MeO*Ph*O-), 164.70 (C4); MS (CI–NH$_3$) *m/e*: 410 ([M + NH$_4^+$], 1.1%), 393 ([MH$^+$], 100), 284 ([M + NH$_4^+$ − ThyH], 4.0), 267 ([MH$^+$ − ThyH], 9.4), 127 ([ThyH + H$^+$], 0.8); HRMS (CI–NH$_3$) *m/e* calcd. for $C_{19}H_{25}N_2O_7$: 393.16618; found: 393.16625.

5′-O-tert-*Butyldimethylsilyl-3′-deoxy-3′*-C-*(2″-hydroxyethyl)-2″*-O-para-*methoxyphenyl-(β-D-ribofuranosyl)thymine (10)*

To a solution of alcohol **9** (1.91 g, 4.00 mmol) in freshly distilled *N,N*-dimethyformamide (4 mL) was added *tert*-butyldimethylsilyl chloride (0.63 g, 4.20 mmol) and imidazole (598 mg, 8.80 mmol) and the reaction was stirred at room temperature under a nitrogen atmosphere. After 18 h the solvent was removed *in vacuo* and the residue was extracted with ethyl acetate (2 × 300 mL) and washed with water (300 mL). The combined organic layers were then dried (Na_2SO_4), filtered, and evaporated *in vacuo* yielding a white foam that was chromatographed over silica gel (2:1 ethyl acetate/hexanes) to give silyl ether **10** as a white solid (2.12 g, 86% yield): ^{1}H NMR (300 MHz, $CDCl_3$) δ: 0.12 and 0.14 (two s, 6H, Si*Me*$_2$), 0.95 (s, 9H, C*Me*$_3$), 1.91 (s, 3H, 5-Me), 1.71–1.81 (m, 1H, H1″$_A$), 2.05–2.18 (m, 1H, H1″$_B$), 2.37 (h7, 1H, H3′), 3.74–3.80 (overlapping s and m, 4H, H5′$_A$ and O*Me*), 4.01 (br t, 2H, H2″$_{AB}$), 4.14–4.20 (m, 2H, H4′ and H5′$_B$), 4.36 (apparent t, 1H, H2′), 4.81 (s, 1H, -O*H*), 5.75 (s, 1H, H1′), 6.80 (s, 4H, MeO*Ph*O-), 7.81 (s, 1H, H6), 10.08 (s, 1H, N*H*), $J_{H1'-H2'}$ ~ 0; ^{13}C NMR ($CDCl_3$): 12.72 ppm (5-Me), 18.64 (*C*Me$_3$), 23.76 (C1″), 26.03 (*CMe*$_3$ and Si*Me*$_2$), 36.71 (C3′), 55.69 (O*Me*), 61.47 (C5′), 66.33 (C2″), 76.58 (C2′), 85.61 (C4′), 92.97 (C1′), 109.82 (C5), 114.59 and 115.61 (*C*H of MeO*Ph*O-), 135.89 (C6), 150.74; 152.88 and 153.73 (C2 and 4° of MeO*Ph*O-), 164.77 (C4); MS (FAB–glycerol) *m/e*: 507 ([MH$^+$], 1.8%), 171 (22), 127 ([ThyH + H$^+$], 3.6); HRMS (FAB–glycerol) *m/e* calcd. for $C_{25}H_{39}O_7N_2Si$: 507.25265; found 507.25277. Anal. calcd. for $C_{25}H_{38}O_7N_2Si$: C 59.26, H 7.56, N 5.53; found: C 58.87, H 7.83, N 5.30.

5′-O-tert-*Butyldimethylsilyl-3′-deoxy-3′*-C-*(2″-hydroxyethyl)-2″*-O-para-*methoxyphenyl-2′*-O-*phenoxythiocarbonyl-(β-D-ribofuranosyl)thymine (11)*

Phenyl chlorothionoformate (595 μL, 4.30 mmol) was added dropwise to a stirred solution of nucleoside **10** (1.98 g, 3.91 mmol) in dry dichloromethane (10 mL), containing dry pyridine (2.5 mL) and the reaction was stirred under a nitrogen atmosphere at 0.°C.

Can. J. Chem. Downloaded from www.nrcresearchpress.com by 217.78.4.112 on 09/08/12
For personal use only.

After 1 h the brown solution was placed in a refrigerator for 20 h. The solvents were then removed *in vacuo* yielding a red syrup to which water (200 mL) was added and the resulting suspension shaken vigorously. The product was extracted with ether (2 × 200 mL) and washed with dilute sulphuric acid (2% w/v, 200 mL), aqueous sodium bicarbonate (saturated, 200 mL), and water (300 mL). The combined ether phases were then dried (Na_2SO_4), filtered, and evaporated *in vacuo* to an orange solid that was chromatographed over silica (2:1 hexanes/ethyl acetate, v/v) to afford thiocarbonate **11** as a pale orange solid (2.20 g, 87% yield): ^{1}H NMR (300 MHz, $CDCl_3$) δ: 0.13 (s, 6H, Si*Me*$_2$), 0.94 (s, 9H, C*Me*$_3$), 1.93 (fine d, 3H, J = 1.1 Hz, 5-Me), 1.84–1.94 (m, 1H, H1″$_A$), 2.04–2.16 (m, 1H, H1″$_B$), 2.91 (m[9], 1H, H3′), 3.76 (s, 3H, O*Me*), 3.80 (dd, 1H, H5′$_A$), 3.98–4.14 (m, 4H, H5′$_B$; H4′ and H2″$_{AB}$), 5.94 (dd, 1H, H2′), 6.08 (d, 1H, H1′), 6.83 (s, 4H, MeO*Ph*O-), 7.08–7.41 (three m, 5H, CSO*Ph*), 7.43 (fine q, 1H, J = 1.1 Hz, H6), 8.28 (br s, 1H, N*H*), $J_{H1'-H2'}$ = 2.4, $J_{H2'-H3'}$ = 6.4; ^{13}C NMR ($CDCl_3$): 12.47 ppm (5-Me), 18.37 (*C*Me$_3$), 24.88 (C1″), 25.87 (C*Me*$_3$ and Si*Me*$_2$), 38.41 (C3′), 55.56 (O*Me*), 62.33 (C5′), 66.38 (C2″), 84.33 (C4′), 86.36 (C1′), 89.14 (C2′), 111.02 (C5), 114.56 and 115.16 (*C*H of MeO*Ph*O-), 121.64 (*o*-*C*H of Ph), 126.60 (*p*-*C*H of Ph), 129.44 (*m*-*C*H of Ph), 135.69 (C6), 150.08; 152.55; 153.20 and 153.81 (C2 and 4° of MeO*Ph*O- and Ph), 163.96 (C4), 193.69 (*C*SOPh): MS (FAB – nitrobenzyl alcohol) *m/e*: 643 ([MH$^+$], 6.7%), 527 ([MH$^+$ – ThyH], 14), 489 ([MH$^+$ – PhOCSOH], 100), 163 (73), 137 ([PhO=C=S$^+$], 73), 127 ([ThyH + H$^+$], 27). Anal. calcd. for $C_{32}H_{42}O_8N_2SiS$: C 59.79, H 6.58, N 4.36, S 4.99; found: C 59.47, H 6.70, N 4.43, S 4.87.

5′-O-tert-*Butyldimethylsilyl-3′-deoxy-3′*-C-*(2″-hydroxyethyl)-2″*-O-(para-*methoxyphenyl)thymidine (12)*

Tri-*n*-butyltin hydride (2.48 mL, 6.06 mmol) was added to a solution of thiocarbonate **11** (1.94 g, 3.03 mmol) and AIBN (0.61 g, 2.42 mmol) in dry toluene (15 mL). A stream of nitrogen was passed through the reaction for 20 min and the solution was heated to 75°C for 4 h. The solvent was then removed *in vacuo* and the residue chromatographed over silica (1:1 hexanes/ethyl acetate, v/v) to yield the 2′-deoxy nucleoside **12** as a white solid (1.38 g, 93% yield): ^{1}H NMR (300 MHz, $CDCl_3$) δ: 0.116 and 0.120 (two s, 6H, Si*Me*$_2$), 0.94 (s, 9H, C*Me*$_3$), 1.92 (d, 3H, J = 1.0 Hz, 5-Me), 1.71–1.78 (m, 1H, H1″$_A$), 1.95–2.06 (m, 1H, H1″$_B$), 2.14–2.31 (m, 2H, H2′$_{AB}$), 2.47–2.56 (m, 1H, H3′), 3.75–3.83 and 3.92–4.06 (two m, 5H and 3H, -O*Me*; H5′$_{AB}$; H4′; and H2″$_{AB}$), 6.12 (dd, 1H, H1′), 6.82 (apparent d, 4H, MeO*Ph*O-), 7.61 (fine 9, 1H, J = 1.0 Hz, H6), 8.77 (br s, 1H, NH), $J_{H1'-H2'}$ = 3.9 and 6.5; ^{13}C NMR ($CDCl_3$): 12.55 ppm (5-Me), 18.41 (C*Me*$_3$), 25.87 (C*Me*$_3$ and Si*Me*$_2$), 31.65 (C1″), 34.32 (C3′), 39.12 (C2′), 55.58 (O*Me*), 62.60 (C5′), 66.39 (C2″), 84.83 and 86.18 (C4′ and C1′), 110.07 (C5), 114.56 and 115.10 (*C*H of MeOPhO-), 135.56 (C6), 150.52; 152.59 and 153.77 (C2 and 4° of MeOPhO-), 164.18 (C4); MS (FAB – nitrobenzyl alcohol) *m/e* 491 ([MH$^+$], 16%), 365 ([MH$^+$ – ThyH], 77), 163 (100), 127 ([ThyH + H$^+$], 51; HRMS (FAB–glycerol) *m/e* calcd. for $C_{25}H_{39}O_6N_2Si$: 491.25774; found: 491.25772.

3′-5′-Dideoxy-3′-C-*(2″-hydroxyethyl)-2″*-O-para-*methoxyphenyl-5′-thiothymidine (13)*

A solution of thiolester **16** (455 mg, 1.05 mmol) in dry methanol (5 mL), previously saturated with nitrogen gas, was cooled to 0°C and a stream of ammonia gas passed through for 15 min. The ice bath was removed and the reaction was stirred for 20 h. The solvent was then evaporated *in vacuo* yielding a white solid that was chromatographed over silica (4:1 ethyl acetate/hexanes, v/v) to afford thiol **13** as a white solid (410 mg, 98% yield): ^{1}H NMR (300 MHz, $CDCl_3$) δ: 1.59 (t, 1H, -S*H*), 1.72–1.83 (m, 1H, H1″$_A$), 1.94 (d, 3H, J = 1.2 Hz, 5-Me), 1.96–2.03 (m, 1H, H1″$_B$), 2.24–2.29 (m, 2H, H2′$_{AB}$), 2.38–2.52 (m, 1H, H3′), 2.83 (A of ABX with an additional coupling to SH, 1H, H5′$_A$), 3.01 (B of ABX with an additional coupling to SH, 1H, H5′$_B$), 3.77 (s, 3H, O*Me*), 3.86–3.92 (m, 1H, H4′), 3.94–4.00 (m, 2H, H2″$_{AB}$), 6.16 (t, 1H, H1′), 6.93 (apparent d, 4H, MeO*Ph*O-), 7.51 (fine q, 1H, J = 1.2 Hz, H6), 8.43 (br s, 1H, N*H*), $J_{H1'-H2'}$ ~ 5.4, $J_{H4'-H5'A}$ = 5.0, $J_{H4'-H5'B}$ = 3.7, $^2J_{H5'A-H5'B}$ = −14.4, $J_{H5'A-SH}$ = 8.0, $J_{H5'B-SH}$ = 8.9; ^{13}C NMR ($CDCl_3$): 12.45 ppm (5-Me), 27.11 (C1″), 31.45 (C2′), 37.59 (C3′), 38.61 (C5′), 55.47 (O*Me*), 66.35 (C2″), 84.03 and 84.77 (C1′ and C4′), 110.63 (C5), 114.49 and 115.11 (*C*H of MeO*Ph*O-), 135.47 (C6), 150.48; 152.30 and 153.75 (C2 and 4° of MeO*Ph*O-), 163.99 (C4); MS (FAB – nitrobenzyl alcohol) *m/e*: 393 ([MH$^+$], 12%), 267 ([MH$^+$ – ThyH], 4.3), 154 (100), 137 ([MeOPhOCH$_2^+$], 65), 136 (68), 127 ([ThyH + H$^+$], 25); HRMS (FAB–glycerol) *m/e* calcd. for $C_{19}H_{25}O_5N_2S$: 393.14842; found: 393.14849. Anal. calcd. for $C_{19}H_{24}O_5N_2S$: C 58.15, H 6.16, N 7.14, S 8.17; found: C 57.84, H 6.54, N 7.17, S 7.88.

5′-S-*Acetyl-3′,5′-dideoxy-3′*-C-*(2″-hydroxyethyl)-2″*-O-para-*methoxyphenyl-5′-thiothymidine (16)*

Diisopropyl azodicarboxylate (1.05 mL, 5.32 mmol) was added dropwise to a stirred solution of triphenylphosphine (1.39 g, 5.32 mmol) in dry tetrahydrofuran (10 mL) cooled to 0°C under nitrogen, resulting in a milky suspension. After 0.5 h a solution of nucleoside **17** (1.00 g, 2.66 mmol) and thiolacetic acid (0.38 mL, 5.32 mmol) in dry tetrahydrofuran (20 mL) was slowly added and the stirring at 0°C continued for 0.5 h after which time the reaction was allowed to warm to room temperature. After 40 min the solvent was removed *in vacuo* and the resulting yellow syrup was chromatographed over silica (25:1 dichloromethane/methanol, v/v) affording thiolester **16** as a white solid (1.00 g, 87% yield): ^{1}H NMR (300 MHz, $CDCl_3$) δ: 1.96 (s, 3H, 5-Me), 1.69–1.80 (m, 1H, H1″$_A$), 2.02–2.12 (m, 1H, H1″$_B$), 2.16–2.31 (m, 3H, H3′ and H2″$_{AB}$), 2.38 (s, 3H, SAc), 3.26 (A of ABX, 1H, H5′$_A$), 3.36 (B of ABX, 1H, H5′$_B$), 3.76 (s, 3H, O*Me*), 3.88 (m[6], 1H, H4′), 3.96 (apparent t, 2H, H2″$_{AB}$, J = 5.9), 6.08 (dd, 1H, H1′), 6.82 (s, 4H, MeO*Ph*O-), 7.36 (s, 1H, H6), 9.16 (br s, 1H, N*H*), $J_{H1'-H2'}$ = 4.2 and 6.0, $J_{H4'-H5'A}$ = 6.5, $J_{H4'-H5'B}$ = 3.5, $^2J_{H5'A-H5'B}$ = −14.4; ^{13}C NMR ($CDCl_3$): 12.62 ppm (5-Me), 30.52 (SCO*Me*), 31.56 and 31.67 (C1″ and C2′), 38.96 and 39.06 (C3′ and C5′), 55.66 (O*Me*), 66.50 (C2″), 83.74 and 84.75 (C1′ and C4′), 110.67 (C5), 114.63 and 115.22 (*C*H of MeO*Ph*O-), 135.40 (C6), 150.31; 152.54 and 153.89 (C2 and 4° of MeO*Ph*O-), 163.85 (C4), 194.71 (S*C*OMe); MS (CI–NH$_3$), *m/e*: 452 ([M + NH$_4^+$], 8.3%), 435 ([MH$^+$], 100), 326 ([M + NH$_4^+$ – ThyH], 3.6), 309 ([MH$^+$ – ThyH], 53), 127 ([ThyH + H$^+$], 2.8); HRMS (CI–NH$_3$) *m/e* calcd. for $C_{21}H_{27}N_2O_6S$: 435.15898; found: 435.15889.

3′-Deoxy-3′-C-*(2″-hydroxyethyl)-2″*-O-(para-*methoxyphenyl)thymidine (17)*

A stock solution of tetra-*n*-butylammonium fluoride (1 N in THF, 7.9 mL, 7.9 mmol) was added to stirred solution of nucleoside **12** (1.29 g, 2.64 mmol) in dry tetrahydrofuran (5 mL) and the resulting solution was stirred at room temperature under a nitrogen atmosphere. After 1.5 h the solvent was evaporated *in vacuo* and the residue chromatographed over silica (20:1 dichloromethane/methanol, v/v) affording nucleoside **17** as a white solid (0.99 g, quantitative): ^{1}H NMR (200 MHz, CD_3OD) δ: 1.86 (s, 3H, 5-Me), 1.63–1.80 (m, 1H, H1″$_A$), 1.91–2.07 (m, 1H, H1″$_B$), 2.14–2.35 (m, 2H, H2′$_{AB}$), 2.38–2.53 (m, 1H, H3′), 3.69–3.81 and 3.89–4.00 (two m, 5H and 3H, -O*Me*; H5′$_{AB}$; H4′; and H2″$_{AB}$), 6.04 (dd, 1H, H1′), 6.81 (s, 4H, MeO*Ph*O-), 8.00 (s, 1H, H6), $J_{H1'-H2'}$ = 3.2 and 6.7; ^{13}C NMR ($CDCl_3$): 12.40 ppm (5-Me), 31.45 (C1″), 34.53 (C3′), 39.09 (C2′), 55.59 (O*Me*), 61.50 (C5′), 66.74 (C2″), 84.95 and 86.41 (C1′ and C4′), 110.19 (C5), 114.57 and 115.23 (CH of MeOPhO-), 136.37 (C6), 150.45; 152.48 and 153.80 (C2 and 4° of MeOPhO-), 164.22 (C4); MS (CI–NH$_3$) *m/e*: 394 ([M + NH$_4^+$], 2.5%), 377 ([MH$_4^+$], 87), 268 ([M + NH$_4^+$ – ThyH], 23), 251 ([MH$^+$ – ThyH], 100), 127 ([ThyH + H$^+$], 16); HRMS (CI–NH$_3$) *m/e* calcd. for $C_{19}H_{25}N_2O_6$: 377.17126; found: 377.17114. Anal. calcd. for $C_{19}H_{25}N_2O_6$: C 60.63, H 6.43, N 7.44; found: C 60.23, H 6.77, N 7.30.

5′-S-*Acetyl-5′-deoxy-5′-thiothymidine (18)*

Diisopropyl azodicarboxylate (1.62 mL, 8.26 mmol) was added dropwise to a stirred solution of triphenylphosphine (2.16 g, 8.26 mmol) in dry tetrahydrofuran (18 mL) cooled to 0°C under

Can. J. Chem. Downloaded from www.nrcresearchpress.com by 217.78.4.112 on 09/08/12
For personal use only.

nitrogen resulting in a milky suspension. After 0.5 h a solution of thymidine (1.00 g, 4.13 mmol) and thiolacetic acid (0.59 mL, 8.26 mmol) in dry *N,N*-dimethylformamide (15 mL) was slowly added and the stirring at 0°C continued for 0.5 h after which time the reaction was allowed to warm to room temperature. After 0.5 h the solvent was removed *in vacuo* and the resulting brown syrup pumped for 2 h. The resulting glass was chromatographed over silica (25:1 to 15:1 dichloromethane/methanol, v/v) affording thiolester **16** as a white solid (650 mg, 52% yield): ^{1}H NMR (300 MHz, CD_3OD) δ: 1.90 (fine d, 3H, J = 1.2 Hz, 5-Me), 2.25 (dd, 2H, H2′$_{AB}$), 2.35 (s, 3H, SAc), 3.23 (d, 2H, H5′$_{AB}$), 3.93 (td, 1H, H4′), 4.20 (td, 1H, H3′), 6.19 (t, 1H, H1′), 7.44 (fine q^4, 1H, J = 1.2 Hz, H6), $J_{H1'-H2'AB}$ = 6.8 Hz, $J_{H2'AB-H3'}$ = 5.0, $J_{H3'-H4'}$ = 3.5, $J_{H4'-H5'AB}$ = 6.2; ^{13}C NMR (CD_3OD): 12.38 ppm (5-Me), 30.43 (CO*Me*), 32.30 (C5′), 40.09 (C2′), 74.37 (C3′), 86.46 (2C, C1′ and C4′), 111.83 (C5), 137.66 (C6), 152.25 (C2), 166.26 (C4), 196.46 (*C*OMe); MS (CI–NH_3) m/e: 318 ([M + NH_4^+], 14%), 301 ([MH^+], 100), 175 ([MH^+ − ThyH], 1.1), 127 ([ThyH + H^+], 17); HRMS (CI–NH_3) m/e calcd. for $C_{12}H_{17}N_2O_5S$: 301.08582; found: 301.08574.

*5′-S-Acetyl-3′-*O*-tert-butyldimethylsilyl-5′-deoxy-5′-thiothymidine (19)*

tert-Butylchlorodimethylsilane (309 mg, 2.05 mmol) and imidazole (280 mg, 4.10 mmol) were successively added to a stirred solution of nucleoside **18** (560 mg, 1.86 mmol) in dry *N,N*-dimethylformamide (5 mL) and the reaction was stirred at ambient temperature under a nitrogen atmosphere. After 18 h the solution was poured into water (300 mL) and the product was extracted with dichloromethane (2 × 200 mL) and washed with water (2 × 300 mL). The combined organic extracts were then dried (Na_2SO_4), filtered, and the solvent removed *in vacuo* yielding a yellow syrup. Chromatography over silica gel (25:1 dichloromethane/methanol, v/v) afforded the silyl ether **19** as a colorless solid (709 mg, 92% yield): ^{1}H NMR (300 MHz, $CDCl_3$) δ: 0.08 and 0.10 (two s, 6H, Si*Me*$_2$), 0.90 (s, 9H, *t*-Bu), 1.96 (fine d, J = 1.2 Hz, 5-Me), 2.10 (A of ABXY, 1H, H2′$_A$), 2.28 (B of ABXY, 1H, H2′$_B$), 2.40 (s, 3H, SAc), 3.21 (d, 2H, H5′$_{AB}$), 3.99 (td, 1H, H4′), 4.17 (dt, 1H, H3′), 6.21 (dd, 1H, H1′), 7.23 (find q^4, 1H, J = 1.2 Hz, H6), 8.62 (br s, 1H, N*H*), $J_{H1'-H2'A}$ = 7.5 Hz, $J_{H1'-H2'B}$ = 6.1, $^2J_{H2'A-H2'B}$ = −13.8, $J_{H2'A-H3'}$ = 6.5, $J_{H2'B-H3'}$ = 3.2, $J_{H3'-H4'}$ = 3.5, $J_{H4'-H5'AB}$ = 5.8; ^{13}C NMR ($CDCl_3$): 12.60 ppm (5-Me), 17.87 (Si*C*Me$_3$), 25.64 (Si*Me*$_2$ and Si*C*Me$_3$), 30.56 (CO*Me*), 31.13 (C5′), 40.44 (C2′), 73.84 (C3′), 85.13 and 85.17 (C1′ and C4′), 111.10 (C5), 135.32 (C6), 150.16 (C2), 163.74 (C4), 194.48 (*C*OMe); MS (CI–NH_3), m/e: 432 ([M + NH_4^+], 4.9%), 415 ([MH^+], 100), 306 ([M + NH_4^+ − ThyH], 1.8), 289 ([MH^+ − ThyH], 11), 127 ([ThyH + H^+], 13); HRMS (CI–NH_3) m/e calcd. for $C_{18}H_{31}N_2O_5SSi$: 415.17230; found: 415.17213.

*3′-*O*-tert-Butyldimethylsilyl-5′-deoxy-5′-thiothymidine (20)*

Methanolic sodium hydroxide solution (0.50 N, 7.7 mL, 3.86 mmol), previously saturated with N_2 gas, was slowly added to a stirred solution of thiolester **19** (800 mg, 1.93 mmol) in methanol (30 mL, deoxygenated) and the reaction allowed to stir at ambient temperature under nitrogen. After 1 h, the base was neutralized with Amberlite H^+ resin, which was filtered and washed thoroughly with methanol. Evaporation of the alcohol *in vacuo* afforded the thiol **20**, a colorless glass that crystallized upon standing (738 mg, quantitative): mp 116–119°C (dec.); ^{1}H NMR (300 Mhz, $CDCl_3$) δ: 0.098 and 0.10 (two s, 6H, Si*Me*$_2$), 0.90 (s, 9H, *t*-Bu), 1.95 (fine d, 3H, J = 1.2 Hz, 5-Me), 1.53 (t, exchangeable, 1H, S*H*), 2.16 (A of ABXY, 1H, H2′$_A$), 2.30 (B of ABXY, 1H, H2′$_B$), 2.78 (A of ABXY, 1H, H5′$_A$), 2.89 (B of ABXY, 1H, H5′$_B$), 3.95 (apparent q^4, 1H, H4′), 4.36 (dt, 1H, H3′), 6.25 (t, 1H, H1′), 7.34 (fine q^4, 1H, J = 1.2 Hz, H5), 8.41 (br s, 1H, N*H*), $J_{H1'-H2'A}$ = $J_{H1'-H2'B}$ = 6.7 Hz, $J_{H2'A-H3'}$ = 7.1, $J_{H2'B-H3'}$ = 4.3, $^2J_{H2'A-H2'B}$ = −13.7, $J_{H3'-H4'}$ = 4.6, $J_{H4'-H5'A}$ = $J_{H4'-H5'B}$ = 4.6, $^2J_{H5'A-H5'B}$ = −14.2, $J_{SH-H5'AB}$ = 8.3; ^{13}C NMR ($CDCl_3$): 12.65 ppm (5-Me), 17.87 (Si*C*Me$_3$), 25.66 (Si*Me*$_2$ and Si*C*Me$_3$), 26.41 (C5′), 40.54 (C2′), 72.50 (C3′), 84.46 and 85.97 (C1′ and C4′), 111.24 (C5), 135.51 (C6), 150.20 (C2), 163.65 (C4); MS (CI–NH_3) m/e: 390 ([M + NH_4^+], 1.4%), 373 ([MH^+], 100), 247 ([MH^+ − ThyH], 2.7), 127 ([ThyH + H^+], 28); HRMS (CI–NH_3) m/e calcd. for $C_{16}H_{29}N_2O_4SSi$: 373.161733; found: 373.161730. Anal. calcd. for $C_{16}H_{27}N_2O_4SSi$: C 51.58, H 7.58, N 7.52, S 8.60; found: C 51.19, H 7.59, N 7.36, S 8.32.

It was found that chromatography of the thiol over silica immediately after the reaction (1:1 hexanes/ethyl acetate, v/v) removes a small amount of impurity that accelerates the oxidation of the product to the symmetrical disulfide: ^{1}H NMR (300 MHz, CD_3OD) δ: 0.096 and 0.101 (two s, 6H, Si*Me*$_2$), 0.90 (s, 9H, *t*-Bu), 1.94 (fine d, 3H, J = 1.2 Hz, 5-Me), 2.16 (A of ABXY, 1H, H2′$_A$), 2.30 (B of ABXY, 1H, H2′$_B$), 3.02 (A of ABX, 1H, H5′$_A$), 3.07 (B of ABX, 1H, H5′$_B$), 4.10 (td, 1H, H4′), 4.35 (dt, 1H, H3′), 6.19 (apparent t, 1H, H1′), 7.23 (fine q, 1H, J = 1.2 Hz, H6), 8.95 (br s, 1H, nH), $J_{H1'-H2'A}$ = 7.1, $J_{H1'-H2'B}$ = 6.3, $^2J_{H2'A-H2'B}$ = −13.6, $J_{H2'A-H3'}$ = 6.7, $J_{H2'B-H3'}$ = 3.5, $J_{H3'-H4'}$ = 3.8, $J_{H4'-H5'A}$ = 6.0, $J_{H4'-H5'B}$ = 5.4, $^2J_{H5'A-H5'B}$ = −14.0; ^{13}C NMR ($CDCl_3$): 12.59 ppm (5-Me), 17.85 (Si*C*Me$_3$), 25.64 (Si*Me*$_2$ and Si*C*Me$_3$), 40.21 and 41.88 (C2′ and C5′), 73.56 (C3′), 85.01 and 85.54 (C1′ and C4′), 111.11 (C5), 135.59 (C6), 150.26 (C2), 163.95 (C4); MS (FAB–glycerol) m/e: 743 ([MH^+], 8.4%), 437 (46).

Acknowledgements

This work was supported by the Natural Sciences and Engineering Research Council of Canada, the Ministère de l'éducation du Québec (FCAR), and IAF BioChem International Inc. We are grateful to Professor O. A. Mamer (McGill University Biomedical Mass Spectrometry Unit) for the measurement of mass spectra.

1. E. Uhlmann and A. Peyman. Chem. Rev. **90**, 543 (1990).
2. P. S. Miller, J. Yano, E. Yano, C. Carroll, K. Jayaraman, and P. O. P. Ts'o. Biochem. **23**, 5134 (1979).
3. J. M. Dagle, M. E. Andracki, R. J. DeVine, and J. A. Walder, Nucleic Acids Res. **19**, 1805 (1991).
4. B. C. Froehler. Tetrahedron Lett. **27**, 5575 (1986).
5. H. Vu and B. L. Hirschbein. Tetrahedron Lett. **32**, 3005 (1991).
6. B. Froehler, P. Ng, and M. Matteucci. Nucleic Acids Res. **16**, 4831 (1988).
7. F. Morvan, B. Rayner, J.-L. Imbach, M. Lee, J. A. Hartley, D.-K. Chang, and J. W. Lown. Nucleic Acids Res. **15**, 7027 (1987).
8. M. Koga, M. F. Moore, and S. L. Beaucage. J. Org. Chem. **56**, 3757 (1991).
9. S. Fujimori, K. Shudo, and Y. Hashimoto. J. Am. Chem. Soc. **112**, 7436, (1990).
10. M. J. Damha, P. A. Giannaris, P. Marfey, and L. S. Reid. Tetrahedron Lett. **32**, 2573 (1991).
11. Z. Huang, K. C. Schneider, and S. A. Benner. J. Org. Chem. **56**, 3869 (1991).
12. B. Musicki and T. S. Widlanski. Tetrahedron Lett. **32**, 1267 (1991).
13. S. H. Kawai and G. Just. Nucleosides Nucleotides, **10**, 1485 (1991).
14. M. Matteucci. Tetrahedron Lett. **31**, 2385 (1990).
15. C. A. Stein, C. Subasinghe, K. Shinozuka, and J. S. Cohen. Nucleic Acids Res. **16**, 3209 (1988).
16. L. Svansson, I. Kvarnström, B. Classon, and B. Samuelsson. J. Org. Chem. **56**, 2993 (1991).
17. C. K. Chu, B. Doboszewski, W. Schmidt, and G. V. Ullas. J. Org. Chem. **54**, 2767 (1989).
18. J. Fiandor and S. Y. Tam. Tetrahedron Lett. **31**, 597 (1990).

19. R. Pappo, D. S. Allen Jr., R. U. Lemieux, and W. S. Johnson. J. Org. Chem. **21**, 478 (1956).
20. S. H. Kawai, J. Chin, and G. Just. Carbohydr. Res. **211**, 245 (1991).
21. H. Vorbrüggen and K. Krolikiewicz. Angew. Chem. Int. Ed. Engl. **14**, 421 (1975).
22. T. Nishimura and I. Iwai. Chem. Pharm. Bull. **12**, 352 (1964).
23. M. J. Robins and J. S. Wilson. J. Am. Chem. Soc. **103**, 932 (1981).
24. G. Just and J.-F. Lavallée. Tetrahedron Lett. **32**, 3469 (1991).
25. R. P. Volante. Tetrahedron Lett. **22**, 3119 (1981).
26. B. Bannister and F. Kagan. J. Am. Chem. Soc. **82**, 3363 (1960).

Can. J. Chem. Downloaded from www.nrcresearchpress.com by 217.78.4.112 on 09/08/12
For personal use only.

Micellar rate enhancement studies in mixed sodium fluorocarbon/hydrocarbon surfactant solutions

TERRENCE J. CONNOLLY AND VINCENT C. REINSBOROUGH[1]
Department of Chemistry, Mount Allison University, Sackville, N.B., Canada E0A 3C0

Received August 7, 1991

TERRENCE J. CONNOLLY and VINCENT C. REINSBOROUGH. Can. J. Chem. **70**, 1581 (1992).

Stopped-flow kinetic studies were conducted in mixed micellar solutions of fluorocarbon and hydrocarbon anionic surfactants to determine the prevalent micellar form. The probe reaction was the Ni_{aq}^{2+}/pyridine-2-azo-*p*-dimethylaniline (PADA) complexation, which is many times accelerated in the presence of anionic micelles. Binding constants for Ni_{aq}^{2+} and PADA partitioning between bulk solution and micelles were determined through the murexide technique and solubility measurements respectively and the molar reaction volume was obtained from the Robinson equation. The three binary surfactant systems investigated had sodium perfluoroheptanoate as the fluorocarbon surfactant while the hydrocarbon surfactants were sodium decylsulfate, sodium nonanesulfonate, and sodium octanesulfonate. The kinetic results were consistent with unimicellar composition in all three systems which was not the behaviour previously found with the sodium octane sulfonate / sodium perfluoroctanoate system. The difference was attributed to closer similarity in the surfactant pair hydrophobicities as revealed through their critical micelle concentrations. Another finding was that mixed micelles synergistically can lead to a much greater solubilization of PADA than is possible through either of the pure surfactants.

TERRENCE J. CONNOLLY et VINCENT C. REINSBOROUGH. Can. J. Chem. **70**, 1581 (1992).

Dans le but de déterminer la forme micellaire prévalante, on a réalisé des études cinétiques à flux stoppé sur des solutions micellaires d'agents de surface anioniques fluoro- et hydro-carbonés. La réaction indicatrice utilisée est la complexation Ni_{aq}^{2+}/pyridine-2-azo-*p*-diméthylaniline (PADA) qui est fortement accélérée en présence de micelles anioniques. Les constantes de fixation du Ni_{aq}^{2+} et de partition du PADA entre la masse de la solution et les micelles ont été déterminées respectivement à l'aide de la technique du murexide et de mesures de solubilité et on a évalué le volume molaire de la réaction grâce à l'équation de Robinson. Les trois systèmes binaires d'agents de surface étudiés contenaient du perfluoroheptanoate de sodium comme agent de surface fluorocarboné alors que les agents de surface hydrocarbonés étaient le décylsulfate de sodium, nonanesulfonate de sodium et octanesulfonate de sodium. Dans les trois systèmes, les résultats cinétiques sont en accord avec la composition unimicellaire; ce comportement est différent de celui observé antérieurement avec le système octanesulfonate de sodium / perfluorooctanoate de sodium. On attribue la différence à la plus grande similarité dans les hydrophobicités des paires d'agents de surface qui sont révélées par leurs concentrations micellaires critiques. Une autre observation a trait au fait que les micelles mixtes peuvent agir par synergie pour conduire à une solubilisation beaucoup plus grande du PADA que celle possible par chacun des agents de surface agissant seuls.

[Traduit par la rédaction]

Introduction

Mixing hydrocarbon and fluorocarbon surfactants is commonplace in industry to achieve better wash results but the constitution and structure of the micelles responsible for this enhanced detergency are still not well understood. Models for binary surfactant mixes range from the extremes of two one-component micelles and a single two-component micelle to intermediate scenarios of two micelles with one richer than the other in one surfactant (refs. 1–4 and references cited therein). Impinging lately upon the situation is the growing realization that fluorocarbon micelles differ quite markedly from hydrocarbon micelles (5, 6). Recently, we investigated the rate enhancements that the complexation reaction between Ni_{aq}^{2+} and the bidentate ligand pyridine-2-azo-*p*-dimethylaniline (PADA) experienced in the presence of mixed sodium perfluorooctanoate (SPFO) / sodium octanesulfonate (SOS) micellar solutions (4). The kinetic results we obtained were consistent with there being two separate micelles of pure or almost pure composition present in solution. In this surfactant mixture, the fluorocarbon surfactant had the greater hydrophobicity, the lower critical micelle concentration (CMC), and presumably the greater influence in determining properties of the mixed solutions. In the first phase of the present study, the roles of the surfactant types were switched by conducting the same kinetic studies in sodium perfluoroheptanoate (SPFH) / sodium decylsulfate (SDeS) micellar solutions. SPFH and SDeS have CMC values of 0.068 mol dm^{-3} and 0.024 mol dm^{-3} respectively in millimolar nickel ion solutions. In this micellization situation, the hydrocarbon surfactant is dominant and any differences in micellar structure between the two mixed surfactant situations should be clear from the kinetic behaviour. Rate enhancements in micellar solution of the Ni_{aq}^{2+}/PADA complexation reaction find a ready explanation in the model of Robinson and co-workers (7–11) which is sufficiently refined to reveal major micellar structural differences. In the second part of this work, the system sodium perfluoroheptanoate (SFPH) / sodium octanesulfonate(SOS) was investigated kinetically. This combination of short-chained surfactants reverts to having the fluorocarbon dominant (CMC = 0.070 mol dm^{-3}) with the hydrocarbon surfactant having a CMC of 0.15 mol dm^{-3}. This second system is similar to the SPFO/SOS system investigated previously (4) except that the CMC values of the pure surfactants are closer together. The data from this second system suggested that a third hydrocarbon/fluorocarbon surfactant combination where the CMC values were almost coincident should be examined. The system chosen in the third section was sodium perfluoroheptanoate / sodium nonanesulfonate (SPFH/SNS).

Experimental

A Cantech stopped-flow apparatus (deadtime 3 ms) with spectrophotometric detection was used to obtain rate constants under

[1]Author to whom correspondence may be addressed.

Can. J. Chem. Downloaded from www.nrcresearchpress.com by 217.78.4.112 on 09/08/12
For personal use only.

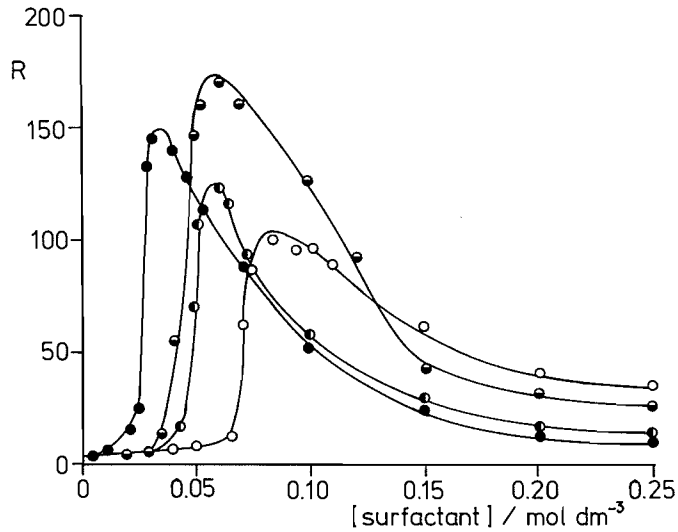

FIG. 1. Rate enhancements R of of the Ni_{aq}^{2+}/PADA complexation reaction in SDeS/SPFH solutions: (●) pure SDeS, (◐) 1:1 SDeS/SPFH, (◒) 1:3 SDeS/SPFH, (○) pure SPFH. [surfactant] = total surfactant concentration.

pseudo-first-order conditions for the formation of the Ni_{aq}^{2+}/PADA complex and the Ni_{aq}^{2+}/murexide complex in the mixed micellar solutions. The dye and Ni_{aq}^{2+} reactant solutions were adjusted to pH 7.2 ± 0.1 before mixing in the PADA runs and to pH 6.0 ± 0.1 in the murexide runs. Equal concentrations of surfactant were used in both reactant syringes to avoid surfactant concentration jumps. Solubility measurements of PADA (Sigma) in surfactant solutions were carried out spectrophotometrically as described previously (8, 9). Solutions of the fluorocarbon surfactants were prepared *in situ* by neutralizing the acids (Aldrich and Fluka) with the highest quality sodium hydroxide (Aldrich). Sodium decylsulfate or SDeS (Lancaster), sodium nonanesulfonate or SNS (Sigma), and sodium octanesulfonate or SOS (Sigma) were dried at room temperature in vacuum and used without further purification. All solutions were made from triply distilled water.

Results and discussion

SDeS/SPFH system

In Fig. 1 the observed rate constants (k_{obs}) for the complexation of Ni_{aq}^{2+} with the dye ligand PADA in pure SDeS, pure SPFH, in 1:3 SDeS/SPFH, and in 1:1 SDeS/SPFH solutions at 25.0°C at various surfactant concentrations are given as R, the ratio of k_{obs} in solution to k_{obs} in pure water (9), which is (1.2 ± 0.1) × 10^3 dm^3 mol^{-1} s^{-1} (11). In addition to the 1:3 and 1:1 SDeS/SPFH systems, three other mixed systems were studied kinetically: the 3:1, 1:2, and 1:6 mole ratios. The general concentration dependence of R was similar to that observed previously in other micellar systems, i.e., little change from unity until close to the CMC and then a more or less sharp rise to a maximum just beyond the CMC followed in turn by a more gradual decline to a plateau in concentrated micellar solution. The increase in rate is a concentrative effect brought about when both reactants, metal cation and hydrophobic dye, are attracted strongly into the micellar surface region (7). Properly speaking, the micelles are not acting as catalysts since no new path is being provided for the reaction with the activation energy for the complexation reaction remaining the same with or without surfactant (7, 8). The values of R_{max} for all six systems investigated are listed in Table 1.

R values for pure SDeS solutions agreed with previously published results with an R_{max} of 150 ± 20 and a CMC of 24 mmol dm^{-3} as determined from the beginning of the steeply rising slope (9). Pure SPFH had not been investigated before in this context but its R_{max} value of 115 was consistent with the R_{max} value of 400 reported for the longer chained sodium perfluorooctanoate or SPFO (4). The reported CMC values for SPFH lie in the range 80–85 mmol dm^{-3} (5, 13) and the value obtained in this work, of 70 mmol dm^{-3}, undoubtedly reflects a slight lowering of the CMC due to the background 10^{-3} mol dm^{-3} Ni_{aq}^{2+} in solution (increasing the ionic strength of surfactant solutions generally lowers the CMC).

For the first mixed system, 3:1 SDeS/SPFH, substituting each fourth SDeS with a SPFH molecule made little difference to the observed rate enhancements. Even though pure SPFH has a higher CMC than does pure SDeS, R_{max} for the 3:1 SDeS/SPFH system was the same as for pure SDeS and the combined CMC was 28 mmol dm^{-3} in total surfactant. The 1:1 SDeS/SPFH system showed more the effect of adding the "weaker" surfactant as the R_{max} declined to 130 and the mixed CMC rose to 43 mmol dm^{-3}. The 1:3 SDeS/SPFH system dramatically reversed this trend with R_{max} rising to 170 and the mixed CMC remaining unchanged. The R_{max} value for the 1:6 SDeS/SPFH system declined slightly to 152 but still was large in view of the 115 reading for pure SPFH. The mixed CMC for the 1:6 system of 62 mmol dm^{-3} total surfactant also was low in view of the CMC of pure SPFH. It is clear that the 1:3 and the 1:6 systems demonstrate synergistic effects (14). Minor synergistic effects have been reported for some mixed anionic hydrocarbon micellar systems (12) but these were not found in the previously studied mixed fluorocarbon/hydrocarbon surfactant system (4).

The Robinson model accounts quantitatively for micellar rate enhancements by the expression (8, 9, 11)

$$k^s_{obs} = k^s_f [Ni^{2+}]/\{CV[1 + (CK_{Ni})^{-1}][1 + (CK_{PADA})^{-1}]\}$$

where k^s_{obs} is the observed rate constant in surfactant solution, k^s_f is the second-order forward rate constant for the complexation in surfactant solution, C is the concentration of the surfactant in the form of micelles, i.e., the total concentration less the CMC, and V is the molar reaction volume of the surfactant. The parameter V is a measure of the tightness or density of the micellar surface region in which the probe reaction occurs. K_{Ni} and K_{PADA} represent partitioning coeficients for each reactant going on and coming off the micelles, e.g., $K_{Ni} = [Ni^{2+}]_s/C[Ni^{2+}]_b$ where subscripts s and b denote the micellar surface and bulk solution pseudophases respectively. K_{PADA} is defined analogously. The value of k^s_f is assumed equal to the rate constant in pure water (1. 2 × 10^3 dm^3 mol^{-1} s^{-1}) (8). Values of K_{Ni} and K_{PADA} are obtained independently by the murexide technique (4, 15) and by solubility measurements respectively (8, 9). Curve-fitting of the kinetic data yields parameter V and (or) K_{Ni}. The values of K_{Ni} (experimental and fitted), K_{PADA}, and V are found in Table 1.

First of all, the fitted binding constants of nickel ion to the micelles in all the pure and mixed surfactant systems agreed reasonably well with those obtained through the murexide technique, which speaks well for the kinetic model. Secondly, K_{Ni} for pure SPFH of 55 was reasonable since K_{Ni} for sodium perfluorooctanoate was 250 (4). Rather surpris-

Can. J. Chem. Downloaded from www.nrcresearchpress.com by 217.78.4.112 on 09/08/12
For personal use only.

TABLE 1. Binding constants, reaction volumes, and R_{max} values for micellar hydrocarbon/fluorocarbon surfactant systems

System	K_{PADA} ($dm^3\ mol^{-1}$)	K_{Ni}[a] ($dm^3\ mol^{-1}$)	K_{Ni}[b] ($dm^3\ mol^{-1}$)	V ($dm^3\ mol^{-1}$)	R_{max}
(*a*) SDeS/SPFH					
Pure SDeS	1065	101	120	0.37	150
3:1	760	90	—	0.26	150
1:1	700	85	120	0.25	127
1:3	380	73	85	0.17	170
1:6	365	73	—	0.16	152
Pure SPFH	100	44	55	0.15	115
(*b*) SOS/SPFH					
Pure SOS	85	22	6	0.71	19
1:1	400	30	—	0.18	90
Pure SPFH	100	44	55	0.15	115
(*c*) SNS/SPFH					
Pure SNS	200	170	—	0.80	55
1:1	695	52	—	0.30	100
Pure SPFH	100	44	55	0.15	115

[a]Fitted values.
[b]Experimental values.

ingly, the binding of the dye PADA to pure SPFH micelles (K_{PADA}) was equally as strong as it was to the presumably larger pure SPFO micelles (4). This may be related to the anomalous nature of perfluorinated surfactants (5). A consistency with sodium perfluorooctanoate did develop, however, in the remarkably low value of the reaction volume of 0.15 $dm^3\ mol^{-1}$ for pure SPFH. The value of V for sodium heptanesulfonate of the same chain length is 0.89 $dm^3\ mol^{-1}$ (10) and, even allowing for the 1.5 factor Shinoda *et al.* (16) found should be used when comparing the properties of fluorocarbon surfactants with their hydrocarbon counterparts, values of reaction volumes of 0.15 $dm^3\ mol^{-1}$ or 0.16 $dm^3\ mol^{-1}$ as found with sodium perfluorooctanoate micelles seem grossly out of line (V for sodium dodecylsulfate is 0.40 $dm^3\ mol^{-1}$ for the same reaction (11)). However, the reaction volume should approximate the molar volume of the surfactant according to theory (17) and for SPFO this should be slightly less than the reported value of 0.22 $dm^3\ mol^{-1}$ for sodium perfluorononanoate at 30°C (18). With short-chained hydrocarbon surfactants, V values often exceed the molar volume of the surfactant many times, suggesting that such micelles are loosely held together and (or) the reaction zone extends considerably into the solution from the micelle surface (10). Fluorinated surfactants on the other hand appear to maintain the tightness of micellar surface region even with a seven-membered tail. Guo *et al.* (5) have noted that the so-called Stern layer of the perfluoroheptanoic micelle is very compact as compared with ordinary or hydrocarbon surfactants, which is in agreement with our results. The better than expected micellar "catalysis" effected by fluorocarbon surfactants on the Ni_{aq}^{2+}/PADA complexation reaction thus is not a result of any greater attraction of either of the reactants Ni_{aq}^{2+} or PADA into the micellar surface region but rather of a pronounced constriction of this part of the micelle.

Remarkably, this contraction of the micellar surface region persists when SDeS is added to pure SPFH micelles to at least 25 mol% SDeS where V is 0.17 $dm^3\ mol^{-1}$ (Table 1). At this concentation, both K_{Ni} and K_{PADA} have increased in keeping with the presence of 25 mol% SDeS for which these partitioning constants are higher. Thus, with increased K values and V remaining the same, the rate enhancement increases overall as compared with the pure SPFH situation. At 50 mol% SDeS, the partitioning constants and the V values both increase, thus negating any overall increase in R as compared with the 25 mol% SDeS system. Thus, a maximum in R_{max} occurs around 25 mol% SDeS in the SDeS/SPFH system. R_{max} values should be a practical indicator of the efficiency of anionic detergents because according to the kinetic analysis the value of R is decided by the effectiveness with which the micellar surfactant is able to attract metallic ions and organic material, and these constitute two important types of materials good detergents should remove from solution. In applications where this is desired, a mixed SDeS/SPFH soap with 25 mol% SDeS should be a more effective dirt remover than either of the pure surfactants.

When SPFO was added to micellar SOS solutions to constitute a 10 mol% SPFO system, the rate enhancements increased dramatically, despite a countering decrease in K_{PADA}. This increase resulted because the reaction volume underwent an eightfold decrease (4). This together with other evidence such as the common occurrence of two CMC's in many of the mixed systems was interpreted to indicate that relatively pure perfluorooctanoate micelles were formed, perhaps together with pure or almost pure octylsulfate micelles, and that the former micelles were almost entirely responsible for the observed rate enhancements. On the other hand, in the mixed system reported here, the kinetic parameters of even the 25 mol% SPFH system seem simply to reflect more or less proportionately the mole ratios of each surfactant. Moreover, no systems gave evidence of having more than one CMC. Thus, it would appear that in the SDeS/SPFH system one mixed-micelle was responsible for the observed rate enhancements. Perfluoroheptanoate monomers are apparently adsorbed and absorbed into decylsul-

Can. J. Chem. Downloaded from www.nrcresearchpress.com by 217.78.4.112 on 09/08/12
For personal use only.

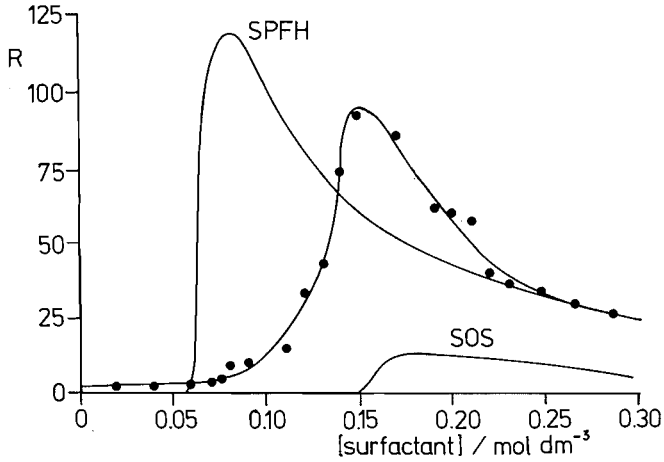

FIG. 2. Rate enhancements R of the Ni_{aq}^{2+}/PADA complexation reaction in 1:1 SOS/SPFH solutions. Fitted curves for R are also shown for the pure surfactants. [surfactant] = total surfactant concentration.

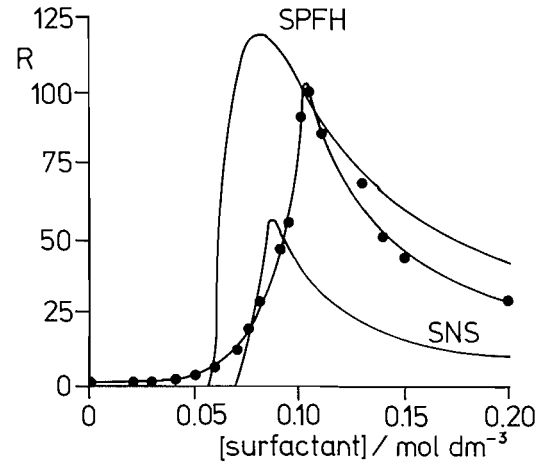

FIG. 3. Rate enhancements R of the Ni_{aq}^{2+}/PADA complexation reaction in 1:1 SNS/SPFH solutions. Fitted curves for R for the pure surfactants are also shown. [surfactant] = total surfactant concentration.

fate micelles where they bring about a roughly proportional diminution in the attraction experienced by each reactant into the micelle but cause an inordinately large shrinking of the micellar surface region in respect to the Ni_{aq}^{2+}/PADA complexation reaction.

SOS/SPFH system

The rate enhancement plots for the 1:1 SPFH/SOS system as compared with the curves for pure SPFH and pure SOS are displayed in Fig. 2. The kinetic parameters for the system as obtained through stopped-flow murexide runs (K_{Ni}), solubility measurements (K_{PADA}), and computer curve-fitting (V) are listed in Table 1. Three features especially are notable and these cause this sytem to resemble more closely the SPFH/SDeS system than the SPFO/SOS system. First of all, R_{max} for the 1:1 combination is 75% of the R_{max} value for pure SPFH or about nine times that for pure SOS. Secondly, the reaction volume of the equimolar mixture in solution is remarkedly close to the reaction volume for pure SPFH. The fluorocarbon surfactant monomer controls this parameter, reducing it to a value four times lower than in pure SOS. Thirdly, the K_{PADA} values indicate that the mixed system is a much more efficient PADA scavenger than either of the pure components, an observation not noted before in mixed surfactant systems. The solubility and the murexide curves gave no sign either of any second CMC's so that all indicators point to a one-micelle system as with the SDeS/SPFH situation.

SNS/SPFH system

From the results with the foregoing perfluorocarbon/hydrocarbon surfactant combinations, whether one or two micelles were formed in these mixed systems seemed to depend on how close were the CMC values for the two pure surfactants. The CMC values for SOS and SPFO in 10^{-3} mol dm^{-3} Ni_{aq}^{2+} were 0.15 mol dm^{-3} and around 0.02 mol dm^{-3} respectively (4) and two micelles were apparently formed in the micellar solutions of the mixtures. SDeS and SPFH had CMC's of 0.024 mol dm^{-3} and 0.070 mol dm^{-3} respectively and their mixtures indicated only one micellar form was prevalent in solution. In the first case, the CMC's differed by a factor of seven while in the second case the factor was three. With the SOS/SPFH system, the CMC ratio was two and simply one micelle formed. To test this closeness-of-CMC hypothesis further, a hydrocarbon surfactant was mixed equimolarly with a fluorocarbon surfactant where the CMC values of the two pure components were even closer and rate enhancements for the probe reaction were obtained in these solutions. The selected two were sodium nonanesulfonate (SNS) and sodium perfluoroheptanoate (SPFH) with CMC's of 0.081 mol dm^{-3} (10) and 0.070 mol dm^{-3}, respectively, or a CMC ratio of 1.2. The data (Fig. 3) and the kinetic parameters from the Robinson analysis (Table 1) for the 1:1 SNS/SPFH system are best consistent with unimicellar composition. The molar reaction volume, in its intermediate position between those of the pure surfactants, reflects a more equal input by each surfactant into its determination. Apparently, as the hydrocarbon and the fluorocarbon surfactant approach each other in their CMC's and hence hydrophobicities (the actual value of the CMC is usually viewed as a trade-off between the polarity of the ionic head of the surfactant and its hydrophobicity (19); changing ionic heads from sulfate to sulfonate or carboxylate is not as influential in modifying the CMC as changing the tail length), the two are more compatible in the micellar assembly. Our results indicate that a ratio in CMC values of the two pure short-chained surfactants of about five or greater is required for two types of micelles to be formed, whereas below five one mixed micelle is to be expected. Shinoda and Nomura state that micellar incompatibility or two micelles will be the case when the chain lengths of both surfactants are sufficiently long (20). For short-chained surfactant mixtures such as we are concerned with here, our work shows that a further condition for a single micellar form in solution is that the CMC's of the pure surfactants be close together.

This mixed micelle formed in sufficiently concentrated hydrocarbon/fluorocarbon surfactant solutions has interesting properties born of synergism that may recommend its use for various applications. For example, in a 1:1 SNS/SPFH micellar solution, the organic dye PADA is solubilized much more effectively than in either of the pure micellar solutions and this increase in solubilization is more dramatic as the CMC values of the pure surfactant components approach each

Can. J. Chem. Downloaded from www.nrcresearchpress.com by 217.78.4.112 on 09/08/12
For personal use only.

other. Also curious is the dominant role often played by the fluorocabon surfactant in mixtures in compressing the micellar surface region to a value differing little from that of the pure fluorocarbon surfactant. On the other hand, it is somewhat difficult to picture fluorocarbon and hydrocarbon chains with their different sizes and electron-withdrawing powers lining up amicably in a mixed micelle. Therefore, it may not be surprising that these differences are reconciled by the fluorocarbon having principal control over the forces at work in the micellar surface region.

Acknowledgement

We are grateful to the Natural Sciences and Engineering Research Council of Canada for funding for this research.

1. T. Asakawa, T. Imae, S. Ikeda, S. Miyagishi, and M. Nishida. Langmuir, **7** 262 (1991).
2. F. H. Haegel and H. Hoffmann. Prog. Colloid Polym. Sci. **76**, 132 (1988).
3. Y. Wada, Y. Ikawa, H. Igimi, T. Makihara, S. Nagadome, and G. Sugihara. Fukuoka Univ. Sci. Rep. **19**, 173 (1989).
4. V. C. Reinsborough, T. D. M. Stultz, and X. Xiang. Aust. J. Chem. **43**, 11 (1990).
5. W. Guo, T. A. Brown, and B. M. Fung. J. Phys. Chem. **95**, 1829 (1991).
6. P. Mukerjee, M. J. Gumkowski, C. C. Chan, and R. Sharma. J. Phys. Chem. **94**, 8832 (1990).
7. A. D. James and B. H. Robinson. J. Chem. Soc. Faraday Trans. 1, **74**, 10 (1978).
8. V. C. Reinsborough and B. H. Robinson. J. Chem. Soc. Faraday Trans. 1, **75**, 2395 (1979).
9. P. D. I. Fletcher and V. C. Reinsborough. Can. J. Chem. **59**, 1361 (1981).
10. J. R. Hicks and V. C. Reinsborough. Aust. J. Chem. **35**, 15 (1982).
11. P. D. I. Fletcher and B. H. Robinson. J. Chem. Soc. Faraday Trans. 1, **80**, 2417 (1984).
12. P. D. I. Fletcher, J. R. Hicks, and V. C. Reinsborough. Can. J. Chem. **61**, 1594 (1983).
13. K. Tamaki, Y. Ohara, and S. Watanabe. Bull. Chem. Soc. Jpn. **62**, 2497 (1989).
14. M. J. Rosen. Langmuir, **7**, 885 (1991).
15. M. Fischer, W. Knoche, P. D. I. Fletcher, B. H. Robinson, and N. C. White. Colloid Polym. Sci. **258**, 733 (1980).
16. K. Shinoda, M. Hato, and T. Hayashi. J. Phys. Chem. **76**, 909 (1972).
17. K. Martinek, A. K. Yatsimiriski, A. V. Levashov, and I. V. Berezin. *In* Micellization, solubilization and microemulsions. Vol. 2. *Edited by* K. L. Mittal. Plenum Press, New York. 1977. p. 489.
18. I. Johnson and G. Olofsson. J. Chem. Soc. Faraday Trans. 1, **84**, 551 (1988).
19. D. F. Evans and B. W. Ninham. J. Phys. Chem. **90**, 226 (1986).
20. K. Shinoda and T. Nomura. J. Phys. Chem. **84**, 365 (1980).

Can. J. Chem. Downloaded from www.nrcresearchpress.com by 217.78.4.112 on 09/08/12
For personal use only.

Enthalpies of solution of naphthalene, *N*,*N*-dimethyl-1-naphthylamine, and 1,8-bis(dimethylamino)naphthalene in 16 organic solvents

DANIEL FIGEYS,[1] MAŁGORZATA KOSCHMIDDER,[2] AND ROBERT L. BENOIT[3]

Département de chimie, Université de Montréal, C.P. 6128, Succ. "A", Montréal (Qué.), Canada H3C 3J7

Received May 8, 1991[4]

DANIEL FIGEYS, MAŁGORZATA KOSCHMIDDER, and ROBERT L. BENOIT. Can. J. Chem. **70**, 1586 (1992).

The enthalpies of solution of naphthalene, *N*,*N*-dimethyl-1-naphthylamine, and 1,8-bis(dimethylamino)naphthalene (proton sponge) were determined at 298.15 K in 16 organic solvents (*n*-hexane, cyclohexane, carbon tetrachloride, chloroform, 1,2-dichloroethane, benzene, chlorobenzene, dimethyl sulfoxide, *N*,*N*-dimethylformamide, ethyl acetate, 1,4-dioxane, anisole, nitrobenzene, benzonitrile, methanol, ethanol). Additional determinations were made with benzene. Useful linear relationships are observed between the molar enthalpies of solution of the four compounds in the solvents. The molar enthalpies of solution were correlated with the solvatochromic parameters of the solvents. The presence of $N(CH_3)_2$ groups on naphthalene does not significantly contribute to the solute–solvent interactions.

DANIEL FIGEYS, MAŁGORZATA KOSCHMIDDER et ROBERT L. BENOIT. Can. J. Chem. **70**, 1586 (1992).

Opérant à 298.15 K, on a déterminé les enthalpies de solution du naphtalène, de la *N*,*N*-diméthyl-1-naphtylamine et du 1,8-bis(diméthylamino)naphtalène (éponge à protons) dans 16 solvants organiques (*n*-hexane, cyclohexane, tétrachlorure de carbone, chloroforme, 1,2-dichloroéthane, benzène, chlorobenzène, diméthylsulfoxyde, *N*,*N*-diméthylformamide, acétate d'éthyle, 1,4-dioxane, anisole, nitrobenzène, benzonitrile, méthanol et éthanol). On a effectué des mesures supplémentaires dans le benzène. On a observé des relations linéaires utiles entre les enthalpies molaires de solution des quatre composés dans les solvants. Il existe une corrélation entre les enthalpies molaires et les paramètres solvatochromiques des solvants. La présence de groupes $N(CH_3)_2$ sur le naphtalène ne contribue pas d'une façon significative aux interactions solutés–solvants.

[Traduit par la rédaction]

Introduction

The unusual structure of the aromatic diamine 1,8-bis-(dimethylamino)naphthalene (proton sponge, PS) confers to its conjugated cation, PSH^+, a nonspecific solvation. This property has been used to formulate an extrathermodynamic assumption leading to valuable single-ion enthalpies of transfer between solvents (1). To assess the validity of the assumption, we had to ascertain the absence of specific interactions between PS as a solute and the solvents, such as H-bonding between protogenic solvents and the $-NMe_2$ group of PS. We therefore determined the standard molar enthalpy of solution of PS in a wide range of organic solvents. We present here the corresponding calorimetric data and their analysis in terms of solute–solvent interactions. To this effect we looked for correlations between the molar enthalpy of solution of PS and the solvatochromic parameters of the solvents (2). We also considered another approach related to that of Fuchs and Rodewald (3), who studied the difference between the molar enthalpy of solution of substituted aromatic solutes and that of the parent compound. Thus we also determined the standard molar enthalpy of solution of *N*,*N*-dimethyl-1-naphthylamine (DMNA) and that of naphthalene (NA) in the same series of solvents. The solvents used were selected so that their solvatochromic parameters would cover a wide range of values. The poor solubility of NA and PS, however, imposed some restrictions on our choice of solvents.

Experimental

Proton sponge (Aldrich, 99%) was purified according to the procedure of de Groot and Sikkema (4). *N*,*N*-Dimethyl-1-naphthylamine (Aldrich, 99%) was used as received and naphthalene (Aldrich, 99%) was recrystallized from ethanol. Benzene (99.9%+), chlorobenzene (99.9%+), nitrobenzene (99%), benzonitrile (99%), ethyl acetate (99.9%+), 1,2-dichloroethane (99.8%), 1,4-dioxane (99.8%), anisol (99%), *n*-hexane (99%+), and carbon tetrachloride (Spectrograde) were supplied by Aldrich. Dimethyl sulfoxide (99.9%) was obtained from BDH, ethanol (anhydrous) from Anachemia. *N*,*N*-Dimethylformamide (reagent grade), cyclohexane (Spectrograde), and chloroform (spectrograde) were from ACP and methanol (spectrograde) from American Chemicals. Chloroform was treated with 4A molecular sieves and distilled.

The enthalpies of solution were measured at 298.15 ± 0.01 K with an LKB model 8721-1 isoperibol calorimeter as previously described (1); the nul detector was connected to a digital–analog circuit and a Zenith computer. The amounts of compounds dissolved in 0.100 dm^3 of solvent were obtained from the weights of the 0.001 dm^3 reaction ampoules. Two different types of ampoules were used, either a glass one whose neck was closed with Parafilm for unreactive solvents, or a small Teflon cylinder tightly closed with thin glass caps at both ends (5). The calorimetric measurements were made at different final solute concentrations, 0.001–0.02 mol dm^{-3}.

Results and discussion

The molar enthalpies of solution were calculated from a linear regression correlation of the heat change against solute concentration. The uncertainties quoted are the standard deviations of the slopes. The enthalpy values obtained for each of the compounds are taken to be equal to the infinite dilution values $\Delta_{sol}H^0_m$ because no concentration dependence was observed in the low concentration range studied, 0.001–0.02 mol dm^{-3}. The standard molar enthalpies of solution at 298.15 K are listed in Table 1 for naphthalene, *N*,*N*-dimethyl-1-naphthylamine, and proton sponge. Our results for the solution of NA in dimethylformamide and methanol are in good agreement with previous values (3).

We note that the three sets of $\Delta_{sol}H^0_m$ values for NA, DMNA, and PS in Table 1 vary within a narrow range of

[1]Present address: Department of Chemistry, University of Alberta, Edmonton, Alta., Canada T6G 2G2.

[2]On leave from: Technical University, Gdańsk, Poland.

[3]Author to whom correspondence may be addressed.

[4]Revision received December 18, 1991.

Can. J. Chem. Downloaded from www.nrcresearchpress.com by 217.78.4.112 on 09/08/12
For personal use only.

TABLE 1. Standard molar enthalpies of solution of naphthalene, proton sponge, *N*,*N*-dimethyl-1-naphthylamine, and benzene at 298.15 K

Solvent	Π^{*a}	$\delta_H{}^a$ ($J^{1/2}$ cm$^{3/2}$)	$\Delta_{sol}H^0_m$ (NA) (kJ mol^{-1})	$\Delta_{sol}H^0_m$ (PS) (kJ mol^{-1})	$\Delta_{sol}H^0_m$ (DMNA,l) (kJ mol^{-1})	$\Delta_{sol}H^0_m$ (Bz,l) (kJ mol^{-1})
n-Hexane	−0.08	14.9	21.2 ± 0.2	18 ± 1.5	4.94 ± 0.09	3.31[b,c]
Cyclohexane	0	16.8	22.3 ± 0.4	21.4 ± 0.2	6.3 ± 0.1	3.81[b]
Carbon tetrachloride	0.28	17.6	18.6 ± 0.5	16.3 ± 0.3	1.11 ± 0.07	0.54[b]
Chloroform	0.58	19.3	15.4 ± 0.2	10.9 ± 0.5	−4.4 ± 0.1	
1,2-Dichloroethane	0.81	20.3	18.1 ± 0.2	17.6 ± 0.5	1.14 ± 0.06	
Benzene	0.59	18.7	17.8 ± 0.4	15.9 ± 0.6	0.86 ± 0.02	0
Chlorobenzene	0.71	19.8	17.7 ± 0.2	14.1 ± 0.5	−0.71 ± 0.05	0.06 ± 0.02
Dimethylsulfoxide	1.00	26.6	19.7 ± 0.3	23.1 ± 0.5	5.2 ± 0.1	
N,*N*-Dimethylformamide	0.88	24.1	16.3 ± 0.3	19.2 ± 0.3	1.14 ± 0.01	
Ethylacetate	0.55	18.2	17.0 ± 0.1	18.6 ± 0.2	1.45 ± 0.07	
1,4-Dioxane	0.55	20.5	16.8 ± 0.5	19.0 ± 0.1	1.6 ± 0.1	
Anisole	0.73	19.7	16.7 ± 0.5	16.0 ± 0.1	−0.08 ± 0.05	0.16 ± 0.02
Nitrobenzene	1.01	22.6	18.6 ± 0.2	18.2 ± 0.1	1.14 ± 0.03	1.07 ± 0.07
Benzonitrile	0.90	22.7	17.8 ± 0.4	16.3 ± 0.1	0.00 ± 0.01[d]	0.15 ± 0.01
Methanol	0.60	29.3	19.1 ± 0.3	20.7 ± 0.5	4.30 ± 0.06	
Ethanol	0.54	26.0	18.8 ± 0.2	20.5 ± 0.6	4.18 ± 0.07	

[a]Reference 2.
[b]Reference 7.[c]In *n*-heptane.
[d]Estimated error.

Can. J. Chem. Downloaded from www.nrcresearchpress.com by 217.78.4.112 on 09/08/12
For personal use only.

approximately 7 kJ mol^{-1} (excluding the $CHCl_3$ values) in spite of the widely different properties of the solvents as can be assessed from their solvatochromic parameters (2). The solvents' parameters of interest for our set of solutes are: δ_H, the Hildebrand solubility parameter, Π^*, a measure of the solvents dipolarity/polarizability, and α, the hydrogen-bond donor ability. The values of δ_H and Π^* are listed in Table 1; the values of α are 0 except for chloroform (0.44), methanol (0.93), and ethanol (0.83), and the values of δ_{cor} (a polarizability correction) are 1 for the aromatic solvents, 0.5 for the chloro solvents, and 0 for the other solvents. The $\Delta_{sol}H^0_m$ values for DMNA are consistently some 15–20 kJ mol^{-1} more exothermic than those for NA and PS. This is because at 298.15 K DMNA is a liquid while NA and PS are both solids. As a matter of fact, if we subtract the enthalpy of fusion of NA (+18.0 kJ mol^{-1}) (6), the calculated values of the enthalpy of solution of supercooled liquid NA in the various solvents are now within a few kJ mol^{-1} of the corresponding values for liquid DMNA.

Correlation between enthalpies of solution

The plot of the molar enthalpies of solution of DMNA in the 16 solvents against those of NA in the same solvents shows some interesting features. If we attempt to use all the data the correlation is rather poor (r = 0.85, s.d. = 1.5) but if we divide the solvents into two groups we obtain two essentially parallel lines:

Line a:

$$[1]\quad \Delta_{sol}H^0_m\,(\text{DMNA, l}) = (1.21 \pm 0.09)\,\Delta_{sol}H^0_m\,(\text{NA}) - (21 \pm 1.5)$$

with N = 9, r = 0.982, s.d. = 0.5, where N is the number of solvents in the correlation; r denotes the correlation coefficient; s.d. is the standard deviation of the estimate. The nine solvents include *n*-hexane and cyclohexane, and the aromatic and chlorosolvents (excluding $CHCl_3$). For the remaining six solvents we have

Line b:

$$[2]\quad \Delta_{sol}H^0_m\,(\text{DMNA,l}) = (1.24 \pm 0.07)\,\Delta_{sol}H^0_m\,(\text{NA}) - (19 \pm 1.3)$$

with N = 6, r = 0.994, s.d. = 0.22.

The correlations between the molar enthalpies of solution of PS and NA are not as good. We find

Line a:

$$[3]\quad \Delta_{sol}H^0_m\,(\text{PS}) = (1.2 \pm 0.2)\,\Delta_{sol}H^0_m\,(\text{NA}) - (5 \pm 4)$$

with N = 9, r = 0.866, s.d. = 1.5.

Line b:

$$[4]\quad \Delta_{sol}H^0_m\,(\text{PS}) = (1.0 \pm 0.3)\,\Delta_{sol}H^0_m\,(\text{NA}) + (2 \pm 5)$$

with N = 6, r = 0.889, s.d. = 0.85.

Finally, for benzene we obtain

Line a:

$$[5]\quad \Delta_{sol}H^0_m\,(\text{Bz,l}) = (0.78 \pm 0.07)\,\Delta_{sol}H^0_m\,(\text{NA}) - (14 \pm 1)$$

with N = 9, r = 0.972, s.d. = 0.37.

These correlations are clearly of practical interest. For example, for the solvent water, from a value of $\Delta_{sol}H^0_m$ (NA) = + 29.9 kJ mol^{-1} (6) and eq. [4] we calculate $\Delta_{sol}H^0_m$ (PS) = + 32 kJ mol^{-1} to be compared with the experimental 30 ± 5 kJ mol^{-1} (1). However, the significance of these correlations is unclear since the two groups of solvents do not form well-defined families. Furthermore, the experimental uncertainties on the enthalpies do not account for the scatter of the points.

Correlations between enthalpies of solution and solvent parameters

The enthalpy of solvation of a solute, i.e., its transfer from the gas phase to the solvent, can be taken to include a number of additive enthalpy contributions that correspond to the creation of a cavity in the solvent, the solute–solvent dis-

Can. J. Chem. Downloaded from www.nrcresearchpress.com by 217.78.4.112 on 09/08/12
For personal use only.

persion and polar interactions, the structural changes produced by the solute in the solvent, and specific interactions, such as H-bonding, between the solute and the solvent. Clearly, isolating the different contributions will lead to a better understanding of solute–solvent interactions and various approaches have been tried to solve the problem (7). Recently, considerable success has been achieved in correlating a large number of physicochemical properties and reactivity parameters to solute and solvent properties through linear relationships (2). We have applied multiple linear regression analysis to correlate our molar enthalpies of solution, and other derived enthalpies, to the solvatochromic parameters of the solvents listed in Table 1.

We obtained for solid NA and PS, and liquid DMNA the following equations where all the coefficients are statistically significant at the confidence level of 95% according to Student's *t*-test.

$$[6] \quad \Delta_{sol}H^0_m\,(NA) = (1.28 \pm 0.05)\,\delta_H - (14 \pm 2)\,(\Pi^* - 0.21\,\delta_{cor}) - (9 \pm 2)\,\alpha$$

where $N = 16$, $R^2 = 0.9950$, s.d. = 1.5.

$$[7] \quad \Delta_{sol}H^0_m\,(PS) = (1.19 \pm 0.06)\,\delta_H - (10 \pm 2)\,\Pi^* - (8 \pm 1)\,\alpha$$

where $N = 16$, $R^2 = 0.9946$, s.d. = 1.5.

$$[8] \quad \Delta_{sol}H^0_m\,(DMNA,l) = (0.26 \pm 0.04)\delta_H - (4 \pm 1.5)\,(\Pi^* + 0.44\,\delta_{cor})$$

where $N = 15$ ($CHCl_3$ excluded), $R^2 = 0.847$, s.d. = 1.3.

For benzene there is no satisfactory correlation since R^2 is only 0.65.

The coefficients of the parameters δ_H, Π^*, and α of the equations make chemical sense in that the cavity term adds a positive contribution to $\Delta_{sol}H^0_m$ while the expected negative contributions come from both polar interactions and H-bond interactions between the solutes and the H-bond donor solvents. Somewhat unexpectedly, the equations have no constant term; when the multiple regression program was run with a constant the R^2 value dropped to ~0.3. Using δ_H^2, which may be preferable to δ_H (7), also gave poorer correlations. The equations do not include a term to account for possible electron donor–acceptor (EDA) interactions of the solutes with the chloro and aromatic solvents, in part because there is no simple way to account for such interactions (8). At any rate the linear relationships between the $\Delta_{sol}H^0_m$ values of naphthalene and those of PS and DMNA would suggest that EDA interactions would only involve the solute's Π electrons and not the nitrogen lone pair. It may be that EDA interactions are accounted for, at least in part, in the Π^* term. It is somewhat difficult to compare the values of the coefficients of the parameters for the three solutes. For NA and PS, which are both solids and with similar enthalpies of sublimation, the coefficients of δ_H and α are nearly the same while those of Π^* are somewhat different, but there is a δ_{cor} term that is significant for NA but not for PS. If we omit δ_{cor} from the NA correlation we obtain:

$$[9] \quad \Delta_{sol}H^0_m\,(NA) = (1.28 \pm 0.07)\,\delta_H - (12 \pm 2)\,\Pi^* - (10 \pm 2)\,\alpha$$

where $N = 16$, $R^2 = 0.991$, s.d. = 1.9.

This time the Π^* coefficients are the same within error for NA and PS. The closeness of the α coefficients for NA and PS would imply that H-bonding between the solvents and the $-NMe_2$ groups plays only a minor role, if any, and that Π electron – hydrogen bond interactions are more important. To obtain a comparable equation for solid DMNA we added 18 kJ mol^{-1}, an estimated value of the molar enthalpy of fusion of DMNA, to the values of $\Delta_{sol}H^0_m$ (DMNA,l) and we found

$$[10] \quad \Delta_{sol}H^0_m\,(DMNA) = (1.40 \pm 0.05)\,\delta_H - (14 \pm 2)\,\Pi^* - (10 \pm 1.5)\,\alpha$$

where $N = 15$, $R^2 = 0.996$, s.d. = 1.5.

The coefficients of δ_H, Π^*, and α are now near those for solid NA and PS. It is puzzling that eq. [10] has no constant term, particularly in view of the fact that current work on the solution of pyridines leads to equations with constant terms whose values are related to the physical state of pyridines, whether gaseous, liquid, or solid. At any rate the terms in eq. [6], [7], [9], and [10] should be regarded as measuring the differences between the solute–solvent interactions formed and the solute–solute interactions disrupted (9). Within these limitations the correlations between the molar enthalpies of solution and the solvatochromic parameters of the solvents permit us to estimate the respective contributions of cavity, polar, and H-bonding terms. For example, for naphthalene the positive cavity contribution would vary between 20 and 40 kJ mol^{-1} and would be counterbalanced by the negative contributions of 0–10 kJ mol^{-1} each for polar and H-bonding terms. The correlations have also a good predictive value. Thus for the solution of NA in the solvent water, we calculate from the solvatochromic parameters and eq. [6] $\Delta_{sol}H^0_m = +34$ kJ mol^{-1}, to be compared with a +29.9 kJ mol^{-1} experimental value (6). For the solution of PS in pyridine we calculate +19 kJ mol^{-1} while a recent experiment gave +17.35 kJ mol^{-1}.

We also looked at correlations between the enthalpy of solvation (gas to solvent) and the solvatochromic parameters of the solvents, but the standard deviations were too high for good predictive value. Similarly, the correlations between the heats of transfer of the solutes (taking cyclohexane as reference solvent) and the differences between the solvatochromic parameters were not satisfactory. Taking naphthalene as the parent compound for PS and correlating the differenes between the heats of transfer of both solutes (3) also lead to no meaningful results. Finally the comparison of correlation, eqs. [7], [9], between $\Delta_{sol}H^0_m$ (NA) and $\Delta_{sol}H^0_m$ (PS), and the solvatochromic parameters on the one hand, and the direct linear relation between $\Delta_{sol}H^0_m$ (PS) and $\Delta_{sol}H^0_m$ (NA), eqs. [3], [4], on the other hand shows that these relations are not strictly compatible and this may account for the fact that the linear relation between $\Delta_{sol}H^0_m$ (PS) and $\Delta_{sol}H^0_m$ (NA) is only approximate.

Acknowledgements

A grant and a scholarship (D.F.) from the Natural Sciences and Engineering Research Council of Canada are gratefully acknowledged. The authors thank Professor M. D'Amboise for his advice on the use of some statistical methods.

1. R. L. Benoit, D. Lefebvre, and M. Fréchette. Can. J. Chem. **65**, 996 (1987).
2. M. H. Abraham, P. L. Grellier, J.-L. Abboud, R. M. Doherty, and R. W. Taft. Can. J. Chem. **66**, 2673 (1988).
3. R. Fuchs and R. F. Rodewald. J. Am. Chem. Soc. **94**, 5897 (1973).
4. R. L. De Groot and D. J. Sikkema. Recl. Trav. Chim. Pays-Bas, **95**, 10 (1976).
5. I. Uruska and M. Koschmidder. J. Chem. Soc. Perkin Trans. 2, 1845 (1989).
6. R. L. Bohon and W. F. Claussen. J. Am. Chem. Soc. **73**, 1571 (1951).
7. R. Fuchs and W. K. Stephenson. Can. J. Chem. **63**, 2529 (1985).
8. K. Morokuma and K. Kitaura. *In* Molecular interactions. Vol. 1. *Edited by* H. Ratajczak and W. J. Orville-Thomas. Wiley, New York. 1980. p. 21.
9. M. J. Kamlet, R. M. Doherty, M. H. Abraham, Y. Marcus, and R. W. Taft. J. Phys. Chem. **92**, 5244 (1988).

Can. J. Chem. Downloaded from www.nrcresearchpress.com by 217.78.4.112 on 09/08/12
For personal use only.

Atrazine in mineral soil: the analytical chemistry of speciation[1]

DONALD S. GAMBLE[2] AND L. ALI ISMAILY
Land Resource Research Centre, Research Branch Agriculture Canada, Ottawa, Ont., Canada K1A 0C6

Received December 2, 1991

DONALD S. GAMBLE and L. ALI ISMAILY. Can. J. Chem. **70**, 1590 (1992).

The HPLC–microfiltration method previously described for determining atrazine and hydroxyatrazine species in organic soil has been adapted to a mineral soil. The method was able to monitor atrazine concentrations of less than 1.0×10^{-6} M, which is over 40 times lower than the atrazine concentrations measured in the earlier organic soil experiments. During kinetics experiments, it also monitored four free and sorbed chemical species instead of only one. Measurements were obtained with much better accuracy and productivity than can be obtained by conventional methods. The atrazine sorption capacity of the mineral soil was also measured. The analytical chemical data produced can support heterogeneous chemical kinetics calculations.

DONALD S. GAMBLE et L. ALI ISMAILY. Can. J. Chem. **70**, 1590 (1992).

Dans le but de déterminer des espèces atrazine et hydroxyatrazine dans des sols organiques, on a adapté à une huile minérale la méthode de CLHP/microfiltration décrite antérieurement. La méthode permet d'évaluer des concentrations d'atrazine de moins de $1{,}0 \times 10^{-6}$ M, soit 40 fois moins que les concentrations d'atrazine mesurées lors des expériences antérieures avec des sols organiques. Au cours d'expériences cinétiques, on peut aussi déterminer quatre espèces chimiques libres et sorbées au lieu d'une seule. Des mesures ont été réalisées avec une meilleure précision et une meilleure productivité que celle possible avec des méthodes conventionnelles. On a aussi measuré la capacité de sorption de l'atrazine à partir de l'huile minérale. Les données analytiques chimiques ainsi produites peuvent supporter des calculs de cinétique chimique.

[Traduit par la rédaction]

Introduction

The herbicide atrazine, used extensively to control weeds in corn, has become associated with a number of environmental problems. Contamination of soil and groundwater is an example (2–4), and its plant toxicity is influenced by the extent to which it is free in solution or sorbed (5, 6). Mathematical models for its persistence and mobility in soils must account for sorption–desorption kinetics and equilibria, and chemical degradation (7, 8). Hydrology models, which seek to predict movement and concentrations of contaminants in groundwater and soil, will consequently require analytical chemical data. The first requirement is that the chemical properties, including speciation, of the atrazine must be quantitatively known. A number of authors have already contributed information on the chemical reactions and speciation of atrazine (9–17). The next requirement is that the relevant physical chemistry properties of particular soils must be measured. They include numbers and acid strengths of carboxyl groups, and atrazine sorption capacities. These physical chemical properties must then be monitored over the course of experiments with a particular soil and atrazine. Variables needed for the supporting calculations should be measured experimentally. It is not sufficient to measure total atrazine in an experimental sample because the calculations of parameters for hydrology models can only be done with measurements of free and bound forms. The physical nature and chemical reactivity of the soil will make a large contribution to the manner and rate of pesticide–soil interactions. In light of this, it is not practical to attempt to solve pesticide–soil interaction problems using only information about the chemistry of the pesticide, without information about the chemistry of the soils. To avoid experimental artifacts the analytical chemical method for measuring the distribution of atrazine between a solution and the suspended solids must not disturb the distribution being measured. This is equally true for both equilibrium and nonequilibrium distributions.

A combination of acid–base titrations and HPLC with microfiltration has been designed to meet such requirements. The basic HPLC–microfiltration method for chemical kinetics speciation experiments was reported previously by us for organic soil (1). The analytical chemical methods must next be adapted to monitor the chemical speciation of atrazine as a function of time when mineral soils are used, because of their greater economic and environmental importance. With mineral soils two experimental problems are encountered that are not encountered with organic soils (1). The soil particles are harder to slurry properly because they are somewhat more dense than organic soil particles. In addition it was anticipated that their sorption capacities and chemical reactivities would be substantially smaller than those of organic soil, because of smaller carboxyl group contents. Preliminary experiments have confirmed this.

A conventional sorption experiment typically uses several samples, each of which has to be separately filtered or centrifuged and extracted for analysis. Each extraction commonly uses only 50–100 mL of extractant for each gram of soil. The preparation for HPLC or GC injection requires 2 days for shaking, separation, volume reduction with a rotary evaporator, and adjustment of the residue to a known volume. This produces only about a dozen low-precision data points for the whole experiment, and the small-volume batch extractions would tend to disturb the solution–solid distributions of pesticide that they were supposed to measure. Such a method is not only labour intensive, but it also produces data that do not support detailed chemical kinetics calculations very well.

The objective of this work was to adapt the analytical chemical methods developed for atrazine interactions with an organic soil to the investigation of its interactions with a mineral soil.

[1]LRRC Contribution No. 90-91.
[2]Author to whom correspondence may be addressed.

Can. J. Chem. Downloaded from www.nrcresearchpress.com by 217.78.4.112 on 09/08/12
For personal use only.

TABLE 1. Mineral soil analyses. Components and some chemical properties of a New Brunswick Mineral Soil[a]

Minerals	%	Organic matter	%	Metal ion extractants	(μmol/g of soil) Fe	Al	Exchangeable metal ions	(mequiv./g of soil)
Sand	42.6	Organic	C 8.18%	Pyrophospate	0.2955	0.8006	Ca^{2+}	0.0090
Silt	45.7			Oxalate	0.2975	1.0081	Mg^{2+}	0.0019
Clay	11.7			Dithionite	0.5694	0.9599	K^{+}	0.0016
							Al^{3+}	0.0440
							Total	0.0565

[a]See Wang and McKeague (19).

Theory

The extraction method used in this study involves injection of an aqueous slurry of soil into an HPLC fitted with inline microfilters. The inline filters trap the soil particles and the flow of the mobile phase results in extraction of atrazine. Analysis of the chromatogram shows the total concentration of a pesticide that was distributed between the solution and quickly accessible sorption sites on the suspended particles. In a typical atrazine – mineral soil experiment, a 20.0 μL injection of slurry contains approximately 4×10^{-4} g of particles, which are trapped on the inline filters. With a mobile phase flow rate of 1.0 mL/min, a typical peak retention time of 6.0 min would give a ratio of extractant to sample approximately equal to 15.0 L/g of soil. The subtraction of solution concentrations determines concentrations of labile sorbed pesticide. The inline extraction distinguishes between desorption that is fast, relative to the extraction time, and desorption that is slow. This distinction should be directly relevant to bioavailability, since very slow desorption rates could limit plant uptake.

Experimental section

Equipment

Titrations

The automatic titrator used has been previously described (18).

Chemical kinetics and speciation

A Varian high-pressure liquid chromatograph was used. It consisted of a Star 9010 variable wavelength UV–visible detector, and a model 4400 Beckman integrator. The column was a Beckman C-18 Ultrasphere ODS, 5 μm particle size, 4.6 mm × 25.0 cm. They were protected with Altech Guard Column Cartridges, C-18 Adsorbosphere. Hamilton microliter syringes ranged in size from 50 to 250 μL. A B-D 1-cm^3 26G 3/7 Tuberculin syringe and precision glide needle, and a B-D Yale 20 needle were also used. Preinjection filtration was done with MSI Cameo Nylon filters, 3 mm diameter, 0.45 μm pore size. Samples were thermostated at 25.00°C in water-jacketed reaction vessels.

Materials and reagents

Mineral soil

The location and properties of the B horizon mineral soil from Central New Brunswick were similar to the Sunbury soil documented by Wang and McKeague (19). Some additional properties are listed in Table 1.

Reagents and standard solutions

Atrazine and hydroxyatrazine reagents and standard stock solutions were the same as previously described (1). Analytical chemical standards contained either 1.000×10^{-6} M or 1.000×10^{-5} M atrazine.

Procedures

Titrations

About 1.0 g of mineral soil weighed to four decimal places was added to 10 mL of 1.0 N NaCl, and titrated with 0.1 N standard NaOH, at 25.0°C. The titrator was programmed to deliver 0.1 mL every 3.0 mins. Titrations using 0.1 N HCl were done in a similar way. Standard buffers were used.

Kinetics chemical speciation experiments

A 0.5 g portion of mineral soil was suspended with stirring in approximately 15 mL of redistilled H_2O for about 2 days. This wetted all of the surfaces and sorbed H_2O into soil particles. The hydrolysis reaction was started by the addition of atrazine standard stock solution, with the total sample volume being adjusted to 25.0 mL. Some sorption experiments were done with high initial concentration of atrazine (5.0×10^{-5} M) in order to saturate the sorption sites and yield a measure of the atrazine sorption capacity of the soil. Subsaturation experiments had an initial atrazine concentration of 1.0×10^{-6} M. From these experiments the rate of the sorption process was examined. Vigorous stirring maintained a uniform suspension of soil particles throughout the whole solution and thermostated water jackets maintained the slurry temperature at 25.0°C. Microfiltrate (0.45 μm) and whole slurry analyses were done as functions of time, essentially as previously described (1). The detector wavelength was set at 220 nm for atrazine, and 240 nm for hydroxyatrazine. An additional inline filter, a 2-μm stainless steel frit, ahead of the guard column was used to prevent excess system pressures by catching some of the soil particles. The system of inline microfilters and guard column was cleaned at the end of each work day. A methanol/H_2O mobile phase, 80:20, with 1.58×10^{-3} M HCl was used with a flow rate of 1.0 mL/min. Microcomputer spreadsheets were used for converting raw analytical chemical measurements and clock and calendar readings into chemical kinetics data for free and reversibly sorbed forms of atrazine and hydroxyatrazine. Table 2 summarizes the experimental conditions for the two types of kinetics–speciation experiments with atrazine and mineral soil.

The determination of parameters

Solution phase concentrations were determined by measuring filtrates obtained with 0.45 μm Nylon 66 disposable filters. Sorption was determined by injecting first the 0.45 μm filtrate and next the whole slurries, and then calculation of the differences. Site saturation gave the sorption capacity, measured on the plateau of the sorption vs. solution concentration curve. Sorption equilibrium functions were calculated from subsaturation experiments and the measured capacity. The early approach to sorption equilibrium was used for the calculation of sorption and desorption rate constants.

Results and discussion

The high organic carbon content of the New Brunswick soil implies a relatively high total content of carboxyl and carboxylate groups. Several authors have demonstrated the central importance of humic carboxyl groups to pesticide –

Can. J. Chem. Downloaded from www.nrcresearchpress.com by 217.78.4.112 on 09/08/12
For personal use only.

TABLE 2. New Brunswick mineral soil: acid–base properties in 1.0 N NaCl

Initial values before titration:	
Apparent cation exchange capacity[a]	0.0565 (mequiv./g)
Upper limit, mole fraction of acidic sites neutralized[a]	0.246
Degree of ionization	0.35
K_A	5.59×10^{-5}
σ	0.06×10^{-5}

Titrant	Calculation method	Equivalence point (mequiv./g)
0.1 N NaOH	Gran's plot	0.149
0.1 N HCl	Titration curve plot	0.0805
Total		0.23
σ		0.05

[a]From Table 1.

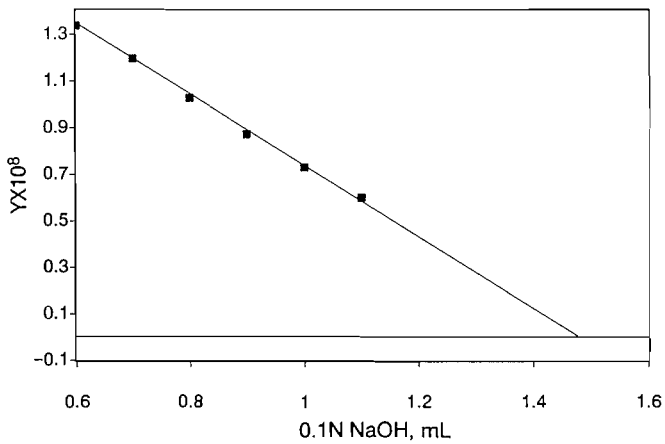

FIG. 1. $M_H V_B$, Gran's function plot for the New Brunswick mineral soil, 1.0 N NaCl. $Y = (V_{sl} - V_B)\text{antilog}(-16.9 \times E_{obs})$ where V_{sl} and V_B are the volumes of the slurry and the base, respectively, and E_{obs} is the observed potential.

soil interactions (1, 20–31). The extent to which the extractable iron and aluminum of this New Brunswick soil might be blocking carboxyl or clay sorption sites is unknown. The best analytical chemical option available for this question is direct titration of the whole soil by standard base. The significance of the exchangeable metal ions is that the portion of them not held by inorganic cation exchange sites equals the number of carboxylate anions. The relative amounts of them held by carboxylate and clay sites were unknown, however, and the upper limit to the number of possible carboxylate anions corresponds to the case in which none of the exchangeable metal ions was held by clay or hydrous metal oxide ion exchange sites.

The conventional appearance of the Gran's plot for titration with standard base shown in Fig. 1 is important evidence indicating that the analytical chemical method is not susceptible to serious interference from the complicated mixture of components in a natural mineral soil. For example, it did not suffer from the type of weak acid polyelectrolyte buffering that makes sharp equivalence points impossible in fulvic acid titrations (32). The purpose of the 1.0 N NaCl was to prevent the Donnan potential restriction of proton movement from particles into the external solution. If an

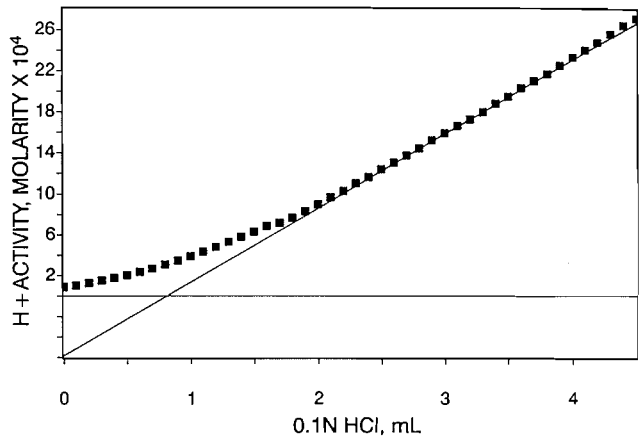

FIG. 2. HCl titration curve for the New Brunswick mineral soil, 1.0 N NaCl.

equivalence point can also be obtained for the titration of the soil with standard acid, it should be a measure of all of the sites that can be protonated. This might include carboxylate anions and such inorganic bases as carbonates, bicarbonates, and hydrous metal oxides. A comparison of this equivalence point with the total ion exchangeable metal ions in Table 1 should be a useful clue to the nature of the sites being titrated. A satisfactory Gran's plot was not obtained for the titration with a standard acid. However, titration with standard HCl produced a clearly defined equivalence point as shown in Fig. 2. The limiting slope of the curve after the early proton binding phase represents a simple dilution of the added H^+. The equivalence point is the boundary between the H^+ binding and H^+ dilution regions of the curve. This is essentially the same type of dilution curve used previously (33, 34) for the titration of fulvic acid with atrazine. In the absence of CO_2 evolution from carbonate or bicarbonate decomposition, the equivalence point should represent a total for carboxylates and hydrous metal oxides. It gives an upper limit for the number of carboxylate anions, for the particular case in which no hydrous metal oxides are being titrated.

A plot of the weighted average equilibrium function for the acid dissociation of acidic sites (35, 36), $\bar{K}_A$ vs. α, is shown in Fig. 3. The use of 1.0 N NaCl ensured that a_{H^+} was approximately the same in and on the soil particles as it was in the external solution (37, 38). Any experimental error in the determination of the number of protonated acid sites will be reflected in the numerical values of $\bar{K}_A$. In the present case, it cannot be assumed that the nonlinear regions of the two ends of the plot have real chemical meaning. Only the linear middle region was used for subsequent calculations.

If a mixture of carboxyl groups has a wide range of weak acid K_A values, the $\bar{K}_A$ determined macroscopically for the whole mixture can sometimes differ by one or two orders of magnitude from the K_A values of individual components (39). This could confuse any attempt at molecular level interpretations of such phenomena as hydrogen-bonded sorption and Brönsted acid catalysis. This problem may be resolved by using the differential equilibrium function, calculated with the equation

$$K_A = -\frac{d(\alpha M_{H^+})}{d\alpha}$$

M_{H^+} and α are the H^+ molarity and the degree of ionization.

Can. J. Chem. Downloaded from www.nrcresearchpress.com by 217.78.4.112 on 09/08/12
For personal use only.

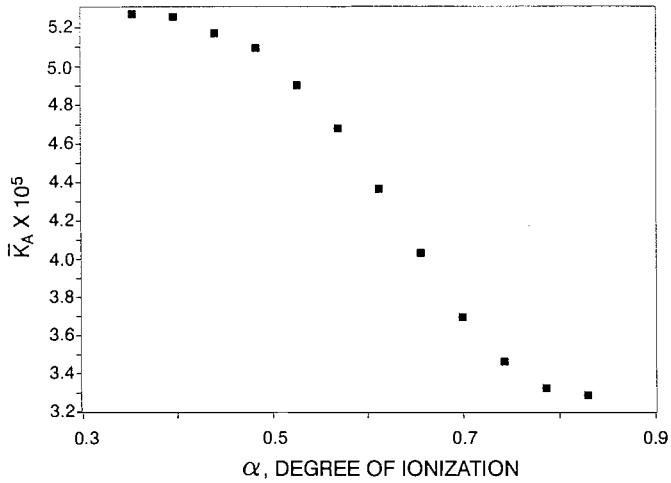

FIG. 3. The weighted average equilibrium function ($\bar{K}_A$) vs. degree of ionization (α), for the acidic sites of the New Brunswick mineral soil.

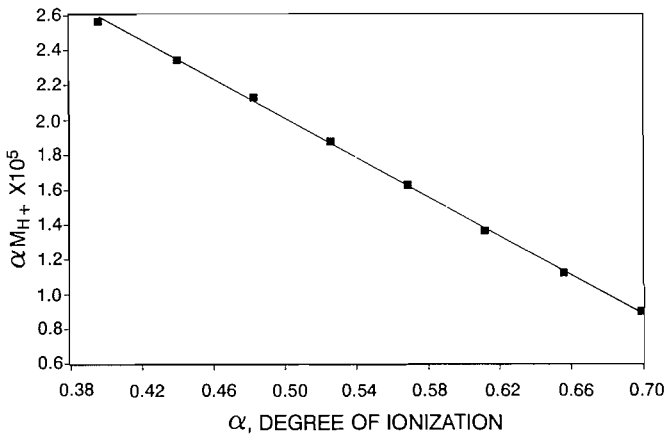

FIG. 4. The calculation of the differential equilibrium function for acid dissociation of the acidic sites in the New Brunswick mineral soil. $\bar{K}_A = -[d(\alpha M_{H^+})/d\alpha]$.

In the present case, this is simply the slope of the straight line for which the least-squares fit is illustrated in Fig. 4. Although the K_A cannot be identified with individual components of the mixture, it is much more directly related to them than is the $\bar{K}_A$ (39). In particular, the numerical values of K_A will not be wrong by one or two orders of magnitude. They may therefore be used for the molecular level interpretations of hydrogen-bonding and acid catalysis effects without major numerical errors. This is expected to remove some causes of data scatter and to improve the effectiveness of predictive calculations.

The data from the acid and base titrations that are directly related to some of the causes of pesticide interactions with soil are listed in Table 2. For example, the K_A, α, and base titration equivalence point govern hydrogen-bonded sorption and Brönsted acid catalysis of atrazine. The acid titration endpoint indicates the expected carboxylate contribution to the cation exchange capacity. The apparent ion exchange capacity from Table 1 and the HCl titration equivalence point from Table 2 are consistent with each other. At present there is no direct evidence that the apparent ion exchange capacity corresponds exactly to the number of carboxylate anions, and the most general case is that clays and hydrous

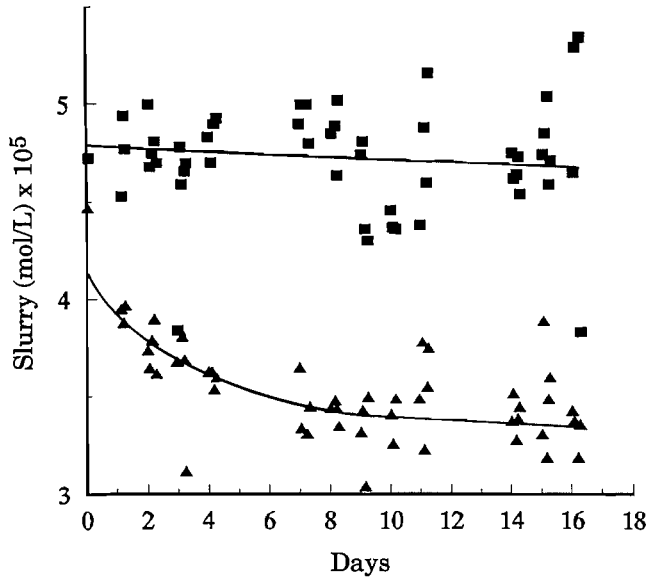

FIG. 5. Chemical analysis of the slurry, using the HPLC–microfiltration method, for a site saturation experiment. Concentration of atrazine vs. time for —■—, whole slurry, $\sigma = 2.0 \times 10^{-6}$; and —▲—, microfiltrate, 0.45 μm, $\sigma = 1.1 \times 10^{-6}$.

metal oxides might contribute to the observed cation exchange capacity. It is therefore only an upper limit for the number of free carboxylate anions. Carboxylate ligands in very stable transition metal chelates would not be free. Within the limits of experimental uncertainty, the apparent cation exchange capacity and the HCl titration equivalence point cannot be assumed to differ significantly. While the HCl equivalence point would be relevant to the ion exchange uptake of cationic pesticides such as Paraquat (20, 21, 40), it is the NaOH equivalence point that is appropriately used for the calculation of $\bar{K}_A$ and K_A. Because the plot in Fig. 4 is linear, it produced the single numerical value for K_A that is recorded in Table 2. There are two indications that the range of K_A values in the New Brunswick mineral soil must be quite narrow. One is that only the single numerical value was obtainable from the data presented in Fig. 4. The other is that K_A is only 1.1–1.7 times larger than the $\bar{K}_A$ value for K_A values in Fig. 3. There are at least two possible reasons for this in the natural, chemically unprocessed, mineral soil. One is that humic acids tend to have a narrower range of K_A values than fulvic acids. Another is that a substantial fraction of the more strongly acidic carboxyl groups may be blocked by chelated Fe(III) and Al(III). Assuming the typical values of 50% organic carbon in humic materials and approximately 3 mequiv./g of carboxyl groups in humic acid, the organic carbon analysis indicates that it would be reasonable to expect about 0.5 mequiv./g total carboxyl groups in the New Brunswick mineral soil. According to the Gran's equivalence point, no more than 30% of that amount was found to be protonated. If only a portion of the total carboxyl groups were protonated, it would have been the most weakly acidic portion.

The results of this atrazine analyses for a site saturation experiment obtained directly by the HPLC–microfiltration method are presented in Fig. 5. The raw data were fitted to polynomials by the method of least squares. The standard deviation for the slurry curve was 2.0×10^{-6}, and for the filtrate curve it was 1.1×10^{-6}. Atrazine recoverable from

Can. J. Chem. Downloaded from www.nrcresearchpress.com by 217.78.4.112 on 09/08/12
For personal use only.

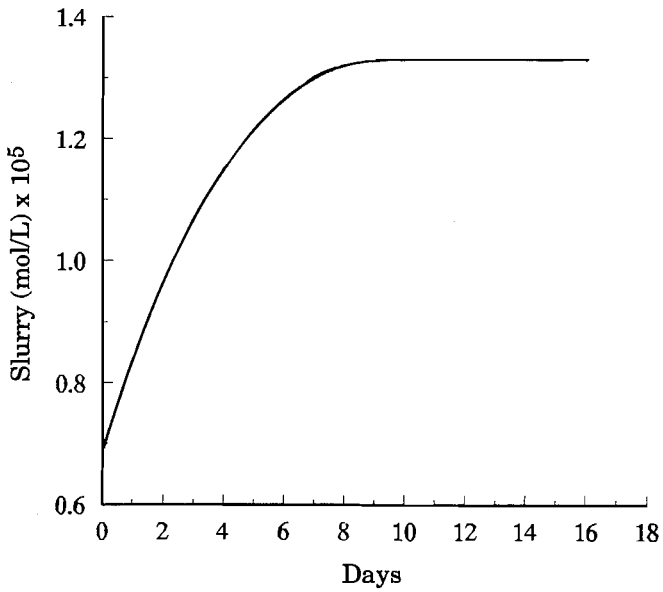

FIG. 6. The amount of atrazine reversibly sorbed vs. time. The plateau region of the curve gives the atrazine sorption capacity of the soil. The sorption sites were saturated with atrazine.

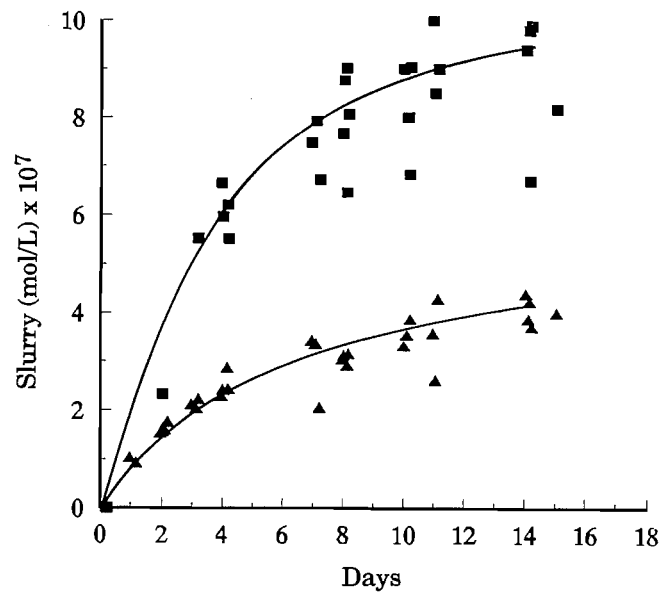

FIG. 7. Chemical analysis of the slurry, using the HPLC–microfiltration method, for a site saturation experiment. Concentration of hydroxyatrazine vs. time for —■—, whole slurry, $\sigma = 1.8 \times 10^{-7}$; and —▲—, microfiltrate 0.45 μm, $\sigma = 4.9 \times 10^{-8}$.

TABLE 3. Atrazine sorption capacity of the New Brunswick soil

Experiment no.	Capacity (μmol/g)
NBV	0.650
NBVI	0.646
NBVII	0.672
Mean	0.656
σ	0.014
Relative σ	2.2%

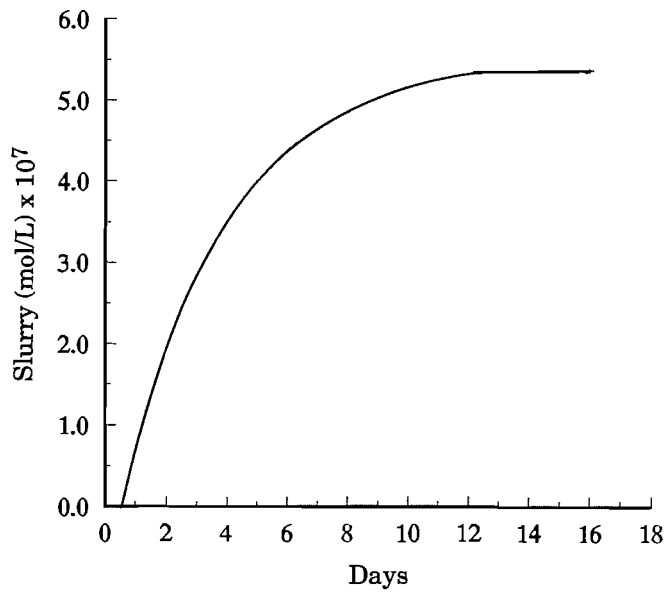

FIG. 8. The amount of hydroxyatrazine reversibly sorbed vs. time. The atrazine sorption sites were saturated with atrazine.

the whole slurry decreased slowly as a linear function of time, within the limits of experimental error. The solution phase concentration of atrazine decreased substantially during the first 8 days, after which there was a linear decrease. An apparent early drop in solution concentration was too fast to be monitored. Subtraction of the two fitted curves shown in Fig. 5 gives the atrazine sorption curve shown in Fig. 6. It reveals two important pieces of information. The first is that not all of the sorption was instantaneous. Several authors have reported that sorption and desorption of pesticides by soils can be slow, so that sorption–desorption kinetics should be accounted for (7, 27, 41–43). The data presented in Fig. 6 clearly show an equilibration time of approximately 8 days. The other important information is that the plateau showed no net decrease. The total atrazine in the whole experimental sample was somewhat greater than the amount required for maintaining site saturation. The results of the determination of atrazine sorption capacity in this way for the New Brunswick mineral soil are summarized in Table 3. Its numerical value is critically important for the subsequent calculations of sorption equilibrium, sorption kinetics, and catalysed chemical reaction kinetics.

The results of chemical analyses for hydroxyatrazine in a site saturation experiment shown in Figs. 7 and 8 are quite different from the corresponding atrazine curves. The standard deviations for the slurry and filtrate curves are 1.8×10^{-7} and 4.9×10^{-8} respectively. The hydroxyatrazine analyses are more difficult than the atrazine analyses, and consequently less useful for subsequent calculations. Significant information is obtained from them, however. In contrast to the atrazine, which must initially be sorbed from the solution onto sorption sites, the hydroxyatrazine, from the hydrolysis of atrazine, initially appears on the catalytic sorption sites. Some of it then desorbs to appear in solution for the first time. At least 4 days were required for the es-

Can. J. Chem. Downloaded from www.nrcresearchpress.com by 217.78.4.112 on 09/08/12
For personal use only.

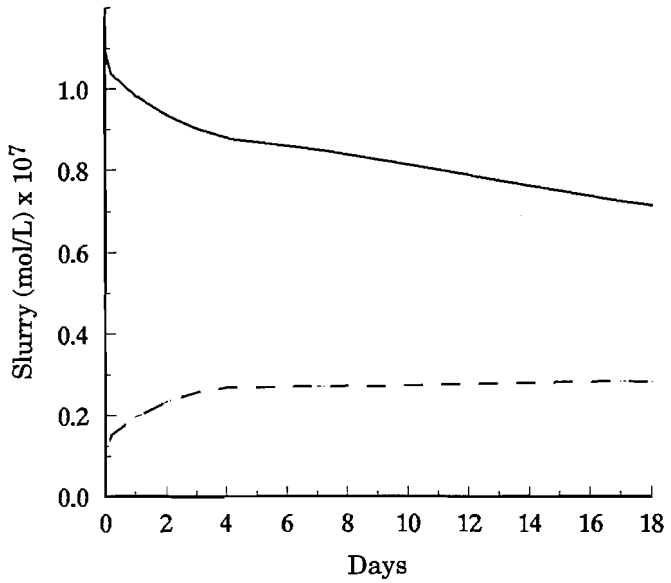

FIG. 9. Concentration of free and reversibly sorbed atrazine vs. time for a subsaturation experiment: ——, in solution; and – – – –, reversibly sorbed.

tablishment of sorption equilibrium. All three curves clearly reflect the continuous production of hydroxyatrazine; however, not enough hydroxatrazine was produced to saturate its sorption sites. The site saturation experiments (Figs. 5–8) revealed four chemical species plus a material balance loss, all of which were monitored simultaneously during the kinetics experiments. The material balance loss increased continuously with time and at 14 days it was equal to 1.3 mol% of the initial atrazine concentration for a site saturation experiment.

A test of the experimental method with an initial atrazine concentration more than 40 times lower than the site saturation experiment gave slurry and filtrate analyses for atrazine similar to those in Fig. 5. The standard deviations for the slurry and filtrate curves were 5.7×10^{-8} and 2.8×10^{-8} respectively. The solution phase and reversibly sorbed atrazine determined as before are shown in Fig. 9. In these experiments, only 1–2 mol% of sorption sites were covered by atrazine. While sorption was clearly observed, no evidence was found for the production of hydroxyatrazine. This does not prove, however, that none was produced. If, as expected, hydroxyatrazine was present, then its total amount must have been quite small. Some of it may have been irreversibly sorbed, and the concentrations of the remainder may simply have been below the detection limits of the analytical chemical method. The material balance loss for this experiment is 16.3 mol% after 14 days reaction time. This material balance loss is an order of magnitude larger than that for the site saturation experiment. The mol% of the material balance loss is evidently not proportional to the amount of reversibly sorbed atrazine; the processes governing the material balance loss warrant further investigation.

Conclusions

The experimental results presented here prove that the analytical chemical method with HPLC and microfiltration previously demonstrated for free and sorbed chemical species in an atrazine organic soil system (1) can be successfully adapted to the environmentally more important case of atrazine in mineral soil systems.

It is also concluded from these results that the method has a number of important advantages. Instead of only one free chemical species being monitored during kinetics experiment, as is common in heterogeneous catalysis research, all four of the free and reversibly sorbed chemical species were monitored simultaneously (1). In addition, the usual material balance loss was monitored. This simultaneous monitoring of five directly relevant experimental variables should substantially improve the subsequent chemical kinetics calculations. Each slurry injection completes an extraction with chemical analysis in only a matter of minutes, using approximately 15 litres of mobile phase as extractant per gram of soil sample. Each kinetics experiment typically has 30–50 such extractions with analyses during its course. Sorption equilibration is monitored as it happens, using only one experimental sample.

Acknowledgement

Dr. S. S. Singh and Mr. D. Hindle provided the important acid and base titrations of the New Brunswick mineral soil.

1. D. S. Gamble and S. U. Khan. J. Agric. Food Chem. **38**, 297 (1990).
2. H. Behrendt, H. Matthies, H. Gildmeister, and G. Gorlitz. Environ. Toxicol. Chem. **9**, 541 (1990).
3. Carl J. Miles, K. Yanagihara, S. Ogata, G. Van De Verg, and R. Boesch. Bull. Environ. Contam. Toxicol. **44**, 955 (1990).
4. W. F. Ritter. J. Environ. Sci. Health, Part B: **B25**, 1 (1990).
5. A. Walker. Pestic. Sci. **3**, 139 (1972).
6. F. Colbert, V. V. Volk, and A. P. Appleby. Weed Sci. **23**, 390 (1975).
7. R. E. Green, V. K. Yamnae, and S. R. Obien. Transport of atrazine in a latoscolic soil in relation to absorption, degradation, and soil water variables. Trans. Int. Congr. Soil Sci. 9th, Adelaide, Australia. Vol. 1. 1968. p. 195.
8. T. Mill. Data needed to predict the environmental fate of organic chemicals. *In* Dynamics, exposure and hazard assessment of toxic chemicals. Vol. 9. *Edited by* R. Haque. Ann Arbor Science, Ann Arbor, Mich. 1980. p. 297.
9. S. J. Horrobin. J. Chem. Soc. 4130 (1963).
10. F. E. Armstrong, G. Chesters, and R. R. Harris. Soil Sci. Soc. Am. Proc. **31**, 61 (1967).
11. C. I. J. Harris. J. Agric. Food Chem. **15**, 157 (1967).
12. J. D. Sullivan and G. T. Felbeck. Soil Sci. **106**, 42 (1968).
13. G. Li and G. T. Felbeck. Soil Sci. **114**, 201 (1972).
14. S. U. Khan. Pest. Sci. **9**, 39 (1978).
15. N. Burkhard and J. A. Guth. Pestic. Sci. **12**, 45 (1981).
16. S. J. Plust, J. R. Loehe, F. J. Fehr, J. H. Benedict, and H. F. Herbrandson. Pestic. Sci. **12**, 45 (1981).
17. D. S. Gamble, S. U. Khan, and O. S. Tee. Pestic. Sci. **14**, 537 (1983).
18. D. S. Gamble. Can. J. Soil Sci. **69**, 313 (1989).
19. C. Wang and J. A. McKeague. Can. J. Soil Sci. **62**, 79 (1982).
20. I. G. Burns, M. H. B. Hayes, and M. Stacey. Weed Res. **13**, 67 (1973).
21. I. G. Burns, M. H. B. Hayes, and M. Stacey. Weed Res. **13**, 79 (1973).
22. D. S. Gamble and S. U. Khan. Can. J. Chem. **66**, 2605 (1988).
23. Z.-d. Wang, D. S. Gamble, and C. H. Langford. Anal. Chim. Acta, **244**, 135 (1991).
24. M. I. Haniff, R. H. Zienus, C. H. Langford, and D. S. Gamble. J. Environ. Sci. Health. Part B: **B20**, 215 (1985).
25. E. M. Perdue and N. L. Wolfe. Environ. Sci. Technol. **16**, 847 (1982).

Can. J. Chem. Downloaded from www.nrcresearchpress.com by 217.78.4.112 on 09/08/12
For personal use only.

26. E. M. Perdue and N. L. Wolfe. Environ. Sci. Technol. **17**, 632 (1983).
27. Z.-d. Wang, D. S. Gamble, and C. H. Langford. Anal. Chim. Acta, **232**, 181 (1990).
28. N. L. Wolfe. Determining the role of hydrolysis in the fate of organics in natural waters. *In* Dynamics, exposure and hazard assessment of toxic chemicals. *Edited by* R. Haque. Ann Arbor Science, Ann Arbor, Mich. 1980. p. 163.
29. O. K. Borggaard and J. C. Streibig. Acta Agric. Scand. **38**, 293 (1988).
30. N. Senesi and C. Testini. Geoderma, **28**, 129 (1982).
31. M. H. B. Hayes. Residue Rev. **32**, 131 (1970).
32. D. S. Gamble. Can. J. Chem. **50**, 2680 (1972).
33. D. S. Gamble, M. I. Haniff, and R. H. Zienius. Anal. Chem. **54**, 727 (1986).
34. D. S. Gamble, M. I. Haniff, and R. H. Zienius. Anal. Chem. **54**, 732 (1986).
35. J. Buffle. Complexation reactions in aquatic systems: an analytical approach. Wiley, New York. 1988.
36. R. D. Burch, C. H. Langford, and D. S. Gamble. Can. J. Chem. **56**, 1196 (1978).
37. D. S. Gamble. Can. J. Chem. **69**, 313 (1989).
38. F. Helfferich. Ion exchange. McGraw–Hill Book Company, Inc., New York. 1962.
39. D. S. Gamble and C. H. Langford. Environ. Sci. Technol. **22**, 1325 (1988).
40. L. E. Sojo, D. S. Gamble, C. H. Langford, and R. H. Zienius. Environ. Sci. Health. Part B: **B24**, 619 (1989).
41. S. W. Karickhoff and K. R. Morris. Environ. Toxicol. Chem. **4**, 469 (1985).
42. M. L. Brusseau and P. S. C. Rao. Crit. Rev. Environ. Control. **19** (1989).
43. B. T. Bowman and W. W. Sans. J. Environ. Qual. **14**, 270 (1985).

Can. J. Chem. Downloaded from www.nrcresearchpress.com by 217.78.4.112 on 09/08/12
For personal use only.

Atrazine in mineral soil: chemical species and catalysed hydrolysis[1]

DONALD S. GAMBLE[2] AND SHAHAMAT U. KHAN
Land Resource Research Centre, Research Branch, Agriculture Canada, Ottawa, Ont., Canada K1A 0C6

Revised December 2, 1991

DONALD S. GAMBLE and SHAHAMAT U. KHAN. Can. J. Chem. **70**, 1597 (1992).

Equilibrium and kinetics parameters have been evaluated at 25.0°C for the heterogeneous catalysis of atrazine hydrolysis in slurries of a chemically characterized mineral soil. The fraction of acidic sites that accounts for sorption capacity, and the sorption equilibrium function resemble those for humic acid and organic soil. Sorption and desorption half-lives increased with increasing coverage of sorption sites. The sorption half-lives ranged from 3.6 to 735 days. The desorption half-lives ranged from 1 to 11 days. The hydrolysis half-lives ranged from 9.6 to 168 days and are consistent with Brönsted acid catalysis theory. The relationship of independent variables to data scatter has been analyzed. The information obtained should be useful for water and solute transport models.

DONALD S. GAMBLE et SHAHAMAT U. KHAN. Can. J. Chem. **70**, 1597 (1992).

Opérant à 25°C, on a évalué l'équilibre et les paramètres cinétiques de la catalyse hétérogène de l'hydrolyse de l'atrazine, délayée dans une huile minérale de composition chimique définie. La fraction des sites acides qui explique la capacité de sorption anisi que la fonction d'équilibre de la sorption ressemblent à celles de l'acide humique et des sols organiques. Les temps de demi-vies de la sorption et de la désorption augmentent avec une augmentation de la couverture des sites de sorption. Les demi-vies de sorption varient de 3,6 à 735 jours. La demi-vies de désorption varient de 1 à 11 jours. Les temps de demi-vies d'hydrolyse varient de 9,6 à 168 jours et ils sont en accord avec la théorie de la catalyse acide de Brønsted. On a analysé la relation entre les variables indépendantes et l'éparpillement des données. L'information obtenue devrait être utile pour des modèles de transport par de l'eau et des solutés.

[Traduit par la rédaction]

Can. J. Chem. Downloaded from www.nrcresearchpress.com by 217.78.4.112 on 09/08/12
For personal use only.

Introduction

Villeneuve *et al.* (1) have observed that the increasing use of deterministic hydrology models for the persistence and leaching of pesticides in soils has increased the requirement for knowledge of pesticide sorption and degradation rate constants. Analysis of the sensitivity of the computed pesticide concentrations and distributions to the empirical parameters used in computation (sensitivity analysis) has been reported by Villeneuve *et al.* (1). This sensitivity analysis (1) indicates that errors of 15–24% in the degradation constant or an error of 24% in the adsorption constant can cause a 100% error in model predictions. A contributing cause to these large errors is the use of oversimplified theories for sorption and degradation. The physical and chemical phenomena responsible for sorption and degradation of pesticides need to be identified, measured, and accounted for in interpretive and predictive calculations.

In a review of sorption theory for dilute solutions, Jaroniec and Madey (4) described both a distribution coefficient and an isotherm equation based on the law of mass action. However, the distribution coefficient does not account for the number of unoccupied sorption sites or for sorption capacity and the isotherm did not account for site heterogeneity.

The literature reviewed by Jaroniec and Madey (4) does not describes a theory that uses both the weighted average concept to account for sorption site heterogeneity, and sorption capacity with the law of mass action to account for the effect of empty sorption sites. The present work seeks to develop such a theory with a single mathematical description. The type of theoretical description being used determines the types and amounts of experimental data that are required. An analytical chemical method similar to that described earlier for an organic soil has been developed for this purpose (2, 3). It has been shown that organic matter dominates pesticide interactions with soils, and carboxyl groups have been identified as being important in these interactions (3, 5, 6).

The objective of this work was to obtain separate numerical values for these sorption and chemical reaction parameters that are required by hydrology models, such as PRZM. Villeneuve *et al.* (1) for example, have discussed its application to the pesticide aldecarb. Atrazine interactions with the aqueous slurry of a mineral soil were used as a case study for the present work. In this study parameters for the persistence and leaching of atrazine in mineral soil were obtained which include the sorption equilibrium function, sorption and desorption rate constants, and a pseudo-first-order reaction rate constant for catalysed hydrolysis. Over the last 30 years atrazine has been the most heavily used herbicide in Canada and in the U.S.A. Residues of atrazine have been found in 4,123 of 10,942 surface water samples and in 343 of 3,208 ground water samples analysed (STORET, 1988, STORET water quality file, Office of Water, U.S. Environmental Protection Agency).

Theory

Atrazine sorption equilibrium

When reversible sorption equilibrium has been established in an aqueous slurry of soil particles, the law of mass action may be applied to give the weighted average equilibrium constant, $\bar{K}_1$, as described previously (3).

$$[1] \qquad \bar{K}_1 = \frac{C_{At}}{C_0 M_{At}} = \frac{\theta_{At}}{\theta_0 M_{At}}$$

M_{At} is atrazine molarity. C_{At} and θ_{At} are sorption sites on soil occupied by atrazine, in mol/L of slurry and mol/g of soil, respectively. C_0 and θ_0 are unoccupied sorption sites, in the

[1]LRRC Contribution No. 91-17.
[2]Author to whom correspondence may be addressed.

same units as those of C_{At} and θ_{At}. The numerical values of empty site variables C_0 and θ_0 depend on the definitions of sorption capacity:

$$[2] \quad C_c = C_{At} + C_0$$

$$[3] \quad \theta_c = \theta_{At} + \theta_0$$

In the previous work with organic soil (3), C_c and θ_c were defined in terms of the number of protonated carboxyl groups in the soil. It has since been found, however, that generally only about 1 mol % or less of the protonated carboxyl groups act at any instant as sorption sites (7, 8). In the present mineral soil study, C_c and θ_c are therefore defined in terms of experimentally measured apparent sorption capacities. This causes corresponding changes in the definitions and numerical values of $\bar{K}_l$ and χ_l, the mole fraction of sorption sites covered, according to eqs. [4] and [5].

$$[4] \quad C_0 = C_c - C_{At}$$

$$[5] \quad \chi_l = C_{At}/C_c$$

To provide a valid comparison of organic soil results to those for the mineral soil used in the present study, $\bar{K}_l$ and χ_l values must be translated to the revised definition of C_c (or θ_c). Otherwise, the numerical values would differ by about two orders of magnitude.

The distribution coefficient K_D that is in general use for pesticide sorption by soils and sediments may be defined in terms of moles of pesticide by eq. [6].

$$[6] \quad K_D = (\theta_{At}/M_{At})$$

This is commonly used as an empirical constant. The correct meaning and real properties of K_D can be deduced, however, by the use of eqs. [1] and [3] with its definition, eq. [6]. Eq. [7] gives the simple relationship

$$[7] \quad K_D = \bar{K}_l(\theta_c - \theta_{At})$$

It should be noted that under certain conditions $\bar{K}_l$ might be approximately constant. If for example, hydrogen bonding sites had a narrow range of weak acid strengths, it might be difficult to observe changes in $\bar{K}_l$. Even if $\bar{K}_l$ is approximately constant, however, K_D must decrease when the site coverage θ_{At} increases. Since the sorption capacity θ_c is now known to be a quite small portion of the protonated carboxyl groups, this effect is somewhat more important than previously expected. Not only will different soils have different sorption capacities θ_c, but also a given soil can have different θ_c values if different amounts of its carboxyl sites are neutralized. Lime applications, for example, could affect the amount of carboxyl groups neutralized. The practical consequence is that the empirical use of K_D without any consideration of sorption capacity or site loading will cause unnecessary data scatter. Brouwer *et al.* (9) have demonstrated that K_D values can be scattered by factors of 20–50. It is important to note that this is not made necessary by the properties of soils. It is instead caused by the incorrect use of the parameter K_D. Published correlations that work roughly with K_D to give data scattered by factors of 20–50 (9) should work somewhat better if $\bar{K}_l$ is used. Even the K_{om} coefficient which has been normalized to constant amounts of soil organic matter has data scattered by factors of 2–6 (200–600%) (9).

Atrazine sorption–desorption kinetics

The sorption–desorption rate law described by eqs. [8]–[10] has been previously used for atrazine–organic soil experiments (3).

$$[8] \quad \frac{dM_{At}}{dt} = -k_{S1}M_{At} + k_{S1}C_{At}$$

$$[9] \quad k_{S1} = k_{B1}C_0$$

$$[10] \quad k_{S2} = k_{B1}/\bar{K}_l$$

k_{S1} is the pseudo-first-order rate constant for atrazine sorption and k_{B1} is the corresponding second-order rate constant. k_{S2} is the first-order rate constant for atrazine desorption. It is evident that k_{S1} depends on the extent of site loading as shown below:

$$[11] \quad k_{S1} = k_{B1}(C_c - C_{At})$$

In addition it cannot be assumed that k_{B1} is a constant. Instead, it might very well have a distribution of values that represents sorption site heterogeneity. To account for these effects, especially when sorption site coverage is extensive, the integral rate law has been used in the form of eqs. [12] and [13].

$$[12] \quad F(t) = k_{B1}(t_2 - t_1)$$

$$[13] \quad F(t) = \int_{M_1}^{M_2} \{1/[(C_{At}/\bar{K}_l) - C_0M_{At}]\}dM_{At}$$

M_1 and M_2 are the integration limits for the atrazine molarity, M_{At}. A spreadsheet and a curve-fitting program readily yield a value for k_{B1}. k_{S1} and k_{S2} are then obtained from eqs. [9] and [10].

Atrazine hydrolysis kinetics

The integral rate law in equations [14] and [15] has been used previously for atrazine hydrolysis in slurries of organic soil (3).

$$[14] \quad \int_{c_1}^{c_2} (1/M_{At})dC_{Tl} = -k_{rl}(t_2 - t_1)$$

$$[15] \quad k_{r2} = \left(\frac{V_S}{W_S\bar{K}_l\theta_0}\right) k_{rl}$$

C_{Tl} is the total measurable atrazine as described by eq. [16],

$$[16] \quad C_{Tl} = M_{At} + C_{At}$$

V_S and W_S are solution volume and weight of soil sample. k_{r2} is the first-order rate constant for the hydrolysis of atrazine on the catalytic sorption sites. It is important to note that C_{Tl}, M_{At}, V_S, and W_S are all direct experimental measurements. $\bar{K}_l$ and θ_0 are determined from direct measurements of the capacity C_c and reversibly sorbed atrazine C_{At}. The practical significance of this is that k_{r2} must be used for correlations and predictive calculations, because k_{rl} is only an artifact of the experimental method. One can obtain any arbitrary value of k_{rl} by manipulating the experimental ratio (V_S/W_S). Karickhoff and Morris (10) have stated that apparent rate constants depend on experimental methodology. Perdue and Wolfe (11, 12) pointed out that humic carboxyl groups are Brönsted acid catalysts. Therefore, k_{r2} is expected to depend on the weak acid constants, K_A, of those

Can. J. Chem. Downloaded from www.nrcresearchpress.com by 217.78.4.112 on 09/08/12
For personal use only.

carboxyl groups. The relationship could be obscured or lost in plots with k_{r1}.

According to eq. [15], the numerical value of k_{r2} will depend on the definitions used in $\bar{K}_1\theta_0 = (\theta_{At}/M_{At})$. The comparison of the humic acid and organic soil results (3, 6) with present mineral soil results therefore requires that they be translated accordingly.

Hydroxyatrazine appearance kinetics

The apparent rate constant k_{p3} for the appearance of hydroxyatrazine may be calculated with eq. [17] which has been used for organic soil experiments (3).

$$[17] \quad \int_{C_1}^{C_2} (1/C_{AT})dC_{T2} = k_{p3}(t_2 - t_1)$$

C_{T2} is the total measurable hydroxyatrazine. The molecular level interpretation of k_{p3} and its relationship to k_{p2} cannot be determined until the capacity and equilibrium function for hydroxyatrazine are known. According to Wang *et al.* (7), the structure, sorption capacity, and the sorption equilibrium function $\bar{K}_2$ for hydroxyatrazine should be different from those for atrazine. If this were the case, then the conversion of atrazine to hydroxyatrazine on the sorption sites would change the structure and properties of the sites. An implication of this is that it cannot be assumed that monitoring atrazine disappearance and monitoring hydroxyatrazine appearance will give the same information. Separate hydroxyatrazine sorption–desorption experiments might therefore be useful.

Categories of variables

Three categories of variables should be clearly distinguished from each other for the conduct, calculations, and molecular level interpretation of experiments with these environmental chemistry systems. They are described below.

Inner variables

Inner variables are those identified by theory as being required for totally specifying the state of a chemical system. They should be used for correlations, molecular level interpretive calculations, and predictive calculations. Typical examples include the numbers or concentrations of protonated carboxyl groups, and the mole fraction of sorption sites occupied by a sorbed pesticide.

Outer variables

Outer variables are the type that are manipulated operationally for the conduct of an experiment. Typical examples include pH, total moles of pesticide or metal ion added to a sample, and the ratio of weight of solid sample to volume of experimental solution. They are more practical than inner variables for running many types of experiments, and frequently inner variables cannot be used for that purpose.

Background description variables

These variables are useful as general background information, for developing qualitative insight or for making practical decisions. They are not used in chemical calculations, and do not appear in the mathematical descriptions of the system. Typical examples include elemental analysis, and percent organic matter in a mineral soil.

Incorrect use of the three types of variables can cause unnecessary data scatter and some confusion. For example, hydrogen-bonded structure formation (12) might cause a sorption rate constant to be a function of the mole fraction of the sorption sites covered by pesticide molecules. A plot of the rate constants for several soils against pH would likely show excessive data scatter. At one and the same pH, different soils would have different numbers of protonated carboxyl groups and therefore different mole fractions of their sites covered. The outer variable pH would be no more than a pale, indirect reflection of the correct inner variable — the mole fraction of the sorption sites covered. If in this case pH were used for an empirical black box correlation, the resulting fitted curve would represent only the particular experiment from which it had come. Because it would not represent the actual molecular level phenomena, it would lack the generality necessary for good predictive calculations. For the above reasons, it is important to compare experimentally measured dependent variables with the proper independent variable or at least be aware of the danger of using a variable from the wrong category.

Materials and methods

The reagents, New Brunswick mineral soil, and the adaptation of the speciation–kinetics method to the mineral soil are reported in a separate article (2).

Results and discussion

The fraction of acidic sites on mineral soil that is available for binding atrazine was calculated. It was observed that about 0.44 mol% of the carboxyl groups accounted for the experimentally observed sorption on both mineral soil and dissolved fluvic acid while humic acid gave the higher value of 1.1 mol% (2). Since the value for the soil is less than the value for humic acid this observation is consistent with the postulate that a fraction of the humic acid carboxyl groups in the soil was the primary cause of atrazine sorption.

Sorption capacities are unavailable for the humic acid and organic soil used in previous studies (3, 6). It is important, however, to test the results for generality. Demonstration values have therefore been obtained for the humic acid and organic soil. This was done for the hypothetical case of 1 mol% of carboxyl groups available as sorption sites. Table 1 presents these estimates. The comparison of sorption capacities for different types of soil and organic matter warrants further investigation.

A number of authors have reported pesticide–soil sorption equilibration times that range from hours to weeks (10, 14–16). The sorption process has usually been assumed to follow first-order kinetics (15). According to the rate-law expressions previously developed (eqs. [8]–[13]) the kinetics are intrinsically second order, but should be pseudo-first order under appropriate experimental conditions. Figure 1 shows results of kinetic experiments obtained using the HPLC-microfiltration method (2) for the present case. The second-order rate constant k_{B1} has been calculated from these data. Any apparent deviation from linearity is less than the experimental errors. The function $F(t)$ is defined by eq. [13], and the calculations were done with a spreadsheet. The most general case is that the k_{B1} rate constants calculated as described above should depend on the mole fraction of sorption sites covered, because the sites would have a mixture of structural and chemical properties. Figure 2 shows that k_{B1} is dependent on the mole fraction of sorption sites covered. Duplicate subsaturation experiments, having site coverage of about 2 mol%, gave k_{B1} values an order of magnitude

Can. J. Chem. Downloaded from www.nrcresearchpress.com by 217.78.4.112 on 09/08/12
For personal use only.

TABLE 1. Atrazine sorption equilibrium function, $\bar{K}_1$ defined for sorption capacities which are small portions of the carboxyl groups

Experiment No.	$\bar{K}_1$ $\sigma = 0.20 \times 10^4$	χ_1 Mole fraction of sites covered $\sigma = 0.10 \times 10^{-2}$	Atrazine sorption capacity (μmol/g)	Comments
Mineral soil NBVIII	2.17×10^4	2.01×10^{-2}	0.656 $\sigma = 0.014$	Present work
Mineral soil NBIX	2.31×10^4	1.99×10^{-2}	0.656 $\sigma = 0.014$	Present work
Chernozem Humic acid	3.5×10^4	0.5	28.3	Demonstration values of K_1, estimated for the hypothetical capacities as 1% of protonated carboxyls.
Organic soil	4.7×10^4	0.5	7.08	Real K_1 values could be higher.

greater than the saturation experiments also shown in Fig. 2. For comparison, a value from previous organic soil work (3) has been added. Now that the effectiveness of the experimental method has been demonstrated, it should be possible to check the generality of this trend and to map it out over the whole range of site coverages. That would permit the extrapolation of laboratory measurements to field conditions.

The pseudo-first order rate constant k_{S1} for atrazine sorption is inherently less rigorously correct than the second-order constant k_{B1}, especially at high site loadings. Figure 3 shows the plot of k_{S1} vs. χ_1 which is useful for two reasons. One is that the data scatter is less because of the partial cancellation of measurement errors. The other is that it provides a fast, convenient way of estimating sorption half-lives. The resulting list of sorption half-lives in Table 2 demonstrates a strong dependence on site loading. Two practical implications must be emphasized. The first is that sorption equilibrium is not instantaneous. The second is that any attempt to use a single, all purpose "black box" value of the half-life for modelling would almost certainly give flawed model predictions. The reason is that numerical values of the half-life would usually be wrong. The comparison of k_{S1} with k_{B1} can be made by multiplying k_{B1} by the number of vacant sorption sites in the slurry. For this mineral soil the sorption capacity is 6.56×10^{-7} mol/g of soil and the slurry contains 20 g of soil/L of water. Comparison shows that the k_{S1} value is dependent on the W_S/V_S ratio, and is thus an artifact of the experimental method.

The first-order rate constant for atrazine desorption in Fig. 4 has an appearance very similar to that of the first-order sorption rate constant. Desorption is evidently faster, however, as is indicated by the desorption half-lives in Table 3.

Perdue and Wolfe (11, 12) presented both theory and ex-

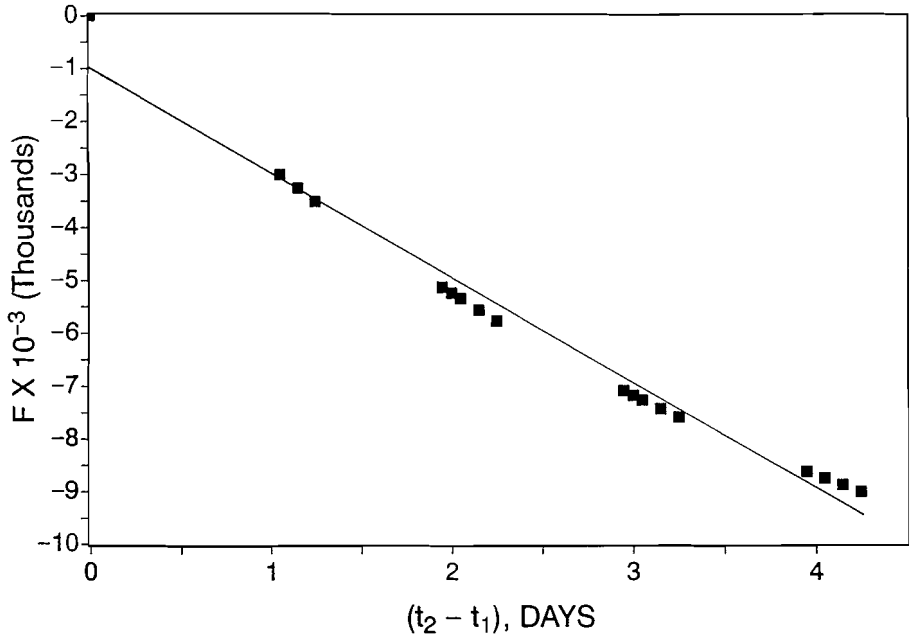

FIG. 1. Kinetic plot for atrazine sorption in a site saturation experiment. The slope gives the second-order rate constant, k_{B1}, at 25.0°C. The plot is based on eq. [12], with F defined by eq. [13].

Can. J. Chem. Downloaded from www.nrcresearchpress.com by 217.78.4.112 on 09/08/12
For personal use only.

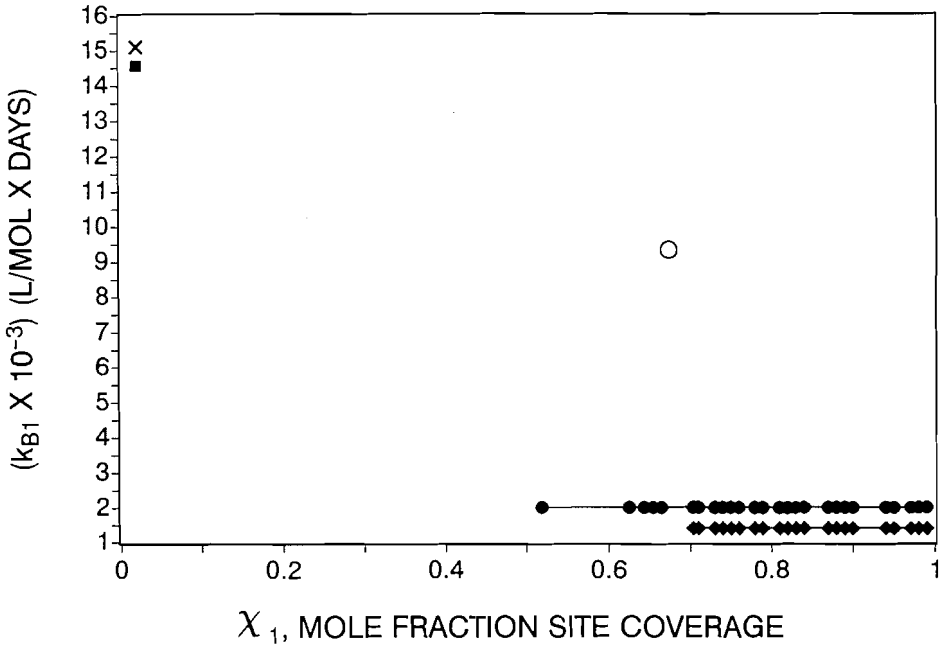

FIG. 2. Second-order rate constants for atrazine sorption at 25.0°C. ×, ■, Duplicate subsaturation experiments. ●, ◆, Duplicate site saturation experiments. ○, Organic soil value, from published study (3).

perimental proof for the Brönsted acid catalyst properties of humic carboxyl groups. The pseudo-first-order rate constants for atrazine hydrolysis catalysed by humic carboxyl groups determined in this work are given in Table 4, together with K_A estimated for the corresponding soil. Table 4 shows that the higher K_A value of the organic matter gives a higher rate constant for atrazine hydrolysis which is consistent with the work of Perdue and Wolfe. The above correlation suggests that the Brönsted acid catalyst properties of the humic carboxyl groups in mineral soils should be systematically measured for correlation to the hydrolysis of atrazine. There is a possibility that this could contribute to the development of practical methods for predictive calculations. If hydroxyatrazine desorption were sufficiently fast

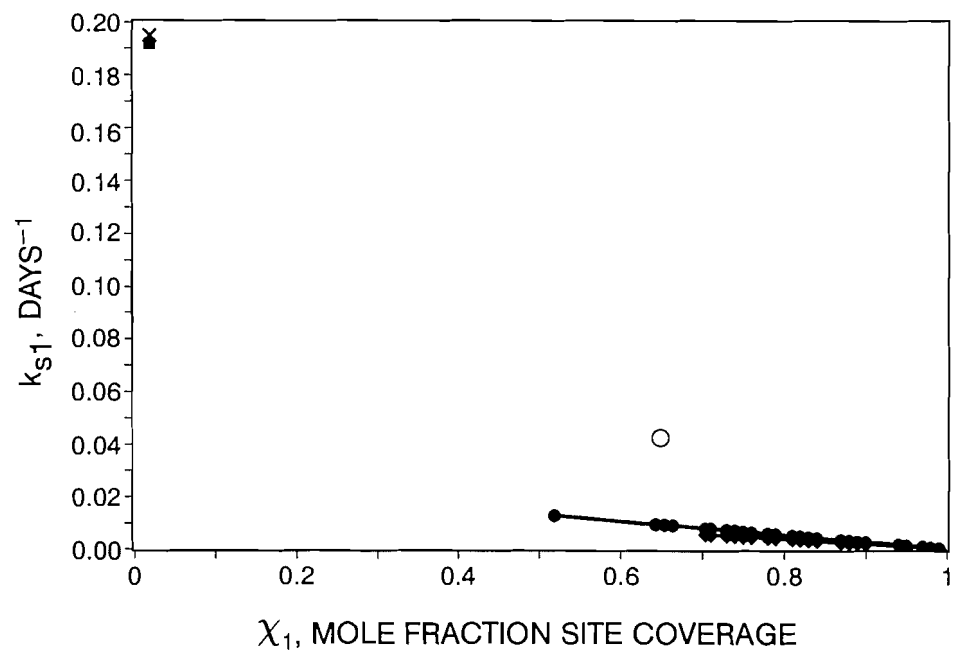

FIG. 3. Pseudo-first-order rate constants for atrazine sorption at 25.0°C. ×, ■, Duplicate subsaturation experiments. ●, ◆, Chord plots for duplicate site saturation experiments. ○, Organic soil value, from published work (3).

Can. J. Chem. Downloaded from www.nrcresearchpress.com by 217.78.4.112 on 09/08/12
For personal use only.

TABLE 2. Atrazine sorption half-lives at 25.0°C: the effect of site coverage

Experiment	Half-lives Days	Half-lives ±σ	Site coverage
NBIX	3.56	0.05	0.0199
NBVIII	3.62	0.05	0.0201
Organic soil	13.8	2.80	0.626
NBVI	523	150	0.95
NBVIII	735	150	0.95

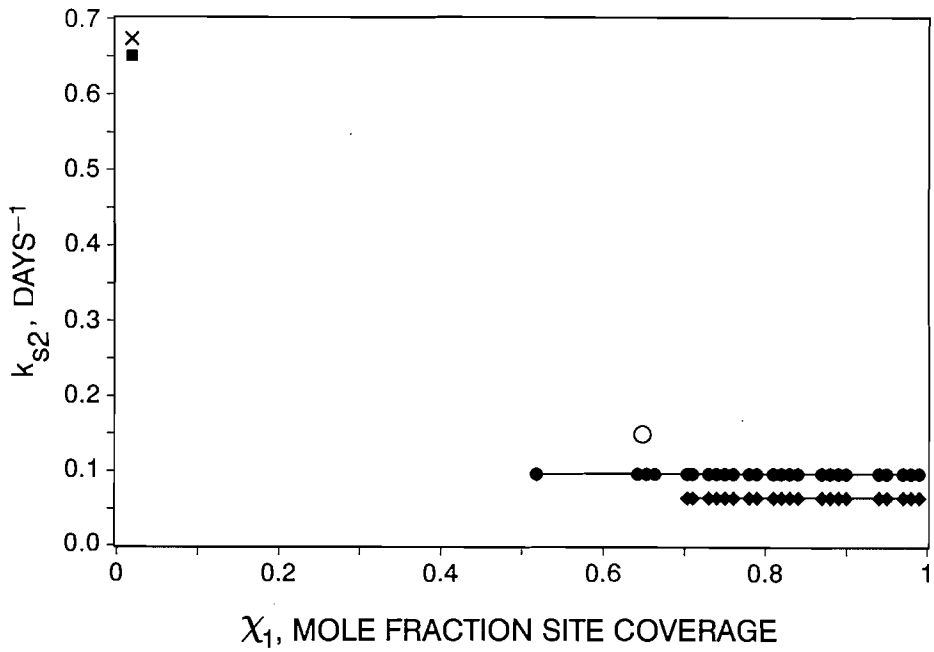

FIG. 4. First-order rate constants for atrazine desorption at 25.0°C. ×, ■, Duplicate subsaturation experiments. ●, ◆, chord plots for duplicate site saturation experiments. ○, Organic soil value, from published work (3).

TABLE 3. Atrazine desorption half-lives at 25.0°C: the effect of site coverage

Experiment	Half-lives Days	Half-lives ±σ	Site coverage
NBIX	1.03	0.03	0.0199
NBVIII	1.07	0.03	0.0201
Organic Soil	4.6	0.93	0.626
NBVI	7.7	2.2	0.95
NBVIII	10.9	2.2	0.95

relative to its rate of production on the catalytic sorption sites, then its apparent rate constant k_{p3} would be described by eq. [18]:

$$[18] \quad k_{p3} = \left(\frac{W_S}{V_S}\right) \bar{K}_2 \theta_0 k_{r2}$$

There are three reasons why k_{r2} cannot at present be calculated from k_{p3} using eq. [18]. The first is that there is some doubt about whether the hydrolysis reaction rather than the desorption is rate determining in this case. The next reason is that the sorption sites and sorption capacity might very well be different from those for atrazine, and the chemical reaction did not produce enough hydroxyatrazine to saturate its sorption sites. The θ_c value for hydroxyatrazine could therefore not be measured. The third reason is a consequence of the other two. Without a numerical value for θ_c, $\bar{K}_2$ cannot be calculated. The apparent k_{p2} listed in Table 4 cannot of course be compared directly with k_{r2}.

Systematic material balance losses were always observed

Can. J. Chem. Downloaded from www.nrcresearchpress.com by 217.78.4.112 on 09/08/12
For personal use only.

TABLE 4. Atrazine hydrolysis rate constants in mineral soil slurries, 25.0°C; mole fraction of sites covered, $\chi_1 = 1.0$

Compound	Acidic catalyst sites K_A	σ	Type of first-order constant	Rate constant $(days)^{-1}$ Value	σ	Half-life (days) $t^{1/2}$	σ	Type of determination
Atrazine	5.59×10^{-5}	$\pm 0.06 \times 10^{-5}$	k_{r2}	4.13×10^{-3}	$\pm 0.32 \times 10^{-3}$	168	±13	Average of 3 experiments
Atrazine	76×10^{-4}	$\pm 1.4 \times 10^{-4}$	k_{r2}	72.1×10^{-3}	$\pm 10 \times 10^{-3}$	9.6	±1.3	Organic matter, published curve (3)
Hydroxyatrazine	5.59×10^{-5}	$\pm 0.06 \times 10^{-5}$	k_{p3}	3.65×10^{-3}	$\pm 0.42 \times 10^{-3}$	190	±22	Average of 2 experiments

in atrazine experiments with both the mineral soil used in the present study and the organic soil described earlier (3). As with the previous organic soil the loss was found, within the limits of analytical chemical errors, to be a linear function of time. While the site saturation experiments gave only qualitative results, the duplicate subsaturation experiments produced the rates, which compare favorably with each other as shown in Table 5. A ^{14}C atrazine experiment with the New Brunswick soil gave qualitative confirmation of the data in Table 5. Also, the use of a ^{14}C labelled atrazine sample in the organic soil experiments gave evidence that the material balance loss corresponded to a bound residue. While it might be thermal diffusion into the interiors of particles as some authors have suggested, the nature of this phenomenon requires further investigation.

Hydrology models such as those investigated by Villeneuve *et al.* (1) typically have two empirical parameters with which to account for the distribution of species and the rate of reaction. The distribution coefficient K_D, unlike the law of mass action function $\bar{K}_1$, does not account for changes in either sorption capacity or site coverage and thus leads to unnecessary data scatter. Use of $\bar{K}_1$ and its quantitative relationship to K_D should lead to a substantial reduction in data scatter. The other parameter is the rate constant k for the loss of a chemical species from solution. Without quantitative knowledge of the sorption, desorption, and catalysed chemical reaction rates, changes in these rates under field conditions cannot be predicted from laboratory column experiments. The practical solution to this problem is to develop mathematical equations that describe this k in terms of the quantitative behavior of the rate constants for sorption, desorption, and chemical reactions. The present work describes the sorption equilibrium function, sorption and desorption rate constants, and a pseudo-first-order reaction rate constant which results in a substantial reduction in data scatter and provides practical solutions for making the hydrology models more effective for prediction.

Future research should seek to determine the exact effects of humic carboxyl K_A values and sorption site loading on the various sorption and chemical reaction parameters. Much more information is needed on the relationship between sorption capacities and numbers of protonated carboxyl groups. In addition, the secondary effects of clays on the parameters should be assessed.

TABLE 5. Rate of material balance loss, 25.0°C

Experiment No.	dQ/dt (μmol/g)/day
NBVIII	4.68×10^{-4}
NBIX	4.95×10^{-4}
Mean	4.81×10^{-4}
σ	0.19×10^{-4}
Relative σ (%)	4.0

1. J.-P. Villeneuve, P. Lafrance, O. Banton, P. Frechette, and C. Robet. J. Contam. Hydrol. **3**, 77 (1988).
2. D. S. Gamble and L. A. Ismaily. Can. J. Chem. **70**, 1590 (1992).
3. D. S. Gamble and S. U. Khan. J. Agric. Food Chem. **38**, 297 (1990).
4. M. Jaroniec and R. Madey. Physical adsorption on heterogeneous solids. Elsevier, Amsterdam. 1988. Chap. 7.
5. M. H. B. Hayes. Residue Rev. **32**, 131 (1970).
6. D. S. Gamble and S. U. Khan. Can. J. Chem. **66**, 2605 (1988).
7. Z.-Di-Wang, D. S. Gamble, and C. H. Langford. Anal. Chim. Acta, **232**, 181 (1990).
8. D. S. Gamble, M. I. Haniff, and R. H. Zienius. Anal. Chem. **54**, 727 (1986).
9. W. W. M. Brouwer, J. J. T. I. Boesten, and W. G. Siegers. Weed Res. **30**, 123 (1990).
10. S. W. Karickhoff and K. R. Morris. Environ. Toxicol. Chem. **4**, 469 (1985).
11. E. M. Perdue and N. L. Wolfe. Environ. Sci. Technol. **16**, 847 (1982).
12. E. M. Perdue and N. L. Wolfe. Environ. Sci. Technol. **17**, 635 (1983).
13. D. S. Gamble. Can. J. Soil Sci. **69**, 313 (1989).
14. R. J. Hance. Weed Res. **7**, 29 (1967).
15. B. T. Bowman and W. W. Sans. J. Environ. Qual. **14**, 270 (1985).
16. M. L. Brusseau and P. S. C. Rao. Sorption nonideality during organic contaminant transport in porous media. *In* Critical reviews in environmental control. Vol. 19. *Edited by* Conrad P. Straub. CRC Press, Inc., Boca Raton, Florida. 1989.

Can. J. Chem. Downloaded from www.nrcresearchpress.com by 217.78.4.112 on 09/08/12
For personal use only.

Mathematical analysis of reactive ion transport in dynamic equilibrium: The case of two ionic species

KOICHI IINUMA AND MASAHIRO TAKEBE
Department of Nuclear Engineering, Tohoku University, Sendai 980, Japan

Received August 19, 1991

KOICHI IINUMA and MASAHIRO TAKEBE. Can. J. Chem. **70**, 1604 (1992).

An exact solution for the transport of two reacting ion species in a drift tube is developed. The calculation of the temporal variation of ion fluxes is simplified using an approximate formulation in terms of the reaction frequencies, drift velocities, and longitudinal diffusion coefficients. The exact and approximate formulations are compared for the case of $(N_2^+, N_4^+)/N_2$ with a view to establishing the approach to equilibrium.

KOICHI IINUMA et MASAHIRO TAKEBE. Can. J. Chem. **70**, 1604 (1992).

On a développé une solution exacte pour le transport de deux espèces ioniques qui réagissent dans un tube à déplacement. Utilisant une formulation approximative en termes de fréquences de réaction, de vitesses de déplacement et de coefficients de diffusion longitudinaux, on a simplifié le calcul de la variation des flux ioniques en fonction du temps. Dans le but d'établir l'approche à l'équilibre, on a comparé les formulations exactes et approximatives pour le cas du $(N_2^+, N_4^+)/N_2$.

[Traduit par la rédaction]

Can. J. Chem. Downloaded from www.nrcresearchpress.com by 217.78.4.112 on 09/08/12
For personal use only.

Introduction

The drift tube technique is a standard time-of-flight method for ion swarm experiments, where an instantaneous burst of ion swarms is released from a source and travels through the gas under the influence of an external electric field applied in a cylindrical tube. The times of arrival of the ions at the detector are measured and the data accumulated over many cycles until a statistically satisfactory spectrum of arrival times is obtained. Dynamic equilibrium is the final phase of the space-time evolution of interreacting ion swarms, where they reach stationary concentrations because of the dynamic balance between the forward and reverse reactions occurring in the system. One often observes in drift-tube experiments with mass spectrometers that the arrival time spectra (ATS) in this phase have similar Gaussian profiles at the same position with the same full width at half-maximum (FWHM). This similarity of profiles occasionally makes it difficult to determine accurately the kinetic coefficients of each ionic species. Another experimental difficulty arises from the fact that the profiles start to broaden so that the current intensities become much smaller than those in the nondynamic equilibrium phase. These difficulties have forced experimentalists to conclude that analysis in dynamic equilibrium should not be expected to be valid for determination of transport coefficients and that it is even incapable of fixing the forward and reverse reaction rates (see ref. 1 pp. 40–51 and the references cited therein). The conclusion is theoretically attributed to insufficient quantitative understanding of the ion-swarm behavior subject to inseparable interplay between their transport properties and reactions. If a better mathematical formulation is established, it may give us new insights that we have overlooked in the past in the analysis of reactive ion transport.

We recently developed a general solution of the coupled transport equations for the analysis of multiple ion swarms in gases (2). A noteworthy result derived therefrom is that any information on the initial conditions including flux will vanish completely in the dynamic equilibrium phase. This is useful in drift-tube analysis because the kinetic coefficients only characterize the shape and width of the ATS. Neither the initial number density of the ionic species, nor the geometrical form of an initial pulse of the ion swarm, need be considered. For this purpose we have explicitly derived the analytical expression of the ATS of two ionic species according to the general solution. This expansion–truncation technique is rather tedious, but an approximate solution yields surprisingly accurate profiles in the limit of infinite drift distance. This paper compares the approximate and exact solutions including a number of related formulas and their application to the $(N_2^+, N_4^+)/N_2$ system.

General analysis of two ion swarms

The general scheme of reactions of two ionic species is depicted as follows:

$$[1] \qquad \rho_1 \underset{\alpha_{12}}{\overset{\alpha_{21}}{\rightleftharpoons}} \rho_2$$

where ρ_1 and ρ_2 are the number densities of first and second species, respectively, and α_{ij} is the reaction frequency from species j to i ($i, j = 1, 2; i \neq j$). The space-time behavior of two ion swarms is governed by a coupled transport equation,

$$[2] \qquad \begin{cases} \dfrac{\partial \rho_1}{\partial t} = \nabla \cdot (\mathbf{D}_1 \cdot \nabla \rho_1) - v_{d1} \cdot \nabla \rho_1 - \alpha_{21}\rho_1 + \alpha_{12}\rho_2 \\ \dfrac{\partial \rho_2}{\partial t} = \nabla \cdot (\mathbf{D}_2 \cdot \nabla \rho_2) - v_{d2} \cdot \nabla \rho_2 - \alpha_{12}\rho_2 + \alpha_{21}\rho_1 \end{cases}$$

where $\mathbf{D}_i$ and v_{di} are the diffusion tensor and the drift velocity of the ith species, respectively. By introducing cylindrical coordinates (r,z) where the z axis is chosen to lie in the electric field direction, and using the method of separation of variables, we represent the solution as

$$[3] \qquad \rho_i(\boldsymbol{r},t) = \sum_{m=1}^{\infty} a_{im} J_0\left(\frac{\beta_m r}{r_0}\right) Z_{im}(z,t)$$

where a_{im} are constants to be determined from the initial

conditions, J_0 is the zeroth-order Bessel function, β_m is the mth root of the Bessel function, and r_0 is the drift-tube radius. Following the mathematical procedure in ref. 2, we solve the partial differential equation of $Z_{im}(z,t)$ by means of a Fourier transform. The solution is

$$[4] \quad Z_{im}(z,t) = \frac{1}{2\pi}\int_{-\infty}^{\infty} \mathcal{Z}_{im}(\omega,t)\exp(\iota\omega z)\,d\omega$$

where ι is the imaginary unit and

$$[5] \quad \mathcal{Z}_{1m}(\omega,t) = \frac{N_1(\lambda_1 - T_2) + N_2\alpha_{12}}{\lambda_1 - \lambda_2}\exp(\lambda_1 t) + \frac{N_1(\lambda_2 - T_2) + N_2\alpha_{12}}{\lambda_2 - \lambda_1}\exp(\lambda_2 t)$$

$$[6] \quad \mathcal{Z}_{2m}(\omega,t) = \frac{N_2(\lambda_1 - T_1) + N_1\alpha_{21}}{\lambda_1 - \lambda_2}\exp(\lambda_1 t) + \frac{N_2(\lambda_2 - T_1) + N_1\alpha_{21}}{\lambda_2 - \lambda_1}\exp(\lambda_2 t)$$

N_1 and N_2 are the transformed initial conditions of the first and second species, respectively, and λ_1 and λ_2 are

$$[7] \quad \lambda_{1,2} = \frac{[T_1 + T_2 \pm \sqrt{(T_1 - T_2)^2 + 4\alpha_{12}\alpha_{21}}]}{2}$$

where subscripts, 1 and 2, attached to λ correspond to the plus and minus sign in the brackets respectively. T_1 and T_2 are expressed as

$$[8] \quad \begin{cases} T_1 = -D_{z1}\omega^2 - \iota v_{d1}\omega - \alpha_{21} - \left(\dfrac{\beta_m}{r_0}\right)^2 D_{r1} \\ T_2 = -D_{z2}\omega^2 - \iota v_{d2}\omega - \alpha_{12} - \left(\dfrac{\beta_m}{r_0}\right)^2 D_{r2} \end{cases}$$

where D_{zi} and D_{ri} are longitudinal and transverse diffusion coefficients of ith species, respectively. By applying the expansion technique in [5] and [6], we can derive an explicit form of the solutions as follows:

$$[9] \quad Z_{1m}(z,t) = f_m(z,t)\sum_{p=0}^{\infty}\sum_{q=0}^{p}\sum_{s=0}^{2q} A_{pqs}(t)\left\{\left[N_1 + \frac{t}{2p+1}\left(\frac{N_1\zeta}{2} + N_2\alpha_{12}\right)\right]H_{2s}\left(\frac{\eta t - z)}{\sqrt{D_{za}t}}\right) - \frac{N_1 D_{zd}}{2(2p+1)D_{za}}H_{2s+2}\left(\frac{\eta t - z}{\sqrt{D_{za}t}}\right)\right\}$$

$$[10] \quad Z_{2m}(z,t) = f_m(z,t)\sum_{p=0}^{\infty}\sum_{q=0}^{p}\sum_{s=0}^{2q} A_{pqs}(t)\left\{\left[N_2 - \frac{t}{2p+1}\left(\frac{N_2\zeta}{2} - N_1\alpha_{21}\right)\right]H_{2s}\left(\frac{\eta t - z}{\sqrt{D_{za}t}}\right) + \frac{N_2 D_{zd}}{2(2p+1)D_{za}}H_{2s+2}\left(\frac{\eta t - z}{\sqrt{D_{za}t}}\right)\right\}$$

where the two delta-functions are adopted as the initial conditions so that N_1 and N_2 simply represent the input numbers of the first and second species, respectively.

$$[11] \quad f_m(z,t) = \frac{1}{\sqrt{2\pi D_{za}t}}\exp\left[\frac{v_{dd}}{2D_{zd}}z + \xi t - \frac{(z - \eta t)^2}{2D_{za}t}\right]$$

and H_{2s} and H_{2s+2} are the Hermite polynomials of $2s$th and $2s+2$th order, respectively. Other coefficients involved in [9]–[11] are listed below:

$$v_{dd} = v_{d2} - v_{d1}, \qquad v_{da} = v_{d1} + v_{d2}, \qquad D_{zd} = D_{z2} - D_{z1}, \qquad D_{za} = D_{z1} + D_{z2}, \qquad \xi = \frac{D_{za}v_{dd}^2}{8D_{zd}^2} - \frac{v_{da}v_{dd}}{4D_{zd}} - \frac{\alpha_a}{2}$$

$$[12] \quad \alpha_a = \alpha_{12} + \alpha_{21} + \left(\frac{\beta_m}{r_0}\right)^2 (D_{r1} + D_{r2}), \qquad \eta = \frac{[v_{da} - (D_{za}v_{dd}/D_{zd})]}{2}, \qquad \zeta = \alpha_{12} - \alpha_{21} + \left(\frac{\beta_m}{r_0}\right)^2 (D_{r2} - D_{r1}) + \frac{v_{dd}^2}{4D_{zd}}$$

$$A_{pqs}(t) = \frac{{}_pC_q\,{}_{2q}C_s}{(-1)^s 2^{2q}(2p)!}(\alpha_{12}\alpha_{21})^{p-q}\left(\frac{D_{zd}}{D_{za}}\right)^s \zeta^{2q-s}t^{2p-s}$$

Analysis in dynamic equilibrium

Owing to insufficient convergence of [9] and [10] we have to take into account an enormous number of terms (several tens of terms even for a normal spectrum profile) in the infinite sum to generate two realistic spectra. However, the solutions suggest an analytical expression of the ATS entirely independent of the initial condition in dynamic equilibrium. Namely, every term connected to N_1 and N_2 will automatically be cancelled, with the exception of the fundamental mode of the solution, $f_m(z,t)$. This mode generates a skewed Gaussian profile, similar to but not exactly the same as that we seek in this

Can. J. Chem. Downloaded from www.nrcresearchpress.com by 217.78.4.112 on 09/08/12
For personal use only.

phase. The reason may be attributed to the problem of the infinite sum in m in [3]. The final solution will therefore assume an appreciably different mathematical form even if the Gaussian shape still holds. We can infer the actual form from the solution of one ionic species accompanied by a depleting reaction as

$$[13]\quad \lim_{z\to\infty} \mathscr{J}_{im} = (K_{i0} + \iota K_{i1}\omega + \cdots) \times \exp(-D_{\text{eff}}t\omega^2 - \iota v_{\text{deff}}t\omega - \alpha_{\text{eff}}t)$$

Note that only the first terms in [5] and [6] will dominate the dynamical behavior of two ion swarms, because $\exp(\lambda_2 t)$ decreases much faster than $\exp(\lambda_1 t)$. The resulting coefficients are listed below:

$$[14]\quad K_{10} = \frac{(N_1 + N_2)\alpha_{12}}{(\alpha_{12} + \alpha_{21})}$$

$$K_{20} = \frac{(N_1 + N_2)\alpha_{21}}{(\alpha_{12} + \alpha_{21})}$$

$$K_{11} = v_{dd}\alpha_{12}\frac{[2N_1\alpha_{21} - N_2(\alpha_{12} - \alpha_{21})]}{(\alpha_{12} + \alpha_{21})^3}$$

$$K_{21} = -v_{dd}\alpha_{21}\frac{[2N_2\alpha_{12} + N_1(\alpha_{12} - \alpha_{21})]}{(\alpha_{12} + \alpha_{21})^3}$$

$$[15]\quad D_{\text{eff}} = \frac{D_{z1}\alpha_{12} + D_{z2}\alpha_{21}}{\alpha_{12} + \alpha_{21}} + \frac{v_{dd}^2}{4(\alpha_{12} + \alpha_{21})}$$

$$[16]\quad v_{\text{deff}} = v_{dm} = \frac{v_{d1}\alpha_{12} + v_{d2}\alpha_{21}}{\alpha_{12} + \alpha_{21}}$$

$$[17]\quad \alpha_{\text{eff}} = \left(\frac{\beta_m}{r_0}\right)^2 \frac{(D_{r1} + D_{r2})}{2}$$

An inverse Fourier transform of [13] is straightforward and the solution is

$$[18]\quad Z_{im}(z,t) = \frac{1}{\sqrt{4\pi D_{\text{eff}}t}}\left[\frac{K_{i1}(v_{dm}t - z)}{2D_{\text{eff}}t} + K_{i0}\right] \times \exp\left[-\frac{(z - v_{dm}t)^2}{4D_{\text{eff}}t} - \alpha_{\text{eff}}t\right]$$

A remarkable feature of [18] is that the effective drift velocity, v_{dm}, is exactly the same as that proposed by Voshall *et al.* (3) in their experimental analysis of negative ions in oxygen gas, because in the dynamic equilibrium phase the ratio of concentrations of two ionic species is in accord with the reaction-frequency ratio. Somewhat unexpected is the appearance of the second term in D_{eff}, [15], which is very much larger than the first term under the usual experimental conditions, and dominates the "apparent" diffusive effect.

The solution [18] gives us the following insights;

(*i*) the K_{i0}th term (i = 1, 2) is a fundamental term to determine the basic structure of the Gaussian profile

(*ii*) the ratio, K_{10}/K_{20}, yields the equilibrium constant independent of the initial conditions

(*iii*) the diminution of the ions arises only from the transverse-diffusion loss

(*iv*) the K_{i1}th term, which weakly depends on the initial conditions, is a subordinate term, producing a subtle shift in the peak position in the K_{i0}th term

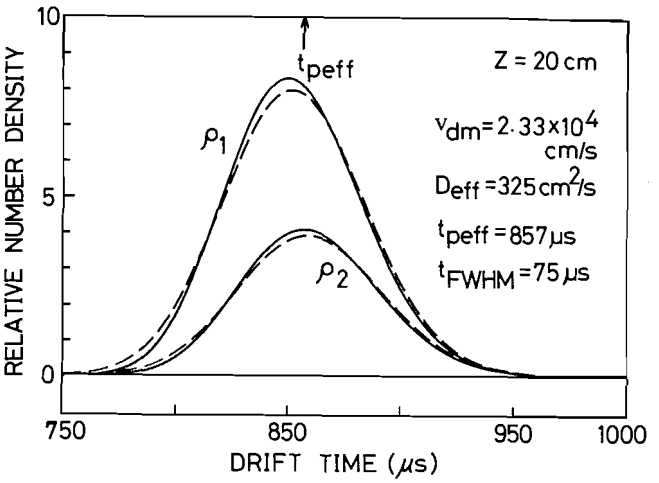

FIG. 1. Comparison of two sets of ATS in a dynamic equilibrium phase. $v_{d1} = 2.5 \times 10^4$ cm s^{-1}, $v_{d2} = 2 \times 10^4$ cm s^{-1}, $D_{z1} = D_{r1} = 125$ cm^2 s^{-1}, $D_{z2} = D_{r2} = 100$ cm^2 s^{-1}, $\alpha_{21} = 10^4$ s^{-1}, $\alpha_{12} = 2 \times 10^4$ s^{-1}. Two solid-line curves are exact arrival time spectra generated from [4]–[6] by using a numerical quadrature. The two broken-line curves are approximate ATS calculated from [18]. A delta-function was adopted as the initial condition for the first species.

(*v*) the FWHM of the arrival time spectrum, t_{FWHM}, is mainly determined by the K_{i0}th term and the influence of the K_{i1}th term is negligible,

$$[19]\quad t_{\text{FWHM}} \simeq \frac{3.33\sqrt{D_{\text{eff}}t_{\text{peff}}}}{v_{dm}}$$

$$[20]\quad t_{\text{peff}} = \frac{z}{v_{dm}}$$

and

(*vi*) the magnitude of the peak difference is independent of the initial conditions on account of the symmetric expression of K_{11} and K_{21} with respect to the ionic species.

A typical comparison of two hypothetical ATS generated from [4]–[6] (two solid-line curves) with those calculated from [18] (two broken-line curves) is shown in Fig. 1. Except for a slight decrease in the peak height in the approximate solution the agreement is quite good. Note that these are number density profiles, the area-ratio of which yields the reaction-frequency ratio; $\rho_1 : \rho_2 = \alpha_{12} : \alpha_{21} = 2 : 1$. Figure 2 depicts their component spectra calculated separately from each term in [13], in which the K_{i0}th, K_{i1}th, and K_{i2}th terms describe the first, second, and third component of each arrival time spectrum, respectively. As mentioned above, no peak difference between two first-component spectra can be observed. The FWHM of the composite arrival time spectra of primary ions agrees with that of secondary ions and is not seriously affected by the second and third components.

The expression of the peak difference can explicitly be derived from [18] as

$$[21]\quad \Delta t_{\text{peak}} = \frac{|v_{d1} - v_{d2}|}{v_{d1}\alpha_{12} + v_{d2}\alpha_{21}}$$

Can. J. Chem. Downloaded from www.nrcresearchpress.com by 217.78.4.112 on 09/08/12
For personal use only.

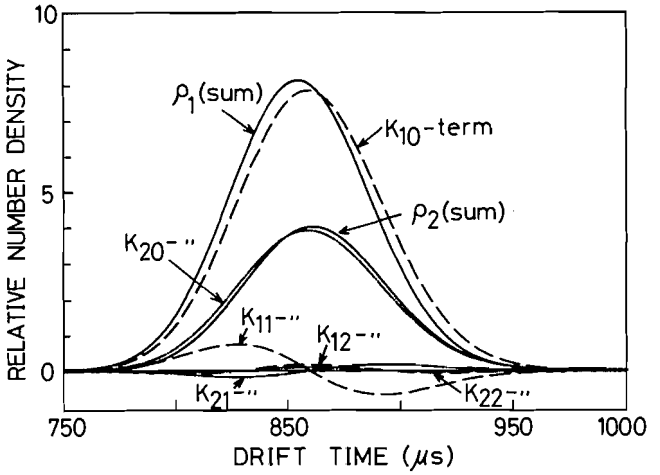

FIG. 2. Two composite ATS (two solid-line curves) and their components. ρ_1(sum) is composed of three subcomponents (three broken-line curves), K_{10}th, K_{11}th, and K_{12}th terms. 0, 1, and 2 refer to the first, second, and third component, respectively. ρ_2(sum) is also composed of K_{20}th, K_{21}th, and K_{22}th term (three dot–dash curves). Each subcomponent spectrum was generated from the corresponding term in [13] by using the quadrature with the same kinetic coefficients as those of Fig. 1.

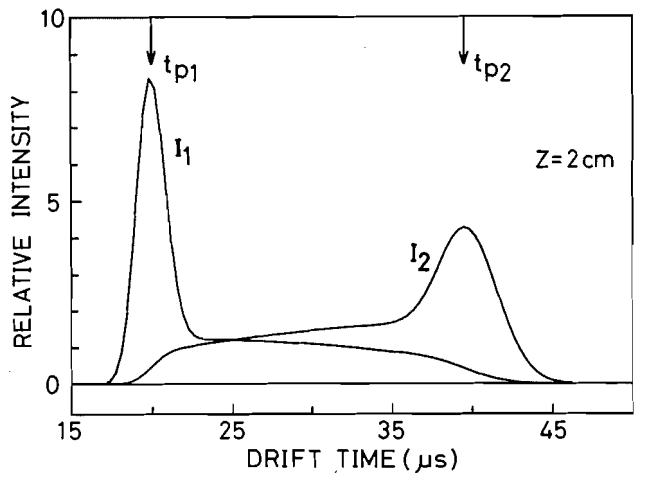

FIG. 3. Two ATS in a nondynamic equilibrium phase generated from [4]–[6]. z = 2 cm, $v_{d1} = 10^5$ cm s^{-1}, $v_{d2} = 5 \times 10^4$ cm s^{-1}, $D_{z1} = D_{r1} = 200$ cm^2 s^{-1}, $D_{z2} = D_{r2} = 100$ cm^2 s^{-1}, $\alpha_{21} = 5 \times 10^4$ s^{-1}, $\alpha_{12} = 2 \times 10^4$ s^{-1}. The ratio of the number densities adopted for the initial conditions was $I_1 : I_2 = 1 : 0.7$. $t_{p1} = 20$ and $t_{p2} = 39.5$ μs, which are peak times determined from the Gaussian components (two peaks on both sides) of I_1 and I_2, respectively.

The Δt_{peak} is a constant determined only from the drift velocities and reaction frequencies, and is completely independent of the initial conditions as well as the diffusion coefficients. As the drift distance increases, a peak difference between two general ATS asymptotically converges to the Δt_{peak}, which is substantial in the limit of infinite drift distance.

This formula is useful for determining the forward and reverse reaction frequencies. We now demonstrate this using two groups of simulation spectra calculated numerically from [4]–[6] with the same kinetic coefficients. The ATS in the first group shown in Fig. 3 correspond to the initial-phase (or

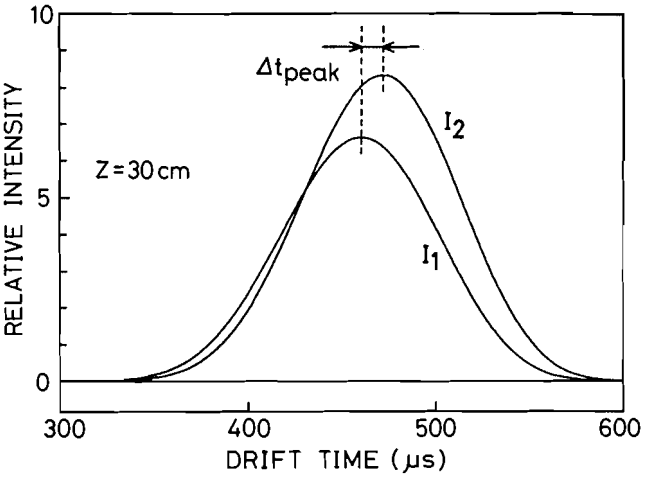

FIG. 4. Two ATS in a dynamic equilibrium phase. z = 30 cm, and other kinetic coefficients are the same as those of Fig. 3. Δt_{peak} = 11.4 μs.

nondynamic equilibrium phase) spectra computed at the drift distance of 2 cm, while those in the second group in Fig. 4 are the spectra in the dynamic equilibrium phase at 30 cm drift distance.

In Fig. 3 two sharp peaks on both sides arise from the initially injected ions of first kind (the left peak) and second kind (the right peak), which give us their approximate drift velocities. They are calculated from the drift distance divided by the peak time in each arrival time spectrum as $v_{d1} = 1.00 \times 10^5$ and $v_{d2} = 5.06 \times 10^4$ cm s^{-1}. The area-ratio of two profiles in Fig. 4 is evaluated as $I_1 : I_2 = 1 : 1.26$, which agrees with the ratio, $N_{1s}v_{d1} : N_{2s}v_{d2}$, provided that the drift component current dominates the arrival time spectrum profile. N_{1s} and N_{2s} are stationary concentrations of the first and second ionic species, respectively, in the dynamic equilibrium phase. This assumption holds in typical experimental conditions (2). By using the above drift velocities we can evaluate the ratio of the concentrations as $N_{1s} : N_{2s} = 1 : 2.49$, which is equivalent to the ratio, $\alpha_{12} : \alpha_{21}$. The magnitude of the peak difference is read from Fig. 4 as 11.4 μs. Substituting the value back into [21] and using the ratio $\alpha_{12} : \alpha_{21} = 1 : 2.49$, we determine the reaction frequencies to be $\alpha_{21} = 4.80 \times 10^4$ and $\alpha_{12} = 1.93 \times 10^4$ s^{-1}. The errors arising from this direct determination from the figures are −4% for α_{21} and −3.5% for α_{12}.

Despite its rather crude analysis, this method gives us surprisingly accurate reaction frequencies. If we require more precise measurements of the drift velocities, which are indispensable for the accurate determination of reaction frequencies, we can always resort to more sophisticated experimental techniques, including the use of a movable ion source and a suitable choice of the experimental conditions.

We now examine the final problem in this part. It is one of the most difficult problems in reactive ion transport analysis to predict exactly how long it takes before equilibrium is achieved. One seeks a relation between the kinetic coefficients and the drift distance where the dynamic equilibrium develops. For this purpose we first introduce an average drift velocity of two general ATS, which may asymptotically converge to v_{dm} as the drift distance increases. We define the velocity, $\langle v_d \rangle(z)$, as

Can. J. Chem. Downloaded from www.nrcresearchpress.com by 217.78.4.112 on 09/08/12
For personal use only.

$$[22]\quad \langle v_d\rangle(z) = \frac{\int_{-\infty}^{\infty}\int_{0}^{\infty} [\mathscr{J}_{1m}(\omega,t)v_{d1} + \mathscr{J}_{2m}(\omega,t)v_{d2}] \exp(\iota\omega z)\, d\omega\, dt}{\int_{-\infty}^{\infty}\int_{0}^{\infty} [\mathscr{J}_{1m}(\omega,t) + \mathscr{J}_{2m}(\omega,t)] \exp(\iota\omega z)\, d\omega\, dt} = \frac{I_n}{I_d}$$

Assuming the drift-tube radius to be infinite, we can obtain explicit forms of I_n and I_d as

$$[23]\quad I_n = \frac{(N_1 + N_2)}{2} + \frac{1}{2\pi}\int_{-\infty}^{\infty} \frac{e^{\iota\omega z}}{g(\omega)} (B_{n2}\omega^2 + \iota B_{n1}\omega + B_{n0})\, d\omega$$

$$[24]\quad I_d = \frac{(N_1 + N_2)}{2v_{dm}} + \frac{1}{2\pi}\int_{-\infty}^{\infty} \frac{e^{\iota\omega z}}{g(\omega)} (B_{d2}\omega^2 + \iota B_{d1}\omega + B_{d0})\, d\omega$$

where the resulting coefficients in the integrands are

$$B_{n2} = (N_1 + N_2)D_{z1}D_{z2}$$

$$[25]\quad B_{n1} = N_1 D_{z1}v_{d2} + N_2 D_{z2}v_{d1}$$

$$B_{n0} = (N_1 + N_2)(D_{z1}\alpha_{12} + D_{z2}\alpha_{21})$$

$$B_{d2} = \frac{B_{n2}}{v_{dm}}$$

$$[26]\quad B_{d1} = (N_1 + N_2)\frac{(D_{z1}v_{d2} + D_{z2}v_{d1})}{v_{dm}} - N_1 D_{z2} - N_2 D_{z1}$$

$$B_{d0} = (N_1 + N_2)\frac{(D_{z1}\alpha_{12} + D_{z2}\alpha_{21} - v_{d1}v_{d2})}{v_{dm}} + N_1 v_{d2} + N_2 v_{d1}$$

The $g(\omega)$ is expressed as

$$[27]\quad g(\omega) = -\iota D_{z1}D_{z2}\omega^3 + (D_{z1}v_{d2} + D_{z2}v_{d1})\omega^2 + \iota(v_{d1}v_{d2} - D_{z1}\alpha_{12} - D_{z2}\alpha_{21})\omega + v_{d1}\alpha_{12} + v_{d2}\alpha_{21}$$

Equation [27] states that the three singular points in I_n and I_d are all purely imaginary, and only one root, $\iota\omega_s(\omega_s > 0)$ for $g(\omega) = 0$, provides for the appropriate formula of $\langle v_d\rangle(z)$. Under typical experimental conditions, we can adopt the following approximate expression for the root as

$$[28]\quad \omega_s = \frac{v_{d1}\alpha_{12} + v_{d2}\alpha_{21}}{v_{d1}v_{d2} - D_{z1}\alpha_{12} - D_{z2}\alpha_{21}}$$

The percentage deviation of $\langle v_d\rangle(z)$ from v_{dm} is derived from [23], [24], and [28] as

$$[29]\quad \%\text{dev} = 100\,\frac{[\langle v_d\rangle(z) - v_{dm}]}{v_{dm}} \simeq \kappa \exp\left(\frac{-z}{z_s}\right)$$

where κ is a constant determined from both the initial conditions and the kinetic coefficients. The other constant, z_s, is

$$[30]\quad z_s = \frac{1}{\omega_s}$$

It has the capability of becoming an important measure for estimating the drift distance required to achieve the dynamic equilibrium phase. However, as will be discussed later, z_s appears to be much smaller than expected so that the ATS at this drift distance will not be close to the complete Gaussian shape. More realistic parameters can be derived from [19] and [21]. The ratio of Δt_{peak} to t_{FWHM}, which is expected to vanish in the limit of infinite drift distance, is a plausible parameter for this prediction. By setting the ratio equal to an appropriately small value as

$$[31]\quad \frac{\Delta t_{peak}}{t_{FWHM}} = \varepsilon$$

we can derive therefrom the drift distance z_r. If we set ε to be 0.1, z_r is expressed as follows:

$$[32]\quad z_r = \frac{9.02\,(v_{d1} - v_{d2})^2 v_{dm}}{D_{eff}(\alpha_{12} + \alpha_{21})^2}$$

Adopting a rather crude but reasonable approximation for [15] as

$$[33]\quad D_{eff} = \frac{(v_{d1} - v_{d2})^2}{4(\alpha_{12} + \alpha_{21})}$$

we obtain an extremely simple formula

$$[34]\quad z_r \simeq \frac{36\, v_{dm}}{\alpha_{12} + \alpha_{21}}$$

The magnitude of the first term in [15] is, in general, much less than one tenth of that of the second term. So, [34] certainly yields the expected drift distance and can be used as a rule of thumb.

The only problem left is the derivative of the time required to achieve dynamic equilibrium. Although [34] may suggest it to be $36/(\alpha_{12} + \alpha_{21})$, this is incorrect owing to the fact that the average drift velocity is a function of drift distance. An important clue is given by [29], which is considered to be a differential equation of drift distance with respect to time. The mathematical analysis is rather cumbersome and is now underway.

Application to experimental analysis

We now analyze reactive ion transport for a real ion–molecule combination. The determination of mobilities, diffusion coefficients, and reaction rates of nitrogen ions in

Can. J. Chem. Downloaded from www.nrcresearchpress.com by 217.78.4.112 on 09/08/12
For personal use only.

Can. J. Chem. Downloaded from www.nrcresearchpress.com by 217.78.4.112 on 09/08/12
For personal use only.

nitrogen has been the subject of a large number of investigations since 1930 (4–13), among which the $(N_2^+, N_4^+)/N_2$ system is one of the most extensively analyzed. It is well known that the dynamic balance between the forward and reverse reactions for N_2^+ and N_4^+ ions,

$$[35] \quad N_2^+ + 2N_2 \underset{k_{12}}{\overset{k_{21}}{\rightleftharpoons}} N_4^+ + N_2$$

occurs in the intermediate energy range.

Using the analysis in the nonequilibrium phase, McKnight *et al.* (5) and McDaniel and co-workers (6, 14, 15) measured the kinetic coefficients in a wide energy range. By using a flow-drift tube, Lindinger *et al.* (8) measured mobilities of N_4^+ in N_2. Böhringer and Arnold (11) also determined mobilities of N_2^+ and N_4^+ in the temperature range 20–420 K using a low-temperature drift tube. The comparison between those mobility data indicates that those of McDaniel and co-workers appear to be the more accurate. As far as the reaction rates of N_2^+ and N_4^+ are concerned, however, controversy still remains regarding their accuracy. So in this analysis we adopted the transport coefficients determined by McDaniel and co-workers and the reaction rates determined by McKnight *et al.* (5). Several useful ion-current profiles for the $(N_2^+, N_4^+)/N_2$ system were obtained by McKnight *et al.* (5), from which we find that the dynamic balance develops at E/N = 150 Td (1 Td = 10^{-17} V cm^2). E/N is the ratio of the electric field strength to the neutral drift gas number density. Unfortunately, no real current profiles at this energy are available so we numerically generate two hypothetical ATS from the data. Then, we examine whether their shape and width reproduce the same data according to the appropriate formulas. In fact this kind of procedure is not an adequate analysis for determining the unknown kinetic coefficients, because two groups of ATS should be measured and analyzed separately in two different phases in actual experiments. Nevertheless, it will lead us to confirm that the present formulation is consistent and useful.

Two ATS for N_2^+ and N_4^+ ions in the initial phase at 150 Td are shown in Fig. 5. We adopted a delta-function as the initial condition for N_2^+ ions only. By increasing the drift distance from 3 to 10 cm and the gas pressure from 0.845 to 2.0 Torr (1 Torr = 133.3 Pa), we can shift the initial phase of Fig. 5 into a dynamic equilibrium phase of Fig. 6. In this procedure two reaction rates were kept constant, viz. k_{21} = 2.7×10^{-29} cm^6 s^{-1} and $k_{12} = 2.0 \times 10^{-12}$ cm^3 s^{-1}. From the ATS in Fig. 6 four kinetic coefficients, α_{21}, α_{12}, D_{z1}, and D_{z2} can be determined directly with the help of [15], [16], and [19]–[21], provided that the two drift velocities are known. The following relation is also assumed;

$$[36] \quad v_{d1} : v_{d2} = D_{z1} : D_{z2}$$

The Δt_{peak} and t_{FWHM} in Fig. 6 are 2.1 and 20.0 μs, respectively. Using the method applied to Figs. 3 and 4, we obtain the reaction-frequency ratio as $\alpha_{21}:\alpha_{12}$ = 0.87:1. Determination of α_{21} and α_{12} by use of [21] is straightforward, and the calculated values are $\alpha_{21} = 1.14 \times 10^5$ and $\alpha_{12} = 1.31 \times 10^5$ s^{-1}. The corresponding values for generating the ATS were 1.12×10^5 and 1.29×10^5 s^{-1}, respectively. Moreover, determination of D_{z1} and D_{z2} is possible according to [15], [19], and [20]. The values evaluated are D_{z1} = 54.4 and D_{z2} = 91.1 cm^2 s^{-1}. The adopted D_{z1} and D_{z2} are 43.2 and 72.2 cm^2 s^{-1}, respectively. As far as the accuracy of the reaction frequency in this case is concerned, the discrepancy of less than 2% is surprisingly small, whereas that of the longitudinal diffusion coefficient exceeds 25%. Again, we emphasize that this test only proves the present method to be consistent. Without carrying out the separate measurements in different phases, we are not at the moment able to say anything about the measurement error of the kinetic coefficients.

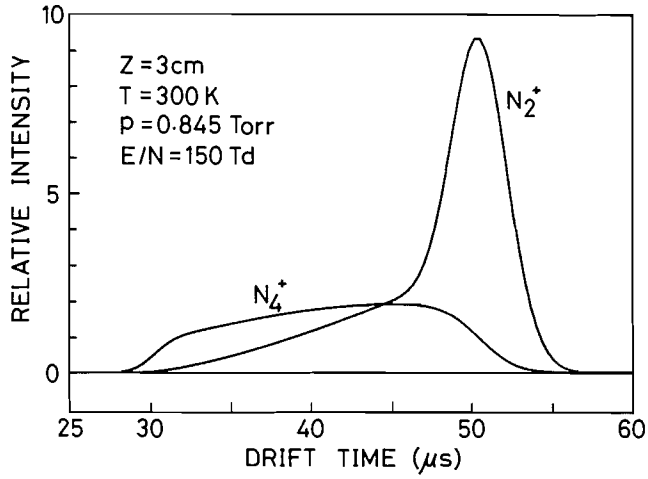

FIG. 5. The ATS of N_2^+ and N_4^+ ions in nitrogen in an initial phase. They were numerically generated from [4]–[6] by introducing the experimental data; v_{d1} = 5.92 × 10^4 cm s^{-1}, v_{d2} 9.91 × 10^4 cm s^{-1}, D_{z1} = 102 cm^2 s^{-1}, D_{z2} = 171 cm^2 s^{-1}, D_{r1} = 74 cm^2 s^{-1}, D_{r2} = 123 cm^2 s^{-1}, α_{21} = 2 × 10^4 s^{-1}, and α_{12} = 5.44 × 10^4 s^{-1}. A delta-function was adopted as the initial condition for the first species (N_2^+ ions; the labelled number as 1).

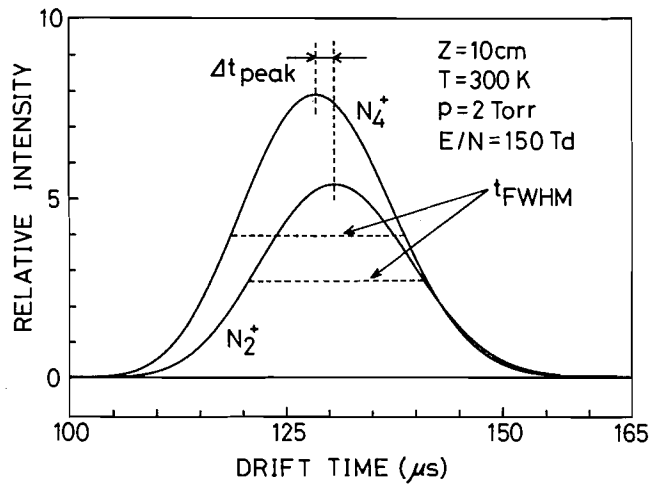

FIG. 6. The ATS of N_2^+ and N_4^+ ions in nitrogen in a dynamic equilibrium phase. The kinetic coefficients were D_{z1} = 43.2 cm^2 s^{-1}, D_{z2} = 72.2 cm^2 s^{-1}, D_{r1} = 31.1 cm^2 s^{-1}, D_{r2} = 52 cm^2 s^{-1}, $\alpha_{21} = 1.12 \times 10^5$ s^{-1}, and $\alpha_{12} = 1.29 \times 10^5$ s^{-1}. Two drift velocities were the same as those of Fig. 5. Δt_{peak} = 2.1 μs and t_{FWHM} = 20.0 μs.

Figure 7 presents the percent deviation of $\langle v_d \rangle(z)$ from v_{dm} as a function of drift length. The approximate formula [29] works well under the present conditions, although only the case where the initial condition is set as (N_1, N_2) = (0,1) appears to be unsatisfactory. The agreement between the re-

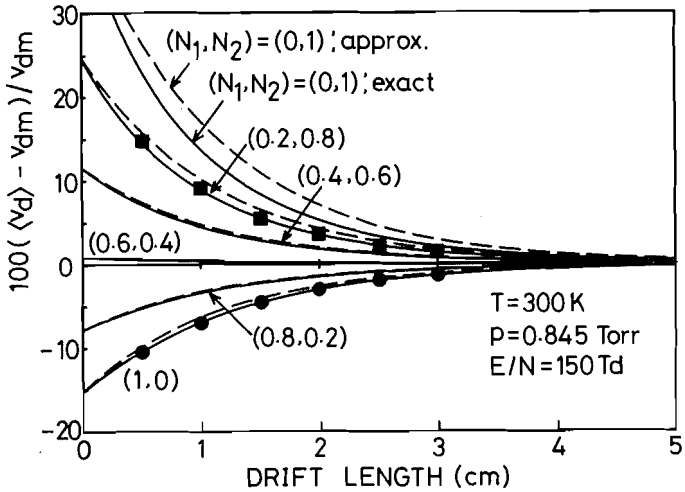

FIG. 7. The percent deviation of $\langle v_d \rangle(z)$ from v_{dm} as a function of drift length. The kinetic coefficients adopted are the same as those of Fig. 5 except for the ratio of the initial number densities of N_2^+ and N_4^+, which is represented as (N_1, N_2) on the drawing. The solid-line curves are the results calculated exactly from the solution according to [22]–[27]. The broken-line curves are from the approximate formula [29]. The filled circles and squares are obtained directly from the two arrival time spectra, the initial conditions of which are (1,0) and (0.2, 0.8), respectively.

sults calculated from the exact solution (the solid-line curves) and the values obtained directly from the ATS (the filled circles and squares) is excellent.

The percent deviation of the filled circle at $z = 3$ cm is -1.28%, which is calculated from the ATS in Fig. 5. Although this deviation is small enough to expect the ATS to be sufficiently close to equilibrium, the two profiles in Fig. 5 are far from those we expect in this phase. This is a clear indication that the z_s of [30] are not a suitable measure for predicting whether equilibrium has been achieved. The z_r, on the other hand, yields a much more appropriate value than z_s. The z_r calculated from [32] and that from [34] by using the same parameters are 33.2 and 33.8 cm, respectively. In fact we have confirmed that the dynamic equilibrium phase is reached at these drift distances.

Discussion

The accurate measurement of reaction frequencies is one of the long-standing aims in the field of reactive ion transport and gas-phase ion chemistry. In contemporary drift-tube experiments, ion mobilities (or drift velocities) can be determined with an accuracy of about $\pm 1\%$ in simple cases (1). Although measurement of longitudinal diffusion coefficients is much more difficult than that of mobilities, its experimental uncertainty is, in general, estimated to be less than $\pm 25\%$ (15). Reaction rates are very much more difficult to measure than the transport coefficients, and the total experimental error may exceed $\pm 50\%$ at mean collision energies ranging from thermal to several electronvolts (16). This may be attributed simply to the fact that most experimentalists have limited their measurements to the nondynamic equilibrium phase, where the appropriate estimation of the initial condition would become indeed troublesome. The difficulty is encountered in various kinds of apparatus, especially in the case of flow drift-tube instruments.

The peak-time difference method in the dynamic equilibrium phase has the potential to be useful in this respect. Even when the difference is difficult to measure under specific experimental conditions, we can resort to a numerical differential technique to determine the peak position in each ATS. Moreover, it has the advantage that the reaction frequency obtained from [21] is not very sensitive to the measured difference. On the contrary, the longitudinal diffusion coefficient calculated from [15], [19], and [20] is very sensitive to the FWHM of the ATS. If we fail to measure it accurately, the D_{eff} may occasionally be negative. This deficiency may suggest a further improvement in the present method.

This means that the diffusive effect in dynamic equilibrium is mainly dominated by the second term in [15], which is a function of the drift velocities and reaction frequencies. In other words, there is a possibility to determine the reaction frequencies from the FWHM of the observed spectrum. The accuracy anticipated therefrom would be within $\pm 5\%$ over a wide range of E/N. The most important conclusion to be drawn from the present analysis in dynamic equilibrium is that the shape and width of ATS depend strongly on the drift velocity and reaction frequency, and that the influence of the longitudinal diffusion coefficient is negligible. Again, the precise determination of the drift velocity is indispensable in carrying out the above procedure. As a final remark we strongly recommend a suitable choice of the above two methods, the initial phase analysis and the dynamic equilibrium phase analysis, for the sake of an accurate determination of the kinetic coefficients. The observation of reactive ion transport phenomena from two different aspects will certainly lead to much deeper understanding.

Conclusions

A method for analyzing the space-time behavior of two ion swarms in dynamic equilibrium has been proposed. The analytic solution of ATS in this phase has been explicitly derived. Two important parameters are the effective diffusion coefficient and the effective drift velocity. By combining these parameters with the peak-time difference and the FWHM of the ATS, the forward and reverse reaction frequencies and the longitudinal diffusion coefficients can be determined. Moreover, a measure of the drift distance where the dynamic equilibrium develops has been examined. The reactive transport process of the $(N_2^+, N_4^+)/N_2$ system has been tested to find out whether the present method has the potential to be useful in drift-tube analysis.

Acknowledgements

The authors wish to thank Dr. K. Seto for introducing them to this interesting field.

1. E. A. Mason and E. W. McDaniel. Transport properties of ions in gases. John Wiley and Sons, New York. 1988.
2. K. Iinuma. Can. J. Chem. **69**, 1090 (1991).
3. R. E. Voshall, J. L. Pack, and A. V. Phelps. J. Chem. Phys. **43**, 1990 (1965).
4. A. M. Tyndall and C. F. Powell. Proc. R. Soc. London A, **129**, 162 (1930).
5. L. G. McKnight, K. B. McAfee, and D. P. Sipler. Phys. Rev. **164**, 62 (1967).
6. J. T. Moseley, R. M. Snuggs, D. W. Martin, and E. W. McDaniel. Phys. Rev. **178**, 240 (1969).
7. W. Lindinger. J. Chem. Phys. **64**, 3720 (1976).

Can. J. Chem. Downloaded from www.nrcresearchpress.com by 217.78.4.112 on 09/08/12
For personal use only.

8. W. Lindinger, I. Dotan, D. L. Albritton, and F. C. Fehsenfeld. J. Chem. Phys. **68**, 2607 (1978).
9. D. Smith, N. G. Adams, and T. M. Miller. J. Chem. Phys. **69**, 308 (1978).
10. H. Böhringer and F. Arnold. J. Chem. Phys. **77**, 5534 (1982).
11. H. Böhringer and F. Arnold. Int. J. Mass Spectrum. Ion Processes, **49**, 61 (1983).
12. P. A. M. van Koppen, P. R. Kemper, A. J. Illies, and M. T. Bowers. Int. J. Mass Spectrom. Ion Processes, **54**, 263 (1983).
13. P. A. M. van Koppen, M. F. Jarrold, M. T. Bowers, L. M. Bass, and K. R. Jennings. J. Chem. Phys. **81**, 288 (1984).
14. H. W. Ellis, R. Y. Pai, E. W. McDaniel, E. A. Mason, and L. A. Viehland. At. Data Nucl. Data Tables, **17**, 177 (1976).
15. H. W. Ellis, E. W. McDaniel, D. L. Albritton, L. A. Viehland, S. L. Lin, and E. A. Mason. At. Data Nucl. Tables, **22**, 179 (1978).
16. M. T. Bowers (*Editor*). Gas phase ion chemistry. Vol. 1. Academic Press Inc., New York. 1979.

Can. J. Chem. Downloaded from www.nrcresearchpress.com by 217.78.4.112 on 09/08/12
For personal use only.

NMR kinetic study of ethyl silicate hydrolysis by ammonia in alcoholic solvents

IDRISS EL BAKALI, ESSAÏD EL RHESS, CHRISTOPHE ROUSSELOT, AND RENÉ MERCIER[1]

Laboratoire d'électrochimie des solides, Unité Associée au Centre National de la recherche scientifique, n° 436, Université de Franche-Comté, 25030 Besançon CEDEX, France

AND

MARIE-FRANCE MERCIER

Centre de spectrométrie, Université de Franche-Comté, 25030 Besançon CEDEX, France

Received June 11, 1991[2]

IDRISS EL BAKALI, ESSAÏD EL RHESS, CHRISTOPHE ROUSSELOT, RENÉ MERCIER, and MARIE-FRANCE MERCIER. Can. J. Chem. **70**, 1612 (1992).

Hydrolysis of $Si(OC_2H_5)_4$ by ammonia has been investigated using ^1H and ^{13}C NMR measurements in alcoholic media. Use of deuterated CD_3CD_2OD and CD_3OD solvents proves the absence of transesterification by alkoxy exchange between silicate and alcohols. The rate constant increases when CD_3OD replaces CD_3CD_2OD as the solvent ($k = 2.8 \times 10^{-3}$ L mol^{-1} min^{-1} in CD_3CD_2OD; 7.5×10^{-3} L mol^{-1} min^{-1} in CD_3OD for similar experiments).

IDRISS EL BAKALI, ESSAÏD EL RHESS, CHRISTOPHE ROUSSELOT, RENÉ MERCIER et MARIE-FRANCE MERCIER. Can. J. Chem. **70**, 1612 (1992).

Opérant en milieu alcoolique et utilisant des techniques de RMN du ^1H et du ^{13}C, on a étudié l'hydrolyse du $Si(OC_2H_5)_4$. L'utilisation du CD_3CD_2OD et du CD_3OD comme solvants permet de démontrer qu'il n'y a pas de transestérification par échange de groupes alcoxyles entre le silicate et les alcools. La constante de vitesse augmente lorsqu'on remplace le CD_3CD_2OD par du CD_3OD comme solvant ($k = 2{,}8 \times 10^{-3}$ L mol^{-1} min^{-1} dans le CD_3CD_2OD; $7{,}5 \times 10^{-3}$ L mol^{-1} min^{-1} dans le CD_3OD, pour des conditions expérimentales semblables).

[Traduit par la rédaction]

Introduction

Obtaining sol–gel materials has been extensively studied in the last decade. In particular, Stöber *et al.* (1) studied the hydrolysis of tetraethylorthosilicate $Si(OC_2H_5)_4$ as reported in a paper on colloidal silica synthesis. He used an ammonia reactant to obtain homodispersed particles in the range of 0.1–1 μm. He varied the ammonia and water concentrations, as well as the solvents, to obtain particles having final diameters that could be measured. Shimohira and Tomuro (2), Shimoda *et al.* (3), and Tan *et al.* (4) studied the effect of temperature on final-diameter size. They found that when temperature increases, the final-diameter size decreases. The influence of all of the above parameters acting on the hydrolysis and condensation of $Si(OC_2H_5)_4$ was reviewed in our laboratory by El Rhess (5). He studied the kinetics of the evolution of both particle diameter and particle concentration for silica particles having an initial diameter of 10 nm.

We wanted to observe the first steps of the hydrolysis and condensation of different alkoxyl silicates. The most efficient technique for this type of study is ^{29}Si Nuclear Magnetic Resonance (NMR). This technique has already been used by various researchers to follow the hydrolysis and condensation reaction of both methyl and ethyl silicate (in particular, Lin and Basil (6) for $Si(OC_2H_5)_4$ and Artaki *et al.* (7), Balfe and Martinez (8), and Klemperer *et al.* (9) for $Si(OCH_3)_4$). ^{29}Si NMR reveals the identity of hydrolyzed molecules such as $Si(OH)(OR)_3$, $Si(OH)_2(OR)_2$, $Si(OH)_3(OR)$, and $Si(OH)_4$ by a characteristic resonance line and the appearance of dimeric (Si-O-Si) and oligomeric species at distinct ranges of frequency. The experimental conditions used to study these hydrolyzed molecules do not, in general, coincide with the experimental conditions used in the synthesis of silica. This paper compares the kinetics of the hydrolysis of $Si(OC_2H_5)_4$ in two alcoholic media, CD_3OD and CD_3CD_2OD, using ^1H NMR spectroscopy. Our experimental conditions are the same as those required to obtain silica colloids by adding ammonia to alcoholic media. Assink and Kay (10–12) studied $Si(OC_2H_5)_4$ and $Si(OCH_3)_4$ using ^1H NMR, first in an acid medium and then in a basic (NH_4OH) medium.

We also wanted to determine if silicate and alcohol exchange alkoxy groups and thus cause transesterification

$$Si(OC_2H_5)_4 + 4\ CD_3OD \rightarrow Si(OCD_3)_4 + 4\ C_2H_5OD$$

This reaction could occur in competition with the hydrolysis reaction.

$$Si(OC_2H_5)_4 + 2\ H_2O \rightarrow Si(OH)_4 + 4\ C_2H_5OH$$

It is not possible, using solely ^1H NMR, to determine if there is competition because deuterical species such as $Si(O\text{-}CD_3)$ do not produce signals. Therefore, in certain experiments, we used ^{13}C NMR because it allowed us to distinguish $Si\text{-}OCD_3$ from $SiOCH_3$ using proton coupling techniques, which produce singlets for $^{13}CH_3$ and multiplets for $^{13}CD_3$.

Experimental conditions

We used wholly deuterated anhydrous alcohols (CD_3OD and C_2D_5OD from Aldrich) as solvents. The silicate and the ammonia solution (NH_3, H_2O) are in their protonated forms. Freshly distilled ethyl silicate was used to avoid atmospheric hydrolysis. $Si(OR)_4$, R'OD, and concentrated ammonia were successively added to NMR tubes at 20°C, for example: 500 μL C_2D_5OD + 15 μL $Si(OEt)_4$ + 90 μL NH_4OH (13.5 M). The different experiments are summarized in Table 1.

Immediately after adding NH_4OH, the tubes were stirred for 15 s and then placed in the NMR instrument (Bruker Spectroscopic AC 200 spectrometer linked to an ASPECT 3000 computer). The ^1H spectra were recorded at 200 MHz. The spectrum produced by the results of 16 pulses was immediately recorded,

[1]Author to whom correspondence may be addressed.

[2]Revision received December 18, 1991.

Can. J. Chem. Downloaded from www.nrcresearchpress.com by 217.78.4.112 on 09/08/12
For personal use only.

TABLE 1. Designation of characteristics of the ^1H NMR experiments

Code	Solvent	Silicate	[Silicate] ($M\ L^{-1}$)	[NH_3] ($M\ L^{-1}$)	[H_2O] ($M\ L^{-1}$)	[H_2O]/[-O-C_2H_5]
ETET1	C_2D_5OD	$Si(OC_2H_5)_4$	0.4	0.56	1.64	1.025
ETET2	C_2D_5OD	$Si(OC_2H_5)_4$	0.12	2.0	5.9	12.3
MEET1	CD_3OD	$Si(OC_2H_5)_4$	0.4	0.56	1.64	1.025
MEET2	CD_3OD	$Si(OC_2H_5)_4$	0.2	0.59	1.72	2.15

giving a spectral record of 2 min. The ^{13}C spectra were recorded at 50 MHz by using ^1H broad-band decoupling: 256 pulses were recorded with a 5 s delay between each pulse. It took 30 min to record the ^{13}C spectrum. The NMR apparatus was calibrated for D resonances for the alcohol chosen, by using anhydrous mixtures (silicate + alcohol).

In Table 1, the four experiments are for the hydrolysis of $Si(OC_2H_5)_4$. The concentration of the solvent is about 14 $M\ L^{-1}$ (C_2D_5OD) and 20 $M\ L^{-1}$ (CD_3OD).

Chemical shifts, δ, are expressed in ppm (for ^{13}C and ^1H NMR), with respect to the zero value of TMS (1%). Using ^1H NMR, we can easily follow the disappearance of silicate species and the appearance of alcohol species formed during hydrolysis.

$$Si(OR)_4 + 2\ H_2O \rightarrow SiO_2 + 4\ ROH$$

At the beginning of the kinetic study, ^1H NMR signals correspond to Si-O-CH_2-CH_3 or Si-O-CH_3 protons and to only one broad peak for both NH_3 and H_2O protons. During hydrolysis, this last peak encompasses all hydroxyl groups (R-OH, Si(OH)).

Precise intensity measurements enable one to determine the exact [O-H]/[Si-O-R] ratio, as well as the evolution of [Si-O-R] groups as a function of time.

The ETET 2 mixture corresponds to experimental conditions required for the synthesis of 300-nm silica particles at 20°C (12 times more H_2O than (OC_2H_5) in concentration).

Results

^{13}C NMR

ETET 1

With C_2D_5OD, the solvent is characterized by a quintuplet at 56.8 ppm (CD_2) and a heptaplet at 17.5 ppm (CD_3). $Si(OC_2H_5)_4$ presents singlets at 59.74 and 18.39 ppm. After hydrolysis, there are CH_3-CH_2OH singlets at 57.68 ppm (CH_2) and 18.32 ppm (CH_3). If transesterification were to occur, one should note the appearance of a Si(O-CD_2-CD_3) quintuplet at about 59.7 ppm at the beginning of the experiment. We never observed quintuplets in this case.

MEET 1

By using CD_3OD as alcohol and $Si(OC_2H_5)_4$, a fast transesterification could be expected. CD_3OD is characterized by a heptaplet at 49.0 ppm and $Si(OC_2H_5)_4$ by singlets at 60.20 ppm (-OCH_2-) and 18.40 ppm (-O-CH_2-CH_3). After 8 days, without adding NH_4OH, the spectrum did not change. This indicates that no substitution was detected. Adding NH_4OH does not enhance substitution; only the hydrolysis of Si-OCH_2CH_3 is detected by ^1H NMR. When 80% of $Si(OC_2H_5)_4$ is hydrolyzed, the ^{13}C NMR spectrum shows only the appearance of a CH_3CH_2OH peak at 58.26 ppm and the residue of a Si(-OCH_2CH_3) peak at 60.20 ppm.

These experiments demonstrate that alkoxy groups do not substitute from the solvent to the silicate. The hydrolysis and condensation of $Si(OR)_4$ in R'OH as alcohol correspond to the following equation:

$$Si(OR)_4 + 2\ H_2O \xrightarrow{R'OH} SiO_2 + 4\ ROH$$

The solvent acts only as a solvent and not as a reactant, because the alkoxy group is not substituted.

^1H NMR

The solvents used for these experiments were C_2D_5OD and CD_3OD.

Because the solvents are deuterated, they are not detected by NMR. Therefore, the NMR spectra are very clear (Fig. 1) and they present the Si-O-CH_2-CH_3 quadruplet (J = 7 Hz; 3.870, 3.835, 3.800, 3.765 ppm) and the Si-O-CH_2-CH_3 triplet (1.242, 1.207, and 1.172 ppm). To determine if water vapor contaminated the preparation, test tubes without NH_3 were monitored during several weeks. After 1 month, only 4–6% of the solution was hydrolyzed, depending on the solvent. This contamination was not taken into account in the following kinetic studies, when adding NH_3.

In these four experiments, the evolution of the spectrum is identical. After adding NH_3, the mobile O-H species are characterized by a line at 4.8, 4.9 ppm and do not interfere with other ^1H signals. The quadruplet for CH_2 silicate does not shift, except for a slight shoulder on each quadruplet line for experiments 3 and 4. The same phenomenon occurs for the -OCH_2CH_3 triplet. The CH_3CH_2O H molecules appear as a quadruplet (3.63–3.53 ppm) and a triplet (1.20–1.13 ppm).

The two quadruplets are in separate ranges. This simplifies the kinetic study. Intensities are integrated for each quadruplet, and the sum total is kept constant (+/−1%) during the reaction.

To discuss the kinetic laws, a and b designate respectively the initial concentrations in $Si(OC_2H_5)_4$ and in H_2O. Many equations can be used to follow both the hydrolysis and the condensation. The simplest way is to consider the overall reaction.

$$\underset{a}{Si(OC_2H_5)_4} + 2\ \underset{b}{H_2O} \xrightarrow{k} SiO_2 + 4\ C_2H_5OH$$

If x is the molar concentration in SiO_2, one can imagine a kinetic law, in which v is the rate of the reaction:

$$v = k(a - x)\ (b - 2x) = dx/dt = -d(a - x)/dt$$

Integration of this differential equation gives rise to:

$$\ln \frac{(b/2) - x}{a - x} = 2(b/2 - a)\ kt + \ln(b/2a)$$

If the water concentration is much greater than that of the silicate, we find the classical law:

Can. J. Chem. Downloaded from www.nrcresearchpress.com by 217.78.4.112 on 09/08/12
For personal use only.

Can. J. Chem. Downloaded from www.nrcresearchpress.com by 217.78.4.112 on 09/08/12
For personal use only.

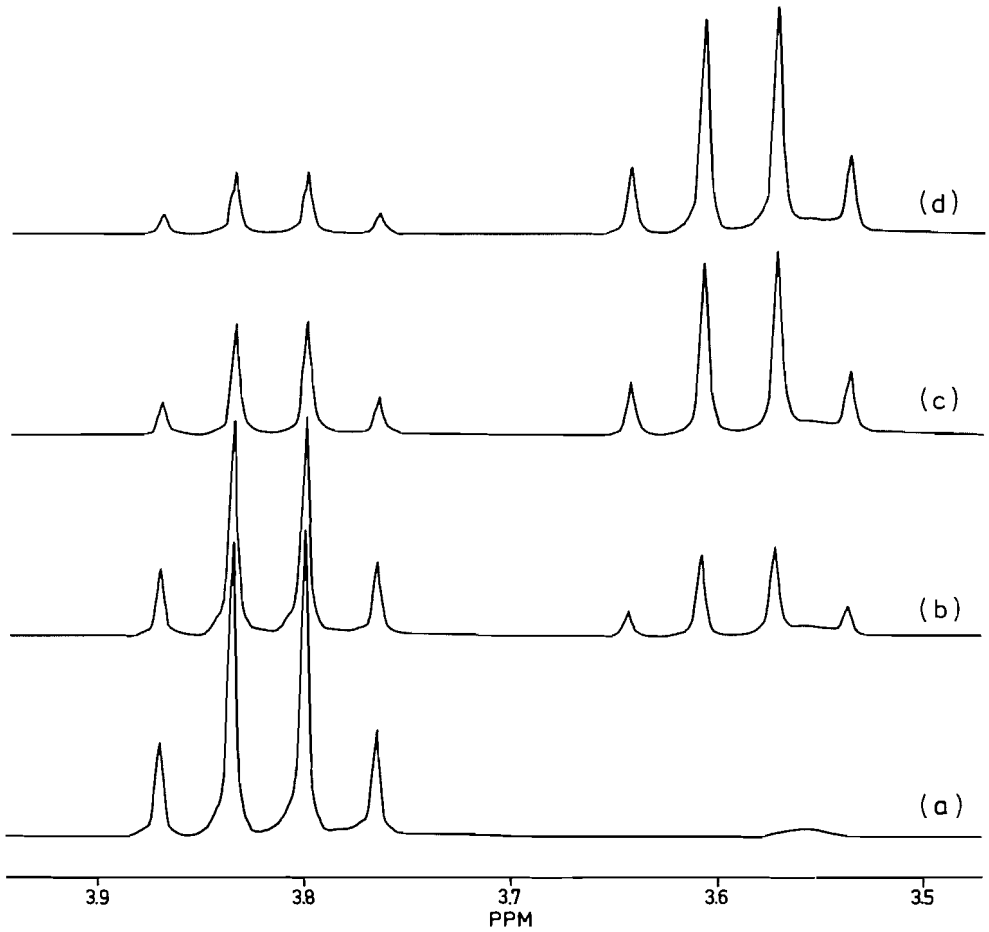

FIG. 1. ^{1}H NMR of $Si(OC_2H_5)_4$ hydrolysis in C_2D_5OD (ETET 1) after (*a*) 2 min; (*b*) 66 min; (*c*) 276 min; (*d*) 456 min.

$$\ln \frac{a}{a-x} \sim b'kt \quad \text{or}$$

$$\ln \frac{a-x}{a} \sim -b'kt \quad \text{with} \quad b' \sim b$$

As an example, Fig. 2 shows plots of the evolution of the silicate concentration (in ln units) as a function of time for the two experiments ETET 1 and ETET 2. In each experiment, more than 80% of the initial silicate has disappeared.

Two straight lines are obtained, which give rise to apparent rate constants $k' = 0.0033$ min^{-1} (ETET 1) and $k' = 0.043$ min^{-1} (ETET 2). The ratio of 12 between them should correspond to a mean ratio of 12 between the "mean" b' values. The initial b values are in the ratio 3.6 and the value 4.7 is obtained from the $(b\text{-}a)$ ratio.

For ETET 2 only, this approximation can be used ($b/a \sim 49$) and the linearity of the plot is a proof that the law is indeed of order 1 versus the silicate concentration.

In Fig. 2, we have plotted the comparison of the experiments ETET 1 and MEET 1 in which the concentrations of both silicate and water (and NH_3) are the same, the solvent being the only distinct parameter. The slopes of the lines show that, in CD_3OD, the apparent rate constant k' is three times greater than for C_2D_5OD (MEET 1, $k' = 9 \times 10^{-3}$ min^{-1}; ETET 1, $k' = 3.3 \times 10^{-3}$ min^{-1}). The k' values for all experiments are listed in Table 2.

As mentioned above and in Table 1, the ratio b/a is not very great for ETET 1, MEET 1, and MEET 2 and it could be four times smaller if we consider the ratio (H_2O/(Si-OC_2H_5 group).

We have imagined four reactions and the most probable kinetic laws:

[1] $\underset{a}{Si(OC_2H_5)_4} + \underset{b}{H_2O} \xrightarrow{k} SiOH(OC_2H_5)_3 + C_2H_5OH$

$$v = k(a\text{-}x)\,(b\text{-}x) = dx/dt$$

[2] $\underset{4a}{Si\text{-}OC_2H_5} + \underset{b}{H_2O} \xrightarrow{k} Si\text{-}OH + C_2H_5OH$

$$v = k(4a\text{-}x)\,(b\text{-}x) = dx/dt$$

[3] $\underset{a}{Si(OC_2H_5)_4} + 4\,\underset{b}{H_2O} \xrightarrow{k} Si(OH)_4 + 4\,C_2H_5OH$

(total hydrolysis)

$$v = k(a\text{-}x)\,(b\text{-}4x) = dx/dt$$

[4] $\underset{a}{Si(OC_2H_5)_4} + 2\,\underset{b}{H_2O} \xrightarrow{k} SiO_2 + 4\,C_2H_5OH$

hydrolysis + condensation

$$v = k(a\text{-}x)\,(b\text{-}2x) = dx/dt$$

or

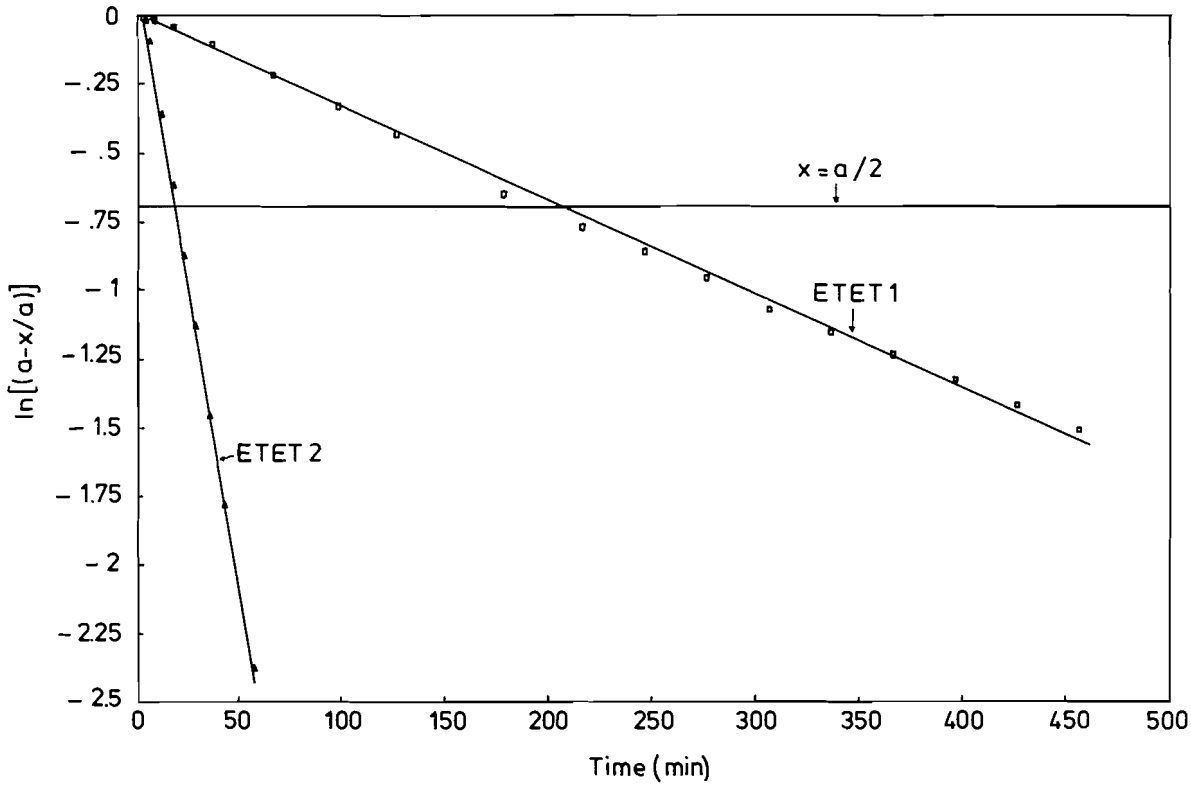

FIG. 2. Evolution of the ethyl silicate concentration during NH_3–H_2O hydrolysis in C_2D_5OD:$[H_2O]/[Si\text{-}OC_2H_5]$ = □, 12.3; Δ, 1.025.

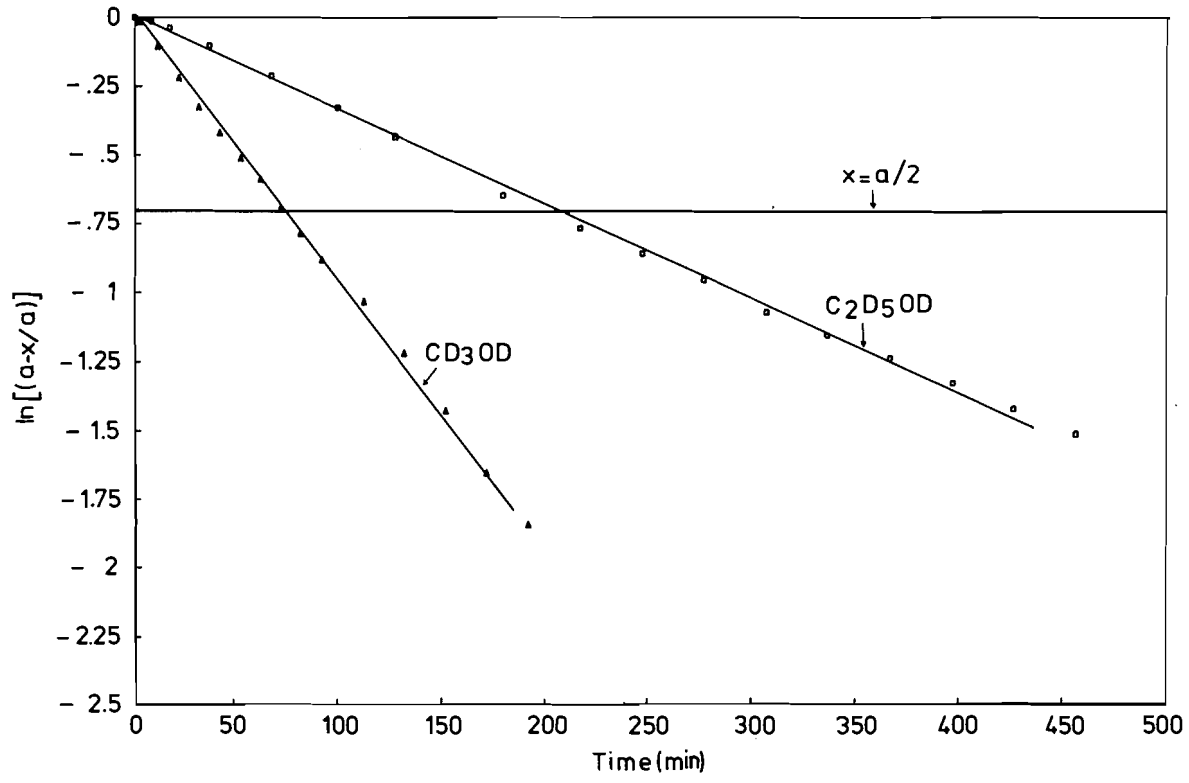

FIG. 3. Evolution of the ethyl silicate concentration during hydrolysis by NH_3–H_2O in Δ, CD_3OD and □, C_2D_5OD:$[H_2O]/[Si\text{-}OC_2H_5]$ = 1.025).

Can. J. Chem. Downloaded from www.nrcresearchpress.com by 217.78.4.112 on 09/08/12
For personal use only.

TABLE 2. Kinetic results of $Si(OC_2H_5)_4$ hydrolysis

Experiment	Solvent	$Si(OC_2H_5)$ ($M\ L^{-1}$)	$[H_2O]/[Si\text{-}OR]$	k' (min^{-1})	k $L\ mol^{-1}\ min^{-1}$
ETET1	C_2D_5OD	0.40	1.025	0.0033	0.0028
ETET2	C_2D_5OD	0.12	12.3	0.0430	0.0075
MEET1	CD_3OD	0.40	1.025	0.0096	0.0075
MEET2	CD_3OD	0.20	2.15	0.0134	0.0079

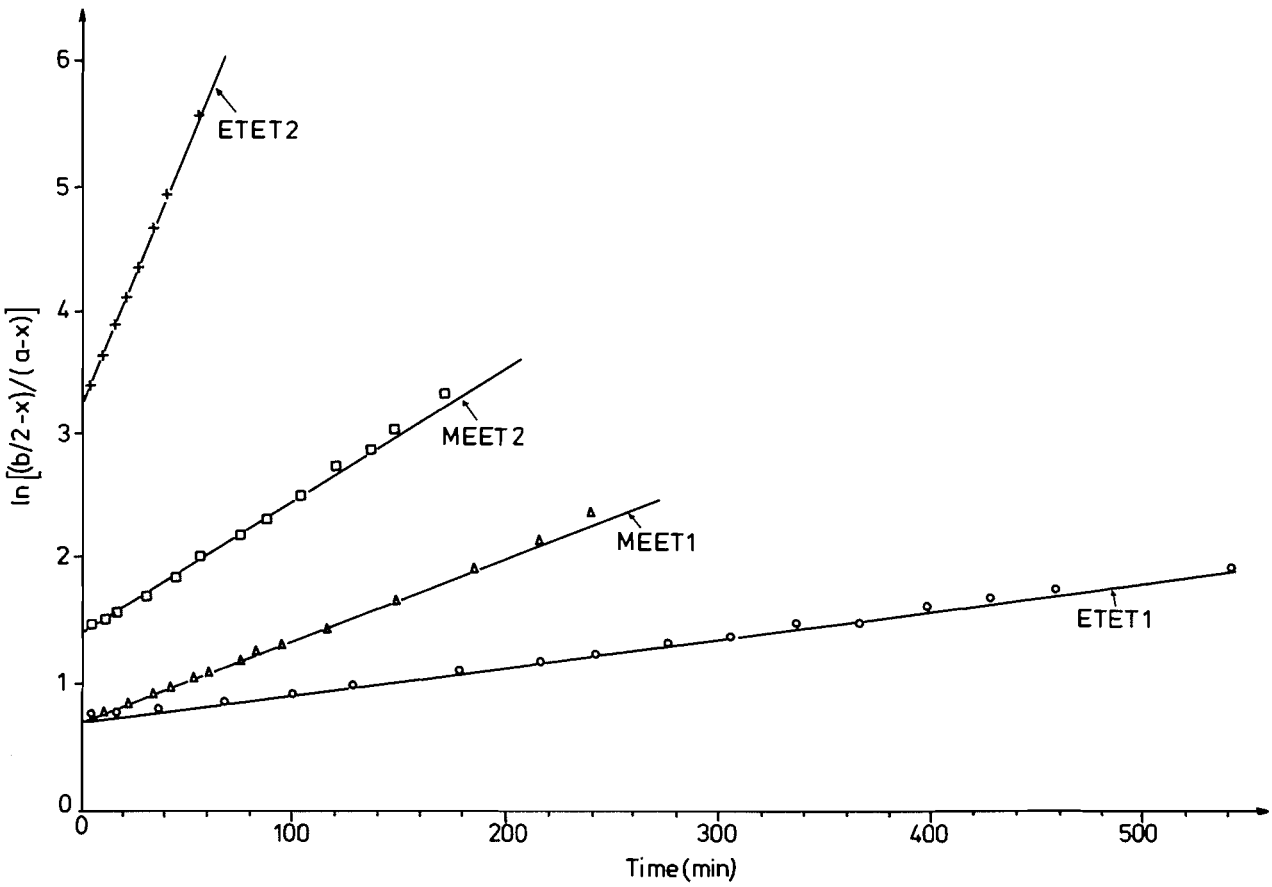

FIG. 4. Plots of $\ln[(b/2\text{-}x)/(a/x)]$ as a function of time for the four experiments corresponding to the global equation: $Si(OC_2H_5)_4 + 2H_2O \rightarrow SiO_2 + 4C_2H_5OH$. $v = k[Si(OC_2H_5)_4]\,[H_2O]$; $a = [Si(OC_2H_5)_4]_{initial}$; $b = [H_2O]_{initial}$.

$$v = k(a\text{-}x)\,(b\text{-}2x)^2 = dx/dt.$$

We have plotted, for these five kinetic laws, the evolution of a term that is linear versus time (example: case [1]: $\ln[(b\text{-}x)/(a\text{-}x)] = (b\text{-}a)kt + \ln(b/a)$.

The best linearity for the four experiments was obtained by using eq. [4] and the kinetic law $v = k(a\text{-}x)\,(b\text{-}2x) = dx/dt = -d(a\text{-}x)/dt$.

The four plots are collected in Fig. 4, in which $\ln[(b/2\text{-}x)/(a\text{-}x)]$ is plotted as a function of time; the mean slope of each fitted straight line corresponds to $2(b/2\text{-}a)k$. These values of k are listed in the last column of Table 2.

The experimental equation $v = k(a\text{-}x)\,(b\text{-}2x)$ followed by NMR measurements proves that the overall reaction [4] is not the elementary mechanism. It corresponds surely to a second-order hydrolysis reaction such as [1]. The decrease in silicate concentration, as measured by NMR, is slow compared to further condensation steps that release water.

Discussion

The solvent plays a considerable role. Hydrolysis rate increases by a factor of 3 when CD_3OD is used instead of C_2D_5OD.

We would expect two separate steps for Si-OCH-2-CH_3: (*i*) hydrolysis leading to monomeric or oligomeric Si-OH species; (*ii*) condensation of these hydrolyzed species leading to siloxane Si-O-Si bridges and to the growth of silica particles.

But at mid-stage, the liquid is already milky. Therefore, during the synthesis of homodispersed silica particles ($Si(OC_2H_5)_4 + C_2D_5OD$), particles grow during the hydrolysis step.

The presence of large particles ($\phi \sim 50$ nm) leading to a milky aspect is accompanied by nonhydrolyzed Si-O-CH_2-CH_3 groups. The Ostwald (13) ripening model, described by Fischmeister and Grimwall (14), implies that nuclei are

Can. J. Chem. Downloaded from www.nrcresearchpress.com by 217.78.4.112 on 09/08/12
For personal use only.

formed as they grow. As particles smaller than a critical size dissolve, they are surrounded by a zone of excess solute that finds its way to particles larger than r^*. This model does not seem in accordance with our experimental results in which large particles exist with Si-OR groups. Condensation and particle growth occur at the same time as hydrolysis.

One can suppose that condensation reactions leading to dimers, polymers, and particles occur very rapidly after SiOH groups are formed by hydrolysis. The hydrolysis rate is therefore the slow step, but the water concentration does not follow eq. [3] for hydrolysis because condensation gives rise to water. If the condensation rate was very slow, the kinetic law should follow reaction [3]. This last model gives rise to curves instead of straight lines, which suggests that condensation is the fast step. A similar point of view has been developed (8) in the case of the hydrolysis of $Si(OCH_3)_4$ in alkaline media (KOH 1 M) because the ^{29}Si NMR signals do not display any intermediate molecules which apparent Si-OH group. Even if the final state in basic media when $Si(OCH_3)_4$ is used is a gel, which we have also seen in kinetic experiments with much greater rates than for $Si(OC_2H_5)_4$, and even if homodispersed SiO_2 particles are obtained when $Si(OC_2H_5)_4$ is used as the starting material, this experiment suggests that, in both cases, condensation is the fast step, which enables one to give evidence of nonhydrolyzed Si-OC_2H_5 groups in silica particles. Even after a long time, such groups are still present and are only broken by a thermal treatment at 400°C (5).

Increase of the rate constant k by increasing the ratio H_2O/silicate in ETET 2 could result from differences in growth kinetics of the silica microparticles, because it has been proven[3] that smaller concentrations of NH_3 and H_2O give rise to smaller particles at the end of the experiments. The heterogeneity of these systems may therefore contribute to different rate constants. Nevertheless, we have definitely established that the role of the solvent (substitution of CD_3CD_2OD by CD_3OD) strongly modifies the kinetics law although we have proved that ethyl silicate does not lead to methyl silicate in CD_3OD by transesterification. The role of the solvent should involve the ionization of OH^- in these NH_3–H_2O solutions. The speciation of the protonic groups (OH^-, NH_3, H_2O) can be different in C_2D_5OD and CD_3OD, arising from different dielectric constants (ε methanol ~ 33; ε ethanol ~ 24); the viscosity of the solvent could be another factor explaining this behaviour difference (20°C; $\eta_{CH_3OH} \sim 6 \times 10^{-4}$ Pa s; $\eta_{CH_3CH_2OH} \sim 12 \times 10^{-4}$ Pa s).

[3]E. El Rhess, I. El Bakali, and R. Mercier. Manuscript submitted for publication.

Conclusion

The solvent affects the kinetics of hydrolysis. CD_3OD is more effective than C_2D_5OD. ^{13}C NMR demonstrates that no transesterification occurs between the silicate and the alcohol. $Si(OC_2H_5)_4$ produces stable colloidal systems with SiO_2 particles in the 0.1–0.5 μm range. The relative rates of hydrolysis and condensation differ for both systems; the condensation rate is much faster than the second-order hydrolysis reaction rate. A complete ^{29}Si NMR study in alkaline media should provide further information about hydrolysis and condensation.

1. W. Stöber, A. Fink, and E. Bohn. J. Colloid Interface Sci. **26**, 62 (1968).
2. T. Shimohira and N. Tomuro. Funtai Oyali Funmatsuyakin, **4**, 19 (1976).
3. K. Shimada, Y. Fukushige, Y. Hirata, and K. Nishimuta. Kogoshina Daigku Kogakubu Kenkya Mokoku, **26**, 53 (1984).
4. G. G. Tan, B. D. Bowen, and N. Epstein. J. Colloid Interface Sci. **118**, 290 (1987).
5. E. El Rhess. Doctoral Thesis, Université de Franche-Comté. 1988.
6. C. C. Lin and J. D. Basil. Mater. Res. Soc. Symp. Proc. **73**, 585 (1986).
7. I. Artaki, M. Bradley, T. W. Zerda, and J. Jonas. J. Phys. Chem. **89**, 4399 (1985).
8. C. A. Balfe and S. L. Martinez. Mater. Res. Soc. Symp. Proc. **73**, 261 (1986).
9. W. G. Klemperer, V. V. Mainz, and D. M. Millar. Mater. Res. Soc. Symp. Proc. **73**, 3 (1986).
10. R. A. Assink and B. D. Kay. Mater. Res. Soc. Symp. Proc. **32**, 301 (1984).
11. R. A. Assink and B. D. Kay. J. Non-Cryst. Solids, **99**, 359 (1988).
12. B. D. Kay and R. A. Assink. Mater. Res. Soc. Symp. Proc. **73**, 157 (1986).
13. W. Ostwald. Z. Phys. Chem. **34**, 495 (1900).
14. M. Fischmeister and G. Grimvall. Mater. Sci. Res. **6**, 119 (1973).

Can. J. Chem. Downloaded from www.nrcresearchpress.com by 217.78.4.112 on 09/08/12
For personal use only.

Electron thermalization distances and free-ion yields in dense gaseous and liquid benzene

NORMAN GEE AND GORDON R. FREEMAN[1]

Chemistry Department and Radiation Research Centre, University of Alberta, Edmonton, Alta., Canada T6G 2G2

Received December 16, 1991

NORMAN GEE and GORDON R. FREEMAN. Can J. Chem. **70**, 1618 (1992).

Electron thermalization has been studied in gaseous and liquid benzene at $4.1 \leq d/\text{kg m}^{-3} \leq 878$ (temperatures 295–560 K) using measurements of the free-ion yield G_{fi}^{E} as a function of electric field strength E and temperature T. The measured (G_{fi}^{E}, E) values at each T were compared to those calculated using an extended Onsager model. Assumption of a three-dimensional Gaussian distribution of secondary electron thermalization distances YG resulted in too large a field dependence. The Gaussian with the small added tail, YGP, gave the correct dependence. Values of the yield extrapolated to zero field, G_{fi}^{0}, and of the most probable thermalization distance b_{GP} were obtained. Variation of the density-normalized distance $b_{\text{GP}}d$ with reduced density d/d_{c} (d_{c} = critical fluid density) was expected to be similar to that in ethene, due to the π-electrons in the two compounds. Instead, it was similar to that in ethane. Throughout the liquid range, epithermal electrons were de-energized less efficiently than in the gas at $d < 0.5\ d_{\text{c}}$ where the benzene molecules are further apart. As the density increases above $2\ d_{\text{c}}$ the values of $b_{\text{GP}}d$ decreased as in other hydrocarbons, rather than like those in hexafluorobenzene, which increased sharply. Dielectric constants were also measured up to 560 K.

NORMAN GEE et GORDON R. FREEMAN. Can. J. Chem. **70**, 1618 (1992).

On a étudié la thermalisation électronique en opérant en phase gazeuse et dans le benzène liquide, à $4{,}1 \leq d/\text{kg m}^{-3} \leq 878$ (températures de 295 à 560 K), en faisant appel à des mesures de rendement en ions libres, G_{fi}^{E}, en fonction de la force E du champ électrique et de la température T. On a comparé les valeurs mesurées (G_{fi}^{E} et E) à chaque température avec celles calculées en utilisant le modèle élargi de Onsager. En faisant l'hypothèse qu'il existe une distribution gaussienne tridimensionnelle des distances YG de thermalisation des électrons secondaires, on obtient une dépendance trop importante par rapport au champ. La gaussienne à laquelle on a ajouté une petite traînée conduit à la bonne dépendance. On a obtenu les valeurs des rendements extrapolés jusqu'à un champ nul, G_{fi}^{0}, ainsi que la distance de thermalisation la plus probable, b_{GP}. À cause de la présence d'électrons π dans les deux systèmes, on s'attendait à ce que la variation de la distance normalisée pour la densité, $b_{\text{GP}}d$, en fonction de la densité réduite, d/d_{c}(d_{c} = densité fluide critique) soit semblable à celle de l'éthène. Toutefois, elle est semblable à celle de l'éthane. Dans toute la phase liquide, les électrons épithermiques perdent leur énergie moins facilement que dans le gaz, à $d < 0{,}5\ d_{\text{c}}$, où les molécules de benzène sont plus éloignées les unes des autres. Lorsque la densité augmente au dessus de $2\ d_{\text{c}}$, les valeurs de $b_{\text{GP}}d$ diminuent comme dans les autres hydrocarbures plutôt que comme dans l'hexafluorobenzène dans lequel elles augmentent rapidement. On a aussi mesuré les constantes diélectriques jusqu'à 560 K.

[Traduit par la rédaction]

I. Introduction

Under irradiation by γ-rays or high-energy electrons, some molecules of a fluid ionize, ejecting secondary electrons with excess kinetic energy. These secondary electrons move away from their sibling cations, undergoing in the course of their flight energy-transfer collisions with the surrounding fluid molecules, and eventually become thermalized at distances y from the cations (1*a*). The thermalization distances have a distribution $F(y)$. The shape of $[F(y),y]$ can be examined using measurements of the free ion yield G_{fi}^{E} over wide ranges of applied field strength E and temperature T, because the shape of $F(y)$ affects the shape of the (G_{fi}^{E}, E) curve at each T(1*b*).

For over 100 liquids the most suitable form for $F(y)$ was found to be a hybrid function that is mainly a three-dimensional Gaussian, with a power tail that represents the outermost 5% of electrons (1*c*). This function, designated YGP, will be discussed further in Sect. III. The most probable thermalization distance b_{GP} is determined largely by the ability of the fluid to de-energize electrons from energies of ~200 zJ to ~10 zJ (160 zJ = 1 eV; z = zepto = 10^{-21});[2] stronger scattering of the electrons at these energies produces a smaller b_{GP} (2, 3). The thermalization distance is often inversely proportional to the mass density d (1*c*, 3), so variations in bd can be used to assess differences in the ability of fluids to de-energize (thermalize) epithermal electrons. It is assumed that any effects of temperature (other than that on the densities of liquids and vapors at equilibrium) are small. This assumption is supported by measurements in the *n*-alkanes: (*a*) In moderately dense gases of methane, ethane, propane, and *n*-butane away from the critical region, so that gas molecules were too far apart for conduction band formation, values of $b_{\text{GP}}d$ were constant, $(5.5 \pm 0.2) \times 10^{-6}$ kg m^{-2}, over ~4-fold variation in density, although the temperature ranges were quite different (158–183 K in methane compared with 365–409 K in *n*-butane) (4, 5). (*b*) In liquid *n*-undecane and in liquid *n*-tetradecane, $b_{\text{GP}}d$ values were constant (Δ_{av} ~3%) as densities were decreased ~25% and temperatures were concomitantly increased from 296 to 472 and 506 K respectively (6).

Electron thermalization has recently been studied in hexafluorobenzene (7). As the fluid density was increased from $0.5\ d_{\text{c}}$, values of $b_{\text{GP}}d$ increased monotonically. An especially sharp increase occurred in the dense liquid at $d > 2d_{\text{c}}$. This behavior is somewhat different from that in most hydrocarbons (1*c*). Measurements in its hydrocarbon analog, benzene, have been limited to $T < 370$ K ($d > 2.6\ d_{\text{c}}$), and reported free-ion yields have differed by up to 1.8-fold (3, 8).

[1]Author to whom correspondence may be addressed.

[2]H. Preston-Thomas, private communication. The following prefixes were accepted by the Comité International des Poids et Mesures in Oct., 1990 to be put forward to the Conférence Générale des Poids et Mesures for adoption in Oct., 1991: 10^{-21}, zepto, z; 10^{21}, zetta, Z; 10^{-24}, yocto, y; 10^{24}, yotta, Y.

Can. J. Chem. Downloaded from www.nrcresearchpress.com by 217.78.4.112 on 09/08/12
For personal use only.

Can. J. Chem. Downloaded from www.nrcresearchpress.com by 217.78.4.112 on 09/08/12
For personal use only.

In this work free-ion yields are given at densities of 4.1–878 kg m^{-3} (temperatures 295–560 K). Values of b_{GP} were then obtained using the extended Onsager model (1*b*), and thermalization of epithermal electrons in benzene, C_6H_6, is used to bridge the comparison of thermalization in hydrocarbons to that in hexaflurobenzene, C_6F_6.

II. Experimental

Materials and sample preparation

Benzene from Aldrich (HPLC grade, 99.9+%) was received stored under nitrogen. The liquid was poured into a storage bulb attached to a grease-free glass vacuum line, closed from the atmosphere, and degassed using two freeze–pump–thaw cycles. The liquid was then transferred, in turn, into storage bulbs containing sulfuric acid, lithium aluminum hydride, and sodium–potassium alloy. To effect the transfers, the source bulb was surrounded with a water bath at ~315 K and the receiver bulb was cooled using ice/water slurry. The benzene sample was stirred slowly on the acid for 1 day, on the $LiAlH_4$ for 4 days, and on the Na–K alloy for 7 days. The liquid was then held on the alloy until transfer to the conductance cell.

Apparatus and techniques

Details of the conductance cells, temperature control and measurement, irradiation and dosimetry procedure, and data collection are in, or cited in, refs. 6 and 7.

Physical properties

Values of liquid densities were compiled from refs. 9–13. The agreement between data sets was ~0.1% at $T < 380$ K and ~0.3% at $T < 559$ K. It might be noted that liquid densities reported in ref. 14 (not used here) were 0.9% higher than those in the other works. Critical fluid parameters reported by different sources varied widely but most values (refs. 9–14 and others cited by them) are within the limits $d_c = 303 \pm 3$ kg m^{-3} at $T_c = 562.3 \pm 0.4$ K. Vapor densities reported in refs. 9, 11, and 14 agreed within ~2%. Exceptions were densities from ref. 11 at 379–433 K, which oscillated about the values of refs. 9 and 14, and densities reported in ref. 14 at $T > 478$ K, which were up to 20% lower than those of refs. 9 and 11 at the same temperatures. The discordant values were not used.

Relative dielectric permittivity ε values reported in the literature (15–18) did not cover the complete range of the present experimental conditions, so values were measured as described in ref. 19. The most recent works concentrated on measurements at constant temperature and increasing density (17, 18). The most extensive earlier measurements in the liquid along the coexistence curve reported permittivities up to 473 K (15). The present measurements agreed with these values within 0.3%. Quadratic interpolation of the present data gave $\varepsilon = 2.274$ at 298.15 K, which is also the value recommended by the National Bureau of Standards (U.S.A.) at that temperature (20).

III. Results and discussion

Electron mobility

The radiation-induced electron conductance transient (ECT) was measured at 295 K as a check on the purity of the liquid. At $0.4 \leq E/\text{MV m}^{-1} \leq 1.3$ the ECT signals decayed with a half life $t_{1/2} = 2.2$ μs. Analysis by the conductance method (Appendix of ref. 19) gave the electron mobility $\mu_0 = 1.1 \times 10^{-5}$ m^2 V^{-1} s^{-1}, in reasonable agreement with previously reported values, 1.1×10^{-5} (21), 1.2×10^{-5} (22), and 1.4×10^{-5} m^2 V^{-1} s^{-1} (23).

Electron thermalization and the extended Onsager model

The passage of a high-energy (> 1 fJ) electron through a liquid results in a widely spaced sequence of activated microzones with diameters of a few nanometers and separated by a few hundreds of nanometers (1*d*). Each microzone contains one or more spatially correlated ion-electron pairs. (We previously called these microzones by the traditional jargon name "spur." The name microzone (1) seems to be clearer to nonspecialists.) The ion-electron separation distance y at which the electron thermalizes determines the probability that the electron will be drawn back to the cation to recombine (geminate neutralization), or will escape the cation to diffuse freely in the bulk medium (free-ion formation). The free ions can be collected at electrodes and measured. The process can be represented as:

[1] $M \rightsquigarrow [M^+ + e^-]$

[2] $[M^+ + e^-] \rightarrow M$ (geminate neutralization)

[3] $[M^+ + e^-] \rightarrow M^+ + e^-$ (free-ion formation)

[4] $\left.\begin{matrix} M^+ \xrightarrow{E} \\ e^- \xrightarrow{E} \end{matrix}\right\}$ electrodes

in which the wavy arrow indicates ionization and the square brackets indicate Coulombic attraction between the electron and the ion that is not negligible in comparison with k_BT. The total yield G_{tot} of reaction [1] (expressed as the number of ion pairs formed per 16 aJ (100 eV) of energy absorbed by the fluid) can be measured chemically in the liquid or electrically in the gas phase. For ion pairs formed in dense media by X or β rays, the competition between eqs. [2] and [3] was first treated by Onsager (1*d*, 24). The competition depends on the relative dielectric permittivity, temperature, and collecting field E as well as on y. An extended Onsager model expressed the free-ion yield as (1*d*)

$$[5] \qquad G_{fi}^{E} = G_{tot} \int_0^\infty F(y)\phi_{fi}^0(y)[1 + f(\varepsilon, E, y, T)]dy$$

where $\phi_{fi}^0(y)$ is the probability that an ion pair that becomes thermalized at a separation y will separate to form free ions when $E = 0$, $f(\varepsilon, E, y, T)$ is a field enhancement term, and $F(y)$ is the distribution of thermalization distances. Explicit forms for these terms and detailed discussions of them are given in ref. 1*d*, and in shortened form in refs. 5, 21, and 25. The most commonly used forms of $F(y)$ are based on a Gaussian or an exponential (1*b*, 3, 25–33). Comparison of free-ion yields calculated from eq. [5] with measured yields allows extrapolation to $E = 0$ to give G_{fi}^0, and gives information about $F(y)$ and thereby about electron energy-transfer interactions with the fluid.

In most liquids where both E and T have been varied over wide ranges a modified Gaussian (see YGP below) is most suitable, whereas at a single T more than one $F(y)$ might provide a fitting to the set of $[G_{fi}^E, E]$ data (25, 27–29). For example, either a one-dimensional exponential or a three-dimensional Gaussian fits the data from neopentane at 295 K (27). The problem was to find an $F(y)$ distribution that would fit the largest number of systems over the widest range of conditions.

The calculation of yields using eq. [5] also requires the value of G_{tot}. Most measurements were done in liquids below their normal boiling points, and often near 295 K. In such liquids, constant values of G_{fi}^E at high field identifiable with G_{tot} were not obtained even at $E \sim 20$ MV m^{-1} (29). Application of yet higher fields causes the ionization pulse to trigger dielectric breakdown. Thus G_{tot} can be used as a free parameter, but in most cases the low-density gas value was

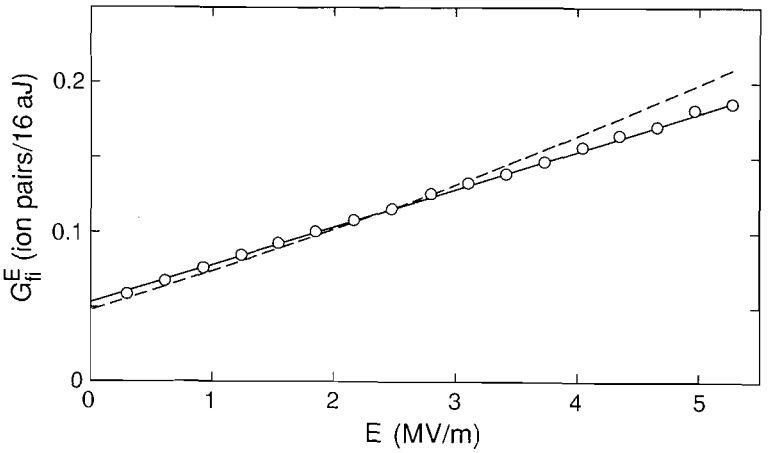

FIG 1. Free-ion yields in liquid benzene at 295 K and 878 kg m^{-3} plotted against electric field strength. ○, measurements. ——— and — — — were calculated from eq. [5], using G_{tot} = 4.3 (33) and $F(y)$ = YGP with b_{GP} = 3.4 × 10^{-9} m, and $F(y)$ = YG with b_G = 4.1 × 10^{-9} m, respectively.

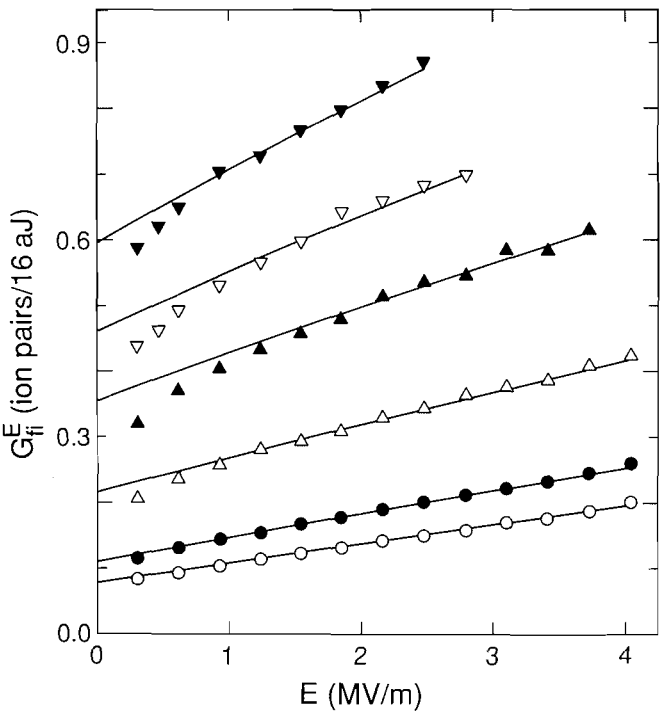

FIG. 2 Free-ion yields in liquid benzene against electric field strength at (T/K, d/kg m^{-3}): ○ (330, 841), ● (367, 798), △ (443, 703), ▲ (503, 609), ▽ (534, 530), and ▼ (556, 430). Lines were calculated from eq. [5], using G_{tot} = 4.3, $F(y)$ = YGP, and b_{GP} of Table 1.

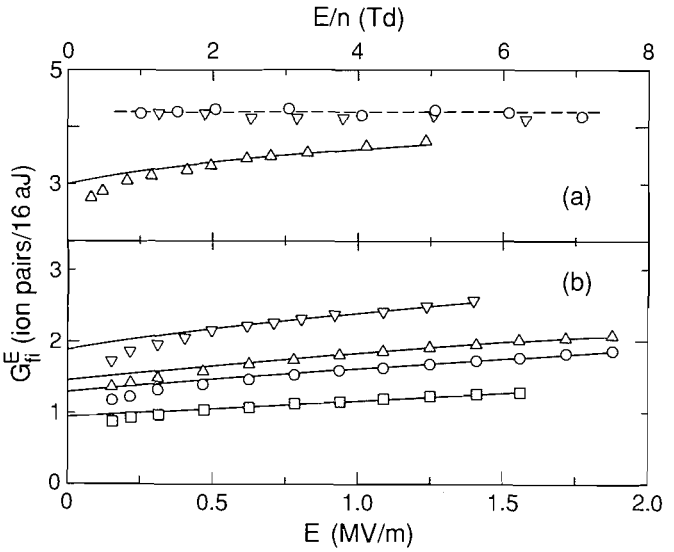

FIG. 3. Free-ion yields in gaseous benzene at (T/K, d/kg m^{-3}): (*a*) ○ (367, 4.1), ▽ (386, 6.5), and △ (453, 25) against electric field strength normalized by number density (Td = 10^{-21} V m^2 $molecule^{-1}$); (*b*) ▽ (514, 73), △ (535, 111), ○ (549, 148), and □ (560, 227). Solid lines calculated as in Fig. 2. Dashed line indicates low density gas G_{tot} = 4.3 (32).

used. Reference 1*f* and the entire Chap. 2 of ref. 1 should be read to understand this problem. If the value used for G_{tot} were 20% too small, the estimated value of b_{GP} would be 5–10% too large.

Measurements

The free-ion yield in liquid benzene at 295 K increases linearly with increasing field strength (Fig. 1). Using eq. [5] and taking $F(y)$ to be a three-dimensional Gaussian, designated YG,

$$[6] \qquad F(y) = \left(\frac{4y^2}{\pi^{1/2} b_G^3}\right) \exp\left(-\frac{y^2}{b_G^2}\right),$$

and G_{tot} = 4.3 (34), the best-fit value b_G = 4.1 × 10^{-9} m (where b_G is the dispersion parameter for the distribution and the most probable value of y) gave the dashed line in Fig. 1. The calculated field effect is greater than that observed experimentally. This means that $F(y)$ should extend more gradually to higher values of y than YG. The distribution YGP does this (1*b*):

$$[7] \qquad F(y) = \begin{cases} 0.96\ \text{YG}, & y < 2.4\ b_{GP} \\ 0.96[\text{YG} + 0.5\ (b_{GP}^2/y^3)], & y > 2.4\ b_{GP} \end{cases}$$

where b_{GP} has replaced b_G. This distribution with b_{GP} = 3.4 × 10^{-9} m and eq. [5] gave the solid line in Fig. 1. The extrapolated value for G_{fi}^0 is 0.053, which is the same as that measured directly in ref. 3. Hence the present set of measurements (examples of which are given in Figs. 2 and 3) was

Can. J. Chem. Downloaded from www.nrcresearchpress.com by 217.78.4.112 on 09/08/12
For personal use only.

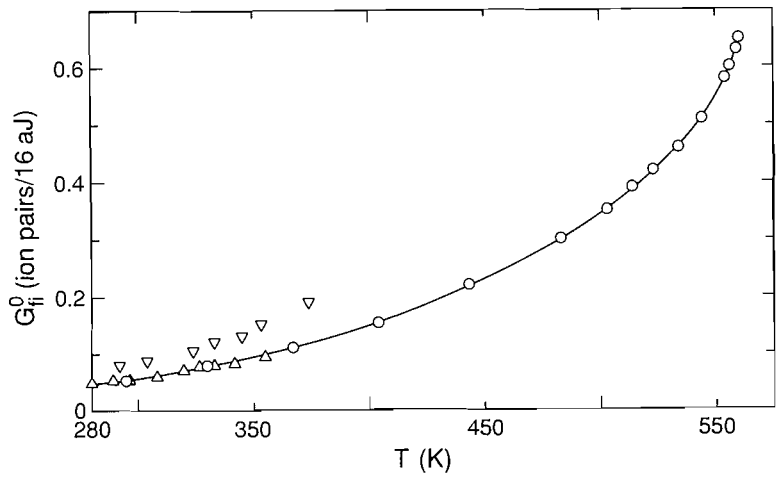

FIG. 4. Temperature dependence of free-ion yields at zero field strength: ○, Table 1; △, ref. 3; ▽, ref. 21.

TABLE 1. Summary of results

T (K)	d^a (kg m^{-3})	ε^b	G_{fi}^{0c}	$b_{GP}{}^c$ (nm)
		Liquid		
295	878	2.28	0.053	3.4
330	841	2.21	0.077	3.6
367	798	2.14	0.110	3.9
404	757	2.07	0.154	4.2
443	703	1.98	0.22	4.6
483	647	1.88	0.30	5.2
503	609	1.82	0.35	5.6
514	580	1.78	0.39	5.9
523	557	1.75	0.42	6.2
534	530	1.70	0.46	6.5
544	497	1.67	0.51	6.8
554	450	1.62	0.58	7.5
556	430	1.61	0.60	7.7
559	405	1.59	0.63	8.0
560[d]	390[d]	1.58	0.65	8.2
		Gas		
560[d]	227[d]	1.19	0.94	14.2
558	198	1.18	1.02	15.3
555	176	1.17	1.08	16.3
549	148	1.16	1.29	19.5
545	135	1.15	1.36	20.8
535	111	1.12	1.45	24.2
525	90	1.10	1.65	28.7
514	73	1.08	1.88	34.2
493	50	1.06	2.27	48.3
453	25	1.03	3.00	101
386	6.5	1.007		
367	4.1	1.004		

[a]Mass density.
[b]Static relative permittivity.
[c]Free ion yield at $E = 0$ and most probable thermalization distance of $F(y)$ = YGP. Assumed $G_{tot} = 4.3$, the experimental value in the low density gas (32). Yields are in ion pairs/16 aJ (100 eV).
[d]Critical fluid values are $T_c = 562.3 \pm 0.4$ K and $d_c = 303 \pm 3$ kg m^{-3} (9–14).

fitted using eq. [5] with $F(y)$ = YGP. The required values for b_{GP} and extrapolated G_{fi}^0 values are summarized in Table 1. In Fig. 4 the present values of G_{fi}^0 are compared to those of refs. 3 and 21. Agreement with ref. 3 is within an average deviation of 3%. Values from ref. 21 were too high, likely due to inaccurate dosimetry (6).

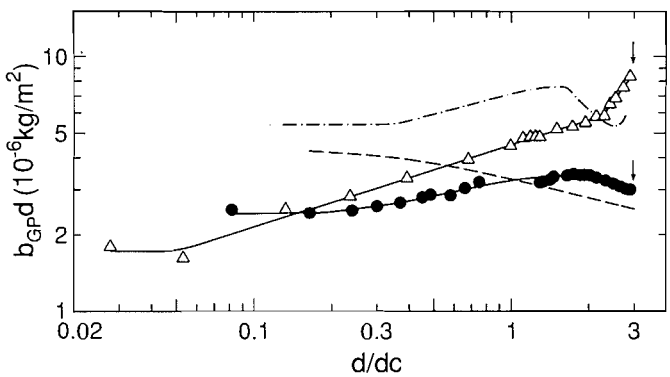

FIG. 5. Product of most probable thermalization distance and density, $b_{GP}d$, plotted against d/d_c for electrons in ethane (ref. 4, — · —), ethene (ref. 5, — — —), benzene (●), and hexafluorobenzene (ref. 7, △). Solid lines are visual aides. Arrows indicate liquid densities at freezing points.

It might be noted that the physical basis of $F(y)$ = YGP is the same as that of the Gaussian $F(y)$ = YG. Over 90% of the ion-pair thermalization distances are in the Gaussian core of YGP (1*b*). The tail is a correction to the Onsager model, which assumes that only one ion pair is formed in each microzone. This is the case in ~75% of the microzones but in ~15% two ion pairs are formed and in ~10% three or more are formed (1*b*). In these multipair microzones, the innermost electrons of the distribution are rapidly drawn back to the cluster of positive ions at the center (1*d*). Only one cation and the outermost electron remains. It is the separation distances of these surviving ion pairs that is represented by the tail of YGP. The inverse cube dependence of the tail was determined empirically by varying x in tails of y^{-x}. Examples of functions y^{-x} are given in refs. 1*b* and 26. In liquids where the values of ϕ_{fi}^0 are low, x converged towards 3. The crossover point $y > 2.4\ b_{GP}$ is related to the percent of contribution of the tail to $F(y)$ and affects d G_{fi}^E/dE. This point was also obtained experimentally. Hence both the power of the tail portion and the crossover point are simply empirical parameters.

In Fig. 3*a* the yields are shown against E/n(n = number

Can. J. Chem. Downloaded from www.nrcresearchpress.com by 217.78.4.112 on 09/08/12
For personal use only.

density), although E rather than E/n appears in the field enhancement term of eq. [5]. The reason is that in lower density gases the interval τ between collisions becomes significant because the space between molecules becomes large. The electrons are accelerated by the field during this time and the energy gained from the field depends on E/n (35). Hence in lower density gases the density-normalized field strength is a more suitable representation of the field strength.

Thermalizing ability

The ability of the fluid to de-energize epithermal electrons (thermalizing ability) is inversely proportional to $b_{GP}d$. In Fig. 5 values of $b_{GP}d$ are plotted against d/d_c for electrons in ethane (4), ethene (5), benzene (Table 1), and hexafluorobenzene (7). The lower $b_{GP}d$ values in ethene than in ethane indicate that the carbon-carbon π-bond in ethene de-energizes hot electrons more readily than does the carbon-carbon σ-bond in ethane. In ethene the thermalizing ability of the fluid increases monotonically with density. In ethane the behavior is complex.

Benzene molecules contain π-bonds. Hence it might be expected that the $b_{GP}d$ curve would be similar to that in ethene. Instead the variation of $b_{GP}d$ with d/d_c resembled that in ethane (Fig. 5). At liquid densities the $b_{GP}d$ values in benzene were larger than those in liquid ethene. The ability of benzene molecules to de-energize hot electrons is less when the molecules are close together than when they are far apart.

Replacing all of the hydrogen atoms in benzene with fluorine atoms decreases $b_{GP}d$ in the low-density gas, but increases it in the dense gas and liquid (Fig. 5). The curves for C_6F_6 and C_6H_6 are qualitatively similar up to $d \approx 2d_c$. However, as the density is further increased the molecules are squeezed closer together, and $b_{GP}d$ values in hexafluorobenzene increase sharply while those in benzene decrease as in other hydrocarbons. This is not a freezing point transition. In hydrocarbons the decrease in $b_{GP}d$ with increasing d/d_c has been attributed to stronger short-range interactions of the electron with the repulsive cores of the molecules, since the spaces between molecular cores are being decreased (1*e*, 25). In hexafluorobenzene, it might be that as the molecules are being squeezed together the fluorine atoms form a separate conduction band from that of the aromatic rings (36), so that the thermalizing electrons can travel further away from their cations before losing their excess kinetic energy. One might expect similar behavior in hexamethylbenzene. Unfortunately, that high-melting-point compound (T_m = 440 K) is difficult to purify sufficiently to obtain measurements over a wide range of temperatures (21).

Acknowledgement

We thank the staff of the Radiation Research Centre for providing and maintaining the experimental facilities.

1. G. R. Freeman. *In* Kinetics of nonhomogeneous processes. *Edited by* G. R. Freeman. Wiley–Interscience, New York. 1987. (*a*) pp. 37–43; (*b*) pp. 53–59; (*c*) pp. 66–87; (*d*) pp. 48–53; (*e*) pp. 62–64; (*f*) p. 293.
2. A. Mozumder and J. L. Magee. J. Chem. Phys. **47**, 939 (1967).
3. W. F. Schmidt and A. O. Allen. J. Chem. Phys. **52**, 2345 (1970).
4. I. György and G. R. Freeman. J. Appl. Phys. **60**, 3188 (1986).
5. N. Gee and G. R. Freeman. IEEE Trans. Electr. Insul. **EI-23**, 505 (1988).
6. N. Gee, P. C. Senanayake, and G. R. Freeman. J. Chem. Phys. **89**, 3710 (1988); erratum, **90**, 2530 (1989).
7. N. Gee and G. R. Freeman. Can. J. Phys. **68**, 930 (1990).
8. A. O. Allen. Yields of free ions formed in liquids by radiation. NBS-NSRDS 57. U.S. Government Printing Office, Washington, D.C. 1976. p. 5.
9. S. Young. Sci. Proc. Soc. Dublin, N.S. **XII**, 374 (1909–1910). *In* Physico-chemical constants of pure organic compounds. *Edited by* J. Timmermans. Elsevier, New York. 1960. p. 141.
10. L. S. Schraiber and N. G. Pechenyuk. Russ. J. Phys. Chem. **39**, 219 (1965).
11. A. N. Campbell and R. M. Chatterjee. Can. J. Chem. **46**, 575 (1968).
12. J. L. Hales and R. Townsend. J. Chem. Thermodyn. **4**, 763 (1972).
13. I. A. Tugarev, Z. I. Avduś, and V. F. Nozdrev. Russ. J. Phys. Chem. **49**, 732 (1975).
14. N. B. Vargaftik. Tables on the thermophysical properties of liquids and gases. 2nd ed. J. Wiley and Sons, Halsted Press, New York. 1975. p. 342.
15. H. Isnardi. Z. Phys. **9**, 153 (1922).
16. A. P. Altschuller. J. Phys. Chem. **58**, 392 (1954).
17. J. K. Vij and W. G. S. Scaife. J. Chem. Phys. **64**, 2226 (1976).
18. R. Deul, S. Rosenweig, and E. U. Franck. Ber. Bunsen-ges. Phys. Chem. **95**, 515 (1991).
19. N. Gee and G. R. Freeman. J. Chem. Phys. **90**, 5399 (1989).
20. A. A. Maryott and E. R. Smith. Tables of dielectric constants of pure liquids. NBS Circular 514. U.S. Government Printing Office, Washington, D.C. 1951. p. 1.
21. K. Shinsaka and G. R. Freeman. Can. J. Chem. **52**, 3495 (1974).
22. S. S.-S. Huang and G. R. Freeman. J. Chem. Phys. **72**, 2849 (1980).
23. K. Itoh and R. Holroyd. J. Phys. Chem. **94**, 8850 (1990).
24. L. Onsager. Phys. Rev. **54**, 554 (1938).
25. (*a*) G. Ramanan, N. Gee, and G. R. Freeman. Can. J. Phys. **68**, 925 (1990); (*b*) N. Gee and G. R. Freeman. J. Chem. Phys. **91**, 586 (1992).
26. J.-P. Dodelet, P. G. Fuochi, and G. R. Freeman. Can. J. Chem. **50**, 1617 (1972).
27. J.-P. Dodelet and G. R. Freeman. J. Chem. Phys. **60**, 4657 (1974).
28. G. C. Abell and K. Funabashi. J. Chem. Phys. **58**, 1079 (1973).
29. (*a*) J. Casanovas, R. Grob, D. Blanc, G. Brunet, and J. Mathieu. J. Chem. Phys. **63**, 3673 (1975); (*b*) J. Casanovas, R. Grob, J. Ortet, and A. Shamsalbin. J. Chim. Phys. **80**, 325 (1983).
30. (*a*) C. L. Braun and T. W. Scott. J. Phys. Chem. **91**, 4436 (1987); (*b*) C. L. Braun, S. N. Smirnov, S. S. Brown, and T. W. Scott. J. Phys. Chem. **95**, 5529 (1991).
31. C. Ferradini and J.-P. Jay-Gerin. J. Chem. Phys. **89**, 6719 (1988).
32. N. J. B. Green and S. M. Pimblott. J. Phys. Chem. **94**, 2922 (1990).
33. A. Hummel. Can. J. Phys. **68**, 858 (1990).
34. R. M. Leblanc and J. A. Herman. J. Chim. Phys. **63**, 1055 (1966).
35. E. W. McDaniel. Collision phenomena in ionized gases. J. Wiley and Sons, New York. 1964. Chap. 9.
36. J. M. Warman. *In* Proc. 8th Int. Conf. Rad. Res. Vol. 2. *Edited by* E. M. Fielden, J. F. Fowler, J. H. Hendry, and D. Scott. Taylor and Francis, London. 1987. pp. 272–277.

Can. J. Chem. Downloaded from www.nrcresearchpress.com by 217.78.4.112 on 09/08/12
For personal use only.

The crystal structure of methyl 4,6-*O*-benzylidene-2,3-*O*-dibutylstannylene-α-D-glucopyranoside

T. STANLEY CAMERON,[1] PRADIP K. BAKSHI, RASIAH THANGARASA, AND T. BRUCE GRINDLEY[1]
Department of Chemistry, Dalhousie University, Halifax, N.S., Canada B3H 4J3

Received June 13, 1991

T. STANLEY CAMERON, PRADIP K. BAKSHI, RASIAH THANGARASA, and T. BRUCE GRINDLEY. Can. J. Chem. **70**, 1623 (1992).

The determination of the crystal structure of methyl 4,6-*O*-benzylidene-2,3-*O*-dibutylstannylene-α-D-glucopyranoside (**1**) was repeated from data collected at −70°C because the previous assignment had a large *R* value (10.9%) and because this structure was the key link in assignment of structures of all stannylene acetals in solution. Crystals of **1** are orthorhombic, of space group $P2_12_12_1$, with $a = 12.479(2)$, $b = 19.202(5)$, $c = 19.654(6)$ Å, $Z = 4$, $R = 0.0597$ ($R_w = 0.0612$) for 3623 independent reflections with $I > 3\sigma(I)$. Compound **1** is a dimer linked together by a four-membered 1,3-dioxa-2,4-distannetane ring containing the O-3 atoms from the two glucose units. Deviations from C_2 symmetry are much smaller than reported earlier and lie mainly in the orientations of the butyl groups. The butyl groups are still significantly disordered at −70°C. It is suggested that steric effects of these flexible butyl groups may be an important factor in the selectivity for dicoordinate oxygens previously observed in reactions of stannylene acetal dimers with electrophiles.

T. STANLEY CAMERON, PRADIP K. BAKSHI, RASIAH THANGARASA et T. BRUCE GRINDLEY. Can. J. Chem. **70**, 1623 (1992).

On a redéterminé la structure cristalline du 4,6-*O*-benzylidène-2,3-*O*-dibutylstannylène-α-D-glucopyranoside de méthyle (**1**) à partir de données recueillies à −70°C parce que l'attribution antérieure n'avait été déterminée qu'avec une valeur élevée de *R* (10,9%) et que cette structure est un lien important dans l'attribution des structures de tous les acétals de stannylène, en solution. Les cristaux du composé **1** sont orthorhombiques, groupe d'espace $P2_12_12_1$, avec $a = 12{,}479(2)$, $b = 19{,}202(5)$ et $c = 19{,}654(6)$ Å, $Z = 4$, $R = 0{,}0597$ ($R_w = 0{,}0612$) pour 3623 réflexions indépendantes avec $I > 3\sigma(I)$. Le composé **1** est un dimère relié par un cycle à quatre chaînons 1,3-dioxa-2,4-distannetane contenant les atomes O-3 de deux unités de glucose. Les déviations par rapport à la symétrie C_2 sont beaucoup plus faibles que celles rapportées antérieurement et elles se situent principalement dans les orientations des groupes butyles. Même à −70°C, les groupes butyles sont encore assez désordonnés. On suggère que les effets stériques de ces groupes butyles flexibles peuvent être un facteur important dans la sélectivité pour les oxygènes dicoordonnés observée antérieurement dans les réactions des dimères d'acétal stannylène avec les électrophiles.

[Traduit par la rédaction]

Introduction

Since the first reports of their use in 1974 (1), stannylene acetals have become widely employed as intermediates for the regioselective monosubstitution of diols and polyols (2). Interest in the use of these compounds continues (3).

Stannylene acetals exist as dimers and (or) higher oligomers in solution (4–6). When the two oxygen atoms in the stannylene acetal are diastereotopic, three dimers can be formed. We have shown that in many of the reactions of stannylene acetals where high regioselectivity is obtained, only one of the three possible dimers is present in solution at concentrations detectable by ^{119}Sn nmr spectroscopy (6). Only one of the several dibutylstannylene acetals studied by X-ray crystallography exists as a dimer in the solid state (7); the others are present as polymers (8–10) or, in one case, as a pentamer (11).

The one stannylene acetal that has been studied by X-ray crystallography and found to be a dimer was methyl 4,6-*O*-benzylidene-2,3-*O*-dibutylstannylene-α-D-glucopyranoside (**1**). This compound was also present as a single dimer in solution and its structure was shown to be the same as that in the solid by comparison of the ^{119}Sn and ^{13}C nmr spectra of **1** from the two phases (6). Identification of the structures of the dimers present for other stannylene acetals were made by correlations of their spectral results with that of **1** and by reactivity arguments (6). The regioselectivities obtained in reactions of all stannylene acetals were then related to the structures of the dimers present. Thus, the conclusions drawn about the cause of the regioselectivity in the reactions of all stannylene acetals depend on the assignment of the structure of **1** in the solid state made by X-ray diffraction.

Unfortunately, there are several difficulties with this determination (7). The *R* value obtained was 10.9% and three carbon atoms were not located. We therefore considered it important to redetermine this structure using low-temperature data so that a better solution could be obtained. We also wanted accurate structural parameters for tin in this type of compound to obtain parameters for use in molecular mechanics calculations.

Experimental

Methyl 4,6-*O*-benzylidene-α-D-glucopyranoside was prepared as previously and had physical constants in accord with literature values (6). It was converted to its 2,3-*O*-dibutylstannylene acetal by refluxing with an equivalent amount of dibutyltin oxide in benzene in an apparatus for the azeotropic removal of water (5, 6). Evaporation of the solvent on a vacuum line yielded a white powder. Distillation of dried hexane and toluene onto the sample, followed by heating and cooling cycles, gave colourless crystals suitable for study by X-ray diffraction. The crystals were transferred into capillaries in a dry box and the capillaries were sealed. Crystal data and other experimental details are summarized in Table 1. The data were collected on an Enraf–Nonius CAD4 diffractometer using graphite monochromated MoK_α radiation ($\lambda = 0.70926$ Å) on crystals maintained at 203 ± 3 K. The temperature was maintained by heating a stream of very cold nitrogen gas at a rate determined by a thermister and a feedback loop using a modified Varian NMR temperature controller. Cell dimensions were calcu-

[1]Authors to whom correspondence may be addressed.

Can. J. Chem. Downloaded from www.nrcresearchpress.com by 217.78.4.112 on 09/08/12
For personal use only.

Can. J. Chem. Downloaded from www.nrcresearchpress.com by 217.78.4.112 on 09/08/12
For personal use only.

TABLE 1. Crystal data for methyl 4,6-*O*-benzylidene-2,3-*O*-dibutylstannylene-α-D-glucopyranoside (**1**)

Formula	$(C_{22}H_{34}O_6Sn)_2$
FW	1026.209
Crystal system	Orthorhombic
Space group	$P2_12_12_1$
a(Å)	12.479(2)
b(Å)	19.202(5)
c(Å)	19.654(6)
V(Å^3)	4710(12)
Z	4 (dimers)
D_{calod} (g cm^{-3})	1.447
T	203 K
μ(MoKα) (cm^{-1})	11.175
F(000)	2112
Crystal dimensions (mm)	0.15 × 0.2 × 0.4
Scan type	ω/2θ
ω scan width (deg)	1.0 + 0.35 tan θ
θ range (deg)	3–23
Range of h, k, l (deg)	−1–13, 0–21, 0–21
Measured reflections	4038
Unique observed reflections $\{I > 3\sigma(I)\}$	3623
Parameters refined	627
Final R, R_w indices[a]	0.0597, 0.0612
Weighting scheme	$w = k/[\sigma^2F + 0.00035F^2]$, $k = 5.9570$
S[b]	7.62
Highest peak (e Å^{-3})	1.15
Lowest peak (e Å^{-3})	−2.08

[a] $R = [\Sigma||F_o|-|F_c||/\Sigma|F_o|$; $R_w = (\Sigma w(|F_o|-|F_c|)^2/\Sigma wF_o^2)^{1/2}$.
[b] $S = (\Sigma w(|F_o|-|F_c|)^2/(m-n)^{1/2}$; m = No. of reflections, n = No. of variables.

lated from 25 reflections with 2θ angles in the range 26–30°. The structure was solved by the direct (SHELXS-86) method (12). All non-hydrogen atoms were refined with anisotropic thermal parameters. One atom, C(20), was found to be 50% disordered and was assigned two positions C(20) and C(20′). Hydrogen atoms were placed geometrically and refined with individual isotropic thermal parameters. No correction was made for extinction but an absorption correction was applied using the program DIFABS (13). Atomic scattering factors for all atoms and corrections for anomalous dispersion for Sn, C, and O were taken from the International Tables for X-ray crystallography, Vol. IV (14), and applied by the program SHELX-76 (12).[2] Refinement using the program SHELX-76 (12) minimized the function $\Sigma w(|F_o|-|F_c|)$.[2] Structures were drawn with the program CHEMGRAF (15).

Results and discussion

The structure of the compound showing thermal ellipsoids is shown in Fig. 1; a different perspective is presented in Fig. 2. The crystal data, atomic coordinates, and selected bond lengths, interbond angles, and torsional angles are listed in Tables 1–4. The numbering system used is based on carbohydrate numbering; in the dimer unit, one monomer unit starts with C-1 as C(1). The tin atom in this first unit is Sn(1). The other monomer unit contains Sn(2) and numbering starts

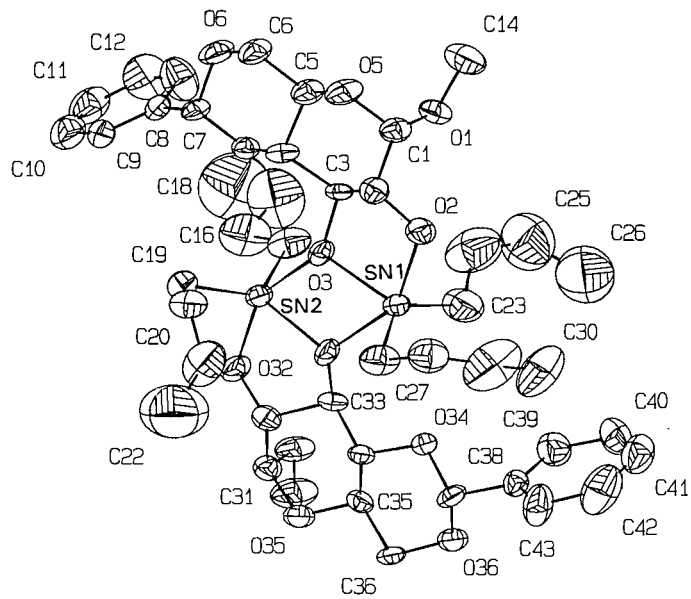

FIG. 1. The structure of methyl 4,6-*O*-benzylidene-2,3-*O*-dibutylstannylene-α-D-glucopyranoside (**1**). Only one position is shown for the disordered atom, C(20).

[2]Supplementary tables providing full crystal data, anisotropic thermal parameters, hydrogen atom positions, all heavy-atom bond lengths, bond angles, and torsional angles, observed and calculated structure factors, and a comparison of the atomic positions from the previous study (7) with positions obtained from those in the current work transformed to the cell dimensions from the previous study may be purchased from: The Depository of Unpublished Data, Document Delivery, CISTI, National Research Council Canada, Ottawa, Canada K2A 0S2.

Tables of full crystal data, hydrogen atom positions, and bond lengths and angles have also been deposited with the Cambridge Crystallographic Data Centre and can be obtained on request from The Director, Cambridge Crystallographic Data Centre, University Chemical Laboratory, Lensfield Road, Cambridge, CB2 1EW, U.K.

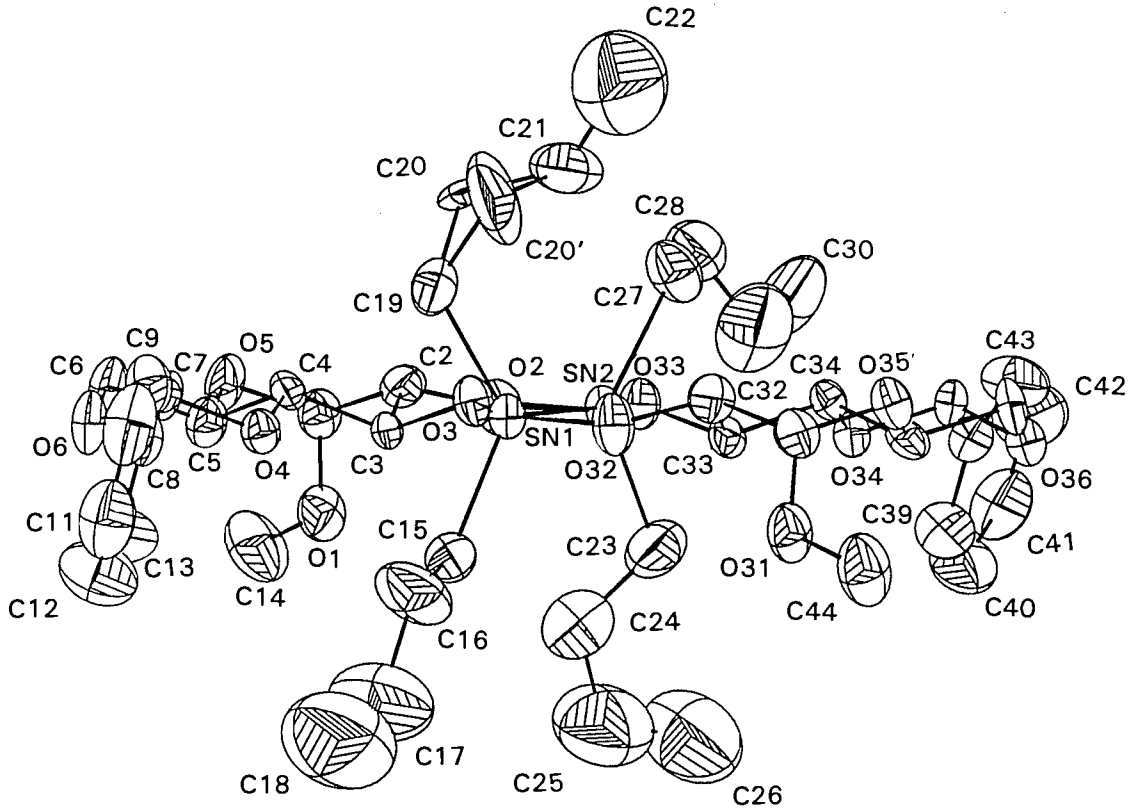

FIG. 2. A second view of the structure of methyl 4,6-*O*-benzylidene-2,3-*O*-dibutylstannylene-α-D-glucopyranoside (**1**), showing both positions for the disordered atom, C(20).

with its carbohydrate C-1 as C(31). In Tables 3–5, values from the same locations in the two monomer units are placed on the same line.

Although the space group and crystal dimensions are very similar here to the values obtained earlier (7), the atom positions calculated here are different mainly because we have chosen to label the cell dimensions in the conventional order. A supplementary table gives a comparison of the atomic positions from the earlier study (7) with the atomic positions from this study transformed to give positions based on the previous order of cell dimensions.[3] The resulting atomic positions are fairly similar to those from ref. 7 except for atoms in one of the butyl groups and the gross features of the present structure are the same as that obtained earlier (7). However, the small differences in atomic positions result in considerable differences in the structural details.

Two major differences can be noted first. The differences between the two monomer units constituting the dimer are smaller in this determination than in the previous one. Recording the data at low temperature yielded more than twice as many unique reflections with $I > 3\sigma(I)$. Because of the additional data and the lesser degree of motion at 203 K, it was possible to find all of the carbon atoms.

The three carbon atoms not found in the previous determination were on two of the butyl groups. A particularly clear representation of the structure found previously (7) is given as Fig. 2 in ref. 8. Comparison of this figure with Fig. 2 here shows that the carbon atoms not located are among those with the largest anisotropic thermal parameters. The disorder observed for one of the β-carbon atoms on a butyl group (C-20) was such that two positions could be defined for it. Although no other disordered atoms were resolved into two positions, it is evident from the large thermal ellipsoids for the terminal two or three atoms in each butyl group that these atoms occupy considerable regions of space. As will be discussed later, the thermal disorder is also evident in the value of one torsional angle. As a result, the value obtained for the goodness-of-fit parameter, S, is still rather high.

Compound **1** is present as a dimer. Formation of a dimer requires that one oxygen in each monomer unit becomes tricoordinate and dimer structures have been named by means of the numbers of the tricoordinate oxygens (6). Three different dimer structures are possible for **1**. The dimer observed here and previously (7) has the 3,3-structure. In theory, a 3,3-dimer has a C_2 axis of symmetry perpendicular to the plane of the central 1,3-dioxa-2,4-distannetane ring that relates the two tin atoms and the two glucose units. However, there are enough differences between the structures of the two monomer segments of the dimer in the crystal (see Tables 3 and 4) to explain the observation of two peaks in the ^{119}Sn nmr spectrum of **1** in the solid and the doubling of several of the peaks in the ^{13}C nmr spectrum of the solid (6).

The structure is composed of two sets of three fused rings from the two monomer units held together by a central 1,3-dioxa-2,4-distannetane ring plus terminal phenyl, butyl, and methoxy groups. The atoms in the seven fused rings have relatively small anisotropic thermal parameters. The aniso-

[3]The transformation used was $-0.25 - z$, $0.75 + y$, $0.75 + x$. We thank a referee for suggesting that we perform this comparison.

Can. J. Chem. Downloaded from www.nrcresearchpress.com by 217.78.4.112 on 09/08/12
For personal use only.

Can. J. Chem. Downloaded from www.nrcresearchpress.com by 217.78.4.112 on 09/08/12
For personal use only.

TABLE 2. Fractional atomic coordinates, with estimated standard deviations in parentheses[a]

Atom	x/a	y/b	z/c	U(mod)[b]
Sn(1)	−46203(5)	−54267(4)	−64005(4)	372
Sn(2)	−17638(5)	−54836(3)	−64841(3)	341
O(3)	−3210 (5)	−4895 (3)	−6147 (3)	38
C(3)	−3438 (7)	−4445 (5)	−5556 (4)	29
C(4)	−2644 (8)	−3842 (5)	−5511 (5)	35
O(2)	−5249 (5)	−4634 (4)	−5831 (3)	46
C(2)	−4505 (8)	−4121 (5)	−5680 (5)	40
C(1)	−4818 (8)	−3663 (5)	−5096 (5)	41
O(1)	−4907 (6)	−4076 (4)	−4510 (4)	52
C(14)	−5335 (12)	−3727 (9)	−3953 (7)	85
O(5)	−4047 (6)	−3121 (3)	−5013 (4)	50
C(5)	−3002 (8)	−3403 (5)	−4905 (6)	43
C(6)	−2259 (9)	−2804 (5)	−4827 (7)	48
O(6)	−1179 (6)	−3080 (4)	−4736 (4)	56
C(7)	−873 (9)	−3508 (5)	−5290 (5)	42
O(4)	−1572 (5)	−4085 (3)	−5359 (3)	35
C(8)	245 (8)	−3798 (5)	−5148 (6)	42
C(9)	1017 (8)	−3766 (6)	−5636 (6)	52
C(10)	2001 (11)	−4031 (7)	−5508 (9)	83
C(11)	2249 (10)	−4345 (7)	−4906 (8)	80
C(12)	1466 (12)	−4350 (9)	−4408 (9)	95
C(13)	490 (11)	−4099 (8)	−4533 (8)	82
O(32)	−1115 (5)	−6303 (4)	−7022 (4)	49
C(32)	−1882 (8)	−6620 (5)	−7450 (5)	40
O(33)	−3170 (5)	−5928 (3)	−6865 (3)	39
C(33)	−2966 (7)	−6641 (5)	−7087 (5)	32
C(34)	−3762 (8)	−6922 (5)	−7589 (5)	32
C(35)	−3376 (7)	−7646 (5)	−7780 (5)	35
O(35)	−2379 (6)	−7618 (4)	−8110 (3)	43
C(31)	−1568 (8)	−7348 (5)	−7678 (5)	40
O(31)	−1393 (6)	−7766 (4)	−7106 (4)	54
C(44)	−1036 (11)	−8447 (6)	−7283 (8)	74
C(36)	−4191 (8)	−7958 (6)	−8262 (5)	42
O(36)	−5217 (5)	−7972 (3)	−7923 (3)	41
C(37)	−5553 (8)	−7282 (5)	−7760 (6)	39
O(34)	−4814 (5)	−6980 (3)	−7288 (3)	34
C(38)	−6610 (7)	−7327 (5)	−7438 (5)	36
C(39)	−6729 (10)	−7532 (7)	−6770 (7)	62
C(40)	−7755 (12)	−7559 (8)	−6461 (7)	82
C(41)	−8640 (11)	−7343 (7)	−6798 (8)	74
C(42)	−8521 (12)	−7167 (9)	−7465 (9)	99
C(43)	−7472 (9)	−7165 (7)	−7797 (7)	69
C(15)	−1372 (10)	−5819 (6)	−5493 (6)	63
C(16)	−206 (11)	−5997 (10)	−5351 (7)	98
C(17)	−77 (13)	−6273 (14)	−4622 (10)	158
C(18)	1053 (17)	−6421 (14)	−4439 (14)	226
C(19)	−1180 (9)	−4619 (6)	−7022 (5)	54
C(20)	−1979 (18)	−4228 (9)	−7520 (9)	51
C(20′)[c]	−1230 (21)	−4604 (18)	−7779 (12)	154
C(21)	−2421 (13)	−4660 (9)	−8040 (7)	106
C(22)	−2377 (19)	−4637 (13)	−8770 (9)	217
C(23)	−4925 (13)	−6259 (7)	−5756 (6)	81
C(24)	−4665 (16)	−6158 (9)	−5039 (8)	132
C(25)	−5022 (16)	−6647 (14)	−4515 (10)	180
C(26)	−6064 (16)	−7001 (13)	−4633 (11)	179
C(27)	−5243 (8)	−5130 (7)	−7377 (6)	62
C(28)	−6418 (9)	−4915 (7)	−7359 (7)	71
C(29)	−7139 (11)	−5435 (9)	−7040 (11)	130
C(30)	−8343 (10)	−5262 (8)	−7143 (10)	110

[a]Sn atoms × 10^5, C and O atoms × 10^4.
[b]$U_{mod} = 1/3\ (U_{11} + U_{22} + U_{33})$; U_{mod} values for Sn atoms × 10^4, for other atoms × 10^3.
[c]C(20) has a 1 : 1 disorder.

TABLE 3. Selected bond lengths (Å), with estimated standard deviations in parentheses[a]

Bond	Length	Bond		Length	
Sn(1)—O(2)	2.045(7)	Sn(2)—O(32)		2.060(7)	
Sn(1)—O(3)	2.095(7)	Sn(2)—O(33)		2.091(7)	
Sn(1)—O(33)	2.244(7)	Sn(2)—O(3)		2.229(7)	
Sn(1)—C(23)	2.074(14)	Sn(2)—C(15)		2.110(12)	
Sn(1)—C(27)	2.148(12)	Sn(2)—C(19)		2.099(11)	
C(1)—O(1)	1.404(13)	C(31)—O(31)		1.398(13)	
C(2)—C(1)	1.496(14)	C(32)—C(31)		1.519(14)	
O(2)—C(2)	1.387(12)	O(32)—C(32)		1.413(12)	
C(3)—C(2)	1.490(13)	C(32)—C(33)		1.529(13)	
O(3)—C(3)	1.476(11)	O(33)—C(33)		1.458(11)	
C(3)—C(4)	1.526(13)	C(33)—C(34)		1.501(13)	
C(4)—O(4)	1.447(12)	C(34)—O(34)		1.444(11)	
C(4)—C(5)	1.526(14)	C(34)—C(35)		1.520(13)	
O(5)—C(5)	1.428(13)	C(35)—O(35)		1.404(12)	
C(1)—O(5)	1.427(13)	O(35)—C(31)		1.419(12)	
O(1)—C(14)	1.39(2)	O(31)—C(44)		1.42(2)	
C(5)—C(6)	1.49(2)	C(35)—C(36)		1.513(14)	
C(6)—O(6)	1.460(14)	C(36)—O(36)		1.444(12)	
O(6)—C(7)	1.417(13)	O(36)—C(37)		1.425(12)	
C(7)—O(4)	1.416(12)	C(37)—O(34)		1.433(12)	
C(7)—C(8)	1.528(15)	C(37)—C(38)		1.466(14)	
C(23)—C(24)	1.46(2)	C(15)—C(16)		1.52(2)	
C(24)—C(25)	1.46(3)	C(16)—C(17)		1.54(3)	
C(25)—C(26)	1.49(3)	C(17)—C(18)		1.48(3)	
C(27)—C(28)	1.52(2)	C(19)—C(20)	1.58(2)	C(19)—C(20′)	1.49(3)
C(28)—C(29)	1.48(2)	C(20)—C(21)	1.43(2)	C(20′)—C(21)	1.58(3)
C(29)—C(30)	1.55(2)	C(21)—C(22)		1.44(3)	

[a]C(20) is disordered.

Can. J. Chem. Downloaded from www.nrcresearchpress.com by 217.78.4.112 on 09/08/12
For personal use only.

tropic thermal parameters for all of the side groups are larger, but those for the butyl groups are particularly large.

The central 1,3-dioxa-2,4-distannetane ring is almost planar with torsional angles averaging 8.6(5)°. The fused 1,3,2-dioxastannolane rings adopt conformations intermediate between twist ($^{C(2)}T_{C(3)}$) and envelope conformations ($E_{C(3)}$). The bond about which the substituents are closest to being eclipsed is Sn(1)—O(2) (or in the other half of the dimer Sn(2)—O(32)) and the other small torsional angle is about the Sn(1)—O(3) (or Sn(2)—O(33)) bond.

Pyranose rings are normally flattened with the smallest torsional angles about the C(2)—C(3) and C(3)—C(4) bonds with values in the 50–55° range (16, 17). In this structure, the two C(1)—C(2)—C(3)—C(4) torsional angles average 61.1(20°). As a result of the ring flattening, the O(2)—C(2)—C(3)—O(3) torsional angle in pyranose rings is normally somewhat larger than 60° (17). Here, this torsional angle averages 52.3(8)°, about 10° smaller than the typical value. These deviations from values normally observed for torsional angles in pyranose rings suggest that formation of stannylene acetals across *trans*-diols on pyranose rings is accompanied by a certain amount of strain.

When carbohydrates having both *cis*- and *trans*-diol units unprotected are reacted with dibutyltin oxide, followed by an electrophile, substitution normally occurs regioselectively on one of the hydroxyls of the *cis*-diol unit (2, 18). These observations suggest that the strain involved in formation of a stannylene acetal across a *trans*-diol is sufficient to cause it to be present in too low concentrations to react to a significant extent when the substrate also contains a *cis*-diol unit.

Coordination about tin

The tin atoms are pentacoordinate in severely distorted trigonal bipyramids. The butyl carbon atoms are equatorial but the average C—Sn—C bond angle is large, 131.0(31)°. The two dicoordinate oxygen atoms are apical to the tin atoms while the tricoordinate oxygen atoms are apical to one tin atom but equatorial to the other. The average O—Sn—O bond angle involving the apical oxygens is 148.6(6)°, far from the ideal 180° value. The apical–equatorial O—Sn—O bond angles average 80.4(4)° inside the five-membered ring and 68.4(3)° inside the four-membered rings. The O—Sn—C bond angles between the dicoordinate oxygen atoms and the α-butyl carbon atoms average 99.8(17)° but in an ideal trigonal bipyramid would be 90°. The O—Sn—C bond angles between the apical tricoordinate oxygen atoms and the α-butyl carbon atoms have average values closer to ideal, 93.0(12)°. The O—Sn—C bond angles between the equatorial tricoordinate oxygen atoms and the α-butyl carbon atoms average 113.7(15)°, less than the expected 120° value.

The bond lengths inside the monomer units are shorter (average 2.073(25) Å) than those between monomer units (average 2.237(13) Å) but the difference is not nearly as large as in dibutylstannylene acetals in which the tin atom is hexacoordinate (8, 10).

Each of the four butyl groups adopt different conformations. The two butyl groups on Sn(1) assume *anti*, *gauche* and *gauche*, *anti* conformations about the C-α, C-β, and C-β, C-γ bonds respectively. As can be seen from Fig. 2, the carbon atoms become increasingly disordered away from the tin atom. One butyl group on Sn(2) adopts an *anti*, *anti* conformation while the other is disordered, adopting

TABLE 4. Selected bond angles (°), with estimated standard deviations in parentheses

Bonds	Angle	Bonds	Angle
O(3)—Sn(1)—O(2)	80.2(3)	O(32)—Sn(2)—O(33)	80.5(3)
O(2)—Sn(1)—O(33)	148.3(3)	O(3)—Sn(2)—O(32)	149.0(3)
O(3)—Sn(1)—O(33)	68.2(2)	O(3)—Sn(2)—O(33)	68.5(2)
O(2)—Sn(1)—C(23)	99.7(4)	O(32)—Sn(2)—C(15)	98.6(4)
O(2)—SN(1)—C(27)	98.8(4)	O(32)—Sn(2)—C(19)	102.1(4)
O(3)—Sn(1)—C(23)	112.6(4)	O(33)—Sn(2)—C(15)	113.6(4)
O(3)—Sn(1)—C(27)	112.8(4)	O(33)—Sn(2)—C(19)	115.7(3)
O(33)—Sn(1)—C(23)	93.8(4)	O(3)—Sn(2)—C(15)	93.9(4)
O(33)—Sn(1)—C(27)	92.4(4)	O(3)—Sn(2)—C(19)	91.7(3)
C(23)—Sn(1)—C(27)	133.2(5)	C(15)—Sn(2)—C(19)	128.8(4)
Sn(1)—O(3)—Sn(2)	111.3(3)	Sn(1)—O(33)—Sn(2)	110.8(3)
Sn(1)—O(2)—C(2)	113.0(6)	Sn(2)—O(32)—C(32)	111.6(6)
Sn(1)—O(3)—C(3)	108.1(5)	Sn(2)—O(33)—C(33)	110.1(5)
Sn(2)—O(3)—C(3)	133.4(5)	Sn(1)—O(33)—C(33)	131.7(5)
C(3)—C(2)—C(1)	110.7(8)	C(33)—C(32)—C(31)	110.0(8)
C(4)—C(3)—C(2)	105.8(8)	C(32)—C(33)—C(34)	106.8(8)
C(3)—C(4)—C(5)	105.9(8)	C(33)—C(34)—C(35)	106.3(8)
C(4)—C(5)—O(5)	111.2(8)	C(34)—C(35)—O(35)	111.1(8)
C(1)—O(5)—C(5)	110.8(8)	C(35)—O(35)—C(31)	111.7(7)
C(2)—C(1)—O(5)	109.9(8)	C(32)—C(31)—O(35)	109.2(8)
C(2)—C(1)—O(1)	108.5(8)	C(32)—C(31)—O(31)	109.3(8)
O(1)—C(1)—O(5)	111.8(8)	O(35)—C(31)—O(31)	112.5(8)
O(2)—C(2)—C(1)	114.1(8)	O(32)—C(32)—C(31)	113.5(8)
C(3)—C(2)—O(2)	109.6(8)	O(32)—C(32)—C(33)	109.4(8)
O(3)—C(3)—C(2)	106.8(7)	C(32)—C(33)—O(33)	105.7(7)
O(3)—C(3)—C(4)	111.4(7)	O(33)—C(33)—C(34)	114.7(7)
C(3)—C(4)—O(4)	111.6(7)	C(33)—C(34)—O(34)	111.1(7)
C(1)—O(1)—C(14)	113.9(9)	C(31)—O(31)—C(44)	112.3(9)
Sn(1)—C(23)—C(24)	116.5(10)	Sn(2)—C(15)—C(16)	117.3(9)
C(23)—C(24)—C(25)	122.0(2)	C(15)—C(16)—C(17)	110.4(13)
C(24)—C(25)—C(26)	117.0(2)	C(16)—C(17)—C(18)	113.0(2)
Sn(1)—C(27)—C(28)	113.5(8)	Sn(2)—C(19)—C(20)	117.8(9)
		Sn(2)—C(19)—C(20′)	120.2(12)
C(27)—C(28)—C(29)	114.4(12)	C(19)—C(20)—C(21)	114.3(14)
		C(19)—C(20′)—C(21)	111.0(2)
C(28)—C(29)—C(30)	112.9(13)	C(20)—C(21)—C(22)	133.0(2)
		C(20′)—C(21)—C(22)	107.0(2)

(+)-*gauche*, *eclipsed* and (−)-*gauche*, *anti* conformations equally. The observed *eclipsed* conformation probably arises from 1:1 disordered arrangements between *gauche* and *anti* conformations of the terminal methyl with respect to C-α in the half of the butyl chains that have Sn and C-γ in the (+)-*gauche* conformation. These results suggest that each butyl group will rotate relatively freely among a number of conformational minima in solution.

Glucose units

The methoxy group adopts the conformation expected from the *exo*-anomeric effect and normally observed with methyl glycosides (16, 17). The normal pattern for 1,3-dioxane rings is to be puckered near the acetal centre but flattened at the other end (19, 20). One benzylidene ring fits this pattern exactly, the other to a lesser extent. The thermal parameters for the two phenyl rings suggest there is some motion occurring about the C(7)—C(8) and C(37)—C(38) bonds. The torsional angles about these bonds indicate that the average conformation of each of the phenyl rings is slightly different than the most favourable (19, 21) "parallel" conformation, which has the acetal hydrogen eclipsed with the phenyl ring. An angle of tilt can be calculated by averaging the differences between the torsional angles about the acetal carbon – phenyl ipso carbon and the ideal torsional angle for a parallel conformation, e.g. the difference between the O(6)—C(7)—C(8)—C(9) torsional angle and 120° or between the O(4)—C(7)—C(8)—C(13) torsional angle and 60°. The angles of tilt away from the parallel conformation calculated were 11.7 ± 0.3 and 17.7 ± 0.8° starting with the ring with the lower numbered atoms. The tilts of the two phenyl rings are in opposite directions; the phenyl ring tilted further from the parallel conformation had the carbon from the edge of its benzene ring on the same face of the molecule as the anomeric oxygen closer to O(34) than to O(36).

Cause of regioselectivity

Compound **1** was found to give exclusive reactions at O-2 under a variety of conditions: with benzoyl chloride in benzene or in dioxane containing triethylamine (22–24); with toluenesulfonyl chloride in dioxane containing triethylamine (22); and with bromine in dichloromethane to give the 2-keto derivative (23). Under more forcing conditions, specifically, on heating in *N,N*-dimethylformamide, it gave selective benzylation (7:2) (25) and methylation (57:30) (23) at O-2.

The regioselectivity obtained has been linked to the structures of the stannylene acetals present in solution. Highly

Can. J. Chem. Downloaded from www.nrcresearchpress.com by 217.78.4.112 on 09/08/12
For personal use only.

TABLE 5. Selected torsional angles (°), with estimated standard deviations in parentheses

Atoms	Angle	Atoms	Angle
(*a*) Around the 1,3-dioxa-2,4-distannetane ring			
O(3)—Sn(1)—O(33)—Sn(2)	8.8(3)	O(33)—Sn(2)—O(3)—Sn(1)	8.9(3)
O(33)—Sn(1)—O(3)—Sn(2)	−8.3(3)	O(3)—Sn(2)—O(33)—Sn(1)	−8.2(3)
O(2)—Sn(1)—O(33)—Sn(2)	11.4(6)	O(32)—Sn(2)—O(3)—Sn(1)	8.8(7)
C(23)—Sn(1)—O(3)—C(3)	−77.9(6)	C(15)—Sn(2)—O(33)—C(33)	−77.4(6)
C(27)—Sn(1)—O(3)—C(3)	114.1(6)	C(19)—Sn(2)—O(33)—C(33)	116.7(6)
C(15)—Sn(2)—O(3)—C(3)	40.7(8)	C(23)—Sn(1)—O(33)—C(33)	42.2(8)
C(19)—Sn(2)—O(3)—C(3)	−88.4(8)	C(27)—Sn(1)—O(33)—C(33)	−91.3(8)
O(32)—Sn(2)—O(3)—C(3)	154.5(7)	O(2)—Sn(1)—O(33)—C(33)	157.6(7)
(*b*) In the 1,3,2-dioxastannolane rings			
O(2)—Sn(1)—O(3)—C(3)	18.6(5)	O(32)—Sn(2)—O(33)—C(33)	17.9(5)
Sn(1)—O(3)—C(3)—C(2)	−42.0(7)	Sn(2)—O(33)—C(33)—C(32)	−41.4(7)
O(3)—C(3)—C(2)—O(2)	52.1(8)	O(32)—C(32)—C(33)—O(33)	52.4(8)
Sn(1)—O(2)—C(2)—C(3)	−36.7(8)	Sn(2)—O(32)—C(32)—C(33)	−38.1(8)
O(3)—Sn(1)—O(2)—C(2)	10.0(6)	O(33)—Sn(2)—O(32)—C(32)	11.8(6)
(*c*) In the butyl groups			
Sn(1)—C(23)—C(24)—C(25)	168.4(14)	Sn(2)—C(15)—C(16)—C(17)	−176.5(10)
C(23)—C(24)—C(25)—C(26)	−32.1(23)	C(15)—C(16)—C(17)—C(18)	−176.9(15)
Sn(1)—C(27)—C(28)—C(29)	−53.1(12)	Sn(2)—C(19)—C(20)—C(21)	−58.2(15)
		Sn(2)—C(19)—C(20′)—C(21)	60.3(20)
C(27)—C(28)—C(29)—C(30)	−169.9(11)	C(19)—C(20)—C(21)—C(22)	−119.4(19)
		C(19)—C(20′)—C(21)—C22)	179.6(12)
(*d*) Around the pyranose rings			
C(4)—C(3)—C(2)—C(1)	−62.4(9)	C(31)—C(32)—C(33)—C(34)	−59.8(8)
C(2)—C(3)—C(4)—C(5)	61.6(9)	C(32)—C(33)—C(34)—C(35)	60.4(8)
C(3)—C(4)—C(5)—O(5)	−62.9(9)	C(33)—C(34)—C(35)—O(35)	−63.5(8)
C(1)—O(5)—C(5)—C(4)	60.9(9)	C(34)—C(35)—O(35)—C(31)	63.3(8)
C(2)—C(1)—O(5)—C(5)	−57.8(9)	C(35)—O(35)—C(31)—C(32)	−59.1(9)
C(3)—C(2)—C(1)—O(5)	60.2(9)	C(33)—C(32)—C(31)—O(35)	57.7(9)
O(2)—C(2)—C(1)—O(1)	61.8(9)	O(32)—C(32)—C(31)—O(31)	57.2(9)
O(3)—C(3)—C(2)—O(2)	52.1(8)	O(32)—C(32)—C(33)—O(33)	52.4(8)
O(3)—C(3)—C(4)—O(4)	−67.0(8)	O(33)—C(33)—C(34)—O(34)	−64.9(8)
C(6)—O(6)—C(7)—O(4)	−60.4(9)	O(34)—C(34)—C(35)—C(36)	57.7(8)
C(2)—C(1)—O(1)—C(14)	−171.7(9)	C(32)—C(31)—O(31)—C(44)	−176.7(8)
O(5)—C(1)—O(1)—C(14)	66.8(10)	O(35)—C(31)—O(31)—C(44)	61.8(9)

regioselective reactions of *trans*-diols on pyranose rings are obtained when one dimer predominates in the reaction mixture and the product results from substitution on the dicoordinate oxygen in the dimer as has been observed for **1** (6). One possible explanation for the regioselectivity was that the tricoordinate oxygen became positively charged on dimer formation as expected on the basis of Lewis structures and hence unreactive with electrophiles, whereas the dicoordinate oxygen atoms assumed apical positions at tin and became more reactive on dimer formation (4). This suggestion of positive tricoordinate oxygen atoms in dimeric structures was not supported by changes in the ^{13}C nmr chemical shifts of attached carbon atoms on stannylene acetal formation (6). An alternative suggestion was that electron shifts only took place in the transition state for reaction (6).

The present X-ray structure demonstrates that the two butyl groups on each tin atom are approximately perpendicular to the plane of the 1,3-dioxa-2,4-distannetane ring and are highly mobile. Another possible explanation of the regioselectivity is that the tricoordinate oxygens are simply better shielded from electrophiles by the four butyl groups on the two adjacent tin atoms than are the dicoordinate oxygens by the two butyl groups on their single adjacent tin atom. This explanation is currently being tested.

Acknowledgements

T. Stanley Cameron and T. Bruce Grindley are grateful to the Natural Sciences and Engineering Research Council of Canada for financial support.

1. D. Wagner, J. Verheyden, and J. G. Moffat. J. Org. Chem. **39**, 24 (1974); S. David. C. R. Acad. Sci. Ser. C, **278**, 1051 (1974).
2. S. David and S. Hanessian. Tetrahedron, **41**, 643 (1985); M. Pereyre, J.-P. Quintard, and A. Rahm. Tin in organic synthesis. Butterworths, London. 1987. Chap. 11; S. J. Blunden, P. A. Cusak, and P. J. Smith. J. Organomet. Chem. **325**, 141 (1987).
3. G. Reginato, A. Ricci, S. Roelens, and S. Scapecchi. J. Org. Chem. **55**, 5132 (1990); A. Dureault, M. Portal, and J. C. Depezay. Synlett, **4**, 225 (1991); V. Gopalakrishnan, H. Mereyala, A. G. Samuel, and K. N. Ganesh. Tetrahedron Lett. **31**, 1613 (1990).
4. S. David, A. Thieffry, and A. Forchioni. Tetrahedron Lett. **22**, 2647 (1981).

Can. J. Chem. Downloaded from www.nrcresearchpress.com by 217.78.4.112 on 09/08/12
For personal use only.

5. T. B. Grindley and R. Thangarasa. J. Am. Chem. Soc. **112**, 1364 (1990).
6. T. B. Grindley and R. Thangarasa. Can. J. Chem. **68**, 1007 (1990).
7. S. David, C. Pascard, and M. Cesario. Nouv. J. Chim. **3**, 63 (1979).
8. A. G. Davies, A. J. Price, H. M. Dawes, and M. B. Hursthouse. J. Chem. Soc. Dalton Trans. 297 (1986).
9. J. C. Pommier, E. Mendes, J. Valade, and J. Housty. J. Organomet. Chem. **55**, C19 (1973).
10. T. B. Grindley, R. Thangarasa, P. K. Bakshi, and T. S. Cameron. Can. J. Chem. **70**, 197 (1992).
11. C. W. Holzapfel, J. M. Koekemoer, C. F. Marais, G. J. Kruger, and J. A. Pretorius. S. Afr. J. Chem. **35**, 80 (1982).
12. G. M. Sheldrick. SHELX. A system of computer programs for crystal structure determination. Cambridge University, Cambridge, U.K. 1976; G. M. Sheldrick *In* Crystallographic computing 3. Edited by G. M. Sheldrick, C. Kruger, and R. Goddard. Oxford University Press. Oxford, U.K. 1985. pp. 175–189.
13. N. Walker and D. N. Stuart. Acta Crystallogr. Sect. A: Found. Crystallogr. **A39**, 158 (1983).
14. International Tables for X-ray crystallography. Vol. IV. Kynoch Press, Birmingham, U.K. 1974.
15. J. R. Carruthers and D. L. Watkins. Crystals, Issue 8 (revised 1989). Chemical Crystallography Laboratory, Oxford, U.K. 1984.
16. G. A. Jeffrey, R. K. McMullan, and S. Takagi. Acta Crystallogr. Sect. B: Struct. Crystallogr. Cryst. Chem. **B33**, 728 (1977).
17. S. Arnott and W. E. Scott. J. Chem. Soc. Perkin Trans. 2, 324 (1972).
18. J. Alais, A. Maranduba, and A. Veyrieres. Tetrahedron Lett. **23**, 2383 (1983).
19. T. B. Grindley, S. Kusuma, T. S. Cameron, and A. Kumari. Carbohydr. Res. **159**, 171 (1987).
20. A. J. de Kok and C. Romers. Recl. Trav. Chim. Pays-Bas, **89**, 313 (1970).
21. T. Schaefer and C. S. Takeguchi. Can. J. Chem. **67**, 1022 (1989).
22. R. M. Munavu and H. H. Szmant. J. Org. Chem. **41**, 1832 (1976).
23. S. David and A. Thieffry. J. Chem. Soc. Perkin Trans. 1, 1568 (1979).
24. C. W. Holzapfel, J. M. Koekemoer, and C. F. Marais. S. Afr. J. Chem. **37**, 19 (1984).
25. T. Ogawa and K. Shibata. Carbohydr. Res. **103**, 53 (1982).

Can. J. Chem. Downloaded from www.nrcresearchpress.com by 217.78.4.112 on 09/08/12
For personal use only.

A model of nonelectrolytic behaviour: activity coefficients

PREM P. SINGH[1] AND SANJEEV MAKEN
Department of Chemistry, Maharshi Dayanand University, Rohtak-124001, Haryana, India

Received January 3, 1991[2]

PREM P. SINGH and SANJEEV MAKEN. Can. J. Chem. **70**, 1631 (1992).

A model is presented for binary mixtures of nonelectrolytes that reproduces successfully the activity coefficient (γ_i, γ_j; x_i) data for even those ($i + j$) mixtures that are known to be characterized by the presence of 1:1 or 1:1 and 1:2 molecular complexes or have components that differ appreciably in their molar volumes when only limited (γ_i^c, γ_j^c; x_i = 0.5) or (γ_i^∞; γ_i^c, x_i = 0.5) or (γ_i^∞) data are available).

PREM P. SINGH et SANJEEV MAKEN. Can. J. Chem. **70**, 1631 (1992).

On présente un modèle pour les mélanges binaires de non-électrolytes qui reproduit bien les données relatives aux coefficients d'activité (γ_i γ_j; x_i). Le modèle s'applique même aux mélanges ($i + j$) qui sont connus pour contenir des complexes moléculaires 1 : 1 ou 1 : 1 et 1 : 2 ou ceux qui contiennent des composants dont les volumes molaires diffèrent beaucoup et pour lesquels il n'y a que des données fragmentaires (γ_i^c, γ_j^c; x_i = 0,5) ou (γ_i^∞; γ_i^c, x_i = 0,5) ou (γ_i^∞) de disponibles.

[Traduit par la rédaction]

Can. J. Chem. Downloaded from www.nrcresearchpress.com by 217.78.4.112 on 09/08/12
For personal use only.

Introduction

A binary ($i + j$) mixture is characterized by the replacement of like contacts in the pure components by unlike i–j contacts in the mixture. The activity coefficient of component i in such a mixture would then depend primarily on the i–j interactions and can, in principle; be computed (1) from the conventional molar excess Gibbs free energy G^E, provided a reliable equation of state is available for the mixture. The development (2) of the equation of state for a mixture via its canonical partition function involves the use of assumptions of doubtful validity (3–6) with the result that we are still far away (1*b*) from a general theory of liquid mixtures. Activity coefficients of the components of a binary mixture have, however, been evaluated from the compositional dependence of its G^E data, but most of the equations that relate G^E to the composition of the mixture are empirical (1) in nature. This calls for an alternative approach.

Theoretical aspects of the approach and results

If we consider the component i in the ($i + j$) mixture then the interaction of i with j would depend directly not only on the surface fraction of j that comes into effective i–j contacts but also on the magnitude of the molar i–j interaction energy, χ_{ij}. The thermal energy would also influence the magnitude of the χ_{ij} energy. Based on these considerations we expressed (7) the activity coefficient of i, γ_i, in an ($i + j$) mixture by the expression [1]

$$[1] \qquad \ln \gamma_i = \chi_{ij} x_j V_j / RT \Sigma x_i V_i$$

where the standard state of i is that of pure i. The activity coefficient of the jth component in the ($i + j$) mixture was then evaluated (7) via the Gibbs–Duhem equation, in the form

$$[2] \qquad \ln \gamma_j = (\chi_{ij} V_j / RTV_i)\left[\ln\left(\frac{\Sigma x_i V_i}{x_j V_j}\right) - x_i V_i / \Sigma x_i V_i\right]$$

In deriving eqs. [1] and [2] it was asumed that the ith and the jth components of the ($i + j$) mixture have nearly the same molar volumes so that the introduction of the jth component into the ith component does not cause drastic changes in their surroundings. This assumption is bound to fail if the components of the binary mixture differ in their molar volumes. In such a situation the activity coefficient of component i would be determined not only by the i–j interactions but also by the work done in accommodating the jth component into the matrix of the ith component. The introduction of the jth component into the matrix of the ith component would require that an appropriate cavity be first created in the matrix of i. This would then bring the jth component into i–j contact with the surrounding i molecules. The work necessary to accommodate the jth component into the matrix of the ith component would then be proportional not only to the difference ($V_i - V_j$) in the molar volumes of i and j but also to the interaction of the jth component with the i components in the cavity. The interaction of the jth component with the surrounding i components in the cavity would evidently be dictated by the mole fraction x_i of i so that if S_j is the surface fraction of j that is brought into i–j contact with the surrounding i molecules then the work due to i–j interactions between j and i components in the cavity will be proportional to $x_i S_j$. The net work done, G_W^E, to accommodate the jth component into the matrix of the ith component over and above the i–i or j–j interactions could then be expressed by $G_W^E \propto x_i S_j (V_i - V_j)$. But $S_j = x_j V_j / \Sigma x_i V_i$ (8), so that G_W^E would be given by

$$[3] \qquad G_W^E = \beta\, x_i x_j V_i V_j (1 - V_j/V_i)/(\Sigma x_i V_i)$$

where β is a constant. The activity coefficients of i and j in an ($i + j$) mixture, due to this effect, would then be given by

$$[4] \qquad RT(\ln \gamma_i)_W = [\partial(n_T G_W^E)/\partial n_i]_{n_j,T,P}$$

and

$$[5] \qquad RT(\ln \gamma_j)_W = [\partial(n_T G_W^E)/\partial n_j]_{n_i,T,P}$$

If the effects due to i–j interactions above (neglecting the difference in molar volumes of i and j) (eq. [1]) and that due to the difference in the molar volumes of i and j are assumed to make independent contributions to the activity

Author to whom correspondence may be addressed.
[2]Revision received January 23, 1992.

Can. J. Chem. Downloaded from www.nrcresearchpress.com by 217.78.4.112 on 09/08/12
For personal use only.

coefficients of the components of a binary $(i + j)$ mixture, then $\ln \gamma_i$ and $\ln \gamma_j$ would be given by

$$[6] \quad \ln \gamma_i = (\ln \gamma_i)_{i-j,V_i=V_j} + (\ln \gamma_i)_{W,V_i \neq V_j}$$

and

$$[7] \quad \ln \gamma_j = (\ln \gamma_j)_{i-j,V_i=V_j} + (\ln \gamma_j)_{W,V_i \neq V_j}$$

Substitution of eq. [3] into eqs. [4] and [5] then yields (in view of eqs. [6] and [7])

$$[8] \quad RT \ln(\gamma_i) = [\chi_{ij} x_j V_j / \Sigma x_i V_i] + \beta V_i V_j^2 x_j^2 (1 - V_j/V_i)/(\Sigma x_i V_i)^2$$

and

$$[9] \quad RT \ln (\gamma_j) = (\chi_{ij} V_j/V_i)[\ln (\Sigma x_i V_i / x_j V_j) - x_i V_i / \Sigma x_i V_i] + \beta x_i^2 V_i^2 V_j (1 - V_j/V_i)/(\Sigma x_i V_i)^2$$

It thus appears that if the two variables χ_{ij} and β of a binary $(i + j)$ mixture are evaluated from eqs. [8] and [9] using the activity coefficient data of its components at a single composition, then it should be possible to evaluate the activity coefficient data of these components of the binary mixture at any other composition. Such $(\gamma_i, \gamma_j; x_i)$ data[3] at various x_i values for some selected $(i + j)$ mixtures are recorded in Table 1 and are also compared with their corresponding experimental (γ_i^e, γ_j^e) values (9–13).

Examination of Table 1 clearly shows that such $(\gamma_i, \gamma_j; x_i)$ data for the components of the various $(i + j)$ mixtures compare well with their corresponding experimental $(\gamma_i^e, \gamma_i^e; x_i)$ values, even for those $(i + j)$ mixture that contain 1:1 or 1:1 and 1:2 molecular complexes though no direct cognizance has been taken of them in deriving eqs. [8] and [9]. The success of these expressions in reproducing well the $(\gamma_i^e, \gamma_j^e; x_i)$ data of the components of these mixtures may be ascribed to the fact that the use of the $(\gamma_i^e, \gamma_j^e; x_i = 0.5)$ data to evaluate them using eqs. [8] and [9] takes sufficient account of them.

Alternatively, as $x_i \rightarrow 0$, $x_j \rightarrow 1$ so that the activity coefficient of i at infinite dilution in j would be given (in view of eq. [8]) by

$$[10] \quad \ln \gamma_i^\infty = \chi_{ij}/RT + \beta V_i (1 - V_j/V_i)/RT$$

The activity coefficients of the ith and the jth components of an $(i + j)$ mixture can then be expressed in terms of $\ln \gamma_i^\infty$ by

$$[11] \quad \ln \gamma_i = (\chi_{ij} x_j V_j / RT \Sigma x_i V_i)[1 - x_j V_j / \Sigma x_i V_i] + (\ln \gamma_i^\infty) x_j^2 V_j^2 / (\Sigma x_i V_i)^2$$

and

$$[12] \quad \ln \gamma_j = (\chi_{ij} V_j / RTV_i)[\ln (\Sigma x_i V_i / x_j V_j) - x_i V_i / \Sigma x_i V_i - x_i^2 V_i^2 / (\Sigma x_i V_i)^2] + (\ln \gamma_i^\infty) x_i^2 V_i V_j / (\Sigma x_i V_i)^2$$

Consequently if the γ_i datum of i at any x_i is avaialble (or can be determined by appropriate experimentation) and as γ_i^∞ can be determined easily (14, 15) by gas–liquid chromatography, eqs. [11] and [12] should provide a convenient method to predict γ_i and γ_j data of both the components of an $(i + j)$ mixture at any x_i value. (The functional form of eq. [9] is such that it is not possible to derive an expression for $\ln \gamma_j^\infty$ analogous to $\ln \gamma_i^\infty$). Since it is the usual practice to report γ_i and γ_j data as functions of x_i, γ_i^∞ has to first be evaluated for the mixture by either plotting the experimental γ_i data (9–13) for the various $(j + j)$ mixtures as functions of x_i and then interpolating them to infinite dilution or from the compositional dependence of G^E data utilizing the reported compositional parameters. Such γ_i^∞ data for an $(i + j)$ mixture can next be combined with $(\gamma_i; x_i = 0.5$, arbitrary composition) data to calculate (via eqs. [10] and [11]) not only its χ_{ij}^+ and β^+ parameters but also the γ_i and γ_j data for both components of the mixture at various other x_i values. Such $(\gamma_i, \gamma_j; x_i)$ data for some selected $(i + j)$ mixtures are reported (as $\gamma_i^+, \gamma_j^+; x_i$) in Table 1 and are also compared with their corresponding experimental values (9–13).

Examination of Table 1 shows that such $(\gamma_i^+, \gamma_j^+; x_i)$ data for an $(i + j)$ mixture compare as closely with the corresponding experimental $(\gamma_i^e, \gamma_j^e; x_i)$ data as do those evaluated for it from the $(\gamma_i^e, \gamma_j^e; x_i = 0.5)$ data via eqs. [8] and [9], even for those binary mixtures that are known to be characterized by the presence of either 1:1 or 1:1 and 1:2 molecular complexes. The success of eqs. [11] and [12] to reproduce the experimental activity coefficient data may again be traced to the same reasons as were advanced to deduce them from $(\gamma_i^e, \gamma_j^e; x_i = 0.5)$ data using eqs. [8] and [9].

On the other hand, since the standard state of i in eq. [1] has been taken (7) to be that of the pure i, i.e., $\gamma_i = 1$ at $x_i = 1$, it may still be possible to predict $(\gamma_i, \gamma_j; x_i)$ data via eqs. [10]–[12] for an $(i + j)$ mixture when its γ_i^∞ datum alone is available or can be determined experimentally by gas–liquid chromatography.

To test this hypothesis we utilized (γ_i^∞) with $\gamma_i = 1$ at $x_i = 0.9999$ (the functional form of eq. [11] is such that we have to make this assumption about the γ_i value for an $(i + j)$ mixture) to evaluate its χ_{ij} and β parameters (via eqs. [10] and [11]), which were subsequently used to predict its $(\gamma_i, \gamma_j; x_i)$ data using eqs. [11] and [12]. Such $(\gamma_i, \gamma_j; x_i)$ data for some selected mixtures are recorded (as γ_i^*, γ_j^*) in Table 1 and are also compared with their corresponding experimental values, and it is apparent from Table 1 that such $(\gamma_i^*, \gamma_j^*; x_i)$ data compare well with the corresponding experimental data for those $(i + j)$ mixturees that are not characterized by specific interactions between their components. Examination of Table 1 further reveals that, barring the two extreme ends of the composition scale, the $(\gamma_i^*, \gamma_j^*; x_i)$ data calculated from eqs. [10]–[12] compare reasonably well with the corresponding experimental $(\gamma_i^e, \gamma_j^e; x_i)$ data even for those $(i + j)$ mixture that are known to contain 1:1 or 1:1 and 1:2 molecular complexes.

Again, if the boiling temperatures of i and j in an $(i + j)$ mixture do not differ significantly, the χ_{ij} and β_{ij} parameters may be taken, for practical applications, to be independent of temperature; the effect of pressure on liquid phase properties is usually small except at higher pressures and at conditions near the critical temperature. In that event, the V_i and V_j data at any temperature T coupled with the $(\gamma_i^e, \gamma_j^e; x_i =$ 0,5) or $\gamma_i^\infty; \gamma_i^e; x_i = 0.5)$ or $(\gamma_i^\infty; \gamma_i^e = 1, x_i = 0.9999)$ data at moderate pressures should be expected to yield a reasonably good estimate of the activity coefficient data of the

[3]Tables comparing $(\gamma_i, \gamma_j; x_i)$ data (evaluated from the experimental $(\gamma_i^e, \gamma_j^e; x_i = 0.5)$, $(\gamma_i^\infty; \gamma_i^e, x_i = 0.5)$, and $(\gamma_i^\infty; \gamma_i = 1, x_i = 0.9999)$ data) with their corresponding experimental $(\gamma_i^e, \gamma_j^e; x_i)$ data for some 30 mixturees may be purchased from: The Depository of Unpublished Data, Document Delivery CISTI, National Research Council Canada, Ottawa, Canada K1A 0S2.

TABLE 1. Comparison of (γ_i, γ_j, x_i) data (evaluated from eqs. [8]–[12] (see text) utilizing (γ_i^e, γ_j^e; $x_i = 0.5$), (γ_i^∞; γ_i^e, $x_i = 0.5$), and (γ_i^∞; $\gamma_i = 1$, $x_i = 0.9999$) data) with their corresponding experimental data for the components of ($i + j$) mixtures; also included are the corresponding χ_{ij}, etc. and β, etc. parameters.

Property	Mole fraction x_i 0.1	0.2	0.3	0.4	0.6	0.7	0.8	0.9	χ_{ij}, cal mol^{-1}	β, cal cm^{-3}
Cyclooctane (i) + 2,3-dimethylbutane (j), T = 288.15 K										
γ_i^e (13)	1.2821	1.2142	1.1573	1.1145	1.0463	1.0265	1.0102	1.0032		
γ_j^e (13)	1.0032	1.0125	1.0272	1.0483	1.1141	1.1552	1.2071	1.2654		
γ_i	1.2840	1.2177	1.1625	1.1169	1.0508	1.2087	1.0131	1.0036	4.5024	41.7423
γ_j	1.0031	1.0126	1.0283	1.0507	1.1168	1.1618	1.2164	1.2831		
γ_i^+	1.2752	1.2122	1.1594	1.1157	1.0516	1.0298	1.0142	1.0043	9.7773	19.1422
γ_j^+	1.0030	1.0120	1.0271	1.0486	1.1125	1.1566	1.2110	1.2804		
γ_i^*	1.2732	1.2088	1.1552	1.1111	1.0473	1.0262	1.0115	1.0028	−0.0017	41.5043
γ_j^*	1.0030	1.0123	1.0277	1.0495	1.1133	1.1563	1.2076	1.2675		
Pyridine (i) + chloroform (j), T = 303.15 K										
γ_i^e (10, 11)	0.3993	0.4998	0.6092	0.7188	0.8996	0.9560	0.9874	0.9989		
γ_j^e (10, 11)	0.9871	0.9488	0.8883	0.8127	0.6517	0.5827	0.5297	0.4978		
γ_i	0.4008	0.5018	0.6092	0.7172	0.9062	0.9727	1.0124	1.0218	222.75	92740.68
γ_j	0.9867	0.9484	0.8890	0.8143	0.6458	0.5666	0.5035	0.4826		
γ_i^+	0.4034	0.5039	0.6107	0.7179	0.9056	0.9718	1.0114	1.0211	217.74	18340.52
γ_j^+	0.9868	0.9488	0.8900	0.8159	0.6480	0.5689	0.5056	0.4835		
γ_i^*	0.3905	0.4756	0.5661	0.6583	0.8304	0.9007	0.9546	0.9884	0.0070	11985.87
γ_j^*	0.9885	0.9546	0.9008	0.8306	0.6584	0.5661	0.4756	0.3903		
Acetone (i) + chloroform (j), T = 323.15 K										
γ_i^e (12)	0.5225	0.6094	0.6938	0.7721	0.8993	0.9444	0.9760	0.9942		
γ_j^e (12)	0.9906	0.9640	0.9235	0.8719	0.7494	0.6844	0.6203	0.5587		
γ_i	0.5294	0.6085	0.6890	0.7678	0.9057	0.9571	0.9918	1.8068	106.36	92.53
γ_j	0.9919	0.9678	0.9285	0.8760	0.7428	0.6705	0.6031	0.5566		
γ_i^+	0.5143	0.5967	0.6810	0.7639	0.9089	0.9622	0.9972	1.0105	133.77	100.63
γ_j^+	0.9914	0.9657	0.9241	0.8687	0.7305	0.6573	0.5912	0.5516		
γ_i^*	0.5054	0.5381	0.6529	0.7273	0.8639	0.9197	0.9629	0.9904	0.0058	80.4278
γ_j^*	0.9923	0.9690	0.9304	0.8778	0.7386	0.6575	0.5729	0.4881		
Chloroform (i) + 1,4-dioxane (j), T = 303.15 K										
γ_i^e (10, 11)	0.4660	0.4877	0.5306	0.5918	0.7542	0.8426	0.9218	0.9786		
γ_j^e (10, 11)	0.9999	0.9913	0.9632	0.9076	0.7074	0.5753	0.4388	0.3319		
γ_i	0.4398	0.4917	0.5473	0.6061	0.7323	0.7985	0.8658	0.9333	−374.73	39.4222
γ_j	0.9938	0.9744	0.9401	0.8896	0.7335	0.6238	0.4876	0.3131		
γ_i^+	0.5021	0.5377	0.5769	0.6202	0.7210	0.7799	0.8454	0.9184	−490.76	−7.3812
γ_j^+	0.9964	0.9843	0.9613	0.9244	0.7913	0.6829	0.5336	0.3262		
γ_i^*	0.5385	0.6098	0.6818	0.7523	0.8786	0.9290	0.9674	0.9917	0.0048	94.4365
γ_j^*	0.9928	0.9712	0.9357	0.8874	0.7596	0.6848	0.6063	0.5269		
n-Pronanol (i) + water (j)										
γ_i^e (13)	5.2020	2.8515	0.9331	1.4992	1.1402	1.0662	1.0253	1.0055		
γ_j^e (13)	1.0480	1.1626	1.3212	1.5130	1.9725	2.2322	2.5077	2.7963		
γ_i	5.4986	2.6580	1.8142	1.4549	1.1621	1.0951	1.0510	1.0210	433.18	26.7624
γ_j	1.0757	1.2171	1.3788	1.5504	1.9277	2.1518	2.4346	2.8802		
γ_i	4.1019	2.3408	1.7222	1.4310	1.1700	1.1041	1.0582	1.0249	533.57	17.6743
γ_j^+	1.0561	1.1620	1.2848	1.4179	1.7259	1.9217	2.1842	2.6313		
γ_i^*	3.3765	1.8690	1.3996	1.2007	1.0509	1.0230	1.0084	1.0018	−0.0037	27.0419
γ_j^*	1.0644	1.1764	1.2925	1.4018	1.5914	1.6722	1.7448	1.8103		

components of the mixture at any composition. Since the boiling temperatures for the components of the n-propanol (i) + water (j) mixture vary from 87.8 to 100°C at a constant pressure of 1.013 bar (1 bar = 100 kPa), it would be an ideal mixture to test the validity of this hypothesis.

For this purpose we utilized density data (16, 17) at 298.15 K to evaluate V_i and V_j data for the n-propanol (i) + water (j) mixture. These values of V_i and V_j were next coupled with the (γ_i^e, γ_j^e; $x_i = 0.5$) or (γ_i^∞; γ_i^e, $x_i = 0.5$) or (γ_i^∞; $\gamma_i = 1$, $x_i = 0.9999$) data (in the manner explained above) to yield activity coefficient (γ_i, γ_j; x_i) or (γ_i^+, γ_j^+; x_i) or (γ_i^*, γ_j^*; x_i) data. Such data are recorded in Table 1, and are also compared with the corresponding experimental data (13). It is apparent that the activity coefficient data evaluated by either of the present approaches reproduce reasonably well the corresponding experimental activity coefficient data.

Can. J. Chem. Downloaded from www.nrcresearchpress.com by 217.78.4.112 on 09/08/12
For personal use only.

The present study thus provides, for the first time, a very simple method that successfully reproduces the experimental (γ_i^e, γ_j^e; x_i) data for the components of an ($i + j$) mixture when only limited (γ_i^e, γ_j^e; $x_i = 0.5$) or (γ_i^∞; γ_i^e, $x_i = 0.5$) or (γ_i^∞; $\gamma_i = 1$, $x_i = 0.9999$) data are available.

Acknowledgements

The authors express their thanks to the Head of the Chemistry Department for providing the necessary research facilities. S.M. thanks the Council for Scientific and Industrial Research (CSIR), New Delhi, for the award of a Research Associateship.

1. J. M. Prausnitz, R. N. Lichtenthaler, and E. Gomez de Azevedo. *In* Molecular thermodynamics of fluid phase equilibria. 2nd ed. Prentice–Hall, Englewood Cliffs, N.J. 1986. (*a*) p. 291; (*b*) p. 361.
2. T. L. Hill. *In* An introduction to statistical thermodynamics. Addison–Wesley, Reading, Mass. 1976.
3. G. C. Maitland, M. Rigby, and W. A. Wakeham. *In* Intermolecular forces. Clarendon, Oxford. 1981. p. 519.
4. J. W. Leland, J. S. Rowlinson, and G. A. Sather. Trans. Faraday Soc. **64**, 1447 (1968).
5. G. H. Hudson and J. C. McCoubrey. Trans. Faraday Soc. **56**, 761 (1960).
6. B. E. F. Fender and G. D. Halsey. J. Chem. Phys. **3**, 1881 (1962).
7. P. P. Singh, H. P. Dahiya, and S. Dager. Z. Phys. Chem. (Leipzig), **269**, 817 (1988).
8. M. L. Huggins. J. Phys. Chem. **74**, 371 (1970).
9. M. B. Ewing and K. N. Marsh. J. Chem. Thermodyn. **2**, 689 (1970).
10. S. M. Byer, R. E. Gibbs, and H. C. van Ness. A.I.Ch. E. J. **19**, 238 (1973).
11. M. M. Abbott and H. C. van Ness. A.I.Ch. E.J. **21**, 62 (1975).
12. W. H. Severns, A. Sesonske, R. H. Perry, and R. L. Pigford. A.I.Ch. E.J. **1**, 401 (1955).
13. T. A. Gadwa. Dissertation, Massachusetts Institute of Technology. 1936. *Quoted by* H. C. Carlson and A. P. Colburn. Ind. Eng. Chem. **34**, 581 (1942).
14. H. Hackenburg and A. P. Schmidt. *In* Gas chromatographic head space analysis. Heydon and Sons, Ltd., London. 1976.
15. T. G. Kiechbusch and C. J. King. Chromatogr. Sci. **17**, 273 (1979).
16. R. F. Brunel. J. Am. Chem. Soc. **45**, 1334 (1923).
17. P. Chappuis. Trav. Mem. Bur. Int. Poids Mes. **13**, D-40 (1907).

Can. J. Chem. Downloaded from www.nrcresearchpress.com by 217.78.4.112 on 09/08/12
For personal use only.

The thermodynamics of the ionization of 3-hydroxypyridine and pyridoxine in water–dioxane mixtures

SALVADOR B. ASENSIO, ENRIQUE LOPEZ-CANTARERO, and JUAN LLOR[1]

Departamento de Quimica-Fisica, Facultad de Ciencias, Universidad de Granada, 18003 Granada, Spain

Received August 12, 1991

SALVADOR B. ASENSIO, ENRIQUE LOPEZ-CANTARERO, and JUAN LLOR. Can. J. Chem. **70**, 1635 (1992).

A potentiometric method has been used to determine the thermodynamic equilibrium constants for the macroscopic ionization processes of 3-hydroxypyridine and pyridoxine in water–dioxane mixtures (0–70% weight fraction in dioxane) at temperatures from 10 to 50°C. From these data the reaction standard thermodynamic function changes were obtained for the processes in various water–dioxane mixtures at 25°C. It was found, in both molecules, that during the first ionization process the contributions of entropy and enthalpy to free energy are similar but that during the second ionization the main contribution comes from entropy, especially in mixtures with a high dioxane content. The effect of the solvent on the tautomeric equilibrium in the net zero charge specie could explain this behaviour.

SALVADOR B. ASENSIO, ENRIQUE LOPEZ-CANTARERO et JUAN LLOR. Can. J. Chem. **70**, 1635 (1992).

On a fait appel à une méthode potentiométrique pour déterminer les constantes thermodynamiques d'équilibre des processus macroscopiques d'ionisation de la 3-hydroxypyridine et de la pyridoxine, dans des mélanges eau–dioxane (0–70% en poids de dioxane), à des températures allant de 10 à 50°C. À partir de ces données, on a évalué les changements dans la fonction thermodynamique standard de la réaction pour les processus qui se produisent dans des mélanges eau–dioxane, à 25°C. On a trouvé que, pour les deux molécules, les contributions de l'entropie et de l'enthalpie à l'énergie libre du premier processus d'ionisation sont semblables, mais que dans la deuxième ionisation la contribution principale provient de l'entropie, spécialement dans des mélanges contenant une grande quantité de dioxane. Ce comportement peut être expliqué par l'effet de solvant sur l'equilibre tautomérique sur la charge nette zéro.

[Traduit par la rédaction]

Introduction

We have reported in recent papers on the solution equilibria of compounds belonging to the vitamin B_6 group and other analogous compounds in water–dioxane, with special emphasis on the ionization processes (1–6). To carry out these studies we designed an experimental method that allows us to calculate the macroscopic ionization equilibrium constants corrected to zero ionic strength, that is to say, the thermodynamic ionization equilibrium constants (1–3), with great saving in time and materials.

Many of the studies carried out on vitamin B_6 dependent enzymes were directed to an understanding of the roles played by the chemical groups of the coenzyme in the catalytic mechanism. Since one important way that the enzyme can influence the reactivity of the coenzyme is through selective protonation or deprotonation of the various functional groups, it is important to understand these effects in the vitamin B_6 group.

A study of the ionization of this group of molecules in water and other solvents with less polarity than water, such as water–organic solvent mixtures, is of interest (7). Relatively little work has been done in general on the thermodynamics of the dissociation processes of acids in mixed solvent systems. These results are also of interest in order to know the properties and the solute–solvent interactions in these media.

In this paper we report the macroscopic ionization equilibrium constants of 3-hydroxypyridine and pyridoxine (pK_1 and pK_2 (see Scheme 1)) in water–dioxane mixtures (0–70% weight fraction in dioxane) at temperatures ranging from 10 to 50°C, from which we have obtained the standard thermodynamic function changes of the macroscopic ionization processes.

[1]Author to whom correspondence may be addressed.

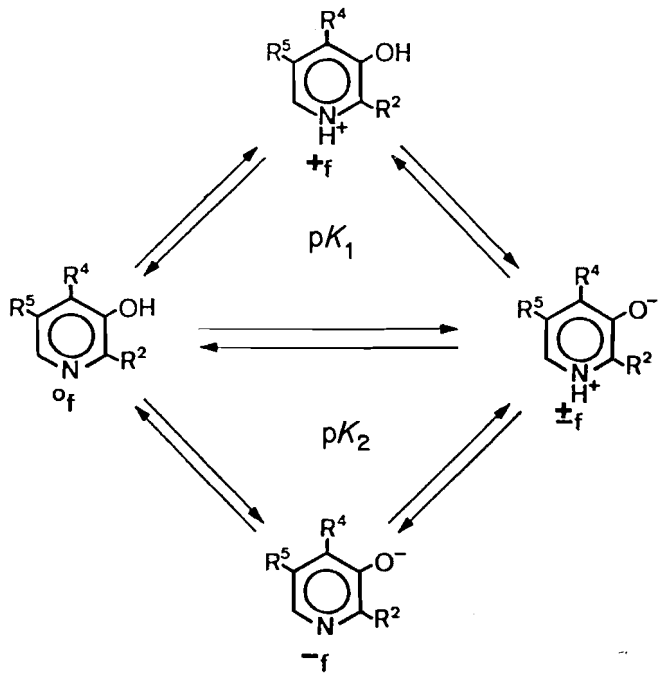

SCHEME 1. 3-Hydroxypyridine, $R^2 = R^4 = R^5 = H$; pyridoxine, $R^2 = CH_3$; $R^4 = R^5 = CH_2OH$.

Experimental

Materials

Dioxane (Ferosa) was purified by the method described in ref. 1. 3-Hydroxypyridine (Merck–Schuchardt, synthesis grade) was transformed into its hydrochloride salt and crystallized by adding acetone–ethanol–ether. Pyridoxine hydrochloride (Fluka Puriss.) was dissolved in hydrochloric acid and recrystallized in a cold ethanol–ether mixture. Carbonate-free KOH was prepared as described elsewhere (8, 9). All the other chemicals used were of the

Can. J. Chem. Downloaded from www.nrcresearchpress.com by 217.78.4.112 on 09/08/12
For personal use only.

Can. J. Chem. Downloaded from www.nrcresearchpress.com by 217.78.4.112 on 09/08/12
For personal use only.

best quality available. All measurements were made under nitrogen.

3-Hydroxypyridine concentrations were obtained by weight. Pyridoxine concentrations were determined by dilution in 0.1 M NaOH (ϵ = 7000 M^{-1} cm^{-1} at 308 nm) (10). Concentrations of KOH and HCl were determined by titration with potassium acid phthalate and KOH, respectively. Three separate measurements were made each time.

pH measurements

The pH measurements were made with an Ingold EA 120 combined electrode and a Crison Digit 501 pH-meter, capable of detecting 0.01 pH units. The scale of the pH-meter was adjusted using standard aqueous buffers (Radiometer).

The pH-meter readings in dioxane–water mixtures (B) were corrected into pH ($-\log a_H$) according to van Uitert and Haas (11), using eq. [1]:

$$[1] \quad \mathrm{pH} = B + \log U_H^0$$

where $\log U_H^0$ is the correction factor (11, 12). This correction factor is a function of the temperature and solvent, but not of the ionic strength. The $\log U_H^0$ values in the different mixtures and temperatures were taken from ref. 13. All the pH values used in this work were calculated from the pH-meter reading (B) and the subsequent application of eq. [1].

Potentiometric measurements

The potentiometric data were obtained by a method similar to that described by Woolley and co-workers (14–16) based on the dilution of an aqueous solution with the organic cosolvent (1, 2). The advantage of this experimental procedure is that it makes it possible to determine the ionization equilibrium constants in a wide range of water–dioxane mixtures in one single experiment, saving both time and cosolvent.

Results and discussion

The thermodynamic ionization constants of acids in water–dioxane mixtures can be determined from pH measurements of solutions containing concentrations similar to the conjugated acidic and basic species. In this way the pH values are close to the pK value, thus reducing experimental error to a minimum.

The proper equation to be used for the calculation of pK depends upon the ionization to be measured (pK_1 and pK_2) and the initial ionic species of the substance in question (hydrochloride salt, free base, etc.) (2).

The calculation of pK_1 for both compounds was carried out using eq. [2],

$$[2] \quad \mathrm{p}K_1 = B + \log U_H^0 + \log \gamma_\pm + \log \left(\frac{a - b + \dfrac{K_W}{a_H \gamma_\pm} - \dfrac{a_H}{\gamma_\pm}}{b + \dfrac{a_H}{\gamma_\pm} - \dfrac{K_W}{a_H \gamma_\pm}} \right)$$

while eq. [3] was used to calculate pK_2:

$$[3] \quad \mathrm{p}K_2 = B + \log U_H^0 - \log \gamma_\pm + \log \left(\frac{2a - b + \dfrac{K_W}{a_H \gamma_\pm} - \dfrac{a_H}{\gamma_\pm}}{b - a + \dfrac{a_H}{\gamma_\pm} - \dfrac{K_W}{a_H \gamma_\pm}} \right)$$

TABLE 1. Selected values[a] of pK_1 and pK_2 (molar scale) of 3-hydroxypyridine and pyridoxine in water and water–dioxane mixtures at 20°C and at 50°C. X_D, weight fraction of dioxane

	3-Hydroxypyridine				Pyridoxine			
	pK_1		pK_2		pK_1		pK_2	
X_D	20°C	50°C	20°C	50°C	20°C	50°C	20°C	50°C
0.0000	4.86	4.69	8.67	8.54	4.90	4.82	9.05	8.73
0.1213	4.80	4.58	8.82	8.73	4.92	4.78	9.11	8.80
0.2565	4.67	4.44	9.10	9.04	4.95	4.77	9.26	8.98
0.3697	4.51	4.30	9.43	9.36	4.97	4.73	9.49	9.21
0.5086	4.28	4.11	9.95	9.93	4.94	4.73	9.89	9.69
0.6330	4.13	4.05	10.66	10.62	4.96	4.75	10.52	10.36
0.7072	4.03	4.00	11.19	11.22	4.97	4.85	11.04	10.94

[a]See footnote 2 in text.

where, for both eqs. [2] and [3], a is the analytical concentration of the compound to be studied and b that of the KOH added to the solution to make the conjugated acid and base concentrations analogous. Equations [2] and [3] were obtained from the corresponding defining expressions for the thermodynamic ionization constants and the charge and material balances. The activity coefficients of the uncharged species were always taken as being 1 and those of the chemical species with a net charge +1 and −1 were assumed to be equal to the average ionic activity coefficients of HCl ($\gamma\pm$) at the same ionic strength and in the same media and were calculated by Debye–Hückel's equation:

$$[4] \quad \log \gamma_\pm = -\frac{(1.825 \times 10^6)\sqrt{(d_0/\epsilon^3 T^3)}I}{1 + 229.8\sqrt{(d_0/\epsilon T)}I}$$

where d_0 is the density, ϵ the dielectric constant of the solvent, and I the ionic strength on the molal scale. The ionization constant of water (K_W) and the dielectric constants for the various water–dioxane mixtures and temperatures were taken from Harned and Owen (17). The densities of the mixtures come from Hovorka *et al.* (18).

This method is valid for both monoprotic and polyprotic acids whenever the successive pK's are sufficiently far apart (about 4 units or more), as is the case with 3-hydroxypyridine and pyridoxine in all of the water–dioxane mixtures and at all of the temperatures studied.

We determined the macroscopic ionization equilibrium constants for 3-hydroxypyridine and pyridoxine in water–dioxane mixtures between 0 and 0.7072 (expressed as a weight fraction of dioxane) at 10, 20, 30, 40, and 50°C (Table 1).[2] All these constants have been corrected to an ionic strength of zero, and thus are thermodynamic in character.

All the pK values are the average of at least two, and usually three, measurements carried out with solutions containing various concentrations of the substance in question (between 2×10^{-3} and 5×10^{-3} M), and thus different ionic

[2]Tables of pK_1 and pK_2 values for 3-hydroxypyridine and pyridoxine vs. temperature and the weight fraction of dioxane in water–dioxane mixtures may be purchased from the Depository of Unpublished Data, Document Delivery, CISTI, National Research Council Canada, Ottawa, Canada K1A 0S2.

Can. J. Chem. Downloaded from www.nrcresearchpress.com by 217.78.4.112 on 09/08/12
For personal use only.

strengths. The mean errors in the measurements were always less than 0.05 pK units. According to Panichajakul and Woolley (16) discrepancies of around 0.08 unit are to be expected with this method and thus our error range is acceptable.

In the equations used to calculate the pK values the log(acid/base) term is usually close to zero because the conjugated acid and base concentrations are approximately the same. As the log $\gamma\pm$ term is also generally small it is clear that B and log U_H^0 are the measurements that have the greatest effect on the precision of the macroscopic ionization constants. Our pK_1 and pK_2 values (Table 1) (see footnote 2) for 3-hydroxypyridine and pyridoxine agree with those previously reported in the literature (19–22) in pure water. We have not found data for these compounds in water–dioxane or other water–organic solvent mixtures.

The uncharged species of 3-hydroxypyridine and pyridoxine are mixtures of two tautomeric forms (see Scheme 1). For this reason the pK values obtained are in fact macroscopic, i.e., they cannot be attributed to any particular ionizable group. By calculating the constants for the tautomerization processes we can then arrive at the microscopic ionization equilibrium constants, i.e., those attributable to a specific group. In general, the pK values corresponding to phenol ionization increase with the proportions of dioxane owing to the fact that two ions are generated for each neutral molecule. On the other hand, the pK's for the ionization of the pyridium ions either do not change or else diminish slightly with an increase in dioxane because no change in the number of ions occurs (23). In our case pK_1 for 3-hydroxypyridine decreases as dioxane increases while pK_1 for pyridoxine increases slightly under the same conditions (Table 1; see also footnote 2). pK_2, however, increases in both cases, more so with for 3-hydroxypyridine (Table 1; see also footnote 2).

As pK_1 is macroscopic (and thus reflects simultaneously the ionization of NH^+ and OH in the form ^+f (see Scheme 1)) we may say that the pK_1 values for 3-hydroxypyridine are mainly due to the ionization of NH^+ while for pyridoxine they are due to that of OH. This is confirmed by the tautomerization constant values for the equilibrium $^0f{=\!=}^{\pm}f$ (see Scheme 1) at 25°C for these two compounds (1), which indicate that the proportion of dipolar form is greater in pyridoxine than in 3-hydroxypyridine for the same water–dioxane mixture. The same reasoning is sufficient to explain the rise in the pK_2 values in both cases and that this increase is greater for 3-hydroxypyridine than for pyridoxine.

As the pK values are macroscopic, we have not studied the quantitative effect of the solvent on the equilibrium constants.

Using the pK_1 and pK_2 values for different temperatures we calculated the standard thermodynamic function changes for the first and second ionization of both compounds in the various water–dioxane mixtures. A general equation has been developed by Clarke and Glew (24) to represent the temperature dependence of reaction equilibrium constants in terms of the standard thermodynamic function changes at a chosen reference temperature, θ. This equation can be rewritten as

$$[5] \quad R \ln K = b_0 + b_1 t_1 + b_2 t_2 + b_3 t_3$$

where the terms t_i are a function of the temperature (25), and the b_i terms are directly proportional to the standard thermodynamic function changes at θ = 298.15 K. Equation [5] gives us a general representation of $R \ln K$ as a function of temperature and four undetermined constants containing ΔG_θ^0, ΔH_θ^0, $\Delta C_{p\theta}^0$, and $(d\Delta C_{p\theta}^0/dT)_\theta$.

We have made a regression analysis, successively increasing the number of terms in Eq. [5] and stopping when an F-test (25) revealed that the confidence level in the introduction of a new term was less than 95%.

To apply eq. [5] it is essential that the concentration scale used should not depend on temperature. Throughout the study, however, we have used the temperature-dependent molar scale and so it is necessary to obtain the equilibrium constants in the molal scale using

$$[6] \quad R \ln K(m) = R \ln K(c) - nR \ln d_0$$

where n is the increase in the stoichiometric number of particles whose activity is involved in the equilibrium constant, $K(m)$ and $K(c)$ are the equilibrium constants in the molal and molar scales, respectively, and d_0 the density of the solvent.

We obtained the values and the standard errors for the standard thermodynamic function changes by a least-squares fitting (26, 27). Typical standard errors in the determination of ΔG_θ^0, ΔH_θ^0, and $-\theta\Delta S_\theta^0$ turned out to be ± 0.12, ± 2, and ± 2 kJ mol^{-1}, respectively.

The optimum values, in the molar scale, of the standard thermodynamic function changes calculated in this way are given in Figs. 1–4. Because of the limited precision of our experimental pK values and the requirement of at least 95% confidence level, we have not calculated either the $\Delta C_{p\theta}^0$ values or their derivatives.

The dissociations of the two compounds studied have very similar characteristics. In the first ionization (Figs. 1 and 3) ΔH_θ^0 and $-\theta\Delta S_\theta^0$ are analogous, with $-\theta\Delta S_\theta^0$ somewhat higher in mixtures with high dioxane content and ΔH_θ^0 in low dioxane content. In the second ionization (Figs. 2 and 4), however, $-\theta\Delta S_\theta^0$ is always much higher than ΔH_θ^0 in all the water–dioxane mixtures studied. We may conclude that the values for $-\theta\Delta S_\theta^0$ are practically always larger than the corresponding ΔH_θ^0 and thus established the trend in ΔG_θ^0. Both components always contribute to the free energy in the same direction.

We can see that the $-\theta\Delta S_\theta^0$ values are partially compensated by the ΔH_θ^0 values so that changes in ΔG_θ^0 are smaller than the increments in either enthalpy or entropy with changes in the chemical systems. This sort of compensation has been observed many times before for other ionization reactions and also for other reactions in solution (14).

The similarity between the ΔH_θ^0 of the dissociation process of these acids in water and in water–dioxane mixtures indicates a similar pattern of solvation in these solvents. The $\theta\Delta S_\theta^0$ values are always negative but are more so in water–dioxane mixtures (except for the first ionization at low dioxane content). This may be due to the fact that the degree of reorientation and partial immobilization of the dioxane and water molecules by H^+ and the neutral and anionic species is greater in water–dioxane mixtures than in pure water.

It is difficult to interpret the effect of the solvent upon the ΔH_θ^0 and $-\theta\Delta S_\theta^0$ values. The trends in ΔH_θ^0 and $-\theta\Delta S_\theta^0$ (Figs. 1–4) could be interpreted in terms of the solvation of the reactant and products (16) but it must not be forgotten that these values correspond to the macroscopic ionization pro-

Can. J. Chem. Downloaded from www.nrcresearchpress.com by 217.78.4.112 on 09/08/12
For personal use only.

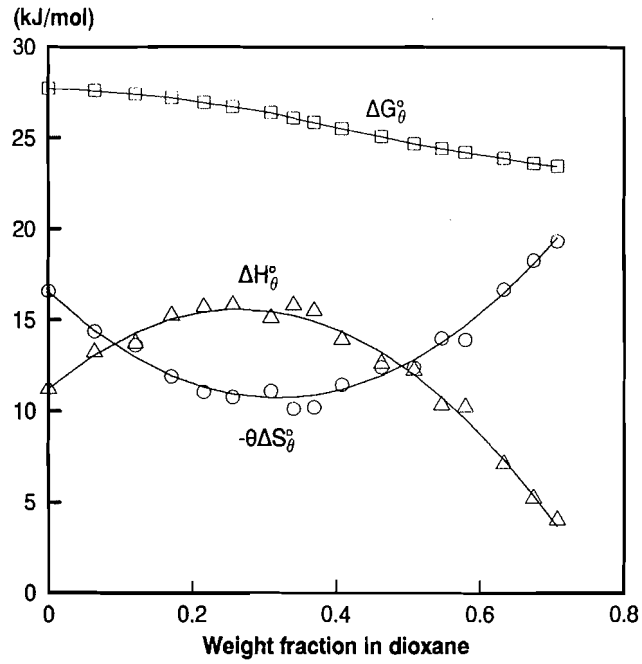

FIG. 1. Standard thermodynamic function changes corresponding to the first macroscopic ionization process of 3-hydroxypyridine versus the weight fraction in dioxane, in water–dioxane mixtures, at 25°C.

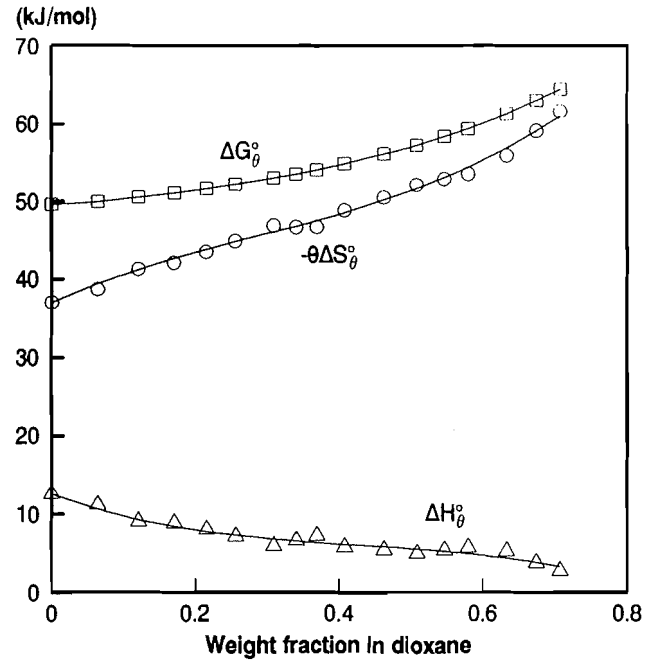

FIG. 2. Standard thermodynamic function changes corresponding to the second macroscopic ionization process of 3-hydroxypyridine versus the weight fraction in dioxane, in water–dioxane mixtures, at 25°C.

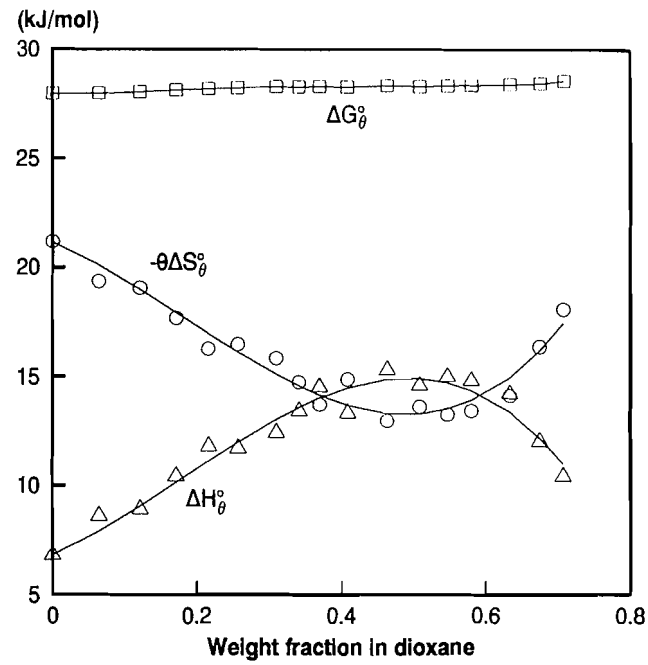

FIG. 3. Standard thermodynamic function changes corresponding to the first macroscopic ionization process of pyridoxine versus the weight fraction in dioxane, in water–dioxane mixtures, at 25°C.

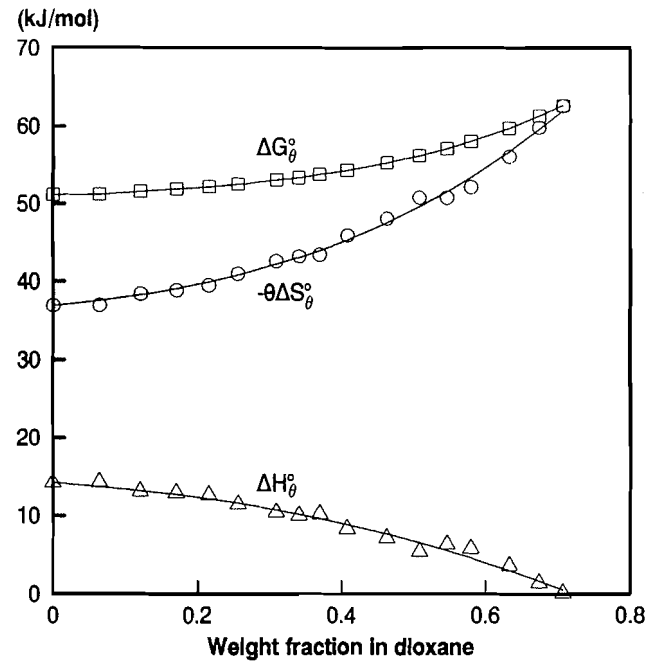

FIG. 4. Standard thermodynamic function changes corresponding to the second macroscopic ionization process of pyridoxine versus the weight fraction in dioxane, in water–dioxane mixtures, at 25°C.

cesses and that the species with a zero net charge exists in two forms (neutral and dipolar (see Scheme 1), the proportion of which changes according to the solvent composition. The different effects of the solvent upon the two microscopic ionizations (NH^+ and OH) and the tautomeric process may explain the overall effect shown in Figs. 1–4.

Since polar solvents per se are usually more structured than apolar solvents, proportionally fewer negative entropy changes are obtained in the more polar solvent such as water (28). This occurs during the second ionization but not during the first (Figs. 1 and 3) where the values of $\theta\Delta S^0_\theta$, although negative, initially increase and then decrease with the

rise in dioxane content. This may be explained qualitatively if we accept that the overall effect upon entropy and enthalpy is the sum of two contributory factors: (*a*) the "normal" effect of the solvent, as mentioned above; (*b*) the effect of the solvent upon the tautomerization equilibrium ${}^{0}f = {}^{\pm}f$.

If we take into account the equations defining ΔS^0_θ for the first and second macroscopic ionization we get:

$$[7] \quad (\Delta S^0_\theta)_{1\text{st ion}} = (f({}^{\pm}f)S({}^{\pm}f) + f({}^{0}f)S({}^{0}f)) + S(H^+) - S({}^{+}f)$$

$$[8] \quad (\Delta S^0_\theta)_{2\text{nd ion}} = S({}^{-}f) + S(H^+) - (f({}^{\pm}f)S({}^{\pm}f) + f({}^{0}f)S({}^{0}f))$$

and thus:

$$[9] \quad (\Delta S^0_\theta)_{1\text{st ion}} - (\Delta S^0_\theta)_{2\text{nd ion}} = 2(f({}^{\pm}f)S({}^{\pm}f) + f({}^{0}f)S({}^{0}f)) - S({}^{+}f) - S({}^{-}f)$$

where $f(i)$ is the molar fraction of the i form in the net zero charge species (see Scheme 1).

This difference is always positive and increases, in both compounds, with increasing proportion of dioxane. Bearing in mind that $f({}^{0}f)$ rises with the quantity of dioxane (1) it would be appear that $S({}^{0}f) > S({}^{\pm}f)$, and that this disparity increases with the proportion of dioxane.

If this be the case, the effect of the tautomeric equilibrium for the first ionization (eq. [7]) should give rise to an increase in $(\Delta S^0_\theta)_{1\text{st ion}}$. This is in fact seen with low dioxane contents, whilst with high dioxane proportions $(\Delta S^0_\theta)_{1\text{st ion}}$ diminishes notably, owing to the fact that $f({}^{\pm}f)$ becomes very small and the "normal" effect of the solvent predominates.

With the second protonation (eq. [8]) the same line of reasoning leads us to believe that the $(\Delta S^0_\theta)_{2\text{nd ion}}$ should diminish because of the tautomerization equilibria, which, together with the decrease brought about by the "normal" effect of the solvent, causes its value to diminish steadily and significantly as the proportion of dioxane increases, and, in fact, this is what we observed experimentally.

Thus the above hypotheses (*a*) and (*b*) would explain the general behaviour of the thermodynamic magnitudes for the first and second macroscopic protonation (Figs. 1–4) and also the differences between the values of ΔH^0_θ and $-\theta\Delta S^0_\theta$ for both protonations (Figs. 1 and 2; Figs. 3 and 4).

Acknowledgements

We thank Dr. J. Trout for the English text. This research was supported by grants from the Comision Asesora de Investìgaciòn Cìentìfica y Techìca (CAICYT) and the "Junta de Andalucia."

1. J. M. Sanchez-Ruiz, J. Llor, and M. Cortijo. J. Chem. Soc. Perkin Trans. 2, 2047 (1984).
2. J. Llor, J. M. Sanchez-Ruiz, and M. Cortijo. Acta Cient. Compostelana, **22**, 231 (1985).
3. J. M. Sánchez-Ruiz, M. Cortijo, and J. Llor. An. Quim. **82**, 165 (1986).
4. J. M. Sánchez-Ruiz, S. Asensio, J. Llor, and M. Cortijo. J. Chem. Soc. Perkin Trans. 2, 169 (1987).
5. J. Llor, J. M. Sánchez-Ruiz, and M. Cortijo. J. Chem. Soc. Perkin Trans. 2, 951 (1988).
6. M. Cortijo, J. Llor, and J. M. Sánchez-Ruiz. J. Biol. Chem. **263**, 17960 (1988).
7. P. Christen and D. E. Metzler (*Editors*). Transaminases. Wiley, New York. 1985. p. 65.
8. J. Steinbach and H. Freiser. Anal. Chem. **24**, 1027 (1952).
9. B. W. Grunbaum, W. Shoeniger, and P. L. Kirk. Anal. Chem. **24**, 1857 (1952).
10. E. A. Peterson and H. A. Sober. J. Am. Chem. Soc. **76**, 169 (1954).
11. L. G. van Uitert and C. E. Haas. J. Am. Chem. Soc. **75**, 451 (1953).
12. L. G. Van Uitert and W. C. Fernelius. J. Am. Chem. Soc. **76**, 5887 (1954).
13. J. Llor, M. Sánchez-Nevado, S. Asensio, and M. Cortijo. An. Quim. **83**, 317 (1987).
14. E. M. Woolley, D. G. Hurkot, and L. H. Hepler. J. Phys. Chem. **74**, 3908 (1970).
15. C. C. Panichajakul and E. M. Woolley. Anal. Chem. **47**, 1870 (1975).
16. C. C. Panichajakul and E. M. Woolley. Adv. Chem. Ser. **155**, 263 (1976).
17. H. S. Harned and B. B. Owen. The physical chemistry of electrolytic solutions. 3rd ed. Reinhold, New York. 1958.
18. F. Hovorka, R. A. Schaeffer, and D. Dreisbach. J. Am. Chem. Soc. **58**, 2264 (1936).
19. J. J. Christensen, L. D. Hansen, and R. M. Izatt. Handbook of proton ionization heats and related thermodynamics quantities. Wiley–Interscience, New York. 1976.
20. D. E. Metzler, C. M. Harris, R. J. Johnson, C. B. Siano, and J. A. Thomson. Biochemistry, **12**, 5377 (1973).
21. H. A. Sober (*Editor*). Handbook of biochemistry and selected data for molecular biology. 2nd ed. The Chemical Ruber Co., Cleveland, Ohio. 1973.
22. P. N. Moorthy and E. Hayon. J. Am. Chem. Soc. **97**, 2048 (1975).
23. D. D. Perrin, B. Dempsey, and E. P. Sarjeant. pK_a prediction for organic acid and bases. Chapman and Hall, London. 1981.
24. E. C. W. Clarke and D. N. Glew. Trans. Faraday Soc. **62**, 539 (1966).
25. P. D. Bolton. J. Chem. Educ. **47**, 638 (1970).
26. W. E. Wentworth. J. Chem. Educ. **42**, 96 (1965).
27. J. Sands. J. Chem. Educ. **54**, 90 (1977).
28. C. Reichardt. Solvent effects in organic chemistry. Verlag Chemie, New York. 1979. p. 76.

Can. J. Chem. Downloaded from www.nrcresearchpress.com by 217.78.4.112 on 09/08/12
For personal use only.

Intramolecular hydrogen bonding in ribonucleoside sugar hydroxyls. An *ab initio* study

ENRIC BOSCH, MIQUEL MORENO, AND JOSÉ M. LLUCH[1]

Departament de Química, Universitat Autònoma de Barcelona, 08193 Bellaterra, Catalonia, Spain

Received October 21, 1991

ENRIC BOSCH, MIQUEL MORENO, and JOSÉ M. LLUCH. Can. J. Chem. **70**, 1640 (1992).

Ab initio self-consistent field (SCF) calculations were done for a model of a ribonucleoside where only the ring part of the furanoside form of D-ribose is considered. Full geometry optimization and direct location of stationary points were used in order to characterize the geometry of the minimum energy structure and of the transition state for the proton transfer reaction in the anion. Topological analysis of the charge density and its Laplacian for the minimum energy structure allow us to find clear electronic and geometrical evidence of an intramolecular hydrogen bond. On the other hand, our results show a very low energy barrier for the proton transfer so that the proton jumps easily between the two oxygen atoms.

ENRIC BOSCH, MIQUEL MORENO et JOSÉ M. LLUCH. Can. J. Chem. **70**, 1640 (1992).

On a effectué des calculs *ab initio* en champ auto-cohérent (SCF) sur un modèle de ribonucléoside dans lequel on ne considère que la partie cyclique de la forme furanoside du D-ribose. On a utilisé une optimisation complète de la géométrie et une location directe des points stationnaires pour caractériser la géométrie de la structure possédant une énergie minimale et de l'état de transition de la réaction du transfert de proton dans l'anion. Une analyse topologique de la densité de charge et de son laplacien pour la structure d'énergie minimale nous permet d'obtenir des données électronique et géométrique non-ambiguës concernant une liaison hydrogène intramoléculaire. Par ailleurs, nos résultats montrent que la barrière d'énergie pour le transfert du proton est faible; il en résulte que le proton passe facilement d'un oxygène à l'autre.

[Traduit par la rédaction]

Can. J. Chem. Downloaded from www.nrcresearchpress.com by 217.78.4.112 on 09/08/12
For personal use only.

Introduction

It is well known that the sugar hydroxyls of ribonucleosides have enhanced acidities (1–3). This fact has been attributed to the presence of the vicinal *cis* 2'-OH and 3'-OH groups and the ability of these to stabilize the anionic form via an intramolecular hydrogen bond O(3')—H $\cdots$ O(2') or O(3') $\cdots$ H—O(2') (see Fig. 1).

The main goal of this paper is to present theoretical evidence of the existence of such an intramolecular hydrogen bond. This kind of work is of relevance given that Izatt *et al.* (1) have suggested that the acidity of the ribose in RNA is a result of the combined effect of both hydroxyl groups. Since the known chemical reactivity of the 2'- and 3'-positions in nucleic acids would be expected to parallel the acidity of the OH group, the different biological functions of RNA and DNA may be closely related to the acidity differences arising from the lack of the second hydroxyl group in DNA.

Analysis of the results will be performed by means of the theory of molecular structure proposed by Bader and coworkers (4–11). According to this methodology, the total electronic charge density $\rho(\boldsymbol{r})$ and its Laplacian $\nabla^2\rho(\boldsymbol{r})$ are considered.

The Laplacian of the charge density is defined as the sum of the three principal curvatures of the function at each point in space. That is:

$$\nabla^2\rho(\boldsymbol{r}) = \frac{\delta^2\rho}{\delta x^2} + \frac{\delta^2\rho}{\delta y^2} + \frac{\delta^2\rho}{\delta z^2}$$

When two neighbouring atoms are chemically bonded to one another, a bond critical point ($\boldsymbol{r}_c$) in the charge density appears between them. At the bond critical point $\nabla\rho(\boldsymbol{r}_c) = 0$, the charge density being a minimum at $\boldsymbol{r}_c$ along the bond path but a maximum along any orthogonal displacement. In turn, the Laplacian of the charge density at a point $\boldsymbol{r}$ in space determines where electronic charge is locally concentrated ($\nabla^2\rho(\boldsymbol{r}) < 0$) or depleted ($\nabla^2\rho(\boldsymbol{r}) > 0$). So when $\nabla^2\rho(\boldsymbol{r}_c)$ is negative the electronic charge is locally concentrated in the internuclear region. This occurs due to shared (covalent) interactions. Conversely, for closed-shell interactions $\nabla^2\rho(\boldsymbol{r}_c)$ is positive. These last kind of interactions are dominated by the contraction of charge away from the interatomic surface towards each of the nuclei. In a closed-shell interaction the atoms are bonded as a consequence of the charge that is concentrated within the basin of each atom. Taking all this into account, a hydrogen bond (11) is defined as one in which a hydrogen atom is bound to the acid fragment by a shared interaction and to the base by a closed-shell interaction.

Method of calculation

Ab initio self-consistent field (SCF) calculations were carried out with the GAUSSIAN 86 series of programs (12) using the split valence basis set 3-21+G (13, 14), which contains a diffuse *sp* shell on atoms other than hydrogens. To obtain a computationally available model of a ribonucleoside, only the ring part of the furanoside form of the D-ribose was considered. That is, we took into account neither the 5' carbon nor the heterocyclic nitrogenated base (see Fig 1).

Full geometry optimization and direct location of stationary points were done by means of the Schlegel gradient optimization algorithm (15). Analytical second derivatives of the energy with respect to the Cartesian coordinates (16) were computed to test the nature of each stationary point.

The influence of the correlation energy was determined by using the Møller–Plesset perturbation theory up to second order (MP2) (17).

Topological analysis of the charge density was performed by means of programs developed in our group that make use of the density matrix as obtained from a GAUSSIAN 86 run.

[1]Author to whom correspondence may be addressed.

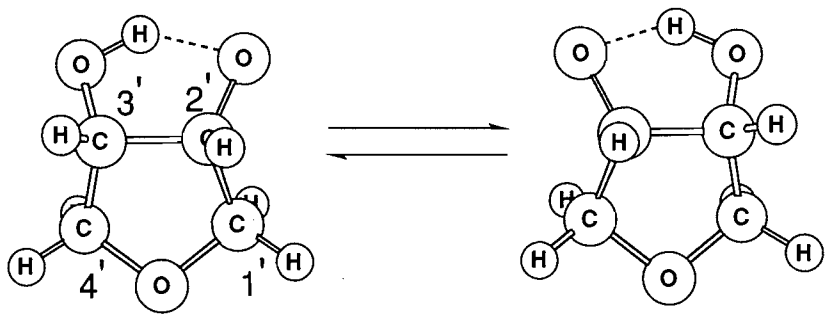

FIG. 1. Model of the ribonucleoside used and scheme of the proton transfer reaction. Numeration of atoms is used in the text.

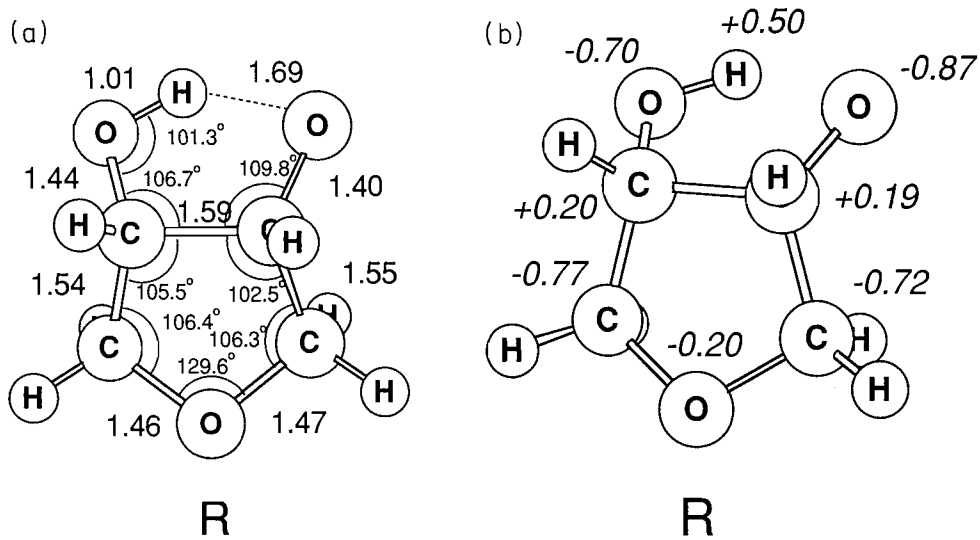

FIG. 2. Geometry of the minimum energy structure located at 3-21+G level. (*a*) Bond lengths (Å) and angles (deg) are given. (*b*) Mulliken atomic charges on heavy atoms and the oxygen-attached hydrogen are given in au. The charges in the rest of the hydrogen atoms range from +0.20 to +0.26 au.

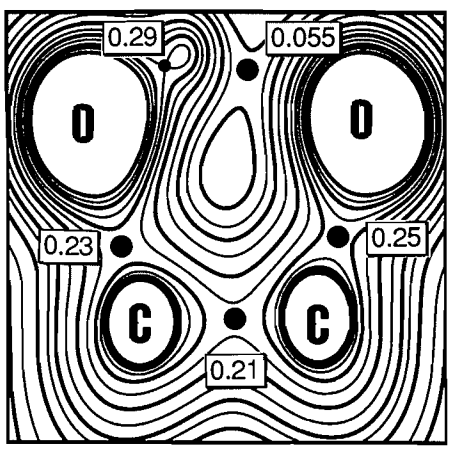

FIG. 3. Isodensity contour plots of $\rho(r)$ in the O(3′)—H···O(2′) plane at the minimum energy structure for the ribonucleoside model. Numbers indicate the $\rho(r)$ values at the bond critical points in au.

Results and discussion

In Fig. 2*a* the structure of minimum energy found for the anion is depicted along with the more significant bond lengths and angles. It has to be noted that the molecule is not planar, belonging to the C_1 symmetry group. The four carbon atoms lie almost in a plane but the oxygen in the furanoside ring is above this plane whereas the O(2′) and O(3′) atoms are placed below it.

Two facts seem to indicate the existence of a hydrogen bond. First, from a geometrical point of view, the short distance between hydrogen and oxygen (2′) is noteworthy (see Figure 2*a*). Second, the Mulliken population analysis (18) discloses that oxygen O(2′) and hydrogen atoms possess net charges of opposite sign (see Fig. 2*b*). This last point is of special importance as a reminder that hydrogen bonds are mainly due to electrostatic interactions.

Figures 3 and 4, respectively, present the isodensity contour plots of $\rho(r)$ and $\nabla^2\rho(r)$ in the O(3′)—H···O(2′) plane at the structure of minimum energy shown in Fig. 2. The positions of the bond critical points are marked with a dot in Figs. 3 and 4. Simultaneous inspection of topological properties of $\rho(r)$ and $\nabla^2\rho(r)$ allow us to identify four covalent bonds in the molecular region represented in Figs. 3 and 4: two C—O, one C—C, and the O(3′)—H bonds. In addition, a clear hydrogen bond H···O(2′) appears, its bond critical point being found clearly inside the positive region of the Laplacian.

As noted by Boyd and Choi (19), the charge density at the bond critical point of the hydrogen bond is paralleled by the increase in the hydrogen bond strength. In this sense, the

Can. J. Chem. Downloaded from www.nrcresearchpress.com by 217.78.4.112 on 09/08/12
For personal use only.

TABLE 1. Energies (au) for the proton transfer reaction

	E_{SCF} (3-21+G)	ZPE[a]	MP2/3-21+G//3-21+G[b]
Reactant	−378.06894	0.11961	−0.76388
Transition state	−378.06431	0.11593	−0.76855

[a]Zero point energy correction.
[b]Second order Møller–Plesset correction.

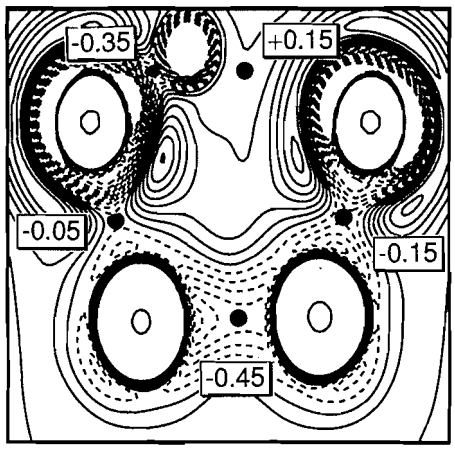

FIG. 4. Isodensity contour plots of the Laplacian $\nabla^2\rho(r)$ in the O(3′)—H · · · O(2′) plane at the minimum energy structure for the ribonucleoside model. Dashed lines correspond to regions in which $\nabla^2\rho(r) < 0$ and solid lines correspond to regions in which $\nabla^2\rho(r) > 0$. Numbers indicate the $\nabla^2\rho(r)$ values at the bond critical points in au. The solid line closest to the dashed lines corresponds to the zero value. The increment between consecutive lines is 0.1 au.

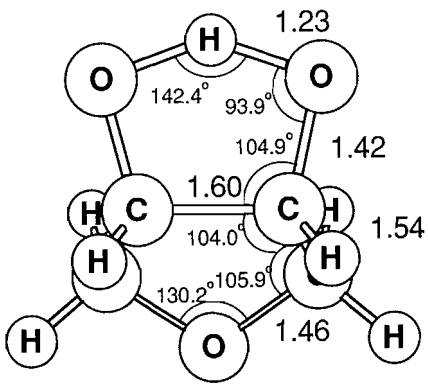

TS

FIG. 5. Geometry of the transition state for intramolecular proton transfer reaction in the ribonucleoside model. Bond lengths are given in Å and angles in degrees.

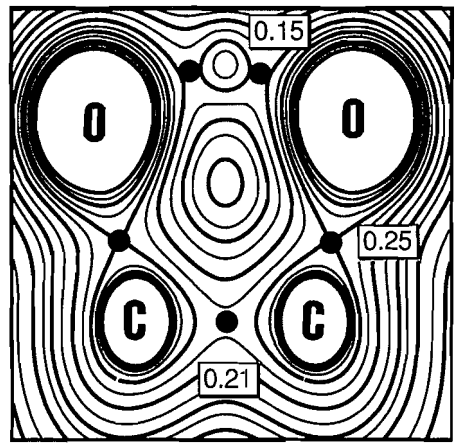

FIG. 6. Isodensity contour plots of $\rho(r)$ in the O(3′)—H · · · O(2′) plane at the transition state for intramolecular proton transfer reaction in the ribonucleoside model. Numbers indicate the $\rho(r)$ values at the bond critical points in au.

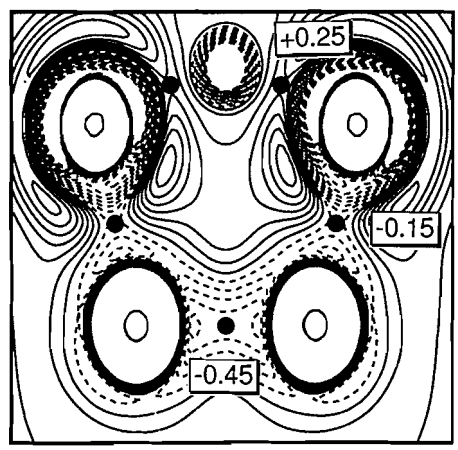

FIG. 7. Isodensity contour plots of the Laplacian $\nabla^2\rho(r)$ in the O(3′)—H · · · O(2′) plane at the transition state for intramolecular proton transfer in the ribonucleoside model. Dashed lines correspond to regions in which $\nabla^2\rho(r) < 0$, and solid lines correspond to regions in which $\nabla^2\rho(r) > 0$. Numbers indicate the $\nabla^2\rho(r)$ values at the bond critical points in au. The solid line closest to the dashed lines corresponds to the zero value. The increment between consecutive lines is 0.1 au.

present value of 0.055 is intermediate between the values we obtained for the water dimer (0.035) and the $H_2O \cdots OH^-$ hydrogen bond (0.15) at the same 3-21+G basis set level by using the corresponding optimized geometries. These values are always low when compared with the typical values of covalent bonds, as is readily seen by inspection of Fig. 3.

Interestingly, we have also seen that the proton is not attached to one oxygen but it may easily switch between oxygens O(2′) and O(3′). In fact a transition state for the intramolecular proton transfer has been localized (Fig. 5). This structure belongs to the C_s symmetry group as now both oxygen–hydrogen distances are equal.

Table 1 shows the total energies for the minimum energy

Can. J. Chem. Downloaded from www.nrcresearchpress.com by 217.78.4.112 on 09/08/12
For personal use only.

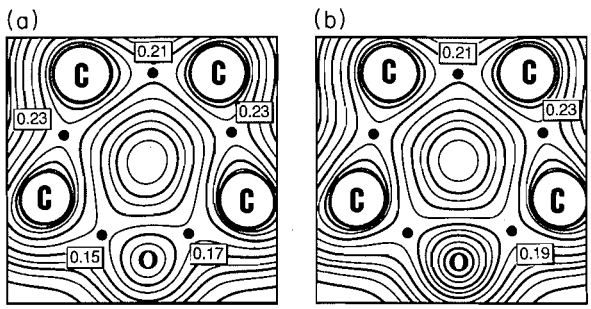

FIG. 8. Isodensity contour plots of $\rho(r)$ in the C(1′), C(2′), and C(3′) plane at the minimum energy structure (*a*) and the transition state (*b*) for intramolecular proton transfer reaction in the ribonucleoside model. Numbers indicate the $\rho(r)$ values at the bond critical points in au.

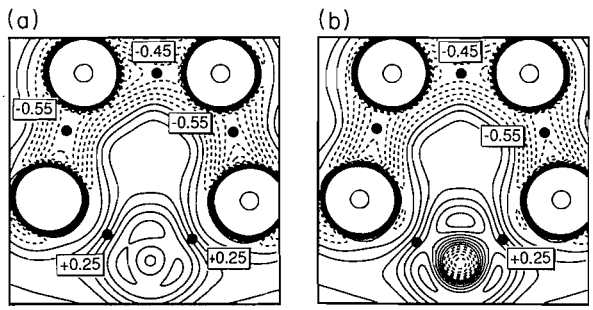

FIG. 9. Isodensity contour plots of the Laplacian $\nabla^2\rho(r)$ in the C(1′), C(2′), and C(3′) plane at the minimum energy structure (*a*) and the transition state (*b*) for intramolecular proton transfer in the ribonucleoside model. Dashed lines correspond to regions in which $\nabla^2\rho(r) < 0$, and solid lines correspond to regions in which $\nabla^2\rho(r) > 0$. Numbers indicate the $\nabla^2\rho(r)$ values at the bond critical points in au. The solid line closest to the dashed lines corresponds to the zero value. The increment between consecutive lines is 0.1 au.

structure and the transition state at the SCF 3-21+G level. Zero Point Energy (ZPE) and correlation energy corrections are also presented. From the data presented in Table 1 the energy barrier obtained for the proton transfer through this transition state is only 2.91 kcal/mol at the 3-21+G level, which reduces to 0.59 kcal/mol when ZPE is calculated through the harmonic frequencies obtained by diagonalizing the energy second derivatives matrix (20). This small barrier disappears when correlation energy is introduced within the Møller–Plesset perturbation theory up to second order (MP2), 3-21+G geometries being kept unchanged. Though it is known that the MP2 level tends to exaggerate the effect of electron correlation (21–23), this result confirms that the proton jumping between both oxygen atoms O(2′) and O(3′) is very easy.

To discuss the electronic distribution of the transition state, the isodensity contour plots of $\rho(r)$ and $\nabla^2\rho(r)$ in the O(3′)—H···O(2′) plane are respectively depicted in Figs. 6 and 7.

As seen in the figures, the transferring hydrogen is bonded with the same strength to both oxygens. In addition, the Laplacian plot discloses that the corresponding bond critical points are now inside the positive region of the Laplacian, so that these two bonds have a closed-shell character and the transferring hydrogen behaves as a proton. This situation is quite different to the one found for the minimum energy structure.

Another interesting point is to see what is happening in the rest of the anion while proton transfer is occurring. To this aim, in Figs. 8 and 9 we show the isodensity contour plots of $\rho(r)$ and $\nabla^2\rho(r)$, respectively, in the plane of the C(1′), C(2′), and C(3′) carbon atoms for both the minimum energy structure and the transition state. It has to be recalled here that the oxygen in the furanoside ring is above this plane in both structures. It is seen that the electronic distribution in the furanoside ring does not noticeably change along the reaction. Only minor modifications appear, due to the fact that the furanoside oxygen is closer to the plane in the transition state than in the minimum energy structure.

Conclusions

In this paper we have presented high level *ab initio* calculations for a model of a ribonucleoside. By analizing the topology of the total electronic charge density and its Laplacian, we have found clear evidence of the existence of an intramolecular hydrogen bond.

We have also seen that the hydroxylic hydrogen is not attached to one oxygen but it jumps between oxygens O(2′) and O(3′), through a small or null barrier. Analysis of the transition state reveals that the transferring hydrogen behaves as a proton.

Acknowledgements

We thank Dr. Miquel Duran and Dr. Feliu Maseras for supplying us the programs to perform the topological analysis.

1. R. M. Izatt, L. D. Hansen, J. H. Rytting, and J. J. Christensen. J. Am. Chem. Soc. **87**, 2760 (1965).
2. G. I. Birnbaum, J. Giziewicz, C. P. Huber, and D. Shugar. J. Am. Chem. Soc. **98**, 4640 (1976).
3. W. Saenger. Principles of nucleic acid structure. Springer Verlag, New York. 1984. p. 108.
4. R. F. W. Bader, Y. Tal, S. G. Anderson, and T. T. Nguyen-Dang. Isr. J. Chem. **19**, 8 (1980).
5. R. F. W. Bader and H. Essen. J. Chem. Phys. **80**, 1943 (1984).
6. R. F. W. Bader, P. J. McDougall, and C. D. H. Lau. J. Am. Chem. Soc. **106**, 1594 (1984).
7. R. F. W. Bader and P. J. McDougall. J. Am. Chem. Soc. **107**, 6788 (1985).
8. R. F. W. Bader, M. T. Carroll, J. R. Cheeseman, and C. Chang. J. Am. Chem. Soc. **109**, 7968 (1987).
9. Z. Shi and R. J. Boyd. J. Chem. Phys. **88**, 4375 (1988).
10. R. P. Sagar, A. C. T. Ku, and V. H. Smith, Jr. J. Chem. Phys. **88**, 4367 (1988).
11. R. F. W. Bader. Atoms in molecules. A quantum theory. Oxford University Press, New York. 1990.
12. M. J. Frisch, J. S. Binkley, H. B. Schlegel, *et al.* Gaussian 86. Carnegie–Mellon Quantum Chemistry Publishing Unit, Pittsburgh, Pa. 1984.
13. G. W. Spitznagel, T. Clark, J. Chandrasekhar, and P. von R. Schleyer. J. Comput. Chem. **3**, 363 (1982).
14. T. Clark, J. Chandrasekhar, G. W. Spitznagel, and P. von R. Schleyer. J. Comput. Chem. **4**, 294 (1983).
15. H. B. Schlegel. J. Comput. Chem. **3**, 214 (1982).
16. J. A. Pople, R. A. Krishnan, H. B. Schlegel, and J. S. Binkley. Int. J. Quantum Chem. Quantum Chem. Symp. **13**, 225 (1979).
17. J. A. Pople, J. S. Binkley, and R. Seeger. Int. J. Quantum Chem. Quantum Chem. Symp. **10**, 1 (1976).

Can. J. Chem. Downloaded from www.nrcresearchpress.com by 217.78.4.112 on 09/08/12
For personal use only.

18. R. S. Mulliken. J. Chem. Phys., **23**, 1833 (1955); **23**, 1841 (1955); **23**, 2338 (1955); **23**, 2343 (1955).
19. R. J. Boyd and S. C. Choi. Chem. Phys. Lett. **120**, 80 (1985); **129**, 62 (1986).
20. W. J. Hehre, L. Radom, P. v. R. Schleyer, and J. A. Pople. Ab initio molecular orbital theory. John Wiley & Sons, New York. 1986.
21. M. M. Szczesniak and S. Scheiner. J. Chem. Phys. **77**, 4586 (1982).
22. S. Scheiner, M. M. Szczesniak, and L. D. Bigham. Int. J. Quantum Chem. **23**, 739 (1983).
23. M. Moreno, J. M. Lluch, A. Oliva, and J. Bertran. J. Phys. Chem. **92**, 4180 (1988).

Can. J. Chem. Downloaded from www.nrcresearchpress.com by 217.78.4.112 on 09/08/12
For personal use only.

Integral method for infinite dilution activity coefficients calculation

A. C. CHIALVO
Programa de Electroquímica Aplicada e Ingeniería Electroquímica (PRELINE), Facultad de Ingeniería Química (UNL), Santiago del Estero 2829, (3000) Santa Fe, Argentina

Received September 27, 1990

A. C. CHIALVO. Can. J. Chem. **70**, 1645 (1992).

An integral method to determine infinite dilution activity coefficients (γ_i^∞) from data sets of finite concentration activity coefficients is proposed for binary systems. This method is based upon the integration of the experimental dependence of $\ln \gamma_i/x_j^2$ over different composition ranges. The limiting behavior of this function is analysed, in order to improve the precision of its integration. The accuracy of this method is demonstrated by the calculation of γ_i^∞ for several systems.

A. C. CHIALVO. Can. J. Chem. **70**, 1645 (1992).

On propose une méthode d'intégration permettant, pour les systèmes binaires, de déterminer les coefficients d'activité à dilution infinie (γ_i^∞) à partir des données relatives aux coefficients d'activité à concentrations finies. La méthode est basée sur l'intégration de la relation expérimentale de $\ln \gamma_i/x_j^2$ sur différents ensembles de composition. Afin d'améliorer la précision de l'intégration, on a analysé le comportement limitant de cette fonction. On a démontré l'exactitude de la méthode par le calcul du γ_i^∞ de plusieurs systèmes.

[Traduit par la rédaction]

Can. J. Chem. Downloaded from www.nrcresearchpress.com by 217.78.4.112 on 09/08/12
For personal use only.

Introduction

One of the sources more commonly used to obtain the infinite dilution activity coefficients (γ_i^∞) is undoubtedly the vapor–liquid equilibrium (VLE). The reduction of VLE data to obtain the γ_i^∞ values varies from the graphical or analytical extrapolation of a $\ln \gamma_i - x_i$ data set (1) to the determination of the limiting slope of temperature or pressure with respect to the liquid phase composition (2–6). All of these processes require experimental determinations in the composition range near to that of the pure components. However, a method that allows us to verify the thermodynamic consistency of these data is not available. The present work intends to cover these important aspects by the development of a process that permits us to evaluate the γ_i^∞ value starting from an entire or partial $\ln \gamma_i - x_i$ data set.

Fundamentals

The Gibbs–Dühem equation for activity coefficients at constant temperature and pressure in a binary system can be written in the form:

$$[1] \quad d \ln \gamma_j = -d\left(\frac{x_i}{x_j} \ln \gamma_i\right) + \frac{\ln \gamma_i}{x_j^2} dx_i$$

The integration of eq. [1] can be carried out using different limits. Taking into account the limiting behaviour of the activity coefficients (7), it is possible to arrive at the following useful expressions:

$$[2] \quad \ln \gamma_j^\infty = \int_{x_i=0}^{x_i=1} \frac{\ln \gamma_i}{x_j^2} dx_i$$

$$[3] \quad \ln \gamma_j^\infty = \frac{g^E}{x_j} + \int_{x_i=x_i}^{x_i=1} \frac{\ln \gamma_i}{x_j^2} dx_i$$

where $g^E = G^E/RT$ and G^E is the excess Gibbs energy.

These equations allow us to determine the infinite dilution activity coefficients. Nevertheless, in order to improve the evaluation of the integrals in eqs. [2] and [3] it is convenient to analyze the limiting behavior of the integrand function.

Limiting behaviour of the function ln γ_i/x_j^2

Taking into account that, when $x_i = 1$, $\ln \gamma_i = 0$ and $d \ln \gamma_i/dx_i = 0$:

$$[4] \quad \lim_{x_i \to 1}\left[\frac{\ln \gamma_i}{x_j^2}\right] = -\lim_{x_i \to 1}\left[\frac{\frac{d \ln \gamma_i}{dx_i}}{2x_j}\right] = \frac{1}{2}\lim_{x_i \to 1}\left[\frac{d^2 \ln \gamma_i}{dx_i^2}\right]$$

The right-hand side of eq. [4] can be evaluated by derivation of the classical form of the Gibbs–Dühem equation and application of limiting conditions:

$$[5] \quad \lim_{x_i \to 1}\left[\frac{d^2 \ln \gamma_i}{dx_i^2}\right] = -\left[\frac{d \ln \gamma_j}{dx_j}\right]^\infty$$

Substituting into eq. [4]:

$$[6] \quad \lim_{x_i \to 1}\left[\frac{\ln \gamma_i}{x_j^2}\right] = -\frac{1}{2}\left[\frac{d \ln \gamma_j}{dx_j}\right]^\infty$$

The behaviour of the integrand function on the other integration limit is

$$[7] \quad \lim_{x_i \to 0}\left[\frac{\ln \gamma_i}{x_j^2}\right] = \ln \gamma_i^\infty$$

Besides, by derivation of the integrand function with respect to x_i,

$$[8] \quad \frac{d}{dx_i}\left[\frac{\ln \gamma_i}{x_j^2}\right] = \frac{x_j\left[\frac{d \ln \gamma_i}{dx_i}\right] + 2 \ln \gamma_i}{x_j^3}$$

the limiting slopes can be found. For $x_i \to 0$:

$$[9] \quad \lim_{x_i \to 0} \frac{d}{dx_i}\left[\frac{\ln \gamma_i}{x_j^2}\right] = \left[\frac{d \ln \gamma_i}{dx_i}\right]^\infty + 2 \ln \gamma_i^\infty$$

TABLE 1. Limiting behavior of the integrand functions

$\ln \gamma_1/x_2^2$	$\ln \gamma_2/x_1^2$
$\lim_{x_1\to 0}\left[\frac{\ln \gamma_1}{x_2^2}\right] = \lim_{x_1\to 0}\left[\frac{g^E}{x_1}\right] = \ln \gamma_1^\infty$	$\lim_{x_2\to 0}\left[\frac{\ln \gamma_2}{x_1^2}\right] = \lim_{x_2\to 0}\left[\frac{g^E}{x_2}\right] = \ln \gamma_2^\infty$
$\lim_{x_1\to 1}\left[\frac{\ln \gamma_1}{x_2^2}\right] = -\lim_{x_2\to 0}\frac{d\left(\frac{g^E}{x_2}\right)}{dx_2} = -\frac{1}{2}\left[\frac{d \ln \gamma_2}{dx_2}\right]^\infty$	$\lim_{x_2\to 1}\left[\frac{\ln \gamma_2}{x_1^2}\right] = -\lim_{x_1\to 0}\frac{d\left(\frac{g^E}{x_1}\right)}{dx_1} = -\frac{1}{2}\left[\frac{d \ln \gamma_1}{dx_1}\right]^\infty$
$\lim_{x_1\to 0}\frac{d\left(\frac{\ln \gamma_1}{x_2^2}\right)}{dx_1} = 2\lim_{x_1\to 0}\left\{\frac{g^E}{x_1} + \frac{d}{dx_1}\left(\frac{g^E}{x_1}\right)\right\} = \left[\frac{d \ln \gamma_1}{dx_1}\right]^\infty + 2 \ln \gamma_1^\infty$	$\lim_{x_2\to 0}\frac{d\left(\frac{\ln \gamma_2}{x_1^2}\right)}{dx_2} = 2\lim_{x_2\to 0}\left\{\frac{g^E}{x_2} + \frac{d}{dx_2}\left(\frac{g^E}{x_2}\right)\right\} = \left[\frac{d \ln \gamma_2}{dx_2}\right]^\infty + 2 \ln \gamma_2^\infty$
$\lim_{x_1\to 1}\frac{d\left(\frac{\ln \gamma_1}{x_2^2}\right)}{dx_1} = \frac{1}{6}\left[\frac{d^3 \ln \gamma_1}{dx_1^3}\right]^\infty$	$\lim_{x_2\to 1}\frac{d\left(\frac{\ln \gamma_2}{x_1^2}\right)}{dx_2} = \frac{1}{6}\left[\frac{d^3 \ln \gamma_2}{dx_2^3}\right]^\infty$

TABLE 2. Calculated and experimental infinite dilution activity coefficients

System	$\ln \gamma_1^\infty$ (γ_1^∞)			$\ln \gamma_2^\infty$ (γ_2^∞)		
	Present work	Experimental	$\lim_{x_1\to 0} g^E/x_1$	Present work	Experimental	$\lim_{x_2\to 0} g^E/x_2$
Dichloromethane(1)–methanol(2) 25°C (ref. 8)	1.0717 (2.920)	1.0777 (ref. 8) (2.938)	1.08 (2.945)	2.3140 (10.115)	2.3343 (ref. 8) (10.322)	2.18 (8.846)
Ethanol(1)–toluene(2) 45°C (9)	2.482 (11.965)	2.531 (9) (12.566)	2.50 (12.182)	1.725 (5.612)	1.725 (9) (5.612) 1.723 (10) (5.601)	1.715 (5.557)
Methanol(1)–cyclohexene(2) 45°C (11)	3.043 (20.968)	3.6375 (4) (37.996) 3.0782 (12) (21.719)	3.04 (20.905)	2.889 (17.975)	2.8545 (4) (17.366) 2.8909 (12) (18.009)	2.90 (18.174)
Benzene(1)–acetonitrile (2) 25°C (13)	1.189 (3.284)	1.160 (5) (3.190) 1.1886 (13) (3.282)	1.19 (3.287)	1.263 (3.536)	1.2441 (20°C) (5) (3.470) 1.2529 (13) (3.500)	1.27 (3.561)
Ethanol(1)–chlorobenzene(2) 75.2°C (14)	1.590 (4.904)	1.466 (14) (4.334)	1.57 (4.807)	1.1575 (3.182)	1.1323 (14) (3.103)	1.15 (3.158)
Diisopropylamine(1)–water(2) 20°C (15)	3.5037 (33.238)	—	3.50 (33.115)	2.0454 (7.732)	—	2.03 (7.614)
1-Propanol(1)–*n*-heptane(2) 45°C (9)	3.325 (27.799)	3.287 (9) (26.762)	3.28 (26.576)	1.978 (7.228)	1.987 (9) (7.294)	1.98 (7.243)

For $x_i \to 1$, the right-hand side of eq. [8] becomes indeterminant. Through the application of L'Hopital's rule twice, the following limit is obtained:

$$[10]\quad \lim_{x_i\to 1}\frac{d}{dx_i}\left[\frac{\ln \gamma_i}{x_j^2}\right] = \lim_{x_i\to 1}\left[\frac{\frac{d^3 \ln \gamma_i}{dx_i^3}}{6}\right] = \frac{1}{6}\left[\frac{d^3 \ln \gamma_i}{dx_i^3}\right]^\infty$$

Estimate of the limiting values

As stated before, the evaluation of eqs. [2] and [3] can be improved if the limiting values of the integrand function are known. For such an estimate, the supplementary function g^E/x_i is used. It provides the following relationships:

$$[11]\quad \lim_{x_i\to 0}\left[\frac{g^E}{x_i}\right] = \ln \gamma_i^\infty = \lim_{x_i\to o}\left[\frac{\ln \gamma_i}{x_j^2}\right]$$

Can. J. Chem. Downloaded from www.nrcresearchpress.com by 217.78.4.112 on 09/08/12
For personal use only.

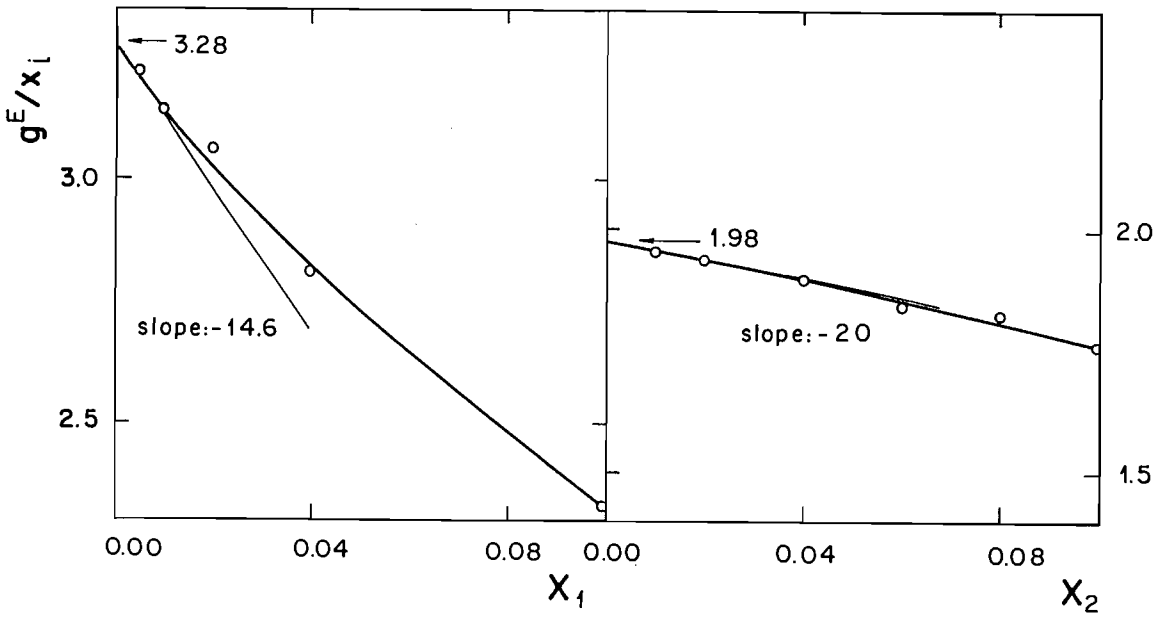

FIG. 1. Dependence of the function g^E/x_i upon the composition for the system 1-propanol(1)–*n*-heptane(2) at 45°C.

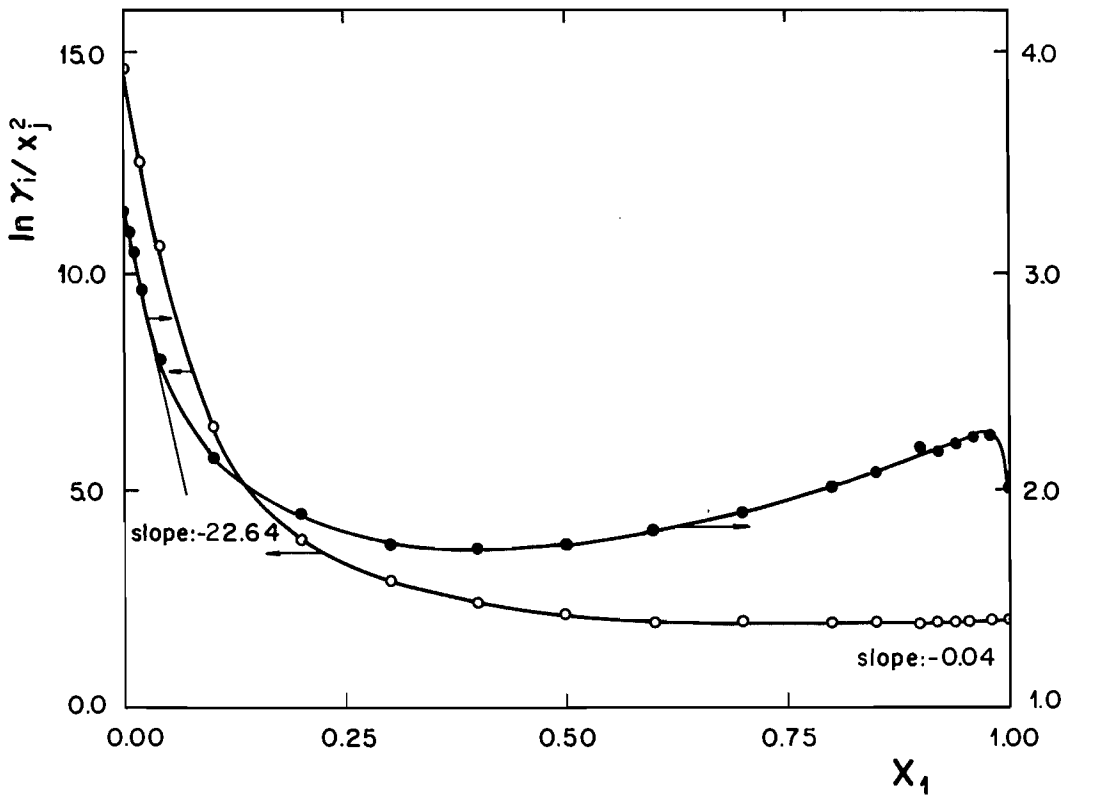

FIG. 2. Dependence of the integrand function upon the composition for the system 1-propanol(1)–*n*-heptane(2) at 45°C. (●) $i = 1$; (○) $i = 2$.

$$[12]\quad \lim_{x_i \to 0} \frac{d}{dx_i}\left[\frac{g^E}{x_i}\right] = \frac{1}{2}\left[\frac{d \ln \gamma_i}{dx_i}\right]^{\infty} = -\lim_{x_i \to o}\left[\frac{\ln \gamma_j}{x_i^2}\right]$$

Hence, eq. [9] can be rewritten as follows:

$$[13]\quad \lim_{x_i \to o} \frac{d}{dx_i}\left[\frac{\ln \gamma_i}{x_j^2}\right] = 2 \lim_{x_i \to 0}\left\{\frac{g^E}{x_i} + \frac{d}{dx_i}\left[\frac{g^E}{x_i}\right]\right\}$$

A summary of the limiting equations derived here is shown in Table 1. These expressions can be applied to evaluate the γ_i^{∞} from experimental isobaric (P) or isothermic (T) activity coefficient data, obtained from VLE studies. These data require a point-to-point temperature or pressure correction and therefore information about the excess enthalpy (h^E) or excess volume (v^E) function under the same conditions as the VLE measurements is necessary. However, the weak de-

Can. J. Chem. Downloaded from www.nrcresearchpress.com by 217.78.4.112 on 09/08/12
For personal use only.

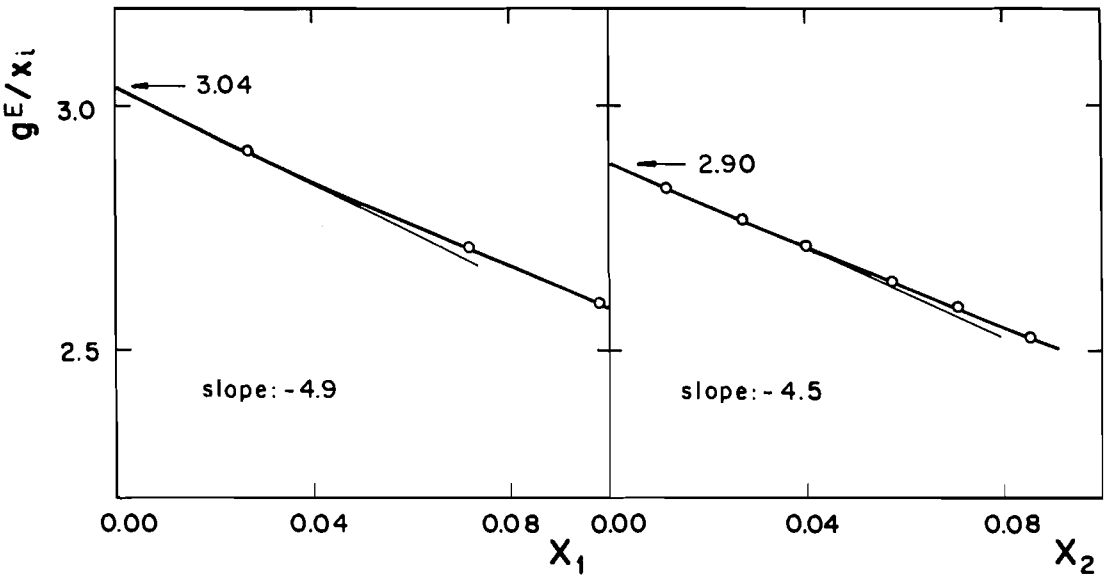

FIG. 3. Dependence of the function g^E/x_i upon the composition for the system methanol(1)–cyclohexene(2) at 45°C.

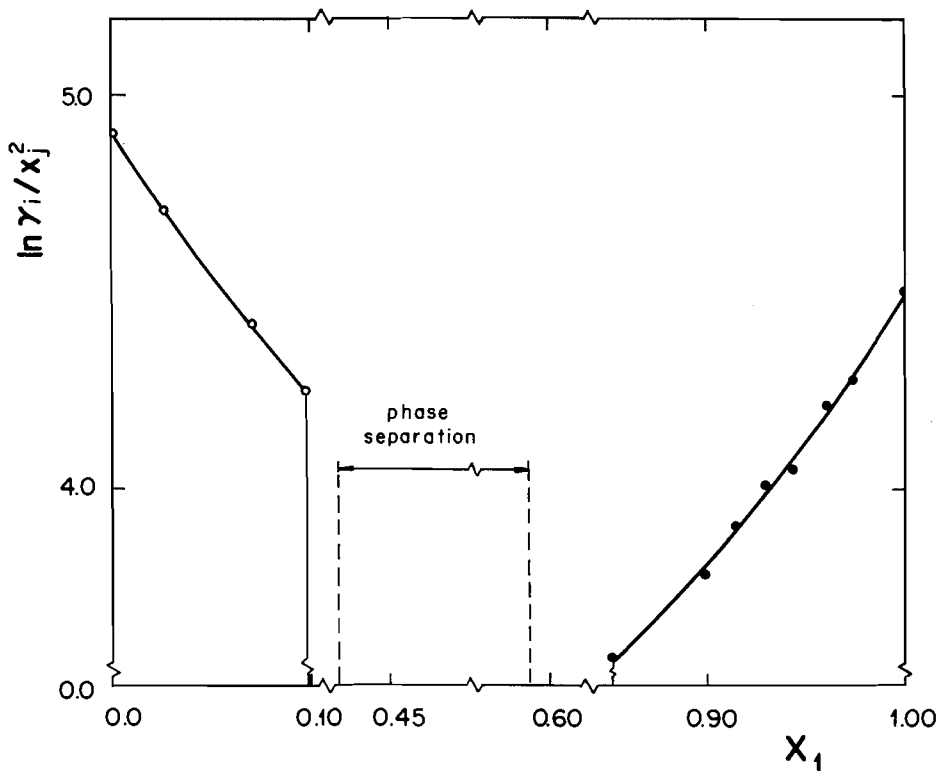

FIG. 4. Dependence of the integrand function upon the composition for the system methanol(1)–cyclohexene(2) at 45°C. (●) $i = 1$; (○) $i = 2$.

pendence of the activity coefficient on pressure makes the correction for isothermic data quite negligible. For this reason, isothermic data were used in this paper to illustrate the expressions obtained.

Applications

The following general procedure is proposed for the calculation of the infinite dilution activity coefficients on the basis of the expressions deduced above: (*i*) Estimation of the limiting behavior of the integrand function starting from the limiting behavior of g^E/x_i, through eqs. [11]–[13]. (*ii*) Evaluation of the integrand function from the corrected $\ln \gamma_i - x_i$ data set. (*iii*) Calculation of γ_i^∞ through eqs. [2] or [3] according to the data set used.

The proposed procedure was used to calculate γ_i^∞ for several systems. The experimental data were obtained from the literature and the results are summarized in Table 2. The calculations for two of these systems are described here in

Can. J. Chem. Downloaded from www.nrcresearchpress.com by 217.78.4.112 on 09/08/12
For personal use only.

order to illustrate the procedure. From data of Van Ness *et al.* (9) for the system 1-propanol(1)–*n*-Heptane(2) at 45°C, the auxiliary plots were drawn for the estimation of the limiting integrand functions (Fig. 1). With these values, the ln γ_i/x_j^2 vs. x_i plot was completed (Fig. 2). The following values were obtained from the integration: ln $\gamma_1^\infty = 3.325$ ($\gamma_1^\infty = 27.798$) and ln $\gamma_2^\infty = 1.978$ ($\gamma_2^\infty = 7.228$).

The second example is the methanol(1)–cyclohexane(2) system at 45°C reported by Madhovan and Murti (11). This mixture exhibits phase separation with the compositions (16): $x_1' = 0.425$ and $x_1'' = 0.590$. The g^E/x_i vs. x_i and ln γ_i/x_j^2 vs. x_i plots are shown in Figs. 3 and 4, respectively. The following integration limits were used: (*i*) for ln γ_1^∞, $x_2 = 0.902$ ($g^E = 0.25426$) and $x_2 = 1$, and (*ii*) for ln γ_2^∞, $x_1 = 0.8515$ ($g^E = 0.3407$) and $x_1 = 1$ (Fig. 4). The application of eq. [3] gave the following results: ln $\gamma_1^\infty = 3.043$ ($\gamma_1^\infty = 20.968$) and ln $\gamma_2^\infty = 2.889$ ($\gamma_2^\infty = 17.975$).

Discussion

The proposed method is based on a suitable solution of the Gibbs–Dühem equation at constant temperature (T) and pressure (P). It provides thermodynamically consistent $\gamma_i^\infty(T,P)$ values from corrected $\gamma_i(T,P^{exp},x_i)$ or $\gamma_i(T^{exp},P,x_i)$ data sets. In this work the calculations that illustrate the proposed procedure were made from isothermic data without pressure correction. The error of this approximation can be estimated with the following expression:

$$[14] \quad \ln \frac{\gamma_i(T,P,x_i)}{\gamma_i(T,P^{exp},x_i)} = \frac{(\bar{v}_i - v_i^0)}{RT}(P - P^{exp})$$

For the different systems analysed, eq. [14] shows that this correction term is less than 10^{-3} and therefore negligible compared to the ln γ_i values. Nevertheless, in the case where the pressure variation is appreciable, the correction should be made.

It is important to note that the limiting values were estimated from the g^E/x_i vs. x_i plot, which exhibits a limiting slope value that is one-half of that of the ln γ_i vs. x_i plot (eq. [12]) and consequently represents a better extrapolation condition. The accuracy obtained in the analysed systems was good, as can be observed in Table 2, for the final evaluation of the γ_i^∞.

A different approach could be made in order to take into account, for example, the pressure effect. In this case, eq. [1] becomes

$$[15] \quad d \ln \gamma_j = -d\left(\frac{x_i}{x_j} \ln \gamma_i\right) + \left[\frac{\ln \gamma_i}{x_j^2} + \frac{v^E}{x_j RT}\frac{\partial P}{\partial x_i}\bigg|_T\right] dx_i$$

The use of this expression is similar to that derived above and, in this case, information about the $v^E(x_i)$ at similar conditions of the activity coefficient data and the total vapor pressure dependence upon the composition of VLE is necessary. The corresponding form of eq. [6] is now

$$[16] \quad \lim_{x_i \to 1}\left(\frac{\ln \gamma_i}{x_j^2}\right) = \frac{1}{2}\left[\frac{\partial \ln \gamma_j}{\partial x_j}\bigg|_T + \frac{v^E}{x_j RT}\frac{\partial P}{\partial x_j}\bigg|_T\right]^\infty$$

It can be concluded, on the basis of the results obtained, that the proposed method allows us to evaluate the activity coefficient at infinite dilution with accuracy and reliability.

1. L. B. Schreiber and C. A. Eckert. Ind. Eng. Chem. Process Des. Develop. **10**, 572 (1971).
2. M. F. Gautreaux and J. Coates. AIChE J. **1**, 496 (1955).
3. S. R. M. Ellis and P. A. Jonah. Chem. Eng. Sci. **17**, 971 (1962).
4. G. M. Loblen and J. M. Prausnitz. Ind. Eng. Chem. Fundam. **21**, 109 (1981).
5. E. R. Thomas, B. A. Newman, G. L. Nicolaides, and C. E. Eckert. J. Chem. Eng. Data, **27**, 233 (1982).
6. K. A. Pividal and S. Sandler. J. Chem. Eng. Data, **33**, 438 (1988).
7. A. C. Chialvo. An. Asoc. Quim. Argent. **73**, 531 (1985).
8. J. R. Khurma, O. Muthu, S. Munjal, and B. O. Smith. J. Chem. Eng. Data, **28**, 412 (1983).
9. H. C. Van Ness, C. A. Soczak, G. L. Peloquin, and R. L. Machado. J. Chem. Eng. Data, **3**, 217 (1967).
10. C. A. Eckert, B. A. Newman, G. L. Nicolaides, and T. C. Long. AIChE J. **27**, 33 (1981).
11. S. Madhavan and P. S. Murti. Chem. Eng. Sci. **21**, 465 (1966).
12. J. Gmehling and U. Onken. Vapor–liquid equilibrium data collection. DECHEMA, Vol. 1. Part 2.a. 1977. p. 237.
13. R. Srivastava and B. D. Smith. J. Chem. Eng. Data, **31**, 94 (1986).
14. J. R. Khurma, O. Muthu, S. Munjal, and B. O. Smith. J. Chem. Eng. Data, **28**, 100 (1983).
15. R. R. Davison. J. Chem. Eng. Data, **13**, 348 (1968).
16. T. Nitta, S. Takeuchi, and T. Katayama. Chem. Eng. Sci. **29**, 2213 (1974).

Can. J. Chem. Downloaded from www.nrcresearchpress.com by 217.78.4.112 on 09/08/12
For personal use only.

Molecular geometry of $M(NO)_2$ complexes: single crystal X-ray structure of $Co(NO)_2(C_5H_5N)_2^+BF_4^-$, lability of the pyridine ligands of $Co(NO)_2(C_5H_5N)_2^+$, and its relevance to the formation of the $Co_2(NO)_3^+$ bimetallic core

JEAN-LOUIS ROUSTAN[1] AND NASRIN ANSARI
Department of Chemistry, University of Ottawa, Ottawa, Ont., Canada K1N 6N5

AND

YVON LE PAGE[1] AND JEAN-PIERRE CHARLAND
Division of Chemistry, National Research Council of Canada, Ottawa, Ont., Canada K1A OR9

Received May 21, 1991[2]

JEAN-LOUIS ROUSTAN, NASRIN ANSARI, YVON LE PAGE, and JEAN-PIERRE CHARLAND. Can. J. Chem. **70**, 1650 (1992).

The BPh_4^- and BF_4^- derivatives of $Co(NO)_2(Py)_2^+$ **3** (Py = pyridine) have been prepared. In solution, whereas $Co(NO)_2(L)_2^+BPh_4^-$ (L = phosphane) and **3**-BF_4^- are inert, **3**-BPh_4^- decomposes rapidly in the absence of an excess of Py. Complex **3**-BF_4^- crystallizes in the monoclinic system with two independent molecules, A and B, in the asymmetric unit, space group $P2_1/a$, a = 14.7633(6) Å, b = 13.9739(5) Å, c = 15.1667(6) Å, β = 109.334(4)°, 2225 reflections, R = 0.054, Rw = 0.023. The cobalt coordination polyhedron is a distorted tetrahedron. The comparison of the (O)N—Co—N(O) angles of 115.6(3)° (molecule A) and 115.9(3)° (molecule B) with those of other $D^{8+2}_{NO(M)}$ pseudotetrahedral dinitrosyl complexes suggests that the lability of the Py ligands of cation **3** reflects the compression experienced by the $Co(NO)_2^+$ molecular portion.

JEAN-LOUISE ROUSTAN, NASRIN ANSARI, YVON LE PAGE et JEAN-PIERRE CHARLAND. Can. J. Chem. **70**, 1650 (1992).

Les dérivés BPh_4^- et BF_4^- de $Co(NO)_2(Py)_2^+$ **3** (Py = pyridine) ont été préparés. En solution, alors que $Co(NO)_2(L)_2^+BPh_4^-$ (L = phosphane) et **3**-BF_4^- sont inertes, **3**-BPh_4^- est décomposé rapidement en l'absence d'un excès de Py. Le complexe **3**-BF_4^- cristallise dans le système monoclinique avec deux molécules indépendantes, A et B, dans l'unité asymétrique, groupe d'espace $P2_1/a$, a = 14,7633(6) Å, b = 13,9739(5) Å, c = 15,1667(6) Å, β = 109,334(4)°, 2225 réflexions, R = 0,054, Rw = 0,023. Le polyèdre de coordination du cobalt est un tétraèdre déformé. La comparaison des angles (O)N—Co—N(O) de 115,6(3)° (molécule A) et 115,9(3)° (molécule B) avec ceux d'autres complexes dinitrosyles pseudotétraédriques du type $D^{8+2}_{NO(M)}$ suggère que la labilité des ligands Py du cation **3** est la conséquence de la compression à laquelle est soumis le fragment moléculaire $Co(NO)_2^+$.

Introduction

Recently, the reaction of BPh_4^- with $Co(NO)_2(PN)I$ **1** containing the diphenyl(2-pyridyl)phosphine ligand $P(C_6H_5)_2$-(2-C_5H_4N) (abbreviated as PN henceforth) was shown (1) to yield the Co—Co bonded bimetallic $Co_2(NO)_3(PN)_2^+BPh_4^-$ **2**. Complex **2** can be viewed as containing two $Co(NO)_2$ subunits sharing the same μ_2-NO bridging ligand with one cobalt further bounded to two pyridyl N atoms and the other to two P atoms. To obtain information suggestive of a possible mode of formation, the previously unknown cobalt dinitrosyl bispyridine cation $Co(NO)_2(Py)_2^+$ **3** was synthesized with either BF_4^- or BPh_4^- as the gegenanion. In this paper, we report the observations pertaining to the behavior in solution of these complexes and the single crystal X-ray structure of the BF_4^- derivative that allow us to comment upon the possible role of BPh_4^- in the reactions ultimately yielding bimetallic **2**.

Experimental

All operations were conducted under argon or vacuum with argon saturated solvents. The IR spectra were recorded on a Perkin–Elmer 783. ^{11}B NMR spectra were recorded on a Varian FT80 with $BF_3(Et_2O)$ as external reference. Elemental analyses were performed by Guelph Chemical Laboratories Ltd, Guelph, Ontario.

Preparation of $Co(NO)_2(Py)_2^+BF_4^-$,3-BF_4^-

$(Co(NO)_2I)_2$ (2.38 g) (2) and 1.6 mL of pyridine (Py) were dissolved in 20 mL of absolute ethanol at 20°C. To the stirred solution was added dropwise 1.88 g of $AgBF_4$ in 10 mL of ethanol. After stirring an additional hour, solid AgI was separated by filtration and the solution was evaporated to dryness under vacuum at 20°C. The residue was recrystallized in CH_2Cl_2–hexane to yield 2.68 g of dark microcrystalline crystals. νNO (CH_2Cl_2) = 1876, 1798 cm^{-1}. Anal. calcd. (found) for $C_{10}H_{10}BCoF_4N_4O_2$: %C 33.0(33.2), %H 2.8(3.1), %N 15.4(15.0). In the solid state, the complex can be handled in air for a brief period of time, but is very air sensitive in solution. Under argon, it is stable in CH_2Cl_2 in the absence of added pyridine.

Preparation of $Co(NO)_2(Py)_2^+BPh_4^-$,3-BPh_4^-

To a stirred solution of 0.55 g of $(Co(NO)_2I)_2$ and 0.37 mL of pyridine in 22 mL of absolute ethanol was added dropwise 0.77 g of $NaBPh_4$ in 15 mL of ethanol. Olive-green microcrystals precipitated rapidly. After an additional 30 min of stirring, the crystals were separated by filtration and dried under vacuum (1.18 g). The compound was recrystallized in CH_2Cl_2–hexane in the presence of an excess of pyridine. νNO(CH_2Cl_2) = 1870, 1790 cm^{-1} (unstable in solution in the absence of added pyridine). (Anal. calcd.(found) for $C_{34}H_{30}BCoN_4O_2.CH_2Cl_2$: %C 61.7(62.4), %H 4.7(5.1), %N 8.2(9.0)).

Preparation of $Co(NO)_2(PN)_2^+BPh_4^-$

To a solution of 0.54 g of $(Co(NO)_2I)_2$ in 30 mL of absolute ethanol heated at 50°C in a water bath was added 0.30 g of $P(C_6H_5)_2$(2-C_5H_4N) (PN) (3). After stirring 20 min at the same temperature, 0.59 g of $NaBPh_4$ in 10 mL of ethanol was added dropwise. The reaction mixture was stirred an additional 20 min and subsequently cooled down to 20°C. The precipitate that had formed was separated by filtration and dried under vacuum to yield 0.49 g of product, recrystallized in CH_2Cl_2–ether. νNO(CH_2Cl_2) = 1845, 1795 cm^{-1} (stable in solution in the absence of added ligand). Anal. calcd. (found) for $C_{58}H_{48}BCoN_4O_2P_2.CH_2Cl_2$: %C 67.4 (67.7) %H 4.8(5.0), %N 5.5(5.4).

Crystallographic studies

Single crystals of $Co(NO)_2(Py)_2^+BF_4^-$ were grown by slow dif-

[1]Authors to whom correspondence may be addressed.
[2]Revision received January 2, 1992.

Can. J. Chem. Downloaded from www.nrcresearchpress.com by 217.78.4.112 on 09/08/12
For personal use only.

TABLE 1. Crystal data and refinement indicators for $C_{10}H_{10}BCoF_4O_2$

Parameter	Value	Parameter	Value
fw	363.83	Radiation	MoKα
Crystal system	Monoclinic	μ, mm^{-1}	1.21
Minimum transmission factor	0.87	Maximum transmission factor	0.90
Space group	$P2_1/a$	$2\theta_{max}$, deg	45
a, Å	14.7633(6)	Measured reflections	6038
b, Å	13.9739(5)	Un. reflections	3820
c, Å	15.1667(6)	Observed reflections (m)[a]	2225
β, deg	109.334(4)	Parameters varied (n)	458
V, $Å^3$	2952.5	R_F[b]	0.054
Z	8	wR_F[c]	0.023
D_{calcd}, g cm^{-3}	1.638	GOF[d]	2.462
$F(000)$	1455.63	max(Δ/σ)	0.1

[a] $I \geq 2.5\ \sigma(I_{net})$.
[b] $R_F = \Sigma[|F_o| - |F_c|]/\Sigma|F_o|$.
[c] $wR_F = [\Sigma w(|F_o| - |F_c|)^2/\Sigma w|F_o|^2]^{1/2}$.
[d] $GOF = [\Sigma w(|F_o| - |F_c|)^2/(m - n)]^{1/2}$.

fusion of an upper layer of toluene into a concentrated solution of the complex in methylene chloride. Crystals were mounted on a glass rod and subsequently coated with a protective layer of epoxy resin.

A dark crystal, 0.15 × 0.15 × 0.30 mm, was selected for intensity measurement at 296 K up to 2θ 45° with graphite monochromatized MoKα radiation on an Enraf–Nonius CAD-4 diffractometer (4). A total of 6038 intensity measurements were performed, which reduced to 3820 unique reflections. Among these, 2225 reflections having I_{net} larger than 2.5 counting statistic stigmas were considered to be observed. The $P2_1/a$ space-group assignment was made from the systematic absence of the classes of reflections $0k0$ with k odd and $h0l$ with h odd. The data reduction assuming this space group comprised corrections for Lorentz and polarization effects using the measured polarization ratio of 0.97 for the monochromator used, but no absorption correction (μ = 1.21/mm). The cell parameters (Table 1) were derived from the angular settings of 45 strong reflections in the 2θ range 40–45° using $MoK\alpha_1$ wavelength (0.70930 Å).

The initial positions for the heavy atoms were proposed by the MULTAN program (5). Successive refinement and difference-Fourier cycles progressively disclosed all atoms, including the hydrogens. The final refinement with full matrix was performed on all atoms minimizing $\Sigma w(|F_c|-|F_o|)^2$ where $w^{-1} = \sigma^2(F_0)$, with fixed isotropic thermal motion for the hydrogens and refined anisotropic motion for the other ones, and included an extinction correction. The scattering factors were those of Cromer and Mann (6). The final residuals on the 2225 observed reflections were R_F = 0.054 and wR_F = 0.023. The largest shift was 0.1σ in the final cycle and the highest residual density was 0.47 e/$Å^3$. All calculations were performed with the NRCVAX system of programs (7). The final atomic positions are given in Table 2. The list of observed and calculated structure amplitudes, parameters for the H atoms, and U_{ij}'s for the non-hydrogen atoms have been deposited as supplementary material.[3]

[3]These data may be purchased from: The Depository of Unpublished Data, Document Delivery, CISTI, National Research Council Canada, Ottawa, Canada K1A 052.

Tables of H-atom parameters and bond lengths and angles associated with the pyridine and NO ligands have also been deposited with the Cambridge Crystallographic Data Centre and can be obtained on request from the Director, Cambridge Crystallographic Centre, University Chemical Laboratory, Lensfield Road, Cambridge CB2 1EW, U.K.

Results

Reactivity of cationic Co/NO/Py complexes

The cobalt dinitrosyl bispyridine cation $Co(NO)_2(Py)_2^+$ **3** was prepared by the room temperature reaction of an ethanolic solution of $(Co(NO)_2I)_2$ and pyridine in excess, with either $AgBF_4$ or $NaBPh_4$. The nature of the counteranion had a marked influence on the stability of cation **3** in solution. Whereas the BF_4^- derivative, **3**-BF_4^-, was inert in CH_2Cl_2 at room temperature, the BPh_4^- derivative, **3**-BPh_4^-, decomposed rapidly. Infrared monitoring of the decomposition showed the formation of a transient intermediate with at least one νNO at 1720 cm^{-1} clearly separated from those of **3**-BPh_4^- at 1870 and 1790 cm^{-1}. The magnitude of the νNO shift toward lower frequencies points to the formation of an uncharged intermediate. However, the latter is also very labile for after a few minutes no absorption remained in the 1900–1700 cm^{-1} region. No cobalt derivative could be isolated from the decomposed solutions. Under the same conditions, in the ^{11}B NMR spectra, the initial sharp BPh_4^- resonance of **3**-BPh_4^- at −5.9 ppm was rapidly replaced by a broad resonance centered at +6.0 ppm suggestive (8) of the formation of BPh_3.

Alternatively, **3**-BPh_4^- could be recrystallized without decomposition in CH_2Cl_2–hexane provided an excess of pyridine was also present. From this inhibitory effect of pyridine, it can be concluded that dissociation of a Py ligand from $Co(NO)_2(Py)_2^+$ is a prerequisite for the decomposition to proceed. Moreover, when dissociation occurs, the only ligand available in the medium for occupying the vacated coordination site has to come from BPh_4^-. Consequently, in line with the documented ability of BPh_4^- to phenylate metallic centers (9), the decomposition is likely to involve the formation of an uncharged σ-phenyl derivative such as $Co(NO)_2(Py)$-Ph with BPh_3 as a co-product. For comparison, with no excess of free ligand present, $Co(NO)_2(PN)_2^+BPh_4^-$, in which the two PN ligands should be P-bonded to Co, as in the structurally characterized BF_4^- derivative (10), was stable in solution, as well as $Co(NO)_2(PPh_3)_2^+BPh_4^-$(11) and $Co(NO)_2(P(OMe)_3)_2^+$ BPh_4^- (12). To identify a possible cause for the lability of the pyridine ligands of $Co(NO)_2(Py)_2^+$, an X-ray diffraction study was

Can. J. Chem. Downloaded from www.nrcresearchpress.com by 217.78.4.112 on 09/08/12
For personal use only.

Can. J. Chem. Downloaded from www.nrcresearchpress.com by 217.78.4.112 on 09/08/12
For personal use only.

TABLE 2. Atomic parameters x, y, z, and B_{iso} for $[CO(NO)_2(C_5H_5N)_2]^+$ $[BF_4]^-$; esd's refer to the last digit printed

	x	y	z	B_{iso}[a]
CO A	0.06232(8)	0.29287(7)	0.84672(7)	4.93(6)
N 1 A	0.0348 (6)	0.1544 (4)	0.8640 (4)	5.3 (4)
N 2 A	−0.0165 (4)	0.3404 (5)	0.9235 (5)	4.5 (4)
N 3 A	0.1768 (4)	0.3196 (5)	0.8985 (4)	6.5 (5)
N 4 A	0.0163 (4)	0.3260 (4)	0.7368 (4)	5.8 (4)
O 1 A	0.2538 (4)	0.3452 (5)	0.9227 (4)	10.6 (5)
O 2 A	−0.0037 (4)	0.3565 (4)	0.6620 (3)	8.3 (4)
C 1 A	0.1056 (6)	0.0889 (9)	0.8827 (6)	6.8 (6)
C 2 A	0.0899 (8)	−0.0072 (8)	0.8867 (7)	8.8 (8)
C 3 A	−0.0020 (11)	−0.0387 (7)	0.8749 (7)	8.0 (8)
C 4 A	−0.0736 (6)	0.0256 (9)	0.8555 (6)	6.4 (6)
C 5 A	−0.0531 (7)	0.1221 (7)	0.8503 (5)	5.5 (6)
C 6 A	−0.0125 (6)	0.3011 (6)	1.0057 (7)	5.4 (6)
C 7 A	−0.0644 (8)	0.3349 (8)	1.0590 (6)	6.6 (6)
C 8 A	−0.1250 (7)	0.4127 (8)	1.0270 (7)	6.5 (6)
C 9 A	−0.1288 (6)	0.4550 (6)	0.9468 (7)	5.9 (6)
C10 A	−0.0759 (7)	0.4171 (7)	0.8962 (5)	6.2 (6)
CO B	0.28679(7)	0.06856(7)	0.40512(7)	4.72(6)
N 1 B	0.3391 (5)	−0.0166 (4)	0.5176 (4)	4.6 (4)
N 2 B	0.1494 (4)	0.0363 (5)	0.3903 (4)	4.8 (4)
N 3 B	0.3165 (4)	0.0303 (5)	0.3154 (4)	5.5 (4)
N 4 B	0.3122 (5)	0.1814 (4)	0.4348 (4)	6.1 (4)
O 1 B	0.3433 (4)	0.0154 (4)	0.2538 (3)	8.1 (4)
O 2 B	0.3335 (5)	0.2603 (3)	0.4427 (4)	9.9 (5)
C 1 B	0.4092 (7)	−0.0805 (7)	0.5247 (6)	6.0 (6)
C 2 B	0.4459 (7)	−0.1356 (7)	0.6038 (10)	8.0 (8)
C 3 B	0.4136 (10)	−0.1245 (10)	0.6756 (8)	8.8 (9)
C 4 B	0.3409 (8)	−0.0618 (9)	0.6691 (7)	7.5 (7)
C 5 B	0.3058 (6)	−0.0077 (6)	0.5897 (8)	5.7 (6)
C 6 B	0.1196 (6)	−0.0531 (6)	0.3947 (5)	5.3 (5)
C 7 B	0.0259 (8)	−0.0764 (6)	0.3813 (6)	6.6 (6)
C 8 B	−0.0414 (7)	−0.0048 (9)	0.3619 (7)	7.6 (7)
C 9 B	−0.0136 (7)	0.0864 (8)	0.3579 (7)	8.5 (7)
C10 B	0.0810 (8)	0.1052 (5)	0.3721 (6)	6.9 (6)
B A	0.2272 (10)	0.2303 (9)	0.6698 (10)	7.1 (9)
F 1 A	0.3060 (5)	0.2281 (4)	0.6491 (6)	16.8 (7)
F 2 A	0.2323 (5)	0.1674 (4)	0.7307 (4)	16.4 (6)
F 3 A	0.1582 (4)	0.2093 (4)	0.5964 (4)	17.0 (5)
F 4 A	0.2193 (4)	0.3197 (3)	0.6947 (4)	11.1 (4)
B B	0.2409 (9)	0.2539 (10)	0.1687 (8)	6.4 (8)
F 1 B	0.3309 (3)	0.2330 (3)	0.2234 (3)	9.6 (3)
F 2 B	0.2173 (4)	0.1931 (4)	0.0947 (4)	13.1 (4)
F 3 B	0.1795 (4)	0.2284 (4)	0.2130 (4)	11.3 (4)
F 4 B	0.2279 (4)	0.3394 (4)	0.1410 (4)	14.7 (5)

[a] B_{iso} is the mean of the principal axes of the thermal ellipsoid.

undertaken with $Co(NO)_2(Py)_2{}^+BF_4{}^-$, which provided suitable crystals.

Single crystal structure of $Co(NO)_2(Py)_2{}^+BF_4{}^-$

The crystal structure consists of discrete $Co(NO)_2(Py)_2{}^+$ cations and $BF_4{}^-$ anions. The compound crystallizes with two independent molecules, A and B, in the asymmetric unit. A perspective view is presented in Fig. 1 together with the numbering scheme, and a summary of selected bond lengths and angles is given in Table 3. An ordered model for the $BF_4{}^-$ anion was considered as satisfactory, although a slight disorder of the F atoms around the calculated positions given in Table 2 might actually exist, in light of the values of their thermal parameters.

The general features are consistent in molecules A and B. Each cobalt is coordinated to two pyridyl and two nitrosylic N atoms located at the corners of a distorted tetrahedron. The (Py)N—Co—N(Py) and (O)N—Co—N(O) planes are perpendicular, with dihedral angles of 89.3(3)° and 89.2(3)° for molecules A and B respectively. The aromatic rings are planar within experimental errors (supplementary material, footnote 3). The Co—N(Py) distances of 2.012(6) Å for molecule A and 2.013(6) and 2.016(6) Å for molecule B fall near the lower range of the reported values for Co—N(Py) bond lengths, which can vary by ca. 0.2 Å, as shown for example by the values 1.917(2) and 2.203(10) Å for, respectively, $(\eta^5\text{-}C_5Me_5)CoCl(Py)$ (13) and $Co_2(DBA)_2(Py)_4$ (14) (DBA = 1,5-diphenyl-1,3,5-pentadionato). The Co—N and N—O bond lengths (Table 3) are normal when they are compared to other cobalt nitrosyl complexes (see for ex-

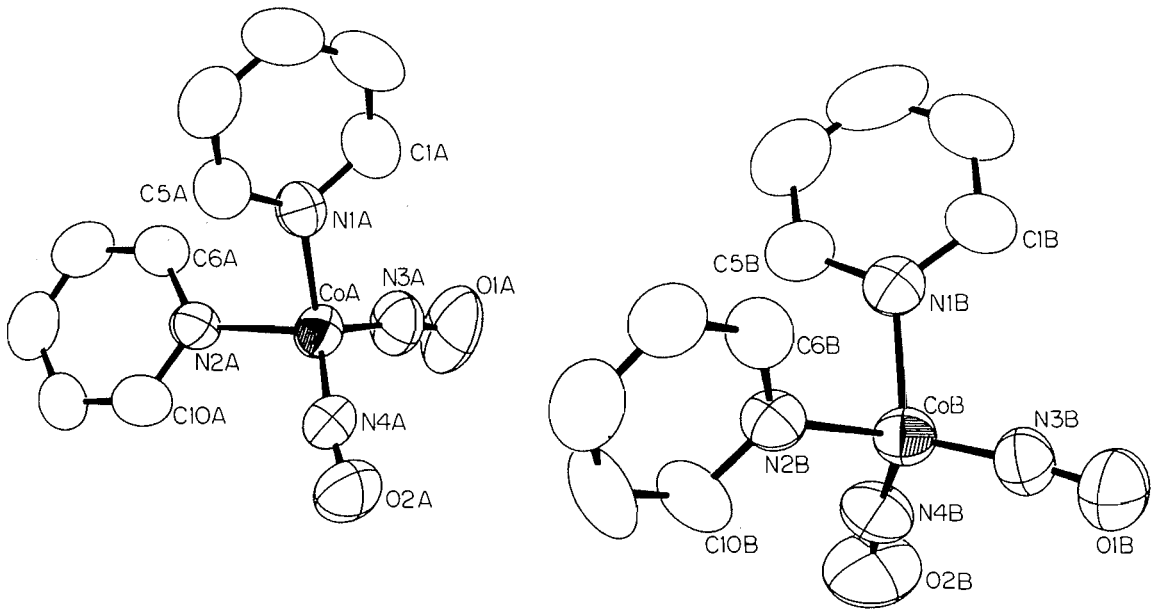

FIG. 1. Perspective view of the two independent cations of $Co(NO)_2(Py)_2^+$ **3** with the numbering scheme (the BF_4^- anions have been omitted for clarity).

ample the compilation in Table IV of Ref. 15 with ranges of 1.645(3)–1.68(2) Å for Co—N and 1.05(2)—1.174(6) Å for N—O). In both molecules, the O(N)..Co..(N)O angle sustended at Co by the two nitrosylic O atoms and the (O)N-Co-N(O) angle nicely follow the linear relationship of Martin and Taylor (16).

The shortest intramolecular nonbonded contacts (Table 3) involve the nitrosylic N atoms and the *ortho* H atoms of the Py ligands. They fall in the range 2.65(6)–2.86(7) Å, not significantly different from that of 2.66–2.89 Å reported (17) for the H(phenyl)...C/N intramolecular separations in $Co(CO)_x(NO)(PPH_3)_y$ ($x + y = 3$; $x = 1,2$). The latter have been regarded as reflecting short H...C/N contacts.

Discussion

The structural result of interest pertains to the values of the (O)N—Co—N(O) angles of 115.6(3)° (molecule A) and 115.9(3)° (molecule B) when they are compared to that of 128.0(8)° reported (18) for $Co(NO)_2(P(OMe)_3)_2^+$ BPh_4^-, which, together with $Co(NO)_2(Py)_2^+BF_4^-$, is a member of the $D^{8+2}_{NO(M)}$ family of pseudotetrahedral monometallic dinitrosyl complexes of general formula $M(NO)_2(L)_2^x$ ($x = 0$, $+1$).[4]

In $D^{8+2}_{NO(M)}$ complexes, the standard model (16, 21–23) to account for the variations of the (O)N—M—N(O) angle (abbreviated as the α angle henceforth) places the emphasis on the electronic influence of the $M(L)_2$ molecular portion of the $M(NO)_2$ moiety. According to this model, an increase in the M to NO π back-bonding, as it increases the electronic population of the M···NO bonds, enhances their mutual electrostatic repulsions, which favors an opening of the α angle. The nonbonded repulsive influence of a NO ligand can therefore be considered as a sensitive increasing function of the M to NO back-bonding. In this model, the variations of α are considered to be largely independent of the steric requirement of the supporting ligands L (16).

Some observations are in agreement with this proposal. For example the closing of α from 136.7(4)° in $Co(NO)_2(PPh_3)_2^+PF_6^-$ (24) (νNO(Nujol) = 1836, 1784 cm^{-1} (25)) to 128.0(8)° in $Co(NO)_2(P(OMe)_3)_2^+BPh_4^-$ (18) (νNO(CH_2Cl_2) = 1876, 1817 cm^{-1} (12)) has been interpreted (18) in terms of a decrease in the ligand σ-donor/π-acceptor ratio.

However, other results are not as readily interpreted. For example, from $Fe(NO)_2(PPh_3)_2$(νNO(C_2Cl_4) = 1724, 1678 cm^{-1} (26)) to $Co(NO)_2(PPh_3)_2^+PF_6^-$, whereas the M to NO back-bonding decreases, as shown by an increase in the νNO values, the α angle opens up by ca. 13° from 123.8(4) (22) to 136.7(4)° (24). The same observation applies upon going from the neutral to the cationic complex of the isoelectronic pairs $\{M(NO)_2(PPh_3)_2$, $M'(NO)_2(PPh_3)_2^+\}$ containing second (Ru, Rh^+) or third row (Os, Ir^+) metallic elements (see the data in Table VIII of Ref. 27). We suggest that these angular variations are more easily accounted for by taking the alternate view that the nonbonded repulsions in the M(NO)(L) moieties might be at least as important as those in the $M(NO)_2$ molecular portion, and might eventually provide the controlling factor.

In Fig. 2 is shown an idealized representation of a pseudotetrahedral $D^{8+2}_{NO(M)}$ complex with *mm*2 point symmetry at M. A chemical change that would lessen the NO repulsive

[4] A monometallic complex $[M](NO)_n$ contains a $D^{a+n}_{NO(M)}$ metallic center M, when the formal removal of the *n* NO ligands as neutral NO leaves a $d^a = D^{a+0}_{NO(M)}$ metallic element in the NO-free species [M]. The numbers "*a*" and "*n*" are respectively the electronic and structural parameters; any change in the value of "*a*" during a reaction implies the occurence of a non-temporary redox change at M (see ref. 19). To derive the d^a configuration, the non-nitrosylic ligands are separated from the metal according to the usual rules (see for example ref. 20). By extension, the cation $[Co_2(NO)_3(PN)_2]^+$ contains a $D^{17+3}_{NO(2Co)}$ bimetallic core, for CO_2^+ with 17 valence electrons would be obtained following the formal removal of three NO molecules and of the two PN ligands.

Can. J. Chem. Downloaded from www.nrcresearchpress.com by 217.78.4.112 on 09/08/12
For personal use only.

TABLE 3. Selected bond distances (Å) and angles (°) with esd's for the two independent molecules A and B of $Co(NO)_2(Py)_2^+BF_4^-$

	Molecule A range (average[a])		Molecule B range (average[a])
Pyridine ligand			
C—N	1.324(14)–1.360(13) (1.344[15])		1.333(12)–1.356(12) (1.344[10])
C—C	1.338(17)–1.390(16) (1.368[19])		1.347(16)–1.377(17) (1.362[13])
C—H	0.69(5)–1.25(6) (1.04[11])		0.85(6)–1.24(5) (1.05[11])
N—C—C	122.8(8)–124.3(7) (123.3[7])		120.8(8)–123.3(7) (122.4[1.2])
C—C—C	118.6(8)–119.5(8) (119.1[4])		118.7(1.0)–120.1(1.1) (119.4[6])
N—C—H	110(5)–117(3) (112[3])		105(3)–116(3) (113[6])
C—C—H	107(5)–133(5) (120[7])		103(4)–126(4) (121[9])
C1A—N1A—C5A	115.4(7)	C1B—N1B—C5B	116.1(7)
C6A—N2A—C10A	117.0(7)	C6B—N2B—C10B	118.4(7)
Nitrosyl ligands			
N3A—O1A	1.130(8)	N3B—O1B	1.149(8)
N4A—O2A	1.156(8)	N4B—O2B	1.142(7)
CoA—N3A—O1A	170.2(6)	CoB—N3B—O1B	170.7(6)
CoA—N4A—O2A	170.1(6)	CoB—N4B—O2B	169.1(7)
Cobalt coordination sphere			
CoA—N1A	2.012(6)	CoB—N1B	2.013(6)
CoA—N2A	2.012(6)	CoB—N2B	2.016(6)
CoA—N3A	1.654(6)	CoB—N3B	1.650(6)
CoA—N4A	1.644(6)	CoB—N4B	1.648(6)
N1A—CoA—N2A	93.5(3)	N1B—CoB—N2B	93.0(3)
N3A—CoA—N4A	115.6(3)	N3B—CoB—N4B	115.9(3)
N1A—CoA—N3A	112.0(3)	N1B—CoB—N3B	112.1(3)
N1A—CoA—N4A	111.6(3)	N1B—CoB—N4B	110.2(3)
N2A—CoA—N3A	110.2(3)	N2B—CoB—N3B	111.6(3)
N2A—CoA—N4A	111.7(3)	N2B—CoB—N4B	111.9(3)
O1A..CoA..O2A	107.6(2)	O1B..CoB..O2B	107.7(2)
BF_4^- anion			
B—F	1.259(15)–1.322(14) (1.288[29])		1.260(14)–1.357(13) (1.327[45])
F—B—F	105.2(10)–116.0(11) (109[4])		102.5(9)–115.0(10) (109[4])
Selected nonbonded intramolecular contacts (Å)			
N1A..N3A	3.045(3)	N1B..N3B	3.044(9)
N1A..N4A	3.032(8)	N1B..N4B	3.010(8)
N2A..N3A	3.014(9)	N2B..N3B	3.038(9)
N2A..N4A	3.033(9)	N2B..N4B	3.041(11)
N3A..H1A	2.81(6)	N3B..H1B	2.77(5)
N4A..H10A	2.86(7)	N4B..H10B	2.65(6)

[a]Standard deviations of mean values are calculated as $\sigma(\bar{x}) = \left[\sum_{i=1}^{n} (x_i - \bar{x})^2/(n-1)\right]^{1/2}$.

influence, but leave invariant parameters r_N, r_L, and β, would result in either a decrease in the $d_{N..N}$ separation, and consequently a closing of α (eq. [1]), if the repulsions in $M(NO)_2$ are the predominant factor involved, or a decrease in $d_{L..N}$, and an opening of α (eq. [2]), if the M(NO)(L) repulsions are the most influential. Taking the structures of $Fe(NO)_2(PPh_3)_2$ and $Co(NO)_2(PPh_3)_2^+PF_6^-$ as a specific example, upon going from the Fe to the Co^+ derivative, the values of r_N, r_L, and β vary little, as shown by a comparison of the data given in refs. 22 and 24. The observed increase in α by ca.

Can. J. Chem. Downloaded from www.nrcresearchpress.com by 217.78.4.112 on 09/08/12
For personal use only.

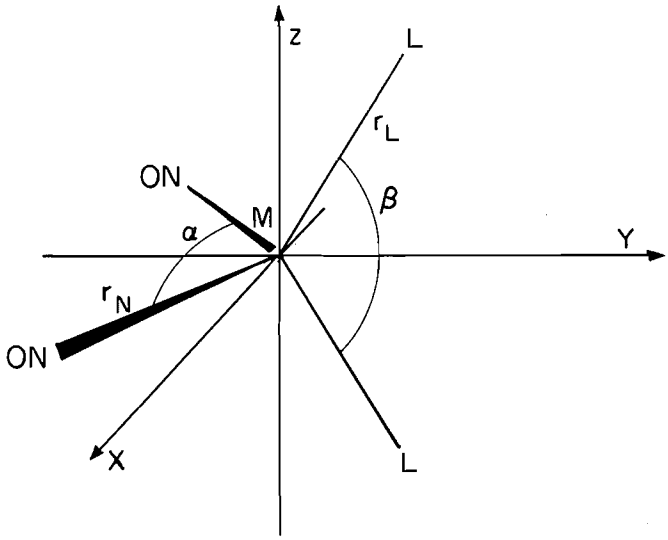

$$[1]\quad d_{NN} = 2 \cdot r_N \cdot \sin(\alpha/2)$$

$$[2]\quad d^2_{LN} = r^2_L + r^2_N + 2.r_N.r_L.\cos(\alpha/2).\cos(\beta/2)$$

FIG. 2. Distances and angles involving the L and NO ligands of a pseudotetrahedral $M(NO)_2(L)_2$ complex with C_{2v} symmetry.

13° supports the view that the repulsive interactions in M(NO)(L) have a predominent role.[5]

A similar situation is encountered in comparing the structure of $Co(NO)_2(P(OMe)_3)_2^+BPh_4^-$ ($\nu NO(CH_2Cl_2)$ = 1876, 1817 cm^{-1}) and $Co(NO)_2(Py)_2^+BF_4^-$ ($\nu NO(CH_2Cl_2)$ = 1876, 1798 cm^{-1}). Upon replacing the $P(OMe_3)$ ligands by pyridine, the closing of the α angle by ca. 13° from 128.0(8)° to 115.6(3)°/115.9(3)° is not associated with a decrease in the extent of Co to NO back-bonding, as inferred from the νNO values. Consequently, there should be no lessening of the nonbonded influence of the NO ligands. This implies that in the pyridine complex (*i*) the $Co(NO)_2$ moiety is more compressed than in the $P(OMe)_3$ derivative, (*ii*) the repulsions in $Co(NO)_2$ do not predominate over the Co(NO)(Py) ones in fixing the value of the α angle. This closing of α is interpreted as the response of the $Co(NO)_2$ moiety to the large decrease in the Co—L bond lengths from 2.209(4)–2.214(5) Å in the $P(OMe)_3$ complex (18) to 2.012(6)–2.016(6) Å in the pyridine derivative, in order to prevent an excessive buildup of compression in the Co(NO)(Py) fragments. The facile dissociation of a Py ligand from $Co(NO)_2(Py)_2^+$ becomes then easily understandable as a means to provide a decompression of the $Co(NO)_2$ molecular portion.

The lability of a Py ligand, when it is bound to a $Co(NO)_2^+$ functional group, might be a key factor for the synthesis of $Co_2(NO)_3(PN)_2^+BPh_4^-$ **2**. The formation of complex **2**, a $D^{17+3}_{NO(2Co)}$ bimetallic (see footnote 4), requires the condensation of two monometallic fragments derived from the $D^{8+2}_{NO(Co)}$ monometallic iodo reactant $Co(NO)_2(PN)I$ **1**. In addition, a reductive denitrosylation is necessarily involved, for a simple condensation of two $D^{8+2}_{NO(Co)}$ monometallic species would yield a $D^{16+4}_{NO(2Co)}$ bimetallic with an electronic parameter one unit less than in the observed product **2**, and the converse for the structural parameter (footnote 4).

An already documented (11), but less involved, case of a reductive denitrosylation also involving cobalt complexes of the same type as **1** is provided by the nearly quantitative formation of $Co(NO)(PPh_3)_3$ ($D^{9+1}_{NO(Co)}$) from a room temperature reaction in THF of $NaBH_4$ with a mixture of the $D^{8+2}_{NO(Co)}$ derivatives $Co(NO)_2(PPh_3)Cl$ and $Co(NO)_2(PPh_3)_2^+$-Cl^- in the presence of an excess of PPh_3. Together with the contrasting solution behaviour of $Co(NO)_2(L)_2^+$ (L = Py, phosphane), this allows us to consider the reaction scheme of Fig. 3 as a viable reaction pathway for the BPh_4^- induced transformation of complex **1** into bimetallic **2**. In an intermediate such as **4**, one of the two possible bimetallics that could result from the ionisation of the Co—I bond of **1**, only the cobalt center attached to the N sites of the PN ligand would be prone to a phenyl transfer involving BPh_4^-. However, contrary to $Co(NO)_2(Py)_2^+$ **3**, due to the geometry of the PN ligand, the pyridinyl moiety that has to dissociate prior to the phenylation step is forced to stay in the vicinity of the metallic center and remains available for recomplexation at a latter stage. It is recognized that alternatives in which formation of the Co—Co bond and (or) the μ_2-NO bridge precedes the reductive denitrosylation step cannot be dismissed at present, and synthesis of more stable analogs of the postulated intermediate **4** is therefore of interest.

Conclusion

In the single crystal X-ray structure of the two independent molecules of $Co(NO)_2(Py)_2^+BF_4^-$, the values of the (O)N—Co—N(O) angles, when they are compared to those of closely related structures, are not readily accounted for in terms of the usual assumption that in $M(NO)_2(L)_2^x$ (x = 0, +1) the repulsions in the $M(NO)_2$ portion are the most influential factor. Instead, the observed changes from one structure to another are more consistent with the notion that the repulsions in the M(NO)(L) fragments are the predominant ones, the same applies to pentacoordinated complexes containing one M(XO)(CO) (X=C, N) moiety (32).

[5]In the series of $M(NO)_2(L)_2^x$ (L = PPh_3, x = 0, +1) derivatives, the behaviour of both the α (N—M—N) and β (P—M—P) angles upon replacing a first row metal by the better back-bonder second row metal of the same group is of interest. Whereas α increases in every case, β is little affected in the cationic series (113.5(2)° (Co^+ (24)), 115.8(5)° (Rh^+ (28))), but decreases significantly in the neutral series (from 111.9(1)° (Fe (22)), to 103.85(6)° (Ru (21))), which increases the compression in $M(L)_2$. A simple rationalization would be to assume that in the Ru complex, in which the M to NO back-bonding should be the most intense, the nonbonded influence of a NO ligand has reached a threshold forcing the β angle to close, in order to achieve a more favorable rebalancing of the nonbonded forces within the $M(NO)_2$, M(NO)(L), and $M(L)_2$ moieties. In support of this hypothesis, based on the νNO values, the nonbonded influence of the NO ligands in $Ir(NO)(CO)(PPh_3)_2$ (νNO ($CHCl_3$) = 1640 cm^{-1} (29)) and in $Ru(NO)_2(PPh_3)_2$ (νNO (Nujol) = 1665, 1615 cm^{-1} (28), $\langle \nu NO \rangle$ = 1640 cm^{-1}) should be comparable, and the P—Ir—P angle of the Ir complex is found at 103.9(1)° (30), identical to the equivalent angle in the Ru derivative. In sharp contrast, in $Ir(NO)_2(PPh_3)_2^+$ with fewer electron-rich, and consequently fewer sterically demanding, NO ligands (νNO (Nujol) = 1760, 1715 cm^{-1} (28), $\langle \nu NO \rangle$ = 1738 cm^{-1}), the P—Ir—P angle has expanded to 116.3(2)° (31).

Can. J. Chem. Downloaded from www.nrcresearchpress.com by 217.78.4.112 on 09/08/12
For personal use only.

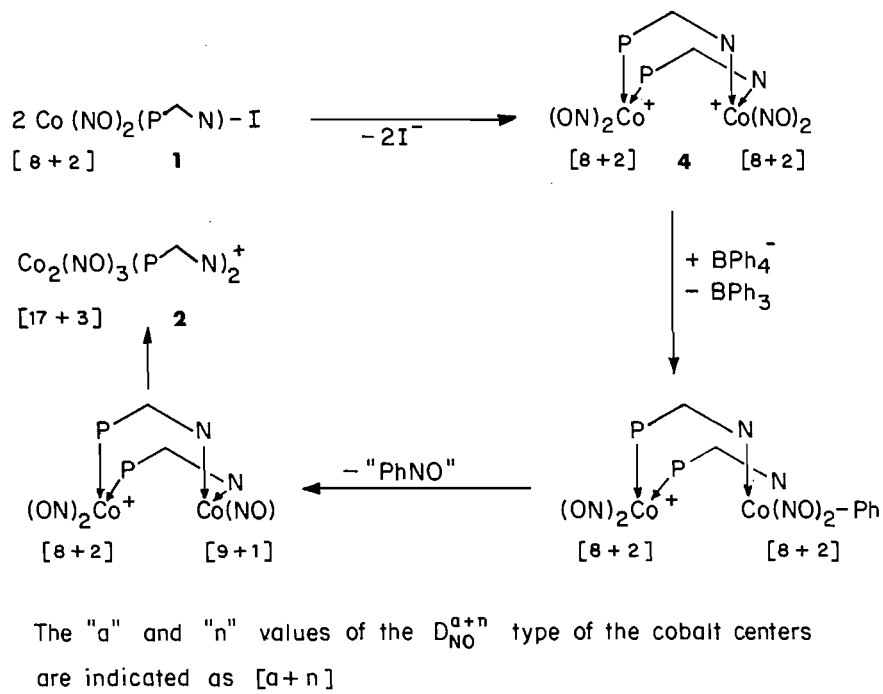

FIG. 3. Suggested reaction pathway for the formation of $Co_2(NO)_3(PN)_2^+BPh_4^-$ **2** in the BPh_4^- induced partial denitrosylation of $Co(NO)_2(PN)I$ **1**.

With respect to the reactivity of nitrosyl complexes, the facile dissociation of the Py ligand from $Co(NO)_2(Py)_2^+$ offers interesting prospects for catalysis (for example, BPh_4^- has a beneficial influence for the catalytic dimerization of norbornadiene in the presence of $(Co(NO)_2Cl)_2$ (33)). In addition, regarding the synthesis of polymetallics containing pyridylphosphines as bridging ligands (see for example the references quoted in ref. 34), the functionalization of their N(Py) donor sites with M(NO) first row metallic fragments might result in nonbonded repulsions within the M(NO)(Py) moieties that are sufficiently destabilizing for opening up reaction pathways leading to the formation of unusual structures, as exemplified by the formation of $Co_2(NO)_3(PN)_2^+BP_4^-$.

Acknowledgment

The authors wish to thank the Natural Sciences and Engineering Research Council of Canada for financial support to one of us (J.L.R.).

1. J. L. Roustan, N. Ansari, and F. R. Ahmed. Inorg. Chim. Acta, **129**, L11 (1987).
2. B. Haymore and R. D. Feltham. Inorg. Synth. **14**, 81 (1973).
3. A. Maisonnet, J. P. Farr, M. M. Olmstead, C. T. Hunt, and A. L. Balch. Inorg. Chem. **21**, 3961 (1982).
4. Y. Le Page, P. S. White, and E. J. Gabe. Proc. Am. Crystallogr. Assoc., Hamilton Meeting, Abstract PA 23. 1986.
5. G. Germain, P. Main, and M. M. Wolfson. Acta Crystallogr. Sect. A: Cryst. Phys. Diffr. Theor. Gen. Crystallogr. **A27**, 368 (1971).
6. D. T. Cromer and J. B. Mann. J. B. Acta Crystallogr. Sect. A: Cryst. Phys. Diffr. Theor. Gen. Crystallogr. **A24**, 321 (1968).
7. E. J. Gabe, F. L. Lee, and Y. Le Page. *In* Crystallographic computing III. *Edited by* G. M. Sheldrick, C. Krüger, and R. Goddard. Clarendon Press, Oxford. 1985.
8. L. Mordenti, J. L. Roustan, and J. G. Riess. Inorg. Chem. **23**, 4503 (1984).
9. R. J. Haines and A. L. Du Prez. J. Organomet. Chem. **84**, 357 (1975).
10. J. L. Roustan, N. Ansari and J. P. Charland. Manuscript in preparation.
11. T. Bianco, M. Rossi, and L. Uva. Inorg. Chim. Acta, **3**, 443 (1969).
12. G. Albertin, E. Bordignon, L. Canovese, and A. A. Orio. Inorg. Chim. Acta, **38**, 77 (1980).
13. E. Raabe and U. Koelle. J. Organomet. Chem. **279**, C29 (1985).
14. J. M. Kuszaj, B. P. Tomlovonic, D. P. Murtha, R. L. Lintvedt, and M. D. Glick. Inorg. Chem. **12**, 1297 (1973).
15. B. L. Haymore, J. C. Huffman, and N. E. Butler. Inorg. Chem. **22**, 168 (1983).
16. R. L. Martin and D. Taylor. Inorg. Chem. **15**, 2970 (1976).
17. V. G. Albano, P. L. Bellon, and G. J. Ciani. J. Organomet. Chem. **38**, 155 (1972).
18. M. A. Manotti Lanfredi, A. Tirpicchio, and M. Tiripicchio Camellini. Acta Crystallogr. Sect. C: Cryst. Struct. Commun. **C39**, 1633 (1983).
19. J. L. Roustan and B. A. Morrow. Inorg. Chem. **27**, 1666 (1988).
20. J. P. Collman and L. S. Hegedus. *In* Principles and applications of organo transition metal chemistry. University Science Books, Oxford University Press. 1980. Chap. II.
21. A. P. Caughan, B. J. Corden, R. Eisenberg, and J. A. Ibers. Inorg. Chem. **13**, 786 (1974).
22. V. G. Albano, A. Araneo, P. L. Bellon, G. Ciani, and M. Manassero. J. Organomet. Chem. **67**, 413 (1974).
23. (*a*) J. H. Enemark and R. D. Feltham. Coord. Chem. Rev. **13**, 335 (1974); (*b*) R. H. Summerville and R. Hoffman. J. Am. Chem. Soc. **98**, 7240 (1976).
24. B. E. Reichert. Acta Crystallogr. Sect. B: Struct. Crystallogr. Cryst. Chem. **B32**, 1934 (1976).
25. J. A. Kaduk and J. A. Ibers. Inorg. Chem. **16**, 3283 (1977).

Can. J. Chem. Downloaded from www.nrcresearchpress.com by 217.78.4.112 on 09/08/12
For personal use only.

26. D. W. McBride, S. L. Stafford, and F. G. A. Stone. Inorg. Chem. **1**, 386 (1962).
27. G. Leborgne, L. Mordenti, J. G. Riess, and J. L. Roustan. Nouv. J. Chem. **10**, 97 (1986).
28. J. A. Kaduk and J. A. Ibers. Inorg. Chem. **14**, 3070 (1975).
29. C. A. Reed and W. J. Roper. J. Chem. Soc. (A), 3054 (1970).
30. C. Pratt Brock and J. A. Ibers. Inorg. Chem. **11**, 2812 (1972).
31. D. M. P. Mingos and J. A. Ibers. Inorg. Chem. **9**, 1105 (1970).
32. J. L. Roustan, N. Ansari, J. P. Charland, and Y. Le Page. Can. J. Chem. **67**, 2016 (1989).
33. D. Ballivet and I. Tkatchenko. J. Mol. Catal. **1**, 322 (1976).
34. P. J. McNair and L. H. Pignolet. Inorg. Chem. **25**, 4717 (1986).

Can. J. Chem. Downloaded from www.nrcresearchpress.com by 217.78.4.112 on 09/08/12
For personal use only.

A pulse radiolysis study of the reaction of OH with I_2 and the decay of I_2^-

A. JOHN ELLIOT

AECL Research, System Chemistry and Corrosion Branch, Chalk River Laboratories, Chalk River, Ont., Canada K0J 1J0

Received January 16, 1992

A. JOHN ELLIOT. Can. J. Chem. **70**, 1658 (1992).

The rate constant for the reaction of the hydroxyl radical with iodine was estimated to be $(9.5 \pm 1.0) \times 10^9$ dm^3 mol^{-1} s^{-1} at 20°C from fitting the time dependence of the decrease in the absorption of iodine at 460 nm. A number of rate constants associated with the decay of I_2^- that were required for this fitting process were also determined. They were the reaction of I_2^- with I_2^-($2k = (4.60 \pm 0.05) \times 10^9$ dm^3 mol^{-1} s^{-1}) at an ionic strength of 1.2×10^{-2} mol dm^{-3}; I_2^- with I ($k = (4.6 \pm 1.6) \times 10^9$ dm^3 mol^{-1} s^{-1}); and I with I ($2k = (3.0 \pm 1.0) \times 10^{10}$ dm^3 mol^{-1} s^{-1}).

A. JOHN ELLIOT. Can. J. Chem. **70**, *1658* (1992).

En se basant sur un ajustement de la diminution de l'absorption de l'iode à 460 nm en fonction du temps, on a évalué que, à 20°C, la constante de vitesse de la réaction du radical hydroxyle avec l'iode est égale à $(9,5 \pm 1,0) \times 10^9$ dm^3 mol^{-1} s^{-1}. On a aussi déterminé un grand nombre de constantes de vitesses associées à la décroissance de I_2^- qui étaient nécessaires pour le processus d'ajustement. Il s'agit de la réaction de I_2^- avec I_2^- ($2k = 4,60 \pm 0,05) \times 10^9$ dm^3 mol^{-1} s^{-1}), à une force ionique de $1,2 \times 10^{-2}$ mol dm^{-3}; de I_2^- avec I ($k = 4,6 \pm 1,6) \times 10^9$ dm^3 mol^{-1} s^{-1}) et de I avec I ($2k = 3,0 \pm 1,0) \times 10^{10}$ dm^3 mol^{-1} s^{-1}).

[*Traduit par la rédaction*]

Introduction

Since the release of radioactive iodine compounds to the environment represents one of the hazards in a nuclear accident, considerable effort has been expended to understand iodine chemistry in order to contain these species. An intermediate goal of this research is to develop a computer simulation package that can be used to model the experimental results from such large-scale experiments as the Radioiodine Test Facility (RTF) at Whiteshell Laboratories in Manitoba, Canada (1, 2). Once this is successful, the simulation package can then be used to help develop containment procedures. As kinetic simulations are only as good as the rate constants which are used, many of the rate constants reported in the early literature of flash and pulse radiolysis need to be re-evaluated or confirmed in the light of the current understandings in iodine chemistry.

In this publication we report on the rate constants for reactions [1] and [5]–[7] at 20°C.

[1] $OH + I_2 \rightarrow I + HOI$

$k_1 = 9.5 \times 10^9$ dm^3 mol^{-1} s^{-1} (this work)

[2] $OH + I^- \rightarrow HOI^-$ $\quad k_2 = 1.1 \times 10^{10}$ dm^3 mol^{-1} s^{-1} (3)

[3] $HOI^- \rightarrow I + OH^-$ $\quad k_3 = 1.2 \times 10^8$ s^{-1} (4)

[4] $I + I^- \rightleftarrows I_2^-$ $\quad K_4 = 1.28 \times 10^5$ dm^3 mol^{-1} (see text)

$k_{4f} = 8.8 \times 10^9$ dm^3 mol^{-1} s^{-1} (this work)

[5] $I_2^- + I_2^- \rightarrow I_3^- + I^-$

$2k_5 = 4.6 \times 10^9$ dm^3 mol^{-1} s^{-1} (this work)

[6] $I_2^- + I \rightarrow I_3^-$

$k_6 = 4.6 \times 10^9$ dm^3 mol^{-1} s^{-1} (this work)

[7] $I + I \rightarrow I_2$ $\quad 2k_7 = 3.0 \times 10^{10}$ dm^3 mol^{-1} s^{-1} (this work)

[8] $I^- + I_2 \rightleftarrows I_3^-$ $\quad K_8 = 747$ dm^3 mol^{-1} (2)

$k_{8f} = 5.6 \times 10^9$ dm^3 mol^{-1} s^{-1} (2)

Based on the minimal loss of I_2 in steady-state γ-radiolysis of deaerated I_2 solutions, it was initially assumed that OH did not react with I_2 (5). However, Schwartz and Bielski (6), in a pulse radiolysis study on N_2O-saturated I_2 solutions, reported a rate constant of 1.1×10^{10} dm^3 mol^{-1} s^{-1} for reaction [1]. In their experiment they monitored the build-up of the absorption at 280 nm where HOI ($\epsilon = 200$ dm^3 mol^{-1} cm^{-1}) (7) and I ($\epsilon = 750$ dm^3 mol^{-1} cm^{-1}) (8) both absorb, but mentioned no measurements made at 460 nm, the λ_{max} for I_2.

This system was reinvestigated because the kinetics might have been distorted by the production of small amounts of I_3^- which absorbs strongly at 280 nm ($\epsilon = 37\,000$ dm^3 mol^{-1} cm^{-1}) (9). I_3^- can be produced through reactions [5] and [6] from I_2^- formed in equilibrium [4] and in reaction [9] from the atomic hydrogen formed in the radiolysis of water.

[9] $H + I_2 \rightarrow I_2^- + H^+$ $\quad k_9 = 3.5 \times 10^{10}$ mol dm^{-3} s^{-1} (6)

Furthermore, the solutions in this pulse radiolysis study (6) were multiply-pulsed for signal averaging purposes (dose per pulse about 3 Gy) so that other iodine species were also present during the experiments (Private communication from H.A. Schwartz to N.H. Sagert).

Experimental

Potassium iodide, sodium sulphate, and iodine (resublimed) were reagent grade quality and were purchased from Anachemia; perchloric acid (69–72%) was Baker Instra-analysed grade; all chemicals were used as supplied. The water used to prepare the solutions was distilled once, passed through a Millipore Milli-Q2 system, and then redistilled from alkaline permanganate.

The iodine solutions were prepared by stirring iodine crystals in perchloric acid solutions (pH 3.3) for about half an hour in the dark. Acidic solutions were used to minimize the hydrolysis of the iodine (reactions [10] and [11]) (7).

[10] $I_2 + H_2O \rightleftarrows HOI + I^- + H^+$

[11] $3HOI \rightarrow 2I^- + IO_3^- + 3H^+$

Immediately after the iodine solutions were prepared, they were saturated with N_2O by the syringe-bubbler technique. The concentrations of the iodine, I_3^-, and I^- in the solution were calculated from the UV-vis spectra recorded on a Hewlett-Packard HP

Can. J. Chem. Downloaded from www.nrcresearchpress.com by 217.78.4.112 on 09/08/12
For personal use only.

8450A diode array spectrometer. These spectra were run before and after the pulse radiolysis experiment using the solution from the syringe. For the calculations, the extinction coefficients of I_2 at 350 and 460 nm were taken to be 30 and 746 $dm^3\ mol^{-1}\ cm^{-1}$ respectively (J. Paquette, private communication); for I_3^-, values of 2.5×10^4 and 980 $dm^3\ mol^{-1}\ cm^{-1}$ (6), respectively, were taken. The value for K_8 of 747 $dm^3\ mol^{-1}$ was used (2). For the solutions used in rate constant calculations, the I^- concentration was always about 1% of the I_2 concentration.

Some studies were made with N_2O-saturated potassium iodide solutions. In these experiments, sodium sulphate was added to the KI solutions of concentration $3.7 \times 10^{-5} - 1.2 \times 10^{-2}$ mol dm^{-3} (natural pH) to keep the ionic strength constant at 1.2×10^{-2} mol dm^{-3}.

The solutions were irradiated with 3×10^{-7} s pulses of 2.25 MeV electrons from a van de Graaff generator at 20 ± 2°C in a 2-cm pathlength optical cell. Between pulses the cell was drained and filled twice to minimize contamination of the sample with products from the previous pulse (10). The optical detection system has been described elsewhere (11). The dosimeter was O_2-saturated 10^{-2} mol dm^{-3} KSCN solution; a $G^*\epsilon_{475}$ of 2.25×10^4 was assumed (11).

Results and discussion

Pulse radiolysis of N_2O-saturated KI solutions

The rate constants for reactions [6] and [7] are required to fit the experimental data for the reaction of OH with I_2 (next section). The only reported values appear to be those published by Grossweiner and Matheson (12) from a flash photolysis of iodide solutions in 1957. However, these data were measured at 405 nm where both I_2^- and I_3^- absorb and the rate constants calculations were based on incorrect values for K_4 and for the extinction coefficient for I_2^-. For this reason it was decided to remeasure k_6 and k_7.

N_2O-saturated solutions containing either 1.2×10^{-2}, 1.2×10^{-3}, 1.2×10^{-4}, or 3.7×10^{-5} mol dm^{-3} KI (at a fixed ionic strength of 1.2×10^{-2} mol dm^{-3}) were pulse irradiated (dose of 9–10 Gy) and the decay of I_2^- was monitored at 725 nm where I_2^- is the only absorbing species (13). Some representative decay profiles are shown in Fig. 1. The *observed* bimolecular rate constants for the two highest iodide concentrations, where reaction [5] is the only important reaction, were identical within experimental error. This confirms that ionic strength effects accounted for the differences observed in k_5 for 10^{-2} and 10^{-3} mol dm^{-3} iodide reported in an earlier publication from this laboratory (13).

The kinetic simulation package FACSIMILE/CHECKMATE (14) was used to fit the *total* absorbance profile of the pulse radiolysis traces so that no assumption needed to be made that equilibrium [4] is always maintained during the I_2^- decay (12). The reaction sequence [2]–[8] and [12] was used to describe the chemistry involved.

[12] $OH + OH \rightarrow H_2O_2$ $\quad k_{12} = 4.2 \times 10^9\ dm^3\ mol^{-1}\ s^{-1}$ (18)

The extinction coefficient for I_2^- at 725 nm was assumed to be 2560 $dm^3\ mol^{-1}\ cm^{-1}$ (13) and the yields of OH were taken from the scavenging curve given by Schuler and coworkers (15). K_4 at 20°C was calculated from the value of Schwartz and Bielski (6) at 25°C using a ΔH of −23 kJ mol^{-1} (16). In order to get the fits in Fig. 1, k_{4f} was allowed to vary in the fitting procedure (with k_{4b} being calculated from K_4 and k_{4f}). A value of k_{4f} of $8.8 \times 10^9\ dm^3\ mol^{-1}\ s^{-1}$ was obtained this way. This 20°C value can be compared to the 25°C value of $1.2 \times 10^{10}\ dm^3\ mol^{-1}\ s^{-1}$ reported by Schwartz and Bielski (6) and the value by Nagarajan and Fessenden (17) of $1.1 \times 10^{10}\ dm^3\ mol^{-1}\ s^{-1}$ where the temperature was not given.

The values for $2k_5$, k_6, and $2k_7$ were $(4.60 \pm 0.05) \times 10^9$, $(4.6 \pm 1.6)\ 10^9$, and $(3.0 \pm 1.0) \times 10^{10}\ dm^3\ mol^{-1}\ s^{-1}$, respectively. The fits to the experimental data can be seen in Fig. 1. While the rate constants, $2k_5$ and k_6, are consistent with those expected for a nearly diffusion-controlled reaction, the value for $2k_7$ appears somewhat high. From the Smoluchowski equation (18), a value for $2k_7$ of $1.6 \times 10^{10}\ dm^3\ mol^{-1}\ s^{-1}$ was calculated using the estimated values of $2.5 \times 10^{-9}\ m^2\ s^{-1}$ and 0.215 nm for the diffusion coefficient and reaction radius, respectively, of the iodine atom.

Pulse radiolysis of N_2O-saturated iodine solutions

The kinetic data for reaction [1] were acquired at 385 nm as well as at 460 nm since the I_2^- produced in reaction [9] contributes significantly to the absorption changes at 460 nm. Two iodine concentrations of 6.7×10^{-5} and 1.1×10^{-4} mol dm^{-3} were studied. Representative traces observed for the later solution are shown in Fig. 2. Data was also acquired at 280 nm, but the poor signal-to-noise character of the signals precluded any quantitative kinetic analysis. In general, the dose per pulse fell in the range 6.5–10 Gy.

The FACSIMILE/CHECKMATE program was used to fit the data. For the simulations, the G values (number formed per 100 eV of energy absorbed) used for the primary species formed at the end of the spur reactions are given in parentheses in reaction [13] (19).

[13] H_2O -radn →

e_{aq} −(2.6), OH(2.7), H(0.55), H_2(0.42), H_2O_2(0.7)

The reactions [1]–[9], [12], [14] and [15] formed the chemical reaction set.

[14] $e_{aq}^- + N_2O - H_2O \rightarrow OH + OH^- + N_2$

$k_{14} = 9.1 \times 10^9\ dm^3\ mol^{-1}\ s^{-1}$ (3)

[15] $e_{aq}^- + H^+ \rightarrow H$ $\quad k_{15} = 2.3 \times 10^{10}\ dm^3\ mol^{-1}\ s^{-1}$ (3)

The extinction coefficients used at 285 and 460 nm, respectively, for I_2^- were 10 000 and 2100 $dm^3\ mol^{-1}\ cm^{-1}$ (13); for I_2, 746 and 106 $dm^3\ mol^{-1}\ cm^{-1}$ (J. Paquette, private communication); and for I_3^- 10 000 (9) and 980 $dm^3\ mol^{-1}\ cm^{-1}$ (6).

The procedure entailed fitting the 385-nm profile first as this predominantly arises from the I_2^- absorption. The time profile of the I_2^- absorption after the initial build-up is sensitive to the iodide ion concentration. This can be seen in Fig. 2 where simulations for three different iodide ion concentrations are given. The best fit was for 1.25×10^{-6} mol dm^{-3} which can be compared to the estimate of the concentration of iodide ion in the 1.1×10^{-4} mol dm^{-3} iodine solution of $(1.1 \pm 0.1) \times 10^{-6}$ mol dm^{-6} mol dm^{-3} made from the UV-vis spectrum. So, in practice, the iodide concentration was finally determined by the fit of the 285-nm kinetic data and this value was used in the fit of the 460-nm data. From these fits an estimate for k_1 of $(9 \pm 1) \times 10^9\ dm^3\ mol^{-1}\ s^{-1}$ can be made for the 1.1×10^{-4} mol dm^{-3} iodine solution (see Fig. 2) and $(10 \pm 1) \times 10^9\ dm^3\ mol^{-1}\ s^{-1}$ for the 6.7×10^{-5} mol dm^{-3} iodine solution. A best estimate for k_1 at 20°C would be $9.5 \times 10^9\ dm^3\ mol^{-1}\ s^{-1}$ with a 10% error, which is in reasonable agreement with the value of $1.1 \times 10^{10}\ dm^3\ mol^{-1}\ s^{-1}$ reported by Schwartz and Bielski (6) for 25°C.

Can. J. Chem. Downloaded from www.nrcresearchpress.com by 217.78.4.112 on 09/08/12
For personal use only.

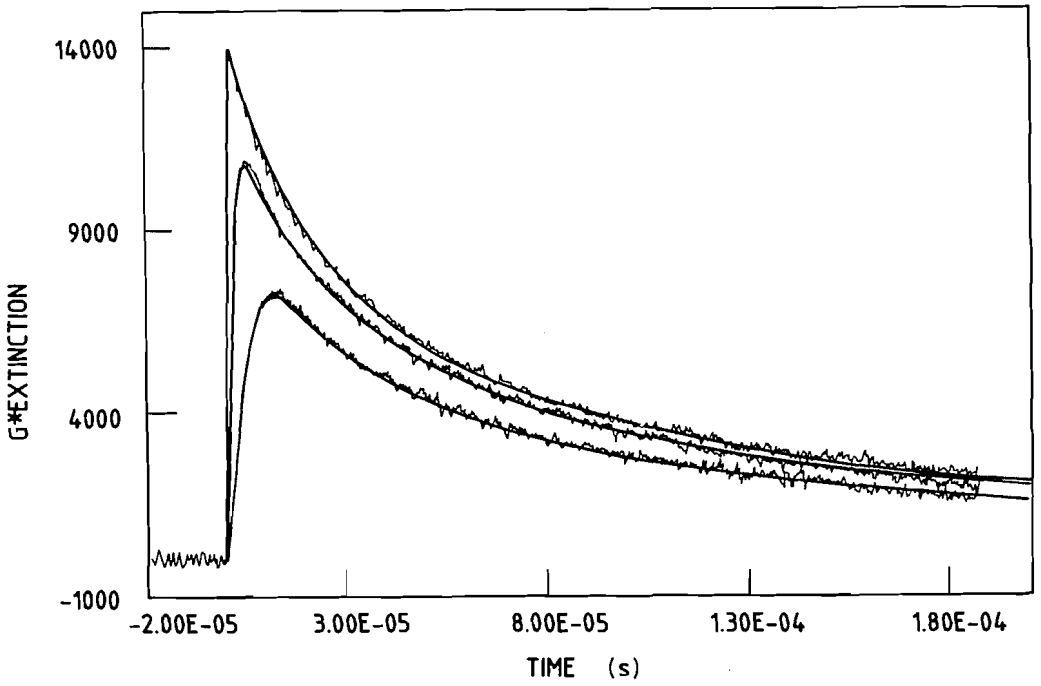

FIG. 1. The experimental and fitted time profile of the formation and decay of I_2^- at 725 nm in N_2O-saturated potassium iodide solutions. The iodide concentration and dose per pulse for upper, middle, and lower traces were: 1.2×10^{-3} mol dm^{-3} and 10.4 Gy; 1.2×10^{-4} mol dm^{-3} and 9.9 Gy; and 3.7×10^{-5} mol dm^{-3} and 9.2 Gy, respectively. The ionic strength was adjusted to 1.2×10^{-2} mol dm^{-3} with sodium sulphate.

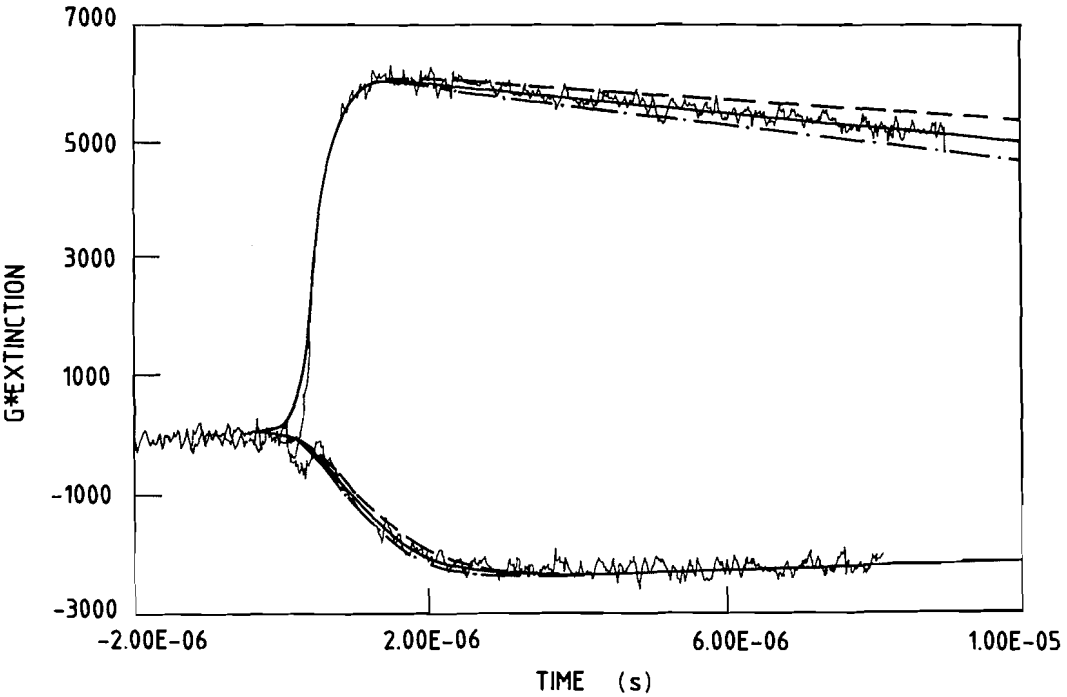

FIG. 2. The experimental and fitted time profiles of the absorption at 385 nm (upper) and 460 nm (lower) observed in N_2O-saturated 1.1×10^{-4} mol dm^{-3} iodine solution after a 9.8 and 7.8 Gy pulse, respectively. For the simulations of the 385-nm (upper) trace, the concentration of iodide ion was 1.0×10^{-6} mol dm^{-3} (–·–·–), 1.25×10^{-6} mol dm^{-3} (—), 1.5×10^{-6} mol dm^{-3} (– – –). For simulations of the 460-nm (lower) trace the value for k_1 was 10×10^9 dm^3 mol^{-1} s^{-1} (–·–·–), 9×10^9 dm^3 mol^{-1} s^{-1} (—), 8×10^9 dm^3 mol^{-1} s^{-1} (– – –), respectively.

Can. J. Chem. Downloaded from www.nrcresearchpress.com by 217.78.4.112 on 09/08/12
For personal use only.

Conclusions

The principal conclusion from this work is that the hydroxyl radical does react rapidly with iodine, in agreement with Schwartz and Bielski (6). However, the minimal loss of iodine observed in the γ-radiolysis of deaerated solutions of iodine referred to by Sellers (5) can be accounted for by regeneration of iodine from the overall reactions [16] and [17] (20) and the reduction of the iodate by the radiolytically generated hydrogen peroxide to iodine (20).

[16] $5HOI \rightarrow 2I_2 + IO_3^- + 2H_2O + H^+$

[17] $10HOI + 10I \rightarrow 9I_2 + 2IO_3^- + 4H_2O + 2H^+$

Acknowledgements

The author would like to thank N. H. Sagert and J. Paquette for discussions. The work was funded jointly by AECL Research and Ontario Hydro, Hydro Quebec, and the New Brunswick Electric Power Commission under the CANDU Owners Group (COG) program, Working Party 06, Work Package 425.

1. A. V. Vikis, F. Garistro, W. C. H. Kupperschmidt, and N. H. Sagert. Proc. Am. Nucl. Soc. React. Saf. Washington. 1990. p. 204.
2. G. J. Evans, A. Melnyk, J. Paquette, and N. H. Sagert. Proc. Int. Conf. Containment Design and Operation 2nd, Toronto. 1990.
3. G. V. Buxton, C. L. Greenstock, W. P. Helman, and A. B. Ross. J. Phys. Chem. Ref. Data, **17**, 513 (1988).
4. D. H. Elision, G. A. Salmon, and F. Wilkinson. Proc. R. Soc. London A, **328**, 23 (1972).
5. R. M. Sellers. CEGB Rep. RD/B/N4009. 1977.
6. H. A. Schwartz and H. J. Bielski. J. Phys. Chem. **90**, 1445 (1986).
7. J. Paquette and B. L. Ford. Can. J. Chem. **63**, 2444 (1985).
8. G. L. Hug. Natl. Stand. Ref. Data Ser. Natl. Bur. Stand. (U.S.) Rep. NSRDS-NBS 69. 1981.
9. A. D. Awtrey and R. E. Connick. J. Am. Chem. Soc. **73**, 1842 (1951).
10. W. A. Seddon and E. B. Selkirk. Int. J. Radiat. Phys. Chem. **3**, 447 (1971).
11. A. J. Elliot and D. R. McCracken. Radiat. Phys. Chem. **33**, 69 (1989).
12. L. I. Grossweiner and M. S. Matheson. J. Phys. Chem. **61**, 1089 (1957).
13. A. J. Elliot and F. C. Sopchyshyn. Int. J. Chem. Kinet. **16**, 1247 (1984).
14. A. R. Curtis and W. P. Sweetenham. Harwell Rep. AERE-R 12805. 1987.
15. R. H. Schuler, A. L. Hartzell, and B. Behar. J. Phys. Chem. **85**, 192 (1981).
16. J. H. Baxendale and P. L. T. Bevan. J. Chem. Soc. A, 2240 (1969).
17. V. Nagarajan and R. W. Fessenden. J. Phys. Chem. **89**, 2330 (1985).
18. A. J. Elliot, D. R. McCracken, G. V. Buxton, and N. D. Wood. J. Chem. Soc. Faraday Trans. **86**, 1539 (1990).
19. J. W. T. Spinks and R. J. Woods. An introduction to radiation chemistry. 2nd ed. John Wiley & Sons, New York. 1976.
20. J. Paquette and B. L. Ford. Radiat. Phys. Chem. **36**, 353 (1990).

Can. J. Chem. Downloaded from www.nrcresearchpress.com by 217.78.4.112 on 09/08/12
For personal use only.

Synthesis of sugar-glutarimide combinations

HEE MOON PARK AND DAVID M. PIATAK[1]
Department of Chemistry, Northern Illinois University, DeKalb, IL 60115, U.S.A.

AND

JOHN R. PETERSON[2] AND ALICE M. CLARK
Department of Pharmacognosy, University of Mississippi, University, MS 38677, U.S.A.

Received September 24, 1991

HEE MOON PARK, DAVID M. PIATAK, JOHN R. PETERSON, and ALICE M. CLARK. Can. J. Chem. **70**, 1662 (1992).

Several sugar glutaramide combinations, wherein the aldehyde group of the sugar was incorporated as C-4 of the imide ring, were prepared to provide molecules with chemotherapeutic potential. The most interesting bioassay results were seen in the inhibition of the bacteria *Mycobacterium intracellularae* by the glutarimide combinations with D- and L-xylose.

HEE MOON PARK, DAVID M. PIATAK, JOHN R. PETERSON et ALICE M. CLARK. Can. J. Chem. **70**, 1662 (1992).

Dans le but d'obtenir des molécules possédant un pouvoir chemothérapeutique, on a préparé plusieurs combinaisons de glutarimides de sucre dans lesquelles le groupe aldéhydique du sucre a été incorporé à la poisition C-4 du cycle imide. Les résultats d'essais biologiques les plus intéressants ont été obtenus lors de l'inhibition de la bactérie *Mycobacterium intracellularae* par les combinaisons de la glutarimide avec les D- et L-xyloses.

[Traduit par la rédaction]

Can. J. Chem. Downloaded from www.nrcresearchpress.com by 217.78.4.112 on 09/08/12
For personal use only.

In an effort to identify new molecules with potential as chemotherapeutic agents, combination of the glutarimide ring, a salient feature of the antibiotic cycloheximide and the antineoplastic sesbanimide, with sugars seemed attractive. It was envisioned that such combinations might increase the solubility characteristics of molecules possessing a glutarimide ring and simulate a modified A/B ring partial structure of sesbanimide for evaluation. Although it has been demonstrated (1) that rings A and B of sesbanimide possess no antineoplastic activity, other biological properties, such as antibacterial and (or) anticonvulsant action, were envisaged. Our previous experience (2, 3) and reports by Makaiyama *et al.* (4) and Yamashita and co-workers (5) with cycloheximide analogues in this context, as well as a recent paper (6) on anticonvulsant activity for 2-benzylglutarimides, further stimulated exploration of other synthetic combinations incorporating a glutarimide ring.

To ensure appropriate inertness of the sugar hydroxyls in subsequent manipulations of the aldehyde group and to afford reasonable solubility in reaction media, the synthetic procedure began with protection of these moieties. Benzylation was most attractive since catalytic reduction could be employed in the final step for their removal without affecting the other functional groups. We had noted earlier (2, 3) that aqueous acidic or basic conditions that are often used to remove many other protecting groups sever the glutarimide ring amide linkage and generate a lactone ring in the presence of available hydroxyl groups. Accordingly, the aldehyde groups of the sugars **1** were first protected as di(ethylthio)acetals **2**, the hydroxyls were completely benzylated with NaH and benzyl chloride in DMSO, and then the aldehyde groups were regenerated with mercuric chloride and cadmium carbonate to finally afford the benzylated sugars **3***.

To provide for the incorporation of glyceraldehyde into the glutarimide ring 2,3-*O*,*O*-dibenzyl-D-glyceraldehyde **3***g** * was secured from D-mannitol by selective protection of the hydroxyl moieties, benzylation of the free hydroxyl groups, and periodate oxidation (7).

Construction of the glutarimide ring fragment was now begun as patterned after procedures used in the total synthesis of sesbanimide (8). First, the carbon chain was extended through Wittig condensation of the free aldehyde with $Ph_3P{=}CHCO_2Me$. Although both *Z* and *E* isomers **5*** ensued, the *E* form represented over 90% of the product as established by ^{1}H NMR signals at δ 6.88 (d, 1H, J = 7.9 Hz) and 5.99 (d, 1H, J = 7.9 Hz). Introduction of the remaining glutarimide ring components and closure to the imide ring **6*** was achieved in a one-pot procedure initiated by Michael condensation of the unsaturated ester and *tert*-butyl malonamide. These products **6*** were mixtures of diastereoisomers owing to the creation of new epimeric chiral centers at the *tert*-butyl ester group attachment site. Multiplicity of NMR signals, in particular, the ^{13}C NMR signals at δ 165–171 for the two orientations of the *tert*-butyl ester (see Table 2), permitted this evaluation.

Removal of the *tert*-butyl ester to yield **7*** proceeded in good yield by, first, expulsion of isobutylene with trifluoroacetic acid and then decarboxylation of the resultant acid by heating in 1,2-dimethoxyethane. It was noted later that the decarboxylation was best accomplished by stirring at room temperature for 16 h since this obviated glutarimide cleavage. Spectral characteristics of products **7*** included IR absorptions at 1720 and 1695 cm^{-1} for the imide system and two ^{13}C NMR signals at ca. δ 172 for the imide carbonyls.

To complete the synthetic sequence to the final products **8*** the benzyl protective groups were removed by catalytic reduction. The usual procedure utilizing 5% Pd–C was found to proceed very slowly, most likely owing to the multiple functionalities present. A more efficient catalytic transfer procedure (9) using 20% palladium hydroxide on carbon and cyclohexene as the hydrogen donor was eventually adopted. Complete displacement of the benzyl groups was established by the appearance of broad OH absorption in the infrared and the absence of any aromatic proton signals in ^{1}H NMR spectra. Signals at ca. δ 174 confirmed that the glutarimide ring remained intact (see Table 2).

[1]Author to whom correspondence may be addressed.
[2]Present address: Panlabs Inc., 11804 N. Creek Parkway South, Bothell, WA 98011-8805, U.S.A.

To determine the type of biological action of the sugar-glutarimide ring combination, in vitro assays for anti-candidal, antifungal, antibacterial, anti-Rhino viral, and anti-Herpes properties were undertaken. In the anticandidal test marginal activity was seen in a 48 h period, while in the antifungal procedures *Aspergillus flavus, Aspergillus fumigatus, Tricophyton mentagrophytes,* and *Sacchromyces cerevisiae* were unaffected. No effect was seen with both viral agents.

The most interesting results occurred with the bacteria *M. intracellularae* (see Table 3). Four of the six D- and L-xylose combinations had strong antibacterial action within the 72 h test period. Two of the target combinations **8***b* and **8***c* had reasonable activity, but the L-xylose intermediate **6***c** with the glutarimide ring epimerically substituted by the *tert*-butyl ester and the sugar portion fully benzylated exhibited the highest degree of inhibition. The structure–activity correlations are not yet fully apparent although it can be noted that combination with L-xylose appears to be favored. With the other bacterial agents employed, *Candida neoformans, Escherichia coli, Staphylococcus aureus, Bacillis subtilis,* or *Pseudomonas aeruginosa,* no positive results were seen.

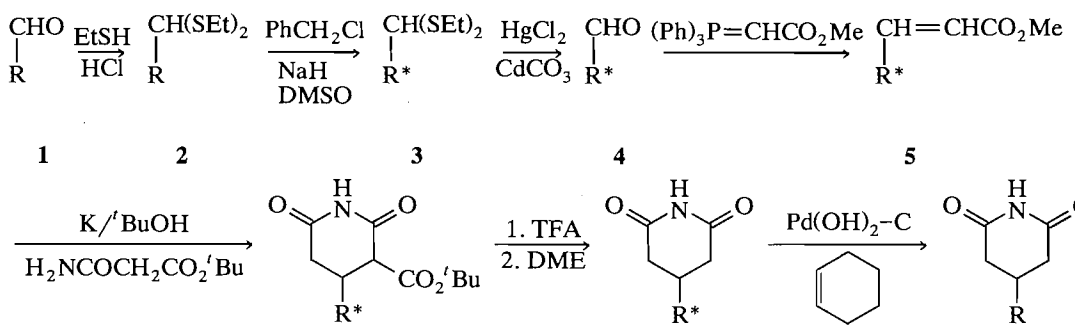

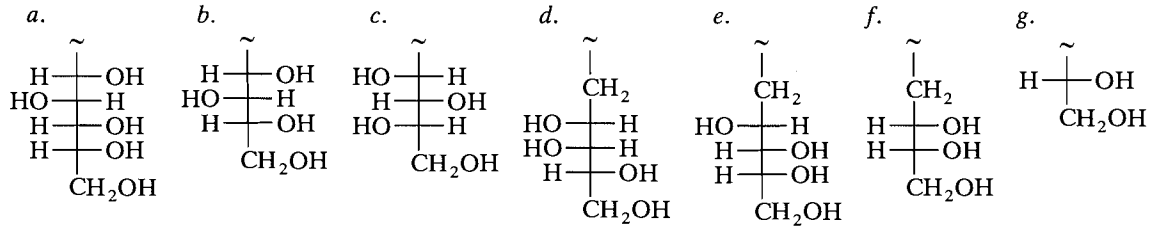

Experimental

All commercial reagents were used as obtained unless otherwise specified. Melting points (mp) were taken on a Fisher–Johns block and are uncorrected. IR spectra were recorded with a Sargent-Welch 3-200 spectrophotometer as KBr pellets or neat; ^{1}H and ^{13}C NMR spectra were obtained with an IBM-NR 200 spectrometer on samples dissolved in deuteriochloroform with tetramethylsilane as an internal standard unless otherwise stated; and elemental analyses were performed on a Perkin–Elmer 240 elemental analyzer by Ms. P. Rider.

Column chromatography was done on Silica Gel 60, and analytical TLC on precoated sheets of Silica Gel 60 F_{254} supplied by EM Reagents. All solvents were redistilled in glass systems. Organic phases were dried over magnesium sulfate before solvent removal.

Formation of di(ethylthio)acetals

The thioacetals **2** were formed by reported procedures (10–13) using ethyl mercaptan and concentrated HCl (see Table 1).

Benzylation of thioacetals

In a typical experiment NaH (2.5 g, 50% oil dispersion) was added to DMSO (10 mL) under nitrogen. The dithioacetal of D-glucose (**1***a*, 2.0 g) dissolved in DMSO (10 mL) was added dropwise, then stirred for 40 min, after which benzyl chloride (4.8 mL) was added. The excess NaH was destroyed with methanol (2 mL) after 2.5 h, followed by 20 mL of water. The product was extracted into ethyl acetate (3 × 30 mL) and washed with water (2 × 20 mL). Purification of the oily syrup (4.2 g) by column chromatography afforded 3.4 g of product **2***a**. See Tables 1 and 2 for yield and spectral data for this compound and others.

Removal of the thioacetal moieties

Although mercuric perchlorate (13) reacted more quickly and gave somewhat better yields, mercuric chloride–cadmium carbonate was found to be less expensive for larger scale reactions. Typically, benzylated D-xylose thioacetal **3***b** (46.26 g), mercuric chloride (100 g), cadmium carbonate (100 g), acetone (750 mL), and water (125 mL) were stirred at ambient temperature for 22 h. The solids were removed by filtration, the residual oil from the filtrate was taken up into ethyl acetate, and the organic layer was washed with water, 10% potassium iodide, and water. The product was purified by column chromatography (20% ethyl acetate/hexane) to yield **4***b** as a colorless oil (30.6 g; 76%). See Tables 1 and 2 for additional data and other examples.

Wittig reaction with benzylated sugars

In a typical experiment a mixture of benzylated D-xylose **4***b** (685 mg) and methyl(triphenylphosphoranylidene)acetate (538 mg; 1.1 equiv.) in benzene (15 mL) was stirred in a nitrogen atmosphere at reflux for 24 h. The solution was filtered through a short silica gel column to remove triphenylphosphine oxide. Removal of the solvent gave an oily product, which was column chromatographed (10% ethyl acetate/hexane) to afford 671 mg (88%; R_f 0.35) of syrupy **5***b**. See Tables 1 and 2 for additional data and other examples.

Can. J. Chem. Downloaded from www.nrcresearchpress.com by 217.78.4.112 on 09/08/12
For personal use only.

TABLE 1. Reaction yields (%) and physical data for products[a]

Base sugar used	Thioketal removal 4*	Wittig product 5*	Michael reaction: Product 6*	Michael reaction: Recovered 5*	*tert*-Butyl removal 7*	Benzyl removal 8	Melting point of final product (°C) 8
D-Glucose *a*	72%	95	29	35	87	53	170–171
D-Xylose *b*	76	87	44	29	82	75	129–131
L-Xylose *c*	51	70	59	32	95	72	130–133
2-Deoxy-D-galactose *d*	84	96	70	29	95	85	168–169
2-Deoxy-D-glucose *e*	56	98	68	31	97	71	157–160
2-Deoxy-D-ribose *f*	78	99	56	27	68	76	125–127
D-Glyceraldehyde *g*	—	85	61	27	97	76	129–130

[a]CHN elemental analyses of products were with ±0.4.

TABLE 2. Selected ^{13}C NMR data for intermediates and products[a]

Base sugar used	Thioketal removal 4*: (C=O)	Thioketal removal 4*: (CH_2)	Wittig product 5*: (CH=)	Wittig product 5*: (C=O) (CH_3)	Wittig product 5*: (CH_2)	Michael product[b,c] 6*: (COO)	Michael product[b,c] 6*: (CH_2)	*tert*-Butyl removal 7*: (C=O)	*tert*-Butyl removal 7*: (C-4 H)	*tert*-Butyl removal 7*: (CH_2)	Final product[b] 8: (C=O)	Final product[b] 8: (C-4 H)	Final product[b] 8: (CH_2OH)
D-Glucose *a*	200.6		145.6	166.3		168.6		172.3	31.6		174.1	32.4	63.5
			122.4	51.4				172.1			173.9		
D-Xylose *b*	201.0		145.5	166.4		168.1		172.5	31.7		173.6	32.6	62.7
			122.5	51.5				172.3			173.3		
L-Xylose *c*	201.0		145.5	165.6		167.3		172.4	31.6		173.6	32.6	62.3
			122.5	51.5				172.2			173.3		
2-Deoxy-D-galactose *d*	200.2	45.3	146.5	166.7	33.6	168.6	35.6	172.4	26.9	35.8	173.4	26.7	63.0
			122.7	51.3		165.6	35.0	172.3			173.3		
2-Deoxy-D-glucose *e*	200.9	45.6	145.6	166.6	34.2	168.3	35.3	172.4	27.1		173.7	27.0	63.8
			123.0	51.3		165.9	33.4	172.2			173.6		
2-Deoxy-D-ribose *f*	200.7	45.0	145.9	166.7	33.6	168.6	35.8	172.1	27.0	35.5	173.5	26.9	62.5
			123.1	51.3		166.1	32.9	171.9			173.3		
D-glyceraldehyde *g*	200.8		147.3	166.2		169.1		172.7	32.2		173.5	32.1	63.0
			122.4	51.3		167.1		172.6			173.4		

[a]Signals for -*C*HOCH_2- were δ 68.5–81.5 and, for -C_6H_5, 126.8–138.7 for most derivatives.
[b]Taken in DMSO-d_6 solution.
[c]Multiple signals were seen in most instances owing to diastereomers formed.

Michael condensation of unsaturated sugar ester

Freshly cut potassium metal (17.2 mg; 0.44 mmol) was added to *tert*-butyl alcohol (3 mL) distilled from calcium hydride. After the metal had reacted, *tert*-butyl α-aminocarbonyl acetate (83.4 mg; 0.53 mmol) was added. After 30 min a solution of the 2-deoxy-D-ribose unsaturated methyl ester **5***f** (30 mg; 0.44 mmol) in *tert*-butyl alcohol (1.0 mL) was added and the reaction was stirred overnight under argon.

The reaction was quenched with acetic acid (1 mL), then with water (10 mL). The product was extracted into ethyl acetate (2 × 5 mL), washed with water (2 × 5 mL) and saturated sodium bicarbonate, and dried. The resultant yellow syrup was purified by column chromatography (30% ethyl acetate/hexane) to yield pure **6***f** (169 mg; 56%; R_f 0.40). See Tables 1 and 2 for additional data and other examples.

Removal of the tert*-butoxycarbonyl moiety*

In a typical experiment, the Michael product from 2-deoxy-D-ribose **6***f** (5.74 g) in methylene chloride (100 mL) was introduced into trifluoroacetic acid (50 mL) and the mixture was stirred at ambient temperature for 16 h. The solvent was then removed *in vacuo* overnight, and the residue was dissolved in dimethoxyethane (100 mL) and stirred at room temperature for 16 h. The crude benzylated sugar glutarimide was purified by column chromatography (10% acetone/chloroform) to give syrupy **7***f** (3.06 g; 68%). Additional data and other examples may be found in Tables 1 and 2.

Removal of benzyl protecting groups

Palladium hydroxide on carbon (14) (20%; 50 mg; usually 10:1 or 4:1 substrate:catalyst ratio by weight) was introduced into a solution of the benzylated L-xylose glutarimide **7***c** (441 mg) in ethanol (8 mL) and cyclohexene (4 mL). The suspension was stirred under reflux and monitored by TLC. The catalyst was removed by filtration, the filtrate evaporated to dryness, and the product crystallized directly or purified by column chromatography (30% methanol/chloroform). The yield of **8***c* was 321 mg (72%); mp 130–133°C. Tables 1 and 2 contain additional data and other examples.

Bioassays

Activity of a synthetic agent was measured with an in vitro assay in which the measure of effectiveness was achieved by the inhibition of candidal, fungal, microbial, or viral growth with a known amount of the agent. Antifungal and antimicrobial assays were conducted by an agar-well diffusion assay as described in ref. 15

Can. J. Chem. Downloaded from www.nrcresearchpress.com by 217.78.4.112 on 09/08/12
For personal use only.

TABLE 3. Significant antibacterial results with *M. intracellularae*

Compound	48 h	72 h	MIC[a] (μg/mL)
D-Glucose[b]			
tert-butoxyimide **6***a**	—	5[c]	
D-Xylose			
tert-butoxyimide **6***b**	—	2	
benzyl product **7***b**	—	3	
final product **8***b*	—	10	50
L-Xylose			
tert-butoxyimide **6***c**	—	10	<0.2
benzyl product **7***c**	—	23	1.56
final product **8***c*	—	15	100
Standard			
Rifampin		24	

[a]Minimum inhibitory concentration.
[b]Initial sugar used.
[c]Zone of inhibition in mm.

with some minor modifications. Qualitative activity is reported as the average of the zone of inhibition measured in millimetres from the edge of the well containing the compound to the edge of the zone. A zone of 1–3 mm = marginal activity; 4–7 mm = moderate–good; 8–12 mm = good; and >12 = excellent.

Pure compounds were tested at 1 mg/mL with 100 μL applied, and the test was conducted for a specified time interval. The minimum inhibitory concentration (MIC) was also a factor since lower concentrations with similar zones of inhibition would denote a more active compound. The method used for the MIC determination was the twofold serial broth dilution assay (16). Test data were compared with standards such as amphotericin B and ketoconazole. See Table 3 for test data of compounds with more than marginal activity.

Antiviral assays (17) were performed on confluent monolayers of Vero cells infected by virus diluted with Eagle's Minimum Essential Medium (EMEM) in 6% bovine serum in microtiter plates wells. After 1 h adsorption time, 150 μL/well of each sample dilution was added and the plates incubated. Activity of a compound was defined as 50% or greater inhibition of the cytopathic effect, by comparison with viral controls, in at least one dilution of sample. For anti-Rhino assays, disoxiral was used as the positive control, and for anti-Herpes assays, ganciclovir was employed. Further details about either type of assay may be obtained from the authors.

Acknowledgements

We wish to acknowledge contract NO1-AI-7268 and grant RO1-AI-27094 from the Division of AIDS, National Institute of Allergy and Infectious Diseases, and support by the American Society of Pharmacognosy and the University of Mississippi Graduate School for development of the bioassays. We are also grateful to Marjorie Richardson and her fine laboratory skills for evaluation of the compounds.

1. F. Matsuda, M. Kawasaki, and S. Terashima. Tetrahedron Lett. **26**, 4639 (1985).
2. D. M. Piatak, P. L. Tang, and C. C. Yen. J. Med. Chem. **29**, 50 (1986).
3. D. M. Piatak and P. L. Tang. Can. J. Chem. **65**, 1327 (1987).
4. (*a*) T. Makaiyama, Y. Morita, J. Oya, and K. Wagatsuma. Japanese Patent 76 65 769, 1976; Chem. Abstr. **85**, P 177260 (1976); (*b*) T. Makaiyama, Y. Morita, and J. Oya. Japanese Patent 77 83 571, 1978; Chem. Abstr. **88**, 22638 (1978).
5. (*a*) S. Kudo, T. Oritani, and K. Yamashita. Agric. Biol. Chem. **48**, 2315 (1984); (*b*) **48**, 2739 (1984); (*c*) **49**, 2919 (1985); (*d*) T. Oritani, H. Kondo, and K. Yamashita. Agric. Biol. Chem. **51**, 263 (1987).
6. R. R. Goehring, T. D. Greenwood, G. C. Nwokogu, J. S. Pisipati, T. G. Rogers, and J. F. Wolfe. J. Med. Chem. **33**, 926 (1990).
7. L. F. Wiggins. J. Chem. Soc. 13 (1946).
8. (*a*) G. W. J. Fleet and T. K. M. Shing. J. Chem. Soc. Chem. Commun. 835 (1984); (*b*) M. J. Wanner, G. J. Kooman, and U. K. Pandit. Heterocycles, **22**, 1483 (1984).
9. S. Hanessian, T. J. Liak, and G. Vanasse. Synthesis, **5**, 396 (1981).
10. J. L. Barclay, A. J. Cleaver, A. B. Foster, and W. G. Overend. J. Chem. Soc. 789 (1956).
11. L. Hough and M. I. Taha. J. Chem. Soc. 3994 (1957).
12. M. Smrz and A. Farkas. Collect. Czech. Chem. Commun. **33**, 3803 (1968).
13. E. Fujita, Y. Nagao, and K. Kaneko. Chem. Pharm. Bull. **26**, 3743 (1978).
14. W. M. Pearlman. Tetrahedron Lett. 1663 (1967).
15. A. M. Clark, F. S. El-Feraly, and W. S. Li. J. Pharm. Sci. **70**, 951 (1981).
16. S. Liu, B. Oguntimein, C. D. Hufford, and A. M. Clark. Antimicrob. Agents Chemother. **34**, 529 (1990).
17. M. D. Richardson, J. R. Peterson, and A. M. Clark. Phytother. Res. In press.

Can. J. Chem. Downloaded from www.nrcresearchpress.com by 217.78.4.112 on 09/08/12
For personal use only.

Single-ion enthalpies and entropies of transfer from water to aqueous urea solutions at 298.15 K

ANDREW W. HAKIN[1] AND COLIN L. BESWICK
Department of Chemistry, University of Lethbridge, Lethbridge, Alta., Canada T1K 3M4

Received April 11, 1991[2]

ANDREW W. HAKIN and COLIN L. BESWICK. Can. J. Chem. **70**, 1666 (1992).

In this paper we report enthalpies of solution at infinite dilution (ΔH_s^θ) at 298.15 K for tetraphenylarsonium chloride (Ph_4AsCl), sodium tetraphenylborate ($NaBPh_4$), sodium chloride (NaCl), sodium bromide (NaBr), and sodium iodide (NaI) in water and aqueous solutions containing 5, 10, 20, and 30% urea by weight. Enthalpies of transfer from water to aqueous urea solutions are reported. Single-ion enthalpies of transfer (ΔH_t^θ) have been calculated using the tetraphenylarsonium tetraphenylborate, (TATB) reference electrolyte assumption. These single-ion enthalpy data have been combined with single-ion Gibbs functions of transfer (ΔG_t^θ) reported in the literature to obtain single-ion entropies of transfer (ΔS_t^θ) for the urea + water mixed solvent system. The results of this single-ion analysis are discussed in terms of the impact of electrolytes on the structure of aqueous urea solutions.

ANDREW W. HAKIN et COLIN L. BESWICK. Can. J. Chem. **70**, 1666 (1992).

Dans ce travail, on a mesuré les enthalpies de solution à dilution infinie (ΔH_s^θ), à 298,15 K, des chlorure de tétraphénylarsonium (Ph_4AsCl), tétraphénylborate de sodium ($NaBPh_4$), chlorure de sodium (NaCl), bromure de sodium (NaBr) et iodure de sodium (NaI) dans l'eau et dans des solutions aqueuses contenant 5, 10, 20 et 30% d'urée en poids. On rapporte aussi les enthalpies de transfert de l'eau vers les solutions aqueuses d'urée. On a calculé les enthalpies de transfert des ions uniques (ΔH_t^θ) utilisant l'hypothèse de l'électrolyte de référence tétraphénylborate de tétraphénylarsonium (TBTA). Dans le but d'obtenir les entropies de transfert pour ions uniques (ΔS_t^θ) pour le système de solvant mixte urée/eau, on a combiné ces données d'enthalpie pour ions uniques avec les fonctions de transfert de Gibbs pour des ions uniques (ΔG_t^θ) rapportées dans la littérature. On discute des résultats de cette analyse pour ions uniques en fonction de l'impact des électrolytes sur la structure des solutions aqueuses de l'urée.

[Traduit par la rédaction]

Introduction

Single-ion thermodynamic transfer functions of solutes from one solvent (often water) to another find applications in many areas of chemistry. By far the most studied of these thermodynamic properties are Gibbs energies of transfer (1–4). These data have been used to interpret patterns observed in rate constants (5), and also to relate pH values in a given solvent to the conventional aqueous pH scale (3). Less extensive compilations of single-ion data exist for enthalpies (6–8) and entropies (8–10) of transfer. These data provide information on the structural interactions of ions with surrounding solvent.

In this paper we concentrate on enthalpies and entropies of transfer for solutes in the urea + water solvent system. ΔG_t^θ data (5*a*, 10, 11), and the ΔH_t^θ and ΔS_t^θ data reported in this paper are some of the essential building blocks that provide a basis for a critical analysis of extrathermodynamic assumptions used in the calculation of single-ion thermodynamic properties, with particular emphasis on temperature and pressure derivatives of Gibbs energies (H, S, C_p).

This paper reports enthalpies of solution at infinite dilution (ΔH_s^θ) at 298.15 K for NaCl, NaBr, NaI, Ph_4AsCl, and $NaBPh_4$ in water and aqueous urea solutions containing 5, 10, 20, and 30% urea by weight. These data have been used to calculate enthalpies of transfer and subsequently single-ion enthalpies of transfer (ΔH_t^θ), using the tetraphenylarsonium tetraphenylborate (TATB) reference electrolyte assumption. In addition we report single-ion entropies of transfer (ΔS_t^θ) for solutes from water to aqueous urea solutions; these entropies have been calculated from the combination of our single-ion enthalpies with published (11–13) single-ion Gibbs energies.

Extensive thermodynamic functions of transfer for a 1:1 salt MX transferred from water (1) to another solvent, or solvent mixture (2), are defined by

$$[1]\quad \Delta Y_t^\theta(\mathrm{MX}: (1) \rightarrow (2)) = \Delta Y_s^\theta(\mathrm{MX}: (2)) - \Delta Y_s^\theta(\mathrm{MX}: (1))$$

where Y represents the extensive thermodynamic function of interest, for example Gibbs energy, enthalpy, or volume; subscript t indicates a transfer property, and subscript s refers to a solid → solution property. The symbol θ indicates that we are dealing with thermodynamic functions for infinitely dilute solutions.

Various extrathermodynamic assumptions have been used to convert the bulk thermodynamic functions of eq. [1] into single-ion properties (1). Of these we are especially concerned with the TATB reference electrolyte extrathermodynamic assumption (1).

The reference electrolytye assumption is based on the idea that specific, oppositely charged, large ions of equal size and similar structure have equal interactions with the solvent. The TATB reference electrolyte extrathermodynamic assumption method is summarized by eq. [2]:

$$[2]\quad \Delta Y_t^\theta(Ph_4As^+: (1) \rightarrow (2)) = \Delta Y_t^\theta(Ph_4B^-: (1) \rightarrow (2)) = (1/2)\,\Delta Y_t^\theta(Ph_4AsBPh_4: (1) \rightarrow (2))$$

Unfortunately Ph_4AsBPh_4 is only sparingly soluble in water and aqueous urea solutions, which complicates calorimetric measurements. It is convenient to obtain transfer data for

[1]Author to whom correspondence may be addressed.
[2]Revision received January 6, 1992.

Can. J. Chem. Downloaded from www.nrcresearchpress.com by 217.78.4.112 on 09/08/12
For personal use only.

this salt by combining relevant transfer data for Ph_4AsCl, $NaBPh_4$, and NaCl using eq. [3].:

[3] $\Delta Y_t^\theta(Ph_4AsBPh_4: (1) \rightarrow (2))$
$= \Delta Y_t^\theta(NaBPh_4: (1) \rightarrow (2))$
$+ \Delta Y_t^\theta(Ph_4AsCl: (1) \rightarrow (2)) - \Delta Y_t^\theta(NaCl: (1) \rightarrow (2))$

Experimental

Urea (certified A.C.S. grade, Fisher Chemicals Ltd.) was used without further purification, after drying for 24 h in a vacuum oven at 50°C over phosphorus pentoxide. Sodium tetraphenylborate (99.5% +, Aldrich Chemical Company) was used without further purification. Tetraphenylarsonium chloride (K & K laboratories) was recrystallized several times, using the method of Kalfoglou and Bowen (14). NaI (Aldrich Chemical Company) was recrystallized from water and dried *in vacuo* at 100°C. NaCl and NaBr (Aldrich Chemical Company) were both 99.99% pure and were used without further purification. All of these inorganic salts were stored in a vacuum oven at 70°C over phosphorus pentoxide.

Doubly distilled water was used in all of our experiments.

Enthalpies of solution were measured with a homemade isoperibol solution calorimeter (15) and with a LKB 8700-1 precision calorimetry system. Both systems were tested at regular intervals by measuring the enthalpy of solution of tris(hydroxymethyl)-aminomethane in excess 0.1 M hydrochloric acid at 25°C (16). Results of these tests are reflected in estimates of our calorimetric uncertainties. Enthalpies of solution, at 298.15 K, were measured for tetraphenylarsonium chloride, sodium tetraphenylborate, sodium chloride, sodium bromide, and sodium iodide in water and in solutions containing 5, 10, 20, and 30% urea by weight. The molalities (defined as the number of moles of salt in 1 kg of mixed solvent) of the electrolyte solutions investigated were in the range $5 \times 10^{-4} - 5 \times 10^{-3}$ mol kg^{-1}. This focus on ions at low concentration provides information about ion–solvent interactions, and excludes effects of ion–ion interactions, which become increasingly important at higher concentrations.

Results

Single-ion enthalpies of transfer (ΔH_t^θ)

Enthalpies of solution at infinite dilution (ΔH_s^θ), were obtained from measured enthalpies of solution at finite concentration by using the extended Debye–Hückel extrapolation method proposed by Guggenheim and Prue (17) and developed by others (18, 19).

$$[4] \quad \rho = \Delta H_s^\theta - 2 \cdot 303\, RT^2 \left(\frac{dB}{dT}\right) (\upsilon_+ \upsilon_- m)$$

where

$$[5] \quad \rho = \Delta H_s - \frac{\upsilon}{2} |z_+ z_-|\, A_H \sqrt{I}\, \alpha$$

$$[6] \quad \alpha = \left[\frac{1}{(1 + \sqrt{I})} - \frac{\sigma(\sqrt{I})}{3}\right]$$

and

$$[7] \quad \sigma(\sqrt{I}) = \frac{3}{I^{1.5}}\left[1 + \sqrt{I} - \frac{1}{1 + \sqrt{I}} - 2 \ln (1 + \sqrt{I})\right]$$

Where $\sigma(\sqrt{I})$ is a function of the ionic strength, I, and B is a constant at a given temperature. Debye–Hückel limiting slopes, A_H, for aqueous urea solutions were interpolated from the data of Verrall and Dickson (20). Values for ΔH_s^θ obtained from plots of ρ vs. m are reported in Table 1, along with ΔH_s^θ values previously reported by others. We estimate that our total uncertainties (calorimetry, chemicals, and extrapolation) are about 0.25 kJ mol^{-1} for Ph_4AsCl and about 0.10 kJ mol^{-1} for the other salts. Our results are in good agreement with the few ΔH_s^θ values previously reported. Our ΔH_s^θ data were used in conjunction with eq. [1] to calculate the enthalpies of transfer reported in Table 2. Figure 1 illustrates the dependence of the transfer enthalpies for the salts investigated on the weight per cent of urea present in solution.

Single-ion enthalpy of transfer values reported in Table 3 were calculated using the TATB assumption (see eq. [2]). Although this method of calculation has been recommended, it should be noted that it represents only one approach to the calculation of single-ion thermodynamic quantities. The adoption of other assumptions (1) may lead to different single-ion values.

Included in Table 3 are single-ion enthalpies of transfer for other ions calculated from the combination of our own single-ion parameters with additional enthalpy of transfer data available in the literature (8, 33). Trends in these enthalpy data as functions of weight per cent urea present in solution are shown in Figs. 2–4.

Single-ion entropies of transfer (ΔS_t^θ)

Gibbs functions of transfer at 298.15 K have been calculated, on the molar (c) scale, using the solubility product data at 298.15 K reported by Kundu and co-workers (11, 12), and eq. [8]:

$$[8] \quad \Delta G_t^\theta(c) = 2.303RT(p_s K_{sp} - p_w K_{sp})$$

The TATB reference electrolyte assumption has been used to divide bulk Gibbs energies of transfer into single-ion contributions. Single-ion enthalpies of transfer for solutions containing 11.52, 20.31, and 29.64 wt.% urea pertinent to Kundu's ΔG_s^θ values were interpolated from our enthalpies. Single-ion entropies of transfer (molar scale), $\Delta S_t^\theta(c)$, were calculated by combining these enthalpies with single-ion Gibbs energies of transfer (molar scale), $\Delta G_t^\theta(c)$. The single-ion entropies calculated from this procedure are reported in Table 4.

Discussion

Comparison of our single-ion enthalpies of transfer with those that can be calculated from Gibbs energy and entropy data reported by Kundu and co-workers (11) identifies differences that are larger than the sum of estimated uncertainties in their results and ours. These discrepancies cannot be attributed to the choice of reference electrolyte assumption. In general, single-ion enthalpies calculated from calorimetric enthalpy data are supposed to be more reliable than their estimation from Gibbs energy data collected at various temperatures.

Several authors (20, 33, 34) have used changes in solvent organization brought about by cosphere overlap between cosolvent and transferred ion to explain patterns observed in single-ion entropies and enthalpies of transfer.

Urea is regarded as a hydrophilic structure disrupter in aqueous solution (21–23), the amount of structure disruption increasing with increased urea concentration. Hydrophilic cosolvent, hydrophobic ion cosphere overlap results in an overall loss of water molecules from the structured

Can. J. Chem. Downloaded from www.nrcresearchpress.com by 217.78.4.112 on 09/08/12
For personal use only.

TABLE 1. Enthalpies of solution at infinite dilution for aqueous urea solutions at 298.15 K (kJ mol^{-1})

Salt	Weight % urea 0	5	10	20	30
Ph_4AsCl	−10.62 −10.75 ± 0.25[g]	−9.93	−10.26	−10.83	−11.10
$NaBPh_4$	−19.26 −19.29 ± 0.08[a] −18.79 ± 0.42[c] −20.00 ± 0.08[h]	−18.15	−16.90	−15.17	−13.72
NaCl	3.90 3.90 ± 0.08[h] 4.12 ± 0.08[c] 3.883[d] 3.85 ± 0.21[e]	3.00	2.16 2.24 ± 0.21[e]	0.93 0.92 ± 0.21[e]	−0.13 −0.12 ± 0.21[e]
NaBr	−0.53 −0.63 ± 0.08[a] −0.50 ± 0.04[b] −0.60[d]	−1.55	−2.49	−4.15	−5.28
NaI	−7.54 −7.53[d]	−8.60	−9.43 −10.18 ± 0.04[f]	−11.17 −11.59 ± 0.04[f]	−12.61 −13.36 ± 0.08[f]

[a]Reference 7.
[b]Reference 29.
[c]Reference 22.
[d]Reference 30.
[e]Reference 8.
[f]Reference 31.
[g]Reference 32.
[h]Reference 6.

TABLE 2. Enthalpies of transfer from water to aqueous urea solutions at 298.15 K (kJ mol^{-1})

Salt	Weight % urea 5%	10%	20%	30%
Ph_4AsCl	0.69	0.36	−0.21	−0.48
$NaBPh_4$	1.11	2.36	4.09	5.54
Ph_4AsBPh_4	2.69	4.47	6.86	9.09
NaCl	−0.90	−1.75	−2.98	−4.03
NaBr	−1.02	−1.96	−3.62	−4.75
NaI	−1.07	−1.90	−3.63	−5.08

hydration zones. In effect, the presence of urea diminishes the structure-promoting capacity of the hydrophobic ion. In the transfer processes water is released from the structured cosphere environment to the bulk solvent, hence increasing the disorder of the solvent system, which results in positive entropies of transfer. A loss of water molecules from the cospheres is accompanied by hydrogen bond breaking and therefore positive enthalpies of transfer are observed. Hydrophilic cosolvent, hydrophilic ion cosphere overlap results in an incorporation of water molecules from the bulk solvent into the more structured cosphere environment. This overlap process decreases the degree of disorder in the solvent system (i.e., negative entropies of transfer) and promotes hydrogen bonding in the cospheres (i.e., negative enthalpies of transfer). In other words both urea and the transferred ion disrupt water structure; therefore in aqueous urea solution the structure disrupting capacity of the ion is decreased.

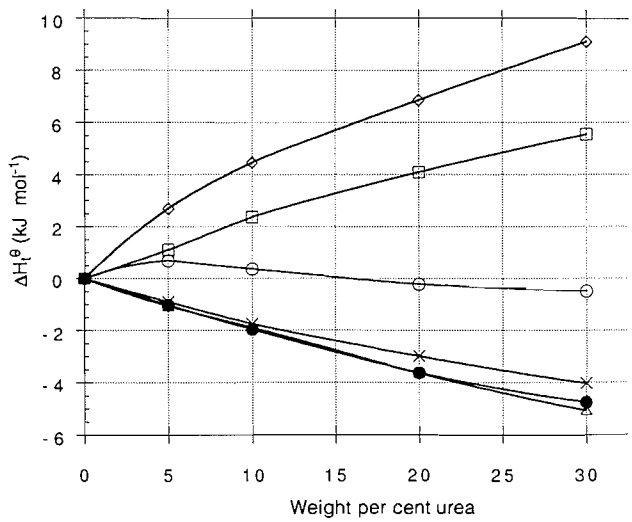

FIG. 1. Enthalpies of transfer (kJ mol^{-1}) from water to aqueous urea solutions at 298.15 K for selected electrolytes. (○) Ph_4AsCl; (□) $NaBPh_4$; (◇) Ph_4AsBPh_4; (×) NaCl; (●) NaBr; (△) NaI.

Figure 1 reports enthalpies of transfer for several salts as a function of urea concentration in aqueous solution. Four of these salts contain the same cation (sodium) and there-

Can. J. Chem. Downloaded from www.nrcresearchpress.com by 217.78.4.112 on 09/08/12
For personal use only.

TABLE 3. Single-ion enthalpies of transfer from water to aqueous urea solutions at 298.15 K (kJ mol^{-1})

Ion	Weight % urea			
	5%	10%	20%	30%
Ph_4As^+	1.35	2.23	3.43	4.55
BPh_4^-	1.35	2.23	3.43	4.55
Na^+	−0.24	0.13	0.66	0.99
Cl^-	−0.66	−1.87	−3.64	−5.03
Br^-	−0.78	−2.09	−4.28	−5.75
I^-	−0.83	−2.02	−4.29	−6.07
K^{+a}	—	0.19	0.52	0.89
Rb^{+a}	—	−0.28	−0.14	0.05
Cs^{+a}	—	−1.02	−1.09	−1.11
NH_4^{+a}	—	0.19	0.60	0.81
Me_4N^{+b}	−0.47	−0.33	−0.21	—
Et_4N^{+b}	−0.54	−0.44	−0.17	—
Bu_4N^{+b}	2.08	4.54	8.77	11.92

[a]Calculated from data contained in ref. 8.
[b]Calculated from data contained in ref. 33.

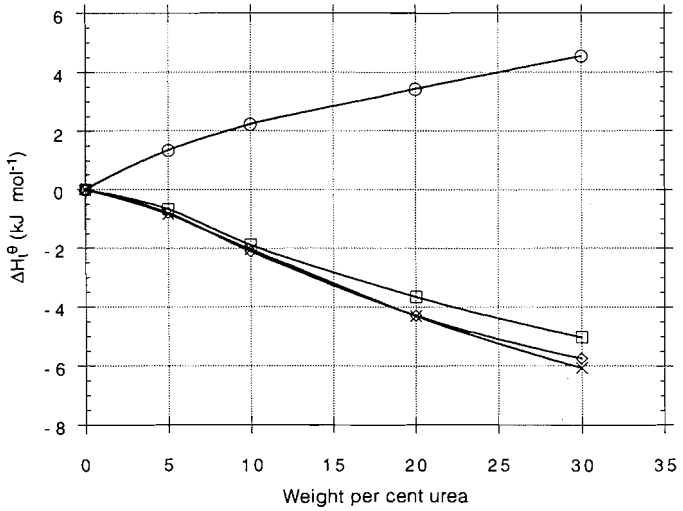

FIG. 2. Single-ion enthalpies of transfer (kJ mol^{-1}) from water to aqueous urea solutions at 298.15 K for selected anions. (○) BPh_4^-; (□) Cl^-; (◇) Br^-; (×) I^-.

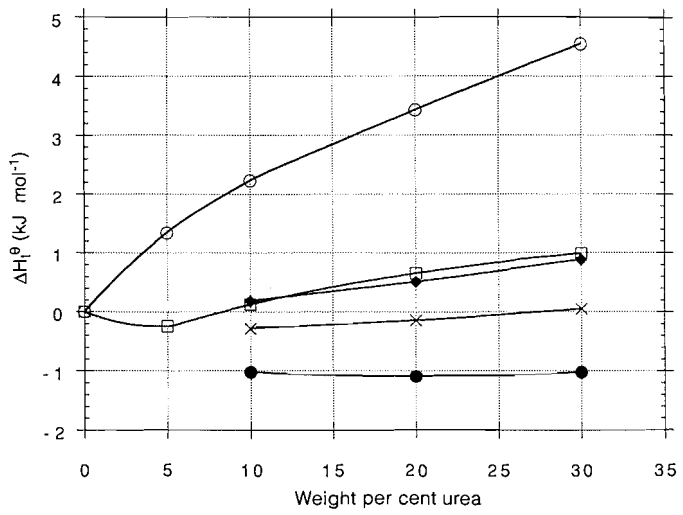

FIG. 3. Single-ion enthalpies of transfer (kJ mol^{-1}) from water to aqueous urea solutions at 298.15 K for selected cations. (○) Ph_4As^+; (□) Na^+; (◆) K^+; (×) Rb^+; (●) Cs^+.

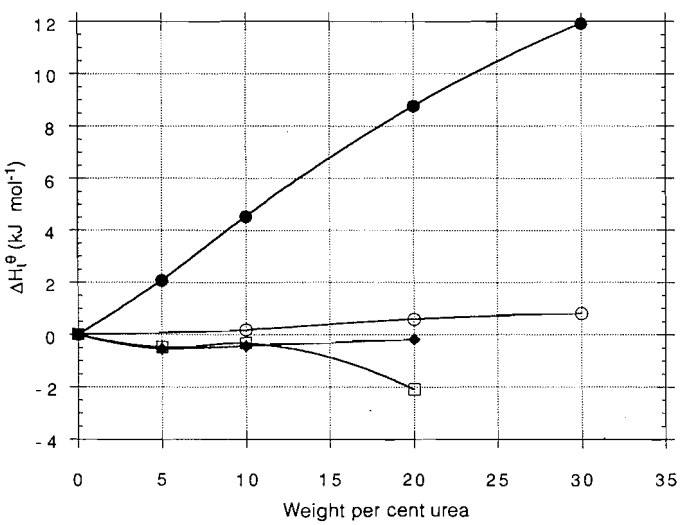

FIG. 4. Single-ion enthalpies of transfer (kJ mol^{-1}) from water to aqueous urea solutions at 298.15 K for the ammonium cation and alkylammonium cations. (○) NH_4^+; (□) Me_4N^+; (◆) Et_4N^+; (●) Bu_4N^+.

fore the differences observed in their enthalpies of transfer can be attributed to the effects of the anion. From this viewpoint it is clear that aqueous urea solutions accommodate Ph_4B^- ions in a different manner from the way in which they accommodate halide ions. Single-ion enthalpies of transfer calculated using the TATB assumption are reported for several anions and cations in Figs. 2 and 3 respectively. These figures indicate that Ph_4As^+ and Ph_4B^- can be regarded as structure enhancers (positive ΔH_t^θ) whereas the halide anions should be classed as structure disrupters (negative ΔH_t^θ) in aqueous urea solutions. The structuring capacity of the alkali metal cations appears to be linked to cation size. The structure disruption capacity following the order $Na^+ < K^+ < Rb^+ < Cs^+$. This relationship between ion size and structure disruption capacity appears to be paralleled by the halide ions. Figure 4 displays trends in single-ion enthalpies of transfer for ammonium and alkylammonium cations as a function of urea concentration in aqueous solution. The trends observed suggest that Me_4N^+ and Et_4N^+ behave as structure disrupters whereas Bu_4N^+ behaves as a structure enhancer in aqueous urea solutions. Such classifications are in agreement with previous studies (24–27). The trends observed in single-ion entropies reported in Table 4 are consistent with the structure enhancing/disrupting classifications described above.

The transfer of a halide ion from water to an aqueous urea solution is a spontaneous process, as indicated by a negative Gibbs energy of transfer (5*a*, 11). Halide ions are stabilized in aqueous urea solutions, and enthalpy/entropy compensation calculations suggest that the transfer processes are enthalpy controlled. However, the transfer of an alkali metal ion from water to an aqueous urea solution is a non-spontaneous process, i.e., positive ΔG_t^θ (5*a*, 11). Alkali metal cations are destabilized in aqueous urea solutions and enthalpy/entropy compensation calculations suggest that

Can. J. Chem. Downloaded from www.nrcresearchpress.com by 217.78.4.112 on 09/08/12
For personal use only.

TABLE 4. Single-ion entropies of transfer (molar scale) from water to aqueous urea solutions at 298.15 K (J K^{-1} mol^{-1})

Ion	Weight % urea		
	11.52%	20.31%	29.64%
Ph_4As^+	11.13	20.39	25.75
Ph_4B^-	11.13	20.39	25.75
Na^+	−7.47	−9.20	−7.44
K^+	−6.77	−9.34	−7.11
Rb^+	−8.34	−10.90	−9.24
Cs^+	−10.38	−13.42	−11.81
Cl^-	−0.27	−2.06	−8.07
Br^-	0.00	−3.42	−9.34
I^-	0.41	−2.73	−8.46

the transfer processes are entropy controlled. These results indicate that aqueous urea solutions accommodate anions differently from the manner in which they accommodate cations. Such an observation is common to other aqueous solvent mixtures (6, 28).

Acknowledgements

The author would like to thank the Natural Sciences and Engineering Research Council of Canada for operating support and C. Dobrogowska and L. G. Hepler for providing access to the calorimeter used for some of the reported measurements.

1. Y. Marcus. Pure Appl. Chem. **58**, 1721 (1986).
2. Y. Marcus, M. J. Kamlet, and R. W. Taft. J. Phys. Chem. **92**, 3613 (1988).
3. Y. Marcus. Rev. Anal. Chem. **5**, 53 (1980).
4. A. Kontturi, K. Kontturi, L. Murtomäki, and D. J. Schiffrin, J. Chem. Soc. Faraday Trans. **86**, 819 (1990).
5. (*a*) M. J. Blandamer, J. Burgess, A. W. Hakin, P. Guardado, S. Nuttall, and S. Radulovic. J. Chem. Soc. Faraday Trans. 1, **83**, 559 (1987); (*b*) M. J. Blandamer, J. Burgess, B. Clark, P. P. Duce, A. W. Hakin, N. Gosal, S. Radulovic, P. Guardado, F. Sanchez, C. D. Hubbard, and E. A. Abu-Gharib. J. Chem. Soc. Faraday Trans. 1, **82**, 1471 (1986); (*c*) M. J. Blandamer, B. Briggs, J. Burgess, D. Elvidge, P. Guardado, A. W. Hakin, S. Radulovic, and C. D. Hubbard. J. Chem. Soc. Faraday Trans. 1, **84**, 2703 (1988).
6. M. H. Abraham, T. Hill, H. C. Ling, R. A. Schulz, and R. A. C. Watt. J. Chem. Soc. Faraday Trans. 1, **80**, 489 (1984).
7. M. Booij and G. Somsen. Electrochim. Acta, **28**, 1883 (1983).
8. Y. Pointud and J. Juillard. J. Chem. Soc. Faraday Trans. 1, **73**, 1048 (1977).
9. A. F. Danil de Namor and H. Beroa de Ponce. J. Chem. Soc. Faraday Trans. 1, **84**, 1671 (1988).
10. A. F. Danil de Namor and L. Ghousseini. J. Chem. Soc. Faraday Trans. 1, **82** 3275 (1986).
11. H. Talukdar, S. Rudra, and K. K. Kundu. Can. J. Chem. **67**, 321 (1989).
12. S. Rudra, H. Talukdar, and K. K. Kundu. Can. J. Chem. **65**, 2595 (1987).
13. A. K. Das and K. K. Kundu. J. Solution Chem. **5**, 431 (1976).
14. G. Kalfoglou and L. H. Bowen. J. Phys. Chem. **73**, 2728 (1969).
15. C. Dobrogowska and L. G. Hepler. Manuscript in preparation.
16. J. H. Fossum, P. C. Markunas, and J. A. Riddick. Anal. Chem. **23**, 491 (1951).
17. E. A. Guggenheim and J. E. Prue. Trans. Faraday Soc. **50**, 710 (1954).
18. C. M. Criss and J. W. Cobble. J. Am. Chem. Soc. **83**, 3223 (1961).
19. O. M. Bhatnager and A. N. Campbell. Can. J. Chem. **52**, 203 (1974).
20. R. E. Verrall and L. W. Dickson. J. Solution Chem. **5**, 203 (1976).
21. H. S. Frank and F. Franks. J. Chem. Phys. **48**, 4746 (1968).
22. J. H. Stern and J. D. Kulluk. J. Phys. Chem. **73**, 2795 (1969).
23. L. L. Bright and J. R. Jezorek. J. Phys. Chem. **79**, 800 (1975).
24. R. L. Kay and D. F. Evans. J. Phys. Chem. **69**, 4216 (1965).
25. R. L. Kay and D. F. Evans. J. Phys. Chem. **70**, 366 (1966).
26. K. W. Bunzl. J. Phys. Chem. **71**, 1358 (1967).
27. R. L. Kay, T. Vittucio, C. Zawoyski, and D. F. Evans. J. Phys. Chem. **70**, 2336 (1966).
28. J. Juillard. J. Chem. Soc. Faraday Trans. 1, **78**, 43 (1982).
29. R. Fuchs and C. P. Hagan. J. Phys. Chem. **77**, 1797 (1973).
30. V. B. Parker. Thermal properties of univalent electrolytes. NSRDS-NBS 2. National Bureau of Standards, Washington, D.C. 1969.
31. M. Woldan. Thermochim. Acta, **120**, 97 (1987).
32. C. V. Krishnan and H. L. Friedman. J. Phys. Chem. **73**, 3934 (1969).
33. R. B. Cassel and W-Y. Wen. J. Phys. Chem. **76**, 1369 (1972).
34. J. P. Chatterjee and I. N. Basumallick. J. Chem. Soc. Faraday Trans. **86**, 3107 (1990).

Can. J. Chem. Downloaded from www.nrcresearchpress.com by 217.78.4.112 on 09/08/12
For personal use only.

Equilibrium constants and heats of formation of methyl esters and *N*,*N*-dimethyl amides of substituted benzoic acids

J. PETER GUTHRIE,[1] DAVID C. PIKE, AND YIU-CHUNG LEE
Department of Chemistry, University of Western Ontario, London, Ont., Canada N6A 5B7

Received July 15, 1991

J. PETER GUTHRIE, DAVID C. PIKE, and YIU-CHUNG LEE. Can. J. Chem. **70**, 1671 (1992).

Heats of methanolysis and dimethylaminolysis of substituted benzoyl chlorides (4-X-C_6H_4-COCl, X = H, CH_3, OCH_3, Cl, NO_2) have been measured, as have the heats of hydrolysis of the esters, permitting the calculation of the heats of formation of the benzoyl chlorides (4-X-C_6H_4-COCl, X, DH_f: CH_3O, −80.29 ± 0.70; CH_3, −48.10 ± 1.46; NO_2, −47.70 ± 0.87), methyl benzoate esters (4-X-C_6H_4-$COOCH_3$, X, DH_f: CH_3O, −124.50 ± 0.39; CH_3, −93.99 ± 0.58; Cl, −92.09 ± 0.53; NO_2, −92.55 ± 0.31), and *N*,*N*-dimethylbenzamides (4-X-C_6H_4-$CON(CH_3)_2$, X, DH_f: CH_3O, −75.87 ± 1.42; CH_3, −46.62 ± 1.99; H, −40.96 ± 1.41; Cl, −49.33 ± 1.09; NO_2, −48.05 ± 1.53). Free energies of transfer from methanol to water and from gas to water were determined for the esters and amides. Free energies of formation in aqueous solution were calculated for the acids, esters and amides, making use of thermodynamic estimation procedures where necessary. Equilibrium constants were measured for ester formation in water (X, K (M^{-1}): CH_3O, 0.14; CH_3, 0.14; H, 0.12; Cl, 0.15; NO_2, 0.13) and *N*,*N*-dimethylaminolysis in methanol (X, K (M^{-1}): CH_3O, 8.16; CH_3, 17.5; H, 26.5; Cl, 22.6; NO_2, 41.0). Partition constants for esters and amides were measured for methanol/dodecane and dodecane/water, permitting calculation of the free energy of transfer from methanol to water (4-X-C_6H_4-$COOCH_3$, X, DG_{mw}: CH_3O, 3.12; CH_3, 3.17; H, 3.01; Cl, 3.43; NO_2, 2.89; 4-X-C_6H_4-$CON(CH_3)_2$, X, DG_{mw}: CH_3O, 0.96; CH_3, 1.48; H, 0.92; Cl, 1.77; NO_2, 0.99). These data permit calculation of the equilibrium constants for dimethylaminolysis of substituted methyl benzoates in water, and for amide formation in water (4-X-C_6H_4-$CON(CH_3)_2$, X, K(M^{-1}, reactants and products as neutral molecules): CH_3O, 767; CH_3, 752; H, 2050; Cl, 1020; NO_2, 2350). In the course of our calorimetric measurements we derived an improved value for the heat of solution of HCl in methanol.

J. PETER GUTHRIE, DAVID C. PIKE et YIU-CHUNG LEE. Can. J. Chem. **70**, 1671 (1992).

On a mesuré les chaleurs de méthanolyse et de diméthylaminolyse de chlorures de benzyles substitués (4-X-C_6H_4-COCl, X = H, CH_3, OCH_3, Cl et NO_2) ainsi que les chaleurs d'hydrolyse des esters, permettant de calculer les chaleurs de formation des chlorures de benzoyles (4-X-C_6H_4-COCl, X, DH_f : CH_3O, −80,29 ± 0,70; CH_3, −48,10 ± 1,46; NO_2, −47,70 ± 0,87), des benzoates de méthyle (4-X-C_6H_4-$COOCH_3$, X, DH_f : CH_3O, −124,50 ± 0,39; CH_3, −93,99 ± 0,58; Cl, −92,09 ± 0,53; NO_2, −92,55 ± 0,31) et des *N*,*N*-diméthylbenzamides (4-X-C_6H_4-$CON(CH_3)_2$, X, DH_f : CH_3O, −75,87 ± 1,42; CH_3, −46, 62 ± 1,99; H, −40,96 ± 1,41; Cl, −49,33 ± 1,09; NO_2, −48,05 ± 1,53). On a aussi déterminé les énergies libre de transfert du méthanol à l'eau et de la phase gazeuse à l'eau pour les esters et les amides. Faisant appel à des méthodes d'évaluations thermodynamiques lorsque nécessaire, on a calculé les énergies de formation en solution aqueuse pour les acides, les esters et les amides. On a mesuré les constantes d'équilibre pour la formation des esters dans l'eau (X, K (M^{-1})) : CH_3), 0,14; CH_3, 0,14; H, 0,12; Cl, 0,15; NO_2, 0,13) et pour la diméthylaminolyse dans le méthanol (X, K (M^{-1})) : CH_3O, 8,16; CH_3, 17,5; H, 26,5; Cl, 22,6; NO_2, 41,0). On a mesuré les constantes de partition des esters et des amides entre le méthanol/dodécane et le dodécane/eau, ce qui permet de calculer les énergies libres de transfert du méthanol à l'eau (4-X-C_6H_4-$COOCH_3$, X, DG_{me} : CH_3O, 3,12; CH_3, 3,17; H, 3,01; Cl, 3,43; NO_2, 2,89; 4-X-C_6H_4-$CON(CH_3)_2$, X, DG_{me} : CH_3O, 0,96; CH_3, 1,48; H, 0,92; Cl, 1,77; NO_2, 0,99). Ces données permettent de calculer les constantes d'équilibre pour la diméthylaminolyse de benzoates de méthyle substitués dans l'eau et pour la formation des amides dans l'eau (4-X-C_6H_4-$CON(CH_3)_2$, X, K (M^{-1}), réactifs et produits sous la forme de molécules neutres) : CH_3O, 767; CH_3, 752; H, 2050; Cl, 1020; NO_2, 2350). Dans le cadre de nos mesures calorimétriques, on a obtenu une valeur améliorée pour la chaleur de solution du HCl dans le méthanol.

[Traduit par la rédaction]

Introduction

We have been interested for some time in the energetics of acyl transfer reactions (1) and in the energy levels of tetrahedral intermediates in ester (2, 3) and amide (4) hydrolyses. As part of a project aimed at extending this study to a series of substituted benzamides, we determined heats of formation of several *N*,*N*-dimethylbenzamides and methyl benzoates. These data permit calculation of the heats of aminolysis. Ester aminolysis is a curious reaction, which is not often useful because it is slow, even though it should be thermodynamically favorable. We find that the heats of dimethyl aminolysis for substituted methyl benzoates are small and not very sensitive to substituents. We also measured equilibrium constants for ester formation in water, and of dimethylaminolysis of the methyl esters in methanol, together with partition coefficients permitting the calculation of equilibrium constants for dimethylaminolysis in water. From equilibrium constants for ester formation and dimethylaminolysis we can calculate equilibrium constants for *N*,*N*-dimethylbenzamide formation.

Results

Heats of formation

In all cases the heat of formation of the substituted benzoic acid was known; methyl benzoate was the only ester for which a heat of formation had been reported (3). Heats of formation of the substituted methyl benzoates were determined by measuring the heat of reaction with tetraethylammonium hydroxide in aqueous DMSO. Heats of formation for benzoyl chloride and *p*-chlorobenzoyl chloride are known (14); for the others we determined the heat of formation by measuring the heat of reaction with methanol. The reaction of substituted benzoyl chlorides with methanol was slow; in

[1]Author to whom correspondence may be addressed.

Can. J. Chem. Downloaded from www.nrcresearchpress.com by 217.78.4.112 on 09/08/12
For personal use only.

Can. J. Chem. Downloaded from www.nrcresearchpress.com by 217.78.4.112 on 09/08/12
For personal use only.

TABLE 1. Heats of reaction and solution determined in this work[a]

Compound	ΔH(MeOH)	ΔH(Me_2NH/MeOH)	ΔH(TEAH/DMSO)
(*a*) Heats of reaction with methanol and methanolic dimethylamine			
CH_3-CO-Cl (l)	−20.77 (0.23)		
*p*MeO-C_6H_4-CO-Cl (s)	−16.29 (0.78)	−32.70 (0.22)	
*p*Me-C_6H_4-CO-Cl (l)	−20.44 (1.30)	−38.60 (0.84)	
C_6H_5-CO-Cl (l)	−19.47 (1.20)	−39.89 (0.92)	
*p*Cl-C_6H_4-CO-Cl (l)	−21.23 (0.66)	−39.89 (0.09)	
pNO_2-C_6H_4-CO-Cl (s)	−18.55 (0.72)	−35.66 (0.68)	
(*b*) Heats of solution in methanolic dimethylamine			
*p*MeO-C_6H_4-CO-NMe_2 (l)		0.07 (0.04)	
*p*Me-C_6H_4-CO-NMe_2 (l)		−0.11 (0.03)	
C_6H_5-CO-NMe_2 (s)		3.37 (0.11)	
*p*Cl-C_6H_4-CO-NMe_2 (s)		3.60 (0.06)	
pNO_2-C_6H_4-CO-NMe_2 (s)		4.66 (0.11)	
Me_2NH (l)		−3.26 (0.17)	
Me_2NH·HCl (s)		1.67 (0.02)	
(*c*) Heats of reaction with tetraethylammonium hydroxide in aqueous DMSO and heats of solution in methanol			
CH_3-CO-OMe (l)	0.76 (0.06)		
*p*MeO-C_6H_4-CO-OMe (s)	5.71 (0.10)		−11.28 (0.18)
*p*Me-C_6H_4-CO-OMe (s)	5.41 (0.04)		−11.09 (0.14)
C_6H_5-CO-OMe (l)	0.79 (0.05)		−17.44 (0.45)[b]
*p*Cl-C_6H_4-CO-OMe (s)	5.50 (0.06)		−12.41 (0.21)
pNO_2-C_6H_4-CO-OMe (s)	6.56 (0.20)		−12.48 (0.20)
(*d*) Heats of solution/reaction with tetraethylammonium hydroxide in aqueous dimethyl sulfoxide			
*p*MeO-C_6H_4-CO-OH (s)			−12.51 (0.31)
*p*Me-C_6H_4-CO-OH (s)			−13.35 (0.44)
C_6H_5-CO-OH (s)			−14.09 (0.54)[b]
*p*Cl-C_6H_4-CO-OH (s)			−12.98 (0.41)
pNO_2-C_6H_4-CO-OH (s)			−13.99 (0.07)
MeOH (l)			−1.53 (0.04)[b]
H_2O (l)			−1.36 (0.03)[b]

[a]All at 25°C; solvents made up as described in the experimental section. Values in parentheses are standard deviations calculated from replicate determinations. Units are kcal mol^{-1}.
[b]Reference 3.

fact this was a serious source of experimental error. Although a heat of solution for HCl in methanol was available from the literature, this value led to inconsistent results. Accordingly we evaluated it by measuring the heat of reaction of several acid chlorides, (acetyl chloride, benzoyl chloride, and *p*-chlorobenzoyl chloride) with methanol; when the heat of formation of the acid chloride is known, the only unknown quantity is the heat of solution of HCl in methanol. Heats of formation of the amides were determined by measuring the heat of reaction of the substituted benzoyl chloride with methanolic dimethylamine. The reaction of substituted benzoyl chlorides with dimethylamine in methanol was fast. HPLC analysis showed that the product of reaction with methanolic dimethylamine was the amide. Heats of reaction and solution are found in Table 1. In this way we completed the set of heats of formation of the acid chlorides, esters, and *N*,*N*-dimethylamides of the five benzoic acids that we have studied. This allowed calculation of the heats of formation in Table 2.

Estimation of boiling points

For several of the solid esters, amides, and acid chlorides used in this work, no atmospheric pressure boiling points could be found in the literature, and, particularly for the nitro derivatives, the compounds are expected to be very high boiling. We endeavored to estimate approximate boiling points as a starting point for later estimation of the vapor pressure at 25°C, using the boiling point number approach of Kinney (5, 6). To do this we calculated the boiling point numbers for benzene, chlorobenzene, toluene, anisole, nitrobenzene, methyl benzoate, *N*,*N*-dimethylbenzamide, and benzoyl chloride using boiling points from ref. (7) and Kinney's formula (5).

$$bp = (230.14 \sqrt[3]{BPN}) - 543$$

$$BPN = ((bp + 543)/230.14)^3$$

We then calculated the increments for replacement of H on a benzene ring by Cl, 5.38; CH_3, 3.06; CH_3O, 8.05; NO_2, 15.31; $COOCH_3$, 13.75; $CON(CH_3)_2$, 24.56; and COCl, 13.40. With these values it was straightforward to estimate boiling points for the substituted derivatives as: ester, X = Cl, 234; X = CH_3, 217 (obs. 217 (8)); X = CH_3O, 250 (obs. 256 (8)); X = NO_2, 295; amide, X = Cl, 305; X = CH_3, 291; X = CH_3O, 319; X = NO_2, 357; acid chloride, X = Cl, 235 (obs. 221 (9)); X = CH_3, 219 (obs. 216 (10)); X = CH_3O,

TABLE 2. Thermodynamic quantities for compounds discussed in this paper[a]

Compound	ΔH_f^0 (l or s)[b]	ΔH_{vap}[c]	ΔH_f^0 (g)[d]	S^0 (g)[e]	ΔG_f^0 (g)[f]	ΔG_t[g]	ΔG_f^0 (aq)[h]
(*a*) Compounds for which ΔG_f^0 (aq) has not been reported previously							
4-X-C_6H_4-COCl							
CH_3O	−80.29 ± 0.70	17.71 ± 1.00	−62.58 ± 1.22	106.46 ± 2.00	−35.96 ± 1.64		
CH_3	−48.10 ± 1.46	14.71 ± 1.00	−33.39 ± 1.77	96.09 ± 2.00	−10.98 ± 2.08		
H	−37.67 ± 0.14[i]	13.00 ± 1.02[i]	−24.67 ± 1.03	87.36 ± 0.15	−9.36 ± 1.03		
Cl	−45.81 ± 0.26	15.00 ± 1.00[i,j]	−30.81 ± 1.03	94.37 ± 2.00	−14.30 ± 1.50		
NO_2	−47.70 ± 0.87	23.64 ± 1.50	−24.06 ± 1.74	102.03 ± 2.00	3.65 ± 2.05		
4-X-C_6H_4-$COOCH_3$							
CH_3O	−124.50 ± 0.39	21.02 ± 1.50	−103.49 ± 1.55	112.96 ± 2.00	−65.08 ± 1.90	−3.43 ± 0.50	−68.50 ± 1.96
CH_3	−93.99 ± 0.58	19.27 ± 1.50	−74.71 ± 1.61	102.59 ± 2.00	−40.51 ± 1.94	−1.88 ± 0.50	−42.39 ± 2.01
H	−77.51 ± 0.72[k]	13.28 ± 0.01	−64.23 ± 0.72	93.86 ± 0.15[l]	−37.14 ± 0.72	−2.38 ± 0.10	−39.52 ± 0.73
Cl	−92.09 ± 0.53	19.29 ± 2.50	−72.80 ± 2.55	100.87 ± 2.00	−44.50 ± 2.78	−1.75 ± 0.50	−46.26 ± 2.82
NO_2	−92.55 ± 0.31	23.89 ± 2.50	−68.66 ± 2.52	108.53 ± 2.00	−29.16 ± 2.75	−4.98 ± 0.50	−34.14 ± 2.79
4-X-C_6H_4-$CON(CH_3)_2$							
CH_3O	−75.87 ± 1.42	22.19 ± 1.50	−53.67 ± 2.07	115.74 ± 2.00	−2.21 ± 2.34	−9.11 ± 0.50	−11.32 ± 2.39 −18.16 ± 1.98[m]
CH_3	−46.62 ± 1.99	19.69 ± 1.50	−26.93 ± 2.49	105.37 ± 2.00	20.32 ± 2.72	−7.86 ± 0.50	12.46 ± 2.76 7.91 ± 2.02[m]
H	−40.96 ± 1.41	21.08 ± 1.50	−19.89 ± 2.06	96.64 ± 0.50	20.25 ± 2.08	−7.39 ± 0.50	12.86 ± 2.14 10.22 ± 0.77[m]
Cl	−49.33 ± 1.09	22.88 ± 2.50	−26.45 ± 2.73	103.65 ± 2.00	14.89 ± 2.94	−7.38 ± 0.50	7.51 ± 2.98 4.12 ± 2.83[m]
NO_2	−48.05 ± 1.53	27.48 ± 2.50	−20.57 ± 2.93	111.31 ± 2.00	31.98 ± 3.13	−10.05 ± 0.50	21.93 ± 3.17 15.61 ± 2.80[m]
4-X-C_6H_4-COOH							
CH_3O	−134.25 ± 0.19[n]	26.24 ± 0.14[n]	−108.01 ± 0.24	107.25 ± 2.00	−77.61 ± 1.12	−5.92 ± 0.50	−83.53 ± 1.22
CH_3	−102.50 ± 0.24[i]	23.21 ± 0.13[o]	−79.37 ± 0.27	96.88 ± 2.00	−53.18 ± 1.12	−5.76 ± 0.50	−58.94 ± 1.23
H	−92.07 ± 0.12[i]	21.78 ± 0.52[i]	−70.29 ± 0.53	88.15 ± 0.50	−51.21 ± 0.60	−5.80 ± 0.19	−57.01 ± 0.63
Cl	−102.51 ± 0.24[p]	24.51 ± 0.09[q]	−78.00 ± 0.26	95.16 ± 2.00	−57.72 ± 1.12	−5.89 ± 0.50	−63.61 ± 1.23
NO_2	−102.03 ± 0.22[i]	28.33 ± 2.00[r]	−73.70 ± 2.01	102.82 ± 2.00	−42.21 ± 2.29	−9.02 ± 0.50	−51.23 ± 2.34
(*b*) Compounds needed for estimation of additivity parameters							
C_6H_5-X							
CH_3O	−27.44 ± 0.19[i]	11.21 ± 0.05[i]	−16.23 ± 0.22[i]	87.01 ± 0.15[t]	5.19 ± 0.23	0.86 ± 0.10[s]	6.05 ± 0.26
CH_3	2.96 ± 0.14[i]	9.08 ± 0.01[i]	12.05 ± 0.14[i]	76.64 ± 0.15[t]	29.26 ± 0.16	1.01 ± 0.10[s]	30.27 ± 0.19
H	11.71 ± 0.14[i]	8.03 ± 0.01[i]	19.74 ± 0.17[i]	64.34 ± 0.15[t]	30.91 ± 0.19	1.03 ± 0.10[s]	31.94 ± 0.21
Cl	2.63 ± 0.31[i]	9.80 ± 0.01[i]	12.43 ± 0.31[i]	74.92 ± 0.15[t]	23.73 ± 0.32	0.89 ± 0.15[s]	24.62 ± 0.35
NO_2	2.99 ± 0.12[i]	13.15 ± 0.04[i]	16.13 ± 0.14[i]	77.28 ± 0.15	40.22 ± 0.17	−2.22 ± 0.15[s]	38.00 ± 0.22

(*c*) Compounds for which ΔH_f or ΔG_f^0 (aq) has been reported previously

Compound	ΔH_f^0 (l or s)	ΔG_f^0 (aq)
CH_3OH	−57.15 ± 0.05[i]	−41.88[v]
$(CH_3)_2NH$	−10.4 ± 0.1[i]	13.84[u]
$(CH_3)_2NH_2Cl$	−69.57 ± 0.02[w]	
HCl (g)	−22.06 ± 0.02 (g)[i]	
H_2O		−56.69[w]

[a]All at 25°C; standard states are pure liquid, pure crystalline solid, ideal gas at 1 atm (101.3 KPa) pressure, and 1 M aqueous solution with an infinitely dilute reference state; units are kcal mol^{-1}, and cal deg^{-1} mol^{-1}.

[b]Heat of formation for the liquid or crystalline solid; determined in this work, Table 1, unless otherwise noted.

[c]Heat of vaporization for a liquid or heat of sublimation for a solid; evaluated as described in the text and Table 3 unless otherwise noted.

[d]Heat of formation of the ideal gas; calculated from the heat of formation in condensed phase and the heat of vaporization or sublimation.

[e]Standard entropy of the ideal gas; evaluated as described in the text unless otherwise noted.

[f]Free energy of formation of the ideal gas; calculated from the heat of formation and the standard entropy.

[g]Free energy of transfer from the ideal gas at 1 atm to 1 M aqueous solution. Values for esters and amides are from Table 7. Values for carboxylic acids are based on the values for benzoic acid (3) and the group contributions in Table 9.

[h]Free energy of formation in aqueous solution; calculated from the free energy of formation in the gas phase and the free energy of transfer.

[i]Reference 14.

Can. J. Chem. Downloaded from www.nrcresearchpress.com by 217.78.4.112 on 09/08/12
For personal use only.

TABLE 2 (*concluded*)

[j]Reference 55.
[k]Reference 3.
[l]Reference 28.
[m]Based on the equilibrium constant for dimethylaminolysis of the corresponding methyl ester (Table 10) and the free energies of formation of methanol, dimethylamine, and the ester, from this table.
[n]Reference 57.
[o]Reference 56.
[p]Reference 61.
[q]Reference 58.
[r]Estimated as described in the text.
[s]Reference 2.
[t]Reference 21.
[u]Reference 4.
[v]Reference 59.
[w]Reference 60.

Can. J. Chem. Downloaded from www.nrcresearchpress.com by 217.78.4.112 on 09/08/12
For personal use only.

252 (obs. 260 (11)); X = NO_2, 297. For the cases where atmospheric pressure boiling points were available the agreement is good.

Estimation of heats of vaporization

We estimated heats of vaporization from the boiling point data, using a method that we had previously devised to use boiling points at various pressures (12). The boiling points and derived heats of vaporization are found in Table 3. The expected error for this estimation procedure is 0.28 kcal mol^{-1} (12); the uncertainty limits in Table 3 are taken as 0.28 kcal mol^{-1} or the standard deviation of the various estimates from different boiling point values, whichever is larger. As a check and in order to estimate values where no vapor pressure data were available, we used an additivity scheme derived from the group additivity scheme we recently published (13). The value for the benzene nucleus with two *para* substituents was taken as 4[C_BH]; contributions for H and Cl were taken as [C_BH] and [C_BCl] respectively; the contribution for CH_3 was taken as [$C_B(C)$] + [$CH_3(C_B)$]; the contributions for O-CH_3, $-NO_2$, $-COOCH_3$, and $CON(CH_3)_2$ were calculated from the heats of vaporization of anisole (14), nitrobenzene (14), methyl benzoate (14), *N*,*N*-dimethylbenzamide (calculated from the boiling point, as already described), and benzoyl chloride (calculated from the boiling point, as already described). The values so obtained were: *p*-C_6H_4, 5.36; H, 1.34; Cl, 2.91; CH_3, 2.47; OCH_3, 4.49; NO_2, 6.45; $COOCH_3$, 6.58; $CON(CH_3)_2$, 11.30; COCl, 6.30. Using these values we could estimate heats of vaporization for the remaining compounds; the values so estimated are found in Table 3. Comparison of heats of vaporization estimated by additivity and corresponding values estimated from the boiling points at various pressures shows that the agreement is generally good, but differences can be as large as 1.5 kcal mol^{-1}; this is taken as the uncertainty in estimates based on additivity.

Estimation of heats of fusion

Fuchs and Rodewald have reported heats of solution of aromatic compounds in methanol (15). For the liquids, the heat of solution is invariably small, with a magnitude less than 1 kcal mol^{-1}. For solids the heat of solution is larger. For two 1,4-disubstituted benzenes both heat of solution and heat of fusion are available, allowing the calculation of the heat of solution for the hypothetical supercooled liquid; the values so calculated are again small, with magnitudes less than 1 kcal mol^{-1}. To obtain approximate values for the heats of fusion of the solid esters and amides studied here, we subtracted the average heat of solution of the liquid analog(s) from the observed heat of solution of the solid compounds. The values so obtained are found in Table 4. As a check we estimated the heats of fusion from the melting points, using the average value for the entropy of fusion, 13.0 cal deg^{-1} mol^{-1}, reported by Yalkowsky and co-workers (16). Yalkowsky and co-workers could find no dependence of the entropy of fusion upon structural features. The values of ΔS_{fus} ranged from 9.1 to 18.9 cal deg^{-1} mol^{-1} for disubstituted benzenes. The agreement between the two estimates for our compounds must be considered satisfactory, and the entropies of fusion calculated assuming the enthalpy values derived from heats of solution are not unreasonable. We consider the uncertainty in these estimated heats of fusion to be 1 kcal mol^{-1}, the approximate scatter in heats of solution in methanol for liquid aromatic compounds similar to those of interest here.

For *p*-nitrobenzoic acid we needed to estimate a heat of sublimation at 25°C. We have procedures for estimating the heat of vaporization of the liquid by atomic additivity (13), but need a heat of fusion. The heat of fusion has been reported at the melting point, 239.2°C (17), but this must be corrected to 25°C. To do this we need the heat capacity of fusion. The heat capacity of the solid at 25°C is available: 43.02 cal deg^{-1} mol^{-1} (17). We can estimate the heat capacity change on vaporization by additivity (18) as −28.48. To estimate the heat capacity of gaseous *p*-nitrobenzoic acid we need a contribution for the group [C_BNO_2]. This was calculated from C_p for nitrobenzene, which in turn was calculated by statistical mechanics from the vibrational spectrum (19) and barriers to internal rotation (20), as was done for entropy; *vide infra*. In this way we obtained: C_p (g, 25°C) [Ph-NO_2] = 28.56 cal deg^{-1} mol^{-1}; [C_BNO_2] = 12.36 cal deg^{-1} mol^{-1}; C_p (g, 25°C) [*p*-NO_2-C_6H_4-COOH] = 33.85 cal deg^{-1} mol^{-1} using a contribution for COOH based on C_p(g) for benzoic acid (21); C_p(1, 25°C) [*p*-NO_2-C_6H_4-COOH] = 62.33 cal deg^{-1} mol^{-1}; ΔC_p(fusion) [*p*-NO_2-C_6H_4-COOH] = 19.31 cal deg^{-1} mol^{-1}. Since ΔH_{fusion} (239°C) [*p*-NO_2-C_6H_4-COOH] = 8.84 kcal mol^{-1} (17), we can now calculate that ΔH_{fusion} (25°C) [*p*-NO_2-C_6H_4-COOH] = 4.71 kcal mol^{-1}. A similar calculation for benzoic acid using the heat of fusion (17), C_p(s) (17), C_p(g) (21), and ΔH_{sub} (14), leads to ΔC_p(fusion) = 10.70 cal deg^{-1} mol^{-1}, ΔH_{fusion}(25°C) = 3.76 kcal mol^{-1}, and, for the hypothetical supercooled liquid at 25°C, ΔH_{vap} = 18.52 kcal mol^{-1}. Then by group additivity estimation we arrive at a value, for the hypothetical

TABLE 3. Data permitting estimation of vapor pressures and heats of vaporization[a]

Compound	Melting point[b]	ΔH_{fus}[c]	Boiling point[d] t	Boiling point[d] p	ΔH_{vap}[e]	ΔC_{vap}[f]	p_{25}[g]
4-X-C_6H_4-$COOCH_3$							
CH_3O	48[h,i]	4.17	123	12[j]	16.67 ± 0.28[k,l]	−28.44	0.0090
CH_3	33[h,m]	3.98	91	8[n]	14.62 ± 0.28[k,o]	−23.75	0.091
H			83	10[p]	13.28 ± 0.01[q,r]	−22.10	0.31
Cl	44[h,s]	4.12	234	760[t]	14.85 ± 1.50[u]	−24.32	0.052
NO_2	96[h,v]	4.80	295	760[t]	18.39 ± 1.50[u]	−29.53	1.3×10^{-4}
4-X-C_6H_4-$CON(CH_3)_2$							
CH_3O	32[h,w]	3.97	107	0.25[x]	22.19 ± 0.43[k,y]	−31.03	1.1×10^{-5}
CH_3	40[h,z]	4.07	97	0.32[aa]	19.69 ± 0.42[k,ab]	−26.34	6.0×10^{-4}
H	43[h,ac]	4.11	130	11[ad]	17.71 ± 0.28[k,ae]	−24.69	4.4×10^{-3}
Cl	58[h,af]	4.30	305	760[t]	19.28 ± 1.50[u]	−26.91	3.0×10^{-4}
NO_2	97[h,ag]	4.81	357	760[t]	23.82 ± 1.50[u]	−37.42	1.03×10^{-6}
4-X-C_6H_4-COCl							
CH_3O			91	1.[ah]	17.71 ± 0.32[k,ai]	−24.32	5.7×10^{-3}
CH_3			73	4.5[aj]	14.71 ± 0.36[k,ak]	−20.20	0.17
H			50	2.7[al]	13.30 ± 0.18[k,am]	−17.98	0.50
Cl			80	2.0[an]	15.00 ± 0.34[k,ao]	−19.63	0.046
NO_2	75[h,ap]	3.13	136	4.[aq]	19.11 ± 0.52[k,ar]	−25.41	2.5×10^{-4}

[a]Many of the data are from Beilstein, "Handbuch der organischen chemie", for which references are given in short form as: Beil, volume, supplement, page. All thermodynamic quantities refer to 25°C.

[b]Selected value.

[c]Estimated from the melting point as described in the text.

[d]Selected value; the literature bp at the lowest pressure that led to a heat of vaporization consistent with the rest of the data was used where possible. When no literature value was available, a value was estimated by the Boiling Point Number method as described in the text.

[e]Selected value or selected estimate; for all compounds, values estimated by additivity are given in the footnotes. Uncertainties based on standard deviations for values estimated from bp data as described in the text and documented in the footnotes.

[f]Estimated by atomic additivity as described in the text.

[g]Vapor pressure at 25°C, in Torr, estimated as described in the text, using the selected values of boiling point, pressure, heat of vaporization, heat of fusion if appropriate, heat capacity of vaporization, and heat capacity of sublimation if appropriate.

[h]Selected value.

[i]Literature values of mp (°C) were as follows: 45, 46, 46–47, Beil 10 H 159; 48.5–49.5, this work; 49, ref. 7; 48.3, 46, Beil 10 I 71; 49–49.5, 48, Beil 10 II 95; 48, Beil 10 III 297.

[j]Beil, 10, III, 297.

[k]Estimated from the boiling point as described in the text.

[l]Literature values of bp (°C) [and associated heats of vaporization] were as follows: 254–255 at 760, Beil 10 H 159 [16.96[k]]; 160 at 20 (7) [18.96[k]; omitted from the average]; 244–245 at 760, Beil 10 III 297; [16.25[k]]; 123.8 at 12, Beil 10 III 297; [16.75[k]]; average 16.67 ± 0.28; additivity 16.80[u].

[m]Literature values of mp were 32, 33, 34, 34–35, Beil 9 H 484; 33.2, Beil 9 I 193; 33, Beil 9 III 2337; 35.5–36, Beil 9 IV 1726; 34–35, this work; 33.2 (7).

[n]Beil 9 III 2337.

[o]Literature values of bp (°C) [and associated heats of vaporization] were 103.2–103.5 at 15, Beil 9 III 2337, [14.71[k]]; 91 at 8, Beil 9 III 2337, [14.72[k]]; 69.5 at 0.4, Beil 9 IV 1726, [17.12[k]]; average 14.62 ± 0.10; additivity 14.70[u].

[p]Beil, 9, III, 381.

[q]Reference 14.

[r]Literature values of bp (°C) [and associated heats of vaporization] were 199.6 at 760. (7) [13.43[k]] 199.35 at 760., Beil, 9, IV, 283, [13.45[k]] 130. at 100., Beil, 9, IV, 283, [13.29[k]]; 81. at 16., Beil, 9, IV, 283, [12.97[k]]; 86. at 15., Beil, 9, IV, 283, [13.41[k]]; 52. at 1., Beil, 9, IV, 283, [14.40[k]]; 183.3 at 507.5, Beil, 9, III, 381, [13.37[k]]; 110.3 at 57., Beil, 9, III, 381, [12.98[k]]; 95. at 25., Beil, 9, III, 381, [13.27[k]]; 83. at 10., Beil, 9, III, 381, [13.79[k]]; average 13.33 ± 0.24.

[s]Literature values of mp (°C) were 44, Beil 9 H 340; 43–43.5, Beil 9 H 340; 43, Beil 9 H 340; 42, Beil 9 H 340; 43–44, this work; 44 (7).

[t]Estimated using boiling point numbers as described in the text.

[u]Estimated by the modified group additivity scheme described in the text.

[v]Literature values of mp (°C) were 96, Beil 9, H, 390; 97, Beil 9, III, 1710; 94.5–95.5, this work; 96 (7).

[w]Literature values of mp (°C) were 29–32, Beil 9 H 340; 29–32 (43).

[x]Reference 49.

[y]Literature values of bp (°C) [and associated heats of vaporization] were 124–126 at 0.16, Beil 9 H 340, [24.79[k]]; 107–108 at 0.25 (49), [21.87[k]]; 122–123 at 0.4 (50), [22.96[k]]; average 22.19 ± 0.43; additivity 20.88[u].

[z]Literature values of mp were: 37–40°C (43).

Can. J. Chem. Downloaded from www.nrcresearchpress.com by 217.78.4.112 on 09/08/12
For personal use only.

TABLE 3 (*concluded*)

[aa]This work.

[ab]Literature values of bp (°C) [and associated heats of vaporization] were 95–98 at 0.32, this work, [20.42[k]]; 148–151 at 10 (48), [19.52[k]]; 151–152 at 13 (49), [19.06[k]]; 108 at 0.8 (50), [20.02[k]]; average 19.69 ± 0.42; additivity 18.48[u].

[ac]Literature values of mp (°C) were 40–43, this work; 43–44 (43); 43 (44).

[ad]Beil 9 III 1068.

[ae]Literature values of bp (°C) [and associated heats of vaporization] were 132–133 at 15, Beil 9 III 1068, [17.04[k]]; 142 at 14, Beil 9 III 1068, [18.07[k]]; 130–131 at 11, Beil 9 III 1068, [17.47[k]]; average 17.71 ± 0.42; additivity 18.00[u].

[af]Literature values of mp (°C) were 57–58, Beil 9 IV 985; 57.5–58.5, this work; 59–60 (48); 58–59 (43); 58–59 (49).

[ag]Literature values of mp (°C) were 97–98, this work; 96, ref. 48; 95–97, ref. 43; 97, refs. 51, 52; 96–97, ref. 49.

[ah]Beil, 10, III, 337.

[ai]Literature values of bp (°C) [and associated heats of vaporization] were 260. at 760., Beil, 10, III, 337, [17.31[k]]; 163. at 40., Beil, 10, III, 337, [17.66[k]]; 137.7 at 14., Beil, 10, III, 337, [17.68[k]]; 127.5 at 4., Beil, 10, III, 337, [19.15[k]; omitted from the average]; 158. at 30., Beil, 10, III, 337, [17.87[k]]; 143. at 13., Beil, 10, III, 337, [18.31[k]]; 134. at 12., Beil, 10, III, 337, [17.66[k]]; 90.8 at 1., Beil, 10, III, 337, [17.89[k]]; 145. at 20., Beil, 10, IV, 430, [17.60[k]]; 142. at 20., Beil, 10, IV, 430, [17.34[k]]; 106.5 at 4., Beil, 10, IV, 430, [17.16[k]]; 137. at 15., Beil, 10, II, 100, [17.48[k]]; 140. at 14., Beil, 10, II, 100, [17.89[k]]; 136. at 12., Beil, 10, II, 100, [17.84[k]]; 145. at 14., Beil, 10, H, 163, [18.34[k]]; 162. at 35., Beil, 10, H, 163, [17.88[k]]; 263. at 760., Beil, 10, H, 163, [17.52[k]]; average 17.71 ± 0.32; additivity 16.17[u].

[aj]Beil, 9, III, 2342.

[ak]Literature values of bp (°C) [and associated heats of vaporization] were 216. at 760., Beil, 9, II, 329, [14.44[k]]; 184. at 260., Beil, 9, II, 329, [14.92[k]]; 125. at 36., Beil, 9, II, 329, [14.83[k]]; 102. at 16., Beil, 9, II, 329, [14.49[k]]; 102.7 at 14., Beil, 9, III, 2342, [14.76[k]]; 72.9 at 4.5, Beil, 9, III, 2342, [14.14[k]]; 118. at 20., Beil, 9, IV, 1733, [15.35[k]]; 57. at 0.3, Beil, 9, IV, 1733, [16.29[k]; omitted from the average]; average 14.71 ± 0.36; additivity 14.13[u].

[al]Beil, 9, III, 1058.

[am]Literature values of bp (°C) [and associated heats of vaporization] were 196.4 at 761.3, Beil, 9, III, 1058, [13.28[k]]; 198. at 760., Beil, 9, III, 1058, [13.37[k]]; 197.3 at 754., Beil, 9, III, 1058, [13.35[k]]; 196.8 at 745., Beil, 9, III, 1058, [13.35[k]]; 82. at 12., Beil, 9, III, 1058, [13.45[k]]; 74.1 at 9.5, Beil, 9, III, 1058, [13.21[k]]; 78. at 8., Beil, 9, III, 1058, [13.73[k]]; 67.70 at 7.5, Beil, 9, III, 1058, [13.07[k]]; 50. at 2.7, Beil, 9, III, 1058, [13.07[k]]; 77. at 2., Beil, 9, III, 1058, [15.60[k]; omitted from the average]; 71. at 9., Beil, 9, II, 159, [13.07[k]]; 122. at 35.5, Beil, 9, II, 159, [14.63[k]; omitted from the average]; 197.2 at 760., Beil, 9, H, 182, [13.33[k]]; 198. at 749.4, Beil, 9, H, 182, [13.40[k]]; 194. at 747.2, Beil, 9, H, 182, [13.18[k]]; average, 13.30 ± 0.18.

[an]Beil, 9, III, 1362.

[ao]Literature values of bp (°C) [and associated heats of vaporization] were 100.2 at 12.5, Beil, 9, III, 1362, [14.75[k]]; 99.6 at 11., Beil, 9, III, 1362, [14.91[k]]; 93.8 at 9., Beil, 9, III, 1362, [14.77[k]]; 79.6 at 2., Beil, 9, III, 1362, [15.83[k]]; 97.5 at 10.5, Beil, 9, II, 227, [14.82[k]]; 119. at 27.5, Beil, 9, II, 227, [14.86[k]]; 119.5 at 22., Beil, 9, II, 227, [15.30[k]]; 221. at 760., Beil, 9, H, 341, [14.74[k]]; 111.5 at 18., Beil, 9, H, 341, [15.03[k]]; average 15.00 ± 0.34; additivity 14.57[u].

[ap]Literature values of mp (°C) were 75, Beil, 9, III, 1709; 74, Beil, 9, III, 1709; 73, Beil, 9, III, 1709; 71.5–71.7, Beil, 9, III, 1709; 75, Beil, 9, H, 394.

[aq]Beil, 9, III, 1709.

[ar]Literature values of bp (°C) [and associated heats of vaporization] were 154. at 12., Beil, 9, I, 162, [19.52[k]]; 197. at 73., Beil, 9, III, 1709, [19.13[k]]; 155. at 20., Beil, 9, III, 1709, [18.50[k]]; 136.1 at 4., Beil, 9, III, 1709, [20.02[k]]; 204. at 105., Beil, 9, H, 394, [18.75[k]]; 151. at 15., Beil, 9, H, 394, [18.75[k]]; average 19.11 ± 0.52; additivity 18.11[u].

supercooled liquid *p*-nitrobenzoic acid, of $\Delta H_{vap}(25°C)$ = 23.63 kcal mol^{-1}, and finally ΔH_{sub} = 28.33 kcal mol^{-1}.

Entropies

The entropy of gaseous nitrobenzene could be calculated by statistical mechanics from the vibrational spectrum (19), moments of inertia (22), and barrier to internal rotation (20).

The entropy of gaseous *N*,*N*-dimethylbenzamide was estimated, following Benson (23), by using estimated vibrational frequencies and rotational barriers. We took frequencies associated with the $N(CH_3)_2$ group from the assignment for *N*,*N*-dimethylacetamide (24) and the frequencies associated with the benzoyl portion from the assignment for methyl benzoate (25). The hindered rotations were assigned barriers of 20, CO-N; 5, C_B-CO; 3, N-CH_3. Moments of inertia for the molecule and fragments of it were calculated from the MM2 geometry.

For benzoyl chloride we calculated the entropy from the published frequencies (26), and the rotational barrier (27).

To estimate entropies for substituted benzoyl chlorides, benzoic acids, methyl benzoates, and *N*,*N*-dimethylbenzamides, we evaluated additivity contributions for the substituents, assuming no significant interactions. From the entropies for benzene, 64.34 (21), toluene, 76.64 (21), anisole, 87.01 (28), chlorobenzene, 74.92 (21), nitrobenzene, 77.28 (this work), methyl benzoate, 93.86 (28), benzoyl chloride, 87.36 (this work), *N*,*N*-dimethylbenzamide, 96.64 (this work), we evaluate the following increments in entropy for replacement of H: CH_3, 10.92; CH_3O, 21.29; Cl, 7.01; NO_2, 10.75; $COOCH_3$, 28.14; COCl, 19.45; $CON(CH_3)_2$, 34.49. In these calculations it is necessary to make suitable corrections for symmetry (23). The entropies so estimated are found in Table 2.

Equilibrium constants for ester formation

For each of the esters, the equilibrium constant was determined by direct analysis, approaching the equilibrium both from the acid and from the ester. The concentration of ester was determined by HPLC analysis, and from ester concentrations as a function of time, fitted to a pseudo-first-order rate law, we could calculate the equilibrium constant from the infinity values. The agreement for the two directions was good in each case. The results of these experiments are summarized in Table 5. The equilibrium constants for methyl

Can. J. Chem. Downloaded from www.nrcresearchpress.com by 217.78.4.112 on 09/08/12
For personal use only.

TABLE 4. Enthalpies of fusion[a]

X	ΔH_{fus}[b]	ΔH_{soln}[c]	ΔH_{fus}[d]	ΔS_{fus}[e]
4-X-$C_6H_4COOCH_3$				
CH_3O	4.17	5.71 (0.10)	4.92	14.4
CH_3	3.98	5.41 (0.04)	4.62	16.1
H		0.79 (0.05)		
Cl	4.12	5.50 (0.06)	4.71	14.9
NO_2	4.80	6.56 (0.20)	5.77	15.6
4-X-$C_6H_4CON(CH_3)_2$				
CH_3O	3.97	0.07 (0.04)		
CH_3	4.07	−0.11 (0.03)		
H	4.11	3.37 (0.11)	3.37	10.7
Cl	4.30	3.60 (0.06)	3.60	10.9
NO_2	4.81	4.66 (0.11)	4.66	12.6

[a]All at 25°C; units are kcal mol^{-1} and cal deg^{-1} mol^{-1}.
[b]Estimated using an average value for ΔS_{fus} = 13.0 cal deg^{-1} mol^{-1} (16); Table 3.
[c]Heat of solution in methanol; from Table 1.
[d]Calculated using the average value for the liquid esters or amides as the value for all, as $\Delta H_{fus} = \Delta H_{soln}(solid) - \Delta H_{soln}(liq)$.
[e]Calculated from the mp (Table 3) and the value of ΔH_{fus} derived from ΔH_{soln} as described in the text.

ester formation show negligible effects of the substituent on the benzene ring ($\rho = -0.01 \pm 0.05$), in striking contrast to the strong dependence of ester formation equilibrium constants upon the nature of the alcohol (29).

Equilibrium constants for ester aminolysis

For each of the esters, we determined the equilibrium constant for dimethylaminolysis in methanol, using HPLC analysis. Analyses were carried out at intervals, and equilibrium constants calculated by the method of Fersht and Requenna (30), as well as being calculated from the final results when equilibrium could be attained. It was necessary to correct for a small amount of accompanying hydrolysis. The results of these experiments are summarized in Table 6. The equilibrium constants for aminolysis are, unlike the equilibrium constants for ester formation, moderately sensitive to the nature of the substituent upon the benzene ring; $\rho = 0.59 \pm 0.19$.

Free energies of transfer

Values for methyl benzoate and benzoic acid have been reported previously (3). To calculate the free energies of transfer we need solubilities and vapor pressures for each compound. The solubilities of the esters and amides were measured by determining the UV absorbance of saturated solutions; the values that we determined are found in Table 7. Vapor pressures were estimated as previously proposed (12) by a modification of an equation derived by Prausnitz and co-workers (31), using the boiling point at the lowest available pressure, the heat of vaporization, and the heat capacity of vaporization. The latter were estimated by atomic additivity as previously proposed (18). Where a compound is solid at room temperature, the vapor pressure was calculated at the melting point using the heat of vaporization and heat capacity of vaporization for the liquid to gas transition, and then from the melting point to 25°C the calculations were done in the same way, using the heat of sublimation, calculated as heat of vaporization + heat of fusion, and the heat capacity of sublimation, taken as $-2R$ (32, 33). Vapor pressures so calculated, and the values used to obtain them (Table 3), are found in Table 7, as are the free energies of transfer. Free energies of transfer for substituted benzoic acids were estimated using group additivity corrections, assuming no interactions of the *para* substituents.

For dimethylamine we could find no data in the literature for the activity of dimethylamine in methanol at low concentrations, but suitable data were available for a number of amines, including diethylamine (34), for which $\Delta G_{H_2O\text{-}MeOH} = -1.41$ kcal mol^{-1}. From the data in ref. 34 we could evaluate the contribution for $[CH_2(X)_2] = -0.67$ kcal mol^{-1}. This allowed the calculation of $\Delta G_{H_2O\text{-}MeOH} = -0.07$ kcal mol^{-1} for dimethylamine.

To calculate equilibrium constants in water from equilibrium constants in methanol it was necessary to determine free energies of transfer from methanol to water. This was done by the method of Toullec and El Alaoui (35), using dodecane as an intermediary solvent, immiscible with both water

TABLE 5. Time dependence of ester concentrations, and derived equilibrium constants for ester formation[a]

X-Ph-$COOCH_3$	$[Acid]_0$	$[Ester]_0$	a_1	a_2	a_3	K[b]	K_{avg}[c]
H[d]	2050.00	0.0	27. (0.002)	−28. (0.002)	0.0594 (0.011)	0.13	
H	2020.00	0.0	231. (0.006)	−233. (0.007)	0.0730 (0.005)	0.13	
H[d]	0.00	2190.0	33. (0.013)	2250. (0.088)	0.0585 (0.003)	0.15	
H	0.00	2190.0	165. (0.121)	2060. (0.10)	0.0549 (0.009)	0.08	0.12
p-NO_2	200.50		22.15 (0.46)	−22.15 (0.46)	0.0612 (0.004)	0.12	
p-NO_2		202.6	23.37 (0.45)	182.8 (4.2)	0.0575 (0.002)	0.13	0.13
p-MeO	201.80		23.46 (0.64)	−23.46 (0.64)	0.0353 (0.002)	0.13	
p-MeO		200.4	24.53 (1.7)	164.9 (5.7)	0.0315 (0.002)	0.14	0.14
p-Me	206.40		24.27 (0.65)	−24.27 (0.65)	0.0517 (0.004)	0.13	
p-Me		204.8	25.38 (1.8)	173.9 (13.8)	0.0588 (0.006)	0.14	0.14
p-Cl	200.80		27.39 (1.6)	−27.39 (1.6)	0.0224 (0.003)	0.16	
p-Cl		201.5	25.49 (0.84)	176.0 (0.95)	0.0682 (0.004)	0.14	0.15

[a]All in water at 25°C. All concentrations in μM. Methanol concentration was 1.0 M unless otherwise noted. The unit for time is days, and for rate constants is $days^{-1}$. Concentration-time data were fitted to: conc. = $a_1 + a_2 \exp(-a_3 t)$ by nonlinear least squares.
[b]K = [Ester]/[Acid][MeOH], M^{-1}.
[c]Average equilibrium constant for an ester.
[d][MeOH] = 0.1 M.

Can. J. Chem. Downloaded from www.nrcresearchpress.com by 217.78.4.112 on 09/08/12
For personal use only.

TABLE 6. Equilibrium constants for dimethylaminolysis of 4-substituted methyl benzoates in methanol[a]

X	$[Ester]_0$ (10^4 M)	$[Amide]_0$ (10^4 M)	$[Me_2NH]$ (10^2 M)	[MeO-] (M)	t (days)	$[Ester]_t$ (10^4 M)	$[Amide]_t$ (10^4 M)	$[Acid]_t$ (10^4 M)	K (M^{-1})	K (best) (M^{-1})
H	4.99	0.00	5.98	0.504	49	1.46	2.312	1.22	26.4	26.5 ± 0.1
	0.00	5.00				1.57	2.49	0.945	26.6	
Cl	5.00	0.00	5.27	0.504	27	1.27	1.49	1.93	22.3	22.62 ± 0.31
	0.00	5.01	5.27	0.504		1.38	1.66	1.90	22.9	
MeO	5.00	0.00	5.27	0.504	145	2.41	1.04	1.55	8.17	8.16 ± 0.01
	0.00	5.01				3.08	1.32	0.604	8.15	
Me	5.00	0.00	5.27	0.504	104	1.84	1.68	1.47	17.4	17.49 ± 0.13
	0.00	4.99				1.70	1.58	1.71	17.6	
NO_2	5.00	0.00	4.21	0.0524	16	1.03	1.80	2.14	41.5	40.96 ± 0.53
	0.00	5.00				1.51	2.57	1.14	40.4	

[a]At 25°C in dry methanol. K = [amide]/[ester] $[Me_2NH]$.

TABLE 7. Free energies of transfer from gas phase to water[a]

Compound	p^b (atm)	c^c (mM)	ΔG_t^d
4-X-C_6H_4-COOMe			
H	4.04×10^{-04}	12.4	−2.03
Me	1.20×10^{-04}	2.83	−1.88
MeO	1.18×10^{-05}	3.84	−3.43
Cl	6.89×10^{-05}	1.33	−1.75
NO_2	1.72×10^{-07}	0.922	−4.98
4-X-C_6H_4-$CONMe_2$			
H	5.76×10^{-06}	1490.[e]	−7.39
Me	7.89×10^{-07}	449.	−7.86
MeO	1.46×10^{-07}	685.	−9.11
Cl	3.99×10^{-07}	101.	−7.38
NO_2	1.35×10^{-09}	54.1	−10.05

[a]All at 25°C; standard states are the ideal gas at 1 atm, and 1 M aqueous solution with an infinitely dilute reference state.

[b]Vapor pressure at 25°C, estimated as described in the text.

[c]Solubility in water at 25°C, measured as described in the text.

[d]Free energy of transfer from gas at 1 atm to 1M ideal aqueous solution with an infinitely dilute reference state.

[e]Because the solubilities of *N,N*-dimethylbenzamide and *N,N*-dimethyl-*p*-methoxybenzamide were high, we calculated the "ideal solubility" from the experimentally determined solubilities in dodecane, 0.188 and 0.0693 M respectively, and the partition constants for transfer from dodecane to water (Table 8).

and methanol. Partition coefficients for water to dodecane and methanol to dodecane were determined, and from these we could determine partition coefficients from methanol to water; the values so determined are found in Table 8. Since methanol is not totally insoluble in dodecane (it is soluble to the extent of 0.3%, w/w (estimated), <0.5% (detection limit) (36)), it was important to determine whether it was necessary to make a correction for the difference in the nature of the dodecane solvent between experiments involving partition with methanol and water. We did this by determining the partition coefficient from water to dodecane and from water to dodecane containing 0.5% 1-octanol. This latter solvent would have the same hydroxyl group concentration as methanol-saturated dodecane, but would not lose any of the alcohol molecules upon extraction with water (34). In the event we found that the effect of the octanol cosolvent was negligible for the esters but not quite negligible for the amides. We made a small correction for the amides, assuming that the effect of the alcohol would be linear in alcohol content and in σ, from the values determined for *N,N*-dimethyl-*p*-methoxybenzamide and *N,N*-dimethyl-*p*-nitrobenzamide. The corrections were made for 0.3% alcohol in dodecane, based on a reasonable estimate of the unmeasurably low solubility (36). The correction is quite small, so even in the worst case the effect on the final result is essentially trivial.

Dodecane is appreciably soluble in methanol (8% w/w (36)) so that there could be a free energy of transfer from methanol to methanol saturated with dodecane. Our compounds are very soluble in methanol, so it is not easy to do direct experiments to determine the magnitude of this effect. Toullec *et al.* (36) demonstrated that the free energy correction was trivial (0.003 kcal mol^{-1} for 4-nitroacetophenone and 0.08 kcal mol^{-1} for 4-nitroacetophenone dimethyl acetal (36)). Since these model compounds are closely related to the compounds used in this work, we assume that the effects of dodecane in methanol will be similarly negligible. Because of these small errors we assign errors of 0.20 kcal mol^{-1} to the free energies of transfer from water to methanol.

As a check on the thermodynamic quantities evaluated in this work, we have calculated the appropriate group contributions to $\Delta H_f^0(g)$, ΔH_{vap}, ΔG_t, and $\Delta G_f^0(aq)$. These are preliminary values, because in many cases they are based on only one compound, but should be useful guides until more firmly established values become available. The source data are included in Table 2. The group contributions used for these checks on internal consistency of our values are found in Table 9.

Discussion

We have reported above experimental measurements of the heats of formation of a series of substituted benzoic acid esters and amides as the solid or liquid, and heats of solution in methanol permitting calculation of the heats of formation in methanolic solution. These values permit calculation of the heats of aminolysis of the esters for the reaction:

$$Ar\text{-}COOMe + HNMe_2 = Ar\text{-}CONMe_2 + HOMe$$

The values so calculated are found in Table 10. The average value is −1.97 ± 1.54 kcal mol^{-1}, and there is no discernible dependence upon substituents: ρ = 0.13 ± 2.4. The major impression is one of scatter, which caused us concern

Can. J. Chem. Downloaded from www.nrcresearchpress.com by 217.78.4.112 on 09/08/12
For personal use only.

TABLE 8. Free energies of transfer from methanol to water[a]

Compound	Partition coefficients[b] MeOH/DOD	DOD/water	MeOH/water	ΔG_{MeOH-H_2O}[c]
X-C_6H_4-COOMe				
H	2.14 ± 0.02	75.16 ± 0.99	160.54 ± 2.12	3.01 ± 0.01
Cl	1.47 ± 0.01	219.63 ± 3.00	323.45 ± 4.42	3.43 ± 0.01
MeO	3.31 ± 0.01	58.24 ± 0.94	193.05 ± 3.13	3.12 ± 0.01
Me	1.72 ± 0.01	121.50 ± 2.86	208.39 ± 4.90	3.17 ± 0.01
NO_2	4.74 ± 0.03	27.73 ± 0.34	131.44 ± 1.63	2.89 ± 0.01
X-C_6H_4-$CONMe_2$				
H	25.68 ± 0.68[d]	0.126 ± 0.004	3.23 ± 0.17	0.70 ± 0.20
Cl	17.90 ± 0.64[d]	0.786 ± 0.009	14.15 ± 0.63	1.57 ± 0.20
MeO	32.87 ± 0.86[d]	0.101 ± 0.002	3.33 ± 0.13	0.71 ± 0.20
Me	17.14 ± 0.49[d]	0.475 ± 0.011	8.14 ± 0.40	1.24 ± 0.20
NO_2	67.51 ± 0.93[d]	0.061 ± 0.001	4.13 ± 0.08	0.84 ± 0.20
Me_2NH				−0.07[e]
MeOH				−0.26[f]

[a]All at 25°C.
[b]MeOH/DOD means $[compound]_{MeOH}/[compound]_{DOD}$; DOD is dodecane.
[c]Free energy of transfer from methanol to water; standard states are 1 M ideal solutions in each solvent.
[d]Corrected for the presence of methanol in the dodecane phase as described in the text. The partition constants from water to dodecane containing 0.5% 1-octanol were as follows: *p*-NO_2-C_6H_4-COOMe, 29.4; *p*-MeO-C_6H_4-$CONMe_2$, 0.143; *p*-NO_2-C_6H_4-$CONMe_2$, 0.0752.
[e]Calculated as described in the text.
[f]Calculated from the free energies of formation of liquid methanol and 1 M aqueous methanol (60).

TABLE 9. Group contributions to thermodynamic quantities for substituted benzenes[a]

Group	ΔH_{vap}	ΔH_f (g)	S^0 (g)	ΔG_f^0 (g)	ΔG_t	ΔG_f^0 (aq)
$[C_BH]$	1.34	3.30	11.53	4.92	−0.15	4.77
$[C_BCH_3]$	2.47	−4.69	22.72	3.43	−0.11	3.32
$[C_BOCH_3]$[b]	4.51	−34.10	32.82[c]	−21.72	−0.27[c]	−21.99
$[C_BCl]$	2.91	−3.8	18.54	−1.09	−0.24	−1.33
$[C_BNO_2]$	6.45[d]	−0.37[d]	22.28[d]	13.21	−3.37	5.07

[a]All at 25°C. Dimensions are kcal mol^{-1} for enthalpy and free energy, and cal deg^{-1} mol^{-1} for entropy. For convenience the "groups" $[C_BCH_3]$ and $[C_BOCH_3]$ are defined by adding the contributions of the contributing groups, $[C_B(C)]$ + $[CH_3(C_B)]$ and $[C_B(O)]$ + $[O(C_B)(C)]$ + $[CH_3(O)]$ respectively. Unless otherwise noted, values for ΔH_f(g) and S^0(g) are from ref. 23, values for ΔG_t are calculated from values for log γ in ref. 37, and values for ΔG_f(g) and ΔG_f(aq) are calculated from other values in the table.
[b]Based on ΔH_{vap} for anisole: Table 2.
[c]Reference 28.
[d]This work.

about possible errors. As a check we examined the data at each stage in the calculation procedure to see if our results were credible.

First we will look at the heats of formation in solution. Heats of formation in the standard state are not directly comparable because some of the compounds are solids, with contributions from the heat of fusion. We use instead the heat of formation in methanol, which can be calculated from data in Tables 1 and 2. We made the approximation that since $\Delta H_{solution}$ is small for the liquids, group contributions to ΔH_f(solution) will be equal to the contributions to ΔH_f(g) + ΔH_{vap}. We will compare the observed and expected increments in ΔH_f(solution) for replacement of 4-H by the various substituents. These increments are mostly within 1 kcal mol^{-1} or so of the expected value, which may be as much as can be expected, although for *p*-CH_3-$C_6H_4COOCH_3$, *p*-$CH_3OC_6H_4CON(CH_3)_2$, and *p*-$NO_2C_6H_4CON(CH_3)_2$ the deviations are larger. Only for *p*-CH_3-$C_6H_4COOCH_3$ is the deviation larger than twice the standard deviation.

It should be noted that in using Benson additivity for disubstituted benzenes we are in effect assuming negligible substituent effects, which may not be correct.

This assumption of Benson additivity also leads to an expectation of a constant value of $\Delta H_{aminolysis}$, which is approximately what we observe, though with considerable scatter.

Now we turn to the heats of formation in the gas phase. Here there is a test, since literature values are available for all but one of the acids. For the substituted benzoic acids the agreement with Benson additivity is quite good. For the acid chlorides, using our estimated heats of vaporization for the compounds for which experimental values are not avail-

Can. J. Chem. Downloaded from www.nrcresearchpress.com by 217.78.4.112 on 09/08/12
For personal use only.

TABLE 10. Enthalpies and free energies of ester hydrolysis, ester aminolysis, and amide formation for *p*-substituted benzoic acid derivatives[a]

(*a*) Methanol

Compound	Ester aminolysis				
	K (M^{-1})[b]	K[c]	$\Delta G^{0d,e}$	ΔH^{0f}	$\Delta S^{0d,g}$
CH_3O	8.16 ± 0.01	202.71 ± 0.31	−3.15 ± 0.01	−0.11 ± 1.49	10.22 ± 5.00
CH_3	17.49 ± 0.13	434.41 ± 3.21	−3.60 ± 0.01	−1.86 ± 2.08	5.87 ± 6.99
H	26.52 ± 0.11	658.86 ± 2.65	−3.85 ± 0.01	−3.62 ± 1.61	−2.33 ± 5.38
Cl	22.62 ± 0.31	561.93 ± 7.82	−3.75 ± 0.01	−2.55 ± 1.23	4.05 ± 4.13
NO_2	40.96 ± 0.53	1017.38 ± 13.08	−4.11 ± 0.01	−0.81 ± 1.59	11.08 ± 5.35

(*b*) Water

Compound	Ester hydrolysis		Ester aminolysis		Amide formation	
	K (M)[h]	ΔG^{0i}	K[c]	$\Delta G^{0d,e}$	K[j]	ΔG^{0i}
CH_3O	7.83 ± 0.22	−1.19 ± 0.02	8610. ± 2920.	−5.37 ± 0.20	1160. ± 738.	−4.19 ± 0.20
CH_3	7.28 ± 0.22	−1.18 ± 0.02	8140. ± 2770.	−5.34 ± 0.20	1110. ± 649.	−4.16 ± 0.20
H	8.05 ± 1.70	−1.24 ± 0.13	23900. ± 8130.	−5.98 ± 0.20	2960. ± 1180.	−4.74 ± 0.24
Cl	6.61 ± 0.29	−1.12 ± 0.03	9400. ± 3190.	−5.42 ± 0.20	1420. ± 828.	−4.31 ± 0.20
NO_2	7.86 ± 0.19	−1.22 ± 0.01	23700. ± 8010.	−5.97 ± 0.20	3000. ± 1750.	−4.75 ± 0.20

[a]Standard states are 1 M ideal solution in the solvent indicated, with infinitely dilute reference states. The standard state for the solvent is either pure liquid or "1 M solution" in itself. Units are kcal mol^{-1} for free energies and enthalpies and cal deg^{-1} mol^{-1} for entropies.

[b]K = [amide]/[ester] [Me_2NH].

[c]K = [amide] [MeOH]/[ester] [Me_2NH].

[d]ΔG^0 and ΔS^0 refer to the 1 M standard state for methanol.

[e]Calculated from the equilibrium constant.

[f]Calculated from the heats of solution and reaction in Table 1.

[g]Calculated from the ΔG^0 and ΔH^0 values in this table.

[h]K = [acid] [MeOH]/[ester].

[i]ΔG^0 refers to the pure liquid standard state for water.

[j]K = [amide]/[acid] [amine], all reactants and products as the neutral molecules.

able, we again find good agreement, except for *p*-nitrobenzoyl chloride where the deviation from expectation is 4 kcal mol^{-1}. For the esters the agreement is reasonable except for methyl *p*-methylbenzoate, which deviates from expectation by 2.5 kcal mol^{-1}. For the amides both *N*,*N*-dimethyl-*p*-methoxybenzamide and *N*,*N*-dimethyl-*p*-nitrobenzamide differ from expectation by more than 3 kcal mol^{-1}.

Free energies of transfer were found to be in satisfactory agreement with expectation except for the *p*-methoxy compounds, where ΔG_t is more negative than expected by simple additivity. Since conjugative interactions might well lead to a distant polar interaction (37) for this substituent, this behavior is not necessarily surprising.

The striking feature of ester aminolysis is that the reaction is exergonic, yet is known to be a poor reaction synthetically. For unactivated alkyl esters the reaction with primary or secondary amines is generally quite slow, and must be accelerated either by heating (as in formation of benzylamides by boiling with benzylamine (38)) or by addition of base (as in the use of methoxide in methanol to catalyze aminolysis, and in the case of primary amines, to displace the equilibrium by salt formation from the secondary amide (39)). For formate esters, esters of α-haloacids, or esters with good leaving groups, the reaction is generally fast (40). Labelle and Gravel reported an unusually rapid reaction of β-ketoesters, the novelty of which emphasizes the normal unreactivity of simple esters (41). What we have found is that the equilibrium is favorable by about 4 kcal mol^{-1}, so that under synthetic conditions the amide would be overwhelmingly favored, i.e., over 99.9% at 1 M dimethylamine, but the reaction is quite slow at room temperature. In the case of *p*-CH_3O-C_6H_4-$COOCH_3$, attainment of equilibrium required months even with 0.5 M NaOMe. The equilibrium is dependent on the nature of the acyl substituent, even though ρ for benzoate esters seems quite small, 0.59 ± 0.19, because the equilibrium free energy changes for the dimethylaminolysis of methyl formate, methyl acetate, and methyl benzoate are −11.3 (4), −6.8 (4), and −5.0. This is in striking contrast to the analogous equilibrium for methyl ester formation, for which the free energy changes are 1.38 (42), 1.30 (42), and 1.26.

Free energies of ester hydrolysis in water are available both from direct measurement of equilibrium constants and from the free energies of formation of the esters and acids calculated, as summarized in Table 2. The values so calculated are found in Table 11. The agreement is quite reasonable in terms of the uncertainties in the thermochemical data.

Free energies of dimethylaminolysis in water are available both from direct measurements of the equilibrium constants, corrected from methanol to water using free energies of transfer, and by free energies of formation of the esters and amides, calculated as summarized in Table 2. The two sets of values are found in Table 11. The agreement is poorer than one would wish, though in fact about as good as can be expected given the cumulation of errors in calculating free energies of formation in aqueous solution from the avail-

Can. J. Chem. Downloaded from www.nrcresearchpress.com by 217.78.4.112 on 09/08/12
For personal use only.

TABLE 11. Free energies of dimethylaminolysis and esterification in aqueous solution[a]

(*a*) Free energies of dimethylaminolysis

Ester X-PhCOOMe	ΔG^0, thermochemical	ΔG^0, direct measurement
MeO	1.46 ± 3.09	−5.37 ± 0.20
Me	−0.87 ± 3.42	−5.34 ± 0.20
H	−3.34 ± 2.26	−5.98 ± 0.20
Cl	−1.93 ± 4.11	−5.42 ± 0.20
NO_2	0.35 ± 4.22	−5.97 ± 0.20

(*b*) Free energies of esterification

Ester X-PhCOOMe	ΔG^0, thermochemical	ΔG^0, direct measurement
MeO	0.21 ± 2.31	1.19
Me	1.74 ± 2.36	1.22
H	2.68 ± 0.97	1.24
Cl	2.54 ± 3.08	1.18
NO_2	2.28 ± 3.65	1.12

[a]All in aqueous solution at 25°C; standard state for all species except water is 1 M ideal solution with an infinitely dilute reference state. For water the standard state is the pure liquid.

able information. Although we have tried to make realistic assessments of the uncertainties in the thermochemical calculations, the disagreements are in all but one case greater than the sum of the estimated standard deviations for the thermochemical and the equilibrium values. Thus we must consider the possibility of systematic errors.

Although we cannot see any source of systematic error in our measurements, there are some disturbing inconsistencies, particularly in the amide data. For the moment we conclude that the best values for the free energies of formation of substituted *N,N*-dimethylbenzamides in aqueous solution will come from the free energies of formation of the esters by way of the equilibrium constants for dimethylaminolysis. Values so calculated are included in Table 2.

From our measurements of equilibrium constants for methyl ester formation and dimethylaminolysis, we can calculate equilibrium constants and free energy changes for *N,N*-dimethylbenzamide formation. These are, we believe, the first measurements of equilibrium constants for benzamide formation. Attempts at direct measurement were carried out, but the amount of amide formed at equilibrium in alkaline solution was very small, and the reactions were slow, even at elevated temperatures.[2]

In the course of our investigations we found that we did not obtain consistent results using the heat of solution for HCl in methanol reported some years ago based on direct calorimetric studies. An indirect determination of the heat of solution of HCl, using the heats of methanolysis of three acyl chlorides, led to a value that gave us internally consistent results. We are forced to conclude that the earlier value is in error; the directly measured value is too high, suggesting that there might be a systematic error from carrying droplets of H_2SO_4 from the gas buret into the calorimeter. In any case we recommend our value for the heat of solution of HCl into pure methanol.

[2]D. C. Pike, unpublished observations.

Experimental

Materials

Benzoyl chloride (BDH) was redistilled, bp 79–80°C (13 Torr; 1 Torr = 133.3 Pa) (lit. (7) bp 71°C (9 Torr)). *N,N*-Dimethylbenzamide (Pfaltz and Bauer) was redistilled, bp 76–78°C (0.3 Torr), mp 40–43°C (lit. (43) mp 43–44°C, (44) mp 43°C). *p*-Chlorobenzoyl chloride (Aldrich) was redistilled, bp 96–98°C (10 Torr) (lit. (45) bp 99.6°C (11 Torr)). *p*-Methylbenzoyl chloride (Aldrich) was redistilled, bp 102–104°C (15 Torr) (lit. (46) bp 102.7°C (14 Torr)). *p*-Nitrobenzoyl chloride (Aldrich), was sublimed, mp 71–72°C (lit. (47) mp 75°C).

N,N-Dimethyl *p*-chlorobenzamide was prepared from *p*-chlorobenzoyl chloride and dimethylamine, crystallized from CH_2Cl_2, and sublimed, mp 57.5–58.5°C (lit. (48) mp 59–60°C, (43) mp 58–59°C, (49) mp 58–59°C); ^{1}H nmr (200 MHz, $CDCl_3$/TMS) δ: 3.032 (d, 6H), 7.37 (d, 4H). *N,N*-Dimethyl *p*-methoxybenzamide was prepared from *p*-methoxybenzoyl chloride and dimethylamine, bp 107–108°C (0.25 Torr) (lit. (49) bp 122–123°C (0.4 Torr), (43) mp 29–32°C); ^{1}H nmr (60 MHz, $CDCl_3$/TMS) δ: 3.02 (s, 6H), 7.37 (d, 4H). Methyl *p*-methylbenzoate was prepared from *p*-methylbenzoyl chloride and methanol, mp 34–35°C (lit. (7) mp 33.2°C); ^{1}H nmr (200 MHz, $CDCl_3$/TMS) δ: 2.363 (s, 3H), 3.865 (s, 3H), 7.195 (d, 2H), 7.916 (d, 2H). *N-N*-Dimethyl-*p*-methylbenzamide was prepared from *p*-methylbenzoyl chloride and dimethylamine, bp 95–98°C (0.32 Torr) (lit. (48) bp 148–151°C (10 Torr), (49) bp 151–152°C (13 Torr), (50) bp 108°C (0.8 Torr); lit. (43) mp 37–40°C); ^{1}H nmr (200 MHz, $CDCl_3$/TMS) δ: 2.327 (s, 3H), 2.993 (d, 6H), 7.228 (dd, 4H). *N,N*-Dimethyl-*p*-nitrobenzamide was prepared from *p*-nitrobenzoyl chloride and dimethylamine, crystallized from ethanol, and sublimed, mp 97–98°C (lit. (48) mp 96°C, (43) 95–97°C, (51, 52) 97°C, (49) 96–97°C); ^{1}H nmr (60 MHz, $CDCl_3$/TMS) δ: 3.05 (bd, 6H), 7.85 (dd, 4H).

Methyl benzoate (Matheson), methyl *p*-chlorobenzoate (Aldrich), *p*-methoxybenzoyl chloride (Aldrich), methyl *p*-methoxybenzoate (Aldrich), methyl *p*-nitrobenzoate (Aldrich), dimethylamine (Eastman), and dimethylamine hydrochloride (Eastman) were used without further purification.

Calorimetry solvents: 0.1 M dimethylamine in methanol was prepared by adding 2.70 mL dimethylamine to 400 mL methanol with stirring. 0.1 M Tetraethylammonium hydroxide in aqueous DMSO was prepared by adding 70 mL tetraethylammonium hydroxide (Aldrich, 20 wt.%), and 30 mL water to enough DMSO to make up to 1.0 L. Methanol was Baker or BDH reagent grade, used without further purification.

Methods

Solubility: Saturated solutions were prepared in aqueous pH 7 phosphate buffer or dodecane, and equilibrated at 25°C with occasional shaking for 11 days. The solutions were centrifuged, and a sample of the supernatant was withdrawn. Analysis by uv spectroscopy, after suitable dilution, gave the concentration of the saturated solutions.

Calorimetry was carried out as previously described (4). Boiling points at various pressures were determined as previously described (53).

Equilibrium constants for ester formation in aqueous solution

$$\text{X-Ph-COOH} + \text{MeOH} \rightleftharpoons \text{X-Ph-COOMe} + H_2O$$

Four solutions were prepared by dissolving benzoic acid or methylbenzoate with methanol and hydrochloric acid in 100.0 mL with water. Six 2-mL aliquots of each of these solutions were sealed into glass tubes and immersed in a 25°C water bath. For each of the other esters, four pairs of solutions were prepared. For the nitro, methoxyl, and methyl *para*-substituted methyl benzoates and benzoic acids the acid or ester was weighed into a 1.0 L volumetric flask and the volume made up with 40.5 mL methanol, 80 mL concentrated hydrochloric acid, and water. Solution required several hours stirring. Because of the slower solution rate for *p*-chloro

Can. J. Chem. Downloaded from www.nrcresearchpress.com by 217.78.4.112 on 09/08/12
For personal use only.

TABLE 12. Analytical conditions for benzoate esters and *N*,*N*-dimethylbenzamides[a]

X-Ph-COY	Wavelength (nm)	HPLC solvent % Buffer[b]	HPLC solvent % Methanol
(*a*) Esterification reactions			
MeO	260	40	60
Me	240	35	65
H	230	45	55
Cl	240	32	68
NO2	265	40	60
(*b*) Aminolysis reactions			
MeO	250	50	50
Me	235	40	60
H	230	50	50
Cl	235	40	60
NO2	265	50	50

[a]Eluted at 3.0 (esterifications) or 2.0 (aminolyses) mL min^{-1} through a C18 Waters radial Pak column. The effluent was monitored by a Waters 490 uv detector and the peak height for the ester in the resulting trace compared to the peak height from a standard solution.

[b]10 mM Aqueous ammonium phosphate pH 4.0 for analysis of esterifications, 20 mM aqueous ammonium phosphate pH 6.6 for analysis of aminolyses.

methyl benzoate and *p*-chlorobenzoic acid, the acid and ester were each dissolved in 100 mL methanol and then 25 mL diluted with 15.5 mL methanol, 80 mL concentrated hydrochloric acid, and water to 1.0 L. The initial concentration of reagents in the eight reaction mixtures was 1.0 M methanol, 1.0 M hydrochloric acid, and *para*-substituted methyl benzoate or benzoic acid as listed below. Seven 1-mL aliquots of each of these solutions were sealed into glass tubes and immersed in a 25°C water bath.

The concentrations of *para*-substituted methyl benzoates were determined by HPLC using the solvent mixtures and wavelengths listed in Table 12, with a C18 Waters radial Pak column and a flow rate of 3.0 mL min^{-1}. The effluent was monitored by a Waters 490 uv detector and the peak height for the ester in the resulting trace compared to the peak height from a standard solution. The criteria for the choice of an HPLC elution solvent were, first, that the peak height per mole of ester be as large as possible for maximum sensitivity and, second, that the ester peak be separate from that of other components. Each of the reaction solutions contains 1.0 M HCl. Injection of 1.0 M HCl into the HPLC system produces two peaks, a sharp one at 2–3 min, just after the void volume, and a broad peak at 5–7 min with a long tail. The exact retention times depended on the elution solvent. The peak heights increased with decreasing detector wavelength over the range 270–230 nm. The composition of these peaks is unknown although it is suspected that they are derived from an interaction between the acid and the pre-column or column packing material.

The concentration of substituted methyl benzoate in the reaction mixtures was assayed by HPLC every few days. The equilibrium constants were estimated at each time by the method of Fersht (30). These values were in good agreement with the final values calculated as described below.

We fitted the ester concentration vs. time data to equations of the form;

$$[\text{Ester}] = a_1 + a_2 \exp(-a_3 t)$$

Ester concentrations are in μM. Reaction pairs consist of those initiated with benzoate esters and those initiated with benzoic acids.

The equilibrium constants were calculated from the above data, using the infinity values of ester concentration, i.e., the a_1 values, and the final acid concentrations, calculated from the initial acid or ester concentration and the final ester concentration. The equilibrium constants so calculated are given in Table 5.

Equilibrium constants for dimethylaminolysis in methanol

Methanol was dried using magnesium (54). Dimethylamine was dried by passing as a stream of gas through a drying tower filled with sodium hydroxide pellets. Solutions of dimethylamine, sodium methoxide, and ester or amide were made up, and sealed in ampoules. The ampoules were incubated at 25°C, and analyzed at suitable times by HPLC. The analytical conditions are given in Table 12. To avoid interference between the acid and the amide it was necessary to use pH 6.6 buffer as the aqueous component of the mixed solvent for elution; this caused the acid to elute at or near the solvent peak, so that direct quantitation of the acid was not accurate. Hydrolysis to the acid was a side reaction, presumably the result of traces of water. This poses a problem for the calculation of equilibrium constants from data before equilibration was complete (30) because these calculations assume identical initial concentrations, yet hydrolysis at short times is more important for reactions starting with ester than with amide. We corrected for hydrolysis by scaling from the peak observed at a particular [ester] + [amide] to the hypothetical peak that would have been observed with no acid formation. Equilibrium constants calculated in this way are in good agreement with those calculated from data for fully equilibrated solutions. The equilibrium constants derived from these experiments are found in Table 6.

Acknowledgments

We thank the Natural Sciences and Engineering Research Council of Canada for financial support of this work.

1. J. P. Guthrie. Acc. Chem. Res. **16**, 122 (1983).
2. J. P. Guthrie. J. Am. Chem. Soc. **95**, 6999 (1973).
3. J. P. Guthrie and P. A. Cullimore. Can. J. Chem. **58**, 1281 (1980).
4. J. P. Guthrie, J. Am. Chem. Soc, **96**, 3608 (1974).
5. C. R. Kinney. J. Am. Chem. Soc. **60**, 3032 (1938); Ind. Eng. Chem. **32**, 559 (1940).
6. K. B. Wiberg. Laboratory technique in organic chemistry. McGraw-Hill, New York. 1960. p. 17.
7. R. C. Weast (*Editor*). Handbook of chemistry and physics. 52nd ed. Chemical Rubber Co., Cleveland, Ohio. 1971.
8. R. C. Weast (*Editor*). Handbook of chemistry and physics. 48th ed. Chemical Rubber Co., Cleveland, Ohio. 1967.
9. Beilstein. Handbuch der organischen Chemie, 9, H, 341.
10. Beilstein. Handbuch der organischen Chemie, 9, II, 329.
11. Beilstein. Handbuch der organischen Chemie, 10, III, p. 337.
12. J. P. Guthrie. Can. J. Chem. **64**, 635 (1986).
13. J. P. Guthrie and K. F. Taylor. Can. J. Chem. **61**, 602 (1983).
14. J. B. Pedley, R. D. Naylor, and S. P. Kirby. Thermochemical data of organic compounds. 2nd ed. Chapman and Hall, London. 1986.
15. R. Fuchs and R. F. Rodewald. J. Am. Chem. Soc. **95**, 5897 (1973).
16. E. Martin, S. H. Yalkowsky, and J. E. Wells. J. Pharm. Sci. **68**, 565 (1979).
17. K. Schafer and E. Lax (*Editors*). Landolt-Bornstein Zahlenwerte und Funktionen aus Physik, Chemie, Astronomie, Geophysik, und Technik. Band II.4, Springer Verlag, Berlin. 1961.
18. J. P. Guthrie and K. F. Taylor. Can. J. Chem. **62**, 363 (1984).
19. A. Kuwae and K. Machida. Spectrochim. Acta, Part A: **35A**, 27 (1979).
20. L. A. Carreira and T. G. Towns. J. Mol. Struct. **41**, 1, (1977).
21. D. R. Stull, E. F. Westrum, Jr., and G. C. Sinke. The chemical thermodynamics of organic compounds. Wiley, New York. 1967.
22. K. E. Reinert. Z. Naturforsch. A: **15**, 85 (1960).

Can. J. Chem. Downloaded from www.nrcresearchpress.com by 217.78.4.112 on 09/08/12
For personal use only.

23. S. W. Benson. Thermochemical kinetics. 2nd ed. Wiley, New York. 1976.
24. A. M. Dwivedi, S. Krimm, and S. Mierson. Spectrochim. Acta, Part A: **45A**, 271 (1989).
25. J. H. S. Green and D. J. Harrison. Spectrochim. Acta, Part A: **33A**, 583 (1977).
26. D. A. Condit, S. M. Craven, and J. E. Katon. Appl. Spectrosc. **28**, 420 (1974).
27. J. R. Durig, H. D. Bist, K. Furic, J. Qiu, and T. S. Little. J. Mol. Struct. **129**, 45 (1985).
28. J. P. Guthrie. Can. J. Chem. **70**, 1042 (1992).
29. J. Gerstein and W. P. Jencks. J. Am. Chem. Soc. **86**, 4655 (1964).
30. A. R. Fersht and Y. Requenna. J. Am. Chem. Soc. **93**, 3499 (1971).
31. D. S. Abrams, H. A. Massaldi, and J. M. Prausnitz. Ind. Eng. Chem. Fundam. **13**, 259 (1974). A. B. Macknick, J. Winnik, and J. M. Prausnitz. Ind. Eng. Chem. Fundam. **16**, 392 (1977).
32. J. S. Chickos. Heats of sublimation. *In* Molecular structure and energetics. Vol. 2. VCH Publishers, Deerfield Beach, Fla. 1987.
33. D. J. Sandman, A. J. Epstein, J. S. Chickos, J. Ketchum, J. S. Fu, and H. A. Scheraga. J. Chem. Phys. **70**, 305 (1979).
34. G. L. Starobinets, E. M. Rakhmanko, S. M. Leshchev, and I. Y. Rumyantsev. Russ. J. Phys. Chem. **60**, 674 (1986).
35. J. Toullec and M. El-Alaoui. J. Org. Chem. **51**, 4054 (1986).
36. J. Toullec, M. El-Alaoui, and P. Kleffert. J. Org. Chem. **48**, 4808 (1983).
37. J. Hine and P. K. Mookerjee. J. Org. Chem. **40**, 292 (1975).
38. N. D. Cheronis and J. B. Entrikin. Semimicro qualitative organic analysis. 2nd ed. Interscience, New York. 1960. p. 442.
39. R. J. De Feoand and P. D. Strickler. J. Org. Chem. **28**, 2915 (1963).
40. A. L. J. Beckwith. *In* The chemistry of amides. *Edited by* J. Zabicky. Wiley, New York. 1970. p. 96 ff.
41. M. Labelle and D. Gravel. J. Chem. Soc. Chem. Commun. 105 (1985).
42. J. P. Guthrie. Can. J. Chem. **56**, 2342 (1978).
43. G. P. Schiemenz and G. Stein. Tetrahedron, **26**, 2007 (1970).
44. C. A. Bunton, B. Nayak, and C. O'Connor. J. Org. Chem. **33**, 572 (1968).
45. Beilstein. Handbuch der organischen Chemie, 9, III, p. 1362.
46. Beilstein. Handbuch der organischen Chemie, 9, III, p. 2342.
47. Beilstein. Handbuch der organischen Chemie, 9, III, p. 1709.
48. A. E. Kulikova, E. N. Zil'Berman, and F. A. Ekstrin. Zh. Vses. Khim. Oa. im. D. I. Mendeleeva, **11**, 704, (1966); Chem. Abstr. **66**, 115426y (1967).
49. L. M. Jackman, T. E. Kavanagh, and R. C. Haddon, Org. Magn. Reson. **1**, 109 (1969).
50. A. M. Lewin and M. Frucht. Org. Magn. Reson. **7**, 206 (1975).
51. H. Wenker. J. Am. Chem. Soc. **80**, 1081 (1938).
52. I. Kojo, S. Awazu, and M. Hanano. Chem. Pharm. Bull. **22**, 864 (1974).
53. J. P. Guthrie and D. C. Pike. Can. J. Chem. **65**, 1951 (1987).
54. B. S. Furniss, A. J. Hannaford, P. W. G. Smith, and A. R. Tatchell. Vogel's textbook of practical organic chemistry. 5th ed. Longman Scientific and Technical, London. 1989. p. 400.
55. G. M. Moselhy and H. O. Pritchard. J. Chem. Thermodyn. **7**, 977 (1975).
56. M. Colomina, P. Jiminez, R. Perez-Ossorio, and C. Turrion. J. Chem. Thermodyn. **8**, 439 (1976).
57. M. Colomina, P. Jiminez, M. V. Roux, and C. Turrion. J. Chem. Thermodynam. **10**, 661 (1978).
58. R. Sabbah and H. Hirtz. Bull. Soc. Chim. Fr. **127**, 26 (1991).
59. J. W. Wilson. J. Chem. Soc. Dalton Trans. 890 (1976).
60. D. D. Wagman, W. H. Evans, V. B. Parker, R. H. Schumm, I. Halow, S. M. Bailey, K. L. Churney, and R. L. Nuttal. J. Phys. Chem. Ref. Data, **11**, 1982. Suppl. 2.
61. A. T. Hu, G. C. Sinke, M. Mannsson, and B. Ringner. J. Chem. Thermodyn. **4**, 283 (1972).

Can. J. Chem. Downloaded from www.nrcresearchpress.com by 217.78.4.112 on 09/08/12
For personal use only.

Medium effect on the second-stage dissociation constant of *N*-(2-acetamido)imino diacetic acid (H_2ADA)

AHMED HASSAN,[1] H. A. AZAB, S. A. EL GYAR, AND Z. A. KHAFAGY
Chemistry Department, Faculty of Science, Assiut University, Assiut, Egypt

Received August 6, 1991

AHMED HASSAN, H. A. AZAB, S. A. EL GYAR, and Z. A. KHAFAGY. Can. J. Chem. **70**, 1684 (1992).

The second-stage dissociation constant values of *N*-(2-acetamido)imino diacetic acid (H_2ADA) were determined at 25 ± 0.1°C by potentiometric titration in different mixed-solvent mixtures (methanol, ethanol, dimethylformamide (DMF), dimethyl sulfoxide (DMSO), acetone, and dioxane). It was observed that the pK_a value is slightly influenced as the solvent is enriched in methanol and ethanol, and remains practically constant in the presence of different amounts of DMF and DMSO. A prounounced change in the pK_a value was observed as the solvent is enriched in acetone or dioxane. These results are discussed in terms of various solvent characteristics. It is concluded that the electrostatic effect has only a relatively small influence on the dissociation equilibrium of the imino group ($-NH^+<$). Other solvent effects such as solvent basicity, different stabilization of the free base of the conjugate acid by hydrogen bonding interactions in aquo-organic solvent media relative to pure aqueous media, as well as proton–solvent interaction play an important role in the acid dissociation equilibrium.

AHMED HASSAN, H. A. AZAB, S. A. EL GYAR et Z. A. KHAFAGY. Can. J. Chem. **70**, 1684 (1992).

Opérant à 25 ± 0,1°C et faisant appel à un titrage potentiométrique, on a déterminé le deuxième stade des valeurs des constantes de dissociation de l'acide *N*-(2-acétamido)iminodiacétique (H_2ADA) dans divers mélanges de solvants mixtes (méthanol, éthanol, diméthylformamide (DMF), diméthylsulfoxyde (DMSO), acétone et dioxane). On a observé que la valeur du pK_a est légèrement influencée lorsque le solvant est enrichi en méthanol ou en éthanol et qu'elle demeure pratiquement constante avec des concentrations de plus en plus grandes de DMF ou de DMSO. On observe une changement prononcé de la valeur du pK_a lorsqu'on enrichit le solvant en acétone ou en dioxane. On discute de ces résultats en fonction de diverses caractéristiques des solvants. On en conclut que l'effet électrostatique n'a qu'une légère influence sur l'équilibre de dissociation du groupe imino ($-NH^+<$). D'autres effets de solvant, tels la basicité du solvant, des stabilisations différentes de la base libre de l'acide conjugué par des liaisons hydrogènes dans les solvants mixtes organiques/eau par rapport au milieu aqueux pur ainsi que l'interaction proton/solvant, jouent un rôle important dans l'équilibre de dissociation de l'acide.

[Traduit par la rédaction]

Introduction

N-(2-Acetamido)imino diacetic acid (H_2ADA) was first prepared, by Schwarzenbach *et al.* (1), in 1955. The choice of alternative buffers has increased with the commercial availability of zwitterionic amino acids, mainly *N*-substituted taurines or *N*-substituted glycines prepared by Good *et al.* (2), so that organic buffers suitable for use in biochemistry now include *N*-(2-acetamido)imino diacetic acid (H_2ADA). Zwitterionic buffers, comparable to amino acids, show significant advantages over conventional buffers: insignificant penetration through biological membrane, maximum buffer capacity at physiological pH range 6–8.50, and no enzyme substrate or enzyme inhibitor properties. Though studies on the dissociation constants of acids and bases in mixed and nonaqueous solvents have been extensive, relatively little work has been done to determine the dissociation constants of the biologically important zwitterionic buffers (3–7).

In this paper the effect of the medium on the second dissociation constant of *N*-(2-acetamido)imino diacetic acid (H_2ADA) has been reported using potentiometric titrations. The organic solvents used are amphiprotic solvents (methanol and ethanol), dipolar aprotic solvents (DMF and DMSO), a low basic aprotic solvent (acetone), and a nonpolar solvent (dioxane).

Experimental

Chemicals and solutions: $H_2N\text{-}CO\text{-}CH_2\text{-}N(CH_2COOH)_2$ (H_2ADA) was analytical grade (BDH) with purity 98% and was used without further purification. Since the solubility of free acid *N*-(2-acetamido)imino diacetic acid is very low, the monosodium salt (NaHADA) was prepared by dissolving 0.1902 g H_2ADA in 10 mL NaOH (0.1 mol dm^{-3}) and diluting to 100 mL with bidistilled water.

The organic solvents methanol, ethanol, dimethylformamide, dimethyl sulfoxide, acetone, and dioxane were of high purity (A.R. or Spectrograde products).

Carbonate-free NaOH was prepared and was standardized by titration with KH-phthalate. The molarity of HNO_3 was checked by titration with standard NaOH solution. Generally, dilute solutions were prepared by appropriate dilution of the stock.

Procedure

The pK_{a_2} values of *N*-(2-acetamido)imino diacetic acid in the different organic solvent–water mixtures under investigation were determined by adopting the Irving and Rossotti pH-titration technique (8, 9). The following solutions were titrated potentiometrically against standard carbonate-free sodium hydroxide (0.1 mol dm^{-3}) solution: (a) 4×10^{-3} mol dm^{-3} HNO_3; (b) solution (a) in the presence of 1×10^{-3} mol dm^{-3} NaHADA. Both the solutions (a) and (b) contain the same proportion (w/w) of the different organic solvents studied.

The total volume was adjusted to 50 cm^3 in each case by adding double-distilled water. The titrations were performed at 25 ± 0.1°C and μ = 0.1 mol dm^{-3} (KNO_3). A Fisher Accumet pH/ion meter model 2301 was used for potentiometric measurements and calibrated by using two aqueous buffer solutions at pH 4.01 and 9.18.

The pH-meter readings were corrected in accordance with the method described by Douheret (10, 11). This was done to account for the difference in acidity, basicity, dielectric constant, and ion activities in partially aqueous solutions relative to the pure solvent.

The pK_{a_2} values were calculated by a graphical method (aver-

[1]Author to whom correspondence may be addressed.

Can. J. Chem. Downloaded from www.nrcresearchpress.com by 217.78.4.112 on 09/08/12
For personal use only.

TABLE 1. The mean $pK^*_{a_2}$ values[a] of H_2ADA in the different organic solvent–water mixtures

Organic solvent	% w/w solvent	pK_{a_2}	$pK^*_{a_2}$
Methanol	00.0	6.560	6.560 ± 0.02
	10.0	6.362	6.357 ± 0.02
	20.0	6.425	6.410 ± 0.04
	30.0	6.425	6.385 ± 0.05
	40.0	6.350	6.260 ± 0.02
	50.0	6.400	6.275 ± 0.04
Ethanol	00.0	6.560	6.560 ± 0.02
	10.0	6.437	6.427 ± 0.04
	20.0	6.412	6.377 ± 0.03
	30.0	6.580	6.500 ± 0.02
	40.0	6.612	6.480 ± 0.03
	50.0	6.612	6.407 ± 0.04
DMF	00.0	6.560	6.560 ± 0.02
	10.0	6.555	6.493 ± 0.03
	20.0	6.625	6.495 ± 0.04
	30.0	6.662	6.437 ± 0.05
	40.0	6.825	6.495 ± 0.03
	50.0	6.975	6.523 ± 0.04
DMSO	00.0	6.560	6.560 ± 0.02
	10.0	6.562	6.530 ± 0.04
	20.0	6.650	6.575 ± 0.05
	30.0	6.737	6.577 ± 0.06
	40.0	6.962	6.682 ± 0.03
	50.0	7.025	6.600 ± 0.02
	55.0	7.137	6.627 ± 0.03
Acetone	00.0	6.560	6.560 ± 0.02
	10.0	6.612	6.632 ± 0.03
	20.0	6.775	6.815 ± 0.03
	30.0	6.800	6.850 ± 0.04
	40.0	6.850	6.920 ± 0.02
	50.0	6.966	7.081 ± 0.02
Dioxane	00.0	6.560	6.560 ± 0.02
	10.0	6.587	6.607 ± 0.05
	20.0	6.662	6.702 ± 0.06
	30.0	6.837	6.917 ± 0.05
	40.0	6.937	7.057 ± 0.04
	50.0	7.250	7.420 ± 0.03
	55.0	7.350	7.545 ± 0.04

[a] $pK^*_{a_2}$: corrected pK_{a_2} values according to Douheret (10, 11).

age value method) and the linear plot method. A PDP-81E minicomputer was programmed to calculate pK_{a_2} values from simultaneous equations.

Results and discussion

The mean pK_{a_2} values of *N*-(2-acetamido)imino diacetic acid in the different aquo-organic solvent mixtures are given in Table 1. Careful examination of the results reveals three important features:

1. With an increase in amphiprotic methanol or ethanol solvent concentration in aqueous medium, the change in pK_{a_2} is quite small, in most cases it decreases slightly.

2. With an increase in the DMF or DMSO content, the pK_{a_2} remains practically constant.

3. By increasing the concentration of acetone or dioxane (nonpolar solvents) in aqueous medium, the pK_{a_2} value increases.

Effect of the amphiprotic solvent

Solvent effects on acid–base phenomena in amphiprotic media of intermediate and high dielectric constant (methanol, ethanol) are often successfully interpreted in terms of changes in the dielectric constant (electrostatic effects) and in the basicity (non-electrostatic effects).

Consider an acid HA at molality m in mixed amphiprotic solvent (SH). It is assumed that the dielectric constant of the mixed solvent is sufficiently large to permit a certain amount of ionization. The proton activity a_H, as a measure of acidity, can be expressed (12) in terms of K_{HA} and K_{SH}, which are, respectively, the acidity constants of HA and SH_2^+; ν is the activity coefficient:

$$[1] \quad a_H = \sqrt{m\, K_{HA}\, K_{SH}\, \frac{\nu_{SH_2^+}\, \nu_{HA}}{\nu_{SH}\, \nu_{A^-}}}$$

A decrease in the dielectric constant usually causes $\nu_{SH_2^+}/\nu_{HA}$ and ν_{A^-}/ν_{HA} to increase, and it is possible that both of these ratios will increase by about the same amount (13). Hence, according to eq. [1], a lowering of the dielectric constant due to addition of methanol or ethanol may have a small effect on the acidity of an unbuffered solution of *N*-(2-acetamido)imino diacetic acid. With respect to the solvent basicity effect, the autoprotolysis constant of water is slightly influenced by addition of methanol or ethanol (pK of pure water is changed from 14.0 to 14.90 mol dm^{-3} for a 50% w/w ethanol–water mixture ($HA + SH \rightleftharpoons SH_2^+ + A^+$). Accordingly, one can deduce that changing the basicity of the medium by increasing additions of methanol or ethanol to the aqueous medium has a small influence on the second-stage dissociation constant of *N*-(2-acetamido)imino diacetic acid.

Generally, it is recognized that properties of solvents such as dielectric constant, acidic or basic strengths, play a major but not exclusive role. Other factors such as stabilization of the different species existing in equilibrium through hydrogen bonding together with ion–solvent interaction and dispersion forces play an important role in the ionization of weak acids. Accordingly, the observed slight changes in pK_{a_2} of H_2ADA as the solvent is enriched in methanol or ethanol can be mainly interpreted as resulting from the following two factors:

1. The relatively high stabilization of the conjugate base

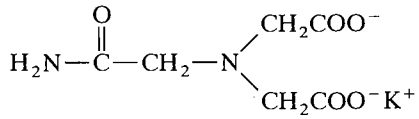

by a donor hydrogen bond in a pure aqueous medium relative to that in the presence of methanol or ethanol. This is due to the greater tendency of water molecules as compared with other solvent molecules to donate hydrogen (14). Thus, an increase in the proportion of methanol or ethanol in the aqueous medium will result in an increase in the activity coefficient of the conjugate base, thereby causing a slight increase in the pK_{a_2} value.

2. The greater stabilization of the proton in methanol–water or ethanol–water mixtures relative to that in pure water through ion–solvent interaction (15, 16). This effect will generate a low activity coefficient of the proton in alcohol–

Can. J. Chem. Downloaded from www.nrcresearchpress.com by 217.78.4.112 on 09/08/12
For personal use only.

water mixtures compared to that in pure aqueous medium, therefore causing a slight decrease in pK_{a_2}.

Effect of dipolar aprotic solvents (DMF and DMSO)

The observed constancy in the pK_{a_2} value of H_2ADA in the presence of varying amounts of DMF and DMSO can mainly be explained as resulting from the following two opposing effects:

1. A DMF–water or DMSO–water mixture is considered to be more basic than water (17). This behaviour is then based on the building up of a strong acceptor hydrogen bond from the $-NH^+$ group of the *N*-(2-acetamido)imino diacetic acid in the former medium as compared to that in water, thus facilitating the ionization process of the imino group i.e., a low pK_{a_2} value.

2. The expected low stabilization of the conjugate *N*-(2-acetamido)imino diacetic acid free base by hydrogen bonding with solvent molecules in the DMF–water or DMSO–water mixtures compared to its stabilization due to hydrogen bonding with water molecules in pure aqueous medium. This in turn results in a high pK_{a_2} value.

Effect of a low basic aprotic acetone solvent

The presence of acetone as co-organic solvent exerts a pronounced effect on the pK_{a_2} of H_2ADA as compared to the effect of the other co-organic solvents studied (methanol, ethanol, dimethyl sulfoxide, and DMF). Though ethanol and acetone have nearly the same dielectric constant (24.30 and 20.70, respectively), the pK_{a_2} values of H_2ADA in ethanol–water and in acetone–water mixtures of the same composition are different. This behaviour can be considered as convincing evidence for the above conclusion that the electrostatic effect will have a relatively small influence on the second-stage dissociation constant of *N*-(2-acetamido)imino diacetic acid. Thus, the observed increase in pK_{a_2} when the amount of the co-organic solvent acetone in the medium is increased can be mainly attributed to the following effects.

1. Solvent basicity effect: acetone is considered to be a very weakly basic solvent (18–21), therefore one can expect that the basicity of acetone mixtures with water is lower than that of a pure aqueous medium (17). This leads to lower ionization of the NH^+ group in the former media as compared to that in the latter one, i.e., a high pK_{a_2} value.

2. Solute–solvent interactions effect: acetone is considered to be both a poorer acceptor as well as donor of hydrogen bonds than is water (22). Thus, one may expect a low stabilization of the free H_2ADA conjugate base by hydrogen bonding interactions in the presence of this co-organic solvent. This leads to higher pK_{a_2} values in such media than those obtained in pure aqueous solution.

3. Proton–solvent interaction effect: it has been recognized that the special type of solvation of the H^+ ion, namely, hydrogen ion–solvent interaction, plays a vital role in acid–base equilibria (21). Since acetone is a weakly basic solvent, one must therefore expect that the H^+ ion becomes less stabilized in the presence of this co-organic solvent. Thus, increasing the acetone proportion in the aqueous medium results in a high activity coefficient of the proton, i.e., a high pK_{a_2} value.

Effect of an aprotic nonionizing dioxane solvent

The observed increase in the pK_{a_2} value of H_2ADA as the solvent is enriched in dioxane may be attributed to lowering of the dielectric constant, which increases the fraction of associated ions to form Bjerrum ion pairs (23) and higher aggregates such as triple ions and dipole aggregates (24). In this aprotic nonionizing medium, the concentration of free ions is very low and acidity phenomena are governed largely by ionic association reactions, as Kolthoff and Bruckenstein have shown so convincingly (25).

Conclusion

H_2ADA (pK_{a_2} 6.60) is a diprotic organic acid in the class of Good buffers (2). It is a potentially useful zwitterionic buffer for use in biochemistry in the physiological pH range (6–8.50), because of its low toxicity. This paper describes solvent effects on the measured ionization constants of H_2ADA. The organic solvents used are methanol, ethanol, DMF, DMSO, and acetone. Methanol and ethanol were chosen as representatives of amphiprotic solvents. We have chosen *N,N*-dimethylformamide (DMF) and dimethyl sulfoxide (DMSO) as aprotic polar solvents to study the pK_{a_2} variations of H_2ADA because their dielectric constants are relatively high, but lower than that of water. Acetone and dioxane have been chosen as a low basic aprotic solvent and an aprotic nonionizing solvent. All the solvents chosen are of frequent use in biochemistry and biology. The new experimental pH and pK_{a_2} data reported in this paper for H_2ADA dissolved in the above-mentioned binary aqueous–organic solvent mixtures should be of great use in a number of areas of chemistry, biochemistry, and biology.

Acknowledgment

We thank Professor M. R. Mahmoud, Professor of Physical and Inorganic Chemistry, Dean of the Faculty of Science, Assiut University, for helpful discussion and valuable advice during this work.

1. G. Schwarzenbach, G. Anderegg, W. Scheneider, and H. Senn. Helv. Chim. Acta, **38**, 1147 (1955).
2. N. E. Good, G. D. Winget, W. Winter, T. N. Connolly, S. Izawa, and R. M. M. Singh. Biochemistry. **5**, 467 (1966).
3. R. N. Roy, J. J. Gibbons, J. L. Padron, and R. G. Casebolt. Anal. Chim. Acta, **129**, 247 (1981).
4. J. T. Michael. J. Chem. Eng. Data, **24**, 230 (1979).
5. R. N. Roy, J. J. Gibbons, and G. E. Baker. Cryobiology, **22**, 589 (1985).
6. R. N. Roy, J. J. Gibbons, K. Buechter, and S. Faszholz. J. Chem. Soc. Faraday Trans. 1, **80**, 3167 (1984).
7. R. N. Roy, J. J. Gibbons, K. Buechter, and S. Faszholz. J. Chem. Thermodyn. **14**, 1011 (1982).
8. H. Irving and H. S. Rossotti. J. Chem. Soc. 3397 (1953); 2904 (1954).
9. H. Rossotti. The study of ionic equilibria. Longman, London. 1978. Chap. 1. p. 38.
10. G. Douheret. Bull. Soc. Chem. Fr. 14125 (1967).
11. G. Douheret. Bull. Soc. Chem. Fr. 33122 (1968).
12. R. G. Bates. Determination of pH theory and practice. John Wiley & Sons, Inc., New York. 1964. p. 198.
13. L. P. Hammett. J. Am. Chem. Soc. **50**, 2666 (1928).
14. F. Franks and D. J. G. Ives. Q. Rev. **20**, 1 (1966).
15. H. P. Bennetto, D. Feakins, and D. L. Turner. J. Chem. Soc. 1211 (1966).
16. D. Feakins, K. G. Lawrence, and R. P. T. Tomkins. J. Chem. Soc. A: (5), 753 (1967).
17. B. Tremillon. Chemistry in non-aqueous solvents. D. Reidel, Dordrecht. p. 68. 1974.
18. E. M. Arnett. Prog. Phys. Org. Chem. **1**, 223 (1963).
19. N. C. Deno and M. J. Wisotsky. J. Am. Chem. Soc. **85**, 1735 (1963).

Can. J. Chem. Downloaded from www.nrcresearchpress.com by 217.78.4.112 on 09/08/12
For personal use only.

20. J. F. Coetzee and G. R. Padmanobhan. J. Phys. Chem. **69**, 3193 (1965).
21. G. R. Bates. *In* Solute–solvent interactions. Edited by J. F. Coetzee and C. D. Ritchie. Marcel Dekker, New York. pp. 51, 72. 1969.
22. C. D. Ritchie. *In* Solute–solvent interactions. Edited by J. F. Coetzee and C. D. Ritchie. Marcel Dekker, New York. 1969. pp. 219–221, 223, 227.
23. N. Bjerrum. K. Dan. Vidensk. Selsk. Mat.-Fys. Medd. **7**, 9 (1926).
24. R. M. Fuoss and C. A. Kraus. J. Am. Chem. Soc. **55**, 2387 (1933); **57**, 1 (1935).
25. I. M. Kolthoff and S. Bruckenstein. J. Am. Chem. Soc. **78**, 1 (1956); **79**, 1 (1957); S. Bruckenstein and I. M. Kolthoff. J. Am. Chem. Soc. **78**, 2974 (1956).

Can. J. Chem. Downloaded from www.nrcresearchpress.com by 217.78.4.112 on 09/08/12
For personal use only.

The sodium perchlorate complex of *cis-syn-cis* dicyclohexano-24-crown-8 ether. X-ray crystal structure and solution conformations as studied by variable temperature ^{13}C NMR spectroscopy at 125 MHz. An example of eight-coordinate sodium[1]

G. W. Buchanan,[2] Y. Lear, and C. Bensimon

Ottawa–Carleton Chemistry Institute, Department of Chemistry, Carleton University, Ottawa, Ont., Canada K1S 5B6

Received November 28, 1991

G. W. Buchanan, Y. Lear, and C. Bensimon. Can. J. Chem. **70**, 1688 (1992).

The major isomer obtained by hydrogenation of dibenzo-24-crown-8 ether is shown to have the *cis-syn-cis* configuration as determined from the crystal structure of its sodium perchlorate complex. This material possesses eight-coordinate sodium with Na—O distances ranging from 2.54 to 2.78 Å. The complex is shown to exist in a single asymmetric conformation below 240 K as determined by ^{13}C NMR at 125 MHz. From NMR coalescence temperature measurement, the free energy of activation for cyclohexane ring inversion in this complex has been determined to be 51.0 ± 0.6 kJ/mol.

G. W. Buchanan, Y. Lear et C. Bensimon. Can. J. Chem. **70**, 1688 (1992).

En se basant sur la structure cristalline du perchlorate, on a déterminé que l'isomère majeur obtenu par hydrogénation de l'éther dibenzo-24-couronne-8 possède la configuration *cis-syn-cis*. Dans ce produit, il y a huit atomes de sodium de cordonnés et les distances Na—O varient de 2,54 à 2,78 Å. Grâce à la RMN du ^{13}C à 125 MHz, on a démontré que, à une température inférieure à 240 K, le complexe existe sous une seule conformation asymétrique. Sur la base de mesures de températures de coalescence, on a déterminé que l'énergie libre d'interconversion du cyclohexane est égale à 51,0 ± 0,6 kJ/mol.

[Traduit par la rédaction]

Introduction

Although the dibenzo-24-crown-8 ether system shown below has been known since the pioneering work of Pedersen (1), the only report of its dicyclohexano derivatives is confined to that describing a mixture of isomers (2)

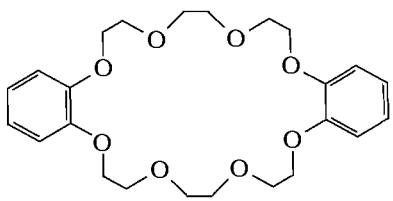

In view of our continuing interest in the solution and solid state stereochemistry of related molecules with a variety of macrocyclic ring sizes (3–7), we wish to report the determination of the configuration of the major isomer obtained from catalytic hydrogenation of dibenzo-24-crown-8. This isomer has been identified as the *cis-syn-cis* form (below) via the X-ray crystal structure of its sodium perchlorate complex.

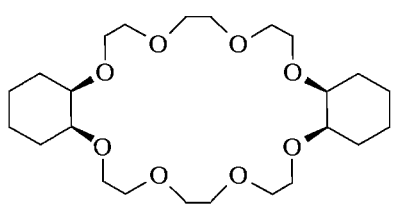

High-field ^{13}C NMR measurements as a function of temperature have permitted assignment of the preferred conformation of this complex at low temperature in solution as well as representing a measure of the free energy for conformational interconversion.

Results and discussion

Figure 1 contains the structural formula and numbering scheme for the $NaClO_4$ complex of *cis-syn-cis*-dicyclohexano-24-crown-8 ether (**1**). Figure 2 shows the ORTEP plot for this complex, while Fig. 3 shows the ^{13}C NMR spectra of **1** at ambient temperature in CD_2Cl_2 solution as well as in the slow exchange limit of 240 K. Bond lengths and angles for **1** are listed in Table 1 while torsional angles involving ring skeletal atoms and the sodium ion are collected in Table 2. The ^{13}C chemical shifts are presented in Table 3, with the crystallographic data in Table 4 and the atomic parameters in Table 5. Lists of structure factors and anisotropic temperature factors are available as supplementary material.[3]

(i) X-ray crystallographic structure

The ORTEP diagram in Fig. 2 clearly shows that, in the crystal, the 24-membered ring adopts a conformation that allows all eight crown ether oxygens to be coordinated to the sodium ion. *This type of coordination of a sodium cation within a single crown ether appears to be unique*. The range of Na—O distances is from 2.54 to 2.78 Å. In the case of both 1:1 and 1:2 complexes of dibenzo-24-crown-8 with

[1]Taken in part from the B.Sc. Honours Thesis of Yvonne Lear, Department of Chemistry, Carleton University, April 1990.

[2]Author to whom correspondence may be addressed.

[3]These tables may be purchased from: The Depository of Unpublished Data, Document Delivery, CISTI, National Research Council Canada, Ottawa, Canada K1A 0S2.

A table of hydrogen atom parameters has also been deposited with the Cambridge Crystallographic Data Centre and can be obtained on request from The Director, Cambridge Crystallographic Data Centre, University Chemical Laboratory, Lensfield Road, Cambridge CB2 1EW, U.K.

Can. J. Chem. Downloaded from www.nrcresearchpress.com by 217.78.4.112 on 09/08/12
For personal use only.

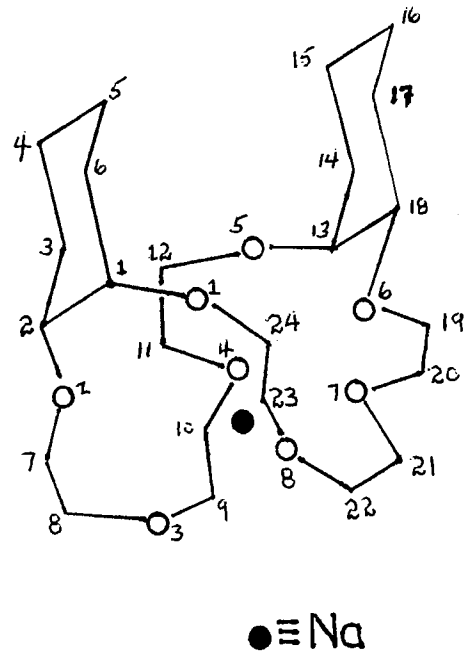

FIG. 1. Structure and numbering scheme

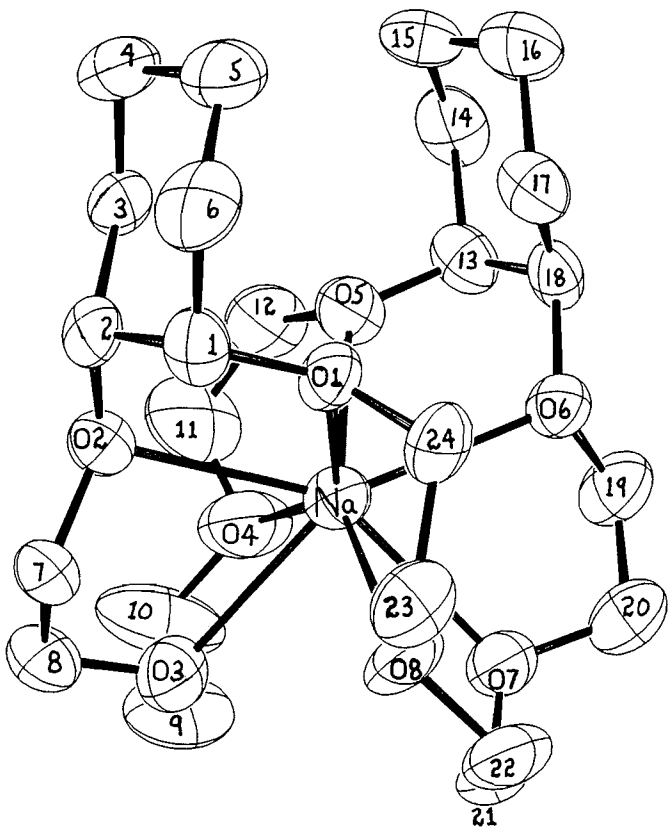

FIG 2. ORTEP diagram for **1**

sodium *o*-nitrophenolate, the coordination number is six, with distances from the crown ether oxygens to the Na^+ ion ranging from 2.47 to 2.61 Å (8). In the 18-crown-6 complex with $NaNCS \cdot H_2O$ (9) the Na^+ ion is heptacoordinate with the water molecule providing the extra coordination site, and the range of Na—O distances is from 2.32 to 2.62 Å. The only reported instance of eight-coordinate sodium in crown ether chemistry occurs in the 2:1 octahydrate complex of 12-crown-4 ether with NaOH (10). In this case the sodium ion forms an eight-coordinated sandwich complex of approximate D_4 symmetry with the two crown ether rings. The oxygen atoms are arranged at the corners of a square antiprism-type structure with an average Na—O distance of 2.49 Å. Thus in **1**, the Na—O distances are significantly longer than in other crown ether complexes involving sodium ions. Considering the atomic radii of Na^+ (0.97 Å) and O (1.40 Å), one would expect the optimal Na—O distance to be near the sum of these values, i.e., 2.37 Å. The stability of **1** in spite of the longer Na—O distances is, accordingly, remarkable.

With respect to the conformation of the crown ether moiety in **1**, the eight O—C—C—O networks of the macrocycle have torsional angles ranging from 49.9° for the O8—C23—C24—O1 unit to 62° for the O6—C19—C20—O7 case. These values are in the normal range for crown ethers where *gauche* O—C—C—O networks are energetically favoured (11). By contrast, the C—O—C—C networks, which in "ideal" crown ether conformations are *transoid* (11), show a wide range of values in **1**. In fact, of the 16 such networks in the macrocyclic portion of **1**, only eight have *transoid* geometries (i.e., 160–180°). Five others exhibit *gauche*-type geometries (70–79°) with the remaining three having dihedral angles of 117.6, 138.4, and 145.6° respectively. Despite the difference in coordination number at sodium, there are some common features between the macrocyclic ring conformation of **1** and that present in the 2:1 sodium-*o*-nitrophenolate complex of dibenzo-24-crown-8 ether (8). In both cases, there is a "propellor" type conformation present in the central portion of the macrocycle as depicted in Fig. 1.

Unfortunately, the free ligand is an oil, so that no direct comparison of "free" vs. complexed macrocyclic ring conformations can be made for this *cis-syn-cis*-dicyclohexano-24-crown-8 ether system.

(ii) ^{13}C NMR spectra

Figure 3 illustrates the 125.76 MHz ^{13}C NMR spectra of **1** in CD_2Cl_2 solution at 303 and 240 K. The spectrum recorded at 303 K is consistent with a situation in which all conformational interconversions in **1** are fast on the NMR time scale, giving rise to only six singlet resonances. The broadened high-field and low-field lines represent sites whose rates of conformational interchange are beginning to approach their slow exchange chemical shift differences (in Hz). From results of the APT test (12) the lowest-field resonance at 76.01 ppm arises from the methine carbons 1, 2, 13, and 18. From well-documented effects of oxygenated substituents on cyclohexyl carbon shifts (13), the highest-field line at 22.11 ppm can be confidently assigned to the carbons most remote from the oxygen atoms, namely C-4, 5, 15, and 16. By elimination, the resonance at 27.32 ppm can be attributed to the C-3, 6, 14, and 17 sites. In the ^1H spectrum at

Can. J. Chem. Downloaded from www.nrcresearchpress.com by 217.78.4.112 on 09/08/12
For personal use only.

Can. J. Chem. Downloaded from www.nrcresearchpress.com by 217.78.4.112 on 09/08/12
For personal use only.

TABLE 1. (*a*) Atomic distances in Å

Na—O(1)	2.578(7)	Na—O(2)	2.560(7)	Na—O(3)	2.539(7)
Na—O(4)	2.585(7)	Na—O(5)	2.600(6)	Na—O(6)	2.614(7)
Na—O(7)	2.557(7)	Na—O(8)	2.775(9)		
Cl—O(9)	1.303(9)	Cl—O(10)	1.412(10)	Cl—O(11)	1.376(10)
Cl—O(12)	1.419(11)				
O(1)—C(1)	1.441(12)	O(1)—C(24)	1.447(12)	O(2)—C(2)	1.446(11)
O(2)—C(7)	1.423(12)	O(3)—C(8)	1.428(14)	O(3)—C(9)	1.439(13)
O(4)—C(10)	1.403(12)	O(4)—C(11)	1.431(11)	O(5)—C(12)	1.424(10)
O(5)—C(13)	1.447(11)	O(6)—C(18)	1.435(10)	O(6)—C(19)	1.450(11)
O(7)—C(20)	1.415(13)	O(7)—C(21)	1.465(14)	O(8)—C(22)	1.453(16)
O(8)—C(23)	1.334(16)				
C(1)—C(2)	1.513(14)	C(1)—C(6)	1.526(15)	C(2)—C(3)	1.510(14)
C(3)—C(4)	1.518(14)	C(4)—C(5)	1.503(16)	C(5)—C(6)	1.529(16)
C(7)—C(8)	1.485(15)	C(9)—C(10)	1.505(16)	C(11)—C(12)	1.496(14)
C(13)—C(14)	1.509(13)	C(13)—C(18)	1.548(13)	C(14)—C(15)	1.518(14)
C(15)—C(16)	1.507(14)	C(16)—C(17)	1.522(13)	C(17)—C(18)	1.552(13)
C(19)—C(20)	1.521(14)	C(21)—C(22)	1.392(19)	C(23)—C(24)	1.388(18)

(*b*) Bond angles in degrees

O(1)—Na—O(2)	63.69(22)	O(1)—Na—O(3)	111.0(3)
O(1)—Na—O(4)	157.61(24)	O(1)—Na—O(5)	101.36(21)
O(1)—Na—O(6)	96.09(22)	O(1)—Na—O(7)	121.70(24)
O(1)—Na—O(8)	63.23(23)	O(2)—Na—O(3)	66.05(23)
O(2)—Na—O(4)	96.73(22)	O(2)—Na—O(5)	89.70(21)
O(2)—Na—O(6)	143.72(23)	O(2)—Na—O(7)	150.9(3)
O(2)—Na—O(8)	104.1(3)	O(3)—Na—O(4)	66.33(23)
O(3)—Na—O(5)	122.44(22)	O(3)—Na—O(6)	148.7(3)
O(3)—Na—O(7)	86.79(24)	O(3)—Na—O(8)	87.79(24)
O(4)—Na—O(5)	65.98(20)	O(4)—Na—O(6)	94.36(23)
O(4)—Na—O(7)	80.67(22)	O(4)—Na—O(8)	136.38(25)
O(5)—Na—O(6)	63.79(20)	O(5)—Na—O(7)	114.86(25)
O(5)—Na—O(8)	149.77(25)	O(6)—Na—O(7)	65.14(22)
O(6)—Na—O(8)	90.88(24)	O(7)—Na—O(8)	62.60(24)
O(9)—Cl—O(10)	111.9(6)	O(9)—Cl—O(11)	111.4(7)
O(9)—Cl—O(12)	111.7(6)	O(10)—Cl—O(11)	106.3(6)
O(10)—Cl—O(12)	110.0(6)	O(11)—Cl—O(12)	105.4(6)
Na—O(1)—C(1)	121.4(5)	Na—O(1)—C(24)	113.1(6)
C(1)—O(1)—C(24)	114.5(8)	Na—O(2)—C(2)	113.8(2)
Na—O(2)—C(7)	108.0(5)	C(2)—O(2)—C(7)	115.6(7)
Na—O(3)—C(8)	114.8(5)	Na—O(3)—C(9)	108.0(6)
C(8)—O(3)—C(9)	113.8(7)	Na—O(4)—C(10)	117.9(6)
Na—O(4)—C(11)	116.6(5)	C(10)—O(4)—C(11)	113.2(7)
Na—O(5)—C(12)	106.1(5)	Na—O(5)—C(13)	122.0(5)
C(12)—O(5)—C(13)	114.6(6)	Na—O(6)—C(18)	113.8(5)
Na—O(6)—C(19)	104.3(5)	C(18)—O(6)—C(19)	115.3(6)
Na—O(7)—C(20)	118.0(5)	Na—O(7)—C(21)	112.1(6)
C(20)—O(7)—C(21)	114.0(8)	Na—O(8)—C(22)	115.1(7)
Na—O(8)—C(23)	99.7(6)	C(22)—O(8)—C(23)	110.5(10)
O(1)—C(1)—C(2)	106.5(8)	O(1)—C(1)—C(6)	112.2(8)
C(2)—C(1)—C(6)	110.8(8)	O(2)—C(2)—C(1)	111.1(7)
O(2)—C(2)—C(3)	107.8(7)	C(1)—C(2)—C(3)	114.1(8)
O(3)—C(9)—C(10)	114.5(7)	O(4)—C(9)—C(10)	106.1(7)
O(4)—C(11)—C(12)	109.2(7)	O(5)—C(12)—C(11)	112.6(7)
O(5)—C(13)—C(14)	113.0(7)	O(5)—C(13)—C(18)	105.8(7)
C(14)—C(13)—C(18)	110.4(7)	C(13)—C(14)—C(15)	112.3(8)
C(14)—C(15)—C(16)	112.7(8)	C(15)—C(16)—C(17)	111.0(7)
C(16)—C(17)—C(18)	110.8(7)	O(6)—C(18)—C(13)	112.7(7)
O(6)—C(18)—C(17)	106.6(7)	C(13)—C(18)—C(17)	112.3(7)
O(6)—C(19)—C(20)	108.0(7)	C(2)—C(3)—C(4)	111.1(8)
C(3)—C(4)—C(5)	111.4(8)	C(4)—C(5)—C(6)	110.6(8)
C(1)—C(6)—C(5)	111.5(8)	O(2)—C(7)—C(8)	108.0(8)
O(3)—C(8)—C(7)	107.4(8)	O(7)—C(20)—C(19)	107.3(7)
O(7)—C(21)—C(22)	115.1(9)	O(8)—C(22)—C(21)	108.3(10)
O(8)—C(23)—C(24)	116.3(11)	O(1)—C(24)—C(23)	116.3(9)

TABLE 2. Torsion angles

O2—Na—O1—C1	3.0(5)	O2—Na—O1—C24	143.6(8)
O3—Na—O1—C1	−44.5(6)	O3—Na—O1—C24	96.1(7)
O4—Na—O1—C1	33.8(6)	O4—Na—O1—C24	174.4(8)
O5—Na—O1—C1	87.1(6)	O5—Na—O1—C24	−132.3(7)
O6—Na—O1—C1	151.6(7)	O6—Na—O1—C24	−67.8(7)
O7—Na—O1—C1	−144.3(7)	O7—Na—O1—C24	−3.7(6)
O8—Na—O1—C1	−120.4(7)	O8—Na—O1—C24	20.2(6)
O1—Na—O2—C2	26.1(5)	O1—Na—O2—C7	−103.8(7)
O3—Na—O2—C2	157.2(7)	O3—Na—O2—C7	27.4(6)
O4—Na—O2—C2	−142.7(7)	O4—Na—O2—C7	87.5(6)
O5—Na—O2—C2	−76.9(6)	O5—Na—O2—C7	153.2(7)
O6—Na—O2—C2	−35.7(5)	O6—Na—O2—C7	−165.6(7)
O7—Na—O2—C2	134.9(7)	O7—Na—O2—C7	5.1(5)
O8—Na—O2—C2	76.4(6)	O8—Na—O2—C7	−53.3(6)
O1—Na—O3—C8	53.3(6)	O1—Na—O3—C9	−178.7(8)
O2—Na—O3—C8	6.9(6)	O2—Na—O3—C9	134.8(7)
O4—Na—O3—C8	−102.8(7)	O4—Na—O3—C9	25.2(6)
O5—Na—O3—C8	−66.5(6)	O5—Na—O3—C9	61.4(6)
O6—Na—O3—C8	−158.5(8)	O6—Na—O3—C9	−30.5(6)
O7—Na—O3—C8	176.3(8)	O7—Na—O3—C9	−55.8(6)
O8—Na—O3—C8	113.5(7)	O8—Na—O3—C9	−118.5(7)
O1—Na—O4—C10	−83.5(7)	O1—Na—O4—C11	55.3(6)
O2—Na—O4—C10	−55.9(6)	O2—Na—O4—C11	82.9(6)
O3—Na—O4—C10	4.0(6)	O3—Na—O4—C11	142.8(7)
O5—Na—O4—C10	−142.8(7)	O5—Na—O4—C11	−4.0(5)
O6—Na—O4—C10	158.4(8)	O6—Na—O4—C11	−62.8(6)
O7—Na—O4—C10	94.8(7)	O7—Na—O4—C11	−126.4(7)
O8—Na—O4—C10	62.4(6)	O8—Na—O4—C11	−158.7(7)
O1—Na—O5—C12	−129.4(6)	O1—Na—O5—C13	96.5(6)
O2—Na—O5—C12	−66.2(6)	O2—Na—O5—C13	159.8(7)
O3—Na—O5—C12	−5.2(5)	O3—Na—O5—C13	−139.2(7)
O4—Na—O5—C12	31.1(5)	O4—Na—O5—C13	−102.9(6)
O6—Na—O5—C12	139.4(7)	O6—Na—O5—C13	5.4(5)
O7—Na—O5—C12	97.4(6)	O7—Na—O5—C13	−36.6(5)
O8—Na—O5—C12	174.7(7)	O8—Na—O5—C13	40.7(5)
O1—Na—O6—C18	−76.6(6)	O1—Na—O6—C19	157.0(7)
O2—Na—O6—C18	−23.8(5)	O2—Na—O6—C19	−150.2(7)
O3—Na—O6—C18	133.1(6)	O3—Na—O6—C19	6.7(5)
O4—Na—O6—C18	83.8(6)	O4—Na—O6—C19	−42.6(5)
O5—Na—O6—C18	23.4(5)	O5—Na—O6—C19	−103.0(6)
O7—Na—O6—C18	161.2(7)	O7—Na—O6—C19	34.8(5)
O8—Na—O6—C18	−139.8(6)	O8—Na—O6—C19	93.8(6)
O1—Na—O7—C20	−84.5(6)	O1—Na—O7—C21	52.2(7)
O2—Na—O7—C20	−177.2(8)	O2—Na—O7—C21	−40.4(6)
O3—Na—O7—C20	162.5(8)	O3—Na—O7—C21	−60.7(7)
O4—Na—O7—C20	96.2(7)	O4—Na—O7—C21	−127.0(8)
O5—Na—O7—C20	38.3(6)	O5—Na—O7—C21	175.0(8)
O6—Na—O7—C20	−3.2(5)	O6—Na—O7—C21	133.5(8)
O8—Na—O7—C20	−108.5(7)	O8—Na—O7—C21	28.3(6)
O1—Na—O8—C22	−158.5(9)	O1—Na—O8—C23	−41.2(8)
O2—Na—O8—C22	150.9(9)	O2—Na—O8—C23	−91.8(9)
O3—Na—O8—C22	86.5(8)	O3—Na—O8—C23	−156.2(10)
O4—Na—O8—C22	35.2(7)	O4—Na—O8—C23	152.6(10)
O5—Na—O8—C22	−93.4(8)	O5—Na—O8—C23	23.9(7)
O6—Na—O8—C22	−62.1(8)	O6—Na—O8—C23	55.2(8)
O7—Na—O8—C22	−1.3(7)	O7—Na—O8—C23	116.1(9)
Na—O1—C1—C2	−29.1(5)	Na—O1—C1—C6	−149.1(10)
C24—O1—C1—C2	−169.4(13)	C24—O1—C1—C6	70.5(10)
Na—O1—C24—C23	1.9(7)	C1—O1—C24—C23	145.6(15)
Na—O2—C2—C1	−53.1(6)	Na—O2—C2—C3	73.2(7)
C7—O2—C2—C1	73.0(9)	C7—O2—C2—C3	−160.7(12)
Na—O2—C7—C8	−58.6(7)	C2—O2—C7—C8	172.7(13)
Na—O3—C8—C7	−38.8(6)	C9—O3—C8—C7	−163.8(14)
Na—O3—C9—C10	−55.6(7)	C8—O3—C9—C10	72.9(10)

Can. J. Chem. Downloaded from www.nrcresearchpress.com by 217.78.4.112 on 09/08/12
For personal use only.

TABLE 2 (*concluded*)

Na—O4—C10—C9	−30.6(6)	C11—O4—C10—C9	−170.4(13)
Na—O4—C11—C12	−23.2(5)	C10—O4—C11—C12	117.6(11)
Na—O5—C12—C11	−59.0(6)	C13—O5—C12—C11	78.7(9)
Na—O5—C13—C14	−150.2(9)	Na—O5—C13—C18	−29.7(5)
C12—O5—C13—C14	79.3(9)	C12—O5—C13—C18	−160.2(11)
Na—O6—C18—C13	−48.9(5)	Na—O6—C18—C17	73.4(6)
C19—O6—C18—C13	72.3(8)	C19—O6—C18—C17	−165.5(11)
Na—O6—C19—C20	−64.2(6)	C18—O6—C19—C20	169.6(12)
Na—O7—C20—C19	−26.9(5)	C21—O7—C20—C19	−162.7(13)
Na—O7—C21—C22	−60.5(9)	C20—O7—C21—C22	78.5(12)
Na—O8—C22—C21	−27.0(8)	C23—O8—C22—C21	−138.4(18)
Na—O8—C23—C24	63.1(9)	C22—O8—C23—C24	−176.0(17)
O1—C1—C2—O2	52.0(7)	O1—C1—C2—C3	−70.6(9)
C6—C1—C2—O2	173.3(14)	C6—C1—C2—C3	50.7(8)
O1—C1—C6—C5	65.5(9)	C2—C1—C6—C5	−52.3(9)
O2—C2—C3—C4	−176.2(14)	C1—C2—C3—C4	−52.3(9)
C2—C3—C4—C5	55.5(9)	C3—C4—C5—C6	−59.0(9)
C4—C5—C6—C1	56.8(9)	O2—C7—C8—O3	66.1(9)
O3—C9—C10—O4	58.5(8)	O4—C11—C12—O5	57.1(7)
O5—C13—C14—C15	64.7(8)	C18—C13—C14—C15	−54.2(8)
O5—C13—C18—O6	50.3(6)	O5—C13—C18—C17	−69.2(8)
C14—C13—C18—O6	173.1(13)	C14—C13—C18—C17	53.7(8)
C13—C14—C15—C16	56.6(8)	C14—C15—C16—C17	−56.8(8)
C15—C16—C17—C18	55.8(8)	C16—C17—C18—O6	−177.8(13)
C16—C17—C18—C13	−55.4(8)	O6—C19—C20—O7	62.0(8)
O7—C21—C22—O8	57.1(10)	O8—C23—C24—O1	−49.9(9)

TABLE 3. ^{13}C NMR chemical shifts (ppm from TMS ∓ 0.01)[a]

Carbon	**1** (303 K)	**1** (240 K)
1	76.01	(69.75)[d]
2	76.01	(78.17)[c]
3	27.32	(27.08)[e]
4	22.11	23.87
5	22.11	18.75
6	27.32	(25.58)[f]
7	(67.88)[b]	(66.27)[g]
8	(68.23)[b]	(66.67)[g]
9	66.62	(64.81)[g]
10	66.62	(65.91)[g]
11	(68.23)[b]	(67.10)[g]
12	(67.88)[b]	(66.67)[g]
13	76.01	(70.68)[d]
14	27.32	(25.35)[f]
15	22.11	18.75
16	22.11	23.87
17	27.32	(26.74)[e]
18	76.01	(78.45)[c]
19	(67.88)[b]	(66.27)[g]
20	(68.23)[b]	(67.43)[g]
21	66.62	(65.34)[g]
22	66.62	(65.47)[g]
23	(68.23)[b]	(66.67)[g]
24	(67.88)[b]	(66.27)[g]

[a]0.05 M in CD_2Cl_2 solution.
[b-h]Denote possible interchange of assignments.

TABLE 4. Crystal data for **1**

Empirical formula	$NaClO_{12}C_{24}H_{44}$
Formula weight	583.04
Crystal shape	plate
Crystal dimensions	0.3 × 0.2 × 0.4
Crystal system	Monoclinic
No. reflections used for unit cell dimension (2θ range)	25 40,47
Lattice parameters	a = 13,214 b = 13.821 c = 15.830 β = 94.06
Space group	$P21/n$
Z value	4
D_{calc}	1.343 mg/cm^{-3}
$F(000)$	1249.23
μ	0.20
No. of reflections measured	4480
No. of reflections unique	4273
No. of reflections observed	1986
No. of atoms	82
No. of variables	343
R_f (sign. refl.)	0.077
R_w (sign. refl.)	0.039
R_f (all refl.)	0.176
R_w (all refl.)	0.040
Goodness of fit	3.51
Last difference Fourier map	
max peak	0.410
min peak	−0.360

Can. J. Chem. Downloaded from www.nrcresearchpress.com by 217.78.4.112 on 09/08/12
For personal use only.

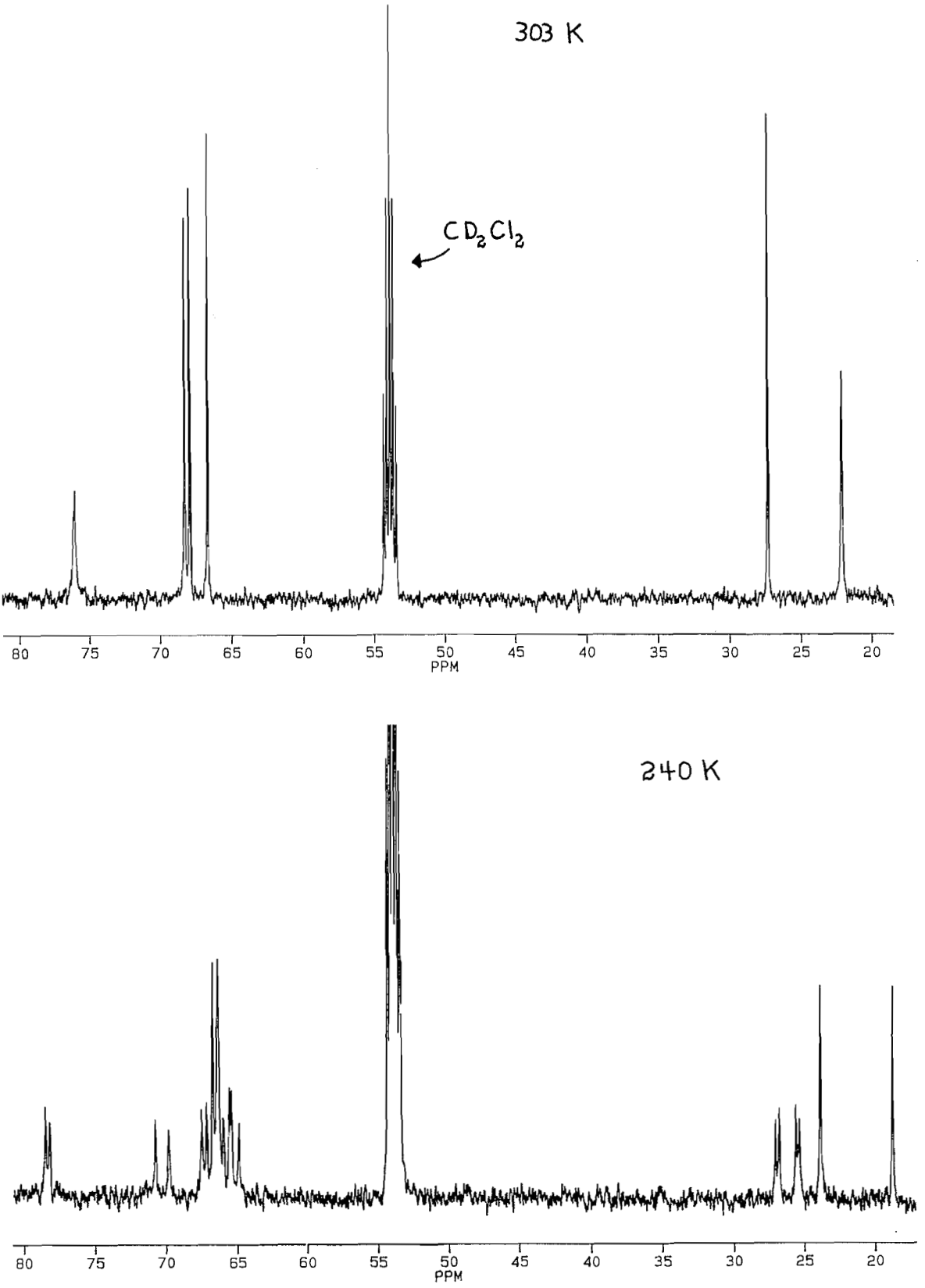

FIG. 3. 125.76 MHz ^{13}C NMR spectra of **1** at 303 and 240 K.

Can. J. Chem. Downloaded from www.nrcresearchpress.com by 217.78.4.112 on 09/08/12
For personal use only.

TABLE 5. Atomic parameters x, y, z and B_{iso} for **1**; esds refer to the last digit printed

Atom	x	y	z	B_{iso}[a]
Na	0.49479(24)	0.2492(3)	0.13199(21)	4.12(19)
Cl1	−0.0311 (3)	0.2697(3)	0.2174 (3)	6.73(21)
O1	0.3846 (4)	0.3716(5)	0.2074 (4)	4.9 (4)
O2	0.5811 (4)	0.4080(4)	0.1793 (4)	3.9 (3)
O3	0.5891 (4)	0.3315(5)	0.0176 (4)	4.9 (4)
O4	0.6576 (4)	0.1592(5)	0.0956 (4)	5.3 (4)
O5	0.5881 (4)	0.1614(4)	0.2602 (3)	3.5 (3)
O6	0.4066 (4)	0.0941(4)	0.1863 (4)	3.8 (3)
O7	0.4189 (5)	0.1372(5)	0.0155 (4)	5.1 (4)
O8	0.3154 (6)	0.3073(6)	0.0450 (5)	8.0 (6)
O9	0.0528 (7)	0.3147(7)	0.2409 (7)	15.5 (8)
O10	−0.0272 (7)	0.2272(8)	0.1366 (5)	14.6 (9)
O11	−0.0499 (7)	0.1955(6)	0.2721 (5)	11.3 (7)
O12	−0.1165 (7)	0.3319(6)	0.2184 (7)	14.8 (9)
C1	0.4236 (8)	0.4649(7)	0.2339 (6)	4.6 (6)
C2	0.5371 (7)	0.4533(7)	0.2505 (6)	4.1 (6)
C3	0.5682 (7)	0.3949(6)	0.3286 (6)	4.3 (6)
C4	0.5190 (8)	0.4338(8)	0.4055 (6)	5.9 (7)
C5	0.4055 (9)	0.4387(8)	0.3900 (6)	5.9 (7)
C6	0.3759 (7)	0.5018(7)	0.3128 (7)	5.8 (6)
C7	0.5877 (7)	0.4674(7)	0.1065 (6)	5.5 (6)
C8	0.6472 (8)	0.4142(8)	0.0453 (6)	6.0 (7)
C9	0.6471 (8)	0.2590(9)	−0.0229 (6)	5.9 (7)
C10	0.7181 (7)	0.2020(8)	0.0367 (6)	5.6 (7)
C11	0.7153 (6)	0.1140(7)	0.1646 (6)	4.7 (6)
C12	0.6931 (6)	0.1632(7)	0.2454 (6)	4.4 (6)
C13	0.5527 (7)	0.0701(6)	0.2918 (6)	3.7 (5)
C14	0.5790 (7)	0.0563(7)	0.3853 (6)	5.0 (6)
C15	0.5261 (7)	0.1295(7)	0.4387 (5)	4.8 (6)
C16	0.4125 (7)	0.1283(7)	0.4218 (6)	4.9 (6)
C17	0.3826 (6)	0.1446(6)	0.3282 (6)	3.7 (5)
C18	0.4361 (7)	0.0704(6)	0.2728 (5)	3.6 (5)
C19	0.4275 (7)	0.0202(7)	0.1249 (6)	4.5 (6)
C20	0.3749 (7)	0.0492(8)	0.0401 (6)	5.3 (6)
C21	0.3579 (9)	0.1902(11)	−0.0501 (7)	8.3 (9)
C22	0.2766 (10)	0.2418(12)	−0.0214 (8)	10.5 (10)
C23	0.2543 (9)	0.3081(11)	0.1086 (8)	9.1 (9)
C24	0.2797 (8)	0.3721(9)	0.1742 (7)	7.4 (8)

[a] B_{iso} is the mean of the principal axes of the thermal ellipsoid.

303 K, the protons on the central carbons of the macrocycle, namely C-9, 10, 21, and 22 appear as a sharp singlet at 3.60 ppm. From the ^{1}J HETCOR experiment, these can be shown to correlate with the ^{13}C resonance at 66.62 ppm. By contrast, the protons on carbons 7, 8; 11, 12; 19, 20; and 23,24 give rise to complex AA′BB′ spin systems and extensive overlap is present even at 500 MHz, thereby precluding unambiguous assignment of the attached carbons.

As the temperature is lowered, decoalescence occurs, starting with the resonance for C-1, 2, 13, and 18 at 76.01 ppm. At 240 K, the limiting low-temperature spectrum is obtained wherein four resonances of approximately equal intensity are observed at 78.45, 78.17, 70.68, and 69.75 ppm. Based on well-documented trends of axial and equatorial substituent effects on oxygenated carbon chemical shifts (14, 15), one can attribute the most deshielded resonances to C-2 and C-18, i.e., the carbons bearing equatorial substituents. No unambiguous distinction between these, however, can be made, as is indicated in Table 3. The methine carbons bearing axial oxygen give rise to lines at 70.68 and 69.75 ppm, again with no distinction between C-1 and C-13 being possible at this time. The fact that four equally intense resonances are seen in the methine carbon region suggests that **1** exists at 240 K in a single conformation that lacks any symmetry elements.

The region of the spectrum (64.81–67.43 ppm) that contains the CH_2-O resonances shows eight resolved lines at 240 K in the ratio of 1:1:1:1:3:3:1:1 (high-field to low-field direction). The small chemical shift differences coupled with several instances of accidental chemical shift equivalence preclude any unambiguous assignment of resonances, but the pattern of relative intensities is consistent with the aforementioned conformational postulate. The cyclohexyl carbons β to oxygen show four resonances of approximately equal intensity in the range of 25.35–27.08 ppm at 240 K. This is also consistent with the notion of a single preferred asymmetric conformer at this temperature. The more deshielded pair are attributed to sites β to equatorial oxygen by analogy with earlier work (14, 15), although again no distinction between C-3 and C-17 is possible.

Can. J. Chem. Downloaded from www.nrcresearchpress.com by 217.78.4.112 on 09/08/12
For personal use only.

Finally, the cyclohexyl sites most remote from the oxygen show only two separate resonances at 240 K. The most shielded, at 18.75 ppm, is attributed to the C-5,15 pair, which are γ-*gauche* to axial oxygen and thus most shielded (13–15). The corresponding C-4,16 sites, being *trans*-γ to the equatorial oxygens, are deshielded by ca. 5 ppm. Apparently the shift differences between C-5 vs. C-15 and C-4 vs. C-16 are too small to be resolved even at 125 MHz.

From the coalescence temperature of this upfield resonance (278 K) and the limiting low-temperature chemical shift difference of 5.11 ppm (642.9 Hz), one can employ the Eyring equation to obtain a free energy of activation, $\Delta G^{\pm}$, for the conformational interconversion process. With a temperature uncertainty of ∓3 K, $\Delta G^{\pm}$ is calculated to be 51.0 ∓ 0.6 kJ/mol. This value is ca. 8 kJ/mol higher than that for cycylohexane ring inversion in *cis*-1,2-disubstituted cyclohexanes (16) and 4 kJ/mol higher than for K^+ complexes of related dicyclohexano-18-crown-6 systems (15). The enhanced value of $\Delta G^{\pm}$ here can be attributed to the rigidity imposed on the macrocyclic portion of the molecule due to the coordination of all eight oxygen atoms with the Na^+ ion. Since conformational reorganization of the macrocycle must accompany cyclohexane ring reversal, any factors that retard the flexibility of the 24-membered ring will also retard the rate of chair–chair interconversion of the cyclohexyl moieties.

Experimental

(i) Materials

Dibenzo-24-crown-8 ether (**2**) was purchased from the Aldrich Chemical Co. Hydrogenation of **2** was accomplished using an American Instrument Co. 50 000 psi (1 psi = 6.9 kPa) maximum pressure high-pressure apparatus. In 60 mL of distilled 1-butanol, 1.0 g (0.0022 mol) of **2** and 0.75 g of 5% ruthenium on alumina catalyst were dissolved. A pressure of 1000 psi was used and the reaction was continued for 16 h at a temperature of 100°C. The catalyst was removed via filtration and the butanol by rotary evaporation at 70°C to yield 0.9 g of a yellow-brown oil. From ^{13}C NMR there appeared to be two configurational isomers present in the ratio of ca. 3:1. Column chromatography of the crude product using activated silica gel of mesh size 100–200 and a mixture of 25% hexane, 25% dichloromethane, and 50% diethyl ether afforded 0.1 g of an oil as the first fraction eluted. This material was deemed to be at least 90% pure by ^{13}C NMR, with characteristic resonances at 78.53, 71.64, 71.56, 69.07, 28.57, and 23.02 ppm. An equimolar amount of this material and $NaClO_4$ were dissolved in a minimum amount of dry ethanol. After allowing the mixture to stand for 3 h, the solvent was removed by rotary evaporation. Recrystallization from hexane – methylene chloride solvent pair yielded **1**, mp. 165–166°C.

(ii) Crystallographic measurements and structure solution

In Table 4 are collected the complete set of crystal data for **1**. A single crystal of **1** was mounted on a glass capillary and studied at 23°C on a Rigaku diffractometer with MoKα radiation. Cell constants and an orientation matrix for data collection were obtained from a least-squares refinement using the setting angles of 25 reflections in the range $40 < 2\theta < 47$ corresponding to a monoclinic cell of dimensions as described in Table 4. Based on systematic absences the space group was determined to be $P21/n$. A total of 4480 reflections were collected. The unique data set contains only 4273 reflections. The standards were measured after every 150 reflections and no crystal decay was noticed. Data were corrected for Lorentz and polarization effects (17).

The structure was solved by direct methods. All the atoms were refined anisotropically except hydrogen. The hydrogen atom positions were calculated but not refined. Weights based on counting statistics were used and all calculations were performed using the NRCVAX crystallographic software package (18).

(iii) ^{13}C NMR spectra

The ^{13}C NMR spectra at 125.76 MHz were obtained on a Bruker AM-500 spectrometer under conditions of complete ^1H noise decoupling. The sample was at a concentration of 0.05 M in CD_2Cl_2 solution. Typical sweep width was 10 000 Hz, and acquisition time 1.6 s with 32 K data points, with a pulse delay of 1 s. Line broadening was 2.0 Hz. With 45° observed pulses under these conditions, satisfactory signal-to-noise ratios were obtained at 240 K after 200 accumulations. Temperatures are deemed accurate to ∓3° and chemical shifts are referenced to internal TMS.

Acknowledgements

G.W.B. thanks the Natural Sciences and Engineering Research Council of Canada (NSERC) for continuing financial support via operating grants. We thank Dr. B. Blackwell and J. Nikiforuk of Agriculture Canada for access to the 500 MHz system.

1. C. J. Pedersen. J. Am. Chem. Soc. **89**, 7017 (1967).
2. S. Z. Kusov, E. G. Lubenets, V. A. Semikolenov, and V. S. Kobrin. Izv. Sib. Otd. Akad. Nauk SSSR Ser. Khim. Nauk. **4**, 62 (1989).
3. G. W. Buchanan, M. Z. Khan, J. A. Ripmeester, J. W. Bovenkamp, and A. Rodrigue. Can. J. Chem. **65**, 2564 (1987).
4. G. W. Buchanan, R. A. Kirby, and J. P. Charland. J. Am. Chem. Soc. **110**, 2477 (1988).
5. G. W. Buchanan, R. A. Kirby, and J. P. Charland. Can. J. Chem. **68**, 49 (1990).
6. G. W. Buchanan, R. A. Kirby, J. P. Charland, and C. I. Ratcliffe. J. Org. Chem. **56**, 203 (1991).
7. G. W. Buchanan, S. Mathias, Y. Lear, and C. Bensmon. Can. J. Chem. **69**, 404 (1991).
8. D. L. Hughes. J. Chem. Soc. Dalton Trans. 2374 (1975).
9. M. Dobler, J. D. Dunitz, and P. Seiler. Acta Cryst. Sect. B: Struct. Crystallogr. Cryst. Chem. **B30**, 2741 (1974).
10. F. P. Boer, M. A. Neuman, F. P. van Remoortere, and E. C. Steiner. Inorg. Chem. **13**, 2826 (1974).
11. A. C. Coxon, D. A. Laidler, R. B. Pettman, and J. F. Stoddart. J. Am. Chem. Soc. **100**, 8260 (1978).
12. S. L. Patt and J. N. Shoolery. J. Magn. Reson. **46**, 535 (1982).
13. H.-J. Schneider and V. Hoppen. Tetrahedron Lett. 579 (1974).
14. N. K. Wilson and J. B. Stothers. Top. Stereochem. **8**, 1 (1973).
15. G. W. Buchanan, K. Bourque, J. W. Bovenkamp, A. Rodrigue, and R. A. B. Bannard. Tetrahedron Lett. **25**, 3963 (1984).
16. S. Wolfe and J. R. Campbell. Chem. Commun. 874 (1967).
17. D. F. Grant and E. J. Gabe. J. Appl. Crystallogr. **11**, 14 (1978).
18. E. J. Gabe, F. L. Lee, and Y. Lepage. J. Appl. Crystallogr. **22**, 384 (1989).

Can. J. Chem. Downloaded from www.nrcresearchpress.com by 217.78.4.112 on 09/08/12
For personal use only.

The duodecet rule: Part 3. Fluoro species of the third period elements

E. A. ROBINSON

Department of Chemistry and the J. T. Wilson Research Laboratories, Erindale College, University of Toronto, Mississauga, Ont., Canada L5L 1C6

Received July 29, 1991

This paper is dedicated to the memory of Professor Thomas Birchall

E. A. ROBINSON. Can. J. Chem. **70**, 1696 (1992).

On the basis of the suggested new value of 54 pm for the single bond covalent radius of fluorine, the previously established *duodecet rule* for period 3 elements in molecular species with highly electronegative ligands is extended to fluorides. It is shown, for species such as SiF_4, $(F_3Si)_2O$, F_3SiNH_2, F_3PO, and PF_5, that the observed bond lengths are consistent with significant partial double bonding involving all the ligands, including fluorine, and with a total of six electron pairs in the valence shell of the central atom. Empirical rules based on d/d_1, the ratio of an observed bond length to the corresponding single bond length calculated from the sum of covalent radii, are developed as a simple approximate guide to the extent of partial double bonding in bonds to third period elements. It is also shown that bond lengths in species such as Al_2F_6, AlO_4^{5-}, and $Al(NH_2)_4^-$ are consistent with a duodecet rule.

E. A. ROBINSON. Can. J. Chem. **70**, 1696 (1992).

En se basant sur la nouvelle valeur de 54 pm pour le rayon covalent d'une liaison simple du fluor, on a étendu au fluor la règle du duodécet établie antérieurement pour les éléments de la période 3 dans des espèces moléculaires comportant des ligands fortement électronégatifs. Pour les espèces comme SiF_4, $(F_3Si)_2O$, F_3SiNH_2, F_3PO et PF_5, on montre que les longueurs de liaisons observées sont en accord avec la présence d'une double liaison partielle importante impliquant tous les ligands, y compris le fluor, et un total de six paires d'électrons dans la couche de valence de l'atome central. On a développé les règles empiriques basées sur d/d_1, le rapport d'une longueur de liaison observée sur la longueur de la simple liaison correspondante calculée à partir de la somme des rayons covalents, comme guide approximatif simple de l'étendue de la double liaison partielle dans les éléments de la troisième période. On montre aussi que les longueurs de liaison dans des espèces comme Al_2F_6, AlO_4^{5-} et $Al(NH_2)_4^-$ sont en accord avec une règle du duodécet.

[Traduit par la rédaction]

Can. J. Chem. Downloaded from www.nrcresearchpress.com by 217.78.4.112 on 09/08/12
For personal use only.

Introduction

In previous papers, by combining linear relationships between log d and log k, and bond order, n, and k, where d is the observed length of a bond, k is its stretching force constant, and n is defined as the average number of electron pairs per bond, we estimated bond orders, n, from the observed bond lengths in many group 3 species (2). While the bond length – force constant relationships are established entirely on the basis of experimental results, the bond order – force constant relationships are based on the judicious choice of appropriate force constants for a minimum of at least two bonds of assumed order, most conveniently a single bond and a double bond. Justification for our choice was given previously (2). These calculations demonstrated that for a large number of species containing Si—O, P—O, S—O, Cl—O, Si—N, P—N, S—N, and S—C bonds, the calculated *total* bond order of all the bonds to the central atom was close to 6 when there are no unshared electron pairs in the valence shell of the central atom, as in Si(IV), P(V), S(VI), and Cl(VII) species. In other words, the structures are consistent with a *duodecet rule* rather than the octet rule.

This result is consistent with the generalized valence bond description proposed by Messmer (3), in contrast to the molecular orbital description of Reed and Schleyer (4), which gives a description of the bonding in isoelectronic species such as F_3PO, SO_4^{2-}, and SO_2Cl_2 in terms of four polar σ-bonds and partial π-bonding due to strong $n \rightarrow \sigma^*$ negative hyperconjugation as a consequence of donation of ligand lone pairs into the σ-antiboding orbitals concentrated between the central atom and adjacent ligands.

We noted previously (2), that a duodecet rule is consistent with the occurrence of species such as AlF_6^{3-}, SiF_6^{2-}, PF_6^-, SF_6, and $:ClF_5$. We also drew attention to the great variation in, for example, P—F bond lengths in a variety of P(V) and P(III) species, but were unable to further analyze X—F bond lengths because there was uncertainty about what length to assign to a single X—F bond. Single bond lengths calculated using either Pauling's value of 64 pm for the covalent radius of F, or half the bond length in the F_2 molecule of 72 pm, and other standard single bond covalent radii are much longer than those observed for the majority of fluoro species (Table 1). Recently, we proposed the new value of 54 pm for the covalent single bond radius of fluorine (1), which clears up many of the difficulties previously encountered in the interpretation of X—F bond lengths (Table 1) and enables observed bond lengths to fluorine to be discussed systematically.

Results and discussion

We have previously shown that the Douglas–Clark linear log d/log k relationship,

$$\log k_{XY} + A \log d_{XY} = \text{constant}$$

where k_{XY} is the stretching force constant of a bond XY of length d_{XY}, and A is a constant (5), is valid for many bond types (2), and that by combining it with our linear bond order, n_{XY}, force constant, k_{XY}, relationship (6),

$$n_{XY} = B_{XY} + \text{constant}$$

where B is a constant, correlations between bond lengths and bond orders can be obtained for a number of bond types. Unfortunately, it has previously not been possible to apply this approach to all bonds of interest because of the lack of

TABLE 1. Some observed and predicted normal X—F single bond lengths

X—F bond	d_{X-F}	r_X cov[a]	d_{X-F} (pred) (pm)			Δ (pm)[b]			Ref.
			[c]	[d]	[e]	[c]	[d]	[e]	
B—F	141	86	158	150	140	+17	+9	−1	[f]
C—F	132	77	149	141	131	+17	+9	−1	[g]
N—F	126	70	142	134	124	+20	+12	−2	[h]
Al—F	181	126	198	190	180	+17	+9	−1	[i]
Si—F	171	117	189	181	171	+18	+10	0	[j]
P—F	164	110	182	174	164	+18	+10	0	[k]
S—F	156	104	176	168	158	+20	+12	+2	[l]
Cl—F	156	99	171	163	153	+15	+7	−3	[m]
Ga—F	178	125	197	189	179	+19	+11	+1	[n]
Ge—F	175	122	194	186	176	+19	+11	+1	[o]
As—F	176	122	194	186	176	+18	+10	0	[p]
Se—F	169	116	188	180	170	+19	+11	+1	[q]
Br—F	170	114	186	178	168	+16	+8	−2	[r]

[a] r_X = covalent radius of X.
[b] Difference between d_{X-F} (predicted) and d_{X-F} (observed).
[c] r_F (covalent radius of F) = 72 pm.
[d] r_F = 64 pm.
[e] r_F = 54 pm.
[f] 140.6 pm in NH_4BF_4 and 141 pm in $NaBF_4$ (ref. 8).
[g] 132.0 pm in CF_4. Tables of interatomic distances. Edited by L. Sutton. Chem. Soc. Special Pub. Nos. 11 and 18.
[h] (1) 130 pm in $NF_4^+BF_4^-$ (ref. 9); (2) 122 pm in $N_2F^+AsF_6^-$ (ref. 17).
[i] (1) 181 pm in Na_3AlF_6 (ref. 18); (2) 181.2(3) pm in $[(CH_3)_2AlF]_4$ (ref. 19); (3) 181 pm (avg.) in linked AlF_6 octahedra in $Hg_2AlF_5 \cdot 2H_2O$ (ref. 20); (4) 178.2 pm in $K[Me_3Al—F—AlMe_3]$ (ref. 21); (5) 182 pm (avg.) in AlO_4F_2 octahedra in $[Sr_2Al_2F_8(OH)_2] \cdot 2H_2O$ (ref. 22).
[j] 171 pm in M_2SiF_6 (M = Cs, K, NH_4, Rb, Tl) (ref. 23).
[k] (1) 163.0 pm in $PO_2F_2^-$ (ref. 24); (2) 163.8 pm in $(C_6H_5)_3PF_2$ (ref. 25); (3) 164 pm (avg.) in $NaPF_6 \cdot H_2O$ (ref. 26).
[l] (1) 156.2 pm in SF_6. H. Kelly and M. Fink (ref. 27); (2) 156.0 (avg.) in $(SF_5)_2O$ (ref. 28); (3) 156.5 pm (avg.) in SOF_4 (ref. 29).
[m] (1) 157 pm for axial bond in ClF_5 (ref. 12, p. 151); (2) 158 pm in $ClF_2^+SbF_6^-$ (ref. 10); (3) 156.6 pm in $ClF_2^+RuF_6^-$ Inorg. Chem. **30**, (ref. 30); (4) 154.1 pm in $ClF_2^+AsCl_6^-$ (ref. 31).
[n] (1) 190 pm (avg.) in $LiMnGaF_6$ (ref. 32); (2) 177.5 pm in GaF (ref. 33).
[o] (1) 177 pm in Rb_2GeF_6 (ref. 34); (2) 176 pm (avg.) in GeF_6 octahedra in Ge_5F_{12} (ref. 35); (3) 174 pm in $[Co(H_2O)_6]GeF_6$ (ref. 36).
[p] (1) 177 pm in $C_5H_6N^+AsF_6^-$. (ref. 8); (2) 180(5) in $KAsF_6$ (ref. 37); (3) 171.9(3) in $KAsF_6$ (ref. 38); (4) 172 pm in $HON(CH_2)CF_3^+AsF_6^-$ (ref. 39); (5) 173 pm (avg.) in $H_3O^+AsF_6^-$ (ref. 40); (6) 176 pm (avg.) in $(Cs^+)_2(F_5As)_2O^{2-}$ (ref. 41).
[q] (1) 168.4 pm in SeF_6 (ref. 42); (2) 173 pm (avg.) in SeF_4 (ref. 43); (3) 167.4 pm (avg.) in $(F_5Se)_2O$ (ref. 44).
[r] (1) 168.9(4) pm for axial bond in BrF_5 (ref. 45); (2) 171.8(10) pm in BrO_3F (ref. 46); (3) 169 pm in $BrF_2^+SbF_6^-$ (ref. 10).

TABLE 2. Constancy of d/d_1 ratios for bonds of the same bond order[a]

Bond order	BN	CC	CN	CO	NN	NO	SiX	PX	SX	ClX
$1\frac{1}{3}$	—	0.92	0.91	0.92	—	—	0.92	0.92	0.92	0.92
$1\frac{1}{2}$	—	—	—	—	—	—	0.90	0.90	0.90	0.90
$1\frac{2}{3}$	—	—	—	—	—	—	0.88	0.88	0.88	0.88
2	0.86	0.87	0.87	0.85	0.88	0.85	0.86	0.85	0.85	0.84
3	0.80	0.78	0.79	0.79	0.79	0.79	0.81	0.79	0.79	0.78

[a] See ref. 1 and Table 11.

comprehensive stretching force constant data. However, it has been apparent from our work that most X—Y bonds of the same bond order have very similar values of the ratio d/d_1, where d is an observed bond length and d_1 is the single bond length calculated from the sum of the single bond covalent radii of X and Y, provided the Y atoms are from the same period (1, 2). This is illustrated in Table 2. Thus, it seems reasonable to extrapolate some of the relationships already established, for example those for X—O bonds, to X—N, X—C, and X—F bonds. In this paper we present some bond orders calculated using this method. Standard single bond lengths are calculated from standard single bond

Can. J. Chem. Downloaded from www.nrcresearchpress.com by 217.78.4.112 on 09/08/12
For personal use only.

TABLE 3. Some species with standard single bond lengths[a]

Bond	Species	d_{XY} (pm)	Bond	Species	d_{XY} (pm)
S—O	$^{-}O_3S\text{-}ONH_3^{+}$	168	S—N	$^{-}O_3S\text{-}NH_3^{+}$	177
	$(F_5S\text{-}O)_2$	166		$(F_5S)_2NH$	168
	$(^{-}O_3S)_2O$	165		$(F_5S)_2NF$	169
	$HO\text{-}SO_3^{-}$	165	Si—O	[b]	177
	$F_5S\text{-}OF$	164	Si—N	[c]	186
C—S	$F_3C\text{-}SF_5$	186	Cl—O	$HO\text{-}ClO_3$	164
P—O	[d]	172		$(O_3Cl)_2O$	171
P—N	$H_3N^{+}\text{-}PO_3^{2-}$	180		Cl_2O	170

[a]For X—F bonds, see Table 1.
[b]Octahedrally coordinated Si in $Si_3O(PO_4)_6$.
[c]See ref. 47.
[d]In tris(*o*-phenylenedioxy)phosphate.

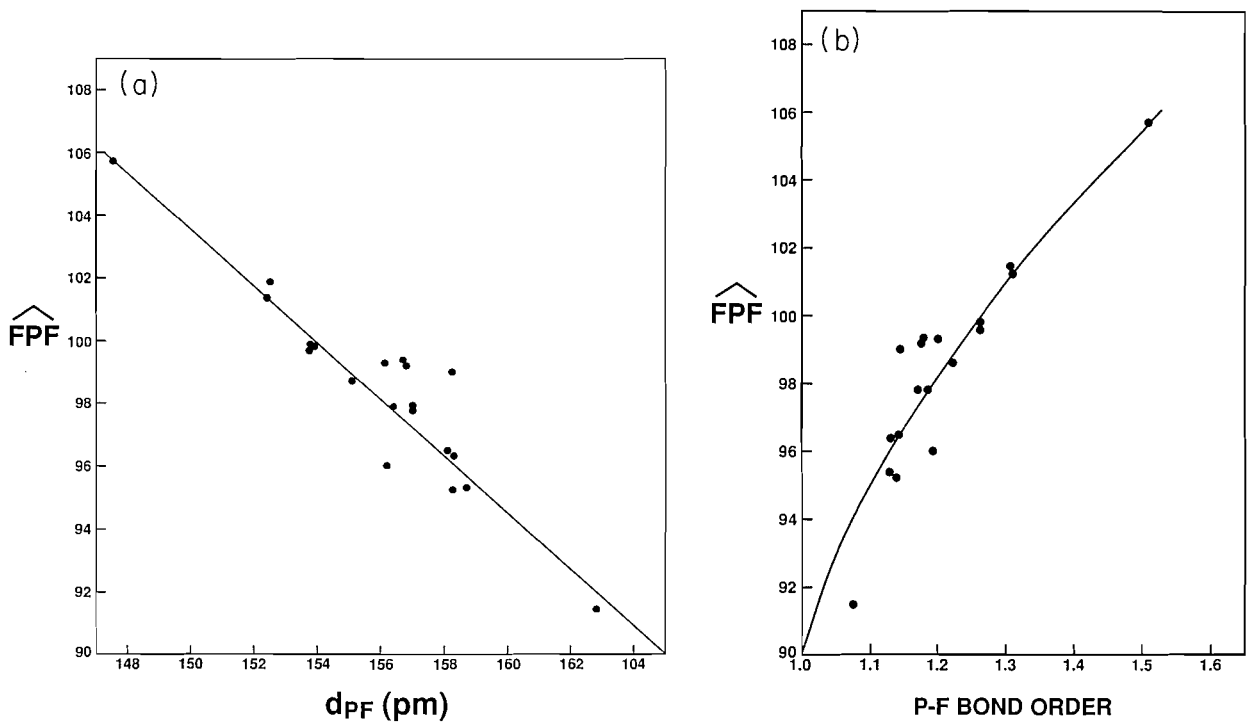

FIG. 1. (*a*) P—F bond length versus FPF bond angle; (*b*) P—F bond order versus FPF bond angle.

covalent radii, except that we use the values 62 pm, and 54 pm for the radii of O, and F, respectively.[1]

Phosphorus(V) and fluorophosphorus species

On the basis of a single bond length of (110 + 62) = 172 pm for a PO single bond, and our previous analysis of PO bonds (2), we obtain the relationship

$$n = 0.35\left(\frac{d}{d_1}\right)^{-8.0} + 0.65$$

and we assume that the same equation applies to P—N bonds (d_1 = 180 pm), and to P—F bonds (d_1 = 164 pm). The choice of these standard single bond lengths is amply justified by the observed bond lengths in species where it seems reasonable to assume that the bonds are normal single bonds (Table 3). Bond orders calculated using this equation are give in Table 4. In all cases the total bond order at the central P(V) atom is close to six. Similar calculation of bond orders for P—F bonds in some P(III) species are shown in Table 5, which also lists the observed FPF bond angles in a variety of fluorophosphorus species. PF bond length and PF bond order are plotted against ∠FPF in Fig. 1. There is a steady increase in bond angle with increasing PF bond order, and diminishing bond length, as might be anticipated and has been shown to be the case previously for, for example, S—O bonds (7). As has also been observed for the O . . . . O distance in SO_2 groups (7), the F . . . . F distance in PF_2 groups is approximately constant (at about 235 ± 2 pm), which undoubtedly warrants further investigation. For P(V) species, when ligands with atoms such as N, O, and F compete for partial lone electron pair delocalization onto a central phosphorus atom, the extent of lone pair delocalization decreases in the order of increasing electronegativity, N > O

[1]Based upon a correlation of electronegativity with covalent radius, 62 pm for r_O is consistent with 54 pm for r_F, 70 pm for r_N, and 77 pm for r_C, and with the data in Table 3 (E. A. Robinson, unpublished).

Can. J. Chem. Downloaded from www.nrcresearchpress.com by 217.78.4.112 on 09/08/12
For personal use only.

TABLE 4. Bond lengths, bond orders, and total bond orders at phosphorus for some P(V) species

Species	Bond Length, d (pm)[a]			d/d_1	Bond order, n	Σn[b]	Ref.
P_4O_{10}	PO	142.9	(1)	0.831	2.19	6.0	8
(cage)	POP	160.4	(3)	0.933	1.26		
P_4O_{10}	PO	149	(1)	0.866	1.75	6.0	8
(layer)	POP	156	(3)	0.907	1.41		
$(MeO)_3PO$	PO	147.7	(1)	0.859	1.83	5.9	48
	POC	158.0	(3)	0.919	1.34		
$P(OC_6H_5)_5$	PO	166.2	(2)	0.966	1.11	6.0	49
	PO	159.8	(3)	0.929	1.27		
$(HNPO_2^-)_3$	PO	149	(2)	0.866	1.75	6.0	8
	PN	168	(2)	0.933	1.26		
$(HNPO_2^-)_4$	PO	149.9	(2)	0.872	1.70	5.9	50
	PN	167.5	(2)	0.930	1.27		
$HN(PO_3^{2-})_2$	PO	152	(3)	0.884	1.59	6.0	8
	PN	168	(1)	0.933	1.26		
F_3PO	PO	143.6	(1)	0.835	2.13	6.0	51
	PF	152.4	(3)	0.929	1.28		
PF_5	PF	153.4	(3)	0.935	1.25	6.0	52
	PF	157.7	(2)	0.962	1.13		
$F_2PO_2^-$	PO	147.0	(2)	0.855	1.88	6.0	8
	PF	157.5	(2)	0.960	1.13		
FPO_3^{2-}	PO	150.6	(3)	0.876	1.66	6.1	8
	PF	158.5	(1)	0.966	1.11		
$F_3P(NH_2)_2$	PN	164.4	(2)	0.913	1.37		
	PF	161.6	(2)	0.985	1.04	6.0	53
	PF	155.6	(1)	0.949	1.18		
$F_2P(NMe_2)_3$	PF	159.0	(2)	0.970	1.10	5.9	54
	PN	168.5	(3)	0.936	1.24		
$(F_2PN)_3$	PF	151	(2)	0.915	1.33	6.2	55
	PN	156	(2)	0.867	1.75		
	PF	154.8	(2)	0.938	1.21	5.6	56
	PN	158.6	(2)	0.881	1.61		
$F_2(H)PO$	PO	144	(1)	0.837	2.10		
	PF	154	(2)	0.939	1.23	5.6	57
	PH	—	(1)	—	(1.00)		
$S_3N_5PF_2$[c]	PF	149.9	(1)	0.914	1.37		
	PF	152.8	(1)	0.932	1.27	6.1	58
	PN	156.2	(2)	0.868	1.74		
$C_5H_5N \cdot PF_5$	PN	189.8	(1)	1.054	0.88		
	PF	159.4	(1)	0.972	1.09	6.1	59
	PF	160.7	(4)	0.980	1.06		
CF_3PF_4	PF	157.3	(2)	0.959	1.14		
	PF	153.7	(2)	0.937	1.24	5.8	60
	PC	188.1	(1)	(1.000)	1.00		
CH_3PF_4	PF	161.2	(2)	0.983	1.05		
	PF	154.3	(2)	0.941	1.22	5.7	61
	PC	179.8	(1)	0.961	1.13		

[a]Bond type, bond length, and number of bonds of this length.
[b]Total bond order at phosphorus.
[c]

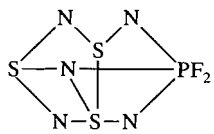

Can. J. Chem. Downloaded from www.nrcresearchpress.com by 217.78.4.112 on 09/08/12
For personal use only.

TABLE 5. Observed bond lengths and bond angles, and calculated bond orders for some fluorophosphorus species

Species	d_{PF} (pm)	Bond order, n	∠FPF(°)	Ref.
PF_3	157.0	1.14_6	97.8	62
OPF_3	152.4	1.27_9	101.3	63
RbF_2PO_2	156.2	1.16_7	96	64
HPF_2	158.2	1.11_7	99.0	65
$HP(O)F_2$	153.9	1.23_2	99.8	66
$F_2P\text{-}PF_2$	158.7	1.10_5	99.1	67
$F_2P\text{-}O\text{-}PF_2$	156.8	1.15_1	99.2	68
$POF_3 \cdot 2SbF_5$	147.5	1.46_7	105.7	69
$F_3P \cdot BH_3$	153.8	1.23_5	99.8	70
$Ni(PF_3)_4$	156.1	1.17_0	99.3	71
H_2NPF_2	158.3	1.10_4	95.3	72
Me_2NPF_2	162.8	1.02_1	91.5	72
$Me_2NPF_2 \cdot B_4H_8$	158.3	1.11_4	96.4	73
$F_3P \cdot B_4F_6$	152.5	1.27_6	101.5	74
F_3PS	153.8	1.23_5	99.6	75
HF_2PS	155.1	1.19_7	98.6	76
$(F_2PO)_3PO$	158.1	1.11_9	96.5	77
F_2PCN	157.0	1.14_6	97.9	78
F_2PCNO	156.4	1.16_2	97.9	79
F_2PNCS	156.7	1.15_4	99.4	79

> F. Moreover, for all the P(V) species, the calculated total bond order at phosphorus is found to be in the range 6.0 ± 0.1, in accord with the duodecet rule.[2] Although PF_4^+ salts have not yet been synthesized, the predicted bond length is close to 148 pm.

Silicon and fluorosilicon species

On the basis of a value of (62 + 117) = 179 pm for a single Si—O bond, our previous correlation for Si—O bonds (2) gives the equation

$$n = 0.30\left(\frac{d}{d_1}\right)^{-9.5} + 0.70$$

We will assume that the same equation also applies to Si—F bonds (d_1 = 171 pm), to Si—N bonds (d_1 = 187 pm), and to Si—C bonds (d_1 = 194 pm), (Table 3). Analysis of bond length data for some silicon species is shown in Table 6. In all cases the total bond order at silicon is close to six (average 5.9 ± 0.2).

Sulfur(VI) and fluorosulfur species

The calculated S—F single bond length is d_1 = (104 + 54) = 158 pm, and in most fluorosulfur species the S—F bond lengths are within 7% percent of this value (Table 7), compared to a variation of 10–11% for P—F bonds and Si—F bonds. Apparently lone pair delocalization from F to S is normally of lesser importance, consistent with the trend in which the extent of lone pair delocalization into an X—F bond diminishes with the increasing electronegativity of X, presumably as a consequence of the decreasing size of the valence shell of X with increasing electronegativity. Unlike SiF and PF species where bond lengths are always either equal or less than d_1, S—F bonds in molecules with lone pairs on sulfur, such as FSSF, NSF, and the axial bonds in SF_4 and $(CF_3)_2SF_2$ (Table 7), are anomalously long; there are more lone pairs, and the increased crowding in the valence shell of sulfur compared to that in Si or P lengthens the S—F bonds. Nevertheless, there are a few notably short S—F bond

[2]The calculated bond order is very sensitive to d/d_1. For most bonds an error of 1% in d/d_1 translates into a change in bond order of about 5%, or 0.2–0.3 for all the bonds to a central atom. Thus, a calculated total bond order of say 6.0 ± 0.2 may certainly be taken as consistent with a duodecet rule.

TABLE 6. Bond lengths, bond orders, and total bond orders at silicon for some Si(IV) species

Species	Bond length d (pm)[a]			d/d_1	Bond order, n	Σn[b]	Ref.
$(SiO_2)_n$	SiO	161	(4)	0.899	1.52	6.1	8
SiO_4^{4-}	SiO	162	(4)	0.905	1.47	5.9	8
$Si(OMe)_4$	SiO	161	(4)	0.899	1.52	6.1	80
$Si(CO_2Me)_4$	SiO	162.5	(4)	0.908	1.45	5.8	81
$HOSiO_3^{3-}$	SiO	162	(3)	0.905	1.47	5.7	82
	SiOH	168	(1)	0.938	1.25		
$(HO)_2SiO_2^{2-}$	SiO	160.1	(2)	0.894	1.57	5.7	83
	SiOH	166.5	(2)	0.934	1.27		
$(SiO_3^{2-})_n$	SiO	157	(2)	0.877	1.74	6.0	84
	SiOSi	168	(2)	0.938	1.25		
$Si_6O_{18}^{12-}$	SiO	159.3	(2)	0.890	1.61	5.9	85
	SiOSi	164.7	(2)	0.920	1.36		
SiF_4	SiF	155.5	(4)	0.909	1.44	5.8	86
	SiF	155.2	(4)	0.908	1.45	5.8	87
$(F_3Si)_2O$	SiF	155.6	(3)	0.910	1.44	6.0	88
	SiO	158.1	(1)	0.883	1.68		
F_3SiOMe	SiF	156.1	(3)	0.912	1.41	5.9	89
	SiO	158.1	(1)	0.883	1.67		
F_3SiNMe_2	SiF	156.9	(3)	0.918	1.38	5.8	90
	SiN	165.6	(1)	0.886	1.65		

[a]Bond type, bond length, and number of bonds of this length.
[b]Total bond order at silicon.

Can. J. Chem. Downloaded from www.nrcresearchpress.com by 217.78.4.112 on 09/08/12
For personal use only.

TABLE 7. Observed S—F bond lengths[a] (r = 158 pm)

Species	r_{SF} (pm)	Species	r_{SF} (pm)	Species	r_{SF} (pm)
$S{=}SF_2$	159.8	$F_3CN{=}SF_2$	158.3	$F_2S(O)NH_2$	154.9
SF_2	158.9	SF_4	164.6 154.5	$F_2S(O)NCl$	154.8
FS—SF	163.5	$(CF_3)_2SC_2$	168.1	F_4SO	159.6 153.3
$N{\equiv}S$-F	164.3	$F_3S{\equiv}N$	155.2	SF_6	156.1
F_2SO	158.7	F_2SO_2	153	SF_5Cl	158.8 156.6
$ClN{=}SF_2$	159.6	$FClSO_2$	155	$(F_5S)_2O$	157.2 155.5
CH_3OSO_2F	154.5	CH_3SO_2F	156.1	F_5SNF_2	156.0 154.6

[a]Data from ref. 91.

TABLE 8. Bond lengths, bond orders, and total bond orders at sulfur for some S(VI) species

Species	Bond length, d (pm)[a]			d/d_1	Bond order, n	Σn^b	Ref.
SO_4^{2-}	SO	149	(4)	0.898	1.50	6.0	8
$HOSO_3^-K^+$	SO	147	(3)	0.886	1.60	6.0	8
	SOH	156	(1)	0.940	1.24		
$H_3N^+SO_3^-$	SO	145	(3)	0.873	1.71	6.1	8
	SN	170	(1)	1.000	1.00		
$(HO)_2SO_2$	SO	142.2	(2)	0.857	1.88	6.2	91
	SOH	157.4	(2)	0.948	1.20		
SO_3	SO	141.8	(3)	0.855	1.90	5.7	92
S_3O_9	SO	142.8	(1)	0.860	1.84	6.3	93
	SO	136.7	(1)	0.823	2.32		
	SOS	162.6	(2)	0.980	1.07		
$(SO_3)_n$	SO	141	(2)	0.849	1.96	6.1	8
	SOS	161	(2)	0.970	1.10		
$(NH_2)_2SO_2$	SO	160	(2)	0.920	1.35	6.2	94
	SOS	144	(2)	0.867	1.76		
$(Me_2N)_2SO_2$	SN	165.1	(2)	0.949	1.19	6.0	91
	SO	143.2	(2)	0.863	1.81		
$:N(SO_3^-)_3$	SN	162.1	(1)	0.932	1.28	5.9	8
	SO	148.2	(3)	0.893	1.54		
F_2SO_2	SF	153.0	(2)	0.968	1.11	6.2	95
	SO	140.5	(2)	0.846	2.00		
F_4SO	SF	159.6	(2)	1.010	0.97		
	SF	153.3	(2)	0.968	1.11	6.2	19
	SO	140.5	(1)	0.846	2.00		
F_3SO^+	SF	145.5	(3)	0.921	1.34	6.3	96
	SO	137.0	(1)	0.825	2.29		
$HC(SO_2F)_3$	SF	155.8	(1)	0.986	1.04		
	SO	141.6	(2)	0.853	1.92	6.0	97
	SC	183.1	(1)	0.974	1.09		
ME_2SO_2	SC	177.1	(2)	0.952	1.18	5.9	98
	SO	143.5	(2)	0.864	1.79		
$F_3S{\equiv}N$	SF	155.2	(3)	0.982	1.06	5.7	99
	SN	141.6	(1)	0.814	2.47		

[a]Bond type, bond length, and number of bonds of this length.
[b]Total bond order at sulfur.

Can. J. Chem. Downloaded from www.nrcresearchpress.com by 217.78.4.112 on 09/08/12
For personal use only.

TABLE 9. Observed Cl=F bond lengths (d_1 = 153 pm)

Species	r_{ClF} (pm)		Ref.	Species	r_{ClF} (pm)	Ref.
ClF	162.8		100	$FClO_2$	169.7	10
ClF_3	159.8	(eq)	101	$ClF_2^+AsCl_6^-$	154	103
	169.8	(ax)				
ClF_5	167	(eq)	12	$ClF_2^+SbF_6^-$	158	10
	157	(ax)				
$FClO_3$	162.0		102	$ClF_2^+RuF_6^-$	156.6	104

TABLE 10. Bond lengths, bond orders, and total bond orders at chlorine for some Cl(VII) species

Species		Bond length, d(pm)[a]		d/d_1	Bond order, n	Σn[b]	Ref.
ClO_4^-	ClO	144	(4)	0.894	1.50	6.0	8
$HOClO_3$	ClO	140.8	(3)	0.875	1.65	6.0	105
	ClOH	163.5	(1)	1.016	(1.00)		
Cl_2O_7	ClO	140.6	(3)	0.873	1.67	6.0	106
	ClOCl	171.1	(1)	1.062	(1.00)		
$FClO_3$	ClO	140.5	(3)	0.872	1.67	6.0	107
	ClF	162.0	(1)	—	(1.00)		
[c]	ClO	139	(1)	0.863	1.75	6.1	108
	ClOM	145	(3)	0.900	1.46		
[d]	ClO	138	(2)	0.857	1.81	6.3	109
	ClOM	148	(2)	0.919	1.34		
[e] I	ClO	150.7	(1)	0.936	1.25		
	ClO	152.0	(1)	0.944	1.21	5.9	110
	ClOM	138.0	(1)	0.857	1.81		
	ClOM	140.8	(1)	0.875	1.65		
II	ClO	150.0	(1)	0.932	1.27		
	ClO	151.2	(1)	0.939	1.25	6.0	
	ClOM	139.2	(1)	0.865	1.74		
	ClOM	139.9	(1)	0.869	1.70		

[a]Bond type, bond length, and number of bonds of this length.
[b]Total bond order at chlorine.
[c]Tridentate ClO_4^- in $Ni(ClO_4)_3$.
[d]ClO_4 in

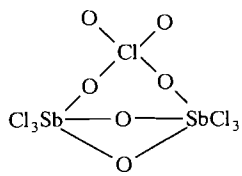

[e]Bidentate ClO_4^- in $Ti(ClO_4)_4$; two different ClO_4 groups, I and II.

TABLE 11. Calculated d/d_1 ratios for bonds of specific bond order

Bond order, n	Bond Si—X	Bond P—X	Bond S—X	Bond Cl—X	d/d_1 average
1.00	1.000	1.000	1.000	1.000	1.00
1.25	0.938	0.935	0.938	0.936	0.94
1.33	0.924	0.920	0.923	0.921	0.92
1.50	0.902	0.895	0.898	0.895	0.90
1.67	0.884	0.875	0.878	0.873	0.88
2.00	0.857	0.845	0.846	0.839	0.85
2.50	0.828	0.812	0.812	0.802	0.81
3.00	0.807	0.788	0.787	0.775	0.79

lengths, for example, in the ion OSF_3^+, and perhaps in molecules such as SO_2F_2 and the equatorial bonds in molecules such as SOF_4 (Table 7).

On the basis of d_1 (SO) = 166 pm and our previous correlation for SO bonds (2), we obtain

$$n = 0.41\left(\frac{d}{d_1}\right)^{-7.4} + 0.59$$

Assuming that this equation is also valid for S—C, S—N, and S—F bonds, with d_1(SC) = 186 (3), d_1(SN) = 174, d_1(SO) = 166, and d_1(SF) = 158 pm, some calculated bond orders are shown in Table 8. The average total bond order is 6.0 ± 0.05.

Can. J. Chem. Downloaded from www.nrcresearchpress.com by 217.78.4.112 on 09/08/12
For personal use only.

TABLE 12. Some presumed Al—O and Al—N single bond lengths

Species		d_{AlO} (pm)	Ref.
$Cs_2Al(NO_3)_5$[a]		189–193[b]	111
		198[b]	
$KAlO_2O_7$[a]		189	112
$AlPO_4 \cdot 2H_2O$[a]	AlO	186–189	113
(metavariscite)	AlOH	189–195	
Tris-tropolonato		188.4	114
aluminum[a]		189.0	
$Al[C_6(CO_2)_6] \cdot 16H_2O$[a]		186–190	115
$Sr_2Al_2F_8(OH)_2 \cdot 2H_2O$[c]	AlO	189–190	116
	AlF	180–183	

Species	d_{AlN} (pm)	Ref.
$(CH_3)_3N$-Al$(CH_3)_3$	210.2	117
$(CH_3)_3N$-AlH_3	206.6	118
Cl_3Al-NH_3	199.6	119
Cl_3Al-N$(CH_3)_3$	194.5	120
$\{Cl_2AlN(CH_3)_2\}_2$	196.1	121
$\{[(CH_3)_3Si]_2Al(NH_2)_2\}_3Al$	202.0	122
$Cs[(CH_3)_3Al]_2N_3$	200–203	123
$[(CH_3)_2Tl]$ $[(CH_3)_3$Al-NCS$]$	208	124
$I(CH_3)_2$Al-N$(CH_3)_3$	202	125
Br_3AlNH_3	199.7	126

[a]AlO_6 octahedra.
[b]Monodentate $AlONO_2$ (191 pm avg.) and bidentate AlO_2NO groups.
[c]Contains AlO_2F_4 octahedra.

Chlorine(VII) and fluorochlorine species

Because chlorine is the most electronegative of the third period elements, substantial crowding of electron pairs is anticipated in its valence shell and almost all Cl—F bond lengths are longer than the sum of the covalent single bond radii, $d_1 = (99 + 54) = 153$ pm (Table 9). Only $ClF_2^+AsF_6^-$ (10), and for the apical bond in ClF_5, does the ClF bond length have the single bond value (1). Based on the previous correlations for Cl—O bonds, with d_1(ClO) = 161 pm, we derive the correlation

$$n = 0.47\left(\frac{d}{d_1}\right)^{-6.5} + 0.53$$

Assuming that this equation is valid for both Cl—O and Cl—F bonds, some calculated bond orders are given in Table 10; the total bond order at Cl(VII) is close to six.

Extension to some aluminum species

Since a duodecet rule seems to be justified for Si(IV), P(V), S(VI), and Cl(VII) species with electronegative ligands, such as N, O, and F, we will now consider some aluminum species.

Table 11 shows that for third period central atoms, bonds to second period atoms with a particular bond order, n, have essentially the same bond length/single bond length ratio, d/d_1. We will assume that the average values given in Table 11 are also valid for calculating bond orders for AlF, AlO, and AlN bonds. The sum of the single bond covalent radii of Al and F is (126 + 54) = 180 pm, which is the observed bond length in the AlF_6^{3-} ion (11), and this same distance is found for the Al—F bond in a number of species with presumed single Al—F bonds (Table 12). In dimeric Al_2F_6, the terminal and bridge Al—F bonds have lengths 160 pm and 172 pm, respectively (12). Applying the simple rules developed above to Al_2F_6, we obtain the following results: Al—$F_{terminal}$, $d/d_1 = 0.88$, $n = 1.7$; Al—F_{bridge}, $d/d_1 = 0.94$, $n = 1.2_5$, for a total bond order at Al of 5.8, strongly suggesting that, in Al_2F_6, aluminum also obeys the duodecet rule.

For AlO bonds, the AlO bond length in βLi_5AlO_4 containing the AlO_5^{5-} ion is 172 pm (13), and in a number of substances containing AlO_6 octahedra the bond length is close to 190 pm (Table 12). Thus, the predicted value for an AlO bond of order $1^1/_2$ is (0.90 × 190) = 171 pm. Apparently AlO_4^{5-}, isoelectronic with SiO_4^{4-}, PO_4^{3-}, SO_4^{2-}, and ClO_4^-, also obeys the duodecet rule.

For Al—N bonds, taking r_1 as 200 pm (Table 12), the expected length of a bond of order $1^1/_2$ is 180 pm, which is to be compared with 178 pm observed in cyclic $[CH_3AlNR_2]_3$, where R is 2,6-isopropylphenyl (14), and 180 pm in $MAl(NH_2)_4$ salts (M^+ = Na^+, K^+, and Cs^+) (15); apparently Al in $Al(NH_2)_4^-$ obeys the duodecet rule. In lithium tetrakis(di-*tert*-butylmethyleneamino)aluminate, two of the AlN bonds have lengths of 187 pm, and the other two have lengths of 178 pm (16). The corresponding d/d_1 values of 0.93 and 0.89 give bond orders of approximately 1.3 and 1.6, for an estimated total bond order at aluminum of close to six.

Conclusions

An estimate of the extent of partial X—F double bonding in many fluorosilicon and fluorophosphorus species, and a few fluorosulfur species, provides support for the extension to them of a duodecet rule for the third period elements. Apparently, when the valence shell of X is formally incomplete, ligands containing atoms such as N, O, and F delocalize unshared electron pairs into the valence shell of X until it contains 12 electrons. When these ligands compete, the extent of lone pair delocalization decreases in the order of their increasing electronegativities; N > O > F. We have also demonstrated that consideration should be given to a duodecet rule in interpreting bond length data for some aluminum species. Despite the controversy surrounding the theoretical treatment of bonding in third period species (3, 4), there seems to be growing support for the empirical interpretation of bond lengths for many species formed by the elements of the third period in terms of a duodecet rule, rather than the octet rule.

Acknowledgments

Professor R. J. Gillespie of McMaster University is thanked for helpful discussion.

1. R. J. Gillespie and E. A. Robinson. Inorg. Chem. **31**, 1960 (1992).
2. E. A. Robinson. J. Mol. Struct. (Theochem), **186**, 9 (1989); **186**, 41 (1989).
3. R. P. Messmer, J. Am. Chem. Soc. **113**, 433, (1991).
4. A. E. Reed and P. v. R. Schleyer, J. Am. Chem. Soc. **112**, 1434, (1990).
5. C. H. Douglas-Clark. Philos. Mag. **18**, 459 (1934); **22**, 1137 (1936).
6. E. A. Robinson and M. W. Lister. Can. J. Chem. **41**, 2988 (1963).
7. R. J. Gillespie and E. A. Robinson. Can. J. Chem. **41**, 2074 (1963); I. Hargittai. The structure of volatile sulfur compounds. D. Reidel, Dordrecht. 1985. (*a*) p. 240; (*b*) p. 212.
8. A. F. Wells. Structural inorganic chemistry. 5th ed. Oxford University Press, 1984.

Can. J. Chem. Downloaded from www.nrcresearchpress.com by 217.78.4.112 on 09/08/12
For personal use only.

Can. J. Chem. Downloaded from www.nrcresearchpress.com by 217.78.4.112 on 09/08/12
For personal use only.

9. K. O. Christe, M. D. Lind, N. Thorup, D. R. Russell, J. Fawcett, and R. Bau. Inorg. Chem. **27**, 2450 (1988).
10. A. J. Edwards and K. O. Christe. J. Chem. Soc. Dalton Trans. 175 (1976).
11. S. Naray Szabo and K. Susvari. Z. Kristallogr. **99**, 27 (1938).
12. R. J. Gillespie and I. Hargittai. The VSEPR model of molecular geometry. Allyn and Bacon, Boston, Mass. 1991. p. 105.
13. F. Stewner and R. Hoppe, Z. Anorg. Chem. **381**, 91 (1971).
14. K. M. Waggoner, H. Hope, and P. P. Power. Angew. Chem. Int. Ed. Engl. **27**, 1699 (1988).
15. P. Molinie, R. Brec, J. Rouxel, and P. Herpin. Acta Crystallogr. Sect. B: Struct. Crystallogr. Cryst. Chem. **B29**, 925 (1973).
16. H. M. M. Shearer, R. Snaith, J. D. Sowerby, and K. Wade. J. Chem. Soc. Chem. Commun. 1275 (1971).
17. K. O. Christe, R. D. Wilson, W. W. Wilson, R. Bau, S. Sukumar, and D. A. Dixon. J. Am. Chem. Soc. **113**, 3795 (1991).
18. S. Naray Szabo and K. Susvari. Z. Kristallogr. **99**, 27 (1938).
19. G. Gundersen, T. Haugen, and A. J. Haaland. J. Organomet. Chem. **54**, 77 (1973).
20. R. S. Nohr, P. M. Kuznesof, K. J. Wynne, M. E. Kenney, and P. G. Siebenman. J. Am. Chem. Soc. **103**, 4371 (1981).
21. J. L. Atwood and W. R. Newberry. J. Organomet. Chem. **66**, 15 (1974).
22. Z. U. Puddovkina, N. M. Chemitsova, and Y. A. Pyatanko. J. Struct. Chem. **14**, 445 (1973).
23. J. Ketelaar. Z. Kristallogr. **92**, 155 (1935).
24. W. Granier, J. Durand, L. Cot, and J. L. Galigne. Acta Crystallogr. Sect. B: Struct. Crystallogr. Cryst. Chem. **B30**, 1565 (1975).
25. W. Sheldrick. Acta Crystallogr. Sect. B: Struct. Crystallogr. Cyrst. Chem. **B31**, 1776 (1975).
26. H. Bode and G. Teufer. Acta Crystallogr. **9**, 825 (1956).
27. H. Kelly and M. Fink. J. Chem. Phys. **77**, 1813 (1982).
28. H. Oberhammer and K. Seppelt. Angew. Chem. Int. Ed. Engl. **17**, 69 (1978); Inorg. Chem. **17**, 1435 (1978).
29. G. Gundersen and K. J. Hedberg. J. Chem. Phys. **51**, 2500 (1969).
30. R. Bougon, W. V. Cicha, M. Lance, L. Meublat, M. Nierlich, and J. Vigner. Inorg. Chem. **30**, 102 (1991).
31. H. Lynton and J. Passmore. Can. J. Chem. **49**, 2539 (1971).
32. W. Viebahn. Z. Anorg. Chem. **413**, 77 (1975).
33. R. F. Barrow, P. G. Dodsworth, and P. B. Zeeman. Proc. Phys. Soc. **70A**, 34 (1957).
34. W. B. Vincent and J. L. Hoard. J. Am. Chem. Soc. **64**, 1233 (1942).
35. J. C. Taylor and P. W. Wilson. J. Am. Chem. Soc. **95**, 1834 (1973).
36. T. S. Kodashova. Krystallografiya, **2**, 609 (1957).
37. J. A. Ibers. Acta Crystallogr. **9**, 967 (1956).
38. G. Gafner and G. J. Kruger. Acta Crystallogr. Sect. B: Struct. Crystallogr. Cryst. Chem. **B30**, 458 (1974).
39. R. Minkwitz, D. Bernstein, H. Bent, and P. Sartore. Inorg. Chem. **30**, 2157 (1991).
40. D. M. Mootz Wiebeke. Inorg. Chem. **25**, 3095 (1986).
41. W. Haase. Z. Anorg. Chem. **397**, 258 (1973).
42. L. Bartell and A. Jin. J. Mol. Struct. **118**, 47 (1984).
43. I. C. Bowater, R. D. Brown, and R. F. Burden. J. Mol. Spectrosc. **28**, 454 (1968).
44. H. Oberhammer and K. Seppelt. Inorg. Chem. **17**, 1435 (1978).
45. A. G. Robiette, R. H. Bradley, and P. N. Brier. J. Chem. Soc. Chem. Commun. 1567 (1971).
46. E. H. Appelman, B. Beigley, D. W. J. Cruickshank, A. Foord, S. Rustad, and V. Ulbrecht. J. Mol. Struct. **35**, 139 (1976).
47. H. Mayer. Monatsh. **105**, 46 (1974).
48. H. Oberhammer. Z. Naturforsch. A, **28**, 1140 (1973).
49. R. Sarma, F. Ramirez, B. McKeever, J. F. Maracek, and S. Lee. J. Am. Chem. Sco. **98**, 581 (1976).
50. B. Berking and D. Mootz. Acta Crystallogr. Sect B: Struct. Crystallogr. Cryst. Chem. **B27**, 740 (1971).
51. T. Moritani, K. Kuchitsu, and Y. Morino. Inorg. Chem. **10**, 344 (1971).
52. K. W. Hansen and L. S. Bartell. Inorg. Chem. **4**, 1775 (1965).
53. C. J. Marsden, K. Hedberg, J. M. Shreeve, and J. D. Gupta. Inorg. Chem. **23**, 3659 (1984).
54. H. Oberhammer and R. Schmultler. J. Chem. Soc. Dalton Trans. 1454 (1976).
55. N. N. Greenwood and A. Earnshaw. Chemistry of the elements. Pergamon Press, London. 1984.
56. M. I. Davis and J. W. Paul, Jr. J. Mol. Struct. **9**, 478 (1971).
57. L. F. Centotani and R. L. Kuczkowski. Inorg. Chem. **7**, 2582 (1968).
58. J. Weiss, I. Ruppert, and R. Appel. Z. Anorg. Chem. **406**, 329 (1974).
59. W. S. Sheldrick, J. Chem. Soc. Dalton Trans. 1402 (1974).
60. H. Oberhammer, J. Grobe, and D. LeVan. Inorg. Chem. **21**, 275 (1982).
61. L. Bartell and K. W. Hansen. Inorg. Chem. **4**, 1777 (1965).
62. Y. Morino, K. Kuchitsu, and T. Moritani. Inorg. Chem. **8**, 867 (1969).
63. T. Moritani, K. Kuchitsu, and Y. Morino. Inorg. Chem. **10**, 344 (1971).
64. W. Granier, J. Durand, L. Cot, and J. L. Galigne. Acta Crystallogr. Sect. B: Struct. Crystallogr. Cryst. Chem. **B31**, 2506 (1975).
65. R. L. Kuczkowski. J. Am. Chem. Soc. **90**, 1705 (1968).
66. L. F. Centofani and R. L. Kuczkowski. Inorg. Chem. **7**, 2582 (1968).
67. H. L. Hodges, L. S. Su, and L. S. Bartell. Inorg. Chem. **14**, 599 (1975).
68. D. E. J. Arnold and D. W. H. Rankin. J. Fluorine Chem. **2**, 405 (1973); Y. Y. Hsuikang, R. W. Rudolph, and L. S. Bartell. J. Mol. Struct. **28**, 205 (1975).
69. A. J. Edwards and K. I. Khallow. J. Chem. Soc. Dalton Trans. 2541 (1984).
70. R. L. Kuczkowski and D. R. Lide. J. Chem. Phys. **46**, 357 (1967).
71. J. F. Nixon. Adv. Inorg. Chem. Radiochem. **13**, 436 (1970).
72. G. C. Holywell, D. W. H. Rankin, B. Beagley, and J. M. Freeman. J. Chem. Soc. A, 785 (1971).
73. M. D. LaPrade and C. E. Nordman. Inorg. Chem. **8**, 1669 (1969).
74. B. G. De Boer, A. Zalkin, and D. H. Templeton. Inorg. Chem. **8**, 836 (1969).
75. K. Karakida and K. Kuchitsu. Inorg. Chim. Acta, **16**, 29 (1976).
76. C. R. Nave and J. Sheridan. J. Mol. Struct. **15**, 391 (1973).
77. D. W. H. Rankin, A. J. Blake, M. J. Davis, E. A. V. Ebsworth, and A. J. Welch. J. Chem. Soc. Dalton Trans. 223 (1989).
78. G. C. Holywell and D. W. H. Rankin. J. Mol. Struct. **9**, 11 (1971).
79. D. W. H. Rankin and S. J. Cyvin. J. Chem. Soc. Dalton Trans. 869 (1972).
80. K. Yamasaki, A. Kobera, M. Yokoi, and Y. Ueda. J. Chem. Phys. **18**, 1414 (1950).
81. B. Kamenar and M. Bruvo, Z. Kristallogr. **141**, 97 (1975).
82. K. M. A. Malik and J. W. Jeffrey. Acta Crystallogr. Sect. B: Struct. Crystallogr. Cryst. Chem. **B32**, 475 (1976).
83. L. S. Dent Glasser and P. B. Jamieson. Acta Crystallogr. Sect. B: Struct. Crystallogr. Cryst. Chem. **B32**, 705 (1976).
84. A. Grund and M. M. Pizy. Acta Crystallogr. **5**, 837 (1952).

85. J. J. Pluth and J. V. Smith. Acta Crystallogr. Sect. B: Struct. Crystallogr. Cryst. Chem. **B29**, 73 (1973).
86. B. Beagley, D. P. Brown, and J. M. Freeman. J. Mol. Struct. **18**, 337 (1973).
87. K. Hagen and K. Hedberg. J. Chem. Phys. **59**, 1549 (1977).
88. W. Airey, C. Glidewell, D. W. H. Rankin, A. G. Robiette, G. M. Sheldrick, and D. W. J. Cruickshank. Trans. Faraday Soc. **66**, 551 (1970).
89. W. Airey, C. Glidewell, A. G. Robiette, and G. M. Sheldrick. J. Mol. Struct. **8**, 413 (1971).
90. W. Airey, C. Glidewell, A. G. Robiette, G. M. Sheldrick, and J. M. Freeman. J. Mol. Struct. **8**, 423 (1971).
91. I. Hargittai. The structure of volatile sulfur compounds. Reidel, Dordrecht. 1985.
92. A. H. Clark and B. Beagley. Trans. Faraday Soc. **67**, 2216 (1971).
93. W. S. McDonald and D. W. J. Cruickshank. Acta Crystallogr. **22**, 48 (1967).
94. D. P. Desmarteau, H. H. Eyssel, H. Oberhammer, and H. Gunther. Inorg. Chem. **21**, 1607 (1982).
95. D. R. Lide, D. E. Mann, and R. M. Fristrom. J. Chem. Phys. **26**, 734 (1957).
96. C. Lau, H. Lynton, J. Passmore, and P. Y. Siew. J. Chem. Soc. Dalton Trans. 2535 (1973).
97. J. Brunvoll, M. Kolonits, C. Bliefert, K. Seppelt, and I. Hargittai. J. Mol. Struct. **78**, 307 (1982).
98. M. Hargittai and I. Hargittai. J. Mol. Struct. **20**, 283 (1974).
99. O. Glemser and R. Mews. Angew. Chem. Int. Ed. Engl. **19**, 883 (1980).
100. D. A. Gilbert, A. Roberts, and P. A. Griswold. Phys. Rev. **76**, 1723 (1949).
101. C. J. Marsden. J. Chem. Soc. Chem. Commun. 786 (1985).
102. A. H. Clark, B. Beagley, D. W. J. Cruickshank, and T. G. Hewitt. J. Chem. Soc. A, 872 (1970).
103. H. Lynton and J. Passmore. Can. J. Chem. **49**, 2539 (1971).
104. R. Bougon, W. V. Cicha, M. Lance, L. Meublat, M. Nierlich, and J. Vigner. Inorg. Chem. **30**, 102 (1991).
105. A. H. Clark, B. Beagley, D. W. J. Cruickshank, and T. G. Hewitt. J. Chem. Soc. A, 1613 (1970).
106. B. Beagley. Trans. Faraday Soc. **61**, 1821 (1965).
107. A. H. Clark, B. Beagley, D. W. J. Cruickshank, and T. G. Hewitt. J. Chem. Soc. A, 872 (1970).
108. J. L. Pascal, J. Potier, D. J. Jones, J. Roziere, and A. Michelowicz. Inorg. Chem. **24**, 238 (1985).
109. C. H. Belin, M. Charbouni, J. L. Pascal, and J. Potier. Inorg. Chem. **21**, 3557 (1982).
110. M. Fourate, M. Chaabouni, C. H. Belin, M. Charbonnel, J. L. Pascal, and J. Potier. Inorg. Chem. **25**, 1386 (1985).
111. O. A. Dyachenko, L. O. Atovmyan, G. L. Shirokova, and V. Ya. Rosolovskii. J. Chem. Soc. Chem. Commun. 595 (1973).
112. H. N. Ng and C. Calvo. Can. J. Chem. **51**, 2613 (1973).
113. R. Kniep and D. Mootz. Acta Crystallogr. Sect. B: Struct. Crystallogr. Cryst. Chem. **B29**, 2292 (1973).
114. E. L. Muetterties and L. J. Guggenberger. J. Am. Chem. Soc. **94**, 8046 (1972).
115. C. Giacovazzo, S. Menchetti, and F. Scordari. Acta Crystallogr. Sect. B: Struct. Crystallogr. Cryst. Chem. **B29**, 26 (1973).
116. Z. V. Pudovkina, N. M. Chernitsova, and Y. A. Pyatenko. J. Struct. Chem. **14**, 445 (1973).
117. G. A. Anderson, F. R. Forgaard, and A. Haaland. Acta Chem. Scand. **26**, 1947 (1972).
118. A. Almenningen, G. Gundersen, T. Haugen, and A. Haaland. Acta Chem. Scand. **26**, 3928 (1972).
119. M. Hargittai, I. Hargittai, V. P. Spirodonov, M. Pelissier, and J. F. Labarre. J. Mol. Struct. **24**, 27 (1975).
120. A. Almenningen, A. Haaland, T. Haugen, and D. P. Novak. Acta Chem. Scand. **27**, 1821 (1973).
121. T. Bartke, A. Haaland, and N. P. Novak. Acta Chem. Scand. A, **29**, 273 (1975).
122. J. F. Janik, E. N. Dicester, and R. T. Paine. Inorg. Chem. **27**, 4335 (1988).
123. J. L. Atwood and W. R. Newberry. J. Organomet. Chem. **87**, 1 (1975).
124. S. K. Seale and J. L. Atwood. J. Organomet. Chem. **64**, 57 (1974).
125. J. L. Atwood and P. A. Milton. J. Organomet. Chem. **52**, 275 (1973).
126. M. Hargittai, I. Hargittai, V. P. Spiridonov, and A. A. Ivanov. J. Mol. Struct. **39**, 225 (1977).

Can. J. Chem. Downloaded from www.nrcresearchpress.com by 217.78.4.112 on 09/08/12
For personal use only.

Reactions of lignin model compounds with pulp bleaching chemicals. Cannizzaro-type reaction of tetrachloro-*o*-benzoquinone with alkali

A. BRUCE MCKAGUE[1] AND DOUGLAS W. REEVE

Pulp and Paper Centre and Department of Chemical Engineering and Applied Chemistry, University of Toronto, Toronto, Ont., Canada M5S 1A4

AND

STEVEN J. RETTIG AND JAMES TROTTER

Department of Chemistry, University of British Columbia, 2036 Main Mall, Vancouver, B.C., Canada V6T 1Z1

Received October 18, 1991

A. BRUCE MCKAGUE, DOUGLAS W. REEVE, STEVEN J. RETTIG, and JAMES TROTTER. Can. J. Chem. **70**, 1706 (1992).

Reaction of tetrachloro-*o*-benzoquinone **1** with aqueous sodium hydroxide resulted in a Cannizzaro-type disproportionation into tetrachloromuconic acid and tetrachlorocatechol. The tetrachloromuconic acid was isolated and identified by X-ray crystallography as the methyl ester of the cyclized lactone **3**. Crystals of $C_7H_3Cl_3O_4$, **4**, are orthorhombic, a = 9.991 (2), b = 7.981 (1), c = 24.626(2) Å, Z = 8, space group $Pna2_1$. The structure was solved by direct methods and was refined by full-matrix least-squares procedures to R = 0.033 for 1609 reflections with $I \geq 3\sigma(I)$.

A. BRUCE MCKAGUE, DOUGLAS W. REEVE, STEVEN J. RETTIG et JAMES TROTTER. Can. J. Chem. **70**, 1706 (1992).

La réaction de la tétrachloro-*o*-benzoquinone (**1**) avec une solution aqueuse d'hydroxyde de sodium donne lieu à une réaction de dismutation du type de Cannizzaro conduisant à de l'acide tétrachloromuconique et à du tétrachlorocatéchol. On a isolé l'acide tétrachloromuconique et, par diffraction des rayons X, l'a identifié comme l'ester méthylique de la lactone cyclique **3**. Les cristaux de $C_7H_3Cl_3O_4$, **4**, sont orthorhombiques, avec a = 9,991(2), b = 7,981(1) et c = 24,626(2) Å, Z = 8 et groupe d'espace $Pna2_1$. On a résolu la structure par des méthodes directes et on l'a affinée par la méthode des moindres carrés jusqu'à une valeur de R = 0,033 pour 1609 réflexions avec $I \geq 3\sigma(I)$.

[Traduit par la rédaction]

Introduction

Muconic acids can be produced from phenols or quinones by chemical or enzymatic oxidation (1–5). Depending on the substituents present and the geometry of the double bonds, the muconic acids may cyclize to form lactones. In the case of pulp bleaching with chlorine, chlorinated muconic acids have been proposed as the terminal products of chlorination of lignin-type phenols (6). To date, neither chlorinated muconic acids nor their cyclized lactone counterparts have been identified in effluents from chlorine bleaching. In the case of one report in which trichloro-β-methylmuconic acid was identified as a chlorination product of the model compound 4-methylguaiacol, firm structural evidence was not provided (7).

The chemistry of pulp bleaching with chlorine is extremely intriging and complicated. Regulatory and market pressures have now driven the pulp and paper industry to replace chlorine with bleaching agents such as chlorine dioxide and oxygen. As a result, chlorine bleaching may be phased out before its chemistry is well understood. In the accompanying paper (8) we report the conversion of the model compound 4-methyltrichlorocatechol to an unusual chlorohydroxycyclohexenone by aqueous chlorine. Treatment of the latter with aqueous sodium hydroxide results in a benzilic acid rearrangement to a chlorohydroxycyclopentenecarboxylic acid. This paper reports the conversion of tetrachloro-*o*-benzoquinone, a product of classical chlorine bleaching, to tetrachloromuconic acid via a Cannizzaro-type reaction with alkali in the absence of any oxidant.

[1]Author to whom correspondence may be addressed. Also with CanSyn Chem. Corp., Toronto, Canada.

Experimental

Melting points were taken on a Fisher Johns melting point apparatus and are uncorrected. Infrared (IR) spectra were recorded on a Perkin Elmer model 598 infrared spectrophotometer and ultraviolet (UV) spectra on a Beckman model DU-7U spectrophotometer. Carbon magnetic resonance (^{13}C NMR) spectra were recorded in CD_3OD or $CDCl_3$ solution using a Bruker AM 500 MHz high resolution spectrometer. Signal positions are given in ppm (δ) relative to Me_4Si. Mass spectra were obtained on a VG analytical ZAB-SE high-mass high-resolution mass spectrometer. Silica gel used for chromatography was 100–200 mesh. Gas chromatography (GC) was done on a Hewlett Packard HP 5890 gas chromatograph equipped with a flame ionization detector and 25 m HP1 capillary column. Temperature was programmed from 185 to 260°C at 10°/min.

*Reaction of tetrachloro-***o***-benzoquinone 1 with alkali*

Tetrachloro-*o*-benzoquinone (3.0 g) was added to 2.5% NaOH (300 mL) with stirring at 60°C. The resultant mixture was stirred 20 min at 60°C, then cooled to room temperature. Sodium chloride (30 g) was added, the product acidified with concentrated hydrochloric acid and extracted with ether (5 × 100 mL). The combined extracts were washed with water (3 × 25 mL), dried ($MgSO_4$), and evaporated to give the crude product (3.1 g). GC analysis showed the two products **3** and **5** with retention times of 2.5 and 5.3 min respectively. Fractionation on silica gel (250 g) and elution with hexane:ether, 2:1 gave the furanone **3** (0.8 g) as a light brown oil. Crystallization from hexane containing a little ether gave tan prisms of **3**; mp 164–165°C; IR (Nujol): 1815, 1720 cm^{-1}; UV (ethanol) λ_{max}: 310 nm (ε 20 800); ^{13}C NMR δ: 163.6 (C1 or C5), 160.9 (C1 or C5), 145.5, 139.9, 126.4, 112.6 (C3); MS *m/e*: 246 (7%), 244 (21), 242 (22), 200 (38), 198 (40), 165 (22), 163 (36), 122 (20), 89 (33), 87 (100). Anal. calcd. for $C_6HCl_3O_4$: C 29.60, H 0.41, Cl43.69; found: C 29.79, H < 0.5, Cl 42.78. Continued elution with the same solvent and hex-

Can. J. Chem. Downloaded from www.nrcresearchpress.com by 217.78.4.112 on 09/08/12
For personal use only.

Can. J. Chem. Downloaded from www.nrcresearchpress.com by 217.78.4.112 on 09/08/12
For personal use only.

TABLE 1. Crystallographic data[a]

Compound	**4**
Formula	$C_7H_3Cl_3O_4$
fw	257.46
Color, habit	Colorless, prism
Crystal size, mm	0.07 × 0.20 × 0.40
Crystal system	Orthorhombic
Space group	$Pna2_1$
a, Å	9.991(2)
b, Å	7.981(1)
c, Å	24.626(2)
V, Å^3	1963.6(4)
Z	8 (two molecules per asymmetric unit)
ρ_{calc}, g/cm^3	1.742
F(000)	1024
μ(Cu-K_α), cm^{-1}	85.75
Transmission factors	0.39–1.00
Scan type	ω–2θ
Scan range, deg in ω	1.05 + 0.20 tan θ
Scan speed, deg/min	32
Data collected	$+h,+k,+l$
$2\phi_{max}$, deg	155
Crystal decay	5.5%
Total reflections	2289
Unique reflections	2289
Reflcns. with $I \geq 3\sigma(I)$	1609
No. of variables	253
R	0.033
R_w	0.036
gof	1.94
Max Δ/σ (final cycle)	0.26
Residual density, e/Å^3	−0.21 to +0.20

[a]Temperature 294 K, Rigaku AFC6S diffractometer, Cu-K_α radiation (λ = 1.54178 Å), graphite monochromator, takeoff angle 6.0°, aperture 6.0 × 6.0 mm at a distance of 285 mm from the crystal, stationary background counts at each end of the scan (scan/background time ratio 2:1, up to 8 rescans), $\sigma^2(F^2) = [S^2(C + 4B) + (0.01F^2)^2]/Lp^2$ (S = scan rate, C = scan count, B = normalized background count), function minimized $\Sigma w(|F_o|-|F_c|)^2$ where $w = 4F_o^2/\sigma^2(F_o^2)$, $R = \Sigma||F_o|-|F_c||/\Sigma|F_o|$, $R_w = (\Sigma w(|F_o|-|F_c|)^2/\Sigma w|F_o|^2)^{1/2}$, and gof = $[\Sigma w(|F_o|-|F_c|)^2/(m-n)]^{1/2}$. Values given for R, R_w, and gof are based on those reflections with $I \geq 3\sigma(I)$.

TABLE 2. Final atomic coordinates (fractional) and B_{eq} (Å^2)[a]

Atom	*x*	*y*	*z*	B_{eq}
Cl(1A)	0.8261(2)	0.7866(2)	0.2281	4.73(8)
Cl(2A)	0.6572(2)	0.4826(2)	0.1606(1)	4.35(7)
Cl(3A)	0.3706(2)	0.8400(2)	0.0385(1)	5.02(8)
O(1A)	0.5595(4)	0.9446(4)	0.1234(2)	3.5(2)
O(2A)	0.6792(4)	1.1109(5)	0.1792(2)	4.4(2)
O(3A)	0.3479(4)	0.4656(5)	0.0751(2)	4.7(2)
O(4A)	0.5537(4)	0.4568(5)	0.0387(2)	4.5(2)
C(1A)	0.6540(6)	0.9724(7)	0.1639(3)	3.4(3)
C(2A)	0.7050(6)	0.8106(8)	0.1805(3)	3.2(2)
C(3A)	0.6424(6)	0.6909(7)	0.1525(3)	3.4(3)
C(4A)	0.5524(7)	0.7726(7)	0.1145(3)	3.1(3)
C(5A)	0.4722(6)	0.7128(7)	0.0760(3)	3.1(3)
C(6A)	0.4656(6)	0.5281(7)	0.0611(3)	3.3(3)
C(7A)	0.3317(8)	0.2880(9)	0.0627(4)	5.9(4)
C1(1B)	0.4061(2)	0.2282(2)	0.24757(8)	4.72(8)
Cl(2B)	0.5827(2)	0.5213(2)	0.3170(1)	4.52(8)
C1(3B)	0.8675(2)	0.1395(2)	0.4324(1)	4.49(7)
O(1B)	0.6733(4)	0.0535(5)	0.3483(2)	3.5(2)
O(2B)	0.5457(5)	−0.1062(5)	0.2933(2)	4.9(2)
O(3B)	0.8979(5)	0.5140(6)	0.4055(3)	6.3(3)
O(4B)	0.6918(5)	0.5268(6)	0.4390(3)	6.0(3)
C(1B)	0.5752(6)	0.0315(8)	0.3093(3)	3.8(3)
C(2B)	0.5270(6)	0.1978(8)	0.2939(3)	3.4(3)
C(3B)	0.5943(6)	0.3107(7)	0.3229(3)	3.1(2)
C(4B)	0.6845(6)	0.2233(7)	0.3593(3)	3.2(3)
C(5B)	0.7690(7)	0.2760(8)	0.3973(3)	3.3(3)
C(6B)	0.7785(7)	0.4546(8)	0.4161(3)	4.0(3)
C(7B)	0.925(1)	0.684(1)	0.4241(6)	9.7(7)

[a]$B_{eq} = (8/3)\pi^2\Sigma\Sigma U_{ij}a_i^*a_j^*(a_i \cdot a_j)$.

ane:ether 1:1 gave a mixture of **3** and **5** (0.2 g) followed by **5** (1.6 g), identical to an authentic sample prepared by the chlorination of catechol.

Preparation of the methylester 4

The furanone **3** (150 mg) was dissolved in methanol (2 mL) and treated with a solution of diazomethane in ether (20 mL). The solution was allowed to stand at room temperature 1 h, then washed with water, dried ($MgSO_4$), and evaporated to give the product. Crystallization from hexane containing a little ether gave colourless prisms of **4**; mp 100–101°C; IR (Nujol): 1805, 1740 cm^{-1}; UV (ethanol) λ_{max}: 296 nm (ϵ 23 700); ^{13}C NMR δ: 161.3 (C1 or C5), 159.3 (C1 or C5), 145.1, 139.0, 125.6, 110.8 (C3), 54.0 (OCH_3); MS *m/e*: 258 (21), 256 (22), 225 (20), 227 (18), 141 (41), 143 (40), 87 (68), 59 (100). Anal. calcd. for $C_7H_3Cl_3O_4$: C 32.65, H 1.17, Cl 41.31; found: C 32.68, H 1.25, Cl 40.75.

X-ray crystallographic analyses of 4

Crystallographic data appear in Table 1. The final unit-cell parameters were obtained by least-squares on the setting angles for 25 reflections with 2θ = 55.0–86.4°. The intensities of three standard reflections, measured every 200 reflections throughout the data collections, decreased uniformly by 5.5%. The data were processed[2] and corrected for Lorentz and polarization effects, decay, and absorption (empirical, based on azimuthal scans for four reflections).

The structure analysis was initiated in the noncentrosymmetric space group $Pna2_1$ on the basis of the *E*-statistics, this choice being confirmed by the subsequent successful solution and refinement of the structure. The structure was solved by direct methods, the coordinates of the non-hydrogen atoms being determined from an *E*-map. There are two molecules in the asymmetric unit, related to one another by a pseudo-inversion centre. The non-hydrogen atoms were refined with anisotropic thermal parameters and the hydrogen atoms were fixed in calculated positions (orientation based on observed Fourier map positions, C—H = 0.98 Å, $B_H = 1.2\ B_{bonded\ atom}$). A correction for secondary extinction was applied, the final value of the extinction coefficient being 1.69×10^{-4}. Neutral atom scattering factors for all atoms and anomalous dispersion corrections for the non-hydrogen atoms were taken from the *International tables for X-ray crystallography* (9). A parallel refinement of the structure having the opposite polarity gave higher residuals, the *R* and R_w factor ratios being 1.05 and 1.04, respectively. Final atomic coordinates and equivalent isotropic thermal parameters, bond lengths, and bond angles appear in Tables 2–4, respectively. A stereoview of the packing arrangement, hydrogen atom parameters, anisotropic thermal parameters, bond lengths and bond angles involving hydrogen, torsion angles, intermolecular con-

[2]TEXSAN/TEXRAY structure analysis package (Molecular Structure Corp., 1985) which includes versions of the following: DIRDIF, direct methods for difference structures, by P. T. Beurskens; ORFLS, full-matrix least squares, and ORFFE, function and errors, by W. R. Busing, K. O. Martin, and H. A. Levy; ORTEP II, illustrations, by C. K. Johnson.

TABLE 3. Bond lengths (Å) with estimated standard deviations

Atoms	Distance	Atoms	Distance
Cl(1A) — C(2A)	1.696(6)	Cl(1B) — C(2B)	1.680(7)
Cl(2A) — C(3A)	1.681(6)	Cl(2B) — C(3B)	1.691(6)
Cl(3A) — C(5A)	1.708(7)	Cl(3B) — C(5B)	1.704(7)
O(1A) — C(1A)	1.390(8)	O(1B) — C(1B)	1.383(8)
O(1A) — C(4A)	1.392(6)	O(1B) — C(4B)	1.387(7)
O(2A) — C(1A)	1.194(7)	O(2B) — C(1B)	1.204(7)
O(3A) — C(6A)	1.323(7)	O(3B) — C(6B)	1.310(8)
O(3A) — C(7A)	1.459(8)	O(3B) — C(7B)	1.460(8)
O(4A) — C(6A)	1.185(7)	O(4B) — C(6B)	1.184(7)
C(1A) — C(2A)	1.448(8)	C(1B) — C(2B)	1.462(8)
C(2A) — C(3A)	1.333(9)	C(2B) — C(3B)	1.331(9)
C(3A) — C(4A)	1.45(1)	C(3B) — C(4B)	1.450(9)
C(4A) — C(5A)	1.329(9)	C(4B) — C(5B)	1.33(1)
C(5A) — C(6A)	1.521(8)	C(5B) — C(6B)	1.502(9)

tacts, least-squares planes, and measured and calculated structure factor amplitudes have been supplied as supplementary material.[3]

Results and discussion

The product resulting from treatment of tetrachloro-*o*-benzoquinone with alkali was found to consist of two components by GC analysis. Neither of the components had a retention time that matched that of chloranilic acid, a compound suggested as a possible product of this reaction (10). The retention time of one of the components matched that of tetrachlorocatechol and the identity of this component was confirmed by subsequent comparison of material isolated by fractionation of the product on SiO_2 with a standard. The other product eluted from SiO_2 prior to tetrachlorocatechol and gave crystals having melting point 164–165°C. This compound and its methyl derivative had infrared absorption bands at 1815 and 1805 cm^{-1} respectively, which suggested they were five-membered ring lactones. The structure of the methyl derivative was determined as the methyl ester **4** by X-ray crystallography described below.

Identification of the methyl derivative of one of the two major reaction products as the methyl ester of the lactone **3** indicated tetrachloro-*o*-benzoquinone **1** had undergone a simple oxidation–reduction with alkali, most likely via a Cannizzaro-type reaction as shown in Scheme 1. The intermediate muconic acid 2 has previously been reported to cyclize to the lactone (1).

The melting point of the lactone **3** obtained in this work is 164–165°C, close to that reported in the literature for the lactone formed on melting tetrachloromuconic acid and which was reported (1) to be a mixture of the two possible geometrical isomers of **3**. The melting point is also lower than that of 182°C reported by Karrer and Testa for the lactone obtained by peracetic acid oxidation of **1** (11). The material reported in the present work appeared homogeneous by GC and ^{13}C NMR, and gave almost entirely one product on methylation that had a melting point of 100–101°C, slightly lower than that of 107°C reported by Karrer and Testa for the methyl ester obtained in their work. Since the structure was determined as the isomer **4** by X-ray crystallography, it is not possible to explain the differences in the reported melting points for the lactone **3**.

The observation that tetrachloro-*o*-benzoquinone undergoes a Cannizzaro-type oxidation–reduction reaction with alkali indicates that chloromuconic acids may be formed in

[3]Supplementary material mentioned in the text may be purchased from: The Depository of Unpublished Data, Document Delivery, CISTI, National Research Council of Canada, Ottawa, Canada K1A 0R6.

Tables of hydrogen atom parameters, bond lengths and angles involving hydrogen, and intermolecular distances for non-hydrogen atoms have also been deposited with the Cambridge Crystallographic Data Centre and can be obtained on request from The Director, Cambridge Crystallographic Data Centre, University Chemical Laboratory, Lensfield Road, Cambridge, CB2 1EW, U.K.

TABLE 4. Bond angles (deg) with estimated standard deviations

Atoms	Angle	Atoms	Angle
C(1A)—O(1A)—C(4A)	107.8(5)	C(1B)—O(1B)—C(4B)	108.5(5)
C(6A)—O(3A)—C(7A)	114.2(5)	C(6B)—O(3B)—C(7B)	116.1(6)
O(1A)—C(1A)—O(2A)	121.1(6)	O(1B)—C(1B)—O(2B)	121.1(6)
O(1A)—C(1A)—C(2A)	107.4(5)	O(1B)—C(1B)—C(2B)	107.4(5)
O(2A)—C(1A)—C(2A)	131.5(7)	O(2B)—C(1B)—C(2B)	131.5(7)
Cl(1A)—C(2A)—C(1A)	123.2(5)	C1(1B)—C(2B)—C(1B)	123.0(5)
Cl(1A)—C(2A)—C(3A)	127.7(5)	Cl(1B)—C(2B)—C(3B)	129.0(5)
C(1A)—C(2A) —C(3A)	109.2(6)	C(1B)—C(2B)—C(3B)	108.0(6)
Cl(2A)—C(3A)—C(2A)	127.3(6)	Cl(2B)—C(3B)—C(2B)	126.3(5)
Cl(2A)—C(3A)—C(4A)	125.0(5)	Cl(2B)—C(3B)—C(4B)	125.0(5)
C(2A)—C(3A)—C(4A)	107.6(5)	C(2B)—C(3B)—C(4B)	108.7(5)
O(1A)—C(4A)—C(3A)	107.9(6)	O(1B)—C(4B)—C(3B)	107.4(6)
O(1A)—C(4A)—C(5A)	119.9(6)	O(1B)—C(4B)—C(5B)	119.9(6)
C(3A)—C(4A)—C(5A)	132.2(6)	C(3B)—C(4B)—C(5B)	132.7(6)
Cl(3A)—C(5A)—C(4A)	122.0(5)	Cl(3B)—C(5B)—C(4B)	121.5(5)
Cl(3A)—C(5A)—C(6A)	114.8(5)	Cl(3B)—C(5B)—C(6B)	114.4(5)
C(4A)—C(5A)—C(6A)	123.2(6)	C(4B)—C(5B)—C(6B)	123.9(6)
O(3A)—C(6A)—O(4A)	127.0(5)	O(3B)—C(6B)—O(4B)	125.9(6)
O(3A)—C(6A)—C(5A)	109.9(5)	O(3B)—C(6B)—C(5B)	109.9(6)
O(4A)—C(6A)—C(5A)	123.1(6)	O(4B)—C(6B)—C(5B)	124.2(6)

Can. J. Chem. Downloaded from www.nrcresearchpress.com by 217.78.4.112 on 09/08/12
For personal use only.

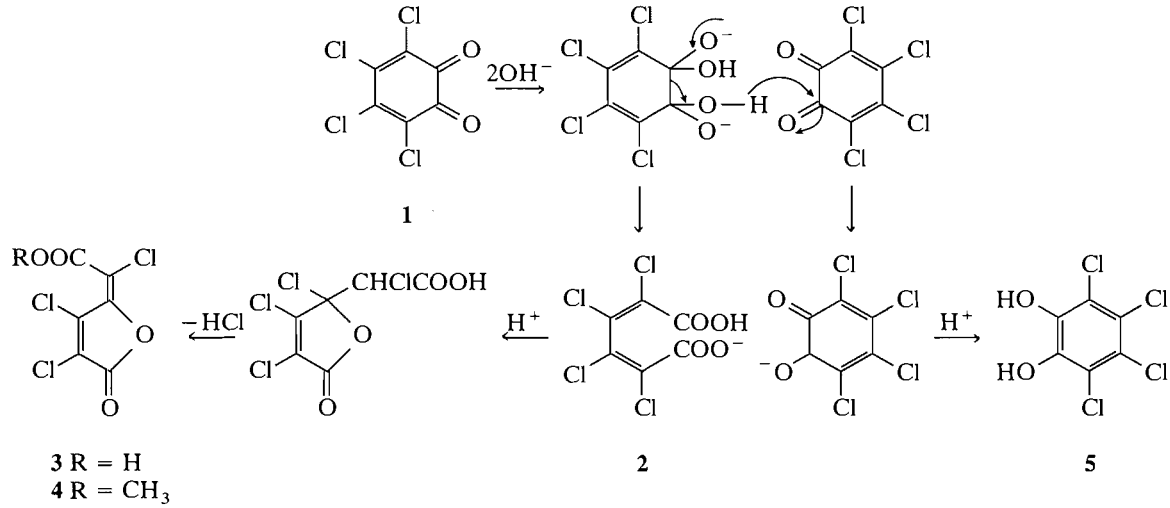

SCHEME 1

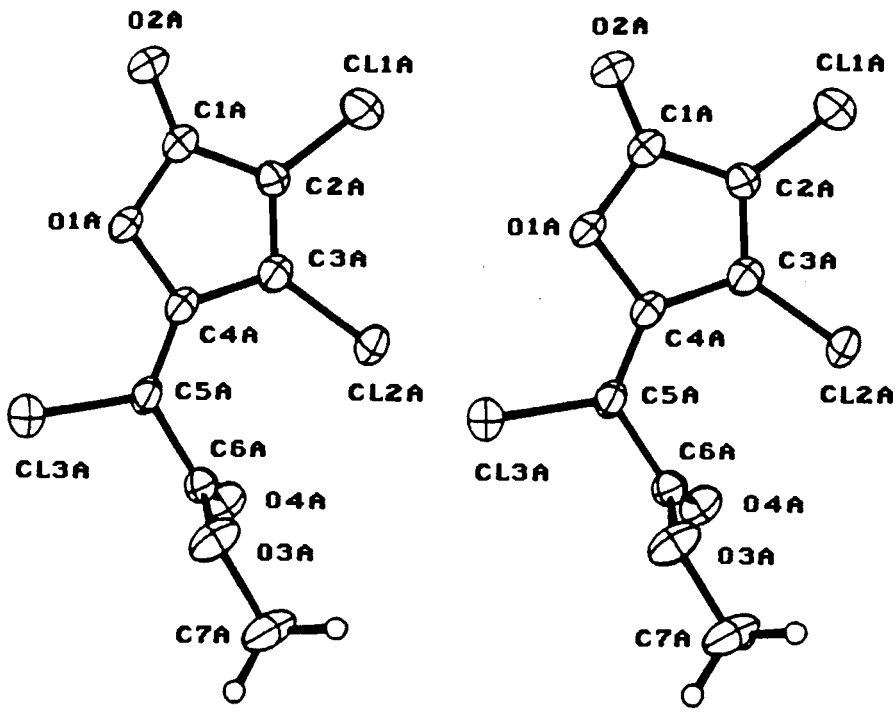

FIG. 1. Stereoscopic view of one of the two crystallographically independent molecules of **4** showing atom labelling; 33% probability thermal ellipsoids are shown for the non-hydrogen atoms.

the alkaline (E) stage of bleaching rather than in the chlorination (C) stage.

Bond lengths and angles for the two crystallographically independent molecules of **4** (side-by-side in Tables 3 and 4 for ease of comparison, Fig. 1) are generally equal within experimental error and are as expected. The five-membered rings are planar within 0.020(7) and 0.025(7) Å in the A and B molecules respectively. The ester functions are planar within experimental error for both molecules and are oriented roughly perpendicular to the five-membered rings (angles between normals to the mean planes are 112.1° and 113.7° for the A and B molecules). The packing is dominated by a herring-bone arrangement of slipped stacks, the five-membered rings of one layer interacting with chlorine atoms or ester groups of the adjacent layer. The shortest intermolecular distances between adjacent layers are O(3A) ··· C(1A) = 2.963(8), O(3B) ··· C(1B) = 2.979(9), Cl(1A) ··· O(2A) = 3.076(5), and Cl(1B) ··· O(2B) = 3.010(4) Å.

Acknowledgements

This work has been supported by a consortium of companies including Albright & Wilson Americas; Aracruz Cellulose S.A.; Champion International Corporation; CRS

Can. J. Chem. Downloaded from www.nrcresearchpress.com by 217.78.4.112 on 09/08/12
For personal use only.

Sirrine, Inc.; Fletcher Challenge Canada Ltd.; International Paper; ITT Rayonier; James River Corporation; Jujo Paper Company Ltd.; Kymmene Corporation; Noranda Inc; The Procter & Gamble Cellulose Co.; Weyerhaeuser Company, and the University Research Incentive Fund.

The authors also thank the Natural Sciences and Engineering Research Council of Canada for financial support. NMR and mass spectrometry services were provided by Dr. A. A. Grey and Dr. H. Pang, respectively, at the University of Toronto Carbohydrate Research Centre.

1. A. T. Shulgin. Recl. Trav. Chim. Pays-Bas, **83**, 897 (1964).
2. J. Tsuji and H. Takayanagi. Tetrahedron, **34**, 641 (1978).
3. E. Schmidt, G. Remberg, and H-J, Knackmuss. Biochem. J. **192**, 331 (1980).
4. G. M. Strunz, M. Kakushima, A. D. Gibson, A. W. McCulloch, and P. S. White. Can. J. Chem. **58**, 2765 (1980).
5. A. J. Pandell. J. Org. Chem. **48**, 3908 (1983).
6. J. B. Van Buren and C. W. Dence. Tappi, **53**, 2246 (1970).
7. J. M. Gess and C. W. Dence. Tappi, **54**, 1114 (1971).
8. A. B. McKague, D. W. Reeve, S. J. Rettig, and J. Trotter. Can. J. Chem. **70**, 1711 (1992).
9. International tables for X-ray crystallography. Vol. IV. Kynoch Press. Birmingham, U.K. (Present distributor: Kluwer Academic Publishers. Dordrecht, The Netherlands). 1974. pp. 99–102 and 149.
10. S. A. Braddon and C. W. Dence. Tappi, **51**, 249 (1968).
11. P. Karrer and E. Testa. Helv. Chim. Acta, **32**, 1019 (1949).

Can. J. Chem. Downloaded from www.nrcresearchpress.com by 217.78.4.112 on 09/08/12
For personal use only.

Reactions of lignin model compounds with pulp bleaching chemicals. Reactions of 4-methyltrichlorocatechol

A. BRUCE MCKAGUE[1] AND DOUGLAS W. REEVE

Pulp and Paper Centre and Department of Chemical Engineering and Applied Chemistry, University of Toronto, Toronto, Ont., Canada M5S 1A4

AND

STEVEN J. RETTIG AND JAMES TROTTER

Department of Chemistry, University of British Columbia, 2036 Main Mall, Vancouver, B.C., Canada V6T 1Z1

Received October 22, 1991

A. BRUCE MCKAGUE, DOUGLAS W. REEVE, STEVEN J. RETTIG, and JAMES TROTTER. Can. J. Chem. **70**, 1711 (1992).

Aqueous chlorination of 4-methyltrichlorocatechol **2** gave the tetrachlorohydroxycyclohexenone **4**, which crystallized as the hydrate **5**. Reaction of **4** with aqueous sodium hydroxide resulted in a benzilic acid rearrangement to the tetrachlorodihydroxycyclopentenecarboxylic acid **6**. These reactions have important implications with respect to understanding how lignin is removed during pulp bleaching. Crystals of the tetrachlorotrihydroxycyclohexenone **5** are monoclinic, a = 11.4420(6), b = 7.5873(9), c = 12.6443(6) Å, β = 101.266(4)°, Z = 4, space group $P2_1/c$, and those of the methyl tetrachlorodihydroxycyclopentenecarboxylate **7** are monoclinic, a = 28.447(1), b = 6.929(1), c = 12.597(1) Å, β = 103.074(5)°, Z = 8, space group $C2/c$. The structures were solved by direct methods and were refined by full-matrix least-squares procedures to R = 0.028 and 0.034 for 1716 and 2164 reflections with $I \geq 3\sigma(I)$, respectively.

A. BRUCE MCKAGUE, DOUGLAS W. REEVE, STEVEN J. RETTIG et JAMES TROTTER. Can. J. Chem. **70**, 1711 (1992).

La chloration aqueuse du 4-méthyltrichlorocatéchol, **2**, conduit à la tétrachlorohydroxycyclohexénone, **4**, qui cristallise sous la forme de l'hydrate **5**. La réaction du composé **4** avec de l'hydroxyde de sodium aqueux donne lieu à un réarrangement benzylique conduisant à l'acide tétrachlorodihydroxycyclopentanecarboxylique, **6**. Ces réactions ont des implications importantes pour la compréhension de la façon dont la lignine est enlevée au cours du blanchiment de la pulpe. Les cristaux de la tétrachlorohydroxycyclohexénone, **5**, sont monocliniques, a = 11,4420(6), b = 7,5873(9) et c = 12,6443(6) Å, β = 101,266(4)°, Z = 4, groupe d'espace $P2_1/c$, et ceux du tétrachlorodihydroxycyclopentènecarboxylate de méthyle, **7**, sont monocliniques, a = 28,447(1), b = 6,929(1) et c = 12,597(1) Å, β = 103,074(5)°, Z = 8, groupe d'espace $C2/c$. On a résolu les structures par des méthodes directes et on les affinées par la méthode des moindres carrés (matrice complète) jusqu'à des valeurs de R = 0,028 et 0,034 respectivement pour 1716 et 2164 réflexions avec $I \geq 3\sigma(I)$.

[Traduit par la rédaction]

Introduction

The chemistry of classical chlorine bleaching of wood pulp has been a subject of extensive study over the past 30 years. A number of reviews that describe our current understanding of how residual lignin is removed from pulp by bleaching (1–3) have been published in textbooks and scientific journals.

In spite of the large number of studies performed, there is still a basic lack of information regarding the mechanism of degradation of aromatic structures present in lignin. There are many examples in the literature that establish that loss of aromaticity can occur via chlorination and oxidation to quinones, but further reactions of the quinones have not been defined and it is not known whether other reaction mechanisms play a significant role in removing aromaticity. The proposed conversion of chlorinated quinones to muconic acids is supported by only one example in which the structure of the muconic acid was not rigorously established (4). Also it was recently reported that tetrachlorocatechol and tetrachloro-*o*-benzoquinone are converted to 2,2,4,5-tetrachlorocyclopentene-1,3-dione by aqueous chlorine (5), which indicates another mechanism is involved in this case.

In connection with studies designed to provide more information on the chemical structure of lignin degraded by chlorine bleaching, we have initiated studies to determine the fate of the more generalized lignin model structure **1**. In this paper we report the identification of products obtained by reacting 4-methyltrichlorocatechol **2** successively with aqueous chlorine and sodium hydroxide.

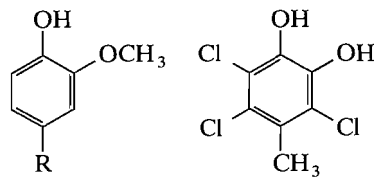

1 **2**

Experimental

Melting points were taken on a Fisher Johns melting point apparatus and are uncorrected. Infrared (IR) spectra were recorded on a Perkin Elmer model 598 infrared spectrophotometer and ultraviolet (UV) spectra on a Beckman model DU-7U spectrophotometer. Proton magnetic resonance (^{1}H NMR) spectra were recorded in $CDCl_3$ solution using a Bruker AM 500 MHz high resolution spectrometer. Signal positions are given in ppm (δ) relative to Me_4Si. Mass spectra were obtained on a VG analytical ZAB-SE high-mass high-resolution mass spectrometer. Silica gel used for chromatography was 100–200 mesh. Methyltrichlorocatechol was prepared by chlorinating 4-methylcatechol as described in the literature (4).

[1]Author to whom correspondence may be addressed. Also with CanSyn Chem. Corp., Toronto, Canada.

Can. J. Chem. Downloaded from www.nrcresearchpress.com by 217.78.4.112 on 09/08/12
For personal use only.

Can. J. Chem. Downloaded from www.nrcresearchpress.com by 217.78.4.112 on 09/08/12
For personal use only.

TABLE 1. Crystallographic data[a]

Compound	**5**	**7**
Formula	$C_7H_6Cl_4O_4$	$C_8H_8Cl_4O_4$
fw	295.93	309.96
Color, habit	Colorless, prism	Colorless, prism
Crystal size, mm	0.08 × 0.10 × 0.35	0.25 × 0.35 × 0.45
Crystal system	Monoclinic	Monoclinic
Space group	$P2_1/c$	$C2/c$
a, Å	11.4420(6)	28.447(1)
b, Å	7.5873(9)	6.929(1)
c, Å	12.6443(6)	12.597(1)
β°	101.266(4)	103.074(5)
V, Å^3	1076.6(1)	2418.7(8)
Z	4	8
ρcalc, g/cm^3	1.826	1.702
$F(000)$	592	1248
μ(Cu-K_α), cm^{-1}	102.09	91.17
Transmission factors	0.76–1.00	0.45–1.00
Scan type	ω–2θ	ω–2θ
Scan range, deg in ω	1.15 + 0.20 tan θ	1.26 + 0.20 tan θ
Scan speed, deg/min	16	32
Data collected	$\pm h$, $+k$, $+l$	$\pm h$, $+k$, $+l$
$2\theta_{max}$, deg	155	155
Crystal decay	4.6%	Negligible
Total reflections	2493	2705
Unique reflections	2206	2428
R_{merge}	0.014	0.033
Reflcns. with $I \geq 3\sigma(I)$	1716	2164
No. of variables	161	178
R	0.028	0.034
R_w	0.030	0.042
gof	2.33	3.81
Max Δ/σ (final cycle)	0.01	0.13
Residual density, e/Å^3	−0.26 to +0.27	−0.43 to +0.28

[a]Temperature 294 K, Rigaku AFC6S diffractometer, Cu-K_α radiation (λ = 1.54178 Å), graphite monochromator, takeoff angle 6.0°, aperture 6.0 × 6.0 mm at a distance of 285 mm from the crystal, stationary background counts at each end of the scan (scan/background time ratio 2:1, up to 8 rescans), $\sigma^2(F^2) = [S^2(C + 4B)]/Lp^2$($S$ = scan rate, C = scan count, B = normalized background count), function minimized $\Sigma w(|F_o| - |F_c|)^2$ where $w = 4F_o^2/\sigma^2(F_o^2)$, $R = \Sigma||F_o| - |F_c||/\Sigma|F_o|$, $R_w = (\Sigma w(|F_o| - |F_c|)^2/\Sigma w|F_o|^2)^{1/2}$, and gof = $[\Sigma w(|F_o| - |F_c|)^2/(m - n)]^{1/2}$. Values given for R, R_w, and gof are based on those reflections with $I \geq 3\sigma(I)$.

Chlorination of 4-methyltrichlorocatechol 2

Chlorine was gently bubbled through a stirred suspension of 4-methyltrichlorocatechol **2** (1.0 g) in water (500 mL) at 50°C for 15 min. After cooling to room temperature, the solution was extracted with ether. The combined extracts were washed with water, dried ($MgSO_4$), and evaporated to give a red gum (1.1 g). The product was fractionated on silica gel (50 g) and 4-methyltrichlorobenzoquinone **3** (130 mg, 13% yield) eluted with hexane:ether, 4:1. Treatment with ether gave **3** as a bright red powder, mp 103–104°C (lit. (6) mp 104–104.5°C); MS, *m/e*: 226 (21%), 224 (21), 200 (32), 198 (97), 196 (100), 191 (25), 189 (38), 170 (32), 168 (33), 163 (24), 161 (37), 135 (48), 133 (75). Reduction of **3** with $NaBH_4$ gave back **2**. Elution with hexane:ether, 1:1, then gave **4** (800 mg, 62% yield), which solidified on cooling. Crystallization from hexane gave tan needles of **4** as the hydrate **5**, mp 91–93°C; IR (Nujol):3460, 3370, 3270, 1720, 1570 cm^{-1}; UV ($CHCl_3$) λ_{max}: 266 nm (ε 11 400); ^{1}H NMR δ: 1.91 (s, 3H), 4.29, 4.49, 5.34 (s, s, s, 1H each, D_2O exchangeable); MS, *m/e*: 217 (32), 215 (97), 213 (100), 168 (40), 166 (57). Anal. calcd. for $C_7H_6Cl_4O_4$: C 28.41, H 2.04, Cl 47.92; found: C 28.70, H 1.95, Cl 47.50.

The same product **4** was obtained by chlorinating the quinone **3**.

Reaction of 4 with sodium hydroxide

A mixture of the crude chlorination product obtained above (1.1 g) and 2.5% NaOH (100 mL) was stirred in a bath at 60°C for 20 min. The product was cooled, acidified with concentrated hydrochloric acid, and extracted as described above to give a light brown gum (600 mg). One half the crude product **6** was treated with diazomethane in ether:methanol 9:1 (25 mL) for 1 h. After evaporation of the solvent the crude product was fractionated on silica gel (25 g) and the product **7** (205 mg) eluted with hexane:ether, 4:1. Crystallization from hexane gave colourless prisms of **7** mp 93–94°C; IR (Nujol):3300, 1720, 1630 cm^{-1}; ^{1}H NMR δ: 1.67 (s, 3H), 3.98 (s, 3H), 4.08 (s, 1H, D_2O exchangeable), 4.17 (m, 1H, D_2O exchangeable). Anal. calcd. for $C_8H_8Cl_4O_4$: C 31.00 H 2.60, Cl 45.76; found: C 30.84, H 2.40, Cl 45.92. The same product was obtained from crystallized **4** by the above procedure.

X-ray crystallographic analyses of the tetrachlorotrihydroxycyclohexenone, 5, and the methyl tetrachlorodihydroxycyclopentenecarboxylate, 7

Crystallographic data for **5** and **7** appear in Table 1. The final unit-cell parameters were obtained by least-squares on the setting angles for 25 reflections with 2θ = 80.9°–100.0° and 109.8°–114.0°, respectively. The intensities of three standard reflections, measured every 200 reflections throughout the data collections, showed only small random variations. The data were

TABLE 2. Final atomic coordinates (fractional) and B_{eq}(Å^2)[a]

Atom	x	y	z	B_{eq}
		5		
Cl(1)	0.40312(7)	0.5607(1)	0.80288(7)	5.8
Cl(2)	0.48504(5)	0.2215(1)	0.93605(5)	4.9
Cl(3)	0.26059(5)	0.0988(1)	0.57765(5)	4.5
Cl(4)	0.01758(5)	0.2069(1)	0.57796(5)	4.4
O(1)	0.3241(2)	−0.0758(3)	0.8652(2)	5.4
O(2)	0.1239(2)	−0.0934(3)	0.7187(2)	4.3
O(3)	0.0961(1)	0.1482(2)	0.8231(1)	3.6
O(4)	0.1241(1)	0.4749(3)	0.7416(1)	3.8
C(1)	0.3233(2)	0.3699(3)	0.7786(2)	3.3
C(2)	0.3589(2)	0.2266(3)	0.8376(2)	3.4
C(3)	0.2908(2)	0.0627(3)	0.8222(2)	3.6
C(4)	0.1643(2)	0.0726(3)	0.7529(2)	3.3
C(5)	0.1640(2)	0.1951(3)	0.6563(2)	3.3
C(6)	0.2089(2)	0.3848(3)	0.6922(2)	3.2
C(7)	0.2260(3)	0.4974(5)	0.5975(2)	4.5
		7		
Cl(1)	0.26376(3)	0.0244(1)	0.39781(7)	5.1
Cl(2)	0.30522(2)	0.4667(1)	0.36944(6)	4.0
Cl(3)	0.36802(2)	0.2421(1)	0.71819(4)	3.3
Cl(4)	0.44838(2)	0.0717(1)	0.65085(6)	3.6
O(1)	0.39349(7)	0.4975(3)	0.5749(1)	2.8
O(2)	0.37693(7)	−0.1374(3)	0.4871(2)	3.1
O(3)	0.42041(8)	0.1442(3)	0.3922(2)	4.2
O(4)	0.44174(7)	0.4498(3)	0.4277(1)	3.3
C(1)	0.31750(8)	0.1162(4)	0.4668(2)	2.6
C(2)	0.33363(8)	0.2904(4)	0.4550(2)	2.2
C(3)	0.38473(7)	0.3235(3)	0.5203(2)	2.0
C(4)	0.38840(7)	0.1541(3)	0.6042(2)	2.0
C(5)	0.35326(8)	−0.0090(3)	0.5455(2)	2.3
C(6)	0.41819(8)	0.2925(4)	0.4402(2)	2.3
C(7)	0.3312(1)	−0.1345(5)	0.6204(2)	3.3
C(8)	0.4716(1)	0.4379(6)	0.3476(3)	4.4

[a] $B_{eq} = (\frac{8}{3})\pi^2\Sigma\Sigma U_{ij}a_i^*a_j^*(a_i \cdot a_j)$.

processed[2] and corrected for Lorentz and polarization effects, decay (for **5**), and absorption (empirical, based on azimuthal scans for four reflections).

The structure analysis of **7** was initiated in the centrosymmetric space group $C2/c$ on the basis of the E-statistics, this choice being confirmed by the subsequent successful solution and refinement of the structure. Both structures were solved by direct methods, the coordinates of the non-hydrogen atoms being determined from E-maps and those of the hydrogen atoms from subsequent difference Fourier syntheses. The non-hydrogen atoms were refined with anisotropic thermal parameters and the hydrogen atoms were refined with isotropic thermal parameters. Corrections for secondary extinction were applied for both compounds, the final values of the extinction coefficients being 4.58×10^{-4} for **5** and 2.48×10^{-4} for **7**. Neutral atom scattering factors and anomalous dispersion corrections for the non-hydrogen atoms were taken from the *International tables for X-ray crystallography* (7). Final atomic coordinates and equivalent isotropic thermal parameters, bond lengths, bond angles, and hydrogen bonding parameters appear in Tables 2–5, respectively. Hydrogen atom parameters, anisotropic thermal parameters, tables of bond lengths and bond angles involving hydrogen, torsion angles, intermolecular contacts, least-squares planes, and measured and calculated structure factor amplitudes are included as supplementary materials.[3]

Results and discussion

Chlorination of 4-methyltrichlorocatechol **2** gave the quinone **3** and the tetrachlorohydroxycyclohexenone **4** (Scheme 1), which crystallized as the hydrate **5** in yields of 13 and 62% respectively. The quinone **3** was readily identified by its melting point, which agreed with the literature, its mass spectrum, and reduction back to the starting catechol **2**. The hydrate **5** had hydrogen-bonded hydroxyl absorption at 3200–3500 cm^{-1} in the IR spectrum. Carbonyl absorption occurred at 1720 cm^{-1} and olefinic absorption at 1570 cm^{-1}. Ultraviolet absorption occurred at 266 nm, in good agreement for a substituted α, β-unsaturated ketone, but the presence of three D_2O exchangeable protons in the ^{1}H NMR spectrum initially caused some difficulty in determining the structure. As a result of a complete structure determination by X-ray crystallography described in the following pages, crystals of compound **4** were found to be in the hydrated form **5**. Isolation as the hydrate indicates that the electron-withdrawing chlorine atoms on the α-carbon atom activate the carbonyl group toward hydrate formation in a manner similar to that of the aldehyde chloral.

Formation of main product **4** is most easily explained by addition of hypochlorous acid to the quinone **3** as shown in Scheme 1. This is supported by the fact that chlorination of the quinone **3** also yields **4** as the major product. Other mechanisms involving chlorination of the catechol **2** at the carbon bearing the methyl group followed by displacement of the chlorine by water may also be involved in formation of the product **4**. A similar mechanism was previously proposed to account for the formation of a spirocyclohexenone obtained by chlorination of dihydroconiferyl alcohol (8).

Reaction of the cyclohexenone **4** with aqueous NaOH at 60°C rapidly produced a clear solution. The product of **6** could not be obtained crystalline but formed the methyl-ester **7** when derivatized with diazomethane. The ester had hydroxyl absorption at 3300 cm^{-1}, ester absorption at 1720 cm^{-1}, and olefinic absorption at 1630 cm^{-1} in the IR spectrum. The ^{1}H NMR had methyl singlets at δ 1.67 and 3.98, and D_2O-exchangeable hydroxyl groups at δ 4.08 and 4.17. The complete structure was determined by X-ray crystallography as described below.

The tetrachlorocyclohexenone **4** evidently undergoes a benzilic acid rearrangement in alkaline solution rather than displacement of chlorine at the position α to the hydrated carbonyl group as might be expected. This suggests the carbonyl group retains its geminal diol structure in solution, thus

[2] TEXSAN/TEXRAY structure analysis package (Molecular Structure Corp., 1985), which includes versions of the following: DIRDIF, direct methods for difference structures, by P. T. Beurskens; ORFLS, full-matrix least squares, and ORFFE, function and errors, by W. R. Busing, K. O. Martin, and H. A. Levy; ORTEP II, illustrations, by C. K. Johnson.

[3] Supplementary material mentioned in the text may be purchased from: The Depository of Unpublished Data, Document Delivery, CISTI, National Research Council Canada, Ottawa, Canada K1A 0R6.

Tables of hydrogen atom coordinates, distances and angles involving the hydrogen atoms, and intermolecular distances involving the non-hydrogen atoms for **5** and **7** have also been deposited with the Cambridge Crystallographic Data Centre and can be obtained on request from The Director, Cambridge Crystallographic Data Centre, University Chemical Laboratory, Lensfield Road, Cambridge, CB2 1EW, U.K.

Can. J. Chem. Downloaded from www.nrcresearchpress.com by 217.78.4.112 on 09/08/12
For personal use only.

TABLE 3. (*a*) Bond lengths (Å) and (*b*) angles (deg) with estimated standard deviations for **5**

(*a*)

Atoms	Distance	Atoms	Distance
Cl(1)—C(1)	1.707(2)	C(1)—C(2)	1.336(3)
Cl(2)—C(2)	1.713(2)	C(1)—C(6)	1.536(3)
Cl(3)—C(5)	1.782(2)	C(2)—C(3)	1.460(3)
Cl(4)—C(5)	1.774(2)	C(3)—C(4)	1.540(3)
O(1)—C(3)	1.210(3)	C(4)—C(5)	1.534(3)
O(2)—C(4)	1.382(3)	C(5)—C(6)	1.566(3)
O(3)—C(4)	1.414(3)	C(6)—C(7)	1.516(4)
O(4)—C(6)	1.427(3)		

(*b*)

Atoms	Angle	Atoms	Angle
Cl(1)—C(1)—C(2)	119.7(2)	C(3)—C(4)—C(5)	109.8(2)
Cl(1)—C(1)—C(6)	114.7(2)	Cl(3)—C(5)—Cl(4)	109.3(1)
C(2)—C(1)—C(6)	125.5(2)	Cl(3)—C(5)—C(4)	106.9(2)
Cl(2)—C(2)—C(1)	123.1(2)	Cl(3)—C(5)—C(6)	109.5(1)
Cl(2)—C(2)—C(3)	115.4(2)	Cl(4)—C(5)—C(4)	109.3(1)
C(1)—C(2)—C(3)	121.5(2)	Cl(4)—C(5)—C(6)	109.6(2)
O(1)—C(3)—C(2)	124.5(2)	C(4)—C(5)—C(6)	112.1(2)
O(1)—C(3)—C(4)	118.5(2)	O(4)—C(6)—C(1)	106.4(2)
C(2)—C(3)—C(4)	116.8(2)	O(4)—C(6)—C(5)	110.8(2)
O(2)—C(4)—O(3)	112.0(2)	O(4)—C(6)—C(7)	106.2(2)
O(2)—C(4)—C(3)	110.7(2)	C(1)—C(6)—C(5)	108.9(2)
O(2)—C(4)—C(5)	110.8(2)	C(1)—C(6)—C(7)	112.3(2)
O(3)—C(4)—C(3)	103.6(2)	C(5)—C(6)—C(7)	112.0(2)
O(3)—C(4)—C(5)	109.8(2)		

TABLE 4. (*a*) Bond lengths (Å) and (*b*) angles (deg) with estimated standard deviations for **7**

(*a*)

Atoms	Distance	Atoms	Distance
Cl(1)—C(1)	1.702(2)	O(4)—C(8)	1.460(3)
Cl(2)—C(2)	1.707(2)	C(1)—C(2)	1.312(4)
Cl(3)—C(4)	1.774(2)	C(1)—C(5)	1.521(3)
Cl(4)—C(4)	1.769(2)	C(2)—C(3)	1.517(3)
O(1)—C(3)	1.382(3)	C(3)—C(4)	1.567(3)
O(2)—C(5)	1.419(3)	C(3)—C(6)	1.551(3)
O(3)—C(6)	1.201(3)	C(4)—C(5)	1.577(3)
O(4)—C(6)	1.308(3)	C(5)—C(7)	1.519(3)

(*b*)

Atoms	Angle	Atoms	Angle
C(6)—O(4)—C(8)	115.5(2)	Cl(3)—C(4)—C(3)	107.7(1)
Cl(1)—C(1)—C(2)	125.6(2)	Cl(3)—C(4)—C(5)	109.7(1)
Cl(1)—C(1)—C(5)	120.7(2)	Cl(4)—C(4)—C(3)	112.2(1)
C(2)—C(1)—C(5)	113.5(2)	Cl(4)—C(4)—C(5)	112.7(2)
Cl(2)—C(2)—C(1)	127.1(2)	C(3)—C(4)—C(5)	106.4(2)
Cl(2)—C(2)—C(3)	119.5(2)	O(2)—C(5)—C(1)	110.2(2)
C(1)—C(2)—C(3)	113.2(2)	O(2)—C(5)—C(4)	111.6(2)
O(1)—C(3)—C(2)	116.4(2)	O(2)—C(5)—C(7)	105.9(2)
O(1)—C(3)—C(4)	110.0(2)	C(1)—C(5)—C(4)	99.0(2)
O(1)—C(3)—C(6)	112.1(2)	C(1)—C(5)—C(7)	115.0(2)
C(2)—C(3)—C(4)	99.3(2)	C(4)—C(5)—C(7)	115.2(2)
C(2)—C(3)—C(6)	106.3(2)	O(3)—C(6)—O(4)	124.4(2)
C(4)—C(3)—C(6)	112.2(2)	O(3)—C(6)—C(3)	123.8(2)
Cl(3)—C(4)—Cl(4)	108.0(1)	O(4)—C(6)—C(3)	111.7(2)

Can. J. Chem. Downloaded from www.nrcresearchpress.com by 217.78.4.112 on 09/08/12
For personal use only.

TABLE 5. Hydrogen bond geometry

Interaction	O—H (Å)	H···O (Å)	O···O (Å)	O—H···O (°)
	5			
O(2)—H(1)···O(1)	0.74(4)	2.18(4)	2.652(3)	122(4)
O(3)—H(2)···O(4)($-x$, $y - 1/2$, $3/2 - z$)	0.77(3)	2.06(3)	2.818(2)	166(3)
O(4)—H(3)···O(3)	0.80(3)	2.05(3)	2.728(3)	142(3)
	7			
O(1)—H(1)···O(2)(x, $1 + y$, z)	0.73(3)	2.06(3)	2.758(3)	160(3)
O(2)—H(2)···O(3)	0.80(3)	1.97(3)	2.727(3)	158(3)

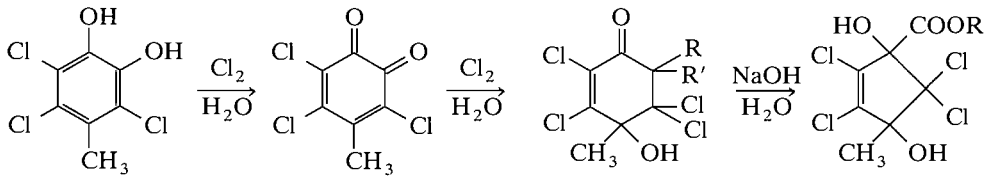

2 **3** **4** R,R′ = carbonyl; **5** R = R′ = OH **6** R = H; **7** R = CH_3

SCHEME 1

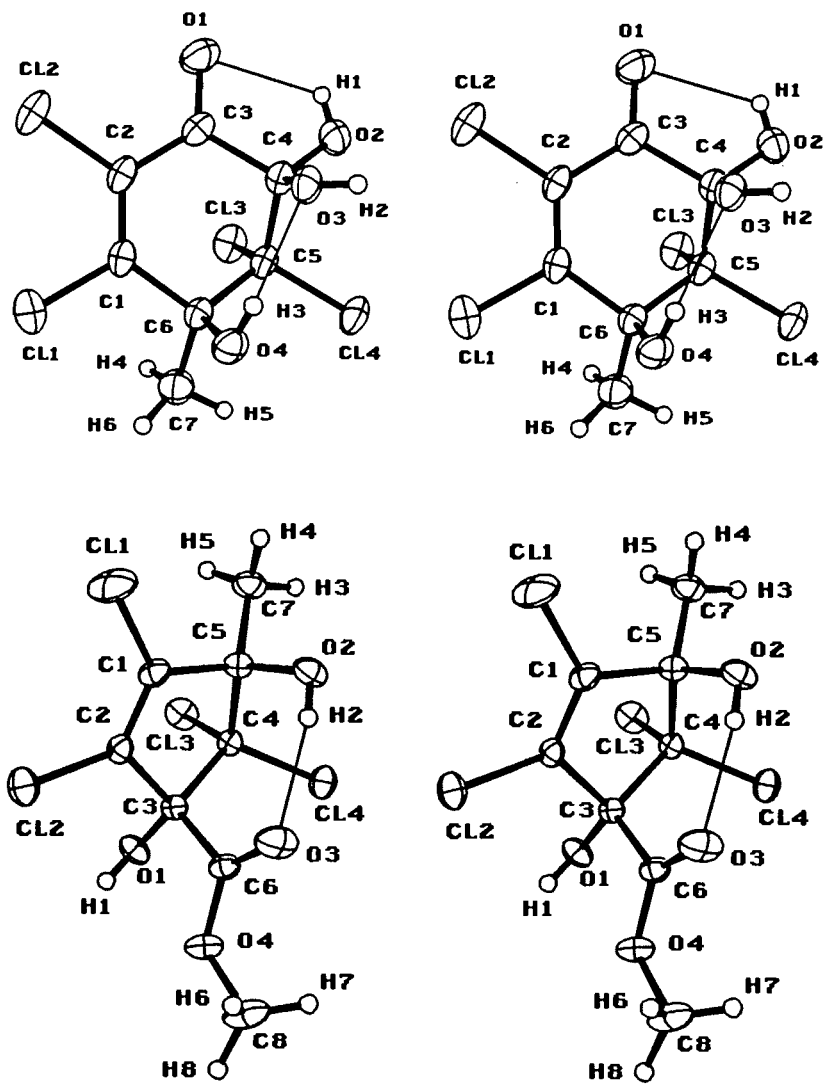

FIG 1. Stereoscopic views of **5** (top) and **7** (bottom) showing atom labelling; 33% probability thermal ellipsoids are shown for the non-hydrogen atoms.

Can. J. Chem. Downloaded from www.nrcresearchpress.com by 217.78.4.112 on 09/08/12
For personal use only.

protecting the chlorine atoms on the adjacent carbon atoms from simple nucleophilic displacement. The ^1H NMR spectrum had indicated that three D_2O-exchangeable protons were present. Also surprising was the fact that epoxide formation was not observed.

Elucidation of the reaction pathway of 4-methyltrichlorocatechol **2** under conditions of classical chlorine bleaching indicates further research on mechanisms for the degradation of aromatic structures in lignin is needed. Formation of the quinone **3** by chlorination of 4-methylguaiacol **1** (R = CH_3) and its subsequent conversion to 3-methyltrichloromuconic acid has been previously reported although, as mentioned in the introduction, structural proof was not provided. The results of the present study, as well as the previous report on the conversion of tetrachlorocatechol and tetrachloro-*o*-benzoquinone to 2,2,4,5-tetrachlorocyclopentene-1, 3-dione, indicate chlorinated muconic acids are not necessarily formed during chlorine bleaching. Further studies are presently underway to determine reaction pathways of the more generalized lignin model **1**.

Bond lengths and angles for the tetrachlorotrihydroxycyclohexenone **5** (Table 3, Fig. 1) are as expected, showing some lengthening of ring bonds between fully substituted carbon atoms. The cyclohexene ring has a C(5)-envelope conformation, C(5) being displaced 0.62 Å from the mean plane of the remaining five ring carbon atoms, which are coplanar to within 0.10 Å. There are two intramolecular O—H···O hydrogen bonds (see Table 5). In the solid state, molecules are linked into infinite chains about the twofold screw axis by O—H···O hydrogen bonding, all other intermolecular distances corresponding to normal van der Waals interactions.

The structure of the rearrangement product **7** is shown in Fig. 1. As noted above for **5**, bond lengths and angles for **7** (Table 4) are generally as expected with bonds between fully substituted carbon atoms showing significant lengthening (particularly those involving C(3) and C(4)). The cyclopentene ring has a C(4)-envelope conformation and the molecule is stabilized by by an intramolecular O—H···O hydrogen bond between the pseudo-axial hydroxyl substituent on C(5) and the carbonyl oxygen atom of the pseudo-axial carbomethoxy substituent on C(3) (see Table 5). In the solid, molecules are O—H···O hydrogen-bonded to form infinite chains along *b*, all other intermolecular distances corresponding to van der Waals interactions.

Acknowledgements

This work has been supported by a consortium of companies including Albright & Wilson Americas; Aracruz Cellulose S. A.; Champion International Corporation; CRS Sirrine, Inc.; Fletcher Challenge Canada Ltd.; International Paper; ITT Rayonier; James River Corporation; Jujo Paper Company Ltd.; Kymmene Corporation; Noranda Inc; The Procter & Gamble Cellulose Co.; Weyerhaeuser Company, and the University Research Incentive Fund.

The authors also thank the Natural Sciences and Engineering Research Council of Canada for financial support. NMR and mass spectrometry services were provided by Dr. A. A. Grey and Dr. H. Pang, respectively, at the University of Toronto Carbohydrate Research Centre.

1. K. V. Sarkanen and C. H. Ludwig. Lignins, occurrence, formation, structure and reactions. Wiley–Interscience, New York. 1971.
2. J. P. Casey. Pulp and paper, chemistry and chemical technology. 3rd ed. Vol. 1. Wiley–Interscience, New York. 1980.
3. J. Gierer. Wood Sci. Technol. **20**, 1 (1986).
4. J. M. Gess and C. W. Dence. Tappi, **54**, 1114 (1971).
5. A. B. McKague, F. de Sousa, L. M. Strömberg, and K. P. Kringstad. Holzforschung, **41**, 191 (1987).
6. M. J. Gray, M. P. Hartshorn, J. Vaughan, and G. J. Wright. Aust. J. Chem. **37**, 2027 (1984).
7. International tables for X-ray crystallography. Vol. IV. Kynoch Press, Birmingham, U.K. (present distributor: Kluwer Academic Publishers. Dordrecht, The Netherlands). 1974. pp. 99–102 and 149.
8. A. B. McKague, S. J. Rettig, J. Trotter, G. R. Douglas, and E. R. Nestmann. Can. J. Chem. **61**, 545 (1983).

Can. J. Chem. Downloaded from www.nrcresearchpress.com by 217.78.4.112 on 09/08/12
For personal use only.

Reactions of 2-phenyl-4*H*-1,3,2-benzodioxaborin, a stable *ortho*-quinone methide precursor

JEFFREY D. CHAMBERS, JASON CRAWFORD, HAYDN W. R. WILLIAMS, CLAUDE DUFRESNE, JOHN SCHEIGETZ, MICHAEL A. BERNSTEIN, AND CHEUK K. LAU[1]

Medicinal Chemistry Department, Merck Frosst Centre for Therapeutic Research, P.O. Box 1005, Pointe Claire-Dorval, Que., Canada H9R 4P8

Received September 17, 1991

JEFFREY D. CHAMBERS, JASON CRAWFORD, HAYDN W. R. WILLIAMS, CLAUDE DUFRESNE, JOHN SCHEIGETZ, MICHAEL A. BERNSTEIN, and CHEUK K. LAU. Can. J. Chem. **70**, 1717 (1992).

Thermolysis of 1-phenyl-4*H*-1,3,2-benzodioxaborins generated the corresponding *ortho*-quinone methides, which were found to undergo intermolecular cycloaddition reactions with ethyl vinyl ether, dihydropyran, β-methylstyrene, cyclohexene, and 1-ethoxy-1-*z*-trimethylsiloxy-1-propenes to give various substituted chromans. Intramolecular trapping of the quinone methides with an olefin led to the syntheses of several analogs of tetrahydrocannabinols. *ortho*-Quinone methides, generated by treatment of the 2-phenyl-4*H*-1,3,2-benzodioxaborins with a Lewis acid, react with various nucleophiles to give the corresponding 1,4-addition products. Thus, alkyl and aryl thiols, alcohols, amine, hydride, allyl trimethylsilane, acetophenone, and diethylmalonate as well as some aryl compounds react with the quinone methide to give various 2-substituted phenols. Intramolecular reaction of the quinone methide with an aryl group led to the preparation of some 4-phenylchromans and tetralins.

JEFFREY D. CHAMBERS, JASON CRAWFORD, HAYDN W. R. WILLIAMS, CLAUDE DUFRESNE, JOHN SCHEIGETZ, MICHAEL A. BERNSTEIN et CHEUK K. LAU. Can. J. Chem. **70**, 1717 (1992).

La thermolyse des 2-phényl-4*H*-1,3,2-benzodioxaborines conduit aux *ortho*-quinométhanes correspondantes qui subissent des réactions de cycloaddition intermoléculaires avec l'éthoxyéthène, le dihydropyrane, le β-méthylstyrène, le cyclohexène et les 1-éthoxy-1-*z*-triméthylsiloxyprop-1-ènes pour conduire à divers chromanes substitués. Le piégeage intramoléculaire des quinométhanes avec une oléfine permet la synthèse de plusieurs analogues des tétrahydrocannabinols. Les *ortho*-quinométhanes, préparés par traitement des 2-phényl-4*H*-1,3,2-benzodioxaborines avec un acide de Lewis, réagissent avec divers nucléophiles pour donner les produits d'additions-1,4 correspondants. Ainsi, les alkyl- et aryl-thiols, les alcools, les amines, les hydrures, l'allyltriméthylsilane, l'acétophénone et le malonate d'éthyle ainsi que certains composés aromatiques réagissent avec le quinométhane pour conduire à divers phénols substitués en position 2. La réaction intramoléculaire des quinométhanes avec un groupe aryle conduit à la préparation de quelques 4-phénylchromanes et de tétralines.

[Traduit par la rédaction]

Can. J. Chem. Downloaded from www.nrcresearchpress.com by 217.78.4.112 on 09/08/12
For personal use only.

Introduction

ortho-Quinone methides **1** are known to be very reactive and unstable intermediates in synthesis (1, 2). As a consequence of this reactivity, di- or trimerization in which one molecule acts as heterodiene and another as dienophile has led to some interesting chroman fused-ring systems (3–6). However, in the presence of electron-rich dienophiles they often react preferentially with these species to form potentially complex chromans (7–11). Intramolecular trapping of these quinone methides by otherwise unreactive dienophiles has also been documented (12–18). In the presence of nucleophiles, *ortho*-quinone methides generated *in situ* undergo Michael addition to give *ortho*-substituted phenols (5, 17, 19).

A variety of methods of *ortho*-quinone methide generation have been reported (2), including pyrolysis of *ortho*-(methoxyalkyl)- or *ortho*-(hydroxyalkyl)phenols (3, 6–8, 12, 13), dehydrohalogenation of 2-chloromethylphenol (4, 20), one-electron oxidation of *ortho*-substituted phenols (5, 9), desilylation of disilylated *ortho*-hydroxybenzyl alcohol (15), photochemical decarbonylation of benzofuran-2(3*H*)-one (10) and treatment of *ortho*-(1-(alkylthio)alkyl)phenols with a variety of metal oxides under mild conditions (11, 16, 17). Recently we reported the preparation of a variety of *ortho*-alkyl, *ortho*-alkoxalkyl, and *ortho*-thioalkyl phenols from 2-phenyl-4*H*-1,3,2-benzodioxaborins, presumably via the quinone methide intermediate (21). Substituted 2-phenyl-4*H*-1,3,2-benzodioxaborins are stable compounds that can be stored indefinitely at room temperature. They are prepared by refluxing a mixture of the corresponding phenol, aldehyde, and phenyl boronic acid in the presence of a catalytic amount of propionic acid in toluene (22, 23). We now report the successful use of these benzodioxaborins as stable precursors of quinone methides in inter- and intramolecular cycloaddition reactions with different dienophiles under pyrolytic conditions as well as their reactions with aryl and alkyl nucleophiles under Lewis acid condition (Scheme 1).

[1]Author to whom correspondence may be addressed.

Results and discussion

Cycloaddition of ortho-quinone methides

ortho-Quinone methide has been generated by pyrolysis of the sulfite ester of 2-hydroxymethylphenol with elimination of sulphur dioxide (24). It was rationalized that 2-phenyl-4*H*-1,3,2-dioxaborin might eliminate phenylboronic anhydride in a similar fashion under pyrolytic condition to give the corresponding quinone methide. Thus, pyrolysis of the unsubstituted 2-phenyl-4*H*-1,3,2-benzodioxaborin **2***a* in the presence of various dienophiles was studied first, to examine the scope and limitation of the reaction. Ethyl vinyl ether was known to trap *ortho*-quinone methides in a [4+2] cycloaddition fashion to give 2-ethoxy chromans (7–11). Heating a solution of **2***a* in ethyl vinyl ether in a base-washed degassed heavy-walled Pyrex tube at 300°C for 72 h gave a 75% yield of the corresponding 2-ethoxychroman **3***a* after chromatography. Similarly, pyrolysis of

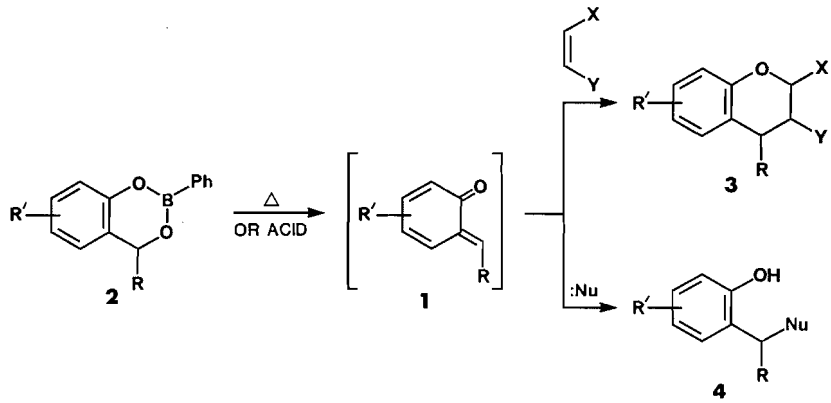

SCHEME 1

2*a* in dihydropyran gave the expected tetrahydropyranobenzopyran **3***b* (4) in a 52% yield in only 5 h. As expected for a cycloaddition reaction, only the *cis*-fused ring compound was obtained. Thus the feasibility of the method as well as the quinone methide intermediacy was established. The results are summarized in Table 1. Attempts to trap the quinone methide with 1-ethoxy-1-trimethylsiloxypropene initially met with some difficulty, due to the extensive polymerization of the dienophile that made the isolation of the initial cycloadduct **3***c* impossible. Eventually, a solution of **2***a* and 1-ethoxy-1-trimethylsiloxypropene in benzene was heated in a sealed tube at 230°C for 18 h. After removal of the volatiles, the crude mixture was treated with tetra-*n*-butylammonium fluoride in tetrahydrofuran. Chromatography of the resulting crude product after normal work-up gave a 23% yield of 3-methyl-2-chromanone **3***d* and 10% of the ethyl 3-(2-hydroxyphenyl)-2-methyl propionate **4***a*. Both **3***d* and **4***a* are the expected desilylation products of the initially formed silyl orthoester **3***c*, as shown in Scheme 2. Pyrolysis of **2***a* with the less electron-rich dienophile, β-methylstyrene, in benzene at 240°C for 48 h in a stainless steel bomb gave the expected *trans*-3-methyl-2-phenylchroman **3***e* in a 50% yield. An unexpected product, 2-benzylphenol (**4***b*), was also isolated in a 20% yield. It is not unlikely that the solvent benzene may have participated in the reaction with the *ortho*-quinone methide to give **4***b*. The reaction was repeated in cyclohexane. Again, **3***e* was isolated in 50% yield and **4***b* was obtained in 20% yield. Similarly, reaction of **2***a* with cyclohexene in cyclohexane at 240°C for 48 h gave 22% of the expected hexahydrodibenzopyran **3***f* having a *cis*-fused ring junction, and 11% of 2-benzylphenol **4***b*. These results indicate that the phenyl group must have been derived from the benzodioxaborin. This was confirmed by thermolysis of **2***a* in cyclohexane at 240°C for 20 h, which gave **4***b* in ~20% yield. Scheme 3 outlines a proposed mechanism of the formation of **4***b* from **2***a*; this may also shed some light on the mechanism of the cycloaddition reaction. Presumably, thermolysis of **2***a* could generate the intermediate **5**, which could expel phenylboronic anhydride to give the free *ortho*-quinone method **1**. In the presence of electron-rich dienophile, either **1** or **5** could react to give the corresponding chroman. In the presence of a less reactive dienophile, compound **5** could undergo a phenyl migration analogous to a [1, 5] sigmatropic phenyl shift (25–29) to give intermediate **6**, which upon work-up gave compound **4***b*. Compound **6** most likely exists as the trimer **7** similar to the formation of trimethoxyboroxine (30). It is interesting to note that no dimer or trimer of the *ortho*-quinone methide was ever isolated in this study. It is likely that intermediate **5** is the reactive species in the cycloaddition reaction instead of the free quinone methide **1**, analogous to the Lewis-acid catalyzed Diels–Alder reaction. The bulky phenyl group on boron may hinder the formation of dimers and trimers.

Indole has been utilized as dienophile in inverse electron demand Diels–Alder reactions (31–33). It is of interest to see if indole would undergo cycloaddition with *ortho*-quinone methide. Pyrolysis of a solution of **2***a* and 5-methoxyindole in cyclohexane at 245°C for 6 h gave a 41% yield of 3-(2-hydroxyphenyl)methyl-5-methoxyindole **4***c* and 11% of 2-(2-hydroxyphenyl)methyl-5-methoxyindole **4***d*. Compound **4***c* may have formed directly from 1,4-addition of the indole to the *ortho*-quinone methide, or via ring opening of the cycloadduct **3***g* (Scheme 4). If the reaction is truly a [4+2] cycloadditon, the ring opening reaction of the resulting cycloadduct may be blocked by placing a substituent on the position 3 of indole. However, thermolysis of **2***a* with methyl 3-indolepropionate gave only methyl 3-(2-(2-hydroxyphenyl)methylindole)propionate **4***f* in a 40% yield. None of the cycloadduct **3***h* was obtained. Presumably, Michael addition of the indole to the *ortho*-quinone methide gave the 3,3-disubstituted compound **4***e*, which rearranged to give **4***f* (Scheme 4). Similarly, compound **4***d* is most likely the rearranged product of **4***c*.

The effect of substituents on the 2-phenyl-4*H*-1,3,2-benzodioxaborin upon the reactivity of the resulting *ortho*-quinone methide was also studied. Several substituted benzodioxaborin derivatives were pyrolized in the presence of ethyl vinyl ether and dihydropyran. The results are summarized in Table 1. Thus, reaction of 2-phenyl-4-ethyl-1,3,2-benzodioxaborin **2***b* with ethyl vinyl ether gave the expected 2-ethoxy-4-ethylchroman **3***i* in 90% yield as a 1:1 mixture of *cis*/*trans* isomers. In contrast, a predominant *cis* isomer was obtained by Inoue *et al.* (11, 17), and Arduini *et al.* (7) who prepared similar compounds using different methods of quinone methide generation. This is probably due to the presence of the phenylboron group on the *ortho*-quinone methide intermediate **5** (Scheme 3) that perturbed the normal *endo* approach of the ethyl vinyl ether towards the quinone methide in the transition state (7). When **2***b* was allowed to react with dihydropyran at various temperatures, no cycloaddition product was obtained. Instead, a 60:40 mixture of 2-(1-propenyl)phenol **8** and its corresponding

Can. J. Chem. Downloaded from www.nrcresearchpress.com by 217.78.4.112 on 09/08/12
For personal use only.

TABLE 1. Thermolysis of 2-phenyl-4*H*-1,3,2-benzodioxaborins in various dienophiles

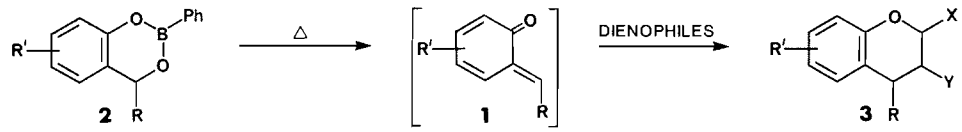

	R	R'	DIENOPHILE	TEMP (°C)	TIME (h)	PRODUCTS (YIELD,[a] %)
2*a*	H	H	CH_2=CHOEt	300	72	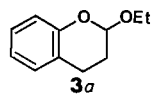 (75) **3***a*
			DHP[b]	300	5	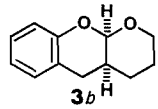 (52) **3***b*
			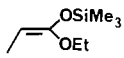	230	13	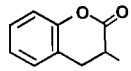 (23) **3***d* + 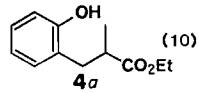 (10) **4***a*
			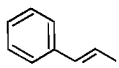	240	48	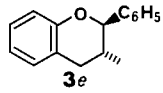 (50) **3***e* + 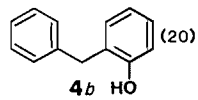 (20) **4***b*
				240	48	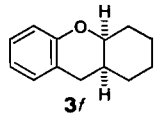 (22) **3***f* + 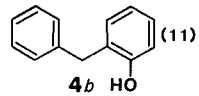 (11) **4***b*
			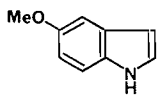	245	6	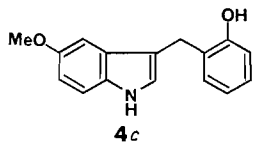 (41) **4***c* + 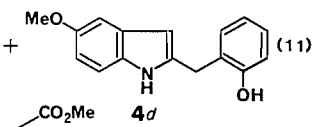 (11) **4***d*
			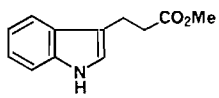	245	4	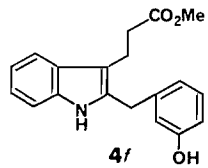 (40) **4***f*
2*b*	CH_2CH_3	H	CH_2=CHOEt	300	18	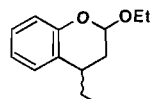 (90) **3***i*
			DHP	250	9.5	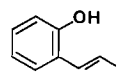 + 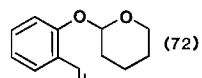 (72) **8** 3 : 2 **9**
2*c*	$CH_2CH_2OC_6H_5$	H	CH_2=CHOEt	250	5.5	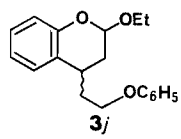 (56) **3***j*
2*d*	H	6-Cl	CH_2=CHOEt	225	18	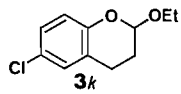 (77) **3***k*
			DHP	235	18	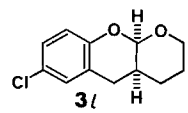 (10) **3***l*

Can. J. Chem. Downloaded from www.nrcresearchpress.com by 217.78.4.112 on 09/08/12
For personal use only.

TABLE 1 (*concluded*)

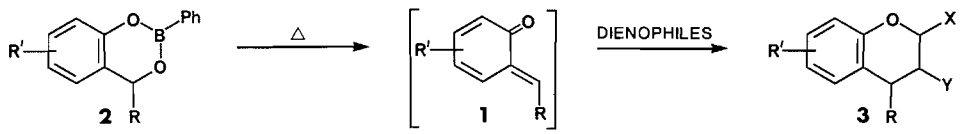

	R	R'	DIENOPHILE	TEMP (°C)	TIME (h)	PRODUCTS (YIELD,[a] %)
2e	CH_2CH_3	6-OMe	CH_2=CHOEt	300	3	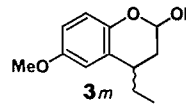 (56)
						3m
2g	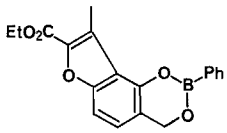		CH_2=CHOEt	300	0.5	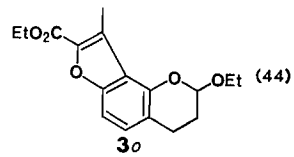 (44)
						3o
			DHP	260	5.5	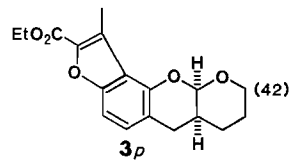 (42)
						3p

[a]ISOLATED YIELD, [b]DIHYDROPYRAN

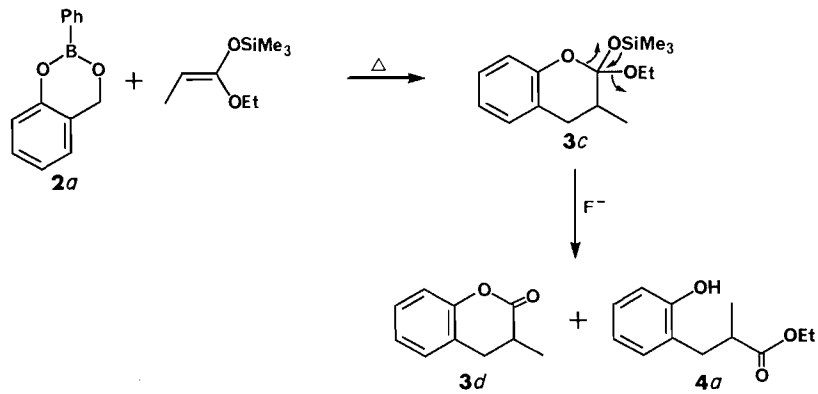

SCHEME 2

tetrahydropyranyl ether **9** was isolated in 72% combined yield. The reactivity of 2-phenyl-4-(2-phenoxyethyl)-1,3,2-benzodioxaborin **2***c* is very similar to the 4-ethyl analog just described. Reaction of **2***c* with ethyl vinyl ether at 250°C for 5.5 h gave 2-ethoxy-4-(2-phenoxyethyl)chroman **3***j* in 56% yield as a 1:1 mixture of *cis*/*trans* isomers. As well, no desired cycloaddition product was obtained with dihydropyran. The ^{1}H NMR spectra of **3***i* and **3***j* ($CDCl_3$ solution) were in accord with the observations made previously on similar compounds (7). Here, rapid interconversion of the half-chair conformation of the *cis* product results in smaller $J_{2,3}$ couplings being observed. In both cases spectral complexity precluded the measurement of $J_{3,4}$ and $J_{3,4'}$ at this field (300 MHz). Thus, $J_{2,3}$ = 4.4 Hz and $J_{2,3'}$ = 2.7 Hz for *trans* **3***j* ($\delta_{H\text{-}2}$ = 5.25), and $J_{2,3}$ = 4.9 Hz and $J_{2,3'}$ = 2.9 Hz for *cis* **3***j* ($\delta_{H\text{-}2}$ = 5.23). The relative stereochemistry was determined in a series of nuclear Overhauser effect (nOe) experiments. When the higher-field H-4 signal (δ 3.20) was irradiated, a 1.6% nOe was observed in that diastereomer's H-2 signal (δ 5.23). This must result from the close contact between these protons in the *cis* molecule where the involved protons are both pseudoaxial. No nOe resulting from such a 1,3 interaction was observed when the H-4 proton of the other diastereomer (δ 3.30) was irradiated. 2D COSY experiments confirmed the overall structure of the molecules.

An electron-withdrawing substituent like chlorine on the phenolic ring (**2***d*) appears to have no significant effect on the reactivity of the cycloaddition reaction with ethyl vinyl ether. The corresponding 2-ethoxychroman **3***k* was isolated in 77% yield. However, reaction of **2***d* with dihydropyran under various reaction conditions gave at best 10% yield of the corresponding tetrahydropyranobenzopyran **3***l*. Electron-donating groups on the phenolic ring seem to in-

Can. J. Chem. Downloaded from www.nrcresearchpress.com by 217.78.4.112 on 09/08/12
For personal use only.

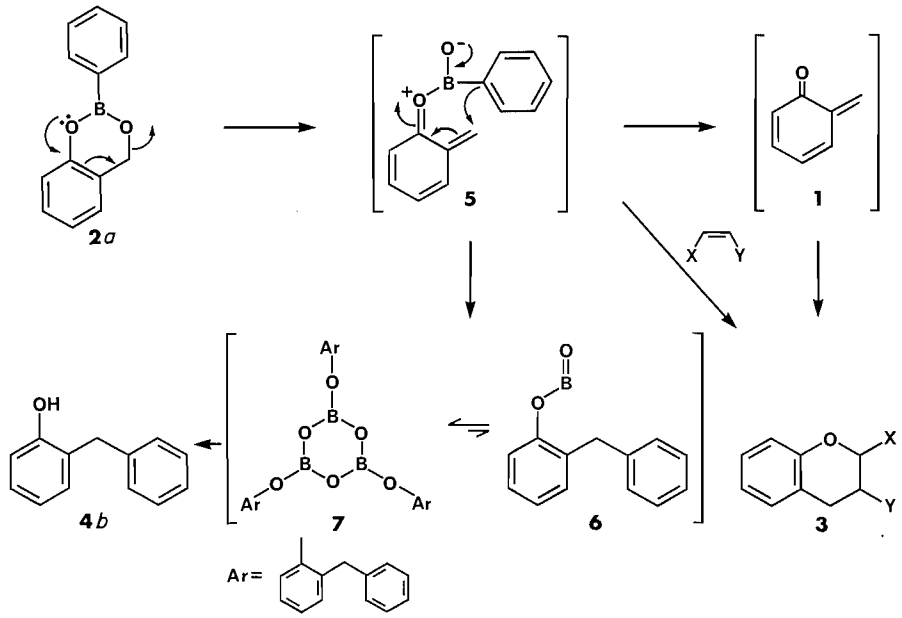

SCHEME 3

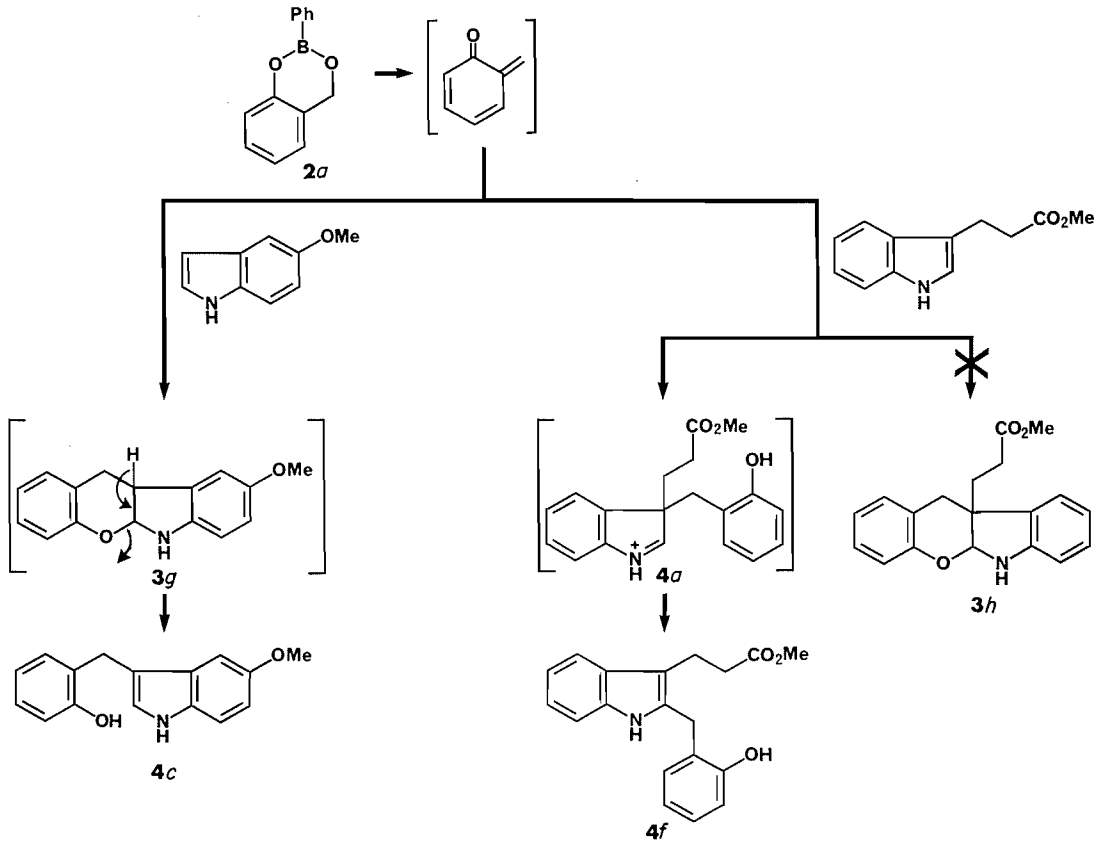

SCHEME 4

crease the reactivity of **2** in the cycloaddition reaction. Complete reaction of 4-ethyl-6-methoxy-2-phenyl-4*H*-1,3,2-benzodioxaborin **2***e* with ethyl vinyl ether occurred in only 3 h at 300°C compared to 72 h for **2***a* or 18 h for **2***b*. The desired product **3***m* was obtained in 56% yield as a 1:1 mixture of *cis*/*trans* isomers. Again, like other 4-substituted benzodioxaborins, **2***e* did not give any cycloadduct when reacted with dihydropyran. The more complex substrate methyl 9-methyl-2-phenyl-1,3,2-dioxaborinbenzofuran-8-carboxylate, **2***g*, was found to react readily with both ethyl vinyl ether and dihydropyran to give the corresponding benzopyran **3***o* and tetrahydropyranobenzopyran **3***p* in 44 and

Can. J. Chem. Downloaded from www.nrcresearchpress.com by 217.78.4.112 on 09/08/12
For personal use only.

TABLE 2. Intramolecular cyclization of 2-phenyl-4*H*-4-(4-pentenyl)-1,3,2-benzodioxaborins

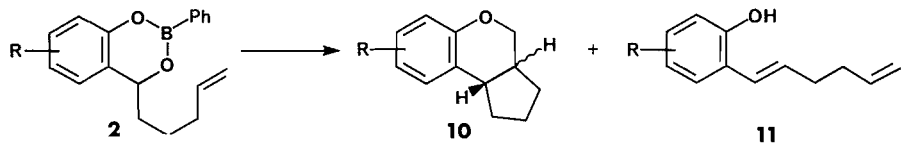

	R	SOLVENT	TEMP (°C)	TIME (h)	PRODUCTS (YIELD, %)	
2*h*	H	$C_6H_5N(Et)_2$	270	0.5	**10***a* (44)	**11** (30)
		BENZENE	300	33	**10***a* (15)	**11** (32)
		$C_6H_4Cl_2$	230	7		**11** (48)
2*i*	7-OMe	BENZENE	230	48	**10***b* (43)	**11** (27)

42% yield respectively in less than 6 h. Again, compound **3***p* has the expected *cis* ring junction. The success of the latter reaction exemplifies the potential utility of the 2-phenyl-4*H*-1,3,2-benzodiozaborins in the formation of highly complex, functionalized fused-ring systems.

Intramolecular trapping of the *ortho*-quinone methide generated by this method was also achieved by heating 4-(4-pentenyl)-1,3,2-benzodioxaborin **2***h* in *N*,*N*-diethylaniline at 270°C for 0.5 h to give the hexahydrocyclopentabenzopyran **10***a* in 44% yield as a mixture of *cis*/*trans* (ratio, 15:85) isomers. A significant amount (30%) of *ortho*-(1,5-hexadienyl)phenol **11***a* was also isolated. The result is in contrast to the report by Hug *et al.* (12) that thermolysis of *ortho*-(1,5-hexadienyl)phenol at 270°C in diethylaniline yields a mixture of 2,6-methanol-3,4,5,6-tetrahydro-2*H*-1-benzoxocin and hexahydrocyclopentabenzopyran of almost equal proportion. The thermolysis of **2***h* in different solvents was studied and the results are summarized in Table 2. In benzene, at 300°C, only 15% yield of the desired cyclopentabenzopyran **10***a* was obtained after 33 h. The major product is diene **11***a* (32%). In *meta*-dichlorobenzene, after 7 h at 230°C, the only product isolated was the diene **11***a* (48%). At higher temperature and prolonged heating, extensive decomposition resulted. With an electron-donating group on the phenol ring, as in the 7-methoxy compound **2***i*, the increased reactivity due to the substituent allowed the reaction to be performed in benzene at lower temperature (230°C) to give 43% of the cyclopentabenzopyran **10***b* as a mixture of *cis*/*trans* isomers (ratio, 1:4) with only 27% yield of the diene **11***b*. The ring-junction stereochemistry of the major isomer of **10***b* was confirmed to be *trans* with ^{1}H NMR experiments. The two $J_{2,3}$ values were 11.3 and 4.1 Hz and this left the literature values (12) ambiguous. There, values of 10 and 4 Hz for these protons indicated a *trans*, and 9 and 5 Hz indicated a *cis*, ring junction. Careful analysis identified H-3 (δ 2.37) as having two large couplings of about 11.5 Hz, and a 6.8 Hz and a 1.25 Hz coupling. Upon irradiation of H-4 (δ 1.73), one of the large couplings collapsed. Molecular models predicted the *trans* isomer would have a 12.2 Hz coupling for the ring-junction protons, and 8.0 Hz for the *cis* compound.

Synthesis of cannabinoids

The successs with the intramolecular [4+2] cycloaddition of the *ortho*-quinone methides generated from the 2-phenyl-4*H*-1,3,2-benzodioxaborins described above prompted us to investigate its application to the synthesis of hexahydrocannabinol analogs. Stereocontrolled syntheses of enantiomeric pure (+)- and (−)-hexahydrocannabinols (HHC) and analogs via intramolecular Diels–Alder reactions of *ortho*-quinone methide have previously been rpeorted (2, 13, 15–18). Using the normal procedure to prepare 2-phenyl-4*H*-1,3,2-benzodioxaborins, reaction of 3-methoxyphenol with (*R*)-(+)-citronelal[2] gave a 70% isolated yield of the optically active (−)-hexahydrodibenzo[*b*,*d*]pyran **12***a* ($[\alpha]_D^{25}$ − 31 (*c* 0.7, $CHCl_3$)) in only 1.5 h. The expected initial product of this reaction, the dioxaborin derivative **2***m*, was also isolated in 10% yield as a mixture of diastereomers. Refluxing the latter in dichlorobenzene gave the same compound, **12***a*. The optical rotation of **12***a* is consistent with other HHC analogs (18). The stereochemistry of **12***a* was confirmed with NMR experiments and references to the analysis of similar compounds described elsewhere (34–36). The deshielded aliphatic signals corresponding to H-10a and H-10eq ($CDCl_3$ solution) at about δ 2.4 suffered considerable overlap and the vicinal coupling constant across the ring junction, *J*(6a, 10a) was measured to be 11.2 Hz from the H-6a signal (δ 1.34); this is consistent with a *trans* ring junction. The equatorial orientation of the 9-Me group and boat conformation of the saturated carbonaceous ring was deduced from analysis of the (highest field) H-10ax (δ 0.88). This proton signal appears as a quartet, due to approximately equal geminal and two *trans* diaxial vicinal *J*'s. H-9 is therefore axial, and the methyl substituent is equatorial. The nOe experiments (data not given) confirm these assignments and show H-10a clearly to be a doubleted triplet, as expected. Finally, ^{13}C NMR spectral analysis was consistent with the given structure (18).

Reaction of orcinol with (*R*)-(+)-citronellal gave a mixture of two regioisomers of the dioxaborin derivatives **2***o* and **2***p* in 82% yield, in the ratio of 2:3. Thermolysis of the mixture in benzene at 215°C for 18 h gave the desired HHC analogs **12***b* and **12***c* in 60% yield in the same ratio as the starting dioxaborin. Analytical samples of **12***b* and **12***c* were

Can. J. Chem. Downloaded from www.nrcresearchpress.com by 217.78.4.112 on 09/08/12
For personal use only.

obtained. The spectral data of **12***b* are virtually identically to those reported (18*b*). The results are summarized in Scheme 5.

Reaction of 3-methoxyphenol with citral gave 45% yield of the cannabichromene analog **13***a*. Similarly with farnesal, compound **13***b* was obtained in 80% yield. No trace of the corresponding dioxaborin intermediate was observed in either case. The formation of **13***a* and **13***b* has been interpreted as proceeding via the electrocyclization of the intermediate *ortho*-quinone methide with the α-double bond as shown in structure **14** of Scheme 5 (37, 38).

Alkylation of ortho-*quinone methides*

ortho-Quinone methide is known to react not only as heterodiene in the Diels–Alder reaction but also as a Michael acceptor (5, 17, 19). Previously we reported the reaction of 2-phenyl-1,3,2-benzodioxaborins with an alcohol, an alkylthiol, or *tert*-butylamine borane in the presence of a Lewis acid or protic acid to give the corresponding 2-substituted phenols (21). Presumably, the reaction involves Michael addition of nucleophiles to the *ortho*-quinone methide intermediate. We now report the alkylation of the *ortho*-quinone methide with carbon nucleophiles to give 2-alkyl phenols. Thus reaction of **2***b*, **2***e*, **2***d*, and **2***j* with allyl trimethylsilane in the presence of boron trifluoride etherate gave the corresponding 2-(3-butenyl)phenol derivatives **4***g*–**4***j*. The results are summarized in Table 3. With the exception of the 6-chloro derivative **2***d*, the yields are reasonable, between 70 and 80%. Reaction of **2***a* with acetophenone in the pres-

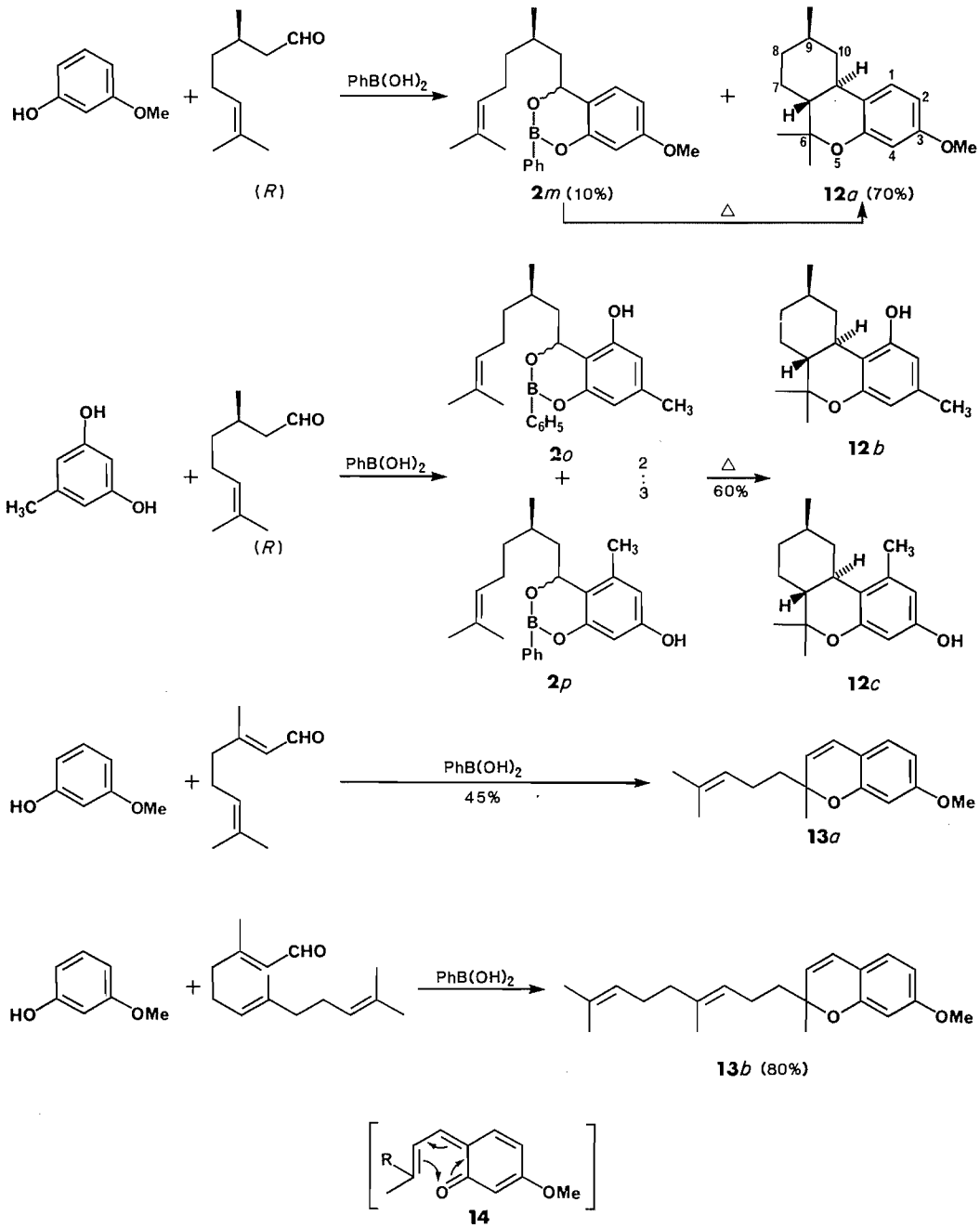

SCHEME 5

Can. J. Chem. Downloaded from www.nrcresearchpress.com by 217.78.4.112 on 09/08/12
For personal use only.

TABLE 3. Reaction of 2-phenyl-4*H*-1,3,2-benzodioxaborins with aliphatic nucleophiles

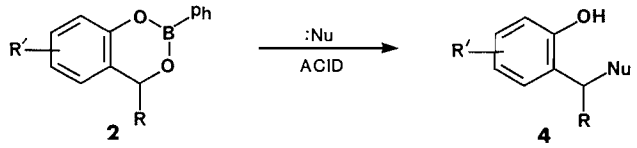

	NUCLEOPHILES	SOLVENT	TEMP (°C)	TIME (h)	ACID (MOL EQUIV.)	PRODUCTS (YIELD %)
2*b*	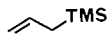	CH_2ClCH_2Cl	70	18	$BF_3{\cdot}Et_2O$ (4)	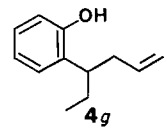 (77) **4***g*
2*e*	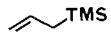	CH_2ClCH_2Cl	70	18	$BF_3{\cdot}Et_2O$ (4)	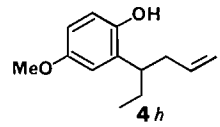 (70) **4***h*
2*d*	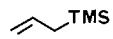	CH_2ClCH_2Cl	70	18	$BF_3{\cdot}Et_2O$ (4)	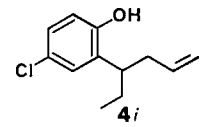 (21) **4***i*
2*j*	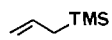	CH_2ClCH_2Cl	70	18	$BF_3{\cdot}Et_2O$ (4)	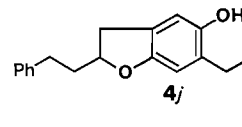 (80) **4***j*
2*a*	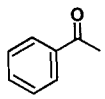	CH_2ClCH_2Cl	70	0.5	$BF_3{\cdot}Et_2O$ (5)	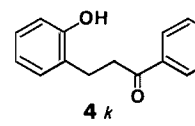 (31) **4***k*
2*f*	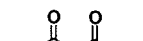	CH_2Cl_2	20	48	$TiCl_4$ (2)	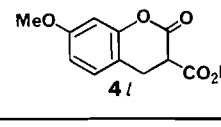 (25) **4***l*

ence of boron trifluoride etherate gave 31% of 2-(3-oxo-3-phenylpropyl)phenol **4***k*. Reaction of **2***f* with diethyl malonate in the presence of titanium tetrachloride gave ethyl 2-oxo-7-methoxybenzopyran-3-carboxylate **4***l* in 25% isolated yield. The latter is the result of lactonization of the initially formed 2-alkylphenol.

Arylation of ortho-*quinone methide*

ortho-Quinone methide generated from 2-phenyl-4*H*-1,3,2-benzodioxaborin under acidic conditions can be viewed as either a protonated quinone methide or a stabilized benzylic cation. Friedel-Crafts alkylations of aromatic systems with benzylic cations are well documented (39). It is thus expected that 2-phenyl-4*H*-1,3,2-benzodioxaborins should react readily with aromatic compounds under acidic conditions to give 2-arylmethyl phenols. Treatment of **2***a* with a Lewis acid in the presence of various aryl substrates gave the expected 2-substituted phenols **4***m*–**4***t*. The results are summarized in Table 4. With a less reactive substrate such as benzene or toluene, which also serves as the solvent, a stronger Lewis acid, titanium tetrachloride, was used as the catalyst. At room temperature after 1.5 h, benzene reacted with 2-phenyl-1,3,2-benzodioxaborin to give 2-benzyl phenol **4***b* in 23% yield. Toluene under similar conditions gave 76% of the 2-(4-methylbenzyl)phenol **4***m*. With the electron-rich anisole and phenol, the reaction was performed in dichloroethane at room temperature with boron trifluoride etherate as catalyst. Both gave a mixture of *ortho*- and *para*-substituted 2-benzyl phenol in the ratio of 1:4 and 1:2 respectively. With thiophene, the reaction was performed at 0°C using aluminum chloride as catalyst. The corresponding product **4***t* was isolated in 56% yield. Reaction of 4-ethyl-2-phenyl-1,3,2-benzodioxaborin **2***b* with toluene, anisol, and thiophene gave similar results to those obtained with **2***a* (Table 4). Reaction of the dioxaborin derivative of 2-(2-phenylethyl)-5-hydroxy-2,3-dihydrobenzofuran **2***j* with thiophene in trifluoroacetic acid at room temperature gave 54% of the desired 6-thiopenyl methyl derivative **4***y*.

Intramolecular alkylation of phenols via trapping of the *ortho*-quinone methide intermediate has been described (40). It was found that the *ortho*-quinone methides generated from 2-phenyl-1,3,2-benzodioxaborins under acidic conditions also react very readily intramolecularly with an aryl substituent. Treatment of 2-phenyl-4-(2-phenoxyethyl)-1,3,2-benzodioxaborin **2***c* with boron trifluoride etherate in dichloromethane at room temperature for 72 h gave the corresponding

Can. J. Chem. Downloaded from www.nrcresearchpress.com by 217.78.4.112 on 09/08/12
For personal use only.

TABLE 4. Reaction of 2-phenyl-4*H*-1,3,2-benzodioxaborins with aryl substrates

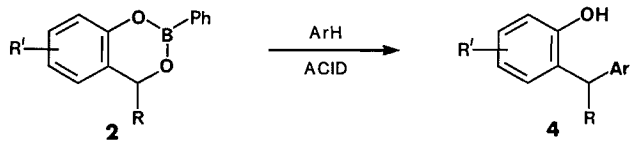

	ArH	SOLVENT	TEMP (°C)	TIME (h)	ACID (MOL EQUIV.)	PRODUCTS (YIELD, %)
2*a*		BENZENE	20	1.5	$TiCl_4$ (5)	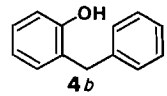 **4***b* (23)
		TOLUENE	20	0.75	$TiCl_4$ (2)	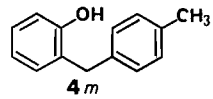 **4***m* (76)
		CH_2ClCH_2Cl	20	72	$BF_3{\cdot}Et_2O$ (5)	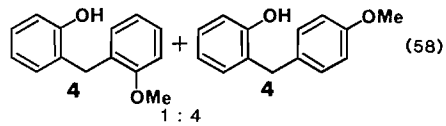 4 : 4 (58)
		CH_2ClCH_2Cl	20	24	$BF_3{\cdot}Et_2O$ (5)	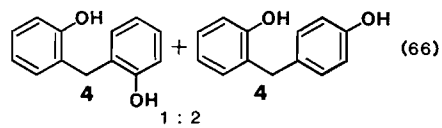 1 : 2 (66)
		CH_2Cl_2	0	0.16	$AlCl_3$ (3)	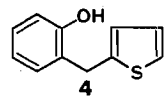 **4** (56)
2*b*		TOLUENE	0	0.75	$TiCl_4$ (2)	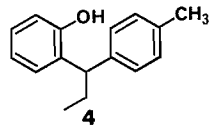 **4** (75)
		CH_2Cl_2	20	21	$BF_3{\cdot}Et_2O$ (5)	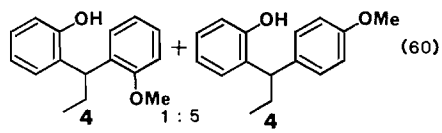 1 : 5 (60)
		CH_2Cl_2	0	0.16	$AlCl_3$ (3)	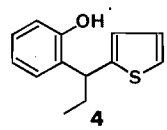 **4** (75)
2*j*		TFA	20	2	—	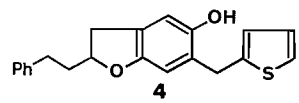 **4** (54)

4-(2-hydroxyphenyl)chroman **16***a* in 99% yield (Table 5). Similarly, with the dihydrobenzofuran derivative **2***k*, the corresponding 4-substituted chroman **16***b* was obtained in 78% yield. With 7-methoxy-2-phenyl-4-(3-(3-*tert*-butyldiphenylsiloxphenyl)propyl)-4*H*-1,3,2-benzodioxaborin **2***l*, the resulting tetraline **16***c* was obtained in 53% yield as a mixture of 6- and 8-*tert*-butyldiphenylsiloxy derivatives in the ratio of 1:3. These reactions represent a very efficient route to 4-phenyl substituted chromans and tetralins.

In summary, we have shown that 2-phenyl-1,3,2-benzodioxaborins serve as stable quinone methide precursors that can be prepared readily from phenols and aldehydes with varying degrees of substitution. These highly substituted benzodioxaborins can react inter- and intramolecularly with different dienophiles to generate potentially complex polycyclic chroman systems without any dimer- or trimerization of the corresponding quinone methide intermediate. Trapping of the *ortho*-quinone methide intermediates generated under acidic conditions with various carbon nucleophiles or an aryl substrate expands the utility of 2-phenyl-1-3,2-benzodioxaborins in the *ortho*-alkylation of phenols (20). Intramolecular trapping of the quinone methides with an aryl

Can. J. Chem. Downloaded from www.nrcresearchpress.com by 217.78.4.112 on 09/08/12
For personal use only.

TABLE 5. Intramolecular reactions of 2-phenyl-1,3,2-benzodioxaborins with aryl substituents

SUBSTRATE	SOLVENT	TEMP. °C	TIME (h)	LEWIS ACID (MOL EQUIV.)	PRODUCTS (YIELD %)
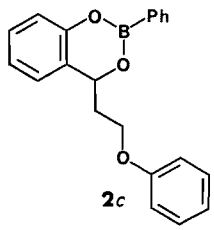 **2c**	CH_2Cl_2	20	72	$BF_3{\cdot}Et_2O$ (1.3)	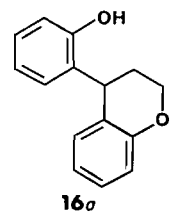 **16a** (98)
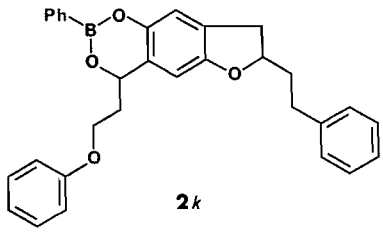 **2k**	CH_2Cl_2	20	20	$BF_3{\cdot}Et_2O$ (1.3)	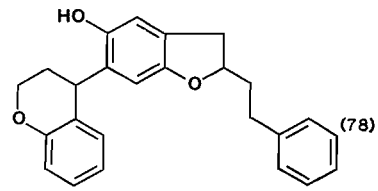 **16b** (78)
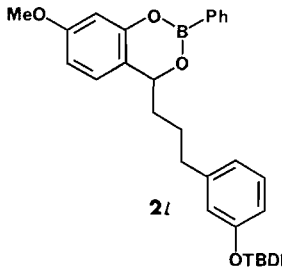 **2l**	CH_2Cl_2	20	20	TFA	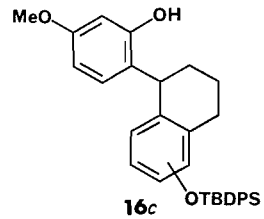 **16c** 75 : 25 ORTHO/PARA (53)

substituent provides an efficient route to 4-phenyl-substituted chromans and tetralines (Scheme 6).

Experimental

General information

Proton nuclear magnetic resonance spectra were obtained on a Bruker AM250 spectrometer or AM300 spectrometer. Reported boiling points are those observed during distillation with a Kugelrohr apparatus and are uncorrected. Melting points were measured on a Buchi 510 melting point apparatus and are uncorrected. Low-resolution mass spectral analyses were performed by the Morgan-Schaffer Corporation, Montreal. Exact masses were obtained by high-resolution mass spectroscopy performed by Dr. O. Maimer of McGill University, Montreal, Quebec. Elemental analyses were performed by Guelph Chemical Laboratories Ltd., Guelph, Ontario. Flash chromatography was performed using Merck silica gel 60, 230–400 mesh, and tlc using Merck silica gel 60F 254 sheets.

General procedure A

Preparation of 4-ethyl-2-phenyl-4H-1,3,2-benzodioxaborin (2b)

A mixture of phenol (31 g, 0.33 mol), phenylboronic acid (64.5 g, 0.527 mol), propionaldehyde (58 g, 1 mol), and propionic acid (7.3 g, 0.1 mol) in toluene was heated under reflux for 20 h, with azeotropic removal of water using a Dean-Stark trap. The reaction mixture was concentrated and the resulting oil was chromatographed (eluting with 5% ethyl acetate in hexane) to give 64 g (82%) of the title compound; mp 43–45°C; ^{1}H nmr (250 MHz, $CDCl_3$), δ: 1.05 (t, 3H, J = 8.34 Hz, CH_3), 1.75–2.1 (m, 2H, CH_2), 5.25 (dd, 1H, J = 8.34 Hz, J' = 4.1 Hz, benzylic), 7.00–7.55 (m, 7H), 8.0 (dd, 2H, J = 9.38 Hz, J' = 2.1 Hz). Anal. calcd. for $C_{15}H_{15}BO_2$: C 75.66, H 6.35, B 4.54; found: C 75.56, H 6.64, B 4.68.

4-(2-Phenoxyethyl)-2-phenyl-4H-1,3,2-benzodioxaborin (2c)

According to the general procedure A, using 3-phenoxypropionaldehyde, the title compound was obtained in 80% yield after chromatography; mp 91–93°C; ^{1}H nmr (250 MHz, $CDCl_3$), δ: 2.18–2.35 (m, 1H), 2.35–2.51 (m, 1H), 4.08–4.20 (m, 1H, OCH_2), 4.26–4.40 (m, 1H, OCH_2), 5.50 (dd, 1H, J = 9.3 Hz, J' = 4 Hz, PhCH), 6.85–7.55 (m, 12H, 7.98, dd, 2H, J = 7.5 Hz, J' = 1.7 Hz). Exact Mass calcd. for $C_{21}H_{19}BO_3$: 330.1427; found: 330.1423.

6-Chloro-2-phenyl-4H-1,3,2-benzodioxaborin (2d)

According to the general procedure A, using 4-chlorophenol and paraformaldehyde, the title compound was obtained in 59% yield after chromatography; mp 86–90°C; ^{1}H nmr (250 MHz, $CDCl_3$), δ: 5.34 (s, 2H, PhCH), 7.15–7.65 (6H, m), 8.05–8.10 (m, 2H), Anal. calcd. for $C_{13}H_{10}O_2BCl$: C 63.87, H 4.12, B 4.42, Cl 14.50; found: C 63.17, H 4.13, B 4.34, Cl 14.62.

4-Ethyl-6-methoxy-2-phenyl-4H-1,3,2-benzodioxaborin (2e)

According to the general procedure A, using 4-methoxyphenol, the title compound was obtained as an oil in 56% yield after chromatography on silica gel; ^{1}H nmr (250 MHz, $CDCl_3$), δ: 1.05 (t, 3H, J = 7 Hz), 1.70–2.15 (m, 2H), 3.80 (s, 3H, OCH_3), 5.20 (t, 1H, J = 5.7 Hz, PhCH), 6.55 (d, 1H, J = 3 Hz), 6.75 (dd, 1H, J = 10 Hz, J' = 3 Hz), 7.0 (d, 1H, J = 10 Hz), 7.35–7.6 (m, 3H), 8.0 (d, 2H, J = 8 Hz). Anal. calcd. for $C_{16}H_{17}O_3B$: C 71.68, H 6.39, B 4.03; found: C 71.89, H 6.53, B 4.10.

4-Ethyl-7-methoxy-2-phenyl-1,3,2-benzodioxaborin (2f)

According to the general procedure A, using 4-methoxyphenol, the title compound was obtained as an oil in 56% yield after chromatography; ^{1}H nmr (250 MHz, $CDCl_3$), δ: 1.00 (t, 3H, J =

Can. J. Chem. Downloaded from www.nrcresearchpress.com by 217.78.4.112 on 09/08/12
For personal use only.

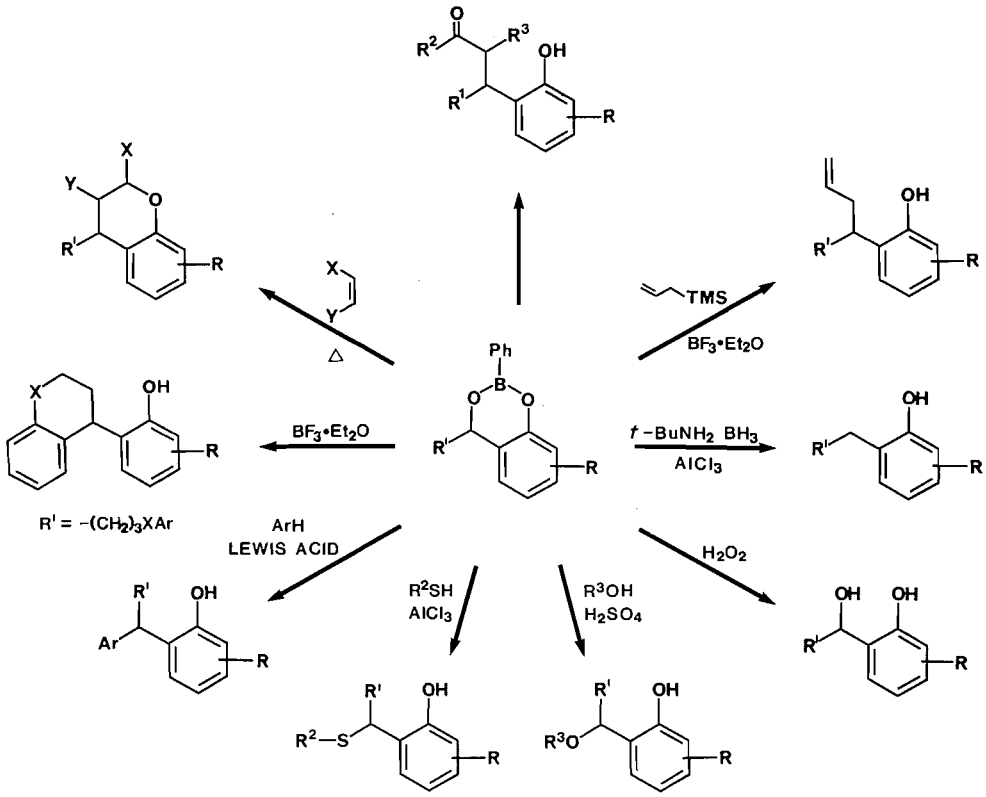

SCHEME 6

6.25 Hz), 1.69–2.05 (m, 2H), 3.8 (s, 3H, OCH_3), 5.19 (dd, 1H, J = 12.5 Hz, J' = 6.25 Hz, benzylic), 6.6 (dd, 1H, J = 12.5 Hz, J' = 3 Hz), 6.65 (d, 1H, J = 3 Hz), 6.9 (d, 1H, J = 12 Hz), 7.3–7.55 (m, 3H), 7.95 (d, 2H, J = 9.37 Hz). Exact Mass calcd. for $C_{16}H_{18}O_3B$ (M + 1): 269.1348; found: 269.1346.

4-(4-Pentenyl)-2-phenyl-1,3,2-benzodioxaborin (2h)

According to the general procedure A, using 5-heptenal, the title compound was obtained as an oil in 44% yield after chromatography; ^{1}H nmr (250 MHz, $CDCl_3$), δ: 1.54–2.22 (m, 6H), 4.90–5.10 (m, 2H, $=CH_2$), 5.25 (dd, 1H, J = 7.8 Hz, J' = 3.8 Hz, PhCH), 5.70–5.90 (m, 1H, CH=), 7.0–7.6 (m, 7H), 7.97 (d, 2H, J = 8 Hz). Exact. Mass calcd. for $C_{18}H_{19}BO_2$: 278.1478; found: 278.1475.

7-Methoxy-4-(4-pentenyl)-2-phenyl-4H-1,3,2-benzodioxaborin (2i)

According to the general procedure A, using 5-heptenal and 3-methoxyphenol, the title compound was obtained as an oil in 85% yield after chromatography; ^{1}H nmr (250 MHz, $CDCl_3$), δ: 1.55–2.2 (m, 6H), 3.78 (s, 3H), 4.95 (m, 2H, olefinic), 5.25 (dd, 1H, J = 9.37 Hz, J' = 6.25 Hz), 5.7–5.9 (m, 1H, olefinic), 6.62 (dd, 1H, J = 12.5 Hz, J' = 3 Hz), 6.65 (d, 1H, J = Hz), 6.95 (d, 1H, J = 10.9 Hz), 7.38–7.55 (m, 3H, aromatic), 8.0 (dd, 2H, J = 9.37, J' = 3 Hz). Exact Mass calcd. for $C_{19}H_{22}O_3B$(M + 1): 309.1662; found: 309.1658.

7,8-Dihydro-2-phenyl-2-(2-phenylethyl)-4H-furo[2,3-g]-1,3,2-benzodioxaborin (2j)

According to the general procedure A, using 2,3-dihydro-2-(2-phenyethyl)5-benzofuranol and paraformaldehyde, the title compound was obtained in 94% yield; mp 93–96°C; ^{1}H nmr (250 MHz, $CDCl_3$), δ: 1.88–2.25 (m, 2H), 2,7–2.92 (m, 3H), 3.28 (dd, 1H, J = 7.5 Hz), 4.79 (m, 1H), 5.18 (s, 2H), 6.41 (s, 1H), 6.91 (s, 1H), 7.14–7.35 (m, 5H), 7.35–7.55 (m, 5H), 7.95 (d, 2H, J = 6 Hz). Anal. calcd. for $C_{23}H_{21}BO_3$: C 77.52, H 5.89, B 3.03; found: C 77.69, H 5.85, B 3.09. Exact Mass calcd. for $C_{23}H_{22}BO_3$(M + 1): 357.1662; found: 357.1659.

7,8-Dihydro-2-phenyl-7-(2-phenylethyl)-4-(2-phenoxyethyl)-4H-furo[2,3-g]-1,3,2-benzodioxaborin (2k)

According to the general procedure A, using 2,3-dihydro-2-(2-phenyethyl)5-benzofuranol and 3-phenoxypropionaldehyde, the title compound was obtained in 90% yield after chromatography; mp 90–92°C; ^{1}H nmr (250 MHz, $CDCl_3$), δ: 1.88–2.07 (m, 1H), 2.07–2.27 (m, 2H), 2.34–2.48 (m, 1H), 2.70–2.91 (m, 3H), 3.27 (dd, J = 15 Hz, J' = 9 Hz), 4.09–4.18 (m, 1H), 4.25–4.36 (m, 1H), 4.70–4.75 (m, 1H), 5.45 (d br, 1H, PhCOH), 6.49 (d, 1H J = 2Hz), 6.90–6.97 (m, 3H), 7.16–7.52 (m, 11H), 7.94 (dd, 2H, J = 7 Hz, J' = 2 Hz). Exact Mass calcd. for $C_{31}H_{29}O_4B + NH_4^+$: 494.2502; found: 494.2499.

4-[3-(3-tert-Butyldiphenylsiloxphenyl)propyl]-4-phenyl-4H-1,3,2-benzodioxaborin (2l)

According to the general procedure A, using 3-methoxyphenol and 4-(3-*tert*-butyldiphenyl)butylaldehyde, the title compound was obtained in 66% yield; ^{1}H nmr (250 MHz, $CDCl_3$), δ: 1.1 (s, 9H, *tert*-butyl), 1.6–1.85 (m, 4H), 2.45 (m, 2H), 3.75 (s, 3H, OCH_3), 5.15 (m, 1H, benzylic), 6.55–6.70 (m, 5H), 6.82 (d, 1H, J = 9.3 Hz), 6.95 (t, 1H, J = 7.5 Hz), 7.25–7.55 (m, 9H), 7.7 (d, 4H, J = 9.3 Hz), 7.95 (d, 2H, J = 9.3 Hz). Anal. calcd. for $C_{39}H_{41}O_4SiB$: C 76.47, H 6.70, B 1.76, Si 4.58; found: C 76.41, H 6.98, B 2.01, Si 4.75. Exact Mass calcd. for $C_{39}H_{41}O_4SiB$ − (*t*-Bu): 555.2162; found: 555.2162.

General procedure B

Thermolysis of 2-phenyl-4H-1,3,2-benzodioxaborin (2a) in ethyl vinyl ether and dihydropyran

A solution of the dioxaborin **2a** (0.212 g, 1 mmol) in ethyl vinyl ether (3 mL) was placed in a base-washed heavy-walled Pyrex tube equipped with a Teflon stopper. The solution was degassed for 2 min and then sealed under nitrogen. The tube was heated at 300°C for 72 h. Upon cooling, the reaction mixture was concen-

Can. J. Chem. Downloaded from www.nrcresearchpress.com by 217.78.4.112 on 09/08/12
For personal use only.

Can. J. Chem. Downloaded from www.nrcresearchpress.com by 217.78.4.112 on 09/08/12
For personal use only.

trated under vacuum. The residual oil was chromatographed on silica gel (eluted with 2.5% ethyl acetate in hexane) to give 2-ethoxychroman **3***a* (0.134 g, 75%) (17); ^{1}H nmr (300 MHz, $CDCl_3$), δ 1.19 (t, 3H, J = 7 Hz), 1.89–2.10 (m, 2H), 2.57–2.72 (m, 1H), 2.90–3.07 (m, 1H), 3.57–3.71 (m, 1H), 3.83–3.97 (m, 1H), 5.26 (t, 1H, J = 3 Hz, OCHO), 6.80–6.92 (m, 2H), 7.02–7.17 (m, 2H). Anal. calcd. for $C_{11}H_{14}O_2$: C 74.13, H 7.92; found: C 74.14, H 8.15. Similarly, pyrolysis of **2***a* in dihydropyran for 5 h at 300°C gave the expected 3,4,4a,10a-tetrahydro-*cis*-2*H*, 5*H*-pyrano[2,3-*b*][1]benzopyran **3***b* (3) in 52% yield; ^{1}H nmr (300 MHz, $CDCl_3$), δ: 1.59–1.77 (m, 4H), 2.10–2.26 (m, 1H), 2.66 (dd, 1H, J = 16.6 Hz, J' = 4.8 Hz), 2.89–3.01 (dd, 1H, J = 16.6 Hz, J' = 4.8 Hz), 3.69–3.79 (m, 1H), 3.96–4.11 (m, 1H), 5.34 (d, 1H, J = 2.6 Hz, OCHO, *cis*-fused), 6.81–6.93 (m, 2H), 7.00–7.17 (m, 2H), Exact Mass calcd. for $C_{12}H_{14}O_2$: 190.0993; found: 190.0993.

*Thermolysis of 2-phenyl-4*H*-1,3,2-benzodioxaborin (**2**a) in 1-ethoxy-1-trimethylsiloxy-1-propene*

According to the general procedure B, a mixture of 2-phenyl-4*H*-1,3,2-benzodioxaborin **2***a* (318 mg, 1.5 mmol) and 1-ethoxy-1-trimethylsiloxy-1-propene (1.04 g, 6 mmol) in benzene (6 mL) was heated to 230°C for 18 h in a stainless steel bomb. The crude reaction mixture was treated with 1 equivalent of tetra-*n*-butyl ammonium fluoride, followed by normal work-up and chromatography, to give a mixture of 3-methyl-2-chromanone **3***d* (23%) and ethyl 3-(2-hydroxyphenyl)-2-methylpropionate **4***a* (10%). **3***d*: mp 57–59°C; ir (film): 1770 (C=O) cm^{-1}; ^{1}H nmr (250 MHz, $CDCl_3$), δ: 1.29 (d, 3H, J = 6.2 Hz, CH_3), 2.7–3.1 (m, 3H), 6.9–7.4 (m, 4H). Anal. calcd. for $C_{10}H_{10}O_2$: C 74.06; H 6.21; found: C 74.09, H 6.33. **4***a*: ir (film): 3400 (OH), 1710 (C=O) cm^{-1}; ^{1}H nmr (250 MHz, CD_3COCD_3), δ: 1.10 (t, 3H, J = 7 Hz, CH_3), 2.6–3.0 (m, 3H), 4.01 (q, 2H, J = 7 Hz), 6.60–7.10 (m, 2H), 8.28 (s, 1H, OH).

*Thermolysis of 2-phenyl-4*H*-1,3,2-benzodioxaborin (**2**a) in the presence of trans-β-methylstyrene*

According to the general procedure B, a mixture of 2-phenyl-4*H*-1,3,2-benzodioxaborin **2***a* (420 mg, 2 mmol) and *trans*-β-methylstyrene (708 mg, 6 mmol) in benzene (6 mL) was heated to 240°C for 48 h in a stainless steel bomb. The *trans*-3-methyl-2-phenylchroman **3***e* was isolated in 50% yield after chromatography. Another product, the 2-benzylphenol **4***b* was obtained in 20% yield. **3***e*: mp 68–70°C; ^{1}H nmr (250 MHz, $CDCl_3$), δ: 0.85 (d, 3H, J = 6.3 Hz, CH_3), 2.20 (m, 1H), 2.65 (dd, 1H, J = 16.8 Hz, J' = 11 Hz, PhCH), 2.87 (dd, 1H, J = 16.8 Hz, J' = 6.2 Hz, PhCH), 4.61 (d, 1H, J = 8.7 Hz, OCH), 6.7–7.5 (m, 9H). Anal. calcd. for $C_{16}H_{16}O$: C 85.68, H 7.19; found: C 85.73, H 7.27. **4***b*: ir (film): 3530 (OH) cm^{-1}; ^{1}H nmr (250 MH_3, $CDCl_3$), δ: 3.99 (s, 2H), 6.7–7.4 (m, 9H). Spectral data identical to commercial material.

The reaction was repeated in cyclohexane under identical condition. Compound **3***e* was obtained in 48% and **4***b* was isolated in 17% yield.

*Thermolysis of 2-phenyl-4*H*-1,3,2-benzodioxaborin (**2**a) in the presence of cyclohexene*

According to the general procedure B, a mixture of 2-phenyl-4*H*-1,3,2-benzodioxaborin **2***a* (420 mg, 2 mmol) and cyclohexene (492 mg, 6 mmol) in cyclohexane (6 mL) was heated to 240°C for 48 h in a stainless steel bomb. The 1,2,3,4,4a,10a-hexahydrodibenzopyran **3***f* was isolated in 22% yield after chromatography on silica gel; mp 78–79°C; ^{1}H nmr (250 MHz, $CDCl_3$), δ: 1.3–1.8 (m, 8H), 2.0 (m, 1H), 2.48 (dd, 1H, J = 16.7 Hz, J' = 2.6 Hz, PhCH), 3.0 (dd, 1H, J = 16.7 Hz, J' = 6 Hz, PhCH), 4.2 (m, 1H, OCH), 6.7–6.9 (m, 2H), 6.95–7.20 (m, 2H). Anal. calcd. for $C_{13}H_{16}O$: C 82.94, H 8.57; found: C 82.88, H 8.83. Compound **4***b* was also isolated in 11%.

*Thermolysis of 2-phenyl-4*H*-1,3,2-benzodioxaborin (**2**a) in the presence of 5-methoxy indole*

According to the general procedure B, a mixture of 2-phenyl-4*H*-1,3,2-benzodioxaborin **2***a* (420 mg, 2 mmol) and 5-methoxyindole (883 mg, 6 mmol) in cyclohexane (6 mL) was heated to 245°C for 6 h in a stainless steel bomb. 3-(2-Hydroxyphenyl)methyl-5-methoxyindole **4***c* was isolated in 41% yield and 2-(2-hydroxyphenyl)methyl-5-methoxyindole **4***d* was obtained in 11% yield after chromatography of the crude mixture. Compound **4***c*: ^{1}H nmr (250 MHz, CD_3COCD_3), δ: 3.75 (s, 3H, OCH_3), 4.05 (s, 2H, $PhCH_2$), 6.65–7.20 (m, 7H), 7.25 (d, 1H, J = 8.9 Hz), 8.25 (s, 1H, OH), 9.85 (bs, 1H, NH). Exact Mass calcd. for $C_{16}H_{16}NO_2$(M + 1): 254.1181; found 254.1181. **4***d*: ^{1}H nmr (250 MHz, CD_3COCD_3), δ: 3.72 (s, 3H, OCH_3), 4.08 (s, 2H, $PhCH_2$), 6.12 (s, 1H, H-3 indole), 6.6–7.3 (m, 7H), 8.46 (bs, 1H, OH), 9.26 (bs, 1H, NH). Exact Mass calcd. for $C_{16}H_{16}NO_2$(M + 1): 254.1181; found 254.1181.

*Thermolysis of 2-phenyl-4*H*-1,3,2-benzodioxaborin (**2**a) in the presence of methyl 3-(3-indole)propionate*

According to the general procedure B, a mixture of 2-phenyl-4*H*-1,3,2-benzodioxaborin **2***a* (420 mg, 2 mmol) and methyl 3-(3-indole) propionate (406 mg, 2 mmol) in cyclohexane (6 mL) was heated to 245°C for 4 h to give, after chromatography, 241 mg (40%) of methyl 3-(2-(2-hydroxyphenyl)methylindole)propionate **4***f*: ir (film): 3410 (OH, NH), 1715 (C=O) cm^{-1}; ^{1}H nmr (250 MHz, $CDCl_3$), δ: 2.58 (t, 2H, J = 8 Hz), 3.10 (t, 2H, J = 8 Hz), 3.57 (s, 3H, OCH_3), 4.11 (s, 2H, PhCH), 6.65–7.10 (m, 6H), 7.26 (dd, 1H, J = 6 Hz, J' = 1.8 Hz), 7.47 (dd, J = 6 Hz, J' = 1.8 Hz), 8.55 (s, 1H, OH), 9.71 (s, 1H, NH). Anal. calcd. for $C_{19}H_{19}O_3N$: C 73.77, H 6.19, N 4.53; found: C 73.23, H 6.06, N 4.49. Exact Mass calcd. for $C_{19}H_{20}NO_3$(M + 1): 310.1443; found 310.1442.

*Thermolysis of 4-ethyl-2-phenyl-4*H*-1,3,2-benzodioxaborin (**2**b) in ethyl vinyl ether*

According to the general procedure B, thermolysis of **2***b* in ethyl vinyl ether at 300°C for 18 h gave 90% yield after chromatography of 2-ethoxy-4-ethylchroman **3***i* as a mixture of 1:1 *cis*/*trans* isomers (17); ^{1}H nmr (300 MHz, $CDCl_3$) assignment was based on nOe experiments; resolved signals of *cis*-**3***i*: δ: 2.75–2.88 (m, 1H, PhCH), 5.16 (dd, 1H, J = 7 Hz, J' = 3 Hz, OCHO); resolved signals of *trans*-**3***i*: δ: 2.90–3.03 (m, 1H, PhCH), 5.26 (t, 1H, J = 3 Hz). Other resonances: 0.94–1.05 (m, 3H), 1.15–1.33 (m, 3H), 1.53–2.23 (m, 4H), 3.56–3.73 (m, 1H), 3.83–4.10 (m, 1H), 6.80–6.99 (m, 2H), 7.06–7.29 (m, 2H). Anal. calcd. for $C_{13}H_{18}O_2$: C 75.69, H 8.80; found: C 75.71, H 8.82.

*Thermolysis of 4-ethyl-2-phenyl-4*H*-1,3,2-benzodioxaborin (**2**b) in dihydropyran*

According to the general procedure B, thermolysis of **2***b* in dihydropyran at 250°C for 9.5 h gave a mixture of *trans*-2-(1-propenyl)phenol **8** and its corresponding tetrahydropyranyl ether **9** in a ratio of 60:40 and a combined yield of 72%. Spectral data of compound **8** are identical to commercial material.

*Thermolysis of 4-(3-phenoxypropyl)-2-phenyl-4*H*-1,3,2-benzodioxaborin (**2**c) in ethyl vinyl ether*

According to the general procedure B, thermolysis of **2***c* in ethyl vinyl ether at 250°C for 5.5 h gave 56% yield of 2-ethoxy-4-(2-phenoxyethyl)chroman **3***j* as a 1:1 mixture of *cis-trans* isomer after chromatography; ^{1}H nmr (300 MHz, $CDCl_3$) assignment was based on nOe experiment; *trans*-**3***j*: δ: 1.21 (t, 3H, J = 3 Hz), 1.80–2.24 (m, 4H), 2.49–2.54 (m, 1H), 3.16–3.36 (m, 1H, 3.51–3.71 (m, 1H), 3.82–4.00 (m, 1H), 4.09 (t, 2H, J = 7 Hz), 5.25 (dd, 1H, J = 4.4 Hz, J' = 2.7 Hz), 6.73–7.39 (m, 9H); *cis*-**3***j*: δ: 1.19 (t, 3H, J = 7 Hz), 1.88–2.06 (m, 1H), 2.09–2.28 (m, 2H), 2.33–2.49 (m, 1H), 3.12–3.28 (m, 1H), 3.52-3.67 (m, 1H), 3.87–4.03 (m, 1H), 4.11 (t, 2H, J = 7 Hz), 5.23 (dd, 1H, J = 4.9 Hz, J' = 2.9 Hz), 6.76–7.37 (m, 9H); ms, *m*/*z*: 298 (M^+, 1.7), 253 (91), 177 (28), 159 (37), 133 (100), 131 (26). Exact Mass calcd. for $C_{17}H_{17}O_2$: (M − OC_2H_5): 253.1227; found: 253.1228.

*Thermolysis of 6-chloro-2-phenyl-4*H*-1,3,2-benzodioxaborin (**2**d) in ethyl vinyl ether*

According to the general procedure B, thermolysis of **2***d* in ethyl vinyl ether in a stainless steel bomb at 225°C for 18 h gave, after

Can. J. Chem. Downloaded from www.nrcresearchpress.com by 217.78.4.112 on 09/08/12
For personal use only.

chromatography, 77% yield of 6-chloro-2-ethoxychroman **3***k* as an oil; ^{1}H nmr (250 MHz, $CDCl_3$), δ: 1.18 (t, 3H, J = 7 Hz), 1.85–2.15 (m, 2H), 2.59 (ddd, 1H, J = 16.3 Hz, J' = 5.8 Hz, J'' = 3.5 Hz, PhCH), 2.93 (m, 1H), 3.5–4.0 (m, 2H, OCH_2), 5.24 (t, 1H, J = 2.8 Hz, OCH), 6.74 (d, 1H, J = 8.4 Hz), 7.0–7.1 (m, 2H). Exact Mass calcd. for $C_{11}H_{13}ClO_2{\cdot}NH_4^+$: 230.0947; found: 230.0947.

*Thermolysis of 6-chloro-2-phenyl-4*H*-1,3,2-benzodioxaborin (2*d*) in dihydropyran*

According to the general procedure B, thermolysis of **2***d* in dihydropyran in a stainless steel bomb at 235°C for 18 h gave 10% yield of 7-chloro-3,4,4a,10a-tetrahydro-*cis*-2*H*,5*H*-pyrano[2,3-*b*][1]benzopyran **3***l* as an oil after chromatography; ^{1}H nmr (250 MHz, CD_3COCD_3), δ: 1.44–1.8 (m, 4H), 2.1–2.3 (m, 1H), 2.65 (dd, 1H, OCHO, J = 16.8 Hz, J' = 5 Hz, PhCH), 2.93 (dd, J = 16.8 Hz, J' = 5.8 Hz, PhCH), 3.55–3.70 (m, 1H, OCH), 3.80–4.00 (m, 1H, OCH), 3.80–4.00 (m, 1H, OCH), 5.30 (d, 1H, J = 2 Hz, OCHO), 6.77 (d, 1H, J = 8.5 Hz), 7.06 (s, 1H), 7.07 (d, 1H, J = 8.5 Hz). Exact Mass calcd. for $C_{12}H_{14}O_2Cl(M + 1)$: 225.0682; found: 225.0682.

*Thermolysis of 6-methoxy-2-phenyl-4*H*-1,3,2-benzodioxaborin (2*e*) in ethyl vinyl ether*

According to the general procedure B, thermolysis of **2***e* in ethyl vinyl ether at 300°C for 3 h gave, after chromatography, 56% yield of 2-ethoxy-4-ethyl-6-methoxychroman **3***m* as a mixture of 1:1 *cis/trans* isomers; ^{1}H nmr (250 MHz, $CDCl_3$), resolved signals of *cis*-**3***m*: δ: 2.75 (m, 1H, PhCH), 5.11 (dd, J = 7 Hz, J' = 2.7 Hz, OCHO); resolved signals of *trans*-**3***m*: δ: 2.95 (m, 1H, PhCH), 5.22 (t, 1H, J = 2.9 Hz, OCHO). Other resonances: 0.93–1.0 (3H, m), 1.15–1.27 (3H, m, J = 7 Hz), 1.57–2.20 (4H, m), 2.7–3.0 (1H, m), 3.55–4.10 (2H, m), 3.76 (3H, s), 5.10–5.25 (1H, m), 6.67–6.80 (3H, m). Anal. calcd. for $C_{14}H_{20}O_3$: C 71.16, H 8.53; found: C 71.08, H 8.54.

*Thermolysis of 9-methyl-2-phenyl-4*H*-1,3,2-dioxaborin[6,5-*e*]-benzofuran-8-carboxylate (2*g*) in ethyl vinyl ether*

According to the general procedure B, thermolysis of **2***g* in ethyl vinyl ether at 300°C for 0.5 h gave 44% yield of ethyl 3,4-dihydro-2-ethyoxy-9-methyl-2*H*-furo[2,3-*h*]-1-benzopyran-8-carboxylate **3***o* as an oil after chromatography; ^{1}H nmr (250 MHz, $CDCl_3$), δ: 1.22 (t, 3H, J = 7 Hz), 1.43 (t, 3H, J = 7 Hz), 1.93–2.17 (m, 2H), 2.62–2.80 (m, 1H), 2.76 (s, 3H), 2.91–3.08 (m, 1H), 3.62–3.77 (m, 1H), 3.86–4.02 (m, 1H), 4.42 (q, 2H, J = 7 Hz), 5.30 (t, 1H, J = 3 Hz, OCHO), 7.00–7.10 (m, 2H). Anal. calcd. for $C_{17}H_{20}O_5$: C 67.09, H 6.62; found: C 66.92, H 6.56.

*Thermolysis of 9-methyl-2-phenyl-4*H*-1,3,2-dioxaborin[6,5-*e*]-benzofuran-8-carboxylate (2*g*) in dihydropyran*

According to the general procedure B, thermolysis of **2***g* in dihydropyran at 260°C for 5.5 h gave, after chromatography, 42% yield of ethyl-10-methyl-2*H*,5*H*-furo[2,3-*h*]pyrano[2,3-*b*][1]benzopyran-9-carboyxlate **3***p* as an oil; ^{1}H nmr (250 MHz, $CDCl_3$), δ: 1.44 (t, 3H, J = 7 Hz), 1.58–1.78 (m, 4H), 2.17–2.31 (m, 1H), 2.63 (dd, 1H, J = 16 Hz, J' = 4.5 Hz), 2.79 (s, 3H), 3.01 (dd, 1H, J = 16 Hz, J' = 4.5 Hz), 3.70–3.85 (m, 1H), 3.97–4.13 (m, 1H), 4.42 (q, 2H, J = 7 Hz), 5.47 (d, 1H, J = 2 Hz, OCHO), 7.00–7.10 (m, 2H). Anal. calcd. for $C_{18}H_{20}O_5$: C 68.34, H 6.37; found: C 68.63, H 6.74.

*Thermolysis of 4-(4-pentenyl)-2-phenyl-4*H*-1,3,2-benzodioxaborin (2*h*)*

According to the general procedure B, thermolysis of **2***h* in *N*,*N*-diethylaniline at 270°C for 0.5 h gave, after chromatography, a mixture of *trans*-2-(1,5-hexadienyl)phenol **11***a* (30% yield) (12) and 1,2,3,3a,4,9b-hexahydrocyclopenta[*c*][1]benzopyran **10***a* (44% yield) as a mixture of *cis/trans* isomers (ratio 1:3)(6, 12); ^{1}H nmr (250 MHz, $CDCl_3$), resolved signals of *trans*-**10***a*: δ: 4.05 (dd, 1H, J = 10 Hz, J' = 10 Hz, OCH_2), 4.54 (dd, 1H, J = 10 Hz, J' = 4 Hz, OCH_2); resolved signal of *cis*-**10***a*: δ: 3.60 (t, 1H, J = 10 Hz, OCH_2); other resonances: 1.15–2.60 (m, 8H), 6.80–7.25 (m, 4H); ms, *m/z*: 174 (M^+, 100), 159 (35), 145 (65), 131 (98), 120 (30), 115 (20), 107 (35).

Thermolysis of **2***h* in benzene at 300°C for 33 h gave 15% yield of the 3,4-propanochroman **10***a* and 33% of the diene **11***a*. Thermolysis of **2***h* in *o*-dichlorobenzene at 230°C for 7 h gave only the diene **11***a* in 45% yield.

*Thermolysis of 7-methoxy-4-(4-pentenyl)2-phenyl-4*H*-1,3,2-benzodioxaborin (2*i*)*

According to the general procedure B, thermolysis of **2***i* in benzene (0.1 M) at 230°C for 48 h gave, after chromatography, 43% of the 7-methoxy-1,2,3,3a,4-9b-hexahydroxyclopenta[*c*][1]benzopyran **10***b* as a mixture of *cis/trans* isomers in the ratio of 1:4 respectively and 27% yield of the *trans*-2-(1.5-hexadienyl)-5-methoxyphenol **11***b*; ^{1}H nmr (250 MHz, $CDCl_3$), resolved signal of *trans*-**10***b*: δ: 1.73 (m, 1H, H-4, $J_{3,4}$ = 11 Hz), 2.37 (m, 1H, H-3), 2.80 (s, 3H, OCH_3), 3.97 (m, 1H, H-2a, $J_{2a,3}$ = 11.3 Hz), 4.45 (m, 1H, H-2e, $J_{2e,3}$ = 4.1 Hz); other resonances: δ 6.31 (dd, J = 2.7 Hz, J' = 2.7 Hz), 6.37 (ddd, J = 8.3 Hz, J' = 2.6 Hz, J'' = 2.6 Hz), 6.89 (dd, 1H, J = 8.3 Hz, J' = 1.1 Hz). Exact Mass calcd. for $C_{13}H_{17}O_2$ (M + 1): 205.1228; found: 205.1228. **11***b*: ^{1}H nmr (250 MHz, $CDCl_3$), δ: 1.95–2.4 (m, 4H), 3.75 (s, 3H, OMe), 4.9–5.05 (m, 2H), 5.7–6.10 (m, 1H), 6.3–6.55 (m, 2H), 7.15–7.30 (m, 3H).

*Preparation of (6a*R*,9*R*,10a*R*)-6,6,9-trimethyl-3-methoxy-6a,7,8,9,10,10a-hexahydro-6*H*-dibenzo[*b,d*]pyran (12*a*)*

According to the general procedure A, using 4-methoxyphenol and (*R*)-citronellal, the title compound **12***a* was obtained, after chromatography, as an oil in 70% yield after 1.5 h reflux in toluene; ^{1}H nmr (250 MHz, $CDCl_3$), δ: 0.8–0.95 (m, 1H), 0.98 (d, 3H, J = 6.25 Hz), 1.0–1.1 (m, 1H), 1.05 (s, 3H), 1.2–1.35 (m, 1H), 1.38 (s, 3H), 1.5–1.7 (m, 1H), 1.8 (m, 2H), 2.35 (m, 2H), 3.75 (s, 3H, OCH_3), 6.35 (d, 1H, J = 3 Hz), 6.45 (dd, 1H, J = 12.5, J' = 3 Hz), 7.1 (d, 1H, J = 12.5 Hz). Exact Mass calcd. for $C_{17}H_{25}O_2$ (M + 1): 261.1854; found: 261.1853. The intermediate 2-phenyl-4*H*-1,3,2-benzodioxaborin **2***m* was also isolated in 10% yield. Thermolysis of the dioxaborin **2***m* in refluxing *o*-dichlorobenzene for 18 h resulted in complete conversion to the title compound.

*Preparation of (6a*R*,9*R*,10a*R*)-1-hydroxy-3,6,6,9-tetramethyl-6a,7,8,9,10,10a-hexadyro-6*H*-dibenzo[*b,d*]pyran (12*b*) and (6a*R*,9*R*,10a*R*)-3-hydroxy-1,6,6,9-tetramethyl-6a,7,8,9,10,10a-hexahydro-6*H*-dibenzo[b,d]pyran (12*c*)*

According to the general procedure A, a mixture of orcinol (1.0 g, 7 mmol), citronelal (2.5 g, 14 mmol), phenyl boronic acid (1.36 g, 11.2 mmol), and propionic acid (30 μL, 0.35 mmol) in benzene (45 mL) was refluxed for 20 h. The reaction was quenched with NH_4OAc (100 mL) and extracted with ethyl acetate. The organic extract was dried over Na_2SO_4 and concentrated *in vacuo*. The residue was chromatographed on silica gel using 15% ethyl acetate/hexane as eluent to yield 3.3 g of a mixture of regioiosomer boronate (**2***o* and **2***p*) contaminated with citronelal. Flash distillation of the mixture (100°C, 0.1 Torr; 1 Torr = 133.3 Pa) gave 1.98 (77% yield) of boronates **2***o* and **2***p* in the ratio of 2:3. The mixture was pyrolyzed in benzene (36 mL) at 220°C in a stainless steel bomb for 2 days. After cooling, the mixture was chromatographed on silica gel and eluted with 2% ethyl acetate in hexane, yielding 0.33 g of **12***b* and 0.54 g of **12***c* (61% combined yield); ^{1}H nmr (500 MHz, $CDCL_3$) of **12***b*: δ: 0.78 (q, 1H, H-10_{ax}, J (10_{ax}, 10_{eq}) ≃ J (10_{ax}, 9) ≃ J (10_{ax}, 10a) ≃ 11.7 Hz), 0.95 (d, 3H, 9-Me, J = 6.5 Hz), 1.07 (s, 3H, 6-Me), 1.10 (m, 2H, 7_{ax}, 8_{ax}), 1.37 (s, 3H, 6-Me), 1.45 (dt, 1H, H-6a, J (6a, 10a) ≃ J (6a, 7_{ax} = 12.0 Hz), 1.6 (m, 1H, H-9), 1.8 (m, 2H, H-7, H-8), 2.19 (s, 3H, 3-Me), 2.45 (dt, 1H, H-10a, J (10a,6a) ≃ J (10a,10_{ax}) ≃11.0 Hz), 3.03 (br d, 1H, H-10_{eq}, J = 12.9 Hz), 6.08 (s, 1H, H-2 or H-4), 6.25 (s, 1H, H-2 or H-4); ^{13}C nmr (125 MHz, $CDCl_3$), δ: 19.0 (q, Me), 20.9 (q, Me), 22.6 (q, 9-Me), 27.7 (q, Me), 28.1 (t, C-7), 32.9 (d, C-9), 35.4 (d, C-10a), 35.5 (t, C-8), 39.0 (t, C-10), 49.2 (d, C-6a), 108.3 (d), 110.1 (s), 110.8 (d), 137.4 (s), 154.8 (s),

Can. J. Chem. Downloaded from www.nrcresearchpress.com by 217.78.4.112 on 09/08/12
For personal use only.

155.1 (s). Exact Mass calcd. for $C_{17}H_{25}O_2$ (M + 1): 261.1855; found: 261.1853. **12***c*, ^{1}H nmr (500 MHz, $CDCl_3$), δ: 0.79 (q, 1H, H-10_{ax}, J (10_{ax}, 10_{eq}) = J (10_{ax}, 9) ≃ J (10_{ax}, 10a) = 11.5 Hz), 0.95 (d, 3H, 9-Me, J = 6.6 Hz), 1.03 (s, 3H, 6-Me), 1.10 (m, 2H, H-7_{ax}, H-8_{ax}), 1.36 (s, 3H, 6-Me), 1.50 (dt, 1H, 6a, J (6a, 10a) ≃ J (6a, 7_{ax}) ≃ 10.9 Hz, J (6a, 7_{eq}) = 2.2 Hz), 1.64 (m, 1H, H-9), 1.8 (m, 2H, H-7_{eq} and H-8_{eq}), 2.30 (s, 3H, 3-Me), 2.38 (dt, 1H, H-10a, J(10a, 6a) = J(10a, 10_{ax}) ≃ 10.9 Hz, J (10a, 10_{eq}) = 2.3 Hz), 2.47 (br d, 1H, H-10_{eq}, J = 13.0 Hz), 4.46 (br s, 1H, OH), 6.13 (d, 1H, J = 2.6 Hz), 6.22 (d, 1H, J = 2.6 Hz); ^{13}C nmr (125 MHz, $CDCl_3$), δ: 18.8 (q, Ar-Me), 21.8 (q, Me), 22.8 (q, Me), 27.8 (q, Me), 28.5 (t, C-7), 33.1 (d, C-9), 35.7 (t, C-8), 37.4 (d, C-10a), 40.9 (t, C-10), 50.4 (d, C6a), 102.1 (d), 110.5 (d), 117.6 (s), 138.7 (s), 154.3 (s), 155.2 (s). Exact Mass calcd. for $C_{17}H_{25}O_2$ (M + 1): 261.1855; found: 261.1853.

*Preparation of 7-methoxy-2-(4-methyl-3-pentenyl)-2H-1-benzopyran (**13**a)*

According to the general procedure A, using 4-methoxyphenol and citral, the title compound was obtained in 45% yield, after chromatography, as an oil after 1.5 h reflux in toluene; ^{1}H nmr (250 MHz, $CDCl_3$), δ: 1.4 (s, 3H), 1.55 (s, 3H), 1.7 (m, 5H), 2.05–2.2 (m, 2H), 3.78 (s, 3H, OCH_3), 5.1 (t, 1H, J = 6.25 Hz), 5.45 (d, 1H, J = 12.5 Hz), 6.30 (d, 1H, J = 12.5 Hz), 6.35 (s, 1H), 6.38 (dd, 1H, J = 12.5, J' = 3 Hz), 6.85 (d, 1H, J = 12.5 Hz). Anal. calcd. for $C_{17}H_{22}O_2$: C 79.06, H 8.52; found: C 78.61, H 8.68. Exact Mass calcd. for $C_{17}H_{23}O_2$ (M + 1): 259.1696; found: 259.1698.

*Preparation of 7-methoxy-2-(4,8-dimethyl-3,7-nonadienyl)-2-H-1-benzopyran (**13**b)*

According to the general procedure A, using 4-methoxyphenol and farnesal, the title compound was obtained in 80% yield as an oil after 1.5 h reflux in toluene; ^{1}H nmr (250 MHz, $CDCl_3$), δ: 1.38 (s, 3H), 1.55–1.75 (m, 13H), 1.90–2.2 (m, 4H), 3.75 (s, 3H, OCH_3), 5.1 (m, 2H), 5.45 (dd, 1H, J = 12.5 Hz, J' = 3 Hz), 6.35 (d, 1H, J = 12.5 Hz), 6.40 (m, 2H), 6.85 (d, 1H, J = 9.4 Hz).

General Procedure C

*Preparation of 2-(1-ethylbut-3-enyl)phenol (**4**g)*

To a solution of 4-ethyl-2-phenyl-1,3,2-benzodioxaborin (**2***b*) (0.238 g, 1.0 mmol) and allyltrimethylsilane (0.456 g, 4.0 mmol) in dichloroethane (10 mL) was added boron trifluoride etherate (0.568 g, 4.0 mmol). The mixture was warmed to 70°C for 20 h. The resulting solution was cooled, and then poured into an aqueous solution of ammonium acetate (20%). Extraction with ethyl acetate followed by chromatography of the concentrated extracts gave 136 mg (77%) of the title compound as an oil; ^{1}H nmr (250 MHz, $CDCl_3$), δ: 0.82 (t, 3H, J = 7.3 Hz), 1.55–1.80 (m, 2H), 2.33–2.40 (m, 2H), 2.80–2.95 (m, 1H, PhCH), 4.60 (s, 1H), 4.70–5.0 (m, 2H, =CH_2), 5.55–5.80 (m, 1H, =CH), 6.5–7.2 (m, 4H). Exact Mass calcd. for $C_{12}H_{16}O{\cdot}NH_4^+$: 194.1544; found: 194.1544.

*2-(1-Ethylbut-3-ene)-4-methoxyphenol (**4**h)*

According to the general procedure C, from **2***e*, the title compound was obtained in 70% yield as an oil; ^{1}H nmr (250 MHz, $CDCl_3$), δ: 0.82 (t, 3H, J = 7.3 Hz), 1.50–1.80 (m, 2H), 2.33–2.40 (m, 2H), 2.80–3.00 (m, 1H, PhCH), 3.76 (s, 3H, OCH_3), 4.67 (s, 1H, OH), 4.96 (m, 2H, =CH_2), 5.65–5.85 (m, 1H, =CH), 6.58–6.72 (m, 3H). Exact Mass calcd. for $C_{13}H_{18}O_2{\cdot}NH_4^+$: 224.1650; found: 224.1650.

*4-Chloro-2-(1-ethylbut-3-eneyl)phenol (**4**i)*

According to the general procedure C, from **2***d*, the title compound was obtained in 21% as an oil; ^{1}H nmr (300 MHz, $CDCl_3$), δ: 2.29–2.43 (m, 2H), 2.62–2.75 (m, 2H), 4.68 (s, 1H, OH), 4.97–5.15 (m, 2H, =CH_2), 5.78–5.97 (m, 1H, =CH), 6.69 (d, 1H, J = 7.5 Hz), 7.04 (dd, 1H, J = 7.5 Hz, J' = 2 Hz), 7.10 (d, 1H, J = 2 Hz). Anal. calcd for $C_{10}H_{11}ClO$: C 65.76, H 6.07, Cl 19.41; found: C 65.03 H 5.97, Cl 19.42.

*6-Butenyl-2,3-dihydro-2(2-phenylethyl)-5-benzofuranol (**4**j)*

According to the general procedure C, from **2***j*, the title compound was obtained in 80% as an oil; ir (film): 3401 (OH) cm^{-1}; ^{1}H nmr (250 MHz, $CDCl_3$), δ: 1.85–2.20 (m, 2H), 2.30–2.45 (m, 2H), 2.60–2.90 (m, 5H), 3.50 (dd, 1H, J = 15.4 Hz, J' = 8.7 Hz), 4.31 (s, 1H, OH), 4.65–4.85 (m, 1H, OCH), 4.97–5.12 (m, 2H, =CH_2), 5.84–5.95 (m, 1H, =CH), 6.56 (s, 1H), 6.62 (s, 1H), 7.16–7.32 (m, 5H). Exact Mass calcd. for $C_{20}H_{22}O_2{\cdot}NH_4^+$: 312.1963; found: 312.1965.

*Preparation of 2-(3-oxo-3-phenylpropyl)phenol (**4**k)*

Boron trifluoride etherate (3.0 mL, 25 mmol) was added to a solution of 2-phenyl-4*H*-1,3,2-benzodioxaborin **2***a* (1.05 g, 5 mmol) and acetophenone (1.8 g, 15 mmol) in 1,2-dichloroethane (15 mL). The mixture was refluxed for 30 min and then washed with water. The organic layer was dried ($MgSO_4$), filtered, concentrated, and the residue chromatographed using 5% ethyl acetate in hexane to give 350 mg (31%) of the title compound as an oil; ir (film): 1655 (C=O) cm^{-1}; ^{1}H nmr (250 MHz, $CDCl_3$), δ: 2.6 (s, 4H), 7.1–8.1 (m, 9H).

*Preparation of ethyl 4-ethyl-2-oxo-7-methoxybenzopyran-3-carboxylate (**4**l)*

To a cooled (0°C) solution of $TiCl_4$ (90 μL, 0.82 mmol) in CH_2Cl_2 (10 mL) was added diethylmalonate (113 μL, 0.746 mmol). The mixture was stirred for 10 min at 0°C, then 4-ethyl-7-methoxy-2-phenyl-1,3,2-benzodioxaborin (0.2 g, 0.746 mmol) was added. After stirring for another 5 min, triethylamine (113 μL, 0.858 mmol) was added. The mixture was stirred at 9°C for 30 min and then overnight at room temperature. Another equivalent of $TiCl_4$ (0.746 μL, 82 mmol) was added. The mixture was stirred at room temperature overnight. The reaction mixture was quenched with cold ammonium acetate (20%) and extracted with ethyl acetate. The extract was dried over Na_2SO_4 and evaporated to dryness. The residue was chromatographed, eluting with 5% ethyl acetate/hexane. The title compound was obtained as an oil in 25% yield; ^{1}H nmr (250 MHz, $CDCl_3$) δ: 0.95 (t, 3H, J = 9.4 Hz), 1.05 (t, 3H, J = 9.4 Hz), 1.5–1.75 (m, 2H), 3.2 (m, 1H), 3.75 (d, 1H, J = 3 Hz), 3.80 (s, 3H, methoxy), 4.05 (m, 2H), 6.65–6.7 (m, 2H), 7.05 (d, 1H, J = 9.4 Hz). Exact Mass calcd. for $C_{15}H_{19}O_5$ (M + 1); 279.1232; found: 279.1232.

General Procedure D

*Preparation of 2-benzyl phenol (**4**b)*

Titanium tetrachloride (0.94 g, 5 mmol) was added to a solution of 2-phenyl-4*H*-1,3,2-benzodioxaborin **2***a* (1.05 g, 5 mmol) in benzene (15 mL) and the resultant solution stirred for 1.5 h at room temperature. The solution was cooled to 5°C and excess 1 N HCl added. The mixture was stirred until two clear layers were formed. The organic layers was separated, dried ($MgSO_4$), filtered, and concentrated. The resulting oil was chromatographed on silica gel using 10% ethyl acetate in hexane as eluent to give 0.21 g (23%) of the title compound as an oil; ^{1}H nmr (250 MHz, $CDCl_3$), δ: 3.99 (s, 2H, $PhCH_2$), 6.7–7.4 (m, 9H). Spectral data identical to commercial material.

*Preparation of 2-(4-methylbenzyl)phenol (**4**m)*

According to the general procedure D, using toluene as solvent, the title compound was obtained in 76% yield as an oil after 45 min at room temperature with only 2 mol equivalent of titanium tetrachloride; ^{1}H nmr (250 MHz, CDCl3), δ: 2.3 (s, 3H, CH_3), 3.9 (s, 2H, $PhCH_2$), 6.7–7.3 (m, 8H). Exact Mass calcd. for $C_{14}H_{15}O$ (M + 1): 199.1122; found: 199.1122.

*Preparation of 2-[1-(4-methylphenyl)propyl]phenol (**4**u)*

According to the general procedure D, using **2***b* in toluene as solvent, the title compound was obtained in 75% yield as an oil after 45 min at 0°C with only 2 mol equivalent of titanium tetrachloride; ^{1}H nmr (250 MHz, CDCl3), δ: 0.93 (t, 3H, J = 7 Hz), 1.9–2.2 (m, 2H), 4.01 (t, 1H, J = 7 Hz, PhCH), 4.61 (s, 1H, OH), 6.7–7.3 (m, 8H). Exact Mass calcd. for $C_{16}H_{19}O$ (M + 1): 227.1436; found: 227.1435.

Can. J. Chem. Downloaded from www.nrcresearchpress.com by 217.78.4.112 on 09/08/12
For personal use only.

General Procedure E

Preparation of 2-(4-methyoxybenzyl)phenol (4q) and 2-(2-methoxybenzyl)phenol (4p)

Boron trifluoride etherate (3.0 mL, 25 mmol) was added to a solution of 2-phenyl-4*H*-1,3,2-benzodioxaborin **2***a* (1.0 g, 5 mmol) and anisole (1.6 g, 15 mmol) in 1,2-dichloroethane (15 mL). After stirring for 2 days at room temperature the mixture was washed with H_2O, dried ($MgSO_4$), filtered, and concentrated. The residue was chromatographed using 15% ethyl acetate in hexane to give 0.63 g (58%) of an isomeric mixture of the title compounds in a ratio of 4:1 in favor of the more polar *para* isomer **4***q*: mp 80–82°C; ^{1}H nmr (250 MHz, $CDCl_3$), δ: 3.8 (s, 3H, OCH_3), 3.9 (s, 2H, $PhCH_2$), 6.7–7.4 (m, 8H). Anal. calcd. for $C_{14}H_{14}O_2$: C 78.47, H 6.58; found: C 78.08, H 7.06; *ortho* isomer **4***p*: oil; ^{1}H nmr (250 MHz, $CDCl_3$), δ: 3.92 (s, 2H, $PhCH_2$), 3.97 (s, 3H, OCH_3), 6.8–7.4 (m, 8H). Exact Mass calcd. for $C_{14}H_{15}O_2$ (M + 1): 215.1072; found: 215.1072.

Preparation of 2-(4-hydroxy)benzyl phenol (4s) and 2-(2-hydroxy)benzyl phenol (4r)

According to the general procedure E, using phenol, after 24 h an isomeric mixture of the title compounds was isolated in 66% yield in a ratio of 2:1 in favor of the more polar *para* isomer **4***s*: mp 115–117°C; ^{1}H nmr (250 MHz, $CDCl_3$), δ: 3.9 (s, 2H, $PhCH_2$), 6.7–7.2 (m, 8H). Anal. calcd. for $C_{13}H_{12}O_2$: C 77.97, H 6.04; found: C 77.98, H 5.87; *ortho* isomer **4***r*: mp 112–114°C; ^{1}H nmr (250 MHz, $CDCl_3$), δ: 3.9 (s, 2H, $PhCH_2$), 6.7–7.22 (m, 8H). Anal. calcd. for $C_{13}H_{12}O_2$: C 77.97, H 6.04; found: C 77.76, H 6.70.

Preparation of 2-[1-(4-methoxyphenyl)propyl]phenol (4w) and 2-[1-(2-methoxypheny)propyl]phenol (4v)

According to the general procedure E, using **2***b* and anisol, after 21 h an isomeric mixture of the title compounds was isolated in 60% yield in a ratio of 5:1 in favor of the more polar *para* isomer **4***w*: mp 69–71%C; ir (KBr): 3403 (OH) cm^{-1}; ^{1}H nmr (250 MHz, $CDCl_3$), δ: 0.92 (t, 3H, J = 7 Hz), 1.90–2.20 (m, 2H), 4.0 (t, 1H, J = 7 Hz, PhCH), 4.68 (s, 1H, OH), 6.75 (d, 1H, J = 7.5 Hz), 6.82 (d, 2H, J = 8 Hz), 6.90–8.0 (m, 1H), 7.05–7.30 (m, 2H), 7.16 (d, 2H, J = 8 Hz). Anal calcd. for $C_{16}H_{16}O_2$: C 79.30, H 7.48; found: C 79.60, H 7.52. Exact Mass calcd. for $C_{16}H_{19}O_2$ (M + 1): 243.1385; found: 243.1385. *ortho* Isomer: oil; ir (film): 3432 (OH) cm^{-1}; ^{1}H nmr (250 MHz, $CDCl_3$), δ: 0.91 (t, 3H, J = 7 Hz), 1.90–2.20 (m, 2H), 4.38 (t, 3H, J = 7 Hz, PhCH), 4.65 (s, 1H, OH), 6.7–7.3 (m, 8H). Exact Mass calcd. for $C_{16}H_{19}O_2$ (M + 1): 243.1385; found: 243.1384.

Preparation of 2-(2-thiophenylmethyl)phenol (4t)

To a solution of 2-phenyl-4*H*-1,3,2-benzodioxaborin **2***a* (0.848 g, 4 mmol) and thiophene (1.01 g, 12 mmol) in dichloromethane (12 mL) at 0°C was added aluminum chloride (1.6 g, 12 mmol) in portions. The reaction mixture was stirred at room temperature for 10 min. Ammonium acetate solution (20%) was added slowly and the mixture was extracted with ethyl acetate. The combined organic extract was dried over $MgSO_4$ and then concentrated *in vacuo*. Chromatography of the residue on silica gel, eluting with 10% ethyl acetate in hexane, gave 420 mg (56%) of the title compound as an oil; ir (film): 3459 (OH) cm^{-1}; ^{1}H nmr (250 MHz, $CDCl_3$), δ: 4.18 (s, 2H, $PhCH_2$), 4.78 (s, 1H), 6.75–7.0 (m, 4H), 7.1–7.3 (m, 3H). Exact Mass calcd. for $C_{11}H_{10}OS$: 190.0452; found: 190.0453.

Preparation of 2-[1-(2-thiophenyl)propyl]phenol (4x)

Following the same procedure described for the preparation of **4***t*, using 4-ethyl-2phenyl-4*H*-1,3,2-benzodioxaborin **2***b* as starting material, the title compound was obtained as an oil in 75% yield; ^{1}H nmr (250 MHz, $CDCl_3$), δ: 0.95 (t, 3H, J = 3.75 Hz), 2.15 (m, 2H), 4.35 (t, 1H, J = 11.25 Hz, PhCH), 4.85 (s, 1H), 6.75 (d, 1H, J = 7.5 Hz), 6.92 (m, 3H), 7.1–7.2 (m, 2H), 7.25 (d, 1H, J = 7.5 Hz). Anal. calcd. for $C_{13}H_{14}OS$: C 71.55, H 6.42, S 14.67; found: C 71.62, H 6.39, S 14.85.

Preparation of 2,3-dihydro-2-(2-phenylethyl)-6-(2-thiophenyl)methyl-5-benzofuranol (4y)

To a solution of **2***j* (1.3 g, 3.66 mmol) in trifluoroacetic acid (20 mL) was added thiophene (0.92 g, 10.98 mmol). The reaction mixture was stirred at room temperature for 2 h. The mixture was diluted with H_2O (50 mL) and neutralized with solid potassium carbonate. The mixture was extracted with ethyl acetate and the combined organic extract was concentrated *in vacuo* after drying over anhydrous $MgSO_4$. Chromatography of the residue on silica gel (eluted with 10% ethyl acetate) gave 600 mg (54%) of the title compound; ^{1}H nmr (250 MHz, $CDCl_3$), δ: 1.9–2.05 (m, 1H), 2.05–2.25 (m, 1H), 2.7–2.95 (m, 3H), 3.22 (dd, 1H, J = 9.4 Hz), 4.1 (s, 2H, $PhCH_2$), 4.75 (m, 1H, OCH), 6.6 (m, 2H), 6.8–7.0 (m, 2H), 7.1–7.35 (m, 6H), Anal. calcd. for $C_{21}H_{20}O_2S$: C 74.97, H 5.99, S 9.52; found: C 74.88, H 6.32, S 9.60.

General Procedure F

Preparation of 2,3-dihydro-4-(2-hydroxyphenyl)benzopyran (16a)

Boron trifluoride etherate (0.5 mL, 4 mmol) was added to a solution of 2-phenyl-4-(2-phenoxyethyl)-4*H*-1,3,2-dioxaborin **2***c* (1.0 g, 3 mmol) in dichloromethane (10 mL). The mixture was stirred at room temperature for 72 h and then diluted with 1 N hydrochloric acid. After stirring for 5 min the organic layer was separated, dried ($MgSO_4$), filtered, and concentrated. The residue was chromatographed using 10% ethyl acetate in hexane to obtain 67 mg (99%) of the title compound; mp 81–86°C; ^{1}H nmr (250 MHz, $CDCl_3$), δ: 2.1–2.4 (m, 2H), 4.19 (t, 2H, J = 4.5 Hz, OCH_2), 4.4 (t, 1H, J = 5.5 Hz, PhCH), 4.75 (s, 1H, OH), 6.7–7.2 (m, 8H). Anal. calcd. for $C_{15}H_{14}O_2$: C 79.62, H 6.23; found: C 79.38, H 6.33.

2,3-Dihydro-6-(4-benzopyranyl)-2-(2-phenylethyl)-5-benzofuranol (16b)

According to the general procedure F, using **2***k*, the title compound was obtained in 78% as an oil; ^{1}H nmr (300 MHz, $CDCl_3$), δ: 1.87–2.01 (m, 1H), 2.03–2.30 (m, 3H), 2.65–2.89 (m, 3H), 3.20 (dd, 1H, J = 14.9 Hz, J' = 8.2 Hz), 4.10–4.28 (m, 2H, OCH_2), 4.38 (t, 1H, J = 5.6 Hz, PhCHPh), 4.63–4.77 (m, 1H, OCH), 6.34 (s, 1H), 6.61 (s, 1H, 6.76–6.95 (m, 3H), 7.08–7.32 (m, 6H); ^{13}C nmr ($CDCl_3$), δ: 155.25, 153.37, 147.00, 141.40, 131.13, 130.29, 128.40, 127.86, 125.91, 125.57, 123.94, 123.89, 120.56, 116.82, 112.58, 110.72, 82.53, 64.05, 63.99, 37.73, 37.67, 35.72, 35.44, 31.83, 29.05. Exact Mass calcd. for $C_{25}H_{24}O_3$: 372.1725; found: 372.1726.

3-Methoxy-6-(6-tert-butyldiphenylsiloxy-1,2,3,4-hexahydronaphthalenyl)phenol (16c) and 3-methoxy-6-(8-tert-butyldiphenylsiloxy-1,2,3,4-hexahydronaphthalenyl)phenol (16d)

According to the general procedure F, using **2***l*, the title compounds **16***c* and **16***d* were obtained in 53% yield as an oil in the ratio of 3:1 respectively; **16***c*: ^{1}H nmr (250 MHz, $CDCl_3$), δ: 1.1 (s, 9H), 1.55–2.0 (m, 4H), 2.6 (m, 2H), 3.75 (s, 3H, OCH_3), 4.35 (t, 1H, J = 6.25 Hz), 4.75 (s, 1H, OH), 6.25 (dd, 1H, J = 12.5, J' = 3 Hz), 6.35–6.60 (m, 5H), 7.3–7.45 (m, 6H), 7.75 (d, 4H, J = 9.4 Hz). Exact Mass calcd. for $C_{33}H_{37}O_3Si$ (M + 1): 509.2511; found: 509.2513. **16***d*: ^{1}H nmr (250 MHz, $CDCl_3$) δ: 1.1 (s, 9H), 1.6–2.05 (m, 4H), 2.6–2.75 (m, 2H), 3.75 (s, 3H, OCH_3), 4.05 (m, 1H), 4.6 (s, 1H, OH), 6.35–6.50 (m, 3H), 6.6 (d, 1H, J = 3 Hz), 6.7 (d, 1H, J = 9.4 Hz), 6.8 (d, 1H, J = 9.4 Hz), 7.4 (m, 6H), 7.7 (d, 4H, J = 9.4 Hz). Exact Mass calcd. for $C_{33}H_{37}O_3Si$ (M + 1): 509.2511; found: 509.2513.

1. G. Desimoni and G. Tacconi. Chem. Rev. **75**, 651 (1975).
2. D. L. Boger and S. N. Weinreb. Hetero Diels-Alder methodology in organic synthesis. Academic Press, New York. 1987.
3. P. D. Gardener, H. Sarrafuzadeg, and R. L. Brandon. J. Am. Chem. Soc. **81**, 5515 (1959).

4. M. S. Chauhan, F. M. Dean, S. McDonald, and M. S. Robinson. J. Chem. Soc. Perkin Trans. 1, 359 (1973).
5. D. A. Bolon. J. Org. Chem. **35**, 715 (1970).
6. Y. L. Mao and Boekelheide. Proc. Natl. Acad. Sci. U.S.A. **77**, 1731 (1980).
7. A. Arduini, A. Bosi, A. Pochini, and R. Ungaro. Tetrahedron, **41**, 3095 (1985).
8. M. Moreau, R. Quagliaro, R. Longeray, and J. Dreux. Bull. Soc. Chim. Fr. 4251 (1968).
9. D. A. Bolon. J. Org. Chem. **35**, 3666 (1970).
10. O. L. Chapman and C. L. McIntosh. Chem. Commun. 383 (1971).
11. T. Inoue, S. Inoue, and K. Sato. Chem. Lett. 653 (1989).
12. R. Hug, H.-J. Hansen, and H. Schmid. Helv. Chim. Acta, **55**, 1675 (1972).
13. J. J. Talley. J. Org. Chem. **50**, 1695 (1985).
14. O. L. Chapman, M. R. Engel, J. P. Springer, and J. C. Clardy. J. Am. Chem. Soc. **93**, 6696 (1971).
15. J. P. Marino and S. L. Dax, J. Org. Chem. **49**, 3671 (1984).
16. T. Inoue, S. Inoue, and K. Sato. Chem. Lett. 55 (1990).
17. T. Inoue, S. Inoue, and K. Sato. Bull. Chem. Soc. Jpn. **63**, 1647 (1990).
18. (*a*) G. Casraghi, M. Cornia, G. Casnati, G. G. Fava, and M. F. Belicchi. Chem. Commun. 271 (1986); (*b*) M. Cornia, G. Casraghi, G. Casnati, and L. Zetta. Gazz. Chim. Ital. **119**, 329 (1989).
19. B. Loubinoux, J. Miazimbakana, and P. Geradine. Tetrahedron Lett. 1939 (1989).
20. M. Wakselman and M. Vilkas. C. R. Hebd. Seances, Acad. Sci. **258**, 1526 (1964).
21. C. K. Lau, H. W. R. Williams, S. Tardiff, C. Dufresne, J. Scheigetz and P. C. Belanger. Can. J. Chem. **67**, 1384 (1989).
22. H. G. Peer. Recl. Trav. Chim. Pays-Bas, **79**, 825 (1960).
23. W. Nagata, K. Okada, and T. Aoki. Synthesis, 365 (1979).
24. W. A. Sheppard. J. Org. Chem. **33**, 3297 (1968).
25. J. Van Alphen. Recl. Trav. Chim. Pays-Bas, **62**, 485 (1943).
26. R. Huttel, J. Reidl, H. Martin, and K. Franke. Chem. Ber. **93**, 1425 (1960).
27. W. A. Pettit and J. W. Wilson. J. Am. Chem. Soc. **99**, 6372 (1977).
28. G. B. Oldaker III, T. A. Perfetti, and M. A. Ogliaruso. J. Org. Chem. **45**, 3912 (1980).
29. P. K. Freeman, A. M. Tafesh, and G. E. Clapp. J. Org. Chem. **54**, 782 (1989).
30. N. M. Yoon, C. S. Pak, H. C. Brown, S. Krishnamurthy, and T. P. Stocky. J. Org. Chem. **38**, 2786 (1973).
31. M. Takahashi, H. Ishida, and M. Kohmoto. Bull. Chem. Soc. Jpn. **49**, 1725 (1976).
32. S. C. Benson, C. A. Palabrica and J. K. Snyder. J. Org. Chem. **52**, 4610 (1987).
33. E. Wenkert, P. D. R. Moeller, and S. R. Piettre. J. Am. Chem. Soc. **110**, 7188 (1988).
34. R. A. Archer, D. B. Boyd, P. V. Demarco, I. J. Tyminski, and N. L. Allinger, J. Am. Chem. Soc. **92**, 5200 (1970).
35. A. Demarco, L. Zetta, R. Consonni, and M. Ragazzi. Tetrahedron, **44**, 2329 (1988).
36. L. Zetta, A. Demarco, C. Anklin, M. Cornia, and G. Casiraghi. Magn. Reson. Chem. **25**, 1081 (1987).
37. V. V. Kane and R. K. Razdan. J. Am. Chem. Soc. **90**, 6551 (1968).
38. M. J. Begley, L. Crombie, D. A. Slack, and D. A. Whiting. J. Chem. Soc. Perkin Trans. 1, 2406 (1977), and references cited therein.
39. G. Olah (*Editor*). Friedel Craft and related reactions. Interscience, New York. 1964.
40. W. S. Murphy and S. Wattanasin. J. Chem. Soc., Perkin Trans. 1, 1567 (1980), and references cited therein.

Can. J. Chem. Downloaded from www.nrcresearchpress.com by 217.78.4.112 on 09/08/12
For personal use only.

Chiral organosilicon compounds in synthesis. Preparation and stereoselective alkylations of silylcinnamyl carbanions[1]

S. LAMOTHE,[2] K. L. COOK,[3] AND T. H. CHAN[4]
Department of Chemistry, McGill University, Montreal, P.Q., Canada, H3A 2K6

Received November 13, 1991

S. LAMOTHE, K. L. COOK, and T. H. CHAN. Can. J. Chem. **70**, 1733 (1992).

Silylallyl carbanions of type **13** bearing a chiral lithium complexing substituent remote from silicon can be alkylated regio- and stereoselectively at the α-position by small electrophiles in nonpolar solvents. The regiochemical outcome of the reaction was found to be highly dependent on the size of the incoming electrophile. Secondary alkyl halides react preferentially at the γ-center and good levels of stereoselectivity are still obtained in nonpolar solvents despite the rather long distance between the reacting center and the chiral auxiliary. Transformation of the alkylated allylsilanes into optically active alcohols and carboxylic acids may represent a potential synthetic application of the method.

S. LAMOTHE, K. L. COOK et T. H. CHAN. Can. J. Chem. **70**, 1733 (1992).

Des carbanions allyliques siliciés de type **13** porteur d'un substituant chiral pouvant complexer le lithium et distant de l'atome de silicium peuvent être alkylés régio- et stéréoselectivement à la position α par de petits électrophiles dans des solvants non-polaires. La régiosélectivité de la réaction est fortement influencée par le volume stérique de l'électrophile. Les halogénures d'alkyle secondaires réagissent préférentiellement à la position γ offrant tout de même de hauts niveaux de stéréosélectivité dans les solvants non-polaires malgré la grande distance entre le centre réactif et l'auxiliaire chiral. La transformation des allylsilanes alkylés en alcools et acides carboxyliques optiquement actifs représente une application synthétique potentielle pour la méthode.

Can. J. Chem. Downloaded from www.nrcresearchpress.com by 217.78.4.112 on 09/08/12
For personal use only.

Introduction

The extensive use of allylsilanes in organic chemistry clearly demonstrates the power of that synthetic tool (2). Among the various possible reactions available to these compounds are alkylations of their derived carbanions.[5] It is well-known that allylsilanes **1** (Scheme 1) can be deprotonated to give the corresponding silylallyl carbanions **2** which react with alkylating agents preferentialy at the γ-position yielding vinylsilanes **3** as major products (3).

However, it was recently demonstrated in this laboratory that the use of chelating substituents on silicon can favor the formation of α-alkylated derivatives **4** through internal complexation of lithium (4). Moreover, preliminary results have shown that in addition to regioselectivity, stereoselectivity of alkylations can also be controlled when using a chiral ligand. As an example, when proline derived ligand in **5** (Scheme 2) was used, the α-alkylated allylsilanes **6** were obtained as single diastereoisomers. Such an approach has also been used to control stereoselectivity in the alkylations of benzylic silane **7** (5). The alkylated derivatives **8** could then be transformed into alcohols **9** (>95% ee) via oxidative cleavage of the carbon-silicon bond with retention of stereochemical integrity (6). To extend the scope of this method we decided to investigate the alkylations of chiral silylcinnamyl carbanions.

Results

Preparation and methylations of **10**

Our first target was the chiral cinnamylsilane **10** (Scheme 3) which was readily prepared in two steps from commercially available starting materials.[6] In the event, allylbenzene (**11**) was metallated (7) with *sec*-BuLi in ether and the resulting allylanion was quenched with chloro(chloromethyl)dimethylsilane affording **12** in 90% yield. Condensation of **12** with (*S*)-(+)-methoxymethylpyrrolidine[7] gave the requisite chiral allylsilane **10** in 80% yield.

Deprotonation of **10** with *sec*-BuLi presumably leads to an internally chelated carbanion **13** (Scheme 4) on which lithium would lie closer to the α-position (4). Upon alkylation with various electrophiles, α-silylcinnamyl carbanion **13** can lead to 8 stereoisomers, depending on olefin stereochemistry and absolute configuration at the alkylated center. In all the reactions that were carried out, the α-*E* and γ-*E* isomers **14***a–d* and **15***a–d* accounted for most of the alkylated products balance. The remainder consisted of *Z*-isomers which were apparent by spectral analysis although further characterisation was not pursued.

Alkylation of **10** was first carried out in THF using methyl iodide as the electrophile (Table 1, entry 1). Deprotonation of **10** using *sec*-BuLi went smoothly at −78°C and alkylation was instantaneous at that same temperature. Although quite clean in giving essentially the α-*E* (**14***a*) and γ-*E* (**15***a*) isomers in high combined yield, the reaction showed disappointing regio- and stereochemical control. However, when THF was replaced by diethyl ether as the solvent (entry 2), the increase in α-regioselectivity was quite spectacular. Moreover, the α-*E* isomer was essentially obtained as a pure diastereoisomer and the absolute configuration of the newly created stereocenter was determined by oxidative cleavage of the carbon-silicon bond (*vide infra*). The fact that some starting material was recovered could have been due to the reduced rate of either deprotonation or alkylation in ether relative to THF. By carrying out the deprotonation over a longer period of time (3 h instead of 0.5, entry 3) we obtained after 0.5 h alkylation time essentially the same amount of starting material, showing that the alkylation process was the one that had slowed down upon solvent change. To speed

[1]For a preliminary account of this work, see ref. 1.
[2]NSERC postdoctoral fellow (1990–1991).
[3]NSERC undergraduate research program participant (summer 1990).
[4]Author to whom correspondence may be addressed.
[5]For a review on the subject, see ref. 17.
[6]Aldrich Chemical Co.
[7]Both enantiomers are available by preparation from (D)- or (L)-proline (see ref. 8).

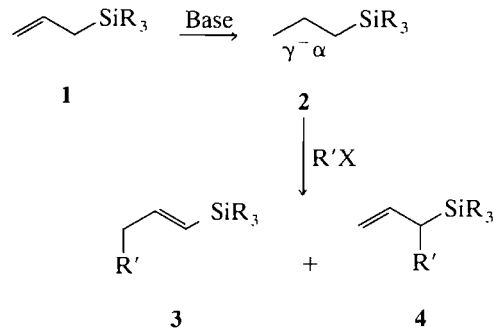

SCHEME 1

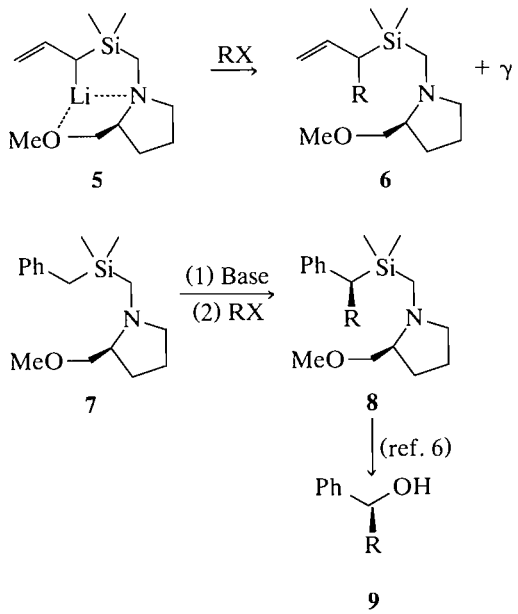

SCHEME 2

up the reaction, the mixture was allowed to warm up to room temperature after the addition of methyl iodide (entry 4). This procedure led to slightly lower α-selectivity while maintaining a high level of diastereoselectivity.

Another way to obtain a sufficient rate of alkylation at −78°C was to add a large excess of alkylating agent (entry 5). Under these conditions, the reaction was completed within 0.5 h at −78°C, thereby insuring excellent α-regio- and diastereoselectivity.

Among other solvents investigated, DME (entry 6) gave results comparable to THF while diisopropyl ether (entry 7) was comparable to diethyl ether. Since decreasing solvent polarity (or complexing ability) seemed to be the key to better control, the reaction was carried out in nonpolar media. While hexanes (entry 8) led to results comparable to ether, some solubility problems were encountered. However, when toluene was used (entry 9), the best overall results were obtained as the α-*E* adduct **14***a* accounted for 90% of the alkylation products. Moreover, excellent diastereoselectivity was obtained for this isomer. Since regioisomers can be separated easily by column chromatography on silica gel, pure α-*E* isomer can thus be obtained in high overall yield.

Other alkylations of **10**

Regioselectivity in the alkylation of the carbanion derived from **10** shows great dependence on the size of the incoming electrophile[8] (4). Reaction of carbanion **13** with ethyl iodide in THF (Table 2, entry 1) results in low regio- and diastereoselection reminiscent of the methyl iodide case. Use of ether (entry 2), again increased the ratio of α-*E* isomer **14***b* (68%) and at the same time provided excellent diastereoselectivity. To improve the extent of α-alkylation, leaving group ability was briefly examined as a potential source of regiochemical control. Reaction with ethyl bromide resulted in low yields and decreased α-selectivity (not shown in Table 2) while ethyl triflate (entry 3) gave α:γ (**14***b*:**15***b*) ratios comparable to those obtained with the corresponding iodide under similar conditions.

Equilibration of the carbanion by warming it up to room temperature prior to alkylation at −78°C (entry 4) did not affect the outcome of the reaction.

As in the case of methylation, it was found that alkylation with ethyl iodide at −78°C (entry 5) could improve α-selectivity at the expense of using a large excess of alkylating agent (20 equiv.) and longer reaction time.

Alkylations in DME (entry 6), diisopropyl ether (entry 7), and pentane (entry 8) followed the same trend as the methylation reactions. Again, use of toluene (entry 9) led to the cleanest reaction as only α-*E* (**14***b*) and γ-*E* (**15***b*) isomers were detected. In this case, α-selectivity was around 4:1 with excellent diastereoselection (>90%).

Alkylation of **10** with *n*-hexyl iodide (entries 10, 11) led to regioisomer as well as diastereoisomer ratios (**14***c*:**15***c*) similar to those obtained with ethyl iodide under similar conditions.

When a secondary iodide such as isopropyl iodide was used as the electrophile, the reaction showed a totally different outcome. As the bulk of the alkylating agent is increased, γ-alkylation takes over as the major pathway. Performing the reaction in THF (entry 12) offered as high as

[8]For similar observations see ref. 9.

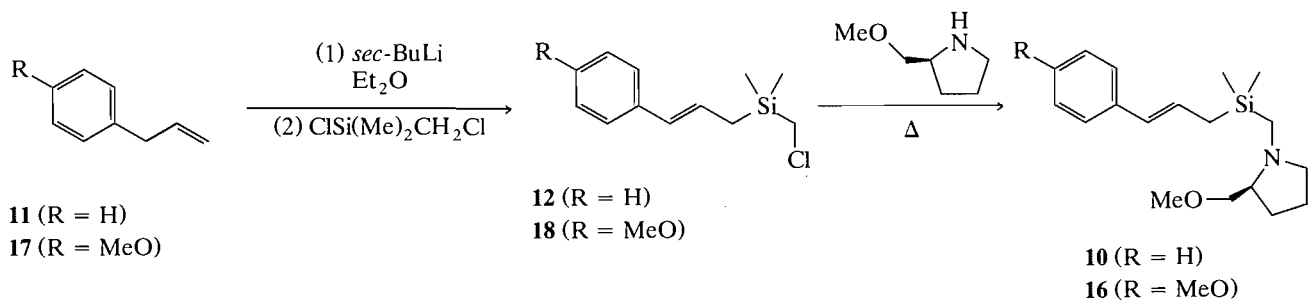

SCHEME 3

Can. J. Chem. Downloaded from www.nrcresearchpress.com by 217.78.4.112 on 09/08/12
For personal use only.

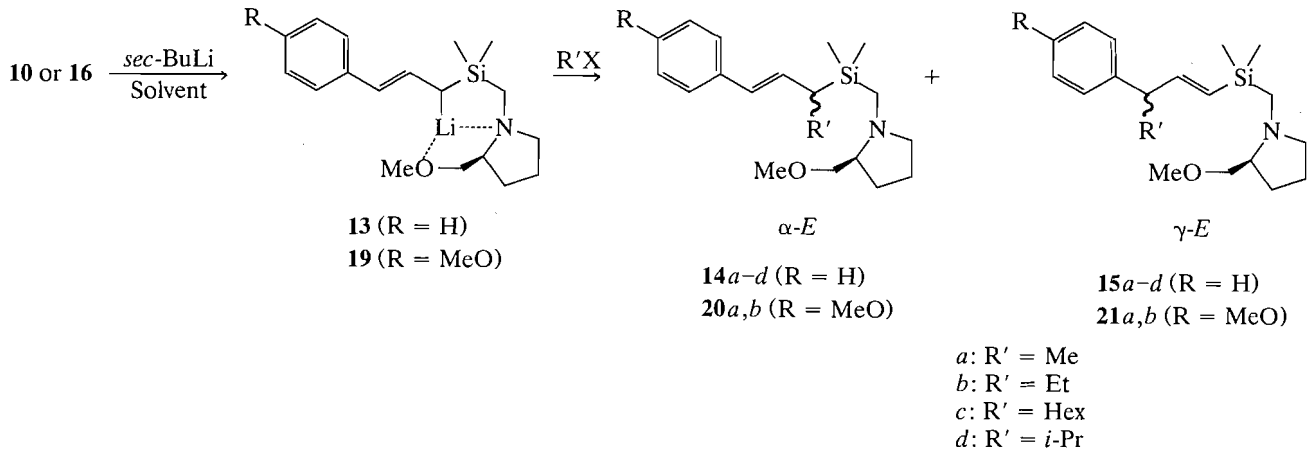

13 (R = H)
19 (R = MeO)

α-*E*

14*a–d* (R = H)
20*a,b* (R = MeO)

γ-*E*

15*a–d* (R = H)
21*a,b* (R = MeO)

a: R′ = Me
b: R′ = Et
c: R′ = Hex
d: R′ = *i*-Pr

SCHEME 4

TABLE 1. Alkylations of **10** with methyl iodide

Entry	Deprotonation[1] conditions (solvent)	Alkylation[2] conditions	Yield[3] (%)	Product distribution (%)[4] α-*E* (de (%)[5], config.[6])	Product distribution (%)[4] γ-*E* (de (%)[5], config.[6])	Product distribution (%)[4] Others
1	A (THF)	A	99	46 (18, *R*)	52 (17, *S*)	2
2	A (ether)	B	93	88 (>90, *S*)	7	5[7]
3	B (ether)	B	100	86 (>90, *S*)	10	5[8]
4	A (ether)	C	84	77 (>90, *S*)	14	9
5	A (ether)	D	89	89 (>90, *S*)	5	6
6	A (DME)	E	89	41 (18, *R*)	53	6
7	A (*i*-Pr_2O)	E	89	75 (>90, *S*)	10	15
8	A (hexane)	F	100	85 (>90, *S*)	9	5[9]
9	A (toluene)	F	89	90 (>90, *S*)	9	1

[1]A: 1.5–2 equiv. *sec*-BuLi, −78°C, 30–60 min. B: 2 equiv. *sec*-BuLi, −78°C, 3 h.
[2]A: 2 equiv. MeI, −78°C, 5 min. B: 2 equiv. MeI, −78°C, 30 min. C: 2 equiv. MeI, −78°C, 5 min to 10 min. D: 10 equiv. MeI, −78°C, 1 h. E: 5 equiv. MeI, −78°C, 5 min to 15 min. F: 10 equiv. MeI, −78°C, 30 min to 5 min.
[3]Crude yield of isomer mixture.
[4]Determined by capillary GC and (or) ^{1}H NMR analysis.
[5]Determined by ^{1}H NMR analysis; >90% indicates that only one diastereomer was found.
[6]Absolute configuration of alkylated center was determined as described in the text.
[7]Ratios based on 15% starting material recovered.
[8]Ratios based on 17% starting material recovered.
[9]Ratios based on 25% starting material recovered.

90% γ-selectivity, but as for other reactions in that solvent, low diastereoselectivity (4%) was observed for the major adduct. Interestingly, changing the solvent to ether (entry 13) increased diastereocontrol on γ-adduct **15***d*, which was still the favored regioisomer. This control was even better in toluene (entry 14) where 85% γ-selectivity was observed with the major regioisomer obtained as an 8:1 mixture of diastereoisomers.

Effect of substitution on the aromatic ring

To improve α-regioselectivity we briefly examined the effect of adding an electron-releasing substituent on the aromatic ring. According to the allopolarisation concept on regioselectivity in reactions of ambident nucleophiles (10), the presence of such a substituent should drive alkylation away from its point of attachment which is in this case the γ-position. Allylsilane **16** bearing a *para*-methoxy group (Scheme 3) was prepared from *para*-methoxyallylbenzene (**17**) through chlorosilane **18** using the same strategy as before. In this case, however, yields were lower in the initial step leading to **18** due to problems associated with increased reactivity of the allylanion.

Nevertheless, methylation of silylallyl carbanion **19** (Scheme 4) in THF (Table 3, entry 1) afforded, as expected, increased α-selectivity relative to the parent non-methoxylated derivative as α-*E* isomer **20***a* accounted for 75% of the alkylated product mixture. However, as was noted in previous alkylations using this solvent, diastereoselection was poor. Using ether as the solvent (entry 2) increased stereoselectivity on all levels. Interestingly, alkylation with ethyl iodide (entry 3) furnished the α-*E* adduct **20***b* with 88% selectivity which represents an improvement in regioselectivity compared to ethylation of the parent unsubstituted derivative **10**.

Variations in the chiral auxiliary

Effects of the variations in the chiral auxiliary of the allylsilane were also investigated. Condensation of chlorosilane **12** (Scheme 5) with *O*-methylated (−)-ephedrin **22** (11) furnished allylsilane **23** using the standard procedure. Al-

Can. J. Chem. Downloaded from www.nrcresearchpress.com by 217.78.4.112 on 09/08/12
For personal use only.

TABLE 2. Other alkylations of **10**

Entry	Deprotonation[1] conditions (solvent)	Alkylation[2] conditions (electrophile)	Yield[3] (%)	Product distribution (%)[4] α-*E* (de (%)[5], config.[6])	Product distribution (%)[4] γ-*E* (de (%)[5], config.[6])	Product distribution (%)[4] Others
1	A (THF)	A (EtI)	92	40 (10, *R*)	60	—
2	A (ether)	B (EtI)	99	68 (92[7], *S*)	19	13
3	A (ether)	B (EtOTf)	98	65 (>90, *S*)	22	13
4	B (ether)	B (EtI)	89	63 (>90, *S*)	26	11
5	A (ether)	C (EtI)	83	82 (>90, *S*)	11	7[9]
6	A (DME)	B (EtI)	100	37 (14, *R*)	63	—
7	A (*i*-Pr_2O)	B (EtI)	100	66 (>90, *S*)	17	17
8	A (pentane)	D (EtI)	83	66 (>90, *S*)	16	18
9	A (toluene)	E (EtI)	81	79 (>90, *S*)	21	—
10	A (toluene)	F (HexI)	100	77 (>90, *S*[8])	21	2
11	A (ether)	D (HexI)	70	84 (>90, *S*[8])	9	7[10]
12	A (THF)	G (*i*-PrI)	87	5	90 (4, *S*)	5
13	A (ether)	C (*i*-PrI)	89	15	68 (64, *R*)	17
14	A (toluene)	E (*i*-PrI)	89	8	85 (78, *R*)	7

[1]A: 1.5 –2 equiv. *sec*-BuLi, −78°C, 30–60 min. B: 2 equiv. *sec*-BuLi, −78°C, 5 min to room temperature, 15 min.
[2]A: 2 equiv. RX, −78°C, 5 min. B: 2 equiv. RX, −78°C, 5 min to room temperature, 10 min. C: 20 equiv. RX, −78°C, 3 h. D: 10 equiv. RX, −78°C, 30–60 min. E: 10 equiv. RX, −78°C, 30 min to room temperature, 10 min. F: 1.5 equiv. RX, −78°C, 15 min. G: 2 equiv. RX, −78°C, 30 min.
[3]Crude yield of isomer mixture.
[4]Determined by capillary GC and (or) ^{1}H NMR analysis.
[5]Determined by ^{1}H NMR analysis unless otherwise stated; >90% indicates that only one diastereomer was found.
[6]Absolute configuration of alkylated center was determined as described in the text.
[7]Value obtained from derived alcohol **33**.
[8]Assumed stereochemistry based on spectral correlation with methyl and ethyl derivatives.
[9]Ratios based on 11% starting material recovered.
[10]Ratios based on 30% starting material recovered.

TABLE 3. Alkylations of various allylsilanes

Entry	Starting material	Deprotonation[1] conditions (solvent)	Alkylation[2] conditions (electrophile)	Yield[3] (%)	Product distribution (%)[4] α-*E* (de (%)[5], config.[6])	Product distribution (%)[4] γ-*E*	Product distribution (%)[4] Others
1	**16**	A (THF)	A (MeI)	82	75 (14)	18	7
2	**16**	A (ether)	A (MeI)	94	90 (>90)	3	7
3	**16**	A (ether)	A (EtI)	79	88 (>90)	8	4
4	**23**	B (ether)	B (MeI)	98	81 (14, *R*)	19	—
5	**23**	B (THF)	C (MeI)	92	39 (6, *S*)	41	20
6	**26**	A (ether)	D (MeI)	88	69 (>90)	25	6
7	**28**	C (THF)	A (MeI)	82	46	53	1
8	**28**	C (ether)	E (MeI)	76	40	46	7

[1]A: 2 equiv. *sec*-BuLi, −78°C, 30–60 min. B: 1.5 equiv. *sec*-BuLi, −78°C, 30 min. C: 2 equiv. *sec*-BuLi, −78°C, 30 min to −40°C, 15 min.
[2]A: 2 equiv. RX, −78°C, 15–60 min. B: 1.5 equiv. RX, −78°C, 5 min to room temperature, 20 min. C: 1.5 equiv. RX, −78°C, 10 min. D: 10 equiv. RX, −78°C, 30 min to room temperature. E: 2 equiv. RX, −78°C, 15 min to room temperature.
[3]Crude yield of isomer mixture.
[4]Determined by capillary GC and (or) ^{1}H NMR analysis.
[5]Determined by ^{1}H NMR analysis; >90% indicates that only one diastereomer was found.
[6]Absolute configuration of alkylated center was determined as described in text.

kylations of this compound with methyl iodide in ether or THF (Table 3, entries 4 and 5) followed a regioselectivity pattern similar to the one observed for compound **10**. However, the diastereoselectivity of these reactions was poor in both solvents, making this auxiliary much less satisfactory than the pyrrolidine derivative.

Alternatively, (*S*)-(+)-1-(2-pyrrolidinylmethyl)pyrrolidine (**25**, Scheme 5) was used to prepare chiral allylsilane **26**. Unfortunately, its alkylation with methyl iodide in ether (Table 3, entry 6) led to no improvement in α-regioselectivity. On the other hand, diastereoselectivity of α-alkylation was maintained.

Can. J. Chem. Downloaded from www.nrcresearchpress.com by 217.78.4.112 on 09/08/12
For personal use only.

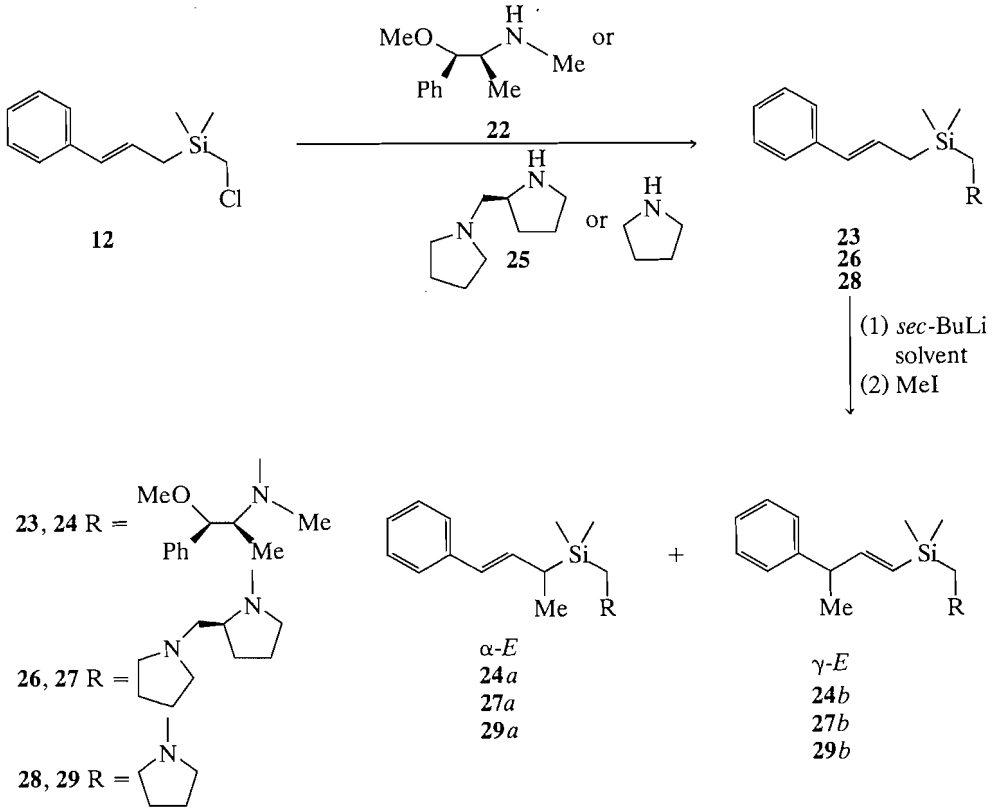

SCHEME 5

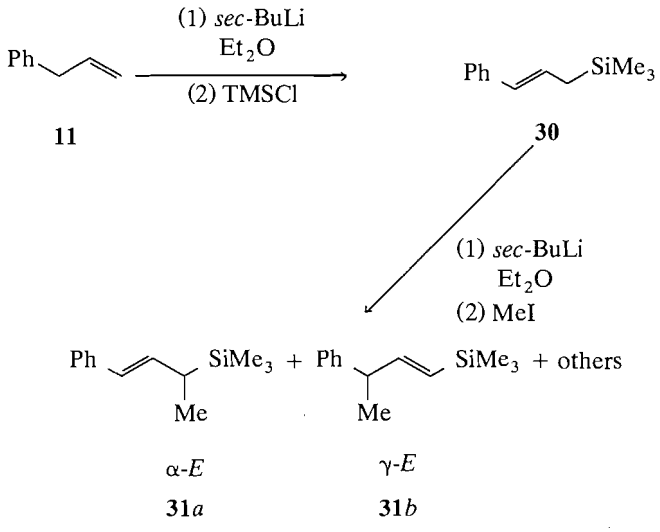

SCHEME 6

Determination of absolute configuration at alkylated centers

The absolute stereochemistry of the newly created asymmetric centers in alkylated allylsilanes was determined by chemical transformations into derivatives of known stereochemistry. The α-adducts were treated according to the procedure described for alkylated benzylic silanes **7** (Scheme 2) (5, 6). Methylated derivatives **14***a* and **24***a* (Scheme 7) afforded alcohol **32** (12) while ethyl alkylated derivative **14***b* gave alcohol **33** (13). For both **14***a* and **14***b* obtained by reaction in toluene or ether, the absolute configuration of the resulting alcohol was found to be "*S*" showing that reaction in these solvents afforded isomers **34** (Scheme 8).[9]

In the case of the γ-adducts **15***a* and **15***d* (Scheme 6), the olefin was cleaved by oxidation with $RuCl_3/NaIO_4$ according to the procedure described by Sharpless *et al.* (14). This reaction afforded substituted phenylacetic acids **35** and **36** (15) for which optical rotation values were compared with previously reported ones. As it turned out, the major enantiomer obtained for product **36** issued from alkylation in toluene or ether had the "*S*" configuration. This implies that the precursor allylsilane had the "*R*" configuration at the alkylated center[9] as shown in structure **37** (Scheme 8).

Reactions of achiral silylcinnamyl carbanions

We have also examined the alkylation reactions of simple silylcinnamyl carbanions in order to understand the factors controlling the regioselection in these systems. The allylsilane **28** (Scheme 5) was prepared from pyrrolidine and **12**. When compound **28** was reacted with methyl iodide in THF (Table 3, entry 7), the α-*E* and γ-*E* adducts **29***a* and **29***b* were obtained in a ratio (1:1.15) similar to the one observed with the methoxymethyl group present on the ring (i.e., 1:1.13). However, when this same reaction was carried out in ether (entry 8) and contrary to the case where oxygen function is present, the α:γ ratio remains essentially unchanged.

Furthermore, the alkylation of the carbanion derived from cinnamyltrimethylsilane **30** (prepared from **11**, Scheme 6) was also examined. Methylation under similar conditions

[9]The absolute configuration for the alkylated center in **15***d* and **36** have opposite "*R*, *S*" designations due to a change in priority sequence.

Can. J. Chem. Downloaded from www.nrcresearchpress.com by 217.78.4.112 on 09/08/12
For personal use only.

Can. J. Chem. Downloaded from www.nrcresearchpress.com by 217.78.4.112 on 09/08/12
For personal use only.

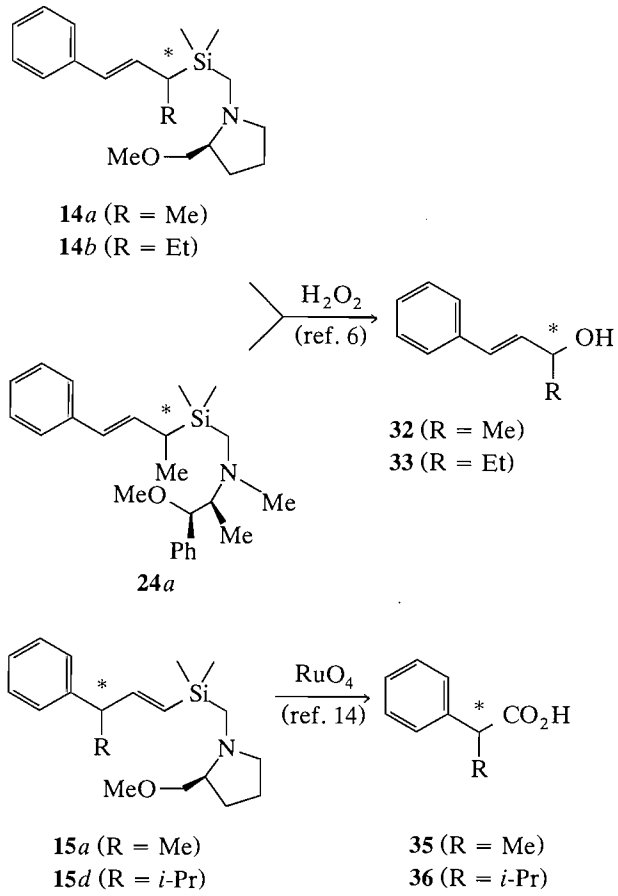

SCHEME 7

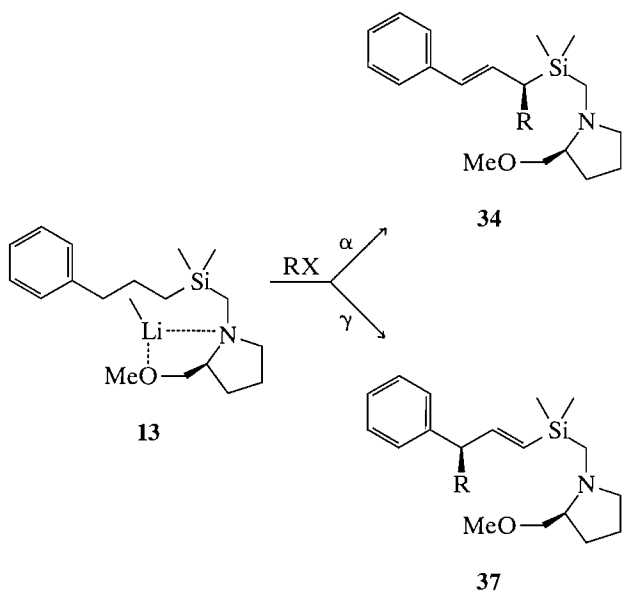

SCHEME 8

gave a low yield of the alkylated products due to competing reactions by addition of the base to the styrene system. Nevertheless, the alkylated products still showed an α-*E*:γ-*E* ratio (**31***a*:**31***b*) close to 1:1.

Discussion

In our previous study on the alkylation of silylallyl anions, we have demonstrated that the regioselectivity of the reactions can be controlled by having metal-ion complexing substituents on silicon (4). In the silylcinnamyl carbanions, the presence of the phenyl substituent on the allylic system modulates the regioselection somewhat. Whereas methylation of simple trimethylsilylallyl anion gives predominantly the γ-*E* alkylated product, the same methylation of trimethylsilylcinnamyl anion **30** gives an α-*E*:γ-*E* ratio close to 1:1. Regioselectivity of the reaction can be similarly affected by internal complexation with the introduction of metal-ion complexing substituents on silicon. The effective substituents seem to require a bidentate ligand since pyrrolidine itself in **28** does not give enhanced α-regioselection. Of the three carbanions with bidentate ligands derived from **10**, **23**, and **26**, the preference for α-alkylation is in fact poorer for **26** even though it is generally assumed that the diamino-type ligand complexes more strongly with lithium ion. A possible explanation is that the pyrrolidinylmethyl group in **26** is sterically bulkier, and it is well established that sterically bulky substituents on silicon favors γ-regioselection (3). Solvent plays an important role. In general, ether, toluene, and hexane favour higher α-alkylation whereas THF and DME reduce α-selection. This can be attributed to the competition of solvent with the internal complexation of the lithium ion. Of the three chiral auxiliaries used in **10**, **23**, and **26**, it is clear that the ephedrine ligand is relatively ineffective in conferring high stereoselectivity even though it is quite effective in controlling regioselectivity. All in all, methoxymethylprrolidine appears to be the ligand of choice in giving the best regioselection as well as stereoselection. In ether or toluene as the solvent, the carbanion derived from **10** alkylates with primary alkyl halides to give mainly the α-*E* alkylated products with excellent stereoselection (>90% de). Alkylation with isopropyl iodide gives mainly the γ-*E*-alkylated product with high stereoselection (78% de). This stereoselectivity is quite remarkable because the newly created asymmetric center is separated from the resident chiral center by a chain of 7 atoms. The absolute configurations of the major enantiomers obtained for the alkylation products **34** and **37** (Scheme 8) issued from alkylation in toluene or ether have "*S*" and "*R*" configurations respectively. These results show that for reactions occuring in less coordinating solvents (toluene or ether), the transoid silylallyl carbanion **13** is alkylated from the same face whether the electrophile is large (γ-selective) or small (α-selective).

Conclusion

This work shows that the use of chiral coordinating substituents remote from silicon can efficiently control alkylation pathways of silylallyl carbanions. The best substrate for that purpose was found to be allylsilane **10** bearing a proline derived chiral ligand. Alkylations of this compound with small electrophiles in non-polar solvents were highly α-selective and diastereoselectivity was excellent in all cases. Reaction with larger electrophiles favored γ-alkylation but still gave good diastereocontrol despite the distance between the chiral auxiliary and the reacting center. Transformation of the alkylated materials into optically active alcohols and carboxylic acids represents a potential synthetic application of the method.

Experimental

All reactions were carried out under argon atmosphere. The infrared spectra (IR) were recorded on an Analect FT, AQS-18 instrument. ^{1}H and ^{13}C NMR spectra were recorded on Varian XL-200

Can. J. Chem. Downloaded from www.nrcresearchpress.com by 217.78.4.112 on 09/08/12
For personal use only.

or XL-300 or on a Gemini-200 instruments. All NMR spectra were recorded in $CDCl_3$ as solvent and internal standard. Abbreviations used are m, multiplet, br, broad, s, singlet, d, doublet, t, triplet, q, quartet, qn, quintet, dd, double doublets, dt, double triplets. Low resolution mass spectra were recorded on a Kratos MS25RFA or on a HP-5980A instruments and are reported as mass (% intensity). High resolution mass spectra were recorded on a ZAB 2F HS spectrometer. Capillary gas chromatographic analysis was performed on a Hewlett-Packard 5890A instrument fitted with a 25 m × 0.2 mm high performance column (cross-linked methylsilicon, film thickness of 0.33 μm). GC/MS analysis were obtained using a Finnigan Mat 700 ion trap detector coupled to a Varian 3500 capillary gas chromatograph. Column chromatography purifications were performed on Merck silica gel 60 (230–400 mesh ASTM).

Cinnamyldimethyl-[(Ŝ)-2'-methoxymethylpyrrolidinyl]-methylsilane ***10***

A mixture of chloride **12** (1.53 g, 6.8 mmol) and (*S*)-2-methoxymethylpyrrolidine (1.57 g, 13.6 mmol) was heated at 80°C (oil bath temperature) for 24 h. After cooling to room temperature, ether and brine were added and the layers were separated. The aqueous layer was extracted with ether and the combined organic layers were dried over $MgSO_4$, filtered, and concentrated under reduced pressure to afford an oil which was purified by flash chromatography (25–100% ethyl acetate in hexane) yielding pure aminosilane **10** (1.69 g, 81%) as a pale yellow oil: $[\alpha]^{25}_D$ −77.8 (*c* 2.54, $CHCl_3$); IR ($CHCl_3$): 3023, 2955, 2875, 1113 cm^{-1}; ^1H NMR (200 MHz, $CDCl_3$) δ: 7.40–7.10 (5H, m), 6.40–6.20 (2H, m), 3.42 (1H, dd, *J* = 9 and 4.5 Hz), 3.34 (3H, s), 3.24 (1H, dd, *J* = 9 and 6.5 Hz), 3.09 (1H, m), 2.53 (1H, d, *J* = 14 Hz), 2.37 (1H, m), 2.09 (1H, q, *J* = 8.5 Hz), 2.00–1.50 (7H, m), 0.11 (3H, s), 0.08 (3H, s); ^{13}C NMR (75.4 MHz, $CDCl_3$) δ: 138.32, 128.31, 128.26, 127.46, 126.04, 125.34, 76.34, 67.40, 58.90, 57.40, 44.70, 28.30, 23.10, 22.20, −3.10, −3.30; HRMS (CI, NH_3) calcd. for $C_{18}H_{29}ONSi + H^+$: 304.2098; found: 304.2097.

Chloromethyl(cinnamyl)dimethylsilane (12)

To a solution of allylbenzene (**11**) (1.0 g, 8.5 mmol) in ether (15 mL) at 0°C was added *sec*-BuLi (1.3 M in cyclohexane, 8.1 mL, 10.6 mmol). After the addition, the mixture was warmed to room temperature and stirred for 2 h after which time it was cooled to −78°C. Chloro(chloromethyl)dimethylsilane (1.34 g, 9.3 mmol) was added and the mixture was stirred for 30 min at −78°C. Saturated NH_4Cl was then added followed by ether. The layers were separated and the aqueous layer was extracted twice with ether. The combined organic layers were washed with brine, dried over $MgSO_4$, filtered, and concentrated under reduced pressure (0.1 Torr; 1 Torr = 133.3 Pa) to afford crude chloride **12** (1.7 g, 90%) as a pale yellow oil; IR (neat): 3082, 3060, 3023, 2960, 2925, 1643, 1598, 1496, 1250 cm^{-1}; ^1H NMR (200 MHz, $CDCl_3$) δ: 7.1–7.4 (5H, m), 6.15–6.40 (2H, m), 2.86 (2H, s), 1.85 (2H, d, *J* = 7 Hz), 0.20 (6H, s); ^{13}C NMR (75.4 MHz, $CDCl_3$) δ: 138.2, 129.5, 128.6, 126.6, 126.1, 125.7, 29.5, 20.38, −5.06; HRMS (CI, NH_3) calcd. for $C_{12}H_{17}SiCl + NH_4^+$: 242.1132; found: 242.1133.

General procedure for allylsilane alkylations

To a solution of allylsilane (50 mg) in solvent (1 mL) at −78°C was added *sec*-BuLi (1.3 M in cyclohexane). The amount of base and length of time needed for deprotonation are listed in Tables 1–3. The electrophile was then added and the various conditions used for alkylations are also listed in Tables 1–3. The resulting mixture was quenched with saturated NH_4Cl solution and was extracted with ether. The combined organic layers were washed with brine and dried over $MgSO_4$. Evaporation of the solvents gave crude alkylation products mixtures which were anlaysed by ^1H NMR as well as capillary GC and (or) GCMS. If desired, in most instances, regioisomers could be separated by column chromatography on silica gel using hexane/ethyl acetate mixtures as eluent. The following is a representative example.

Methyl alkylated derivatives ***14***a *("S"),* ***14***a *("R") and* ***15***a[10]

To a solution of allylsilane **10** (50 mg) in ether (1 ml) at −78°C was added *sec*-BuLi (2 equiv., 1.3 M in cyclohexane). The mixture was stirred for 60 min. To the mixture, methyl iodide (10 equiv.) was added and stirred for 1 h at −78°C. The resulting mixture was quenched with saturated NH_4Cl solution and extracted with ether. The combined organic layers were washed with brine and dried over $MgSO_4$. Evaporation of solvents gave the crude alkylation products mixture which was chromatographed on silica gel using hexane/ethyl acetate as eluent to give the methyl alkylated derivative **14***a* and **15***a* in 89 and 5% yield respectively based on GC and ^1H NMR analyses. ^1H NMR (300 MHz, $CDCl_3$) δ: 7.40–7.10 (5H, m, **14***a* ("*S*"), **14***a* ("*R*"), **15***a*), 6.38 (1H, dd, *J* = 16.0 and 8.0 Hz, **14***a* ("*S*"), **14***a* ("*R*")), 6.24 (1H, dd, *J* = 18.5 and 6.0 Hz, **15***a*), 6.21 (1H, dm, *J* = 16.0 Hz, **14***a* ("*S*"), **14***a* ("*R*")), 5.70 (1H, dd, *J* = 18.5 and 1.5 Hz, **15***a*), 3.48 (1H, qn, *J* = 7.1 Hz, **15***a*), 3.50–3.40 (1H, m, **14***a* ("*S*"), **14***a* ("*R*"), **15***a*), 3.34 (3H, s, **15***a*), 3.33 (3H, s, **14***a* ("*S*"), **14***a* ("*R*")), 3.30–3.15 (1H, m, **14***a* ("*S*"), **14***a* ("*R*"), **15***a*), 3.06 (1H, m, **14***a* ("*S*"), **14***a* ("*R*"), **15***a*), 2.57 (1H, d, *J* = 14.5 Hz, **14***a* ("*S*"), **14***a* ("*R*")), 2.48 (1H, d, *J* = 14.5 Hz, **15***a*), 2.37 (1H, m, **14***a* ("*S*"), **14***a* ("*R*"), **15***a*), 2.11 (1H, m, **14***a* ("*S*"), **14***a* ("*R*"), **15***a*), 2.00–1.50 (5H, m, **15***a* and 6H, m, **14***a* ("*S*"), **14***a* ("*R*")), 1.36 (3H, d, *J* = 7.0 Hz, **15***a*), 1.21 (3H, d, *J* = 7.0 Hz, **14***a* ("*R*")), 1.20 (3H, d, *J* = 7.0 Hz, **14***a* ("*S*")), 0.12 (3H, s, **15***a*), 0.11 (3H, s, **14***a* ("*S*")), 0.10 (3H, s, **14***a* ("*R*"), **15***a*), 0.04 (3H, s, **14***a* ("*R*")), 0.03 (3H, s, **14***a* ("*S*")); GCMS *m/e* (EI): isomers **14***a* ("*S*"), **14***a* ("*R*") (not resolved), 272 ($M^+ - CH_2OCH_3$, 100), 186 (81), 154 (38), 131 (26), 128 (56); isomers **15***a*, 272 ($M^+ - CH_2OCH_3$, 100), 166 (7), 131 (7), 128 (22).

Ethyl alkylated derivatives ***14***b *("S"),* ***14***b *("R") and* ***15***b

The general procedure was followed; for additional details see Table 2. ^1H NMR (200 MHz, $CDCl_3$) δ: 7.40–7.10 (5H, m, **14***b* ("*S*"), **14***b* ("*R*"), **15***b*), 6.26 (1H, d, *J* = 16.0, **14***b* ("*S*")), 6.25 (1H, d, *J* = 16.0, **14***b* ("*R*")), 6.17 (1H, dd, *J* = 18.5 and 7.0 Hz, **15***b*), 6.13 (1H, dd, *J* = 16.0 and 8.5 Hz, **14***b* ("*S*")), 6.09 (1H, dd, *J* = 16.0 and 9.0 Hz, **14***b* ("*R*")), 5.67 (1H, dd, *J* = 18.5 and 1.0 Hz, **15***b*), 3.50–3.35 (1H, m, **14***b* ("*S*"), **14***b* ("*R*"), **15***b*), 3.33 (3H, s, **15***b*), 3.32 (3H, s, **14***b* ("*R*")), 3.31 (3H, s, **14***b* ("*S*")), 3.30–2.95 (2H, m, **14***b* ("*S*"), **14***b* ("*R*") and 3H, m, **15***b*), 2.55 (1H, d, *J* = 14.0 Hz, **14***b* ("*S*"), **14***b* ("*R*")), 2.46 (1H, d, *J* = 14.5 Hz, **15***b*), 2.35–2.25 (1H, m, **14***b* ("*S*"), **14***b* ("*R*"), **15***b*), 2.20–2.00 (1H, m, **14***b* ("*S*"), **14***b* ("*R*"), **15***b*), 2.00–1.40 (7H, m, **15***b* and 8H, m, **14***b* ("*S*"), **14***b* ("*R*")), 0.95 (3H, t, *J* = 7.0 Hz, **14***b* ("*S*"), **14***b* ("*R*")), 0.85 (3H, t, *J* = 7.5 Hz, **15***b*), 0.11 (3H, s, **15***b*), 0.10 (3H, s, **14***b* ("*S*") and **15***b**), 0.08 (3H, s, **14***b* ("*R*"), **15***b*), 0.07 (3H, s, **15***b**), 0.04 (3H, s, **14***b* ("*R*")), 0.02 (3H, s, **14***b* ("*S*")); GCMS *m/e* (EI): isomers **14***b* ("*S*"), **14***b* ("*R*") (not resolved), 286 ($M^+ - CH_2OCH_3$, 89), 186 (91), 154 (40), 145 (15), 144 (17), 128 (100); isomers **15***b*, 286 ($M^+ - CH_2OCH_3$, 100), 166 (6), 135 (10), 128 (18), 115 (6).

Hexyl alkylated derivatives ***14***c *("S"),* ***14***c *("R") and* ***15***c

The general procedure was followed; for additional details see Table 2. ^1H NMR (200 MHz, $CDCl_3$) δ: 7.40–7.10 (5H, m, **14***c* ("*S*"), **14***c* ("*R*"), **15***c*), 6.24 (1H, d, *J* = 16.0, **14***c* ("*S*")), 6.23 (1H, d, *J* = 16.0, **14***c* ("*R*")), 6.16 (1H, dd, *J* = 18.5 and 7.5 Hz, **15***c*), 6.13 (1H, dd, *J* = 16.0 and 8.5 Hz, **14***c* ("*S*")), 6.09 (1H, dd, *J* = 16.0 and 9.0 Hz, **14***c* ("*R*")), 5.65 (1H, dd, *J* = 18.5 and 1.0 Hz, **15***c*), 3.45–3.35 (1H, m, **14***c* ("*S*"), **14***c* ("*R*"), **15***c*), 3.33 (3H, s, **15***c*), 3.32 (3H, s, **14***c* ("*R*")), 3.31 (3H, s, **14***c* ("*S*")), 3.30–3.15 (1H, m, **14***c* ("*S*"), **14***c* ("*R*") and 2H, m, **15***c*), 3.04 (1H, m, **14***c* ("*S*"), **14***c* ("*R*"), **15***c*), 2.55 (1H, d, *J* = 14.5 Hz, **14***c* ("*S*"), **14***c* ("*R*")), 2.46 (1H, d, *J* = 14.0 Hz, **15***c*), 2.40–2.25 (1H, m, **14***c* ("*S*"), **14***c* ("*R*"), **15***c*), 2.20–1.40 (5H, m, **15***c* and 6H, m, **14***c* ("*S*"), **14***c* ("*R*")), 1.35–1.10 (8H, m, **14***c* ("*S*"), **14***c* ("*R*"), **15***c*), 0.95–0.80 (3H, m, **14***c* ("*S*"), **14***c* ("*R*"), **15***c*), 0.11

[10]The "*S*", "*R*" designation refers to absolute configuration at the alkylated center.

Can. J. Chem. Downloaded from www.nrcresearchpress.com by 217.78.4.112 on 09/08/12
For personal use only.

(3H, s, **15***c*), 0.10 (3H, s, **14***c* ("*S*") and **15***c**), 0.08 (3H, s, **14***c* ("*R*"), **15***c*), 0.07 (3H, s, **15***c**), 0.04 (3H, s, **14***c* ("*R*")), 0.02 (3H, s, **14***c* ("*S*")); GCMS *m/e* (EI): isomers **14***c* ("*S*"), **14***c* ("*R*") (not resolved), 342 ($M^+ - CH_2OCH_3$, 100), 186 (91), 154 (24), 128 (36), 59 (40); isomers **15***c*, 342 ($M^+ - CH_2OCH_3$, 100), 285 (4), 207 (14), 128 (24), 84 (65).

*Isopropyl alkylated derivatives **14**d, **15**d ("R") and **15**d ("S")*

The general procedure was followed; for additional details see Table 2. ^{1}H NMR (200 MHz, $CDCl_3$) δ: 7.40–7.10 (5H, m, **15***d* ("*R*"), **15***d* ("*S*"), **14***d*), 6.35–6.20 (2H, m, **14***d*), 6.23 (1H, dd, *J* = 18.5 and 8.5 Hz, **15***d* ("*S*")), 6.22 (1H, dd, *J* = 18.5 and 8.5 Hz, **15***d* ("*R*")), 5.66 (1H, dd, *J* = 18.5 and 1.0 Hz, **15***d* ("*R*"), **15***d* ("*S*")), 3.40 (1H, dd, *J* = 9.5 and 4.5 Hz, **15***d* ("*R*")), 3.45–3.34 (1H, m, **15***d* ("*S*"), **14***d*), 3.33 (3H, s, **15***d* ("*R*"), **15***d* ("*S*")), 3.30 (3H, s, **14***d*), 3.19 (1H, dd, *J* = 9.5 and 6.5 Hz, **15***d* ("*R*")), 3.30–3.10 (1H, m, **15***d* ("*S*"), **14***d*), 3.10–2.92 (1H, m, **15***d* ("*R*"), **15***d* ("*S*"), **14***d*), 2.90 (1H, t, *J* = 8.5 Hz, **15***d* ("*R*"), **15***d* ("*S*")), 2.58 (1H, d, *J* = 14.5 Hz, **14***d*), 2.46 (1H, d, *J* = 14.5 Hz, **15***d* ("*R*"), **15***d* ("*S*")), 2.42–2.25 (1H, m, **15***d* (*R*), **15***d* ("*S*"), **14***d*), 2.20–1.40 (6H, m, **15***d* ("*R*"), 7H, m, **15***d* ("*S*"), 8H, m, **14***d*)), 1.74 (1H, d, *J* = 14.2 Hz, **15***d* ("*R*")), 1.00 (3H, d, *J* = 5.0 Hz, **14***d*), 0.97 (3H, d, *J* = 4.5 Hz, **14***d*), 0.94 (3H, d, *J* = 6.5 Hz, **15***d* ("*R*"), **15***d* ("*S*")), 0.75 (3H, d, *J* = 6.5 Hz, **15***d* ("*R*"), **15***d* ("*S*")), 0.15 (3H, s, **14***d*), 0.10 (3H, s, **15***d* ("*S*")), 0.09 (3H, s, **15***d* ("*R*")), 0.08 (3H, s, **15***d* ("*R*")), 0.07 (3H, s, **15***d* ("*S*")), 0.06 (3H, s, **14***d*); GCMS *m/e* (EI): isomers **15***d* ("*R*"), **15***d* ("*S*") (not resolved), 346 ($M^+ + H^+$, 10), 345 (M^+, 3), 330 (6), 314 (12), 300 (100), 257 (1), 186 (3), 166 (4), 128 (20); isomers **14***d* (resolved): isomer 1, 300 ($M^+ - CH_2OCH_3$, 99), 186 (100), 154 (41), 128 (65), 115 (20), 89 (25), 73 (48), 59 (50); isomer 2, 300 ($M^+ - CH_2OCH_3$, 100), 186 (98), 154 (38), 128 (56), 115 (20), 89 (24), 73 (39), 59 (54).

*Dimethyl-(*p*-methoxylcinnamyl)-[(S)-2'-methoxymethylpyrrolidinylmethyl]silane **16***

A mixture of chloride **18** (100 mg, 0.39 mmol) and methoxymethylpyrrolidine (91 mg, 0.79 mmol) was heated at 80°C (oil bath temperature) for 20 h. After cooling to room temperature, ether and brine were added and the layers were separated. The aqueous layer was extracted with ether and the combined organic layers were dried over $MgSO_4$, filtered, and concentrated under reduced pressure to afford an oil which was purified by column chromatography (25–100% ethyl acetate in hexane) yielding pure aminosilane **16** (112 mg, 85%) as a pale yellow oil: $[\alpha]^{25}_D$ -66.4 (*c* 2.49, $CHCl_3$); IR (neat): 3029, 3016, 2952, 2918, 2876, 2835, 2808, 1609, 1509, 1247, 839 cm^{-1}; ^{1}H NMR (200 MHz, $CDCl_3$) δ: 7.25 (2H, m), 6.84 (2H, m), 6.21 (1H, d, *J* = 15.5 Hz), 6.10 (1H, dt, *J* = 15.5 and 7 Hz), 3.79 (3H, s), 3.41 (1H, dd, *J* = 9 and 4.5 Hz), 3.33 (3H, s), 3.23 (1H, dd, *J* = 9 and 6.5 Hz), 3.10 (1H, m), 2.50 (1H, d, *J* = 14 Hz), 2.38 (1H, m), 2.12 (1H, q, *J* = 8.5 Hz), 1.50–2.00 (7H, m), 0.09 (3H, s), 0.06 (3H, s); ^{13}C NMR (50.3 MHz, $CDCl_3$) δ: 158.4, 131.5, 127.9, 125.4, 113.9, 76.3, 67.5, 59.0, 57.4, 55.1, 44.8, 28.2, 23.0, 21.9, −3.4, −3.5; MS *m/e* (CI, NH_3): 334 (MH^+, 100), 302 (0.1), 288 (2.3); HRMS (CI, NH_3) calcd. for $C_{19}H_{31}NO_2Si + H^+$:334.2202; found: 334.2202.

*Chloromethyl-dimethyl-(*p*-methoxycinnamyl)silane **18***

To a solution of 4-allylanisole (**17**) (10.0 g, 67 mmol) in ether (100 mL) at 0°C was added *sec*-BuLi (1.3 M in cyclohexane, 67.5 mL, 87 mmol). After the addition, the mixture was warmed to room temperature and stirred for 5 h after which time it was cooled to −78°C. Chloro(chloromethyl)dimethylsilane (11.6 mL, 87 mmol) was added dropwise and the mixture was stirred for 30 min at −78°C. Saturated NH_4Cl was then added followed by ether. The layers were separated and the aqueous layer was extracted twice with ether. The combined organic layers were washed with brine, dried over $MgSO_4$, filtered, and concentrated under reduced pressure (0.1 Torr, oil bath 85–90°C) to afford crude chloride **18**. This material was purified by column chromatography on silica gel (2% ethyl acetate in hexane) yielding pure **18** (1.94 g, 11%) as a pale yellow oil: IR (neat): 3005, 2958, 2933, 2913, 2836, 1609, 1577, 1514, 1509, 1260, 847, 815 cm^{-1}; ^{1}H NMR (200 MHz, $CDCl_3$) δ: 7.25 (2H, m), 6.84 (2H, m), 6.25 (1H, br d, *J* = 16 Hz), 6.06 (1H, dt, *J* = 16 and 8 Hz), 3.80 (3H, s), 2.82 (2H, s), 1.78 (2H, dd, *J* = 8 and 1 Hz), 0.16 (6H, s); ^{13}C NMR (75.4 MHz, $CDCl_3$) δ: 158.6, 131.1, 128.8, 126.7, 123.7, 113.9, 55.1, 29.5, 20.1, −5.1; GC/MS *m/e* (EI): 254 (M^+, 75), 239 (44), 219 (33), 205 (6), 147 (100); HRMS (CI, NH_3) calcd. for $C_{12}H_{17}SiCl + H^+$: 255.0973; found: 255.0972.

*Methyl alkylated derivatives **20**a ("S"), **20***a* ("R") and **21**a*

The general procedure was followed; for additional details see Table 3. ^{1}H NMR (200 MHz, $CDCl_3$) δ: 7.25 (2H, m, **20***a* ("*S*"), **20***a* ("*R*")), 7.10 (2H, m, **21***a*), 6.83 (2H, m, **21***a*), 6.82 (2H, m, **20***a* ("*S*"), **20***a* ("*R*")), 6.30–6.10 (2H, m, **20***a* ("*S*"), **20***a* ("*R*")), 6.20 (1H, dd, *J* = 18.5 and 6.0 Hz, **21***a*), 5.65 (1H, dd, *J* = 18.5 and 1.5 Hz, **21***a*), 3.79 (3H, s **20***a* ("*S*"), **20***a* ("*R*")), 3.78 (3H, s, **21***a*), 3.42 (1H, m, **20***a* ("*S*"), **20***a* ("*R*") and 2H, m, **21***a*), 3.34 and 3.33 (3H, 2s, both diastereomers of **21***a*), 3.32 (3H, s, **20***a* ("*S*"), **20***a* ("*R*")), 3.22 (1H, m, **20***a* ("*S*"), **20***a* ("*R*"), **21***a*), 3.05 (1H, m, **20***a* ("*S*"), **20***a* ("*R*"), **21***a*), 2.55 (1H, d, *J* = 14.5 Hz, **20***a* ("*S*"), **20***a* ("*R*")), 2.47 (1H, d, *J* = 14.5 Hz, **21***a*), 2.37 (1H, m, **20***a* ("*S*"), **20***a* ("*R*"), **21***a*), 2.10 (1H, m, **20***a* ("*S*"), **20***a* ("*R*"), **21***a*), 2.00–1.45 (5H, m, **21***a* and 6H, m, **20***a* ("*S*"), **20***a* ("*R*")), 1.31 (3H, d, *J* = 7.0 Hz, **21***a*), 1.18 (3H, d, *J* = 7.0 Hz, **20***a* ("*R*")), 1.17 (3H, d, *J* = 7.0 Hz, **20***a* ("*S*")), 0.11 (3H, s, **21***a*), 0.08 (3H, s, **20***a* ("*S*"), **21***a*), 0.078 (3H, s, **20***a* ("*R*")), 0.02 (3H, s, **20***a* ("*R*")), 0.01 (3H, s, **20***a* ("*S*")).

*Ethyl alkylated derivatives **20**b ("S") and **21**b*

The general procedure was followed; for additional details see Table 3. ^{1}H NMR (200 MHz, $CDCl_3$) δ: 7.26 (2H, m, **20***b* ("*S*")), 7.07 (2H, m, **21***b*), 6.83 (2H, m, **20***b* ("*S*"), **21***b*), 6.30–6.00 (1H, m, **21***b*), 6.19 (1H, d, *J* = 16.0, **20***b* ("*S*")), 5.96 (1H, dd, *J* = 16.0 and 9.0 Hz, **20***b* ("*S*")), 5.63 (1H, dd, *J* = 19.0 and 1.0 Hz, **21***b*), 3.79 (3H, s, **20***b* ("*S*")), 3.78 (3H, s, **21***b*), 3.41 (1H, dd, *J* = 9.5 and 4.6 Hz, **20***b* ("*S*") and 2H, m, **21***b*), 3.33 (3H, s, **21***b*), 3.31 (3H, s, **20***b*) ("*S*")), 3.22 (1H, dd, *J* = 9.0 and 7.0 Hz, **20***b* ("*S*") and 1H, m, **21***b*), 3.05 (1H, m, **20***b* ("*S*"), **21***b*), 2.54 (1H, d, *J* = 14.5 Hz, **20***b* ("*S*")), 2.37 (1H, m, **20***b* ("*S*")), 2.08 (1H, q, *J* = 8.5 Hz, **20***b* ("*S*")), 1.70 (1H, d, *J* = 14.0 Hz, **20***b* ("*S*")), 2.00–1.30 (7H, m, **20***b* ("*S*")), 2.50–1.30 (7H, m, **21***b*), 0.94 (3H, t, *J* = 6.5 Hz, **20***b* ("*S*")), 0.83 (3H, t, *J* = 7.0 Hz, **21***b*), 0.09 (3H, s, **20***b* ("*S*")), 0.01 (3H, s, **20***b* ("*S*")), the singlets for methyl groups on silicon for isomer **21***b* were not characterised precisely but occur between 0.05 and 0.15 ppm.

*Cinnamyldimethyl-[1'-(R)-methyl-2'-(S)-phenyl-2-methoxyethyl-N-methylaminomethyl]silane **23***

A mixture of chloride **12** (467 mg, 2.1 mmol) and *O*-methylated (−) ephedrine (**22**) (11) (1.3 g, 7.3 mmol; this compound was contaminated with the bis-*O*,*N*-methylated derivative of (−) ephedrine) was heated at 135°C (oil bath temperature) for 15 h. After cooling to room temperature, ether and brine were added and the layers were separated. The aqueous layer was extracted with ether and the combined organic layers were dried over $MgSO_4$, filtered, and concentrated under reduced pressure to afford an oil (1.32 g). The remaining starting materials were distilled off (0.05 Torr, 40–45°C) and the residue was purified by column chromatography (10–50% ethyl acetate in hexane) yielding pure aminosilane **23** (285 mg, 37%) as a pale yellow oil: $[\alpha]^{25}_D$ −31.8 (*c* 2.0, $CHCl_3$); IR (neat): 3083, 3063, 3023, 2986, 2960, 2859, 2819, 1641, 1601, 1496, 1248, 1097, 835 cm^{-1}; ^{1}H NMR (200 MHz, $CDCl_3$) δ: 7.10–7.45 (10H, m), 6.05–6.30 (2H, m), 4.17 (1H, d, *J* = 6 Hz), 3.21 (3H, s), 2.72 (1H, qn, *J* = 6.5 Hz), 2.24 (3H, s), 2.03 (2H, d, *J* = 3.5 Hz), 1.57 (2H, m), 1.05 (3H, d, *J* = 6.5 Hz), −0.03 (6H, s); ^{13}C NMR (50.3 MHz, $CDCl_3$) δ: 141.7, 138.5, 128.7, 128.2, 128.0, 127.8, 127.1, 126.1, 125.5, 85.8, 66.7, 56.7, 44.3, 41.0, 22.2, 7.6, −3.2, −3.4; MS *m/e* (EI): 367 (M^+, 0.1), 352 (0.6), 336 (0.3), 246 (100); HRMS (EI) calcd. for $C_{23}H_{33}ONSi - CH_3$: 352.2098; found: 352.2097.

Can. J. Chem. Downloaded from www.nrcresearchpress.com by 217.78.4.112 on 09/08/12
For personal use only.

Methyl alkylated derivatives ***24****a ("R"), **24**a ("S"), and **24**b*

The general procedure was followed; for additional details see Table 3. ^{1}H NMR (200 MHz, $CDCl_3$) (in some sections of the NMR spectrum, the diastereoisomers of **24***b* could be distinguished and are designated as maj (major) and min (minor) δ: 7.45–7.10 (10H, m, **24***a* ("*R*"), **24***a* ("*S*"), **24***b*), 6.25 (1H, dd, *J* = 16.0 and 7.0 Hz, **24***a* ("*R*")), 6.23 (1H, dd, *J* = 16.0 and 6.5 Hz, **24***a* ("*S*")), 6.17 (1H, dd, *J* = 18.5 and 6.0 Hz, **24***b*maj), 6.16 (1H, dd, *J* = 18.5 and 6.0 Hz, **24***b*min), 6.12 (1H, d, *J* = 16.0 Hz, **24***a* ("*R*"), **24***a* ("*S*")), 5.61 (1H, dd, *J* = 18.5 and 1.5 Hz, **24***b*min), 5.60 (1H, dd, *J* = 18.5 and 1.5 Hz, **24***b*maj), 4.18 (1H, d, *J* = 6.0 Hz, **24***b*), 3.21 (3H, s, **24***b*), 3.20 (3H, s, **24***a* ("*R*"), **24***a* ("*S*")), 2.72 (1H, m, **24***a* ("*R*"), **24***a* ("*S*"), **24***b*), 2.23 (3H, s, **24***a* ("*R*"), **24***a* ("*S*")), 2.22 (3H, s, **24***b*), 2.10 (2H, m, **24***a* ("*R*"), **24***a* ("*S*"), **24***b*), 1.73 (1H, qn, *J* = 6.5 Hz, **24***a* ("*S*")), 1.70 (1H, qn, *J* = 7.0 Hz, **24***a* ("*R*")), 1.33 (3H, d, *J* = 7.0 Hz, **24***b*), 1.10 (3H, *d*, *J* = 7.0 Hz, **24***a* ("*S*")), 1.08 (3H, d, *J* = 6.0 Hz, **24***a* ("*R*")), 1.04 (3H, d, *J* = 6.5 Hz, **24***a* ("*R*"), **24***a* ("*S*")), 1.00 (3H, d, *J* = 6.5 Hz, **24***b*), −0.02 and −0.03 (6H, 4s, **24***b*), −0.05 (3H, s, **24***a* ("*S*")), −0.07 (6H, s, **24***a* ("*R*")), −0.08 (3H, s, **24***a* ("*S*")).

Cinnamyldimethyl-[(S)-2′-(pyrrolidinylmethyl)-pyrrolidinylmethyl]silane ***26***

A mixture of chloride **12** (280 mg, 1.29 mmol) and (*S*)-(+)-2-(1′-pyrrolidinylmethyl)pyrrolidine (**25**) (400 mg, 2.60 mmol) was heated at 80°C (oil bath temperature) for 15 h. After cooling to room temperature, ether and brine were added and the layers were separated. The aqueous layer was extracted with ether and the combined organic layers were dried over $MgSO_4$, filtered, and concentrated under reduced pressure to afford an oil which was purified by flash chromatography (hexane:EtOAc:CH_2Cl_2 80:10:10 then EtOAc:MeOH 50:50) yielding pure aminosilane **26** (174 mg, 40%) as a pale yellow oil: $[\alpha]^{25}_D$ −90.7 (*c* 1.7, $CHCl_3$); IR (neat): 3082, 3058, 3023, 2965, 2960, 2939, 2905, 2875, 2785, 1641, 1601, 1496, 1248, 862, 835 cm^{-1}; ^{1}H NMR (200 MHz, $CDCl_3$) δ: 7.40–7.10 (5H, m), 6.40–6.15 (2H, m), 3.10 (1H, m), 2.75–1.50 (20H, m), 0.11 (3H, s), 0.07 (3H, s); ^{13}C NMR (50.3 MHz, $CDCl_3$) δ: 138.6, 128.5 (2C), 127.8, 126.3, 125.6, 67.9, 61.5, 57.2, 54.9, 44.4, 30.2, 23.2, 22.8, 22.2, −3.2, −3.4; MS *m/e* (EI): 342 (M^+, 0.1), 327 (0.6), 258 (100), 226 (17); HRMS (EI) calcd. for $C_{21}H_{34}N_2Si - CH_3$: 327.2256; found: 327.2256.

Methyl alkylated derivatives ***27****a, **27**b*

The general procedure was followed; for additional details see Table 3. ^{1}H NMR (200 MHz, $CDCl_3$) δ: 7.40–7.10 (5H, m, **27***a*, **27***b*), 6.38 (1H, dd, *J* = 16.0 and 7.5 Hz, **27***a*), 6.23 (1H, dd, *J* = 18.5 and 6.0 Hz, **27***b*), 6.20 (1H, dd, *J* = 16.0 and 1.0 Hz, **27***a*), 5.68 (1H, dd, *J* = 18.5 and 1.5 Hz, **27***b*), 3.48 (1H, m, **27***b*), 3.06 (1H, m, **27***a*, **27***b*), 2.70–1.50 (19H, m, **27***a* and 18H, m, **27***b*), 1.34 (3H, d, *J* = 7.0 Hz, **27***b*), 1.18 (3H, d, *J* = 7.0 Hz, **27***a*), 0.11 (3H, s, **27***b*), 0.10 (3H, s, **27***a*), 0.09 (3H, s, **27***b*), 0.01 (3H, s, **27***a*).

Cinnamyldimethylpyrrolidinylmethylsilane ***28***

A mixture of chloride **12** (11.0 g, 49.0 mmol) and pyrrolidine (13.9 g, 196 mmol) was heated at 80°C (oil bath temperature) for 20 h. After cooling to room temperature, ether and brine were added and the layers were separated. The aqueous layer was extracted with ether and the combined organic layers were dried over $MgSO_4$, filtered, and concentrated under reduced pressure to afford crude **28** (11.6 g, 91%) as an oil which was suitable for use in the next reaction. If desired, the compound could be purified by column chromatography (10–50% EtOAc in hexane); IR (neat): 3023, 2986, 2962, 2952, 2904, 2773, 1641, 1601, 1496, 1247, 861, 835 cm^{-1}; ^{1}H NMR (200 MHz, $CDCl_3$) δ: 7.40–7.10 (5H, m), 6.40–6.15 (2H, m), 2.48 (4H, m), 2.08 (2H, s), 1.75 (6H, m), 0.12 (6H, s); ^{13}C NMR (50.3 MHz, $CDCl_3$) δ: 138.5, 128.7, 128.5, 127.6, 126.3, 125.6, 58.1, 46.0, 23.7, 22.3, −3.4; MS *m/e* (EI): 259 (M^+, 1), 244 (1.1), 175 (0.5), 142 (100), 84 (76).

Methyl alkylated derivatives ***29****a, **29**b*

The general procedure was followed; for additional details see Table 3. ^{1}H NMR (200 MHz, $CDCl_3$) δ: 7.40–7.10 (5H, m, **29***a*, **29***b*), 6.35 (1H, dd, *J* = 16.0 and 7.0 Hz, **29***a*), 6.23 (1H, dd, *J* = 18.5 and 6.0 Hz, **29***b*), 6.20 (1H, d, *J* = 16.0 Hz, **29***a*), 5.70 (1H, dd, *J* = 18.5 Hz, **29***b*), 3.48 (1H, br qn, *J* = 6.0 Hz, **29***b*), 2.45 (4H, m, **29***a*, **29***b*), 2.08 (2H, s, **29***a*), 2.06 (2H, s, **29***b*), 1.89 (1H, qn, *J* = 6.8 Hz, **29***a*), 1.75 (4H, m, **29***a*, **29***b*), 1.35 (3H, d, *J* = 7.0 Hz, **29***b*), 1.19 (3H, d, *J* = 7.0 Hz, **29***a*), 0.13 and 0.12 (3H, s, **29***b*), 0.10 and 0.09 (3H, s, **29***a*).

Cinnamyltrimethylsilane ***(30)*** *(16)*

To a solution of allylbenzene (**11**) (1.0 g, 8.5 mmol) in ether (15 mL) at 0°C was added *sec*-BuLi (1.3 M in cyclohexane, 8.1 mL, 10.6 mmol). After the addition, the mixture was warmed up to room temperature and stirred for 2 h after which time it was cooled to −78°C. Chlorotrimethylsilane (1.01 g, 9.3 mmol) was added and the mixture was stirred for 45 min at −78°C. Saturated NH_4Cl was then added followed by ether. The layers were separated and the aqueous layer was extracted twice with ether. The combined organic layers were washed with brine, dried over $MgSO_4$, filtered, and concentrated under reduced pressure (0.1 Torr overnight) to afford allylsilane **30** (1.29 g, 80%) as a pale yellow oil: IR (neat): 3082, 3060, 3023, 2955, 2917, 2896, 1643, 1599, 1496, 1248, 962, 863, 841, 740, 694 cm^{-1}; ^{1}H NMR (200 MHz, $CDCl_3$) δ: 7.40–7.10 (5H, m), 6.40–6.15 (2H, m), 1.68 (2H, m), 0.08 (9H, s); ^{13}C NMR (50.3 MHz,$CDCl_3$) δ: 138.6, 128.5, 128.4, 127.9, 126.3, 125.6, 23.7, −2.1; MS *m/e* (EI): 190 (M^+, 9.3), 175 (2.4), 117 (2.5), 73 (100).

Methyl alkylated derivatives ***31****a, **31**b*

The general procedure was followed. ^{1}H NMR (200 MHz, $CDCl_3$) δ: 7.40–7.10 (5H, m, **31***a*, **31***b*), 6.32 (1H, dd, *J* = 16.0 and 7.0 Hz, **31***a*), 6.20 (1H, d, *J* = 16.0, **31***a*), 6.20 (1H, dd, *J* = 18.5 and 6.0 Hz, **31***b*), 5.68 (1H, dd, *J* = 18.5 Hz, **31***b*), 3.48 (1H, m, **31***b*), 1.80 (1H, m, **31***a*), 1.36 (3H, d, *J* = 7.0 Hz, **31***b*), 1.18 (3H, d, *J* = 7.5 Hz, **31***a*), 0.06 (9H, s, **31***b*), 0.03 (9H, s, **31***a*); other compounds owing to addition of the base to the starting olefin were detected in this reaction but did not interfere with the evaluation of the α/γ ratio.

Typical procedure for the oxidative degradation of α-alkylated derivatives

To a solution of allylsilane **14***a* (42 mg, 0.132 mmol) in methanol (0.5 mL) and THF (0.5 mL) were added potassium bicarbonate (26 mg, 0.26 mmol) and potassium fluoride (15 mg, 0.26 mmol) followed by hydrogen peroxide (30%, 0.125 mL). The resulting mixture was stirred at room temperature for 24 h after which time it was diluted with brine and ether. The layers were separated and the aqueous layer was extracted twice with ether. The combined organic layers were washed with bisulfite and brine and were dried over $MgSO_4$. The residue obtained after evaporation was purified by column chromatography on silica gel (eluent 25% ethyl acetate in hexane) to afford alcohol **32** (9.4 mg, 48%) as an amorphous solid; the $[\alpha]^{25}_D$ value was compared with values obtained elsewhere (12, 13) (see text).

Typical procedure for the oxidative degradation of γ-alkylated derivatives

To a solution of vinylsilane **15***d* (62 mg, 0.18 mmol) in acetonitrile (0.5 mL), water (0.5 mL), and carbon tetrachloride (0.5 mL) were added sodium periodate (232 mg, 1.07 mmol) and ruthenium trichloride heptahydrate (0.8 mg, 0.004 mmol). The resulting mixture was stirred at room temperature for 2 h after which time it was diluted with dichloromethane. The layers were separated and the aqueous layer was extracted twice with dichloromethane. The combined organic layers were washed with brine and were dried over $MgSO_4$. The residue obtained after evaporation was purified by column chromatography on silica gel (eluent 10–50% ethyl acetate in hexane) to afford acid **36** (12.2 mg, 42%); the $[\alpha]^{25}_D$ value was compared with values obtained elsewhere (15) (see text).

Acknowledgments

Financial support for this work by the Natural Sciences and Engineering Research Council of Canada (NSERC) and Fonds pour la formation de chercheurs et l'aide à la recherche (Québec) (FCAR) is gratefully acknowledged.

1. S. Lamothe and T. H. Chan. Tetrahedron Lett. **32**, 1847 (1991).
2. E. Colvin. Silicon in organic synthesis. Krieger, Florida. 1985. Chap. 9; W. P. Weber. Silicon reagents in organic synthesis. Springer-Verlag, Berlin. 1983. Chap. 11.
3. K. Koumaglo and T. H. Chan. Tetrahedron Lett. **25**, 717 (1984).
4. R. F. Horvath and T. H. Chan. J. Org. Chem. **54**, 317 (1989).
5. T. H. Chan and P. Pellon. J. Am. Chem. Soc. *111*, 8737 (1989).
6. K. Tamao, N. Ishida, T. Tanaka, and M. Kumada. Organometallics, **2**, 1694 (1983).
7. H. F. Herbrandon and D. S. Mooney. J. Am. Chem. Soc. **57**, 5809 (1957).
8. D. Enders, P. Fey, and H. Kipphardt. Org. Synth. **65**, 173 (1987).
9. E. Schaumann and A. Kirshning. Tetrahedron Lett. **29**, 4281 (1988).
10. R. Gompper and H. U. Wagner. Angew. Chem. Int. Ed. Engl. **15**, 321 (1976).
11. K. Tamao, R. Kanatani, and M. Kumada. Tetrahedron Lett. **25**, 1913 (1984).
12. M. Kawasaki, Y. Suzuki, and S. Terashima. Chem. Lett. 239 (1984).
13. M. Kitamura, S. Suga, K. Kawai, and R. Noyori. J. Am. Chem. Soc. **108**, 6071 (1986).
14. P. H. J. Carlsen, T. Katsuki, V. S. Martin, and K. B. Sharpless. J. Org. Chem. **46**, 3936 (1981).
15. R. Aaron, D. Dull, J. L. Schmiegel, D. Jaeger, Y. Ohashi, and H. S. Mosher. J. Org. Chem. **32**, 2797 (1967).
16. D. Seyferth, K. R. Wursthorn, and R. E. Mammarella. J. Org. Chem. **42**, 3104 (1977).
17. S. Lamothe and T. H. Chan. *In* Advances in carbanion chemistry. Vol. 2. *Edited by* V. Snieckus. JAI Press, Conn. In press.

Can. J. Chem. Downloaded from www.nrcresearchpress.com by 217.78.4.112 on 09/08/12
For personal use only.

A variable-temperature ^{13}C NMR study of $(\eta^5\text{-}C_5H_5)_2Mo_2(CO)_4$ complexes of chiral alkynes derived from a terpene or a hormonal steroid: interconversion of diastereomers via exchange of terminal and semi-bridging carbonyls[1]

SYLVIE TONDU AND GÉRARD JAOUEN[2]
École nationale supérieure de chimie, 11, Rue Pierre et Marie Curie, 75231 Paris CEDEX 05, France

AND

MICHAEL F. D'AGOSTINO, KRISZTINA L. MALISZA, AND MICHAEL J. MCGLINCHEY[2]
Department of Chemistry, McMaster University, Hamilton, Ont., Canada L8S 4M1

Received September 25, 1991

SYLVIE TONDU, GÉRARD JAOUEN, MICHAEL F. D'AGOSTINO, KRISZTINA L. MALISZA, and MICHAEL J. MCGLINCHEY. Can. J. Chem. **70**, 1743 (1992).

The reaction of $(C_5H_5)_2Mo_2(CO)_4$ with the steroidal hormone 11β-(4-dimethylaminophenyl)-17β-hydroxy-17α-(1-propynyl)-estra-4,9-dien-3-one (RU 38486) or with propynylborneol yields in each case a chiral cluster that exhibits two cyclopentadienyl resonances in both the ^1H and ^{13}C NMR regimes. At low temperature the interconversion of diastereomers arising from the different orientations of the semi-bridging carbonyl ligand can be slowed on the NMR time scale. The barrier to diastereomer interchange has been determined for the terpenoid cluster and the mechanism of this process is discussed.

SYLVIE TONDU, GÉRARD JAOUEN, MICHAEL F. D'AGOSTINO, KRISZTINA L. MALISZA et MICHAEL J. MCGLINCHEY. Can. J. Chem. **70**, 1743 (1992).

La réaction du $(C_5H_5)_2Mo_2(CO)_4$ avec l'hormone stéroidale 11β-(4-diméthylamino)-17β-hydroxy-17α-(1-propynyl)-estra-4,9-dièn-3-one (RU 38486) ou avec le propynylborméol conduit dans chaque cas à un cluster chiral qui présente deux résonances de cyclopentadiényles en RMN tant du ^1H que du ^{13}C. À basses températures, sur l'échelle de temps de la RMN, on peut ralentir l'interconversion des diastéréoisomères provenant des différentes orientations dans le ligand carbonyle agissant comme demi-pont.

[Traduit par la rédaction]

Can. J. Chem. Downloaded from www.nrcresearchpress.com by 217.78.4.112 on 09/08/12
For personal use only.

Introduction

In continuation of our studies on metal complexes of hormonal steroids and related systems (1–6), we have synthesized a number of dimetalla-alkyne clusters, e.g., **1**, **2**, and **3**. These molecules, in which the M_2C_2 tetrahedral moiety is situated on the α-face of the steroid, are known to bind to various steroidal receptor sites (7, 8). Moreover, it has been demonstrated that one can take advantage of the intense metal carbonyl infrared stretching absorptions to assay the receptor sites without any of the inconveniences associated with radio-labels (9, 10). Perhaps the most fascinating of these is the dimolybdenum complex **3**, which is derived from 11β-(4-dimethylaminophenyl)-17β-hydroxy-17α-(1-propynyl)-estra-4,9-dien-3-one, **4**, the now famous "morning-after pill" originally known as RU 38486 and recently marketed by Roussel-Uclaf as Mifepristone.

Any attempts to carry out substitution reactions on these systems (either to displace a carbonyl ligand or to replace an entire metal vertex with an isolobal group) must take account of the chiral nature of the molecules and consequent diastereotopic character of the metal centers (11–13). This phenomenon is clearly reflected in the NMR spectra of molecules **2** and **3**, each of which give rise to two cyclopentadienyl resonances in both the ^1H and ^{13}C regimes (14). We were particularly intrigued by the observation that these pairs of cyclopentadienyl peaks were further split on cooling, thus indicating the presence of more than one diastereomer. We here describe a variable-temperature NMR study carried out to clarify and extend these observations.

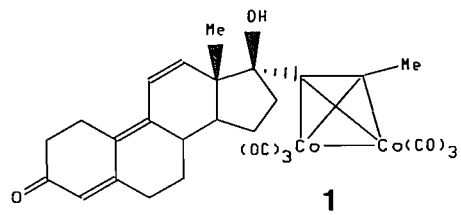

1

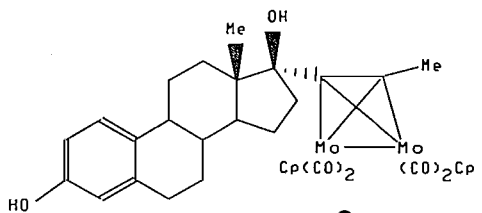

2

Results and discussion

The molecular structures and fluxional behavior of clusters of the type $Cp_2(CO)_4M_2(R^1C{\equiv}CR^2)$, where M = Mo or W, were first described by Cotton and co-workers (15). In the solid state, three of the carbonyl ligands are terminally bonded while the fourth is in a semi-bridging environment. This situation also obtains in solution and the asymmetric nature of the bonding renders all four carbonyls nonequivalent as evidenced by the ^{13}C NMR spectrum at low temperature. Now, for those cases where $R^1 = R^2$, increasing the

[1]Dedicated to the memory of our friend and colleague Tom Birchall.

[2]Authors to whom correspondence may be addressed.

Can. J. Chem. Downloaded from www.nrcresearchpress.com by 217.78.4.112 on 09/08/12
For personal use only.

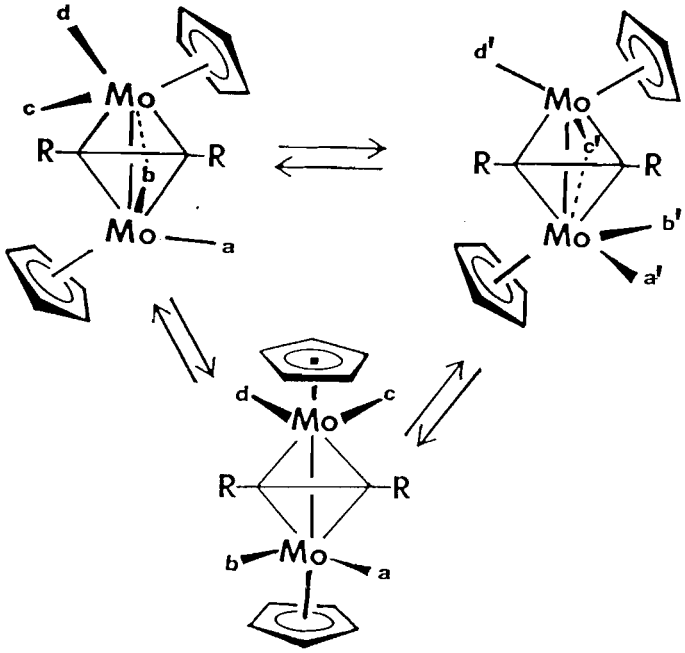

SCHEME 1. Exchange process that interconverts carbonyl ligands in semi-bridging and in terminal environments.

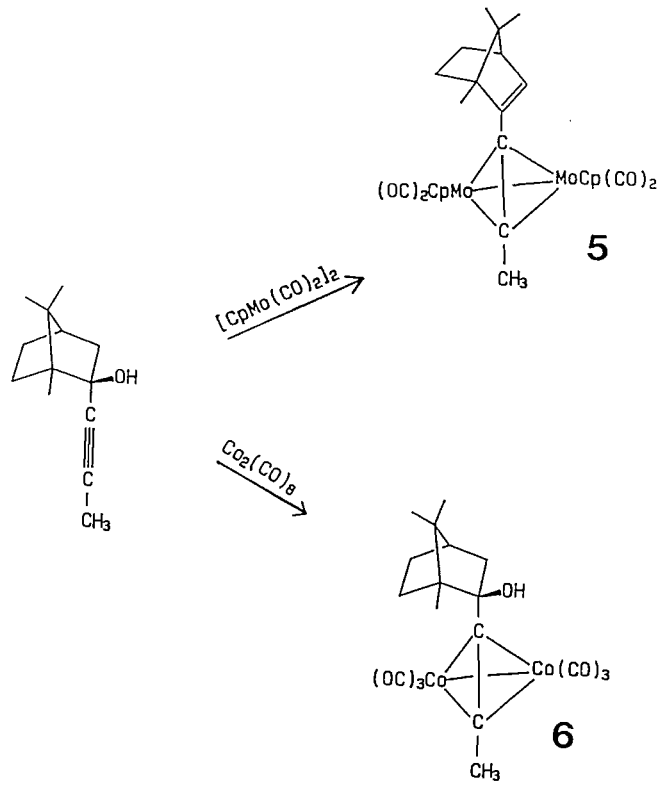

SCHEME 2. Synthetic routes to chiral clusters.

temperature brings about a coalescence of the four ^{13}CO NMR signals to two, and ultimately yields a single resonance. The first exchange process, which has an activation energy of approximately 8 kcal mol^{-1}, was suggested to involve a twitching motion by which the semi-bridging carbonyl on one molybdenum and a terminal CO ligand on the other molybdenum are equilibrated; the effective symmetry would then be C_2 rather than C_1 and this process would also interconvert the two cyclopentadienyl environments, as in Scheme 1. The observation of a single ^{13}CO peak requires that the time-averaged symmetry be raised to C_{2v} as would be the case if partial rotation of the $CpMo(CO)_2$ groups were to occur; this latter process has a barrier ranging from 9.5 to 12.5 kcal mol^{-1} depending on the steric bulk of the substituents borne by the cyclopentadienyl ligands (16, 17). A moment's reflection leads to the realization that for those systems where $R^1 \neq R^2$ the maximum symmetry attainable is C_s and so the four ^{13}CO resonances at low temperature can at best become two even when both fluxional processes are fast on the NMR time scale. It is further apparent that when one of the alkyne substituents is chiral the four carbonyl ligands are *always* nonequivalent. Likewise, in a molecule such as **3**, where the alkyne bears a hormonal steroid as one substituent, the cyclopentadienyl groups will also retain their chemical shift difference.

As shown in Fig. 1, the ^1H NMR spectrum of **3** in the cyclopentadienyl region changes quite noticeably upon raising the temperature from −40°C to +20°C. The low-temperature spectrum shows the presence of two molecular species in an approximate 80:20 ratio. Upon increasing the temperature, these two species are equilibrated and the four cyclopentadienyl resonances coalesce to yield only two peaks.

As shown in Fig. 2, the ^{13}C NMR spectrum of **3**, recorded at −40°C, reveals the anticipated eight resonances in the metal carbonyl region; four of these ^{13}CO peaks are assigned to the major diastereomer and the other four to its less abundant partner. Further examination of the ^1H spectra reveals that one of the C_5H_5 rings in the major diastereomer is markedly deshielded from the remaining cyclopentadienyl protons; one is led to the suspicion that this particular Cp ring may be situated near the edge of the aromatic ring attached

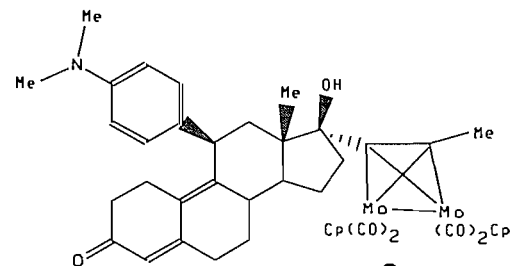

3

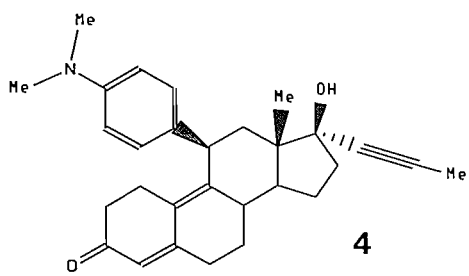

4

to C-11 of the steroid and so lies in the deshielding region of the diamagnetic anisotropy associated with the arene. This idea is buttressed by the observation that the resonances attributable to the Me_2N group and also the ring protons *ortho* to this substituent are clearly separated in the two diastereomers. Furthermore, these chemical shift differences are

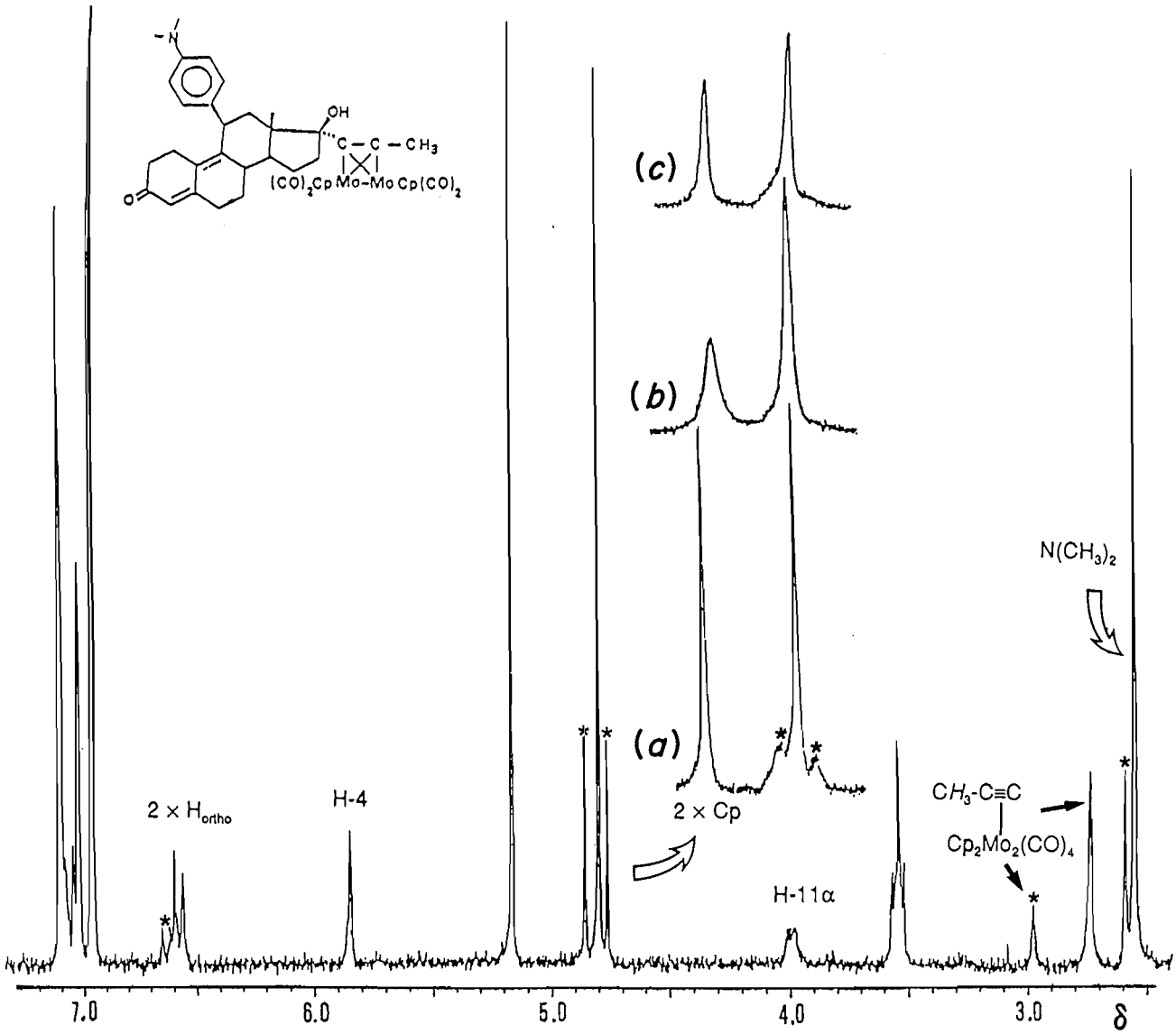

FIG. 1. Section of the 250 MHz ^{1}H NMR spectrum of **3** at 233 K. Peaks attributable to the minor diastereomer are marked with an asterisk (*). The cyclopentadienyl resonances are also shown (*a*) at 275 K, (*b*) at 283 K, and (*c*) at 293 K.

detectable not only for the methyl groups situated at C-13 but also for the CH_3's attached to the alkyne that are likewise split in a 4:1 ratio at low temperature. Clearly, X-ray crystallographic data would be valuable in elucidating the detailed structures of these diastereomers. These observations are relevant to the recent report describing the variable-temperature NMR spectra of the alkyne cluster $[(C_5H_5)_2Mo_2(HC{\equiv}CR)]^+$, where R is a cationic steroidal substituent (18). In this cation there are intimations of a very low-energy fluxional process in which extra cyclopentadienyl resonances are observed. Subsequently, there has been speculation about the possibility of evaluating the barrier to rotation of the $(C_5H_5)Mo(CO)_2$ vertices (19).

The results of these variable-temperature NMR experiments prompted us to look in more detail at another di-molybdenum cluster in which the alkyne possessed a chiral substituent. We recently described convenient routes to a variety of chiral di-cobalt, di-molybdenum, or di-tungsten clusters as well as those containing Co–Mo or Co–W units (12, 20). Molecules such as **5** or **6** are obtainable in multigram quantities by reaction of the appropriate organometallic precursor with 2-propynylborneol, as shown in Scheme 2. Furthermore, ^{13}CO enrichment of **5** is a straightforward process and greatly facilitates the acquisition of the variable-temperature spectra.

The ^{13}C NMR spectrum of **5** has been recorded over the temperature range +30°C to −80°C and a selection of these spectra appear in Fig. 3, together with those simulated by using the program EXCHANGE. We note immediately that there is a coalescence phenomenon that interchanges pairs of ^{13}CO resonances in quite different environments (see Fig. 4). This is in complete accord with Cotton's original proposal in which a semi-bridging carbonyl on one metal exchanges with a terminal CO ligand on the other metal. The X-ray crystal structure of **5** appears as Fig. 5 and reveals that the three terminal carbonyl ligands are oriented very differently with respect to the terpenoid substituent (20) and so would be expected to have noticeably different chemical shifts. The

Can. J. Chem. Downloaded from www.nrcresearchpress.com by 217.78.4.112 on 09/08/12
For personal use only.

Can. J. Chem. Downloaded from www.nrcresearchpress.com by 217.78.4.112 on 09/08/12
For personal use only.

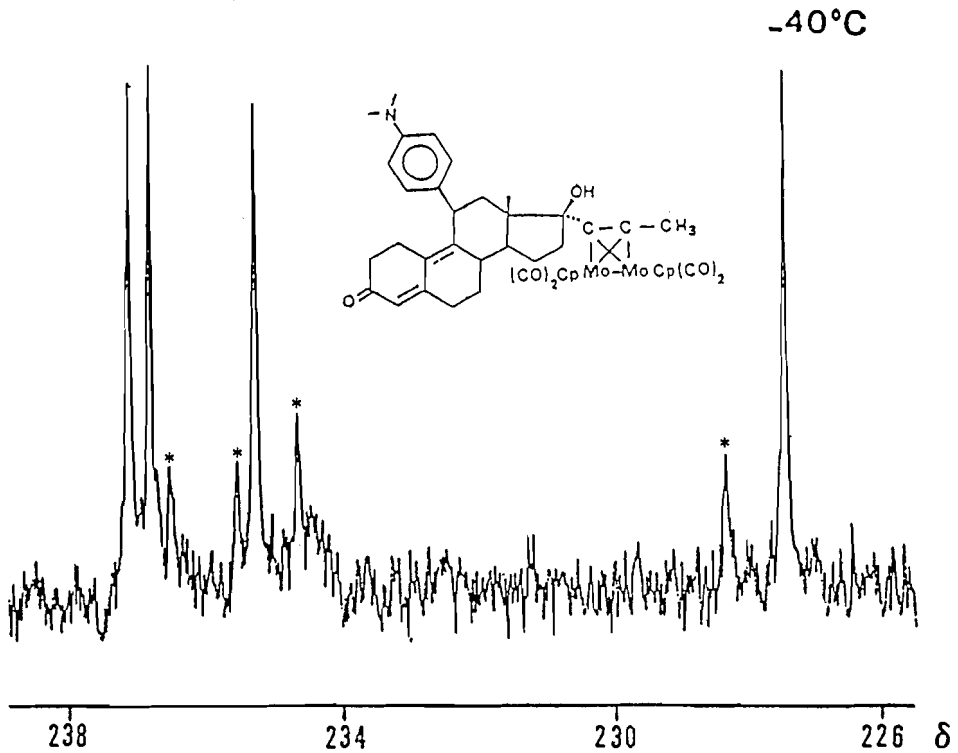

FIG. 2. Section of the 62.86 MHz ^{13}C NMR spectrum of **3**, in the metal carbonyl region, recorded at 233 K; data collection time 12 h.

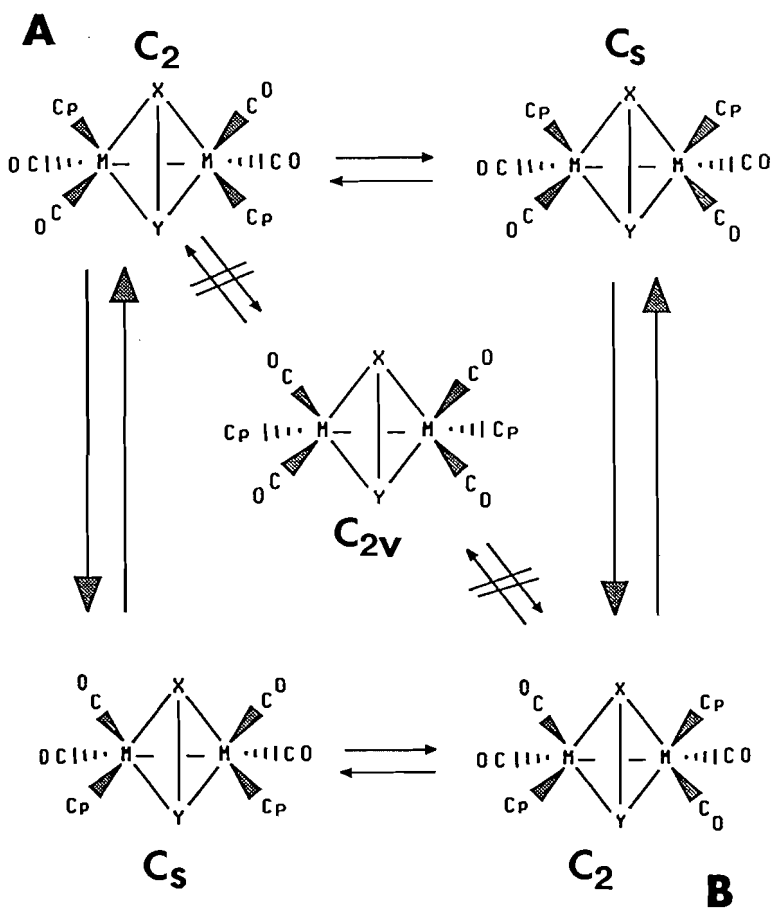

SCHEME 3. Proposed mechanism of interconversion of enantiomeric clusters via C_s rather than C_{2v} intermediates.

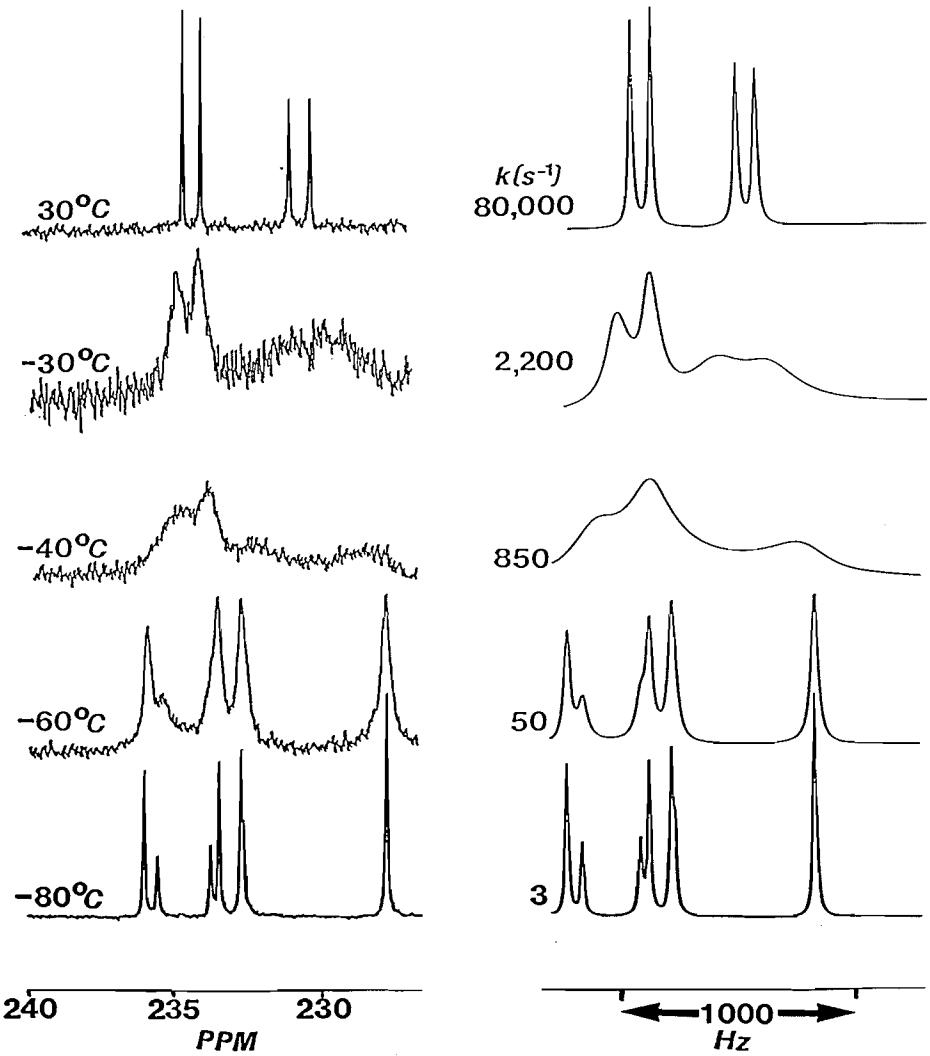

FIG. 3. Experimental and simulated 125.7 MHz ^{13}C variable-temperature NMR spectra of **5** in the metal carbonyl region.

crystallographically characterized molecule is presumably the major diastereomer and the minor isomer can arise simply by invoking semi-bridging of a different carbonyl ligand. The activation energy barrier for this fluxional process (obtained from a knowledge of the experimental temperatures and the rate constants given by the spectral simulations) is 11.2 ± 0.4 kcal mol^{-1} and is in the range found for other systems with modestly large steric requirements (16).

In this case the simulation is decidedly non-trivial since the relative populations of major and minor diastereomers change with temperature; that is, the simulation requires a knowledge not only of the rate constant but also of the equilibrium constant at each temperature for which experimental data are available. The ratio at the low-temperature limit is of course directly measurable from peak intensities; the diastereomer ratio at +30°C is calculable from the peak positions, which reflect the weighted average of the chemical shifts of the individual molecules. The equilibrium constants for the intermediate temperatures were obtained by interpolation of the measured values at −80°C and +30°C; these data allowed the simulation of the variable-temperature NMR spectra, shown in Fig. 3, and yielded the above-mentioned activation energy of 11.2 ± 0.4 kcal mol^{-1}. The variation of K_{eq} with temperature corresponds to a preferential stabilization of one of the two diastereomers by ≈0.2 kcal mol^{-1}.

As noted already, this chemical exchange process involves not merely the carbonyl ligands but also requires the swivelling of the $CpMo(CO)_2$ fragments so as to interconvert enantiomers (when $R^1 = R^2$) or diastereomers (when one of the R groups is chiral, as in the present case). The more fundamental question perhaps concerns the course of the molecular rearrangement that interconverts the rotamers **A** and **B** in Scheme 3. The low-energy twitching process generates a pair of molecules, each of which has effective C_2 symmetry; that is, when $R^1 = R^2$ we have an enantiomeric pair, that must be equilibrated by the high-energy process. Thus when both processes have large rate constants the time-averaged symmetry is C_{2v}. However, this does not mandate that the molecule actually adopt the C_{2v} geometry during the course of the rearrangement. Indeed, such a transition state would be disfavored on entropic grounds since this would require a synchronous swivelling motion of both $CpMo(CO)_2$ groups about imaginary axes joining each molybdenum to the tetrahedral center. One possible technique is to use the Bürgi–Dunitz approach in which the crystal structures of a

Can. J. Chem. Downloaded from www.nrcresearchpress.com by 217.78.4.112 on 09/08/12
For personal use only.

Can. J. Chem. Downloaded from www.nrcresearchpress.com by 217.78.4.112 on 09/08/12
For personal use only.

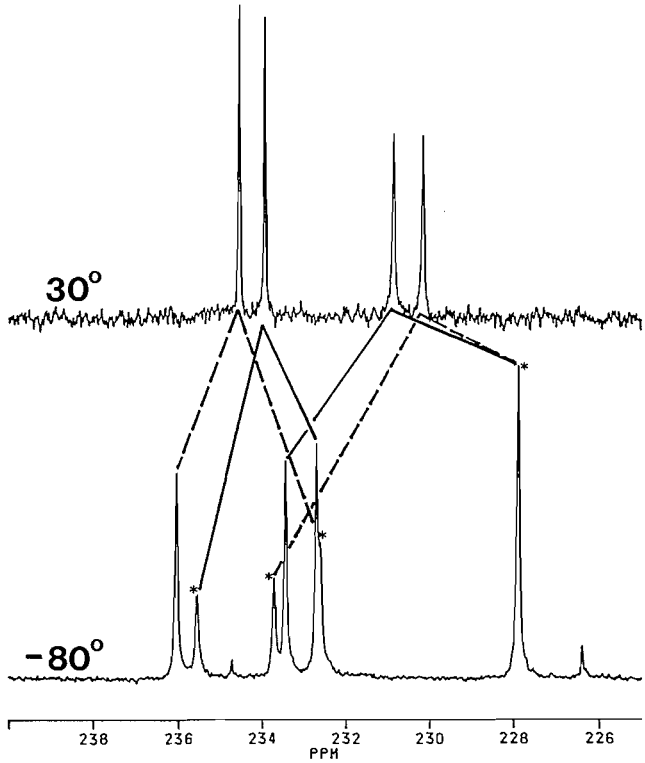

FIG. 4. Coalescence pattern of the metal carbonyl resonances of **5** over the temperature range −80°C to +30°C, showing equilibration of CO ligands in very different environments. Peaks of the minor diastereomer are labelled with an asterisk (*).

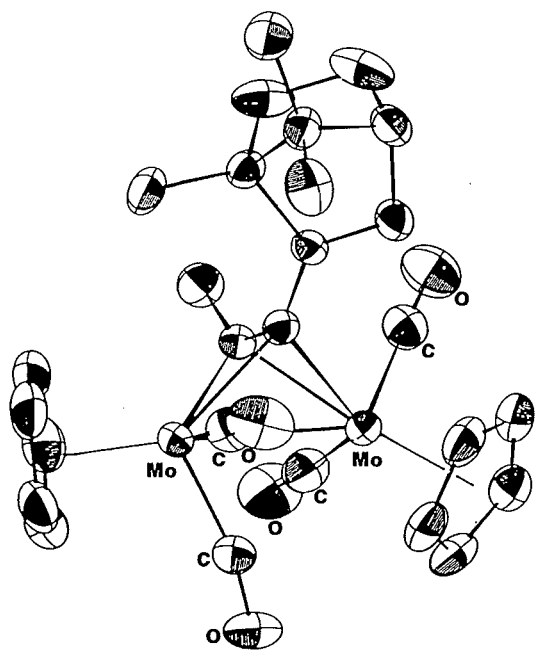

FIG. 5. X-ray crystal structure of **5** using data taken from ref. 20.

large number of closely related molecules are analyzed (21). By this means one can obtain a profile of the reaction pathway whereby a suitably arranged series of structures maps out the trajectory followed by the interacting species. This method has been adopted by Crabtree and Lavin who showed that there is a gradual bending of a carbonyl ligand (i.e., a decrease in the M═C═O bond angle) as it migrates from a terminal to a bridging environment (22). While the detailed analysis of more than 30 crystal structures is deferred to another paper,[3] we note that the published data on molecules of the type $[CpM(CO)_2]_2(X{\equiv}Y)$, where M = Mo or W, and X≡Y can be RC≡CR, RC≡ML_n, As≡As, P≡P, RN≡C, etc., are of the C_2 or C_S types than the C_{2v} structures (see Scheme 3). One might conclude that the reaction proceeds via successive rotations of single $CpM(CO)_2$ vertices rather than by concerted motion of both. These conclusions are supported by EHMO calculations, which likewise favor the stepwise process (23).

In summary, we present the first direct observations on chiral dimetal–alkyne clusters in which equilibration of a semi-bridging carbonyl on one metal and a terminal carbonyl ligand on the other brings about diastereomerization. The observation of four CO resonances at room temperature also provides definitive evidence that there is no intermetallic carbonyl migration.

Experimental

All reactions were carried out under an atmosphere of dry nitrogen employing conventional benchtop and glovebag techniques. All solvents were dried according to standard procedures before use (24). NMR spectra were recorded using Bruker AM500 and WM250 spectrometers; chemical shifts reported were referenced to tetramethylsilane. The ^{13}C spectra of **3** were acquired on a Bruker **WM** 250 spectrometer operating at 62.86 MHz at 5.87 T. The spectrum of the metal carbonyl region of **3** at 233 K was obtained as the result of an overnight run; the sample was not enriched in ^{13}CO. The ^{13}C spectra of **5** were acquired on a Bruker AM 500 spectrometer operating at 125.7 MHz at 11.74 T. Typically, 5000 scans were required to achieve adequate signal-to-noise with a digital resolution of 1.9 Hz/point. The complexes **3** and **5** were prepared via reaction of freshly prepared $(C_5H_5)_2Mo_2(CO)_4$ and the appropriate alkyne as described previously (10, 20); to facilitate the observation of minor isomers, in the ^{13}C spectra, **5** was enriched by stirring a dichloromethane solution for 1 week under an atmosphere of ^{13}CO. NMR spectral simulations were carried out on an IBM PS50 personal computer by using the multisite EXCHANGE program generously provided by Professor R.E.D. McClung (University of Alberta at Edmonton).

Acknowledgments

We thank the Natural Sciences and Engineering Research Council of Canada (NSERC) and le Centre national de la recherche scientifique (France) (CNRS) for financial support, Roussel-Uclaf for a generous gift of RU 38486, Dr. Ted McClung (Edmonton) for the EXCHANGE program, and IBM (Canada) Ltd. for the donation of computers. M.F.D. and K.L.M. were the recipients of NSERC postgraduate scholarships.

1. G. Jaouen and A. Vessières. Pure Appl. Chem. **61**, 565 (1989).
2. H. El-Amouri, M. Gruselle, P. A. Jackson, G. Jaouen, and J. Vaissermann. Organometallics, **9**, 2871 (1990).
3. R. M. Moriarty, Y-Y. Ku, U. S. Gill, R. Gilardi, R. E. Perrier, and M. J. McGlinchey. Organometallics, **8**, 960 (1989).
4. A. Vessières, S. Tondu, G. Jaouen, S. Top, A. A. Ismail, G. Teutsch, and M. Moguilewsky. Inorg. Chem. **27**, 1852 (1988).
5. M. Gruselle, P. Deprez, A. Vessières, S. Greenfield, G.

[3]K. L. Malisza and M. J. McGlinchey, manuscript in preparation.

Jaouen, J-P. Larue, and D. Thouvenot J. Organoment. Chem. **359**, C53 (1989).
6. C. Cordier, M. Gruselle, G. Jaouen, D. W. Hughes, and M. J. McGlinchey, Magn. Reson. Chem., **28**, 835 (1990).
7. G. Jaouen, A. Vessières, S. Top, A. A. Ismail, and I. S. Butler. J. Am. Chem. Soc. **107**, 4778 (1985).
8. A. Vessières, S. Top, A. A. Ismail, I. S. Butler, and G. Jaouen. Biochemistry, **27**, 6659 (1988).
9. G. Jaouen, A. Vessières, S. Top, M. Savignac, A. A. Ismail, and I. S. Butler. Organometallics, **6**, 1985 (1987).
10. A. Vessières, G. Jaouen, M. Gruselle, J. L. Rossignol, M. Savignac, S. Top, and S. Greenfield. J. Steroid Biochem. **30**, 301 (1988).
11. D. H. Bradley, A. K. Masood, and K. M. Nicholas. Organometallics, **8**, 554 (1989).
12. M. F. D'Agostino, C. S. Frampton, and M. J. McGlinchey. Organometallics, **9**, 2972 (1990).
13. D. T. Clark, K. A. Sutin, R. E. Perrier, and M. J. McGlinchey. Polyhedron, **7**, 2297 (1988).
14. M. Savignac, G. Jaouen, C. A. Rodger, R. E. Perrier, B. G. Sayer, and M. J. McGlinchey J. Org. Chem. **51**, 2328 (1986).
15. W. I. Bailey, Jr., M. H. Chisholm, F. A. Cotton, and L. A. Rankin. J. Am. Chem. Soc. **100**, 5764 (1978).
16. P. Bougeard, S. Peng, M. Mlekuz, and M. J. McGlinchey. J. Organomet. Chem. **296**, 383 (1985), and references therein.
17. G. A. Carriedo, J. A. K. Howard, D. B. Lewis, G. E. Lewis, and F. G. A. Stone. J. Chem. Soc. Dalton Trans. 905 (1985).
18. C. Cordier, M. Gruselle, G. Jaouen, V. I. Bakhmutov, M. V. Galakhov, L. L. Troitskaya, and V. I. Sokolov. Organometallics, **10**, 2303 (1991).
19. M. V. Galakhov, V. I. Bakhmutov, I. V. Barinov, and O. A. Reutov. J. Organomet. Chem. **421**, 65 (1991).
20. M. F. D'Agostino, C. S. Frampton, and M. J. McGlinchey. J. Organomet. Chem. **394**, 145 (1990).
21. H.-B. Bürgi and J. D. Dunitz. Acc. Chem. Res. **16**, 153 (1983).
22. R. H. Crabtree and M. Lavin. Inorg. Chem. **25**, 805 (1986).
23. K. L. Malisza, M. F. D'Agostino, L. Li, and M. J. McGlinchey. Organometallics. Submitted for publication.
24. D. D. Perrin, W. L. F. Armarego, and D. R. Perrin. Purification of laboratory chemicals. Pergamon Press, New York. 1980.

Can. J. Chem. Downloaded from www.nrcresearchpress.com by 217.78.4.112 on 09/08/12
For personal use only.

The solvent dependence of the small internal barrier to rotation in 3,5-dichlorobenzyl fluoride

TED SCHAEFER,[1] JAMES R. MANSFIELD, FRANK E. HRUSKA, AND RUDY SEBASTIAN
Department of Chemistry, University of Manitoba, Winnipeg, Man., Canada R3T 2N2

Received February 17, 1992

TED SCHAEFER, JAMES R. MANSFIELD, FRANK E. HRUSKA, and RUDY SEBASTIAN. Can. J. Chem. **70**, 1750 (1992).

The ^1H and ^{19}F nuclear magnetic resonance spectra of 3,5-dichlorobenzyl fluoride, dissolved in solvents of varying polarity, are analyzed to yield precise values of the long-range coupling constants between ring protons and the nuclei in the fluoromethyl group. The conformational properties of these coupling constants, dependent on the angle by which the C—H and C—F bonds of the side chain twist out of the aromatic plane, are used to determine the solvent dependence of the predominantly twofold barrier to rotation about the Csp^2—Csp^3 bond. In all solvents, the conformer in which the C—F bond lies in the aromatic plane represents the minimum in the internal rotational potential. The magnitude of the twofold potential changes from 3.2(2) kJ/mol in the nonpolar medium, C_6D_{12}, to 0.6(2) kJ/mol in the polar solvent, CD_3CN. Intermediate magnitudes occur for solvents of intermediate dielectric constant. Comparisons are made with the parent molecule, benzyl fluoride, for which the perpendicular conformer is most stable in the same solvents. Such comparisons indicate that for the free molecules, the in-plane conformer of the dichloro derivative is also more stable than the same conformer of benzyl fluoride. This indication is in qualitative agreement with molecular orbital predictions.

TED SCHAEFER, JAMES R. MANSFIELD, FRANK E. HRUSKA et RUDY SEBASTIAN. Can. J. Chem. **70**, 1750 (1992).

On a analysé les spectres en résonance magnétique nucléaire du ^1H et du ^{19}F du fluorure de 3,5-dichlorobenzyle dissous dans des solvants de polarités différentes pour obtenir des valeurs précises pour les constantes de couplage à longue distance entre les protons du cycles et les noyaux du groupe fluorométhyle. On utilise les propriétés conformationnelles de ces constantes de couplage, qui varient avec l'angle de torsion qui existe entre les liaisons C—H et C—F de la chaîne latérale et le plan du noyau aromatique, pour déterminer l'influence du solvant sur la barrière principalement binaire à la rotation autour de la liaison Csp^2—Csp^3. Dans tous les solvants, le conformère dans lequel la liaison C—F se trouve dans le plan du noyau aromatique correspond à un minimum dans le potentiel de la rotation interne. L'amplitude des potentiels binaires varie de 3,2(2) kJ/mol dans un solvant non-polaire, le C_6D_{12}, à 0,6(2) kJ/mol dans un solvant polaire, CD_3CN. Avec des solvants de constante diélectrique intermédiaire, on observe des amplitudes intermédiaires. On a effectué des comparaisons avec la molécule parente, le fluorure de benzyle, dans laquelle le conformère perpendiculaire est le plus stable dans les mêmes solvants. Ces comparaisons indiquent que, pour les molécules libres, le conformère dans le plan du dérivé dichloré est aussi plus stable que le même conformère du fluorure de benzyle. Cette indication est en accord qualitatif avec les prédictions faites à l'aide de calculs d'orbitales moléculaires.

[Traduit par la rédaction]

Can. J. Chem. Downloaded from www.nrcresearchpress.com by 217.78.4.112 on 09/08/12
For personal use only.

Introduction

The internal barrier to rotation in benzyl fluoride, **1**, is small and solvent dependent (1, 2). In solution, long-range

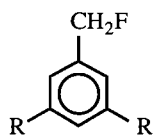

1 R = H
2 R = Cl

spin–spin coupling constants, between nuclei in the side chain and those in the phenyl group, imply an apparent twofold barrier to rotation about the Csp^2—Csp^3 bond that ranges from 3.2 ± 0.2 kJ/mol in the polar solvent, CD_3CN, to 0.7 ± 0.2 kJ/mol in the nonpolar solvent, C_6D_{12} (2). In both instances, the conformer corresponding to the minimum in the internal rotational potential is **3**. Such an interpretation

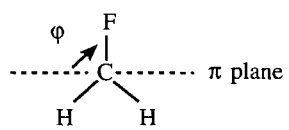

3

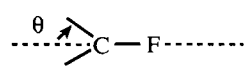

4

is consistent with motionally averaged dipolar coupling constants measured for **1** in liquid crystalline solvents. These measurements yield twofold barriers of 0.30 ± 0.02 and 1.50 ± 0.08 kJ/mol in two such solvents; the former number applies to the less polar solvent (1). Again, the temperature dependence of the ^{19}F chemical shift in acetone solution suggests **3** as the conformer of lowest energy (3). An extrapolation of the twofold barrier magnitudes, based on a dielectric model, yields **4** as the most stable conformer for the free molecule, perhaps by about 1 kJ/mol (2). This result agrees qualitatively with *ab initio* molecular orbital computations, various bases yielding **4** as the stable conformer but with large variations in the barrier height (2). Electron diffraction patterns of the vapor imply a conformer of minimum energy near a φ of 60° and a barrier height near 1.7 kJ/mol (4). Furthermore, excitation spectroscopy, mass-resolved, of a supersonic jet of benzyl fluoride has **3** as the conformation at very low temperatures (5), based on certain similarities in the spectra of **1** and benzyl alcohol. In view of all these results, it would be of interest to have rather higher level molecular orbital calculations on **1**, preferably those including (expensive) allowance for electron correlation, as well as studies using techniques such as far infrared and high-resolution microwave spectroscopies. A recent temperature-dependent, low-resolution, microwave study of the benzyl halides in the vapor phase (6) showed that the

[1]Author to whom correspondence may be addressed.

TABLE 1. The ^1H and ^{19}F nmr spectral parameters for 3,5-dichlorobenzyl fluoride at 300 K in various solvents

Parameter	C_6D_{12}[a]	CS_2[b]	CCl_4[c]	CD_2Cl_2[d]	$(CD_3)_2C{=}O$[e]	CD_3CN[f]
ν_F[g]	14696.969[h]	14452.983	14672.862	14124.955	13805.411	13649.018
$\nu(CH_2)$[i] 1545.584	1571.106	1579.701	1598.238	1637.024	1643.634	
$\nu_{2,6}$	2132.364	2144.841	2155.496	2179.649	2224.542	2237.210
ν_4	2164.657	2172.092	2188.344	2206.643	2237.213	2259.256
^2J(H, F)	47.201	47.137	47.101	47.024	47.077	47.014
$^4J_{24}$[j]	1.902	1.907	1.904	1.912	1.928	1.952
^4J(H, F)	−1.244	−1.248	−1.293	−1.444	−1.482	−1.527
^4J(H, H)	−0.709	−0.705	−0.697	−0.664	−0.658	−0.647
^6J(H, F)	−1.033	−1.038	−1.076	−1.233	−1.256	−1.307
^6J(H, H)	−0.537	−0.534	−0.531	−0.503	−0.499	−0.489
Calcd. transitions	128	128	128	128	128	128
Assigned trans.	116	119	118	110	119	112
Peaks observed	116	120	118	110	121	113
Largest difference	0.004	0.007	0.011	0.006	0.009	0.009
Root mean square deviation	0.001	0.002	0.003	0.003	0.003	0.004

[a]5.2 mol% in C_6D_{12}, containing also 0.5 mol% of tetramethylsilane (TMS) and 0.25 mol% of C_6F_6.
[b]5.0 mol% in CS_2, containing also 10 mol% of C_6D_{12}, 0.25 mol% of C_6F_6, and TMS as in [a].
[c]5.1 mol% in CCl_4, containing also 10 mol% of C_6D_{12}, 0.25 mol% of C_6F_6, and TMS as in [a].
[d]4.4 mol% in CD_2Cl_2, also containing TMS and C_6F_6 as in [c].
[e]5.0 mol% in acetone-d_6, with TMS and C_6F_6 as in [c].
[f]5.6 mol% in CD_3CN, with TMS and C_6F_6 as in [c].
[g]In Hz at 282.36264 MHz to low frequency (more shielded) of internal C_6F_6.
[h]All standard deviations in the spectral parameters are ≤0.001 Hz, as given by the iterative analyses.
[i]In Hz at 300.13493 MHz to high frequency of internal TMS.
[j]The coupling constant between the ring protons, *ortho* and *para* to CH_2F.

heavier halides are nonplanar, but that the conformation of the fluoride was not deducible.

Now, the minimal basis set, of all those used, appears to agree best with the experimental indications of a very low barrier to internal rotation in **1**. Furthermore, this basis predicts a significant substituent dependence of the barrier height. Specifically, the twofold barrier is computed as 2.4 kJ/mol for **2**, R = Cl, that is, that **4** is about 1 kJ/mol lower in energy in **2** than in the parent molecule, **1**. Hence, depending on the accuracy of the computations and also on the extent by which the solvent shifts the minimum in the internal potential, perhaps towards **3** from **4**, the possibility arises that, in **2**, the lowest internal barrier will exist in the most polar solvent, in direct contrast to the behaviour of **1**. We report here the results of such experiments on **2** in six solvents, polar and nonpolar, using long-range ^1H, ^1H and ^1H, ^{19}F coupling constants.

Experimental

The fluorination of 3,5-dichlorobenzyl alcohol with morpholinosulfur trifluoride (morph-DAST), both compounds coming from Aldrich, followed the literature procedure (7) to give 3,5-dichlorobenzyl fluoride, **2**. Dilute solutions of **2** in various solvent mixtures (see Table 1 for details) were filtered into 5 mm o.d. nmr sample tubes, degassed by at least four freeze–pump–thaw cycles, and were then flame-sealed under vacuum.

The ^1H and ^{19}F nmr spectra were obtained with a $^1H/^{19}F$ probe on a Bruker AM300 spectrometer using acquisition times of 41 s and, typically, 32 free induction decays were coadded. The digital resolution was 0.012 Hz/point, followed by zero-filling to four times the original data table (8). A small amount of resolution enhancement produced line widths at half-height of as little as 0.05 Hz. Final shimming procedures used the free induction decays from the internal reference compounds. The probe temperature was maintained at 300 K.

Results and discussion

Spectral analyses

The ^1H and ^{19}F nmr spectra arise from an AB_2X_2R spin system. Relatively straightforward iterative analyses with the substantially modified algorithm, NUMARIT (9), produce the spectral parameters in Table 1. The standard deviations in chemical shifts and coupling constants are less than or equal to 0.001 Hz.

^6J(H,F) and ^6J(H,H) as indicators of the internal barriers

Previous, detailed, discussions concluded that ^6J(H,F) and ^6J(H,H) are σ–π coupling constants and, as such, are proportional, respectively, to $\sin^2\varphi$ and $\sin^2\theta$ (2, 10), as in eqs. [1] and [2].

$$[1]\quad {}^6J(H,H) = {}^6J_{90}(H,H)\,\langle\sin^2\theta\rangle$$

$$[2]\quad {}^6J(H,F) = {}^6J_{90}(H,F)\,\langle\sin^2\varphi\rangle$$

Together with the approximation, $\langle\sin^2\theta\rangle = 0.75 - 0.5\,\langle\sin^2\varphi\rangle$, obviously holding rigorously for a tetrahedral geometry at the side chain, angular brackets indicating expectation values arising from the internal rotation, only the extema in ^6J(H,F) and ^6J(H,H)), those for φ and θ at 90°, are needed to deduce $\langle\sin^2\theta\rangle$ and $\langle\sin^2\varphi\rangle$ in the various solvents. The extrema follow from simultaneous equations applicable to the different solvents. Picking a nonpolar solvent, say CS_2, and a polar solvent, say acetone-d_6, and noting that the expectation values are different in the two solvents, yields $^6J_{90}$(H,F) as −2.909(2) Hz and $^6J_{90}$(H,H) as −0.934(2) Hz for the two solutions. On the assumption that these extreme values are applicable to all the solvents in Table 1, values

Can. J. Chem. Downloaded from www.nrcresearchpress.com by 217.78.4.112 on 09/08/12
For personal use only.

TABLE 2. Apparent twofold barriers to internal rotation in 3,5-dichlorobenzyl fluoride, **2**, and benzyl fluoride, **1**, in various solutions

Solvent[a]	$\langle \sin^2\varphi \rangle$[b]	$\langle \sin^2\theta \rangle$[c]	V_2, **2**[e]	V_2, **1**[f]
C_6D_{12}	0.335	0.575	3.2(2)	0.7(2)
CS_2/C_6D_{12}	0.357[d]	0.572[d]	3.0	0.9
CCl_4/C_6D_{12}	0.370	0.569	2.7	1.1
CD_2Cl_2	0.424	0.539	1.6	2.8
$(CD_3)_2C{=}O$	0.432[d]	0.534[d]	1.4	2.6
CD_3CN	0.449	0.524	0.6	3.2

[a]See Table 1 for solvent details.
[b]Based on ^6J(H, F) in Table 1 and a $^6J_{90}$ (H, F) of −2.909 Hz, but see [d].
[c]Based on ^6J(H, H) in Table 1 and a $^6J_{90}$ (H, H) of −0.934 Hz, but see [d].
[d]These values obey exactly the equation, $\langle \sin^2\theta \rangle = 0.75 - 0.5 \langle \sin^2\varphi \rangle$, see text. The other values in these columns also satisfy this relationship to within an average deviation of 0.002.
[e]The formal error is less than 0.1 kJ/mol, but is quoted as 0.2 kJ/mol.
[f]From ref. 2.

of $\langle \sin^2\theta \rangle$ and $\langle \sin^2\varphi \rangle$ follow immediately from the ratio of the measured coupling constants, e.g., $\langle \sin^2\theta \rangle = {}^6J(\mathrm{H,H})/{}^6J_{90}(\mathrm{H,H})$. A check on self-consistency is then provided by the relationship above between $\langle \sin^2\theta \rangle$ and $\langle \sin^2\varphi \rangle$ (see footnotes to Table 2).

The $^6J_{90}$(H,H) of −0.934(2) Hz for 3,5-dichlorobenzyl fluoride differs by very little from that of −0.941(4) Hz deduced for benzyl fluoride (2), as expected from a large data set indicating that ^6J(H,H) in toluene and benzyl derivatives is sensitive to the electronegativity of the α substituent but insensitive to ring substitution. For benzyl fluoride, $^6J_{90}$(H,F) is −2.856(4) Hz (2), somewhat smaller in magnitude than the −2.909(2) Hz in the 3,5-dichloro derivative. It is anticipated that the composite, σ−π, hyperfine parameter for the C—F bond will evince a greater sensitivity to substitution than will that of a C—H bond.

The apparent twofold barrier to rotation about the Csp^2—Csp^3 bond follows from a hindered rotor model (11, 12), or from a classical averaging procedure, relating $\langle \sin^2\theta \rangle$ and $\langle \sin^2\varphi \rangle$ to the barrier magnitude. The two procedures yield the same barriers in the present instance, very likely because thermal energies at 300 K are large compared to the discrete spacings of the hindered rotor energies. The STO-3G MO computations (2) for **2** yield the internal rotational potential as $2.41(2) \sin^2\varphi + 0.13(2) \sin^2 2\varphi$, so that the fourfold is only about 5% of the twofold component.

The solvent dependence of the barrier

The apparent twofold barriers, V_2, are given in Table 2. With reference to the in-plane, **4**, and perpendicular, **3**, conformers, the $\langle \sin^2\varphi \rangle$ numbers demonstrate **4** as lying at the minimum of the twofold potential. A rigid **4** corresponds to a vanishing $\langle \sin^2\varphi \rangle$, a rigid **3** to unity, and a value of 0.5 to a negligible internal barrier. Similarly, $\langle \sin^2\theta \rangle$ for a rigid **3** is 0.25 and, for **4**, it is 0.75. The most polar solvent, CD_3CN, causes a decrease of 2.6(4) kJ/mol in V_2, reflecting the tendency, also seen for V_2 of benzyl fluoride, to shift the phase of V_2 by 90°. In other words, a medium of high dielectric constant stabilizes **3** relative to **4** for both molecules.

The opposite trend in V_2 for the two molecules in Table 2 simply reflects the greater stability of the in-plane conformer of 3,5-dichlorobenzyl fluoride, **2**, in the nonpolar solvents. For benzyl fluoride, the perpendicular conformer is most stable even in C_6D_{12} solution. If an extrapolation to a medium of unit dielectric constant is valid (2), then the free molecule of **2** is more stable in the in-plane than in the perpendicular conformation by 4.5–5.5 kJ/mol. For benzyl fluoride, **1**, this relative stability was estimated as 1.1 ± 0.7 kJ/mol (2). Qualitatively, the relative stability agrees with the STO-3G MO data (2).

Increased barriers to internal rotation, due to *meta* halogen substituents, are known experimentally for thioanisoles (13, 14), thiophenols (15), and theoretically for phenols (16). The hydroxyl and thiomethyl groups are π electron donors; the substituent effects on the barriers have been discussed in terms of perturbational molecular orbital (PMO) theory (15, 16). *meta* Substitution by fluorine in benzaldehyde causes a decrease in the internal barrier (17–19); the formyl group is a π electron acceptor. For benzyl fluoride, an interpretation of a stable in-plane conformer for the free molecule in terms of PMO theory is somewhat ambiguous; an attraction between C^+—F^- and *ortho* C^-—H^+ dipoles has been invoked (20). If this interpretation is correct, then it is possible that the electronegative chlorine substituents enhance the polarity of the *ortho* C—H bonds, accounting for the increased stability of the planar conformer.

According to Table 2, the stabilization by solvents of the perpendicular conformer is roughly the same for benzyl fluoride and its 3,5-dichloro derivative. The best estimates of the dipole moments of the perpendicular, 2.10 D, and in-plane, 1.74 D, conformers of **1** come from a 6–31G* basis (2). The difference is not large enough to account for the observed solvent stabilization of the perpendicular conformer in polar solvents (21, 22), so that quadrupolar terms in reaction field theory may be important. Similar remarks must apply to the 3,5-dichloro derivative, for which the minimal basis set predicts a dipole moment lower by 0.1 D for the perpendicular, relative to the in-plane, conformer.

The coupling constants, ^4J(H,F) and ^4J(H,H)

The *ortho* benzylic coupling constant, ^4J(H,H), in toluene has σ−π and σ components (23), written as $^4J(\mathrm{H,H}) = {}^4J_{90} \sin^2\theta + {}^4J^\sigma \cos^2\theta$, $^4J_{90}$ being −1.08 Hz and ^4J, −0.32 Hz (23, 24). Because $\langle \sin^2\theta \rangle$ is known for 3,5-dichlorobenzyl fluoride, derivations of $^4J_{90}$(H,H) and $^4J^\sigma$ are possible, assuming the applicability of such a relationship to this molecule. It turns out that $^4J_{90}(\mathrm{H,H})$ is -1.23_4Hz, while $^4J^\sigma$ is 0.002 Hz or less. Neglect of $^4J^\sigma$ and use of $\langle \sin^2\theta \rangle$ deduced from ^6J(H,H), together with this $^4J_{90}$(H,H), reproduces the ^4J(H,H) values in Table 1 to within a mean deviation of 0.002 Hz (for the CCl_4 solution the deviation is 0.005 Hz). The range of ^4J(H,H) is 0.062(2) Hz. The increase in magnitude of $^4J_{90}$(H,H) relative to toluene, whereas that of $^6J_{90}$(H,H) decreases (23), is perhaps unexpected, as is the apparent absence of a σ component of ^4J(H,H). The present compound may be unique in this respect; further work is indicated.

Turning to ^4J(H,F), the *assumption* of a θ dependence similar to ^4J(H,H) yields $^4J(\mathrm{H,F})/\mathrm{Hz} = -3.25_3 \langle \sin^2\varphi \rangle - 0.134_8 \langle \cos^2\varphi \rangle$. The values of $\langle \sin^2\varphi \rangle$ in Table 2, derived from ^6J(H,F), reproduce ^4J(H,F) in Table 1 with an average deviation of 0.004_6 Hz; the range of ^4J(H,F) is 0.283(2) Hz. Of course, this result does not prove the relationship, although a large σ−π component, proportional to $\sin^2\varphi$, is expected.

Can. J. Chem. Downloaded from www.nrcresearchpress.com by 217.78.4.112 on 09/08/12
For personal use only.

Nevertheless, this discussion of ^4J(H,H) and ^4J(H,F) suggests the possibility of the derivation of internal rotational potentials in various solvents for a series of *para*-substituted benzyl fluorides; ^6J(H,H) and ^6J(H,F) are not present in such compounds.

The solvent dependence of $^4J_{24}$

This intraring coupling constant is sensitive to the polarity of the medium, increasing by 0.050(2) Hz between the solvents, C_6D_{12} and CD_3CN. A solvent dependence of[3,4,5] J(H,H) in various monosubstituted benzenes is known from unpublished work in this laboratory. A regular pattern is observed, apparently independent of the polarity of the substituent, X, being the same, for example, for phenylacetylene and phenyl cyanide. The magnitudes of the changes in these coupling constants are comparable to those of $^4J_{24}$ in **2**. This point is made to allay suspicion that the variation of $^4J_{24}$ in **2** might be an artifact of the analyses.

Acknowledgements

We are grateful to the Natural Sciences and Engineering Research Council of Canada for financial assistance.

1. G. Celebre, G. DeLuca, M. Longeri, and J. W. Emsley. Mol. Phys. **67**, 239 (1989).
2. T. Schaefer, C. Beaulieu, R. Sebastian, and G. H. Penner. Can. J. Chem. **68**, 581 (1990).
3. R. T. C. Brownlee and D. J. Craik. Tetrahedron Lett. **21**, 1681 (1980).
4. R. J. Abraham, R. A. Hearmon, M. Traetteberg, and P. Bakken. J. Mol. Struct. **57**, 149 (1979).
5. H.-S. Im, E. R. Bernstein, H. V. Secor, and J. I. Seeman. J. Am. Chem. Soc. **113**, 4422 (1991).
6. S. A. Sorenson and N. S. True. J. Mol. Struct. **263**, 21 (1991).
7. P. Messina, K. Mange, and W. J. Middleton, J. Fluorine Chem. **42**, 137 (1989).
8. R. Freeman. A handbook of nuclear magnetic resonance. J. Wiley & Sons, New York. 1988 p. 302.
9. J. S. Martin, A. R. Quirt, and K. E. Worvill. The NMR program library. Daresbury Laboratory, Daresbury, U.K.
10. T. Schaefer, J. Peeling, and R. Sebastian. Can. J. Chem. **63**, 3219 (1985).
11. P. B. Ayscough, M. S. Brice, and R. E. D. McClung. Mol. Phys. **20**, 41 (1971).
12. W. J. E. Parr and T. Schaefer. Acc. Chem. Res. **13**, 400 (1980).
13. T. Schaefer and J. D. Baleja. Can. J. Chem. **64**, 1376 (1986).
14. T. Schaefer and G. H. Penner. Can. J. Chem. **66**, 1229 (1988).
15. T. Schaefer, J. D. Baleja, and G. H. Penner. Can. J. Chem. **63**, 2471 (1985).
16. A. Pross and L. Radom. Prog. Phys. Org. Chem. **13**, 1 (1981).
17. F. A. L. Anet and M. Ahmad. J. Am. Chem. Soc. **86**, 119 (1964).
18. T. Drakenberg, R. Jost, and J. M. Sommer. J. Chem. Soc. Perkin Trans. 2, 1682 (1975).
19. T. Schaefer and C. S. Takeuchi. Can. J. Chem. **67**, 827 (1989).
20. G. H. Penner, T. Schaefer, R. Sebastian, and S. Wolfe. Can. J. Chem. **65**, 1845 (1987).
21. R. J. Abraham and E. Bretschneider. *In* Internal rotation in molecules. *Edited by* W. J. Orville Thomas. J. Wiley & Sons, London. 1974. Chap. 13.
22. M. W. Wong, M. J. Frisch, and K. B. Wiberg. J. Am. Chem. Soc. **113**, 4776 (1991).
23. M. Barfield, C. J. Fallick, K. Hata, S. Sternhell, and P. W. Westerman. J. Am. Chem. Soc. **105**, 2178 (1983).
24. T. Schaefer, R. Sebastian, and G. H. Penner. Can. J. Chem. **63**, 2597 (1985).

Can. J. Chem. Downloaded from www.nrcresearchpress.com by 217.78.4.112 on 09/08/12
For personal use only.

Synthesis of β-*O*-4 lignin model dimers and their chlorinated derivatives

XINHUA SHEN[1] AND ADRIAAN VAN HEININGEN[2]

Papricon and McGill Pulp and Paper Research Centre, 3420 University Street, Montreal, Que., Canada H3A 2A7

Received October 21, 1991

XINHUA SHEN and ADRIAAN VAN HEININGEN. Can. J. Chem. **70,** 1754 (1992).

The unknown lignin model dimers with hydroxymethyl group at the *para* position of the phenoxy moiety and their chlorinated derivatives (compounds **1**–**13**, except **8**) have been synthesized. During the preparation of **6** from **5**, a by-product was isolated and identified as **9**. The compounds **4**, **7**, and **8** were obtained as a mixture of *erythro* and *threo* isomers in the ratio of about 5:4, estimated from their ^{13}C NMR spectra, and the *erythro* isomer **8***a* was crystallized from the mixture. Chlorinated derivatives **12***a* (*erythro*) and **12***b* (*threo*) were also isolated. Their relative configuration was assigned on the basis of both ^{13}C and ^{1}H NMR spectroscopy.

XINHUA SHEN et ADRIAAN VAN HEININGEN. Can. J. Chem. **70**, 1754 (1992).

On a réalisé la synthèse des dimères modèles de la lignine inconnue portant un groupe hydroxyméthyle en position *para* de la portion phénoxy et de ses dérivés chlorés (composés **1**–**13**, à l'exception du produit **8**). Au cours de la préparation du composé **6** à partir du composé **5**, on a isolé un produit secondaire que l'on a identifié au composé **9**. On a obtenu les composés **4**, **7** et **8** sous la forme des isomères *érythro* et *thréo* qui, d'après la RMN du ^{13}C, sont présents dans un rapport de 5 : 4; on a isolé l'isomère *érythro* **8***a* du mélange. On a aussi isolé les dérivés chlorés **12***a* (*érythro*) et **12***b* (*thréo*). Les configurations relatives ont été attribuées à l'aide de la RMN du ^{13}C et du ^{1}H.

[Traduit par la rédaction]

Can. J. Chem. Downloaded from www.nrcresearchpress.com by 217.78.4.112 on 09/08/12
For personal use only.

Introduction

Lignin is a crosslinked polymer with phenylpropane as the most prevalent monomer unit. The phenylpropane units are linked by ether and carbon–carbon bonds. Approximately half of all softwood lignin interunit linkages are of the arylglycerol-β-aryl ether (β-O-4) type. Therefore, synthesis of β-O-4 substructure models is very important for the study of chemical structure, reactivity, and biodegradation of lignin. Guaiacylglycerol-β-guaiacyl ether and veratrylglycerol-β-guaiacyl ether, widely used as model compounds for various reactions of lignin (1–3), were first synthesized by Adler *et al.* (4, 5). Since then, β-O-4 models have been synthesized by many investigators (6–11). During recent years, Hauteville and Duclos-Jordan (12) reported the synthesis of a series of syringyl type of β-O-4 lignin models. At the moment highly toxic organic chlorinated compounds released from bleach plant effluent make a notable impact on the environment. The present work reports the synthesis of non-phenolic and phenolic β-O-4 dimers with a hydroxymethyl group at the *para* position of the phenoxy moiety, as well as their chlorinated derivatives.

Results and discussion

The synthesis of compounds **1–4** in Scheme 1 was carried out by a modified Adler's procedure (4, 5). Acetoveratrone, commercially available, was brominated to α-bromoacetoveratrone (13), which was subsequently reacted with vanillyl alcohol in the presence of anhydrous potassium carbonate in absolute alcohol to yield a dimer **1**. Condensation of **1** with formaldehyde gave ketol derivative **2**. The ketones **1** and **2** were respectively reduced using sodium borohydride to give the corresponding compounds **3**, a crystalline product, and **4**, a mixture of two diastereomers. Compounds **5–8** were synthesized using acetovanillone as starting material. First, the phenolic hydroxyl group of acetovanillone was protected by benzylation (7) and then, via a similar reaction route to that used for the synthesis of compound **4**, compounds **5–7** were obtained. Compound **7** was a mixture of two diastereomers. Debenzylation of **7** by catalytic hydrogenation with 5% palladium on barium sulfate yielded compound **8**. The phenolic compound 8 was synthesized by Nimz (8) using a different method, in which the hydroxymethyl group was introduced by reduction of the aldehyde at a late stage, and also synthesized by Katayama *et al.* (11) using a different synthetic approach. Both of them obtained only the mixture of two isomers in viscous syrup or glass form. In the present work *erythro* isomer **8***a* was crystallized from the mixture of the two diastereomers in ethyl acetate. In the preparation of **6**, a by-product was isolated when **5** was treated with formaldehyde in the presence of potassium carbonate at a temperature over 40°C and identified as **9** by means of ^{1}H NMR, IR, mass spectra, and elemental analysis. This demonstrates that the ketol derivatives **6** or **2** were unstable during the reaction in alkaline solution at temperatures over 40°C and easily underwent dehydration to form α, β-unsaturated ketone compounds. Therefore, this reaction step should be carried out at low temperature in aqueous alcohol. The analytical and spectroscopic data for compounds **1–9** are listed in Tables 1–3.

The ratios of *erythro* and *threo* isomers of diastereomers **4**, **7**, and **8** were estimated to be about 5:4 by ^{13}C NMR spectroscopy (Table 4). The assignment of relative configuration was based on both ^{13}C NMR chemical shifts for α-C and β-C (Table 4) and ^{1}H NMR coupling constants, for α-H and β-H, and chemical shifts for β-H (Table 5). For ^{13}C NMR spectra the upfield shifts were attributed to the *erythro* isomer and downfield shifts were attributed to the *threo* isomer. For ^{1}H NMR spectra the smaller *J* values and downfield shifts (β-H) were attributed to the *erythro* isomer and the large values and upfield shifts (β-H) were attributed to the *threo* isomer; Similar assignments have been made in the literature (14–17) for analogous structures of β-O-4 lignin model compounds.

[1]Author to whom correspondence may be addressed. Present address: Pulp and Paper Centre, University of Toronto, 200 College Street, Toronto, Ont., Canada M5S 1A4.

[2]Present address: Industrial Research Chair in Pulping Technology, Incutech Centre, Mckay Drive, University of New Brunswick, P.O. Box 69000, Fredericton, N.B., Canada E3B 6C2.

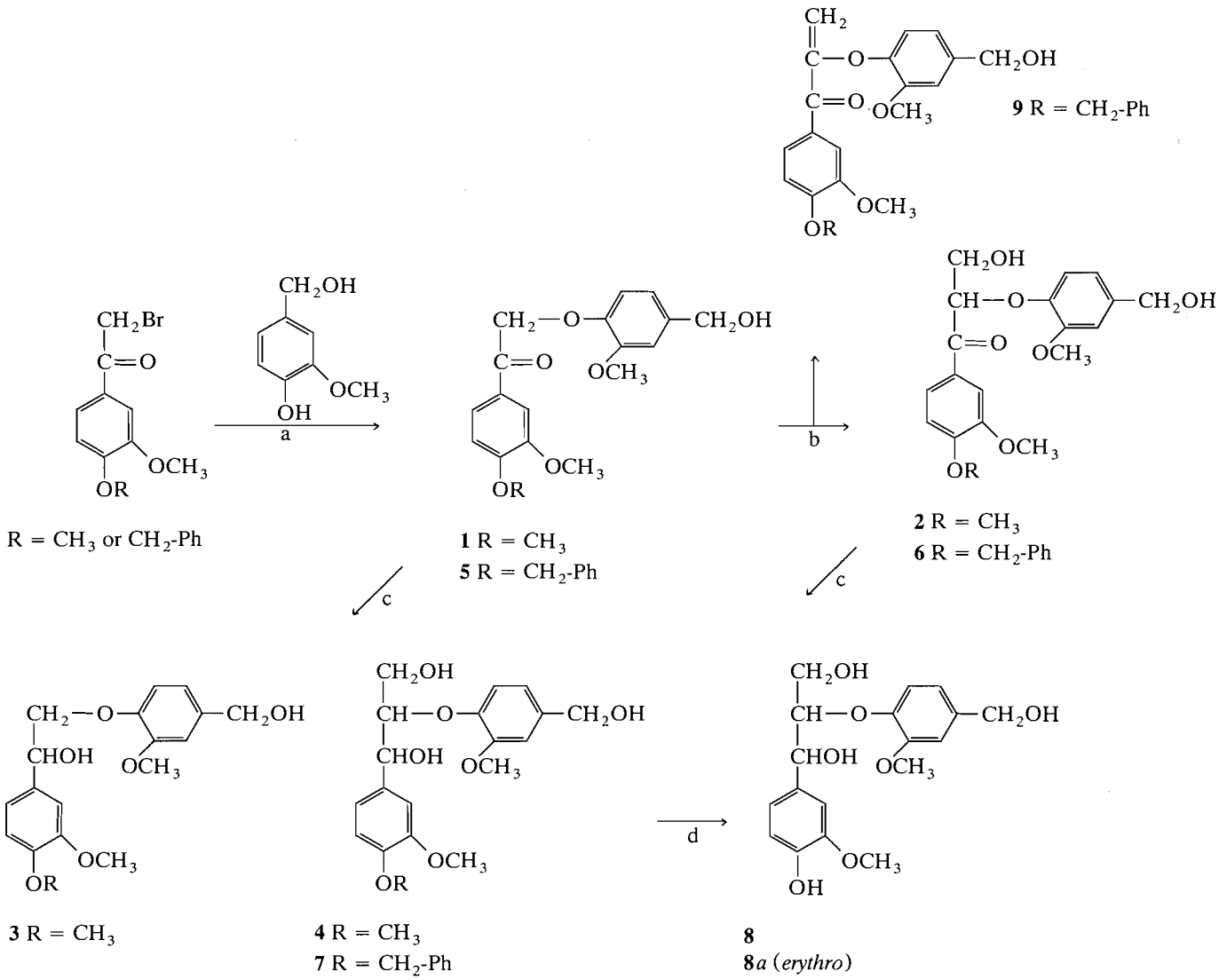

a. anhydrous K_2CO_3, absolute EtOH, reflux, 1 h; b. formalin, K_2CO_3, EtOH, 35°C, 1.5 h; c. $NaBH_4$, EtOH, r.t. 1 h; d. 5%Pd–$BaSO_4$/H_2, r.t. 2 h.

SCHEME 1

To prepare some chloro-organic products that are closer to those generated during pulp bleaching, compounds **3** and **4** were chlorinated with different ratios of chlorine in aqueous solution containing a small amount of alcohol at room temperature. The corresponding chlorinated derivatives **10**, **11**, **12***a*, **12***b*, and **13** in Scheme 2 were isolated from the chlorination products by column chromatography using toluene–ethyl acetate as eluent. Their analytical and spectroscopic data are summarized in Tables 1 and 3. The dichlorinated dimers **10** and **12** resulted from electrophilic substitution by chlorine, which took place predominantly at positions *para* to the methoxyl groups in both aromatic rings. No products substituted at the *ortho* positions were isolated. This demonstrates that the *para* position relative to the methoxyl group is much more reactive than the *ortho* position. The structures of compounds **10** and **12** (Fig. 1) were assigned by comparison of their ^{1}H NMR spectra with those of known monomers (18), chlorovanillyl alcohol diacetylated derivatives **14** and **15** (Fig. 1). It is found that when chlorine is substituted at the 6 position, as in **14**, no long-range coupling is observed between protons H-2 and H-5 of the aromatic ring, because these two protons are *para*. When the chlorine is substituted at the 5 position, as in **15**, because the two protons H-2 and H-6, are *meta*, their signals are split into a doublet in which $J_{2,6}$ = 1.7 Hz. The peak patterns of the protons of the two aromatic rings for compound **10** or **12** are similar to those of 6-chlorinated compound **14**. Furthermore, the results previously obtained for chlorination of the nonphenolic monomer, veratryl alcohol, in aqueous solution also showed that substitution by chlorine occurred at the position *para* to the methoxyl group (18). With increasing chlorine ratio, **11** and **13** were formed by electrophilic displacement of the hydroxymethyl group of **10** and **12** by chlorine. The chlorinated derivative, **13**, was obtained as a mixture of two diastereoisomers and **12** as pure isomers, **12***a* (*erythro* form) and **12***b* (*threo* form), respectively. Their configuration was assigned according to ^{13}C and ^{1}H NMR spectroscopy by comparison with the spectra of

Can. J. Chem. Downloaded from www.nrcresearchpress.com by 217.78.4.112 on 09/08/12
For personal use only.

TABLE 1. Analytical and spectroscopic data for the compounds

Compound	Melting point (°C)	Yield (%)	Formula	Anal. calcd. C	Anal. calcd. H	found C	found H	MS m/e (M^+)
α-(4-Hydroxymethyl-2-methoxyphenoxy)-3,4-dimethoxyacetophenone **1**	105–106	87	$C_{18}H_{20}O_6$	65.04	6.08	65.33	6.31	
α-(4-Hydroxymethyl-2-methoxyphenoxy)-β-hydroxy-3,4-dimethoxypropiophenone **2**	148–149	80	$C_{19}H_{22}O_7$	62.96	6.13	62.72	6.09	362
1-(3,4-Dimethoxyphenyl)-2-(4-hydroxymethyl-2-methoxyphenoxy)-1-ethanol **3**	100–102	92	$C_{18}H_{22}O_6$	64.65	6.64	64.73	6.69	334
1-(3,4-Dimethoxyphenyl)-2-(4-hydroxymethyl-2-methoxyphenoxy)-1,3-propanediol **4**	Syrup	94	$C_{19}H_{24}O_7$	62.62	6.65	62.42	6.54	
α-(4-Hydroxymethyl-2-methoxyphenoxy)-4-benzyloxy-3-methoxyacetophenone **5**	105–106	88	$C_{24}H_{24}O_6$	70.56	5.93	70.77	5.71	
α-(4-Hydroxymethyl-2-methoxyphenoxy)-β-hydroxy-4-benzyloxy-3-methoxypropiophenone **6**	73–75	79	$C_{25}H_{26}O_7$	68.47	5.99	68.52	6.13	
1-(4-Benzyloxy-3-methoxyphenyl)-2-(4-hydroxymethyl-2-methoxyphenoxy)-1,3-propanediol **7**	Syrup	95	$C_{25}H_{28}O_7$	68.16	6.42	68.03	6.41	
1-(4-Hydroxy-3-methoxyphenyl)-2-(4-hydroxymethyl-2-methoxyphenoxy)-1,3-propanediol **8**	Syrup	96	$C_{18}H_{22}O_7$	61.70	6.34	61.36	5.72	
8*a* (*erythro*)	106–107		$C_{18}H_{22}O_7$	61.70	6.34	61.77	6.52	
1-(4-Benzyloxy-3-methoxyphenyl)-2-(4-hydroxymethyl-2-methoxyphenoxy)-2-propen-1-one **9**	104–105		$C_{25}H_{24}O_6$	71.40	5.76	71.72	6.00	420
1-(6-Chloro-3,4-dimethoxyphenyl)-2-(5-chloro-4-hydroxymethyl-2-methoxyphenoxy)-1-ethanol **10**	153–155	46	$C_{18}H_{20}Cl_2O_6$					406, 404, 402
1-(6-Chloro-3,4-dimethoxyphenyl)-2-(4,5-dichloro-2-methoxyphenoxy)-1-ethanol **11**	128–130	38	$C_{17}H_{17}Cl_3O_5$					410, 408, 406
1-(6-Chloro-3,4-dimethoxyphenyl)-2-(5-chloro-4-hydroxymethyl-2-methoxyphenoxy-1,3-propanediol **12***a* (*erythro*)	58–60	25	$C_{19}H_{22}Cl_2O_7$					436, 434, 432
12*b* (*threo*)	66–68	20	$C_{19}H_{22}Cl_2O_7$					436, 434, 432
1-(6-Chloro-3,4-dimethoxyphenyl)-2-(4,5-dichloro-2-methoxyphenoxy)-1,3-propanediol **13**	Syrup	36	$C_{18}H_{19}Cl_3O_6$					440, 438, 436

compounds **4**, **7**, and **8**. Their ^{13}C and ^1H NMR data are listed, respectively, in Tables 4 and 5.

Experimental

General methods

Solutions were usually evaporated under diminished pressure at a bath temperature not exceeding 40°C. Melting points were determined with a Fisher–Johns melting-point apparatus, and are uncorrected. Elemental analyses were performed with a CEC model 240XA CHN analyzer. Thin-layer chromatography (TLC) was carried out with precoated silica gel plates using toluene and ethyl acetate in different ratios as developing solvent, and the spots were detected by charring with 8% aqueous sulfuric acid. All reactions were monitored by TLC. Column chromatography was performed on silica gel (Merck 230–240 mesh ASTM). ^1H and ^{13}C NMR spectra were recorded at 25°C with a Varian XL 200 or XL 300 NMR spectrometer and tetramethylsilane as an internal standard. Solid state infrared spectra were recorded using an FT-IR spectrometer (Mattson Instruments, model IR10100) equipped with a photoacoustic detector. Mass spectra were obtained with a Kratos MS25RFA analytic spectrometer with a direct insertion probe (70 eV at 250°C).

Analytical and spectroscopic data for the following compounds are summarized in Tables 1–3.

*α-(4-Hydroxymethyl-2-methoxyphenoxy)-3,4-dimethoxy acetophenone **1***

To a solution of α-bromo-acetoveratrone (18 g, 0.069 mol) (13) and vanillyl alcohol (12.8 g, 0.083 mol) in absolute alcohol

Can. J. Chem. Downloaded from www.nrcresearchpress.com by 217.78.4.112 on 09/08/12
For personal use only.

Can. J. Chem. Downloaded from www.nrcresearchpress.com by 217.78.4.112 on 09/08/12
For personal use only.

TABLE 2. ^{1}H NMR spectroscopic data for the compounds (chemical shift[a]/ppm)

Compound no.	α-H	β-H	γ-H	α-OH β or γ-OH	α′-H	α′-OH	OCH_3			Ar-H					
										6′H	5′H	5H	3′H	2H	6H
1	5.30(s)				4.61(d) $J_{\alpha',OH}$ = 5.7	1.78 (t)	3.90 (s)	3.94 (s)	3.96 (s)	6.79 (d)	6.83 (dd)	6.91 (d)	6.97 (d)	7.60 (d)	7.68 (dd)
										$J_{5',6'}$ = 8.0, $J_{3',5'}$ = 1.6, $J_{5,6}$ = 8.4, $J_{2,6}$ = 2.0					
2	5.43(t) $J_{\alpha,\beta}$ = 5.1	4.09(dd) $J_{\beta,OH}$ = 6.8		3.30(t)	4.62(d) $J_{\alpha',OH}$ = 5.2	1.97 (t)	3.85 (s)	3.93 (s)	3.96 (s)	6.84 (d)	6.79 (dd)	6.90 (d)	6.96 (d)	7.62 (d)	7.76 (dd)
										$J_{5',6'}$ = 8.0, $J_{3',5'}$ = 1.6, $J_{5,6}$ = 8.5, $J_{2,6}$ = 2.0					
3[b]	5.05(dd) $J_{\alpha,\beta1}$ = 9.08	3.96(dd, β1H) $J_{\beta1,\beta2}$ = 9.93	4.13(dd, β2H) $J_{\alpha,\beta2}$ = 2.95		4.61(s)		3.84 (s)	3.88 (s)	3.90 (s)	6.84–7.03 (m, 6H)					
4	4.93(dd) $J_{\alpha,\beta}$ = 4.8 (*erythro*)	4.01 (m, *threo*) 4.11 (m, *erythro*) $J_{\alpha,\beta}$ = 7.8 (*threo*)	3.30–3.92 (m)	2.84(m) 3.30–3.92(m)	4.66(d) $J_{\alpha',OH}$ = 5.4	2.02 (t)	3.30–3.92 (m)			6.80–7.30 (m, 6H)					
5	5.28(s)				4.61(d) $J_{\alpha',OH}$ = 5.6	1.61 (t)	3.89 (s)	3.94 (s)	5.24 (s,OCH_2)	6.78 (d)	6.81 (dd)	6.90 (d)	6.95 (d)	7.60 (d)	7.58 (dd)
										$J_{5',6'}$ = 8.2, $J_{3',5'}$ = 1.6, $J_{5,6}$ = 8.3, $J_{2,6}$ = 2.0 7.29–7.45 (m, 5H, Ph)					
6	5.41(t) $J_{\alpha,\beta}$ = 5.2	4.06(dd) $J_{\beta,OH}$ = 6.6		3.28(t)	4.61(d) $J_{\alpha',OH}$ = 5.7	1.96 (t)	3.83 (s)	3.93 (s)	5.24 (s,OCH_2)	6.82 (d)	6.77 (dd)	6.90 (d)	6.94 (d)	7.63 (d)	7.67 (dd)
										$J_{5',6'}$ = 8.0, $J_{3',5'}$ = 1.5, $J_{5,6}$ = 8.3, $J_{2,6}$ = 2.0 7.29–7.46 (m, 5H, Ph)					
7[b]	4.96(d) $J_{\alpha,\beta}$ = 4.8 (*erythro*)	4.04(m, *threo*) 4.15(m, *erythro*) $J_{\alpha,\beta}$ = 7.7 (*threo*)	3.20–3.88 (m)		4.62(s)		3.20–3.88 (m)		5.15 (s,OCH_2)	6.80–7.30 (m, 6H, 2Ar)			7.30–7.50 (m, 5H, Ph)		

[a]Solvent: $CDCl_3$.
[b]Solvent: $CDCl_3$ + D_2O.

Can. J. Chem. Downloaded from www.nrcresearchpress.com by 217.78.4.112 on 09/08/12
For personal use only.

TABLE 3. ^{1}H NMR spectroscopic data for the compounds (chemical shift[a]/ppm)

Compound no.	α-H	β-H	γ-H	α-OH β or γ-OH	α′-H	α′-OH	OCH_3			Ar-H 6′H	5′H	5H	3′H	2H	6H
8	4.97(dd) $J_{\alpha,\beta}$ = 5.0 (*erythro*)	4.04(m, *threo*) 4.15(m, *erythro*) $J_{\alpha,\beta}$ = 7.7 (*threo*)	3.46–3.98 (m)	3.46–3.98 (m) 2.68(m)	4.67(d) $J_{\alpha',OH}$ = 5.4	1.86 (t) 5.66(2s, PhOH)	3.46–3.98(m)			6.80–7.30 (m, 6H)					
8*a*[b]	4.96(d) $J_{\alpha,\beta}$ = 5.0	4.15(m) $J_{\beta,\gamma1}$ = 3.40	3.66(dd, γ2H) $J_{\gamma1,\gamma2}$ = 12.11	3.90 (m, γ1H)	4.67(s)		3.90(m)			6.82–7.01 (m, 6H)					
9		4.74(d, β1H) J_{gem} = 2.4	5.21(d, β2H)		4.68(d) $J_{\alpha',OH}$ = 5.7	1.84 (t)	3.87 (s)	3.96 (s)	5.25 (s, OCH_2)	6.92 (d)	6.91 (dd)	7.04 (d)	7.03 (d)	7.65 (d)	7.74 (dd)
										$J_{5',6'}$ = 8.2, $J_{3',5'}$ = 2.0, $J_{5,6}$ = 8.3, $J_{2,6}$ = 2.0					
10[b]	5.44(dd) $J_{\alpha,\beta1}$ = 2.49	3.82 (dd, β2H) $J_{\alpha,\beta2}$ = 9.07	4.25(dd,β1H) $J_{\beta1,\beta2}$ = 9.87		4.72(s)		3.88 (s)	3.89 (s)	3.91 (s)		6.85	6.93 (4s,	7.04 4H)	7.22	
11[b]	5.44 (dd) $J_{\alpha,\beta1}$ = 2.40	3.81(dd, β2H) $J_{\alpha,\beta2}$ = 9.10	4.20 (dd, β1H) $J_{\beta1,\beta2}$ = 9.82				3.85 (s)	3.87 (s)	3.90 (s)		6.88	6.93 (4s,	6.97 4H)	7.19	
12*a*[b]	5.31(d) $J_{\alpha,\beta}$ = 3.50	4.39(m) $J_{\beta,\gamma2}$ = 2.54	3.64(dd, γ2H) $J_{\gamma1,\gamma2}$ = 12.38	3.79–3.90 (m, γ1H)	4.66(s)		3.79–3.90(m)				6.79	6.99 (4s,	7.11 4H)	7.14	
12*b*[b]	5.33(d) $J_{\alpha,\beta}$ = 5.54	4.26(m) $J_{\beta,\gamma2}$ = 3.64	3.75(dd,γ2H) $J_{\gamma1,\gamma2}$ = 12.38	3.84–3.87 (m, γ1H)	4.65 (s)		3.84–3.87(m)				6.84	6.87 (4s,	7.01 4H)	7.06	
13*a*[b]	5.33(d) $J_{\alpha,\beta}$ = 3.66	4.40(m) $J_{\beta,\gamma2}$ = 3.21	3.67(dd,γ2H) $J_{\gamma1,\gamma2}$ = 12.34	3.84–3.87 (m, γ1H)			3.81–3.94(m)				6.81	7.00 (4s,	7.15 4H)	7.19	
13*b*[b]	5.34(d) $J_{\alpha,\beta}$ = 5.72	4.23(m) $J_{\beta,\gamma2}$ = 3.54	3.73(dd,γ2H) $J_{\gamma1,\gamma2}$ = 12.41	3.81–3.91 (m, γ1H)			3.81–3.91(m)				6.84	6.94 (4s,	6.98 4H)	7.06	

[a]Solvent: $CDCl_3$.
[b]Solvent: $CDCl_3$ + D_2O.

TABLE 4. ^{13}C NMR data for some model compounds and chlorinated derivatives

Compound	Isomer	Chemical shift (ppm)[a] β-C	α-C	α'-C	γ-C
3		76.21	72.32	64.60	
4[b]	E	86.53	73.09	64.76	61.15
	T	88.49	73.87	64.76	61.15
7[b]	E	86.29	72.86	64.63	60.81
	T	88.35	73.66	64.63	60.97
8*a*	E	88.01	73.15	65.45	61.11
8[b]	T	89.89	74.33	65.27	61.38
11		73.90	68.98		
12*a*	E	83.92	70.34	62.30	60.67
12*b*	T	87.38	70.76	62.25	62.25
13	E	84.65	70.88		61.17
	T	88.23	71.25		62.73

[a]Solvent: $CDCl_3$.
[b]From analysis of a diastereomeric mixture.

TABLE 5. ^1H NMR data for some model compounds and chlorinated derivatives

Compound	Isomer	Chemical shift/ppm (*J*/Hz)[a] α-H		β-H
4[c]	E	4.93	(4.8)	4.11
	T	4.93	(7.8)	4.01
7[c]	E	4.96	(4.8)	4.15
	T	4.96	(7.7)	4.04
8*a*	E	4.96	(5.0)	4.15
8[c]	T	4.97	(7.7)	4.04
12*a*	E	5.31	(3.5)	4.39
12*b*	T	5.33	(5.5)	4.26
13	E	5.33	(3.7)	4.40
	T	5.34	(5.7)	4.23

[a]Solvent: $CDCl_3$ + D_2O.
[b]Multiplet.
[c]From analysis of a diastereomeric mixture.

(100 mL), anhydrous potassium carbonate (18 g, 0.13 mol) was added, and the mixture was refluxed with vigorous stirring for about 1 h, then diluted with water and extracted with methylene chloride. The extract was freed from excess vanillyl alcohol by washing with sodium hydroxide solution, then with water, dried over anhydrous sodium sulfate, and evaporated to gave a yellow residue, which was recrystallized from methanol or methylene chloride–petroleum ether (bp 30–60°C) to yield 20 g (87%) of white crystalline **1**.

α-(4-Hydroxymethyl-2-methoxyphenoxy)-β-hydroxy-3,4-dimethoxypropiophenone 2

To a suspension of **1** (20.6 g, 0.062 mol) in ethanol (150 mL), potassium carbonate (1.1 g, 0.008 mol) and formalin (10 mL, 37%) were added and the reaction mixture was vigorously stirred for 1.5 h at about 35°C, then diluted with water and extracted with methylene chloride. The extract was washed, dried, and evaporated to yield a colorless syrup, which was crystallized from toluene–ethyl acetate to give 18 g (80%) of white crystalline **2**.

1-(3,4-Dimethoxyphenyl)-2-(4-hydroxymethyl-2-methoxyphenoxy)-1-ethanol 3

Sodium borohydride (1.6 g, 0.042 mol) was added to a suspension of compound **1** (20 g, 0.06 mol) in ethanol (160 mL) and the mixture was stirred at room temperature for approximately 1 h. The reaction solution was diluted with water and neutralized with diluted acetic acid, then extracted several times with methylene chloride. The extract was washed with aqueous sodium bicarbonate solution, then water, dried, and evaporated. The colorless residue was crystallized from acetone–petroleum ether (bp 30–60°C) to give 18.5 g (92%) of white crystalline **3**.

1-(3,4-Dimethoxyphenyl)-2-(4-hydroxymethyl-2-methoxyphenoxy)-1,3-propanediol 4

Compound **2** (18 g, 0.05 mol) was treated in the same way as for the synthesis of **3** and purified by column chromatography using toluene–ethyl acetate (1:4) as eluent to give 17.1 g (94%) of colorless foaming substance, **4** (a mixture of two diastereomers).

α-(4-Hydroxymethyl-2-methoxyphenoxy)-4-benzyloxy-3-methoxyacetophenone 5

A mixture of *O*-benzyl-α-bromo-acetovanillone (17 g, 0.051 mol) (7), vanillyl alcohol (9.4 g, 0.061 mol), and anhydrous potassium carbonate (13.8 g, 0.1 mol) in absolute alcohol (150 mL) was treated in the same way as for the preparation of **1** to yield 18.3 g (88%) of colorless prisms, **5**, from methanol.

α-(4-Hydroxymethyl-2-methoxyphenoxy)-β-hydroxy)-4-benzyloxy-3-methoxypropiophenone 6

A white powder **6** (14.9 g, 79%) was obtained from **5** (17.5 g, 0.043 mol) according to the procedure described for the preparation of **2**.

1-(4-Benzyloxy-3-methoxyphenyl)-2-(4-hydroxymethyl-2-methoxyphenoxy)-1,3-propanediol 7

The ketol derivative **6** (13.8 g, 0.031 mol) was treated in the same way as **4** to give 13 g (95%) of colorless foaming substance, **7**, a mixture of two diastereomers.

1-(4-Hydroxy-3-methoxyphenyl)-2-(4-hydroxymethyl-2-methoxyphenoxy)-1,3-propanediol 8

Compound **7** (10 g, 0.023 mol) was dissolved in methanol (100 mL) and 5% palladium on barium sulfate (10 g) was added.

Can. J. Chem. Downloaded from www.nrcresearchpress.com by 217.78.4.112 on 09/08/12
For personal use only.

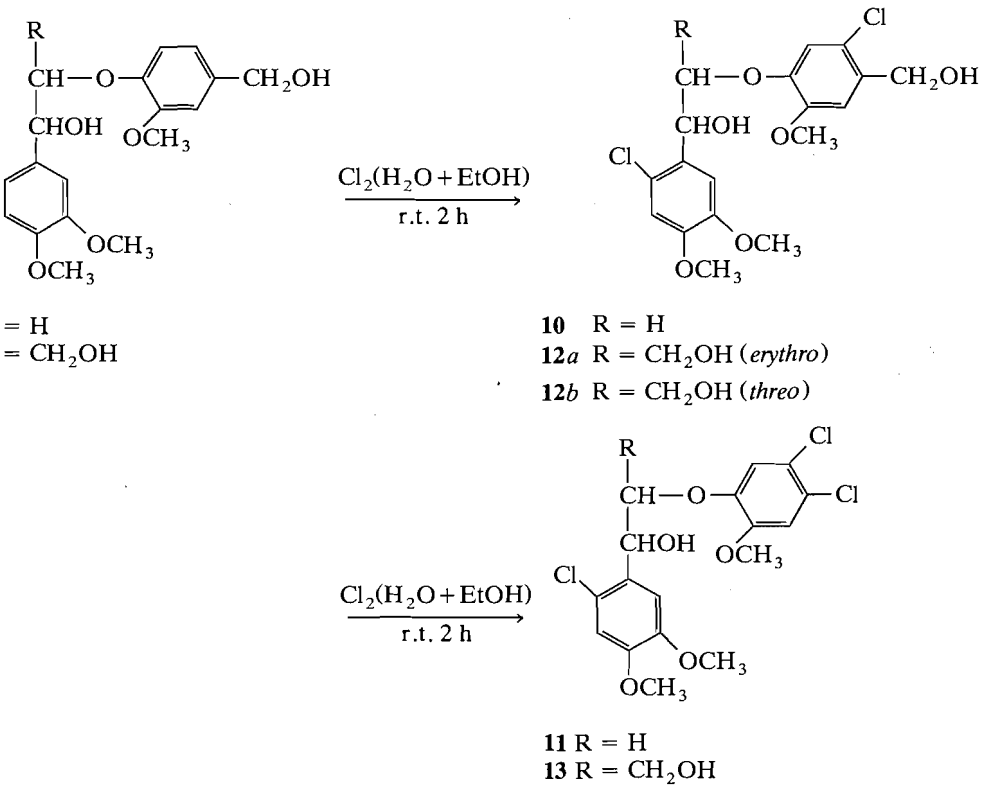

SCHEME 2

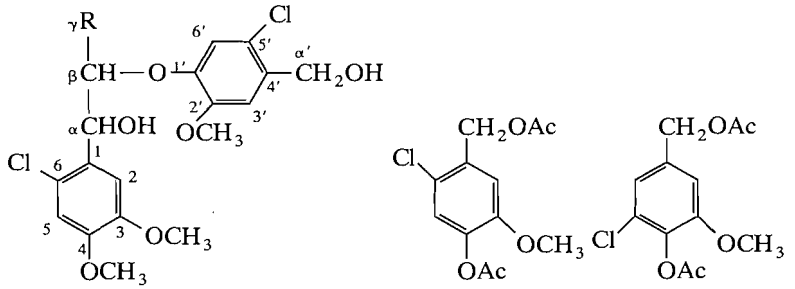

FIG. 1

The mixture was shaken for 2 h at room temperature under hydrogen. The catalyst was then filtered off and washed with methanol. The filtrate and the washings were combined and concentrated under reduced pressure to yield a colorless glass **8** (7.7 g, 96%), a mixture of two diastereomers. A white crystalline *erythro* isomer **8***a* (mp 106–107°C) was crystallized from the mixture of two diastereomers by adding ethyl acetate.

Chlorination treatment of compounds 3 and 4

Compound **4** (0.364 g, 1 mmol) was dissolved in ethanol (10 mL), diluted with distilled water (50 mL), and aqueous chlorine solution was added under vigorous stirring. The mixture was stirred at room temperature for 2 h. The reaction was stopped by adding a small amount of sodium sulfite and extracted with methylene chloride. The extract was washed with water, dried over anhydrous sodium sulfate, and evaporated. The mixture residue was separated by column chromatography with toluene–ethyl acetate (1:2) as eluent. White crystalline **12***a* (*erythro*) (0.108 g, 25%) and **12***b* (*threo*) (0.086 g, 20%) were sequentialy obtained as major products in a molar ratio of 2.5 (Cl_2:**4**). A colorless glass **13**, a mixture of two diastereomers (0.158 g, 36%), was isolated as a major product at a molar ratio of 3.5 (Cl_2:**4**).

Compound **3** (0.334 g, 1 mmol) was treated in the same way as for the preparation of **12** and **13**, and was separated by column chromatography with toluene–ethyl acetate (1:1) as eluent to yield compound **10** (0.185 g, 46%), at a molar ratio of 2.5 (Cl_2:**3**), and **11** (0.155 g, 38%), at a molar ratio of 3.5 (Cl_2:**3**).

Acknowledgements

The authors wish to express their thanks to Professor Arthur S. Perlin for valuable criticism of the manuscript and to Mr. Yonghao Ni for his assistance with the elemental analyses.

1. J. Gierer and H. F. Huber. Acta Chem. Scand. **18**, 1237 (1964).
2. J. Gierer and L. Sundholm. Svensk Papperstid. **74**, 345 (1971).
3. K. Lundquist and R. Lundgren. Acta Chem. Scand. **26**, 2005 (1972).

Can. J. Chem. Downloaded from www.nrcresearchpress.com by 217.78.4.112 on 09/08/12
For personal use only.

4. E. Adler, B. O. Lindgren and U. Saeden. Svensk Papperstid. **55**, 245 (1952).
5. E. Adler and E. Erikson. Acta Chem. Scand. **9**, 341 (1955).
6. E. M. Gerhard. Acta Chem. Scand. **20**, 1038 (1966).
7. K. Kratzl, W. Kisser, J. Gratzl, and H. Silbernagel. Monatsh. Chem. **90**, 771 (1959).
8. H. Nimz. Chem. **Ber**. **102**, 3803 (1969).
9. F. Nakatsubo, K. Sato, and T. Higuchi. Holzforschung, **29**, 165 (1975).
10. S. Hosoyo, K. Kanazawa, H. Kaneko, and J. Nakano. Mokuzai Gakkaishi, **26**, 118 (1980).
11. T. Katayama, F. Nakatsubo, and T. Higuchi. Mokuzai Gakkaishi, **27**, 223 (1981).
12. P. M. Hauteville and M. C. Duclos-Jordan. Holzforschung, **40**, 293 (1986).
13. H. Erdtman and B. Leopold. Acta Chem. Scand. **3**, 1358 (1949).
14. E. Adler, G. Brunow, and K. Lundquist. Holzforschung. **41**, 199 (1987).
15. K. Lundquist. Acta Chem. Scand. Ser. B: **B33**, 418 (1979).
16. G. E. Hawkes, C. Z. Smith, and J. H. P. Utley, and H. L. Chum. Holzforschung, **40** (suppl.), 115 (1986).
17. H. H. Nimz, U. Tschirner, M. Stahle, R. Lehmann, and M. Schlosser. J. Wood Chem. Technol. **4**, 265 (1984).
18. X. Shen and A. R. P. van Heiningen. 6th Int. Symp. Wood Pulping Chem. 1991, p. 557.

Can. J. Chem. Downloaded from www.nrcresearchpress.com by 217.78.4.112 on 09/08/12
For personal use only.

Hydrogen bonding and internal rotation barriers of glycine and its zwitterion (hypothetical) in the gas phase

DAKE YU, DAVID A. ARMSTRONG, AND ARVI RAUK[1]
Department of Chemistry, The University of Calgary, Calgary, Alta., Canada T2N 1N4

Received November 29, 1991

DAKE YU, DAVID A. ARMSTRONG, and ARVI RAUK. Can. J. Chem. **70**, 1762 (1992).

The structures of the major glycine conformers, and several transition state structures, were optimized at HF/6-31G* and HF/6-31+G* levels of theory and the correlation energies were calculated at MP2/6-31G* and MP2/6-31+G** levels on these geometries, respectively. The heat of formation of gas phase glycine is calculated to be ΔH_f^0 (298.15) = −389.6 kJ/mol. Thermodynamic properties, C_p^0, S^0, $H^0 - H_0^0$, ΔH_f^0, etc. are calculated as functions of temperature using standard statistical thermodynamic methods. MP2/6-31+G* optimization was carried out on the zwitterion, found by HF/6-31+G* optimization to be a local minimum. The results suggest that glycine in the zwitterionic form in the gas phase is *not* a stationary point. Zwitterionic glycine does not exist in the gas phase.

DAKE YU, DAVID A. ARMSTRONG et ARVI RAUK. Can. J. Chem. **70**, 1762 (1992).

Opérant aux niveaux HF/6-31G* et HF/6-31+G*, on a optimisé les structures des principaux conformères de la glycine et de plusieurs états de transition et on a calculé les énergies de corrélation de ces géométries aux niveau MP2/6-31G* et MP2/6-31+G** respectivement. On a évalué que la chaleur de formation de la phase gazeuse de la glycine est ΔH_f^0(298,15) = −389,6 kJ/mol. Utilisant les méthodes standard de la thermodynamique statistique, on a calculé les propriétés thermodynamiques, C_p^0, S^0, $H^0 - H_0^0$, ΔH_f^0, etc. en fonction de la température. Opérant au niveau MP2/6-31+G*, on a effectué une optimisation du zwitterion qui, par une optimisation HF/6-31+G*, correspond à un minimum local. Les résultats suggèrent que la forme zwitterionique de la glycine en phase gazeuse *n'est pas* un point stationnaire. La glycine sous la forme zwitterionique n'existe pas en phase gazeuse.

[Traduit par la rédaction]

1. Introduction

Amino acids are the fundamental structural units of proteins. Glycine is the simplest of the α-amino acids and one of the first to be isolated. It serves as an important model compound in biophysics and biochemistry and, because of its small size, has been the subject of numerous theoretical investigations, by both semi-empirical (1–11), and *ab initio* (7–25) methods. Although it is the smallest amino acid, glycine is nevertheless sufficiently large and has enough conformational flexibility that its complete description poses a formidable challenge to computational chemists. All of the early work suffered to some extent or other from the necessity to use approximate theory or rather small basis sets, or from the inability to carry out complete searches of the conformational space. Indeed, specific knowledge of major aspects of its potential energy surface and its thermochemistry even in the gas phase are as yet lacking. Both are necessary for an understanding of protein conformations and dynamics (26). We review briefly below current theoretical and experimental knowledge of the structures and energetics of glycine and its zwitterion. The purpose of this communication is to extend the quantitative knowledge of the structures of glycine in the gas phase, specifically addressing the interplay of intramolecular hydrogen bonding as a structure determining factor. We also provide a detailed analysis of the thermodynamics of glycine. The work is directly relevant to the search for glycine in interstellar space (27) and is intended to lay the groundwork for a study of glycine in solution which is in progress. This study also serves to provide comparisons with experimental results.

Glycine is known to exist in a variety of structures depending on its environment. In water at neutral pH, it exists as the zwitterion, $H_3N^+CH_2COO^-$; at high pH, it exists as glycinate, $H_2NCH_2COO^-$; at low pH, as glycinium, $H_3N^+CH_2COOH$. In the solid state, glycine is zwitterionic. Measurements of the dielectric properties of amino acids in nonaqueous solutions suggests that the dominant form is probably the intermolecularly hydrogen-bonded neutral species (28). The insolubility of glycine in nonpolar solvents may be largely due to its crystal lattice strength. In the isolated state, glycine adopts the neutral form, H_2NCH_2COOH, as found by several independent millimeter wave (13, 14, 29) and microwave investigations (30), and by spectroscopic studies on the low-temperature matrix-isolated products of sublimation (31). Structures **1***a* and **1***c* have been identified as components in the gas phase. The structure deduced from the first spectroscopic experiments, **1***c*, did not correspond to the most stable structure, **1***a*, predicted by virtually all theoretical studies. The discrepancy has been explained (13, 18) as due to the rather weak dipole moment of **1***a* compared with that of the structure responsible for the observed rotational spectrum, **1***c*.

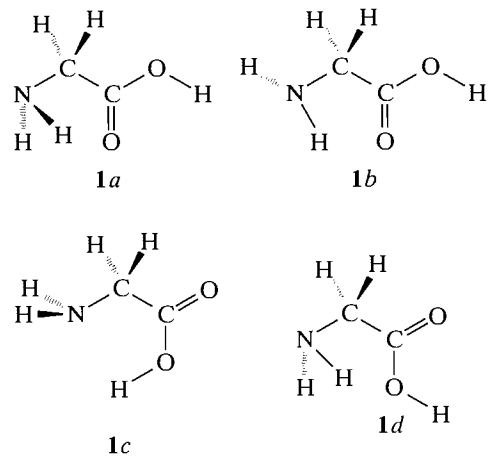

1*a* **1***b* **1***c* **1***d*

Clearly, glycine in the vapor phase exists as two and possibly more conformers. The strength of a hydrogen bond, 20–

[1]Author to whom correspondence may be addressed.

Can. J. Chem. Downloaded from www.nrcresearchpress.com by 217.78.4.112 on 09/08/12
For personal use only.

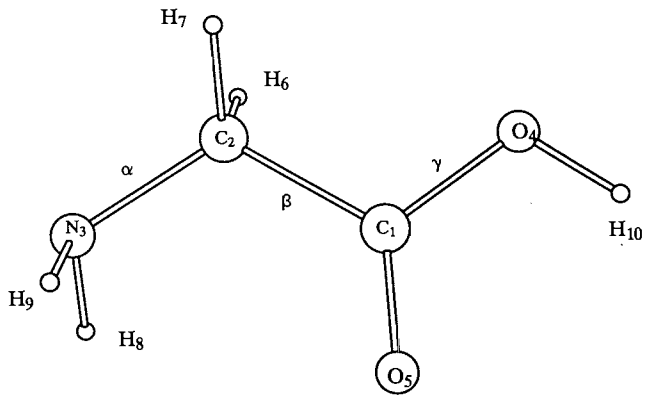

FIG. 1. Nuclear numbering system of glycine and definitions of α, β, and γ for their intermolecular rotations.

30 kJ/mol, is normally larger than rotational barriers about single bonds, which fall in the range 4–15 kJ/mol. Since glycine contains basic units NH_2 and =O, and polar NH and OH bonds, the conformations of glycine would be expected to be governed by several H-bonding possibilities. Relative stabilities of the conformers and magnitudes of internal rotation barriers will reflect the strength of the H bonds. There are three internal rotational degrees of freedom, which we define as α, β, and γ for C—N, C—C, and C—O rotations, respectively, as shown in Fig. 1. The first two correspond to the parameters, Φ and Ψ, respectively, used by biochemists to discuss the conformations of proteins. The structure observed experimentally in the gas phase, **1***c*, is unusual in having an *anti* orientation of the O—H bond relative to the C=O group. By analogy with esters (32), this orientation must be at the expense of approximately 20 kJ/mol stabilization. If it were quasiplanar, an additional cost of 6–8 kJ/mol would ensue from the eclipsing of the NH_2 group with the CH_2 group. Apparently, formation of the N···H—O bond more than compensates for these undesirable features. In the most stable structure, **1***a*, the O—H, NH_2, and CH_2 groups are in their normal orientations and additional stabilization may be obtained from a bifurcated hydrogen-bonding arrangement. The bifurcated arrangement of H bonds is itself unusual, an almost linear arrangement with a single hydrogen bridge being the norm (33).

The most thorough theoretical study to date, which appeared while the present work was in progress, is due to Jensen and Gordon (11) (JG), who determined all of the minima and transition structures at the restricted Hartree-Fock level of theory with the 6-31G* basis set (RHF/6-31G*). Correlation energy contributions were determined at the level of second-order Moller-Plesset perturbation theory. Eight stationary points corresponding to minima on the neutral glycine hypersurface were located. Structure **1***c* was found to be 7.5 kJ/mol less stable than **1***a*, the global minimum. A second structure, **1***d*, at relative energy 7.1 kJ/mol, was also found to be more stable than **1***c*, and a third structure, **1***b*, relative energy 8.9 kJ/mol, is slightly less stable. The population of **1***c* at 298°C in the vapour phase was predicted to be about 5%. Even given the higher dipole moment of **1***c*, it would appear that the spectroscopic data would indicate a higher proportion than the predicted 5%. The comprehensive work of JG follows partial *ab initio* investigations of the glycine potential energy surface by Vishveshwara and Pople (17), Schafer and co-workers (13, 18), Palla and co-workers (7, 22), Luck *et al.* (34), and Ramek and co-workers (24, 25), who investigated at various levels of theory structures **1***a*, **1***c*, **1***d*, and several other structures with C_s symmetry. All investigations agree on the global minimum, **1***a*.

The relationship between the neutral and zwitterionic forms of glycine has been the subject of several investigations. All calculations yield the same gas-phase structure for the zwitterion, namely **2***a*, but depending on the theoretical method, a wide range of values for the gas-phase energy difference has been obtained (kJ/mol): CNDO/2, 421 (2); MNDO, 257 (6); STO-3G, 344 (22); 4-31G, 121 (6, 19); 6-31G, 180 (20); Dunning's DZP, 156 (9). The high values obtained with the semiempirical methods reflect their inability to describe hydrogen bonding correctly. The effect of solvation on the relative stabilities has been simulated by MNDO using an effective charge model (6). Structures **1***a* and **2***a* were found also to be the most stable 'in solution' but the relative energies were reversed from 257 kJ/mol to −46 kJ mol. *Ab initio* calculations, wherein mutual solute–solvent polarization effects are accommodated by an additional potential term added to the Hamiltonian, have yielded accurate values for the heat of solvation at 298 K for the process, neutral (gas) → zwitterion (solution), $\Delta H = -81.6$ kJ/mol (22) at 4-31G level of theory, compared with experiment, -80 ± 4 kJ/mol (35). The relative energy of the two forms in solution by this approach is −79.0 kJ/mol. Specific solvation of three of the neutral forms of glycine by a single water molecule (the 'supermolecule' approach) has been investigated by Basch and Stevens (23) using a DZP basis set and compact effective potentials for the core electrons. The complex **1***a*-H_2O is still the most stable, while **1***c*-H_2O is 20.5 kJ/mol less stable than **1***d*-H_2O. The zwitterionic form was not considered.

In the present work, we have investigated the eight stable neutral glycine conformers and a number of the transition structures in the gas phase with the objective of refining existing estimates of relative stabilities and geometrical differences among glycine conformers. In Sect. 2, we briefly describe the levels of *ab initio* theory used for evaluating the conformational and energetic properties of glycine and its zwitterion. In Sect. 3 we present the results of stationary point calculations, reporting the fully optimized geometries for all of the minima and transition structures at the HF/6-31+G* levels, corrected for correlation effects by MP2/6-31+G** single point calculations on the HF/6-31+G* structures. For zwitterion glycine the results at this level indicated that it might not correspond to a stationary point in the potential energy surface. MP2/6-31+G* optimization was carried out and the results confirmed that the zwitterion form does not exist as a stable molecule in the gas phase at this level of theory. Also presented in this section are some thermodynamic properties, as functions of temperature, calculated with standard statistical thermodynamic methods. Then we discuss the general features of these calculations and the hydrogen bonding and rotation barriers of the glycine conformers. Finally in Sect. 4 we summarize our main results and conclusions.

2. Computational details

All *ab initio* calculations presented here were performed with the Gaussian 88 and Gaussian 90 (36) molecular orbital packages. The geometries were optimized with the

Can. J. Chem. Downloaded from www.nrcresearchpress.com by 217.78.4.112 on 09/08/12
For personal use only.

Can. J. Chem. Downloaded from www.nrcresearchpress.com by 217.78.4.112 on 09/08/12
For personal use only.

standard restricted Hartree-Fock method. Convergence of the geometry was to the limits imposed internally in Gaussian 90, which correspond approximately to ±0.002 Å and ±0.1°. The 6-31G* split-valence basis set was used for the initial evaluations. The larger 6-31+G* basis was used for the final geometry optimizations, as it has been quite successful in studies of hydrogen-bonding systems, where the need for diffuse functions was recognized (37). No symmetry constraints were assumed at the beginning of each geometry optimization, but if the optimization ended with a nearly symmetric structure, the conformer's symmetry was verified. Vibrational frequencies were calculated to confirm the nature of the stationary points and to provide the vibrational zero-point energy (ZPE). The ZPE values were scaled by a factor of 0.9 in considering the relative energies of the conformers to take account of known inadequacies in frequencies calculated at this level (38). The HF/6-31+G* structures were also used for single-point calculations with the 6-31+G** basis set, at the second-order Moller–Plesset (MP2) level of theory. The MP2 method with an extended basis such as 6-31+G** recovers much of the electron correlation energy neglected in HF theory, and significantly improves HF relative energies. For the zwitterionic form of glycine, MP2/6-31+G* optimization was also carried out, since it was apparent from single-point calculations that correlation has a significant effect on the geometry of this isomer.

Ideal gas thermodynamic functions C_p^0, S^0, $H^0 - H_0^0$, and $(G^0 - H_0^0)/T$ in the temperature range 0–1500 K and 1 atm pressure were calculated by standard statistical thermodynamic methods based on the rigid rotor – harmonic oscillator model. The computed vibrational frequencies were scaled by a factor of 0.9 in calculating the vibrational contributions to the above thermodynamic functions. The rotations about angles α and β were treated as hindered internal rotors in the first instance and an improved calculation was carried out by direct summation over the energy levels using rotational potentials as given by $V = \Sigma_n \frac{1}{2}V_n(1 - \cos n\phi)$ (ϕ = α or β). The calculation of the temperature dependence of $\Delta H_f^0(T)$, and hence $\Delta G_f^0(T)$ and $K_f(T)$, for glycine requires knowledge of the enthalpy of formation of at least one of its conformers at a reference temperature. In the absence of an experimental value for the heat of formation for glycine in the gas phase, the method of isodesmic reactions was used to determine a theoretical value. Thus, *ab initio* calculations were performed on the hypothetical reaction

$$H_2NCH_2CH_3 + H_3CCOOH \rightarrow \text{Glycine } (\mathbf{1}a) + C_2H_6$$

The experimental heats of formation for $H_2NCH_2CH_3$, H_3CCOOH, and C_2H_6 are available (39). These can be used together with the reaction energy for the above reaction from *ab initio* calculations (MP2/6-31+G**//6-31+G* + ZPE), to obtain a value for $\Delta H_f^0(T = 0)$. The reliability of such a procedure and the criteria for the choice of components for the hypothetical reaction have been discussed elsewhere (40). The thermodynamic properties listed in Table 4 are derived for the equilibrium mixture at a given temperature, assuming a Boltzman distribution of the conformers.

3. Results and discussion

Optimized geometric parameters of the seven most stable glycine conformers are reported in Table 1(*a* and *b*), in the *Z*-matrix format as actually used in the calculations. The nuclear numbering scheme is defined in Fig. 1 and the structures in Fig. 2. The data for a number of transition structures are also included in Table 1 and Fig. 2. Table 2 collects electronic energies at HF and MP2 levels, the zero-point vibrational energies, and the dipole moments for all of the structures. The transition structures are verified to have one and only one imaginary frequency (Table 2). All of the minimum energy and transition structures described in this work have also been described to some extent by JG (11). In addition, the basis set dependence of the relative SCF energies of structures **1***a*, **1***c*, **1***d*, **1***cc*, and **1***dd* has been investigated by Ramek, Cheng, Frey, Newton, and Schafer (RCFNS) (25). The present results, obtained with a somewhat better basis set than that of JG and approaching the best of RCFNS, are only quantitatively different from JG. Table 3 lists the relative energies at different levels of calculations, including the MP2/6-31G*//6-31G* results of JG and the largest basis set results of RCFNS. A curious consequence of the presence of diffuse functions in the basis set is that the relative (to **1***a*) energies of *all* structures are lower than those of JG. The differences are in the range 0.6–6.1 kJ/mol for the minima, and 1.5–8 kJ/mol for the transition structures (for which comparison could be made). In the few cases where comparison is possible, our results are within 0.3 kJ/mol of those obtained by RCFNS. We discuss the structures in some detail from the point of view of attempting to isolate structure-determining factors, hydrogen bonding, bond–bond repulsions, and special properties of carbonyl groups.

Hydrogen bonding, rotational barriers, and relative stability of neutral glycine conformers

Bifurcated H bonding? The most stable of the neutral glycine conformers is **1***a*, as previously found using other semiempirical and *ab initio* calculations. Structure **1***a* has two NH bonds which are symmetrically disposed to the carbonyl oxygen atom. The molecular point group is C_s. It is tempting to describe the configuration of **1***a* as evidence of bifurcated hydrogen bonding. As alluded to earlier, bifurcated H bonding is not the preferred mode in most H-bonded systems. Deviation of the NCC angle from its normal tetrahedral value, or proximity of the N—H protons to the oxygen atom may be sought as evidence of attractive or repulsive interactions. The extended value of the NCC angle (3-2-1, Table 1) of **1***a*, 115.4° is consistent with the lack of an attractive interaction. According to the calculations, the H···O nonbonded distance, 2.81 Å, is well outside of van der Waals separation, but the O and N, separated by 2.84 Å, are just in van der Waals contact. Indeed it is possible that there is little if any attractive interaction between the NH_2 and the carbonyl O. One must conclude that considerations other than hydrogen bonding are probably responsible for the predominance of **1***a*. It is well documented (for a review, see ref.41) that in compounds of the class, $XCH_2C(O)Y$, where X is a polar group or alkyl and Y is H, alkyl, or alkoxy, the group X tends to adopt a position eclipsing the carbonyl group. This occurs even in nonpolar solvents where the coalignment of bond dipoles is disfavoured. The explanation for this effect is uncertain. It may have little to do with the polar group itself, but rather may be driven by the necessity to optimize the orientation of the best donor group (the CH_2 group) for electron delocalization into the π* orbital of

TABLE 1(*a*). HF/6-31+G* optimized geometries[a] and rotational constants of glycine conformers (minima)[b]

	1*a* C_s	**1***b* C_1	**1***c* C_1	**1***d* C_1	**1***e* C_1	**1***f* C_s	**1***g* C_1	**2***a* C_s
2-1	1.516	1.508	1.525	1.520	1.510	1.524	1.517	1.566
3-2	1.438	1.444	1.454	1.440	1.450	1.436	1.441	1.504
4-1	1.330	1.329	1.186	1.190	1.188	1.336	1.333	1.207
5-1	1.189	1.188	1.320	1.329	1.330	1.182	1.182	1.245
6-2	1.084	1.082	1.084	1.085	1.091	1.087	1.086	1.079
7-2	1.084	1.092	1.083	1.082	1.080	1.087	1.093	1.079
8-3	1.001	1.000	1.000	1.001	1.001	1.001	1.000	1.005
9-3	1.001	1.001	1.001	1.000	1.001	1.001	1.001	1.005
10-3	—	—	—	—	—	—	—	1.053
10-4	0.953	0.953	—	—	—	0.949	0.948	—
10-5	—	—	0.956	0.953	0.952	—	—	—
3-2-1	115.4	110.5	112.0	118.2	111.4	115.5	110.5	105.4
4-1-2	111.7	112.0	121.9	123.7	125.0	115.2	115.6	115.0
5-1-2	125.6	125.2	115.4	113.9	112.4	124.2	123.6	112.0
6-2-1	107.6	108.6	106.1	106.0	106.4	108.1	109.6	111.2
7-2-1	107.6	105.7	107.5	106.6	107.0	108.1	105.8	111.2
8-3-2	111.2	111.3	112.4	111.9	111.7	110.8	111.7	114.1
9-3-2	111.2	111.4	112.1	111.9	110.8	110.8	111.0	114.1
10-3-2	—	—	—	—	—	—	—	98.9
10-4-1	109.1	108.9	—	—	—	112.7	112.8	—
10-5-1	—	—	109.1	108.6	108.9	—	—	—
4-1-2-3	180.0	199.7	166.1	164.8	138.2	180.0	198.6	180.0
5-1-2-3	0.0	22.3	—	—	—	0.0	—	0.0
5-1-2-4	—	—	178.5	178.4	177.2	—	183.1	—
6-2-1-3	—	—	119.2	122.8	125.1	—	—	—
6-2-1-5	123.0	143.2	—	—	—	122.6	—	118.7
7-2-1-3	—	—	—	—	—	—	—	—
7-2-1-5	−123.0	−102.4	—	—	—	−122.6	—	−118.7
7-2-1-6	—	—	114.4	112.9	115.1	—	114.9	—
8-3-2-1	59.4	192.7	—	—	—	59.0	—	117.1
8-3-2-6	—	—	28.6	176.6	−55.8	—	78.2	—
9-3-2-1	−59.4	−45.9	—	—	—	−59.0	—	−117.1
9-3-2-8	—	—	121.5	120.6	120.6	—	121.7	—
10-3-2-1	—	—	—	—	—	—	—	0.0
10-4-1-5	0.0	0.5	—	—	—	180.0	182.5	—
10-5-1-2	—	—	—	—	—	—	—	—
10-5-1-4	—	—	181.2	0.4	−1.8	—	—	—
I_A[c]	10.6289	10.6515	10.2122	10.1327	9.8536	10.4248	10.4681	10.6623
I_B[c]	3.9141	3.9874	4.1179	4.0359	4.1030	3.9391	4.0153	4.2126
I_C[c]	2.9548	2.9936	3.0561	3.0038	3.1046	2.9532	2.9920	3.1284

[a]Bond lengths in Å, angles in deg.
[b]The parameters are listed in Gaussian 90 'Z-matrix' format. See Fig. 1 for the numbering scheme.
[c]Rotational constants in gigahertz.

the carbonyl group. In addition, structure **1***a* has the ideal staggered arrangement of N—H and C—H bonds.

Two other 'bifurcated' structures are shown in Fig. 2. A fourth, found by JG to be 35.1 kJ/mol higher than **1***a*, and GLY5 in their notation, is not considered here. Rotation about the C—C bond (β rotation) yields the 'bifurcated' structure, **1***d*, 6.4 kJ/mol less stable than **1***a*. This structure has an even more extended NCC angle, 118.2°, a consequence of steric repulsion between the NH_2 group and the OH group due to the highly constricted CCO(H) angle of the carboxylate group. Its skeletal point group is C_1. The C_s structure with two symmetric N—H bonds bracketing the OH group **1***dd* is a saddle point between **1***d* and its enantiomer, posing a barrier of only 0.2 kJ/mol for the interconversion. The energy of **1***d* relative to **1***a* may be taken to be the energy cost of assuming the *anti* orientation of the C—N and C=O bonds. The two transition structures between **1***a* and **1***d* have a nearly perpendicular orientation of the —COOH moiety, and present barriers of 10.3 kJ/mol from **1***a* to **1***d* and 3.9 kJ/mol in the reverse direction. Conformer **1***f* also has a bifurcated arrangement of N—H bonds. The NCC angle of **1***f* is almost identical to that found in **1***a*. Conformer **1***f* differs from **1***a* in having an *anti* orientation of the acidic O—H group. This orientation is known to be unfavorable in esters (32) and by extension should be unfavourable in acids as well. This structure lies 24.9 kJ/mol above **1***a*. The energy difference represents the energy cost of assuming the *anti* orientation of the OH group. The energy difference between structures **1***b* and **1***g*, which also differ in this one respect, is similar, 25.4 kJ/mol.

Can. J. Chem. Downloaded from www.nrcresearchpress.com by 217.78.4.112 on 09/08/12
For personal use only.

TABLE 1(*b*). HF/6-31+G* optimized geometries[a] of glycine conformers (transition structures)[b]

	1*ab* C_1	**1***ad* C_1	**1***af* C_1	**1***bb* C_s	**1***be* C_1	**1***be'* C_1	**1***cc* C_s	**1***cd* C_1	**1***c*–**2***a* C_1	**1***dd* C_s	**1***de* C_1	**2***aa* C_s
2-1	1.510	1.518	1.518	1.519	1.515	1.520	1.527	1.513	1.560	1.520	1.514	1.564
3-2	1.446	1.450	1.438	1.438	1.447	1.449	1.456	1.452	1.492	1.440	1.450	1.508
4-1	1.328	1.330	1.360	1.337	1.191	1.186	1.186	1.180	1.201	1.190	1.189	1.211
5-1	1.189	1.190	1.180	1.184	1.323	1.333	1.318	1.357	1.260	1.329	1.329	1.236
6-2	1.087	1.082	1.085	1.086	1.085	1.085	1.083	1.080	1.079	1.084	1.084	1.080
7-2	1.085	1.081	1.086	1.086	1.085	1.083	1.083	1.090	1.079	1.084	1.086	1.080
8-3	0.999	1.001	1.001	0.997	1.001	1.001	0.999	1.001	1.004	1.001	0.999	1.009
9-3	1.001	1.001	1.001	0.997	1.000	1.000	0.999	1.001	1.004	1.001	0.999	1.009
10-3	—	—	—	—	—	—	—	—	—	—	—	1.007
10-4	0.953	0.953	0.950	0.952	—	—	—	—	—	—	—	—
10-5	—	—	—	—	0.952	0.953	0.956	0.951	1.398	0.953	0.953	—
3-2-1	112.1	112.9	116.0	113.4	113.0	110.6	112.5	110.7	103.6	118.4	116.0	106.6
4-1-2	111.7	113.1	113.2	109.8	123.3	125.5	121.5	124.0	117.8	123.4	123.2	114.0
5-1-2	125.4	124.5	124.8	127.7	114.1	112.1	115.6	113.7	110.3	114.2	114.5	112.1
6-2-1	106.5	107.5	107.1	106.4	106.2	108.8	106.7	107.5	111.2	106.2	105.6	112.0
7-2-1	107.3	109.9	108.0	106.4	106.1	106.2	106.7	107.1	111.1	106.2	105.3	112.0
8-3-2	112.1	112.0	111.4	113.6	111.8	111.8	112.8	111.0	114.4	111.9	111.9	108.3
9-3-2	111.1	111.6	111.1	113.6	111.0	111.0	112.8	111.5	114.4	111.9	112.5	108.3
10-3-2	—	—	—	—	—	—	—	—	—	—	—	114.6
10-4-1	109.0	108.9	112.9	108.7	—	—	—	—	—	—	—	—
10-5-1	—	—	—	—	108.4	108.6	108.7	111.5	95.2	108.5	108.7	—
4-1-2-3	186.9	99.9	181.1	180.0	221.0	59.2	180.0	215.6	179.9	180.0	190.2	180.0
5-1-2-3	—	—	—	—	—	—	0.0	—	—	0.0	—	0.0
5-1-2-4	180.3	182.3	176.8	180.0	182.3	178.9	—	183.8	180.0	—	180.7	—
6-2-1-3	−124.0	—	123.1	123.8	126.9	126.4	—	119.9	119.0	—	123.2	—
6-2-1-5	—	119.9	—	—	—	—	123.1	—	—	123.7	—	118.0
7-2-1-3	—	—	—	−123.8	—	—	—	—	—	—	—	—
7-2-1-5	—	—	—	—	—	—	−123.1	—	—	−123.7	—	−118.0
7-2-1-6	−113.6	118.2	113.4	—	114.5	116.3	—	115.4	122.1	—	112.3	—
8-3-2-1	—	—	—	117.0	—	—	118.6	—	—	60.3	—	55.9
8-3-2-6	−9.9	176.8	179.9	—	−49.5	−46.5	—	42.3	−2.6	—	111.7	—
9-3-2-1	—	—	—	−117.0	—	—	−118.6	—	—	−60.3	—	−55.9
9-3-2-8	121.4	121.8	118.8	—	120.3	120.4	—	120.2	126.7	—	121.8	
10-3-2-1	—	—	—	—	—	—	—	—	—	—	—	180.0
10-4-1-5	0.0	0.0	99.5	0.0	—	—	—	—	—	—	—	—
10-5-1-2	—	—	—	—	—	—	0.0	—	—	—	—	—
10-5-1-4	—	—	—	—	0.0	0.3	—	92.2	180.1	0.0	0.6	—

[a]Bond lengths in Å, angles in deg.
[b]The parameters are listed in Gaussian 90 'Z-matrix' format. See Fig. 1 for the numbering scheme.

Each of the structures **1***a*, **1***d*, and **1***f* has a corresponding structure in which a single N—H bond projects more or less toward an oxygen of the carboxylate group. These are **1***b*, **1***e*, and **1***g*, respectively. In each, the corresponding structure is higher in energy than the structure with the 'bifurcated' configuration, by 5.6, 3.3, and 6.2 kJ/mol. Nevertheless, the NCC angle in each case is less, by 4.9, 6.8, and 5.0°, respectively. The contraction of the angle would normally be interpreted as evidence of increased attraction, or decreased repulsion between the NH_2 group and the carboxyl oxygen atom, and a lowering of the energy would be expected. The nonbonded H···O separation in **1***b* is 2.45 Å, a value which is shorter than the sum of van der Waals radii for the two atoms, 2.6 Å. Evidence for a weak bonding interaction may also be gleaned from the observation that both the N—H and C=O bonds are twisted out of the NCC plane in such a way as to maintain contact. The higher energy of each of these three structures relative to the corresponding 'bifurcated' species probably ensues from the imposition of an eclipsing interaction between the N—H bond and the skeletal C—C bond in the 'singly H-bonded' configuration.

Conformer **1***b*, which we find to be second in stability, is connected to **1***a* through an α rotation (107°) without significant change of β and γ. This structure was calculated to be 9.2 kJ/mol above **1***a* by JG (11) and not considered by RCFNS (25). The barrier for conversion of **1***a* to **1***b* is 7.1 kJ/mol but only 1.5 kJ/mol in the reverse direction. Since **1***b* has comparable stability to **1***c*, the reason why **1***b* has not been observed experimentally is probably due to its relatively small dipole moment (Table 2). The enantiomeric form of **1***b*, namely $\overline{\mathbf{1}b}$, is reached via the transition structure **1***bb*, which has C_s symmetry. The rotation from **1***b* to $\overline{\mathbf{1}b}$ is also dominated by the α motion with a barrier of 12.5 kJ/mol. This relatively high barrier for α rotation is due to the eclipsed arrangement of hydrogen atoms in the CH_2 and NH_2 groups in **1***bb*. In fact, the energy difference between **1***bb* and **1***a*, 18 kJ/mol, may be

Can. J. Chem. Downloaded from www.nrcresearchpress.com by 217.78.4.112 on 09/08/12
For personal use only.

TABLE 2. Electronic and vibrational energies of glycine conformers

Conformer[a]	HF (hartree) 6-31+G*//6-31+G*	ZPE[b] (kJ/mol) 6-31+G*		MP2 (hartree) 6-31+G**//6-31+G*	Dipole[c]
Minima					
1*a* C_s	−282.841051	226.98	(79.1)	−283.665217	1.36
1*b*	−282.838249	226.77	(97.0)	−283.662999	2.41
1*c*	−282.836778	228.50	(96.0)	−283.663566	5.87
1*d*	−282.838230	227.03	(21.9)	−283.662804	2.06
1*e*	−282.836911	227.15	(78.3)	−283.661581	2.86
1*f* C_s	−282.829975	226.25	(90.1)	−283.655476	3.48
1*g*	−282.826814	225.75	(95.1)	−283.652958	4.95
2*a* C_s	−282.799146	228.06	(86.4)	−283.634875	10.77
Transition structures					
1*ab*	−282.837434	225.77	(203.6i)	−283.662044	2.15
1*ad*	−282.836560	227.72	(68.1i)	−283.661568	1.68
1*af*	−282.819825	221.76	(552.7i)	−283.644174	2.60
1*bb* C_s	−282.832632	224.30	(269.7i)	−283.657409	3.12
1*be*	−282.833833	226.47	(56.0i)	−283.658265	1.94
1*be'*	−282.831727	226.67	(93.4i)	−283.656994	3.23
1*cc* C_s	−282.836497	227.46	(97.6i)	−283.663429	6.05
1*cd*	−282.819196	222.51	(544.6i)	−283.643588	3.97
1*c*–**2***a*	−282.798249	219.45	(937.8i)	−283.639655	9.64
1*dd* C_s	−282.838214	226.93	(19.4i)	−283.662711	2.09
1*de*	−282.833519	225.76	(271.6i)	−283.658289	2.30
2*aa* C_s	−282.795467	230.37	(174.2i)	−283.625817	11.52

[a]See Fig. 2 for the structures.
[b]The numbers in parentheses are the lowest vibrational frequencies in cm^{-1}.
[c]In Debye, from MP2/6-31+G**//6-31+G*.

taken as a measure of the energy cost of assuming the eclipsed orientation of the CH_2 and NH_2 groups, as opposed to the staggered orientation.

The experimentally observed (29, 30) structure **1***c*, which is the obvious precursor to the zwitterionic form, has almost the same energy as that of **1***b*. The strong hydrogen bond between the basic nitrogen atom and the acidic carboxyl H is evidenced by the short N···H distance (2.06 Å compared with the van der Waals distance 2.7 Å). In **1***c*, the strong H bond is countered by a number of unfavorable interactions between the NH_2 and CH_2 groups (partially eclipsed, +18 kJ/mol), the arrangement of the hydrogen atom of the carboxylic acid group (*anti*, +25 kJ/mol), and the orientation of the C—N bond relative to the C=O (*anti*, +6 kJ/mol). The relative energy of **1***c* is 5.7 kJ/mol. The difference provides an estimate for the strength of the H bond between a carboxylic acid and an amine, approximately 43 kJ/mol. The relative stability of **1***c* is appreciably less than predicted by MNDO (4) and smaller basis set (4-21G) *ab initio* (13) studies and is essentially the same as found by JG (6.3 kJ/mol (11)). The MNDO method is unable to account for hydrogen bonding. The results also emphasize the inadequacy of small basis sets in *ab initio* studies. The only experimental value of relative energy of glycine conformers was for **1***c* (versus **1***a*), given by Schafer *et al.* (13) as 5.86 ± 1.79 kJ/mol. This is in excellent agreement with the present result. It should be noted that without the diffuse functions (i.e., MP2/6-31G*//6-31G*+ZPE, this work or ref. 11), a higher relative energy is predicted for **1***c*, 7.9 kJ/mol (the number listed in Table IV of ref. 11 does not include the ZPE contribution).

Structure **1***c* is isolated on the glycine hypersurface. The nearest conformer, **1***d*, is similar in energy, being less stable by 0.7 kJ/mol, but is separated from **1***c* by a substantial barrier of 46 kJ/mol. The rotational motion involves coupled α and β rotations. The barrier originates from the necessity to disrupt the π-bonding character of the C—O bond in a manner analogous to the C—N rotation of amides, and from the effort required to break the strong H bond in **1***c*. A notable change in NCC angle is found again, the angle decreasing by 6° from **1***d* to **1***c*. Structure **1***c* is chiral. An α rotation leads **1***c* to its mirror image conformer. The transition structure for the interconversion, **1***cc*, which has C_s symmetry, is only 0.4 kJ/mol above **1***c* at the MP2 level. Addition of the ZPE contribution reverses the relative stability to −0.6 kJ/mol, an indication that **1***c* exists in a very shallow double-welled potential and that the actual structure is probably planar in the heavy-atom skeleton. From **1***c* to $\overline{\mathbf{1}c}$ covers about 148° of α rotation with only 15° change in β and 1° in γ.

Parallel to the **1***a*–**1***d* pair, the interchange between **1***b* and **1***e* is also through the β rotation. **1***e* is only 3.3 kJ/mol above **1***b* but they are well separated by a barrier of 9.1 or 11.1 kJ/mol, if rotating along the opposite direction. Another possible change of conformer from **1***e* is through a simultaneous rotation of α and β, passing over a barrier of 7.4 kJ/mol to **1***d*. The β rotation introduces no significant change in bond lengths and bond angles, about 0.05 Å and 2.5° from

Can. J. Chem. Downloaded from www.nrcresearchpress.com by 217.78.4.112 on 09/08/12
For personal use only.

Can. J. Chem. Downloaded from www.nrcresearchpress.com by 217.78.4.112 on 09/08/12
For personal use only.

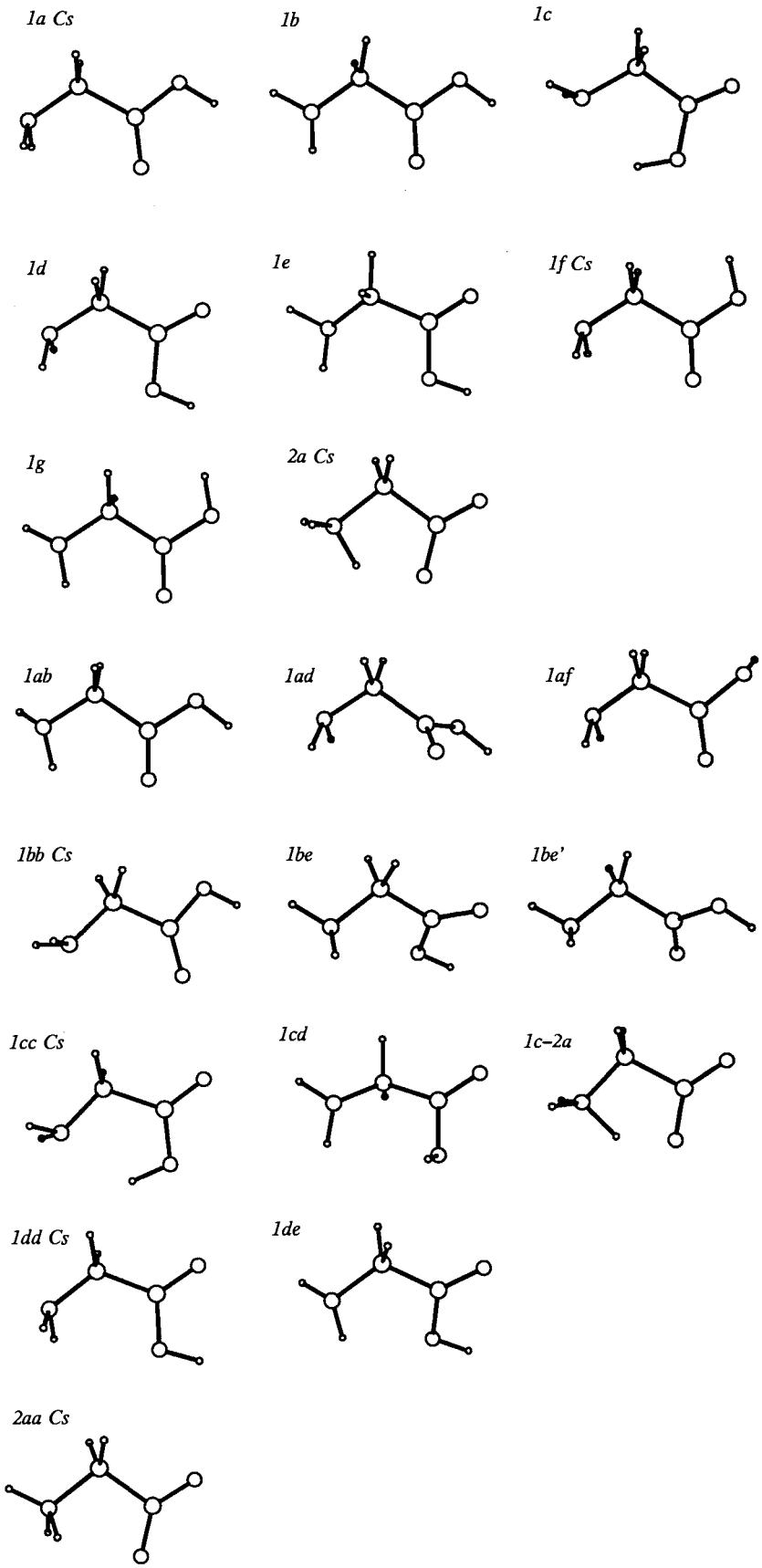

FIG. 2. Glycine conformers. Structures labelled with a single letter correspond to local minima; structures labelled with two letters are transition structures; thus **1***ab* is the transition structure connecting **1***a* and **1***b*. The nuclear numbering can be found in Fig. 1.

TABLE 3. Relative energies (kJ/mol) of glycine conformers

Conformer[a]	HF 6-31+G*//6-31+G*	MP2 6-31+G**//6-31+G*	MP2 + ZPE[a] 6-31+G**//6-31+G*	MP2[b] 6-31G*//6-31G*
Minima				
1*a* C_s	0.00	0.0	0.0	0.0
1*b*	7.36	5.82	5.63	9.2
1*c*	11.22(11.28)[c]	4.33(2.92)[d]	5.70	6.3
1*d*	7.41(7.63)[c]	6.33	6.38	7.1
1*e*	10.87	9.55	9.70	13.4
1*f* C_s	29.08	25.57	24.91	27.2
1*g*	37.38	32.19	31.08	37.2
2*a* C_s	110.02	79.66	80.63	
Transition structures				
1*ab*	9.50	8.33	7.12	10.9
1*ad*	11.79	9.58	10.25	11.7
1*af*	55.73	55.25	50.55	59.0
1*bb* C_s	22.10	20.50	18.09	
1*be*	18.95	18.25	18.76	18.4
1*be'*	24.48	21.59	21.31	24.7
1*cc* C_s	11.96(11.73)[c]	4.69(3.53)[d]	5.12	7.1
1*cd*	57.38	56.79	52.32	
1*c*–**2***a*	112.38	67.11	59.58	
1*dd* C_s	7.45(7.74)[c]	6.58	6.54	
1*de*	19.78	18.19	17.09	21.7
2*aa* C_s	119.68	103.44	106.49	

[a]ZPE from 6-31+G* calculation and scaled uniformly by a factor of 0.9 (38).
[b]Reference 11.
[c]Optimized at the RHF/6-31++G** level, ref. 25.
[d]Optimized at the MP2/6-311G** level, ref. 25.

1*a* to **1***d* or **1***b* to **1***e*. Changing the 'bifurcated' bonds to hydrogen in **1***d* to a single hydrogen bridge in **1***e* narrows the NCC angle by 7°.

The two high-energy conformers **1***f* and **1***g* are characterized by the repulsions between the hydrogens from CH_2 and carbonyl groups. The connections with **1***a* or **1***b* through γ rotation is less likely to happen at room temperature. From **1***a* to **1***f* the rotational barriers are as high as 50.6 or 25.7 kJ/mol from the other side and it is expected that from **1***b* to **1***g* the barrier will be similar, if not higher.

The zwitterionic form of glycine, a hypothetical molecule in the gas phase

A number of theoretical studies on the zwitterionic form of glycine in the gas phase have been carried out. The results depend strongly on the methods or the basis sets used, the relative energy of the zwitterion relative to **1***a* ranging from 121–421 kJ/mol. Tse *et al.* (19) have reported the transition structure for proton transfer from neutral glycine to **2***a*. The barrier for the H migration was found to be only 2 kJ/mol, located at N—H distance 1.18 Å and H—O distance 1.41 Å. In the present work, a stationary point **2***a*, the zwitterion form of glycine was located on the HF potential energy surface by HF/6-31+G* optimization. It is characterized by a hydrogen bond between a single NH bond and one of the carbonyl oxygen atoms. The structure has C_s symmetry. The ammonium group conformation is such that one proton is in the molecular plane. At the present level of theory, the HF structure **2***a*, corresponding to zwitterionic glycine, is 80.6 kJ/mol less stable than the most stable neutral form, **1***a*. A second stationary point, **2***aa*, was also found at this level of calculation. It has one imaginary frequency and corresponds to the saddle point for CN rotation. The transition state for the neutral glycine–zwitterion exchange, **1***c*–**2***a*, was found by HF/6-31+G* geometry optimization. Harmonic frequency analysis shows one fairly large imaginary frequency (Table 2). Transition structure **1***c*–**2***a* is 2.4 kJ/mol above **2***a* and the geometric parameters are essentially the same as found by Tse *et al.* (19). However, at the MP2/6-31+G** level, the energy at this 'saddle point', **1***c*–**2***a*, is 13 kJ/mol *lower* than that of **2***a*! MP2/6-31+g* optimization, started at the HF/6-31+G* geomtry, **2***a*, results in a smooth transition to a structure similar to **1***c*. Thus, the present results suggest that the zwitterionic form of glycine rearranges without activation to conformation **1***c* of neutral glycine.

Effects of basis set, correlation, and zero point energy

A comparison of the relative energies of the glycine minima and transition structures as a function of level of theory is presented in Table 3. Data by the MP2/6-31G*//6-31G* method are those of JG (11). Correlation corrections have been previously shown to have significant effects on the structures and relative energies of H-bonded systems (42). Comparison of columns 2 and 3 of Table 3, reveals that *all* structures are stabilized by electron correlation relative to the global minimum, **1***a*. Stated a different way, structure **1***a* has a smaller correlation energy correction than any of the other structures. In most cases the differences are small, less than

Can. J. Chem. Downloaded from www.nrcresearchpress.com by 217.78.4.112 on 09/08/12
For personal use only.

TABLE 4. Ideal gas thermodynamic properties of glycine

T (K)	C_p^0 (J K^{-1} mol^{-1})	S^0 (J K^{-1} mol^{-1})	$-(G^0 - H^0)/T$ (kJ K^{-1} mol^{-1})	$H^0 - H_0^0$ (kJ mol^{-1})	ΔH_f^0 (kJ mol^{-1})	ΔG_f^0 (kJ mol^{-1})	log K_f
Neutral glycine							
0	0.00	0.00	0.00	0.00	−373.41	−373.41	∞
100	46.94	246.53	207.95	3.86	−381.93	−355.59	185.75
200	67.27	282.77	233.95	9.76	−386.46	−325.49	85.01
298.15	93.04	304.59	244.84	17.81	−389.60	−290.01	50.81
300	87.42	313.97	255.76	17.46	−390.17	−292.54	50.93
400	106.83	341.91	274.01	27.16	−393.22	−258.42	33.75
500	123.67	367.67	290.29	38.69	−395.55	−223.75	23.37
600	137.65	391.53	305.25	51.77	−397.15	−188.76	16.43
700	149.25	413.67	319.22	66.12	−398.12	−153.58	11.46
800	158.98	434.28	332.35	81.54	−398.52	−118.32	7.73
900	167.27	453.52	344.78	97.87	−398.44	−83.03	4.82
1000	174.40	471.53	356.57	114.96	−397.93	−47.77	2.50
1100	180.57	488.47	367.81	132.72	−397.07	12.57	0.60
1200	185.94	504.43	378.55	151.05	−395.90	22.56	−0.98
1300	190.61	519.51	388.83	169.89	−394.52	57.57	−2.31
1400	194.69	533.80	398.68	189.16	−392.93	92.49	−3.45
1500	198.27	547.37	408.15	208.82	−391.19	127.29	−4.43
Zwitterionic form (**2***a*)							
0	0.00	0.00	0.00	0.00	−293.48	−293.48	∞
100	46.00	241.15	202.18	3.90	−301.96	−275.09	143.69
200	63.01	278.09	231.47	9.32	−306.52	−244.61	63.88
298.15	82.03	306.75	251.64	16.43	−309.65	−210.71	36.92
300	82.40	307.25	251.98	16.58	−310.20	−210.55	36.66
400	101.91	333.66	269.14	25.81	−313.25	−175.14	22.87
500	119.35	358.33	284.54	36.89	−315.59	−139.12	14.53
600	134.16	381.43	298.78	49.59	−317.18	−102.73	8.94
700	146.59	403.08	312.15	63.65	−318.14	−66.18	4.94
800	157.09	423.36	324.80	78.84	−318.56	−29.62	1.93
900	166.02	442.39	336.82	95.01	−318.47	6.95	−0.40
1000	173.65	460.28	348.28	112.00	−317.97	43.43	−2.27
1100	180.21	477.15	359.24	129.71	−317.09	79.85	−3.79
1200	185.86	493.08	369.73	148.02	−315.92	116.16	−5.06
1300	190.75	508.15	379.81	166.85	−314.54	152.31	−6.12
1400	194.98	522.45	389.49	186.14	−312.96	188.35	−7.03
1500	198.66	536.03	398.81	205.83	−311.24	224.25	−7.81

Can. J. Chem. Downloaded from www.nrcresearchpress.com by 217.78.4.112 on 09/08/12
For personal use only.

2 kJ/mol. However, in the case of the two structures which have clearly defined H bonds, stabilization due to correlation is very important. The relative energy of **1***c* is reduced from 11.22 to 4.33 kJ/mol (from 12.40 to 2.93 kJ/mol after MP2/6-311G** optimization according to RCFNS (25), and the relative energy of the zwitterionic structure, **2***a*, is lowered by over 30 kJ/mol. The HF 'transition structure' for H transfer, **1***c*–**2***a*, is lowered even more, by 45.27 kJ/mol. In other words, a qualitative change in the nature of the potential energy surface is predicted. Of special interest is the comparison of the effect of the correlation correction on **2***a* and **2***aa*. The former has a strong single H bond, while the latter structure has a bifurcated geometry. Stabilization of the latter by correlation correction is only about half of the former, 16.24 kJ/mol.

The ZPE of neutral glycine conformers vary from 222 to 229 kJ/mol. The largest difference, after scaling (38), corresponds to a change of as much as 6 kJ/mol in relative stability or barrier height. As shown in Table 3, the vibrational contributuion makes **1***b* a more stable conformer than **1***c*, and the transition state **1***cc* for the interconversion of the enantiomeric forms of **1***c* is actually lower in energy than **1***c*. It is clear that it is important to include ZPE in considering the total energy in studies involving a few molecules or conformers with similar electronic energies. The relative energies of the glycine conformers as reported by JG (11), or RCFNS (25), and which are listed in Table 3 do not appear to include the ZPE correction.

The addition of diffuse functions on the heavy atoms and polarization functions on hydrogen atoms is normally not required to achieve qualitatively correct geometries and relative energies. The most pronounced effect of diffuse functions is on species which have nonbonded electron pairs, especially if they are also negatively charged. Polarization functions on H are most important when H bonding is involved. In this sense, glycine which has both nonbonded lone pairs (and a negatively charged region in the zwitterionic form) and H bonds is a worst case for description by use of the normally sufficient 6-31G* basis set. Some measure of the importance of the expansion of the basis set may be garnered by comparison of columns 3 and 5 of Table 3. The latter are the MP2/6-31G*//6-31G* results of JG (11), the former our MP2/6-31+G**//6-31+G* results. The comparison is not precise because our basis set contains the

additional diffuse functions. Neither set of data is corrected for ZPE. In every case, the *relative* energies of the structures are reduced using the larger basis set by amounts ranging from 1–5 kJ/mol. As with the effect of correlation alone, the most stable structure, **1***a*, is least affected by the change of basis set. Thus the extended basis set calculations predict a narrower spread of relative stabilities and lower internal rotation barriers. We illustrate the impact of the energy differences by noting the effect on the rate constants for **1***a*–**1***b* interconversion reactions. The free energy differences for these conformers, and the −2.6 and 0.8 kJ/mol change in barriers will contribute a factor of 2.8 for the forward reaction and 0.7 for the reverse reaction, or a factor of 4 to the equilibrium constant at 300 K.

Thermodynamic properties

Ideal gas thermodynamic functions C_p^0, S^0, $H^0 - H_0^0$, and $(G^0 - H_0^0)/T$ in the temperature range 0–1500 K and 1 atm pressure for the neutral and zwitterionic forms of glycine are listed in Table 4. In the case of the neutral form, the properties correspond to the composite mixture appropriate for a given temperature. The experimental heat of formation of solid-phase glycine at 298.15 K has been reported to be −528.6 kJ/mol (39). The enthalpy of sublimation of glycine has been measured experimentally at 418.93 K to be 136.5 kJ/mol (43). The heat capacity of solid glycine has been determined to be 99.2 J/mol (39). The present investigation provides a theoretical value of 93.0 J/mol (Table 4) for the heat capacity of glycine in the vapour phase at 298.15 K. These data permit the determination of an 'experimental' value for the heat of formation of glycine in the vapour phase, ΔH_f^0 (298.15) = −392.8 kJ/mol, which is in excellent agreement with the theoretical value, ΔH_f^0 (298.15) = −389.6 kJ/mol, derived using the isodesmic reaction described in Sect. 2.

As discussed in the previous section, the zwitterionic form does not exist as a separate species in the gas phase. Nevertheless, in the absence of other information, we have adopted the structure obtained from the 6-31+G* calculations as representative of the solution phase or solid phase structure. The data presented in Table 4 represent the overall thermodynamic properties without contributions from solvent or solid state interactions. The reference value for the heat of formation of zwitterionic glycine is obtained by adding the stability of **2***a* relative to **1***a* to the heat of formation of glycine at 0 K. The thermodynamic data in Table 4 lay the groundwork for a solution phase study which is in progress.

4. Summary

The results of this study show that glycine exists only in the neutral form in the gas phase. The zwitterionic form is not a stationary point at MP2/6-31+G* level of theory. The theoretical 6-31+G* geometries and frequencies were used to calculate the heat of formation of gas phase glycine, ΔH_f^0 (298.15) = −389.6 kJ/mol, in excellent agreement with an estimate derived from experimental solid state and sublimation data.

5. Acknowledgement

The financial support of the Natural Sciences and Engineering Research Council of Canada is gratefully acknowledged. We thank Yonghua Chen for useful discussions in connection with the thermodynamic properties and Kim Wagstaff for assistance with the computers.

Can. J. Chem. Downloaded from www.nrcresearchpress.com by 217.78.4.112 on 09/08/12
For personal use only.

1. W. R. Oegerle and J. R. Sabin. J. Mol. Struct. **15**, 131 (1973).
2. K. Chung, R. M. Hedges, and R. D. MacFarlane. J. Am. Chem. Soc. **98**, 7523 (1976).
3. S. Millefiori and A. Millefiori. J. Mol. Struct. **91**, 391 (1983).
4. M. Masamura. J. Mol. Struct. **152**, 293 (1987).
5. M. Masamura. J. Mol. Struct. **168**, 227 (1988).
6. O. Kikuchi, T. Natsui, and T. Kozaki. J. Mol. Struct. **207**, 103 (1990).
7. P. Palla, C. Petrongolo, and J. Tomasi. J. Phys. Chem. **84**, 435 (1980).
8. P. R. Laurence and C. Thomson. J. Mol. Struct. **88**, 37 (1982).
9. J. Voogd, J. L. Derissen, and F. B. Van Duijneveld. J. Am. Chem. Soc. **103**, 7701 (1981).
10. P. R. Laurence and C. Thomson. Theor. Chim. Acta, **58**, 121 (1981).
11. J. H. Jensen and M. S. Gordon. J. Am. Chem. Soc. **113**, 7917 (1991).
12. L. L. Shipman and R. E. Christoffersen. Theor. Chim. Acta., **31**, 75 (1973).
13. L. Schafer, H. L. Sellers, F. J. Lovas, and R. D. Suenram. J. Am. Chem. Soc. **102**, 6566 (1980).
14. R. D. Suenram and F. J. Lovas. J. Am. Chem. Soc. **102**, 7180 (1980).
15. J. A. Ryan and J. L. Whitten. J. Am. Chem. Soc. **94**, 2396 (1972).
16. M. A. Hermsmeier and T. M. Gund. J. Mol. Graphics, **7**, 150 (1989).
17. S. Vishveshwara and J. A. Pople. J. Am. Chem. Soc. **99**, 2422 (1977).
18. H. L. Sellers and L. Schafer. J. Am. Chem. Soc. **100**, 7728 (1978).
19. Y. C. Tse, M. D. Newton, S. Vishveshwara, and J. A. Pople. J. Am. Chem. Soc. **100**, 4329 (1978).
20. L. R. Wright and R. F. Borkman. J. Am. Chem. Soc. **102**, 6207 (1978).
21. K. Slam, V. J. Klimkowski, J. D. Ewbank, C. Van Alsenoy, and L. Schafer. J. Mol. Struct. **110**, 171 (1984).
22. R. Bonaccorsi, P. Palla, and J. Tomasi. J. Am. Chem. Soc. **106**, 1945 (1984).
23. H. Basch and W. J. Stevens. Chem. Phys. Lett. **169**, 275 (1990).
24. M. Ramek. Int. J. Quantum Chem. Quantum Biol. Symp. **17**, 45 (1990).
25. M. Ramek, V. K. W. Cheng, R. F. Frey, S. Q. Newton, and L. Schafer. J. Mol. Struct. **235**, 1 (1991).
26. T. Head-Gordon, M. Head-Gordon, M. J. Frisch, C. L. Brooks III, and J. A. Pople. J. Am. Chem. Soc. **113**, 5989 (1991) and references therein.
27. R. D. Brown, P. D. Godfrey, J. W. V. Storey, M. P. Bassez, B. J. Robinson, R. A. Bachelor, M. G. McCulloch, O. E. H. Rydbeck, and A. G. Hjalmarson. Mon. Not. R. Astron. Soc. **186**, 5 (1979).
28. J. W. O. Tam and C. P. Nash. J. Phys. Chem. **76**, 4033 (1972).
29. R. D. Suenram and F. J. Lovas, J. Mol. Spectrosc. **72**, 372 (1978).
30. R. D. Brown, P. D. Godfrey, J. W. V. Storey, and M. P. Bassez. Chem. Commun. 547 (1978).
31. Y. Grenie, J. C. Lassegues, and C. Garrigou-Lagrange. J. Chem. Phys. **53**, 2980 (1970); A. Theoret. Spectrochim. Acta, Part A, **27**, 11 (1971).
32. W. O. George, T. E. Houston, and W. C. Harris. Spectrochim. Acta, Part A, **30**, 1035 (1974); E. Knosinger. Ber Bunsen-Ges. **78**, 1199 (1974); J. M. Riveros and E. B. Wilson, Jr. J. Chem. Phys. **46**, 4605 (1967).
33. G. C. Pimentel and A. L. McClellan. The hydrogen bond. W. H. Freeman and Co., San Francisco. 1960; P. Herbine, T. A. Hu, G. Johnson, and T. R. Dyke. J. Chem. Phys. **93**, 5485 (1990).
34. B. T. Luck, A. G. Gupta, G. H. Loew, J. G. Lawless, and

D. H. White. Int. J. Quantum Chem. Quantum Biol. Symp. **11**, 117 (1984).
35. J. S. Gaffney, R. C. Pierce, and L. Freedman. J. Am. Chem. Soc. **99**, 4293 (1977).
36. M. J. Frisch, M. Head-Gordon, H. B. Schlegel, *et al.* Gaussian 88. Gaussian, Inc., Pittsburgh Pa. 1988; M. J. Frisch, M. Head-Gordon, G. W. Trucks, *et al.* Gaussian 90. Gaussian, Inc., Pittsburgh Pa. 1990.
37. M. J. Frisch, J. A. Pople, and J. E. Del Bene. J. Phys. Chem. **89**, 3664 (1985).
38. J. A. Pople, H. B. Schlegel, R. Krishnan, D. J. Defrees, J. B. Binkley, M. J. Frisch, R. A. Whiteside, R. F. Hout, and W. J. Hehre. Int. J. Quantum Chem. Symp. 15, 269 (1981).
39. D. D. Wagner, W. H. Evans, V. B. Parker, R. H. Schumm, I. Halow, S. M. Bailey, K. L. Churney, and R. L. Nuttal. J. Phys. Chem. Ref. Data, **11**, 1982; Supplement No. 2.
40. Y. Chen, A. Rauk, and E. Tschuikow-Roux. J. Chem. Phys., **93**, 1187 (1990).
41. G. J. Karabatsos and D. J. Fenoglio. Top. Stereochem. **5**, 167 (1970).
42. M. M. Szczesniak, S. Scheiner, and Y. Bouteiller. J. Chem. Phys. **81**, 5024 (1984).
43. C. G. Kruif, J. Voogd, and J. C. A. Offringa. J. Chem. Thermodyn. **11**, 651 (1979).

Can. J. Chem. Downloaded from www.nrcresearchpress.com by 217.78.4.112 on 09/08/12
For personal use only.

Structure effects in copper coordination compounds of ligands with thioether, aromatic nitrogen, and ether donors

SHUANG LIU AND C. ROBERT LUCAS[1]
Department of Chemistry, Memorial University of Newfoundland, St. John's, Nfld., Canada A1B 3X7

AND

ROSEMARY C. HYNES[2] AND JEAN-PIERRE CHARLAND[3]
Division of Chemistry, National Research Council of Canada, Ottawa, Ont., Canada K1A 0R9

Received August 25, 1991

SHUANG LIU, C. ROBERT LUCAS, ROSEMARY C. HYNES, and JEAN-PIERRE CHARLAND. Can. J. Chem. **70**, 1773 (1992).

Preparations of the ligands 1,9-bis(2-pyridyl)-2,5,8-trithianonane (L1) and 1,9-bis(2-pyridyl)-5-oxa-2,8-dithianonane (L2) and their copper(II) complex cations $[Cu(L1)]^{2+}$ and $[Cu(L2)]^{2+}$ as ClO_4^-, $CF_3SO_3^-$, or BF_4^- salts are described. X-ray structures of both complex cations as perchlorates are reported. For $[Cu(L1)](ClO_4)_2$: space group *Pbca*, $a = 10.4896(5)$, $b = 12.9376(6)$, $c = 33.3943(13)$ Å, $Z = 8$, $R_f = 0.067$, $R_w = 0.074$ for 1769 reflections. For $[Cu(L2)](ClO_4)_2$: space group $P2_1/c$, $a = 14.388(2)$, $b = 9.990(5)$, $c = 16.076(3)$ Å, $\beta = 107.919(12)°$, $Z = 4$, $R_f = 0.069$, $R_w = 0.089$ for 2813 reflections. Both are slightly distorted square pyramidal species having interactions in the solids between their ClO_4^- anions and one of the pyridine rings in the L1 complex and the copper atom in the L2 complex. The complexes have been examined by electron spin resonance, electronic spectroscopy, and cyclic voltammetry. The effects of anion coordination, solvation, and removal or alteration of the apical donor atom are assessed by comparisons involving the new complexes and published data on related substances.

SHUANG LIU, C. ROBERT LUCAS, ROSEMARY C. HYNES et JEAN-PIERRE CHARLAND. Can. J. Chem. **70**, 1773 (1992).

On décrit la préparation des ligands 1,9-bis(2-pyridyl)-2,5,8-trithianonane (L1) et 1,9-bis(2-pyridyl)-5-oxa-2,8-dithianonane (L2) ainsi que celle de leurs complexes cationiques du cuivre(II), $[CuL1)^{2+}]$ et $[Cu(L2)]^{2+}$, sous forme de sels du ClO_4^-, $CF_3SO_3^-$ ou BF_4^-. On a déterminé les structures cristallographiques des deux complexes cationiques, sous la forme de perchlorates. Pour le $[Cu(L1)](ClO_4)_2$: groupe d'espace *Pbca*, $a = 10{,}4896(5)$, $b = 12{,}9376(6)$ et $c = 33{,}3943(13)$ Å, $Z = 8$, $R_f = 0{,}067$ et $R_w = 0{,}074$ pour 1769 réflexions. Pour le $[Cu(L2)](ClO_4)_2$: groupe d'espace $P2_1/c$, $a = 14{,}388(2)$, $b = 9{,}990(5)$ et $c = 16{,}076(3)$ Å, $\beta = 107{,}919°$, $Z = 4$, $R_f = 0{,}069$ et $R_w = 0{,}089$ pour 2813 réflexions. Les deux cations sont des espèces pyramidales carrées légèrement déformées qui, dans le solide, possèdent des interactions avec leurs anions ClO_4^- et l'un des cycles pyridiniques dans le complexe L1 et avec l'atome de cuivre dans le complexe L2. On a examiné les complexes par résonance paramagnétique électronique, par spectroscopie électronique et par voltampérométrie cyclique. En se basant sur une comparaison de ces nouveaux complexes avec les données publiées pour des substances apparentées, on a évalué les effets de la coordination par l'anion, de la solvatation et de l'enlèvement ou de l'altération de l'atome donneur apical.

[Traduit par la rédaction]

Introduction

Continuing attempts to model the active sites in copper proteins have generated considerable new knowledge of the behaviour of simple coordination compounds of copper (1). Interest in the "type 1" copper site in proteins has led to successful mimicking of several of its distinctive features such as colour, redox potential, electron spin resonance (ESR) parameters, rapid electron transfer kinetics, and specific structural details using simple coordination compounds as models. A short, general discussion of these efforts has been given by Solomon (2) while individual properties of both the enzymes and the model compounds are addressed in greater detail by other authors (1, 2). Knowledge of the specific structural details to mimic in small model molecules has been greatly assisted by the availability of high-resolution X-ray structural determinations of poplar plastocyanin (1.6 Å resolution) (3) and *alcaligenes denitrificans* azurin (1.8 Å resolution) (4), both of which indicate that copper(II) is surrounded by two aromatic N-donors, a mercaptide-S and a thioether-S, and, in the case of the azurin, by a weakly bonded O-donor as well. Careful studies by several groups (5–8) of various specific characteristics of the "blue" or "type 1" copper centers have revealed the factors responsible for each property, with the possible exception of the unique ESR signature for which the explanation is still mostly phenomenological. The ESR properties have been examined in some detail by Addison and co-workers (6, 9, 10), Urbach and co-workers (5), and others (11) and it is clear that donor atom identity, coordination geometry, and, in particular, distortion from regular geometry are important influences, although in model compounds only limited success has been achieved in duplicating simultaneously both the ESR parameters and the other characteristics of the natural materials. As part of our continuing interest in the chemistry of sulfur-containing coordination compounds (12–14), we have examined the influence of adding a fifth donor of changeable type to the coordination sphere of copper atoms already surrounded by a pair of aromatic nitrogens and a pair of thioether sulfurs. Four-coordinate copper(II) surrounded by N_2S_2 ligands has been widely studied as a model of the "blue" copper centers and the literature provides many examples with which to compare our five-coordinate systems. In this report we examine the ESR, electronic spectroscopic, electrochemical, and structural properties of cop-

[1]Author to whom correspondence may be addressed.

[2]Present address: Department of Chemistry, McGill University, 801 Sherbrooke St. W., Montreal, Que., Canada H3A 2K6.

[3]Present address: Canmet, B.C.C. Building 3, Energy Research Labs, 555 Booth Street, Ottawa, Ont., Canada K1A 0G1.

Can. J. Chem. Downloaded from www.nrcresearchpress.com by 217.78.4.112 on 09/08/12
For personal use only.

per(II) complexes of the ligands L1 and L2 and compare them to those of related four-coordinate copper complexes in the literature.

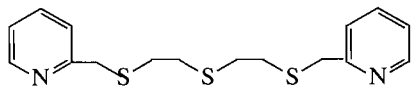

L1

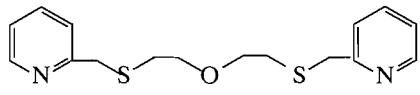

L2

Experimental

Reagents were obtained from the Aldrich Chemical Co. or from Morton Thiokol Alfa Products and were used without further purification. Spectroscopic data were obtained using the following instruments: IR, Perkin Elmer model 283; NMR, General Electric 300-NB; mass spectra, VG micromass 7070 HS; UV/VIS, Cary model 17; ESR, Bruker ESP-300 X-band spectrometer. Cyclic voltammetry data were obtained using a BAS CV27 voltammograph with an electrode configuration designed to minimize *iR* drop and a Houston 2000 Omnigraph *X-Y* recorder. Electrochemical measurements were carried out under a nitrogen atmosphere at room temperature. Solution concentrations were 10^{-3} mol/L in complex and 10^{-1} mol/L in supporting electrolyte (tetraethylammonium perchlorate). Voltammograms were recorded using a glassy carbon working electrode, a platinum counter electrode, and an aqueous saturated calomel reference electrode checked periodically relative to a 1.0×10^{-3} mol/L solution of ferrocene in dimethyl sulfoxide containing 0.1 mol/L tetraethylammonium perchlorate for which the ferrocenium/ferrocene reduction potential was 400 mV and ΔE_p was 72 mV at a scan rate of 100 mV/s. The reference electrode was separated from the bulk of the solution by a porous Vycor tube. Junction potential corrections were not used and potentials reported versus the normal hydrogen electrode were obtained by adding 0.244 V to values obtained versus the saturated calomel electrode. X-ray diffraction data were collected using a Picker diffractometer. Analyses were performed by Canadian Microanalytical Service Ltd.

Preparative

(a) 1,9-Bis(2-pyridyl)-2,5,8-trithianonane (ligand L1)

Sodium (4.6 g, 0.2 mol) was dissolved in commercial absolute ethanol (300 mL) under an atmosphere of dry nitrogen and 2-mercaptoethyl sulfide (7.7 g, 0.05 mol) was added slowly. The resulting mixture was heated to reflux and a solution of 2-picolyl chloride hydrochloride (16.3 g, 0.1 mol) in absolute ethanol (200 mL) was added dropwise with stirring over 2 h. Refluxing and stirring were continued for an additional hour. Volatiles were removed on a rotary evaporator, the residue extracted with chloroform (3 × 50 mL), washed with water several times, dried over anhydrous $CaCl_2$, and taken to dryness to yield a brown oil that was further purified by chromatography on Al_2O_3 in $CHCl_3$/ethyl acetate (50:50) to give 15.5 g (92.2%) of a yellow oil. Attempts to purify the oil by vacuum distillation led only to decomposition. NMR spectrum ($CDCl_3$, ppm from TMS internal standard, assignments from heteronuclear and homonuclear correlation, position identification from Fig. 1), ^{13}C: 30.3 (C7,C10), 30.4 (C6,C11), 36.6 (C8,C9), 120.9 (C2,C15), 122.0 (C4,C13), 135.6 (C3,C14), 148.0 (C1,C16), 157.6 (C5,C12); ^1H: 8.49 (m,2H,C1,C16), 7.63 (m,2H,C3,C14), 7.35 (m,2H,C4,C13), 7.13 (m,2H,C2,C15), 3.84 (s,4H,C6,C11), 2.67 (m,8H,C7,C8,C9,C10). Mass spectrum: parent ion, calcd. for $[C_{16}H_{20}N_2S_3]^+$, m/e = 336; found: m/e = 336.

(b) 1,9-Bis(2-pyridyl)-5-oxa-2,8-dithianonane (Ligand L2)

This preparation was similar to that in (*a*) except that 6.9 g (0.05 mol) of 2-mercaptoethyl ether was used instead of 2-mercaptoethyl sulfide. The yield was 15.3 g (95.5%) of a yellow oil, which was decomposed by attempts at vacuum distillation. NMR spectrum ($CDCl_3$, ppm from TMS internal standard, assignments from heteronuclear and homonuclear correlation, position identification from Fig. 2), ^{13}C: 31.3 (C7,C10), 38.0 (C6,C11), 70.1 (C8,C9), 122.0 (C2,C15), 123.1 (C4,C13), 136.8 (C3,C14), 148.5 (C1,C16), 158.7 (C5,C12); ^1H: 8.51 (m,2H,C1,C16), 7.63 (m,2H,C3,C14), 7.35 (m,2H,C4,C13), 7.15 (m,2H,C2,C15), 3.87 (s,4H,C6,C11), 3.59 (t, J = 6.8 Hz, C8, C9), 2.66 (t, J = 6.8 Hz, C7, C10). Mass spectrum: parent ion, calcd. for $[C_{16}H_{20}N_2OS_2]^+$, m/e = 320; found: m/e = 320.

(c) [Cu(L1)](ClO$_4$)$_2$

CAUTION: *This compound explodes when melted or powdered by grinding. Use of the triflate salt, which appears to be similar in most respects, is recommended instead of the perchlorate.*

Solutions of $Cu(ClO_4)_2 \cdot 6H_2O$ (0.37 g, 1.0 mmol) in methanol (20 mL) and ligand L1 (0.40 g, 1.2 mmol) in acetone (5 mL) were mixed. The resulting deep blue solution was filtered immediately and the filtrate left to evaporate slowly. The blue crystals that formed were separated, washed with acetone, and dried in air to give 0.48 g (80%) of product, mp 181°C (**explodes**). Anal. calcd. for $C_{16}H_{20}Cl_2CuN_2O_8S_3$: C 32.08, H 3.36, Cu 10.61; found: C 32.16, H 3.35, Cu 10.50.

(d) [Cu(L1)](CF$_3$SO$_3$)$_2$

Preparation of this compound is similar to (*c*) except that $Cu(CF_3SO_3)_2$ was used as starting material. Green crystals (mp 187–190°C (dec.)) were obtained in 85% yield. Anal. calcd. for $C_{18}H_{20}CuF_6N_2O_6S_5$: C 30.96, H 2.89, N 4.01; found: C 30.91, H 2.89, N 3.94.

(e) [Cu(L2)](ClO$_4$)$_2$

Solutions of $Cu(ClO_4)_2 \cdot 6H_2O$ (0.19 g, 0.51 mmol) in methanol (15 mL) and ligand L2 (0.19 g, 0.60 mmol) in methanol (5 mL) were mixed by adding the ligand solution to the metal salt solution to give a deep green solution, which was filtered and left to evaporate slowly. The green crystals that formed were separated, washed with dichloromethane, acetone, and a small amount of diethyl ether to give 0.25 g (84%) of product. Anal. calcd. for $C_{16}H_{20}Cl_2CuN_2O_9S_2$: C 32.97, H 3.46, N 4.80, Cu 10.9; found: C 33.03, H 3.47, N 4.80, Cu 11.0.

(f) [Cu(L2)](BF$_4$)$_2$

Preparation of this green crystalline compound is similar to (*e*) except that $Cu(BF_4)_2 \cdot xH_2O$ was used as starting material. Anal. calcd. for $C_{16}H_{20}B_2CuF_8N_2OS_2$: C 34.46, H 3.62, N 5.02, Cu 11.4; found C 34.71, H 3.65, N 5.02, Cu 11.3.

X-ray

A summary of crystallographic data for $[Cu(L1)](ClO_4)_2$ and $[Cu(L2)](ClO_4)_2$ is given in Table 1. The diffraction intensities were collected at 295 K using the $\theta/2\theta$ scan technique with profile analysis (15) at a scan speed of 4°/min. Three standards were measured after every 100 reflections and no significant crystal decay was detected. The space group was determined by systematic absences. Unit cell parameters (Table 1) were determined by a least-squares refinement of the setting angles for 36 reflections ($90° \leq 2\theta \leq 100°$) for $[Cu(L1)](ClO_4)_2$ and of 26 reflections ($90° \leq 2\theta \leq 120°$) for $[Cu(L2)](ClO_4)_2$. Lorentz and polarization factors were applied and corrections were made for absorption. The structures were solved by MULTAN (16) plus a difference Fourier map and refined by full-matrix least squares with unit weights. H-atom positions were calculated but their parameters were not refined. All heavier atoms were refined anisotropically. All calculations were

Can. J. Chem. Downloaded from www.nrcresearchpress.com by 217.78.4.112 on 09/08/12
For personal use only.

TABLE 1. Crystal data for $[Cu(L1)](ClO_4)_2$ and $[Cu(L2)](ClO_4)_2$

Parameter	Value	
	$[Cu(L1)](ClO_4)_2$	$[Cu(L2)](ClO_4)_2$
Empirical formula	$C_{16}H_{20}Cl_2CuN_2O_8S_3$	$C_{16}H_{20}Cl_2CuN_2O_9S_2$
Formula weight	598.57	552.88
Crystal dimensions, mm	0.20 × 0.20 × 0.20	0.20 × 0.20 × 0.15
Space group	Orthorhombic, *Pbca*	Monoclinic, $P2_1/c$
a, Å	10.4896(5)[a]	14.388(2)[a]
b, Å	12.9376(6)	9.990(5)
c, Å	33.3943(13)	16.076(3)
β, deg	90.00	107.919(12)
Z (molecules/cell)	8	4
F (0,0,0) electrons	2303.65	1123.87
V, Å^3	4531.9(3)	2198.7(12)
d_{calc}, g/cm^3	1.756	1.670
Linear absorption coefficient (μ) mm^{-1}	5.42	5.85
Radiation, Å	1.54056 ($CuK\alpha_1$)	1.54056 ($CuK\alpha_1$)
2θ(max), deg	120.0	119.9
No. reflections measured	5716	3920
No. unique reflections	3377	3244
No. unique refl. $I_{net} > n\sigma I_{net}$	1769 (n = 2.5)	2813 (n = 2.5)
Last least-squares cycle calcd. with	52 atoms 290 parameters 1769 reflections	52 atoms 290 parameters 2811 reflections
R_f (sig. refl.)	0.067[b]	0.069[b]
R_w (sig. refl.)	0.074[c]	0.089[c]
Goodness of fit (last cycle)	2.46[d]	10.36[d]
R_f (all refl.)	0.067[b]	0.076[b]
R_w (all refl.)	0.074[c]	0.091[c]
Max. shift/σ	0.208	0.236
Last *D*-map		
deepest hole, e/Å^3	−0.650	−0.670
highest peak, e/Å^3	0.460	1.050
Secondary extinction coeff.	0.192	2.08

[a]Throughout this work esd's are in parentheses and refer to the last digit printed.
[b]$R_f = \Sigma||F_o| - |F_c||/\Sigma|F_o|$.
[c]$R_w = [\Sigma w(|F_o| - |F_c|)^2/\Sigma(w|F_o|)^2]^{1/2}$ where $w = 1/\sigma^2 I$.
[d]Goodness of fit = $[\Sigma w(|F_o| - |F_c|)^2/(\text{no. of reflections} - \text{no. of parameters})]^{1/2}$.

performing with the NRCVAX Crystal Structure Programs (17). Scattering factors were taken from the usual source (18).

Results

The new ligands L1 and L2 and their complexes with copper(II) as perchlorate and triflate salts have been prepared and characterized. The final atomic positional parameters, equivalent isotropic temperature factors, and important bond lengths and angles from X-ray studies of the explosive perchlorate salt of $[Cu(L1)]^{2+}$ and of $[Cu(L2)]^{2+}$ are listed in Tables 2–5. Figures 1 and 2 show views of the cations and their atomic numbering schemes. Anisotropic thermal parameters, a full listing of bond lengths and angles, and final structure factors are available as supplementary data.[4] Electronic spectra in water, *N*,*N*-dimethylformamide, dimethyl sulfoxide, nitromethane, methanol, and acetonitrile, mull IR spectra, and ESR spectra of both microcrystalline samples and *N*,*N*-dimethylformamide solution glasses at 77 K have been determined as have the cyclic voltammograms of the compounds in acetonitrile and water. The spectroscopic and other data are given in Tables 6 and 7 and in Figures 3–6 and will be introduced at appropriate points in the discussion that follows.

Discussion

The cations $[Cu(L1)]^{2+}$ and $[Cu(L2)]^{2+}$ (Figs. 1 and 2) both have distorted square pyramidal arrays of ligand donor atoms about a copper atom. In both, there are N_2S_2 donor sets in the basal planes while the apical sites are occupied either by thioether sulfur S2 of ligand L1 or by the analogous ether oxygen in ligand L2. Although both cations have essentially square pyramidal arrangements of ligand donors about their central copper atoms, the conformations of the two ligands are different, which leads to a facial arrangement of the three sulfur atoms of L1 but a meridional arrangement of the analogous S_2O donor set of L2. For $[Cu(L2)][ClO_4]_2$, there is an interaction between copper and a perchlorate oxygen in the copper's sixth or octahedral coordination site

[4]A complete set of data may be purchased from: The Depository of Unpublished Data, Document Delivery, CISTI, National Research Council Canada, Ottawa, Canada K1A 0S2.

Tables of bond lengths and angles and atomic parameters have also been deposited with the Cambridge Crystallographic Data Centre and can be obtained on request from The Director, Cambridge Crystallographic Data Centre, University Chemical Laboratory, Lensfield Road, Cambridge CB2 1EW, U.K.

Can. J. Chem. Downloaded from www.nrcresearchpress.com by 217.78.4.112 on 09/08/12
For personal use only.

Can. J. Chem. Downloaded from www.nrcresearchpress.com by 217.78.4.112 on 09/08/12
For personal use only.

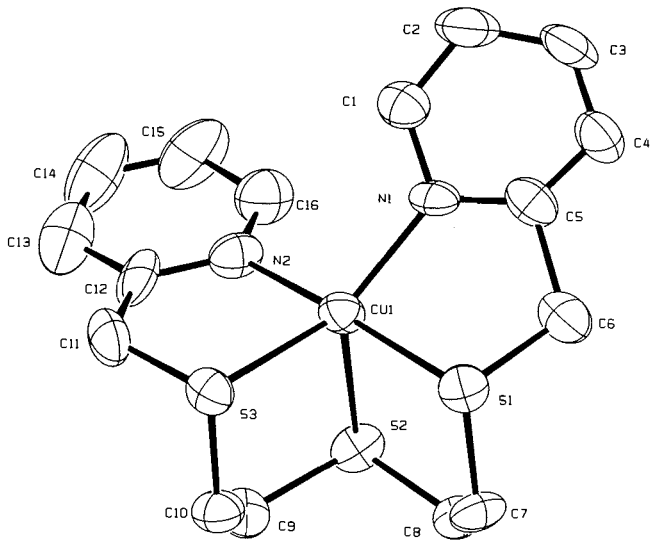

FIG. 1. Structure of $[Cu(L1)]^{2+}$.

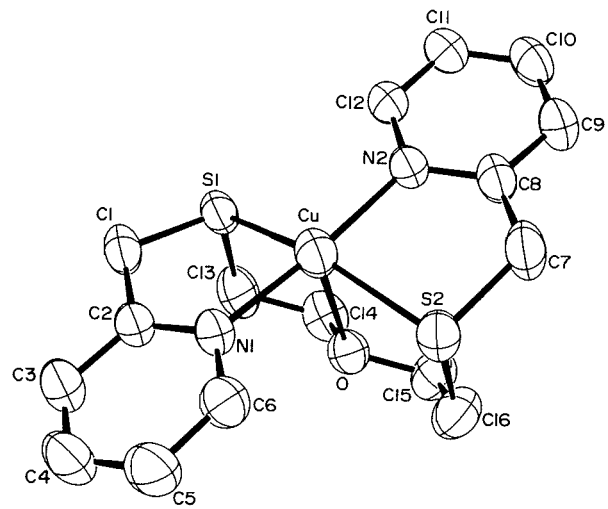

FIG. 2. Structure of $[Cu(L2)]^{2+}$.

that has no parallel in the $[Cu(L1)][ClO_4]_2$ structure. This Cu—O(perchlorate) distance (2.469(10) Å) in $[Cu(L2)][ClO_4]_2$ is roughly comparable to others of its type that are normally in the range 2.52–2.68 Å, but it is significantly longer than the Cu—O(perchlorate) distance of 2.264(5) Å in perchlorato(1,8-bis-(2-pyridyl)-3,6-dithiaoctane)copper(II) ion (19). In the basal planes of the two ions, corresponding bonds are similar in length. For $[Cu(L1)]^{2+}$, Cu—N = 2.017(12) and 1.993(12) Å whereas for $[Cu(L2)]^{2+}$, Cu—N = 2.020(6) and 2.007(6) Å. For $[Cu(L1)]^{2+}$, Cu—S = 2.3324(5) and 2.360(5) Å whereas for $[Cu(L2)]^{2+}$, Cu—S = 2.373(2) and 2.376(3) Å. The apical bond lengths are unremarkable with apical Cu—S = 2.454(4) Å for $[Cu(L1)]^{2+}$ and apical Cu—O = 2.413(5) Å for $[Cu(L2)]^{2+}$.

These distances may be compared with Cu—S(basal) distances of 2.349(3) and 2.358(3) Å in $(CuCl_2 \cdot L)_2$ (L = 2,5,9-trithia[9](2,5)thiophenophane) (20), with Cu—S(apical) distances of 2.814(1) Å in the six-coordinate complex of 1,6-bis(5′-methylimidazol-4′-yl)-2,5-dithiahexane (21) and 2.398(2) Å in the five-coordinate complex of 1,4,7,10,13-pentathiacyclopentadecane (8) and with Cu—N(basal) dis-

TABLE 2. Positional parameters and equivalent isotropic temperature factors for $[Cu(L1)](ClO_4)_2$

Atom	x	y	z	B_{iso}[a]
Cu	0.7493(3)	0.2228(1)	0.11085(5)	3.09(9)
Cl(1)	1.0168(4)	0.4472(3)	0.18323(11)	4.19(18)
Cl(2)	0.2478(5)	0.9576(3)	0.04374(9)	3.98(17)
S(1)	0.9022(4)	0.2020(3)	0.06112(12)	3.38(18)
S(2)	0.7518(5)	0.4091(3)	0.09695(9)	3.49(16)
S(3)	0.5768(4)	0.1965(3)	0.06663(12)	3.31(17)
O(1)	0.9973(20)	0.5008(13)	0.1475(4)	10.6(10)
O(2)	0.9252(16)	0.4764(19)	0.2100(5)	12.2(14)
O(3)	1.1334(14)	0.4609(20)	0.1998(4)	12.5(15)
O(4)	0.993(3)	0.3478(11)	0.1772(6)	14.7(17)
O(5)	0.22335(20)	0.9312(15)	0.0834(4)	11.3(12)
O(6)	0.1429(14)	1.0100(13)	0.0287(5)	8.6(10)
O(7)	0.3594(15)	1.0153(13)	0.0390(5)	8.4(9)
O(8)	0.2595(18)	0.8624(10)	0.0237(5)	9.4(9)
N(1)	0.8791(12)	0.1450(8)	0.1437(3)	3.0(5)
N(2)	0.6149(12)	0.2474(10)	0.1519(3)	3.6(6)
C(1)	0.8476(15)	0.0937(11)	0.1775(4)	3.6(7)
C(2)	0.9361(20)	0.0465(15)	0.2011(5)	5.2(9)
C(3)	1.0644(19)	0.0546(15)	0.1900(6)	5.5(10)
C(4)	1.0962(16)	0.1001(13)	0.1550(5)	4.3(8)
C(5)	1.0025(16)	0.1470(12)	0.1338(4)	3.6(7)
C(6)	1.0347(18)	0.2122(13)	0.0975(5)	4.5(8)
C(7)	0.9064(17)	0.3276(13)	0.0348(4)	3.6(7)
C(8)	0.8751(16)	0.4205(15)	0.0609(5)	4.1(8)
C(9)	0.6023(17)	0.4118(11)	0.0676(5)	3.7(8)
C(10)	0.5739(18)	0.3218(13)	0.0420(5)	3.6(7)
C(11)	0.4503(17)	0.2055(13)	0.1009(6)	4.2(9)
C(12)	0.4884(16)	0.2419(12)	0.1420(5)	4.1(8)
C(13)	0.3977(19)	0.2638(17)	0.1720(7)	6.3(11)
C(14)	0.4387(24)	0.2875(18)	0.2112(7)	7.3(13)
C(15)	0.5640(24)	0.2925(18)	0.2196(5)	6.7(12)
C(16)	0.6530(18)	0.2770(14)	0.1903(5)	5.0(8)

[a] B_{iso} is the mean of the principal axes of the thermal ellipsoid.

TABLE 3. Selected bond lengths and angles in $[Cu(L1)](ClO_4)_2$

Bond	Distance (Å)	Bonds	Angle (deg)
Cu—S(1)	2.324(5)	S(1)—Cu—S(2)	88.38(16)
Cu—S(2)	2.454(4)	S(1)—Cu—S(3)	93.74(16)
Cu—S(3)	2.360(5)	S(1)—Cu—N(1)	82.2(4)
Cu—N(1)	2.017(12)	S(1)—Cu—N(2)	176.9(4)
Cu—N(2)	1.993(12)	S(2)—Cu—S(3)	91.82(17)
S(1)—C(6)	1.851(18)	S(2)—Cu—N(1)	125.8(4)
S(1)—C(7)	1.849(16)	S(2)—Cu—N(2)	88.9(4)
S(2)—C(8)	1.772(17)	S(3)—Cu—N(1)	141.8(3)
S(2)—C(9)	1.850(18)	S(3)—Cu—N(2)	84.9(4)
S(3)—C(10)	1.818(16)	N(1)—Cu—N(2)	100.5(5)
S(3)—C(11)	1.756(19)	Cu—S(1)—C(6)	92.3(6)
N(1)—C(1)	1.350(18)	Cu—S(1)—C(7)	104.7(5)
N(1)—C(5)	1.336(21)	Cu—S(2)—C(8)	102.6(6)
N(2)—C(12)	1.370(21)	Cu—S(2)—C(9)	96.3(5)
N(2)—C(16)	1.395(22)	Cu—S(3)—C(10)	99.6(6)
		Cu—S(3)—C(11)	99.3(6)
		Cu—N(1)—C(1)	122.3(10)
		Cu—N(1)—C(5)	120.7(9)
		Cu—N(2)—C(12)	120.7(10)
		Cu—N(2)—C(16)	118.2(11)

TABLE 4. Positional parameters and equivalent isotropic temperature factors for $[Cu(L2)](ClO_4)_2$

Atom	x	y	z	B_{iso}[a]
Cu	0.23996(7)	0.50614(12)	0.25163(7)	4.38(5)
S(1)	0.32879(15)	0.35312(22)	0.19232(15)	3.95(10)
S(2)	0.15962(14)	0.70701(24)	0.26924(14)	4.21(10)
Cl(1)	0.33866(20)	1.0509(3)	0.34961(17)	5.42(12)
Cl(2)	0.15729(16)	0.4208(3)	0.44309(16)	4.97(11)
O	0.2571(4)	0.6371(6)	0.1311(3)	4.0(3)
O(1)	0.3043(6)	0.9618(9)	0.3986(6)	9.1(5)
O(2)	0.3841(11)	0.9943(15)	0.3002(9)	15.5(11)
O(3)	0.2525(11)	1.0926(17)	0.2830(9)	16.6(11)
O(4)	0.3696(14)	1.1628(17)	0.3865(9)	20.4(13)
O(5)	0.1978(7)	0.3431(15)	0.5110(8)	15.6(9)
O(6)	0.1809(12)	0.5536(16)	0.4600(10)	17.3(12)
O(7)	0.0612(6)	0.4127(14)	0.4055(8)	14.1(8)
O(8)	0.2041(10)	0.4072(15)	0.3792(8)	14.6(10)
N(1)	0.3711(4)	0.5574(7)	0.3356(4)	3.7(3)
N(2)	0.1071(4)	0.4427(7)	0.1797(4)	3.8(3)
C(1)	0.4455(6)	0.3765(10)	0.2727(6)	5.1(5)
C(2)	0.4539(5)	0.4952(9)	0.3315(5)	4.0(4)
C(3)	0.5451(6)	0.5371(10)	0.3846(6)	4.6(4)
C(4)	0.5529(6)	0.6372(10)	0.4434(6)	4.7(4)
C(5)	0.4682(6)	0.6985(10)	0.4487(6)	4.7(4)
C(6)	0.3802(6)	0.6560(9)	0.3941(5)	4.3(4)
C(7)	0.0397(6)	0.6337(10)	0.2359(6)	4.8(4)
C(8)	0.0285(5)	0.5193(9)	0.1755(5)	4.1(4)
C(9)	−0.0637(6)	0.4863(11)	0.1193(6)	5.3(5)
C(10)	−0.0752(7)	0.3758(12)	0.0692(6)	6.0(5)
C(11)	0.0047(7)	0.2959(11)	0.0750(6)	5.4(5)
C(12)	0.0940(6)	0.3328(9)	0.1308(6)	4.6(4)
C(13)	0.3391(7)	0.4477(10)	0.1001(6)	5.2(5)
C(14)	0.3438(7)	0.5981(10)	0.1130(6)	4.8(5)
C(15)	0.2533(6)	0.7753(9)	0.1498(6)	4.9(4)
C(16)	0.1594(6)	0.7980(9)	0.1723(7)	5.2(4)

[a] B_{iso} is the mean of the principal axes of the thermal ellipsoid.

TABLE 5. Selected bond lengths and angles in $[Cu(L2)](ClO_4)_2$

Bond	Distance (Å)	Bonds	Angle (deg)
Cu—O	2.413(5)	S(1)—Cu—O	79.95(15)
Cu—O(8)	2.469(10)	S(1)—Cu—O(8)	110.5(3)
Cu—S(1)	2.373(2)	S(2)—Cu—O	79.14(15)
Cu—S(2)	2.376(3)	S(2)—Cu—O(8)	90.5(3)
Cu—N(1)	2.020(6)	O—Cu—O(8)	169.6(3)
Cu—N(2)	2.007(6)	O—Cu—N(1)	95.37(22)
S(1)—C(1)	1.793(9)	O—Cu—N(2)	91.30(23)
S(1)—C(13)	1.804(10)	O(8)—Cu—N(1)	86.5(4)
S(2)—C(7)	1.798(8)	O(8)—Cu—N(2)	87.0(4)
S(2)—C(16)	1.807(10)	Cu—O—C(14)	109.2(5)
O—C(14)	1.420(10)	Cu—O—C(15)	109.8(5)
O—C(15)	1.418(11)	Cu—O(8)—Cl(2)	147.0(8)
N(1)—C(2)	1.365(10)	S(1)—Cu—S(2)	159.07(10)
N(1)—C(6)	1.343(11)	S(1)—Cu—N(1)	85.64(20)
N(2)—C(8)	1.353(10)	S(1)—Cu—N(2)	95.70(20)
N(2)—C(12)	1.331(11)	S(2)—Cu—N(1)	95.44(20)
		S(2)—Cu—N(2)	85.65(21)
		N(1)—Cu—N(2)	173.3(3)
		Cu—S(1)—C(1)	97.4(3)
		Cu—S(1)—C(13)	100.7(3)
		Cu—S(2)—C(7)	94.5(3)
		Cu—S(2)—C(16)	101.2(3)
		C(14)—O—C(15)	113.8(6)
		Cu—N(1)—C(2)	120.1(5)
		Cu—N(1)—C(6)	121.6(5)
		Cu—N(2)—C(8)	118.9(5)
		Cu—N(2)—C(12)	122.6(5)

tances of 1.997(4) and 1.950(4) Å in the five-coordinate complex of 1,7-bis(*N*-methylbenzimidazol-2′-yl)-2,6-dithiaheptane (22). The basal Cu—S and Cu—N distances are thus normal and the apical Cu—S in the L1 complex, while somewhat longer than the basal Cu—S distances, is significantly less than the sum of the van der Waals' radii (3.20 Å) (23) of copper and sulfur. There is no interaction in $[Cu(L1)][ClO_4]_2$ between copper and the perchlorate anions like that in $[Cu(L2)][ClO_4]_2$ (*vide supra*), the closest approach to copper in the L1 complex by a perchlorate oxygen being 3.727(4) Å. There is, however, a close approach by one of the perchlorate oxygens to hydrogens on both C15 and C16 of the pyridine ring of L1 that lies more or less in the base plane of the ion (Fig. 1). The distances between the perchlorate oxygen atom and both H15 and H16 are approximately equal to the sum of the oxygen and hydrogen van der Waals' radii (2.70 Å) (23). These contacts have a quite profound effect on the structure and properties of the cation (*vide infra*).

The copper atom in $[Cu(L1)]^{2+}$ is displaced 0.091 Å in the direction of N2 from the plane defined by the apical and two basal sites (N1 and S3) of the coordination sphere. The best plane in the ion, however, is that defined by three of the basal donors S1, S3, and N2. The copper atom lies 0.052 Å below that plane while N1, the other basal donor, lies 1.318 Å below the plane, indicating that it is bent down sharply from its expected position thereby giving an angle between the apex and N1 of 125.8(4)°. As usual with coordination number five, the question raised by this distortion is whether the complex is best regarded as trigonal bipyramidal or square pyramidal. The question is answered satisfactorily by the ESR spectrum (*vide infra*), which is that of a distorted square pyramid.

The copper atom in $[Cu(L2)]^{2+}$ is displaced 0.11 Å towards the apex from either of the planes defined by the two nitrogen atoms and one sulfur, while the remaining sulfur is also displaced towards the apex by 1.07 Å in each case. This ion's structure therefore appears less distorted than that of $[Cu(L1)]^{2+}$ and it is of interest that there is no difference near 1025 and 615 cm^{-1}, where perchlorate bands occur, between its perchlorate salt's mull IR spectrum and that of the perchlorate salt of the L1 complex cation. In other words, the perchlorate interaction with copper revealed by the X-ray study of the L2 complex must be weak. Finally, it may be noted that there is a change from *cis*-pyridines in $[Cu(L1)]^{2+}$ to *trans*-pyridines in $[Cu(L2)]^{2+}$ that is caused primarily by the apical bond length requirements and resulting chelate ring strain, which favour meridional coordination by the S—O—S system with its short apical bond while the S—S—S system with a longer apical bond favours facial coordination.

Comparison of ESR and electronic spectra and cyclic voltammetric behaviour of these compounds having N_2S_3, N_2S_2O, or $N_2S_2O_2$ donor sets with literature data from related species containing N_2S_2 donor sets reveals the influence of the added apical thioether or ether donor as well as the influence of anion or solvent interactions in vacant coordination sites. Table 6 contains electronic and ESR spectral data for the new compounds.

The structure of these complex cations is very sensitive to

Can. J. Chem. Downloaded from www.nrcresearchpress.com by 217.78.4.112 on 09/08/12
For personal use only.

TABLE 6. Electronic and ESR spectral data

Compound	Electronic spectrum λ in nm (ε) Solid[a]	Solution[b]	ESR Powder	Glass[c]
$[Cu(L1)](ClO_4)_2$	640 560(sh) 415 360	915(200) 596(400) 350(5 800) 258(11 100)	$g_1 = 2.04$ $g_2 = 2.06$ $g_3 = 2.14$	$g_\parallel = 2.36$ $g_\perp = 2.06$ $\lvert A_\parallel \rvert = 152 \times 10^{-4}$[d]
$[Cu(L1)](CF_3SO_3)_2$	620 400 360	915(200) 596(400) 350(5 800) 260(11 000)	$g_1 = 2.02$ $g_2 = 2.08$ $g_3 = 2.16$	$g_\parallel = 2.36$ $g_\perp = 2.05$ $\lvert A_\parallel \rvert = 152 \times 10^{-4}$[d]
$[Cu(L2)](ClO_4)_2$		900(sh) 675(300) 375(3 500) 265(10 000)	$g_1 = 2.03$ $g_2 = 2.12$ $g_3 = 2.17$	$g_\parallel = 2.25$ $g_\perp = 2.05$ $\lvert A_\parallel \rvert = 150 \times 10^{-4}$[d]
$[Cu(L2)](BF_4)_2$		700(450) 370(3 000) 260(11 000)	$g_\parallel = 2.03$ $g_\perp = 2.19$	$g_\parallel = 2.25$ $g_\perp = 2.04$ $\lvert A_\parallel \rvert = 155 \times 10^{-4}$[d]
$[Cu(pdthx)](ClO_4)_2$[e]		925(165)[e] 610(185) 344(2 260) 263(12 300)		$g_1 = 2.05$[e] $g_2 = 2.12$ $g_3 = 2.28$ $\lvert A_\parallel \rvert = 183 \times 10^{-4}$[d]
$[Cu(pdthp)](ClO_4)_2$[e]		670(342)[e] 360(3 430) 263(11 100)		$g_1 = 2.01$[e] $g_2 = 2.11$ $g_3 = 2.27$ $\lvert A_\parallel \rvert = 180 \times 10^{-4}$[d]
$[Cu(pdto)](ClO_4)_2$[e]		595(902)[e] 360(5 560) 260(11 300)		$g_1 = 2.05$[e] $g_2 = 2.08$ $g_3 = 2.20$ $\lvert A_\parallel \rvert = 202 \times 10^{-4}$[d]

[a]Nujol mull.
[b]In methanol, water, nitromethane, acetonitrile, or *N*,*N*-dimethylformamide.
[c]In *N*,*N*-dimethylformamide at 77 K unless noted.
[d]In cm^{-1}.
[e]Reference 5; UV/VIS in acetonitrile; ESR at 77 K in methanol/ethanol glass; pdthx, pdthp, pdto, pdtn are bis(pyridyl)-dithioether ligands, $py(CH_2)_xS(CH_2)_yS(CH_2)_xpy$; pdthx $x = 1$, $y = 2$; pdthp $x = 1$, $y = 3$; pdto $x = 2$, $y = 2$; pdtn $x = 2$, $y = 3$.

the presence of coordinating anions or solvent. For example, ESR spectra of microcrystalline samples of the L1 complex are quite different depending upon the identity of the anion (Fig. 3, Table 6). When the anion is perchlorate, the spectrum shows only a minor rhombic distortion from a typical axial situation but when the anion is triflate, this distortion is much greater. Based on the X-ray results for $[Cu(L1)](ClO_4)_2$, it seems likely that this cation's preferred coordination geometry, in the absence of a donor in the sixth octahedral site, is that of a square pyramid distorted towards trigonal bipyramidal, as indicated by the ESR for $[Cu(L1)](CF_3SO_3)_2$. In solid state $[Cu(L1)](ClO_4)_2$, however, interaction between a perchlorate oxygen and hydrogens on C15 and C16, mentioned earlier, "lifts" one of the pyridine rings. The structure is then a square pyramid with the "unsupported" pyridine ring drooping. This anion-related structural change in the solid state has ramifications for the electronic structure of the cation that are immediately apparent simply from the colour of the compounds. The perchlorate salt is a deep rich blue in the solid state while the triflate salt is deep green. In the electronic spectra of these substances as Nujol mulls (Table 6), the effect is also apparent as a shift in the frequency of the *d–d* envelope as well as appearance in the spectrum of $[Cu(L1)](ClO_4)_2$ of a shoulder at 560 nm of nearly equal intensity to that of the main peak at 640 nm. Powder ESR spectra of the L2 complex cation (Fig. 4) also vary with the identity of the anion, indicating a rhombic distorted axial coordination sphere when the anion is perchlorate and interacting with copper, but indicating trigonal bipyramidal geometry about copper when the anion is BF_4^- and presumably not interacting.

In frozen solutions, all the ESR spectra (Fig. 5, Table 6) are indicative of axial species, which argues for a change of both $[Cu(L1)](CF_3SO_3)_2$ and $[Cu(L2)](BF_4)_2$ from their geometries in the solid state to pseudo-octahedral as a result of interactions either with solvent or with their anions. As noted above, the impact of this structural change in solution is visually apparent for $[Cu(L1)]^{2+}$. Upon dissolving green crystals of $[Cu(L1)](CF_3SO_3)_2$ in any of a variety of solvents (Table 6), the solution colour becomes blue. Solution elec-

Can. J. Chem. Downloaded from www.nrcresearchpress.com by 217.78.4.112 on 09/08/12
For personal use only.

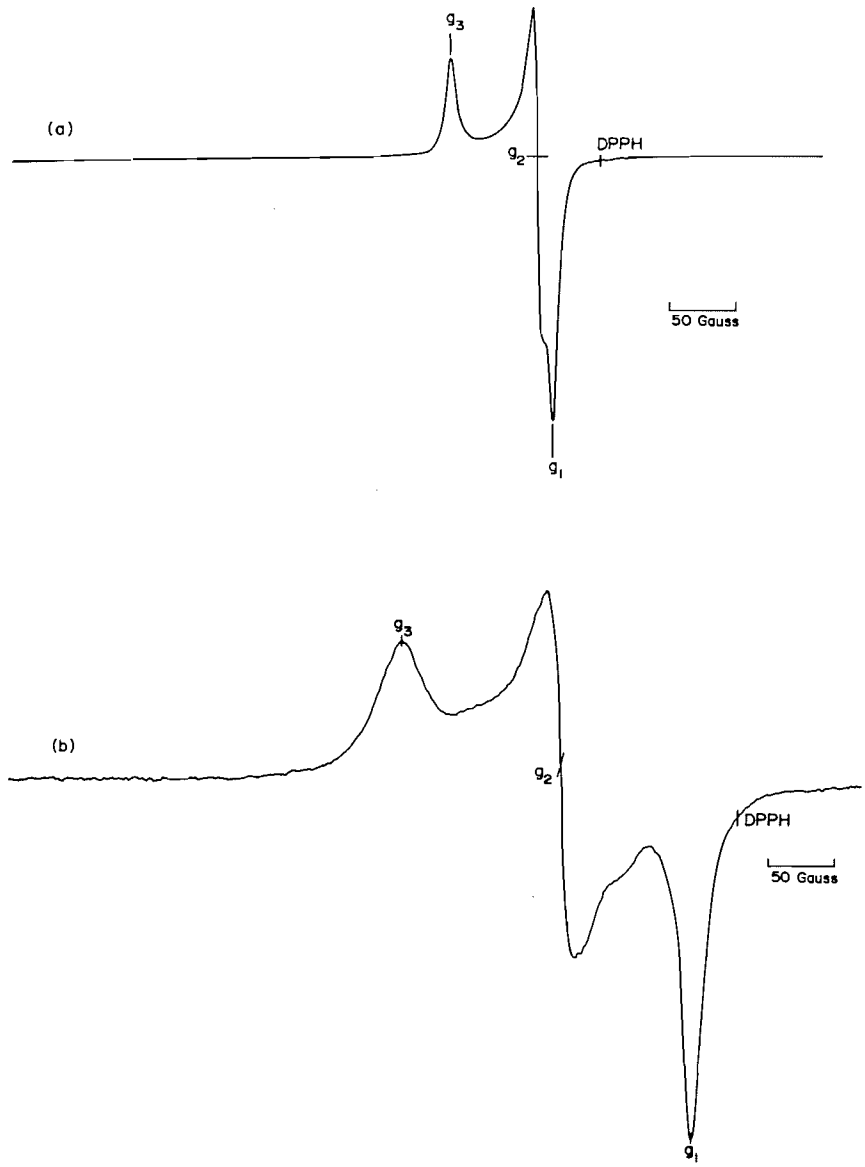

FIG. 3. ESR of microcrystalline samples of $[Cu(L1)^{2+}$ as (*a*) ClO_4^- and (*b*) $CF_3SO_3^-$.

tronic spectra of the triflate and perchlorate salts of $[Cu(L1)]^{2+}$ are indistinguishable and invariant with solvent except for dimethyl sulfoxide, which decomposes them affording green solutions with altered spectral characteristics. Several authors have noted a solvent dependence of the *d–d* band position or intensity in electronic spectra of planar or square pyramidal copper(II) species and have interpreted this as indication of solvent interactions in open coordination sites on copper(II) (5, 20). In this regard, it may be significant that, for $[Cu(L1)]^{2+}$, the electronic spectrum is invariant in the *d–d* region over a range of solvents, suggesting that its anions (ClO_4^- or $CF_3SO_3^-$) are associated with the copper atom in solution even though they are not in the solid state. This interpretation would account both for the axial species in solution detected by ESR and for the invariance of the electronic spectra with solvent. In support of this conclusion, it may be noted that spectra of $[Cu(L2)]^{2+}$ in acetonitrile as its ClO_4^- and BF_4^- salts have different values of λ_{max} in the *d–d* region, suggesting that the perchlorate anion associated with copper in the solid state as revealed by the X-ray study remains associated in solution while the BF_4^-, which is apparently not associated in the solid state, either associates in solution or solvent occupies the sixth coordination site on copper so that the two $[Cu(L2)]^{2+}$ species become different in solution. In this regard, it is relevant that Ochrymowycz, Rorabacher, and co-workers (24–26) have reported evidence for adduct formation between copper complexes and several anions, including both ClO_4^- and BF_4^-, that are normally considered to be noncomplexing. In view of the observation that the electrochemical behaviour of $[Cu(L2)]^{2+}$ as its perchlorate and tetrafluoroborate salts is quite different and yet the ESR behaviour of the two salts in *N*,*N*-dimethylformamide is similar, it seems likely that in acetonitrile the anions remain associated with copper but in *N*,*N*-dimethylformamide they are replaced by solvent.

It is interesting to note (Fig. 5) that at least for $[Cu(L1)]^{2+}$ in dimethylformamide, there is a dissociative equilibrium

Can. J. Chem. Downloaded from www.nrcresearchpress.com by 217.78.4.112 on 09/08/12
For personal use only.

Can. J. Chem. Downloaded from www.nrcresearchpress.com by 217.78.4.112 on 09/08/12
For personal use only.

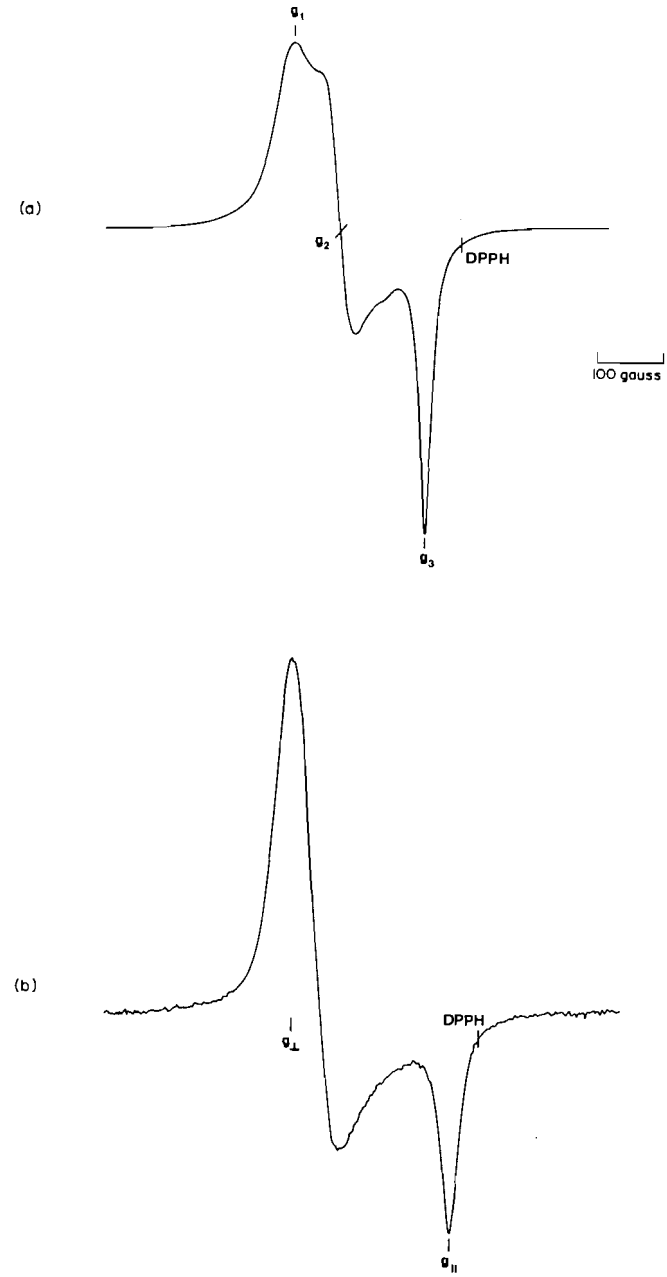

FIG. 4. ESR of microcrystalline samples of $[Cu(L2)]^{2+}$ as (*a*) ClO_4^- and (*b*) BF_4^-.

involving ligand and solvent revealed by the ESR spectra recorded at different concentrations. Spectra at 77 K of glasses formed from these solutions appear as a superpositioning of spectra of the cation and cupric triflate or perchlorate. The spectra show clearly separated peaks in the $g_\parallel$ region that belong to the two species and, as the solution is diluted, those belonging to cupric triflate or perchlorate grow relative to those due to the cation. The glass spectra show no resolved hyperfine structure or rhombic splitting in the $g_\perp$ region although the line width is at least as large as that in the corresponding part of the spectrum of $[Cu(bmdhp)(OH_2)](ClO_4)_2$ (bmdhp = 1,7-bis(*N*-methylbenzimidazol-2′-yl)-2,6-dithiaheptane) under similar conditions (22). For that compound, small rhombic splitting and hyperfine coupling in the $g_\perp$ region were proposed on the basis of spectral simulation. It may be, therefore, that $[Cu(L1)]^{2+}$ is also distorted in solution in a manner similar to the distortion we have shown for its perchlorate salt in the solid state. Unfortunately, the value of $|A_\parallel|$ (152×10^{-4} cm^{-1}) observed for this ion is far too large to be a satisfactory simulation of the values found in "blue" copper proteins (typically, $|A_\parallel| = 31 \times 10^{-4}$–$63 \times 10^{-4}$ cm^{-1}, $g_\parallel = 2.226$–2.288, $g_\perp = 2.052$–2.080) (27) even though other properties of the cation suggest similarities to the natural materials. Assuming the observations concerning the magnitude of $|A_\parallel|$ in four-coordinate structures (28) are applicable in a general way to five-coordinate structures, adjustment of some of the bond angles at copper should help to correct this model's shortcomings. We are addressing this problem and the results will be reported shortly.

Having established both the solid state and solution structures of the two cations, it is useful to compare their properties with each other and with related substances in the literature to observe the effects of replacing or removing axial donors. A similar evaluation of effects in equatorial positions was conducted by Urbach and co-workers (5) and their series of N_2S_2 ligand complexes are convenient for comparison. Electronic spectra of their compounds are similar to ours. Thus, bands near 260 nm are assigned to overlapping pyridine $\pi \rightarrow \pi^*$ and $N(\sigma) \rightarrow Cu(II)$ LMCT transitions; those near 360 nm to an $S(\sigma) \rightarrow Cu(II)$ LMCT, and those of wavelength 600 nm or greater to *d*–*d* transitions enhanced, particularly below 600 nm, by intensity borrowing from nearby charge transfer bands. Urbach and co-workers (5) proposed that $[Cu(pdthx)^{2+}$ consists of a Cu(II) surrounded by two *trans*-aromatic nitrogens, a thioether in the equatorial plane, and one in an axial position. From our work it seems likely there is also an associated perchlorate in the remaining axial position and solvent in the other equatorial site. Comparison of the data for this ion with that of our $[Cu(L1)^{2+}$ (Table 6) shows that adding a thioether to the equatorial plane has surprisingly little effect on the electronic spectrum. Replacing an apical thioether by ether, however, appears to alter significantly the relative spacings of the *d* orbital energies so that the various *d*–*d* transitions are much closer in energy and the longer wavelength transition near 915 nm in $[Cu(L1)]^{2+}$ (as either perchlorate or triflate) moves under other *d*–*d* bands at 675 nm in $[Cu(L2)]^{2+}$. These changes can be understood in terms of the differing abilities of O and S to participate in back-bonding and the differences in the size of their orbitals. Thus, the d_{z^2}–$d_{x^2-y^2}$ gap in $[Cu(L2)]^{2+}$ is somewhat larger than in $[Cu(L1)]^{2+}$ due to a lesser extension of the oxygen orbitals compared to sulfur. There is, hence, a lesser interaction by O than S with the d_{z^2} on copper so that d_{z^2} lies lower in energy. Both the d_{xz} and d_{yz} are less able to participate in back-bonding with O than they are with S so they are raised in energy in $[Cu(L2)]^{2+}$ making the d_{xz},d_{yz}–$d_{x^2-y^2}$ gap smaller and shifting the 596 nm band in $[Cu(L1)]^{2+}$ to 675 nm in $[Cu(L2)]^{2+}$.

Comparison of the electrochemistry of $[Cu(L1)]^{2+}$ with $Cu(pdthx)^{2+}$ (Table 7) shows that removal of a thioether donor causes a change in $E_{1/2}$ in acetonitrile from 734 to 510 mV, which is consistent with the influence of thioether sulfur previously reported (5). Unfortunately, we cannot view by itself the influence of adding a thioether donor in the apical site because changes in chelate ring size are also occurring in the present series of compounds and these are known

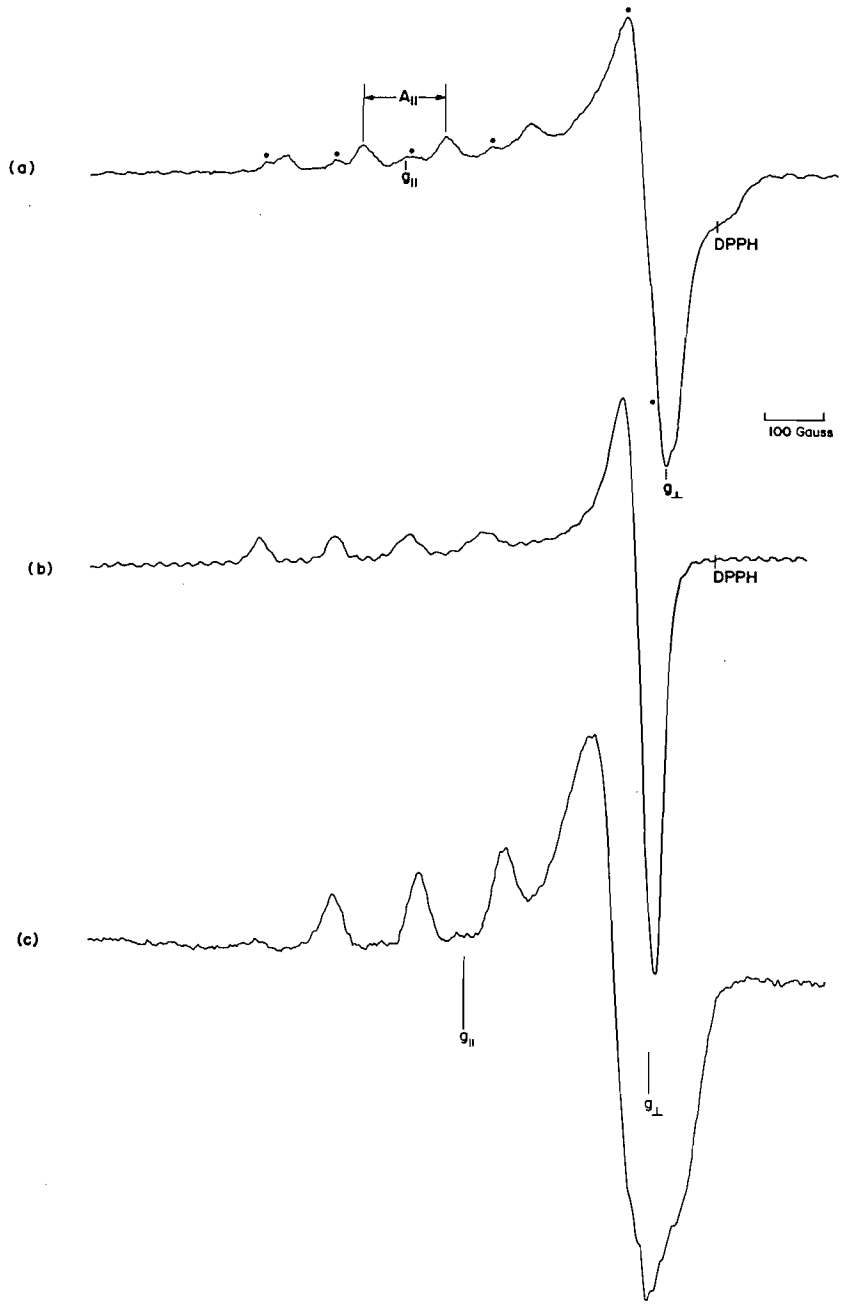

FIG. 5. ESR in DMF glass at 77 K of (*a*) $[Cu(L1)][CF_3SO_3]_2$,* = $Cu(CF_3SO_3)_2$ from dissociation of L1; (*b*) $Cu(CF_3SO_3)_2$ under identical conditions; (*c*) $[Cu(L2)][ClO_4]_2$.

(7) to affect $E_{1/2}$. We can estimate the effect of added apical thioether, however, by recognizing that the change from $Cu(pdthp)^{2+}$ to $Cu(pdtn)^{2+}$ (Table 7) gives a change in $E_{1/2}$ from 547 to 659 mV (or 112 mV) due to the change from 5-, 6-, and 5-membered chelate rings to 6, 6, and 6. Assuming a comparable effect upon changing from $Cu(pdthp)^{2+}$ to $[Cu(L1)]^{2+}$, the total observed change from 547 to 734 mV (or 187 mV) is due in part (~112 mV) to relieved strain between the two equatorial S atoms, and the remainder (~75 mV) is due to addition of an apical thioether donor. Likewise, the change from $[Cu(L1)^{2+}$ to $[Cu(L2)]^{2+}$, or changing apical S into O, changes $E_{1/2}$ from 734 to 696 mV (or −38 mV). These values are substantially smaller than the 150–350 mV changes observed (5, 7) when altering basal or equatorial sites from O or N to S. This observation is perhaps not so surprising if it is the apical donor that is lost when Cu(II) is reduced to Cu(I) and X-ray studies of the Cu(II) and Cu(I) complexes of pdto (19) show folding of the complex and loss of its apical donor on reduction. The cyclic voltammetric behaviour of $[Cu(L1)^{2+}$ in water (Fig. 6) is somewhat different from that in acetonitrile and may be related to solvation or anation changes in the apical sites as a result of the solvent change. Typical voltammograms (Fig. 6, Table 7) show that the potential but not the peak-to-peak separation of the wave is rather sensitive to solvent. In both water and acetonitrile, ΔE_p = 80 mV, but in water, $E_{1/2}$ = 524 mV instead of 734 mV versus NHE as in acetonitrile. These potentials do not match Addison's criteria for con-

Can. J. Chem. Downloaded from www.nrcresearchpress.com by 217.78.4.112 on 09/08/12
For personal use only.

TABLE 7. Cyclic voltammetric data

Compound	$E_{1/2}$[a] (mV)	ΔE_p (mV)[c]
$[Cu(L1)](ClO_4)_2$	734	80
$[Cu(L1)](CF_3SO_3)_2$	702	100
$[Cu(L2)](ClO_4)_2$	696	75
$[Cu(L2)](BF_4)_2$	714	100 at 50 mV/s 210 at 300 mV/s
$[Cu(pdthx)](ClO_4)_2$[b]	510	78
$[Cu(pdthp)](ClO_4)_2$[b]	547	70
$[Cu(pdto)](ClO_4)_2$[b]	609	84
$[Cu(pdtn)](ClO_4)_2$[b]	659	90

[a]In acetonitrile vs. NHE.
[b]Reference 5 and footnote (*e*), Table 6.
[c]At 100 mV/s unless otherwise indicated.

verting potentials in CH_3CN to water (7) but it should also be noted that those criteria probably do not apply in this case because the ratio of i_{pc}/i_{pa} in water is not one, as it is in acetonitrile, although it approaches one as the scan rate is increased. It seems likely that the process in water is different than in acetonitrile and may involve rearrangement of a solvated species that occurs relatively slowly in water and either does not occur at all or is very rapid in acetonitrile. This aspect of the $[Cu(L1)]^{2+}$ cation's properties is under continuing investigation.

It is clear from comparison of the ESR parameters for $Cu(pdto)(ClO_4)^+$ in different solvents (5, 6) that axial solvent interactions affect both $g_\parallel$ and $|A_\parallel|$. This axial effect is apparent in spectra of $[Cu(L1)]^{2+}$ and $[Cu(L2)]^{2+}$ (Table 6) where replacement of apical S by O causes a decrease in $g_\parallel$ from 2.36 to 2.25 and a somewhat smaller decrease in $g_\perp$ from 2.05 to 2.04. Interestingly, there is almost no change in $|A_\parallel|$. Others have noted variations in $g_\parallel$ and $|A_\parallel|$ with structure and have commented on correlations with bond angle distortion at copper, with anionic charge, with thermodynamic stability, or with axial perturbations of the complex species' symmetry (6, 9–11, 29). Usually, there is an inverse relationship between $g_\parallel$ and $|A_\parallel|$ for a given donor set and it is probable that for the L1 and L2 complexes this rule is violated because of the change in ligand donor at the apical position.

Conclusions

Solid state and solution structures of the copper(II) species described in this report are very sensitive to interactions with anions and solvents. Structure changes that accompany anation or solvation may be as minor as small alterations of bond angles in the coordination sphere or they

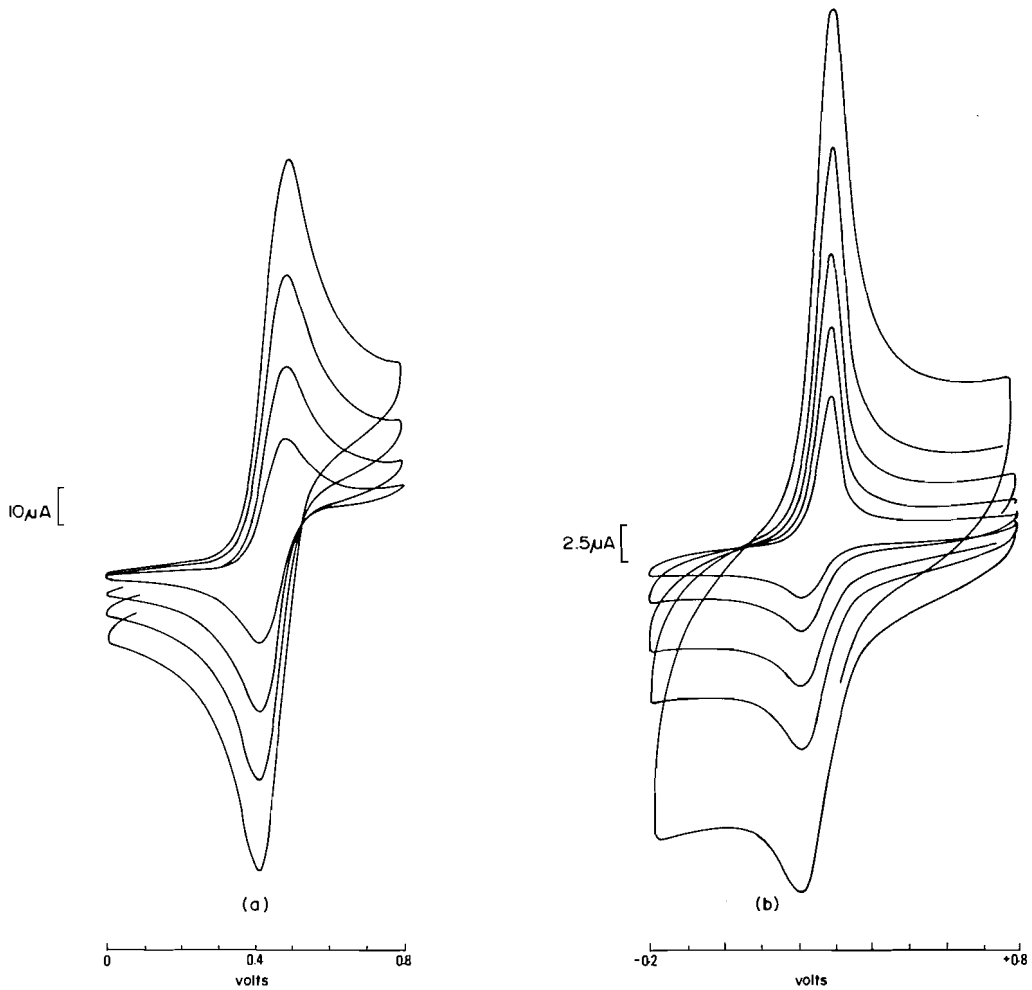

FIG. 6. Cyclic voltammograms of $[Cu(L1)][ClO_4]_2$ (*a*) in acetonitrile at scan rates of 50, 100, 200, and 400 mV s^{-1} and (*b*) in water at scan rates of 20, 50, 100, 200, and 400 mV s^{-1}.

Can. J. Chem. Downloaded from www.nrcresearchpress.com by 217.78.4.112 on 09/08/12
For personal use only.

may be as major as dissociation of the ligand but all affect significantly the electronic and ESR spectra as well as the redox properties of the copper complexes. The greatest effect of changes in ligand donor atom is expressed through the basal or equatorial planes of pseudo-square pyramidal or octahedral complexes while the effect at the apical site is smaller but still detectable by ESR, electronic spectroscopy, or cyclic voltammetry. Changing the apical donor to O from S shortens the metal–apex bond length, which may also change the way in which the ligand surrounds the metal from meridional to facial in order to minimize strain. Increasing the chain length between basal sites while spanning the apical site (or even linking basal sites directly) influences the ease with which tetrahedral geometry in Cu(I) can be achieved upon reduction, and consequently increases the magnitude of $E_{1/2}$. Changing from apical O to S increases $E_{1/2}$ by ~38 mV; it increases the wavelength of the d–d band envelope by ~240 nm; it increases $g_{\|}$ by ~0.11, $g_{\perp}$ by ~0.01, and leaves $|A_{\|}|$ unchanged within experimental error. Adding apical S or O donors, thereby converting formally four-coordinate species into five-coordinate ones, causes the expected appearance of a long-wavelength tail on the d–d band envelope or even appearance of a further low-intensity band at longer wavelength (~925 nm) and an increase in $E_{1/2}$ of 75–190 mV. Although different solvent systems were used for the five-coordinate and four-coordinate ESR studies and therefore conclusions about ESR trends should be treated with caution, a small increase in $g_{\|}$ accompanied by a small decrease in $|A_{\|}|$ while $g_{\perp}$ remains constant within experimental error is noted upon adding an apical donor. ESR evidence suggests that *N*,*N*-dimethylformamide competes with ligand for copper(II) in an equilibrium process.

Can. J. Chem. Downloaded from www.nrcresearchpress.com by 217.78.4.112 on 09/08/12
For personal use only.

Acknowledgments

Assistance with aspects of the X-ray studies by Drs. E. J. Gabe, J. N. Bridson, and M. J. Newlands and loan of electrochemical equipment by Dr. P. G. Pickup are gratefully acknowledged. Financial support was provided by Memorial University of Newfoundland in the form of a Hatcher Scholarship (S.L.) and by the Natural Sciences and Engineering Research Council of Canada in the form of an operating grant (C.R.L.).

1. K. D. Karlin and J. Zubieta (*Editors*). Biological and inorganic copper chemistry. Vols. I and II. Adenine Press, New York. 1986.
2. E. I. Solomon. *In* Copper coordination chemistry: biochemical and inorganic perspectives. *Edited* by K. D. Karlin and J. Zubieta. Adenine Press, New York. 1983.
3. J. M. Guss and H. C. Freeman. J. Mol. Biol. **169**, 521 (1983).
4. G. E. Norris, B. F. Anderson, and E. N. Baker. J. Am. Chem. Soc. **108**, 2784 (1986).
5. D. E. Nikles, M. J. Power, and F. L. Urbach. Inorg. Chem. **22**, 3210 (1983).
6. U. Sakaguchi and A. W. Addison. J. Chem. Soc. Dalton Trans. 600 (1979).
7. A. W. Addison. Inorg. Chim. Acta, **162**, 217 (1989).
8. P. W. R. Corfield, C. Ceccarelli, M. D. Glick, I. Wei-Yu Moy, L. A. Ochrymowycz, and D. B. Rorabacher. J. Am. Chem. Soc. **107**, 2399 (1985).
9. A. W. Addison, M. Carpenter, L. K-M. Lau, and M. Wicholas. Inorg. Chem. **17**, 1545 (1978).
10. H. Yokoi and A. W. Addison. Inorg. Chem. **16**, 1341 (1977).
11. K. Miyoshi, H. Tanaka, E. Kimura, S. T. Ama, S. Murata, H. Shimizu, and K. Ishizu. Inorg. Chim. Acta, **78**, 23 (1983).
12. C. R. Lucas, S. Liu, and L. K. Thompson. Inorg. Chem. **29**, 85 (1990).
13. C. R. Lucas, S. Liu, M. J. Newlands, J. P. Charland, and E. J. Gabe. Can. J. Chem. **68**, 644 (1990).
14. S. Liu, C. R. Lucas, M. J. Newlands, and J. P. Charland. Inorg. Chem. **29**, 4380 (1990).
15. D. F. Grant and E. J. Gabe. J. Appl. Crystallogr. **11**, 114 (1978).
16. G. Germain, P. Main, and M. M. Woolfson. Acta Crystallogr. Sect. A: Cryst. Phys. Diffr. Theor. Gen. Crystallogr. *A27*, 368 (1971).
17. E. J. Gabe, F. L. Lee, and Y. Lepage. *In* Crystallographic computing 3. *Edited by* G. Sheldrick, C. Kruger, and R. Goddard. Clarendon Press, Oxford. 1985. p. 167.
18. International tables for X-ray crystallography. Vol. IV. Kynoch Press, Birmingham, England. 1974. p. 99. Table 2.2B.
19. G. R. Brubaker, J. N. Brown, M. K. Yoo, R. A. Kinsey, T. M. Kutchan, and E. A. Mottel. Inorg. Chem. **18**, 299 (1979).
20. C. R. Lucas, S. Liu, M. J. Newlands, J. P. Charland, and E. J. Gabe. Can. J. Chem. **67**, 639 (1989).
21. E. Bouwman, W. L. Driessen, and J. Reedijk. J. Chem. Soc. Dalton Trans. 1337 (1988).
22. A. W. Addison, T. Rao, J. Reedijk, J. Van Rijn, and G. C. Verschoor. J. Chem. Soc. Dalton Trans. 1349 (1984).
23. A. Bondi. J. Phys. Chem. **68**, 441 (1964).
24. M. M. Bernardo, R. R. Schroeder, and D. B. Rorabacher. Inorg. Chem. **30**, 1241 (1991).
25. L. S. W. L. Sokol, L. A. Ochrymowycz, and D. B. Rorabacher. Inorg. Chem. **20**, 3189 (1981).
26. I. R. Young, L. A. Ochrymowycz, and D. B. Rorabacher. Inorg. Chem. **25**, 2576 (1986).
27. E. I. Ochiai. *In* Bioinorganic chemistry — an introduction. Allyn and Bacon, Boston. 1977. p. 239.
28. A. W. Addison. *In* Copper coordination chemistry: biochemical and inorganic perspectives. *Edited by* K. D. Karlin and J. Zubieta. Adenine Press, New York. 1983. p. 109.
29. A. F. Garito and B. B. Wayland. J. Am. Chem. Soc. **91**, 866 (1969).

Laser flash photolysis studies of the formation and reactivities of phenyl(naphthyl)methyl carbocations generated from phosphonium salt precursors[1]

E. O. ALONSO,[2a] L. J. JOHNSTON, J. C. SCAIANO,[2b] AND V. G. TOSCANO[2a]

Steacie Institute for Molecular Sciences, National Research Council Canada, Ottawa, Ont., Canada K1A 0R6

Received October 7, 1991

E. O. ALONSO, L. J. JOHNSTON, J. C. SCAIANO, and V. G. TOSCANO. Can. J. Chem. **70**, 1784 (1992).

The photolysis of several substituted phenyl(naphthyl)methyl triphenylphosphonium chlorides has been examined using a combination of laser flash photolysis experiments and product studies. Both carbocation and radical intermediates have been characterized in the transient experiments, with the relative yields depending strongly on the solvent. For example, in alcohols, acetonitrile, or aqueous solvents cation formation predominates while acetonitrile/dioxane mixtures (5–10%) are required for the observation of radicals. Quantum yields for cation formation vary from 0.79 in methanol to 0.093 in 1:4 acetonitrile/dioxane, as measured by product studies and transient experiments, respectively. The addition of perchlorate salts leads to dramatic enhancements in the cation lifetimes; the effects are particularly pronounced for acetonitrile/dioxane mixtures where the cation yields also increase by factors of 3–4. In this case the effects are attributed primarily to replacement of chloride by perchlorate in the initial ion pairs. The combined data from both solvent and perchlorate salt effects on the cation lifetimes and yields suggest that the excited state of the phosphonium salt cleaves homolytically, followed by electron transfer within the initial radical/triphenylphosphine radical cation pair to generate carbocation, as opposed to direct heterolytic cleavage. The cation yields also indicate that back reaction to regenerate starting material, as well as product formation within the initial geminate cage, occur in some solvents. The effects of solvent and added perchlorate salts on the rate constants for reaction with nucleophiles have been examined. For example, rate constants that vary by an order of magnitude have been measured for quenching by azide ion in various aqueous acetonitrile and trifluoroethanol mixtures.

E. O. ALONSO, L. J. JOHNSTON, J. C. SCAIANO et V. G. TOSCANO. Can. J. Chem. **70**, 1784 (1992).

Faisant appel à une combinaison d'expériences de photolyse éclair au laser et d'études des produits, on a examiné la photolyse de plusieurs chlorures de phényl(naphtyl)méthyl triphényl phosphonium. On a caractérisé des intermédiaires tant cationiques que radicalaires dans les expériences impliquant les espèces transitoires; les rendements relatifs dépendent beaucoup du solvant. Par exemple, dans les alcools, l'acétonitrile ou des solvants aqueux, il y a formation prédominante de cations alors qu'il faut un mélange d'acétonitrile/dioxane (5–10%) pour observer des radicaux. Les rendements quantiques pour la formation des cations, tels que mesurés respectivement par des études de produits et des expériences sur les espèces transitoires, varient de 0,79 dans le méthanol à 0,093 dans un mélange 1 : 4 d'acétonitrile/dioxane. L'addition de sels de perchlorate conduit à une augmentation dramatique des temps de vie des cations; les effets sont particulièrement prononcés pour les mélanges acétonitrile/dioxane dans lesquels les rendements en cations augmentent aussi par des facteurs de 3–4. Dans ce cas, on attribue les effets principalement à une substitution du chlorure par le perchlorate dans les paires d'ions initiales. Les données combinées des effets tant de solvant que de sel perchlorate sur les temps de vie des cations et sur les rendements suggèrent que l'état excité du phosphonium subit plutôt un clivage homolytique, suivie d'un transfert d'électrons à l'intérieur de la paire initiale radical/cation radicalaire de la triphénylphosphine conduisant à un carbocation qu'un clivage hétérolytique direct. Les rendements de cation indiquent aussi que la rétro-réaction régénérant le produit de départ, ainsi que le formation de produit à l'intérieur de la cage géminée initiale, se produit dans certains solvants. On a aussi examiné les effets du solvant et de l'addition de perchlorate sur les constantes de vitesse pour les réactions avec les nucléophiles. Par exemple, on a mesuré les constantes de vitesse qui varient par un ordre de grandeur en piégeant avec l'ion azoture, dans divers mélanges aqueux d'acétonitrile et de trifluoroéthanol.

[Traduit par la rédaction]

A number of recent reports demonstrate that a variety of di- and triarylmethyl substituted cations can be readily generated by photoheterolysis of suitable precursors. This technique was used to generate transient carbocations and to examine their reactivity using direct time-resolved techniques such as laser flash photolysis and time-resolved conductivity (1–15). These methods have considerable advantages over the use of acidic media to generate stable cations for spectroscopic studies and the examination of reactivities using indirect competitive product studies. The direct examination of transient cations allows the measurement of cation lifetimes and reactivities in a variety of reactive solvents such as alcohols and aqueous mixtures and does not rely on the use of nucleophiles such as azide ion as "clocks."

Precursors with leaving groups such as halide, acetate, tosylate, and 4-cyanophenoxide have been frequently used for the generation of cations via photoheterolysis. For many of these precursors homolysis to generate radicals competes with cation formation. We recently reported that phosphonium salts **1** and **2** show a marked preference for heterolysis to generate cations in a variety of polar solvents (16). Although the competition between homolysis and heterolysis in the photolysis of a variety of naphthylmethyl systems has been examined using conventional steady state techniques (17–22), transient techniques were not previously applied to the study of carbocations in these systems. We have now examined the generation of naphthylphenylmethyl cations and radicals from several phosphonium salts (**1–3**, **11**). The ef-

[1]Issued as NRCC No. 33302.

[2]Present address: (a) Instituto de Quimica, Universidade de Sao Paulo, C.P. 20780, 01498 Sao Paulo, Brazil; (b) Department of Chemistry, University of Ottawa, Ottawa, Ont. Canada K1N 6N5.

Can. J. Chem. Downloaded from www.nrcresearchpress.com by 217.78.4.112 on 09/08/12
For personal use only.

fects of solvent and added salts such as lithium perchlorate on the relative amounts of cation and radical and on the lifetimes of the cations have been examined. Further, we have observed a wide variation in the reactivity of the cation towards nucleophiles such as azide ion. Preliminary results for some of these systems have already been reported (16).

Results

Characterization of cations

Laser excitation of phosphonium salt **1** (~5×10^{-5} M; 308 nm) has been demonstrated to result in efficient formation of cation **4** in a variety of polar solvents such as acetonitrile and 2,2,2-trifluoroethanol (TFE) (16). This cation has λ_{max}

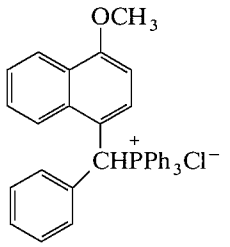

1

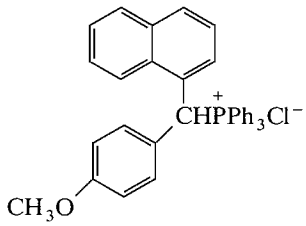

2

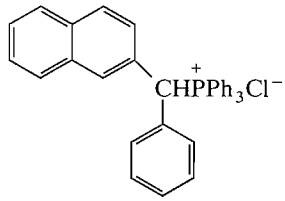

3

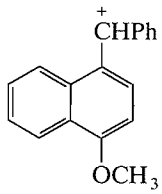

4

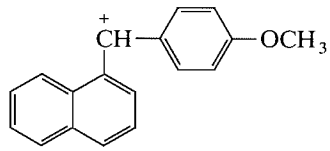

5

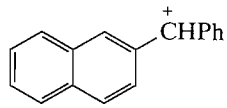

6

at 500 nm with a small second absorption band at ~360 nm and has lifetimes of ~2.5 μs in acetonitrile and in excess of 100 μs in TFE. The cation assignment was confirmed by quenching with nucleophiles such as azide and chloride ions and by the insensitivity of the transient lifetime to the presence of oxygen.

Similar to the results observed with salt **1**, laser excitation of salt **2** (~2.5×10^{-4} M) also produced a strongly absorbing transient with λ_{max} at 550 nm and a weaker absorption band at 370 nm in aerated or deaerated trifluoroethanol as shown in Fig. 1. This species had a lifetime of >35 μs, and was assigned to cation **5.** The same cation could be readily produced as a stable solution from the parent alcohol in TFE/trifluoroacetic acid, and under these conditions the spectrum was identical to that shown in Fig. 1. A similar transient was produced from salt **2** in acetonitrile, although in this case the lifetime was shortened to 350 ns (Table 1).

Excitation (308 nm) of 10^{-3} M salt **3** generated cation **6** with λ_{max} at 445 nm and with a weaker band between 500 and 600 nm (Fig. 1). Decay traces monitored at 445 or 560 nm gave identical lifetimes of 450 ns in TFE and 50 ns in acetonitrile. However, our previous observation of shorter lifetimes for cation **4** at higher concentrations of the precursor salt suggested that these lifetimes were at least partly a reflection of an increased rate for reaction with chloride ion (present as the phosphonium salt counterion) at the higher salt concentration required to obtain sufficient absorption at the laser wavelength. Accordingly, the same cation was produced via 266 nm excitation of 5×10^{-5} M salt **3** in acetonitrile; in this case the spectrum of the cation was identical to that measured using 308 nm excitation but the lifetime was 0.5 μs.

The assignment of the observed transients from salts **2** and **3** to cations **5** and **6**, respectively, was confirmed by their insensitivity towards oxygen and their characteristic quenching by azide ion. Rate constants of 2.4×10^9 and 4.5×10^9 M^{-1} s^{-1} were obtained from plots of the rate constant for cation decay (k_{obs}) versus [azide] for **5** and **6**, respectively, in 10% aqueous TFE (Table 2).

Cation **6** was also generated from 1-naphthyl(phenyl)methyl chloride (**7**) in acetonitrile. The cation spectrum using this precursor was identical to that obtained from the phosphonium salt (**3**) but the lifetime was substantially longer (1.0 μs) and was independent of the precursor concentration. Similarly cation **4** generated from chloride **8** was also longer-lived than that from the phosphonium salt precursor, and no difference in the spectra could be detected. The latter chloride was very rapidly solvolyzed in solvents containing small amounts of either water or alcohols and was, thus, not very suitable for the transient experiments. These observations suggest that reaction with the chloride ion associated with the phosphonium salts is responsible for the shorter cation lifetimes at higher salt concentrations. This is further supported by two additional observations. Firstly, chloride ion added as either the sodium or potassium salt reacted with various cations, as discussed in more detail below. Secondly, the lifetime of cation **6** generated from chloride **7** in acetonitrile decreased substantially in the presence of added phosphonium salts. For example, rate constants of 9×10^9 and ~1×10^{10} M^{-1} s^{-1} were measured for quenching of **6** by di-(4-methoxyphenyl)methyltriphenylphosphonium chloride (**9**) and (1-naphthylmethyl)triphenylphosphonium chloride (**10**) in acetonitrile. Note that excitation of these salts (**9** and **10**) alone in the absence of **7** and at the maximum concentra-

Can. J. Chem. Downloaded from www.nrcresearchpress.com by 217.78.4.112 on 09/08/12
For personal use only.

Can. J. Chem. Downloaded from www.nrcresearchpress.com by 217.78.4.112 on 09/08/12
For personal use only.

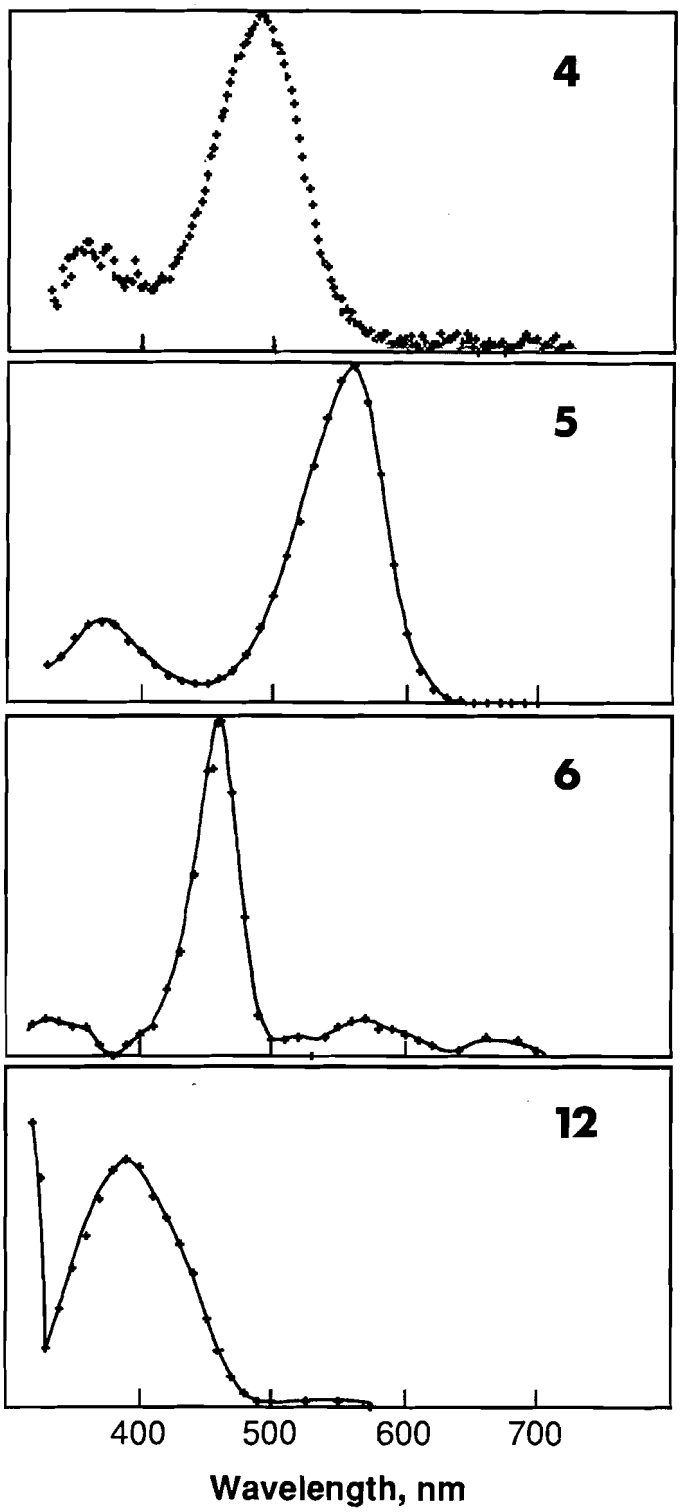

FIG. 1. Transient absorption spectra for cations **4**, **5**, **6** and **12** produced by 308 nm (266 nm for **12**) excitation of aerated or oxygenated TFE solutions of the corresponding phosphonium salts.

tions used in the quenching experiments did not produce any transients since they had very low optical densities at 308 nm. Furthermore, addition of 1-naphthylmethyltriphenylphosphonium tetrafluoroborate had no effect on the lifetime of cation **6**, indicating that a nucleophilic counterion such as chloride is required to observe the effect.

TABLE 1. Room temperature lifetimes of cations **4–6** under a variety of conditions

Cation	Solvent	τ, μs[a]	Precursor, M
4	TFE	>100	**1**, 4.6×10^{-5}
	Acetonitrile	2.5	**1**, 4.2×10^{-5}
	Methanol	0.105	**1**, 8.5×10^{-5}
	1:1 Acetonitrile/dioxane	1.1	**1**, 4.2×10^{-5}
	5% Water/acetonitrile	6.2	**1**, 4×10^{-5}
5	TFE	>35	**2**, 2.6×10^{-4}
	Acetonitrile	0.28	**2**, 2.8×10^{-4}
	Methanol	0.02	**2**, 2.4×10^{-4}
	3:7 Methanol/TFE	0.65	**2**, 2×10^{-4}
	1:1 Acetonitrile/dioxane	0.12	**2**, 2.8×10^{-4}
	5% Water/acetonitrile	0.7	**2**, 2.8×10^{-4}
6	TFE	0.45	**3**, 1.6×10^{-3}
	Acetonitrile[b]	0.05	**3**, 1×10^{-3}
	Acetonitrile[c]	0.6	**3**, 5×10^{-5}
	Acetonitrile[b]	1.1	**7**, 1.9×10^{-3}
	Acetonitrile[c]	0.9	**7**, 8.9×10^{-5}
	1:1 Acetonitrile/dioxane	0.45	**3**, 5.6×10^{-5}
	5% Water/acetonitrile	<0.02	**3**, 5×10^{-5}

[a]Typical errors are ±10%.
[b]308 nm excitation.
[c]266 nm excitation.

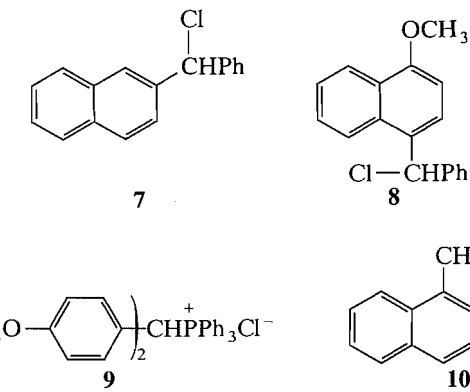

4-Methoxy-1-naphthylmethyltriphenylphosphonium chloride (**11**) was also examined in TFE using both 266 and 308 nm excitation. The spectrum of cation **12** produced by 266 nm excitation of **11** in oxygenated TFE is shown in Fig. 1. Under these conditions the cation lifetime was 7.5 μs. Surprisingly, repeating the same experiment using 308 nm excitation resulted in considerably weaker transient absorption signals due to **12**, despite the fact that the laser energies and optical densities of the precursor at the laser wavelength were comparable in each case. This wavelength dependence may be related to photochemistry from an upper dissociative state in the case of 266 nm excitation.[3]

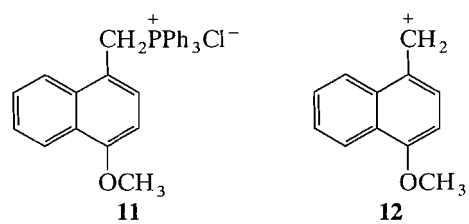

[3]A detailed study of the photochemistry of salt **11** is obviously required to sort out this unusual wavelength dependence.

TABLE 2. Rate constants for quenching of cations **4**, **5**, and **6** with a variety of nucleophiles

Cation	Quencher	Solvent	k_q, M^{-1} s^{-1}
4	NaN_3	5% aq. ACN[a]	$(1.68 \pm 0.05) \times 10^{10}$
		5% aq. ACN + 0.1 M $LiClO_4$	$(3.5 \pm 0.3) \times 10^9$
		5% aq. ACN + 0.01 M $LiClO_4$	$(8.3 \pm 0.5) \times 10^9$
		5% aq. ACN + 0.0012 M $LiClO_4$	$(1.6 \pm 0.1) \times 10^{10}$
		5% aq. TFE	$(1.7 \pm 0.1) \times 10^9$
		5% aq. TFE + 0.0012 M $LiClO_4$	$(1.5 \pm 0.1) \times 10^9$
		10% aq. TFE	$(1.2 \pm 0.1) \times 10^9$
5	NaN_3	10% aq. TFE	$(2.4 \pm 0.2) \times 10^9$
6	NaN_3	10% aq. TFE	$(4.2 \pm 0.2) \times 10^9$
4	NaBr	5% aq. ACN	$(8.1 \pm 0.1) \times 10^9$
		5% aq. ACN + 0.1 M $LiClO_4$	$(5.5 \pm 0.5) \times 10^9$
4	KCl	5% aq. ACN	$(2.2 \pm 0.2) \times 10^9$
		5% aq. ACN + 0.0014 M $LiClO_4$	$(1.8 \pm 0.1) \times 10^9$
		3% aq. ACN	$(5.3 \pm 0.3) \times 10^9$
		10% aq. ACN	$(9.5 \pm 0.5) \times 10^8$
5	KCl	10% aq. ACN	$(1.7 \pm 0.1) \times 10^9$
4	LiCl	5% aq. ACN	$\sim 1.4 \times 10^{9b}$

[a]ACN = acetonitrile.
[b]Plot shown as insert in Fig. 7.

Can. J. Chem. Downloaded from www.nrcresearchpress.com by 217.78.4.112 on 09/08/12
For personal use only.

Table 1 gives lifetimes for cations **4**, **5**, and **6** under a variety of conditions. Since most of these were measured using phosphonium chlorides as precursors, they reflect a combination of reaction of the cation with chloride ion and solvent, with the relative importance of each varying with solvent. Note that the results are further complicated by the fact that the rate of chloride ion quenching is also expected to be solvent dependent (see below). However, the much shorter lifetimes in methanol are attributed to nucleophilic reaction with solvent, which is present in much larger concentration than chloride ion.

One rather surprising observation was the substantially longer lifetimes observed for cations **4** and **5** in aqueous acetonitrile as compared to acetonitrile (Table 1). In contrast, cation **6** generated from either the salt or chloride precursor reacted rapidly with small amounts of water and was too short-lived to measure in >5% water. Since solvolysis of the appropriate naphthylphenylmethyl chlorides in aqueous solvents was rapid, it was not possible to use these substrates to compare results obtained for the two precursors. Therefore, the effect of water on the lifetime of cation **13** produced from **9** was examined as a function of the concentration of water in acetonitrile. In this case literature results are available for the same cation generated from the 4-cyanophenoxy ether in aqueous acetonitrile mixtures (4). As observed for cation **4**, the lifetime of **13** (with **9** as the precursor) initially increased with added water and then levelled off to a constant value of 6 μs at 80% water (Fig. 2). This is in direct contrast to the literature results, which indicated lifetimes of 16.0, 7.3, and 10 μs for the same cation in 7, 17, and 80% aqueous acetonitrile.[4] These results appear to be specific to the phosphonium salt precursors and are thought to be related to variations in the rate constants for chloride quenching of **4** and **5** in the different solvent mixtures, as discussed below. Thus, even in aqueous solvents the lifetimes for **4**, **5**, and **13** are determined by reaction with chloride counterion. In the case of **6**, the cation is more reactive and its lifetime in aqueous acetonitrile is limited by reaction with water rather than chloride ion.

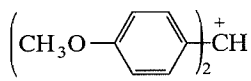

13

Characterization of naphthylphenylmethyl radicals

As previously reported (16), excitation of **1** in less polar solvents than TFE or acetonitrile (e.g., acetonitrile/dioxane

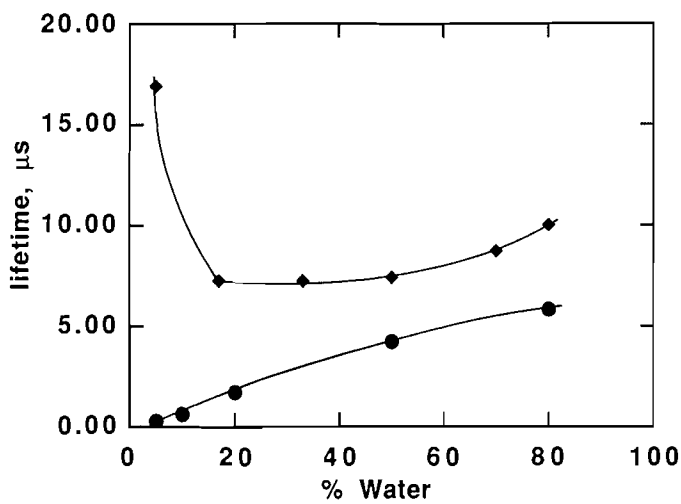

FIG. 2. Effect of water on the lifetime of cation **13** in acetonitrile: (●) this work; (◆) data from ref. 4.

[4]These are approximate values since they were read from a graph in ref. 4.

Can. J. Chem. Downloaded from www.nrcresearchpress.com by 217.78.4.112 on 09/08/12
For personal use only.

mixtures) led to the detection of radical **14** with λ_{max} at 400 nm. The yields of radical varied considerably with the solvent composition with only radical observed between 1 and 5% acetonitrile in dioxane and only cation in pure acetonitrile or in 4:1 acetonitrile/dioxane. As expected, the radical was relatively long-lived (>10 μs), did not decay by first-order kinetics, and reacted efficiently with oxygen, but not with 1,3-cyclohexadiene. The latter served to differentiate the radical from any naphthalene-containing triplet, which would be expected to absorb in a similar region (23) but which would be quenched by dienes. The same radical could be readily generated from (4-methoxy-1-naphthyl)-phenylmethyl chloride in nonpolar solvents such as cyclohexane.

Salt **2** also produced some radical in acetonitrile/dioxane mixtures, as shown in Fig. 3. In contrast to the large shifts that are observed in the cation spectra upon methoxy substitution, the spectrum of radical **15** is very similar to that of **14**. This is to be expected based on the known insensitivity of arylmethyl-substituted radicals to changes in substituents on the aromatic rings (10, 24, 25). Similarly to the results observed with salt **1**, mixtures of both radical and cation were produced by excitation of **2** in acetonitrile/dioxane mixtures.

The spectrum of the (2-naphthyl)phenylmethyl radical (**16**) was obtained by 266 nm excitation of salt **3** in acetonitrile/dioxane mixtures. The radical was clearly visible without interference from cation signals at >1 μs delays after the laser and had λ_{max} at 340 nm with weaker bands at 400 and 680 nm. The decay kinetics measured at the three wavelengths were similar, indicating that all three bands belonged to the same species. Further, this species reacted efficiently with oxygen, demonstrating that the observed transient is not a naphthalene radical cation, which has also been reported to absorb in the 650–700 nm region and which is readily detectable in oxygenated solutions (26*a*).[5] A similar spectrum for radical **16** was also observed from the chloride precursor in cyclohexane and acetonitrile (Fig. 3). The shift in λ_{max} from 400 nm for radicals **14** and **15** to 340 nm for **16** is in line with the reported spectra for the 1- and 2-naphthylmethyl radicals, which have absorption maxima at 365 nm, whereas the (1-bromo-2-naphthyl)methyl radical has λ_{max} at 350 nm (25, 27). The long-wavelength absorption is rather unusual since the lowest energy band in most naphthylmethyl radicals is too weak to be observed in absorption, although its fluorescence is readily detectable in various systems (24).

A variety of naphthalenes have triplet–triplet absorption

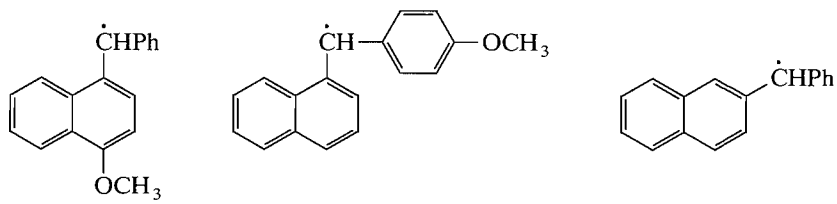

14 **15** **16**

spectra with maxima at ~420 nm (23). However, in none of the transient experiments with salts **1** and **2** did we find any evidence for species other than either the corresponding cations or radicals. Note that it is important to use flow system in these experiments to eliminate the possibility of signals due to the accumulation of photoproducts that have strong triplet absorptions. However, for salt **3** in deaerated acetonitrile/dioxane mixtures there was a weak triplet signal at 420 nm in addition to radical **16**. It was also possible to observe weak and long-lived transients at 420 nm due to the triplets of 2- and 3-methoxy-1-naphthylmethyl triphenylphosphonium chlorides.

Cation yields

Two approaches were used to measure the yields of cations produced by photolysis of the phosphonium salts. The first of these involves determination of quantum yields for product formation. The second method is based on measuring the yields of transient cations using a suitable actinometer.

Photolysis of salt **2** in methanol at low conversions gave a single product that was isolated and shown to be ether **17** (reaction [1]), the expected product of methanol trapping of the intermediate carbocation. Both triphenylphosphine and triphenylphosphine oxide were also observed by HPLC analysis. The latter may result from either the oxidation of triphenylphosphine or the reaction of triphenylphosphine radical cation with water (28). The quantum yield for formation of **17** upon 313 nm photolysis of 3×10^{-3} M **2** in methanol was measured using the formation of acetophenone from valerophenone in cyclohexane ($\Phi_{ACP} = 0.4$) as the actinometer (29, 30). An average of six determinations gave a value of 0.71 ± 0.10 (Table 3). A quantum yield for ether production of 0.39 (two determinations) was measured in 3:7 (v/v) methanol/TFE. This particular solvent was selected since 30% methanol was sufficient to give a clean yield of **17**. Irradiation of **2** in TFE alone gave a number of additional products. Irradiation of **2** in acetonitrile also gave a complex product mixture. Previous studies of diarylmethyl cations have shown that there is the added complication of reversible addition of the cation to the solvent, which results in lower than expected yields of amide products in acetonitrile (4). Therefore, quantitative measurements were not attempted in this solvent.

[5]In a few experiments using high 266 nm power there were some additional broad absorptions at λ > 650 nm that may be due to radical cations generated by photoionization. Note that reactions of radical cations with oxygen are relatively slow (10^6 M^{-1} s^{-1}) and do not compete with other decay pathways (under laser flash photolysis conditions) at the oxygen concentrations present in most organic solvents (26*b*).

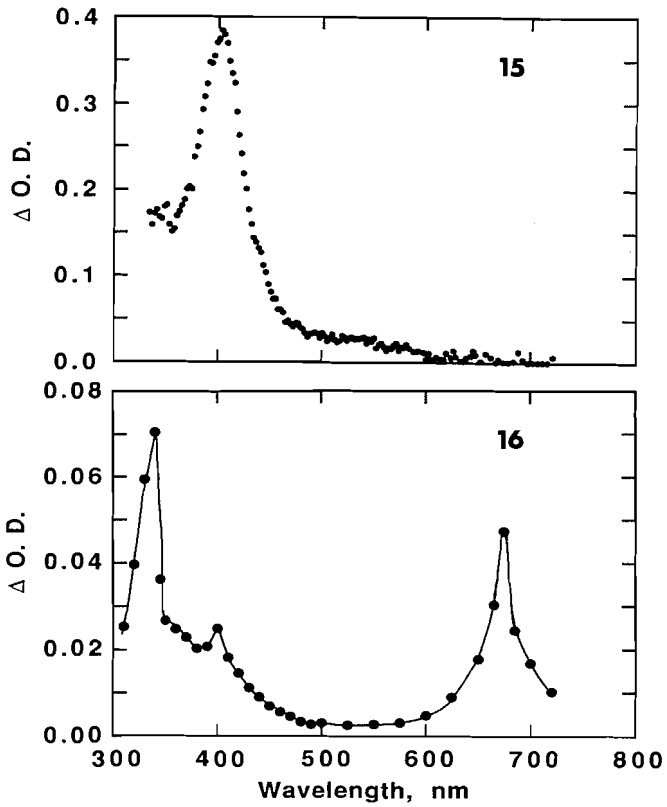

FIG. 3. Spectra of radicals **15** and **16** produced by 308 nm excitation of **2** in deaerated 5% acetonitrile/dioxane and 266 nm excitation of **7** in deaerated acetonitrile, respectively.

[1] 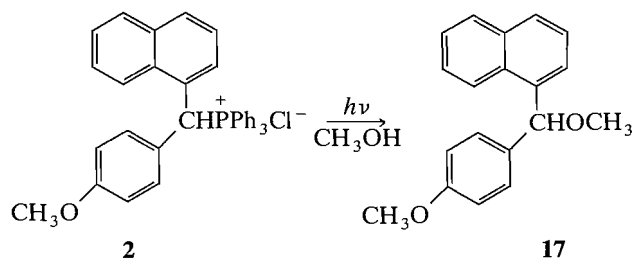

2 **17**

It should be noted that trapping of cation **5** by chloride ion to give **18** might be expected to be a complication in the above quantum yield determinations. However, **18** was not stable in methanol due to its rapid solvolysis to ether **17**. Therefore, the measured quantum yields for ether formation are a suitable measure of the cation yields, since under our reaction conditions trapping by either solvent or chloride will give the same product. Another potential source of error is trapping of the cation by triphenylphosphine accumulated as a product of the reaction. To test whether this was a possible complication the reactivity of cation **6** (generated from chloride **7**) towards triphenylphosphine was examined. A rate constant of 5×10^9 M^{-1} s^{-1} was measured from a plot of the observed rate constant for cation decay as a function of added triphenylphosphine in acetonitrile. However, despite the high rate constant, at low conversions the amount of triphenylphosphine generated would not be able to compete with solvent for trapping of the cation, given the observed 20 ns lifetime for **6** in methanol.[6]

TABLE 3. Yields of cation **5** produced by photolysis of **2** under various conditions

Solvent	Φ	Method[a]
Methanol	0.71	Products
3:7 Methanol/TFE	0.39	Products
3:7 Methanol/TFE	0.18	Transient
TFE	0.15	Transient
Acetonitrile	0.53	Transient
Acetonitrile + 0.1 M $LiClO_4$	0.58	Transient
1:4 Water/acetonitrile	0.53	Transient
1:4 Acetonitrile/dioxane	0.093	Transient
1:4 Acetonitrile/dioxane + 0.1 M $LiClO_4$	0.32	Transient

[a]The quantum yields were determined from product studies or laser flash photolysis measurements.

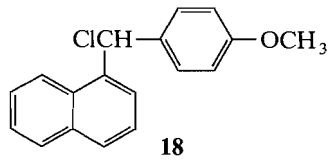

18

The yields of cation **5** in a variety of solvents were measured using transient absorption techniques. This approach has the advantage of being readily applicable to solvents in which complex mixtures of products are formed. The technique requires a suitable actinometer that absorbs in the same region as the cation precursor and knowledge of the extinction coefficient of the cation. Aberchrome-540 (**19**), which undergoes photocyclization with a quantum yield of 0.20 in toluene, was used as the actinometer (31, 32). The extinction coefficient for **5** was measured by generating the cation from the parent alcohol in strong acid. The value of 43 000 M^{-1} cm^{-1} (at 550 nm) used in our experiments was the average of determinations in concentrated sulfuric acid, trifluoroacetic acid, and 1:1 TFE/trifluoroacetic acid, all of which gave similar results. The measured cation yields in various solvents are listed in Table 3. These numbers were calculated assuming that the extinction coefficient of **5** was identical in all the solvents. This is a reasonable assumption based on the fact that the transient spectra in various polar solvents are virtually superimposable with those for the cation in strong acid. Thus, a change in ϵ also implies a change in oscillator strength, which is unlikely (33).

The quantum yields in acetonitrile and aqueous acetonitrile are comparable to the value obtained by product analysis in methanol. It should be noted that the transient measurements are not affected by the decay pathway for the cation, although they will not account for cations that give products within the initial geminate cage. There is a substantial difference between the cation yields measured by transient techniques and product studies for 3:7 methanol/TFE. The lower yields in the transient experiment suggest that, at least in this particular solvent, there is a considerable amount of product formation within the initial geminate cage. Despite this discrepancy between the two methods,

[6]At 5% conversion the concentration of triphenylphosphine would be only 1.5×10^{-4} M, which in combination with the measured rate constant gives $k_{obs} = 7.35 \times 10^5$ s^{-1}. This is almost two orders of magnitude less than the measured rate constant for decay of **5** in methanol (5×10^7 s^{-1}).

Can. J. Chem. Downloaded from www.nrcresearchpress.com by 217.78.4.112 on 09/08/12
For personal use only.

both the transient experiments and the product studies indicate that the cation yields in TFE are significantly lower than those in other solvents. Thus, although TFE stabilizes the cation, less cation is actually generated by photolysis of the phosphonium salt in this solvent.

Salt effects on cation lifetimes and yields

Our previous observation (16) of the remarkable enhancement in cation lifetime in the presence of lithium perchlorate has now been investigated in more detail. Some of these results are tabulated in Table 4 and shown in Fig. 4. For example, the lifetime of **4** increased from 3 to 40 μs in the presence of 0.4 M $LiClO_4$ in acetonitrile, with a concomitant increase of ~80% in the signal intensity. Spectra of the cation in the presence and absence of $LiClO_4$ are shown in Fig. 5 and indicate that there is virtually no effect of the salt on the transient absorption. It should also be noted that the added salt did not have a measurable effect on the ground state absorption of the precursor (**1**). Much more modest effects on both the lifetime and signal intensities were observed in mixed solvents such as 10% aqueous acetonitrile or 15% methanol in acetonitrile and in TFE (Table 4). In acetonitrile, the effect of added $LiClO_4$ starts to appear at ~1×10^{-4} M, at which concentration the cation lifetime has increased by 50%.

The effect of added $LiClO_4$ was also examined in 1:4 acetonitrile/dioxane, under which conditions both radical and cation are readily detectable. In this case the effects were even more dramatic than those outlined above. Figure 6 shows spectra obtained in the mixed solvent with and without 0.2 M $LiClO_4$ under a nitrogen atmosphere. In the presence of perchlorate there is an approximately sevenfold increase in the amount of cation and the radical yield (λ_{max} 400 nm) is substantially lower; most of the radical has disappeared, although overlap of its spectrum with the 360 nm band of the cation would make it difficult to detect a small amount of this species. These results demonstrate that the added salt has a large effect on the processes occurring in the initial geminate cage. Under these conditions the cation lifetime increases from 0.7 μs in the absence of the salt to ~50 μs in the presence of 0.2 M $LiClO_4$. Furthermore, 0.01 M $LiClO_4$ is sufficient to almost completely suppress radical for-

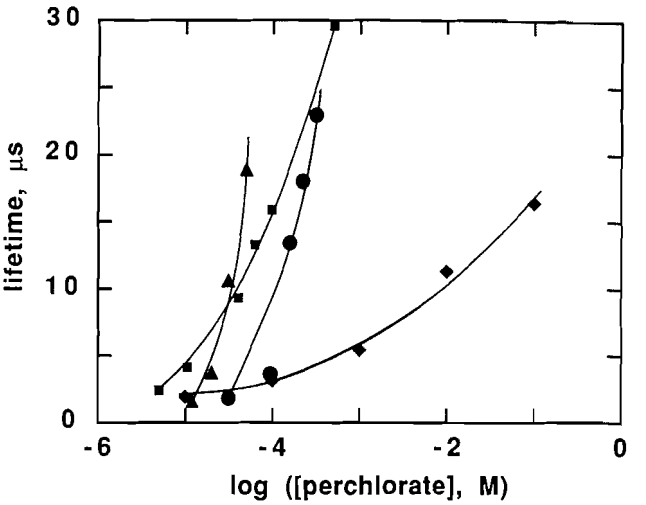

FIG. 4. Effect of added perchlorate salts on the lifetime of **4**: (◆), $LiClO_4$ in acetonitrile; (●) $NaClO_4$ in acetonitrile; (■) $MgClO_4$ in acetonitrile; (▲) $LiClO_4$ in 1:4 acetonitrile/dioxane.

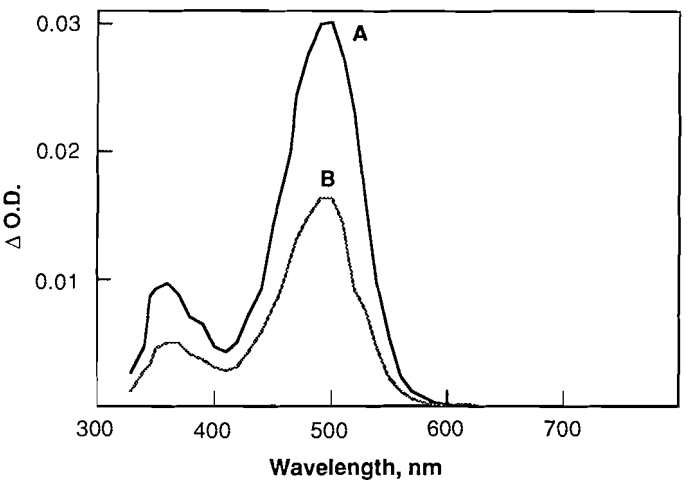

FIG. 5. Transient absorption spectra of **4** in acetonitrile (A) with and (B) without 0.4 M $LiClO_4$.

TABLE 4. Effect of added $LiClO_4$ on the lifetimes and signal intensities of cations **4** and **5** in various solvents

Cation	Solvent	Salt, M	τ, μs[a]	ΔOD
4	Acetonitrile	—	3	0.13
		0.001 M $LiClO_4$	5.4	0.14
		0.4 M $LiClO_4$	40	0.23
	10% Water/ACN	—	7.4	0.15
		0.4 M $LiClO_4$	16	0.19
	15% MeOH/ACN	—	1.6	0.14
		0.4 M $LiClO_4$	4.1	0.175
	20% ACN/dioxane	—	0.7	0.09
		2.9×10^{-4} M $LiClO_4$	16	0.32
		0.2 M $LiClO_4$	48	0.41
	20% Water/TFE	—	25	0.14
		0.4 M $LiClO_4$	27	0.17
5	Acetonitrile	—	0.3	0.34
		0.44 M $LiClO_4$	9.8	0.38
6	Acetonitrile	—	0.55	0.15
		1.4×10^{-3} M $LiClO_4$	0.78	0.17

[a]Typical errors are ±10%.

Can. J. Chem. Downloaded from www.nrcresearchpress.com by 217.78.4.112 on 09/08/12
For personal use only.

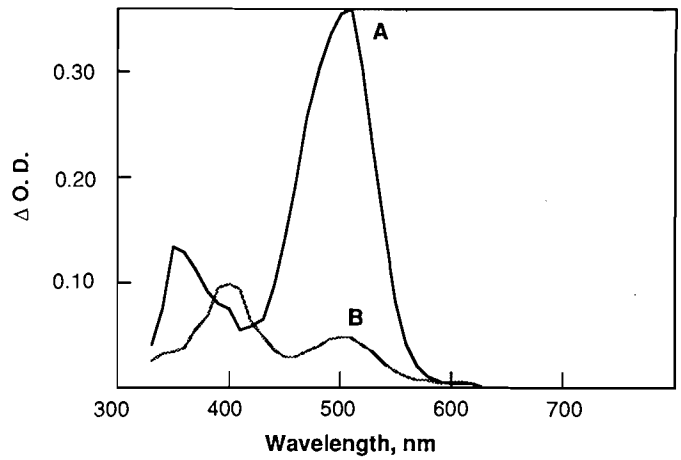

FIG. 6. Transient absorption spectra produced by 308 nm excitation of **1** in 1:4 acetonitrile/dioxane (A) with and (B) without 0.2 M $LiClO_4$.

mation and under these conditions the intensity of the cation signal has only increased by a factor of roughly 2.5. The effects of $LiClO_4$ on the cation lifetime start to appear at much more moderate concentrations than those discussed above. For example, the cation lifetime is already 16 μs at 2.9×10^{-4} M salt (Table 4). The lifetime of the radical is not affected by the addition of salt under any of these conditions.

Similar salt effects were also observed for cation **5**, which had a lifetime of 9.8 μs in the presence of 0.44 M salt in acetonitrile. The quantum yields of cation formation were also measured in acetonitrile and 1:4 acetonitrile/dioxane in the presence of 0.1 M $LiClO_4$ (Table 3). In the former solvent the addition of the salt gave only a modest increase in the yield of cation. In contrast, 0.1 M salt increased the yield of cation by a factor of 3.5 in the mixed solvent.

Sodium and magnesium perchlorates showed similar effects to those discussed above for $LiClO_4$. For the sodium salt the effects of **4** were larger than those for lithium at the same concentration (Fig. 4). This effect is consistent with the degree of dissociation of these salts in acetonitrile (34). A lifetime of 19.5 μs was measured for **4** in acetonitrile containing 10^{-4} M $MgClO_4$. The effect of potassium tetrafluoroborate was also examined. In this case the low solubility of the salt in acetonitrile required the use of a partly aqueous solution. The lifetime for **4** increased from 5.1 μs in 10% aqueous acetonitrile to 5.6 μs in the presence of 3.1×10^{-3} M KBF_4; use of $LiClO_4$ gave identical results.

Reactions of cations with nucleophiles

Rate constants for azide quenching for **4–6** in 10% aqueous trifluoroethanol are listed in Table 2. We also examined the quenching of **4** by azide in other solvents and in the presence of varying amounts of $LiClO_4$; representative plots are shown in Fig. 7. The results demonstrate an order of magnitude difference in the rate constant for azide quenching in going from 5% aqueous acetonitrile (1.8×10^{10} M^{-1} s^{-1}) to 5% aqueous TFE (1.7×10^{9} M^{-1} s^{-1}). Further, the addition of 0.01 and 0.1 M $LiClO_4$ to 5% aqueous acetonitrile causes 2- and 5-fold decreases, respectively, in the azide quenching rate constants.

The effects of the medium on bromide quenching of **4** were also examined and are listed in Table 2. The rate constant in 5% aqueous acetonitrile was close to diffusion controlled and again the measured rate constants were considerably lower in the presence of $LiClO_4$.

Quenching of **4** by chloride ion was examined under a variety of conditions (Table 2). Rate constants of $\sim 2 \times 10^{9}$ M^{-1} s^{-1} were measured for quenching by potassium chloride in 5% aqueous acetonitrile with and without 1.4×10^{-3} M $LiClO_4$. However, the rate constants for chloride quenching were quite sensitive to the water content. For example rate constants of 5.3×10^{9} and 9.5×10^{8} M^{-1} s^{-1} were measured in 3 and 10% aqueous acetonitrile, respectively.

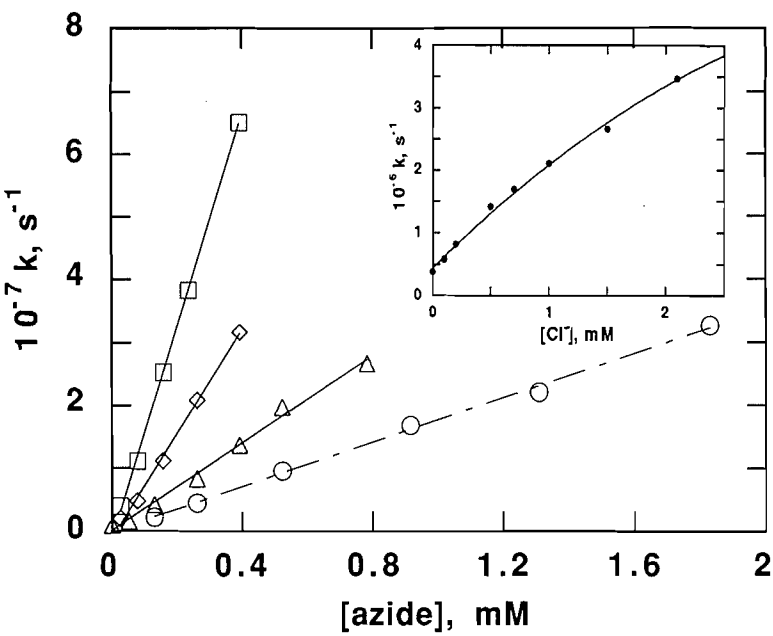

FIG. 7. Plots of the rate constant for decay of **4** as a function of the concentration of azide ion in 5% aqueous acetonitrile (□), 5% aqueous acetonitrile + 0.01 M $LiClO_4$ (◇), 5% aqueous acetonitrile + 0.1 M $LiClO_4$ (△), and 5% aqueous TFE (○); the insert shows the plot obtained for reaction of **4** with lithium chloride in 5% aqueous acetonitrile.

Can. J. Chem. Downloaded from www.nrcresearchpress.com by 217.78.4.112 on 09/08/12
For personal use only.

Can. J. Chem. Downloaded from www.nrcresearchpress.com by 217.78.4.112 on 09/08/12
For personal use only.

In some cases the plots of k_{obs} versus [Cl^-] showed negative curvature at higher concentrations (>1–2 mM; Fig. 7), probably as a result of changes in the ionic strength of the solution due to the addition of the salt. Solubility problems prevented the measurement of a rate constant for chloride quenching in neat acetonitrile. However, addition of 1.3×10^{-4} M lithium chloride to an acetonitrile solution of **1** containing 4.5×10^{-4} M 18-6 crown ether (to solubilize the lithium salt) decreased the lifetime of **4** to 0.56 μs. The crown ether alone had no effect on the cation lifetime. In 5% aqueous acetonitrile a rate constant of $\sim 1.4 \times 10^9$ M^{-1} s^{-1} was measured for quenching by LiCl; a curved quenching plot was obtained in this case and the estimated rate constant is based on the slope (based on a quadratic fit of the data) of the rate constant versus concentration plot at [Cl^-] = 0.

Discussion

The present laser flash photolysis results indicate that photolysis of diarylmethyl triphenylphosphonium salts such as **1–3** produces both radical and cation intermediates, with the relative yields of each depending on the solvent. For example, in polar solvents such as acetonitrile and alcohols these salts give exclusively cation formation, whereas in less polar solvents such as dioxane there are substantial yields of radical. These results are in line with those obtained for irradiation of similar iodonium and sulfonium salts for which heterolytic and homolytic cleavage reactions have been reported (35–37). One advantage of the phosphonium salts is their stability in aqueous and alcohol solvents under conditions where other typically used cation precursors, such as halides, undergo rapid ground state solvolysis.

The various mechanistic possibilities in the photochemistry of the phosphonium salts are outlined in Scheme 1. Note that the phosphonium salts will exist as either fully solvated species or solvent-separated or contact ion pairs, depending on the solvent, although these possibilities are not explicitly shown in the scheme. Cleavage of the C—P bond may occur either homolytically to give a diarylmethyl radical and triphenylphosphine radical cation or heterolytically to yield a diarylmethyl cation and triphenylphosphine. The excited state responsible for the photochemistry must be very short-lived based on the fact that we have been unable to observe any fluorescence that could be reliably assigned to emission from the first excited singlet states of salts **1–3**. This is in line with recent AM1 calculations for substituted arylmethylsulfonium salts that suggest that the lowest excited singlet is a dissociative σ* state centered on the C—S bond rather than a π* state when the aromatic substituent is phenyl, naphthyl, or anthryl (35). A similar ordering of the excited state energy levels has also been postulated for phosphonium salts (35). Further, there is no evidence for the intermediacy of a reactive triplet state for salts **1–3**. In those cases where a triplet has been observed, it is definitely not the precursor to either the cation or radical.

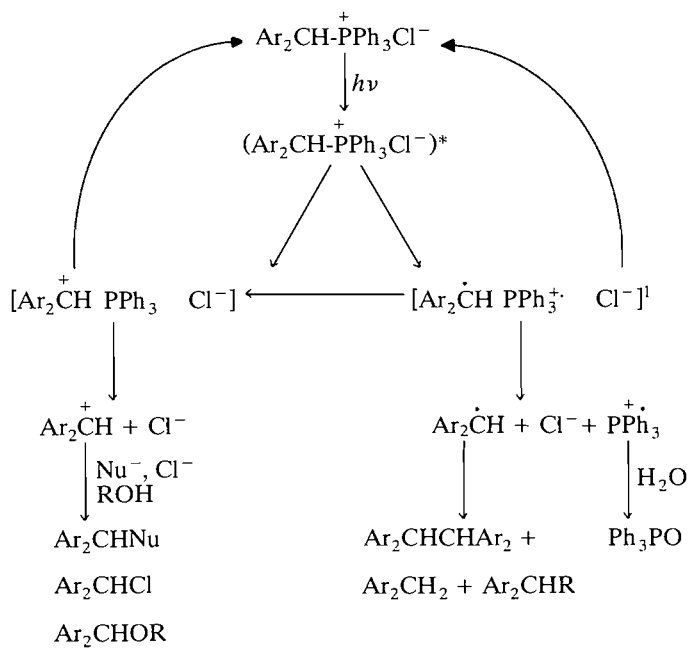

SCHEME 1

An alternate mechanism to heterolytic cleavage to produce the observed diarylmethyl cation is electron transfer within the initial radical/radical cation pair (Scheme 1). Such a pathway has recently been demonstrated to be responsible for cation formation in the photochemical cleavage of a series of substituted 1-naphthylmethyl esters (21). It is therefore of interest to investigate the generality of this process in the formation of carbocation intermediates. In our case an electron transfer pathway would be exothermic by approximately 1 V based on the redox potentials of 1.33 V (acetonitrile, vs. SCE) for triphenylphosphine (38) and 0.2–0.4 V for various substituted diarylmethyl radicals (39). This mechanism would be consistent with the increased yield of carbocation in polar solvents that would stabilize the carbocation. Compare, for example, the data for acetonitrile and 1:4 acetonitrile/dioxane in Table 3.

At first sight the low yield of cation **5** in TFE compared with acetonitrile (Table 3) may appear inconsistent with a mechanism where cation stabilization would determine the efficiency of radical pair to carbocation evolution via electron transfer. However, the dominant effect in this case is probably the difference in viscosity for the two solvents; thus, the viscosity of TFE is 1.99 cP (20°C) compared with 0.36 cP for acetonitrile. Therefore, one should anticipate increased geminate processes (including back reaction) in the case of TFE. The importance of geminate processes in modulating the observable cation yields is also apparent in the differences between "transient" and "product" determinations of quantum yields (see Table 3).

The diarylmethyl cation can decay by a number of pathways. Firstly, recombination with triphenylphosphine within the initial geminate cage can regenerate starting material. Note that the reaction of cation **6** with triphenylphosphine has been shown to occur at close to the diffusion-controlled rate. Secondly, in solvents where the phosphonium salt exists as ion pairs, reaction with chloride ion may also compete with cage escape. The cation can also be trapped with external nucleophiles such as solvent. The discrepancy between the cation yields measured by product studies and transient techniques for **5** in methanol/TFE suggests that there is a substantial fraction of the initial cations that reacts rapidly within the solvent cage to give product and, as a consequence, is not detectable in the transient experiments. This provides support for reaction with chloride before cage escape since trapping by triphenylphosphine would not account for the differences between the two methods for

Can. J. Chem. Downloaded from www.nrcresearchpress.com by 217.78.4.112 on 09/08/12
For personal use only.

estimating the cation yields and since the cation lifetime (0.65 μs, Table 1) in this solvent is too long for methanol trapping to compete efficiently with cage escape.

The present results show that there are substantial effects of solvent and added salts on both the yields and lifetimes of cations **4**–**6**. For example, the yield of cation **5** varies from 0.71 in methanol to 0.093 in the less polar solvent 1:4 acetonitrile/dioxane. These observations could be explained by changes in the rate of the initial cleavage, the electron transfer, or the back reaction to regenerate starting material, or by some combination of these factors. The effects of added perchlorate salt on the cation yields are modest (≤20% increases, Table 4) in alcohols and acetonitrile and aqueous mixtures of these solvents, presumably due to efficient solvation of the ions in these solvents. However, the addition of even low concentrations of perchlorate (e.g., 0.29 mM) to 1:4 acetonitrile/dioxane leads to over a threefold enhancement in the yield of cation. In this less polar solvent the effect is best explained on the basis of replacement of chloride by perchlorate in the initial phosphonium salt ion pairs. The subsequent stabilization of the cation by the nonnucleophilic perchlorate ion prevents reaction with chloride or back reaction with triphenylphosphine. Note that stabilization of the triphenylphosphine radical cation by perchlorate may also lead to less back reaction from the radical/radical ion pair and this may be a factor if some or all of the cation is formed via the electron transfer route. The results shown in Fig. 6 for **4** indicate that the increased cation yield in the presence of perchlorate in acetonitrile/dioxane is accompanied by a concomitant decrease in the radical yield. This is consistent with homolytic cleavage to give a radical/radical cation pair, followed by electron transfer. The results also demonstrate the important role that salts can play in determining the outcome of cage processes.

The cation lifetimes tabulated in Table 1 are in many cases limited by reaction with the chloride counterion of the precursor salt. However, the short lifetimes in methanol reflect predominantly reaction of the cation with solvent. The unusual effects of water on the lifetime of **4** are also explicable on the basis of changes in the rate constants for chloride quenching for the various solvents. For example, the rate constant for reaction of **4** with chloride ion decreases by a factor of 5.6 when the water content is increased from 3 to 10%. Thus, the apparent increases in the cation lifetime in the presence of water are a result of the lower efficiency of chloride ion quenching in aqueous solution. For example, if we assume that in 5% aqueous acetonitrile all of the chloride counterions are available for quenching, then at 4×10^{-5} M salt precursor the rate for chloride quenching would be $\sim 10^6$ s^{-1}. The same calculation for 10% water gives a rate of 7.6×10^4 s^{-1}. The addition of perchlorate ion also has a substantial effect on the lifetimes of **4**–**6**, even at submillimolar concentration. These effects probably reflect a combination of both stabilization of the cation by ion pairing with the nonnucleophilic perchlorate anion and of ionic strength effects at higher salt concentrations.

The data in Table 4 demonstrate that there are very substantial effects of both solvent and added salt on the measured rate constants for reaction of **4** with nucleophiles. For example, even for azide ion the rate constants vary by over an order of magnitude in comparing aqueous acetonitrile and TFE. These effects are in line with those recently reported for substituent and solvent effects on the reactivities of triarylmethyl and diarylmethyl carbocations (40). Further, the addition of 0.1 M perchlorate decreases the rate constant for azide quenching by a factor of five in 5% aqueous acetonitrile. These effects are of considerable importance given the frequent assumption of a diffusion-controlled rate constant of 5×10^9 M^{-1} s^{-1} for reaction of azide with various cations and the use of this number as a "clock" to obtain absolute rate constants from product ratios measured in competitive experiments (41, 42).

Experimental

Materials and general techniques

Spectrograde solvents (Aldrich or BDH) and triphenylphosphine were used as received. Lithium, sodium, and magnesium perchlorates (Aldrich, anhydrous) were stored in a desiccator. Lithium chloride was dried at 160°C for 20 h and stored in a desiccator over P_2O_5. GC analyses were done on a Perkin–Elmer 8320 gas chromatograph with a 12-m BP1 on vitreous silica column. HPLC measurements were carried out on a Hewlett–Packard 1090 liquid chromatograph equipped with a diode array detector and a reverse-phase column (RP-18; 5 μm). Methanol/water solvent mixtures were used; analysis of the phosphonium salts required the addition of 4×10^{-3} M sodium dodecyl sulfate to the methanol. GC/MS measurements were done on a Hewlett–Packard 5995 instrument. NMR spectra were recorded on a Varian 200 MHz instrument. UV–visible spectra were measured using a Hewlett–Packard 8451A diode array spectrometer.

Synthesis

Phosphonium salts were synthesized by refluxing a mixture of the corresponding chlorides and triphenylphosphine (30% excess) for 12 h in benzene or toluene. In most cases the salt precipitated during the reaction or upon cooling and was filtered, washed with benzene or ether, and recrystallized from isopropanol/ethyl ether. The chlorides were obtained by refluxing the corresponding alcohols with thionyl chloride in benzene for 1.5 h and were recrystallized from hexane. The alcohol precursors for salts **1** and **2** were obtained by Grignard reactions of 4-methoxy-1-naphthaldehyde (**1**) with phenylmagnesium bromide and *p*-anisaldehyde (**2**) with 1-naphthylmagnesium bromide. The alcohol precursors for salts **3** and **9** were prepared by sodium borohydride reduction of the commercially available ketones. Analytical data for the various salts and chlorides are listed below.

Salt **1**: mp 183°C (dec.); ^{1}H NMR($CDCl_3$) δ(ppm): 8.6 (d, 1H), 8.3–6.5 (m, 26H), 3.9 (s, 3H). Anal. calcd. for $C_{36}H_{30}OPCl$: C 79.33%, H 5.55%; found: C 79.50%, H 5.66%.

Salt **2**: mp 160°C (dec.); ^{1}H NMR($CDCl_3$) δ(ppm): 8.8 (d, 1H), 7.8–6.6 (m, 26 H), 3.7 (s, 3H). Anal. calcd. for $C_{36}H_{30}OPCl$: C 79.33%, H 5.55%; found: C 79.15%, H 5.61%.

Salt **3**: mp 220°C (dec.); ^{1}H NMR($CDCl_3$) δ(ppm): 8.8 (d, 1H), 7.9–7.2 (m, 27H), 4.0 (s, 1H), 1.2 (d, 6H). Anal. calcd. for $C_{35}H_{28}PCl \cdot C_3H_8O$: C 79.36%, H 6.31%; found: C 79.03%, H 6.39%.

Chloride **7**: mp 70–72°C; ^{1}H NMR($CDCl_3$) δ(ppm): 7.9–7.2 (m, 12H), 6.3 (s, 1H). Anal. calcd. for $C_{17}H_{13}Cl$: C 80.79%, H 5.18%; found: C 81.00%, H 5.34%.

Chloride **8**: mp 117–121°C; ^{1}H NMR($CDCl_3$) δ(ppm): 8.3–6.7 (m, 11 H), 6.8 (s, 1H), 4.0 (s, 3H). Anal. calcd. for $C_{18}H_{15}OCl$: C 76.46%, H 5.35%, found: C 76.35%, H 5.47%.

Salt **9**: mp (dec.); ^{1}H NMR($CDCl_3$) δ(ppm): 8.3 (d, 1H), 7.8–6.6 (m, 23H), 3.7 (s, 6H). Anal. calcd. for $C_{33}H_{30}O_2PCl$: C 75.49%, H 5.76%; found C 73.41%, H 5.78%.

Salt **11**: mp 241–242°C (dec.); ^{1}H NMR($CDCl_3$) δ(ppm): 8.2–6.5 (m, 21H), 5.8 (s, 2H), 3.9 (s, 3H). Anal. calcd. for $C_{30}H_{26}OPCl$: C 76.83%, H 5.59%; found: C 77.09%, H 5.75%.

Laser flash photolysis

Detailed descriptions of the laser flash photolysis system have been published (43, 44). For these experiments either a Lumonics

TE-860-2 excimer laser with a Xe-HCl gas mixture (308 nm; ~5-ns pulses; <20 mJ/pulse) or a Lumonics HY750 Nd:YAG (fourth harmonic, 266 nm; 10-ns pulses; <25 mJ/pulse) was used for excitation. The samples were contained in 7 × 7 mm^2 quartz flow cells. The use of flow samples was essential to prevent signals due to the buildup of photoproducts. Samples were either aerated or were purged with nitrogen. Some of the transient spectra were recorded using an EG&G gated intensified optical multichannel analyzer equipped with a 20-ns gate.

The yields of cation **5** were determined by preparing samples of **2** and the actinometer (Aberchrome-540) with matched optical densities at 308 nm. The signals due to **5** at 550 nm and the colored form of Aberchrome-540 at 494 nm were then measured as a function of the laser intensity. The ratio of optical densities was taken as the slopes of the ΔOD versus laser intensity plots, extrapolated to zero laser intensity.

Product studies

Preparative photolysis of salt 2

A solution of **2** in methanol (250 mL, 3.7 × 10^{-3} M) was deaerated by nitrogen purging and irradiated for 3 h using 300-nm Rayonet lamps. The ether photoproduct (**17**) was isolated by column chromatography on silica using ethyl acetate/hexane mixtures and was further purified by chromatography on a Chromatotron (5% ethyl acetate/hexane). It was obtained as a colorless oil; GC/MS: *m/e* 278 (M^+).

Quantum yields

Samples of salt **2** in methanol (1 mL, 2.9 × 10^{-3} M) and valerophenone in cyclohexane (6.7 × 10^{-2} M) with matched optical densities at 313 nm were degassed by purging with nitrogen. The samples were irradiated in a merry-go-round in front of a Hanovia 200-W Hg/Xe lamp with a neutral density filter and a potassium chromate filter solution to isolate the 313-nm line. The valerophenone actinometer solutions were irradiated 1.5 h and the salt solutions for periods of 2–5 min at the beginning, middle, and end of the actinometer irradiations. An internal standard (biphenyl) was added to the irradiated salt solutions and they were analyzed by HPLC, using mixtures of pure compounds for calibration purposes. The production of acetophenone (Φ = 0.40) from the actinometer samples was measured by GC with hexadecane as the internal standard.

Can. J. Chem. Downloaded from www.nrcresearchpress.com by 217.78.4.112 on 09/08/12
For personal use only.

Acknowledgements

Thanks are due to G. Charette and S. Sugamori for technical assistance and to Dr. R. A. McClelland for a sample of 4-methoxy-1-naphthylmethyl ammonium chloride and for helpful discussions. EOA thanks Capes (Brazil) for a graduate "sandwich" fellowship.

1. L. M. Dorfman, R. J. Sujdak, and B. Bockrath. Acc. Chem. Res. **9**, 352 (1976).
2. F. I. M. V. Ginkel, R. J. Visser, C. A. G. O. Varma, and G. Lodder. J. Photochem. **30**, 453 (1985).
3. R. A. McClelland, N. Banait, and S. Steenken. J. Am. Chem. Soc. **108**, 7023 (1986).
4. R. A. McClelland, V. M. Kanagasabapathy, N. S. Banait, and S. Steenken. J. Am. Chem. Soc. **111**, 3966 (1989).
5. S. L. Mecklenburg and E. F. Hilinski. J. Am. Chem. Soc. **111**, 5471 (1989).
6. R. A. McClelland, N. Banait, and S. Steenken. J. Am. Chem. Soc. **111**, 2929 (1989).
7. S. Steenken and R. A. McClelland. J. Am. Chem. Soc. **111**, 4967 (1989).
8. L. J. Johnston, J. Lobaugh, and V. Wintgens. J. Phys. Chem. **93**, 7370 (1989).
9. E. Gaillard, M. A. Fox, and P. Wan. J. Am. Chem. Soc. **111**, 2180 (1989).
10. J. Bartl, S. Steenken, H. Mayr, and R. A. McClelland. J. Am. Chem. Soc. **112**, 6918 (1990).
11. R. A. McClelland, N. Mathivanan, and S. Steenken. J. Am. Chem. Soc. **112**, 4857 (1990).
12. R. A. McClelland, F. Cozens, and S. Steenken. Tetrahedron, **31**, 2821 (1990).
13. S. Steenken and R. A. McClelland. J. Am. Chem. Soc. **112**, 9648 (1990).
14. V. B. Ivanov. Mol. Photochem. **6**, 125 (1974).
15. R. E. Minto and P. K. Das. J. Am. Chem. Soc. **111**, 8858 (1989).
16. E. O. Alonso, L. J. Johnston, J. C. Scaiano, and V. G. Toscano. J. Am. Chem. Soc. **112**, 1270 (1990).
17. G. H. Slocum, K. Kaufmann, and G. B. Schuster. J. Am. Chem. Soc. **103**, 4625 (1981).
18. G. H. Slocum and G. B. Schuster. J. Org. Chem. **49**, 2177 (1984).
19. B. Arnold, L. Donald, A. Jurgens, and J. A. Pincock. Can. J. Chem. **63**, 3140 (1985).
20. B. Foster, B. Gaillard, N. Mathur, A. L. Pincock, J. A. Pincock, and C. Sehmbey. Can. J. Chem. **65**, 1599 (1987).
21. D. P. DeCosta and J. A. Pincock. J. Am. Chem. Soc. **111**, 8948 (1989).
22. B. Hall and P. Wan. J. Photochem. Photobiol. A: Chem. **56**, 35 (1991).
23. I. Carmichael and G. L. Hug. J. Phys. Chem. Ref. Data, **15**, 1 (1986).
24. L. J. Johnston and J. C. Scaiano. J. Am. Chem. Soc, **107**, 6368 (1985).
25. J. C. Scaiano, M. Tanner, and D. Weir. J. Am. Chem. Soc. **107**, 4396 (1985).
26. (*a*) S. Steenken, C. J. Warren, and B. C. Gilbert. J. Chem. Soc. Perkin Trans. **2**, 335 (1990); (*b*) M. Tsuchiya, T. W. Ebbesen, Y. Nishimura, H. Sakuragi, and K. Tokumaru. Chem. Lett. 2121 (1987).
27. D. Weir, L. J. Johnston, and J. C. Scaiano. J. Phys. Chem. **92**, 1742 (1988).
28. H. Ohmori, S. Nakai, and M. Masui. J. Chem. Soc. Perkin Trans. **1**, 1333 (1978).
29. P. J. Wagner. J. Am. Chem. Soc. **89**, 5898 (1967).
30. P. J. Wagner, P. A. Kelso, A. E. Kemppainen, and R. G. Zepp. J. Am. Chem. Soc. **94**, 7500 (1972).
31. H. G. Heller and J. R. Langan. J. Chem. Soc. Perkin Trans. **2**, 341 (1981).
32. V. Wintgens, L. J. Johnston, and J. C. Scaiano. J. Am. Chem. Soc. **110**, 511 (1988).
33. R. Bensasson and E. J. Land. Trans. Faraday Soc. **67**, 1904 (1971).
34. C. H. Springer, J. F. Coetzee, and R. L. Kay. J. Phys. Chem. **73**, 471 (1969).
35. F. D. Saeva, D. T. Breslin, and P. A. Martic. J. Am. Chem. Soc. **111**, 1328 (1989).
36. R. J. DeVoe and M. R. V. Sahyun. Can. J. Chem. **65**, 2342 (1987).
37. J. L. Dektar and N. P. Hacker. J. Org. Chem. **55**, 639 (1990).
38. M. Culcasi, G. Gronchi, and P. Tordo. Phosphorus Sulfur **30**, 511 (1987).
39. D. D. M. Wayner, D. J. McPhee, and D. Griller. J. Am. Chem. Soc. **110**, 132 (1988).
40. R. A. McClelland, V. M. Kanagasabapathy, N. S. Banait, and S. Steenken. J. Am. Chem. Soc. **113**, 1009 (1991).
41. J. P. Richard. J. Am. Chem. Soc. **111**, 1455 (1989).
42. T. L. Amyes and W. P. Jencks. J. Am. Chem. Soc. **111**, 7888 (1989).
43. J. C. Scaiano. J. Am. Chem. Soc. **102**, 7747 (1980).
44. S. Kazanis, A. Azarani, and L. J. Johnston. J. Phys. Chem. **95**, 4430 (1991).

Crystal structures of $(n\text{-}Pr_4N)_2SnCl_6$, $(n\text{-}Pr_4N)[TeCl_4(OH)]$, $(n\text{-}Pr_4N)_2[Te_2Cl_{10}]$ (nominal), and $(n\text{-}Pr_4N)_2[Se_2O_2Cl_6]$, with observations on $Z_2L_{10}^{2n-}$ and $Z_2L_8^{2-}$ dimers in general

MARGARET ANN JAMES
Chemistry Department, Mount Saint Vincent University, Halifax, N.S., Canada B3M 2J6

AND

OSVALD KNOP[1] AND T. STANLEY CAMERON
Department of Chemistry, Dalhousie University, Halifax, N.S., Canada B3H 4J3

Received June 27, 1991

This paper is dedicated to Professor Kurt Dehnicke on the occasion of his 60th birthday

MARGARET ANN JAMES, OSVALD KNOP, and T. STANLEY CAMERON. Can. J. Chem. **70**, 1795 (1992).

The crystal structures of the following four compounds have been determined: $(n\text{-}Pr_4N)_2SnCl_6$ (**A**; *Pbca*, a = 29.073 Å, b = 15.825 Å, c = 14.851 Å, Z = 8), $(n\text{-}Pr_4N)[TeCl_4(OH)]$ (**B**; $C2/c$ or Cc, a = 10.800 Å, b = 17.429 Å, c = 10.604 Å, β = 93.81°, Z = 4), $(n\text{-}Pr_4N)_2[Te_2Cl_{10}]$ (**C**, nominal composition; $P\bar{1}$, a = 9.635 Å, b = 10.900 Å, c = 11.547 Å, α = 73.34°, β = 70.44°, γ = 68.15°, Z = 1), and $(n\text{-}Pr_4N)_2[Se_2O_2Cl_6]$ (**D**; $P\bar{1}$, a = 9.252 Å, b = 11.691 Å, c = 18.304 Å, α = 110.18°, β = 92.57°, γ = 97.72°, Z = 2). **B** contains a square-pyramidal $TeCl_4(OH)^-$ anion. The actual composition of the centrosymmetric μ_2-dimer in **C** is $Te_2Cl_8(Cl, OH)_2^{2-}$, the replacement of Cl by OH being at the axial ligand positions of the $TeCl_5^-$ halves of the dimer. In the centrosymmetric μ_2-$Se_2O_2Cl_6^{2-}$ dimer in **D** the Se—O bonds are perpendicular to the $Se(Cl)_2Se$ bridge plane and *trans* to the presumed lone-electron pairs on the Se atoms. It is shown that the Z—Hal bonds in the known centrosymmetric homoligand μ_2-$Z_2Hal_{10}^{2n-}$ (Z = Se, Te) and μ_2-$Z_2Hal_8^{2-}$ (Z = As, Sb, Bi) as well as in the μ_2-$Se_2O_2Hal_6^{2-}$ dimers exhibit a uniform stereochemistry, in which the d(Z—Hal) bond lengths in pairs of opposing bonds *trans* to each other are consistently related by the *trans* effect (TE). Empirical quantification of Te for the Se and Te dimers is exploited to authenticate the composition of the dimer in situations where the nature of the ligand is in doubt (in the present case on partial hydrolysis). The asymmetry of the $Z(Hal)_2Z$ double bridge is examined in relation to the overall stereochemistry of the dimer. Also examined are circumstances that may lead to the occurrence, in a crystal, of a $Z_2Hal_{10}^{2n-}$ dimer on the one hand and of a discrete $ZHal_5^{n-}$ monomer on the other, in situations which otherwise are chemically closely similar. TLS analysis of the thermal motion is used to judge the strength of association of the two monomer halves in a μ_2-dimer, with results that are important when correcting bond lengths for the effects of thermal motion. A variety of general observations on μ_2-dimers in crystals is proffered for good measure.

MARGARET ANN JAMES, OSVALD KNOP et T. STANLEY CAMERON. Can. J. Chem. **70**, 1795 (1992).

On a déterminé les structures cristallines des quatre composés suivants: $(n\text{-}Pr_4N)_2SnCl_6$ (**A**; *Pbca*, a = 29,073, b = 15,825 et c = 14,851 Å, Z = 8), $(n\text{-}Pr_4N)[TeCl_4(OH)]$ (**B**; $C2/c$ ou Cc, a = 10,800, b = 17,429 et c = 10,604 Å, β = 93,81°, Z = 4), $(n\text{-}Pr_4N)_2[Te_2Cl_{10}]$ (**C**, composition nominale; $P\bar{1}$, a = 9,635, b = 10,900 et c = 11,547 Å, α = 73,34, β = 70,44 et γ = 68,15°, Z = 1) et $(n\text{-}Pr_4N)[Se_2O_2Cl_6]$ (**D**; $P\bar{1}$, a = 9,252, b = 11,691 et c = 18,304 Å, α = 110,18, β = 92,57 et γ = 97,72°, Z = 2). Le composé **B** contient un anion $TeCl_4(OH)^-$ à pyramide carrée. La composition réelle du dimère-μ_2 centrosymétrique du produit **C** est $Te_2Cl_8(Cl,OH)_2^{2-}$, le OH qui remplace le Cl se trouvant dans les positions des ligands axiaux des portions $TeCl_5^-$ du dimère. Dans le dimère centrosymétrique μ_2-$Se_2O_2Cl_6^{2-}$ du composé **D**, les liaisons Se—O sont perpendiculaires au plan du pont $Se(Cl)_2Se$ et *trans* par rapport aux présumées paires d'électrons libres sur les atomes de Se. On a montré que les liaisons Z—Hal dans les dimères centrosymétriques homoligand μ_2-$Z_2Hal_{10}^{2n-}$ (Z = As, Sb, Bi) et μ_2-$Z_2Hal_8^{2-}$ (Z = Se, Te) connus ainsi que les dimères μ_2-$Se_2O_2Hal_6^{2-}$ présentent une stéréochimie uniforme dans laquelle les longueurs des liaisons d(Z—Hal) dans les paires des liaisons *trans* s'opposant les unes aùx autres sont toujours liées par l'effet *trans* (TE). On exploite une quantification empirique du TE pour les dimères du Se et du Te pour authentifier la composition de dimères dans des situations où la nature du ligand n'est pas certaine (dans le cas examiné ici, il s'agit du produit d'hydrolyse partielle). On a examiné l'asymétrie du double pont $Z(Hal)_2Z$ en rapport avec la stéréochimie globale du dimère. On a aussi examiné les circonstances qui peuvent conduire, dans un cristal, à la présence d'une part d'un dimère $Z_2Hal_{10}^{2n-}$ et d'un monomère $ZHal_5^{n-}$ individuel, dans des conditions chimiques qui sont par ailleurs chimiquement semblables. On a utilisé l'analyse TLS du mouvement thermique pour juger de la force de l'association de deux parties de monomères dans un dimère-μ_2; les résultats sont importants pour corriger les longueurs de liaison pour les effets des mouvements thermiques. On présente aussi un nombre d'observations générales sur dimères-μ_2 dans les cristaux.

[Traduit par la rédaction]

In the course of investigating the actual geometry of octahedral 12- and 14-valence-electron ML_6^{n-} anions in crystals (cf. ref. 1) we obtained, serendipitously, several tetra-*n*-propylammonium salts not useful for the intended purpose but interesting in their own right. Preliminary crystallographic studies showed three of them (see title) to contain uncommon Se(IV)- and Te(IV)-derived anions and thus to merit closer investigation. The crystal structures of these salts, together with that of $(n\text{-}Pr_4N)_2SnCl_6$ (**A**), are described below and the stereochemistry of the anions is compared with that previously reported in the literature. The conditions under which the three salts were formed were ill-

[1]Author to whom correspondence may be addressed.

Can. J. Chem. Downloaded from www.nrcresearchpress.com by 217.78.4.112 on 09/08/12
For personal use only.

Can. J. Chem. Downloaded from www.nrcresearchpress.com by 217.78.4.112 on 09/08/12
For personal use only.

TABLE 1. Crystal data[a] of $(n\text{-Pr}_4N)_2SnCl_6$ (**A**), $(n\text{-Pr}_4N)[TeCl_4(OH)]$ (**B**), $(n\text{-Pr}_4N)_2[Te_2Cl_{10}]$[b] (**C**), and $(n\text{-Pr}_4N)_2[Se_2O_2Cl_6]$ (**D**)

Parameter	A	B	C	D
Formula	$C_{24}H_{56}Cl_6N_2Sn$	$C_{12}H_{29}Cl_4NOTe$[c]	$C_{24}H_{56}Cl_{10}N_2Te_2$	$C_{24}H_{56}Cl_6N_2O_2Se_2$
f.w.	704.1	472.8	982.5	775.2
θ range, deg	2–23	2–23	2–23	3–25
μ_{Mo}, cm^{-1}	12.4	20.3	20.7	24.6
Max/min[d]	1.402/0.779	1.266/0.792	1.426/0.509	1.956/0.525
a, Å	29.073(8)[e]	10.800(3)	9.635(2)	9.252(4)
b, Å	15.826(4)[e]	17.429(3)	10.900(2)	11.691(7)
c, Å	14.851(5)[e]	10.604(2)	11.547(2)	18.304(9)
α, deg	90	90	73.34(1)	110.18(4)
β, deg	90	93.81(2)	70.44(1)	92.57(4)
γ, deg	90	90	68.15(2)	97.72(4)
V, $Å^3$	6833(6)	1992(2)	1042(1)	1833(3)
Z	8	4	1	2
ρ_c, g/cm^3	1.369(1)[f]	1.577(2)	1.566(2)	1.405(2)
Space group	*Pbca* (no. 61)	*C*2/*c* (no. 15)	$P\bar{1}$ (no. 2)	$P\bar{1}$ (no. 2)
F(000), e	2928	944	488	800
Reflections:				
total measured	6168	1703	3037	6703
unique total	4709	1382	2872	6425
unique used	3178[g]	1005[g]	2384[g]	3092[h]
$100R_{merg}$	4.84	3.01	1.23	2.64
d/p	10.6	9.1	13.5	8.1
$100R$; $100R_w$	5.8; 6.7	4.6; 5.4	6.2; 6.9	9.4; 10.0
G.O.F.	1.11	2.16	4.85	0.89

[a]Mo $K\alpha_1$, λ = 0.70926 Å (graphite monochromator); $T \sim 18°C$.
[b]Nominal composition; partially hydrolyzed. In refinement, all ligands assumed to be Cl; for alternative refinements see text.
[c]Disorder in anion. For refinement of the ordered structure in *Cc* see text.
[d]Max/min empirical absorption corrections, cf. ref. 3.
[e]The axial ratio from optical measurements in ref. 4 is 0.7852:1:1.8018.
[f]ρ_o = 1.356 g/cm^3 (21°C). Ries (5) gives 1.314 g/cm^3 for his orthorhombic (D_{2h}) and 1.548 g/cm^3 for his triclinic form.
[g]$I > 2\sigma(I)$.
[h]$I > 3\sigma(I)$.

defined; the complexity of the solution and crystal chemistry of such anionic species, which is reflected in their compositions, can be gleaned from the recent review by Krebs and Ahlers (2) and from the references therein. Nor were the determinations of these three structures without problems, though in the end having to deal with some of the complications was repaid by a broadened chemical insight.

Preliminary observations (Sect. I) are followed by a description and discussion of the crystal structures of the title compounds (Sect. II) and by observations on the structural aspects of $Z_2Hal_{10}^{2n-}$, $Z_2Hal_8^{2-}$, and $Se_2O_2Hal_6^{2-}$ (Z = Se, Te; As, Sb, Bi) dimers (Sect. III). Experimental detail is relegated to the end of the paper (Sect. IV). Where no reference is given the result is from the present investigation. All bond lengths quoted are uncorrected for thermal motion except where stated otherwise; the appropriateness of corrections is discussed in Sect. III. The abbreviations TE and RBM stand for the *trans* effect and for rigid-body motion, respectively.

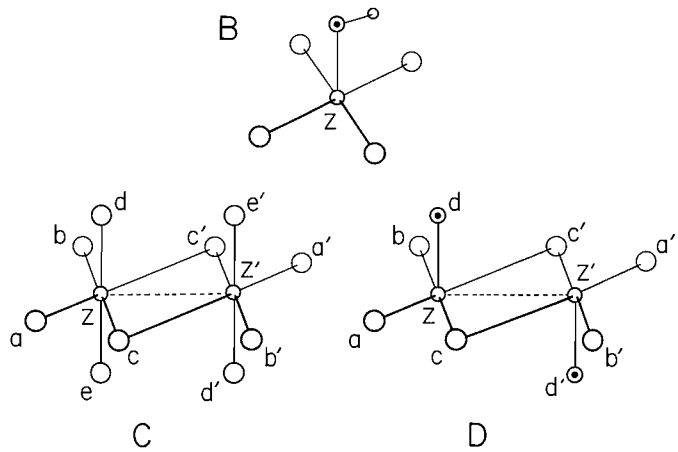

FIG. 1. Standardized anion configurations (schematic): $ZL'L_4^{n-}$ (in **B**, $TeCl_4(OH)^-$), $Z_2L_{10}^{2n-}$ (in **C**, nominally $Te_2Cl_{10}^{2-}$, actually $Te_2Cl_8(Cl, OH)_2^{2-}$ with L_a, L_a' mixed ligands), and $Z_2L'_2L_6^{n-}$ (in **D**, $Se_2O_2Cl_6^{2-}$). The longest Z–L distance in the dimers is Z–L_c'.

I. Preliminary observations

The crystal data of the title compounds are assembled in Table 1. Standard execution of the structure determinations (supported by evidence from ir spectra, see Sect. IV) showed unambiguously that the structures of **A** and **B** corresponded to the stated compositions. The structures of **C** and **D** turned out to contain centrosymmetric dimers $Te_2Cl_{10}^{2-}$ and $Se_2O_2Cl_6^{2-}$, respectively (Fig. 1). This finding was unexpected but accepted as correct, since the existence of these

TABLE 2. Bond lengths and interatomic distances (Å) in $Z_2Hal_{10}^{2-}$ and $Se_2O_2Hal_6^{2-}$ dimers (cf. Fig. 1)

Code	Cation	d_a	d_b	d_c	d_c'	d_d	d_e	Z···Z'
				$SeCl_{10}^{2-}$				
Ca	Ph_4As (−130°C) (14)	2.217(3)	2.306(3)	2.519(2)	2.803(1)	2.401(2)	2.344(2)	3.881
Cb	$C_{14}H_{13}ClN_3$ (13)[a]	2.210(2)	2.208(2)	2.725(2)	2.733(2)	2.384(2)	2.380(2)	3.970
Cc	S_4N_3 (15)	2.189(2)	2.222(3)	2.688(2)	2.816(3)	2.338(2)	2.417(2)	4.113
Cd	Et_4N (−133°C) (*)[b]	2.205(3)	2.265(3)	2.576(3)	2.799(3)	2.382(2)	2.382(2)	4.065
				$Se_2Br_{10}^{2-}$				
Ce	Et_4N (−20°C) (*)	2.393(3)	2.432(4)	2.756(4)	2.877(4)	2.556(3)	2.556(3)	4.239(4)
				Pseudo $Te_2F_{10}^{2-}$				
Cf	Et_4N (2, *)	1.872	1.958	1.961	3.186	1.944	1.936	4.229
Cg	Cs (16)	1.81(2)	1.91(1)	1.95(1)	3.11	1.91(1)	1.95(1)	4.31
				$Te_2Cl_{10}^{2-}$				
Ch	Ph_4As (−130°C) (12)	2.336(1)	2.436(1)	2.653(1)	3.010(1)	2.517(1)	2.478(1)	4.033(1)
Ci	Ph_3PCl (*)	2.353(5)	2.407(5)	2.704(6)	2.950(6)	2.507(5)	2.479(5)	4.040
Cj1	Ph_4As (6, 7, *)[c]	2.162(7)	2.458(4)	2.570(4)	3.306(4)	2.505(3)	2.452(3)	4.430(3)
Cj2		2.310(3)	2.406(4)	2.692(4)	2.945(4)	2.485(3)	2.484(4)	4.153(3)
C	*n*-Pr_4N (this work)[c]	2.312(4)	2.456(3)	2.564(3)	3.241(5)	2.465(3)	2.484(3)	4.418(3)
				$Te_2Br_{10}^{2-}$				
Ck	Ph_4P (8)	2.530(2)	2.579(2)	2.876(2)	3.000(2)	2.698(2)	2.648(2)	4.213
Cm	Et_4N (2, *)	2.569	2.566	2.920	2.930	2.671	2.689	4.327
				$Te_2I_{10}^{2-}$				
Cn	(*p*-tolyl)Et_3N (2, *)	2.791	2.841	3.069	3.186	2.933	2.946	4.609
Co	Et_4N (*)	2.822	2.824	3.096	3.129	2.916	2.943	4.575
				$Se_2O_2Cl_6^{2-}$				
Da	Et_4N (11)	2.270(1)	2.351(2)	2.698(1)	2.920(1)	1.589(4)[d]	—	4.288
Db	Ph_4P (10)	2.266 (2)	2.329(2)	2.667(1)	2.851(1)	1.597(4)[d]	—	4.133
D1	*n*-Pr_4N (this work)	2.278(5)	2.357(4)	2.645(4)	2.940(5)	1.59(1)[d]	—	4.163(3)
D2		2.249(5)	2.382(4)	2.605(4)	3.064(5)	1.57(1)[d]	—	4.142(3)
				$Se_2O_2Br_6^{2-}$				
Dc	Ph_4P (9, 10)	2.469(1)	2.464(1)	2.878(1)	2.980(1)	1.584(6)[d]	—	4.289
Dd	Ph_4As (10)[e]							
				Related to $Se_2O_2Cl_6^{2-}$				
De	Ph_4As (−135°C) (9, 11)[f]	2.234(1)	2.430(1)	2.475(1)	—	1.601(3)[d]	—	see text
Df	C_9H_8NO (17)[g]	2.234(4)	2.271(4)	2.963(3)	2.992(3)	1.594(9)[d]	[3.380(4)][h]	4.471(2)

[a] [*N*-(*N*-Chlorobenzimidoyl)benzamidium] $[Se_2Cl_{10}] \cdot 2MeCN$.
[b] $(Et_4N)_4[Se_2Hal_{10}][Se_2Hal_9]_2$.
[c] Partially hydrolyzed, see text. Structure refined on assumption that all ligands are Cl.
[d] Se—O bond.
[e] Isostructural with **Db**.
[f] $(Ph_4As)SeOCl_3$; contains $SeOCl_3^-$ monomer.
[g] (8-Hydroxyquinolinium)$SeOCl_3$; contains chains of $[SeOCl_5]$ quasi-octahedra sharing two Cl–Cl edges.
[h] *trans* to the oxygen atom.
*B. Krebs. Personal communication to O.K.

and related dimers had been previously (2, 6–13) reported in salts of these anions with several organic cations. However, the thermal parameters of some of the anion ligand atoms in **C** were large and the Te···Te' distance, 4.418(1) Å, was well in excess of the corresponding distances in the Ph_4As^+ (**Ch**, Table 2) and Ph_3PCl^+ (**Ci**) salts, 4.033(1) and 4.040(1) Å, respectively. Closer attention to this difficulty revealed a precedent: the Te···Te' distance in **Cj** (originally reported as having the composition $(Ph_4As)_2[Te_2Cl_{10}]$, refs. 6 and 7) was 4.430(3) Å in one (**Cj1**) and 4.153(3) Å in the other (**Cj2**) of the two nonequivalent $Te_2Cl_{10}^{2-}$ anions in the unit cell. Moreover, the shortest bond, Te—Cl_a, was significantly shorter in **Cj** than in **Ch** and **Ci**, while the longest bond, Te—Cl_c' (bridging bond *trans* to Te—Cl_a), was significantly longer in **Cj** than in **Ch** and **Ci**. Because of these discrepancies the structure of **Cj** was later (B. Krebs, personal communication) reformulated as corresponding to $(Ph_4As)_4[Te_2Cl_{10}][Te_2Cl_8Cl_x(OH)_{2-x}]$, i.e., to partially hydrolyzed $(Ph_4As)_2[Te_2Cl_{10}]$. In view of this it appeared indispensable for a proper interpretation of our own results for **C** to establish a standard for the variation of the Z—Cl bond lengths in $Z_2Cl_{10}^{2-}$ and $Se_2O_2Cl_6^{2-}$ dimers with which the bond lengths observed in **C** and **D** could be compared. For this an analysis of the observed complete geometries of the

Can. J. Chem. Downloaded from www.nrcresearchpress.com by 217.78.4.112 on 09/08/12
For personal use only.

Can. J. Chem. Downloaded from www.nrcresearchpress.com by 217.78.4.112 on 09/08/12
For personal use only.

dimers is required. Two questions will be asked: (1) Are differences in the Z—Hal bond lengths within a dimer and between nonidentical dimers of the same composition random (i.e., due to accidents of crystal packing and interion interaction) or systematic? (2) If the differences are systematic, do relationships between the bond lengths exist and, if they do, can they be used to authenticate Z—Hal bond lengths in crystals?

Differences in bond lengths

The geometries of the $Z_2Hal_{10}^{2-}$ (Z = Se, Te) and $Se_2O_2Hal_6^{2-}$ dimers are standardized in Fig. 1, and Table 2 contains a synoptic presentation of the reported Z—Hal, Z···Z′, and Se—O distances ($d_a = d$(Z—Hal$_a$) etc.).

By and large, d_a appears to be the shortest and d_c' the longest of the Z—Hal bonds in a $Z_2Hal_{10}^{2-}$ dimer, the latter bond in $Te_2Cl_{10}^{2-}$ being at least 0.2 Å longer than any of the other bonds in this ion. The dimer may thus be regarded, at least formally at this point, as a pair of square-pyramidal $TeHal_5^-$ ions, with Hal$_a$ and Hal$_a$′ as the axial ligands, and weakly bonded through Z—Hal$_c$′. This is consistent with the observation that in the square-pyramidal TeF_5^- monomer the axial Te—F bond (corresponding to Z—Hal$_a$) is about 0.1 Å shorter than the equatorial Te—F bonds.[2] Furthermore, as pointed out by Krebs *et al.* (2, 10), the difference between the bridging bonds in a $Te_2Hal_{10}^{2-}$ dimer (and thus the asymmetry of the double bridge) increases with the decreasing atomic number of Hal, until ultimately for Hal = F the dimer becomes a centrosymmetric pair of TeF_5^- monomers with the Te···F$_c$′ distance (in **Cf**) about 60% longer than Te—F$_c$ and with the Te—F bond lengths in the monomer virtually indistinguishable from those in the discrete TeF_5^- ion.[3] In such circumstances one might expect the equatorial Te—Hal bond lengths in each $TeHal_5^-$ monomer half to be the same, save for possible differences arising from accidents of packing in each particular crystal structure.

In $Te_2Cl_{10}^{2-}$, for which three sets of authentic Te—Cl bond lengths are available (**Ch**, **Ci**, **Cj2**),[4] analysis of variance and *t* tests show that the following hypotheses can be *rejected* at the 99.5% significance level or better: (*i*) the means $\langle d_b\rangle$ = 2.416(17) Å, $\langle d_g\rangle$ = 2.683(27) Å, $\langle d_d\rangle$ = 2.503(16) Å, and $\langle d_e\rangle$ = 2.480(3) Å are from the same population; (*ii*) $\langle d_b\rangle$, $\langle d_d\rangle$, and $\langle d_e\rangle$ are from the same population; (*iii*) $\langle d_b\rangle$ and $\langle d_e\rangle$ are from the same population. Conclusions *ii* and *iii* in fact hold for the entire set **Ch**, **Ci**, **Cj1**, **Cj2**, and **C**. However, the hypothesis that $\langle d_d\rangle$ and $\langle d_e\rangle$ come from the same population can be rejected at only the 8% significance level for **Ch**, **Ci**, and **Cj2**, and at the 10% level for all five $Te_2Cl_{10}^{2-}$ sets in Table 2.

In sum, then, the differences between d_b, d_c, and (d_d, d_e) persist regardless of the nature of the counter cation and may be regarded as stereochemical class differences reflecting the existence of an underlying bonding scheme for the dimer. Significant for the view that the differentiation of the equatorial bonds in the monomer halves is due to the bridge formation is the fact that the bonds Te—Cl$_d$ and Te—Cl$_e$ perpendicular to the bridge plane remain undifferentiated between themselves, whereas those *in* the bridge plane and *trans* to each other, Te—Cl$_b$ and Te—Cl$_c$, now belong to different classes (contrast this with the lack of differentiation in the pseudo dimer $Te_2F_{10}^{2-}$ in **Cf**).[2,5]

Corresponding statistical scrutiny of the Se—Cl bond lengths in $Se_2O_2Cl_6^{2-}$ (**D1**, **D2**, **Da**, **Db**) shows that the means $\langle d_a\rangle$ = 2.266(12) Å, $\langle d_b\rangle$ = 2.355(22) Å, and $\langle d_c\rangle$ = 2.654(39) Å do not come from the same population (significance level, >> 99.9%), nor do $\langle d_a\rangle$ and $\langle d_b\rangle$ (significance level, >99.9%). These means differ from the bond lengths observed in the $SeOCl_3^-$ monomer (**De**): $\langle d_a\rangle$ is barely within 3σ of d_a in **De**, but d_b and d_c in **De** differ by 0.045 Å, whereas in the dimer the difference between $\langle d_b\rangle$ and $\langle d_c\rangle$ is 0.30(5) Å, i.e., there is disproportionation in the two *trans* Se—Cl bond lengths in the dimer. In $Se_2O_2Br_6^{2-}$ (**Dc**) the Se—Br$_c$ bond is clearly the longest of the three, but d_a and d_b are now almost identical, the asymmetry of the double bridge notwithstanding.[6]

Relationship between Z—Hal bonds: the trans *effect*

From the preceding it appears that Z—Hal bonds in a dimer that belong to distinct stereochemical classes are also metrically different. Closer examination of the spatial relationships of these bonds reveals that, in bonds *trans* to each other, the shorter the one bond the longer the other. This compensation, which is nonlinear but not severely so over the observed Z—Hal ranges, is referred to as the *trans* effect. The effect is electronic in nature and reflects in part the response of a molecule or molecule-ion to its incorporation in a crystal. The pervasive occurrence of TE in the structural chemistry of Se(IV) and Te(IV) halogeno species has been repeatedly pointed out by Krebs (11, 18, 19) and others (20). However, TE is not confined to these species or to halogens as ligands. It has been empirically quantified for L$_1$—Z—L$_2$ *trans* bonds with chemically nonequivalent ligands (21), and some of its general aspects are discussed in detail in ref. 22.

The regularity of TE, for a given pair of elements, should make it possible to demonstrate whether a set of *d*,*d** bond lengths (*d** ≥ *d*) in pairs of conjugate *trans* bonds[7] conforms to the same bonding principle, and to test whether a particular *d*,*d** pair can legitimately be included in the set.

[2]**Cf**, d(Te—F$_a$) = 1.872 Å; $\langle d$(Te—F$_{eq}$)$\rangle$ = 1.950(10) Å. Means from other monomers, $\langle d$(Te—F$_{ax}$)$\rangle$ = 1.868(33) Å, $\langle d$(Te—F$_{eq}$)$\rangle$ = 1.963(44) Å (cf. Table 10).

[3]The occurrence of the centrosymmetric pairs of TeF_5^- ions in **Cf**, with closest interion F···F approaches equal to or exceeding the sum of the van der Waals radii and with Te···F separations of ~3.2 Å raises the quation, to what extent is the existence of such pairs in $A^+TeHal_5^-$ crystals due to external factors (minimization of lattice energy, maximization of packing density) rather than to an intrinsic tendency of $TeHal_5^-$ to form $Te_2Hal_{10}^{2-}$ dimers (see Sect. III).

[4]The structures of **Ca**, **Ch**, and **De** were determined from low-temperature data (Table 2). It is difficult to know how to adjust the bond lengths obtained from these determinations to room-temperature values. The original bond lengths have therefore been retained throughout. From a qualitative estimate of the magnitude of the required corrections (based on the assumption that dV/dT ~ 0.01%/K and that the bond lengthening is isotropic) it appears doubtful that substitution of the true room-temperature bond lengths would significantly alter any of the conclusions below.

[5]Similar conclusions appear to hold for $Se_2Cl_{10}^{2-}$, $Te_2Br_{10}^{2-}$, $Te_2I_{10}^{2-}$, and also for the corresponding $Z_2Hal_{10}^{4-}$ dimers with Z from Group V (see III for details and further discussion.

[6]In $As_2Br_8^{2-}$ (**3**, **4**, and **5**; Table 9), the hypothesis that $\langle d_a, d_b, d_c\rangle$ comes from the same population as $\langle d_c, d_c'\rangle$ can be rejected absolutely. However, the hypothesis that $\langle d_a\rangle$, $\langle d_b\rangle$, and $\langle d_d\rangle$ come from the same population must be *accepted* at the 30% significance level, and ditto for $\langle d_c\rangle$, $\langle d_c'\rangle$, (21% significance level), and $\langle d_a\rangle$, $\langle d_d\rangle$ (62% significance level).

[7]In bridged species *d* refers to the terminal and *d** to the bridged ligands. In all the cases considered in this paper, $d_{terminal} \leq d_{bridge}$.

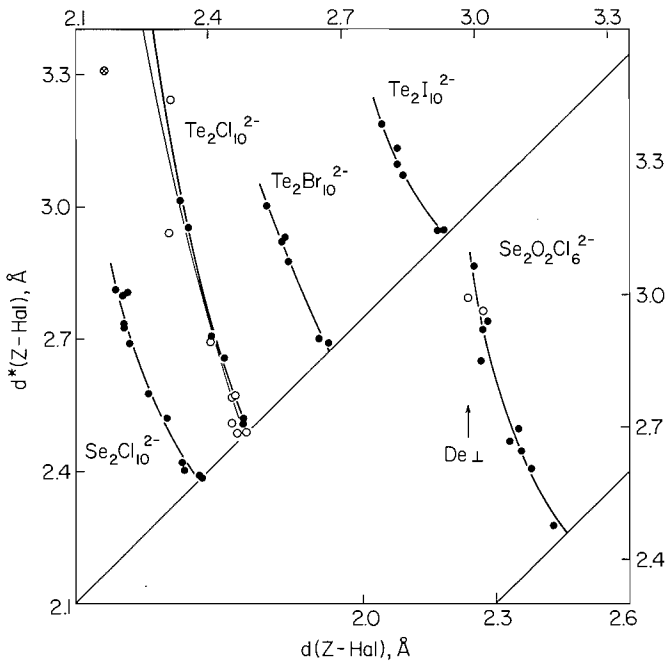

FIG. 2. Variation of the Z—Hal bond lengths d^* with $d \leq d^*$ in pairs of conjugated *trans* bonds in $Z_2Hal_{10}^{2-}$ and $Se_2O_2Cl_6^{2-}$ anions (cf. Table 2). The curves represent the DPF regressions of Table 3. $Te_2Cl_{10}^{2-}$: thick line and full circles, data set *a* ($n = 6$); thin line and full and open circles, data set *b* ($n = 14$); crossed circle, **Cjl**(d_a, d_c'), mixed-ligand Te—(Cl, OH) bond. $Se_2O_2Cl_6^{2-}$: the two open circles are for **Df** (not included in the regressions).

Specifically, TE should be able to indicate whether or not some of the bonds assumed in the structure refinement of **Cj** and **C** to be Te—Cl bonds had in fact undergone hydrolysis.

To date no satisfactory theory-based general function $d^* = f(d)$ appears to have been proposed. However, TE in Z(III)—Hal (AsBr, SbBr, SbI) bonds has recently been successfully quantified by Sheldrick et al. (23, 57), who modified Pauling's (24) relation $D(n) = D(1) - B \log n$ to

$$[1] \quad d^* = d_0 - B \ln s^*$$

assuming in addition that, for a d,d^* pair, $s + s^* = 1$ and $B = b_0 + b_1 (d - d_0)$. Here d_0 is the Z—Hal bond length in $ZHal_3(g)$, s and s^* are the conjugate bond orders, and b_0 and b_1 are parameters of least-squares refinement.[8] This treatment is referred to in the following as CSBO (constant sum of bond orders). A purely empirical alternative to CSBO, free from particular model assumptions, is the function

$$[2] \quad d^* - d_0 = K(d - d_0)^{-c}$$

(difference power fit, DPF; see ref. 22). To determine which of the bond lengths in **Cj** and **C** quality as proper Te—Cl bond lengths we examined the DPF, CSBO, and other schemes (Table 3, Fig. 2), using in the regressions (*a*) the Te—Cl distances in **Ch** and **Ci**, and (*b*) all the pairs of Te—Cl distances in Table 2 except d_a,d_c' in **Cj1**, which produced a gross visual misfit in the d^* vs. d plot and for which the reported d was unacceptably short for a Te—Cl bond length. Since the Te—Cl bond lengths in the free $TeCl_4$ molecule are not known, the limiting d_0 (Te—Cl) bond length was treated as a parameter of regression. The figures of merit resulting from the three-parameter nonlinear optimizations (Table 3 and Sect. IV) indicate that both CSBO and DPF (as well as PF2) are good approximations to the variation of d^* with d in $Te_2Cl_{10}^{2-}$ and that these regressions describe the variation in each of the two sets equally satisfactorily though not identically.

From Fig. 2 it is clear that the bond length in **Cj1** reported as d(Te—Cl_a) is inconsistent with any of the regressions. If the associated distance d(Te—L_c') is assumed to be the correct distance for L = Cl, then the reported d(Te—L_a) deviates by 57σ from the DPF regression line for data set *a* and by more than 9σ from that for set *b*. This legitimizes Krebs's reinterpretation (personal communication) of this distance as resulting from a partial replacement of Cl in the Te—L_a bond by OH. As for the Te—L_a bonds in **Cj2** and **C**, the point for **Cj2** is ~11σ below the regression line *a* and ~2.2σ below the regression line for *b*. The deviations of the other points for **Cj1** and **C** from the regression lines, however, are within ~3σ for line *a* and ~1σ for line *b*, in a region of the plot which is well determined by points of data set *a*. It thus appears that the partial hydrolysis of anion **Cj1** was sufficiently serious to reduce the apparent Te—L_a = Te—L_{ax} bond length to a value disqualified for inclusion in the d(Te—Cl) data set. However, the hydrolysis was selective in that it affected, preferentially, the axial ligand much more than any of the equatorial ligands; curiously enough, its effect on **Cj2**, the second anion in the same crystal, was considerably less.

If the difference between d(Te—Cl) and d(Te—O) is estimated as ~0.5 Å (see Sect. II), on the average less than one half of the Cl_a in the **Cj1** anions would seem to have been replaced by OH. However, this was sufficient to increase d(T···Te′) by ~0.4 Å relative to **Ch** and **Ci**. Significantly, the lesser degree of Cl_a substitution in **Cj2** is associated with a smaller increase in d(Te···Te′), only about 0.12 Å. Although these changes are relatively small and on the whole affect only one of the two types of anions in a structure otherwise chemically the same as **Ch**, they were sufficient to produce changes in the triclinic crystal structure such that Gretenkord (12) was unable to reconcile the unit cell of **Ch** (−130°C) with that of **Cj** (room temperature).

The implication of these findings is that our own compound **C** may also have undergone partial hydrolysis and that this may have been the reason for some of the unsatisfactory features of the structure refinement that assumed all the ligands to be Cl. The d(Te—L_a) and d(Te···Te′) values (Table 2) would support this possibility, but the position of the point for **C**(d_a,d_c') *above* the regression lines in Fig. 2 poses a contradiction. Attempts to resolve this problem are described in Sect. II.

The operation of TE in $Te_2Cl_{10}^{2-}$ receives support from an examination of the data available for $Se_2Cl_{10}^{2-}$, $Te_2Br_{10}^{2-}$, and $Te_2I_{10}^{2-}$ (Fig. 2, Table 2). The regressions (Table 3) gave on the whole satisfactory agreement for these data sets. Interestingly, the regression line for the $Te_2Br_{10}^{2-}$ set shows very little curvature although a curvature intermediate between $Te_2Cl_{10}^{2-}$ and $Te_2I_{10}^{2-}$ might be expected. Additional $Te_2Br_{10}^{2-}$ dimers are required to see whether the behaviour of the existing set is a real phenomenon or merely a statistical oddity.

The TE in the $Se_2O_2Cl_6^{2-}$ anions also exhibits good internal consistency (Fig. 2, Table 3). The regression line ac-

[8]For the history and limitations of these assumptions see ref. 22.

Can. J. Chem. Downloaded from www.nrcresearchpress.com by 217.78.4.112 on 09/08/12
For personal use only.

TABLE 3. Regressions of $d^* \geq d$ on d for bond lengths in pairs of *trans* Z—Hal bonds in $Z_2Hal_{10}^{2-}$ and $Se_2O_2Cl_6^{2-}$ dimers using different model functions

Model function[a]	Parameter[b]							
	r^2	σ, Å	d_0, Å	K	c	b_0, Å	b_1	d_{equal}, Å
				(*a*) $Te_2Cl_{10}^{2-}$ ($n = 6$)[c]				
LIN	0.9882	0.025	—	—	—	11.120	−3.477	2.484
PF1	0.9922	0.021	—	39.984	3.051	—	—	2.486
PF2	0.9950	0.0196	2.0944	1.7267	0.3927	—	—	2.489
DPF	0.9950	0.0196	1.6458	0.5570	2.4285	—	—	2.489
CSBO	0.9949	0.0196	2.1110	—	—	0.9291	−1.0159[d]	2.489
				(*b*) $Te_2Cl_{10}^{2-}$ ($n = 14$)[e]				
LIN	0.9193	0.071	—	—	—	11.463	−3.626	2.478
PF1	0.9307	0.070	—	42.273	3.122	—	—	2.480
PF2	0.9230	0.0725	1.6893	2.0008	0.9222	—	—	2.481
DPF	0.9230	0.0725	1.0529	3.9344	2.8409	—	—	2.481
CSBO	0.9232	0.0724	1.8833	—	—	1.6460	−1.3087[d]	2.481
				$Se_2O_2Cl_6^{2-}$ ($n = 9$)[f]				
LIN	0.9206	0.057	—	—	—	9.637	−2.958	2.434
PF1	0.9332	0.054	—	22.896	2.512	—	—	2.439
PF2	0.9419	0.0529	2.1705	2.0143	0.1609	—	—	2.459
DPF	0.9403	0.0537	2.0023	0.1643	1.3073	—	—	2.459
CSBO	0.9413	0.0532	2.1696	—	—	0.4824	−0.2168[d]	2.460
				$Se_2Cl_{10}^{2-}$ ($n = 12$)[g]				
PF2	0.9679	0.0350	2.0363	1.8760	0.2188	—	—	2.376
DPF	0.9684	0.0347	1.8223	0.2357	1.4488	—	—	2.376
CSBO	0.9682	0.0348	2.0400	—	—	0.6018	−0.3453[d]	2.376
				$Te_2Br_{10}^{2-}$ ($n = 6$)[h]				
LIN	0.9812	0.0198	—	—	—	9.0014	−2.3707	2.670
PF2	0.9821	0.0223	0.4796	10.8201	1.7826	—	—	2.671
DPF	0.9821	0.0223	0.2898	15.572	2.1639	—	—	2.671
CSBO	0.9821	0.0223	1.5292	—	—	2.6010	−0.8344[d]	2.671
				$Te_2I_{10}^{2-}$ ($n = 6$)[i]				
PF2	0.9849	0.0157	2.6775	2.5532	0.10213	—	—	2.934
DPF	0.9853	0.0154	2.5338	0.1445	1.1130	—	—	2.934
CSBO	0.9851	0.0155	2.6601	—	—	0.4207	−0.0929[d]	2.934

[a]LIN, $d^* = b_0 + b_1 d$; PF1, $d^* = Kd^{-c}$; PF2, $d^* = K(d - d_0)^{-c}$; DPF, difference power fit, $d^* - d_0 = K(d - d_0)^{-c}$; CSBO, constant sum of bond orders fit, $d^* = d_0 - [b_0 + b_1(d - d_0)] \ln [1 - \exp\{-(d - d_0)/[b_0 + b_1(d - d_0)]\}]$.
[b]$d_{equal} = d = d^*$.
[c]**Ch** and **Ci**.
[d]Note that for As(III)—Br, Sb(III)—Br, and Sb(III)—I bonds $b_1 > 0$ (23, 57).
[e]**Ch**, **Ci**, **Cj1**, **Cj2**, and **C** but excluding **Cj1**(d_a, d_c').
[f]**Da**, **Db**, **D1**, **D2**, and **De**(d_b, d_c).
[g]**Ca**, **Cb**, **Cc**, and **Cd**.
[h]**Ck** and **Cm**. The very large probable errors on the regression coefficients render the nonlinear regressions questionable (see text).
[i]**Cn** and **Co**.

commodates well also the two d,d^* pairs in the linear $[SeOCl_2Cl_{2/2}]_\infty^-$ chains in **Df** and the *trans* Se—Cl pairs in the $SeOCl_3^-$ monomer **De**. The Se—Cl bond length involving the unopposed Cl ligand in the latter is at the limit of the $Se_2O_2Cl_6^{2-}$ data set (Fig. 2).

The data sets of Fig. 2 and Table 3 are statistically inadequate for trends in the fitted parameter values to emerge.[9] The exception is d_{equal}, which does not depend critically on the curvature of the regression line (i.e., on the distribution of the d,d^* pairs and the assumed model function), provided there are well-behaved d,d^* pairs sufficiently close to the $d = d^*$ line. Regression of the d_{equal} from the $Te_2Hal_{10}^{2-}$ ($n = 6$) data sets on Shannon's $r(Hal^-)$ radii (25) gave $d_{equal} = 0.4357 + 1.1368r(Hal^-)$, $r^2 = 0.999$, $\sigma = 0.009$ Å; extrapolation to $r(F^-) = 1.33$ Å yielded $d_{equal} = 1.948$ Å, which compares well with the $\langle d(Te—F_{eq})\rangle$ value of 1.964(33) Å (Table 10).

[9]For a discussion of the existence of such trends see ref. 22.

II. Crystal structures

The atom coordinates and thermal parameters of the nonhydrogen atoms in the title compounds are listed in Tables 4–7, and the bond lengths and bond angles for all four are

Can. J. Chem. Downloaded from www.nrcresearchpress.com by 217.78.4.112 on 09/08/12
For personal use only.

Can. J. Chem. Downloaded from www.nrcresearchpress.com by 217.78.4.112 on 09/08/12
For personal use only.

listed in Table 8. The atom coordinates of the hydrogen atoms and tables of structure factors have been deposited (see Sect. IV).

*(n-$Pr_4N)_2SnCl_6$ (**A**)*

The salt investigated here is probably the D_{2h} form of (*n*-$Pr_4N)_2SnCl_6$ of Ries (4, 5), although the density he reports is too low and the axial ratio from his optical measurements bears no obvious relation to the unit-cell dimensions of **A**.[10]

The structure consists of an *anti*-fluorite-type arrangement of fully extended *n*-Pr_4N^+ cations 1 and 2 and only slightly distorted $SnCl_6^{2-}$ octahedra of symmetry C_1 (Fig. 3). The $Pbca \subset Pa\bar{3}$ unit cell may be regarded as an *anti*-fluorite *Pbcm* cell doubled on the *a* axis, the contents of the two *Pbcm* halves being related by a chromatic $a/2$ translation; the chromatic operation on the Bravais P_a lattice is inversion of the ion orientation. The relation between the ion orientations in the structure can thus be described by the dichromatic space group $P_abca - 2Pbcm|Pbca$. This arrangement appears to be novel for A_2MX_6 salts containing small, relatively symmetric cations (cf. refs. 1 and 26).

The U_{ij} values of Sn and Cl are satisfactorily explained on the RBM model (cf. Table 11). The librational motion of the $SnCl_6$ octahedron is quite uniform; the libration axis L_2 is nearly parallel to *a*.

*(n-Pr_4N)[$TeCl_4(OH)$] (**B**)*

As described in Sect. IV, the structure was solved in the centrosymmetric space group $C2/c$ and subsequently refined both in $C2/c$ (with the Te and O atoms each in two-fold positional disorder) and in Cc (as a fully ordered structure). The two refinements differ essentially only in details of the anion structure.

The fully extended *n*-Pr_4N^+ cations and the $TeCl_4(OH)^-$ anions are arranged in an *anti*-NiAs-type packing.[11] The *c* axis of **B** corresponds to the *c* axis of the hexagonal NiAs structure ($P6_3mc \supset Cc \subset C2/c$), and $b(\mathbf{B})/a(\mathbf{B}) = 1.614 \sim \sqrt{3}$. The cations are arranged in columns parallel to *c*.

In the Cc refinement the spread of the Te—Cl bond lengths is considerably smaller than in the $C2/c$ refinement, but the means are the same, 2.49(1) and 2.50(1) Å, respectively. This compares with ⟨2.48(1)⟩ Å in $(Ph_4As)[TeCl_4(OH)]\cdot H_2O$ (56), ⟨2.496⟩ Å in $(H_9O_4)[TeCl_4(OH)]\cdot H_2O$ (2, 18), and ⟨2.51(4)⟩ Å for anion 1 and ⟨2.50(2)⟩ Å for anion 2 in $K(TeCl_4(OH)]\cdot\frac{1}{2}H_2O$ (58), the mean for the five anions being 2.50(10) Å.

The Te atom is on the opposite side of the best plane through the four Cl ligands from the oxygen atom, 0.06 Å from the plane in the Cc and 0.15 Å in the $C2/c$ refinement. This is consistent with the expectation from the VSEPR rules. These two distances are shorter than the corresponding distance in the ordered anion 2 of the K^+ salt, 0.21 Å; in the $C2/c$ refinement of the Ph_4As^+ salt the Te atom was placed at a centre of symmetry and is therefore coplanar with the Cl atoms.

Up to this point the refinements in $C2/c$ and Cc do not differ appreciably. However, the Te—O bond length is 1.87(1) Å in the $C2/c$ and 1.73(2) Å in the Cc refinement, a significant difference. Interestingly, the latter value is the same as in the Ph_4As^+ salt, 1.74(1) Å, whereas the values in the $H_9O_4^+$ and K^+ salts are 1.93 and 1.91(2) Å, respectively. The paucity of known $TeCl_4(OH)^-$ structures makes rationalization of these differences difficult, and there are other obstacles: a similar difficulty of choice between $C2/c$ and Cc was encountered in the structure refinement of the Ph_4As^+ salt; a full account of the $H_9O_4^+$ salt structure is yet to be published; one of the anions in the K^+ salt is partially disordered; and three of the four relevant compounds are hydrated. Nevertheless, since hydrogen bonding was suspected to be a possible factor responsible for the discrepancy, the four structures were examined in detail for whatever evidence for this possibility could be found. The pertinent structural detail is presented in Fig. 4.

In the $H_9O_4^+$ salt the hydroxyl oxygen is involved in an O—H···$O(H_2O)$ bond to the nearest water (*not* $H_9O_4^+$) oxygen. The O···O separation of 2.64 Å indicates a strong H-bonding interaction, comparable to that in $NaOH\cdot H_2O$.[12] The O(OH) oxygen is also hydrogen-bonded to a $H_9O_4^+$ oxygen at 2.84 Å.

In the other structure containing long Te—O bonds, $K[TeCl_4(OH)]\cdot\frac{1}{2}H_2O$, anion 1 is orientationally disordered, *d*[Te(11)—O(11)] = 1.905(17) Å, *d*[Te(12)—O(12)] = 2.15 Å (*sic*). In the ordered anion 2, *d*[Te(2)—O(2)] = 1.908(13) Å. Although the OH hydrogens in this structure have not been located, the direction of the Te(2)—O(2) bond is compatible with the existence of an almost symmetrically bifurcated O(2)—H(2)···Cl(23a),Cl(24b) hydrogen bond, in which *d*[O(2)···Cl(23a)] = 3.66 Å and *d*[O(2)···Cl(24b)] = 3.69 Å (Fig. 4; a, $(-x, -y, -z)$; b, $(-x, 1-y, -z)$). The midpoint M of the Cl(23a)···Cl(24b) distance forms a Te(2)—O(2)—M angle of 113°, i.e., not far from tetrahedral, and is ~2.40 Å from H(2), if the latter is placed in accordance with the geometry normally expected for a Te—O—H group. In that case, the H(2)···Cl(23a),Cl(24a) distance would be ~3.0 Å. which would qualify O(2)—H(2)···Cl(23a),Cl(24b) for at least a moderately strong hydrogen bond.[13,14]

By contrast, consideration of admissible atom···atom separations in the $(Ph_4As)[TeCl_4(OH)]\cdot H_2O$ structure (as refined in $C2/c$, oxygens in half occupancy) shows that the only atom that could conceivably function as an acceptor of the hydroxyl hydrogen H(1) is the water oxygen O(2) (Fig. 4). However, the large O(1)···O(2) distance, 3.04 Å, and the Te—O(1)—O(2) angle of 134° are both unfavourable to the existence of an effective hydrogen bond. The oxygen of the water molecule, O(2), is nominally ~3.2 Å from the nearest chlorines Cl(1′) and Cl(2). Weak O—H···Cl hy-

[10]The second form reported by Ries is triclinic, with the improbably high density of 1.548 g/cm³ (a misprint?).

[11]In the $(Ph_4As)[TeCl_4(OH)]\cdot H_2O$ structure the packing is regular but not clearly related to any of the simple types of 1:1 ionic structures. In $K[TeCl_4(OH)]\cdot\frac{1}{2}H_2O$ the ions are arranged in a distorted CsCl-type packing, with columns of K^+ ions and $O(H_2O)$ atoms parallel to *c*.

[12]In $NaOH\cdot H_2O$ the O(OH)···$O(H_2O)$ distances are reported as 2.64 and 2.66 Å (59, 60).

[13]The disorder proposed in ref. 58 for anion 1 complicates evaluation of the H-bonding engagement of this anion. The distance *d*[O(12)···$O(H_2O)$] = 2.26 Å is too short for any interaction that might occur in that crystal. However, at *d*[O(11)···$O(H_2O)$] = 2.52 Å the Te(11)—O(11)—$O(H_2O)$ angle is ~118°, which strongly implies the existence of a Te(11)—O(11)···$O(H_2O)$ bond of moderate strength.

[14]It should be possible to demonstrate the bifurcated character of this bond from the temperature dependence of the ν(OD) frequency of the weakly deuterated compound (cf. refs. 61 and 62).

Can. J. Chem. Downloaded from www.nrcresearchpress.com by 217.78.4.112 on 09/08/12
For personal use only.

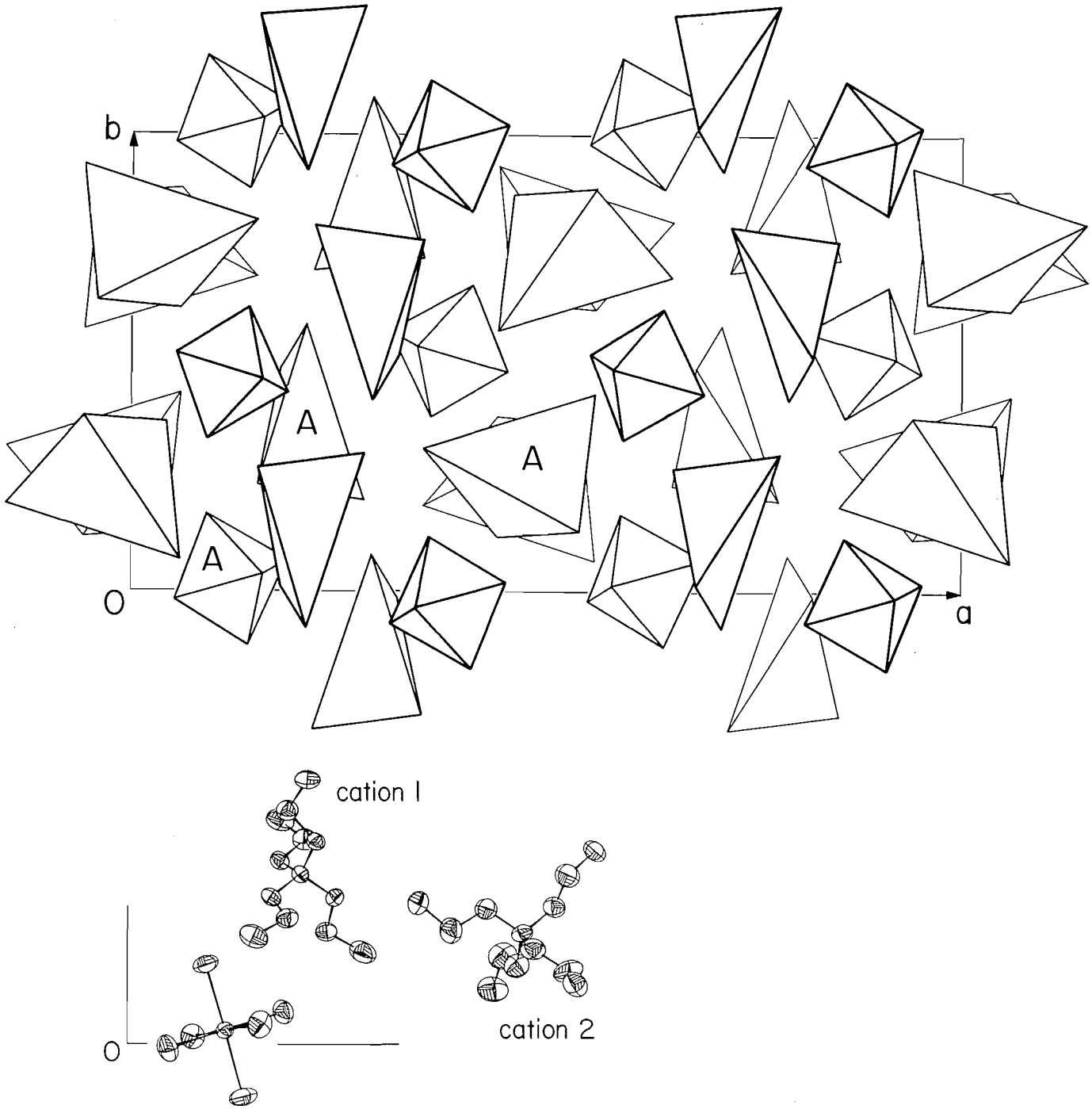

FIG. 3. Projection of the structure of $(n\text{-}Pr_4N)_2SnCl_6$ (**A**) on (001). The octahedra represent $SnCl_6^{2-}$, the tetrahedra $n\text{-}Pr_4N^+$. The anion and the cations in positions listed in Table 4 are marked A.

drogen bonding at this distance is possible, but it is unlikely that both H_2O hydrogens could be simultaneously engaged in hydrogen bonds unless dynamically. The large U_{iso}[O(2)], 0.113 Å^2 compared to 0.059 Å^2 for O(1), would support the latter, though it might be imprudent to place too much weight on the refinement of the water oxygen in half occupancy. It should be noted that although the placement of the oxygen atoms in the anion columns of Fig. 4 requires full order within a column, orientational disorder *between* columns will satisfy the oxygen disorder assumed in ref. 56.

If participation of the hydroxyl oxygen of the Ph_4As^+ salt in a hydrogen bond is improbable, it is no less so in the anhydrous **B**. The only possible H-bond acceptor for the OH group is Cl(2Ac), at 3.20 Å and a Te—O—Cl(2Ac) angle of 142°. This geometry would result at best in a weak O—H···Cl bond.

From this examination of the four structures it would seem that the discrepancy in the reported Te—O bond lengths *could* be explained by the presence or the absence of significant hydrogen bonding that involves the OH group of the anion.

Can. J. Chem. Downloaded from www.nrcresearchpress.com by 217.78.4.112 on 09/08/12
For personal use only.

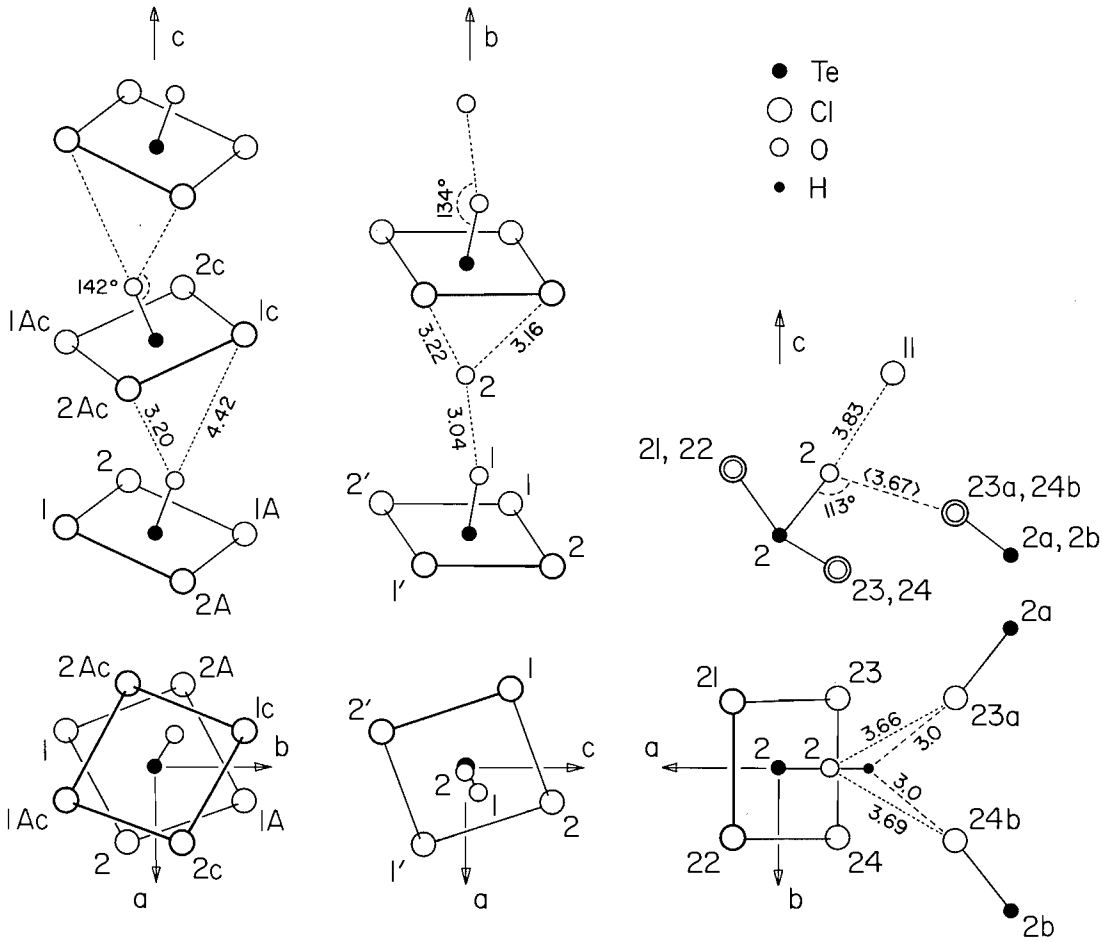

FIG. 4. Hydrogen bonding of the $TeCl_4(OH)^-$ anion in **B** (ordered structure; left), $(Ph_4As)[TeCl_4(OH)] \cdot H_2O$ (disordered oxygens; centre), and $K[TeCl_4(OH)] \cdot \frac{1}{2}H_2O$ (right). Double circles, atoms overlapping in projection; dashed lines, putative hydrogen bonds. Dotted lines indicate distances between atoms.

Still, a Te—O bond length of 1.74 Å seems rather short and the possibility that it may be, to some extent at least, an artefact of refinement cannot be discounted. Clearly, further accumulation of structural information is required. As for **B**, on balance the ordered structure, as refined in *Cc*, appears marginally preferable to the disordered structure as described in *C*2/*c*.

*(n-$Pr_4N)_2[Te_2Cl_{10}]$ (nominal) (**C**)*

The ion packing in **C** is of the *anti*-CdI_2 type (cf. Sect. III). The results of refinement on the assumption that all the Te ligands are Cl atoms are presented in Tables 2, 6, and 8. As pointed out in Sect. I, the short Te—Cl(1) (= "Te—Cl_a") bond length and the large U_{ij} of the Cl atoms were puzzling even for a structure containing the nonrigid *n*-Pr_4N^+ cations until Krebs's reinterpretation (personal communication) of the composition of the anion **Cj**, which had been reported previously (6, 7) as $Te_2Cl_{10}^{2-}$ but which in reality was partially hydrolyzed to $Te_2Cl_8(Cl, OH)_2^{2-}$. Comparison of the Te—Cl bond lengths with those in the **Cj** dimers on the one hand and those in the authentic $Te_2Cl_{10}^{2-}$ dimers **Ch** and **Ci** on the other revealed that only one bond length in **C** was shorter than expected for a Te—Cl bond, namely the presumed Te—Cl(1). It was about the same as d(Te—L_a) in **Cj2** but not nearly as short as d(Te—L_a) in **Cj1**. From this it was assumed that only Cl_a had undergone replacement by OH and then only in a minority of the dimers. The attempts made to refine the occupancy factor at the mixed-ligand site *a* in order to resolve the Cl_a and O_a positions are described in Sect. IV. However, these attempts cannot be regarded as completely successful. The seemingly large U_{ij} values in the "chlorines only" refinement can be accounted for on a RBM model (cf. Sect. III), but since the mixed ligands could not be cleanly resolved, the position of the d_a,d_c' point *above* the regression line in Fig. 2 remains unexplained. Additional elaboration of the mixed-ligands model having been deemed unpromising, further attempts to resolve the site occupancy at *a* were abandoned.

Since the partial hydrolysis made the **C** dimer unsuitable for a discussion of the Te—Cl bond lengths in $Te_2Cl_{10}^{2-}$, in the following we rely on the authentic $Te_2Cl_{10}^{2-}$ dimers **Ch** and **Ci**. A closer look at their geometry shows that in both these anions the Te atom is only 0.10 Å from the centroid of the $Cl_{a,b,c,c',d,e}$ octahedron. In **Ch** the Te atom is only 0.033 Å below the best plane through $Cl_{b,c,d,e}$, i.e., coplanar with these atoms (σ = 0.044 Å; Cl_a is 2.30 Å from this best plane).[15]

It is curious that partial replacement of Cl_a by OH should cause a 10% increase in the Te···Te' distance in $Te_2Cl_{10}^{2-}$ and have a significant effect on the shape of the unit cell

[15]For projections of the $Te_2Cl_{10}^{2-}$ dimer **Ch** see Fig. 12.

TABLE 4. $(n\text{-}Pr_4N)_2SnCl_6$ (**A**): positional ($\times 10^4$) and thermal ($\times 10^3$) parameters of nonhydrogen atoms

Atom	x y z	U_{11} U_{22} U_{33}	U_{12} U_{13} U_{23}	Atom	x y z	U_{11} U_{22} U_{33}	U_{12} U_{13} U_{23}
Sn	1160.6(2)	42.5(4)	1.3(3)	C(141)	2228(3)	56(6)	−6(4)
	0244.1(3)	40.2(4)	−3.5(3)		4471(5)	43(5)	−6(4)
	2378.7(4)	42.0(4)	1.5(3)		4062(6)	42(5)	−5(4)
Cl(1)	0926(1)	87(2)	17(1)	C(142)	1890(3)	64(7)	6(5)
	1722(1)	47(1)	11(2)		5160(5)	51(5)	−10(5)
	2476(2)	87(2)	0(1)		4288(7)	70(7)	−13(5)
Cl(2)	1377(1)	100(2)	14(1)	C(143)	2124(4)	101(8)	−2(5)
	−1236(2)	46(1)	−17(2)		5850(6)	48(6)	−9(6)
	2273(2)	93(2)	−3(2)		4834(7)	72(7)	−16(5)
Cl(3)	0473(1)	63(2)	−18(1)	N(2)	4729(2)	61(5)	6(4)
	−0153(2)	97(2)	11(2)		2419(4)	43(4)	4(4)
	3179(2)	78(2)	15(2)		4662(4)	41(4)	7(3)
Cl(4)	1854(1)	55(2)	−7(2)	C(211)	5111(4)	89(8)	−4(6)
	0654(2)	82(2)	18(2)		2995(6)	57(6)	−5(6)
	1589(2)	82(2)	−9(2)		4291(7)	62(6)	17(6)
Cl(5)	1578(1)	77(2)	4(2)	C(212)	5270(4)	84(8)	−11(6)
	0377(2)	99(2)	−20(2)		3704(7)	66(7)	−16(7)
	3779(2)	54(2)	−10(2)		4865(8)	103(9)	12(7)
Cl(6)	0768(1)	79(2)	0(1)	C(213)	5587(3)	61(6)	−12(5)
	0107(2)	84(2)	−23(1)		4269(6)	59(6)	−13(6)
	0939(2)	56(2)	5(2)		4366(7)	87(8)	7(6)
N(1)	2052(2)	39(4)	−7(3)	C(221)	4290(3)	58(7)	−7(5)
	3733(4)	42(4)	−1(3)		2960(6)	57(6)	9(5)
	3500(4)	47(4)	0(3)		4746(7)	71(6)	−2(5)
C(111)	2456(3)	46(6)	2(4)	C(222)	3860(4)	66(7)	−17(7)
	3212(5)	50(5)	8(5)		2492(6)	88(9)	15(6)
	3248(6)	65(6)	−14(5)		4948(8)	110(10)	−6(8)
C(112)	2363(3)	69(7)	−8(5)	C(223)	3470(3)	61(7)	7(6)
	2450(6)	50(5)	10(5)		3081(6)	72(7)	9(6)
	2670(7)	71(7)	−22(5)		5097(8)	105(9)	−13(7)
C(113)	2814(4)	95(10)	−12(7)	C(231)	4657(4)	76(7)	4(6)
	1978(7)	60(7)	30(8)		1687(6)	74(7)	5(5)
	2439(8)	113(10)	−26(7)		4031(7)	53(6)	−12(6)
C(121)	1799(3)	52(6)	−12(5)	C(232)	4501(5)	99(10)	3(7)
	4045(6)	53(5)	−5(4)		1896(7)	91(9)	−8(8)
	2676(5)	39(5)	−2(4)		3123(8)	85(9)	−11(8)
C(122)	2096(4)	83(7)	−6(6)	C(233)	4375(5)	127(12)	−9(9)
	4537(6)	69(7)	2(5)		1160(8)	102(10)	−22(8)
	2027(6)	43(6)	10(5)		2558(7)	64(8)	−30(7)
C(123)	1804(4)	123(11)	−13(6)	C(241)	4852(3)	74(7)	5(6)
	4946(6)	59(6)	−18(7)		2083(7)	73(7)	2(6)
	1315(8)	66(7)	17(6)		5585(7)	63(7)	10(6)
C(131)	1705(3)	43(5)	−10(4)	C(242)	5281(4)	99(9)	11(8)
	3214(5)	49(5)	7(4)		1591(7)	85(8)	−14(7)
	4039(5)	35(5)	1(4)		5648(8)	82(8)	33(7)
C(132)	1900(3)	75(7)	−1(5)	C(243)	5378(4)	76(8)	−8(7)
	2734(5)	47(5)	−1(5)		1270(8)	89(8)	−18(7)
	4833(6)	58(6)	12(5)		6571(8)	103(10)	28(8)
C(133)	1501(4)	108(10)	−11(7)				
	2346(7)	79(8)	1(7)				
	5347(7)	63(7)	14(6)				

Can. J. Chem. Downloaded from www.nrcresearchpress.com by 217.78.4.112 on 09/08/12
For personal use only.

TABLE 5. (n-Pr_4N)[$TeCl_4(OH)$] (**B**): positional ($\times 10^4$) and thermal ($\times 10^3$) parameters of nonhydrogen atoms (refinements in $C2/c$ and Cc)[a]

Atom	x y z		U_{11} U_{22} U_{33}		U_{12} U_{13} U_{23}	
Te	*0056(12)*	−0008(6)	*59(2)*	63(1)	*−2(2)*	4(1)
	0048(4)	0001(6)	*37(2)*	45(1)	*−12(3)*	−24(1)
	−0151(8)	0009(4)	*59(4)*	91(1)	*17(2)*	2(1)
Cl(1)	−0830(1)	−0835(9)	79(2)	89(6)	−6(1)	−12(3)
	−1322(1)	−1309(3)	52(1)	54(4)	4(1)	0(6)
	0084(2)	0137(9)	98(2)	115(6)	6(1)	19(4)
Cl(1A)		0823(9)		70(5)		0(3)
		1331(3)		51(3)		4(4)
		−0040(8)		86(5)		−6(3)
Cl(2)	1910(2)	1869(8)	74(2)	72(5)	1(1)	−11(4)
	−0417(1)	−0391(5)	80(2)	95(5)	−46(2)	−67(5)
	1299(2)	1374(9)	129(3)	150(7)	24(2)	41(6)
Cl(2A)		−1942(8)		73(5)		11(3)
		0441(4)		69(4)		−27(4)
		−1239(8)		117(6)		13(4)
O	*−0724(13)*	−0726(12)	*122(10)*	126(9)	*11(8)*	18(6)
	0264(7)	0267(6)	*79(8)*	71(6)	*53(8)*	51(6)
	1330(11)	1348(10)	*55(8)*	47(6)	*−12(6)*	−17(5)
N	0	0005(25)	37(4)	35(4)	0	0
	−3363(4)	−3352(3)	33(4)	33(4)	4(4)	2(4)
	$\frac{1}{4}$	2616(25)	48(5)	41(7)	0	0
C(11)	−1087(5)	−1087(22)	34(3)	37(12)	4(3)	−14(11)
	−2833(3)	−2858(14)	47(4)	75(13)	7(3)	16(8)
	2747(7)	2653(21)	49(4)	37(10)	−3(3)	−19(9)
C(11A)		1075(18)		33(10)		−19(7)
		−2814(10)		29(8)		2(8)
		2172(19)		35(10)		2(7)
C(12)	−2242(6)	−2261(21)	39(4)	32(12)	2(4)	−33(13)
	−3238(4)	−3217(12)	70(5)	133(21)	11(4)	13(12)
	3140(8)	3192(24)	62(5)	76(18)	−3(4)	40(15)
C(12A)		2227(20)		55(14)		−24(10)
		−3237(9)		35(11)		−5(11)
		1899(19)		51(14)		23(9)
C(13)	−3287(7)	−3309(18)	49(4)	29(10)	11(5)	−19(11)
	−2659(5)	−2648(13)	95(7)	132(20)	16(5)	38(9)
	3201(9)	3298(21)	86(7)	52(12)	0(6)	−9(13)
C(13A)		3256(27)		67(18)		−49(14)
		−2663(13)		79(15)		−11(18)
		1897(32)		132(24)		−5(17)
C(21)	0320(6)	0299(20)	51(4)	36(10)	4(3)	14(7)
	−3871(3)	−3849(9)	40(4)	26(7)	−2(4)	−7(7)
	3621(6)	3724(16)	46(4)	20(9)	7(3)	1(6)
C(21A)		−0352(27)		75(16)		15(11)
		−3922(13)		59(12)		13(11)
		1514(22)		47(14)		9(10)

Can. J. Chem. Downloaded from www.nrcresearchpress.com by 217.78.4.112 on 09/08/12
For personal use only.

TABLE 5 (*concluded*)

Atom	*x* *y* *z*		U_{11} U_{22} U_{33}		U_{12} U_{13} U_{23}	
C(22)	0701(7)	0715(23)	62(5)	96(15)	4(4)	−3(9)
	−3482(4)	−3408(10)	57(5)	47(11)	0(4)	−12(8)
	4851(7)	4854(16)	50(5)	11(7)	3(4)	8(7)
C(22A)		−0697(18)		36(10)		−5(7)
		−3557(11)		23(7)		16(10)
		0137(25)		108(19)		−19(9)
C(23)	0835(9)	0921(23)	102(7)	59(10)	−8(5)	−3(9)
	−4093(5)	−4078(12)	72(5)	64(12)	4(5)	30(9)
	5893(7)	5835(20)	45(5)	45(12)	18(5)	12(10)
C(23A)		−0682(26)		100(18)		16(13)
		−4098(15)		99(17)		7(11)
		−0961(18)		31(11)		−36(11)

[a]First column, $C2/c$; second column, Cc. Values in italics, occupancy factor $\frac{1}{2}$.

TABLE 6. $(n\text{-}Pr_4)_2[Te_2Cl_{10}]$ (**C**): positional ($\times 10^4$) and thermal ($\times 10^3$) parameters of nonhydrogen atoms

Atom	*x* *y* *z*	U_{11} U_{22} U_{33}	U_{12} U_{13} U_{23}	Atom	*x* *y* *z*	U_{11} U_{22} U_{33}	U_{12} U_{13} U_{23}
Te	0794.5(7)	70.4(4)	−13.7(2)	C(21)	7226(13)	93(8)	−40(6)
	1441.6(4)	69.9(4)	−22.5(2)		8842(10)	87(7)	−36(6)
	3352.5(4)	65.9(4)	−13.8(2)		1568(10)	105(8)	1(6)
Cl(1)	2860(4)	109(3)	−70(2)	C(22)	7404(18)	170(13)	−49(8)
	2288(3)	169(3)	−32(2)		9980(11)	92(8)	−68(10)
	2702(3)	157(3)	−12(3)		1881(13)	128(10)	−4(7)
Cl(2)	−0101(3)	110(2)	−10(2)	C(23)	7119(15)	133(10)	−60(7)
	2841(3)	119(2)	−32(2)		11251(10)	80(7)	−24(7)
	1500(2)	70(2)	−8(2)		0946(10)	98(8)	11(6)
Cl(3)	1828(3)	120(2)	−15(2)	C(31)	6114(12)	102(8)	−46(6)
	0062(2)	88(2)	−63(2)		7681(11)	102(8)	−5(6)
	5263(2)	105(2)	−15(2)		3663(9)	79(7)	−20(6)
Cl(4)	−0681(3)	152(3)	5(2)	C(32)	6114(14)	111(10)	−32(7)
	3349(2)	80(2)	−38(2)		6506(12)	108(9)	11(7)
	4458(2)	91(2)	−26(2)		4657(11)	107(9)	−5(7)
Cl(5)	2498(4)	134(3)	24(2)	C(33)	4765(12)	86(8)	−45(7)
	−0351(3)	127(2)	−54(2)		6786(12)	118(9)	14(6)
	2123(3)	128(2)	−68(2)		5787(9)	79(7)	−3(6)
N	7426(7)	55(4)	−24(3)	C(41)	7410(11)	72(6)	−43(6)
	7517(6)	64(4)	−10(3)		6477(10)	115(8)	−9(5)
	2471(5)	53(4)	−5(3)		1856(9)	89(7)	−31(6)
C(11)	8965(11)	71(7)	−35(5)	C(42)	6000(13)	86(8)	−30(7)
	7044(10)	94(7)	−13(6)		6657(12)	124(9)	−28(7)
	2815(10)	100(7)	−9(6)		1522(12)	139(10)	−53(8)
C(12)	10344(14)	96(9)	−63(10)	C(43)	6271(12)	90(8)	−42(6)
	6865(16)	196(15)	−10(7)		5616(10)	99(7)	−43(7)
	1794(11)	100(9)	−22(9)		0755(10)	128(9)	−28(7)
C(13)	11828(10)	54(6)	−33(6)				
	6288(11)	132(9)	−13(6)				
	2239(10)	109(8)	−27(7)				

[a]Structure refined on the assumption that all the anion ligands are Cl atoms (see text).

Can. J. Chem. Downloaded from www.nrcresearchpress.com by 217.78.4.112 on 09/08/12
For personal use only.

TABLE 7. $(n\text{-}Pr_4N)_2[Se_2O_2Cl_6]$ (**D**): positional ($\times 10^4$) and thermal ($\times 10^3$) parameters of nonhydrogen atoms

Atom	x y z	U_{11} U_{22} U_{33}	U_{12} U_{13} U_{23}	Atom	x y z	U_{11} U_{22} U_{33}	U_{12} U_{13} U_{23}
Se(1)	0960.7(13) 3419.4(11) 4558.5(8)	40.9(7) 48.3(7) 51.3(9)	5.6(5) −0.1(6) 16.2(6)	Se(2)	4595.8(15) 6797.9(12) 0467.6(8)	50.4(7) 57.6(8) 58.0(10)	10.3(6) 7.4(7) 23.6(7)
Cl(11)	0876(5) 1722(3) 4907(2)	126(4) 64(2) 69(3)	31(2) 9(3) 32(2)	Cl(21)	5254(5) 8488(3) 0162(2)	125(4) 59(2) 74(3)	6(2) 1(3) 33(2)
Cl(12)	0973(4) 2216(3) 3228(2)	74(2) 64(2) 50(2)	5(2) 15(1) 12(2)	Cl(22)	5096(4) 8007(3) 1824(2)	82(3) 78(2) 61(3)	18(2) 3(2) 24(2)
Cl(13)	0069(3) 4650(2) 5921(1)	74(2) 61(2) 47(2)	6(2) 0(2) 26(2)	Cl(23)	4798(4) 5359(3) −0960(2)	98(3) 51(2) 49(2)	10(2) 5(2) 21(2)
O(1)	2655(9) 3998(9) 4737(6)	40(5) 91(7) 108(9)	−12(5) 3(6) 37(7)	O(2)	2875(10) 6630(10) 0389(6)	50(6) 118(9) 62(7)	19(6) 30(5) 9(7)
N(1)	0249(10) 7540(8) 2392(6)	39(5) 53(6) 46(7)	0(5) −1(5) 23(6)	N(2)	4331(10) 7285(9) 7304(6)	38(6) 63(6) 58(7)	−8(5) −19(5) 35(6)
C(111)	0303(12) 6217(11) 2353(9)	37(7) 57(8) 86(12)	4(6) 15(8) 36(9)	C(211)	5707(12) 7745(11) 7893(8)	30(7) 63(8) 100(12)	−8(6) −22(8) 46(9)
C(112)	1537(14) 5664(11) 1952(9)	49(8) 59(8) 78(11)	9(7) 15(8) 35(9)	C(212)	6196(14) 9178(12) 8213(8)	47(8) 53(8) 64(10)	0(7) 7(8) −6(7)
C(113)	1345(19) 4303(13) 1882(10)	92(13) 68(10) 78(12)	21(9) 13(11) 33(9)	C(213)	7567(15) 9499(13) 8783(9)	49(9) 78(10) 88(13)	−5(8) −10(9) 33(10)
C(121)	0128(13) 7634(11) 1590(8)	40(7) 59(8) 80(11)	6(6) 6(7) 38(8)	C(221)	3046(14) 7956(12) 7657(8)	47(8) 65(9) 69(11)	14(7) 6(7) 28(8)
C(122)	−1147(18) 6786(14) 1032(8)	62(10) 83(11) 50(10)	−8(8) −16(9) 3(8)	C(222)	2704(16) 7860(17) 8417(10)	44(9) 131(16) 88(14)	27(9) 23(9) 51(13)
C(123)	−1080(21) 6988(18) 0260(9)	86(14) 147(19) 67(14)	26(13) −16(11) 18(13)	C(223)	1592(19) 8714(18) 8753(11)	63(11) 127(17) 88(15)	−1(11) 17(11) 19(13)
C(131)	−1086(14) 7921(11) 2825(8)	53(8) 47(7) 67(10)	14(6) 20(8) 29(8)	C(231)	4631(14) 7540(10) 6573(7)	57(8) 43(7) 47(9)	8(6) 8(7) 12(7)
C(132)	−1285(17) 9246(13) 3002(10)	62(10) 70(10) 94(14)	−3(8) 10(10) 28(10)	C(232)	3442(17) 7017(13) 5912(8)	85(11) 71(9) 52(10)	−8(8) −20(9) 36(8)
C(133)	−2493(18) 9557(14) 3550(9)	76(11) 76(11) 78(13)	26(9) 5(10) 21(10)	C(233)	3932(19) 7261(16) 5195(8)	89(13) 110(14) 39(10)	19(11) −3(9) 23(9)
C(141)	1664(13) 8345(10) 2786(7)	44(7) 46(7) 48(8)	−2(6) 5(6) 15(7)	C(241)	3857(13) 5932(10) 7161(7)	53(8) 38(6) 58(9)	11(6) 15(7) 21(7)
C(142)	2016(15) 8478(12) 3660(7)	52(8) 74(9) 46(9)	−4(7) −2(7) 23(8)	C(242)	4956(17) 5087(11) 6733(9)	72(10) 48(8) 70(11)	−4(7) 18(9) 18(8)
C(143)	3360(17) 9411(14) 4014(14)	53(10) 100(12) 95(14)	−14(9) −35(11) 38(11)	C(243)	4338(18) 3784(9) 6660(8)	120(14) 22(6) 64(10)	38(8) 39(10) 12(7)

Can. J. Chem. Downloaded from www.nrcresearchpress.com by 217.78.4.112 on 09/08/12
For personal use only.

TABLE 8. Interatomic distances (Å) and bond angles (deg) in the anions of compounds **A**, **B**, **C**, and **D**

Atoms	Distance[a]	Atoms	Angle
	Compound **A**[b]		
Sn—Cl(1)	2.442/20	Cl(1)—Sn—Cl(2)	178.7
Sn—Cl(2)	2.430/21	Cl(1)—Sn—Cl(3)	89.4
Sn—Cl(3)	2.410/20	Cl(1)—Sn—Cl(4)	90.3
Sn—Cl(4)	2.420/21	Cl(1)—Sn—Cl(5)	90.4
Sn—Cl(5)	2.418/19	Cl(1)—Sn—Cl(6)	90.3
Sn—Cl(6)	2.434/20	Cl(2)—Sn—Cl(3)	89.7
Mean	2.426(11)/20	Cl(2)—Sn—Cl(4)	90.7
		Cl(2)—Sn—Cl(5)	90.6
		Cl(2)—Sn—Cl(6)	88.8
		Cl(3)—Sn—Cl(4)	179.4
		Cl(3)—Sn—Cl(5)	90.9
		Cl(3)—Sn—Cl(6)	91.2
		Cl(4)—Sn—Cl(5)	88.6
		Cl(4)—Sn—Cl(6)	89.3
		Cl(5)—Sn—Cl(6)	77.8
	Compound **B** (refinement in $C2/c$)[c]		
Te—Cl(1)	2.590(8)	Cl(1)—Te—Cl(1a)	172.4(3)
Te—Cl(1a)	2.372(7)	Cl(1)—Te—Cl(2)	86.0(2)
Te—Cl(2)	2.573(12)	Cl(1)—Te—Cl(2a)	88.7(2)
Te—Cl(2a)	2.461(12)	Cl(1a)—Te—Cl(2)	91.0(2)
Mean	2.50(9)	Cl(1a)—Te—Cl(2a)	93.5(2)
Te—O	1.869(15)	Cl(2)—Te—Cl(2a)	171.8(3)
Te···O(a)	1.581(15)	O—Te—Cl(1)	85.1(5)
Te···Te(a)	0.387(16)	O—Te—Cl(1a)	88.0(5)
Cl(1)···Cl(2)	3.520(3)	O—Te—Cl(2)	86.4(5)
Cl(1)···Cl(2a)	3.531(3)	O—Te—Cl(2a)	86.6(5)
O···Cl(1)	3.062(9)	Te—O—Cl(2b)	146.1(5)
O···Cl(1a)	2.967(17)	O—Te—O(a)	171.4(9)
O···Cl(2)	3.084(14)	Cl(2)—Cl(1)—Cl(2a)	90.8(3)
O···Cl(2a)	3.001(12)	Cl(1)—Cl(2)—Cl(1a)	89.2(3)
*O···Cl(2b)	3.129(12)		
*O···O(b)	2.844(23)		
	Compound **B** (refinement in Cc)[c]		
Te—Cl(1)	2.459(8)	Cl(1)—Te—Cl(1A)	178.0(4)
Te—Cl(1A)	2.489(7)	Cl(1)—Te—Cl(2)	89.9(3)
Te—Cl(2)	2.506(11)	Cl(1)—Te—Cl(2A)	91.2(3)
Te—Cl(2A)	2.517(11)	Cl(1A)—Te—Cl(2)	89.2(3)
Mean	2.493(22)	Cl(1A)—Te—Cl(2A)	89.6(3)
Te—O	1.726(13)	Cl(2)—Te—Cl(2A)	176.3(4)
Cl(1)···Cl(2)	3.508(14)	O—Te—Cl(1)	91.1(5)
Cl(1)···Cl(2A)	3.554(10)	O—Te—Cl(1A)	87.1(4)
Cl(1A)···Cl(2)	3.508(9)	O—Te—Cl(2)	89.4(5)
Cl(1A)···Cl(2A)	3.526(13)	O—Te—Cl(2A)	87.0(5)
O···Cl(1)	3.032(9)	Te—O—Cl(2Ac)	141.7(5)
O···Cl(1A)	2.955(19)	Cl(2)—Cl(1)—Cl(2A)	90.6(3)
O···Cl(2)	3.027(15)	Cl(1)—Cl(2)—Cl(1A)	89.7(3)
O···Cl(2A)	2.977(20)		
*O···Cl(2Ac)	3.200(14)		
	Compound **C**[c,d]		
Te—Cl(1)	2.312(4)	Cl(1)—Te—Cl(2)	89.7(1)
Te—Cl(2)	2.456(3)	Cl(1)—Te—Cl(3)	87.2(1)
Te—Cl(3)	2.564(3)	Cl(1)—Te—Cl(3e)	168.7(1)
Te—Cl(3e)	3.241(4)	Cl(1)—Te—Cl(4)	87.2(1)
Te—Cl(4)	2.465(3)	Cl(1)—Te—Cl(5)	86.7(1)
Te—Cl(5)	2.484(4)	Cl(2)—Te—Cl(3)	176.8(1)
Te··Te(e)	4.418(1)	Cl(2)—Te—Cl(3e)	101.6(1)
		Cl(2)—Te—Cl(4)	88.8(1)
		Cl(2)—Te—Cl(5)	89.9(1)
		Cl(3)—Te—Cl(3e)	81.5(1)
		Cl(3)—Te—Cl(4)	90.2(1)
		Cl(3)—Te—Cl(5)	90.8(1)
		Cl(4)—Te—Cl(5)	173.7(1)

Can. J. Chem. Downloaded from www.nrcresearchpress.com by 217.78.4.112 on 09/08/12
For personal use only.

TABLE 8 (*concluded*)

Atoms	Distance[a]	Atoms	Angle
		Compound **D**[c]	
Se(1)—Cl(11)	2.278(5)	Cl(11)—Se(1)—Cl(12)	91.5(2)
Se(1)—Cl(12)	2.357(4)	Cl(11)—Se(1)—Cl(13)	89.8(1)
Se(1)—Cl(13)	2.645(4)	Cl(11)—Se(1)—Cl(13a)	159.4(1)
Se(1)—Cl(13a)	2.940(4)	Cl(11)—Se(1)—O(1)	102.7(5)
Se(1)—O(1)	1.593(9)	Cl(11)—Se(1)—Se(1a)	131.2(1)
Se(1)···Se(1a)	4.163(2)	Cl(12)—Se(1)—Cl(13)	162.3(1)
Se(2)—Cl(21)	2.249(5)	Cl(12)—Se(1)—Cl(13a)	88.9(2)
Se(2)—Cl(22)	2.382(4)	Cl(12)—Se(1)—O(1)	98.2(4)
Se(2)—Cl(23)	2.605(4)	Cl(12)—Se(1)—Se(1a)	126.3(1)
Se(2)—Cl(23a)	3.064(4)	Cl(13)—Se(1)—Cl(13a)	83.8(2)
Se(2)—O(2)	1.572(10)	Cl(13)—Se(1)—O(1)	98.7(4)
Se(2)···Se(2a)	4.142(2)	Cl(13a)—Se(1)—O(1)	97.6(4)
Cl(11)···Cl(12)	3.320(6)	O(1)—Se(1)—Se(1a)	100.9(3)
Cl(11)···Cl(13)	3.485(5)	Se(1)—Cl(13)—Se(1a)	96.2(1)
Cl(12)···Cl(13a)	3.732(5)	Cl(21)—Se(2)—Cl(22)	90.3(2)
Cl(13)···Cl(13a)	3.735(3)	Cl(21)—Se(2)—Cl(23)	91.3(2)
O(1)···Cl(11)	3.054(12)	Cl(21)—Se(2)—Cl(23a)	154.1(1)
O(1)···Cl(12)	3.027(10)	Cl(21)—Se(2)—O(2)	103.3(5)
O(1)···Cl(13)	3.289(9)	Cl(21)—Se(2)—Se(2a)	132.8(1)
O(1)···Cl(13a)	3.523(12)	Cl(22)—Se(2)—Cl(23)	163.8(2)
Cl(21)···Cl(22)	3.285(7)	Cl(22)—Se(2)—Cl(23a)	85.1(2)
Cl(21)···Cl(23)	3.479(5)	Cl(22)—Se(2)—O(2)	99.8(4)
Cl(22)···Cl(23a)	3.718(5)	Cl(22)—Se(2)—Se(2a)	122.8(1)
Cl(23)···Cl(23a)	3.898(5)	Cl(23)—Se(2)—Cl(23a)	86.5(2)
O(2)···Cl(21)	3.026(12)	Cl(23)—Se(2)—O(2)	95.5(4)
O(2)···Cl(22)	3.070(10)	Cl(23a)—Se(2)—O(2)	102.6(4)
O(2)···Cl(23)	3.169(11)	O(2)—Se(2)—Se(2a)	102.8(3)
O(2)···Cl(23a)	3.736(14)	Se(2)—Cl(23)—Se(2a)	93.6(1)

[a]The number ($\times 10^{-3}$) after the oblique stroke is the correction for thermal motion (RBM model, see text). The standard deviations of the means $\sigma(\bar{d})$ are $[(1/n)\Sigma(d_i - \bar{d})]^{1/2}$. Inter-ion distances are marked *.

[b]esd(bond length) = 0.003 Å; esd(bond angle) = 0.1°.

[c]a, $(-x, -y, -z)$; b, $(-x, y, \frac{1}{2} - z)$; c, $(x, -y, \frac{1}{2} + z)$; d, $(x, -y, z - \frac{1}{2})$; e, $(-x, -y, 1 - z)$.

[d]Structure refined on the assumption that all the ligands are chlorine atoms.

TABLE 9. Group V anion dimers and other species examined in this work

1 $(PhNMeH_2)_2[As_2Cl_8]$ (32)
2 $(Ph_4P)_2[As_2Cl_8]$ (33)
3 $(PhNMeH_2)_2[As_2Br_8]$ (34)
4 $(Ph_4P)_2[As_2Br_8]$ (23)
5 $(n\text{-}Pr_4N)_2[As_2Br_8]$ (23)
6 $(n\text{-}Bu_4N)_2[As_2I_8]$ (35)
7 $(C_{10}H_8N_2H_2)_2[Sb_2Cl_{10}]$ (36)
8 Sb_2Cl_{10} in $[Fe(\pi\text{-}cp)(CO)_2Cl]_4(SbCl_3)_2$, molecule 1 (37)
9 Ditto, molecule 2
10 $K_2[SbCl_5]$ (38)
11 $Sb_2Cl_8^{2-}$ in $(Ph_2NH_2)(SbCl_3)Cl$ (39)
12 $(n\text{-}Pr_4N)_2[Sb_2Cl_8]$, anion 1 (40)
13 Ditto, anion 2
14 $(n\text{-}Bu_4N)_2[cis\text{-}Sb_2Cl_8]$, the Sb(1) half (40)
15 Ditto, the Sb(2) half
16 $(Ph_4P)_2[Sb_2Br_8].MeCN$ (41)
17 $(C_2H_{10}N_4S)_2[Bi_2Cl_{10}].4H_2O$ (42)
18 Bi_2Cl_{10} in $(C_5H_5)_2FeBiCl_4$ (43)
19 Bi_2Cl_{10} in $(pyH)_6Bi_4Cl_{18}$ (44)
20 $Na_7[BiBr_6][Bi_2Br_{10}].18H_2O$ (45)
21 $[Sr(H_2O)_8]_2[Bi_2Br_{10}]$ (46)
22 $K_4[Bi_2Br_{10}].4H_2O$, dimer symmetry C_s (47)
23 $K_4[Tl_2Cl_{10}].4H_2O$ (48)
26 $(PCl_4)_2[Ti_2Cl_{10}]$ (49)
27 $(S_4N_5)_2[Ti_2Cl_{10}]$ (50)
28 $(S_4N_4Cl)_2[Zr_2Cl_{10}]$, anion 1 (51)
29 Ditto, anion 2
30 $(Ph_4P)_2[Mo_2Cl_{10}]$ (52)
31 $(n\text{-}Bu_4N)_2[Os_2Cl_{10}]$ (53)
32 $(n\text{-}Bu_4N)_2[Os_2Br_{10}]$ (54)
33 Nb_2Br_{10} in $\alpha\text{-}NbBr_5$, dimer symmetry C_s (55)

(cf. Sect. I). In our attempts to establish the site occupancy at *a* the Te···Te′ distance was noted to increase slightly with the degree of substitution of Cl by OH, but since the "chlorines only" refinement already gave a Te···Te′ of 4.42 Å, manipulating the Cl/OH ratio further seemed pointless.

Can. J. Chem. Downloaded from www.nrcresearchpress.com by 217.78.4.112 on 09/08/12
For personal use only.

Can. J. Chem. Downloaded from www.nrcresearchpress.com by 217.78.4.112 on 09/08/12
For personal use only.

TABLE 10. Mean Z—Hal bond lengths ⟨Σ⟩ (Å) in $Z_2Hal_{10}^{2n-}$, $Z_2Hal_8^{2-}$, and $Se_2O_2Hal_6^{2-}$ dimers (cf. Fig. 8)[a]

Z	F	Cl	Br	I
		$Z_2Hal_{10}^{2-}$		
Se		2.439(6)/4	2.595	
Te	[2.143][b]	2.564(8)/3	2.723(1)/2	2.958(3)/2
		$Z_2Hal_{10}^{4-}$		
Sb	[c]	2.704(2)/2[d]		
Bi		2.727(4)/2	2.874(6)/2	
Tl		2.596		
		$Z_2Hal_8^{2-}$		
As		2.559(12)/2	2.654(27)/3	2.849
Sb		2.610(12)/3	2.768	
Bi		2.754		
		$Z_2O_2Hal_6^{2-}$		
Se		2.555(17)/4[e]	2.698	

[a]The number after the oblique stroke represents the number n of dimers in the sample. The figure in parentheses is the dispersion (standard deviation) σ of the n individual means.

[b]In the **Cf** monomer half, 1.934(32) Å, the same as in $KTeF_5$ (27). The mean for TeF_5^- in $KTeF_5$, NH_4TeF_5 (two anions) (28), $RbTeF_5$ (two anions) (78), $NaTeF_5$ (77), and $K_2[TeF_5]NO_3$ (29) is 1.943(51) Å (1.941(48) Å with the **Cf** monomer included). Overall means for Te—F_{ax} and Te—F_{eq}, 1.880(15) and 1.964(33) Å, respectively.

[c]In $(NH_4)_2[SbF_5]$, 2.043(64) Å; Sb—F_{ax}, 1.916(4), Sb—F_{eq}, 2.075(3) Å (30).

[d]Mean for $SbCl_5^{2-}$ in **10** and $(NH_4)_2SbCl_5$ (31), 2.628(40) Å; mean in **10** if formulated as containing a pseudo dimer $Sb_2Cl_{10}^{4-}$, 2.80(50) Å. Overall means for Sb—Cl_{ax} and Sb—Cl_{eq}, 2.37(2) and 2.64(9) Å, respectively.

[e]In the $SeOCl_3^-$ monomer (**De**), 2.380 Å.

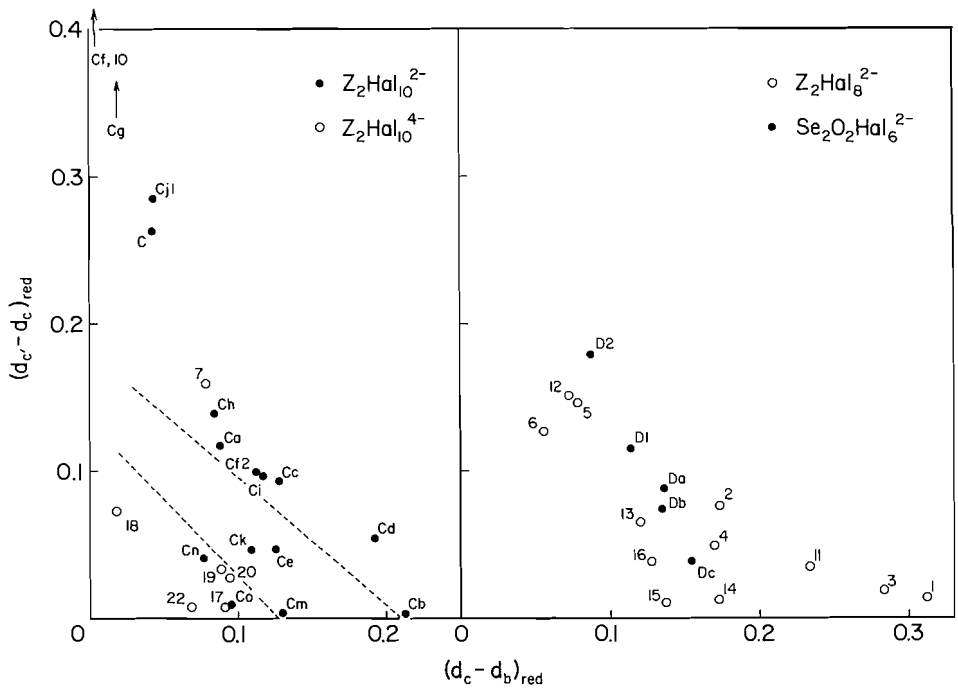

FIG. 5. Variation of the bridge asymmetry parameter $(d_c' - d_c)_{red}$ with $(d_c - d_b)_{red}$ in dimers. For code see Tables 2 and 9.

*(n-$Pr_4N)_2[Se_2O_2Cl_6]$ (**D**)*

The structure consists of *n*-Pr_4N^+ cations 1 and 2 and centrosymmetric $Se_2O_2Cl_6^{2-}$ anion dimers **D1** and **D2** arranged in a distorted *anti*-CdI_2-type packing, with the layers ∥(010). This is the same type of packing as is found, with varying degree of distortion, in the structures containing the **Da**, **Db**, and **Dc** dimers. Both cations have fully extended conformations.

The Cl atoms in the dimers are nearly coplanar, the mean deviation from the best plane p through the chlorines being

Can. J. Chem. Downloaded from www.nrcresearchpress.com by 217.78.4.112 on 09/08/12
For personal use only.

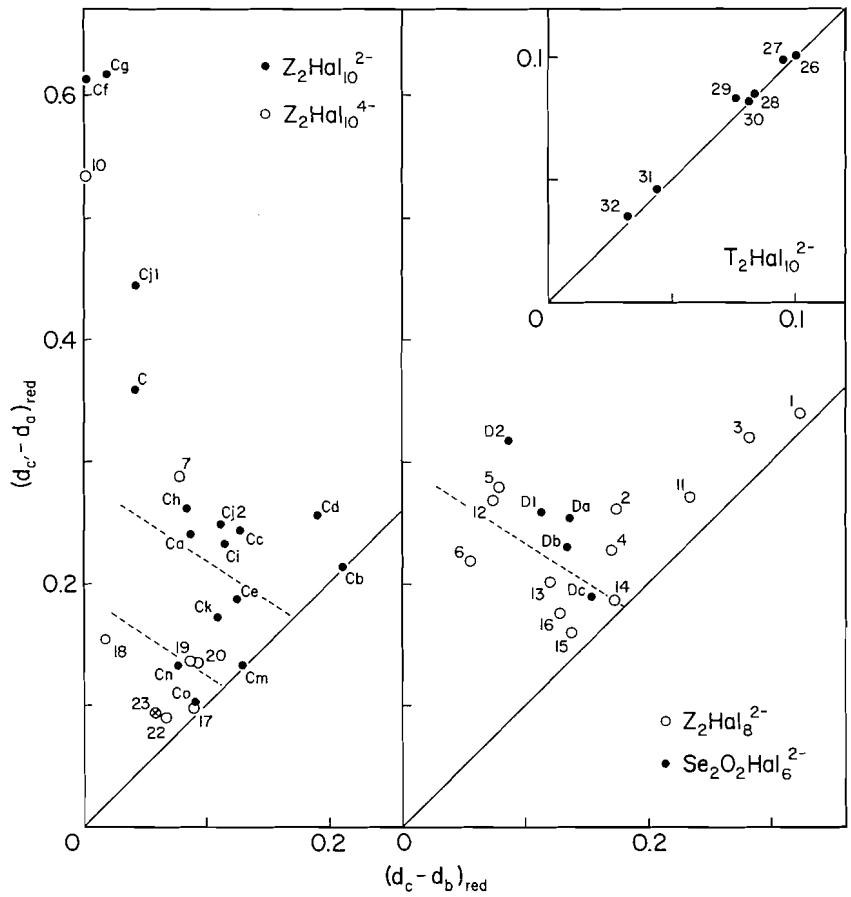

FIG. 6. Variation of $(d_c' - d_a)_{red}$ with $(d_c - d_b)_{red}$ in dimers. For code see Tables 2 and 9. Note the expanded scale in the inset.

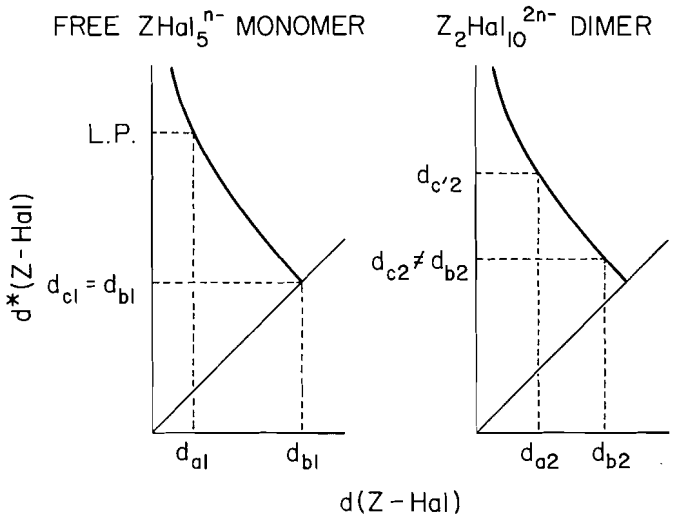

FIG. 7. Effect of dimerization on the Z—Hal bond lengths in $Z_2Hal_{10}^{2n-}$ dimers (cf. the *trans* effect plots of Fig. 2). d_{a1}, d_{a2}, Z—Hal_{ax}; d_{b1}, d_{b2}, d_{c1}, d_{c2}, Z—Hal_{eq}; d_{c2}', Z—Hal_{bridge}.

0.041 Å in **D1** and 0.014 Å in **D2**. The oxygen atom is 2.00 Å above p in **D1** and 1.91 Å in **D2**. The Se atom is on the same side of p as the respective oxygen atom (i.e., inside the distorted OCl_4 square pyramid), at 0.41 Å from p in **D1** and 0.35 Å in **D2**. This compares with 0.41 Å in **Da**, 0.31 Å in **Db**, and 0.39 Å in **Dc**. The angle formed by the Se–O vector with p is 88.6° in **D1** and 86.9° in **D2**. Interestingly, the perpendicular distances of O and Se from p and the p (Se—O) angles are not very different from those relative to the Cl_a—Cl_b—Cl_c plane in the $SeOCl_3^-$ monomer **De**: O–p, 1.90 Å; Se–p, 0.31 Å; p|(Se–O), 83.0°.

The d_a and d_b = d(Se—O) bond lengths in $Se_2O_2Cl_6^{2-}$, averaged over **D1**, **D2**, **Da**, and **Db**, are 2.266(11) and 1.588(10) Å, respectively,[16] and thus quite similar to the corresponding bond lengths in the $SeOCl_3^-$ monomer **De** and in the $[SeOCl_2Cl_{2/2}]_\infty^-$ chains in **Df**. However, the $\langle d_b \rangle$ and $\langle d_c \rangle$ for the dimers are significantly different from d_b and d_c in **De** and **Df**, although the mean $\langle d_a, d_b, d_c \rangle$ in the dimers, 2.43(17) Å, is statistically the same as the d(Se—Cl) mean in the monomer, 2.38(1) Å. These differences are consistent with the operation of TE in Se(IV)—Cl bonds (22).

The means of the O—Se—Cl angles over **D1**, **D2**, **Da**, and **Db** are 102.4(9)° for Cl_a, 98.6(17)° for Cl_b, 95.7(27)° for Cl_c, and 99.2(22)° for Cl_c'. Here again the angle involving Cl_a is the largest and compares to the corresponding (also largest) angles in **De** and **Df**, 105.1(1)° and 104.0(3)°, respectively.

III. Observations on dimers

Earlier on[3] the question was raised, is the formation of $Z_2Hal_{10}^{2n-}$ and $Se_2O_2Hal_6^{2-}$ dimers the result of exigencies of crystal packing, i.e., accidents of crystallization, or is there a genuine tendency of the ZL_5^- or ZL_4^- monomers (which

[16]The d(Se—O) average over **D1**, **D2**, **Da**, **Db**, **Dc**, **De**, and **Df** is 1.590(9) Å, i.e., indistinguishable from the above value.

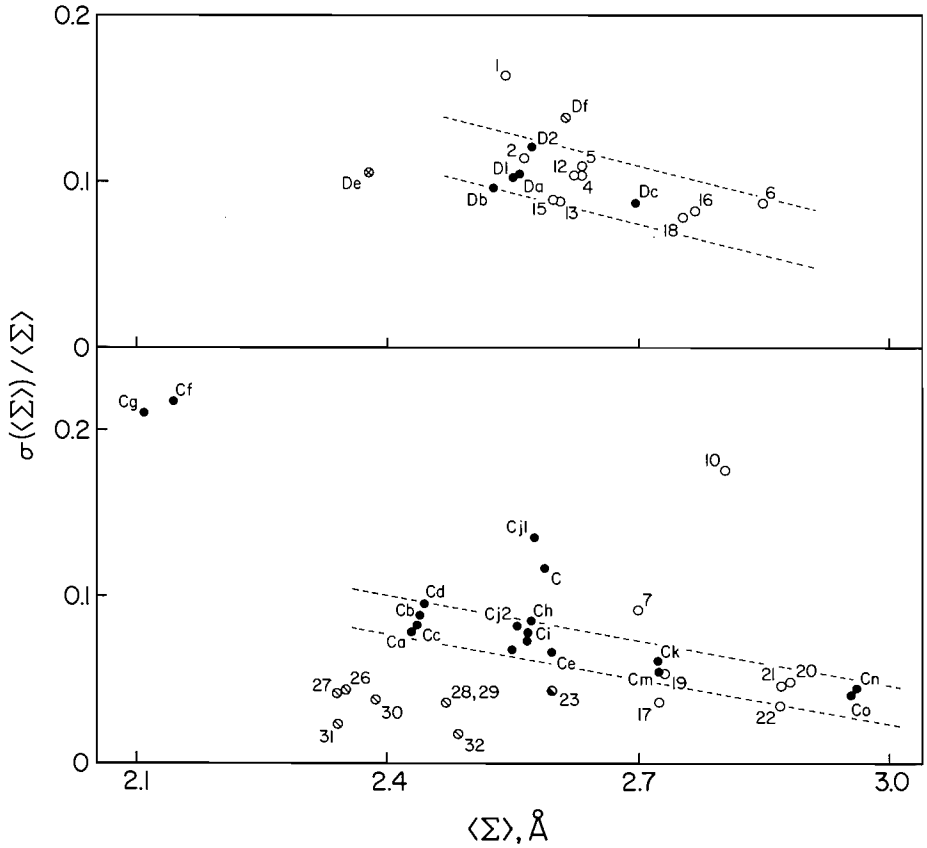

FIG. 8. Variation of the relative standard deviation $\sigma(\langle\Sigma\rangle)/\langle\Sigma\rangle$ with the mean $\langle\Sigma\rangle$ of all the Z—Hal bond lengths in a dimer: Z_2Hal_{10} and T_2Hal_{10} skeletons (bottom); Z_2Hal_8 and $Se_2O_2Hal_6$ skeletons (top). For code see Tables 2 and 9. The widths of the dashed-line bands are 2σ of the respective linear regression (see text).

Can. J. Chem. Downloaded from www.nrcresearchpress.com by 217.78.4.112 on 09/08/12
For personal use only.

may not be known as discrete entities) to associate for reasons that are explicitly chemical? In an attempt to discover what evidence bearing on this question can be obtained from the available crystallographic[17] information, we shall examine (*a*) the asymmetry of the double bridge and (*b*) its rigidity, in so far as the latter is ascertainable from the parameters of thermal motion. In doing so we shall consider not only Group VI dimers but also the more abundant Group V $Z_2Hal_{10}^{4-}$ and $Z_2Hal_8^{2-}$ anion dimers (Table 9).

Bridge asymmetry

As mentioned in Sect. I, the decrease in the asymmetry of the bridge from $Se_2O_2Cl_6^{2-}$ to $Se_2O_2Br_6^{2-}$ has been pointed out by Krebs (10), who also notes (2, 18) that in **Cf** the centrosymmetric $TeF_5^-\cdots TeF_5^-$ pair may be regarded as a pseudo dimer $Te_2F_{10}^{2-}$ with the $Te\cdots F_c'$ distance about 60% longer than $Te—F_c$. This appears to suggest that the bridge asymmetry is a manifestation of a systematic effect that depends on the nature of the Z,Hal combination. It will be convenient to denote the mean of all the Z—Hal bond lengths in a dimer by $\langle\Sigma\rangle$ (Table 10). The asymmetry of the bridge can then be measured by the difference $d_c' - d_c$ or by the corresponding normalized difference $(d_c' - d_c)/\langle\Sigma\rangle = (d_c' - d_c)_{red}$.

The dependence of the bridge asymmetry on the Z,Hal combination emerges when $(d_c' - d_c)_{red}$ is plotted against $(d_c - d_b)_{red}$ (Fig. 5). Keeping in mind the various limitations of the available data set, one is bound to acknowledge that this plot for $Z_2Hal_{10}^{2n-}$ successfully maps the dimers, at first sight according to the type of ligand but more probably according to the mean Z—Hal bond length (see Table 10 and below).[18] The latter view is supported by the segregation of the Se and Te dimers in three clearly defined regions; the points for the Bi dimers appear to be out of place when only the size of the *ligand* is considered.

Since, in normalizing $d_c' - d_c$ and $d_c - d_b$ by $\langle\Sigma\rangle$, account has already been taken of the size disparity of the ligands, it is clear that the segregation of the dimers in Fig. 5 must reflect the effect of dimerization on the strength of the $Z—Hal_{eq}$ bonds, via TE in the $Hal_b—Z—Hal_c$ grouping. Stated differently, the variation in the bridge asymmetry cannot be considered in isolation but must be related to the dimer geometry as a whole and, more particularly, to the normalized magnitudes of TE in the bridge plane.

The interrelation of the bond length adjustments in $Z_2Hal_{10}^{2-}$ (Z = Se, Te) dimers is rendered even more impressive by comparing, instead of the bridge asymmetry, the normalized magnitudes of TE in the axial bond pairs, $(d_c' - d_a)_{red}$, and the equatorial bond pairs, $(d_c - d_b)_{red}$ (Fig. 6). Here again the dimers are segregated in a pattern similar to that in Fig. 5. However, whereas the $(d_c - d_b)_{red}$ and $(d_c' - d_c)_{red}$ values in a dimer are comparable in magnitude,

[17]For ambiguity of evidence from vibrational spectra see ref. 40.

[18]The mean $\langle d_d, d_e\rangle$ of the Z—Hal bond lengths perpendicular to the bridge plane would be an acceptable experimental variable in the present discussion.

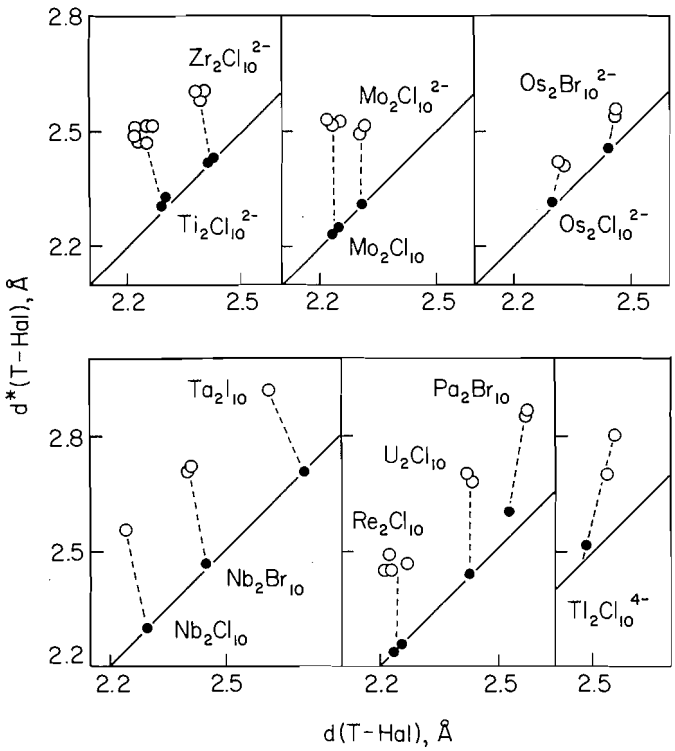

FIG. 9. Variation of d^* with d in $T_2Hal_{10}^{2-}$, T_2Hal_{10}, and $Tl_2Cl_{10}^{4-}$ dimers. Full circles, *trans* bonds perpendicular to bridge plane, T—Hal_d and T—Hal_e; open circles, T—Hal bonds in bridge plane. $T_2Hal_{10}^{2-}$: TiCl, **26**, **27**; ZrCl, **28**, **29**; MoCl, **30**; OsCl, **31**; OsBr, **32**. T_2Hal_{10}: $MoCl_5$ (63), $NbCl_5$ (64), TaI_5 (65); $ReCl_5$ (66), UCl_5 (67), β-$PaBr_5$ (68), α-$NbBr_5$, **33**. $Tl_2Cl_{10}^{4-}$, **23**.

the $(d_c' - d_a)_{red}$ value is significantly larger than the associated $(d_c - d_b)_{red}$ value, the difference decreasing from Cl to I. This indicates that the bridge asymmetry is ultimately determined by the difference in the Z—Hal_{ax} and Z—Hal_{eq} bond lengths in the free monomer limit and by the functional form of TE for Z,Hal (Fig. 7). It is therefore not surprising to find the points for the **C** and **Cj1** dimers in the partially hydrolyzed compounds away from the other $Z_2Cl_{10}^{2-}$ dimers in Fig. 6: replacement of Cl_a by OH in the two dimers further shortens the Te—L_a bond (without significantly affecting the Te—Cl_{eq} bonds) and thus directly affects the $(d_c' - d_a)$ value.

Although only one of the five $Se_2O_2Hal_6^{2-}$ dimers in Table 2 is a bromide, Figs. 5 and 6 seem to suggest that similar trends are followed as for the $Z_2Hal_{10}^{2-}$ dimers.

For the Group V $Z_2Hal_8^{2-}$ dimers the situation is less clear-cut. In some of them there is, in the crystal, covalent or hydrogen-bonding interaction between the bridging halogens and external atoms (**1**?, **3**, **11**).[19] However, even if these contentious cases are disregarded, the segregation is not nearly as well defined as for the Se and Te dimers. It is possible that the geometry of the Z_2Hal_8 skeletons is less rigid than that of the Z_2Hal_{10} (and perhaps even the $Se_2O_2Hal_6$) skeletons because of the incomplete coordination sphere of Z and is thus more susceptible to external influences in the crystal, which would account for the less regular trends.[20]

The desirability of considering the geometry of the whole dimer instead of focusing on the bridge asymmetry alone is demonstrated in yet another way by the variation of the standard deivation σ of ⟨Σ⟩ expressed as a fraction of ⟨Σ⟩. This fraction decreases as ⟨Σ⟩ increases, and although the variation is not strong, the trend is unmistakable (Fig. 8).[21] The distribution of the Z,Hal groups in this plot is well resolved and permits a comparison with $Tl_2Cl_{10}^{4-}$ (**23**) and the transition-element $T_2Hal_{10}^{2-}$ (**26–32**) dimers, none of which contains lone electron pairs on the nonhalogen atom.

Characteristically, the $T_2Hal_{10}^{2-}$ dimers show practically no bridge asymmetry (Fig. 9). Their $\sigma(\langle\Sigma\rangle)/\langle\Sigma\rangle$ values are less than half those encountered with $Z_2Hal_{10}^{2n-}$ dimers of comparable ⟨Σ⟩ (Fig. 8), i.e., the difference between the bridge and terminal bond lengths is small, ≤0.25 Å. The difference between $d_{terminal}$ for bonds in the bridge plane and those perpendicular to the bridge plane is well within 0.1 Å; the difference between T—Hal_d and T—Hal_e is very small, ~0.07 Å or less.

It is interesting that the d,d^* relations for the $T_2Hal_{10}^{2-}$ dimers in Fig. 9 are very similar to those in the neutral T_2Hal_{10} dimers (compare $Mo_2Cl_{10}^{2-}$ and Mo_2Cl_{10}), the more so as the molecular geometry of the neutral dimers results from the filling, by T atoms, of interstices in close-packed arrays of the halogen atoms in $THal_5$ crystals (cf. refs. 65 and 69), whereas the corresponding $T_2Hal_{10}^{2-}$ dimers in **26–32** are discrete anions in ionic structures containing composite univalent counter cations. The question as to whether the existence of a lone electron pair on the central atom is essential for a significant bridge asymmetry to be observed will be touched upon in ref. 22.

While the above account does not explain details of the geometry of the dimers in fundamental terms, it does offer a qualitative insight into the factors involved and sets forth criteria which a detailed model will have to satisfy. Clearly, the existing data set no more than sketches out the distribution of dimers in Figs. 5, 6, and 8. Although it is probable that subtler trends exist, e.g., those differentiating Group VI from Group V and $Se_2O_2Hal_6^{2-}$ dimers, it would be difficult at this stage to extract them with any confidence from the accidental causes of the observed spread (packing, hydrogen-bonding and interion effects, inadequacies of crystal-structure determinations).

Thermal motion: doing what comes naturally

If it is assumed that a centrosymmetric $Z_2Hal_{10}^{2n-}$ dimer consists of two $ZHal_5^-$ monomer halves held together by a $Z\cdots Hal_c'$,$Z'\cdots Hal_c$ interaction of a strength ranging (as measured by the $d_c' - d_c$ difference) from very weak to comparable to that in the Z—Hal_c bond, it is not unreasonable to suppose that the strength of this interaction will be reflected in the thermal motion of the dimer. More specifically, each monomer half by itself would be expected to approximate to RBM behaviour more closely than the dimer as a whole, if indeed the RBM model applies. The closeness of approximation to RBM behaviour is measured

[19]This is also the case for the $Z_2Hal_{10}^{2n-}$ dimers **8** and **9** and possibly also **7** and **17**.

[20]Results of TLS analysis (see below) are inconclusive on this point.

[21]Linear regression on the 21 $Z_2Hal_{10}^{2n-}$ points in Fig. 8 (excluding **Cf**, **Cg**, **10**, and the T dimers) gave $r^2 = 0.67$, $\sigma = 0.010$, $\sigma(\langle\Sigma\rangle)/\langle\Sigma\rangle = 0.317 - 0.0942\langle\Sigma\rangle$.

Can. J. Chem. Downloaded from www.nrcresearchpress.com by 217.78.4.112 on 09/08/12
For personal use only.

Can. J. Chem. Downloaded from www.nrcresearchpress.com by 217.78.4.112 on 09/08/12
For personal use only.

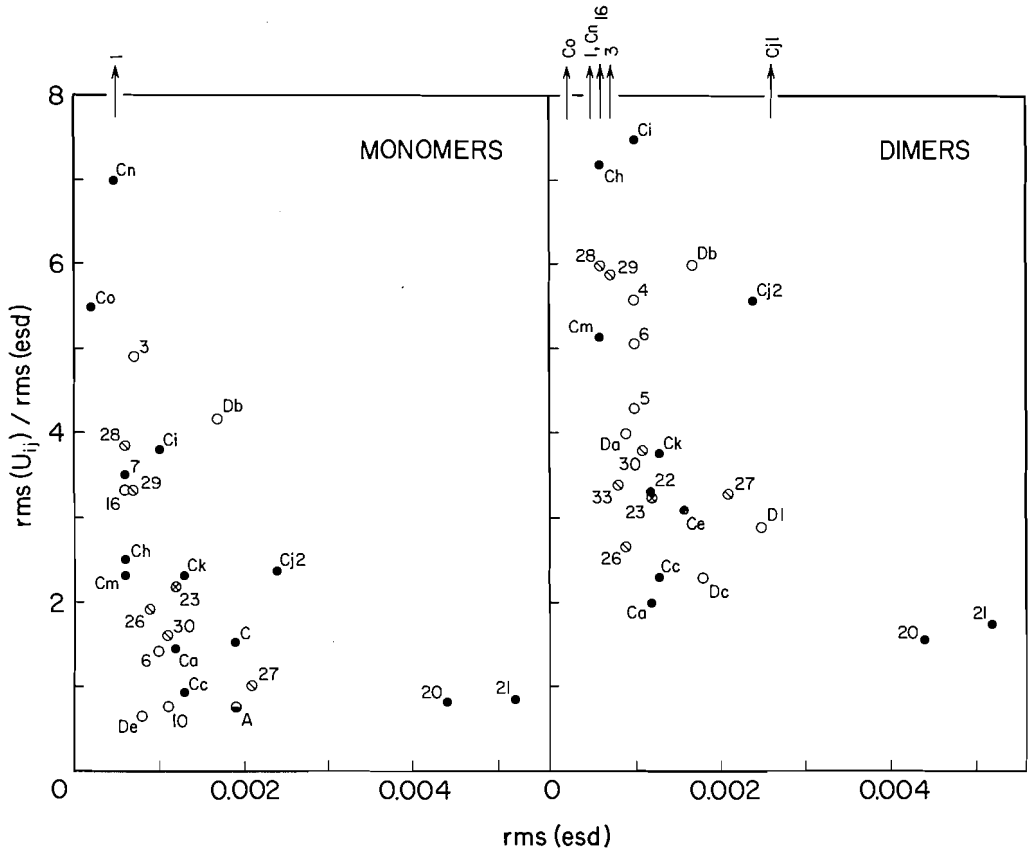

FIG. 10. Applicability of the RBM model to the thermal motion of $Z_2Hal_{10}^{2n-}$, $Z_2Hal_8^{2-}$, and $Se_2O_2Hal_6^{2-}$ anions considered as dimers (right) and as the respective monomer halves (left). For definitions of rms(U_{ij}) and rms(esd) (Å^2) see text. For code see Tables 2 and 9.

by the magnitude of $R(U_{ij})$ or rms(U_{ij}) as obtained from the TLS analysis, and by comparing rms(U_{ij}) = $[(1/n)\Sigma(\Delta U_{ij})^2]^{1/2}$ with the rms[esd(U_{ij})] = $[(1/n)\Sigma[\text{esd}(U_{ij})^2]^{1/2}$ (= rms(esd) for short) from the crystal-structure refinement. The decrease in rigidity of the binuclear unit relative to the monomer can then be estimated from the $\text{rms}_{2/1}$ = $\text{rms}(U_{ij})_{\text{dimer}}/\text{rms}(U_{ij})_{\text{monomer}}$ ratio.[22] The magnitude of this ratio can in turn be examined for dependence on the bridge asymmetry $d_c' - d_c$ or $(d_c' - d_c)_{\text{red}}$.

It must be emphasized that utilization of the results of TLS analysis can be fraught with uncertainties, and considerable caution must be exercised if the interpretation is to have physical meaning. The TLS figures of merit for a particular composite anion may vary widely from one structure to another, both because of real differences in the degree of applicability of the RBM model and because of the uneven quality of the crystal-structure determinations. In the present discussion we shall consider the $SnCl_6^{2-}$ ion in **A** and the undoubted $SeOCl_3^-$ monomer **De** (Fig. 10) as anions for which the TLS criteria of RBM are reasonably well satisfied and which may therefore be regarded as standards for judging the rigidity of the other anions. In neither case is there effective H-bonding interaction between the anion and the counter cation, and the single positive charge on the counter cation is in both crystals so diffuse that directional Coulombic interactions are unlikely to come into play. The $R(U_{ij})$ and rms(U_{ij}) values for both anions are small and the U_{ij} values are accounted for on the RBM model collectively within the experimental rms(esd). Similarly small figures of merit for the $ZHal_5^-$ monomers will therefore be taken to indicate that the RBM model adequately describes the thermal motion of the monomer as an independent inertial unit.

In the following the U_{ij} values of most of the reported $Z_2Hal_{10}^{2n-}$ as well as $Z_2Hal_8^{2-}$ and $Se_2O_2Hal_6^{2-}$ anions will have been subjected to scrutiny, some 35 species in all. The results are presented in Table J (deposited, see Experimental) and Figs. 10 and 11.[23]

[22] $R(U_{ij})$ is less suitable for this purpose than rms(U_{ij}), as the contribution to $R(U_{ij})$ of numerically small U_{ij} ($i \neq j$) values suffering from a large percentage error is out of all proportion to their importance and may create a misleading impression of how well the thermal motion approximates to RBM behaviour.

[23] In a number of cases execution of the standard TLS program (70) ended up in physically unreasonable results (not shown in Table J and Fig. 10), with negative values for the squares of one of the three mean librational amplitudes L about the principal axes of libration, in some instances for the monomer, in others for the dimer, and in yet others for both the monomer and the dimer. The reason for this behaviour appears to be a weak ill-conditioning of the U_{ij} data set. In general, a single minor adjustment of the tolerance criteria (70) will produce a set of positive L values, with only a small increase in rms(U_{ij}). The $\text{rms}_{2/1}$ ratios obtained in this way may, *faute de mieux*, still be considered reasonable indicators of the relative rigidity of the dimers, albeit inferior to $\text{rms}_{2/1}$ obtained from properly behaved U_{ij} sets and within the limitations discussed in the text. Such $\text{rms}_{2/1}$ values are indicated in Fig. 11 by underlining.

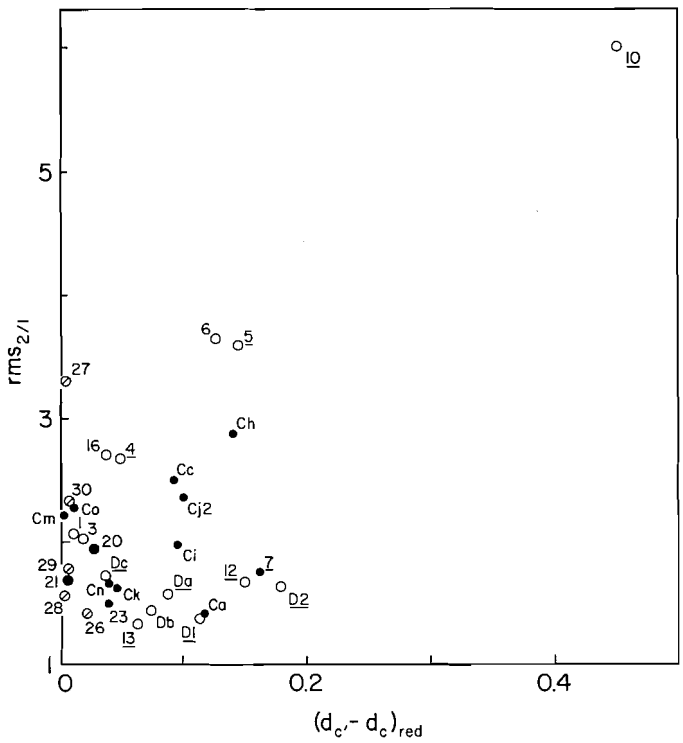

FIG. 11. Variation of the RBM "rigidity indicator" $rms_{2/1}$ = $rms(U_{ij})_{dimer}/rms(U_{ij})_{monomer}$ with the bridge asymmetry $(d_c' - d_c)_{red}$ in dimers. For code see Tables 2 and 9; for the underlined code numbers see text.

The rms(esd) values are, with the exception of **20** and **21**, all smaller than ~0.0025 Å^2, indicating that the quality of the U_{ij} data is generally acceptable. However, the $rms(U_{ij})$/rms(esd) ratio is greater than unity for all but a few of the species examined. This means that the RBM model does not describe the thermal motion of even the monomers adequately, the mismatch being the greater the larger the value of the ratio. This finding thus immediately calls for a scrutiny of the assumption that RBM is an appropriate model on which to correct bond lengths for the effects of thermal motion (see below).

The extent of conformity to the RBM model notwithstanding, the $rms(U_{ij})$/rms(esd) ratio for a dimer is always larger than that for the corresponding monomer, i.e., the rigidity of the dimer is always inferior to that of the monomer. Indeed, none of the dimers with rms(esd) $\leq$ 0.0025 Å^2 in Fig. 10 has an $rms(U_{ij})$/rms(esd) value smaller than 2. There are no clearly discernible trends in Fig. 10, not even between the 6-coordinate and the 5-coordinate Z species: statistical tests show that the probability of the $rms(U_{ij})$/rms(esd) means for the ZL_6 and the ZL_5 coordination classes to come from the same population is high. The incompleteness of the coordination sphere of Z in the ZL_5-type monomers *or* dimers does not therefore appear to be a significant rigidity-determining factor, at least in the present sample.

Since the rms(esd) for a centrosymmetric dimer is the same as for each of the monomer halves, $[rms(U_{ij})/rms(esd)]_{dimer}/[rms(U_{ij})/rms(esd)]_{monomer} = rms_{2/1}$. On plotting $rms_{2/1}$, which ranges from ~1.4 to ~3.6, against the bridge asymmetry parameter $(d_c' - d_c)_{red}$ a considerable scatter results (Fig. 11). The ratio can be claimed to increase with $(d_c' - d_c)_{red}$ if the TLS result for the clearly crystallographic dimer $Sb_2Cl_{10}^{4-}$ dimer in **10** is accepted as legitimizing the direction of the presumed trend.

Obviously, additional experimental data for dimers must be obtained before a statistically valid trend can be claimed. This conclusion is somewhat disappointing vis-à-vis the initial expectation that $rms_{2/1}$ as a measure of decrease of the rigidity of the dimer relative to the monomer varies with the bridge asymmetry, but if the existence of such a trend *is* substantiated, an augmented Fig. 11 would be a useful device for clarifying the relationship between chemical and crystallographic dimers.

Bond-length corrections for thermal motion

From the above it follows that the RBM model describes the motions of the anions only to the extent indicated by $rms(U_{ij})$. The results of a TLS analysis cannot be used as a basis of bond-length corrections unless $rms(U_{ij})$ is small, and where the latter is not stated, the meaning of the corrections is uncertain. However, where the observed U_{ij} *are* satisfactorily explained, collectively, on the assumption of RBM but significantly better so for the separate monomer halves than for the dimer, corrections to bond lengths and angles should be made on the basis of the monomer RBM rather than that of the dimer. This in practice may not make appreciable difference measured against the accuracy of the crystal-structure determination, but *in principle* the distinction of course matters, for the corrections in the two cases arise from RBM's about entirely different centroids and axes (cf. Figs. 12 and 13).

Some idea of the importance of the differences in the corrections to bond lengths calculated on the assumption of RBM in the monomer and the dimer, respectively, can be gained from Table K (deposited, see Experimental). The differences are small, but the corrections to the individual bond lengths in general follow a different pattern as to magnitude for the monomer and the dimer. These findings raise questions about the practical meaning of the corrected bond lengths when these are reported without indication of the comparative figures of merit and physical significance of the underlying TLS analysis.

Chemical or crystallographic dimers?

Where the d_c' distance in Groups VI and V dimers is long but explained without contradiction as a consistent response to TE, it qualifies as corresponding to a weak bonding interaction and the dimers qualify as "chemical" dimers. At the other extreme, a crystal structure may contain widely separated, clearly identifiable discrete monomers in positions and mutual orientations that give no indication of a tendency to dimerize, e.g., $Na^+[TeF_5]^-$ (see below).

We shall now turn to intermediate situations, i.e., to crystal structures in which $ZHal_5^{n-}$ or related anions reported as monomeric occur in centrosymmetric pairs and in mutual orientations such that the two monomers would form an undoubted μ_2-dimer if the distance between them were decreased. Examples of such *pro*-dimer pairs are $TeF_5^- \cdots TeF_5^-$ in **Cf** and **Cg** and the $SbCl_5^{2-} \cdots SbCl_5^{2-}$ pair in **10**; the description of the anions in **Cf** in ref. 2 as "quasi-monomeric pseudo-octahedral anions with almost negligible bonding interaction within the pseudo dimer" testifies to the ambiguity with which such situations are approached.

The centrosymmetric $ZHal_4^{n-}$ pairs in **Cf**, **Cg**, and **10** may be regarded formally as dimers in which d_c' is ~65% longer than the mean of the other five Z—Hal bond lengths in the

Can. J. Chem. Downloaded from www.nrcresearchpress.com by 217.78.4.112 on 09/08/12
For personal use only.

Can. J. Chem. Downloaded from www.nrcresearchpress.com by 217.78.4.112 on 09/08/12
For personal use only.

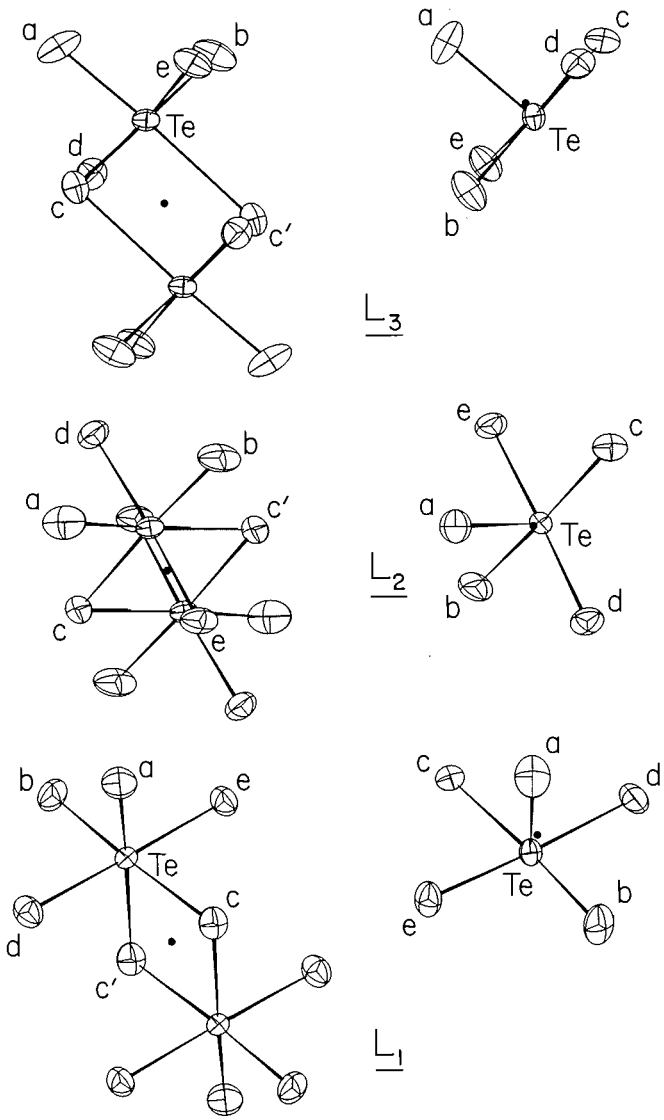

FIG. 12. Librational motions of the $Te_2Cl_{10}^{2-}$ (**Ch**) ion considered as a dimer (left) and as two monomer halves (right). Projection down principal axes of libration, in the decreasing order of the mean librational amplitude ($L_3 > L_2 > L_1$). The centroids of the motions are indicated by black dots.

Cf and **Cg** monomer halves and 50% longer in **10**. The positions of the points for **Cf** and **Cg** (regarded as dimers) in Figs. 5, 6, and 8 are extreme relative to the $Te_2Hal_{10}^{2-}$ (Hal $\neq$ F) dimers. It could conceivably be argued that a nonlinear relationship may exist in these plots that would reconcile the positions of these two points with the rest of the dimers, but such an argument would be difficult to sustain from these two isolated cases alone, no other $Z_2F_{10}^{2n-}$ dimer or pseudo dimer structures being known at present.

In **10** the orientation of the two $SbCl_5^{2-}$ ions is such as to suggest the existence of a highly asymmetric double bridge, but the Sb···Cl$_c$′ separation of 3.88 Å is not consistent with the presence of even a weak Sb···Cl bond. In addition, the very small rms(U_{ij}) and rms(U_{ij})/rms(esd) values for the monomer point to the autonomous character of the $SbCl_5^{2-}$ unit.

In none of the **Cf**, **Cg**, and **10** pairs can d_c' be related to the respective d_a by TE. In **10** this is obvious from the shape of the TE(Sb—Cl) line (22); the d_c'(Sb—Cl) expected for d_a (Sb—Cl) = 2.39 Å would be in the vicinity of 3.2 Å, i.e., ~0.7 Å below the observed d_c'. In **Cf** and **Cg** the d_c' to be expected from TE(Te—F) cannot be assessed, for the curvature of the TE line is very poorly defined by the data currently available. Such indications as there are seem compatible with the conclusion that the observed d_c'(Te—F) is longer than would be expected from TE.

From these observations one could conclude, tentatively, that the centrosymmetric $ZHal_5^{n-}$ pairs found in **Cf**, **Cg**, and **10** are "crystallographic" rather than "chemical" dimers, i.e., $ZHal_5^{n-}$ pairs that owe their existence to external factors and not to a strong intrinsic tendency of the $ZHal_5^{n-}$ units to dimerize. If such tendency exists, it is not sufficiently strong to overcome other forces implicit in the formation of the crystal from solution.

It is significant in this context that the compounds in Tables 2 and 9 that are of the [cation$^+$]$_2$[dimer^{2-}] type and in which the cation is composite but not highly asymmetric crystallize, without exception and regardless of the specific chemistry of the dimer (e.g., $Se_2Hal_{10}^{2-}$, $Se_2O_2Hal_6^{2-}$, $As_2Br_8^{2-}$, $Mo_2Cl_{10}^{2-}$, $Os_2Cl_{10}^{2-}$), in one of the three space groups $P\bar{1}$, $P2_1/c$ ($\equiv P2_1/a$, $P2_1/n$), or $Pbca$; $P\bar{1} \subset P2_1/c \subset Pbca$ ($\supset Pa3$). In *molecular* crystals these space groups (plus $C2/c$) describe the symmetries of closest-packed arrangements of molecules of C_i symmetry, but the $P\bar{1}$ and $P2_1/c$ symmetries can also be realized by close packing of completely asymmetric molecules (71). The close-packed layers are found in one, two, or three systems of planes, depending on the particular space group. The [cation$^+$]$_2$-[dimer^{2-}] crystals of course are not molecular, but the dimers, because of their size relative to the cations,[24] dominate the packing, with the result that the overall structure consists of a close packing of the dimers with the cations interstitial to it. The dimer centres form an oblique layer mesh with a coordination number 6 and a minimum plane-group symmetry $p2$; the Z···Z′ vectors are at an arbitrary tilt to the axial directions of the layer lattice. The cations are situated either between or in the close-packed dimer layers, depending on the cation shape and size and on the number of ligands in the dimer, the latter two factors determining the Z···Z′ tilt. The tendency of the dimers to form such layers explains the preponderance of the *anti*-CdI_2-type structures among these compounds.

When the cation is small, it will not fill the space between the dimers properly. This will result in an inefficient utilization of space. Furthermore, in contrast to composite cations, in which the distribution of ionic charge is diffuse, in a simple univalent cation the full charge is spatially much more concentrated and thus likely to lead to strong local interactions with atoms of the dimers.[25] If the monomer anions were to dimerize, the distribution of ionic charge in such a [cation$^+$]$_2$[dimer^{2-}] crystal would compete with the energetically more favourable as well as better space-filling ar-

[24]The nuclear skeleton of a $Z_2Hal_{10}^{2-}$ dimer may be approximated for the present purpose by an elliptical cylinder about 8 Å long and 4–6 Å in diameter.

[25]This is also the case with composite cations capable of hydrogen bonding, e.g., NH_4^+ and the alkylammonium cations.

Can. J. Chem. Downloaded from www.nrcresearchpress.com by 217.78.4.112 on 09/08/12
For personal use only.

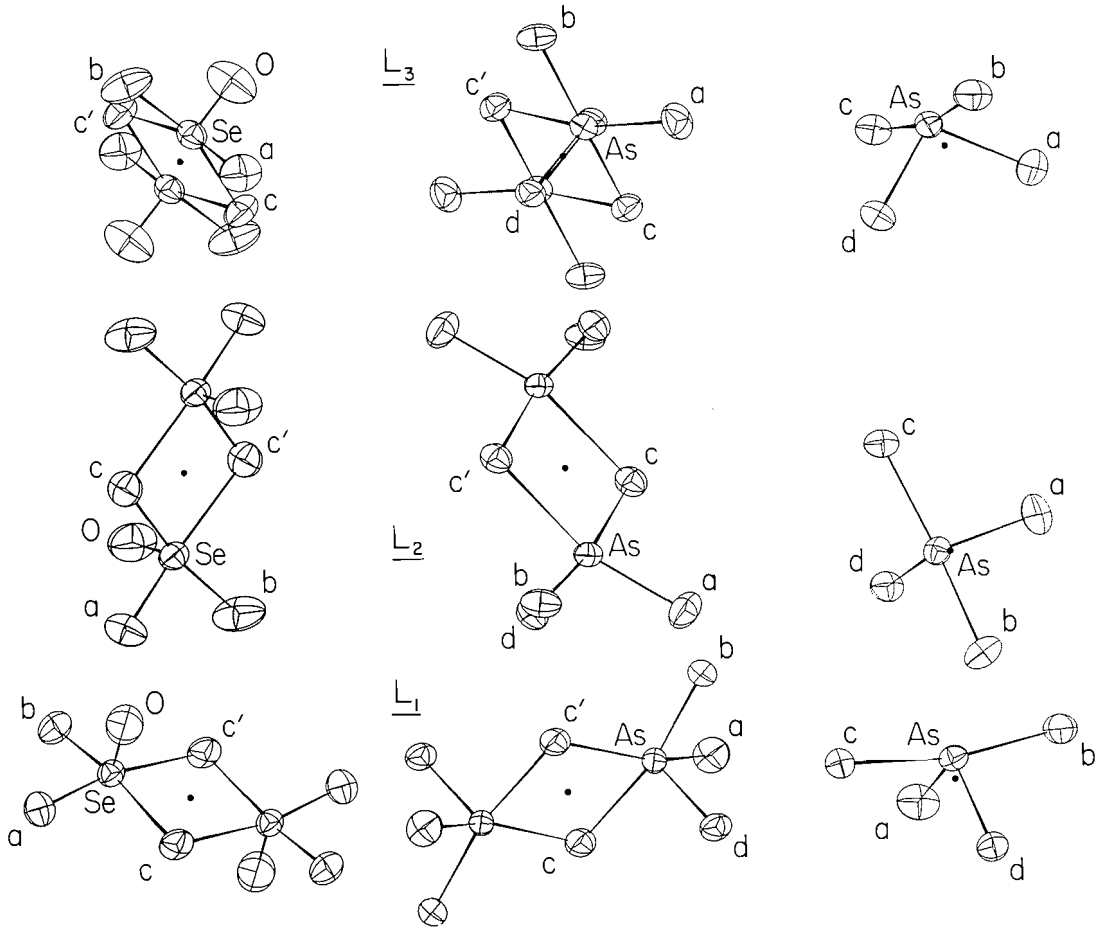

FIG. 13. Librational motions of the $Se_2O_2Cl_6^{2-}$ (**Db**, left) and $As_2I_8^{2-}$ (**6**, centre) dimers and of the monomer half of $As_2I_8^{2-}$ (right). TLS analysis based on parameter values from refs. 10 and 35, respectively. The oxygen atom in $Se_2O_2Cl_6^{2-}$ corresponds to the I_d atom in $As_2I_8^{2-}$. Cf. also caption of Fig. 12.

rangement that is obtained when the monomer halves in the crystal exist as separate anions. The close packing of the anion dimers is then likely to give way to a more typically ionic crystal structure with a regular three-dimensional cation–anion alternation. This is arguably the case with $K[TeF_5]$ (27, 72), which has a distorted (*Pbcm*) CsCl-type packing, and with $Na[TeF_5]$ (77), both of which contain discrete TeF_5^- monomers.

The centrosymmetric $TeF_5^-\cdots TeF_5^-$ pairs in **Cf** ($P2_1/n$) and **Cg** (*Pnma*) as well as the $SbCl_5^{2-}\cdots SbCl_5^{2-}$ pair in **10** ($P2_1/c$) constitute situations intermediate between obvious $Z_2Hal_{10}^{2n-}$ dimers and discrete $ZHal_5^{n-}$ monomers. While the Hal_a—Z—Hal_c' angle in these pairs is small compared to that in the true dimers (148° in **Cf**, 138° in **Cg**, 144° in **10**, but 177° in **Ch**), the relative orientation of the monomer halves is such that it would take only a minor adjustment of the tilt and of $d(Z\cdots Z')$ to convert the pair to a true dimer. These pairs may therefore be regarded as frustrated dimers. In $Rb[TeF_5]$ (*Pnma*, refs. 78 and 79) and $NH_4[TeF_4]$ ($Pn2_1a$, refs. 28 and 80) the situation is more complicated in that the two crystallographically nonequivalent TeF_5^- anions in a pair (d[Te(1)···Te(2)] = 4.40 Å in the Rb and 4.34 Å in the NH_4 compound) are not related by a symmetry operation, and single-bridging Te···F approaches at unfavourable Te···F distances (Te···F ~ 3.0, 3.4 Å) and F—Te—F angles occur between TeF_5^- pairs in the chain-like arrangements of anions. However, rotational adjustments about the Te atoms of the TeF_5^- units would result in pseudo dimer pairs similar to those in **Cf** and **Cg**.

These general arguments do not account completely for the differences between the four chemically closely similar structures containing the centrosymmetric $SeOCl_3^-\cdots SeOCl_3^-$ pairs and formulated (cf. Table 2) as

Db $(Ph_4P)_2[Se_2O_2Cl_6]$, $P\bar{1}$ **Dd** $(Ph_4As)_2[Se_2O_2Br_6]$, $P\bar{1}$

Dc $(Ph_4P)_2[Se_2O_2Br_6]$, $P2_1/c$ **De** $(Ph_4As)[SeOCl_3]$, $P2_1/c$

Examination of these crystal structures may in fact provide a clue to the above title question.

The dimensional and chemical differences between Ph_4P^+ and Ph_4As^+ being trivial, it is not surprising that **Db** and **Dd** are isostructural. They consist of almost close-packed planar layers of identically oriented $Se_2O_2Hal_6^{2-}$ dimers interleaved with planar layers of the cations; the P (or As) atoms in the cation layers are arranged in zigzag chains, d(P···P) ~ 6.5 Å (Fig. 14). The structure containing **Dc** approximates even more closely to the *anti*-CdI_2-type arrangement. The centres of the dimers form a slightly distorted hexagonal planar network with alternating orientations of the di-

Can. J. Chem. Downloaded from www.nrcresearchpress.com by 217.78.4.112 on 09/08/12
For personal use only.

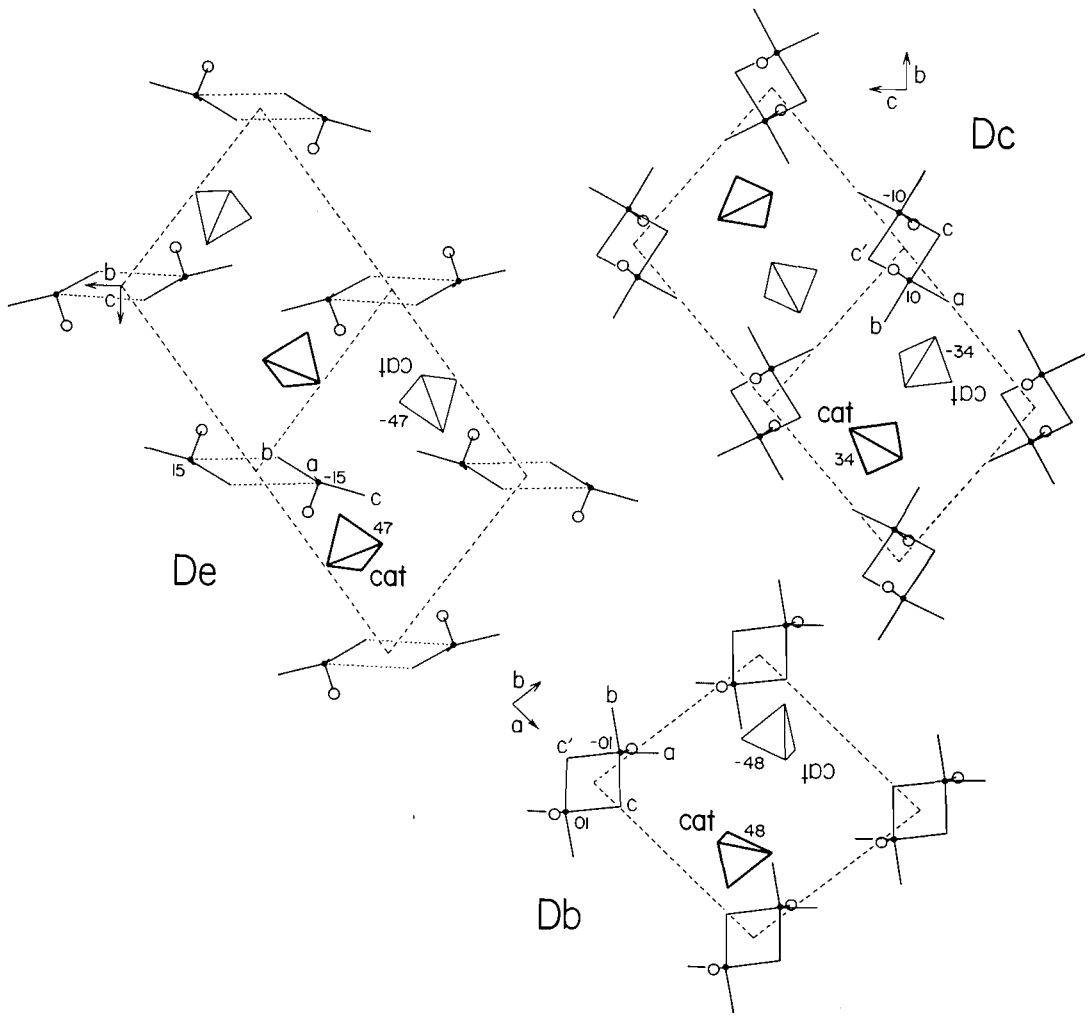

FIG. 14. Projections displaying the *anti*-CdI_2-type packing of cations and $SeOHal_3 \cdots SeOHal_3$ pairs in $(Ph_4P)SeOCl_3$ (**Db**), $(Ph_4P)SeOBr_3$ (**Dc**), and $(Ph_4As)SeOCl_3$ (**De**). Black circles, Se; open circles, oxygen atoms. The centres of the $SeOHal_3 \cdots SeOHal_3$ pairs (at zero elevation) are in the plane of the paper; the elevations of the Se and P (or As) atoms are indicated by the respective fractional coordinates × 100. The cations are represented by the PC_4 and AsC_4 tetrahedra. The basic *anti*-CdI_2-type cell in the $(Ph_4P)_2[SeOHal_3 \cdots SeOHal_3]$ and $(Ph_4As)_2[SeOCl_3 \cdots SeOCl_3]$ structures (dashed lines) contains a centrosymmetric cation pair (marked **cat**); in **Dc** and **De**, columns of these cells $\|a$ alternate in an *antiferro* arrangement.

mers at the corners of the *anti*-CdI_2 cells (Fig. 14), so that two cells are required to define the structure translationally.

When properly presented the structure containing **De** is seen to have an ion packing intermediate between those of **Db** and **Dc** (Fig. 14). The anions are arranged, formally, in centrosymmetric pairs the centres of which define a distorted hexagonal array at relative height $h = 0$, similar to **Db** and **Dc**, and with alternating orientations of these pairs, similar to **Dc**. However, unlike **Dc** but similar to **Db**, the centre atoms of all the cations are found in quasi-planar layers halfway ($h \sim \frac{1}{2}$) between the $h = 0$ layers of the anion-pair centres; in **Dc** half the P atoms are located at $h \sim \frac{1}{3}$, with the other half at $h \sim \frac{2}{3}$. The orientation of the $SeOCl_3^-$ units in these pairs is favourable to dimerization through Cl_b and Cl_b', but the $Se \cdots Cl_b'$,$Se' \cdots Cl_b$ distances are 5.3 Å, i.e., much too long for significant bonding interaction. The next-shortest $Se \cdots Cl$ distances, in centrosymmetric pairs involving other $SeOCl_3^-$ neighbours, are considerably longer, 6.23 and 7.76 Å, with less favourable $SeOCl_3^-$ orientations. The **De** structure, although *pro*-dimer, is therefore properly described as formulated above, viz. a monomer salt.

Comparison of the volumes per formula unit shows that the monomer-containing structure indeed represents a more efficient packing: V_1(**Db**) = 594 Å^3, V_1(**Dc**) = 617 Å^3, and V_1(**Dd**) = 619 Å^3, whereas V_1(**De**, −135°C) = 569 Å^3. The estimated (see footnote 4) room-temperature V_1(**De**) is 580 Å^3, i.e., still significantly inferior to V_1(**Db**).

Since the spatial organization of the ions in these structures is basically the same, one is led to the conclusion that there is no fundamental chemical difference between the $SeOCl_3^-$ monomer and the $Se_2O_2Cl_6^{2-}$ dimer anions in such crystals. Which of the two will prevail in any given situation will be determined by unpredictable details of ion packing. In any event the energy associated with the formation of the dimer from (or its dissocation into) $SeOCl_3^-$ monomer units is of a magnitude such that changes in lattice energy arising from relatively minor positional and orientational displacements of the ions are sufficient to decide

the outcome of the monomer/dimer competition. In other words, the dimer is always a *crystallographic* dimer, but once formed it assumes a chemical identity of its own and behaves like a chemical species in its own right (underlying bonding scheme, conformation to TE).

Conclusions

1. In a free $ZHal_5^{n-}$ (Z = Se, Te; Bi) ion, of symmetry C_{4v}, $d(Z—Hal_{ax}) < d(Z—Hal_{eq})$. When two such ions in a crystal associate to form a centrosymmetric $Z_2Hal_{10}^{2n-}$ dimer, the resulting differentiation in the $d(Z—Hal_{eq})$ and lengthening of $d(Z—Hal_{ax})$ are consistently interrelated through the operation of TE (Figs. 1 and 2). The asymmetry of the double bridge in $Z_2Hal_{10}^{2n-}$ is thus a property of the dimer as a whole; it decreases from Cl to I and with the increasing difference in the Z—Hal_{eq} bond lengths in the bridge plane (Fig. 5). The limits of the bridge asymmetry appear to be set by the $d(Z—Hal_{ax})$ and $d(Z—Hal_{eq})$ values in the free monomer (Fig. 7).

2. The empirical quantification of TE makes it possible to authenticate Z—L bonds as Z—Hal bonds in cases where the nature of the ligand is in doubt, e.g., on partial replacement of a Hal ligand by OH.

3. Where the RBM model is applicable, analysis of the thermal motion of a centrosymmetric $Z_2Hal_{10}^{2n-}$ dimer shows that the rigidity of the dimer is smaller than that of each $ZHal_5^{n-}$ nomoner half. As a consequence, corrections of bond lengths for the effects of thermal motion should be made on the basis of the monomer as the rigid inertial unit. In practice the differences between corrections made for the monomer and for the dimer are not large, but their magnitudes follow different patterns in the two models. There are indications that the rigidity of the dimer relative to the monomer half ($rms_{2/1}$, Fig. 11) may decrease with the increasing asymmetry of the bridge and thus in the direction of decreasing strength of association of the monomer halves.

4. All centrosymmetric $Z_2Hal_{10}^{2n-}$ dimers are crystallographic by virtue of the presence of a crystallographic inversion centre. The difference between a chemical and a crystallographic dimer is probably continuous, the limit for the latter being an inversion-related pair of well-separated monomers, and is believed to be the outcome of a fine balance of crystal forces, unpredictable at present.

IV. Experimental

Structure determination (Table 2)

A CAD-4 four-circle diffractometer (ω:2θ scans) was used in the data acquisition. Lorentz, polarization, and empirical absorption corrections (3) were applied. Scattering factors for neutral atoms and corrections for anomalous scattering were taken from ref. 73. The structures were solved with the SHELX-76 and SHELXS-86 programs (74, 75). After the nonhydrogen atoms had been located, full-matrix least-squares ($w\Delta|F|$ = minimum) refinement was carried out with isotropic temperature factors until R was reduced to a reasonably low value. The hydrogen atoms were then placed, consistent with the difference maps, and the refinement was continued with anisotropic temperature factors on the nonhydrogen and isotropic factors on the hydrogen atoms. The H atoms were constrained to ride on their respective C atoms. The final difference maps were featureless except as noted. The anisotropic temperature factor is defined as $\exp[-2\pi^2(U_{11}h^2a^{*2} + U_{22}k^2b^{*2} + U_{33}l^2c^{*2} + 2U_{23}klb^*c^* + 2U_{13}hla^*c^* + 2U_{12}hka^*b^*)]$. The TLS and best plane calculations were performed with CRYSTALS (70).

The following material has been deposited:[26]

Table A. (n-$Pr_4N)_2SnCl_6$ (**A**): positional parameters and isotropic temperature factors of hydrogen atoms.

Table B. (n-Pr_4N)[$TeCl_4$(OH)] (**B**): positional parameters and isotropic temperature factors of hydrogen atoms.

Table C. (n-$Pr_4N)_2[Te_2Cl_{10}]$ (**C**): positional parameters and isotropic temperature factors of hydrogen atoms.

Table D. (n-$Pr_4N)_2[Se_2O_2Cl_6]$ (**D**): positional parameters of hydrogen atoms.

Table E. Observed and calculated structure factors for **A**.

Table F. Ditto for **B** (refinement in $C2/c$).

Table G. Ditto for **C** (all ligands assumed to be Cl).

Table H. Ditto for **D**.

Table J. TLS analysis of anion dimers treated as monomers or dimers.

Table K. Corrections δd for thermal motion (in 10^{-3} Å) to be added to Z—Hal bond lengths in the anions.

Compound A

This salt was prepared by neutralizing aqueous n-Pr_4NOH with HCl, adding to the resulting solution an equivalent amount of $SnCl_4$ dissolved in water strongly acidified with HCl, and allowing **A** to crystallize by slow evaporation at room temperature.

Systematic absences: $hk0$, h odd; $0kl$, k odd; $h0l$, l odd; consistent with $Pbca$. The Sn position was found from a Patterson map and the remaining nonhydrogen atoms from Fourier syntheses. The isotropic temperature factors on the H atoms were refined, one value reported for each cation. The weighting scheme was $w = 1.18/[\sigma^2(F) + 0.005F^2]$. Two reflections were omitted from the final refinement because of suspected extinction. The highest residual peak in the final difference map, 0.68 e/Å^3, was near the Sn atom.

Compound B

Intended product composition, (n-$Pr_4N)_2TeCl_6$. The solution obtained by dissolving 0.56 g TeO_2 in 5 mL of 6 M HCl was added, with stirring, to 14 mL of a 0.5 M aqueous solution of n-Pr_4NCl. The resulting clear, colourless solution was allowed to crystallize by slow evaporation at room temperature. The crystal used in the structure determination came from the crop of clear, pale yellow crystals that appeared after 1 day.

The systematic absences (hkl, $h + k$ odd; $h0l$, h,l odd) pointed to $C2/c$ or Cc as possible space groups, the E-statistic favouring the centrosymmetric group. The Te atom was found from a Patterson map, at or near the origin. Only four instead of the expected six Cl atoms per Te were located in a Fourier map. The FT-ir spectrum of the product (Fluorolube mull, CaF_2 plates) taken at this stage contained a strong, broad ($\nu_{1/2} \sim 270$ cm^{-1}) OH-stretching absorption at 3397(10) cm^{-1} on a regular background but no discernible $\delta(H_2O)$ absorption. These findings, together with chemical considerations, suggested that the composition of the crystal was (n-Pr_4N)[$TeCl_4$(OH)], with $Z = 4$ and a square-pyramidal [$TeCl_4$(OH)]$^-$ anion. We therefore proceeded with solution of the structure on this assumption, all the remaining nonhydrogen atoms having been located from difference maps. It was clear, however, that for a solution in $C2/c$ the Te and O atoms had to be treated as positionally disordered. Both were placed in general positions with half occupancy, the Te atom close to the origin, and the structure was refined to $R = 4.6\%$, with anisotropic temperature factors on the nonhydrogen atoms and isotropic factors on the hydrogens. The weighting scheme was $w = 2.45/[\sigma^2(F) + 0.0015F^2]$.

[26]These tables may be purchased from: The Depository of Unpublished Data, Document Delivery, CISTI, National Research Council Canada, Ottawa, Canada K1A 0S2.

Tables A–D have also been deposited with the Cambridge Crystallographic Data Centre and can be obtained on request from The Director, Cambridge Crystallographic Data Centre, University Chemical Laboratory, Lensfield Road, Cambridge, CB2 1EW, U.K.

Can. J. Chem. Downloaded from www.nrcresearchpress.com by 217.78.4.112 on 09/08/12
For personal use only.

Can. J. Chem. Downloaded from www.nrcresearchpress.com by 217.78.4.112 on 09/08/12
For personal use only.

Three reflections were omitted from the final refinement because of suspected extinction. The highest residual peak in the final difference map was 0.8 e/Å^3, near Cl(2).

The refined structure with Te and O in disorder gave reasonable bond lengths and confirmed the assumed anion geometry. The H atom of the OH group could not be located, but examination of the O···Cl separations and Te—O—Cl angles revealed that Cl(2) in a neighbouring anion was the only atom at a distance and angle that could qualify as an acceptor in a O—H···Cl hydrogen bond.

Since placing Te and O in the general position of the noncentrosymmetric subgroup *Cc* of *C*2/*c* would result in a fully ordered structure, **B** was also refined in *Cc*. The final *xyz* values from the refinement in *C*2/*c* were used as the initial parameters. With anisotropic temperature factors on the nonhydrogen atoms, one U_{iso} each for H(CH_3) and H(CH_2), and $w = 1.76/[\sigma^2(F) + 0.0015F^2]$, the structure refined to $R = 4.2\%$ ($R_w = 4.7\%$, d/p = 5.7, G.O.F. = 1.53). The highest residual peaks in the final difference map, 0.55 and 0.46 e/Å^3, were near Cl(2) and Cl(2A), respectively. The enantiomorph was also refined but the results were not significantly different.

While the refinement in *Cc* gave a lower *R* value and more uniform Te—Cl bond lengths, the Te—O bond length was significantly shorter than that from the refinement in *C*2/*c*. The ordered and partially disordered structures are compared in Sect. II.

Compound ***C***

Intended product composition, $(n\text{-}Pr_4N)_2TeCl_6$. The canary yellow paste that resulted on adding an equivalent amount of a concentrated aqueous solution of $n\text{-}Pr_4NCl$ to a solution of TeO_2 in a slight excess of concentrated HCl was separated from the mother liquor by decantation and redissolved in concentrated HCl. This solution was concentrated by heating and allowed to stand at room temperature. The deep yellow crystals that formed after 3 days were filtered off, pressed dry between layers of filter paper, and air-dried.

Systematic absences, none; consistent with $P\bar{1}$ and $P1$. The structure was solved in $P\bar{1}$. The Te atom was found in a general position from a Patterson map and the other nonhydrogen atoms from Fourier syntheses. It was clear at this stage that the composition of the crystal did not correspond to the above intended composition. From the combined crystallographic and chemical evidence the crystal was taken to be $(n\text{-}Pr_4N)_2[Te_2Cl_{10}]$, the essential correctness of which assumption was borne out by subsequent refinement. The isotropic temperature factors on the H atoms were refined, one for the methyl hydrogens and another for the remaining hydrogens. The weighting scheme was $w = 4.22/[\sigma^2(F) + 0.000633F^2]$. Six reflections were omitted from the final refinement because of suspected extinction. The highest residual peak in the final difference map, 1.1 e/Å^3, was near the Te atom.

After the realization that the $Te_2Cl_{10}^{2-}$ dimer in **C** was in fact partially hydrolyzed at the L_a site the refinement was repeated in order to estimate the degree of replacement of Cl_a by OH. The Te—O_a and Te—Cl_a distances were fixed to 1.90 and 2.33 Å, respectively, with a tolerance of 0.005 Å. All nonhydrogen atoms were refined with anisotropic temperature factors except Cl_a and O_a, which were refined with equal isotropic temperature factors, initially set at 0.06 Å^2; the site occupancy factor at *a* was fixed at 0.84 Cl + 0.16 O, as estimated from an exploratory refinement. After refinement to convergence the site occupancy factor was allowed to refine, giving 0.52 for Cl and 0.48 for oxygen. A final refinement fixing the site occupancy factor at these values and refining Cl_a and O_a with anisotropic temperature factors ($w = 5.30/[\sigma^2(F) + 0.000633F^2]$) gave the following result: $R = 7.3\%$, $R_w = 8.1\%$, G.O.F. = 6.53, d(Te—O_a) = 1.92(1) Å, d(Te—Cl_a) = 2.35(1) Å; population at site *a*, 0.515(2) Cl + 0.485(2) O; highest residual peak, 1.1 e/Å^3, near the Te atom.

Compound ***D***

Intended product composition, $(n\text{-}Pr_4N)_2SeCl_6$. Equivalent amounts of SeO_2 dissolved in 6 M HCl and a concentrated aqueous solution of $n\text{-}Pr_4NCl$ were combined and the resulting solution was allowed to stand at room temperature. The clear, pale yellow crystals that appeared after 3 months were dried between layers of filter paper and subsequently air-dried.

Systematic absence, none; consistent with $P\bar{1}$ and $P1$. When the two nonequivalent $SeCl_3$ units were found using SHELXS-86 and most of the nonhydrogen atoms were located from Fourier syntheses, it became clear that the cation:Se ratio was not 2:1 as intended but 1:1, with the Se and Cl atoms forming two distinct centrosymmetric μ_2-$Cl_2Se(Cl)_2SeCl_2$ dimers. Further refinement revealed the presence of oxygen as the ligand perpendicular to the bridge plane. This established the composition as $(n\text{-}Pr_4N)_2[Se_2O_2Cl_6]$. The refinement was continued on this basis to convergence at $R = 9.4\%$. The probable cause of this high *R* value was the progressive deterioration of the crystal, which on exposure to the X-ray beam turned black. The intensities of the three standard reflections dropped *unevenly* in the course of the collection by between 15 and 20%, most of the decrease occurring toward the end of the data collection. Omission of a block of these last reflections, deemed to be most affected (ca. 8% of the total used), and re-refinement reduced *R* insignificantly, leaving the final parameter values virtually unchanged. In spite of the large final *R* value the structure appears to be adequately refined (cf. the reasonable esd's on the final parameter values).

The highest residual peaks in the final difference map, 1.2 and 1.4 e/Å^3, were near the Se(1) and Se(2) atoms, respectively. The weighting scheme was $w = 4.17/[\sigma^2(F) + 0.100F^2]$. Ten reflections were omitted from the final refinement because of suspected extinction.

Nonlinear optimization

The model function was fitted to the d,d^* data pairs using a nonlinear least-squares procedure that minimizes SSE = $\Sigma(d^*_{obs} - d^*_{calc})^2$, and a statistical package comprising a Gauss–Newton algorithm described in ref. 76. Approximate standard errors on the parameter estimates were obtained from the inverse of the expected information matrix, which contains sums of squares and cross products of the model partial derivatives with respect to the parameters. A measure of the overall agreement between the observed and fitted values is given by $\hat{r}^2 = 1 - \text{SSE/TSS}$, where TSS = $\Sigma(d^*_{obs} - \overline{d^*}_{obs})^2$.

Acknowledgments

We are greatly indebted to Professor B. Krebs and Dr. F.-P. Ahlers for their generosity in providing us with details of a number of their crystal-structure determinations in advance of publication and with other valuable information. We thank Dr. David C. Hamilton for supplying much of the expertise needed for the statistical treatment of the data, and Mrs. Lorraine Fullum-Bouchard for her assistance with the preparative chemistry. This investigation was supported by grants from the Natural Sciences and Engineering Research Council of Canada to O.K. and T.S.C., and from the Mount Saint Vincent University Committee on Research and Publication to M.A.J.

1. O. Knop, A. Linden, B. R. Vincent, S. C. Choi, T. S. Cameron, and R. J. Boyd. Can. J. Chem. **67**, 1984 (1989).
2. B. Krebs and F.-P. Ahlers. Adv. Inorg. Chem. **35**, 235 (1990).
3. N. Walker and D. Stuart. Acta Crystallogr. Sect. A: Found. Crystallogr. **A39**, 158 (1983).
4. A. Ries. Z. Kristallogr. **39**, 49 (1904).
5. A. Ries. Z. Kristallogr. **36**, 321 (1902).
6. B. Krebs and V. Paulat. Angew. Chem. Int. Ed. Engl. **12**, 666 (1973).
7. V. Paulat. Ph.D. thesis. Universität Bielefeld. 1976.
8. B. Krebs and K. Büscher. Z. Anorg. Allg. Chem. **463**, 56 (1980).

Can. J. Chem. Downloaded from www.nrcresearchpress.com by 217.78.4.112 on 09/08/12
For personal use only.

9. B. Krebs, M. Hucke, and A. Schäffer. Z. Kristallogr. **159**, 84 (1981).
10. B. Krebs, A. Schäffer, and M. Hucke. Z. Naturforsch. **37b**, 1410 (1982).
11. B. Krebs, M. Hucke, M. Hein, and A. Schäffer. Z. Naturforsch. **38b**, 20 (1983).
12. K. Gretenkord. Ph.D. thesis. Universität Münster. 1984.
13. A. J. Privett, S. L. Craig, D. Y. Jeter, A. W. Cordes, R. T. Oakley, and R. W. Reed. Acta Crystallogr. Sect. C: Cryst. Struct. Commun. **C43**, 2023 (1987).
14. B. Krebs, N. Rieskamp, and A. Schäffer. Z. Anorg. Allg. Chem. **532**, 118 (1986).
15. H. G. Stammler and J. Weiss. Z. Naturforsch. **44b**, 1483 (1989).
16. J. C. Jumas, M. Maurin, and E. Philippot. J. Fluor. Chem. **10**, 219 (1977).
17. A. W. Cordes. Inorg. Chem. **6**, 1204 (1967).
18. B. Krebs. Nova Acta Leopoldina, **59**, 131 (1985).
19. K. Büscher, S. Heuer, and B. Krebs. Z. Naturforsch. **36b**, 307 (1981).
20. Yu. E. Gorbunova, Yu. V. Kokunov, and Yu. A. Buslaev. Pure Appl. Chem. **59**, 155 (1987).
21. O. Knop, B. R. Vincent, and T. S. Cameron. Can. J. Chem. **67**, 63 (1989).
22. O. Knop, S. C. Choi, and D. C. Hamilton. Can. J. Chem. In press.
23. W. S. Sheldrick and C. Horn. Z. Naturforsch. **44b**, 405 (1989).
24. L. Pauling. The nature of the chemical bond. 3rd ed. Cornell University Press, Ithaca, N.Y. 1960.
25. R. D. Shannon. Acta Crystallogr. Sect. A: Cryst. Phys. Diffr. Theor. Gen. Crystallogr. **A32**, 751 (1976).
26. O. Knop, T. S. Cameron, M. A. James, and M. Falk. Can. J. Chem. **61**, 1620 (1983); (erratum) **62**, 1227 (1984).
27. S. H. Mastin, R. R. Ryan, and L. B. Asprey. Inorg. Chem. **9**, 2100 (1970).
28. Yu. E. Gorbunova, S. A. Linde, V. I. Pakhomov, Yu. V. Kokunov, M. P. Gustyakova, and Yu. A. Buslaev. Koord. Khim. **12**, 835 (1986).
29. Yu. E. Gorbunova, S. A. Linde, V. I. Pakhomov, Yu. V. Kokunov, M. P. Gustyakova, and Yu. A. Buslaev. Koord. Khim. **9**, 524 (1983).
30. R. R. Ryan and D. T. Cromer. Inorg. Chem. **11**, 2322 (1972).
31. M. Webster and S. Keats. J. Chem. Soc. A, 298 (1971).
32. J. Kaub and W. S. Sheldrick. Z. Naturforsch. **39b**, 1252 (1984).
33. A. T. Mohammed and U. Müller. Acta Crystallogr. Sect. C: Cryst. Struct. Commun. **C41**, 329 (1985).
34. J. Kaub and W. S. Sheldrick. Z. Naturforsch. **39b**, 1257 (1984).
35. W. S. Sheldrick, H.-J. Häusler, and J. Kaub. Z. Natuforsch. **43b**, 789 (1988).
36. A. Lipka. Z. Anorg. Allg. Chem. **469**, 229 (1980).
37. F. W. B. Einstein and A. G. MacGregor. J. Chem. Soc. Dalton Trans. 778 (1974).
38. R. K. Wismer and R. A. Jacobson. Inorg. Chem. **13**, 1678 (1974).
39. A. Lipka and D. Mootz. Z. Anorg. Allg. Chem. **440**, 231 (1978).
40. U. Ensinger, W. Schwarz, and A. Schmidt. Z. Naturforsch. **37b**, 1584 (1982).
41. S. Pohl, W. Saak, R. Lotz, and D. Haase. Z. Naturforsch. **45b**, 1355 (1990).
42. F. Bigoli, M. Lafranchi, and M. A. Pellinghelli. Inorg. Chim. Acta, **90**, 215 (1984).
43. N. J. Mammano, A. Zalkin, A. Landers, and A. L. Rheingold. Inorg. Chem. **16**, 297 (1977).
44. B. Aurivillius and C. Stålhandske. Acta Chem. Scand. A, **32**, 715 (1978).
45. F. Lazarini. Acta Crystallogr. Sect. B: Struct. Crystallogr. Cryst. Chem. **B36**, 2748 (1980).
46. F. Lazarini and I. Leban. Acta Crystallogr. Sect. B: Struct. Crystallogr. Cryst. Chem. **B36**, 2745 (1980).
47. F. Lazarini. Acta Crystallogr. Sect. B: Struct. Crystallogr. Cryst. Chem. **B33**, 1954 (1977).
48. G. Thiele and B. Grunwald. Z. Anorg. Allg. Chem. **498**, 105 (1983).
49. T. J. Kistenmacher and G. D. Stucky. Inorg. Chem. **10**, 122 (1971).
50. J. Eicher, P. Klingelhöfer, U. Müller, and K. Dehnicke. Z. Anorg. Allg. Chem. **514**, 79 (1984).
51. J. Eicher, U. Müller, and K. Dehnicke. Z. Anorg. Allg. Chem. **521**, 37 (1985).
52. E. Hey, F. Weller, and K. Dehnicke. Z. Anorg. Allg. Chem. **508**, 86 (1984).
53. B. Krebs, G. Henkel, M. Dartmann, W. Preetz, and M. Bruns. Z. Naturforsch. **39b**, 843 (1984).
54. F. A. Cotton, S. A. Duraj, C. C. Hinckley, M. Matusz, and W. J. Roth. Inorg. Chem. **23**, 3080 (1984).
55. W. Hönle, S. Furuseth, and H. G. von Schnering. Z. Naturforsch. **45b**, 952 (1990).
56. P. H. Collins and M. Webster. J. Chem. Soc. Dalton Trans. 1545 (1974).
57. W. S. Sheldrick and C. Martin. Z. Naturforsch. **46b**, 639 (1991).
58. J. B. Milne, E. J. Gabe, and C. Bensimon. Can. J. Chem. **69**, 648 (1991).
59. J. A. Wunderlich. Acta Crystallogr. **10**, 462 (1957).
60. J. A. Wunderlich. Bull. Soc. Fr. Mineral. Cristallogr. **81**, 287 (1958).
61. O. Knop, W. J. Westerhaus, and M. Falk. Can. J. Chem. **58**, 270 (1980).
62. O. Knop, W. J. Westerhaus, and M. Falk. Can. J. Chem. **58**, 867 (1980).
63. D. E. Sands and A. Zalkin. Acta Crystallogr. **12**, 723 (1959).
64. A. Zalkin and D. E. Sands. Acta Crystallogr. **11**, 615 (1958).
65. U. Müller. Acta Crystallogr. Sect. B: Struct. Crystallogr. Cryst. Chem. **B35**, 2502 (1979).
66. K. Mucker, G. S. Smith, and Q. Johnson. Acta Crystallogr. Sect. B: Struct. Crystallogr. Cryst. Chem. **B24**, 874 (1968).
67. G. S. Smith, Q. Johnson, and R. E. Elson. Acta Crystallogr. **22**, 300 (1967).
68. D. Brown, T. J. Petcher, and A. J. Smith. Acta Crystallogr. Sect. B: Struct. Crystallogr. Cryst. Chem. **B25**, 178 (1969).
69. A. F. Wells. Structural inorganic chemistry. 5th ed. Clarendon Press, Oxford. 1984.
70. J. R. Carruthers and D. L. Watkins. CRYSTALS, issue 5. Chemical Crystallography Laboratory, Oxford, England. 1981.
71. A. I. Kitaigorodsky. Molecular crystals and molecules. Academic Press, New York and London. 1973. pp. 33–37.
72. A. J. Edwards and M. A. Mouty. J. Chem. Soc. A, 703 (1969).
73. International tables for X-ray crystallography. Vol. IV. The Kynoch Press, Birmingham, England. 1974.
74. G. M. Sheldrick. SHELX system report. University Chemical Laboratories, Lensfield Road, Cambridge, England. 1976.
75. G. M. Sheldrick. SHELXS-86. Program for the solution of crystal structures. Institut für Anorganische Chemie der Universität, Göttingen. 1986.
76. D. M. Bates and D. G. Watts. Nonlinear regression analysis and its applications. Wiley–Interscience, New York. 1988.
77. A. du Bois and W. Abriel. Mater. Res. Bull. **24**, 633 (1989).
78. W. Abriel. Mater. Res. Bull. **24**, 1515 (1989).
79. J. C. Jumas, F. Vermot-Gaud-Daniel, and E. Philippot. C. R. Seances Acad. Sci. Ser. C: **282**, 843 (1976).
80. J.-P. Bastide, P. Germain, J.-M. Létoffé, R. El Mail, and Nguyen Ba Chanh. Mater. Res. Bull. **24**, 293 (1989).

Universal Gaussian basis functions in relativistic quantum chemistry: atomic Dirac–Fock–Coulomb and Dirac–Fock–Breit calculations

G. L. MALLI[1] AND A. B. F. DA SILVA[2]
Department of Chemistry, Simon Fraser University, Burnaby, BC, Canada V5A 1S6

AND

YASUYUKI ISHIKAWA
Department of Chemistry and the Chemical Physics Program, University of Puerto Rico, Rio Piedras, Puerto Rico 00931, U.S.A.

Received January 2, 1992

G. L. MALLI, A. B. F. DA SILVA, and YASUYUKI ISHIKAWA. Can. J. Chem, **70**, 1822 (1992).

Matrix Dirac–Fock–Coulomb and Dirac–Fock–Breit self-consistent field calculations are performed for a number of neutral atoms, He ($Z = 2$) through Xe ($Z = 54$), using the universal Gaussian basis set ($18s$, $12p$, $11d$) reported recently by Da Silva *et al.* The total Dirac–Fock–Coulomb, the Dirac–Fock–Breit, and the Breit interaction energies calculated with this universal Gaussian basis set are in good agreement with the corresponding values obtained by using an extensive well-tempered Gaussian basis set for the He through Ca ($Z = 20$) atoms. Although this universal Gaussian basis set is inadequate for the calculation of total Dirac–Fock–Coulomb and Dirac–Fock–Breit energies for the Kr, Sr, and Xe atoms, the Breit interaction energies calculated with this basis for these three atoms are in very good agreement with the corresponding Breit interaction energies obtained by using the extensive well-tempered Gaussian basis sets. Work is in progress to generate a more extensive and energetically better universal Gaussian basis set for He through Xe for its use in non-relativistic Hartree–Fock as well as Dirac–Fock self-consistent field calculations on polyatomics involving heavy atoms.

G. L. MALLI, A. B. F. DA SILVA et YASUYUKI ISHIKAWA. Can. J. Chem. **70**, 1822 (1992).

Utilisant la base gaussienne universelle ($18s$, $12p$, $11d$) proposée récemment par Da Silva *et al.*, on a effectué des calculs en champ auto-cohérent des matrices de Dirac–Fock–Coulomb et de Dirac–Fock–Breit d'un certain nombre d'atomes neutres, He ($Z = 2$) à Xe ($Z = 54$). Les énergies totales d'interaction de Dirac–Fock–Coulomb, et les énergies d'interaction de Dirac–Fock–Breit et de Breit sont en bon accord avec les valeurs correspondantes obtenues par l'utilisation d'une base gaussienne extensive bien tempérée pour les atomes de He à Ca ($Z = 20$). Même si cette base gaussienne universelle est inadequate pour calculer les énergies totales de Dirac–Fock–Coulomb et de Dirac–Fock–Breit des atomes de Kr, Sr et Xe, les énergies d'interaction de Breit calculées pour ces trois atomes à l'aide de cette base sont en bon accord avec les énergies correspondantes d'interaction de Breit obtenues en utilisant la base gaussienne extensive bien tempérée. Des travaux sont en cours dans le but de générer une base gaussienne universelle plus étendue et meilleure d'un point de vue de l'énergie que l'on pourrait appliquer du He au Xe et qui pourrait être utilisée dans des calculs en champ auto-coherent non-relativiste de Hartree–Fock ainsi que de Dirac–Fock pour des ensembles polyatomiques impliquant des atomes lourds.

[Traduit par la rédaction]

Introduction

Ab initio electronic structure calculations for atoms and especially for molecules in general are mostly carried out within the finite basis set expansion method of Roothaan (1). There is a considerable degree of freedom in choosing the basis functions for atomic and molecular calculations, since any complete set of functions can be employed.

Although Slater-type basis functions (STF) have been widely used for atoms and diatomics, Gaussian-type basis functions (GTF) are invariably the popular choice for polyatomic calculations. The prime reason for the preference of the GTF as basis for polyatomics lies in the fact that all the multicenter integrals can be evaluated exactly by closed analytical formulas. However, a much larger basis set of GTF is needed than the basis set of STF because the GTF's behave incorrectly both in the region near the nucleus (if approximated as a point nucleus) and in the long range.

These deficiencies are, however, relevant to the non-relativistic quantum chemistry based upon the Schrodinger equation where the point nucleus approximation is usually employed. Relativistic quantum chemistry, however, is based on the Dirac equation whose solutions for an electron in a finite nucleus have been shown to be Gaussians (2, 3). Thus the GTF basis set is the natural choice for *ab initio* relativistic quantum chemistry, and spherical Gaussians were introduced as basis sets in relativistic quantum chemistry more than a decade ago (4).

Since the computational cost of finite basis set atomic and molecular calculations increases as $\sim N^4$ (where N is the number of basis functions used), various attempts have been made to economize the cost as much as possible by adopting various strategies. One such approach was the introduction of the universal STF basis set (5) for atoms following the earlier work on the even-tempered STF and GTF basis sets (6, 7). As a result of extensive studies, it was observed that the optimum exponents of the rigorously optimized GTF for *ab initio* non-relativistic Hartree–Fock (HF) atomic calculations could be related by Gaussian rule (8). The existence of such a rule suggested a high degree of universality in the optimum GTF representation of different atoms, and it is obvious that considerable computational savings would accrue if a universal Gaussian basis set were employed for each atom in a molecular calculation. The transferability

[1]Author to whom correspondence may be addressed.
[2]Permanent address: Departamento de Física e Química Molecular, Instituto de Física e Química de São Carlos, Universidade de São Paulo, C.P. 369, 13560 São Carlos, SP, Brazil.

Can. J. Chem. Downloaded from www.nrcresearchpress.com by 217.78.4.112 on 09/08/12
For personal use only.

Can. J. Chem. Downloaded from www.nrcresearchpress.com by 217.78.4.112 on 09/08/12
For personal use only.

alone of all the one- and two-electron integrals over the primitive universal GTF from system to system (with trivial multiplicative scale factors due to change in nuclear charges) would lead to remarkable computational savings. Therefore, there has been a considerable effort involved in the design of the so-called "universal Gaussian basis set" (8–10). A universal basis set is a single, sufficiently flexible basis set that can be used for any atomic or molecular environment without much loss of accuracy (9). Needless to reiterate, it is always possible to construct a basis set for an atom which is smaller and still as accurate as the universal basis set; however, the design of such basis sets involves nonlinear exponent optimization for each atom, which is computationally very expensive and time consuming.

Recently, well-tempered GTF (11), geometrical GTF, and various other GTF basis sets have been used for Dirac–Fock–Coulomb (DFC) and Dirac–Fock–Breit (DFB) (12–15) calculations without exponent reoptimization along with the "kinetic balance" and the finite model of the atomic nucleus. The results have been very encouraging not only for DFC and DFB calculations, but also for relativistic many-body perturbation theory calculations on atoms (16). In this paper, we report the results of the DFC and DFB calculations for a number of atoms, He ($Z = 2$) through Xe ($Z = 54$), using the universal Gaussian type functions (UGTF) (18*s*, 12*p*, 11*d*) basis set reported recently by Da Silva *et al.* (10). The purpose of the present study is to assess the performance of the UGTF in atomic Dirac–Fock calculations. The calculations are performed using the matrix Dirac–Fock–Breit SCF methodology detailed by us previously (15).

Gaussian basis set for relativistic calculations

The basis set expansion method for relativistic calculations was pioneered by Kim (17), who introduced the STF basis set with a non-integer exponent of r and developed the Dirac–Fock–Roothaan SCF method for closed-shell atoms. Kagawa (18) extended Kim's method to open-shell atoms and results were reported for a large number of transition elements (18) and Rn (19). In these studies, the same STF basis set was used for the large and small radial components, and often the problem of so-called variational failure was encountered. The spherical Gaussian basis set was introduced in relativistic atomic structure calculations by Malli (4), and in Dirac–Fock–Roothaan molecular calculations by Matsuoka *et al.* (21). Recently, there has been great interest in the use of GTF as a basis set for Dirac–Fock–Coulomb, Dirac–Fock–Breit, and relativistic many-body perturbation calculations (12–16). This is mainly due to the work of Ishikawa *et al.* (2, 3, 12, 15, 16), who have emphasized that the imposition of finite nuclear boundary conditions for solutions of the Dirac–Fock equation results in a solution that is Gaussian at the origin and, therefore, the GTF of integer power of r are appropriate basis functions for the finite nuclear model. Moreover, it has been shown that the failure to satisfy proper boundary conditions near the origin can lead to a spurious solution. The Gaussian-type functions that satisfy the boundary conditions for the finite nucleus automatically satisfy the condition of the so-called "kinetic balance" for a finite speed of light. This is due to the fact that the exponent of r for the GTF does not depend on the speed of light, c, in contrast to the non-integer STF whose exponent depends on the speed of light and, thus, does not satisfy the kinetic balance conditions for a finite value of c (3). The kinetic balance simply guarantees that the solutions of the matrix DFC and DFB equations approach the correct non-relativistic limit as c approaches infinity (3).

TABLE 1. Orbital exponents of the universal Gaussian basis set (18*s*, 12*p*, 11*d*) taken from ref. 10

18*s*	12*p*	11*d*
451350.74		
172818.99		
66171.160		
25336.466		
9701.1528		
3714.5024	3498.1866	
1422.2565	1339.4308	
544.57191	512.85851	544.57191
208.51271	196.36988	208.51271
79.838033	75.188628	79.838033
30.569415	28.789191	30.569415
11.704812	11.023176	11.704812
4.481689	4.220696	4.481689
1.716007	1.616074	1.716007
0.657047	0.618783	0.657047
0.251579	0.236928	0.251579
0.096328	0.090718	0.096328
0.036883		0.036883

Choice of the universal Gaussian basis set

There are a great variety of GTF's to be used in relativistic atomic and molecular calculations; however, if the GTF basis is sufficiently large and flexible, the particular choice of the GTF basis is not expected to be reflected in the calculated properties. One is forced, however, to use a moderately large basis set, since its flexibility in general increases as it is extended. It is also well established that it is generally more profitable to increase the basis set size rather than optimize the individual basis function exponent since the exponent optimization is computationally very costly. The concept of a universal basis set arose from these considerations and basis set exponent non-optimization has been so far almost the rule in relativistic quantum chemistry. We chose to adopt the UGTF (18*s*, 12*p*, 11*d*) basis set recently reported by Da Silva *et al.* (10), which is based on the earlier work of Mohallem *et al.* (22). The significance of the UGTF basis set (10, 22) lies in the fact that no *a priori* information is forced on an atom, which is characterized in the SCF algorithm only by the atomic number in the Fock operator, i.e., an atom is characterized only by its Hamiltonian. This method of designing a UGTF basis introduces a new algorithm for basis set exponent selection. The basis set exponents are not adjustable parameters to optimize a property (e.g., energy), but values generated by a certain criterion for the integration of the SCF equations for the atom, i.e., the exponent values are generated by discretization of an integral equation (with the best numerical integration as the goal). The number of basis functions, N, is related to the number of discretization points, and as the number N is increased, better numerical integration is achieved. We believe that this procedure of generating UGTF basis has sound theoretical background and deserves further investigation both in non-relativistic and relativistic quantum chemistry.

TABLE 2. Total DFC SCF, DFB SCF, and variational Breit interaction energies of the rare-gas and alkaline-earth atoms (in au)

Atom		UGTF	GTF[a]	Numerical[b]
He	E_{DFC}	−2.861808	−2.861813[c]	−2.8618133
	E_{DFB}	−2.861744	−2.861749[c]	
	E_B(SCF)	+0.000064	+0.000064	
Ne	E_{DFC}	−128.691376	−128.691777	−128.69194
	E_{DFB}	−128.674735	−128.675136	
	E_B(SCF)	+0.016641	+0.016641	
Ar	E_{DFC}	−528.677978	−528.683361	−528.68384
	E_{DFB}	−528.545657	−528.551038	
	E_B (SCF)	+0.132321	+0.132323	
Kr	E_{DFC}	−2788.708324	−2788.856297	−2788.86181
	E_{DFB}	−2787.282844	−2787.430423	
	E_B (SCF)	+1.425480	+1.425874	
Xe	E_{DFC}	−7444.578070	−7446.894950	−7446.9010
	E_{DFB}	−7438.822606	−7441.125194	
	E_B (SFC)	+5.755464	+5.769756	
Be	E_{DFC}	−14.575846	−14.575872	−14.575892
	E_{DFB}	−14.575144	−14.575169	
	E_B (SCF)	+0.000702	+0.000703	
Mg	E_{DFC}	−199.933953	−199.934789	−199.93508
	E_{DFB}	−199.902125	−199.902962	
	E_B (SCF)	+0.031828	+0.031827	
Ca	E_{DFC}	−679.699769	−679.709594	−679.71028
	E_{DFB}	−679.508775	−679.518600	
	E_B(SCF)	+0.190994	+0.190994	
Sr	E_{DFC}	−3177.864761	−3178.074209	−3178.0815
	E_{DFB}	−3176.146877	−3176.355672	
	E_B (SCF)	+1.717884	+1.718537	

[a]Calculated by using well-tempered GTF basis (15).
[b]Numerical finite-difference calculations (15).
[c]Calculated by using even-tempered GTF basis (15).

Can. J. Chem. Downloaded from www.nrcresearchpress.com by 217.78.4.112 on 09/08/12
For personal use only.

Results and discussion

The UGTF (18*s*, 12*p*, 11*d*) basis set was used for the atoms He, Be, Ne, Mg, Ar, Ca, Kr, Sr, and Xe. The exponents of this basis set are derived from the non-relativistic generator coordinate version of the Hartree–Fock equations (22) and are collected in Table 1. The exponents were used in our DFC and DFB SCF calculations without further optimization. The radial functions with different κ quantum number but of the same ℓ quantum number are expanded in terms of the same set of basis functions, e.g., the radial functions of $p_{1/2}$ and $p_{3/2}$ symmetries are expanded in the same set of *p*-type GTF's listed in Table 1. The speed of light used in our calculations is 137.0370 au (atomic units). The nuclei are modeled as spheres as uniform proton charge distribution and the atomic masses used for the rare gas atoms He, Ne, Ar, Kr, and Xe are, respectively, 4.0026, 20.18, 39.948, 83.80, and 131.30. The atomic masses used for the alkaline earth atoms Be, Mg, Ca, and Sr are, respectively, 9.0122, 24.312, 40.08, and 87.62.

The results of the calculated DFC, DFB, and Breit interaction energies (designated as E_{DFC}, E_{DFB}, and E_B, respectively) using the UGTF (18*s*, 12*p*, 11*d*) basis are given in Table 2, where we have also included the results obtained using large well-tempered (11) GTF basis sets (6). In the last column of Table 2, the DFC energies obtained by using the numerical finite-difference Dirac–Fock program (20) are also tabulated. Here, E_B denotes the variational Breit interaction energy computed as the difference $E_{DFB} - E_{DFC}$. The variational Breit energy is the level shift in the total SCF energy due to the inclusion of the Breit term in the SCF process. The results clearly demonstrate that the total DFC and DFB energies computed with the UGTF basis set are in very good agreement with those obtained by using large well-tempered GTF for He, Be, Ne, Mg, Ar, and Ca atoms. However, for Kr, Sr, and Xe atoms, the calculated DFC and DFB energies are relatively poor in comparison with those obtained from the well-tempered GTF basis set calculations (15); the differences in E_{DFC} and E_{DFB} for the case of the Sr atom are 0.209448 and 0.208795 au, respectively. For the Xe atom, these differences are an order of magnitude larger than in the case of the Sr atom, viz., 2.31688 and 2.302588 au, respectively.

Moreover, it turns out that both E_{DFC} and E_{DFB} are in error by almost the same amount for each atom and, therefore, the variational Breit interaction energies predicted by using both the UGTF and well-tempered GTF basis sets are in excellent agreement for all the atoms, He through Xe, treated in this paper.

Although the UGTF (18*s*, 12*p*, 11*d*) basis is inadequate for the calculations of E_{DFC} and E_{DFB} for the Kr, Sr and Xe

TABLE 3. DFC and DFB orbital energies of Xe (in au)

	Orbital energies			
	DFC SCF		DFB SCF	
Orbital	UGTF[a]	GTF[b]	UGTF[a]	GTF[b]
$1s_{1/2}$	−1276.956	−1277.258	−1273.999	−1274.292
$2s_{1/2}$	−202.4716	−202.4650	−202.1914	−202.1845
$2p_{1/2}$	−189.4130	−189.6782	−188.9371	−189.1988
$2p_{3/2}$	−177.7308	−177.7045	−177.4071	−177.3806
$3s_{1/2}$	−43.02494	−43.01036	−42.98454	−42.96991
$3p_{1/2}$	−37.61075	−37.65954	−37.53675	−37.58481
$3p_{3/2}$	−35.34130	−35.32518	−35.29622	−35.28006
$3d_{3/2}$	−26.05303	−26.02329	−26.02987	−26.00013
$3d_{5/2}$	−25.56835	−25.53703	−25.55814	−25.52686
$4s_{1/2}$	−8.430171	−8.429814	−8.424531	−8.424185
$4p_{1/2}$	−6.442612	−6.452325	−6.431199	−6.440767
$4p_{3/2}$	−5.986039	−5.982693	−5.980501	−5.977144
$4d_{3/2}$	−2.718103	−2.711237	−2.717878	−2.711006
$4d_{5/2}$	−2.640786	−2.633670	−2.642697	−2.635577
$5s_{1/2}$	−1.009666	−1.010069	−1.009366	−1.009779
$5p_{1/2}$	−0.4906846	−0.4924893	−0.4899431	−0.4917363
$5p_{3/2}$	−0.4395628	−0.4397307	−0.4394645	−0.4396367

[a]Computed by using UGTF basis set (18*s*, 12*p*, 11*d*) (10)
[b]Computed by using well-tempered 23*s*21*p*14*d* GTF basis set (15).

atoms, E_B calculated with this UGTF basis set is in very good agreement with the corresponding E_B obtained from using an extensive GTF basis set. We also performed calculations for these atomic systems using the UGTF (18*s*, 18*p*, 18*d*) basis set. Although the basis set is much larger for the *p* and *d* symmetries, only a marginal improvement in E_{DFC} and E_{DFB} over the results of UGTF (18*s*, 12*p*, 11*d*) was obtained for the heavier atoms Kr, Sr, and Xe.

The calculated orbital energies for the Xe atom obtained by using the UGTF and well-tempered GTF (15) are collected in Table 3. A comparison of the orbital energies calculated by using these two basis sets indicates significant differences for the innermost shells. An improvement of the UGTF basis is therefore expected to lead to better total DFC and DFB energies and also the orbital energies of the innermost shells.

Conclusion

The universal Gaussian basis set employed in our calculations is fairly good for the DFC and DFB calculations for the atoms He through Ca. However, this basis set needs much improvement for the Kr, Sr, and Xe atoms, since the DFC and DFB energies calculated with this basis set for these three atoms are rather poor. The errors in the calculated DFC and DFB energies are, however, of the same magnitude and, therefore, the calculated Breit interaction energies even for these three atoms are in perfect agreement with those obtained by using the well-tempered GTF basis set (11, 15).

It is clear that there is an urgent need for an improved UGTF basis set for He through Xe atoms. Work is in progress in the design of the improved UGTF basis set that can consistently provide more accurate results for the calculations of E_{DFC} and E_{DFB} for many-electron atoms. The improved UGTF basis set should lead to remarkable savings in computations for non-relativistic as well as relativistic calculations on molecular systems.

Acknowledgments

This work was supported in part by the Natural Sciences and Engineering Research Council of Canada (grant no. A3598 to G. L. Malli), by the Brazilian CNPQ (to A. B. F. Da Silva), and by the National Science Foundation (PHY-9008627 to Y. Ishikawa), which are gratefully acknowledged. All calculations were performed on an IBM RISC/6000 workstation at Simon Fraser University. The authors thank Dr. Steve Kloster of the Academic Computing Services at Simon Fraser University for continuous help with the calculations on the IBM RISC/6000.

1. C. C. J. Roothaan. Rev. Mod. Phys. **23**, 69 (1951).
2. Y. Ishikawa, R. Baretty, and R. C. Binning, Jr. Chem. Phys. Lett. **121**, 130 (1985).
3. Y. Ishikawa and H. M. Quiney. Int. J. Quantum Chem. **S21**, 523 (1987).
4. G. Malli. Chem. Phys. Lett. **68**, 529 (1979).
5. D. M. Silver and W. C. Nieuwpoort. Chem. Phys. Lett. **57**, 421 (1978).
6. K. Ruedenberg, R. C. Raffenetti, and R. D. Bardo. Energy, structure, and reactivity. Proceedings of the 1972 Boulder Seminar Research Conference on Theoretical Chemistry. *Edited by* D. W. Smith. Wiley, New York. 1973. p. 164.
7. R. C. Raffenetti. J. Chem. Phys. **59**, 5936 (1973).
8. P. G. Mezey. Theor. Chim. Acta, **53**, 183 (1979).
9. S. Wilson. Adv. Chem. Phys. **67**, 439 (1987).
10. A. B. F. Da Silva, H. F. M. Da Costa, and M. Trsic. Mol. Phys. **68**, 433 (1989).
11. S. Huzinaga and M. Klobukowski. J. Mol. Struct. Theochem. **167**, 1 (1988); S. Huzinaga, M. Klobukowski, and H. Tatewaki. Can. J. Chem. **63**, 1812 (1985).
12. Y. Ishikawa, H. Sekino, and R. C. Binning, Jr. Chem. Phys. Lett. **160**, 206 (1989).
13. S. Okada and O. Matsuoka. J. Chem. Phys. **91**, 4193 (1989).
14. A. K. Mohanty and E. Clementi. J. Chem. Phys. **93**, 1829 (1990).

Can. J. Chem. Downloaded from www.nrcresearchpress.com by 217.78.4.112 on 09/08/12
For personal use only.

15. Y. Ishikawa, H. M. Quiney, and G. L. Malli. Phys. Rev. A, **43**, 3270 (1991).
16. Y. Ishikawa. Phys. Rev. A, **42**, 1142 (1990).
17. Y.-K. Kim. Phys. Rev. **154**, 17 (1967).
18. T. Kagawa. Phys. Rev. A, **12**, 2245 (1975).
19. T. Kagawa and G. L. Malli. Can. J. Chem. **63**, 1550 (1985).
20. J. P. Desclaux. Comput. Phys. Commun. **9**, 31 (1975).
21. O. Matsuoka, N. Suzuki, T. Aoyama, and G. L. Malli. J. Chem. Phys. **73**, 1320 (1980).
22. J. R. Mohallem and M. Trsic. J. Chem. Phys. **86**, 5043 (1987); H. F. M. Da Costa, M. Trsic, and J. R. Mohallem. Mol. Phys. **62**, 91 (1987).

Can. J. Chem. Downloaded from www.nrcresearchpress.com by 217.78.4.112 on 09/08/12
For personal use only.

Identification of 2-deoxy-D-ribono-1,4-lactone at the site of benzophenone photosensitized release of guanine in 2′-deoxyguanosine and thymidylyl-(3′-5′)-2′-deoxyguanosine

GARRY W. BUCHKO[1] AND JEAN CADET

Laboratoire des lesions des acides nucléiques, Département de recherche fondamentale sur la matière condensée/ Service d'études des systèmes moléculaires, Centre d'études nucléaires de Grenoble, 85 X, F-38041 Grenoble CEDEX, France

Received January 3, 1992

GARRY W. BUCHKO and JEAN CADET. Can. J. Chem. **70**, 1827 (1992).

Benzophenone-mediated photosensitization of 2′-deoxyguanosine (dG) and thymidylyl-(3′-5′)-2′-deoxyguanosine (d(TpG)) at 350 nm in oxygen-saturated aqueous solution produces 2-deoxy-D-ribono-1,4-lactone (dL) and thymidylyl-(3′-5′)-2-deoxy-D-ribono-1,4-lactone (d(TpL)), respectively. These photoproducts have been isolated by reverse phase high-performance liquid chromatography and characterized by proton magnetic resonance spectroscopy and fast atom bombardment mass spectroscopy. Conformational analysis of d(TpG) and d(TpL) in aqueous solution using coupling constant data suggests no major conformational differences between the two dinucleoside monophosphates.

GARRY W. BUCHKO et JEAN CADET. Can. J. Chem. **70**, 1827 (1992).

Les photosensibilisations de la 2′-désoxyguanosine (dG) et de la thymidylyl-(3′, 5′)-2′-désoxyguanosine (d(TpG)), à l'aide de la benzophénone, à 350 nm, dans une solution aqueuse saturée d'oxygène, conduisent respectivement à la 2-désoxy-D-ribono-1,4-lactone (dL) et à la thymidylyl-(3′-5′)-2-désoxy-D-ribono-1,4-lactone ((d(TpL)). On a isolé ces photoproduits par chromatographie liquide à haute performance en phase inversée et on les a caractérisés par spectroscopie de résonance magnétique nucléaire et par spectroscopie de masse avec bombardement avec des atomes rapides. L'analyse conformationnelle du d(TpG) et de la d(TpL) en phase aqueuse, en se basant sur les données relatives aux constantes de couplage, suggère qu'il n'y a aucune différence conformationnelle importante entre les deux monophosphates de dinucléoside.

[Traduit par la rédaction]

Introduction

The exposure of living organisms to solar radiation spanning the near ultraviolet (280–380 nm) to visible regions may induce mutagenic and lethal effects as a result of photooxidative modifications to genomic DNA (1, 2). The type of photochemical modifications that occur depend on the wavelength of the incident radiation. At wavelengths shorter than 290 nm the DNA directly absorbs the energy and the majority of photoproducts produced involve the pyrimidine bases. On the other hand, at wavelengths in the UV-A region (320–400 nm) the primary photochemical target is guanine (2–5). The latter reactions occur through the agency of endogenous and exogenous photosensitizers, which are initially excited to the triplet state and generate oxidation products via their decay to the ground state through two principal competitive mechanisms labelled Type I and Type II (6). Type I mechanisms involve initial electron or hydrogen transfer by the excited photosensitizer to, or from, the substrate. Type II mechanisms involve the initial generation of singlet oxygen by the excited photosensitizer and subsequent reaction with the substrate. The end result of these two mechanisms is a different set of photoproducts (2, 5, 7).

Benzophenone acts primarily through a Type I mechanism (8) and for this reason was chosen to investigate more specifically the formation of the related guanine photooxidation products. Even so, the benzophenone photooxidation of the dinucleoside monophosphate d(TpG) still produced a large variety of photoproducts involving (*i*) modified guanine bases, (*ii*) intrabase thymine–guanine covalent crosslinks, (*iii*) phosphodiester bond cleavages, and (*iv*) glycosylation (9). Our attention here focuses on one product of the later event, thymidylyl-(3′-5′)-2-deoxy-D-ribono-1,4-lactone, d(TpL). A 2-deoxy-D-ribono-1,4-lactone (dL) (Fig. 1) was previously identified at (*i*) the internal residue of d(ApCpA) (10) and d(GpCpG) (11) upon UV irradiation at acidic pH (4.0), (*ii*) the terminal residue of d(ApGpC) following reaction with the neocarzinostatin chromophore (12), and (*iii*) in oligonucleotide duplexes containing 5-bromouracil following photolysis (13). Exposure of 2′-deoxyguanosine (dG) to γ-radiation in oxygen-free aqueous solution (14) and to hydrogen peroxide (15) also produces this lactone. The isolation of dL and d(TpL) from the starting material dG and d(TpG), respectively, constitutes the first examples of the formation of 2-deoxy-D-ribono-1,4-lactone as a product of the photosensitization of DNA components.

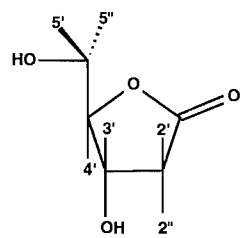

FIG. 1. Structure and proton numbering scheme for 2-deoxy-D-ribono-1,4-lactone, dL, the modified component of d(TpL).

Experimental

Materials and methods

The dinucleoside monophosphate d(TpG) was synthesized in solution by using the phosphotriester approach (16, 17). Benzophenone (1.0 mg) (Merck) was added to 50 mL of 1.0 mM d(TpG) in a flat, round-bottom flask and irradiated for 1 h with 16 350-nm black lamps in a photochemical reactor (Rayonet, Southern New

[1]Author to whom correspondence may be addressed. Present address: Department of Radiobiology, Cross Cancer Institute, 11560 University Ave., Edmonton, Alberta, T6G 1Z2.

Can. J. Chem. Downloaded from www.nrcresearchpress.com by 217.78.4.112 on 09/08/12
For personal use only.

Can. J. Chem. Downloaded from www.nrcresearchpress.com by 217.78.4.112 on 09/08/12
For personal use only.

England Ultraviolet Company, Hander, Conn.). During the irradiation, oxygen was continuously bubbled through the solution to maintain its saturation with oxygen. The water was removed by rotary evaporation (30°C) and the solids resuspended in the minimum volume of water for high-performance liquid chromatography (HPLC). Identical conditions were employed for 2′-deoxyguanosine (Genofit) photosensitization using 50 mL of a 7.5 mM solution irradiated for 16 h. Control experiments with dG and d(TpG) were performed in the absence of photosensitizer.

Chromatography of photoproducts

Samples were injected onto a 5-μm Hypersil (10 mm × 25 cm) semipreparative octadecyl silica gel reverse-phase column. After 1 min of 100% 0.1 M ammonium acetate (pH = 6.0), a linear gradient of methanol was introduced at a rate of change of 0.5%/min and a flow rate of 2.0 mL/min. The product profile was monitored by UV absorbance at 230 nm. The major bands were collected, pooled, and concentrated by rotary evaporation. Fractions containing 2-deoxy-D-ribono-1,4-lactone were further purified by HPLC as described above, using acetonitrile instead of methanol. The products were then lyophilized a minimum of 3× to remove the ammonium acetate.

Fast Atom Bombardment (FAB) mass spectrometry

Negative ion mode FAB mass spectra (glycerol matrix, 8-keV xenon atoms) were obtained on a VG ZAB 2-EQ mass spectrometer. Some of the more prominent peaks are reported here as follows: *m/z*(relative intensity, [ionic species]), with the relative intensity normalized to the molecular ion $[M - H]^-$. *d(TpL)*: 435 (100, $[M - H]^-$), 527 (11, [M + glycerol − H]$^-$), 211 (56, [5′dLMP − H]$^-$), 321 (32, [3′dTMP − H]$^-$). *d(TpG)*: 570 (100, $[M - H]^-$), 346 (20, [5′dGMP − H]$^-$), 321 (42, [3′dTMP − H]$^-$), 150(51, [guanine − H]$^-$), 125 (72, [thymine − H]$^-$. *dL*: no prominent ions.

Proton Nuclear Magnetic Resonance (^{1}H NMR) spectroscopy

Samples were lyophilized twice from 99.8% D_2O prior to resuspension in 400 μL of NMR buffer (pD = 7.0) consisting of 0.1 M sodium chloride, 0.01 M sodium phosphate, and 0.001 M ethylenediaminotetraacetic acid. A trace of *tert*-butanol was added to serve as an internal NMR reference (assigned a chemical shift of 1.231 ppm on the DSS scale). The proton spectra were recorded at 400.135 MHz (Bruker AM400), except for d(TpG), which was obtained at 500.135 MHz (Bruker WM500). Free induction decay data were obtained in 16K of computer memory, processed with a Lorentz-to-Gaussian lineshape transform (GB = 0.2, LB = −2.0), and zero-filling to 32K prior to Fourier transformation. The digital resolution of the processed spectra was 0.23 (400.135 MHz) and 0.30 (500.135 MHz) Hz/point. Conventional homonuclear decoupling, nuclear Overhauser enhancement and two-dimensional coherence (18), and relay coherence spectroscopy (19) experiments were carried out for proton spectral assignments. The H5′ was assigned downfield of H5″ according to Remin and Shugar (20) whereas the H2′/H2″ assignments were based on coupling constant arguments (21, 22). To verify the assignments and to obtain accurate coupling constants, all the spectra were simulated using the Bruker PANIC program.

Results and discussion

Isolation and characterization of the lactone photoproducts

It is not surprising to observe d(TpL) as a final product of benzophenone-sensitized irradiation of d(TpG) after identifying dL as one of the final products of benzophenone photosensitization of dG in oxygen-saturated aqueous solution. Proton NMR evidence for the latter is apparent from the data in Tables 1 and 2 that illustrate the key spectral features of 2-deoxy-D-ribono-1,4-lactone: (*i*) the absence of an anomeric proton resonance, (*ii*) the absence of a downfield nonexchangeable base proton resonance, and (*iii*) a geminal coupling of −18.6 Hz between the 2′ and 2″ protons. The latter observation represents a 4.5 Hz increase relative to dG and is consistent with the addition of a substituent adjacent to C2′ containing a double bond (24, 25). Furthermore, the chemical shifts and coupling constants tabulated herein for dL are nearly identical to those published by Berger and Cadet (14) for authentic dL and dL obtained after γ radiolysis of a deaerated aqueous solution of dG. The only anomalies are misprints by Berger and Cadet that reverse $J(4'5')$ and $J(4'5'')$ and $J(2'3')$ and $J(2''3')$ (this is clearly evident in their published spectrum for dL).

The ^{1}H NMR features that distinguish dL also serve to identify the lactone in the dinucleoside monophosphate as tabulated in Tables 1 and 2 and illustrated in Fig. 2. First, only the H6 and H1′ resonances of the Tp unit appear in the downfield part of the spectrum; the guanine H8 and H1′ are absent. Moreover, these Tp H6 and H1′ resonances of d(TpL) are downfield relative to those of d(TpG) as expected in the absence of ring current effects from the pL unit. Second, the 2′ and 2″ protons assigned to the pL unit by COSY and relay coherence transfer experiments have a geminal coupling of −18.7 Hz and chemical shifts nearly identical to those of the nucleoside, dL. Third, the chemical shifts of the

TABLE 1. Proton chemical shifts (δ, ppm from DSS) of d(TpG), d(TpL), and dL[a]

	d(TpG)		d(TpL)		
	Tp	pG	Tp	pL	dL
1′	6.06	6.18	6.30	—	—
2′	1.64	2.82	2.40	3.09	3.04
2″	2.23	2.50	2.51	2.55	2.57
3′	4.61	4.76	4.72	4.64	4.53
4′	4.05	4.17	4.17	4.70	4.57
5′	3.64	4.05	3.82	4.14	3.86
5″	3.64	4.05	3.77	4.09	3.76
6 or 8	7.41	8.04	7.64	—	—
Me5	1.84	—	1.89	—	—

[a]Data for d(TpG) taken from ref. 23. Spectra obtained in 0.1 M NaCl, d(TpG) at 500.1 MHz (10°C), d(TpL) and dL at 400.1 MHz (23°C).

TABLE 2. Proton coupling constants (*J*, Hz) of d(TpG), d(TpL), and dL[a]

	d(TpG)		d(TpL)		
	Tp	pG	Tp	pL	dL
1′2′	8.9	6.9	7.4	—	—
1′2″	5.6	6.6	6.4	—	—
2′2″	−14.0	−13.9	−14.4	−18.7	−18.6
2′3′	5.9	6.6	7.1	6.9	7.0
2″3′	2.1	4.2	3.3	2.2	2.8
3′4′	2.1	3.7	3.1	2.1	2.7
4′5′	4.2[b]	2.8[b]	3.4	2.9	3.1
4′5″	4.2[b]	2.8[b]	4.9	3.2	4.6
5′5″	−12.8[b]	−11.8[b]	−12.5	−11.8	−12.9
3′P	6.0	—	6.0	—	—
4′P	—	2.8	—	—	—
5′P	—	3.6[b]	—	5.3	—
5″P	—	3.6[b]	—	5.0	—
6(M5)	1.3	—	1.3	—	—

[a]Data for d(TpG) taken from ref. 23. Spectra obtained in 0.1 M NaCl, d(TpG) at 500.1 MHz (10°C), d(TpL) and dL at 400.1 MHz (23°C).
[b]When δ5′ ≅ δ5″, $^2J(5'5'')$ is arbitrary and only the sums of the connected coupling constants are significant.

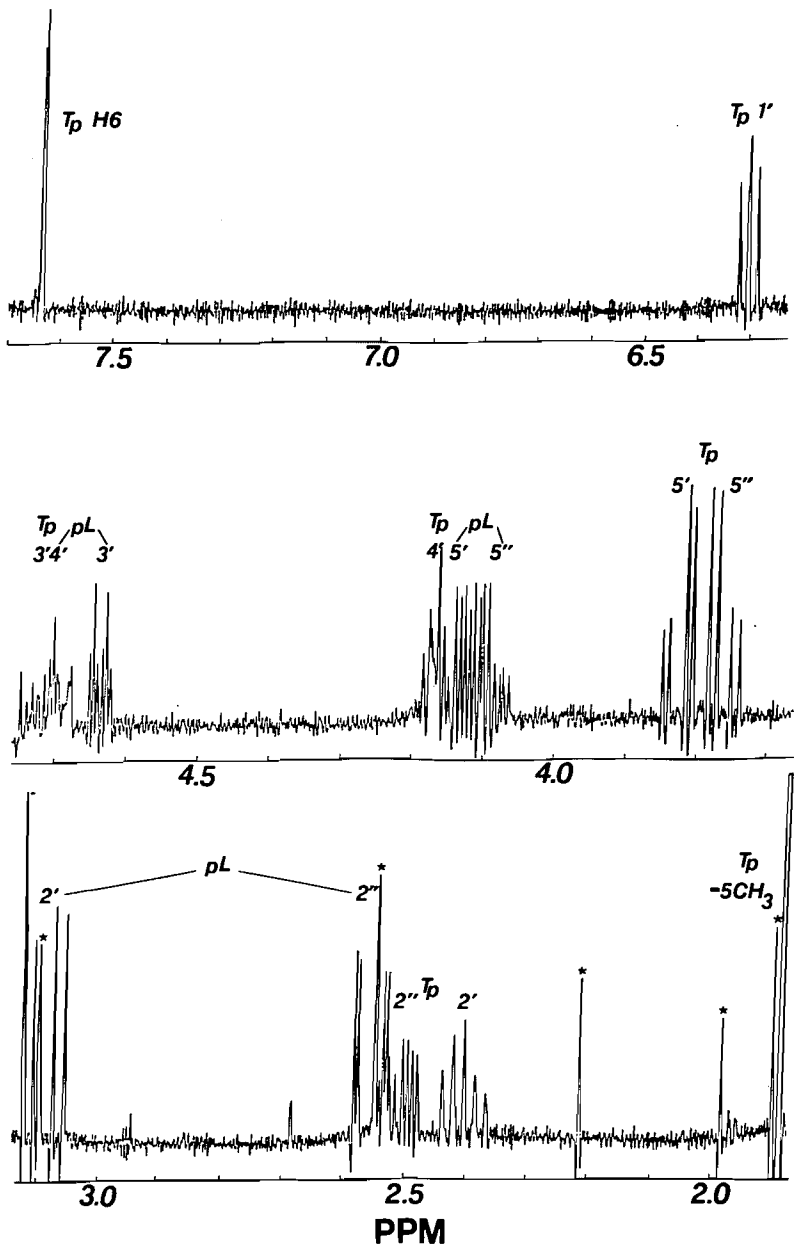

FIG. 2. High-field (top), mid-field (middle), and low-field (bottom) 400 MHz ^{1}H NMR spectra of d(TpL) in 0.1 M NaCl (23°C). Tp and pL represent the 3′- and 5′-linked nucleotidyl units, respectively. Unidentified resonances of impurities are labelled with an asterisk (*).

Can. J. Chem. Downloaded from www.nrcresearchpress.com by 217.78.4.112 on 09/08/12
For personal use only.

pL protons are within 0.1 ppm of those for dL with the exception of H5′/H5″, which are downfield due to the presence of a phosphate group at the 5′ position.

FAB mass spectrometry

Figure 3 contains the negative ion mode FAB mass spectrum of d(TpL). A pseudomolecular ion at m/z 435 (100, $[M - H]^-$) and a glycerol adduct at m/z 527 (11, $[M +$ glycerol $- H]^-$) are indicative of a species with a molecular weight of 436. Fragmentation ions at m/z 211 (56, $[5'dLMP - H]^-$) and m/z 321 (32, $[3'dTMP - H]^-$) further support the structure implied from the ^{1}H NMR data.

Conformational features

(a) Sugar conformation

The 2-deoxyribose ring can be evaluated in terms of a 2′-*endo* (*S*) $\rightleftharpoons$ 3′-*endo* (*N*) equilibrium from the vicinal proton coupling constants $J(1'2')$ through $J(3'4')$, or from certain sums of these couplings (26). In this manner it is possible to estimate the *%S* conformer population from the equation $\%S = [(J(1'2') + J(1'2'')) - 9.8]/5.9$ (26) using the data in Table 2. It is observed (Table 3) that there is a decrease in the *%S* conformer of the Tp unit in going from d(TpG) (80%) to the apurinic d(TpL) (68%). Such an observation suggests more freedom of movement in d(TpL) in comparison to d(TpG), as may be expected in the absence of any possible base-stacking interactions.

The sum of $J(1'2')$ and $J(1'2'')$ cannot be used to analyse the 2-deoxy-D-ribono-1,4-lactone conformation because of the lack of an anomeric proton. However, the X-ray structure of a similar D-pentono-1,4-lactone, D-arabino-1,4-lactone, shows the 5-member ring to exhibit an ^3E envelope conformation with C3′ displaced 0.57 Å above the mean

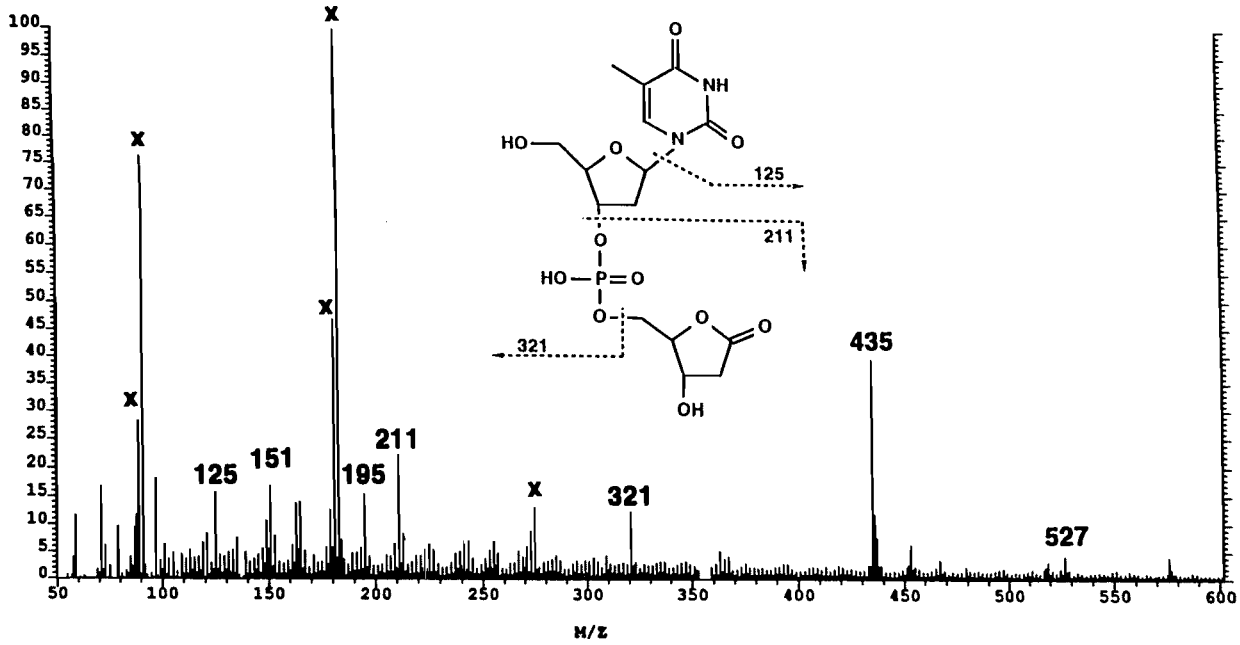

FIG. 3. Negative ion mode fast atom bombardment mass spectrum of d(TpL). Glycerol ions are identified with an x.

TABLE 3. Furanose conformations and exocyclic bonds rotamer distributions for d(TpG), d(TpL), and dL[a]

Molecule	%S	%γ⁻	%γ′	%γ⁺	%β′
Tp	80	21	26	53	—
pG	63	4	15	80	88
Tp	68	11	36	53	—
pL	77[b]	5	19	75	72
dL	71[b]	7	32	58	—

[a]%S and %γ calculated according to ref. 26 and %β calculated according to ref. 31 using the data in Table 2.
[b]Calculated according to ref. 28.

plane of C4′—O1′—C1′—C2′ (27). In solution, the conformation of D-pentono-1,4-lactones has been described in terms of a dynamic equilibrium between this ^3E (*N*) conformer and an other E_3 (*S*) envelope form that has C3′ displaced below the plane of C4′—O1′—C1′—C2′ (14, 28, 29) (Fig. 4). The contribution of the ^3E conformer to the $^3E \rightleftharpoons E_3$ blend may be estimated using the equation $\%^3E = [J(2''3')/9.5] \times 100$ (28) and the data in Table 2. It is observed that the E_3 conformer predominates at both the nucleoside (71%) and the dinucleoside monophosphate level (77%) in the range typical of deoxyribodinucleoside monophosphates (56–81%*S*) (30).

(b) The C4′—C5′ (γ) bond

Table 3 gives the populations for the *gauche*$^+$ (g^+), *trans* (t), and *gauche*$^-$ (g^-) conformers about the γ bond of d(TpG), d(TpL), and dL calculated from the $J(4'5')$ and $J(4'5'')$ data according to Haasnoot *et al.* (31). In all cases there is a preference for g^+ followed by g^t, then g^-, as expected for small DNA oligomers (32). Also expected, and observed, are the smaller g^+ populations for the Tp units (53%) in comparison to the pN units (75 and 80%) due to more freedom of movement at the 5′-end of oligonucleotides (33).

(c) The C5′—O5′ (β) bond

Table 3 gives the populations of the preferred *trans* (t) conformation of the β bond of the pN units estimated from $\Sigma = J(5'P) + J(5''P)$ (32). For d(TpL) the $\%\beta^t$ population is 72% while for d(TpG) it is 88%, the former population below the low end of the range typically observed for deoxyribodinucleoside monophosphates composed of poorly stacking pyrimidine units (74–82%) (30). This observation, together with the γ-bond information, suggests that there are no gross distortions in the sugar-phosphate backbone of d(TpL) relative to d(TpG) but only less order in the former due to the lack of any base-stacking interactions.

Mechanisms and biological significance

Neither dL nor d(TpL) was detected by HPLC chromatography after 350 nm irradiation in the absence of benzophenone, even upon extension of the period of irradiation.

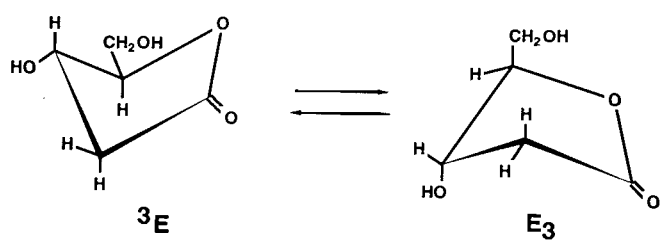

FIG. 4. Structures of the ^3E and E_3 envelope conformers of dL.

Can. J. Chem. Downloaded from www.nrcresearchpress.com by 217.78.4.112 on 09/08/12
For personal use only.

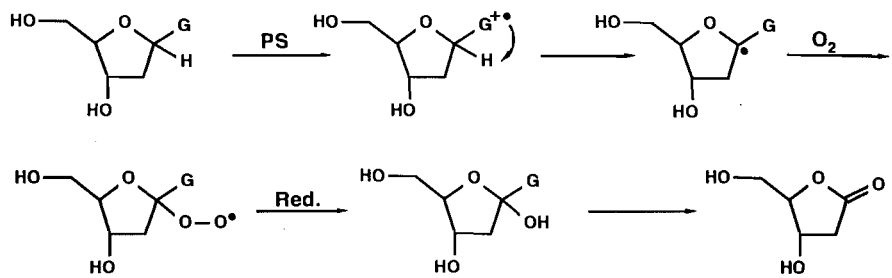

FIG. 5. Proposed mechanism for the free radical mediated formation of 2-deoxy-D-ribono-1,4-lactone. PS = photosensitizer, Red = reduction.

Such an observation dictates that the lactone is generated through a photosensitization process. Furthermore, neither dL nor d(TpL) was observed, at least in detectable quantities, when phthalocyanine derivatives, which generate products primarily through a Type II mechanism, were used as the photosensitizer (34). Hence, while the exact mechanism of lactone formation via benzophenone photosensitization is not clear, if it is occurring through a Type I pathway then proton or electron abstraction from the guanine base is likely the initial step as indicated in Figure 5. The next event may involve deprotonation at C1′ by the guanine radical cation (although another possible mechanism that cannot be ruled out is the photoexcited benzophenone directly abstracting this hydrogen). Molecular oxygen is expected to react with the C1′-centered radical producing a peroxyl radical intermediate, which is converted into the corresponding alcohol. Subsequent hydrolysis of the weakened *N*-glycosidic bond of the latter compound will give rise to the 2-deoxy-D-ribono-1,4-lactone with concomitant release of the free base (35).

While d(TpL) was not the major photoproduct of benzophenone-sensitized irradiation of d(TpG) (9), the biological significance of a DNA lesion is not determined solely by quantity but by its susceptibility to DNA repair systems (36). Lactone lesions show resistance to certain AP and UV endonucleases (37, 38) and, hence, may have great biological significance even though they are produced in low yield. Because the coupling constant data demonstrate no major conformational differences between d(TpG) and d(TpL) in aqueous solution, our data, if extendable to oligonucleotides, suggest such biological consequences are likely due to the presence of the C1′ keto group.

Acknowledgements

We thank Jacques Ulrich (Services d'études analytiques, Centre d'études nucléaires de Grenoble) for recording the mass spectra; Dr. Frank E. Hruska (Chemistry Department, University of Manitoba) for providing some protected d(TpG), and the French government for a postdoctoral fellowship for GWB.

1. C. Helene. Photobiochem. Photobiophys. Suppl. 3(1987).
2. J. Cadet and P. Vigny. In Bioorganic photochemistry. Photochemistry and the nucleic acids. Edited by H. Morrison. John Wiley & Sons, Inc., New York. 1990. p. 1.
3. M. I. Simon and H. Van Vunakis. J. Mol. Biol. **4**, 488(1962).
4. K. S. Sastry and M. P. Gordon. Biochim. Biophys. Acta, **29**, 42(1966).
5. J. Cadet, M. Berger, C. Decarroz, J. R. Wagner, J. E. Van Lier, Y. Ginot, and P. Vigny. Biochimie, **68**, 813(1986).
6. C. S. Foote. In Oxy-radicals in chemistry and biology. Edited by M. A. J. Rodgers and E. L. Powers, Academic Press, New York. 1981. p. 425.
7. J. F. Ennever and W. T. Speck. Pediatr. Res. **15**, 956(1981).
8. K. Uehara and T. Hayakawa. J. Biochem. (Tokyo), **71**, 401(1972).
9. G. W. Buchko, J. Cadet, J-L. Ravanat, and M. Berger. Résumés des Conférences. 4ème Réunion du Groupe Thématique Magnétisme Nucléaire et Biologie, Progrès Méthodologiques de la RMN en Biologie: Structures Macromoléculaires et Metabolisme. Eveux, France, Oct. 23–26, 1990. p. 88.
10. H. Urata, K. Yamamoto, M. Akagi, H. Hiroaki, and S. Uesugi. Biochemistry, **28**, 9566(1989).
11. H. Urata, and M. Akagi. Nucleic Acids Res. **19**, 1773(1991).
12. L. S. Kappen and I. H. Goldberg. Biochemistry, **28**, 1027(1989).
13. H. Sugiyama, Y. Tsutsumi, and I. Saito. J. Am. Chem. Soc. **112**, 6720(1990).
14. M. Berger and J. Cadet. Z. Naturforsch, **40B**, 1519(1985).
15. H-J. Rhaese and E. Freese. Biochem. Biophys. Acta, **155**, 476(1968).
16. C. B. Reese. Tetrahedron, **34** 3143(1978).
17. G. W. Buchko, F. E. Hruska, and K. L. Sadana. Can. J. Chem. **67**, 109(1989).
18. W. P. Aue, E. Bartholdi, and R. R. Ernst. J. Chem. Phys. **64**, 2229(1976).
19. D. W. Hughes, R. A. Bell, T. Neilson, and A. D. Bain. Can. J. Chem. **63**, 3133(1986).
20. M. Remin and D. Shugar. Biochem. Biophys. Res. Commun. **48**, 636(1972).
21. D. J. Wood, F. E. Hruska, and K. K. Ogilvie. Can. J. Chem. **52**, 3353(1974).
22. D. B. Davies and S. S. Danyluk. Biochemistry, **13**, 4417(1974).
23. G. W. Buchko. Ph. D. Thesis, University of Manitoba, Winnipeg, Manitoba. 1989. p. 101.
24. M. Barfeild and D. M. Grant. J. Am. Chem. Soc. **85**, 1899(1963).
25. M. Barfeild, V. J. Hruby and J-P. Meraldi. J. Am. Chem. Soc. **98**, 1308(1976).
26. L. J. Rinkel and C. Altona. J. Biomol. Struct. Dyn. **4**, 621(1987).
27. T. Svinning and H. Sorum. Acta Crystallogr. Sect. B: Struct. Crystallogr. Cryst. Chem. **B35**, 2967(1979).
28. D. Horton and Z. Walaszek. Carbohydr. Res. **105**, 111(1982).
29. H. Wong. Aust. J. Chem. **37**, 327(1984).
30. D. M. Cheng and R. H. Sarma. J. Am. Chem. Soc. **99**, 7333(1977).
31. C. A. G. Haasnoot, F. A. A. M. de Leeuw, H. P. M. de Leeuw, and C. Altona. Recl. Trav. Chim. Pays-Bas, **98**, 576 (1979).
32. C. Altona. Recl. Trav. Chem. Pays-Bas, **101**, 413(1982).

Can. J. Chem. Downloaded from www.nrcresearchpress.com by 217.78.4.112 on 09/08/12
For personal use only.

33. J-R. Mellema, J. M. L. Pieters, G. A. Van Der Marel, J. H. Van Boom, C. A. G. Haasnoot, and C. Altona. Eur. J. Biochem. **143**, 285(1984).
34. J-L. Ravanat, M. Berger, G. W. Buchko, J-F. Benard, J. E. Van Lier, and J. Cadet. J. Chim. Phys. **88**, 1069(1991).
35. G. W. Teebor, R. J. Boorstein, and J. Cadet. Int. J. Radiat. Biol. **54**, 131(1988).
36. D. E. Brash, S. Saraswathy, K. H. Kraemer, M. M. Seidman, and A. Bredberg. Proc. Natl. Acad. Sci. U.S.A. **84**, 3782(1987).
37. L. F. Povirk and I. H. Goldberg. Proc. Natl. Acad. Sci. U.S.A. **82**, 3182(1985).
38. F. Bourre, G. Renault, and A. Sarasin. Nucleic Acids Res. **15**, 8861(1987).

Can. J. Chem. Downloaded from www.nrcresearchpress.com by 217.78.4.112 on 09/08/12
For personal use only.

Electron transport in clay-modified electrodes: study of electron transfer between electrochemically oxidized tris (2,2′-bipyridyl) iron cations and clay structural iron(II) sites

YAN XIANG AND GILLES VILLEMURE[1]

Department of Chemistry, University of New Brunswick, Bag Service #45222, Fredericton, N. B. Canada E3B 6E2

Received July 15, 1991

YAN XIANG and GILLES VILLEMURE. Can. J. Chem. **70**, 1833 (1992).

The cyclic voltammograms of tris (2,2′-bipyridyl) iron(II) ($[Fe(bpy)_3]^{2+}$) adsorbed in clay-modified electrodes made from a range of different smectites were recorded. In all cases, at low scan speed (1 mV/s), the initial anodic peak current was much larger than the initial cathodic peak current. Partial reduction of the clay structural iron further increased the initial anodic to cathodic current ratio, suggesting that the discrepancy between the charge transferred in the anodic and cathodic scans was due to a slow electron transfer between the clay structural Fe(II) and the oxidized bipyridyl cations. However, no clear quantitative relation was found between the measured FeO contents of the different clays and the observed excess anodic currents. In fact, of all the clays tested only one, montmorillonite SWy-1, contained enough Fe(II) for it to account for all of the excess anodic charge transferred in the initial scan.

YAN XIANG et GILLES VILLEMURE. Can. J. Chem. **70**, 1833 (1992).

Une étude par voltamétrie cyclique de l'ion fer(II) tris(2,2′-bipyridyl) ($[Fe(bpy)_3]^{2+}$) adsorbé dans des électrodes modifiées par des films d'argile montre qu'au cours du premier cycle, le courant anodique est plus élevé que le courant cathodique, lorsque la vitesse de balayage est de 1 mV/s. Cette différence augmente lorsque la réduction partielle des sites Fe(III) de l'argile augmente son contenu en fer(II), ce qui suggère que le courant anodique supplémentaire est dû à un transfert d'électron entre les sites fer(II) de l'argile et les ions fer(III)tris(2,2′-bipyridyl). Cependant, il ne semble pas y avoir de relation quantitative entre cette différence et la quantité totale de fer(II) présente dans les argiles. En fait, de toutes les argiles étudiées une seule, la montmorillonite SWy-1, contenait suffisamment de Fe(II) pour que l'on puisse leur attribuer la totalité de l'excédant de charge anodique transférée au cour du premier cycle.

Can. J. Chem. Downloaded from www.nrcresearchpress.com by 217.78.4.112 on 09/08/12
For personal use only.

Introduction

Recently, we found that the anodic peak currents were much larger than the cathodic peak currents in the first scan of the cyclic voltammograms of $[Fe(bpy)_3]^{2+}$ cations adsorbed in electrodes modified with films of montmorillonite (1). Discrepancies between the charge transferred in the cathodic and anodic waves have also been reported for $[Ru(bpy)_3]^{2+}$ (2, 3) and $[Ru(NH_3)_6]^{3+}$ (4, 5) adsorbed in clay-modified electrodes. These differences have generally been attributed to electron transfer between the adsorbed electroactive cations and iron sites in the clay lattices. Iron atoms in clay minerals have been known to act as electron donor/acceptor sites since the work of Solomon, more than 20 years ago (6).

Electron transfer between acceptor/donor sites in the clay lattice and adsorbed cations could help alleviate the problem of electron transport in clay-modified electrodes (CME) (7, 8). The electronic conductivity of clay minerals is low (9). Electron transport in CME must therefore depend on a combination of diffusion of the adsorbates through the films, and electron hopping between adsorbed species. The low mobility of cations in clay films means that only a small fraction of them, only those that are adsorbed in the vicinity of defects in the film structure, can reach the conductive substrate to participate in the electrochemical reaction (1). These small electroactive fractions greatly limit the usefulness of clays as electrode surface modifiers (10, 11). A more efficient electron transport mechanism, one which would be independent of the adsorbate mobility, would greatly increase the usefulness of CME.

One way to improve charge transport in CME would be to make use of the clay lattice acceptor/donor sites as relays to transfer electrons from the adsorbed cations to the conductive substrates. We therefore undertook a systematic investigation of the electrochemical behaviour of $[Fe(bpy)_3]^{2+}$ adsorbed in CME made from a range of smectites containing different Fe(II) concentrations. The objective was to establish the involvement of structural iron(II) in the anomalous initial peak current ratios.

Experimental

Materials

$[Fe(bpy)_3]Cl_2$ was prepared by adding 3 equivalents of 2,2′-bipyridyl (Aldrich) to an aqueous solution of ferrous sulphate (12). Addition of a saturated solution of NaCl gave a dark red solid on cooling.

The clay samples used are listed in Table 1. They were obtained from the Source Clay Minerals Repository (University of Missouri, Columbia, Mo). Sodium forms were prepared and the <0.2 μm (esd) fractions separated by literature procedures (13, 14). The clays' Fe(II) and the total iron contents were determined by a spectrophotometric method using 1,10-phenanthroline according to a published procedure (15, 16). Results are shown in Table 2, along with corresponding literature data.

A fraction of the structural Fe(III) in samples of SWy-1 and STx-1 was reduced to Fe(II) by heating to 70°C with sodium dithionite for 8 days according to a literature procedure (18). For each clay, two identical samples were reduced in the same conditions. One of them was used to determine the iron(II) and the total iron contents of the treated clays by the above method, the other to prepare the clay-modified electrodes.[2]

Methods

Cyclic voltammetry experiments were performed using a Princeton Applied Research (Princeton, N.J.) PARC model 270-1

[1]Author to whom correspondence may be addressed.

[2]During the preparation of the modified electrodes the reduced clays were exposed to air. This could result in partial reoxidation even if clay oxidation by oxygen is slow at room temperature.

Can. J. Chem. Downloaded from www.nrcresearchpress.com by 217.78.4.112 on 09/08/12
For personal use only.

TABLE 1. Clay samples used

Sample	Source
Nontronite	
SWa-1	Grant County, Washington
NG-1	Holen Hagen, Federal Republic of Germany
Montmorillonite	
SWy-1	Cook County, Wyoming
STx-1	Gonzales County, Texas
SAz-1	Apache County, Arizona
Hectorite	
SHCa-1	San Bernardino County, California

TABLE 2. Weight percent of FeO and Fe_2O_3 in the clay samples

	This work		Literature[a]	
Clay	FeO	Fe_2O_3	FeO	Fe_2O_3
Nontronite				
SWa-1	0.23	24.1	0.07	17.6
NG-1	0.12	33.3	0.12	20.0
Montmorillonite				
SWy-1	0.14	4.13	0.12	3.85
STx-1	0.03	1.49	0.04	1.17
SAz-1	0.02	1.75	—	—
Hectorite				
SHCa-1	0.01	0.52	—	—

[a]Values are for the <2.0 μm fractions of the clays. They were taken from ref. 16 for the nontronites and ref. 17 for the montmorillonites.

electrochemical analysis system. All electrochemical experiments were done in an undivided three-electrode cell. The counter electrode was a Pt gauze and the reference electrode was a saturated calomel electrode (SCE). The 0.1 M Na_2SO_4 electrolyte solutions were degassed by bubbling with N_2 prior to the measurements.

The clay-modified electrodes were prepared by spin coating (1, 20). The supports were 1 × 2 cm pieces of indium-doped SnO_2 coated glass (Delta Technologies, Stillwater, Minn.), cleaned by three cycles of sonication in EtOH. One drop of H_2SO_4 (10% v/v) was added to a 10 g/L suspension of the clay in distilled water to make a low-viscosity gel. Drops of the clay gel were spin coated at 3000 rpm (Headway Research, Photo-Resist spinner, Garland, Tex.). This gave films (1 cm^2) with interference colours from purple to yellow with estimated thickness of about 300 nm (1).

All the clay films were presoaked in 0.1 mM solutions of $[Fe(bpy)_3]^{2+}$ overnight. The volumes of the soaking solutions were selected so that the adsorption of the cations by the films would result in a 25–40% decrease of their concentrations. The amounts of $[Fe(bpy)_3]^{2+}$ adsorbed by the films were determined by measuring this decrease by UV–visible spectroscopy. As described in a previous report (19), this method gives more reliable measurements of the total amount of this type of cation adsorbed by clay films.

Results and discussions

The first three scans in the cyclic voltammogram of $[Fe(bpy)_3]^{2+}$ adsorbed in an electrode modified with a film of nontronite SWa-1, recorded at 1 mV/s, are shown in Fig. 1. In the initial scan the ratio of anodic to cathodic current was found to be 2.04. The anodic peak current I_{pa}, was much larger than the cathodic peak current I_{pc}. In subsequent scans this difference became smaller. By the third scan (dashed line) the ratio of I_{pa}/I_{pc} was down to 1.24. Table 3 shows that this was a general result for $[Fe(bpy)_3]^{2+}$ adsorbed in electrodes modified with a range of different montmorillonites and nontronites. Only for the electrode modified with hectorite (SHCa-1) was the initial current ratio close to 1, and for all CME the current ratio decreased in subsequent scans. The waves also became sharper (smaller ΔE) and shifted to lower potentials.

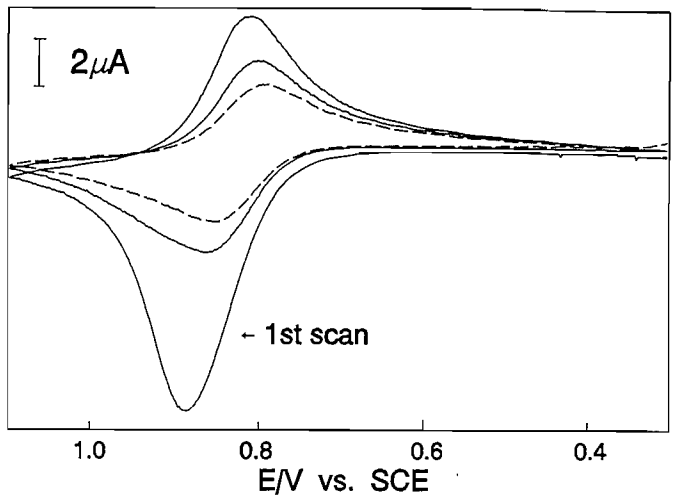

FIG. 1. Cyclic voltammogram of a SWa-1 CME (300 nm thick) presoaked overnight in 0.1 mM $[Fe(bpy)_3]^{2+}$, recorded at 1 mV/s in 0.1 M Na_2SO_4.

TABLE 3. Cyclic voltammetry data of CME containing $[Fe(bpy)_3]^{2+}$ recorded at 1 mV/s in 0.1 M Na_2SO_4

Clay	I_{pa1}/I_{pc1}	I_{pa3}/I_{pc3}	$(E_{1/2})_1$	$(E_{1/2})_3$
Nontronite				
SWa-1	2.04	1.24	0.85	0.82
NG-1	1.92	1.20	0.85	0.82
Montmorillonite				
SWy-1	2.36	1.29	0.86	0.84
STx-1	2.29	1.40	0.85	0.82
SAz-1	2.25	1.26	0.84	0.81
Hectorite				
SHCa-1	1.27	1.12	0.86	0.83

It appears that in the initial scan more electrons were passing during the oxidation than during the reduction of adsorbed $[Fe(bpy)_3]^{2+}$ cations. This would suggest that we are tapping an electron well in the clay films. One possible source of the additional electrons, first suggested by Oyama and Anson (4), is structural iron(II) sites in the clay lattice. To confirm the involvement of structural iron(II) sites in the anomalous initial current ratios, the concentrations of iron(II) in samples of montmorillonites STx-1 and SWy-1 were increased by the partial reduction of their iron(III). Figure 2 and Table 4 show that this resulted in a definite increase of the initial I_{pa}/I_{pc} ratios. However, Table 4 also shows that this increase was much smaller than could have been expected based on the 10-fold increase in the clay iron(II) contents.

That brings up the question of just how much additional anodic current can electron transfer from the clays' structural Fe(II) sites be expected to produce. To answer this

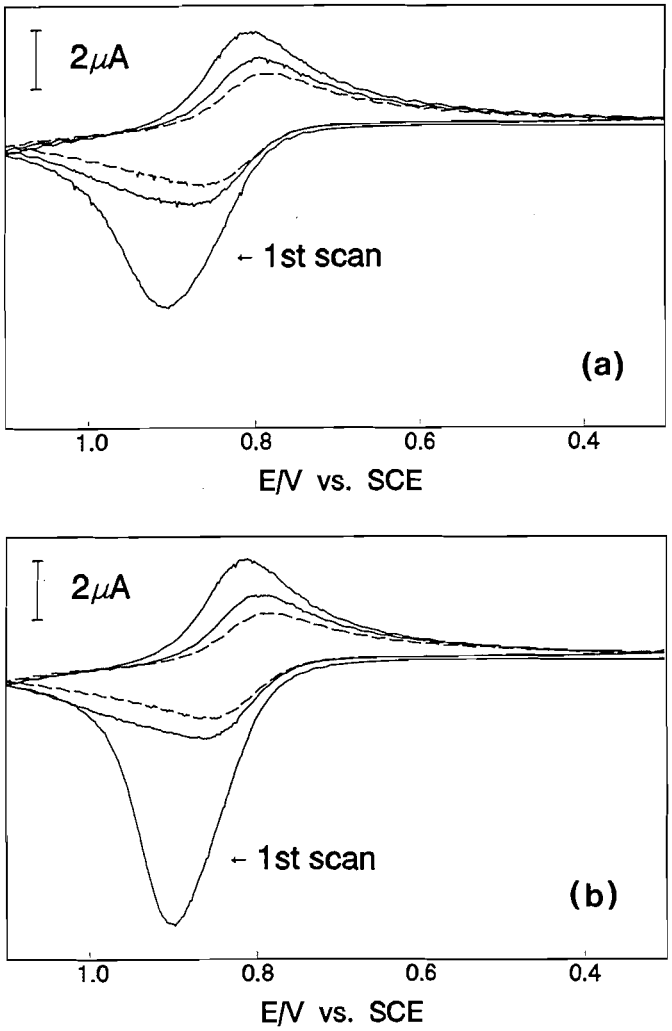

FIG. 2. Cyclic voltammograms of STx-1 CME (300 nm thick) presoaked overnight in 0.1 mM $[Fe(bpy)_3]^{2+}$, recorded at 1 mV/s in 0.1 M Na_2SO_4, prepared from (*a*) untreated and (*b*) partially reduced STx-1 (see Table 4).

TABLE 4. Effect of partial reduction of clay structural iron on the initial anodic to cathodic current ratio.

Clay	%FeO	I_{pa1}/I_{pc1}[a]
SWy-1	0.14	2.36
Reduced SWy-1	1.40	2.80
STx-1	0.03	2.29
Reduced STx-1	0.30	3.10

[a]Values of the current ratio are the averages of duplicate measurements. They were reproducible within ±0.05.

question we have to look, not at the initial current ratio, but at the difference between the first scan anodic and cathodic peak currents. The additional current due to electron transfer from the clay Fe(II) sites can be estimated from the film volume, the clay density, and its iron content, using the thin-layer equation (20).[3] When the results are compared with the observed current differences in Table 5, it is found that, except for SWy-1, the clays contained far too little iron(II) to account for the magnitude of the difference.

TABLE 5. Comparison of the observed difference between the initial I_{pa} and I_{pc} with that estimated from the clay FeO contents

Clay	%FeO	Estimated from %FeO $I_{pa} - I_{pc}/\mu A$	Observed $I_{pa} - I_{pc}/\mu A$
Nontronite			
SWa-1	0.23	2.39	5.8
NG-1	0.12	1.25	4.6
Montmorillonite			
SWy-1	0.14	1.45	1.1
Re-SWy-1	1.40	14.5	1.5
STx-1	0.03	0.31	3.3
Re-STx-1	0.30	3.11	5.8
SAz-1	0.02	0.21	4.9
Hectorite			
SHCa-1	0.01	0.10	0.4

Table 5 also shows that in the case of partially reduced STx-1 the increase in the $I_{pa} - I_{pc}$ difference of 2.5 μA found was close to the increase of 2.8 μA expected. But, in the case of partially reduced SWy-1, the small 0.4 μA increase found was nowhere near the 13 μA expected on the basis of the additional iron(II) present in the clay.

We also investigated the possibility that the discrepancy between the initial anodic and cathodic currents was due not only to an additional source of electrons, but also to the leaching of the adsorbed electroactive cations from the films by the electrolyte. Examination of Figs. 1 and 2 shows that there was a decrease in the magnitudes of both the anodic and cathodic peak currents. In Fig. 1, for example, I_{pc} was 2.7 μA lower in the third scan than in the first scan. Although this decrease was smaller than that of I_{pa}, 7.7 μA, it is not a negligible variation. This observation, combined with the finding that soaking the electrodes in the electrolyte solution for 24 h prior to recording the voltammograms reduced both the cathodic and anodic currents to less than 5% of their original values, suggests that the adsorbed electroactive $[Fe(bpy)_3]^{2+}$ cations were gradually washed away from the clay films by the electrolyte. This lost of activity was essentially unaffected by whether or not the potential was scanned continously, showing that the desorption of $[Fe(bpy)_3]^{3+}$ was not significantly faster than that of $[Fe(bpy)_3]^{2+}$.

A closer examination of the voltammograms, however, shows that the simple loss of electroactive $[Fe(bpy)_3]^{2+}$ cannot account for all of the change in the anodic current. For example, in Fig. 2*a* the second scan anodic peak current (I_{pa2}) is 2.7 μA larger than the first scan cathodic peak current (I_{pc1}), 2.6 μA. This is the reverse of what would be found if the decrease in current was due solely to a slow desorption of the $[Fe(bpy)_3]^{2+}$ cations with soaking time.

More convincing evidence that leaching of the adsorbed cations by the electrolyte does not account for all of the

[3]The additional currents obtained by this method are probably overestimated since the transfer of electron is not expected to be reversible, nor to be completed in the first scan, and the anodic peaks do not have the symmetrical shapes of surface waves.

Can. J. Chem. Downloaded from www.nrcresearchpress.com by 217.78.4.112 on 09/08/12
For personal use only.

Can. J. Chem. Downloaded from www.nrcresearchpress.com by 217.78.4.112 on 09/08/12
For personal use only.

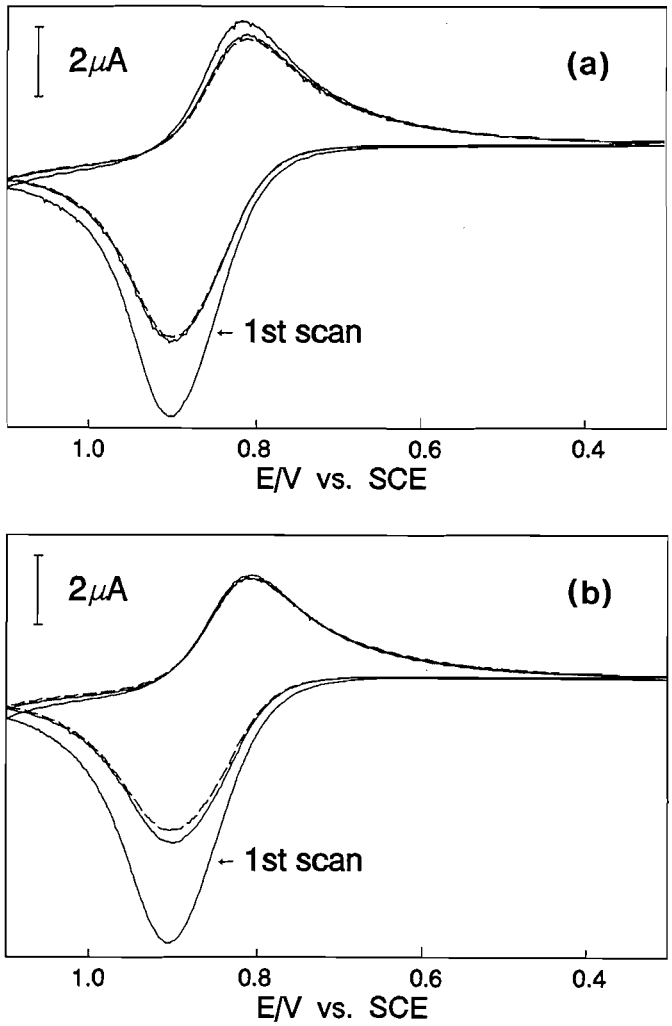

FIG. 3. Cyclic voltammograms of STx-1 CME (300 nm thick) presoaked overnight in 0.1 mM $[Fe(bpy)_3]^{2+}$, recorded at 1 mV/s in 0.1 M Na_2SO_4 electrolyte containing 0.04 mM $[Fe(bpy)_3]^{2+}$;(*a*) first three scans, (*b*) after 24 hours.

variation in anodic current is provided by the results shown in Fig. 3. To remove, or at least reduce, the importance of leaching, $[Fe(bpy)_3]^{2+}$ was added to the electrolyte solution in which the voltammograms were recorded. As expected, the variation of I_{pc} all but disappeared[4,5]. In fact, there was little change in I_{pc} even when the electrode was soaked in the electrolyte for 24 prior to recording the voltammograms (see Fig. 3*b*). As mentioned above, when there was no $[Fe(bpy)_3]^{2+}$ in the electrolyte, soaking of the electrode for 24 reduced I_{pc} by more than 95%. However Figs. 3*a* and 3*b* show that significant differences between the first and second scan I_{pa} remained. In fact the initial I_{pa}/I_{pc} ratio in Fig. 3*a* is 2.26, very close to the value found when there was no $[Fe(bpy)_3]^{2+}$ in the electrolyte solution (see Table 3). Despite the relatively rapid loss of adsorbed electroactive $[Fe(bpy)_3]^{2+}$ cations from CME when there was no $[Fe(bpy)_3]^{2+}$ in the electrolyte solution, this desorption does not appear to have a significant effect on the initial current ratio.

How then can we account for the excess anodic currents observed? Simply assuming that the oxidation of $[Fe(bpy)_3]^{2+}$ in CME is not reversible does not explain our results. Assuming that some of the $[Fe(bpy)_3]^{3+}$ produced is lost, either because of faster leaching or decomposition of the oxidized complex, would explain why I_{pc} is lower than I_{pa}. However, it would not account for the variation of the current ratio. Why would a process that is irreversible in the first scan become more reversible in subsequent scans? Further, an irreversible loss of $[Fe(bpy)_3]^{3+}$ would not allow for the second scan anodic current (I_{pa2}) to be larger than the first scan cathodic current (I_{pc1}). Although the difference between these two peak currents was generally small, it was quite common, especially for the montmorillonite electrodes, for I_{pa2} to be larger than I_{pc1}.

That leaves three possibilities to account for our results. First, there is an additional source of electrons we have not considered. For example, the iron(II) contents measured in the bulk clay powders may not reflect the state of oxidation of the clay in the film electrodes. All clay samples contained enough total iron that the reduction of only a fraction of it would account for the observed current differences.

A second possibility is that there are two types of electroactive $[Fe(bpy)_3]^{2+}$ cations. There are in the clay films a limited number of sites in which adsorbed $[Fe(bpy)_3]^{2+}$ can only be irreversibly oxidized. This irreversible oxidation is slow, so it takes several scans to complete. After it is completed, only the wave for the other type of electroactive cations, those that can be reversibly oxidized, remains.

Finally, we cannot exclude the possibility that the anomalous initial current ratios are due to more complex phenomena. For example, our results can be explained by assuming that there was an irreversible change in the film structure, induced by the electrogenerated $[Fe(bpy)_3]^{3+}$ cations, that was complete after a few scans and that reduced the mobility of the adsorbed cations. This would explain why both the anodic and cathodic current decreased with scanning, and how an oxidation that was initially not reversible becomes more reversible after a few scans, when this change was complete.

Support for the occurrence of an irreversible change of the clay films is provided by the observation that the activity of a CME that is resoaked in the $[Fe(bpy)_3]^{2+}$ solution after recording of the cyclic voltammograms does not recover. For example, the initial I_{pa} found for a STx-1 modified electrode was 5.9 μA. As mentioned above, this current was reduced by more than 95% after 24 h in the electrolyte. The initial anodic current found for this same electrode after it was resoaking in a solution of $[Fe(bpy)_3]^{2+}$ was only 1.5 μA. This change in the film structure would be analogous, in its effect on the current, to an increase in the cross-linking of a polymer-modified electrode (21). The problem with this interpretation is that it does not allow for the second scan anodic current (I_{pa2}) to be larger than the first scan cathodic current (I_{pc1}).

[4]Since the concentration of the $[Fe(bpy)_3]^{2+}$ in the electrolyte was lower than that of the soaking solution, some slight change in I_{pc} remained until complete equilibration occurred.

[5]Except for an increase in the background noise, stirring the solution during the measurement had no significant effect on the cyclic voltammograms, confirming that the waves were due only to the cations adsorbed in the clay films and not to solution cations.

Conclusion

At slow scan speed in the initial scan, the anodic peak current of $[Fe(bpy)_3]^{2+}$ adsorbed in a range of clay-modified electrodes is larger than the cathodic peak current, indicating that more electrons are passing during the oxidation than during the reduction of the adsorbed species. This remains true even after the rapid loss of activity of the films due to leaching is taken into account. Increasing the concentration of structural iron(II) sites in the clays, by the partial reduction of the their structural iron(III), was found to result in a further increase of the initial anodic to cathodic current ratio. However, except for montmorillonite SWy-1, the clays did not contain enough Fe(II) to account for all of the discrepancy between the charge transferred in the cathodic and anodic scans, unless we assume that the bulk FeO contents did not reflect the FeO contents of the clay films used to modify the electrodes.

Unless there is another source of electrons in the clay films that we have not considered, the remaining difference between the initial anodic and cathodic currents must be due to other phenomena. The most straightforward explanation is that the film contained two types of electroactive cations, one for which the oxidation was reversible and one for which the oxidation was irreversible. However, we cannot exclude the possibility of more complex mechanisms, such as changes in the film structure.

We are pursuing our study of the involvement of structural iron in the anomalous initial scan current ratio found for $[Fe(bpy)_3]^{2+}$ adsorbed in CME. Investigations of leaching, decomposition of the redox species, and the effect of oxidation state on transport in the clay films and on the film structures are also underway.

Acknowledgements

Financial support for this work was provided by the Natural Sciences and Engineering Research Council of Canada, the Maritime Provinces Higher Education Council, and the University of New Brunswick.

1. G. Villemure and A. J. Bard. J. Electroanal. Chem. **282**, 107 (1990).
2. W. E. Rudzinski and A. J. Bard. J. Electroanal. Chem. **199**, 232 (1986).
3. D. Ege, P. K. Ghosh, J. R. White, J.-F. Equey, and A. J. Bard. J. Electroanal. Chem. **169**, 315 (1984).
4. N. Oyama and F. C. Anson. J. Electroanal. Chem. **199**, 467 (1986).
5. T. Ohsaka, Y. Yamaguchi, and N. Oyama. Bull. Chem. Soc. Jpn. **63**, 2646 (1990).
6. D. H. Solomon. Clays Clay Miner. **16**, 31 (1968).
7. R. W. Murray, *In* Electroanalytical chemistry. Vol. 13. *Edited by* A. J. Bard. Marcel Dekker, New York. 1984. p. 191, and references therein.
8. A. Fitch. Clays Clay Miner. **38**, 391 (1990).
9. D. Wang, W Yu and B. Zhu. Solid State Ionics, **34**, 129 (1989).
10. A. J. Bard and T. E. Mallouk *In* Molecular design of electrode surfaces. *Edited by* R. Murray. Wiley, New York.
11. P. K. Ghosh and A. J. Bard. J. Am. Chem. Soc. **105**, 5591 (1983).
12. M. H. Ford-Smith and N. Sutin. J. Am. Chem. Soc. **83**, 1830 (1961).
13. C. B. Tanner and M. L. Jackson. Soil Sci. Soc. Am. Proc. **12**, 60 (1947).
14. M. L. Jackson, L. D. Wittig, and R. P. Pennington. Soil Sci. Soc. Am. Proc. **14**, 77 (1949).
15. J. W. Stucki. Soil Sci. Soc. Am. J. **45**, 638 (1981).
16. P. Komadel and J. W. Stucki. Clays Clay Miner. **36**, 379 (1988).
17. H. van Olphen and J. J. Fripiat (*Editors*). Data handbook for clay materials and other non-metallic minerals. Pergamon Press, New York. 1979. p. 128.
18. J. W. Stucki, D. C. Golden, and C. B. Roth. Clays Clay Miner. **32**, 191 (1984).
19. G. Villemure and A. J. Bard. J. Electroanal. Chem. **283**, 403 (1990).
20. A. J. Bard and L. R. Murray *In* Electrochemical methods: fundamentals and applications. John Wiley & Sons, New York. 1980. pp. 406–413.
21. K. Niwa and K. Doblhofer. Electrochim. Acta, **31**, 549 (1986).

Can. J. Chem. Downloaded from www.nrcresearchpress.com by 217.78.4.112 on 09/08/12
For personal use only.

Radical-based syntheses of 5-benzoyl-1,2-dihydro-3H-pyrrolo[1,2-a]pyrrole-1-carboxylic acid (ketorolac)[1]

DEAN R. ARTIS, IN-SEOP CHO,[2] AND JOSEPH M. MUCHOWSKI[3]
Syntex Research, Institute of Organic Chemistry, 3401 Hillview Ave., Palo Alto, CA 94304, U.S.A.

Received January 21, 1992

DEAN R. ARTIS, IN-SEOP CHO, and JOSEPH M. MUCHOWSKI. Can. J. Chem. **70**, 1838 (1992).

Short, efficient, and convergent syntheses of ketorolac (**1**) based on the inter- or intramolecular oxidative addition of malonyl and substituted malonyl radicals to 2-benzoylpyrrole and derivatives thereof are described.

DEAN R. ARTIS, IN-SEOP CHO et JOSEPH M. MUCHOWSKI. Can. J. Chem. **70**, 1838 (1992).

On décrit des synthèses à la fois courtes, efficaces et convergentes du kétorolac **1** qui sont basées sur l'addition oxydante inter- ou intra-moléculaire de radicaux malonyles ou malonyles substitués sur le 2-benzoylpyrrole et ses dérivés.

[Traduit par la rédaction]

Ketorolac (5-benzoyl-1,2-dihydro-3*H*-pyrrolo[1,2-*a*]pyrrole-1-carboxylic acid (**1**, Scheme 1) is a powerful non-narcotic analgesic that is used clinically for the management of moderate to severe pain states (1). Both linear (2) and convergent (3, 4) syntheses of this compound, and its derivatives, based on "ionic" bond formation processes have been reported. This paper describes new synthetic approaches to ketorolac in which the salient feature is the oxidative addition of an "electrophilic" radical species to a 2-benzoylpyrrole derivative.

Malonate anions of type **2** (X = Cl, Br, SO_2Me) readily cyclize to the bicyclic esters **3** and consequently they are valuable intermediates in the synthesis of ketorolac and congeners thereof (3, 4). It seemed to us that the alkylmalonyl radical **4** might add intramolecularly to the relatively electron-rich pyrrole nucleus to give the bicyclic radical **5**, which on oxidation to the cationic species **6** and proton loss therefrom would provide another route to the diester **3**. The recently described manganese(III) acetate induced cyclizations of β-arylethyl-, λ-arylpropyl-, β-aryloxyethyl-, and λ-aryloxypropylmalonates are the first reported examples of just such a process (5).

To ascertain if ketorolac could indeed be obtained by an oxidative radical cyclization process, the known (6) *N*-chloroethylpyrrole **7** (Scheme 2) was converted into the corresponding solvolytically sensitive iodide **8** (sodium iodide in boiling acetonitrile), which was immediately reacted with the sodium salt of diethyl malonate in dimethylformamide (DMF) solution. Reaction of the alkylmalonate **9** thus obtained with 2.5 equivalents of manganese(III) acetate (generated *in situ* from $Mn(OAc)_2 \cdot 4H_2O$),[4] in acetic acid solution at 80°C, gave the cyclic diester **11** in nearly quantitative yield. The amount of Mn(III) could be reduced by 60%, without a diminution in the yield of **11**, by using sodium persulfate (in the presence of Ag(I) as a cocatalyst) to reoxidize Mn(II) to Mn(III) (8). This result indicates that the latter process might well be made catalytic in Mn(III) but this possibility was not examined. Saponification of **11** and decarboxylation of the diacid gave ketorolac (**1**) in over 50% yield based on 2-benzoylpyrrole, the immediate precursor of **7**.

The conversion of **9** to **11** could also be effected by abstraction of Br· from the bromomalonate **10** mediated by the aerial oxidation of triethylborane (9, 10). The nature of the specie(s) responsible for the transformation of the bicyclic radical (i.e., corresponding to **5**) to **11** is not known. Compound **10** was synthesized by bromination of the sodium salt of **9** with *N*-bromosuccinimide.

It was of considerable interest to determine if diethyl 5-benzoylpyrrole-2-malonate (**14**, Scheme 3) could be synthesized by the reaction of the diethyl malonyl radical with 2-benzoylpyrrole (**12**). Compound **14** is of obvious synthetic importance because base-induced alkylation with an appropriate 1,2-disubstituted ethane derivative would most certainly produce the bicyclic ester **11**.

The Mn(III)-induced reaction of diethyl malonate with 2-benzoylpyrrole gave the α-acetoxy derivative **13** as the major product. The formation of this substance was not unexpected (11) nor was it prevented by the use of diethyl chloromalonate, a stratagem that has been utilized to obviate such overoxidation (12, 13). The desired malonate **14** could be obtained from **13**, albeit in modest yield, by triethylsilane – trifluoracetic acid reduction. Compound **14** could, however, be directly prepared from 2-benzoylpyrrole in excellent yield (86%) when the diethyl malonyl radical was generated from diethyl bromomalonate by the triethylborane-autoxidation process.

As expected, potassium carbonate induced alkylation of **14** with 1,2-dichloroethane (reactant and solvent), in the presence of 1 equivalent of tetra-*n*-butylammonium bromide, gave the bicyclic ester **11** in ca. 70% yield.

We have recently shown (14) that electron-rich aromatic systems undergo Mn(III)-induced tri(ethoxycarbonyl)methylation with triethyl methanetricarboxylate and that the triester **15** is formed as the only product (86%) from 2-benzoylpyrrole. The dealkoxycarbonylation of trialkyl alkane-1,1,1-tricarboxylates under basic conditions is known to be facile (15) and the conversion of **15** to **14** could be efficiently effected with sodium ethoxide in DMF at room temperature. Thus, this process not only constitutes a simple solution to the overoxidation problem, it also means that **15** is functionally equivalent to the malonate ester **14**. Indeed, reaction of **15** with 1,2-dichloroethane under conditions identical to those used with **14** gave the bicyclic diester **11**

[1]Contribution no. 832 from the Syntex Institute of Organic Chemistry.

[2]Syntex Research Postdoctorate Fellow, 1989–1990.

[3]Author to whom correspondence may be addressed.

[4]$KMnO_4$ was used as the oxidant (7). This method obviates the need to purchase the costly Mn(III) reagent.

Can. J. Chem. Downloaded from www.nrcresearchpress.com by 217.78.4.112 on 09/08/12
For personal use only.

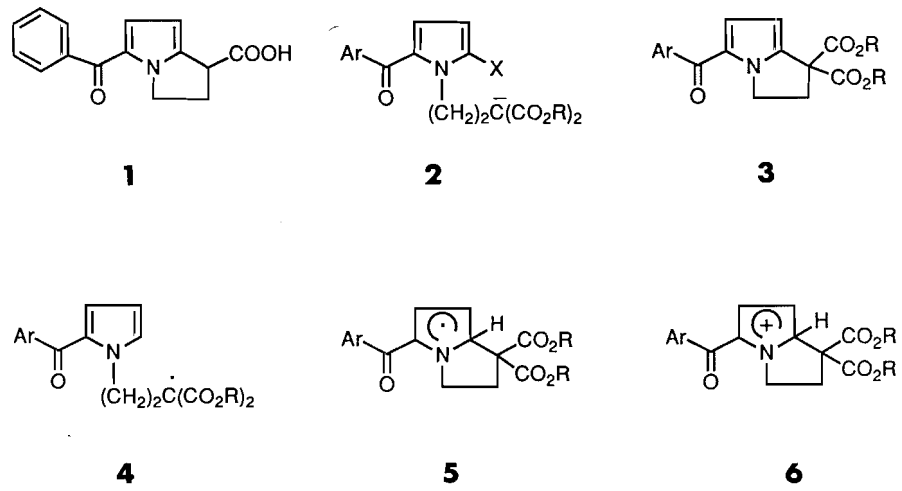

SCHEME 1

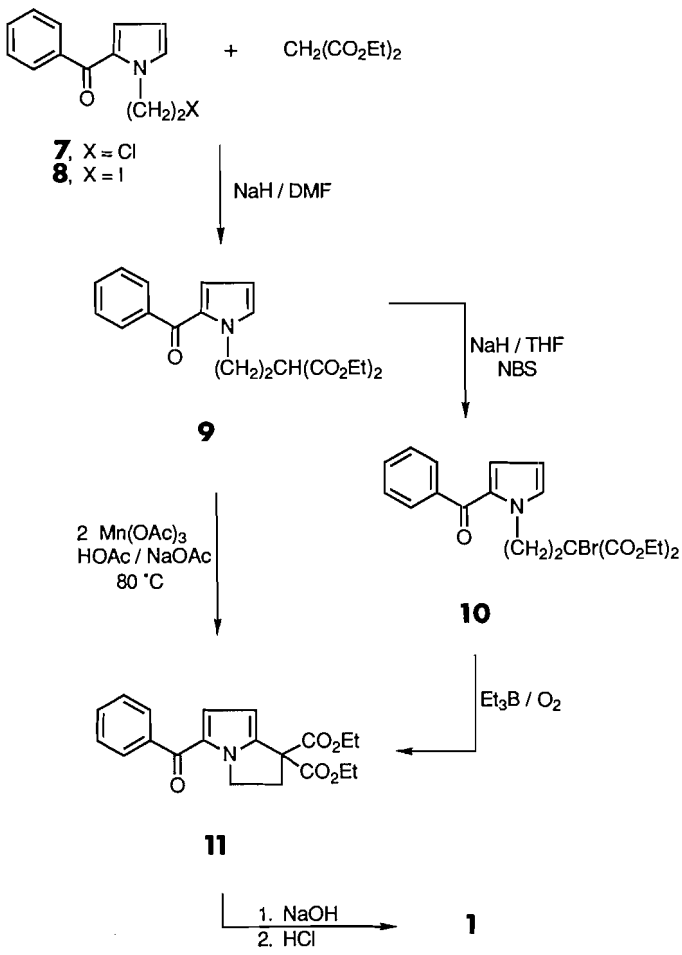

SCHEME 2

directly in 80% yield. This, therefore, is the shortest and most efficient (64% overall yield from 2-benzoylpyrrole) synthesis of ketorolac published to date.

The regiospecificity of the reaction of the diethyl malonyl, diethyl chloromalonyl, and tri(ethoxycarbonyl)methyl radicals with 2-benzoylpyrrole is especially noteworthy. The outcome of these reactions can be accounted for on the basis of the principles of the Frontier Molecular Orbital Theory, the regiospecificity being related to the relative values of the squares of the coefficients of the appropriate molecular orbitals of the potential positions of substitution (16). The attacking radicals are all electron deficient and therefore one would expect that the SOMO's thereof would interact preferentially with the HOMO of 2-benzoylpyrrole. Examination of the squares of the coefficients of both the HOMO and the LUMO of 2-benzoylpyrrole (Table 1) indicates a strong preference for substitution at C-5, as is observed, if the reactions occur through the HOMO.

Experimental

The melting points were determined in a Thomas Hoover "uni melt" capillary melting point apparatus and are not corrected. The infrared spectra were measured with a Nicolet 5 PC FT infrared spectrophotometer. The ^1H nmr spectra were recorded with a Bruker WM 300 or a Bruker AM 500 nmr spectrometer in deuteriochloroform and are expressed as parts per million (δ) from internal tetramethylsilane. The high-resolution mass spectra were obtained with a Finnigan MAT 311A mass spectrometer on samples that were at least 95% pure as judged by nmr spectrometry.

The terms "worked up in the usual manner" or "the usual work-up" signify that the extract was washed with water, dried over sodium sulfate, and evaporated *in vacuo*.

1-(2-Iodoethyl)-2-benzoylpyrrole (8)

A solution of the known (6) chloro compound **7** (11.4 g, 49 mmol) in acetonitrile (250 mL) containing sodium iodide (14.7 g, 98 mmol) was heated at reflux temperature for 24 h. The cooled solution was concentrated to a small volume *in vacuo*, water was added to the residue, and the product was extracted into ethyl acetate. After the usual work-up, the residue was subjected to column chromatographic purification on silica gel using hexane – ethyl acetate (97:3) as the eluting solvent. Compound **8**, which because of its solvolytic sensitivity should be used immediately in the next step, was obtained as an oil (12.7 g, 80%); ir (neat): 1623 cm^{-1}; nmr (300) δ: 3.58 (t, 2H, J = 6.84 Hz, CH_2I), 4.71 (t, 2H, J = 6.84 Hz, NCH_2), 6.20 (dd, 1H, $J_{3,4}$ = 4.06 Hz, $J_{4,5}$ = 2.58 Hz, H-4), 6.81 (dd, 1H, $J_{3,4}$ = 4.06 Hz, $J_{3,5}$ = 1.67 Hz, H-3) 7.04 (t, 1H, H-5), 7.43–7.58 (m, 3H), 7.79 (dd, 2H, J_o = 8.27 Hz, J_m = 1.4 Hz); *m/e* calcd. for $C_{13}H_{12}INO$: 324.9962; found: 324.9960.

1-(3,3-Diethoxycarbonylpropyl)-2-benzoylpyrrole (9)

Sodium hydride (60% in mineral oil, 1.35 g, 34 mmol) was added portionwise to a stirred solution of diethyl malonate (5.4 g,

Can. J. Chem. Downloaded from www.nrcresearchpress.com by 217.78.4.112 on 09/08/12
For personal use only.

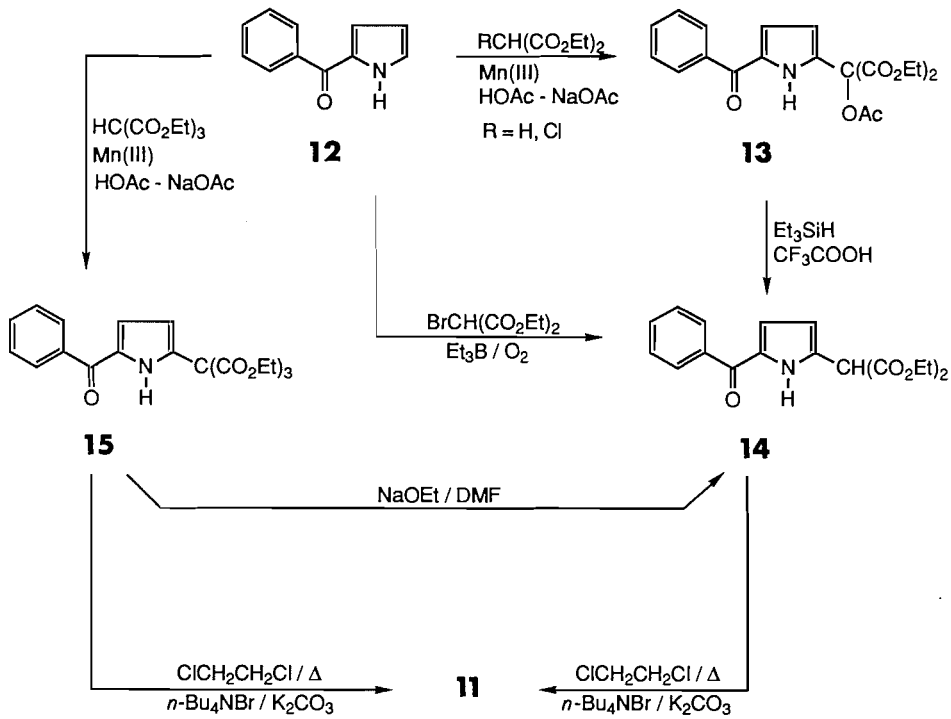

SCHEME 3

TABLE 1. Squares of the coefficients of the pyrrole HOMO's and LUMO's of 2-benzoylpyrrole[a]

Position	HOMO	LUMO
3	0.0920	0.1048
4	0.1483	0.0013
5	0.3347	0.0904

[a]The molecular orbital coefficients are derived from semi-empirical molecular orbital calculations on fully optimized structures. The calculations were carried out using the MNDO Hamiltonian within the implementation of MOPAC 4.0 as released in SYBYL 5.32.

34 mmol) in dry DMF (50 mL) at 0°C. The reaction mixture was then stirred at room temperature for 0.5 h after which time a solution of the iodo compound **8** (11.0 g, 34 mmol) in dry DMF (50 mL) was added. The reaction mixture was stirred at room temperature for 16 h, poured into water, and extracted with ethyl acetate. The extract was washed with water and with saturated NaCl solution, then it was dried (Na_2SO_4) and evaporated *in vacuo*. The residual oil was purified by column chromatography on silica gel using hexane – ethyl acetate (9:1) to elute the malonate ester **9** (9.85 g, 82%) as an oil; ir (neat): 1748, 1732, 1628 cm^{-1}; nmr (500) δ: 1.22 (t, 6H, J = 7.0 Hz, Me), 2.40 (q, 2H, J = 7.2 Hz, CH_2CH), 3.32 (t, 1H, J = 7.3 Hz, CH), 4.15 (q, 4H, J = 7.0 Hz, OCH_2), 4.47 (t, 2H, J = 7.0 Hz, NCH_2), 6.14 (dd, 1H, $J_{3,4}$ = 4.12 Hz, $J_{4,5}$ = 2.58 Hz, H-4), 6.70 (dd, 1H, $J_{3,4}$ = 4.12 Hz, $J_{3,5}$ = 1.76 Hz, H-3), 6.94 (t, 1H, H-5), 7.40 (m, 2H), 7.47 (m, 1H), 7.74 (m, 2H); *m/e* calcd. for $C_{20}H_{23}NO_5$: 357.1576, found: 357.1580.

*1-(3,3-Diethoxycarbonyl-3-bromopropyl)-2-benzoylpyrrole (**10**)*

Sodium hydride (60% in mineral oil, 0.14 g, 3.45 mmol) was added portionwise to a stirred solution of compound **9** (1.12 g, 3.14 mmol) in dry THF (50 mL) at 0°C. The reaction mixture was then agitated at room temperature for 0.5 h after which time *N*-bromosuccinimide (0.64 g, 3.45 mmol) was added. After a further 0.5 h, the reaction mixture was poured into water and the product was extracted into ether. The extract was washed with water and with saturated NaCl solution, and then it was dried and evaporated in *in vacuo*. The residue was subjected to column chromatographic purification on silica gel using hexane – ethyl acetate (9:1) to elute the bromo compound **10** (1.15 g, 84%) as an oil; ir (neat): 1741, 1627 cm^{-1}; nmr (300) δ: 1.29 (t, 6H, J = 7.13 Hz, Me), 2.87 (t, 2H, J = 7.37 Hz, CH_2), 4.26 (m, 4H, OCH_2), 4.61 (d, 2H, J = 7.37; NCH_2), 6.17 (dd, 1H, $J_{3,4}$ = 4.07 Hz, $J_{4,5}$ = 2.55 Hz, H-4), 6.73 (dd, 1H, $J_{3,4}$ = 4.07 Hz, $J_{3,5}$ = 1.68 Hz, H-3), 7.26 (t, 1H, H-5), 7.44–7.56 (m, 3H), 7.77 (dd, 2H, J_o = 8.2 Hz, J_m = 1.4 Hz). Anal. calcd. for $C_{20}H_{22}BrNO_5$: C 55.05; H 5.08, N 3.21; found: C 54.98, H 5.25, N 3.17.

*Diethyl 5-benzoylpyrrol-2-yl-(α-acetoxy)malonate (**13**)*

(a) From 2-benzoylpyrrole and diethyl malonate

A solution of 2-benzoylpyrrole (0.855 g, 5 mmol) and diethyl malonate (0.800 g, 5 mmol) in acetic acid (30 mL) containing manganese triacetate trihydrate (4.56 g, 15 mmol) and sodium acetate (0.820 g, 10 mmol) was stirred at 70°C under a nitrogen atmosphere for 4 h. The reaction mixture was cooled, diluted with ether, and filtered. The filtrate was washed with 10% NaOH solution and saturated NaCl solution, and then it was dried and evaporated *in vacuo*. The residue was subjected to column chromatographic purification on silica gel using hexane – ethyl acetate (7:3) to elute the α-acetoxy compound **13** (1.10 g, 57%) as an oil; ir (neat): 3426, 3263, 1753, 1629 cm^{-1}; nmr (300) δ: 1.30 (t, 6H, J = 7.13 Hz, Me), 2.25 (s, 3H, MeCO), 4.33 (m, 4H, OCH_2), 6.40 (dd, 1H, $J_{3,4}$ = 3.97 Hz, $J_{NH,3}$ = 2.65 Hz, H-3), 6.78 (dd, 1H, $J_{3,4}$ = 3.97 Hz, $J_{NH,4}$ = 2.65 Hz, H-4), 7.47–7.58 (m, 3H), 7.87 (dd, 2H, J_o = 8.30 Hz, J_m = 1.4 Hz), 10.31 (bs, 1H, NH); *m/e* calcd. for $C_{20}H_{21}NO_7$: 387.1318; found: 387.1326.

(b) From 2-benzoylpyrrole and diethyl chloromalonate

The reaction was carried out exactly as in (*a*) and on the same scale but diethyl chloromalonate was used. Compound **13** was obtained in 75% yield.

Can. J. Chem. Downloaded from www.nrcresearchpress.com by 217.78.4.112 on 09/08/12
For personal use only.

Can. J. Chem. Downloaded from www.nrcresearchpress.com by 217.78.4.112 on 09/08/12
For personal use only.

*Diethyl 5-benzoylpyrrole-2-malonate (**14**)*

*(a) By reduction of acetoxy compound **13***

Trifluoroacetic acid (0.168 g, 1.47 mmol) was added to a solution of the acetoxy compound **13** (0.142 g, 0.367 mmol) in dichloromethane (10 mL) containing triethylsilane (0.102 g, 0.440 mmol) and the solution was then stirred at 40°C for 24 h. Additional triethylsilane (0.102 g) and trifluoroacetic acid (0.168 g) were added and stirring at 40°C was continued for a further 24 h. The cooled solution was washed with cold 10% NaOH solution and then worked up in the usual manner. The residue was subjected to column chromatographic purification on silica gel, the product (0.060 g, 50%) being eluted with hexane – ethyl acetate (87:13) as an oil; ir (neat): 3264, 1739, 1611 cm^{1}; nmr (300) δ: 1.30 (t, 6H, J = 7.23 Hz, Me), 4.26 (m, 4H, OCH_2), 4.81 (s, 1H, CH), 6.29 (d, 1H, $J_{3,4}$ = 3.9 Hz, H-3),[5] 6.80 (d, 1H, $J_{3,4}$ = 3.98 Hz, H-4),[5] 7.45–7.56 (m, 3H), 7.88 (m 2H), 10.19 (bs, 1H, NH). Anal. calcd. for $C_{18}H_{19}NO_5$: C 65.64, H 5.81, N 4.25; found: C 65.61, H 5.80, N 4.25.

(b) From 2-benzoylpyrrole and diethyl bromomalonate

A 1.0 M solution of triethylborane in hexane (2 mL) was added to a stirred solution of 2-benzoylpyrrole (0.171 g, 1.0 mmol) and diethyl bromomalonate (1.185 g, 5.0 mmol) in benzene (20 mL) that was open to the atmosphere. Additional triethylborane solution was added at the end of 1 h (2 mL) and 2 h (1 mL) at room temperature. The reaction mixture was poured into water and extracted with ether. The ether extract was washed with saturated NaCl solution and then worked up in the usual manner. After purification of the crude product as described above, the pure malonate **14** was obtained as an oil (0.284 g, 86%) identical to that prepared by method (*a*).

*(c) By deethoxycarbonylation of triester **15***

Ethanol (0.176 mL, 0.138 g, 3.0 mmol) was added to a stirred suspension of 50% sodium hydride in mineral oil (0.048 g, 1.0 mmol) in anhydrous DMF (10 mL). After ca. 10 min a solution of **15** (0.403 g, 1 mmol) in dry DMF (5 mL) was added and stirring was continued for 2 h at room temperature. The reaction mixture was poured into aqueous ammonium chloride solution and the product was extracted into ethyl acetate. After the usual work-up the crude malonate ester **14** was purified by column chromatography on silica gel (40 g) using hexane – ethyl acetate (4:1) as the eluting solvent. Pure **14** was obtained as an oil (0.273 g, 83%) identical to material prepared by methods (*a*) or (*b*).

*Diethyl 5-benzoyl-1,2-dihydro-3H-pyrrolo[1,2-a]pyrrole-1,1-dicarboxylate (**11**)*

*(a) By Mn(III) induced cyclization of **9***

Potassium permanganate (0.138 g, 0.875 mmol), acetic anhydride (1.25 mL, 1.35 g, 10.5 mmol), and sodium acetate (0.420 g, 5 mmol) were added sequentially to a stirred solution of manganese diacetate tetrahydrate (0.858 g, 3.5 mmol) in acetic acid (8 mL) at 80°C. A solution of the malonate ester **9** (0.500 g, 1.40 mmol) in acetic acid (2 mL) was added thereto and the solution was stirred at 80°C for 6 h. The solution was poured into water and the product was extracted into toluene. After the usual work-up the bicyclic ester **11** was obtained as an oil (0.478 g, 96%), which was pure as judged by nmr spectroscopy; ir (neat): 1738, 1626 cm^{-1}; nmr (500) δ: 1.29 (t, 6H, J = 7.10 Hz, Me), 3.13 (t, 2H, J = 7.0 Hz, CH_2C), 4.26 (q, 4H, J = 7.10 Hz, OCH_2), 4.54 (t, 2H, J = 7.0 Hz, NCH_2), 6.27 (d, 1H, $J_{6,7}$ = 4.07 Hz, H-7), 6.84 (d, 1H, $J_{6,7}$ = 4.07 Hz, H-6), 7.43–7.54 (m, 3H), 7.82 (dd, 2H, J_o = 8.3 Hz, J_m = 1.4 Hz); *m/e* calcd. for $C_{20}H_{21}NO_5$: 355.1420; found: 355.1413.

*(b) From **9** using Mn(II) and sodium persulfate*

A solution of manganese diacetate tetrahydrate (0.343 g, 1.40 mmol), silver nitrate (0.024 g, 0.14 mmol), sodium acetate (0.420 g, 5 mmol), acetic anhydride (0.5 mL, 0.54 g, 4.20 mmol), and sodium persulfate (0.333 g, 1.40 mmol) in acetic acid (8 mL) was stirred at 80°C for 0.5 h. A solution of the malonate ester **9** (0.500 g, 1.4 mmol) in acetic acid (2 mL) and additional sodium persulfate (0.333 g, 1.4 mmol) were added and the solution was stirred at 80°C for 12 h. After work-up of the reaction mixture as described in (*a*) compound **11**, identical to that obtained above, was isolated as an oil (0.475 g, 95%).

*(c) By the triethylborane induced cyclization of bromomalonate **10***

This reaction was carried out exactly as described for the synthesis of compound **14** from 2-benzoylpyrrole and diethyl bromomalonate. The crude product was purified by column chromatography on silica gel using hexane – ethyl acetate (85:15). Compound **11** was isolated in 75% yield.

*(d) From malonate ester **14** and 1,2-dichloroethane*

A mixture of tetra-*n*-butylammonium bromide (0.130 g, 0.40 mmol) and potassium carbonate (2.76 g, 20 mmol) in 1,2-dichloroethane (16 mL) containing compound **14** (0.132 g, 0.40 mmol) was stirred at reflux temperature until the starting material had disappeared (~ 24 h). The mixture was filtered and the filtrate was evaporated *in vacuo*. The residue was taken up in ether and after the usual work-up the crude material was purified by column chromatography on silica gel using hexane – ethyl acetate (9:1) as the eluant. The product was isolated in 67% yield.

*(e) From triester **15** and 1,2-dichloroethane*

A reaction performed on a 5 mmol scale exactly as described in (*d*) gave **11** in 80% yield.

*5-Benzoyl-1,2-dihydro-3H-pyrrolo[1,2-a]pyrrole-1-carboxylic acid (**1**, ketorolac)*

A biphasic mixture of the diester **11** (0.600 g, 1.69 mmol) in ether (20 mL) and 20% aqueous NaOH (10 mL) was vigorously stirred at reflux temperature for 24 h. The aqueous layer was washed with ether, carefully made acidic with concentrated hydrochloric acid, and extracted with ethyl acetate. The extract was heated at 70°C for 4 h and then evaporated *in vacuo* to give **1** (0.400 g, 93%) as a solid identical in all respects to an authentic specimen of ketorolac.

[5]After exchange with D_2O.

Acknowledgement

We thank Saul Jaime for converting the triester **15** to the malonate ester **14** and for preparing an analytical specimen of the latter compound.

1. J. M. Muchowski. *In* Advances in medicinal chemistry. Vol. 1. *Edited by* B. A. Maryanoff and C. Maryanoff. JAI Press Inc., Greenwich, Conn. 1992. pp. 109–135.
2. J. M. Muchowski, S. H. Unger, J. Ackrell, P. Cheung, G. F. Cooper, J. Cook, P. Gallegra, O. Halpern, R. Koehler, A. F. Kluge, A. R. Van Horn, Y. Antonio, H. Carpio, F. Franco, E. Galeazzi, I. Garcia, R. Greenhouse, A. Guzman, J. Iriarte, A. Leon, A. Pena, V. Perez, D. Valdez, N. Ackerman, S. A. Ballaron, D. V. Krishna Murthy, J. R. Rovito, A. J. Tomolonis, J. M. Young, and W. H. Rooks. J. Med. Chem. **28**, 1037 (1985).
3. F. Franco, R. Greenhouse, and J. M. Muchowski. J. Org. Chem. **47**, 1682 (1982).
4. J. M. Muchowski and R. Greenhouse. U.S. Patent, 4,873,340 (1989); Chem. Abstr. **112**, 178,658q (1990); J. M. Muchowski and R. Greenhouse. U.S. Patent, 4,988,822 (1991).
5. A. Citterio, D. Fancelli, C. Finzi, L. Pesce, and R. Santi. J. Org. Chem. **54**, 2713 (1989).
6. C. Gonzalez, R. Greenhouse, R. Tallabs, and J. M. Muchowski. Can. J. Chem. **61**, 1697 (1983).
7. E. I. Heiba, R. M. Dessau, A. L. Williams, and P. G. Rodewald. Org. Synth. **61**, 22 (1983)
8. H. Skarzewski. Tetrahedron, **40**, 4997 (1984).

9. B. Giese. *In* Radicals in organic synthesis: formation of carbon–carbon bonds. Pergamon Press, Oxford. 1986. pp. 86–89.
10. P. G. Allies and P. B. Brindley. J. Chem. Soc. (B), 1126 (1969).
11. A. Citterio, R. Santi, T. Fiorani, and S. Strologo. J. Org. Chem. **54**, 2703 (1989).
12. E. J. Corey and A. W. Gross. Tetrahedron Lett. **26**, 4291 (1985).
13. B. B. Snider, J. J. Patricia, and S. A. Kates. J. Org. Chem. **53**, 2137 (1988).
14. I. Cho and J. M. Muchowski. Synthesis, 567 (1991).
15. H. C. Padgett, I. G. Csendes, H. Rapoport. J. Org. Chem. **44**, 3492 (1979).
16. L. Salem. *In* Molecular orbital theory of conjugated systems. W. A. Benjamin, Menlo Park, Calif. 1966. pp. 326–332.

Can. J. Chem. Downloaded from www.nrcresearchpress.com by 217.78.4.112 on 09/08/12
For personal use only.

Détermination par voie électrochimique des propriétés acido-basiques et oxydo-réductrices des solutions concentrées en acide phosphorique progressivement neutralisées par la soude

J. BESSIÈRE[1] ET M. K. AROUA

Laboratoire de chimie et d'électrochimie analytique, Université de Nancy 1, 54506 Vandoeuvre-lès-Nancy, France

Reçu le 25 avril 1991[2]

J. BESSIÈRE et M. K. AROUA. Can. J. Chem. **70**, 1843 (1992).

Les propriétés acido-basiques des milieux H_3PO_4 7 M progressivement neutralisés par la soude sont caractérisés par la fonction d'acidité $R(H)$ et les fonctions basiques $R(H_2PO_4^-)$, $R(HPO_4^{2-})$, $R(PO_4^{3-})$ qui représentent repectivement l'activité du proton et le pouvoir donneur des ions $H_2PO_4^-$, HPO_4^{2-}, PO_4^{3-}. Le niveau d'acidité de ces milieux (Na/P = 0,0–1,6) passe de $R(H) = -2,7$ à $R(H) = +7,5$. Le domaine des potentiels accessibles dans les différents milieux est voisin de 1,23 V. Les valeurs de l'activité en eau des solutions varient entre 0,66 et 0,81. Les domaines d'électroactivité aux électrodes de platine, de carbone et de mercure sont également précisés.

J. BESSIÈRE and M. K. AROUA. Can. J. Chem. **70**, 1843 (1992).

Acid–base properties in 7 M H_3PO_4 medium neutralized by soda are characterized with an $R(H)$ acidity function and $R(H_2PO_4^-)$, $R(HPO_4^{2-})$, $R(PO_4^{3-})$ basicity functions, which respectively represent the H^+ activity in these media and their ability to donate $H_2PO_4^-$, HPO_4^{2-}, PO_4^{3-} ions. The acidity level of these media (Na/P = 0.0–1.6), changes from $R(H) = -2.7$ to $R(H) = +7.5$. The accessible potential domain for the media studied is close to 1.23 V. Activities of these solutions in water vary between 0.66 and 0.81. The ranges of electroactivity for platinum, carbon, and mercury electrodes are also determined.

Can. J. Chem. Downloaded from www.nrcresearchpress.com by 217.78.4.112 on 09/08/12
For personal use only.

Introduction

L'analyse et la prévision des réactions dans les milieux phosphoriques neutralisés présentent un intérêt majeur dans le domaine de la synthèse des engrais et de l'élaboration de produits purs destinés à l'industrie alimentaire et au traitement de surface (1–3). Au cours des opérations de synthèse, la concentration ainsi que le rapport base/acide sont susceptibles de varier dans une large gamme. De la teneur en acide et du rapport base/acide vont dépendre le pouvoir oxydo-réducteur des solutés, la stabilité de nombreux composés, la protonation des bases, la quantitativité des réactions de titrage *in situ*, le pouvoir extractant des agents chelatants en milieu non miscible ou des résines échangeuses d'ions. Les caractéristiques électrochimiques du solvant et des solutés sont également modifiées ainsi que les grandeurs cinétiques.

La prévision de nombreuses réactions dans les milieux concentrés s'effectue à partir des diagrammes potentiel – niveau d'acidité, en adoptant les mêmes raisonnements que dans l'eau (4–11).

On peut à partir de ces diagrammes évaluer les coefficients de transfert de solvatation des différentes espèces et prévoir les constantes thermodynamiques dans ces milieux réactionnels connaissant celles en solutions aqueuses diluées.

Plusieurs auteurs (7, 9) ont signalé l'importance du facteur activité de l'eau dans la fixation du niveau d'acidité des milieux eau–acide.

Comme dans les cas des solutions aqueuses concentrées en sel (12–16), la réctivité des espèces dans les milieux concentrés en acide, neutralisés ou non, dépend à la fois de l'activité de l'eau et de la solvatation spécifique des solutés par les ions du solvant. Il est important d'évaluer la part respective de ces deux influences pour prévoir ensuite les réactions en fonction de taux de neutralisation de l'acide. Cette démarche justifie donc la mesure de l'activité en eau dans une première étape. Il conviendra ensuite de comparer les équilibres dans les milieux phosphoriques et dans les milieux non complexants présentant la même activité en eau (milieux isopiestiques).

Avant d'envisager l'étude de la réactivité des solutés dans les milieux H_2O–H_3PO_4–NaOH, il importe, tant du point de vue industriel que du point de vue fondamental de la connaissance des milieux réactionnels, de préciser les propriétés caractéristiques du solvant : niveau d'acidité, propriétés redox, activité en eau, aptitude à céder les ions phosphate, domaine d'électroactivité aux électrodes de platine, mercure et carbone.

L'examen a porté sur la neutralisation de l'acide H_3PO_4 7 M par une solution de soude 18 M (50% en poids). Ces concentrations correspondent aux conditions habituellement rencontrées dans l'industrie du tripolyphosphate de sodium.

Partie expérimentale

Réactifs

Tous les réactifs utilisés sont de qualité pour analyse.

Acid phosphorique : Prolabo; soude en pastilles : Prolabo; ferrocène : Sigma; 3,4,5,6-tetrachloro-1,2-benzoquinone (*o*-chloranile) : Fluka; réactif de Karl–Fisher : Merck; phosphate acide mercureux : préparé par oxydation électrochimique du mercure dans H_3PO_4 5,5 M.

Préparation des solutions

L'acide phosphorique 7 M est neutralisé par une solution de soude 18 M (environ 50%). L'opération est réalisée à température contrôlée (80°C) et sous reflux. Le taux de neutralisation, exprimé par le rapport molaire Na/P, varie de 0,0 à 1,6. Au delà de cette valeur, il y a cristallisation à température ambiante. Les concentrations des espèces NaH_2PO_4 et Na_2HPO_4 sont alors respectivement égales à 1,7 et 2,6 M.

La solution mère de ferricinium (Fc^+ 0,1 M) est préparée en réalisant l'oxydation du ferrocène par le p-chloranile en milieu biphasique toluène–H_3PO_4 7 M (17).

[1]Auteur correspondant.

[2]Révision reçue le 25 février 1992.

Can. J. Chem. Downloaded from www.nrcresearchpress.com by 217.78.4.112 on 09/08/12
For personal use only.

Equipements

Les mesures potentiométriques à intensité nulle ont été faites au moyen du millivoltmètre Minisis 6000 Tacussel. Les tracés voltampérométriques sur électrodes solides ont été réalisés en utilisant un montage classique à trois électrodes et un ensemble Tipol EPL 2 Tacussel. Le dégazage des milieux réactionnels est effectué par barbotage d'azote.

Les différentes électrodes de travail utilisées sont l'électrode tournante de platine (EDI controvit Tacussel) et l'électrode tournante à pâte de carbone (EDI controvit Tacussel). La vitesse de rotation est de 600 tours/min.

L'électrode au calomel aqueuse, placée dans un compartiment séparé contenant H_3PO_4 0,1 M, est utilisée comme électrode de référence.

L'électrode auxiliaire est constituée par un fil de platine.

L'électrode à pâte de carbone, contenant l'*o*-chloranile peu soluble, est préparée selon le méthode décrite par Adams *et al.* (18, 19). L'*o*-chloranile insérée dans l'électrode est sous la forme quinonique. L'électrode est portée à un potentiel suffisamment réducteur pour que la forme réduite se forme à l'interface solide–liquide. On réalise ensuite les tracés voltampérométriques qui permettent d'apprécier la réversibilité et la rapidité du système considéré. Le mélange *o*-chloranile–hydrochloranile peut également être utilisé directement.

L'électrode à pâte de carbone, à base de phosphate mercureux, est préparée de la même manière que la précédente.

L'activité en eau des différents milieux est déterminée à 25°C par la méthode de transpiration, à partir de la mesure des pressions partielles d'eau. Le dispositif utilisé, représenté figure 1, est similaire à celui décrit par Davis et De Bruin (20), Bent et Francel (21) et Majima et coll. (22). Le capteur d'eau est remplacé par l'appareil Karl–Fisher Metrohm. On peut ainsi réduire considérablement le temps de mesure qui devient inférieur à 3 h.

L'eau contenue dans l'azote est éliminée par passage à travers un tamis moléculaire (3Å). L'azote, régulé à un débit constant, passe dans un présaturateur D, contenant 2–5 cm^3 de la solution à analyser, puis dans le saturateur E et la cellule de dosage coulométrique H. Le saturateur, contenant environ 40 cm^3 de la solution, et le pré-saturateur sont maintenus à température constante (25 ± 0,5°C). Le tube entre le saturateur et la cellule est chauffé pour éviter la condensation de l'eau.

La masse d'eau en gramme (W_{H_2O}) transportée par un volume (V_{N_2}) d'azote est déterminée par dosage coulométrique par la méthode Karl–Fisher.

La pression partielle de l'eau est donnée par la relation :

$$[1] \qquad p_{H_2O} = \frac{W_{H_2O}RT}{18\ V}$$

où W_{H_2O} est la masse d'eau dosée au cours de l'expérience et V est le volume de la phase gaseuse, donné par la relation :

$$[2] \qquad V = V_{N_2} + V_{H_2O}$$

La valeur de V_{N_2} est calculée à partir du débit de gaz et de la durée de l'expérience, alors que V_{H_2O} est déterminé à partir de W_{H_2O} et de la pression atmosphérique pendant l'expérience.

Résultats et discussions

1. Fonction d'acidité R*(H) des milieux H_2O–H_3PO_4–NaOH*

Le niveau d'acidité est caractérisé par la fonction d'acidité R(H) qui peut être déterminée expérimentalement à partir de la mesure du potentiel pris par une électrode indicatrice de pH en utilisant le système ferricinium/ferrocène (Fc^+/Fc) comme référence de potentiel.

Lorsque l'on utilise le système quinone/hydroquinone (Q(s)/QH_2(s)), la fonction R(H) est donnée par la relation :

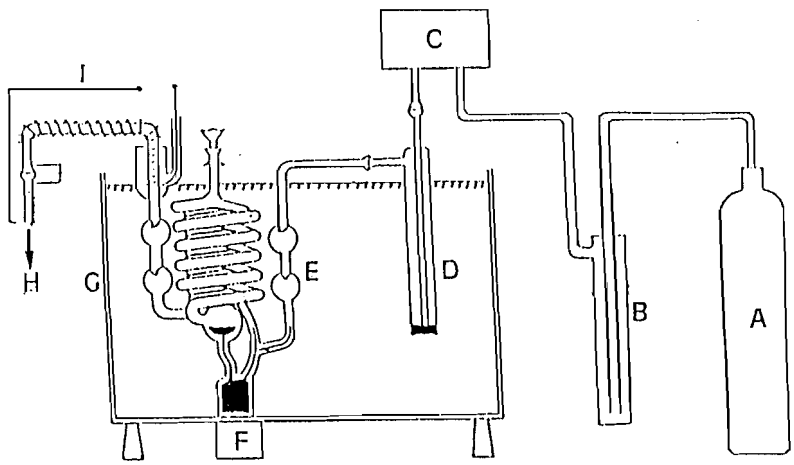

A: Bouteille d'azote

B: Tamis moléculaire (3 Å)

C: Débimètre

D: Pré-saturateur

E: Saturateur

F: Agitateur magnétique

G: Bain thermostaté

H: Vers la cellule de dosage Karl-Fisher

FIG. 1. Schéma du dispositif utilisé pour la mesure de l'activité en eau.

TABLEAU 1. Variation des propriétés acido-basiques des milieux H_3PO_4 7 M progressivement neutralisés par la soude, en fonction du taux de neutralisation (Na/P)

	Na/P									
	0,0	0,2	0,4	0,6	0,8	0,9	1,1	1,2	1,4	1,6
$E_{1/2}$ Fc^+/Fc (mV vs. ECS)	−85	−30	+30	+90	+130	+180	+190	+200	+220	+250
a_{H_2O}	0,66	0,72	0,70	0,75	0,78	0,81	0,80	0,80	0,75	—
R(H)	−2.7	−1.9	−0,8	+0,6	+1,9	+3,3	+4,9	+5,7	+6,9	+7,5
$R(H_2PO_4^-)$	+5,3	+4,5	+3,6	+2,8	+2,2	+1,8	+1,6	+1,5	+1,0	0.0
$R(HPO_4^{2-})$	+15,3	+13,6	+11,6	+9,5	+7,5	+5,6	+3,9	+3,0	+1,3	−0.2
$R(PO_4^{3-})$	+30,4	+27,9	+24,9	+21,3	+18,0	+14,7	+11,4	+9,7	+6,8	+4,7

$$[3] \quad R(\mathrm{H}) = \frac{E^{H_2O}_{Q(s)/QH_2(s)} - E^{S}_{Q(s)/QH_2(s)}}{0{,}058}$$

où $E^{H_2O}_{Q(s)/QH_2(s)}$ est le potentiel standard du système Q(s)/QH_2(s) dans l'eau et $E^{S}_{Q(s)/QH_2(s)}$ son potentiel dans la solution étudiée, exprimés par rapport au système Fc^+/Fc.

La fonction R(H) s'identifie au pH si l'on admet que le potentiel standard du système ferricinium/ferrocène est indépendant de la nature du solvant (23, 24). Dans la relation

$$[4] \quad \mathrm{pH} = R(\mathrm{H}) + \log \frac{f_{Fc}}{f_{Fc^+}}$$

les coefficients d'activité f_{Fc} et f_{Fc^+} sont alors égaux, l'état de réference étant la solution aqueuse infiniment diluée.

1.1. Système de comparaison : ferricinium/ferrocène (Fc^+/Fc)

La rapidité et la réversibilité du système Fc^+/Fc dans les milieux concentrés en acide phosphorique ont été démontrées par voltampérométrie cyclique sur électrode de carbone vitreux ainsi que sur électrode fixe de mercure (9, 28).

Dans tout le domaine Na/P envisagé, seul un signal correspondant à la réduction rapide de l'espèce Fc^+ est mis en évidence en voltampérométrie sur l'électrode tournante de platine : l'analyse mathématique des tracés voltampérométriques donne des pentes comprises entre 55 et 60 mV.

Étant données les caractéristiques de rapidité et de réversibilité du système Fc^+/Fc, son potentiel normal est pris égal au potentiel de demi-vague de réduction de Fc^+. Les valeurs expérimentales figurent dans le tableau 1.

1.2. Système indicateur de H^+ : chloranile/hydrochloranile ($C_{(s)}/CH_{2(s)}$)

Le système indicateur d'acidité engage le couple de l'*o*-chloranile. L'*o*-chloranile et l'hydrochloranile étant insolubles, le potentiel du système

$$[5] \quad C_{(s)} + 2H^+ + 2e^- \rightleftharpoons CH_{2(s)}$$

ne dépend que du niveau d'acidité. Le bon fonctionnement de l'électrode à pâte de carbone dans laquelle est inséré l'*o*-chloranile a été vérifié dans plusieurs milieux acides concentrés (7, 17). Les courbes intensité–potentiel montrent que le potentiel à intensité nulle est bien défini et stable.

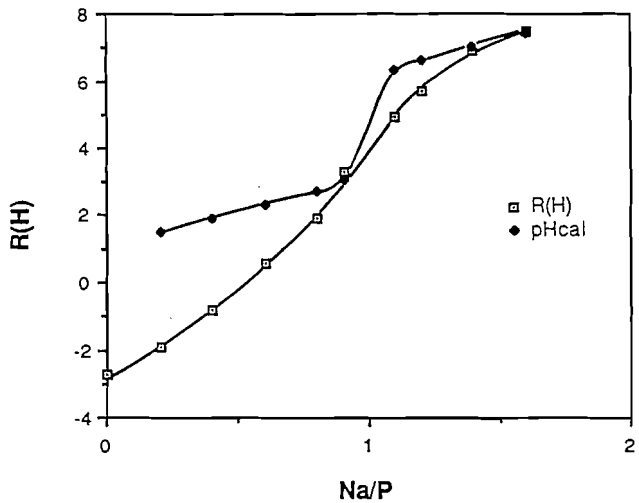

FIG. 2. Variation de la fonction R(H) des milieux H_3PO_4 7 M progressivement neutralisés par la soude, en fonction du rapport Na/P. Comparaison avec la variation de pH calculé.

1.3. Fonction R(H)

La fonction d'acidité R(H), représentée figure 2, varie de 10,2 unités lorsque le rapport Na/P passe de 0,0 à 1,6. Elle rend compte de deux effets : (*i*) le premier est directement lié au taux de neutralisation de l'acide fixé par la valeur du rapport Na/P; (*ii*) le second traduit l'influence de l'eau apportée d'une part par la solution aqueuse de soude et d'autre part par la neutralisation elle même.

Les résultats récents de N. Medouni (27) concernant la neutralisation de H_3PO_4 5,5 M par les pastilles de soude montrent que pour une même valeur du rapport (Na/P = 1,0), le niveau d'acidité est moins élevé (R(H) = +3,2 au lieu de +4,0 environ d'après la figure 2).

Il est intéressant de comparer la fonction R(H) des milieux neutralisés avec les valeurs du pH calculées en utilisant la formule appliquée en solution diluée. Pour un rapport Na/P inférieur à 1,0, on a la relation :

$$[6] \quad \mathrm{pH_{cal}} = 2{,}1 + \log \frac{\mathrm{Na/P}}{1 - \mathrm{Na/P}}$$

pour les rapports Na/P supérieurs à 1,0 et inférieurs à 2,0, on a la relation :

$$[7] \quad \mathrm{pH_{cal}} = 7{,}2 + \log \frac{\mathrm{Na/P} - 1}{2 - \mathrm{Na/P}}$$

Can. J. Chem. Downloaded from www.nrcresearchpress.com by 217.78.4.112 on 09/08/12
For personal use only.

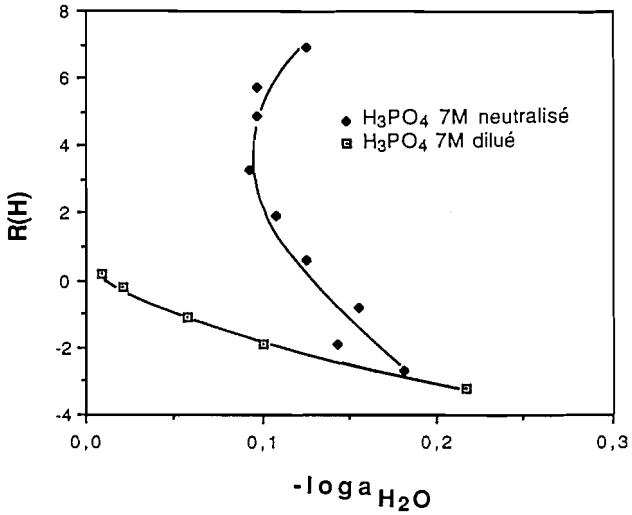

FIG. 3. Variation du niveau d'acidité avec l'activité en eau. Milieux H_3PO_4 7,0 M neutralisé et dilué.

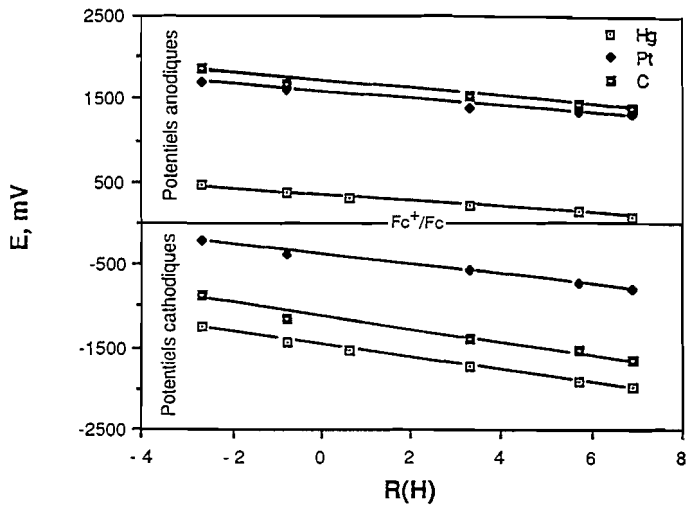

FIG. 4. Domaines d'électroactivité aux électrodes de mercure, carbone vitreux et platine dans les milieux H_3PO_4 7,0 M progressivement neutralisés par la soude (densité maximale de courant 0,2 m A/cm^2).

On constate (figure 2) que la différence $pH_{cal} - R(H)$ devient supérieure à 1,5 unités pour des taux de neutralisation Na/P inférieurs à 0,6. La fonction $R(H)$ ne fait pas apparaître l'effet tampon comme les valeurs du pH_{cal}. Par contre, pour des taux de neutralisation supérieurs à 0,6, on note des écarts réduits au voisinage de la demi-neutralisation de la deuxième fonction acide où les deux courbes sont pratiquement confondues.

2. Activité en eau dans les milieux H_2O–H_3PO_4–NaOH

Les valeurs de a_{H_2O}, regroupées dans le tableau 1, sont données à 5% près. La neutralisation de l'acide H_3PO_4 7 M se traduit par une faible variation de l'activité en eau des solutions. Celle-ci augmente légèrement jusqu'à Na/P = 0,9. Au delà de 1,2, l'activité en eau décroît.

La solution correspondant à Na/P = 1,0 a une molalité en NaH_2PO_4 de 7,3 mol/kg. La valeur correspondante de a_{H_2O} (0,80) est en bon accord avec les données de Robinson et Stokes (0,82) (25). Dans le cas où la neutralisation est réalisée avec de la soude en pastilles, l'activité en eau et le niveau d'acidité sont respectivement égaux à 0,74 et +3,2.

La comparaison des courbes $R(H) = f(\log a_{H_2O})$ (figure 3) relatives aux solutions diluées de l'acide 7 M d'une part et aux solutions neutralisées d'autre part montre que la variation du terme $\log a_{H_2O}$ est inférieur à 0,1 unité pour les solutions neutralisées. On peut dès à présent affirmer que la variation de réactivité des espèces ioniques qui sera observée au cours de la neutralisation est due principalement à une modification de leur solvatation spécifique par les ions phosphate du milieu, l'activité en eau ne variant pratiquement pas, contrairement à ce que l'on observe dans le cas de l'acide 7 M progressivement dilué.

3. Domaines d'électroactivité et de potentiel accessible dans les milieux H_2O–H_3PO_4–NaOH

Les domaines d'électroactivité aux électrodes de mercure, carbone vitreux et platine sont établis pour une densité de courant de 0,2 mA/cm^2. Les résultats sont présentés en fonction de $R(H)$ dans la figure 4. On remarque que l'étendue du domaine d'électroactivité varie légèrement avec le taux de neutralisation (0,3 V de Na/P = 0,0–1,4). Les électrodes étudiées permettent d'explorer un large domaine de potentiel, environ 3 V, peu différent de celui dans l'eau. On utilisera l'électrode de mercure pour explorer les potentiels réducteurs et l'électrode de platine pour les potentiels oxydants.

D'un point de vue thermodynamique, le domaine des potentiels accessibles dans les milieux H_2O–H_3PO_4–NaOH est limité par les propriétés oxydantes du proton et les propriétés réductrices de l'eau. Les limites sont fixées par la variation des potentiels des systèmes $H^+/H_2(g)$ et $O_2(g)/H_2O$ avec le taux de neutralisation.

La variation du pouvoir oxydant du solvant ne dépend que du niveau d'acidité : L'équilibre

[8] $$2H^+ + 2e^- \rightleftharpoons H_2(g)$$

est caractérisé par la relation

[9] $$E = -0{,}400 - 0{,}058\,R(H)$$

où −0,400 V représente le potentiel normal du système de l'hydrogène dans l'eau par rapport au système du ferrocène (23).

La limite thermodynamique des potentiels accessibles en oxydation correspond à l'oxydation des molècules d'eau. Elle dépend donc du niveau d'acidité et de l'activité en eau. À l'equilibre

[10] $$O_2(g)^+ + 4H^+ + 4e^- \rightleftharpoons 2H_2O$$

correspond la relation

[11] $$E = 0{,}829 - 0{,}058\,R(H) - 0{,}029 \log a_{H_2O}$$

La valeur 0,829 représente le potentiel normal de l'oxygène dans l'eau par rapport au ferrocène (9).

Les valeurs calculées à partir des expressions précédentes sont rassemblées dans le tableau 1 et présentées figure 5. L'étendue du domaine thermodynamique reste très proche de 1,23 V compte tenu de la faible variation de l'activité en

Can. J. Chem. Downloaded from www.nrcresearchpress.com by 217.78.4.112 on 09/08/12
For personal use only.

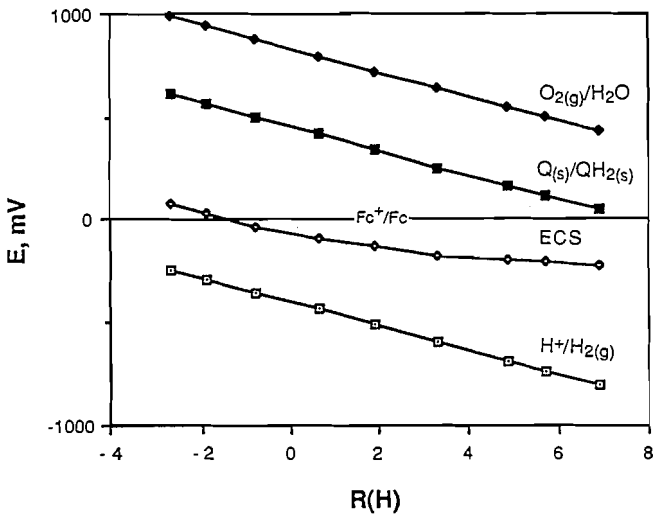

FIG 5. Propriétés oxydo-réductrices, déterminées par voie électrochimique, des milieux H_3PO_4 7,0 M progressivement neutralisés par la soude.

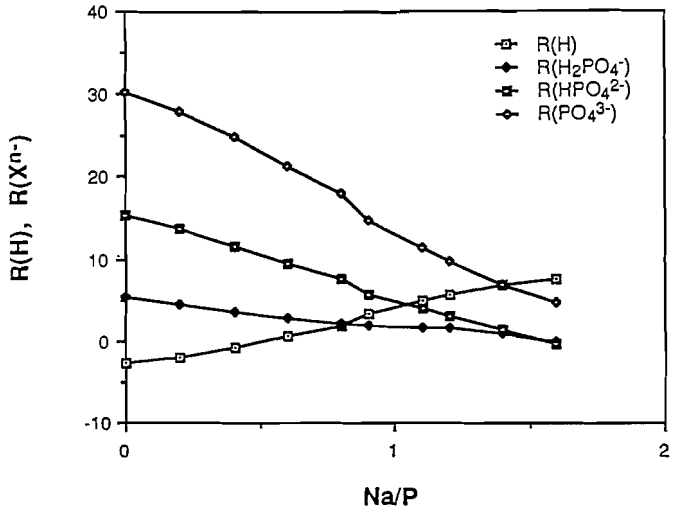

FIG. 6. Aptitude des milieux H_3PO_4 7,0 M progressivement neutralisés par la soude, à céder leurs espèces. Fonction d'acidité et fonctions basiques.

eau. On retrouve un résultat similaire dans les milieux H_2O–H_3PO_4 (7).

4. Fonctions basiques des milieux H_2O–H_3PO_4–NaOH

La fonction $R(H)$ traduit l'aptitude des milieux H_2O–H_3PO_4–NaOH à céder la particule H^+. Par analogie, les fonctions $R(H_2PO_4^-)$, $R(HPO_4^{2-})$ et $R(PO_4^{3-})$ sont définies pour caractériser l'aptitude des milieux H_2O–H_3PO_4–NaOH à céder les particules $H_2PO_4^-$, HPO_4^{2-} et PO_4^{3-}.

Elles peuvent être déterminées expérimentalement à partir de la mesure du potentiel pris par une électrode dont le fonctionnement fait intervenir un équilibre électrochimique engageant l'une des espèces phosphate comme seule espèce soluble. Ainsi, le potentiel d'une électrode phosphate mercureux/mercure, qui correspond à l'équilibre électrochimique

[12] $Hg_2HPO_4(s) + 2e^- \rightleftharpoons 2Hg(s) + HPO_4^{2-}$

ne dépend que de l'activité de l'espèce HPO_4^{2-} (l'état de référence étant la solution infiniment diluée dans l'eau) :

[13] $$E = E^0_{H_2O} - 0{,}029 \log a_{HPO_4^{2-}}$$
$$= E^0_{H_2O} + 0{,}029\, R(HPO_4^{2-})$$

$E^0_{H_2O}$ représente le potentiel normal du système $Hg_2HPO_4(s)$/Hg(s) dans l'eau exprimé par rapport au système Fc^+/Fc.

La connaissance de l'une des fonctions $R(HPO_4^{2-})$, $R(H_2PO_4^-)$ et $R(PO_4^{3-})$ permet de déterminer les deux autres à partir des relations

[14] $$R(H) + R(HPO_4^{2-}) - R(H_2PO_4^-) = 7{,}2$$

[15] $$R(H) + R(PO_4^{3-}) - R(HPO_4^{2-}) = 12{,}4$$

Les valeurs 7,2 et 12,4 représentent les valeurs de pK_2 et pK_3 de l'acide H_3PO_4 dans l'eau (26).

L'ensemble des résultats sont rassemblés dans le tableau 1 et figure 6.

La décroissance des fonctions basiques avec le taux de neutralisation indique clairement l'aptitude plus grande que présente ces milieux à céder les ions phosphate correspondants. Compte tenu de la valeur de $R(H)$ égale à 7,2 pour Na/P égal à 1,5, il est logique que les fonctions $R(HPO_4^{2-})$ et $R(H_2PO_4^-)$ soient dans ce cas égales. Elles sont proches de 0,0.

Ces fonctions sont nécessaires pour prévoir au cours de la neutralisation l'évolution de la solubilité de phosphates minéraux ou des équilibres de partage par solvant lorsque ceux-ci engagent les particules phosphates.

Conclusion

On a caractérisé le niveau d'acidité des solutions d'acide H_3PO_4 7 M progressivement neutralisées par la fonction d'acidité $R(H)$. Sa variation est de 10,2 unités lorsque le rapport Na/P passe de 0,0 à 1,6. Ces résultats permettront de préciser l'influence du niveau d'acidité sur le pouvoir oxydo–réducteur de nombreux systèmes. L'étendue thermodynamique du domaine des potentiels accessibles reste proche de 1,23 V. On dispose ainsi des limites thermodynamiques de stabilité des oxydants et des réducteurs dans ces milieux.

La faible variation de l'activité en eau observée au cours de la neutralisation implique que les changements de réactivité des solutés s'interprèteront essentiellement à partir d'intéractions spécifiques avec les ions du solvant.

L'utilisation du système électrochimique du mercure a permis de déterminer les fonctions $R(H_2PO_4^-)$, $R(HPO_4^{2-})$ et $R(PO_4^{3-})$. Elles seront utiles pour évaluer les variations thermodynamiques de solubilité des phosphates minéraux avec le taux de neutralisation.

1. A. V. Slack. Phosphoric acid. Vol. 1. Marcel Dekker Inc., New York. 1968. Parts 1, 2.
2. P. T. Chiang et R. A. Wiesboeck. Actes du 2ème congrès international sur les composés phosphorés. Boston. 1980. p. 583.
3. J. A. Peterson. Actes du 2ème congrès international sur les composés phosphorés. Boston. 1980. p. 593
4. M. Bauer et M. Bouchet. C. R. Acad. Sci. Ser. C. Paris, **275**, 21 (1972).
5. A. Vaillant, J. Devynck et B. Tremillon. Anal. Lett., **6**, 1095 (1973).
6. D. D. Babale, R Wandji et J. Bessière. J. Chem. Eng. Data, **35**, 345 (1990).

Can. J. Chem. Downloaded from www.nrcresearchpress.com by 217.78.4.112 on 09/08/12
For personal use only.

7. C. Louis, A. Bebba et J. Bessière. Can. J. Chem. **65**, 1353 (1987).
8. C. Louis, A. Bebba et J. Bessière. Can. J. Chem. **66**, 2422 (1988).
9. C. Louis et J. Bessière. Can. J. Chem. **63**, 908 (1985).
10. C. Louis et J. Bessière. Can. J. Chem. **64**, 608 (1986).
11. R. Gaboriaud. Ann. Chim. **2**, 201 (1967).
12. V. M. Vdovenko et M. A. Ryazanov. Zh. Fiz. Khim. **42**, 1936 (1968).
13. M. A. Ryazanov. Zh. Fiz. Khim. **44**, 312 (1970).
14. J. Ly et C. Poitrenaud. Analysis, **14**, 192 (1986).
15. H. Pisch et C. Poitrenaud. Rev. Soc. Quim. Mex. **30**, 152 (1986).
16. H. Pisch et C. Poitrenaud. Rev. Soc. Quim. Mex. **33**, 86 (1989).
17. A. Benayada. Thèse de Doctorat d'État, Université de Nancy 1, France. 1986.
18. R. N. Adams. Anal. Chem. **30**, 1570 (1958).
19. R. N. Adams, L. S. Marcoux et K. B. Pratem. Anal. Chem. **37**, 1446 (1965).
20. Jr. W. Davis et H. J. De Bruin. J. Inorg. Nucl. Chem. **26**, 1069 (1964).
21. H. E. Bent et R. J. Francel. J. Am. Chem. Soc. **70**, 634 (1948).
22. H. Majima, Y. Kawasaki, A. Uno, K. Sato et Y. Awakusa. Hydrometallurgy, **19**, 137 (1987).
23. H. M. Koepp, H. Wendt et H. Strehlow. Z. Electrochem. **64**, 483 (1960).
24. H. Strehlow. The chemistry of non-aqueous solvents. Vol. 1. *Édité par* J. Lagowski. Academic Press, New York. 1966. Chap. 4. p. 129.
25. R. A. Robinson et R. H. Stokes. Electrolyte solutions, 2e édition. Butterworths Scientific Publications, London. 1959. pp. 482–493.
26. G. Charlot. Les réactions chimiques en solution aqueuse. 7e édition. Masson, Paris. 1983. p. 40.
27. N. Medouni. Thèse de Doctorat de l'Université de Nancy 1, France. 1991.
28. T. A. Modro, K. Yates et J. Janata. J. Am. Chem. Soc. **97**, 1492 (1975).

Can. J. Chem. Downloaded from www.nrcresearchpress.com by 217.78.4.112 on 09/08/12
For personal use only.

The *trans–cis* isomerisation of bis(dioxolene)bis(pyridine) ruthenium complexes

YU-HONG TSE, PAMELA R. AUBURN, AND A. B. P. LEVER[1]

Department of Chemistry, York University, 4700 Keele St., North York (Toronto), Ont., Canada M3J 1P3

Received August 23, 1991[2]

YU-HONG TSE, PAMELA R. AUBURN, and A. B. P. LEVER. Can. J. Chem. **70**, 1849 (1992).

The isomerisation of *trans* to *cis* bis(3,5-di-*t*-butylbenzosemiquinonato)bis(R-pyridine)ruthenium, $Ru(R\text{-}Py)_2(DTBDiox)_2$, is induced by warming with an excess of R-pyridine, where R = 3-chloro, 4-methyl, 4-phenyl, or 4-butyl. The rates of these reactions, for the species with R-Py = 3-chloropyridine, were monitored in *o*-dichlorobenzene by UV–visible spectroscopy against varying 3-chloropyridine and varying *trans*-$[Ru(3\text{-}ClPy)_2(DTBDiox)_2]$ concentration. The data were found to obey first-order kinetics, $-d[Ru(3\text{-}ClPy)_2(DTBDiox)_2]/dt = k_{obsd}[Ru(3\text{-}ClPy)_2(DTBDiox)_2]$, over a considerable range of pyridine concentration. A plot of $1/k_{obsd}$ vs. [3-chloropyridine] is linear with a positive intercept. A dissociative mechanism is proposed for the isomerisation reaction. The activation parameters were determined for the specific case of R-Py = 3-chloropyridine. Electronic and electrochemical features of these species are briefly discussed.

YU-HONG TSE, PAMELA R. AUBURN et A. B. P. LEVER. Can. J. Chem. **70**, 1849 (1992).

L'isomérisation du bis(3,5-di-*tert*-butylbenzosemiquinonato)bis(R-pyridine)ruthénium, $Ru(R\text{-}Py)_2(DTBDiox)_2$, *trans* en *cis* est induite par un chauffage avec un excès de R-pyridine, où R = 3-chloro, 4-méthyl, 4-phényl ou 4-butyl. Opérant en solution dans le *o*-dichlorobenzène et faisant appel à la spectroscopie UV–visible, on a déterminé les vitesses de ces réactions, pour les espèces où R-Py = 3-chloropyridine, pour diverses concentrations de 3-chloropyridine et de *trans*-$[Ru(3\text{-}ClPy)_2(DTBDiox)_2]$. On a trouvé que, sur une plage importante de concentrations en pyridine, les données expérimentales peuvent être reliées par l'équation de cinétique du premier ordre, $-d[Ru(3\text{-}ClPy)_2(DTBDiox)_2]/dt = k_{obs}[Ru(3\text{-}ClPy)_2(DTBDiox)_2]$. Une droite de $1/k_{obs}$ vs. [3-chloropyridine] est linéaire, avec une ordonnée à l'origine qui est positive. On propose un mécanisme dissociatif pour la réaction d'isomérisation. On a déterminé les paramètres d'activation pour le cas spécifique de R-Py = 3-chloropyridine. On discute brièvement des caractéristiques électroniques et électrochimiques de ces espèces.

[Traduit par la rédaction]

Introduction

The series of complexes $Ru(NN)_2(diox)$ (1–3) and $Ru(NN)(diox)_2$ (3–7) have been described, where NN may be 2,2′-bipyridine or two substituted pyridines, R-Py, and (diox) is a dioxolene ligand which may exist in the catechol, semiquinone, or quinone oxidation states. These complexes form redox series whose electronic structures have been probed by a range of techniques including X-ray crystallography, NMR, ESR, magnetism and UV–VIS–FTIR, PES, and resonance Raman (rR) spectroscopy. The bipyridine-bis(dioxolene) complexes are necessarily *cis*, where the R-Py analogues could be either *cis* or *trans*.

The previously described *trans*-$Ru(R\text{-}Py)_2(diox)_2$ series of complexes (5, 7) are found to be isomerised to a *cis* configuration when warmed with an excess of pyridine. Here we describe studies of the isomerisation reaction and electrochemical and optical data characterising these new *cis* species.

Experimental section

Equipment

All absorbance measurements were performed on a Hitachi – Perkin Elmer microprocessor model 340 spectrometer equipped with an electrically heated cell compartment connected to a built-in thermostat for temperature measurement and control. Fourier transform infrared (FTIR) data were obtained using a Nicolet SX20 spectrometer. ^1H NMR and ^{13}C NMR spectra were obtained with a Bruker AM300FT NMR spectrometer using samples dissolved in $CDCl_3$.

Electrochemical data were obtained with a Pine Instruments RDE-3 potentiostat. Cyclic voltammetry was carried out, in dichloroethane (DCE), using platinum wires as working and counter electrodes, and a AgCl/Ag quasi-reference electrode with ferrocene (Fc) as an internal standard. The Fc/Fc^+ couple lies at +0.425 V vs. SCE (7).

Materials

Tetrabutylammonium perchlorate (TBAP, Kodak) was recrystallised from absolute ethanol and dried in vacuo at 50°C for 2 days. 1,2-Dichlorobenzene (DCB) (Aldrich, HPLC grade) and toluene-d_8 were used as supplied. 1,2-Dichloroethane (DCE) was fractionally distilled from P_2O_5. 3-Chloropyridine (Aldrich) and 4-methylpyridine (Aldrich) were fractionally distilled under reduced pressure. Other substituted pyridines (Aldrich) were used as supplied without any further purification.

Syntheses

The species *trans*-$Ru(R\text{-}Py)_2(DTBDiox)_2$ were prepared by the methods given previously (5, 7).

cis-*$Ru(R\text{-}Py)_2(DTBDiox)_2$*

Trans-$Ru(R\text{-}Py)_2(DTBDiox)_2$ (36 mg, ca. 5.0×10^{-2} mmol) was dissolved in toluene (10 mL). R-pyridine (R = 3-chloro, 4-methyl, or 4-phenyl) (2.1 mmol) was added. The resulting mixture was refluxed under nitrogen for 12 h, filtered hot, and then concentrated by rotary evaporation; methanol (1 mL) was then added to initiate crystallisation. The products were filtered, washed with cold methanol, and air dried; yield ~80%. Anal. found: C 59.48, H 6.27; N 3.64; calcd.: C 59.37, H 6.29, N 3.64 for R = 3-chloro; found: C 64.70, H 7.44, N 3.88; calcd.: C 64.40, H 7.60, N 3.76 for R = 4-methyl, monohydrate; found: C 68.70, H 6.86, N 3.53; calcd.: C 69.0, H 6.95, N 3.21 for R = 4-phenyl, monohydrate. The *trans* species used for the kinetic measurements had acceptable C, H, N analysis (7).

^1H NMR data for R = 3-chloropyridine species, in $CDCl_3$. Data for the *trans* isomer from ref. 7 (s = singlet, d = doublet, dd = doublet–doublet, m = multiplet): *trans* isomer, 7.74 (d, J = 2.2 Hz, 2H), 7.63 (d, J = 2.0 Hz, 2H), 7.6 (dd, J = 5.4, 1.1 Hz, 2H), 7.23 (m, 2H), 6.87 (dd, J 8.2, 5.7 Hz, 2H), 6.17 (br s, 2H),

[1]Author to whom correspondence may be addressed.

[2]Revision received February 28, 1992.

Can. J. Chem. Downloaded from www.nrcresearchpress.com by 217.78.4.112 on 09/08/12
For personal use only.

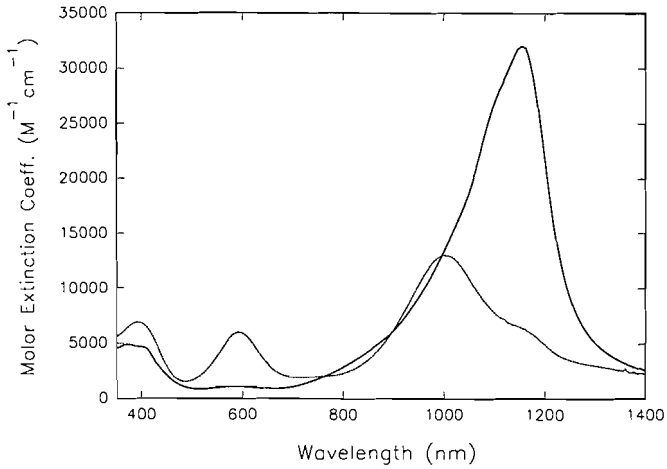

FIG. 1. Visible – near infrared spectra for (·) *cis*- and (-) *trans*-Ru(3-ClPy)$_2$(DTBDiox)$_2$ in 1,2-dichloroethane.

1.62 (s, 18H), 1.35 (s, 18H); *cis* isomer, 8.54 (m), 8.27 (m), 8.04 (d, J = 2.2 Hz), 7.73 (m), 7.57 (m), 7.14 (m), 6.90 (m), 6.80 (m), 6.70 (d, J = 2.1 Hz), 1.77 (s), 1.67 (s), 1.37 (s), 1.36 (s), 1.33 (s), 1.20 (s), 0.89 (s), 0.88 (s).

Kinetic studies

DCB was used as the solvent for the rate studies unless otherwise stated. The liquid 3-chloropyridine (8.40×10^{-5} to 1.05×10^{-3} mol) was mixed with 4 mL of a stock solution of *trans*-Ru(3-ClPy)$_2$(DTBDiox)$_2$ and diluted to 5 mL ((*trans*-Ru(3-ClPy)$_2$(DTBDiox)$_2$ = (2.07×10^{-4} M)). The reaction mixture was transferred to a 1-cm cell which was placed into a preheated cell compartment; the temperature of the solution inside the cell was measured before and after each experiment (variation ±0.25°C). Successive spectra were collected at time intervals from 2.8 to 100 min, depending upon the temperature and concentration range involved.

The isomerisation from *trans*-to *cis*-Ru(3-ClPy)$_2$(DTBDiox)$_2$ was monitored by observing the growth of a new absorption band lying close to 600 nm (6) observed for the *cis* isomer. The *trans* isomer possesses very weak absorption at this wavelength (Fig. 1).

For the pseudo-first-order conditions, the observed rate constants (k_{obsd}) were obtained from the Guggenheim plots (8). The reactions were allowed to proceed for 3–4 half-lives. The delay time was about 2 half-lives.

Rate constants for isomerisation of *trans*-Ru(3-ClPy)$_2$(DTBDiox)$_2$ (2.07×10^{-4} M) in DCB at various temperatures from 91 to 110°C are presented here as a function of the concentration of 3-chloropyridine. Values of [3-chloropyridine] are tabulated, together with k_{obsd} (all values to be multiplied by 10^{-4} s^{-1}), followed by the standard deviation in parentheses.

T (°C)	0.016 M	0.03 M	0.06 M	0.08 M	0.1 M	0.2 M
91	1.64	1.24	0.89	0.857	0.787	0.496
	(0.01)	(0.02)	(0.01)	(0.002)	(0.001)	(0.001)
96	3.19	2.67	2.14	1.87	1.64	1.06
	(0.03)	(0.02)	(0.02)	(0.01)	(0.01)	(0.01)
100	5.97	5.33	3.99	3.71	3.50	2.24
	(0.04)	(0.06)	(0.01)	(0.04)	(0.03)	(0.01)
105	11.4	9.7	7.4	6.41	6.16	4.26
	(0.21)	(0.19)	(0.1)	(0.06)	(0.06)	(0.04)
110	18.89	18.1	14.61	13.3	12.1	9.02
	(0.73)	(0.5)	(0.07)	(0.15)	(0.2)	(0.07)

Data were also obtained, at 90°C, for constant [3-chloropyridine] = 0.16 M and varying [*trans*-Ru(3-ClPy)$_2$(DTBDiox)$_2$] over the range from about 1×10^{-4} to 3.4×10^{-4} M, with no significant variation in k_{obsd}.

The isomerisation of Ru(3-ClPy)$_2$(DTBDiox)$_2$ in toluene-d_8 at 93°C was followed by ^{1}H NMR ([Ru(3-ClPy)$_2$(DTBDiox)$_2$] = 2.72×10^{-3} M; [3-chloropyridine] = 0.5 M).

Results and discussion

The *trans*-Ru(R-Py)$_2$(DTBDiox)$_2$ species are best regarded as fully delocalised *trans*-Ru(III)(R-Py)$_2$(DTBCat(-2))(DTBSq(-1)) species (so-called (S) (starting) species in previous discussions) (3–5, 7). Their electronic spectra are typified by a very intense absorption near 1100 nm attributed to diox (π) → Ru($d\pi$) + diox (π^*) IL + LMCT (Fig. 1). They display only weak absorption in the visible region (near 580 nm (7)).

Synthesis of the cis *complexes and background literature*

When a *trans*-Ru(R-Py)$_2$(DTBDiox)$_2$ complex is warmed with a pyridine, a band near 600 nm (Table 1) grows in at a rate which depends upon temperature, concentration of pyridine, and nature of the R substituent (Fig. 2). Isomerisation proceeds within a fairly narrow range of pyridine concentrations. If a large excess of pyridine (>10^4 [Ru(R-Py)$_2$(DTBDiox)$_2$]) is used, a side reaction takes place, probably forming the tetrapyridine species, and the isosbestic point is lost. The *trans* isomer undergoes another side reaction if insufficient pyridine (<10 [Ru(R-Py)$_2$(DTBDiox)$_2$]) is used. Heating either the *cis* or *trans* isomer in an inert solvent, in the absence of an excess of pyridine ligand, led to eventual decomposition. Isomerisation occurs cleanly when the pyridine to ruthenium ratio lay approximately in the range $10^2 - 10^3$.

The final electronic spectrum has the same overall band envelope as that (6) of *cis*-Ru(bpy)(DTBDiox)$_2$ (save for the absence of the Ru → bpy CT transition), providing evidence that isomerisation has occurred. The absorption near 600 nm (Table 1) corresponds with an $n \rightarrow \pi^*$ semiquinone transition allowed in the *cis* isomer but forbidden in the *trans* isomer (5, 7). Further, *cis* complexes were isolated (see Experimental) and their NMR spectra (see Experimental) leave no doubt that *cis*-Ru(R-Py)$_2$(DTBDiox)$_2$ species have been formed. Under the experimental conditions used to prepare the *trans* isomer, no *cis* isomer is isolated (7).

A number of *cis–trans* isomerisations of ruthenium complexes have been previously reported. It is revealing to contrast their behaviour. The species *cis*-[Ru(bpy)$_2$(H$_2$O)$_2$]$^{2+}$ is photoisomerised to the *trans* species by a dissociative pathway (9), but no thermal route was reported. The species *trans*-Ru(dppm)$_2$Cl$_2$ (dppm = bis-diphenylphosphinomethane) can readily be thermally isomerised to the *cis* isomer in halocarbon solvents (at 83°C (reflux) in DCE) (10). This may be reversed (*cis* → *trans*) photochemically (10). Oxidation of *cis*-Ru^{II}(dppm)$_2$Cl$_2$ leads to isomerisation to the *trans*-Ru^{III} species and the formation of *trans*-Ru(dppm)$_2$Cl$_2$ upon subsequent reduction (10). The complex cation *trans*-[Ru(acac)$_2$(CH$_3$CN)$_2$]$^{2+}$ is thermally isomerised to the *cis* species at 30°C with a half-life of about 9 days (11). Data for *cis*- and *trans*-[RuCl(NO)(bpy)$_2$]$^{2+}$ have been reported (12), but no interconversion experiments were reported. Some bis(dithiocarbamate)nitrosyl complexes of ruthenium, such as *cis*-Ru(NO)(S$_2$CNMe$_2$)SCN, can be thermally converted to the corresponding *trans* isomer, in the solid

Can. J. Chem. Downloaded from www.nrcresearchpress.com by 217.78.4.112 on 09/08/12
For personal use only.

TABLE 1. Electronic spectroscopic data for *cis*-Ru(R-Py)$_2$(DTBDiox)$_2$, (S), and *cis*-[Ru(R-Py)$_2$(DTBDiox)$_2$]$^+$, (O1), complexes[a,b]

Complex	λ_{max} (nm)		
cis-Ru(3-ClPy)$_2$(DTBDiox)$_2$	1001	595	394
cis-Ru(4-MePy)$_2$(DTBDiox)$_2$	1028	587	362(sh)
cis-Ru(4-PhPy)$_2$(DTBDiox)$_2$	1009	597	412
cis-Ru(4-BuPy)$_2$(DTBDiox)$_2$	1017	590	366
cis-Ru(3-ClPy)$_2$(DTBDiox)$_2^+$	738	519	379(sh), 305(sh)
cis-Ru(4-MePy)$_2$(DTBDiox)$_2^+$	748	511	378(sh), 315(sh)
cis-Ru(4-PhPy)$_2$(DTBDiox)$_2^+$	743	526(sh)	369(sh)
cis-Ru(4-BuPy)$_2$(DTBDiox)$_2^+$	761	513	371(sh)

[a]Solvent DCE. Data for the *cis* (S) species from solid starting materials.
[b]Oxidised (O1) species are prepared by the oxidation of S species with Ag^+ ions in DCE, followed by filtration through Celite.

Can. J. Chem. Downloaded from www.nrcresearchpress.com by 217.78.4.112 on 09/08/12
For personal use only.

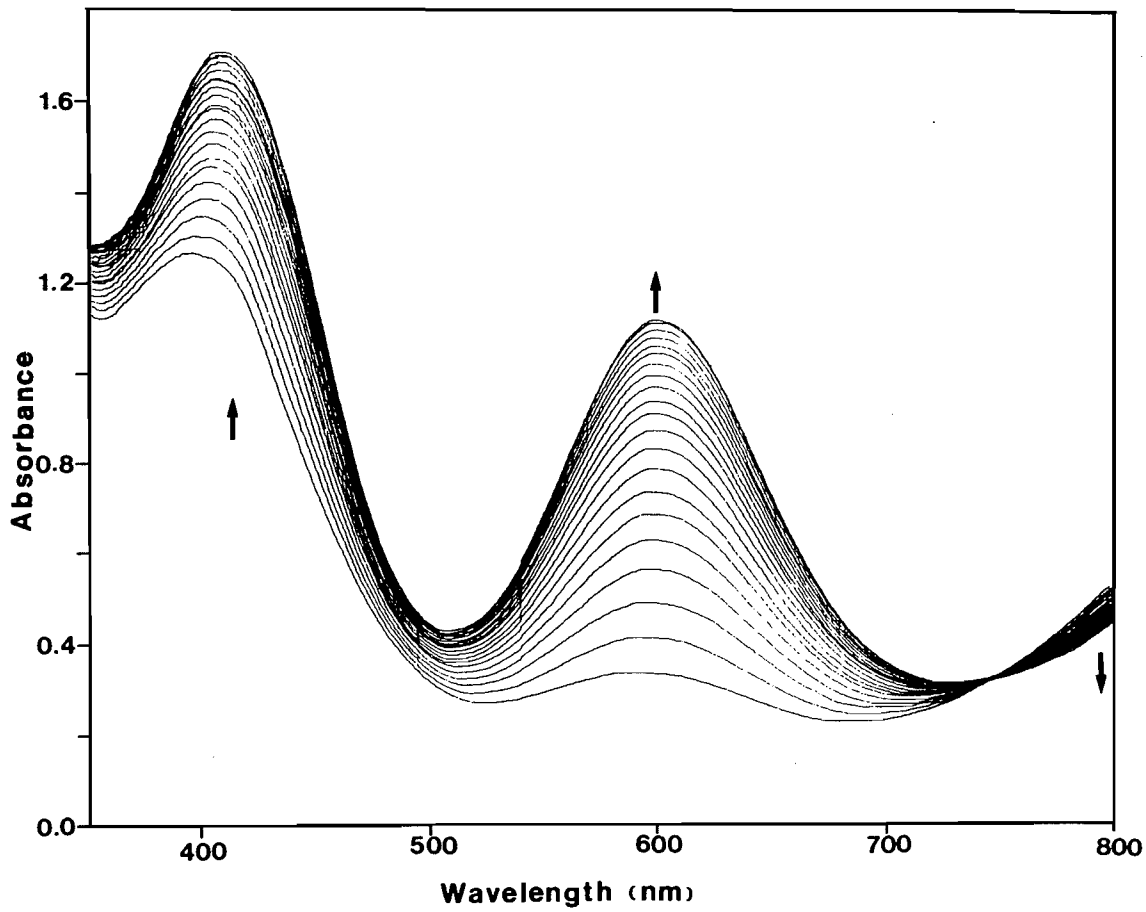

FIG. 2. A typical data set showing successive scans of the visible spectrum during the isomerisation of *trans*-Ru(3-ClPy)$_2$(DTBDiox)$_2$ (2.07×10^{-4} M) in the presence of an excess of 3-chloropyridine (1.0×10^{-1} M) at 100°C in *o*-dichlorobenzene. The first scan in the experiment was not recorded on the spectrum.

state, at 220°C (13). Transformations in the rather more complex Ru(AzPy)$_2$Cl$_2$ (AzPy = 2-phenylazopyridine) have also been explored (14). A very detailed contribution discusses the formation of all *trans*, *ttt*-Ru(CO)$_2$Cl$_2$(PR$_3$)$_2$ species which isomerise in chloroform at from 50°C (actual temperature depending upon the phosphine) to the all *cis*, *ccc*-Ru(CO)$_2$Cl$_2$(PR$_3$)$_2$ species which then isomerise to the thermodynamically stable *cct*-Ru(CO)$_2$Cl$_2$(PR$_3$)$_2$ species (15). Our systems appear to be the first ruthenium species to be reported where isomers may be isolated by addition of an external common ligand (*vide infra*).

Nuclear magnetic resonance studies

trans-Ru(R-Py)$_2$(DTBDiox)$_2$ complexes can exist in two forms with C_{2h} and C_{2v} symmetry depending upon the relative orientation of the *t*-butyl groups. Previously we have demonstrated (7) that for all of these complexes, only two *t*-butyl resonances are observed for the DTBDiox ligands, indicative of a single isomer having been prepared. The X-ray data (3) for both the (S) *trans*-Ru(4-*t*-BuPy)$_2$(DTBDiox)$_2$ and the oxidised (O1) *trans*-[Ru(3-ClPy)$_2$(DTBDiox)$_2$]$^+$ cation show that these *trans* isomers in the solid state have C_{2h} symmetry.

TABLE 2. Rate constants k_1 and k_{-1}/k_r for isomerisation of *trans*-Ru(3-ClPy)$_2$(DTBDiox)$_2$ at different temperatures[a]

T (K)	k_1 ($\times 10^{-4}$ s)	k_{-1}/k_r (M)
91	1.74(0.19)	12.7(2.2)
96	3.76(0.08)	12.7(0.4)
100	6.82(0.41)	10.2(1.0)
105	12.0(0.1)	9.4(1.5)
110	20.7(0.1)	6.7(0.5)

[a]Data derived from the k_{obsd} data cited in the experimental section. Standard deviation in parenthesis.

The *cis*-Ru(R-Py)$_2$(DTBDiox)$_2$ species can exist as three different geometric isomers that could give rise to eight *t*-butyl resonances in their ^{1}H NMR spectra (see Experimental). Four different *t*-butyl resonances arise from two *cis* isomers with same C_2 symmetry (so-called symmetric isomers). Another four different *t*-butyl resonances come from the third *cis* isomer which has C_1 symmetry (asymmetric isomer). In fact, these eight *t*-butyl resonances are observed for *cis*-Ru(3-ClPy)$_2$(DTBDiox)$_2$, although we have been unable to separate these three *cis* isomers.

When isomerisation of the *trans*-Ru(3-ClPy)$_2$(DTBDiox)$_2$ species was followed by NMR, in toluene-d_8, the resonances for all three *cis* isomers grew at approximately the same rate.[3]

Electrochemistry

The electrochemical behaviour of the *cis*-Ru(R-Py)$_2$(DTBDiox)$_2$ species is very similar to that of the *trans* analogues (Table 3). Assignments have been discussed in depth previously (6, 7). Arguments have been expressed in the literature relating differences in the electrochemical behaviour of *cis* and *trans* pairs to differences in electronic structure. Thus the ruthenium-centred waves observed with the *cis*- and *trans*-[RuCl(NO)(bpy)$_2$]$^{2+}$ nitrosyl species (12) differ by only 10 mV, but there is a substantial difference (170 mV) in the nitrosyl reduction wave for these two isomers, implying some marked structurally dependent electronic changes localised on the nitrosyl group. The M^{III}/M^{II} potentials for the pairs of *cis* and *trans* isomers M(dppm)$_2$Cl$_2$ (M = Os, Ru) (10) differ by 370 mV (Ru) and 460 mV (Os) with the *cis* isomers being the most difficult to oxidise, the difference being attributed to the difference in π-backbonding capability in the pairs of isomers. Where more than one π-accepting ligand is present, such as in the series [Ru(dppm)$_2$(CO)X]$^+$ and [Ru(bpy)(dppe)(CO)X]$^+$ (X = Cl, Br, I) (16), the *trans* isomer is more difficult to oxidise by up to 450 mV. In our dioxolene system, couple V (Table 3) is most closely associated with the Ru^{III}/Ru^{II} couple (6, 7). The lack of any shift in this couple between *cis* and *trans* isomer arises because at this oxidation level the Ru^{II} is bound to the non-π-accepting catechol. The remaining couples involve redox processes which are more localised on the dioxolene residues and are, accordingly, less sensitive to the geometry of the isomer.

Kinetic studies

The kinetics of the isomerisation reactions of Ru(3-ClPy)$_2$(DTBDiox)$_2$ (2.07×10^{-4} M) were investigated at various temperatures with 3-chloropyridine concentrations ranging between 1.6×10^{-2} and 2×10^{-1} M (see Experimental). Values of k_{obsd} were derived from a Guggenheim plot (8) (Fig. 3). The reaction followed pseudo-first-order kinetics

$$[1] \quad -d[Ru(3\text{-}ClPy)_2(DTBDiox)_2]/dt = k_{obsd}[Ru(3\text{-}ClPy)_2(DTBDiox)_2]$$

over at least four half-lives. Values of k_{obsd} at constant [3-chloropyridine] were independent of the concentration of Ru(3-ClPy)$_2$(DTBDiox)$_2$.

Plots of $1/k_{obsd}$ against [3-chloropyridine] were linear (Fig. 4). This linearity is consistent with the following mechanism:

$$[2] \quad trans\text{-}Ru(3\text{-}ClPy)_2(DTBDiox)_2 \underset{k_{-1}}{\overset{k_1}{\rightleftharpoons}} Ru(3\text{-}ClPy)(DTBDiox)_2 + 3\text{-}ClPy$$

$$[3] \quad Ru(3\text{-}ClPy)(DTBDiox)_2 \xrightarrow{k_r} [Ru(3\text{-}ClPy)(DTBDiox)_2]^*$$

$$[4] \quad [Ru(3\text{-}ClPy)(DTBDiox)_2]^* + 3\text{-}ClPy \rightleftharpoons cis\text{-}Ru(3\text{-}ClPy)_2(DTBDiox)_2$$

Assuming step [4] is fast and using the steady-state ap-

[3]This in fact differs from the behaviour of the corresponding bipyridine complexes, in which only two of the three possible isomers are obtained. Previously (6), we reported that all three isomers were present. This was in error, the seven peaks in the *t*-butyl region of the ^{1}H NMR spectra being due to two isomers (C_1 and C_2 symmetry) and to water. The presence of only two isomers was clearly confirmed by TLC.

TABLE 3. Electrochemical data for Ru(NN)$_2$(DTBDiox)$_2$ complexes[a]

Complex	$E_{1/2}$ (V) vs. SCE II	III	IV	V
trans-Ru(3-ClPy)$_2$(DTBDiox)$_2$[b]	+1.08	+0.30	−0.60	−1.51qr
cis-Ru(3-ClPy)$_2$(DTBDiox)$_2$	+1.01	+0.35	−0.71	−1.54qr
cis-Ru(bpy)(DTBDiox)$_2$[c]	+1.00	+0.31	−0.71	−1.42

[a]Measurements were made using 1,2-dichloroethane solutions of the starting materials (10^{-3} M) containing 0.2 M TBAP. $E_{1/2}$ values are obtained from cyclic voltammetry at 100 m V s^{-1}; qr = quasi-reversible.

[b,c]For assignment of the redox couples, see refs. 6 and 7: ref. 7[b]; ref. 6[c]. The assumed position of the Fc$^+$/Fc couple used in ref. 6 differed by +0.115 V relative to that assumed here. The potentials taken from ref. 6 have been appropriately corrected.

Can. J. Chem. Downloaded from www.nrcresearchpress.com by 217.78.4.112 on 09/08/12
For personal use only.

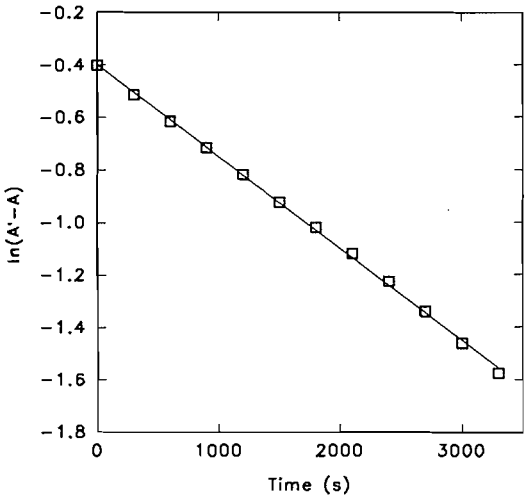

FIG. 3. Guggenheim plot using data from Fig. 2 at wavelength 600 nm for the isomerisation of the *trans*-Ru(3-ClPy)$_2$(DTBDiox)$_2$ complex. The delay time in the Guggenheim plots is approximately two half-lives.

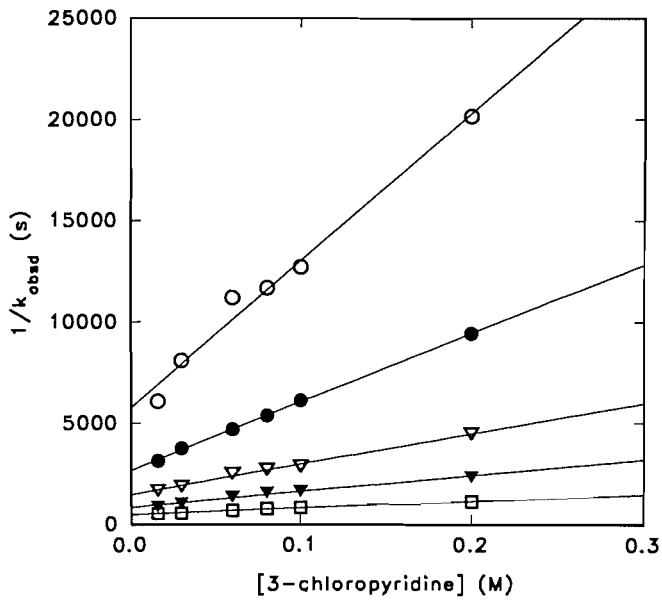

FIG. 4. Plots of $1/k_{obsd}$ vs. [3-chloropyridine] for the isomerisation of Ru(3-ClPy)$_2$(DTBDiox)$_2$ at 100°C in *o*-dichlorobenzene at (from upper to lower) 91, 96, 100, 105, and 110°C.

proximation (8) for [Ru(3-ClPy)(DTBDiox)$_2$], the rate of isomerisation is

$$[5] \quad -\mathrm{d}[\textit{trans}\text{-Ru(3-ClPy)}_2\text{(DTBDiox)}_2]/\mathrm{d}t = \{(k_1k_r/k_{-1}[\text{3-chloropyridine}] + k_r)\} \cdot [\textit{trans}\text{-Ru(3-ClPy)}_2\text{(DTBDiox)}_2] = k_{obsd}[\textit{trans}\text{-Ru(3-ClPy)}_2\text{(DTBDiox)}_2]$$

The calculated k_1 and k_{-1}/k_r derived respectively from the intercept $(1/k_1)$ and the slope (k_{-1}/k_1k_r) are listed in Table 2. An Arrhenius plot of $\ln(k_1)$ versus inverse temperature led to an activation energy of 148 ± 6 kJ/mol and, using the Eyring expression (8), an activation entropy of 88 ± 17 J/mol.

The data (Fig. 4) are consistent with a dissociative mechanism in which a pyridine ligand is lost to form a five-coordinate intermediate which can either reattach the pyridine ligand and return to the *trans* isomer or undergo a twist, first to form two different trigonal bipyramidal intermediates (e.g., see ref. 15) differing in the orientation of the *t*-butyl groups on the dioxolene ligands. These two intermediates can be interchanged by a pseudo-rotation. When the pyridine ligand is reattached to these intermediates, all three *cis* isomers are formed. Ligand loss and formation of the five-coordinate intermediate lead to alternative decomposition pathways when insufficient pyridine is present to trap the intermediate.

The positive activation entropy value associated with reaction [1] is consistent with the dissociative mechanism (15, 17–20). Indeed both the activation enthalpy and entropy have values close to those reported previously for mechanisms involving the loss of a ligand from a six-coordinate ruthenium(II) species (15, 19). Specifically there is a close similarity between the activation data reported here and those detailed for the isomerisation of the Ru(CO)$_2$Cl$_2$(PR$_3$)$_2$ species (15).

A mixed-ligand experiment shows that the rate of isomerisation of *trans*-Ru(3-ClPy)$_2$(DTBDiox)$_2$ in the presence of bulk 4-methylpyridine is different from that with bulk 3-chloropyridine (and vice versa). Although additional kinetic data cannot readily be extracted because the electronic spectra of the various R-Py species do not differ sufficiently, the result supports the proposed mechanism.

Electronic spectra

The electronic spectra of the new *cis* species reveal some subtle but important differences from the previously reported (7) spectra of the *trans* species. The NIR band in the *cis*-S species shifts slightly to lower energy with more electron-donating pyridine ligands (Table 1), consistent with the MLCT Ru(d) → semiquinone (π^*) transition previously assigned in the spectra of the analogous bipyridine species (6). The lower energy of this band in the pyridine series relative to the bipyridine series arises from the greater stabilisation of the d orbitals by the bipyridine ligand. There is no shift with pyridine substituent in the spectra of the *trans*-S species (7) for the corresponding band which has little CT character.

The behaviour of the second band, near 600 nm, is more ambiguous, but does shift to the red with the more electron-accepting 3-chloro substituent. This is an $n \rightarrow \pi^*$ transition that evidently has some LMCT character.

The third band, near 400 nm, is evidently Ru($d\pi$) → R-Py(π^*), since it shifts to lower energy in the sequence 4-methyl > 3-chloro > 4-phenyl, this last having an especially low energy π^* orbital extending over the phenyl group.

To confirm certain subtle conclusions concerning the differences in electronic structure between the *cis* and *trans* series, some of these species were oxidised with silver ion to the O1 species, to obtain their electronic spectra. These O1 complexes, which were not isolated, have spectra more closely related to the spectra of the *cis*-O1 bipyridine analogues (6) than to their *trans*-O1 relatives. Thus the main band has MLCT Ru($d\pi$) → semiquinone(π^*) character and shifts to lower energy with the more electron-donating pyridines. The corresponding band in the *trans* species (transition O1, II) (7) has LMCT character and shifts in the opposite sense with pyridine substituent. The shifts in the second band, near 520 nm, are too small to comment upon.

Can. J. Chem. Downloaded from www.nrcresearchpress.com by 217.78.4.112 on 09/08/12
For personal use only.

These data support previous assignments (6, 7) and indeed add useful corroboratory evidence. The contrasting dependencies upon dioxolene and pyridine substituents arise from changes in the degree of mixing of metal and ligand orbitals owing to the symmetry restrictions imposed by the two geometries (7). The *cis* isomers are concluded to parallel the bipyridine species in having somewhat more Ru^{II} character than their *trans* analogues (7).

Conclusion

The *trans*-$Ru(R\text{-}Py)_2(DTBDiox)_2$ (C_{2h}) species are kinetically favoured products during synthesis and are isomerised to their corresponding *cis* isomers by warming with an excess of a pyridine. A dissociative mechanism for this *trans* → *cis* isomerisation is proposed.

The electrochemical and optical data for the *trans* and *cis* isomers of $Ru(R\text{-}Py)_2(DTBDiox)_2$ are compared. The electronic spectra support previous assignments given for the corresponding *cis*-bpy complexes (6). Detailed analysis further corroborates earlier arguments (5–7, 21) concerning the degree of mixing between metal and ligand orbitals and the formal oxidation states of the species.

Acknowledgments

We thank Dr. Dave Thompson, Dr. Elaine Dodsworth, and Prof. D. V. Stynes for useful discussion, Mr Hitoshi Masui and Mr. Jing Li for technical help, and the Johnson Matthey Company for the loan of ruthenium trichloride. The financial support of the Natural Sciences and Engineering Research Council (NSERC) (Ottawa) and the Office of Naval Research (Washington) is appreciated. Y-H Tse also thanks NSERC for an undergraduate scholarship during his undergraduate summer training at York University.

1. M. A. Haga, E. S. Dodsworth, and A. B. P. Lever. Inorg. Chem. **25**, 447 (1986).
2. D. J. Stufkens, T. L. Snoeck, and A. B. P. Lever. Inorg. Chem. **27**, 953 (1988).
3. S. R. Boone and C. G. Pierpont. Inorg. Chem. **26**, 1769 (1987).
4. S. R. Boone and C. G. Pierpont. Polyhedron, **18**, 2267 (1990).
5. M. A. Haga, E. S. Dodsworth, A. B. P. Lever, S. R. Boone, and C. G. Pierpont. J. Am. Chem. Soc. **108**, 7413 (1986).
6. A. B. P. Lever, P. R. Auburn, E. S. Dodsworth, M. A. Haga, W. Liu, M. Melnik, and W. A. Nevin. J. Am. Chem. Soc. **110**, 8076 (1988).
7. P. R. Auburn, E. S. Dodsworth, M. A. Haga, W. Liu, W. A. Nevin, and A. B. P. Lever. Inorg. Chem. **30**, 3502 (1991).
8. J. W. Moore and R. G. Pearson. Kinetics and mechanism. 3rd. ed. John Wiley and Sons, New York. 1981. p. 1178.
9. B. Durham, S. R. Wilson, D. J. Hodgson, and T. J. Meyer. J. Am. Chem. Soc. **102**, 600 (1980).
10. B. P. Sullivan and T. J. Meyer. Inorg. Chem. **21**, 1037 (1982).
11. T. Hasegawa, T. C. Lau, H. Taube, and W. P. Schaefer. Inorg. Chem. **30**, 2921 (1991).
12. H. Nagao, H. Funato, H. Nishimura, Y. Ichikawa, F. S. Howell, H. Kakihana, and M. Mukaida. Inorg. Chem. **28**, 3955 (1989).
13. J. W. Dubrawski and R. D. Feltham. Inorg. Chem. **19**, 355 (1980).
14. R. A. Krause and K. Krause. Inorg. Chem. **19**, 2600 (1980); T. Bao, K. Krause, and R. A. Krause. Inorg. Chem. **27**, 759 (1988).
15. D. W. Krassowski, J. H. Nelson, K. R. Bower, D. Hauenstein, and R. A. Jacobson. Inorg. Chem. **27**, 4294 (1988).
16. A. M. Popov, M. B. Egorova, V. V. Khorunzhii, and A. V. Drobachenko. Zh. Neorg. Kim. **33**, 2319 (1988); Engl. Transl. Russ. J. Inorg. Chem. **33**, 1324 (1988).
17. R. G. Wilkins. The study of kinetics and mechanism of reactions of transition metal complexes. Allyn and Bacon, Boston, Mass. 1974.
18. T. L. Brown, L. M. Ludwick, and R. S. Stewart. J. Am. Chem. Soc. **94**, 384 (1972).
19. R. G. Linck. Inorg. Chem. **8**, 1016 (1969).
20. F. Pomposo, D. Carruthers, and D. V. Stynes. Inorg. Chem. **21**, 4245 (1982).
21. H. Masui, P. R. Auburn, and A. B. P. Lever. Inorg. Chem. **30**, 2402 (1991).

Can. J. Chem. Downloaded from www.nrcresearchpress.com by 217.78.4.112 on 09/08/12
For personal use only.

The molecular and electronic structure of 1-pyrazolylphosphazenes

KEITH D. GALLICANO, NORMAN L. PADDOCK, STEVEN J. RETTIG, AND JAMES TROTTER
Department of Chemistry, University of British Columbia, 2036 Main Mall, Vancouver, B.C., Canada V6T 1Z1

Received July 25, 1991[1]

KEITH D. GALLICANO, NORMAN L. PADDOCK, STEVEN J. RETTIG, and JAMES TROTTER. Can. J. Chem. **70**, 1855 (1992).

The nature of the interactions between pyrazolyl and phosphazene rings has been investigated through the study of the structures of bis(1-pyrazolyl)methane, $CH_2(H_2pz)_2$, **1**, bis[1-(3,5-dimethylpyrazolyl)]methane, $CH_2(Me_2pz)_2$, **2**, the pyrazolylphosphazenes $N_3P_3(Me_2pz)_6$, **3**, $N_4P_4(H_2pz)_8$, **4**, and $N_4P_4(Me_2pz)_8$, **5**, and the partially substituted *gem*-$N_3P_3Ph_2(Me_2pz)_4$, **6**. Crystal data are as follows: **1**, orthorhombic, $P2_12_12_1$, a = 7.997(2), b = 9.287(2), c = 10.049(2) Å, Z = 4, R = 0.034 for 647 reflections; **2**, monoclinic, $C2/c$, a = 19.115(4), b = 4.2690(8), c = 14.543(3) Å, β = 98.91(2)°, Z = 4, R = 0.064 for 528 reflections; **3**, monoclinic, $C2/c$, a = 16.778(2), b = 12.1083(9), c = 19.269(4) Å, β = 113.885(6)°, Z = 4, R = 0.039 for 2716 reflections; **4**, monoclinic $P2_1/n$, a = 10.4223(9), b = 8.1879(7), c = 19.403(2) Å, β = 94.381(7)°, Z = 2, R = 0.059 for 2937 reflections; **5**, triclinic, $P\bar{1}$, a = 11.516(2), b = 13.121(3), c = 18.142(3) Å, α = 77.96(1), β = 79.20(1), γ = 66.54(2)°, Z = 2, R = 0.036 for 5300 reflections; **6**, monoclinic, $P2_1/c$, a = 10.3598(4), b = 17.8827(4), c = 19.0851(6) Å, β = 94.675(2)°, Z = 4, R = 0.053 for 4867 reflections. Interpretation of the structures through iterative extended Hückel calculations shows that conjugative interactions lead to a quinonoid deformation of the pyrazole ring, similar to that in bis(1-pyrazolyl)carbonyl. π-Electron transfer to the phosphazene ring, facilitated by the use of acceptor *d* orbitals on phosphorus, is accompanied by a synergic σ transfer to the pyrazole ring. The pyrazolyl group acts both as a strongly electronegative group and as a good potential donor. The calculations account satisfactorily for the bond lengths in the pyrazolyl group, the large bond angles at nitrogen in **4** and **5**, the bond length inequalities in the phosphazene ring of **6**, and the reactivity of the pyrazolylphosphazenes.

KEITH D. GALLICANO, NORMAN L. PADDOCK, STEVEN J. RETTIG et JAMES TROTTER. Can J. Chem. **70**, 1855 (1992).

On a déterminé la nature des interactions entre les noyaux pyrazolyle et phosphazène grâce à une étude des structures du bis(1-pyrazolyl)méthane, $CH_2(H_2pz)_2$, **1**, du bis[1-(3,5-diméthylpyrazolyl)]méthane, $CH_2(Me_2pz)_2$, **2**, des pyrazolylphosphazènes $N_3P_3(Me_2pz)_6$, **3**, $N_4P_4(H_2pz)_8$, **4**, et $N_4P_4(Me_2pz)_8$, **5**, et du *gem*-$N_3P_3Ph_2(Me_2pz)_4$, **6**, partiellement substitué. Les données cristallographiques sont les suivantes: **1**, orthorhombique, $P2_12_12_1$, a = 7,997(2), b = 9,287(2) et c = 10,049(2) Å, Z = 4, R = 0,034 pour 647 réflexions; **2**, monoclinique, $C2/c$, a = 19,115(4), b = 4,2690(8) et c = 14,543(3) Å, β = 98,91(2)°, Z = 4, R = 0,064 pour 528 réflexions; **3**, monoclinique, $C2/c$, a = 16,778(2), b = 12,1083(9) et c = 19,269(4) Å, β = 113,885(6)°, Z = 4, R = 0,039 pour 2716 réflexions; **4**, monoclinique, $P2_1/n$, a = 10,4223(9), b = 8,1879(7) et c = 19,403(2) Å, β = 94,381(7)°, Z = 2, R = 0,059 pour 2937 réflexions; **5**, triclinique, $P\bar{1}$, a = 11,516(2), b = 13,121(3) et c = 18,142(3) Å, α = 77,96(1), β = 79,20(1) et γ = 66,54(2)°, Z = 2, R = 0,036 pour 5300 réflexions; **6**, monoclinique, $P2_1/c$, a = 10,3598(4), b = 17,8827(4) et c = 19,0851(6) Å, β = 94,675(2)°, Z = 4, R = 0,053 pour 4867 réflexions. L'interprétation des structures à l'aide de calculs de Hückel étendus montrent que les interactions de conjugaison conduisent à une déformation quinonoïdale du noyau pyrazole, semblable à celle observée dans le bis(1-pyrazolyl)carbonyle. Le transfert d'électrons π vers le noyau phosphazène, facilité par l'utilisation d'un accepteur d'orbitales *d* sur le phosphore, s'accompagne d'un transfert σ synergique vers le noyau pyrazole. Le groupe pyrazolyle agit à la fois comme une groupe fortement électronégatif et comme un bon donneur potentiel. Les calculs rendent bien compte des longueurs des liaisons dans le groupe pyrazolyle, des angles de liaison élargis au niveau de l'azote des composés **4** et **5**, des inégalités dans les longueurs des liaisons dans le cycle phosphazène du produit **6** ainsi que de la réactivité des pyrazolylphosphazènes.

[Traduit par la rédaction]

Introduction

Although the detailed electronic structure of phosphazenes is complex, the interaction of a phosphazene ring with its substituents is usually interpreted simply in terms of induction and conjugation, concepts primarily appropriate to organic molecules. Although such a classification seems valid, the details are different for phosphazenes, because the number of *d* orbitals available at phosphorus exceeds that formally required for π bonding, and their potential interactions are diverse. The balance of σ and π effects is different from that in carbon-based molecules and is an important topic of this paper. Apart from their specific applications, the results obtained may also help in the elucidation of the directional effects found in the substitution reactions of phosphazenes (1).

At the lowest level, Hückel methods applied to $d\pi$ interactions within the ring have proved valuable in the interpretation of the structures and behaviour of phosphazenes (2–4). Notably, the possibility of both homomorphic and heteromorphic interactions in both the in-plane (π) and out-of-plane π systems (π′) has been recognized. The homomorphic π′ system is presumably responsible for the oscillatory behaviour of the ionization energy of $(NPF_2)_n$ as a function of ring size (5), and the heteromorphic π system for the thermochemical stability of the high polymer relative to the halides of smaller ring size (6).

Calculations at this level suggest that ring perturbation involves significant charge transfer, showing the need for a theoretical method with some degree of self-consistency, so allowing for σ–π interaction. EHMO calculations on $(NPCl_2)_3$ showed the d_{xz},d_{yz} contributions to be unequal (7), and the possible importance in $(NPF_2)_4$ of such orbital combinations as $PX_2(\sigma^*)$, as acceptors alternative to atomic *d* functions (8). CNDO/2 calculations (9) show that the order of the π,π′ systems depends on the substituent, the HOMO being π′ in $(NPF_2)_3$ and π in $(NPCl_2)_3$. By the X_αSW method,

[1]Revision received February 20, 1992.

Can. J. Chem. Downloaded from www.nrcresearchpress.com by 217.78.4.112 on 09/08/12
For personal use only.

Can. J. Chem. Downloaded from www.nrcresearchpress.com by 217.78.4.112 on 09/08/12
For personal use only.

the HOMO is found to be homomorphic in both $(NPF_2)_{3,4}$ and $(NPCl_2)_3$, and contributions from $p\pi-p\pi$ and $d\sigma$ bonding were also recognized (10).

The first non-empirical study of cyclotriphosphazenes verfied the significant effect of *d* orbitals, beyond that of ordinary polarization functions, in inducing substantial π contractions; bond lengths and angles were satisfactorily reproduced (11). In later calculations (12) on $(NPH_2)_3$, $(NPF_2)_3$, and $(NPF_2)_4$, using a larger basis set, the *d* contributions were found to be smaller, but nevertheless involved in π and π' bonding, the dependence on substituent electronegativity being confirmed.

The experimental evidence on ring-substituent interactions is more extensive than the calculations relating to them. ^{19}F nmr spectroscopy (13) shows that the withdrawal of electrons from phenyl by a fluorophosphazenyl group is similar to that by a nitro group, but UV (14) and PE spectroscopy (15) suggest that conjugation is weak, the interaction being largely inductive, through the σ system. Experimentally, strong π conjugation requires donation from the substituent (16), inducing a planar configuration of the *exo*-N atoms in alkylamino derivatives, shortening the *exo*-P—N bond, and, in agreement with CNDO calculations of electron density (17), making a ring-nitrogen atom the basic centre (18). A band in the UV spectra of the 1-methyl-2-(fluorophosphazenyl)pyrroles $N_nP_nF_{2n-1}\cdot C_4H_3NMe$ (n = 3–6) is attributed to $d\pi-p\pi$ charge transfer, its variation with ring size and the conformation of the tetrameric molecule being consistent with conjugation to a homomorphic system (19). Later work (20) on the ESR spectrum of a phenalenylphosphazene radical specifically designed to allow spiro conjugation only through the phosphorus d_{xz} orbital showed at least half of the ring nuclei to be ESR active. π Interactions have also been detected by UV spectroscopy (21) between the l-aziridinyl and other groups attached to a phosphazene nucleus, but in this case the detailed mechanism is unknown.

HMO methods, although useful, cannot help if there is significant $\sigma-\pi$ mixing. At the other extreme, in an *ab initio* study of the model compound 1,1-diaminocyclodiphosphazene (22), the substituents were found to stabilize the ring inductively, without much mesomeric conjugation, though these latter contributions would be expected to be strengthened in corresponding halogeno derivatives.

The electronic structure of pyrazolylphosphazenes is of interest, because complex formation takes place through the pyridinic nitrogen atom rather than the phosphazene ring (23, 24), conjugative release being limited by the competition for π electrons between the pyrazolyl ring and the *exo*-P—N bond (Fig. 1). Because the pyrazolyl group is unsymmetrical, its geometry is sensitive to substitution and the changes induced in it by a phosphazenyl ring can be used to discriminate the interactions between the rings.

The structure of pyrazole itself, as determined by microwave spectroscopy (25), has limited comparative value, because the spectroscopic and X-ray diffraction results refer to molecules in different vibrational states (26) and, in the structures determined by X-ray (26) and neutron (27) diffraction, the ring geometry is affected by hydrogen bonding. We have therefore determined the structures of the dipyrazolylmethanes **1** and **2** (in which no conjugation is expected), the pyrazolylphosphazenes **3–5**, and the partially substituted derivative **6**.

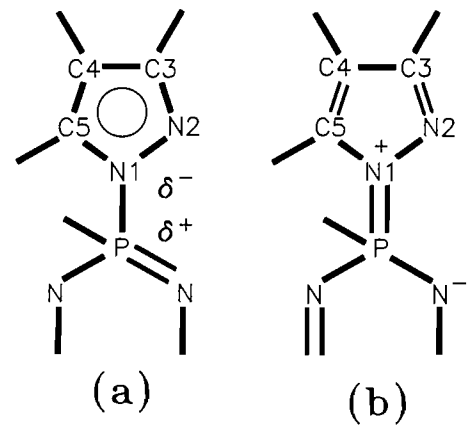

FIG. 1. Inductive (*a*) and conjugative (*b*) interactions of a pyrazolyl group with a phosphazene ring.

Experimental

The preparation of compounds **3–6** is described in ref. 2. Details on the preparation of **1** and **2** are reported in ref. 28.

Crystallographic analyses of 1–6

Crystallographic data for the six compounds appear in Table 1. Final unit-cell parameters were obtained from least-squares refinement of 2 sin θ/λ values for 25 reflections with 2θ = 22–31, 50–83, 35–44, 35–40, 35–41, and 64–84° for **1–6**, respectively. The intensities of three standard reflections, measured each hour of X-ray exposure time, were essentially constant throughout the data collections, except for compound **2** which showed a uniform decay of 32%. Data for compounds **2–4** and **6** were corrected for absorption (numerical integration)[2] and data for **2** were scaled for linear decay.

The structures of **1** and **2** were solved by direct methods and those of **3–6** by conventional heavy-atom methods. For **2**, **3**, and **5**, there were choices between centrosymmetric and noncentrosymmetric space groups, the structure analyses being initiated in the former in each case on the basis of the *E* statistics. These choices were confirmed by the subsequent successful solutions and refinements of the structures. The pyrazole rings in **4** were all found to be disordered, (1:1) twofold disordered models being refined for each ring. Attempts to refine an ordered model of **4** in the lower symmetry space groups $P2_1$ and *Pn* were not successful.

All non-hydrogen atoms were refined with anisotropic thermal parameters. Hydrogen atoms were refined with isotropic thermal parameters (**1–3**) or fixed in idealized positions (**4–6**, methyl orientations based on difference map peaks, $C(sp^3)$—H = 0.98 Å, $C(sp^2)$—H = 0.97 Å, $U_H \propto U_{\text{bonded atom}}$). Isotropic extinction parameters (29–31) were refined for **1** and **6**, the final values of g being $4.4(9)\times10^4$ and $0.66(9)\times10^4$, respectively. Neutral-atom scattering factors and anomalous dispersion corrections (for P) were taken from ref. 32. No attempt was made to determine the absolute configuration of **1**. Final coordinates and equivalent isotropic thermal parameters (U_{eq} = 1/3 trace of diagonalized U) for the non-hydrogen atoms are given in Table 2 (those for the disordered **4** are

[2]The computer programs used include locally written programs for data processing and locally modified versions of the following: ORFLS, full-matrix least-squares, and ORFFE, function and errors, by W. R. Busing, K. O. Martin, and H. A. Levy; FORDAP, Petterson and Fourier syntheses, by A. Zalkin; ORTEP II, illustrations, by C. K. Johnson; AGNOST, absorption corrections, by J. A. Ibers; MULTAN 80, multisolution program, by P. Main, S. J. Fiske, S. E. Hull, L. Lessinger, G. Germain, J. P. Declercq, and M. M. Woolfson.

Can. J. Chem. Downloaded from www.nrcresearchpress.com by 217.78.4.112 on 09/08/12
For personal use only.

TABLE 1. Crystallographic data[a]

Compound	$CH_2(pz)_2$, **1**	$CH_2(Me_2pz)_2$, **2**	$P_3N_3(Me_2pz)_6$, **3**	$P_4N_4(pz)_8$, **4**	$P_4N_4(Me_2pz)_8$, **5**	$P_3N_3(pz)_4Ph_2$, **6**
Formula	$C_7H_8N_4$	$C_{11}H_{16}N_4$	$C_{30}H_{42}N_{15}P_3$	$C_{24}H_{24}N_{20}P_4$	$C_{40}H_{56}N_{20}P_4$	$C_{32}H_{38}N_{11}P_3$
fw	148.17	204.27	705.68	716.49	940.92	669.66
Crystal system	Orthorhombic	Monoclinic	Monoclinic	Monoclinic	Triclinic	Monoclinic
Space group	$P2_12_12_1$	$C2/c$	$C2/c$	$P2_1/n$	$P\bar{1}$	$P2_1/c$
a (Å)	7.997(2)	19.115(4)	16.778(2)	10.4223(9)	11.516(2)	10.3598(4)
b (Å)	9.287(2)	4.2690(8)	12.1083(9)	8.1879(7)	13.121(3)	17.8827(4)
c (Å)	10.049(2)	14.543(3)	19.269(4)	19.403(2)	18.142(3)	19.0851(6)
α (deg)	90	90	90	90	77.96(1)	90
β (deg)	90	98.91(2)	113.885(6)	94.381(7)	79.20(1)	94.675(2)
γ (deg)	90	90	90	90	66.54(2)	90
V(Å^3)	746.3(3)	1172.4(4)	3579.3(7)	1650.9(4)	2442.5(9)	3523.9(3)
Z	4	4	4	2	2	4
D_c (g/cm^3)	1.319	1.157	1.310	1.441	1.279	1.262
F(000)	312	440	1488	736	922	1408
Radiation	Mo	Cu	Mo	Mo	Mo	Cu
μ (cm^{-1})	0.82	5.46	2.05	2.33	1.66	17.6
Crystal dimensions (mm)	0.15 × 0.30 × 0.45	0.08 × 0.23 × 0.53	0.25 × 0.26 × 0.55	0.20 × 0.26 × 0.33	0.30 × 0.35 × 0.40	0.22 × 0.26 × 0.54
Transmission factors	—	0.828–0.959	0.941–0.957	0.950–0.958	—	0.506–0.723
Scan type	ω – 2θ	ω – θ	ω – 2θ	ω – 2θ	ω – 2θ	ω – 2θ
Scan range (deg in ω)	0.70 + 0.35 tan θ	0.75 + 0.14 tan θ	0.60 + 0.35 tan θ	0.50 + 0.35 tan θ	0.50 + 0.35 tan θ	0.75 + 0.20 tan θ
Scan speed (deg/min)	0.7–6.7	1.0–10.1	1.0–10.1	1.2–10.1	0.4–4.0	1.1–6.7
Data collected	$+h, +k, +l$	$\pm h, -k, +l$	$+h, +k, \pm l$	$+h, +k, \pm l$	$\pm h, \pm k, +l$	$+h, +k, \pm l$
$2\theta_{max}$ (deg)	55	150	55	55	50	150
Crystal decay	Negligible	32%	Negligible	Negligible	Negligible	Negligible
Unique reflections	1010	1206	4088	3780	8598	7223
Reflections with $I \geq 3\sigma(I)$	647	528	2716	2937	5300	4867
Number of variables	133	101	302	361	577	416
R	0.034	0.064	0.039	0.059	0.036	0.053
R_w	0.035	0.073	0.049	0.092	0.046	0.068
S	1.486	2.923	1.992	3.350	1.489	1.677
Mean Δ/σ (final cycle)	0.004	0.02	0.04	0.04	0.06	0.03
Max Δ/σ (final cycle)	0.03	0.14	0.22	0.29	0.33	0.20
Residual density (e/Å^3)	0.17	0.42	0.29	0.81	0.26	0.39

[a]Temperature 295 K, Enraf–Nonius CAD4-F diffractometer, graphite monochromatized Mo-K_α radiation ($\lambda_{K\alpha_1}$ = 0.70930, $\lambda_{K\alpha_2}$ = 0.71359 Å), or Cu-K_α radiation ($\lambda_{K\alpha_1}$ = 1.540562, $\lambda_{K\alpha_2}$ = 1.544390 Å), takeoff angle 2.7°, aperture (2.0 + tan θ) × 4.0 mm at a distance of 173 mm from the crystal, scan range extended by 25% on both sides for background measurement, $\sigma^2(I) = C + 2B + |0.04(C - B)|^2$ (C = scan count, B = normalized background count), function minimized: $\Sigma w(|F_o| - |F_c|)^2$ where $w = 1/\sigma^2(F)$, $R = \Sigma||F_o| - |F_c||/\Sigma|F_o|$, $R_w = (\Sigma w(|F_o| - |F_c|)^2/\Sigma w|F_o|^2)^{1/2}$, $S = (\Sigma w|F_o| - |F_c|)^2/(m - n))^{1/2}$. Values given for R, R_w, and S are based on those reflections with $I \geq 3\sigma(I)$.

Can. J. Chem. Downloaded from www.nrcresearchpress.com by 217.78.4.112 on 09/08/12
For personal use only.

TABLE 2. Final positional (fractional × 10^4, $P \times 10^5$) and isotropic thermal parameters ($U \times 10^3$ Å^2) with estimated standard deviations in parentheses

Atom	x	y	z	U_{eq}
		1		
N(1)	3 926(4)	2 506(4)	3 535(4)	46
N(2)	2 632(5)	1 819(4)	2 957(4)	54
N(3)	3 528(5)	5 059(4)	3 290(4)	49
N(4)	3 766(6)	5 747(4)	4 454(4)	63
C(1)	4 426(8)	1 841(6)	4 645(5)	57
C(2)	3 456(8)	679(5)	4 822(6)	63
C(3)	2 377(7)	713(5)	3 763(5)	58
C(4)	2 230(7)	5 605(5)	2 604(6)	60
C(5)	1 605(7)	6 710(5)	3 324(6)	63
C(6)	2 589(8)	6 752(5)	4 458(5)	63
C(7)	4 549(7)	3 823(6)	2 957(6)	58
		2		
N(1)	4 365(2)	3 580(7)	2 446(3)	70
N(2)	4 046(2)	2 584(8)	1 585(2)	73
C(1)	3 500(2)	864(10)	1 775(4)	70
C(2)	3 474(2)	797(13)	2 709(5)	83
C(3)	4 033(2)	2 526(11)	3 138(4)	75
C(4)	5 000	5 441(16)	2 500	79
C(5)	3 005(3)	−544(21)	982(6)	99
C(6)	4 271(5)	3 218(24)	4 119(6)	127
		3 (all × 10^5)		
P(1)	50 000	34 405(6)	25 000	32
P(2)	46 223(3)	54 111(5)	17 161(3)	32
N(1)	46 573(11)	41 097(14)	17 316(9)	33
N(2)	50 000	60 353(20)	25 000	35
N(3)	42 102(12)	25 553(15)	24 616(10)	40
N(4)	44 713(15)	17 897(17)	30 488(11)	55
N(5)	35 923(12)	58 579(15)	12 412(10)	37
N(6)	31 461(12)	53 807(16)	5 348(10)	44
N(7)	51 046(11)	58 426(15)	11 515(9)	35
N(8)	49 028(12)	69 128(15)	8 670(11)	42
C(1)	34 271(16)	22 565(23)	18 986(15)	55
C(2)	31 925(21)	13 195(27)	21 477(18)	69
C(3)	38 514(19)	10 577(21)	28 511(14)	53
C(4)	29 705(32)	28 688(52)	11 807(32)	114
C(5)	39 165(41)	790(34)	33 501(25)	86
C(6)	31 022(16)	66 719(20)	13 795(15)	48
C(7)	23 420(18)	66 865(24)	7 536(18)	61
C(8)	23 915(15)	58 887(20)	2 532(13)	44
C(9)	33 930(29)	73 630(38)	20 793(22)	81
C(10)	17 153(24)	55 695(34)	−5 090(20)	68
C(11)	57 243(13)	53 729(18)	9 385(12)	35
C(12)	58 992(14)	61 381(20)	5 085(13)	40
C(13)	53 880(15)	70 694(18)	4 816(12)	39
C(14)	61 105(19)	42 531(22)	11 712(19)	51
C(15)	53 463(22)	81 362(24)	758(16)	54
		5		
P(1)	47 877(8)	7 906(6)	39 499(5)	35
P(2)	52 836(8)	13 097(6)	53 524(5)	34
P(3)	92 390(7)	66 321(6)	716(5)	33
P(4)	83 595(7)	47 467(6)	5 632(5)	33
N(1)	5 327(2)	1 171(2)	4 516(1)	36
N(2)	4 958(2)	477(2)	6 030(1)	39
N(3)	8 362(2)	5 950(2)	294(2)	38
N(4)	9 624(2)	3 680(2)	569(1)	36
N(5)	5 368(3)	1 222(2)	3 070(1)	41
N(6)	3 202(2)	1 570(2)	3 972(2)	41
N(7)	4 313(2)	2 607(2)	5 532(2)	38
N(8)	6 744(2)	1 314(2)	5 390(2)	39
N(9)	8 283(2)	7 980(2)	−200(2)	38
N(10)	9 711(2)	6 747(2)	874(1)	38
N(11)	7 357(2)	4 653(2)	34(1)	38
N(12)	7 593(2)	4 678(2)	1 444(1)	38
N(13)	6 337(3)	439(2)	2 672(2)	51
N(14)	2 607(3)	2 168(2)	4 568(2)	48
N(15)	4 394(3)	3 463(2)	4 958(2)	49
N(16)	6 894(3)	1 582(2)	6 060(2)	49
N(17)	8 572(3)	8 564(2)	−892(2)	44
N(18)	9 733(3)	5 929(2)	1 502(2)	49
N(19)	7 012(3)	3 724(2)	273(2)	44
N(20)	6 463(3)	5 592(2)	1 552(2)	49
C(1)	5 223(3)	2 310(3)	2 731(2)	43
C(2)	6 077(4)	2 207(3)	2 101(2)	54
C(3)	6 744(4)	1 052(3)	2 087(2)	54
C(4)	2 345(4)	1 686(3)	3 492(2)	54
C(5)	1 200(4)	2 376(3)	3 795(3)	68
C(6)	1 402(4)	2 655(3)	4 437(3)	62
C(7)	3 402(4)	3 023(3)	6 111(2)	53
C(8)	2 901(4)	4 145(3)	5 895(2)	60
C(9)	3 526(3)	4 388(3)	5 191(2)	48
C(10)	7 835(3)	1 141(3)	4 889(2)	48
C(11)	8 677(3)	1 284(3)	5 251(2)	56
C(12)	8 060(3)	1 558(3)	5 966(2)	46
C(13)	7 203(3)	8 637(3)	205(2)	44
C(14)	6 798(3)	9 656(3)	−238(2)	52
C(15)	7 656(4)	9 574(3)	−898(2)	49
C(16)	10 230(3)	7 472(3)	995(2)	42
C(17)	10 556(4)	7 127(3)	1 708(2)	56
C(18)	10 251(4)	6 177(3)	1 995(2)	56
C(19)	6 932(3)	5 216(3)	−655(2)	43
C(20)	6 287(3)	4 650(3)	−837(2)	53
C(21)	6 363(3)	3 744(3)	−258(2)	47
C(22)	7 849(3)	3 948(3)	2 110(2)	46
C(23)	6 872(4)	4 408(3)	2 635(2)	59
C(24)	6 044(4)	5 419(3)	2 271(2)	52
C(25)	4 282(4)	3 327(3)	3 043(2)	58
C(26)	7 819(5)	484(4)	1 525(3)	86
C(27)	2 720(5)	1 128(4)	2 805(3)	79
C(28)	459(4)	3 415(4)	4 975(3)	97
C(29)	3 107(6)	2 327(4)	6 823(3)	107
C(30)	3 326(4)	5 498(3)	4 701(3)	80
C(31)	8 025(4)	821(4)	4 115(2)	78
C(32)	8 564(4)	1 816(4)	6 575(2)	70
C(33)	6 679(4)	8 246(3)	975(2)	61
C(34)	7 656(5)	10 463(3)	−1 569(2)	71
C(35)	10 358(4)	8 420(3)	414(2)	55
C(36)	10 456(5)	5 451(4)	2 756(3)	90
C(37)	7 167(4)	6 224(3)	−1 087(2)	62
C(38)	5 827(4)	2 853(3)	−191(3)	66
C(39)	8 978(4)	2 881(4)	2 183(2)	71
C(40)	4 824(4)	6 249(4)	2 583(3)	77
		6		
P(1)	75 988(8)	50 417(5)	11 368(4)	41
P(2)	89 562(8)	53 441(4)	24 186(4)	39
P(3)	64 456(8)	48 623(5)	23 886(4)	41
N(1)	8 905(3)	5 266(2)	1 601(1)	44
N(2)	7 741(3)	5 104(2)	2 811(1)	46
N(3)	6 388(3)	4 814(2)	1 567(1)	47
N(4)	10 259(3)	4 869(2)	2 769(1)	49

TABLE 2 (*concluded*)

Atom	*x*	*y*	*z*	U_{eq}
N(5)	10 401(4)	4 866(2)	3 497(2)	70
N(6)	9 308(3)	6 240(1)	2 651(1)	45
N(7)	10 055(3)	6 643(2)	2 220(2)	51
N(8)	6 022(3)	4 027(2)	2 722(1)	43
N(9)	5 112(3)	3 621(2)	2 313(2)	50
N(10)	5 231(3)	5 426(2)	2 616(2)	55
N(11)	5 156(4)	5 493(2)	3 334(2)	75
C(1)	7 942(3)	4 266(2)	581(2)	44
C(2)	7 590(4)	3 553(2)	748(2)	63
C(3)	7 972(6)	2 959(2)	340(3)	86
C(4)	8 687(5)	3 077(3)	−222(3)	76
C(5)	9 023(4)	3 776(3)	−396(2)	65
C(6)	8 656(4)	4 380(2)	0(2)	53
C(7)	7 155(3)	5 813(2)	568(2)	47
C(8)	7 564(4)	6 530(2)	753(2)	66
C(9)	7 152(6)	7 128(3)	335(3)	90
C(10)	6 371(5)	7 016(3)	−272(3)	91
C(11)	5 981(5)	6 318(3)	−470(2)	74
C(12)	6 359(4)	5 715(2)	−48(2)	59
C(13)	9 140(4)	6 627(2)	3 264(2)	55
C(14)	9 761(4)	7 289(2)	3 204(2)	65
C(15)	10 306(4)	7 277(2)	2 553(2)	59
C(16)	8 420(5)	6 340(3)	3 857(2)	82
C(17)	11 062(6)	7 875(3)	2 228(3)	95
C(18)	11 282(4)	4 515(2)	2 498(2)	56
C(19)	12 057(5)	4 282(3)	3 063(3)	77
C(20)	11 500(5)	4 512(3)	3 655(2)	75
C(21)	11 451(5)	4 432(3)	1 740(3)	93
C(22)	11 937(7)	4 377(4)	4 425(3)	130
C(23)	6 229(4)	3 730(2)	3 386(2)	52
C(24)	5 450(4)	3 110(2)	3 388(2)	63
C(25)	4 783(4)	3 064(2)	2 721(2)	58
C(26)	7 117(5)	4 049(3)	3 966(2)	74
C(27)	3 793(5)	2 508(3)	2 446(3)	83
C(28)	4 253(4)	5 809(2)	2 249(3)	69
C(29)	3 558(5)	6 126(3)	2 745(4)	94
C(30)	4 131(5)	5 922(3)	3 389(3)	87
C(31)	4 089(5)	5 870(4)	1 474(4)	108
C(32)	3 786(7)	6 137(4)	4 125(4)	144

in the Depository material[3]). Hydrogen-atom coordinates, anisotropic thermal parameters, bond lengths and angles, intra-annular torsion angles, and observed and calculated structure factor amplitudes for all six compounds are included as supplementary material.[3] Bond lengths for compounds **1**, **2**, and **5** have been corrected for thermal libration using the TLS model (33, 34). The structures **1**–**3**, **5**, **6** are shown in Figs. 2–6, respectively (**4** in Depository material[3]). The geometry of the phosphazene rings in **3**–**6** is summarized in Fig. 7 and comparison data for the tetrameric rings are given in Table 3.

[3]These may be purchased from: The Depository of Unpublished Data, Document Delivery, CISTI, National Research Council Canada, Ottawa, Canada, K1A 0S2.

Tables of hydrogen atom coordinates, bond lengths and angles, and positional parameters and view for compound **4** have also been deposited with the Cambridge Crystallographic Data Centre and can be obtained on request from the Director, Cambridge Crystallographic Data Centre, University Chemical Laboratory, Lensfield Road, Cambridge, CB2 1EW, U.K.

Results and discussion

General characteristics of the structures

The geometry of hexakis[1-(3,5-dimethylpyrazolyl)]cyclotriphosphazene, **3**, is based on a nearly planar N_3P_3 framework; the torsion angles about successive ring bonds are −2.0, 3.9, −1.9°, the remaining angles being related by the crystallographic C_2 axis through P(1) and N(2). The mean length of the exocyclic P—N bond (1.682 Å) suggests some exocyclic conjugation. The mean ring bond length (1.577 Å) is closer to the 1.581 Å in $N_3P_3Cl_6$ (35) than to the 1.605 Å in $N_3P_3Me_6$ (36) or 1.597 Å in $N_3P_3Ph_6$ (37), and the similarity of the structural effects of chlorine and the dimethylpyrazolyl group is confirmed by a comparison of the inequalities in the ring bonds of **6**, compared with those in $N_3P_3Ph_2Cl_4$ (38) and $N_3P_3Ph_2F_4$ (39). If methylation reduces electron withdrawal by the pyrazole group, the unsubstituted pyrazolyl group should be even more electronegative, in agreement with the structures of the two tetramers **4** and **5**, which are compared with other tetramers in Table 3. The mean angle at nitrogen in the phosphazene ring is larger in **4** (146.2°) than in **5** (136.8°), and the PN framework is therefore flatter in **4** (mean deviation of the phosphorus atoms from the plane of the nitrogen atoms = 0.08 Å) than in the two crystallographically independent molecules of **5** (mean deviations 0.28, 0.38 Å). The ring geometry of **4** resembles that of $N_4P_4F_8$ (45) more than that of the other tetramers (Table 3) and the possibility that the unsubstituted pyrazolyl group is almost as effectively electronegative as fluorine (to the phosphazene ring) is reinforced by the spectroscopic results (24). Steric interactions may also contribute to the apparent effects of methylation. Calculations of non-bonded interactions show that in the most stable conformations of an isolated $M(pz)_2$ group (M = C, P; pz = H_2pz, Me_2pz), the two pyrazolyl groups are related by a twofold axis, but the conformational energy is, over large ranges, insensitive to the torsion angle about the M—N bonds; measured angles are given in Table 4. The twofold axis is exact in **2** and at P(1) in **3**, and close in **1**. The approximate correspondence otherwise holds except at P(2) in **4** where, because of the disorder, the pyrazolyl groups are related by either an approximate local plane of symmetry or by an approximate twofold axis. In **3** and **6**, the three sets of torsion angles all have the same sign, so that, numerical inequalities apart, **3** approaches threefold symmetry. In **5**, the angles at the phosphazene nitrogen atoms are larger than those in the trimeric phosphazenes, **3** and **6**, tending to decrease Me···Me distances, unacceptably so if the torsion angle is increased. In fact, in **5** (both molecules) the pairs of pyrazolyl groups on alternate phosphorus atoms are enantiomerically related, so preserving locally favourable conformations while relieving steric repulsion between the groups on neighboring phosphorus atoms. Methyl–methyl interactions are still significant in controlling the conformation. In **5** (molecule 1) the shortest Me···Me distances are C(25)···C(27) (4.09 Å, same center) and C(25)···C(30) (4.27 Å, different); in molecule 2 they are C(38)···C(35′) (4.00 Å) and C(37)···C(36′) (4.05 Å) (both different), and C(33)···C(35) (4.25 Å, same). The results as a whole suggest no barrier to rotation about the exocyclic P—N bond other than that arising from non-bonded interactions.

Geometry of the pyrazolyl group

The nature of the electronic interactions between the rings is reflected in the detailed structures of the pyrazolyl groups.

Can. J. Chem. Downloaded from www.nrcresearchpress.com by 217.78.4.112 on 09/08/12
For personal use only.

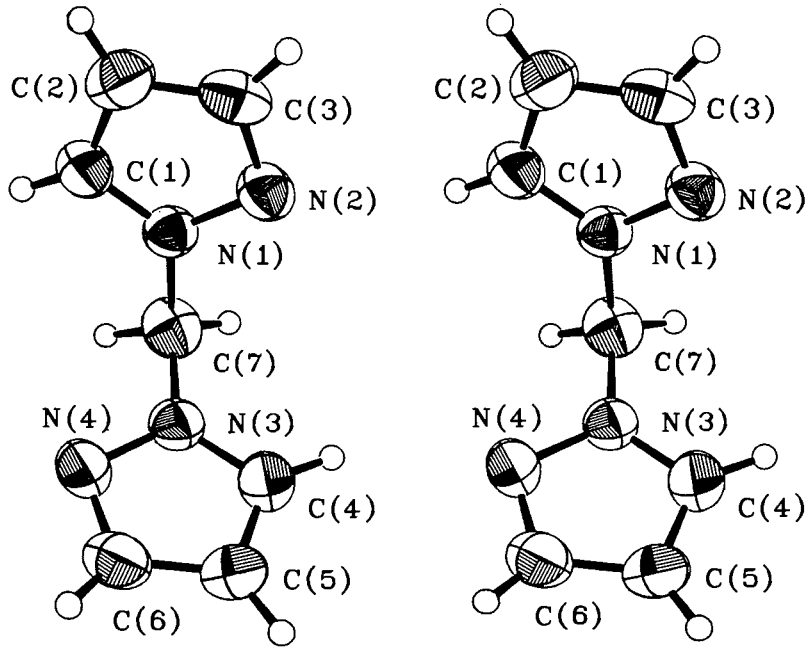

FIG. 2. Stereoview of bis(1-pyrazolyl)methane, **1**; 50% probability thermal ellipsoids are shown for the non-hydrogen atoms.

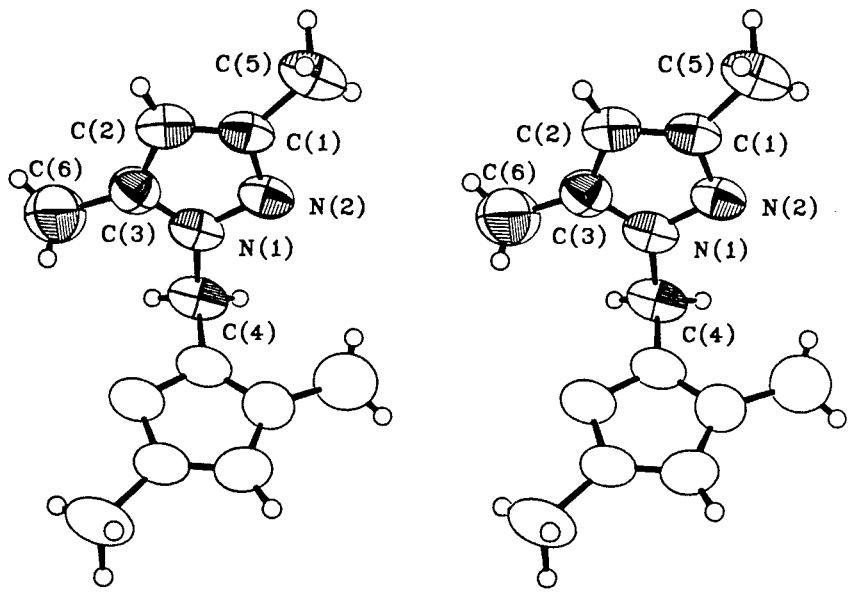

FIG. 3. Stereoview of bis[1-(3,5-dimethylpyrazolyl)]methane, **2**; 50% probability thermal ellipsoids are shown for the non-hydrogen atoms. Shaded non-hydrogen atoms comprise the asymmetric unit.

For each of molecules **1**, **2**, **3**, **5**, **6**, the pyrazolyl groups are insignificantly different; average structures are shown in Fig. 8. The structure of **4** is not included because the pyrazolyl rings are disordered.

Since the pyrazole ring is planar, the σ and π systems are geometrically separable, their mutual influence being indirect, through charge density effects; the π electrons have no direct effect on ring angles. The bond lengths can be expected to be controlled jointly by the electron density in both σ and π bonds. The measured length L is analyzed here in terms of a length L_1 characteristic of the σ bond, the difference $L_2 = L_1 - L$ being attributed solely to π bonding, and referred to below as a π contraction. L_1 is assumed to depend on the σ hybridization state only and, over a limited range, the atomic contribution to the σ-bond length is linearly related to the *p*-electron density in the relevant hybrid orbital (46), calculated from the geometry. This technique, which has been applied to phosphazenes (2), is appropriate to a discussion of the ring bonds; its limitations have been discussed by Salem (47). The molecules contain too many heavy atoms for the π contributions to be determined by non-empirical methods, but since substantial charge migration is involved, simple EHMO calculations are inadequate.

The geometrical changes induced by π bonding, how-

Can. J. Chem. Downloaded from www.nrcresearchpress.com by 217.78.4.112 on 09/08/12
For personal use only.

Can. J. Chem. Downloaded from www.nrcresearchpress.com by 217.78.4.112 on 09/08/12
For personal use only.

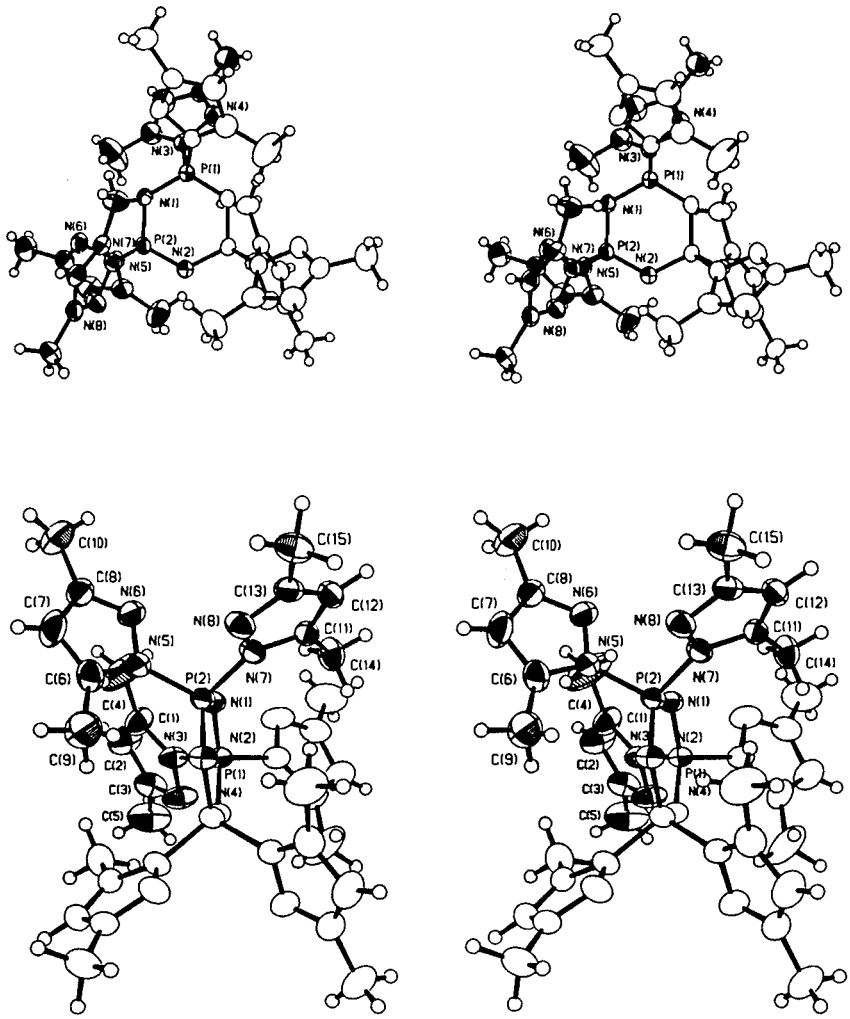

FIG. 4. Two stereoviews of hexakis[1-(3,5-dimethylpyrazolyl)]cyclotriphosphazene, **3**; 50% probability thermal ellipsoids are shown for the non-hydrogen atoms.

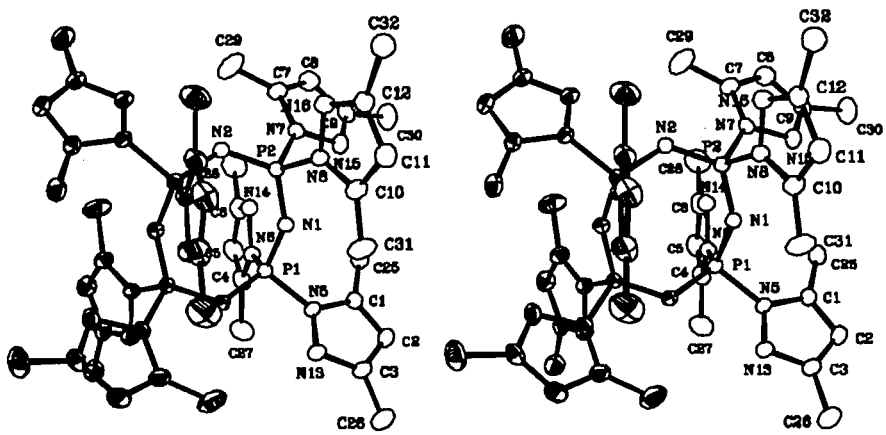

FIG. 5. Stereoview of one of the two crystallographically independent molecules of octakis[1-(3,5-dimethylpyrazolyl)]cyclotetraphosphazene, **5**; 25% probability thermal ellipsoids are shown for the non-hydrogen atoms. Labeled non-hydrogen atoms comprise the asymmetric unit.

ever, have been satisfactorily assessed by iterative EHMO calculations[4] that allow some degree of $\sigma-\pi$ interaction through the dependence of the Coulomb parameters H_{ii} on atomic charge, followed by a Mulliken population analysis. Madelung corrections were applied where appropriate. The coordinates used were based on the structures of **1** and **2**, modelled in the calculations by 1-methylpyrazole and 1,3,5-trimethylpyrazole, respectively. A least-squares anal-

[4]QCPE Program 344, J. Howell, A. Rossi, D. Wallace, and R. Hoffmann and QCMPO11, the same program adapted for personal computers by J. E. Bartmess and D. Thomas.

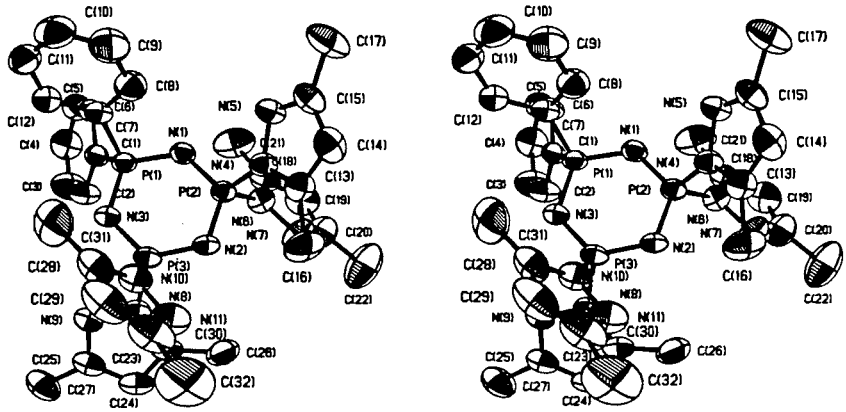

FIG. 6. Stereoview of *gem*-diphenyltetrakis[1-(3,5-dimethylpyrazolyl)]cyclotriphosphazene, **6**; 50% probability thermal ellipsoids are shown for the non-hydrogen atoms.

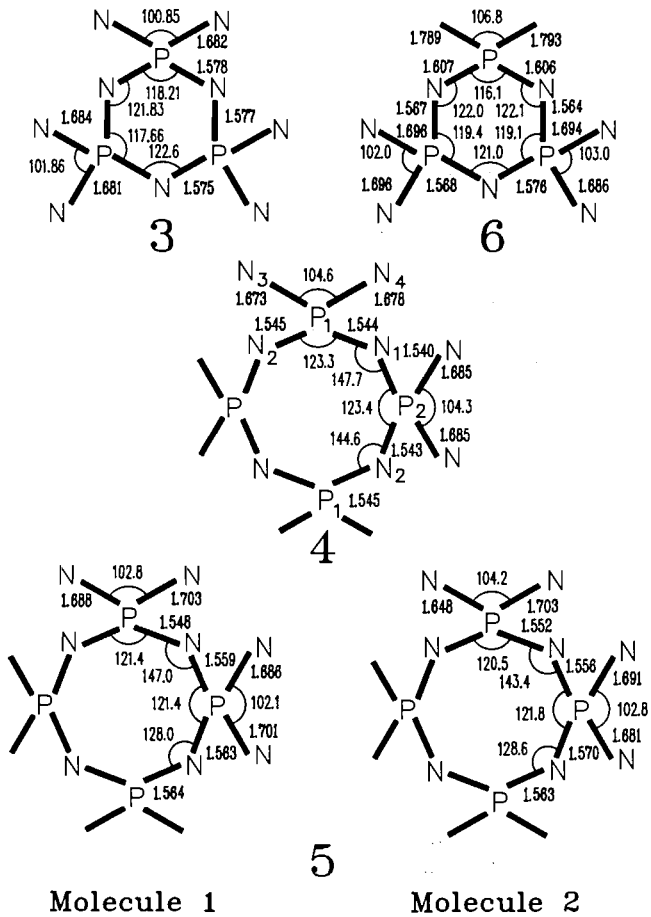

FIG. 7. Summarized phosphazene ring geometry of **3–6**.

ysis (R = 0.997) showed the π populations to be related to the π contractions (L_2) by $L_2 = 0.657 \times (\pi$ popn.), with errors 0.005 Å (mean) and 0.010 Å (max., bond 5–1 in **1**), comparable to the experimental mean standard deviation of 0.005 Å. The individual bond lengths (measd. and calcd.) are given in Table 5. A more stringent test of the theoretical method is provided by the small differences in bond lengths between **1** and **2** that result from 3,5-dimethylation. Except for bond 5–1, for which the discrepancy between calculated and observed bond lengths is greatest, the predicted differences (Table 5) are of the right sign, though on average 0.008 Å too small. This underestimation of bond length changes may well be a limitation of the theoretical method, which nevertheless seems good enough to reproduce the main effects of substituent interactions.

Substituent effects on the pyrazolyl group

We are concerned with the effect of substituents on the pyrazole ring, chiefly at N(1) (where they may have both inductive and conjugative interactions), and at N(2), in relation to complex formation.[5] The effect of an electropositive interaction at N(1) is illustrated by comparative calculations on pyrazole and 1-methylpyrazole. Relative to hydrogen, the methyl group releases 0.068 electrons to the ring, raising α_p at N(1), N(2) by 0.38, 0.29 eV. Other aspects of methyl substitution are shown by the comparative calculated energy levels of pyrazole, 1-methylpyrazole, and 1,3,5-trimethylpyrazole (Fig. 9). All occupied levels are raised without change of order. The HOMO is the N(2) lone-pair orbital; the negative charge on this atom is increased from 0.332 to 0.343 to 0.365 electrons. The effect arises principally from the transfer of 0.174 electrons from the *N*-methyl group to the ring; the 3- and 5-methyl groups are themselves weak acceptors. The general effect of an electropositive perturbation at N(1) is to strengthen bonds 1–2, 3–4, and 5–1 at the expense of 2–3 and 4–5. A purely inductive interaction at N(2) is simulated by protonation of 1,3,5-trimethylpyrazole and is considered briefly at the end of the paper.

Conjugative interactions are to be expected between pyrazolyl and phosphazenyl rings, though they should be smaller than in pyrrolylphosphazenes (19). They are discussed first in relation to the simpler molecule bis(1-pyrazolyl)carbonyl **7** (48). Calculations of electron density are summarized in Table 6 for 1-methypyrazole and 1-formylpyrazole, both with and without[6] exocyclic N–C conjugation. The pyrazole ring is a net acceptor in all cases, the slight decrease (0.013) from (*a*) to (*b*) arising from the greater electronegativity of CHO relative to CH_3. Conjugation, in (*c*), greatly reduces the ring charge, as a result of a large π donation (0.175) to the formyl group, partly offset and facilitated by a σ transfer of 0.060 from the formyl group.

[5]K. D. Gallicano, N. L. Paddock, S. J. Rettig, and J. Trotter. Manuscript in preparation.

[6]Exocyclic (N)$p\pi$–(C)$p\pi$ overlap integral set to zero.

Can. J. Chem. Downloaded from www.nrcresearchpress.com by 217.78.4.112 on 09/08/12
For personal use only.

TABLE 3. Summarized geometry of homogeneously substituted tetraphosphazenes, $N_4P_4X_8$

X	XPX (deg)	NPN (deg)	PNP (deg)	PN (Å)	Conformation	Ref.
Me	104	119.8	132.0	1.595	$\bar{4}$	40
Ph	105.1	119.9	127.9	1.590	$\bar{4}$	41
Br	103.9	120.1	131.0	1.575	$\bar{4}$	42
Cl(K)[a]	102.8	121.2	131.3	1.570	$\bar{4}$	43
Cl(T)[a]	103.1	120.5	135.9	1.559	$\bar{1}$	44
F[b]	99	123	147	1.507	$\bar{1}$	45
Me_2pz	102.4	121.3	136.8	1.557	$\bar{1}$	This work
H_2pz	104.4	123.3	146.2	1.543	1	This work

[a]Two polymorphic forms.
[b]Form stable at room temperature; planar skeleton.

TABLE 4. Torsion angles (deg) about bonds to pyrazolyl group[a]

Compound	Torsion angles
1	−9, −5
2	−177, −177
3, P(1)	−28, −28
3, P(2)	−23, −48
4, P(1)	174, 180
4, P(2)	4, 177
5, molecule 1, P(1)	136, 143
5, molecule 1, P(2)	−22, −34
5, molecule 2, P(3)	30, 43
5, molecule 2, P(4)	−140, −155
6, P(2)	−22, −1
6, P(3)	−2, −26

[a]Pairs of angles θ, ψ are related enantiomerically to those with π−θ, π−ψ. The angles shown are torsion angles about the C—N(pz) or P—N(pz) bond, zero for the open-book conformation, in which the normal to the pyrazolyl ring is coplanar with the N(pz)—P(C)—N(pz) plane.

Structurally, the effect of conjugation is seen in the planarity of the molecule as a whole and in the calculated and measured differences in bond length between **7** and **1** (Table 7). The inductive and conjugative effects are of the same sign and qualitatively indistinguishable; both reproduce the pattern of bond lengths correctly. However, in the absence of conjugation, the characteristic shortening of bonds 2–3 and 4–5, ca. 0.005 Å, would be undetectable. The conjugative effects are not much greater, but correspond fairly well to the measured differences, though again the experimental values are significantly greater than those calculated. The mean error is 0.006 Å. As expected, the inclusion of conjugation decreases the total bond population in the ring (by 0.025) and in the carbonyl group (by 0.043), but the molecule as a whole is stabilized by the additional π population in the exocyclic N—C bond (0.116). The enhanced π donation from the ring makes the ring atoms more electronegative, but the competition for π electrons between the ring and the carbonyl group restricts conjugation, so that the exocyclic N—C (1.393 Å) and C—O (1.195 Å) bonds are, respectively, somewhat longer and shorter than those characteristic of simple amides (1.333, 1.235 Å) (49). The calculations agree with the earlier crystallographic investigation (48) that delocalization is not extensive, but add the point that the partial quinonoid localization is largely a result of conjugation with the carbonyl group.

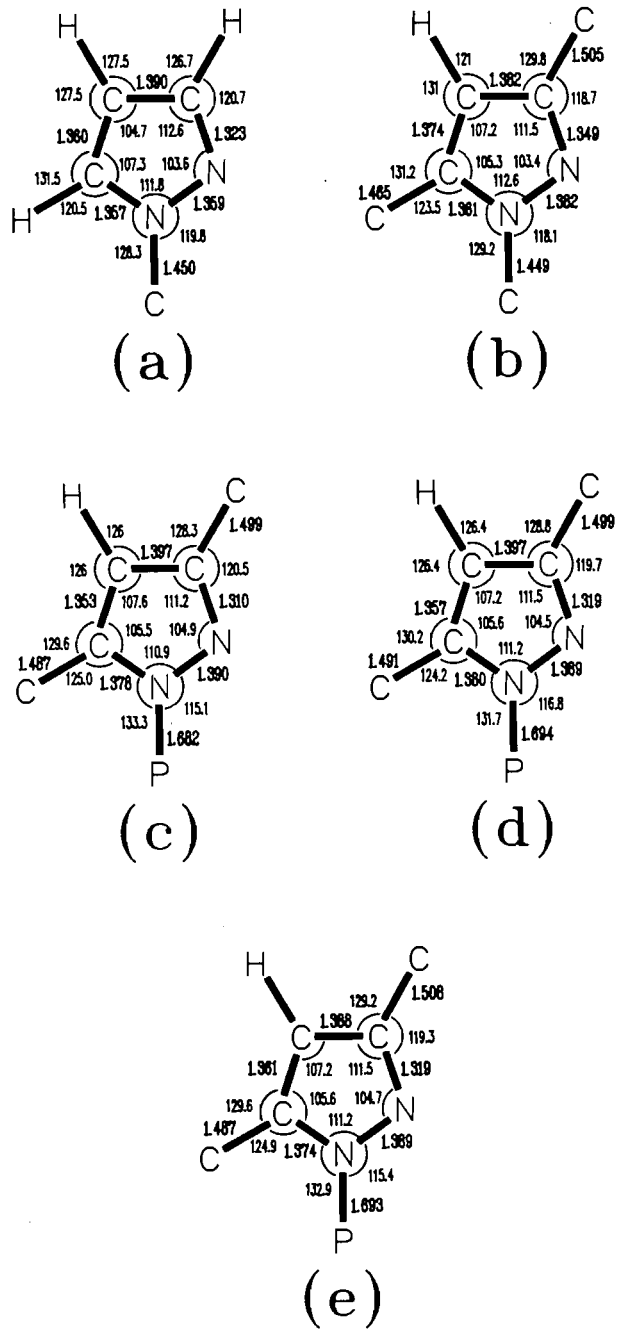

FIG. 8. Summarized pyrazolyl geometry of **1**(*a*), **2**(*b*), **3**(*c*), **5**(*d*), and **6**(*e*).

Can. J. Chem. Downloaded from www.nrcresearchpress.com by 217.78.4.112 on 09/08/12
For personal use only.

TABLE 5. Measured and calculated bond lengths (Å) in $CH_2(H_2pz)_2$, **1**, and $CH_2(Me_2pz)_2$, **2**[a]

Bond	1–2	2–3	3–4	4–5	5–1
Molecule **1**					
Length (calcd.)	1.361	1.327	1.393	1.362	1.367
Length (measd.)	1.359	1.333	1.390	1.360	1.357
Molecule **2**					
Length (calcd.)	1.373	1.343	1.388	1.373	1.359
Length (measd.)	1.382	1.349	1.382	1.374	1.361
Difference **2** − **1**					
Calculated	0.012	0.016	−0.005	0.011	−0.008
Measured	0.023	0.016	−0.008	0.014	0.004

[a]The calculation of σ lengths from atom 2 depends on the lone pair direction, assumed to be along the external bisector of the C—N—N angle.

TABLE 6. Calculated deviations (electrons) from formal charges on ring atoms in 1-methylpyrazole, 1-formylpyrazole, and 1-phosphinylpyrazole, $H_2pzP(H_2)O$[a]

1-Methylpyrazole (*a*)			1-Formylpyrazole, no *exo* conjugation (*b*)			1-Formylpyrazole, with *exo* conjugation (*c*)			1-Phosphinylpyrazole, *s,p*; no *exo* conjugation (*d*)			1-Phosphinylpyrazole, *s,p*; with *exo* conjugation (*e*)			1-Phosphinylpyrazole, *s,p,d*; with *exo* conjugation[b] (*f*)		
σ	π	Total	σ	π	Total	σ	π	Total	σ	π	Total	σ	π	Total	σ	π	Total
0.216	−0.007	0.209	0.201	−0.005	0.196	0.261	−0.180	0.081	0.094	0.188	0.282	0.106	0.157	0.263	0.290	−0.189	0.101

[a]$\alpha_d = -3$ eV.
[b]For $\alpha_d = -1$ eV, σ, π, total are 0.276, −0.128, 0.147 respectively. The total withdrawal is increased, mainly by decreased donations to the π levels.

Pyrazolyl–monophophazene interactions

The dimethylpyrazolyl group attached to a phosphazene ring shows the same structural evidence of bond localization, but the quinonoid shortening of bonds 2–3 and 4–5 is more marked. The pyrazolyl groups in **3** and **5** do not differ significantly, either within or between the separate molecules. Both show significant shortening of the 2–3 and 4–5 bonds relative to **2** (Fig. 10). The pattern of inequalities is the same as in **7**, and, although there are differences in detail, the mean absolute difference between **7** and **1** 0.019 Å) is almost the same as that between **3** and **2** (0.020 Å) and between **5** and **2** (0.018 Å). The interactions between the two rings in **3**, **4**, and **5** evidently have a significant conjugative component, comparable in magnitude to that in **7**. These interactions were modelled initially by calculations on 1-phosphinylpyrazole.

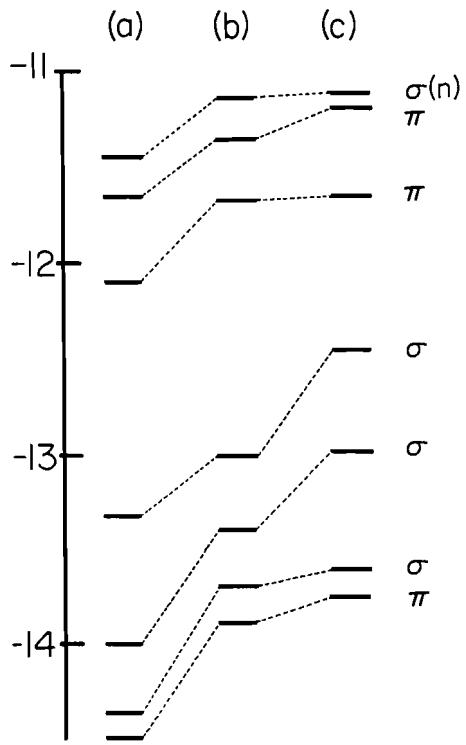

FIG. 9. The calculated highest occupied orbitals (eV) in (*a*) pyrazole, (*b*) 1-methylpyrazole, (*c*) 1,3,5-trimethylpyrazole. The LUMO (π) is higher by 3.58, 3.49, 3.45 eV respectively.

TABLE 7. Bond lengths in bis(1-pyrazolyl)carbonyl (48) relative to **1**

Bond	1–2	2–3	3–4	4–5	5–1
Measured (Å)	0.021	−0.016	0.018	−0.015	0.026
Calculated[a]	0.005	−0.005	0.004	−0.005	0.010
Calculated[b]	0.011	−0.008	0.014	−0.011	0.020

[a]Inductive only.
[b]Inductive plus conjugative effect.

The —H_2PO group differs from the —CHO group in that, in an *sp* basis, σ and π bonding are competitive. In valence-bond terms, all three *p* orbitals are formally required for σ bonding; none are available exclusively for π bonding. Deviations from formal charges are given in Table 6 (*d*, *e*). The ring is now a stronger acceptor, and in the absence of exocyclic N–P conjugation, the phosphinyl group transfers both σ and π electrons. When conjugation is permitted, the electron release to the ring is reduced, but not drastically. The biggest change from 1-formyl to 1-phosphinylpyrazole (*sp* basis, both conjugated) is in the reversal of sign of the large

Can. J. Chem. Downloaded from www.nrcresearchpress.com by 217.78.4.112 on 09/08/12
For personal use only.

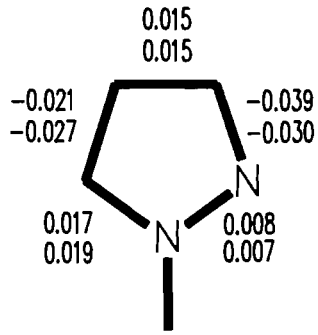

FIG. 10. Differences between average bond lengths (Å) in **3** and **2** (upper figures) and **5** and **2** (lower figures).

component of π charge, from -0.180 to 0.157 electrons (Table 6); the pyrazole ring is now a strong π acceptor. There is little competition from the phosphinyl bond, in which the π population is 0.098, compared with 0.315 for the carbonyl bond. The expected differences from **1** have the wrong pattern and the wrong sign, and are too small numerically. The *sp* basis does not allow the strengthening of the 2–3 and 4–5 bonds found for the dimethylpyrazolylphosphazenes (Fig. 10).

Comparability of phosphinyl and carbonyl compounds is achieved by the introduction of acceptor orbitals at phosphorus, which in the present semiempirical method are valence-shell *d* orbitals. Several comments are required. First, the geometry at phosphorus is non-planar, so that the simple σ/π division loses some of its value; a particular *d* orbital may contibute to bonding of both classes. Second, although π-bond populations can still be defined and assumed proportional to π contraction, the proportionality constant is unlikely to be the same as for $p\pi$–$p\pi$ bonding. Third, there is no agreement on the best *d*-orbital parameters. The exponent was taken to be 1.400, the Coulomb parameters being determined jointly by the assumed VSIE parameters and the electronegativities of the neighboring atoms. The final value, after iteration, was typically 2.5 eV more negative than the initial value (α_d), usually taken to be in the range 0 to -5 eV, the converged value then being about 8–10 eV above the 3*p* orbitals. Although α_d was frequently taken to be -3 eV, the bond populations (as distinct from charge densities) were found to be insensitive to the choice and, in spite of the limitations referred to above, useful conclusions are possible.

TABLE 8. Effect of exocyclic conjugation on π-bond population in $H_2pzP(H_2)O$[a]

	H_2pz ring	N–P	P–O	Total
(*a*)	0.958	0.0	0.106	1.064
(*b*)	0.951	0.043	0.098	1.093
(*c*)	1.020	0.132	0.318	1.470

[a](*a*) No P–N conjugation. (*b*) $p\pi$–$p\pi$ N–P conjugation only. (*c*) $p\pi$–$p\pi$ + $p\pi$–$d\pi$ conjugation: α_d = -1 eV.

We consider the three classes, phosphine oxides, pyrazolyl–monophosphazenes, and the pyrazolylcyclophosphazenes **3–6**. The effect of *d* orbitals on the charge distribution in 1-phosphinylpyrazole $H_2pzP(H_2)O$ is shown in Table 6*f*; compared with the *sp* basis, the phosphoryl group becomes a strong π acceptor rather than a strong π donor, the transfer being coupled with a return of electrons to the σ system of the pyrazole ring. The final distribution is similar to that in 1-formylpyrazole (Table 6). The synergic process by which it is attained is the key to the structural and chemical characteristics of the pyrazolylphosphazenes.

Although no structure of a pyrazolylphosphine oxide has been determined, there is extensive spectroscopic, thermochemical, and structural evidence for conjugative interactions in phosphine oxides R_3PO in which R is an electron-releasing group (50). Table 8 shows that the N–P π population characteristic of a conjugated system is small in an *sp* basis. The introduction of *d* orbitals strengthens this interaction significantly, and the π populations of the phosphoryl bond even more. The calculated π populations in the pyrazole ring show the expected strengthening of the 2–3 and 4–5 bonds, similar to that in 1-formylpyrazole.

More detail on the electronic effects of the pyrazolyl groups is provided by calculations on the monophosphazenes $RP(H_2)NH$ (R = Ph, Cl, Me_2pz) (Table 9) and the methyl derivatives 1-methylpyrazole and 1,3,5-trimethylpyrazole. To a methyl group, the pyrazolyl and dimethylpyrazolyl groups are poorer acceptors than a chlorine atom, their net charges being -0.174, -0.177, and -0.198 (Cl in MeCl). In the monophosphazenes, the negative charge on R increases in the order R = Ph < Cl < Me_2Pz, but although it decreases in the last case as the *d* orbitals are made more electronegative, the pyrazolyl group is still a better acceptor than chlorine. The phenyl group is calculated to be a weak

TABLE 9. Calculated charges and π populations in $RP(H_2)$=NH

R	Ph[b]	Cl[b]	Me_2pz (*sp*)	Me_2pz (*spd*)[a]	Me_2pz (*spd*)[b]
Charge on R	-0.073	-0.106	-0.277	-0.270	-0.208
Charge on P	0.747	0.772	1.271	1.052	0.869
Charge on N(H)	-0.601	-0.539	-0.879	-0.678	-0.577
d population	0.493	0.701	—	0.292	0.611
π populations P—R					
p	0.023	0.030	0.032	0.032	0.040
d	0.036	0.110	—	0.054	0.104
π populations P—N(H)					
p	0.116	0.114	0.096	0.108	0.114
d	0.241	0.254	—	0.185	0.255

[a]α_d = -1 eV.
[b]α_d = -3 eV.

Can. J. Chem. Downloaded from www.nrcresearchpress.com by 217.78.4.112 on 09/08/12
For personal use only.

TABLE 10. Calculated pyrazolyl bond lengths in $Cl_5N_3P_3(H_2pz)$,[a] $F_5N_3P_3(H_2pz)$,[a] and $Me_2pzP(H_2)NH$[b]

Bond	1–2	2–3	3–4	4–5	5–1
$Cl_5N_3P_3(H_2pz)$	1.371	1.332	1.398	1.360	1.370
$F_5N_3P_3(H_2pz)$	1.378	1.330	1.401	1.355	1.378
$Me_2pzP(H_2)NH$	1.383	1.335	1.397	1.364	1.372
Measured (**5**)	1.389	1.319	1.393	1.357	1.380

[a]$\alpha_d = -1.0$ eV.
[b]$\alpha_d = -3.0$ eV.

acceptor, and only weakly conjugated to the phosphazene group (in agreement with experiments (14, 15)). As α_d is made more electronegative, the *d* population and the π components increase greatly, while the positive charge on phosphorus decreases. Conjugation again strengthens, as expected, the 2–3 and 4–5 bonds of the pyrazolyl group at the expense of the others, to an extent which is embodied in the bond-length calculations (Table 10).

Cyclic phosphazenes

The phosphazene ring bonds, also, are affected by interaction with the pyrazolyl group. Although the cyclic phosphazenes **3–6** and even the mono(dimethylpyrazolyl)-cyclotriphosphazene are all too large for direct calculation, their structural and chemical properties can be elucidated by comparison of the effects of chlorine, fluorine, and the pyrazolyl group on the phosphazene ring. Comparative calculations on $N_3P_3H_6$ and $N_3P_3H_5Cl$ show the expected features; electron withdrawal by chlorine (greater than in the monophosphazene) and alternating π-bond populations, the largest being in the bonds to the P(H)Cl group (Table 11). The pyrazolyl group is a better acceptor than chlorine and, for the same α_d, the population alternation is more marked. In $N_3P_3Cl_5(H_2pz)$, the net negative charge on the pyrazolyl group is reduced, but because Cl is more electronegative than H, the scale of the alternation is decreased, though it still has the same sense. In $N_3P_3F_5(H_2pz)$, the negative charge on pyrazole is reduced further, but it is still greater than that on Cl in $N_3P_3H_5Cl$. The most important point is that the sense of the alternation in bond populations is reversed, the π bonds to P(F) (H_2pz) being the weakest. We can conclude that the structural effect of a pyrazolyl group is approximately the mean of those of the chlorine and fluorine atoms, i.e., it behaves as a strongly electronegative group. In view of these results, and the calculated minor effect of dimethylation on the acceptor properties of the pyrazole group, it is surprising that the difference between the Ph_2P—N and N—P $(Me_2pz)_2$ bonds in **6** (0.042 Å) is smaller than the corresponding difference in $Ph_2P_3N_3Cl_4$ (0.060 Å) (38). It may be that the calculational method is inadequate, as it is in predicting the difference between **1** and **2** (Table 5). The calculations nevertheless reproduce satisfactorily the bond lengths in the pyrazole rings of **5** (Table 10).

The remaining structural feature for comment is the length of the inter-ring P—N bond, which should reflect the degree of conjugative interaction between the rings. The (weighted) mean *exo*-P—N bond length in **3**, **4**, and **5** is 1.684 Å (mean derivation 0.009 Å), but the assessment of the π contraction is not straightforward, because the σ-bond length cannot be calculated accurately. We prefer to use a direct comparison, specifically with the structure of (octakisdimethylaminocyclotetraphosphazene)tetracarbonyltungsten (51), in which coordination of one dimethylamido group to tungsten prevents donation of its lone pair to the phosphazene ring. The *exo*-P—N bond length is increased to 1.77 Å. If we take this to be the appropriate σ-bond length, the π contraction in **3**, **4**, and **5** is 0.09 Å, compared with 0.11 Å for the comparison molecule. It is likely that this is an overestimate and we prefer to take 0.06 Å as a probable π contraction, though the quinonoid deformation of the pyrazolyl ring is better evidence of conjugation. The important point, however, is that although the demands of the aromatic sextet reduce the *exo*-P—N π bonding to about half what it might otherwise be, there is still an effective conjugative interaction between the rings.

We discuss two chemical points, reactivity and donor properties. An electronegative substituent on phosphorus increases the mean positive charge on phosphorus and, especially, the charge on the substituted atom. Accelerated nucleophilic attack is thereby promoted and in fact no partially substituted derivatives have yet been reported from the

TABLE 11. Calculated quantities for monosubstituted cyclotriphosphazenes

Substituents on P_3N_3[a]	H_5,Cl [3]	H_5,H_2pz [3]	Cl_5,H_2pz [1]	Cl_5,H_2pz [3]	F_5,H_2pz [1]
Pyrazolyl ring					
Charge on H_2pz	−0.187(Cl)	−0.335	−0.313	−0.265	−0.231
Charge on N(2)(pz)		−0.335	−0.335	−0.331	−0.323
Exo π-bond popn.[b]	0.079	0.125	0.090	0.130	0.136
PN ring: bond P(1)N(1)					
Charge on P(1)[c]	1.012	1.039	1.373	1.133	1.606
π-bond popn.	0.230	0.236	0.199	0.238	0.208
PN ring: bond N(1)P(2)					
Charge on N(1)	−0.745	−0.722	−0.872	−0.731	−0.812
π-bond popn.	0.214	0.212	0.190	0.229	0.232
PN ring: bond P(2)N(2)					
Charge on P(2)	0.941	0.941	1.282	1.046	1.838
π-bond popn.	0.219	0.221	0.192	0.232	0.223
Charge on N(2)	−0.742	−0.738	−0.875	−0.736	−0.812
Mean ring π popn.[c]	0.221	0.223	0.194	0.233	0.221

[a]The number in square brackets is $-\alpha_d$, as used in the VSIE parameters.
[b]For all P—N bonds, $p\pi$–$d\pi$ interactions account for 60–70% of the total bond population.
[c]For $N_3P_3H_6$, P charge = 0.944, ring bond π population = 0.216.

Can. J. Chem. Downloaded from www.nrcresearchpress.com by 217.78.4.112 on 09/08/12
For personal use only.

reaction of a pyrazolide ion with $(NPCl_2)_n$. From Table 11, non-geminal derivatives might be most easily obtainable from reactions with $(NPF_2)_n$. The reactivity of a pyrazolyl–phosphazene bond, once formed, is less simple. In the related compound hexa(imidazolyl)cyclotriphosphazene (**8**), the calculated ligand–PN interactions are almost the same as in the pyrazolyl compounds, as shown by the *exo*-PN bond length (1.680 Å) (52), but **8** is nevertheless much less stable to hydrolysis. The kinetics of the reaction are complex (53), but the first step probably involves the electrophilic interaction of water with the pyridinic nitrogen atom. If the same mechanism applies to the hydrolysis of pyrazolylphosphazenes, the difference between the reactivity of the two series can be ascribed to a difference between electron availability there. Although the calculated negative charge is only 0.04 greater in imidazole, the lone-pair orbital lies 0.82 eV higher (probably because the two nitrogen atoms are further apart) and is expected to interact more strongly with a water molecule. In an apparently similar pair of reactions, *N*-acetylimidazole is hydrolysed 22 times faster than *N*-acetylpyrazole (54), the rates paralleling the base strengths of the parent heterocycles (pK_{BH^+} = 2.47(pzH), 6.95(imH)) (55). The calculations generally support Kauffmann's (56) suggestion that azoles containing more than one N atom bound by way of an N atom correspond to halogen and other good leaving groups.

The same considerations are important to complex formation. Dimethylamidophosphazenes ordinarily coordinate to a positive centre through the nitrogen atoms on the PN ring, the ligands having lost much of their electron density to the ring by conjugation. Such back-donation is sufficiently restricted in **3**–**6** to allow the formation of stable complexes through N(2) (23, 24). We mention two significant features of the calculations. (*a*) Because of the extensive σ withdrawal from the PN ring (simulated in the calculations by a phosphinyl group), the proton affinity of the dimethylpyrazolyl group is greater (by about 0.2 eV) than when it is attached to a methyl group at N(1). (*b*) As the *d* orbitals are made more electronegative, the phosphazene ring tends to be favoured as a protonation site. More detail is given elsewhere (see footnote 5).

Acknowledgements

We are grateful to the Natural Sciences and Engineering Research Council of Canada for financial support and to the University of British Columbia Computing Services for assistance.

1. C. W. Allen. Chem. Rev. **91**, 119 (1991).
2. D. P. Craig and N. L. Paddock. *In* Nonbenzenoid aromatics. Vol. II. *Edited by* J. P. Snyder. Academic Press, New York. 1971. p. 273.
3. N. L. Paddock. Int. Rev. Phys. Chem. **5**, 161 (1986).
4. C. Mihart, M. Mracec, and Z. Simon. Rev. Roum. Chim. **28**, 857 (1983).
5. G. R. Branton, C. E. Brion, D. C. Frost, K. A. R. Mitchell, and N. L. Paddock. J. Chem. Soc. A, 151 (1970).
6. J. K. Jacques, M. F. Mole, and N. L. Paddock. J. Chem. Soc. 2112 (1965).
7. M. Pelavin, D. N. Hendrickson, J. M. Hollander, and W. L. Jolly. J. Phys. Chem. **74**, 1116 (1970).
8. R. A. Wheeler, R. Hoffmann, and J. Strähle. J. Am. Chem. Soc. **108**, 5381 (1986).
9. J.-P. Faucher, J. Devanneaux, C. Leibovici, and J.-F. Labarre. J. Mol. Struct. **10**, 439 (1971).
10. K. A. R. Mitchell, L. Noodleman, and N. L. Paddock. Chem. Phys. Lett. **47**, 265 (1977); L. Noodleman, N. P. C. Westwood, and K. A. R. Mitchell. Chem. Phys. Lett. **58**, 252 (1978).
11. R. C. Haddon. Chem. Phys. Lett. **120**, 372 (1985).
12. K. F. Ferris, P. Friedman, and D. M. Friedrich. Int. J. Quantum Chem. Quantum Chem. Symp. **22**, 207 (1988); K. F. Ferris and C. B. Duke. Int. J. Quantum Chem. Quantum Chem. Symp. **23**, 397 (1989).
13. T. Chivers and N. L. Paddock. Inorg. Chem. **11**, 848 (1972).
14. A. J. Wagner and T. Moeller. J. Inorg. Nucl. Chem. **33**, 1307 (1971).
15. C. W. Allen and J. C. Green. Inorg. Chem. **19**, 1719 (1980).
16. K. D. Gallicano, R. T. Oakley, R. D. Sharma, and N. L. Paddock. ACS Symp. Ser. **171**, 301 (1981).
17. J.-P. Faucher, J.-F. Labarre, and R. A. Shaw. J. Mol. Struct. **25**, 109 (1975).
18. D. Feakins, W. A. Last, and R. A. Shaw. J. Chem. Soc. 4464 (1964).
19. R. D. Sharma, S. J. Rettig, N. L. Paddock, and J. Trotter. Can. J. Chem. **60**, 535 (1982).
20. R. C. Haddon, S. L. Mayo, S. V. Chichester, and J. H. Marshall. J. Am. Chem. Soc. **107**, 7585 (1985).
21. K. Brandt. J. Mol. Struct. **243**, 163 (1991).
22. G. Trinquier. J. Am. Chem. Soc. **108**, 568 (1986).
23. K. D. Gallicano, N. L. Paddock, S. J. Rettig, and J. Trotter. Inorg. Nucl. Chem. Lett. **15**, 417 (1979).
24. K. D. Gallicano and N. L. Paddock. Can. J. Chem. **60**, 521 (1982).
25. L. Nygaard, D. Christen, J. T. Nielsen, E. J. Pedersen, O. Snerling, E. Vestergaard, and G. O. Sørensen. J. Mol. Struct. **22**, 401 (1974).
26. T. La Cour and S. E. Rasmussen. Acta Chem. Scand. **27**, 1845 (1973).
27. F. K. Larsen, M. S. Lehmann, I. Sotofte, and S. E. Rasmussen. Acta Chem. Scand. **24**, 3248 (1970).
28. S. Trofimenko. J. Am. Chem. Soc. **92**, 5118 (1970); S. Juliá, J. Elguero, G.-P. Fayet, and M.-C. Vertut. J. Heterocycl. Chem. **19**, 1141 (1982).
29. P. J. Becker and P. Coppens. Acta Crystallogr. Sect. A: Cryst. Phys. Diffr. Theor. Gen. Crystallogr. **30**, 129 (1974); **30**, 148 (1974); **31**, 417 (1975).
30. P. Coppens and W. C. Hamilton. Acta Crystallogr. Sect. A: Cryst. Phys. Diffr. Theor. Gen. Crystallogr. **26**, 71 (1970).
31. F. R. Thornley and R. J. Nelmes. Acta Crystallogr. Sect. A: Cryst. Phys. Diffr. Theor. Gen. Crystallogr. **30**, 748 (1974).
32. International tables for X-ray crystallography. Vol. IV. Kynoch, Birmingham. 1974, pp. 99–102, 149.
33. V. Schomaker and K. N. Trueblood. Acta Crystallogr. Sect. B: Struct. Crystallogr. Cryst. Chem. **24**, 63 (1968).
34. D. W. J. Cruickshank. Acta Crystallogr. **9**, 747 (1956); **9**, 754 (1956); **14**, 896 (1961).
35. G. J. Bullen. J. Chem. Soc. A, 1450 (1971).
36. R. T. Oakley, N. L. Paddock, S. J. Rettig, and J. Trotter. Can. J. Chem. **55**, 4206 (1977).
37. F. R. Ahmed, P. Singh, and W. H. Barnes. Acta Crystallogr. Sect. B: Struct. Crystallogr. Cryst. Chem. **25**, 316 (1969).
38. N. V. Mani, F. R. Ahmed, and W. H. Barnes. Acta Crystallogr. **19**, 693 (1965).
39. C. W. Allen, J. B. Faught, T. Moeller, and I. C. Paul. Inorg. Chem. **8**, 1719 (1969).
40. M. W. Dougill. J. Chem. Soc. 5471 (1961).
41. M. J. Begley, D. B. Sowerby, and R. J. Tillott. J. Chem. Soc. Dalton Trans. 2527 (1974).
42. H. Zoer and A. J. Wagner. Acta Crystallogr. Sect. B: Struct. Crystallogr. Cryst. Chem. **28**, 252 (1972).
43. R. Hazekamp, T. Migchelsen, and A. Vos. Acta Crystallogr. **15**, 539 (1962).

Can. J. Chem. Downloaded from www.nrcresearchpress.com by 217.78.4.112 on 09/08/12
For personal use only.

44. A. J. Wagner and A. Vos. Acta Crystallogr. Sect. B: Struct. Crystallogr. Cryst. Chem. **24**, 707 (1968).
45. H. McD. McGeachin and F. R. Tromans. J. Chem. Soc. 4777 (1961).
46. M. J. S. Dewar and H. N. Schmeising. Tetrahedron. **11**, 96 (1960).
47. L. Salem. Molecular orbital theory of conjugated systems. W. A. Benjamin, Inc., Reading, Mass. 1966. pp. 139–140.
48. M. Belluce, F. W. B. Einstein, L. Peterson, and P. L. Vogel. Acta Crystallogr. Sect. B: Struct. Crystallogr. Cryst. Chem. **33**, 266 (1977).
49. Interatomic distances. Supplement. Chem. Soc. Spec. Publn. 18, 1965.
50. N. L. Paddock. Q. Rev. Chem. Soc. **18**, 168 (1964).
51. H. P. Calhoun, N. L. Paddock, and J. Trotter. J. Chem. Soc. Dalton Trans. 2708 (1973).
52. R. J. Ritchie, T. J. Fuller, and H. R. Allcock. Inorg. Chem. **19**, 3842 (1980).
53. H. R. Allcock and T. J. Fuller. J. Am. Chem. Soc. **103**, 2250 (1981).
54. H. A. Staab. Angew. Chem. Int. Ed. Engl. **1**, 351 (1962); W. Driessen and P. L. A. Everstijn. Inorg. Chim. Acta, **41**, 179 (1980).
55. A. Albert. *In* Physical methods in heterocyclic chemistry. Vol. 1. Academic Press, New York. 1963. p. 97.
56. T. Kauffmann. Angew. Chem. Int. Ed. Engl. **10**, 743 (1971).

Can. J. Chem. Downloaded from www.nrcresearchpress.com by 217.78.4.112 on 09/08/12
For personal use only.

L'ion positif géminé intervient-il sur le destin de l'électron piégé incomplètement relaxé dans les liquides polaires irradiés?

J.-P. JAY-GERIN

Groupe du Conseil de recherches médicales du Canada en sciences des radiations, Département de médecine nucléaire et de radiobiologie, Faculté de médecine, Université de Sherbrooke, Sherbrooke (Québec), Canada J1H 5N4

ET

C. FERRADINI

Laboratoire de chimie-physique (Unité associée de recherche n° 400 du Centre national de la recherche scientifique), Université René-Descartes, 45, Rue des Saints-Pères, 75270 Paris CEDEX 06, France

Reçu le 8 août 1991[1]

J.-P. JAY-GERIN et C. FERRADINI. Can. J. Chem. **70**, 1869 (1992).

Un modèle concernant l'influence possible de l'ion positif géminé sur le destin de l'électron piégé incomplètement relaxé (e_{ir}^-) dans les liquides polaires irradiés est proposé. Ce modèle est basé sur l'éjection, par un mécanisme d'effet tunnel et (ou) de saut de piège à piège dans le champ coulombien du cation, des électrons occupant des états localisés peu profonds préexistant dans le solvant au-dessous du bas de la bande de conduction de celui-ci. Les électrons éjectés pourraient soit se recombiner avec l'ion positif géminé, soit se piéger à nouveau. Globalement, le vidage des pièges peu profonds se ferait au profit des pièges plus profonds, contribuant ainsi à la diminution de la partie infra-rouge du spectre d'absorption de l'électron traduisant les tout premiers stades de la solvatation. Un tel processus impliquerait donc l'existence d'un maximum du spectre d'absorption de l'électron e_{ir}^-.

J.-P. JAY-GERIN and C. FERRADINI. Can. J. Chem. **70**, 1869 (1992).

A model is proposed concerning the influence of the parent positive ion on the fate of the incompletely relaxed trapped electron (e_{ir}^-) in irradiated polar liquids. This model is based on the release, by a tunneling and (or) a trap-hopping mechanism in the Coulomb field of the cation, of the electrons captured in preexisting shallow localized states below the bottom of the conduction band of the solvent. The released electrons would either recombine with the parent positive ion or get retrapped. The net effect would be an accumulation of electrons in deeper traps. The removal of weakly trapped electrons would contribute to the decrease of the infrared part of the optical absorption spectrum during the very early time dynamics of electron solvation. Such a process would imply, as a consequence, the existence of a maximum of the e_{ir}^- absorption spectrum.

Can. J. Chem. Downloaded from www.nrcresearchpress.com by 217.78.4.112 on 09/08/12
For personal use only.

De nombreux travaux de radiolyse, tant théoriques qu'expérimentaux, concernant le processus de solvatation de l'électron dans les liquides polaires, ont été développés (pour des revues d'ensemble récentes, voir, par exemple, réfs. 1–4) sans toutefois que les mécanismes alors mis en jeu soient complètement élucidés. Bien que la recombinaison entre l'ion positif géminé et l'électron thermalisé ait toujours été considérée comme se produisant à un stade très primaire (voir, par exemple, réf. 2), un tel processus n'a été que rarement invoqué pour expliquer les anomalies spectrales ou cinétiques fréquemment observées dans cette même échelle de temps. Truong (5) a cependant suggéré que, dans certains verres non polaires irradiés, la décroissance rapide d'une partie des électrons piégés pourrait être attribuée au fait que ces électrons se trouvaient au voisinage de l'ion positif géminé et que la recombinaison par effet tunnel se trouvait ainsi facilitée. Une hypothèse analogue a été proposée par van Leeuwen *et al.* (6) pour expliquer le déclin de la composante absorbant dans le rouge du spectre de l'électron piégé mesuré dans un verre 8 M en NaOH. D'autres suggestions reposant sur des bases différentes ont également été émises (pour une revue d'ensemble récente, voir, par exemple, réf. 7), ainsi la partie «rouge» du spectre a été attribuée à l'électron piégé dans un environnement mettant en jeu des molécules d'eau non liées dans le verre (8). Cette dernière hypothèse est néanmoins difficile à généraliser à tous les cas pour lesquels des observations analogues ont été faites et en particulier l'eau et certains alcools en phase liquide.

Nous envisageons ici un modèle, inspiré de celui déjà proposé dans le cas de la radiolyse de solides amorphes (voir, par exemple, réfs. 9–11), visant à prendre en compte l'influence possible de l'ion positif lors de la description du spectre d'absorption de l'entité négative dans les phases liquides pendant les tout premiers stades de la solvatation de celle-ci.

Les conséquences spatiales et temporelles de la présence de l'ion positif peuvent être schématisées de la manière suivante (voir figure 1).

La figure 1*a* représente une distribution typique des distances de thermalisation d'un électron secondaire, l'ion positif géminé étant situé à l'origine des axes. À titre d'exemple, rappelons que, pour l'eau liquide irradiée, la distance (la plus probable) de thermalisation est estimée à environ 20 Å (voir, par exemple, réfs. 2, 12 et 13).

Une fois thermalisé au bas de la bande de conduction du solvant (que l'on dénote généralement par l'énergie V_0 en référence au niveau du vide), l'électron se localise dans un des pièges préexistants de celui-ci. Il devient alors un électron dit «incomplètement relaxé», noté e_{ir}^-, par opposition à l'électron après solvatation dit «complètement relaxé» (2).

[1]Révision reçue le 22 avril 1992.

Can. J. Chem. Downloaded from www.nrcresearchpress.com by 217.78.4.112 on 09/08/12
For personal use only.

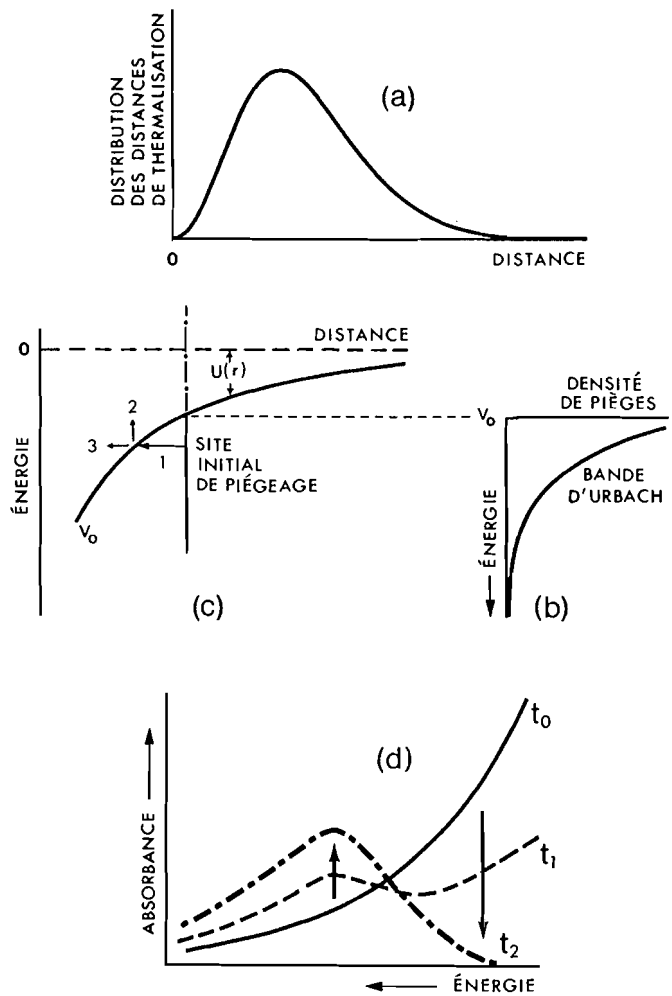

FIG. 1. (*a*) Allure de la distribution des distances de thermalisation en fonction de la distance entre l'électron éjecté et l'ion positif géminé, ce dernier étant supposé à l'origine des axes. (*b*) Allure de la distribution énergétique des pièges préexistants du solvant, décrite par une bande d'Urbach. Cette bande d'états localisés s'étend au-dessous du bas de la bande de conduction, dénoté par V_0, à l'intérieur de la bande d'énergie interdite du liquide. Sa décroissance suit une loi sensiblement exponentielle en fonction de l'énergie des états de piège. Cette loi est, bien sûr, caractéristique du solvant considéré. (*c*) Illustration de l'action de l'ion positif géminé. La courbe en trait plein montre la variation, due au champ coulombien $U(r)$ créé par l'ion positif, du bas de la bande de conduction V_0 du liquide en fonction de la distance r à celui-ci. L'échappement vers la bande de conduction, par effet tunnel et (ou) par saut de piège à piège à travers la barrière de potentiel, d'un électron localisé initialement dans un piège peu profond de la bande d'Urbach est indiqué par la fléche 1. L'électron ainsi éjecté à V_0 est quasi-libre. Il peut alors soit se recombiner avec le cation parent, soit se relocaliser sur un site voisin après un nouvel échantillonnage de l'ensemble de la distribution des pièges de la bande d'Urbach (nous supposons bien sûr que chaque piège possède la même section efficace de capture électronique). Ces deux processus ont été indiqués schématiquement par les fléches 2 et 3. Comme la probabilité d'échappement d'un électron piégé est d'autant plus faible que la profondeur du piège est plus grande, on voit ainsi que, globalement, le processus favorise le vidage des pièges de faible énergie au profit des pièges de grande énergie. (*d*) Évolution du spectre d'absorption de l'électron piégé incomplètement relaxé (e_{ir}^-) en fonction du temps. Le temps initial t_0 correspond au remplissage «primaire» uniforme de tous les pièges préexistants de la bande d'Urbach du solvant. Les temps t_1 et t_2 montrent la diminution progressive de l'absorbance dans la partie «rouge» du spectre par vidage des pièges de faible énergie et l'augmentation concomitante de celle-ci dans la partie «bleue» due au remplissage des pièges de grande énergie. Nous supposons ici que l'absorption optique observée résulte d'une transition électronique directe état lié – continuum à V_0 (voir, par exemple, réf. 19). L'intervention de l'ion positif géminé sur le destin de l'électron avant relaxation impliquerait donc, selon ce processus, l'existence d'un maximum du spectre d'absorption de l'électron e_{ir}^-, de sorte que le passage subséquent de l'électron e_{ir}^- à l'électron solvaté serait facilité.

La distribution énergétique de ces pièges peut être décrite par une bande d'Urbach, caractéristique des milieux désordonnés et située à l'intérieur de la bande d'énergie interdite du liquide, juste au-dessous du bas de la bande de conduction (14–16). De nombreux travaux ont montré que la densité d'états localisés dans cette bande d'Urbach décroissait à partir de V_0 selon une loi sensiblement exponentielle en fonction de l'énergie des états de piège (figure 1*b*) (voir, par exemple, réfs. 17–19).

Un électron ainsi piégé se trouve soumis à l'action de l'ion positif, régie par la loi coulombienne $U(r) = -|e|/(4\pi\varepsilon_0)\varepsilon r$, où e est la charge de l'électron, ε_0 la permittivité du vide, ε la constante diélectrique du milieu et r la distance séparant les deux charges (figure 1*c*). Cette action confère à l'électron e_{ir}^- une probabilité d'être éjecté de son piège par un mécanisme d'effet tunnel et (ou) de saut de piège à piège à travers la barrière de potentiel qui lui est offerte dans le champ coulombien du cation, et d'être ainsi ramené à l'état quasi-libre dans la bande de conduction à une distance plus rapprochée du cation. Compte-tenu de la forme sensiblement «triangulaire» de la barrière, cette probabilité est évidemment d'autant plus grande que la profondeur du piège est plus faible. Chaque fois qu'un électron est ainsi éjecté, il peut soit se recombiner avec l'ion positif géminé, soit se localiser à nouveau dans un piège de la bande d'Urbach après avoir eu une nouvelle chance d'échantillonner l'ensemble de la distribution des pièges existants. En supposant que chaque piège possède la même section efficace de capture électronique, le processus global favorise ainsi le vidage des pièges de faible énergie au profit du remplissage des pièges de grande énergie; l'absorption correspondante manquera donc dans le spectre de l'électron piégé, incomplètement relaxé. Typiquement, on peut estimer qu'un tel processus de vidage interviendrait à des énergies de piège inférieures ou de l'ordre de l'électron-volt.

L'évolution du spectre d'absorption de l'électron e_{ir}^- est schématisée sur la figure 1*d* pour trois temps t_0, t_1 et t_2. Le temps le plus initial, t_0, correspond au remplissage «primaire» uniforme des pièges préexistants de la bande d'Urbach du solvant. Les temps ultérieurs t_1 et t_2 montrent la disparition progressive, selon le processus précédent, des électrons faiblement piégés tandis que la redistribution conduit à une augmentation de la densité optique aux grandes énergies. Un tel processus impliquerait donc l'existence d'un maximum du spectre d'absorption de l'électron e_{ir}^- dans les solvants polaires irradiés. La plupart des expériences menées en radiolyse pulsée, autant dans le cas des alcools liquides à 300 K ou refroidis à basse température (20–24) que dans le cas d'alcools solides (7, 25, 26), n'ont toutefois pas permis, à ce jour, la mise en évidence d'un maximum du spectre des électrons avant relaxation. En raison surtout de leurs limitations à la région infra-rouge en deçà de 800–1300 nm, ces

expériences n'ont en fait montré, aux temps les plus courts, qu'une absorbance croissant de façon monotone dans toute la gamme des longueurs d'onde étudiées. Signalons cependant que Klassen et Teather (27), grâce à des mesures précises s'étendant jusqu'à 2200 nm, semblent avoir nettement établi l'existence d'un tel maximum, vers 2000 nm (~0,62 eV), dans le spectre «initial» à 100 ns des électrons piégés dans des verres irradiés de propanol-1, butanol-1 et pentanol-1 à 6 K.

Le destin des électrons avant relaxation dans les liquides irradiés et principalement l'évolution spectrale aux faibles énergies pourraient donc être expliqués, non pas uniquement par la dynamique de solvatation, mais aussi par l'action de l'ion positif géminé. Un tel effet devrait également être pris en compte dans l'interprétation des résultats concernant la dynamique de la solvatation de l'électron observée en photolyse ultra-rapide, compte-tenu de la proximité, au moment de leur création, de l'électron piégé et du cation parent (28). Le passage de l'électron e_{ir}^- à l'électron solvaté se trouverait ainsi favorisé. Les mesures récentes de Long *et al.* (29) en photolyse femtoseconde semblent d'ailleurs avoir révélé, dans le cas de l'eau, la présence d'un maximum dans le spectre d'absorption de l'électron e_{ir}^- situé vers 900 nm (~1,4 eV) à 180 fs. Ces auteurs ont de plus remarqué que ce spectre présentait une certaine similarité avec celui de l'électron hydraté, ce dernier se formant en 540 fs (29). Il est d'autre part fort probable que l'intervention de l'ion positif géminé dans les tout premiers stades de la solvatation conduirait à une non-conservation du nombre total d'électrons, empêchant ainsi l'observation d'un point isobeste. La possibilité pour l'électron e_{ir}^- de réagir chimiquement avec l'eau et les alcools avant solvatation, telle qu'évoquée précédemment par les auteurs (4, 30), pourrait aussi amplifier la non-conservation du nombre d'électrons. La question de l'existence ou non d'un point isobeste dans le cas de l'eau liquide fait actuellement l'objet d'une controverse (31, 32). Enfin, comme il a déjà été souligné auparavant (28, 33), le modèle proposé ici montre à nouveau l'intérêt d'inclure le rôle de l'ion positif dans les calculs de simulation numérique de la dynamique de solvatation de l'électron.

Remerciements

Les auteurs tiennent à exprimer leurs remerciements au Professeur René Voltz et au Dr Annette Bernas pour de très intéressantes discussions. Ce travail a été réalisé avec l'aide financière du Conseil de Recherches Médicales du Canada et du Programme de Subventions à la Recherche Coopérative de l'OTAN (subvention n° 91/0996).

1. N. V. Klassen. *Dans* Radiation chemistry. Principles and applications. *Éditeurs* : Farhataziz et M. A. J. Rodgers. VCH Publishers, New York, N.Y. 1987. pp. 29–64.
2. G. R. Freeman. *Dans* Kinetics of nonhomogeneous processes. *Éditeur* : G. R. Freeman. Wiley, New York, N.Y. 1987. pp. 19–87 et 277–304.
3. E. M. Itskovitch, A. M. Kuznetsov et J. Ulstrup. *Dans* The chemical physics of solvation. Part C. Solvation phenomena in specific physical, chemical, and biological systems. *Éditeurs* : R. R. Dogonadze, E. Kálmán, A. A. Kornyshev et J. Ulstrup. Elsevier, Amsterdam. 1988. pp. 275–327.
4. J.-P. Jay-Gerin et C. Ferradini. *Dans* Excess electrons in dielectric media. *Éditeurs* : C. Ferradini et J.-P. Jay-Gerin, CRC Press, Boca Raton, Fla. 1991. pp. 259–285.
5. T. B. Truong. Chem. Phys. Lett. **26**, 400 (1974).
6. J. W. van Leeuwen, M. G. J. Heijman, H. Nauta et G. Casteleijn. J. Chem. Phys. **73**, 1483 (1980).
7. J. Kroh. *Dans* Pulse radiolysis. *Éditeur* : Y. Tabata. CRC Press, Boca Raton, Fla. 1991. pp. 357–396.
8. G. V. Buxton, M. Medley, G. A. Salmon, P. J. Baugh, R. Catterall et P. B. Williams. J. Chem. Soc. Faraday Trans. 1, **81**, 3067 (1985).
9. H. Tsujikawa, K. Fueki et Z. Kuri. Bull. Chem. Soc. Jpn. **38**, 2210 (1965).
10. A. J. Doheny et A. C. Albrecht. Can. J. Chem. **55**, 2065 (1977).
11. R. F. Khairutdinov, K. I. Zamaraev et V. P. Zhdanov. *Dans* Electron tunneling in chemistry. Chemical reactions over large distances. *Éditeur* : R. G. Compton. Elsevier, Amsterdam. 1989. pp. 161–224.
12. G. R. Freeman. J. Chim. Phys. **88**, 803 (1991).
13. N. V. Klassen. J. Chim. Phys. **88**, 747 (1991).
14. F. Urbach. Phys. Rev. **92**, 1324 (1953).
15. M. V. Kurik. Phys. Status Solidi A, **8**, 9 (1971).
16. C. E. Krohn, P. R. Antoniewicz et J. C. Thompson. Surf. Sci. **101**, 241 (1980).
17. D. Monroe et M. A. Kastner. Phys. Rev. B, **33**, 8881 (1986).
18. V. Sa-Yakanit et H. R. Glyde. Comments Condens. Matter Phys. **13**, 35 (1987).
19. C. Houée-Levin et J.-P. Jay-Gerin. J. Phys. Chem. **92**, 6454 (1988) et références citées.
20. J. H. Baxendale et P. Wardman. Nature (London), **230**, 449 (1971); J. Chem. Soc. Faraday Trans. 1, **69**, 584 (1973).
21. W. J. Chase et J. W. Hunt. J. Phys. Chem. **79**, 2835 (1975).
22. L. Gilles, M. R. Bono et M. Schmidt. Can. J. Chem. **55**, 2003 (1977).
23. K. Okazaki et G. R. Freeman. Can. J. Chem. **56**, 2305 (1978); **56**, 2313 (1978).
24. G. A. Kenney-Wallace et C. D. Jonah. J. Phys. Chem. **86**, 2572 (1982).
25. J. T. Richards et J. K. Thomas. J. Chem. Phys. **53**, 218 (1970).
26. J. H. Baxendale et P. H. G. Sharpe. Int. J. Radiat. Phys. Chem. **8**, 621 (1976).
27. N. V. Klassen et G. G. Teather. J. Phys. Chem. **87**, 3894 (1983).
28. E. Keszei et J.-P. Jay-Gerin. Can. J. Chem. **70**, 21 (1992) et références citées.
29. F. H. Long, H. Lu et K. B. Eisenthal. Phys. Rev. Lett. **64**, 1469 (1990).
30. C. Ferradini et J.-P. Jay-Gerin. Chem. Phys. Lett. **167**, 371 (1990).
31. F. H. Long, H. Lu, X. Shi et K. B. Eisenthal. Chem. Phys. Lett. **185**, 47 (1991).
32. S. Pommeret, A. Antonetti et Y. Gauduel. J. Am. Chem. Soc. **113**, 9105 (1991) et références citées.
33. E. Keszei, T. Goulet, J.-P. Jay-Gerin et C. Ferradini. J. Chim. Phys. **88**, 759 (1991).

Can. J. Chem. Downloaded from www.nrcresearchpress.com by 217.78.4.112 on 09/08/12
For personal use only.

Ted Schaefer, Kerry J. Cox, and Rudy Sebastian. The conformational distribution of 2-cyanobenzaldehyde and 3-cyanobenzaldehyde in solution and in the vapor. Can. J. Chem **69**, 1039 (1991).

In the fourth column of Table 1 the spectral data are incorrect. The correct Table 1 is presented here. There are two consequences. First, the fractional population of the *o-trans* conformer in CS_2 solution is now 0.55(2) instead of 0.52(2) and, in the vapor, is now 0.58(2) instead of 0.52(2). Second, the solvent dependence of the intraring proton coupling constants in 3-cyanobenzaldehyde, while present, is now similar to that observed for 2-cyanobenzaldehyde and not significantly larger, as previously stated.

TABLE 1. The ^{1}H nmr spectral data for 2-cyanobenzaldehyde and 3-cyanobenzaldehyde at 300 K

Parameter	Compound			
	2CNB (CS_2)[a]	2CNB (acetone)[b]	3CNB (CS_2)[a]	3CNB (acetone)[b]
ν(CHO)	3099.799[c]	3083.554	2999.263	3036.289
ν_2	—	—	2416.034	2493.900
ν_3	2320.561	2400.530	—	—
ν_4	2304.404	2375.044	2345.090	2430.330
ν_5	2312.081	2387.770	2292.051	2356.567
ν_6	2399.714	2439.262	2412.245	2474.964
$^3J_{34}$	7.709(2)[d]	7.703	—	—
$^3J_{45}$	7.520	7.602	7.686	7.735
$^3J_{56}$	7.847	7.797	7.773(2)	7.820
$^4J_{24}$	—	—	1.670	1.701
$^4J_{26}$	—	—	1.620	1.623
$^4J_{35}$	1.229(2)	1.206	—	—
$^4J_{46}$	1.340(2)	1.307	1.248	1.211
$^5J_{25}$	—	—	0.641(2)	0.642
$^5J_{36}$	0.588	0.562	—	—
^4J(2,CHO)	—	—	−0.076	−0.072
^4J(6,CHO)	−0.099	−0.130	−0.112	−0.115
^5J(3,CHO)	0.098	0.378	—	—
^5J(5,CHO)	0.796	0.480	0.476	0.451
^6J(4,CHO)	−0.010(2)[e]	−0.009[f]	−0.003[g]	−0.001[h]
calcd. transitions	100	92	88	80
assigned transitions	72	72	77	73
peaks observed	66	73	63	62
largest difference	0.008	0.005	0.004	0.002
Root-mean-square deviation	0.003	0.002	0.002	0.001

[a]A saturated solution in CS_2, being considerably less than 2 mol% in 2CNB or 3CNB, containing also 10 mol% of C_6D_{12}, and 0.5 mol% of TMS.

[b]4.0 mol% in acetone-d_6, containing also 0.5 mol% of TMS.

[c]The ^{1}H nmr chemical shifts are in Hz at 300.135$_2$ MHz to high frequency of internal TMS.

[d]Standard deviations in the last significant figure are all less than or equal to 0.001, except for those given in parentheses.

[e]Simulations with various values imply that $-0.020 < {}^6J(4,CHO) < 0.00$ Hz.

[f]Appears to be negative or, possibly, zero, by simulation; see Fig. 1.

[g]Simulations suggest $-0.015 < {}^6J(4,CHO) < 0.020$ Hz.

[h] Again, spectral simulations imply that $-0.010 < {}^6J(4,CHO) < 0.010$ Hz.

Can. J. Chem. Downloaded from www.nrcresearchpress.com by 217.78.4.112 on 09/08/12
For personal use only.

0198C0910

Studies of complex formation from permittivity measurements: a statistical reexamination

OTTO EXNER

Institute of Organic Chemistry and Biochemistry, Czechoslovak Academy of Sciences, 166 10 Prague, Czechoslovakia

Received May 1, 1991[1]

OTTO EXNER. Can. J. Chem. **70**, 1873 (1992).

Permittivity measurements on solutions of two compounds present in a variable ratio may reveal complex formation: both the equilibrium constant and the dipole moment of the complex can be in principle estimated. However, an incorrect statistical treatment involving transformation of variables is used quite often, for example, in the classical method of Few and Smith. In this case the estimates obtained are usually biased, or loaded with such a great uncertainty that they are practically worthless. The results of numerous papers, even some recent ones, are thus completely at variance with facts. This is shown in this paper by recalculating equilibrium constants and dipole moments of the complex in 17 examples from the literature. Simultaneously, a correct and simple statistical procedure is suggested. The danger of an incorrect and (or) incomplete statistical treatment may be encountered, for the same reason, even in other, quite different, areas.

OTTO EXNER. Can. J. Chem. **70**, 1873 (1992).

Des mesures de permittivité effectuées sur deux composés présents à des rapports variables peut permettre de déceler la formation de complexes : on peut en principe évaluer la constante d'équilibre ainsi que le moment dipolaire du complexe. Toutefois, un traitement statistique erroné, impliquant la transformation de variables, est souvent utilisé, comme dans la méthode classique de Few et Smith. Dans ce cas, les évaluations obtenues sont généralement biaisées ou elles comportent de telles incertitudes qu'elles sont pratiquement inutiles. Les résultats de plusieurs études antérieures, même de études récentes, diffèrent de la réalité. Dans ce travail, on démontre ce fait en recalculant les constantes d'équilibre et les moments dipolaires de complexes rapportés dans 17 exemples cités dans la littérature. Simultanément, on suggère une méthode statistique simple et correcte. Enfin, le danger d'un traitement statistique incorrect et (ou) incomplet peut être rencontré, pour la même raison, dans d'autres domaines très différents.

[Traduit par la rédaction]

Dielectric measurements have been used many times for detecting complex formation, either of the same or of different molecules (1). In the former case, the permittivity ϵ of a solution is measured by the dependence on concentration (expressed as the weight fraction w_2): three parameters, μ_M, μ_D, K, can be in principle estimated from eq. [1] where the function f has been theoretically derived (2–6). In the latter case (e.g., refs. 7–11) solutions of two components, A and B, are prepared in a variable ratio and eq. [2] contains four parameters, μ_A, μ_B, μ_{AB}, and K.

$$[1] \quad \epsilon = f(w_2, \mu_M, \mu_D, K)$$

$$[2] \quad \epsilon = f(w_A, w_B, \mu_A, \mu_B, \mu_{AB}, K)$$

Of all the parameters the dipole moments of the dimer, μ_D, or of the complex, μ_{AB}, are most valuable while the equilibrium constant K may also be determined by other, possibly more efficient, methods. The dipole moments of the components, μ_A and μ_B, are always obtainable from separate measurements and can be considered as known in eq. [2]: sometimes this holds also for the dipole moment of the monomer, μ_M. Nevertheless, μ_D and K in eq. [1] or μ_{AB} and K in eq. [2] are as a rule estimated simultaneously from the same set of data. This introduces serious statistical problems. Our recent reinvestigation (12, 13) revealed that almost all the values of K and μ_D published to date (e.g., refs. 2–4) are completely wrong due to two defects in the statistical processing. On the one hand eq. [1] was rearranged (2, 4) so that the same variable appeared on both sides; on the other hand the errors of the results were underestimated and their mutual dependence was not accounted for (6).

The whole problem has much broader consequences than those concerning dipole moments or complexes: it is a general problem of correct statistical processing of experimental data, in particular of the use or misuse of the linear regression. For this reason we considered this problem worth one more paper, in which we extend our criticism to the measurements of complex formation according to eq. [2]. Compared to eq. [1], this case seems to be more favourable since the weight fractions w_A and w_B can be varied independently and the data set obtained is more extensive. Nevertheless, some rearrangements of the equation had also been used, with the result that the statistical estimates are biased and their errors underestimated. This is the case with the classical method of Few and Smith (8), which has been used many times in the literature. The approach may be explained using three recent papers from this journal (9–11) that have the advantage of giving explicitly all the necessary data. The measurements are divided into subsets, each with a constant excess (w_B) of the component B. For each subset, the polarization P_A^* is obtained from the experimental permittivities with variable component A, considering B provisionally as a component of the solvent. Values of P_A^* are then input in the regression eq. [3] where P_A' is the value for $w_B = 0$, and P_B is determined separately on pure B. Equation [3] may be viewed as an implicit form of the general equation [2] since P_A^* involves ϵ and w_A.

$$[3] \quad \underbrace{\frac{1}{P_A^* - P_A'}}_{y} = \underbrace{\frac{1}{P_{AB} - P_A' - P_B}}_{\text{intercept}} + \underbrace{\frac{M_B}{K(P_{AB} - P_A' - P_B)}}_{\text{slope}} \underbrace{\frac{1}{w_B d}}_{x}$$

From the intercept of the regression one gets P_{AB} and from it the dipole moment of the complex μ_{AB}. From the slope one

[1]Revision received March 20, 1992.

Can. J. Chem. Downloaded from www.nrcresearchpress.com by 217.78.4.112 on 09/08/12
For personal use only.

Can. J. Chem. Downloaded from www.nrcresearchpress.com by 217.78.4.112 on 09/08/12
For personal use only.

gets K if P_{AB} is already known. The question is whether the premises of a linear regression (see, for example, ref. 14) are met. The explanatory variable x may be considered as a practically exact quantity since its combined error would be less than 0.1% according to the estimated errors (8) of w_B and d. However, the errors in the response function y are not independent of x but increase with decreasing concentration. In the examples of Table 1 this estimated rise might be at least from 1 to 3% in example 4, but from 4 to 100% in example 3. The measurements at the lowest concentrations could be better omitted but the number of degrees of freedom would be reduced too much. Another improvement with the same consequence was estimating P'_A in eq. [3] as the third disposable parameter (10), instead of using the experimental value measured with the pure component A. This value P'_A was essentially arbitrary since optimizing three parameters on the basis of five measurements cannot be trustworthy.

In this paper we have recalculated, according to a statistically correct procedure, several examples from the literature, where the method of Few and Smith (8) was applied. Our intention was to put right the previous erroneous results and to show clearly the difference between a correct and incorrect statistical treatment. Particular attention was given to recent papers (9–11) since it is important to stop proliferation of the error. It was not our intention to recalculate all the examples appearing in the literature: this was not even possible since the original data are not always published.

Results and discussion

Our approach to the problem will proceed in three steps:

1. Checking the calculated values of K and P_{AB} given in the literature (8–11, 15–20).

2. Suggesting an acceptable statistical method for unbiased estimation of these parameters.

3. Estimating the errors of these parameters with respect to their mutual dependence.

1. There is a simple and efficient procedure for testing any theory, with or without optimized parameters. It requires that we calculate back the expected original experimental values, as they should be to correspond to the theory exactly, and to compare with the values actually measured (12, 13, 21, 22). In our case the value of P^*_A may be taken as the original experimental quantity since it is obtained from independent experiments with a reasonably constant error. In this way we calculated the expected values P^*_A in 17 systems from the literature. The standard deviations, s, from the values actually measured are listed in the last column of Table 1, last line in each section. (Table 1 is divided into sections: the first line in each section represents the recalculation we consider our best one, the last line reproduces the parameters given in the literature and the pertinent standard deviation calculated by us.) The values of s range from 0.28 to as much as 206 cm^3. With respect to the estimated experimental error, less than 1 cm^3, values up to 1.5 cm^3 could be acceptable. It follows that in one half of all examples there is no fit of the theory with experiments. Note still that for a comparison not only the overall standard deviation is important but also the distribution of the errors on the individual points (see later Figs. 1 and 2).

2. The suggested statistical treatment is still based on the method of least squares but minimizes the sum of squares (SSQ) in P^*_A according to eq. [4], not in $1/(P^*_A - P'_A)$. The optimum values of the parameters K and P_{AB} can be calculated by successive approximations. For an assumed value of K one gets the corresponding best value of P_{AB} (i.e., optimized for this given K) by differentiating eq. [4] with respect to P_{AB}, eq. [5]. The corresponding SSQ and hence the standard deviation are given by eq. [4]. The procedure is repeated for various values of K to get the minimum SSQ: this may be easily programmed.

$$[4]\quad SSQ = \sum (P^*_A - P^*_A, \text{calc})^2 = \sum \left(P^*_A - P'_A - \frac{K(P_{AB} - P'_A - P_B)}{K + M_B/w_B d}\right)^2 = \min$$

$$[5]\quad P_{AB} = P'_A + P_B + \sum \frac{P^*_A - P'_A}{K + M_B/w_B d} \Big/ K \sum \frac{1}{(K + M_B/w_B d)^2}$$

In this way the optimum values of K and P_{AB} as well as the corresponding standard deviations were calculated for the 17 examples mentioned. The results are given in Table 1, first line of each section. Of course, the standard deviations must be smaller than those based on literature data since they are least-squares estimates (the same criterion both for optimization and estimation of accuracy). However, the difference is sometimes tremendous, e.g., in examples 11, 14, and 15. In these cases the calculations used in the literature have nothing in common with reality, as seen very objectively from a graphical comparison of experimental and calculated P^*_A values in one example (Fig. 1).

In the above calculations P'_A was the experimental quantity for the component A. It would be possible to treat even P'_A as a disposable parameter, but the number of available data (four to eight items) is too small for adjusting three parameters (K, P_{AB}, P'_A) reliably. Only in cases when an optimized P'_A was suggested in the literature (10) have we added calculations with this P'_A and with the optimum values of K and P_{AB} for this given P'_A. The results (Table 1, middle line in examples 3–5) are sometimes more precise than without adjusting P_A (first lines) but they have one less degree of freedom. Use of the third disposable parameter is in our opinion not justified. This conclusion is well demonstrated by the graphical representation (Fig. 2) in which the example selected was relatively the most favourable of those given in ref. 10. To show finer differences, relative P^*_A values were plotted instead of the absolute values as plotted in Fig. 1. The least-squares calculation with two parameters (K and P_{AB}) was chosen as a reference line (line 1, the x-axis). When the experimental points are pictured with an error of ± 2 cm^3, they are well distributed with almost random deviations. The calculations with three parameters (line 2) display only a little better fit for most points: the errors are concentrated on the first, rejected point, pertinent to the pure component A. In our opinion there is no reason for such a treatment. On the contrary, the first point should be known with a better accuracy than the others. Moreover it is not evident from Fig. 1 why P'_A should acquire just the particular value given; by no means can it viewed as an "extrapolated value of P_A to $w_B \rightarrow 0$" (10). Our results, recalculated with P'_A from the literature (10) and K and P_{AB} optimized (Table 1, middle line in example 4), are not much better than in the literature (last line in example 4), they only reveal that calculations with few degrees of freedom are sensitive to small changes. We consider as established that the treatment according to eq. [4],

TABLE 1. Equilibrium constants and dipole moments of the complexes as determined from dielectric measurements according to the method of Few and Smith (8): a recalculation[a]

Example	Compounds A and B	K[b]	P_{AB}[c]	μ_{AB}[d]	s[e]
1	$CH_3COCH_2CONHPh + NEt_3$	<0.1[f]	>330 000[f]	>130	6.8 (3)
	ref. 9	*357 ± 10*	*450 ± 9*	*4.43 ± 0.03*	9.3 (3)
2	$C_6H_5COCH_2CONHPh + NEt_3$	<0.1[g]	>650 000[g]	>180	3.9 (3)
	ref. 9	*600 ± 18*	*654 ± 13*	*5.25 ± 0.03*	35.1 (3)
3	$CH_3COCH_2COCH_3 + NEt_3$	<0.1[f]	>320 000[f]	>130	2.7 (3)
	with P'_A[h]	1875	294	3.37	1.6 (2)
	ref. 10	*1203 ± 36*	*314 ± 6*	*3.74 ± 0.03*	2.0 (2)
4	$C_6H_5COCH_2COCH_3 + NEt_3$	1081 [340–2290]	427 [377–629]	4.11 [3.79–5.17]	2.3 (3)
	with P'_A[h]	1448	410	4.00	2.6 (2)
	ref. 10	*1178 ± 35*	*429 ± 8*	*4.32 ± 0.03*	3.1 (2)
5	$C_6H_5COCH_2COC_6H_5 + NEt_3$	26 [0–1100]	1972 [346–∞]	9.57 [3.44–∞]	1.37 (3)
	with P'_A[h]	994	365	3.57	0.60 (2)
	ref. 10	*777.2 ± 2.3*	*382 ± 8*	*3.87 ± 0.03*	1.05 (2)
6	Acrylonitrile + styrene	705 [520–910]	360 [346–383]	3.88 [3.79–4.02]	0.28 (3)
	ref. 11	*606.6*	*372.2*	*3.98*	0.58 (3)
7	Acrylonitrile + C_6H_6	447 [135–990]	344 [315–462]	3.82 [3.63–4.52]	1.43 (3)
	ref. 11	*457.5*	*342.1*	*3.83*	1.44 (3)
8	Acrylonitrile + $EtOCH{=}CH_2$	40 [0–212]	561 [351–∞]	5.06 [3.91–∞]	0.41 (3)
	ref. 11	*185.1*	*354.7*	*3.93*	0.78 (3)
9	$PhNH_2$ + dioxan	75 [56–97]	136.8 [132–144]	2.00 [1.94–2.09]	0.23 (2)
	ref. 8	*128*	*129.7*	(1.78)	1.16 (2)
	corr.[i]	88 [70–108]	132.1 [129–136]	1.95 [1.91–1.99]	0.19 (2)
	ref. 8[i]	*116*	*126.7*	*1.88*	0.71 (2)
10	$PhNO_2$ + 2-bromoaniline	12 850 [3900–46 000]	635 [599–755]	5.29 [5.06–5.80]	11.8 (6)[j]
	ref. 15[j]	*12 950*	*647.5*	*5.31*	12.2 (6)[j]
11	$PhNO_2 + C_6H_6$	55 [0–190]	2824 [1220–∞]	11.7 [7.6–∞]	7.6 (5)[k]
	ref. 16[k]	*64 ± 3*	*529.2*	*5.00*	206 (5)[k]
12	PhOH + pyridine	36 800 [26 000–53 000]	389 [369–415]	4.05 [3.92–4.20]	4.1 (2)
	ref. 17	*36 000*	*388*	*4.06*	4.7 (2)
13	$CH_3CO_2CH_3$ + PhOH	929 [160–2100]	401 [305–1220]	4.17 [3.55–7.59]	2.8 (3)
	ref. 18	*7150*	*407.5*	*4.50*	143 (3)
14	$CH_3CO_2C_6H_5$ + PhOH	1310 [850–1890]	275 [256–308]	3.19 [2.99–3.43]	0.9 (3)
	ref. 18	*8710*	*274*	*3.70*	51.9 (3)
15	Acetone + PhOH	2305 [1360–3640]	456 [415–532]	4.49 [4.25–4.90]	2.8 (3)
	ref. 19	*143.2*	*516.5*	*5.02*	93.9 (3)
16	n-C_4H_9OH + pyridine	2390 [2060–2770]	270.1 [266–275]	3.30 [3.27–3.34]	0.35 (5)
	ref. 20	*2000*	*278*	*3.37*	1.04 (5)
17	t-C_4H_9OH + pyridine	1885 [1160–2940]	238.8 [233–248]	3.05 [3.01–3.12]	0.65 (4)
	ref. 20	*1200*	*252*	*3.16*	1.7 (4)

[a]Experimental data taken from the references as given in the second column. Our calculations are based on eqs. [4] and [5], confidence intervals for $2s$ given in brackets only if they are of any significance. The results from the original literature given in italics.

[b]Equilibrium constant in $cm^3\ mol^{-1}$.

[c]Polarization of the complex in $cm^3\ mol^{-1}$.

[d]Dipole moment of the complex in D; in our calculations correction for the atomic polarization 5% of R_D.

[e]Standard deviation of the fit, calculated by us according to eq. [4], similarly also for parameters given in the literature (degrees of freedom in parentheses).

[f]No convergence.

[g]No convergence, not improved even when the first point is deleted.

[h]Calculated with P'_A as the third adjustable parameter, its value taken as it was given in the literature (10).

[i]With a special correction for solvent effect (8).

[j]The experimental data are of low quality: particularly, the fourth point is evidently in error and was omitted from the calculations. Omitting the third point still does not improve the precision significantly.

[k]Omitting the third point improves s only to 5.6, the enormous discrepancy with literature parameters is not removed.

Can. J. Chem. Downloaded from www.nrcresearchpress.com by 217.78.4.112 on 09/08/12
For personal use only.

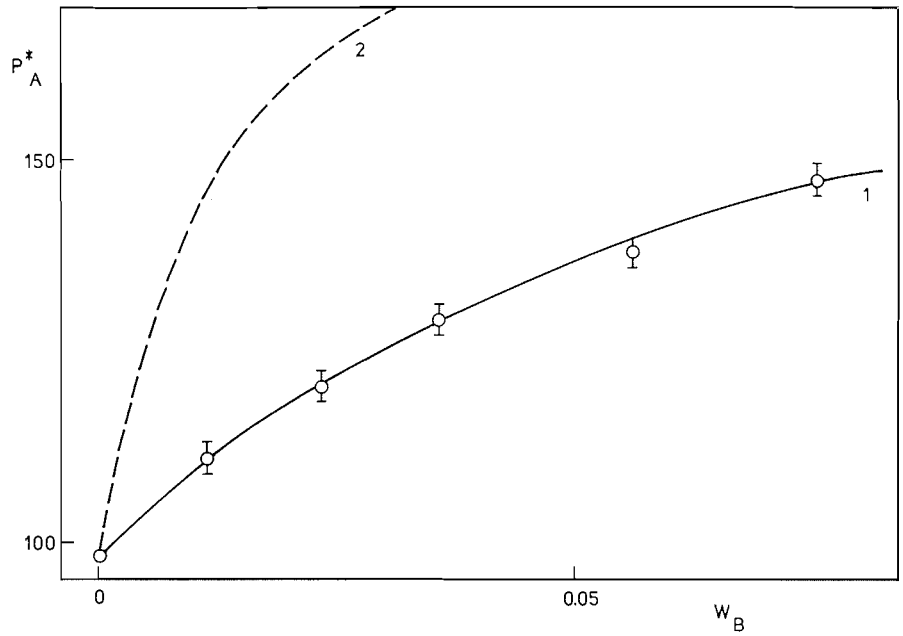

FIG. 1. Comparison of experimental and calculated polarizations P_A^* (absolute values) for complex formation of phenyl acetate with phenol in benzene; 1: the best least-squares fit with K = 1310 cm^3, P_{AB} = 275 cm^3; 2: calculated according to ref. 18. Experimental points (18) are shown with uncertainties ±2 cm^3. (Example 14, Table 1.)

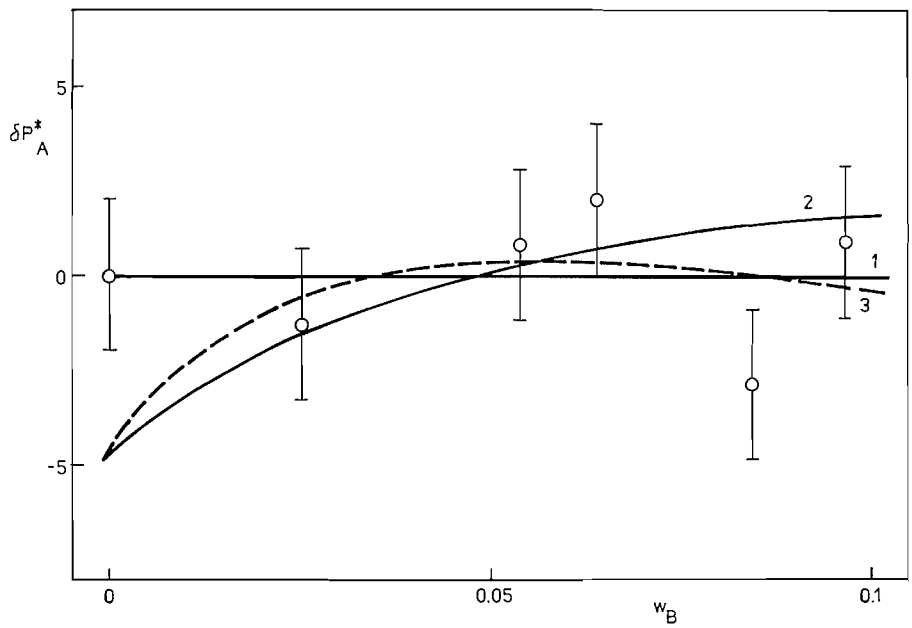

FIG. 2. Comparison of experimental and calculated polarizations P_A^* (relative values) for complex formation of benzoylacetone with triethylamine in cyclohexane; 1: the best least-squares fit with K = 1081 cm^3, P_{AB} = 427 cm^3, as reference line; 2: calculated according to ref. 10 with an arbitrary parameter P'_A = 226.7; 3: calculated with the same parameter and least-squares values for K and P_{AB}. Experimental points (10) are shown with uncertainties of ±2 cm^3. (Example 4, Table 1.)

with only two parameters adjusted, gives the most realistic estimates. It follows that almost one half of the examples of Table 1 do not yield acceptable results with any statistical treatment. Some possible reasons might be low experimental accuracy or too small a value of K (no complex formation).

3. To complete the statistical treatment it is necessary to give at least an estimate of the reliability of the parameters. Since the least-squares problem is not linear, we prefer the following simple and telling procedure (13). If the lowest possible standard deviation (in P_A^*) is known, one can choose its arbitrary multiple, usually between 2s and 3s, and calculate all possible combinations of the parameters (K and P_{AB}) that reproduce the experiments within this accuracy. It is very important that the parameters are strongly dependent on each other: one of them can even be strongly shifted from its op-

Can. J. Chem. Downloaded from www.nrcresearchpress.com by 217.78.4.112 on 09/08/12
For personal use only.

timum value when the second is shifted too (in the opposite direction). Graphical representation of this dependence is a contour diagram (Fig. 3) where the same example was chosen as in Fig. 2, i.e., a relatively favourable one. The pairs of parameters giving the same overall fit (2*s* or 3*s*) are connected by a curve. The confidence interval is given by the extreme points of the whole curve and corresponds to the confidence coefficients 95% or 99.7%, respectively. These intervals are also given in Table 1, but only in those examples when they are actually meaningful. The mutual dependence of parameters is strong: the greatest K belongs to the smallest P_{AB}, and conversely. There is a widespread mistake (in the field of dipole moments, e.g., ref. 6) that the confidence interval of one parameter is given with the condition that the second one be kept constant. In the graphical representation it means to intersect the curve in Fig. 3 by a horizontal or vertical straight line and to read off the distance of the two points of intersection. In this way the actual uncertainty may be badly underestimated, e.g., in Fig. 3 by more than one order of magnitude. See also the unrealistic estimates of the errors in the literature (Table 1) compared to the actual uncertainty.

Until now, K and P_{AB} have been considered as parameters that are to be estimated by the statistical approach. Ultimately, it is necessary to calculate μ_{AB} from P_{AB} and from the molar refraction R_{AB}. We always estimated R_{AB} as the sum of molar refractions of the components: $R_{AB} = R_A + R_B$. The values of R_A and R_B themselves were known either from experimental determination on the liquids or were calculated by us from Vogel's increments (23). In the literature (9–11) a sophisticated procedure was also reported, determining R_{AB} similarly to P_{AB}, with the same statistical shortcoming. The results obtained are quite unreliable but affect the final values of μ_{AB} rather little: this mistake is negligible compared to the much more important mistake in determining P_{AB}. In some other cases our calculations might differ from the literature by applying a 5% correction for atomic polarization: even here the possible error is negligible.

Conclusions

It has been shown here that the method of Few and Smith (8) is principally wrong from the statistical point of view: all the results reported must be considered as untrustworthy. Note, however, that the results of a correct approach must be correct, while the results of an incorrect approach need not be always wrong. This means that they need not differ too much from the best estimates in each particular case. In our case the estimates of K are more sensitive to errors that than those of μ_{AB}. Among the 17 examples of Table 1 we may characterize the following typical cases:

(*a*) The fit in the correct treatment is acceptable in relation to the experimental error (s should be less than 1 cm^3 but we have allowed even 1.4 cm^3). The estimated parameters may be accepted within the given limits of uncertainty. The fit of the Few–Smith procedure is somewhat worse (still $s < 1.7$ cm^3) but the estimated parameters fall within the uncertainty limits (examples 6, 7, and 17 in Table 1), or exceed these limits but slightly (examples 9 and 16). In this case use of the Few–Smith method has no great consequences.

(*b*) The fit of the correct procedure is as good as above ($s < 1$ cm^3) but the Few–Smith procedure gives no fit and very biased estimates of the parameters (example 14). In this treatment the fit usually remains unknown and the results may be completely at variance with reality. On the other hand, we may say that in the six examples cited in (*a*) and (*b*) the parameters K and μ_{AB} have actually been determined when a correct procedure was used. Note that with few degrees of freedom the fit must be very good to accept the result as significant.

(*c*) The fit is as good as above but the uncertainty in the parameters is too great, particularly in K, including even the value $K = 0$ (examples 5 and 8). The reasons for this be-

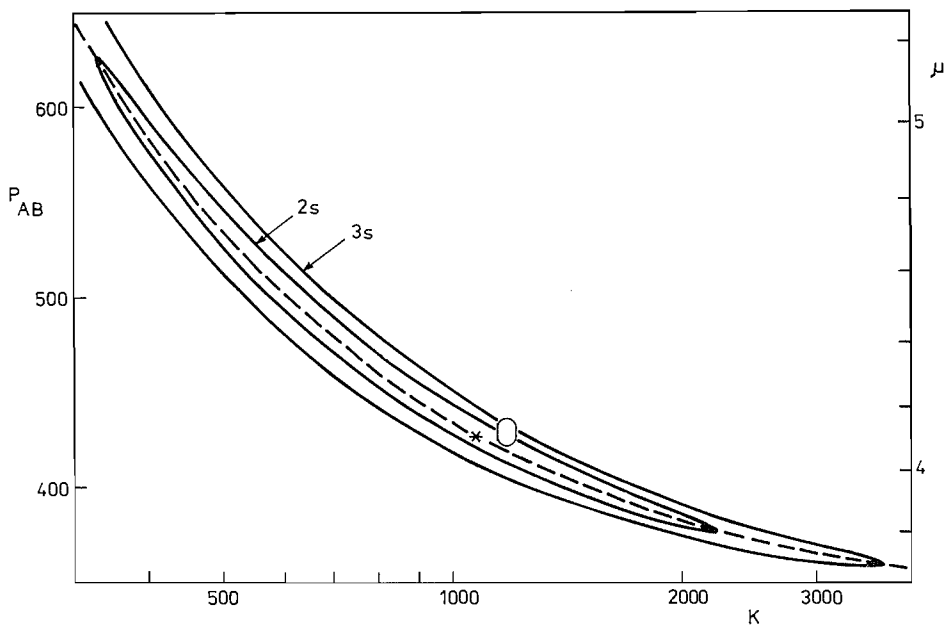

FIG. 3. Mutual dependence of parameters for the same example as in Fig. 2—the contour diagram. Full lines: the dependence of P_{AB} on K for a given standard deviation (twice or three times its minimum value); broken line: the optimum values of P_{AB} for a given K; *: absolute optimum values; empty oval: values from ref. 10, with their given uncertainties.

Can. J. Chem. Downloaded from www.nrcresearchpress.com by 217.78.4.112 on 09/08/12
For personal use only.

haviour are difficult to guess; possibly the experiments are insufficiently precise when K is small. The Few–Smith procedure is again at variance with facts: the estimates are biased and their errors badly underestimated.

(*d*) When a good fit cannot be obtained, there is no sense in discussing the values of the parameters and comparing correct and incorrect procedures (examples 10, 11, and 12). When s can be no longer considered as an estimate of the experimental error, our suggested confidence interval for the parameters has little meaning. The reasons may be bad experiments, sometimes even misprints in the literature, or a bad theoretical model (different stoichiometry of complex formation, large solvent effects of the component B). Again the Few–Smith procedure may be very untrustworthy since it does not reveal that the fit is bad. In two borderline cases the fit evidently exceeded the experimental error (s 2.8 cm^3) but the fit of the Few–Smith procedure was dramatically worsened (examples 13 and 15). In another case (example 4) the fit remained almost unchanged and the parameters were not much shifted. This example is shown in Fig. 2. The reason for this indeterminate behaviour may be that relatively imprecise data are connected with few degrees of freedom.

(*e*) In some cases no convergence was reached and the optimum value of K approached zero (examples 1, 2, and 3); simultaneously P_{AB} grew without limits. It is possible that practically no complex formation occurs but in this case P_A should be constant. The model evidently fails and the observed changes of P_A^* must have another reason, say, too large solvent effects of the component B. This cannot be unraveled within the framework of the Few–Smith approach: apparent values of the parameters that have no real significance are obtained instead.

Still more important than a criticism of the Few–Smith method are general conclusions for processing experimental data using regression analysis. In the time of computers there is no need for rearrangement into linear equations. The least-squares principle must be applied to the sum of squares in the original experimental quantity, not in any function. An additional problem arises when two or more parameters are estimated together from the same set of data: then their confidence intervals must be determined with respect to their mutual dependence. Neglecting these requirements has led to both biased estimates and overestimated reliability: this happened in quite different fields of chemistry (21, 22). The results of many papers are thus completely worthless. We dare to say that this is one of the most widespread mistakes in contemporary science. In same cases it cannot be either revealed or corrected since the original data were not published.

1. O. Exner. Dipole moments in organic chemistry. Thieme, Stuttgart. 1975. Chap. 7.
2. K. Bauge and J. W. Smith. J. Chem. Soc. 4244 (1964).
3. J. O. Jenkins and J. W. Smith. J. Chem. Soc. B, 1538 (1970).
4. C. Treiner, J. F. Skinner, and R. M. Fuoss. J. Phys. Chem. **68**, 3406 (1964).
5. H. Lumbroso, J. Curé, T. Konakahara, and K. Sato. J. Mol. Struct. **98**, 277 (1983).
6. J. A. Walmsley, E. J. Jacob, and H. B. Thompson. J. Phys. Chem. **80**, 2745 (1976).
7. D.-M. Bertin and H. Lumbroso. C. R. Seances Acad. Sci. Ser. C: **263**, 181 (1966).
8. A. V. Few and J. W. Smith. J. Chem. Soc. 2781 (1949).
9. M. M. Naoum, G. R. Saad, M. M. Abdel-Moteleb, H. G. Shinouda, and H. A. Rizk. Can. J. Chem. **65**, 2760 (1987).
10. G. R. Saad, M. M. Naoum, and H. A. Rizk. Can. J. Chem. **67**, 284 (1989).
11. G. R. Saad, M. M. Naoum, and H. A. Rizk. Can. J. Chem. **68**, 480 (1990).
12. O. Exner. J. Mol. Struct. **216**, 153 (1990).
13. O. Exner. Collect. Czech. Chem. Commun. **55**, 1435 (1990).
14. H. Mager. Moderne Regressionsanalyse. Otto Salle, Frankfurt am Main. 1982. Chap. 1.1.
15. N. N. Polle, E. G. Polle, and L. N. Pushnikova. Zh. Obshch. Khim. **40**, 372 (1970).
16. V. N. Nagareva, N. N. Polle, and E. G. Polle. Zh. Obshch. Khim. **40**, 2320 (1970).
17. R. J. Bishop and L. E. Sutton. J. Chem. Soc. 6100 (1964).
18. V. Shanmugasundaram and M. Meyyapan. Indian J. Chem. Sect. A: **17A**, 506 (1979).
19. V. Shanmugasundaram and M. Meyyapan. Indian J. Chem. **10**, 936 (1972).
20. D. Cleverdon, G. B. Collins, and J. W. Smith. J. Chem. Soc. 4499 (1956).
21. O. Exner. Collect. Czech. Chem. Commun. **31**, 3222 (1966).
22. O. Exner. Prog. Phys. Org. Chem. **10**, 411 (1973).
23. A. I. Vogel. J. Chem. Soc. 1842 (1948).

Can. J. Chem. Downloaded from www.nrcresearchpress.com by 217.78.4.112 on 09/08/12
For personal use only.

Intramolecular electron transfer in the photochemistry of substituted 1-naphthylmethyl esters of benzoic acids

D. P. DeCosta and J. A. Pincock[1]

Department of Chemistry, Dalhousie University, Halifax, N.S., Canada B3H 4J3

Received November 15, 1991

D. P. DeCosta and J. A. Pincock. Can. J. Chem. **70**, 1879 (1992).

Direct excitation of the esters **5** in methanol solvent leads to rapid intramolecular exciplex formation ($k_{ex} = 10^{10}$ s^{-1} for X = CH_3O, Y = CN) with electron transfer from the naphthalene to the benzoate ring. This process dominates the usual fluorescence and reaction of the excited singlet state. The rate of this process can be varied over 10^3 by suitable change in the substituents X and Y. The electron-transfer rates can be correlated with the two-parameter Hammett equation: $\log k_{ex} = 8.48 - 1.5\sigma^+ + 0.77\sigma$. For cases where the rate of exciplex formation is slow, the usual homolytic carbon–oxygen bond cleavage occurs from the excited singlet state. The eventual products result from the ion pair since the rate of electron transfer in the radical pair to form the ion pair is considerably faster than the rate of decarboxylation of the benzoyloxy radical.

D. P. DeCosta et J. A. Pincock. Can. J. Chem. **70**, 1879 (1992).

L'excitation directe des esters **5** dans le methanol conduit à une formation intramoléculaire rapide de l'exciplexe ($k_{ex} = 10^{10}$ s^{-1} pour X = CH_3O, Y = CN) impliquant un transfert d'électron du naphtalène vers le noyau benzoate. Ce processus domine la fluorescence habituelle et la réaction de l'état excité singulet. La vitesse de processus peut varier par un facteur de plus de 10^3 en faisant varier convenablement les substituants X et Y. Il existe une corrélation entre les vitesses de transfert de charge et les deux paramètres de l'équation de Hammett: $\log k_{ex} = 8{,}48 - 1{,}5\sigma^+ + 0{,}77\sigma$. Dans les cas où la vitesse de formation de l'exciplexe est lente, il se produit le clivage homolytique habituel de la liaison carbone–oxygène à partir de l'état singulet excité. Les produits éventuels proviennent de la paire d'ions puisque la vitesse de transfert d'électron dans la paire de radicaux, conduisant à la paire d'ions, est beaucoup plus rapide que la vitesse de décarboxylation du radical benzoyloxy.

[Traduit par la rédaction]

Introduction

The photochemistry of benzylic compounds with leaving groups ($ArCH_2$-LG) is well known (1) to give products that result from both arylmethyl cations and radicals. The partitioning between these two intermediates is controlled by a variety of factors such as the leaving group, the structure of the aromatic ring including substituent effects, the nature of the excited state (singlet or triplet), and the solvent. In general, these factors are still so poorly understood that a reliable prediction about the products for any new system is impossible.

Recently, we have reported (2–4) a detailed study of the photochemistry of 1-naphthylmethyl esters, **1**, in the nucleophilic solvent methanol. As shown in eq. [1] (A = $C_{10}H_{7-n}X_n$), three major products are normally observed. The ether **2** and the carboxylic acid **3** are formed by methanol trapping of the 1-naphthylmethyl cation and the carboxylate anion, respectively. The hydrocarbon **4** is formed by in-cage coupling of the 1-naphthylmethyl radical with R which is formed by loss of carbon dioxide from the initially formed acyloxy radical. The product-yield results for a large number of esters where both substituents on the naphthalene ring

$$[1]\quad \underset{\mathbf{1}(A = C_{10}H_{7-n}X_n)}{ACH_2\text{-}O_2C\text{-}R} \xrightarrow[CH_3OH]{h\nu} \underset{\mathbf{2}}{ACH_2\text{-}OCH_3} + \underset{\mathbf{3}}{H\text{-}O_2C\text{-}R} + \underset{\mathbf{4}}{ACH_2\text{-}R}$$

(2) and the structure of the R group (3,4) were varied could best be explained by the mechanism outlined in Scheme 1. We have suggested that for these esters the excited singlet state (the triplet state for 1-naphthylmethyl esters is unreactive (5,6)) cleaves exclusively to the radical pair. Competition between electron transfer converting the radical pair to the ion pair (k_{ET}) and decarboxylation (k_{CO_2}) then controls the product distribution. This proposal is quite different from previously suggested mechanisms that assumed that product distribution was mainly controlled by the initial competition between heterolytic and homolytic cleavage of the benzylic ester bond in the excited state.

During the course of these studies, we observed that 1-naphthylmethyl benzoate (eq. [1], R = Ph, $n = 0$) behaved anomalously. The first fact noticed was the abnormally long time required in preparative scale photolyses for conversion of the ester to products when compared with, e.g., 1-naphthylmethyl phenylacetate (eq. [1], R = $PhCH_2$, $n = 0$). Since the absorbing chromophore for both these esters is the naphthalene ring, a reasonable expectation would be that excited-state carbon–oxygen bond cleavage would occur with about the same efficiency. The second observation was the very low quantum yield of fluorescence for the benzoate esters. Normally unsubstituted 1-naphthylmethyl esters have values of about 0.14 (3,4) independent of the structure of R. However, for the benzoate with R = Ph, a value of 0.005 was obtained. Third, there was no observable phosphorescence although intersystem crossing followed by emission is a

[1]Author to whom correspondence may be addressed.

Can. J. Chem. Downloaded from www.nrcresearchpress.com by 217.78.4.112 on 09/08/12
For personal use only.

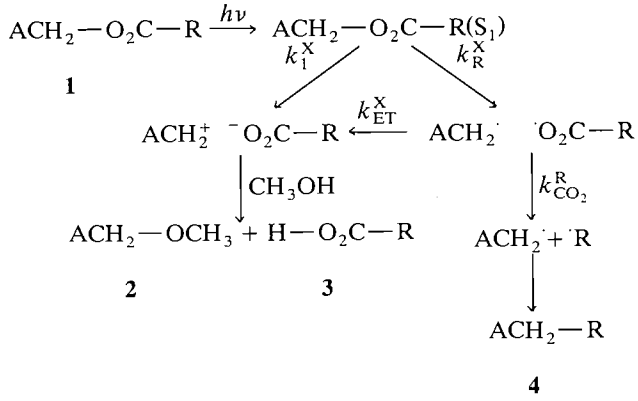

SCHEME 1. General mechanism for the photolysis of 1-naphthylmethyl esters (A = $C_{10}H_{7-n}X_n$) in methanol.

reasonably efficient process for naphthalene derivatives. Finally, the products obtained from the very slow photolysis were almost entirely those resulting from ionic intermediates, i.e., **2** and **3**.

A reasonable suggestion for these observations was that the excited singlet state was being quenched by intramolecular electron transfer, as is well documented for bichromophoric systems where the chromophores are separated by a three-carbon saturated chain (7,8). To investigate this possibility the set of substituted benzoates **5a**–*g* was synthesized and their excited-state behaviour examined. During the course of this work a similar electron-transfer pathway was proposed to explain the fluorescence behaviour of some 1-pyrenylmethyl esters **6** (R being 1-naphthyl, 9-anthryl, and 4-tolyl (9,10)) and **7** (R being 9-anthryl (11)). As will be discussed below these results can be usefully compared to ours.

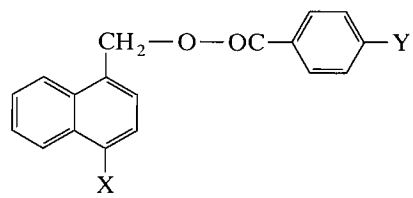

5

a, X = H, Y = H
b, X = H, Y = CH_3O
c, X = H, Y = CN
d, X = CH_3O, Y = H
e, X = CH_3O, Y = CN
f, X = CN, Y = H
g, X = CN, Y = CH_3O

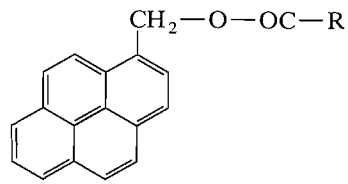

6

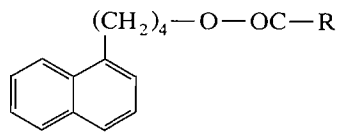

7

Experimental

General experimental

All melting points were determined on a Fisher-Johns melting point apparatus and are uncorrected. Infrared spectra were recorded on a Perkin–Elmer 237B spectrometer and are reported in wavenumbers (cm^{-1}). ^1H nmr spectra were recorded on a Nicolet-360 spectrometer and are reported with chemical shift relative to internal TMS. Mass spectra were obtained on a CEC 21–104 spectrometer; all signals greater than 10% of the base peak are reported as *m/e* (relative intensity). HPLC analyses were performed on a Waters system equipped with model 450 variable wavelength detector. A Brownlee RP-8 analytical column was used with the normal eluting solvent being an 80% methanol–water mixture and detection at 280 nm. Fluorescence spectra were obtained on a Perkin–Elmer MPF 66 spectrometer with samples in methanol that were degassed by three freeze-pump-thaw cycles; quantum yields were determined relative to a value of 0.21 (12) for 1-methylnaphthalene. Fluorescence lifetimes were obtained from the same samples using a PRA system 3000 instrument with a hydrogen flash lamp of pulse width 0.8 ns. Microanalyses were by Canadian Microanalytical Service Ltd., Delta, B.C., Canada.

Preparation of esters

To a solution of the alcohol (20 mmol) in 75 mL of benzene and 1 mL of pyridine was added a solution of the acid chloride (22 mmol) in 20 mL of benzene. After 6 h, the mixture was poured into 50 mL of water and the organic layer was separated, washed with 40 ml each of 10% HCl, 5% NaOH, and water, dried over $MgSO_4$, filtered, and the benzene evaporated. This crude material was chromatographed on silica gel with 30% dichloromethane/hexane as eluant. The esters were then purified by either recrystallization or bulb-to-bulb distillation. Physical properties are given below.

Benzoyl chloride and 4-cyanobenzoyl chloride were from Aldrich; 4-methoxybenzoyl chloride was made from the acid (Aldrich) with thionyl chloride.

1-Naphthylmethanol was from Aldrich; 4-methoxy-1-naphthylmethanol (13) and 4-cyano-1-naphthylmethanol (14) were prepared by literature procedures.

Physical properties of esters

5*a*: mp 36–37°C; ^1H nmr ($CDCl_3$) δ: 8.11 (d, 1H, *J* = 8.3 Hz, H8), 8.05 (d, 2H, *J* = 8.1 Hz, H2′), 7.85 (d, 1H, *J* = 8.0 Hz, H5), 7.86 (d, 1H, *J* = 8.5 Hz, H4), 7.63 (d, 1H, *J* = 6.7 Hz, H4′), 7.57–7.47 (m, 3H, H6, 7, 3), 7.45 (d, 1H, *J* = 7.0 Hz, H2), 7.39 (t, 2H, *J* = 7.7 Hz, H3′), 5.81 (s, 2H, $NpCH_2$); ir (neat): 3060, 2950, 1725, 1275, 1100 cm^{-1}; mass spectrum, *m/e*: 263(15), 262(73), 141(67), 140(30), 139(12), 115(13), 105(100), 77(19). Anal. calcd. for $C_{18}H_{14}O_2$: C 82.42, H 5.34; found: C 82.43, H 5.34.

5*b*: mp 68–69°C; ^1H nmr ($CDCl_3$) δ: 8.07 (d, 1H, *J* = 8.1 Hz, H8), 7.97 (d, 2H, *J* = 8.1 Hz, H2′), 7.84 (d, 1H, *J* = 8.4 Hz, H5), 7.81 (d, 1H, *J* = 8.5 Hz, H4), 7.58 (d, 1H, *J* = 7.0 Hz, H2), 7.51 (t, 1H, *J* = 8.0 Hz, H7), 7.49 (t, 1H, *J* = 8.0 Hz, H6), 7.42 (t,

Can. J. Chem. Downloaded from www.nrcresearchpress.com by 217.78.4.112 on 09/08/12
For personal use only.

1H, J = 7.1 Hz, H3), 6.81 (d, 2H, J = 7.4 Hz, H3′), 5.75 (s, 2H, $NpCH_2$) 3.73 (s, 3H, OCH_3); ir (Nujol): 1695, 1240, 1010 cm^{-1}; mass spectrum, *m/e*: 293 (10), 292 (46), 142 (10), 141 (80), 140 (10), 136 (10), 135 (100), 115 (11). Anal. calcd. for $C_{19}H_{16}O_3$: C 78.06, H 5.52; found: C 77.69; H 5.39.

5*c*: mp 142–143°C; ^{1}H nmr ($CDCl_3$) δ: 8.08 (d, 2H, J = 8.3 Hz, H3′), 8.05 (d, 1H, J = 8.3 Hz, H8), 7.88 (d, 1H, J = 7.6 Hz, H5), 7.86 (d, 1H, J = 7.6 Hz, H4), 7.63 (d, 2H, J = 8.4; H2′), 7.60 (d, 1H, J = 6.7 Hz, H2), 7.56 (t, 1H, J = 6.9 Hz, H6), 7.51 (t, 1H, J = 6.8 Hz, H7), 7.45 (t, 1H, J = 7.3 Hz, H3), 5.81 (s, 2H, $NpCH_2$); ir (Nujol): 2205, 1710, 1270, 1100 cm^{-1}; mass spectrum, *m/e*: 288(13), 287(60), 142(16), 141(100), 128(20), 115(15). Anal. calcd. for $C_{19}H_{13}NO_2$: C 79.43, H 4.56, N 4.88; found: C 79.25, H 4.47, N 4.85.

5*d*: mp 77–78°C; ^{1}H nmr ($CDCl_3$) δ: 8.32 (d, 1H, J = 8.2 Hz, H8), 8.06 (d, 1H, J = 8.3 Hz, H5), 8.01 (d, 2H, J = 7.4 Hz, H2′), 7.58–7.46 (m, 4H, H6, 7, 2, 4′), 7.35 (t, 2H, J = 7.4 Hz, H3′), 6.76 (d, 1H, J = 7.8 Hz, H3), 5.72 (s, $NpCH_2$), 3.98 (s, 3H, OCH_3); ir (Nujol): 1720, 1260, 1080 cm^{-1}; mass spectrum, *m/e*: 293(14), 292(63), 172(14), 171(100), 136(17), 115(14). Anal. calcd. for $C_{20}H_{18}O_3$: C 78.06, H 5.52; found: C 78.17, H 5.66.

5*e*: mp 112–113°C; ^{1}H nmr ($CDCl_3$) δ: 8.33 (d, 1H, J = 8.0 Hz, H8), 8.07 (d, 2H, J = 7.6 Hz, H3′), 8.02 (d, 1H, J = 8.2 Hz, H4), 7.64 (d, 2H, J = 7.6 Hz, H2′), 7.57 (t, 1H, J = 7.5 Hz, H7), 7.52 (d, 1H, J = 7.9 Hz, H2), 7.51 (t, 1H, J = 7.5 Hz, H6), 6.77 (d, 1H, J = 8.0 Hz, H3), 5.74 (s, 2H, $NpCH_2$), 3.99 (s, 3H, OCH_3); ir (Nujol): 2210, 1700, 1240, 1080 cm^{-1}; mass spectrum, *m/e*: 318(14), 317(65), 172(14), 171(100), 128(18), 102(10). Anal. calcd. for $C_{20}H_{15}NO_3$: C 75.70, H 4.76, N 4.41; found: C 75.62, H 4.93, N 4.37.

5*f*: mp 122–123°C; ^{1}H nmr ($CDCl_3$) δ: 8.31 (d, 1H, J = 8.2 Hz, H8), 8.17 (d, 1H, J = 7.9 Hz, H5), 8.07 (d, 2H, J = 7.7 Hz, H2′), 7.92 (d, 1H, J = 7.4 Hz, H3), 7.74 (t, 1H, J = 6.6 Hz, H6), 7.70 (t, 1H, J = 7.3 Hz, H7), 7.70 (d, 1H, J = 7.4 Hz, H2), 7.58 (t, 1H, J = 7.3 Hz, H4′), 7.44 (t, 2H, J = 7.7 Hz, H3′), 5.86 (s, 2H, $NpCH_2$); ir (Nujol): 2200, 1700, 1280, 1105 cm^{-1}; mass spectrum, *m/e*: 288(7), 287(31), 166(32), 165(10), 105(100), 77(24). Anal. calcd. for $C_{19}H_{13}NO_2$: C 79.33, H 4.56, N 4.88; found: C 79.00, H 4.59, N 4.86.

5*g*: mp 140–141°C; ^{1}H nmr ($CDCl_3$) δ: 8.29 (d, 1H, J = 8.2 Hz, H8), 8.15 (d, 1H, J = 8.2 Hz, H5), 8.02 (d, 2H, J = 8.9 Hz, H2′), 7.90 (d, 1H, J = 7.3 Hz, H3), 7.73 (t, 1H, J = 7.2 Hz, H6), 7.69 (t, 1H, J = 7.2 Hz, H7), 7.68 (d, 1H, J = 7.3 Hz, H2), 6.91 (d, 2H, J = 8.9 Hz, H3′), 5.81 (s, 2H, $NpCH_2$), 3.84 (s, 3H, OCH_3); ir (Nujol): 2200, 1700, 1260, 1080 cm^{-1}; mass spectrum, *m/e*: 318(4), 317(20), 166(35), 136(10), 135(100). Anal. calcd. for $C_{20}H_{15}NO_3$: C 75.70, H 4.76, N 4.41; found: C 75.43, H 4.89, N 4.42.

Photolysis of esters

Irradiations were with a 200-W medium pressure Hanovia mercury lamp in a Pyrex immersion well. Normally about 300 mg of the ester was dissolved in 300 mL of methanol and irradiations were continued until more than 90% of the esters was consumed. Reactions were purged with a steady stream of nitrogen gas. Yields were determined by calibrated HPLC using solutions of the products of known concentration. Dark reactions were negligibly slow.

For isolation of the carboxylic acid photoproducts, the reaction mixtures were first concentrated under vacuum to about 10 mL and then dissolved in 30 mL of dichloromethane. The dichloromethane was extracted with 2 × 25 mL of 5% NaOH and the extract acidified with conc. HCl. Extraction and concentration gave the acid which was identified by ^{1}H nmr and the yield determined by weight.

Results and discussion

Fluorescence quantum yields

Fluorescence quantum yields for the esters **5***a–g* are reported in Table 1. Clearly, there is a large range in the values from a maximum of 0.20 for **5***g* to a minimum of 0.003 for **5***e*. If these changes reflect charge-transfer quenching of the excited singlet state by an intramolecular process, then the expected direction of this charge transfer should be towards the benzoate aromatic ring which is the better electron acceptor. This suggestion has been confirmed for **7** (11). The exciplex would have radical anion/radical cation character as in **8**. If this is true the efficiency of formation of this species should be highest when the naphthalene ring has a lower oxidation potential because of an electron-donating substituent (X = CH_3O) and the benzene ring a lower reduction potential because of an electron-withdrawing substituent (X = CN). This is the ester **5***e*, which has the lowest ϕ_F. The reverse case, **5***g* (X = CN, Y = CH_3O), has the highest ϕ_F. The obvious conclusion is that intramolecular charge transfer to form an exciplex in the excited singlet state completes with the usual fluorescence emission of the naphthalene ring.

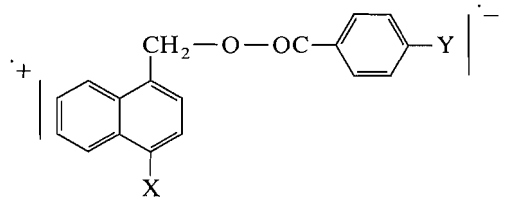

8

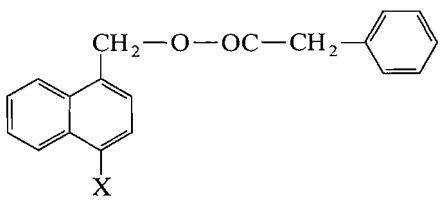

9

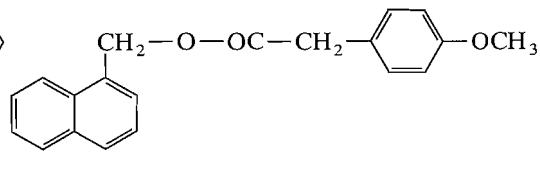

14

Often, intramolecular exciplex formation of this type results in a new fluorescence emission (7). For the esters **5**, in methanol solvent, only **5***d* showed the expected broad structureless band at longer wavelength (λ_{max} ~ 440 nm) than

Can. J. Chem. Downloaded from www.nrcresearchpress.com by 217.78.4.112 on 09/08/12
For personal use only.

TABLE 1. Fluorescence quantum yields for esters **5***a–g*

Ester	X	Y	ϕ_f^5 [a]	ϕ_f^9 [a,b]	$\tau^{PA} \times 10^9$ [b] (s^{-1})	log k_{ex} [c]
5*a*	H	H	0.005	0.14	49	8.74 (0.08)
5*b*	H	CH_3O	0.030[d] (7.6)	0.14 (49)	49	7.87 (0.10)
5*c*	H	CN	0.004	0.14	49	8.84 (0.08)
5*d*	CH_3O	H	0.005	0.27	7.3	9.86 (0.08)
5*e*	CH_3O	CN	0.003	0.27	7.3	10.1 (0.08)
5*f*	CN	H	0.16 (5.0)	0.21 (5.2)	5.2	7.77 (0.48)
5*g*	CN	CH_3O	0.20 (5.0)	0.21 (5.2)	5.2	6.98 (0.70)

[a]Values in parentheses are singlet lifetimes in nanoseconds.
[b]For the corresponding phenylacetate **9**, see D. P. DeCosta and J. A. Pincock, to be published.
[c]The error in log k_{ex}, given in parentheses underneath, is calculated assuming a ±10% error in both ϕ_f^5 and ϕ_f^9.
[d]A value of 0.05 was obtained in hexane.

the normal fluorescence for 4-methoxy naphthalene derivatives at 340 nm. The intensity of this exciplex emission was about 20% that of the normal emission. The same compound in hexane solvent gave an exciplex band about seven times as strong as that observed in methanol. A more detailed study (10) of solvent effects on excimer emission for **6** (R = 9-anthryl) showed the same effect. In an earlier study (9), the same authors also confirmed that not all intramolecular exciplexes of this general structure are emissive. For **6** (R = 1-naphthyl), the quenching of the normal fluorescence occurred, but no new bands were observed.

The fluorescence quantum yield data for **5***a–g* can be analyzed in a more quantitative way as follows. As a model for the fluorescence of these compounds, the corresponding phenylacetate esters, **9**, seem ideal. The excited singlet-state properties of these substrates should be the same as those of **5**, except now intramolecular exciplex formation is no longer occurring. This must be so since the quantum yield (4) of fluorescence (0.14) of the phenylacetate ester **9***a* is identical to that of the related acetate ester (3) which does not have a good electron-accepting functional group. The quantum yield of fluorescence (ϕ_f^9) of the compounds **9** will be given by eq. [2], where the rate constants are for reactivity of the excited singlet state: fluorescence, radiationless decay (inter-

$$[2] \quad \phi_f^9 = k_f/(k_f + k_d + k_r) = k_f \tau_f^9$$

system crossing and internal conversion), and reaction (carbon-oxygen bond cleavage), respectively. The reciprocal of the denominator of eq. [2] is the singlet lifetime τ_f^9.

A similar expression for the compounds **5** is given in eq. [3], where the only additional term is k_{ex}, the rate of intramolecular exciplex formation.

$$[3] \quad \phi_f^5 = k_f/(k_f + k_d + k_r + k_{ex})$$

Division of eq. [2] by eq. [3] gives eq. [4].

$$[4] \quad \phi_f^9/\phi_f^5 = 1 + \tau_f^9 k_{ex}$$

Values for the fluorescence quantum yields and singlet lifetimes for **9***a–c* are given in Table 1, as are the calculated values for k_{ex} (in logarithmic form). The values of k_{ex} span almost three orders of magnitude and, as expected, the fastest rate is for **5***e* and the slowest for **5***g*. For **5***e*, therefore, exciplex formation dominates the processes available to the excited singlet, whereas for **5***g* exciplex formation is too slow to compete with normal emission.

Some comment is necessary concerning the accuracy of this method for determining k_{ex} values. For some cases, the ϕ_f values are very small (≤0.005). Determining accurate fluorescence efficiencies for weakly emissive compounds is inherently difficult but perhaps even more so for these cases. All the esters were made from the corresponding 1-naphthylmethanols which have high quantum yields of fluorescence (0.2–0.4). Therefore, if the alcohols (or other highly emissive naphthalene derivatives) are present as even very low percentage impurities in the esters, significant error in the quantum yields could result. We have, of course, used highly purified samples and made measurements on more than one sample of each compound. We therefore feel confident that the values reported are accurate within the ±10% error limits given in Table 1. Even these error limits can lead to quite large errors in the values estimated for log k_{ex}, particularly where ϕ_f^5 and ϕ_f^9 are quite similar as for **5***f* and **5***g*. A better experimental way to arrive at these values might be to use singlet lifetimes. Unfortunately most of the compounds studied here have singlet lifetimes which are shorter than the limit of ~1 ns for our single-photon counting equipment. For those cases (**5***b*, **5***f*, and **5***g*) where singlet lifetimes are available, the ratio of τ_f^9/τ_f^5 is, within experimental error, close enough to ϕ_f^9/ϕ_f^5 to give us confidence in the accuracy of the fluorescence quantum yields.

The values for log k_{ex} can be put on a more quantitative basis by application of a linear free energy approach. Assuming that the exciplex can be represented by a charge-separated structure like **8**, then the rates of its formation might be expected to follow a two-parameter Hammett function as in eq. [5].

Can. J. Chem. Downloaded from www.nrcresearchpress.com by 217.78.4.112 on 09/08/12
For personal use only.

Can. J. Chem. Downloaded from www.nrcresearchpress.com by 217.78.4.112 on 09/08/12
For personal use only.

[5] $\log k_{ex} = K + \rho^+\sigma^+ + \rho\sigma$

The $\rho^+\sigma^+$ term would be for the oxidation of the naphthalene ring. Recent results (15) for the electrochemical oxidation of substituted methylnaphthalenes show a good correlation of E_{ox} (CH_3CN vs. SCE) with σ^+ ($\rho^+ = -8.4$ *V*/σ^+). The $\rho\sigma$ term would be for the reduction of the benzoate functional group. There is some question of what sigma value to use here. The available literature data (16) for the reduction potentials of substituted benzoates or even substituted acetophenones or benzaldehydes with resonance electron-withdrawing groups is insufficient to decide if the reduction process should correlate with σ or σ^-. Recent *ab initio* calculations at the STO-3G level (17) for the radical anion of 4-cyanobenzaldehyde indicate that 27% of the negative charge is on the carbonyl oxygen and a similar amount is on the nitrile nitrogen.

A plot of the data in Table 1 according to eq. [5] is shown in Fig. 1. The calculated line is eq. [6] ($R^2 = 0.95$), where the values in parentheses are the standard deviations.[2] The

[6] $\log k_{ex} = 8.48(0.12) - 1.5(0.2)\sigma^+ + 0.77(0.37)\sigma$

correlation is reasonably good and certainly shows the expected trend with a negative ρ^+ value for the naphthalene ring and a positive ρ for the benzoate ring.

As a confirmation of this electron-transfer quenching process, the intermolecular quenching of 1-methoxynaphthalene by methyl benzoate was examined. The fluorescence intensity results gave a good Stern-Volmer plot ($k_q\tau = 13.7 \pm 0.8\ M^{-1}$) which along with the measured singlet lifetime ($\tau = 11$ ns) gives a quenching rate constant $k_q = 1.2 \times 10^9\ M^{-1}\ s^{-1}$. The value for the similar intramolecular case, **5***d* is somewhat faster ($7.2 \times 10^9\ s^{-1}$). However, the two processes may not, in fact, be too closely related. The mechanism for intramolecular electron transfer in **7** has been suggested (11) to occur through the bonds followed by a Coulombic attraction that enables rotation about the ester functional group to the conformation with the two chromophores sitting face-to-face as required for a stable exciplex. The conclusion from this section is that for suitably substituted derivatives of **5**, intramolecular exciplex formation by charge transfer can be fast enough to dominate other possible processes of the excited singlet state. The effect that this process has on actual photoreactivity will be discussed next.

Photolysis of esters **5**

The products for the photolysis of the esters **5***b*, *d*, *f*, *g* are given in eq. [7] and the product yields in Table 2. The products **10** and **11** are those expected from the photolysis

[7]

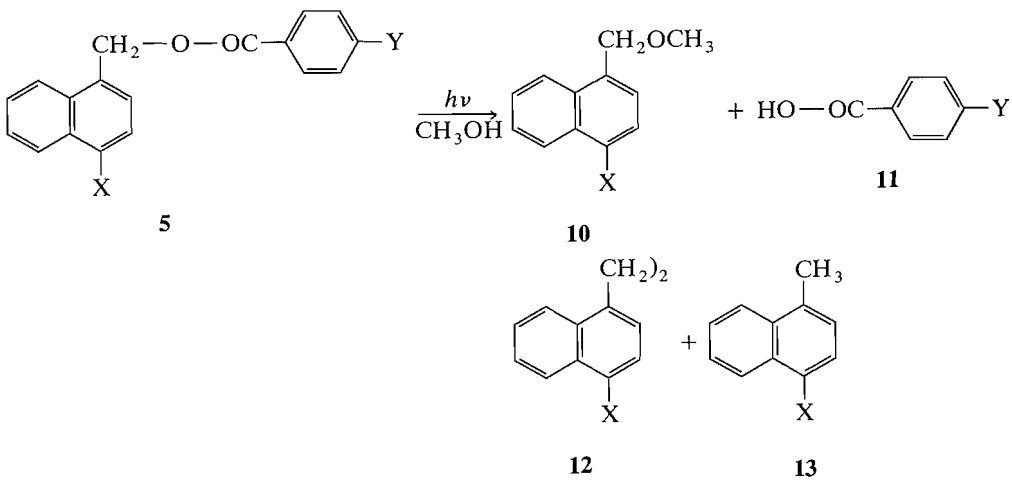

5 **10** **11**

12 **13**

of other esters (eq. [1] and Scheme 1). However, the products **12** and **13** derived from the 1-naphthylmethyl radical intermediate are no longer resulting from decarboxylation of the acyloxy radical. This is not surprising since aromatic acyloxy radicals are known (18) to decarboxylate quite slowly ($k_{CO_2} \sim 10^6\ s^{-1}$). Therefore in Scheme 1, k_{ET} should dominate k_{CO_2}. Normally, this would lead to products resulting entirely from the 1-naphthylmethyl cation and the acyloxy anion. This is seen to be true for **5***b* and **5***d* where k_{ET} is expected to be relatively fast (2) because of the stability of the 1-naphthylmethyl cation that is formed. Note that the yield determined for the carboxylic acid **11** is lower than expected, but this is explicable since the value is obtained by weight of isolated material after extraction. The yield of the ether **10**, determined by calibrated HPLC on the photolysis solutions, gives a better measure of the intervention of ionic intermediates.

For the esters **5***f* and **5***g* significant yields of products derived from the 1-naphthylmethyl radical are now formed. As mentioned above, the coupling product **4** is not formed because decarboxylation of the aromatic acyloxy radical is slow. However, now k_{ET} is also expected to be slower because of the effect the 4-cyano group has on the oxidation potential of the 1-naphthylmethyl radical (2,15). Therefore, the process that competes with electron transfer in the radical pair is cage escape. Since the 1-naphthylmethyl radical is not expected to efficiently abstract a hydrogen atom from methanol (the process is endothermic by about 46 kJ mol^{-1}) (5), the product formed is the dimer. 1-Methylnaphthalene, **13**, is formed in low yield but the source of the hydrogen atom is likely the reactive methylene group in either the starting ester **5** or the product ether **10**. This conclusion is substan-

[2]The corresponding equation for σ^- ($\log k_{ex} = 8.43\ (0.16) - 1.6\ (0.3\ \sigma^+ + 0.55\ (0.36)\ \sigma^-$; $R^2 = 0.93$) is not significantly different.

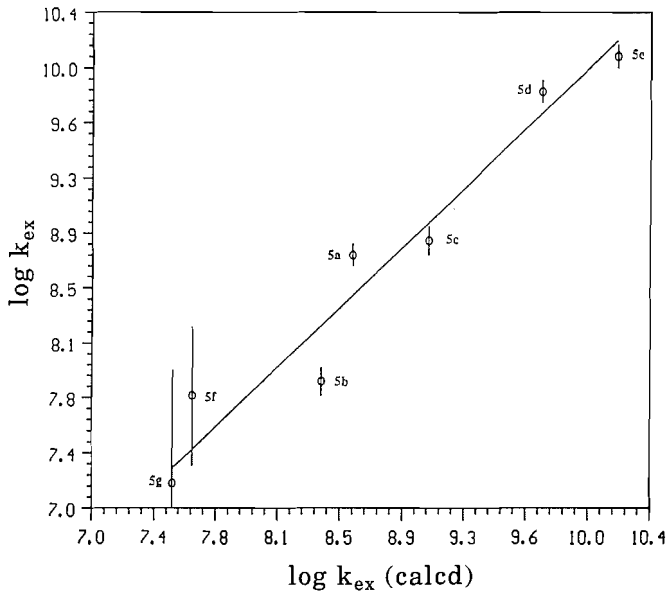

FIG. 1. Plot of log k_{ex} versus log k_{ex} (calcd.) = 8.48 − 1.5 σ^+ + 0.77 σ (R^2 = 0.95, s = 0.31) for intramolecular exciplex formation for the esters **5***a*–**5***g*. The error bars assume a ±10% error in the measurement of ϕ_f.

TABLE 2. Product yields (%) for photolysis of esters **5** in methanol

Substrate	**10**[a]	**11**[b]	**12**[a]	**13**[a]
5*b* (X = H, Y = CH_3O)	88	70	<2	<2
5*d* (X = CH_3O, Y = H)	92	80	<2	<2
5*f* (X = CN, Y = H)	66[c]	55	22	5
	55[d]	40	2	40
5*g* (X = CN, Y = CH_3O)	66[e]	100	22	5
	60[f]	61	2	39

[a]Yield determined by calibrated HPLC.
[b]Yield determined by weight of acid isolated by basic extraction of the phosolysis reaction mixture.
[c]Molarity of **5***f*: 8.1×10^{-4}.
[d]Molarity of **5***f*: 3.5×10^{-3}.
[e]Molarity of **5***g*: 6.4×10^{-4}.
[f]Molarity of **5***g*: 2.2×10^{-3}.

tiated by the observation that the yield of **13** rises dramatically if the starting concentration of the ester **5** is increased (footnotes *d* and *f* in Table 2).

The conclusion from this section is that the product yields from these esters can be explained by the normal mechanism outlined in Scheme 1 with the change that k_{CO_2} is too slow to have any importance. For substrates like **5***b* and **5***d* where intramolecular exciplex formation (k_{ex}) is fast, the quantum efficiency for bond cleavage is very low but those molecules that do react behave normally. Inefficiency of bond cleavage for substrates **6** where intramolecular exciplex formation leads to fluorescence quenching has also been observed (9). For **5***f* and **5***g* where k_{ex} is small, normal efficiencies for the excited singlet-state carbon–oxygen bond cleavage reaction are observed.

It is perhaps surprising that the intramolecular exciplex, as described by structure **8**, does not react by efficient cleavage of the carbon–oxygen bond of the ester. We know this is not true since substrates like **5***b* and **5***d* must be forming **8** with efficiencies approaching 100%, but the reaction efficiency is extremely low (quantum efficiencies well below 1%). The process of bond cleavage in charge-transfer species has been well documented (19) for the intramolecular radical anion/radical cation pairs of highly substituted ethane carbon–carbon bonds. As the authors state, "Radical ion pairs of the kind described herein (and related ones) can, in principle, cleave to yield either a pair of ions or neutral radicals. This is easy to describe (on paper, at least) in terms of electron "pushing".[3] If the carbon–oxygen bond electron pair in **8** is shifted to the naphthalene side (heterolytic cleavage), then the radical pair results; if one electron is shifted to the naphthalene and one to the benzoate side (homolytic cleavage), then the ion pair results.

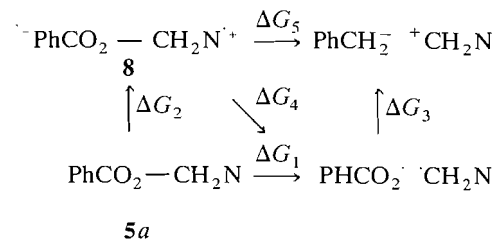

SCHEME 2. Thermodynamic cycle for estimating ΔG_4 (heterolytic cleavage) and ΔG_5 (homolytic cleavage) of the intramolecular exciplex **8**.

An estimate for the thermodynamic feasibility of these two processes can be made by the now very commonly used cycle shown in Scheme 2. The values of interest are ΔG_4 (heterolytic cleavage) and ΔG_5 (homolytic cleavage). A value of ΔG_1 = 268 kJ mol^{-1} can be estimated from the carbon–oxygen bond dissociation energy of 280 kJ mol^{-1} (20) for benzyl acetate minus 12 kJ mol^{-1} for the stabilization (21) of the 1-naphthylmethyl radical relative to the benzyl radical. A value of ΔG_2 = 355 kJ mol^{-1} is estimated from the oxidation potential of 1-methylnaphthalene (1.59 V vs. SCE in CH_3CN) (15) and the reduction potential of methyl benzoate (2.12 V vs. SCE in ethanol) (16). This ignores the electrostatic stabilization of **8**. Molecular models show that the two rings in **8** can be coplanar as close as 2 Å. Assuming the dielectric constant to be used is that the bulk medium, methanol, the value of this term[4] ($e^2/\epsilon r$) is about 21 kJ mol^{-1}. A value of ΔG_3 = −105 kJ mol^{-1} (in acetonitrile) can be estimated (15) from the oxidation potential of the 1-naphthylmethyl radical and the reduction potential of the acetyloxy radical. This leads to values of ΔG_4 = −66 kJ mol^{-1} and ΔG_5 = −192 kJ mol^{-1}. Both bond cleavage possibilities (heterolytic or homolytic) are clearly thermodynamically possible. The most reasonable explanation for lack of efficient bond cleavage in **8** is that back electron transfer to regenerate the ground state is faster. Note that molecular models indicate that there is no particular stereo-electronic inhibition to bond cleavage, as has been observed for some radical cations (22). Finally, as mentioned above, the

[3]Note that the authors have the electron "pushing" facts reversed in the rest of the paragraph and in Scheme II (19). If one apportions one electron of the central bond to each of the two parts, the result is the ion pair not the radical pair.

[4]NOTE ADDED IN PROOF: Suppan (23) recently proposed a very different model for contact ion pairs that gives this term a much larger value of ~150 kJ mol^{-1}. This, of course, leads to a very different conclusion about the stability of **8**.

Can. J. Chem. Downloaded from www.nrcresearchpress.com by 217.78.4.112 on 09/08/12
For personal use only.

phenylacetate esters **9** do not form intramolecular exciplexes. However, if an electron-donating group such as 4-CH_3O is on the benzene ring as in **14**, decreased fluorescence is again observed (3). The explanation again is intramolecular exciplex formation, but from the benzene ring to the naphthalene ring. Moreover, in this case, bond cleavage to radical pairs competes efficiently with back electron transfer.

Acknowledgements

We thank the Natural Sciences and Engineering Research Council of Canada for financial support.

1. S. J. Cristol and T. H. Bindel. Organic photochemistry. Vol. 6. Marcel Dekker, New York. 1983. p. 327.
2. D. P. DeCosta and J. A. Pincock. J. Am. Chem. Soc. **111**, 8948 (1989).
3. J. W. Hilborn and J. A. Pincock. J. Am. Chem. Soc. **113**, 2683 (1991).
4. J. W. Hilborn and J. A. Pincock. Can. J. Chem. **70**, 992 (1992).
5. B. Arnold, L. Donald, A. Jurgens, and J. A. Pincock. Can J. Chem. **63**, 3140 (1985).
6. R. S. Givens, G. Matuszewski, and C. V. Neywick. J. Am. Chem. Soc. **96**, 5547 (1974).
7. F. C. De Schriver, P. Collart, J. Vanderdriessche, R. Goldeweek, A. Swinen, and M. V. Auweraer. Acc. Chem. Res. **20**, 159 (1987).
8. P. Hirayama. J. Chem. Phys. **42**, 3163 (1965).
9. M. Iwamura, K. Tokuda, N. Koga, and H. Iwamura. Chem. Lett. 1729 (1987).
10. M. Iwamura, K. Takuma, N. Koga, and H. Iwamura. Chem. Lett. 1249 (1988).
11. T. Kamisuki, N. Akamatsu, Y. Adachi, C. Hirose, N. Yamamoto, K. Takuma, and M. Iwamura. Bull. Chem. Soc. Jpn. **62**, 1415 (1989).
12. P. Lenz, H. Blunre, and D. Schulte-Frohlinde. Ber. Bunsen-Ges. Phys. Chem. **74**, 484 (1970).
13. N. P. Buu-Hoi and D. Lavit. J. Chem. Soc. 2776 (1955).
14. B. Foster, B. Gaillard, N. Mathur, A. L. Pincock, J. A. Pincock, and C. Sehmbey. Can. J. Chem. **65**, 1599 (1987).
15. P. H. Milne, D. D. M. Wayner, D. P. DeCosta, and J. A. Pincock. Can. J. Chem. **70**, 121 (1992).
16. A. J. Bard. Encyclopedia of electrochemistry of the elements. Vol. XII. Marcel Dekker, New York. 1978. p. 261.
17. K. McMahon. Ph.D. Thesis, Dalhousie University, Halifax, 1991.
18. J. Chateauneuf, J. Lusztyk, and K. U. Ingold. J. Am. Chem. Soc. **110**, 2886 (1988).
19. N. J. Pienta, R. J. Kessler, K. S. Petus, E. D. O'Driscoll, E. M. Arnett, and K. E. Molter. J. Am. Chem. Soc. **113**, 3773 (1991).
20. D. F. McMillen and D. M. Golden. Annu. Rev. Phys. Chem. **33**, 493 (1982).
21. W. C. Herndon. J. Org. Chem. **46**, 2119 (1981).
22. A. L. Perrott and D. R. Arnold. Can. J. Chem. **70**, 272 (1992).
23. P. Suppan. Chimia, **42**, 320 (1988).

Can. J. Chem. Downloaded from www.nrcresearchpress.com by 217.78.4.112 on 09/08/12
For personal use only.

Coordination chemistry of thioether–pyridazine macrocycles. I. Synthetic, structural, and spectroscopic studies of Cu(II) and Cu(I) complexes of novel thioether–pyridazine macrocycles that contain two or three pyridazine subunits

LIQIN CHEN, LAURENCE K. THOMPSON,[1] AND JOHN N. BRIDSON
Department of Chemistry, Memorial University of Newfoundland, St. John's, Nfld., Canada A1B 3X7

Received January 15, 1992

LIQIN CHEN, LAURENCE K. THOMPSON, and JOHN N. BRIDSON. Can. J. Chem. **70**, 1886 (1992).

The preparations of thioether–pyridazine macrocycles containing three (L1) and two (L2) pyridazine subunits and their copper complexes are described. The ligands are characterized by ^{1}H nuclear magnetic resonance and mass spectrometry and in one case by X-ray crystallography, and the complexes by infrared, electronic, and electron spin resonance (esr) spectra and in some cases by X-ray crystallography. The complex $[Cu_3(L1)_2Cl_6] \cdot 2CHCl_3$ (**1**) crystallized in the triclinic system, space group $P\bar{1}$ with a = 13.661(2) Å, b = 14.174(3) Å, c = 9.412(2) Å, α = 101.08(2)°, β = 96.94(2)°, γ = 75.76(2)°, V = 1728.2(6) Å^3, and Z = 2 (R = 0.056, R_w = 0.048 for 2080 reflections). Two monodentate pyridazine rings in each ligand bind to one square-planar copper centre with the third monodentate pyridazine in each ligand linking the two to the central square-planar copper. The complex $[Cu(L2)Cl_2]$ (**2**) crystallized in the orthorhombic system, space group *Pnma*, with a = 8.571(1) Å, b = 16.104(3) Å, c = 13.961(2) Å, V = 1927(1) Å^3, and Z = 4 (R = 0.037, R_w = 0.033 for 1070 reflections). A *cis* square-planar structure exists for **2** with monodentate pyridazines. $[Cu(L2)_2] \cdot (ClO_4)_2 \cdot CH_3CN \cdot CHCl_3$ (**5**) crystallized in the triclinic system, space group $P\bar{1}$, with a = 12.888(4) Å, b = 17.462(6) Å, c = 10.906(1) Å, α = 96.07(2)°, β = 104.18(2)°, γ = 94.51(2)°, V = 2352(1) Å^3, and Z = 2 (R = 0.053, R_w = 0.044 for 2941 reflections). Two ligands involving monodentate pyridazine rings bind to a square-planar copper(II) centre. The protonated ligand salt $[L2H](ClO_4) \cdot H_2O$ (**6**) crystallized in the monoclinic system, space group $P2_1/n$, with a = 14.762(4) Å, b = 8.637(5) Å, c = 16.267(4) Å, β = 92.78(2)°, V = 2072(1) Å^3, and Z = 4 (R = 0.064, R_w = 0.053 for 1456 reflections). No sulfur coordination is observed in these complexes and there is no apparent spin exchange in the trinuclear derivative.

LIQIN CHEN, LAURENCE K. THOMPSON et JOHN N. BRIDSON. Can. J. Chem. **70**, 1886 (1992).

On décrit les préparations de macrocyles de thioéther–pyridazine contenant trois sous-unités (L1) et deux (L2) et de leurs complexes de cuivre. Les coordinats ont été caractérisés par résonance magnitique nucléaire du ^{1}H et par spectrométrie de masse et, dans un cas, par diffraction des rayons X; les complexes ont été caractérisés par leurs spectres infrarouges, électroniques et résonance paramagnétique électronique et, dans quelques cas, par diffraction des rayons X. Le complexe $[Cu_3(L1)_2Cl_6] \cdot 2CHCl_3$ (**1**) cristallise dans le système triclinique, groupe d'espace $P\bar{1}$ avec a = 13,661(2), b = 14,174(3) et c = 9,412 Å, α = 101,08(2), β = 96,94(2) et γ = 75,76(2)°, V = 1728,2(6) Å^3 et Z = 2 (R = 0,056, R_w = 0,048 pour 2080 réflexions). Deux cycles pyridazines monodentates dans chaque coordinat se lient à un cuivre central plan-carré alors que la troisième pyridazine monodentate de chaque coordinat relie les deux au cuivre central du plan-carré. Le complexe $[Cu(L2)Cl_2]$ (**2**) cristallise dans le système orthorhombique, groupe d'espace *Pnma*, avec a = 8,571(1), b = 16,104(3) et c = 13,961(2) Å, V = 1927(1) Å^3 et Z = 4 (R = 0,037 et R_w = 0,033 pour 1070 réflexions). Pour le composé **2**, il existe une structure plan carré *cis* portant des pyridazines monodentates. Le $[Cu(L2)_2] \cdot (ClO_4)_2 \cdot CH_3CN \cdot CHCl_3$ (**5**) cristallise dans le système triclinique, groupe d'espace, $P\bar{1}$, avec a = 12,888(4), b = 17,462(6) et c = 10,906(1) Å, α = 96,07(2), β = 104,18(2) et γ = 94,51(2)°, V = 2352(1) Å^3 et Z = 2 (R = 0,053 et R_w = 0,044 pour 2941 réflexions). Deux coordinats impliquant les cycles pyridazines monodentates se lient à une cuivre(II) central plan-carré. Le sel du ligand protoné $[L2H](ClO_4) \cdot H_2O$ (**6**) cristallise dans le système monoclinique, groupe d'espace $P2_1/n$, avec a = 14,762(4), b = 8,637(5) et c = 16,267(4) Å, β = 92,78(2)°, V = 2072(1) Å^3 et Z = 4 (R = 0,064 et R_w = 0,053 pour 1456 réflexions). Aucun de ces complexes ne présente de coordination par le soufre et il ne semble pas se produire d'échange de spin dans le dérivé trinucléaire.

[Traduit par la rédaction]

Introduction

The discovery of the structure of the "blue" copper proteins plastocyanin (1, 2) and azurin (3, 4) has demonstrated thioether sulfur coordination to the copper ion and although the intense visible absorption in these systems is associated with cysteine (thiolate) to copper charge transfer (5), the high reduction potentials are likely to be a function of both types of sulfur site. To clarify the relationship between electronic and molecular structure numerous studies have been directed towards the synthesis of copper complexes with coordination spheres similar to those of the proteins (6–15). Homoleptic thioether complexes represent the most promising synthetic systems to explain the electronic consequences of thioether coordination. For this reason a considerable number of homoleptic, thioether complexes of four, five, and six-coordinate copper have been studied (16–23). In addition, the coordination chemistry of chelating agents with built-in thioether and azole groups (15), and macrocyclic ligands with thioether and amino, amido, pyridine, furan, and thiophene subunits, has also been explored (24–33).

Our interest in mixed sulfur–nitrogen ligands involving thioether and diazine linkages stems from our earlier studies on open-chain tetradentate (N_4) thioether–pyridazine ligands (34–39), which involved non-coordinating thioether linkages and formed binuclear copper(II) complexes with, in some cases, positive (0 → + 0.5 V vs. SCE) reduction potentials. The combination of pyridazine and thioether groups, suitably disposed for simultaneous coordination, might be expected to produce binuclear copper(II) com-

[1]Author to whom correspondence may be addressed.

Can. J. Chem. Downloaded from www.nrcresearchpress.com by 217.78.4.112 on 09/08/12
For personal use only.

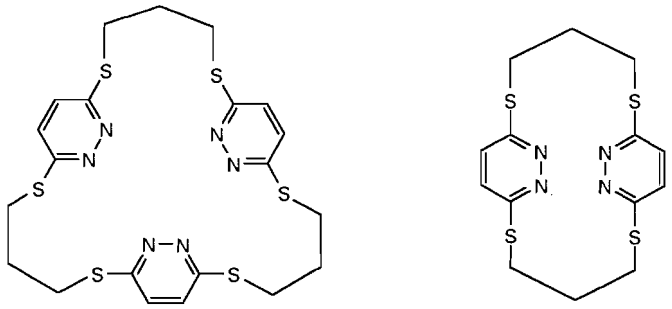

FIG. 1. Structural representation of the ligands.

plexes with more positive reduction potentials. Our initial studies in this area have involved the synthesis of a series of new macrocyclic thioether–pyridazine ligands and this paper describes the spectroscopic and structural investigation of copper(II) and copper(I) complexes of two oligomeric ligands (L1, L2, Fig. 1) derived from the reaction of 3,6-dichloropyridazine and 1,3-propanedithiol.

Experimental section

Commercially available reagents (Aldrich) were used without further purification. Infrared spectra were recorded using a Mattson Polaris FT instrument and electronic spectra with a Cary 17 spectrometer. The epr spectra were recorded with a Bruker ESP 300 X-band spectrometer at room temperature and 77 K. Mass spectra were obtained using a VG Micromass 7070 HS spectrometer and nmr spectra using a GE 300 MHz instrument. X-ray diffraction data were collected using a Rigaku AFC6S instrument and magnetic susceptibility data were measured by the Faraday method using a Cahn 7600 magnetic susceptibility system. Elemental analyses were performed by Canadian Microanalytical Service, Delta, British Columbia, Canada.

Synthesis of ligands and complexes

L1 and L2

1,3-Propanedithiol (2.82 g, 25 mmol) was added to anhydrous ethanol (100 mL), in which sodium metal (1.15 g, 50 mmol) had been dissolved and the resulting solution was stirred for 1 h. 3,6-Dichloropyridazine (3.84 g, 26 mmol) was dissolved in anhydrous ethanol (100 mL) and both solutions were added dropwise, simultaneously, to refluxing anhydrous ethanol (500 mL) by using pressure equalizing funnels, under a dry nitrogen atmosphere. The addition took place over a period of 6 h, during which time a white precipitate formed. The mixture was stirred and refluxed for a further 2 h and then stirred at room temperature overnight. The white solid (L1) was filtered off, washed with anhydrous ethanol (3 × 80 mL), and deionized water (3 × 100 mL), dried *in vacuo*, and recrystallized twice from $CHCl_3$. Yield: 150 mg (3.2%); mp 190–210°C. Further recrystallization from $MeNO_2$ produced white crystals, mp 188–190°C; ^1H nmr ($CDCl_3$) (δ (relative intensity)):2.25 (6) (multiplet, CH_2a), 3.36(12) (multiplet, CH_2b), 7.00 (6) (singlet, pyridazine). Mass spectrum, major mass peaks (*m/e* (relative intensity)):552(5) P, 519(4),367(7), 218(22), 184(43), 144(40), 106(39), 73(40), 41(100).

The initial filtrate obtained after isolation of L1 was removed on a rotary evaporator and the residual solid extracted with $CHCl_3$; the extract was washed several times with water and dried over Na_2SO_4. The concentrated extract was chromatographed on silica gel, eluted with $CHCl_3$, and the volume of the solution reduced to a few millilitres on a rotary evaporator and placed in a refrigerator. Colourless crystals of L2 were obtained. Yield: 0.52 g (11.3%); mp 215–217°C; ^1H nmr ($CDCl_3$) (δ (relative intensity)):2.43(4) (multiplet, CH_2a), 3.34(8) (multiplet, CH_2b), 7.00(4) (singlet, pyridazine). Mass spectrum, major mass peaks (*m/e* (relative intensity)):368(88) P, 217(33), 191(31), 185(66), 151(100), 144(81), 114(62), 96(34), 79(49), 73(66).

$[Cu_3(L1)_2Cl_6]\cdot 2CHCl_3$ (1)

$CuCl_2\cdot 2H_2O$ (0.17 g, 1.0 mmol) was dissolved in CH_3CN (20 mL) and added to a solution of L1 (0.11 g, 0.2 mmol) in $CHCl_3$ (20 mL). The resulting deep-green solution was filtered immediately and allowed to stand at room temperature overnight. A very small amount of an unidentified green solid formed, that was filtered off and the filtrate allowed to stand at room temperature for 1 week. Bluish-green crystals formed, which were filtered off, washed with CH_3CN and $CHCl_3$, and air dried (yield 31 mg). Anal. calcd. for $[C_{42}H_{56}N_{12}S_{12}Cl_6Cu_3]\cdot 2CHCl_3$: C 30.24, H 2.88, N 9.62; found: C 30.66, H 3.04, N 9.81.

$[Cu(L2)Cl_2]$ (2)

$CuCl_2\cdot 2H_2O$ (0.14 g, 0.80 mmol) was dissolved in CH_3CN (20 mL) and added to a solution of L2 (0.14 g, 0.38 mmol) in $CHCl_3$ (20 mL). The resulting dark-green solution was filtered immediately and allowed to stand at room temperature overnight. Bright green crystals formed, which were filtered off, washed with CH_3CN and $CHCl_3$, and air dried (yield 0.16 g). Anal. calcd. for $[C_{14}H_{16}N_4S_4Cl_2Cu]$: C 33.43, H 3.21, N 11.14; found: C 33.38, H 3.19, N 11.19.

$[Cu(L2)Br_2]$ (**3**) and $[Cu(L2)(NO_3)_2]$ (**4**) were prepared in a similar manner. Anal. calcd. for $[C_{14}H_{16}N_4S_4Br_2Cu]$ (**3**): C 28.41, H 2.72, N 9.47; found: C 28.31, H 2.67, N 9.49. Anal. calcd. for $[C_{14}H_{16}N_6O_6S_4Cu]$ (**4**): C 30.35, H 2.90, N 15.11 found: C 30.24, H 2.91, N 15.31.

$[Cu(L2)_2](ClO_4)_2\cdot CH_3CN\cdot CHCl_3$ (5), $[L2H](ClO_4)\cdot H_2O$ (6)

$Cu(ClO_4)_2\cdot 6H_2O$ (0.15 g, 0.40 mmol) was dissolved in CH_3CN (10 mL) and added to a solution of L2 (0.15 g, 0.40 mmol) in $CHCl_3$ (10 mL). The resulting brown solution was filtered and allowed to stand at room temperature for several days. A small quantity (15 mg) of pale yellow crystals (**6**) formed, which were filtered off and the brown filtrate evaporated slowly at room temperature. Red-brown crystals (**5**) formed, which were filtered off, washed with CH_3CN and $CHCl_3$, and air dried (yield 0.10 g). Anal. calcd. for $[C_{28}H_{32}N_8S_8Cu]\cdot(ClO_4)_2\cdot CH_3CN\cdot CHCl_3$ (**5**): C 32.10, H 3.13, N 10.87; found: C 32.11, H 3.20, N 10.90. Anal. calcd. for $[C_{14}H_{17}N_4](ClO_4)\cdot H_2O$ (**6**): C 34.53, H 3.93, N 11.50; found: C 34.23, H 3.96, N 11.46.

$[Cu(L2)Cl]$ (6)

Copper powder (0.19 g, 3.0 mmol) was added to a solution of $CuCl_2\cdot 2H_2O$ (0.051 g, 0.30 mmol) in CH_3CN (20 mL), the mixture stirred under a nitrogen atmosphere until the solution became colourless, and then filtered into a solution of L2 (0.074 g, 0.20 mmol) in $CHCl_3$ (20 mL) under a nitrogen atmosphere. The resulting orange solution was allowed to stand at room temperature overnight. Red crystals formed, which were filtered off, washed with CH_3CN and $CHCl_3$, and air dried (yield 0.058 g). Anal. calcd. for $[C_{14}N_{16}N_4S_4ClCu]$: C 35.96, H 3.45, N 11.98; found: C 36.06, H 3.44, N 11.94. [Cu(L2)Br] (**7**) was prepared in a similar manner and obtained as red-brown crystals. Anal. calcd. for $[C_{14}H_{16}N_4S_4BrCu]\cdot 0.5H_2O$: C 32.30, H 3.27, N 10.76; found: C 32.40, H 2.97, N 10.78.

X-ray crystallographic analysis of $[Cu(L2)Cl_2]$ (2)

The diffraction intensities of a green parallelepiped crystal of $[Cu(L2)Cl_2]$ of approximate dimensions 0.2 × 0.15 × 0.05 mm were collected using a Rigaku AFC6S diffractometer with graphite monochromatized MoKα radiation. Cell constants and the orientation matrix were obtained by the least-squares refinement of the setting angles of 25 carefully centred reflections in the range $26.23° < 2\theta < 38.84°$. Based on systematic absences, packing considerations, a statistical analysis of the intensity distribution, and the successful solution and refinement of the structure, the space group was determined to be *Pnma*. Machine and data collection

Can. J. Chem. Downloaded from www.nrcresearchpress.com by 217.78.4.112 on 09/08/12
For personal use only.

TABLE 1. Summary of crystal data, intensity collection, and structure refinement for **1**, **2**, **5**, and **6**

	$[Cu_3(L1)_2Cl_6] \cdot 2CHCl_3$ (**1**)	$[Cu(L2)Cl_2]$ (**2**)	$[Cu(L2)_2](ClO_4)_2 \cdot CH_3CN \cdot CHCl_3$ (**5**)	$[L2H](ClO_4) \cdot H_2O$ (**6**)
Formula	$C_{22}H_{25}Cu_{1.5}Cl_6N_6S_6$	$C_{14}H_{16}CuCl_2N_4S_4$	$C_{31}H_{36}CuCl_5N_9O_8S_8$	$C_{14}H_{19}ClN_4O_5S_4$
Crystal colour	Blue-green	Green	Brown	Pale yellow
(habit)	(regular polyhedron)	(parallelepiped)	(regular polyhedron)	(polyhedron)
Formula weight	873.88	503.00	1159.97	487.02
Crystal system	Triclinic	Orthorhombic	Triclinic	Monoclinic
Space group	$P\bar{1}$ (No. 2)	*Pnma* (No. 62)	$P\bar{1}$ (No. 2)	$P2_1/n$ (No. 14)
a (Å)	13.661(2)	8.571(1)	12.888(4)	14.762(4)
b (Å)	14.174(3)	16.104(3)	17.462(6)	8.637(5)
c (Å)	9.412(2)	13.961(2)	10.906(1)	16.267(4)
α (deg)	101.08(2)	—	96.07(2)	—
β (deg)	96.94(2)	—	104.18(2)	92.78(2)
γ (deg)	75.76(3)	—	94.51(2)	—
Volume (Å^3)	1728.2(6)	1927(1)	2352(1)	2072(1)
Density (g cm^{-3})				
calcd.	1.679	1.734	1.638	1.561
Z	2	4	2	4
Absorption coeff.,				
μ (cm^{-1})	17.77	18.39	11.47	6.03
Radiation, λ (Å)	MoKα, 0.71069	MoKα, 0.71069	MoKα, 0.71069	MoKα, 0.71069
Temperature (°C)	26	25	25	25
F_{000}	881	1020	1182	1008
Scan rate (deg min^{-1})	4.0 (ω scan)	8.0 (ω scan)	16.0 (ω scan)	16.0 (ω scan)
$2\theta_{max}$ (deg)	45.0	50.0	50.0	50.1
Data collected	4754	1979	8673	4083
Number of unique				
data ($I > 3.0\sigma(I)$)	2080	1070	2941	1456 ($I > 2.0\sigma(I)$)
Number of variables	373	119	545	266
Goodness of fit	1.77	1.39	1.55	1.95
R	0.056	0.037	0.053	0.063
R_w	0.048	0.033	0.044	0.052

parameters and crystal data are given in Table 1. The data were collected at 25 ± 1°C using the ω–2θ scan technique to a maximum 2θ value of 50.0°. Omega scans of several intense reflections, made prior to data collection, had an average width at half-height of 0.26° with a take-off angle of 6.0°. Scans of $(1.15 + 0.30 \tan\theta)°$ were made at a speed of 8.0°/min (in ω). The weak reflections ($I < 10.0\ \sigma(I)$) were rescanned (maximum of two rescans) and the counts were accumulated to assure good counting statistics. Stationary background counts were recorded on each side of the reflection. The ratio of peak counting time to background counting time was 2:1.

A total of 1979 reflections were collected. The intensities of three representative reflections, which were measured after every 150 reflections, remained constant during data collection (no decay correction applied). An empirical absorption correction was applied, using the program DIFABS (40), which resulted in transmission factors ranging from 0.94 to 1.08. The data were corrected for Lorentz and polarization effects.

The structure was solved by direct methods (41, 42). The non-hydrogen atoms were refined anisotropically. The final cycle of full-matrix least-squares refinement was based on 1070 observed reflections ($I > 3.00\ \sigma(I)$) and 119 variable parameters and converged with unweighted and weighted agreement factors of $R = \Sigma||F_o| - |F_c||/\Sigma|F_o| = 0.037$ and $R_w = [(\Sigma w(|F_o| - |F_c|)^2/\Sigma wF_o^2)]^{1/2} = 0.033$. The standard deviation of an observation of unit weight was 1.26. The weighting scheme was based on counting statistics and included a factor ($p = 0.01$) to downweight the intense reflections. Plots of $\Sigma w(|F_o| - |F_c|)^2$ versus $|F_o|$, reflection order in data collection, $\sin\theta/\lambda$, and various classes of indices showed no unusual trends. The maximum and minimum peaks on the final difference Fourier map corresponded to 0.40 and −0.43 electrons/Å^3 respectively and have no chemical significance. Neutral atom scattering factors (43) and anomalous dispersion terms (44, 45) were taken from the usual sources. All calculations were performed using the TEXSAN (46) crystallographic software package using a VAX 3100 workstation. Hydrogen atoms were located in a difference map but not refined. Thermal parameters were set at 1.2 times the isotropic thermal parameter of the bonded C atoms.

TABLE 2. Positional parameters and B(eq) values (esd's) for $[Cu(L2)Cl_2]$ (**2**)

Atom	x	y	z	B(eq)
Cu(1)	0.3348(1)	1/4	0.51675(6)	2.17(4)
Cl(1)	0.1683(2)	0.35231(8)	0.5555(1)	3.18(6)
S(1)	0.5594(2)	0.1393(1)	0.6496(1)	3.31(7)
S(2)	0.5765(2)	0.0787(1)	0.2121(1)	3.87(8)
N(1)	0.4868(5)	0.1628(3)	0.4691(3)	2.5(2)
N(2)	0.4821(5)	0.1505(3)	0.3733(3)	2.7(2)
C(1)	0.817(1)	1/4	0.6327(6)	3.8(4)
C(2)	0.7605(7)	0.1705(4)	0.6773(4)	4.1(3)
C(3)	0.5772(6)	0.1178(3)	0.5264(4)	2.6(3)
C(4)	0.6723(7)	0.0561(3)	0.4883(4)	3.3(3)
C(5)	0.6719(7)	0.0418(3)	0.3926(4)	3.3(3)
C(6)	0.5734(6)	0.0921(3)	0.3364(4)	2.7(3)
C(7)	0.4805(7)	0.1720(4)	0.1725(4)	3.5(3)
C(8)	0.5752(9)	1/4	0.1914(5)	2.8(4)

Atomic positional parameters are given in Table 2 and selected bond distances and angles are given in Table 5. Thermal parame-

Can. J. Chem. Downloaded from www.nrcresearchpress.com by 217.78.4.112 on 09/08/12
For personal use only.

Can. J. Chem. Downloaded from www.nrcresearchpress.com by 217.78.4.112 on 09/08/12
For personal use only.

ters (Table S-1), hydrogen atom parameters (Table S-2), a full listing of bond distances and angles (Table S-3), and observed and calculated structure factors ($10|F_o|$ and $10|F_c|$) (Table S-4) are deposited as supplementary material.[2]

X-ray crystallographic analysis of $[Cu_3(L1)_2Cl_6]\cdot 2CHCl_3$ (1)

The diffraction intensities of a blue-green regular polyhedral crystal of **1** of approximate dimensions 0.30 × 0.25 × 0.15 mm were collected in a similar manner to **2**. Crystal data, intensity collection, and refinement details are summarized in Table 1. Hydrogen atoms were placed in calculated positions (C—H 0.95Å) and not refined. Thermal parameters were set at 1.2 times the isotropic thermal parameter of the bonded C atoms. The chloroform molecule was disordered and was modelled with two chlorines and the carbon disordered over two positions with 50% occupancy. Atomic positional parameters are given in Table 3 and selected bond distances and angles are given in Table 6. Thermal parameters (Table S-5), hydrogen atom parameters (Table S-6), a full listing of bond distances and angles (Table S-7), and observed and calculated structure factors ($10|F_o|$ and $10|F_c|$) (Table S-8) are deposited as supplementary material.[2]

Least-squares planes data for **2**, **5**, **6**, (Tables S-17 to S-19 respectively) and torsional angles data for **1**, **2**, **5**, **6** (Tables S-20 to S-23 respectively) are deposited as supplementary material.[2]

X-ray crystallographic analysis of $[Cu(L2)_2](ClO_4)_2\cdot 2CH_3CN\cdot CHCl_3$ (5)

The diffraction intensities of a brown, regular polyhedral crystal of **5** of approximate dimensions 0.30 × 0.25 × 0.15 mm were collected in a similar manner to **2**. Crystal data, intensity collection, and refinement details are summarized in Table 1. Hydrogen atoms were placed in calculated positions (C—H 0.95 Å) and not refined. Thermal parameters were set at 1.2 times the isotropic thermal parameter of the bonded C atoms. Atomic positional parameters are given in Table 4 and selected bond distances and angles are given in Table 8. Thermal parameters (Table S-9), hydrogen atom parameters (Table S-10), a full listing of bond distances and angles (Table S-11), and observed and calculated structure factors ($10|F_o|$ and $10|F_c|$) (Table S-12) are deposited as supplementary material.[2]

X-ray crystallographic analysis of $[L2H](ClO_4)\cdot H_2O$ (6)

The diffraction intensities of a colourless, polyhedral crystal of **6** of approximate dimensions 0.25 × 0.25 × 0.20 mm were collected in a similar manner to 2. Crystal data, intensity collection, and refinement details are summarized in Table 1. Hydrogens on the water molecule and on N4 were located from difference maps. The position of HN4 was allowed to refine during an early round of least squares, where it remained in a sensible position. However, because of a somewhat limited data set, this hydrogen was fixed in final rounds. Other hydrogens including that at N1 were put in calculated positions (C—H 0.95 Å and isotropic thermal parameters set at 1.2 times the isotropic value of the bonded carbon). Occupancy of the hydrogens on N1 and N4 was set at 0.5, but no attempt was made to refine this. The final round of least squares included all hydrogen atoms, none of which were refined. The perchlorate ion appears to be disordered around the Cl—O1 axis and the occupancies of the two images used to model the disorder were arbitrarily set at 0.7 and 0.3. A limited data set was obtained for this compound and a sigma cut-off of 2.0 was chosen to give a better ratio of data to refined variables. Atomic positional parameters are given in Table 5 and selected bond distances and angles are given in Table 9. Thermal parameters (Table S-13), hydrogen atom parameters (Table S-14), a full listing of bond distances and angles (Table S-15), and observed and calculated structure factors ($10|F_o|$ and $10|F_c|$) (Table S-16) are deposited as supplementary material.[2]

TABLE 3. Positional parameters and B(eq) values (esd's) for $[Cu_3(L1)_2Cl_6]\cdot 2CHCl_3$ (**1**)

Atom	x	Y	z	B(eq)
Cu(1)	0	0	1.0000	2.7(1)
Cu(2)	0.3263(1)	0.3148(1)	0.8764(2)	2.5(1)
Cl(1)	−0.0508(3)	0.1608(3)	1.0929(5)	4.4(2)
Cl(2)	0.3377(3)	0.2680(3)	0.6404(4)	5.5(3)
Cl(3)	0.4529(3)	0.1924(3)	0.9350(4)	4.3(2)
Cl(4)	0.6807(5)	0.1358(4)	0.5761(6)	8.9(4)
Cl(5)	0.615(3)	0.229(3)	0.358(4)	30.8
Cl(6)	0.545(5)	0.129(7)	0.31(1)	69.4
Cl(7)	0.5397(7)	0.0267(7)	0.448(1)	6.6
Cl(8)	0.5494(9)	0.1915(7)	0.321(1)	5.9
S(1)	0.0649(4)	0.1169(3)	0.5100(5)	5.0(3)
S(2)	−0.0826(3)	0.4326(3)	0.8056(6)	6.0(3)
S(3)	0.3310(3)	0.5367(3)	0.8076(5)	4.3(2)
S(4)	0.4131(3)	0.5888(3)	1.3233(5)	4.9(3)
S(5)	0.2018(3)	0.2469(3)	1.1036(4)	3.5(2)
S(6)	0.2428(3)	−0.0421(3)	1.0760(4)	3.7(2)
N(1)	0.100(1)	0.0277(8)	0.887(1)	3.1(7)
N(2)	0.0556(8)	0.0613(8)	0.762(1)	3.1(7)
N(3)	0.118(1)	0.3994(8)	0.830(1)	3.6(8)
N(4)	0.207(1)	0.4257(8)	0.835(1)	3.0(7)
N(5)	0.3570(8)	0.4443(9)	1.130(1)	3.3(7)
N(6)	0.3128(8)	0.3674(8)	1.088(1)	2.2(6)
C(1)	0.200(1)	0.010(1)	0.920(1)	2.8(8)
C(2)	0.264(1)	0.031(1)	0.830(2)	4(1)
C(3)	0.220(1)	0.067(1)	0.707(2)	4(1)
C(4)	0.117(1)	0.078(1)	0.674(2)	3.4(9)
C(5)	−0.069(1)	0.161(1)	0.535(2)	5(1)
C(6)	−0.098(1)	0.274(1)	0.592(2)	5(1)
C(7)	−0.052(1)	0.300(1)	0.749(2)	4(1)
C(8)	0.033(1)	0.468(1)	0.808(2)	4(1)
C(9)	0.033(1)	0.562(1)	0.794(2)	6(1)
C(10)	0.124(1)	0.586(1)	0.797(2)	5(1)
C(11)	0.211(1)	0.514(1)	0.819(1)	4(1)
C(12)	0.321(1)	0.660(1)	0.913(2)	5(1)
C(13)	0.315(1)	0.666(1)	1.074(2)	5(1)
C(14)	0.416(1)	0.622(1)	1.150(2)	5(1)
C(15)	0.363(1)	0.481(1)	1.269(2)	3.3(9)
C(16)	0.332(1)	0.441(1)	1.375(2)	4(1)
C(17)	0.287(1)	0.366(1)	1.332(2)	2.9(8)
C(18)	0.274(1)	0.333(1)	1.182(2)	2.8(8)
C(19)	0.196(1)	0.184(1)	1.249(1)	3.2(8)
C(20)	0.292(1)	0.110(1)	1.289(2)	4(1)
C(21)	0.334(1)	0.030(1)	1.164(2)	3.6(9)
C(22)	0.55(1)	0.17(1)	0.52(2)	18.3
C(23)	0.568(3)	0.149(3)	0.479(4)	4.6

Results and discussion

Although macrocyclic thioether ligands containing aromatic and heterocyclic rings, e.g., pyridine, are well known (28, 31, 47), we are not aware of any reports of such thioether macrocycles involving pyridazine subunits. Polythia(3,6)-pyridazinophanes can be synthesized, usually in reasonable

[2]Supplementary Tables S-1 to S-23 may be purchased from: The Depository of Unpublished Data, Document Delivery, CISTI, National Research Council Canada, Ottawa, Canada K1A OS2.

Tables of atomic positional parameters and bond distances and angles for **1**, **2**, **5**, and **6** have also been deposited with the Cambridge Crystallographic Data Centre and can be obtained on request from the Director, Cambridge Crystallographic Data Centre, University Chemical Laboratory, 12 Union Road, Cambridge, CB2 1EZ, U.K.

Can. J. Chem. Downloaded from www.nrcresearchpress.com by 217.78.4.112 on 09/08/12
For personal use only.

TABLE 4. Positional parameters and B(eq) values (esd's) for $[Cu(L2)_2](ClO_4)_2 \cdot CH_3CN \cdot CHCl_3$ (**5**)

Atom	*x*	*Y*	*z*	*B*(eq)
Cu(1)	0.8072(1)	0.25610(8)	0.4367(1)	2.06(6)
Cl(1)	0.1566(3)	0.3602(2)	0.0741(4)	4.4(2)
Cl(2)	0.4380(3)	0.1891(2)	0.7563(3)	3.8(2)
Cl(3)	0.4677(3)	0.0870(2)	0.2098(4)	7.1(2)
Cl(4)	0.2696(4)	0.1229(3)	0.0561(4)	8.3(3)
Cl(5)	0.3474(3)	−0.0221(3)	−0.0011(4)	6.9(2)
S(1)	0.7951(3)	0.2581(2)	0.1315(3)	3.7(1)
S(2)	0.4000(3)	0.3170(2)	0.3430(4)	5.2(2)
S(3)	0.7342(3)	0.3538(2)	0.6744(3)	3.6(1)
S(4)	0.9113(3)	0.5279(2)	0.2906(4)	4.7(2)
S(5)	1.0620(3)	0.2739(2)	0.4248(3)	3.8(1)
S(6)	0.9313(3)	0.1689(2)	0.8949(3)	4.8(2)
S(7)	0.6337(3)	0.1268(2)	0.5158(3)	3.6(1)
S(8)	0.9533(3)	0.0167(2)	0.2104(4)	5.6(2)
O(1)	0.0694(8)	0.3697(6)	−0.028(1)	6.9(5)
O(2)	0.118(1)	0.3381(7)	0.174(1)	10.3(7)
O(3)	0.2205(8)	0.3070(7)	0.037(1)	9.3(6)
O(4)	0.3905(9)	0.1656(5)	0.6262(8)	8.0(6)
O(5)	0.533(1)	0.2372(7)	0.775(1)	9.1(6)
O(6)	0.467(1)	0.1229(7)	0.815(1)	9.8(7)
O(7)	0.221(1)	0.4310(7)	0.120(1)	10.0(7)
O(8)	0.368(1)	0.221(1)	0.813(1)	14(1)
N(1)	0.6803(7)	0.2706(5)	0.2987(8)	2.4(4)
N(2)	0.5970(8)	0.2833(5)	0.3504(8)	2.8(4)
N(3)	0.8226(7)	0.3708(5)	0.4847(9)	2.4(4)
N(4)	0.8644(7)	0.4059(6)	0.4000(8)	2.9(4)
N(5)	0.9359(7)	0.2398(5)	0.5685(8)	2.7(4)
N(6)	0.9024(7)	0.2180(5)	0.6719(9)	2.7(4)
N(7)	0.7844(7)	0.1402(5)	0.3934(8)	2.4(4)
N(8)	0.8547(8)	0.1197(5)	0.3260(9)	3.1(4)
N(9)	0.598(1)	0.4809(8)	0.258(1)	8.2(4)
C(1)	0.675(1)	0.2722(6)	0.176(1)	2.7(5)
C(2)	0.576(1)	0.2842(7)	0.095(1)	3.8(6)
C(3)	0.491(1)	0.2956(8)	0.143(1)	4.2(6)
C(4)	0.505(1)	0.2973(7)	0.274(1)	3.4(6)
C(5)	0.471(1)	0.3279(8)	0.511(1)	4.1(6)
C(6)	0.539(1)	0.4060(8)	0.559(1)	4.1(6)
C(7)	0.621(1)	0.4057(8)	0.686(1)	4.8(7)
C(8)	0.7878(9)	0.4098(7)	0.575(1)	2.6(5)
C(9)	0.796(1)	0.4912(7)	0.587(1)	3.7(6)
C(10)	0.834(1)	0.5254(7)	0.498(1)	4.4(6)
C(11)	0.867(1)	0.4807(7)	0.405(1)	3.1(6)
C(12)	0.916(1)	0.4469(7)	0.177(1)	4.0(6)
C(13)	0.805(1)	0.4166(7)	0.091(1)	4.0(6)
C(14)	0.798(1)	0.3323(8)	0.029(1)	4.7(7)
C(15)	1.0377(9)	0.2456(5)	0.565(1)	2.3(4)
C(16)	1.118(1)	0.2308(7)	0.672(1)	3.6(6)
C(17)	1.085(1)	0.2109(8)	0.774(1)	4.0(6)
C(18)	0.977(1)	0.2023(6)	0.770(1)	3.1(5)
C(19)	0.789(1)	0.1443(8)	0.818(1)	4.8(7)
C(20)	0.763(1)	0.0703(7)	0.727(1)	4.0(6)
C(21)	0.649(1)	0.0626(7)	0.637(1)	4.5(6)
C(22)	0.7195(9)	0.0898(7)	0.428(1)	2.6(5)
C(23)	0.718(1)	0.0095(7)	0.389(1)	3.9(6)
C(24)	0.788(1)	−0.0130(7)	0.321(1)	3.6(6)
C(25)	0.858(1)	0.0449(8)	0.291(1)	3.6(6)
C(26)	1.035(1)	0.1062(8)	0.231(1)	4.3(6)
C(27)	1.113(1)	0.1252(8)	0.360(1)	4.2(6)
C(28)	1.159(1)	0.2116(8)	0.395(1)	4.6(6)
C(29)	0.382(1)	0.0752(8)	0.055(1)	5.1(7)
C(30)	0.605(1)	0.525(1)	0.193(2)	7.2(4)
C(31)	0.626(2)	0.580(1)	0.110(2)	11.4(6)

TABLE 5. Positional parameters and *B*(eq) values (esd's) for [L2H] $(ClO_4) \cdot H_2O$ (**6**)

Atom	*x*	*y*	*z*	*B*(eq)
Cl(1)	0.7333(2)	0.4569(4)	0.4696(2)	4.6(2)
S(1)	−0.0047(2)	0.2591(4)	0.3538(2)	4.2(2)
S(2)	0.1086(2)	0.1281(4)	0.7187(2)	4.4(2)
S(3)	0.4711(2)	0.1147(4)	0.6397(2)	4.5(2)
S(4)	0.3582(2)	0.2652(4)	0.2768(2)	4.3(2)
O(1)	0.6567(5)	0.509(1)	0.4230(5)	7.5(6)
O(2)	0.766(1)	0.312(2)	0.442(1)	8(1)
O(3)	0.800(1)	0.571(2)	0.477(1)	8(1)
O(4)	0.703(1)	0.426(2)	0.5509(7)	9(1)
O(5)	0.742(4)	0.536(7)	0.526(4)	17(2)
O(6)	0.810(2)	0.492(5)	0.422(2)	8(1)
O(7)	0.724(2)	0.303(6)	0.466(3)	7(1)
O(8)	0.7934(4)	0.0878(8)	0.5899(3)	3.3(3)
N(1)	0.0887(5)	0.116(1)	0.4788(5)	3.3(4)
N(2)	0.1152(5)	0.085(1)	0.5575(5)	3.4(5)
N(3)	0.3684(5)	0.087(1)	0.5022(5)	3.5(5)
N(4)	0.3462(5)	0.122(1)	0.4229(5)	3.2(4)
C(1)	0.0258(6)	0.220(1)	0.4573(6)	3.0(5)
C(2)	−0.0172(6)	0.306(1)	0.5185(7)	3.8(6)
C(3)	0.0067(7)	0.275(1)	0.5975(7)	3.8(6)
C(4)	0.0749(7)	0.164(1)	0.6153(6)	3.3(6)
C(5)	0.2103(7)	0.015(1)	0.7092(5)	4.2(6)
C(6)	0.2906(7)	0.112(1)	0.6848(6)	3.5(5)
C(7)	0.3746(8)	0.009(1)	0.6719(6)	4.2(6)
C(8)	0.4405(7)	0.156(1)	0.5353(6)	3.6(6)
C(9)	0.4931(7)	0.263(2)	0.4937(8)	4.1(6)
C(10)	0.4690(7)	0.296(1)	0.4146(7)	4.3(7)
C(11)	0.3912(7)	0.222(1)	0.3797(6)	3.8(6)
C(12)	0.2490(8)	0.176(1)	0.2625(6)	4.3(6)
C(13)	0.1738(7)	0.257(1)	0.3074(6)	4.1(6)
C(14)	0.0847(7)	0.167(1)	0.3001(6)	4.2(6)

TABLE 6. Selected bond distances (Å) and angles (deg) for $[Cu(L2)Cl_2]$ (**2**)

Cu(1)—Cl(1)	2.246(2)
Cu(1)—N(1)	2.028(4)
Cl(1)—Cu(1)—Cl(1)a	94.39(8)
Cl(1)—Cu(1)—N(1)	174.5(1)
Cl(1)—Cu(1)—N(1)a	88.8(1)
Cl(1)a—Cu(1)—N(1)a	174.5(1)
N(1)—Cu(1)—N(1)a	87.7(2)

yields, by the condensation of 3,6-dichloropyridazine with a dithiol under high-dilution conditions in basic media. In this report we examine the copper coordination chemistry of two low-yield, oligomeric (3:3, L1; 2:2, L2; Fig. 1) thiapyridazinophanes derived from the reaction of 1,3-propane-dithiol with 3,6-dichloropyridazine. Other longer chain S_3 and S_4 α, ω-dithiols produce just 1:1 or 2:2 macrocycles on reaction with 3,6-dichloropyridazine and their coordination chemistry will be described elsewhere.[3]

The appearance of the perchlorate salt of L2 as a minor product during the synthesis of $[Cu(L2)_2](ClO_4)_2 \cdot CH_3CN \cdot CHCl_3$ (**5**) was a surprise, but nevertheless a fortuitous one since crystals of L2 itself, obtained after several recrystallizations, were found to be unsuitable for structural analy-

[3]L. Chen and L. K. Thompson, unpublished results.

TABLE 7. Selected bond distances (Å) and angles (deg) for $[Cu_3(L1)_2Cl_6] \cdot 2CHCl_3$ (**1**)

Cu(1)—N(1)	1.99(1)	Cu(1)—N(1)a	1.99(1)
Cu(1)—Cl(1)	2.246(4)	Cu(1)—Cl(1)a	2.246(4)
Cu(1)—N(4)	2.02(1)		
Cu(2)—N(6)	2.00(1)		
Cu(2)—Cl(2)	2.206(4)		
Cu(2)—Cl(3)	2.229(4)		
Cl(1)—Cu(1)—N(1)	91.5(3)		
Cl(1)—Cu(1)—Cl(1)a	180.00		
N(1)—Cu(1)—N(1)a	180.00		
Cl(1)a—Cu(1)—N(1)a	88.5(3)		
N(4)—Cu(2)—N(6)	87.7(4)		
N(6)—Cu(2)—Cl(3)	89.2(3)		
Cl(3)—Cu(2)—Cl(2)	94.3(2)		
Cl(2)—Cu(2)—N(4)	88.9(3)		
N(4)—Cu(2)—N(6)	87.7(4)		
N(4)—Cu(2)—Cl(3)	176.3(4)		
N(6)—Cu(2)—Cl(2)	175.9(3)		

TABLE 8. Selected bond distances (Å) and angles (deg) for $[Cu(L2)_2] (ClO_4)_2 \cdot CH_3CN \cdot CHCl_3$ (**5**)

Cu(1)—N(1)	1.986(8)
Cu(1)—N(3)	1.997(9)
Cu(1)—N(5)	1.973(9)
Cu(1)—N(7)	2.010(9)
N(1)—Cu(1)—N(3)	86.6(4)
N(3)—Cu(1)—N(5)	94.6(4)
N(5)—Cu(1)—N(7)	86.3(4)
N(7)—Cu(1)—N(1)	92.6(4)
N(1)—Cu(1)—N(5)	177.6(4)
N(3)—Cu(1)—N(7)	176.6(4)

TABLE 9. Selected bond distances (Å) and angles (deg) for $[L2H](ClO_4) \cdot H_2O$ (**6**)

N(1)—C(1)	1.33(1)	N(4)—C(11)	1.31(1)
N(1)—N(2)	1.35(1)	N(3)—N(4)	1.35(1)
N(2)—C(4)	1.33(1)	N(3)—C(8)	1.31(1)
C(11)—N(4)—N(3)	123.8(9)	C(1)—N(1)—N(2)	123.7(9)
N(4)—N(3)—C(8)	116.1(9)	N(1)—N(2)—C(4)	116.6(9)

sis. We attribute the formation of the salt to the presence of residual perchloric acid impurity in the commercial copper(II) perchlorate.

Description of the structures of $[Cu_3(L1)_2Cl_6] \cdot 2CHCl_3$ (I), $Cu(L2)Cl_2$ (2), $[Cu(L2)_2](ClO_4)_2 \cdot CH_3CN \cdot CHCl_3$ (5), and $[L2H](ClO_4 \cdot H_2O$ (6)

The structure of $[Cu_3(L1)_2Cl_6]$ (**1**) is unique (Fig. 2) in that it contains a trinuclear arrangement of copper(II) centres in which the central copper (Cu1) bridges two ligands that encompass one copper each. The molecule has a centre of symmetry at Cu1 with the result that the three coppers are colinear. The Cu1—Cu2 separation is 7.360(2) Å. The central copper has an almost square-planar *trans*-CuN_2Cl_2 arrangement of ligand donors involving one pyridazine nitrogen from each ligand. Copper–nitrogen and copper–chlorine distances are normal for ligands of this sort. In contrast the terminal coppers (Cu2) have an almost square-planar *cis* structure, with comparable Cu—N and Cu—Cl separations to those around Cu1. Each ligand coordinates in a tridentate (N_3) fashion, with each pyridazine fragment utilizing one nitrogen only. L1 is a 27-membered macrocycle and effectively uses just two pyridazine nitrogens in coordination to the endocyclic metal (Cu2). This creates a most unusual situation where the ligand forms two very large chelate rings, one involving 11 atoms and the other 20. This is seen, in part, as a consequence of the juxtaposition of the sulfur and nitrogen centres, such that simultaneous coordination of adjacent sulfur and nitrogen atoms would be highly unlikely due to the formation of a four-membered chelate ring. The hard nature of the copper(II) centre and the presence of relatively strong chlorine ligands would also mitigate against sulfur coordination.

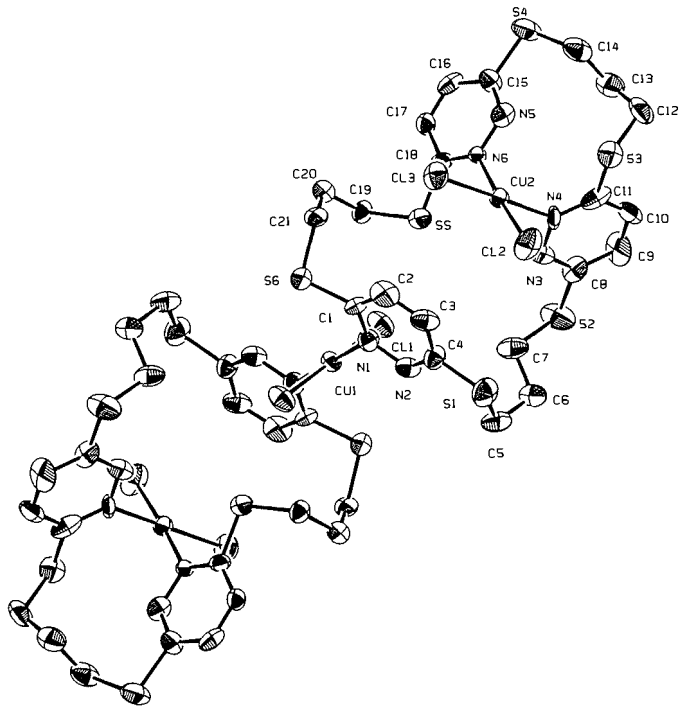

FIG. 2. Molecular structure of $[Cu_3(L1)_2Cl_6]$ (**1**) (40% probability ellipsoids).

The structure of $[CuL2Cl_2]$ (**2**) is illustrated in Fig. 3 and consists of an almost square-planar *cis* copper(II) centre bound by two pyridazine nitrogens, one from each pyridazine ring. Copper–chlorine (2.246(2) Å) and copper–nitrogen (2.028(4) Å) distances are normal and the square plane is slightly compressed (Cl1—Cu1—Cl1 94.39(8)°, Cl1—Cu1—N1 88.8(1)°) with the copper centre displaced by 0.082 Å from the mean Cl_2N_2 plane. The tetrathiapyridazinophane ligand L2 utilizes two nitrogen donor atoms on the same relative side of the macrocyclic ring as opposed to opposite sides for each *endo*-macrocyclic copper centre in **1**. This results in the creation of two chelate rings of different size (10-membered and 12-membered). The two pyridazine ring least-squares planes are separated by a dihedral angle of 83.5°.

The structure of $[Cu(L2)_2]^{2+}$ (**6**) is illustrated in Fig. 4 and involves two *cis*-bidentate N_2 ligands bound to a slightly distorted square-planar copper(II) centre. Each ligand uti-

Can. J. Chem. Downloaded from www.nrcresearchpress.com by 217.78.4.112 on 09/08/12
For personal use only.

Can. J. Chem. Downloaded from www.nrcresearchpress.com by 217.78.4.112 on 09/08/12
For personal use only.

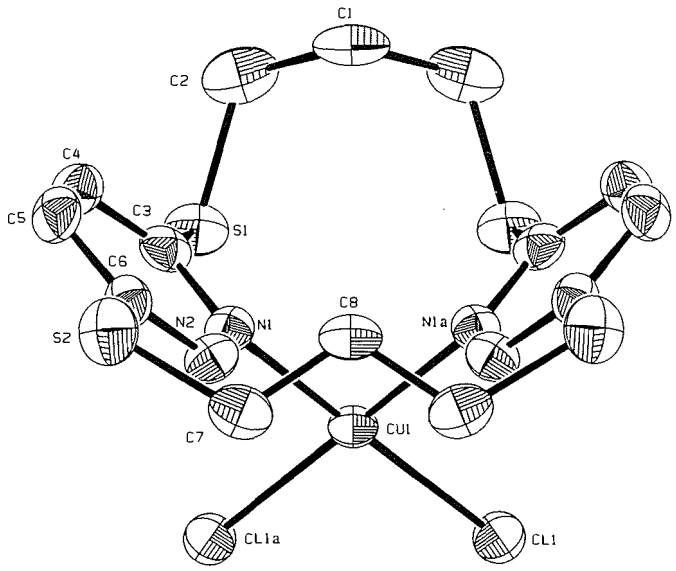

FIG. 3. Molecular structure of $[Cu(L2)Cl_2]$ (**2**) (40% probability ellipsoids).

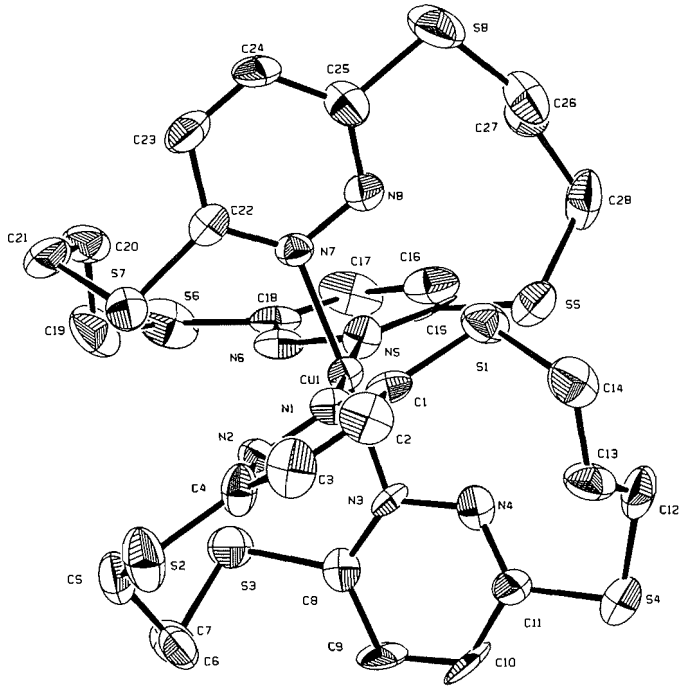

FIG. 4. Molecular structure of $[Cu(L2)_2]^{2+}$ (**5**) (40% probability ellipsoids).

lizes one nitrogen donor per pyridazine ring but, unlike the situation in **2**, opposite pyridazine nitrogens are involved. This produces a situation where the two chelate rings within each macrocyclic half are 11-membered. The four copper–nitrogen bond distances are very similar and the copper square plane is compressed slightly within each chelating half (N1—Cu1—N2 86.6(4)°, N5—Cu1—N7 86.3(4)°). The copper centre is displaced slightly from the mean N_4 plane by 0.011 Å. A packing diagram (Fig. 5) shows that there are no significant associations between cations and that perchlorate oxygens are not involved in coordination. The dihedral angle between the pyridazine rings defined by N1 and

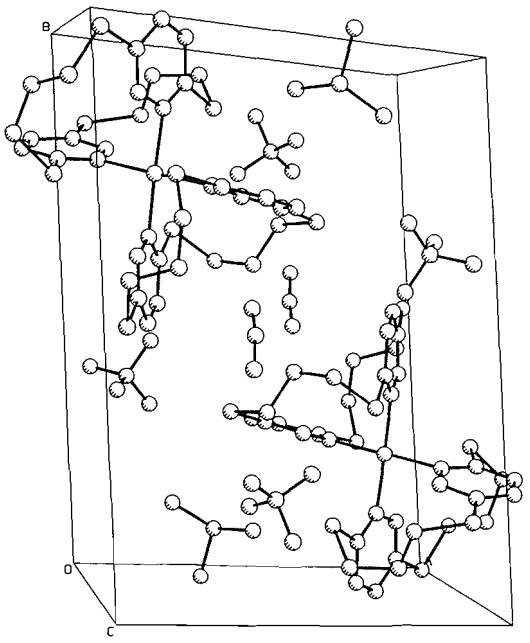

FIG. 5. Packing diagram for $[Cu(L2)_2](ClO_4)_2 \cdot CH_3CN \cdot CHCl_3$ (**5**).

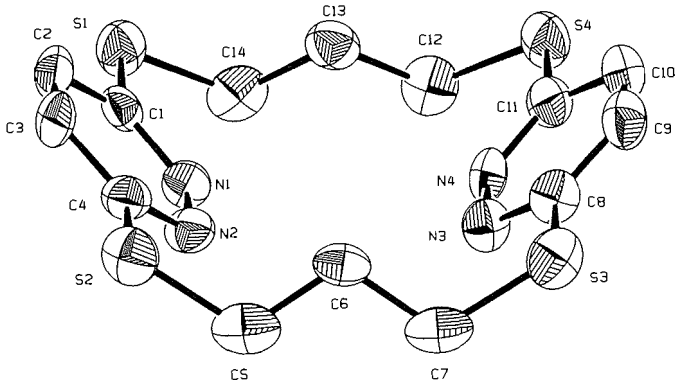

FIG. 6. Molecular structure of $[L2H]^+$ (hydrogens omitted) (40% probability ellipsoids).

N3 is 76.1°, while that between the pyridazine rings defined by N5 and N7 is 81.8°.

The structure of $[L2H]^+$ is illustrated in Fig. 6. The protonated ligand adopts a crownlike conformation with the pyridazine rings canted inwards such that the nitrogen lone pairs point towards the roof of the crown, and with a dihedral angle of 95.7° between the pyridazine least-squares planes. The sulfur lone pairs are exodentate to the ring. Torsional angles N1—C1—S1—C14 (−13(1)°), N2—C4—S2—C5 (12(1)°), N3—C8—S3—C7 (−10(1)°), and N4—C11—S4—C12 (11(1)°) indicate a slight twisting of the aliphatic C—S bonds relative to the pyridazine planes. The inward canting of the pyridazine rings appears to present the nitrogen lone pairs in a favourable orientation for coordination as a tetradentate N_4 ligand to two metal centres. Molecular models confirm these possibilities, although some reorganization of the aliphatic chains would be required to prevent serious steric problems involving the C—H bonds. However, even with anionic groups (e.g., Cl, Br) that could occupy vacant copper coordination sites, such binuclear

Can. J. Chem. Downloaded from www.nrcresearchpress.com by 217.78.4.112 on 09/08/12
For personal use only.

structures have not occurred with L2. This is somewhat surprising because for $[Cu(L2)Cl_2]$ (**2**) (Fig. 3) the torsional angle N1—C3—S1—C2 of −120.1(5)° indicates quite clearly that the aliphatic fragment can readily reorient to accommodate one planar copper(II) centre bound to nitrogen atoms N1. The other torsional angle, N2—C6—S2—C7 (13.6(6)°) is comparable with that in $L2H^+$. Molecular models indicate that an N—C—S—C torsional angle of about 120° at both ends of each pyridazine would be sufficient to accommodate two metals. The foregoing discussion makes the assumption that the conformation of the free ligand, L2, would be comparable with that in **6**.

The hydrogen atoms on the water molecule and that on N4 were located from difference maps and the location of H-N4 was tested by allowing its position to refine during an early round of least squares, where it remained at a sensible position and no peaks were seen at other possible protonation sites. Refinement was completed with the nitrogen-hydrogen located at N4 and a reasonable result was obtained (R = 0.064, R_w = 0.053, GOF = 1.99). However, significant differences in pyridazine nitrogen ring angles resulted in both pyridazine rings (C11—N4—N3 124.9(9)°, N4—N3—C8 115.2(9)°, N2—N1—C1 122.4(9)°, N1—N2—C4 117.4(9)°). This situation would not be anticipated if the N-H proton were located on just one pyridazine nitrogen. The unprotonated ligand 3,6-bis-(2-pyridylthio)pyridazine has two virtually identical ring nitrogen angles (119.3(2)°, 119.4(2)°) (39) and in compounds **1**, **2**, and **5** significant differences are observed in the pyridazine nitrogen ring angles with the larger angle occurring at the coordinated ring nitrogen site. With all these factors taken into account the refinement was redone with an arbitrarily chosen half occupancy of the N-H proton at N1 and N4, with a resulting slight improvement in R values. The pyridazine nitrogen ring angles (C11—N4—N3 123.8(9)°, N4—N3—C8 116.1(9)°, N2—N1—C1 123.7(9)°, N1—N2—C4 116.6(9)°) are again found to be significantly different consistent with this new model.

Spectroscopy and magnetism

Both ligands L1 and L2 have simple infrared spectra with weak νCN bands at 1573 and 1570 cm^{-1} respectively, strong bands at 1146 and 1150 cm^{-1} respectively, and weaker absorptions in the range 720–820 cm^{-1}. Coordination of the pyridazine rings, all of which are ligands in the compounds that have been structurally characterized, does not cause a major shift in the CN stretching frequency. Shifts of −10 (**1**), −11 (**2**), and −5 (**5**) cm^{-1} are observed for those cases where the pyridazine rings have been shown to coordinate via one nitrogen atom. In each case the absorption appears as a single, sharp band, even though two different CN groups would be expected in the coordinated ligand.

The infrared spectra of $[Cu(L2)Cl_2]$ (**2**) and $[Cu(L2)Br_2]$ (**3**) are identical in the range 4000–500 cm^{-1}, indicating an identical *cis* structure. The nitrate complex $[Cu(L2)(NO_3)_2]$ (**5**) exhibits a νCN band at 1564 cm^{-1}, shifted by 6 cm^{-1} to lower energy than the free ligand, indicating coordinated pyridazine. Prominent combination ($\nu_1 + \nu_4$) nitrate bands are observed at 1708 and 1747 cm^{-1} (48), and the difference between these bands (39 cm^{-1}) strongly suggests a bidentate role for coordinated nitrate. In view of the *cis* coordination of L2 in compounds **2** and **5** a similar bonding situation would be expected for **4** with a six-coordinate *cis* structural arrangement.

The copper(I) complexes Cu(L2)Cl (**6**) and Cu(L2)Br (**7**) have virtually identical infrared spectra, with a very slight increase in energy of the νCN band (+2, +1 cm^{-1} respectively) compared with the free ligand. This suggests that the pyridazine rings are not bound to the copper centres and that the likely donors are sulfur atoms. No structural data are available for these compounds, but the copper(I) chloride complex of the 1:1 macrocyclic ligand formed by condensation of 3,6-dichloropyridazine and 1,4,7,11-tetrathiaundecane involves a polymeric structure with just sulfur coordination and tetrahedral CuS_2Cl_2 metal centres (see footnote 3).

A comparison of the far infrared spectrum of **1** (Table 10) with that of the free ligand L1 reveals three strong bands associated with copper–ligand stretching. The bands at 320 and 308 cm^{-1} are assigned to Cu–Cl stretch, while the single band at 288 cm^{-1} is assigned to Cu–N stretch. A *cis*-CuN_2Cl_2 system, with local C_{2v} symmetry, would require the presence of two Cu–Cl stretching bands, while the *trans* square-planar CuN_2Cl_2 system, with local C_{2h} symmetry would require just one Cu–Cl stretch. Although **1** contains two pseudo *cis* square-planar centres and one pseudo *trans* square-planar centre, it does not appear to be reflected in the far-infrared spectrum and the third absorption is probably hidden in the general Cu–Cl stretching envelope.

The *cis* square-planar structure of $[Cu(L2)Cl_2]$ (**2**) is clearly reflected in the far infrared with two strong bands at 320, 304 cm^{-1} assigned to Cu–Cl stretch and two bands at 287, 273 cm^{-1} assigned to Cu–N stretch. The analogous bromo-complex (**3**) shows two pairs of bands at 264, 257 cm^{-1} (νCu–N) and 248, 235 cm^{-1} (νCu–Br) consistent with a *cis*-CuN_2Br_2 structure. The nitrate complex exhibits three very strong far-infrared bands associated with Cu–O stretch and two bands associated with Cu–N stretch, nominally consistent with the proposed structure. The perchlorate complex, $[Cu(L2)_2](ClO_4)_2 \cdot CH_3CN \cdot CHCl_3$ (**5**) involves a slightly compressed square-planar arrangement of four monodentate pyridazine rings from two ligands. The presence of two far infrared bands at 270, 264 cm^{-1}, assigned to Cu–N stretch, is consistent with such a structure, and assumes an idealized C_{2v} local site symmetry.

Room temperature magnetic moments for compounds **1**–**5** all exceed the spin-only value for a one-unpaired electron system and suggest the presence of dilute copper(II) centres in all cases, with no spin exchange. Solid state, mull transmittance electronic spectra are characterized by the presence of one major visible absorption for compounds **1**–**4**, while **5** exhibits two high-energy bands. No distinction can be made between the different CuN_2Cl_2 sites in **1**, while the slightly lower energy bands associated with $[CuL2Br_2]$, compared with $[CuL2Cl_2]$, are consistent with a structurally analogous bromo complex. The lower energy absorption associated with **4** is consistent with a six-coordinate copper(II) centre, especially when compared with the square-planar complex **5**.

The room temperature, solid state esr spectrum of **1** (Fig. 7) (Table 10) is rather complicated, but can be considered as the superposition of two axial species. A consideration of the solid spectrum of **2** is useful in assigning the g values. **2** exhibits an axial spectrum associated with a *cis*-CuN_2Cl_2, square-planar species, with $g_\parallel$ = 2.155 and $g_\perp$ = 2.081. Assuming that the *cis*-CuN_2Cl_2 centre in **1** is comparable with that in **2**, then the resonance with $g_\parallel$ = 2.125 and $g_\perp$ = 2.043

TABLE 10. Infrared, magnetic, electronic spectral, and esr data

Compound	Colour	Infrared bands (cm^{-1})	μ_{eff} (BM)(RT)	UV/VIS (cm^{-1})[a]	ESR
$[Cu_3(L1)_2Cl_6]$ $\cdot 2CHCl_3$ (**1**)	Blue-green	1563 (νCN), 320,308 (νCu–Cl), 288 (νCu–N)	1.87	16 000	$g_{\parallel} = 2.166, 2.125$[b] $g_{\perp} = 2.078, 2.043$
$[Cu(L2)Cl_2]$ (**2**)	Green	1559 (νCN), 320, 304 (νCu–Cl) 287, 273 (νCu–N)	1.77	15 900, (14 500)	$g_{\parallel} = 2.155, g_{\perp} = 2.081$[b]
$[Cu(L2)Br_2]$ (**3**)	Yellow-brown	1558 (νCN), 264, 257 (νCu–N), 248, 235 (νCu–Br)	1.88	15 600, (14 300)	$g_{av} = 2.08$[b]
$[Cu(L2)(NO_3)_2]$ (**4**)	Green	1564 (νCN), 1747, 1708 ($\nu_1 + \nu_4\ NO_3^-$), 334, 320, 298 (νCu–O), 284, 270 sh (νCu–N)	1.78	14 800	$g_{av} = 2.07$[b]
$[Cu(L2)_2](ClO_4)_2$ $\cdot CH_3CN \cdot CHCl_3$ (**5**)	Brown	1565 (νCN), 1090 ($\nu_3\ ClO_4^-$), 2297, 2253 (CH_3CN), 270, 264 (νCu–N)	1.77	20 000, 18 200	$g_{\parallel} = 2.215, g_{\perp} = 2.065$[c] $A_{\parallel} = 210 \times 10^{-4}\ cm^{-1}, A_{\perp} = 35.7 \times 10^{-4}\ cm^{-1}$ $g_{\parallel} = 2.22, g_{\perp} = 2.05, A_{\parallel} = 207 \times 10^{-4}\ cm^{-1}$[b]
$[L2H](ClO_4)$ $\cdot H_2O$ (**6**)	Pale yellow		—	—	
$[Cu(L2)Cl]$ (**7**)	Red	1572 (νCN)	—	—	
$[Cu(L2)Br]$ $\cdot 0.5H_2O$ (**8**)	Red-brown	1571 (νCN)	—	—	

[a]Mull transmittance (shoulder).
[b]Solid (RT).
[c]$MeNO_2$ solution.

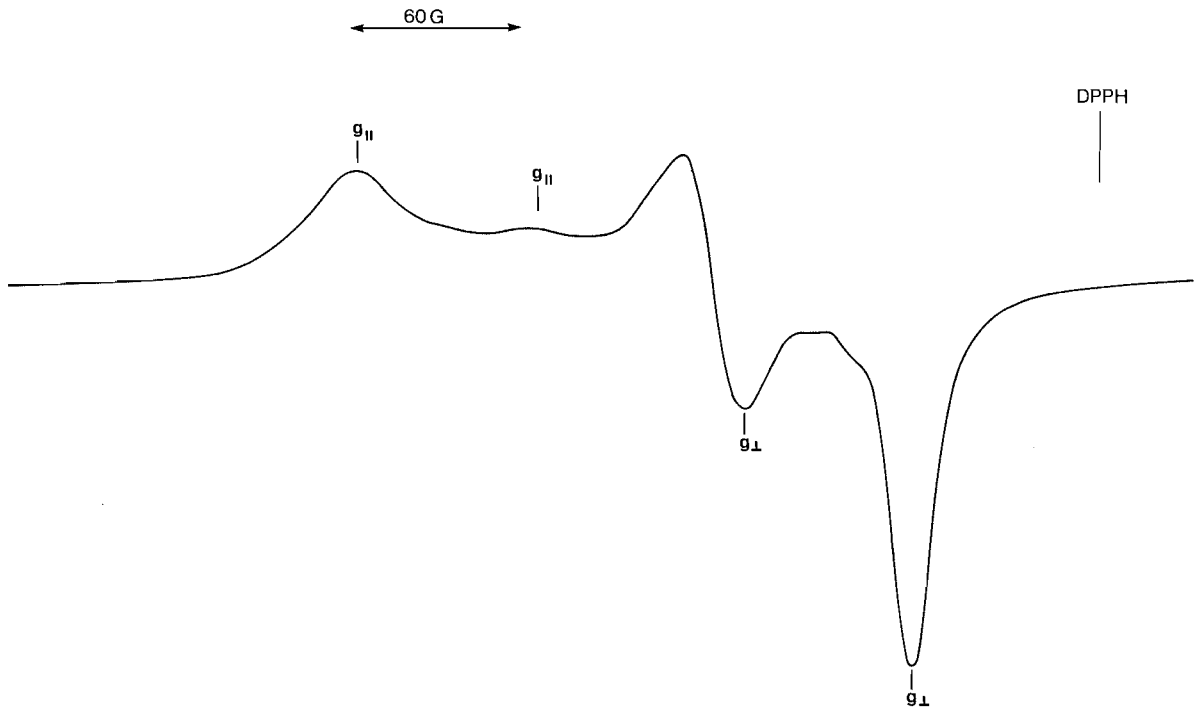

FIG. 7. Solid state esr spectrum (9.77 GHz) (room temperature) of $[Cu_3(L1)_2Cl_6] \cdot 2CHCl_3$ (**1**).

is assigned to the *trans*-CuN_2Cl_2 centre in **1**. Compounds **3** and **4** have uninformative isotropic spectra at both room temperature and at 77 K.

The square-planar perchlorate complex (**5**) exhibits a most unusual solid state spectrum (Fig. 8) at room temperature, which is not an averaged spectrum, but appears to be due to a unique axial species. A similar spectrum is also observed at 77 K. It closely resembles the frozen nitromethane glass (77 K) spectrum (Fig. 9) of the same compound. In fact values of $g_{\parallel}$, $g_{\perp}$, and $A_{\parallel}$ observed in the solid state are very close to those observed in the frozen glass (Table 10). The high values of $g_{\parallel}$ and $A_{\parallel}$ are typical of square-planar CuN_4

Can. J. Chem. Downloaded from www.nrcresearchpress.com by 217.78.4.112 on 09/08/12
For personal use only.

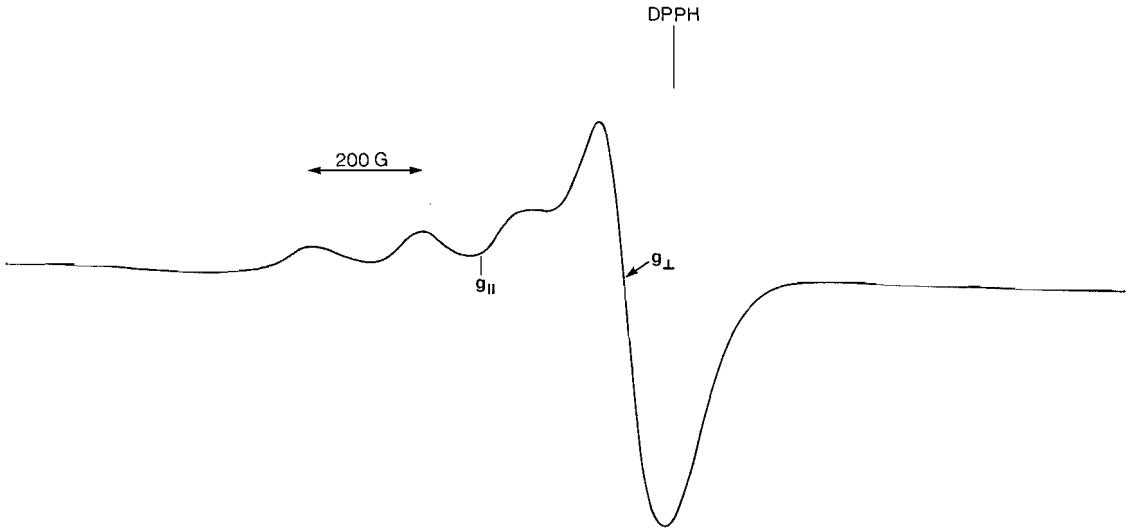

FIG. 8. Solid state esr spectrum (9.76 GHz, room temperature) of $[Cu(L2)_2](ClO_4)_2 \cdot CH_3CN \cdot CHCl_3$ (**5**).

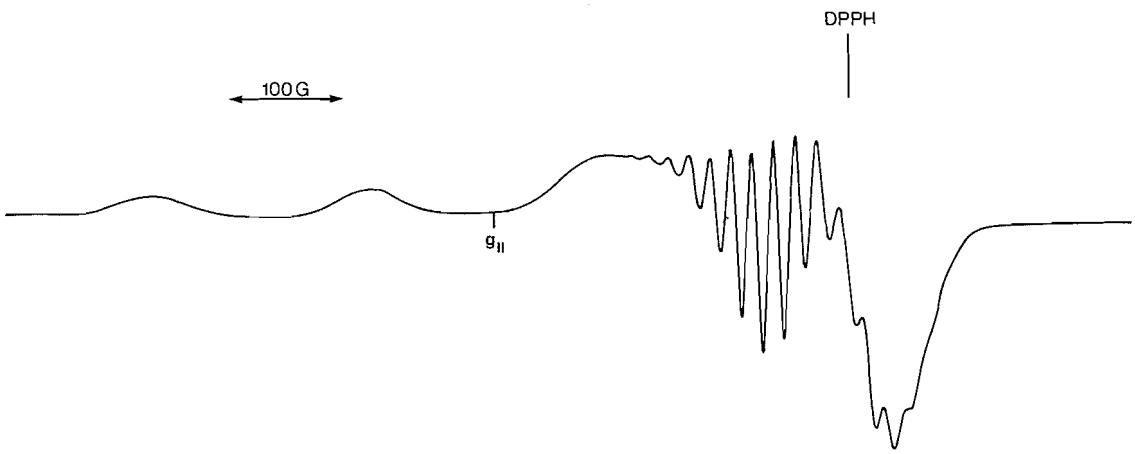

FIG. 9. Frozen glass (nitromethane, 77 K) esr spectrum (9.52 GHz) of $[Cu(L2)_2](ClO_4)_2 \cdot CH_3CN \cdot CHCl_3$ (**5**).

chromophores and the values of g and the hyperfine coupling constants are comparable with those observed for the square-planar complex $[Cu(LP)_2](ClO_4)_2$ (LP = 1,2-bis (4,5-dihydroimidazol-2-yl) benzene), which has comparable dimensions ($g_{\parallel} = 2.232$, $g_{\perp} = 2.044$, $A_{\parallel} = 198 \times 10^{-4}$ cm^{-1}, $A_{\perp} = 46.7 \times 10^{-4}$ cm^{-1}) (49).

Acknowledgements

We thank the Natural Sciences and Engineering Research Council of Canada for financial support for this study, and for funds to purchase the Rigaku AFC6S X-ray diffractometer.

1. P. M. Colman, H. C. Freeman, J. M. Guss, M. Murata, V. A. Norris, J. A. M. Ramshaw, and M. P. Venkatappa. Nature, **272**, 319 (1978).
2. J. M. Guss and H. C. Freeman. J. Mol. Biol. **169**, 521 (1983).
3. E. T. Adman and L. H. Jensen. Isr. J. Chem. **21**, 8 (1981).
4. G. E. Norris, B. F. Anderson, and E. N. Baker. J. Am. Chem. Soc. **108**, 2784 (1986).
5. K. W. Penfield, A. W. Gewirth, and E. I. Solomon. J. Am. Chem. Soc. **107**, 4519 (1985).
6. H. J. Prochaska, W. F. Schwindinger, M. Schwartz, M. J. Burk, E. Berneducci, R. A. Lalancette, J. A. Potenza, and H. J. Schugar. J. Am. Chem. Soc. **103**, 3446 (1981).
7. J. Van Rijn, W. L. Driessen, J. Reedijk, and J-M. Lehn. Inorg. Chem. **23**, 3584 (1984).
8. J. V. Dagidigian, V. McKee, and C. A. Reed. Inorg. Chem. **21**, 1332 (1982).
9. P. J. M. W. L. Birker, J. Helder, G. Henkel, B. Krebs, and J. Reedijk. Inorg. Chem. **21**, 357 (1982).
10. M. J. Schilstra, P. J. M. W. L. Birker, G. C. Verschoor, and J. Reedijk. Inorg. Chem. **21**, 2637 (1982).
11. N. Aoi, G. E. Matsubayashi, and T. J. Tanaka. J. Chem. Soc. Dalton Trans. 1059 (1983).
12. A. W. Addison, T. N. Rao, J. Reedijk, J. Van Rijn, and G. C. Verschoor. J. Chem. Soc. Dalton Trans. 1349 (1984).
13. J. V. Dagdigian and C. A. Reed. Inorg. Chem. **18**, 2623 (1979).
14. J. F. Richardson and N. C. Payne. Inorg. Chem. **17**, 2111 (1978).
15. E. Bouwman, W. L. Driessen, and J. Reedjik. Coord. Chem. Rev. **104**, 143 (1990).
16. T. E. Jones, L. A. Ochrymowycz, and D. B. Rorabacher. J. Am. Chem. Soc. **98**, 4322 (1976).
17. M. D. Glick, D. P. Gravel, L. L. Diaddario, Jr., and D. B. Rorabacher. Inorg. Chem. **15**, 1190 (1976).

Can. J. Chem. Downloaded from www.nrcresearchpress.com by 217.78.4.112 on 09/08/12
For personal use only.

18. E. R. Dockal, L. L. Diaddario, Jr., M. D. Glick, and D. B. Rorabacher. J. Am. Chem. Soc. **99**, 4530 (1977).
19. P. W. R. Corfield, C. Ceccarelli, M. D. Glick, I. W-Y. Moy, L. A. Ochrymowycz, and D. B. Rorabacher. J. Am. Chem. Soc. **107**, 2399 (1985).
20. L. L. Diaddario, Jr., E. R. Dockal, M. D. Glick, L. A. Ochrymowycz, and D. B. Rorabacher. Inorg. Chem. **24**, 356 (1985).
21. V. B. Pett, L. L. Diaddario, Jr., P. W. Corfield, C. Ceccarelli, M. D. Glick, L. A. Ochrymowycz, and D. B. Rorabacher. Inorg. Chem. **22**, 3661 (1983).
22. J. R. Hartman and S. R. Cooper. J. Am. Chem. Soc. **108**, 1202 (1986).
23. S. C. Rowle, G. A. Admans, and S. R. Cooper. J. Chem. Soc. Dalton Trans. 93 (1988).
24. N. Atkinson, A. J. Blake, M. G. B. Drew, G. Forsyth, A. J. Lavery, G. Reid, and M. Schröder. J. Chem. Soc. Chem. Commun. 984 (1989).
25. P. D. Beer, J. E. Nation, S. L. W. McWhinnie, M. E. Harman, M. B. Hursthouse, M. I. Ogden, and A. H. White. J. Chem. Soc. Dalton Trans. 2485 (1991).
26. A. J. Blake, G. Reid, and M. Schröder. J. Chem. Soc. Dalton Trans. 615 (1991).
27. E. Kimura, Y. Kurogi, T. Tojo, M. Shionoya, and M. Shiro. J. Am. Chem. Soc. **113**, 4857 (1991).
28. I. M. Helps, K. E. Matthes, D. Parker, and G. Ferguson. J. Chem. Soc. Dalton Trans. 915 (1989).
29. E. Weber and F. Vögtle. Liebigs Ann. Chem. 891 (1976).
30. J. S. Bradshaw and J. Y. K. Hui. J. Heterocycl. Chem. **11**, 649 (1974).
31. G. R. Newkome, J. D. Sauer, J. M. Roper, and D. C. Hager. Chem. Rev. 77, 513 (1977).
32. C. R. Lucas, S. Liu, and M. J. Newlands. Can. J. Chem. **67**, 639 (1989).
33. C. R. Lucas, S. Liu, and L. K. Thompson. Inorg. Chem. **29**, 85 (1990).
34. S. K. Mandal, L. K. Thompson, E. J. Gabe, J-P. Charland, and F. L. Lee. Inorg. Chem. **27**, 855 (1988).
35. L. K. Thompson, S. K. Mandal, J-P. Charland, and E. J. Gabe. Can. J. Chem. **66**, 348 (1988).
36. L. K. Thompson, S. K. Mandal, L. Rosenberg, F. L. Lee, and E. J. Gabe. Inorg. Chim. Acta, **133**, 81 (1987).
37. S. K. Mandal, L. K. Thompson, E. J. Gabe, F. L. Lee, and J-P. Charland. Inorg. Chem. **26**, 2384 (1987).
38. T. C. Woon, R. McDonald, S. K. Mandal, L. K. Thompson, S. P. Connors, and A. W. Addison. J. Chem. Soc. Dalton Trans, 2381 (1986).
39. S. K. Mandal, L. K. Thompson, M. J. Newlands, F. L. Lee, Y. Lepage, J-P. Charland, and E. J. Gabe. Inorg. Chim. Acta, **122**, 199 (1986).
40. N. Walker and D. Stuart. Acta Crystallogr. **A39**, 158 (1983).
41. C. J. Gilmore. J. Appl. Crystallogr. **17**, 42 (1984).
42. P. T. Beurskens. Dirdif: Technical Report 1984/1, Crystallography Laboratory, Toernooiveld, 6525 Ed Nijmegen, Netherlands.
43. D. T. Cromer and J. T. Waber. International tables for X-ray crystallography. Vol. IV. The Kynoch Press, Birmingham, U.K. 1974. Table 2.2A.
44. J. A. Ibers and W. C. Hamilton. Acta Crystallogr. **17**, 781 (1974).
45. D. T. Cromer. International tables for X-ray crystallography. Vol. IV. The Kynoch Press, Birmingham, U.K. 1974. Table 2.3.1.
46. Texsan–Texray structure analysis package, Molecular Structure Corporation, 1985.
47. J. S. Bradshaw and J. Y. K. Hui. J. Heterocycl. Chem., **11**, 649 (1974).
48. A. B. P. Lever, E. Mantovani, and B. S. Ramaswamy. Can. J. Chem. **49**, 1957 (1971).
49. S. K. Mandal, L. K. Thompson, M. J. Newlands, E. J. Gabe, and F. L. Lee. Inorg. Chem. **29**, 3556 (1990).

Can. J. Chem. Downloaded from www.nrcresearchpress.com by 217.78.4.112 on 09/08/12
For personal use only.

Reaction path Hamiltonian for the association reactions CH_3 + H and CH_3 + D

DAVID M. WARDLAW[1]
Department of Chemistry, Queen's University, Kingston, Ont., Canada K7L 3N6

Received January 21, 1992

DAVID M. WARDLAW. Can J. Chem. **70**, 1897 (1992).

Coupling coefficients and normal mode frequencies appearing in the reaction path Hamiltonian formulated by Miller, Handy, and Adams have been calculated for the title reactions as a function of distance along the reaction path. The calculation of the coupling coefficients requires the use of symmetry coordinates which are described herein. It is found that the carbon–hydrogen separation provides an excellent representation of the reaction path coordinate, being linearly related to it. The coupling coefficients for CH_3 + H and CH_3 + D are approximately the same in the region of variational transition states and do not support the suggestion that an apparent isotope anomaly in the experimentally derived rates of these reactions might be attributable to different dynamics along the reaction path. The relative magnitudes of coupling coefficients for CH_3 + H are used to assess some of the usual assumptions in variational transition state theory concerning separability of different types of motion in the transition state region.

DAVID M. WARDLAW. Can. J. Chem. **70**, 1897 (1992).

On a calculé les coefficients de couplage et les fréquences du mode normal apparaissant dans l'hamiltonien de la voie réactionnelle formulée par Miller, Handy et Adams pour les réactions mentionnées dans le titre, en fonction de la distance parcourue sur la voie réactionnelle. Pour calculer les coefficients de couplage, il est nécessaire d'utiliser les coordonnées de symétrie présentées ici. On a trouvé que la séparation carbone–hydrogène fournit une excellente représentation des coordonnées de la voie réactionnelle puisqu'elle lui est reliée d'une façon linéaire. Les coefficients de couplage pour les réactions CH_3 + H et CH_3 + D sont approximativement les mêmes dans la région des états de vibration variationnels et ils ne supportent pas la suggestion à l'effet qu'une anomalie isotopique apparente dans les vitesses obtenues expérimentalement pour ces réactions peut être attribuable à des dynamiques le long de la voie réactionnelle. On a utilisé les amplitudes relatives des coefficients de couplage pour CH_3 + H pour évaluer les hypothèses usuelles de la théorie de l'état de transition variationnel concernant la possibilité de séparer les divers types de mouvements dans la région de l'état de transition.

[Traduit par la rédaction]

Introduction

The reaction path (RP) Hamiltonian, as formulated by Miller *et al.* (1) in 1980, has provided a useful framework, both conceptual and practical, for theoretical treatments of chemical reaction dynamics. This approximation to the full Hamiltonian is parameterized by a reaction coordinate s which is defined as the distance along the steepest descent/ascent path (in mass-weighted Cartesian coordinates) from reactants to products. For an N-atom system with zero total angular momentum, the RP Hamiltonian is

$$[1]\quad H(p_s, s, \{P_i, Q_i\}) = V_o(s) + \sum_{i=1}^{3N-7} \frac{1}{2}(P_i^2 + \omega_i^2(s)Q_i^2) + \frac{1}{2}\frac{\left[p_s - \sum_{i,j=1}^{3N-7} Q_i P_j B_{i,j}(s)\right]^2}{\left[1 + \sum_{i=1}^{3N-7} Q_i B_{i,3N-6}(s)\right]^2}$$

Here p_s is the momentum conjugate to s (labelled as the $3N - 6$th degree of freedom) and $V_o(s)$ is the potential energy along the RP. $\{Q_i; i = 1,2,\ldots,3N - 7\}$ are normal mode displacement coordinates for the $3N - 7$ vibrations orthogonal to the RP and $\{P_i\}$ are the corresponding conjugate momenta. The six degrees of freedom not represented in eq. [1] are center-of-mass translation and rotation of the entire system about the center-of-mass ($i = 3N - 5,3N - 4,\ldots,3N$).

The normal mode frequencies $\{\omega_i(s); k = 1,2,\ldots,3N - 7\}$ are obtained by diagonalizing the projected force constant matrix

$$[2]\quad F^P(s) = [1 - P(s)] \cdot F(s) \cdot [1 - P(s)]$$

where F is the $3N \times 3N$ mass-weighted, Cartesian force constant matrix and P is a $3N \times 3N$ matrix which projects out motion directed along the normalized gradient vector (which locally defines the RP) and along unit vectors corresponding to infinitesimal rotations and translations of the entire system. The eigenvalues of F^P for these seven degrees of freedom ($i = 3N - 6,\ldots,3N$) are zero. Explicit forms for the gradient vector, the force constant matrix, and the projection matrix are provided in ref. 1. The sets of coefficients $\{B_{i,j}(s)\}$ and $\{B_{i,3N-6}(s)\}$ appearing in the last term of eq. [1] describe coupling between the pairs of normal modes induced by reaction coordinate motion, and between the reaction coordinate and individual normal modes, respectively. These coupling coefficients are defined in terms of the frequencies ω_i and eigenvectors $\mathbf{L}_i = (L_{1,i}, L_{2,i},\ldots,L_{3N,i})$ associated (1, 2) with the ith eigenvalue, ω_i^2, of F^P:

$$[3a]\quad B_{i,j}(s) = \sum_{k=1}^{3N} \frac{\partial L_{k,i}(s)}{\partial s} L_{k,j}(s), \quad i < j$$

$$[3b]\quad B_{i,i}(s) = -\frac{\partial \omega_i(s)}{\partial s} \Big/ (2\omega_i(s)), \quad \omega_i \neq 0$$

$$i = 1,2,\ldots,3N - 7$$

$$j = 1,2,\ldots,3N - 6$$

[1]Natural Sciences and Engineering Research Council of Canada University Research Fellow.

Can. J. Chem. Downloaded from www.nrcresearchpress.com by 217.78.4.112 on 09/08/12
For personal use only.

Can. J. Chem. Downloaded from www.nrcresearchpress.com by 217.78.4.112 on 09/08/12
For personal use only.

The general case of nonzero total angular momentum ($J \neq 0$) is treated in ref. 1; rotational effects within the RP Hamiltonian framework are under study in this laboratory but are not considered here.

In many applications it is satisfactory to retain only the first two terms of eq. [1], i.e., the coupling coefficients are implicitly set equal to zero, resulting in a separable approximation to the RP Hamiltonian,

$$[4] \quad H(p_s,s,\{P_i,Q_i\}) \approx \frac{p_s^2}{2} + V_o(s) + \sum_{i=1}^{3N-7} \frac{1}{2}(P_i^2 + \omega_i^2(s)Q_i^2)$$

A noteworthy example of this approach is the thorough RP Hamiltonian study of the isomerization of the methoxy radical by Colwell (3). Less effort has been made to exploit the dynamical information contained in the coupling coefficients. Miller (2, 4) has shown how symmetry along the RP leads to selection rules in the coupling embodied in the third term of eq. [1] and hence to a symmetry-adapted transition state theory (TST). For the particular case of formaldehyde decomposition the difference between symmetry-adapted and ordinary TST rate coefficients is found to be most pronounced at low energies just below and above threshold and to vanish at high energies. Miller has also demonstrated the role of the $B_{i,3N-6}$ coefficients in estimating a critical energy up to which TST is exact (5). Ryaboy (6) has shown how strong coupling of transverse vibrations to each other and to the reaction coordinate can significantly affect the kinetics of gas-phase nucleophilic substitution (S_N2) reactions. Explicit calculations of coupling coefficients for particular systems include $H^- + CH_3F \rightarrow CH_4 + F^-$ by Ryaboy (6), HNC → HCN isomerization by Gray *et al.* (7), three-dimensional $H + H_2$ by Shwartz and Miller (8), and vinylidene → acetylene isomerization by Carrington, Jr. *et al.* (9).

In this paper coupling coefficients for the radical recombination reactions

$$CH_3 + H \rightarrow CH_4$$

$$CH_3 + D \rightarrow CH_3D$$

on the so-called Hirst potential energy surface (10, 11) are presented and discussed. The motivation is twofold. First, it is of interest to compare coupling coefficients for these two reactions to assess the possibility that differential dynamical effects along the RP are responsible for an apparent isotope anomaly in the high-pressure rate coefficients determined by Pilling and co-workers (12, 13). Second, knowledge of the relative magnitude of the coupling coefficients for $CH_3 + H \rightarrow CH_4$ is useful in assessing assumptions about mode separability inherent in several versions of variational transition state theory (VTST) that have been applied to this reaction employing the same potential energy surface (10, 14, 15). In order to obtain $\{B_{i,j}\}$ and $\{B_{i,3N-6}\}$ for these reactions it is necessary to transform from Cartesian coordinates to symmetry coordinates; these are derived and discussed in Sect. 2. Symmetry coordinates are appealing because, as has been pointed out by Miller (2), coupling coefficients between modes belonging to different irreducible representations are identically zero. In the particular case of $CH_3 + X$ (X = H, D), which has C_{3v} symmetry along the RP and hence a doubly degenerate irreducible representation (E), it is essential to use them. Otherwise the (arbitrary) orientation of a pair of degenerate eigenvectors ($\boldsymbol{L}_i,\boldsymbol{L}_{i+1}$) in their two-dimensional subspace evolves erratically as a function of s and the derivative $\partial L_{k,i}/\partial s$ in eq. [3] is ill-defined. The results of the coupling coefficient calculation are presented in Sect. 3 and the implications discussed in Sect. 4.

Symmetry coordinates for $CH_3 + X$

The use and derivation of symmetry coordinates is standard practice in the field of molecular spectroscopy but this does not appear to be the case in the field of reaction dynamics where they are rarely required. Since symmetry coordinates are necessary for the calculation of RP coupling coefficients and since no details of the associated methodology have previously appeared in the literature on the RP Hamiltonian, their derivation is presented here for $CH_3 + X$. Adaptation of the method to systems having different symmetry along the reaction path should be straightforward.

The symmetry coordinates listed in Table 1 are linear combinations of the mass-weighted Cartesian atomic displacement coordinates $\boldsymbol{r}_i = (x_i,y_i,z_i)$ where $i = 1$ denotes the carbon atom, $i = 2,3,4$ denote the three (equivalent) hydrogen atoms, and $i = 5$ denotes atom X (X = H or D). The z axis is aligned with the C_3 axis of the $CH_3\ldots X$ reaction path structure and the orientation of the CH_3 about the z axis is chosen such that $y_2 = 0$. The 15 symmetry coordinates constitute an orthogonal set of unit displacement vectors and are related to the original mass-weighted Cartesian displacements by a 15×15 orthogonal transformation matrix S. In Table 1 the symmetry coordinates are labeled $\boldsymbol{S}_i^{(\gamma)}$, $i = 1,\ldots,n_\gamma$ where n_γ is the number of coordinates belonging to irreducible representation (species) $\gamma = A_1, A_2, E$. Coordinates belonging to irreducible representation E are further classified as $\boldsymbol{S}_{ia}^{(\gamma)}$ or $\boldsymbol{S}_{ib}^{(\gamma)}$ depending on the coordinate being even (a) or odd (b) with respect to reflection in the x–z plane. The derivation of the symmetry coordinates is described in the Appendix and follows the method of Wilson, Jr. *et al.* (16).

Since center-of-mass translation does not couple to any of the internal motions nor to overall rotation, it is expedient to construct a modified set of symmetry coordinates of which three are unit vectors $\boldsymbol{T}_x,\boldsymbol{T}_y,\boldsymbol{T}_z$ for infinitesimal translations. Explicit expressions for $\boldsymbol{T}_x,\boldsymbol{T}_y,\boldsymbol{T}_z$ are readily obtained as linear combinations within the respective subsets $\{\boldsymbol{S}_{ia}^{(E)}\}$, $\{\boldsymbol{S}_{ib}^{(E)}\}$, $\{\boldsymbol{S}_i^{(A_1)}\}$ ($i = 1,2,3$) of original symmetry coordinates by noting that the general form of $\boldsymbol{T}_\lambda$ ($\lambda = x,y,z$) is

$$[5] \quad \boldsymbol{T}_\lambda = \frac{1}{\sqrt{M}} \sum_{i=1}^{N} \sqrt{m_i}\,\lambda_i; \quad M = \sum_{i=1}^{N} m_i$$

where N is the number of atoms and m_i is the mass of the ith atom. The two remaining modified symmetry coordinates within each subset were obtained by inspection. The complete set of modified symmetry coordinates, expressed as linear combinations of the original symmetry coordinates, is provided in the lower portion of Table 1. The associated modified orthogonal transformation matrix S' which links the Cartesian displacement coordinates to the modified symmetry coordinates is used in Sect. 3.

TABLE 1. Symmetry coordinates for CH_3X

Original set in terms of mass-weighted Cartesian displacement coordinates

$$S_1^{(A_1)} = \frac{1}{\sqrt{3}}(z_2 + z_3 + z_4) \qquad S_2^{(A_1)} = z_1 \qquad S_3^{(A_1)} = z_5$$

$$S_4^{(A_1)} = \frac{1}{\sqrt{12}}(2x_2 - x_3 + \sqrt{3}y_3 - x_4 - \sqrt{3}y_4)$$

$$S_1^{(A_2)} = \frac{1}{\sqrt{12}}(2y_2 - \sqrt{3}x_3 - y_3 + \sqrt{3}x_4 - y_4)$$

$$S_{1a}^{(E)} = \frac{1}{\sqrt{3}}(x_2 + x_3 + x_4) \qquad S_{1b}^{(E)} = \frac{1}{\sqrt{3}}(y_2 + y_3 + y_4)$$

$$S_{2a}^{(E)} = x_1 \qquad S_{2b}^{(E)} = y_1$$

$$S_{3a}^{(E)} = x_5 \qquad S_{3b}^{(E)} = y_5$$

$$S_{4a}^{(E)} = \frac{1}{\sqrt{12}}(-2x_2 + x_3 + \sqrt{3}y_3 + x_4 - \sqrt{3}y_4) \qquad S_{4b}^{(E)} = \frac{1}{\sqrt{12}}(2y_2 + \sqrt{3}x_3 - y_3 - \sqrt{3}x_4 - y_4)$$

$$S_{5a}^{(E)} = \frac{1}{\sqrt{6}}(2z_2 - z_3 - z_4) \qquad S_{5b}^{(E)} = \frac{1}{\sqrt{2}}(z_3 - z_4)$$

Unit vectors for infinitesimal rotations

$$R_x = \frac{1}{\sqrt{I_{xx}}}\left(-\sqrt{m_H}\, a_{2z}\, S_{1b}^{(E)} - \sqrt{m_C}\, a_{1z}\, S_{2b}^{(E)} - \sqrt{m_X}\, a_{5z}\, S_{3b}^{(E)} + \frac{\sqrt{3m_H}}{2}\, a_{2x}\, S_{5b}^{(E)}\right)$$

$$R_y = \frac{1}{\sqrt{I_{yy}}}\left(+\sqrt{m_H}\, a_{2z}\, S_{1a}^{(E)} + \sqrt{m_C}\, a_{1z}\, S_{2a}^{(E)} + \sqrt{m_X}\, a_{5z}\, S_{3a}^{(E)} - \frac{\sqrt{3m_H}}{2}\, a_{2x}\, S_{5a}^{(E)}\right)$$

$$R_z = \sqrt{m_H}\, S_1^{(A_2)}$$

Modified set in terms of original set

$$S_1'^{(A_1)} = T_z = \frac{1}{\sqrt{M}}(\sqrt{3m_H}\, S_1^{(A_1)} + \sqrt{m_C}\, S_2^{(A_1)} + \sqrt{m_X}\, S_3^{(A_1)})$$

$$S_2'^{(A_1)} = \frac{1}{\sqrt{m_c+m_x}}(\sqrt{m_X}\, S_2^{(A_1)} - \sqrt{m_C}\, S_3^{(A_1)})$$

$$S_3'^{(A_1)} = \sqrt{3m_H/M/(m_C+m_X)}\left(-\frac{m_C+m_X}{\sqrt{3m_H}}\, S_1^{(A_1)} + \sqrt{m_C}\, S_2^{(A_1)} + \sqrt{m_X}\, S_3^{(A_1)}\right)$$

$$S_4'^{(A_1)} = S_4^{(A_1)})$$

$$S_1'^{(A_2)} = S_1^{(A_2)})$$

$$S_{1a}'^{(E)} = T_x = \frac{1}{\sqrt{M}}(\sqrt{3m_H}\, S_{1a}^{(E)} + \sqrt{m_C}\, S_{2a}^{(E)} + \sqrt{m_X}\, S_{3a}^{(E)})$$

$$S_{2a}'^{(E)} = \frac{1}{\sqrt{m_c + m_x}}(\sqrt{m_X}\, S_{2a}^{(E)} - \sqrt{m_C}\, S_{3a}^{(E)})$$

$$S_{3a}'^{(E)} = \sqrt{3m_H/M/(m_C+m_X)}\left(-\frac{m_C+m_X}{\sqrt{3m_H}}\, S_{1a}^{(E)} + \sqrt{m_C}\, S_{2a}^{(E)} + \sqrt{m_X}\, S_{3a}^{(E)}\right)$$

$$S_{4a}'^{(E)} = S_{4a}^{(E)}$$

$$S_{5a}'^{(E)} = S_{5a}^{(E)}$$

$$S_{1b}'^{(E)} = T_y = \frac{1}{\sqrt{M}}(\sqrt{3m_H}\, S_{1b}^{(E)} + \sqrt{m_C}\, S_{2b}^{(E)} + \sqrt{m_X}\, S_{3b}^{(E)})$$

$$S_{2b}'^{(E)} = \frac{1}{\sqrt{m_c + m_x}}(\sqrt{m_X}\, S_{2b}^{(E)} - \sqrt{m_C}\, S_{3b}^{(E)})$$

$$S_{3b}'^{(E)} = \sqrt{3m_H/M/(m_C + m_X)}\left(-\frac{m_C+m_X}{\sqrt{3m_H}}\, S_{1b}^{(E)} + \sqrt{m_C}\, S_{2b}^{(E)} + \sqrt{m_X}\, S_{3b}^{(E)}\right)$$

$$S_{4b}'^{(E)} = S_{4b}^{(E)}$$

$$S_{5b}'^{(E)} = S_{5b}^{(E)}$$

For completeness, the unit vectors $\boldsymbol{R}_x,\boldsymbol{R}_y,\boldsymbol{R}_z$ corresponding to infinitesimal rotations of the entire system are expressed as linear combinations of the original symmetry coordinates in the middle portion of Table 1. Note that $\boldsymbol{R}_z$ corresponds to the only symmetry coordinate belonging to A_2 whereas $\boldsymbol{R}_x$ and $\boldsymbol{R}_y$ form a doubly degenerate pair. Explicitly evaluating the expressions for $\boldsymbol{R}_x,\boldsymbol{R}_y,\boldsymbol{R}_z$ in Table 1 in terms of mass-weighted Cartesian displacements yields the

Can. J. Chem. Downloaded from www.nrcresearchpress.com by 217.78.4.112 on 09/08/12
For personal use only.

Can. J. Chem. Downloaded from www.nrcresearchpress.com by 217.78.4.112 on 09/08/12
For personal use only.

standard result (e.g., eq. (4.8*a*) of ref. 1, or p. 22 of ref. 16),

$$[6] \qquad \vec{\mathbf{R}} = (\mathbf{R}_x,\mathbf{R}_y,\mathbf{R}_z) = I_0^{-1} \sum_{i=1}^{5} \vec{\mathbf{a}}_i \times \vec{\mathbf{r}}_i$$

where I_o is the inertia tensor for the reaction path configuration which is specified by $\mathbf{a}_i$ (i = 1,...,5) in mass-weighted Cartesian coordinates.

Calculations

All numerical results reported herein were obtained by following the negative gradient vector (reaction path) on the Hirst potential energy surface for CH_3 + H using the VENUS program[2] with several modifications. The first modification consisted of applying a similarity transformation to F^P (eq. [2]) to yield the "symmetrized" projected force constant matrix $(F^P)_{S'}$ arising from the modified symmetry coordinate basis:

$$[7] \qquad (F^P)_{S'} = S' \cdot F^P \cdot (S')^{-1}$$

The matrix $(F_P)_{S'}$ has the anticipated block diagonal structure: one 1×1 block containing a zero and corresponding to $\boldsymbol{R}_z = \boldsymbol{S}_1'^{(A_2)}$; three 1×1 blocks each containing a zero and corresponding to $\boldsymbol{T}_x = \boldsymbol{S}_{1a}'^{(E)}$, $\boldsymbol{T}_y = \boldsymbol{S}_{1b}'^{(E)}$, and $\boldsymbol{T}_z = \boldsymbol{S}_1'^{(A_1)}$; one 3×3 block corresponding to the remaining coordinates of A_1 type; two identical 4×4 blocks corresponding to the remaining coordinates of E type. The evaluation of frequencies and coupling coefficients is now substantially simplified since it is only necessary to diagonalize one 3×3 and one 4×4 matrix. The square roots of the seven eigenvalues yield frequencies which will be labeled here by symmetry type and arranged in order of increasing magnitude: $\{\omega_1^{(A_1)},\omega_2^{(A_1)},\omega_3^{(A_1)}\}$, $\{\omega_1^{(E)},\omega_2^{(E)},\omega_3^{(E)},\omega_4^{(E)}\}$. In all calculations undertaken it was found, as expected, that one frequency in each group ($\omega_1^{(A_1)}$ and $\omega_1^{(E)}$) was zero (to two decimal place accuracy). The corresponding eigenvectors $\boldsymbol{S}_1''^{(A_1)}$ and $\boldsymbol{S}_1''^{(E)}$ are accordingly associated with reaction path motion (which always belongs to the totally symmetric representation) and rotational motion about the x (or y) axis. The remaining five nonzero frequencies agreed with values obtained from our previous reaction path analysis on the Hirst surface (14) in which symmetry coordinates were not employed and F^P was diagonalized. Equation [3a] for the coupling coefficients can be rewritten in terms of the eigenvectors $\{\boldsymbol{S}_1''^{(A_1)}\}$ and $\{\boldsymbol{S}_1''^{(E)}\}$ resulting from diagonalization of the 3×3 and 4×4 blocks, respectively, as

$$[8] \qquad B_{i,j}^{(A_1)} = \sum_{k=1}^{15} \frac{\partial S_{k,i}''^{(A_1)}}{\partial s} \cdot S_{k,j}''^{(A_1)}, \quad (i,j = 1,2,3;\ i < j)$$

$$B_{i,j}^{(E)} = \sum_{k=1}^{15} \frac{\partial S_{k,i}''^{(E)}}{\partial s} \cdot S_{k,j}''^{(E)}, \quad (i,j = 1,2,3,4;\ i < j)$$

where $S_{k,n}''^{(\gamma)}$ is the coefficient of the kth symmetry displacement coordinate of the eigenvector $S_n''^{(\gamma)}$. The diagonal coupling coefficients are given by eq. [3*b*] but, since $\omega_1^{(A_1)} = \omega_1^{(E)} = 0$, $B_{1,1}^{(A_1)}$ and $B_{1,1}^{(E)}$ are not defined. There are thus nine off-diagonal and five diagonal nonzero coupling coefficients to report and their evaluation required a second modification of the VENUS program as described immediately below.

Numerical values of $\omega_1^{(\gamma)}$ and $B_{i,j}^{(\gamma)}$ were determined on a grid of 31 values of the reaction coordinate, the grid corresponding to 0.1 Å increments of the C···X distance r_{CX} from 1.4 to 4.4 Å. To assess the suitability of r_{CX} as a convenient substitute for s, the derivative $\partial r_{CX}/\partial s$ was also determined. All derivatives $\partial f(s)/\partial s$ ($f = \omega_i^{(\gamma)}$, $S_{k,i}''^{(\gamma)}$, or r_{CX}) were approximated by

$$[9] \qquad \frac{\partial f(s)}{\partial s} \approx \frac{\Delta f}{\Delta s} = \frac{f(s + n\delta) - f(s - n\delta)}{2n\delta}, \quad n = 1, 2, 3$$

where $\delta = -0.000125$ amu$^{1/2}$ Å is the (fixed) step size supplied to the VENUS program for integration along the RP beginning at r_{CX} = 4.5 Å. At each grid value of s each coupling coefficient (eqs. [3b] and [9]), as well as $\partial r_{CX}/\partial s$, was calculated via eq. [10] for each of the three Δs values (2δ,4δ,6δ) to establish the accuracy of this approach.[3] For each quantity, the results for the three Δs values agreed to four significant figures. It was observed that r_{CX} and s are linearly related for both reactions: $\partial r_{CX}/\partial s$ = 1.034 ± 0.003 and 0.758 ± 0.003 for CH_3 + H and CH_3 + D, respectively, over the range of r_{CX} considered (1.4–4.4 Å). Note that the ratio of slopes $[\partial r_{CH}/\partial s]/[\partial r_{CD}/\partial s]$ = 1.36 is close to the mass ratio $\sqrt{m_D/m_H}$ = 1.41 of the mass scaled Cartesian coordinates for atom X. In applications of VTST to recombination processes having no intrinsic barrier to the reverse dissociation process, it is quite common to use a bond coordinate to represent distance along the RP. For CH_3 + H/D, such a substitution is certainly justified and is used in Sect. 4 to provide a common reaction coordinate to facilitate the comparison of CH_3 + H and CH_3 + D frequencies and coupling coefficients. The latter are thus re-expressed as

$$[10] \qquad B_{i,j}^{(\gamma)}(r_{CX}) = B_{i,j}^{(\gamma)}(s)/(\partial r_{CX}/\partial s) \approx \sum_k \frac{\partial S_{k,i}''^{(\gamma)}}{\partial r_{CX}} \cdot S_{k,j}''^{(\gamma)}$$

However, it must be emphasized that the more subtle and complex issue of the physically correct description of the transitional modes within VTST is not addressed by a simple change of variable (17). Within a RP Hamiltonian framework, the information pertinent to this issue is contained in the eigenvectors $S_i''^{(\gamma)}$ whose s-dependent composition requires an appropriate and detailed analysis.

Results and discussion

Frequencies

Figure 1 displays the five nonzero frequencies for CH_3 + H (solid curves) and CH_3 + D (dashed curves) as a function of r_{CX} (X = H,D) on the range 1.4–4.4 Å. The reaction path dependence of the CH_3 + H frequencies has been displayed and discussed elsewhere (15), but the comparison to the CH_3 + D frequencies has not previously been considered.

[2]W. L. Hase, R. J. Duchovic, X. Hu, K. F. Lim, D.-H. Lu, K. N. Swamy, S. R. Vande Linde, and R. J. Wolf. *VENUS*. to be submitted to QCPE.

[3]With $f = S_{k,i}''^{(\gamma)}$ a minor technical difficulty was encountered. The sign of the coefficients $S_{k,i}''^{(\gamma)}$ was found to alternate unpredictably as a function of s because of the sign ambiguity in the eigenvectors $S_i''^{(\gamma)}$, i.e., the sets $+\{S_i''^{(\gamma)}\}$ and $-\{S_i''^{(\gamma)}\}$ are both acceptable, being physically indistinguishable. This ambiguity was removed by arbitrarily selecting a sign convention at a grid value of the reaction coordinate and requiring that the coefficients of adjacent eigenvectors at $s \pm \delta$, $s \pm 2\delta$, $s \pm 3\delta$ evolve smoothly as a function of s.

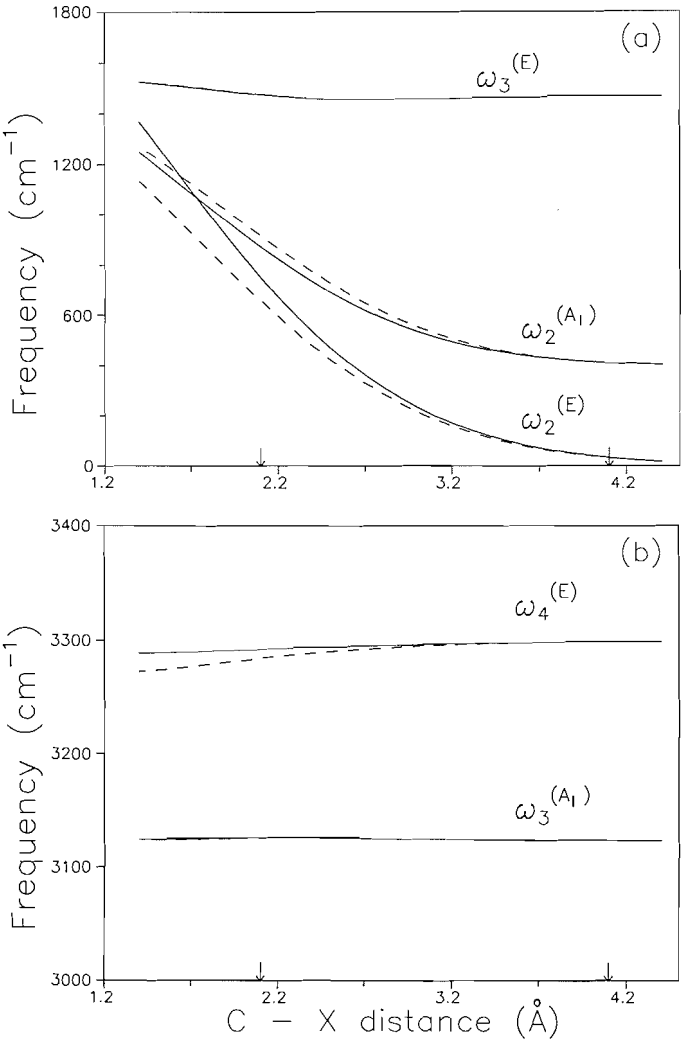

FIG. 1. Harmonic frequencies of modes orthogonal to the reaction path for CH_3 + H (solid curves) and CH_3 + D (dashed curves) as a function of distance along the reaction path as parameterized by the C–X distance (X = H or D).

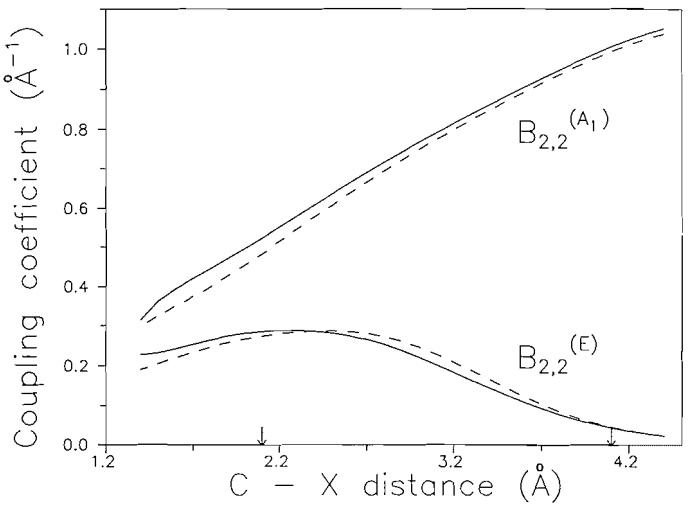

FIG. 2. Reaction path Hamiltonian coupling coefficients for CH_3 + H (solid curves) and CH_3 + D (dashed curves) as a function of C–X distance. The arrows on the abscissa indicate lower and upper bounds to the range of variational transition state locations as determined by flexible transition state theory.

At large separations, the frequencies are those of the normal modes of CH_3 reactant and are independent of the identity of X. A comparison of these methyl radical frequencies with experimentally derived ones and with another set of theoretical ones is provided in ref. 14. Small differences between some pairs of H and D frequencies appear as r_{CX} is decreased to the smallest value considered (1.4 Å). Between 1.4 Å and the equilibrium value in CH_3X (~1.1 Å), one anticipates a relatively rapid variation of some frequencies in order that the magnitudes and symmetry types of the CH_4 and CH_3D product frequencies be reproduced (19). Reaction path calculations were stopped at 1.4 Å since the fitting of $V_o(r_{CX})$ to Hirst's *ab initio* data was designed to be accurate only for r_{CX} larger than this value, i.e., the potential energy surface is intended to be reliable in the region of variational transition state locations. Three of the frequencies ($\omega_4^{(E)}$, $\omega_3^{(A_1)}$, $\omega_3^{(E)}$) are almost independent of r_{CX} and the remaining two ($\omega_2^{(A_1)}$, $\omega_2^{(E)}$) vary substantially with r_{CX}. Of the latter two frequencies, one ($\omega_2^{(E)}$) goes to zero as r_{CX} increases.

In a particular version of VTST, known as flexible transition state theory (FTST) and described elsewhere (15, 20), modes orthogonal to the reaction path are classified as conserved or transitional and coupling between a mode of one type and any mode of the other type is assumed neglible. Conserved modes are vibrations whose character is qualitatively the same in reactants and products, whereas transitional modes are inter-fragment relative motions whose attributes change drastically in going from reactants to products. On these grounds, the CH_3 umbrella vibration ($\omega_2^{(A_1)}$), the CH_3 in-plane bending ($\omega_3^{(E)}$), and the CH stretching ($\omega_3^{(A_1)}$, $\omega_3^{(E)}$) can be classified as conserved modes; the two transitional modes correspond to free relative rotation of reactants (with a frequency of zero and to degenerate CH_3 deformation in CH_3X. Within the RP Hamiltonian description, which is valid in the vicinity of the minimum energy path, the two transitional modes are doubly degenerate harmonic CH_3 rocking vibrations of frequency $\omega_2^{(E)}$. At intermediate and large separations the transitional motion is generally 2-*d* hindered rotation and 2-*d* free rotation, respectively. It is well known that such large amplitude motion renders the RP Hamiltonian treatment of the transitional modes invalid. A reliable treatment of these modes within the RP Hamiltonian framework can be achieved by the *ad hoc* replacement of their normal mode description with a hindered rotor model in which the dependence of the hindering barrier height on the reaction coordinate is obtained from the full potential energy surface. Several applications of VTST to CH_3 + X have adopted this approach (21, 22).

Coupling coefficients

Figures 2–6 display 12 of 14 coupling coefficients for CH_3 + H (solid curves) and CH_3 + D (dashed curves) versus r_{CX} in the range 1.4–4.4 Å. The two missing coefficients, $B_{3,3}^{(A_1)}$ and $B_{4,4}^{(E)}$, are each an order of magnitude less than the smallest coefficient included, $B_{3,3}^{(E)}$ in Fig. 6. The arrows in Figs. 1–6 indicate upper and lower bounds to the range of transition state locations $r_{CX}^{\dagger}$ ($2.1 < r_{CX}^{\dagger} < 4.1$ Å) determined by Aubanel and Wardlaw (14) in their application of microcanonical FTST to these reactions on the Hirst surface. This range of $r_{CX}^{\dagger}$ arose from the minimization, with respect to variation in the reaction coordinate, of the sum of states for motion orthogonal to the RP for the wide range of

Can. J. Chem. Downloaded from www.nrcresearchpress.com by 217.78.4.112 on 09/08/12
For personal use only.

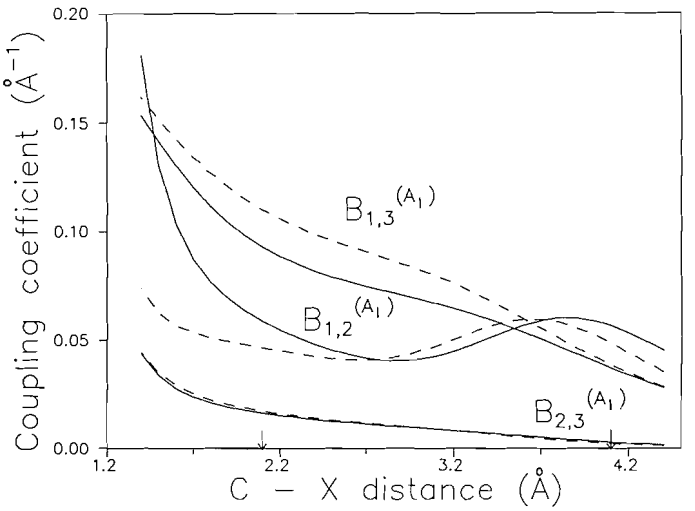

FIG. 3. Same as Fig. 2 except for different scale of ordinate.

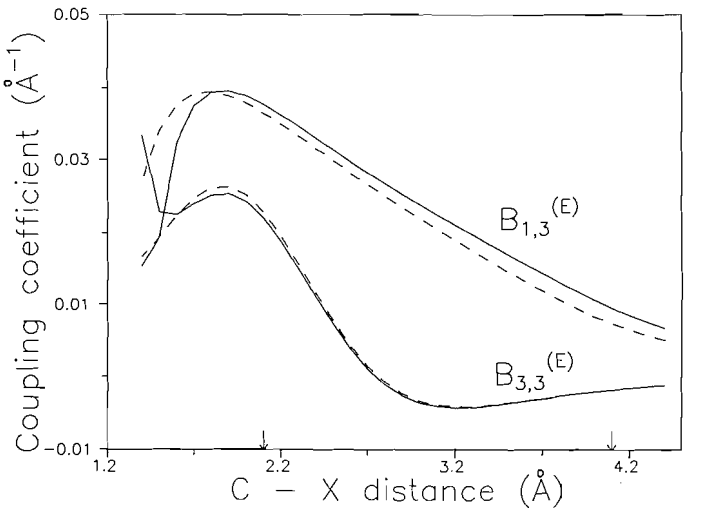

FIG. 6. Same as Fig. 2 except for different scale of ordinate.

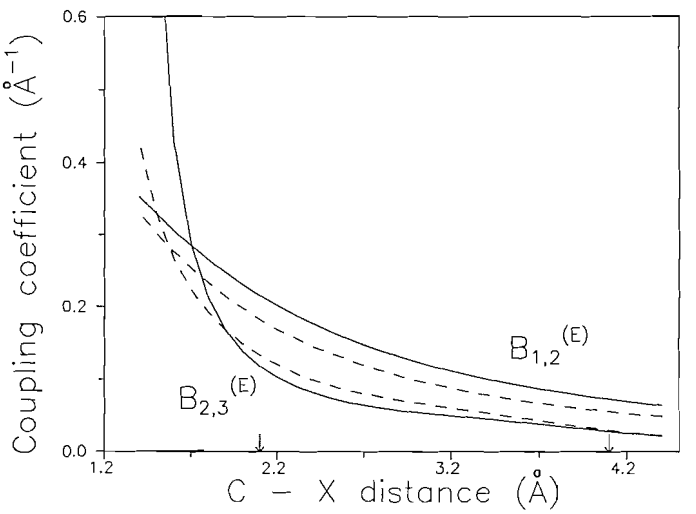

FIG. 4. Same as Fig. 2 except for different scale of ordinate.

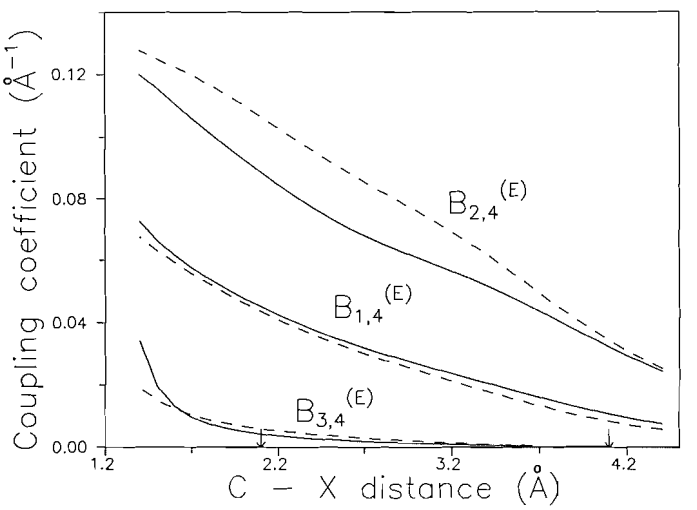

FIG. 5. Same as Fig. 2 except for different scale of ordinate.

energy and angular momentum values involved in the calculation of thermally averaged rate coefficients in the 300–2500 K temperature range.

Examination of Figs. 1–6 reveals no major differences in magnitude or r_{CX} dependence of the frequencies or coupling coefficients for these two related reactions on the range of variational transition states and does not support the conjecture that different dynamics along the RP might lead to "differences in recrossing of the dividing surface separating reactants and products" (12). This suggestion is one of several made by Pilling and co-workers as possible explanations of an apparent isotope anomaly in the experimental value of the ratio $\rho = k_H/k_D$ of thermal rate coefficients k_H and k_D for these two reactions. Specifically, these authors find (12, 13) the experimental ratio $\rho_{expt} \approx 2.5$ in the 300–400 K range, whereas VTST treatments on several potential energy surfaces by Hase *et al.* (10) and our FTST treatment on the Hirst surface (14) yield $\rho_{VTST} \approx 1.4 \approx \sqrt{m_D/m_H}$. In absolute terms, the VTST and experimental values for k_D agree but the experimental values for k_H in this temperature range significantly exceed the VTST values, contrary to the expectation that transition state theory should provide an upper bound to the rate. It is apparent from Figs. 1–6 that a sum-of-states calculation based on the RP Hamiltonian of eq. [1] would yield approximately the same results for CH_3 + H and CH_3 + D anywhere in the transition state range 2.1–4.1 Å. Such sums of states could then be used to determine VTST rate coefficients k_H and k_D whose ratio ρ_{RP} would be essentially determined by the ratio of reactant state densities. This latter ratio reduces to the ratio of partition functions for relative translation and thus $\rho_{RP} \approx \sqrt{m_D/m_H}$, in agreement with ρ_{VTST}. It is still conceivable, as suggested in ref. 12, that coupling differences in the product molecules CH_4 and CH_3D could be responsible for the isotope anomaly. Some coupling differences in CH_4 and CH_3D are certainly expected and indeed begin to appear in the 1.4–2.0 Å range in Figs. 2–6. Dynamical coupling mechanisms between C–H stretching vibrations and other normal modes in CHD_3, CHT_3, and CH_3D have been examined in a theoretical treatment by Voth *et al.* (23) who discuss the implications for intramolecular vibrational energy redistribution. Whether such differences can account for the anomaly in the

Can. J. Chem. Downloaded from www.nrcresearchpress.com by 217.78.4.112 on 09/08/12
For personal use only.

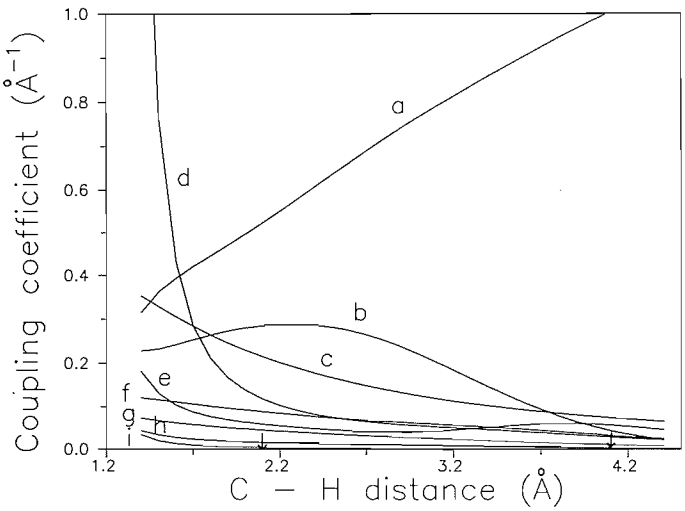

FIG. 7. The nine largest coupling coefficients for CH_3 + H as a function of r_{CH}. The arrows on the abscissa are as in Fig. 2. The connection between the alphabetic labels and coupling coefficients is as follows: (*a*) $B^{(A_1)}_{2,2}$, (*b*) $B^{(E)}_{2,2}$, (*c*) $B^{(E)}_{1,2}$, (*d*) $B^{(E)}_{2,3}$, (*e*) $B^{(A_1)}_{1,2}$, (*f*) $B^{(A_1)}_{1,3}$, (*g*) $B^{(E)}_{2,4}$, (*h*) $B^{(E)}_{1,4}$, (*i*) $B^{(E)}_{3,4}$.

observed rates for CH_3 + H and CH_3 + D cannot be ascertained from the present study since RP calculations were not done for $r_{CX} < 1.4$ Å, the region in which the potential is not accurately fit to the *ab initio* data. A recent trajectory study by Hu and Hase (24) on a modified version of the Hirst potential (so that it has proper asymptotic behavior at large r_{CX}) yields thermal rate coefficients (at 300 and 1000 K for CH_3 + H and at 300 K for CH_3 + D) that are in excellent agreement with microcanonical FTST values obtained by Aubanel and Wardlaw (14) and whose ratio $\rho_{traj} \approx 1.3$ at 300 K is close to $\rho_{VTST} \approx 1.4$. The trajectory results do not account for the isotope anomaly as characterized by $\rho_{expt} \approx 2.5$ on 300–400 K and suggest that the coupling differences in CH_4 and CH_3D are not responsible for it.

The paper concludes with an assessment of the relative magnitudes of the larger coupling coefficients for CH_3 + H $\rightarrow$ CH_4. The nine largest coefficients are presented in Fig. 7 where they are labeled (*a*)–(*i*); the arrows at 2.1 and 4.1 Å on the abscissa again denote the FTST range of transition states for this system. The two largest coupling coefficients in this range are the diagonal ones $B^{(A_1)}_{2,2}$ (curve *a*) and $B^{(E)}_{2,2}$ (curve *b*) arising from the variation in frequency with r_{CX} of the CH_3 umbrella motion and the transitional modes, respectively. That these two coefficients would be the largest diagonal ones is immediately evident from Fig. 1. The three remaining diagonal coefficients are sufficiently small on the scale of the ordinate in Fig. 7 that they could not be distinguished from the abscissa and were not included. The relatively large value of $B^{(A_1)}_{2,2}$ (curve *a*) indicates that, within a harmonic description of the umbrella mode, it may be important to observe semiclassical vibrational selection rules arising from the term involving $B^{(A_1)}_{2,2}$ in the RP Hamiltonian (2). Namely, if all other couplings among A_1-type modes (the next largest of which are $B^{(A_1)}_{1,2}$ and $B^{(A_1)}_{1,3}$ (curves *e*, *f*)) are ignored, then umbrella vibrational states with even and odd quantum numbers are uncoupled. The associated even and odd sums of states for motion orthogonal to the RP lead to even and odd microcanonical rate coefficients. The influence on thermal rate coefficients $k_H(T)$ is unknown but is likely small in the 300–2500 K temperature range. In any case, the umbrella mode is highly anharmonic in isolated CH_3 and becomes progressively more harmonic (for the Hirst potential) as r_{CX} is decreased to its equilibrium value in CH_4. Inclusion of this behavior in microcanonical FTST has been shown to affect significantly the magnitude and temperature dependence of $k_H(T)$.

Among off-diagonal coefficients of *E* type, we first examine those involving the transitional modes (mode 2): $B^{(E)}_{1,2}$ (curve *c*), $B^{(E)}_{2,3}$ (curve *d*), $B^{(E)}_{2,4}$ (curve *g*) which describe coupling of the transitional modes to overall rotation, to the degenerate CH_3 in-plane bend, and to degenerate C–H stretching, respectively. Notwithstanding the poor description of the transitional modes provided by the normal mode treatment of the RP Hamiltonian, the relative magnitudes agree with intuitive predictions based on the type and frequency of the modes involved. In all implementations of VTST for this reaction, coupling between transitional and conserved modes is assumed negligible. From a RP Hamiltonian perspective this corresponds to setting $B^{(E)}_{2,3}$ and $B^{(E)}_{2,4}$ to zero. The largest off-diagonal coefficient involving the transitional modes is $B^{(E)}_{1,2}$, which most implementations of VTST also ignore except for FTST which implicitly includes coupling between the transitional modes and overall rotation via a rigorous treatment of conservation of angular momentum. The two remaining off-diagonal *E*-type coefficients in Fig. 7 are $B^{(E)}_{1,4}$ (curve *h*) and $B^{(E)}_{3,4}$ (curve *i*). They describe coupling of (high frequency) C–H stretching to overall rotation and to CH_3 bending, respectively, and are relatively small on the entire range of r_{CX} values, as would be expected. The two off-diagonal A_1-type coefficients included in Fig. 7 are $B^{(A_1)}_{1,2}$ (curve *e*) and $B^{(A_1)}_{1,3}$ (curve *f*) describing coupling of the reaction path to the CH_3 umbrella mode and to (nondegenerate) C–H stretching, respectively. The fact that they are nonzero indicates that RP motion induces changes in the vibrational state of these two modes, an effect which is ignored in existing implementations of VTST but whose significance therein is unknown.

Acknowledgments

The author is grateful to Geoff Anderson for preliminary work in the form of a senior undergraduate research project and to Prof. R. D. Gordon for fruitful discussions concerning symmetry coordinates. This work was supported by an operating grant from the Natural Sciences and Engineering Research Council of Canada.

1. W. H. Miller, N. C. Handy, and J. E. Adams. J. Chem. Phys. **72**, 99 (1980).
2. W. H. Miller. J. Am. Chem. Soc. **105**, 216 (1983).
3. S. C. Colwell. Mol. Phys. **51**, 1217 (1984).
4. W. H. Miller. J. Phys. Chem. **87**, 2731 (1983).
5. W. H. Miller. J. Chem. Phys. **76**, 4904 (1982).
6. V. M. Ryaboy. Chem. Phys. Lett. **159**, 371 (1989).
7. S. K. Gray, W. H. Miller, Y. Yamaguchi, and H. F. Schaefer. J. Chem. Phys. **73**, 2733 (1980).
8. S. D. Schwartz and W. H. Miller. J. Chem. Phys. **79**, 3759 (1983).
9. T. Carrington, Jr., L. M. Hubbard, H. F. Schaefer, and W. H. Miller. J. Chem. Phys. **80**, 4347 (1984).
10. W. L. Hase, S. L. Mondro, R. J. Duchovic, and D. M. Hirst. J. Am. Chem. Soc. **109**, 2916 (1987).

Can. J. Chem. Downloaded from www.nrcresearchpress.com by 217.78.4.112 on 09/08/12
For personal use only.

11. D. M. Hirst. Chem. Phys. Lett. **122**, 225 (1985).
12. M. Brouard, M. T. Macpherson, and M. J. Pilling. J. Phys. Chem. **93**, 4047 (1989).
13. M. Brouard and M. J. Pilling. Chem. Phys. Lett. **129**, 439 (1986).
14. E. E. Aubanel and D. M. Wardlaw. J. Phys. Chem. **93**, 3118 (1989).
15. W. L. Hase and D. M. Wardlaw. *In* Bimolecular collisions. *Edited by* J. E. Baggott and M. N. Ashfold. Burlington House, London, UK. 1989.
16. E. B. Wilson, Jr., J. C. Decius, and P. C. Cross. Molecular vibrations. Dover, New York. 1980.
17. S. J. Klippenstein. Chem. Phys. Lett. **170**, 71 (1990); J. Chem. Phys. **94**, 6469 (1991); **96**, 367 (1992).
18. E. E. Aubanel, D. M. Wardlaw, L. Zhu, and W. L. Hase. Int. Rev. Phys. Chem. **10**, 249 (1991).
19. G. C. Schatz, A. F. Wagner, and T. H. Dunning. J. Phys. Chem. **88**, 221 (1984).
20. D. M. Wardlaw and R. A. Marcus. Adv. Chem. Phys. **70**, Part I, 231 (1988).
21. E. E. Aubanel, S. H. Robertson, and D. M. Wardlaw. J. Chem. Soc. Faraday Trans. **87**, 2291 (1991).
22. S. C. King, J. F. Leblanc, and P. D. Pacey. Chem. Phys. **123**, 329 (1988).
23. G. A. Voth, R. A. Marcus, and A. H. Zewail. J. Chem. Phys. **81**, 5494 (1984).
24. X. Hu and W. L. Hase. J. Chem. Phys. **95**, 8073 (1991).

Appendix

The construction of symmetry coordinates is based on eq. [1] of Sect. 6–5 in ref. 16:

$$[A1] \quad S_k^{(\gamma)} = N \sum_R \chi_R^{(\gamma)} \hat{R}\xi$$

Here N is a normalization constant, $\hat{R}$ (= E, C_3, C_3^2, σ_v, σ_v', or σ_v'') is a symmetry operation of C_{3v}, $\chi_R^{(\gamma)}$ is the character of R in irreducible representation γ, and ξ is one of, or a simple linear combination of, the mass-weighted Cartesian displacement coordinates. $\hat{R}\xi$ is the result of operating on ξ with the symmetry operation $\hat{R}$ and, in this case, was determined diagramatically following Fig. 6–6 of ref. 16. The procedure is considerably simplified by identifying sets of atoms whose Cartesian displacements are not mixed by the group's symmetry operations. In the present case there are three such sets: $\{x_1,y_1,z_1\}$, $\{x_5,y_5,z_5\}$, and $\{x_2,y_2,z_2,x_3,\ldots,z_4\}$. A further simplification is achieved by subdividing each set into two groups on the grounds that none of the z coordinates are mixed with x or y coordinates by application of any of the symmetry operations of C_{3v}. This results in six sets: $\{x_1,y_1\}$, $\{x_5,y_5\}$, $\{x_2,y_2,x_3,y_3,x_4,y_4\}$, $\{z_1\}$, $\{z_5\}$, and $\{z_2,z_3,z_4\}$. For A_1, the symmetry coordinates are generated by applying eq. [A1] with $\gamma = A_1$ to x_1,x_5,x_2,z_1,z_5, and z_2; for A_2 to y_1,y_5,y_2,z_1,z_5, and z_2. This yields six symmetry coordinates for each species. However, two of these are zero for A_1 and five are zero for A_2; the surviving coordinates appear in Table 1. Applying eq. [A1] to all coordinates in a set with two or more members is unnecessary since no additional nonzero symmetry coordinates result. To generate symmetry coordinates belonging to the two-dimensional E representation it is necessary to select within each of the six sets listed above pairs (a, b) of Cartesian coordinates, or of linear combinations of Cartesian coordinates, that are orthogonal and are symmetric or antisymmetric with respect to a chosen set of group operations constituting a subgroup. This procedure removes the aforementioned ambiguity in the orientation of degenerate sets of symmetry coordinates belonging to species E. In this case we chose the subgroup (E, σ_v). Clearly such a pair which is even(a)/odd(b) with respect to σ_v cannot be created from the one element sets $\{z_1\}$ or $\{z_5\}$. The elements of the sets $\{x_1,y_1\}$, $\{x_5,y_5\}$ themselves provide two such pairs. The set $\{z_2,z_3,z_4\}$ provides the pair $(z_2,z_3 - z_4)$ and the set $\{x_2,y_2,\ldots,y_4\}$ provides two pairs: $(x_2 + x_3 + x_4,y_3 - y_4)$ and $(y_2 + y_3 + y_4,x_3 - x_4)$. Alternative combinations such as $(x_2,y_3 - y_4)$ or $(z_2 + z_3 + z_4,z_3 - z_4)$ satisfying the stated criteria are possible but not useful. Applying eq. [A1] with $\gamma = E$ to these five pairs yields the 10 E-type symmetry coordinates in Table 1.

Can. J. Chem. Downloaded from www.nrcresearchpress.com by 217.78.4.112 on 09/08/12
For personal use only.

Sirosterol and dehydroazasirosterol, unusual steroidal adducts from a *Sirococcus* species

WILLIAM A. AYER[1] AND YU-TING MA
Department of Chemistry, University of Alberta, Edmonton, Alta., Canada T6G 2G2

Received November 20, 1991

WILLIAM A. AYER and YU-TING MA. J. Chem. **70**, 1905 (1992).

Two unusual compounds, which are made up of a sterol portion fused at C-5 and C-6 to an atrovenetin-like part, have been isolated from a fungus that causes Sirococcus shoot blight of spruce. The structures of these compounds, sirosterol (**4**) and dehydroazasirosterol (**13**), were determined by spectroscopic methods and comparison with appropriate model compounds. Sirosterol is an adduct of ergosterol and atrovenetin (**5**) and dehydroazasirosterol is an adduct of 9(11)-dehydroergosterol and an azaatrovenetin. Both compounds give a monomethyl ether when treated with diazomethane and both have been transformed to the corresponding 3-ketosteroids. The preparation of the triol **6** resulting from the selective hydroxylation of the 5,6-double bond in ergosterol is described. A possible biogenesis of sirosterol from ergosterol endoperoxide and a desoxyatrovenetin is discussed.

WILLIAM A. AYER et YU-TING MA. Can. J. Chem. **70**, 1905 (1992).

On a isolé deux composés inhabituels, faits d'une portion stéroïdale condensée par les carbones 5 et 6 à une partie de type atrovénétine, à partir d'un champignon qui provoque la rouille des pousses de l'épinette par le Sirococcus. On a déterminé la structure de ces composés, le sirostérol (**4**) et le déhydroazasirostérol (**13**), grâce à des méthodes spectroscopiques et par comparaison avec des composés modèles appropriés. Le sirostérol est un adduit de l'ergostérol avec l'atrovénétine (**5**) alors que le déhydroazasirostérol est un adduit du 9(11)-déhydroergostérol avec une azaatrovénétine. Lorsqu'on les traite avec du diazométhane, les deux composés fournissent un éther méthylique; on a aussi pu les transformer tous les deux dans les 3-cétostéroïdes correspondants. On décrit la préparation du triol **6** qui résulte de l'hydroxylation sélective de la double liaison en 5,6 de l'ergostérol. On discute d'une voie de biogenèse possible à partir de l'endoperoxyde de l'ergostérol et d'une désoxyatrovénétine.

[Traduit par la rédaction]

Can. J. Chem. Downloaded from www.nrcresearchpress.com by 109.225.110.28 on 09/08/12
For personal use only.

Introduction

We previously reported on the metabolites produced by two strains of fungi responsible for the so-called Sirococcus shoot blight of spruce (1). Our interest in these fungi arose from our work on the related disease of pine known as Scleroderris canker (2). We now report on two new metabolites isolated from the mycelium of a strain (strain 35B) of the Sirococcus disease fungus from the mountains of southern Germany.[2] In addition to the two previously unreported compounds, racemic sclerodin (**1**), atrovenetinone (**2**, as its acetone adduct), Scleroderris blue (**3**) (3), and the ubiquitous fungal sterols ergosterol and 9(11)-dehydroergosterol endoperoxide, were isolated from this stain.

Results and discussion

The methylene chloride extract of the mycelium of Sirococcus 35B (UAMH 5401) was separated by silica gel column chromatography into nonpolar, intermediate, and polar fractions and these fractions were further separated by flash chromatography to provide the individual components. When the yellow sirosterol (**4**) was initially isolated it appeared to be a mixture of a sterol and a phenalenone type compound. High-resolution electron impact mass spectrometry (hrms) and chemical ionization mass spectrometry (cims) gave confusing results. Methylation (diazomethane) provided a new material, which also showed a single spot on thin-layer chromatography (tlc). Fast atom bombardment mass spectrometry (fabms) of sirosterol (**4**) showed a peak at 737 $[M + H]^+$ corresponding to a molecular formula of $C_{47}H_{60}O_7$, suggesting that the compound was an adduct of a sterol and an atrovenitin (**5**) related compound. The ir spectrum of sirosterol shows hydroxyl absorption and a strongly chelated carbonyl at 1611 cm^{-1}. The phenalenone portion of the molecule gives rise to signals for: two exchangeable phenolic hydrogens, one strongly chelated (δ 17.16), one free (δ 9.56); an aromatic methyl (δ 2.83) and hydrogen (δ 6.93); signals due to the isopentyl portion (methyl singlets at δ 1.56 and δ 1.32, doublet at δ 1.47, methine quartet at δ 4.65). These chemical shifts are very similar to those of atrovenitin trimethyl ether (**5***a*) (4). The "sterol" portion of the molecule gave rise to ^1H nmr signals very similar to those of the triol **6** prepared (see below) from ergosterol. Thus, the methyl groups of the sterol portion give rise to singlets at δ 0.57 (C-18 in **6**, δ 0.57) and δ 1.14 (C-19 in **6**, 0.98), doublets at δ 0.80, 0.81, 0.88, and 1.00 (0.83, 0.84, 0.93, and 1.03 in **6**). The two side-chain alkenic hydrogens give rise to an unresolved multiplet at δ 5.15 in **4** and at δ 5.20 in **6**, and the steroidal C-7 hydrogen appears at δ 4.99 in **4** and δ 5.03 in **6**. The C-7″ hydrogen in **4** is vicinally coupled to the methine signal (H-6″) at δ 4.91. In **6**, the C-6 hydrogen appears at δ 3.98, indicating a difference in the C-6 substituent. The broad methine doublet at δ 4.05 in **4** and δ 4.01 in **6** has the normal complexity of a steroidal 3α-carbinol hydrogen. The downfield shift of the 3α hydrogen is characteristic of 3β-hydroxysterols bearing a 5α oxygen substituent (5). It seemed clear at this stage that sirosterol consisted

[1]Author to whom correspondence may be addressed.

[2]These cultures were provided by Prof. O. Kander, Botanisches Institute der Universität München, and are deposited at the University of Alberta Microfungus Herbarium as Sirococcus 35B (UAMH 5401).

Can. J. Chem. Downloaded from www.nrcresearchpress.com by 109.225.110.28 on 09/08/12
For personal use only.

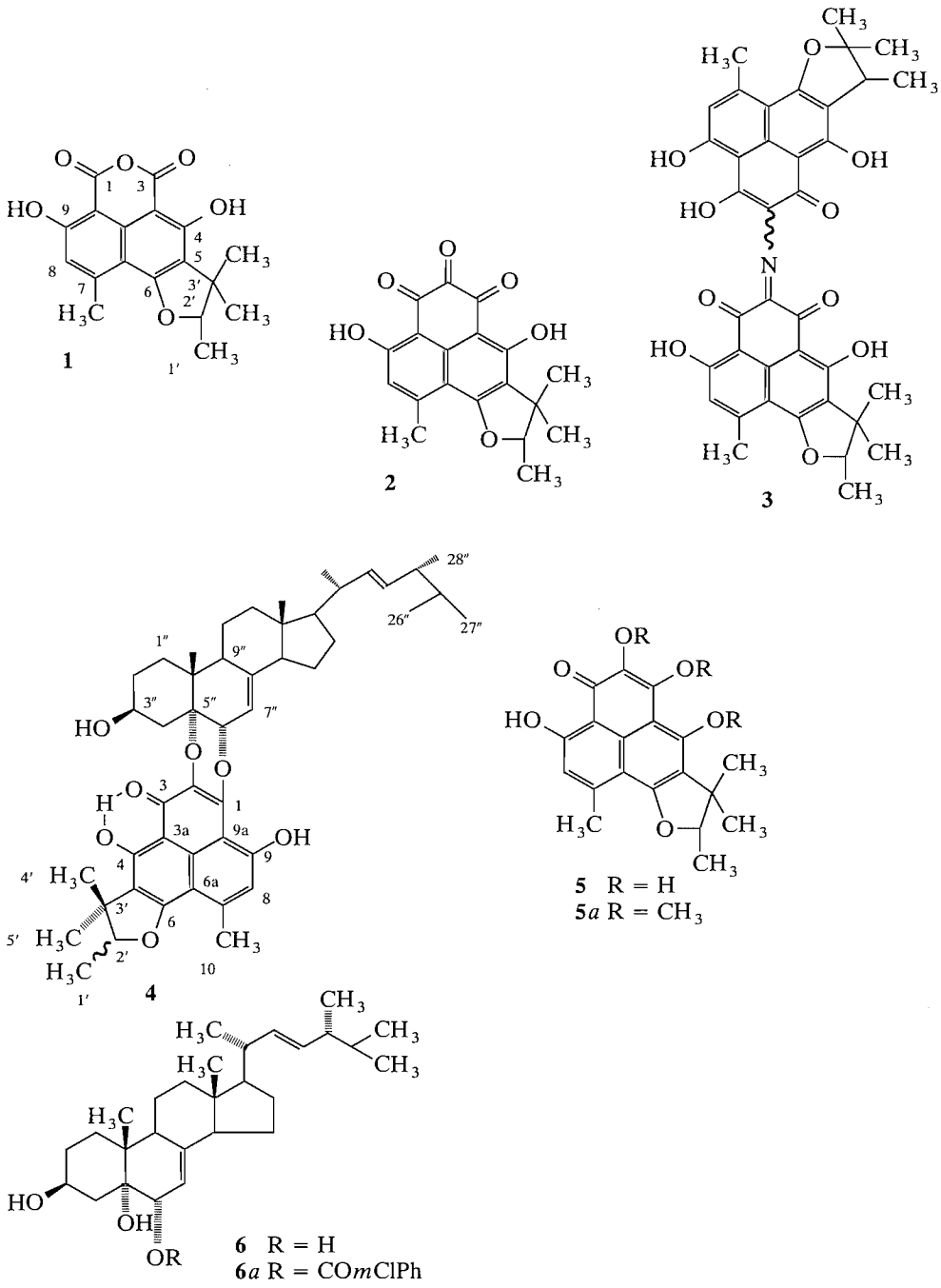

of an "atrovenitin" portion fused to an ergosterol-derived sterol portion through ether linkages at C-5 and C-6 of the sterol portion to C-1 and C-2 (or C-2 and C-3 of the tautomeric form) of atrovenitin. A strong nuclear Overhauser enhancement (nOe) effect between the hydrogen at C-6″ and the 19 methyl group in **4**, along with the very small coupling between this hydrogen and the C-7 hydrogen, indicates that the C-6″ substituent is in the α-orientation. To distinguish between **4** and the other structural isomers possible (**7**, **8**, and **9**), several derivatives of sirosterol were prepared.

Treatment of sirosterol with diazomethane in ether provided the monomethyl ether **10**. The fabms indicated a molecular weight of 750 amu. The ir spectrum shows the presence of hydroxyl (3300 cm^{-1}) and strongly chelated carbonyl (1611 cm^{-1}), and the ^1H nmr spectrum shows the hydrogen of the chelated carbonyl at δ 17.95, indicating that the non-chelated phenolic hydroxyl is the one methylated. The methoxyl hydrogens appear at δ 4.05. The remainder of the spectrum is very similar to that of sirosterol itself. Strong nOe enhancement of the aromatic hydrogen is observed when the methoxyl hydrogens are irradiated and when the aromatic methyl hydrogens are irradiated. This indicates that the methoxyl is located at C-9, thus the non-chelated phenolic hydrogen in **4** is at C-9. On this basis, structures **8** and **9** for sirosterol are ruled out. The nOe results with **10** also serve to confirm the stereochemistry at C-6″. Irradiation of the C-19″ methyl causes enhancement (10.4%) of the signal at

δ 4.83 (C-6″). Irradiation of the hydrogen at δ 4.83 also causes enhancement of the alkenic hydrogen at δ 4.99 (C-7″), and vice versa. This further supports the proximate relationship of these two hydrogens. The ^{13}C nmr spectrum of **10** adds further support to the structural assignment. As shown in Table 1, the signals for the "atrovenitin" portion correspond much better with those of atrovenitin trimethyl yellow (**11**) than with those of atrovenitin trimethyl orange (**5***a*) (4). A comparison of the ^{13}C nmr signals of the "sterol" portion of **10** with those of the triol **6** is provided in Table 2. The upfield shifts of C-1, C-4, C-7, and C-10 relative to those of **6** are consistent with the expected substituent steric effects (6).

Acetylation of sirosterol methyl ether (**10**) provided the acetyl derivative **10***a*. The C-3″ hydrogen is shifted downfield to δ 5.05, indicating the position of acetylation. Acetylation of sirosterol (**4**) itself provided the diacetyl derivative **10***b*. The ir spectrum of **10***b* shows chelated carbonyl (1620 cm^{-1}), alkyl acetate (1734 cm^{-1}), and aryl acetate (1753 cm^{-1}) absorption. The signal for the chelated phenolic hydrogen appears at δ 17.41 in the ^1H nmr spectrum. Comparison of the ^1H nmr spectra of sirosterol (**4**) and its derivatives **10**, **10***a*, and **10***b* leads us to favor structure **4** over structure **7** for the metabolites. Table 3 provides a comparison of the chemical shifts of H-6″ and H-7″ in these four compounds and Fig. 1 shows conformation drawings of **4** and

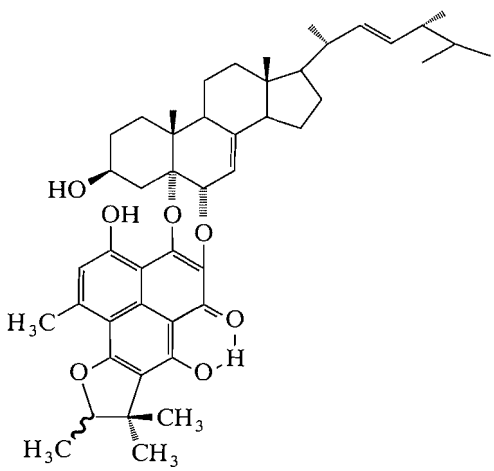

7

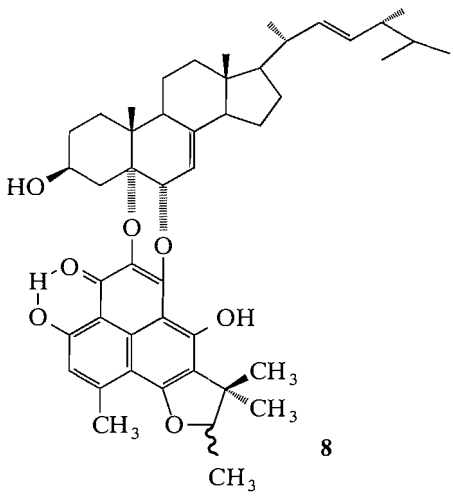

8

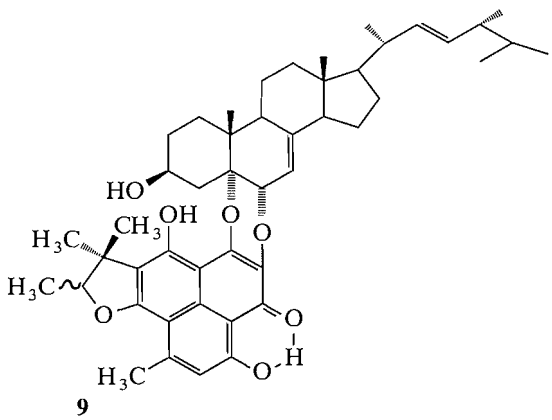

9

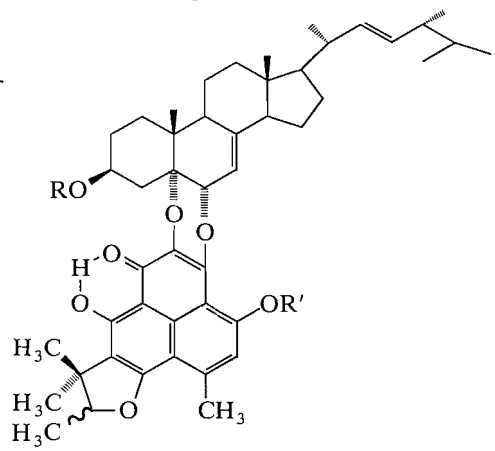

10 R = H, R′ = CH_3
10*a* R = Ac, R′ = CH_3
10*b* R = R′ = Ac

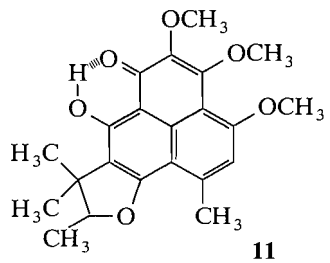

11

7. As can be seen in Fig. 1, the unchelated phenolic hydroxyl group (at C-9 in **4**) is much closer to H-6″ and H-7″ in **4** than in **7**. Methylation and, particularly, acetylation of the C-9 hydroxyl induces significant chemical shifts of H-6″ and, to a lesser extent, H-7″. We feel that these anisotropic shifts are best explained if sirosterol possesses structure **4**

Can. J. Chem. Downloaded from www.nrcresearchpress.com by 109.225.110.28 on 09/08/12
For personal use only.

Can. J. Chem. Downloaded from www.nrcresearchpress.com by 109.225.110.28 on 09/08/12
For personal use only.

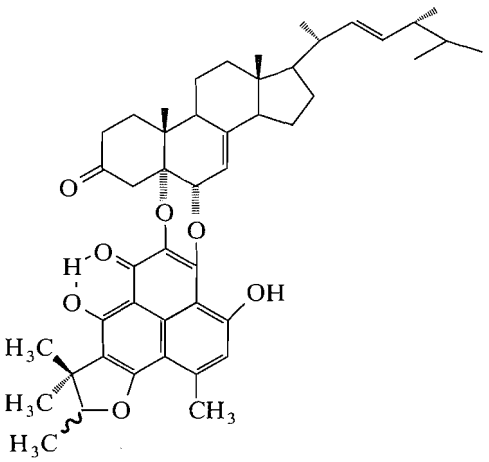

12

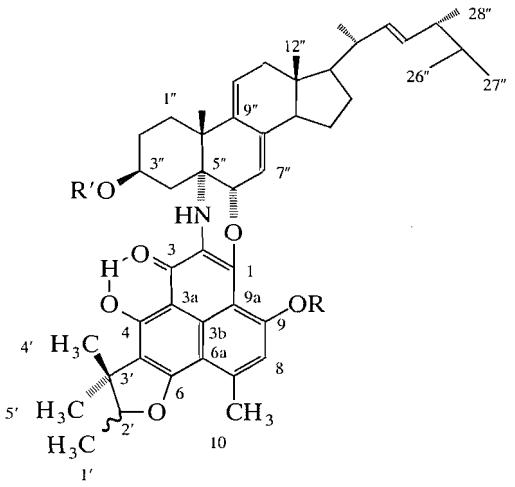

13 R = R′ = H
13*a* R = CH_3, R′ = H
13*b* R = R′ = Ac
13*c* R = CH_3, R′ = Ac

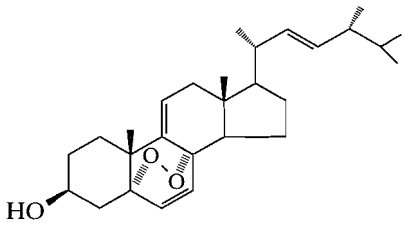

14

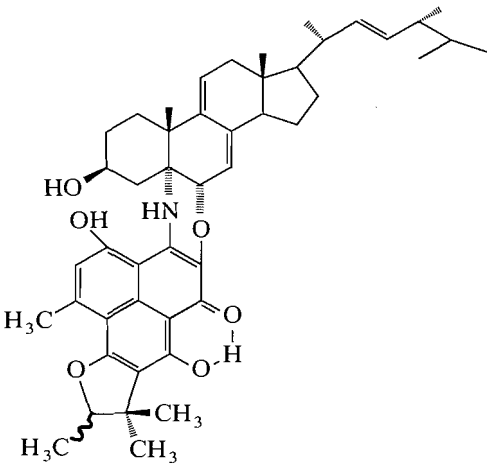

15

rather than **7**. Since sirosterol was not available in large quantities (approximately 1 mg/L of culture broth) we carried out only a limited number of further experiments.[3] All attempts to bring about acid-catalyzed hydrolysis (aqueous trifluoroacetic acid, 50% sulphuric acid, *p*-toluenesulfonic acid in acetone) of sirosterol methyl ether (**10**) were unsuccessful. Aqueous base had no effect. Attempted hydrogenolysis of the allylic ether at C-6″ was unsuccessful, both with the ether **10** and the diacetate **10***b* and utilizing both platinum and palladium catalysts. In every case the side-chain double bond was hydrogenated and the corresponding dihydro compound was obtained. The C-7″, 8″ double bond was not reduced and no hydrogenolysis was observed. Oxidation of sirosterol using the Swern procedure (7) provided ketone **12**, which shows carbonyl absorption at 1722 cm^{-1} in the ir. The ^1H nmr spectrum of **12** is similar to that of sirosterol except that the signal at δ 4.05 (C-3″ H) is not present. Attempts to bring about (acid and base catalyzed) β-elimination of the C-5″ functionality in ketone **12** were not successful.

Sirosterol (**4**), which is optically active, is a mixture of diastereoisomers at C-2′ (ca. 2:1) as indicated by the multiplicity of the signal for H-2′ (two superimposed quartets, $J \approx 6$ Hz) in sirosterol and its derivatives. These diastereoisomers could not be separated (tlc, hplc). Since the phenalenone metabolites from Sirococcus are partially racemic (1), it is not surprising that sirosterol exists in diastereomeric forms.

A second yellow phenalenone-sterol adduct, which we call dehydroazasirosterol, was present (ca. 0.4 mg/L of culture) among the metabolites of Sirococcus 35B. The fabms showed an M + H^+ peak at 734 amu corresponding to a molecular formula $C_{47}H_{59}O_6N$. The ^1H nmr spectrum of dehydroazasirosterol (**13**) was very similar to that of sirosterol (**4**) with the exception of signals at δ 5.73 (1 H, d, $J \approx 6$ Hz) and at δ 4.01 (1 H, s, D_2O exchangeable). Since all the sig-

[3]Sirosterol and its derivatives are obtained as amorphous powders. All attempts to prepare suitable crystals for X-ray crystallographic studies were unsuccessful.

Can. J. Chem. Downloaded from www.nrcresearchpress.com by 109.225.110.28 on 09/08/12
For personal use only.

TABLE 1. The ^{13}C nmr spectra of sirosterol methyl ether **10** (non-steroidal portion), atrovenitin trimethyl yellow (**11**), and atrovenitin orange (**5***a*) in $CDCl_3$

Compound	**10**	**11**[a]	**5***b*[a]
C-1	145.69	157.28	177.31
C-2	130.26	142.37	140.35
C-3	173.96	176.01	160.48
C-3a	107.09	108.19	109.93
C-3b	125.49	127.38	127.85
C-4	172.09	173.93	157.60
C-5	118.99	119.42	126.97
C-6	166.07	166.99	163.34
C-6a	109.20	109.42	108.35
C-7	144.87	144.70	149.96
C-8	111.28	110.66	121.30
C-9	161.06	161.19	174.75
C-9a	105.93	109.23	109.34
C-10	24.06	24.07	24.53
C-1′	14.69	14.65	14.39
C-2′	91.18	91.40	90.48
C-3′	43.38	43.30	44.35
C-4′	25.89	25.87	26.19
C-5′	20.57	20.49	22.09
OCH_3	56.69	56.49, 60.80, 61.61	60.97, 62.29, 64.38

[a]From ref. 4.

TABLE 2. The ^{13}C nmr spectra of sirosterol methyl ether **10** (steroidal portion) and triol **6** in $CDCl_3$

Compound	**10**[a]	**6**[b]	Compound	**10**[b]	**6**[b]
C-1	27.97*	30.68*	C-15	22.67	22.70
C-2	30.61	31.60	C-16	29.75*	28.04*
C-3	66.90	67.44	C-17	55.75	55.89
C-4	31.16	38.72	C-18	12.30	12.19
C-5	75.96	76.05	C-19	17.54	17.77
C-6	73.42	70.35	C-29	40.42	40.39
C-7	115.35	119.52	C-21	21.17	21.11
C-8	143.42	142.08	C-22	135.57	135.40
C-9	42.86	42.81	C-23	132.07	132.14
C-10	35.43	38.51	C-24	42.99	43.76
C-11	21.23	21.41	C-25	33.13	33.08
C-12	39.03	39.23	C-26	19.97	19.94
C-13	43.72	43.33	C-27	19.67	19.64
C-14	54.29	54.70	C-28	17.67	17.58

*Signals interchangeable within the column.
[a]Determined at 75 MHz.
[b]Determined at 90 MHz.

TABLE 3. Comparison of ^1H nmr spectral data for H-6″ and H-7″ in compounds **4**, **10**, **10***a*, **10***b*

Compound	**4**	**10**	**10***a*	**10***b*
H-6″	4.91	4.83	4.82	4.68
H-7″	4.99	4.99	4.96	4.91

nals for the "atrovenitin" portion of the molecule were observed, the signal at δ 5.73 appeared to arise from the sterol portion of the molecule. The presence of an additional olefinic double bond was apparent from the ^{13}C nmr spectrum of **13**. Since 9(11)-dehydroergosterol endoperoxide (**14**) is

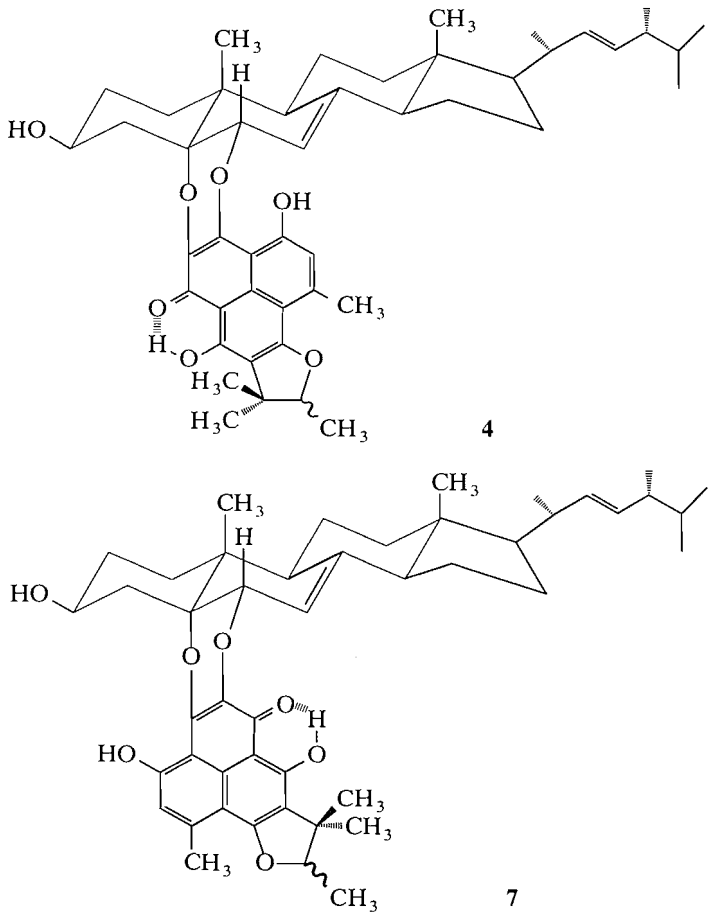

FIG. 1. Conformational drawings of possible structures of sirosterol.

present among the metabolites of this fungus, the location of the additional unsaturation at C-9, C-11 seemed reasonable. In fact, the chemical shifts (Table 4) of the non-side-chain alkenic carbons (δ 117.1, 124.8, 139.2, 140.6) suggest a conjugated diene (8). Whereas the ^{13}C nmr spectrum of **4** shows the presence of three oxygenated sterol carbons (δ 76.0 (s), 73.4 (d), 66.9 (d)), the spectrum of **13** (Table 4) shows only the secondary oxygenated carbons (δ 75.7, 66.9) and a new quaternary carbon signal at δ 55.7, consistent with the replacement of oxygen by nitrogen. The exchangeable hydrogen at δ 4.01 may then be assigned to NH and structure **13** (or **15**) results for dehydroazasirosterol.

Treatment of dehydroazasirosterol (**13**) with ethereal diazomethane provided the monomethyl ether **13***a*. The fabms shows the protonated molecular ion at 748 amu and the ^1H nmr spectrum shows an aromatic methoxyl (δ 4.07) and a chelated OH (δ 17.65). In the COSY 2D nmr spectrum the alkenic hydrogen at δ 5.67 (H-11″) is weakly correlated with a hydrogen at δ 5.03 (H-7″) and this in turn is coupled to the hydrogen at δ 4.81 (H-6″). The latter hydrogen is correlated with the NH hydrogen (δ 3.99). As with sirosterol methyl ether, nOe experiments confirmed the position of methylation and the stereochemistry at C-6″. Irradiation of the C-11″ hydrogen and the NH hydrogen did not lead to observable nOe enhancements. Acetylation of dehydroazasirosterol **13** provides the *O*, *O*-diacetyl derivative **13***b* and acetylation of methyl ether **13***a* provides the monoacetyl ether **13***c*. The *O*, *O*-diacetyl derivative **13***b* shows ir absorption bands for ar-

Can. J. Chem. Downloaded from www.nrcresearchpress.com by 109.225.110.28 on 09/08/12
For personal use only.

TABLE 4. The ^{13}C nmr spectra of dehydroazasirosterol (**13**) and its monomethyl ether (**13***a*)

	Compound			Compound	
Carbon	**13**[a]	**13***a*[b]	Carbon	**13**[a]	**13***a*[b]
C-1	140.61	141.73	C-5″	55.66	55.37
C-2	124.18	123.75	C-6″	75.73	74.17
C-3	174.89	172.56	C-7″	117.05	118.06
C-3a	105.50	104.96	C-8″	139.17	139.17
C-3b	121.04	121.65	C-9″	140.61	139.70
C-4	170.07	172.39	C-10″	37.17	37.59
C-5	118.29	119.09	C-11″	124.81	124.32
C-6	166.23	165.76	C-12″	40.22	40.15
C-6a	108.58	108.17	C-13″	42.43	42.33
C-7	142.37	142.73	C-14″	51.03	50.95
C-8	116.43	111.76	C-15″	22.99	23.02
C-9	158.51	160.34	C-16″	29.45	29.53
C-9a	104.17	109.32	C-17″	55.85	55.84
C-10	23.49	23.69	C-18″	11.63	11.58
C-1′	14.68	14.62	C-19″	23.67	23.89
C-2′	91.27	91.12	C-20″	40.33	40.30
C-3′	43.29	43.32	C-21″	20.75	20.70
C-4′	25.85	25.86	C-22″	135.31	135.40
C-5′	20.65	20.57	C-23″	132.30	132.15
OMe		56.86	C-24″	42.86	42.82
C-1″	28.65	28.63	C-25″	33.10	33.08
C-2″	30.36	30.39	C-26″	19.66	19.60
C-3″	66.84	67.11	C-27″	19.98	19.92
C-4″	42.03	42.08	C-28″	17.67	17.64

[a]APT spectrum measured at 75 MHz.
[b]Obtained at 90 MHz.

omatic acetate (1770 cm^{-1}) and aliphatic acetate (1739 cm^{-1}). The ^1H nmr spectrum shows acetate methyls at δ 2.40 and 1.96 and the chelated OH at δ 17.01. The remaining signals are similar to those of the parent compound **13**. As is the case with sirosterol (**4**, Fig. 1), the signals for H-6″ and H-7″ are shifted upfield in the derivatives **13***a*, **13***b*, and **13***c*, favoring structure **13** over structure **15** for dehydroazasirosterol. Biogenetic precedent for the location of nitrogen at C-2 in the atrovenitin portion of the molecule, as in Scleroderris blue (**3**), also argues in favor of this arrangement.

Oxidation of dehydroazasirosterol (**13**) using the Swern procedure (7) gave the 3″-ketone **16**, ir 1720 cm^{-1}. Attempts to bring about β-elimination to give the α,β-unsaturated enone **17** were unsuccessful. Considering that the "open" form **17** might be thermodynamically less favored than the "closed" form **16**, we heated **16** in acetic anhydride in the presence of triethylamine for 2 h in an attempt to trap **17** as the *N*-acetyl derivative. Only the *O*-acetyl derivative **16***a* and the $\Delta^{2''}$ enol acetate of **16***a* were obtained. The enol acetate does not show ketonic carbonyl absorption in the ir, only ester absorption (1753 cm^{-1}). The ^1H nmr spectrum of the enol acetate shows a signal for H-2″ at δ 5.50 (d, $J \approx 5$ Hz) and two acetyl methyls (δ 2.04, 2.41).

As is the case with sirosterol (**4**), dehydroazasirosterol (**13**) is isolated as a mixture of diastereoisomers at C-2′. This is indicated by two pairs of signals for the phenolic hydrogens at δ 17.84 and 9.76. The ratio of the two epimers for dehydroazasirosterol (ca. 5:1) is different than that for sirosterol (ca. 2:1).

Sirosterol (**4**) and dehydroazasirosterol (**13**) represent a unique combination of two different classes of natural products. We are not aware of other examples where sterols and phenalenones are fused by means of dioxene or dihydro-1,4-oxazine ring systems. A simplistic scheme that illustrates a possible biogenetic pathway uniting ergosterol endoperoxide and an atrovenitin-type molecule is shown in Scheme 1. A related free radical pathway may be written to achieve the same result.

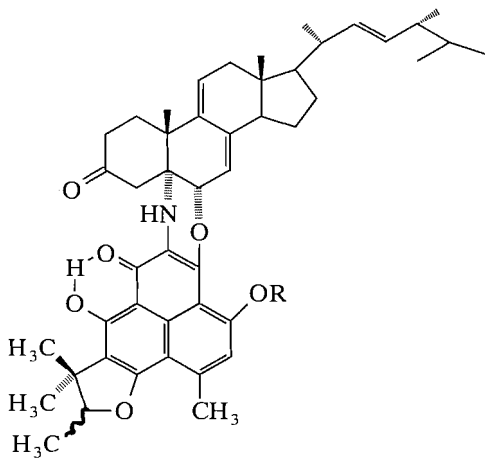

16 R = H
16*a* R = Ac

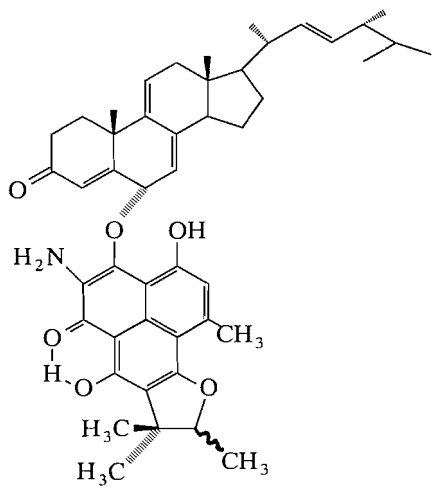

17

The triol **6** mentioned earlier was prepared by *m*-chloroperbenzoic acid oxidation of ergosterol that provides the ester **6***a*. Hydrolysis of **6***a* (KOH, methanol) gives triol **6**. Triol **6** was first prepared by Windaus and Luttringhaus in 1930 (9) by perbenzoic acid oxidation of ergosterol followed by hydrolysis of the benzoate thus obtained and later by Criegee *et al.* (10) by osmium tetroxide oxidation of ergosterol.[4] In agreement with the assigned stereochemistry, irradiation of the methyl group at C-10 in **6** gives rise to a nOe effect (7.5%) on the signal for H-6.

[4]For an interesting discussion of the proof of the stereochemistry of **6** see ref. 11.

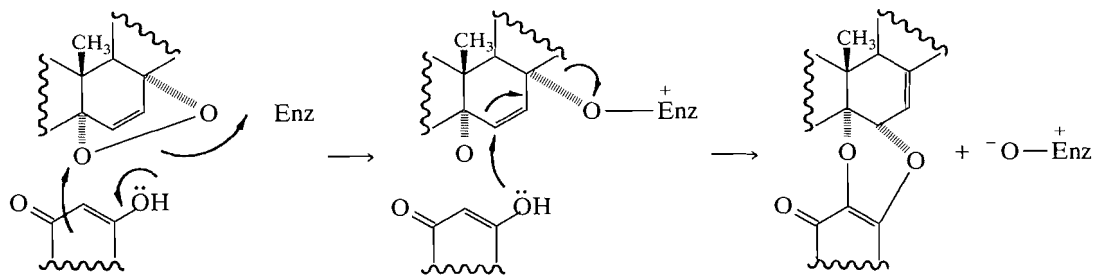

SCHEME 1

Experimental

For general experimental details see ref. 1.

Growth and harvesting of the fungi

Stock cultures of Sirococcus 35B (UAMH 5401) were maintained in slant tube culture on potato dextrose agar at 4°C. To initiate large-scale cultures, small fragments of agar containing the mycelium were aseptically transferred to Erlenmeyer flasks containing sterile culture medium (200 mL). The medium used was Difco potato dextrose broth containing 0.04% (w/v) yeast extract. The cultures were shaken for 10 days at 15–17°C, then used to inoculate five 2.8-L Fernbach flasks containing the same liquid medium (1 L, still culture). After 50–60 days at 15–17°C, the mycelium was separated from the broth by gravity filtration through cheese cloth. The air-dried mycelium was extracted with methylene chloride in a Soxhlet extractor for 2 days. Concentration of the methylene chloride extracts gave the crude mycelial extract (3.0 g). Most of the metabolites were present in the mycelial extract and only a small amount (ca. 0.04 g) in the broth extract.

Separation of the metabolites

The methylene chloride extract (3.0 g) from the mycelium was separated into nonpolar, medium polar, and polar fractions by silica gel column chromatography (gradient elution; hexanes-toluene-ethyl acetate-methanol). The nonpolar and medium polar fractions were separated by repeated flash chromatography over silica gel. Fatty acids, triglycerides, sclerodin (**1**, 140 mg), ergosterol (36 mg), 9(11)-dehydroergosterol endoperoxide (3 mg), ergosta-4,6,8(14),22-tetraen-3-one (3 mg), sirocodilide (17 mg), sirosterol (**4**, 5 mg), and dehydroazasirosterol (**13**, 2mg) were isolated. Scleroderris blue (**3**, 3 mg) was isolated from the polar fraction by flash chromatography. Atrovenetinone (**2**) was isolated as its acetone adduct from the metabolites grown on Wort medium. Compounds **4** and **13** were not isolated from the Wort medium growth.

*Sirosterol (**4**)*

Sirosterol was isolated as an amorphous powder that showed a single spot on tlc. However, the ^{1}H nmr spectrum indicates that it is a mixture of diastereoisomers (both configurations at C-2′, superimposed quartets at δ 4.65 in $CDCl_3$); ir ν_{max}: 3390, 3384, 1730 (w), 1660 (w), 1611, 1576, 1444, 1416, 1375, 1339, 1307, 1281, 1239, 1190 cm^{-1}; ^{1}H nmr (360 MHz) δ: 0.57 (3 H, s, 18″-CH_3), 0.80 (3 H, d, 5.3 Hz, 26″-CH_3), 0.81 (3 H, d, 5.3 Hz, 27″-CH_3), 0.88 (3 H, d, 6 Hz, 28″-CH_3), 1.00 (3 H, d, 6 Hz, 21″-CH_3), 1.14 (3 H, s, 19″-CH_3), 1.25 (1 H, brs, OH), 1.32 (3 H, s, 4′-CH_3), 1.47 (3 H, d, 6 Hz, 1′-CH_3), 1.56 (3 H, s 5′-CH_3), 2.82 (3 H, s, ArCH_3), 4.05 (1 H, m, H-3″), 4.65 (1 H, q, 6 Hz, H-2′), 4.91 (1 H, brs, H-6″), 4.99 (1 H, brs, H-7″), 5.15 (2 H, m, H-22″, 23″), 6.83 (1 H, s, ArH), 9.56 (1 H, s, 9-OH), 17.16 (1 H, s, 4-OH); ^{1}H nmr ($CDCl_3$ + C_5D_5N, 360 MHz) δ: 0.57 (3H, s, 18″-CH_3), 0.80 (3 H, d, 5.3 Hz, 26″-CH_3), 0.82 (3 H, d, 5.3 Hz, 27″-CH_3), 0.90 (3 H, d, 6 Hz, 28″-CH_3), 1.02 (3 H, d, 6 Hz, 21″-CH_3), 1.14 (3 H, s, 19″-CH_3), 1.27 (1 H, brs, OH), 1.31 (3 H, s, 4′-CH_3), 1.45 (3 H, d, 6 Hz, 1′-CH_3), 1.59 (3 H, s, 5′-CH_3), 2.83 (3 H, s, ArCH_3), 4.16 (1 H, m, H-3″), 4.66 (1 H, q, 6 Hz, H-2′), 4.90 (1 H, brs, H-6″), 5.05 (1 H, brs, H-7″), 5.20 (2 H, m, H-22″, 23″), 6.88 (1 H, s, ArH), 9.82 (1 H, s, 9-OH), 17.55 (1 H, s, 4-OH); fabms, *m/z*: 737.48 (M + H$^+$, calcd. for $C_{47}H_{61}O_7$: 737.4417, 2.67%), 341 (6), 309 (9).

*Methylsirosterol (**10**)*

Sirosterol (5 mg) was treated with an excess of diazomethane in ether solution at room temperature for 24 hs. The solvent was evaporated and the residue was purified by flash chromatography (hexanes–acetone 3:1) to give an amorphous solid (**10**, 5 mg), [α]$_D$ + 79.1 (c 0.22, $CHCl_3$); ir ν_{max}: 3300, 2956, 2932, 1718 (w), 1642 (w), 1611, 1444, 1375, 1220, 1181, 1162, 1106, 1060, 1037, 1012 cm^{-1}; ^{1}H nmr (360 MHz) δ: 0.57 (3 H, s, 18″-CH_3), 0.81 (3 H, d, 5.3 H, 26″-CH_3), 0.82 (3 H, d, 5.3 Hz, 27″-CH_3), 0.89 (3 H, d, 6 Hz, 28″-CH_3), 1.09 (3 H, d, 6 Hz, 21″-CH_3), 1.13 (3 H, s, 19″-CH_3), 1.26 (1 H, brs, OH), 1.32 (3 H, s, 4′-CH_3), 1.48 (3 H, d, 6 Hz, 1′-CH_3), 1.57 (3 H, s, 5′-CH_3), 2.89 (3 H, s, ArCH_3), 4.05 (1 H, m, H-3″), 4.05 (3 H, s, OCH_3), 4.65 (1 H, q, 6 Hz, H-2′), 4.83 (1 H, brs, H-6″), 4.99 (1 H, brs, H-7″), 5.14 (2 H, m, H-22″, 23″), 6.85 (1 H, s, ArH), 17.95 (1 H, s, 4-OH); ^{13}C nmr (75 MHz) see Tables 1 and 2; hrms, *m/z*: 396.3385 (calcd. for $C_{28}H_{44}O$: 396.3392, (28%), 376 ($C_{28}H_{40}$, 13), 356 ($C_{20}H_{20}O_6$, 63), 341 ($C_{19}H_{17}O_6$, 100), 323 (20), 251 (33); fabms, *m/z*: 751.64 (M + H$^+$, calcd. for $C_{48}H_{63}O_7$: 751.4574, 10.1%), 377.53 (1.97), 357.14 (8.94), 341.07 (5.19).

*Methylacetylsirosterol (**10**a)*

Acetic anhydride (1 mL) and pyridine (1 mL) were added to a solution of methyl sirosterol (1 mg) in methylene chloride (2 mL). The mixture was stirred at room temperature for 18 hs. The solution was concentrated and the residue was purified by flash chromatography (hexanes–acetone 4:1) to give **10***a* (1 mg) as an oil, ir ν_{max}: 3320, 2957, 2936, 2933, 2870, 1736, 1614, 1590 cm^{-1}; ^{1}H nmr (360 MHz) δ: 0.56 (3 H, s, 18″-CH_3), 0.80 (3 H, d, 5.3 Hz, 26″-CH_3), 0.81 (3 H, d, 5.3 Hz, 27″-CH_3), 0.89 (3 H, d, 6 Hz, 28″-CH_3), 1.01 (3 H, d, 6 Hz, 21″-CH_3), 1.15 (3 H, s, 19″-CH_3), 1.32 (3 H, s, 4′-CH_3), 1.47 (3 H, d, 6 H, 1′-CH_3), 1.57 (3 H, s, 5′-CH_3), 1.91 (3 H, s, $COCH_3$), 2.90 (3 H, s, ArCH_3), 4.04 (3 H, s, OCH_3), 4.63 (1 H, q, 6 Hz, H-2′), 4.82 (1 H, brs, H-6″), 4.96 (1 H, brs, H-7″), 5.05 (1 H, m, H-3″), 5.16 (2 H, m, H-22″, 23″), 6.85 (1 H, s, ArH), 17.97 (1 H, s, 4-OH); fabms, *m/z*: 793.59 (M + H$^+$, calcd. for $C_{50}H_{65}O_8$: 793.4679, 2.46%), 356.85 (2.72), 340.80 (1.62), 308.80 (5.62).

*Diacetylsirosterol (**10**b)*

Sirosterol (0.5 mg) was dissolved in a solution of acetic anhydride (1 mL) and pyridine (1 mL) in methylene chloride (2 mL). The mixture was stirred at room temperature for 17 hs. The solvent was coevaporated with ethanol and the residue was purified by flash chromatography (hexane–acetone 5:1) providing **10***b* (0.5 mg); ir ν_{max}: 3400, 2975, 2927, 1753, 1734, 1620, 1593, 1456, 1443, 1376, 1366, 1265, 1242, 1226, 1195, 1176 cm^{-1}; ^{1}H nmr (360 MHz) δ: 0.56 (3 H, s, 18″-CH_3), 0.80 (3 H, d, 5.3 Hz, 26″-CH_3), 0.81 (3 H, d, 5.3 Hz, 27″-CH_3), 0.88 (3 H, d, 6 Hz, 28″-CH_3), 1.00 (3 H, d, 6 Hz, 21″-CH_3), 1.15 (3 H, s, 19″-CH_3), 1.32 (3 H, s, 4′-CH_3), 1.47 (3 H, d, 6 Hz, 1′-CH_3), 1.57 (3 H, s, 5′-CH_3), 1.96 (3 H, s, $COCH_3$), 2.38 (3 H, s, $COCH_3$), 2.86 (3 H, s, ArCH_3), 4.66 (1 H, q, 6 Hz, H-2′), 4.68 (1 H, brs, H-6″),

Can. J. Chem. Downloaded from www.nrcresearchpress.com by 109.225.110.28 on 09/08/12
For personal use only.

Can. J. Chem. Downloaded from www.nrcresearchpress.com by 109.225.110.28 on 09/08/12
For personal use only.

4.91 (1 H, brs, H-7″), 5.02 (1 H, m, H-3″), 5.16 (2 H, m, H-22″, 23″), 6.94 (1 H, s, ArH), 17.41 (1 H, s, 4-OH); fabms, *m/z*: 821.56 ($M + H^+$, calcd. for $C_{51}H_{65}O_9$: 821.5107, 0.87%).

*Dehydrosirosterol (**12**)*

Trifluoroacetic anhydride (10 μL) was added dropwise to a stirred solution of dimethyl sulfoxide (10 μL) in 3 mL of methylene chloride at −78°C. After 10 min, sirosterol (1 mg) in methylene chloride (2 mL) was added and the solution was stirred for 40 min at the same temperature. Triethylamine (50 μL) was then added and the reaction was kept for another 40 min at −78°C. The reaction mixture was allowed to warm to room temperature and water (3 mL) was added. The aqueous layer was separated and extracted twice with methylene chloride. The combined organic extracts were washed, dried, and evaporated. The residue was purified by flash chromatography (hexanes – ethyl acetate 7:3) providing **12** (0.8 mg) as an amorphous solid; ir ν_{max}: 3390, 2957, 2927, 2871, 2855, 1722, 1610, 1454, 1445, 1377, 1306, 1280, 1237, 1223, 1189, 1171, 1157, 1135, 1101, 1063, 1036 cm^{-1}; ^1H nmr (360 MHz) δ: 0.60 (3 H, s, 18″-CH_3), 0.81 (3 H, d, 6 Hz, 26″-CH_3), 0.83 (3 H, d, 6 H, 27″-CH_3), 0.90 (3 H, d, 6.5 Hz, 28″-CH_3), 1.02 (3 H, d, 6.5 H, 21″-CH_3), 1.31 (3 H, s, 19″-CH_3), 1.34 (3 H, s, 4′-CH_3), 1.49 (3 H, d, 6.5 Hz, 1′-CH_3), 1.56 (3 H, s, 5′-CH_3), 2.82 (3 H, s, $ArCH_3$), 4.65 (1 H, q, 6.5 Hz, H-2′), 5.03 (2 H, brs, H-6″ and H-7″), 5.18 (2 H, m, H-22″, 23″), 6.83 (1 H, s, ArH), 9.43 (1 H, s, 9-OH), 17.03 (1 H, s, 4-OH); fabms, *m/z*: 735.17 ($M + H^+$, calcd. for $C_{47}H_{59}O_7$: 735.4261, 6%), 394.16 (2), 340.68 (29).

*Dehydroazasirosterol (**13**)*

Dehydroazasirosterol (**13**) was isolated as an amorphous powder that showed a single spot on tlc. The ^1H nmr spectrum shows that it is a mixture of diastereoisomers (at C-2′). This is indicated by the fact that the phenolic hydrogens at δ 17.84 and δ 9.76 each appear as two closely spaced singlets. This is also true of the low-field chelated phenol signal in **13***a* and **13***b*. Dehydroazasirosterol shows the following spectral properties: ir ν_{max}: 3398, 3388, 3380, 2956, 2869, 1610, 1569, 1455, 1428, 1384, 1371, 1296, 1249, 1226, 1193, 1134, 1101, 1048, 1032 cm^{-1}; ^1H nmr (360 MHz) δ: 0.55 (3 H, s, 18″-CH_3), 0.80 (3 H, d, 6 Hz, 26″-CH_3), 0.82 (3 H, d, 6 Hz, 27″-CH_3), 0.89 (3 H, d, 6 Hz, 28″-CH_3), 1.00 (3 H, d, 6.5 Hz, 21″-CH_3), 1.29 (3 H, s, 19″-CH_3), 1.30 (3 H, s, 4′-CH_3), 1.48 (3 H, d, 6.5 Hz, 1′-CH_3), 1.57 (3 H, s, 5′-CH_3), 2.82 (3 H, s, $ArCH_3$), 4.01 (1 H, s, NH), 4.12 (1 H, m, H-3″), 4.89 (1 H, brs, H-6″), 5.04 (1 H, brs, H-7″), 5.16 (2 H, m, H-22″, 23″), 5.73 (1 H, d, 6 Hz, H-11″), 6.84 (1 H, s, ArH), 9.76 (1 H, s, 9-OH), 17.84 (1 H, s, 4-OH); ^{13}C nmr (75 MHz) see Table 4; fabms, *m/z*: 734.55 ($M + H^+$, calcd. for $C_{47}H_{60}O_6N$: 734.4421, 0.72%), 733.55 (0.81), 375.30 (2), 339.89 (9).

*Methyl dehydroazasirosterol (**13**a)*

Dehydroazasirosterol (**13***a*, 5 mg) was treated with an excess of diazomethane in ether at room temperature for 24 hs. Evaporation of the solvent and purification of the residue by flash chromatography (hexanes – ethyl acetate 5:1) provided **13***a* (5 mg) as an amorphous solid, ir ν_{max}: 3400, 2957, 2924, 2850, 1612, 1590, 1552 cm^{-1}; ^1H nmr (360 MHz) δ: 0.54 (3 H, s, 18″-CH_3), 0.80 (3 H, d, 6 Hz, 26″-CH_3), 0.81 (3 H, d, 6 Hz, 27″-CH_3), 0.89 (3 H, d, 6 Hz, 28″-CH_3), 1.00 (3 H, d, 6 Hz, 21″-CH_3), 1.27 (3 H, s, 19″-CH_3), 1.32 (3 H, s, 4′-CH_3), 1.48 (3 H, d, 6 Hz, 1′-CH_3), 1.55 (3 H, s, 5′-CH_3), 2.88 (3H, s, $ArCh_3$), 3.99 (1 H, s, NH), 4.07 (3 H, s, OCH_3), 4.13 (1 H, m, H-3″), 4.64 (1 H, q, 6 Hz, H-2′), 4.81 (1 H, brs, H-6″), 5.03 (1 H, brs, H-7″), 5.16 (2 H, m, H-2″, 23″), 5.67 (1 H, d, 6 Hz, H-11″), 6.90 (1 H, s, ArH), 17.65 (1 H, s, 4-OH); ^{13}C nmr (90 MHz) see Table 4; hrms, *m/z*: 394.3231 ($C_{28}H_{42}O$, 14%), 376 ($C_{28}H_{40}$, 16), 355.1419 ($C_{20}H_{21}O_5N$, 54), 340 ($C_{19}H_{18}O_5N$, 41), 251 (74), 57 (100); fabms, *m/z*: 748.33 ($M + H^+$, calcd. for $C_{48}H_{62}O_6N$: 748.4577, 7.27%), 747.32 (6.5), 354.19 (15).

*Methyl acetyldehydroazasirosterol (**13**c)*

Methyl dehydroazasirosterol (1 mg) was dissolved in acetic anhydride (2 mL), pyridine (1 mL), and methylene chloride (2 mL). The mixture was stirred at room temperature for 22 h. The solvent was coevaporated with ethanol. The residue was purified by flash chromatography (hexanes – ethyl acetate 5:1) providing **13***c* (0.9 mg). ir ν_{max}: 3398, 2956, 1729, 1610, 1590 cm^{-1}; ^1H nmr (360 MHz) δ: 0.53 (3 H, s, 18″-CH_3), 0.79 (3 H, d, 5.3 Hz, 26″-CH_3), 0.81 (3 H, d, 5.3 Hz, 27″-CH_3), 0.88 (3 H, d, 6 Hz, 28″-CH_3), 0.99 (3 H, d, 6 Hz, 21″-CH_3), 1.26 (3 H, s, 19″-CH_3), 1.30 (3 H, s, 4′-CH_3), 1.48 (3 H, d, 6.5 Hz, 1′-CH_3), 1.56 (3 H, s, 5′-CH_3), 1.94 (3 H, s, $COCH_3$), 2.87 (3 H, s, $ArCH_3$), 4.03 (1 H, s, NH), 4.06 (3 H, s, OCH_3), 4.62 (1 H, q, 6.5 Hz, H-2′), 4.81 (1 H, brs, H-6″), 5.01 (1 H, brs, H-7″), 5.15 (2 H, m, H-22″, 23″), 5.68 (1 H, d, 6 Hz, H-11″), 6.88 (1 H, s, ArH), 17.66 (1 H, s, 4-OH); fabms, *m/z*: 790.77 ($M + H^+$, calcd. for $C_{50}H_{64}O_7N$: 790.4683, 2.56%), 789.74 (2.36), 355.98 (7), 353.95 (8).

*Diacetyldehydroazasirosterol (**13**b)*

Acetic anhydride (1 mL) were added to a solution of sirocodinine (0.5 mg) in methylene chloride (1 mL). The mixture was stirred at room temperature for 16 hs. The solvent was evaporated and the residue was redissolved in methylene chloride. The organic phase was washed with 5% HCl, and then evaporated to dryness. The residue was purified by passing through a short Florisil column giving **13***b* (0.4 mg), ir ν_{max}: 3400, 2955, 2870, 1770, 1739, 1619, 1596 cm^{-1}; ^1H nmr (360 MHz) δ: 0.53 (3 H, s, 18″-CH_3), 0.78 (3 H, d, 6 Hz, 26″-CH_3), 0.80 (3 H, d, 6 Hz, 27″-CH_3), 0.91 (3 H, d, 6 Hz, 28″-CH_3), 0.99 (3 H, d, 6.5 Hz, 21″-CH_3), 1.31 (3 H, s, 19″-CH_3), 1.32 (3 H, s, 4′-CH_3), 1.48 (3 H, d, 6.5 Hz, 1′-CH_3), 1.57 (3 H, s, 5′-CH_3), 1.96 (3 H, s, $COCH_3$), 2.40 (3 H, s, $COCH_3$), 2.85 (3 H, s, $ArCH_3$), 4.06 (1 H, s, NH), 4.64 (1 H, brs, H-6″), 4.66 (1 H, q, 6.5 Hz, H-2′), 4.99 (1 H, brs, H-7″), 5.15 (2 H, m, H-22″, 23″), 5.68 (1 H, d, 6 Hz, H-11″), 6.93 (1 H, s, ArH), 17.01 (1 H, s, 4-OH); fabms, *m/z*: 818.80 ($M + H^+$, calcd. for $C_{51}H_{64}O_8N$: 818.4632, 0.99%), 817.78 (1.06), 382.33 (6), 368.37 (11), 340.12 (12).

*Oxidation of dehydroazasirosterol (**13**)*

Trifluoroacetic anhydride (30 μL) was added dropwise to a stirred solution of dimethyl sulfoxide (30 μL) in 3 mL of methylene chloride at −78°C. After 10 min, dehydroazasirosterol (2 mg) in methylene chloride (2 mL) was added and the solution was allowed to stir at the same temperature for 40 min. Triethylamine (100 μL) was then added and the mixture was kept at −78°C for another 40 min. The reaction mixture was allowed to warm up to room temperature. Water (3 mL) was added and the aqueous layer was separated and extracted twice with methylene chloride. The combined organic extracts were washed with brine, dried, and evaporated. Purification of the crude product by flash chromatography (hexanes – ethyl acetate 70:30) yielded **16** (1.2 mg), ir ν_{max}: 3420, 2958, 2927, 2871, 1720, 1607, 1571 cm^{-1}; ^1H nmr (360 MHz) δ: 0.57 (3 H, s, 18″-CH_3), 0.80 (3 H, d, 6 Hz, 26″-CH_3), 0.82 (3 H, d, 6 Hz, 27″-CH_3), 0.89 (3 H, d, 6.5 Hz, 28″-CH_3), 1.01 (3 H, d, 6.5 Hz, 21″-CH_3), 1.30 (3 H, s, 19″-CH_3), 1.32 (3 H, s, 4′-CH_3), 1.47 (3 H, d, 6.5 Hz, 1′-CH_3), 1.54 (3 H, s, 5′-CH_3), 2.82 (3 H, s, $ArCH_3$), 4.00 (1 H, s, NH), 4.66 (1 H, q, 6.5 Hz, H-2′), 5.01 (1 H, brs, H-6″), 5.10 (1 H, brs, H-7″), 5.20 (2 H, m, H-22″, 23″), 5.83 (1 H, d, 6 Hz, H-11″), 6.84 (1 H, s, ArH), 9.63 (1 H, s, 9-OH), 16.70 (1 H, s, 4-OH); fabms, *m/z*: 732.62 ($M + H^+$, calcd. for $C_{47}H_{58}O_6N$: 732.4264, 0.67%), 731.63 (1.02), 341.44 (11), 340.43 (11), 339.43 (21).

*Monoacetate **16**a and enol acetate of **16**a*

Ketone **16** (1.2 mg) in acetic anhydride (2 mL) and triethylamine (2 mL) was heated under reflux for 2 hs. The mixture was poured onto crushed ice. The aqueous layer was extracted with methylene chloride twice and the organic layer was washed with brine, dried, and evaporated. The residue was separated by silica gel chromatography (hexanes – ethyl acetate 70:30) giving monoacetate **16***a* (0.5 mg) and the $\Delta^{2\prime\prime}$ enol acetate (0.6 mg). **16***a*: ir ν_{max}: 3400, 2929, 1767, 1744, 1717, 1620, 1594 cm^{-1}; ^1H nmr (360 MHz) δ: 0.57 (3 H, s, 18″-CH_3), 0.80 (3 H, d, 6 Hz, 26″-CH_3), 0.81 (3 H, d, 6 Hz, 27″-CH_3), 0.88 (3 H, d, 6.5 Hz, 28″-CH_3), 1.00 (3

H, d, 6.5 Hz, 21″-CH_3), 1.30 (3 H, s, 19″-CH_3), 1.32 (3 H, s, 4-CH_3), 1.45 (3 H, d, 6.5 Hz, 1′-CH_3), 1.50 (3 H, s, 5′-CH_3), 2.38 (3 H, s, $OCOCH_3$), 2.85 (3 H, s, $ArCH_3$), 4.10 (1 H, s, NH), 4.67 (1 H, q, 6.5 Hz, H-2′), 4.78 (1 H, brs, H-6″), 5.05 (1 H, brs, H-7″), 5.20 (2 H, m, H-22″, 23″), 5.79 (1 H, d, 6 Hz, H-11″), 6.94 (1 H, s, ArH), 16.88 (1 H, s, 4-OH); fabms, *m/z*: 774.53 ($M + H^+$, calcd. for $C_{49}H_{60}O_7N$: 774.4370, 2.15%), 773.55 (1.65), 339.86 (6), 308.85 (9). *Enol acetate*: ir ν_{max}: 3400, 2957, 2925, 2869, 2853, 1753, 1621, 1596 cm^{-1}; ^1H nmr (360 MHz) δ: 0.55 (3 H, s, 18″-CH_3), 0.80 (3 H, d, 6 Hz, 26″-CH_3), 0.82 (3 H, d, 6 Hz, 27″-CH_3), 0.89 (3 H, d, 6.5 Hz, 28″-CH_3), 1.00 (3 H, d, 6.5 Hz, 21″-CH_3), 1.24 (3 H, s, 19″-CH_3), 1.32 (3 H, s, 4′-CH_3), 1.48 (3 H, d, 6.5 Hz, 1′-CH_3), 1.54 (3 H, s, 5′-CH_3), 2.04 (3 H, s, $COCH_3$), 2.41 (3 H, s, $COCH_3$), 2.85 (3 H, s, $ArCH_3$), 4.48 (1 H, s, NH), 4.67 (1 H, q, 6.5 Hz, H-2′), 4.83 (1 H, brs, H-6″), 5.09 (1 H, brs, H-7″), 5.16 (2 H, m, H-22″, 23″), 5.50 (1 H, d, 5 Hz, H-2″), 5.66 (1 H, d, H-11″), 6.95 (1 H, s, ArH), 16.96 (1 H, s, 4-OH); fabms, *m/z*: 816.67 ($M + H^+$, calcd. for $C_{51}H_{62}O_8N$: 816.4475, 0.28%), 815.68 (0.35), 339.89 (2).

*Preparation of 5α, 6α-dihydroxydihydroergosterol (**6**)*

m-Chloroperbenzoic acid (81 mg of 80%, 0.376 mmol) was added to a solution of ergosterol (149 mg, 0.376 mmol) in methylene chloride (12 mL). The mixture was stirred at room temperature for 5 hs, then further *m*-chloroperbenzoic acid (20 mg) was added and the mixture was stirred for 19 hs. The solution was washed twice with sodium thiosulfate solution, then twice with sodium bicarbonate solution. The organic layer was dried and evaporated. The residue was separated by flash chromatography (hexanes – ethyl acetate 8:3) to give the 6-*O*-*m*-chlorobenzoate **6***a* (95 mg): mp 196–198°C; ir ν_{max}: 3560, 3220, 2956, 2870, 1705, 1660, 1575 cm^{-1}; ^1H nmr (360 MHz) δ: 0.60 (3 H, s, 18-CH_3), 0.83 (3 H, d, 6 Hz, 26-CH_3), 0.84 (3 H, d, 6 Hz, 27-CH_3), 0.92 (3 H, d, 6.5 Hz, 28-CH_3), 1.04 (3 H, d, 6.5 Hz, 21-CH_3), 1.09 (3 H, s, 19-CH_3), 4.03 (1 H, m, H-3), 5.03 (1 H, brs, H-7), 5.19 (2 H, m, H-22, 23), 5.55 (1 H, brs, H-6), 7.40 (1 H, dd, 8, 8 Hz), 7.55 (1 H, ddd, 2, 2, 8 Hz), 7.95 (1 H, ddd, 2, 2, 8 Hz), 8.03 (1 H, dd, 2,2 Hz); ^1H nmr (C_6D_6, 360 MHz) δ: 0.47 (3 H, s, 18-CH_3), 0.84 (9 H, m), 0.91 (3 H, d, 7 Hz, 28-CH_3), 1.00 (3 H, d, 6 Hz, 21-CH_3), 4.07 (1 H, m, H-3), 5.11 (1 H, brs, H-7), 5.18 (2 H, m, H-22, 23), 5.72 (1 H, brs, H-6), 6.80 (1 H, dd, 8, 8 Hz), 7.12 (1 H, brd, 8 Hz), 7.89 (1 H, d, 8 Hz), 8.18 (1 H, brs); hrms, *m/z*: 412.3348 ($M^+ - C_7H_5O_2Cl$, calcd. for $C_{28}H_{44}O_2$: 412.3341, 4%), 394 ($M^+ - C_7H_5O_2Cl - H_2O$, 12), 376 ($M^+ - C_7H_5O_2Cl - 2\,H_2O$, 18), 251 (36), 158 (17), 156 (53), 139 (58), 69 (100). The *m*-chlorobenzoate **6***a* (61 mg) was stirred with 5% KOH in methanol for 24 hs. Removal of the methanol, addition of water, and extraction with ethyl acetate provided the crude product. Triol **6** (33 mg) was obtained after flash chromatography (methylene chloride – acetone 50:50) and crystallization from methanol: 227–229°C; $[\alpha]_D$ + 13.3 (c 0.18, $CHCl_3$); ir ν_{max}: 3323, 3273, 2889, 2870, 2850, 1660 cm^{-1}; ^1H nmr (360 MHz) δ 0.57 (3 H, s, 18-CH_3), 0.83 (3 H, d, 6 Hz, 26-CH_3), 0.84 (3 H, d, 6Hz, 27-CH_3), 0.93 (3 H, d, 7 Hz, 28-CH_3), 0.98 (3 H, s, 19-CH_3), 1.03 (3 H, d, 6.5 Hz, 21-CH_3), 3.98 (1 H, brs, H-6), 4.01 (1 H, m, H-3), 5.03 (1 H, brs, H-7), 5.20 (2 H, m, H-22, 23); ^{13}C nmr (90 MHz) see Table 2; hrms, *m/z*: 412.3341 ($M - H_2O$, calcd. for $C_{28}H_{44}O_2$: 412.3341, 100%), 394 ($M - 2\,H_2O$, 13), 379 (26), 269 (11), 251 (17).

Acknowledgements

We thank the Natural Sciences and Engineering Research Council for financial support. We also thank Lynne Sigler, University of Alberta Microfungus Herbarium, for taxonomical work and valuable discussion, and M. Kamada for preliminary experiments.

1. W. A. Ayer, M. Kamada, and Y. Ma. Can. J. Chem. **67**, 2089 (1989).
2. W. A. Ayer, M. S. Pedras, and D. E. Ward. Can. J. Chem. **65**, 760 (1987), and references therein.
3. W. A. Ayer, Y. Hoyano, M. S. Pedras, and I. van Altena. Can. J. Chem. **64**, 1585 (1986).
4. W. A. Ayer, M. S. Pedras, and D. E. Ward. Can. J. Chem. **65**, 760 (1987).
5. V. Piccialli and D. Sica. J. Nat. Prod. **50**, 915 (1987).
6. F. W. Wehrli and T. Nishida. *In* Progress in the chemistry of organic natural products. Vol. 36. *Edited by* W. Herz, H. Grisebach, and G. W. Kirby. Springer-Verlag, New York. 1979. pp. 104–121.
7. D. Swern and A. J. Mancuso. Synthesis, 165 (1981).
8. E. Breitmaier and W. Voelter. Carbon-13 NMR spectroscopy. 3rd ed. VCH Publishers, New York. 1987. p. 114.
9. A. Windaus and A. Luttringhaus. Ann. **481**, 119 (1930).
10. R. Criegee, B. Marchand, and H. Wannowius. Ann. **550**, 114 (1942).
11. L. F. Fieser and M. Fieser. Steroids. Reinhold, New York. 1959. pp. 98–101.

Can. J. Chem. Downloaded from www.nrcresearchpress.com by 109.225.110.28 on 09/08/12
For personal use only.

Reduction of two-component $CuO–Cr_2O_3$ mixed oxides and their catalytic activity

V. MÚČKA

Technical University of Prague, Department of Nuclear Science and Physical Engineering, 115 19 Prague 1, Czechoslovakia

Received July 10, 1991.[1]

V. MÚČKA. Can. J. Chem. **70**, 1914 (1992).

The reduction with hydrogen of the two-component mixed oxides $CuO–Cr_2O_3$ containing various amounts of both components in the whole range from 0 to 100% was studied, as well as some physico-chemical and catalytic properties. The hydrogen peroxide decomposition served as a test catalytic reaction. A significant effect of the reduction on the rate constant of the test reaction was found, as well as on the value of its apparent activation energy. Pronounced changes were observed, especially in the border ranges of the composition. This fact may be connected with the mutual influence of both components in the catalyst.

V. MÚČKA. Can. J. Chem. **70**, 1914 (1992).

On a étudié quelques propriétés physico-chimiques et catalytiques ainsi que la réduction par de l'hydrogène des oxydes mixtes $CuO–Cr_2O_3$ à deux composants contenant diverses quantités de chacun sur l'ensemble des compositions allant de 0 à 100%. On a utilisé le décomposition du peroxyde d'hydrogène comme réaction catalytique témoin. On a trouvé qu'il existe un effet important de la réduction sur la constante de vitesse de la réaction témoin ainsi que sur la valeur de son énergie d'activation apparente. On a observé des changements importants, spécialement dans les régions de composition limite. On peut relier ce fait avec l'influence mutuelle des deux composants dans le catalyseur.

[Traduit par la rédaction]

Introduction

A notable effect of the degree of reduction on the catalytic properties of the $CuO–Cr_2O_3$ catalyst containing about 77 wt.% of CuO was found earlier (1). This phenomenon may be due to the changes in the oxidation state of both metals present in the catalyst after its reduction. The catalytic activity of the mixture composed of cupric and cuprous oxides was found (2) to be higher than the activity of the oxides CuO or Cu_2O separately. Hence, the catalytic sites of the CuO may be connected in some way with the redox $CuO–Cu_2O$ system (3). The catalytic activity of the chromium sesquioxide was found to be proportional to surface over-stoichiometric oxygen (4, 5), which is probably compensated by the presence of hexavalent chromium in the form of insoluble chromate (6–8). That is probably why the oxidized chromic catalysts showed notably higher activity than the reduced ones (9). Hence, one can assume (10) that the Cr^{3+} and Cr^{6+} ions serve as donor and acceptor sites, respectively. Nevertheless, no linear relation was found between the concentration of Cr^{6+} ions present in the chromium sesquioxide and the rate constant of hydrogen peroxide decomposition.

For this reason it seemed of interest to investigate systematically the catalytic properties of $CuO–Cr_2O_3$ two-component catalysts of various composition after reduction and to compare them with those of nonreduced samples.

Experimental

The mixed catalysts were prepared from the solutions of the respective nitrates (analytical grade) mixed in such ratios that the resulting catalysts covered the whole range of composition, i.e., from 0 to 100%. The nitrates were precipitated using a solution of sodium carbonate (analytical grade). After washing (until no sodium carbonate was detected) and after filtering, the precipitate was dried and calcinated for 4 h in air at a temperature of 400°C. The completeness of the decomposition of the carbonates under these conditions were confirmed by means of the study of thermal decomposition of the uncalcinated samples (the thermoanalyser of Netzsch was used for this purpose). The soluble chromates were washed out of the samples by distilled water. The washed samples were dried at room temperature for 7–10 days. Prior to their use all samples were reduced with hydrogen (at a hydrogen flow rate of 56 mL min^{-1}) at a constant temperature of 400°C. The reduction was performed in a glass basket hanging on the arm of a microbalance (Sartorius) and immersed in a hydrogen stream, up to the maximum loss in weight of the sample (maximum degree of reduction). The maximum degree of reduction R (%) was defined by the following relation

$$R = \frac{a - b}{p\,a\,[1 - (M_{Cu}/M_{CuO})]} \times 10^4$$

where a and b are the weights of the sample before and after the reduction, respectively, p is the percentage content of the CuO in the sample, and M_{Cu} and M_{CuO} represent the molecular weights of copper and cupric oxide, respectively. The decrease in the weight of the sample was monitored during its reduction. The reduction was stopped by introducing nitrogen instead of hydrogen afrer which weight loss was no longer detectable (the precision of this operation was determined by the sensitivity of the microbalance and was ±0.1 mg). After reduction, the samples were cooled to room temperature in a flow of nitrogen.

The catalytic activity of the samples was measured by the decomposition of the aqueous solution of hydrogen peroxide (analytical grade) in a concentration of 1.2 mol L^{-1} at temperatures of 30, 35, 40, and 45°C.

A more detailed description of the methods used for preparation, chemical analysis, measurement of some physical properties, and catalytic activities of the samples was reported earlier (1).

Results and discussion

The prepared catalysts were found to be composed mainly of cupric oxide, CuO, and chromium sesquioxide, Cr_2O_3 (Table 1). It is evident from the results of X-ray diffraction that the system also contains both the cubic and the tetragonal spinel structure of $CuCr_2O_4$ (Table 1), mainly in the middle region (samples 6–14) of composition of the sam-

[1]Revision received January 28, 1992.

Can. J. Chem. Downloaded from www.nrcresearchpress.com by 217.78.4.112 on 09/08/12
For personal use only.

TABLE 1. Results of the chemical and X-ray analysis of the catalysts

Sample	CuO (wt.%)	Cr_2O_3 (wt.%)	Phase[a]
1	1.8	88.5	Cr_2O_3
2	4.0	88.4	Cr_2O_3
3	5.7	90.2	Cr_2O_3
4	7.9	90.7	Cr_2O_3
5	9.9	83.8	Cr_2O_3
6	18.8	74.6	Cr_2O_3,$CuCr_2O_4$ (T)
7	28.7	62.9	Cr_2O_3,$CuCr_2O_4$ (T), partly $CuCr_2O_4$ (C)
8	40.3	55.6	Defective $CuCr_2O_4$ (C), traces of $CuCr_2O_4$ (T)
9	48.7	47.2	$CuCr_2O_4$ (C), CuO
10	59.0	40.8	↓ decreasing ↓ increasing
11	67.6	32.8	↓ conc. ↓ conc.
12	77.3	19.9	
13	88.8	10.2	CuO, traces of $CuCr_2O_4$ (C)
14	90.2	8.2	CuO, traces of $CuCr_2O_4$ (C)
15	91.1	6.5	CuO
16	95.3	3.9	CuO
17	97.1	2.0	CuO
18	99.0	0.0	CuO

[a](T), tetragonal, (C), cubic.

Can. J. Chem. Downloaded from www.nrcresearchpress.com by 217.78.4.112 on 09/08/12
For personal use only.

ples (the creation of this substance has, of course, no effect on the weight of the reduced sample).

The reduction of the system studied leads, under the given conditions, just to the reduction of the cupric oxide to metallic copper while the Cr_2O_3 oxide remains unreduced. This was confirmed earlier (11) by thermal analysis of the samples. Nevertheless, the Cr^{6+} ions present in the chromium sesquioxide may be reduced to Cr^{3+} ions (8). As can be seen from the nonmonotonic and rather complicated dependence of the maximum degree of reduction on the catalyst composition (Fig. 1), the reduction of the CuO was, nevertheless, significantly affected by the presence of the Cr_2O_3 in the catalyst. According to earlier results (11) the samples containing a high excess of cupric oxide were fully reduced under these conditions. The degree of reduction dropped rapidly and nonmonotonically to a value of 10% for the sample containing about 70 wt.% of Cr_2O_3 with increasing content of Cr_2O_3 in the sample. The chromium sesquioxide probably blocks those centers serving as the sites initiating the reduction of the CuO. Further increase in the Cr_2O_3 content led, of course, to a higher degree of reduction, up to the maximum of 40% for the sample containing about 90 wt.% of Cr_2O_3 (i.e. of 10 wt.% of CuO). After this maximum the degree of reduction increased again with increasing content of the Cr_2O_3. The abovementioned maximum shows that the manner in which the chromium sesquioxide affects the cupric oxide reduction is probably more complicated than just the blocking of the reduction sites.

The reduction of the system studied resulted in an increase in values of the specific surface area of the samples. But the general character of the dependence of specific surface areas on sample composition was found to be maintained after the reduction (Fig. 2). That means that the mu-

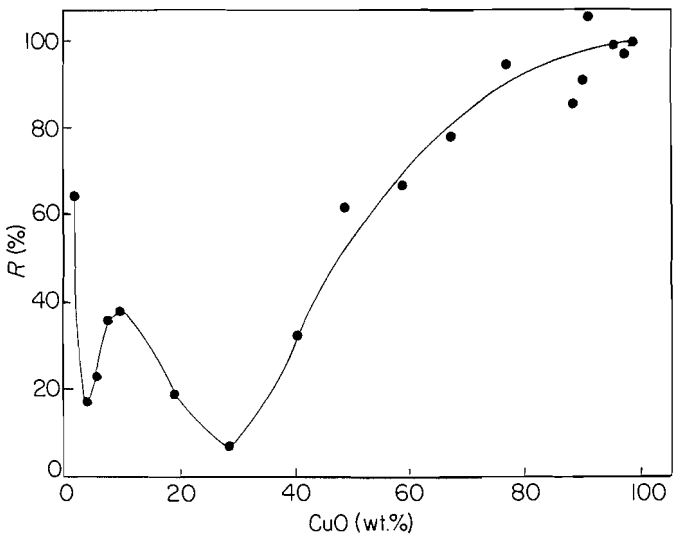

FIG. 1. Dependence of the maximum degree of reduction R on composition of the catalysts.

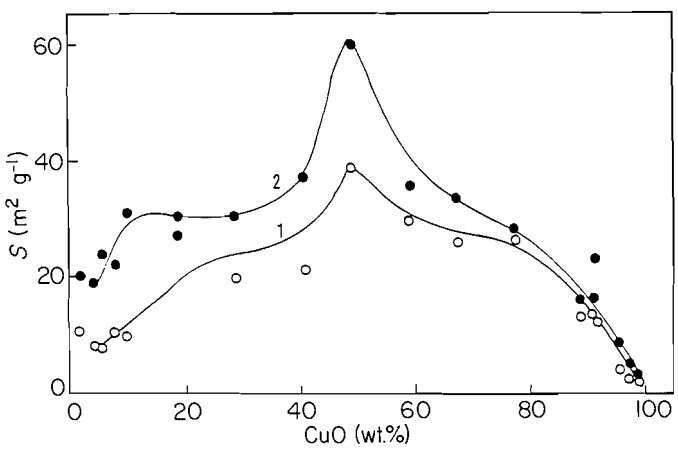

FIG. 2. Specific surface area values S of nonreduced (1) and reduced (2) samples of various composition.

Can. J. Chem. Downloaded from www.nrcresearchpress.com by 217.78.4.112 on 09/08/12
For personal use only.

tual interaction between the oxides, resulting also in the creation of spinel structures with a higher specific surface area, survives also after the reduction of the oxide.

The catalytic activity of the reduced samples (characterized by the first-order rate constant of the hydrogen peroxide decomposition normalized to the surface area of the catalysts) increased notably and nonlinearly with increasing content of the cupric oxide in the catalyst (Fig. 3, curve 2). Therefore one may assume that, similar to the case of nonreduced samples (Fig. 3, curve 1), the mutual influence of the catalytic properties of both oxides also takes place after the reduction of the samples. Hence, the resulting catalytic activities of the two-component reduced catalysts seem to be non-additive. As well, the catalytic activity values of most of the reduced samples were found practically unchanged. On the other hand, a significant difference in the extent of the catalytic activities of both reduced and the nonreduced samples of various compositions was observed: non-typical maxima at 10 and 95 wt.% of CuO were observed in the case of reduced samples (Fig. 3, curve 2) in contrast to the nonreduced ones (Fig. 3, curve 1). The maxima at 10 and 95 wt.% of CuO may be due to the mutual influence of the two basic oxides. The reduction leads, probably, to a system without this influence. As the reduction of the samples with 10 and 95 wt.% of CuO leads simultaneously to lower values of the apparent activation energy of the test reaction (Fig. 4), we may assume that some new catalytic centres with a higher efficiency are created in the course of the reduction. Their concentration is, of course, lower than those of the centres active before reduction. The stability of the newly created centres seems to be relatively high because the catalytic activity of the reduced samples remains unchanged during their storage at room temperature in air for a few months (Fig. 3, ⊙). These observations show that the catalysts with 10 and 95 wt.% of CuO possess the highest sensitivity to reduction.

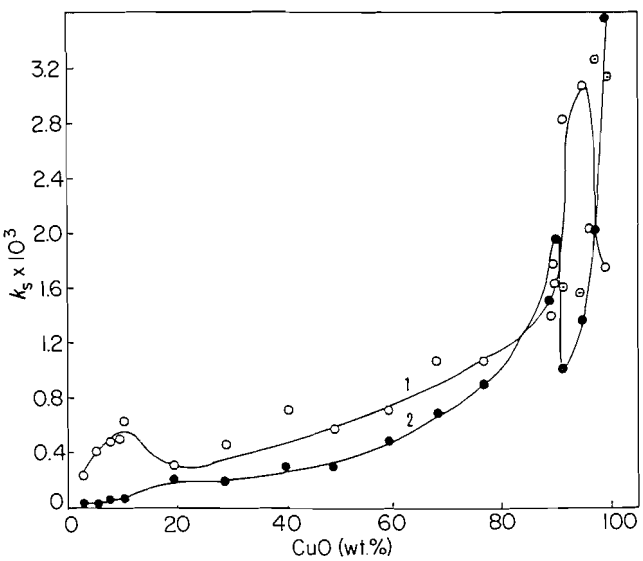

FIG. 3. Specific catalytic activity k_s (L m^{-2} min^{-1}) at 40°C prior to (1) and after (2) reduction of the catalysts of different composition; ⊙, stored reduced samples.

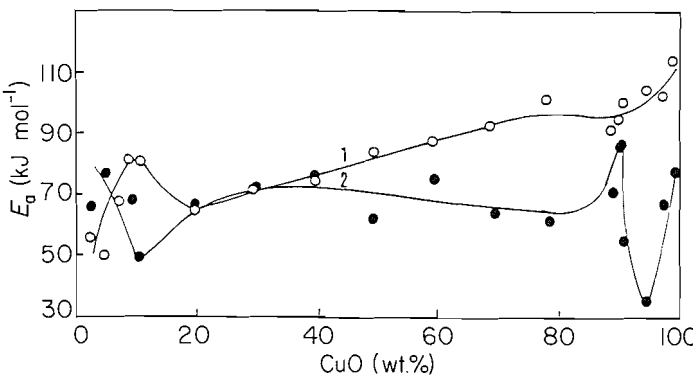

FIG. 4. Apparent activation energies E_a of the test reaction carried out on nonreduced (1) and reduced (2) catalysts of different composition.

Conclusions

The following conclusions can be drawn from the study of the two-component $CuO–Cr_2O_3$ catalysts after their reduction:

1. The presence of the chromium sesquioxide in the two-component $CuO–Cr_2O_3$ catalyst significantly affects the reducibility of the cupric oxide.

2. The changes in the oxidation state of the metal ions present in catalysts result in significant changes in the catalytic properties of the system studied.

1. V. Múčka. Collect. Czech. Chem. Commun. **53**, 1636 (1988).
2. I. A. Legenchenko, N. F. Semizorova, and V. E. Polishchek. Zh. Fiz. Khim. **51**, 102 (1977).
3. M. M. Selim and N. A. Youssef. J. Serb. Chem. Soc. **52**, 543 (1987).
4. S. E. Voltz and S. W. Weller. J. Am. Chem. Soc. **75**, 5227 (1953).
5. Y. Matsunaga. Bull. Chem. Soc. Jpn. **30**, 984 (1957).
6. S. W. Weller and S. E. Voltz. J. Am. Chem. Soc. **76**, 4695 (1954).
7. S. E. Voltz and S. W. Weller. J. Phys. Chem. **59**, 569 (1955).
8. D. Mihajlova and A. Andrejev. Izv. Khim. **9**, 265 (1976).
9. S. E. Voltz and S. W. Weller. J. Am. Chem. Soc. **76**, 1586 (1954).
10. J. Deren, J. Haber, A. Podgorecka, and J. Burzyk. J. Catal. **2**, 161 (1963).
11. M. Pospíšil. Thermochim. Acta, **119**, 261 (1987).

Electronic configuration and structure of paramagnetic iron dinitrosyl complexes[1]

TRACI R. BRYAR AND DONALD R. EATON[2]
Department of Chemistry, McMaster University, Hamilton, Ont., Canada L8S 4M1

Received September 18, 1991

TRACI R. BRYAR and DONALD R. EATON. Can. J. Chem. **70**, 1917 (1992).

The electronic and geometric structures of paramagnetic iron dinitrosyl complexes have been investigated using electron spin resonance, infrared spectroscopy, and X-ray crystallography. It is concluded that these compounds are best described as 17 electron complexes with a d^9 configuration rather than the d^7 configuration assumed by most previous investigators. The anisotropy of the g values, determined from the electron spin resonance spectra of frozen solutions, varies considerably from complex to complex. The results are consistent with the supposition that all of the complexes have a distorted tetrahedral geometry, but the nature of the distortion changes as the ligands are varied. As a result of this variation there are changes in the nature of the spin-containing d orbital. Ligands containing hard, nonpolarizable donor atoms such as oxygen or fluorine produce a distortion towards a planar geometry, placing the odd electron in a predominantly $d_{x^2-y^2}$ orbital, while those containing softer donor atoms such as phosphorus or sulfur give complexes with a different type of distortion, leading to placement of the odd electron in a predominantly d_{z^2} orbital. Nitrogen and halide donor ligands produce smaller distortions, leading to spin-containing molecular orbitals with contributions from a mixture of d orbitals. In accordance with this model, the crystal structure of $[Fe(NO)_2I_2]^-$ has been found to be only slightly distorted from regular tetrahedral coordination about the iron atom.

TRACI R. BRYAR et DONALD R. EATON. Can. J. Chem. **70**, 1917 (1992).

Faisant appel à la résonance paramagnétique électronique (rpe), à la spectroscopie infrarouge et à la diffraction des rayons X, on a étudié les structures électroniques et géométriques des complexes paramagnétiques du dinitrosyl fer. On en conclut que la meilleure façon de décrire ces composés est de les considérer comme des complexes à 17 électrons possédant une configuration d^9 plutôt que la configuration d^7 utilisée par la plupart des auteurs qui en ont traité antérieurement. L'anisotropie des valeurs g, déterminée par les spectres rpe de solutions congelées, varie beaucoup d'un complexe à l'autre. Les résultats sont en accord avec l'hypothèse selon laquelle tous les complexes possédent une géométrie tétraédrique déformée, mais que la nature de la distorsion varie avec la nature des ligands. Un résultat de cette variation amène des changements dans la nature de l'orbitale contenant le spin. Les ligands contenant des atomes donneurs durs et non-polarisables, comme l'oxygène ou le fluor, provoquent une distorsion vers une géométrie plane forçant l'électron célibataire à occuper une orbitale principalement $d_{x^2-y^2}$ alors que ceux qui contient des atomes donneurs plus mous, comme le phosphore ou le soufre, donnent des complexes avec un type de distorsion différent, conduisant à une présence de l'électron célibataire dans une orbitale qui est principalement d_{z^2}. Les ligands contenant des atomes d'azote et d'halogénure comme donneurs provoquent des distortions plus faibles conduisant à des orbitales moléculaires contenant le spin dans lesquelles un mélange d'orbitales d contribuent. En accord avec ce modèle, on a trouvé que la structure cristalline du $[Fe(NO)_2I_2]^-$ n'est que légèrement déformée par rapport à la coordination tétraédrique régulière autour de l'atome de fer.

[Traduit par la rédaction]

Introduction

The structure of paramagnetic iron dinitrosyl complexes was first investigated by McDonald, Phillips, and Mower in 1965 (1). These compounds are easily produced in aqueous solution from Fe(II) salts and nitric oxide. However, they have been found to be fairly unstable and difficult to isolate. The majority of researchers have used Electron Paramagnetic Resonance (EPR) spectroscopy to study the complexes (2). Most of these investigations were carried out at room temperature and in solution since the compounds were prepared in an aqueous medium. A wide variety of ligands, including halides, phosphines, mercaptans, and various nitrogen-bonded ligands, will complex to the $Fe(NO)_2$ group. The hyperfine coupling observed indicates that the complexes are four-coordinate with the general stoichiometry $[Fe(NO)_2XY]^n$. The only notable exception, established by the fluorine hyperfine coupling, is the six-coordinate complex, $[Fe(NO)_2F_4]^{3-}$, which can be prepared in solution if the fluoride concentration is high. The solution EPR spectra also have been used to demonstrate that the complexes are quite labile. The $Fe(NO)_2$ unit remains intact while the other two ligands exchange.

Potentially, solid state EPR studies are more informative than solution studies. Only a limited number of such studies, all carried out on frozen solutions, have been reported (3). In general, the components of the g tensor vary considerably for different dinitrosyl complexes, indicating the possibility of more than one structure for these compounds. The EPR data were interpreted on the basis of a d^7 electronic configuration for iron and the possible geometries suggested by these authors included tetrahedral, octahedral with *trans* NO groups, octahedral with *cis* NO groups, square-planar, and square-pyramidal.

The first successful isolation of one of these compounds occurred in 1973 when deep purple crystals of $Fe(NO)_2(PPh_3)Cl$ were prepared by the reaction of triphenylphosphine with $[Fe(NO)_2Cl_2]^-$ (4). In 1976, Connelly and Gardner reported the isolation and characterization of $[N(PPh_3)_2)][FE(NO)_2X_2]$ where X = Cl, Br, or I (5). The analytical data confirmed the stoichiometry and the EPR spectra were consistent with those obtained with dinitrosyl

[1]A preliminary description of these structures, based on data available in the literature, was presented at the 69th Conference of the Canadian Institute of Chemistry and is contained in the proceedings of an ESR symposium published as Electron Magnetic Resonance of the Solid State, edited by J. A. Weil.

[2]Author to whom correspondence may be addressed.

Can. J. Chem. Downloaded from www.nrcresearchpress.com by 217.78.4.112 on 09/08/12
For personal use only.

Can. J. Chem. Downloaded from www.nrcresearchpress.com by 217.78.4.112 on 09/08/12
For personal use only.

complexes prepared in solution. Magnetic susceptibility measurements indicated the presence of one unpaired electron and revealed the absence of dimerization in the solid state. In 1986, black crystals of $[NEt_4][Fe(NO)_2(SPh)_2]$ (6) were synthesized from the diamagnetic cluster, $[Fe_4S_3(NO)_7]^-$ (2*k*). Only two other paramagnetic iron dinitrosyl compounds have been isolated. Both of these have the stoichiometry $Fe(NO)_2L$ where L is a bidentate ligand. In one case, the ligand is coordinated through sulfur atoms [-SCH_2CH_2NH-$(CH_3)CH_2CH_2CH_2N(CH_3)CH_2CH_2S$-] (7), while in the other molecule, the 2-methyl-8-quinolinolate ion is coordinated through N and O (8). X-ray structure determinations have been reported for only three of the six crystalline solids. The geometry of the $Fe(NO)_2$ complex with the bidentate sulfur ligand was found to be pseudotetrahedral, with the angles showing only small deviations from the true tetrahedral values (7). The $[Fe(NO)_2(SPh)_2]^-$ anion was described to be a distorted tetrahedron, but the deviations from tetrahedral were larger than for the other sulfur complex (6). Kopf and Schmidt described the structure of $Fe(NO)_2(PPh_3)Cl$ as a trigonal bipyramid with one axial ligand missing, although the angles deviate somewhat from this idealized geometry (9).

Although the stoichiometry of the paramagnetic iron dinitrosyl complexes has been clearly established, the literature contains ambiguous and conflicting reports for both the electronic and geometric structure. The question concerning the electronic structure revolves around the formal oxidation state of the iron atom. These are clearly 17-electron compounds, but it is plausible to assign either 7 *d* electrons to the metal atom, giving an Fe^{+1} ion, or 9 d electrons giving an Fe^{-1} ion. The original investigators of these complexes preferred the d^7 formulation, but three arguments have been used to favour the d^9 alternative. These arguments are based on Fe—N—O bond angles, on infrared NO stretching frequencies, and on the small values of the nitrogen hyperfine coupling constants observed by solution EPR. None of these arguments are unambiguous since the ranges of possible parameters tend to overlap. Thus the uncertainties caused by the use of infrared data to infer the bonding in the NO ligand, and by inference the oxidation state of Fe, have been discussed by Mingos and Ibexs (10). Most EPR investigators have opted for a d^7 configuration, although one recent group of publications, concerned with dinitrosyls with sulfur-containing ligands, assumed d^9 (2*k*–2*o*). The only evidence quoted was the small nitrogen hyperfine coupling constant compared to compounds of known d^7 configuration; this argument is not completely convincing. There are 17 electrons to be assigned to molecular orbitals whether the complex is regarded as d^7 or d^9, and so the nitrogen hyperfine coupling constant is determined by the detailed nature of the spin-containing molecular orbital. MO calculations (2*m*, 30), particularly at the EHMO level, are probably not sufficiently reliable to answer the question with certainty.

In the present paper we will use the *g* value anisotropies obtained from frozen solution EPR to argue for a d^9 configuration. This approach has two advantages. Firstly it relies on qualitative arguments on the relative magnitudes of the different components of the *g* tensor, rather than on quantitative calculations. The reliability of qualitative crystal field arguments in transition metal chemistry is generally accepted. Secondly it enables us to correlate electronic structure with molecular geometry. X-ray crystallographic evidence has proved the existence of at least two different structures in the solid state. At least one of these complexes has been shown to exhibit catalytic activity (11) and it is of interest to enquire whether this activity is related to structure. The objective of this paper is therefore to confirm the previously suggested d^9 configuration of these iron dinitrosyl complexes and to relate their electronic and molecular structures. Frozen solution EPR spectroscopy has been the primary method of investigation, but supporting data from X-ray crystallography and from IR spectroscopy will also be presented.

Experimental

All complexes were prepared using established literature techniques. Nitric oxide gas (Matheson) was purified by passage through aqueous NaOH and a −78°C trap. All reactions were carried out under argon or nitrogen atmospheres in dry, degassed organic solvents. $HNEt_3[Fe(NO)_2Cl_2]$ and $Fe(NO)_2(PPh_3)Cl$ were prepared using the method of Gwost and Caulton (4). $[N(PPh_3)_2][Fe(NO)_2I_2]$ and its precursor $[N(PPh_3)_2][Fe(CO)_3NO]$ were prepared by the method of Connelly and Gardner (5). $Fe(NO)_2$(thiourea)I was prepared from the addition of excess thiourea to $[Fe(NO)_2I_2]^-$ in CH_2Cl_2. $Fe(NO)_2$(thiourea)Cl was prepared in an analogous manner from $[Fe(NO)_2Cl_2]^-$ in ethanol. The identity of the two thiourea complexes prepared using this technique was confirmed by EPR spectroscopy but no analytical data are available since the compounds could not be isolated as pure crystalline solids. Solutions of the remaining complexes in methanol or ethanol were prepared by adding excess anionic ligand to 10^{-2} M $FeCl_2$ followed by the passage of NO gas for 5 min (2). The ligands used were MeO^-, EtO^-, and anions of urea and 4-nitroimidazole.

All EPR spectra were recorded on a Bruker ER-100D spectrometer, operated in the X-band microwave region. The wavemeter allowed measurements of microwave frequency to 0.08% precision. 10^{-2} M solutions of each complex in organic solvents were analyzed in 3 mm quartz tubes at ambient temperature and again at 125 K. The solvents used are listed in Table 4 with the EPR data. Aqueous solutions were avoided to circumvent experimental difficulties at 125 K. Each spectrum was simulated to confirm the choice of parameters (12). The same 10^{-2} M solutions of the $Fe(NO)_2$ complexes were then examined using a Nicolet model 7199 FT-IR spectrometer with 0.1 mm solution cells. Most of the vibration modes were masked by the solvent but in all cases the NO stretching bands were visible and provide significant information.

The X-ray crystal structure of $[N(PPh_3)_2][Fe(NO)_2I_2]$ was determined. Crystals of $[N(PPh_3)_2][Fe(NO)_2I_2]$ were grown from CH_2Cl_2/ethanol. The density was determined by suspension in CCl_4/$C_2H_2Br_4$. Red-black plate-shaped crystals were examined under a polarizing microscope for homogeneity. A well-formed crystal, 0.3 mm × 0.2 mm × 0.133 mm, was selected and sealed in a Lindemann capillary. Unit cell parameters were obtained from a least-squares fit of χ, ϕ' and 2θ for 15 reflections in the range $19.5° < 2\theta < 23.5°$, recorded on a Nicolet $P2_1$ diffractometer with the use of graphite monochromated MoKα radiation ($\lambda = 0.71069$ Å) at 22°C. Intensity data were also recorded on a Nicolet $P2_1$ diffractometer with a coupled θ(crystal)–2θ(counter) scan, over h, $\pm k$, $\pm l$ resulting in 4999 reflections with $2\theta \leq 45°$. Corrections for Lorentz–polarization effects and absorption were applied to all reflections. Two standard reflections (−4,3,4; 1.54% and 6,1,−7; 1.47%) monitored every 48 reflections showed no sign of crystal decomposition or instrument instability. After reduction and averaging of redundant data (agreement factor $R_{int} = 0.017$) there were 4791 unique reflections, and 4514 reflections with $I > 3\sigma(I)$. Maximum error in F_o was calculated to be 9.5%. Empirical absorption corrections were estimated from psi-scan observations on 19 selected reflections. The crystal data are summarized in Table 1.

The structure was solved by determination of the phases by direct methods with the use of 46 reflections with $E > |1.2|$ and 12 sets of starting phases. The positional parameters for the iodine and

TABLE 1. Crystal data for $[N(PPh_3)_2][Fe(NO)_2I_2]$

Formula	$FeC_{36}H_{30}N_3O_2P$
F.W.	908.26
Crystal shape; size, mm	Plate; 0.30 × 0.20 × 0.133
System	Triclinic
Systematic absences	None
Space group	$P\bar{1}$
a, Å	11.943(3)
b, Å	10.090(3)
c, Å	17.590(4)
α	113.09(2)°
β	105.43(2)°
γ	92.87(2)°
V, Å^3	1850.9(9)
Z	2
D(calc), g cm^{-3}	1.63
D(obs), g cm^{-3}	1.64
F(000)	888.31
Diffractometer	Nicolet $P2_1$
Temperature	22°C
Radiation	MoKα, λ = 0.71069 Å
μ(MoKα), cm^{-1}	22.26
Absorption coefficient limits	$1.29 \leq A^* \leq 1.56$
No. reflections for cell detn.	15 ($19.5° \leq 2\theta \leq 23.5°$)
Standard reflections (%)	−4,3,4 (1.54)
	6,1,−7 (1.47)
Data collected	$h, \pm k, \pm l$
Max. 2θ reflections collected	45°
No. reflections collected	4999
No. independent reflections	4791
R_{int}[a]	0.017
No. with $I > 3\sigma(I)$	4514
Final shift/error max. (ave.); No. variables	Block 1: 0.240 (0.034); 65
	Block 2: 0.053 (0.008); 353
R_1[b],R_2[c]	0.040, 0.047
Weighting scheme	$w = (\sigma^2F + 0.000323F^2)^{-1}$
Error in obsv. of unit weight[d]	Block 1: 1.19
	Block 2: 1.23
Secondary extinction, x[e]	0.00016
Highest peak, e Å^{-3}	0.476
Location	0.0819, 0.7979, 0.6816
Lowest valley, e Å^{-3}	−0.576

[a] $R_{int} = \sqrt{\frac{\Sigma[N\Sigma(\omega(\langle F\rangle - F)^2)]}{\Sigma(N-1)\Sigma\omega F_o^2}}$.

[b] $R_1 = \frac{\Sigma\|F_o| - |F_c\|}{\Sigma|F_o|}$.

[c] $R_2 = \sqrt{\frac{\Sigma\omega(|F_o| - |F_c|)^2}{\Sigma\omega F_o^2}}$.

[d] $S = \sqrt{\frac{\Sigma\omega(|F_o| - |F_c|)^2}{m-n}}$; m = no. of reflections; n = no. of variables.

[e] $F^* = F\left(\frac{1 - 0.0001 \times F^2}{\sin\theta}\right)$.

iron atoms were found in the subsequent E-map. A series of full-matrix least-squares refinements that minimized $\Sigma w(|F_o| - |F_c|)^2$ ($w = 1/[\sigma^2F_o + 0.000323F_o^2]$) revealed the positional parameters of all non-hydrogen atoms. Temperature factors of all non-hydrogen atoms were then made anisotropic. Further least-squares refinement required the use of two block-matrices, one for $[N(PPh_3)_2]^+$ and the other for $[Fe(NO)_2I_2]^-$. Corrections were made for secondary extinction by the method in SHELX (13). Refinement was complete when the maximum shift/error reached 0.240 for the anion and 0.053 for the cation. Final $R^1 = 0.040$, $R^2 = 0.047$, and $S = 1.19$ for the iron dinitrosyl anion. The final difference map revealed no significant regions of electron density with a maximum of 0.476 and a minimum of −0.576 e Å^{-3}. Throughout refinement, scattering factors were taken from ref. 14 and anomalous dispersion corrections from ref. 15 were applied to the curve for iron. All calculations were performed on a VAX 8600 computer. Programs used: XTAL (16) for data reduction, TAPER (17) for absorption correction, SHELX-86 (13) for structure solution, SHELX-76 (18) for structure refinement, MOLGEOM (19) for molecular geometry and SNOOPI (20) for diagrams. The atomic positions are listed in Table 2, while the structure of $[Fe(NO)_2I_2]^-$ is shown in Fig. 1. Selected bond angles and bond lengths are listed in Table 3. An-

Can. J. Chem. Downloaded from www.nrcresearchpress.com by 217.78.4.112 on 09/08/12
For personal use only.

TABLE 2. Positional parameters ($\times 10^5$) and U_{eq} ($\times 10^4$) for $[N(PPh_3)_2][Fe(NO)_2I_2]$ (standard errors in parentheses)

Atom	x	y	z	$U_{eq}(Å^2)^a$
I1	33173(3)	82562(4)	85172(2)	480(1)
I2	−512(4)	66580(4)	66255(3)	534(1)
Fe	13809(7)	64137(8)	79431(5)	421(2)
N1	16334(45)	46865(56)	75664(33)	544(21)
O1	17226(48)	34979(52)	74212(35)	844(25)
N2	8915(40)	69053(49)	88115(32)	456(19)
O2	6835(43)	69828(49)	94276(30)	703(21)
P1	36935(11)	56715(13)	24807(8)	259(4)
P2	23314(11)	80095(13)	30607(8)	248(4)
N3	27094(34)	64477(39)	28422(25)	293(14)
C11	15925(50)	75810(59)	43131(35)	412(22)
C12	12707(58)	80204(85)	50574(45)	603(30)
C13	13679(61)	95002(99)	55650(41)	661(33)
C14	17659(61)	105403(71)	53427(40)	560(28)
C15	20878(50)	100998(56)	45923(33)	404(21)
C16	19931(42)	86093(51)	40751(30)	289(18)
C21	5229(49)	65929(59)	15139(33)	404(21)
C22	−5224(58)	65113(73)	9030(39)	575(27)
C23	−10878(56)	77092(86)	10264(45)	587(28)
C24	−6221(53)	89842(74)	17413(48)	560(27)
C25	4198(50)	91072(56)	23665(39)	455(23)
C26	9960(42)	79061(50)	22445(30)	282(18)
C41	58872(47)	50926(55)	31837(32)	363(19)
C42	68082(49)	51030(59)	38684(37)	427(22)
C43	67634(52)	57248(62)	47064(37)	457(23)
C44	58059(56)	63353(60)	48751(34)	469(24)
C45	48683(49)	63294(53)	42089(31)	367(20)
C46	49112(42)	57086(47)	33585(29)	263(18)
C51	35939(48)	29470(53)	11802(30)	361(20)
C52	30995(62)	14688(62)	6638(35)	484(25)
C53	21160(65)	8621(59)	7451(40)	529(25)
C54	16013(51)	16873(63)	13473(46)	511(25)
C55	20720(48)	31540(55)	18641(35)	382(21)
C56	30618(44)	37923(49)	17807(29)	294(18)
C61	53719(52)	72506(56)	21578(35)	416(22)
C62	57377(60)	78345(71)	16412(47)	600(29)
C63	49885(76)	75730(81)	8445(49)	672(34)
C64	39032(71)	67504(84)	5326(43)	686(32)
C65	35206(52)	61409(66)	10248(37)	485(24)
C66	42688(44)	63921(50)	18390(30)	290(18)
C31	45130(47)	97339(52)	38390(30)	334(19)
C32	54549(47)	106819(58)	39197(33)	392(20)
C33	53466(52)	112835(60)	33235(37)	444(23)
C34	43132(56)	109412(67)	26620(40)	522(25)
C35	33503(48)	99982(58)	25774(35)	407(21)
C36	34428(41)	93841(47)	31711(28)	251(16)

$^a U_{eq} = \frac{1}{3}(U_{11} + U_{22} + U_{33} + 2\cos\alpha U_{23} + 2\cos\beta U_{13} + 2\cos\gamma U_{12})$.

isotropic temperature factors (Table S1), H-atom coordinates (Table S2), and a listing of structure factor amplitudes (Table S3) are available as supplementary material.[3]

An attempt to correlate the conclusions based on EPR results with

[3]A complete set of supplementary material may be purchased from the Depository of Unpublished Data, Document Delivery, CISTI, National Research Council Canada, Ottawa, Canada K1A 0S2.

Table S2 has also been deposited with the Cambridge Crystallographic Data Centre and can be obtained on request from The Director, Cambridge Crystallographic Data Centre, University Chemical Laboratory, Lensfield Road, Cambridge CB2 1EW, U.K.

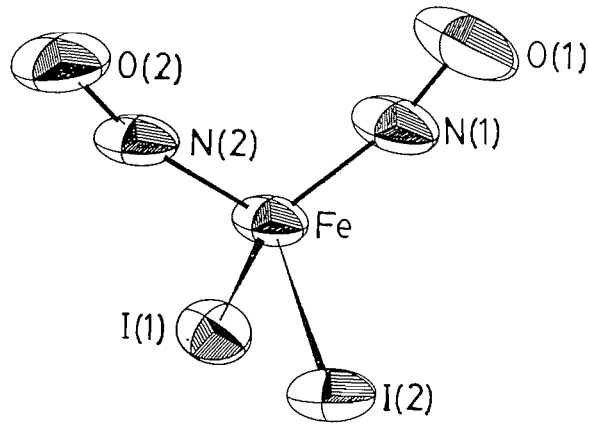

FIG. 1. ORTEP view of $[Fe(NO)_2I_2]^-$.

Extended Hückel molecular orbital calculations was made. The calculations were performed using the ICON8 package (21) with weighted H_{ij}'s (22). The d orbital exponents have been removed for Cl, I, and P. EHMO calculations were carried out for representative complexes of each geometry. Crystal structure parameters provided the positional coordinates for $Fe(NO)_2(PPh_3)Cl$ and $[Fe(NO)_2I_2]^-$, but it was necessary to estimate the Cartesian coordinates for $[Fe(NO)_2F_2]^-$.

Results

EPR spectra of each complex were recorded at ambient temperature and at 125 K. The g values and hyperfine coupling constants are given in Table 4 along with those for a few relevant complexes from the literature. The isotropic solution g values vary from 2.02 to 2.08 with no obvious correlation between g value and the type of ligand coordinated to iron. Examination of the hyperfine coupling constants in Table 4 reveals the presence of two NO groups and coupling from two other ligands can be resolved in some cases. The spectra for $[Fe(NO)_2I_2]^-$ are shown in Fig. 2 along with their simulations. The 11-line solution spectrum shows coupling from two iodine atoms ($I = 5/2$). The frozen solution EPR spectrum of $[Fe(NO)_2I_2]^-$ is much more complicated than the room temperature spectrum and simulation of the spectrum was necessary to confirm the correct choice of the three g values. Most frozen EPR spectra were far less complex than this, allowing unambiguous interpretation of the spectra. Two additional frozen solution EPR spectra are illustrated in Fig. 3. The spectrum for $[Fe(NO)_2Cl_2]^-$ (Fig. 3*a*) has three different g values, just like $[Fe(NO)_2I_2]^-$, but the spectrum is quite simple because the hyperfine coupling is not resolved. Not all spectra had three different principal values for the g matrix. Figure 3*b* illustrates the frozen solution spectrum of $[Fe(NO)_2(MeO)_2]^-$, which has only two g values. In this spectrum $g_\perp$ is upfield of $g_\parallel$, which indicates that $g_\parallel > g_\perp$. Overall, it was found that the frozen solution EPR spectra of all of the complexes fell into three categories. These are listed as parts A, B, and C of Table 4. Type A spectra had $g_\perp > g_\parallel$. Only complexes containing ligands bonded through phosphorus or sulfur gave this type of frozen solution spectrum. Dinitrosyl complexes with the halides, Cl, Br, I, or ligands bonded through nitrogen are listed in part B of the table. All of these spectra have three different principal values of the g matrix. Finally, the spectra in part C of Table 4 have $g_\parallel > g_\perp$. Only complexes containing fluoride or ligands bonded through oxygen have this

Can. J. Chem. Downloaded from www.nrcresearchpress.com by 217.78.4.112 on 09/08/12
For personal use only.

TABLE 3. Selected intramolecular distances and angles for the $[Fe(NO)_2I_2]^-$ anion

(*a*) Intramolecular distances

Atom	Atom	Distance (Å)	Atom	Atom	Distance (Å)
Fe	I1	2.584(1)	Fe	I2	2.596(1)
Fe	N1	1.679(5)	Fe	N2	1.682(6)
N1	O1	1.141(8)	N2	O2	1.149(8)

(*b*) Intramolecular angles

Atom	Atom	Atom	Angle (deg)	Atom	Atom	Atom	Angle (deg)
I1	Fe	I2	109.41(4)	N1	Fe	N2	114.3(3)
Fe	N1	O1	167.6(6)	Fe	N2	O2	164.1(5)
N1	Fe	I1	110.8(2)	N1	Fe	I2	106.0(2)
N2	Fe	I1	103.1(1)	N2	Fe	I2	113.4(2)

TABLE 4. EPR *g* values and hyperfine coupling constants of paramagnetic iron dinitrosyl complexes

Part A: $g_\perp > g_\parallel$

Compound	Solvent	g_{iso}[a]	A_{iso} (G)[a]	$g_\perp$[b]	$g_\parallel$[b]	A (G)[b]
$Fe(NO)_2(PPh_3)Cl$	MeOH	2.037	A_P = 49 G	2.046	2.016	A_P = 46 G
$Fe(NO)_2$(thiourea)Cl	EtOH	2.035	A_N = 2.2	2.042	2.015	—
$Fe(NO)_2$(thiourea)I	CH_2Cl_2	2.059	A_I = 17.5	2.085	2.010	A_I = 19
$[Fe(NO)_2$(*n*-propylthiol)$_2]^-$[c]	Isoamyl alcohol[d]	2.028	—	2.039	2.013	—

Part B: $g_1 > g_2 > g_3$

Compound	Solvent	g_{iso}	A_{iso} (G)	g_1	g_2	g_3	*A* (G)
$[N(PPh_3)_2][Fe(NO)_2I]$	THF	2.077	A_I = 20.2	2.125	2.074	2.015	A_I = 20.5
$HNEt_3[Fe(NO)_2Cl_2]$	MeOH	2.033	$A_{^{35}Cl}$ = 6.0 $A_{^{37}Cl}$ = 5.0	2.042	2.032	2.015	—
$[Fe(NO)_2(4\text{-}NO_2\text{-}C_3H_3N_2)_2]^-$	MeOH	2.028	—	2.047	2.025	2.013	—
$[Fe(NO)_2(NCS)_2]^-$[e]	Isoamyl alcohol	2.034	A_N = 2.6	2.055	2.027	2.011	—

Part C: $g_\parallel > g_\perp$

Compound	Solvent	g_{iso}	A_{iso} (G)	$g_\perp$	$g_\parallel$	*A* (G)
$Na[Fe(NO)_2(MeO)_2]$	MeOH	2.020	—	2.036	2.011	—
$Na[Fe(NO)_2(EtO)_2]$	EtOH	2.025	—	2.040	2.017	—
$Na[Fe(NO)_2(urea)_2]$	EtOH	2.024	—	2.041	2.013	—
$[Fe(NO)_2F_4]^{3-}$[f]	80% EtOH[g]	2.033	A_F = 20.4	2.017	2.052	—

[a] *g* and *A* values from solution EPR spectra.
[b] *g* and *A* values from frozen solution EPR spectra at 125 K.
[c] Reference 3*c*.
[d] Isoamyl alcohol.
[e] Reference 2*f*.
[f] Solution EPR parameters from ref. 2*a*. Solid state EPR parameters from ref. 3*e*.
[g] 80% Ethanol, 20% water.

type of spectrum. In general, the nature of a frozen solution EPR spectrum depends upon the type of orbital that contains the unpaired electron. Therefore, to have three different types of frozen solution EPR spectra for a homologous series of complexes, there must be corresponding differences in the spin-containing orbital. If all the paramagnetic iron dinitrosyl complexes have the same electronic configuration, then there must be three different geometries for these compounds.

Further information on the structure and bonding of these complexes can be obtained from infrared spectroscopy and from X-ray crystallography. The NO^+ ion has a stretching

Can. J. Chem. Downloaded from www.nrcresearchpress.com by 217.78.4.112 on 09/08/12
For personal use only.

Can. J. Chem. Downloaded from www.nrcresearchpress.com by 217.78.4.112 on 09/08/12
For personal use only.

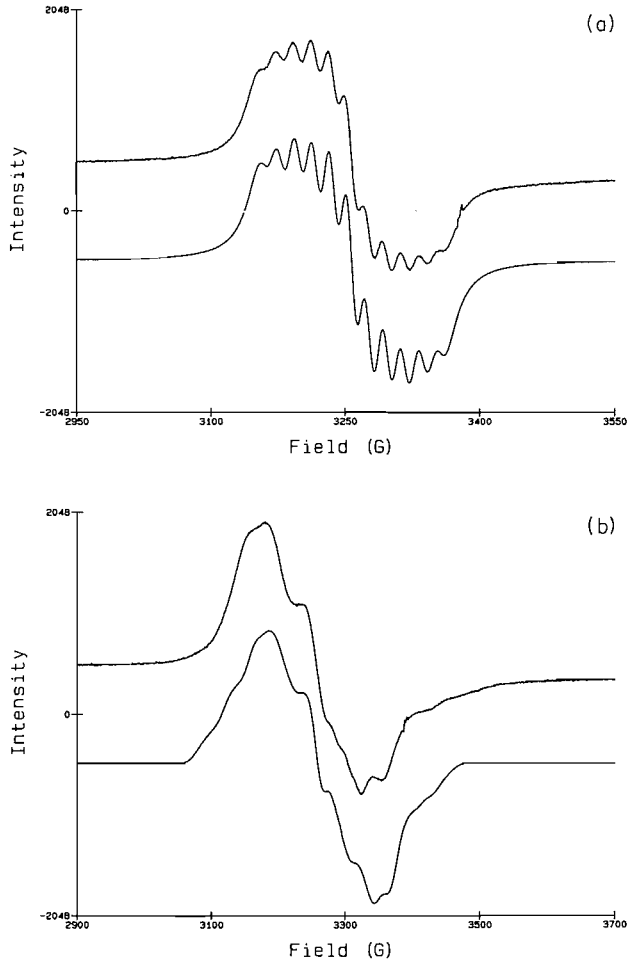

FIG. 2 Electron paramagnetic spectra of $[Fe(NO)_2I_2]^-$ (with simulated spectra shown below) (*a*) at ambient temperature; (*b*) at 125 K.

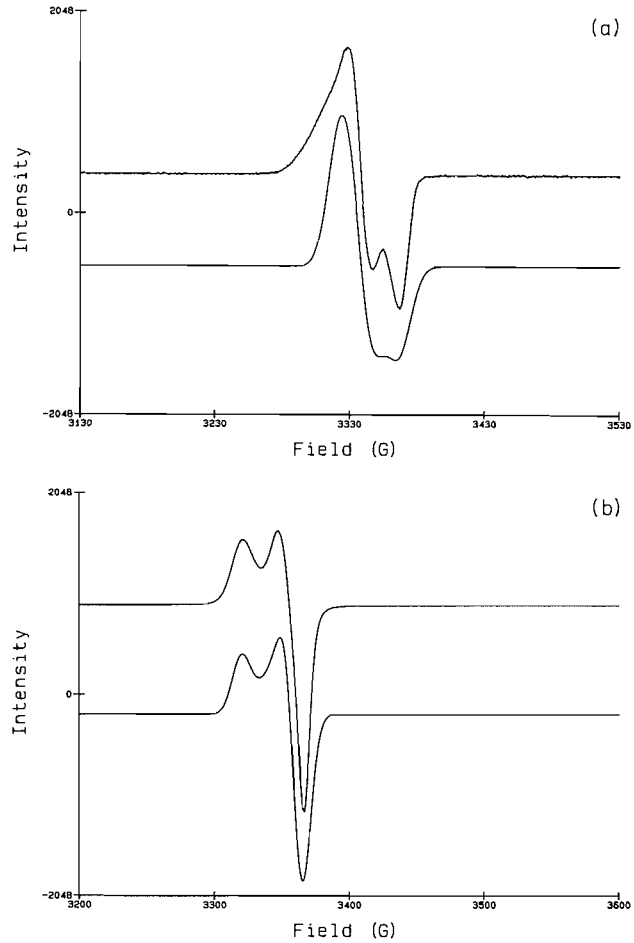

FIG. 3. Electron paramagnetic spectra at 125 K (with simulated powder spectra shown below) (*a*) $[Fe(NO)_2I_2]^-$; (*b*) $[Fe(NO)_2(OCH_3)_2]^-$.

frequency of 2220 cm^{-1} while the frequency for the neutral NO molecule, with the extra electron in a π^* orbital, is 1876 cm^{-1} (23). These data reflect the increased multiple bond character in the cation. Complexation considerably reduces these frequencies since backbonding, increasing the positive charge on the nitrosyl group, is possible. Stretching frequencies in the range of 1940 to 1650 cm^{-1} are indicative of complexed NO^+, while neutral or negatively charged NO ligands have stretching frequencies even lower (1525–1690 cm^{-1}) (23, 24). Since there is considerable overlap in these frequencies, discretion must be used when attempting to determine the nature of NO ligands from IR data. The NO stretching frequencies for a selection of paramagnetic iron dinitrosyl complexes are shown in Table 5, with those for some diamagnetic complexes included for comparison. The paramagnetic dinitrosyls show two bands in the NO region corresponding to the symmetric and asymmetric stretches of the NO ligands. There is some variation in the frequencies for the different dinitrosyl complexes but, in general, the range of frequencies is reasonably small (1690–1808 cm^{-1}). In comparison, the nitroprusside ion, a diamagnetic, Fe^{2+} complex with formally NO^+ ligands, has an NO stretching frequency of 1939 cm^{-1} (25). If nitroprusside is reduced, $[Fe(CN)_5NO]^{3-}$, which has 19-electron configuration, is formed. Not surprisingly, the electron does not remain on the

TABLE 5. Infrared NO stretching frequencies of paramagnetic iron dinitrosyl complexes

Compound	NO frequency (cm^{-1})
$Fe(NO)_2$(thiourea)Cl	1800, 1738
$Fe(NO)_2$(thiourea)I	1787, 1730
$Fe(NO)_2(PPh_3)Cl$	1789, 1731[a]
$Na[Fe(NO)_2(4\text{-}NO_2\text{-imidazole})_2]$	1804, 1740
$[N(PPh_3)_2][Fe(NO)_2I_2]$	1775, 1719
$HNEt_3[Fe(NO)_2Cl_2]$	1779, 1706[b]
$Na[Fe(NO)_2(EtO)_2]$	1755, 1686
$Na[Fe(NO)_2(MeO)_2]$	1756, 1695
$Na[Fe(NO)_2(urea)_2]$	1755, 1690
$[Fe(NO)_2(CN)_2]^-$	1808, 1730[c]
$[Fe(CN)_5NO]^{2-}$	1939[d] NO^+, d^6
$[Fe(CN)_4NO]^{2-}$	1755[e] NO^+, d^7
$[Fe(CN)_5NO]^{3-}$	1580[e] NO, d^6

[a]Reference 2*h*.
[b]Reference 4.
[c]Reference 34.
[d]Reference 25.
[e]Reference 26.

TABLE 6. Comparison of $[Fe(NO)_2I_2]^-$ bond angles to $Fe(NO)_2(PPh_3)Cl$ and trigonal bipyramid and tetrahedral geometries

Bond angle	$[Fe(NO)_2I_2]^-$	$[Fe(NO)_2(SPh)_2]^-$	$Fe(NO)_2(PPh_3)Cl$	Trigonal bipyramidal	Tetrahedral
			(all angles in degrees)		
N—Fe—N	114.3	117.4	115.6	120	109.5
N—Fe—X	113.4	111.5	115.8	120	109.5
	110.8	110.8	116.0	120	109.5
N—Fe—Y	106.0	103.9	96.9	90	109.5
	103.1	103.6	98.0	90	109.5
X—Fe—X	109.4	109.7	111.0	90	109.5

metal but moves to the NO ligand. This formally reduces the NO^+ group to NO, leaving the iron in the +2 oxidation state. Accordingly, the stretching frequency for the NO group drops to 1580 wavenumbers (26). Usually, stretching frequencies for iron nitrosyl compounds are not quite as high as that for nitroprusside. For example, nitroprusside can also be reduced to five-coordinate $[Fe(CN)_4NO]^{2-}$ (26). The complex has lost a cyanide group and the nitrosyl group remains as NO^+. The NO stretching frequency for this complex is 1755 cm^{-1}. The NO stretching frequencies for the paramagnetic iron dinitrosyl compounds compare closely with this frequency. Overall, the frequencies are too high for the NO groups to be considered neutral or NO^-.

Data pertaining to the crystal structure determination of the $[Fe(NO)_2I_2]^-$ ion are given in Tables 1–3. The $[Fe(NO)_2I_2]^-$ anion is illustrated in Fig. 1. Bond lengths and bond angles are compared with those reported for $Fe(NO)_2(PPh_3)Cl$, $[Fe(NO)_2(SPh)_2]^-$, and for idealized geometries in Table 6. The structure of $[Fe(NO)_2I_2]^-$ obtained differs only slightly from that of a regular tetrahedral array of ligands around the iron atom. The deviations are markedly less than those found for $Fe(NO)_2(PPh_3)Cl$ and $[Fe(NO)_2(SPh)_2]^-$. It is notable that this complex occurs in part B of Table 4, showing three distinct g values. We would anticipate that other compounds in this group, with chloride or nitrogen-bonded ligands, would have similar close to regular tetrahedral geometries.

The relationship between molecular geometry and the EPR parameters

The components of the g tensor for a paramagnetic transition metal complex are determined by the nature of the orbital(s) containing the unpaired electron(s). The ordering of the metal d orbitals is in turn determined by the molecular geometry and can be predicted from crystal field theory. In the present section simple crystal field considerations are used to make qualitative predictions concerning the g tensor.

The geometries possible for a four-coordinated complex are square-planar, tetrahedral, and various distortions of these simple geometries. If the complex has a formula MX_4, the relevant point groups are T_d (tetrahedral) or D_{4h} (square-planar). If, as in the present case, the formula is MX_2L_2 the point group becomes C_{2v} (tetrahedral), D_{2h} (*trans*-square-planar), or C_{2v} (*cis*-square-planar). If the complex is of the form $MXYL_2$, or if the geometry is not regular tetrahedral or square-planar, less symmetry is present and any degeneracy of the d orbitals is completely removed. This is the case for the complexes under present consideration. As far as the g tensor is concerned, to zero-order approximation all the components will have a value equal to the free electron g value, g_e. To a first-order approximation, spin orbit coupling mixes the different d orbitals and deviations from the g_e will occur. This potentially leads to different values for different components of the g tensor. If the distortions are not too great, we would still expect to observe an EPR spectrum corresponding to separate $g_\parallel$ and $g_\perp$, if this is required by the undistorted symmetry. The differences in g values vary according to the geometry assumed, and this allows deductions concerning the molecular geometry to be made from qualitative observations on the form of the g tensor.

The necessary calculations involve first determining the nature of the orbital containing the odd electron, and then considering the contribution of spin orbit coupling for the different orientations of the molecule in the magnetic field. The theory for all the cases of interest is available in the literature (27). The resulting conclusions concerning the g value anisotropies are contained in Table 7. Thus for example, in a d^9 complex with a square-planar geometry, the odd electron will occupy the $d_{x^2-y^2}$ orbital and spin orbit coupling mixes this orbital with d_{xy}, leading to the prediction that $g_\parallel > g_\perp > g_e$. If the complex had a d^7 configuration, the odd electron would be in the d_{xy} orbital and the prediction becomes $g_\perp > g_e > g_\parallel$. A qualitative measurement of the g tensor will clearly distinguish between these possibilities. It should be noted that this result is also applicable to a tetragonally distorted octahedral complex, a conclusion that is pertinent to consideration of the complex $[Fe(NO)_2F_4]^{3-}$.

The situation is a little more complex for compounds that have an overall tetrahedral geometry. Even for an MX_4 complex, distortion from T_d symmetry will occur due to the Jahn–Teller effect. For a d^9 complex there can only be a single unpaired electron. Since the maximum symmetry is C_{2v}, the odd electron must be in an orbitally non-degenerate orbital. Three different g values are predicted, all of them being greater than g_e. The ordering of these g values depends on the nature of the distortion from T_d symmetry. A special case arises if the distortion is towards a complex with basically the geometry of a trigonal bipyramid that is missing an axial ligand, as has been suggested by an X-ray crystal structure (9). For this case the approximate threefold symmetry leads to the prediction of only two observable g values with $g_\perp > g_e$ and $g_\parallel = g_e$ (see Table 7). For a d^7 complex the nature of the spectrum depends on the magnitude of the distortion. If a threefold axis remains, there will be a very large positive shift in $g_\parallel$ and, if the molecule is fluxional, very rapid electron spin relaxation, preventing the

Can. J. Chem. Downloaded from www.nrcresearchpress.com by 217.78.4.112 on 09/08/12
For personal use only.

TABLE 7. Summary of conclusions for the EPR spectra of $Fe(NO)_2LX$ complexes

Configuration	Geometry	Conclusion
d^9	Square planar[a]	$g_1 > g_\parallel > g_\perp$
d^9	Distorted tetrahedral	$g_1 > g_2 > g_\perp > g_\perp$
d^9	Tetrahedral distorted towards tbp	$g_\perp > g_\parallel = g_e$
d^7	Square planar[a]	$g_\perp > g_e > g_\parallel$
d^7	Distorted tetrahedral (low symmetry)[b]	$g_1 > g_e > g_2 > g_3$
d^7	Distorted tetrahedral with 3-fold axis[b]	$g_\parallel \gg g_e > g_\perp$

[a]The same conclusion is true for tetragonally distorted octahedral complexes.
[b]If the molecule is fluxional the EPR spectrum will be unobservable as a result of very rapid spin relaxation.

observation of a solution EPR spectrum.[4] If the distortions are large and the symmetry is low, it is predicted that two of the g values will be less than g_e and one greater. For the special case of a d^7 complex with a distortion towards a pyramidal structure the most likely outcome is that the solution spectrum will be unobservable, contrary to experiment, due to rapid electron spin relaxation as noted above. All these deductions are summarized in Table 7.

Discussion

Our strategy for the interpretation of the present results is to first establish the d electron configuration of the complexes, to next use the EPR data to deduce the geometries, and to finally examine the data for internal consistency. We note initially that all the g values reported in Table 4 are comfortably greater than g_e, which considerably limits the geometries possible for a d^7 configuration. However, supporting evidence for the configuration is provided by the infrared results.

From an examination of the IR stretching frequencies, it can be concluded that the nitrosyl ligands in the paramagnetic $Fe(NO)_2$ complexes are better regarded as NO^+ rather than neutral or negatively charged NO. NO stretching frequencies vary considerably from compound to compound, even when the charges on the ligands are formally the same, and are therefore not reliable indicators of bond type. However, the frequencies reported in Table 5 are clearly closer to the literature examples containing formally positively charged NO than those containing formally neutral NO. This implies that the iron is formally Fe(−I) in these compounds, and the electronic configuration is d^9.

This conclusion has some structural implications. Nitrosyl ligands that are formally NO^- or NO^0 would theoretically result in a 120° Fe—N—O angle, while the Fe—N—O angle would be linear for NO with a formal +1 charge. In practice, the angles in dinitrosyl complexes tend to deviate from these theoretical values by as much as 20°. For example, the bent M—N—O group in $Ru(NO)_2(PPh_3)_2Cl$ is 138° rather than 120° (28). Linear Fe—N—O angles also show large deviations from 180° especially for dinitrosyl complexes with *cis* NO groups (29). Summerville and Hoffmann found that the large deviations were a direct result of the acute N—M—N angle in these dinitrosyl complexes (30). The bending of the NO ligand occurs to stabilize the interaction between the NO ligand and the metal. Crystallographic evidence shows that the Fe—N—O angles in paramagnetic iron dinitrosyl complexes range from 164° to 170°. These angles are indicative of the linear bonded nitrosyl with a +1 formal charge. Therefore, as inferred from the infrared results, $[Fe^{1-}(NO)^+(NO)^+]$ is the most appropriate representation of the complexes, resulting in a d^9 electronic configuration for iron.

Interpretation of the solid state EPR data by earlier authors was based on the assumption that all of the complexes had a d^7 electronic configuration. This led to some interpretational difficulties. These occurred particularly for frozen solution EPR spectra for complexes with F or O bonded ligands (3). These compounds all have EPR spectra with $g_\parallel > g_\perp > g_e$. If it is assumed that the iron complexes had a d^7 configuration, none of the geometries described above gave the appropriate EPR spectrum and it was necessary to postulate a compressed octahedral geometry with *trans*-NO groups for these complexes. However, this structure is not consistent with the available data because a complex with D_{4h} symmetry would have only a single NO stretching frequency in the infrared spectrum. All the paramagnetic iron dinitrosyl complexes have two NO stretching frequencies. These difficulties are removed if the iron dinitrosyl compounds are described as d^9 complexes. The EPR spectra of the fluorine and oxygen complexes then match that calculated for square-planar geometry. A coordination number of six is possible for complexes with the fluoride ion. Therefore, it is important to note that a tetragonally elongated octahedron with a d^9 electron configuration also results in a frozen EPR spectrum with $g_\parallel > g_\perp > g_e$ as is observed.

A second class of iron dinitrosyl compounds have completely different EPR spectra. For complexes with S or P bonded ligands, $g_\perp > g_\parallel > g_e$. The unpaired electron must occupy an orbital other than $d_{x^2-y^2}$. An example of a complex with $g_\perp > g_\parallel$ is $Fe(NO)_2(PPh_3)Cl$. Examination of the crystal structure of this compound shows a geometry that can be loosely described as a trigonal bipyramid with one axial ligand missing. This can be regarded as a distorted tetrahedron but the nature of the distortion differs from that observed with "hard" ligands. The phosphine is in the axial position, so that the d_{z^2} orbital becomes the highest energy metal orbital. If the paramagnetic iron dinitrosyl complexes have a d^9 configuration, the pyramidal structure predicts an EPR spectrum with $g_\perp > g_\parallel$ as observed. It is plausible that all paramagnetic iron dinitrosyl compounds with $g_\perp > g_\parallel$ have a similar structure.

The two suggested geometries represent the extremes of the possible distortions from a regular tetrahedron. The complexes with fluoride or oxygen are formed from a tetrahedron that is flattened towards a square-planar geometry

[4]We are indebted to a referee for drawing our attention to this case.

Can. J. Chem. Downloaded from www.nrcresearchpress.com by 217.78.4.112 on 09/08/12
For personal use only.

Can. J. Chem. Downloaded from www.nrcresearchpress.com by 217.78.4.112 on 09/08/12
For personal use only.

with increased solvent interaction. For the complexes with sulfur or phosphorus ligands, the tetrahedron is distorted by dropping the metal atom onto a triangular face with the nitrosyls at two of the apices of the triangle. The geometry does not fit this idealized geometry exactly. An examination of the bond angles in $Fe(NO)_2(PPh_3)Cl$ given in Table 6 indicates that the complex is better described as a tetrahedron distorted towards the trigonal bipyramidal (tbp) geometry. The existence of a third group of $Fe(NO)_2$ complexes, with three different principal values of the g matrix, suggests that intermediate geometries are also possible. These complexes would have low symmetry and could only be described as distorted tetrahedra. The considerations of the previous section confirm that d^9 complexes with this geometry do in fact have EPR spectra with three g values all greater than g_e.

Some extended Hückel calculations have been carried out to obtain further insight into the bonding in these complexes. The calculations indicate that the spin-containing molecular orbital (SOMO) is composed of approximately 70% d orbital character. This was expected since the hyperfine coupling constant A_N was only 2 G. Hyperfine coupling is normally much larger (ca. 10–14 G) in nitrosyls where nitrogen orbitals hold the unpaired electron. These results are in agreement with EHMO calculations carried out by Butler *et al.* for $[Fe(NO)_2(SR)_2]^-$ (2*m*). They found that the SOMO was a π-type orbital with respect to the Fe—N bonds. For $Fe(NO)_2(PPh_3)Cl$, the calculations indicate that the molecular orbital (MO) containing the unpaired electron is primarily composed of the d_{z^2} metal orbital as predicted. Since the geometry is not a perfect triangular pyramid, the MO also contains some d_{yz} orbital. This tilts the d_{z^2} to more effectively overlap with the Cl ligand. The spin-containing MO includes a slight bonding interaction between iron and the NO groups but iron is antibonding with respect to phosphorus and chloride. The unpaired electron in $[Fe(NO)_2I_2]^-$ resides in a molecular orbital that is primarily a mixture of metal d_{yz}, $d_{x^2-y^2}$, and d_{z^2} orbitals. This is also in agreement with predictions based on EPR data. The results obtained for $[Fe(NO)_2F_2]^-$ in a planar geometry were almost identical to those for tetragonally distorted $[Fe(NO)_2F_4]^{3-}$. In both of these complexes, the metal orbital containing the unpaired electron was $d_{x^2-y^2}$ as predicted. In addition, there was a slightly larger contribution to the singly occupied MO from the NO orbitals. There was a small bonding interaction between iron and nitrogen, but the N–O interaction was antibonding. In general, the molecular orbital calculations for the representative molecules support the conclusions drawn about the structure of the paramagnetic iron dinitrosyl complexes.

The chemistry of the iron dinitrosyl complexes is comparable to other first row d^9 transition metal compounds. Structural information for d^9 complexes is relatively rare compared to other first row transition metal configurations. Copper(II) compounds are the most common. These complexes are generally square-planar with weak interactions with fifth and sixth ligands (31). The iron dinitrosyl complexes with hard, ionic ligands such as fluoride, hydroxide, and methoxide are analogous to these Cu^{2+} compounds. In fact, it is possible to prepare six-coordinate $[Fe(NO)_2F_4]^{3-}$ under conditions with high fluoride concentrations. Softer donor ligands such as the halides and N-bonded ligands encourage more π bonding to the NO ligands. There is a subsequent change in the nature of the distortion to accommodate better π bonding. This case is analogous to nickel(I) complexes, which, although rare, are known to adopt tetrahedral geometries (32). X-ray crystal structure data have shown that a trigonal bipyramidal structure with one axial ligand missing is the approximate geometry adopted by the $Fe(NO)_2(PPh_3)Cl$ complex. With this arrangement, d_{xy} and $d_{x^2-y^2}$ can form in-plane π bonds with the nitrosyl ligands and d_{xz} and d_{yz} participate in out-of-plane π bonding. In this way, the d_{z^2} orbital is available to interact with the triphenylphosphine ligand. It is possible that another reason for the distortion from the tetrahedral shape is the maximization of π bonding within the $Fe(NO)_2$ moiety. Evidence in support of this is the higher NO stretching frequencies for $Fe(NO)_2$ complexes with π acceptor ligands such as CN^- or PPh_3, compared to those observed for the complexes with methoxide and ethoxide. Cobalt(0) complexes also have the d^9 electronic configuration. However, the structure and bonding in Co(0) compounds does not parallel that of Fe(−I) complexes as do the Cu(II) and Ni(I) species. Co–Co bonds tend to be formed in cobalt chemistry in accordance with the 18-electron rule. The paramagnetic iron dinitrosyls also dimerize to form diamagnetic compounds such as $[Fe(NO)_2(\mu-I)]_2$. However, the interaction is not as strong as in the case of cobalt. The interaction is better compared to Cu(II) dimers with carboxylate or triazinate bridges, in which there are antiferromagnetic couplings of the unpaired spins (33).

1. C. C. McDonald, W. D. Phillips, and H. F. Mower. J. Am. Chem. Soc. **87**, 3319 (1965).
2. (*a*) L. Burlamacchi, G. Martini, and E. Tiezzi. Inorg. Chem. **8**, 2021 (1969); (*b*) G. Martini and E. Tiezzi. Trans. Faraday Soc. **67**, 2538 (1971); (*c*) G. Martini and E. Tiezzi. Z. Naturforsch. **28B**, 300 (1973); (*d*) R. Basosi, E. Gagelli, E. Tiezzi, and G. Valensin. J. Chem. Soc. Perkin Trans. 2, 423 (1975); (*e*) R. Basosi, F. Laschi, and C. Rossi. J. Chem. Soc. Perkin Trans. 2, 875 (1978); (*f*) N. S. Garif'yanov and S. A. Luchkina. Str. Mol. Kvantovaya Khim. 62 (1970). Quoted in Landolt-Bornstein, New Series, Vol. 10, Suppl. 2; Springer-Verlag, Berlin. 1979; (*g*) R. Kramolowsky and J. Schmidt. Z. Naturforsch. **25B**, 1487 (1970); (*h*) J. Schmidt. Z. Naturforsch. **27B**, 600 (1972); (*i*) J. P. Crow, W. R. Cullen, F. G. Herring, J. R. Sams, and R. L. Tapping. Inorg. Chem. **10**, 1616 (1971); (*j*) E. Miki, M. Motonaga, K. Mizumachi, T. Ishimori, and M. Katada. Bull. Chem. Soc. Jpn. **55**, 2858 (1982); (*k*) A. R. Butler, C. Glidewell, A. R. Hyde, and J. C. Walton. Polyhedron, **4**, 797 (1985); (*l*) Polyhedron, **4**, 303 (1985); (*m*) A. R. Butler, C. Glidewell, I. L. Johnson, and J. C. Walton. Polyhedron, **6**, 2085 (1987); (*n*) A. R. Butler, C. Glidewell, and I. L. Johnson. Polyhedron, **6**, 2091 (1987); (*o*) C. Glidewell and I. L. Johnson. Polyhedron, **7**, 1371 (1988).
3. (*a*) N. S. Garif'yanov and S. A. Luchkina. Dokl. Akad. Nauk SSSR, **189**, 951 (1969); (*b*) B. A. Goodman and J. B. Raynor. J. Chem. Soc. (A), 2038 (1970); (*c*) B. Jezowska-Trezebiatowska and A. Jezierski. J. Mol. Struct. **19**, 635 (1973); (*d*) D. S. Burbaev, A. F. Vanin, and L. A. Blyumenfel'd. Russ. J. Struct. Chem. **12**, 230 (1971); (*e*) R. Basosi, L. Burlamacchi, G. Martini, and E. Tiezzi. J. Chim. Phys. **72**, 89 (1975).
4. D. Gwost and K. G. Caulton. Inorg. Chem. **12**, 2095 (1973).
5. N. G. Connelly and C. Gardner. J. Chem. Soc. Dalton Trans. 1525 (1976).
6. H. Strasdeit, B. Krebs, and G. Henkel. Z. Naturforsch. **41B**, 1357 (1986).
7. L. M. Baltusis, K. D. Karlin, H. N. Rabinowitz, J. C. Dewan, and S. J. Lippard. Inorg. Chem. **19**, 2627 (1980).

8. E. Miki, M. Motonaga, K. Mizumachi, T. Ishimori, and M. Katada. Bull. Chem. Soc. Jpn. **55**, 2858 (1982).
9. J. Kopf and J. Schmidt. Z. Naturforsch. **30B**, 149 (1975).
10. D. M. P. Mingos and J. A. Ibers. Inorg. Chem. **10**, 1479 (1971).
11. (*a*) D. Ballivet, C. Billard, and I. Tkatchenko. J. Organomet. Chem. **124**, C9 (1977); (*b*) D. Ballivet-Tkatchenko, C. Billard, and A. Revillon. J. Polym. Sci. Part A: Polym. Chem. **19**, 1697 (1981).
12. D. B. Fulton. MCEPR, Monte Carlo calculation of electron paramagnetic powder spectra. McMaster University, Canada. 1989.
13. G. M. Sheldrick. SHELX-86, Program for crystal structure solution. University of Göttingen, Federal Republic of Germany. 1986.
14. K. Yamamoto, S. Homma, and N. Kato. Acta Crystallogr. Sect. A: Cryst. Phys. Diffr. Theor. Gen. Crystallogr. **A24**, 232 (1968).
15. D. T. Cromer and D. Liberman. J. Chem. Phys. **53**, 1891 (1970).
16. J. M. Stewart and S. R. Hall. The XTAL system of crystallographic programs. Tech. Rept. TR-1364, University of Maryland, College Park, Md. 1983.
17. J. C. Calabrese and R. M. Burnett. TAPER, locally modified by Z. Tun with the permission of the Nicolet XRD Corp., 1980.
18. G. M. Sheldrick. SHELX-76, Program for crystal structure determination. University of Cambridge, England. 1976.
19. J. Stephens. MOLGEOM adapted from CUDLS. McMaster University, Canada. 1973.
20. K. Davies. CHEMGRAF suite: SNOOPI. Chemical Design Ltd., Oxford, England. 1983.
21. J. Howell, A. Rossi, D. Wallace, and R. Hoffmann. ICON8. Department of Chemistry, Cornell University, Ithaca, N.Y.
22. J. H. Ammeter, H. B. Bürgi, J. C. Thibeault, and R. Hoffmann. J. Am. Chem. Soc. **100**, 3686 (1978).
23. K. Nakamoto. Infrared spectra of inorganic coordination compounds. 2nd ed. Wiley–Interscience, New York. 1970. p. 200.
24. N. N. Greenwood and A. Earnshaw. Chemistry of the elements. Pergamon, Oxford. 517 (1984).
25. J. Lewis, R. J. Irving, and G. Wilkinson. J. Inorg. Nucl. Chem. **7**, 32 (1958).
26. J. Schmidt, H. Kühr, W. L. Dorn, and J. Kopf. Inorg. Nucl. Chem. Lett. **10**, 55 (1974).
27. (*a*) A. Abragam and B. Bleaney. Electron paramagnetic resonance of transition ions. Dover Publications, New York. 1986. Chapter 7 provides an in-depth survey of the EPR spectra of the 3*d* ions in intermediate ligand fields; (*b*) M. Symons. Chemical and Biological aspects of electron-spin resonance spectroscopy. John Wiley & Sons, New York, 1978. Chapter 2 provides a simple summary of qualitative interpretation of powder EPR spectra.
28. C. G. Pierpont and R. Eisenberg. Inorg. Chem. **11**, 1088 (1972).
29. (*a*) J. H. Enemark and R. D. Feltham. Coord. Chem. Rev. **13** 339 (1974); (*b*) R. D. Feltham and J. H. Enemark. Top. Stereochem. **12**, 155 (1981).
30. R. H. Summerville and R. Hoffmann. J. Am. Chem. Soc. **98** 7240 (1976).
31. (*a*) J. Gazo, I. B. Bersuker, J. Garaj, M. Kabesova, J. Kohout H. Langfelderova, M. Melnik, M. Serator, and F. Valach Coord. Chem. Rev. **18**, 253 (1976); (*b*) B. J. Hathaway and D. E. Billig. Coord. Chem. Rev. **5**, 143 (1970).
32. P. Dapporto, G. Fallani, and L. Sacconi. Inorg. Chem. **13** 2847 (1974).
33. R. J. Doedens. Prog. Inorg. Chem. **21**, 209 (1976).
34. J. Schmidt. Transition Met. Chem. (London), **1**, 256 (1976)

Can. J. Chem. Downloaded from www.nrcresearchpress.com by 217.78.4.112 on 09/08/12
For personal use only.

Thermally stable coordination compounds intercalated in montmorillonite clay mineral

N. K. LABHSETWAR AND O. P. SHRIVASTAVA[1]
Department of Chemistry, Dr. H. S. Gour University, Sagar-470 003 (M. P.), India

Received January 9, 1991[2]

N. K. LABHSETWAR and O. P. SHRIVASTAVA. Can. J. Chem. **70**, 1927 (1992).

Montmorillonite is a natural layered clay mineral having myriad applications due mainly to its remarkable ion exchange, intercalation, and swelling properties. It can act as a good host for several compounds. Two intercalated coordination compounds of Cu(II) and Ni(II) with 2,2′-bipyridyl have been prepared in the interlayer spaces of montmorillonite structure. They are characterized on the basis of elemental analysis, infrared spectroscopy, magnetic studies, and X-ray diffraction. Both compounds show similarity in their structure and properties with the respective normal complexes of similar composition. These compounds show good thermal stability. The present intercalated compounds might be useful for their nitrogen-immobilizing properties and high-temperature applications.

N. K. LABHSETWAR et O. P. SHRIVASTAVA. Can. J. Chem. **70**, 1927 (1992).

La montmorillonite est une argile minérale naturelle en couche qui a des myriades d'applications reliées à ses propriétés remarquables pour l'échange ionique, l'intercalation et le gonflement. Elle peut agir comme hôte pour plusieurs composés. Dans les espaces interstitiels de la structure de la montmorillonite, on a préparé deux composés de coordination intercalés du Cu(II) et du Ni(II) avec le 2,2′-pyridyle. On les a caractérisés par des analyses élémentaires, par spectroscopie infrarouge, des études magnétiques et par diffraction des rayons X. Les deux composés ont des similarités de structure et de propriétés par rapport à leurs complexes respectifs normaux de composition semblable. Ces composés présentent une bonne stabilité thermique. Ces composés pourraient s'avérer utiles à cause de leurs propriétés permettant d'immobiliser l'azote et de leurs applications à hautes températures.

[Traduit par la rédaction]

Introduction

Ion exchange properties of clay minerals have been investigated by several workers with different cations and also with charged large organic moieties (1–5). The montmorillonite group of clays having the general formula $Al_4Si_8O_{20}(OH)_4 \cdot nH_2O$ show cation exchange and can also take up extraneous molecules between the structural layers (6, 7). Intercalation behaviour of montmorillonite clay is of interest and many attempts have been made to introduce macromolecules in the interlayer spaces of this layered clay mineral (7–30). Earlier Traynor *et al.* also reported tris-bipyridyl–metal complexes supported on the layer-lattice-silicate hectorite (31). Cruz *et al.* investigated the Ru-(bipyridyl)$_2$-$(H_2O)^{2+}$ complex adsorbed on hectorite (32). These compounds were prepared by ion exchange or adsorption of charged complex ions with layered clay. Traynor *et al.* observed that a metal–bipyridyl complex can be supported on hectorite beyond its ion-exchange capacity. This additional binding of the metal complex to the mineral occurs through intercalation of the metal complex salt. The present paper reports physicochemical data on intercalated coordination compounds of Cu(II)- and Ni(II)-exchanged montmorillonites with 2,2′-bipyridyl.

Experimental

Cu(II)- and Ni(II)-exchanged montmorillonites were prepared by shaking 5.0 g of finely powdered (mesh size 150) USGS montmorillonite clay sample with 0.5 M aqueous metal-ion solution at 25°C for 10 days (30). The metal-exchanged clay was separated and thoroughly washed with deionized water before drying at 70°C for 8 h. Cu(II)- and Ni(II)-saturated montmorillonites were thus obtained. The metal–bipyridyl complexes were prepared by refluxing the metal-exchanged montmorillonite with 0.5 M 2,2′-bipyridyl solution in acetone for 15 h. By the end of the reaction the colour of both compounds had changed completely. The products thus obtained were washed with acetone and dried over P_4O_{10} before analysis. In earlier studies most of the clay-supported coordination compounds were prepared either by ion-exchange of charged complex molecules with interlayer exchangeable cations of clay mineral or adsorption of complex molecules on a large surface area of clay. In the present case uptake of the bound metal–bipyridyl complex to the montmorillonite is within its ion-exchange capacity where the cation-exchanged clay is treated with a stoichiometric quantity of ligands.

The metal content was determined spectrophotometrically in both compounds using standard methods (33). Nitrogen was estimated using a Coleman Analyser. The IR absorption spectra of the compounds were recorded on a Perkin–Elmer-397 IR spectrophotometer. The sample was used as KBr pellets. Room temperature magnetic susceptibilities of the compounds were determined by Gouy's method using $Hg[Co(NCS)_4]$ as the standard. X-ray powder diffraction patterns of the compounds were recorded on a Phillips X-ray machine attached to a microprocessed PW-1700 diffractometric system using Cu-K_α radiation of wavelength 1.542 Å Thermogravimetric analysis was carried out on a Perkin–Elmer thermal analyser using inert atmosphere. The heating rate was maintained at 12.5°C min^{-1} in the temperature range 60–1000°C. All chemicals used were of A. R./E. Merck grade.

Results and discussion

The montmorillonite clay mineral consists of negatively charged aluminosilicate layers with interlayer cations compensating the positive charge deficiency. The empirical formula of the present montmorillonite sample is

$$(Ca_{0.90}Na_{0.16}K_{0.03})(Al_{1.48}Fe_{0.13}Mg_{0.4})\,[Si_{3.99}Al_{0.01}]O_{10}(OH)_2 \cdot nH_2O$$

The charge deficiency in montmorillonite is mainly due to isomorphous substitution of Si^{4+} by Al^{3+}. The interlayer spaces in montmorillonite clay are substantial enough for it

[1]Author to whom correspondence may be addressed.
[2]Revision received March 23, 1992.

Can. J. Chem. Downloaded from www.nrcresearchpress.com by 217.78.4.112 on 09/08/12
For personal use only.

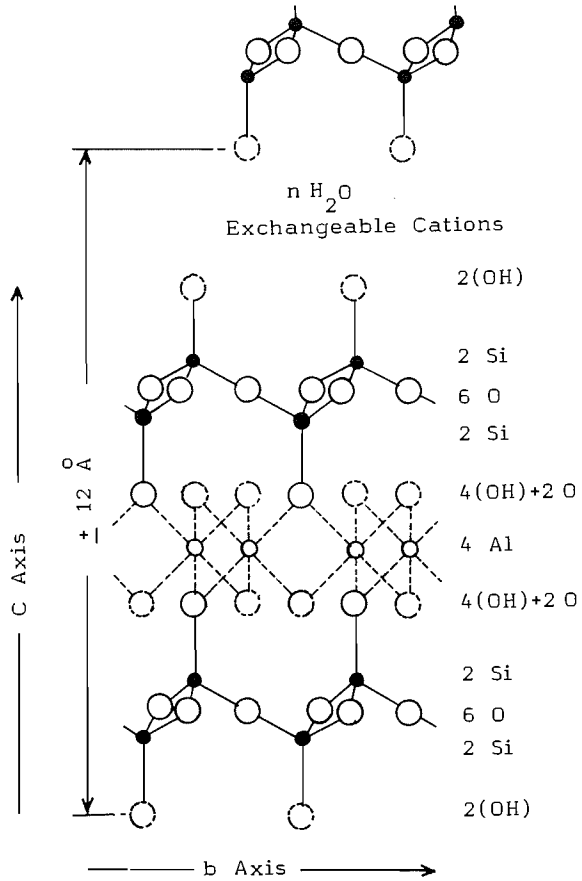

FIG. 1. Schematic presentation of the structure of montmorillonite (ref. 14).

to act as a host compound, and, therefore, it is possible to prepare intercalation compounds of the exchanged cations that are formed in the interlayer spaces along with water molecules (6, 30, 34, 35) (Fig. 1).

The treatment with 2,2′-bipyridyl (hereafter bipy) turns Cu(II)-montmorillonite to violet and Ni(II)-montmorillonite to pink-coloured materials. This indicates the interaction of the ligand molecules with cation-exchanged montmorillonite clay. Chemical analysis of the compounds is summarized in Table 1. The metal to ligand molar ratio is observed as 1:2 in both cases. This stoichiometric ligand content of intercalated compounds shows the formation of coordination compounds of Cu(II) and Ni(II) in montmorillonite. The IR absorption spectra of metal-exchanged montmorillonite show all the characteristic absorptions of montmorillonite clay (hereafter mnt) (Table 2). In addition to this, absorption due to coordinated water also appears in the case of metal-exchanged clay (Fig. 2). IR absorption spectra of intercalated compounds consist of several prominent absorptions, characteristic of bipy-complex with metal ions (Figs. 2, 3). These data have been presented in Table 2 along with their assignments. On comparison of IR spectra of the intercalated compounds with those of the free ligand (36–38) it is observed that the ring vibrations and other modes are shifted towards the higher energy side. This shift towards lower wavelength indicates the tightening of the ring on coordination through the nitrogen atoms of the ligand molecules. The Ni(II)-mnt compound also shows IR absorption due to coordinated water. A remarkable feature of the IR spectra of intercalated compounds is the broadening of the characteristic Si—O stretching absorption in comparison to that in metal-exchanged mnt. This absorption is directly related to the composition and structure of the silicate layers in mnt and is thus expected to alter with the changes in silicate layer (34, 39, 40). It is also established that the exchanged cations are present on the interlayer surfaces of the mnt (30, 34, 35). Chemical and IR absorption data suggest the formation of coordination compounds of the exchanged metal ions; therefore, the formation of these coordination compounds in the interlayer space of the clay structure may be predicted.

A significant increase in magnetic susceptibility of mnt is observed after exchange of metal ions (Table 1). This could be due to the incorporation of Cu^{2+} ions in mnt. The observed Bohr magneton value (μ_B) for bipy–Cu(II)-mnt is 2.18. Analytical data (Table 1) give the metal to ligand stoichiometry as 1:2. This ratio fits in well with the bidentate nature of the bipy ligand, satisfying the coordination number [4] for Cu(II). Square-planar is the most favourable geometry in a tetracoordinated Cu(II) complex. The presence of coordinated water in a Ni(II)-mnt intercalated compound suggests hexacoordinated nickel. The bipy adduct of Ni(II)-mnt has a μ_B value of 2.98. This value suggests the intercalated Ni ion in octahedral field corresponding to two unpaired electrons. Thus it may be concluded that the pres-

TABLE 1. Analytical, magnetic, and thermal data

Compound	Chemical analysis (mmol/100 g) Metal	Ligand	Bohr magneton at 300 K (μ_B)	Weight loss in wt.% (Temperature range, °C)		
Montmorillonite	—	—	0.56	18.05 (60–175)	5.50 (550–720)	
Cu(II)-montmorillonite	50.1	—	2.07	18.00 (60–175)	2.00 (510–780)	
Ni(II)-montmorillonite	55.2	—	2.92	20.00 (60–180)	4.75 (530–785)	
Bipy–Cu(II)-montmorillonite	43.42	88.10	2.18	3.0 (60–120)	13.5 (360–530)	3.0 (550–760)
Bipy–Ni(II)-montmorillonite	46.29	94.21	2.98	6.8 (60–180)	13.2 (470–725)	3.9 (725–890)

Can. J. Chem. Downloaded from www.nrcresearchpress.com by 217.78.4.112 on 09/08/12
For personal use only.

TABLE 2. Infrared absorption bands (in cm^{-1}) of metal-exchanged montmorillonites and their 2,2′-bipyridyl derivatives

Assignments	Bipy–Cu(II)-montmorillonite (Cu(II)-montmorillonite)	Bipy–Ni(II)-montmorillonite (Ni(II)-montmorillonite)
O—H stretching	3600 s (3600 s)	3600 s (3605 s)
H—O—H bending	1630 s (1625 m)	1635 s (1630 m)
C=C, C=N, and ring stretching	1595 w 1565 vs	1605 s 1530 m
Si—O stretching	1200–840 br (1000 br)	1190–810 br (1005 br)
C—H out-of-plane deformation due to three adjacent hydrogens	765 s	770 s
Out-of-plane ring deformation	730 w	—
H—O—H (coordinated) rocking	— (710 m)	710 m (705 m)

vs = very sharp, s = sharp, m = medium, w = weak, br = broad.

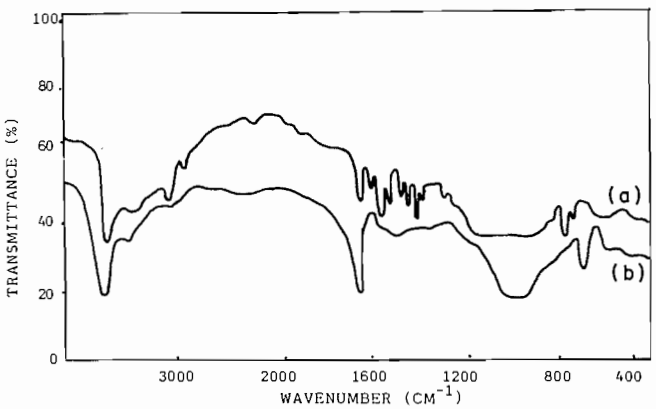

FIG. 2. IR absorption spectra: (*a*) 2,2′-bipyridyl–Cu(II)-montmorillonite and (*b*) Cu(II)-montmorillonite.

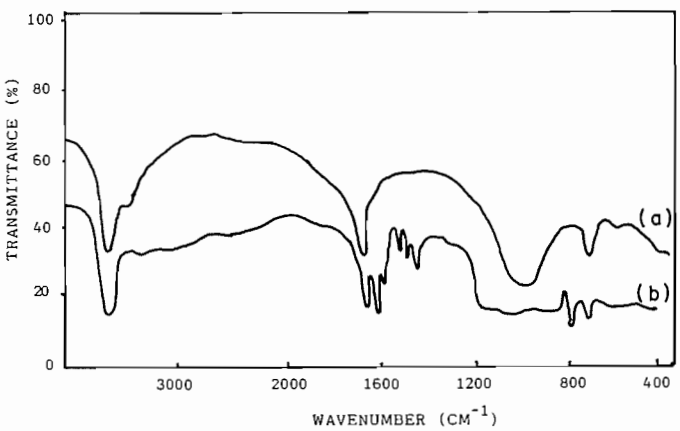

FIG. 3. IR absorption spectra: (*a*) Ni(II)-montmorillonite and (*b*) 2,2′-bipyridyl–Ni(II)-montmorillonite.

ent intercalated compounds show similarity in their magnetic behaviour to those of normal complexes of similar composition.

The position and orientation of intercalated compounds in layered clays can be investigated on the basis of X-ray diffraction patterns. The *c* lattice parameter (d_{001}) for a monoclinic cell of montmorillonite is dependent on its interlayer content, normally the interlayer water. A significant change in *c* value is reported with the change in interlayer content because of the inclusion of different cations/molecules in such available spaces of layered clays (9, 13, 17, 19–21, 30–32). In the present study the d_{001} spacing of montmorillonite clay is also, observed to be significantly changed after treatment with 2,2′-bipyridyl. The observed d_{001} spacing for 2,2′-bipyridyl–Cu(II)-montmorillonite is 18.3 Å. This shows that the interlayer is increased by 6.2 Å when compared with Cu(II)-exchanged montmorillonite (Table 3). Analytical and magnetic data for the $Cu(bipy)_2$-intercalated complex suggest square-planar geometry and bipyridyl planes parallel to the clay surface. Traynor *et al.* have also reported similar d_{001} spacing for bis-bipyridyl–copper complexes with hectorite, prepared by heating of a tris-bipyridyl–copper complex. The d_{001} value for 2,2′-bipyridyl–Ni(II)-montmorillonite is 18.8 Å. Thus an increase of 6.9 Å in the d_{001} spacing is observed after inclusion of 2,2′-bipyridyl molecules in Ni(II)-exchanged montmorillonite clay. Our analytical magnetic, thermal, and infrared absorption data suggest the formation of a hexacoordinated octahedral Ni(II) complex with chemical composition $[Ni(bipy)_2(H_2O)_2]^{2+}$. The estimated interlayer distance from the interatomic distances and the van der Waals radii (32, 45, 46) would be 6.40 Å for a pseudo-octahedral molecular model of the *cis* isomer of a complex molecule intercalated between two clay sheets with the bipyridyl planes parallel to the surface. X-ray diffraction and other investigations suggest that this is the most probable orientation of the Ni–bipy complex among the various possible orientations suggested by Cruz *et al.* (32). The Na-montmorillonite shows a d_{001} value of 10.3 Å while Ni(II)-

Can. J. Chem. Downloaded from www.nrcresearchpress.com by 217.78.4.112 on 09/08/12
For personal use only.

TABLE 3. d_{001} layer spacings of metal-exchanged montmorillonites and 2,2′-bipyridyl derivatives

Sample no.	Compound	d_{001} spacing (Å)
1.	Cu(II)-montmorillonite	12.1
2.	2,2′-Bipyridyl–Cu(II)-montmorillonite	18.3
3.	Ni(II)-montmorillonite	11.9
4.	2,2′-Bipyridyl–Ni(II)-montmorillonite	18.8

exchanged montmorillonite with interlayer-coordinated water gives d_{001} = 11.9 Å. This small difference in d_{001} could be due to "keying" of water molecules into the ditrigonal holes of the clay surface, as it is of small molecular size (7). Thus replacement of water molecules from interlayer spaces does not make a significant change in the interlayer spacings of the clay, as is evident from the thermal and X-ray diffraction data (Tables 1 and 3) of the intercalated compounds.

Thermogravimetric analyses of the intercalated compounds were carried out in order to investigate their thermal stability. Cu(II)- and Ni(II)-exchanged mnt show almost similar thermal decomposition patterns with about 19% weight loss up to ~180°C. This can be attributed to the loss of interlayer and coordinated water. The second weight loss step between 480 and 780°C is due to structural loss, i.e., breaking of OH groups (34, 41, 42). Intercalated compounds show an additional weight loss, which starts from 360°C in the case of the Cu(II) compound and from 470°C for the Ni(II) compound. In this major decomposition step the intercalated complex molecules break and oxidation of ligand takes place. The interlayer water content of metal-exchanged mnt is found to be significantly decreased after formation of intercalation compounds. This suggests the replacement of interlayer water of cation-exchanged montmorillonite by the bipy molecules. These intercalation compounds are observed to be thermally very stable in comparison to the corresponding complexes of Cu(II) and Ni(II) with similar composition (43, 44). This might be due to the silicate shielding of intercalated coordination compounds in the interlayer spaces of montmorillonite clay mineral.

Owing to the large-scale applications of intercalation and complex compounds in catalysis, N-fixation, medicines, and other important areas, the intercalation compounds of cation-exchanged expandable clays need to be explored thoroughly. Such compounds promise application as nitrogen-immobilizing and microencapsulating agents. It has been established that montmorillonite clay has extraordinary intercalation and retention properties; however, reported work (8–13, 19, 24, 25, 30) and the present study infer that these properties are even better in the case of a metal-exchanged clay mineral, particularly in respect of the substances that can form coordination compounds with those exchanged metal ions. High thermal stability of the intercalated compounds can be exploited in industrial applications. In this regard, the normal behaviour of the intercalated coordination compounds is remarkable.

Acknowledgements

The authors are grateful to the Council of Scientific and Industrial Research for their financial support (to N.K.L.). Thanks are also due to the Head, Department of Chemistry, Dr. H.S. Gour University, Sagar, for providing research facilities.

1. H. Van Olphen and C. T. Deeds. Nature, **194**, 176 (1962).
2. R. Greene Keley. Trans. Faraday Soc. **51**, 425 (1955).
3. M. Patel. J. Mater. Sci. Lett. **5**, 1279 (1986).
4. M. Tsuji and S. Komarneni. J. Mater. Sci. **4**, 698 (1989).
5. W. Bodenheimer and L. Heiler. Clay Miner. Bull. **5**, 145 (1962).
6. B. Mason and C. B. Moore. Principles of geochemistry. 4th ed. Wiley Eastern Ltd., New Delhi. 4th ed. 1985. p. 156.
7. B. K. G. Theng. The chemistry of clay organic reactions. Adam–Hilger, London. 1974. p. 1.
8. W. Bodenheimer, B. Kirson, and SH. Yariv. Isr. J. Chem. **1**, 69 (1963).
9. W. Bodenheimer, L. Heller, B. Kirson, and SH. Yariv. Clay Miner. Bull. **5**, 145 (1962).
10. W. Bodenheimer, L. Heller, B. Kirson, and SH. Yariv. Proc. Int. Clay Conf. Stockholm, **2**, 351 (1963).
11. W. Bodenheimer, L. Heller, B. Kirson, and SH. Yariv. Isr. J. Chem. **1**, 391 (1963).
12. W. Bodenheimer, L. Heller, and SH. Yariv. Isr. J. Chem. **2**, 201 (1964).
13. W. Bodenheimer, L. Heller, and SH. Yariv. Proc. Int. Clay Conf. Jerusalem, **1** 251 (1966).
14. W. Bodenheimer, L. Heller, and SH. Yariv. Clay Miner. **6**, 167 (1966).
15. D. Yamamato, N. Wakasugi, and K. Ono. Proc. Int. Clay Conf. Tokyo, **1**, 735 (1969).
16. S. Yariv, J. D. Russel, and V. C. Farmer. Isr. J. Chem. **4**, 201 (1966).
17. W. Bodenheimer and L. Heller. Clay Miner. **7**, 167 (1967).
18. S. Yariv and L. Heller, Clays Clay Miner. **17**, 301 (1969).
19. L. Heller and S. Yariv. Proc. Int. Clay Conf. Tokyo, **1**, 741 (1969).
20. Z. Sofer, L. Heller, and S. Yariv. Isr. J. Chem. **7**, 697 (1969).
21. L. Heller and S. Yariv. Isr. J. Chem. **8**, 391 (1970).
22. L. Heller, S. Yariv, and M. Riemer. Proc. Int. Clay Conf. Madrid, 651 (1972).
23. L. Heller-Kallai, S. Yariv, and M. Riemer. Clay Miner. **10**, 35 (1973).
24. S. Son, S. Ueda, F. Kanamaru, and M. Kolzumi. J. Phys. Chem. **80**, 1780 (1976).
25. V. C. Farmer and M. M. Mortland. J. Phys. Chem. **69**, 683 (1985).
26. Y. Fukushima, A. Okada, M. Kawasumi, T. Kurauchi, and O. Kamigaito. Clay Miner. **23**, 27 (1988).
27. S. Shoval and S. Yariv. Clays Clay Miner. **27**, 19 (1979).
28. S. Yariv, G. Kahr, and A. Rub. Thermochim. Acta, **135**, 299 (1988).
29. S. Yariv, M. Muller Vonmoos, G. Kahr, and A. Rub. J. Therm. Anal. **35**, 1997 (1989).
30. T. Kijima, J. Tanaka, M. Goto, and Y. Matsui. Nature (London), **310**, 45 (1984).

Can. J. Chem. Downloaded from www.nrcresearchpress.com by 217.78.4.112 on 09/08/12
For personal use only.

31. F. S. E. Traynor, M. M. Mortland, and T. J. Pinnavaia. Clays Clay Miner. **26**, 318 (1978).
32. M. I. Cruz, H. Nijs, J. J. Fripiat, and H. Van Damme. J. Chim. Phys. **79**, 753 (1982).
33. A. I. Vogel. Textbook of quantitative inorganic analysis. 4th ed. ELBS, London. 1978. p. 740.
34. R. E. Grim. Clay mineralogy, 2nd ed. McGraw–Hill, New York 1968. p. 83.
35. H. A. Deer, R. H. Howie, and J. Zussman. Rock forming minerals Vol. **3**. Longman, London. 1976. p. 226.
36. P. C. H. Mitchell. J. Inorg. Nucl. Chem. **25**, 963 (1963).
37. C. Postmus, J. R. Ferrore, A. Quattrochi, K. Shobatake, and K. Nakamato. Inorg. Chem. 1851 (1966).
38. J. S. Strucki and J. L. Walter. Spectrochim Acta, Part A: **A27**, 223 (1971).
39. V. C. Farmer and J. D. Russel. Spectrochim. Acta, **20**, 1149 (1964).
40. V. C. Farmer. Clay Miner. **7**, 373 (1968).
41. D. Mc. Conell. Am. Miner. **35**, 166 (1950).
42. J. B. Page. Soil Sci. **56**, 273 (1943).
43. A. B. Khare. Ph.D. Thesis, Sagar University (India). (1989).
44. A. K. Shakya. Ph.D. Thesis, Sagar University (India). (1981).
45. L. Pauling, The nature of the chemical bond. 3rd ed. Cornell Univ. Press, Ithaca, N.Y. 1960.
46. R. D. Shannon. Acta Crystallogr. Sect. A: Cryst. Phys. Diffr. Theor. Gen. Crystallogr. **A32**, 751 (1976).

Can. J. Chem. Downloaded from www.nrcresearchpress.com by 217.78.4.112 on 09/08/12
For personal use only.

Ground and excited state dipole moments of planar vs. twisted *p-N,N*-(dimethylamino)benzonitrile systems: maximum charge transfer for minimum overlap

HEMANT K. SINHA,[1] S. MURALIDHARAN, AND KEITH YATES

Department of Chemistry, Lash Miller Chemical Laboratories, University of Toronto, Toronto, Ont., Canada M5S 1A1

Received February 26, 1992

HEMANT K. SINHA, S. MURALIDHARAN, and KEITH YATES. Can. J. Chem. **70**, 1932 (1992).

Electric field induced change in the absorption spectrum (electrochromism) has been employed to obtain the ground and excited state dipole moments of planar and sterically hindered (twisted) *p-N,N*-(dimethylamino)benzonitriles in dioxane solution. These studies support the twisted intramolecular charge transfer (TICT) hypothesis and provide additional insight to the TICT concept. The charge transfer nature of the excited state has been found to directly depend on the torsional angle of the *N,N*-dimethylamino group with respect to the benzonitrile moiety. It is suggested that solvent coupling is essential to initiate twisting by affecting the intramolecular degrees of freedom and the existence of the highly dipolar excited state is a result of such twisting of the donor–acceptor bond. Theoretical calculations have been performed to explain the observed changes in dipole moment values.

HEMANT K. SINHA, S. MURALIDHARAN et KEITH YATES. Can J. Chem. **70**, 1932 (1992).

On a utilisé le changement induit de champ électrique dans le spectre d'absorption (électrochromisme) pour obtenir les moments polaires des états fondamental et excité des conformations plane et stériquement empêchée (déformée) des *p-N,N*-(diméthylamino)benzonitriles, en solution dans le dioxane. Les résultats obtenus sont en accord avec l'hypothèse d'un transfert de charge intramoléculaire déformé (TCID) et ils fournissent des données supplémentaires pour comprendre le concept de TCID. On a trouvé que la nature du transfert de charge de l'état excité dépend directement de l'angle de torsion du groupe *N,N*-diméthylaminé par rapport à la portion benzonitrile. On suggère que le couplage de solvant est essentiel pour initier la déformation en affectant les degrés de liberté intramoléculaire et que l'existence d'états dipolaires hautement excités est un résultat d'une telle déformation de la liaison donneur/accepteur. On a effectué des calculs théorique pour expliquer les changements observés dans les valeurs des moments dipolaires.

[Traduit par la rédaction]

Introduction

The concept of twisted intramolecular charge transfer (TICT) has received considerable attention in the recent past owing to its intriguing characteristics (1). The most remarkable one is the idea that the charge transfer can be of maximum limiting value (complete one-electron transfer) when the molecular orbitals involved are orthogonally positioned rather than in the same plane, which was believed to be the case prior to the discovery of the TICT concept. This led to the proposition of a *minimum overlap rule*, which operates in certain types of molecules exhibiting TICT character.

The molecule that led to the foundation of TICT concept is *p-N,N*-(dimethylamino) benzonitrile (DMABN). This dates back almost to three decades when Lippert *et al.* reported the unusual nature of fluorescence from this molecule (2). However, the correct interpretation of results from Lippert's report was demonstrated by Grabowski *et al.* much later by their elegant experimental studies on the TICT concept (3). This mechanism suggests that the intramolecular charge transfer of the DMABN molecule is induced by rotation around the C—NMe_2 bond. The short-wavelength emitting species, identified with the planar form of DMABN, and the long-wavelength emitting species, the perpendicular form, are in equilibrium in the excited (S_1) state. Since then there have been numerous studies that have given this mechanism a strong basis.

However, controversy still exists regarding the role of solvent molecules in creating the TICT state (4, 5). For example, it has been proposed that local coupling of solvent molecules, with a particular local configuration, and the reactant (DMABN) is essential for the twisting of the C—NMe_2 bond (4*e*, 5). This is very clear from the fact that isolated DMABN molecules in the gas phase do not emit from the TICT state even when they are allowed to complex with a specific number of solvent molecules (6). On the other hand, the fact that 2,6-*N,N*-(tetramethylamino)benzonitrile (TMABN), which has the -NMe_2 group already twisted in the ground state, shows distinct TICT emission in the gas phase proves beyond reasonable doubt that internal twisting of the C—NMe_2 bond is the sole reason behind TICT emission (7). Recent results from advanced spectroscopic techniques suggest that solvent fluctuation plays a minor role, whereas the dominant contribution to intramolecular charge transfer involves fluctuations in the intramolecular degrees of freedom (8). If this is true, then the primary function of polar solvents in the formation of the TICT state is to induce twisting rather than charge transfer by disturbing the intramolecular vibrational modes. Once the twisting is achieved the resultant dipolar molecule can further interact electrostatically with solvent dipoles to produce strongly Stokes-shifted solvent dependent emission.

This paper attempts to clarify the above concept on the basis of experimental results obtained from electrochromic measurements. Electrochromism has been claimed to be the best method to probe the charge transfer characteristics of suitable molecules both in the ground and excited states (9). Both absorption and fluorescence electrochromic measurements are well documented in the literature (9, 10). The former method is employed here to examine the effect of internal twisting of the C—NMe_2 bond on the magnitude of

[1]Author to whom correspondence may be addressed at the Department of Chemistry, University of Saskatchewan, Saskatoon, Sask., Canada S7N 0W0

Can. J. Chem. Downloaded from www.nrcresearchpress.com by 109.225.110.28 on 09/08/12
For personal use only.

Can. J. Chem. Downloaded from www.nrcresearchpress.com by 109.225.110.28 on 09/08/12
For personal use only.

intramolecular charge transfer. Since this method looks at the vertical excited state, any contribution from solvent fluctuation modes to intramolecular charge transfer can be totally avoided. This has the advantage over fluorescence electrochromic methods because the latter probe the thermally relaxed excited state where the perturbation due to solvent coupling, if at all present, has already been manifested. However, comparison of results obtained from both methods will be useful in analysing the changes that take place when the molecule relaxes from its initially created vertical excited state to its thermally relaxed excited state. Our results mainly focus on the change in the dipole moment upon electronic excitation of planar vs. twisted DMABN systems and present a coherent picture that sudden polarization upon excitation can be achieved by orbitally decoupling the donor and acceptor groups and thereby affecting the intramolecular degrees of freedom. This study particularly emphasizes the fact that torsional motion of the C—NMe_2 bond should be initiated by solvent coupling during the relaxation from the initially created excited state. Theoretical dipole moments were also obtained from simple molecular orbital calculations and compared with the experimental values.

Theory of electrochromism

An intense electric field affects the intensity of both absorption and fluorescence, and such electric field effects were first quantitatively interpreted by Labhart (11), Czekalla (12), and Liptay (13) independently. The basic principles of electrochromic measurements with appropriate theoretical reasoning were reviewed by Liptay (*9b*). In addition, our previous papers also present a complete experimental and physical description of electro-optical absorption measurements on macroscopic systems (14). Hence this will not be repeated, but the basic principles will be summarized here.

For a dipolar molecule the perturbation due to the presence of an external electric field on the electronic absorption intensity is mainly due to two factors; (*i*) anisotropic molecular distribution and (*ii*) change in the electronic transition energy if the ground state dipole moment μ_g is different from the excited state dipole moment μ_e. The theoretical expression relating the change in extinction coefficient $\Delta\epsilon$ to the frequency ν of the incident light, the internal field strength F_{int}, and the angle χ between the direction of the applied field and the polarization direction of incident light, according to Liptay (*9b*), is

$$[1]\quad \Delta\epsilon = F_{int}^2\epsilon\left[A_\chi + B_\chi/15h\,\frac{\partial/\partial\nu(\epsilon/\nu)}{(\epsilon/\nu)} + C_\chi/30h^2\,\frac{\partial^2/\partial\nu^2(\epsilon/\nu)}{(\epsilon/\nu)}\right]$$

where

$$[2]\quad A_\chi = 1/30(3\cos^2\chi - 1)\beta^2[3(\hat{p}\cdot\mu_g)^2 - \mu_g^2]$$

$$[3]\quad B_\chi = 5\beta(\mu_g\cdot\Delta\mu) + (3\cos^2\chi - 1) \times \beta[3(\hat{p}\cdot\mu_g)(\hat{p}\cdot\Delta\mu) - (\mu_g\cdot\Delta\mu)]$$

$$[4]\quad C_\chi = 5\Delta\mu^2 + (3\cos^2\chi - 1)[3(\hat{p}\cdot\Delta\mu)^2 - \Delta\mu^2]$$

In these equations, $\hat{p}$ is a unit vector in the direction of the molecular transition moment, h is Planck's constant, and $\beta = (kT)^{-1}$ where k is Boltzmann's constant and T is the temperature.

TABLE 1. Ground state dipole moment data obtained from dielectric measurements

	DMABN	DMMBN	TMABN
a	42.83 ± 0.01	30.82 ± 0.04	21.2 ± 1.6
c	0.29 ± 0.01	0.116 ± 0.009	0.085 ± 0.008
μ_g	6.2	5.1	4.5

Materials and methods

p-N,N-(Dimethylamino)benzonitrile (DMABN) was obtained from Aldrich chemicals. *N,N*-Dimethyl-2-(methylamino)benzonitrile (DMMBN) and *N,N*-2,6-(tetramethylamino)benzonitrile (TMABN) were prepared from the corresponding *p*-bromoaniline derivatives (obtained from Aldrich) by treating with CuCN, followed by *N*-methylation with freshly distilled dimethyl sulphate (15, 20*a*). All the compounds were recrystallized from appropriate solvents and the purity was checked by standard spectroscopic methods. Spectrograde dioxane and cyclohexane from Aldrich were used without further purification. Absorption spectra were recorded on a Cary 2000 spectrometer and their first and second derivatives (see eq. [1]) were computed numerically.

Ground state dipole moments

Dielectric constants and refractive indices of solutions were measured with a Dekameter (WTW GmbH DK 03), which uses resonance technique to measure cell capacitance, and a refractometer (Valentine 800) respectively. The μ_g's were calculated by the method of Guggenheim (16) as modified by Smith (17). Cyclohexane was used as solvent and all the measurements were done at 22°C. Assuming that $\xi \approx n_1^2$, Smith's equation for μ_g becomes

$$\frac{4\pi N}{9kT}\mu^2 = \frac{3M_1}{\rho_1}\left[\frac{a}{(\xi_1 + 2)^2} - \frac{c}{(n_1^2 + 2)^2}\right]$$

The subscript refers to the solvent, N is Avogadro's number, T is the temperature in K, M is the molecular weight in grams, ρ is the density in g/cm^3, ξ is the measured dielectric constant, and n is the refractive index. The parameters a and c are determined by assuming that the solution dielectric constant and refractive index vary linearly with mole fraction of the solute X_2 for dilute solutions, as

$$\xi_{solution} = \xi_1 + aX_2$$

$$n^2_{solution} = n_1^2 + cX_2$$

The complete dielectric constant data for the three compounds are compiled in Table 1.

Excited state dipole moments

The apparatus used for the μ_e determination has been described in detail elsewhere (14). The value of the effective external field F_{ext} is 3.768 × 10^4 V/cm for each molecule. The externally applied field was converted to an internal field by using the spherical cavity approximation (18), given by

$$F_{int} = F_{ext}\,\frac{3\xi}{2\xi + 1}$$

where ξ is the dielectric constant of the solvent. Since dioxane (ξ = 2.209) was used as solvent in the electric field experiment F_{int} = 1.224 F_{ext}.

For each molecule the electric field signals were collected at three different values of χ and for several wavelengths λ within the absorption band of interest. The experimentally obtained $\Delta\epsilon$, which is obtained from the equation

TABLE 2. Heteroatom parameters used in the HMO calculation

H_{ii}	H_{ij}
$N(NMe_2) = 0.95$	$C—N(C—NMe_2) = 0.8$
$N(C\equiv N) = 0.5$	$C\equiv N = 1.66$

TABLE 3. Molecular parameters obtained from theoretical calculations

θ^a	μ_g	$\Delta\mu$	μ_e	M^b	γ^c
0	3.9	9.9	13.9	M_z	0
45	2.8	10.4	13.1	M_z	0
90	1.6	18.9	20.5	—	—

[a]Angle between the dimethylamino group and the benzene ring.
[b]Transition moment direction.
[c]Angle between the transition moment and dipole moment vectors.

$$\Delta\epsilon = -\frac{1}{2.303cl}\frac{\Delta I}{I}$$

where ΔI is the difference in the transmitted light intensities in the presence and absence of the electric field, I is the transmitted light intensity in absence of the electric field, c is the concentration, and l is the path length of the electric field cell, was least-squares-fitted with the derivative terms, as shown in eq [1], to obtain the values of A_χ, B_χ, and C_χ. The contribution from the second derivative term (see eq. [1]) to the electric field signal was found to be very small, as observed for several other polar molecule (14, 19). Therefore this term has been neglected in the regression analysis. Finally, the molecular parameters were calculated from the slopes and intercepts of least-squares plots of A_χ and B_χ versus $(3\cos^2\chi - 1)$.

No correction was made for the effect of dipole reaction field or for the contribution of molecular polarizability to the electric field signal in the calculation of dipole moment parameters. Since these will be approximately of the same order of magnitude for each molecule studied here, direct comparison of their dipolar character will not be subject to serious error due to lack of the above corrections. In fact, a more detailed investigation on similar molecules shows that polarizability effects can be neglected as compared to dipole moments (20). Furthermore, recent electric field measurements comparing the gas phase and solution phase results on similar molecules show that the combined error due to lack of the above corrections amounts to less than 10% (21).

Theoretical calculations

The basic Hückel molecular orbital method was modified empirically as described earlier (14). The Coulomb integral H_{ii} and the bond integral H_{ij} terms used for heteroatoms, obtained after empirical modification, are given in Table 2. For the aromatic ring, standard values of H_{ii} and H_{ij} were used unmodified. The electron density distribution in the HOMO was used to calculate the ground state dipole moments. Excited state dipole moments were calculated by promoting one electron from the HOMO to the LUMO and recalculating the q_i terms. The calculated dipole moments are shown in Table 3. In addition, the symmetries of the calculated HOMO and LUMO could be used to predict the directions of the transition moments.

Results

The electric field signals for DMABN and TMABN at polarization angle $\chi = 0$ are shown in Fig. 1. The continuous lines in these figures were computed from the least-squares values of A_χ and B_χ using eq. [1]. The excellent agreement between the observed and calculated electric field spectrum suggests that eq. [1] adequately describes the field-induced changes in the absorption spectrum. The molecular parameters obtained from electric field experiments are compiled in Table 4. The dipole moment values reported from electro-optical emission measurements by Baumann and co-workers (20*b*, 22) are also shown in Table 4 for the sake of comparison.

The intensity of the strong charge transfer (CT) transition of DMABN (λ_{max} = 290 mm; ϵ = 26 870) was found to decrease significantly with a simultaneous red shift in the long wavelength absorption maxima upon twisting the C—NMe_2 bond by substituting the methyl group(s) at the *ortho* positions. Similar observations have also been reported for the *N*,*N*-dimethyl-4-nitroaniline system (19*b*). For DMMBN and TMABN the absorption maxima and the ϵ values are, respectively, 286 nm; 12 900 and 310 nm; 3450. Substitution of methyl group(s) at the 2 and 6 positions, as in TMABN, results in a ground state configuration where the -NMe_2 group lies in a plane that is twisted nearly 80° with respect to the phenyl plane (23). This angle would be close to 90° in the solution phase because of minimum steric repulsion. In the case of DMMBN, where only one *ortho* methyl group is substituted, this angle has been predicted to be nearly 40° (24), which is intermediate between 0° (DMABN) and 90° (TMABN) twist. The gradual decrease in the intensity of CT absorption upon increasing the twist angle could be explained on the basis of orbital decoupling of donor (D) and acceptor (A) groups, which inhibits the mixing of CT and LE (locally elicited) wave functions, consequently affecting the oscillator strength of the CT transition.

Further evidence for such decoupling comes from the μ_g values (see Tables 1, 3, and 4). Maximum resonance interaction in the planar form, where the D and A groups have maximum overlap of molecular orbitals, is the main reason for the high μ_g values observed for such systems. As a result, in such systems, μ_g generally exceeds the value predicted by the addition of corresponding group moments of the substituents. The μ_g values obtained by dielectric measurements, as shown in Table 1, indicate that μ_g decreases as the twisting angle increases. This behaviour is expected, since the contribution of ionic forms to the molecular wave functions in the HOMO will be maximum in the planar form (DMABN) and minimum for the perpendicular form (TMABN). This is also reflected in the calculated μ_g's obtained by the HMO method (see Table 3).

Assuming that these molecules belong to point groups of C_{2v} symmetry, which seems to be valid for DMABN and TMABN, the μ_g can be calculated from eq. [2]. This is because the dipole moment and the transition moment vectors must be either parallel or perpendicular in such a case. The μ_g values obtained by electrochromic measurements also manifest a similar trend (see Table 4); however, the magnitudes are smaller than those obtained from dielectric method. This discrepancy could be due to the uncertainty in the transition moment direction with respect to the dipole moment. However, a similar calculation done by Varma and co-workers using Baumann's experimental data shows better agreement in the μ_g's in the case of DMABN (25). The difference between the μ_g reported here and that by Varma for DMABN using the same method is nearly

Can. J. Chem. Downloaded from www.nrcresearchpress.com by 109.225.110.28 on 09/08/12
For personal use only.

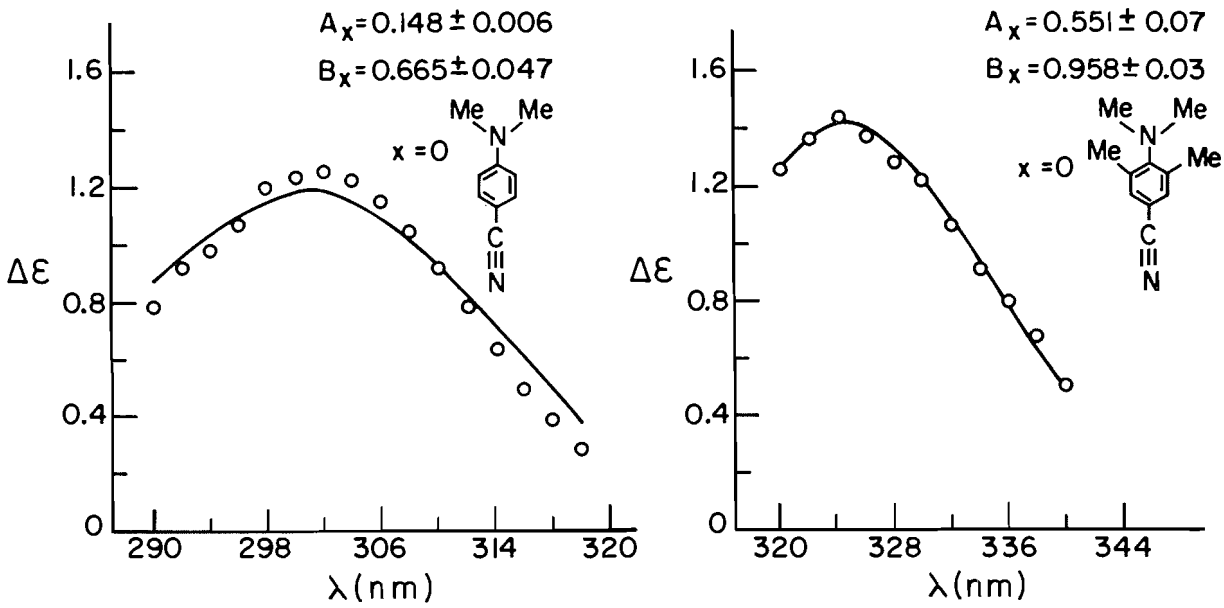

FIG. 1. Electric field spectra of DMABN and TMABN ($\chi = 0$) in dioxane solution at 298 K.

TABLE 4. Molecular parameters obtained from electric field study

Compound	μ_g[a]	$\Delta\mu \cdot \mu_g$	$\Delta\mu$	μ_e(FC)	γ
DMABN	4.5 ± 0.5	29.8 ± 2	4.8 ± 0.5	11.0 ± 0.5 (11.2,[b] 16.2[c])	0
DMMBN	2.9 ± 0.4	34.8 ± 2	6.8 ± 0.6	11.9 ± 0.6 (10.7)[c]	0
TMABN	2.8 ± 0.5	42.1 ± 2	10.0 ± 0.5	14.5 ± 0.6 (15.2)[c]	0

[a]Obtained by assuming the $\hat{p}$ and μ_g are parallel (see eq 2).
[b]Obtained by electrochromism on the *b*-fluorescence band (S_1(sr) state) (see ref. 1*b*).
[c]Obtained by electrochromism on the *a*-fluorescence band (S_1(tict:sr) state) (see refs, 1*b*, 20*b* and 24). The μ_e value of DMMBN reported by Rotkiewicz (24) may have a large error due to strong overlap of *a*- and *b*-fluorescence.

5×10^{-30} C · m, which could arise due to the experimental uncertainties. This observation of decrease of dipole moment on deconjugation is in line with the generally accepted *maximum overlap rule*, which has always been understood to be the necessary condition for maximum charge transfer to occur.

However, μ_e values obtained by electrochromic measurements show a dramatically reversed trend (see Table 4). Similar results have also been reported from electro-optical fluorescence measurements (20). For example, the $\Delta\mu$ value, which is an absolute measure of the change in the charge distribution due to electronic excitation, reveals that CT is at a maximum when the orbitals involved are orthogonally positioned. Furthermore, comparison of values of $\Delta\mu$'s for the three compounds, where the twist angle is varied systematically, suggests that the extent of charge transfer in the excited state is directly related to the twist angle of the C—NMe_2 bond with respect to the benzene ring.

In all three cases the dipole moment and the transition moment vectors are found to be nearly in the same direction, i.e., along the direction of the long molecular axis. This

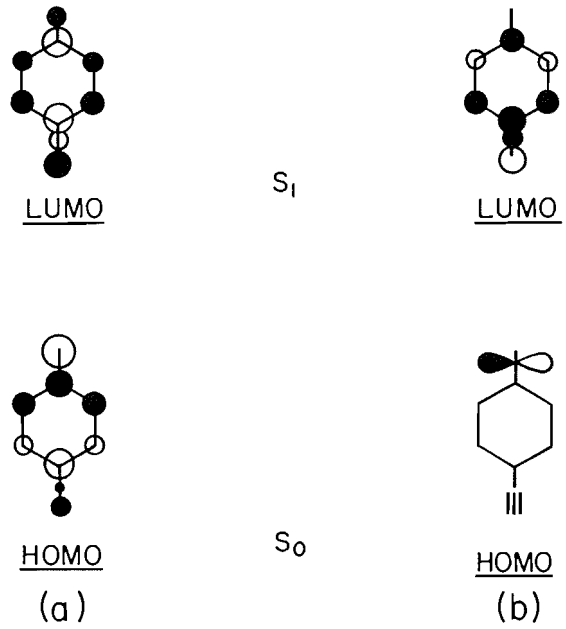

FIG. 2. Schematic drawings of the HOMO and LUMO of DMABN in both the planar (*a*) and perpendicular (*b*) conformations.

conclusion is made from the fact that for all three molecules the slope of A_χ vs. $(3\cos^2\chi - 1)$ plot was positive and large.

Even though a number of different types of semiempirical theoretical calculations have been reported, to rationalize the energetics of TICT formation (26), our attempt here employs a simple method to offer an explanation for the observed change in the dipole moments upon electronic excitation based on the molecular orbital diagram. The molecular orbital (MO) diagrams of planar and twisted DMABN systems are shown in Fig. 2. The symmetry characteristics of the HOMO and the LUMO obtained by this simple method are essentially the same as predicted by several other au-

Can. J. Chem. Downloaded from www.nrcresearchpress.com by 109.225.110.28 on 09/08/12
For personal use only.

Can. J. Chem. Downloaded from www.nrcresearchpress.com by 109.225.110.28 on 09/08/12
For personal use only.

thors (1*b*, 26), by adopting more sophisticated methods, such as PPP, CNDO, AM1, etc. It is apparent that the difference in the CT characteristics of the planar and twisted conformations arises primarily because of the specific localization of the HOMO and LUMO upon twisting the NMe_2 group. In the twisted conformation the electron density is completely localized on the NMe_2 group and the electronic excitation results in a LUMO where the charge localization is predominantly on the benzonitrile group. Therefore, electronic excitation results in extensive charge transfer from a pure -NMe_2 orbital to an antibonding orbital of the benzonitrile group. On the other hand, in the planar conformation both the HOMO and the LUMO have mixed character, where the charge is delocalized over the whole molecular skeleton. Hence the charge transfer upon electronic excitation is moderate. This is also indicated experimentally by a moderate change in the dipole moment upon electronic excitation. The calculated and the observed dipole moments (μ_g and $\Delta\mu$) essentially follow the same trend (see Tables 3 and 4).

As shown in Fig. 2, in the planar form the HOMO(b_2) to the LUMO(b_2) transition is A_1 type and hence, should be polarized along the M_z direction i.e., along the long molecular axis. However, other semiempirical methods that take into consideration configuration interaction (CI) predict that a B_1 type transition (M_x polarized), having a very low oscillator strength, will be the lowest energy transition and that the second transition is A_1 type with a very high oscillator strength (1*b*). The calculations also show that upon deconjugating the -NMe_2 group (twisted form) the ICT character of the ^1L_a state becomes more pronounced while the lowest energy transition becomes forbidden (A_2 type). This behaviour is also consistent with those predicted by other methods (1*b*, 26). It is worth pointing out that the simple calculations provide results that are very similar to those obtained by other theoretical methods, particularly in terms of the nature of the HOMO and the LUMO.

Discussion

The absorption and fluorescence characteristics of DMABN and TMABN can essentially be represented by the schematics shown in Fig. 3. The excitation of DMABN (initially planar) results in the normal fluorescence (F_b) from the state S_1(sr) (sr: solvent relaxed) and the second anomalous emission (F_a) originates from the state S_1(tict:sr) in polar solvents. From the solvent-dependent study (solvatochromism) it is evident that the intrinsic difference between these two emitting states is mainly in terms of polarity. This has also been directly identified by fluorescence electrochromic studies (20*b*, 22), which reveal that indeed the S_1(tict:sr) state is significantly more polar (16.2 D) than the S_1(sr) state (11.2 D). However, excitation of TMABN (initially nonplanar) results in direct population of the TICT state, and therefore only the band corresponding to F_a in DMABN is observed both in polar and nonpolar solvents (Fig. 3*b*). The observed μ_e ($\approx$15 D) from electrochromic fluorescence measurements also reflects a magnitude similar to that observed for the S_1 (tict:sr) state of DMABN. These observations provide clear evidence for the fact that F_a originates from a geometry that is twisted in the excited state and has a large intramolecular charge transfer character.

However, what is still ambiguous is the question of how the role of solvent can be defined in creating the TICT state

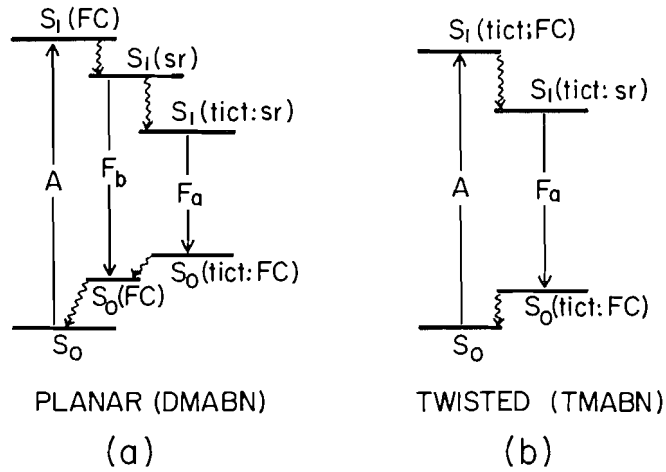

FIG. 3. Schematic representations of the absorption and fluorescence processes in planar and sterically hindered (twisted) conformations of DMABN showing the origin of the normal (F_b) and anomalous (F_a) fluorescence. (*a*) In planar DMABN, absorption of photons results in a planar Franck–Condon excited state (S_1(FC)). Emissions F_b and F_a occur from a solvent-relaxed planar excited state (S_1(sr)) and a solvent-relaxed twisted excited state (S_1(tict:sr)) respectively to give a FC ground state having a planar geometry (S_0(FC)) and a FC ground state having twisted geometry (S_0(tict:FC)). (*b*) In twisted DMABN (TMABN), absorption of photons results in a twisted FC excited state (S_1(tict:FC)) and the only emission F_a occurs from a solvent-relaxed twisted excited state (S_1(tict:sr)).

from the planar molecule. Does it have a direct role or an indirect one? The fact that solvent plays a direct role comes from the following experiments. Experimental studies on DMABN in a supersonic jet expansion show that isolated molecules show only F_b fluorescence and hence do not undergo twisting (6). Further evidence from spectroscopic and picosecond studies indicates that a short-range coupling interaction between a specific number of solvent molecules and the solute, either in the ground or exited state, is essential for TICT formation (4*e*, 5).

On the other hand, the fact that solvent does not play a major role can be argued on the basis of the fact that excitation of TMABN in a supersonic jet expansion gives prompt TICT emission even in the absence of the solvent (7). Furthermore, recent time-resolved emission studies to determine the electron transfer rate in DMABN indicate that the dominant contribution to the electron transfer rate comes from the fluctuation in intramolecular degrees of freedom and solvent fluctuation seems to play a minor role, though this seems to depend on the nature of the solvent (8).

Our results on experimental dipole moments may be considered as a method of resolving the above question and provide additional insight into the TICT concept. Since the measurements were done on the absorption spectrum, here we deal only with the Franck–Condon (FC) excited state. This is unlike the electro-optical fluorescence studies, which investigate the solvent-relaxed excited state, where all information concerning the transition from the S_1(FC) to the S_1(tict) state may be lost. In the FC excited state one would expect that the surrounding medium would be in the same arrangement as in the solvent-equilibrated ground state. Therefore, the solvent fluctuation mode, which would contribute to fluorescence electrochromic measurements, will not be of concern here.

Can. J. Chem. Downloaded from www.nrcresearchpress.com by 109.225.110.28 on 09/08/12
For personal use only.

The three model molecules studied here have different torsional angles between the -NMe_2 group and the phenyl ring, which range from 0° in the case of DMABN to nearly 80° in the case of TMABN. It can be clearly seen from Table 4 that as the torsional angle increases μ_g decreases, whereas $\Delta\mu$ and μ_e increase significantly. These dipole moments are a direct measure of the charge transfer. Since the solvent system remains the same, it can be concluded that it is the torsional angle which directly influences $\Delta\mu$. This observation is in agreement with the gas phase measurements, which clearly indicate that CT in the excited state is linked to the twisting of the phenyl–dimethylamino bond (6, 7).

Since the charge separation can be directly achieved in the vertical excited state it could be termed a sudden polarization, as indicated earlier by Salem (27). It is also clear that sudden polarization is more effective when the orbitals involved in charge transfer are totally decoupled. A direct comparison between our results and those from fluorescence electrochromism measurements (see Table 4) indicates that the solvent relaxation around the excited state dipole does not drastically affect the magnitude of charge transfer. In fact, within experimental uncertainty, μ_e(FC $\approx$ μ_e(sr) and μ_e(tict: FC) $\approx$ μ_e(tict: sr).

These results seem to provide a clear picture in regard to the role of the solvent in the TICT formation in DMABN. Since the charge transfer, as evident from $\Delta\mu$ and μ_e, is induced by twisting, it is not unreasonable to conclude that a polar solvent induces twisting motion by affecting the intramolecular degrees of freedom, and the result of such twisting motion is extensive charge transfer. Our explanation is in accord with those results reported by Su and Simon based on time-dependent spectroscopic studies (5), in which they suggested that fluctuations in the sorrounding solvent polarization may not play a dominant role in the rate of electron transfer in DMABN and the main contribution to the rate comes from the fluctuations in intramolecular vibrational coordinates. These results were interpreted in terms of the dynamical electron transfer theories of Nadler and Marcus (28), which address the influence of fluctuations in both solvent polarization and intramolecular vibrational coordinates on the rate of electron transfer. We would stress that this is different from solvent-induced charge transfer, where the solvent is directly involved, i.e., in cases where the rate of electron transfer correlates directly with the inverse of longitudinal relaxation time of the solvent (29). Since, μ_e(FC) is different from μ_e(tict), the TICT state should continuously evolve along the solvent relaxation coordinate in DMABN, which would be the prime reason for the time-dependent shift in the emission spectrum. Finally, the charge-separated species will be further stabilized by strong electrostatic interaction with the solvent, which would account for the strong solvent dependency of the emission spectrum of DMABN. This explanation also fits well with the recent theoretical model by Schenter and Duke, which was used to simulate the twisting dynamics of DMABN in polar solvent (30). In the case of TMABN, the TICT state charge distribution is directly produced in the FC excited state and then it responds to the electrostatic interaction with solvent. This phenomenon is strongly corroborated by the results obtained by Baumann and co-workers (20, 22). The strong solvent-dependent dipole moment obtained by electro-optical emission studies (20) can only be explained on the basis of a solvent-polarity-dependent average torsional angle around the phenyl to dimethylamino group bond since the magnitude of induced dipole moment has been found to be very small. Their results show excellent agreement with the results reported here.

It is very apparent from these results that the disturbance in the intramolecular degrees of freedom, which results in twisting, comes as a result of coupling of polar solvent molecules with the DMABN. *The solvent coupling is essential for the twisting motion and twisting is the requirement for strong charge transfer*. This explanation provides a consistent picture that the TICT state originates from a conformation where the -NMe_2 group is forced into a position nearly orthogonal to the phenyl plane.

The theoretical results reported here are almost parallel to those predicted by other methods, except for the fact that our approach is very simple. The dipole moments calculated are in fair to good agreement with the observed values and show similar trends. These values, combined with those recently obtained for several nitroaromatics (14*b*, 19*b*,*c*) suggest that this method can be used as a tool in predicting the charge transfer behaviour of molecules both in the ground and excited states. The difference in the charge transfer nature of the planar and twisted systems is a reflection of the nature of the HOMO and LUMO involved in the electronic transition. This can be seen from the fact that charge transfer can be directly related to the ionization potential (IP) and electron affinity (EA), whose values are dependent upon the nature of the HOMO and LUMO respectively (19*b*). A change in these values, which can be produced by deconjugating the functional groups, makes a direct impact on the charge transfer characteristics.

Acknowledgement

We are grateful to the Natural Sciences and Engineering Research Council of Canada (NSERC) for continued financial support.

1. (*a*) K. Rotkiewicz, K. H. Grellman, and Z. R. Grabowski. Chem. Phys. Lett. **19**, 315 (1973); (*b*) Z. R. Grabowski, K. Rotkiewicz, A. Siemiarczuk, D. J. Cowley, and W. Baumann, Nouv. J. Chim. **3**, 443 (1979); (*c*) Z. R. Grabowski, and J. Dobkowski. Pure Appl. Chem. **55**, 245 (1983); (*d*) W. Rettig, Angew. Chem. Int. Ed. Engl. **25**, 971 (1986); (*e*) K. Rotkiewicz, W. Rubaszewska. J. Lumin. **27**, 221 (1982); (*f*) D. Huppert, S. D. Rand, P. M. Rentzepis, P. F. Barbara, W. S. Struve, and Z. R. Grabowski. J. Chem. Phys. **75**, 5714 (1981); (*g*) F. Heisel, and J. A. Miehe. Chem. Phys. **98**, 233 (1985); (*h*) W. Rettig. Appl. Phys. B: **B45**, 145 (1988); (*i*) Y. Wang, M. McAuliffe, F. Novak, and K. B. Eisenthal. J. Phys. Chem. **85**, 3736 (1981); (*j*) E. Lippert, W. Rettig, B. Bonacic-Koutecky, F. Heisel, and J. A. Miehe. Adv. Chem. Phys. **68**, 1 (1987); (*k*) K. Rotkiewicz, H. Leismann, and W. Rettig. J. Photochem. Photobiol. **49**, 347 (1989).
2. E. Lippert, W. Lüder, and H. Boos. *In* Advances in molecular spectroscopy. *Edited by* A. Mangini, Pergamon, Oxford. 1962. p. 443.
3. Z. R. Grabowski, K. Rotkiewicz, W. Rubaszewska, and E. Kirkor-Kaminska. Acta Phys. Pol. A, **A54**, 767 (1978).
4. (*a*) R. J. Visser, and C. A. G. O. Varma. J. Chem. Soc. Faraday Trans. 2, **76**, 453 (1980); (*b*) R. J. Visser, C. A. G. O. Varma, J. Konijnenberg, and P. Bergwerf. J. Chem. Soc. Faraday Trans. 2, **79**, 347 (1983); (*c*) R. J. Visser, P. C. M. Weisenborn, and C. A. G. O. Varma. Chem. Phys. Lett. **104**, 38 (1984); (*d*) R. J. Visser, P. C. M. Weisenborn, J. Konijnenberg, B. H. Huizer, and C. A. G. O. Varma. J.

Photochem. **32**, 217 (1986); (*e*) C. Cazeau-Dubroca, S. Ait Lyazidi, P. Cambou, A. Peirigua, Ph. Cazeau, and M. Pesquer. J. Phys. Chem. **93**, 2347 (1989).
5. (*a*) Y. Wang, and K. B. Eisenthal. J. Chem. Phys. **77**, 6076 (1982); (*b*) J. Hicks, M. Vandersall, Z. Babarogic, and K. B. Eisenthal. Chem. Phys. Lett. **116**, 18 (1985); (*c*) J. M. Hicks, M. T. Vandersall, E. V. Sitzmann, and K. B. Eisenthal. Chem. Phys. Lett. **135**, 413 (1987).
6. (*a*) L. W. Peng, M. Dantus, A. H. Zewail, K. Kemnitz, J. M. Hicks, and K. B. Eisenthal. J. Phys. Chem. **91**, 6162 (1987); (*b*) E. M. Gibson, A. C. Jones, and D. Phillips. Chem. Phys. Lett. **136**, 454 (1987).
7. T. Kobayashi, M. Futakami, and O. Kajimoto. Chem. Phys. Lett. **141**, 450 (1987).
8. S-G. Su and J. D. Simon. J. Chem. Phys. **89**, 908 (1988).
9. (*a*) N. G. Bakhshiev, V. I. Knyazhanskii, V. I. Minkin, O. A. Osipov, and V. G. Saidov. Russ. Chem. Rev. **38**, 740 (1969); (*b*) W. Liptay. *In* Excited states. *Edited by* E. C. Lim. Academic Press, New York. 1974. p. 129.
10. (*a*) W. Baumann and H. Decker. Ber. Bunsen-ges. Phys. Chem. **81**, 786 (1977); (*b*) W. Baumann and H. J. Bischof. J. Mol. Struct. **84**, 181 (1982); (*c*) W. Baumann, F. Petzke, and K. D. Loosen. Z. Naturforsch. **34a**, 1070 (1979); (*d*) R. Mathies, and A. C. Albretch. J. Chem. Phys. **60**, 2500 (1974); (*e*) W. Liptay, R. Wortman, H. Schaffrin, O. Burkhard, W. Reitinger, and N. Detzer. Chem. Phys. **120**, 429 (1988).
11. H. Labhart, Chimia, **15**, 20 (1961); Helv. Chim. Acta, **44**, 447 (1961).
12. J. Czekalla. Chimia, **15**, 26 (1961); J. Czekalla and G. Wick. Ber. Bunsen-ges. Phys. Chem. **65**, 727 (1961).
13. W. Liptay, and J. Czekalla. Z. Naturforsch. **15a**, 1072 (1960); Ber. Bunsen-ges. Phys. Chem. **65**, 721 (1961).
14. H. K. Sinha, P. C. P. Thomson, and K. Yates. Can. J. Chem. **68**, 1507 (1990); H. K. Sinha and K. Yates. J. Chem. Phys. **93**, 7085 (1990).
15. B. M. Wepster. Recl. Trav. Chim. Pays-Bas, **76**, 357 (1957).
16. E. A. Guggenheim. Trans. Faraday Soc. **45**, 714 (1950).
17. J. W. Smith. Trans. Faraday Soc. **46**, 394 (1950).
18. C. J. F. Böttcher. *In* Theory of electric polarization. Vols. 1 and 2. Elsevier, Amsterdam. 1973.
19. (*a*) W. Liptay, W. Eberlein, H. Weidenberg, and O. Elflein. Ber. Bunsen-ges. Phys. Chem. **71**, 548 (1967); (*b*) H. K. Sinha and K. Yates. Can. J. Chem. **69**, 550 (1991); (*c*) J. Am. Chem. Soc. **110**, 6062 (1991).
20. (*a*) H. Bischof, W. Baumann, N. Detzer, and K. Rotkiewicz. Chem. Phys. Lett. **116**, 180 (1985); (*b*) C. Brittinger, A. K. Maiti, W. Baumann, and N. Detzer, Z. Naturforsch. **45a**, 883 (1990).
21. A. Kriebel and H. Labhart. Z. Phys. Chem. (Frankfurt am Main), **92**, 247 (1974).
22. W. Baumann. Z. Naturforsch. **36a**, 868 (1981).
23. H. Albrecht, E. O. Duber, J. Epsztajn, and R. M. K. Marcinkowski. Tetrahedron, **40**, 1157 (1984).
24. K. Rotkiewicz. Spectrochim. Acta, **42A**, 575 (1986).
25. R. J. Visser, P. C. M. Weisenborn, C. A. G. O. Varma, M. P. De Hass, and J. M. Warman. J. Mol. Struct. **104**, 38 (1984).
26. D. J. Cowley and A. J. Peoples. J. Chem. Soc. Chem. Commun. 352 (1977); W. Rettig and V. Bonacic-Koutecky. Chem. Phys. Lett. **62**, 115 (1979); J. P. LaFemina, C. B. Duke, and A. J. Paton. Chem. Phys. **87**, 2 151 (1987); P. Ertl. Collect. Czech. Chem. Commun. **55**, 1891 (1990).
27. L. Salem. Acc. Chem. Res. **12**, 87 (1979).
28. W. Nadler and R. A. Marcus. J. Chem. Phys. **86**, 3906 (1987).
29. E. M. Kosower, H. Dodiuk, K. Tanizawa, M. Ottolenghi, and N. Orbach. J. Am. Chem. Soc. **97**, 2167 (1975).
30. G. K. Schenter and C. B. Duke. Chem. Phys. Lett. **176**, 563 (1991).

Can. J. Chem. Downloaded from www.nrcresearchpress.com by 109.225.110.28 on 09/08/12
For personal use only.

Stereocontrolled synthesis of optically active 14β-hydroxy steroids and other steroid derivatives

RÉJEAN RUEL AND PIERRE DESLONGCHAMPS[1]

Laboratoire de synthèse organique, Département de chimie, Faculté des sciences, Université de Sherbrooke, Sherbrooke (Québec), Canada J1K 2R1

Received January 2, 1992

RÉJEAN RUEL and PIERRE DESLONGCHAMPS. Can. J. Chem. **70**, 1939 (1992).

The synthesis of optically active 14β-hydroxy steroids via base-catalyzed reactions is reported.

RÉJEAN RUEL et PIERRE DESLONGCHAMPS. Can J. Chem **70**, 1939 (1992).

On décrit la synthèse de stéroïdes 14β-hydroxylés optiquement actifs via des réactions catalysées par des bases.

Can. J. Chem. Downloaded from www.nrcresearchpress.com by 109.225.110.28 on 09/08/12
For personal use only.

Introduction

Steroidal cardiotonic glycosides are of considerable importance in the treatment of heart disease (1, 2). However, the naturally occurring cardenolides show a rather narrow margin of safety as most patients receive 60% of the toxic dose (3). Cardenolides have thus stimulated several structural (4) and synthetic (5, 6) studies. In most synthetic studies, steroidal starting materials were employed (5) while in others (6), the construction of the skeleton was carried out by total synthesis via an intramolecular aldol addition of ABD tricyclic compounds. In the last approach, the tricyclic aldol precursors used were all synthesized via a modification of the original Torgov sequence (7).

An original report from our laboratories described the one-step stereocontrolled synthesis of 14α-hydroxy steroid **3** (Scheme 1) via a new polycyclization method (8). Anionic cycloaddition of 2-carbomethoxycyclohex-2-en-1-one (**1**) and cyclopentane-1,3-dione β-ketoester **2** first gave enolate **4** bearing three new stereocontrolled centers (9). This enolate was then trapped *in situ* to give tetracyclic compound **5** which gave 14α-hydroxy steroid **3** after selective decarboxylation. Further investigations allowed us to find two ways to correct the stereochemistries of the C13 and C14 carbon centers into the more desired 13β-methyl 14β-hydroxy configuration. The first way involved aldol addition of dienol **6** that gave a 3:2 mixture of steroids **7** and **8** as previously described in this journal (10). We also synthesized optically active 14β-hydroxy steroid **11** from anionic cycloaddition of chiral precursors **9** and **10***a* (11). This account describes the detailed synthesis of (+)-methyl 17β-benzoyloxy-14β-hydroxy-3β-methylethenyl-1,7-dioxo-5β-androstan-19-oate (**11**) as well as other results observed in the synthesis of related compounds. Preliminary results indicating that optically active 14β-hydroxy steroids can be synthesized from achiral cyclopentane-1,3-dione β-ketoester **2** and chiral cyclohexenone **9** are also included.

Results and discussion

1. Synthesis of substituted Nazarov reagents ***10****a and* ***10****b*

The synthesis of the requisite chiral substituted Nazarov reagent **10***a* (R = COPh) is depicted in Scheme 2. The sequence was also applied to *tert*-butyl ether **10***b* (R = $C(CH_3)_3$). Ozonolysis (12) of chiral enone **12** (13) gave ketoacid **13** in 71% yield. Selective borane reduction (14) of ketoacid **13** gave ketoalcohol **14** existing in solution as a 4:1 mixture of ketone-hemiketal forms. Diol **15***a* (**14***a*: **15***a*, 5.6:1) was also isolated from the reaction. This was obviously not a problem since the following oxidation step involving **14** and **15** gave the same desired ketoaldehyde **17**. Nevertheless, the absolute configuration assigned to the secondary carbinolic center in **15***a* was secured with the formation of its tribenzoylated derivative.

Dibenzoylation of diol **15***a* gave indeed tribenzoate **16**. The alternative *meso* structure was ruled out based on the following arguments. The methynes of the five-membered ring are not equivalent in the ^1H nmr spectrum and compound **16** is optically active ($[\alpha]_D^{25}$ +80.8 (*c* 1.3, $CHCl_3$)). Oxidation of the 5.6:1 mixture of alcohols **14** and **15** with pyridinium chlorochromate (15) then gave ketoaldehyde **17** in 50% yield from enone **12**. This aldehyde was treated with (formylmethylene)triphenylphosphorane (16) to give *trans* unsaturated aldehyde **18** along with traces of undesired *cis* isomer. The Reformatsky reagent of *tert*-butylbromoacetate was then added to unsaturated aldehyde **18** and the resulting diastereoisomeric allylic alcohols **19** were converted into the desired substituted Nazarov reagent **10** upon oxidation with manganese dioxide. Comparable yields for the transformation of enone **12** to β-ketoester **10** were obtained in both series (*a*, R = COPh and *b*, R = $C(CH_3)_3$) (25% overall).

2. Cycloadditions of 2-carbomethoxycyclohexenones with substituted Nazarov reagents

To compare the reactivity of substituted Nazarov reagents **10** with cyclopentanedione β-ketoester **2** (8), we first carried out the cycloaddition of *tert*-butyl ether **10***b* with 2-carbomethoxycyclohex-2-en-1-one (**1**) (Scheme 3). As will be evidenced by the following results, this model experiment clearly shows that, contrary to the case involving reagent **2**, polycyclization did not occur since no tetracyclic compound was obtained from the reaction. The reaction of precursors **1** and **10***b* with cesium carbonate in chloroform gave (after acid treatment that induced decarboxylation and cleavage of the *tert*-butyl ether) a ≈1:1 mixture of two diastereoisomers in 44% yield (two steps). One diastereoisomer has structure **20** whereas the other has the same absolute configuration around the five-membered ring, but with the opposite configuration at C5, C9, and C10. Upon oxidation with tetrapropylammonium perruthenate (17), this diastereoisomeric mixture led to racemic tetraketone **21** in 61% yield. Thus, while anionic cycloaddition of reagents **1** and **2** gave tetracyclic compound **5** (8), reaction of **1** and **10***b* did not yield directly any steroidal skeleton.

Cycloaddition of **1** and **10***b* generated enolate **22**, which,

[1]Author to whom correspondence may be addressed.

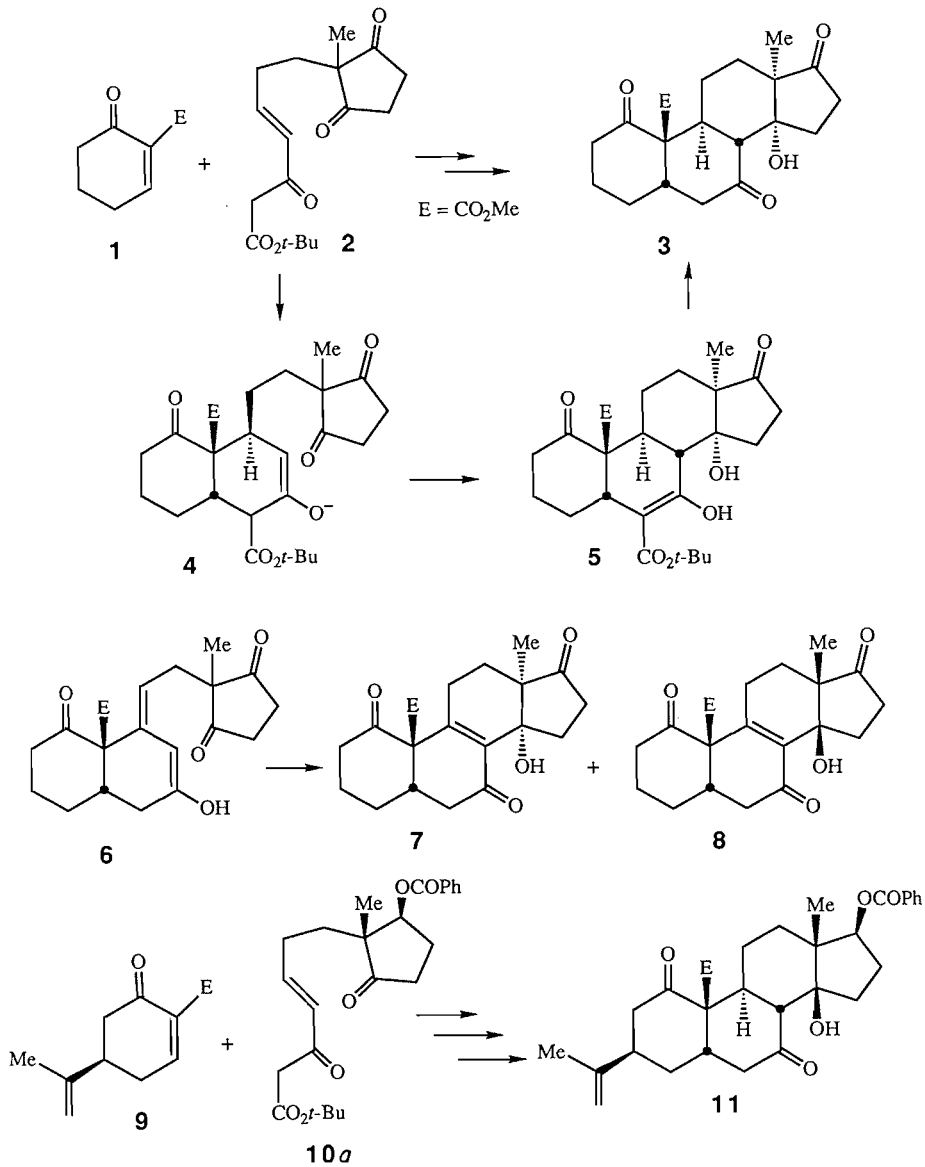

SCHEME 1

unlike enolate **4**, did not cyclize *in situ*, probably because isomerization to conjugated enolate **23** took place predominantly. Enolates related to **4** also failed to react in the polycyclization process as indicated by other results obtained in our laboratory (18).[2] The above results led us to reexamine the original polycyclization result (**1** + **2** → **5**). Although the direct formation of tetracyclic compound **5** was supported by strong spectroscopic arguments (19), these new results prompted us to find supplementary evidence. The crude compound obtained from cycloaddition of **1** and **2** was directly treated with sodium hydride and diethyl chlorophosphate in tetrahydrofuran (20, 21) to yield enol phosphate **24** in 76% yield (based on recovered starting material, see Experimental). Compound **5** was thus directly formed in a polycyclization process.

The chiral cyclohexenone **9** (Scheme 4), synthesized as previously described (18, 22), and compound **10***a* were treated with cesium carbonate in chloroform giving, after decarboxylation, triketone **25** (60% yield), which was obtained pure by chromatography. The cesium carbonate-catalyzed aldol condensation was then carried out in refluxing acetonitrile and produced 14β-hydroxy steroid **11** in 32% yield (47% based on recovered starting material). Although this reaction proceeded in low yield, it should be pointed out here that steroid **11** was the only new product formed in the aldol reaction we found to be at equilibrium. In fact, when the purified steroid **11** was resubmitted to the reaction conditions, a 1:1 mixture of compounds **25** and **11** was obtained. Structure **11** was secured by a single crystal X-ray analysis.[3]

Our next task then consisted in finding ways to improve the yield of the aldol reaction carried out on triketone **25**. All attempts to improve the yield by modifications of reaction conditions proved unsuccessful, but one case led to a very

[2]Also, C. Spino. Unpublished results. Université de Sherbrooke, 1990.

[3]M. Drouin and A. G. Michel. Structure determination to be submitted to Acta Crystallogr. Sect. C.

Can. J. Chem. Downloaded from www.nrcresearchpress.com by 109.225.110.28 on 09/08/12
For personal use only.

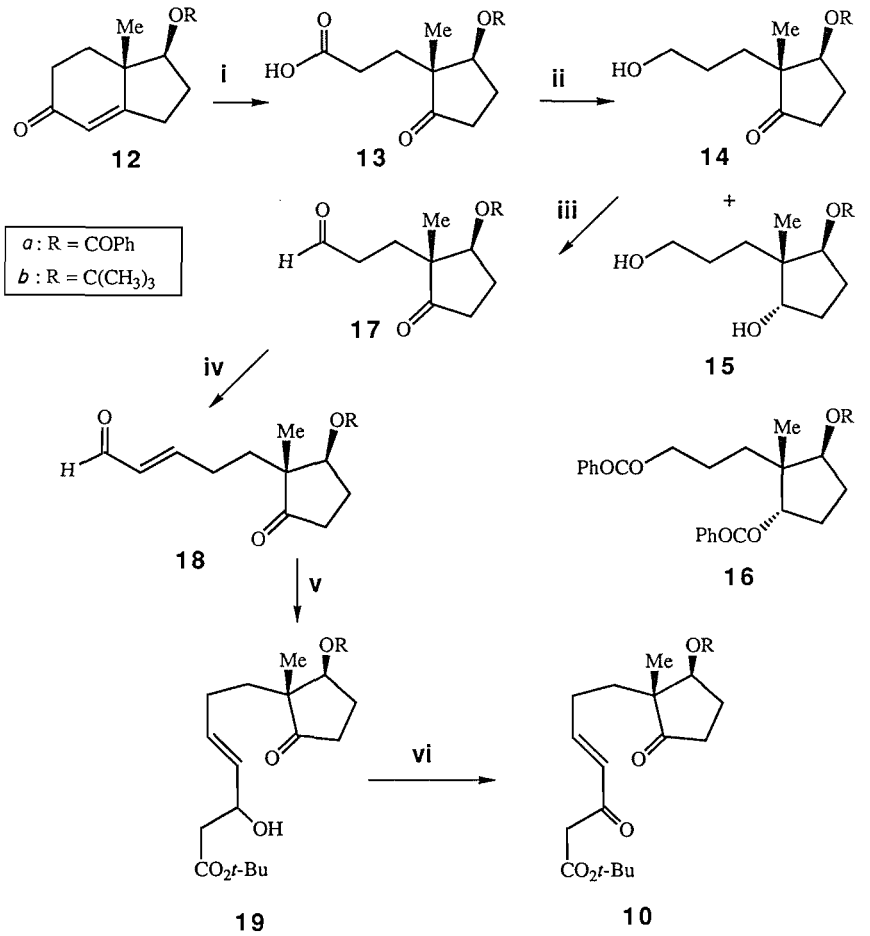

i: (1) O_3, MeOH, −78°C; (2) $NaIO_4$, H_2O; ii: $BH_3 \cdot THF$, THF; iii: PCC, CH_2Cl_2; iv: $Ph_3PCHCHO$, C_6H_6,Δ; v: $BrZnCH_2CO_2t$-Bu, THF; vi; MnO_2, AcOEt

SCHEME 2

interesting observation. Thus, warming a solution of potassium bis(trimethysilyl)amide and triketone **25** in tetrahydrofuran did not afford the expected *trans* (C8—C9) steroid **11**, but a new aldol product for which we have proposed structure **26** having the *cis* C8—C9 junction. Compound **26** was converted to **11** (Cs_2CO_3, CH_3CN, reflux) while dehydration under acidic conditions (PTSA, benzene, reflux) of both **11** and **26** gave the same compound **33** (Scheme 5). Also, compound **26** was further characterized through its conversion to the silyl ether derivative **27**. The implications of this observation on the aldol reaction transition state will be discussed in Sec. 3. To improve the yield of the aldol reaction, we also considered modifications on triketone **25**. Compounds **28** and **29** were then synthesized from benzoylated triketone **25**. Thus benzoate cleavage (MeONa, MeOH) gave alcohol **28** (73%), which afforded carbonate **29** (71%) upon treatment with phenyl chloroformate in pyridine. The cesium carbonate-catalyzed aldol condensation carried out on alcohol **28** gave diol **30** in low yield (30%). It was hoped that intramolecular hydrogen bonding between hydroxyl groups in **30** could eventually shift the equilibrium aldol reaction but starting material was again recovered as a result of the reversibility of this reaction. This idea was, however, the basis for the synthesis of carbonate **29**. Upon aldol condensation, the equilibrium reaction would hopefully be shifted through formation of six-membered ring carbonate **31**. Therefore, the cesium carbonate-catalyzed aldol condensation was then carried out on carbonate **29** and, as expected, starting material was totally consumed. However, six-membered ring carbonate **31** could not be isolated because of an elimination that gave allylic alcohol **32** (51%) and carbon dioxide.

Acid-catalyzed aldol condensation was also carried out on benzoate **25** and carbonate **29** (Scheme 5). Reaction of **25** and *p*-toluenesulfonic acid in refluxing benzene gave compound **33** in 77% yield. In this case, not only did dehydration occur but the C3 isopropenyl substituent also isomerized to the cyclohex-2-en-1-one **33**. Acid-catalyzed aldol condensation of carbonate **29** gave bis-enones **34** (74%) in a similar manner.

*3. Cycloaddition of chiral 2-carbomethoxycyclohexenone **9** with achiral substituted Nazarov reagent **2***
Application to the synthesis of 14β-hydroxy steroids

We described in Scheme 1 the one-step stereocontrolled construction of a 14α-hydroxy steroid from cycloaddition of compounds **1** and **2** (8). Our next goal was then to study the reactivity of chiral cyclohexenone **9** with achiral substituted Nazarov reagent **2**. Thus, a 1:1 mixture of tetraketone **35** and 14α-hydroxy steroid **36** (44% total yield, two steps) was obtained from selective decarboxylation of the cycloaddition product resulting from the reaction of precursors **2** and

Can. J. Chem. Downloaded from www.nrcresearchpress.com by 109.225.110.28 on 09/08/12
For personal use only.

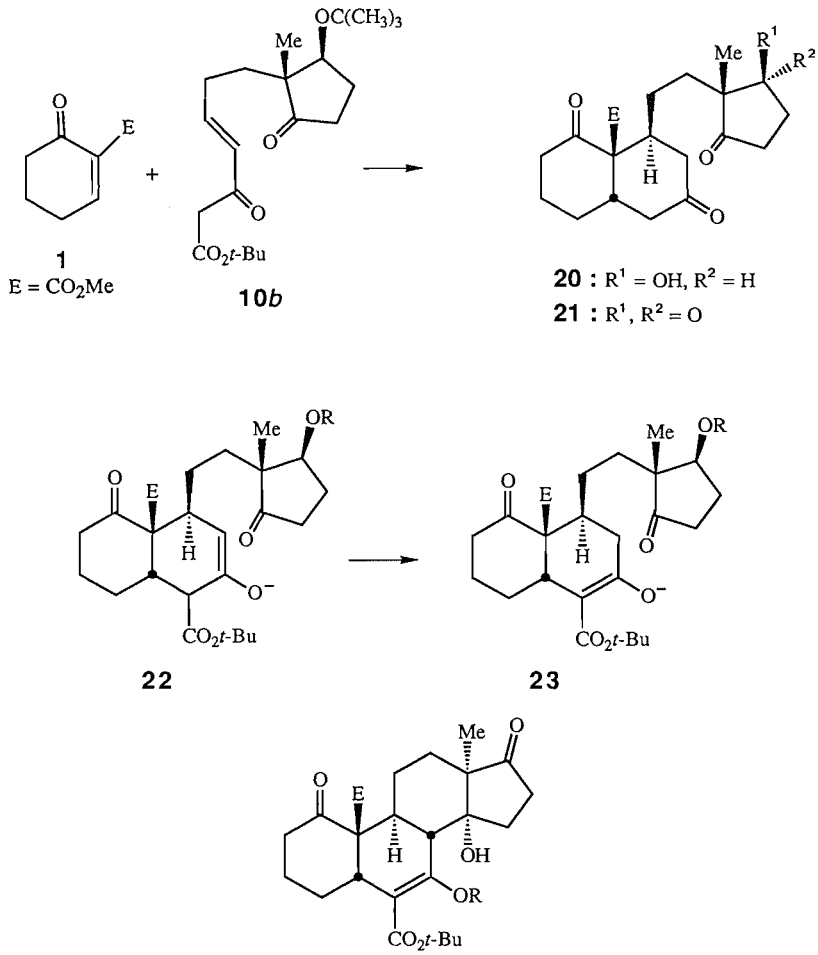

SCHEME 3

9 (Scheme 6). No tetraketone product (like **35**) was obtained in the previous reaction (**1** + **2** → **3**). This difference in reactivity might be explained on the following basis: as previously stated (8), tetracyclic compound **5** is likely to be formed from intermediate enolate **39** (Scheme 7); similarly, steroid **41** would arise from enolate **40** and decarboxylation of **41** would then give steroid **36**. The C3 isopropenyl substituent in **40** may, however, induce conformational change to **42**. If so, such conformational bias may then allow sufficient time for isomerization of the enolate to the more stable (C6—C7) position and a tetracyclic compound cannot be formed if such isomerization occurs.

With respect to the synthesis of 14β-hydroxy steroids, tricyclic compounds like **35** may be of considerable importance as suggested by the following preliminary results. Base-catalyzed aldol condensation (6) of tetraketone **35** gave 14β-hydroxy steroid **37** having a *cis* relationship between C8 and C9 carbon centers (Scheme 6). Equilibration of steroid **37** gave 14β-hydroxy steroid **38**. The structure of the latter compound was ascertained by chemical correlation since it was obtained from 14β-hydroxy steroid **11** by methanolysis and oxidation (see Experimental). Although the yield (29%) of the aldol condensation reaction (**35** → **37**) remains yet to be optimized, the synthesis of enantiomerically pure 14β-hydroxy steroid **37** (or **38**) is of interest since six new stereocenters were controlled starting from a single asymmetric center (i.e., **9** + **2** → **35** → **37**). Also, *cis* (C8—C9) isomer **37** could, like **26**, be effectively isolated. Compounds **26** and **37** were both showing a rather interesting characteristic in their ^{1}H nmr spectrum. They both displayed a doublet ($J \approx$ 2 Hz) for the tertiary alcohol, that usually stands as a singlet. A possible explanation for this is apparent considering the rigid structure **43** (Scheme 8). This phenomenon could originate from a W-type coupling between Hα at C15 and the hydroxyl group that would be involved in hydrogen bonding with the C7 carbonyl oxygen.

The formation of the *cis* B–C ring junction in products **26** and **37** must involve aldol addition on the β face of enolate **44**. Such aldol reaction would be precluded in the case of enolate **45** because of severe steric interactions involving the axial *tert*-butyl ester group (Scheme 8). Aldol addition on the β face of enolate **46** to give the *cis* B–C ring junction could also take place following stereoelectronic control requirements (23). However, the formation of *cis* B–C ring products **26** and **37** probably comes from the reaction on conformation **44** rather than **46**, because the resulting aldol

Can. J. Chem. Downloaded from www.nrcresearchpress.com by 109.225.110.28 on 09/08/12
For personal use only.

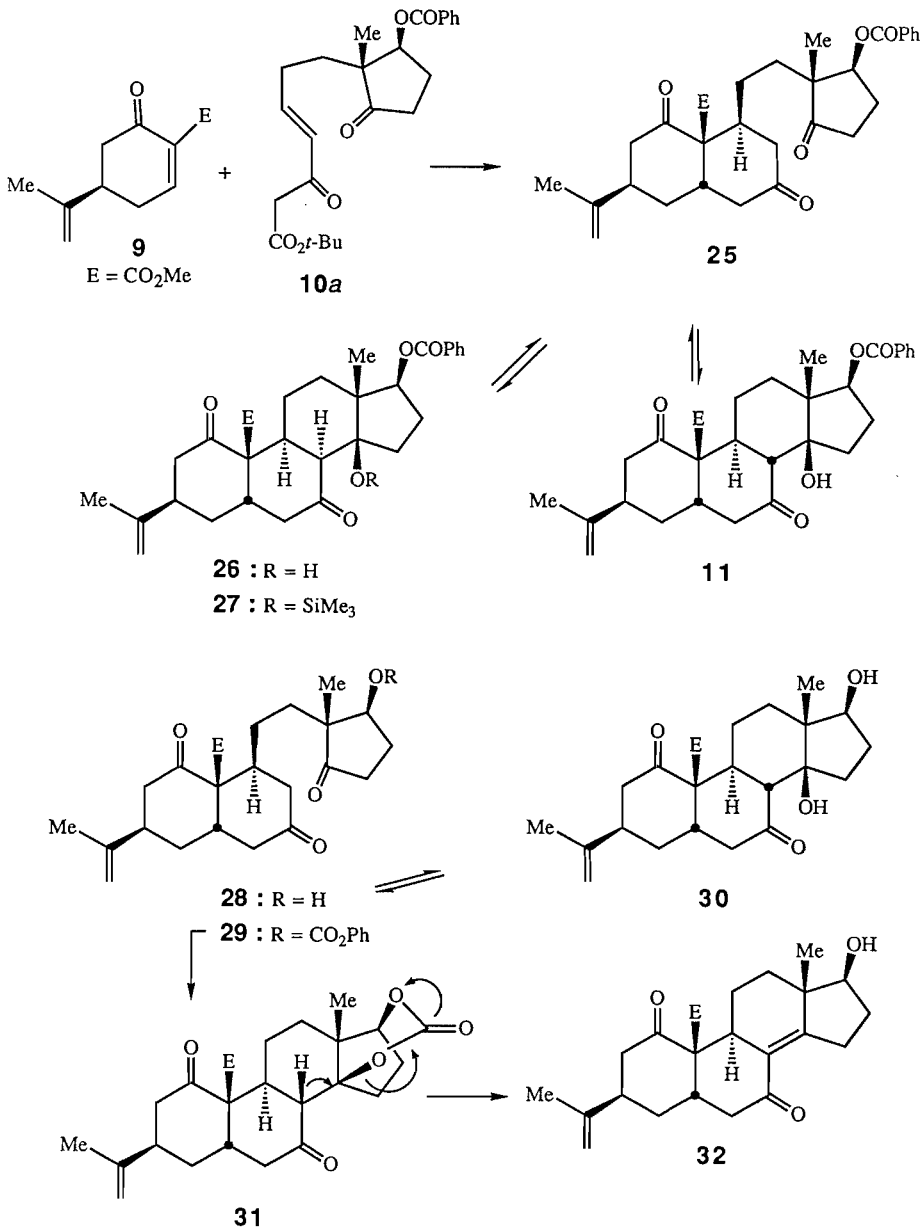

SCHEME 4

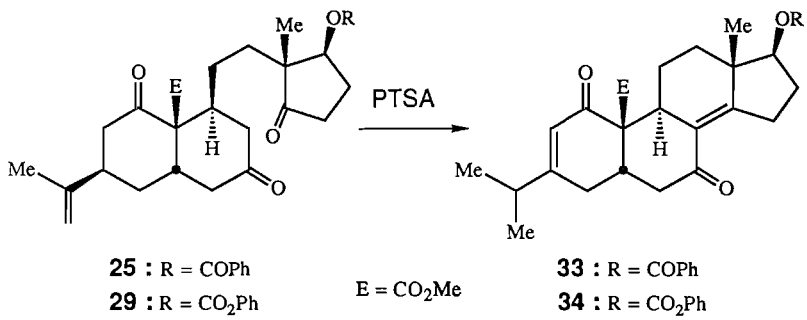

SCHEME 5

Can. J. Chem. Downloaded from www.nrcresearchpress.com by 109.225.110.28 on 09/08/12
For personal use only.

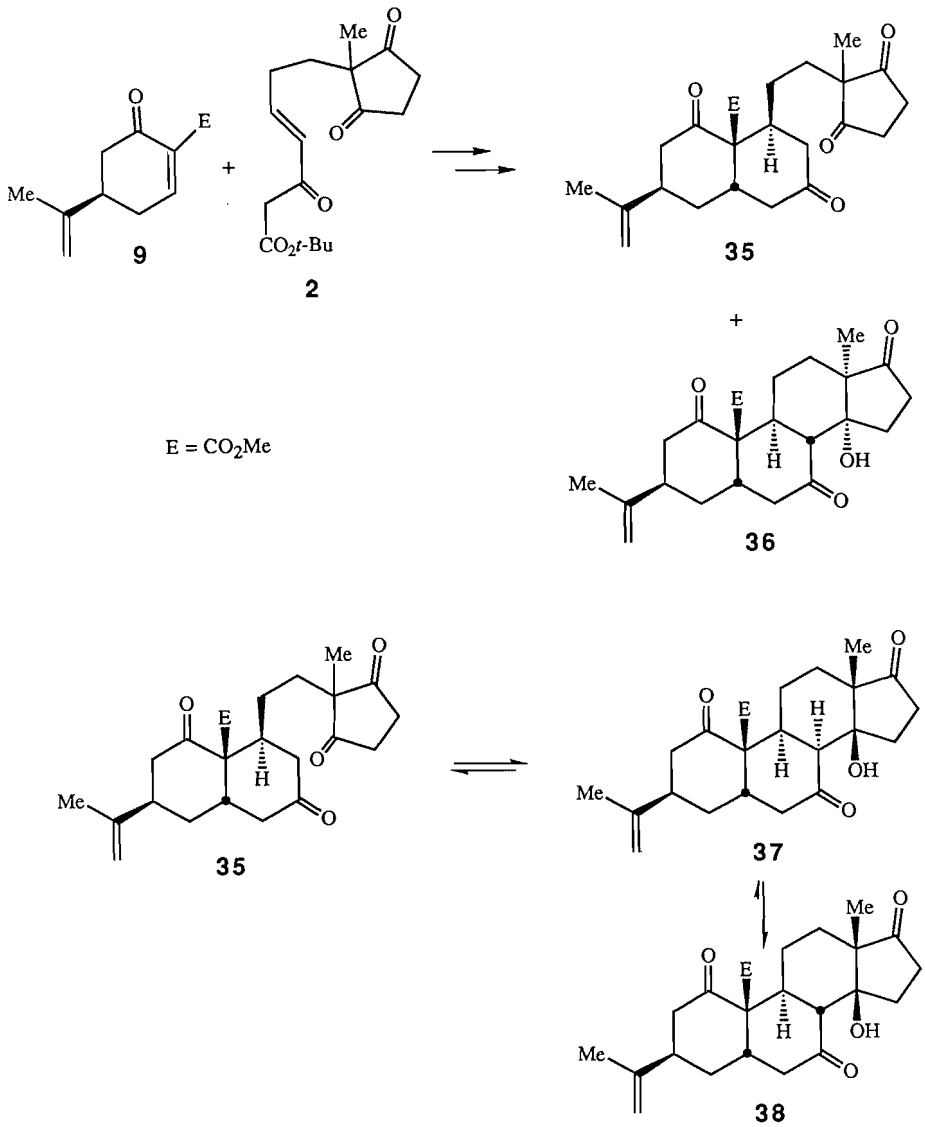

SCHEME 6

compound is produced having rings B and C in a chair conformation in the former case and in a boat conformation in the latter. In conclusion, the above considerations show that the stepwise synthesis of tetracyclic compounds **37** and **38** was by far more advantageous than the (synchronous) polycyclization leading to **41** (and **36** after decarboxylation) as only the former afforded 14β-hydroxy steroids.

Experimental

Melting points were determined on a Reichert Hot Stage apparatus and are uncorrected. Chromatographic separations were made using Merck Kieselgel 60 (230–400 mesh ASTM). The infrared (ir) spectra were taken on a Perkin–Elmer 681 spectrophotometer. Proton nuclear magnetic resonance (^{1}H nmr) and carbon (^{13}C nmr) spectra were recorded on a Bruker WM-250 instrument. Chemical shifts are reported in δ values relative to chloroform as internal standard. The following abbreviations have been used: s, singlet; d, doublet; t, triplet, dd, double doublets; m, multiplet; br, broad. Mass spectral assays were obtained using a VG Micromass ZAB-1F spectrometer. Optical rotation values ($[\alpha]_D$) were determined at 25°C in a 1-dm cell on a Perkin–Elmer 141-B polarimeter with chloroform as solvent. All reactions were carried out under an argon atmosphere unless otherwise noted.

*Ketoacid 13*a

Ozone is bubbled into a cold (−78°C) solution of enone **12***a* (10 g, 37.0 mmol) in methanol (200 mL) for 2.5 h (although the solution becomes bluish after 5 min, ozone bubbling is maintained until TLC analysis shows disappearance of starting material). Dimethyl sulfide (13.6 mL, 0.19 mol) is then added and the resulting yellow solution is stirred at room temperature for 12 h. Saturated sodium bicarbonate solution is then added until pH reaches 7 and the solution volume is reduced to 25% by evaporation under reduced pressure. Water (100 mL) and sodium periodate (9.0 g, 42.1 mmol) are added to the resulting mixture and the new mixture is vigorously stirred at room temperature for 2 h. The mixture is extracted with methylene chloride (5 × 100 mL) and the combined organic layers are washed with brine, dried ($MgSO_4$), filtered, and evaporated. The crude ketoacid **13***a* can be used without purification but pure material can be obtained by liquid–liquid extraction involving the carboxylic acid salt of **13***a*: 1 N sodium hydroxide solution (37 mL) is added at 0°C to the crude ketoacid **13***a* (10.7 g, 37 mmol) in methylene chloride. The separated aqueous layer is acidified (pH = 2) with hydrochloric acid and ex-

Can. J. Chem. Downloaded from www.nrcresearchpress.com by 109.225.110.28 on 09/08/12
For personal use only.

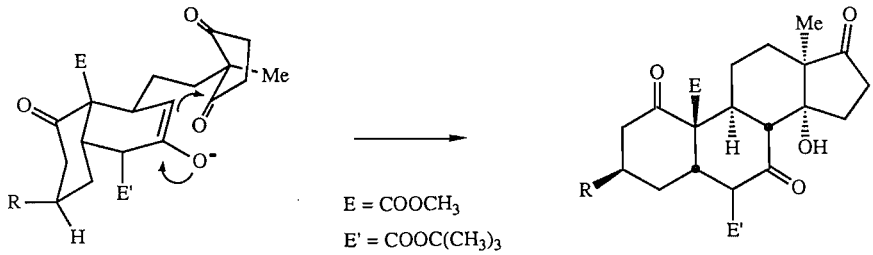

39 : R = H
40 : R = $C(CH_3)=CH_2$

5 : R = H
41 : R = $C(CH_3)=CH_2$

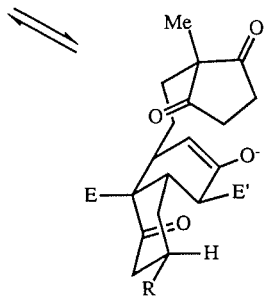

42 : R = $C(CH_3)=CH_2$

SCHEME 7

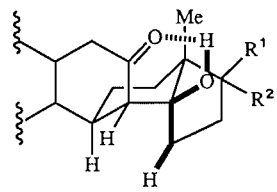

43

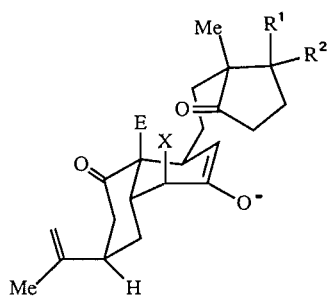

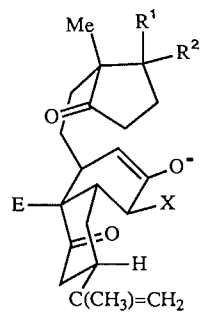

44 : X = H
45 : X = CO_2t-Bu

46

SCHEME 8

tracted with methylene chloride. This extraction yields 7.6 g (71%) of pure ketoacid **13***a*; ir (CH_2Cl_2, ν cm^{-1}): 3620–2400 (OH), 1740 (C=O ester), 1720 (C=O ketone and acid); ^{1}H nmr (250 MHz, $CDCl_3$) δ ppm: 8.04, 7.57, 7.45 (5H, 3m, -C_6H_5, 5.45 (1H, t, J = 4.7 Hz, -C*H*OCOC_6H_5), 2.47–1.86 (8H, m), 1.13 (3H, s, -CH_3); ms, *m/e*: 290 (M^+), 275 (M^+-CH_3), 272 (M^+-H_2O), 262 (M^+-CO). Exact Mass calcd. for $C_{16}H_{18}O_5$ (M^+): 290.1154; found: 290.1149.

Can. J. Chem. Downloaded from www.nrcresearchpress.com by 109.225.110.28 on 09/08/12
For personal use only.

Can. J. Chem. Downloaded from www.nrcresearchpress.com by 109.225.110.28 on 09/08/12
For personal use only.

Ketoacid ***13****b*

Ketoacid **13***b* is synthesized from enone **12***b* following the same procedure; ir (CH_2Cl_2, ν cm^{-1}): 3680–2400 (OH), 1750–1700 (C=O ketone and acid); ^1H nmr (250 MHz, $CDCl_3$) δ ppm: 3.87 (1H, t, J = 5.8 Hz, -C*H*OC(CH_3)$_3$), 2.53–1.71 (8H, m), 1.19 (9H, s, -C(C*H*$_3$)$_3$), 0.96 (3H, s, -C*H*$_3$); ms, *m/e*: 242 (weak, M^+), 186 ($MH^+-C_4H_9$). Exact Mass calcd. for $C_9H_{14}O_4$ ($MH^+-C_4H_9$): 186.0892; found: 186.0891.

Ketoalcohol ***14****a*

A solution of carboxylic acid **13***a* (11.3 g, 39.0 mmol) in tetrahydrofuran (250 mL) is added to a cold (0°C) stirred solution of borane–THF complex (1 M/THF, 40 mL) in tetrahydrofuran (250 mL). After stirring for 2 h at 0°C, water (100 mL) is added and the separated aqueous layer is extracted with ethyl acetate (5 × 200 mL). The combined organic layers are washed with brine, dried ($MgSO_4$), filtered, and evaporated. The crude product is used without further purification. Pure materials may, however, be obtained by flash chromatography (ethyl acetate – hexane, 4:1) of a portion of the residue which yields a 5.6:1 mixture of alcohol **14***a* and diol **15***a*. Ketoalcohol **14***a*: $[\alpha]_D$ +36.3 (*c* 1); ir (CH_2Cl_2, ν cm^{-1}): 3620, 3500 (OH), 1745 (C=O ester), 1720 (C=O ketone); ^1H nmr (250 MHz, $CDCl_3$) δ ppm: 8.01, 7.56, 7.45 (5H, 3m, -C$_6$*H*$_5$), 5.52 (1H, t, J = 5.0 Hz, -C*H*OCOC$_6$H$_5$), 3.62 (2H, m, -C*H*$_2$OH, becomes t, J = 5.9 Hz upon exchange with D_2O), 2.45–1.56 (8H, m), 1.13 (3H, s, -C*H*$_3$), and the following signals can be attributed to the hemiketal form: 5.65 (<1H, br t, J = 6.2 Hz, -C*H*OCOC$_6$H$_5$), 1.11 (<3H, s, -C*H*$_3$); ^{13}C nmr (62.9 MHz, $CDCl_3$) δ ppm: 218.9, 165.8, 133.2, 129.5, 128.5, 103.5, 77.9, 76.5, 62.6, 60.9, 52.3, 35.7, 34.7, 31.5, 27.3, 27.1, 25.5, 25.3, 20.9, 18.5, 15.9; ms, *m/e*: 277 (MH^+), 261 (M^+-CH_3), 258 (M^+-H_2O). Exact Mass calcd. for $C_{16}H_{21}O_4$ (MH^+): 277.1440; found: 277.1434. Diol **15***a*: ir (CH_2Cl_2, ν cm^{-1}): 3620, 3400 (OH), 1715 (C=O ester); ^1H nmr (250 MHz, $CDCl_3$) δ ppm: 8.03, 7.55, 7.44 (5H, 3m, -C$_6$*H*$_5$), 5.24 (1H, dd, J = 8.5, 6.5 Hz, -C*H*OCOC$_6$H$_5$), 4.00 (1H, dd, J = 6.0, 2.4 Hz, -C*H*OH), 3.67 (2H, m, -C*H*$_2$OH), 2.45–1.47 (8H, m), 1.04 (3H, s, -C*H*$_3$); ms, *m/e*: 279 (MH^+). Dibenzoylation of this diol **15***a* gives tribenzoylated derivative **16**. Tribenzoate **16**: $[\alpha]_D$ +80.8 (*c* 1.3); ^1H nmr (250 MHz, $CDCl_3$) δ ppm: 8.04, 7.90, 7.45 (15H, m, 3 × -C$_6$*H*$_5$), 5.36, 5.26 (2H, 2m, 2 × -C*H*OCOC$_6$H$_5$), 4.26 (2H, m, -C*H*$_2$OCOC$_6$H$_5$), 2.60–1.60 (8H, m), 1.22 (3H, s, -C*H*$_3$); ms, *m/e*: 486 (M^+), 381 ($M^+-COC_6H_5$), 365 ($M^+-OCOC_6H_5$). Exact Mass calcd. for $C_{30}H_{30}O_6$ (M^+): 486.2042; found: 486.2038.

Ketoalcohol ***14****b*

Ketoalcohol **14***b* is synthesized from ketoacid **13***b* following the procedure described for the synthesis of ketoalcohol **14***a*. Ketoalcohol **14***b*: ^1H nmr (250 MHz, $CDCl_3$) δ ppm: 3.95 (1H, t, J = 6.0 Hz, -C*H*OCC(CH_3)$_3$), 3.60 (2H, m, -C*H*$_2$OH), 2.53–2.40 (8H, m), 1.19 (9H, s, -C(C*H*$_3$)$_3$), 1.15 (<9H, s, -C(C*H*$_3$)$_3$, hemiketal form), 0.96 (3H, s, -C*H*$_3$), 0.88 (<3H, s, -C*H*$_3$, hemiketal form).

Aldehyde ***17****a*

To a stirred solution of crude alcohol **14***a* (10.8 g, 39.1 mmol) in methylene chloride (200 mL) at room temperature is added pyridinium chlorochromate (25.2 g, 117.4 mmol). After stirring at room temperature for 3 h, the mixture is diluted with ether (1.5 mL) and filtered on silica gel. Concentration under reduced pressure and flash chromatography (ethyl acetate – hexane, 2:3) of the resulting residue yields 5.4 g (50% from enone **12***a*) of aldehyde **17***a*; $[\alpha]_D$ +43.1 (*c* 4); ir (CH_2Cl_2, ν cm^{-1}): 1740 (C=O ester), 1720 (C=O ketone and aldehyde); ^1H nmr (250 MHz, $CDCl_3$) δ ppm: 9.76 (1H, s, -C*H*O), 8.01, 7.59, 7.45 (5H, 3m, -C$_6$*H*$_5$), 5.44 (1H, t, J = 5.0 Hz, -C*H*OCOC$_6$H$_5$), 2.73–1.80 (8H, m), 1.11 (3H, s, -C*H*$_3$); ms, *m/e*: 274 (M^+). exact mass calculated for $C_{16}H_{18}O_4$ (M^+): 274.1205; found: 274.1199.

Aldehyde **17**b: ir (CH_2Cl_2, ν cm^{-1}): 1730 (C=O ketone and aldehyde); ^1H nmr (250 MHz, $CDCl_3$) δ ppm: 9.75 (1H, t, J = 1.3 Hz, -C*H*O), 3.86 (1H, t, J = 5.9 Hz, -C*H*OC(CH_3)$_3$), 2.62–1.57 (8H,m), 1.19 (9H, s, -C(C*H*$_3$)$_3$), 0.96 (3H, s, -C*H*$_3$).

Unsaturated aldehyde ***18****a*

To a stirred solution of aldehyde **17***a* (1.0 g, 3.6 mmol) in benzene (70 mL) at room temperature is added (formylmethylene) triphenylphosphorane (1.3 g, 4.4 mmol). The mixture is heated at reflux for 48 h and then cooled down at room temperature. Concentration under reduced pressure and flash chromatography (ethyl acetate – hexane, 2:3) of the resulting residue yields 799 mg of the desired *trans* unsaturated aldehyde (73%) and a minor amount (<5%) of undesired *cis* isomer; $[\alpha]_D$ +65.9 (*c* 1); ir (CH_2Cl_2, ν cm^{-1}): 2880 (CH aldehyde), 1740–1720 C=O ester and ketone), 1680 (C=O conjugated aldehyde); ^1H nmr (250 MHz, $CDCl_3$) δ ppm: 9.48 (1H, d, J = 7.8 Hz, -CH=CH-C*H*O), 8.03, 7.58, 7.47 (5H, 3m, -C$_6$*H*$_5$), 6.80 (1H, dt, J = 15.7, 6.8 Hz, -C*H*=CH-CHO), 6.16 (1H, ddt, J = 15.7, 7.8, 1.5 Hz, -CH=C*H*-CHO), 5.52 (1H, t, J = 6.1 Hz, -C*H*OCOC$_6$H$_5$), 2.65–1.66 (8H, m), 1.16 (3H, s, -C*H*$_3$); ms, *m/e*: 298 (M^+-2H), 273 (MH^+-CO), 231 ($M^+-C_4H_5O$). Exact Mass calcd. for $C_{18}H_{18}O_4$ (M^+-2H): 298.1205; found: 298.1202.

Unsaturated aldehyde **18**b: ^1H nmr (250 MHz, $CDCl_3$) δ ppm: 9.48 (1H, d, J = 7.8 Hz, -CH=CH—C*H*O), 6.81 (1H, dt, J = 15.6, 6.8 Hz, -C*H*=CH—CHO), 6.10 (1H, ddt, J = 15.7, 7.8, 1.5 Hz, -CH=C*H*—CHO), 3.92 (1H, m, -C*H*OC(CH_3)$_3$), 2.60–1.51 (8H, m), 1.20 (9H, s, -C(C*H*$_3$)$_3$), 0.98 (3H, s, -C*H*$_3$).

β-Hydroxyester ***19****a*

To a suspension of granular zinc (549 mg, 8.4 mmol) in tetrahydrofuran (20 mL) at room temperature are added *tert*-butyl bromoacetate (0.9 mL, 5.6 mmol) and one crystal of iodine. The resulting mixture is heated at reflux for 1 h and then cooled down at 0°C. A solution of *trans* unsaturated aldehyde **18***a* (1.1 g, 3.7 mmol) in tetrahydrofuran (20 mL) is then added to the reaction mixture at 0°C. After stirring at 0°C for 90 min, saturated aqueous ammonium chloride (20 mL), water (5 mL), and ether (20 mL) are added. The separated aqueous layer is extracted with ethyl acetate (4 × 15 mL) and the combined organic layers are washed with brine, dried ($MgSO_4$), filtered, and evaporated. Flash chromatography (ethyl acetate – hexane, 2:3 to 3:2) of the residue yields 1.3 g (85%) of an unseparated (1:1) mixture of diastereomers; ir (neat, ν cm^{-1}): 3480 (OH), 1730 (C=O ester and ketone); ^1H nmr (250 MHz, $CDCl_3$) δ ppm: 8.01, 7.59, 7.45 (10H, 3m, 2 × -C$_6$*H*$_5$), 5.56 (6H, m, 2 × -C*H*=C*H* and -C*H*OCOC$_6$H$_5$), 4.43 (2H, m, 2 × -C*H*OH), 3.09, 3.07 (2 × 1H, 2d, J = 3.7 Hz, 2 × -O*H*), 2.60–1.50 (20H, m, 2 × -C*H*$_2$)), 1.46 (9H, s, -C(C*H*$_3$)$_3$), 1.45 (9H, s, -C(C*H*$_3$)$_3$), 1.12 (3H, s, -C*H*$_3$), 1.11 (3H, s, -C*H*$_3$); ms, *m/e*: 343 ($M^+-OC(CH_3)_3$).

β-Hydroxyester ***19****b:* ir (neat, ν cm^{-1}); 3460 (OH), 1730 (C=O ester and ketone); ^1H nmr (250 MHz, $CDCl_3$) δ ppm: 5.73–5.40 (4H, m, 2 × -C*H*=C*H*), 4.42 (2H, m, 2 × -C*H*OH), 3.92 (2H, m, 2 × -C*H*OC(CH_3)$_3$), 3.09 (2H, br s, 2 × -O*H*), 2.55–1.70 (20H, m, 2 × (5 × -C*H*$_2$)), 1.46 (9H, s, -OC(C*H*$_3$)$_3$), 1.45 (9H, s, -OC(C*H*3)$_3$), 1.20 (9H, s, -C(C*H*$_3$)$_3$), 1.19 (9H, s, -C(C*H*$_3$)$_3$), 0.94 (6H, s, 2 × -C*H*$_3$).

β-Ketoester ***10****a*

To a stirred solution of β-hydroxyester **19***a* (802 mg, 1.93 mmol) in ethyl acetate (80 mL) at room temperature was added manganese dioxide (3.35 g, 38.5 mmol). After vigorous stirring at room temperature for 8 h, the mixture is filtered on silica gel and evaporated under reduced pressure. Flash chromatography (ethyl acetate – hexane, 2:3) of the residue yields 464 mg (58%) of β-ketoester **10***a* along with 27% of recovered starting material; ir (neat, ν cm^{-1}): 1735 (C=O ester), 1690 (C=O conjugated ketone); ^1H nmr (250 MHz, $CDCl_3$) δ ppm: 12.00 (<1H, br s, -O*H*, enol form), 8.01, 7.57, 7.45 (5H, 3m, -C$_6$*H*$_5$), 6.85–6.55 (1H, 2dt, J = 15.9, 6.8 Hz, -CH$_2$C*H*=CH-, β-ketoester and enol forms), 6.15–5.75 (1H, 2m, -CH$_2$CH=C*H*-), 5.51 (1H, m, -C*H*OCOC$_6$H$_5$), 4.86 (<1H, s, -C=C*H*CO$_2$-, enol form), 3.45 (<2H, s, -COC*H*$_2$CO$_2$-), 2.65–1.58 (8H, m), 1.48, 1.47 (9H, 2s, -C(C*H*$_3$)$_3$, β-ketoester and enol forms), 1.14 (3H, s, -C*H*$_3$); ms,

Can. J. Chem. Downloaded from www.nrcresearchpress.com by 109.225.110.28 on 09/08/12
For personal use only.

m/e: 383 (M^+-OCH_3), 357 ($M^+-C_4H_9$). Exact Mass calcd. for $C_{20}H_{21}O_6$ ($M^+-C_4H_9$): 357.1338; found: 357.1333.

β-Ketoester ***10****b*: ir (neat, ν cm^{-1}): 1735 (C=O ester), 1690 (C=O conjugated ketone); ^1H nmr (250 MHz, $CDCl_3$) δ ppm: 12.00 (<1H, m, -O*H*, enol form), 6.85–6.51 (1H, 2dt, *J* = 15.9, 6.8 Hz, β-ketoester and enol forms), 6.17–5.70 (1H, 2m, $-CH_2-CH=CH-$), 4.88 (<1H, s, $-C=CHCO_2$, enol form), 3.92 (1H, 2t, *J* = 6.0 Hz, $-CHOC(CH_3)_3$), 3.47 (2H, s, $-COCH_2CO_2-$), 2.60–1.40 (8H, m), 1.49, 1.45 (9H, 2s, $-CO_2C(CH_3)_3$, β-ketoester and enol forms), 1.20 (9H, s, $-OC(CH_3)_3$), 0.96 (3H, s, $-CH_3$).

Triketone ***20***

A solution of 2-carbomethoxycyclohex-2-en-1-one (**1**) (42 mg, 0.27 mmol) in chloroform (2.0 mL) is added to a stirred mixture of β-ketoester ***10****b* (72 mg, 0.2 mmol) and cesium carbonate (32 mg, 0.1 mmol) in chloroform (3.0 mL) at room temperature over 20 mins. After stirring for 1 h at room temperature, the mixture is filtered on silica gel and evaporated under reduced pressure. The residue is dissolved in trifluoroacetic acid (4 mL) and evaporated under reduced pressure. The new residue is then dissolved in benzene (10 mL) and heated at reflux for 2 h. The solution is cooled down at room temperature and evaporated under reduced pressure. Flash chromatography (ethyl acetate – hexane, 9:1) of the residue yields 31.2 mg (44%) of a 1:1 mixture of diastereomers; ir (neat, ν cm^{-1}): 3450 (OH), 1740–1720 (C=O ester and ketones); ^1H nmr (250 MHz, $CDCl_3$) δ ppm: 4.10 (1H, m, -C*H*OH), 3.77, 3.76 (3H, s, $-CO_2CH_3$), 3.10 (1H, m, $-CH_2CH(CO_2CH_3)$), 2.74–0.95 (19H, m), 0.93, 0.92 (3H, s, $-CH_3$); ms, *m/e*: 364 (M^+), 346 (M^+-H_2O), 305 ($M^+-CO_2CH_3$).

Tetraketone ***21***

Tetrapropylammonium perruthenate (0.001 mmol) is added to a vigorously stirred mixture of alcohol **20** (9 mg, 0.025 mmol), 4Å molecular sieves (5 mg), and 4-methylmorpholine *N*-oxide (4.3 mg, 0.03 mmol) in methylene chloride (1 mL) at room temperature. After stirring for 15 h at room temperature, methylene chloride (20 mL), 5% aqueous sodium sulfite solution (10 mL), and brine (10 mL) are added. The separated organic layer is dried ($MgSO_4$), filtered, and evaporated. Flash chromatography (ethyl acetate – hexane, 3:2) of the residue yields 5.4 mg (61%) of tetraketone **21**: ir (CH_2Cl_2, ν cm^{-1}): 1740–1720 (C=O ester and ketones); ^1H nmr (250 MHz, $CDCl_3$) δ ppm: 3.76 (3H, s, $-CO_2CH_3$), 3.05 (1H, m, $-CH_2CH(CH_2CO-)$, 2.73 (4H, m, $-OC(CH_2)_2CO-$), 2.65–0.93 (15H, m), 1.07 (3H, s, $-CH_3$); ms, *m/e*: 362 (M^+), 344 (M^+-H_2O), 330 (M^+-CH_3OH). Exact Mass calcd. for $C_{20}H_{26}O_6$ (M^+): 362.1729; found: 362.1727.

Enol phosphate ***24***

A solution of crude compound **5** (60 mg, 0.13 mmol) in tetrahydrofuran is added to a stirred suspension of sodium hydride (6 mg, 0.26 mmol) in tetrahydrofuran (1 mL) at 0°C. Diethyl chlorophosphate (28 μL, 0.19 mmol) is then added to the resulting yellow solution at 0°C and the mixture is stirred at room temperature for 16 h. Saturated aqueous ammonium chloride (5 mL) and ethyl acetate (5 mL) are added and the separated aqueous layer is extracted with ethyl acetate (4 × 10 mL). The combined organic layers are washed with brine, dried ($MgSO_4$), filtered, and evaporated. Flash chromatography (ethyl acetate – hexane, 4:1) of the residue yields 21.6 mg (28%) of enol phosphate **24** along with 63% of recovered starting material. Recovered starting material could be recycled to give the same compound **24** in comparable yield (to ascertain that the aldol reaction was not observed using these conditions, a control experiment was run without diethyl chlorophosphate. In this case, starting material remained unchanged); ir (CH_2Cl_2, ν cm^{-1}): 3580, 3470 (OH), 1740 (C=O ester), 1730–1710 (C=O ketones and conjugated ester); ^1H nmr (250 MHz, $CDCl_3$) δ ppm: 4.16 (4H, qd, *J* = 7.1, 4.0 Hz, $-OP(O)(OCH_2CH_3)_2$), 4.15 (1H, s, -O*H*), 3.69 (3H, s, $-CO_2CH_3$), 3.65 (1H, m, HβC5), 3.00–1.10 (16H, m), 1.50 (9H, s, $-CO_2C(CH_3)_3$), 1.35 (6H, td, *J* = 7.1, 1.1 Hz, $-OP(O)(OCH_2CH_3)_2$), 1.06 (3H, s, $-CH_3$); ms, *m/e*: 598 (M^+), 584 (MH^+-CH_3), 567 (M^+-OCH_3), 542 ($MH^+-C_4H_9$).

Triketone ***25***

A solution of chiral cyclohexenone **9** (567 mg, 2.9 mmol) in chloroform (18 mL) is added to a stirred mixture of β-ketoester ***10****a* (803 mg, 1.9 mmol) and cesium carbonate (285 mg, 0.9 mmol) in chloroform (30 mL) at room temperature. After stirring for 6 h at room temperature, the mixture is filtered on silica gel and evaporated under reduced pressure. The residue is dissolved in trifluoroacetic acid (20 mL) and evaporated under reduced pressure. The new residue is then dissolved in benzene (30 mL) and heated at reflux for 5 h. The solution is cooled down at room temperature and evaporated under reduced pressure. Flash chromatography (ethyl acetate – hexane, 1:3 to 2:3) of the residue yields 587 mg (60%) of compound **25** along with 104 mg (11%) of uncharacterized diastereomer; $[\alpha]_D$ +83.6 (*c* 1); ir (CH_2Cl_2, ν cm^{-1}): 1740 (C=O ester), 1720, 1710 (C=O ketones); ^1H nmr (250 MHz, $CDCl_3$) δ ppm: 7.99, 7.58, 7.43 (5H, m, $-C_6H_5$), 5.37 (1H, t, *J* = 5.6 Hz, $-CHOCOC_6H_5$), 4.80, 4.72 (2H, 2 br s, $-C=CH_2$), 3.73 (3H, s, $-CO_2CH_3$), 3.15 (1H, m, $-CH_2CH(C\text{-}COOCH_3)CH_2-$), 2.76–1.10 (18H, m), 1.71 (3H, s, $=C\text{-}CH_3$), 1.06 (3H, s, $-CH_3$); ms, *m/e*: 508 (M^+), 490 (M^+-H_2O), 476 (M^+-CH_3OH). Exact Mass calcd. for $C_{30}H_{36}O_7$ (M^+): 508.2461; found: 508.2457. Diastereoisomer: ^1H nmr (250 MHz, $CDCl_3$) δ ppm: 8.01, 7.57, 7.45 (5H, 3m, $-C_6H_5$), 5.46 (1H, t, *J* = 6.7 Hz, $-CHOCOC_6H_5$), 4.82, 4.78 (2H, 2 br s, $-C=CH_2$), 3.73 (3H, s, $-CO_2CH_3$), 3.10 (1H, m, $-CH_2CH(C\text{-}CO_2Ch_3)CH_2-$), 2.46–1.20 (18H, m), 1.75 (3H, s, $=C\text{-}CH_3$), 1.06 (3H, s, $-CH_3$).

*Methyl 17β-benzoyloxy-14β-hydroxy-3β-methylethenyl-1,7-dioxo-5β-androstan-19-oate (****11****)*

To a stirred solution of triketone **25** (94 mg, 0.19 mmol) in acetonitrile (5 mL) at room temperature is added cesium carbonate (36 mg, 0.11 mmol). The mixture is heated at reflux for 20 h, cooled down at room temperature, filtered on silica gel, and evaporated under reduced pressure. Flash chromatography of the residue (ethyl acetate – hexane, 7:13) yields 30 mg (32%) of steroid **11** along with 31% recovered starting material; mp 156–157°C; $[\alpha]_D$ +61.5 (*c* 1); ir (CH_2Cl_2, ν cm^{-1}): 3520–3500 (OH), 1740 (C=O ester), 1720–1710 (C=O ketones); ^1H nmr (250 MHz, $CDCl_3$) δ ppm: 8.08, 7.53, 7.42 (5H, 3m, $-C_6H_5$), 5.01 (1H, m, HαC17), 4.84, 4.73 (2H, 2s, $-C=CH_2$), 4.01 (1H, s, -O*H*), 3.81 (3H, s, $-CO_2CH_3$), 3.19 (1H, m, HβC5), 2.79 (1H, d, *J* = 13.6 Hz, HβC8), 2.64–1.35 (16H, m), 1.72 (3H, s, $=C\text{-}CH_3$), 1.07 (3H, s, $-CH3$); ^{13}C nmr (62.9 MHz, $CDCl_3$) δ ppm: 214.8, 206.3, 171.5, 166.5, 146.0, 132.7, 129.6, 128.3, 111.1, 84.1, 82.9, 82.3, 62.8, 52.7, 52.4, 50.5, 45.2, 42.5, 40.8, 36.6, 35.1, 34.1, 32.6, 28.9, 28.0, 23.5, 20.7, 13.2; ms, *m/e*: 508 (M^+), 490 (M^+-H_2O), 476 (M^+-CH_3OH), 449 ($M^+-COOCH_3$). Exact Mass calcd. for $C_{30}H_{36}O_7$ (M^+): 508.2461; found: 508.2472.

Compound ***11*** *is also obtained from* ***26*** *under the same conditions.*

*Methyl 17β-benzoyloxy-14β-hydroxy-3β-methylethenyl-1,7-dioxo-5β,8α-androstan-19-oate (****26****)*

To a stirred solution of triketone **25** (16 mg, 0.03 mmol) in tetrahydrofuran (1 mL), at −78°C, is added a solution of potassium bis(trimethylsilyl)amide (82 μL, 0.5 M, 0.04 mmol) in toluene. After stirring for 30 min at −78°C, the reaction mixture is warmed to room temperature and, after an additional 20 min, quenched with saturated aqueous ammonium chloride (2 mL). Ethyl acetate (10 mL) is added and the separated aqueous layer is extracted with a 1:1 mixture of ether and ethyl acetate (4 × 10 mL). The combined organic layers are washed with brine, dried ($MgSO_4$), filtered, and evaporated. Flash chromatography (ethyl acetate – hexane, 3:7) of the residue yields 4 mg (25%) of steroid **26** along with 30% recovered starting material; ir (CH_2Cl_2, ν cm^{-1}): 3500 (OH), 1740–1700 (C=O ketones and ester); ^1H nmr (250 MHz, $CDCl_3$) δ ppm: 8.07, 7.53, 7.43 (5H, 3m, $-C_6H_5$), 5.03 (1H, dd, *J* = 7.5, 2.5 Hz, $-CHOCOC_6H_5$), 4.82, 475 (2H, 2 br s, $-C=CH_2$),

Can. J. Chem. Downloaded from www.nrcresearchpress.com by 109.225.110.28 on 09/08/12
For personal use only.

4.64 (1H, d, J = 2.0 Hz, -O*H*), 3.78 (3H, s, -CO_2CH_3) 3.30–1.00 (18H, m), 1.71 (3H, s, -C(CH_3)=CH_2), 1.09 (3H, s, -CH_3).

Methyl 17β-benzoyloxy-2β-methylethenyl-1,7-dioxo-14β-trimethylsilyloxy-5β,8α-androstan-19-aote (27)

Trimethylsilylchloride (5 μL, 0.04 mmol) is added to a stirred solution of alcohol **26** (9 mg, 0.02 mmol) and imidazole (3 mg, 0.04 mmol) in dimethylformamide (0.1 mL) at room temperature. After stirring for 12 h at room temperature, saturated aqueous ammonium chloride (1 mL) and ether (1 mL) are added. The separated aqueous layer is extracted with ether (3 × 10 mL) and the combined organic layers are washed with brine, dried ($MgSO_4$), filtered, and evaporated. Flash chromatography (ethyl acetate – hexane, 1:4) of the residue yields 8 mg (79%) of trimethylsilyl ether **27**; ^{1}H nmr (250 MHz, $CDCl_3$) δ ppm: 8.08, 7.55, 7.44 (5H, 3m, -C_6H_5), 4.90 (1H, m, C*H*OCOC_6H_5), 4.81, 4.74 (2H, 2 br s, -C=CH_2), 3.76 (3H, s, -CO_2CH_3), 3.40–0.80 (18H, m), 1.72 (3H, s, -C(CH_3)=CH_2), 1.15 (3H, s, -CH_3), 0.08 (9H, s, -Si(CH_3)$_3$); ms, *m/e*: 580 (M^+), 565 (M^+-CH_3).

Tricyclic alcohol 28

To a stirred solution of benzoate **25** (95 mg, 0.19 mmol) in methanol (2 mL) at room temperature is added a solution of sodium methoxide (190 μL, 0.5 M) in methanol. After stirring for 15 h at room temperature, the mixture is neutralized with weakly acidic Dowex IRC-50 resin, filtered, and evaporated. Flash chromatography (ethyl acetate – hexane, 7:3) of the residue yields 55 mg (73%) of alcohol **28**; ^{1}H nmr (250 MHz, $CDCl_3$) δ ppm: 4.81, 4.73 (2H, 2 br s, -C=CH_2), 4.08 (1H, m, -*CH*OH) 3.76 (3H, s, -CO_2CH_3), 3.15 (1H, m, -CH_2CH(C-$COOCH_3$)CH_2-), 2.81–0.98 (19H, m), 1.72 (3H, s, -C=C(CH_3)), 0.94 (3H, s, -CH_3); ms, *m/e*: 404 (M^+), 386 (M^+-H_2O), 372 (M^+-CH_3OH). Exact Mass calcd. for $C_{23}H_{32}O_6$ (M^+): 404.2199; found: 404.2191.

Tricyclic carbonate 29

To a stirred solution of alcohol **28** (50 mg, 0.12 mmol) in pyridine (0.2 mL) at room temperature, is added phenyl chloroformate (23 μL, 0.18 mmol). After stirring for 24 h at room temperature, the mixture is quenched with ice and saturated aqueous sodium bicarbonate (10 mL) and ether (10 mL) are added. The separated aqueous layer is extracted with ether (3 × 10 mL) and the combined organic layers are washed with brine, dried ($MgSO_4$), filtered, and evaporated. Flash chromatography (ethyl acetate – hexane, 7:13) of the residue yields 46 mg (71%) of carbonate **29**; ^{1}H nmr (250 MHz, $CDCl_3$) δ ppm: 7.40, 7.24 (5H, 2m, -C_6H_5), 5.07 (1H, br t, J = 6.0 Hz, -*CH*O$CO_2C_6H_5$), 4.81, 4.71 (2H, br s, -C=CH_2), 3.74 (3H, s, -CO_2CH_3), 3.18 (1H, m, -CH_2CH(C-CO_2CH_3)CH_2-), 2.72–1.20 (18H, m), 1.72 (3H, s, C=C(CH_3)), 1.04 (3H, s, -CH_3); ms, *m/e*: 524 (M^+), 506 (M^+-H_2O), 492 (M^+-CH_3OH). Exact Mass calcd. for $C_{30}H_{36}O_8$ (M^+): 524.2410; found: 524.2405.

Methyl 14β,17β-dihydroxy-3β-methylethenyl-1,7-dioxo-5β-androstan-19-oate (30)

To a stirred solution of triketone **28** (60 mg, 0.15 mmol) in acetonitrile (4 mL) at room temperature is added cesium carbonate (36 mg, 0.11 mmol). The mixture is heated at reflux for 20 h, cooled down at room temperature, filtered, and evaporated under reduced pressure. Flash chromatography (ethyl acetate – hexane, 7:3) of the residue yields 18 mg (30%) of steroid **30** along with 30% recovered starting material; ^{1}H nmr (250 MHz, $CDCl_3$) δ ppm: 4.84, 4.73 (2H, 2s, -C=CH_2), 4.21 (1H, s, -O*H* tertiary), 3.82 (3H, s, -CO_2CH_3), 3.55 (1H, m, HαC17), 3.16 (1H, d, J = 11.3 Hz, -O*H* secondary), 3.15 (1H, m, HβC5), 2.75 (1H, d, J = 13.6 Hz, HβC8), 2.60–1.20 (16H, m), 1.72 (3H, s, C=C(CH_3)), 1.10 (3H, s, -CH_3); ms, *m/e*: 386 (M^+-H_2O); 368 (M^+-2H_2O). Exact Mass calcd. for $C_{23}H_{30}O_5$ (M^+-H_2O): 386.2093; found: 386.2100.

Methyl 17β-hydroxy-3β-methylethenyl-1,7-dioxo-5β-androst-8(14)-en-19-oate (32)

Cesium carbonate (25 mg, 0.08 mmol) is added to a stirred solution of tricyclic carbonate **29** (100 mg, 0.19 mmol) in acetonitrile (15 mL) at room temperature. The mixture is heated at reflux for 6 h, cooled down at room temperature, filtered, and evaporated under reduced pressure. Flash chromatography (ethyl acetate – hexane, 1:1) of the residue yields 37.5 mg (51%) of allylic alcohol **32**; ir (CH_2Cl_2, ν cm^{-1}): 3600, 3500 (OH), 1740 (C=O ester), 1710 (C=O ketone), 1690 (C=O conjugated ketone); ^{1}H nmr (250 MHz, $CDCl_3$) δ ppm: 4.82, 4.73 (2H, 2s, -C=CH_2), 3.78 (3H, s, -CO_2CH_3), 3.71 (1H, m, HαC17), 3.43 (1H, m, HβC5), 3.15–1.23 (17H, m), 1.72 (3H, s, -C=C(CH_3)), 0.98 (3H, s, -CH_3); ms, *m/e*: 386 (M^+), 368 (M^+-H_2O), 354 (M^+-CH_3OH).

Tetraketone 35 and methyl 14α-hydroxy-3β-methylethenyl-1,7,17-trioxo-5β-13α-androstan-19-oate (36)

To a stirred mixture of cyclopentanedione β-ketoester **2** (80 mg, 0.3 mmol) and cesium carbonate (50 mg, 0.2 mmol) in chloroform (3 mL) at room temperature is added a solution of chiral cyclohexenone **9** (101 mg, 0.5 mmol) in chloroform (3 mL). After stirring for 6 h at room temperature, the mixture is filtered on silica gel and evaporated under reduced pressure. The residue is dissolved in trifluoroacetic acid (5 mL) and evaporated under reduced pressure. The new residue is then dissolved in benzene (15 mL) and heated at reflux for 5 h. The solution is cooled down at room temperature and evaporated under reduced pressure. Flash chromatography (ethyl acetate – hexane, 1:1) of the residue yields 22.5 mg (22%) of tricyclic compound **35** and 22.5 mg (22%) of steroid **36**. Tricyclic tetraketone **35** (R_f 0.31): ir (CH_2Cl_2, ν cm^{-1}): 1770 (C=O β-diketone), 1750–1710 (C=O ester and ketones); ^{1}H nmr (250 MHz, $CDCl_3$) δ ppm: 4.81, 4.72 (2H, 2 br s, -C(CH_3)=CH_2), 3.77 (3H, s, -CO_2CH_3), 3.10 (1H, m, -CH_2-$CHCH_2$-), 2.74 (4H, m, -OC(CH_2)$_2$CO-), 2.70–1.00 (18H, m), 1.71 (3H, s, -C(CH_3)=CH_2), 1.07 (3H, s, -CH_3); ms, *m/e*: 402 (M^+), 384 (M^+-H_2O), 352 (M^+-H_2O-CH_3OH); a minor diastereomeric compound corresponding to **35** was not isolated. 14α-Hydroxy steroid **36** (R_f 0.43): ir (CH_2Cl_2, ν cm^{-1}): 3500 (OH), 1735 (C=O ester), 1710 (C=O ketones); ^{1}H nmr (250 MHz, $CDCl_3$) δ ppm: 4.91, 4.72 (2H, 2br s, -C(CH_3)=CH_2), 4.15 (1H, s, -O*H*; exchanges upon treatment with D_2O), 3.73 (3H, s, -$COOCH_3$), 3.10 (1H, m, HβC5), 2.77 (1H, d, J = 12.4 Hz, HβC8), 2.70–1.15 (16H, m), 1.73 (3H, s, -C(CH_3)=CH_2), 1.01 (3H, s, -CH_3); ms *m/e*: 402 (M^+), 384 (M^+-H_2O). Steroid **36** was accompanied by a minor diastereomeric compound: its corresponding signals could be seen in the ^{1}H nmr spectrum at δ ppm: 4.82, 4.74 (2H, 2br s, -C(CH_3=CH_2), 4.32 (1H, s, -O*H*; exchanges upon treatment with D_2O), 3.76 (3H, s, -COl_2CH_3), 1.05 (3H, s, -CH_3).

Methyl 14β-hydroxy-3β-methylethenyl-1,7,17-trioxo-5β,8α-androstan-19-oate (37)

Potassium *tert* butoxide (44 mg, 0.4 mmol) is added to a stirred solution of tetraketone **35** (40 mg, 0.1 mmol) in a mixture of *tert*-butanol (0.3 mL), tetrahydrofuran (0.3 mL), and benzene (0.3 mL) at room temperature. After stirring for 15 min at room temperature, saturated aqueous ammonium chloride (5 mL) is added and the separated aqueous layer is extracted with ethyl acetate (4 × 10 mL). The combined organic layers are washed with brine, dried ($MgSO_4$), filtered, and evaporated under reduced pressure. Flash chromatography (ethyl acetate – hexane, 3:7) of the residue yields 11.6 mg (29%) of 14β-hydroxy steroid **37** and traces of isomer **38**; ir (CH_2Cl_2, ν cm^{-1}): 3500 (OH), 1750–1700 (C=O ester and ketones); ^{1}H nmr (250 MHz, $CDCl_3$) δ ppm: 4.82, 4.74 (2H, 2s, -C(CH_3)=CH_2), 4.66 (1H, d, J = 2.5 Hz, -O*H*), 3.77 (3H, s, -CO_2CH_3), 3.25–0.98 (18H, m), 1.72 (3H, s, -C(CH_3)=CH_2), 1.11 (3H, s, -CH_3); ms, *m/e*: 402 (M^+), 384 (M^+-H_2O), 369 (M^+-H_2O-CH_3).

Methyl 14β-hydroxy-3β-methylethenyl-1,7,17-trioxo-5β-androstan-19-oate (38)

From isomerization of 37

To a stirred solution of steroid **37** (8 mg, 0.02 mmol) in acetonitrile (2 mL) at room temperature is added cesium carbonate (6 mg, 0.02 mmol). The mixture is heated at reflux for 2 h, cooled down

Can. J. Chem. Downloaded from www.nrcresearchpress.com by 109.225.110.28 on 09/08/12
For personal use only.

at room temperature, filtered, and evaporated. Flash chromatography (ethyl acetate – hexane, 2:3) of the residue yields 3.5 mg (45%) of steroid **38** along with 13% of recovered starting material.

*From methanolysis and oxidation of steroid **11***

To a stirred solution of steroid **11** (20 mg, 0.04 mmol) in methanol (0.1 mL) at room temperature is added a solution of sodium methoxide (40 μL, 0.5 M) in methanol. After stirring for 16 at room temperature, weakly acidic Dowex IRC-50 resin is added to the reaction mixture until pH reaches ~7. The mixture is then filtered on Celite and evaporated under reduced pressure. The residue is dissolved in methylene chloride (5 mL) and pyridinium chlorochromate (25 mg, 0.12 mmol) is added portionwise. After stirring for 2 h at room temperature, ether (50 mL) is added and the mixture is filtered on silica gel and evaporated. Flash chromatography (ethyl acetate – hexane, 2:3) of the residue yields 4.5 mg (30%, 2 steps) of a material identical to that obtained from isomerization of **37**; ir (CH_2Cl_2, ν cm^{-1}): 3500 (OH), 1740 (C=O ester), 1715 (C=O ketones); ^1H nmr (250 MHz, $CDCl_3$) δ ppm: 4.85, 4.74 (2H, 2s, -C(CH_3)=CH_2), 3.97 (1H, s, -O*H*; exchanges upon treatment with D_2O), 3.82 (3H, s, -CO_2CH_3), 2.80 (1H, d, J = 12.3 Hz, HβC8), 3.15–1.00 (17H, m), 1.73 (3H, s, -C(CH_3=CH_2), 1.05 (3H, s, -CH_3); ms, *m/e*: 402 (M^+).

*Methyl 17β-benzoyloxy-3-isopropyl-1,7-dioxo-5β-androsta-2,8(14)-dien-19-oate (**33**)*

To a stirred solution of triketone **25** (60 mg, 0.12 mmol) in benzene (10 mL) at room temperature is added *p*-toluenesulfonic acid (34 mg, 0.18 mmol). The mixture is heated at reflux for 16 h and then cooled down at room temperature, Water (10 mL) is added and the separated aqueous layer is extracted with ether (3 × 10 mL). The combined organic layers are washed with saturated aqueous sodium bicarbonate (10 mL), brine, dried ($MgSO_4$), filtered, and evaporated. Flash chromatography (ethyl acetate – hexane, 2:3) of the residue yields 44.5 mg (77%) of **33**, which may be recrystallized from heptane; mp 137–139°C; $[\alpha]_D$ −106.4 (*c* 1); ir (CH_2Cl_2, ν cm^{-1}): 1740, 1720 (C=O esters), 1670 (C=O conjugated ketones); ^1H nmr (250 MHz, $CDCl_3$) δ ppm: 8.05, 7.55, 7.45 (5H, 3m, −C_6H_5), 5.94 (1H, br s, HC2), 4.99 (1H, dd, J = 10.4, 7.6 Hz, HαC17), 3.75 (3H, s, -CO_2CH_3), 3.32–3.07 (2H, m, HβC5 and HαC9), 2.89–1.34 (13H, m), 1.36 (3H, s, -CH_3), 1.13, 1.12 (6H, 2d, J = 6.8 Hz, -CH(CH_3)$_2$); ms, *m/e*: 490 (M^+), 459 M^+−OCH_3), 431 (M^+−CO_2CH_3). Exact Mass calcd. for $C_{30}H_{34}O_6$ (M^+): 490.2355; found: 490.2352.

*This compound is also obtained by submitting **26** or **11** to the same conditions.*

*Methyl 3-isopropyl-1,7-dioxo-17β-phenyloxycarbonyloxy-5β-androsta-2,8(14)-dien-19-oate (**34**)*

The preceding procedure is applied using carbonate **29** (25 mg, 0.05 mmol) and *p*-toluenesulfonic acid (13.6 mg, 0.07 mmol) in benzene (5 mL). Flash chromatography (ethyl acetate – hexane, 2:3) of the residue yields 17.8 mg (74%) of compound **34**; ^1H nmr (250 MHz, $CDCl_3$) δ ppm: 7.38, 7.20 (5H, 2m, -OC_6H_5), 5.95 (1H, br s, HC2), 4.72 (1H, dd, J = 10.5, 7.4 Hz, HαC17), 3.75 (3H, s, -CO_2CH_3), 3.22–3.10 (2H, m, HβC5 and HαC9), 2.87–1.16 (13H, m), 1.30 (3H, s, -CH_3), 1.12 (6H, d, J = 6.8 Hz, -CH(CH_3)$_2$).

Acknowledgements

We are grateful to the Natural Sciences and Engineering Research Council of Canada and to Fonds pour la Formation de Chercheurs et l'Aide à la Recherche (Québec) for financial support of this work. We also thank Dr. Keith T. Hogan for the large-scale synthesis of compound **9**. We acknowledge the help of Dr. Solo Goldstein in writing this manuscript.

1. W. H. Lewis and M. P. F. Elvin-Lewis. *In* Medical botany: plants affecting man's health. John Wiley and Sons, New York. 1977.
2. T. W. Guntert and H. H. A. Linde. *In* Cardiac glycosides. *Edited by* K. Greef. Springer-Verlag, Berlin. 1981.
3. K. Wiesner and T. Y. R. Tsai. Pure Appl. Chem. **58**, 799 (1986).
4. T. Drakenberg, P. Brodelius, D. D. McIntyre, and H. J. Vogel. Can. J. Chem. **68**, 272 (1990), and refs. cited therein.
5. S. Lociuro, T. Y. R. Tsai, and K. Wiesner. Tetrahedron, **44**, 35 (1988); J. P. Kutney, K. Piotrowska, J. Somerville, S.-P. Huang, and S. J. Rettig. Can. J. Chem. **67**, 580 (1989), and refs. 5–17 cited therein; G. Groszek, A. Kurek-Tyrlik, and J. Wicha. Tetrahedron, **45**, 2223 (1989); G. Kirsch, R. Golde, and G. Neef. Tetrahedron Lett. **30**, 4497 (1989); P. Kocovsky and I. Stieborova. Tetrahedron Lett. **30**, 4295 (1989).
6. P. Yates, S. P. Douglas, S. K. Datta, and J. F. Sawyer. Can. J. Chem. **66**, 2268 (1989); A. R. Daniewski, Z. Valenta, and P. S. White. Bull. Pol. Acad. Sci. Chem. **32**, 29 (1984); A. R. Daniewski, M. M. Kabat, M. Masnyk, J. Wicha, and W. Wojciechowska. J. Org. Chem. **53**, 4855 (1988).
7. I. N. Nazarov, S. N. Ananchenko, and I. V. Torgov. Izv. Akad. Nauk SSR, Otd. Khim. 103 (1959); Chem. Abstr. **59**, 16088i (1959); I. N. Nazarov, I. V. Torgov, and G. N. Verkholetova. Dokl. Akad. Nauk SSR, **112**, 1067 (1957); Chem. Abstr. **51**, 14647d (1957).
8. J.-F. Lavallée and P. Deslongchamps. Tetrahedron Lett. **29**, 6033 (1988).
9. J.-F. Lavallée and P. Deslongchamps. Tetrahedron Lett. **29**, 5117 (1988).
10. R. Ruel and P. Deslongchamps. Can. J. Chem. **68**, 1917 (1990).
11. R. Ruel and P. Deslongchamps. Tetrahedron Lett. **31**, 3961 (1990).
12. P. Deslongchamps, A. Bélanger, D. J. F. Berney, H.-J. Borschberg, H. Katayama, R. Lapalme, D. M. Leturc, C.-C. Liao, F. N. MacLachlan, J.-P. Maffrand, F. Marazza, R. Martino, C. Moreau, L. Ruest, L. Saint-Laurent, R. Saintonge, and P. Soucy. Can. J. Chem. **68**, 127 (1990); T. Kitahara, H. Kurata, T. Matsuoka, and K. Mori. Tetrahedron, **41**, 5475 (1985).
13. Z. G. Hajos, D. R. Parrish, and E. P. Olivetto. Tetrahedron, **24**, 2039 (1968); R. A. Micheli, Z. G. Hajos, N. Cohen, D. R. Parrish, L. A. Portland, W. Sciamanna, M. A. Scott, and P. A. Wehrli. J. Org. Chem. **40**, 675 (1975); Z. G. Hajos and D. R. Parrish. J. Org. Chem. **39**, 1612 (1974); **39**, 1615 (1974).
14. N. M. Yoon, C. S. Pak, H. C. Brown, S. Krishnamurthy, and T. P. Stocky. J. Org. Chem. **38**, 2786 (1973).
15. E. J. Corey and J. W. Suggs. Tetrahedron Lett. 2647 (1975).
16. S. Trippett and D. M. Walker. J. Chem. Soc. 1266 (1961).
17. W. P. Griffith, S. V. Ley, G. P. Whitcombe, and A. D. White. J. Chem. Soc. Chem. Commun. 1625 (1987).
18. J.-F. Lavallée, C. Spino, R. Ruel, K. T. Hogan, and P. Deslongchamps. Can. J. Chem. **70**, 1406 (1992).
19. J.-F. Lavallée. Ph.D. Thesis, Université de Sherbrooke, 1988. pp. 130–137.
20. M. Alderdice, F. W. Sum and L. Weiler. Org. Synth. **62**, 14 (1984).
21. R. Ruel. Ph.D. Thesis, Université de Sherbrooke, 1990. pp. 157–158.
22. R. Ruel, K. T. Hogan, and P. Deslongchamps. Synlett. **9**, 516 (1990).
23. P. Deslongchamps. *In* Stereoelectronic effects in organic chemistry. *Edited by* J. E. Baldwin. Pergamon Press, Oxford. 1983. pp. 221–242.

Combined use of NMR, distance geometry, and restrained energy minimization for the conformational analysis of 8-lysine–vasopressin

CHIN YU,[1] TA-HORNG YANG, CHAO-JUNG YEH, AND LI-CHIN CHUANG
Chemistry Department, National Tsing Hua University, Hsin Chu, Taiwan 30043, Republic of China

Received September 4, 1991

CHIN YU, TA-HORNG YANG, CHAO-JUNG YEH, and LI-CHIN CHUANG. Can. J. Chem. **70,** 1950 (1992).

The conformation of the neurohypophyseal hormone, 8-lysine–vasopressin, in DMSO solution has been determined from 2D-NMR and distance geometry followed by the restrained energy minimization calculation. The conformation of 8-lysin-vasopressin in the 20-membered ring region is well defined but the acyclic tripeptide tail region is disordered.

CHIN YU, TA-HORNG YANG, CHAO-JUNG YEH et LI-CHIN CHUANG. Can. J. Chem. **70,** 1950 (1992).

En se basant sur les spectres RMN-2D et la géométrie des distances, suivie de calculs de minimisation des énergies restreintes, on a déterminé la conformation de l'hormone neurohypophysaire, 8-lysine–vasopressine. La conformation de ce composé est bien définie dans la région du cycle à 20 chaînon; elle est toutefois désordonnée dans la région de queue comportant le tripeptide acyclique.

[Traduit par la rédaction]

Can. J. Chem. Downloaded from www.nrcresearchpress.com by 217.78.4.112 on 09/08/12
For personal use only.

Introduction

8-Lysine–vasopressin (LysVP) consists of nine amino acid residues with the following sequence:

$$Cys^1\text{-}Tyr^2\text{-}Phe^3\text{-}Gln^4\text{-}Asn^5\text{-}Cys^6\text{-}Pro^7\text{-}Lys^8\text{-}Gly^9(NH_2)$$

It has a 20-membered disulfide-containing ring and an acylic tripeptide tail. LysVP has important biological properties (1, 2) such as milk ejecting, uterine contracting, and antidiuretic functions. It also interacts noncovalently with neurophysin protein (MW approx. 10 000) within the neurosecretory granules of the hypothalamo-neurohypophyseal tract (3). Many different models have been proposed for the 3D structure of LysVP on the basis of potential energy minimization (4), and NMR (5–11) and CD (12) spectroscopies. However, determination of the detailed structure of the LysVP molecule is incomplete and thus remains to be solved.

Recently, two-dimensional nuclear magnetic resonance (2D NMR) (13) and distance geometry (DG) (14–17) techniques have been combined to determine 3D molecular structure in solution. In DG techniques, a complete distance matrix is set up using a random choice of atom–atom distance (obtained by nuclear Overhauser enhancement (NOE) measurements and the covalent structure of the molecule). The matrix obtained is then embedded in 3D space and the resulting 3D structure is optimized to reduce the remaining atom–atom distance violations.

In the present study, the conformational properties of LysVP in DMSO solution were examined by NMR data and distance geometry calculation followed by restrained energy minimization.

Experimental

LysVP was obtain commercially (Auspep). LysVP (10 mg) was dissolved in 500 μL DMSO-d_6 (Aldrich) solution to make the concentration ~20 mmol L^{-1}. 4,4-Dimethyl-4-silapentane-1-sulfonate was used as an internal standard. The NMR tube was degassed and sealed. Phase-sensitive NOESY (18) spectra with four different mixing periods (τ_m = 60, 100, 180, and 300 ms) were recorded on a 400 MHz spectrometer (Bruker AM-400). Quadrature detection in w_1 was achieved using time-proportional phase incrementation (19); 512 t_1 increments were recorded, with 2048 complex data points. For each free induction, the decays were Fourier transformed in w_2 using a Kaiser window and in w_1 using a 45° phase-shifted sine-bell window. All two-dimensional data were processed on a computer (μVax III), using FTNMR software provided by Dr. D. Hare.

To plot the NOE buildup curves, the cross peaks of four NOESY spectra were volume integrated, and the curves were best fitted by least squares. The interproton distances, d_{ij}, were calculated according to the following relation (20)

$$d_{ij} = d_{lm}(\sigma_{lm}/\sigma_{ij})^{1/6}$$

in which d_{lm} stands for a known calibrated distance (1.78 Å for geminal protons), and σ_{lm}, σ_{ij} stand for the cross relaxation (NOE buildup) rate for spin l, m and spin i, j respectively (obtained from the initial slope of the NOE buildup curve). The DGEOM (21) program was acquired from QCPE, and pseudo atoms were taken into account in setting upper and lower bounds for the DG calculation (22). Restrained energy minimization calculations were performed on a Silicon Graphic 4D/25G computer by the program CHARMM (22). The molecular graphic program QUANTA (Polygen, Version 3.0) was used for displaying, analyzing, and plotting the structures.

A potential energy term representing the interproton distance restraints, $E_{NOE}(r_{ij})$, was added to the total energy of the system given by

$$E_{NOE} = \begin{cases} C_1(r_{ij} - r_{ij}^0), & \text{if } r_{ij} > r_{ij}^0 \\ C_2(r_{ij} - r_{ij}^0), & \text{if } r_{ij} < r_{ij}^0 \end{cases}$$

where r_{ij} and r_{ij}^0 are the calculated and target interproton distances respectively, and C_1 and C_2 are force constants given by

$$C_1 = \frac{k_B TS}{2(\Delta_{ij}^+)^2}, \qquad C_2 = \frac{k_B TS}{2(\Delta_{ij}^-)^2}$$

where k_B is the Boltzmann constant, T the absolute temperature, S a scale factor, and Δ_{ij}^+ and Δ_{ij}^- the positive and negative error estimates, respectively, of r_{ij}.

Structures were minimized by using the adopted basis Newton–Raphson algorithm (23). All hydrogen atoms capable of forming hydrogen bonds were included explicitly, but molecular bond lengths involving these atoms were kept fixed through the use of the constraint procedure SHAKE (24).

Results and discussion

Extraction of the NMR parameters

The ^{1}H NMR resonances were previously assigned (5–11). The NOESY spectra were particularly helpful in identifying

[1]Author to whom correspondence may be addressed.

Can. J. Chem. Downloaded from www.nrcresearchpress.com by 217.78.4.112 on 09/08/12
For personal use only.

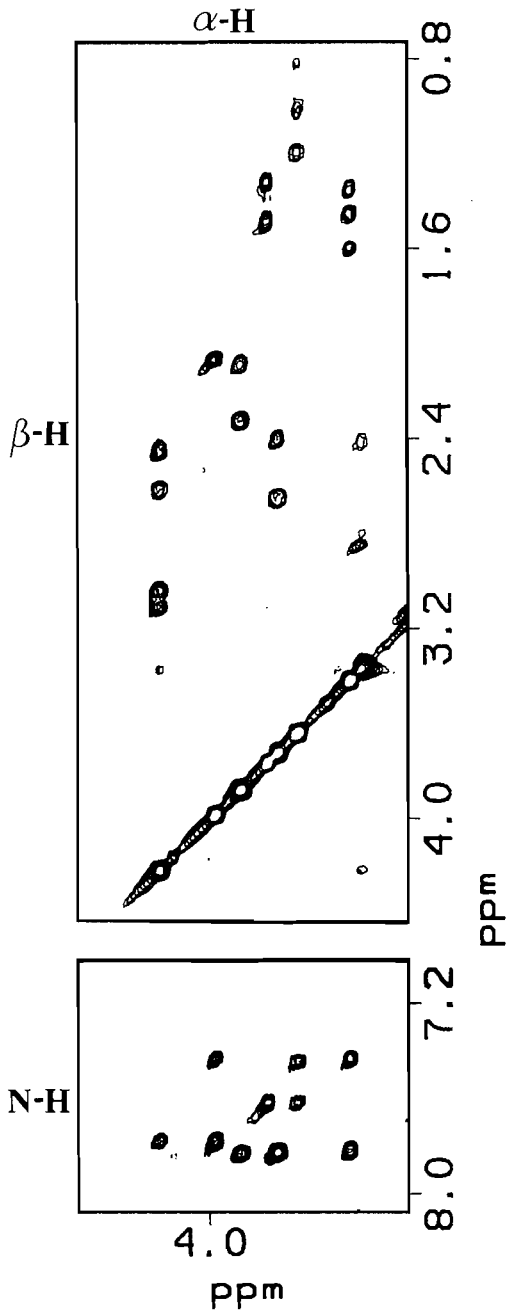

FIG. 1. NOESY spectrum (τ_m = 180 ms) of LysVP. Only amide protons are shown.

the conformation of LysVP. A contour plot of the NOESY (τ_m = 180 ms) spectrum observed for the amide proton range (w_2) is shown in Fig. 1. A total of 57 observable NOE's were used to set up distance constraints to define the conformation of the LysVP.

Initial cross-relaxation rates for each proton pair of NOE's were obtained from NOESY spectra recorded with four different mixing times and the interproton distances were calculated as described in the experimental section. The time dependence of some NOE's measured from NOESY spectra are shown in Fig. 2. Evaluation of the dependence of these cross peaks showed that the first few points were still in the domain in which buildup is linear with time.

The distances obtained by this approach were estimated

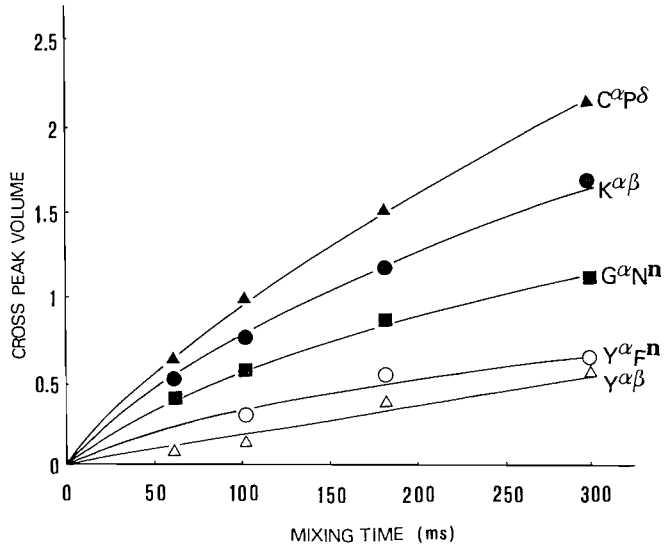

FIG. 2. Time dependence of some NOE's in LysVP measured from four different mixing times of NOESY spectra. The NOE buildup curves for corresponding cross peaks are identified by the IUPAC–IUB one-letter symbols for amino acids. The plot is of the volume of cross peaks against mixing time. The vertical scale is arbitrary since the cross-peak volumes were only measured relative to each other.

to have a precision better than ±0.5 Å, and the distance contraints used in the DG calculation are listed in Table 1. Pseudo atoms were taken into consideration as described by Wüthrich *et al.* (22).

Distance geometry structures

The distance geometry technique was repeatedly applied to LysVP using the 57 distance constraints given in Table 1. The 29 structures obtained were grouped into nine general conformational families by the SAS cluster analysis method (25). As shown in Table 2, root-mean-square distance (RMSD) values between all pairs among conformers are listed. The conformers correlated within a family are set off as rectangular sections.

Restrained energy minimization (REM)

For each of the nine families, we chose the structure nearest the center of the cluster as a representative,[2] and it was subjected to a final energy minimization with 57 distance restraints as described in the experimental section.

The results obtained by this procedure show that the coordinates of the side-chain atoms after restrained energy minimization (REM) vary somewhat from those of the DG structures, implying that the side chains move to energetically more favored positions. Figure 3 shows these nine REM structures (thin lines) superposed over the X-ray crystal structure (26) of pressionic acid (thick line), the cyclic moiety of vasopressin. It reveals clearly the similarities of solution conformations in the ring region of vasopressin with those of the crystal structure of pressionic acid. Table 3 shows the RMS difference values among nine REM structures. The positions of the backbone atoms of nine REM structures show smaller RMSD values in Table 3, indicating that the NMR constraints define the basic backbone folding of the molecule. From the superposition of nine REM structures (Fig.

[2]J. M. Blaney, private communication.

TABLE 1. Input distance constraints (Å) for distance geometry calculation on LysVP

Cys-1				Asn-5			
$C^{\alpha}H$	Cys-1	$C^{\beta}H$	2.00–5.60 c	NH	Asn-5	$C^{\beta}H$	2.00–5.60 c
$C^{\alpha}H$	Cys-6	$C^{\alpha}H$	2.00–5.00	NH	Asn-5	$C^{\alpha}H$	2.70–3.96
				$C^{\alpha}H$	Asn-5	$C^{\beta}H$	2.33–4.23 c
Tyr-2				$C^{\beta}H$	Asn-5	$C^{\delta}H$	2.29–4.09 a,c
NH	Tyr-2	$C^{\alpha}H$	2.00–500	$C^{\alpha}H$	Cys-6	NH	2.47–3.27
NH	Tyr-2	$C^{\delta}H$	2.00–7.40 d	NH	Cys-6	NH	2.34–3.34
$C^{\beta}H$	Tyr-2	$C^{\delta}H$	2.92–7.22 c,d	NH	Gln-4	$C^{\beta}H$	2.00–6.00 b
$C^{\alpha}H$	Tyr-2	$C^{\beta}H$	2.75–5.10 c	NH	Gln-4	$C^{\gamma}H$	2.00–6.00 b
$C^{\alpha}H$	Tyr-2	$C^{\delta}H$	2.03–5.40 d				
$C^{\alpha}H$	Phe-3	NH	2.79–3.39	Cys-6			
				NH	Cys-6	$C^{\alpha}H$	2.80–4.10
Phe-3				$C^{\alpha}H$	Cys-6	$C^{\beta}H$	2.40–4.59 c
NH	Phe-3	$C^{\alpha}H$	2.40–3.00	NH	Cys-6	$C^{\beta}H$	2.79–4.39 c
$C^{\alpha}H$	Phe-3	$C^{\delta}H$	2.00–7.40 d	$C^{\alpha}H$	Pro-7	$C^{\delta}H$	2.79–4.02 c
$C^{\beta}H$	Phe-3	$C^{\delta}H$	2.00–8.00 c,d	NH	Pro-7	$C^{\delta}H$	2.00–6.00 d
$C^{\delta}H$	Asn-5	$C^{\beta}H$	2.00–8.40 b,d	NH	Asn-5	$C^{\beta}H$	2.00–6.00 d
NH	Tyr-2	$C^{\beta}H$	2.00–6.00 b	$C^{\beta}H$	Gln-4	$C^{\epsilon}H$	2.00–7.00 a,c
$C^{\beta}H$	Asn-5	NH	2.00–6.00 b	NH	Asn-5	NH	2.00–5.00
$C^{\alpha}H$	Phe-3	$C^{\beta}H$	2.70–5.03 c				
NH	Phe-3	$C^{\beta}H$	2.00–5.60 c	Pro-7			
$C^{\alpha}H$	Gln-4	NH	2.00–5.00	$C^{\alpha}H$	Pro-7	$C^{\beta}H$	2.98–4.56 c
$C^{\epsilon}H$	Asn-5	NH	2.00–7.40 d	$C^{\gamma}H$	Pro-7	$C^{\delta}H$	2.00–6.20 c,c
				$C^{\alpha}H$	Lys-8	NH	2.00–5.00
Gln-4							
$C^{\alpha}H$	Gln-4	NH	2.50–3.62	Lys-8			
NH	Gln-4	$C^{\beta}H$	3.70–5.10 c	NH	Lys-8	$C^{\alpha}H$	3.21–4.01
$C^{\alpha}H$	Gln-4	$C^{\gamma}H$	3.00–5.28 c	NH	Lys-8	$C^{\beta}H$	3.71–5.11 c
$C^{\alpha}H$	Gln-4	$C^{\beta}H$	2.05–5.56 c	NH	Lys-8	$C^{\gamma}H$	1.80–2.90 c
$C^{\gamma}H$	Gln-4	$C^{\epsilon}H$	3.26–5.13 c,d	$C^{\alpha}H$	Lys-8	$C^{\beta}H$	2.70–5.28 c
$C^{\beta}H$	Gln-4	$C^{\gamma}H$	1.88–5.48 c,d	NH	Pro-7	$C^{\beta}H$	1.80–3.48 b
$C^{\alpha}H$	Asn-5	NH	2.88–3.48	$C^{\alpha}H$	Gly-9	NH	2.79–3.39
				$C^{\alpha}H$	Lys-8	$C^{\gamma}H$	2.00–5.60 c
				$C^{\beta}H$	Lys-8	$C^{\gamma}H$	2.00–6.20 c,c
				NH	Gly-9	NH	2.00–5.00
				$C^{\alpha}H$	Lys-8	$C^{\beta}H$	2.00–5.60 c
				Gly-9			
				NH	Gly-9	NH	2.73–3.23

Lower and upper bounds are given for each constraint. The letters a, b, c, and d after the upper distance bounds indicate that additional factors 1.0, 1.0, 0.6, and 2.4 Å, respectively, were added to the upper distance bounds. The additional terms corresponding to the letters a, b, c, and d account for lack of stereospecific assignments for methyl, methylene (long range), methylene (intraresidue), and ring protons, respectively.

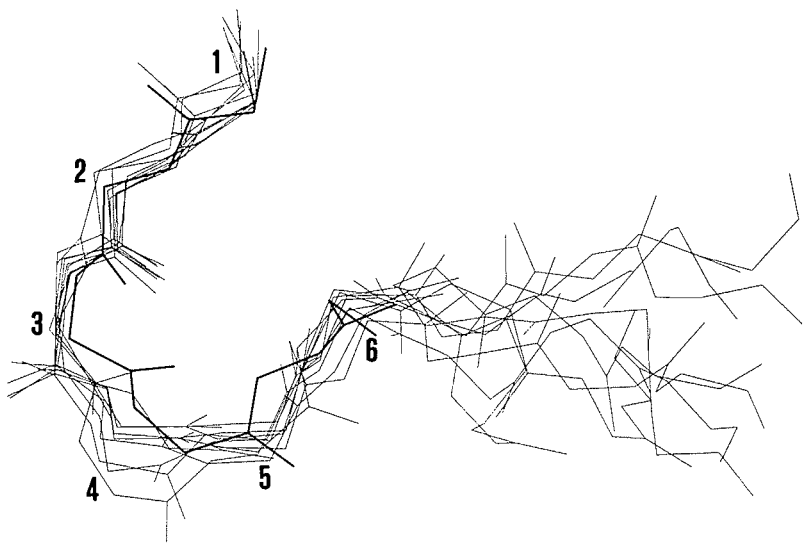

FIG. 3. Superposition of backbone atoms for nine restrained energy-minimized (REM) structures of LysVP (thin lines) and the X-ray crystal structure of pressionic acid (thick line), the cyclic moiety of LysVP. The sequence numbers are labeled at the C^{α} carbons in the 20-membered tocin ring. The disulfide bond is not shown.

Can. J. Chem. Downloaded from www.nrcresearchpress.com by 217.78.4.112 on 09/08/12
For personal use only.

Can. J. Chem. Downloaded from www.nrcresearchpress.com by 217.78.4.112 on 09/08/12
For personal use only.

TABLE 2. Families of geometrical structures

	I		II			III					IV			V		VI			VII			VIII				IX		
I	0.00	0.77	1.44	1.41	1.50	1.27	1.31	1.02	1.08	1.16	1.25	1.40	1.02	1.83	1.81	2.12	1.90	1.92	2.27	2.24	2.06	2.14	2.40	2.16	2.37	2.32	2.67	2.43	2.59
	0.77	0.00	1.37	1.48	1.53	1.20	1.30	1.02	1.14	1.34	1.26	1.25	0.99	1.73	1.69	2.05	1.87	1.83	2.35	2.26	2.10	2.08	2.32	2.15	2.30	2.27	2.85	2.57	2.63
	1.44	1.37	0.00	1.10	1.23	1.21	1.05	1.13	1.20	1.48	1.49	1.42	1.58	1.93	1.98	2.76	2.35	2.40	2.86	2.73	2.66	2.40	2.49	2.51	2.61	2.64	3.09	2.94	2.93
II	1.41	1.48	1.10	0.00	0.82	1.13	1.00	1.19	1.10	1.25	1.45	1.48	1.32	1.91	1.90	2.52	2.19	2.29	2.57	2.46	2.39	2.15	2.38	2.30	2.40	2.38	2.79	2.64	2.75
	1.50	1.53	1.23	0.82	0.00	1.14	1.02	1.28	1.21	1.12	1.56	1.52	1.40	1.84	1.98	2.47	2.07	2.23	2.56	2.38	2.31	2.10	2.23	2.25	2.24	2.28	2.68	2.56	2.47
	1.27	1.20	1.21	1.13	1.14	0.00	0.76	0.81	0.69	0.78	0.88	1.08	1.20	1.60	1.68	2.18	1.94	2.00	2.19	2.08	1.93	1.84	2.09	2.03	2.14	2.04	2.56	2.37	2.38
	1.31	1.30	1.05	1.00	1.02	0.76	0.00	0.90	0.74	0.93	1.05	1.13	1.30	1.63	1.73	2.38	2.12	2.14	2.31	2.23	2.13	2.07	2.20	2.16	2.31	2.17	2.66	2.50	2.55
III	1.02	1.02	1.13	1.19	1.28	0.81	0.90	0.00	0.61	0.79	0.99	1.11	1.09	1.80	1.88	2.23	2.02	2.07	2.23	2.16	2.06	2.16	2.24	2.09	2.23	2.20	2.71	2.50	2.59
	1.08	1.14	1.20	1.10	1.21	0.69	0.74	0.61	0.00	0.61	0.86	1.04	1.15	1.66	1.73	2.20	2.03	2.08	2.08	2.07	1.89	2.01	2.23	2.02	2.22	2.08	2.58	2.40	2.50
	1.16	1.34	1.48	1.25	1.12	0.78	0.93	0.79	0.61	0.00	1.13	1.29	1.25	1.70	1.89	2.12	1.92	2.04	1.95	1.95	1.75	1.97	2.15	1.98	2.11	2.00	2.38	2.23	2.28
	1.25	1.26	1.49	1.45	1.56	0.88	1.05	0.99	0.86	1.13	0.00	0.56	0.97	1.55	1.53	1.96	1.82	1.82	2.00	1.97	1.76	1.74	1.96	1.74	1.96	1.76	2.40	2.19	2.24
IV	1.40	1.25	1.42	1.48	1.52	1.08	1.13	1.11	1.04	1.29	0.56	0.00	0.94	1.47	1.49	1.97	1.77	1.76	2.09	2.02	1.81	1.70	1.88	1.69	1.85	1.75	2.47	2.28	2.23
	1.02	0.99	1.58	1.32	1.40	1.20	1.30	1.09	1.15	1.25	0.97	0.94	0.00	1.67	1.69	1.76	1.59	1.56	2.15	1.99	1.86	1.76	1.94	1.70	1.79	1.85	2.47	2.18	2.22
	1.83	1.73	1.93	1.91	1.84	1.60	1.63	1.80	1.66	1.70	1.55	1.47	1.67	0.00	0.71	1.55	1.25	1.26	1.55	1.47	1.32	1.08	1.31	1.25	1.49	1.31	1.93	1.66	1.66
V	1.81	1.69	1.98	1.90	1.98	1.68	1.73	1.88	1.73	1.89	1.53	1.49	1.69	0.71	0.00	1.71	1.49	1.46	1.75	1.77	1.58	1.18	1.66	1.49	1.74	1.57	2.16	1.86	1.93
	2.12	2.05	2.76	2.52	2.47	2.18	2.38	2.23	2.20	2.12	1.96	1.97	1.76	1.55	1.71	0.00	0.87	0.94	1.30	1.07	1.03	1.31	1.28	1.08	1.21	1.17	1.60	1.29	1.37
VI	1.90	1.87	2.35	2.19	2.07	1.94	2.12	2.02	2.03	1.92	1.82	1.77	1.59	1.25	1.49	0.87	0.00	0.76	1.53	1.20	1.13	1.07	1.18	1.03	1.12	1.24	1.69	1.45	1.42
	1.92	1.83	2.40	2.29	2.23	2.00	2.14	2.07	2.08	2.04	1.82	1.76	1.56	1.26	1.46	0.94	0.76	0.00	1.54	1.18	1.18	1.15	1.09	0.98	1.10	1.17	1.76	1.35	1.44
	2.27	2.35	2.86	2.57	2.56	2.19	2.31	2.23	2.08	1.95	2.00	2.09	2.15	1.55	1.75	1.30	1.53	1.54	0.00	0.96	0.92	1.51	1.44	1.20	1.48	1.29	1.18	1.09	1.28
VII	2.24	2.26	2.73	2.46	2.38	2.08	2.23	2.16	2.07	1.95	1.97	2.02	1.99	1.47	1.77	1.07	1.20	1.18	0.96	0.00	0.83	1.20	1.02	0.86	1.10	1.03	1.18	1.03	1.14
	2.06	2.10	2.66	2.39	2.31	1.93	2.13	2.06	1.89	1.75	1.76	1.81	1.86	1.32	1.58	1.03	1.13	1.18	0.92	0.83	0.00	1.05	1.28	0.90	1.17	0.90	1.35	1.12	1.17
	2.14	2.08	2.40	2.15	2.10	1.84	2.07	2.16	2.01	1.97	1.74	1.70	1.76	1.08	1.18	1.31	1.07	1.15	1.51	1.20	1.05	0.00	1.17	0.88	1.07	0.98	1.60	1.36	1.29
	2.40	2.32	2.49	2.38	2.23	2.09	2.20	2.24	2.23	2.15	1.96	1.88	1.94	1.31	1.66	1.28	1.18	1.09	1.44	1.02	1.28	1.17	0.00	0.88	0.79	0.97	1.36	1.24	1.10
VIII	2.16	2.15	2.51	2.30	2.25	2.03	2.16	2.09	2.02	1.98	1.74	1.69	1.70	1.25	1.49	1.08	1.03	0.98	1.20	0.86	0.90	0.88	0.88	0.00	0.64	0.70	1.38	1.11	1.13
	2.37	2.30	2.61	2.40	2.24	2.14	2.31	2.23	2.22	2.11	1.96	1.85	1.79	1.49	1.74	1.21	1.12	1.10	1.48	1.10	1.17	1.07	0.79	0.64	0.00	0.91	1.47	1.25	1.02
	2.32	2.27	2.64	2.38	2.28	2.04	2.17	2.20	2.08	2.00	1.76	1.75	1.85	1.31	1.57	1.17	1.24	1.17	1.29	1.03	0.90	0.98	0.97	0.70	0.91	0.00	1.40	1.09	1.07
	2.67	2.85	3.09	2.79	2.68	2.56	2.66	2.71	2.58	2.38	2.40	2.47	2.47	1.93	2.16	1.60	1.69	1.76	1.18	1.18	1.35	1.60	1.36	1.38	1.47	1.40	0.00	0.80	0.91
IX	2.43	2.57	2.94	2.64	2.56	2.37	2.50	2.50	2.40	2.23	2.19	2.28	2.18	1.66	1.86	1.29	1.45	1.35	1.09	1.03	1.12	1.36	1.24	1.11	1.25	1.09	0.80	0.00	0.88
	2.59	2.63	2.93	2.75	2.47	2.38	2.55	2.59	2.50	2.28	2.24	2.23	2.22	1.66	1.93	1.37	1.42	1.44	1.28	1.14	1.17	1.29	1.10	1.13	1.02	1.07	0.91	0.88	0.00

Differences (Å) for the positions of all atoms of 29 conformations generated by distance geometry; they can be subdivided into nine conformational families indicated by the Roman numerals. "Rectangles" indicate correlation within a family.

TABLE 3. The RMS differences for nine energy-minimized structures of vasopressin computed for the main chain atoms

	R M D structures								
	I	II	III	IV	V	VI	VII	VIII	IX
		←					For cyclic residues[a]		
I		1.62	1.08	1.07	1.23	1.33	0.87	1.54	1.22
II	1.72		1.64	1.46	1.60	1.60	1.33	1.70	1.36
III	1.97	2.00		0.73	0.79	0.67	1.05	1.25	1.36
IV	1.52	1.54	1.78		0.93	0.90	0.80	1.53	1.15
V	1.70	1.78	2.27	1.40		0.58	1.06	1.19	1.51
VI	2.22	2.45	1.53	2.24	2.60		1.12	1.12	1.43
VII	1.30	1.40	1.89	1.59	1.53	2.32		1.36	1.03
VIII	1.64	1.79	1.90	1.83	1.87	2.15	1.71		1.49
IX	2.05	2.31	1.79	2.37	2.84	1.60	2.27	2.31	
	for all residues →								

[a]The upper triangular values were computed for the cyclic (six) residues. The lower triangular values refer to all residues.

TABLE 4. Backbone dihedral angles of the nine selected structures of 8-lysine-vasopressin

Residue	Dihedral angle	I	II	III	IV	V	VI	VII	VIII	IX
Cys 1	ψ	163	164	−80	−62	−55	−130	96	72	128
Tyr 2	ϕ	−79	−101	−50	−11	−6	−177	−141	−122	−94
Tyr 2	ψ	−172	−131	−148	−143	−145	−146	−174	−56	−177
Phe 3	ϕ	64	52	60	54	67	69	54	−78	−78
Phe 3	ψ	−109	−125	−90	−133	−71	−69	−99	61	−166
Gln 4	ϕ	−151	−136	−166	−90	−178	−172	−75	68	72
Gln 4	ψ	−50	26	−53	−46	−50	−50	56	−47	−71
Asn 5	ϕ	−104	−147	−70	−133	−63	−86	56	−63	−161
Asn 5	ψ	138	109	138	143	81	106	75	73	162
Cys 6	ϕ	−174	−125	−160	−110	−127	−113	−86	−128	−169
Cys 6	ψ	−48	−49	−51	−45	70	126	105	77	−61
Pro 7	ϕ	−65	−66	−46	−4	−112	−14	−97	−54	−65
Pro 7	ψ	163	−180	−73	−124	−70	−134	−171	−65	−47
Lys 8	ϕ	54	−35	50	−176	−153	−143	−62	66	64
Lys 8	ψ	51	−69	51	68	159	31	−47	48	38
Gly 9	ϕ	−70	71	−73	−72	−65	177	72	−175	63

3, thin lines), it is readily apparent that the overall shape of the vasopressin fold is well reproduced. To emphasize this, the backbone dihedral angles of the nine REM structures are listed in Table 4. All REM structures in Fig. 3 show a somewhat similar pattern of backbone folding in the 20-membered ring, forming a β-turn comprising the sequence Tyr^2-Phe^3-Gln^4-Asn^5. This is consistent with the observation of long-term stability of the 20-membered tocin ring in the vasopressin molecule by molecular dynamics simulation (27). On the other hand, the acyclic tripeptide tail does not have a defined conformation and there are no specific interactions between the core and tail regions. The disorder of the acyclic tripeptide tail might be due to its conformational freedom, and this is consistent with observations in thin-film dialysis (28) and ^{13}C spin-lattice relaxation studies (29).

Acknowledgments

We thank Dr. D. Hare for providing FTNMR software and Dr. Blaney for helpful discussion. This work was supported by research grants from the National Science Council of the Republic of China (NSC81-0208-M007-81).

1. J. Rudinger. Recent Prog. Horm. Res. **28**, 131 (1972).
2. E. Breslow. Cell biology of secretory processes. *Edited by* M. Kautin. Karger, Basel. 1984.
3. I. M. Caiken, D. M. Abercrombie, T. Kanmera, and R. P. Sequiera. Pept. Protein Rev. **1**, 113 (1983).
4. B. Honig, E. A. Kabat, L. Katz, C. Levinthal, and T. T. Wu. J. Mol. Biol. **80**, 277 (1973).
5. D. H. Live and D. Cowburn. Biochemistry, **26**, 6415 (1987).
6. R. Deslauriers, I. C. P. Smith, and R. Walter. J. Am. Chem. Soc. **96**, 2289 (1974).
7. R. Walter, K. U. M. Prasad, R. Deslauriers, and I. C. P. Smith. Proc. Natl. Acad. Sci. U.S.A. **70**, 2086 (1973).
8. J. Lyerla and M. H. Freeman. J. Biol. Chem. **247**, 8183 (1972).
9. J. D. Glickson, D. W. Urry, and R. Walter. Proc. Natl. Acad. Sci. U.S.A., **69**, 2566 (1972).
10. P. H. Von Dreele, A. I. Brewster, J. Dadok, H. A. Scheraga, and F. A. Bovey. Proc. Natl. Acad. Sci. U.S.A. **69**, 2169 (1972).

Can. J. Chem. Downloaded from www.nrcresearchpress.com by 217.78.4.112 on 09/08/12
For personal use only.

11. P. H. Von Dreele, A. I. Brewster, M. F. Ferger, and V. Du Vigneaud. Proc. Natl. Acad. Sci. U.S.A. **68**, 1028 (1971).
12. V. J. Hruby, K. K. Deb, J. Fox, J. Bjarnason, and A. T. Tu. J. Biol. Chem. **253**, 6060 (1978).
13. K. Wüthrich. NMR of proteins and nucleic acids. John Wiley & Sons, New York. 1986.
14. G. M. Crippen and T. F. Havel. Acta Crystallogr. Sect. A: Cryst. Phys. Diffr. Theor. Gen. Crystallogr. **A34**, 282 (1978).
15. I. D. Kuntz, G. M. Crippen, and P. A. Kollman. Biopolymers, **18**, 939 (1979).
16. W. Braun and N. Go. J. Mol. Biol. **186**, 611 (1985).
17. T. F. Havel and K. Wüthrich. J. Mol. Biol. **182**, 281 (1985).
18. Anil-Kumar, G. Wagner, R. R. Ernst, and K. Wüthrich. J. Am. Chem. Soc. **103**, 3654 (1981).
19. D. Marion and K. Wüthrich. Biochem. Biophys. Commun. **113**, 967 (1983).
20. D. Gondol and G. Van Binst. Biopolymers, **25**, 977 (1986).
21. J. M. Blaney, G. M. Crippen, A. Dearing, and J. S. Dixon. DGEOM, Quantum Chemistry Program Exchange No. 590, Indiana University, Bloomington, Ind.
22. K. Wüthrich, M. Billeter, and W. Braun. J. Mol. Biol. **169**, 949 (1983).
23. O. Ermer. Struct. Bonding (Berlin), **27**, 161 (1976).
24. W. F. van Gunsteren and H. J. C. Berendsen. Mol. Phys. **34**, 1311 (1977).
25. SAS user's guide: statistics, version 5 edition. Cary, N.C. Institute Inc. 1985.
26. D. A. Langs, G. D. Smith, J. J. Stezowski, and R. E. Hughes. Science, **232**, 1240 (1986).
27. J. R. Somoza and J. W. Brady. Biopolymers, **27**, 939 (1988).
28. L. C. Craig, E. J. Harfenist, and A. C. Paladini. Biochemistry, **3**, 764 (1964).
29. R. Deslauriers, I. C. P. Smith, and R. Walter. J. Am. Chem. Soc. **96**, 2289 (1974).

Can. J. Chem. Downloaded from www.nrcresearchpress.com by 217.78.4.112 on 09/08/12
For personal use only.

Synthèses du β-L-rhamnopyranoside d'hordénine et d'acylgluco-L-rhamnopyranoses peracétylés

NADIA BOUGHANDJIOUA,[1] LIN RUI CHAO, ALEXIOS-LEANDROS SKALTSOUNIS, ELISABETH SEGUIN, FRANÇOIS TILLEQUIN ET MICHEL KOCH[2]

Laboratoire de pharmacognosie de l'Université René-Descartes, Unité associée au Centre national de la recherche scientifique, n° 1310, Faculté de pharmacie, 4, Avenue de l'Observatoire, 75006 Paris, France

Reçu le 5 décembre 1991

NADIA BOUGHANDJIOUA, LIN RUI CHAO, ALEXIOS-LEANDROS SKALTSOUNIS, ELISABETH SEGUIN, FRANÇOIS TILLEQUIN et MICHEL KOCH. Can. J. Chem. **70**, 1956 (1992).

La synthèse stéréosélective du β-L-rhamnopyranoside d'hordénine (**3**) a été possible grâce à l'emploi du bromure de 4-*O*-acétyl-2,3-*O*-carbonyl-α-L-rhamnopyranosyle (**14**). Les synthèses régiospécifiques des peracétyl-(*E*)-*O*-(6-*O*-cinnamoyl-β-D-glucopyranosyl)-(1 → 2)-, (1 → 3)- et (1 → 4)-α-L-rhamnopyranoses et de leurs homologues 4-acétoxycinnamiques ont été réalisées grâce à l'emploi de dérivés du rhamnose de type 1,2-*O*-orthoester pour la série (1 → 2), 2,3-*O*-orthoester pour la série (1 → 3) et 2,3-*O*-isopropylidène pour la série (1 → 4).

NADIA BOUGHANDJIOUA, LIN RUI CHAO, ALEXIOS-LEANDROS SKALTSOUNIS, ELISABETH SEGUIN, FRANÇOIS TILLEQUIN, and MICHEL KOCH. Can. J. Chem. **70**, 1956 (1992).

The stereoselective synthesis of hordenine β-L-rhamnopyranoside (**3**) was achieved using 4-*O*-acetyl-2,3-*O*-carbonyl-α-L-rhamnopyranosyl bromide (**14**) as key intermediate. The regiospecific syntheses of the peracetyl derivatives of (*E*)-*O*-(6-*O*-cinnamoyl-β-D-glucopyranosyl)-(1 → 2)-, (1 → 3)-, and (1 → 4)-α-L-rhamnopyranoses and of their 4-acetoxycinnamoyl counterparts were achieved through the use of various types of rhamnose-derived intermediates, i.e., 1,2-*O*-orthoester for the (1 → 2) series, 2,3-*O*-orthoester for the (1 → 3) series, and 2,3-*O*-isopropylidene for the (1 → 4) series.

L'étude chimique de *Selaginella doederleinii* Hieron, plante largement utilisée en médecine traditionnelle chinoise pour le traitement de diverses affections cardiovasculaires (1), a conduit antérieurement à l'isolement de divers glucoalcaloïdes dérivés de l'hordénine (2). Les deux constituants majoritaires sont l'α-L-rhamnopyranoside d'hordénine (**1**) et le (*E*)-*O*-(6-*O*-cinnamoyl-β-D-glucopyranosyl)-(1 → 3)-α-L-rhamnopyranoside d'hordénine (**2**). La structure de ce dernier a été définitivement établie à la suite d'une synthèse totale non régiospécifique de son dérivé acétylé (3). Par ailleurs, le mélange naturel des glucoalcaloïdes isolés de la plante montre, après administration orale chez le rat, une activité hypertensive marquée à rapprocher des effets thérapeutiques observés en médecine traditionnelle chinoise (4). Souhaitant disposer de glucoalcaloïdes purs et d'analogues en quantité suffisante pour étudier l'influence de divers paramètres structuraux sur l'activité pharmacologique, nous décrivons ici, d'une part la synthèse du β-L-rhamnopyranoside d'hordénine (**3**), d'autre part la synthèse régiospécifique des (*E*)-*O*-(6-*O*-cinnamoyl-β-D-glucopyranosyl)-(1 → 2)-, (1 → 3)- et (1 → 4)-α-L-rhamnopyranoses et des (*E*)-*O*-[6-*O*-(4-hydroxycinnamoyl)-β-D-glucopyranosyl]-(1 → 2)-, (1 → 3)- et (1 → 4)-α-L-rhamnopyranoses, sous forme de leurs dérivés peracétylés, précurseurs des glucoalcaloïdes correspondants, **4**, **5**, **6**, **7**, **8** et **9** (3).

La condensation de l'hordénine (**10**) avec le 1,2,3,4-tétra-*O*-acétyl-α,β-L-rhamnopyranose en présence de tétrachlorure d'étain avait conduit au 2,3,4-tri-*O*-acétyl-α-L-rhamnopyranoside d'hordénine (**11**) avec un rendement de 46% (3). L'étude des produits secondaires de cette réaction a permis ultérieurement l'isolement d'une faible quantité (rendement : 4%) de l'anomère β correspondant, **12**. Nous avons donc réalisé la même réaction en utilisant comme donneur de glycosyle le 1,4-di-*O*-acétyl-2,3-*O*-carbonyl-α,β-L-rhamnopyranose (**13**) (5), dépourvu de groupement acétyle participant en position 2, afin de favoriser la formation de l'anomère β (5–11). Le rendement global médiocre de cette dernière réaction (29%) et sa faible stéréosélectivité (α/β 7 : 3) nous ont conduit à envisager l'emploi du bromure de 4-*O*-acétyl-2,3-*O*-carbonyl-α-L-rhamnopyranosyle (**14**) (5) comme agent glycosylant. En effet, des réactifs associant des groupements 1-bromo et 2,3-*O*-carbonyl sur une unité rhamnose avaient été précédemment utilisés avec succès lors des synthèses des deux *O*-β-L-rhamnopyranosides d'aryle antérieurement décrits : ceux de 4-nitrophényle (12) et de quercet-3-yle (13). La condensation de l'hordénine (**10**) avec **14**, dans des conditions de transfert de phase, précédemment employées pour l'obtention de β-D-mannopyranosides d'aryle (14) et de β-L-rhamnopyranosides d'aryle (13), n'a toutefois pas conduit au produit escompté, mais au seul 4-*O*-acétyl-2,3-*O*-carbonyl-α-L-rhamnopyranoside d'hordénine (**15**) avec un rendement de 60%. Il semble donc probable que, sous l'influence du bromure de benzyltriéthylammonium, le bromure de 4-*O*-acétyl-2,3-*O*-carbonyl-α-L-rhamnopyranosyle (**14**) se soit transformé en anomère β correspondant avant la réaction de glycosidation. De telles inversions de configuration en position anomérique sous l'influence d'ammoniums quaternaires ont d'ailleurs été antérieurement observées en séries D-glucose, D-galactose et L-fucose (15). Finalement, la condensation de l'hordénine (**10**) avec le bromure **14**, en présence de carbonate d'argent (16, 17) a permis l'obtention, avec un rendement global de 83%, du mélange des glycosides anomères **15** (α) et **16** (β), dans un rapport 1 : 9, en faveur de l'anomère β. Les glycosides **15** et **16**, inséparables, ont été déprotégés par méthanolyse, puis acétylés pour donner les deux glycosides acétylés **11** (α) et **12** (β) qui ont pu alors être aisément séparés par chromatographie sur colonne de silice. Ils se différencient nettement

1. Adresse permanente : Département de pharmacie, Institut national d'enseignement supérieur en sciences médicales, B.P. 205, 23000 Annaba, Algérie.

2. Auteur correspondant.

Can. J. Chem. Downloaded from www.nrcresearchpress.com by 109.225.110.28 on 09/08/12
For personal use only.

par leurs spectres de rmn ^1H. Les signaux des protons H-1′ et H-5′ de l'anomère β (**12**) apparaissent comme prévu (18) à champs plus forts que les signaux homologues de **11**. De plus, des expériences de COSY à acquisition retardée effectuées sur **11** et **12** ont permis, dans le cas de l'anomére α, l'observation de couplages à longue distance entre H-1′ et H-4′ d'une part et H-1′ et H-6′ d'autre part, couplages qui n'ont pas été observés dans le cas de l'anomère β (**12**) (19). La méthanolyse du dérivé acétylé **12** a fourni le β-L-rhamnopyranoside d'hordénine (**3**) recherché.

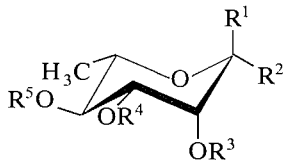

1	R^1 = 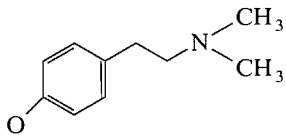		$R^2 = R^3 = R^4 = R^5 = H$	
3	$R^1 = R^3 = R^4 = R^5 = H$		R^2 = 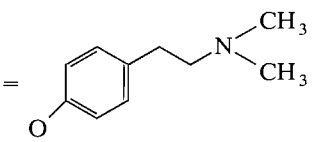	
11	R^1 = 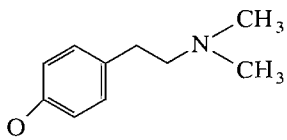	$R^2 = H$	$R^3 = R^4 = R^5 = COCH_3$	
12	$R^1 = H$	R^2 = 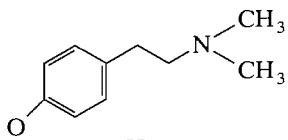	$R^3 = R^4 = R^5 = COCH_3$	
15	R^1 = 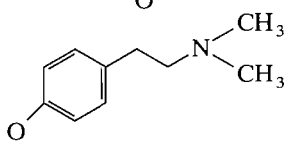	$R^2 = H$	$R^3 + R^4 = CO$	$R^5 = COCH_3$
16	$R^1 = H$	R^2 = 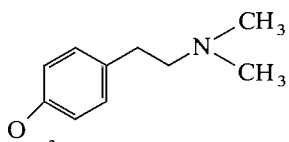	$R^3 + R^4 = CO$	$R^5 = COCH_3$
13	$R^1 = OCOCH_3$ $R^1 = H$	$R^2 = H$ $R^2 = OCOCH_3$	$R^3 + R^4 = CO$	$R^5 = COCH_3$
14	$R^1 = Br$	$R^2 = H$	$R^3 + R^4 = CO$	$R^5 = COCH_3$
18	$R^1 = OCH_3$	$R^2 = H$ $R^3 = COCH_3$	$R^4 = R^5 = CH_2C_6H_5$	
19	$R^1 = OCH_3$	$R^2 = R^3 = H$	$R^4 = R^5 = CH_2C_6H_5$	
28	$R^1 = OCH_3$	$R^2 = R^4 = H$	$R^3 = R^5 = COC_6H_5$	
29	$R^1 = OCH_3$	$R^2 = R^3 = R^4 = R^5 = H$		
40	$R^1 = OCH_3$	$R^2 = R^4 = H$	$R^3 = R^5 = COCH_3$	
43	$R^1 = OCH_3$	$R^2 = R^5 = H$	$R^3 + R^4 = C(CH_3)_2$	

La synthèse régiospécifique des composés **4** et **7** suppose la synthèse préalable d'un dérivé du rhamnose convenablement protégé en positions 1, 3 et 4. Un tel dérivé peut être obtenu à partir d'un 1,2-*O*-alkylorthoester, selon une approche initialement développée en série mannose (20, 21). Le traitement du *O-exo*-3,4-di-*O*-benzyl-1,2-*O*-(1-méthoxyéthylidène)-β-L-rhamnopyranose (**17**) (22), par le tétrachlorure d'étain dans le dichlorométhane (23) a fourni le 2-*O*-acétyl-3,4-di-*O*-benzyl-α-L-rhamnopyranoside de méthyle (**18**) qui a été désacétylé par la méthode de Zemplén pour conduire au 3,4-di-*O*-benzyl-α-L-rhamnopyranoside de méthyle (**19**) (24). La glycosylation de ce dernier par le bromure de 2,3,4-tri-*O*-acétyl-6-*O*-chloroacétyl-α-D-glucopyranosyle (**20**) (25, 26), en présence de cyanure mercurique n'a permis l'obtention du disaccharide recherché **21** que lorsque la réaction a été effectuée dans le nitrométhane anhydre (27, 28). Tous les autres essais de couplage réalisés, en particulier dans l'acétonitrile, n'ont en effet permis l'obtention que du seul orthoester **22**. L'hydrogénolyse de **21** a fourni le diol **23**, aisément transformé en dérivé acétylé **24** par acétolyse–acétylation (5, 29). La déprotection sélective du groupement chloroacétyle de **24**, réalisée par action de la

Can. J. Chem. Downloaded from www.nrcresearchpress.com by 109.225.110.28 on 09/08/12
For personal use only.

thiourée dans le méthanol (26), a permis l'obtention du disaccharide **25** qui, traité soit par le chlorure de (*E*)-cinnamoyle, soit par le chlorure de (*E*)-4-acétoxycinnamoyle (30), a conduit aux disaccharides recherchés **26** et **27**.

La synthèse régiosélective des composés **5** et **8** nécessite la préparation d'un dérivé du rhamnose protégé en positions 1, 2 et 4. Les seuls composés de ce type antérieurement décrits au début de ce travail étaient des 2,4-di-*O*-benzoyl-

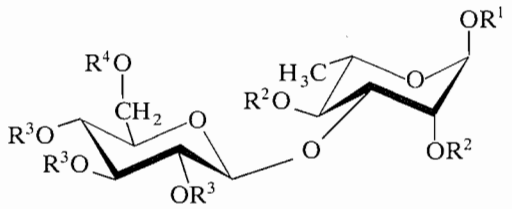

2 R^1 = 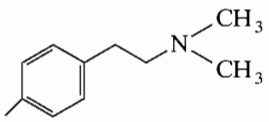 $R^2 = R^3 = H$ R^4 = 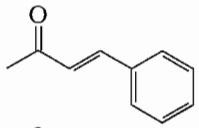

5 R^1 = 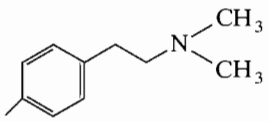 $R^2 = R^3 = COCH_3$ R^4 = 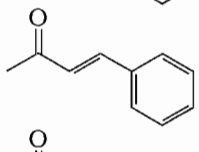

8 R^1 = 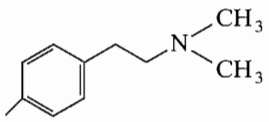 $R^2 = R^3 = COCH_3$ R^4 = 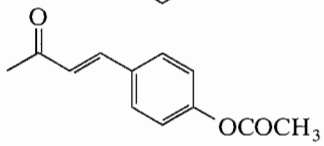

31 $R^1 = CH_3$ $R^2 = COC_6H_5$ $R^3 = R^4 = COCH_3$

33 $R^1 = CH_3$ $R^2 = R^3 = R^4 = H$

34 $R^1 = CH_3$ $R^2 = R^3 = COCH_3$ $R^4 = C(C_6H_5)_3$

35 $R^1 = CH_3$ $R^2 = R^3 = COCH_3$ $R^4 = H$

36 $R^1 = CH_3$ $R^2 = R^3 = COCH_3$ R^4 = 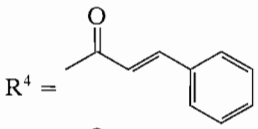

37 $R^1 = CH_3$ $R^2 = R^3 = COCH_3$ R^4 = 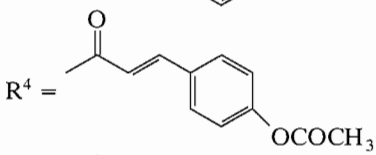

38 $R^1 = R^2 = R^3 = COCH_3$ R^4 = 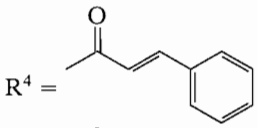

39 $R^1 = R^2 = R^3 = COCH_3$ R^4 = 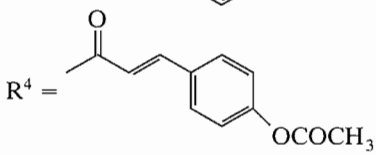

α-L-rhamnopyranosides (31, 32), préparés par benzoylation en 4 puis clivage sélectif, en milieu acide faible, de 2,3-*O*-orthobenzoates intermédiaires. Le 2,4-di-*O*-benzoyl-α-L-rhamnopyranoside de méthyle (**28**) (33) a été préparé à partir de l'α-L-rhamnopyranoside de méthyle (**29**) (29, 34) en utilisant cette méthode. Sa glycosylation par le bromure de 2,3,4,6-tétra-*O*-acétyl-α-D-glucopyranosyle (**30**), en présence de cyanure mercurique dans le nitrométhane (27, 28), a fourni le β-glucoside **31**, accompagné de traces de l'α-glucoside **32**. Le disaccharide **31** a été désacétylé pour donner **33** qui a été sélectivement tritylé en position 6′ par le chlorure de triphénylméthyle, puis peracétylé par l'anhydride acétique pour donner **34**. L'hydrogénolyse du trityle a permis l'accès à **35**, précurseur commun aux glucorhamnosides acylés **36** et **37**, par acylation avec le chlorure de (*E*)-cinnamoyle ou de (*E*)-4-acétoxycinnamoyle. L'acétolyse de **36** et **37** (5, 29) a finalement permis l'obtention des disaccharides **38** et **39** recherchés. Toutefois, le rendement global de cette suite de réactions est très faible. Nous avons donc tenté d'utiliser une approche similaire, mais en utilisant l'ouverture d'un orthoacétate au premier stade de la synthèse compte-tenu de données précédemment publiées sur le comportement en milieu acide de 3,4-*O*-orthoacétates de série galactose (36). Le traitement de l'α-L-rhamnopyranoside de

Can. J. Chem. Downloaded from www.nrcresearchpress.com by 109.225.110.28 on 09/08/12
For personal use only.

méthyle (**29**) par le triméthylorthoacétate, suivi de l'acétylation de l'orthoester intermédiaire et de son hydrolyse acide a conduit au 2,4-di-*O*-acétyl-α-L-rhamnopyranoside de méthyle (**40**), avec un rendement de 85%, en accord avec des données publiées très récemment en série rhamnose (37). La glycosylation de **40** par le bromure de (*E*)-2,3,4-tri-*O*-acétyl-6-*O*-cinnamoyl-α-D-glucopyranosyle (**41**) (3) ou de (*E*)-6-*O*-(4-acétoxycinnamoyl)-2,3,4-tri-*O*-acétyl-α-D-glucopyranosyle (**42**) (3) a donné ensuite les glucorhamnosides acylés **36** et **37** qui ont été soumis à une acétolyse pour fournir les disaccharides peracétylés **38** et **39**.

La synthèse régiospécifique des disaccharides peracétylés précurseurs des composés **6** et **9** (3) a mis à profit la condensation du 2,3-*O*-isopropylidène-α-L-rhamnopyranoside de méthyle (**43**) antérieurement décrit (29) avec les bromures de glucopyranosyle **41** ou **42** (3), en présence de cyanure mercurique dans l'acétonitrile. Les groupements isopropylidène des glucorhamnosides de méthyle **44** et **45** obtenus ont été ensuite hydrolysés par l'acide trifluoroacétique dans le chloroforme (29) pour conduire aux diols **46** et **47**. L'acétolyse–acétylation de ces derniers (5, 29) a fourni les disaccharides acétylés recherchés **48** et **49**.

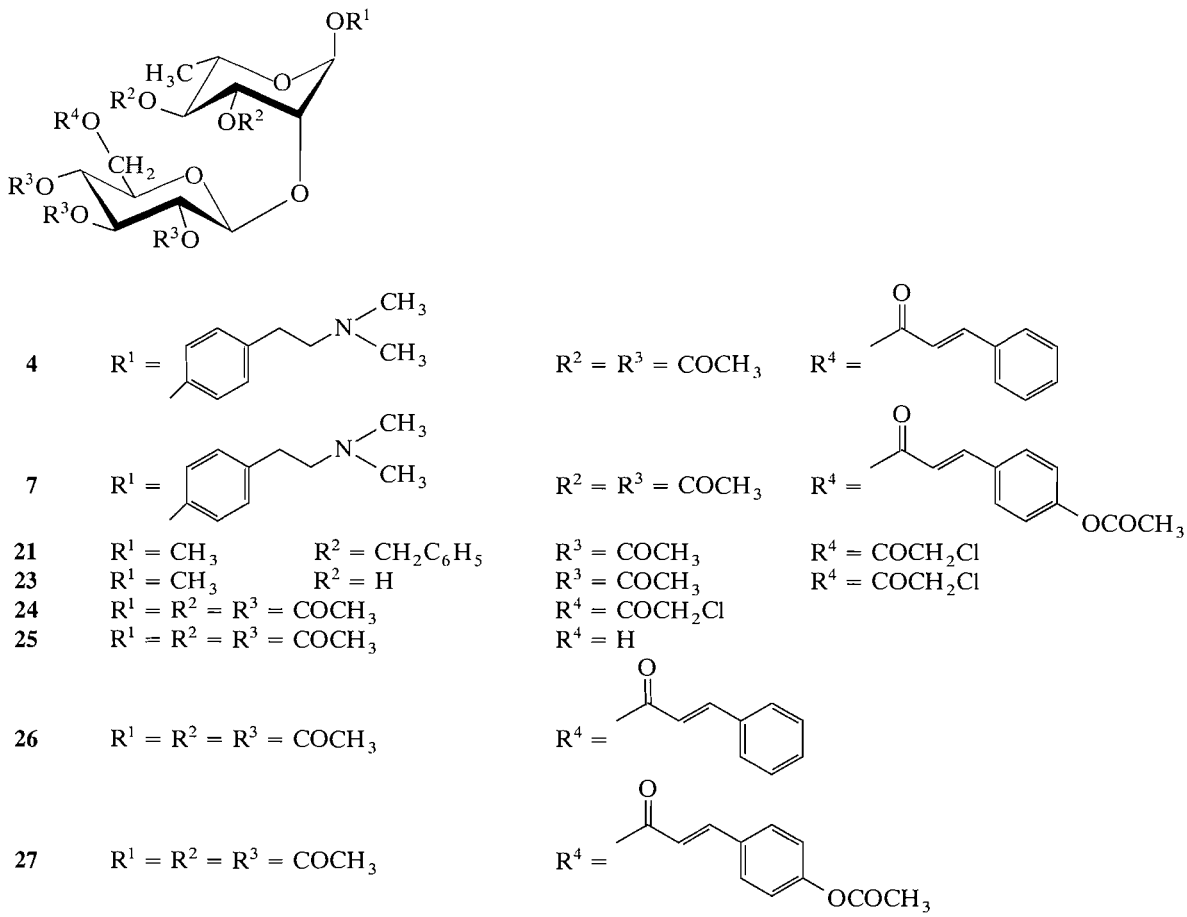

Partie expérimentale

Méthodes générales

Les points de fusion sont déterminés au moyen d'un microscope à platine chauffante Reichert et ne sont pas corrigés. Les pouvoirs rotatoires sont mesurés à 20°C à l'aide d'un polarimètre Perkin–Elmer 241, les spectres ir enregistrés sur un appareil Unicam SP 3-200. Les spectres de masse sont effectués en désorption – ionisation chimique (dic) sur un spectromètre Nermag R10-10C, en utilisant l'ammoniac comme gaz réactant. Les spectres de rmn du proton sont réalisés en solution dans le $CDCl_3$ (sauf indication contraire), en utilisant le tétraméthylsilane comme étalon interne, à l'aide d'un appareil Bruker HX 270 (270 MHz).

Après extraction des milieux réactionnels, les solvants organiques sont séchés sur Na_2SO_4 et évaporés sous pression réduite à 40°C. Les chromatographies sur colonne sont réalisées à l'aide de gel de silice Merck 60 (230–400 mesh) ou 60H.

2,3,4-Tri-O-acétyl-β-L-rhamnopyranoside d'hordénine (12)

On ajoute, sous agitation magnétique, une solution de bromure de 4-*O*-acétyl-2,3-*O*-carbonyl-α-L-rhamnopyranosyle (**14**) (5) (0,6 g) dans le dichlorométhane anhydre (5 mL) à un mélange d'hordénine (**10**) (0,088 g, 0,53 mmol), de carbonate d'argent (0,7 g) et de tamis moléculaire 4 Å (1 g) dans du dichlorométhane anhydre (10 mL). Le milieu réactionnel est maintenu sous agitation à 20°C pendant 14 h, puis filtré et évaporé à sec. Après chromatographie (CH_2Cl_2–CH_3OH–ammoniaque à 34%, 90 : 10 : 1), on obtient 0,116 g (83%) d'un mélange non séparable de rhamnosides **15** et **16**. Ce mélange est additionné de méthanolate de sodium 0,1 N dans le méthanol (2 mL) puis maintenu 30 min sous agitation magnétique. La solution est neutralisée par addition de résine Amberlite IRC 50 H^+, filtrée et évaporée à sec. On obtient 0,130 g d'un mélange de rhamnosides **1** et **3** non séparables. Ce mélange, dissous dans la pyridine (1 mL), est additionné d'anhydride acétique (1 mL), abandonné 24 h à 20°C, puis évaporé à sec. Après chromatographie (CH_2Cl_2–CH_3OH, 95 : 5), on obtient successivement le 2,3,4-tri-*O*-acétyl-α-L-rhamnopyranoside

Can. J. Chem. Downloaded from www.nrcresearchpress.com by 109.225.110.28 on 09/08/12
For personal use only.

d'hordénine (**11**) (0,016 g, 7%) et le 2,3,4-tri-*O*-acétyl-β-L-rhamnopyranoside d'hordénine (**12**) (0,144 g, 74%) : $[\alpha]_D$ −2 (*c* 0,5, $CHCl_3$); ir (KBr) : 2960, 1750, 1610, 1510, 1375, 1225, 1130, 1020, 920, 830, cm^{-1}; rmn ^1H : 7,11 (2H, d, *J* 8,5 Hz, H-3, H-5), 6,91 (2H d, *J* 8,5 Hz, H-2, H-6), 5,62 (1H, dd, *J* 3, 0,5 Hz, H-2′), 5,15 (1H, d, *J* 0,5 Hz, H-1′), 5,11 (1H, t, *J* 9 Hz, H-4′), 5,05 (1H, dd, *J* 9, 3 Hz, H-3′), 3,65 (1H dq, *J* 9, 6 Hz, H-5′), 2,73 (2H, m, CH_2-7), 2,49 (2H, m, CH_2-8), 2,27 (6H, s, $N(CH_3)_2$), 2,23 2,06, 2,01 (3×3H, 3s, $3OCOCH_3$), 1,33 (3H, d, *J* 6 Hz, CH_3-6′); sm (dic) *m/z* : 438 $(M + H)^+$, 396, 166. Anal. calc. pour $C_{22}H_{31}NO_8$: C 60,40; H 7,14; N 3,20; trouvé : C 60,61; H 7,12; N 3,23.

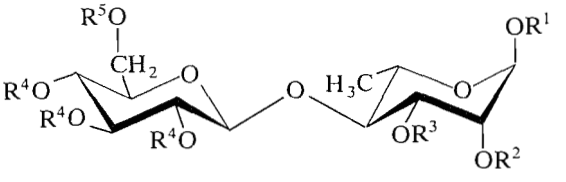

6 R^1 = 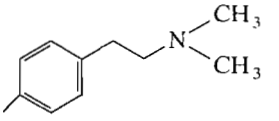 $R^2 = R^3 = R^4 = COCH_3$ R^5 = 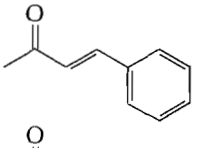

9 R^1 = 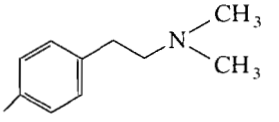 $R^2 = R^3 = R^4 = COCH_3$ R^5 = 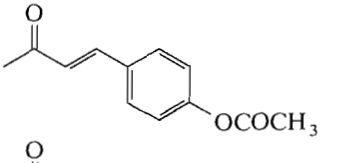

44 $R^1 = CH_3$ $R^2 + R^3 = C(CH_3)_2$ $R^4 = COCH_3$ R^5 = 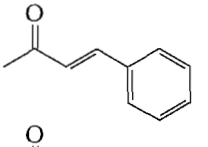

45 $R^1 = CH_3$ $R^2 + R^3 = C(CH_3)_2$ $R^4 = COCH_3$ R^5 = 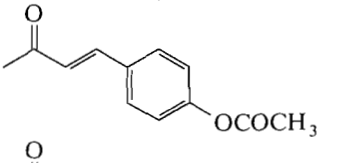

46 $R^1 = CH_3$ $R^2 = R^3 = H$ $R^4 = COCH_3$ R^5 = 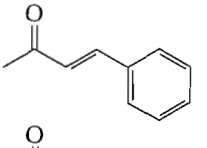

47 $R^1 = CH_3$ $R^2 = R^3 = H$ $R^4 = COCH_3$ R^5 = 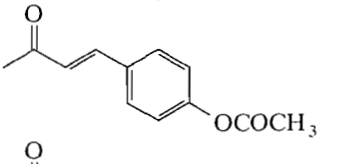

48 $R^1 = R^2 = R^3 = R^4 = COCH_3$ R^5 = 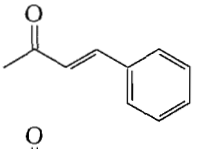

49 $R^1 = R^2 = R^3 = R^4 = COCH_3$ R^5 = 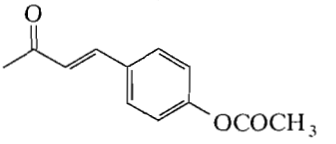

*β-L-Rhamnopyranoside d'hordénine (**3**)*

Une solution de 2,3,4-tri-*O*-acétyl-β-L-rhamnopyranoside d'hordénine (**12**) (0,04 g, 0.09 mmol) dans le méthanolate de sodium 0,1 N dans le méthanol (2 mL) est maintenue sous agitation magnétique à 20°C pendant 30 min. Après neutralisation par addition de résine Amberlite IRC 50 H^+, filtration et évaporation sous pression réduite on obtient le β-L-rhamnopyranoside d'hordénine (**3**) (0,025 g, 89%) : $[\alpha]_D$ +44 (*c* 0,4, EtOH); ir (KBr) : 3400, 2940, 1620, 1520, 1240, 1130, 1070, 1025, 990, 830 cm^{-1} ; rmn ^1H (DMSO-d_6) : 7,33 (2H, d, *J* 9 Hz, H-3, H-5), 6,88 (2H, d, *J* 9 Hz, H-2, H-6), 5,12 (1H, d, *J* 0,5 Hz, H-1′), 3,86 (1H, dd, *J* 3, 0,5 Hz, H-2′), 3,37 (1H, dd, *J* 9, 3 Hz, H-3′), 3,30 (1H, dq, *J* 9, 6 Hz, H-5′), 3,20 (1H, t, *J* 9 Hz, H-4′), 2,65 (2H, t, *J* 9 Hz CH_2-7), 2,43 (2H, t, *J* 9 Hz, CH_2-8), 2,24 (6H, s, $N(CH_3)_2$), 1,15 (3H, d, *J* 6 Hz, CH_3-6′); sm (dic) *m/z* : 312 $(M + H)^+$, 222, 166 Anal. calc. pour $C_{16}H_{25}NO_5$: C 61,71; H 8,09; N 4,50; trouvé : C 61,67; H 8,12; N 4,47.

*3,4-Di-O-benzyl-2-(2,3,4-tri-O-acétyl-6-O-chloroacétyl-β-D-glucopyranosyl)-α-L-rhamnopyranoside de méthyle (**21**)*

Une solution de 3,4-di-*O*-benzyl-α-L-rhamnoside de méthyle (**19**) (24) (0,358 g, 1 mmol) dans un mélange de benzène anhydre (20 mL) et de nitrométhane (20 mL) est distillée à pression atmosphérique jusqu'à élimination de la moitié du mélange solvant

Can. J. Chem. Downloaded from www.nrcresearchpress.com by 109.225.110.28 on 09/08/12
For personal use only.

Après refroidissement à 45°C, on ajoute du cyanure mercurique (0,5 g) et du bromure de 2,3,4-tri-*O*-acétyl-6-*O*-chloroacétyl-α-D-glucopyranosyle (**20**) (25, 26) (0,9 g, 2 mmol). Le milieu réactionnel est agité 24 h à température ambiante, dilué par addition de chloroforme (20 mL), puis évaporé à sec. Le résidu est dissous dans le chloroforme (50 mL), filtré, puis lavé par une solution aqueuse de KI à 5% (2 × 25 mL) et par de l'eau (5 × 25 mL). La phase organique fournit un résidu qui, après chromatographie (hexane-EtOAc, 85 : 15), permet d'obtenir le disaccharide **21** (0,197 g, 27%) : $[\alpha]_D$ +27 (*c* 2, MeOH); ir ($CHCl_3$) : 2920, 1750, 1600, 1500, 1440, 1365, 1310, 1130, 1030, 975, 885 cm^{-1}; rmn ^1H : 7,35–7,30 (10H, m, Ar-*H*), 5,22 (1H, t, *J* 9 Hz, H-3′), 5,06 (1H, dd, *J* 9, 8 Hz, H-2′), 5,02 (1H, t, *J* 9 Hz, H-4′), 4,79, 4,69, 4,59, 4,58 (4 × 1H, 4d, *J* 11 Hz, $2OCH_2$-Ar), 4,68 (1H, d, *J* 2 Hz, H-1), 4,60 (1H, d, *J* 8 Hz, H-1′), 4,29 (2H, m, CH_2-6′), 4,09 (2H, s, $OCOCH_2Cl$), 3,85 (1H, dd, *J* 3, 2 Hz, H-2), 3,80 (1H, dd, *J* 9, 3 Hz, H-3), 3,62 (2H, m, H-5, H-5′), 3,34 (1H, t, *J* 9 Hz, H-4), 3,31 (3H, s, OCH_3), 2,03, 2,01, 1,97 (3 × 3H, 3s, $3OCOCH_3$), 1,30 (3H, d, *J* 6,5 Hz, CH_3-6); sm (dic) *m/z* : 742 $(M + NH_4)^+$, 740 $(M + NH_4)^+$, 708, 706, 376, 367, 365, 108, 91. Anal. calc. pour $C_{35}H_{43}O_{14}Cl$: C 58,13; H 5,99; Cl 4,90; trouvé : C 58,05; H 6,01; Cl 4,93.

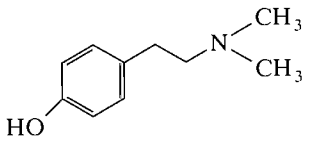

10

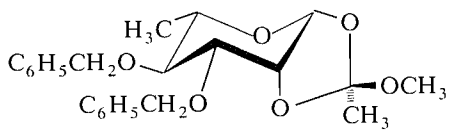

17

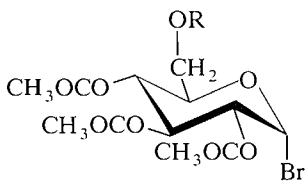

20 R = $COCH_2Cl$

30 R = $COCH_3$

41 R =

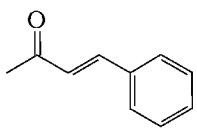

42 R =

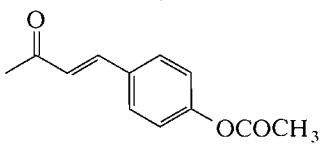

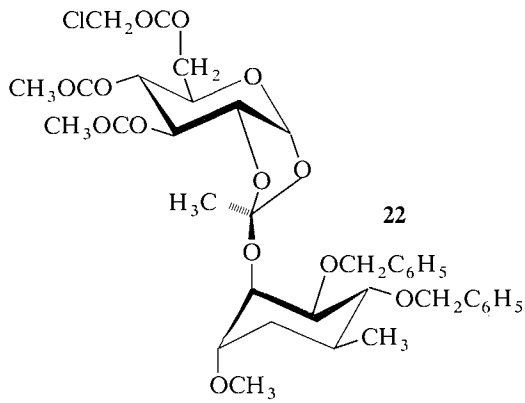

22

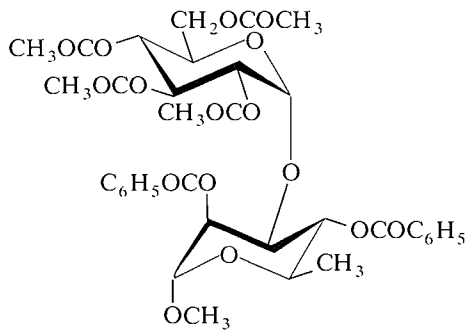

32

3,4-Di-O-acétyl-6-O-chloroacétyl-1,2-O-(3,4-di-O-benzyl-α-L-rhamnopyranoside-2-yl de méthyle)-orthoacétyl-α-D-glucopyranose (22)

On ajoute du cyanure mercurique (0,125 g), puis du bromure de 2,3,4-tri-*O*-acétyl-6-*O*-chloroacétyl-α-D-glucopyranosyle (**20**) (25, 26) (0,45 g, 1 mmol) et du tamis moléculaire 3 Å (0,5 g) à une solution de 3,4-di-*O*-benzyl-α-L-rhamnopyranoside de méthyle (**19**) (24) (0,115 g, 0,3 mmol) dans l'acétonitrile anhydre (5 mL). Après agitation pendant 6 h à température ambiante, on ajoute du chlorure mercurique sec (0,125 g). L'agitation est poursuivie pendant 24 h, puis le milieu réactionnel est filtré sur Célite, concentré et le résidu sirupeux obtenu, en solution dans du dichlorométhane (20 mL), est lavé successivement par une solution aqueuse saturée de $NaHCO_3$ (2 × 15 mL), une solution aqueuse de KI à 10% (15 mL) et par de l'eau (3 × 15 mL). La phase organique est séchée et concentrée. Par chromatographie (hexane–EtOAc, 85 : 15) du résidu, on obtient l'orthoester **22** (0,093 g, 43%) : $[\alpha]_D$ +24 (*c* 2, MeOH); ir ($CHCl_3$) : 2920, 2840, 1750, 1600, 1370, 1110, 1045, 985, 905 cm^{-1}; rmn ^1H : 7,29–7,24 (10H, m, Ar-*H*), 5,68 (1H, d, *J* 5 Hz, H-1′), 5,05 (1H, t, *J* 3 Hz, H-3′), 4,88, 4,75, 4,64, 4,60,

Can. J. Chem. Downloaded from www.nrcresearchpress.com by 109.225.110.28 on 09/08/12
For personal use only.

Can. J. Chem. Downloaded from www.nrcresearchpress.com by 109.225.110.28 on 09/08/12
For personal use only.

(4 × 1H, 4d, *J* 11 Hz, 2O-CH_2-Ar), 4,84 (1H, dd, *J* 9, 3 Hz, H-4'), 4,57 (1H, d, *J* 2 Hz, H-1), 4,50 (1H, dd, *J* 5, 3 Hz, H-2'), 4,26 (2H, m, CH_2-6'), 4,09 (2H, s, OCOCH_2Cl), 4,00 (1H, dd, *J* 3, 2 Hz, H-2), 3,91 (1H, ddd, *J* 9, 5, 2,5 Hz, H-5') 3,80 (1H, dd, *J*9, 3 Hz, H-3), 3,62 (1H, dq, *J* 9, 6,5 Hz, H-5), 3,43 (1H, t, *J* 9 Hz, H-4), 3,30 (3H, s, OCH_3), 2,10, 2,02 (2 × 3H, 2s, 2OCOCH_3), 1,71 (3H, s, CCH_3), 1,32 (3H, d, *J* 6,5 Hz, CH_3-6); sm (dic) *m/z* : 742 $(M + NH_4)^+$, 740 $(M + NH_4)^+$, 427, 376, 367, 365, 344, 108, 91. Anal. calc. pour $C_{35}H_{43}O_{14}Cl$: C 58,13; H 5,99; Cl 4,90; trouvé : C58,29; H 5,97; Cl 4,88.

2-O-(2,3,4-Tri-O-acétyl-6-O-chloroacétyl-β-D-glucopyranosyl)-α-L-rhamnopyranoside de méthyle (23)

Une solution du disaccharide **21** (0,256 g, 0,35 mmol) dans le méthanol (10 mL) est additionnée de palladium à 10% sur charbon (0,2 g), puis maintenue 2 h sous atmosphère d'hydrogène à la pression atmosphérique. Le catalyseur est éliminé par filtration et la solution concentrée. Le résidu obtenu fournit, après chromatographie (CH_2Cl_2–CH_3OH, 98 : 2), le diol **23** (0,12 g, 62%) : $[\alpha]_D$ +21 (*c* 1,5, MeOH) ; ir ($CHCl_3$) : 3580, 2920, 2840, 1750, 1605, 1370, 1135, 1060, 970, 895 cm^{-1} ; rmn ^1H : 5,19 (1H, t, *J* 9 Hz, H-3'), 5,03 (1H, t, *J* 9 Hz, H-4'), 5,03 (1H, dd, *J* 9, 8 Hz, H-2'), 4,78 (1H, d, *J* 1 Hz, H-1), 4,65 (1H, d, *J* 8 Hz, H-1'), 4,23 (2H, m, CH_2-6'), 4,10 (2H, s, OCOCH_2Cl), 3,82 (1H, dd, *J* 3, 1 Hz, H-2), 3,71 (2H, m, H-3, H-5'), 3,56 (1H, dq, *J* 9, 6,5 Hz, H-5), 3,33 (3H, s, OCH_3), 3,30 (1H, t, *J* 9 Hz, H-4), 2,30 (1H, s, large, éch. D_2O, O*H*), 2,02, 2,00, 1,99 (3 × 3H, 3s, 3OCOCH_3), 1,66 (1H, s large, éch. D_2O, O*H*), 1,30 (3H, d, *J* 6,5 Hz, CH_3-6); sm (dic) *m/z* : 562 $(M + NH_4)^+$, 560 $(M + NH_4)^+$, 526, 366, 362, 337, 289, 178. Anal. calc. pour $C_{21}H_{31}O_{14}Cl$: C 46,45; H 5,75; Cl 6,52; Trouvé : C 46,28; H 5,73; Cl 6,55.

1,3,4-Tri-O-acétyl-2-O-(2,3,4-tri-O-acétyl-6-O-chloroacétyl-β-D-glucopyranosyl)-α-L-rhamnopyranose (24)

Une solution de diol **23** (0,100 g, 0,18 mmol) dans l'anhydride acétique (0,3 mL) est additionnée d'anhydride acétique contenant 1% d'H_2SO_4 (0,3 mL), puis agitée 1 h à 20°C. Après addition d'eau (20 mL), l'agitation est poursuivie pendant 2 h, puis la solution extraite par le dichlorométhane (2 × 20 mL). La solution organique est lavée par une solution aqueuse saturée de $NaHCO_3$ (2 × 20 mL), par de l'eau (20 mL), séchée, puis concentrée pour donner le disaccharide **24** (0,095 g, 77%) : $[\alpha]_D$ ±0 (*c* 1, MeOH); ir ($CHCl_3$) : 2920, 2840, 1750, 1600, 1370, 1130, 1035, 980, 910 cm^{-1}; rmn ^1H : 6,11 (1H, d, *J* 2 Hz, H-1), 5,22 (1H, t, *J* 9 Hz, H-3'), 5,16 (1H, dd, *J* 9, 3 Hz, H-3), 5,05 (2H, m, H-2', H-4'), 4,97 (1H, t, *J* 9 Hz, H-4), 4,53 (1H, d, *J* 8 Hz, H-1'), 4,33 (1H, dd, *J* 12, 7,5 Hz, H-6'a), 4,18 (1H, dd, *J* 12, 2 Hz, H-6'b), 4.14 (2H, s, OCOCH_2Cl), 4,01 (1H, dd, *J* 3, 2 Hz, H-2), 3,89 (1H, dq, *J* 9, 6,5 Hz, H-5), 3,75 (1H, ddd, *J* 9, 7,5, 2 Hz, H-5'), 2,11, 2,06, 1,99 (3 × 6 H, 3s, 6OCOCH_3), 1,19 (3H, d, *J* 6,5 Hz, CH_3-6); sm (dic) *m/z* : 674 $(M + NH_4)^+$, 672 $(M + NH_4)^+$, 638, 596, 480, 408, 365, 331, 155. Anal. calc. pour $C_{26}H_{35}O_{17}Cl$: C 47,67; H 5,38; Cl 5,41; trouvé : C 47,74; H 5,40; Cl 5,42.

1,3,4-Tri-O-acétyl-2-O-(2,3,4-tri-O-acétyl-β-D-glucopyranosyl)-α-L-rhamnopyranose (25)

On ajoute de la thiourée (0,1 g) dans le méthanol (5 mL) à une solution du disaccharide **24** (0,070 g, 0,11 mmol) dans le méthanol (18 mL). Le milieu réactionnel est agité 60 h à 20°C, puis évaporé à sec. Le résidu obtenu fournit, après chromatographie (CH_2Cl_2–CH_3OH, 99 : 1), l'alcool **25** (0,031 g, 50%) : $[\alpha]_D$ −19 (*c* 0,5, MeOH); ir ($CHCl_3$) : 3540, 1750, 1600, 1370, 1135, 1030, 950, cm^{-1}; rmn ^1H : 6,16 (1H, d, *J* 1,5 Hz, H-1), 5,24 (1H, t, *J* 9 Hz, H-3'), 5,14 (1H, dd, *J* 9, 2,5 Hz, H-3), 5,03 (1H, t, *J* 9 Hz, H-4'), 4,97 (1H, dd, *J* 9, 8 Hz, H-2'), 4,87 (1H, t, *J* 9 Hz, H-4), 4,49 (1H, d, *J* 8 Hz, H-1'), 4,01 (1H, dd, *J* 2,5, 1,5 Hz, H-2), 3,94 (1H, dq, *J* 9, 6,5 Hz, H-5), 3,59 (3H, m, H-5', H-6'a, H-6'b), 2,12, 2,06, 2,02 (3 × 6H, 3s, 6OCOCH_3), 1,21 (3H, d, *J* 6,5 Hz, CH_3-6); sm (dic) *m/z* : 596 $(M + NH_4)^+$, 306, 231. Anal. calc. pour $C_{24}H_{34}O_{16}$: C, 49,82; H, 5,92; trouvé : C, 49,91; H, 5,89.

(E)-1,3,4-Tri-O-acétyl-2-O-(2,3,4-tri-O-acétyl-6-O-cinnamoyl-β-D-glucopyranosyl)-α-L-rhamnopyranose (26)

On ajoute, à 0°C, du chlorure de (*E*)-cinnamoyle (0,10 g) et de la 4-diméthylaminopyridine (0,01 g) à une solution de l'alcool **25** (0,058 g, 0,1 mmol) dans la pyridine (3 mL). Le milieu réactionnel est agité à 20°C pendant 5 jours, puis évaporé à siccité. Le résidu obtenu fournit, après chromatographie (hexane–EtOAc, 90 : 10, 70 : 30, 50 : 50), le cinnamate **26** (0,059 g, 83%), identique à un échantillon authentique (3).

(E)-1,3,4-Tri-O-acétyl-2-O-[6-O-(4-acétoxycinnamoyl)-2,3,4-tri-O-acétyl-β-D-glucopyranosyl]-α-L-rhamnopyranose (27)

La technique décrite pour la préparation de **26** appliquée à **25** (0,058 g, 0,1 mmol) et au chlorure de (*E*)-4-acétoxycinnamoyle (0,10 g), permet d'obtenir le 4-acétoxycinnamate **27** (0,067 g, 87%), identique à un échantillon authentique (3).

2,4-Di-O-benzoyl-3-O-(2,3,4,6-tétra-O-acétyl-β-D-glucopyranosyl)-α-L-rhamnopyranoside de méthyle (31) et 2,4-di-O-benzoyl-3-O-(2,3,4,6-tétra-O-acétyl-α-D-glucopyranosyl)-α-L-rhamnopyranoside de méthyle (32)

La condensation du 2,4-di-*O*-benzoyl-α-L-rhamnopyranoside de méthyle (**28**) (33) (1,9 g, 5 mmol) avec le bromure de 2,3,4,6-tétra-*O*-acétyl-α-D-glucopyranosyle (**30**) (5 g), dans des conditions analogues à celles décrites pour la préparation de **21**, permit d'obtenir un résidu qui fournit successivement, après chromatographie (CH_2Cl_2), les deux disaccharides suivants.

(*i*) L'anomère α (**32**) (0,103 g, 2,8%) : $[\alpha]_D$ +86 (*c* 1,5, $CHCl_3$); ir (KBr) : 2995, 2940, 1755, 1725, 1600, 1450, 1370, 1270, 1220, 1180, 1110, 1070, 1040, 920, 800, 715 cm^{-1}; rmn ^1H : 8,15–7,46 (10H, m, 10Ar-*H*), 5,60 (1H, t, *J* 10 Hz, H-4), 5,51 (1H, dd, *J* 3, 1,5 Hz, H-2), 5,23 (1H, d, *J* 4 Hz, H-1'), 5,14 (1H, t, *J* 9 Hz, H-3'), 4,84 (2H, m, H-2', H-4'), 4,81 (1H, d, *J* 1,5 Hz, H-1), 4,40 (1H, dd, *J* 10, 3 Hz, H-3), 4,06 (1H, dq, *J* 10, 6 Hz, H-5), 3,86 (3H, m, H-5', H-6'a, H-6'b), 3,46 (3H, s, OCH_3), 2,07, 1,87, 1,64, 1,50, (4 × 3H, 4s, 4OCOCH_3), 1,35 (3H, d, *J* 6 Hz, CH_3-6); sm (dic) *m/z* : 734 $(M + NH_4)^+$, 331, 105. Anal. calc. pour $C_{35}H_{40}O_{16}$: C 58,65; H 5,62; Trouvé : C 58,57; H 5,65.

(*ii*) L'anomère β (**31**) (1,45 g, 55%) : $[\alpha]_D$ +38 (*c* 1, $CHCl_3$); ir (KBr) : 2990, 2940, 1755, 1720, 1600, 1450, 1370, 1320, 1265, 1220, 1180, 1110, 1070, 980, 910, 800, 715, cm^{-1}; rmn ^1H : 8,11–7,51 (10H, m, 10 Ar-*H*), 5,48 (1H, t, *J* 9 Hz, H-4), 5,44 (1H, dd, *J* 2,5, 1 Hz, H-2), 5,01 (1H, t, *J* 8 Hz, H-3'), 4,94 (1H, t, *J* 8 Hz, H-4'), 4,87 (1H, d, *J* 1 Hz, H-1), 4,86 (1H, t, *J* 8 Hz, H-2'), 4,67 (1H, d, *J* 8 Hz, H-1'), 4,35 (1H, dd, *J* 9, 2,5 Hz, H-3), 4,14 (1H, dd, *J* 12, 5 Hz, H-6'a), 4,08 (1H, dd, *J* 12, 2 Hz, H-6'b), 4,02 (1H, dq, *J* 9, 6 Hz, H-5), 3,66 (1H, ddd, *J* 8, 5, 2 Hz, H-5'), 3,48 (3H, s, OCH_3), 1,96, 1,94, 1,88, 1,38, (4 × 3H, 4s, 4OCOCH_3), 1,31 (3H, d, *J* 6 Hz, CH_3-6); sm (dic) *m/z* : 734 $(M + NH_4)^+$, 614, 331, 105. Anal. calc. pour $C_{35}H_{40}O_{16}$: C 58,65; H 5,62; trouvé : C 58,71; H 5,64.

O-β-D-Glucopyranosyl-(1 → 3)-α-L-rhamnopyranoside de méthyle (33)

Le disaccharide **31** (1,43 g, 2 mmol) est dissout dans une solution méthanolique de méthanolate de sodium (0,4 N, 6 mL) et le mélange est agité pendant 2 h à 20°C. La solution est neutralisée par addition de résine Amberlite IRC 50 H^+, filtrée et évaporée à sec. Après chromatographie du résidu obtenu sur silice greffée en phase inverse (Lichroprep RP 18, solvant : H_2O), on obtient le β-D-glucopyranosyl-α-L-rhamnopyranoside de méthyle (**33**) (0,666 g, 98%) : $[\alpha]_D$ −48 (*c* 0,5 EtOH); ir (KBr) : 3400, 2910, 1450, 1390, 1200, 1130, 1080, 1050, 980, 900, cm^{-1}; rmn ^1H (CD_3OD) : 4,63 (1H, d, *J* 1 Hz, H-1), 4,55 (1H, d, *J* 8 Hz, H-1'), 4,14 (1H, dd *J* 3, 1 Hz, H-2), 3,87 (1H, dd, *J* 12, 2 Hz, H-6'a), 3,77 (1H, dd, *J* 12, 4 Hz, H-6'b), 3,75–3,25 (7H, m, H-3, H-4, H-5, H-2', H-3', H-4', H-5'), 1,20 (3H, d, *J* 6 Hz, CH_3-6); sm (dic) *m/z* : 358 $(M + NH_4)^+$, 196, 180, 164. Anal. calc. pour $C_{13}H_{24}O_{10}$: C 45,88; H 7,11; trouvé : C 45,67; H 7,08.

Can. J. Chem. Downloaded from www.nrcresearchpress.com by 109.225.110.28 on 09/08/12
For personal use only.

2,4-Di-O-acétyl-3-O-(2,3,4-tri-O-acétyl-6-O-triphénylméthyl-β-D-glucopyranosyl)-α-L-rhamnopyranoside de méthyle (34)

On ajoute, sous agitation, du chlorure de triphénylméthyle (0,837 g, 3 mmol) à une solution de β-D-glucopyranosyl-(1 → 3)-α-L-rhamnopyranoside de méthyle (**33**) (0,438 g, 1,28 mmol) dans la pyridine (3 mL). L'agitation est poursuivie 15 h à 40°C. Après refroidissement à 25°C, le mélange est additionné d'anhydride acétique (2 mL), puis agité 4 h à température ambiante et concentré. Une chromatographie (CH_2Cl_2) du résidu donne le disaccharide **34** qui cristallise dans CH_2Cl_2 (0,62 g, 61%) : *F* 246–247°C; $[\alpha]_D$ +12,5 (*c* 1, $CHCl_3$); ir (KBr) : 3080, 3000, 2940, 1750, 1600, 1490, 1450, 1380, 1240, 1140, 1055, 980, 900, 770, 750, 710, 640 cm^{-1}; rmn ^1H : 7,51–7,28 (15H, m, 15 Ar-*H*), 5,33 (1H, dd, *J* 3, 1 Hz, H-2), 5,06 (4H, m, H-4, H-2′, H-3′, H-4′), 4,72 (1H, d, *J* 1 Hz, H-1), 4,64 (1H, d, *J* 8 Hz, H-1′), 4,24 (1H, dd, *J* 10, 3 Hz, H-3), 3,80 (1H, dq, *J* 10, 6 Hz, H-5), 3,58 (1H, m, H-5′), 3,28 (3H, s, OCH_3), 3,14 (2H, m, H-6′a, H-6′b), 2,16, 2,13, 2,04, 1,97, 1,73, (5 × 3H, 5s, 5-$OCOCH_3$), 1,24 (3H, d, *J* 6 Hz, CH_3-6); sm (dic) *m/z* : 810 $(M + NH_4)^+$, 568, 262, 243. Anal. calc. pour $C_{42}H_{48}O_{15}$: C 63,62; H 6,10; trouvé : C 63,67; H 6,12.

2,4-Di-O-acétyl-3-O-(2,3,4-tri-O-acétyl-β-D-glucopyranosyl)-α-L-rhamnopyranoside de méthyle (35)

Une solution du disaccharide **34** (0,3 g, 0,38 mmol) dans l'éthanol (15 mL) est additionnée de palladium à 10% sur charbon (0,2 g), puis maintenue sous atmosphère d'hydrogène, pendant 24 h, à la pression atmosphérique. Le mélange réactionnel est filtré, concentré et une chromatographie (CH_2Cl_2–CH_3OH, 99 : 1) du résidu donne l'alcool **35** qui cristallise dans CH_2CL_2 (0,18 g, 84%) : *F* 225°C; $[\alpha]_D$ +3 (*c* 1, $CHCl_3$); ir (KBr) : 3575, 2995, 2950, 1750, 1380, 1260, 1230, 1140, 1080, 1050, 980 cm^{-1}; rmn ^1H : 5,35 (1H, dd, *J* 3, 1 Hz, H-2), 5,23 (1H, t, *J* 9 Hz, H-3′), 5,04 (1H, t, *J* 10 Hz, H-4), 4,98 (1H, t, *J* 9 Hz, H-4′), 4,90 (1H, dd, *J* 9, 8 Hz, H-2′), 4,64 (1H, d, *J* 8 Hz, H-1′), 4,55 (1H, d, *J* 1 Hz, H-1), 4,02 (1H, dd, *J* 10, 3 Hz, H-3), 3,73 (1H, dq, *J* 10, 6 Hz, H-5), 3,67 (1H, m, H-5′), 3,55 (2H, m, H-6′a, H-6′b), 3,38 (3H, s, OCH_3), 2,16, 2,07, 2,05, 2,04, 2,01 (5 × 3H, 5s, 5$OCOCH_3$), 1,26 (3H, d, *J* 6 Hz, CH_3-6); sm (dic) *m/z* : 567 $(M + H)^+$. Anal. calc. pour $C_{23}H_{34}O_{15}$: C 48,76; H 6,04; trouvé : C 48,74; H 6,02.

2,4-Di-O-acétyl-α-L-rhamnopyranoside de méthyle (40)

Une solution d'α-L-rhamnopyranoside de méthyle (**29**) (29, 34) (3,8 g, 21,8 mmol) de triméthylorthoacétate (3,0 mL, 25,6 mmol) et d'acide toluène-4-sulfonique (0,05 g) dans la diméthylformamide (50 mL) est agitée 6 h à température ambiante. La solution est concentrée et on ajoute de l'anhydride acétique (5 mL) à une solution du résidu dans la pyridine (10 mL). Cette solution est agitée 18 h à température ambiante, diluée par du dichlorométhane (200 mL), lavée par une solution aqueuse d'HCl/N à 0°C (2 × 100 mL), par une solution aqueuse saturée de $NaHCO_3$ (2 × 100 mL), par l'eau glacée (2 × 100 mL), puis séchée et évaporée à sec. Le produit sirupeux obtenu est dissout dans l'acide acétique à 80% et la solution est agitée 30 min à température ambiante, puis évaporée. Le résidu d'évaporation permet d'isoler, après chromatographie (hexane-EtOAc, 70 : 30), le 2,4-di-*O*-acétyl-α-L-rhamnopyranoside de méthyle (**40**) qui cristallise dans EtOAc (4,74 g, 85%) : *F* 94°C; $[\alpha]_D$ −26 (*c* 1, MeOH); ir (KBr) : 3530, 2980, 2940, 2890, 1720, 1370, 1235, 1130, 1065, 1040, 970 cm^{-1}; rmn ^1H : 5,04 (1H, dd, *J* 3, 1 Hz, H-2), 4,85 (1H, t, *J* 9 Hz, H-4), 4,64 (1H, d, *J* 1 Hz, H-1), 3,98 (1H, ddd, *J* 9, 7, 3 Hz, H-3) 3,76 (1H, dq, *J* 9, 6 Hz, H-5), 3,39 (3H, s, OCH_3), 3,12 (1H, d, *J* 7 Hz, éch. D_2O, O*H*-3), 2,14, 2,09 (2 × 3H, 2s, 2$OCOCH_3$), 1,23 (3H, d, *J* 6 Hz, CH_3-6); sm (dic) *m/z* : 280 $(M + NH_4)^+$, 263 $(M + H)^+$. Anal. calc. pour $C_{11}H_{18}O_7$: C 50,37; H 6.92; trouvé : C 50,41; H 6,92.

(E)-2,4-Di-O-acétyl-3-O-(2,3,4-tri-O-acétyl-6-O-cinnamoyl-β-D-glucopyranosyl)-α-L-rhamnopyranoside de méthyle (36)

(*a*) L'acylation de l'alcool **35** (0,165 g, 0,3 mmol) par le chlorure de (*E*)-cinnamoyle (0,35 g), dans des conditions analogues à celles décrites pour la synthèse de **26**, fournit un résidu qui, après chromatographie (CH_2Cl_2), donne le cinnamate **36** (0,195 g, 96%) : $[\alpha]_D$ −9 (*c* 1, $CHCl_3$); ir (KBr) : 2950, 1760, 1710, 1640, 1380, 1250, 1225, 1070, 1055, 980, 910, 775 cm^{-1}; rmn ^1H: 7,82 (1H, d, *J* 16 Hz, H-7″), 7,62 (2H, m, H-2″, H-6″), 7,44 (3H, m, H-3″, H-4″, H-5″), 6,53 (1H, d, *J* 16 Hz, H-8″), 5,19 (1H, dd, *J* 3, 1 Hz, H-2), 5,14 (1H, t, *J* 9 Hz, H-3′), 5,09 (1H, t, *J* 9 Hz, H-4′), 5,05 (1H, t, *J* 10 Hz, H-4), 4,97 (1H, dd, *J* 9, 8 Hz, H-2′), 4,66 (1H, d, *J* 8 Hz, H-1′), 4,62 (1H, d, *J* 1 Hz, H-1), 4,35 (2H, m, H-6′a, H-6′b), 4,11 (1H, dd, *J* 10, 3 Hz, H-3), 3,81 (2H, m, H-5, H-5′), 3,28 (3H, s, OCH_3), 2,12, 2,11, 2,05, 2,04, 2,00 (5 × 3H, 5s, 5$OCOCH_3$), 1,21 (3H, d, *J* 6 Hz, CH_3-6); sm (dic) *m/z* : 698 $(M + NH_4)^+$, 280, 263, 245, 231. Anal. calc. pour $C_{32}H_{40}O_{16}$: C 56,47; H 5,92; trouvé : C 56,43; H 5,91.

(*b*) La condensation du 2,4-di-*O*-acétyl-α-L-rhamnopyranoside de méthyle (**40**) (0,262 g, 1 mmol) avec le bromure **41** (1 g, 2,1 mmol) dans des conditions analogues à celles décrites pour la préparation de **21**, permet d'obtenir un résidu qui donne, après chromatographie (CH_2Cl_2), le disaccharide **36** (0,414 g, 61%).

(E)-2,4-Di-O-acétyl-3-O-[6-O-(4-acétoxycinnamoyl)-2,3,4-tri-O-acétyl-β-D-glucopyranosyl]-α-L-rhamnopyranoside de méthyle (37)

(*a*) L'acylation de l'alcool **35** (0,165 g, 0,3 mmol) par le chlorure de (*E*)-4-acétoxycinnamoyle (0,45 g), dans des conditions analogues à celles décrites pour la synthèse de **26**, donne un résidu qui permet d'isoler, après chromatographie (CH_2Cl_2), l'acétoxycinnamate **37** (0,201 g, 94%) : $[\alpha]_D$ −8 (*c* 1 $CHCl_3$); ir (KBr) : 3000, 2950, 1830, 1790, 1740, 1710, 1610, 1540, 1480, 1330, 1270, 1165, 1035, 960, 910, 850, 775, cm^{-1}; rmn ^1H : 7,76 (1H, d, *J* 16 Hz, H-7″), 7,62 (2H, d, *J* 8 Hz, H-2″, H-6″), 7,13 (2H, d, *J* 8 Hz, H-3″, H-5″), 6,46 (1H, d, *J* 16 Hz, H-8″), 5,18 (1H, dd, *J* 3, 1 Hz, H-2), 5,15 (1H, t, *J* 9 Hz, H-3′), 5,09 (1H, t, *J* 9 Hz, H-4′), 5,05 (1H, t, *J* 10 Hz, H-4), 4,97 (1H, dd, *J* 9, 8 Hz, H-2′), 4,64 (1H, d, *J* 8 Hz, H-1′), 4,61 (1H, d, *J* 1 Hz, H-1), 4.33 (2H, m, H-6′a, H-6′b), 4,07 (1H, dd, *J* 10, 3 Hz, H-3), 3,75 (2H, m, H-5, H-5′), 3,26 (3H, s, OCH_3), 2,33 (3H, s, Ar$OCOCH_3$), 2,11, 2,10, 2,05, 2,04, 2,00, (5 × 3H, 5s, 5R$OCOCH_3$), 1,21 (3H, d, *J* 6 Hz, CH_3-6); sm (dic) *m/z* : 756 $(M + NH_4)^+$, 477, 245, 189, 147. Anal. calc. pour $C_{34}H_{42}O_{18}$: C 55,28; H 5,73; trouvé : C 55,21; H 5,77.

(*b*) La condensation du 2,4-di-*O*-acétyl-α-L-rhamnopyranoside de méthyle (**40**) (0,262 g, 1 mmol) avec le bromure **42** (1,2 g), dans des conditions analogues à celles décrites pour la préparation de **21**, permet d'obtenir un résidu qui, après chromatographie (CH_2Cl_2), donne le disaccharide **37** (0,435 g; 59%).

(E)-1,2,4-Tri-O-acétyl-3-O-(2,3,4-tri-O-acétyl-6-O-cinnamoyl-β-D-glucopyranosyl)-α-L-rhamnopyranose (38)

L'acétolyse du méthylglycoside **36** (0,100 g, 0,15 mmol), dans des conditions analogues à celles décrites pour la préparation de **24**, fournit un résidu qui, après chromatographie (hexane–EtOAc, 60 : 40), permet l'obtention du disaccharide **38** (0,082 g, 80%), identique à un échantillon authentique (3).

(E)-1,2,4-Tri-O-acétyl-3-O-[6-O-(4-acétoxycinnamoyl)-2,3,4-tri-O-acétyl-β-D-glucopyranosyl]-α-L-rhamnopyranose (39)

L'acétolyse du méthylglycoside **37** (0,120 g, 0,16 mmol), dans les conditions identiques à celles décrites pour la préparation de **24**, donne, après chromatographie (hexane–EtOAc, 60 : 40), donne le disaccharide **39** (0,094 g, 77%), identique à un échantillon authentique (3).

(E)-2,3-O-Isopropylidène-4-O-(2,3,4-tri-O-acétyl-6-O-cinnamoyl-β-D-glucopyranosyl)-α-L-rhamnopyranoside de méthyle (44)

On ajoute sous agitation du bromure **41** (1 g, 2,1 mmol) et du tamis moléculaire 3 Å (1 g) à une solution de 2,3-*O*-isopropylidène-α-L-rhamnopyranoside de méthyle (**43**) (29) (0,35 g, 1,6 mmol) et de cyanure mercurique (0,37 g) dans l'acétonitrile anhydre (10 mL). L'agitation est poursuivie pendant 5 h, puis le milieu réactionnel est filtré et concentré pour donner un résidu si-

Can. J. Chem. Downloaded from www.nrcresearchpress.com by 109.225.110.28 on 09/08/12
For personal use only.

rupeux qui est dissous dans du dichlorométhane (20 mL), puis lavé par une solution aqueuse 1 M de KBr (2 × 10 mL), par une solution aqueuse saturée de $NaHCO_3$ (10 mL), par de l'eau (2 × 10 mL), puis séché et concentré. Après chromatographie (hexane–EtOAc, 80 : 20), on obtient le disaccharide **44** (0,865 g, 85%) : $[\alpha]_D$ −8 (*c* 0,5, $CHCl_3$); ir (KBr) : 3000, 2950, 1760, 1720, 1640, 1455, 1380, 1250, 1225, 1170, 1090, 1045, 980, 910, 875, 775, 690 cm^{-1}; rmn ^1H : 7,72 (1H, d, *J* 16 Hz, H-7″), 7,56 (2H, m, H-2″, H-6″), 7,40 (3H, m, H-3″, H-4″, H-5″), 6,43 (1H, d, *J* 16 Hz, H-8″), 5,28 (1H, t, *J* 9 Hz, H-3′), 5,11 (1H, t, *J* 9 Hz, H-4′), 5,01 (2H, m, H-1′, H-2′), 4,86 (1H, d, *J* 1 Hz, H-1), 4,39 (1H, dd, *J* 12, 2 Hz, H-6′b), 4,28 (1H, dd, *J* 12, 5 Hz, H-6′a), 4,08 (2H, m, H-2, H-3), 3,79 (1H, ddd, *J* 9, 5, 2 Hz, H-5′), 3,59 (2H, m, H-4, H-5), 3,34 (3H, s, OCH_3), 2,07, 2,06, 2,05 (3 × 3H, 3s, $3OCOCH_3$), 1,54, 1,36 (2 × 3H, 2s, $C(CH_3)_2$), 1,29 (3H, d, *J* 6 Hz, CH_3-6); sm (dic) *m/z* : 654 $(M + NH_4)^+$, 234, 201, 143, 131. Anal. calc. pour $C_{31}H_{40}O_{14}$: C 58,48; H 6,33; trouvé : C 58,42; H 6,36.

(E)-2,3-O-Isopropylidène-4-O-[6-O-(4-acétoxycinnamoyl)-2,3,4-tri-O-acétyl-β-D-glucopyranosyl]-α-L-rhamnopyranoside de méthyle (45)

La condensation du 2,3-*O*-isopropylidène-α-L-rhamnopyranoside de méthyle (**43**) (29) (0,33 g, 1,5 mmol) avec le bromure **42** (1 g, 2,1 mmol), dans des conditions analogues à celles décrites pour la synthèse de **44** permet d'obtenir, après chromatographie (hexane–EtOAc, 80 : 20), le disaccharide **45** (0,780 g, 75%) : $[\alpha]_D$ −3 (*c* 1, $CHCl_3$); ir (KBr) : 3000, 2950, 1760, 1720, 1640, 1605, 1510, 1375, 1250, 1225, 1170, 1095, 1045, 1025, 985, 915, 865, 790, 740 cm^{-1}; rmn ^1H : 7,77 (1H, d, *J* 16 Hz, H-7″), 7,60 (2H, d, *J* 9 Hz, H-2″, H-6″), 7,19 (2H, d, *J* 9 Hz, H-3″, H-5″), 6.41 (1H, d, *J* 16 Hz, H-8″), 5,33 (1H, t, *J* 9 Hz, H-3′), 5,17 (1H, t, *J* 9 Hz, H-4′), 5,05 (2H, m, H-1′, H-2′), 4,88 (1H, d, *J* 1 Hz, H-1), 4,44 (1H, dd, *J* 12, 2 Hz, H-6′b), 4,29 (1H, dd, *J* 12, 6 Hz, H-6′a), 4,12 (2H, m, H-2, H-3), 3,81 (1H, ddd, *J* 9, 6, 2 Hz, H-5′), 3,61 (2H, m, H-4, H-5), 3,38 (3H, s, OCH_3), 2,35 (3H, s, $ArOCOCH_3$), 2,09, 2,08, 2,04 (3 × 3H, 3s, $3ROCOCH_3$), 1,55, 1,36 (2 × 3H, 2s, $C(CH_3)_2$), 1,29 (3H, d, *J* 6 Hz, CH_3-6). sm (dic) *m/z* : 712 $(M + NH_4)^+$, 234, 210, 143. Anal. calc. pour $C_{33}H_{42}O_{16}$: C 57,06; H 6,09; trouvé : C 56,98; H 6,10.

(E)-4-O-(2,3,4-Tri-O-acétyl-6-O-cinnamoyl-β-D-glucopyranosyl)-α-L-rhamnopyranoside de méthyle (46)

Une solution de l'acétal **44** (0,64 g, 1 mmol) dans le chloroforme (31,5 mL), est additionnée d'acide trifluoroacétique contenant 1% d'eau (3,5 mL), puis abandonnée 1 h à température ambiante. Le solvant est éliminé par évaporation et l'acide trifluoroacétique par codistillation avec le benzène. Le résidu obtenu fournit, après chromatographie (hexane–EtOAc, 80 : 20, 50 : 50), le diol **46** (0,44 g, 73%) : $[\alpha]_D$ −41 (*c* 0,5, $CHCl_3$); ir (KBr) : 3500, 2950, 1760, 1715, 1640, 1455, 1380, 1250, 1225, 1170, 1065, 1040, 980, 910, 775, 690 cm^{-1}; rmn ^1H : 7,74 (1H, d, *J* 16 Hz, H-7″), 7,57 (2H, m, H-2″, H-6″), 7,41 (3H, m, H-3″, H-4″, H-5″), 6,46 (1H, d, *J* 16 Hz, H-8″), 5,24 (1H, t, *J* 9 Hz, H-3′), 5,12 (1H, t, *J* 9 Hz, H-4′), 5,01 (1H, dd, *J* 9, 8 Hz, H-2′), 4,89 (1H, d, *J* 8 Hz, H-1′), 4,66 (1H, d, *J* 1,5 Hz, H-1), 4,41 (1H, dd, *J* 12, 2 Hz, H-6′b), 4,26 (1H, dd, *J* 12, 6 Hz, H-6′a), 3,92 (1H, dd, *J* 5, 1,5 Hz, H-2), 3,89 (2H, m, H-5, H-5′), 3,67 (1H, dd, *J* 9, 5 Hz, H-3), 3,56 (1H, t, *J* 9 Hz, H-4), 3,34 (3H, s, OCH_3), 2,80, 2,39 (2 × 1H, 2s larges, éch. D_2O, O*H*-2, O*H*-3), 2,08, 2,06, 2,01 (3 × 3H, 3s, $3OCOCH_3$), 1,31 (3H, d, *J* 6 Hz, CH_3-6); sm (dic) *m/z* : 614 $(M + NH_4)^+$. Anal. calc. pour $C_{28}H_{36}O_{14}$: C 56,37; H 6,08; trouvé : C 56,41; H 6,07.

(E)-4-O-[6-O-(4-Acétoxycinnamoyl)-2,3,4-tri-O-acétyl-β-D-glucopyranosyl]-α-L-rhamnopyranoside de méthyle (47)

Le traitement de l'acétal **45** (0.70 g, 1 mmol), dans des conditions analogues à celles décrites pour l'obtention de **46**, donne, après chromatographie (hexane–EtOAc, 60 : 40), le diol **47** (0,51 g, 78%) : $[\alpha]_D$ −32 (*c* 0,5, $CHCl_3$); ir (KBr) : 3500, 3000, 2950, 1760, 1710, 1640, 1455, 1380, 1310, 1250, 1225, 1160, 1060, 1040, 980, 910, 790, 740 cm^{-1}; rmn ^1H : 7,70 (1H, d, *J* 16 Hz, H-7″), 7,59 (2H, d, *J* 9 Hz, H-2″, H-6″), 7,14 (2H, d, *J* 9 Hz, H-3″, H-5″), 6,42 (1H, d, *J* 16 Hz, H-8″), 5,28 (1H, t, *J* 9 Hz, H-3′), 5,14 (1H, t, *J* 9 Hz, H-4′), 5,01 (1H, dd, *J* 9, 8 Hz, H-2′), 4,92 (1H, d, *J* 8 Hz, H-1′) 4,63 (1H, d, *J* 1,5 Hz, H-1), 4,42 (1H, dd, *J* 12, 2 Hz, H-6′b), 4,27 (1H, dd, *J* 12, 5 Hz, H-6′a), 3,90 (1H, dd, *J* 3, 1,5 Hz, H-2), 3,82 (2H, m, H-5, H-5′), 3,64 (1H, dd, *J* 9, 3 Hz, H-3), 3,55 (1H, t, *J* 9 Hz, H-4), 3,35 (3H, s, OCH_3), 2,92 (2H, m large, éch. D_2O, O*H*-2, O*H*-3), 2,31 (3H, s, $ArOCOCH_3$), 2,08, 2,06, 2,01 (3 × 3H, 3s, 3 $ROCOCH_3$), 1,30 (3H, d, *J* 6 Hz, CH_3-6). sm (dic) *m/z* : 672 $(M + NH_4)^+$. Anal. calc. pour $C_{30}H_{38}O_{16}$: C 55,04; H 5 85; trouvé : C 55,09; H 5,85.

(E)-1,2,3-Tri-O-acétyl-4-O-(2,3,4,-tri-O-acétyl-6-O-cinnamoyl-β-D-glucopyranosyl)-α-L-rhamnopyranose (48)

Le traitement du diol **46** (0,40 g, 0,67 mmol), dans des conditions identiques à celles décrites pour la préparation de **24**, fournit, après chromatographie (hexane–EtOAc, 60 : 40), le disaccharide **48** (0,325 g, 68%), identique à un échantillon authentique (3).

(E)-1,2,3-Tri-O-acétyl-4-O-[6-O-(4-acétoxycinnamoyl)-2,3,4-tri-O-acétyl-β-D-glucopyranosyl]-α-L-rhamnopyranose (49)

Le traitement du diol **47** (0,45 g, 0.68 mmol), dans des conditions analogues à celles décrites pour la préparation de **24**, fournit, après chromatographie (hexane–EtOAc, 60 : 40), le disaccharide **49** (0,344 g, 68%), identique à un échantillon authentique (3).

Remerciements

Nous remercions les Drs. G. Massiot et C. Lavaud (Laboratoire de pharmacognosie, Faculté de pharmacie, Université de Reims) pour de fructueuses discussions sur les expériences de COSY à acquisition retardée.

1. Jian Su Xin Hi Xue Yuan. Zhong Yao Da Ci Dian. Vol 1. Shangai People's Editor, Shangai. 1977.
2. R. C. Lin, E. Seguin, F. Tillequin et M. Koch. J. Nat. Prod. **50**, 422 (1987).
3. R. C. Lin, A.-L. Skaltsounis, E. Seguin, F. Tillequin et M. Koch. J. Nat. Prod. **53**, 882 (1990).
4. R. C. Lin, J. Peyroux, E. Seguin et M. Koch. Phytother. Res. **5**, 188 (1991).
5. L. V. Backinowsky, N. F. Balan, A. S. Shashkov et N. K. Kochetkov. Carbohydr. Res. **84**, 225, (1980).
6. P. A. J. Gorin et A. S. Perlin. Can. J. Chem. **39**, 2474 (1961).
7. K. L. Matta et J. J. Barlow. Carbohydr. Res. **48**, 294 (1976).
8. G. M. Bebault et G. G. S. Dutton. Carbohydr. Res. **37**, 309 (1974).
9. T. Iversen et D. R. Bundle. Carbohydr. Res. **84**, C13 (1980).
10. P. Garegg et T. Iversen. Carbohydr. Res. **70**, C13 (1979).
11. S. Kamiya, S. Esaki et N. Shiba. Agric. Biol. Chem. **51**, 2207 (1987).
12. R. Kasai, M. Okihara, J. Asakawa, K. Mizutani et O. Tanaka. Tetrahedron, **35**, 1427 (1979).
13. C. Demetzos, A.-L. Skaltsounis, F. Tillequin et M. Koch. Carbohydr. Res. **207**, 131 (1990).
14. H. P. Kleine et R. S. Sidhu. Carbohydr. Res. **188**, 307 (1988).
15. R. U. Lemieux, K. B. Hendriks, R. V. Stick et K. James. J. Am. Chem. Soc. **97**, 4056 (1975).
16. W. Konigs et E. Knorr. Ber. Dtsch. Chem. Ges. **34**, 957 (1901).
17. K. Szekely, B. Vermes, L. Farkas et M. Nogradi. Acta Chim. Acad. Sci. Hung. **98**, 241 (1978).
18. C. Laffite, A.-M. Nguyen Phuoc Du, F. Winternitz, R. Wylde et F. Pratviel-Sosa. Carbohydr. Res. **67**, 91 (1978).
19. G. Massiot, C. Lavaud et V. Besson. Bull. Soc. Chim. Fr. **127**, 440 (1990).
20. N. K. Kochetkov, A. J. Khorlin et A. F. Bochkov. Tetrahedron, **23**, 693 (1967).
21. H. B. Boren, G. Ekborg, K. Eklind, P. J. Garegg, A. Pilotti et C.-G. Swahn. Acta Chem. Scand. **27**, 2639 (1973).

22. D. R. Bundle et S. Josephson. Can. J. Chem. **57**, 662 (1979).
23. S. Hanessian et J. Banoub. Carbohydr. Res. **44**, C14 (1975).
24. T. Iversen et D. R. Bundle. J. Org. Chem. **46**, 5389 (1981).
25. D. Y. Gagnaire et P. J. A. Vottero. Carbohydr. Res. **28**, 165 (1973).
26. B. Vermes, V. M. Chari et H. Wagner. Helv. Chim. Acta, **64**, 1964 (1981).
27. A. Liptak, P. Nanasi, A. Neszmelyi et H. Wagner. Tetrahedron, **36**, 1261 (1980).
28. A. Liptak, P. Nanasi, A. Neszmelyi, I. Riessmaurer et H. Wagner. Carbohydr. Res. **93**, 43 (1981).
29. G. M. Bebault et G. G. S. Dutton. Can. J. Chem. **50**, 3373 (1972).
30. S. Ogawa. Bull. Chem. Soc. Jpn. **2**, 20 (1927).
31. P. J. Garegg et H. Hultberg. Carbohydr. Res. **72**, 276 (1979).
32. S. Josephson et D. R. Bundle. J. Chem. Soc. Perkin Trans. 1, 297 (1980).
33. H.-P. Wessel et D. R. Bundle. Carbohydr. Res. **124**, 301 (1983).
34. P. A. Levene et I. E. Muskat. J. Biol. Chem. **105**, 413 (1934).
35. R. L. Whistler, L. W. Doner et M. Kosik. *Dans* Methods in carbohydrate chemistry. Vol. 6. *Éditeurs* : R. L. Whistler et J. N. Bemiller. Academic Press, New York. 1972. pp. 411–412.
36. R. U. Lemieux et H. Driguez. J. Am. Chem. Soc, **97**, 4069 (1975).
37. S. Ramesh et R. W. Frank. Tetrahedron: Asymmetry, **1**, 137 (1990).

Can. J. Chem. Downloaded from www.nrcresearchpress.com by 109.225.110.28 on 09/08/12
For personal use only.

Diurnal and seasonal modelling of the tropospheric half-lives of polycyclic aromatic hydrocarbons

NIGEL J. BUNCE[1] AND HELENA G. DRYFHOUT
Department of Chemistry and Biochemistry, University of Guelph, Guelph, Ont., Canada, N1G 2W1

Received December 6, 1991

NIGEL J. BUNCE and HELENA G. DRYFHOUT. Can. J. Chem. **70**, 1966 (1992).

The half-lives of polycyclic aromatic hydrocarbons (PAH) were calculated under different conditions of location, season, and time of day, based on the reaction of PAH with the hydroxyl radical OH as the major sink. The calculations required a method of estimating the diurnal variation in the concentration of OH, which is not normally available experimentally. For naphthalene as a prototype PAH, the half-lives were of the order of several hours, but varied by more than an order of magnitude with season and geographical location. The previously developed model applicable to rural atmospheres was modified to estimate the half-lives of PAH in the urban troposphere by including of the reaction of OH with NO_2 as a major urban sink for OH. The half-lives of several PAH were estimated for North York, Ontario, under different conditions of NO_2 and ozone concentrations during a period of high tropospheric air pollution in July 1988.

NIGEL J. BUNCE et HELENA G. DRYFHOUT. Can. J. Chem. **70**, 1966 (1992).

Utilisant le réaction des HAP avec le radical OH comme modèle pour leur mode principal d'élimination, on a calculé les demi-vies des hydrocarbures aromatiques polycycliques (HAP) dans diverses conditions, comme le lieu, la saison et l'heure du jour. Pour ces calculs, il a été nécessaire d'évaluer la variation diurne de la concentration en OH; cette valeur n'est généralement pas disponible d'une façon expérimentale. Pour le naphtalène comme prototype des HAP, les demi-vies sont de l'ordre de plusieurs heures; elles varient toutefois par plus d'un ordre de grandeur avec la saison et l'emplacement géographique. Dans le but d'évaluer les demi-vies de HAP dans des troposphères urbaines, on a modifié le modèle développé antérieurement et applicable aux atmosphères ruraux en incluant le réaction de OH avec NO_2 comme piège urbain principal pour les OH. Utilisant diverses concentrations de NO_2 et d'ozone durant une période de haute pollution de l'air troposphérique, en juillet 1988, on a évalué les demi-vies de plusieurs HAP pour North York, Ontario.
[Traduit par la rédaction]

Introduction

Tropospheric pollutants may be removed from a given region of the atmosphere by physical removal involving either wet or dry deposition, by transport out of the area through the movement of air masses, and by chemical reaction. The tropospheric lifetime of the pollutant depends on the rates of all three processes, whereas the rate of chemical reaction relative to those of the other processes determines whether the pollutant will eventually be deposited in its original form or as a secondary pollutant.

Chemical transformation in the lower atmosphere may occur through photolysis by sunlight, provided that the pollutant contains a chromophore that absorbs in the range of wavelengths of tropospheric solar radiation ($\lambda > 290$ nm). Alternatively, a substrate may react with one of several reactive substances which are present at low concentrations in the troposphere. These include hydroxyl radicals, ozone, and nitrate radicals, the latter being significant only at night.

In daylight hours, the predominant reactive substance is usually the hydroxyl radical, whose characteristic reactions are hydrogen-atom abstraction and addition to an unsaturated centre, the latter process occurring both for inorganic molecules such as NO_2 and SO_2, and for unsaturated organic substances (alkenes and aromatics). The reaction with OH is normally second-order kinetically, and so both the rate constant and the concentration of OH must be known in order to estimate the rate of the reaction or the half-life of the substance (eq. [1]).

$$[1] \quad \text{rate} = k\,[\text{substrate}]\,[\text{OH}]$$

Many gas-phase rate constants of interest have been measured in the laboratory (1). Rates of reaction have often been calculated by using globally, seasonally, and diurnally averaged estimates of OH concentrations (2), an approach which is appropriate for long-lived tropospheric gases. However, the assumption of a constant concentration of OH fails for short-lived gases: the concentration of OH in the troposphere varies diurnally, seasonally, and geographically according to the solar photon intensity, since OH is formed by a photochemical reaction sequence (Scheme 1). These dependencies of the concentration of OH must be known in order to estimate the lifetimes of short-lived substrates. Unfortunately, the OH concentration is difficult to obtain in the field, because OH has few convenient absorption bands that are easily distinguished from those of other chemicals in the atmosphere and also because its concentration is always extremely low ($<10^{-14}$ atm).

$$[2] \quad NO_2 \xrightarrow{h\nu,\ \lambda < 400\ \text{nm}} NO + O(^3P)$$
$$[3] \quad O(^3P) + O_2 \longrightarrow O_3$$
$$[4] \quad O_3 \xrightarrow{h\nu,\ \lambda < 320\ \text{nm}} O_2(^1\Delta_g) + O(^1D)$$
$$[5] \quad O(^1D) + H_2O \longrightarrow 2OH$$

SCHEME 1

Polycyclic aromatic hydrocarbons (PAH) are tropospheric pollutants that result from incomplete combustion of fuels, notably vehicular emissions (e.g., ref. 3), and hence are present at higher concentrations in the urban troposphere than in the rural troposphere. PAH containing four or fewer benzene rings exist almost exclusively in the gas phase under tropospheric conditions. Previous research has shown that PAH are rather short lived in the troposphere and that

[1]Author to whom correspondence may be addressed.

Can. J. Chem. Downloaded from www.nrcresearchpress.com by 217.78.4.112 on 09/08/12
For personal use only.

they react predominantly by way of hydroxyl radical attack (4).

The fate of PAH in the troposphere is important because of the well-documented toxicity of some members of the family and because they are transformed in the troposphere into a wide variety of secondary pollutants, including phenolics, nitro-PAH, and nitrophenols. Although the complete spectrum of products has not yet been identified, even for reactants as simple as toluene and naphthalene (4), some of the known secondary products are more toxic than the parent PAH on the basis of mutagenicity assays (5).

Methodology

We recently developed a simple computational model to estimate the half-lives of pollutants in the atmosphere with respect to photolysis and (or) reaction with OH radicals (6). The model was developed following observations by Platt *et al.* (7) which imply that the OH concentration in the rural troposphere is directly proportional to the rate of photolysis of (tropospheric) ozone (eq. [6]).

$$[6] \quad [OH] = \text{constant} \times J(O_3) \times [O_3]$$

$J(O_3)$ is the rate constant for the photolysis of ozone, which depends on the intensity of sunlight. $J(O_3)$ can be calculated at any time of day for any location and date by making use of tables of tropospheric intensity vs. wavelength for defined zenith angles (8). The zenith angle can be calculated for any time, date, and location, and the solar intensities at each wavelength interpolated from the tabulated data. $J(O_3)$ can then be calculated at a single wavelength, knowing the absorption cross section of ozone σ_λ and the quantum yield ϕ_λ for reaction [4] at that wavelength (eq. [7]).

$$[7] \quad J(O_3)_\lambda = I_\lambda \cdot \sigma_\lambda \cdot \phi_\lambda$$

$J(O_3)_\lambda$ must then be summed over all the tropospheric wavelengths at which ozone absorbs. Once $J(O_3)$ is known, the rate of reaction of the pollutant with OH follows by application of eq. [6] and [1].

Equation [8] is the expression for the concentration of [OH], assuming an instantaneous steady state.

$$[8] \quad [OH] = \frac{\alpha J(O_3)[O_3] + \Sigma k_f[Y]}{\Sigma k_l[X]}$$

In eq. [8], α is the proportionality constant to convert the rate of photolysis of ozone to the rate of formation of OH, $\Sigma k_f[Y]$ is the rate of other source reactions of OH, and $\Sigma k_l[X]$ is the combined rate of all sink reactions (eq. [1]). The experimental finding that $[OH] \propto J(O_3)$, eq. [6], implies that the predominant source of OH is the photolysis of ozone ($\alpha J(O_3)[O_3] >> \Sigma k_f[Y]$), at least in the rural area where the measurements were made (7). Under these conditions, eq. [8] simplifies to eq. [9].

$$[9] \quad [OH]_r = \frac{\alpha J(O_3)[O_3]}{\Sigma k_l[X]}$$

The hydroxyl radical reacts rapidly and irreversibly with NO_2, eq. [10]. This reaction is relatively unimportant in the unpolluted troposphere where $[NO_2]$ is low, but becomes a major sink for OH in the urban troposphere whenever $[NO_2]$ exceeds a few ppbv (9).

$$[10] \quad NO_2 + OH \rightarrow HNO_3$$

$$k = 1.16 \times 10^{-11} \text{ cm}^3 \text{ molec}^{-1} \text{ s}^{-1}$$

The relationship between $[NO_2]$ and [OH] is therefore complex; NO_2 is both a precursor of OH (Scheme 1) and a sink (eq. [10]). The inclusion of reaction [10] as a major sink for OH changes eq. [9] to eq. [11], in which subscripts u and r refer to urban and rural.

$$[11] \quad [OH]_u = \frac{\alpha J(O_3)[O_3]}{\Sigma k_l[X] + k[NO_2]}$$

By equating $\Sigma k_l[X]$ in eqs. [9] and [11], the urban OH concentration can be approximated by eq. [12].

$$[12] \quad [OH]_u = \frac{\alpha J(O_3)[O_3][OH]_r}{\alpha J(O_3)[O_3] + k[NO_2][OH]_r}$$

This equation was incorporated into the model developed for rural atmospheres (6). An attempt to validate the revised model was made by using it to estimate the OH concentration for the data set reported by Dorn *et al.* (9).

TABLE 1. Rate constants for reaction of PAH with OH

Chemical	k (cm^3/(molec s))	$t_{1/2}$(h)
Acenaphthene	1.03×10^{-10}[a]	1.6
Acenapthylene	1.10×10^{-10}[a]	1.5
Anthracene	1.1×10^{-10}[b]	1.5
Biphenyl	8.1×10^{-11}[b]	1.9
Fluoranthene	5.0×10^{-11}[c]	2.5
Naphthalene	2.2×10^{-11}[b]	3.9
Phenanthrene	3.4×10^{-11}[b]	3.4
Pyrene	5.0×10^{-11}[c]	2.5
Styrene	5.9×10^{-11}[a]	2.2

[a]Reference 9.
[b]Reference 14.
[c]Estimated as described in ref. 15.

Results and discussion

Although PAH can in principle be altered chemically both by photolysis and reaction with OH, the latter reaction is their principal chemical sink (4) and so quantum yields of photolysis were taken to be zero.

The half-lives of several PAH were estimated under different conditions of time, place, and date. Rate constants for the reaction of OH with several PAH are given in Table 1 along with half-life estimates for various PAH at latitude 43.70°N, the same latitude as Toronto, Ontario (43.70°N, 79.47°W) on March 21, starting at 8:00 a.m., and assuming a single, instantaneous emission of the PAH. These initial calculations employed the original (rural) model and hence apply to the latitude of Toronto, rather than to Toronto itself. Because of the high rate constants of OH with PAH, all the half-lives are very short, a few hours, hence a globally and seasonally averaged concentration of OH would be inappropriate for modelling the behaviour of PAH.

Figures 1–3 show the results of calculations involving naphthalene as a prototype PAH, again using the rural model. Figure 1 shows the half-life of naphthalene at 43.70°N on

Can. J. Chem. Downloaded from www.nrcresearchpress.com by 217.78.4.112 on 09/08/12
For personal use only.

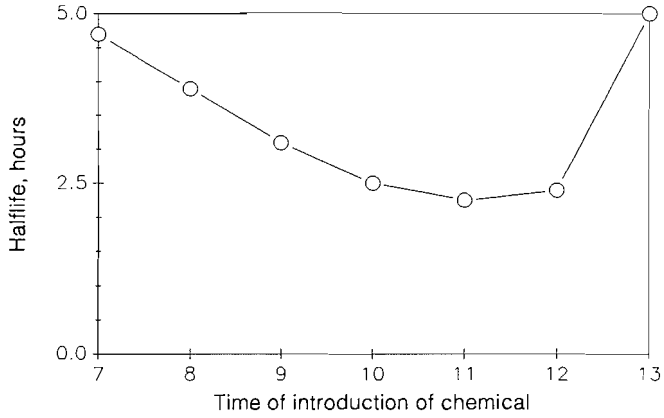

FIG. 1 Variation of the half-life of naphthalene using rural model at 43.7°N on March 21 according to the time of emission.

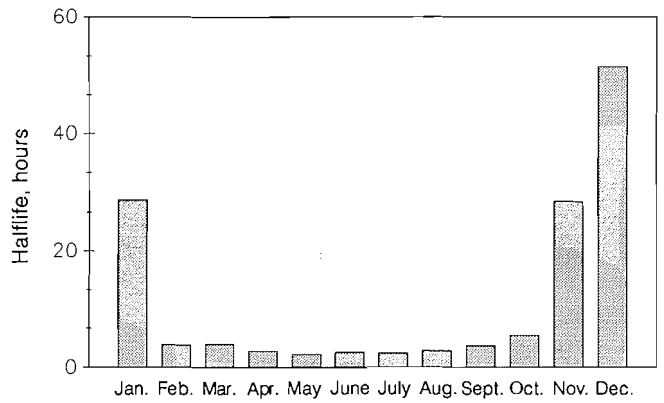

FIG. 2 Monthly variation of the half-life of naphthalene at 43.7°N using rural model: emission at 8:00 a.m. on the 21st of the month.

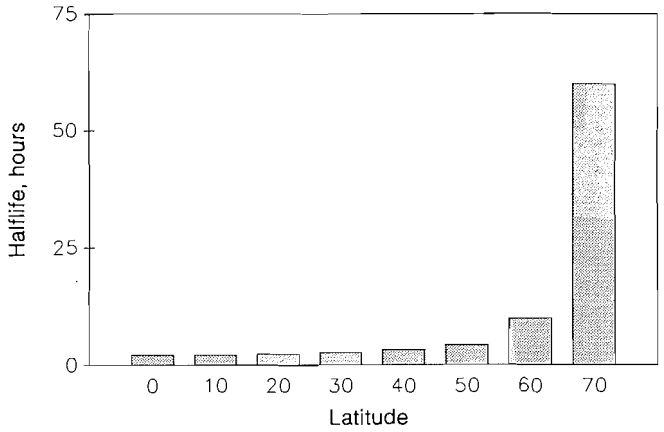

FIG. 3 Estimate of half-life of naphthalene at different latitudes using the rural model: emission at 8:00 a.m. on March 21.

March 21, with the single emission of naphthalene occurring at different times of the day. The half-life is, as expected, shortest when there is the maximum exposure to the highest solar intensities near noon. A late afternoon emission gives a longer lifetime, because any PAH not destroyed by sunset will survive the night unchanged.[2]

[2]In practice, this statement is an approximation, because the model does not take account of the nighttime reaction of PAH with the NO_3 radical.

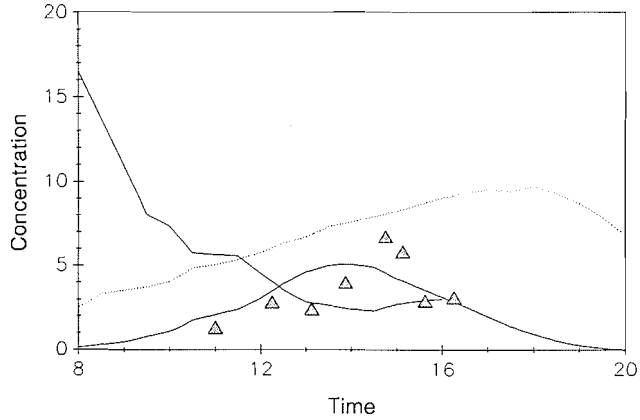

FIG. 4 Verification of urban model using experimental measurements from Dorn *et al.* (9) in Julich, Germany, on July 14, 1987. Symbols represent experimental measurements. Lower solid line, calculated OH concentration ($\times 10^{-6}$ radicals cm^{-3}); dotted line, ozone concentration ($\times 10^{-1}$ ppbv); upper solid line NO_2 concentration (ppbv).

Figure 2 is a similar calculation for a single emission of naphthalene at 8:00 a.m. at different seasons, again at 43.70°N. A substantial difference exists between winter ($t_{1/2}$ ~ 2 days) and summer ($t_{1/2}$ ~ 2–3 h). In winter the zenith angle of the sun is greater, leading to a slower rate of photolysis of ozone and therefore a lower OH concentration. Other calculations (not shown) demonstrate that the divergence between winter and summer increases at higher latitudes. Figure 3 illustrates the variation in half-life with latitude, again for a single emission of naphthalene at 8:00 a.m. on March 21. These calculations with the rural model exemplify the variation of half-life with time of day, season, and place for a short-lived tropospheric component such as PAH, but do not attempt to simulate urban conditions.

Verification of the urban model

The NO_2 and ozone concentrations reported by Dorn *et al.* (9) for Julich, Germany, for July 14, 1987, were used to determine how well the model reproduced the experimental concentrations of OH. The importance of this data set is that the diurnal variations of OH, NO_2, and O_3 were all measured. The calculated concentration of OH is shown in Fig. 4 along with the experimental values for the concentrations of NO_2, ozone, and OH. For purposes of calculation, the concentrations of NO_2 and O_3 from the paper were approximated by the functions below (t = hours elapsed since 8 a.m.).

$$O_3 \text{ (ppbv)} = 20 + 9.2t \text{ (time} < 1700 \text{ h)}$$

$$= 130 \text{ (time} > 1700 \text{ h)}$$

$$NO_2 \text{ (ppbv)} = 16.5 - 5.33t + 0.53t^2 \text{ (time} < 1320 \text{ h)}$$

$$= 3.0 \text{ ppb (time} > 1320 \text{ h)}$$

Figure 4 shows an acceptable concordance between the calculated and the experimental values of [OH]. In this context, acceptable means that the experimental trend in OH was reproduced and the quantitative agreement between calculation and experiment was within a factor of 2. As we have stated previously (10), the models presented here were designed to provide a rapid estimate of tropospheric lifetimes

Can. J. Chem. Downloaded from www.nrcresearchpress.com by 217.78.4.112 on 09/08/12
For personal use only.

Can. J. Chem. Downloaded from www.nrcresearchpress.com by 217.78.4.112 on 09/08/12
For personal use only.

using only spreadsheet software, and that additional precision would be computationally much more intensive.[3]

Reaction [10] is important in regulating the concentration of OH. The high NO_2 concentrations early in the day in Fig. 4 result from early morning rush hour traffic, which produces NO, subsequently oxidized to NO_2 by agents such as O_3 and HO_2. The OH concentration remains very low during this period due to low photon intensity (slow reaction [4]) coupled with high [NO_2] (fast reaction [10]). As the morning proceeds, rising solar intensity increases the rate of formation of OH, and the removal of NO_2 by reaction [10] outstrips its rate of emission. The concentration of NO_2 therefore falls, allowing the OH radical concentration to build up. The afternoon rush hour does not greatly increase the concentration of NO_2, since reaction [10] removes NO_2 as it forms.

A serious limitation of the present model is the lack of data with which to validate it—so far, only the set of measurements of OH concentrations in the urban troposphere reported by Dorn *et al.* (9). More measurements of this sort are clearly needed.

Application of the urban model

The data set of Dorn *et al.* (9) is unique in providing experimental measurements of the diurnal variation of O_3, NO_2, and OH. As stated earlier, [OH] cannot yet be routinely measured, and so its concentration must be calculated in order to estimate the half-lives of pollutants such as PAH. Calculations with the urban model require time-dependent concentrations of O_3 and NO_2 to be provided in order to calculate the time-dependent concentration of OH. The diurnal variations of O_3 and NO_2 are only available for a limited number of locations. An especially useful data set has been collected by the Ontario Ministry of the Environment.[4] The data used in the present paper are from the monitoring station at North York and relate to a period in July 1988 when Southern Ontario experienced a protracted hot, dry spell with severe air pollution. Three days were modelled on which very different NO_2 (actually measured as [NO_x – NO]) and ozone concentrations were recorded. The experimental and calculated OH concentrations for July 27, July 7, and July 18 are shown in Figs. 5–7.

The NO_2 and O_3 concentrations for July 27 (Fig. 5) exemplify a normal summer day. The pattern is similar both to the validation data set from Julich, Germany (except that the concentration of NO_2 increases in the afternoon rather than decreases), and to the "textbook" diurnal patterns of pollutants which have been observed in Los Angeles, California, since the late 1940's. The calculated OH concentration peaks at about 6×10^6 molec cm^{-3}.

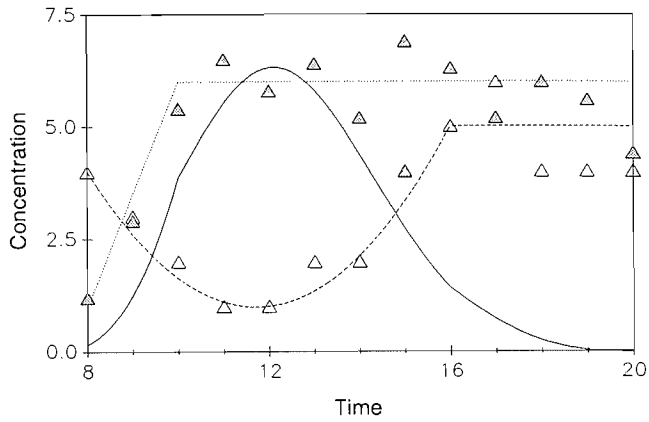

FIG. 5 Estimate of OH concentration in North York, Ont., on July 27, 1988. Symbols represent actual experimental measurements; symbols represent experimental measurements. Solid line (no symbols), calculated OH concentration ($\times 10^{-6}$ radicals cm^{-3}); symbols: dotted line and filled triangles, ozone concentration ($\times 10^{-1}$ ppbv); dashed line and open triangles, NO_2 concentration (ppbv).

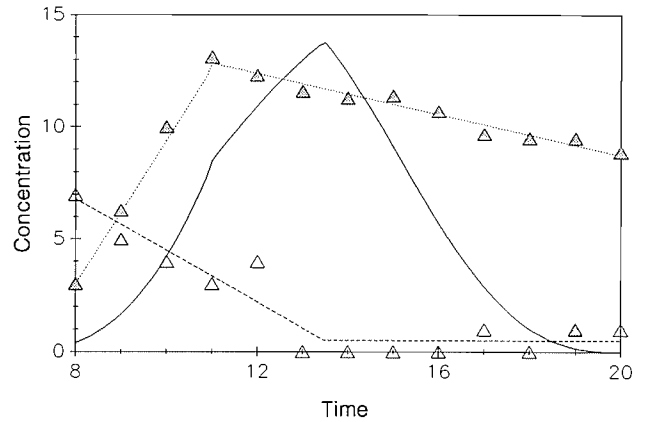

FIG. 6 Estimate of OH concentration in North York, Ont., on July 7, 1988. Symbols and lines as in Fig. 5.

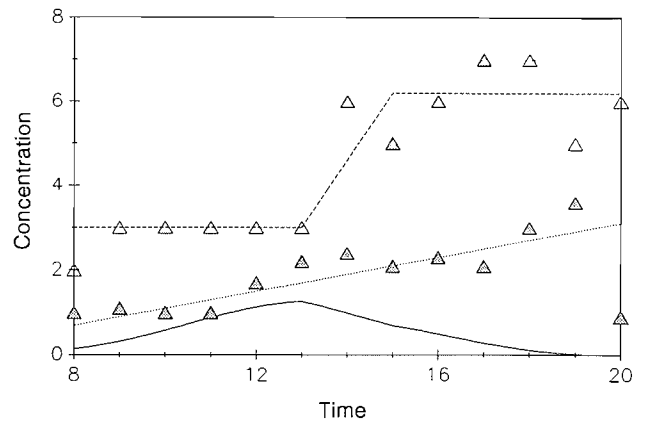

FIG. 7 Estimate of OH concentration in North York, Ont., on July 18, 1988. Symbols and lines as in Fig. 5.

[3]In particular, eq. [11] and [12] do not account for all sources and sinks of OH. For example, the photolysis of HONO is sometimes the chief source of OH in the early morning, and under some conditions reaction cycles involving OH-initiated reactions of hydrocarbons can be a net producer of OH. Under conditions of high [NO], the reaction of OH with CO may not lead to a net loss of OH due to the cycle below.

$$CO + OH \rightarrow CO_2 + H$$
$$H + O_2 \rightarrow HO_2$$
$$HO_2 + NO \rightarrow NO_2 + OH$$

Likewise, we have not included in the model the effect of the partial pressure of water (which affects the source strength of OH; Scheme 1) or other sinks for PAH such as reaction with NO_3 during darkness.

[4]Personal communication from Annette Deane, Air Resources Branch, Ontario Ministry of the Environment.

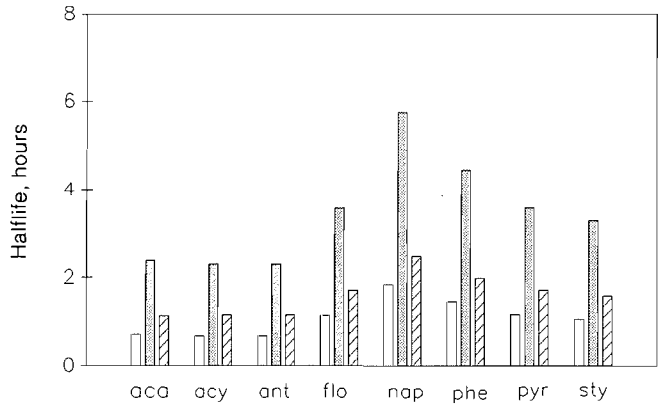

FIG. 8 Estimate of half-life of several PAH using the urban model in North York for the dates July 7, 18, and 27, 1988: emission of PAH at 8:00 a.m. Abbreviations: aca, acenaphthene; acy, acenaphthylene; ant, anthracene; flo, fluoranthrene; nap, naphthalene; phe, phenanthrene; pyr, pyrene; sty, styrene.

The ozone concentrations on July 7 (Fig. 6) were unusually high. This produced very high concentrations of OH because the rate of photolysis of ozone is proportional to the concentration of ozone. This is consistent with an experimental data set reported from Glendora, California, for August 1986 when, during a protracted period of high air pollution, 12-h average concentrations of OH of 2×10^6 radicals cm^{-3} were recorded (11). The negligible concentration of NO_2 in the afternoon of July 7 was presumably due to the efficient removal of NO_2 by the high concentration of OH (reaction [10]).

On July 18 (Fig. 7), the ozone concentration was unusually low and $[NO_2]$ increased as the day progressed. These factors combined to limit the rate of formation of OH and to maximize its rate of removal, and so on July 18 the OH concentration was unusually low.

The estimated half-lives of several PAH under these urban conditions are shown in Fig. 8. For example, the value for the half-life of naphthalene calculated on the "typical" day July 27 is about 2.5 h. On July 7, when the concentrations of OH were extremely high, the half-life was less than 2 h. Conversely on July 18, when concentrations of OH were very low, the half-life tripled to just under 6 h.

The OH concentration depends in a complex manner on the composition of the urban troposphere. According to Scheme 1, high $[NO_2]$ leads to high $[O_3]$, and hence to increased rates of formation of OH. High concentrations of NO_2 and PAH provide sinks for OH, while reactions with substances involved in cyclic reactions of OH (e.g., CO and aliphatic hydrocarbons) may cause a net increase or decrease in the concentration of OH, depending on the conditions. The instantaneous steady-state concentration of OH thus depends on the interplay of these factors. Recent work (12) implies that the long term *global* trend in [OH] may be downward, owing to greater sink strengths, especially increased global concentrations of methane. In the polluted urban troposphere, the trend in [OH] is predicted to be upward, due to high levels of ground level ozone.

Urban concentrations of PAH are important because of concerns over the toxicity of the parent PAH and some of their tropospheric products. The present work suggests that high levels of ozone should be associated with a greater sink strength for PAH, due to increased production of OH. A different explanation was provided by Flessel and Levaggi (13), who noted that high levels of ground level ozone were associated with low levels of PAH, and concluded that reaction with ozone itself must be a strong sink for PAH. However, later work (4) suggested that reaction with ozone is rapid only for five-membered ring PAH such as acenaphthylene. Trends in the concentration of PAH are important in assessing the success of vehicular emission controls; however, a lower ambient level of PAH could be achieved either by reduced emission, reducing the source strength, or by faster reaction due to a higher concentration of OH, increasing the sink strength. To distinguish these possibilities it will be necessary to monitor concurrently the diurnal variation of [PAH] and $[O_3]$ at different seasons, thus allowing the concentration of OH, and hence the sink strength, to be estimated.

Acknowledgement

We thank the Atmospheric Environment Service of Environment Canada for financial support.

1. R. Atkinson. Chem. Rev. **86**, 69 (1986).
2. P. J. Crutzen. *In* Atmospheric chemistry. *Edited by* D. G. Goldberg. Ann Arbor Press, Michigan. 1982. pp. 313–328; R. Prinn, D. Cunnold, R. Rasmussen, P. Simmonds, F. Alyea, A. Crawford, P. Fraser, and R. Rosen. Science, **238**, 945 (1987).
3. T. Dann. Polycyclic aromatic hydrocarbons in the ambient air of Toronto, Ontario and Monreal, Quebec. Environment Canada Report PMD 89–14. 1989. pp. 89–98.
4. R. Atkinson. Atmos. Environ. A, **24**, 1 (1990).
5. H. Tokiwa and Y. Ohnishi. CRC Crit. Rev. Toxicol. **17**, 23 (1986).
6. N. J. Bunce, J. S. Nakai, and M. Yawching. Chemosphere, **22**, 305 (1991).
7. U. Platt, M. Rateike, W. Junkermann, J. Rudolph, and D. H. Ehhalt. J. Geophys. Res. **93**, 5159 (1988).
8. B. J. Finlayson-Pitts and J. N. Pitts, Jr. Atmospheric chemistry. Wiley, New York, N.Y. 1986. Sect. 3-A-2 and 3-C-2.
9. H. P. Dorn, J. Callies, U. Platt, and D. H. Ehhalt. Tellus, **40**, Ser. B, 437 (1988).
10. N. J. Bunce, J. S. Nakai, and M. Yawching. J. Photochem. Photobiol. A, **57**, 429 (1991).
11. J. Arey, R. Atkinson, B. Zielinska, and P. A. McElroy. Environ. Sci. Technol. **23**, 321 (1989).
12. R. A. Kerr. Science, **253**, 1210 (1991).
13. P. Flessel and D. A. Levaggi. Monitoring for PAH and criteria pollutants in Contra Costa County, CA., 1979–1986. Proc. APCA Annu. Meet. 80th, 1987. Paper 87–96.4
14. H. W. Biermann, H. Mac Leod, R. Atkinson, A. M. Winer, and J. N. Pitts, Jr. Environ. Sci. Technol. **19**, 244 (1985).
15. R. Atkinson, J. Arey, B. Zielinska, and S. M. Aschmann. Int. J. Chem. Kinet. **22**, 999 (1990).

Can. J. Chem. Downloaded from www.nrcresearchpress.com by 217.78.4.112 on 09/08/12
For personal use only.

Computational and ultraviolet photoelectron spectroscopic evidence that (*Z*)-2-methyl-1,3-pentadiene prefers twisted *s-cis* conformers in the gas phase

NICK HENRY WERSTIUK,[1] GEORGE TIMMINS, JIANGONG MA, AND TIMOTHY A. WILDMAN[1]
Department of Chemistry, McMaster University, Hamilton, Ont., Canada L8S 4M1

Received June 6, 1991[2]

NICK HENRY WERSTIUK, GEORGE TIMMINS, JIANGONG MA, and TIMOTHY A. WILDMAN. Can. J. Chem. **70**, 1971 (1992).

A redetermination of the ultraviolet photoelectron (pe) spectrum of (*Z*)-2-methyl-1,3-pentadiene has led to a correction of the published spectrum. By studying (*Z*)-2-methyl-1,3,-pentadiene (**1***a*) and (*E*)-2-methyl-1,3-pentadiene (**1***b*) with MMX, MNDO, AM1, and *ab initio* MO computational methods and pe spectroscopy, we have shown that a combination of these methods provides useful insights on the conformational behaviour of methyl-substituted 1,3-dienes in the gas phase. Synthetic pe spectra, derived from the computed potential energy surfaces and angle-dependent orbital energies, are in good agreement with experiment. Thus, the *E* isomer prefers the *s-trans* conformer but the *Z* isomer prefers twisted *s-cis* conformations in the gas phase.

NICK HENRY WERSTIUK, GEORGE TIMMINS, JIANGONG MA et TIMOTHY A. WILDMAN. Can. J. Chem. **70**, 1971 (1992).

Une redétermination du spectre photoélectronique ultraviolet (pe) du (*Z*)-2-méthylpenta-1,3-diène a conduit à une correction du spectre publié antérieurement. En étudiant les (*Z*) et (*E*)-2-méthylpenta-1,3-diènes, respectivement **1***a* et **1***b*, par des méthodes de calculs d'orbitales moléculaires MMX, MNDO, AM1 et *ab initio* et par spectroscopie pe, on a montré qu'une combinaison de ces méthodes permet d'avoir des idées utiles sur le comportement conformationnel en phase gazeuse de ces 1,3-diènes substitués par des méthyles. Les spectres pe synthétiques, calculés à partir des surfaces d'énergie potentielle et des énergies orbitalaires qui dépendent des angles, sont en bon accord avec les valeurs expérimentales. Ainsi, en phase gazeuse, l'isomère *E* existe préférentiellement comme conformère *s-trans* alors que l'isomère *Z* préfère les conformations *s-cis* déformées.

[Traduit par la rédaction]

Introduction

A comprehensive study of the effect of methyl and ethyl substituents on the conformations of conjugated dienes by ultraviolet photoelectron spectroscopy (UPS) and by empirical (MMX), semiempirical (AM1, MNDO), and *ab initio* MO calculations was initiated recently (1, 2). This work was undertaken for several reasons. The primary goal was to establish whether or not AM1 (3) is useful for carrying out conformational analyses and for detailing conjugative and homoconjugative interactions in dienes. In our view, this research is timely because there is renewed interest (4–8) in the conformational analysis of dienes, a subject which occupied the attention of experimentalists and theoreticians for decades.[3] Our plan was to study a series of alkyl-substituted 1,3-dienes computationally to calculate heats of formation or total energies as a function of the dihedral (twist) angle between the double bonds in order to identify the stable conformations and to calculate the π_-, π_+ splittings of planar (*s-cis* and *s-trans*) and twisted conformations. By comparing the latter values with the splittings obtained experimentally by UPS, we hoped to establish whether combined AM1/UPS could be of general use in the study of conformational behaviour and of conjugative or homoconjugative interactions of alkyl-substituted polyenes in the gas phase. Moreover, because structure determines the conformational behaviour of these molecules, these studies would establish whether AM1/UPS could be used to elucidate the geometrical structure of highly alkylated dienes and polyenes, especially where there are no vicinal protons on the double bonds; the classical approach of using ^{1}H coupling constants to determine stereochemistry cannot be used in these cases. We were motivated to undertake this comprehensive study primarily by a report that the three lowest ionization energies of (*Z*)-2-methyl-1,3-pentadiene (**1***a*) and (*E*)-2-methyl-1,3-pentadiene (**1***b*) are identical within experimental error (8.43, 10.49, 11.53 eV for **1***a* and 8.42, 10.46, and 11.50 eV for **1***b*) (9). In preparing **1***a* in order to repeat the work of Masclet and co-workers (9), we established that the commercial product claimed to be predominantly (*Z*)-2-methyl-1,3-pentadiene was in fact the *E* isomer. The photoelectron (pe) spectra of **1***a* (Fig. 1A) and **1***b* (Fig. 1B) are different. On the basis of the π_+, π_- splitting and MMX calculations, we concluded that twisted *s-cis* conformers of **1***a* are preferentially populated in the gas phase and published a communication to document the results.

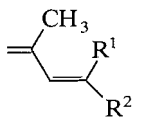

1

a, $R^1 = CH_3$, $R^2 = H$

b, $R^1 = H$, $R^2 = CH_3$

In this paper, we give a full account of our study of **1***a* and **1***b* that includes comprehensive computational studies and synthetic pe spectra derived from those studies.

Results and discussion

Preparation and pe spectroscopy of (Z)-2-methyl-1,3-pentadiene (1a) and (E)-2-methyl-1,3-pentadiene (1b)

Samples that were supposedly **1***a* and **1***b* were first isolated from a commercial product that was labelled as 80% **1***a* and 20% **1***b* by Aldrich Chemical Co. The major com-

[1]Authors to whom correspondence may be addressed.
[2]Revision received February 20, 1992.
[3]See ref. 4 for a comprehensive list.

Can. J. Chem. Downloaded from www.nrcresearchpress.com by 217.78.4.112 on 09/08/12
For personal use only.

Can. J. Chem. Downloaded from www.nrcresearchpress.com by 217.78.4.112 on 09/08/12
For personal use only.

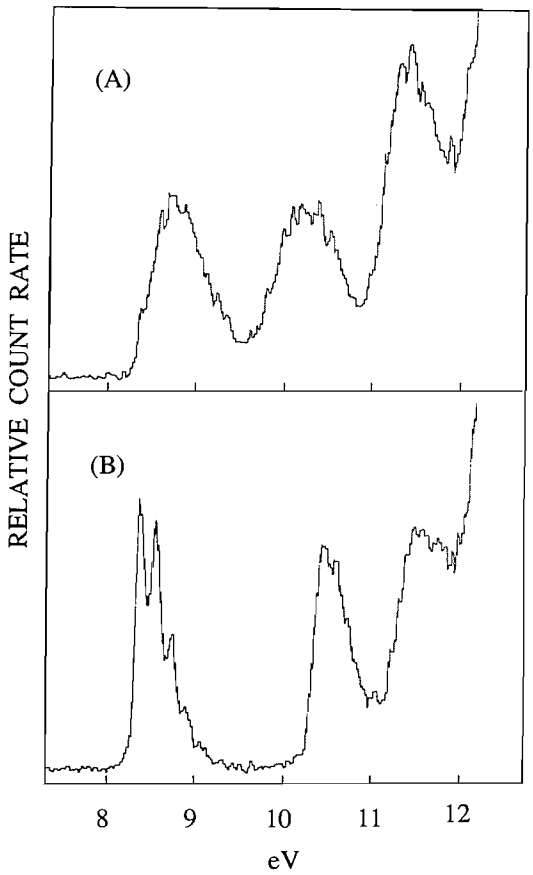

FIG 1. Partial ultraviolet photoelectron spectra of (*Z*)-2-methyl-1,3-pentadiene (A) and (*E*)-2-methyl-1,3-pentadiene (B) recorded at 300 ± 5 K.

ponent exhibited three discernable low-IE bands at 8.42 (π_-), 10.46 (π_+), and 11.50 eV, in agreement with the pe spectrum reported by Masclet and co-workers (9). The π_-, π_+ splitting was 2.04 ± 0.05 eV. However, the ^{1}H NMR spectrum of this sample corresponded closely to the spectrum of (*E*)-2-methyl-1,3-pentadiene (10). The key feature was that the vicinal vinylic ^{1}H coupling constant of 15.6 Hz fell in the range expected for *trans* vinylic hydrogens (11). Furthermore, the ^{1}H NMR spectrum of the sample which was supposedly **1***b* (20% of the commercial material) corresponded to the spectrum of 4-methyl-1,3-pentadiene (10). Here the key feature was a broad singlet at 1.75 ppm of relative area six. As was reported in the preliminary account of this work (1), different conformational preferences for **1***a* (crosses in Fig. 2) and **1***b* (circles in Fig. 2) were indicated by MMX calculations in which the nonplanar option was used for the double bonds. Unlike **1***b*, for which the planar *s-trans* conformation is the most stable structure, *s-cis* conformations with dihedral angles in the region of 60° are predicted to be the most stable structures of **1***a*. On this basis, a π_-, π_+ splitting less than the observed value of 2.04 eV would be expected for **1***a* (12). The NMR data and the MMX calculations coupled with the magnitude of the π_-, π_+ splitting indicated that the major component of the commercial material was not **1***a* and that the pe spectrum reported previously (9) was not the spectrum of (*Z*)-2-methyl-1,3-pentadiene (**1***a*).

Analysis of the Aldrich product on a 1,2,3-tris-(2-cyanoethoxy)-propane (TCEP) column at ambient temperature

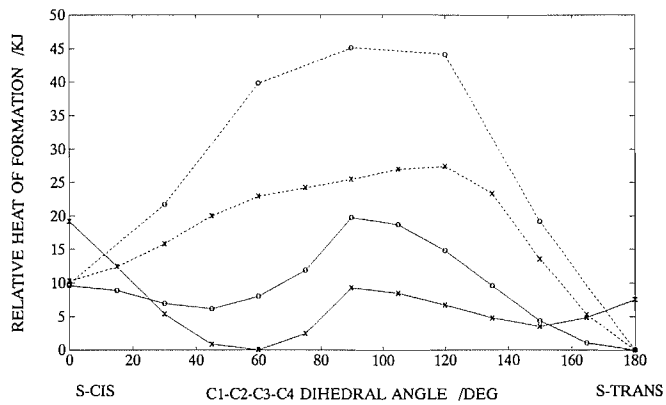

FIG. 2. Calculated relative heat of formation of 2-methyl-1,3-pentadiene from MMX. Dashed lines correspond to planar double bonds and solid lines correspond to twisted, nonplanar double bonds. Crosses correspond to **1***a*, circles to **1***b*.

established that three components, A, B, and C, with relative retention times of 1:1.40:1.55 were present in a ratio of 1 (2%): 39 (78%): 10 (20%) respectively. Based on the assumption that the commercial material was actually composed predominately of a mixture of (*E*)-2-methyl-1,3-pentadiene (**1***b*) (78%) and 4-methyl-1,3-pentadiene (20%), an attempt was made to prepare **1***a* by photochemical isomerization of **1***b* (13). To that end, the commercial product was photolyzed at 300 nm in pentane in a Rayonet reactor in the presence of acetophenone as a sensitizer. Photolysis reactions were monitored by gc (TCEP) and stopped when the yield of peak A reached a maximum, usually after 8–10 h. For one photolysis, the ratio of peaks A:B:C was 1:1.84:0.87 after 9 h. These components were isolated by preparative gc (TCEP) and ^{1}H NMR spectra were obtained. Because the ^{1}H NMR spectra of the compounds A, B, and C correspond closely to the spectra reported for **1***a* (14), **1***b* (10), and 4-methyl-1,3-pentadiene (10), the commerical product was deemed to be a mixture of **1***b* and 4-methyl-1,3-pentadiene, not **1***a* and **1***b* as indicated on the label. The partial pe spectra of **1***a* and **1***b* are shown as Fig. 1(A and B), respectively.

Computational studies of dienes **1***a and* **1***b*

The heats of formation (ΔH_f) of **1***a* and **1***b* were computed with MMX as the C1—C2—C3—C4 dihedral angle was driven from 180° to 0° in 15° increments. When planarity of the double bonds was enforced, planar *s-trans* conformations were computed to be the most stable structures of **1***a* and **1***b*, as shown by dashed lines in Fig. 2. On the other hand, when the non-planar optimization option was used, torsional distortion of the double bonds of **1***a* occurred and twisted *s-cis* conformers with C1—C2—C3—C4 dihedral angles in the region of 60° were the most stable structures, as shown by crosses on solid lines in Fig. 2. Clearly, this version of MMX (15) is not generally useful for studying conformational preferences of highly substituted 1,3-dienes.

MNDO and AM1 calculations were also carried out to compute ΔH_f as a function of the C1—C2—C3—C4 dihedral angle. The keyword PRECISE was specified in order to tighten the convergence criteria. As shown by the dashed lines in Fig.3(A and B), the MNDO results wrongly indicate that 90° conformations are the most stable structures of **1***a* and **1***b*. This is presumably a consequence of the underestimation of the resonance stabilization of the planar con-

TABLE 1. Heats of formation of diene conformers computed with AM1

C1—C2—C3—C4 dihedral angle	Diene[a]	
	1*a*	**1***b*
180 (*s-trans*)	68.33	55.65
165	67.88	56.01
150	66.93	57.19
135	66.48	58.62
120	65.26	59.96
105	64.77	61.24
90	64.98	61.63
75	64.42	60.77
60	62.93	58.92
45	61.64	56.74
30	61.89	55.35
15	63.95	55.11
0 (*s-cis*)	65.28	55.22

[a]Heat of formation is given in kJ/mol.

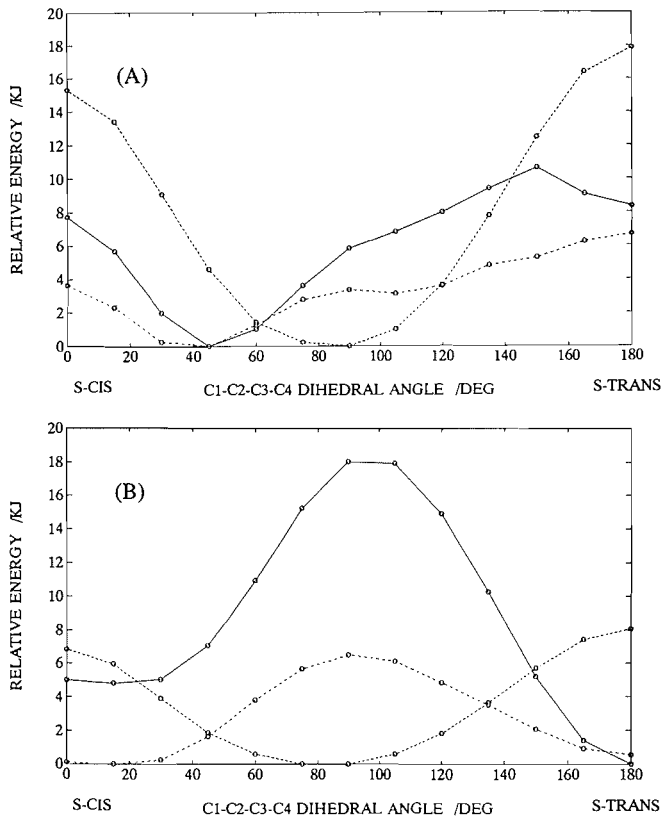

FIG. 3. Calculated heat of formation or relative total energy of 2-methyl-1,3-pentadiene from MNDO (dashed line), AM1 (dot–dashed line), and STO-3G (solid line): *Z* isomer (**1***a*) in A, *E* isomer (**1***b*) in B.

formations and the consistent overestimation of steric repulsions in MNDO (3).

According to the AM1 results (see Table 1 and the dot–dashed lines in Fig. 3) the planar *s-trans* conformation of **1***b* is only marginally less stable than the *s-cis* structure. The AM1 barrier to interconversion of the planar *s-trans* to the planar *s-cis* conformation is only 6.5 kJ/mol. This low barrier is consistent with the results of a previous AM1 computational study of butadiene (2). AM1 underestimates the torsional barrier in 1,3-butadiene by approximately 12 kJ/mol and $\Delta\Delta H_f$ between the planar *s-trans* and planar *s-cis* conformations by approximately 4 kJ/mol. Twisted (45°) *s-cis* conformations of **1***a* are computed to be more stable than the planar *s-trans* and *s-cis* conformations (Fig. 3A). Contrary to the MMX results, there is no significant torsional distortion of the double bonds at the AM1 level. It is not clear why the AM1 surface for **1***a* compares closely to the 4-31G// STO-3G surface (*vide infra*) and yet AM1 fails to reproduce the relative stabilities of the planar *s-cis* and planar *s-trans* conformations of **1***b*. A possible explanation runs as follows. As with MNDO, the AM1 torsional barrier for butadiene is low, probably because the resonance stabilization of the planar *s-cis* and planar *s-trans* conformations is underestimated. If the 1,3-methyl–methyl and methyl–vinyl steric interactions in the planar *s-trans* and planar *s-cis* conformations are also underestimated, a fortuitous cancellation of errors may occur for **1***a* but not for **1***b*, in which steric repulsions are less important.

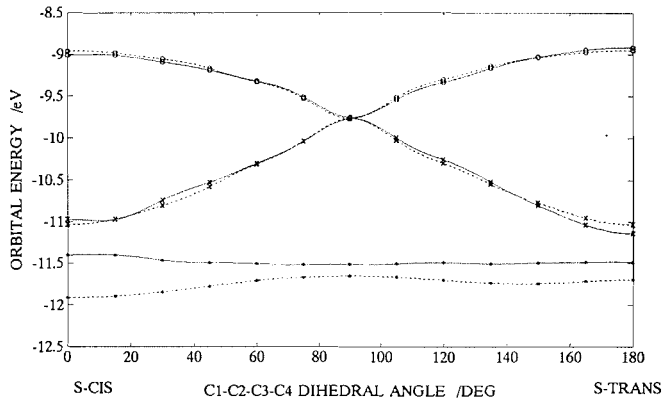

FIG. 4. Calculated angle dependence of the π_-, π_+ and highest σ MO energies of (*Z*)-2-methyl-1,3-pentadiene (solid lines) and (*E*)-2-methyl-1,3-pentadiene (dashed lines) from AM1.

Figure 4 shows how the π_-, π_+ and highest σ orbital energies of **1***a* and **1***b* change as a function of the C1—C2—C3—C4 dihedral angle with AM1. As for 2,3- and 2,4-dimethyl-2,4-hexadiene (2), π_- is less sensitive to twist angle than π_+. This can be rationalized on the basis of a homohyperconjugative interaction between the methyl group at C2 and the π system of the diene (16).

At the STO-3G level, the computed torsional barrier for conversion of *s-trans*-**1***b* to *s-cis*-**1***b* is 18 kJ/mol and ΔE for the planar *s-trans* and planar *s-cis* conformations is 5 kJ/mol, shown in Fig. 3B) as the solid-line plot. Like the AM1 results, the STO-3G calculations indicate that twisted *s-cis* conformers of **1***a* are the most stable. The results are shown graphically on the solid-line plot in Fig. 3A. The optimum STO-3G structures of four conformations of **1***a* (**1***a* (180°), **1***a* (90°), **1***a* (45°), and **1***a* (0°)) and three conformations of **1***b* (**1***b* (180°), **1***b* (90°), **1***b* (0°)) are given in Fig. 5. The point here is that the terminal methyl of **1***a* undergoes a 180° rotation as the C1—C2—C3—C4 dihedral is driven from 180° to 0°. The total energies are given in Table 2. The π_-, π_+ splittings from STO-3G, 4-31G//STO-3G, and AM1 calculations on **1***a* and **1***b* appear in Tables 3 and 4. On the basis of the STO-3G results, the π_-, π_+ splitting expected for **1***b* is about 2.99 eV. The experimental value is only 2.04 ±

Can. J. Chem. Downloaded from www.nrcresearchpress.com by 217.78.4.112 on 09/08/12
For personal use only.

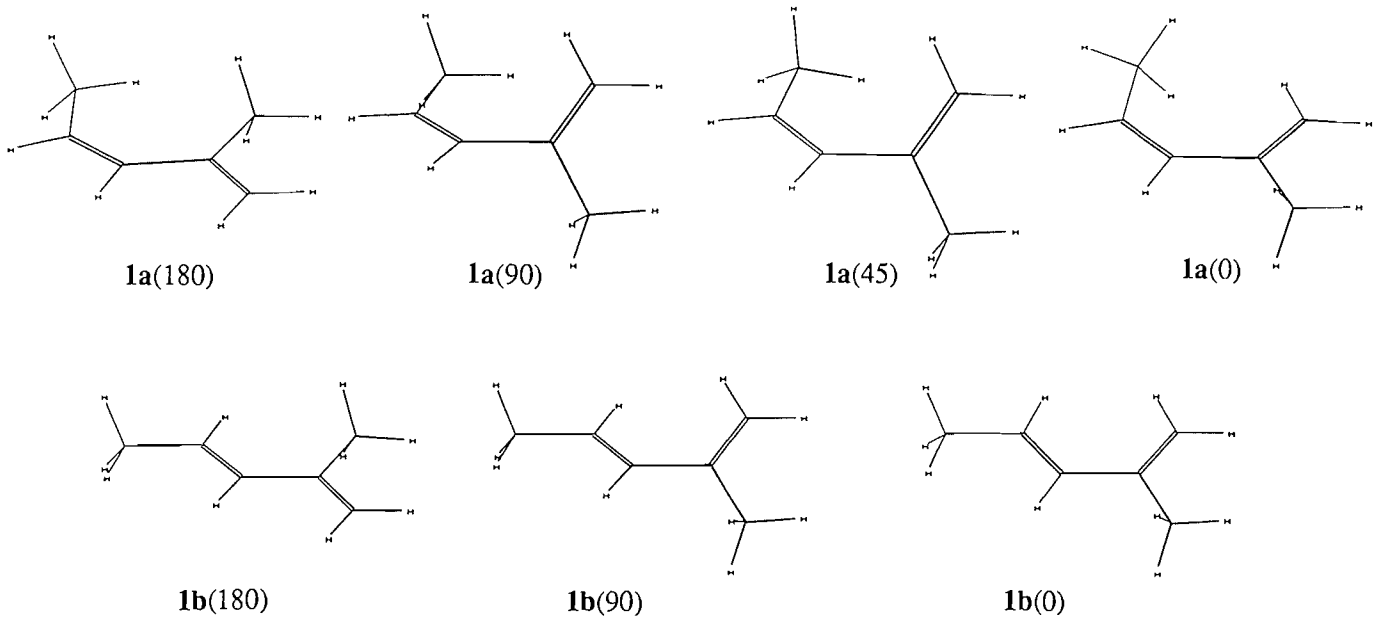

FIG. 5. Geometry-optimized STO-3G structures of **1***a* at C1—C2—C3—C4 dihedral angles of 180°, 90°, 45°, and 0°, and of **1***b* at 180°, 90°, and 0°. Notice the internal rotation about C4—C5 in **1***a*.

TABLE 2. Total energies of diene conformers

C1—C2—C3—C4 dihedral angle	Diene[a]			
	1*a*		**1***b*	
	STO-3G	4-31G//STO-3G	STO-3G	4-31G//STO-3G
	−230.0	−232.0	−230.0	−232.0
180 (*s-trans*)	0.1817222	0.6530438	0.1902794	0.6618328
165	0.1817222	0.6525809	0.1897488	
150	0.1808472	0.6515456	0.1882993	
135	0.1807147	0.6509167	0.1863788	
120	0.1818440	0.6523471	0.1846027	
105	0.1822838	0.6529486	0.1834577	
90	0.1826767	0.6536642	0.1834136	0.6544666
75	0.1835276	0.6547404	0.1844816	
60	0.1845056	0.6556451	0.1861227	
45	0.1848932	0.6557317	0.1875981	
30	0.1841380	0.6547006	0.1883709	
15	0.1827381	0.6530675	0.1884532	
0 (*s-cis*)	0.1819599	0.6520826	0.1883809	0.6571411

[a]Total energies are given in hartrees; 1H corresponds to 2625.5001 kJ/mol.

0.05 eV.[4] Computations with the 4-31G basis at the STO-3G optimum geometry provide some reduction in the π_-, π_+ splitting, but the values are still significantly larger than that observed. On the other hand, AM1 provides 2.08 eV, in splendid agreement with the experimental value. All of the methods indicate that the π_-, π_+ splitting for **1***a* should be smaller than that for **1***b*. The AM1 orbital energies are used in the pe spectrum syntheses for two reasons: (*i*) STO-3G overestimates the π_-, π_+ splitting and (*ii*) AM1 computes these splittings with good accuracy for methyl-substituted 1,3-dienes (2). The AM1 π_-, π_+ splitting of the 45°-twisted *s-cis* conformation of **1***a* is 1.34 eV, in modest agreement with the experimental value of 1.50 ± 0.05 eV. The STO-3G and 4-31G//STO-3G values are 1.98 eV and 1.86 eV, respectively. However, such direct comparisons fail to account for conformational distribution.

Synthesis of photoelectron spectra

In this work, the bands of primary interest show sensitivity to conformational behaviour. The spectral intensity $S(I)$ at ionization energy I due to a particular conformation, corresponding to a dihedral angle ϕ, depends upon the thermal population density of conformations about ϕ and upon the angular dependence of I itself (17–19). Thus if I were independent of ϕ, the spectrum would consist of a sharp line

[4]This differs slightly from the value we reported previously (2.14 eV).

Can. J. Chem. Downloaded from www.nrcresearchpress.com by 217.78.4.112 on 09/08/12
For personal use only.

Can. J. Chem. Downloaded from www.nrcresearchpress.com by 217.78.4.112 on 09/08/12
For personal use only.

TABLE 3. Computed π_-, π_+ splitting (eV) of (*Z*)-2-methyl-1,3-pentadiene

C1—C2—C3—C4 dihedral angle	AM1	4-31G//STO-3G	STO-3G
180 (*s-trans*)	2.22	2.83	3.02
165	2.10	2.73	2.91
150	1.77	2.42	2.57
135	1.35	1.87	1.96
120	0.92	1.19	1.24
105	0.46	0.60	0.61
90	0.02	0.08	0.09
75	0.53	0.78	0.83
60	0.98	1.37	1.45
45	1.33	1.86	1.98
30	1.65	2.24	2.40
15	1.87	2.51	2.68
0 (*s-cis*)	1.96	2.62	2.81

TABLE 4. Computed π_-, π_+ splittings (eV) of (*E*)-2-methyl-1,3-pentadiene

C1—C2—C3—C4 dihedral angle	AM1	4-31G//STO-3G	STO-3G
180 (*s-trans*)	2.08	2.78	2.99
165	1.98		2.90
150	1.74		2.65
135	1.40		2.20
120	1.00		1.57
105	0.51		0.78
90	0.01	0.03	0.03
75	0.50		0.83
60	0.98		1.51
45	1.40		2.09
30	1.75		2.54
15	1.99		2.85
0	2.07	2.83	2.96

at this ionization energy, but if I were strongly angle dependent, the intensity would be distributed over a range of ionization energies, although the integrated intensity would be the same.

To provide a comparison between the experimental observations and the computational results, the relative conformational energies and angle-dependent orbital energies from the MO calculations were used to synthesize photoelectron spectra. Because these computational results form a discrete set, it was necessary to construct interpolating functions to represent them. The scheme is similar to one proposed by Honegger and Heilbronner (19), but more general.

Relative conformational energies and orbital energies are periodic functions of ϕ and can be expressed as Fourier series. For the molecules of present interest, these functions must also have even parity, i.e., they are symmetric with respect to reflection through $\phi = 0°$.

$$V(\phi) = \sum_{m=0}^{M} V_m \cos(m\phi)$$

and similarly

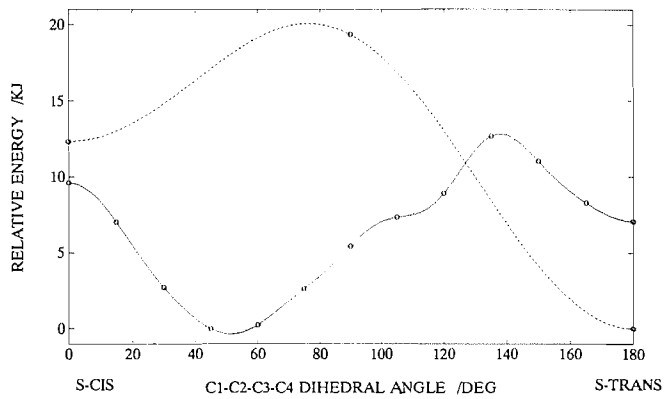

FIG. 6. Relative total energy of **1***a* and **1***b* (circles) from 4-31G//STO-3G calculations as a function of the C1—C2—C3—C4 dihedral angle. The interpolated angle dependence used in the synthesis of spectra is represented by a solid line for **1***a* and a dashed line for **1***b*.

$$I_a(\phi) = \sum_{n=0}^{N} c_{an} \cos(n\phi)$$

where a is an orbital label and V_m, c_{an} are coefficients. For a dataset $\{\{\phi\}, \{V(\phi)\}, \{I_a(\phi)\}, \{I_b(\phi)\},\ldots\}$, the coefficients are found by solution of the appropriate set of linear equations. In this work, $M = N$ is the number of angles for which data is available. Clearly, the dataset must include sufficient angles to define the features of $V(\phi)$ and all of the $I(\phi)$.

Spectral bands for each orbital, $s_a(I)$, were generated separately and then summed. For a particular spectral range, the ionization energy I was scanned at the desired digital resolution. When I fell within the range of $i_a(\phi)$, the corresponding angles were found as the zeros of $f(\phi) = I_a(\phi) - I$. In general, $\phi(I_a)$ is not single valued so the algorithm searches for a maximum of $2N$ angles. The spectral intensity due to orbital a, $s_a(I)\,dI$, is proportional to the Boltzmann population density, $\exp[-V(\phi)/k_BT]\,d\phi$, summed over all of the angles found. The intensity $s_a(I)$ in the digitized spectrum is given by

$$s_a(I) = \int_{\phi_1}^{\phi_2} \exp[-V(\phi)/k_BT]\,d\phi$$

where ϕ_1 and ϕ_2 correspond to the energies $I + \Delta I/2$, where ΔI is the digital resolution. The intensity distribution is folded with a Gaussian lineshape (FWHH = 0.3 eV) to approximate the Franck–Condon profile. The integrated intensity of each band $s_a(I)$ is normalized. Admittedly the Gaussian convolution is quite crude, but normal coordinate analyses for the electronic ground state and for each corresponding ion would be required in order to calculate Franck–Condon factors and thus more realistic vibrational fine structure. Such calculations are beyond our resources.

For **1***a*, $V(\phi)$ was satisfactorily defined by data at 15° increments on the interval [0°, 180°]. Relative energies from 4-31G//STO-3G calculations and relative heats of formation from AM1 were used. The *ab initio* potential energy surface appears in Fig. 6 (solid-line plot). Fourier coefficients appear in Table 5. The corresponding STO-3G energies are given in Table 2. The AM1 energies of the three highest occupied MOs appear in Fig. 4 and were used in the

TABLE 5. Fourier coefficients for computed diene potentials

	V_m/(kJ/mol)			
	1*a*		**1***b*	
m	AM1	4-31G//STO-3G	AM1	4-31G//STO-3G
0	3.19	6.20	2.97	12.76
1	−2.39	−3.61	−0.78	6.16
2	0.74	1.64	−3.13	−6.60
3	0.28	3.55	0.31	
4	0.95	0.38	0.43	
5	0.62	1.36	0.25	
6	0.20	−0.28	0.03	
7	−0.07	0.01	0.03	
8	0.15	0.40	0.03	
9	−0.01	−0.24	−0.03	
10	−0.02	0.09	0.01	
11	0.04	0.19	0.00	
12	−0.03	−0.11	0.00	

spectrum calculation, for reasons given above. Because the potential energy surface for **1***b* is adequately described by one- and two-fold components, only the data for $\phi = 0°$, 90°, and 180° were used to define the interpolating functions, as shown by the dashed-line plot of Fig. 6.

The synthetic spectra of **1***a* and **1***b* appear in Figs. 7A and 7B, respectively. The solid lines correspond to the 4-31G// STO-3G potentials and the dashed lines correspond to the AM1 potentials in Fig. 3. The spectra are clearly sensitive to details of the potentials. particularly if the thermal distribution of conformers is wide, as expected from Fig. 3A. Comparison of Fig. 1 and Fig. 7 suggests that the synthetic spectra from the 4-31G//STO-3G potentials correspond more closely to the experimental spectra than do those from AM1 potentials. The π_-, π_+ splitting for **1***a* is only 1.3 eV, both π bands are broader than for **1***b*, and the lower intensity maximum for the π_+ band indicates that π_+ has a stronger angle dependence than π_-.

Thermal [1,5] sigmatropic shifts in (Z)-1,3-pentadiene and ***1****a*

The thermal [1,5] sigmatropic hydrogen shift in (*Z*)-1,3-pentadiene has been the subject of much attention because the reaction proceeds via vibrationally assisted hydrogen transfer (20). Calculations on this molecule suggest that the twisted *s-cis* conformer, which is a secondary minimum on the potential energy surface, is the reactive species rather than the *s-trans*. The conformational equilibrium masks any indications of non-Arrhenius temperature dependence in the rate constant. However, if our understanding of the hydrogen transfer process in (*Z*)-1,3-pentadiene is good, we would predict more rapid intramolecular hydrogen transfer in (*Z*)-2-methyl-1,3-pentadiene. On the basis of the AM1 potential, k_{obs}^{H} for the 2-methyl derivative should be an order of magnitude larger (10^{-5}/s) at 475 K and two orders of magnitude larger (10^{-9}/s) at room temperature. The primary deuterium isotope effect should be near 5 at 475 K, as for (*Z*)-1.3-pentadiene itself, but it should increase dramatically as *T* decreases (20). Because the twisted *s-cis* conformer is preferred, non-Arrhenius behaviour should occur below 75 K, but k_{obs}^{H} is expected to be on the order of 10^{-19}/s at 75 K, which implies unobservably slow exchange.

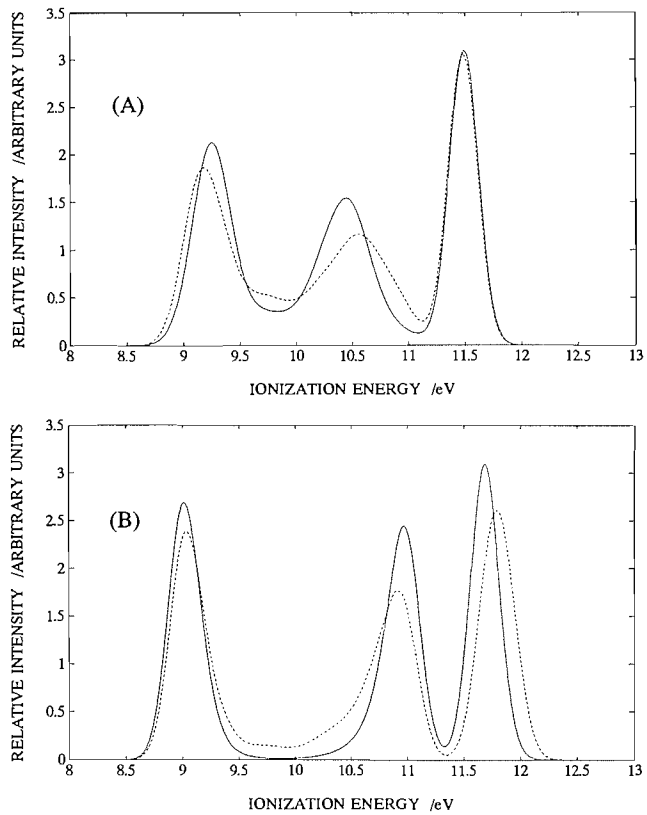

FIG. 7. Synthetic photoelectron spectra of **1***a* (A) and **1***b* (B) derived from the angle-dependent relative energies and orbital energies in Fig. 6. Solid lines are from 431G//STO-3G potentials. Dashed lines are from AM1 potentials. Spectra have been convoluted with a Gaussian lineshape with a full width at half height of 0.3 eV. The sample temperature was taken to be 300 K.

Conclusions

This study has shown that a combination of AM1, *ab initio*, and UPS studies coupled with synthesis of pe spectra will be generally useful for studying the conformational behaviour of alkyl-substituted 1,3-dienes. The results also confirm that the previous conclusions reached about the conformational behaviour of 2,3- and 2,4-dimethyl-2,4-hexadienes based solely on an AM1/UPS study are valid (2). Synthetic pe spectra derived from the computed potential energy surfaces and angle-dependent orbital energies are in good agreement with experiment. Thus, the *E* isomer prefers the *s-trans* conformer but the *Z* isomer prefers twisted *s-cis* conformations in the gas phase.

Experimental

*Preparation of (Z)-2-methyl-1,3-pentadiene (****1****a)*

A mixture of (*E*)-2-methyl-1,3-pentadiene (785), 4-methyl-1,3-pentadiene (20%), and (*Z*)-2-methyl-1,3-pentadiene (2%) (0.25 g) from Aldrich Chemical Co. and acetophenone (0.036 g) were dissolved in spectral grade pentane (30 mL) in a quartz vessel. The solution was cooled with ice-water, deoxygenated with N_2 for 20 min, and photolyzed at 300 nm for 9 h in a Rayonet reactor equipped with 8 lamps. Gc analysis of the mixture on a 3.3 m × 5 mm 18% TCEP on Supelcoport 100/120 column (He flow rate 40 mL/min) maintained at ambient temperature (~30°) showed that three major components, corresponding to peaks A (24.1%), B (44.4%), and C (21.1%), were present. These had the same relative retention times as the starting components (1:1.40:1.55). An

Can. J. Chem. Downloaded from www.nrcresearchpress.com by 217.78.4.112 on 09/08/12
For personal use only.

additional product (10.4%) not present in the starting material had a retention time only slightly longer than solvent pentane. The major components were separated and purified using the TCEP column. Peak A (**1***a*) exhibited resonances (500 MHz, $CDCl_3$) at 5.85 (d, J = 11.7 Hz, 1H), 5.51 (d of q, J = 11.7, 6.5 Hz, 1H), 4.96 (s, 1H), 4.83 (s, 1H), 1.88 (s, 3H), and 1.81 (d, 6.5 Hz, 3H) ppm. Peak B (**1***b*) exhibited resonances (200 MHz, $CDCl_3$) at 6.15 (d with fine structure, J = 15.6 Hz, 1H), 5.66 (d of 1, J = 15.6, 6.6 Hz, 1H), 4.83 (s, 2H), 1.82 (s, 3H), and 1.77 (d, J = 6.6, Hz, 3H) ppm. Peak C (4-methyl-1,3-pentadiene) exhibited resonances (200 MHz, $CDCl_3$) 6.55 (d of t, J = 16.8, 9.8 Hz, 1H), 5.81 (d, J = 10.8 Hz, 1H), 5.05 (d, J = 16.8 Hz, 1H), 4.94 (d, J = 9.8 Hz, 1H), and 1.75 (b, 3H) ppm.

Photoelectron spectra of **1**a *and* **1**b

The pe spectra of **1***a* and **1***b* were obtained on a non-commercial instrument (21). The spectra were obtained by signal averaging 20–30 scans and argon was used as a calibrant.

Computational studies

The MMX calculations were carried out using MMX Version 87.200 (15) running on an IBM PS/2 55Z microcomputer equipped with a math coprocessor. The MNDO and AM1 calculations were carried out using AMPAC Version 2.10 (22) ported to a MIPS 2030 workstation. All optimizations were carried out using the keyword PRECISE to tighten the convergence criteria. The *ab initio* calculations were carried out using GAMESS (23) ported to a MIPS 2030 workstation equipped with 16 MB RAM and a 1.2 GB Wren VII SCSI hard drive.

Synthetic spectra were calculated from the MO results using a FORTRAN program (PESPEC) written by TAW and running on a microcomputer or a Sun3/60 workstation. For convenience, the results were output in Matlab™ (The MathWorks Inc., 24 Prime Pkwy, Natick, MA 01760) file format for plotting.

Acknowledgements

We thank the Natural Sciences and Engineering Research Council of Canada and IBM Canada Ltd. for financial support. The IBM RT and PS/2 computers used in this study were provided by IBM Canada Ltd. under the auspices of the McMaster University – IBM Canada Ltd. Cooperative Project.

1. N. H. Werstiuk and G. Timmins. Can. J. Chem. **66**, 2954 (1988).
2. N. H. Werstiuk, K. B. Clark, and W. J. Leigh. Can J. Chem. **68**, 2078 (1990).
3. M. J. S. Dewar, E. G. Zoebisch, E. F. Healy, and J. J. P. Stewart. J. Am. Chem. Soc. **107**, 3902 (1985).
4. J. J. Fisher and J. Michl. J. Am. Chem. Soc. **109**, 1056 (1987).
5. M. E. Squillacote, T. C. Semple, and P. W. Mui. J. Am. Chem. Soc. **107**, 6842 (1985).
6. M. E. Squillacote, R. S. Sheridan, O. L. Chapman, and F. A. L. Anet, J. Am. Chem. Soc. **101**, 3657 (1979), and references therein.
7. P. W. Mui and E. Grundwald. J. Am. Chem. Soc. **104**, 6562 (1982).
8. E. Honegger, Yang Zhong-Zhi, E. Heilbronner, W. V. E. Doering, and J. C. Schmidhauser. Helv. Chim. Acta, **67**, 640 (1984).
9. P. Masclet, G. Mouvier, and J. F. Bocquet. J. Chim. Phys. **78**, 99 (1981).
10. R. S. Bly and R. T. Swindell. J. Org. Chem. **30**, 10 (1965).
11. R. M. Silverstein and G. C. Bassler. Spectroscopic identification of organic compounds. 2nd. ed. J. Wiley, New York. 1968.
12. R. S. Brown and F. S. Jorgensen. Electron Spectrosc. **5**, 1 (1984).
13. H. M. Frey and R. J. Ellis. J. Chem. Soc. 4770 (1965).
14. H. Yasuda, Y. Ohnuma, M. Yamauchi, H. Tani, and A. Nakamura. Bull. Chem. Soc. Jpn. **52**, 2036 (1979).
15. MMX, Version 87.200 of PCMODEL: A molecular mechanics package including MM2 (Allinger-QCPE 395), MMP1 Pi (Allinger-QCPE 318), MODEL parameters (Still) plus more atoms and constants by K. E. Gilbert and J. J. Gajewski, Indiana University. Available from Dr. K. E. Gilbert, Serena Software, P.O. Box 3096, Bloomington, IN, 47402.
16. M. Beez, G. Bieri, H. Bock, and E. Heilbronner. Helv. Chim. Acta, **56**, 1028 (1973).
17. T. A. Wildman. Chem. Phys. Lett. **75**, 383 (1980).
18. T. A. Wildman. Chem. Phys. Lett. **80**, 210 (1981).
19. E. Honegger and E. Heilbronner. Chem. Phys. Lett. **81**, 615 (1981).
20. L. Chantranupong and T. A. Wildman. J. Am. Chem. Soc. **112**, 4151 (1990), and references therein.
21. N. H. Werstiuk, D. N. Butler, and E. Shahid. Can. J. Chem. **65**, 760 (1986).
22. Dewar Research Group and J. J. P. Stewart. QCPE Bull. **6**, 2 (1986).
23. GAMESS: An *ab initio* computational package. August 5, 1989 Version. NRCC Staff: M. Dupuis, D. Spangler, and J. J. Wendoloski; M. W. Schmidt, North Dakota State University; S. T. Elbert, Iowa State University.

Can. J. Chem. Downloaded from www.nrcresearchpress.com by 217.78.4.112 on 09/08/12
For personal use only.

Mathematical modelling of atom loss in delivery tubing

R. SCOTT DANIELS AND DONALD C. WIGFIELD[1]
The Ottawa–Carleton Chemistry Institute, Department of Chemistry, Carleton University, Ottawa, Ont., Canada K1S 5B6

AND

KENNETH S. WILLIAMS
Department of Mathematics and Statistics, Carleton University, Ottawa, Ont., Canada K1S 5B6

Received July 10, 1991[2]

R. SCOTT DANIELS, DONALD C. WIGFIELD, and KENNETH S. WILLIAMS. Can. J. Chem. **70**, 1978 (1992).

A mathematical model is presented to establish a relationship between the quantity of trace analyte vapor lost to the surface of delivery tubing and the tubing diameter, while in transit between stages of an instrument. Cold-vapor atomic absorption spectrometry for mercury, hydride generation techniques, and interfaces like the interface between electrothermal vaporization and inductively coupled plasma mass spectrometry all risk significant analyte loss before measurement. The results of this modelling substantiate the results of limited experimental work published elsewhere suggesting the use of the smallest possible tubing diameter for the delivery of atomic vapor through a tube. This diameter is calculable using Poiseuille's formula. Using this model, kinetic theory, and experimental data, the sticking probability for mercury on latex tubing is calculated to be approximately 1.6×10^{-6}.

R. SCOTT DANIELS, DONALD C. WIGFIELD et KENNETH S. WILLIAMS. Can. J. Chem. **70**, 1978 (1992).

On présente un modèle mathématique permettant d'établir une relation entre le diamètre du tube et la quantité d'une trace à analyser en phase vapeur qui est perdue sur la surface du tube de transfert entre deux stades d'un instrument. Dans les techniques de génération d'hydrure de la spectroscopie d'absorption atomique de vapeurs froides pour le mercure et dans les interfaces comme celle qui existe entre la vaporisation électrothermique et la spectrométrie de masse aux plasmas couplés d'une façon inductive, il existe des risques importants de perte des produits à analyser. Les résultats de notre modèle permettent de circonstancier les résultats expérimentaux limités qui ont été publiés ailleurs et qui suggèrent qu'il est utile d'utiliser des tubes ayant des diamètres les plus faibles que possible pour transférer une vapeur atomique à travers un tube. On peut calculer ce diamètre à l'aide de la formule de Poiseuille. Utilisant ce modèle, la théorie cinétique et les données expérimentales, on a calculé que le probabilité d'adhérence du mercure sur un tube de latex est approximativement $1{,}6 \times 10^{6}$.

[Traduit par la rédaction]

I. Introduction

The substance of this communication lies in a single question; that is, for a given standard flow rate of a carrier gas containing a trace analyte, which is the best for minimizing analyte loss to the surface of the delivery tubing: a small diameter tube, a large diameter tube, or is there an optimum diameter?[3]

Cold-vapor atomic absorption spectrometry, hydride generation techniques, electrothermal vaporization inductively coupled plasma mass spectrometry, and gas chromatography graphite furnace atomic absorption share one thing in common: the transport of trace molecular or atomic vapor, or aerosols, through delivery tubing. To ensure optimum analytical sensitivity, it is necessary to provide conditions to minimize analyte loss due to surface interactions along the walls of the delivery tubing. An earlier communication addressed the question of tubing type and optimum tubing diameter from an experimental perspective (1). Due to a limited number of available tubing diameters for testing, it was felt that a mathematical model of atom loss in tubing, particularly as a function of tubing diameter and flow rate, would add further justification to, and understanding of, the trends observed for the limited number of diameters tested. In addition, this model would permit predictions beyond the scope of readily available tubing diameters. A brief summary of transport efficiency and particle size is given by Lubman (2). Although omitting a sticking probability factor that is introduced in this model, a solution to the ratio of the number of particles at the exit of a tube to the number at the entrance is given by Gormley and Kennedy (3). Their model is most applicable to mass transport of larger particles and aerosols transported by a carrier gas through a horizontal tube.

The presentation of this model will be in two parts: a simple intuitive approach will be given, followed by a more detailed model of atom loss.

II. Experimental section

An evaluation of the atom loss dependence on the tubing diameter used 3.7 m lengths of latex tubing (Fisher Cat. No. 14-150) of varying diameters. While the tube was attached to the inlet of the spectrometer, and ambient air was being drawn by a pump through the tubing, 10 μL Hg^0 vapor (21–23°C, approximately 0.15 ng) injections were made alternately at a port directly adjacent to the inlet to the spectrometer and at an injection port attached to the end of the 3.7 m length of tubing.

Apparatus

A Laboratory Data Control/Milton Roy UVD 253.7 nm spectrometer was used for measuring the integrated absorbance signals. The fluid flow cell from the UVD monitor was removed and the detector was fixed to the end of a 30-cm double beam gas flow cell. Data acquisition was performed using a Jones Chromatography 6000 data system. Mercury vapor injections were performed using a 10-μL gas-tight syringe (Hamilton, 1801RN-3). The mercury vapor was housed in a septum-sealed 25-mL volumetric flask

[1]Author to whom correspondence may be addressed.

[2]Revision received March 2, 1992.

[3]There is an analogous question, and an apparent lack of a scientific answer for this question, pertaining to minimizing the heat loss during the transport of a warm gas through optimum piping diameters.

Can. J. Chem. Downloaded from www.nrcresearchpress.com by 217.78.4.112 on 09/08/12
For personal use only.

containing 5 mL of elemental mercury. Temperature-sensitive fluctuations of the vapor pressure of mercury were minimized by partially immersing the volumetric flask in water contained in a double-insulated 200-mL beaker. The flow rate was monitored using a bubble-meter calibrated mass flow meter (Matheson 0–2000 standard mL min^{-1}, model 81111-0423).

III. Results and discussion

III.1. A simplified perspective of atom loss

Consider a segment of tubing of length l (cm), diameter d (cm), standard flow rate f (mL min^{-1}), volume v (cm^3), and internal surface area, s (cm^2). As a plug of vapor traverses the length of the tube there is some function h, describing atom loss, that depends both on the mean atom residence time τ (s) (4), and the tube surface to volume ratio s/v, eq. [1].

$$[1] \quad \text{loss} = h\left(\tau, \frac{s}{v}\right) = h\left(\frac{\pi l d^2}{4f}, \frac{4}{d}\right)$$

$$[2] \quad \text{loss} = h_1(d)$$

Since the standard flow rate is to be considered constant, then the new loss function h_1, eq. [2], is some unknown function of the delivery tube diameter. In eq. [1] it is not immediately clear how τ and s/v will be a function of atom loss, but it is reasonable to argue that an increased atom residence time, and (or) an increased surface to volume ratio (i.e., decreased diameter), would result in increased atom loss. A longer atom residence time would give a higher probability of a surface adsorption, and the greater the amount of surface, the higher would be the probability of a surface interaction. Clearly then, as the tube diameter is varied, these two factors act in opposition insofar as atom loss is concerned. To illustrate this Fig. 1 shows how τ and s/v vary with the tube diameter at a constant flow rate. If the loss function is an algebraic sum of the contributions from τ and s/v (curve 3, a simplistic view, yet mathematically incorrect), then there would be a local minimum in the loss function versus tube radius. This will be shown to be incorrect.

To overcome the inadequacies of this simplified view of atom loss, a detailed model of atom loss will permit a rigorous evaluation of h_1.

III.2. A detailed model of atom loss

The development of this detailed atom loss model entails 12 assumptions listed below:

1. N_0 mercury atoms are instantaneously injected into a flow of ambient nitrogen carrier gas such that the mercury atoms are evenly distributed across a plug volume of radius r and length x.

2. In the time increment $1/Z$, all atoms a distance λ or less from the tube surface are lost to the tube wall. Z is the collision frequency and λ is the mean free path of mercury atoms with nitrogen molecules under ambient conditions. This assumption disregards the sticking probability ρ, and the kinetic geometry term, g. See Appendix.

3. No pressure drop occurs along the tube length, for all tube radii and flow rates, omitting the Poiseuille pressure drop.

4. Following each $1/Z$ increment, the remaining atoms instantaneously redistribute themselves across the plug volume v.

5. No axial diffusional broadening of the plug occurs as it moves along the length of the tube.

6. There will exist a uniform non-parabolic velocity distribution along the tube cross section.

7. The tube wall surface is ideal: no eddies.

8. Syringe injection produces a homogeneous disk distribution of mercury vapor in nitrogen.

9. Nitrogen, N_2(g), and mercury, Hg^0(g), behave as ideal gases.

10. Flow is generated by draw from the atmosphere, through the tubing, to a vacuum pump.

11. The tube radius will not be less than the mean free path λ.

12. The tube wall is flat, not curved. See Appendix.

The philosophy adopted for developing this model has been to obtain a mathematical solution for the simplest case: making all the assumptions above, for model 1, then removing the assumptions sequentially until it is felt that there is sufficient agreement with experimental data. This outlook has resulted in three models presented in the order of making (1) all the assumptions above, (2) assumptions 3–8 above, and (3) assumptions 4–8 above.

III.3. Model 1

The goal of model 1 is to obtain a mathematical expression for the ratio of the number of atoms lost at the tube sur-

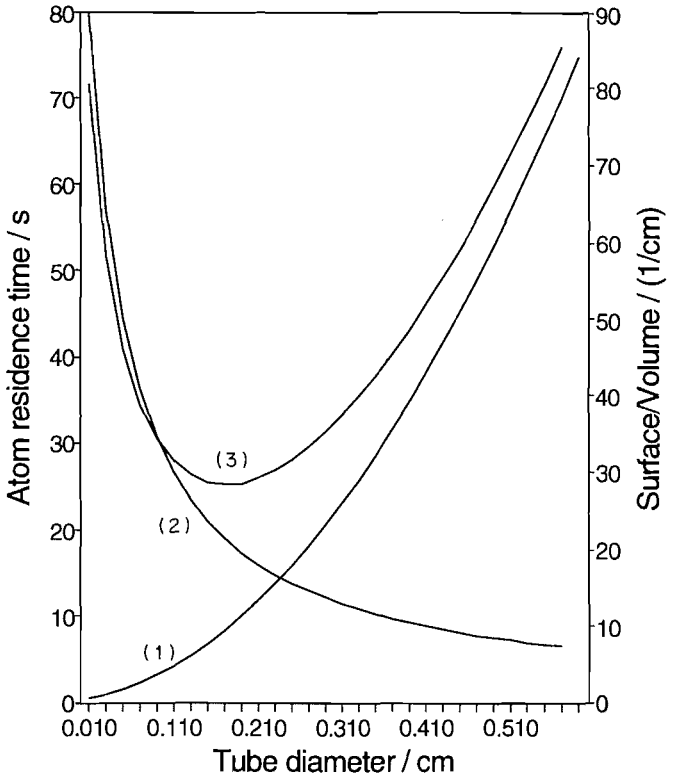

FIG. 1. Variation of atom residence time (1); surface to volume ratio (2); and their sum[4] (3); with tube diameter at 100 mL min^{-1}.

[4]Arithmetically incorrect, but presented for illustrative purposes.

Can. J. Chem. Downloaded from www.nrcresearchpress.com by 217.78.4.112 on 09/08/12
For personal use only.

TABLE 1. Model 1: incremental atom loss

Time	Number of atoms lost, N	Number of atoms remaining
0	0	N_0
$1/Z$	Atom density × rim volume $\frac{N_0}{v}[x\pi\{r^2 - (r-\lambda)^2\}] = N_0K$ where $K = \left[\frac{x\pi\{r^2 - (r-\lambda)^2}{v}\right]$ $= \frac{\text{rim volume}}{\text{plug volume}}$	$N_0(1-K)$
$2/Z$	$N_0K(1-K)$	$N_0(1-K)^2$
$3/Z$	$N_0K(1-K)^2$	$N_0(1-K)^3$
$4/Z$	$N_0K(1-K)^3$	$N_0(1-K)^4$

face to the number of atoms before any loss, N/N_0. The following notation will be used:

Term	Symbol	Units
Carrier gas	N_2	
Carrier gas viscosity	μ	kg m^{-1} s^{-1}
Flow rate	f	m^3 s^{-1}
Tube length	l	m
Tube radius	r	m
Plug length	x	m
Plug volume	v	m^3
Plug, atom residence time	τ	s
Mean free path of $Hg^0(g)$ in $N_2(g)$	λ	m
Collision frequency, $Hg^0(g)$ with $N_2(g)$	Z	s^{-1}

The total number of atoms lost is the sum of the number of atoms lost in each of η time increments of $1/Z$, where η is the floor[5] of the product of the collision frequency Z and the plug residence time τ. Table 1 lists the number of atoms lost to the tube wall, and the number of atoms remaining, for each of the first four of η, $1/Z$ increments of time. The number of atoms lost in the first time increment of $1/Z$ is the number of atoms contained in the rim of the disk whose thickness is λ, the mean free path of a mercury atom in nitrogen (approximately 45.7 nm, for 20°C), and whose length is x. This number is the product of the rim volume, $x\pi\{r^2 - (r-\lambda)^2\}$ and the initial atom density N_0/v.

Similarly, the number of atoms lost at the time $2/Z$ is the product of the new atom density $(N_0 - N_0K)/v$ and the rim volume. As shown in Table 1, this number is merely the product of the remaining number of atoms in the plug volume $(N_0 - N_0K)$ and K, where K is the ratio of the rim volume to the plug volume.

The total number N of atoms lost is

$$[3] \quad N_0K\sum_{n=0}^{n=\eta}(1-K)^n$$

where

$$[4] \quad \eta = \lfloor Z \times \tau \rfloor = \left\lfloor \frac{Z\pi l r^2}{f} \right\rfloor$$

Summing the geometric series gives eq. [5],

$$[5] \quad \frac{N}{N_0} = 1 - [1-K]^{\eta+1}$$
$$= 1 - \left\{1 - \frac{x\pi[r^2 - (r-\lambda)^2]}{v}\right\}^{\eta+1}$$
$$= 1 - \left[1 - \frac{(2r\lambda - \lambda^2)}{r^2}\right]^{\lfloor Z\pi l r^2/f \rfloor + 1}$$

where $v = x\pi r^2$.

Figure 2 is a plot of the adsorptional loss, N/N_0, versus the log of the tube radius. This model, like the simplified view of Fig. 1, also predicts a local minimum in the loss function versus tube radius. In model 1, increased tube length has two effects: a shift in optimum diameter to larger radii, and greater losses at all radii.

III.4. Model 2

Model 2 corrects for the certainty that not every atom striking the tube surface is lost. It also corrects for the fact that not all atoms at a distance λ or less from the tube wall will have trajectories in the direction of the wall. The correction terms will be ρ and g respectively. In fact, only one quarter of the atoms within the distance λ from the wall will strike the wall ($g = \frac{1}{4}$, Appendix). Table 2 is a modification of Table 1, taking into account the sticking probability ρ, and the geometry factor, g.

Summing the geometric series as in model 1, and substitution of $\frac{1}{4}$ for g, gives eq. [6],

$$[6] \quad \frac{N}{N_0} = 1 - \left[1 - \frac{\rho(2r\lambda - \lambda^2)}{4r^2}\right]^{\lfloor Z\pi l r^2/f \rfloor + 1}$$

Figure 3 is a plot of the adsorptional loss, N/N_0, versus the log of the tube radius, for ρ values of 10^{-4}, 10^{-2}, and 1. Like the previous model, this model also predicts the existence of a local minimum in the loss functions of Fig. 3 at radii of 7.6λ.

According to this intermediate and still very naive model,

[5]The floor operator ($[x]$) takes the integer portion of its argument; for example, $[3.7] = 3$.

Can. J. Chem. Downloaded from www.nrcresearchpress.com by 217.78.4.112 on 09/08/12
For personal use only.

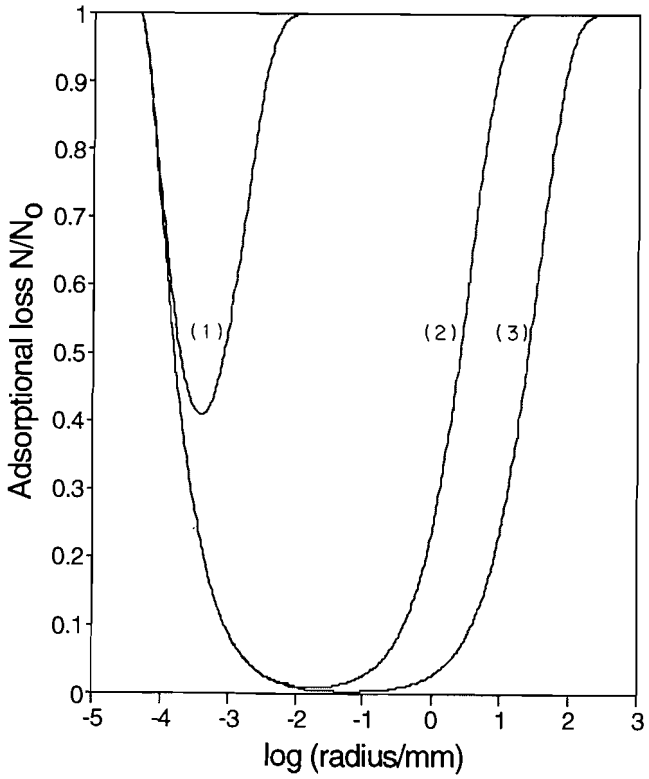

FIG. 2. Atom loss model 1. Plot of N/N_0 versus log(tube radius) for 100 mL min^{-1} and tube lengths/nm: (1) 10^{-6}; (2) 40; (3) 400.

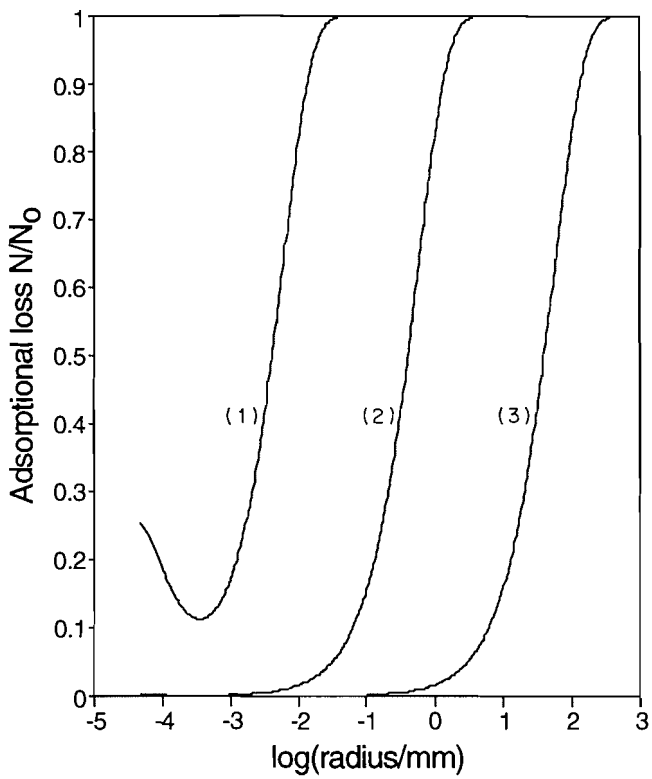

FIG. 3. Atom loss model 2. Plot of N/N_0 versus log(tube radius) for: f = 100 mL min^{-1}, l = 1.0 mm, and sticking probability, ρ: (1) 1; (2) 10^{-2}; (3) 10^{-4}.

TABLE 2. Model 2: incremental atom loss

Time	Number of atoms lost, N
$1/Z$	$g\rho \times$ atom density $\times$ rim volume
	$g\rho \frac{N_0}{v}\{x\pi[r^2 - (r-\lambda)^2]\} = \rho N_0 K$
	where $K = \left\{\frac{x\pi[r^2 - (r-\lambda)^2]}{v}\right\}$
$2/Z$	$g\rho N_0 K(1 - g\rho K)$
$3/Z$	$g\rho N_0 K(1 - g\rho K)^2$
$4/Z$	$g\rho N_0 K(1 - g\rho K)^3$

the limiting tube radius would be λ, when, in this limit, the loss, N/N_0, would approach a value of ρg. Very small diameters lead to the ludicrous situation of linear atomic trajectories surpassing the speed of light: in fact, $3c$, for a flow rate of 100 mL min^{-1} and a tube radius of $\lambda/2$! The real limiting diameter would be the diameter, calculable from the Poiseuille equation, for a given standard flow rate through a defined length of tubing, and the condition of a pressure drop of 1 atmosphere along the length of the tube. This limiting diameter is best illustrated in Model 3.

III.5. Model 3

This, the third and final model, takes into account the pressure drop at some distance y along the tube length l. As the pressure drops in the direction of the vacuum pump, from ambient pressure P_1 at the open end of the tube to some lower pressure P_2 at the pump end of the tube, the kinetic properties Z, the flow rate f, and λ change. P_2 is a function of y.

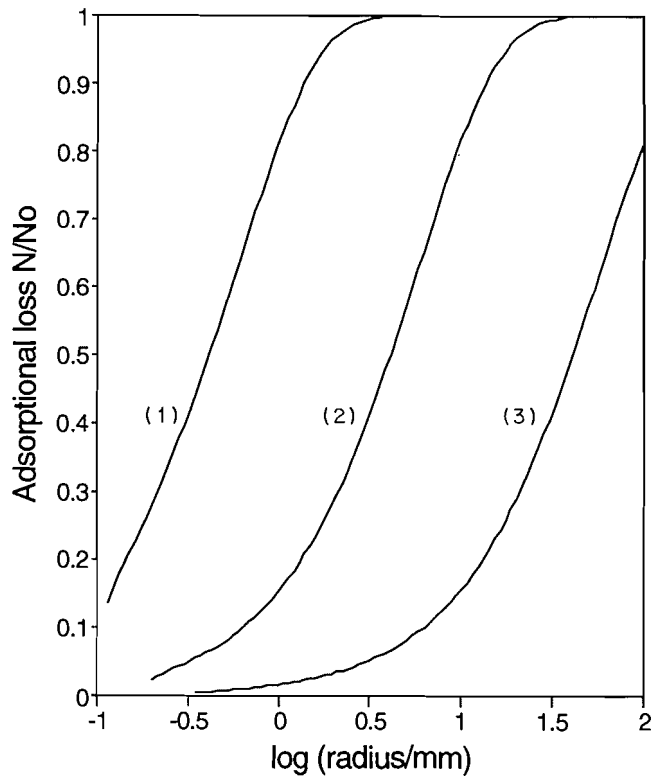

FIG. 4. Atom loss model 3. Plot of N/N_0 versus log(tube radius) for: l = 1.0 m, ρ = 10^{-6}, and f/(mL min^{-1}): (1) 10; (2) 100; (3) 1000.

Can. J. Chem. Downloaded from www.nrcresearchpress.com by 217.78.4.112 on 09/08/12
For personal use only.

To correct for this, the mean values of Z, f, and λ are calculated and used in place of the fixed values in model 2. The variables Z', f', and λ', are the values of Z, f, and λ respectively under ambient conditions, and are defined collectively in eq. [7] as follows:

$$\bar{Z} = \frac{1}{l}\int_{y=0}^{y=l} Z'\frac{P_2}{P_1}\,dy, \qquad Z = Z' \times \left(\frac{P_2}{P_1}\right)$$

$$[7] \qquad \bar{f} = \frac{1}{l}\int_{y=0}^{y=l} f'\frac{P_1}{P_2}\,dy, \qquad f = f' \times \left(\frac{P_1}{P_2}\right)$$

$$\bar{\lambda} = \frac{1}{l}\int_{y=0}^{y=l} \lambda'\frac{P_1}{P_2}\,dy, \qquad \lambda = \lambda' \times \left(\frac{P_1}{P_2}\right)$$

and dy is some infinitesimal of the tube length l. Solving the Poiseuille equation:

$$[8] \qquad f' = \frac{(P_1^2 - P_2^2)\pi r^4}{16y\mu P_1}$$

for P_2, and substitution into the previous integral eqs. [7] gives equation set [9].

$$\bar{Z} = \frac{Z'}{P_1 l}\int_{y=0}^{y=l}\sqrt{P_1^2 - \frac{16\mu P_1 f' y}{\pi r^4}}\,dy$$

$$[9] \qquad \bar{f} = \frac{f'P_1}{l}\int_{y=0}^{y=l}\frac{1}{\sqrt{P_1^2 - \frac{16\mu P_1 f' y}{\pi r^4}}}\,dy$$

$$\bar{\lambda} = \frac{\lambda' P_1}{l}\int_{y=0}^{y=l}\frac{1}{\sqrt{P_1^2 - \frac{16\mu P_1 f' y}{\pi r^4}}}\,dy$$

The solution for these integral equations is given in eq. [10].

$$\bar{Z} = \frac{Z'\pi r^4}{24P_1^2 l\mu f'}\left[P_1^3 - \left(P_1^2 - \frac{16\mu P_1 f' l}{\pi r^4}\right)^{3/2}\right]$$

$$[10] \qquad \bar{f} = \frac{\pi r^4}{8l\mu}\left[P_1 - \sqrt{P_1^2 - \frac{16\mu P_1 f' l}{\pi r^4}}\right]$$

$$\bar{\lambda} = \frac{\lambda'\pi r^4}{8\mu l f'}\left[P_1 - \sqrt{P_1^2 - \frac{16\mu P_1 f' l}{\pi r^4}}\right]$$

Substitution of these average values of Z, f, and λ into the general solution from model 2 gives eq. [11], the general solution for model 3.

$$[11] \qquad \frac{N}{N_0} = 1 - \left\{1 - \frac{\rho a r^4\left[P_1 - \sqrt{P_1^2 - \frac{b}{r^4}}\right]\left[2r - ar^4\left(P_1 - \sqrt{P_1^2 - \frac{b}{r^4}}\right)\right]}{4r^2}\right\}^{[cr^2\{2P_1^2 + P_1\sqrt{P_1^2 - (b/r^2)} - (b/r^2)\}]+1}$$

where

$$[12] \qquad a = \frac{\lambda'\pi}{8\mu l f'}, \qquad b = \frac{16\mu P_1 f' l}{\pi}, \qquad c = \frac{Z'\pi l}{3P_1^2 f'}$$

A plot of this equation using $l = 1.0$ m, $\rho = 10^{-6}$, and $\mu = 1.76 \times 10^{-5}$ kg m^{-1} s^{-1} is given in Fig. 4 for $f' = 10$, 100, and 1000 mL min^{-1}. The model 3 functions are truncated at radii predicted by the Poiseuille equation. These limiting radii get

Can. J. Chem. Downloaded from www.nrcresearchpress.com by 217.78.4.112 on 09/08/12
For personal use only.

TABLE 3. Estimation of the latex sticking probability, ρ, by comparison of experimental and theoretical loss data

Flow rate (mL min^{-1})	Internal radius (mm)	Loss N/N_0			
		Experimental		Theory: model 3	
		Day 1	Day 2	$\rho = 1.6 \times 10^{-6}$	$\rho = 1.6 \times 10^{-7}$
50	0.8	0.77±0.01	0.82±0.02	0.80	0.18
	1.6	0.84±0.01	0.87±0.01	0.96	0.33
	3.95	0.93±0.01	0.96±0.01	1.00	0.63
100	0.8	0.65±0.01	0.67±0.02	0.55	
	1.6	0.73±0.01	0.78±0.01	0.80	
	3.95	0.79±0.01	0.86±0.01	0.98	
200	0.8	0.48±0.01	0.51±0.02	0.33	
	1.6	0.52±0.03	0.62±0.01	0.53	
	3.95	0.59±0.01	0.63±0.02	0.86	
500	0.8	0.39±0.01	0.40±0.03	0.14	
	1.6	0.36±0.01	0.47±0.01	0.27	
	3.95	0.33±0.01	0.48±0.02	0.54	
1000	0.8	0.07±0.06	0.28±0.02	0.07	
	1.6	0.16±0.04	0.28±0.03	0.15	
	3.95	0.20±0.03	0.29±0.06	0.32	
1500	0.8	0.03±0.05	0.16±0.07	0.05	
	1.6	0.15±0.04	0.18±0.01	0.10	
	3.95	0.27±0.01	0.19±0.02	0.23	

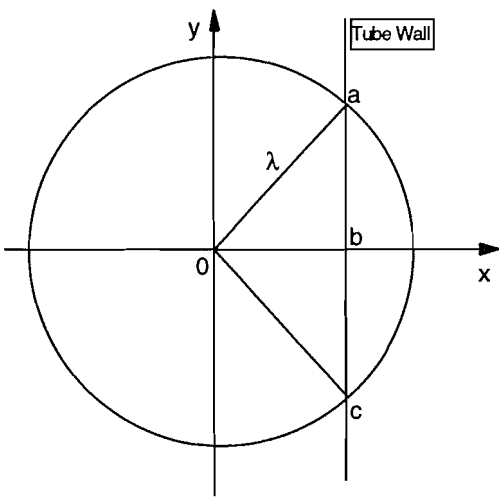

FIG. 5. Solution for the geometry term *g*: the fraction of atoms within the distance λ from the tube wall that strike the wall.

smaller as the flow rate decreases. Just as predicted by the experimental data of Table 3, the ideal conditions to minimize analyte loss to tubing surfaces are (1) use the smallest tube diameter possible, and (2) use the highest flow rate possible.

III.6. Estimating a value of ρ, the sticking probability for latex

Using the general solution of model 3 above, combined with experimental data for N/N_0, an estimate of the real value of ρ may finally be made. Variables are used in the model 3 solution of Table 3 according to the conditions that prevailed while data was collected. An estimate of $\rho = 1.6 \times 10^{-6}$ gives model 3 solutions for N/N_0 that agree satisfactorily with experimental values shown in Table 3. The mathematical model is more sensitive to a change in loss, with changing tube radii, than is observed experimentally. At higher flow rates, there is a larger uncertainty and poor reproducibility between days, in experimental values of N/N_0. This model, in addition to predicting trends, was expected to give values of ρ, at best, to within an order of magnitude of its real value. Calculated values are listed in Table 3 showing the model 3 estimates for N/N_0 at 50 mL min^{-1} and for three radii, when a value of ρ 1.6×10^{-7} was used, which varies by an order of magnitude from the best estimate of ρ.

IV. Conclusions

The atom loss model has been developed to the point at which it predicts loss trends as a function of varied tube radii for all possible flow rates, sticking probabilities, and tube lengths. The primary trend, that is, trace analyte loss increases with increasing tube diameter, was confirmed with this model, and corroborates inferences by the solution proposed by Gormley and Kennedy (2). Further to this and in conjunction with experimental data, the model allowed the estimation of a sticking probability. For latex tubing it was found that only one mercury atom in 0.83 million ($\rho = 1.2 \times 10^{-6}$) that strikes the tube wall surface actually remains adsorbed for a sufficient length of time to be termed "lost."

V. Acknowledgements

We are grateful to Dr. Steve Brooks of the Department of Biology, Carleton University, and Mr. Andrew Forrest, P.Eng., for extensive discussions and contributions to this work.

Can. J. Chem. Downloaded from www.nrcresearchpress.com by 217.78.4.112 on 09/08/12
For personal use only.

1. R. S. Daniels and D. C. Wigfield. Anal. Chim. Acta, **248**, 575 (1991).
2. D. M. Lubman, Lasers and mass spectrometry. Oxford University Press, New York. 1990.
3. P. G. Gormley and M. Kennedy. Proc. R. Irish Acad. **52A**, 163 (1949).
4. J. Dedina. Prog. Anal. Spectrosc. **11**, 251 (1988).

Appendix

Solution for the geometry term *g*: the fraction of atoms within the distance λ from the tube wall that strike the wall

In Fig. 5, consider a wall at some distance b, $0 \leq b \leq \lambda$, from an atom at the origin.[6] On this microscale, where λ is the mean free distance travelled by a mercury atom before collision with a nitrogen molecule, the tube wall will be considered to be flat and not curved.

The geometry term, g, represents the probability that an atom, at some distance less than or equal to λ from a wall, will strike the wall before hitting a nitrogen molecule. g is the ratio of the average sector-area of a sphere swept out by revolving the curve $y = (\lambda^2 - x^2)^{1/2}$, $b \leq x \leq \lambda$, for $0 \leq b \leq \lambda$, about the x-axis to the total sphere surface area $4\pi\lambda^2$.

The general area of a surface, a sector-area of a sphere, swept out by revolving the curve $y = f(x)$, $a \leq x \leq b$, about the x-axis (5) is given in eq. [13].

$$[13] \quad \int_a^b 2\pi y \sqrt{1 + (y')^2}\, dx$$

Therefore eq. [14] gives the sector-area of a sphere swept out by revolving the curve $y = (\lambda^2 - x^2)^{1/2}$, $b \leq x \leq \lambda$, about the x-axis, where λ is the sphere radius, and eq. [15] gives the general sector-area A_s swept out by revolving the curve $y = (\lambda^2 - x^2)^{1/2}$ about the x-axis.

[6]It is more convenient to consider an atom at the origin and the wall at different distances from the origin, than the reverse case.

$$[14] \quad \int_b^\lambda 2\pi \sqrt{\lambda^2 - x^2} \sqrt{1 + \frac{x^2}{\lambda^2 - x^2}}\, dx$$

$$= \int_b^\lambda 2\pi \sqrt{\lambda^2 - x^2} \sqrt{\frac{\lambda^2}{\lambda^2 - x^2}}\, dx$$

$$= \int_b^\lambda 2\pi\lambda\, dx$$

$$= 2\pi\lambda(\lambda - b)$$

$$[15] \quad A_s = 2\pi\lambda(\lambda - x), \qquad 0 \leq x \leq \lambda$$

Equation [16] gives the average $\bar{A}_s$ of the general sector-area A_s swept out by revolving the curve $y = (\lambda^2 - x^2)^{1/2}$ about the x-axis, for $0 \leq x \leq \lambda$.

$$[16] \quad \bar{A}_s = \frac{1}{\lambda}\int_0^\lambda A_s\, dx$$

$$= \frac{1}{\lambda}\int_0^\lambda 2\pi\lambda(\lambda - x)\, dx$$

$$= 2\pi\left[\int_0^\lambda \lambda\, dx - \int_0^\lambda x\, dx\right]$$

$$= 2\pi\left[\lambda^2 - \frac{\lambda^2}{2}\right]$$

$$= \pi\lambda^2$$

Therefore, g, eq. [17], is the ratio of $\bar{A}_s$ to the total sphere surface area $4\pi\lambda^2$

$$[17] \quad g = \frac{\bar{A}_s}{4\pi\lambda^2} = \frac{1}{4}$$

Can. J. Chem. Downloaded from www.nrcresearchpress.com by 217.78.4.112 on 09/08/12
For personal use only.

Mechanism of Wittig reaction with cyclic anhydrides

MARGARET M. KAYSER[1] AND KRISTA L. HATT
Department of Chemistry, University of New Brunswick, P. O. Box 5050, Saint John, N. B., Canada E2L 4L5

AND

DONALD L. HOOPER
Department of Chemistry, Dalhousie University, Halifax, N. S., Canada B3H 4J3

Received November 19, 1991

MARGARET M. KAYSER, KRISTA L. HATT, and DONALD L. HOOPER. Can. J. Chem. **70**, 1985 (1992).

The reactions of stabilized phosphoranes with cyclic anhydrides give enol-lactones as final products. The initial condensation, however, leads to the formation of acyclic adducts that are observable by NMR, can be easily trapped, and, in some cases, can be isolated. A study of the mechanism of these condensations by NMR spectroscopic methods and by various trapping experiments is described and the reaction pathway is proposed.

MARGARET M. KAYSER, KRISTA L. HATT et DONALD L. HOOPER. Can. J. Chem. **70**, 1985 (1992).

Les réactions des phosphoranes stabilisés avec des anhydrides cycliques fournissent des énol-lactones comme produit finals. Toutefois, la condensation initiale conduit à la formation d'adduits acycliques que l'on peut observer par RMN, qui peuvent facilement être piégés et qui, dans quelques cas, peuvent être isolés. On décrit une étude du mécanisme de ces condensations basée sur des méthodes de RMN et sur diverses expériences de piégeages et on propose la voie réactionnelle.

[Traduit par la rédaction]

Can. J. Chem. Downloaded from www.nrcresearchpress.com by 217.78.4.112 on 09/08/12
For personal use only.

Introduction

Originally, the reaction of an ylide and a simple aldehyde or ketone was described as a stepwise ionic process involving a betaine intermediate (1, 2). This mechanism, however, was challenged when studies on the solvent effects in Wittig condensations showed a nonpolar transition state for the reactions of stabilized ylides (3). Since lithium-free betaine intermediates have not been detected in the course of Wittig condensations, it was questioned whether such species could even exist in a "salt-free" environment (4). This problem was settled when independently generated lithium-free betaines were found to collapse to alkenes too rapidly to be detected by NMR (4–6).

While betaine in the "salt-free" environment remained elusive, for reactions of an ylide with aldehyde or ketone, experimental evidence was obtained for the formation of an oxaphosphetane (5, 7–9). *Ab initio* studies of a model reaction between $H_3P{=}CH_2$ and HCHO further supported the mechanism involving a direct formation of the oxaphosphetane via a concerted-low-energy addition of the ylide to the carbonyl substrate (10, 11).

Recently, Vedejs and Marth (7) demonstrated through a series of equilibrium studies on independently generated betaines, that betaines are unlikely intermediates in Wittig reactions for aldehydes and ketones, and that these condensations proceed via a "4-centre mechanism" leading directly to formation of more or less stable oxaphosphetane intermediates (7, 12, 13).

Carbonyl-stabilized phosphoranes are unreactive vis-à-vis ketones but are readily condensed with aldehydes and with 5-member cyclic anhydrides, the latter reactions leading to synthetically and biologically important enol-lactones (14). Although a number of researchers have employed these condensations as a route to enol-lactones (15), there has been no systematic investigation of their mechanism comparable to the studies carried out for the Wittig olefination of aldehydes and ketones (4–7).

The condensations of phthalic anhydride with various carbonyl-stabilized ylides were first investigated by Chopard *et al.* (reaction [1]). The enol-lactones produced in these reactions showed a surprisingly high stereoselectivity in favour of *E* geometry (16).

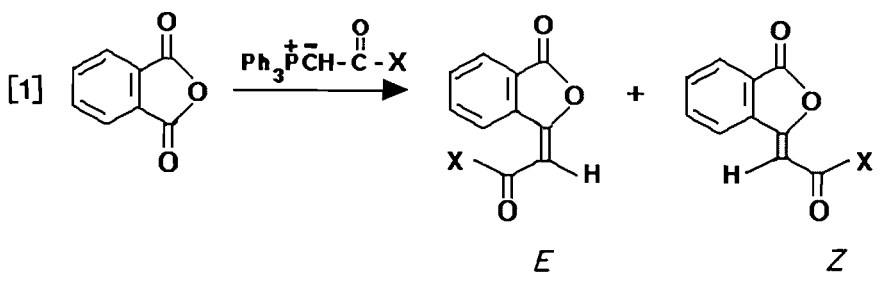

To account for this selectivity, Chopard suggested a cyclic transition state with the COX group of the ylide in the plane parallel to the phenyl ring of phthalic anhydride, Fig. 1.

According to this scheme, the electron-rich system interacts with the electron-deficient aromatic ring to give preferentially the *E* product (16). The fact that *E* selectivity was shown to increase with the electron-donating capacity of the X group gave support for the proposed transition state.

[1]Author to whom correspondence may be addressed.

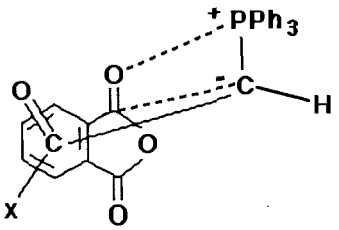

FIG. 1. Transition state proposed for the addition of stabilized ylides to phthalic anhydride (16).

Chopard's hypothesis appeared to be further strengthened by subsequent studies, indicating that the 4-centre mechanism is the only obligatory route in the kinetically controlled reactions of aldehydes with carbonyl-stabilized ylides, *vide supra* (7, 12, 13).

Two pieces of experimental evidence, however, put in question this interpretation. Firstly, it was soon discovered that the condensations of stabilized ylides with succinic and maleic anhydrides gave also *E* enol-lactones as major products (17). Secondly, open-ring acylated phosphoranes such as **3***b*. Scheme 1, were observed as intermediates in the condensations with cyclic anhydrides (16–20). The latter discovery suggested a mechanism that included betaine as an obligatory (albeit, possibly, very short-lived) intermediate (17).

The topic of the reversibility of Wittig reactions has been discussed extensively in relation to the stereochemistry of the products (21–24). The crossover experiments carried out by several groups showed that the formation of oxaphosphetane intermediates is reversible in the reactions of non-stabilized ylides with aromatic aldehydes (21) and appears to be irreversible with aliphatic aldehydes and ketones (22–24). Recently, parallel behaviour was observed for the reactions of moderated and ester-stabilized ylides with aromatic and aliphatic aldehydes (12).

Reversibility (or irreversibility) and its effects on the stereo- and regioselectivity of reactions is equally important in condensations of cyclic anhydrides with stabilized phosphoranes. Here an additional complication arises from the fact that acyclic adducts are produced as intermediates and consequently betaine as well as oxaphosphetane must be considered as an obligatory intermediate along the mechanistic pathway (26).

In this paper we report an NMR study of Wittig condensations between carbonyl-stabilized ylides and phthalic, phenyl maleic, and succinic anhydrides, all of which were found to be reversible at the stage of an acyclic intermediate. Various trapping experiments that support and refine the mechanistic pathway of these reactions are also discussed.

Results and discussion

Structural studies

During a low-temperature ^{1}H NMR study of the reaction between methyl (triphenylphosphoranylidene)acetate **2** and phthalic anhydride **1**, an intermediate with a signal for the methoxy group at an unusually high field (2.98 ppm) was observed and identified, from trapping experiments, as corresponding to the rapidly exchanging **3***a*–**3***b* pair produced as a result of the opening of the anhydride ring.

All trapping experiments, outlined in Schemes 1–4 *were carried out at the time of the highest build-up of the intermediate (70% after 30 min at 0°C)* as established from sev-

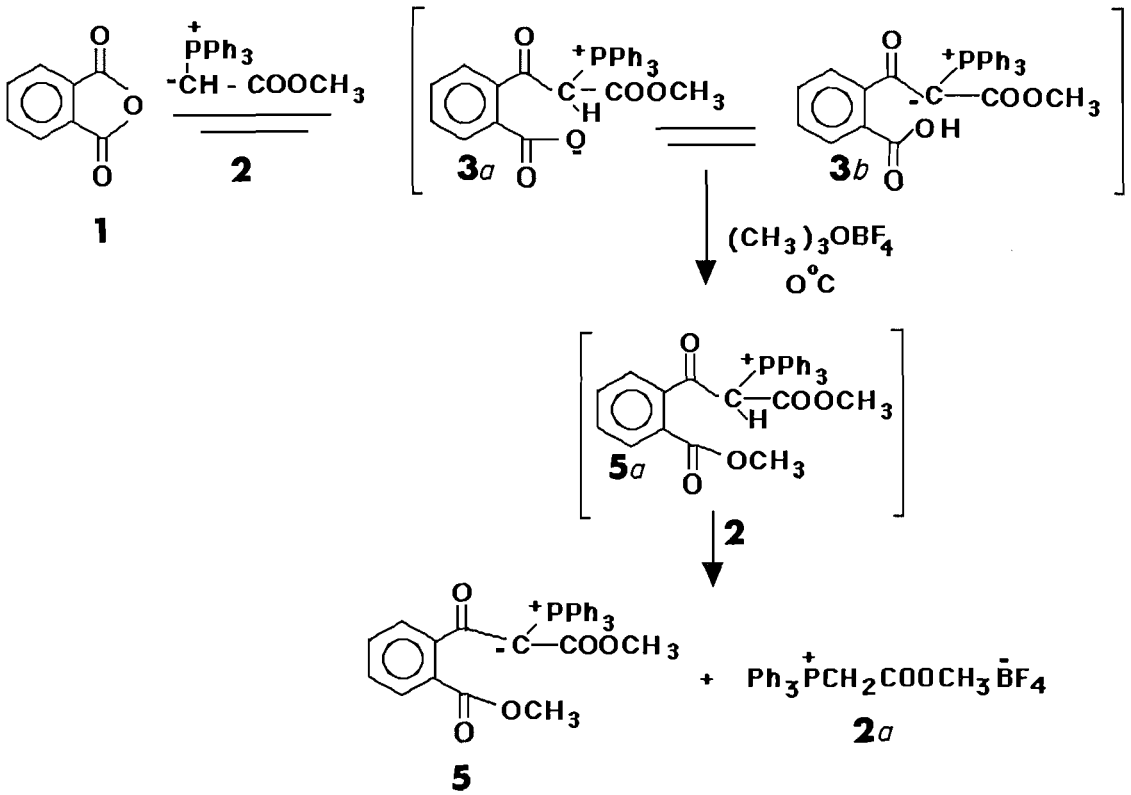

SCHEME 1

Can. J. Chem. Downloaded from www.nrcresearchpress.com by 217.78.4.112 on 09/08/12
For personal use only.

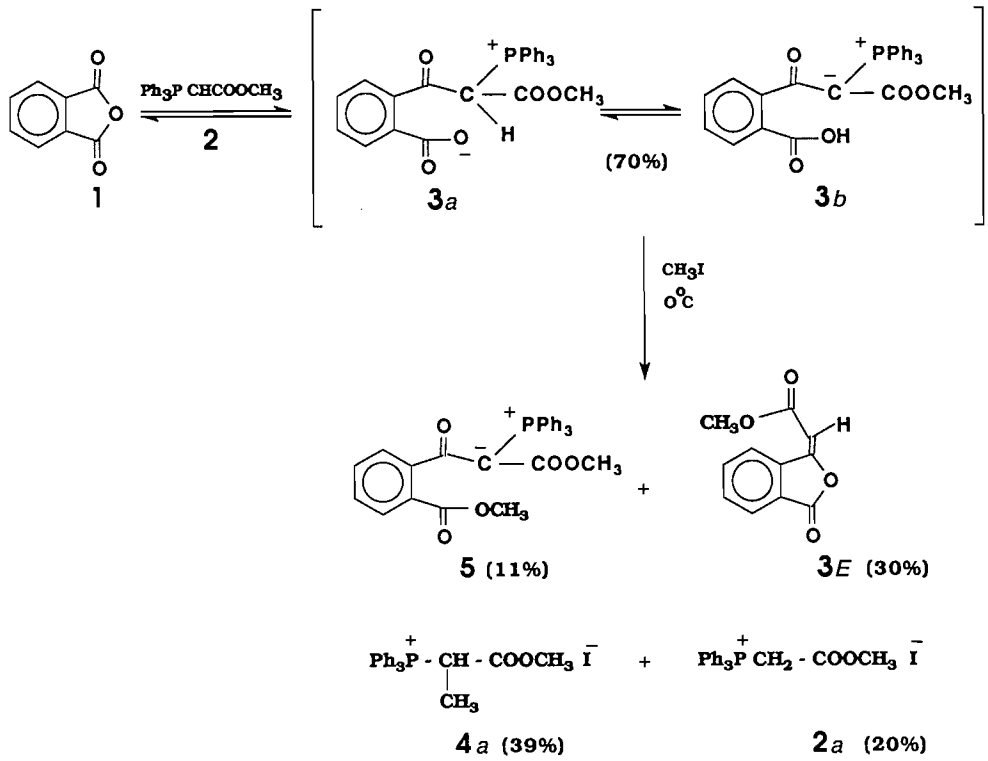

SCHEME 2

eral prior low-temperature studies. The reaction of the intermediate **3***a* with trimethyloxonium tetrafluoroborate, $(CH_3)_3OBF_4$, gave the *O*-alkylated compound **5** and some conjugate acid **2***a*, the latter resulting from proton exchange between the short-lived intermediate **5***a* and ylide **2** (Scheme 1).

The softer alkylating agent, methyl iodide, was expected to give the *C*-alkylated acid **6** (Scheme 2). However, under conditions similar to those for the reaction with $(CH_3)_3OBF_4$, trapping with methyl iodide produced a mixture consisting of **5** (11%), enol-lactone **3***E* (30%), and conjugate acids **2***a* (20%) and **4***a* (39%), the last resulting from the *C*-alkylation of **4** (Scheme 3). The large proportion of **2***a* and **4***a* (59% total) trapped at the time when the concentration of ylide **2** was reduced to 30%, indicates that the formation of acyclic intermediates is a reversible process.

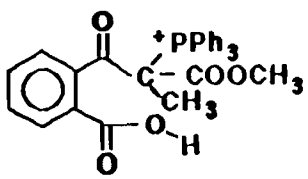

6

The trapping with diazomethane, which reacts rapidly with acidic intermediate **3***b*, gave phosphorane **5** as the only product (Scheme 3). The above results indicate that the addition of ylide **2** to phthalic anhydride leading to the acyclic intermediates (**3***a* and **3***b*) is an equilibrium. Trimethyloxonium tetrafluoroborate reacts preferentially at the carboxylate oxygen atom, shifting the equilibrium from **3***b* to **3***a*. On the other hand, diazomethane reacts with **3***b*, shifting the equilibrium in the opposite direction. Methyl iodide does not react with **3***b* because the highly delocalized charge on the ylide's carbon atom is slow to *C*-alkylate, permitting the competing reactions, *O*-alkylation of **3***a* and *C*-alkylation of ylide **2**, to occur.

The reaction of phthalic anhydride with freshly crystallized ylide 4 leads to an intermediate, **7***a*, which does not possess an exchangeable proton. This unstable species (observable as a broad transient signal at 27.58 ppm in the ^{31}P NMR spectrum) exists at low temperatures (−35 to −30°C) in equilibrium with the reagents, but we were unable to trap it as its ethyl ester with triethyloxonium tetrafluoroborate. As **7***a* collapses to the product, only **7***E* and a slight excess of the conjugate acid of ylide **4** can be detected in the ^1H NMR spectrum of the reaction mixture (Scheme 4).

The structure of the *O*-methylated product **5** was verified by NMR studies and by derivatization. The methoxy group from the ylide appears at a relatively high field (3.01 ppm). In solution it apparently occupies the space in the shielding region of the phenyl rings similar to its conformation shown in the X-ray crystal structure of compound **5**, Fig. 2.[2] The low-field ^{13}C NMR signal for C1 of phosphorane **5** (71.17 ppm) suggests that ylide **5** should be quite unreactive (25). In fact all attempted condensations with benzaldehyde failed as only the starting materials were recovered, even after 24 h reflux in toluene.

Since the highly shielded methoxy group appears to be fixed in the vicinity of the triphenylphosphorane group, we expected an important contribution of the *trans*-enolate structure with the oxygen atom bearing a significant nega-

[2]X-ray crystal structure, M. M. Kayser and F. Rochon. Unpublished results.

Can. J. Chem. Downloaded from www.nrcresearchpress.com by 217.78.4.112 on 09/08/12
For personal use only.

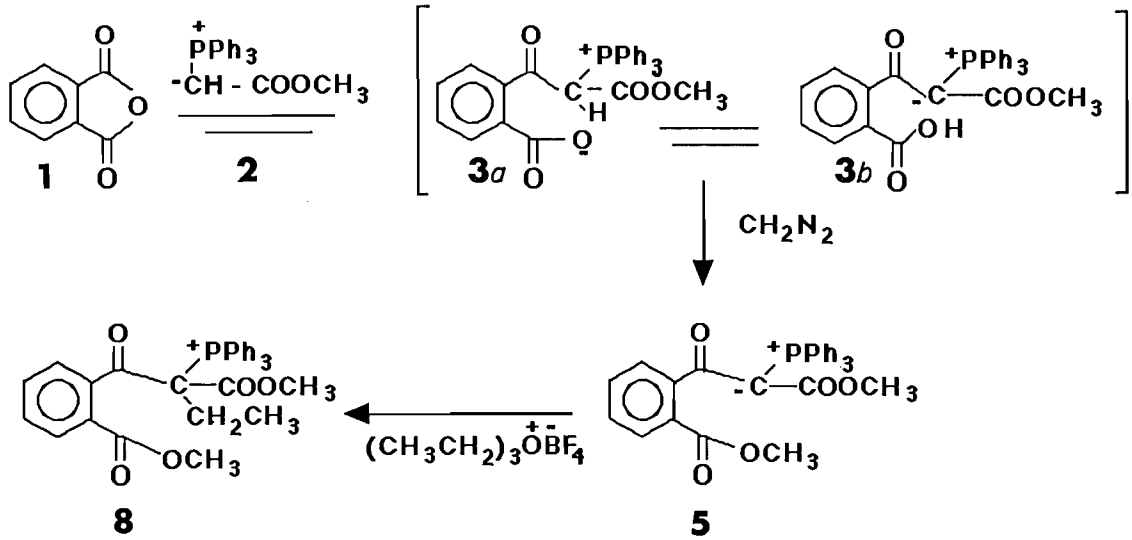

SCHEME 3

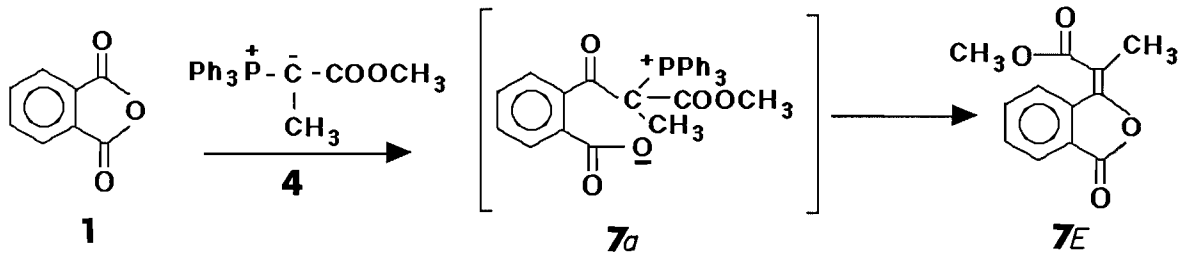

SCHEME 4

tive charge as shown in **9**. However, trapping with triethyloxonium tetrafluoroborane at 0 and −78°C gave only the *C*-alkylated product **8** as shown by ^1H and ^{13}C NMR, Fig. 3.

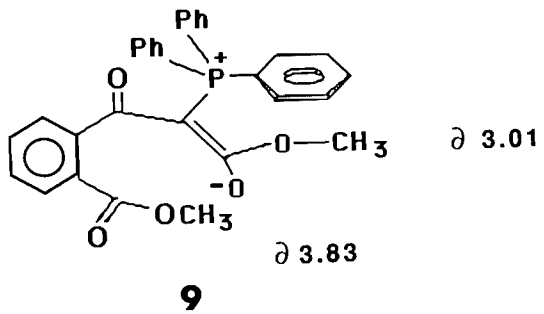

9

X-ray crystallographic analysis of the parent compound **5** provided some insight into its structure and the resulting preference for *C*-alkylation. Judging from the bond lengths, there is more delocalization of the negative charge into the neighbouring (C3—O3) keto group than toward the ester function. Predictably, the keto function occupies a position *cis* to the positively charged triphenylphospho group. As a result of such electron delocalization, if an *O*-alkylation were to occur, it should occur at O3 rather than O2. It appears, however, that the charge is too diffused for the *O*-alkylation to take place since only *C*-alkylation is observed.

Comparison of bond lengths in compound **5** with those reported for the related compound **11***b* (Table 1) shows that although the C1—C3 bonds are shorter than C1—C3 in both **5** and **11***b* the C3—O3 bond is significantly longer in the latter ylide. This suggests more single bond character and higher negative charge on the O3 atom of the keto carbonyl function in **11***b*, which should lead to a more facile *O*-alkylation. A series of parallel experiments carried out for the succinic anhydride **10** supports this forecast, as the alkylation with triethyloxonium tetrafluoroborate gives only one product, the *O*-alkylated compound **13** in 83% yield, Scheme 5.

Reactivities of stabilized ylides in condensations with phthalic anhydride

Once the identities of the observable intermediates were confirmed, we monitored by NMR the course of the reaction leading to their formation and we studied the conditions necessary for the re-cyclization to the corresponding enol-lactones. In the course of the reaction of phthalic anhydride with phosphorane **2**, followed by ^1H NMR, after 10 min at −30°C the mixture consisted of the acyclic intermediate (42%) and the ylide (52%). A typical run is shown in Table 2. When the temperature was not allowed to rise above 0°C, only 4% of the final product was formed after 2 h, while the intermediate and the ylide accounted for 66% and 30%, respectively.

The same reaction proceeded to completion quite rapidly at room temperature. Within 5 min at 25°C, 33% of the intermediate and 6% of the product could be observed in the ^1H NMR spectrum. After 90 min the reaction mixture contained 35% product, 20% intermediate, and 45% ylide. The signal for the ylide was broadened and had shifted to a

Can. J. Chem. Downloaded from www.nrcresearchpress.com by 217.78.4.112 on 09/08/12
For personal use only.

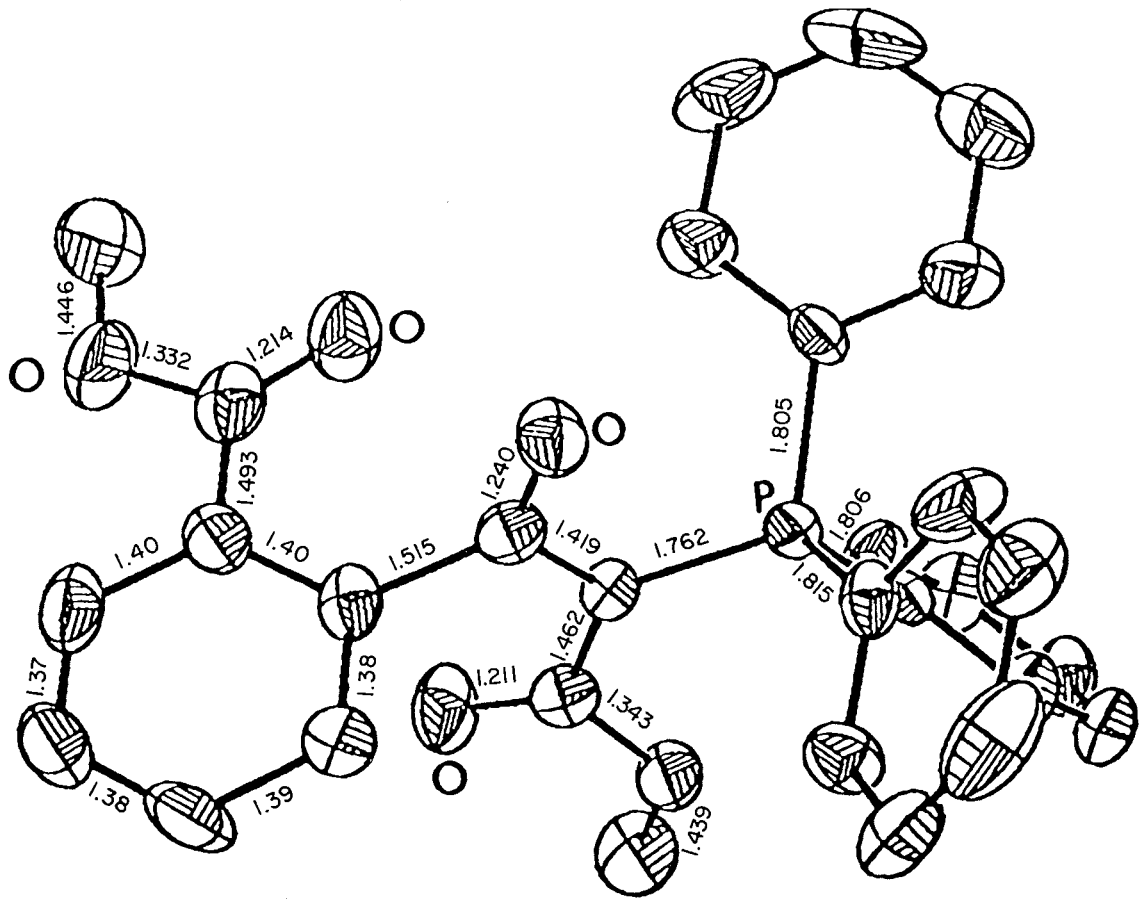

FIG. 2. The crystal structure of compound **5**.

slightly lower field, suggesting that equilibria are set up among the ylide, acyclic intermediates (**3***a* and **3***b*), and the conjugate acid **2***a*, formed as a by-product during the condensation reaction. After 18 h, the product accounted for 65%, the intermediate was gone, and so was the ylide, which had been converted completely into its conjugate acid **2***a*.

The downfield shifts of the ylide's signal were more pronounced during the experiments in which no particular precaution was taken to dry the solvent and to purify the ylide and phthalic anhydride. During several runs monitored by ^{31}P NMR, the ylide's signal drifted visibly downfield as shown in Fig. 4. When such a reaction was left overnight, the only signals remaining the following morning were the product Ph_3PO and the conjugate acid **2***a*.

The condensation carried out under anhydrous conditions between freshly recrystallized phthalic anhydride and ylide **2**, pretreated with BuLi (or NaH) to remove traces of its conjugate acid **2***a*, was initially slightly slower; however, as the reaction progressed, the rate became comparable to that measured in previous studies, as illustrated in Fig. 5.

This experiment supports the previously postulated catalytic effect of acidic protons on the reactivity of stabilized ylides (25*a*, *b*). In a prior communication we discussed experiments that established that removing all sources of acidic protons, including traces of the conjugated acid, results in a considerable slowing down of the reaction between a stabilized ylide and benzaldehyde (25*a*). In the absence of acidic protons, the stabilized ylides, $Ph_3PCHCOOR$, exist as the slow-reacting *cis–trans* enolate mixture. The presence of Li^+ or Na^+ counterions appears to stabilize the enolic forms, hence retarding rather than accelerating the reactions with aldehydes (25, 27). However, during the condensations of ylides such as **2** with anhydrides, even after *all sources of acidic protons are removed*, the first step generates an equilibrating pair of acyclic structures (**3***b* and **3***b*), each bearing an acidic proton that can serve as a catalyst. Thus, the reaction is self-catalyzed.

To further confirm the catalytic role of a proton, we studied the condensation of phthalic anhydride with ylide **4**, which leads to the formation of an intermediate lacking an acidic proton. Ylide **4** is more moisture sensitive than **2**, and commercial samples always contain small quantities of its conjugate acid **4***a*. The room temperature reaction between phthalic anhydride and **4**, in the presence of traces of **4***a*, is 50% complete in 5 mins. In contrast, when **4** is pretreated to remove traces of the conjugate acid **4***a* immediately prior to the addition of phthalic anhydride, the reaction run under anhydrous conditions is considerably slower. After 3 h at 25°C, only 40% of the enol-lactone is observable in the reaction mixture as shown in Fig. 6.

It is important to note that in the reaction of ylide **2** with phthalic anhydride, each of the intermediates within the **3***a*,**3***b* pair can be expected to undergo proton transfer to give the other member of the pair, at a rate very much faster than the recyclization and the cleavage to the products, enol-lactones and triphenylphosphine oxide. In view of the above, the lifetime of the **3***a*,**3***b* pair should be much longer than the lifetime of an intermediate with no internal proton transfer

Can. J. Chem. Downloaded from www.nrcresearchpress.com by 217.78.4.112 on 09/08/12
For personal use only.

Can. J. Chem. Downloaded from www.nrcresearchpress.com by 217.78.4.112 on 09/08/12
For personal use only.

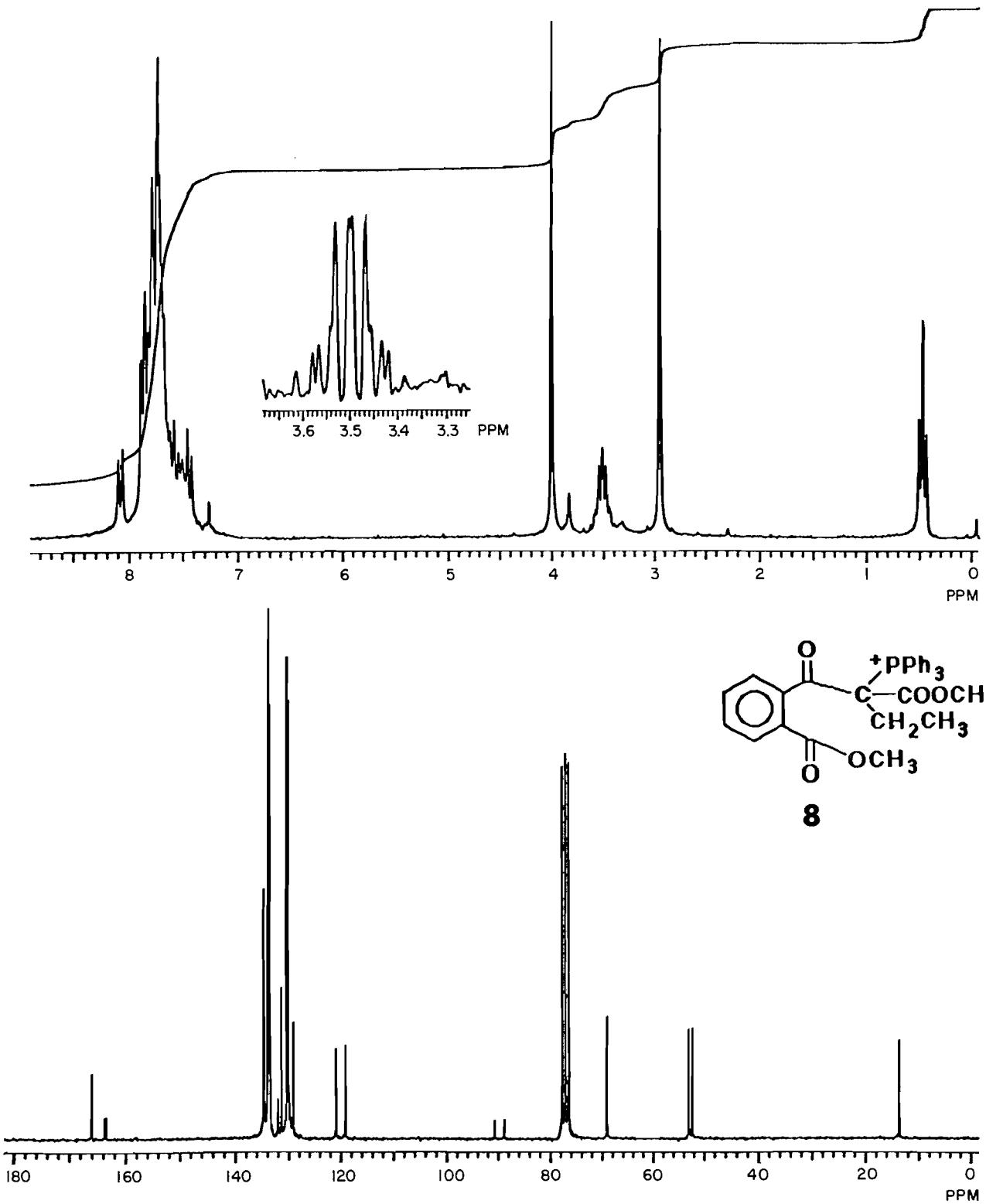

FIG. 3. The ^{1}H and ^{13}C NMR spectra of compound **8**.

to compete with the reaction leading to the Wittig product. The latter case is illustrated by the reaction of ylide **4**; here, the intermediate **7***a* is observable only as a transient species in the ^{31}P spectrum at $-35°C$ (a broad peak at 27.50 ppm). At $-20°C$ this intermediate exists in equilibrium with ylide **4** (a broad signal centred on 24.55 ppm) and collapses rapidly to the products. In this case the sluggishness of the reaction carried out *in the absence of acidic protons* can be directly linked to the slower initial attack of the ylide on the carbonyl group of the anhydride.

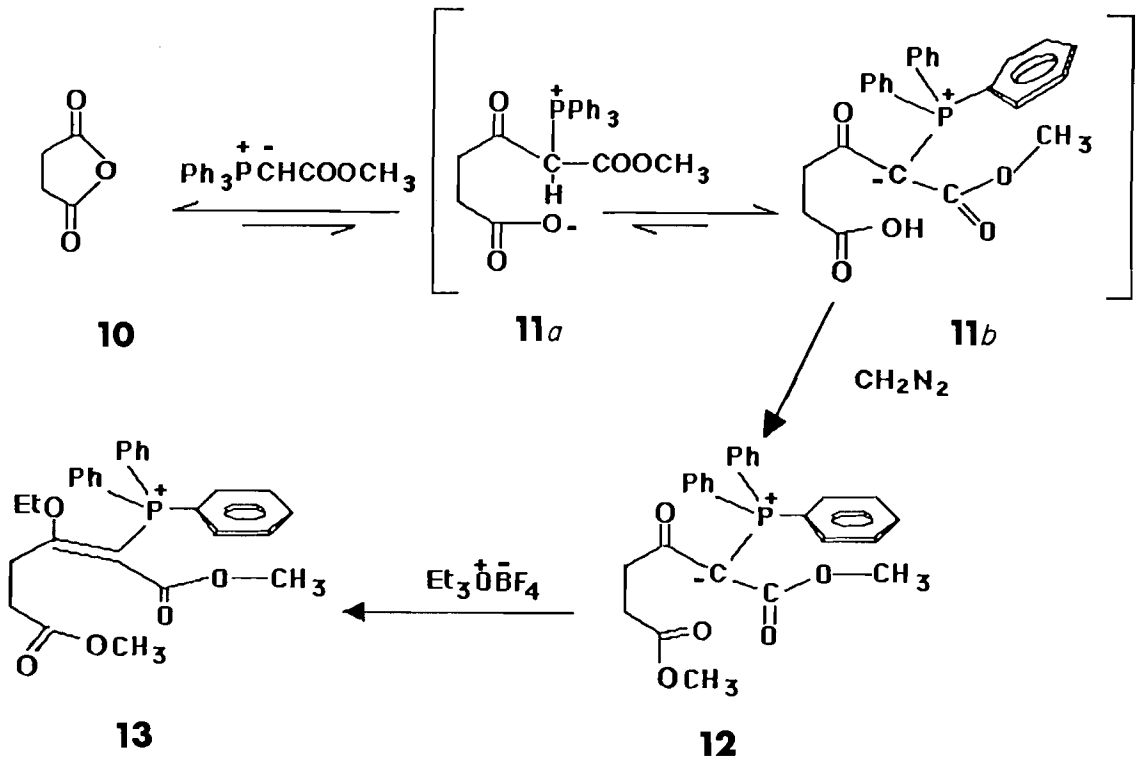

SCHEME 5

TABLE 1. Selected bond lengths (Å) for compounds **5** and **11***b*

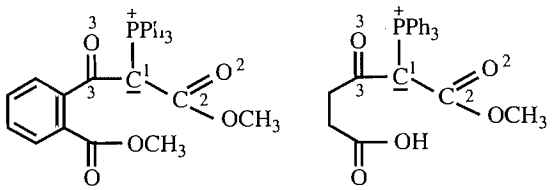

Atoms	Ylide **5**	Ylide **11***b*
P—C1	1.762	1.75
C1—C2	1.462	1.452
C1—C3	1.419	1.425
C2—O2	1.211	1.205
C3—O3	1.240	1.256

Study of the reversibility of the reaction between ylide 2 and 5-member cyclic anhydrides

The condensation of ylide **2** with several cyclic anhydrides was initially investigated by Abell and Westropp (18), who reported that the formation of an acyclic intermediate was reversible for the reaction with phthalic anhydride and irreversible with succinic anhydride. Our studies of the condensation of phthalic anhydride with ylide **2** monitored by NMR suggested that formation of the acyclic intermediate pair **3***a* and **3***b* is an equilibrium and hence reversible. Unequivocal proof for reversibility was provided by the following experiment.

Under the conditions corresponding to the maximum buildup of acyclic intermediates (**3***a* and **3***b*, 70%), a solution of freshly distilled benzaldehyde in $CHCl_3$ was added at 0°C, and the reaction, warmed to room temperature, was followed by NMR. After 2 h only methyl cinnamate and traces of products **3***E* and **3***Z* could be detected. Upon chromatography, methyl cinnamate was isolated in 87% yield (based on benzaldehyde).[3]

In a similar series of experiments we were able to establish the reversibility of phenyl maleic and succinic anhydrides; the last result is in contrast to the earlier report of Abell and Westropp (18). The condensation of succinic anhydride with ylide **2** was followed by ^1H NMR until the acyclic intermediates constituted 90% of the reaction mixture. At that stage freshly distilled benzaldehyde was added, and the room-temperature reaction was monitored by ^1H NMR. The reappearance of the succinic anhydride and the formation of cinnamate could be readily observed. After 70 h the reaction mixture consisted of methyl cinnamate, succinic anhydride, and traces of enol-lactone **11***E*, see Scheme 6.

The condensation of ylide **2** with unsubstituted maleic anhydride at −30°C leads to the formation of an acyclic intermediate, as witnessed by an instantaneous appearance of a new, highly shielded methoxy signal at 3.10 ppm. The reaction, however, does not lead to the corresponding enol-lactone since rapid polymerization competitively consumes the reagents, shifting the equilibrium and depleting the intermediate. Consequently, trapping experiments and re-

[3]One referee suggested a double crossover experiment to further confirm reversibility of these condensations. However, such an experiment, in which phthalic anhydride reacts with $Ph_3P{=}CHCOOMe$ to give intermediate A and 3-chlorophthalic anhydride reacts with $Ph_3P{=}CHCOOEt$ to give two intermediates B and C, leads to 12 overlapping products upon mixing of the A, B, and C, and is difficult to interpret.

Can. J. Chem. Downloaded from www.nrcresearchpress.com by 217.78.4.112 on 09/08/12
For personal use only.

TABLE 2. ^{1}H NMR followed reaction of phthalic anhydride **1** with ylide **2**

Temperature (°C)	Time (min)	Ylide **2** (ppm)	%	Intermediate **3** (ppm)	%	Product (ppm)	%
−30	10	3.49	56	2.98	42	3.86	2
−20	50	3.49	35	3.01	63	3.86	2
−15	60	3.49	31	3.01	67	3.85	2
−10	80	3.49	28	3.02	70	3.85	2
0	100	3.50	29	3.02	69	3.84	2
0	130	3.50	30	3.02	67	3.84	4

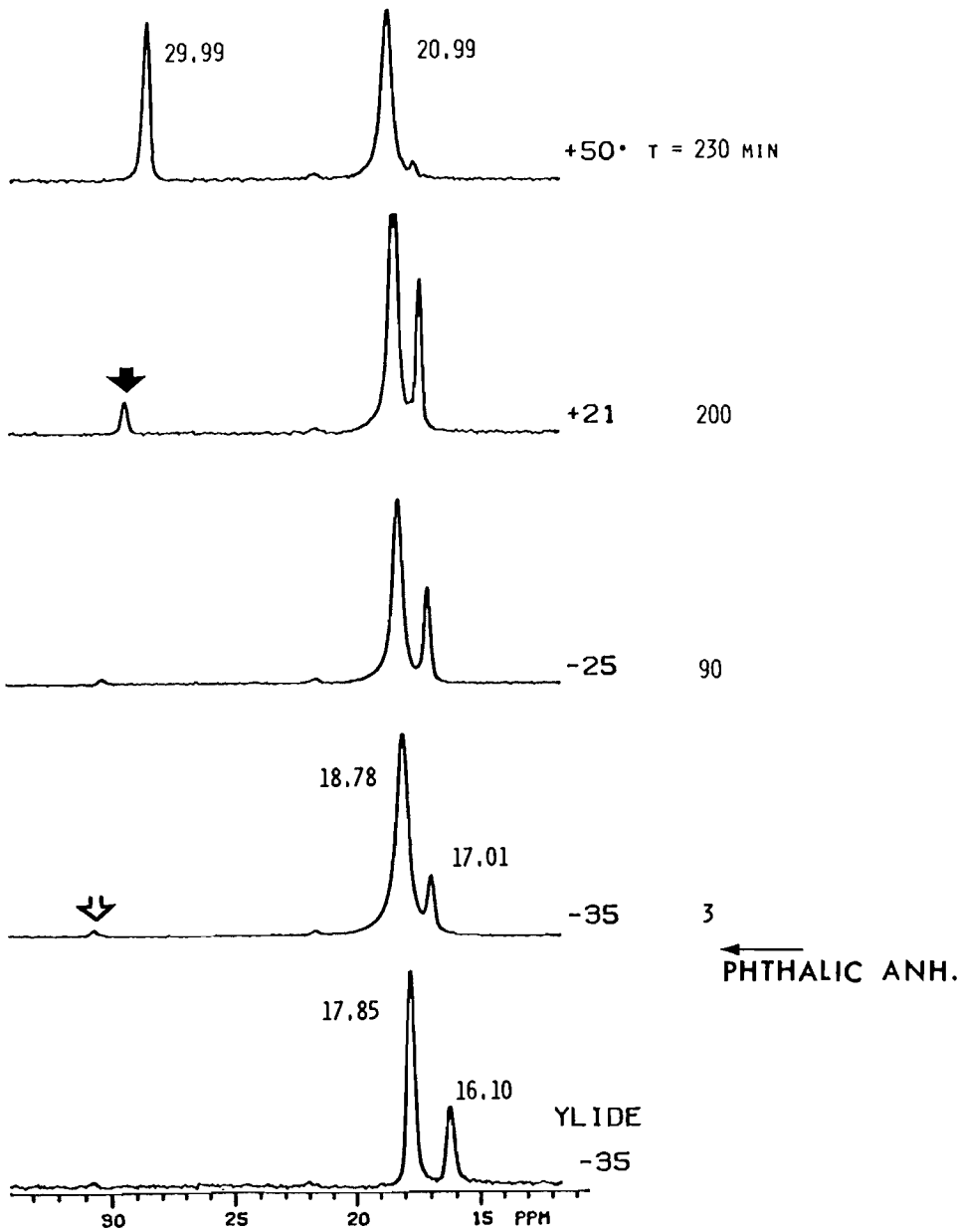

FIG. 4. Reaction of ylide **2** with phthalic anhydride monitored by ^{31}P NMR. In this experiment no precaution was taken to eliminate acidic protons. Here, the ylide's signal formed at 18.78 ppm upon mixing is visibly drifting downfield during the reaction.

Can. J. Chem. Downloaded from www.nrcresearchpress.com by 217.78.4.112 on 09/08/12
For personal use only.

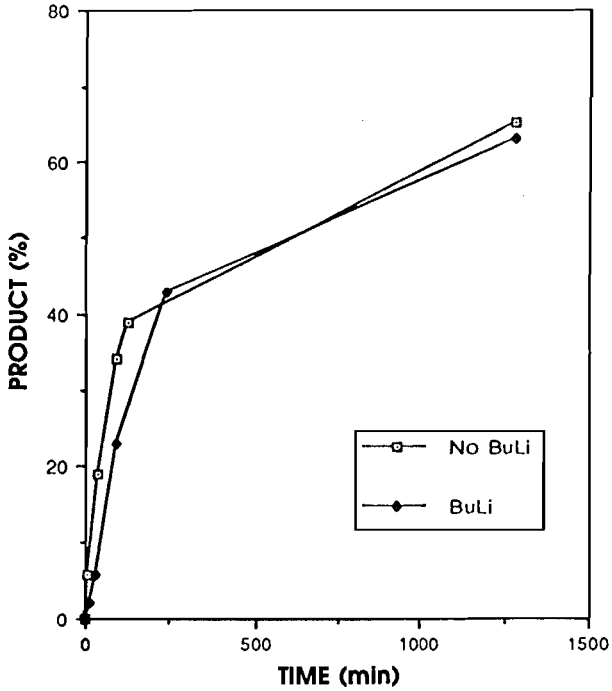

FIG. 5. Room temperature reaction of phthalic anhydride with ylide **2**, as obtained from the supplier –⊡–, and pretreated with BuLi –◆–.

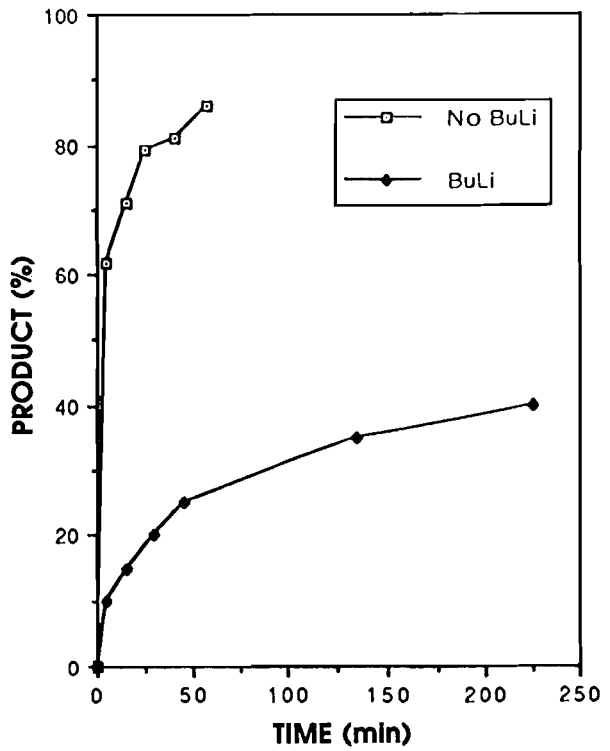

FIG. 6. Room temperature reaction of phthalic anhydride with ylide **4** obtained from the supplier –⊡–, and pretreated with BuLi –◆–.

versibility studies were carried out on phenylmaleic anhydride **14**. The principle acyclic intermediate **15***b* was trapped when the reaction carried out at −5°C for 35 min was treated with diazomethane to give the corresponding ester **16**. When acetaldehyde, instead of diazomethane, was added at that time, the product mixture consisted of methylcrotonate **17**, phenylmaleic anhydride **14**, and a small quantity of enol-lactone **18**, confirming that the reversibility of the first condensation step is general to the three classes of cyclic anhydrides, Scheme 7.

Conclusion

The principal goal of this study was to investigate the mechanism of the condensation of stabilized phosphoylides, such as $Ph_3PCHCOOCH_3$, **2**, with cyclic anhydrides. To accomplish that, the observable intermediates were trapped and their identity was established. The reversibility of the condensation step, leading to the formation of acyclic intermediates, was demonstrated for phthalic, phenyl maleic, and succinic anhydrides, in a series of reverse reactions between the acyclic intermediates and highly reactive aldehydes such as benzaldehyde or acetaldehyde.

Trapping experiments also confirmed that an equilibrium is established between reactants and acyclic intermediates and that the intermediates themselves are in equilibrium with a strong bias toward the stabilized ylide forms such as **3***b*, **11***b*, or **15***b*.

We were unable to observe directly any oxaphosphetane or betaine intermediates. This is not particularly surprising in view of unsuccessful efforts of other investigators to observe such species in the reactions between aldehydes and stabilized ylides (4, 12). Although the betaine intermediate was calculated to be of considerably higher energy than the corresponding oxaphosphetane for the model reaction of aldehyde with ylide (11), it seems to us that the most feasible route to the acyclic intermediates in the reactions of stabilized ylides with 5-member cyclic anhydrides is through a very short-lived betaine or a betaine-like transition state.

In all cases studied, the reversible formation of cyclic adducts is a lower energy process than the formation of product enol-lactones. This suggests that in the condensations of stabilized phosphoranes with cyclic anhydrides, the oxaphosphetane is formed either through betaine or a betaine-like transition state, or that there is an independent, competing, slightly higher energy pathway to enol-lactones via a 4-centre transition.[4] At this stage it is not possible to distinguish between the two mechanistic pathways.

The study of condensations of cyclic anhydrides with methyl (triphenylphosphoranylidene) acetate **2** and (carboethoxy-ethylidene) triphenylphosphorane **4** in the absence of all external sources of acidic protons (including traces of the corresponding conjugate acids), strengthens our earlier observation that Wittig condensations with stabilized ylides appear to be catalyzed by traces of protic acids (25, 27).

Experimental

Nuclear magnetic resonance spectra were recorded at 361 MHz (^1H), 91 MHz (^{13}C), and 146 MHz (^{31}P) on the Nicolet 360 NB spectrometer of the Atlantic Region Magnetic Resonance Centre, and some ^{31}P spectra were recorded at 81 MHz on the Varian XL-200 spectrometer of the University of New Brunswick. All spectra were in $CDCl_3$ solutions unless otherwise indicated. Calibration of the spectra was done with respect to TMS as internal

[4]M. M. Kayser, K. L. Hatt, and D. Hooper. Manuscript in preparation.

Can. J. Chem. Downloaded from www.nrcresearchpress.com by 217.78.4.112 on 09/08/12
For personal use only.

Can. J. Chem. Downloaded from www.nrcresearchpress.com by 217.78.4.112 on 09/08/12
For personal use only.

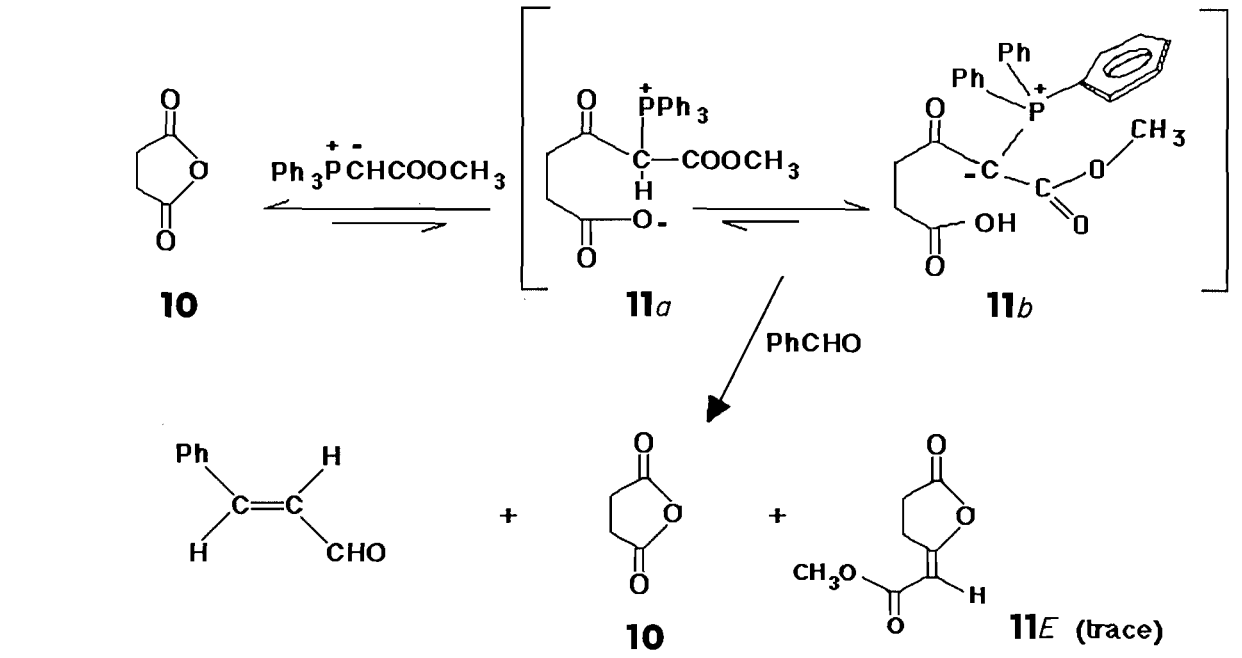

SCHEME 6

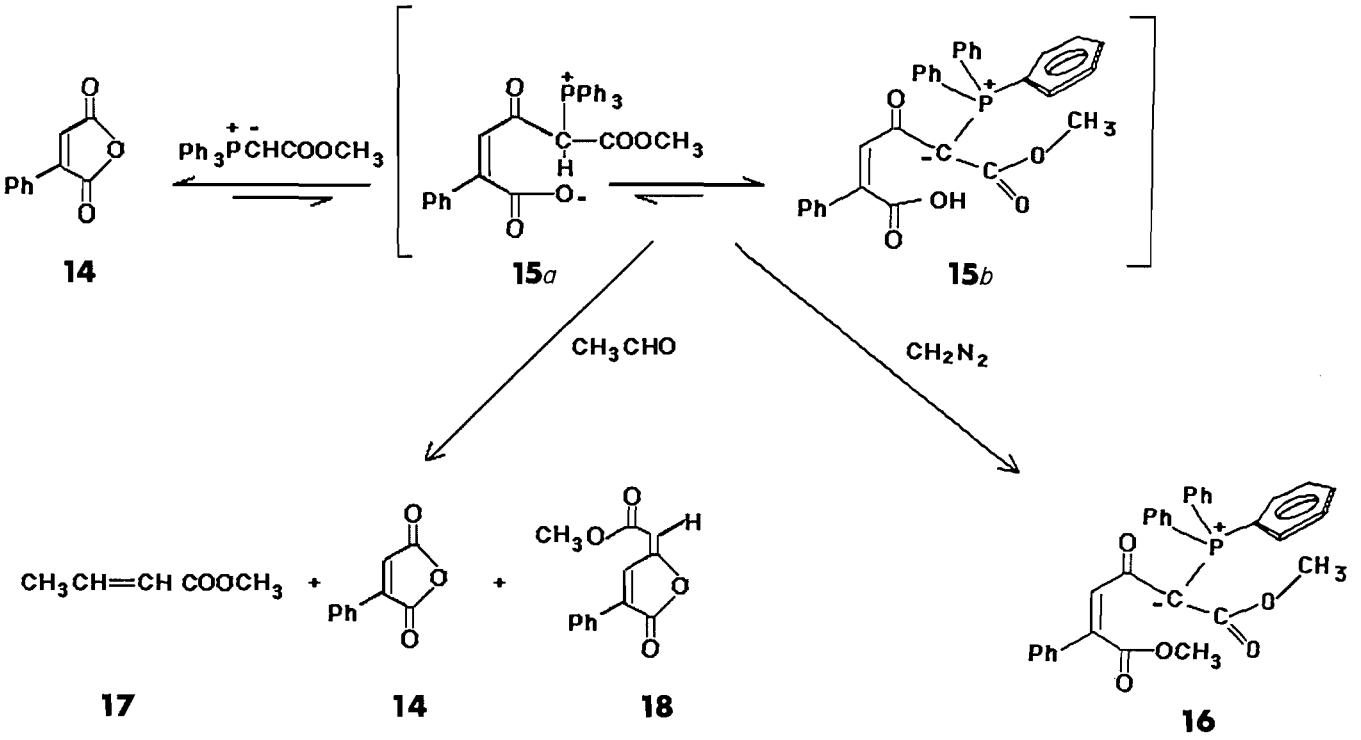

SCHEME 7

reference (^{1}H and ^{13}C) or 85% H_3PO_4 as external standard (^{31}P). Temperature control was by the usual Nicolet method. Calibration of the thermocouple showed an estimated error of less than 1°C in the temperature range used.

For all experiments carried out under anhydrous conditions, anhydrides were freshly crystallized from dry chloroform; methyl (triphenylphosphoranylidene)acetate **2** (obtained from Aldrich) and (carboethoxyethylidene)-triphenylphosphorane **4** (obtained from Lancaster) were subjected to azeotropic drying with benzene. To remove traces of conjugate acids, treatment with BuLi or MeLi was necessary. $CDCl_3$ (Silanor C*) was dried over molecular sieves and all glassware and NMR tubes were oven-dried at 150°C for 2 h and cooled under stream of argon.

*Room temperature reaction of phthalic anhydride **1** with ylide **2** monitored by ^{1}H NMR. Formation of 3E and 3Z*

Methyl(triphenylphosphoranylidene)acetate **2** (100.5 mg, 0.3 mmol) was dissolved in 0.3 mL of $CDCl_3$, and the spectrum of the ylide was recorded. Phthalic anhydride **1** (44.5 mg, 0.3 mmol) suspended in 0.5 mL of $CDCl_3$ was added to the ylide solution and the spectrum was recorded immediately. The composition of the reaction mixture was established from the integration of ^{1}H NMR

Can. J. Chem. Downloaded from www.nrcresearchpress.com by 217.78.4.112 on 09/08/12
For personal use only.

spectra taken at regular intervals for 24 h. After approximately 20 h at room temperature the reaction was completed. The product, the (*E*/*Z*) mixture of enol-lactones (65%), was separated from the conjugate acid **2***a* (35%) and triphenylphosphine oxide by chromatography on silica gel. The major (*E*) isomer (80%) was eluted first (10:90 ether:petroleum ether) followed by the minor (*Z*) isomer (20%) (50:50 ether:petroleum ether). Methyl (*E*)-3-oxo-1,3-dihydro-isobenzofuran-1-ylideneacetate **3***E*, ^{1}H NMR δ: 3.77 (s, 3H, OCH_3), 6.09 (s, 1H, CH), 7.92–7.60 (m, 4H, aromatic), 9.05 (d, 1H, *o*-aromatic). Methyl (*Z*)-3-oxo-1,3-dihydroisobenzofuran-1-ylideneacetate **3***Z*, ^{1}H NMR δ: 3.79 (s, 3H, OCH_3), 5.83 (s, 1H, CH), 7.92–7.60 (m, 4H, aromatic).

*Room temperature reaction of phthalic anhydride **1** with ylide **2** pretreated with BuLi, monitored by ^{1}H NMR*

The solution of ylide **2** (100 mg, 0.3 mmol in 0.3 mL of $CDCl_3$) was treated with a few drops of BuLi until the spectrum resolved into two isomeric forms. At that point the suspension of phthalic anhydride (44.4 mg, 0.3 mmol) in $CDCl_3$ (0.5 mL) was added and the reaction was monitored by ^{1}H NMR as described above.

*Room temperature reaction of phthalic anhydride **1** with ylide **4** monitored by ^{1}H NMR Formation of 7*E

(Carbethoxyethylidene)triphenylphosphorane **4** (109 mg, 0.3 mmol) was dissolved in 0.3 mL of $CDCl_3$ and the spectrum was taken. Phthalic anhydride **1** (45 mg, 0.3 mmol) suspended in 0.5 mL of $CDCl_3$ was added to the ylide solution and a spectrum was recorded immediately after mixing. At this point, approximately half of the ylide was already converted to product. After 1 h all ylide was consumed. The products, (*E*) enol-lactone and triphenylphosphine oxide, were isolated by chromatography on silica gel. Ethyl (*E*)-3-oxo-1,3-dihydroiso-benzofuran-1-ylidene(2′-propanoate) **7***E*, 40 mg (61%) was eluted with ether:petroleum ether (20:80) ^{1}H NMR δ: 1.39 (t, 3H, OCH_2,CH_3), 2.27 (s, 3H, CH_3), 4.36 (q, 2H, OCH_2CH_3), 8.57–7.58 (m, 4H, aromatic); triphenylphosphine oxide, 67 mg (80%), was eluted with ether.

*Room temperature reaction of phthalic anhydride **1** with ylide **4** pretreated with BuLi, monitored by ^{1}H NMR*

The solution of **4** (109 mg, 0.3 mmol) in $CDCl_3$ (0.3 mL) was treated with a few drops of BuLi until the spectrum indicated presence of the two isomeric forms. At that point a suspension of phthalic anhydride (45 mg, 0.3 mmol) in $CDCl_3$ (0.5 mL) was added and the reaction was monitored by ^{1}H NMR as described above.

*Trapping with Me_3OBF_4: phthalic anhydride **1** + ylide **2***

Ylide **2** (571 mg, 1.71 mmol) dissolved in 15 mL of $CHCl_3$ and cooled to 0°C was added to an ice-cold suspension of phthalic anhydride **1** (253 mg, 1.71 mmol) in 15 mL $CHCl_3$. The reaction was allowed to proceed for 30 min at 0°C under N_2 atmosphere. After addition of Me_3OBF_4 (253 mg, 1.71 mmol) the reaction was stirred at 0°C for another 30 min. The solution was warmed to room temperature and the solvent was evaporated. The products were identified by ^{1}H NMR as a 50:50 mixture of the conjugate acid **2***a* and the *O*-alkylated acyclic intermediate **5**: ^{1}H NMR δ: 3.01 (s, 3H, OCH_3), 3.81 (s, 3H, OCH_3), 7.86–7.26 (aromatic H's).

*Trapping with MeI: phthalic anhydride **1** + ylide **2***

Ylide **2** (388 mg, 1.16 mmol) dissolved in 15 mL of $CHCl_3$ and cooled to 0°C was added to phthalic anhydride **1** (172 mg, 1.16 mmol) suspended in 15 mL $CHCl_3$ at 0°C. After 30 min at 0°C, the reaction mixture was treated with excess MeI (0.1 mL); and stirring was continued at that temperature for additional 30 mins. The solution was allowed to warm to room temperature and the solvent was evaporated. The products were identified by ^{1}H NMR as: conjugate acid **2***a* (20%), **4***a* (39%), **3***E*/*Z* mixture of enol-lactones (30%), and acyclic intermediate **5** (11%). **2***a*: ^{1}H NMR δ: 3.59 (s, 3H, OCH_3), 5.22 (d, 2H, 2, J_{PH} = 13.6 Hz, I^- counterion), 7.86–7.26 (aromatic H's); for **4***a*, 1.68 (dd, 3H, CH_3, J_{PH} = 18.3 Hz, J_{PH} = 7.3 Hz), 3.56 (s, 3H, OCH_3), 6.20 (m, 1H, CH, I^- counterion), 7.86–7.26 (aromatic H's); for **3***E* and **3***Z* enol-lactones; δ: 3.84 (s, 3H, OCH_3, *E* + *Z*), 5.96 (s, 1H, CH, *Z*), 6.13 (s, 1H, CH, E), 7.86–7.26 (Aromatic H's); **5**: ^{1}H NMR δ: 3.01 (s, 3H, OCH_3), 3.81 (s, 3H, OCH_3), 7.86–7.26 aromatic H's).

*Trapping with CH_2N_2: phthalic anhydride **1** + ylide **2**. Formation of **5***

Ylide **2** (670 mg, 2.0 mmol) was added to phthalic anhydride **1** (297 mg, 2.0 mmol) suspended in 10 mL $CHCl_3$ and cooled to 0°C. The reaction mixture was stirred for 30 mins at 0°C before quenching with excess ethereal solution of diazomethane (0.2 M in Et_2O). The product **5** was isolated by chromatography on silica gel using 100% ether as elutant and was subsequently recrystallized from ether to give pure **5** as white crystals, 660 mg (66%), mp 182–184°C; ^{1}H NMR δ: 3.01 (s, 3H, OCH_3), 3.83 (s, 3H, OCH_3), 7.25–7.92 (aromatic H's); ^{13}C NMR δ: 49.57, 51.85, 71.17 (J_{PC} 112 Hz), 133.4–125.3 (aromatic), 146.57 (J_{PC} 8.2 Hz), 167.12, 167.57 (J_{PC} 14.8 Hz), 192.68 (J_{PC} 5:4 Hz); ^{31}P NMR δ: 17.73; HRMS: *m*/*e* 496.1465; (M^+) requires 496.1439; 463, 437, 361, 262, 201, 183, 163.

*Trapping of compound **5** with Et_3OBF_4. Formation of **8***

1-Methoxycarbonyl-2-(2′-methoxy-carbonylphenyl)-2-oxoethylidene-triphenylphosphorane **5**, (225 mg, 0.45 mmol) was dissolved in 20 mL of CH_2Cl_2 (distilled from CaH_2) and cooled to 0°C in a dry three-necked flask under N_2 atmosphere. An excess of triethyloxonium tetrafluoroborate (300 mg, 1.6 mmol), dissolved in dry CH_2Cl_2, was added to the solution. The reaction mixture was stirred for 10 min at 0°C, then was allowed to warm to room temperature and the solvent was evaporated. The resulting creamy-white solid was recrystallized from ether to give 1-methoxycarbonyl-2-(2-methoxy-carbonylphenyl)-1-oxobutan-2-triphenylphosphonium tetrafluoroborate **8**, 195 mg (82%), mp 169–171°C; ^{1}H NMR δ: 0.46 (t, 3H, CH_2CH_3), 2.94 (s, 3H, OCH_3), 3.45 (dq, 2H, CH_2CH_3), 3.99 (s, 3H, OCH_3), 8.09–7.41 (aromatic H's); ^{13}C NMR δ: −13.62, 52.28, 53.03, 69.03, 89.73 (J_{PC} 92.5 Hz), 119.00, 120.84, 129.04–134.57 (aromatic), 163.53 (J_{PC} 10.0 Hz), 165.87, 182.22; ^{31}P NMR δ: 14.84; HRMS: *m*/*e* 496.1413; (M^+ − 29) requires 496.1439, 463, 277, 201, 187. The reaction carried out at −78°C for 3 h gave the identical product. Note: C7 was shown to be the correct assignment by APT experiments.

*Trapping with CH_2N_2: succinic anhydride **10** + ylide **2**. Formation of **12***

Ylide **2** (2.1 g, 6.3 mmol) was added to succinic anhydride **10** (631 mg, 6.3 mmol) suspended in 50 mL of $CHCl_3$. The reaction mixture was stirred for 2 h at room temperature, quenched with excess diazomethane, and left overnight to allow the excess diazomethane to escape. After evaporation of the solvent, the product mixture consisted of **12** (60%), dimethyl succinate (10%), and small quantities of unreacted ylide **2** and the conjugate acid **2***a* in addition to triphenylphosphine oxide. Triphenylphosphine oxide was removed by crystallization from ether. The trapped intermediate, dimethyl 3-oxo-2-(triphenylphosphoranylidene)adipate **12**, was isolated by chromatography on silica gel with 100% ether. The isolated yield was 914 mg (32%); mp 113–115°C; ^{1}H NMR δ: 2.53 (t, 2H, CH_2), 3.13 (s, 3H, OCH_3), 3.24 (t, 2H, CH_2), 3.53 (s, 3H, OCH_3), 7.70–7.34 (aromatic); ^{13}C NMR δ: 28.15, 34.32 (J_{PC} 3.8 Hz), 48.45, 50.23, 69.6 (J_{PC}, 110 Hz), 132.71–124.98 (aromatic), 167.05 (J_{PC} 15.4 Hz), 173.09, 193.97; ^{31}P NMR δ: 16.46; HRMS: *m*/*e*: 448.1560; (M^+) requires 448.1439, 417, 361, 277, 201, 183, 77.

*Trapping of compound **12** with Et_3OBF_4. Formation of **13***

Triethyloxonium tetrafluoroborate (0.25 mL, 0.25 mmol) was added to the solution of compound **12** (100 mg, 0.22 mmol) dissolved in 10 mL CH_2Cl_2 (freshly distilled from CaH_2) and cooled to −78°C under N_2. The reaction mixture was stirred for 1 h at −78°C, then warned to room temperature. The solvent was evaporated to give single product identified from its NMR spectra as O3 alkylated compound **13**. ^{1}H NMR δ: 0.51 (t, 3H, CH_3), 2.79 (t, 2H, CH_2), 3.24 (t, 2H, CH_2), 3.28 (s, 3H, OCH_3), 3.71 (s, 3H, OCH_3),

4.07 (q, 2H, OCH_2), 7.54–7.79 (m, 15H, aromatic H's); ^{13}C NMR δ: 13.49, 25.81, 31.61, 52.33, 52.49, 67.68, 91.00 ($^1J_{PC}$ 100 Hz), 117.74–135.27 (aromatic), 164.07 ($^2J_{PC}$ = 8.7 Hz), 171.89, 184.83 ($^2J_{PC}$ = 8.9 Hz).

*Trapping with CH_2N_2: phenylmaleic anhydride **14** + ylide **2**. Formation of **16***

Ylide **2** (835 mg, 2.5 mmol) was added to phenylmaleic anhydride **14** (435 mg, 2.5 mmol) suspended in 20 mL of $CHCl_3$ at −5°C. The reaction mixture was stirred for 35 min at 0°C. At that point only the intermediate pair **15***a*, **15***b* and the product **18** were observable in the ^1H NMR spectrum. After quenching with excess diazomethane, the reaction mixture was left overnight to allow the excess diazomethane to escape. The solvent was evaporated and triphenylphosphine oxide was removed by crystallization from ether. The remaining products were separated by chromatography on silica gel. The enol-lactone **18** was eluted first, followed by **16** eluted with ether: petroleum ether (50:50) to give 417 mg (32%): ^1H NMR δ: 3.17 (s.3H), 3.47 (s, 3H), 7.2–7.7 (m. 20H), 7.93 (s, 1H); ^{31}P NMR δ: 17.11; *m/e*: 522 (M^+), 277, 262, 201, 199, 174, 102.

*Reversibility study: phthalic anhydride **1** + ylide **2***

Phthalic anhydride **1** (100 mg, 0.7 mmol) was added to the solution of **2** (227 mg, 0.7 mmol) in 50 mL $CHCl_3$ cooled to 0°C. After 30 min at 0°C, the reaction was quenched with benzaldehyde and was stirred for an additional 2 h at 0°C. After evaporation of the solvent, the products were separated by chromatography on silica gel. *trans*-Methylcinnamate, 96 mg (87%), was eluted first with ether: petroleum ether (5:95); ^1H NMR δ: 3.79 (s, 3H, OCH_3), 6.44 (d, 1H, C*H*), 8.00–7.20 (m, 6H, aromatic + C*H*), followed by trace amounts of enol-lactone(s) eluted with ether: petroleum ether (10:90) and triphenylphosphine oxide 189 mg (79%) eluted with 100% ether.

Acknowledgement

Financial support by the Natural Sciences and Engineering Research Council of Canada (NSERC) is gratefully acknowledged. The NMR spectra were, in large part, recorded at the Atlantic Region Magnetic Resonance Centre, an NSERC supported facility.

1. A. W. Johnson. Organic chemistry, A series of monographs. Ylide chemistry, Vol. **7**. Academic Press, New York, 1966; I. Gosney and A. G. Rowley. *In* Organophosphorus reagents in organic synthesis. *Edited by* J. I. G. Cadogen. Academic Press, New York. 1979.
2. S. Trippett. Adv. Org. Chem. **1**, 83 (1960); S. Trippett. Q. Rev. Chem. Soc. **17**, 406 (1963).
3. P. Froyen. Acta Chem. Scand. **26**, 2163 (1972).
4. B. E. Maryanoff and A. B. Reitz. Chem. Rev. **89**, 863 (1989).
5. E. Vedejs, K. A. J. Snoble, and P. L. Fuchs. J. Org. Chem. **38**, 118 (1973).
6. E. Vedejs, C. F. Marth, and R. Ruggeri. J. Am. Chem. Soc. **110**, 3940 (1988).
7. E. Vedejs and C. F. Marth. J. Am. Chem. Soc. **112**, 3905 (1990).
8. V. Samano and M. J. Robins. Synthesis 238 (1991).
9. F. Ramirez, C. P. Smith, and J. F. Pilot. J. Am. Chem. Soc. **90**, 6726 (1968).
10. R. Holler and H. Lischka. J. Am. Chem. Soc. **102**, 4632 (1980).
11. F. Volatron and O. Eisenstein. J. Am. Chem. Soc. **109**, 1 (1987); **106**, 6117 (1984).
12. E. Vedejs and T. J. Fleck. J. Am. Chem. Soc. **111**, 5861 (1989).
13. E. Vedejs, T. J. Fleck, and S. Hara. J. Org. Chem. **52**, 4637 (1987).
14. G. Pattenden. Fortschr. Chem. Org. Naturst. **35**, 133 (1978); S. B. Daniels and J. A. Katzenellenbogen. Biochemistry, **25**, 1436, (1986), and references cited therein.
15. D. W. Knight and G. Pattenden. J. Chem. Soc. Perkin Trans. **1**, 62 (1979); D. W. Knight and G. Pattenden. J. Chem. Soc. Perkin Trans. **1**, 635 (1975).
16. P. A. Chopard, R. F. Hudson, and R. J. G. Searle. Tetrahedron Lett. 2357 (1965); P. A. Chopard, R. F. J., Searle, and F. H. Devitt. J. Org. Chem. **30**, 1015 (1965).
17. C. F. Ingham, R. A. Massy-Westropp, G. D. Reynolds, and W. D. Thorpe. Aust. J. Chem. **28**, 2499 (1975).
18. A. D. Abell and R. A. Massy-Westropp. Aust. J. Chem. **35**, 2077 (1982).
19. L. Breau. M. Sc. Thesis, Mount Allison University (1986).
20. A. D. Abell, B. M. Clark, and W. T. Robinson. Aust. J. Chem. **41**, 1243 (1988).
21. E. Vedejs, G. P. Meier, and K. A. J. Snoble. J. Am. Chem. Soc. **103**, 2823 (1981).
22. M. Schlosser and K. F. Chrisitmann. Ann. Chem. **708**, 1 (1967).
23. M. Schlosser. Top. Stereochem. **5**, 1 (1970).
24. R. J. Anderson and C. A. Henrich. J. Am. Chem. Soc. **97**, 4327 (1975).
25. (*a*) M. M. Kayser and D. Hooper. Can. J. Chem. **68**, 2123 (1990); (*b*) C. Rüchardt, S. Eichler, and P. Panse. Angew. Chem. Int. Ed. Engl. **21**, 619 (1963).
26. A. D. Abell and J. D. Trent. J. Chem. Soc. Chem. Commun. 409 (1989).
27. M. M. Kayser, K. L. Hatt, and D. Hooper. Can. J. Chem. **69**, 1929 (1991).

Can. J. Chem. Downloaded from www.nrcresearchpress.com by 217.78.4.112 on 09/08/12
For personal use only.

A study of the nonstationary character of the methanol-to-hydrocarbons conversion

V. KANAZIREV[1] AND T. TSONCHEVA

Institute of Organic Chemistry with Centre of Phytochemistry, Bulgarian Academy of Sciences, Sofia 1040, Bulgaria

Received May 29, 1991[2]

V. KANAZIREV and T. TSONCHEVA. Can. J. Chem. **70**, 1997 (1992).

An important characteristic of the methanol-to-hydrocarbons reaction is its autocatalytic behaviour under certain conditions. In this paper, self-acceleration in the conversion of MeOH over various zeolites, e.g., H-ZSM-5, H-CaY, H-offretite, and H-mordenite, in a flow reactor is examined. Self-acceleration is considered as a step of the nonstationary state changes taking place as a result of the interaction between the reaction medium and the catalyst. The effect on this process of factors such as partial pressure of methanol and the presence of hydrogen in the reaction mixture are investigated. Conclusions regarding the mechanism of C—C bond formation are considered. The course of the nonstationary process may be used for preliminary selection of catalysts for synthesis of hydrocarbons from methanol.

V. KANAZIREV et T. TSONCHEVA. Can. J. Chem. **70**, 1997 (1992).

Une caractéristique importante de la réaction du méthanol en hydrocarbures est son comportement autocatalytique, dans certaines conditions. Dans ce travail, on a examiné l'auto-accélération de la conversion du MeOH sur divers zéolites, comme la H-ZSM-5, la H-CaY, la H-offretite et la H-mordenite dans un récteur à écoulement. L'auto-accélération est considérée comme une étape des changements de l'état non-stationnaire qui se produit par l'interaction entre le milieu réactionnel et le catalyseur. On a aussi examiné l'effet, sur ce processus, de facteurs comme la pression partielle du méthanol et la présence d'hydrogène dans le milieu réactionnel. On considère les conclusions à tirer au sujet du mécanisme de la formation de la liaison C—C. On peut utiliser le cours du processus non-stationnaire pour la sélection préliminaire des catalyseurs à utiliser pour la synthèse d'hydrocarbure à partir du méthanol.

[Traduit par la rédaction]

Can. J. Chem. Downloaded from www.nrcresearchpress.com by 217.78.4.112 on 09/08/12
For personal use only.

Introduction

The methanol-to-hydrocarbons conversion is one of the most intensively studied catalytic processes because of its scientific interest and practical significance.

An important characteristic of this reaction is its self-acceleration, i.e., autocatalytic course under certain conditions (1–5). Self-acceleration during the conversion of methanol has been observed for different zeolites, i.e., ZSM-5 (1–3); X (5), Y (4), as well as for copper dodecatungstophosphate (6). Self-acceleration takes place in a recirculation system (3) as well as in an open flow reactor (1, 2, 4, 5), and has been indicated by characteristic temperature dependence (3–5), existence of an induction period (3–5), and an increase of activity during the experiments (5, 7). Additional evidence for the autocatalytic character of the conversion is the shortening of the induction period in the presence of certain substances, such as olefins (3, 21, 23) and alcohols (7). The induction period is also affected by the acidity of the catalyst (1, 21, 22), its particle size, methanol pressure, reaction temperature, and the presence of water in the reaction mixture (2).

The mechanism of self-acceleration is not completely known. In the case of zeolite catalysts, the autocatalytic course of the reaction is associated with the formation and generation of reactive intermediates (C_1 particles), which react at a high rate with olefins (or aromatics) (1–3, 7, 8, 21, 24). An alternative possibility is discussed by Baba and Ono (6). They show an increase in the number of acidic centres during the reaction on the copper dodecatungstophosphate catalyst due to the reductive influence of hydrogen molecules (or atoms) produced by the decomposition of methanol. Prinz and Riekert (22) assume that the formation of some reactive hydrocarbons in the zeolite is a necessary intermediate step in the reaction. Espinoza (25, 26) considers that C-containing particles modify the catalyst and because of that the reaction deviates into a faster course.

In the present investigation, self-acceleration is considered as a step in the nonstationary state changes taking place as a result of the interaction between the reaction medium and the catalyst. Also discussed is the extent to which the nonstationary process is indicative of the intrinsic capability of different zeolites to accelerate C—C bond formation from methanol. The effect on the nonstationary process of factors such as the partial pressure of methanol and the presence of hydrogen in the reaction flow is also investigated.

Experimental

Catalysts

H-ZSM-5

The sample was obtained via crystallization in the presence of tetrapropylammonium cations (9); SiO_2/Al_2O_3-89; (98% degree of decationization).

H-offretite (H-off)

The sample was obtained via crystallization in a tetramethylammonium cations medium according to known procedure (10); SiO_2/Al_2O_3-9, 9; (90% degree of decationization).

H-mordenite (H-mord)

The sample was prepared on the basis of synthetic mordenite kindly provided by Leuna, Germany; SiO_2/Al_2O_3-10; (90% degree of decationazation).

H-CaY

This was obtained on the basis of the sodium form of the zeolite kindly provided by Leuna, Germany; the content of each of the cations (H^+ and Ca^{2+}) is 36% equivalents, respectively.

The H-modifications of all samples were prepared via ion exchange with NH_4^+ followed by thermal decomposition of the ammonium at 813 K. The H-CaY sample was prepared via ion exchange in the presence of NH_4^+ and Ca^{2+} ions. The organic cations in the cases of H-ZSM-5 and H-off were removed beforehand by heating in an air flow at 813 K for 6 h. In the catalytic reactor all samples were subjected to additional thermal treatment

[1]Author to whom correspondence may be addressed.

[2]Revision received April 13, 1992.

TABLE 1. Temperature dependence of the selective dehydration of methanol to DME, R_{CH_3OH} = 3.85 kPa

Catalyst	Temperature, K	Yield DME, %
	481	39.8
H-ZSM-5	517	76.0
	539	79.7
	419	18.9
	445	60.5
H-mordenite	458	74.7
	431	61.0
H-offretite	443	77.8
	486	50.2
	493	56.0
H-CaY	501	60.0
	559	70.0

by means of consecutive heating at 703 K for 6 h in air, argon, and hydrogen flow.

Procedure and apparatus

The flow system consists of a glass microreactor, a calibrated saturator, and a gas inlet system (for argon and hydrogen) (11). This instrumental setup permits easy variation of the temperature, flow rate, and partial pressure of the components; it also allows a periodic check of the catalyst activity under standard conditions, as well as monitoring colour changes in the catalyst during the experiments. The reaction mixture is analysed on-line by means of gas chromatography using a 2-m Porapak Q column. The quantitative evaluation was conducted using an absolute calibration with automatic computation of the chromatographic data. A carbon base was used for the product yield calculation.

The experiment includes the following stages: preliminary thermal treatment of the catalyst; adjustment and determination of the methanol partial pressure in a by-pass line; running the reaction mixture through the reactor, followed by chromatographic analysis at 4–7 min intervals. The catalytic experiments were carried out in a temperature range of 400–650 K at a weight hourly space velocity (WHSV) 1.5 h^{-1} and partial pressure of methanol 1.57–3.85 kPa. The catalyst (0.1 g), with a particle size of 0.2–0.8 mm, was diluted threefold with glass of the same particle size.

Results

Start and course of the nonstationary process

The temperature dependence of methanol (MeOH)-to-dimethyl ether (DME) conversion is registered for each sample (Table 1). With all samples examined, a near-equilibrium conversion into DME is reached. The nonstationary process under isothermal conditions (the temperature in the catalyst bed is kept constant within 1°) begins in all cases after the appearance of the first hydrocarbon products in the gas phase. As can be seen in Fig. 1, in the example of H-CaY and H-off zeolites the nonstationary process includes the following steps: (*i*) rapid increase of the hydrocarbon products, mainly C_2—C_4 olefins (only C_2—C_3 hydrocarbons are given in Fig. 1); (*ii*) decrease in the DME and methanol content; (*iii*) subsequent complex changes in the distribution of the products. The nonstationary process reveals in its course specific characteristics for each of the catalysts examined. Lower initial temperature, appearance of CH_4, significantly lower yields of C_2—C_3 hydrocarbons, and a specific change in the DME content are typical for the H-off sample. The H-mordenite catalyst behaves (Fig. 2) in a manner similar to that of the H-CaY and H-off samples. However, the changes take place more rapidly and in 1 h the catalytic activity is totally lost. In comparison with the other samples, the high methane concentration and the continuous decrease of the DME with time on-stream are worth noting. Among the hydrocarbons in the gas phase, the C_1—C_3 ones predominate (over 90%). The temperature at which the nonstationary process starts is higher than that for H-off but lower than for H-CaY.

In Fig. 3 data are presented for the H-ZSM-5 catalyst at three different temperatures. It can be seen that the C_2—C_3 hydrocarbons appear in the gas phase for the first time at 547 K, the ethylene yield being about 50% greater than the propylene yield; thus after 15 min there are 0.1% of C_2^{2-} and 0.06% of C_3^{2-}, while after 40 min there are 0.25% and 0.18%, respectively. The rate of composition change grows when the temperature is increased to 561 K: the C_2^{2-}/C_3^{2-} ratio is already in favour of propylene and small amounts of C_4 are also present. For example, 14 min after the temperature increase the amounts of C_2, C_3, and C_4 hydrocarbons are 2.88, 4.43, and 0.53% respectively, but after 38 min they are 3.87, 6.23, and 0.83%. A very sharp change in the product distribution is observed after further raising the temperature to 593 K.

Influence of the partial pressure (P) of MeOH and the presence of H_2 in the reaction flow

The effect of the partial pressure of MeOH was examined in the case of the H-CaY sample. The decrease of *P* from 3.6 down to 1.2 kPa was achieved by dilution with Ar or H_2 (Fig. 4).

Comparison of the data from Fig. 1 and Fig. 4 shows that the decrease in the methanol partial pressure and the presence of H_2 in the reaction mixture do not affect significantly the basic characteristics of the nonstationary process. A trend towards a smoother running of this process is, however, noticeable. The effect of H_2 is more pronounced in the formation of C_2—C_3 hydrocarbons when their yield decreases with a corresponding increase of C_4^+ hydrocarbons between the 20th and 120th minutes of the experiment (Table 2).

However, no increase of methane in the gas phase is observed. Its concentration remains, as in the case of Ar-dilution, lower than 0.5%.

Deposition of nondesorbable products during the experiment

The material balance during the experiments can be followed with an accuracy of about 5% using absolute calibration of the chromatographic signals. The material balance data indicate that a part of the carbon content of the reactant flow remains deposited on the catalyst, when the self-acceleration of the methanol conversion proceeds under isothermal conditions. The deposit formation, as evaluated from the deficiency of the material balance, decreases in the sequence: H-mord > H-off > H-CaY > H-ZSM-5, and can be determined with sufficient accuracy only in the case of the H-mord catalyst. The loss in the material balance together with the changes in the CH_4 concentration (Ar or H_2 as diluent gas) are shown in Fig. 5. It can be clearly seen that the rate of deposit formation follows the course of the nonstationary process, as presented with the typical changes in the methane content of the gas phase. The inclusion of H_2 in the reaction flow has no significant effect on this phenomenon.

It should also be mentioned that the deposition of nondesorbable products and the nonstationary state process are

Can. J. Chem. Downloaded from www.nrcresearchpress.com by 217.78.4.112 on 09/08/12
For personal use only.

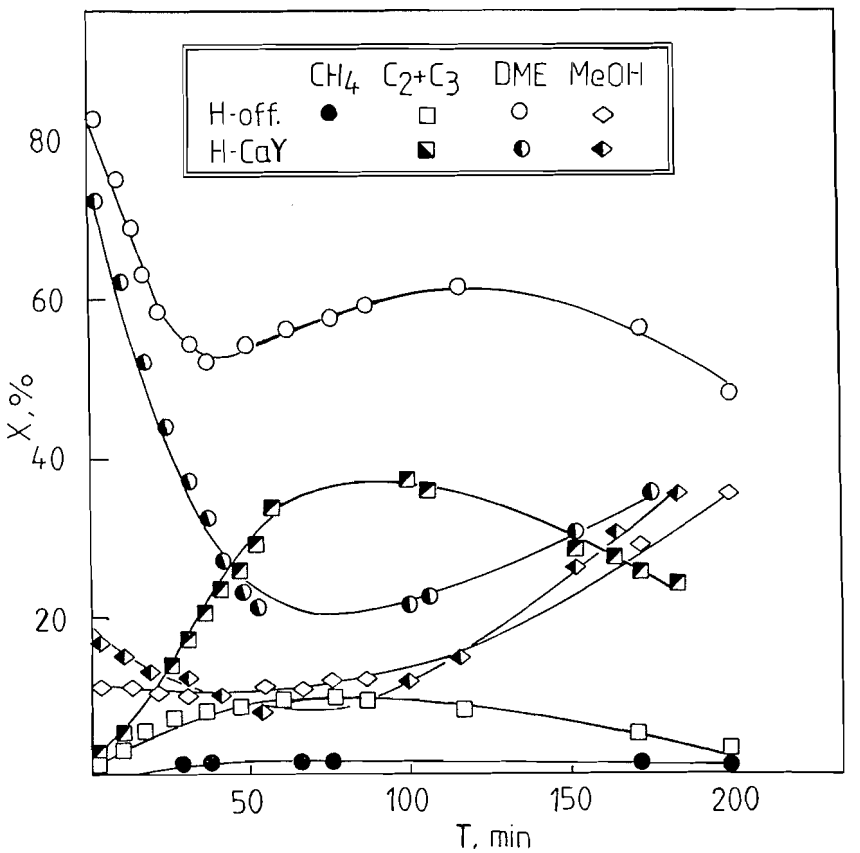

FIG. 1. Change in the distribution of the products (x, mol%) with time on-stream (t, min) in the MeOH conversion over H-off (T = 517 K) and H-CaY (T = 560 K), $P_{CH\,OH}$ = 3.85 kPa.

accompanied, in the case of all zeolites studied, by a series of colour changes of the catalyst, i.e., from light-yellow through dark-yellow to orange, also various shades of brown to dark-brown, dark-gray, and finally black. The rate of the colour changes generally follows the dynamics of the nonstationary process and, accordingly, is highest in the case of H-mord. The process is not so intensive and the colour changes are especially slow in the case of H-ZSM-5 zeolite.

Discussion

Autocatalysis during the methanol-to-hydrocarbons conversion was first observed in the case of ZSM-5 zeolites (1–3). It is found in the present study that this phenomenon may be even more marked in the presence of acidic forms of other structural types of zeolites. Moreover, the self-acceleration (autocatalysis) can be considered as one stage in the complex sequence of interactions between the reaction flow and the catalyst. The following stages of this nonstationary process can be distinguished under isothermal conditions:

A. An increase in the hydrocarbon concentration and simultaneous decrease in the MeOH and DME content (autocatalysis, self-acceleration).

B. A period of stable catalytic activity and selectivity.

C. A deactivation with respect to hydrocarbon formation. At the same time the activity in the dehydration of MeOH to DME resumes (H-off, H-CaY).

D. A continuing deactivation in both hydrocarbon as well as DME formation (H-off, H-mord).

The indicated stages take place to a different degree for the catalysts studied. The whole process in the case of H-mordenite is so fast that step B cannot practically be observed, while in the presence of the H-ZSM-5 sample step A is rather prolonged and hydrocarbons take several hours to form.

We assume that the self-acceleration and the deactivation during the methanol conversion are two sides of one and the same nonstationary process. There are some indications that deposits on the catalyst play an important role in this process: (*ii*) there is parallelism between the rate of deposit formation and the colour changes of the catalyst on the one hand and the changes in the composition of the gas phase with time on the other hand; (*ii*) the nonstationary process can be repeated in all its details after burning of the deposits in the presence of air; (*iii*) the autocatalytic stage can be stopped and even reversed in the presence of H_2 in the case of Pt-containing zeolites (11).

The chosen conditions, i.e., small amounts of catalyst diluted with an inert material, low partial pressure of methanol, and a high flow rate, preclude the influence of macrofactors, such as temperature and concentration gradients, and limit the process to the formation mainly of C_2—C_4 hydrocarbons. The general assumption in this paper is that the self-acceleration of the methanol conversion is closely associated with a buildup of reactive deposits on the zeolite catalyst. Similar, to some proposals in the relevant literature (29), we suggest that the carboneous residues at different stages of their growth may possess proton-donating capability and hence enhanced catalytic activity in the

Can. J. Chem. Downloaded from www.nrcresearchpress.com by 217.78.4.112 on 09/08/12
For personal use only.

Can. J. Chem. Downloaded from www.nrcresearchpress.com by 217.78.4.112 on 09/08/12
For personal use only.

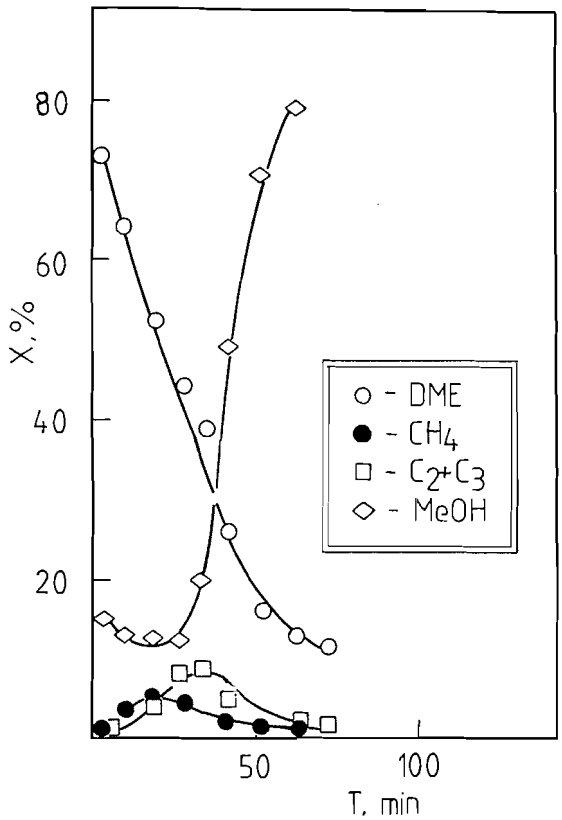

FIG. 2. Product distribution (x, mol%) in the MeOH conversion over H-mor vs. time on-stream (t, min) at 547 K.

methanol conversion. The increase of the catalytic activity with time on-stream is a well-known phenomenon in the case of the conversion of aromatic hydrocarbons on zeolite catalysts (30, 31). The following steps of the nonstationary process, i.e., the deactivation, can be envisaged as a further transformation of the deposits via hydrogen depletion. The observed decrease in the rate of deactivation, i.e., mordenite > offretite > type Y > ZSM-5, fully corresponds to the decrease in the tendency toward coke-formation, which is the same for other acid–base reactions (4).

The course of the nonstationary process in principle contains information regarding the capability of the catalyst to accelerate C—C bond formation from methanol. Ono *et al.* (1), on the basis of the observation that the autocatalytic reaction begins at different temperatures, concluded that the ZSM-5 sample with SiO_2/Al_2O_3-134 is less active than similar zeolites with a lower SiO_2/Al_2O_3 ratio.

In the present study the samples differ in the initial temperature at which, under isothermal conditions, an increase of the hydrocarbons formation starts:

H-offretite	H-mordenite	H-CaY	H-ZSM-5
517	547	559	561/593

Judging from this, it can be assumed that the capability of initiating and conducting the process of C—C bond formation from methanol is most pronounced in the case of the zeolite H-offretite. On the other hand, the behaviour of the ZSM-5 catalytic systems is characterized by a rather moderate rate of the nonstationary process. A much higher temperature, i.e., 593 K, is needed for the completion of the above process. Information regarding the primary products was obtained in the present study. All investigated zeolite catalysts favour ethylene production at the beginning of the self-acceleration, but the C_2/C_3 ratio quickly diminishes to finally become less than unity.

The H-mordenite catalyst only leads to methane preponderance after the initial appearance of C_2 and C_3 for a cer-

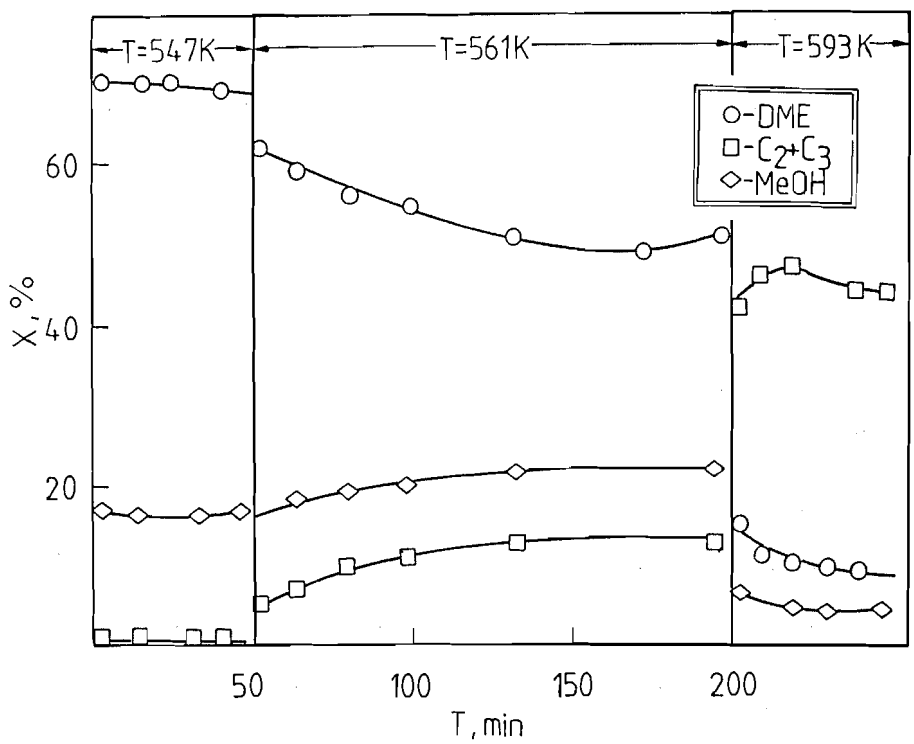

FIG. 3. Product distribution (x, mol%) in the MeOH conversion over H-ZSM-5 vs. time (t, min) at different temperatures.

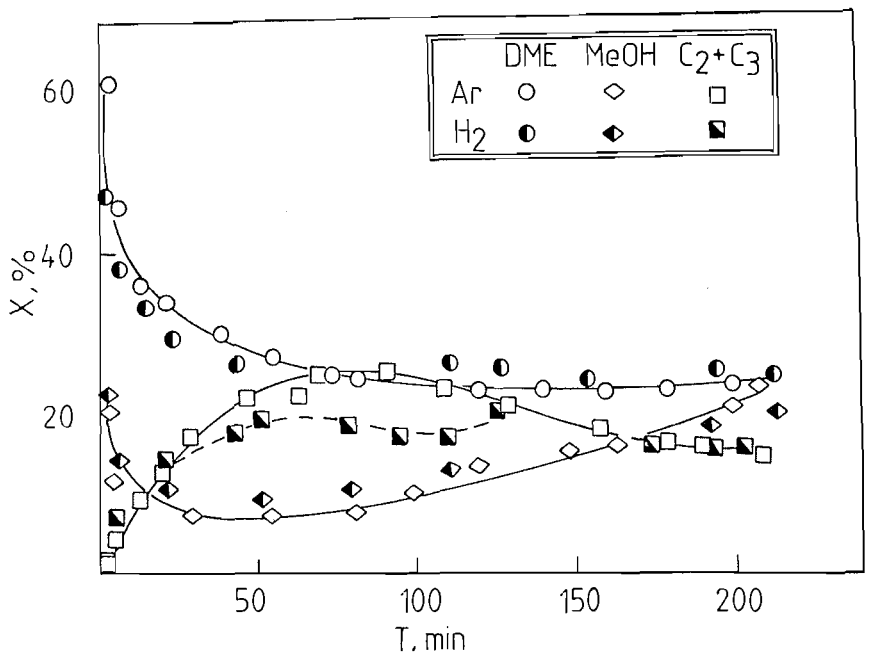

FIG. 4. The effect of presence of hydrogen on the product distribution in the MeOH conversion over H-CaY at 563 K; $P_{CH\,OH}$ = 1.57 kPa.

TABLE 2. Content of C_4 hydrocarbons (mol%) in the reactor effluent (the same experimental conditions as in Fig. 4)

Diluent gas	Time on-stream (min)				
	24	57	85	104	113
Ar	26.5	30.1	29.2	25.7	23.1
H	30.0	32.2	32.4	33.4	33.2

tain time period, after which the C_2—C_3 hydrocarbons begin to predominate. The results obtained from conducting the process under nonstationary conditions support the assumption that evolution of ethylene in the gas phase is favoured in the initial stage of the process. Under the reaction conditions employed in the present study, the partial pressure exerted by hydrogen exceeds that of methanol by about a factor of 20 and can therefore affect significantly the reaction steps proceeding with absorption or evolution of hydrogen. The observation that with the catalysts H-mordenite and H-CaY the reaction course remained essentially unaffected, the basic features of the nonstationary process being retained, indicates that hydrogen is unlikely to participate in the key step, directly or via adsorption–chemical equilibria. The observed changes in the product composition occurring during a part of the activity interval of the H-CaY catalyst can be explained by peculiarities in the secondary conversions undergone by olefins in the presence of hydrogen, as reported recently by Blackmond *et al.* (19) on the basis of IR data. In the literature (12–18) are discussed such key reactions and intermediates as should be significantly affected by the presence of hydrogen in the reaction mixture. Thus, the interaction between carbenes and hydrogen should shift the process towards methane formation, as illustrated in the photolysis reaction of ketene and diazomethane (20), or in the interaction between methylene and sodium vapours in a hydrogen atmosphere (11, 27, 28). The fact that the process

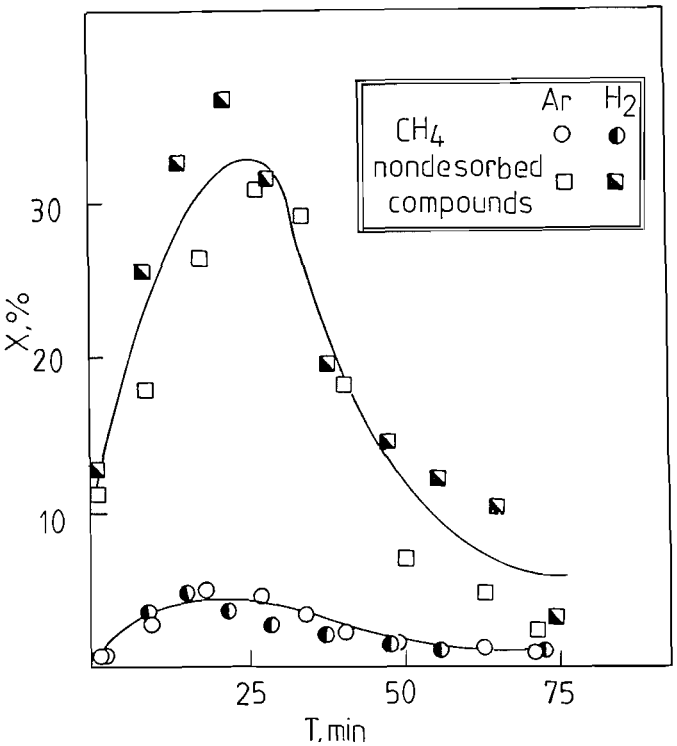

FIG. 5. Conversion of MeOH (x, mol%) to CH_4 and nondesorbable compounds during experiments in Ar or H_2 as diluent gases (T = 547 K).

preserves its nonstationary character in the presence of hydrogen also indicates a lower degree of dehydrogenation and hydrogenation reactions in the mechanistic route of the methanol-to-hydrocarbons reaction.

Conclusion

Self-acceleration in the methanol-to-hydrocarbons conversion is considered as one step of the nonstationary process taking place in the interaction between zeolite catalyst,

Can. J. Chem. Downloaded from www.nrcresearchpress.com by 217.78.4.112 on 09/08/12
For personal use only.

methanol, and DME. This nonstationary process is more pronounced with catalytic systems possessing a higher density of active centers than in the case of high silica zeolites. The course of the nonstationary process over various catalysts reflects the importance of some surface reactions leading to the formation and conversion of coke precursors on the catalyst surface. The investigation of the nonstationary process and the tracing out of the influence of H_2 can be an important source of information about the mechanism of C—C bond formation and the choice of an appropriate catalyst for methanol-to-hydrocarbons conversion.

Acknowledgements

The authors are grateful to Dr. H. Minchev and L. Kozova for the preparation of the catalysts. We acknowledge with appreciation the useful ideas and comments from the colleagues of our group. We also thank the Bulgarian Academy of Sciences for financial support.

1. Y. Ono, E. Imai, and T. Mori. Z. Phys. Chem. (Neue Folge), **115**, 99 (1979).
2. N. Y. Chen and W. J. Reagan. J. Catal. **59**, 123 (1979).
3. Y. Ono and T. Mori. J. Chem. Soc. Faraday Trans. 1, **77**, 2209 (1981).
4. B. E. Langner. Appl. Catal. **2**, 289 (1982).
5. N. Jaeger, A. Jahn, and G. Schulz-Ekloff. React. Kinet. Catal. Lett. **19**, 79 (1982).
6. T. Baba and Y. Ono. Appl. Catal. **8**, 315 (1983).
7. T. Mole. J. Catal. **84**, 423 (1983).
8. C. D. Chang. Chem. Eng. Sci. **35**, 619 (1980).
9. W. Maiwald, W. D. Basler, and H. T. Lechert. Proceedings of the 5th International Conference of Molecular Sieves, Heyden. 1980, pp. 562–570.
10. W. D. Breck. Zeolite molecular sieves, John Wiley & Sons, New York. 1974.
11. V. Kanazirev and T. Tsoncheva. Proceedings of the 5th International Symposium of Heterogeneous Catalysis. Varna. 1983. p. 423.
12. K. G. Ione, G. V. Echevskii, and G. N. Nosyreva. J. Catal. **85**, 287 (1984).
13. C. D. Chang and A. J. Silvestri. J. Catal. **47**, 249 (1977).
14. E. G. Derouane, J. B. Nagy, P. Dejaifve, J. H. C. van Hoof, B. P. Spekmam, J. C. Vedrine, and C. Naccache. J. Catal. **53**, 40 (1978).
15. J. P. van den Berg. The conversion of methanol to gasoline on ZSM-5. Doctoral Dissertation, Eindhoven. 1981.
16. W. W. Kaeding and S. A. Butter. J. Catal. **61**, 155 (1980).
17. B. J. Ahn, J. Armando, G. Perot, and M. Guisnet. C. R. Seances Acad. Sci. Ser. C: **288**, 245 (1979).
18. J. R. Anderson, K. Foger, R. Mole, R. A. Rajadhyaksha, and J. V. Sanders. J. Catal. **58**, 114 (1979).
19. D. G. Blackmond, J. G. Goodwin, Jr., and Y. E. Lester. J. Catal. **78**, 247 (1982).
20. V. Kirmse. Khimia Karbenov (in Russian). MIR Publishing House. 1966.
21. J. G. Robinson, P. W. F. Riemer, and G. Marr. Appl. Catal. **23**, 207 (1986).
22. D. Prinz and L. Riekert. Appl. Catal. **37**, 139 (1988).
23. T. Inui, T. Hagiwars, and Y. Tarumoto. Sekiyu Gakkashi. **28**, 341 (1985).
24. C. T.-W. Chu and C. D. Chang. J. Catal. **86**, 297 (1984).
25. R. L. Espinoza. Appl. Catal. **26**, 203 (1986).
26. R. L. Espinoza. Actas Symp. Iberoam. Catal. 9th, Lisbon. **2**, 1003 (1984).
27. V. Kanazirev and T. Tsoncheva. Neftechimia, **29**, 384 (1989).
28. R. Hunter and G. J. Hutchings. J. Chem. Soc. Chem. Commun. 377 (1987).
29. N. W. Cant and W. K. Hall. J. Catal. **25**, 161 (1972).
30. H. G. Karge, K. Hatada, Y. Zhang, and R. Fiedorou. Zeolites, **3**, 13 (1983).
31. J. Weitkamp, S. Ernst, P. A. Jacobs, and H. G. Karge. Erdoel und Kohle. **30**, 13 (1986).

Can. J. Chem. Downloaded from www.nrcresearchpress.com by 217.78.4.112 on 09/08/12
For personal use only.

Volumes of mixing of ternary alkane mixtures with branched chain components

SHEN WEIGUO
Department of Chemistry, Lanzhou University, Lanzhou, People's Republic of China
AND
ARTHUR G. WILLIAMSON[1]
Department of Chemical and Process Engineering, University of Canterbury, Christchurch, New Zealand

Received September 20, 1991

SHEN WEIGUO and ARTHUR G. WILLIAMSON. Can. J. Chem. **70**, 2003 (1992).

Measurements at 25°C are reported for the volumes of mixing of binary mixtures of *n*-dodecane + 2 methyl pentane and of ternary mixtures created by mixing an equimolar mixture of (*n*-decane + *n*-tetradecane) with each of the isomers of hexane. The results are compared with the work of Hamam *et al.* for binary mixtures of *n*-dodecane with the hexane isomers and shown to be in accord with the principle of congruence within the limits of experimental accuracy of the measurements.

SHEN WEIGUO et ARTHUR G. WILLIAMSON. Can. J. Chem. **70**, 2003 (1992).

Opérant à 25°C, on a effectué des mesures de volumes de mélanges binaries du *n*-dodécane avec le 2-méthylhexane et des mélanges ternaires obtenus par mélange d'une quantité équimoléculaire de (*n*-décane + *n*-tétradécane) avec chacun des isomères de l'hexane. On compare les résultats avec ceux obtenus par Hamam *et al.* pour des mélanges binaires du *n*-dodécane avec les isomères de l'hexane et on montre que, dans les limites de l'exactitude expérimentale des mesures, ces résultats sont en accord avec le principe de congruence.

[Traduit par la rédaction]

Introduction

As a part of the study of the applicability of the principle of congruence to ternary mixtures (1), this work reports the excess volumes of *n*-dodecane + 2-methylpentane and of pseudo *n*-dodecane prepared from equimolar quantities of *n*-decane and *n*-tetradecane + each of the four branched hexane isomers at 298.15 K.

Experimental

Volumes of mixing were deduced from accurate density measurements using a vibrating tube densimeter. As was pointed out by previous authors (2), a major problem with such measurements on mixtures of volatile components is the preparation of mixtures whose compositions are known to an accuracy consistent with that of the density measurements.

In an attempt to eliminate errors due to vaporization of volatile components we examined two methods of preparing mixtures. In the first procedure, the mixture was prepared by weighing the liquids into an evacuated cell shown in Fig. 1(*a*).

The weighing cell, which had two septa, was initially evacuated by inserting a hypodermic needle through one of the septa and drawing air out of the cell with a vacuum pump. The liquids were then injected into the weighed cell in succession and the cell was weighed after each addition. For any chosen composition the amounts of liquids were chosen so as to almost completely fill the cell. When the mixture was withdrawn from the cell through one septum with a hypodermic syringe a hypodermic needle was inserted into other septum and mercury was drawn into the vessel as the liquid was withdrawn. With these procedures buoyancy corrections and vapour corrections were kept to a minimum.

A second procedure used a Precision Safety Corporation "pressure lok" gas-tight glass and Teflon syringe with a built-in slide valve as shown in Fig. 1(*b*). In this case the syringe was weighed, then the liquids were drawn into the syringe in succession and the syringe was weighed after each addition. After mixing in the syringe, the mixture was injected directly into the densimeter. With both of these techniques of preparation of mixtures, the mole fraction is believed to be accurate to about 5×10^{-5}.

Pseudo dodecane was prepared in a stoppered flask by weighing an empty flask, then the flask with *n*-tetradecane, and finally the flask with *n*-decane + *n*-tetradecane.

Density measurements were made using a Mettler DMA 60/DMA 602H vibrating tube densimeter with a precision of $\pm 1.5 \times 10^{-6}$ g cm^{-3}. The stability of temperature in the sample chamber of the densimeter was ±0.003 K. The period of vibration τ for the vibrating capillary tube in the densimeter is related to the density ρ of the fluid in the tube by

$$[1] \quad \rho = a + b\tau$$

where a and b are constants. Degassed distilled water and air were used to calibrate the densimeter to obtain the instrument constants a and b. The density of water was taken from ref. 3 and the density of moist air was calculated by the following equation (3)

$$[2] \quad \rho_a/\text{g cm}^{-3} = 1.2929\,(273.13/T)(B - 0.3783e)/760$$

where B is the barometric pressure (Torr; 1 Torr = 133.3 Pa), T is absolute temperature (K), and e is the vapour pressure of the moisture in the air (Torr); which can be determined by the measurement of dew point (3). In this work the dew point was measured with an EG & G Digital Humidity Analyzer, model 911, with an accuracy of ±0.5 K.

To reduce the errors caused by the drift of the densimeter and the density change of the pseudo alkanes due to vaporization of volatile component, the densimeter was recalibrated and the densities of the "pure" components were measured again after each two or three measurements of the densities of mixtures.

To test the methods, measurements were made on the system benzene and cyclohexane at 298.15 K. The results for the system are believed to be reproducible to ±0.002 cm^3 mol^{-1}.

Materials

Benzene and cyclohexane were analytical reagents from M & B, and BDH, respectively, with quoted purities better than 99.8 and 99.5%. Branched hexanes were from Aldrich with quoted purities better than 98% for 2,2-dimethylpentane, 97% for 2,3-dimethylbutane, 99% for 2-methylpentane and 3-methylpentane, and *n*-al-

[1]Author to whom correspondence may be addressed.

Can. J. Chem. Downloaded from www.nrcresearchpress.com by 217.78.4.112 on 09/08/12
For personal use only.

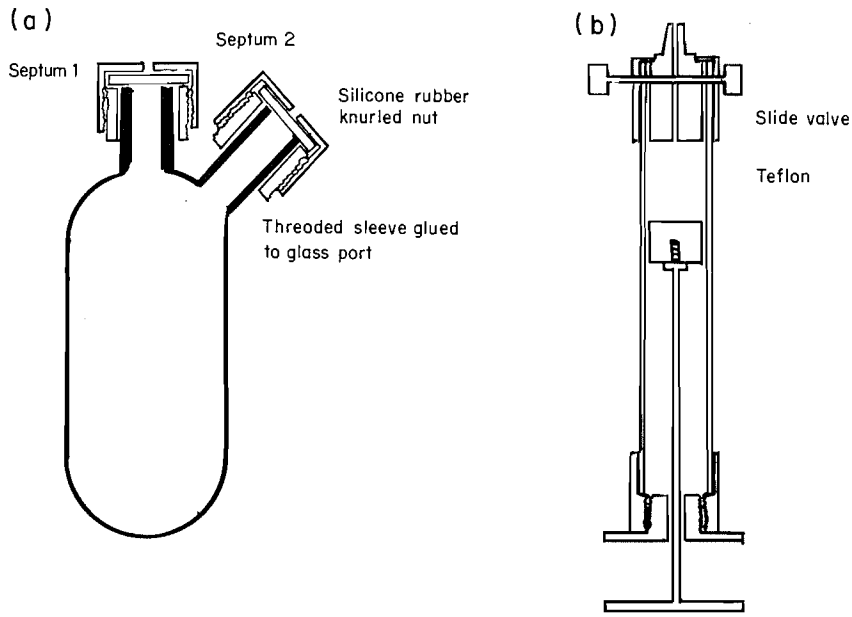

FIG. 1. Diagram of (*a*) weighing cell; (*b*) gas-tight glass and Teflon syringe.

TABLE 1. Densities/g cm^{-3} of chemicals used in this work at 298.15 K

	Source of data					
Compound	This work	Ref. 5	Ref. 6	Ref. 7	Ref. 8	Ref. 9
Benzene	0.873369				0.87370	
Cyclohexane	0.773645				0.77389	
Decane	0.726004	0.72622	0.72609	0.72588	0.72625	0.72635
Dodecane	0.745097			0.74519	0.74516	0.74518
Tetradecane	0.759052			0.75906		0.75920
2-MP	0.648526 0.648613[a]				0.64852	
3-MP	0.659602				0.65976	
2,3-DMB	0.656768				0.65702	
2,2-DMB	0.644314				0.64446	

[a]The density of 2-MP used in measurement of V^E of *n*-dodecane + 2-MP. Both samples came from the same company.

TABLE 2. Experimental densities and excess volumes for cyclohexane (1)

$x(1)$	ρ (g/cm^3)	V^E (cm^3/mol)	R (cm^3/mol)	$x(1)$	ρ (g/cm^3)	V^E (cm^3/mol)	R (cm^3/mol)
			Mixing cell				
0	0.873367			0.54438	0.809031	0.6505	−0.0014
0.14758	0.853101	0.3188	0.0004	0.59061	0.804792	0.6359	−0.0001
0.23363	0.842319	0.4575	−0.0009	0.70218	0.795160	0.5549	0.0018
0.30795	0.833698	0.5449	0.0015	0.78747	0.788438	0.4495	0.0005
0.39868	0.823620	0.6200	−0.0009	0.90021	0.780178	0.2469	−0.0018
0.45077	0.818224	0.6419	0.0003	1	0.773645		
			Syringe				
0	0.873368			0.48489	0.814760	0.6536	−0.0010
0.10945	0.858089	0.2486	−0.0008	0.63489	0.800849	0.6119	0.0007
0.16324	0.851055	0.3477	0.0013	0.73431	0.792500	0.5213	−0.0005
0.22158	0.843759	0.4426	0.0002	0.80318	0.787175	0.4259	−0.0003
0.31269	0.830991	0.5574	−0.0020	0.90936	0.779557	0.2250	0.0005
0.40719	0.822701	0.6256	0.0020	1	0.773645		

Can. J. Chem. Downloaded from www.nrcresearchpress.com by 217.78.4.112 on 09/08/12
For personal use only.

TABLE 3. Values of parameters in eq. [4] for cyclohexane + benzene (298.15 K)

N	A1	A2	A3	A4	R	Source
10	2.6099	−0.0958	0.0444	−0.0136	0.0004[a]	Ref. 2
29	2.61313	−0.10497			0.0017	Ref. 10
10	2.6059	−0.1236	0.0367		0.0013	Mixing cell
10	2.6156	−0.0891	0.0315	−0.0484	0.0014	Syringe

[a]Average deviation.

kanes were "puriss" grade from Koch-Light, with quoted purities of 99% minimum.

Their measured densities are compared with literature values in Table 1.

Results and discussion

Excess volumes were calculated from the densities of the two "pure" components and their mixtures in the whole range of mole fractions by the equation

$$[3] \quad V^E = x_1M_1\,(1/\rho - 1/\rho_1) + x_2M_2\,(1/\rho - 1/\rho_2)$$

where ρ, ρ_1, ρ_2 are the densities of mixture, component 1, and component 2, respectively, and x_1 is the mole fraction of component 1.

An equation of the type

$$[4] \quad V^E/\text{cm}^3\,\text{mol}^{-1} = x_i(1 - x_i)\,\Sigma\,A_j(1 - 2x_i)^{j-1}$$

was fitted to each set of results by the method of least squares with all points weighted equally.

The densities of mixtures of cyclohexane + benzene prepared by the mixing cell and syringe methods were measured separately and the excess volumes were determined from the measured densities of the pure components and their mixtures by eq. [3]. The results are listed in Table 2. The excess volumes were fitted to eq. [4] for which the parameters and the standard deviations (R) are listed and compared with the literature values in Table 3 in which N is the number of measurements in each set. The differences between the results of our work and those of other workers and between our two methods of preparation of mixtures were less than 4×10^{-3} cm^3 mol^{-1}. The deviations of the fitting eq. [4] are compared with literature data in Fig. 2.

The densities and the excess volumes of *n*-dodecane + 2-methylpentane (2-MP) determined by using the syringe method are listed in Table 4. The parameters in eq. [4] and the standard deviation (R) are listed and compared with those obtained by Hamam *et al.* (4) in rows 1 and 2 of Table 5. The two sets of measurements agreed within 5×10^{-3} cm^3

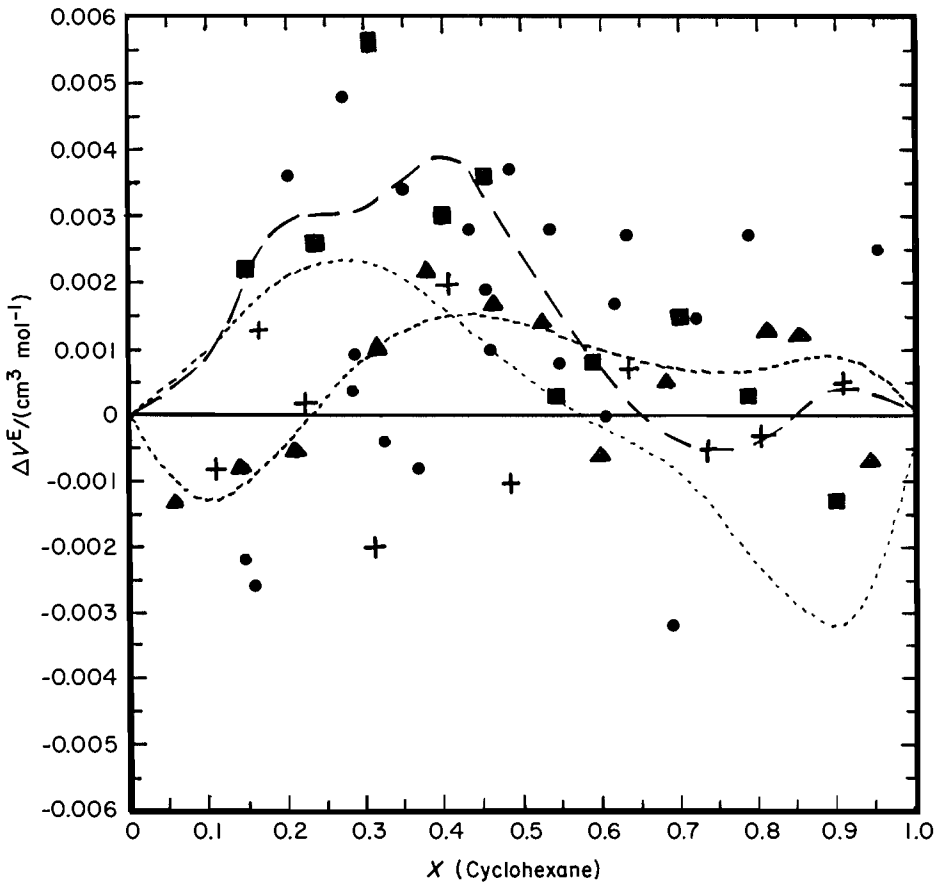

FIG. 2. Deviations of excess volumes for cyclohexane + benzene at 298.15 K. Curves: calculated with eq. [4] are (1) V^E (syringe method) − V^E (mixing cell); (2) V^E (syringe method) − V^E (Kiyohara *et al.*); (3) V^E (syringe method) − V^E (Goates *et al.*). +, V^E calculated with eq. [4] (syringe method) − V^E (exp) (syringe); ■, V^E calculated with eq. [4] (syringe method) − V^E (exp) (mixing cell); ●, V^E calculated with eq. [4] (syringe method) − V^E (exp) (Kiyohara *et al.*); ▲, V^E calculated with eq. [4] (syringe method) − V^E (exp) (Goates *et al.*).

Can. J. Chem. Downloaded from www.nrcresearchpress.com by 217.78.4.112 on 09/08/12
For personal use only.

TABLE 4. Experimental densities and excess volumes for *n*-dodecane + hexane isomers at 298.15 K

$x_{(1)}$	ρ (g/cm^3)	V^E (cm^3/mol)	R (cm^3/mol)	$x_{(1)}$	ρ (g/cm^3)	V^E (cm^3/mol)	R (cm^3/mol)
			n-dodecane$_{(1)}$ + 2-MP$_{(2)}$				
0	0.648613			0.63046	0.722080	−0.3934	0.0015
0.11102	0.666910	−0.2610	0.0001	0.70458	0.727378	−0.3306	−0.0012
0.25050	0.685786	−0.4409	−0.0003	0.82028	0.734964	−0.2193	0.0012
0.34763	0.696826	−0.4882	0.0003	0.86913	0.737880	−0.1626	−0.0008
0.49401	0.710964	−0.4712	0.0006	1	0.745097		
0.55943	0.716462	−0.4373	−0.0014				
			(0.500 *n*-Decane + 0.500 *n*-tetradecane)$_{(1)}$ + 2-MP$_{(2)}$				
0	0.648526			0.55575	0.716149	−0.4425	0.0020
0.10447	0.665845	−0.2534	−0.0003	0.62089	0.721277	−0.3983	−0.0015
0.19053	0.678074	−0.3834	−0.0012	0.71076	0.727788	−0.3267	−0.0009
0.29181	0.690559	−0.4615	−0.0018	0.75091	0.730507	−0.2914	0.0013
0.40122	0.702228	−0.4844	0.0013	0.89030	0.739088	−0.1381	−0.0002
0.51252	0.712502	−0.4601	−0.0011	1	0.745072		
			(0.500 *n*-Decane + 0.500 *n*-tetradecane)$_{(1)}$ + 3-MP$_{(2)}$				
0	0.659602			0.59701	0.722436	−0.3002	0.0003
0.09883	0.674212	−0.1763	−0.0013	0.69308	0.728733	−0.2486	0.0012
0.20678	0.687704	−0.2914	0.0018	0.80843	0.735465	−0.1642	−0.0015
0.29558	0.697254	−0.3351	−0.0003	0.91040	0.748070	−0.0813	0.0007
0.42063	0.708869	−0.3489	−0.0007	1	0.745085		
0.49307	0.714790	−0.3371	−0.0004				
			(0.500 *n*-Decane + 0.500 *n*-tetradecane)$_{(1)}$ + 2,3-DMB$_{(2)}$				
0	0.656768			0.57750	0.720397	−0.3733	−0.0043
0.09996	0.672129	−0.2171	0.0010	0.68273	0.727622	−0.3096	0.0005
0.19630	0.684679	−0.3388	−0.0013	0.70236	0.728872	−0.2938	0.0002
0.29587	0.695866	−0.4067	0.0002	0.78190	0.733681	−0.2242	0.0009
0.41934	0.707727	−0.4260	−0.0002	0.89197	0.739712	−0.1114	−0.0006
0.49767	0.714327	−0.4129	0.0018	1	0.745073		
0.52294	0.716320	−0.4043	0.0019				
			(0.500 *n*-Decane + 0.500 *n*-tetradecane)$_{(1)}$ + 2,2-DMB$_{(2)}$				
0	0.644314			0.56867	0.716279	−0.5689	0.0012
0.10041	0.661931	−0.3189	0.0004	0.69146	0.725845	−0.4478	−0.0011
0.19842	0.676518	−0.5071	−0.0016	0.74679	0.729766	−0.3828	0.0015
0.28459	0.687670	−0.6020	0.0018	0.84940	0.736427	−0.2382	0.0001
0.42029	0.702654	−0.6372	0.0005	0.91892	0.740578	−0.1302	0.0008
0.50004	0.710276	−0.6091	−0.0022	1	0.745071		

TABLE 5. Values of parameters in eq. [4] for *n*-dodecane + hexane isomers at 298.15 K

Systems[a]	$-A1$	$-A2$	$-A3$	$-A4$	$A5$	$A6$
1*	1.8745	0.7534	0.2752	0.0666		0.0010
2	1.8728	0.8217	0.3391	−0.0672	0.1410	0.0014
3	1.8647	0.7574	0.3144	0.1031		0.0017
4*	1.3476	0.5567	0.2407	0.0964		0.0008
5	1.3428	0.5375	0.2363	0.1321		0.0014
6*	1.6282	0.6940	0.2891	0.0776		0.0012
7	1.6417	0.6338	0.2099	0.2314		0.0021
8*	2.4410	0.9983	0.4252	0.1646		0.0007
9	2.4454	0.9972	0.3310	0.1427		0.0017

[a]Systems: 1,2: *n*-dodecane + 2-MP; 3: pseudo *n*-dodecane + 2-MP; 4: *n*-dodecane + 3-MP; 5: pseudo *n*-dodecane + 3-MP; 6: *n*-dodecane + 2,3-DMB; 7: pseudo *n*-dodecane + 2,3-DMB; 8: *n*-dodecane + 2,2-DMB; 9: pseudo *n*-dodecane + 2,2-DMB; *: from Hamam *et al.* (4).

Can. J. Chem. Downloaded from www.nrcresearchpress.com by 217.78.4.112 on 09/08/12
For personal use only.

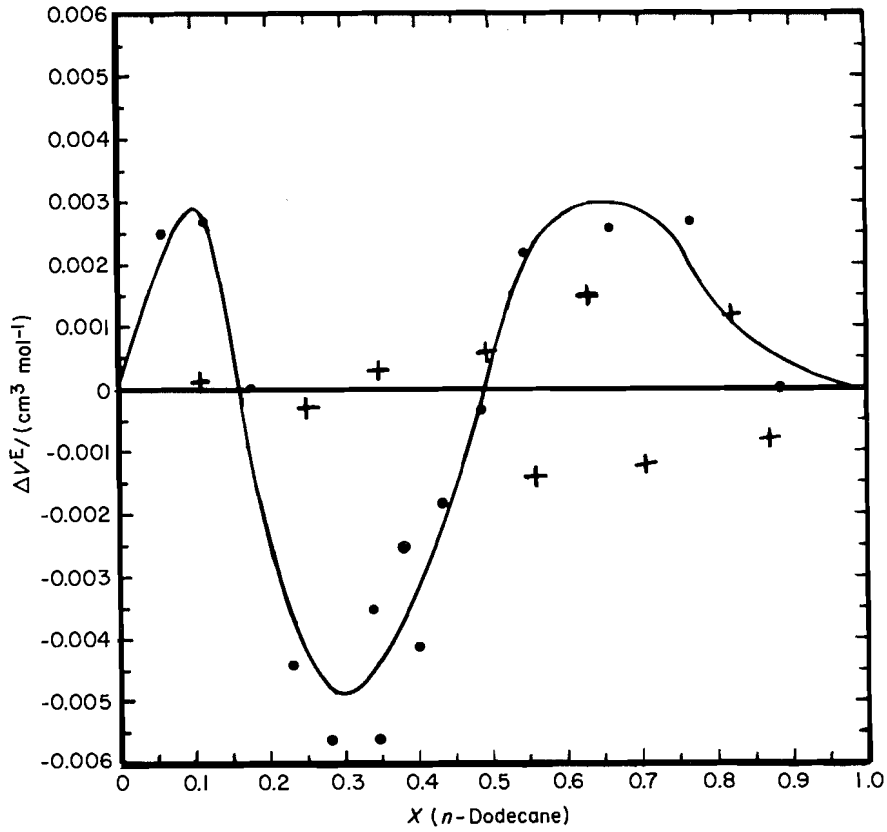

FIG 3. Deviations of excess volumes for *n*-dodecane + 2-MP at 298.15 K. Curve V^E calculated with eq. [4] (syringe method) − V^E calculated with eq. [4] (Hamam *et al.*). +, V^E calculated with eq. [4] (syringe method) − V^E (exp) (syringe); ●, V^E calculated with eq. [4] (syringe method) − V^E (exp) (Hamam *et al.*).

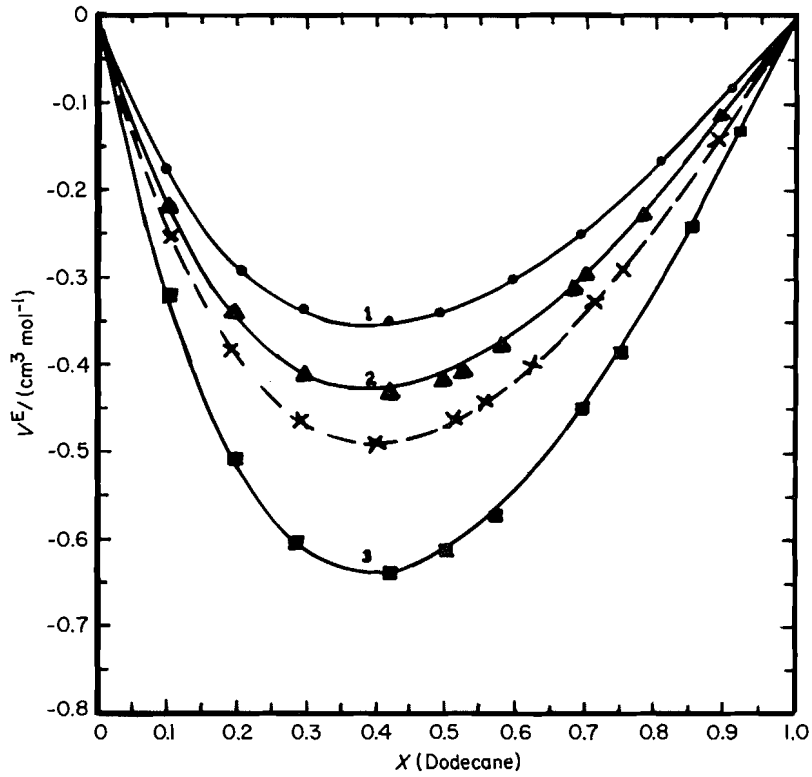

FIG. 4. Excess volumes for *n*-dodecane and hexane isomers. Dotted curve: eq. [4] with parameters from Table 5, system 2, for *n*-dodecane + 2-MP; solid curve: eq. [4] with parameters from Table 5, for (1) *n*-dodecane + 3-MP (system 4), (2) *n*-dodecane + 2,3-DMB (system 6), (3) *n*-dodecane + 2,2-DMB (system 8). Experimental results: ×, pseudo *n*-dodecane (10:14) + 2-MP; ●, pseudo *n*-dodecane (10:14) + 3-MP; ▲, pseudo *n*-dodecane (10:14) + 2,3-DMB; ■, pseudo *n*-dodecane (10:14) + 2,2-DMB.

Can. J. Chem. Downloaded from www.nrcresearchpress.com by 217.78.4.112 on 09/08/12
For personal use only.

mol^{-1}. The deviations from eq. [4] are compared with those of Hamam *et al.* in Fig. 3.

The measured densities and excess volumes of pseudo *n*-dodecanes + 2-MP are also listed in Table 4 and the parameters in eq. [4] and standard deviations are listed in Table 5. The magnitude of the excess volumes of pseudo *n*-dodecane + isomers of hexane decreases in order: 2,2-DMB > 2-MP > 2,3 DMB > 3-MP, just as Hamam *et al.* observed from their measurements for *n*-dodecane + hexane isomers.

We believe that the agreement of our results and those of Hamam *et al.* justifies direct comparison of our measurement for ternary mixtures with the corresponding binary data of Hamam *et al.* within 5×10^{-3} cm^3 mol^{-1}. These comparisons are shown in Fig. 4. The curves are from values calculated by eq. [4] with the parameters from this work for *n*-dodecane + 2-MP (dotted curve), and from Hamam *et al.* for *n*-dodecane + the other three hexane isomers (solid curve). The points are the experimental volumes for the ternary mixtures. The difference of less than 1% seems to be random in the range of experimental errors. This excellent agreement between binary and ternary mixture behaviour is consistent with the principle of congruence in its broader sense (11).

Acknowledgement

This work was supported by the grants from Lanzhou University, People's Republic of China, and The New Zealand University Grants Committee.

1. W. G. Shen and A. G. Williamson. Can. J. Chem. **66**, 904 (1988).
2. J. R. Goates, J. B. Ott, and R. B. Grigg. J. Chem. Thermodyn. **11**, 497 (1979).
3. R. C. Weast (*Editor*), Handbook of chemistry and physics. 56th ed. CRC Press, Boca Raton, Fla. 1975.
4. S. E. M. Hamam *et al.* J. Chem. Thermodyn. **16**, 537 (1984).
5. R. S. Hutchings and W. A. Van Hook. Fluid Phase Equilib. **21**, 165 (1985).
6. J. R. Goates *et al.* J. Chem. Thermodyn. **13**, 907 (1981).
7. A. M. Awwad and E. I. Allos. Fluid Phase Equilib. **22**, 353 (1985).
8. J. A. Riddick and W. B. Bunger. Techniques of Chemistry. Vol. 2. Organic Solvents. Wiley–Interscience, New York. 1970.
9. TRC thermodynamic tables. Thermodynamics Research Centre, Texas A & M University, College Station, Tex.
10. O. Kiyohara and G. C. Benson. Can. J. Chem. **51**, 2489 (1973).
11. S. P. Koh and A. G. Williamson. Chem. Eng. J. **19**, 85 (1980).

Can. J. Chem. Downloaded from www.nrcresearchpress.com by 217.78.4.112 on 09/08/12
For personal use only.

Structure–reactivity correlations of substituted 2-phenylthiazolidines

R. UMARANI[1]
Chemistry Department, Anna University, Madras, India

AND

G. RADHAKRISHNAN
Central Leather Research Institute, Madras, India

Received October 15, 1991

R. UMARANI and G. RADHAKRISHNAN. Can. J. Chem. **70**, 2009 (1992).

Systematic investigations of the kinetics of the reactions of ethyl bromoacetate (EBA) and of picryl bromide (PB) with 2-phenylthiazolidines (PT) in 100% ethanol were undertaken at 30, 35, 40, and 45°C. The most incisive information concerning the Hammett equation comes from the extensive studies on the substituted 2-phenylthiazolidines, establishing linear Hammett plots with negative ρ values. The kinetic data, plotted in a Brønsted fashion against pK_a of the corresponding thiazolidinium ions, yield linear relationships. The activation parameters were computed. The linear relationships between $\Delta H^{\neq}$ and $\Delta S^{\neq}$ signify a consistent mechanism throughout the series.

R. UMARANI et G. RADHAKRISHNAN. Can. J. Chem. **70**, 2009 (1992).

Opérant à 30, 35, 40 et 45°C, dans des solutions d'éthanol à 100%, on a entrepris une étude systématique de la cinétique des réactions du bromoacétate d'éthyle (BAE) et du bromure de picryle (BP) avec les 2-phénylthiazolidines (PT). L'information la plus pertinente concernant l'équation de Hammett provient d'études extensives sur les 2-phénylthiazolidines substituées qui permettent d'établir des courbes de Hammett linéaires comportant des valeurs de ρ négatives. Le graphique des données cinétiques, établi de la manière de Brønsted en fonction des pK_a des ions thiazolidinium correspondants, conduit à des relations linéaires. Les relations linéaires entre $\Delta H^{\neq}$ et $\Delta S^{\neq}$ signifient que le mécanisme est le même dans toute la série.

[Traduit par la rédaction]

Introduction

Studies of thiazolidines are of great interest because of the presence of the thiazolidine moiety in the important antibiotic, penicillin. 2-Phenylthiazolidine (PT) is a potential radioprotectant. (1) Antiradiation activity has been reported for a variety of thiazolidines, which could provide a means of latentiating a typical radioprotective thiol (NCS linkage) (2).

The transmission of electronic effects from the substituents to the thiazolidine heterocycle in substituted 2-phenylthiazolidines has been analyzed by ^{1}H NMR(3) and ^{13}C NMR. (4) Electron-withdrawing groups substituted at the nitrogen stabilize the thiazolidine ring. Because of their stability and their biological importance, (5) studies of *N*-substituted thiazolidines have assumed particular significance. Synthetic aspects of the acylation of the thiazolidines by benzoyl chloride, (6) acetic anhydride, (7) *N*-glycylation, (8) etc. have been studied so far. Detailed work on the kinetics of acidic and alkaline hydrolysis of *N*-butyl, *N*-phenyl, and *N*-acyl 2-phenyl-1, 3-thiazolidine derivatives has been presented by T. H. Fife *et al.* (9) and the alkaline hydrolysis of *N*-methyl compounds and its mechanistic aspects were studied by Luhowy and Meneghini (10). Recently the thiazolidine ring opening in penicillin derivatives was studied by A. M. Davis *et al.* (11) In the literature considerable interest has been focused on S_NAr reactions with amine nucleophiles, (12) and the most suitable mechanism has been the one that passes through Meisenheimer-type intermediates. Aminolysis of α-haloketones and α-halogeno esters with amines was studied by Pearson *et al.* (13*b*) and Mohanty *et al.* (13*a*) Because of the higher reactivity of α-halogeno esters towards nucleophiles, ethyl bromoacetate (EBA) was chosen for the reaction with 2-phenylthiazolidines. To compare the mechanistic aspects with the S_NAr reaction, the kinetics of PT with picryl bromide (PB) were also investigated. The detailed kinetic analysis of these reactions provides insight into the modified reactivities and activities of substituted thiazolidine rings.

Experimental

2-Phenylthiazolidine and its *meta*- and *para*-substituted compounds (**1***a*–**10***a*) were prepared by Tsukermann's general procedure, which is reported elsewhere. (3) Crystalline picryl bromide was synthesized and had a melting point of 120°C. (13) Ethyl bromoacetate (Fluka) was used after distillation. Studies of the kinetics of the reaction of ethyl bromoacetate with 2-phenylthiazolidines were carried out in 100% ethanol at 30, 35, 40, and 45°C. The experiments were done under second-order rate conditions, [PT] = 0.04 M; [EBA] = 0.01 M; and the rate of the reaction was monitored by Volhard's method. The rate constants were calculated using the second-order rate equation (eq. [1]) where a is the concentration of thiazolidine (PT), b is the concentration of ethyl bromoacetate (EBA), and x is the concentration of EBA reacted in time t.

$$[1] \quad k_2 = \frac{2.303}{t(a-b)} \log \frac{b(a-2x)}{a(b-x)}$$

The stoichiometry of the reaction was determined for the reaction of 2-phenylthiazolidine with ethyl bromoacetate by taking a known excess of EBA relative to the PT. Upon completion of the reaction the amount of EBA consumed was estimated by Volhard's method and the stoichiometry was found to be in the ratio 2:1 for PT:EBA. For product analysis the substrate and EBA were taken in the same proportion as used in the kinetic measurements, and were kept at 40°C in 100% ethanol for several days. The material obtained after work-up was purified by column chromatography on silica gel (1:1 petroleum ether – ethyl acetate). The low-melting products were characterized by elemental analysis and identified

[1]Author to whom correspondence may be addressed. Present address: Chemistry Department, Queen's University, Kingston, Ont. Canada K7L 3N6.

Can. J. Chem. Downloaded from www.nrcresearchpress.com by 109.225.110.28 on 09/08/12
For personal use only.

Can. J. Chem. Downloaded from www.nrcresearchpress.com by 109.225.110.28 on 09/08/12
For personal use only.

as *N*-carbethoxymethylene-2-phenylthiazolidines (**1***b*–**10***b*). The details of their elemental analysis and spectral data are given below.

N-Carbethoxymethylene-2-phenylthiazolidine, ***1****b:* ^{1}H NMR ($CD-Cl_3$) δ: 1.1–1.3 (t, 3H, $NCH_2COOCH_2CH_3$), 2.7–3.1 (m, 4H, NCH_2CH_2S), 3.52 (s, 2H, NCH_2COO-), 3.9–4.2 (q, 2H, $COOCH_2CH_3$), 5.3 (s, 1H, SCHNPh), 7.2–7.4 (m, 5H, Ph). Anal. calcd.:C 62.12, H 6.82; found: C 62.6, H 6.7%.

N-Carbethoxymethylene-2(4′-methoxyphenyl)thiazolidine, ***2****b:* ^{1}H NMR ($CDCl_3$) δ: 1.1–1.3 (t, 3H), 2.2–3.2 (m, 4H), 3.5 (s, 2H), 3.8 (s, 3H), 4.0–4.3 (q, 2H), 5.4 (s, 1H), 7.2–7.7 (m, 4H). Anal. Calcd.: C 57.75, H 6.81; found: C 59.7, H 6.8%.

N-Carbethoxymethylene-2(4′-methylphenyl)thiazolidine, ***3****b:* ^{1}H NMR ($CDCl_3$) δ: 1.2–1.3 (t, 3H), 2.4 (s, 3), 2.6–3.3 (m, 4H), 3.32 (s.2H), 3.8 (s, 3H), 4.0–4.3 (q, 2H), 5.5 (s, 1H), 7.1–7.4 (m, 4H). Anal. calcd.: C 63.36, H 7.2; found: C 63.28, H 7.25%.

N-Carbethoxymethylene-2(4′-chlorophenyl)thiazolidine, ***7****b:* ^{1}H NMR ($CDCl_3$) δ: 1.2–1.4 (t, 3H), 2.2–3.4 (m, 4H), 3.3 (s, 2H), 4.1–4.4 (q, 2H), 5.4 (s, 1H), 7.2–7.7 (m, 4H). Anal. calcd.: C 54.63, H 5.64; found: C 54, 69, H 5.58%.

N-Carbethoxymethylene-2(4′-nitrophenyl)thiazolidine, ***10****b:* ^{1}H NMR ($CDCl_3$) δ: 1.2–1.4 (t, 3H); 3.2–3.5 (m, 4H); 2.42 (s, 2H); 4.1–4.4 (q, 2H); 5.5 (s, 1H); 7.1–8.5 (m, 4H). Anal. calcd.: C 52.58, H 5.44; found: C 52.58, H 5.49%.

The missing frequency at 3215 cm^{-1} in the IR spectra of these compounds shows that the substitution has taken place at the nitrogen atom. Due to the solubility problem in preparing a 0.04 M solution of 2(4′-nitrophenyl)thiazolidine in ethanol at 30 and 35°C, the kinetics measurements were not carried out for this compound at these temperatures and the activation parameters are not calculated for the reaction with 2(4′-nitrophenyl)thiazolidine.

The kinetics of the reaction of 2-phenylthiazolidines with picryl bromide was studied spectrophotometrically. A double-beam 810 UV/VIS Kontron spectrometer was used with 1 cm quartz cells. In all cases pseudo-first-order kinetics ([PT] = 5×10^{-3} M; [PB] = 0.8×10^{-4} M) were observed. The kinetics was followed by monitoring the increase in absorption at 400 nm corresponding to the products formed. The rate constants k_{obs} were calculated using eq. [2]:

$$[2] \quad k_{obs}\, t = \ln E_\infty - \ln(E_\infty - E_t)$$

where E_∞ is the optical density at infinite time, which was taken after at least 10 half-lives. E_t is the absorption at time t. The stoichiometry was determined by studying the reaction of 2-phenylthiazolidine with excess picryl bromide relative to 2-phenylthiazolidine at 45°C. After the completion of the reaction, the consumed picryl bromide was estimated by Volhard's method and it was found that 2 moles of PT reacted with 1 mole of PB, establishing a 2:1 stoichiometry. For the product analysis the substrate and picryl bromide were taken in the same proportion as that used in the kinetic measurements and allowed to react at 45°C for several days. After completion of the reaction, the product was purified by column chromatography on silica gel (petroleum ether – benzene (3:1)) as eluent. The products were identified as *N*-(2′,4′,6′-trinitrophenyl)-2-phenylthiazolidines (**1***c*–**10***c*) and their elemental analyses and ^{1}H NMR spectral values are as follows.

N-(2′,4′,6′-Trinitrophenyl-2-phenylthiazolidine, ***1****c:* ^{1}H NMR ($CDCl_3$) δ: 3.3–34.4 (m, 4H, NCH_2CH_2S), 3.9–4.2, 5.7 (s, 1H, SCHNPh), 7.0–7.4 (m, 5H, Ph), 3.7 (s, 2H, picryl). Anal. calcd.: C 47.87, H 3.19; found: C 47.58, H 3.23%.

N-(2′,4′,6′-Trinitrophenyl)-2(4′-methoxyphenyl)thiazolidine, ***2****c:* ^{1}H NMR ($CDCl_3$) δ: 3.1–3.7 (m, 4H), 3.93 (s, 2H), 5.7 (s, 1H), 7.0–7.8 (m, 4H), 9.1 (s, 2H). Anal. calcd.: C 47.28, H 3.47; found: C 47.2, H 3.51%.

N-(2′,4′,6′-Trinitrophenyl)-2(4′-methylphenyl)thiazolidine, ***3****c:* ^{1}H NMR ($CDCl_3$) δ: 2.4 (s, 3), 3.3–4.3 (m, 4H), 5.75 (s, 1H), 7.1–7.4 (m, 4H), 8.75 (s, 2H). Anal. calcd.: C 49.22, H 3.61; found: C 49.02, H 3.62%.

N-(2′,4′,6′-Trinitrophenyl)-2(4′-chlorophenyl)thiazolidine, ***7****c:* ^{1}H NMR ($CDCl_3$) δ: 2.3–2.4 and 3.2–3.4 (m, 4H), 5.7 (s, 1H), 7.2–7.7 (m, 4H), 3.65 (s, 2H). Anal. calcd.: C 43.75, H 2.86; found: C 43.6, H 2.7%.

N-(2′,4′,6′-Trinitrophenyl)-2(4′-nitrophenyl)thiazolidine, ***10****c:* ^{1}H NMR ($CDCl_3$) δ: 2.4–3.6 (m, 4H), 5.8 (s, 1H), 7.3–8.2 (m, 4H), 9.1 (s, 2H). Anal. calcd.: C 42.75, H 2.61; found: C 42.6, H 2.3%.

The UV spectra of these compounds in ethanol show λ_{max} at 260, 330, and 400 nm.

The energies of activation were calculated from the linear regression of ln k_2 versus $1/T$ by the least-squares method, and the entropies of activation $\Delta S^{\neq}$ and collision frequency factor (log PZ) were calculated by the standard formula derived from the absolute theory of reaction rates.

The dissociation constants (pK_a) of the conjugate acids of the substituted 2-phenylthiazolidines were determined by a potentiometric titration method. The pH meter was periodically calibrated by using a buffer solution of 0.05 M potassium hydrogen phthalate of pH 4.00 and a solution of 0.02 M KH_2PO_4 and 0.025 M Na_2HPO_4 with pH = 6.8. 2-Phenylthiazolidine was dissolved in HCl of known concentration and the ionic strength of the solution was maintained at 0.1 M using KCl. The temperature was held constant at 27°C. The acid dissociation constants were determined by titrating the acid in the absence and in the presence of a known concentration of the 2-phenylthiazolidines with a standard KOH titrant. The pK_a values of the conjugate acid were read from the half-neutralization point and were accurate to within ±0.02 units. The values for the different thiazolidines are shown in Table 1.

TABLE 1. The pK_a values of 2-phenylthiazolidinium ions at 27°C in water

Compound no.	Substituent X	pK_a
1	H	5.20
2	4′-OH	5.50
3	4′-OMe	5.45
4	4′-Me	5.35
5	3′-Me	5.26
6	3′-OMe	5.12
7	4′-Br	5.05
8	4′-Cl	5.01
9	3′-I	4.93
10	3′-NO_2	4.63
11	4′-NO_2	4.55

Results and discussion

It was observed that these nucleophilic substitution reactions of (*i*) picryl bromide (*ii*) ethyl bromoacetate with 2-phenylthiazolidines followed second-order kinetics, first order in each reactant. Since the stoichiometry is 2:1, it is supposed that 2-phenylthiazolidine protonated preferentially by the acid liberated in the reaction, so that a second molecule reacts, but following the rate-determining step. The above situation describes that the reactions (eqs. [3] and [4]) are stoichiometrically termolecular but kinetically second order and the expected rate equation is then eq. [5], where a is the concentration of the nucleophiles (PT), b is the concentration of the EBA or PB, and x is the concentration of EBA or PB reacted in time t. The rate constants for various *meta*- and *para*-substituted 2-phenylthiazolidines reveal that electron-donating substituents increase the reaction rate while electron-attracting substituents decrease it. The observed rate conforms to the following order of reactivity for both reactions: 4′-OH > 4′-OMe > 4′-Me > 3′-Me > H > 3′-OMe > 4′-Br, 4′-Cl > 3′-I > 3′-NO_2 > 4′-NO_2.

TABLE 2. Second-order rate constants and activation parameters for the reaction between substituted 2-phenylthiazolidines and ethyl bromoacetate

Substituent	$k_2 \times 10^4$(L mol^{-1} s^{-1}) 30°C	35°C	40°C	45°C	E_a (kJ M^{-1})	$\Delta H^{\neq}$ (kJ M^{-1})	$-\Delta S^{\neq}$ (J M^{-1} K^{-1})	log PZ
H	3.90	6.06	11.60	16.30	76.76	74.12	65.77	9.82
4′-OMe	7.92	10.60	18.00	24.90	61.63	58.99	109.83	7.52
4′-Me	5.61	8.36	16.40	21.60	73.35	70.70	74.18	9.38
3′-Me	4.61	7.10	13.60	19.50	77.31	74.67	62.55	9.99
3′-OMe	3.29	5.31	9.97	14.20	77.96	75.32	63.13	9.96
4′-Br	—	3.82	6.39	12.10	86.02	83.38	39.11	11.90
4′-Cl	2.36	3.90	7.92	11.60	85.09	82.45	42.40	11.04
3′-I	—	3.04	5.63	9.89	92.64	90.00	19.97	13.88
3′-NO_2	0.82	1.59	3.63	5.78	104.20	101.56	11.91	5.60
4′-NO_2	—	—	2.83	5.41	—	—	—	—

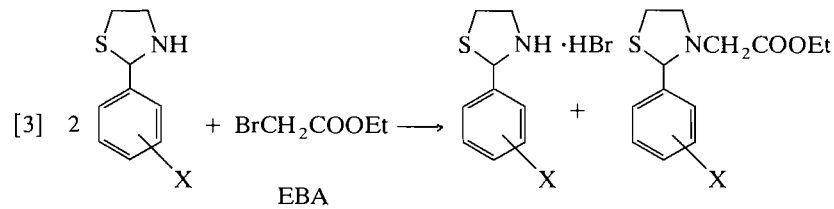

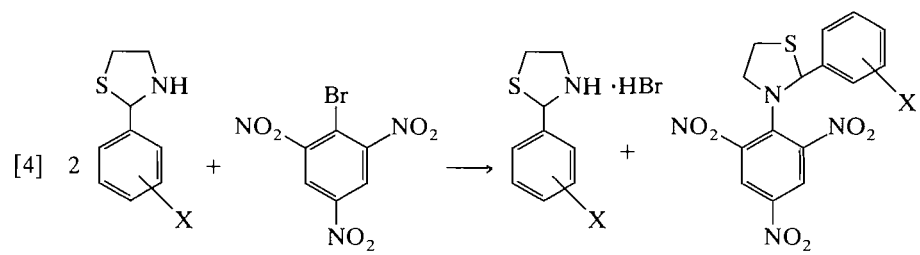

Compound no.	1	2	3	4	5	6	7	8	9	10	11
Substituent X	H	4′-OH	4′-OMe	4′-Me	3′-Me	3′-OMe	4′-Br	4′-Cl	3′-I	3′-NO_2	4′-NO_2

$$[5] \quad \frac{dx}{dt} = k(a - 2x)(b - x)$$

The activation energies in both reactions thus show a regular variation with substituents: electron-releasing substituents decrease and electron-withdrawing substituents increase E_a as shown in Tables 2 and 3.

The entropies of activation are found to be negative as expected for bimolecular reactions with a highly polar transition state (ranges from −11.9 to 109.83 J M^{-1} K^{-1} in the EBA reaction and ranges from −169 to −223 J M^{-1} K^{-1} in the PB reaction). This is consistent with the fact that charge is developed in the transition state formed from neutral reactant molecules. Since the activated complex is more highly solvated than the neutral reactants, it is evident that the spontaneous process of solvation tends to reduce the potential energy. This type of solvent participation must, however, lower the entropy of activation because more molecules are now involved in the structure of the transition state species, and considerable loss of freedom of the solvent occurs. The transition state (Scheme 1) for the α-halogeno ester and amine analogous to the transition state for the aminolysis of α-halogeno ketone(13) has been formulated.

The transition state for the reaction of picryl bromide with 2-phenylthiazolidine has been assigned as in Scheme 2. This is similar to a mechanism suggested for related reactions(14). Some degree of hydrogen bonding between amino and *ortho*-nitro groups further decreases the entropy of activation and, as shown in Table 3, the $\Delta S^{\neq}$ for picryl bromide reactions (e.g., for compound **1**, $\Delta S^{\neq}$ −208.32 J M^{-1} K^{-1}) are more negative than those for the ethyl bromoacetate reactions (Table 2, for compound **1**, $\Delta S^{\neq}$ = −65.77 J M^{-1} K^{-1}).

Brønsted correlation

The magnitude of the Brønsted coefficient in the Brønsted relationship has usually been related to the extent of bond

Can. J. Chem. Downloaded from www.nrcresearchpress.com by 109.225.110.28 on 09/08/12
For personal use only.

TABLE 3. Second-order rate constants and activation parameters for the reaction between picryi bromide and substituted 2-phenylthiazolidines

Substituent	$k_2 \times 10^2$ (L mol^{-1} s^{-1}) 35°C	40°C	45°C	E_a (kJ M^{-1})	$\Delta H^{\neq}$ (kJ M^{-1})	$-\Delta S^{\neq}$ (J M^{-1} K^{-1})	log PZ
H	2.43	3.27	3.97	38.02	35.42	208.32	4.84
4′-OH	3.85	4.72	5.84	32.20	29.60	223.80	4.06
4′-OMe	3.23	4.03	5.01	34.48	31.56	218.82	4.36
4′-Me	2.93	3.76	4.57	34.16	31.88	218.45	4.27
3′-OMe	2.34	3.03	3.82	38.02	35.28	209.37	4.83
4′-Cl	1.94	2.53	3.34	42.38	39.78	196.44	5.49
4′-Br	1.95	2.55	3.24	39.33	36.72	206.19	4.97
3′-I	1.85	2.41	2.94	40.54	37.94	202.74	5.14
3′-NO_2	1.08	1.43	2.04	49.62	47.02	178.05	6.46
4′-NO_2	0.92	1.22	1.82	53.39	50.79	169.82	7.03

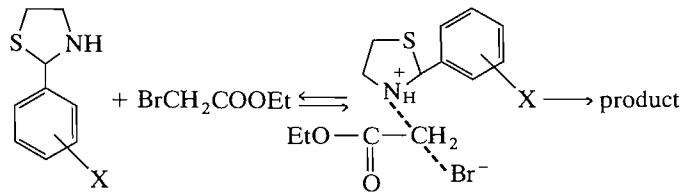

SCHEME 1

formation in the transition state, and when an intermediate is formed along the reaction path, a large Brønsted coefficient is expected. The correlation has been represented graphically by plotting the logarithm of the rate constants against the pK_a values of the corresponding conjugate acids in 100% water. A good Brønsted plot was obtained for these reactions, as shown in Fig 1.

The value of β, the Brønsted coefficient was found to be 0.584 for the PB reaction and 0.918 for the EBA reaction at 40°C. The positive value of β is in accordance with the expectation for the bimolecular nucleophilic substitution reaction, i.e., the rate increases with increasing basicity of the molecule. According to the significance generally attached to the Brønsted coefficient (15–17), $\beta > 0.3$ indicates that the bond formation between the nucleophile and the reaction centre at the rate-limiting transition state is pronounced in both the picryl bromide and the ethyl bromoacetate reactions.

Hammett plot

The rate constants for reactions involving *meta*- and *para*-substituted 2-phenylthiazolidines very closely fit the Hammett equation ($\log k/k_0 = \rho\sigma$) for both reactions; the ρ values are negative in both cases, implying that a similar electronic transfer occurs from the nucleophile to the substrate. The ρ values are −0.647, −0.771, −0.843, and −0.959 at 45, 40, 35, and 30°C, respectively, for the EBA reaction and −0.418, −0.485, and −0.505 at 45, 40 and 35°C for the PB reaction. These values, according to the significance generally attached to them, seem to indicate that the substituent effect in the EBA reaction is greater than that in the PB reaction. A Plot of the logarithm of the rate constants of the nucleophilic substitution reaction of PB against the logarithm of the rate constants of the reaction of EBA of the correspondingly substituted 2-phenylthiazolidines at 45°C is shown as a straight line. The existence of a linear relationship in this case indicates that the charge delocalization that occurs with various substituents in the EBA reaction parallels that in the PB reaction. The positive slope of the plot indicates that the factors that favour the EBA reaction play a parallel role in the PB reaction.

Arrhenius plot

Linear relationships between the enthalpies of activation $\Delta H^{\neq}$ and the entropies of activation $\Delta S^{\neq}$ have been observed for the reactions of ethyl bromoacetate and picryl bromide with 2-phenylthiazolidines. In the Arrhenius equation $\Delta H^{\neq} = \Delta H^{\neq} + \beta\Delta S^{\neq}$; β has a value of 400 K in the ethyl bromoacetate reaction and 385 K for the picryl bromide reaction. The continuous relationship shown by the majority of the substituents signifies a mechanism constant in its main detail (18).

By Exner analysis (19), a plot of log k_2 (45°C) against log k_2 (35°C) for the PB reaction gives a least-squares slope of 0.836 ($r = 0.99$, $s = 0.061$). Using eq. [6]

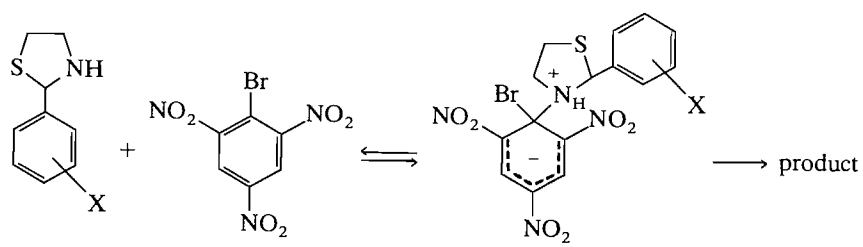

SCHEME 2

Can. J. Chem. Downloaded from www.nrcresearchpress.com by 109.225.110.28 on 09/08/12
For personal use only.

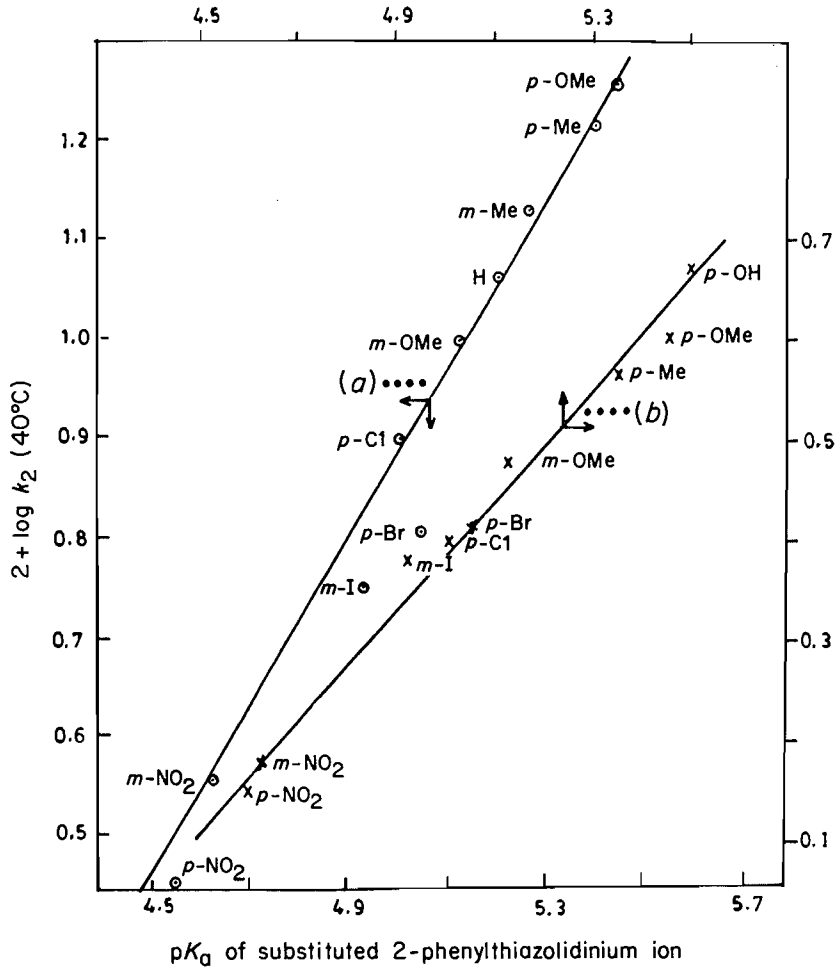

FIG. 1. (*a*) Brønsted plot for EBA reaction with PT; (*b*) Brønsted plot for PB reaction with PT.

$$[6] \quad \beta = T_2 \cdot \frac{1 - b}{1 - \tau b}$$

where $\tau b = T_2/T_1$, $T_2 > T_1$, β is predicted to be 379.8 K, which is in adequate agreement with the least-squares value of 385 K from the $\Delta S^{\neq}$ versus $\Delta H^{\neq}$ plot. From the plot of log k_2 (45°C) against log k_2 (40°C) for the EBA reaction, the least-squares slope b is 0.928 and therefore β is calculated to be 399 K (r = 0.986, s = 0.038), which closely corresponds to the value of 400 K obtained from the $\Delta H^{\neq}$ versus $\Delta S^{\neq}$ plot. These results indicate the experimental temperatures are well below the isokinetic temperature, and the mechanism for these reactions remains constant over the temperature range studied.

Conclusions

The Hammett relationship, Brønsted correlation, and activation parameters obtained in both reactions indicate that there is a constant mechanism in these reactions and that the reactivity depends on the substituents in the phenyl ring and the nature of the substrate.

1. Y. Robbe, J. P. Fernandez, G. Subra, J. P. Chapat, H. Sentenac-Roumanou, and M. Fatome. Eur. J. Med. Chem. **23**, 155 (1988).
2. B. J. Sweetman, M. Bellas, and L. Field. J. Med. Chem. **12**, 888 (1969).
3. R. Umarani. Magn. Reson. Chem. **28**, 743 (1990).
4. R. Umarani. Magn. Reson. Chem. In press.
5. (*a*) F. Banci. J. Med. Chem. **14**, 82 (1971); (*b*) M. Oya, T. Baba, E. Kato, Y. Kawashima, and T. Watanabe. Chem. Pharm. Bull. **30**, 484 (1982); (*c*) R. D. Westland, M. H. Lin, R. A. Cooley, Jr., M. L. Zwiesler, and M. M. Grenan. J. Med. Chem. **16**, 328 (1973).
6. A. H. Cook and I. M. Heilbron. The chemistry of penicillin. Princeton University Press, Princeton, N.J. 1949. p. 921.
7. S. Ratner and H. T. Clarke. J. Am. Chem. Soc. **59**, 200 (1937).
8. O. Aboulwafa, J. Oiry, and J. L. Imbach. Eur. J. Med. Chem. **21**, 493 (1986).
9. T. H. Fife, R. Natarajan, C. C. Shen, and R. Bembi. J. Am. Chem. Soc. **113**, 3071 (1991).
10. R. Luhowy and F. Meneghini. J. Am. Chem. Soc. **101**, 420 (1979).
11. A. M. Davis, N. J. Layland, M. I. Page, F. Martin, and R. M. O'Ferrall. J. Chem. Soc. Perkin Trans 2, 1225 (1991).
12. (*a*) C. F. Bernasconi. Acc. Chem. Res. **11**, 147 (1978); (*b*) Chimia, **1**, 34 (1980); (*c*) T. A. Emokpae and J. Hirst. J. Chem. Soc. Perkin Trans 2, 829 (1980); (*d*) S. K. Das, A. Sharma, and B. K. Sinha. Indian J. Chem. **14B**, 108 (1976).
13. (*a*) R. K. Mohanty, G. Behera, and M. K. Rout. Indian J. Chem. **5**, 259 (1967); (*b*) R. G. Pearson, S. H. Langer, F. V. Williams, and W. J. McGuire. J. Am. Chem. Soc. **74**, 5130 (1952).

Can. J. Chem. Downloaded from www.nrcresearchpress.com by 109.225.110.28 on 09/08/12
For personal use only.

14. (*a*) L. M. Litvinenko, G. D. Titskii, and A. E. Shumeiko. Zh. Org. Khim. **13**, 767 (1977); (*b*) R. E. Parker and T. O. Read. J. Chem. Soc. 9 (1962); (*c*) J. Bunnett and R. Garst. J. Am. Chem. Soc. **87**, 3875 (1965).
15. G. Biggi and F. Pietra. J. Chem. Soc(B), 44 (1971).
16. M. J. Gregory and T. C. Bruice. J. Am. Chem. Soc. **89**, 4400 (1967).
17. L. Senatore, E. Gluffarin, and A. Fava. J. Am. Chem. Soc. **92**, 3035 (1970).
18. K. Bowden, N. B. Chapman, and J. Shorter. J. Chem. Soc. 3370 (1964).
19. J. E. Leffler and E. Grunwald. Rates and equilibria of organic reactions. John Wiley and Sons, New York. 1963.

Can. J. Chem. Downloaded from www.nrcresearchpress.com by 109.225.110.28 on 09/08/12
For personal use only.

Structural studies of organoboron compounds. LII.[1] *N*-Ethylhydroxylamine-(*O-B*)1,7-diethyl-3,5-diphenyl-2,4,6-trioxa-7-aza-1-azonia-3-bora-5-boratabicyclo[3.3.0]octane[2]

WOLFGANG KLIEGEL AND GOTTFRIED LUBKOWITZ

Institut für Pharmazeutische Chemie der Technischen Universität Braunschweig, Beethovenstrasse 55, 3300 Braunschweig, Germany

AND

STEVEN J. RETTIG AND JAMES TROTTER

Department of Chemistry, University of British Columbia, 2036 Main Mall, Vancouver, B.C., Canada V6T 1Z1

Received March 14, 1991

WOLFGANG KLIEGEL, GOTTFRIED LUBKOWITZ, STEVEN J. RETTIG, and JAMES TROTTER. Can. J. Chem. **70**, 2015 (1992).

The reaction of *N,N'*-diethyl-*N,N'*-dihydroxymethanediamine with oxybis(diphenylborane) in absolute ethanol yields *N*-ethylhydroxylamine(*O-B*)1,7-diethyl-3,5-diphenyl-2,4,6-trioxa-7-aza-1-azonia-3-bora-5-boratabicyclo[3.3.0]octane [3-(1-oxa-2-azoniabutyl)-1,7-diethyl-3,5-diphenyl-2,4,6-trioxa-7-aza-1-azonia-3,5-diboratabicyclo[3.3.0]octane], **7***b*, in good yield. Crystals of this material are monoclinic, $a = 16.396(2)$, $b = 11.303(2)$, $c = 22.898(4)$ Å, $\beta = 92.78(1)°$, $Z = 8$ (two molecules per asymmetric unit), space group $P2_1/a$. The structure was solved by direct methods and was refined by full-matrix least-squares procedures to $R = 0.041$ and $R_w = 0.050$ for 3602 reflections with $I \geq 3\sigma(I)$. The product **7***b* is formed by O→B coordination between *N*-ethylhydroxylamine and the bicyclic bis-phenylboronate of *N,N'*-diethyl-*N,N'*-dihydroxymethanediamine. Compound **7***b* is only the second structurally characterized example of an *N*-alkylhydroxylamine(*O-B*)boron complex having an open-chain *B,N*-betaine structure. Bond lengths about boron are: B—O(N) = 1.467(4)–1.527(4), B—O(B) = 1.433(4)–1.451(4), B—N = 1.688(4) and 1.707(4), B—C = 1.586(4)–1.606(5) Å.

WOLFGANG KLIEGEL, GOTTFRIED LUBKOWITZ, STEVEN J. RETTIG et JAMES TROTTER. Can. J. Chem. **70**, 2015 (1992).

La réaction de la *N,N'*-diéthyl-*N,N'*-dihydroxyméthanediamine avec l'oxybis(diphénylborane), dans l'éthanol absolu, fournit la *N*-éthylhydroxylamine(*O-B*)1,7-diéthyl-3,5-diphényl-2,4,6-trioxa-7-aza-1-azonia-3-bora-5-boratabicyclo-[3.3.0]octane[3-(1-oxa-2-azoniabutyl)-1,7-diéthyl-3,5-diphényl-2,4,6-trioxa-7-aza-1-azonia-3,5-diboratabicyclo[3.3.0]octane], **7***b*, avec un bon rendement. Les cristaux de ce produit sont monocliniques, $a = 16,396(2)$, $b = 11,303(2)$, $c = 22,898(4)$ Å, $\beta = 92,78(1)°$, $Z = 8$ (deux molécules par unité asymétrique) et groupe d'espace $P2_1/a$. On a résolu la structure par des méthodes directes et on l'a affinée par la méthode des moindres carrés jusqu'à des valeurs de $R = 0,041$ et $R_w = 0,050$ pour 3602 réflexions avec $I \geq 3\sigma(I)$. Le produit **7***b* est formé par une coordination O→B entre la *N*-éthylhydroxylamine et le bis-phénylboronate bicyclique de la *N,N'*-diéthyl-*N,N'*-dihydroxyméthanediamine. Le composé **7***b* n'est que le deuxième exemple de structure caractérisée d'un complexe *N*-alkylhydroxylamine(*O→B*)bore possédant une structure *B,N*-bétaïne en chaîne ouverte. Les longueurs des liaisons autour du bore sont : B—O(N) = 1,467(4)–1,527(4), B—O(B) = 1,433(4)–1,451(4), B—N = 1,688(4) et 1,707(4), B—C = 1,586(4)–1.606(5) Å.

[Traduit par la rédaction]

Introduction

The *N,N'*-dihydroxyaminal **1** was reacted with the anhydride of diphenylborinic acid in absolute ethanol with the intention of synthesizing the six-membered diphenylboron chelate **2**. Compound **2** would be analogous to the seven-membered ring derivative **3** which had been obtained by a similar method from an *N,N'*-dihydroxy-1,2-ethanediamine and diphenylborinic acid. The structure of **3** has been established by X-ray analysis (1). Contrary to expectations, the crystalline material obtained from the reaction of **1** and oxybis(diphenylborane) did not give the typical blue color reaction with diphenylcarbazone (2) which would indicate the presence of an intact diphenylboron moiety (by trapping of Ph_2B^+). The reddish color of this reaction solution indicated the presence of a monophenyl substitution at boron (2) suggesting that a dephenylation had taken place. The elemental analysis, however, did not agree with a simple cyclic phenylboronate **4** that could result from **2** by the elimination of 1 mol of benzene, but shows an additional content of 1 mol "PhBO" and 1 mol "EtNHOH". The ^{1}H nmr spectrum displays two signals for exchangeable OH/NH protons, one appearing at fairly low field ($\delta = 11.57$ ppm) as is usually observed for acidic protons and (or) strongly hydrogen-bonded protons. This is also confirmed by the infrared spectrum with lowered O—H/N—H stretching frequencies (between 2500 and 2700 cm^{-1}).

The analytical data are in agreement with several possible condensation and addition products. The six-membered cycloboronate **4** is not expected to be stable with respect to the substitution pattern. Stability of a type **4** compound could be achieved by reducing the basicity of the aminal nitrogen atoms (e.g., by α-cyanoalkyl or by β-nitroalkyl substitution) and, furthermore, by impeding the Lewis acidity of the boronic acid itself by a combination of steric and inductive/mesomeric effects (3). At best, an adduct of **4** to the phenylborinic monoester of *N*-ethylhydroxylamine could exist in the BONBON form **5***a* or in the BNOBON form **5***b*, the former

[1]Previous paper in this series: ref. 11.

[2]3-(1-Oxa-2-azoniabutyl)-1,7-diethyl-3,5-diphenyl-2,4,6-trioxa-7-aza-1-azonia-3,5-diboratabicyclo[3.3.0]octane.

Can. J. Chem. Downloaded from www.nrcresearchpress.com by 109.225.110.28 on 09/08/12
For personal use only.

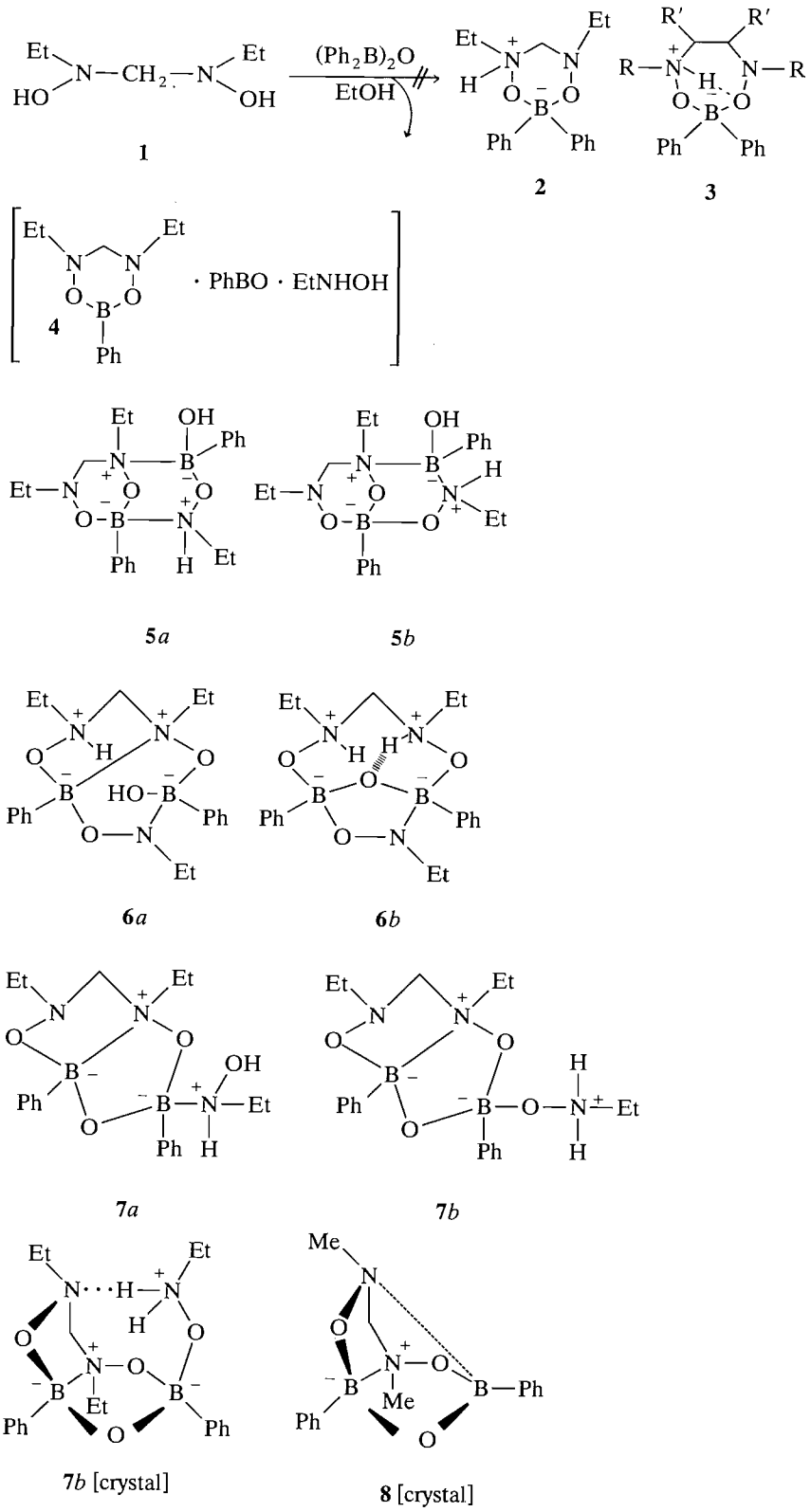

ring system being well documented in the literature (4). Other possible isomers that would be supported by the spectroscopic data are the bicyclic structures **6***a* (with a transannular N—B bridge) or **6***b* (containing a pyroboronate BOB bridge). Finally, an adduct of *N*-ethylhydroxylamine to an eight-membered bicyclic ring system, in which the hydroxylamine would coordinate either through the nitrogen atom (**7***a*) or through the oxygen atom (**7***b*) to the trigonal planar boron centre of the bicyclic compound, must also be considered. The structure of the bicyclic skeleton has been established by an X-ray crystallographic analysis of the *N*-methyl derivative **8** [crystal] (5). For a definite structural assignment (at least in the solid state) an X-ray analysis was undertaken.

Can. J. Chem. Downloaded from www.nrcresearchpress.com by 109.225.110.28 on 09/08/12
For personal use only.

TABLE 1. Final atomic coordinates (fractional) and B_{eq} (Å^2)[a]

Atom	x	y	z	B_{eq}	Occ.
O(1)	0.3007(1)	0.0651(2)	0.55797(8)	4.0	
O(2)	o.4442(1)	0.0556(2)	0.56640(7)	3.5	
O(3)	0.4428(1)	0.2649(2)	0.53517(8)	3.9	
O(4)	0.3715(1)	−0.0586(2)	0.48926(8)	4.1	
O(5)	−0.0203(1)	0.2352(2)	0.1054(1)	5.8	
O(6)	0.0252(1)	0.0454(2)	0.08018(8)	4.6	
O(7)	0.1479(1)	0.1522(2)	0.0497(1)	6.0	
O(8)	−0.0916(1)	0.1299(2)	0.0256(1)	5.8	
N(1)	0.3263(1)	0.1786(2)	0.5792(1)	3.7	
N(2)	0.3720(1)	0.2591(2)	0.4947(1)	4.1	
N(3)	0.4000(1)	0.0270(2)	0.4498(1)	3.7	
N(4)	0.0641(2)	0.2321(2)	0.1232(1)	5.2	
N(5)	0.1147(2)	0.2673(3)	0.0332(1)	6.7	
N(6)	−0.0388(2)	0.1624(2)	−0.0187(1)	5.6	
C(1)	0.3051(2)	0.2671(3)	0.5336(1)	4.5	
C(2)	0.2875(2)	0.2015(3)	0.6353(1)	4.9	
C(3)	0.1953(2)	0.1882(3)	0.6312(2)	6.7	
C(4)	0.3768(2)	0.3627(3)	0.4555(2)	6.1	
C(5)	0.3888(2)	0.4804(3)	0.4843(2)	7.7	
C(6)	0.3542(2)	0.0178(3)	0.3931(1)	5.5	
C(7)	0.3834(2)	0.1078(3)	0.3506(1)	6.7	
C(8)	0.3646(2)	−0.1339(2)	0.5896(1)	3.9	
C(9)	0.4054(2)	−0.2371(3)	0.5766(2)	6.1	
C(10)	0.4023(3)	−0.3363(3)	0.6119(2)	7.8	
C(11)	0.3578(3)	−0.3374(4)	0.6604(2)	7.1	
C(12)	0.3163(2)	−0.2382(4)	0.6741(1)	6.3	
C(13)	0.3197(2)	−0.1387(3)	0.6397(1)	5.1	
C(14)	0.4703(2)	0.2224(2)	0.6416(1)	3.4	
C(15)	0.4877(2)	0.1456(3)	0.6879(1)	4.4	
C(16)	0.5218(2)	0.1849(3)	0.7409(1)	5.6	
C(17)	0.5386(2)	0.3029(4)	0.7491(1)	5.5	
C(18)	0.5214(2)	0.3819(3)	0.7045(2)	5.2	
C(19)	0.4876(2)	0.3410(3)	0.6519(1)	4.2	
C(20)	0.1067(2)	0.3226(3)	0.0901(2)	6.8	
C(21)	0.0720(2)	0.2513(3)	0.1872(1)	6.4	
C(22)	0.0374(3)	0.3682(4)	0.2072(2)	8.8	
C(23)	0.1839(3)	0.3239(4)	0.0012(2)	10.1	
C(24)	0.1670(4)	0.4496(6)	−0.0107(3)	14.6	
C(25)	−0.0818(3)	0.2480(4)	−0.0577(2)	8.3	
C(26)	−0.0289(4)	0.2951(5)	−0.1017(2)	9.3	0.835
C(26A)	−0.083(2)	0.360(3)	−0.034(1)	9.3	0.165
C(27)	−0.1179(2)	0.0581(3)	0.1231(1)	5.2	
C(28)	−0.1583(2)	−0.0440(4)	0.1057(2)	6.8	
C(29)	−0.2156(3)	−0.0980(4)	0.1386(2)	8.2	
C(30	−0.2352(3)	−0.0499(5)	0.1905(2)	8.7	
C(31)	−0.1970(3)	0.0506(5)	0.2100(2)	8.8	
C(32)	−0.1393(3)	0.1045(3)	0.1758(2)	7.4	
C(33)	0.1588(2)	0.0342(3)	0.1430(1)	4.5	
C(34)	0.1276(2)	−0.0487(3)	0.1801(1)	5.1	
C(35)	0.1755(2)	−0.1111(3)	0.2205(2)	6.2	
C(36)	0.2572(3)	−0.0908(4)	0.2252(2)	7.6	
C(37)	0.2909(2)	−0.0087(4)	0.1900(2)	8.1	
C(38)	0.2426(2)	0.0544(3)	0.1492(2)	6.4	
B(1)	0.3727(2)	−0.0162(3)	0.5518(1)	3.6	
B(2)	0.4305(2)	0.1772(3)	0.5811(1)	3.5	
B(3)	−0.0486(2)	0.1133(3)	0.0840(2)	4.8	
B(4)	0.1003(2)	0.1038(3)	0.0969(2)	4.8	

[a] $B_{eq} = (8/3)\pi^2\Sigma\Sigma U_{ij} a_i^* a_j^* (a_i \cdot a_j)$.

Can. J. Chem. Downloaded from www.nrcresearchpress.com by 109.225.110.28 on 09/08/12
For personal use only.

Can. J. Chem. Downloaded from www.nrcresearchpress.com by 109.225.110.28 on 09/08/12
For personal use only.

TABLE 2. Bond lengths (Å) with estimated standard deviations in parentheses

Molecule 1		Molecule 2	
Atoms	Distance	Atoms	Distance
O(1)—N(1)	1.427(3)	O(5)—N(4)	1.424(3)
O(1)—B(1)	1.508(3)	O(5)—B(3)	1.527(4)
O(2)—B(1)	1.451(4)	O(6)—B(3)	1.440(4)
O(2)—B(2)	1.435(4)	O(6)—B(4)	1.433(4)
O(3)—N(2)	1.451(3)	O(7)—N(5)	1.454(3)
O(3)—B(2)	1.467(4)	O(7)—B(4)	1.470(4)
O(4)—N(3)	1.418(3)	O(8)—N(6)	1.415(3)
O(4)—B(1)	1.508(4)	O(8)—B(3)	1.494(4)
N(1)—C(1)	1.476(4)	N(4)—C(20)	1.468(4)
N(1)—C(2)	1.484(3)	N(4)—C(21)	1.481(4)
N(1)—B(2)	1.707(4)	N(4)—B(4)	1.688(4)
N(2)—C(1)	1.448(4)	N(5)—C(20)	1.458(4)
N(2)—C(4)	1.481(4)	N(5)—C(23)	1.521(5)
N(3)—C(6)	1.471(4)	N(6)—C(25)	1.472(4)
C(2)—C(3)	1.517(4)	C(21)—C(22)	1.518(5)
C(4)—C(5)	1.494(5)	C(23)—C(24)	1.472(7)
C(6)—C(7)	1.503(5)	C(25)—C(26)	1.461(7)
		C(25)—C(26A)	1.37(3)
C(8)—C(9)	1.384(4)	C(27)—C(28)	1.381(5)
C(8)—C(13)	1.393(4)	C(27)—C(32)	1.376(5)
C(8)—B(1)	1.598(4)	C(27)—B(3)	1.606(5)
C(9)—C(10)	1.385(5)	C(28)—C(29)	1.376(5)
C(10)—C(11)	1.359(5)	C(29)—C(30)	1.358(6)
C(11)—C(12)	1.356(5)	C(30)—C(31)	1.362(6)
C(12)—C(13)	1.376(4)	C(31)—C(32)	1.397(6)
C(14)—C(15)	1.389(4)	C(33)—C(34)	1.379(4)
C(14)—C(19)	1.388(4)	C(33)—C(38)	1.393(4)
C(14)—B(2)	1.586(4)	C(33)—B(4)	1.599(5)
C(15)—C(16)	1.384(4)	C(34)—C(35)	1.379(4)
C(16)—C(17)	1.373(5)	C(35)—C(36)	1.358(5)
C(17)—C(18)	1.377(4)	C(36)—C(37)	1.364(5)
C(18)—C(19)	1.380(4)	C(37)—C(38)	1.392(5)

Experimental

N-*Ethylhydroxylamine(*O-B*)1,7-diethyl-3,5-diphenyl-2,4,6-trioxa-7-aza-1-azonia-3-bora-5-boratabicyclo[3.3.0]-octane,* 7b

N,N'-Diethyl-*N,N'*-dihydroxymethanediamine, **1**, (6, 7) (0.54 g, 4 mmol) and oxybis(diphenylborane) (0.69 g, 2 mmol) was dissolved in 5 mL absolute ethanol and the reaction mixture was heated for several minutes until crystallization commenced.[3] Cooling of the solution yielded 0.55 g (71%, corresponding to 2 mmol $(Ph_2B)_2O$) of colorless material which was recrystallized from ethanol: mp 140–143°C. Infrared (KBr): 2700, 2550 cm^{-1} (N—H). ^1H nmr (400 MHz, $CDCl_3$/TMS) δ (ppm): 0.97–1.06 (m, $2CH_3$), 1.14–1.23 (m, CH_3), 2.29–2.41 (m, 1H, CH_2N^+), 3.01–3.09 (m, 1H, CH_2N^+), 3.12/4.14 (d/d, J = 7 Hz, N—CH_2—N), 7.08–7.29 (m, 6 arom. H and NH), 7.48 (s, broad, 2 arom. *ortho*-H), 7.78 (d, 2 arom. *ortho*-H), 11.57 (s, NH). ^{11}B nmr (64 MHz, $CDCl_3/Et_2OBF_3$) δ (ppm): 10.0 (broad). Anal. calcd. for $C_{19}H_{29}B_2N_3O_4$: C 59.26, H 7.95, B 5.61, N 10.91; found: C 59.26, H 7.67, B 5.53, N 10.82.

The substance gives a reddish color reaction with diphenylcarbazone in methanol, indicating a phenylboronic acid component (2). Crystals suitable for X-ray analysis were obtained by recrystallization from absolute ethanol.

X-ray crystallographic analysis of 7b

A crystal ca. 0.40 × 0.45 × 0.50 mm in size was mounted on a glass fiber. Unit-cell parameters were refined by least-squares on setting angles for 25 reflections (2θ = 20.0–24.1°) measured on a diffractometer with Mo-K_α radiation (λ = 0.71069 Å). Crystal data at 21°C are as follows

$C_{19}H_{29}B_2N_3O_4$ fw = 385.08

Monoclinic, a = 16.396(2), b = 11.303(2), c = 22.898(4) Å, β = 92.78(1)°, V = 4239(1) $Å^3$, Z = 8, ρ_c = 1.207 Mg m^{-3}, $F(000)$ = 1648, μ(Mo-K_α) = 0.77 cm^{-1}. Absent reflections $0k0$, k odd, and $h0l$, h odd, uniquely indicate the space group $P2_1/a$ (No. 14).

Intensities were measured with graphite-monochromated Mo-K_α radiation on a Rigaku AFC6S diffractometer. An ω–2θ scan at 32° min^{-1} over a range of (1.25 + 0.35 tan θ)° in ω (with up to 8 rescans, background/scan time ratio = 0.5) was employed. Data were measured to 2θ = 50°. The intensities of three check reflections, measured every 150 reflections throughout the data collection, showed only small random variations. After data reduction,[4] an empirical absorption correction, based on azimuthal scans for three reflections, was applied. Transmission factors range from 0.97 to 1.00. Of the 8146 reflections measured, 7893 were unique (R_{int} = 0.026) and 3602 had intensities greater than or equal to $3\sigma(F^2)$ above background where $\sigma^2(F^2) = [S^2(C + 4B) + (0.03F^2)^2]/Lp^2$ with S = scan speed, C = scan count, B = total background count, and Lp = Lorentz-polarization factor.

The structure was solved by direct methods. Minor disordering of the terminal carbon atom of the C(25)—C(26) ethyl group was modelled by split-atom refinement. The relative site occupancy factors were estimated from Fourier map peak heights and were subsequently adjusted to give approximately equal equivalent isotropic thermal parameters for the two component atoms. All non-hydrogen atoms except the low-occupancy carbon atom C(26A) were refined with anisotropic thermal parameters and the hydrogen atoms were fixed in idealized positions (N—H/C—H = 0.98 Å, $B_H = 1.2\ B_{\text{bonded atom}}$). A correction for secondary extinction was applied, the final value of the extinction coefficient being 1.49×10^{-7}. Scattering factors for all atoms and anomalous dispersion corrections for the non-hydrogen atoms were taken from ref. 8. The weighting scheme $w = 4F_o^2/\sigma^2(F_o^2)$ gave uniform average values of $w(|F_o| - |F_c|)^2$ over ranges of both $|F_o|$ and sin θ/λ and was employed in the final stages of full-matrix least-squares refinement of 506 variables. Reflections with $I < 3\sigma(I)$ were not included in the refinement. Convergence was reached at R = 0.041 and R_w = 0.050 for 3602 reflections with $I \geq 3\sigma(I)$. The function minimized was $\Sigma w(|F_o| - |F_c|)^2$, $R = \Sigma||F_o| - |F_c||\Sigma w|F_o|$, $R_w = (\Sigma w(|F_o| - |F_c|)^2/\Sigma w|F_o|^2)^{1/2}$.

On the final cycle of refinement the maximum parameter shift corresponded to 0.01σ. The mean error in an observation of unit weight was 1.86. The final difference map showed maximum fluctuations of ±0.17 e $Å^{-3}$. The final positional and (equivalent) isotropic thermal parameters for the non-hydrogen atoms appear in Table 1. Bond lengths and angles are given in Tables 2 and 3 and intra-annular torsion angles in Table 4. Hydrogen-atom parameters, anisotropic thermal parameters, torsion angles, intermolecular contacts, least-squares planes, and structure factors have been deposited.[5]

[3]The reaction can also be carried out at room temperature, but more solvent and more time are required. The yield of crystals obtained from the cooled solution is smaller in this case.

[4]TEXSAN/TEXRAY structure analysis package which includes versions of the following: MITHRIL, integrated direct methods, by C. J. Gilmore; DIRDIF, direct methods for difference structures, by P. T. Beurskens; ORFLS, full-matrix least-squares, and ORFFE, function and errors, by W. R. Busing, K. O. Martin, and H. A. Levy; ORTEP II, illustrations, by C. K. Johnson.

[5]Supplementary material mentioned in the text may be purchased from the Depository of Unpublished Data, Document Delivery, CISTI, National Research Council Canada, Ottawa, Canada K1A 0R6.

Tables of hydrogen atom coordinates and intermolecular distances have also been deposited with the Cambridge Crystallographic Data Centre and can be obtained on request from the Director, Cambridge Crystallographic Data Centre, University Chemical Laboratory, Lensfield Road, Cambridge, CB2 1EW, U.K.

TABLE 3. Bond angles (deg) with estimated standard deviations in parentheses

Molecule 1		Molecule 2	
Atoms	Angle	Atoms	Angle
N(1)—O(1)—B(1)	111.2(2)	N(4)—O(5)—B(3)	110.3(2)
B(1)—O(2)—B(2)	117.1(2)	B(3)—O(6)—B(4)	116.9(3)
N(2)—O(3)—B(2)	107.1(2)	N(5)—O(7)—B(4)	108.6(2)
N(3)—O(4)—B(1)	113.4(2)	N(6)—O(8)—B(3)	113.4(2)
O(1)—N(1)—C(1)	108.2(2)	O(5)—N(4)—C(20)	108.3(2)
O(1)—N(1)—C(2)	108.7(2)	O(5)—N(4)—C(21)	108.5(2)
O(1)—N(1)—B(2)	106.2(2)	O(5)—N(4)—B(4)	105.8(2)
C(1)—N(1)—C(2)	113.4(2)	C(20)—N(4)—C(21)	112.8(3)
C(1)—N(1)—B(2)	103.1(2)	C(20)—N(4)—B(4)	103.4(2)
C(2)—N(1)—B(2)	116.8(2)	C(21)—N(4)—B(4)	117.6(3)
O(3)—N(2)—C(1)	102.2(2)	O(7)—N(5)—C(20)	101.5(2)
O(3)—N(2)—C(4)	106.7(2)	O(7)—N(5)—C(23)	102.9(3)
C(1)—N(2)—C(4)	112.8(2)	C(20)—N(5)—C(23)	110.7(3)
O(4)—N(3)—C(6)	110.1(2)	O(8)—N(6)—C(25)	108.3(3)
N(1)—C(1)—N(2)	103.5(2)	N(4)—C(20)—N(5)	103.2(3)
N(1)—C(2)—C(3)	113.4(2)	N(4)—C(21)—C(22)	114.3(3)
N(2)—C(4)—C(5)	116.5(3)	N(5)—C(23)—C(24)	110.9(4)
N(3)—C(6)—C(7)	111.0(3)	N(6)—C(25)—C(26)	112.0(4)
		N(6)—C(25)—C(26A)	113(1)
C(9)—C(8)—C(13)	115.2(3)	C(28)—C(27)—C(32)	115.7(3)
C(9)—C(8)—B(1)	122.0(3)	C(28)—C(27)—B(3)	120.4(3)
C(13)—C(8)—B(1)	122.7(3)	C(32)—C(27)—B(3)	123.9(3)
C(8)—C(9)—C(10)	121.6(3)	C(27)—C(28)—C(29)	122.9(4)
C(9)—C(10)—C(11)	121.4(4)	C(28)—C(29)—C(30)	119.9(4)
C(10)—C(11)—C(12)	118.5(3)	C(29)—C(30)—C(31)	119.7(4)
C(11)—C(12)—C(13)	120.6(3)	C(30)—C(31)—C(32)	119.6(4)
C(8)—C(13)—C(12)	122.7(3)	C(27)—C(32)—C(31)	122.2(4)
C(15)—C(14)—C(19)	116.2(3)	C(34)—C(33)—C(38)	116.3(3)
C(15)—C(14)—B(2)	121.7(2)	C(34)—C(33)—B(4)	120.8(3)
C(19)—C(14)—B(2)	122.1(3)	C(38)—C(33)—B(4)	122.9(3)
C(14)—C(15)—C(16)	121.9(3)	C(33)—C(34)—C(35)	122.9(3)
C(15)—C(16)—C(17)	120.1(3)	C(34)—C(35)—C(36)	119.6(3)
C(16)—C(17)—C(18)	119.8(3)	C(35)—C(36)—C(37)	119.7(4)
C(17)—C(18)—C(19)	119.3(3)	C(36)—C(37)—C(38)	120.8(3)
C(14)—C(19)—C(18)	122.8(3)	C(33)—C(38)—C(37)	120.7(3)
O(1)—B(1)—O(2)	105.3(2)	O(5)—B(3)—O(6)	104.9(3)
O(1)—B(1)—O(4)	108.0(2)	O(5)—B(3)—O(8)	107.2(3)
O(1)—B(1)—C(8)	111.7(2)	O(5)—B(3)—C(27)	112.6(3)
O(2)—B(1)—O(4)	111.7(2)	O(6)—B(3)—O(8)	111.9(3)
O(2)—B(1)—C(8)	115.3(2)	O(6)—B(3)—C(27)	116.5(3)
O(4)—B(1)—C(8)	104.6(2)	O(8)—B(3)—C(27)	103.4(3)
O(2)—B(2)—O(3)	116.7(2)	O(6)—B(4)—O(7)	117.0(3)
O(2)—B(2)—N(1)	99.8(2)	O(6)—B(4)—N(4)	100.3(3)
O(2)—B(2)—C(14)	116.8(2)	O(6)—B(4)—C(33)	115.5(3)
O(3)—B(2)—N(1)	98.5(2)	O(7)—B(4)—N(4)	98.7(2)
O(3)—B(2)—C(14)	110.1(2)	O(7)—B(4)—C(33)	110.2(3)
N(1)—B(2)—C(14)	112.9(2)	N(4)—B(4)—C(33)	113.5(3)

Can. J. Chem. Downloaded from www.nrcresearchpress.com by 109.225.110.28 on 09/08/12
For personal use only.

Results and discussion

The X-ray analysis confirms the solid-state structure **7***b* (Fig. 1), formed by O→B coordination between *N*-ethylhydroxylamine and the bicyclic bis-phenylboronate of the *N,N'*-diethyl-*N,N'*-dihydroxyaminal **1**. If benzene is used as solvent (20 mL, 5 min reflux), and the product recrystallized from toluene/petroleum ether, only the bicyclic bisphenylboronate[6] (7) is isolated (70% yield) and not the *N*-ethylhydroxylamine adduct **7***b*. The two crystallographically independent molecules show some small, but statistically significant, geometrical differences (see Tables 2–4). The centrosymmetric crystal structure contains equal numbers of the (1*R*,3*R*,5*S*,7*R*) and (1*S*,3*S*,5*R*,7*S*) enantiomers, the former being depicted in Fig. 1.[7] The yield of the reaction between **1** and oxybis(diphenylborane) (over 70%) suggests that an extensive dephenylation of the diphenylborinic acid or of its primary reaction product (possibly the chelate **2**) has taken place. The subsequent formation of the

[6]The synthesis of the bicyclic bis-phenylboronate (1,7-diethyl-3,5-diphenyl-2,4,6-trioxa-7-aza-3-bora-5-boratabicyclo[3.3.0]-octane) has already been described (7).

[7]The chiral centres correspond to atoms N(1), B(1), B(2), and N(2) in molecule 1 and N(4), B(3), B(4), and N(5) in molecule 2.

TABLE 4. Intra-annular torsion angles (deg) with estimated standard deviations in parentheses

Molecule 1		Molecule 2	
Atoms	Value (deg)	Atoms	Value (deg)
B(1)—O(1)—N(1)—B(2)	6.2(3)	B(3)—O(5)—N(4)—B(4)	13.8(3)
O(1)—N(1)—B(2)—O(2)	−6.2(2)	O(5)—N(4)—B(4)—O(6)	−12.4(3)
N(1)—B(2)—O(2)—B(1)	4.3(3)	N(4)—B(4)—O(6)—B(3)	6.7(3)
B(2)—O(2)—B(1)—O(1)	−0.9(3)	B(4)—O(6)—B(3)—O(5)	1.0(3)
O(2)—B(1)—O(1)—N(1)	−3.8(3)	O(6)—B(3)—O(5)—N(4)	−10.1(3)
B(2)—N(1)—C(1)—N(2)	29.6(3)	B(4)—N(4)—C(20)—N(5)	33.7(3)
N(1)—C(1)—N(2)—O(3)	−49.0(2)	N(4)—C(20)—N(5)—O(7)	−49.3(3)
C(1)—N(2)—O(3)—B(2)	50.4(2)	C(20)—N(5)—O(7)—B(4)	46.7(3)
N(2)—O(3)—B(2)—N(1)	−28.8(2)	N(5)—O(7)—B(4)—N(4)	−23.7(3)
O(3)—B(2)—N(1)—C(1)	−0.8(2)	O(7)—B(4)—N(4)—C(20)	−6.5(3)

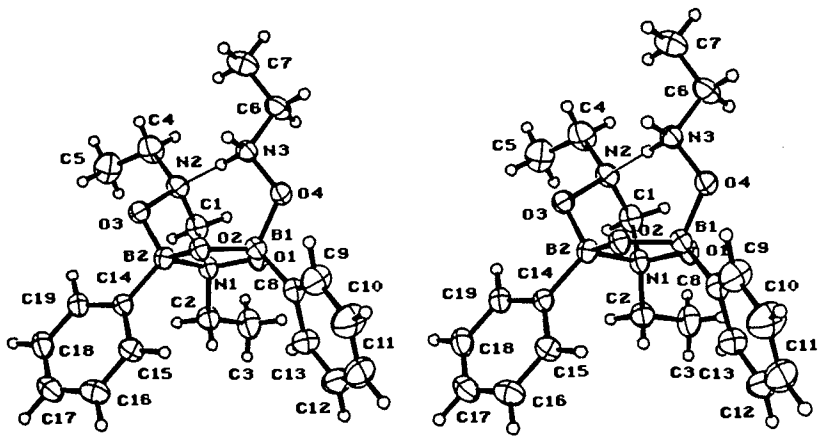

FIG. 1. Stereoview of one of the two independent *N*-ethylhydroxylamine(*O*-*B*)1,7-diethyl-3,5-diphenyl-2,4,6-trioxa-7-aza-1-azonia-3-bora-5-boratabicyclo[3.3.0]octane molecules; 33% probability thermal ellipsoids are shown for the non-hydrogen atoms. Fine line represents a hydrogen bond.

bicyclo[3.3.0]octane skeleton via the incorporation of a second molar equivalent of phenylboronic acid into the dephenylation product (a monophenylboronate of **1**) would liberate one mol of the dihydroxyaminal **1** as a potential source of the free *N*-ethylhydroxylamine base (7).

The O→B coordinated addition product is further stabilized by an intramolecular N—H···N hydrogen bond (N(3)—H(1)···N(2) and N(6)—H(3)···N(5), N···H = 1.88 and 1.97 Å, N···N = 2.863(3) and 2.977(4) Å, N—H···N = 177 and 178°, respectively), at least in the solid state of **7***b* (cf. formula **7***b*[crystal]). The N···N distances for the $^{+}$N—H···N interactions in **7***b* are longer than those observed for $^{+}$N—H···N hydrogen bonds in monocationic "proton sponge" compounds which range up to 2.626 Å for linear systems (9) and similar to the mean value of 2.949 Å for noncationic N—H···N hydrogen bonds in crystalline organic compounds (10). The remaining hydrogen atom of each protonated hydroxylamine nitrogen atom is hydrogen bonded to a pyroboronate oxygen atom to result in hydrogen-bonded, centrosymmetric dimers (N(3)—H(2)···O(2)(1 − *x*,−*y*,1 − *z*) and N(6)—H(4)···O(6)(−*x*,−*y*,−*z*), H···O = 1.81 and 1.79 Å, N···O = 2.762(3) and 2.753(3) Å, N—H···O = 163 and 165°, respectively).

Compared with the bicyclic compound **8** (5) containing one tetracoordinated sp^3 boron atom and one nearly planar trigonal sp^2 boron atom in a pyroboronate linkage with a typical short (sp^2)B—O(B) bond (typically about 1.34 Å in most BOBON rings of this type (5)) and a longer (sp^3)B—O(B) bond (about 1.46 Å), the hydroxylamine adduct **7***b* possesses a (sp^3)B—O—(sp^3)B system with two slightly different B—O bonds (1.435(4) and 1.451(3), 1.433(4) and 1.440(4) Å, respectively, for the two molecules). This demonstrates once again the strength of the O—B *pp*(π) interaction for trigonal planar boron, and the marked O—B bond length increase associated with tetracoordination of the boron atom. The transannular N—B bond in **7***b* (1.707(4) and 1.688(4) Å in the two molecules) is slightly shorter than the corresponding bond (mean 1.733(4) Å) in the bicyclic "parent" compound **8** (5). The intramolecular non-bonding distances N(2)···B(1) = 3.374(4) and N(5)···B(3) = 3.444(5) Å in **7***b*, however, are lengthened relative to the corresponding N···B distance in **8** (mean 3.083 Å) by the insertion of the *N*-ethylhydroxylamine moiety. The dihedral angles between the normals to the mean planes of the BOBON and the approximately planar OBNC portions of the BONCN rings average 113.6° in **8** whereas the corresponding values for the two molecules of **7***b* are 116.3 and 116.7°, the slightly larger value for molecule 2 of **7***b* being consistent with the longer N···N distance in the intramolecular N—H···N hydrogen bond. The five-membered BOBON

Can. J. Chem. Downloaded from www.nrcresearchpress.com by 109.225.110.28 on 09/08/12
For personal use only.

ring is nearly planar (mean deviations from the mean plane = 0.028 and 0.059 Å for the two molecules), whereas the BONCN ring has a slightly irregular N(2)/N(5)-envelope conformation (see Table 4). The degree of pyramidalization at N(2) and N(5) in **7***b* (bond angles sums = 321.7 and 315.1°) is essentially the same as that observed for the trivalent nitrogen atoms in **8** (bond angles sums = 319.3 and 317.5°).

The central N—C bond distances of the aminal group of **7***b* are different from one another, the differences being marginally smaller than those observed for **8** (5) (the mean N—C, mean C—N^+, and the difference between them are 1.447(4), 1.475(4), 0.028(6) Å for **8**; 1.448(4), 1.476(4), 0.028(6) Å for **7***b* (molecule 1); and 1.458(4), 1.468(4), and 0.010(6) Å for **7***b* (molecule 2)). The strength of the interaction between the tertiary amine function and the Lewis-acid boronate function in **8** appears to be similar to that between the tertiary amine and the proton-acid in **7***b*. The N—O bond lengths in the two molecules of **7***b* differ by less than one standard deviation. The longest of the N—O bonds is that involving the trivalent nitrogen atom in the BONCN ring (mean 1.453(2) Å for **7***b*, mean 1.459(1) Å for **8**), that in the BOBON ring being shorter (mean 1.426(2) Å for **7***b*, mean 1.447(4) Å for **8**), while the shortest N—O bond is that in the added *N*-ethylhydroxylamine base of the **7***b* molecule (mean 1.417(2) Å). As expected, the B—O bonds to the differently bound *N*-ethylhydroxylamines show the opposite trend, but there are some statistically significant differences between corresponding bonds in the two independent molecules. The longest B—O(N) bond involves the added *N*-ethylhydroxylamine base (1.508(4) and 1.494(4) Å) and is similar in length to the corresponding mean B—O(N) distance of 1.490(6) Å in the *N*-methylhydroxylamine complex **9** (11). The B—O(N) distances of 1.508(3) and 1.527(4) Å in the five-membered BOBON ring are somewhat shorter, whereas those in the five-membered BONCN ring are the shortest (1.467(4) and 1.470(4) Å). The B—C(phenyl) bond lengths range from 1.586(4) to 1.606(5) Å, typical values for compounds of this type (e.g., 1.581(5) Å in **8** (5) and 1.589(6) Å in **9** (11)).

The sum of bond lengths about B(1) and B(3), having "$PhBO_3$" ligand sets, are 6.065 and 6.067 Å, respectively. These values are similar to that of 6.100 Å for the "$PhBO_3$" compound **9** (11) and values of 6.083 to 6.101 Å reported for other related compounds (11 and references therein).

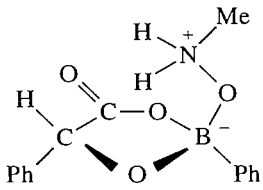

9

Acknowledgements

We thank the Natural Sciences and Engineering Research Council of Canada and the Fonds der Chemischen Industrie, Frankfurt am Main, for financial support.

1. H. Amt, W. Kliegel, S. J. Rettig, and J. Trotter. Can J. Chem. **68**, 1797 (1990).
2. R. Neu. Z. Anal. Chem. **176**, 334 (1960).
3. W. Kliegel, G. Lubkowitz, S. J. Rettig, and J. Trotter. Can. J. Chem. **69**, 234 (1991); **69**, 1217 (1991); **69**, 1227 (1991).
4. L. P. Kuhn and M. Inatome. J. Am. Chem. Soc. **85**, 1206 (1963); H. J. Roth and B. Miller. Arch. Pharm. Ber. Dtsch. Pharm. Ges. **297**, 744 (1964); A. Singh, V. D. Gupta, G. Srivastava, and R. C. Mehrotra. J. Organomet. Chem. **64**, 145 (1974); E. Hohaus. Z. Anorg. Allg. Chem. **484**, 41 (1982); W. Kliegel and D. Nanninga. Monatsh. Chem. **114**, 465 (1983); S. J. Rettig and J. Trotter. Can J. Chem. **61**, 206 (1983); H. Amt, W. Kliegel, S. J. Rettig, and J. Trotter. Can. J. Chem. **66**, 1117 (1988).
5. W. Kliegel, S. J. Rettig, and J. Trotter. Can. J. Chem. **62**, 515 (1984).
6. G. Zinner and W. Kliegel. Chem. Ber. **99**, 2686 (1966).
7. W. Kliegel. J. Organomet. Chem. **253**, 9 (1983).
8. International tables for X-ray crystallography. Kynoch Press, Birmingham, U.K. (present distributor Kluwer Academic Publishers, Dordrecht, The Netherlands). Vol. IV. 1974. pp. 99–102 and 149.
9. H. A. Staab and T. Saupe. Angew. Chem. **100**, 895 (1988).
10. A. L. Llamas Saiz and C. Foces-Foces. J. Mol. Struct. **238**, 367 (1990).
11. W. Kliegel, U. Schumacher, S. J. Rettig, and J. Trotter. Can. J. Chem. **70**, 1188 (1992).

Can. J. Chem. Downloaded from www.nrcresearchpress.com by 109.225.110.28 on 09/08/12
For personal use only.

Structural studies of organoboron compounds. LIII.[1] *N,N*-Diethylhydroxylamine-(*O-B*)1,7-dimethyl-3,5-diphenyl-2,4,6-trioxa-7-aza-1-azonia-3-bora-5-boratabicyclo[3.3.0]octane[2]

WOLFGANG KLIEGEL AND GOTTFRIED LUBKOWITZ

Institut für Pharmazeutische Chemie der Technischen Universität Braunschweig, Beethovenstrasse 55, 3300 Braunschweig, Germany

AND

STEVEN J. RETTIG AND JAMES TROTTER

Department of Chemistry, University of British Columbia, 2036 Main Mall, Vancouver, B.C., Canada V6T 1Z1

Received April 2, 1991

WOLFGANG KLIEGEL, GOTTFRIED LUBKOWITZ, STEVEN J. RETTIG, and JAMES TROTTER. Can. J. Chem. **70**, 2022 (1992).

Reaction of the condensation product of *N,N'*-dimethyl-*N,N'*-dihydroxymethanediamine and phenylboronic acid with *N,N*-diethylhydroxylamine gives *N,N*-diethylhydroxylamine(*O-B*)1,7-dimethyl-3,5-diphenyl-2,4,6-trioxa-7-aza-1-azonia-3-bora-5-boratabicyclo[3.3.0]octane [3-(2-ethyl-1-oxa-2-azoniabutyl)-1,7-dimethyl-3,5-diphenyl-2,4,6-trioxa-7-aza-1-azonia-3,5-diboratabicyclo[3.3.0]octane, **3**] in high yield. Crystals of **3** are orthorhombic, a = 11.8132(11), b = 15.4768(11), c = 11.7325(16) Å, Z = 4, space group $P2_12_12_1$. The structure was solved by direct methods and was refined by full-matrix least-squares procedures to R = 0.039 and R_w = 0.044 for 1729 reflections with $I \geq 2\sigma(I)$. The title compound is the second example of this recently characterized class of O-B coordinated hydroxylamine complexes, stabilized by an intramolecular $^+$N—H···N hydrogen bond (N···N = 2.796(6) Å). Bond lengths about boron are: B—O(N) = 1.482(4)–1.526(4), B—O(B) = 1.412(4) and 1.420(4), B—N = 1.712(4), B—C = 1.591(5) and 1.602(5) Å.

WOLFGANG KLIEGEL, GOTTFRIED LUBKOWITZ, STEVEN J. RETTIG et JAMES TROTTER. Can. J. Chem. **70**, 2022 (1992).

La réaction du produit de condensation de la *N,N'*-diméthyl-*N,N'*-dihydroxyméthanediamine et de l'acide phénylboronique avec la *N,N*-diéthylhydroxylamine fournit la *N,N*-diéthylhydroxylamine(*O-B*)1,7-diméthyl-3,5-diphényl-2,4,6-trioxa-7-aza-1-azonia-3-bora-5-boratabicyclo[3.3.0]octane [3-(2-éthyl-1-oxa-2-azoniabutyl)-1,7-diméthyl-3,5-diphényl-2,4,6-trioxa-7-aza-1-azonia-3,5-diboratabicyclo[3.3.0]octane], **3**, avec un excellent rendement. Les cristaux de ce produit sont orthorhombiques, a = 11,8132(11), b = 15,4768(11), c = 11,7325(16) Å, Z = 4 et groupe d'espace $P2_12_12_1$. On a résolu la structure par des méthodes directes et on l'a affinée par la méthode des moindres carrés jusqu'à des valeurs de R = 0,039 et R_w = 0,044 pour 1729 réflexions avec $I \geq 2\sigma(I)$. Le composé **3** n'est que le deuxième exemple la classe des complexes de l'hydroxylamine comportant une coordination O-B qui a été caractérisée récemment et qui sont stabilisés par une liaison hydrogène intramoléculaire $^+$N—H···N (N···N = 2,796(6) Å). Les longueurs des liaisons autour du bore sont: B—O(N) = 1,482(4)–1,526(4), B—O(B) = 1,412(4) et 1,420(4), B—N = 1,712(4), B—C = 1,591(5) et 1,602(5) Å.

[Traduit par la rédaction]

Introduction

The findings reported in the preceding work (1) prompted us to attempt the addition of some Lewis bases to the bicyclic compound **2** synthesized by condensation of the *N,N'*-dihydroxyaminal **1** and phenylboronic acid (2, 3). The reaction of **2** with *N,N*-diethylhydroxylamine yielded a crystalline product having the elemental analysis of a 1:1 adduct and was expected to be a further example of an O-B coordinated hydroxylamine complex stabilized by an intramolecular hydrogen bond with the postulated structure **3**. Experiments with *tert*-amine *N*-oxides having no hydrogen available at the nitrogen atom for the formation of the intramolecular $^+$N—H···N interaction failed to give stable complexes by coordination of the *N*-oxide to the sp^2 boron centre at the trigonal boronate function of **2**. No adducts of this type have thus far been obtained from the reaction of **2** with simple primary or secondary amines that do offer an N—H group for intramolecular hydrogen bonding. Presumably an intramolecular $^+$N—H···N hydrogen bond is precluded on steric grounds in this case, disallowing the formation of stable crystalline addition compounds. In contrast, the reaction product of **2** and *N,N*-diethylhydroxylamine could be isolated in good yield.

Infrared and ^{1}H nmr spectra of the reaction product confirm the existence of a relatively strong hydrogen bond with a broad low-frequency band for the N—H stretch and a low-field signal for associated NH protons, respectively. The ^{11}B nmr spectrum displays one main broadened signal at $\delta(Et_2OBF_3)$ = 9.6 ppm which is consistent with tetracoordinated boron, comparable to the δ value observed for the *N*-ethylhydroxylamine derivative (1). A second less intense signal at 21.0 ppm is indicative of the presence of a small amount of the free bicyclic compound **2** which could originate from a dissociation process in solution.[3] Parallel ^{1}H nmr spin-decoupling experiments suggest that in $CDCl_3$ solution 27% of

[1]Previous paper in this series: ref. 1.

[2]3-(2-Ethyl-1-oxa-2-azoniabutyl)-1,7-dimethyl-3,5-diphenyl-2,4,6-trioxa-7-aza-1-azonia-3,5-diboratabicyclo[3.3.0]octane.

[3]An even less intense signal in the ^{11}B nmr spectrum, at $\delta(Et_2OBF_3)$ = 30.0 ppm, is consistent with the presence of a minor component containing a trigonal planar sp^2 boron (4), such as that in a trigonal planar phenylboronate grouping.

Can. J. Chem. Downloaded from www.nrcresearchpress.com by 217.78.4.112 on 09/08/12
For personal use only.

Can. J. Chem. Downloaded from www.nrcresearchpress.com by 217.78.4.112 on 09/08/12
For personal use only.

TABLE 1. Final atomic coordinates (fractional) and B_{eq} (Å^2)[a]

Atom	x	y	z	B_{eq}	Occ.
O(1)	0.1503(2)	0.1644(1)	0.6034(2)	6.7	
O(2)	0.0936(2)	0.1610(1)	0.3299(2)	5.8	
O(3)	0.2594(2)	0.1975(1)	0.4295(2)	5.4	
O(4)	0.2572(2)	0.0659(1)	0.3132(2)	7.4	
N(1)	0.0801(3)	0.0968(2)	0.5555(3)	7.7	
N(2)	0.0564(2)	0.2067(2)	0.4288(2)	5.5	
N(3)	0.2394(4)	0.0170(2)	0.4142(4)	9.8	
C(1)	−0.0087(3)	0.1465(3)	0.5004(3)	7.5	
C(2)	0.0350(5)	0.0470(3)	0.6512(4)	11.3	
C(3)	−0.0135(3)	0.2794(2)	0.3906(3)	7.1	
C(4)	0.1980(6)	−0.0692(2)	0.3832(5)	11.7	
C(5)	0.0772(6)	−0.0658(3)	0.3464(5)	13.1	
C(6A)	0.383(1)	0.0179(5)	0.4442(8)	6.5	0.50
C(6B)	0.3157(7)	0.0105(5)	0.5164(8)	6.0	0.50
C(7A)	0.386(1)	−0.0088(7)	0.5632(9)	8.5	0.50
C(7B)	0.4198(9)	−0.0317(8)	0.471(1)	8.9	0.50
C(8)	0.1882(2)	0.3197(2)	0.5563(3)	5.2	
C(9)	0.1818(3)	0.3385(2)	0.6711(3)	7.0	
C(10)	0.1965(4)	0.4217(3)	0.7123(4)	8.8	
C(11)	0.2178(4)	0.4885(3)	0.6402(5)	8.8	
C(12)	0.2241(4)	0.4729(2)	0.5258(4)	7.5	
C(13)	0.2109(3)	0.3892(2)	0.4853(3)	6.2	
C(14)	0.2676(3)	0.2047(2)	0.2117(3)	5.6	
C(15)	0.2001(3)	0.2397(2)	0.1277(3)	6.4	
C(16)	0.2424(4)	0.2801(2)	0.0317(4)	7.8	
C(17)	0.3572(5)	0.2863(3)	0.0180(4)	8.9	
C(18)	0.4272(4)	0.2535(4)	0.0980(5)	10.0	
C(19)	0.3843(3)	0.2127(3)	0.1931(4)	8.2	
B(1)	0.1758(3)	0.2241(2)	0.5081(3)	5.3	
B(2)	0.2214(3)	0.1602(2)	0.3258(4)	5.4	

[a] $B_{eq} = (8/3)\pi^2\Sigma\Sigma U_{ij} a_i^* a_j^* (a_i \cdot a_j)$.

TABLE 2. Bond lengths (Å) with estimated standard deviations

Atom	Atom	Distance	Atom	Atom	Distance
O(1)	N(1)	1.448(4)	C(6A)	C(7A)	1.46(1)
O(1)	B(1)	1.482(4)	C(6B)	C(7B)	1.49(1)
O(2)	N(2)	1.428(3)	C(8)	C(9)	1.380(5)
O(2)	B(2)	1.510(4)	C(8)	C(13)	1.386(4)
O(3)	B(1)	1.412(4)	C(8)	B(1)	1.591(5)
O(3)	B(2)	1.420(4)	C(9)	C(10)	1.387(5)
O(4)	N(3)	1.421(4)	C(10)	C(11)	1.359(6)
O(4)	B(2)	1.526(4)	C(11)	C(12)	1.366(6)
N(1)	C(1)	1.452(5)	C(12)	C(13)	1.388(5)
N(1)	C(2)	1.463(5)	C(14)	C(15)	1.378(5)
N(2)	C(1)	1.471(4)	C(14)	C(19)	1.402(5)
N(2)	C(3)	1.466(4)	C(14)	B(2)	1.602(5)
N(2)	B(1)	1.712(4)	C(15)	C(16)	1.381(5)
N(3)	C(4)	1.468(5)	C(16)	C(17)	1.369(7)
N(3)	C(6A)	1.73(1)	C(17)	C(18)	1.350(7)
N(3)	C(6B)	1.50(1)	C(18)	C(19)	1.378(6)
C(4)	C(5)	1.492(8)			

the uncoordinated species **2** and 27% of free *N,N*-diethylhydroxylamine accompany 73% of the intact 1 : 1 complex. To be sure that the postulated structure **3** is realized, rather than the possible alternatives discussed before (1) (an N-B coordinated adduct, for example), an X-ray crystallographic analysis has been carried out to allow an unambiguous assignment of the solid-state molecular structure.

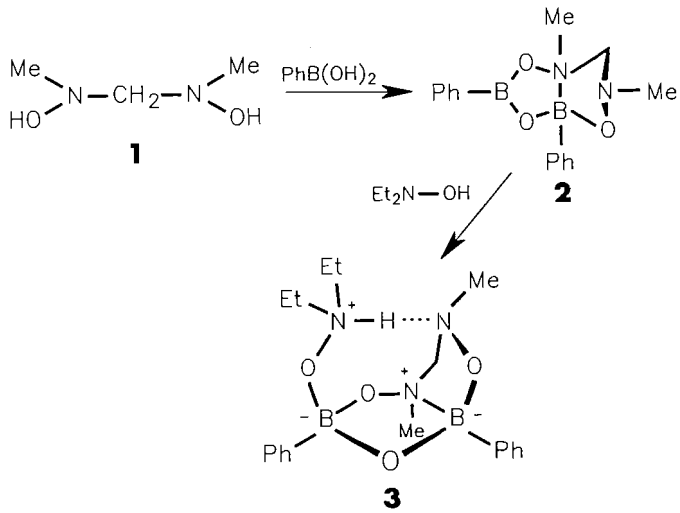

Experimental

N,N-*Diethylhydroxylamine*(O-B)*1,7-dimethyl-3,5-diphenyl-2,4,6-trioxa-7-aza-1-azonia-3-bora-5-boratabicyclo[3.3.0]octane, 3*

Compound **2**, prepared by condensation of **1** and phenylboronic acid as previously reported (2), (0.59 g, 2 mmol) and *N,N*-diethylhydroxylamine (0.18 g, 2 mmol) were dissolved in 3 mL boiling ethanol. The hot solution was filtered, cooled, and kept at −18°C for 6 h. The precipitated substance was recrystallized from absolute ethanol. Yield: 0.65 g (84%); mp 125–126°C (from EtOH). Infrared (KBr): 2100–2800 cm^{-1} (N—H). ^{1}H nmr (400 MHz, $CDCl_3$/TMS) δ (ppm): 1.09–1.19 (m, 27% of 6H, $2CH_2CH_3$), 1.36 (t, J = 7.3 Hz, 73% of 3H, CH_2CH_3), 1.38 (t, J = 7.4 Hz, 73% of 3H, CH_2CH_3), 2.44 (s, 73% of 3H, N—CH_3), 2.67–2.74 (m, 27% of 4H, CH_2CH_3), 2.76 (s, 27% of 6H, 2N—CH_3), 2.84 (s, 73% of 3H, $^+$N—CH_3), 3.11–3.22 (m, 73% of 1H, CH_2CH_3), 3.22–3.31 (m, 73% of 1H, CH_2CH_3), 3.29 and 4.16 (d and d, J = 7.8 Hz, 73% of 2H, N—CH_2—N), 3.49–3.61 (m, 73% of 1H, CH_2CH_3), 3.71–3.84 (m, 73% of 1H, CH_2CH_3), 3.74 (s, 27% of 2H, N—CH_2—N), 7.19–7.45 (m, 6 arom. H), 7.65–7.85 (m, 4 arom. H), 12.40 (s, broad, 73% of 1H, $^+$NH, exchangeable).[4] ^{11}B nmr (64 MHz, $CDCl_3/Et_2OBF_3$) δ (ppm): 9.6 (broad, highest intensity), 21.0 (broad, small), 30.0 (broad, very small). Anal. calcd. for $C_{19}H_{29}B_2N_3O_4$: C 59.26, H 7.59, B 5.61, N 10.91; found: C 59.17, H 7.62, B 5.89, N 10.85.

X-ray crystallographic analysis of 3

A crystal ca. 0.25 × 0.35 × 0.45 mm in size was mounted on a glass fiber. Unit-cell parameters were refined by least-squares on setting angles for 25 reflections (2θ = 54.9–88.6°) measured on a diffractometer with Cu-K_α radiation (λ = 1.54178 Å). Crystal data at 21°C are as follows

$C_{19}H_{29}B_2N_3O_4$ fw = 385.08

Orthorhombic, a = 11.8132(11), b = 15.4768(11), c = 11.7325(16) Å, V = 2145.0(3) Å^3, Z = 4, ρ_c = 1.192 Mg m^{-3}, $F(000)$ = 824, μ(Cu-K_α) = 6.27 cm^{-1}. Absent reflections: $h00$, h odd, $0k0$, k odd, and $00l$, l odd, uniquely indicate the space group $P2_12_12_1$ (No. 19).

Intensities were measured with graphite-monochromated Cu-K_α radiation on a Rigaku AFC6S diffractometer. An ω–2θ scan at 32° min^{-1} over a range of (1.00 + 0.20 tan θ)° in ω (with up to 8 rescans, background/scan time ratio = 0.5) was employed. Data were

[4] 27% of 1H (free or otherwise associated Et_2NOH base) remained undetected.

Can. J. Chem. Downloaded from www.nrcresearchpress.com by 217.78.4.112 on 09/08/12
For personal use only.

TABLE 3. Bond angles (deg) with estimated standard deviations

Atom	Atom	Atom	Angle	Atom	Atom	Atom	Angle
N(1)	O(1)	B(1)	105.9(2)	C(8)	C(9)	C(10)	121.9(4)
N(2)	O(2)	B(2)	109.7(2)	C(9)	C(10)	C(11)	120.9(4)
B(1)	O(3)	B(2)	117.2(2)	C(10)	C(11)	C(12)	119.1(4)
N(3)	O(4)	B(2)	112.8(3)	C(11)	C(12)	C(13)	119.7(4)
O(1)	N(1)	C(1)	101.8(3)	C(8)	C(13)	C(12)	122.7(3)
O(1)	N(1)	C(2)	106.9(3)	C(15)	C(14)	C(19)	115.0(4)
C(1)	N(1)	C(2)	111.0(4)	C(15)	C(14)	B(2)	124.8(3)
O(2)	N(2)	C(1)	108.1(3)	C(19)	C(14)	B(2)	120.2(4)
O(2)	N(2)	C(3)	107.8(2)	C(14)	C(15)	C(16)	123.5(4)
O(2)	N(2)	B(1)	105.4(2)	C(15)	C(16)	C(17)	119.1(4)
C(1)	N(2)	C(3)	111.5(3)	C(16)	C(17)	C(18)	119.9(5)
C(1)	N(2)	B(1)	102.7(2)	C(17)	C(18)	C(19)	120.7(4)
C(3)	N(2)	B(1)	120.6(2)	C(14)	C(19)	C(18)	121.9(4)
O(4)	N(3)	C(4)	109.1(3)	O(1)	B(1)	O(3)	116.9(3)
O(4)	N(3)	C(6A)	91.2(4)	O(1)	B(1)	N(2)	98.3(2)
O(4)	N(3)	C(6B)	127.8(5)	O(1)	B(1)	C(8)	109.3(3)
C(4)	N(3)	C(6A)	112.6(5)	O(3)	B(1)	N(2)	100.1(2)
C(4)	N(3)	C(6B)	109.7(4)	O(3)	B(1)	C(8)	116.1(3)
N(1)	C(1)	N(2)	102.2(3)	N(2)	B(1)	C(8)	114.5(2)
N(3)	C(4)	C(5)	111.0(5)	O(2)	B(2)	O(3)	106.6(3)
N(3)	C(6A)	C(7A)	103(1)	O(2)	B(2)	O(4)	106.7(3)
N(3)	C(6B)	C(7B)	103.7(9)	O(2)	B(2)	C(14)	111.3(3)
C(9)	C(8)	C(13)	115.7(3)	O(3)	B(2)	O(4)	112.6(3)
C(9)	C(8)	B(1)	122.5(3)	O(3)	B(2)	C(14)	115.7(3)
C(13)	C(8)	B(1)	121.8(3)	O(4)	B(2)	C(14)	103.6(3)

TABLE 4. Intra-annular torsion angles (deg) with estimated standard deviations in parentheses

Atoms	Value (deg)
B(1)—N(2)—O(2)—B(2)	−9.5(3)
N(2)—O(2)—B(2)—O(3)	6.3(3)
O(2)—B(2)—O(3)—B(1)	0.7(4)
B(2)—O(3)—B(1)—N(2)	−5.9(3)
O(3)—B(1)—N(2)—O(2)	9.3(3)
B(1)—N(2)—C(1)—N(1)	−32.8(3)
N(2)—C(1)—N(1)—O(1)	52.8(3)
C(1)—N(1)—O(1)—B(1)	−52.3(4)
N(1)—O(1)—B(1)—N(2)	28.5(3)
O(1)—B(1)—N(2)—C(1)	3.0(3)

measured to $2\theta = 155°$. The intensities of three check reflections, measured every 200 reflections throughout the data collection, showed a linear decline of 7.8%. After data reduction,[5] an empirical absorption correction, based on azimuthal scans for three reflections, and a linear decay correction were applied. Transmission factors range from 0.96 to 1.00. Of the 2269 independent reflections measured, 1729 had intensities greater than or equal to $2\sigma(F^2)$ above background, where $\sigma^2(F^2) = [S^2(C + 4B) + (0.01F^2)^2]/Lp^2$ with S = scan speed, C = scan count, B = total background count, and Lp = Lorentz-polarization factor.

[5]TEXSAN/TEXRAY structure analysis package which includes versions of the following: MITHRIL, integrated direct methods, by C. J. Gilmore; DIRDIF, direct methods for difference structures, by P. T. Beurskens; ORFLS, full-matrix least-squares, and ORFFE, function and errors, by W. R. Busing, K. O. Martin, and H. A. Levy; ORTEP II, illustrations, by C. K. Johnson.

The structure was solved by direct methods. The non-hydrogen atoms were refined with anisotropic thermal parameters, the N–H proton was refined with an isotropic thermal parameter, and the remaining hydrogen atoms were fixed in idealized positions (C—H = 0.98 Å, $B_H = 1.2B_{\text{bonded atom}}$). The C(6),C(7) ethyl group of the *N,N*-diethylhydroxylamine moiety was found to be 1 : 1 disordered over two positions; the split carbon atoms were refined with anisotropic thermal parameters. The site occcupancy factor of C(6A) was initially refined with the constraints that the occupancy factors for C(6A) and C(6B) sum to 1.00 and that site occupancies of the β-carbons (C(7A) and C(7B)) be equal to those of the α-carbons. The refined occupancy of C(6A) converged at 0.501. In the final stages of the refinement the occupancy factors were fixed at 0.50. The geometry at N(3) suggests that the entire Et_2NH^+ moiety may be disordered, but attempts to refine a disordered model for atoms N(3), C(4), C(5), and H(1) were not successful. A correction for secondary extinction was applied, the final value of the extinction coefficient being 8.43×10^{-6}. Scattering factors for all atoms and anomalous dispersion corrections for the non-hydrogen atoms were taken from ref. 5. The weighting scheme $w = 4F_o^2/\sigma^2(F_o^2)$ gave uniform average values of $w(|F_o| - |F_c|)^2$ over ranges of both $|F_o|$ and $\sin\theta/\lambda$ and was employed in the final stages of full-matrix least-squares refinement of 276 variables. Reflections with $I < 2\sigma(I)$ were not included in the refinement. Convergence was reached at $R = 0.039$, $R_w = 0.044$, and $S = 2.50$ for 1729 reflections with $I \geq 2\sigma(I)$. The function minimized was $\Sigma w(|F_o| - |F_c|)^2$, $R = \Sigma||F_o| - |F_c||/\Sigma|F_o|$, $R_w = (\Sigma w(|F_o| - |F_c|)^2/\Sigma w|F_o|^2)^{1/2}$, $S = (\Sigma w(|F_o| - |F_c|)^2/(m - n))^{1/2}$ (where m = number of observations and n = number of variables).

On the final cycle of refinement the maximum parameter shift corresponded to 0.31σ. The final difference map showed maximum fluctuations of −0.10 to +0.13 e Å^{-3}. A parallel refinement of the opposite enantiomer resulted in marginally higher residuals, the R and R_w factors ratios being 1.002 and 1.003, respectively. The final positional and (equivalent) isotropic thermal parameters for the non-hydrogen atoms appear in Table 1. Bond

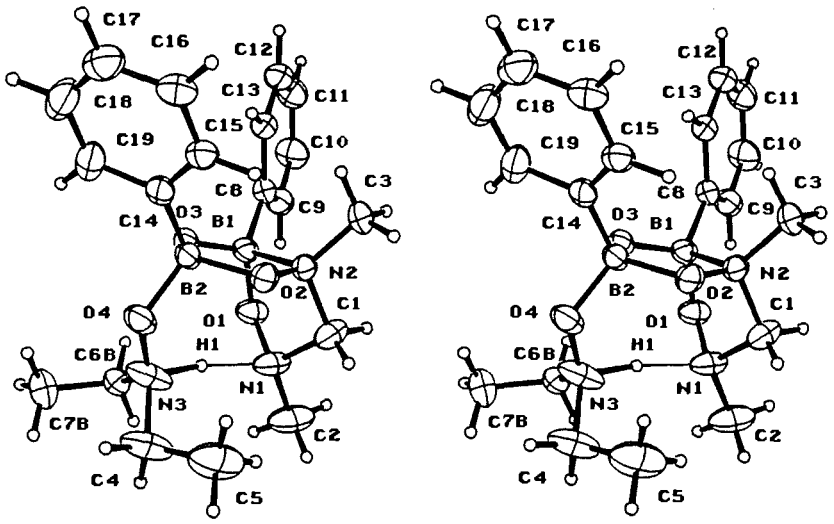

FIG. 1. Stereoview of **3**; 20% probability thermal ellipsoids are shown for the non-hydrogen atoms. For the sake of clarity, only one component of the disordered C(6),C(7) ethyl group is shown.

Can. J. Chem. Downloaded from www.nrcresearchpress.com by 217.78.4.112 on 09/08/12
For personal use only.

lengths and angles are given in Tables 2 and 3 and intra-annular torsion angles in Table 4. Hydrogen-atom parameters, anisotropic thermal parameters, torsion angles, intermolecular contacts, least-squares planes, and structure factors have been deposited.[6]

Results and discussion

The postulated structure **3**, featuring O-B coordination of the *N,N*-diethylhydroxylamine, is established by the X-ray analysis. The molecule shown in Fig. 1 is the (1*S*,3*S*,5*R*,7*S*) enantiomer (chiral centres N(2), B(2), B(1), and N(1) respectively) and is the only one present in the particular crystal chosen for the X-ray analysis; the bulk sample is racemic. This type of adduct is essentially the same as that found for the *N*-monoethylhydroxylamine complex, **4**, reported in the preceding paper (1), the hydroxylamine being bonded through the oxygen atom of the *N*-oxide form to the acceptor boronate group. The complex is stabilized by a relatively strong intramolecular $^{+}$N—H···N hydrogen bond (N(3)–H(1)···N(1), N–H = 1.27(6) Å, N···H = 1.54(6) Å, N···N = 2.796(6) Å, N—H···N = 166(5)°). There are no additional *inter*-molecular hydrogen bonds involving the protonated nitrogen atom of **3** as were observed in the structure of **4** (1) which has two NH protons associated with the hydroxylamine ligand. All intermolecular distances correspond to normal van der Waals interactions, the shortest intermolecular contact involving non-hydrogen atoms being C(1)···C(13) = 3.363(5) Å.

The overall geometry of the ring system of **3** is quite similar to that reported for **4** (1) but there are several significant differences between the two molecules. The bonds at the pyroboronate connection are shorter in **3** than in **4**[7] (O—B = 1.412(4) and 1.420(4) vs. 1.434(4) and 1.446(4) Å), whereas the (N)O—B bond involving the hydroxylamine ligand is longer in the present complex (1.526(4) vs. 1.501(4) Å). The intramolecular $^{+}$N—H···N hydrogen bond is significantly stronger in **3**, the N···N distance being 0.124 Å shorter than the mean distance of 2.920 Å reported for **4**. The transannular non-bonding distance between N(1) and B(2) in **3** (3.318(5) Å) is shorter than the corresponding mean of 3.409 Å in the *N*-ethylhydroxylamine complex **4** (1), whereas both of these distances are longer than that in the parent compound **2** (3.083 Å) (3). Both the stronger $^{+}$N—H···N hydrogen bond and the shorter transannular non-bonding N···B distance in **3** relative to those in **4** may be a result of the absence of a second hydrogen (and the associated intermolecular hydrogen bonding) at the hydroxylamine nitrogen atom.

The five-membered BOBON ring in **3** has a flattened N(2)-envelope conformation (see Table 4) and is planar to within 0.083(3) Å, similar to the corresponding ring in **4**. The five-membered BONCN ring has a slightly distorted N(1)-envelope conformation. The angle between the normals to the mean planes of the BOBON ring and the approximately (to within 0.023(4) Å) planar O(1)B(1)N(2)C(1) portion of the BONCN ring of 116.0° is identical to the value reported for **2** (3). The degree of pyramidalization at N(1) in **3** is comparable to that observed for **4** (1), the sums of bond angles about N(1) being 319.7 and 318.4° (mean), respectively. The sum of the bond distances about B(2) (6.058 Å) is similar to those reported for **4** and other anionic $PhBO_3$ complexes (ref. 1 and references therein).

Acknowledgements

We thank the Natural Sciences and Engineering Research Council of Canada and the Fonds der Chemischen Industrie, Frankfurt am Main, for financial support.

[6]Supplementary material mentioned in the text may be purchased from the Depository of Unpublished Data, Document Delivery, CISTI, National Research Council Canada, Ottawa, Canada K1A 0R6.

Tables of hydrogen atom coordinates and intermolecular distances have also been deposited with the Cambridge Crystallographic Data Centre and can be obtained on request from the Director, Cambridge Crystallographic Data Centre, University Chemical Laboratory, Lensfield Road, Cambridge, CB2 1EW, U.K.

[7]Distances quoted for compound **4** are average values for the two crystallographically independent molecules and the standard deviations are the larger of the two individual values.

1. W. Kliegel, G. Lubkowitz, S. J. Rettig, and J. Trotter. Can. J. Chem. **70**, 2015 (1992).
2. W. Kliegel. J. Organomet. Chem. **253**, 9 (1983).
3. W. Kliegel, S. J. Rettig, and J. Trotter. Can. J. Chem. **62**. 515 (1984).
4. H. Nöth and B. Wrackmeyer. Nuclear magnetic resonance spectroscopy of boron compounds. Springer-Verlag, Berlin. 1978; B. Wrackmeyer. Annu. Rep. NMR Spectrosc. **20**, 61 (1988); A. R. Siedle. Annu. Rep. NMR Spectrosc. **20**, 205 (1988).
5. International tables for X-ray crystallography. Kynoch Press, Birmingham, U.K. (present distributor Kluwer Academic Publishers, Dordrecht, The Netherlands). Vol. IV. 1974. pp. 99–102 and 149.

Can. J. Chem. Downloaded from www.nrcresearchpress.com by 217.78.4.112 on 09/08/12
For personal use only.

Structural studies of organoboron compounds. LIV.[1] 4-Cyclohexyl-2-methyl-3,6,8-triphenyl-5,7,9-trioxa-4-aza-1-azonia-8-bora-6-boratabicyclo[4.3.0]nonane

WOLFGANG KLIEGEL AND GOTTFRIED LUBKOWITZ

Institut für Pharmazeutische Chemie der Technischen Universität Braunschweig, Beethovenstrasse 55, 3300 Braunschweig, Germany

AND

STEVEN J. RETTIG AND JAMES TROTTER

Department of Chemistry, University of British Columbia, 2036 Main Mall, Vancouver, B.C., Canada V6T IZI

Received April 30, 1991

WOLFGANG KLIEGEL, GOTTFRIED LUBKOWITZ, STEVEN J. RETTIG, and JAMES TROTTER. Can. J. Chem. **70**, 2027 (1992).

The synthesis of N^1-cyclohexyl-N^1,N^2-dihydroxy-1-phenyl-1,2-propanediamine and its reaction with phenylboronic acid to produce 4-cyclohexyl-2-methyl-3,6,8-triphenyl-5,7,9-trioxa-4-aza-1-azonia-8-bora-6-boratabicyclo[4.3.0]nonane, **5**, in moderate yield are described. Crystals of the organoboron derivative **5** are triclinic, a = 11.4142(8), b = 12.4719(8), c = 10.2154(6) Å, α = 75.177(6), β = 112.306(5), γ = 105.000(6)°, Z = 2, space group $P\bar{1}$. The structure was solved by direct methods and was refined by full-matrix least-squares procedures to R = 0.037 and R_w = 0.053 for 4232 reflections with $I \geq 3\sigma(I)$. The bicyclo[4.3.0]nonane system consists of a six-membered BONCNN ring and a five-membered BOBON ring *cis*-fused about the transannular N→B bond. Bond lengths involving boron are: (sp^2)B—O(B) = 1.336(2), (sp^2)B—O(N) = 1.411(2), (sp^2)B—C(aryl) = 1.557(2), (sp^3)B—O(B) = 1.457(2), (sp^3)B—O(N) = 1.434(2), (sp^3)B—N = 1.706(2), and (sp^3)B—C(aryl) = 1.593(2) Å.

WOLFGANG KLIEGEL, GOTTFRIED LUBKOWITZ, STEVEN J. RETTIG et JAMES TROTTER. Can. J. Chem. **70**, 2027 (1992).

On décrit la synthèse de la N^1-cyclohexyl-N^1,N^2-dihydroxy-1-phényl-propane-1,2-diamine et sa réaction avec l'acide phénylboronique pour donner le 4-cyclohexyl-2-méthyl-3,6,8-triphényl-5,7,9-trioxa-4-aza-1-azonia-8-bora-6-boratabicyclo[4.3.0]nonane, **5**, avec un modeste rendement. Les cristaux de ce produit sont tricliniques, a = 11,4142(8), b = 12,4719(8), c = 10,2154(6) Å, α = 75,177(6), β = 112,306(5), γ = 105,000(6)°, Z = 2 et groupe d'espace $P\bar{1}$. On a résolu la structure par des méthodes directes et on l'a affinée par la méthode des moindres carrés jusqu'à des valeurs de R = 0,037 et R_w = 0.053 pour 4232 réflexions avec $I \geq 3\sigma(I)$. Le système bicyclo[4.3.0]nonane comprend un cycle à six chaînons BONCCN et un cycle à cinq chaînons BOBON condensés d'une façon *cis* avec une liaison transannulaire N→B. Les longueurs des liaisons impliquant le bore sont: (sp^2)B—O(B) = 1,336(2), (sp^2)B—O(N) = 1,411(2), (sp^2)B—C(aryl) = 1,557(2), (sp^3)B—O(B) = 1,457(2), (sp^3)B—O(N) = 1,434(2), (sp^3)B—N = 1,706(2) et (sp^3)B—C(aryl) = 1,593(2) Å.

[Traduit par la rédaction]

Introduction

As part of our continuing study of polycyclic boron complexes with hydroxylamine ligands the N^1-substituted 1,2-bishydroxylamine **3** has been synthesized from the nitropropene derivative **1** (1) followed by the addition of *N*-cyclohexylhydroxylamine and a subsequent reduction of the nitro group of the addition product **2**.[2]

The bishydroxylamine **3** was then reacted with 2 molar equivalents of phenylboronic acid targeting the preparation of a cyclic pyroboronate with transannular N→B coordination, similar to the bicyclic compound **7** which had been obtained from a symmetrically substituted bishydroxylamine (3). A crystalline compound with an elemental analysis consistent with the desired 2:1 condensate of phenylboronic acid and **3** was isolated from this reaction, the infrared and ^{1}H nmr spectra confirming a bisphenylboronate constitution. Based on the crystallographically established structure **7** (3), a similar bicyclononane skeleton was also expected for this product. In contrast to compound **7**, the unsymmetrically substituted ligand of the new derivative allows two alternative transannular bonds between different nitrogen and boron bridgeheads, as in **4** and **5**, respectively. Structure **5** would furthermore offer another site for protonation and could isomerize by proton migration to **6**.[3]

Infrared and ^{1}H nmr data are insufficient for a definitive structural assignment. In the solid state (KBr tablet) infrared spectrum a sharp absorption band at 3210 cm^{-1} could be assigned to an N—H stretching mode, consistent with the ammonium function present in both **5** and **6**. Related hydroxylamine derivatives with quaternized nitrogen like **8** (4, 5) or **9** (6) also display distinct N—H bands in their infrared spectra, though at somewhat lower frequencies between 3050 and 3150 cm^{-1}. A compound of structure **4** would be expected to display an N—H stretching frequency similar to, but not as distinct as, those reported for O,N-disubstituted hydroxylamine derivatives which absorb at about 3200 cm^{-1} (7, 8). The ^{1}H nmr spectrum displays a signal for one exchangeable proton at δ = 6.50 ppm in $CDCl_3$ solu-

[1]Previous paper in this series: ref. 12.

[2]The addition of the *N*-cyclohexylhydroxylamine seems to be quite stereoselective since only one of the possible diastereomers of **2** was obtained (61%). Narrow melting ranges and unambiguous ^{1}H nmr spectra of **2** (as well as of the reduction product **3**) indicate the formation of only one of the diastereomers which should be present as a racemate. Similar diastereoselectivity has been reported for the addition of cyclohexylamine to 2-nitro-1-phenylpropene (2).

[3]Other less probable polycyclic skeleton isomers that could be formed have been discussed in a previous report (2) and will not be dealt with here.

Can. J. Chem. Downloaded from www.nrcresearchpress.com by 217.78.4.112 on 09/08/12
For personal use only.

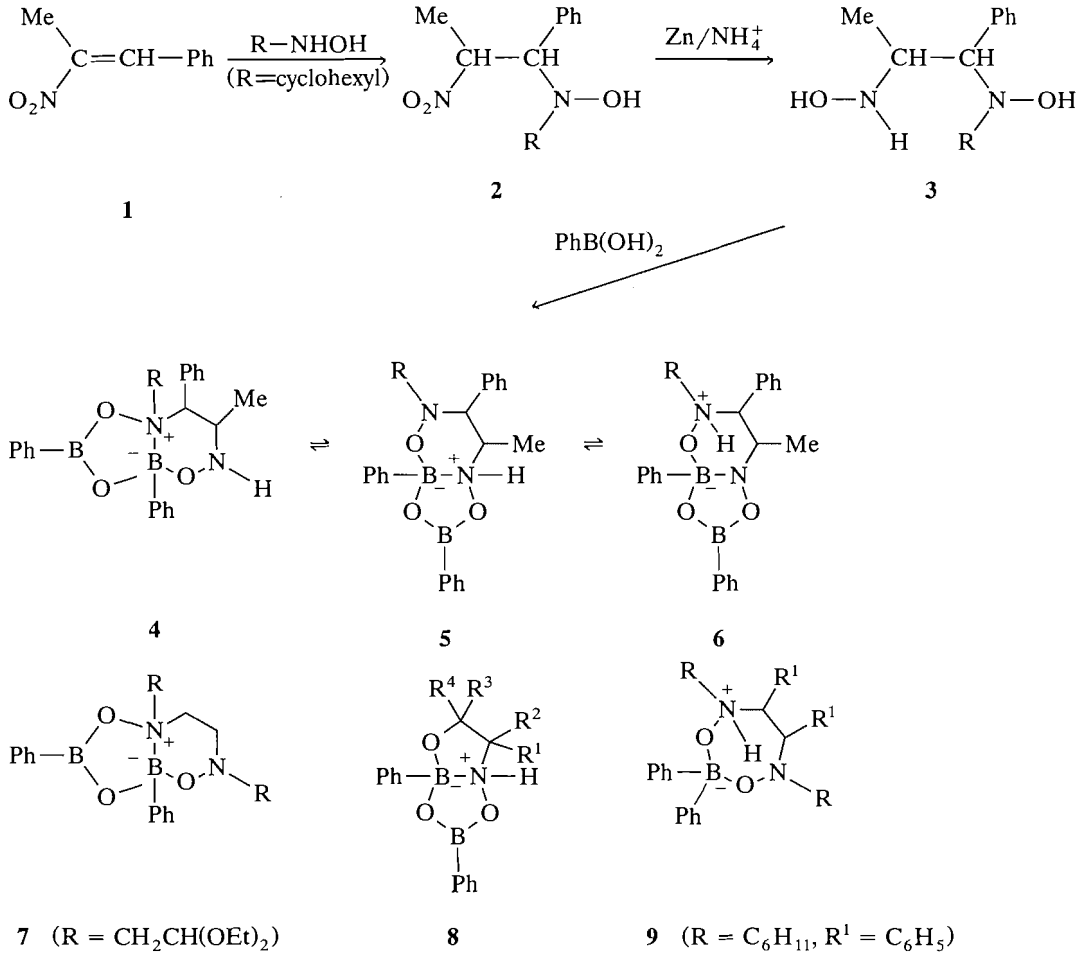

tion and at 10.02 ppm in DMSO-d_6 solution. No coupling is observed between the N—H proton and the vicinal C—H proton which could be possible for all three structures **4**, **5**, and **6**. All of these isomers have structures consistent with the entire ^{1}H nmr spectra produced in either solvent. The possible temperature-dependent fluxional processes of topomerization (**4**↔**5**) and (or) prototropy (**5**↔**6**) could cause signal coalescence in the nmr experiments and must be taken into consideration.

The question of which of the three isomers **4**, **5**, or **6** would be "frozen" in a single crystal of this material was therefore of great interest. An X-ray crystallographic analysis was undertaken to establish the solid-state molecular structure.

Experimental

N-*Cyclohexyl*-N-*hydroxy-2-nitro-1-phenylpropanamine, 2 ($R = C_6H_{11}$)*

2-Nitro-1-phenylpropene (1) (4.89 g, 30 mmol) and cyclohexylhydroxylamine (3.46 g, 30 mmol) were dissolved in 50 mL of methanol and refluxed for 2 h. The solvent was removed *in vacuo* and the remaining oil was dissolved in 10 mL of absolute ethanol. Crystallization at −30°C yields 5.10 g (61%) of a colorless substance, mp 100–101°C (from absolute ethanol). Infrared (KBr): 3510 (O—H), 1550 cm^{-1} (NO_2). ^{1}H nmr ($CDCl_3$/TMS) δ (ppm): 0.85–2.05 (m, $(CH_2)_5$), 1.29 (d, J = 6 Hz, CH_3), 2.16–2.48 (m, N—C*H*$(CH_2)_5$), 4.30 (d, J = 11 Hz, C*H*—Ph), 4.80 (s, exchangeable, OH), 5.38 (m_c, C*H*—Me), 7.2–8.5 (m, C_6H_5). Anal. calcd. for $C_{15}H_{22}N_2O_3$: C 64.73, H 7.97, N 10.06; found: C 64.66, H 8.00, N 10.12.

N^1-*Cyclohexyl*-N^1,N^2-*dihydroxy-1-phenyl-1,2-propanediamine, 3 ($R = C_6H_{11}$)*

N-Cyclohexyl-*N*-hydroxy-2-nitro-1-phenylpropanamine, **2** (8.34 g, 30 mmol) was dissolved in 100 mL ethanol (96%). After addition of a solution of ammonium chloride (6 g) in 25 mL water, zinc dust (11 g) was added in small portions under vigorous stirring such that the temperature of the solution did not exceed 30°C. Stirring was continued for 2 h, the precipitate was filtered off and washed with boiling tetrahydrofuran (2 × 150 mL). The combined solutions were evaporated *in vacuo*, and the dry residue recrystallized from tetrahydrofuran. Yield: 5.91 g (75%), mp 168–169°C (from THF). Infrared (KBr): 3370 (O—H), 2260 cm^{-1} (broad, O—H, associated). ^{1}H nmr (DMSO-d_6/TMS) δ (ppm): 0.72 (d, J = 7 Hz, CH_3), 0.85–1.93 (m, $(CH_2)_5$), 1.98–2.30 (m, N—C*H*$(CH_2)_5$), 3.54 (m_c, C*H*—Me), 3.79 (d, J = 9 Hz, C*H*—Ph), 6.01, 6.89, and 7.58 (3 s, exchangeable, 2OH and NH), 7.1–7.4 (m, C_6H_5). Anal. calcd. for $C_{15}H_{24}N_2O_2$: C 68.15, H 9.15, N 10.60; found: C 68.04, H 9.27, N 10.44.

4-*Cyclohexyl-2-methyl-3,6,8-triphenyl-5,7,9-trioxa-4-aza-1-azonia-8-bora-6-boratabicyclo[4.3.0]nonane, 5 ($R = C_6H_{11}$)*

N^1-Cyclohexyl-N^1,N^2-dihydroxy-1-phenyl-1,2-propanediamine, **3** (0.53 g, 2 mmol) and phenylboronic acid (0.49 g, 4 mmol) were suspended in 10 mL of tetrachloromethane and refluxed for 1.5 h with continuous removal of reaction water. The solution was evaporated *in vacuo* to half of its original volume and diluted with 170 mL of petroleum ether (bp 30–70°C). At −18°C a colorless

Can. J. Chem. Downloaded from www.nrcresearchpress.com by 217.78.4.112 on 09/08/12
For personal use only.

Can. J. Chem. Downloaded from www.nrcresearchpress.com by 217.78.4.112 on 09/08/12
For personal use only.

TABLE 1. Final atomic coordinates (fractional) and B_{eq} (Å^2)[a]

Atom	x	y	z	B_{eq}
O(1)	0.32575(8)	0.25495(7)	0.66569(9)	4.1
O(2)	0.37248(9)	0.43204(7)	0.8783(1)	4.6
O(3)	0.47492(9)	0.43086(7)	0.7199(1)	4.6
N(1)	0.2244(1)	0.31656(7)	0.6403(1)	3.6
N(2)	0.3857(1)	0.31641(8)	0.8979(1)	4.3
C(1)	0.1595(1)	0.2593(1)	0.7469(1)	3.9
C(2)	0.2628(1)	0.2384(1)	0.8956(1)	4.3
C(3)	0.1425(1)	0.3226(1)	0.4889(1)	3.8
C(4)	0.2228(1)	0.3790(1)	0.3923(1)	4.8
C(5)	0.1399(2)	0.4003(2)	0.2347(2)	5.9
C(6)	0.0400(2)	0.4698(2)	0.2105(2)	6.6
C(7)	−0.0423(2)	0.4122(2)	0.3030(2)	5.8
C(8)	0.0393(1)	0.3902(1)	0.4612(1)	4.6
C(9)	0.0641(1)	0.1502(1)	0.7183(1)	4.2
C(10)	0.1010(2)	0.0579(1)	0.7021(2)	4.9
C(11)	0.0142(2)	−0.0415(1)	0.6781(2)	6.1
C(12)	−0.1105(2)	−0.0508(2)	0.6710(2)	6.7
C(13)	−0.1485(2)	0.0391(2)	0.6863(2)	7.1
C(14)	−0.0617(2)	0.1397(1)	0.7102(2)	5.8
C(15)	0.2195(2)	0.2426(2)	1.0169(2)	6.2
C(16)	0.4193(1)	0.6189(1)	0.7182(1)	4.6
C(17)	0.4596(2)	0.6786(1)	0.6027(2)	6.0
C(18)	0.4629(3)	0.7939(2)	0.5612(2)	7.9
C(19)	0.4252(2)	0.8504(2)	0.6337(2)	8.0
C(20)	0.3827(2)	0.7929(1)	0.7467(2)	6.6
C(21)	0.3795(1)	0.6778(1)	0.7880(2)	5.2
C(22)	0.5518(1)	0.2394(1)	0.8292(1)	4.5
C(23)	0.5284(2)	0.1233(1)	0.8374(2)	5.5
C(24)	0.6274(2)	0.0620(1)	0.8959(2)	6.4
C(25)	0.7523(2)	0.1151(2)	0.9494(2)	6.3
C(26)	0.7788(2)	0.2293(2)	0.9435(2)	6.8
C(27)	0.6795(2)	0.2910(1)	0.8836(2)	6.0
B(1)	0.4220(1)	0.4904(1)	0.7670(2)	4.4
B(2)	0.4381(1)	0.3101(1)	0.7648(2)	4.2

[a]$B_{eq} = (8/3)\pi^2\Sigma\Sigma U_{ij} a_i^* a_j^* (a_i \cdot a_j)$.

substance crystallized. Yield: 0.60 g (66%), mp 168–171°C (from CCl_4/petroleum ether). Infrared (KBr): 3210 (sharp, N—H), 1595 cm^{-1} (aromatic C=C). ^{1}H nmr ($CDCl_3$/TMS δ (ppm): 0.6–2.5 (m, C_6H_{11}), 1.39 (d, J = 6 Hz, CH_3), 3.55 (m_c, C*H*—Me), 3.94 (d, 8 Hz, C*H*—Ph), 6.50 (s, exchangeable, NH), 7.1–7.5 (m, 9 arom. H), 7.5–7.7 (m, 4 arom. H), 7.8–7.9 (m, 2 arom. H); (DMSO-d_6) δ (ppm): 0.5–2.4 (m, C_6H_{11}), 1.30 (d, J = 6 Hz, CH_3), 3.43 (m_c, C*H*—Me), 3.95 (d, 8 Hz, C*H*—Ph), 7.2–7.5 (m, 9 arom. H), 7.6–7.9 (m, 6 arom. H), 10.02 (s, exchangeable, NH). Anal. calcd. for $C_{27}H_{32}B_2N_2O_3$: C 71.40, H 7.10, B 4.76, N 6.17; found: C 71.48, H 7.22, B 4.86, N 6.14.

Crystals suitable for X-ray analysis were obtained by recrystallization from toluene/petroleum ether.

X-ray crystallographic analysis of 5 (R = C_6H_{11})

A crystal ca. 0.15 × 0.25 × 0.35 mm in size was mounted on a glass fiber. Unit-cell parameters were refined by least-squares on setting angles for 25 reflections (2θ = 101.7–120.6°) measured on a diffractometer with Cu-K_α radiation (λ = 1.54178 Å). Crystal data at 21°C are as follows

$C_{27}H_{32}B_2N_2O_3$ fw = 454.19

Triclinic, a = 11.4142(8), b = 12.4719(8), c = 10.2154(6) Å, α = 75.177(6), β = 112.306(5), γ = 105.000(6)°, V = 1279.2(2) Å^3, Z = 2, ρ_c = 1.179 Mg m^{-3}, $F(000)$ = 484, μ(Cu-K_α) = 5.60 cm^{-1}. Absent reflections: none, space group $P\bar{1}$ (No. 2) from structure analysis.

Intensities were measured with graphite-monochromated Cu-K_α radiation on a Rigaku AFC6S diffractometer. An ω–2θ scan at 32° min^{-1} over a range of (1.26 + 0.25 tan θ)° in ω (with up to 8 rescans, background/scan time ratio = 0.5) was employed. Data were measured to 2θ = 155°. The intensities of three check reflections, measured every 150 reflections throughout the data collection, showed only small random variations. After data reduction,[4] an empirical absorption correction, based on azimuthal scans for three reflections, was applied. Transmission factors range from 0.89 to 1.00. Of the 5486 reflections measured, 5206 were unique (R_{int} = 0.007), and 4232 had intensities greater than or equal to $3\sigma(F^2)$ above background where $\sigma^2(F^2) = [S^2(C + 4B) + (0.025F^2)^2]/Lp^2$ with S = scan speed, C = scan count, B = total background count, and Lp = Lorentz-polarization factor.

The structure was solved by direct methods. The non-hydrogen atoms were refined with anisotropic thermal parameters and the hydrogen atoms with isotropic thermal parameters. A correction for secondary extinction was applied, the final value of the extinction coefficient being 2.21 × 10^{-5}. Scattering factors for all atoms and anomalous dispersion corrections for the non-hydrogen atoms were taken from ref. 9. The weighting scheme $w = 4F_o^2/\sigma^2(F_o^2)$ gave uniform average values of $w(|F_o| - |F_c|)^2$ over ranges of both $|F_o|$ and sin θ/λ and was employed in the final stages of full-matrix least-squares refinement of 436 variables. Reflections with $I < 3\sigma(F_o^2)$ were not included in the refinement. Convergence was reached at R = 0.037 and R_w = 0.053 for 4232 reflections with $I \geq 3\sigma(F_o^2)$. The function minimized was $\Sigma w(|F_o| - |F_c|)^2$, $R = \Sigma||F_o| - |F_c||/\Sigma|F_o|$, $R_w = (\Sigma w(|F_o| - |F_c|)^2/\Sigma w|F_o|^2)^{1/2}$.

On the final cycle of refinement the maximum parameter shift corresponded to 0.006σ. The mean error in an observation of unit weight was 2.65. The final difference map showed maximum fluctuations of −0.12 to +0.14 e Å^{-3}. The final positional and (equivalent) isotropic thermal parameters for the non-hydrogen atoms appear in Table 1. Bond lengths and angles are given in Tables 2 and 3 and intra-annular torsion angles in Table 4. Hydrogen atom parameters, anisotropic thermal parameters, torsion angles, intermolecular contacts, least-squares planes, bond lengths and angles involving hydrogen, and structure factors have been deposited.[5]

Results and discussion

The structure analysis shows that in the solid state the bicyclic form **5** is present (Fig. 1). The transannular N→B coordinative bond dividing the cyclononane system into a six-membered BONCCN ring and a five-membered BOBON ring originates from the unsubstituted nitrogen atom N(2), presumably due to the presence of less steric hindrance (less "F-strain" (10)) at this Lewis-basic centre relative to that at N(1). The overall geometry of the bicyclo[4.3.0]nonane skeleton resembles that of compound **7** (3). The BOBON ring is axially fused to the side of the slightly distorted boat of the BONCCN ring, the annellation site being the coordinative B(2)–N(2) bond. The five-membered BOBON ring has a

[4]TEXSAN/TEXRAY structure analysis package which includes versions of the following: MITHRIL, integrated direct methods, by C. J. Gilmore; DIRDIF, direct methods for difference structures, by P. T. Beurskens; ORFLS, full-matrix least-squares, and ORFFE, function and errors, by W. R. Busing, K. O. Martin, and H. A. Levy; ORTEP II, illustrations, by C. K. Johnson.

[5]Supplementary material mentioned in the text may be purchased from the Depository of Unpublished Data, Document Delivery, CISTI, National Research Council Canada, Ottawa, Canada K1A 0R6.

Tables of hydrogen atom parameters, intermolecular contacts, and bond lengths and angles involving hydrogen have also been deposited with the Cambridge Crystallographic Data Centre and can be obtained on request from The Director, Cambridge Crystallographic Data Centre, University Chemical Laboratory, Lensfield Road, Cambridge, CB2 1EW, U.K.

TABLE 2. Bond lengths (Å) with estimated standard deviations in parentheses

Atom	Atom	Distance	Atom	Atom	Distance
O(1)	B(2)	1.434(2)	C(9)	C(10)	1.390(2)
O(1)	N(1)	1.458(1)	C(10)	C(11)	1.383(2)
O(2)	B(1)	1.411(2)	C(11)	C(12)	1.374(3)
O(2)	N(2)	1.444(1)	C(12)	C(13)	1.364(3)
O(3)	B(1)	1.336(2)	C(13)	C(14)	1.395(2)
O(3)	B(2)	1.457(2)	C(16)	C(21)	1.394(2)
N(1)	C(3)	1.467(1)	C(16)	C(17)	1.394(2)
N(1)	C(1)	1.478(1)	C(16)	B(1)	1.557(2)
N(2)	C(2)	1.482(2)	C(17)	C(18)	1.387(2)
N(2)	B(2)	1.706(2)	C(18)	C(19)	1.377(3)
C(1)	C(9)	1.522(2)	C(19)	C(20)	1.380(3)
C(1)	C(2)	1.537(2)	C(20)	C(21)	1.383(2)
C(2)	C(15)	1.515(2)	C(22)	C(27)	1.389(2)
C(3)	C(4)	1.518(2)	C(22)	C(23)	1.390(2)
C(3)	C(8)	1.523(2)	C(22)	B(2)	1.593(2)
C(4)	C(5)	1.521(2)	C(23)	C(24)	1.385(2)
C(5)	C(6)	1.517(3)	C(24)	C(25)	1.369(3)
C(6)	C(7)	1.506(3)	C(25)	C(26)	1.368(3)
C(7)	C(8)	1.522(2)	C(26)	C(27)	1.390(2)
C(9)	C(14)	1.380(2)			

TABLE 3. Bond angles (deg) with estimated standard deviations in parentheses

Atom	Atom	Atom	Angle	Atom	Atom	Atom	Angle
B(2)	O(1)	N(1)	105.06(8)	C(11)	C(10)	C(9)	121.1(2)
B(1)	O(2)	N(2)	105.1(1)	C(12)	C(11)	C(10)	120.2(2)
B(1)	O(3)	B(2)	111.6(1)	C(13)	C(12)	C(11)	119.5(2)
O(1)	N(1)	C(3)	108.25(8)	C(12)	C(13)	C(14)	120.6(2)
O(1)	N(1)	C(1)	106.88(8)	C(9)	C(14)	C(13)	120.6(2)
C(3)	N(1)	C(1)	115.96(9)	C(21)	C(16)	C(17)	118.2(1)
O(2)	N(2)	C(2)	111.0(1)	C(21)	C(16)	B(1)	122.1(1)
O(2)	N(2)	B(2)	106.22(9)	C(17)	C(16)	B(1)	119.8(1)
C(2)	N(2)	B(2)	113.0(1)	C(18)	C(17)	C(16)	120.7(2)
N(1)	C(1)	C(9)	117.5(1)	C(19)	C(18)	C(17)	119.9(2)
N(1)	C(1)	C(2)	108.6(1)	C(18)	C(19)	C(20)	120.5(2)
C(9)	C(1)	C(2)	109.5(1)	C(19)	C(20)	C(21)	119.5(2)
N(2)	C(2)	C(15)	112.4(1)	C(20)	C(21)	C(16)	121.2(2)
N(2)	C(2)	C(1)	110.4(1)	C(27)	C(22)	C(23)	116.6(1)
C(15)	C(2)	C(1)	112.9(1)	C(27)	C(22)	B(2)	121.4(1)
N(1)	C(3)	C(4)	110.1(1)	C(23)	C(22)	B(2)	122.0(1)
N(1)	C(3)	C(8)	108.23(9)	C(24)	C(23)	C(22)	121.7(2)
C(4)	C(3)	C(8)	110.3(1)	C(25)	C(24)	C(23)	120.3(2)
C(3)	C(4)	C(5)	112.0(1)	C(26)	C(25)	C(24)	119.5(2)
C(6)	C(5)	C(4)	111.4(1)	C(25)	C(26)	C(27)	120.2(2)
C(7)	C(6)	C(5)	110.2(1)	C(22)	C(27)	C(26)	121.7(2)
C(6)	C(7)	C(8)	111.3(1)	O(3)	B(1)	O(2)	116.2(1)
C(7)	C(8)	C(3)	112.3(1)	O(3)	B(1)	C(16)	125.9(1)
C(14)	C(9)	C(10)	117.9(1)	O(2)	B(1)	C(16)	117.7(1)
C(14)	C(9)	C(1)	120.6(1)	O(1)	B(2)	O(3)	115.7(1)
C(10)	C(9)	C(1)	121.4(1)	O(1)	B(2)	C(22)	112.0(1)
				O(1)	B(2)	N(2)	103.5(1)
				O(3)	B(2)	C(22)	116.0(1)
				O(3)	B(2)	N(2)	97.8(1)
				C(22)	B(2)	N(2)	109.9(1)

flattened B(2)-envelope conformation. The alkyl and aryl substituents of the six-membered BONCCN ring all occupy equatorial positions.

The bond lengths in the BOBON ring, B(2)—O(3)—B(1)—O(2)—N(2) = 1.457, 1.336, 1.411, 1.444 Å, respectively, are similar to those reported for compounds **7** (3) (1.451, 1.332, 1.401, 1.451 Å), **8** ($R^1 = R^2 = Me$, $R^3 = R^4 = H$) (4) (1.467, 1.337, 1.404, 1.440 Å), and other similar compounds cited in ref. 3. The shortest bond in this type of BOBON ring is the (sp^2)B—O bond in the anhydridic

Can. J. Chem. Downloaded from www.nrcresearchpress.com by 217.78.4.112 on 09/08/12
For personal use only.

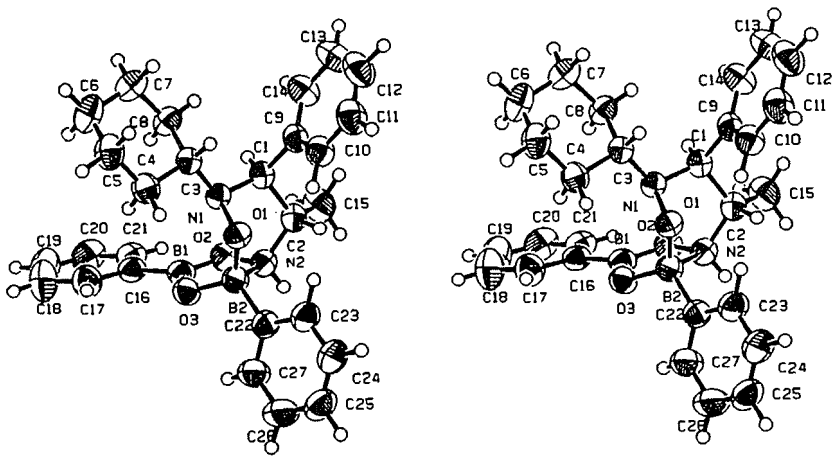

FIG 1. Stereoview of **5**; 50% probability thermal ellipsoids are shown for the nonhydrogen atoms.

TABLE 4. Intra-annular torsion angles (deg) with estimated standard deviations in parentheses

Atoms	Value (deg)
B(2)—O(1)—N(1)—C(1)	−91.4(1)
O(1)—N(1)—C(1)—C(2)	47.3(1)
N(1)—C(1)—C(2)—N(2)	21.5(1)
C(1)—C(2)—N(2)—B(2)	−54.7(1)
C(2)—N(2)—B(2)—O(1)	16.9(1)
N(2)—B(2)—O(1)—N(1)	50.2(1)
B(2)—N(2)—O(2)—B(1)	−6.1(1)
N(2)—O(2)—B(1)—O(3)	−5.2(1)
O(2)—B(1)—O(3)—B(2)	16.3(2)
B(1)—O(3)—B(2)—N(2)	−17.2(1)
O(3)—B(2)—N(2)—O(2)	13.9(1)

(sp^2)B—O—(sp^3)B segment in all cases reported to date, this distance ranging from 1.329 to 1.339 Å (3). The B—O π-bond order can be estimated as about 0.7 from a bond length versus π-bond order plot (11); this can be regarded as evidence for a considerable O—B pp(π) back-donation. Partial π-bond character can also be seen at the B(1)—O(2) bond, although it is of lesser magnitude in this portion of the ring. This is consistent with relative bond lengths observed for comparable B—O bonds in the BOBON rings of **7** (3), **8** (4), and the other structurally characterized BOBON rings (3). The approximate (or actual) planarity of these five-membered BOBON rings is consistent with the assumption of significant π-interactions.

The phenyl substituent at B(1) is nearly coplanar with the BOBON ring (dihedral angle between the normals to the mean planes = 5.6°), and the B(1)—C(16) bond length is exactly the same as the (sp^2)B—C(aryl) bond lengths in **7** (3) and **8** ($R^1 = R^2$ = Me, $R^3 = R^4$ = H) (4): 1.557 Å. The distance between B(2) and C(22) in **5** (1.593(2) Å), however, is longer than the (sp^3)B—C(aryl) distance in **7** (1.579 Å) (3). This corresponds to the short (1.706 Å) transannular N→B bond in **5** relative to that in **7** (1.756 Å), and is consistent with the previously noted observation (ref.3 and references therein) that, for a given set of ligand atoms, the sum of bond lengths about boron remains essentially constant. There is nearly no pyramidalization at B(1), the sum of bond angles at the trigonal planar boron centre being 359.8°. At N(1) the bond angle sum is 331.1°. The geometry at N(1) would allow a coordinative interaction with B(1), the non-bonding distance N(1)···B(1) of 2.855(2) Å being significantly shorter than the sum of van der Waals radii (~3.15 Å) and also shorter than the corresponding non-bonding distance of 2.972 Å in **7**. The bicyclic skeleton of **5** appears to be more compact than that of **7**, with both the transannular N—B bond and transannular non-bonding N···B contact shorter, possibly a result of reduced steric repulsion in **5**.

Unlike compound **8** ($R^1 = R^2$ = Me, $R^3 = R^4$ = H) (4) in which the $^+$N—H moiety forms an intermolecular hydrogen bond with a ring (B)O(C) oxygen atom, the $^+$N—H proton in **5** is *not* involved in any hydrogen bonding. This is presumably the result of steric blocking, both intramolecular and intermolecular, of the possible acceptor oxygen atoms by bulky phenyl and cyclohexyl groups. The crystal structure of **5** consists of molecules separated by normal van der Waals distances, the shortest intermolecular distance between non-hydrogen atoms being N(2)···C(21) = 3.313(2) Å.

Acknowledgements

We thank the Natural Sciences and Engineering Research Council of Canada and the Fonds der Chemischen Industrie, Frankfurt am Main, for financial support.

1. M. Koremura, H. Oku, T. Shono, and T. Nakanishi. Takamine Keukyusho Nempo, **13**, 212 (1961); Chem. Abstr. **57**, 16451*a* (1962).
2. P. L. Southwick and J. E. Anderson. J. Am. Chem. Soc. **79**, 6222 (1957).
3. H. Amt, W. Kliegel, S. J. Rettig, and J. Trotter. Can. J. Chem. **68**, 1791 (1990).
4. S. J. Rettig, J. Trotter, W. Kliegel, and H. Becker. Can. J. Chem. **54**, 3142 (1976).
5. W. Kliegel, B. Enders, and H. Becker. Liebigs Ann. Chem. 1712 (1982).
6. H. Amt, W. Kliegel, S. J. Rettig, and J. Trotter. Can. J. Chem. **68**, 1797 (1990).
7. M. Davies and N. A. Spiers. J. Chem. Soc. 3971 (1959).

Can. J. Chem. Downloaded from www.nrcresearchpress.com by 217.78.4.112 on 09/08/12
For personal use only.

8. R. Mathis-Noel, A. Munoz, and F. Mathis. Ann. Fac. Sci. Univ. Toulouse, Sci. Math. Sci. Phys. **25**, 111 (1963).
9. International tables for x-ray crystallography. Kynoch Press, Birmingham, U.K. (present distributor Kluwer Academic Publishers, Dordrecht, The Netherlands), Vol. IV. 1974. pp. 99–102 and 149.
10. H. C. Brown. J. Chem. Soc. 1248 (1956); Boranes in organic chemistry. Ithaca, London. 1972. p. 102.
11. C. A. Coulson and T. W. Dingle. Acta. Crystallogr. Sect. B, **24**, 153 (1968).
12. W. Kliegel, G. Lubkowitz, S. J. Rettig, and J. Trotter. Can. J. Chem. **70**, 2022 (1992).

Can. J. Chem. Downloaded from www.nrcresearchpress.com by 217.78.4.112 on 09/08/12
For personal use only.

Structural studies of organoboron compounds. LV.[1] *N,N'*-Di-*tert*-butyl-*N,N'*-dihydroxypropane-1,3-diamine(*O-B*)ethoxydiphenylborane[2] and N^1,N^2-di-*tert*-butyl-N^1,N^2-dihydroxy-1-phenylpropane-1,3-diamine(N^2-*O-B*)hydroxydiphenylborane[3]

WOLFGANG KLIEGEL AND GOTTFRIED LUBKOWITZ

Institut für Pharmazeutische Chemie der Technischen Universität Braunschweig, Beethovenstrasse 55, 3300 Braunschweig, Germany

AND

STEVEN J. RETTIG AND JAMES TROTTER

Department of Chemistry, University of British Columbia, 2036 Main Mall, Vancouver, B.C., Canada V6T 1Z1

Received October 22, 1991

WOLFGANG KLIEGEL, GOTTFRIED LUBKOWITZ, STEVEN J. RETTIG, and JAMES TROTTER. Can. J. Chem. **70**, 2033 (1992).

The 1,3-propanediamine derivatives *N,N'*-di-*tert*-butyl-*N,N'*-dihydroxy-1,3-propanediamine and *N,N'*-di-*tert*-butyl-*N,N'*-dihydroxy-1-phenyl-1,3-propanediamine have been prepared and reacted with oxybis(diphenylborane) to yield, respectively, the crystalline organoboron compounds *N,N'*-di-*tert*-butyl-*N,N'*-dihydroxypropane-1,3-diamine(*O-B*)-ethoxydiphenylborane, **5***a*, and N^1,N^2-di-*tert*-butyl-N^1,N^2-dihydroxy-1-phenylpropane-1,3-diamine(N^2-*O-B*)-hydroxydiphenylborane, **5***b*. Crystals of **5***a* are monoclinic, *C*2/*c*, a = 35.402(1), b = 9.212(2), c = 18.101(2) Å, β = 116.688(3)°, Z = 8, ρ_c = 1.079 g cm^{-3}, and crystals of **5***b* are monoclinic, $P2_1/c$, a = 12.899(4), b = 12.571(4), c = 17.412(3) Å, β = 90.02(2)°, Z = 4, ρ_c = 1.121 g cm^{-3}. The structures were solved by direct methods and were refined by full-matrix least-squares procedures to final R values of 0.047 and 0.041 for 2492 and 3334 reflections with $I \geq 3\sigma(I)$, respectively. Compounds **5***a* and **5***b* are open-chain hydroxylamine adducts of diphenylborinic acid and ethyl diphenylborinate, respectively. Both of these compounds are stabilized by a system of three intramolecular hydrogen bonds (O—H···O, N—H···O, and N—H···N). Bond lengths involving the tetrahedrally coordinated boron atoms are: (C)O—B = 1.457(3), (N)O—B = 1.558(3), and C—B = 1.613(4) and 1.615(4) Å for **5***a*; (H)O—B = 1.475(3), (N)O—B = 1.562(2), and C—B = 1.618(3) and 1.619(3) Å for **5***b*.

WOLFGANG KLIEGEL, GOTTFRIED LUBKOWITZ, STEVEN J. RETTIG et JAMES TROTTER. Can. J. Chem. **70**, 2033 (1992).

On a préparé les dérivés de la propane-1,3-diamine, *N,N'*-di-*tert*-butyl-*N,N'*-dihydroxypropane-1,3-diamine et la *N,N'*-di-*tert*-butyl-*N,N'*-dihydroxy-1-phényl-propane-1,3-diamine, et on les a fait réagir avec l'oxybis(diphénylborane) pour obtenir respectivement les composés organoborés, le *N,N'*-di-*tert*-butyl-*N,N'*-dihydroxypropane-1,3-diamine-(*O-B*)éthoxydiphénylborane, **5***a*, et le *N,N'*-di-*tert*-butyl-*N,N'*-dihydroxy-1-phényl-propane-1,3-diamine(N^2-*O-B*)hydroxydiphénylborane, **5***b*. Les cristaux du produit **5***a* sont monocliniques, *C*2/*c* avec a = 35,402(1), b = 9,212(2), et c = 18,101(2) Å, β = 116,688(3)°, Z = 8 et ρ_c = 1,079 g cm^{-3} alors que les cristaux du composé **5***b* sont monocliniques, $P2_1/c$ avec a = 12,899(4), b = 12,571(4) et c = 17,412(3) Å, β = 90,02(2)°, Z = 4 et ρ_c = 1,121 g cm^{-3}. On a résolu les structures par les méthodes directes et on les a affinées par la méthode des moindres carrés (matrice entière) jusqu'à des valeurs de R de 0,047 et 0,041 respectivement pour 2492 et 3334 réflexions avec $I \geq 3\sigma(I)$. Les composés **5***a* et **5***b* existent sous la forme des chaînes ouvertes d'adduits d'hydroxylamine sur respectivement l'acide diphénylborinique et le diphénylborinate d'éthyle. Ces deux composés sont stabilisés par un système de trois liaisons hydrogènes (O—H···O, N—H···O, et N—H···N). Les longueurs des liaisons impliquant les atomes de bore coordonnés d'une façon tétraédrique sont : (C)O—B = 1,457(3), (N)O—B = 1,558(3), et C—B = 1,613(4) et 1,615(4) Å pour le composé **5***a*; (H)O—B = 1,475(3), (N)O—B = 1,562(2), et C—B = 1,618(4) et 1,619(3) Å pour le composé **5***b*.

[Traduit par la rédaction]

Introduction

Our investigation of boron chelates of alkylene-bis-hydroxylamines led to the preparation of the 1,3-propanediamine derivatives **2** by reduction of the nitrone **1** (1) with either $NaBH_4$ or phenylmagnesium bromide. The 1,3-bis-hydroxylamines **2** (R = H or C_6H_5) were then reacted with oxybis(diphenylborane) in ethanolic solution in order to prepare the eight-membered diphenylboron chelates **3**. These compounds would be analogous to the seven-membered chelate **4** that is obtained under the same conditions from a 1,2-bis-hydroxylamine (2). The crystalline reaction products derived from **2***a* and **2***b* show the elemental analyses and ^{1}H nmr spectra of the expected derivatives plus 1 molar equivalent of ethanol in the case of **3***a*, and 1 molar equivalent of water in the case of **3***b*. These supposed "solvate" components could not be removed by recrystallization or by drying *in vacuo*. The nature of the bonding or association of the ethanol and water molecules, respectively, in these compounds cannot be ascertained from the infrared and ^{1}H nmr spectral data. In addition to the assumed solvate structures of both diphenylboron chelates (**3***a* · EtOH and **3***b* · H_2O) the 1:1 adducts, **2***a* · Ph_2BOEt and **2***b* · Ph_2BOH, had to be considered as isomeric structural alternatives. These adducts could arise from complex formation through the oxygen atom of one of the hydroxylamine groups of **2***a* leading to **5***a*, or of **2***b* leading to **5***b* or **5***b'*, respectively. Furthermore, the coordination of the hydroxylamine function via the nitrogen atom to boron, leading to the isomeric N→B coordinated complexes **6***a* and **6***b* or **6***b'*, had to be considered. This possibility has already been discussed for other adducts of hydroxylamines (3).

[1]Previous paper in this series: ref. 13.

[2]Alternative nomenclature: 3,7-di-*tert*-butyl-1-ethoxy-1,1-diphenyl-2,8-dioxa-7-aza-3-azonia-1-borataoctane.

[3]Alternative nomenclature: 3,7-di-*tert*-butyl-1-hydroxy-1,1,6-triphenyl-2,8-dioxa-7-aza-3-azonia-1-borataoctane.

Can. J. Chem. Downloaded from www.nrcresearchpress.com by 217.78.4.112 on 09/08/12
For personal use only.

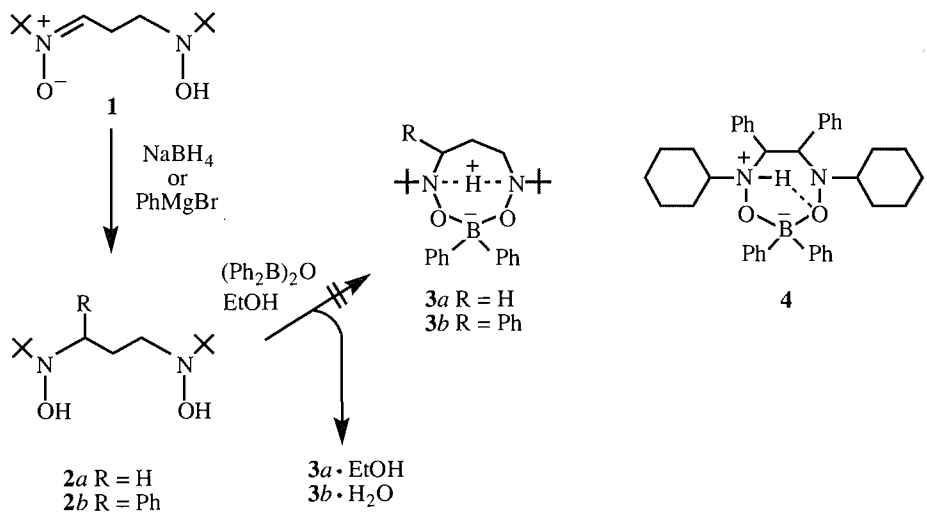

X-ray crystallographic analyses have been carried out for both compounds to distinguish between the three possible molecular structures in the solid state: the "solvate" (**3***a* · EtOH and **3***b* · H_2O), the O→B coordinated complex (**5***a* and **5***b* or **5***b*′), and the N→B coordinated complex (**6***a* and **6***b* or **6***b*′).

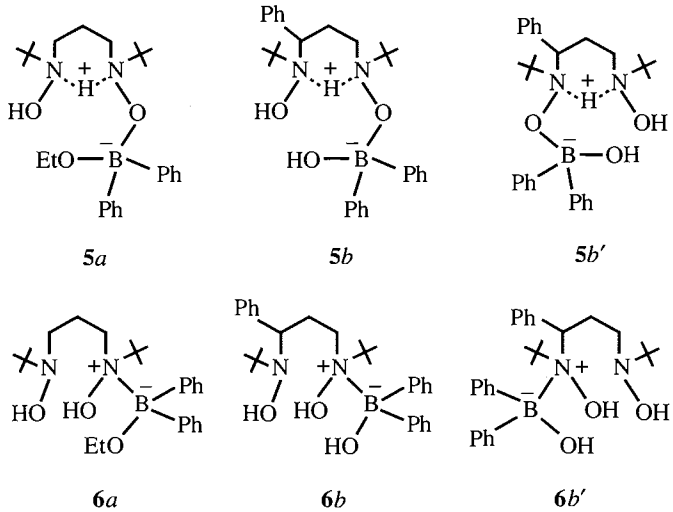

Experimental

N,N′-*Di*-tert-*butyl*-N,N′-*dihydroxy-1,3-propanediamine*, **2**a

N-tert-Butyl-3-[*tert*-butyl-(hydroxy)amino]propylidenamine-*N*-oxide, **1** (1), (1.08 g, 5 mmol) is dissolved in 60 mL of isopropanol and 10 mL of water. After addition of $NaBH_4$ (0.38 g, 10 mmol), the solution is refluxed for 2 h. Excess $NaBH_4$ is decomposed with tartaric acid, and the solution is adjusted to pH 9–10 using a solution of Na_2CO_3. Evaporation to a small volume induces crystallization of a colorless substance. Yield: 1.02 g (93%); mp 87–88°C (from petroleum ether, bp 30–75°C). Infrared (KBr): 3360 cm^{-1} (broad, O-H); ^1H nmr (90 MHz, $CDCl_3$/TMS) δ (ppm): 1.15 (s, 2 $(CH_3)_3C$), 1.70–1.99 (m, C-CH_2-C), 2.80 (t, J = 6 Hz, 2 CH_2N), 7.00 (s, very broad, exchangeable, 2 OH). Anal. calcd. for $C_{11}H_{26}N_2O_2$: C 60.51, H 12.00, N 12.83; found: C 60.57, H 12.19, N 12.83.

N,N′-*Di*-tert-*butyl*-N,N′-*dihydroxy-1-phenyl-1,3-propanediamine*, **2**b

N-tert-Butyl-3-[*tert*-butyl-(hydroxy)amino]propylidenamine-*N*-oxide, **1** (1), (2.16 g, 10 mmol) is dissolved in 100 mL of absolute ether and mixed, under vigorous stirring within 15 min, with a Grignard reagent prepared from bromobenzene (9.42 g, 60 mmol) and magnesium (1.46 g, 60 mmol) in 100 mL of absolute ether. After refluxing for 1 h the reaction mixture is hydrolyzed with water under cooling with ice, the precipitated magnesium hydroxide dissolved with 2 N HCl, and the acid solution neutralized with $NaHCO_3$. The ether layer is separated, and the aqueous solution extracted twice with 50 mL of ether. The combined ether solutions are dried with $MgSO_4$ and evaporated to a small volume. At −18°C a colorless substance crystallizes. Yield: 1.65 g (56%); mp 81°C (from ether). Infrared (KBr): 3380 cm^{-1} (broad, O-H); ^1H nmr (90 MHz, $CDCl_3$/TMS) δ (ppm): 0.97 (s, $(CH_3)_3C$), 1.18 (s, $(CH_3)_3C$), 1.49–3.23 (m, CH_2-CH_2N), 3.95 and 4.06 (d and d, N-C*H*-Ph), 6.20 (s, very broad, exchangeable, 2 OH), 7.13–7.28 (m, 3 aromatic H), 7.39–7.55 (m, 2 aromatic H). Anal. calcd. for $C_{17}H_{30}N_2O_2$: C 69.35, H 10.27, N 9.51; found: C 69.37, H 10.30, N 9.51.

N,N′-*Di*-tert-*butyl*-N,N′-*dihydroxypropane-1,3-diamine* (O-B) *ethoxydiphenylborane*, **5**a

2*a* (0.22 g, 1 mmol) is dissolved in 1 mL of absolute ethanol and mixed, stirring continuously, with a solution of oxybis(diphenylborane) (0.17 g, 0.5 mmol) in 0.5 mL of ethanol. The reaction mixture is cooled to −18°C for 24 h, and the precipitate is recrystallized from ethanol. Yield: 0.30 g (70%); mp 74°C (from ethanol). Infrared (KBr): 3570 (sharp, O-H/N-H), 3460 and 3210 cm^{-1} (broadened, O-H/N-H); ^1H nmr (DMSO-d_6/TMS) δ (ppm): 1.01 (s, 2 $(CH_3)_3C$), 1.09 (t, CH_3CH_2), 1.51–1.88 (m, C-CH_2-C), 2.42–2.65 (m, 2 CH_2N), 3.35–3.65 (m, CH_2CH_3), 4.25 and 6.92 (s and s, broad exchangeable, OH and NH), 7.09–7.72 (m, 2 C_6H_5). Anal. calcd. for $C_{25}H_{41}BN_2O_3$: C 70.09, H 9.65, B 2.52, N 6.54; found: C 69.89, H 9.68, B 2.57, N 6.40.

Crystals suitable for X-ray analysis were obtained by recrystallization from absolute ethanol.

N^1,N^2-*Di*-tert-*butyl*-N^1,N^2-*dihydroxy-1-phenylpropane-1,3-diamine* (N^2-O-B) *hydroxydiphenylborane*, **5**b

2*b* (0.59 g, 2 mmol) in 2 mL of ethanol and oxybis(diphenylborane) (0.35 g, 1 mmol) in 1 mL of ethanol are reacted as described above. Yield: 0.59 g (62%); mp 105–107°C (from benzene).[4] Infrared (KBr): 3650 (sharp, O-H/N-H), 3250 cm^{-1} (broadened, O-H/N-H); ^1H nmr (DMSO-d_6/TMS) δ (ppm): 0.90 (s, $(CH_3)_3C$), 1.00 (s, $(CH_3)_3C$), 1.68–1.88 and 2.06–2.24 (m and m, C-CH_2-C), 2.39–2.68 (m, CH_2N), 3.89–4.13 (m, N-C*H*-Ph), 7.12–7.79 (m, 3 C_6H_5, 2 OH, NH). Anal. calcd. for $C_{29}H_{41}BN_2O_3$: C 73.10, H 8.67, N 5.88; found: C 73.05, H 8.66, N 5.69.

[4]Recrystallization of **5***b* from ethanol yielded an unstable compound (mp 101–102°C, dec.) whose elemental analysis and ^1H nmr spectrum suggest the incorporation of 1 mol of ethanol, analogous to **5***a*.

Can. J. Chem. Downloaded from www.nrcresearchpress.com by 217.78.4.112 on 09/08/12
For personal use only.

Can. J. Chem. Downloaded from www.nrcresearchpress.com by 217.78.4.112 on 09/08/12
For personal use only.

Table 1. Crystallographic data[a]

Compound	**5***a*	**5***b*
Formula	$C_{25}H_{41}BN_2O_3$	$C_{29}H_{41}BN_2O_3$
fw	428.42	476.46
Crystal system	Monoclinic	Monoclinic
Space group	$C2/c$	$P2_1/c$
a, Å	35.402(1)	12.899(4)
b, Å	9.212(2)	12.571(4)
c, Å	18.101(2)	17.412(3)
β, °	116.688(3)	90.02(2)
V, Å^3	5274(1)	2824(1)
Z	8	4
ρ_{calc}, g/cm^3	1.079	1.121
$F(000)$	1872	1032
μ(Cu-K$_\alpha$), cm^{-1}	5.13	5.27
Crystal size, mm	0.15 × 0.35 × 0.35	0.25 × 0.35 × 0.45
Relative transmission factors	0.73–1.00	0.79–1.00
Scan type	ω–2θ	ω–2θ
Scan range, deg in ω	1.10 + 0.20 tan θ	0.94 + 0.20 tan θ
Scan speed, deg/min	32 (8 rescans)	32 (8 rescans)
Data collected	$+h$, $+k$, $\pm l$	$+h$, $+k$, $\pm l$
$2\theta_{max}$, deg	155	155
Crystal decay	15.0%	6.9%
Total reflections	5661	6196
Total unique reflections	5566	5939
R_{merge}	0.015	0.042
No. of reflcns with $I \geq 3\sigma(I)$	2492	3334
No. of variables	289	329
R	0.047	0.041
R_w	0.058	0.053
gof	2.15	1.66
Max Δ/σ (final cycle)	0.08	0.02
Residual density e/Å^3	−0.26 to +0.11	−0.11 to +0.15

[a]Temperature 294 K, Rigaku AFC6S diffractometer, Cu-K$_\alpha$ radiation (λ = 1.54178 Å), graphite monochromator, takeoff angle 6.0°, aperture 6.0 × 6.0 mm at a distance of 285 mm from the crystal, stationary background counts at each end of the scan (scan/background time ratio 2:1), $\sigma^2(F^2) = [S^2(C + 4B) + (0.03F^2)^2]/Lp^2$ (S = scan rate, C = scan count, B = normalized background count), function minimized $\Sigma w(|F_o|-|F_c|)^2$ where $w = 4F_o^2/\sigma^2(F_o^2)$, $R = \Sigma||F_o|-|F_c||/\Sigma|F_o|$, $R_w = (\Sigma w(|F_o|-|F_c|)^2/\Sigma w|F_o|^2)^{1/2}$ and gof = $[\Sigma w(|F_o|-|F_c|)^2/(m-n])^{1/2}$. Values given for R, R_w, and gof are based on those reflections with $I \geq 3\sigma(I)$.

Crystals suitable for X-ray analysis were obtained by recrystallization from absolute benzene.

X-ray crystallographic analyses of **5**a and **5**b

Crystallographic data for the two complexes appear in Table 1. The final unit-cell parameters were obtained by least squares on the setting angles for 25 reflections with 2θ = 55.0–78.5° for **5***a* and 45.5–64.5° for **5***b*. Although the β angle for compound **5***b* (90.02(2)°) suggests an orthorhombic unit cell, a check of the Laue symmetry clearly indicated monoclinic rather than orthorhombic symmetry. The intensities of three standard reflections, measured every 200 reflections throughout the data collections, showed linear decays of 15.0% for **5***a* and 6.9% for **5***b*. The data were processed,[5] and corrected for Lorentz and polarization effects, decay, and absorption (empirical, based on azimuthal scans for four reflections).

The structure analysis of **5***a* was initiated in the centrosymmetric space group $C2/c$ on the basis of E-statistics, this choice being confirmed by subsequent calculations. The structures were solved by direct methods, the coordinates of the non-hydrogen atoms being determined from E-maps or from subsequent difference Fourier syntheses. The non-hydrogen atoms were refined with anisotropic thermal parameters, OH and NH hydrogen atoms were refined with isotropic thermal parameters, and carbon-bound hydrogen atoms were fixed in idealized positions (C—H = 0.98 Å, B_H = 1.2 $B_{bonded\ atom}$). Neutral atom scattering factors and anomalous dispersion corrections for the non-hydrogen atoms were taken from the *International tables for X-ray crystallography* (4). Final atomic coordinates and equivalent isotropic thermal parameters, bond lengths, and bond angles appear in Tables 2–4, respectively. Hydrogen atom parameters, anisotropic thermal parameters, torsion angles, intermolecular contacts, and least-squares planes, and measured and calculated structure factor amplitudes for the both structures are available as supplementary material.[6]

[5]TEXSAN/TEXRAY structure analysis package which includes versions of the following: DIRDIF, direct methods for difference structures, by P. T. Beurskens; ORFLS, full-matrix least-squares, and ORFFE, function and errors, by W. R. Busing, K. O. Martin, and H. A. Levy; ORTEP II, illustrations, by C. K. Johnson.

[6]Supplementary material mentioned in the text may be purchased from: The Depository of Unpublished Data, Document Delivery, CISTI, National Research Council Canada, Ottawa, Canada K1A 0R6.

Tables of hydrogen atom parameters and inter- and intramolecular contacts involving hydrogen have also been deposited with the Cambridge Crystallographic Data Centre and can be obtained on request from The Director, Cambridge Crystallographic Data Centre, University Chemical Laboratory, 11 Union Road, Cambridge CB2 1EZ U.K.

TABLE 2. Final atomic coordinates (fractional) and B_{eq} (Å^2)[a]

Atom	x	y	z	B_{eq}
		5a		
O(1)	0.35455(5)	0.0246(2)	0.0862(1)	5.6
O(2)	0.42751(7)	0.3957(3)	0.1777(2)	9.0
O(3)	0.35460(5)	0.2602(2)	0.1499(1)	6.1
N(1)	0.37101(6)	0.0989(3)	0.0396(1)	5.0
N(2)	0.42726(7)	0.3636(3)	0.0988(2)	7.5
C(1)	0.41457(8)	0.0415(3)	0.0610(2)	6.1
C(2)	0.44926(8)	0.1130(4)	0.1361(2)	6.4
C(3)	0.46212(9)	0.2610(4)	0.1192(2)	7.4
C(4)	0.33934(8)	0.0820(4)	−0.0524(2)	5.9
C(5)	0.2968(1)	0.1349(4)	−0.0613(2)	8.3
C(6)	0.3375(1)	−0.0768(4)	−0.0754(2)	7.8
C(7)	0.3529(1)	0.1756(4)	−0.1044(2)	8.4
C(8)	0.4331(1)	0.5057(5)	0.0642(4)	10.4
C(9)	0.3933(2)	0.5934(4)	0.0463(4)	15.0
C(10)	0.4713(2)	0.5894(5)	0.1247(4)	15.6
C(11)	0.4370(2)	0.4764(6)	−0.0144(4)	13.5
C(12)	0.3200(1)	0.3620(4)	0.1122(3)	8.7
C(13)	0.3234(2)	0.4851(5)	0.1698(4)	14.2
C(14)	0.30683(8)	0.0462(3)	0.1538(2)	5.2
C(15)	0.2859(1)	−0.0754(4)	0.1085(2)	7.8
C(16)	0.2494(1)	−0.1272(5)	0.1097(3)	9.9
C(17)	0.2327(1)	−0.0614(5)	0.1555(3)	8.5
C(18)	0.2521(1)	0.0580(4)	0.2007(2)	7.2
C(19)	0.28881(8)	0.1093(4)	0.2001(2)	6.2
C(20)	0.38988(8)	0.0501(3)	0.2433(2)	5.3
C(21)	0.41081(8)	0.1386(4)	0.3114(2)	6.5
C(22)	0.4438(1)	0.0886(5)	0.3843(2)	8.1
C(23)	0.4567(1)	−0.0503(6)	0.3900(2)	9.0
C(24)	0.4368(1)	−0.1447(5)	0.3244(2)	8.3
C(25)	0.4034(1)	−0.0938(4)	0.2522(2)	6.5
B(1)	0.35093(9)	0.1043(4)	0.1587(2)	4.9
		5b		
O(1)	0.1239(1)	0.2430(1)	0.32992(7)	4.6
O(2)	0.3151(1)	0.4969(1)	0.36990(8)	4.7
O(3)	0.1291(1)	0.4127(1)	0.40005(9)	4.8
N(1)	0.1626(1)	0.3040(2)	0.26851(9)	3.8
N(2)	0.3155(1)	0.4877(1)	0.2868(1)	4.0
C(1)	0.2646(2)	0.2590(2)	0.2436(1)	4.7
C(2)	0.3561(1)	0.2980(2)	0.2904(1)	4.2
C(3)	0.3966(1)	0.4082(2)	0.2676(1)	4.1
C(4)	0.5055(2)	0.4254(2)	0.2988(1)	4.7
C(5)	0.5285(2)	0.4116(2)	0.3757(2)	6.2
C(6)	0.6296(2)	0.4210(3)	0.4015(2)	8.5
C(7)	0.7082(2)	0.4433(3)	0.3517(3)	9.2
C(8)	0.6875(2)	0.4572(2)	0.2756(2)	7.7
C(9)	0.5864(2)	0.4487(2)	0.2487(2)	5.8
C(10)	0.0791(2)	0.3076(2)	0.2057(1)	4.8
C(11)	0.1174(2)	0.3794(3)	0.1415(1)	7.2
C(12)	−0.0172(2)	0.3553(2)	0.2423(1)	6.4
C(13)	0.0592(2)	0.1955(2)	0.1781(1)	6.8
C(14)	0.3287(2)	0.5988(2)	0.2569(1)	5.2
C(15)	0.3556(2)	0.5947(2)	0.1718(2)	7.2
C(16)	0.2228(2)	0.6514(2)	0.2656(2)	6.8
C(17)	0.4095(2)	0.6635(2)	0.3010(2)	6.9
C(18)	0.0105(2)	0.2611(2)	0.4474(1)	4.1
C(19)	−0.0556(2)	0.3330(2)	0.4825(1)	5.0
C(20)	−0.1493(2)	0.3038(2)	0.5149(1)	6.0
C(21)	−0.1793(2)	0.1987(3)	0.5135(1)	6.5
C(22)	−0.1163(2)	0.1248(2)	0.4792(2)	6.5
C(23)	−0.0233(2)	0.1561(2)	0.4464(1)	5.6
C(24)	0.2199(2)	0.2538(2)	0.4583(1)	4.5
C(25)	0.2748(2)	0.3187(2)	0.5091(1)	5.6
C(26)	0.3624(2)	0.2840(3)	0.5470(2)	7.7
C(27)	0.3979(2)	0.1828(4)	0.5370(2)	8.8
C(28)	0.3444(2)	0.1147(3)	0.4885(2)	7.8
C(29)	0.2566(2)	0.1508(2)	0.4501(1)	5.8
B(1)	0.1205(2)	0.2967(2)	0.4108(1)	4.1

[a] $B_{eq} = (8/3)\pi^2 \Sigma\Sigma U_{ij} a_i * a_j * (a_i \cdot a_j)$.

TABLE 3. Bond lengths (Å) with estimated standard deviations

Atom	Atom	Distance	Atom	Atom	Distance
			5a		
O(1)	N(1)	1.401(3)	C(8)	C(11)	1.514(6)
O(1)	B(1)	1.558(3)	C(12)	C(13)	1.509(6)
O(2)	N(2)	1.456(4)	C(14)	C(15)	1.389(4)
O(3)	C(12)	1.447(4)	C(14)	C(19)	1.389(4)
O(3)	B(1)	1.457(3)	C(14)	B(1)	1.615(4)
N(1)	C(1)	1.507(3)	C(15)	C(16)	1.388(5)
N(1)	C(4)	1.541(3)	C(16)	C(17)	1.359(5)
N(2)	C(3)	1.464(4)	C(17)	C(18)	1.358(5)
N(2)	C(8)	1.505(5)	C(18)	C(19)	1.387(4)
C(1)	C(2)	1.513(4)	C(20)	C(21)	1.383(4)
C(2)	C(3)	1.512(4)	C(20)	C(25)	1.394(4)
C(4)	C(5)	1.519(4)	C(20)	B(1)	1.613(4)
C(4)	C(6)	1.515(4)	C(21)	C(22)	1.390(4)
C(4)	C(7)	1.505(4)	C(22)	C(23)	1.346(5)
C(8)	C(9)	1.528(6)	C(23)	C(24)	1.382(5)
C(8)	C(10)	1.515(6)	C(24)	C(25)	1.392(4)
			5b		
O(1)	N(1)	1.407(2)	C(10)	C(13)	1.510(3)
O(1)	B(1)	1.562(2)	C(14)	C(15)	1.523(3)
O(2)	N(2)	1.451(2)	C(14)	C(16)	1.525(3)
O(3)	B(1)	1.475(3)	C(14)	C(17)	1.529(3)
N(1)	C(1)	1.496(3)	C(18)	C(19)	1.386(3)
N(1)	C(10)	1.536(3)	C(18)	C(23)	1.390(3)
N(2)	C(3)	1.486(2)	C(18)	B(1)	1.619(3)
N(2)	C(14)	1.500(3)	C(19)	C(20)	1.384(3)
C(1)	C(2)	1.515(3)	C(20)	C(21)	1.377(4)
C(2)	C(3)	1.533(3)	C(21)	C(22)	1.371(4)
C(3)	C(4)	1.522(3)	C(22)	C(23)	1.385(3)
C(4)	C(5)	1.382(3)	C(24)	C(25)	1.396(3)
C(4)	C(9)	1.392(3)	C(24)	C(29)	1.386(3)
C(5)	C(6)	1.384(3)	C(24)	B(1)	1.618(3)
C(6)	C(7)	1.365(5)	C(25)	C(26)	1.379(4)
C(7)	C(8)	1.364(4)	C(26)	C(27)	1.364(5)
C(8)	C(9)	1.390(4)	C(27)	C(28)	1.385(5)
C(10)	C(11)	1.519(3)	C(28)	C(29)	1.392(4)
C(10)	C(12)	1.521(3)			

Results and discussion

The X-ray analyses confirm the suggested constitutions **5a** and **5b**, respectively, for the crystalline adducts (see Fig. 1). In both compounds one of the hydroxylamine groups coordinates the borinic acid derivative via the oxygen atom. This results in a *B,N*-betainic complex structure similar to those reported for the related hydroxylamine-boron adducts **8** (5) and **9** (3). In compounds **8** and **9** the hydroxylamine-boron

Can. J. Chem. Downloaded from www.nrcresearchpress.com by 217.78.4.112 on 09/08/12
For personal use only.

TABLE 4. Bond angles (deg) with estimated standard deviations

Atom	Atom	Atom	Angle	Atom	Atom	Atom	Angle
				5a			
N(1)	O(1)	B(1)	119.4(2)	O(3)	C(12)	C(13)	111.9(4)
C(12)	O(3)	B(1)	126.3(2)	C(15)	C(14)	C(19)	115.2(3)
O(1)	N(1)	C(1)	109.2(2)	C(15)	C(14)	B(1)	123.0(3)
O(1)	N(1)	C(4)	107.7(2)	C(19)	C(14)	B(1)	121.6(3)
C(1)	N(1)	C(4)	114.0(2)	C(14)	C(15)	C(16)	121.4(3)
O(2)	N(2)	C(3)	104.5(3)	C(15)	C(16)	C(17)	121.4(4)
O(2)	N(2)	C(8)	106.9(3)	C(16)	C(17)	C(18)	119.1(3)
C(3)	N(2)	C(8)	114.1(3)	C(17)	C(18)	C(19)	119.6(3)
N(1)	C(1)	C(2)	113.8(2)	C(14)	C(19)	C(18)	123.2(3)
C(1)	C(2)	C(3)	114.0(3)	C(21)	C(20)	C(25)	116.0(3)
N(2)	C(3)	C(2)	109.7(2)	C(21)	C(20)	B(1)	123.5(3)
N(1)	C(4)	C(5)	106.7(2)	C(25)	C(20)	B(1)	120.5(3)
N(1)	C(4)	C(6)	108.4(2)	C(20)	C(21)	C(22)	122.4(3)
N(1)	C(4)	C(7)	109.6(2)	C(21)	C(22)	C(23)	119.9(3)
C(5)	C(4)	C(6)	111.3(3)	C(22)	C(23)	C(24)	120.6(3)
C(5)	C(4)	C(7)	109.2(3)	C(23)	C(24)	C(25)	118.9(4)
C(6)	C(4)	C(7)	111.5(3)	C(20)	C(25)	C(24)	122.1(3)
N(2)	C(8)	C(9)	105.2(3)	O(1)	B(1)	O(3)	109.1(2)
N(2)	C(8)	C(10)	112.8(4)	O(1)	B(1)	C(14)	103.9(2)
N(2)	C(8)	C(11)	108.9(4)	O(1)	B(1)	C(20)	107.2(2)
C(9)	C(8)	C(10)	108.9(4)	O(3)	B(1)	C(14)	116.9(2)
C(9)	C(8)	C(11)	111.1(5)	O(3)	B(1)	C(20)	109.2(2)
C(10)	C(8)	C(11)	109.9(4)	C(14)	B(1)	C(20)	110.0(2)
				5b			
N(1)	O(1)	B(1)	117.4(1)	N(2)	C(14)	C(16)	105.5(2)
O(1)	N(1)	C(1)	109.0(2)	N(2)	C(14)	C(17)	113.5(2)
O(1)	N(1)	C(10)	107.9(1)	C(15)	C(14)	C(16)	108.4(2)
C(1)	N(1)	C(10)	114.9(2)	C(15)	C(14)	C(17)	110.5(2)
O(2)	N(2)	C(3)	106.3(1)	C(16)	C(14)	C(17)	109.3(2)
O(2)	N(2)	C(14)	105.8(2)	C(19)	C(18)	C(23)	115.6(2)
C(3)	N(2)	C(14)	117.9(2)	C(19)	C(18)	B(1)	122.2(2)
N(1)	C(1)	C(2)	114.0(2)	C(23)	C(18)	B(1)	122.2(2)
C(1)	C(2)	C(3)	114.7(2)	C(18)	C(19)	C(20)	122.9(2)
N(2)	C(3)	C(2)	108.0(1)	C(19)	C(20)	C(21)	119.5(2)
N(2)	C(3)	C(4)	118.3(2)	C(20)	C(21)	C(22)	119.5(2)
C(2)	C(3)	C(4)	110.5(2)	C(21)	C(22)	C(23)	120.0(2)
C(3)	C(4)	C(5)	121.8(2)	C(18)	C(23)	C(22)	122.5(2)
C(3)	C(4)	C(9)	119.8(2)	C(25)	C(24)	C(29)	116.0(2)
C(5)	C(4)	C(9)	118.3(2)	C(25)	C(24)	B(1)	122.1(2)
C(4)	C(5)	C(6)	120.4(3)	C(29)	C(24)	B(1)	121.9(2)
C(5)	C(6)	C(7)	120.7(3)	C(24)	C(25)	C(26)	122.3(3)
C(6)	C(7)	C(8)	120.0(3)	C(25)	C(26)	C(27)	120.5(3)
C(7)	C(8)	C(9)	120.1(3)	C(26)	C(27)	C(28)	119.2(3)
C(4)	C(9)	C(8)	120.6(3)	C(27)	C(28)	C(29)	119.8(3)
N(1)	C(10)	C(11)	108.2(2)	C(24)	C(29)	C(28)	122.2(3)
N(1)	C(10)	C(12)	106.6(2)	O(1)	B(1)	C(3)	108.1(2)
N(1)	C(10)	C(13)	108.6(2)	O(1)	B(1)	C(18)	105.1(2)
C(11)	C(10)	C(12)	109.9(2)	O(1)	B(1)	C(24)	107.2(2)
C(11)	C(10)	C(13)	112.0(2)	O(3)	B(1)	C(18)	112.9(2)
C(12)	C(10)	C(13)	111.3(2)	O(3)	B(1)	C(24)	109.5(2)
N(2)	C(14)	C(15)	109.4(2)	C(18)	B(1)	C(24)	113.6(2)

(*O-B*) adducts are stabilized by hydrogen bonding involving the quaternized nitrogen atoms: intramolecular in **8**, and intermolecular (to form dimers) in **9**, at least in the solid state. In compounds **5***a* and **5***b*, stabilization is achieved by the formation of three intramolecular hydrogen bonds (cf. the general formula **7**) resulting in a basic skeletal structure that is geometrically similar in the two derivatives. The manifold intramolecular hydrogen bonding is a consequence of the polyfunctionality of this type of compound, containing five nucleophilic centres available for interaction with the acidic functions within the same molecule. The O—H···O hydrogen bonds are strongest in both compounds (O(2)—H···O(3), O—H = 1.07(5) and 0.92(3), H···O = 1.65(5) and 1.76(3), O···O = 2.703(3) and 2.674(2) Å, O—H···O = 167(4) and 170(2)°, respectively for **5***a* and **5***b*), the N—H···O interactions are of intermediate strength (N(1)—

Can. J. Chem. Downloaded from www.nrcresearchpress.com by 217.78.4.112 on 09/08/12
For personal use only.

Can. J. Chem. Downloaded from www.nrcresearchpress.com by 217.78.4.112 on 09/08/12
For personal use only.

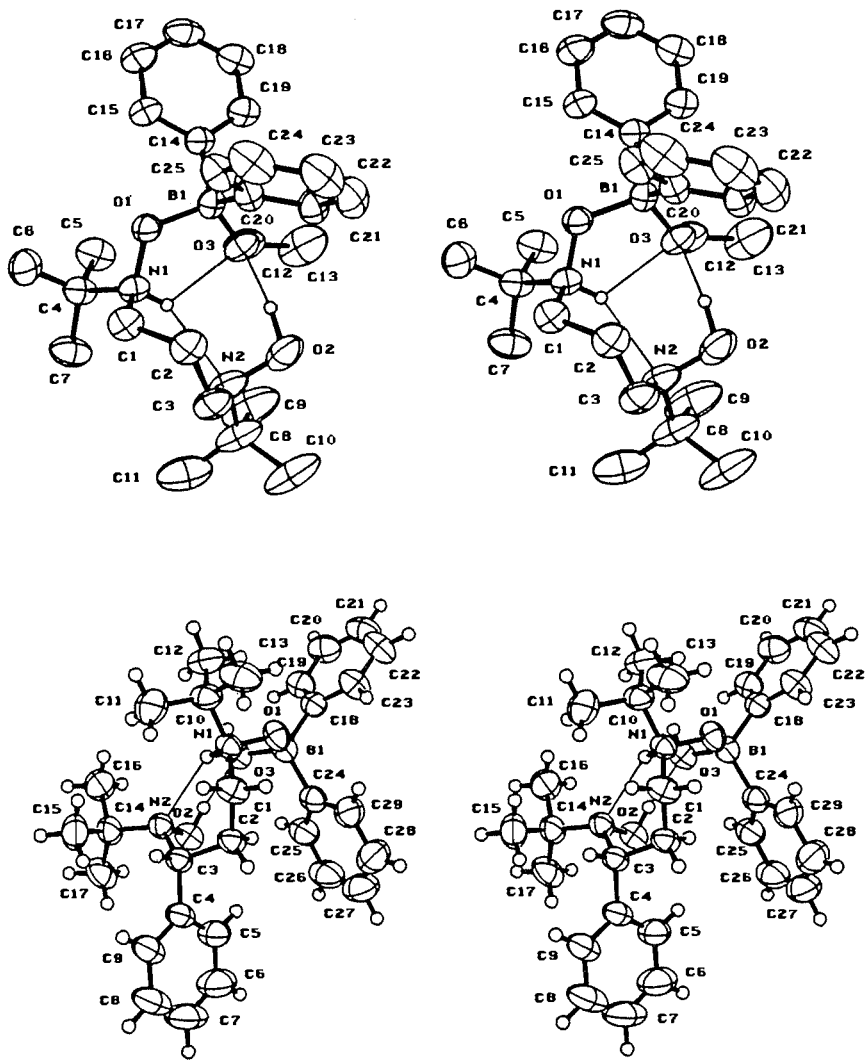

FIG. 1. Stereoviews of **5***a* (top) and **5***b* (bottom); 33% probability thermal ellipsoids are shown for the non-hydrogen atoms.

H···O(3), N—H = 0.93(2) and 0.97(2), H···O = 2.20(3) and 2.13(2), N···O = 2.752(3) and 2.702(2) Å, N—H···O = 117(2) and 116(2)°), while the N—H···N interactions are weakest (N(1)—H···N(2), N—H = 0.93(2) and 0.97(2), H···N = 2.29(3) and 2.30(2), N···N = 3.024(4) and 3.054(2) Å, N—H···N = 135(2) and 133(2)°). The intramolecular hydrogen-bonding system in each compound contains a bifurcation at the N(1)-positioned proton (H(2) in **5***a*, H(3) in **5***b*) that interacts simultaneously with both O(3) and N(2); the oxygen atom O(3) accepts two hydrogen atoms (H(1) and H(2) in **5***a*, H(1) and H(3) in **5***b*).

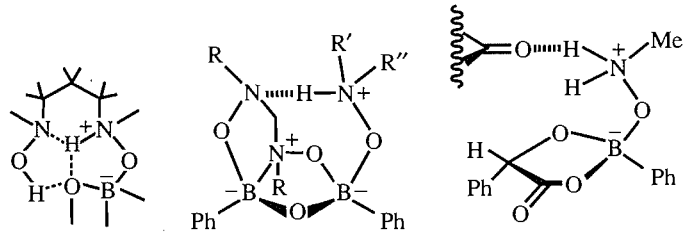

7 **8** **9**

The 1,3-diamine moieties of both molecules are cyclized by the hydrogen bridges to form six-membered proton chelates C(1)—N(1)—H···N(2)—C(3)—C(2). These rings have distorted "envelope"-like conformations with C(2) on the flap in both compounds. All of the *tert*-butyl groups in **5***a* and **5***b*, and the phenyl substituent in **5***b*, occupy (pseudo)equatorial positions, while the oxygen atoms O(1) and O(2) both occupy (pseudo)axial positions with respect to these proton chelate rings. Thus the two fused five-membered ring systems, also formed by hydrogen bonds (H···O—B—O—N and H···O···H—O—N), are connected (pseudo)axially to the six-membered ring system of the 1,3-diamine moiety in both compounds.

Bonds lengths are similar in the two derivatives **5***a* and **5***b* (see Table 3). A significant difference is noted for the B(1)—O(3) bond: in **5***a* this bond is 0.018(4) Å shorter than that in **5***b* reflecting the increased nucleophilicity of the EtO^- ligand in **5***a* relative to that of the HO^- ligand in **5***b*. This influence also manifests itself in the O(3)···H(1) distance, which is nearly 0.1 Å shorter in **5***a* than in **5***b*. Not surprisingly, the phenyl substituent at C(3) in compound **5***b* causes

lengthening of the adjacent bonds relative to those in **5***a*: C(3)—C(2) and C(3)—N(2) = 1.512(4) and 1.464(4) Å for **5***a*, 1.533(3) and 1.486(2) Å for **5***b*. In both of the compounds the N—O bonds at the quaternized nitrogen atom N(1) (1.401(3) and 1.407(2) Å) are about 0.05 Å shorter than those at the trivalent nitrogen N(2) (1.456(4) and 1.451(2) Å). Correspondingly, the N—C bonds at N(1) are about 0.04 Å longer than those at N(2) in both compounds. The geminal *B*-phenyl groups of both **5***a* and **5***b* show nearly equal B—C bond lengths, averaging 1.614 Å in the former and 1.619 Å in the latter. These B—C distances can be compared to the mean values of 1.624 Å in **4** (2), 1.600 Å in compounds of the type **8** (5), 1.589 Å in **9** (3), and similar values reported for other diphenylboron chelates (6–11). The (N)O—B distances (O(1)—B(1) = 1.558(3) and 1.562(2) Å for **5***a* and **5***b*, respectively) are longer than the corresponding bonds in other hydroxylamine(*O-B*)boron complexes such as **8** (average 1.509 Å) (5) or **9** (average 1.494 Å) (3), but resemble the O—B bond lengths in diphenylboron chelates of hydroxylamine derivatives like **4** (2) and other related compounds (6–11) having cyclic $^{+}$N—O—B^{-} betaine structures.

The tetracoordination at B(1) arising from the adduct formation causes, as expected, rehybridization of the trigonal planar (sp^2) boron atom in diphenylborinic acid (12) to a tetrahedral sp^3 boron atom in both the diphenylborinic ester complex **5***a* and the diphenylborinic acid complex **5***b*. Associated with this rehybridization is the usual lengthening of both the B—C and O—B bonds.

Acknowledgements

We thank the Natural Sciences and Engineering Research Council of Canada and the Fonds der Chemischen Industrie, Frankfurt am Main, for financial support.

1. H. G. Aurich, J. Eidel, and M. Schmidt. Chem. Ber. **119**, 18 (1986).
2. H. Amt, W. Kliegel, S. J. Rettig, and J. Trotter. Can. J. Chem. **68**, 1797 (1990).
3. W. Kliegel, U. Schumacher, S. J. Rettig, and J. Trotter. Can. J. Chem. **70**, 1188 (1992).
4. International tables for X-ray crystallography. Vol. IV. Kynoch Press, Birmingham, U.K. (present distributor: Kluwer Academic Publishers. Dordrecht, The Netherlands). 1974. pp. 99–102 and 149.
5. (a) W. Kliegel, G. Lubkowitz, S. J. Rettig, and J. Trotter. Can. J. Chem. **70**, 2015 (1992); (b) W. Kliegel, G. Lubkowitz, S. J. Rettig, and J. Trotter. Can. J. Chem. **70**, 2022 (1992).
6. S. J. Rettig, J. Trotter, and W. Kliegel. Can. J. Chem. **52**, 2531 (1974).
7. S. J. Rettig, J. Trotter, W. Kliegel, and D. Nanninga. Can. J. Chem. **56**, 1676 (1978).
8. W. Kliegel, D. Nanninga, S. J. Rettig, and J. Trotter. Can. J. Chem. **61**, 2493 (1983).
9. W. Kliegel, U. Lauterbach, S. J. Rettig, and J. Trotter. Can. J. Chem. **65**, 1457 (1987).
10. E. Ebeling, W. Kliegel, S. J. Rettig, and J. Trotter. Can. J. Chem. **67**, 933 (1989).
11. W. Kliegel, M. Tajerbashi, S. J. Rettig, and J. Trotter. Can. J. Chem. **68**, 69 (1990).
12. S. J. Rettig and J. Trotter. Can. J. Chem. **61**, 2334 (1983).
13. W. Kliegel, G. Lubkowitz, S. J. Rettig, and J. Trotter. Can. J. Chem. **70**, 2027 (1992).

Can. J. Chem. Downloaded from www.nrcresearchpress.com by 217.78.4.112 on 09/08/12
For personal use only.

Reactions of unactivated olefins with Vilsmeier reagents

ALAN R. KATRITZKY[1] AND IRINA V. SHCHERBAKOVA
Center for Heterocyclic Compounds, Department of Chemistry, University of Florida, Gainesville, FL 32611-2046, U.S.A.

ROBERT D. TACK
Paramins Division, Exxon Chemical, Linden, NJ 07036, U.S.A.

AND

PETER J. STEEL
Department of Chemistry, University of Canterbury, Christchurch, New Zealand

Received September 26, 1991

ALAN R. KATRITZKY, IRINA V. SHCHERBAKOVA, ROBERT D. TACK, and PETER J. STEEL. Can J. Chem. **70**, 2040 (1992).

Reactions of *N*-formylmorpholine/$POCl_3$ with several unactivated olefins yield the corresponding α,β-unsaturated aldehydes. Norbornene affords with dimethylformamide/$POCl_3$ a product formed by a novel inverse-electron demand Diels–Alder reaction of an acyclic 2-azoniodiene. The structure of this product was confirmed by X-ray analysis. Crystals are monoclinic: a = 8.025(3), b = 11.670(3), c = 9.309(4) Å, β = 108.03(3)°, $P2_1$,Z = 2; the structure was refined to R = 0.044 for 1379 independent observed reflections.

ALAN R. KATRITZKY, IRINA V. SHCHERBAKOVA, ROBERT D. TACK et PETER J. STEEL. Can. J. Chem. **70**, 2040 (1992).

Les réactions du couple *N*-formylmorpholine/$POCl_3$ avec plusieurs oléfines inactives fournit les aldéhydes α,β-insaturés correspondants. Le norbornène qui réagit avec le couple diméthylformamide/$POCl_3$ par une nouvelle réaction de Diels–Alder comportant une demande inverse d'électrons fournit un 2-azoniodiène acyclique dont on a déterminé la structure par diffraction des rayons-X. Les cristaux sont monocliniques, groupe d'espace $P2_1$, avec a = 8,025(3), b = 11,670(3) et c = 9,309(4) Å, β = 108,03(3)° et Z = 2; on a affiné la structure jusqu'à une valeur de R = 0,044 pour 1379 réflexions indépendantes observées.

[Traduit par la rédaction]

Introduction

Vilsmeier reagents have been used for the formylation of aromatic secondary and tertiary amines (1, 2), and applied in numerous synthetic transformations of carbonyl compounds to give β-chlorovinylaldehydes (3, 4) and derived cyanines (5, 6). Both vinyl ketones (7, 8) on the one hand and olefinic systems activated towards electrophilic attack (vinyl ethers (9), vinylamines (10), and vinyl halides (11)) on the other have all been thus employed. Terminal olefins and 1,1-disubstituted ethylenes can also be formylated; however, for these compounds further reactions often take place and the nature of the product depends on the environment of the vinyl or vinylidine group. Methylenecyclohexane consumed 2 mol of the Vilsmeier reagent to produce 1-dimethylamino-3-dimethylimmonio-2-[cyclohexen-1-yl]prop-1-ene, isolated as the perchlorate (12). 2-Methylenebornane underwent triformylation and subsequent transformation to furnish a formylpyridine derivative (12). Similarly, isobutene and 2-phenylpropene afford 2,7-naphthyridine-4-aldehyde and 4-phenylpyridine-3-aldehyde, respectively, each involving triformylation (13). However, in terminal olefins and 1,1-disubstituted ethylenes in which migration of the double bond to the adjacent position is blocked, Vilsmeier reactions favour monoformylation. Thus, camphene or 1,1,2,3,5,6-hexamethyl-4-methylene cyclohexa-2,5-diene (13) undergo monoformylation to α,β-unsaturated aldehydes. The monoformylation of steroids having an exocyclic methylene group (12, 14) is known. Monoformylation (40% yield) of a nonexocyclic methylene group in limonene along with isomerization to terpinolene (37% yield) was reported (15). Mono-, bi-, and tri-formylations of vinylcyclopropane derivatives have been intensively studied (16, 17). The present paper is concerned with a more general procedure for the preparation of α,β-unsaturated aldehydes by the monoformylation of unactivated olefins with an excess of the Vilsmeier reagent. We also describe an interesting example of a hetero Diels–Alder reaction of novel type under conditions of the Vilsmeier reaction: the course of the last transformation was supported by an X-ray analysis of the product.

Results and discussion

α,β-Unsaturated aldehydes are important in synthetic organic chemistry (18) and previous preparations include: (*i*) from ketones by one-carbon homologation procedures (19, 20); (*ii*) from methyl vinyl ethers by photooxidation (18); (*iii*) from aldehydes via organolithium derivatives (20, 22–24) or by oxidation via α-chloroaldimines (18); (*iv*) from α-bromoaldehydes via *N*,*N*-dimethylhydrazones (25) or piperidine enamines (26); (*v*) from α-lithiated allenic sulfides (27); and (*vi*) a single example (for 1-cyclohexenecarboxaldehyde) from a nitromethylolefin (28).

We now report that the Vilsmeier reagent *N*-formylmorpholine/phosphorus oxychloride, previously applied to the formylation of vinyl ketones (8), readily converts the unactivated olefines **1**, **3**, **4**, and **6** into the α,β-unsaturated aldehydes **2**, **5**, and **7** (Scheme 1). However, two alternative Vilsmeier reagents (dimethylformamide/phosphorus oxychloride or *N*-formylmethylaniline/phosphorus oxychloride) failed to effect these transformations, although they had earlier (12, 13) successfully monoformylated exocyclic methylene groups in hydrocarbons.

The present reactions were conducted in trichloroethyl-

[1]Author to whom correspondence may be addressed.

Can. J. Chem. Downloaded from www.nrcresearchpress.com by 217.78.4.112 on 09/08/12
For personal use only.

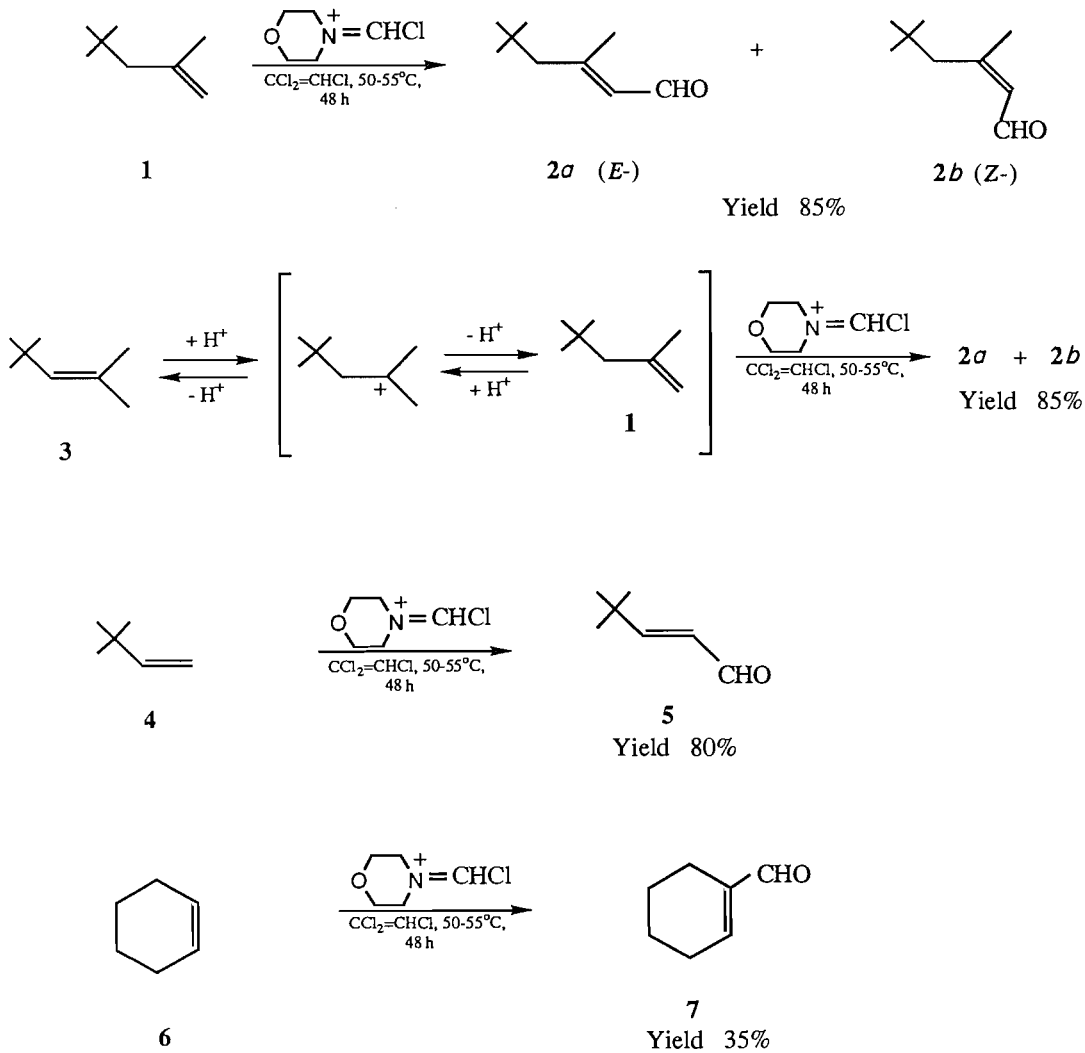

SCHEME 1

ene solution at 50°C for 48 h. Olefin, *N*-formylmorpholine, and $POCl_3$ were used in a molar ratio of 1:2.5:1.5, and the yields of aldehydes **2**, **5**, and **7** were 85, 80, and 35% respectively. When the reaction was carried out at 70–80°C for 24 hs, the yields of aldehydes **2** and **5** decreased somewhere to 60–70%, and cyclohexene gave a low yield of aldehyde **7** (15%). Interestingly, the use of stoichiometric amounts of 2,4,4-trimethylpent-1-ene (**1**), *N*-formylmorpholine, and $POCl_3$ in the absence of solvent at 80°C for 12 h yielded 55% of the corresponding aldehyde **2**.

The formylations of 2,4,4-trimethylpent-1-ene (**1**) and the -2-ene (**3**) both yield mixtures of the *E*-(**2***a*) and the *Z*-(**2***b*) isomers. The ^1H nmr integrals and the gc data show an approximate ratio of 2:1 for the isomers. The spectroscopic assignments are presented in Table 1. The preparation of 3,5,5-trimethyl-2-hexenal **2** as an unseparated mixture of *E*/*Z* isomers in a 7:3 ratio (^1H nmr data) has recently been reported (27). The isomerization of **3** to **1** is easily explained as shown in Scheme 1. Some traces of air moisture can initiate the proton formation. The similar isomerization was observed also for some vinylcyclopropane derivatives on conditions of the Vilsmeier reaction (17) and was explained by the tendency of a double bond to have less steric hindrance. The formylation of 3,3-dimethylbut-1-ene **4** yields only the *E* isomer **5** as is clearly indicated by the coupling constant for the vinyl protons (J = 16 Hz, Table 1). The chemical shifts of the proton and carbon signals in **7** (Table 1) clearly established the structure as 1-cyclohexene carboxaldehyde.

Norbornene **8** did not give the expected aldehyde (21, 29) under the conditions described above. We isolated an unstable colourless viscous oil that decomposed on keeping. The nmr spectra of this oil in $CDCl_3$, recorded immediately after isolation, showed signals for two aldehyde groups at δ 9.85 and 10.15 (^1H nmr) and at 198.50 and 199.15 (^{13}C nmr) and clearly indicated the presence of two bicyclo[2.2.1]heptyl residues. We failed to isolate any solid aldehyde derivative from this oil. Surprisingly, in contrast to its lack of reactivity with olefins **1**, **3**, **4**, and **6**, the use of DMF/$POCl_3$ as a formylating agent was effective for norbornene **8**. Treatment of the hydrolyzed reaction mixture with 70% perchloric acid yielded a stable colourless crystalline perchlorate (85% yield) of such low solubility that nmr spectra could not be obtained. The low resolution mass spectrum gave a molecular ion at m/z 244, and along with the elemental analysis data demonstrated the composition $C_{17}H_{26}N^+ClO_4^-$.

Can. J. Chem. Downloaded from www.nrcresearchpress.com by 217.78.4.112 on 09/08/12
For personal use only.

TABLE 1. α,β-Unsaturated aldehydes

Compound	Boiling point (°C/Torr)	Infrared (cm^{-1})	^1H nmr	^{13}C nmr	Yield (%)	Literature
2*a*(*E*)[a]	79–80/14	1675, 1635	0.97 (s, 9H), 2.23 (d, *J* = 1 Hz, 3H), 2.13 (m, 2H), 5.81 (d, *J* = 8 Hz, 1H), 10.00 (d, *J* = 8 Hz, 1H)	20.02 (27.92), 29.90 (30.18), 32.17 (32.28), 45.56 (54.13), 130.20 (130.38), 161.94 (162.04), 190.75 (191.15)	85	27
2*b*(*Z*)[a]			1.01 (s, 9H), 2.03 (d, *J* = 1 Hz, 3H), 2.52 (m, 2H), 5.99 (d, *J* = 8 Hz, 1H), 9.87 (d, *J* = 8 Hz, 1H)			
5	45–50/14	1695, 1638	1.15 (s, 9H), 6.03 (dd, *J* = 7.3 and 16 Hz, 1H) 6.83 (d, *J* = 16 Hz, 1H), 9.56 (d, *J* = 7.3 Hz, 1H)	30.02, 46.63, 130.20, 160.02, 190.30	80	24
7	72/15	1685, 1645	1.65 (m, 4H), 2.21 (m, 4H), 6.66 (m, 1H), 9.35 (s, 1H)	27.00, 30.05, 32.06, 127.21, 135.16, 191.50	35	28

[a]The isomers have not been separated; the mixtures of **2***a* and **2***b* in a ratio of 2:1 were obtained from **1** and **3**.

Structure determination by X-ray crystallography revealed the spiro dimeric azinium salt **11** (Scheme 2 and Fig. 1). The proposed mechanism for the formation of **11** is shown in Scheme 2. The expected intermediate cation **9** is postulated to undergo a thermally allowed suprafacial [1,5]-hydrogen shift to give the isomeric cation **10** which then undergoes Diels–Alder reaction with more norbornene to give **11**. The X-ray structure determination demonstrates that the Diels–Alder reaction occurs in a diastereofacially selective manner on the *exo* face of both diene and dienophile. Diels–Alder reactions with inverse electron demand involving a 2-azoniobutadiene unit as part of a quaternary heteroaromatic ring (30, 31) or of *N*-arylimmonium ions (32) are well recognized, but we have not found any previous example in which the azoniobutadiene unit is acyclic.

The interaction of perchlorate **11** with aqueous alkali solution yields the hydroxide adduct **12** (Scheme 2) which is easily reconverted into **11** by treatment with 70% perchloric acid in ethanol solution. The structure **12** was established on the basis of elemental analysis and its ir spectrum (a hydroxyl band at 3350 cm^{-1}). The electron impact mass spectrum showed self-chemical ionization of the molecular ion to give the cation **11**, whereas the chemical ionization mass spectrum at high resolution gives the molecular ion of **12**. We failed to obtain the nmr spectra of **12** in DMSO-d_6, the only solvent which allows a sufficient concentration. It gives an unstable solution and the compound decomposed before a spectrum could be acquired.

Experimental

Apparatus, materials, and methods

Melting points were determined on a Thomas–Hoover capillary mp apparatus and are uncorrected. ^1H and ^{13}C nmr spectra were recorded on a Varian VXR 300 spectrometer (300 and 75 MHz,

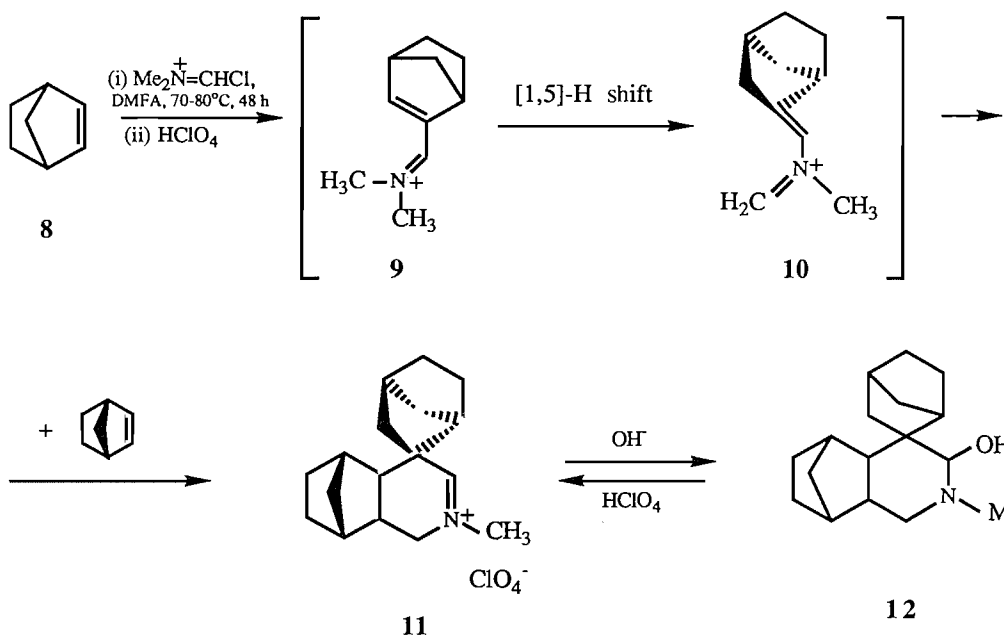

SCHEME 2

Can. J. Chem. Downloaded from www.nrcresearchpress.com by 217.78.4.112 on 09/08/12
For personal use only.

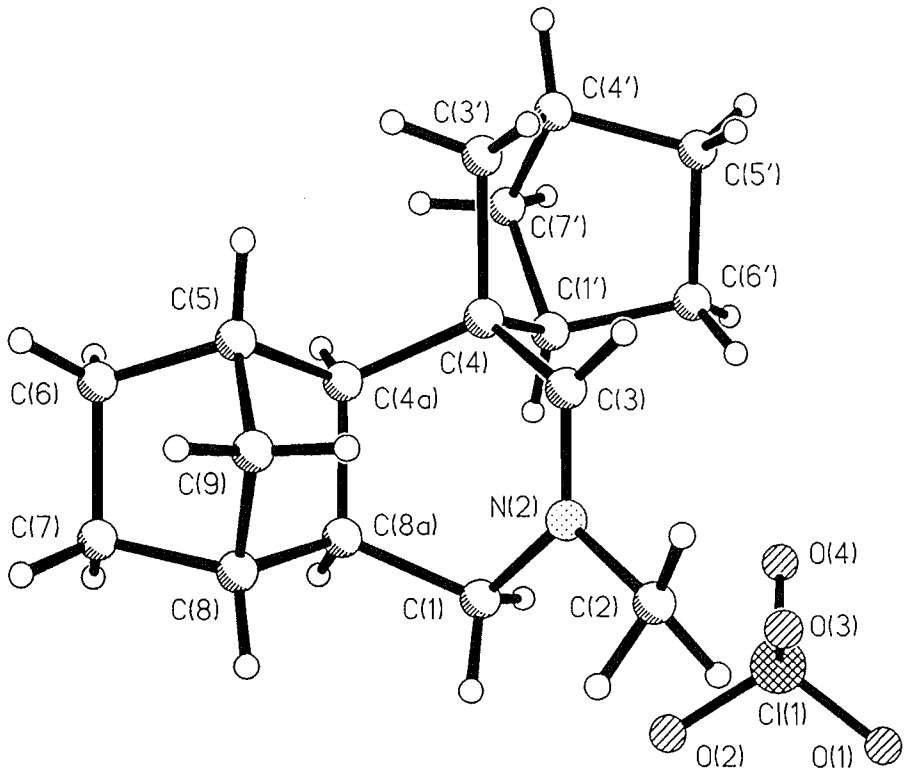

FIG. 1. Perspective view and atom labelling of the X-ray structure.

respectively), using $CDCl_3$ as solvent and tetramethylsilane as an internal reference. Infrared spectra were recorded as neat samples (unless otherwise stated) on a Perkin–Elmer 1600 series FTIR. Mass spectra were recorded on a Krafts AEI MS 30 spectrometer. Elemental analyses were performed on a Carbo Erba 1106 elemental analyser. Commercially available reagent grade solvents were dried over BDH-type 4A molecular sieves prior to use. Flash column chromatography was run over silica gel (EM Merck 60, 230–400 mesh).

X-ray crystallographic analysis

A colorless crystal with approximate dimensions 0.46 × 0.14 × 0.08 mm was cooled to approximately −100°C in a stream of cold nitrogen (controlled boil-off system) in a Nicolet R3/m four-circle diffractometer. Unit cell dimensions were determined by least-squares refinement of 25 accurately centred reflections (2θ = 13–33°). Crystal data are:

$C_{17}H_{26}ClNO_4$ fw = 343.8

Monoclinic, a = 8.025(3), b = 11.670(3), c = 9.309(4), β = 108.03(3), V = 829.0(5), Z = 2, ρ_c = 1.377 Mg m^{-3}, F(000) = 368, μ(Mo-Kα) = 2.47 cm^{-1}, space group $P2_1$.

Intensities were measured using graphite-monochromated Mo-Kα (λ = 0.7107 Å) radiation with ω–2θ scans to 2θ = 60° (±h, +k, +l). The intensities of three check reflections (210, 051, 005), measured every 100 reflections throughout the data collection, showed only small random fluctuations. The data were corrected for Lorentz and polarization effects but no correction for absorption was deemed necessary. Of the 2645 reflections measured, 2511 were unique (R_{int} = 0.020) and 1379 had intensities greater than three times their standard deviations.

The structure was solved[2] by direct methods and refined by full-

[2]All calculations, including the drawing of diagrams, were performed with SHELXTL PC™, Version 4.1 (1990), by G. M. Sheldrick and available from Siemens Analytical X-Ray Instruments Inc. The scattering factors used were those employed by SHELXTL PC™.

TABLE 2. Atomic coordinates (× 10^4) and equivalent isotropic displacement coefficients (Å^2 × 10^3) with esd's in parentheses for 4-methyl-4-aziniumtricyclo[6.2.1.0^{2,7}]undec-4-ene-6-spiro-2′-bicyclo[2.2.1]heptane perchlorate (**11**)

Atom	x	y	z	U_{eq}[a]
C(1)	6328(5)	6511(4)	8524(5)	25
N(2)	8209(5)	6561(3)	9451(4)	25
C(2)	8610(6)	6329(5)	11081(5)	39
C(3)	9383(6)	6805(4)	8836(5)	24
C(4)	8935(5)	7028(4)	7182(5)	21
C(4a)	7293(5)	7824(4)	6662(4)	21
C(5)	7595(6)	9105(4)	7051(5)	29
C(6)	5975(6)	9773(4)	6094(5)	36
C(7)	4568(6)	9460(4)	6860(5)	35
C(8)	5558(7)	8648(4)	8132(6)	32
C(8a)	5832(6)	7515(4)	7403(5)	24
C(9)	7365(6)	9197(4)	8638(5)	34
C(1′)	8566(6)	5876(4)	6270(4)	24
C(3′)	10562(5)	7506(4)	6740(5)	31
C(4′)	10976(6)	6578(5)	5782(5)	34
C(5′)	11695(6)	5525(5)	6815(5)	38
C(6′)	9990(6)	4996(4)	7032(5)	32
C(7′)	9172(6)	6181(5)	4876(5)	32
Cl(1)	6411(2)	3003[b]	8311(1)	30
O(1)	6343(5)	1998(3)	9183(4)	40
O(2)	7587(5)	3811(3)	9315(4)	57
O(3)	4705(6)	3508(4)	7781(5)	81
O(4)	7024(6)	2734(4)	7075(5)	77

[a]Equivalent isotropic U defined as one third of the trace of the orthogonalized U_{ij} tensor.

[b]Origin-defining coordinate.

Can. J. Chem. Downloaded from www.nrcresearchpress.com by 217.78.4.112 on 09/08/12
For personal use only.

TABLE 3. Bond lengths (Å) and angles (°) with esd's in parentheses

C(1)-N(2)	1.490(5)	C(1)-C(8a)	1.537(6)	N(2)-C(2)	1.475(6)
N(2)-C(3)	1.277(7)	C(3)-C(4)	1.491(6)	C(4)-C(4a)	1.562(6)
C(4)-C(1′)	1.568(6)	C(4)-C(3′)	1.586(7)	C(4a)-C(5)	1.539(7)
C(4a)-C(8a)	1.575(7)	C(5)-C(6)	1.541(6)	C(5)-C(9)	1.548(8)
C(6)-C(7)	1.554(8)	C(7)-C(8)	1.532(7)	C(8)-C(8a)	1.534(7)
C(8)-C(9)	1.521(7)	C(1′)-C(6′)	1.536(6)	C(1′)-C(7′)	1.562(7)
C(3′)-C(4′)	1.505(8)	C(4′)-C(5′)	1.556(7)	C(4′)-C(7′)	1.505(6)
C(5′)-C(6′)	1.570(7)	Cl(1)-O(1)	1.438(4)	Cl(1)-O(2)	1.452(4)
Cl(1)-O(3)	1.430(4)	Cl(1)-O(4)	1.419(5)		
N(2)-C(1)-C(8a)		111.5(4)	C(1)-N(2)-C(2)		116.6(4)
C(1)-N(2)-C(3)		120.3(4)	C(2)-N(2)-C(3)		123.1(4)
N(2)-C(3)-C(4)		121.8(4)	C(3)-C(4)-C(4a)		109.5(4)
C(3)-C(4)-C(1′)		110.7(4)	C(4a)-C(4)-C(1′)		110.0(3)
C(3)-C(4)-C(3′)		112.0(3)	C(4a)-C(4)-C(3′)		113.2(4)
C(1′)-C(4)-C(3′)		101.2(4)	C(4)-C(4a)-C(5)		116.6(3)
C(4)-C(4a)-C(8a)		113.5(4)	C(5)-C(4a)-C(8a)		101.8(4)
C(4a)-C(5)-C(6)		108.2(3)	C(4a)-C(5)-C(9)		103.6(4)
C(6)-C(5)-C(9)		100.9(4)	C(5)-C(6)-C(7)		102.6(4)
C(6)-C(7)-C(8)		102.9(4)	C(7)-C(8)-C(8a)		107.6(4)
C(7)-C(8)-C(9)		101.3(4)	C(8A)-C(8)-C(9)		104.3(4)
C(1)-C(8a)-C(4a)		113.6(4)	C(1)-C(8a)-C(8)		113.5(4)
C(4a)-C(8a)-C(8)		102.9(4)	C(5)-C(9)-C(8)		93.4(4)
C(4)-C(1′)-C(6′)		109.5(3)	C(4)-C(1′)-C(7′)		101.5(4)
C(6′)-C(1′)-C(7′)		99.0(4)	C(4)-C(3′)-C(4′)		104.5(4)
C(3′)-C(4′)-C(5′)		108.0(4)	C(3′)-C(4′)-C(7′)		101.7(4)
C(5′)-C(4′)-C(7′)		102.2(4)	C(4′)-C(5′)-C(6′)		102.6(4)
C(1′)-C(6′)-C(5′)		103.4(4)	C(1′)-C(7′)-C(4′)		95.6(3)
O(1)-Cl(1)-O(2)		107.3(2)	O(1)-Cl(1)-O(3)		109.4(3)
O(2)-Cl(1)-O(3)		108.4(2)	O(1)-Cl(1)-O(4)		111.2(2)
O(2)-Cl(1)-O(4)		110.3(3)	O(3)-Cl(1)-O(4)		110.3(3)

matrix least-squares procedures. All non-hydrogen atoms were refined with anisotropic displacement parameters and hydrogen atoms were included in calculated positions (C—H = 0.96 Å) with fixed isotropic parameters (the orientations of the methyl group hydrogens were based on difference map peaks). The function minimized was $\Sigma w(|F_o| - |F_c|)^2$, with $w = [\Sigma^2(F_o)+0.00005F_o^2]^{-1}$. The absolute configuration was deemed to be that which gave the better of two otherwise identical refinements. In the final cycles of refinement the maximum parameter shift corresponded to 0.005 σ. A final difference map showed no features >0.35 e^- Å^{-3}. Refinement converged[3] with $R = 0.044$, $wR = 0.036$ and $S = 1.41$ for the 1379 reflections with $I > 3\sigma(I)$.

The final positional and equivalent isotropic displacement parameters for the non-hydrogen atoms are given in Table 2. Bond lengths and angles are listed in Table 3. Anisotropic displacement parameters and tables of observed and calculated structure factors have been deposited.[4] The bonding geometries at N(2) and C(3) (Table 3) clearly locate the double bond between these two atoms. It is also noteworthy that the bonds to C(4) are somewhat elongated, which reflects the steric congestion about this spiro-center.

[3] $R = \Sigma(|F_o| - |F_c|)/\Sigma|F_o|$; $wR = \{\Sigma w(|F_o| - |F_c|)^2/\Sigma w(|F_o|)^2\}^{1/2}$; $S = \{\Sigma w(|F_o| - |F_c|)^2/n - m\}^{1/2}$.

[4] A complete set of tables may be purchased from: The Depository of Unpublished Data, Document Delivery, CISTI, National Research Council Canada, Ottawa, Canada K1A 0S2.

A table of hydrogen atom coordinates has also been deposited with the Cambridge Crystallographic Data Centre and can be obtained on request from The Director, Cambridge Crystallographic Data Centre, University Chemical Laboratory, 12 Union Road, Cambridge, CB2, 1EZ, U.K.

General procedure for preparation of α,β-unsaturated aldehydes

Freshly distilled phosphorus oxychloride (7.0 g, 45.8 mmol) was added to a stirred mixture of *N*-formylmorpholine (6.9 g, 60 mmol) and trichloroethylene (10 mL) over 5 min at 5°C. After stirring the resultant solution for 10 min at 20°C, the appropriate olefin (24 mmol) was added dropwise at 15–20°C. The mixture was then stirred at 50–55°C for 48 h and cooled. Methylene chloride (25 mL) was added, and the reaction mixture was brought to pH 7 with a solution of sodium carbonate (12.5 g, 0.12 M) in water (75 mL). The aqueous layer was extracted with methylene chloride (3 × 50 mL). The combined organic layers were washed with water (60 mL) and dried over $MgSO_4$. The solvent was removed under vacuum at room temperature and the residue distilled under vacuum or purified by flash column chromatography with ether as eluent. The spectroscopic data of aldehydes **2**, **5**, and **7** are presented in Table 1.

*4-Methyl-4-aziniumtricyclo[6.2.1.0^{2,7}]undec-4-ene-6-spiro-2′-bicyclo[2.2.1]heptane perchlorate (**11**)*

A solution of $POCl_3$ (4.5 mL, 50 mmol) in DMF (5 mL) was slowly added to DMF (10 mL) at 5°C. After stirring the resultant mixture for 5 min at 5°C, a solution of norbornene **8** (4.7 g, 50 mmol) in DMF (5 mL) was added dropwise at 15–20°C. The mixture was stirred at room temperature for 48 h and at 70–80°C for 2 h. The product was poured onto ice (150 g) and treated with 70% perchloric acid (5 mL). The colourless crystalline precipitate was filtered off, dried, and recrystallized from ethanol to give 7.30 g (85%) of **11**, mp 253°C. Anal. calcd. for $C_{17}H_{26}ClNO_4$: C 59.38, H 7.52, N 4.00; found: C 59.38, H 7.82, N 3.63.

*4-Methyl-4-aza-5-hydroxytricyclo[6.2.1.0^{2,7}]undecan-6-spiro-2′-bicyclo[2.2.1]heptane (**12**)*

A suspension of perchlorate **11** (0.34 g, 0.001 M) in 25% aqueous NaOH solution (10 mL) and ether (10 mL) was stirred for

Can. J. Chem. Downloaded from www.nrcresearchpress.com by 217.78.4.112 on 09/08/12
For personal use only.

2 h at room temperature. The ether layer was separated, washed with water (10 mL), and dried over $MgSO_4$. The solvent was removed under vacuum to give colourless crystals of **12** (0.25 g, 98%), mp 157–158°C after recrystallization from ethanol; ir (ν_{max}, Nujol): 3350 (OH) cm^{-1}. Anal. calcd. for $C_{17}H_{27}NO$: C 79.16, H 10.54, N 5.36; found: C 79.38, H 10.80, N 5.32. Exact mass (hrms/ci) calcd. for $C_{17}H_{27}NO$: 261.2092; found: 261.2105.

1. O. Fischer, A. Müller, and A. Vilsmeier. J. Prakt. Chem. **109**, 69 (1925).
2. A. Vilsmeier and A. Haack. Chem. Ber. **60**, 119 (1927).
3. Z. Arnold and J. Zemlicka. Proc. Chem. Soc. 227 (1958).
4. P. R. Giles and C. M. Marson. Tetrahedron Lett. **21**, 5227 (1990).
5. H. E. Nikolajewski, S. Dähne, and B. Hirsch. Chem. Ber. **100**, 2616 (1967).
6. P. R. Giles and C. M. Marson. Tetrahedron, **47**, 1303 (1991).
7. A. R. Katritzky and C. M. Marson. J. Org. Chem. **52**, 2726 (1987).
8. A. R. Katritzky, C. M. Marson, and Z. Wang. J. Org. Chem. **52**, 2730 (1987).
9. D. Burn, G. Cooley, M. T. Davies, J. W. Ducker, B. Ellis, P. Feather, A. K. Hiscock, D. N. Kirk, A. P. Leftwick, V. Petrow, and D. M. Williamson. Tetrahedron, **20**, 597 (1964).
10. A. Consonni, U. Pallini, and R. Sciaky. Gazz. Chim. Ital. **96**, 1284 (1966).
11. R. Sciaky and F. Mancini, Tetrahedron Lett. 137 (1965).
12. C. Jutz and W. Müller. Chem. Ber. **100**, 1536 (1967).
13. C. Jutz, W. Müller, and E. Müller. Chem. Ber. **99**, 2479 (1966).
14. M. J. Grimwade and M. G. Lester. Tetrahedron, **25**, 4535 (1969).
15. G. Dauphin. Synthesis, 799 (1979).
16. P. C. Traas and H. Boelens. Rec. Trav. Chim. **92**, 985 (1973).
17. P. C. Traas, H. Boelens, and H. J. Takken. Rec. Trav. Chim. **95**, 57 (1976).
18. N. De Kimpe and C. Stevens. Bull. Soc. Chim. Belg. **99**, 41 (1990).
19. J. N. Denis, W. Dumont, and A. Krief. Tetrahedron Lett. 453 (1976).
20. P. C. Traas, H. Boelens, and H. J. Takken. Tetrahedron Lett. 2287 (1976).
21. G. Rousseau, P. Le Perchec, and J. M. Conia. Synthesis, 67 (1978).
22. H. Taguchi, S. Tanaka, H. Yamamoto, and H. Nozaki. Tetrahedron Lett. 2465 (1973).
23. K. S. Y. Lau and M. Schlosser. J. Org. Chem. **43**, 1595 (1978).
24. L. Duhamel and F. Tombret. J. Organomet. Chem. **280**, 1 (1985).
25. L. Duhamel and J.-Y. Valnot. C. R. Acad. Sci. Paris, **286(C)**, 47 (1978).
26. D. R. Williams and K. Nishitani. Tetrahedron Lett. 4417 (1980).
27. E. Guittet, C. Bibang Bi Ekogha, and S. A. Julia. Bull. Soc. Chim. Fr. 325 (1986).
28. J. L. Hogg, T. E. Goodwin, and D. W. Nave. Org. Prep. Proced. Int. **10**, 9 (1978).
29. J. J. Riehl and F. Jung. Tetrahedron Lett. 3139 (1969).
30. C. K. Bradsher. Adv. Heterocycl. Chem. **16**, 289 (1974).
31. D. L. Boger. Chem. Rev. **86**, 781 (1986).
32. K.-D. Hesse. Liebigs Ann. Chem. **741**, 117 (1970).

Can. J. Chem. Downloaded from www.nrcresearchpress.com by 217.78.4.112 on 09/08/12
For personal use only.

Oxidation of L-rhamnose and D-mannose by Cr(VI) in perchloric acid. A comparative study[1]

LUIS F. SALA,[2] SANDRA R. SIGNORELLA, MARCELA RIZZOTTO, MARÍA I. FRASCAROLI, AND FABIO GANDOLFO

Departamento de Ciencias Exactas, Facultad de Ciencias Bioquímicas (UNR), Suipacha 531, 2000 Rosario, Argentina

Received August 26, 1991[3]

LUIS F. SALA, SANDRA R. SIGNORELLA, MARCELA RIZZOTTO, MARÍA I. FRASCAROLI, and FABIO GANDOLFO. Can. J. Chem. **70**, 2046 (1992).

The oxidation of L-rhamnose and D-mannose by Cr(VI) in perchloric acid follows the rate law:

$$-\frac{d[Cr(VI)]}{dt} = \frac{(k_0 + k_1 [h_0]^2) K [\text{aldose}] [Cr(VI)]}{1 + K [\text{aldose}]}$$

$K = 5.40$, $k_0 = 0.00138\ M^{-1}\ s^{-1}$, $k_1 = 6.71 \times 10^{-4}\ M^{-3}\ s^{-1}$ for D-mannose and $K = 2.63$, $k_0 = 2.51 \times 10^{-3}\ M^{-1}\ s^{-1}$, $k_1 = 2.74 \times 10^{-3}\ M^{-3}\ s^{-1}$ for L-rhamnose. This rate law corresponds to the reaction leading to the formation of L-1,4-rhamnonelactone and D-1,4-mannonelactone. No cleavage to carbon dioxide takes place when a 20-fold or higher excess of aldose over Cr(VI) is employed. Relative values of kinetic constants are interpreted in terms of primary hydroxyl group participation in the chromic ester formed in the first reaction step. The free radicals formed during the reaction react with Cr(VI) to yield Cr(V). Two signals ($g_{iso} = 1.977$ and $g_{iso} = 1.970$) ascribed to intermediate Cr(V) complexes were observed by electron paramagnetic resonance (epr) of 0.25–1 N $HClO_4$ solutions saturated with L-rhamnose and $Cr_2O_7^{2-}$. At higher pH (3–7), only the signal at $g = 1.977$ was detected. For D-mannose only one signal at $g = 1.978$ was observed over the whole range of $HClO_4$ concentrations.

LUIS F. SALA, SANDRA R. SIGNORELLA, MARCELA RIZZOTTO, MARÍA I. FRASCAROLI et FABIO GANDOLFO. Can. J. Chem. **70**, 2046 (1992).

L'oxydation du L-rhamnose et du D-mannose par le Cr(VI), dans l'acide perchlorique, suit l'équation de vitesse suivante :

$$-\frac{d[Cr(VI)]}{dt} = \frac{(k_0 + k_1 [h_0]^2) K [\text{aldose}] [Cr(VI)]}{1 + K [\text{aldose}]}$$

dans laquelle $K = 5{,}40$, $k_0 = 0{,}00138\ M^{-1}\ s^{-1}$, $k_1 = 6{,}71 \times 10^{-4}\ M^{-3}\ s^{-1}$ pour le D-mannose et $K = 2{,}63$, $k_0 = 2{,}51 \times 10^{-3}\ M^{-1}\ s^{-1}$, $k_1 = 2{,}74 \times 10^{-4}\ M^{-3}\ s^{-1}$ pour le L-rhamnose. Cette équation de vitesse correspond à la réaction conduisant à la formation de la L-1,4-rhamnonelactone et de la D-1,4-mannonelactone. Il ne se produit pas de clivage en dioxyde de carbone lorsque la quantité d'aldose utilisée dépasse de 20 fois ou plus la quantité de Cr(VI). On interprète les valeurs relatives des constantes cinétiques en fonction d'une participation du groupe hydroxyle primaire dans l'ester chromique qui se forme au cours de la première étape de la réaction. Les radicaux libres qui se forment au cours de la réaction réagissent avec le Cr(VI) pour former du Cr(V). On attribue deux signaux ($g_{iso} = 1{,}977$ et $g_{iso} = 1{,}970$) observés par resonance paramagnétique électronique (rpe) sur des solutions de 0,25 à 1 N de $HClO_4$ saturées en L-rhamnose et en $Cr_2O_7^{2-}$, aux complexes du Cr(V) intermédiaire. À des pH supérieurs (3–7), on n'a détecté que le signal à $g = 1{,}977$. Pour le D-mannose, on n'observe que le signal à $g = 1{,}978$ à toutes les concentrations de $HClO_4$.

[Traduit par la rédaction]

Introduction

Sugars are very attractive natural ligands for both toxic and essential metal ions. Besides acting simply as effective chelators (1), in many cases they are also reducing agents; e.g., for metal ions such as Ce(IV), V(V), Co(III), Fe(III) (refs. 2, 3, 4, 5 respectively), depending on the acidity of the medium. There is also an indication that some sugars, or their derivatives, may play an important role in the chemistry of chromium, specially in the environment (6–8), where Cr(VI) may present a serious hazard because of its mutagenic and carcinogenic activity. It has recently been reported that the major coordination sites involved in chromium binding in natural systems may be the hydroxyl (e.g., nucleic acids, polysaccharides) and thiol (in peptides and proteins) donors (9). They form stable esters or thioesters with chromate and stabilize Cr(V) intermediates after further interaction with biological reductants such as glutathione.

It was considered worthwhile to revise the degradative oxidation of aldoses by action of Cr(VI) (10–15) in order to determine: (*a*) the extension of ester chromate formation; (*b*) the detection of Cr(V) (not yet reported for the oxidation of aldoses); (*c*) the availability of the hydroxyl groups to bind Cr(VI).

We started by studying the degradative oxidation of two aldohexoses: L-rhamnose and D-mannose.

Experimental

L-Rhamnose and D-Mannose (Sigma pure) were used without further purification. Potassium dichromate (BDH reagent) was used for the kinetic runs, while the sodium salt (BDH reagent) was used for the products analysis, where the high concentrations cause precipitation of potassium perchlorate. Mixtures of sodium perchlorate (Aldrich puriss.) and perchloric acid (Merck reagent) were used to maintain a constant ionic strength of 2.0 M at different hydrogen ion concentrations. Stock solutions of perchloric acid were analyzed by titration employing standard analytical methods (16).

[1]The present work was presented at the XIX Latin American Meeting on Chemistry, Buenos Aires, Argentina (1990).

[2]Author to whom correspondence may be addressed.

[3]Revision received April 15, 1992.

Can. J. Chem. Downloaded from www.nrcresearchpress.com by 109.225.110.28 on 09/08/12
For personal use only.

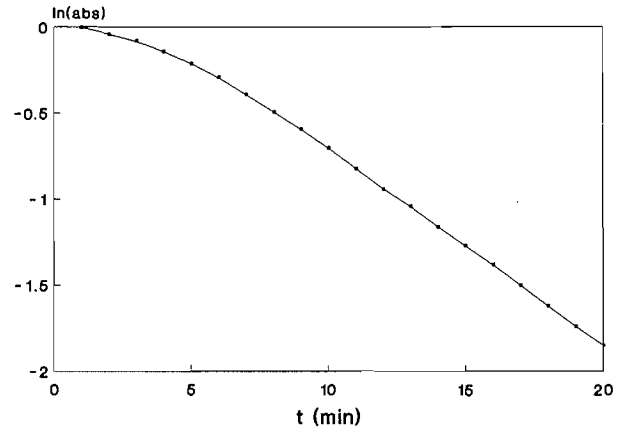

FIG. 1. Time dependence of ln(abs) at 350 nm. T = 33°C; [Cr(VI)] = 0.0008 M, [rhamnose] = 0.016 M, [$HClO_4$] = 1.75 M; I = 2.0 M.

Kinetics

Kinetic measurements were made at 350 nm by monitoring the absorbance changes on a Guilford Response II spectrophotometer with fully thermostated cell compartments. The concentration of Cr(VI) was kept constant at a 8×10^{-4} M, while the aldose concentrations were varied between 0.016 and 0.16 M (0.28 M in some cases), at a constant ionic strength of 2.0 M.

For both D-mannose and L-rhamnose, pseudo-first-order rate constants were calculated from the slopes of the linear part of the ln(abs) vs. time plots (Fig. 1). Rate constants obtained from multiple determinations were within ±5% of each other.

Products analysis

The stoichiometry of the chromic oxidation of L-rhamnose and D-mannose was determined by mixing chromic acid and aldose solutions to final concentrations of 0.112 M and 0.0158 M respectively, in 2 N $HClO_4$ at 80°C, during 2 days. After the reaction went to completion, yield of carbon dioxide per mole of aldose was determined as follows.

A slow stream of pure nitrogen was flushed through the reaction mixture to sweep the carbon dioxide formed into a barium hydroxide solution. The barium carbonate was filtered and the filtrate titrated against standard potassium hydrogen phthalate. The molar amount of barium hydroxide consumed and the barium carbonate weighed were always the same. On successive experiments carbon dioxide was also trapped in a sodium hydroxide solution of known titre and back-titrated, obtaining the same yield of carbon dioxide as by the previous method.

In this way, 4 moles of CO_2 were produced per mole of L-rhamnose and 6 moles of CO_2 per mole of D-mannose.

The amount of reacted Cr(VI) was determined spectrophotometrically. Six moles of Cr(VI) were consumed per mole of L-rhamnose, while 3 moles of D-mannose consumed 22 moles of Cr(VI).

From these experimental data, the stoichiometry for total oxidative degradation of L-rhamnose and D-mannose by Cr(VI) is:

$$[1] \quad C_6O_5H_{12} + 6Cr(VI) \rightarrow 4CO_2 + CH_3COOH + 6Cr(III)$$

$$[2] \quad 3C_6O_6H_{12} + 22Cr(VI) \rightarrow 18CO_2 + 22Cr(III)$$

Under conditions used in the kinetic measurements CO_2 was never detected. In excess of substrate (ratios of aldose over Cr(VI) from 20 to 200), qualitative identification of reaction products was carried out by paper chromatography. L-1,4-Rhamnonelactone and D-1,4-mannonelactone were identified against authentic samples, using *n*-butanol – acetic acid – water (4:1:5) as eluent. Paper chromatograms were visualized by two kinds of development reagents: a three-stage dip of silver nitrate, sodium hydroxide, and sodium thiosulfate (17) and *p*-anisidine reagent, specific for aldoses detection (18).

TABLE 1. Effect of oxidant on the oxidation of L-rhamnose and D-mannose. [aldose] = 0.08 M; [$HClO_4$] = 2 N; T = 35°C

$[Cr(VI)]_0/M \times 10^4$	$10^2 k_{obs}$ [Cr(VI)] / $[Cr_2O_7^{2-}]$
L-Rhamnose	
4.0	3.48
14	3.47
20	3.48
26	3.45
D-Mannose	
8.0	2.44
14	2.46
20	2.46
26	2.47

The EPR measurements

The epr spectra were recorded with a Bruker spectrometer model ER-200. g values were measured by refence to diphenylpicrylhydracyl (DPPH, g = 2.0036). Spectra were acquired at a frequency of ca. 9.8 GHz with a center field of 3550 G, a sweep width of 20–1000 G, and a variable modulation amplitude. The cavity and sample tube were kept at 25°C. 0.25–1 N $HClO_4$ solutions saturated with $Cr_2O_7^{2-}$ were used for Cr(V) detection. Under these experimental conditions the reaction went to completion in ca. 30 h, but Cr(V) could be followed during no longer than 30 min.

Results and discussion

Kinetic results

The observed rate constants were deduced from absorbance data obtained at 350 nm. The pseudo-first-order rate constants were calculated at various $[Cr(VI)]_0$ but at constant $[aldose]_0$, ionic strength (I = 2 N), and temperature. The rate was found to increase with increase in $[Cr(VI)]_0$. The values of k_{obs} $[Cr(VI)]_0/[Cr_2O_7^{2-}]$ at various $[Cr(VI)]_0$ were calculated at 35°C. The results (Table 1) indicate that the dimeric species, viz. $Cr_2O_7^{2-}$ is the effective oxidant. The equilibrium $HCrO_4^-/Cr_2O_7^{2-}$ (K = 76 (19)) was used to calculate $[Cr_2O_7^{2-}]$, neglecting the subsidiary equilibrium $HCrO_4^-/CrO_4^{2-}$ because of the high [$HClO_4$] employed. Table 2 summarizes values of k_{obs} for various concentrations of aldoses at fixed concentrations of perchloric acid. Plots of $1/k_{obs}$ vs. 1/[aldose], for both L-rhamnose and D-mannose, are given in Figs. 2 and 3. Effect of the aldose concentration on k_{obs} can be written as:

$$[3] \quad k_{obs} = \frac{kK\,[\text{aldose}]}{1 + K\,[\text{aldose}]}$$

Values of k and K for different perchloric acid concentrations are given in Table 3. It is observed that while K is clearly acidity independent over the whole range of hydrogen ion concentrations, k varies with acidity between 0.5 M and 2.0 M. Due to the high acidities employed in this study, the concentration of hydrogen ions was replaced by the acidity function h_0 (20). Plots of k vs. h_0^2 give straight lines with a positive intercept (Fig. 4) for both L-rhamnose and D-

Can. J. Chem. Downloaded from www.nrcresearchpress.com by 109.225.110.28 on 09/08/12
For personal use only.

TABLE 2. Pseudo-first-order rate constants for the oxidation of L-rhamnose and D-mannose by Cr(VI). T = 33°C; $[Cr(VI)]_{tot} = 8 \times 10^{-4}$ M; I = 2 M; λ = 350 nm

	$k_{obs}{}^a \times 10^4$ (s^{-1}) for $[HClO_4]$/M of				
[Rham]/M	0.5	0.75	1.00	1.25	1.50
0.016	1.74	4.00	6.50	8.90	17.2
0.04	3.95	9.30	14.3	20.7	35.9
0.08	7.20	16.9	26.7	40.1	67.6
0.12	10.5	22.5	38.2	52.0	115
0.16	15.9	30.4	43.9	64.0	147
0.20		29.9	60.1		
0.24		41.0	70.2		
0.28		42.0			

	$k_{obs}{}^a \times 10^4$ (s^{-1}) for $[HClO_4]$/M of				
[Mann]/M	0.75	1.00	1.25	1.50	1.75
0.016	2.02	3.40	5.88	8.61	10.9
0.04	4.00	7.56	11.6	17.2	22.4
0.08	7.56	12.3	21.2	31.0	42.3
0.12	10.6	17.4	30.2	43.6	60.2
0.16	12.9	20.0	38.7	58.3	74.9

[a]Rate constants obtained from multiple determinations.

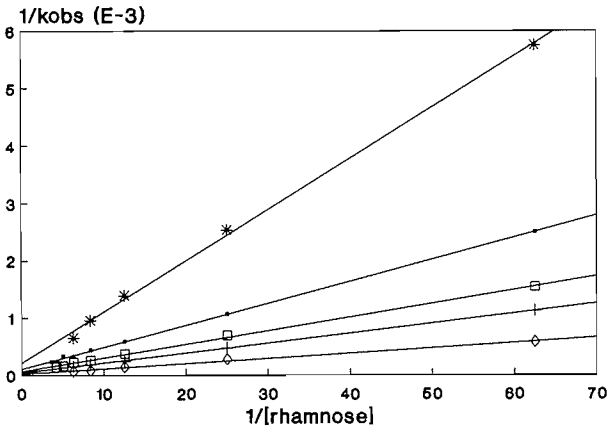

FIG. 2. Effect of [rhamnose] on k_{obs}. T = 33°C; I = 2.0 M; $[HClO_4]$ = (*) 0.5 M, (■) 0.75 M, (□) 1.0 M, (+) 1.25 M, (◇) 1.5 M.

mannose, showing that the acidity dependence of k can be written as:

$$[4] \quad k = k_0 + k_1 h_0^2$$

where $k_0 = 2.51 \times 10^{-3}$ M^{-1} s^{-1}, $k_1 = 2.74 \times 10^{-3}$ M^{-3} s^{-1} for L-rhamnose and $k_0 = 1.38 \times 10^{-3}$ M^{-1} s^{-1}, $k_1 = 6.71 \times 10^{-4}$ M^{-3} s^{-1} for D-mannose.

The complete rate law for the reaction thus is given by:

$$[5] \quad -\frac{d[Cr(VI)]}{dt} = k_{obs}[Cr(VI)]_0 = \frac{(k_0 + k_1 h_0^2) K [aldose][Cr(VI)]_0}{1 + K [aldose]}$$

where $[Cr(VI)]_0$ represents the total Cr(VI) concentration.

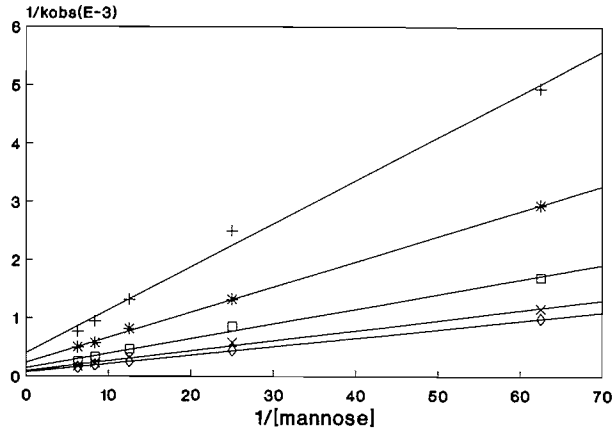

FIG. 3. Effect of [mannose] on k_{obs}. T = 33°C; I = 2.0 M; $[HClO_4]$ = (+) 0.75 M, (*) 1.0 M, (□) 1.25 M, (×) 1.5 M, (◇) 1.75 M.

TABLE 3. Rate constants for the oxidation of L-rhamnose and D-mannose by Cr(VI). T = 33°C; $[Cr(VI)] = 8 \times 10^{-4}$ M; I = 2.00 M

h_0	$k(M^{-1} s^{-1})$	K
L-Rhamnose		
1.17	0.00495	2.26
1.51	0.00909	2.87
2.13	0.0158	2.65
2.63	0.0221	2.62
3.72	0.0399	2.77
		$K = 2.63 \pm 0.21$
D-Mannose		
1.51	0.00250	5.42
2.13	0.00420	5.49
2.63	0.00699	5.63
3.72	0.0104	5.54
4.67	0.016	4.94
		$K = 5.40 \pm 0.24$

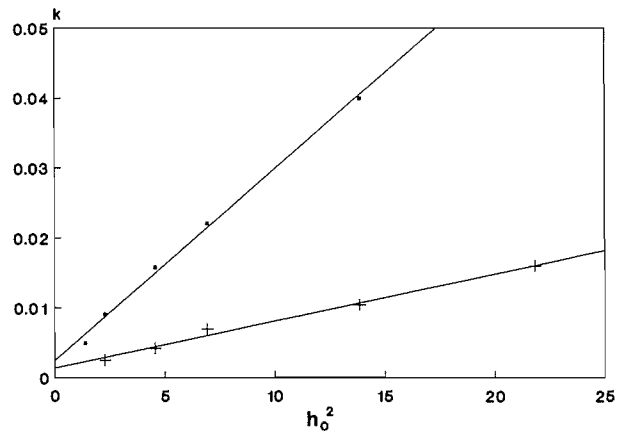

FIG. 4. Effect of acidity (h_0) on k. T = 33°C; I = 2.0 M; (+) D-mannose; (■) L-rhamnose.

Detection of Cr(V)

No Cr(V) epr signals were detected in the dilute solutions used for kinetic measurements. The fact that no signals were

Can. J. Chem. Downloaded from www.nrcresearchpress.com by 109.225.110.28 on 09/08/12
For personal use only.

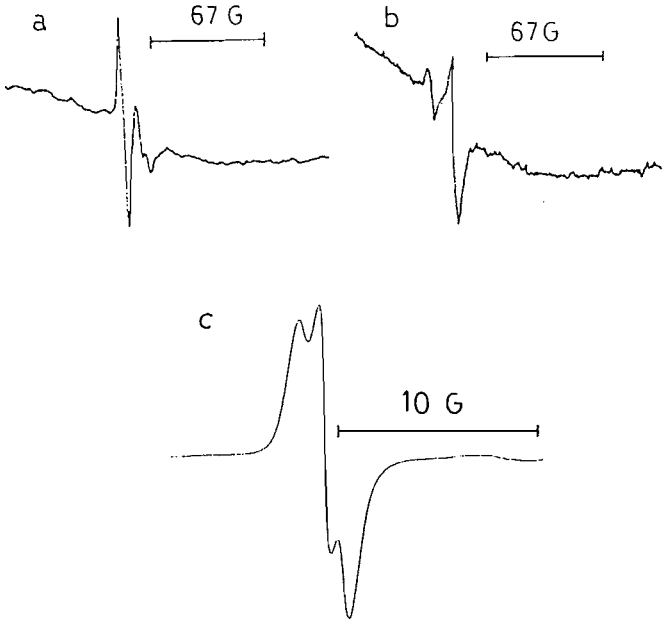

FIG. 5. The epr signal of a mixture of L-rhamnose and Cr(VI) (10:1 mole ratio) in $HClO_4$ (a) 0.25 N, 5 min after solution preparation; (b) 1 N, 3 min after mixing; and (c) 0.01 N, 3 h after solution preparation. T = 25°C.

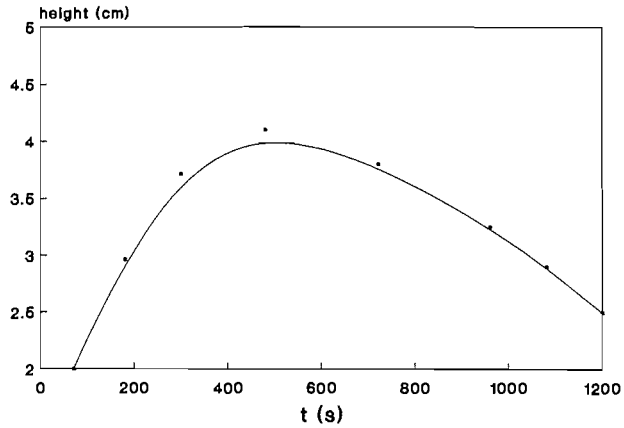

FIG. 6. Peak-to-peak heights of epr signal due to Cr(V) at g = 1.977 vs. time. $[HClO_4]$ = 0.25 N, [Cr(VI)] = 0.34 M, [rhamnose] = 0.77 M; T = 25°C.

observed does not necessarily mean that they are not present. All it means is that the sensivity of the instrumentation used was not sufficient to detect them, if they were present. Given the high concentrations of chromium that were required to detect the signals in other experiments, we believe that it is highly likely that Cr(V) signals are present in all of the experiments, but that they were not detected due to sensitivity problems of the measurements. When aldose and Cr(VI) saturated solutions were used, two different patterns of signals were observed for L-rhamnose–Cr(V) and D-mannose–Cr(V) complexes. Figure 5 shows the epr spectrum of an aqueous solution of Cr(VI) and rhamnose in 10:1 mole ratio in 0.25 N $HClO_4$. This spectrum was measured 5 min after solution preparation. The spectrum is dominated by a band at g_{iso} = 1.977, with its four weak ^{53}Cr (9.55% abundance, I = 3/2) hyperfine bands at 17.8 G spacing, and a superhyperfine (shf) splitting value of 0.90 G. The shf pattern clearly indicates that the Cr(V) ion coordinates to one sugar molecule via two hydroxyl oxygens and that the shf structure derives from the coupling with the two protons bound to the carbons. At this $[HClO_4]$ a minor band (g_{iso} = 1.970) is observed.

As the rhamnose:Cr(VI) ratio was decreased (10:1 to 1:1), the signal at g = 1.977 was always the major one. Both signals decayed with time, but the major band decayed faster than the band at g = 1.970.

Variation of the solution pH within the range 3–7 afforded the signal at g = 1.977, which remains during ca. 1 week. However, extra bands were not detected, even when different rhamnose:Cr(VI) mole ratios were used (Fig. 5).

In the range of 0.25–1 N $[HClO_4]$ the signal at g = 1.970 grew and became the dominant feature (Fig. 5).

These results show that interaction of L-rhamnose and Cr(VI) in perchloric acid solution produces at least two relatively long-lived Cr(V) species, characterized by their epr bands at g = 1.977 and g = 1.970, with the latter being strongly dependent upon $[HClO_4]$.

g_{iso} = 1.977 and A_{iso} = 17.8 are typical of five-coordinate oxochromate(V) complexes (21, 22) and the structure of this complex is most likely a square-pyramidal $[Cr{=}O]^{3+}$ species with the molecule of aldohexose bound in bidentate fashion through two *syn*-hydroxyl groups. Analysis of the signal at g = 1.970 is very difficult because of the low intensity of this signal and its badly resolved superhyperfine structure.

Figure 6 shows a typical growth and decay curve for peak-to-peak heights of the Cr(V) epr signal at g = 1.977 vs. time, obtained on a reacting solution. This signal grows and decays in a very short time (t_{max} = 8 min). This means that at high hydrogen ion concentrations the L-rhamnose/Cr(V) complex behaves like stationary stage that decomposes as it is formed.

An epr signal (g = 1.978) assigned to the Cr(V)–D-mannose complex has already been reported for the Cr(VI)/D-mannose reaction mixture at pH = 7.4 (23). We observed this signal in 0.25 N $HClO_4$ solution saturated with reactants, and, unlike L-rhamnose, no other signal was detected. This complex had been ascribed to Cr(V) coordinated to one sugar molecule via the two hydroxyl oxygens at C2 and C3. We propose a different structure for this species observed in the reaction of Cr(VI) with D-mannose. D-Mannose differs from L-rhamnose in the C6 hydroxyl group, so a different behavior in forming complexes with Cr(V) could be related to this structural difference. Examination of CPK models showed that, if the sugar is in the boat conformation, spatial disposition of hydroxyl groups on C1, C2, and C6 is appropriate to form a square-pyramidal $[Cr{=}O]^{3+}$ complex bound to the D-mannose, acting as tridentate ligand, and a water molecule in the fourth site of coordination. This structure seems to better reflect the formation of only one Cr(V) complex, such as proposed in Fig. 7, and it should be considered as a tentative hypothesis.

Mechanism

The observed deviation from first-order decay of ln(abs) at 350 nm at short times (Fig. 1) has already been observed in other systems where Cr(V) was detected (24). However,

Can. J. Chem. Downloaded from www.nrcresearchpress.com by 109.225.110.28 on 09/08/12
For personal use only.

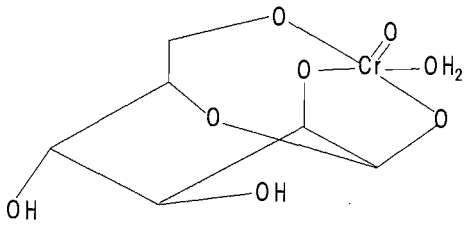

FIG. 7. Proposed structure for Cr(V)/mannose complex.

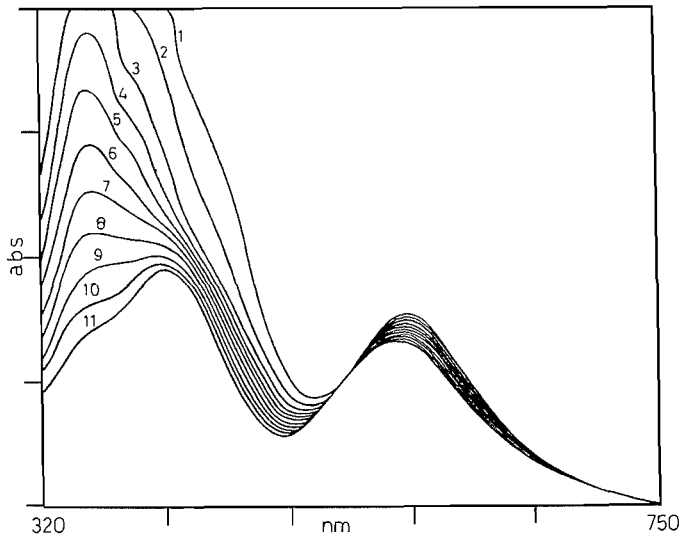

FIG. 8. Time evolution of UV/VIS spectrum of a mixture of D-mannose (0.18 M) and Cr(VI) (0.018 M). $[HClO_4]$ = 0.55 M; T = 30°C. Spectra 1–11 represent measurements taken over a period of ca. 70 min.

neither L-rhamnose nor D-mannose forms Cr(V) complexes stable enough to be detected under conditions used in the kinetic measurements. All attempts to observe Cr(V) at 750 nm were unsuccessful, even when saturated solutions were used. Besides, it was not possible to detect such a complex by epr measurements of dilute solutions of aldose/Cr(VI) mixtures. It might be observed by employing more sophisticated equipment. Only when aldose/Cr(VI) saturated solutions were mixed, could Cr(V) complexes be observed by epr. On the other hand, these Cr(V) complexes grow and decay in a very short time compared to Cr(VI) decay under the same reaction conditions. These results mean that the decomposition rate of Cr(V) has to be much larger than that of Cr(VI), and that Cr(V) concentration is not high enough to interfere significantly with the absorbances observed at 350 nm over a very short time, whereas k_{obs} values obtained from the linear part of the ln(abs) vs. time plot should not be further modified by Cr(V) absorbance.

Another suitable explanation for this initial deviation from linearity may be the formation of the chromic ester with aldose in a pre-equilibrium process. The maximum absorbance of these esters must not differ too much from that of chromic acid. The shoulder at 380 nm in the spectra obtained from wavelength scanning of aldose/Cr(VI) mixtures at different times may be attributed to the chromic ester (Fig. 8). Effect of the substrate concentration on the absorbance of Cr(VI) at 350 nm in the presence of either L-rhamnose or D-mannose in the kinetic studies supports this hypothesis.

From all experimental data, the following mechanism is deduced:

$$[6]\quad Cr_2O_7^{2-} + \text{aldose} \overset{K_1}{\rightleftharpoons} \underset{A}{[Cr_2O_7 - \text{aldose}]^-}$$

$$[7]\quad A \overset{k_2}{\rightarrow} Cr(IV) + RC_5O_5H_7 + HCrO_4^-$$

$$[8]\quad A + 2H^+ \overset{k_3}{\rightarrow} [AH_2]^+ \rightarrow Cr(IV) + RC_5O_5H_7 + HCrO_4^-$$

$$[9]\quad 2HCrO_4^- \rightleftharpoons Cr_2O_7^{2-} + H_2O$$

where R = CH_3 for L-rhamnose or R = CH_2OH for D-mannose.

The first step represents the formation of the rather stable anionic complex between Cr(VI) and the aldohexose (25). Possibly several linkage isomers might be formed by coordination of the sugar with Cr(VI) via any properly disposed hydroxyl group. In eq. [6] A (with the anomeric hydroxyl bound to Cr(VI)) has been chosen, since it should be the precursor of the lactone. This complex may decompose, directly to the products or may be doubly protonated to form a new complex in the slow step, which decomposes rapidly to the products. We propose that redox paths, involving either the anionic or the cationic complex, are two-electron steps, and Cr(IV) is formed with the lactone.

According to the proposed mechanism, the full rate law for the chromic acid oxidation of aldoses, under conditions studied in the kinetic measurements, can be written (eq. [10]):

$$[10]\quad -\frac{dCr(VI)}{dt} = (k_2 + k_3[H^+]^2)[A]$$
$$= (k_2 + k_3[H^+]^2) K_1 [\text{aldose}] [Cr_2O_7^{2-}]$$

Since

$$[11]\quad [Cr(VI)]_T = Cr_2O_7^{2-} + [A]$$
$$= [Cr_2O_7^{2-}]\{1 + K_1[\text{aldose}]\}$$

Replacing $[Cr_2O_7^{2-}]$ in eq. [10]

$$[12]\quad -\frac{dCr(VI)}{dt} = \frac{(k_2 + k_3[H^+]^2) K_1 [\text{aldose}]}{1 + K_1[\text{aldose}]} [Cr(VI)]_T$$

There are at least three possible explanations for the observed rate law:

1. $HCrO_4^-$ is the major Cr(VI) species in solution (which is inconsistent with other data).
2. The reactive complex is a monoester of dichromate instead of chromate.
3. The reactive intermediate is a diester of Cr(VI).

The experimental data are better fixed for possibility number two according to the proposed observed rate law. After the slow step, reactions [13], [14], and [15] may take place:

$$[13]\quad Cr(IV) + \text{aldose} \rightarrow Cr(III) + \text{aldose}^\bullet$$

$$[14]\quad \text{Aldose}^\bullet + Cr(VI) \rightarrow Cr(V) + \text{lactone}$$

$$[15]\quad Cr(V) + \text{aldose} \rightleftharpoons [\text{aldose} - Cr(V)] \rightarrow Cr(III) + \text{lactone}$$

Because under the conditions used in the kinetic measurements (20 to 200-fold ratio of aldohexose to Cr(VI)) the

Can. J. Chem. Downloaded from www.nrcresearchpress.com by 109.225.110.28 on 09/08/12
For personal use only.

TABLE 4. Effect of acrylonitrile on the yield of carbon dioxide. T = 70°C; [L-rhamnose] = 4×10^{-4} M; [Cr(VI)] = 6×10^{-3} M; [$HClO_4$] = 1 M; time = 24 h

Moles of acrylonitrile	—	0.2	0.5	0.9	1.7	2.0	2.3
Moles of CO_2/mole L-rhamnose	4.0	3.4	2.7	2.3	1.7	1.4	1.4

only product detected is the lactone, eqs. [6]–[9] and [13]–[15] represent the total reaction:

[16] $2H^+ + 3\text{aldose} + 2Cr(VI) \rightarrow 3\text{lactone} + 2Cr(III)$

However, when a 10-fold ratio of substrate to Cr(VI) was employed, the α-keto acid was observed by paper chromatography as a minor product, as well as the lactone (main product). Oxidation of the secondary hydroxyl group to ketone requires a two-electron step. Equations [17]–[20] are proposed to explain this reaction product:

[17] $\text{Lactone} + Cr(VI) \rightarrow Cr(IV) + RCOCOOH$

[18] $Cr(IV) + \text{lactone} \rightarrow Cr(III) + R'COOH^{\cdot}$

[19] $R'COOH^{\cdot} + Cr(VI) \rightarrow Cr(V) + RCOCOOH$

[20] $Cr(V) + \text{lactone} \rightarrow Cr(III) + RCOCOOH$

where lactone refers either to L-1,4-rhamnonelactone or D-1,4-mannonelactone; R = $C_4O_3H_9$ or $C_4O_4H_9$ and R′ = $C_5O_4H_{11}$ or $C_5O_5H_{11}$.

Test for free radicals

If the oxidation is carried out in the presence of acrylonitrile (free-radical scavenger) the formation of polymers indicates the presence of free-radical intermediates. We investigated the effect of the concentration of acrylonitrile on the yield of carbon dioxide in order to check if carbon dioxide formation involves the proposed free-radical steps. The blank experiments in absence of aldose or potassium dichromate did not show the formation of any precipitate. The yield of carbon dioxide is reduced in the presence of acrylonitrile and a limiting value is reached when the yield of CO_2 is reduced to one third of the stoichiometric amount (Table 4). These results fit well with a mechanism given by eqs. [6]–[9] and [13]–[24] for degradation of aldose to the lower carboxylic acid and eqs. [25]–[27] for total degradation of L-rhamnose in excess of Cr(VI).

[21] $RCOCOOH + Cr(VI) \rightarrow Cr(IV) + CO_2 + RCOOH$

[22] $Cr(IV) + RCOCOOH \rightarrow Cr(III) + RCOCOOH^{\cdot}$

[23] $RCOCOOH^{\cdot} + Cr(VI) \rightarrow Cr(V) + CO_2 + RCOOH$

[24] $Cr(V) + RCOCOOH \rightarrow Cr(III) + CO_2 + RCOOH$

[25] $3RCOOH + 4Cr(VI) \rightarrow 3CO_2 + 3R_1COOH + 4Cr(III)$

[26] $3R_1COOH + 4Cr(VI) \rightarrow 3CO_2 + 3R_2COOH + 4Cr(III)$

[27] $3R_2COOH + 4Cr(VI) \rightarrow 3CO_2 + 3R_3COOH + 4Cr(III)$

where R = $C_4O_3H_9$, R_1 = $C_3O_2H_7$, R_2 = C_2OH_5, and R_3 = CH_3.

Under these conditions, L-rhamnose undergoes a quantitative oxidation to CO_2 and acetic acid following the stoichiometry given in eq. [28]. When acrylonitrile is added, two thirds of the carbon dioxide, starting from the radical steps, is not produced.

[28] $3\,\text{Rhamnose} + 18Cr(VI) \rightarrow 12CO_2 + 3CH_3COOH + 18Cr(III)$

Thus, in the presence of a sufficient excess of free-radical scavenger to trap all $RCOOH^{\cdot}$ radicals, the yield of carbon dioxide should be reduced from 12 molecules to four molecules per three molecules of L-rhamnose.

These results may be extended to the total degradation of D-mannose.

Conclusions

From the previous results, it is evident that both D-mannose and L-rhamnose react in a similar fashion with Cr(VI) in perchloric acid. However, an important difference must be pointed out. The equilibrium constant K is twice as high for the D-mannose/Cr(VI) complex as for L-rhamnose, while the oxidation rate is faster for the L-rhamnose/Cr(VI) complex. This difference has to be related to a difference in structural features between these complexes. Additional work is in progress to determine the structure of such complexes exactly.

Since either glyceraldehyde (11, 26) or lower sugars without possibility of cyclic forms (15), under the same experimental conditions, do not show kinetic evidence of chromic-ester formation, we propose cyclic hemiacetal forms as the reactive forms for aldohexoses, where hydroxyl groups are better disposed to bind Cr(VI) (27). This is in agreement with the great stability observed for Cr(V)/aldohexose complexes at higher pH (23): oxidation rates of both aldose/Cr(VI) and aldose/ Cr(V) complexes (as can be deduced from epr measurements) are strongly pH dependent; so, at higher pH, oxidation is negligible and aldohexoses coordinate to Cr(VI) or Cr(V) without reducing them.

Finally, we are in a position to state that, when an excess of Cr(VI) over the sugar is used, further oxidation of the lactone formed in the first reaction stages occurs by abstraction of the *a*-H to yield the *a*-keto acid, preceding the decarboxylation process.

Acknowledgements

We wish to thank the National Research Council of Argentina (CONICET) and the National University of Rosario for financial support. M. Rizzotto also thanks The Research Council of the National University of Rosario for a fellowship.

1. S. Angyal. Adv. Carbohydr. Chem. Biochem. **47**, 1 (1989).
2. L. Sala, A. Cirelli, and R. Lederkremer. J. Chem. Soc. Perkin Trans. 2, 685 (1977).
3. L. Sala, A. Cirelli, and R. Lederkremer. Anal. Asoc. Quim. Arg. **66**, 57 (1978).
4. M. Gupta, S. Saha, and P. Banerjee. J. Chem. Soc. Perkin Trans. 2, 1781 (1988).
5. J. Barrek, A. Berka, and A. Pokormá-Haladiková. Collect. Czech. Chem. Commun. **47**, 2466 (1982).
6. D. Goodgame and M. Joy. Inorg. Chim. Acta, **135**, L5 (1987).
7. M. Branca, G. Micera, and A. Dessi. Inorg. Chim. Acta, **153**, 61 (1988).
8. G. Micera and A. Dessi. J. Inorg. Biochem. **34**, 157 (1988).
9. S. Brauer and K. Wetterhahn. J. Am. Chem. Soc. **113**, 3001 (1991).

Can. J. Chem. Downloaded from www.nrcresearchpress.com by 109.225.110.28 on 09/08/12
For personal use only.

10. K. Gupta, S. Gupta, and S. Basu. Carbohydr. Res. **71**, 75 (1979).
11. K. Gupta and S. Basu. Carbohydr. Res. **86**, 7 (1980).
12. K. Gupta and S. Basu. Carbohydr. Res. **80**, 223 (1980).
13. K. Gupta and S. Basu. Carbohydr. Res. **97**, 1 (1981).
14. K. Sharma, V. Sharma, and R. Rai. J. Indian Chem. Soc. **60**, 747 (1983).
15. P. Virtanen and R. Lindroos-Heinanen. Acta Chim. Scand. **B42**, 411 (1988).
16. R. Fischer and D. Peter. A brief introduction to quantitative chemical analysis. Internat. Copywright Union, Mexico. 1969, p. 224.
17. W. Travelyan, D. Proctor and J. Harrison. Nature, **166**, 444 (1950).
18. L. Haugh, J. Jones, and N. Wadman. J. Chem. Soc. 1702 (1950).
19. H. Spenson and R. Kinney. Inorg. Chem. **10**, 1376 (1971).
20. A. Gordon and R. Ford. The chemist's companion. A handbook of practical data techniques and references. J. Wiley & Sons, New York. 1972. p. 65.
21. R. Bramley, J. Ji, R. Judd, and P. Lay. Inorg. Chem. **29**, 3089 (1990).
22. R. Bramley, R. Farrell, J. Ji, and P. Lay. Aust. J. Chem. **43**, 263 (1990).
23. M. Branca, A. Dessi, H. Kozlowski, and G. Micera. J. Inorg. Biochem. **39**, 217 (1990).
24. F. Hasan and J. Rocek. J. Am. Chem. Soc. **94**, 9073 (1972).
25. K. K. Sengupta, T. Samanta, and S. N. Basu. Tetrahedron, **41**, 205 (1985).
26. L. Sala, M. Rizzotto, S. Signorella, M. Frascaroli, and S. Acebal. Oxid. Commun. **14**, 56 (1991).
27. M. Rizzotto, L. Sala, N. Feito, and M. Frascaroli. Anal. Asoc. Quim. Arg. **78**, 75 (1990).

Can. J. Chem. Downloaded from www.nrcresearchpress.com by 109.225.110.28 on 09/08/12
For personal use only.

Complexes of Cu(II) with D-aldonic and D-alduronic acids in aqueous solution

GRACIELA M. ESCANDAR
Departamento de Quimica Analitica, Facultad de Ciencias Bioquímicas y Farmacéuticas
Universidad Nacional de Rosario, Suipacha 531, (2000) Rosario, Argentina

AND

LUIS F. SALA[1]
Departamento de Ciencias Exactas, Facultad de Ciencias Bioquímicas y Farmacéuticas,
Universidad Nacional de Rosario,Suipacha 531, (2000) Rosario, Argentina

Received December 3, 1991

GRACIELA M. ESCANDAR and LUIS F. SALA. Can. J. Chem. **70**, 2053 (1992).

A quantitative study of the equilibria involved in the interaction of Cu(II) ion with D-glucoheptonic, D-gluconic, D-galactonic, D-ribonic, D-glucuronic, and D-galacturonic acids in aqueous medium has been carried out by means of potentiometric measurements of hydrogen ion concentrations at a constant temperature of 20°C and an ionic strength of 0.10 ($NaNO_3$). The equilibrium data were processed with the FORTRAN computer program BEST. It was found that Cu(II) interacts with D-aldonic acids to form 1:1, 2:2, and 1:2 (M/L) complexes. The copper(II) complexes with D-galacturonic and D-glucuronic acids are considerably weaker than those of D-aldonic acid. Possible structures of the complex species formed are discussed.

GRACIELA M. ESCANDAR et LUIS F. SALA. Can. J. Chem. **70**, 2053 (1992).

Faisant appel à des mesures potentiométriques de concentrations en ion hydrogène, à une température constante de 20°C et à une force ionique de 0,10 ($NaNO_3$), on a effectué une étude quantitative des équilibres impliqués dans l'interaction du Cu(II) avec les acides D-glucoheptonique, D-gluconique, D-galactonique, D-ribonique, D-glucoronique et D-galacturonique en milieu aqueux. On a examiné les données à l'aide du programme d'ordinateur BEST écrit en FORTRAN. On a trouvé que le Cu(II) interagit avec les acides D-aldoniques pour former des complexes 1 : 1, 2 : 2 et 1 : 2 (M/L). Les complexes du Cu(II) avec les acides D-galacturonique et D-glucuronique sont beaucoup plus faibles que ceux avec les acides D-aldoniques. On discute des structures possibles pour les espèces complexes qui se forment.

[Traduit par la rédaction]

Introduction

The aldonic and uronic acids (Scheme 1) play an important role in carbohydrate metabolism and they are components of many polysaccharides of biological importance. These sugars, characterized by a terminal carboxylate group, are able to bind both essential and toxic metal ions, forming soluble complexes (1). Uronic acids, present in plant cells, activate the solubilization of metal ions through complex formation, mobilizing them from poorly soluble salts (2). Besides, D-gluconic acid is used as sequestering agent for metal ions in medical, industrial, and agricultural areas (3). Recently, following a study of the chemical speciation of metal ions in aquatic environments, Haas made an investigation of sugar–metal complexes in seawater and their significance in marine processes (4).

The purpose of the present discussion, as part of a general program of analysis of metal–sugar acid chelates, is to define the quantitative interaction between these ligands and Cu(II) ion. A complete study of the cupric complexes formed by D-aldonic acid has not yet been made, and the results reported for D-alduronic acid by different authors are conflicting (5–8).

The computer program selected to process the data, allowed us to provide an accurate description of the aqueous coordination chemistry of Cu(II) for this series of saccharides. At the same time the stability constant values of the different species present in the systems under study were computed.

[1]Author to whom correspondence may be addressed.

Experimental section

Reagents

All the sugars were obtained commercially from Sigma Chemical Co. The lactones of the D-aldonic acids investigated were opened to the sodium salt in order to work with the carboxylate form. In the case of D-gluconic acid both the sodium salt and the 1,5 lactone were employed, obtaining the same results. The D-alduronic acids were purchased as D-galacturonic acid monohydrate and D-glucuronic acid free form. The purity of ligands was checked by pH titration. Stock solutions of $Cu(NO_3)_2$, Na(OH), and HNO_3 were prepared and standardized according to the method reported earlier (9).

Potentiometry

The procedures and apparatus used for potentiometric measurements were described previously in detail (10). Briefly, measurements were made at 20.0 ± 0.1°C and 0.10 M ($NaNO_3$) ionic strength. The pH meter was standardized by titrations of HNO_3 and acetic acid to read $-\log[H^+]$ rather than hydrogen ion activity. Concentrations of reactants in the experimental solutions were of the order of 2×10^{-3} M for each component. D-Aldonic acids were investigated at 1:1 and 1:2 (M/L) ratios. Because of the low stability of the cupric complexes with D-alduronic acids, potentiometric titrations were performed at a high ligand-to-metal ratio.

The lactones were dissolved in standard base and the lower end of the equilibrium curves developed from a back titration, by stepwise addition of standard acid.

Computations

Since the chelates studied are not completely formed at low pH, their stability constants were obtained directly by potentiometric measurements with the program BEST (11).

Results and discussion

The protonation constants of the ligands studied in this work are listed in Table 1.

Can. J. Chem. Downloaded from www.nrcresearchpress.com by 217.78.4.112 on 09/08/12
For personal use only.

Can. J. Chem. Downloaded from www.nrcresearchpress.com by 217.78.4.112 on 09/08/12
For personal use only.

D-ALDONIC ACIDS

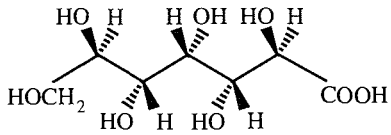

D-glucoheptonic acid

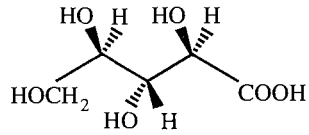

D-ribonic acid

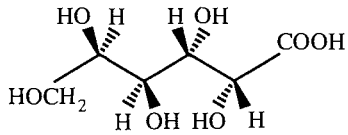

D-galactonic acid

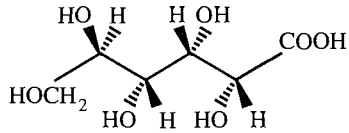

D-gluconic acid

D-ALDURONIC ACIDS

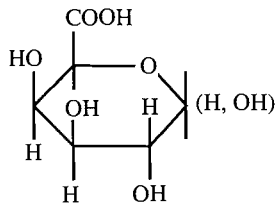

D-galacturonic acid

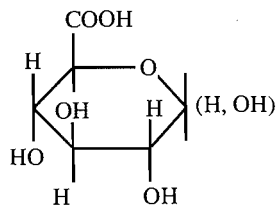

D-glucuronic acid

SCHEME I

TABLE 1. Protonation constants (μ = 0.10 ($NaNO_3$), 20°C)

Ligand	log K	Lit. values
D-Glucoheptonic acid	3.38 ± 0.008	
D-Gluconic acid	3.40 ± 0.01	3.56,[a] 3.439[b]
D-Galactonic acid	3.49 ± 0.01	
D-Ribonic acid	4.02 ± 0.03	
D-Glucuronic acid	2.98 ± 0.01	2.95,[c] 3.07[d]
D-Galacturonic acid	3.19 ± 0.01	3.17,[c] 3.29[d]

[a]Reference 12.
[b]Reference 13.
[c]Reference 5.
[d]Reference 7.

Cu(II) – D-aldonic acid 1:1 systems

The Cu(II) – D-gluconic acid system was studied in strongly basic medium by Pecsok and Juvet, and two different species $Cu_2H_{-3}L_2^-$ and $Cu_2H_{-4}L_2^{2-}$ in less basic solution were proposed by these authors (14). Other D-aldonic acids have not been previously investigated with Cu(II).

The potentiometric behavior of D-gluconic, D-galactonic, and D-ribonic acids with Cu(II) was found to be similar. To explain the potentiometric results of these systems, it was necessary to introduce the macroscopic equilibria [1]–[4]:

[1] $Cu^{2+} + L^- = CuL^+$

[2] $CuL^+ = CuH_{-2}L^- + 2\,H^+$

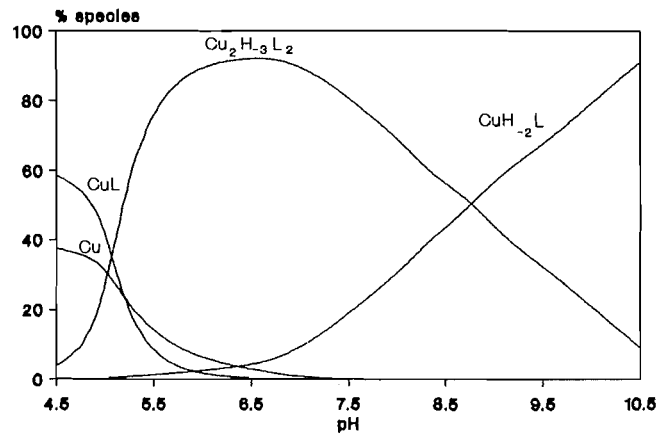

FIG. 1. Distribution of species as a function of p[H^+] in a 1:1 Cu(II)–D-gluconic acid system. Concentration of ligand and metal ion ≈ 2.00×10^{-3} M; μ = 0.10 ($NaNO_3$); t = 20.0°C

[3] $CuH_{-2}L^- = CuH_{-3}L^{2-} + H^+$

[4] $2\,Cu^{2+} + 2\,L^- = Cu_2H_{-3}L_2^- + 3\,H^+$

where the negative stoichiometric coefficient for H represents the protons displaced in the complex formation.

A comparison of the relative positions of the titration curves at different concentration levels of Cu(II) and ligand was employed as a qualitative indication of dimer forma-

TABLE 2. Stability constants and deprotonation constants of chelates between D-aldonic acids and Cu(II) at 20°C and μ = 0.10 M ($NaNO_3$)

Quotient	log K			
	D-Glucoheptonic acid	D-Gluconic acid	D-Galactonic acid	D-Ribonic acid
$[CuL^+]/[Cu^{2+}][L^-]$	—	3.02	3.04	3.52
$[CuH_{-2}L^-][H^+]^2/[CuL^+]$	—	−11.96	−11.33	−11.85
$[CuH_{-3}L^{2-}][H^+]/[CuH_{-2}L^-]$	—	—	(−10.86)	(−10.30)
$[Cu_2H_{-3}L_2^-][H^+]^3/[Cu^{2+}]^2[L^-]^2$	—	−6.58	−7.54	−7.26
$[CuH_{-3}L^{2-}][H^+]^3/[Cu^{2+}][L^-]$	(−18.6)[a]			
σ fit		0.04	0.05	0.04
$[CuL_2]/[Cu^{2+}][L^-]^2$	5.33	6.08	4.84	6.10
$[CuH_{-1}L_2^-][H^+]/[CuL_2]$	—	−5.55	—	−6.09
$[CuH_{-3}L^{2-}][H^+]^2/[CuL_2]$	−10.20	−11.34	−10.99	−11.50
σ fit	0.03	0.03	0.06	0.04

[a]Calculated from the 1:2 (M/L) system.
( )See text.

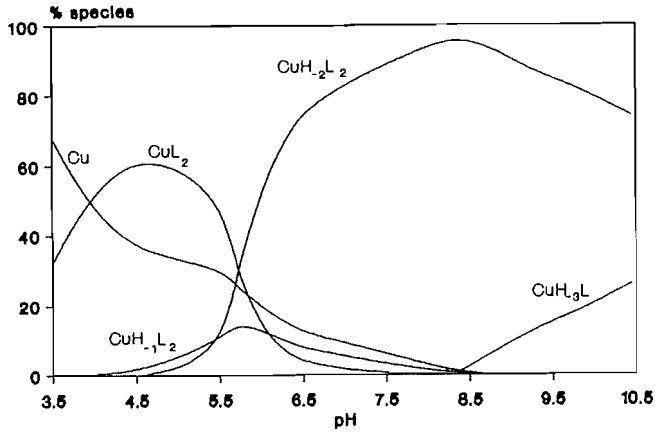

FIG. 2. Distribution of species as a function of p[H^+] in a 1:2 Cu(II)–D-ribonic acid system. Concentration of Cu(II) ≈ 2.00 × 10^{-3} M; μ = 0.10 ($NaNO_3$); t = 20.0°C.

tion (15). Polymeric copper(II) chelates have been reported previously (16). It was found that $CuH_{-1}L$ does not possess enough stability to be important relative to the strong tendency to form $CuH_{-2}L^-$. The dimer $Cu_2H_{-4}L_2^{-2}$ was not found in the systems investigated.

The species distribution – pH diagram in Fig. 1 points out the interplay of the above equilibria for the Cu(II) – D-gluconic acid (1:1) system. The stability constants are listed in Table 2. Since the presence of the more deprotonated $CuH_{-3}L^{2-}$ complex is found at high pH, where potentiometric measurements become less accurate, the last deprotonation constant values are reported within parentheses.

The titration curve for the Cu(II) – D-glucoheptonic acid (1:1) system showed precipitate formation above $a \approx 0.5$ (a : mol of NaOH added per mol of ligand or metal ion). Beyond $a \approx 2$ the insoluble species (probably the neutral $CuH_{-1}L^-$complex) dissolved to give a completely clear, green solution. The measurement of useful potentiometric data for a stability constant computation was not possible.

Cu(II) – D-aldonic acid (1:2) systems

Analysis of the equilibrium data for Cu(II) – D-aldonic acids (1:2) showed the formation of complexes with this ratio. Figure 2 shows the distribution diagram for the Cu(II) – D-ribonic acid (1:2) system.

It is interesting to point out the presence of the $CuH_{-3}L^{2-}$ 1:1 complex in very basic solutions in all the 1:2 systems. The dimer $Cu_2H_{-3}L_2^-$ complex is only detected in the D-gluconic acid system, over a wide range of pH. The corresponding equilibrium constants are shown in Table 2.

Cu(II) – D-alduronic acid systems

In recent years, the Cu(II) – D-uronic acid systems have been studied by different authors (5–8). Although the CuL^+ complex formation is generally accepted, the other species in equilibrium and the coordination centers with the metal ion are controversial (see Table 3).

The potentiometric curves of the Cu(II) – D-galacturonic acid (Fig. 3) and Cu(II) – D-glucuronic acid in a ratio 1:5 (M/L) show a first jump at a = 5 and another one at a = 6.8. Since precipitate formation occurs about a = 5.5 and equilibrium analysis in the presence of solid phase is difficult, constant computations were found necessary in each soluble region. The solid phase present in both systems is attributed to $Cu(OH)_2$ and prevents the evaluation of complex formation in alkaline medium.

The species formed in the D-galacturonic system at low pH are CuL^+ and $CuH_{-1}L$ and their stability constants are listed in Table 3. In our working conditions, the CuL^+ D-glucuronic acid complex was not found. The $CuH_{-1}L$ complex was detected at very low concentration just before precipitation occurred, therefore its stability constant value could not be determined. Cu(II) – D-alduronic acid 1:2 complexes were not found in the pH range investigated.

Conclusions

In the Cu(II) – D-aldonic acids (1:1) systems, the CuL^+ formation may be explained by the interaction of the Cu(II) with the carboxylate and α-hydroxyl groups (Scheme 2). The fact that the formation constant of this complex is more than

Can. J. Chem. Downloaded from www.nrcresearchpress.com by 217.78.4.112 on 09/08/12
For personal use only.

TABLE 3. Stability constants of Cu(II) with D-galacturonic acid

Complex stoichiometry ($Cu_pL_qH_r$)	log K				
p q r	Ref. 5[a]	Ref. 6[a]	Ref. 7[a]	Ref. 8[a]	This work[b]
1 1 0	1.81 (0.02)	1.81 (0.02)	1.80	3.39(0.03)	2.08(0.01)
1 1–1				−2.60(0.02)	−3.75(0.01)
1 2 0			3.00(0.03)	5.99(0.01)	
1 2–1			−3.02(0.08)		
1 2–2			−10.06(0.10)		
1 2–4			−26.69(0.20)		

[a]25°C and μ = 1 M.
[b]20°C and μ = 0.10 M ($NaNO_3$).
Standard deviation is given in parentheses.
K refers to the reaction p Cu + q L + r H = $Cu_pL_qH_r$.

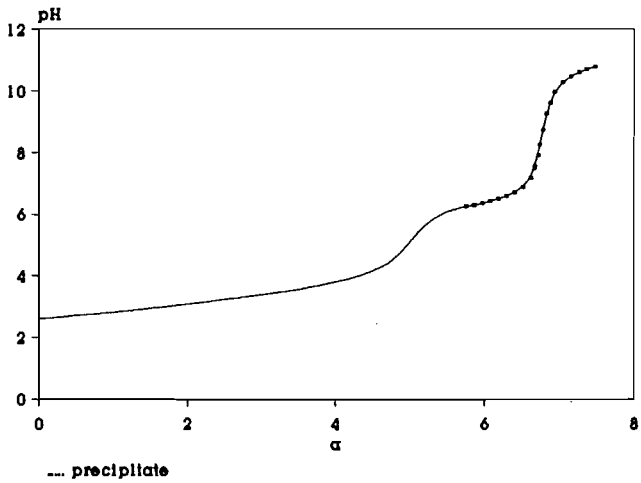

FIG. 3. Potentiometric equilibrium curve of Cu(II)–D-galacturonic acid (1:5) system; μ = 0.10 ($NaNO_3$); t = 20.0°C.

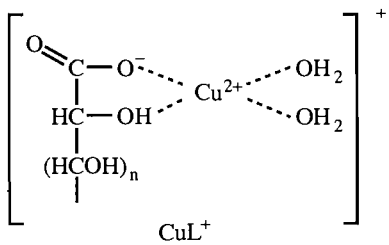

SCHEME 2

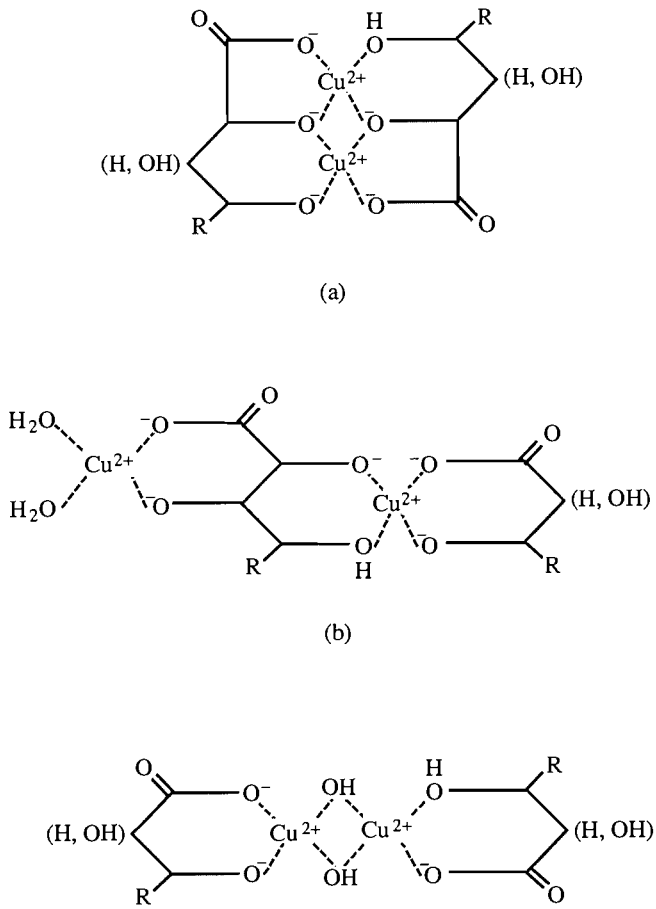

SCHEME 3

one log unit higher than the copper acetate complex (log K_{ML} = 1.83 at 25°C and μ = 0.1 M) (12) supports the conclusion that the α-hydroxyl group of the ligands interacts with the metal center. In addition, the magnitude of the D-hydroxypropanoic acid constant formation (log K_{ML} = 3.02 at 25°C and μ = 0) (12) compares more favorably to the D-aldonic acids. The subsequent deprotonation reactions in the 1:1 systems should be associated with the hydroxyl groups of the sugar chain with chelate ring formation. A large chelate effect should explain the high stability of the $CuH_{-3}L^{2-}$ complex, which is even detected in the 1:2 M/L systems. Examination of CPK models suggests different possibilities of binding with the metal center to form square-planar complexes. To get more rigorous structural information, spectroscopic studies should be made. The structure of the $Cu_2H_{-3}L_2^-$ dimer may be as proposed in Scheme 3. The coordinate bonding structures for the complexes involving two moles of ligand to copper ion could be represented by Scheme 4. The cupric-D-aldonic acid chelates are stable enough to avoid the precipitation of the hydroxide. By contrast, the D-alduronic complexes are considerably weaker than the former, and $Cu(OH)_2$ is separated in basic solution.

It is interesting to note that while some authors postulate

Can. J. Chem. Downloaded from www.nrcresearchpress.com by 217.78.4.112 on 09/08/12
For personal use only.

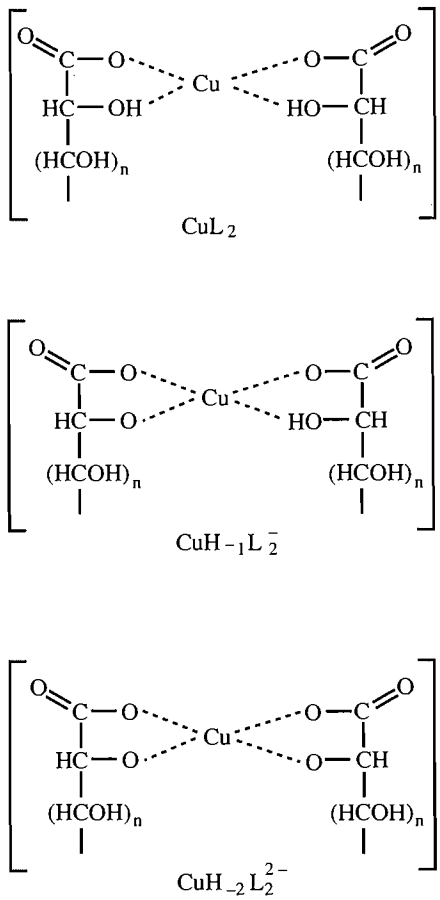

Cu(II) – D-galacturonic acid 1:2 complex formation, in the present work it was found necessary to introduce only two 1:1 Cu(II)-to-ligand species to bring the calculated and experimental p[H] values into line, at low pH.

The generally accepted bindings in the CuL^+ galacturonic acid complex involve the carboxylate group and the endocyclic sugar oxygen. The position of the proton liberated in the $CuH_{-1}L$ complex cannot be decided by potentiometric data. Studies of complex formation of various metal ions with alduronic acids have demonstrated that D-galacturonic acid complexes are more stable than D-glucuronic acid complexes (5). This fact suggests that the oxygen atom on C-4 is probably involved in the metal–ligand binding.

Acknowledgments

We thank Dr R. J. Motekaitis, Chemistry Department, Texas A & M University, U.S.A., for helpful comments, and CONICET and the University of Rosario for financial support.

1. H. A. Tajmir-Riahi. J. Inorg. Biochem. **26**, 23 (1986).
2. G. G. Leppard and S. Ramamoorthy. Can. J. Bot. **53**, 1729 (1975).
3. D. T. Sawyer. Chem. Rev. 633 (1964).
4. J. W. Hass, Jr. Mar. Chem. **19**, 299 (1986).
5. C. Makridou, M. Cromer-Morin, and J. Sharff. Bull. Soc. Chim. Fr. 59 (1977).
6. R. Aruga. Bull. Chem. Soc. Jpn. **54**, 1233 (1981).
7. G. Micera, A. Dessi, H. Kozlowski, B. Radomska, J. Urbanska, P. Decock, B. Dubois, and I. Olivier. Carbohydr. Res. **188**, 25 (1989).
8. S. Deiana, C. Gessa, B. Manunza, P. Piu, and R. Seeber. J. Inorg. Biochem. **39**, 25 (1990).
9. G. M. Escandar and L. F. Sala. Can. J. Chem. **69**, 1994 (1991).
10. G. M. Escandar and L. F. Sala. An. Asoc. Quim. Argent. **78**, 37 (1990).
11. A. E. Martell and R. J. Motekaitis. The determination and use of stability constants. VCH Publishers, Inc., New York. 1988.
12. A. E. Martell and R. M. Smith. Critical stability constants. Vol. 3. Plenum Press, New York. 1989.
13. R. J. Motekaitis and A. E. Martell. Inorg. Chem. **23**, 18 (1984).
14. R. L. Pecsok and R. S. Juvet, Jr. J. Am. Chem. Soc. **77**, 202 (1955).
15. S. Chaberek and A. E. Martell. Organic sequestering agents. John Wiley & Sons, Inc., New York. 1959. pp. 76–78.
16. K. S. Rajan and A. E. Martell. J. Inorg. Nucl. Chem. **29**, 463 (1967).

Can. J. Chem. Downloaded from www.nrcresearchpress.com by 217.78.4.112 on 09/08/12
For personal use only.

Use of lithium (trimethylstannyl)(cyano)cuprate for the conversion of alkyl 2-alkynoates into alkyl (*Z*)- and (*E*)-3-trimethylstannyl-2-alkenoates

EDWARD PIERS,[1] TIMOTHY WONG, AND KEITH A. ELLIS

Department of Chemistry, University of British Columbia, 2036 Main Mall, University Campus, Vancouver, B.C., Canada V6T 1Z1

Received February 20, 1992

EDWARD PIERS, TIMOTHY WONG, and KEITH A. ELLIS. Can. J. Chem. **70**, 2058 (1992).

Reaction of functionalized alkyl 2-alkynoates (e.g., **13**–**19**) with lithium (trimethylstannyl)(cyano)cuprate (**3**) under two sets of carefully defined experimental conditions provides, efficiently and stereoselectively, either alkyl (*Z*)- or (*E*)-3-trimethylstannyl-2-alkenoates (e.g., **23**, **26**–**31** and **24**, **32**–**37**, respectively).

EDWARD PIERS, TIMOTHY WONG et KEITH A. ELLIS. Can. J. Chem. **70**, 2058 (1992).

La réaction de 2-alcynoates d'alkyles fonctionnalisés (comme **13**–**19**) avec le (triméthylstannyl)(cyano)cuprate de lithium (**3**), dans deux ensembles de conditions expérimentales bien définies, fournit soit les (*Z*)- ou (*E*)-3-triméthylstannyl-2-alcènoates d'alkyles (comme **23**, **26**–**31** et **24**, **32**–**37**, respectivement) d'une façon à la fois efficace et stéréosélective.

[Traduit par la rédaction]

Introduction

We previously reported (1), *inter alia*, that reaction (tetrahydrofuran (THF), −78°C) of α,β-acetylenic esters **5** with lithium (phenylthio)(trimethylstannyl)cuprate (**1**) (2) in the presence of a proton source provides, highly stereoselectively, the corresponding alkyl (*E*)-3-trimethylstannyl-2-alkenoates **6** (eq. [1]). Furthermore, it was shown (1) that the stereoselective conversion of **5** into **6** could also be accomplished by use of the (trimethylstannyl)copper(I) reagents **2** (2) and **4** (2) (eq. [2]). Importantly, from a synthetic viewpoint, related investigations disclosed (1) that reaction of **5** with **1** under reaction conditions somewhat different than those given in eq. [1] provides, also highly stereoselectively, alkyl (*Z*)-3-trimethylstannyl-2-alkenoates **7** (eq. [3]). Thus, use of reagent **1**, along with selection of appropriate reaction conditions, allows one to control experimentally the stereochemical outcome of the overall addition of the elements of Me_3Sn–H across the triple bond of **5**. Interestingly, reagents **2** and **4** proved to be ineffective for the stereocontrolled transformation of **5** into **7**.

Recently, we required a number of new β-trimethylstannyl α,β-unsaturated esters of general formula **7**. Although reagent **1** had served quite well for the conversion of **5** into **7**, this method (eq. [3]) does have drawbacks. Phenylthiocopper(I) (PhSCu), which is used to prepare reagent **1** (2), is somewhat tedious to make (3). Furthermore, the latter preparation requires the use of thiophenol, a substance with a notably offensive odour. More importantly, PhSCu, like many copper(I) salts, is not particularly stable. Thus, the occasionally capricious nature of reactions employing the (phenylthio)cuprate **1** can nearly invariably be traced to the fact that PhSCu, after it has been stored for a period of time, no longer serves as a useful material for the preparation of synthetically effective cuprates.

Copper(I) cyanide is readily available, is a reasonably stable substance (CuCN is more stable than copper(II) cyanide (4)), and has been used extensively in organocuprate chemistry (5). Therefore, we have carried out a brief study to determine whether or not the lower order cuprate $[Me_3SnCuCN]Li$ (**3**), which is readily prepared by reaction of Me_3SnLi with CuCN in THF (2), would serve as an effective reagent, alternative to **1**, for the stereoselective conversion of **5** into **7**. The results derived from this study are presented below.

$[Me_3SnCuR]Li$ $\qquad$ $Me_3SnCu{\cdot}Me_2S$

1 R = SPh
2 R = C≡C–C(OMe)Me_2
3 R = CN

4

[1] $R{-}C{\equiv}C{-}CO_2R'$ $\xrightarrow[R'OH,\ -78°C]{\mathbf{1},\ THF}$ Me_3Sn(H)C=C(R)CO_2R'

5 **6**

[2] $R{-}C{\equiv}C{-}CO_2R'$ $\xrightarrow[2.\ NH_4Cl,\ NH_4OH,\ H_2O]{1.\ \mathbf{2}\text{ or }\mathbf{4},\ THF,\ -48°C}$ Me_3Sn(H)C=C(R)CO_2R'

5 **6**

[3] $R{-}C{\equiv}C{-}CO_2R'$ $\xrightarrow[2.\ R'OH]{1.\ \mathbf{1},\ THF,\ -48°C}$ Me_3Sn(CO$_2$R')C=C(H)R

5 **7**

Results and discussion

(a) Preparation of the α,β-acetylenic esters 13–19

The structural formulas of the α,β-acetylenic esters **13**–**19** employed in this investigation are shown in Chart 1. Ethyl 2-pentynoate (**13**) is commercially available. Each of the remaining substances, except **16**, was prepared by treatment of the corresponding 1-alkyne (see **8**–**12**, Chart 1) with methyllithium in THF, followed by reaction of the resultant lithium acetylide with either ethyl or methyl chloroformate. Of the required 1-alkynes **8**–**12**, substances **11** and **12** are commercially available. Compounds **8** and **9** are readily de-

[1]Author to whom correspondence may be addressed.

Can. J. Chem. Downloaded from www.nrcresearchpress.com by 217.78.4.112 on 09/08/12
For personal use only.

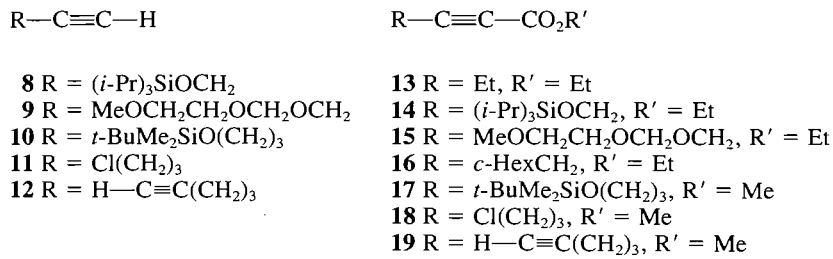

CHART 1

rived from 2-propyn-1-ol, while **10** is similarly prepared from 4-pentyn-1-ol. Details of these preparations are provided in the experimental section. In general, the reactions employed were straightforward and the yields were good to excellent.

Ethyl 4-cyclohexyl-2-butynoate (**16**) was synthesized as shown in eq. [4]. Oxidation of the commercially available alcohol **20** with pyridinium chlorochromate (6), followed by reaction of the resultant aldehyde **21** with dibromomethylenetriphenylphosphorane in dichloromethane (7), gave the 1,1-dibromo-1-alkene **22**. Conversion of **22** into **16** was readily accomplished by means of a published method (7).

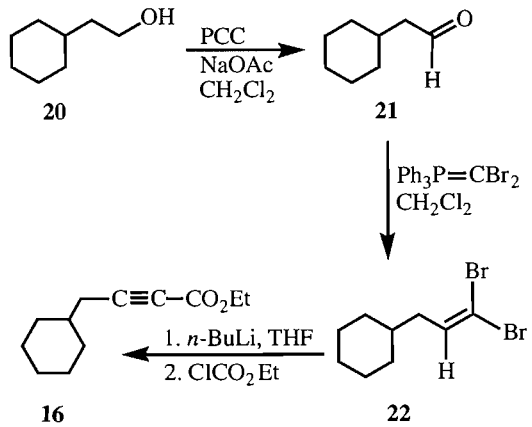

[4]

*(b) Conversion of the α,β-acetylenic esters **13–19** into the alkyl (Z)-3-trimethylstannyl-2-alkenoates **23** and **26–31***

The reaction of $[Me_3SnCuCN]Li$ (**3**) with ethyl 2-pentynoate (**13**) in THF was investigated under a variety of experimental conditions. It was found that when the reaction was carried out at −48°C for fairly short periods of time (≤1 h) and then was warmed to 0°C and subjected to work-up, the major (desired) product **23** was accompanied by minor (<10%) and significant (~20%) amounts of the geometric isomer **24** and ethyl (*E*)-2,3-bis(trimethylstannyl)-2-pentenoate (**25**),[2] respectively. However, further experimentation eventually revealed reaction conditions that effected a relatively clean conversion of **13** into **23**. Thus, reaction of **13** with approximately 1.1 equivalents of the cuprate **3** at −48°C for 2 h and then at 0°C for 2 h, followed by work-up, gave a product that consisted nearly entirely of **23**, accompanied by very minor amounts of **24** and **25**. Purification of this material by a combination of flash chromatography (9) on silica gel (which removed **24**) and distillation (**25** remained in the still-pot) provided the desired *Z* enoate **23** in 72% yield.

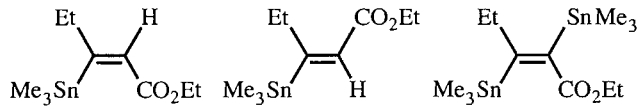

Subjection of the α,β-acetylenic esters **14–19** to reaction conditions very similar to those outlined above afforded the corresponding alkyl (*Z*)-3-trimethylstannyl-2-alkenoates **26–31** in very good yields. The results of these experiments are summarized in Table 1. In each case, the crude product contained minor amounts (<5%), of the corresponding (*E*)-3-trimethylstannyl-2-alkenoate and (*E*)-2,3-bis(trimethylstannyl)-2-alkenoate. The pure desired substances **26–31** could readily be obtained by subjection of the crude products to sequential flash chromatography and distillation.

As shown in Table 1, this procedure for the preparation of alkyl (*Z*)-3-trimethylstannyl-2-alkenoates can be accomplished successfully on substrates containing a variety of functional groups. Thus, silyl ethers (entries 2 and 5), acetals (entry 3), primary alkyl chlorides (entry 6), and terminal alkyne functions (entry 7) are stable to the reaction conditions.

*(c) Conversion of the α,β-acetylenic esters **13–19** into the alkyl (E)-3-trimethylstannyl-2-alkenoates **24** and **32–37***

For other ongoing research projects in our laboratory, we also required the α,β-unsaturated esters that are geometrically isomeric with the *Z* enoates listed in Table 1. Therefore, we carried out a short investigation to determine whether the cyanocuprate **3** could also be employed to effect the efficient, stereoselective conversion of α,β-acetylenic esters into alkyl (*E*)-3-trimethylstannyl-2-alkenoates.

Reaction (THF, −78°C, 4 h) of ethyl 2-pentynoate (**13**) with 1.3 equivalents of reagent **3** in the presence of 1.3 equivalents of ethanol provided a crude product that consisted of a mixture of the *E* and *Z* 2-pentenoates **24** and **23** in a ratio of ~97:3, respectively. Purification of this material by flash chromatography (9) and distillation provided pure **24** in 74% yield.

Reaction of the acetylenic esters **14–19** with the cuprate **3** under conditions similar to those described above produced the corresponding alkyl (*E*)-3-trimethylstannyl-2-alkenoates **32–37** in very good yields (see Table 2). The major, desired products were accompanied by small amounts (1–4%) of the *Z* isomers, but, in each case, the pure *E* isomer could

[2]For a previous report regarding the preparation of alkyl (*E*)-2,3-bis(trimethylstannyl)-2-alkenoates by reaction of α,β-acetylenic esters with $Me_3SnCu \cdot Me_2S$ (**4**), see ref. 8.

Can. J. Chem. Downloaded from www.nrcresearchpress.com by 217.78.4.112 on 09/08/12
For personal use only.

TABLE 1. Preparation of alkyl (*Z*)-3-trimethylstannyl-2-alkenoates

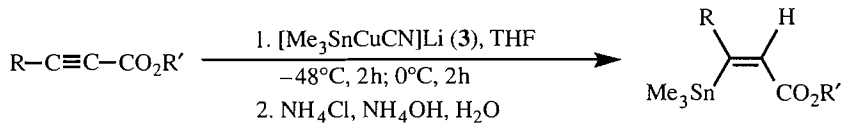

Entry	Acetylenic ester	R	R′	Equiv. of cuprate	Product[a] (yield, %)[b]
1	**13**	Et	Et	1.09	**23** (72)
2	**14**	$(i\text{-Pr})_3SiOCH_2$	Et	1.06	**26** (76)
3	**15**	$MEMOCH_2$[c]	Et	1.06	**27** (72)
4	**16**	$c\text{-HexCH}_2$[d]	Et	1.04	**28** (81)
5	**17**	$t\text{-BuMe}_2SiO(CH_2)_3$	Me	1.05	**29** (78)
6	**18**	$Cl(CH_2)_3$	Me	1.05	**30** (79)
7	**19**	$HC{\equiv}C{-}(CH_2)_3$	Me	1.01	**31** (78)

[a]The isolated crude products contained small amounts (~1–4% and ~1–2%, respectively) of the corresponding alkyl (*E*)-3-trimethylstannyl-2-alkenoates and alkyl (*E*)-2,3-*bis*-trimethylstannyl-2-alkenoates. These minor products could, in each case, be removed by a combination of flash chromatography and distillation.
[b]Yields refer to purified, distilled products.
[c]MEM = $CH_3OCH_2CH_2OCH_2$.
[d]*c*-Hex = cyclohexyl.

TABLE 2. Preparation of alkyl (*E*)-3-trimethylstannyl-2-alkenoates

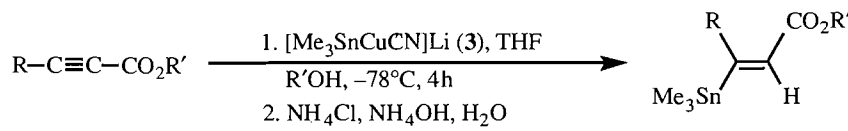

Acetylenic ester	R	R′	Equiv. of cuprate	Equiv. of R′OH	Product[a] (yield, %)[b]
13	Et	Et	1.30	1.31	**24** (74)
14	$(i\text{-Pr})_3SiOCH_2$	Et	1.31	1.31	**32** (74)
15	$MEMOCH_2$[c]	Et	1.30	1.30	**33** (70)
16	$c\text{-HexCH}_2$[d]	Et	1.50	1.50	**34** (81)[e]
17	$t\text{-BuMe}_2SiOCH_2$	Me	1.30	1.35	**35** (77)
18	$Cl(CH_2)_3$	Me	1.30	1.30	**36** (80)
19	$HC{\equiv}C{-}(CH_2)_3$	Me	1.30	1.33	**37** (72)

[a]The isolated crude products contained small amounts (~1–5%) of the corresponding alkyl (*Z*)-3-trimethylstannyl-2-alkenoates. Flash chromatography of these crude materials provided pure desired products.
[b]Yields refer to purified, distilled products.
[c]MEM = $CH_3OCH_2CH_2OCH_2$.
[d]*c*-Hex = cyclohexyl.
[e]The reaction time in this experiment was 7 h rather than 4 h.

readily be obtained by subjection of the mixture to flash chromatography (9) and distillation.

Conclusion

This brief study has disclosed that the lower order cuprate reagent [$Me_3SnCuCN$]Li (**3**) can be used effectively for the synthetically useful, stereoselective conversion of α,β-acetylenic esters (e.g., **13**–**19**) into *either* alkyl (*Z*)-3-trimethylstannyl-2-alkenoates (e.g., **23**, **26**–**31**, respectively, Table 1) or alkyl *E*-3-trimethylstannyl-2-alkenoates (e.g., **24**, **32**–**37**, respectively, Table 2). The advantages of the procedures described herein over those reported earlier (1) are related to the nature of cuprate **3**. This reagent is conveniently prepared (2) from the stable copper(I) salt CuCN and, in terms of reaction efficacy, is significantly less capricious than other lower order (trimethylstannyl)cuprates such as [$Me_3SnCuSPh$]Li (**1**).

Experimental

General information

Distillation temperatures, which refer to short path (Kugelrohr) distillations, and melting points are uncorrected. Proton nuclear magnetic resonance (^1H nmr) spectra were recorded on $CDCl_3$ solutions. Signal positions (δ values) were measured relative to those of tetramethylsilane (δ = 0) or $CHCl_3$ (δ = 7.25). The tin–proton coupling constants (J_{Sn-H}) are given as an average of the ^{117}Sn and ^{119}Sn values. Carbon nuclear magnetic resonance (^{13}C nmr) spectra were taken on $CDCl_3$ solutions and the signal positions are given relative to that of $CDCl_3$ (δ = 77.0). Infrared (ir) spectra were obtained on liquid films (NaCl plates) employing a Perkin–Elmer model 1710 Fourier transform spectrophotometer with internal

Can. J. Chem. Downloaded from www.nrcresearchpress.com by 217.78.4.112 on 09/08/12
For personal use only.

Can. J. Chem. Downloaded from www.nrcresearchpress.com by 217.78.4.112 on 09/08/12
For personal use only.

calibration. For compounds containing the Me_3Sn moiety, high-resolution mass spectrometric measurements are based on ^{120}Sn and were made on the ($M^+ - Me$) peak. Flash chromatography (9) was carried out with 230–400 mesh silica gel (E. Merck). Gas–liquid chromatography (glc) was carried out on an instrument equipped with a flame-ionization detector and a 25 m × 0.32 mm fused silica column coated with cross-linked 5% phenylmethyl silicone. Thin-layer chromatography (tlc) was carried out with commercial, aluminum-backed silica gel plates.

Reagents and solvents were purified and dried using standard methods. Petroleum ether refers to a hydrocarbon mixture with bp 35–60°C. Copper(I) cyanide was purchased from Aldrich Chemical Co., Inc., and was used without further purification.

Aqueous NH_4Cl–NH_4OH (pH 8) refers to a solution prepared by addition of ~50 mL of aqueous NH_4OH (58%) to ~1 L of saturated aqueous NH_4Cl.

Note: All reactions were carried out under an atmosphere of argon in flame- or oven-dried glassware.

3-(Triisopropylsiloxy)propyne (8)

To a stirred solution of 2-propyn-1-ol (1.02 g, 18.2 mmol) in dry CH_2Cl_2 (30 mL) was added sequentially imidazole (1.86 g, 27.3 mmol) and triisopropylsilyl chloride (3.33 g, 17.3 mmol) and the resultant mixture was stirred at room temperature for 2 h. Aqueous NH_4Cl–NH_4OH (pH 8) (25 mL) was added and the mixture was extracted thoroughly with CH_2Cl_2. The combined extracts were washed with brine and then were dried ($MgSO_4$) and concentrated. Flash chromatography (35 g silica gel, hexanes) of the remaining material and distillation (45–47°C/0.15 Torr (1 Torr = 133.3 Pa)) of the acquired oil gave 2.75 g (75%, based on $(i\text{-Pr})_3SiCl$) of **8**, a colorless oil that displayed ir (neat): 3313, 2123, 1465, 1107 cm^{-1}; ^1H nmr (400 MHz) δ: 1.06 (d, 18H, J = 6.0 Hz), 1.10 (m, 3H), 2.46 (t, 1H, J = 2.0 Hz), 4.37 (d, 2H, J = 2.0 Hz); ^{13}C nmr (100.6 MHz) δ: 11.9, 17.8, 51.7, 72.5, 82.4. Anal. calcd. for $C_{12}H_{24}OSi$: C 67.86, H 11.39; found: C 67.86, H 11.43. Exact Mass calcd.: 212.1598; found: 212.1604.

3-[(2-Methoxyethoxy)methoxy] propyne (9)

To a cold (0°C), stirred solution of 2-propyn-1-ol (1.02 g, 18.2 mmol) and $(i\text{-Pr})_2NEt$ (3.53 g, 27.3 mmol) in dry CH_2Cl_2 (30 mL) was added, over a period of 1 min, 2.16 g (17.3 mmol) of $MeOCH_2CH_2OCH_2Cl$ and the resulting mixture was stirred at 0°C for 3.5 h. Hydrochloric acid (2 N, 15 mL) was added and the mixture was extracted with CH_2Cl_2 (3 × 20 mL). The combined extracts were washed with brine, dried ($MgSO_4$), and concentrated. Flash chromatography (50 g silica gel, 4:1 hexanes–Et_2O) of the remaining oil and distillation (65–68°C/10 Torr) of the liquid thus obtained gave 1.98 g (79%) of the alkyne **9**, a colorless oil that showed ir (neat): 3262, 2118, 1454, 1110 cm^{-1}; ^1H nmr (400 MHz) δ: 2.40 (t, 1H, J = 2.0 Hz), 3.38 (s, 3H), 3.54 (m, 2H), 3.70 (m, 2H), 4.22 (d, 2H, J = 2.0 Hz), 4.78 (s, 2H); ^{13}C nmr (100.6 MHz) δ: 54.1, 58.9, 67.1, 71.6, 74.2, 79.3, 93.8. Anal. calcd. for $C_7H_{12}O_3$: C 58.32, H 8.39; found: C 58.56, H 8.49. Exact Mass calcd. for $C_7H_{11}O_3$ (M^+ − H): 143.0704; found: 143.0700.

(5-tert-butyldimethylsiloxy)-1-pentyne (10)

A solution of 4-pentyn-1-ol (1.81 g, 21.5 mmol), *tert*-butyldimethylsilyl chloride (4.25 g, 28.2 mmol), and imidazole (3.70 g, 54.3 mmol) in dry *N*,*N*-dimethylformamide (10 mL) was stirred at room temperature for 16 h. Saturated aqueous $NaHCO_3$ and Et_2O (10 mL) were added and the mixture was extracted with Et_2O (3 × 20 mL). The combined extracts were washed with brine (2 × 60 mL), and then were dried ($MgSO_4$) and concentrated. Flash chromatography (150 g silica gel, 200:3 petroleum ether – Et_2O) of the crude product and distillation (65–90°C/0.2 Torr) of the oil thus obtained afforded 4.04 g (95%) of the 1-pentyne **10**, a colorless liquid that exhibited ir (neat): 3315, 2121, 1109, 632 cm^{-1}; ^1H nmr (400 MHz) δ: 0.03 (s, 6H), 0.87 (s, 9H), 1.69 (quintet, 2H, J = 7.0 Hz), 1.89 (t, 1H, J = 2.5 Hz), 2.24 (dt, 2H, J = 2.5, 7.0 Hz), 3.67 (t, 2H, J = 7.0 Hz); ^{13}C nmr (50.3 MHz) δ: −5.4, 14.8, 18.2, 25.9, 31.5, 61.3, 68.2, 84.1. Anal. calcd. for $C_{11}H_{22}OSi$: C 66.60, H 11.18; found: C 66.80, H 11.30. Exact Mass calcd. for $C_7H_{13}OSi$ (M^+ − *t*-Bu): 141.0736; found: 141.0728.

Ethyl 4-(triisopropylsiloxy)-2-butynoate (14)

To a cold (−78°C), stirred solution of the 1-alkyne **8** (0.5 g, 2.36 mmol) in 15 mL of dry THF was added, dropwise, a solution of methyllithium (2.36 mmol) in Et_2O. After the solution had been stirred at −78°C for 15 min and at −20°C for 1 h, ethyl chloroformate (256 mg, 2.36 mmol) was added. The mixture was stirred at −20°C for 1 h and at room temperature for 1 h. Saturated aqueous $NaHCO_3$ (15 mL) was added and the mixture was extracted thoroughly with Et_2O. The combined extracts were washed twice with brine and then were dried ($MgSO_4$) and concentrated. Distillation (98–99°C/0.11 Torr) of the remaining oil yielded 512 mg (76%) of **14**, a colorless oil that exhibited ir (neat): 2241, 1718, 1465, 1258 cm^{-1}; ^1H nmr (400 MHz) δ: 1.04 (d, 18H, J = 6.0 Hz), 1.10 (m, 3H), 1.29 (t, 3H, J = 7.0 Hz), 4.20 (q, 2H, J = 7.0 Hz), 4.49 (s, 2H); ^{13}C nmr (100.6 MHz) δ: 11.9, 13.9, 17.7, 51.4, 61.9, 76.4, 85.7, 155.5. Anal. calcd. for $C_{15}H_{28}O_3Si$: C 63.33, H 9.92; found: C 63.34, H 9.84. Exact Mass calcd. for $C_{12}H_{21}O_3Si$ (M^+ − *i*-Pr): 241.1260; found: 241.1261.

Ethyl 4-[(2-methoxyethoxy)methoxy]-2-butynoate (15)

This substance was prepared via a procedure very similar to that described above. The quantities of reagents and solvents employed were as follows: starting material **9**, 0.5 g (3.47 mmol); THF, 15 mL; MeLi, 3.47 mmol; EtO_2CCl, 377 mg (3.47 mmol); saturated aqueous $NaHCO_3$, 15 mL. Distillation (85–87°C/0.11 Torr) of the crude product afforded 595 mg (79%) of **15**, a colorless oil that displayed ir (neat): 1718, 1450, 1254, 1045 cm^{-1}; ^1H nmr (400 MHz) δ: 1.30 (t, 3H, J = 7.5 Hz), 3.39 (s, 3H), 3.53 (m, 2H), 3.71 (m, 2H), 4.20 (q, 2H, J = 7.5 Hz), 4.34 (s, 2H), 4.77 (s, 2H); ^{13}C nmr (100.6 MHz) δ: 14.0, 54.0, 59.0, 62.1, 67.4, 71.6, 77.8, 83.0, 94.3, 153.1. Anal. calcd. for $C_{10}H_{16}O_5$: C 55.55, H 7.46; found: C 55.51, H 7.47. Exact Mass calcd.: 215.0920; found: 215.0918.

Methyl 6-(tert-butyldimethylsiloxy)-2-hexynoate (17)

A procedure similar to that given above was employed. The quantities of reagents and solvents used were as follows: substrate **10**, 3.59 g (18.1 mmol); THF, 36 mL; MeLi, 20.3 mmol; MeO_2CCl, 1.65 mL (21.4 mmol); saturated aqueous $NaHCO_3$, 25 mL. Distillation (80–100°C/0.2 Torr) of the crude product gave 3.82 g (82%) of **17**, a colorless oil that showed ir (neat): 2238, 1719, 1260, 1109, 1074 cm^{-1}; ^1H nmr (400 MHz) δ: 0.07 (s, 6H), 0.90 (s, 9H), 1.78 (quintet, 2H, J = 7.0 Hz), 2.44 (t, 2H, J = 7.0 Hz), 3.68 (t, 2H, J = 7.0 Hz), 3.75 (s, 3H); ^{13}C nmr (50.3 MHz) δ: −5.4, 15.2, 18.2, 25.9, 30.6, 52.5, 61.1, 72.9, 89.5, 154.2. Anal. calcd. for $C_{13}H_{24}O_3Si$: C 60.89, H 9.43; found: C 61.10, H 9.60. Exact Mass calcd. for $C_{12}H_{21}O_3Si$ (M^+ − Me): 241.1260; found: 241.1260.

Methyl 6-chloro-2-hexynoate (18)

A procedure similar to that described above was used. The quantities of reagents and solvents used were as follows: substrate **11**, 2.0 mL (18.9 mmol); THF, 40 mL; MeLi, 20.6 mmol; MeO_2CCl, 1.8 mL (23.3 mmol); saturated aqueous $NaHCO_3$, 80 mL. Flash chromatography (40 g silica gel, 9:1 petroleum ether – Et_2O) of the crude product, followed by distillation (50–70°C/0.6 Torr) of the acquired liquid, produced 2.45 g (81%) of **18**, a colorless oil that exhibited ir (neat): 2240, 1718, 1262 cm^{-1}; ^1H nmr (400 MHz) δ: 2.04 (quintet, 2H, J = 7.0 Hz), 2.55 (t, 2H, J = 7.0 Hz), 3.65 (t, 2H, J = 7.0 Hz), 3.78 (s, 3H); ^{13}C nmr (50.3 MHz) δ: 16.0, 30.2, 43.2, 52.3, 73.6, 87.4, 153.9. Anal. calcd. for $C_7H_9ClO_2$: C 52.35, H 5.65, Cl 22.08; found: C 52.42, H 5.72, Cl 21.90. Exact Mass calcd. for $C_7H_9{}^{35}ClO_2$: 160.0292; found: 160.0282.

Methyl 2,7-octadiynoate (19)[3]

This material was prepared via a procedure similar to that outlined above. The quantities of reagents and solvents used were as

[3]This experiment was carried out by Mr. Philip Coish. We are very grateful to Mr. Coish for a generous sample of compound **19**.

Can. J. Chem. Downloaded from www.nrcresearchpress.com by 217.78.4.112 on 09/08/12
For personal use only.

follows: substrate **12**, 10.0 g (109 mmol); THF, 200 mL; MeLi, 109 mmol; MeO_2CCl (rapid addition!), 33.7 mL (436 mmol); saturated aqueous $NaHCO_3$, 150 mL. Distillation (80–100°C/0.3 Torr) of the crude product gave 13.2 g (81%) of **19**, a colorless oil that displayed ir (neat): 3292, 2239, 1714, 1435, 1264, 1078 cm^{-1}; ^1H nmr (400 MHz) δ: 1.78 (quintet, 2H, J = 7.0 Hz), 1.96 (t, 1H, J = 2.5 Hz), 2.32 (dt, 2H, J = 7.0, 2.5 Hz), 2.47 (t, 2H, J = 7.0 Hz), 3.73 (s, 3H); ^{13}C nmr (50.3 MHz) δ: 17.5, 17.6, 26.4, 52.5, 69.4, 73.4, 82.6, 88.4, 154.1. Anal. calcd. for $C_9H_{10}O_2$: C 71.98, H 6.71; found: C 71.72, H 6.78. Exact Mass calcd. for $C_9H_9O_2$ (M^+ − H): 149.0602; found: 149.0593.

1,1-Dibromo-3-cyclohexylpropene (22)

To a stirred mixture of pyridinium chlorochromate (33.7 g, 156 mmol) and sodium acetate (3.2 g, 39 mmol) in dry CH_2Cl_2 (200 mL) was added a solution of 2-cyclohexylethanol (**20**) (10.0 g, 78 mmol) in dry CH_2Cl_2 (300 mL). The mixture was stirred at room temperature for 2 h. Diethyl ether (400 mL) was added and the resultant mixture was filtered through a column of Florisil (6 cm diameter, 7.5 cm depth). The column was eluted with 1 L of Et_2O. Concentration of the combined eluant, followed by distillation (50–56°C/15 Torr) of the remaining liquid, gave 9.03 g (91%) of cyclohexylethanal (**21**), a colorless oil that exhibited ir (neat): 1725 cm^{-1}; ^{13}C nmr (75 MHz) δ: 25.9, 26.0, 33.0, 34.7, 41.7, 51.4, 203.1. Exact Mass calcd. for $C_8H_{14}O$: 125.0966; found: 125.0960.

To a solution of CBr_4 (18.71 g, 56.4 mmol) in dry CH_2Cl_2 (150 mL) was added slowly (at a rate such that the temperature of the reaction mixture remained below 50°C) a solution of triphenylphosphine (29.59 g, 112.8 mmol) in dry CH_2Cl_2 (150 mL). After the resultant mixture had been stirred for 5 min, a solution of the aldehyde **21** (3.55 g, 28.2 mmol) in dry CH_2Cl_2 (300 mL) was added over a period of 10 min and the mixture was then stirred at room temperature for an additional 30 min. Pentane (500 mL) was added and the resultant mixture was filtered through a column of Florisil (6 cm diameter, 7.5 cm depth). The column was washed with 1 L of pentane. The combined eluant was concentrated and the remaining oil was distilled (125–130°C/15 Torr) to provide 6.56 g (86%) of **22**, a colorless oil that displayed ir (neat): 1448, 785 cm^{-1}; ^1H nmr (400 MHz) δ: 0.90–1.05 (m, 2H), 1.10–1.30 (m, 3H), 1.35–1.50 (m, 1H), 1.55–1.90 (m, 5H), 2.05 (t, 2H, J = 7.0 Hz), 6.42 (t, 1H, J = 7.0 Hz); ^{13}C nmr (75 MHz) δ: 26.2, 26.3, 32.9, 37.2, 40.6, 88.7, 137.8. Anal. calcd. for $C_9H_{14}Br_2$: C 38.33, H 5.00; found: C 38.60, H 5.13. Exact Mass calcd.: 281.9443; found: 281.9440.

Ethyl 4-cyclohexyl-2-butynoate (16)

To a cold (−78°C), stirred solution of compound **22** (2.5 g, 8.9 mmol) in dry THF (115 mL) was added, dropwise, a solution of *n*-butyllithium (22.2 mmol) in hexanes. The mixture was stirred at −78°C for 1 h, at room temperature for 1 h, and then was recooled to −20°C. Ethyl chloroformate (1.06 g, 9.76 mmol) was added and the mixture was stirred at −20°C for 1 h and at room temperature for 1 h. Saturated aqueous $NaHCO_3$ (100 mL) was added and the mixture was extracted thoroughly with Et_2O. The combined extracts were washed with brine, dried ($MgSO_4$), and concentrated. Flash chromatography (75 g silica gel, 95:5 petroleum ether – Et_2O) of the crude product and distillation (90–96°C/12 Torr) of the acquired liquid provided 1.55 g (90%) of **16**, a colorless oil that showed ir (neat): 2232, 1713, 1249, 1076 cm^{-1}; ^1H nmr (400 MHz) δ: 0.97–1.08 (m, 2H), 1.12–1.30 (m, 2H), 1.32 (t, 3H, J = 7.0 Hz), 1.50–1.60 (m, 2H), 1.65–1.87 (m, 5H), 2.25 (d, 2H, J = 7.0 Hz), 4.24 (q, 2H, J = 7.0 Hz); ^{13}C nmr (100.6 MHz) δ: 14.1, 25.8, 25.9, 26.4, 32.7, 36.7, 61.8, 74.0, 88.6, 153.8. Anal. calcd. for $C_{12}H_{18}O_2$: C 74.22, H 9.35; found: C 74.40, H 9.41. Exact Mass calcd.: 194.1307; found: 194.1309.

Lithium (trimethylstannyl) (cyano)cuprate (3)

To a cold (−48°C), stirred solution of trimethylstannyllithium in dry THF (2) was added solid copper(I) cyanide (1 equiv.). The resultant mixture was stirred at −48°C for 20 min to produce a pale yellow solution of the cuprate **3**.

General procedure for the conversion of alkyl 2-alkynoates into alkyl (Z)-3-trimethylstannyl-2-alkenoates

To a cold (−48°C), stirred solution of [$Me_3SnCuCN$]Li (**3**) (1.01–1.09 equiv.) in dry THF was added, dropwise, a solution of the α,β-acetylenic ester (1 equiv.) in dry THF. The mixture was stirred at −48°C for 2 h and at 0°C for 2 h. Aqueous NH_4Cl–NH_4OH (pH 8) (one-half the volume of the total volume of the reaction mixture) was added, the mixture was opened to the atmosphere, was allowed to warm to room temperature, and then was stirred until the aqueous phase became deep blue. The organic phase was separated and the aqueous layer was extracted thoroughly with Et_2O. The combined organic phases were washed with brine, dried ($MgSO_4$), and concentrated. The crude product was purified by flash chromatography, followed by distillation.

The following substances were prepared via this general procedure.

Ethyl (Z)-3-trimethylstannyl-2-pentenoate (23)

The following amounts of reagents and solvents were used: [$Me_3SnCuCN$]Li (**3**), 4.38 mmol, in THF, 20 mL; substrate **13**, 507 mg (4.02 mmol), in THF, 4 mL. Flash chromatography (80 g silica gel, 200:3 petroleum ether – Et_2O) of the crude product and distillation (54–84°C/0.6 Torr) of the acquired liquid afforded 843 mg (72%) of the (*Z*)-pentenoate **23**, a colorless oil that displayed ir (neat): 1703, 1601, 1201, 772 cm^{-1}; ^1H nmr (400 MHz) δ: 0.18 (s, 9H, $^2J_{Sn-H}$ = 55 Hz), 1.04 (t, 3H, J = 7.0 Hz), 1.29 (t, 3H, J = 7.0 Hz), 2.45 (qd, 2H, J = 7.0, 1.5 Hz, $^3J_{Sn-H}$ = 43 Hz), 4.18 (q, 2H, J = 7.0 Hz), 6.36 (t, 1H, J = 1.5 Hz, $^3J_{Sn-H}$ = 120 Hz); ^{13}C nmr (50.3 Hz) δ: −7.5, 13.6, 14.3, 32.9, 60.2, 126.9, 168.1, 177.1. Anal. calcd. for $C_{10}H_{20}O_2Sn$: C 41.28, H 6.93; found: C 41.47, H 7.09. Exact Mass calcd. for $C_9H_{17}O_2Sn$ (M^+ − Me): 277.0250; found: 277.0244.

Ethyl (Z)-4-(triisopropylsiloxy)-3-trimethylstannyl-2-butenoate (26)

The following quantities of reagents and solvents were used: [$Me_3SnCuCN$]Li (**3**), 0.37 mmol, in THF, 3 mL; substrate **14**, 100 mg (0.35 mmol), in THF, 0.5 mL. Flash chromatography (10 g silica gel, 97:3 hexanes–Et_2O) of the crude product, followed by distillation (100–104°C/0.11 Torr) of the acquired liquid, provided 120 mg (76%) of **26**, a colorless oil that exhibited ir (neat): 1702, 1609, 1465, 1299, 1191, 1044 cm^{-1}; ^1H nmr (400 MHz) δ: 0.18 (s, 9H, $^2J_{Sn-H}$ = 56 Hz), 1.05 (d, 18H, J = 6.0 Hz), 1.10 (m, 3H), 1.27 (t, 3H, J = 7.0 Hz), 4.15 (q, 2H, J = 7.0 Hz), 4.52 (d, 2H, J = 2.0 Hz, $^3J_{Sn-H}$ = 19 Hz), 6.72 (t, 1H, J = 2 Hz, $^3J_{Sn-H}$ = 114 Hz); ^{13}C nmr (100.6 MHz) δ: −7.9, 11.9, 14.2, 17.9, 60.3, 68.6, 124.6, 168.3, 171.6. Anal. calcd. for $C_{18}H_{38}O_3SiSn$: C 48.12, H 8.52; found: C 48.14, H 8.60. Exact Mass calcd. for $C_{17}H_{35}O_3SiSn$ (M^+ − Me): 435.1376; found: 435.1360.

Ethyl (Z)-4-[(2-methoxyethoxy)methoxy]-3-trimethylstannyl-2-butenoate (27)

The following amounts of reagents and solvents were used: [$Me_3SnCuCN$]Li (**3**), 0.49 mmol, in THF, 4 mL; substrate **15**, 100 mg (0.46 mmol), in THF, 0.5 mL. Flash chromatography (10 g silica gel, 85:15 hexanes–Et_2O) of the crude product and distillation (95–98°C/0.11 Torr) of the liquid thus obtained produced 127 mg (72%) of **27**, a colorless oil that displayed ir (neat): 1702, 1608, 1368, 1198 cm^{-1}; ^1H nmr (400 MHz) δ: 0.18 (s, 9H, $^2J_{Sn-H}$ = 56 Hz), 1.28 (t, 3H, J = 7.5 Hz), 3.37 (s, 3H), 3.52 (m, 2H), 3.71 (m, 2H), 4.17 (q, 2H, J = 7.5 Hz), 4.38 (d, 2H, J = 2.0 Hz, $^3J_{Sn-H}$ = 20 Hz), 4.75 (s, 2H), 6.63 (t, 1H, J = 2.0 Hz, $^3J_{Sn-H}$ = 112 Hz); ^{13}C nmr (100.6 MHz) δ: −7.7, 14.2, 58.9, 60.4, 66.9, 71.7, 72.4, 95.0, 125.8, 167.5, 168.7. Anal. calcd. for $C_{13}H_{26}O_5Sn$: C 40.98, H 6.88; found: C 41.20, H 7.01. Exact Mass calcd. for $C_{12}H_{23}O_5Sn$ (M^+ − Me): 367.0567; found: 367.0575.

Can. J. Chem. Downloaded from www.nrcresearchpress.com by 217.78.4.112 on 09/08/12
For personal use only.

Ethyl (Z)-4-cyclohexyl-3-trimethylstannyl-2-butenoate (28)

The following amounts of reagents and solvents were employed: [$Me_3SnCuCN$]Li (**3**), 0.54 mmol, in THF, 4.5 mL; substrate **16**, 100 mg (0.52 mmol), in THF, 1.0 mL. Flash chromatography (12 g silica gel, 97:3 hexanes–Et_2O) of the crude product and distillation (104–107°C/0.12 Torr) of the acquired liquid afforded 149 mg (81%) of **28**, a colorless oil that exhibited ir (neat): 1703, 1599, 1064 cm^{-1}; ^1H nmr (400 MHz) δ: 0.15 (s, 9H, $^2J_{Sn-H}$ = 55 Hz), 0.84 (m, 2H), 1.10–1.21 (m, 4H), 1.27 (t, 3H, J = 7.0 Hz), 1.30 (m, 1H), 1.63–1.70 (m, 4H), 2.28 (d, 2H, J = 6.0 Hz, $^3J_{Sn-H}$ = 54 Hz), 4.15 (q, 2H, J = 7.0 Hz), 6.25 (s, 1H, $^3J_{Sn-H}$ = 124 Hz); ^{13}C nmr (75 MHz) δ: −7.3, 14.3, 26.4, 26.5, 33.2, 37.5, 47.9, 60.3, 129.1, 167.8, 174.7. Anal. calcd. for $C_{15}H_{28}O_2Sn$: C 50.17, H 7.86; found: C 50.10, H 7.82. Exact Mass calcd. for $C_{14}H_{25}O_2Sn$ (M^+ − Me): 345.0877; found: 345.0871.

*Methyl (Z)-6-(*tert*-butyldimethylsiloxy)-3-trimethylstannyl-2-hexenoate (29)*

The following quantities of reagents and solvents were used: [$Me_3SnCuCN$]Li (**3**), 1.26 mmol, in THF, 6 mL; substrate **17**, 273 mg (1.20 mmol), in THF, 1.2 mL. Flash chromatography (20 g silica gel, 200:3 petroleum ether – Et_2O) of the crude product and distillation (100–130°C/0.6 Torr) of the liquid thus obtained gave 397 mg (78%) of the product **29**, a colorless oil that solidified when cooled and exhibited mp 22–23°C; ir (neat): 1709, 1601, 1329, 1210, 1104, 837, 776 cm^{-1}; ^1H nmr (400 MHz) δ: 0.03 (s, 6H), 0.16 (s, 9H, $^2J_{Sn-H}$ = 55 Hz), 0.88 (s, 9H), 1.53–1.62 (m, 2H), 2.47 (dt, 2H, J = 1.0, 7.0 Hz, $^3J_{Sn-H}$ = 48 Hz), 3.59 (t, 2H, J = 6.0 Hz), 3.70 (s, 3H), 6.36 (t, 1H, J = 1.0 Hz, $^3J_{Sn-H}$ = 120 Hz); ^{13}C nmr (50.3 MHz) δ: −7.4, −5.3, 18.3, 25.9, 32.2, 36.4, 51.4, 62.3, 127.7, 168.3, 175.7. Anal. calcd. for $C_{16}H_{34}O_3SiSn$: C 45.51, H 8.12; found: C 45.80, H 8.21. Exact Mass calcd. for $C_{15}H_{31}O_3SiSn$ (M^+ − Me): 407.1065; found: 407.1071.

Methyl (Z)-6-chloro-3-trimethylstannyl-2-hexenoate (30)

The following amounts of reagents and solvents were used: [$Me_3SnCuCN$]Li (**3**), 2.28 mmol, in THF, 10 mL; substrate **18**, 351 mg (2.18 mmol), in THF, 2 mL. Flash chromatography (45 g silica gel, 200:3 petroleum ether – Et_2O) of the crude product, followed by distillation (75–90°C/0.6 Torr) of the acquired liquid provided 565 mg (79%) of the chloro ester **30**, a colorless oil that exhibited ir (neat): 1708, 1601, 1213, 774 cm^{-1}; ^1H nmr (400 MHz) δ: 0.19 (s, 9H, $^2J_{Sn-H}$ = 55 Hz), 1.87 (quintet, 2H, J = 7.0 Hz), 2.59 (dt, 2H, J = 1.0, 7.0 Hz, $^3J_{Sn-H}$ = 47 Hz), 3.52 (t, 2H, J = 7.0 Hz), 3.73 (s, 3H), 6.40 (t, 1H, J = 1.0 Hz, $^3J_{Sn-H}$ = 116 Hz); ^{13}C nmr (50.3 MHz) δ: −7.4, 31.7, 36.9, 44.0, 51.6, 128.7, 168.1, 174.0. Anal. calcd. for $C_{10}H_{19}ClO_2Sn$: C 36.91, H 5.89, Cl 10.90; found: C 37.10, H 5.96, Cl 10.77. Exact Mass calcd. for $C_9H_{16}{}^{35}ClO_2Sn$ (M^+ − Me): 310.9862; found: 310.9862.

Methyl (Z)-3-trimethylstannyl-2-octen-7-ynoate (31)

The following amounts of reagents and solvents were employed: [$Me_3SnCuCN$]Li (**3**), 1.04 mmol, in THF, 5.5 mL; substrate **19**, 155 mg (1.03 mmol), in THF, 1.0 mL. Flash chromatography (20 g silica gel, 200:3 petroleum ether – Et_2O) of the crude product and distillation (50–70°C/0.6 Torr) of the liquid thus obtained produced 254 mg (78%) of the alkyne ester **31**, a colorless oil that showed ir (neat): 3310, 2120, 1708, 1600, 1212, 774, 636 cm^{-1}; ^1H nmr (400 MHz) δ: 0.20 (s, 9H, $^2J_{Sn-H}$ = 54 Hz), 1.62 (quintet, 2H, J = 7.0 Hz), 1.98 (t, 1H, J = 2.5 Hz), 2.20 (dt, 2H, J = 2.5, 7.0 Hz), 2.55 (dt, 2H, J = 1.0, 7.0 Hz, $^3J_{Sn-H}$ = 48 Hz), 3.73 (s, 3H), 6.39 (t, 1H, J = 1.0 Hz, $^3J_{Sn-H}$ = 119 Hz); ^{13}C nmr (50.3 Hz) δ: −7.4, 17.9, 27.7, 38.7, 51.5, 68.9, 83.7, 128.3, 168.2, 174.8. Anal. calcd. for $C_{12}H_{20}O_2Sn$: C 45.76, H 6.40; found: C 46.03, H 6.49. Exact Mass calcd. for $C_{11}H_{17}O_2Sn$ (M^+ − Me): 301.0251; found: 301.0247.

*General procedure for the conversion of alkyl 2-alkynoates into alkyl (*E*)-3-trimethylstannyl-2-alkenoates*

To a cold (−78°C), stirred solution of [$Me_3SnCuCN$]Li (**3**) (1.30–1.50 equiv.) in dry THF was added dry ethanol (1.30–1.50 equiv., for ethyl ester substrates) or dry methanol (1.30–1.35 equiv., for methyl ester substrates). After 5 min, a solution of the α,β-acetylenic ester (1.0 equiv.) in dry THF was added dropwise over a period of about 2 min and the mixture was stirred at −78°C for 4 h. Aqueous NH_4Cl–NH_4OH (pH 8) (one-half the volume of the total volume of the reaction mixture) was added, the mixture was opened to the atmosphere, was allowed to warm to room temperature, and was stirred vigorously until the aqueous phase became deep blue. The phases were separated and the aqueous phase was extracted thoroughly with Et_2O. The combined organic extracts were washed with brine, dried ($MgSO_4$), and concentrated. The crude product was purified by flash chromatography and distillation.

The following substances were prepared by means of this general procedure.

*Ethyl (*E*)-3-trimethylstannyl-2-pentenoate (24)*

The following amounts of reagents and solvents were used: [$Me_3SnCuCN$]Li (**3**), 64.4 mmol, in THF, 200 mL; EtOH, 3.80 mL (64.7 mmol); substrate **13**, 6.25 g (49.5 mmol), in THF, 30 mL. Flash chromatography (250 g silica gel, 200:3 petroleum ether – Et_2O) of the crude product and distillation (50–70°C/0.6 Torr) of the acquired liquid afforded 10.7 g (74%) of the ester **24**, a colorless oil that displayed ir (neat): 1718, 1598, 1179, 774 cm^{-1}; ^1H nmr (400 MHz) δ: 0.21 (s, 9H, $^2J_{Sn-H}$ = 53 Hz), 1.05 (t, 3H, J = 8.0 Hz), 1.29 (t, 3H, J = 7.0 Hz), 2.89 (qd, 2H, J = 8.0, 1.0 Hz, $^3J_{Sn-H}$ = 64 Hz), 4.16 (q, 2H, J = 7.0 Hz), 5.94 (t, 1H, J = 1.0 Hz, $^3J_{Sn-H}$ = 74 Hz); ^{13}C nmr (50.3 MHz) δ: −9.1, 14.1, 14.3, 27.9, 59.6, 126.9, 164.3, 174.5. Anal. calcd. for $C_{10}H_{20}O_2Sn$: C 41.28, H 6.93; found: C 41.08, H 6.87. Exact Mass calcd. for $C_9H_{17}O_2Sn$ (M^+ − Me): 277.0250; found: 277.0250.

*Ethyl (*E*)-4-(triisopropylsiloxy)-3-trimethylstannyl-2-butenoate (32)*

The following amounts of reagents and solvents were used: [$Me_3SnCuCN$]Li (**3**), 0.46 mmol, in THF, 3 mL; EtOH, 0.027 mL (0.46 mmol); substrate **14**, 100 mg (0.35 mmol), in THF, 0.5 mL. Flash chromatography (10 g silica gel, 97:3 hexanes–Et_2O) of the crude product and distillation (115–120°C/0.11 Torr) of the acquired liquid afforded 117 mg (74%) of the product **32**, a colorless oil that showed ir (neat): 1712, 1603, 1184, 1047 cm^{-1}; ^1H nmr (400 MHz) δ: 0.21 (s, 9H, $^2J_{Sn-H}$ = 57 Hz), 1.05 (d, 18H, J = 6.0 Hz), 1.12 (m, 3H), 1.27 (t, 3H, J = 7.0 Hz), 4.12 (q, 2H, J = 7.0 Hz), 4.95 (d, 2H, J = 2.5 Hz, $^3J_{Sn-H}$ = 30 Hz), 5.79 (t, 1H, J = 2.5 Hz, $^3J_{Sn-H}$ = 78 Hz); ^{13}C nmr (100.6 MHz) δ: −7.9, 11.9, 14.3, 18.0, 59.8, 67.2, 123.4, 161.8, 178.5. Anal. calcd. for $C_{18}H_{38}O_3SiSn$: C 48.12, H 8.52; found: C 48.23, H 8.58. Exact Mass calcd. for $C_{17}H_{35}O_3SiSn$ (M^+ − Me): 435.1376; found: 435.1374.

*Ethyl (*E*)-4-[(2-methoxyethoxy)methoxy]-3-trimethylstannyl-2-butenoate (33)*

The following quantities of reagents and solvents were used: [$Me_3SnCuCN$]Li (**3**), 0.60 mmol, in THF, 4 mL; EtOH, 0. 035 mL (0.60 mmol); substrate **15**, 100 mg (0.46 mmol), in THF, 0.5 mL. Flash chromatography (10 g silica gel, 3:1 hexanes–Et_2O) of the crude product and distillation (85–93°C/0.11 Torr) of the acquired liquid provided 122 mg (70%) of **33**, a colorless oil that displayed ir (neat): 1709, 1608, 1370, 1186 cm^{-1}; ^1H nmr (400 MHz) δ: 0.19 (s, 9H, $^2J_{Sn-H}$ = 56 Hz), 1.26 (t, 3H, J = 7.0 Hz), 3.37 (s, 3H), 3.53 (m, 2H), 3.65 (m, 2H), 4.13 (q, 2H, J = 7.0 Hz), 4.72 (s, 2H), 4.79 (d, 2H, J = 2.5 Hz, $^3J_{Sn-H}$ = 30 Hz), 5.92 (t, 1H, J = 2.5 Hz, $^3J_{Sn-H}$ = 73 Hz); ^{13}C nmr (100.6 MHz) δ: −8.1, 14.2, 59.0, 59.9, 66.9, 71.7, 72.1, 95.2, 124.5, 164.3, 173.6. Anal. calcd. for $C_{13}H_{26}O_5Sn$: C 40.98, H 6.88; found: C 41.23, H 7.01. Exact Mass calcd. for $C_{12}H_{23}O_5Sn$ (M^+ − Me): 367.0567; found: 367.0564.

*Ethyl (*E*)-4-cyclohexyl-3-trimethylstannyl-2-butenoate (34)*

The following quantities of reagents and solvents were employed: [$Me_3SnCuCN$]Li (**3**), 30.9 mmol, in THF, 320 mL; EtOH, 1.4 g (30.9 mmol); substrate **16**, 4.0 g (20.6 mmol), in THF,

10 mL. In this experiment, the reaction time was 7 h instead of 4 h. Flash chromatography (50 g silica gel, 97:3 petroleum ether – Et_2O) of the crude product, followed by distillation (100–110°C/0.12 Torr) of the acquired liquid, gave 5.98 g (81%) of the ester **34**, a colorless oil that showed ir (neat): 1718, 1598, 1177, 770 cm^{-1}; ^1H nmr (400 MHz) δ: 0.19 (s, 9H, $^2J_{Sn-H}$ = 56 Hz), 0.95–1.05 (m, 2H), 1.13–1.23 (m, 3H), 1.29 (t, 3H, J = 7.0 Hz), 1.32–1.40 (m, 1H), 1.60–1.75 (m, 5H), 2.83 (d, 2H, J = 8.0 Hz, $^3J_{Sn-H}$ = 61 Hz), 4.16 (q, 2H, J = 7.0 Hz), 6.03 (s, 1H, $^3J_{Sn-H}$ = 82 Hz); ^{13}C nmr (75 MHz) δ: −9.0, 14.3, 26.4 (3C), 33.2, 38.7, 41.9, 59.6, 128.4, 164.5, 172.4. Anal. calcd. for $C_{15}H_{28}O_2Sn$: C 50.17, H 7.86; found: C 50.40, H 7.88. Exact Mass calcd. for $C_{14}H_{25}O_2Sn$ (M^+ − Me): 345.0877; found: 345.0881.

Methyl (E)*-6-(*tert*-butyldimethylsiloxy)-3-trimethylstannyl-2-hexenoate (35)*

The following amounts of reagents and solvents were used: [$Me_3SnCuCN$]Li (**3**), 1.78 mmol, in THF, 9 mL; MeOH, 0.075 mL (1.85 mmol); substrate **17**, 312 mg (1.37 mmol), in THF, 1.4 mL. Flash chromatography (30 g silica gel, 200:3 petroleum ether – Et_2O) of the crude product and distillation (110–130°C/0.6 Torr) of the acquired oil produced 446 mg (77%) of the ester **35**, a colorless oil that exhibited ir (neat): 1720, 1597, 1256, 1169, 1098, 836, 776 cm^{-1}; ^1H nmr (400 MHz) δ: 0.05 (s, 6H), 0.21 (s, 9H, $^2J_{Sn-H}$ = 54 Hz), 0.90 (s, 9H), 1.58–1.67 (m, 2H), 2.95 (br t, 2H, J = 8.0 Hz, $^3J_{Sn-H}$ = 62 Hz), 3.64 (t, 2H, J = 6.0 Hz), 3.69 (s, 3H), 5.98 (br s, 1H, $^3J_{Sn-H}$ = 73 Hz); ^{13}C nmr (50.3 MHz) δ: −9.1, −5.7, 18.3, 25.9, 31.5, 32.8, 50.8, 63.0, 127.2, 164.6, 173.3. Anal. calcd. for $C_{16}H_{34}O_3SiSn$: C 45.51, H 8.12; found: C 45.80, H 8.08. Exact Mass calcd. for $C_{15}H_{31}O_3SiSn$ (M^+ − Me): 407.1065; found: 407.1070.

Methyl (E)*-6-chloro-3-trimethylstannyl-2-hexenoate (36)*

The following amounts of reagents and solvents were employed: [$Me_3SnCuCN$]Li (**3**), 2.95 mmol, in THF, 15 mL; MeOH, 0.12 mL (2.96 mmol); substrate **18**, 364 mg (2.27 mmol), in THF, 2 mL. Flash chromatography (45 g silica gel, 200:3 petroleum ether – Et_2O) of the crude product and distillation (70–90°C/0.6 Torr) of the liquid thus obtained provided 590 mg (80%) of the ester **36**, a colorless oil that exhibited ir (neat): 1718, 1598, 1176, 1152, 772 cm^{-1}; ^1H nmr (400 MHz) δ: 0.23 (s, 9H, $^2J_{Sn-H}$ = 54 Hz), 1.89 (quintet, 2H, J = 7.0 Hz), 3.01 (dt, 2H, J = 1.0, 7.0 Hz, $^3J_{Sn-H}$ = 60 Hz), 3.56 (t, 2H, J = 7.0 Hz), 3.70 (s, 3H), 6.02 (t, 1H, J = 1.0 Hz, $^3J_{Sn-H}$ = 71 Hz); ^{13}C nmr (50.3 MHz) δ: −9.2, 32.2, 32.5, 44.6, 50.9, 128.2, 164.4, 171.5. Anal. calcd. for $C_{10}H_{19}ClO_2Sn$: C 36.91, H 5.89, Cl 10.90; found: C 37.11, H 5.90, Cl 10.75. Exact Mass calcd. for $C_9H_{16}{}^{35}ClO_2Sn$ (M^+ − Me): 310.9862; found: 310.9860.

Methyl (E)*-3-trimethylstannyl-2-octen-7-ynoate (37)*

The following amounts of reagents and solvents were used: [$Me_3SnCuCN$]Li (**3**), 2.52 mmol, in THF, 12 mL; MeOH, 0.105 mL (2.59 mmol); substrate **19**, 293 mg (1.95 mmol), in THF, 2 mL. Flash chromatography (30 g silica gel, 200:3 petroleum ether – Et_2O) of the crude product and distillation (64–84°C/0.6 Torr) of the acquired liquid afforded 444 mg (72%) of the ester **37**, a colorless oil that displayed ir (neat): 3309, 2218, 1719, 1597, 1262, 1161, 774, 635 cm^{-1}; ^1H nmr (400 MHz) δ: 0.22 (s, 9H, $^2J_{Sn-H}$ = 54 Hz), 1.60–1.72 (m, 2H), 1.96 (t, 1H, J = 2.5 Hz), 2.23 (dt, 2H, J = 2.5, 8.0 Hz), 2.98 (dt, 2H, J = 1.0, 7.0 Hz, $^3J_{Sn-H}$ = 61 Hz), 3.70 (s, 3H), 6.00 (t, 1H, J = 1.0 Hz, $^3J_{Sn-H}$ = 73 Hz); ^{13}C nmr (100.6 MHz) δ: −9.1, 18.5, 28.4, 33.9, 50.9, 68.6, 84.1, 127.8, 164.5, 172.3. Anal. calcd. for $C_{12}H_{20}O_2Sn$: C 45.76, H 6.40; found: C 46.01, H 5.63. Exact Mass calcd. for $C_{11}H_{17}O_2Sn$ (M^+ − Me): 301.0251; found: 301.0253.

Acknowledgements

We are grateful to the Natural Sciences and Engineering Research Council of Canada for financial support and for a postgraduate scholarship (to K.A.E.).

1. E. Piers, J. M. Chong, and H. E. Morton. Tetrahedron, **45**, 363 (1989).
2. E. Piers, H. E. Morton, and J. M. Chong. Can. J. Chem. **78**, 65 (1987).
3. G. H. Posner, D. J. Brunelle, and L. Sinoway. Synthesis, 662 (1974).
4. F. A. Cotton and G. Wilkinson. Advanced inorganic chemistry. 5th ed. John Wiley and Sons, Inc., New York, N.Y. 1988. p. 757.
5. B. H. Lipshutz, R. S. Wilhelm, and J. A. Kozlowski. Tetrahedron, **40**, 5005 (1984).
6. E. J. Corey and J. W. Suggs. Tetrahedron Lett. 2647 (1975).
7. E. J. Corey and P. L. Fuchs. Tetrahedron Lett. 3769 (1972).
8. E. Piers and J. M. Chong. J. Org. Chem. **47**, 1602 (1982).
9. W. C. Still, M. Kahn, and A. Mitra. J. Org. Chem. **43**, 2923 (1978).

Can. J. Chem. Downloaded from www.nrcresearchpress.com by 217.78.4.112 on 09/08/12
For personal use only.

Thermal cyclizations of protonated poly-unsaturated aldehydes

GEORGE R. ELIA, RONALD F. CHILDS,[1] AND GARY S. SHAW
Department of Chemistry, McMaster University, Hamilton, Ont., Canada L8S 4M1

Received November 22, 1991

GEORGE R. ELIA, RONALD F. CHILDS, and GARY S. SHAW. Can. J. Chem. **70**, 2065 (1992).

Protonated 2,4-hexadienal (**1H**) and 2,4,6-octatrienal (**2H**), prepared by protonation of the analogous aldehydes in FSO_3H, isomerized to give cyclized products **3H** and **4H** at 30°C and −20°C respectively. The rate constants for the cyclization of **1H** were measured in both FSO_3H and CF_3SO_3H. It was found that the rate constant for isomerization decreased when CF_3SO_3H was used as the reaction medium. It is suggested that the thermal cyclizations of **1H** and **2H** involve diprotonated species with protonation occurring on oxygen. **1H** and **2H** underwent photoisomerization at −78°C in FSO_3H to yield **5H** and **7H** respectively. It was found that **5H** underwent a cyclization reaction at −40°C to give **6H**, which subsequently rearranged to give **3H** at −10°C. However, **7H** was found to isomerize to **2H** at −50°C. The mechanisms of the thermal isomerization are discussed.

GEORGE R. ELIA, RONALD F. CHILDS et GARY S. SHAW. Can J. Chem **70**, 2065 (1992).

L'hexa-2,4-diènan (**1H**) et l'octa-2,4,6-triènal (**2H** protonés, préparés par protonation des aldéhydes correspondants par le FSO_3H, s'isomérisent pour donner les produits cycliques **3H** et **4H**, à 30°C et −20°C respectivement. On a mesuré les constantes de vitesse pour la cyclisation du produit **1H**, tant dans le FSO_3H que dans le CF_3SO_3H. On a trouvé que la constante de vitesse pour l'isomérisation diminue lorsqu'on utilise le CF_3SO_3H comme milieu réactionnel. Il est suggéré que les cyclisations thermiques des composés **1H** et **2H** impliquent des espèces diprotonées dans lesquelles la protonation se fait sur l'oxygène. Dans le FSO_3H, à −78°C, les composés **1H** et **2H** subissent des photo-isomèrisations qui conduisent respectivement aux composés **5H** et **7H**. On a trouvé que le composé **5H** subit une réaction de cyclisation à −40°C qui conduit au produit **6H** qui se transpose subséquemment pour donner le composé **3H** à −10°C. Toutefois, on a trouvé que, à −50°C, le composé **7H** s'isomérise en composé **2H**. On discute des mécanismes des isomérisations thermiques.

[Traduit par la rédaction]

The chemistry of polyenyl carbocations has been investigated extensively (1–3). The characteristic reaction of this important class of carbenium ions is ring closure of a pentadienyl fragment to form a substituted cyclopentenyl cation. This cyclization reaction has been shown to proceed via a stereoselective 4-π electron electrocyclic ring closure (4, 5). These reactions are generally facile, occurring, for example, at very low temperatures when the ions are generated as long-lived species in strong acid media.

There have been fewer studies reported on the chemistry on the hydroxy- or alkoxy-substituted polyenyl carbenium ions, despite the ease by which these ions can be prepared by the protonation of unsaturated carbonyl compounds and their derivatives (6). One important example is the cyclization of protonated cross-conjugated dienones to form protonated cyclopentenones, a reaction that forms the key step in what has become known as the Nazarov reaction (7). This cationic cyclization reaction parallels the cyclization reactions observed with the parent polyenyl cations referred to above (8). The Nazarov reaction is of synthetic importance as a route to cyclopentenones.

In contrast to the many examples of the thermal isomerization of protonated cross-conjugated dienones, no reports have appeared on the chemistry of the corresponding 1-hydroxy-pentadienyl or higher polyenyl cations. This is surprising given the ready availability of the corresponding unsaturated carbonyl compounds, the importance of this type of functionality in a variety of natural systems[2] and the potential use of cyclization reactions to prepare a variety of cyclopentenones (5). In this work we report on the protonation and isomerization of a variety of such systems.[3]

Results and discussion

The cations selected for study were **1H** and **2H**. These cations were prepared by the protonation of the corresponding carbonyl compounds, **1** and **2**. The ions were characterized by their low-temperature ^1H and ^{13}C NMR spectra, which were consistent with the assigned structures, Tables 1 and 2. The chemical shifts of the various proton resonances and coupling constants corresponded to those reported for the simpler enones (6, 11) and cyclic dienones (12). The *E* conformation about the formal double bonds was clearly shown by the characteristic 14.0 ± 0.4 Hz coupling constant observed between the two protons *trans* to each other on the bonds.

Detailed examination of the ^1H NMR spectra of these ions showed in each case that minor isomers were present. These isomers were shown to be the 4-*Z* isomer in the case of **1** and the 6-*Z* isomer in the case of **2**. In each case the $^1H/^1H$ coupling constant across the *Z* bond was found to be 11.1 ± 0.3 Hz; a value characteristic of a *Z* configuration in comparable cations (11). Both of these *Z* isomers were shown to be present in the neutral aldehydes prior to protonation, Table 3. As can be seen from the data in Table 3, in the case of **2** partial isomerization about the various C=C bonds to form the all-*E* isomer occurred on protonation and NMR characterization of the cation. The all-*E* isomer **2H** is expected to be the most thermodynamically stable conformer of this cation.

Rotational barriers about the formal C—C single bonds of cations comparable to **1H** and **2H** are expected to be low and,

[1]Author to whom correspondence may be addressed.

[2]Indeed, this work was prompted by an enquiry from Drs. P. Yates and J. J. F. Krepinsky about the possible role of carbocation species in accounting for the mutagenic and carcinogenic properties of fecapentaenes (9).

[3]This work was previously presented at a CIC Conference (10).

Can. J. Chem. Downloaded from www.nrcresearchpress.com by 217.78.4.112 on 09/08/12
For personal use only.

TABLE 1. ^{1}H chemical shifts of cations

	Compound[a,b]						
H-atom	**1H**	**5H**[c]	**2H**	**7H**[c]	**6H**[c]	**3H**	**4H**
H1	8.82 d	9.34 d	8.60 d	8.70 d	—	—	—
H2	6.83 dd	6.66 t	6.85 dd	7.08 t	3.93 m	3.26 m	3.84 m
H3	8.45 dd	7.46 t	8.44 dd	8.96 t	6.12 m	3.34 m	3.45 m
H4	7.03 dd	8.41 dd	7.00 dd	7.26 dd	6.10 m	8.80 bs	8.58 bs
H5	7.67 dq	7.64 dq	7.86 dd	7.67 dd	4.05 m	—	—
H6	2.23 d	2.24 d	6.81 dd	6.86 dd	1.50 d	2.17 s	7.15 d
H7	—	—	7.21 dq	7.08 dq	—	—	9.25 d
H8	—	—	2.21 d	2.21 d	—	—	2.17 s

[a]In ppm relative to CD_2Cl_2 (δ = 5.32 ppm) in FSO_3H/CD_2Cl_2; d = doublet, t = triplet, dq = doublet of quartets, m = multiplet, s = singlet, bs = broad singlet, dd = doublet of doublets. Measured at 20°C.
[b]Coupling constants for **1H**, **5H**, **2H**, and **7H** were very similar. H,H_{trans} = 14.0 ± 0.4 Hz; H,H_{cis} = 11.1 ± 0.3 Hz; vinyl H,CH_3 = 7.2 ± 0.1 Hz.
[c]Measured at −60°C.

as such, rotation about these bonds will be fast on the NMR time scale at temperatures above −100°C (13). The thermodynamically preferred conformations about the "single" bonds of **1H** and **2H** are also expected to be *E*. This was shown previously for 1-hydroxyallyl cations and conjugated iminium salts through low-temperature ^{13}C NMR studies (14). A crystallographic study of a dioxolynium cation corresponding to **1H** has shown it has an *E* configuration about each of the formal C—C and C=C bonds (15). Crystal structures of conjugated iminium salts have also shown the all-*E* conformation to be the present in the solid state (16, 17).

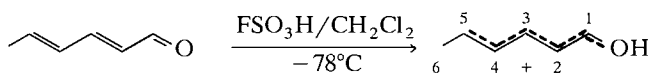

1 **1H**

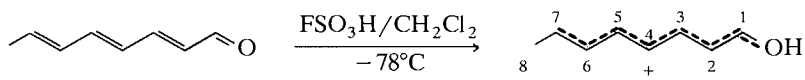

2 **2H**

Thermal isomerizations

The 1-hydroxy cations **1H** and **2H** were stable in FSO_3H for several hours at −60°C. Thermal stability at higher temperatures was assessed using ^{1}H NMR and monitoring the resulting spectrum as the temperature was increased. The samples were maintained at each temperature for about 30 min while spectra were being acquired. From these spectra it was evident that **1H** isomerized to form a second species as the temperature was increased above 30°C. The cation **2H** was found to undergo a more facile reaction, with it forming another species at temperatures as low as −20°C. In both cases the isomerizations proceeded quantitatively.

The thermal products of **1H** and **2H** were identified as the protonated cyclopentenone, **3H**, and the cation, **4H**, respectively, on the basis of their ^{1}H NMR spectra, Table 1. In the case of the isomerization of **1H**, a key feature in the spectrum used in the identification of **3H** was the disappearance of all but one of the vinylic proton resonances. The presence of two methylene groups was evident from the two

TABLE 2. ^{13}C NMR chemical shifts of 1-hydroxyallyl cations and corresponding aldehydes

	Compound[a]			
Position	**1**[b]	**1H**[c]	**2**[b]	**2H**[c]
C1	193.82	198.20	193.20	190.89
C2	129.79	122.92	130.46	132.14
C3	152.55	184.87	152.25	183.51
C4	130.03	134.57	127.42	122.21
C5	141.88	174.96	142.94	171.89
C6	18.87	22.15	131.00	134.37
C7	—	—	136.94	164.10
C8	—	—	19.06	21.01

[a]In ppm.
[b]Referenced to $CDCl_3$ at 77.3 ppm. Measured at 21°C.
[c]Referenced to CD_2Cl_2 at 53.8 ppm in FSO_3H/CD_2Cl_2. Measured at −60°C.

TABLE 3. Isomeric composition of aldehydes and corresponding 1-hydroxyallyl cations

	1	**1H**	**2**	**2H**
All *E*	85.5	87.4	68.5	88.9
2-*Z*	nd[a]	nd	2.7	nd
4-*Z*	14.5	12.6	11.0	nd
6-*Z*	—	—	17.8	11.1

[a]Not detected.

Can. J. Chem. Downloaded from www.nrcresearchpress.com by 217.78.4.112 on 09/08/12
For personal use only.

mutually coupled resonances appearing at 3.26 ppm and 3.34 ppm (18). Elucidation of the structure of **4H** proved to be a more difficult task than in the case of **3H**. The presence of the cyclopentene ring moiety was evidenced by ^{1}H NMR signals arising from two adjacent methylene groups as in the case of **3H**. The doublet at 9.25 ppm, characteristic of an aldehydic proton coupled to an adjacent vinyl proton, indicated that ring closure occurred between C3 and C7. An NOE experiment confirmed that the protonated carbonyl group was *trans* to the methyl group substituted on the cyclopentene ring.

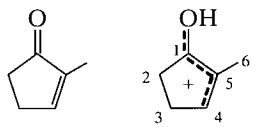

3 **3H**

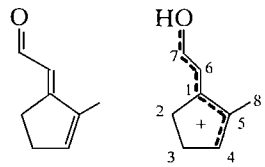

4 **4H**

The acid solutions of **3H** and **4H** were neutralized in order to retrieve the cyclopentene derivatives **3** and **4**. This proved to be a facile task in the case of **3**, which was recovered and purified by gas chromatography. The identification of **3** was confirmed through an independent synthesis following the method of Ho and Liu (19). Protonation of 2-methyl-2-cyclopentenone in FSO_3H afforded a cation with the identical ^{1}H NMR spectrum to that of **3H** derived from the isomerization of **1H**.

Neutralization of an FSO_3H solution containing the cation **4H** led to the formation of a mixture of compounds. The major product was identified as 2-methyl-2-cyclopentylidene acetaldehyde by its ^{1}H NMR spectrum although isolation of a pure sample of this material proved to be difficult. The major product had an identical ^{1}H NMR spectrum to that described by Gilbert and Smith for **4** (20).

The overall steps in the isomerization of **1H** would most reasonably involve *E* to *Z* isomerization about both the C(1)—C(3) formal double and C(3)—C(4) single bonds of the starting cation, Scheme 1. The intermediary 2-*Z* isomer **5H** could then undergo cyclization and subsequent hydride shifts to give **3H**(21).

To test this suggested mechanism the 2-*Z* isomer **5H** was prepared by photoisomerization of **1H** (6, 11). An FSO_3H solution of **1H** (λ_{max} 338 nm (log ε = 4.1)) was irradiated at low temperature for about 6 h. A single isomer of the starting protonated aldehyde was formed (ca. 30% conversion), which was identified as **5H** on the basis of its ^{1}H NMR spectrum, Table 1. The spectrum of **5H** exhibited an 11.2 Hz coupling constant between the two protons attached to the C(2)C(3) partial double bond, clearly indicating the *Z* configuration of this bond. On continued irradiation beyond this point the ^{1}H NMR spectrum of the mixture of cations became more complex, suggesting the formation of other isomers such as the di-*Z* isomers. These cations were not identified.

The thermal isomerization of **5H** was examined by following the reactions by NMR. Heating a mixture of **1H** (70%) and **5H** (30%) to −40°C caused the latter isomer to isomerize to give **6H**. This new cation was identified as **6H** on the basis of its NMR spectrum, Table 1. On further heating the reaction mixture to −10°C, the cation **6H** was found to isomerize to give **3H**.

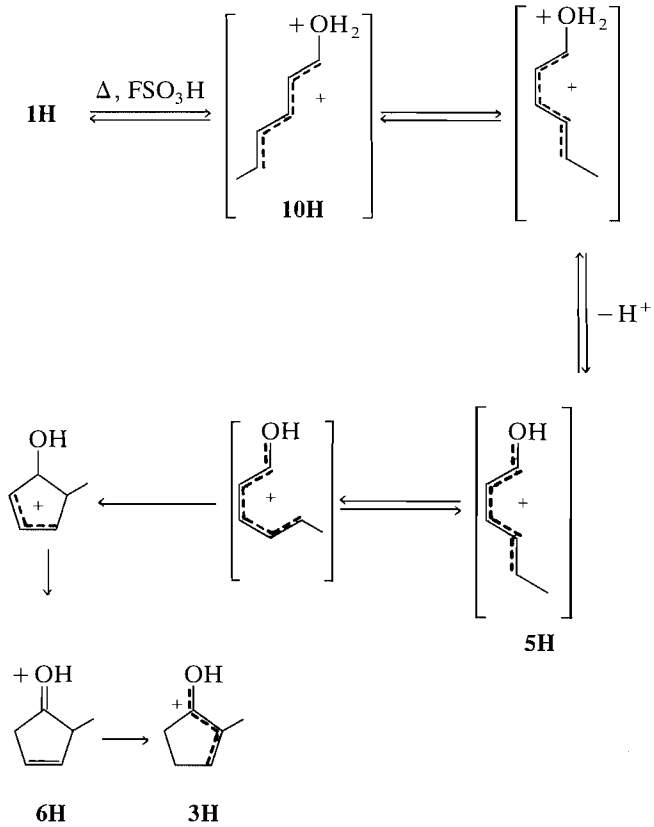

SCHEME 1

It is clear from these results that the isomerization could proceed via the formation of the thermodynamically less stable 2-*Z* isomer **5H**. Given the thermal lability of **5H** and its ring closure product **6H**, these isomers would not be detected at temperatures required for the isomerization of **1H**. The intermediacy of **6H** and its subsequent transformation to the thermodynamically most stable ion **3H** parallels the report of Olah *et al.* on the protonation of 3-cyclopentenone (18).

Further information on the mechanism of the thermal isomerization of **1H** was obtained by examining the reaction in media of different acidity. The rate constants for the isomerization of **1H** to the cyclopentenone cation **3H** were measured in both FSO_3H and CF_3SO_3H. The isomerizations followed first-order kinetics. The rate constants and activation parameters for the isomerizations are given in Table 4.

As can be seen from the data in Table 4, the isomerization of **1H** to **3H** is significantly faster in FSO_3H than in CF_3SO_3H. FSO_3H is a stronger acid than CF_3SO_3H(22). The faster rate of isomerization in the stronger acid medium suggests that the reaction is acid catalysed. The large negative entropy of activation (−42.5 cal K^{-1} mol^{-1} at 60°C) measured for the isomerization of **1H** to **3H** is fully consistent with protonation on oxygen to form a dication, Scheme 1. It is not clear whether it is a dication that undergoes ring closure or if a proton loss to form **5H** occurs prior to cycli-

Can. J. Chem. Downloaded from www.nrcresearchpress.com by 217.78.4.112 on 09/08/12
For personal use only.

TABLE 4. Rate constants and activation parameters for the isomerization of **1H** to **3H**

Temperature, °C	Acid	k ($s^{-1} \times 10^{-4}$)	$\Delta S^{\ddagger}$ (cal $K^{-1}mol^{-1}$)	E (kcal mol^{-1})	$\Delta G^{\ddagger}$ (kcal mol^{-1})
60	CF_3SO_3H	3.01 ± 0.23	—	—	24.9
50	FSO_3H	3.59 ± 0.23			
60	FSO_3H	4.53 ± 0.04	−42.5	10.4	24.6
70	FSO_3H	9.25 ± 0.16			

zation. Earlier work in this group has shown that the *Z* to *E* isomerizations of 3-aryl-1-methoxyallyl (23) and *N*-aryl-3-arylpropenylidene iminium salts (24) can involve protonation on the heteroatom to form a dication. There is growing evidence to suggest that comparable dications are involved in a range of other organic reactions (25).

The surprising feature of the isomerization of **2H** is the regioselectivity of the process. The other product that could have formed is **9H** (26); however, no such product could be detected in the NMR spectrum of the reaction mixture during the isomerization.

To examine this regioselectivity the 2-*Z* isomer of **2H** was prepared by irradiation. The cation **2H** exhibited a UV spectrum with a long-wavelength band at 425 nm (log ε = 4.0). Irradiation of an FSO_3H solution of **2H** at low temperature for about 6 h led to the formation of **7H** (45% conversion). The photoproduct was again identified as the corresponding 2-*Z* isomer **7H** on the basis of its ^1H NMR spectra, Table 1. On continued irradiation of the **2H/7H** mixture, the vinyl region in the ^1H NMR spectrum for both cations became complex suggesting the formation of the di-*Z* isomers. These cations were not identified.

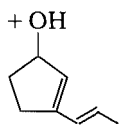

9H

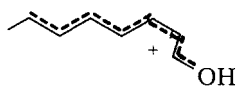

7H

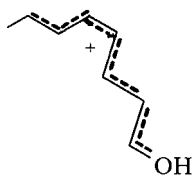

8H

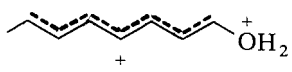

11H

Warming the FSO_3H mixture of **7H** (45%) and **2H** (55%) to −50°C caused this ion to revert completely to **2H**. No cyclic products were formed under these conditions. The all-*Z* isomer **2H** was stable in the acid solution at −50°C and did not isomerize to **4H** until the solution was heated to −20°C. It is clear from these results that, while **7H** might well be thermally accessible from **2H** this isomer does not undergo a ring closure reaction.

The formation of **4H** from **2H** would seem to proceed via the 4-*Z* isomer **8H**. As **2H** is expected to be more basic than **1H**, isomerization about the formal C—C bonds of **2H** will again involve protonation on oxygen to form the dication **11H**. This dication can be considered to be a substituted heptatrienyl cation and should exhibit behaviour more typical of a trienyl cation than δ a protonated heptatrienal. Baird has shown by calculation that the barriers to rotation about the central partial double bonds of trienyl cations are lower than those of the terminal partial double bonds (13). As such it would be expected that **8H** could be produced preferentially in solutions of **2H** in FSO_3H. The lowest energy cyclization process available to **8H** is C(3)—C(7) bonding to eventually form **4H** rather than a C(1)—C(5) bonding reaction.

Experimental section

General

^1H NMR spectra were recorded on a Varian EM-390 or on a Bruker AM-500 spectrometer. The latter was used for all low-temperature studies and ^{13}C NMR spectra (125.78 MHz). UV spectra were recorded on a Hewlett Packard 8451A diode array spectrophotometer using FSO_3H as solvent. Centrifugal chromatography was carried out on silica (Merck Kieselgel $60PF_{254}$) coated plates (coating 2 or 4 mm) spinning in a Chromatotron model 7924T apparatus.

Materials

All solvents were available commercially and were purified by standard procedures. Compound **1** was also commercially available and distilled before use. Purity was checked using ^1H and ^{13}C NMR. FSO_3H and CF_3SO_3H were distilled twice under N_2 before use, and stored in sealed glass ampules.

2,4,6-Octatrienal (2)

A mixture of butenal (11.0 g, 0.16 mol). glacial acetic acid (1.5 mL, 0.025 mol), and piperidine (0.15 mL, 0.0015 mol) was heated over a steam bath for 10 min under an N_2 atmosphere and subsequently cooled in an ice bath. The entire contents of the flask were distilled under 0.05 Torr pressure (1 Torr = 133.3 Pa) and the fraction boiling at 65°C removed. A centrifugal chromatography separation using 10% ether/hexanes as solvent was carried out and the second band (R_F = 0.2) taken. The solvent was removed to give **2** as the major product with a small amount of *cis* isomers representing the minor products. ^1H NMR (CD_2Cl_2) δ: 1.80 (d, J = 7 Hz, CH_3, 3H), 6.05(m, H_2, H_7, 2H), 6.18 (dd, J = 11 Hz, 15 Hz, H_6, 1H), 6.33 (dd, J = 11 Hz, 15 Hz, H_4, 1H), 6.66 (dd, J = 11 Hz, 15 Hz, H_5 1H), 7.14 (dd, J = 11 Hz, 15 Hz, H_3, 1H), 9.46 (d, J = 8 Hz, H_1, 1H).

Preparation of cations

FSO_3H (1 mL) was cooled to −78°C and slowly added to a CD_2Cl_2 solution of the appropriate aldehyde (40–50 mg) also at

Can. J. Chem. Downloaded from www.nrcresearchpress.com by 217.78.4.112 on 09/08/12
For personal use only.

−78°C. CF_3SO_3H was cooled to −5°C and added in a similar manner.

Irradiations

All photoisomerizations were carried out using a photoreactor that consisted of 10 reactor lamps (Southern New England Ultraviolet Co., RPR 3000A or 3500A) arranged in a circle around a quartz Dewar. The samples were placed inside the Dewar and cooled using a FTS Systems Flexi-cooler refrigeration system and methanol. The photoisomerizations were monitored by ^{1}H NMR.

Rate measurements

The isomerization rates of protonated 2,4-hexadienal were determined by placing medium-walled NMR tubes containing the cation in a constant temperature bath. After a given time interval, the reaction was quenched by rapidly cooling the samples in an ice bath, and the reaction assayed by ^{1}H NMR at 20°C. Each spectrum was scanned twice and the extent of reaction determined by the average of integrations of methyl resonance of each species. In each rate determination some six to eight different points were taken, and first-order kinetics were observed. Each rate constant was determined in duplicate using independent samples.

Acknowledgement

This work was supported by the Natural Sciences and Engineering Research Council of Canada. The provision of a sample of **2** by Drs. P. Yates and J. J. F. Krepinsky is gratefully acknowledged.

1. N. C. Deno, C. U. Pittman, Jr., and J. O. Turner. J. Am. Chem. Soc. **87**, 2153 (1965).
2. T. S. Sorensen. J. Am. Chem. Soc. **87**, 5075 (1965).
3. T. S. Sorensen. Carbonium Ions, 1968–1976, *2*, 807 (1970); D. M. Brouwer, E. L. Mackor, and C. Maclean. Carbonium Ions, 1968–1976, *2*, 837 (1970).
4. N. W. K. Chiu and T. S. Sorensen. Can. J. Chem. **51**. 2776 (1973).
5. T. S. Sorensen and A. Rauk. Pericyclic reactions. Vol II. (Edited by Alan P. Marchand and Roland E. Lehr. Academic Press, New York, 1977. p. 21–24.
6. R. F. Childs, T. DiClemente, E. F. Lund-lucas, T. J. Richardson, and C. V. Rogerson. Can. J. Chem. **61**, 856 (1983).
7. I. N. Nazarov, I. I. Zaretskaya, and T. I. Sorkina. Zh. Obsh. Khim. **30** 746 (1960).
8. C. W. Shoppee and B. J. A. Cooke. J. Chem. Soc. Perkin trans. 1, 2271 (1972).
9. I. Gupta, K. Susuki, W. R. Bruce, J. J. Krepinsky, and P. Yates. Science, **225**, 521 (1984).
10. G. R. Elia, R. F. Childs, and G. S. Shaw. 73rd CIC Congress, Halifax, Nova Scotia. 1990. Abstr. 903.
11. R. F. Childs, E. F. Lund, A. G. Marshall, W. J. Morrisey, and C. V. Rogerson. J. Am. Chem. Soc. **98**, 5924 (1976).
12. K. E. Hine and R. F. Childs. J. Am. Chem. Soc. **95**, 3289 (1973).
13. N. C. Baird. Tetrahedron, **28**, 2355 (1972).
14. R. F. Childs, M. Mahendran, C. Blackburn, and G. Antoniadis, Can. J. Chem. **66**, 1355 (1988).
15. R. M. Orgias, M. Sc. Thesis, McMaster University, Hamilton. 1989.
16. S. D. Santarsiero, M. Mahendran, R. F. Childs, and M. N. G. James. J. Am. Chem. Soc. **112**, 9416 (1990).
17. G. R. Elia and R. F. Childs. 74th CCCE Congress, Hamilton, Ontario. 1991. Abstr. 682.
18. G. A. Olah, Y. Halpern, Y. K. Mo, and G. Liang. J. Am. Chem. Soc. **94**, 3554 (1972).
19. T-L Ho and S-H Liu. Chem. Ind. (London), **11**, 371 (1982).
20. J. C. Gilbert and K. R. Smith. J. Org. Chem. **41**, 3883 (1976).
21. G. J. Karabatsos and J. L. Fry. Carbonium Ions, 1968–1976, **2**, 521 (1970).
22. G. A. Olah, G. K. S. Prakash, and J. Sommer. Superacids. Wiley–Interscience, New York. 1985. p. 34.
23. C. Blackburn and R. F. Childs. J. Chem. Soc. Chem. Commun. 812 (1984).
24. M. Pankratz and R. F. Childs. J. Org. Chem. **50**, 4553 (1985).
25. M. Yato, T. Ohwada, and K. Shudo. J. Am. Chem. Soc. **113**, 692 (1991).
26. H. Hart and A. F. Naples. J. Am. Chem. Soc. **94**, 3256 (1972).

Can. J. Chem. Downloaded from www.nrcresearchpress.com by 217.78.4.112 on 09/08/12
For personal use only.

A CAD study of isobaric $(CH_3)_3SiArH^+$ ions (ArH = benzene, toluene) formed by association and protonation

XIAOPING LI[1] AND JOHN A. STONE
Department of Chemistry, Queen's University, Kingston, Ont., Canada K763N6

Received February 11, 1992

XIAOPING LI and JOHN A. STONE. Can. J. Chem. **70**, 2070 (1992).

Collision-assisted dissociation has been used to compare the ions formed by (*a*) the addition of trimethylsilylium ($(CH_3)_3Si^+$) to benzene and toluene, and (*b*) the protonation of trimethylsilyl-substituted aromatics. The spectra of the isobaric ions are essentially identical at both high (8 keV) and low (<15 eV) collision energies. Proton transfer to trimethylamine is observed for all ions at centre of mass collision energies below 1.5 eV. The results show that the decomposing and reacting structures are the same for all these isobaric ions, whether formed by protonation or by addition of trimethylsilylium to aromatic, but they do not definitively resolve the question of the structure of their ground state, i.e., whether $(CH_3)_3Si$ is π or σ bonded.

XIAOPING LI et JOHN A. STONE. Can. J. Chem. **70**, 2070 (1992).

On a utilisé une dissociation assistée par collision pour comparer les ions qui se forment par (*a*) l'addition du triméthylsilylium ($(CH_3)_3Si^+$) au benzène et au toluène et (*b*) la protonation de produits aromatiques substitués par des groupes triméthylsilyles. Les spectres des ions isobares sont pratiquement identiques aux énergies de collision tant élevées (8 keV) que basses (<15 eV). On a observé un transfert de proton vers la triméthylamine pour tous les ions au centre d'énergies de collision de masse inférieures à 1,5 eV. Les résultats montrent que les structures qui réagissent et qui se décomposent sont les mêmes pour tous ces ions isobares, qu'ils se forment par protonation ou par addition de triméthylsilylium à un produit aromatique; toutefois, ils ne permettent pas de résoudre d'une façon définitive la question de la structure de leur état fondamental, à savoir si le $(CH_3)_3Si$ est lié par des électrons δ ou π.

[Traduit par la rédaction]

Introduction

γ-Radiolysis of $CH_4/(CH_3)_4Si/ArH$ mixtures (ArH = aromatic = benzene, toluene, xylene) at pressures of around 1 atmosphere (1 atm = 101.3 kPa) leads to the formation of the silylated aromatics $(CH_3)_3SiAr$ (1, 2). The suggested mechanism has the σ-bonded structure **I** as an intermediate.

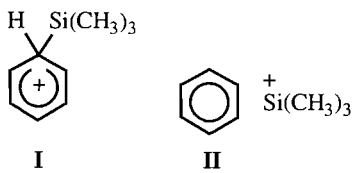

I **II**

For example, in the case of benzene the proposed mechanism involves initial formation of $(CH_3)_3Si^+$ by dissociative protonation of $(CH_3)_4Si$ followed by addition of $(CH_3)_3Si^+$ to benzene and subsequent deprotonation of the adduct by a base B.

[1] $CH_5^+ (C_2H_5^+) + (CH_3)_4Si \rightarrow CH_4 + CH_4(C_2H_4) + (CH_3)_3Si^+$

[2] $(CH_3)_3Si^+ + C_6H_6 \longrightarrow$ 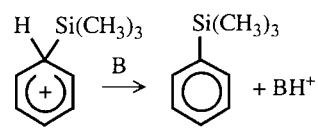 $+ BH^+$

The base employed was $(C_2H_5)_3N$ which has high Brønsted basicity but relatively low nucleophilicity. Preliminary experiments using ion cyclotron resonance spectroscopy showed that molecules with basic oxygen sites, such as cyclohexanone, which might be expected to deprotonate the suggested arenium ion, did not do so and only $(CH_3)_3Si^+$ transfer was observed (2).

[3] $(CH_3)_3SiArH^+ + C_6H_{10}O \rightarrow (CH_3)_3SiOC_6H_{10}^+ + ArH$

Earlier studies of the association of $(CH_3)_3Si^+$ with aromatics in a high-pressure mass spectrometer (HPMS) source (2–4.5 Torr; 1 Torr = 133.3 Pa) led to the suggestion that the observed stabilized $(CH_3)_3SiArH^+$ ions had the π-complex structure **II** rather than being σ-complexes (3). Later HPMS studies failed to find convincing evidence for arenium ion structures (4). Adducts were formed by the addition of either $(CH_3)_3Si^+$ or $(CH_3)_3C^+$ to perdeuterated benzene and toluene and $(C_2H_5)_3N$ was used as a deprotonating agent. The appearance of $(C_2H_5)_3ND^+$ was taken as evidence that deprotonation of an arenium ion had occurred according to reaction [2]. The disappearance of $(CH_3)_3CC_6D_6^+$, for example, was accompanied by an almost equal increase in $(C_2H_5)_3ND^+$, which characterizes $(CH_3)_3C^+$ adducts as arenium ions. Although the $(CH_3)_3Si^+$ adducts of perdeuterated aromatics disappeared as rapidly as did the analogous $(CH_3)_3C^+$ adducts in the presence of $(C_2H_5)_3N$, the accompanying formation of $(C_2H_5)_3ND^+$ was far less than expected; $(C_2H_5)_3NH^+$ was the major product. Therefore, although the results with the $(CH_3)_3C^+$ adducts show that HPMS is able to provide good evidence for the presence of arenium ions, the evidence obtained with the $(CH_3)_3Si^+$ adducts is inconclusive.

In this paper we report on a further investigation of the structures of the $(CH_3)_3SiArH^+$ complexes, this time using collision-assisted dissociation (CAD). In particular, a comparison is made of the CAD spectra of $(CH_3)_3SiArH^+$ ions formed by the addition of $(CH_3)_3Si^+$ to benzene and toluene and the isobaric ions formed by protonation of trimethylsilylbenzene and trimethylsilyltoluene. The evidence suggests that the isobaric $(CH_3)_3SiArH^+$ ions formed by the two dif-

[1]Department of Chemistry, University of Toronto.

Can. J. Chem. Downloaded from www.nrcresearchpress.com by 217.78.4.112 on 09/08/12
For personal use only.

Can. J. Chem. Downloaded from www.nrcresearchpress.com by 217.78.4.112 on 09/08/12
For personal use only.

ferent methods decompose from a common structure and that the ions probably do have the arenium ion structure **I**.

Experimental

All experiments were carried out using the ZAB-2FQ (BEQQ geometry) mass spectrometer located at the Ontario Regional Ion Centre at the University of Toronto. Two different ion sources were employed, the standard VG EI/CI source and a recently constructed high pressure source (HP) (5). The advantage of the latter is that since the electron-emitting filament is ~5 cm from the ion source block there is no heating of the block by the filament and temperatures as low as 300 K may be used. This aids in the formation of usable beams of ions that are susceptible to thermal decomposition. In addition, the HP source was operable at significantly higher pressures, 4 Torr vs. ~0.5 Torr.

Metastable spectra, due to the unimolecular decomposition of ions of unique m/z values in the second field free region between the magnetic and electrostatic sectors were obtained by scanning the electrostatic field at fixed acceleration voltage and magnet field (MIKES scan). Collisional-activated dissociations were carried out in the second field free region (high energy (HE)) or in the first of the two quadrupole mass filters, which was operated in the RF only mode (low energy (LE)). For HE studies the ion beam energy was usually 8 keV while for LE studies the energies of the decelerated ions ranged from 0.5 to 50 eV. Daughter ions from HE dissociations were analyzed using the electric sector and those from LE dissociations by using the second quadrupole analyzer. Helium was used as the collision gas at HE while both nitrogen and trimethylamine were used at LE. This latter collision gas adsorbs strongly on all surfaces and persisted for a considerable length of time in the system after its flow was turned off. The pressure reading of an ionization gauge well downstream was not a reliable measure of the pressure in the collision region. For example, changes in gauge reading did not correlate well with spectral changes and when N_2 was introduced as collision gas immediately after $(CH_3)_3N$ had been used, spectra at low beam energy (<6 eV) contained ions due to collisions with $(CH_3)_3N$. Multiple scans (10–100) were summed in a multichannel analyser to obtain each of the spectra presented in this paper. Pressure readings downstream from the collision cell were used as a rough guide to set up operating conditions for HE CAD studies but the main criterion to be met in obtaining the spectral data was a decrease in main-beam intensity of approximately 10–20%. With this attenuation the problem of multiple collisions was minimized. Of course identical parent ions should yield identical spectra under the same conditions whether they are in the single or multiple collision regime. A range of beam attenuations was used for CAD studies at low pressure to gain information on the observed ion–molecule reactions.

Trimethylsilylbenzene and trimethylsilyltoluene were obtained from PCR Laboratories Ltd. Tetramethylsilane (TMS), benzene-d_5, toluene-d_8, and toluene-α,α,α-d_3 were from Merck Sharpe and Dohme and all other chemicals were from the Aldrich Chemical Company Limited. All chemicals were used as received.

Results

The $(CH_3)_3Si^+$ adducts of benzene, benzene-d_6, toluene and toluene-α,α,α-d_3, and mesitylene were readily formed in both the HP source and the EI/CI source by addition of $(CH_3)_3Si^+$ to the aromatic via reactions [1] and [2]. Higher relative intensities of the adducts were obtained using the HP source because of more efficient third-body stabilization but the observed metastable and CAD spectra obtained were independent of the source employed. Ions of the same m/z values as the $(CH_3)_3Si^+$ adducts of benzene and toluene were also formed by protonation of $(CH_3)_3SiC_6H_5$ and p-$(CH_3)_3SiC_6H_4CH_3$. (Henceforth for convenience, such ions, no matter how formed, with elemental composition $(CH_3)_3$-SiArH$^+$ (ArH = aromatic) will be designated MH$^+$.) MH$^+$ formed by protonation was always of very low intensity even when the HP source was operated at 300 K and this was also the case if either the strong protonating reagent ion CH_5^+ was used or the much weaker i-$C_3H_7^+$ (PA(C_3H_6) = 180 kcal mol^{-1} (6)), generated in CH_4/C_3H_8 mixtures. The reason for the weak signal was that protonization by CH_5^+ can lead to extensive desilylation rather than protonation, while with i-$C_3H_7^+$ displacement of $(CH_3)_3Si^+$ competes with protonation (7). In addition there was always a significant M$^+$ peak (~60% the intensity of MH$^+$), which has a ^{29}Si isotopic component isobaric with MH$^+$. Presumably M$^+$ originated by direct electron impact ionization (8). The possibility was therefore present of metastable decomposition or collisional dissociation of M$^+$ interfering with studies of MH$^+$. M$^+$ was generated in the absence of MH$^+$ by electron impact on $(CH_3)_3SiC_6H_5$ and $(CH_3)_3SiC_6H_4CH_3$ in the EI/CI source at low pressure and the metastable and CAD spectra were recorded. A very intense [M − 15]$^+$ peak was the only metastable decomposition observed and this peak was also dominant in the HE CAD spectrum, constituting >80% total ion intensity.

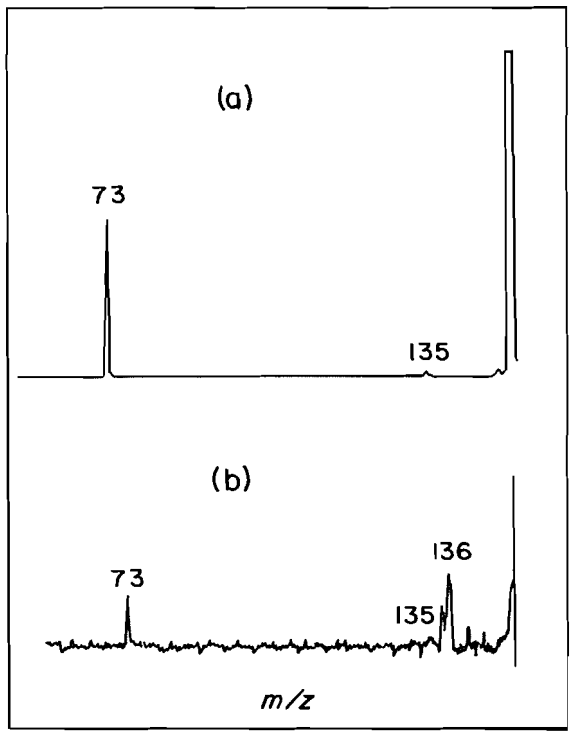

FIG. 1. The metastable spectra for m/z 151 formed by (*a*) the addition of $(CH_3)_3Si^+$ to C_6H_6, and (*b*) the protonation of $(CH_3)_3SiC_6H_5$. Main beam energy 8 keV.

Metastable (unimolecular) decompositions

The metastable decomposition spectra observed in the second field free region of MH$^+$ (ArH = C_6H_6) formed by the two different methods are compared in Fig. 1. The significant difference between the two spectra, apart from the obvious difference in intensity, is the pair of relatively large peaks attributed to loss of CH_3 (m/z 136) and CH_4 (m/z 135) from MH$^+$ formed by protonation. The peak at m/z 136 may be due, wholly or in part, to the unimolecular decomposition of the isobaric M$^+$ containing ^{29}Si, for which CH_3 loss constitutes the major, and very intense, metastable decom-

Can. J. Chem. Downloaded from www.nrcresearchpress.com by 217.78.4.112 on 09/08/12
For personal use only.

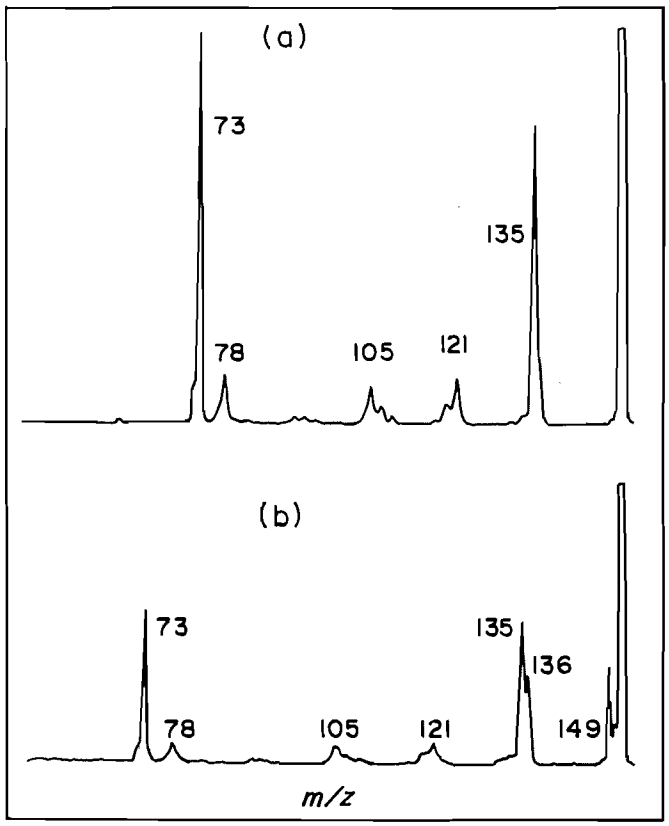

FIG. 2. The CAD spectra of m/z 151 formed by (*a*) the addition of $(CH_3)_3Si^+$ to C_6H_6, and (*b*) the protonation of $(CH_3)_3SiC_6H_5$. Main beam energy 8 keV, target gas He.

position. Loss of CH_4 occurs for all MH^+ but constitutes a greater fraction of the total for ions formed by protonation. This may be due to a slightly different energy content for these ions although most ions from the high-pressure source should be thermalized since the average ion suffers more than 10^4 collisions before exiting the source. The results for the metastable decomposition of MH^+ (ArH = $C_6H_5CH_3$), which are not shown, are similar to the results for MH^+ (ArH = C_6H_6) but the intensity of $[MH - 15]^+$ is only 5% of m/z 73 for the ion formed by protonation and only m/z 73 is observed for MH^+ formed by association.

The metastable spectra from decompositions subsequent to deceleration were observed at ion energies of 50 eV. The results confirm those described above, with loss of aromatic to yield $(CH_3)_3Si^+$ (m/z 73) being the major decomposition path. Peaks due to loss of CH_3 but only from protonated M, (mainly from ^{29}Si containing M^+?) and CH_4 are also observed.

CAD spectra

HE CAD spectra for MH^+ (ArH = C_6H_6) are shown in Fig. 2. The data from these figures are presented in Table 1, as are the data for MH^+ (ArH = $C_6H_5CH_3$). Also shown in the table are the assigned neutral losses. The assignments for MH^+ formed by association could be partially checked using C_6D_6 and $C_6D_5CD_3$. The loss of 16 mass units for the C_6H_6 adduct becomes 17 mass units with C_6D_6, i.e., the methane lost is composed of CH_3 from $(CH_3)_3Si$ and H from the aromatic ring. The CH_3 lost is entirely from the $(CH_3)_3Si$ group as is loss of C_2H_6 (ArH = C_6D_6) but loss of both masses 30 and 33 in almost equal proportions (C_2H_6 and $C_2H_3D_3$) is observed with $C_6D_5CD_3$. This interesting observation of an apparent combination of ring and silicon methyls was not pursued. Losses of masses 46, 44, and 42 from MH^+ (ArH = benzene) becomes losses of 47, 45, and 43 with C_6D_6. The lost neutrals are presumed not to contain silicon (for example 46 amu could be loss of $H_3{}^{28}SiCH_3$) since this implies significant rearrangement, which is not usually encountered in HE CAD.

LE CAD spectra of MH^+ were studied using either N_2 or $(CH_3)_3N$ as collision gas. With a beam energy of 50 eV there was no difference between the results obtained for any MH^+, loss of aromatic to give $(CH_3)_3Si^+$ being the only decomposition path. This path was the only one for N_2 CAD at all lower energies but at very low laboratory energies (<6 eV) other paths opened up with $(CH_3)_3N$. Figure 3 shows representative CAD spectra for MH^+ (ArH = C_6H_6) formed by both protonation of $(CH_3)_3SiC_6H_5$ and by addition of $(CH_3)_3Si^+$ to C_6H_6 with $(CH_3)_3N$ as collision gas. When C_6D_6 rather than C_6H_6 was complexed with $(CH_3)_3Si^+$ to form MH^+, the peaks at m/z 73 and 132 were unchanged and m/z 60 became 61. The major peaks are identified as $(CH_3)_3NH^+$ (m/z 60), $(CH_3)_3Si^+$ (m/z 73), and $(CH_3)_3SiN(CH_3)_3{}^+$ (m/z 132). The minor peak at m/z 119 is the proton-bound dimer $((CH_3)_3N)_2H^+$ but the identity of the small m/z 104 peak is not immediately evident. Although it is present in the two spectra of Fig. 3 it was absent when C_6D_6 was used instead of C_6H_6 in forming the complex with $(CH_3)_3Si^+$. This peak also appeared in the CAD spectrum of the toluene adduct and may be due to an impurity in the $(CH_3)_3N$. For all MH^+, a lowering of ion translational energy to ~0.5 eV resulted in the presence of essentially only two CAD ions, viz. m/z 60 and m/z 132, m/z 73 being of very low intensity.

The $(CH_3)_3Si^+$ adduct of 1,3,5-trimethylbenzene (mesitylene) was also examined in the same manner as those of benzene and toluene. The only metastable decomposition peak was due to loss of aromatic to give $(CH_3)_3Si^+$. The HE CAD spectrum was more intense than for the lower aromatics with large peaks for losses of CH_4, C_2H_6, and $(CH_3)_3Si^+$. An equally large peak at m/z 105 could be loss of $(CH_3)_4Si$. LE CAD with nitrogen as collision gas led only to m/z 73, i.e., loss of mesitylene. The same result occurred with $(CH_3)_3N$ as collision gas at centre of mass energies greater than 1 eV, but below this energy the $(CH_3)_3Si^+$ adduct of trimethylamine was formed. $(CH_3)_3NH^+$ was present but in a far diminished yield (<5% relative abundance) compared with those from the benzene and toluene adducts.

Discussion

Comparison of Figs. 2*a* and 2*b* and the data in Table 1 strongly suggests that the decomposing forms of MH^+ ions for ArH = benzene, whether formed by association or protonation, have the same structure. For ArH = toluene the relative intensities of CAD ions for MH^+ formed by the two methods are not as well matched as those for benzene but the intensity patterns are comparable. The contribution of metastable decomposition to each of the spectra was assessed by biasing the collision cell by 1 kV to separate CAD and metastable ions. Very small metastable contributions (<10% of the intensity of each peak) were observed for m/z 73 in all spectra. Metastable decomposition of MH^+ formed by protonation also showed a small contribution to the ion

TABLE 1. Relative ion abundances (RA) in the CAD spectra of MH^+ formed by the association of $(CH_3)_3Si^+$ with aromatic and by the protonation of trimethylsilyl aromatic

Loss	RA(%)			
	$(CH_3)_3Si^+ + C_6H_6$	$(CH_3)_3SiC_6H_5 + H^+$	$(CH_3)_3Si + C_6H_5CH_3$	$(CH_3)_3SiC_6H_4CH_3 + H^+$
H_2	0.3	13.9	1.5	—
CH_3	6.0	13.6	37.6	50.0
CH_4	3.0	14.9	1.7	15.6
C_2H_6	4.6	11.4	14.5	4.2
C_2H_8	1.9	1.9	3.6	1.9
C_2H_{10}	0.4	0.7	1.3	—
C_3H_6	0.9	0.9	0.7	—
C_3H_8	1.8	1.5	5.0	2.4
C_3H_{10}	3.7	3.4	4.6	2.4
$C_4H_{12}(C_2H_8Si)$	0.4	0.5	0.7	—
$C_4H_{10}(C_2H_4Si)$	0.8	0.6	1.0	0.6
$C_4H_8(C_2H_2Si)$	0.8	1.1	2.3	1.4
C_3H_9Si	4.8	3.3	9.2	2.5
$C_3H_{10}Si$	1.5	1.1	5.9	2.4
ArH	38.6	28.4	8.9	16.5
ArH_2	3.7	2.8	1.3	0.2

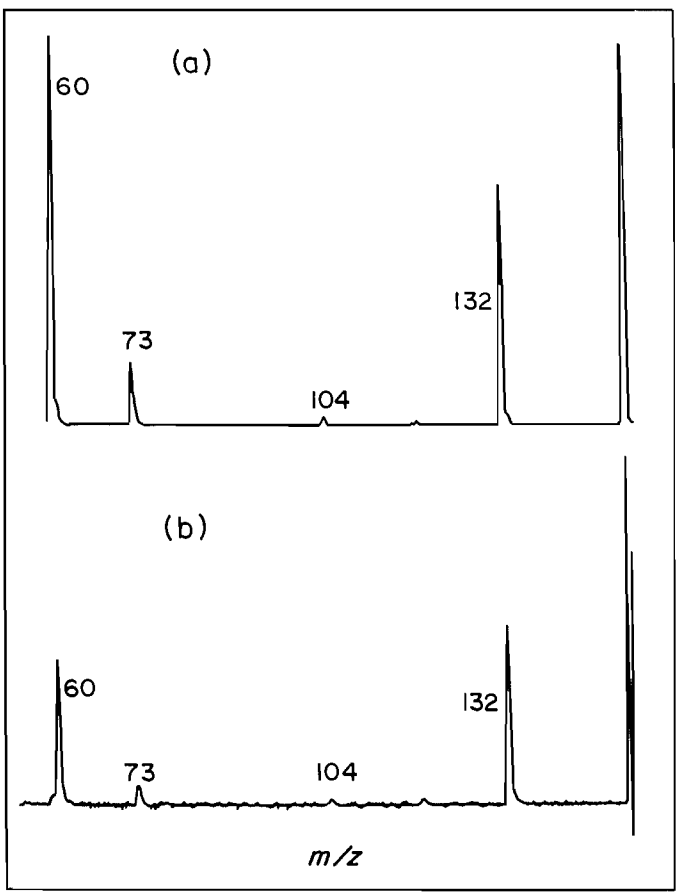

FIG. 3. The CAD spectra of m/z 151 formed by (*a*) the addition of $(CH_3)_3Si^+$ to C_6H_6, and (*b*) the protonation of $(CH_3)_3SiC_6H_5$. Main beam energy 1.5 eV, target gas $(CH_3)_3N$.

formed by loss of 15 amu, i.e., CH_3. The major CAD ion in all spectra is m/z 73 ($(CH_3)_3Si^+$) formed by loss of the aromatic molecule.

[4] $(CH_3)_3SiArH^+ \rightarrow (CH_3)_3Si^+ + ArH$

This is the expected ion if the dissociation is that of either a π or a σ complex since the positive charge will tend to remain with the fragment of lowest ionization energy ($IE(C_6H_6) = 9.25$ eV, IE ($(CH_3)_3Si$) ≈ 6.5 eV (9)). It is to be noted that a small peak corresponding to loss of $(CH_3)_3Si$ as neutral is also observed in all HE CAD spectra. The presence of this ion shows a minimum energy input in the collision process of $IE(C_6H_6) - IE((CH_3)_3Si) + D((CH_3)_3Si^+ - C_6H_6) = 3.76$ eV for $ArH = C_6H_6$. The observation of this ion requires activating collisions leading to excitation to upper electronic states of $(CH_3)_3SiArH^+$.

Most of the He CAD ions not discussed above arise from alkyl and alkene losses from the $(CH_3)_3Si$ group alone; losses of CH_3, C_2H_6, and C_3H_8 are particularly prominent. Of particular note is that loss of CH_4 becomes loss minimum energy input in the collision process of $IE(C_6H_6) - IE((CH_3)_3Si) + D((CH_3)_3Si^+ - C_6H_6) = 3.76$ eV for $ArH = C_6H_6$. The observation of this ion requires activating collisions leading to excitation to upper electronic states of $(CH_3)_3SiArH^+$.

Most of the He CAD ions not discussed above arise from alkyl and alkene losses from the $(CH_3)_3Si$ group alone; losses of CH_3, C_2H_6, and C_3H_8 are particularly prominent. Of particular note is that loss of CH_4 becomes loss of CH_3D for MH^+ formed by association of $(CH_3)_3Si^+$ with a perdeuterated aromatic. This methane loss results in the formation of the very stable $(CH_3)_2SiAr^+$ ion, which is the most intense ion in the electron impact mass spectra of $(CH_3)_3SiAr$ (Ar = C_6H_5, $CH_3C_6H_4$), demonstrating the greater stability of $(CH_3)_2SiAr^+$ compared with $(CH_3)_3Si^+$.

Figure 2*b* shows significant peaks due to loss of one and two mass units that are not present in Fig. 2*a*. We have no explanation for their presence and assume that they are not significant. These peaks were not observed in the LE CAD spectra of this same ion or indeed in any other spectrum. In particular, no such peaks were observed in the HE CAD spectrum of M^+.

The LE CAD spectra with N_2 or $(CH_3)_3N$ as collision gas with laboratory ion energies in the range 6–50 eV show only loss of aromatic for all MH^+. There are no competing dissociation paths. Dissociation under LE conditions is attrib-

Can. J. Chem. Downloaded from www.nrcresearchpress.com by 217.78.4.112 on 09/08/12
For personal use only.

Can. J. Chem. Downloaded from www.nrcresearchpress.com by 217.78.4.112 on 09/08/12
For personal use only.

utable to vibrational excitation of the ground electronic state (10). This is the reverse of the association, which occurs on the ground state electronic energy surface and for which the reversible association has been studied in a high-pressure mass spectrometer to yield $(CH_3)_3Si^+$–ArH binding energies of 23.9 ± 0.4 kcal mol^{-1} (ArH = C_6H_6) (11) and 28.4 ± 0.4 kcal mol^{-1} (ArH = $C_6H_5CH_3$) (4).

Ion–molecule reactions in addition to collisional dissociation occur between MH^+ and $(CH_3)_3N$ below 6 eV laboratory energy; for MH^+ (ArH = C_6H_6) this energy corresponds to a centre of mass energy of 2.8 eV. Proton transfer (reaction [5]) and displacement (reaction [6]) together with collisional dissociation (reaction [7]) are observed. The presence of a small amount of $((CH_3)_2N)_2H^+$ shows that multiple collisions are occurring. This ion is not significant (<1% total ion intensity) at nominal $(CH_3)_3N$ pressures less than 1×10^{-6} Torr.

[5] $(CH_3)_3SiC_6H_6^+ + (CH_3)_3N \rightarrow (CH_3)_3SiC_6H_5 + (CH_3)_3NH^+$

[6] $\rightarrow (CH_3)_3SiN(CH_3)_3^+ + C_6H_6$

[7] $\rightarrow (CH_3)_3Si^+ + C_6H_6 + (CH_3)_3N$

With decreasing energy the $(CH_3)_3Si^+$ peak decreases and is insignificant at a centre of mass energy ~0.14 eV. At this very low energy the relative rates of reactions [5] and [6] appear, within the aforementioned limitations of pressure measurement, to be independent of $(CH_3)_3N$ pressure below a pressure gauge reading of 9×10^{-7} Torr. From the relative peak heights $k_5/k_6 = 1.9 \pm 0.2$ for $(CH_3)_3N$ pressure readings from 1 to 9×10^{-7} Torr. Both reactions [5] and [6] are highly exothermic. The binding energies of $(CH_3)_3Si^+$ to C_6H_6 and $(CH_3)_3N$ are 24 (3) and >60 kcal mol^{-1} (11) respectively. If the proton affinity of $(CH_3)_3SiC_6H_5$ is taken to be roughly that of $(CH_3)_3CC_6H_5$ (193 kcal mol^{-1} (7)) then reaction [5] is exothermic by ~30 kcal mol^{-1}. The important conclusion to be drawn from these LE CAD studies is that they do not differentiate between MH^+ ions formed by the two methods, association and protonation.

The evidence cited in this paper strongly supports the idea that MH^+ has the same structure for a given aromatic whether it is formed by association of $(CH_3)_3Si^+$ with ArH or by protonation of $(CH_3)_3SiAr$. Kebarle and co-workers (12) verified the identity of the $(CH_3)_3C^+$ adduct of benzene and protonated *tert*-butyl benzene by showing the consistency of binding enthalpy with proton affinity. Such a thermochemical proof is not possible for the analogous silicon compounds discussed in this paper because of the lack of the required thermochemical data, namely the proton affinity and enthalpy of formation of $(CH_3)_3SiC_6H_5$. The uncertainties in any estimations of these values are such that no confidence could be placed in the conclusions drawn from their use.

The identity of the HE CAD spectra of protonated isopropyl-*n*-butyl benzene and the ion formed by the addition of the isopropylcarbenium ion to *n*-butyl benzene was taken by Holman and Gross as evidence not only that such reactions produce identical MH^+ species that collisionally decompose from identical structures but also that their ionization-threshold structures are the same (13). They argued that as the size of the alkyl group increases, its ability to accommodate carbenium ion character also increases. This ability also increases with branching in a given alkyl group, for example for butyl in the order *n*-butyl < *sec*-butyl < *tert*-butyl. This is also the order of stability of protonated butylbenzenes, the *n*-butyl and *sec*-butyl members of which, with suitable excitation, can isomerize to the more branched structures. Such an isomerization is presumed to occur via a π-complex and supporting evidence for this statement is the observation of hydrogen scrambling between the aromatic and alkyl hydrogens (13–15). This scrambling is envisaged to occur via the proton-bound structure **V** with the π-complex **IV** as a distinct intermediate on the potential energy surface.

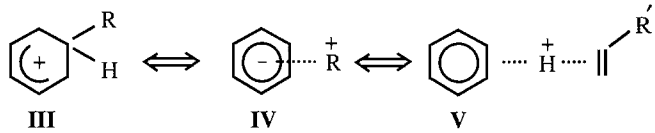

III **IV** **V**

Structure **V** must be of relatively high energy for the $(CH_3)_3Si^+$ and $(CH_3)_3C^+$ adducts of benzene and toluene since no isotopic hydrogen scrambling between the ring and methyl hydrogens of $(CH_3)_3X$ is observed when the equilibrium association is studied using C_6D_6 or $C_6D_5CD_3$ (4). Presumably under the experimental conditions, the much higher proton affinities of $(CH_3)_2X{=}CH_2$ (PA($(CH_3)_2C{=}CH_2$) = 196 kcal mol^{-1} (6), PA($(CH_3)_2Si{=}CH_2$) = 228 kcal mol^{-1} (16)) than of benzene (PA = 181 kcal mol^{-1}) and toluene (190 kcal mol^{-1}) do not allow structures such as **V** to be accessible. A strong Brønsted base such as $(C_2H_5)_3N$ will proton transfer via **I** or **III** for silicon and carbon adducts respectively. A strong oxygen-containing nucleophile such as cyclohexanone but which has much weaker Brønsted basic properties than $(C_2H_5)_3N$ reacts via **II**, the very strong Si—O bond formed favouring a displacement reaction rather than proton transfer.

Little proton transfer is observed from the $(CH_3)_3Si^+$ adduct of 1,3,5-trimethylbenzene to $(C_2H_5)_3N$. This is in agreement with the observation that trimethylsilylation of mesitylene was not observed in the radiolysis of $(CH_3)_4Si/C_6H_3(CH_3)_3/(C_2H_5)_3N$ mixtures (2). The explanation of steric hindrance in the deprotonation step given for the radiolytic result is consistent with our observations. The enthalpy of binding of $(CH_3)_3Si^+$ to mesitylene is 7 kcal mol^{-1} greater than to benzene (3). The proton affinity of 2,4,6-trimethyl-1-trimethylsilylbenzene will be only slightly greater than the 201 kcal mol^{-1} of mesitylene. Reactions analogous to [5] and [6] will therefore still be highly exothermic with mesitylene and should be fast and competitive. The preponderance of the displacement reaction over the proton transfer reaction is indicative of significant steric hindrance in the latter reaction.

Acknowledgements

The authors thank the Natural Sciences and Engineering Research Council of Canada for continuing financial assistance.

1. S. Fornarini. J. Org. Chem. **53**, 1314 (1988).
2. F. Cacace, M. E. Crestoni, S. Fornarini, and R. Gabrielli. Int. J. Mass Spectrom. Ion Processes, **84**, 17 (1988).
3. A. C. M. Wojtyniak and J. A. Stone. Int. J. Mass Spectrom. Ion Processes, **74**, 59 (1986).
4. J. M. Stone and J. A. Stone. Int. J. Mass Spectrom. Ion Processes, **109**, 247 (1991).
5. J. E. Szulejko, A. G. Harrison, C. E. C. A. Hop, T. B. McMahon, J. A. Stone, and A. B. Young. J. Am. Soc. Mass Spectrom. **3**, 33 (1992).

6. S. G. Lias, J. F. Liebman, and R. D. Levin. J. Phys. Chem. Ref. Data, **13**, 695 (1984).
7. F. Cacace, M. E. Crestoni, G. de Petris, S. Fornarini, and F. Grandinetti. Can. J. Chem. **63**, 3099 (1988).
8. S. J. Hazell, R. D. Bowen, and K. R. Jennings. Org. Mass Spectrom. **23**, 597 (1988).
9. S. G. Lias, J. E. Bartmess, J. F. Liebman, J. L. Holmes, R. D. Levin, and G. W. Mallard. J. Phys. Chem. Ref. Data, **17**, 1988. Supplement No. 1.
10. K. L. Busch, G. L. Glish, and S. A. McLuckey. Mass spectrometry/mass spectrometry, techniques and applications of tandem mass spectrometry. VCH Publishers, New York. 1988.
11. X. Li and J. A. Stone. Int. J. Mass Spectrom. Ion Processes, **101**, 149 (1990).
12. D. K. Sensharma, S. Ikuta, and P. Kebarle. Can. J. Chem. **60**, 2329 (1982).
13. R. W. Holman and M. L. Gross. J. Am. Chem. Soc. **111**, 3560 (1989).
14. J. A. Herman and A. G. Harrison. Org. Mass. Spectrom. **16**, 423 (1981).
15. D. Berthomieu, H. Audier, J. P. Denhez, and C. Monteiro. Org. Mass Spectrom. **26**, 271 (1991).
16. C. E. Allison and T. B. McMahon. J. Am. Chem. Soc. **112**, 1672 (1990).

Can. J. Chem. Downloaded from www.nrcresearchpress.com by 217.78.4.112 on 09/08/12
For personal use only.

Electrochemical behavior of *C*-methoxy, amino, cyano, and mercapto nitrones

BRUCE J. ACKEN,[1] DAVID E. GALLIS,[2] JAMES A. WARSHAW, AND DELANSON R. CRIST[3]
Department of Chemistry, Georgetown University, Washington, DC 20057, U.S.A.

Received October 11, 1991

BRUCE J. ACKEN, DAVID E. GALLIS, JAMES A. WARSHAW, and DELANSON R. CRIST. Can. J. Chem. **70**, 2076 (1992).

The redox behavior of various *C*-substituted nitrones was investigated by cyclic voltammetry in acetonitrile. These included *C*-methoxynitrones (MeO)CR = N(O)*t*-Bu with R = C_6H_5(**1***a*), *p*-$MeOC_6H_4$ (**1***b*), *p*-$NO_2C_6H_4$ (**1***c*), and H (**1***d*) and nitrones YCH = N(O)*t*-Bu with Y = n-BuS (**2***a*), CN (**2***b*), and C_6H_5NH (**2***c*). All gave anodic peaks which can be identified as oxidations of the nitrone function. Controlled potential electrolysis of **1***a* at 1.05 V (SCE) showed that its oxidation was a one-electron process. Reduction of **1***a* occurs stepwise at −2.08 and at −2.47 V, the same potential for reduction of methyl *N-tert*-butylbenzimidate (MeO)CPh = N*t*-Bu. With electrochemical windows of ca. 3 V, all of the nitrones studied appear suitable for spin-trapping experiments.

BRUCE J. ACKEN, DAVID E. GALLIS, JAMES A. WARSHAW et DELANSON R. CRIST. Can. J. Chem. **70**, 2076 (1992).

Opérant dans l'acétonitrile et faisant appel à la voltampérométrie cyclique, on a étudié le comportement rédox de diverses nitrones *C*-substituées dont les *C*-méthyoxynitrones (MeO)CR = N(O)*t*-Bu dans lesquelles R = C_6H_5 (**1***a*), *p*-$MeOC_6H_4$ (**1***b*), *p*-$NO_2C_6H_4$ (**1***c*) et H (**1***d*) et les nitrones YCH = N(O)*t*-Bu dans lesquelles Y = *n*-BuS (**2***a*), CN (**2***b*) et C_6H_5NH (**2***c*). Tous ces produits donnent des pics anodiques que l'on peut identifier comme des oxydations de la fonction nitrone. Une électrolyse du composé **1***a* à un potentiel contrôlé de 1,05 V (SCE) montre que cette oxydation est un processus impliquant un électron. La réduction du composé **1***a* se produit par étapes à −2,08 et à −2,47 V, les mêmes potentiels que ceux observés lors de la réduction du N-*tert*-butylbenzimidate de méthyle (MeO)CPh = N*t*-Bu. Avec des plages électrochimiques d'environ 3 V, toutes les nitrones étudiées semblent appropriées pour des études de piégeage de spin.

[Traduit par la rédaction]

Most of the attention devoted to nitrone chemistry in recent years has concerned applications as synthetic intermediates (1) or as spin-trapping agents (2). In connection with spin-trapping applications Blount and co-workers (3) examined nitrone electrochemistry in aqueous and nonaqueous media in order to determine windows of inactivity suitable for electrochemical generation of free radicals. In acetonitrile most aldonitrones were oxidized at potentials greater than 1 V (vs. SCE) and reduced at ca. −2.0 V, a relatively wide window, in one-electron oxidation and two-electron reduction processes.

We now present electrochemical results on nitrones bearing RO, RS, R_2N, or CN at the α position. If the nitronyl function is considered analogous to a carbonyl group, these nitrones are related to esters, thio esters, ketonitriles, and amides, respectively. The effective spin-trapping ability of *C*-methoxy-*C*-aryl-*N-tert*-butylnitrones has previously been reported (4).

Results

Various *C*-methoxynitrones **1** and aldonitrones **2**(*a*–*c*) shown in Scheme 1 were prepared as previously described (5) and their electrochemistry studied by cyclic voltammetry. Also investigated as references were the well-known *C*-phenyl-*N-tert*-butylnitrone (PBN) **2***d*, imine **3***a*, and imidate **3***b*.

Cyclic voltammograms were taken in acetonitrile containing 0.1 M tetraethylammonium perchlorate, with oxidations at a platinum electrode (range ca. 2.5 to −1.8 V vs. SCE) and reductions at a hanging mercury drop electrode (HMDE) (range ca. 0.6 to −2.7 V vs. SCE).

C-Methoxynitrones

Nitrone **1***a* is irreversibly oxidized at 0.91 V at Pt (Fig. 1A). Controlled potential electrolysis showed that this oxidation released 1.06 electrons. Reduction of **1***a* is an irreversible two-step process with $E_{p(c)}$ = −2.08 and −2.47 V (Fig. 1B). The heights of the two reduction peaks in the cyclic voltammogram are essentially the same and the position of the second peak is the same as that for authentic benzimidate **3***b*.

To determine the substituent effect on the electrochemical characteristics of *C*-alkoxynitrones, cyclic voltammograms of **1***b* and **1***c* were also recorded and the data are summarized in Table 1. In the case of the nitro derivative there is an extra multi-step reduction at ca. −1.4 V corresponding (6) to a four-electron reduction of —NO_2 to —NHOH (Fig. 1C). Thus, the nitrone reduced at −2.04 V is *N*-hydroxylaminonitrone **5**, eq. [1], a similar conclusion reached for reduction of *C*-*p*-nitrophenyl-*N*-methylnitrone (7).

Electrochemical oxidation of **1***d* is similar to the other *C*-alkoxynitrones studied. It is oxidized in an irreversible one-step oxidation at 1.00 V (Fig. 1D). However, its reduction is quite different in that it undergoes a quasi-reversible one-step reduction at −1.96 V (Fig. 1E).

Other nitrones

C-n-Butylmercaptonitrone **2***a* undergoes a two-step irreversible oxidation at 1.17 and 1.77 V (Fig. 2A). There was no reduction of this compound prior to the solvent discharge. Sulfides are known to undergo two-electron oxidations to either the sulfoxide or a pseudo-dimer depending on the amount of water present (8). Since the peak at 1.17 V is approximately twice the size of the peak at 1.77 V and since aldonitrones are known to undergo one-electron oxidations in nonaqueous media (3), it is reasonable to assign the peak at 1.17 V to oxidation of the sulfide portion of the molecule and the peak at 1.77 V to nitrone oxidation.

[1]Present address: Pfizer, Inc., Groton, CT 06340, U.S.A.
[2]Present address: Environmental Resources Management, Inc., Exton, PA 19341, U.S.A.
[3]Author to whom correspondence may be addressed.

Can. J. Chem. Downloaded from www.nrcresearchpress.com by 217.78.4.112 on 09/08/12
For personal use only.

[1] 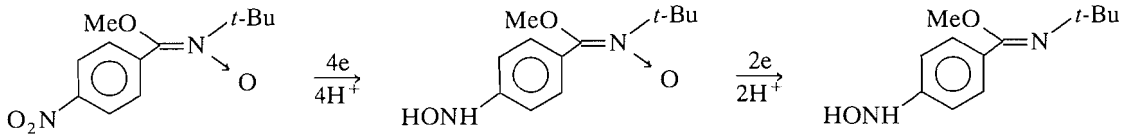

5

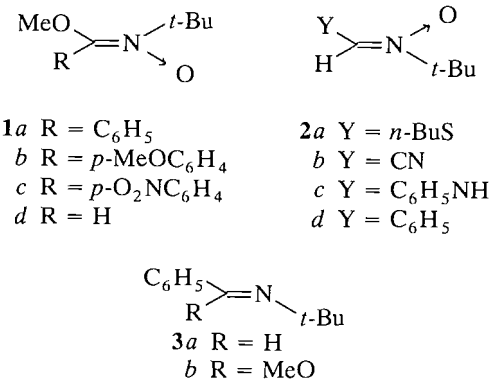

1*a* R = C_6H_5
b R = *p*-$MeOC_6H_4$
c R = *p*-$O_2NC_6H_4$
d R = H

2*a* Y = *n*-BuS
b Y = CN
c Y = C_6H_5NH
d Y = C_6H_5

3*a* R = H
b R = MeO

SCHEME 1

C-Cyanonitrone **2***b* undergoes a one-step irreversible oxidation at 0.88 V (Fig. 2B) and a two-step irreversible reduction at −1.14 and −1.79 V (Fig. 2C). The extra reduction step at −1.14 V, as compared with aldonitrones **1***d* and PBN (see below), is in the region for reduction of CN by various processes (9–11). *C*-Anilinonitrone (**2***c*) undergoes a series of oxidations (Fig. 2D) at 0.63, 1.01, and 1.31 V and an irreversible two-step reduction at −2.06 and −2.66 V (Fig. 2E). Anilines are known (12) to be oxidized in two steps, each with two-electron, coupled anodic and cathodic peaks, so that the quasi-reversible oxidations at 0.63 and 1.31 V probably represent oxidation of the anilino group.

An aldonitrone, PBN (**2***d*), and two model compounds were also studied. PBN undergoes an irreversible one-electron oxidation at 1.34 V and a one-step, two-electron reduction at −2.28 V (Fig. 2F). Benzylidene-*tert*-butylamine (**3***a*) is irreversibly oxidized at 2.04 V and reduced irreversibly at −2.43 V. Methyl *N*-*tert*-butylbenzimidate (**3***b*) is irreversibly oxidized at 2.08 V and reduced at −2.46 V.

Discussion

C-Methoxynitrones

Nitrones **1**, **2***b*, and **2***d* all undergo an irreversible one-electron oxidation as reported for other nitrones in nonaqueous media (3). Oxidation of nitrones **2***a* and **2***c* involves prior oxidation of the *n*-butylmercapto and anilino groups, respectively. Attempts to characterize the product of oxidation of **1***a* were inconclusive. In the case of phenazine-*N*, *N*′-dioxide the radical cation produced dimerized (13).

The process for reduction of *C*-alkoxynitrone **1***a* shown

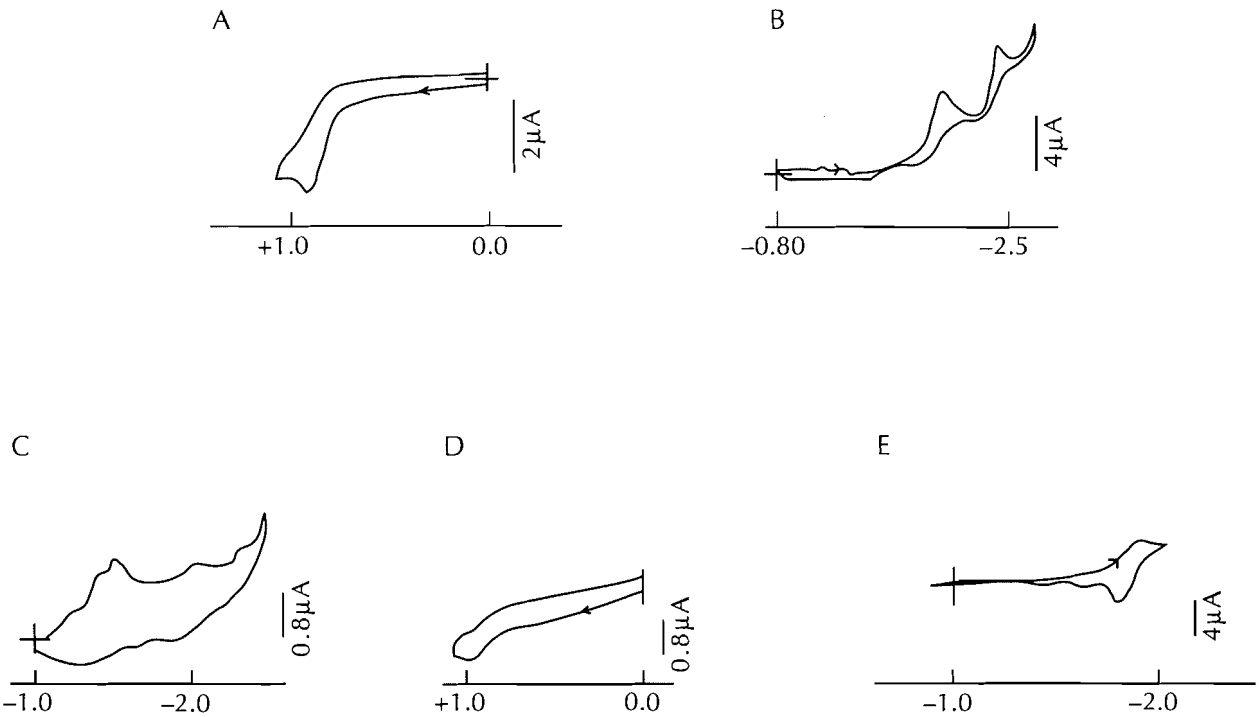

FIG. 1. Cyclic voltammograms of *C*-methoxynitrones **1** in acetonitrile containing 0.1 M Et_4NClO_4, sweep rate 50 mV/s, *x* axis in V vs. SCE. (A and B) **1***a* at Pt and HMDE, respectively; (C) **1***c* at HMDE; (D and E) **1***d* at Pt and HMDE, respectively.

Can. J. Chem. Downloaded from www.nrcresearchpress.com by 217.78.4.112 on 09/08/12
For personal use only.

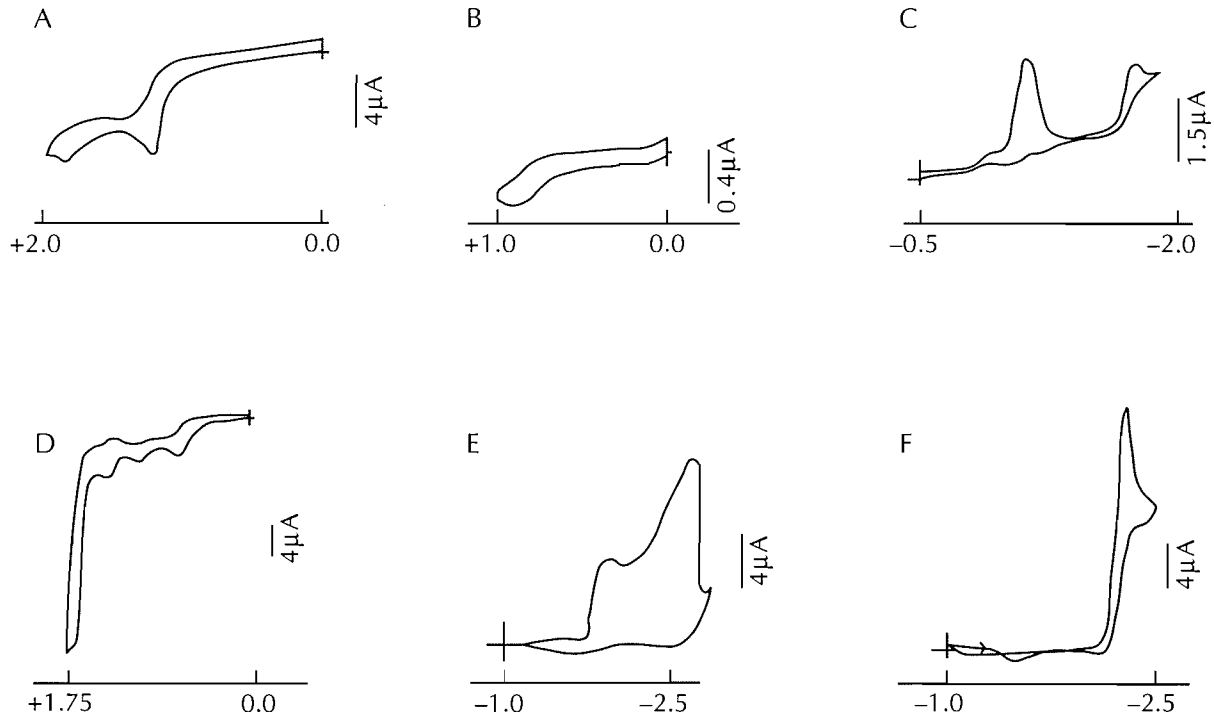

FIG. 2. Cyclic voltammograms of nitrones **2** in acetonitrile containing 0.1 M Et_4NClO_4, sweep rate 50 mV/s, *x* axis in V vs. SCE. (A) **2***a* at Pt; (B and C) **2***b* at Pt and HMDE, respectively; (D and E) **2***c* at Pt and HMDE, respectively; (F) **2***d* at HMDE.

[2] 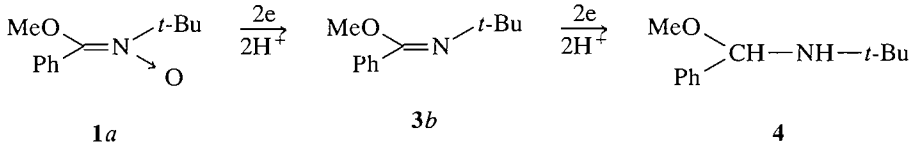

1*a* **3***b* **4**

in eq. [2] is consistent with two reduction peaks of nearly the same heights, and thus involving the same number of electrons (14), and the fact that the second peak occurred at the same potential as that for authentic **3***b*.

The first step is analogous to reduction of *N*-phenylnitrones in aqueous acid (7, 15) and the second to reduction of imidates to aminals (16) and imines to amines (17). Unlike the present case, the double bond is reduced for PBN and other *N-tert*-butylnitrones in acetonitrile giving *N*-hydroxyamines (3) which are not reduced further (6).

Structural effects

Electron-withdrawing groups hindered oxidation of *C*-alkoxynitrones **1**, as shown by increasing $E_{p(a)}$ for the series **1***b*, **1***a*, and **1***c* (see Table 1). This is an expected result, since electron withdrawal from the nitrone function should make it more difficult to remove an electron, as reported for substituted pyridine *N*-oxides (18).

For reduction, the electron-donating *p*-MeO substituent retarded addition of electrons, since $E_{p(c)}$ is −2.26 V for **1***b* compared with −2.08 V for the unsubstituted phenyl **1***a*. The value of −2.04 V for the *p*-NO_2 derivative **1***c* is similar to that for *p*-MeO, since prior reduction of NO_2 gives a nitrone containing the electron-donating *p*-NHOH group on phenyl, eq. [1]. These results are in general agreement with the usual trend that substrates with electron-donating groups have more negative polarographic half-wave potentials (19), as reported specifically for *C*-aryl-*N*-methylnitrones (7).

Model compounds **2***d*, **3***a*, and **3***b* and alkoxynitrone **1***a* have peak potentials (Table 1) that give the following order[4] for ease of oxidation *and* reduction:

imidate < imine < aldonitrone < alkoxynitrone

Aromatic hydrocarbons exhibit the same behavior in that the one more easily oxidized is also more easily reduced (20).

Electrochemical windows

It has been shown (21) that nitrones can be used as spin traps in experiments using electrochemical generation of radicals. For this use, the range of electrochemical inactivity must first be known. For the nitrones in the present study, possible useful potentials would occur between the least positive $E_{p(a)}$ and least negative $E_{p(c)}$ listed in Table 1. A graphical representation of these resulting maximum electrochemical windows is shown in Fig. 3. Also included is *C*-phenyl-*N-tert*-butylnitrone **2***d* for comparison purposes.

The *C*-alkoxynitrones studied all have more narrow electrochemical windows than PBN. In the case of **1***c*, the win-

[4] $E_{p(a)}$ values for these compounds correlated with HOMO energies calculated by MNDO, but $E_{p(c)}$ did not show a relationship with LUMO energies (unpublished work).

Can. J. Chem. Downloaded from www.nrcresearchpress.com by 217.78.4.112 on 09/08/12
For personal use only.

Can. J. Chem. Downloaded from www.nrcresearchpress.com by 217.78.4.112 on 09/08/12
For personal use only.

TABLE 1. Anodic and cathodic peak potentials of nitrone and other functional groups[a]

	$E_{p(a)}$		$E_{p(c)}$	
Compound	Nitrone	Other	Nitrone	Other
1*a*	0.91		−2.08, −2.47	
1*b*	0.80		−2.26, −2.63	
1*c*	0.95		−2.04,[b] −2.34[b]	−1.44[c]
1*d*	1.00		−1.96	
2*a*	1.77[d]	1.17		
2*b*	0.88		−1.79[e]	−1.14[e]
2*c*	1.01[d]	0.63, 1.31		
2*d*	1.34		−2.28	
3*a*		2.04		−2.43
3*b*		2.08		−2.46

[a]In acetonitrile containing 0.1 M Et_4NClO_4 with oxidations at Pt, reductions at a HMDE; all potentials in volts with respect to SCE. See text for tentative assignments of peaks to the nitrone function or to other groups in the molecule.

[b]Reduction of a modified nitrone due to prior reduction of other functional groups (see text).

[c]Part of a complex series.

[d]Oxidation of a modified nitrone due to prior oxidation of other functional group (see text).

[e]Assignments of these functional groups may be interchanged.

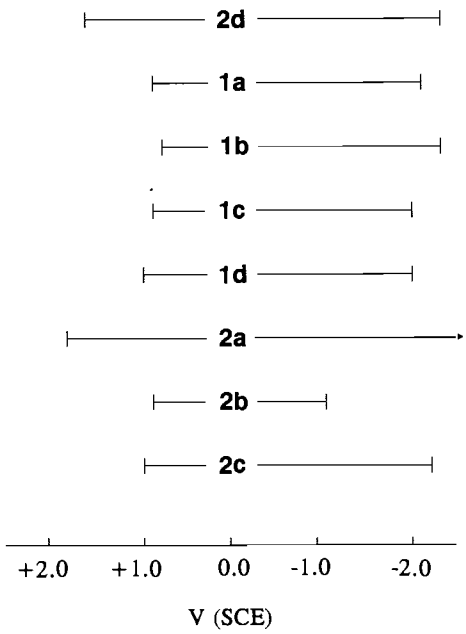

FIG. 3. Electrochemical windows of *C*-substituted nitrones. Limits are defined as the anodic and cathodic peak potentials of nitrone or other electroactive function (see text).

dow is narrowed considerably by reduction of the nitro group (6). Similarly, electrochemical reactions of the Y group in **2***a*, **2***b*, and **2***c* determine the width of the window, not the nitrone function itself. As is apparent from Fig. 3, however, all of the nitrones studied here would be suitable for electrochemical spin-trapping experiments. Most of these compounds have electrochemical windows of 3 V, the greatest being *C*-*n*-butylmercaptonitrone **2***a* which has a window of 3.95 V.

Experimental

Instrumentation

Nuclear magnetic resonance (NMR) spectra were obtained on a Bruker (Aspect 3000) 300 MHz spectrometer with absorptions given in ppm from internal tetramethylsilane. Cyclic voltammograms were obtained on an IBM Instruments EC/225 Voltammetric Analyzer. The working electrodes were either Pt (Bioanalytical Systems) or a HMDE (Metroh E-410). The reference electrode was a double junction, saturated calomel electrode (EG&G). Controlled potential electrolyses were done on a coulometer built by W. Craig, Georgetown University, with Pt gauze or a Hg pool as working electrodes.

Materials

All electrochemical studies were done in acetonitrile (Baker) that had been passed through alumina under Ar and stored over Molecular Sieves (Linde 4 A, previously heated at 400°C for 4 h). Nitrones **1** were prepared by alkylation of the hydroxamic acids with methyl triflate and deprotonation on silica gel/methanol as previously described (5). After evaporation of methanol at 0°C under N_2 the nitrone was taken up in 20 mL of acetonitrile containing 0.1 M Et_4NClO_4 to give a solution ca. 1 mM in nitrone. Nitrones **2***a*, **2***b*, and **2***c*, prepared from **1***d* as previously described (4), were purified by preparative thin-layer chromatography on 0.5 mm silica gel plates (CH_2Cl_2/MeOH 9:1). The nitrone band was scraped and eluted from silica with methanol. Solutions ca. 1 mM in nitrone in acetonitrile with 0.1 M Et_4NClO_4 were made as above. Imine **3***a* (22) and imidate **3***b* (23) were prepared as previously described and nitrone **2***d* was obtained from Kodak.

Cyclic voltammetry

Oxidations were done at a platinum electrode and reductions at a hanging mercury drop electrode (HMDE). In both cases the auxiliary electrode was platinum. All potentials are with respect to an aqueous saturated calomel electrode, separated from the sample solution by a double junction containing 0.1 M Et_4NClO_4 in acetonitrile. The reference electrode was standardized to the reduction of ferrocinium$^+$ to ferrocene, $E_{1/2}$ = 0.307 V in acetonitrile (0.2 M $LiClO_4$). Acetonitrile solutions of the species under study, 1–8 mM in substrate and 0.1 M in Et_4NClO_4, were degassed with Ar for 10–15 min prior to taking a voltammogram. The sweep rate was typically 50 mV/s and the current sensitivity 10 μA.

Cyclic voltammograms were run on similar solutions of methyl benzoate and *N*-*tert*-butylhydroxylamine, possible products of hydrolysis of **1***a*. The ester showed no oxidation prior to solvent discharge and an irreversible reduction with $E_{p(c)}$ = −2.42 V. The hydroxylamine was irreversibly oxidized with $E_{p(a)}$ = 0.59 V but showed no reduction prior to solvent discharge.

Controlled potential electrolysis of **1**a

For oxidation, a solution of 4 mg of **1***a* in 20 mL of acetonitrile 0.1 M in Et_4NClO_4 was degassed for 15 min with Ar. Exhaustive electrolysis was done at +1.05 V vs. SCE at a platinum gauze electrode. The auxiliary electrode was separated from the solution by a glass-fritted chamber containing acetonitrile 0.1 M in Et_4NClO_4. The solution was electrolyzed until the current–time curve reached a plateau. A solution containing only the supporting electrolyte was deoxygenated and electrolyzed. The difference in coulombs between these two currents, when converted to electrons, corresponds to a 1.06 electron oxidation. After removal of solvent at 0°C under a stream of N_2, the residue was taken up in $CDCl_3$. ^1H NMR showed only signals due to methyl benzoate δ ($CDCl_3$): 3.92 (s, 3H, OCH_3), 7.40–7.46 (m, 2H, ArH), 7.52–7.58 (m, 1H, ArH), 8.02–8.05 (m, 2H, ArH) and *N*-*tert*-butylhydroxylamine δ ($CDCl_3$): 1.13 (s, 9H, *N*-*t*-Bu).

For reduction, a solution of 3 mg of **1***a* was made as above. Exhaustive reduction was done at −2.20 V vs. SCE at a mercury pool electrode. The auxiliary electrode was separated from the solution by a glass-fritted chamber containing acetonitrile 0.1 M in

Et_4NClO_4. Electrolysis data indicated an apparent 8 electrons/mol nitrone, but this high value may be caused by reduction of the supporting electrolyte (24). After removal of solvent as described above, the residue was taken up in $CDCl_3$. ^1H NMR of the solution indicated a complex mixture containing a minor amount of methyl *N-tert*-butylbenzimidate δ ($CDCl_3$): 1.21 (s, 9H, *N-t*-Bu), 3.62 (s, 3H, OCH_3), 7.35 (s, 5H, ArH).

Acknowledgment

This research was supported by an NSF Chemical Instrumentation Grant (CHE-8406088) and by an equipment grant from the W. M. Keck Foundation. We especially wish to thank Profs. Vaclav Horak and Miklos Kertesz for valuable discussions and Gilles Frapper for technical assistance.

1. (*a*) E. Breuer. *In* Nitrones, nitronates, and nitroxides. *Edited by* E. Breuer, H. G. Aurich, and A. Nielsen. Wiley, New York, NY. 1989. pp. 139–312; (*b*) K. B. G. Torssell. Nitrile oxides, nitrones, and nitronates in organic synthesis. VCH Publishers, New York, NY. 1988; (*c*) P. DeShong, W. Li, J. W. Kennington, Jr., and H. L. Ammon. J. Org. Chem. **56**, 1364 (1991).
2. (*a*) E. G. Janzen. Methods in enzymology. Vol. 105. Academic Press, Orlando, Fl. 1984. pp. 188–198; (*b*) M. J. Perkins. Adv. Phys. Org. Chem. **17**, 1 (1980).
3. G. L. McIntire, H. N. Blount, H. J. Stronks, R. V. Shetty, and E. G. Janzen. J. Phys. Chem. **84**, 916 (1980).
4. B. J. Acken, J. A. Warshaw, D. E. Gallis, and D. R. Crist. J. Org. Chem. **54**, 1743 (1989).
5. J. A. Warshaw, D. E. Gallis, B. J. Acken, O. J. Gonzalez, and D. R. Crist. J. Org. Chem. **54**, 1736 (1989).
6. H. Lund. Organic electrochemistry. 2nd ed. *Edited by* M. M. Baizer and H. Lund. Marcel Dekker, New York, NY. 1983. pp. 293–295.
7. T. Kubota, H. Miyazaki, and Y. Mori. Bull. Chem. Soc. Jpn. **40**, 245 (1967).
8. K. Uneyama and S. Torii. J. Org. Chem. **37**, 367 (1972).
9. O. Manousek and P. Zuman. J. Chem. Soc. Chem. Commun. 158 (1965).
10. P. H. Rieger, I. Bernal, W. H. Reinmuth, and G. F. Fraenkel. J. Am. Chem. Soc. **85**, 683 (1963).
11. M. M. Baizer. Organic electrochemistry. 2nd ed. *Edited by* M. M. Baizer and H. Lund. Marcel Dekker, New York, NY. 1983. pp. 639–689.
12. R. L. Hand and R. F. Nelson. J. Am. Chem. Soc. **96**, 850 (1974).
13. (*a*) A. Stüwe and H. Baumgärtel. Ber. Bunsen-Ges. Phys. Chem. **78**, 320 (1974); (*b*) A. Stüwe, M. Weber-Schäfer, H. Baumgärtel. Ber. Bunsen-Ges. Phys. Chem. **78**, 309 (1974).
14. A. J. Bard and L. R. Faulkner. Electrochemical methods. Wiley, New York, NY. 1980. pp. 222–224.
15. P. Zuman and O. Exner. Collect. Czech. Chem. Commun. **30**, 1832 (1965).
16. H. Lund. The chemistry of the carbon nitrogen double bond. *Edited by* S. Patai, Wiley, New York, NY. 1970. p. 538.
17. (*a*) D. K. Root and W. H. Smith. J. Electrochem. Soc. **129**, 1231 (1982); (*b*) C. P. Andrieux and J. M. Saveant. J. Electroanal. Chem. **33**, 453 (1971).
18. H. Miyazaki, T. Kubota, and M. Yamakawa. Bull. Chem. Soc. Jpn. **45**, 780 (1972).
19. M. B. Kass, A. P. Borsetti, and D. R. Crist. J. Am. Chem. Soc. **95**, 959 (1973), and references therein.
20. A. Streitwieser, Jr. Molecular theory for organic chemists. Wiley, New York, NY. 1961. pp. 175–186, and references therein.
21. (*a*) A. J. Bard, J. C. Gilbert, and R. D. Goodin. J. Am. Chem. Soc. **96**, 620 (1974); (*b*) T. H. Walter, E. E. Bancroft, G. L. McIntire, E. R. Davis, L. M. Gierasch, H. N. Blount, H. J. Stronks, and E. G. Janzen. Can. J. Chem. **60**, 1621 (1982).
22. B. L. Emling, R. J. Horvath, A. J. Saraceno, E. F. Ellermeyer, L. Haile, and L. D. Hudac. J. Org. Chem. **24**, 657 (1959).
23. O. J. Gonzalez, D. E. Gallis, and D. R. Crist. J. Org. Chem. **51**, 3266 (1986).
24. (*a*) B. C. Southworth, R. Osteryoung, K. D. Fleischer, and F. C. Nachod. Anal. Chem. **33**, 208 (1961); (*b*) J. D. Littlehailes and B. J. Woodhall. J. Chem. Soc. Chem. Commun. 665 (1967).

Can. J. Chem. Downloaded from www.nrcresearchpress.com by 217.78.4.112 on 09/08/12
For personal use only.

Reactions of hydriodic acid with aldonolactones and *n*-alkanolactones. Interconversions between lactones and iodocarboxylic acids

ZHENGCHUN LIU, ALESSANDRO GRANATA, XINHUA SHEN, AND ARTHUR S. PERLIN[1]
Department of Chemistry, McGill University, Montreal, Que., Canada H3A 2A7

Received February 18, 1992

ZHENGCHUN LIU, ALESSANDRO GRANATA, XINHUA SHEN, and ARTHUR S. PERLIN. Can. J. Chem. **70**, 2081 (1992).

Aldonolactones containing from four to eight carbon atoms, and lactones of the related monohydroxy-*n*-alkanoic acids, were subjected to reaction with 57% hydriodic acid at 125°C. As in the classical studies of Kiliani, the reduction of D-*glycero*-D-*ido*-heptono-1,4-lactone yielded mainly γ-heptanolactone. Analogously, the corresponding γ-alkanolactones were obtained as major products from the 1,4-lactones of the D-xylono-, D-allono-, and D-*erythro*-L-*talo*-octono configuration. Monoiodo-*n*-alkanoic acids were also formed in admixture with the lactones in all of these reactions. D-Erythrono-1,4-lactone was unique among the aldonolactones in that it led only to an acid, i.e., 3-iodo-*n*-butanoic acid. The latter was also the product of the non-reductive reaction of hydriodic acid with β-butyrolactone whereas, by contrast, γ-butyrolactone afforded 4-iodobutanoic acid. Among compounds in the five to eight carbon series, it was found that under conditions close to equilibrium the ratio of lactone to iodoacid decreased progressively with the length of the carbon chain; e.g., in the 4 h reactions of γ-valero-, γ-capro-, γ-heptano-, and γ-octanolactone, the ratios were 2.4, 1.2, 0.2, and 0.1, respectively. An accompanying characteristic of these reactions is a progression in the number of isomeric iodoacids formed. Whereas γ-valerolactone was accompanied by 4-iodopentanoic acid, there were two isomers (4- and 5-) of iodohexanoic acid, three monoiodo- (including 6-iodo-) heptanoic acids, and four (including 7-iodo-) octanoic acids. In all instances, the isomer substituted at the penultimate carbon was major. An interplay of several individual reactions, including ring-opening displacements, eliminations–additions, and rearrangements, as well as a probable influence of entropy changes on the lactone-acid equilibria, appear to account largely for these observations.

ZHENGCHUN LIU, ALESSANDRO GRANATA, XINHUA SHEN et ARTHUR S. PERLIN. Can. J. Chem. **70**, 2081 (1992).

On a soumis des aldonolactones contenant de quatre à huit atomes de carbone ainsi que les lactones des acides monohydroxy-*n*-alcanoïques apparentés à une réaction avec de l'acide periodique à 57%, à 125°C. Comme il a été observé dans les études classiques de Kiliani, la réduction de la D-*glycéro*-D-*ido*-heptono-1,4-lactone fournit principalement la γ-heptanolactone. De la même manière, on a obtenu les γ-alcanolactones comme produits principaux à partir des 1,4-lactones de configurations D-xylono, D-allono- et D-*érythro*-L-*talo*-octono. On observe aussi la formation des acides monoiodo-*n*-alcanoïques en mélange avec les lactones obtenues dans toutes ces réactions. La D-érythrono-1,4-lactone est unique parmi les aldonolactones puisqu'elle ne fournit qu'un acide, soit l'acide 3-iodo-*n*-butanoïque. Cet acide est aussi le produit de la réaction non-réductive de l'acide hydriodique avec la β-butyrolactone alors que, par contraste, la γ-butyrolactone fournit l'acide 4-iodobutanoïque. Parmi les composés de la série contenant de cinq à huit atomes de carbone, on a trouvé que, dans des conditions proches de celles de l'équilibre, le rapport entre la quantité lactone et celle d'acide iodé diminue progressivement avec une augmentation de la longueur de la chaîne carbonée; par exemple, dans les réactions de 4 h de γ-valéro-, γ-capro-, γ-heptano- et γ-octanolactone, les rapports sont respectivement de 2,4, 1,2, 0,2 et 0,1. Une autre caractéristique de ces réactions est une progression dans le nombre des acides iodés isomères qui se forment. Alors que la γ-valérolactone est accompagnée par de l'acide 4-iodopentanoïque, il se forme deux isomères (4- et 5-) de l'acide iodohexanoïque, trois acides monoiodo (incluant le 6-iodo-) heptanoïques et quatre acides monoiodo (y compris le 7-iodo-) octanoïques. Dans tous les cas, l'isomère substitué sur le pénultième atome de carbone est l'isomère principal. Il semble que l'interaction de plusieurs réactions individuelles, y compris des substitutions avec ouverture de cycle, des éliminations avec additions et des transpositions, ainsi que l'influence probable de changement entropique sur l'équilibre lactone/acide, soient largement responsables de ces observations.

[Traduit par la rédaction]

Can. J. Chem. Downloaded from www.nrcresearchpress.com by 217.78.4.112 on 09/08/12
For personal use only.

Introduction

One of the early proofs that D-glucose is an *aldo*-hexose (**1**) is attributable to Kiliani (1), who converted the sugar via the cyanohydrin into a heptoglyconic acid (**2**), which on reduction (2) with hydriodic acid (HI), followed by zinc – hydrochloric acid, gave heptanoic acid (**3**). Only a low yield of **3** was obtained (3) from a crystalline γ-(1,4)-lactone form of **2**, i.e., **4**, whereas 60–70% of the product was γ-heptanolactone (**5**). Although this could imply that the lactone ring had remained intact, product **5** has been found subsequently[2] to be racemic, and hence the configuration at C-4 of **4** (and C-3 of **1**) is not retained in the process. This result, and a broader interest in the reactions of HI, led to the present examination of its chemistry as applied to a group of aldonolactones and also to the related lactones of monohydroxy-*n*-alkanoic acids (i.e., dihydro-2 (3*H*) furanone and several of its 5-alkyl derivatives).

Results and discussion

Compounds based on n-*butanoic acid*

Using reaction conditions similar to those in earlier studies (3), D-erythrono-1,4-lactone (**6**) was heated under reflux with 57% HI for 1 h. Extraction into methylene chloride afforded, on evaporation of solvent, a solid in 71% yield that, according to its ^1H and ^{13}C nmr spectra, consisted primarily of one compound (see Fig. 1*a* for the ^1H spectrum). Its mass spectrum indicated that the product was a monoiodobutanoic acid, and the fact that the methyl signal was a doublet (δ 2.0) and the H-3 multiplet was strongly deshielded (δ 4.4), verified that the structure is 3-iodobutanoic acid (**7**). Also consistent with the latter designation is the pair of doublet of doublets at δ ~ 3.1, attributable to diastereotopic H-2 and

[1]Author to whom correspondence may be addressed.
[2]A. S. Perlin and R. K. Hill, unpublished.

Can. J. Chem. Downloaded from www.nrcresearchpress.com by 217.78.4.112 on 09/08/12
For personal use only.

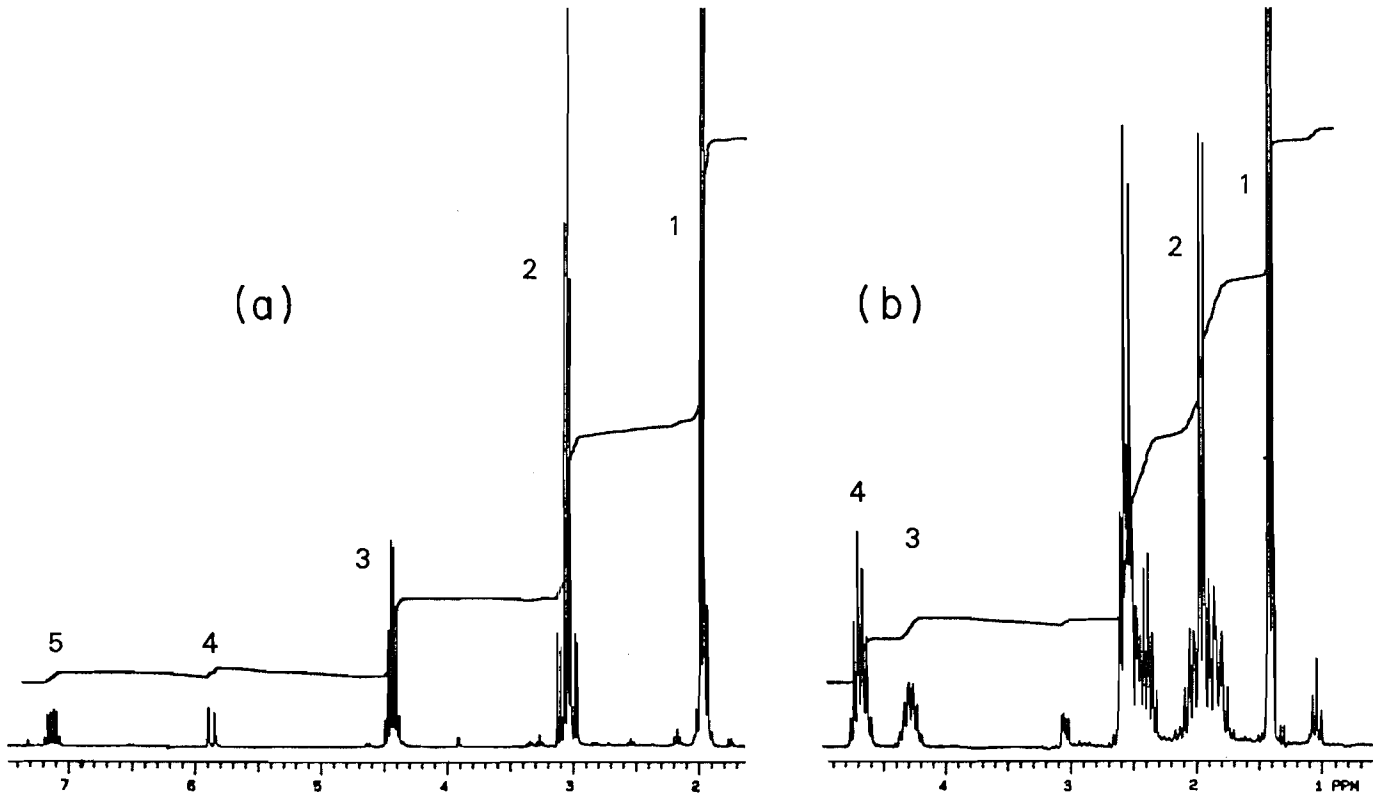

FIG. 1. The ^{1}H nmr spectra of the products (extracted into methylene chloride) from the reaction with 57% HI at 125°C of (*a*) D-erythrono-1,4-lactone (**6**) (1 h reaction); signals 1, 2, and 3 are those of CH_3, H-2,2′, and H-3, respectively, of 3-iodobutanoic acid (**7**), and signals 4 and 5 are those of H-3 and H-2, respectively, of *E*-2-butanoic acid (**12**), (*b*) γ-valerolactone (**14**) (4 h reaction); signals 1 and 4 are due to CH_3 and H-4, respectively, of **14** and signals 2 and 3 are those of CH_3 and H-4, respectively, of 4-iodopentanoic acid (**16**).

H-2′. (The two minor, downfield, signals are referred to later.)

This inference that a four-carbon lactone may be unstable, e.g., relative to the seven-carbon homolog (**5**), received support from three other experiments. First, D-erythronic acid (**8**) gave virtually the same result as **6**, as shown by its ^{1}H nmr spectrum and mass spectral data. Although some isomerization to **6** in the HI solution was to be anticipated, little or no lactone was detected in the product. Second, a similar result, i.e., a 74% yield of **7** was obtained when the reflux period was extended to 4 h. Iodide **7** also was obtained, in 92% yield, from the 1 or 4 h reaction of β-butyrolactone (**9**) with HI. Third, complete ring opening was observed with γ-butyrolactone (**10**) although, in this instance, the product was found to be 4-iodobutanoic acid (**11**), on the basis of its ^{1}H nmr spectrum, ^{13}C nmr spectrum, and mass spectrum.

Formation of the 4-iodo product (**11**) is consistent with observations on macrocyclic ω-lactones, which showed (4, 5) that ring opening with HI affords the corresponding ω-iodocarboxylic acids. The fact that the β-lactone (**9**) was converted into the 3-iodide (**7**) appears (5, 6) to be an analogous example of a ring-opening displacement reaction. However, the formation of **7** from *erythro* derivatives **6** and **8** is clearly not accommodated by the same type of mechanism. Likely, such an intermediate as 2-butenoic acid (**12**) accounts for its formation. The occurrence of **12** as a minor reaction product is shown by the relatively weak signals in Fig. 1*a* at δ 7.15 and 5.90, which are coincident in chemical shift with resonances of the known *E* isomer of **12** (confirmed by introducing some *E* isomer into the solution used to obtain Fig. 1*a*). Electrophilic addition of HI to **12** would be expected (7) to lead regioselectively to the 3-iodide (**7**). Another indication of equilibration between these two species, was the presence (^{1}H nmr evidence) of a trace proportion of **12** in admixture with **7** obtained from β-butyrolactone (**9**), whereas none of it was detected in the reaction product (**11**) of γ-butyrolactone (**10**).

Compounds based on n*-pentanoic acid*

In this series, the lactone – iodocarboxylic acid equilibrium lies mainly in favor of the cyclic form, which contrasts strikingly with that of the four-carbon compounds.

The reaction of D-xylono-1,4-lactone (**13**) with HI for 4 h afforded an oil soluble in methylene chloride, which accounted for about a 70% yield of γ-valerolactone (**14**). That is, both the ^{1}H and ^{13}C nmr spectra of the crude product consisted primarily of signals superimposable on those of authentic **14**, although the presence of minor components, including olefinic ones, was evident as well. By analogy with the comparison of the *erythrono* homologues, when D-xylonic acid (**15**) was subjected to the same reaction for 4 h, its product was indistinguishable from that of **13**. The relative stability of the γ-lactone structure in this series was verified additionally by the finding that when pure γ-valerolactone was heated with HI for 4 h, 63% of it was recovered intact although, as the ^{1}H nmr spectrum (Fig. 1*b*) shows, it was accompanied by 26% of 4-iodopentanoic acid

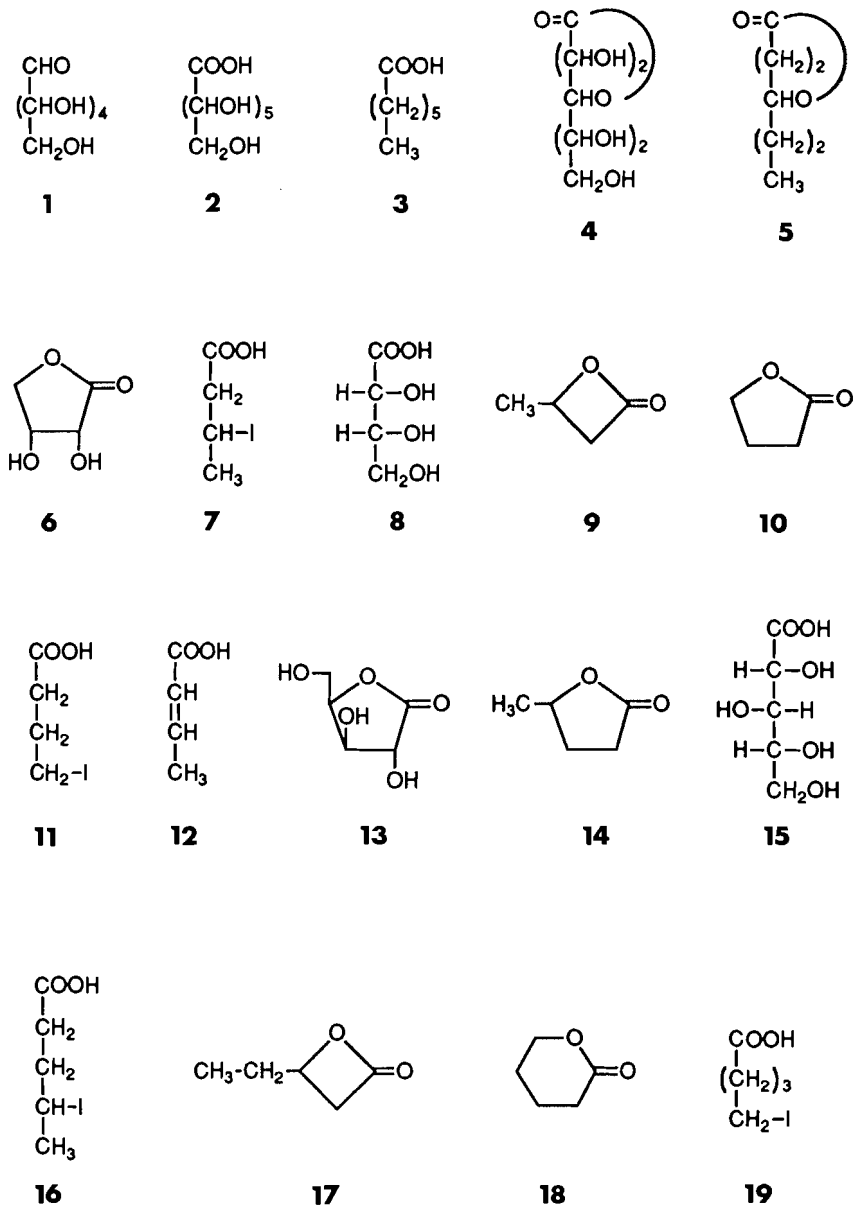

(**16**). The ratio of **14** to **16** is given by the relative intensities of their H-4 signals (δ 4.7 and 4.3, respectively), both being located relatively far downfield due to deshielding by the ring O atom (of **14**) or the I atom (of **16**). Also each CH_3 signal is a doublet, attributable to the presence of only one vicinal ^1H, the signal at δ 1.95 reflecting the particularly strong deshielding effect (~0.9 ppm) of the neighboring I atom. (An analogous signal for CH_3 of **7** is the doublet at δ 1.95 in Fig. 1*a*.) Supporting evidence for the structure of **16** was given by ^{13}C nmr data, presented later, as well as by mass spectrometry (M = 228).

Virtually the same spectrum as represented by Fig. 1*b* was obtained from the product (95% yield) of the 4 h reaction of HI with β-valerolactone (**17**). This showed that **17** had been isomerized into γ-valerolactone (**14**) and, possibly (although see later), that ~25% of the latter had undergone a ring-opening displacement to give 4-iodo-*n*-pentanoic acid (**16**).

Consistent with the reaction of other ω-lactones with HI, δ-valerolactone (**18**) afforded 5-iodopentanoic acid (**19**) in 97% yield (at both 1 and 4 h).

Compounds based on hexa-, hepta-, and octanoic acid

In the reactions of HI with lactones (other than ω) having six, seven, or eight carbon atoms, the product ratios are progressively more in favor of the iodinated carboxylic acids as the number of carbons increases. In 4 h, both D-allono-1,4-lactone (**20**) and D-glucono-1,5-lactone (**21**) (see also ref. 2) were converted into 65–67% of γ-caprolactone (**22**), accompanied by about 20% of mixed iodohexanoic acids. (Lactone **22** was also a major product of the reaction of δ-caprolactone (**23**) with HI.) With a seven-carbon example, i.e., D-*glycero*-D-*ido*-heptanoic-1,4-lactone (**24** = **4**), the yield of γ-heptanolactone (**25**) in 1–4 h was about 60%, in agreement with the earlier results reported (3). A mixture of iodocarboxylic acids made up the remaining 30–34% of the product. The corresponding yields in the reaction of D-*erythrono*-L-*talo*-octono-1,4-lactone (**26**) with HI were 46% of

Can. J. Chem. Downloaded from www.nrcresearchpress.com by 217.78.4.112 on 09/08/12
For personal use only.

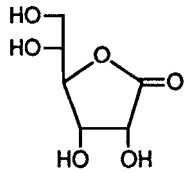
20

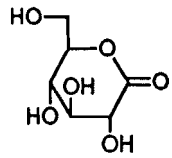
21

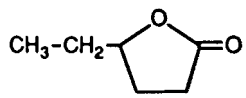
22

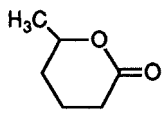
23

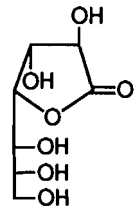
24

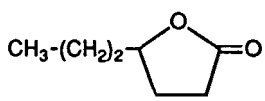
25

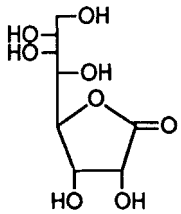
26

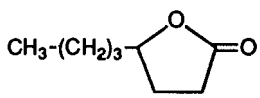
27

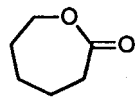
28

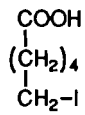
29

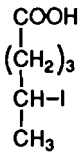
32

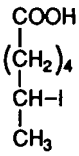
33

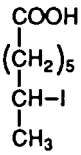
34

γ-octanolactone (**27**) and 35% of a mixture of iodocarboxylic acids.

Turning to the structurally related lactones of the monohydroxy-*n*-alkanoic acids, their reactions with HI show even more clearly the pronounced trend towards the iodoacid in the lactone–acid equilibrium. This is illustrated by ^{1}H nmr spectra of the reaction mixtures produced in 4 h from γ-caprolactone (**22**) and γ-octanolactone (**27**) (Figs. 2*a* and 2*b*, respectively). A comparison of the intensity of the lactone H-4 multiplet (δ 4.5) with that of the broad signal (δ ~4.2) attributable to a proton α to an iodine substituent, gives a lactone-to-iodocarboxylic acid ratio of 1.2 for **22**, and 0.11 for **27**; a ratio of 0.2 was found for γ-heptanolactone (**25**).

A relationship between the number of carbon atoms in the individual γ-lactones, and the percentage of those lactones remaining intact after reaction with HI for 1 h and 4 h, is depicted in Fig. 3. As most of the transformation into iodocarboxylic acid is seen to have taken place during the first period, the 4 h values must be close to equilibrium. Accordingly, the proportion of iodocarboxylic acid becomes progressively greater as the carbon chain is elongated from five to eight atoms.

Comparative data are included in Fig. 3 for the products of reduction of the aldonolactones at 4 h. When these isolated products, in turn, were subjected to reaction with fresh HI for 2 h, the percentage of lactone remaining decreased, and approached the values obtained for the alkanolactones.

*The formation of monoiodo-*n*-alkanoic acids*

Various isomeric iodo-*n*-alkanoic acids were recovered from the reaction of HI with either aldonolactones or aldonic acids, or with *n*-alkanoic lactones. As reported by others, when the lactone ring involved a primary carbon atom, the corresponding ω-iodo carboxylic acid was produced in high yield. Examples of this are described above for γ-butyrolactone and δ-valerolactone, and this also proved to be true for ε-caprolactone (**28**), which afforded 6-iodohexanoic acid (**29**). These correspond to a ring-opening displacement by iodide, as in an S_N2 type reaction. Although the conversion of β-butyrolactone into 3-iodo-*n*-butanoic acid

Can. J. Chem. Downloaded from www.nrcresearchpress.com by 217.78.4.112 on 09/08/12
For personal use only.

Can. J. Chem. Downloaded from www.nrcresearchpress.com by 217.78.4.112 on 09/08/12
For personal use only.

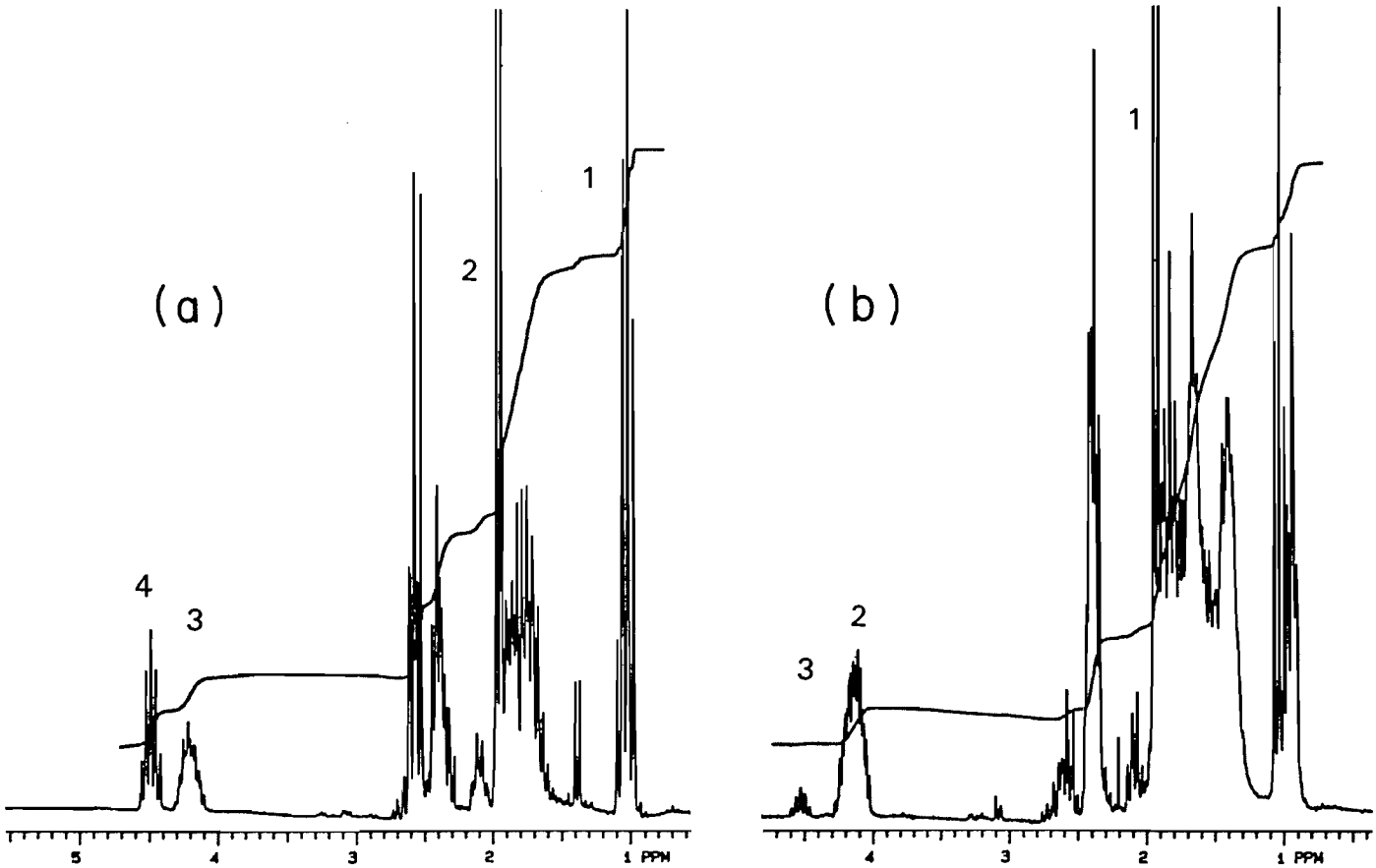

FIG. 2. The ^{1}H nmr spectra of the products (extracted into methylene chloride) from the 4 h reaction with 57% HI at 125°C of (*a*) γ-caprolactone (**22**); signals 1 and 4 are those of CH_3 and H-4, respectively of **22**, signal 2 is that of CH_3 of 5-iodohexanoic acid (**32**), and signal 3 is that of HC-I of the monoiodohexanoic acids, (*b*) γ-octanolactone (**27**); signal 1 is that of CH_3 of 7-iodooctanoic acid (**34**), signal 2 is that of HC-I of the monoiodooctanoic acids, and signal 3 is that of H-4 of **27**.

(**7**) may be accommodated in the same way, the latter was also the product of reduction of D-erythrono-1,4-lactone (as well as the acid form). Had γ-butyrolactone rather than 2-butenoic acid been an intermediate, then 4-iodo-*n*-butanoic acid should have been obtained instead.

With the presence of a fifth carbon atom in the substrate, i.e., D-xylono-1,4-lactone (**13**) (as well as the corresponding acid), the formation of an iodocarboxylic acid was now a minor event, as the preponderant product (71% in 4 h) was γ-valerolactone (**14**). When the latter was subjected to the HI reaction, it gave about 25% 4-iodopentanoic acid (**16**), in what appears to have been a ring-opening displacement. However, as seen with the D-*erythrono* homologues, the location of the iodine atom in the product is not necessarily the same as that of the lactone bridge initially. Another example of this is found in the fact that β-valerolactone (**17**) also yielded the 4-iodide (**16**) as well as γ-valerolactone (**14**) in a ratio of ~1:3. Both of these represent rearrangement products, the formation of which likely involved the 3-iodide (**30**) and perhaps an intermediate such as **31** (Scheme 1). This could account for the finding that both the iodine atom of **16** and the lactone bridge in **14** occur at a position different from that in **17**. Evidence that **30** was a transient product was obtained from ^{1}H and ^{13}C nmr spectra of the reaction components at 1 h, at which time no **17** remained and **30** was the major product. However, at 4 h the ^{1}H nmr spectrum was now essentially the same as that represented by Fig. 1*b*, showing that the final product consisted of a 2.5:1 mixture of **14** and **16**.

Analogous effects are observed in the six-carbon series: 5-iodohexanoic acid (**32**) was the major acid species produced from either D-allono-1,4-lactone (**20**) or γ-caprolactone (**22**), whereas the 4-iodo isomer constituted one third of the acid mixture. These then, are additional examples of a rearrangement accompanying the opening of the lactone ring, as is the fact that the same mixture of acids was obtained from D-glucono-1,5-lactone (**21**) and δ-caprolactone (**23**). The presence of **32** was apparent from its strong CH_3 doublet observable at δ 1.95 (Fig. 2*a*), comparable to that for the CH_3 group of **16** (Fig. 1*b*); supporting data from the ^{13}C nmr spectrum are given later.

The occurrence of isomers bearing an iodine atom at the carbon *adjacent* to the terminal methyl group is found even with the more extended *n*-alkyl chains of the 7- and 8-carbon compounds. Thus, the ^{1}H nmr spectra of the products from the aldoheptono-1,4-lactone (**24**) or γ-heptanolactone (**25**), and from the aldooctono-1,4-lactone (**26**) or γ-octanolactone (**27**) (see Fig. 2*b*), all contain a strong doublet at δ 1.95, diagnostic for the CH_3 group adjacent to the H-C-I group. This corresponds to the formation of 6-iodoheptanoic acid (**33**) and 7-iodooctanoic acid (**34**).

The absence of a 3-iodo-*n*-alkanoic acid, analogous to **7**,

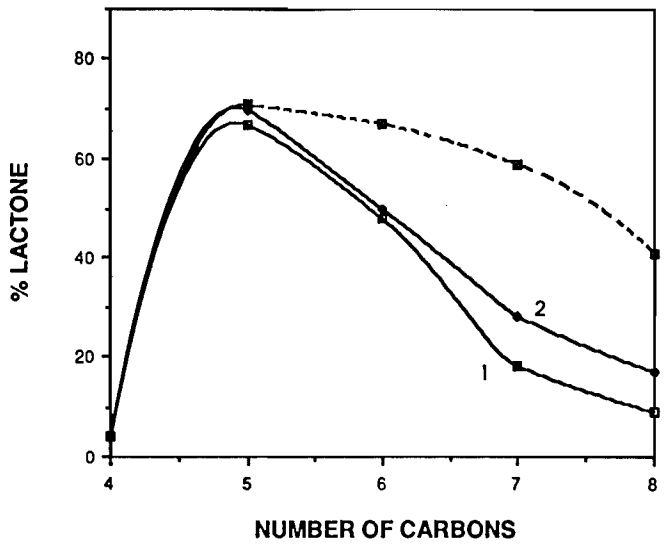

FIG. 3. (Solid lines) Percentages of the initial γ-*n*-alkanolactones, comprising from 4 to 8 carbon atoms, remaining after reaction with 57% HI at 125°C for 4 h (1) and 1 h (2). (Broken line) Comparative values for products of the HI reduction (4 h) of aldonolactones comprising from 4 to 8 carbon atoms. (Here, the joining of the points to form smooth curves is not intended to imply defined mathematical relationships between the parameters used but, rather, to highlight differences.)

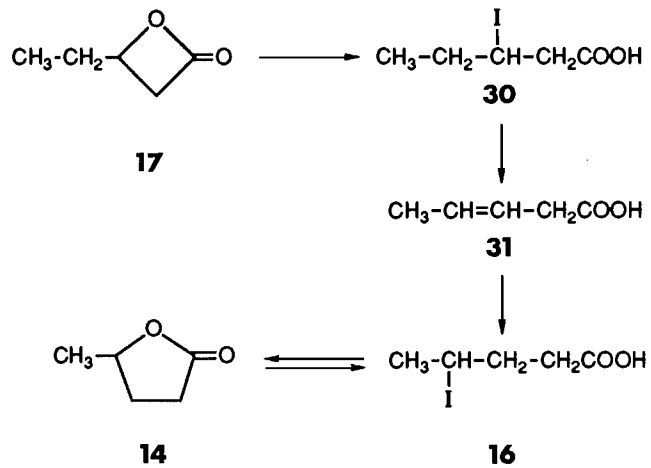

SCHEME 1

among the products from the 5 to 8-carbon aldonolactones is noteworthy in suggesting that electronic factors restrict the iodine atom to positions more remote from the carboxyl group. Whereas it is reasonable to find the iodine at position 4 of **16** in equilibrium with a γ-lactone (**14**), as in Scheme 1, migration of the iodine atom to C-5 would have required the intermediacy of the less stable, Δ-4,5 isomer of **31**, and also anti-Markovnikov addition of HI. The 5-iodocarboxylic acid (**19**) was accessible, nevertheless, through a direct displacement at C-5 of **18**, and hence was not accompanied by rearrangement products.

In the 6-carbon series, the formation of γ-caprolactone (**22**) from δ-lactones **21** and **23** finds precedence in many rearrangements of the δ- to the more stable γ-lactones (see, e.g., ref. 8). However, the occurrence of 5-iodohexanoic acid (**32**) among the products from the γ- as well as the δ-lactones is noteworthy. By analogy with Scheme 1, 4-iodohexanoic acid and 4-hexenoic acid could be feasible intermediates in the formation of **32**, and the fact that there was more of the latter present than of the 4-iodo isomer, may indicate the occurrence of competitive lactone-ring closure reactions in which an iodo substituent on C-4 is more frequently displaced than one on C-5.

More unexpected is the appearance of the 6-iodo- (**33**) and 7-iodo- (**34**) carboxylic acids as major species admixed with γ-heptanolactone (**25**) and γ-octanolactone (**27**), respectively, as well as among the products of the reaction of aldonolactones **24** and **26** with HI. That is, it is unclear why an iodine atom should appear at a location beyond C-4 or C-5, because those positions correspond to the more probable outcome of ring-opening and -closing displacement reactions envisaged for γ- and δ-lactones, respectively.

In all these instances, isomeric iodocarboxylic acids were present in minor proportions. Evidence for the co-occurrence of the minor isomers was most clearly afforded by ^{13}C nmr spectra (see later), based on the total number of resolved ^{13}C resonances and their relatively low intensities. The hexanoic acids were found to comprise a 2:1 mixture of the 5-iodo- (**32**) and 4-iodo isomers, whereas heptanoic and octanoic acid derivatives **33** and **34** were both accompanied by at least two, lesser, isomeric iodides. As would be expected, these minor products were characterized by relatively weak ^{13}C signals in the region δ 13.4–14.3 (and also ^{1}H signals at δ ~1.0), diagnostic for species in which the CH_3 group is more remote from the iodine atom than in **32**, **33**, or **34**. Most likely, therefore, they are 4- and 5-iodoheptanoic acids and 4-, 5-, and (or) 6-iodooctanoic acids.

It is worth noting that none of the parent, non-iodinated, *n*-alkanoic acids were detected among the reaction products. Although this appears to be at variance with the earlier reports (1–3) of such products as *n*-heptanoic acid (**3**), those studies involved an additional step in which the material isolated from the HI reaction was subjected to reduction with zinc/hydrochloric acid (1, 2) or catalytic hydrogenation (3), which would have displaced iodine atoms.

Overall, then, whereas only one secondary iodocarboxylic acid isomer is feasible in the 4-carbon (3-iodo, **7**) and 5-carbon (4-iodo, **16**) series, the higher homologues allow for isomeric secondary iodide structures. This helps to accommodate the formation of *two* 6-, *three* 7-, and *four* 8-carbon isomers. A related characteristic is the striking tendency for migration of the iodine atom toward the penultimate carbon of the carboxylic acid chain, which occurs to a lesser extent as the chain length increases. As to how far from the carboxyl group this tendency occurs remains to be determined, as well as if it also applies for the other halogens. Undoubtedly, the relatively severe conditions that these reactions with HI entail are conducive to extensive rearrangements, as well as to racemization and some decomposition of the aldonolactones.[3] Olefinic products, de-

[3]However, an example of a lactone that is relatively unaffected under these conditions is 3,3-dimethyl-2-hydroxy-γ-butyrolactone (pantolactone) (**35**). In contrast to the quantitative ring-opening reaction of γ-butyrolactone, two thirds of **35** was recovered after treatment for 1 h and 4 h. The product was the 4-iodoacid (**36**), which suggested that the *gem* dimethyl structure hindered not only the displacement at C-4, but also reduction of the hydroxyl group. Even more resistant was the "γ-butyrolactone" ring incorporated within norbornane derivative **37**.

Can. J. Chem. Downloaded from www.nrcresearchpress.com by 217.78.4.112 on 09/08/12
For personal use only.

TABLE 1. ^{13}C chemical shifts for monoiodo derivatives of *n*-alkanoic acids

Carboxylic acid	δ, carbon no. 1	2	3	4	5	6	7	8
Butanoic	179.6	36.3	18.5	13.4				
3-iodo (**7**)	177.0	48.0	17.3	29.0				
4-iodo (**11**)	179.5	34.8	28.3	5.3				
Pentanoic	179.7	34.1	27.0	22.0	13.5			
4-iodo (**16**)	175.1	34.5	37.6	28.8	29.1			
5-iodo (**19**)	180.6	33.2	25.7	32.8	6.0			
Hexanoic	181.0	34.5	25.2	32.6	23.7	14.8		
4-iodo	176.5	34.0	35.0	40.0	34.2	13.4		
5-iodo (**32**)	178.3	32.2	28.9	41.1	29.7	29.1		
6-iodo (**29**)	180.9	34.1	23.8	30.1	33.3	6.6		
Heptanoic	181.1	35.1	26.0	30.5	33.7	24.2	15.4	
6-iodo (**33**)	179.6	(42.1	40.6	33.6	32.9	29.6	28.7)	
4- and 5-iodo	(179.3[a]	39.0	33.4	28.9	24.4	23.5	13.0)	
	(178.5[b]	42.4	37.5	34.9	24.0	22.5	13.5)	
Octanoic								
7-iodo (**34**)	181.0	42.7	40.0	34.2	30.7	29.6	29.1	24.6
4-, 5-, and 6-iodo	180.8							14.3
	180.5			16 signals between δ 41.9 and 22.1				14.2
	179.9							13.4

[a]Signals of lower intensity than those of **33**.
[b]Signals of lowest intensity.

tected in some instances, may be involved as intermediates, although such other possibilities as rearrangements of transient carbocations (or, perhaps, free radicals) may be envisaged as well. The possibility that there are several competing reactions is strengthened by a different type of observation: when a specimen of δ-valerolactone (**23**) deuterated at C-5 (by deuteride reduction of the corresponding 5-ketoacid), was subjected to reaction with HI for 4 h, about 50% of the deuterium was exchanged (MS evidence).

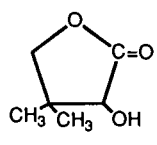

35

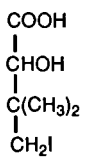

36

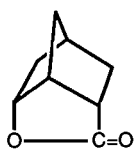

37

Finally, the progressive decrease observed in the ratio of lactone to iodocarboxylic acid with lengthening of the carbon chain may reflect incremental increases in entropy associated with greater numbers of isomeric iodoacid species generated in the lactone–acid equilibria.

^{13}C nuclear magnetic resonance spectral data

This source of information was particularly helpful for the detection and identification of the iodocarboxylic acids. In many instances, the ^{13}C assignments were facilitated by use of the DEPT technique (9).

An iodine substituent introduces distinctive shielding characteristics, some of which have been recognized (10, 11) with other classes of compounds. For example, C-3 and C-4 of 4-iodo-*n*-butanoic acid (**11**) resonate *down*field (by 10 ppm) and *up*field (by 8 ppm), respectively of the corresponding nuclei of butanoic acid (Table 1). Similarly, these opposing effects are found for pentanoic acid and its 5-iodo derivative (**19**), as well as hexanoic acid and its 6-iodide (**29**).

Verification of the structure of 3-iodobutanoic acid (**7**) was provided by evidence (DEPT) that the signals at δ 17.3 and 29.0 (Table 1) are due to methine and methyl groups, respectively. Hence, the presence of an iodine atom at C-3 causes only a small increase in shielding, relative to the C-3 of butanoic acid, whereas the neighboring ^{13}C nuclei experience strong deshielding, by 12 ppm (C-2) and 15 ppm (C-4). In 4-iodopentanoic acid (**16**) the effect of the halogen atom is deshielding, not only for C-3 and C-5, but also for C-4.

Two secondary iodo isomers of hexanoic acid were recognized, in a ratio of ~2:1. The group of major signals was assigned to the 5-iodo isomer (**32**), because the appropriate methyl ^{13}C is strongly deshielded (relative to *n*-hexanoic acid), and hence is adjacent to the methine ^{13}C (C-5). By contrast, the chemical shift of the smaller methyl signal (δ 13.4) is consistent with a CH_3CH_2 structure, and that of the methine ^{13}C with the expectation that C-4 contains the substituent.

There are a total of 20 resolved signals in the spectrum of the product mixture obtained from γ-heptanolactone (**25**) (in addition to minor signals of the lactone), corresponding to three isomeric iodo-*n*-heptanoic acids in a ratio of about 1.5:1.0:0.5. Among the minor signals are two, at δ 13.5 and 13.0, which identifies their origin as $^{13}CH_3CH_2$ groups. However, as all of the major signals appear below δ 28, they must be due to the 6-iodo derivative (**33**), containing a CH_3CHI arrangement for which ^1H data have already been cited. As the individual resonances have not all been assigned, the chemical shifts are listed (Table 1) only according to sets for each isomer.

A similar assessment of the ^{13}C spectrum of the 8-carbon product mixture points to the co-occurrence of four isomeric iodocarboxylic acids. Aside from minor signals due

Can. J. Chem. Downloaded from www.nrcresearchpress.com by 217.78.4.112 on 09/08/12
For personal use only.

to γ-octanolactone (**27**), the spectrum contains 30 resolved resonances out of the 32 required, and their integral values correspond to an isomer ratio of roughly 2:1:1:1. Once again, the minor species were found to possess terminal CH_3CH_2 structures by virtue of their upfield $^{13}CH_3$ resonances, at δ 14.3, 14.2, and 13.4. By elimination, the major set of signals, all of which are found downfield of δ 24, is alloted to the 7-iodo isomer (**34**).

Experimental

Nuclear magnetic resonance spectra were recorded with a Varian XL-200, XL-300, or Gemini 200 spectrometer, operating at 200 MHz or 300 MHz for ^1H, and 50 MHz for ^{13}C. The solvent was $CDCl_3$, and chemical shifts are given with respect to the signal for internal Me_4Si (δ 0.0). Chemical ionization mass spectra were obtained with isobutane as the ionization reagent. Extracts of reaction mixtures were concentrated under diminished pressure at a bath temperature of 40°C. Hydriodic acid (57%) was obtained from Aldrich Chemical Co., as also were samples of β- and γ-butyrolactone, γ- and δ-valerolactone, γ-caprolactone, 5-ketohexanoic acid, ε-caprolactone, and γ-octanolactone. The aldonolactones were prepared by established procedures. Potassium D-erythronate and ammonium D-xylonate were obtained from Pfanstiehl Laboratories, Waukegan, Ill.

Representative of reactions of the lactones with HI are the following:

*Reaction of D-erythrono-1,4-lactone (**6**) with hydriodic acid*

A solution D-erythrono-1,4-lactone (0.60 g, 5.0 mmol) in hydriodic acid (57%, 5 mL) was heated under reflux at 125°C for 1 h. Saturated aqueous NaCl (10 mL) was added after cooling to room temperature and the mixture was extracted into dichloromethane (50 mL). The organic layer was washed successively with saturated aqueous $Na_2S_2O_3$ (10 mL) and saturated aqueous NaCl (3 × 10 mL), dried (anhydrous $MgSO_4$), and concentrated. The dark, solid, residue was recrystallized from dichloroethane – petroleum ether, affording yellow crystals (0.77g, 71%); mp 35–36°C; $[\alpha]_D$ +1.4 (4.6 *c*, $CHCl_3$). ^{13}C nmr data are given in Table 1. The ^1H nmr spectrum of the crude product extracted is shown in Fig. 1*a*; the introduction of authentic *E*-crotonic acid produced an increase in the relative intensities of the signals at σ 7.15 and 5.85. EI-mass spectrum: *m/z* 214 [M, 22.3%], *m/z* 127 [I, 25.0%], *m/z* 87 [(M − I), 100%].

*Reaction of D-allono-1,4-lactone (**20**) with HI*

A solution of the lactone (0.60 g, 3.3 mmol) in HI (57%, 5 mL) was heated under reflux for 4 h. After being cooled to room temperature the reaction mixture was processed as described for **6**. The dichloromethane extract afforded a reddish-brown oil (0.44 g, 88%), which, according to its ^1H and ^{13}C nmr spectra (see Fig. 1*b* and Table 1), consisted primarily of a mixture of γ-caprolactone (**22**) (67%), 5-iodohexanoic acid (**32**) (14%), and 4-iodohexanoic acid (7%). CI-mass spectrum: *m/z* [(M + H, iodoacid), 9.3%], *m/z* 115 [(M + H, lactone and (or) M iodoacid-I), 100%].

*Reaction of γ-octanolactone (**27**) with HI*

A solution of the lactone (0.60 g, 4.2 mmol) in HI (57%, 5 mL) was heated under reflux for 4 h, and the reaction mixture was processed as described for compound (**20**). The dichloromethane extract afforded a yellow oil (1.16 g, 98%), which, according to the ^1H and ^{13}C nmr spectra (see Fig. 2*b* and Table 1) consisted primarily of the lactone (**27**) (9%) and a mixture of monoiodooctanoic acids (89%). CI-mass spectrum: *m/z* 271 [(M + H, iodoacid), 12.2%], *m/z* 143 [(M + H, lactone and (or) M iodoacid-I), 100%].

*5-Iodo-*n*-pentanoic acid (**19**)*

Isolated, as above, from the reaction of δ-valerolactone (**18**) in 90% yield (1.2 g); yellow crystals, mp 59–60°C (lit. (5) mp 58°C); ^{13}C nmr data are given in Table 1.

CI-mass spectral data for iodoacids produced from aldonolactones and δ-caprolactone-5-^2H

D-Xylono-1,4-lactone: *m/z* 229 [(M + H), 15.7%]

D-Glucono-1,4-lactone: *m/z* 243 [(M + H), 4.6%]

D-*Glycero*-D-*ido*heptono-1,4-lactone: *m/z* 257 [(M + H), 2.5%]

D-*Erythro*-L-*talo*octono-1,4-lactone: *m/z* 271 [(M + H), 12.0%]

δ-Caprolactone-5-^2H: *m/z* 244 [(M + H, 6.1%)], 243 [(M − 50% ^2H + H), 61%], 116 [(M − HI), 93.6%], 115 [(M − 50% ^2H − HI), 100%].

Acknowledgements

Generous support by the Natural Sciences and Engineering Research Council of Canada, and McGill University, is gratefully acknowledged. We also thank Jick Chin for very helpful discussion.

1. H. Kiliani. Ber. **19**, 767 (1886); **19**, 1128 (1886).
2. H. Kiliani and S. Kleeman. Ber. **17**, 1296 (1884).
3. A. S. Perlin and C. B. Purves. Can. J. Chem. **31**, 227 (1953).
4. W. H. Kruizinga and R. M. Kellogg. J. Am. Chem. Soc. **103**, 5183 (1981).
5. G. A. Olah, R. Karfeles, and S. C. Narang. Synthesis, 963 (1982).
6. E. Keinan and M. Sahai. J. Org. Chem. **55**, 3922 (1990).
7. T. Sakai, K. Miyata, M. Utaka, and A. Takeda. Bull. Chem. Soc. Jpn. **60**, 1063 (1987).
8. J. T. Edward, E. Cooke, and T. C. Paradellis. Can. J. Chem. **59**, 597 (1981).
9. D. M. Doddrell, D. T. Pegg, and M. R. Bendall. J. Magn. Reson. **48**, 323 (1982).
10. W. M. Litchman and D. M. Grant. J. Am. Chem. Soc. **90**, 1400 (1968).
11. J. B. Stothers, Carbon-13 NMR spectroscopy. Academic, New York. 1972. pp. 128–137.

Can. J. Chem. Downloaded from www.nrcresearchpress.com by 217.78.4.112 on 09/08/12
For personal use only.

Preparation and NMR spectra of $PF_4(N\text{-}N)^+$ and $SiF_4(N\text{-}N)$, where N-N = 2,2′-bipyridine, 4-fluoro-2,2′-bipyridine, and 1,10-phenanthroline

TUAN Q. NGUYEN, FANQI QU,[1] XIAOLING HUANG,[1] AND ALEXANDER F. JANZEN[2]
Department of Chemistry, University of Manitoba, Winnipeg, Man., Canada R3T 2N2

Received January 2, 1992

TUAN Q. NGUYEN, FANQI QU, XIAOLING HUANG, and ALEXANDER F. JANZEN. Can. J. Chem. **70**, 2089 (1992).

Cationic complexes $PF_4(N\text{-}N)^+$, where N-N = 2,2′-bipyridine (bpy), 4-fluoro-2,2′-bipyridine (fbpy), and 1,10-phenanthroline (phen), were prepared in modest yield and identified by their A_2B_2 and A_2BC fluorine NMR spectra, which are similar to those of the isoelectronic $SiF_4(N\text{-}N)$ adducts. The ligands bpy, fbpy, and phen may be useful for monitoring reactions of HF and H_2O, or other fluorinated compounds, with glass apparatus because any liberated SiF_4 is then trapped as $SiF_4(N\text{-}N)$, which can be readily detected by NMR spectroscopy.

TUAN Q. NGUYEN, FANQI QU, XIAOLING HUANG et ALEXANDER F. JANZEN. Can. J. Chem. **70**, 2089 (1992).

On a préparé les complexes cationiques $PF_4(N\text{-}N)^+$, dans lesquels N-N = 2,2′-pyridine (bpy), 4-fluoro-2,2′-bipyridine (fbpy) et 1,10-phénanthroline (phen), avec de modestes rendements et on les a identifiés par leurs spectres RMN A_2B_2 et A_2BC du fluor qui sont semblables à ceux des adduits isoélectroniques $SiF_4(N\text{-}N)$. Dû au fait que tout SiF_4 libéré peut être piégé sous la forme de $SiF_4(N\text{-}N)$ que l'on peut facilement détecter par spectroscopie RMN, les ligands bpy, fbpy et phen peuvent être utiles pour suivre les réactions du HF, de l'eau ou d'autres composés fluorés avec les appareils de verre.

[Traduit par la rédaction]

Fluorophosphonium cations PF_4^+, RPF_3^+, $R_2PF_2^+$, R_3PF^+, and $PF_4(donor)_2^+$ are known (1), but a reported reaction between PF_5 and phenanthroline did not give the expected cation $PF_4(phen)^+$ (2), although $PCl_4(phen)^+$ is stable (2, 3). We have studied the reaction of PF_5 with bidentate ligands N-N, where N-N = 2,2′-bipyridine (bpy), 4-fluoro-2,2′-bipyridine (fbpy), and 1,10-phenanthroline (phen), in an attempt to identify the $PF_4(N\text{-}N)^+$ cation. During the course of this work it was observed that extraneous reactions with glass apparatus produced $SiF_4(N\text{-}N)$; its convenient detection by NMR provides a way of monitoring the reactions of fluorinated compounds with glassware.

The synthesis of 4-fluoro-2,2′-bipyridine (fbpy) was carried out in four stages and fbpy was characterized by means of mass spectrometry, ^{15}N (4), ^{19}F, ^{13}C, ^1H NMR, and by its reactions with iron and cobalt salts (4).

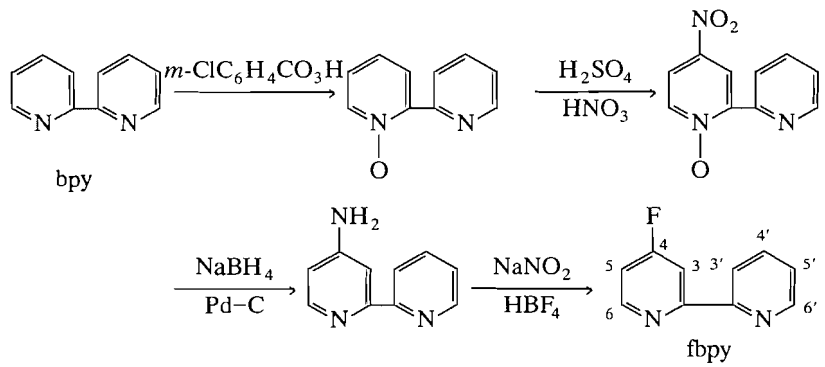

When the reaction of PF_5 with bidentate ligands bpy, fbpy, and phen was carried out in dichloromethane solution, using a glass vacuum line and a glass reaction tube with a PTFE insert, it was found that the cation $PF_4(N\text{-}N)^+$ was prepared in yields of 10–20%. The cations were identified

$$2PF_5 + N\text{-}N \xrightarrow[CH_2Cl_2]{-196 \text{ to } 25^\circ C} PF_4(N\text{-}N)^+PF_6^-$$

(10–20% yield) N-N = bpy, fbpy, phen

by ^{19}F NMR (Table 1) and showed an A_2B_2 spin system for $PF_4(bpy)^+$ and $PF_4(phen)^+$ and an A_2BC pattern for $PF_4(fbpy)^+$, consistent with an octahedral structure of the cation.

The isoelectronic adducts $SiF_4(N\text{-}N)$ were prepared in essentially quantitative yield and their NMR spectra are in agreement with the assignments for $PF_4(N\text{-}N)^+$ (Table 1).

$$SiF_4 + N\text{-}N \xrightarrow[CH_2Cl_2]{-196 \text{ to } 25^\circ C} SiF_4(N\text{-}N)$$

N-N = bpy, fbpy, phen

The crystal structure and the ^{19}F NMR and infrared spectra of $SiF_4(bpy)$ have been reported previously (5). Al-

[1]Visiting scientist. Permanent address: Department of Chemistry, Wuhan University, Wuhan, China.
[2]Author to whom correspondence may be addressed.

Can. J. Chem. Downloaded from www.nrcresearchpress.com by 217.78.4.112 on 09/08/12
For personal use only.

TABLE 1. ^{19}F NMR data of $SiF_4(N\text{-}N)$ and $PF_4(N\text{-}N)^+$, where N-N = bpy, fbpy, and phen[a]

Compound	F spin system	F^A	F^B	F^C	F(fbpy)	$^2J(F^AF^B)$	$^2J(F^AF^C)$	$^2J(F^BF^C)$	$^1J(F^AM)$	$^1J(F^BM)$	$^1J(F^CM)$	Solvent
$SiF_4(bpy)$[b]	A_2B_2	−120.4	−143.9			14			161	141		DMSO
$SiF_4(phen)$	A_2B_2	−120.1	−144.9			17			158	142		DMSO
$SiF_4(fbpy)$[c]	A_2BC	−120.1	−143.3	−144.0	−91.4	14	14	28	161	141	142	DMSO
$PF_4(bpy)^+$	A_2B_2	−52.5	−80.3			62			844	825		DMSO
$PF_4(phen)^+$	A_2B_2	−50.8	−81.5			65			867	833		CD_3CN
$PF_4(fbpy)^+$	A_2BC	−51.3	−79.9	−80.7	−77.9	62	62	62	846	825	827	CD_3CN

[a]Recorded on Bruker AM300 NMR spectrometer. Chemical shifts in ppm and coupling constants in Hz; internal reference is C_6F_6 (−162.9 ppm).
[b]^{29}Si NMR (DMSO): −176 ppm.
[c]^{29}Si NMR (DMSO): −176 ppm.

though the symmetry of the octahedral complexes allows a unique assignment of the F^A ligands, the assignment of F^B versus F^C in $PF_4(fbpy)^+$ and $SiF_4(fbpy)$ remains uncertain.

The reaction of SiF_4 with bpy, fbpy, and phen occurs on warming the reaction mixture from −196 to 25°C, and the mechanism of formation of $SiF_4(bpy)$ was described recently by the coordination model of reaction mechanisms (6) as a two-step pathway, P(4,2), in which the first step is viewed as a diffusion-controlled formation of a five-coordinate SiF_4–bpy adduct, followed by a rapid entropy-favoured five-center step to give the six-coordinate adduct $SiF_4(bpy)$, as illustrated in Scheme 1.

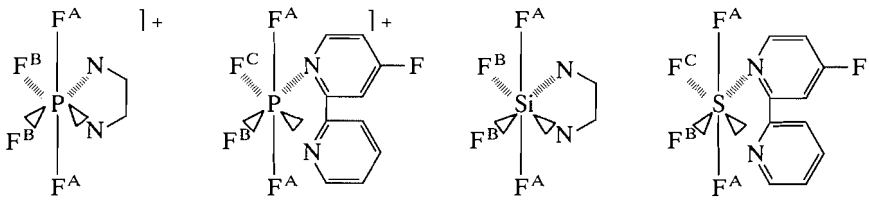

N-N = bpy, phen

N-N = bpy, phen

It is reasonable to propose a similar path for the formation of $PF_4(N\text{-}N)^+$, except that a fluorine ligand must be transferred, presumably via a fluorine-bridged intermediate, as shown in Scheme 2.

The formation of $PF_4(N\text{-}N)^+$ also occurs on warming the reaction mixture from −196 to 25°C but, as seen in Scheme 2, this reaction involves cleavage of a bridging P—F—P bond; however, such cleavage of bridging bonds in phosphorus fluorides is known to be a rapid process, even on the NMR time scale (7). Numerous other four- and five-coordinate metal halides react with bidentate ligands (8) in a manner entirely analogous to that proposed for SiF_4 and PF_5; consequently, pathways P(4,2) and P(8,4) may also be proposed for these reactions.

$$MX_4 + L\text{-}L \rightarrow X_4M(L\text{-}L)$$

$$2MX_5 + L\text{-}L \rightarrow X_4M(L\text{-}L)^+MX_6^-$$

^{31}P and ^{19}F NMR examination showed that the formation of $PF_4(N\text{-}N)^+$ was accompanied by the following products: $(N\text{-}NH)^+PF_6^-$, $F_2P(O)OH$, $FP(O)(OH)_2$, $P(O)(OH)_3$, $SiF_4(N\text{-}N)$, and BF_4^-, thus demonstrating that reaction with glass and moisture was the major reason for the low yield (10–20%) of formation of $PF_4(N\text{-}N)^+$. These reactions were carried out in Teflon-lined tubes; however, PF_5 was handled in a glass vacuum line and there was partial exposure to glass valves during the reaction. Once formed, the cation $PF_4(N\text{-}N)^+$ is stable in the reaction mixture.

No ligand exchange was observed when fbpy was added to $SiF_4(fbpy)$ nor when $SiF_4(fbpy)$ was added to $SiF_4(phen)$,

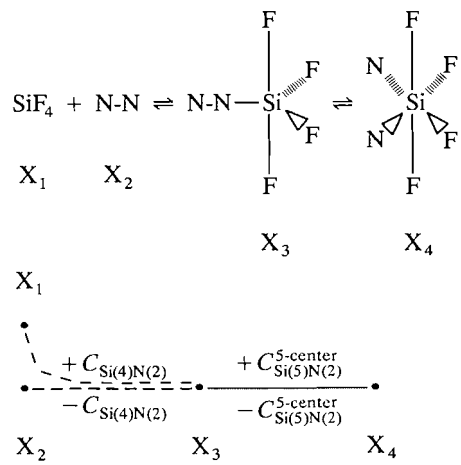

SCHEME 1. Proposed mechanism[3] of reaction of SiF_4 and N-N. Minimum set of CN: Si(4) Si(5) Si(6) N(2) N(3); pathway P(4,2).

nor was there line-broadening in the ^{19}F NMR spectrum of $SiF_4(N\text{-}N)$ or $PF_4(N\text{-}N)^+$ in DMSO solution if 1 equivalent of H_2O, CF_3COOH, or PhCOOH was added. Ligand

[3]Graph P(*X*,*C*) consists of a vertex set *X* of reactants, intermediates, and products, and an edge set *C* consisting of coordination number operators +C, −C, $+C^C$, and $-C^C$, which are drawn above the edges for forward steps and below for reverse steps; dashed lines refer to intermolecular steps and solid lines to intramolecular steps, as described previously (6).

Can. J. Chem. Downloaded from www.nrcresearchpress.com by 217.78.4.112 on 09/08/12
For personal use only.

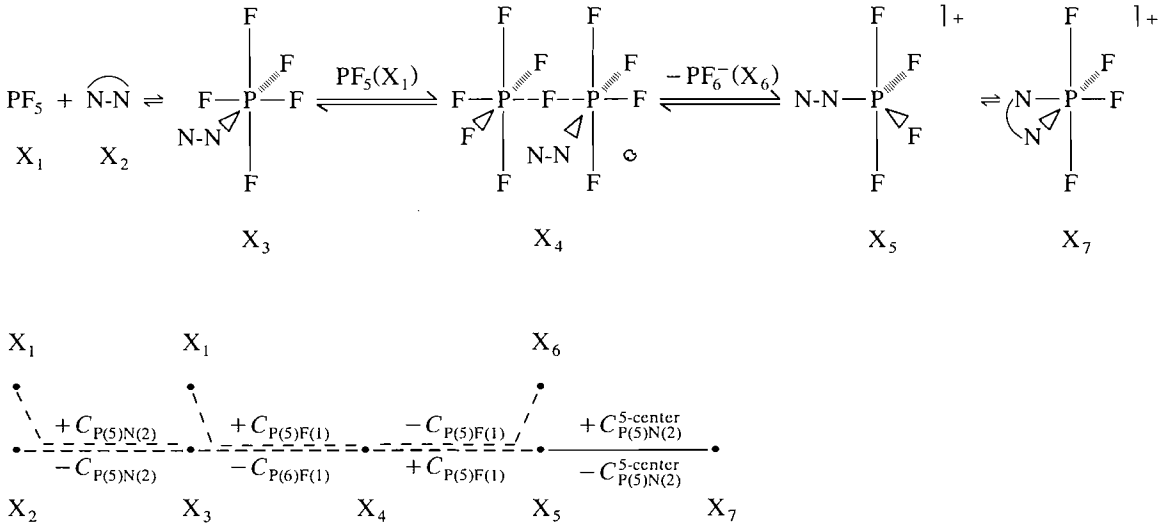

SCHEME 2. Proposed mechanism[3] of formation of $PF_4(N\text{-}N)^+PF_6^-$. N-N is bpy, fbpy, or phen; minimum set of CN: P(5) P(6) N(2) N(3) F(1) F(2); pathway P(8,4).

exchange did occur when excess PF_5 was added to $PF_4(N\text{-}N)^+PF_6^-$ in CH_2Cl_2 solution, but rapid fluorine exchange occurred only between anionic PF_6^- and PF_5, a known process (7), but not between cationic $PF_4(N\text{-}N)^+$ and PF_5, and this difference, as well as the fluorine transfer step of Scheme 2, may be attributed to the selective cleavage of bridging P—F—P bonds in the postulated intermediates, as shown below.

It was found that exchange between PF_6^- and excess PF_5 could be observed in CD_3CN, but not in DMSO solution, and this may be attributed to the relative stability of the PF_5 (solvent) adducts; dissociation of $PF_5(NCCD_3)$ gives free PF_5, however, the PF_5(DMSO) adduct is more stable and therefore PF_5 is not available for exchange with PF_6^-. Exchange between $PF_5(NCCH_3)$ and PF_6^- was also observed by Il'in and co-workers in their study of the interaction of PF_5 with phosphorus oxides (9). The NMR spectra of bpy and phen complexes, but not those of fbpy complexes, were therefore generally recorded in DMSO solution.

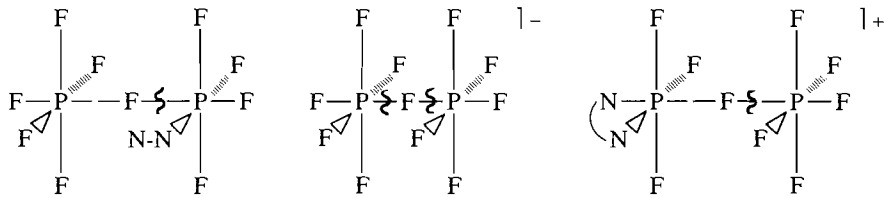

On adding DMSO to the reaction mixture containing $PF_4(fbpy)^+$, there was immediate loss of the fluorine substituent from the bound fbpy ligand and the appearance of a new A_2BC ^{19}F NMR spectrum assigned to $F_4P(Xbpy)^+$; furthermore, any SiF_4(fbpy) was also converted to SiF_4(Xbpy), but the identity of X was not established.

The fluorine chemical shift of free fbpy (−103.2 ppm) differs significantly from that of bound fbpy, e.g., SiF_4(fbpy) (−91.4 ppm) or $PF_4(fbpy)^+$ (−77.9 ppm), and it was possible to show in a qualitative way that adduct formation occurs in 3:1 mixtures of fbpy/$SbCl_5$ (−95 ppm), fbpy/$SnCl_4$ (−87.6 ppm), fbpy/SnI_4 (−87.8 ppm), and fbpy/SiI_4 (−94 ppm), all in acetone solution, and fbpy/$TeCl_4$ (−95 ppm) in $CH_3NO_2/CDCl_3$ solution, but the stoichiometry of the adducts was not investigated further.

Borosilicate glass, Lewis acids, and halogen-bridged intermediates

When alcohols and water are handled in Pyrex or quartz vessels, boron and silicon esters and their hydrolysis products are usually present (10); furthermore, hydrogen fluoride and water, even in minute amounts, also react with borosilicate glass to produce boron and silicon fluorides and removal of these impurities can stop ligand exchange or isomerization reactions of various fluorinated compounds (11).

In some previous NMR studies of ligand exchange, we attempted to identify trace amounts of glass-produced boron and silicon fluorides but, although BF_4^- can be readily detected by NMR because of the characteristic $^{11}BF_4^-/^{10}BF_4^-$ pattern, it is difficult to detect small amounts of silicon fluorides because these compounds can undergo a variety of fluorine exchange processes involving SiF_4, SiF_5^-, SiF_6^{2-}, $SiF_4(donor)_2$ and $SiF_5(donor)^-$(12, 13), which complicates the positive identification of silicon fluorides in solution.

It was therefore of interest to find in this study that during the reactions of PF_5 with bpy, fbpy, and phen, small amounts of SiF_4(bpy), SiF_4(fbpy), and SiF_4(phen), along with BF_4^-, were invariably present, although glass was the only source of silicon and boron in these reactions. These $SiF_4(N\text{-}N)$ complexes are all "rigid" on the NMR time scale,

Can. J. Chem. Downloaded from www.nrcresearchpress.com by 217.78.4.112 on 09/08/12
For personal use only.

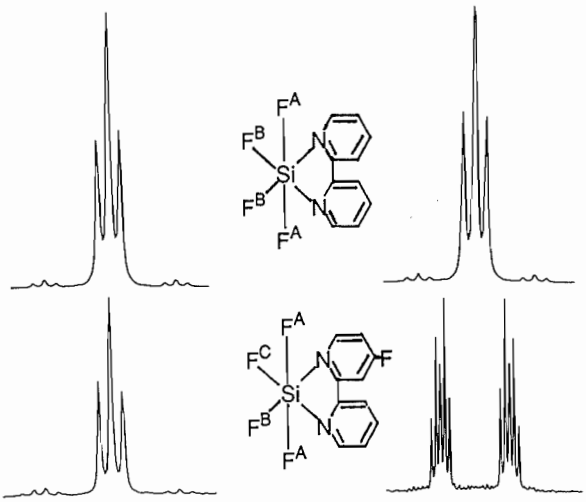

FIG. 1. The A_2B_2 ^{19}F NMR spectrum of SiF_4(bpy) (top) and the A_2BC spectrum of SiF_4(fbpy) (bottom) in DMSO-d_6 solution, recorded on a Bruker AM300 NMR spectrometer. Chemical shifts and coupling constants are given in Table 1.

and fluorine exchange does not interfere with identification by NMR. Therefore, in those reactions involving cleavage of element–halogen bonds, where Lewis acids and halogen-bridged intermediates are suspected (6, 11), but where glass may be the only source of silicon or boron Lewis acids, it may be possible to add small amounts of bidentate ligands such as bpy, fbpy, or phen to a reaction mixture and then use fluorine NMR to detect SiF_4(N-N), along with BF_4^-. Typical A_2B_2 and A_2BC fluorine NMR spectra of SiF_4(bpy) and SiF_4(fbpy) are shown in Fig. 1. For the detection and positive identification of small amounts of SiF_4 by this method, we have carried out parallel reactions using bpy and fbpy and then recorded each ^{19}F NMR spectrum in proton-coupled and proton-decoupled mode on a 300 MHz NMR spectrometer.

Experimental

General

The ^1H, ^{19}F, ^{13}C, ^{29}Si, and ^{31}P NMR spectra were recorded on a Bruker AM300 spectrometer using TMS, C_6F_6(−162.9 w.r.t. $CFCl_3$), and H_3PO_4 as references. High-resolution mass spectra were recorded on a VG7070E instrument.

The following compounds were prepared by literature methods and their NMR spectra were recorded and used to identify reaction products: PF_5(DMSO) (14), PF_5(pyridine) (15), and $PF_5(NCCH_3)$ (14). PF_5(pyridine-*N*-oxide) was prepared by condensing PF_5 (1.1 mmol) onto pyridine-*N*-oxide (1.1 mmol) in CH_2Cl_2 (2 mL) at −196°C and warming the mixture to room temperature. All volatile material was then removed and the remaining white solid identified by ^{19}F and ^{31}P NMR as PF_5(pyridine-*N*-oxide) (70% yield). $SiF_4(DMSO)_2$, prepared from SiF_4 and DMSO (13), gives a very broad ^{19}F NMR peak at about −135 ppm because of rapid fluorine exchange, but it can be detected by either lowering the temperature and thus reducing the line width, or by integrating the broad ^{19}F NMR spectrum in the region −130 to −140 ppm at ambient temperature. $F_2P(O)OH$, $FP(O)(OH)_2$, H_3PO_4, and PF_6^- were identified by ^{31}P and ^{19}F NMR.

4-Nitro-2,2′-bipyridine-N-oxide

2,2′-Bipyridine-*N*-oxide was obtained as an oil (2.6 g) from 2,2′-bipyridine (5.0 g) by the method of Sont and Alper (16). The oil was dissolved in concentrated sulphuric acid (15 mL). Fuming nitric acid (24 mL) in concentrated sulphuric acid (13 mL) was added during 10 min, and the mixture was refluxed for 2.5 h. The solution was poured onto ice (100 g) and neutralized, with cooling, to pH 8 by 38% NaOH. The light yellow precipitate was filtered and washed with water. Recrystallization from hot ethanol gave 4-nitro-2,2′-bipyridine-*N*-oxide (1.45 g, 21%), mp 180–181°C (lit. (17) mp 183–185°C); MS: 217 (M^+), 171 $(M - NO_2)^+$, 155 $(M - NO_2,O)^+$, 143 $(M - NO_2,CN)^+$.

4-Amino-2,2′-bipyridine

4-Nitro-2,2′-bipyridine-*N*-oxide (0.42 g, 1.9 mmol) in methanol (20 mL) was reduced with sodium borohydride (0.85 g, 23 mmol) in the presence of 5% palladium-on-carbon (150 mg) by the method of Neilson *et al.* (18). The solution was filtered, evaporated, extracted with ether, and dried over NaOH pellets. Ether was removed to give 4-amino-2,2′-bipyridine (282 mg, 85%), mp 115–116°C (lit. (17) mp 128–129°C); ^1H NMR ($CDCl_3$): H3 7.66, H5 6.54, H6 8.29, H3′ 8.34, H4′ 7.78, H5′ 7.27, H6′ 8.63; MS: 171 $(M)^+$, 170 $(M - H)^+$, 145 $(M - CN)^+$, 144 $(M - HCN)^+$, 143 $(M - H,HCN)^+$.

4-Fluoro-2,2′-bipyridine (fbpy)

Fluoroboric acid (12.0 g) was added gradually to 4-amino-2,2′-bipyridine (1.0 g), with cooling, and a solution of sodium nitrite (1.10 g) in 10 mL of cold water was added. The solution was then cooled in liquid nitrogen and the precipitate was filtered to give the diazonium salt. After drying, the diazonium salt was decomposed by heating and 20% aqueous sodium hydroxide was added until no more solid was formed.

The brown solid was then filtered, washed with cold water, and extracted with petroleum ether. Removal of solvent gave 4-fluoro-2,2′-bipyridine (fbpy) (0.53 g, 52%), light yellow solid, mp 83–85°C, ^1H NMR ($CDCl_3$): H3 8.17 ($^3J_{HF}$ = 10.4), H5 7.04 ($^3J_{HF}$ = 8.1), H6 8.64 ($^4J_{HF}$ = 8.5), H3′ 8.41, H4′ 7.83, H5′ 7.34, H6′ 8.68; ^{19}F NMR ($CDCl_3$): −103.2 ppm; (CD_3CN): −102.7 ppm; ^{13}C NMR (CD_2Cl_2): C2 159.7 ($^3J_{CF}$ = 7), C3 108.8 ($^2J_{CF}$ = 19.0), C4 169.7 ($^1J_{CF}$ = 261), C5 111.5 ($^2J_{CF}$ = 17), C6 151.5 ($^3J_{CF}$ = 7), C2′ 154.9 ($^4J_{CF}$ = 4), C3′ 121.3, C4′ 137.0, C5′ 124.3, C6′ 149.3; MS: 174 $(M)^+$, 173 $(M - H)^+$, 148 $(M - CN)^+$, 147 $(M - HCN)^+$, 146 $(M - H,HCN)^+$; Mol. Wt. (MS) calcd. for $C_{10}H_7FN_2$, *m/z*: 174.0593; found, *m/z*: 174.0594.

In aqueous sulphuric acid, the ^{19}F NMR peak of protonated fbpy shifts to −92.9 ppm.

Reaction of PF_5 with bpy, fbpy, and phen

PF_5 (3.3 g, 2.6 mmol) was handled in a standard glass vacuum line and condensed onto a solution of bpy (0.10 g, 0.64 mmol) in CH_2Cl_2 at −196°C in a glass reaction tube with a PTFE insert, and the mixture was slowly warmed to room temperature. After 1 h, the solvent was removed under vacuum and a pale yellow solid remained that was dissolved in DMSO-d_6 or CD_3CN and characterized as $PF_4(bpy)^+PF_6^-$ by ^{19}F NMR (Table 1). The reaction was carried out numerous times and the yield of product varied between 10 and 20%, with side products $(bpyH)^+PF_6^-$, $F_2P(O)OH$, $FP(O)(OH)_2$, $P(O)(OH)_3$, and SiF_4(bpy). A similar procedure was used for the preparation of $PF_4(fbpy)^+PF_6^-$ and $PF_4(phen)^+PF_6^-$, which were characterized by ^{19}F NMR (Table 1).

The complexes $PF_4(bpy)^+$ and $PF_4(phen)^+$ are stable in CH_2Cl_2, CH_3CN, and DMSO solution; $PF_4(fbpy)^+$ is also stable in CH_2Cl_2 and CH_3CN, but in DMSO solution the fluorine substituent in the bound fbpy ligand is lost and replaced by substituent X to give the cation $PF_4(Xbpy)^+$; however, X was not identified. $PF_4(Xbpy)^+$; A_2BC ^{19}F NMR (300 MHz; $(CD_3)_2SO$): −51.0 (F^A, J_{AB} = 60, J_{AC} = 62), −78.2 (F^B, J_{BC} = 61), −80.6 (F^C).

Reaction of SiF_4 with bpy, fbpy, and phen

Using standard procedures, SiF_4 (0.31 g, 3.0 mmol, Matheson) was condensed at −196°C onto a solution of bpy (0.28 g, 1.8 mmol)

Can. J. Chem. Downloaded from www.nrcresearchpress.com by 217.78.4.112 on 09/08/12
For personal use only.

in dried and redistilled CH_2Cl_2 in a reaction tube connected to a vacuum line. The mixture was warmed to room temperature and reaction occurred within 5 min. Removal of volatile material gave a white solid in quantitative yield identified as SiF_4(bpy) by ^{19}F and ^{29}Si NMR (Table 1).

A similar procedure was used for the preparation of SiF_4(fbpy) and SiF_4(phen) and their ^{19}F NMR data are found in Table 1. SiF_4(bpy), SiF_4(phen), and SiF_4(fbpy) are stable in CH_2Cl_2, CH_3CN, and DMSO solution; however, a slow conversion of SiF_4(fbpy) to SiF_4(Xbpy) occurs over a period of several weeks in DMSO solution, analogous to the conversion of $PF_4(fbpy)^+$ to $PF_4(fbpy)^+$ in DMSO described above. SiF_4(Xbpy); A_2BC ^{19}F NMR (300 MHz; $(CD_3)_2SO$): -119.4 (F^A, $J_{AB} = 14$, $J_{AC} = 14$), -142.5 (F^B, $J_{BC} = 28$), -143.5 (F^C).

Small amounts of SiF_4(N-N) and BF_4^- were always observed during the reactions of PF_5 and N-N although the only source of silicon and boron was the glass apparatus (see text).

Acknowledgement

The financial assistance of the Natural Sciences and Engineering Research Council of Canada is gratefully acknowledged.

1. J. K. Ruff. Inorg. Chem. **2**, 813 (1963); R. Schmutzler. Angew. Chem. Int. Ed. Engl. **4**, 496 (1965); M. Brownstein and R. Schmutzler. Chem. Commun. 278 (1975); G. S. H. Chen and J. Passmore. J. Chem. Soc. Dalton Trans. 1251 (1979); E. G. Il'in, A. P. Nazarov, and M. N. Shcherbakova. Dokl. Akad. Nauk SSSR, **250**, 367 (1980); H. W. Roesky, K.-L. Weber, and J. Schimkowiak. Angew. Chem. Int. Ed. Engl. **20**, 973 (1981).
2. W. Webster and M. J. Deveney. J. Chem. Soc. (A), 2166 (1968).
3. I. R. Beattie, K. Livingston, and M. Webster. J. Chem. Soc. 7421 (1965).
4. A. F. Janzen, T. Q. Nguyen, Fanqi Qu, and K. Marat. J. Chem. Soc. Chem. Commun. 1274 (1988); X. Huang, F. Qu, J. Yao, and A. F. Janzen. J. Inorg. Chem. (China), **6**, 408 (1990).
5. A. D. Adley, D. F. R. Gilson, and M. Onyszchuk. J. Chem. Soc. Chem. Commun. 813 (1968); A. D. Adley, P. H. Bird, A. R. Fraser, and M. Onyszchuk. Inorg. Chem. **11**, 1402 (1972); L. V. Ostapchuk, L. A. Gavrilova, V. O. Gel'mbol'dt, and A. A. Ennan. Russ. J. Inorg. Chem. **33**, 813 (1988).
6. A. F. Janzen and M. Jang. Can. J. Chem. **67**, 71 (1989).
7. F. N. Tebbe and E. L. Muetterties. Inorg. Chem. **6**, 129 (1967); S. Brownstein and J. Bornais. Can. J. Chem. **46**, 225 (1968); C. Wang and A. F. Janzen. Can. J. Chem. **62**, 1563 (1984).
8. W. R. McWhinnie and J. D. Miller. Adv. Inorg. Chem. Radiochem. **12**, 135 (1969); S. N. Tandura, M. G. Voronkov, and N. V. Alekseev. Top. Curr. Chem. **131**, 99 (1986).
9. E. G. Il'in, M. N. Shcherbakova, Y. A. Buslaev, T. Y. Medved, N. P. Nesterova, and M. I. Kabachnik. Dokl. Akad. Nauk SSSR, **271**, 373 (1983).
10. R. B. Porter. J. Phys. Chem. **61**, 1260 (1957).
11. A. F. Janzen, J. A. Gibson, and D. G. Ibbott. Inorg. Chem. **11**, 2853 (1972); A. S. Secco, K. Alam, B. J. Blackburn, and A. F. Janzen. Inorg. Chem. **25**, 2125 (1986); M. Jang and A. F. Janzen. J. Fluorine Chem. **52**, 45 (1991).
12. R. K. Marat and A. F. Janzen. Can. J. Chem. **55**, 3845 (1977); J. A. Gibson, D. G. Ibbott, and A. F. Janzen. Can. J. Chem. **51**, 3203 (1973).
13. E. L. Muetterties, J. Am. Chem. Soc. **82**, 1082 (1960).
14. E. L. Muetterties, T. A. Bither, M. W. Farlow, and D. D. Coffman. J. Inorg. Nucl. Chem. **16**, 52 (1960).
15. K.-P. John and R. Schmutzler. Z. Naturforsch. **29B**, 730 (1974).
16. W. Sont and H. Alper, Org. Prep. Proced. Int. **12**, 243 (1980).
17. R. A. Jones, B. D. Roney, W. H. F. Sasse, and K. O. Wade. J. Chem. Soc. B, 106 (1967).
18. T. Neilson, H. C. S. Wood, and A. G. Wylie. J. Chem. Soc. 371 (1962).

Can. J. Chem. Downloaded from www.nrcresearchpress.com by 217.78.4.112 on 09/08/12
For personal use only.

The chemistry of thujone. XVI.[1] Versatile and efficient routes to safronitrile, β-cyclogeranonitrile, β-cyclocitral, damascones, and their analogues

JAMES P. KUTNEY,[2] PHILIP J. GUNNING, ROBIN G. CLEWLEY, JOHN SOMERVILLE, AND STEVEN J. RETTIG
Department of Chemistry, University of British Columbia, 2036 Main Mall, Vancouver, B.C., Canada V6T 1Z1

Received October 28, 1991

JAMES P. KUTNEY, PHILIP J. GUNNING, ROBIN G. CLEWLEY, JOHN SOMERVILLE, and STEVEN J. RETTIG. Can. J. Chem. **70**, 2094 (1992).

Thujone, a waste by-product of the Canadian forest industry, has been utilized as a starting material to develop a versatile synthetic route to the damascones (rose oil ketones) and related analogues. The synthetic sequence provides a route to β-cyclocitral (**45**), the latter having been previously converted to β-damascone (**2**). In addition, thujone-derived intermediates are converted to β-damascenone (**48**) and to intermediates that can be utilized for the preparation of damascone analogues. In conjunction with the above, an efficient route to safronitrile (**42**), β-cyclogeranonitrile (**43**), and β-cyclocitral (**45**) from 2,6-dimethylcyclohexanone has been developed. In summary, these studies afford an attractive versatile route to these important perfumery materials.

JAMES P. KUTNEY, PHILIP J. GUNNING, ROBIN G. CLEWLEY, JOHN SOMERVILLE et STEVEN J. RETTIG. Can. J. Chem. **70**, 2094 (1992).

On a utilisé le thuyone, un sous-produit de l'industrie forestière canadienne, comme produit de départ pour développer une voie de synthèse versatile conduisant aux damascones (cétones de l'huile de rose) et à des produits apparentés. La voie de synthèse conduit au β-cyclocitral (**45**) qui a été transformé antérieurement en β-damascone. De plus, des intermédiaires dérivés de la thuyone peuvent être transformés en β-damascénone (**48**) et en d'autres intermédiaires qui peuvent être utilisés pour la préparation d'analogues de la damascone. En relation avec les travaux mentionnés plus haut, on a aussi développé une voie efficace de synthèse du safronitrile (**42**), du β-cyclogéranonitrile (**43**) et du β-cyclocitral à partir de la 2,6-diméthylcyclohexanone. En bref, ces travaux ont permis de développer une voie versatile de synthèse de ces produits importants en parfumerie.

[Traduit par la rédaction]

The damascones or "rose oil ketones," as exemplified by α- and β-damascone (**1** and **2** respectively) are a family of natural products found as minor constituents in tea, tobacco, and in rose and geranium oils (2). Their importance as perfumery agents is well known (2) and the impracticality of their isolation from such natural sources, particularly rose oil, has stimulated interest in their laboratory syntheses. Major efforts by the group at Firmenich in Geneva, Switzerland, have provided commercial routes to these compounds (3–5) and other groups have also made substantial contributions to this field (6–13). In our program directed toward the use of thujone (**3**), a waste by-product of the Canadian forest industry, as a starting material for the syntheses of various natural products, biologically active and commercially important substances, we have directed our attention toward the development of a versatile route to the damascones and, in particular, to novel analogues of these compounds, the latter as potential perfumery agents. This publication presents results that satisfy these objectives.

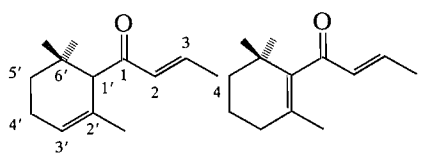

1 **2**

The synthetic strategy for the synthesis of β-damascone (**2**) from thujone (**3**) is summarized in Scheme 1. Methylation of thujone would give a trimethylated bicyclo[3.1.0]cyclohexanone system (**4**) that could serve as a key intermediate. Two routes from this intermediate to the damascones are shown in Scheme 1. The first route, **4** → **5**, **6** → **2** involves attachment of the side chain present in the damascones either through a direct nucleophilic attack on the carbonyl group so as to attach the complete side chain, or by initial attack with a nucleophile, such as cyanide ion, followed by a chain extension. Cyclopropane ring-opening and isopropyl side-chain cleavage would lead to the damascones. The second route, **4** → **7** → **2**, involves cyclopropane ring-opening and isopropyl side-chain cleavage directly after methylation of thujone to obtain a cyclohexenone system to which the desired side chain could be attached. The strategy employed should allow the synthesis of damascone analogues with substitution at C2′, C3′, C4′, C5′, and C6′ positions of the "cyclohexane" part of the damascones, as well as numerous analogues in which the side chain is altered. Even the cyclopropane and isopropyl functionalities present in thujone could be retained for the synthesis of interesting analogues.

A large number of experiments concerning the best route to **4** were conducted. These involved studies with various bases (KOH, NaH, K-*tert*-butoxide) in different solvents (methanol, THF, *tert*-butanol) and iodomethane or dimethyl sulphate as alkylating agents. With KOH, in methanol, the only observed reaction was isomerization of the C-4 methyl group to afford an equilibrium mixture of (−)-isothujone (**3**, C-4 methyl in β-orientation) and (+)-thujone (**3**, C-4 methyl in α-orientation) in a ratio 2:3 respectively. The stronger base, NaH in THF and iodomethane as alkylating agent (3 equivalents of each), afforded a mixture of unreacted **3** (13%), the monomethylated product **8** (58%), and the dialkylated product **9** (14%) while replacement of NaH by potassium *tert*-butoxide (2.5 equivalents) afforded **8** (48%) and the fully alkylated ketone **10** (15%). In all cases, the re-

[1]For Part XV, see ref. 1.
[2]Author to whom correspondence may be addressed.

Can. J. Chem. Downloaded from www.nrcresearchpress.com by 217.78.4.112 on 09/08/12
For personal use only.

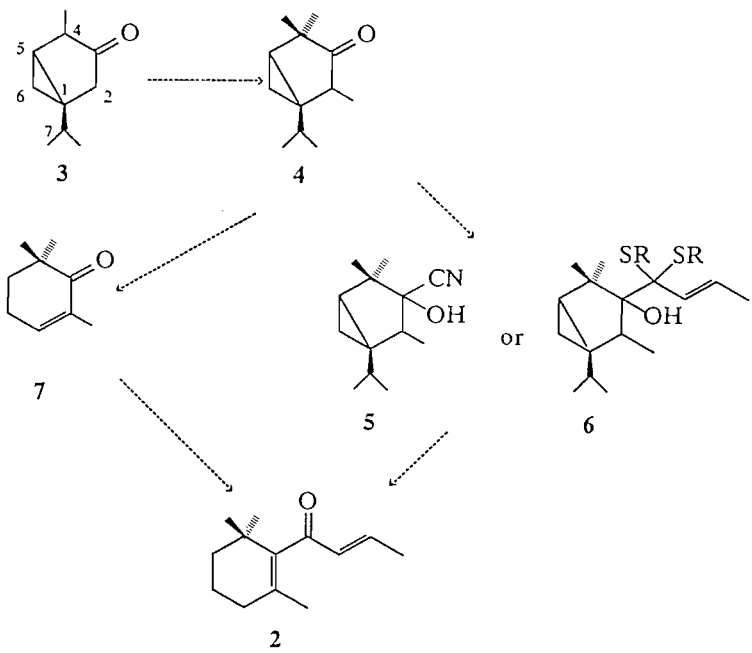

SCHEME 1. Synthetic strategy for synthesis of β-damascone (**2**) from thujone (**3**).

sulting reaction mixture was difficult to separate so a "one-step" alkylation process to provide the desired **9** (or its C-2 isomer) was clearly undesirable. Thus regiospecific monoalkylation of **3** at the C-4 position became the primary focus in the hope that **8** could be converted in higher overall yield to **9** in a subsequent reaction. Table 1 summarizes the

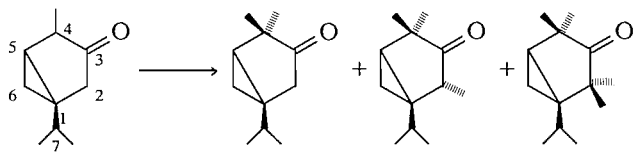

III

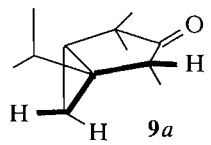

results obtained in studies directed to optimize yields of **8**. The high yields obtained (entries 2 and 3, Table 1) were encouraging and these conditions were employed in all subsequent studies. For purposes of compound characterization, **8** could be separated from **9** by repeated flash chromatography. Since it was expected that the rate of alkylation of **8** to **9** would be higher than **9** to undesired **10**, the mixture of **8** and **9**, as obtained in these studies, could be employed directly in the subsequent alkylation experiments.

The minor component **9**, which was eluted first from the column, showed a molecular ion peak at m/z = 180 in the mass spectrum. The ^{1}H NMR spectrum showed two singlets at δ 0.99 and 1.09 ppm, a doublet at δ 0.98 ppm and two overlapping doublets at δ 1.03 ppm each integrating for three protons, the three cyclopropane protons at high field, and the characteristic septet of the isopropyl group. A quartet of doublets at δ 2.80 ppm, assigned to the C-2 proton, was shown by decoupling to be coupled to one of the methyl doublets at δ 1.03 ppm and also to one of the cyclopropane protons by a W-coupling. Hence the C-2 methyl had to be *cis* to the cyclopropane ring (*endo* form or explicitly the *R* configuration)[3] to allow for a W-coupling of the C-2 proton with a C-6 proton (see **9***a*). Also the C-6 H_{exo} proton at δ 0.54 ppm could be assigned through this W-coupling.

The ^{1}H NMR spectrum of the monomethylated ketone **8** (M^+ at m/z = 166) clearly showed two methyl singlets at δ 1.12 and 1.03 ppm, and an AX system for the protons at C-2 (δ 2.09 and 2.66 ppm). The signal at δ 2.66 ppm has long-range coupling (J = 2.5 Hz) corresponding to a W-coupling with C-6-H_{exo} (δ 0.64 ppm), and so could be assigned as the *exo* C-2 proton.

Given the high yield of monomethylated thujone derivative **8**, a second methylation was required for the production of the desired dimethylated thujone **9**. Since the use of excess potassium tert-butoxide in the methylation of thujone gave rise to significant amounts of product **10**, as well as the desired products, it was decided to use lithium diisopropylamide as the base. Using 1 equivalent of lithium diisopropylamide in tetrahydrofuran in the reaction with **8**, and subsequent alkylation with iodomethane, gave a mixture, separable by spinning band distillation and column chromatography, that contained a predominance of two isomeric dimethylated compounds **9** (25%) and **11** (57%), with

[3]Previous workers (14) have used the term "pseudo-axial" and "pseudo-equatorial" for describing substituents on the thujone system. However, since the five-membered ring is very close to planarity, and so can be distorted by substituents into either a "boat" or "chair"-like conformation, these terms do seem very ambiguous. For this work the terms *exo* and *endo* have been used to describe substituents on the bicyclic system. The term *endo* is used when the substituent is closer to the longer of the two unsubstituted bridges (see **9***a*).

Can. J. Chem. Downloaded from www.nrcresearchpress.com by 217.78.4.112 on 09/08/12
For personal use only.

TABLE 1. Methylation of thujone with potassium *tert*-butoxide and iodomethane

Expt. No.	Equiv. of KO'Bu	Solvent	Equiv. of MeI	Total yield of products	Percent composition[a] 3	8	9	10
1	2.5	THF	2.5	Quantitative	—	37	48	15
2	1.5	THF/'BuOH	1.5	95	—	91	9	—
3	1.0	THF/'BuOH	1.0	81	13	86	—	

[a]Determined by GC analysis.

some starting material **8** (7%) and the fully methylated product **10** (6%). The overall yield of **9** and **11** from this reaction was 77%. It was found that after the methylation reaction had ceased, prolonging the reaction time resulted in an increase in the ratio of **9** to **11** with no change in the amount of **8** or **10**. It was believed that the diisopropylamine present was effecting an isomerization of **11** into **9**. Subsequently, the reaction mixture was treated with alcoholic potassium hydroxide to result in an almost complete isomerization of **11** to **9**. Since the methylation of the enolate generated from **8** is a kinetically controlled process, compounds **11** and **9** are both formed in the methylation of **8**. Approach of iodomethane can occur from either side of the enolate, with the *exo* face preferred (since the C-6-*endo* proton hinders attack from the *endo* face) giving rise to a predominance of **11** over **9**. However, ketone **9** is the more thermodynamically stable compound and thus becomes predominant on equilibration of the mixture. Both **10** and **11** were characterized from the usual spectroscopic data (see Experimental).

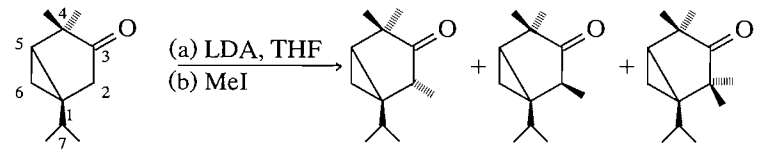

8 **9** **11** **10**

The isomerization of **11** to **9** was investigated. Treatment of either pure **11** or pure **9** with alcoholic potassium hydroxide, resulted in an identical mixture of **9**:**11** = 99:1. Treatment of a mixture of **8**, **9**, **11**, and **10** (**9**:**11** = 38:28) with thionyl chloride in methanol (a source of alcoholic hydrogen chloride) also resulted in isomerization of **11** to **9** (**9**:**11**) = 65:3). The isomerization of **11** to **9** would be expected, since in **11** the near-planarity of the cyclopentane ring forces an eclipsing relationship between the *exo* C-2 methyl group and the isopropyl group. On isomerization to **9**, the C-2 methyl group is *cis* to the cyclopropane ring, which is expected to be less sterically demanding than the isopropyl group.

The above detailed studies provided some understanding of the alkylation of thujone (**3**) to the ultimate desired product (**9** and (or) **11**) and allowed satisfactory yields of these compounds.

In summary, by the use of a two-step alkylation process, using initially potassium *tert*-butoxide and iodomethane to afford **8** as a major component, and without isolation, reaction with lithium diisopropylamide and iodomethane, followed by treatment of the latter mixture with potassium hydroxide, a 77% overall yield of **9** from **3** could be realized.

With the desired **9** in hand, the elaboration of the side chain, as required for the damascone series, and ring-opening of the cyclopropyl group was now considered. Preliminary investigations in our laboratory revealed that direct introduction of the four-carbon side chain, that is, the sequence, **4** → **7** → **2** or **4** → **6** → **2** (Scheme 1) would provide difficulties and the route, **4** → **5** → **2**, shown in Scheme 1 was pursued.

In considering the conversion of **9** (shown in general terms as **4** in Scheme 1) to the cyanohydrin **5**, it was deemed unnecessary to prepare a pure isomer of the two possible cyanohydrins since subsequent elimination of the hydroxyl function to generate the required double bond in **2** would not necessitate a specific stereochemistry in cyanohydrin **5**. For this purpose, studies involving direct addition of cyanide ion to **9** under a variety of conditions were pursued but no formation of **5** could be observed. However, the use of trimethylsilyl cyanide (15–17) (1.05 equivalents) with tetra-*n*-butylammonium cyanide (0.1 equivalent) as catalyst in the absence of solvent at 70–80°C did afford an essentially quantitative yield of the trimethylsilyl cyanides **12** and **13** in a ratio of 70:28 respectively (GC analysis). No attempt was made, either chemically or spectroscopically, to establish the configuration of each compound at this stage, though, following a literature search on the stereochemical outcome of this reaction, some conclusions as to the stereochemistry can be inferred. Evans *et al.* (18) established the stereochemical course of the trimethylsilyl cyanide addition to the relatively unhindered, but conformationally locked, 4-*tert*-butylcyclohexanone. Kinetically the cyanide ion preferentially attacks the carbonyl from its axial face. A thermodynamic equilibrium can be established in which the axial cyanide isomer also predominates. With the trimethylsilyl cyanohydrins from **9**, the isomer with the cyano group *endo* to the cyclopropane ring is likely to predominate in a thermodynamic equilibrium, since the periplanar interaction of the C-2

Can. J. Chem. Downloaded from www.nrcresearchpress.com by 217.78.4.112 on 09/08/12
For personal use only.

methyl and the nitrile would be less than the equivalent interaction of the C-2 methyl and the oxysilyl group. Since the use of tetra-*n*-butylammonium cyanide as a catalyst induces thermodynamic equilibrium (16), the major isomer is likely to be **12**.[4] Separation of the isomers for characterization proved difficult. As the trimethylsilyl group was intended to be eliminated at a later stage, there was no need to separate the isomers for the synthesis of the damascones.

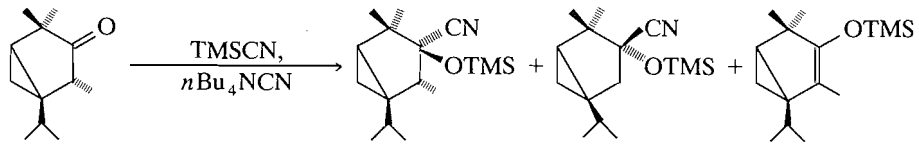

9 **12** **13** **14**

Along with the above mixture of isomeric silyl cyanohydrins we obtained the silyl enol ether **14** as a very minor product (2% by GC). In larger scale reactions, **14** was separated from the silyl cyanohydrins. The generation of silyl enol ethers in the reaction of trimethylsilyl cyanide with ketones has been noted before (15).

With the desired introduction of the nitrile group in hand, attention was focussed on opening the cyclopropane ring to generate a six-membered ring system. The strategy employed here was based on an earlier observation in our laboratory (1) that ozonation of thujone-derived intermediates allows selective introduction of a hydroxyl group exclusively at the tertiary carbon atom of the isopropyl group, and the product thus formed can be elaborated to the desired system by successive treatment with mineral acid and tri-*n*-butyltin hydride. Application of this strategy of cyclopropane-opening/isopropyl cleavage to the present study was highly successful. Treatment of the mixture of silyl cyanohydrins **12/13** in ethyl acetate at 0°C with a stream of ozone for 8 h resulted in complete consumption of the starting material. The products, isolated as three separate mixtures of isomers, were the epimeric olefins **15/16** (1%), the epimeric ketones **17/18** (45%), and the epimeric alcohols **19/20** (21%). Attempts to separate the individual epimers

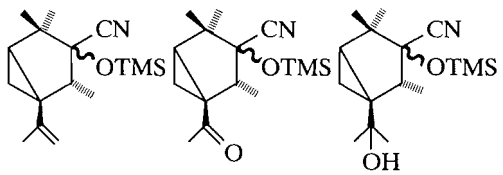

15/16 **17/18** **19/20**

from each of the mixtures by column chromatography for a detailed characterization resulted only in the enrichment of each isomer in the mixture. Pure compounds were not obtained in this study. The mixture of alcohols **19** and **20**, occurring as a white solid, consisted of a 66:34 mixture of the epimers similar to the ratio present in the starting material. The assumption is that the major product has the nitrile group *endo* to the cyclopropane ring. The ratio of isomers was determined by GC, and by integration in the ^{1}H NMR spectrum. Since mixtures greatly enriched in either of the alcohols could be obtained by chromatography, identification of the resonances in the ^{1}H NMR spectrum was possible.

The ketones **17** and **18**, obtained in 45% yield, occurred as an inseparable mixture (71:29) while the third mixture, obtained in 1% yield, was shown to be the alkenes **15** and **16**, present as a 60:40 mixture as determined by integration of the ^{1}H NMR resonances at δ 4.78 and 4.85 ppm corresponding to the terminal methylene protons.

Initial investigation of the ring-opening of the cyclopropane ring began with the alcohols **19** and **20**. Treatment of a mixture of the alcohols dissolved in dichloromethane with concentrated hydrochloric acid gave a mixture of three isomeric chlorides in 52% overall yield, of which **21** was the predominant compound (83% of the mixture). Repeated purification by column chromatography resulted in a pure sample of **21**. The mass spectrum showed it to be a chloride of formula $C_{16}H_{28}ClNOSi$. The ^{1}H NMR spectrum readily established **21** as the isolated product and not the alternative six-membered structure **22**.

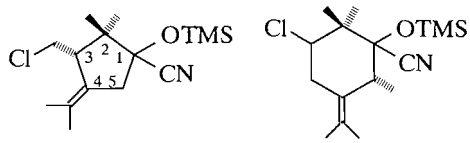

21 **22**

On monitoring the reaction of **19** and **20** with hydrochloric acid by GC, it was found that an initial product was formed, which then decreased as the percentage of the chloride mixture containing **21** increased. By performing the same reaction at 0°C, the initial product could be obtained after careful work-up. The product was a highly unstable 60:40 mixture of the chlorides **23** and **24**, that rapidly decomposed to the alkenes **15** and **16**.

It was subsequently found that performing a sequence of reactions in which the chlorides were not purified led to significant increases in the yields. It was believed that the moderate yield of the chlorination step was due to the purification process.

The five-membered ring chloride **21** was not an unexpected product since, as noted earlier, studies in our laboratory (1) had provided a similar ring-opening reaction.

In parallel experiments, it was found that treatment of the mixture of chlorides (containing **21**) with tri-*n*-butyltin hydride afforded the alkenes **27** and **28** (83:17) in 69% yield. The ^{1}H nmr spectrum of **27** clearly showed that a rearrangement had occurred, since the methyl group doublet that would result from direct replacement of chlorine in **21** was absent.

[4]This argument assumes a near-planarity of the five-membered ring in the products **12** and **13**. It has been shown (19) that in 3-thujone (**3**) the five-membered ring is only slightly distorted from planarity.

Can. J. Chem. Downloaded from www.nrcresearchpress.com by 217.78.4.112 on 09/08/12
For personal use only.

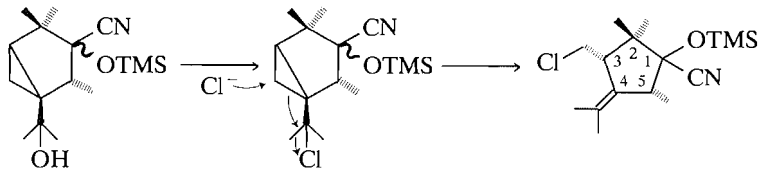

19/20 23/24 21

Such a radical rearrangement had been noted previously (1). Treatment of the chlorides with tri-*n*-butyltin hydride (20) leads to homolytic cleavage of the C—Cl bond to generate a free radical. Usually, this radical abstracts a hydrogen atom from the tin hydride to propagate the free-radical chain reaction. However, the radical can rearrange to a more stable radical before abstraction, as has apparently happened in this case (**21** → **25** → **26** → **27/28**). The primary radical **25** generated from **21** by tri-*n*-butyltin hydride may rearrange

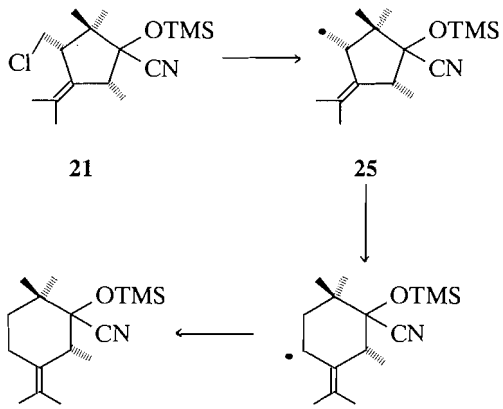

21 25 27/28 26

to the secondary radical **26**. This secondary radical is then trapped by a hydrogen atom. Davies and co-workers (21) and Mariano and Bay (22) investigated cyclopropyl radical rearrangements in which either the primary or secondary radicals were obtained on ring-opening, depending on the conditions and the initial stereochemistry of the cyclopropyl radicals.

At this stage it was decided, since the alcohols **19/20** could be converted to the six-membered ring alkenes **27/28**, which on ozonolysis should be converted to the ketones **29/30**, that a study involving the conversion of the ketones **17/18** into the ketones **29/30** should also be investigated.

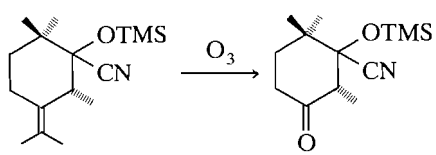

27/28 29/30

As discussed previously, the ketones **17** and **18** (71:29) were produced in 45% yield in the prolonged ozonation of **12** and **13**. Reduction with sodium borohydride gave, in 92% yield, a mixture of four isomeric alcohols **31**, **32**, **33**, and **34** (38:35:14:13 as shown by integration of the C-7 proton resonances in the ^{1}H nmr spectrum). It was not considered necessary to obtain pure alcohols for the subsequent reactions, since it was expected that eventually a common product would be obtained from all of the isomers. Analysis of the product ratios in relation to the composition of the starting material suggested that, for each ketone, the reducing reagent attacked both the *re* or *si* face at equal rates.

Reaction of this mixture of alcohols with hydrochloric acid resulted in the production of two chlorides **35** and **36** (63:37). (63:37). Traces of the five-membered ring chlorides were detected. Compounds **35** and **36** were clearly identified by the presence in the ^{1}H NMR spectrum of the signals corresponding to the cyclopropane protons, and the two signals at δ 3.75 and 4.11 ppm corresponding to the protons attached to the carbon atoms bearing chlorine. The simplification of the mixture from four isomers (for the alcohols) to two isomers (for the chlorides) was somewhat surprising, as was the retention of the cyclopropane functionality since, with the alcohols **19** and **20**, ring-opening to the five-membered ring chloride **21** occurred under the same conditions.

The formation of the chlorides **35** and **36** was of concern, since treatment with tri-*n*-butyltin hydride might result in the eventual retention of the cyclopropane functionality. Fortunately, on treatment with this reagent a rearrangement of the initial radical, formed by the homolytic cleavage of the C—Cl bond, resulted in an efficient conversion of the chloride into the alkenes **37** and **38** (**37**:**38** = 72:28) in 95% yield, possessing the desired six-membered ring. The two alkenes were epimeric about the silyl cyanohydrin functionality. Support for the structures of **37** and **38** was provided by the presence of the two vinylic protons at δ 5.20 and 5.41 ppm, and the absence of resonances corresponding to the cyclopropyl protons in the ^{1}H NMR spectrum. The stereochemistry about the double bond could not be determined from the regular proton spectrum. Since the stereochemistry was to be destroyed in the next step, further experiments to determine this stereochemistry were not undertaken.

Ozonolysis of the mixture **37** and **38** gave, in high yield (93%), the six-membered ring ketone, **29**, contaminated with 5% of the epimer **30** (further purification gave samples of **29** of 98.5% purity). This result was highly surprising. Obviously an epimerisation α to the carbonyl had occurred (Scheme 2). The isomer **29** must consist of a pair of enantiomers to account for the high yield of the reaction after starting with a mixture of diasteroisomers of 72:28 ratio. Although the product had $[\alpha]_D = -28$, it would be expected that **29** was not optically pure. Attempts at using a chiral shift reagent in the separation of the signals in the ^{1}H NMR spectrum were unsuccessful. The determination of the relative stereochemistry of **29** was based on ^{1}H NMR nOe difference experiments performed on **29**, reinforced by an

Can. J. Chem. Downloaded from www.nrcresearchpress.com by 217.78.4.112 on 09/08/12
For personal use only.

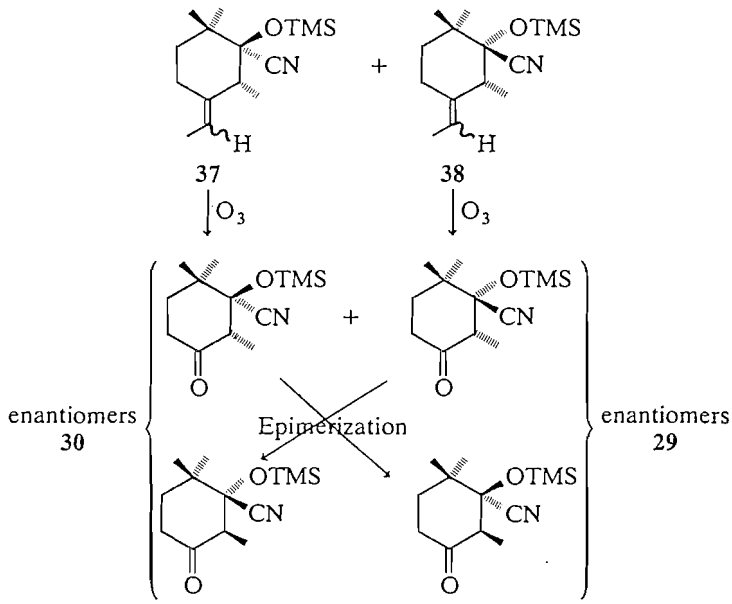

SCHEME 2. Conversion of isomeric trimethylsilyl cyanohydrins **37/38** into ketones **29/30**.

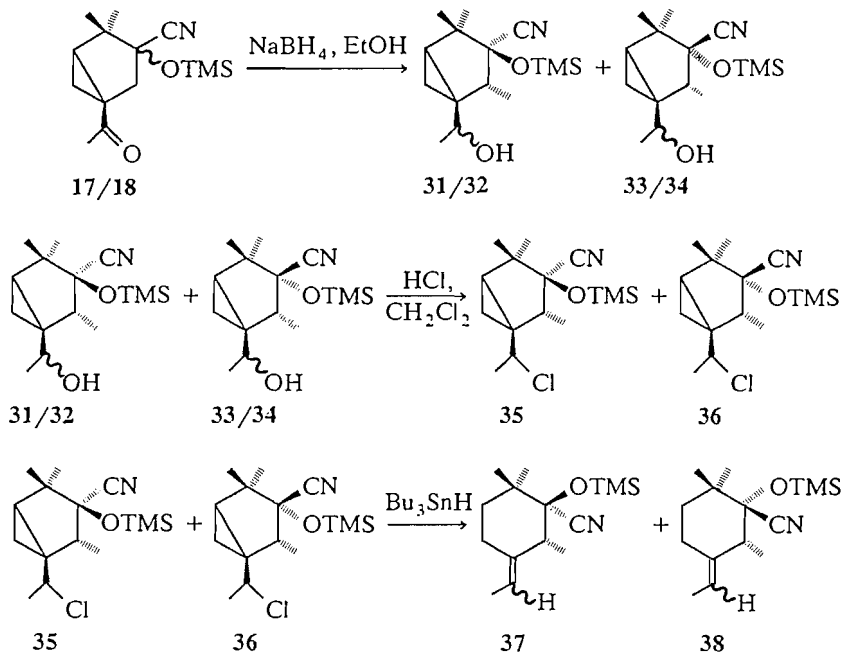

^{1}H NMR nOe difference experiment performed on a subsequent structure derived from **29** (see later).

For preparative purposes, the above studies now afforded the opportunity to develop an efficient route from thujone (**3**), via **9**, to the desired ketones **29** (or **30**). It was clear that isolation of the various intermediates discussed above is not essential since on further reaction these various compounds will lead to the same end product along the sequence. Thus **9** is converted to the mixture of **12** and **13**, the latter is directly treated with ozone to afford a mixture of **15–20** that, without further separation, is reacted successively with sodium borohydride, hydrochloric acid, tri-*n*-butyltin hydride, and finally ozone. The latter mixture, on purification, provides ketones **29** and **30** in a ratio of 95:5 respectively and in 35% overall yield for this six-step process.

A further overall improvement of the above process was developed when it was noted that a crude reaction mixture resulting from the methylation of thujone, that is, conversion of **3** to **9** and **10**, discussed earlier, could be employed in the reaction with trimethylsilyl cyanide. The sterically hindered carbonyl group in **10** does not undergo conversion to the corresponding nitrile and **10** is consequently readily separated from **12** and **13**.

Having obtained ketone **29** via the rather efficient overall reaction sequence from thujone, elaboration of the side chain to afford a versatile route to the damascones and (or) novel

Can. J. Chem. Downloaded from www.nrcresearchpress.com by 217.78.4.112 on 09/08/12
For personal use only.

analogues thereof was now considered. Reduction of the nitrile function in **29** to the corresponding aldehyde by the classical reagent diisobutylaluminum hydride (23) was only moderately successful (41% yield) with reduction of nitrile and carbonyl functions as well as removal of the trimethylsilyl group occurring simultaneously. An alternative route involved treatment of **29** with thionyl chloride in methanol to afford an enone (**39**) and the latter, upon reduction with sodium borohydride in the presence of cerium III salts (24, 25) provided **40** in essentially quantitative yield. These reactions can be accomplished without isolation of intermediates and an overall 92% yield of **40** from **29** is achieved.

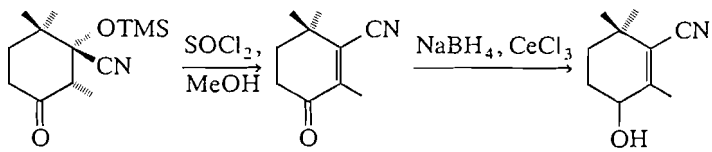

29 **39** **40**

Compound **40** was now envisaged to be a key intermediate in the production of β-damascenone. Elimination of the hydroxyl group to generate the unsaturated nitrile **42** would give access to the damascenones, whilst a reductive elimination would lead to the α,β-unsaturated nitrile **43**, which would give access to the damascone series.

Compound **40** was converted to the bromide **41** in 92% yield by treatment with phosphorus tribromide in petroleum ether at 0°C (molecular ion peaks at m/z = 229 and 227 in the mass spectrum). Reduction of the bromide, accomplished by sodium borohydride in dimethyl sulphoxide (26, 27) gave, in 95% yield, the α,β-unsaturated nitrile **43** and the non-conjugated nitrile **44**, as a 90:10 mixture.

The nitrile **43** has been reported previously in the literature (28, 29). Ohloff and co-workers (29) have mentioned that an equilibrium mixture of **43** and **44** contained 92% **44** and 8% **43**.

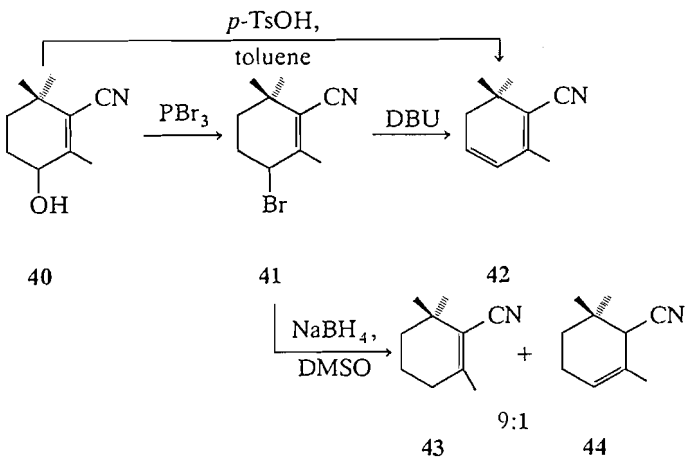

The conversion of **43** into β-cyclocitral (**45**) would constitute a formal synthesis of β-damascone (**2**) since **45** had been already converted to **2** (29, 30). For this purpose, our attention turned to the reduction of **43** with diisobutylaluminum hydride. While this research was in progress, Picard *et al.* (31) published results complementary to procedures we were employing. It was reported that the reduction of **43** by diisobutylaluminum hydride, with a work-up involving 5% sulphuric acid, gave the aldehyde, β-cyclocitral (**45**) in 70% yield. Repetition of this procedure with slight modifications (change in solvent and reaction time) afforded **45** in 90% yield after distillation. The presence of the unsaturated aldehyde functionality was shown by the absorbance at 1665 cm^{-1} in the infrared spectrum, and by the singlet at δ 10.11 ppm in the ^1H nmr spectrum. The facile oxidation of **45** to the corresponding acid required careful manipulation of the reaction mixture in order to obtain optimum yields of **45**. An alternative approach to **45** has also been published (32).

Having completed a formal synthesis of β-damascone, the production of β-damascenone was investigated. Treatment of **41** with 1,8-diazabicyclo[5.4.0]undec-7-ene (DBU) resulted in the formation of the diene **42** in 27% yield. The conjugated diene was characterized by the absorbances at 1640 and 1575 cm^{-1} in the infrared spectrum and by the maximum at 285 nm in the ultraviolet spectrum corresponding to the chromophore of the unsaturated nitrile. The synthesis of **42**, trivially named safronitrile, from the alcohol **40** by acid-catalyzed dehydration has been reported (28), though no yields or procedure were presented. It was found in our laboratory that treatment of **40** with *para*-toluenesulphonic acid (0.18 equivalent) in toluene, with azeotropic removal of water, resulted in dehydration to give the diene **42** in 75% yield.

Elongation of the side chain, utilizing **42** as starting material, was considered via the sequence, **42** → **45** → **46**/**47**. Reduction of **42** with diisobutylaluminum hydride afforded the expected aldehyde **45** (63% yield) and the latter was immediately subjected to reaction with 1-propenylmagnesium bromide to give a 1:1 mixture of the allylic alcohols **46** and **47**. The two alcohols are formed since the commercial supply of 1-bromopropene, used in the generation of the Grignard reagent, exists as a 1:1 mixture of geometric isomers. It was found that the *Z* isomer, **47**, was unstable to chromatography, possibly undergoing an acid-catalyzed rearrangement, while **46** was completely stable and could be isolated pure (43% overall yield) by chromatography of the mixture on silica gel. Assignments of stereochemistry at C-2 and C-3 were made based on conversion to subsequent structures and relating the configuration back through to **46** and **47**.

Mild oxidation of **46** with 20 equivalents of "active" manganese dioxide (33) gave quantitatively β-damascenone (**48**), which had spectral data consistent with the natural product.

Oxidation of the mixture of alcohols **46** and **47** (49:51) under the same conditions afforded a mixture of the ketones β-damascenone (**48**) and its *Z*-isomer (**49**) (49:51) in quan-

Can. J. Chem. Downloaded from www.nrcresearchpress.com by 217.78.4.112 on 09/08/12
For personal use only.

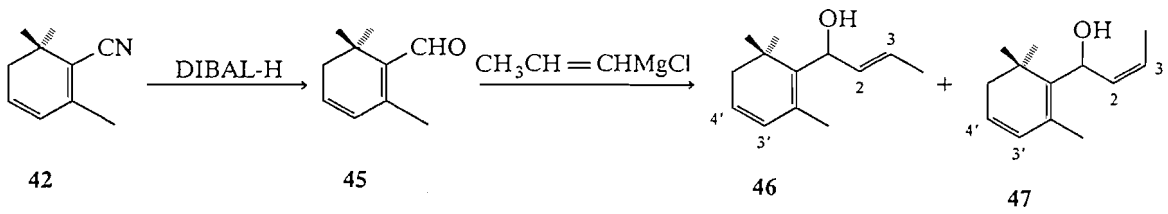

titative yield. β-Damascenone (**48**) showed the two olefinic protons of the side chain at δ 6.20 and 6.85 ppm with a coupling constant of 16 Hz. Ketone **49** showed the equivalent protons as a multiplet resonating at δ 6.20 ppm. The coupling constant indicated that the double bond has the *E* configuration in β-damascenone (**48**).

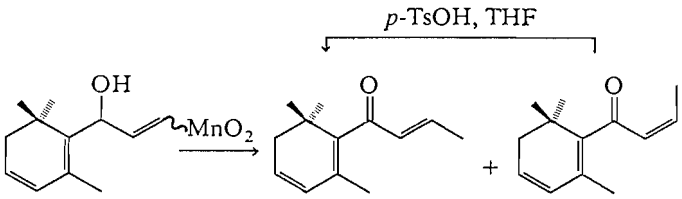

Separation of the mixture **48** and **49** was not required since it has been reported (34) that acid-catalyzed isomerization of **49** to **48** occurs. Treatment of the mixture with *para*-toluenesulphonic acid in tetrahydrofuran resulted in the production of pure β-damascenone (**48**) exclusively, in 76% yield after purification.

In summary, the total synthesis of **48** from thujone has been accomplished in 6% overall yield via the 15-step route outlined in Scheme 3. A majority of the intermediates noted need not be isolated, thereby increasing the efficiency of the overall process. Specifically the synthesis can be accomplished as a "several-pot" process: (*i*) **3** → → **9**; (*ii*) **9** → → **29/30**; (*iii*) **29/30** → **40**; (*iv*) **40** → → **42**; (*v*) **42** → **45**; (*vi*) **45** → → **48**.

As noted at the outset, it was the purpose of this investigation to develop a synthetic route to intermediates that could, in turn, allow the synthesis of novel damascone analogues that may reveal interesting perfumery or aroma properties. The intermediates **12/13**, **19/20**, and **27/28**, obtained in several steps from the readily available and inexpensive thujone, can, in conjunction with the chemistry developed herein, be utilized for this purpose. Studies in this direction will be presented later.

While the above studies were underway, an alternate route to **42** was undertaken from commercially available 2,6-dimethylcyclohexanone (**50**). The sequence under investigation is summarized in Scheme 4.

2,2,6-Trimethylcyclohexanone (**51**) was synthesized in 85% yield from commercially available 2,6-dimethylcyclohexanone (**30**), by treatment with lithium diisopropylamide and iodomethane, by a modification of the procedure reported by Fitjer and Quabeck (35). The product (**51**) contained a minor amount (3%) of 2,2,6,6-tetramethylcyclohexanone (**52**) (as shown by GC). This impurity was tolerated

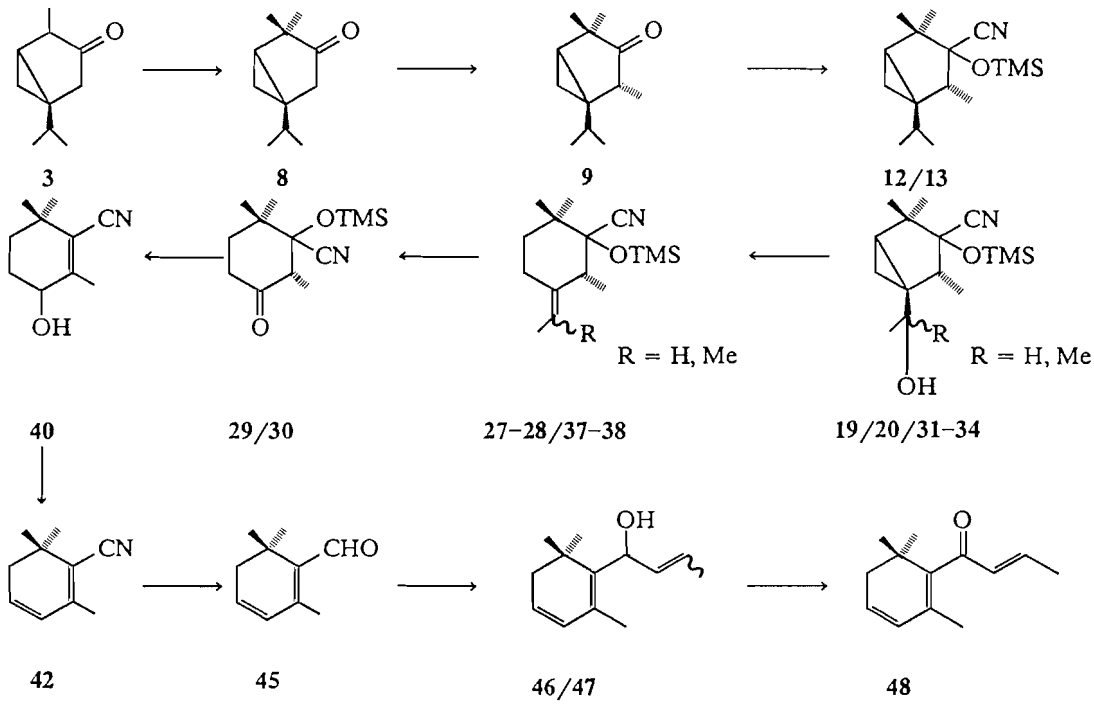

SCHEME 3. Overall summary in conversion of thujone (**3**) to damascenone (**48**).

Can. J. Chem. Downloaded from www.nrcresearchpress.com by 217.78.4.112 on 09/08/12
For personal use only.

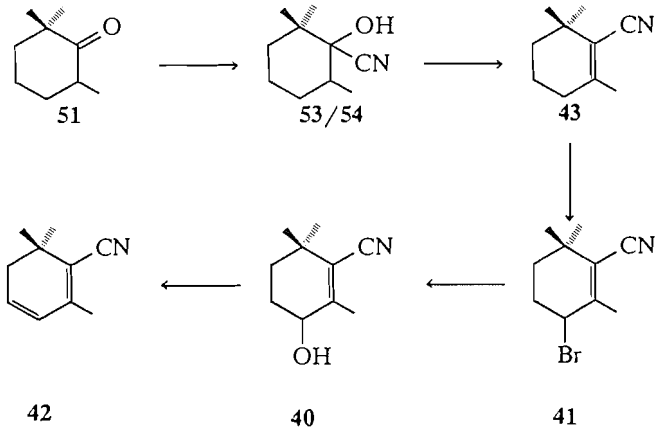

SCHEME 4. Synthesis of safronitrile (**42**) from 2,2,6-trimethylcyclohexanone (**51**).

in preference to the impurity of *cis/trans* 2,6-dimethylcyclohexanone as in the synthesis of trimethylcyclohexanone reported by Fitjer.

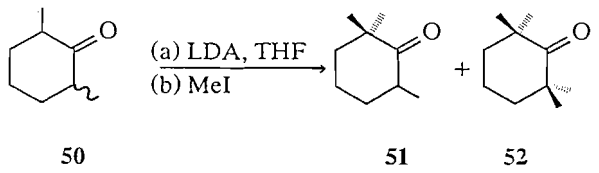

Reaction of **51** with sodium cyanide in aqueous sodium bisulphite solution, a procedure described by Stille and coworkers (36), gave a quantitative yield of a white solid, shown by GC and ^{1}H nmr spectroscopy to contain a 23:77 mixture of the cyanohydrins **53** and **54** respectively.[5] The stereochemistry shown in **53** and **54** follows from a single crystal X-ray analysis of a subsequent product (see later).

The dehydration of the mixture of **53** and **54**, in order to achieve a synthesis of **43**, was attempted with thionyl chloride and pyridine in refluxing benzene and in accord with the procedure employed by Stille (36) in which a high yielding

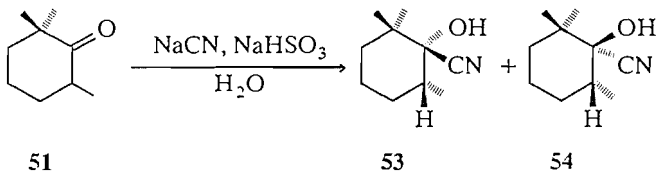

conversion of a closely related cyanohydrin had been obtained. However, in the present study, the mixture of **53** and **54** was shown to convert to a mixture of nitriles **43** and **55** (94% overall yield) and in an unfavorable ratio (**3**:**14** = 26:74). Apart from the spectral data (see Experimental), further proof of the structure of **55** was provided by ozonolysis. The resulting ketone possessed all the characteristic spectral data consistent with **56**.

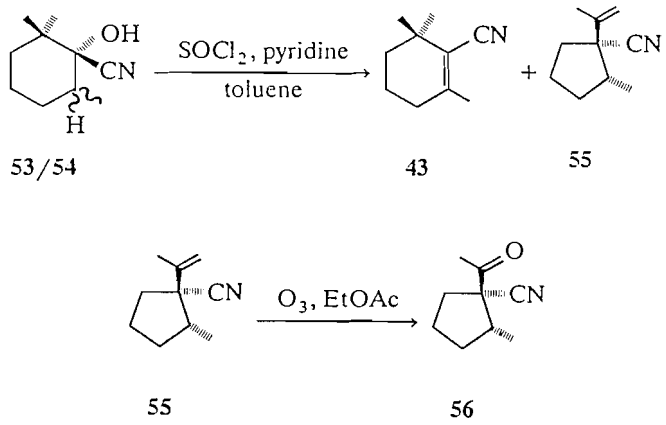

The isolation of **43** and **55** is explicable in conformational terms according to Scheme 5 wherein **43** is obtained via diaxial elimination of water from **53** while **54** undergoes rearrangement due to inaccessibility of the requisite β-hydrogen atom for such an elimination process.

An extensive series of experiments was conducted in the hope of altering the ratio of **43**:**55** in the desired direction (Table 2) but, in all cases studied, **55** was observed as the major product. Consequently, attention was focussed on developing a procedure in which the desired nitrile **43** could be obtained efficiently from the mixture of **53** and **54** and, if possible, without isolation of the individual compounds.

Acetylation of the mixture of **53**/**54** (acetic anhydride, acetyl bromide) afforded a 72:28 mixture of the corresponding acetates **56** and **57** respectively (79% overall yield). Subjecting this mixture to vacuum pyrolysis with a furnace temperature of 450°C afforded the desired nitrile **43** (72% yield) and recovery of starting material (ratio of **56**:**57** of 91:9, 28% yield). This result was encouraging in that it indicated a highly selective *cis* elimination occurring with **57** and thereby a possible route to optimizing the yield of the desired **43** from the original mixture of **53** and **54**.

Reaction of the mixture of **53** and **54** (ratio of **53**:**54** of 20:80) with thionyl chloride and pyridine at 4°C in toluene (17 h) revealed *selective* dehydration of **53** to **43**; the resulting mixture of **43** and **54** is directly acetylated to afford a mixture of **43** and **57** from which the latter could be isolated, for the first time, as a pure crystalline solid. Single crystal X-ray analysis (Fig. 1) established the structure and stereochemistry of **57** and, in turn, the earlier proposed structures for the cyanohydrins **53** and **54**.

Based on the above results, an extremely efficient synthesis of the nitrile **43** from 2,2,6-trimethylcyclohexanone (**51**) was achieved without intermediate purification (Scheme 6). The steps followed were treatment of **51** with cyanide, treatment of the resultant mixture with thionyl chloride and pyridine at 4°C ("*trans*" elimination), followed by acetylation of the remaining "*cis*" isomer and finally "*cis*" pyrolytic elimination to give the desired nitrile **43**. The overall yield of **43**, from this four-step conversion, was 81%.

While the above studies were underway, we became aware of an independent program by Picard *et al.* (37), relating to

[5]Conventionally only one of each pair of enantiomers is drawn. The terms "*cis*" and "*trans*" have been adopted for compounds like **53** and **54** to indicate the stereochemistry of a β-proton relative to the hydroxyl group. A "*cis*" compound would have the hydroxyl group and the β-proton on the same side of the ring plane. This convention has been used by others, i.e., Picard *et al.* (37) and Holm (38).

Can. J. Chem. Downloaded from www.nrcresearchpress.com by 217.78.4.112 on 09/08/12
For personal use only.

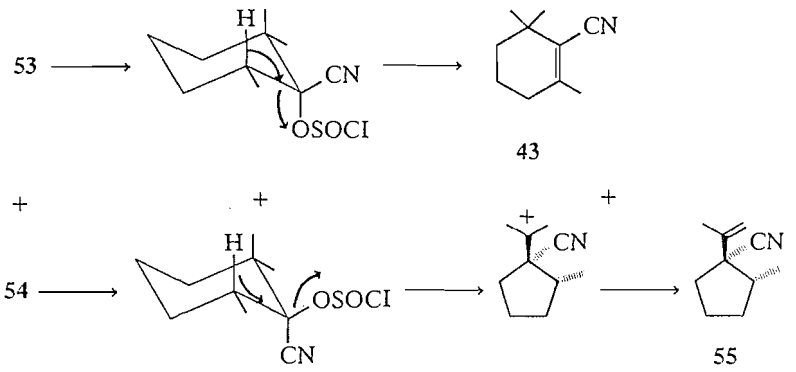

SCHEME 5. Rationale for the conversion of isomeric cyanohydrins **53** and **54** to **43** and **55** respectively.

TABLE 2. Formation of cyanohydrins **53** and **54** from 2,2,6-trimethylcyclohexanone

Expt. No.	Reagent	Temperature (°C)	Yield (%)	*"cis":"trans"*[a]
1	TMSCN	75–80	97	88:12[b]
2	NaCN	0–5	100	80:20
3	NaCN	0–15	100	77:23
4	NaCN	20	100	80:20
5	NaCN	60	97	70:30
6	Et_2AlCN	−15–+5	97	65:35

[a]Ratios determined by ^1H NMR analysis.
[b]Obtained as the trimethylsilyl cyanohydrins. Conversion of these cyanohydrins to **53** and **54** was achieved by reaction with HCl, MeOH.

the above. Through private exchange of information,[6] it is clear that their route involving the reaction of **51** with trimethylsilyl cyanide, separation of the resultant *cis* and *trans* products, and subsequent elaboration of the *trans* isomer to **43** is completely different from the sequence described herein.

In conclusion, the process involving the "one-pot" conversion of **51** to **43** (81% overall yield), which in turn affords **42** (47% overall yield from **51**) and **45**, when coupled with the earlier described chemistry provides a highly attractive route to the various damascones from cyclohexanone. In addition, these compounds are important building units; for example, **43** can be efficiently converted to the widespread natural terpenoid β-cyclocitral (**45**) and the latter, in turn, serves as a starting material in the syntheses of various natural products: thujopsene (39), safranal (32, 40, damascenone (**48**) (41), and widdrol (42) as examples.

[6]We are very grateful to Dr. Picard for informing us of his unpublished results.

Experimental

Melting points (with the recrystallization solvents given in parentheses) were determined using a Kofler block melting point apparatus and are uncorrected. Optical rotations were recorded on a Perkin–Elmer 141 automatic polarimeter in chloroform solution using a quartz cell of 10 cm pathlength with the concentration (in g/100 mL) given in parentheses. The infrared spectra were recorded on Perkin–Elmer 710, 710B, and 1710 spectrometers in chloroform solution (using NaCl cells of 0.1 mm pathlength) or as thin film (using NaCl plates). The ultraviolet spectra were recorded on Cary 15 or Unicam SP800 spectrometers using quartz cells of 1 cm pathlength. The ^1H NMR spectra were recorded on Bruker WH-400, AE-200, or Varian XL-300 spectrometers (with solvent given in parentheses) and the chemical shifts are reported on the delta (δ) scale in ppm relative to tetramethylsilane. Assignments, where given, are based on a combination of chemical shift,

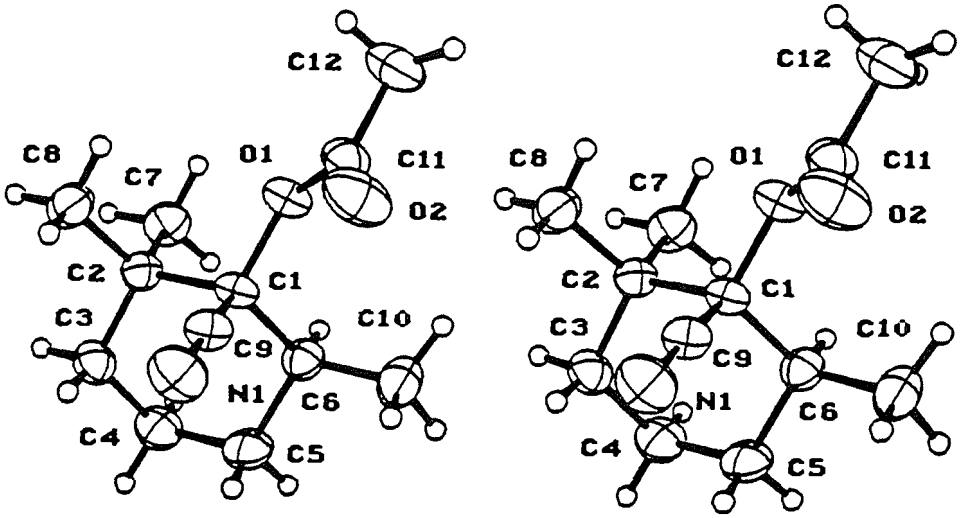

FIG. 1. Stereoview of **57**; 33% probability thermal ellipsoids are shown for the non-hydrogen atoms.

Can. J. Chem. Downloaded from www.nrcresearchpress.com by 217.78.4.112 on 09/08/12
For personal use only.

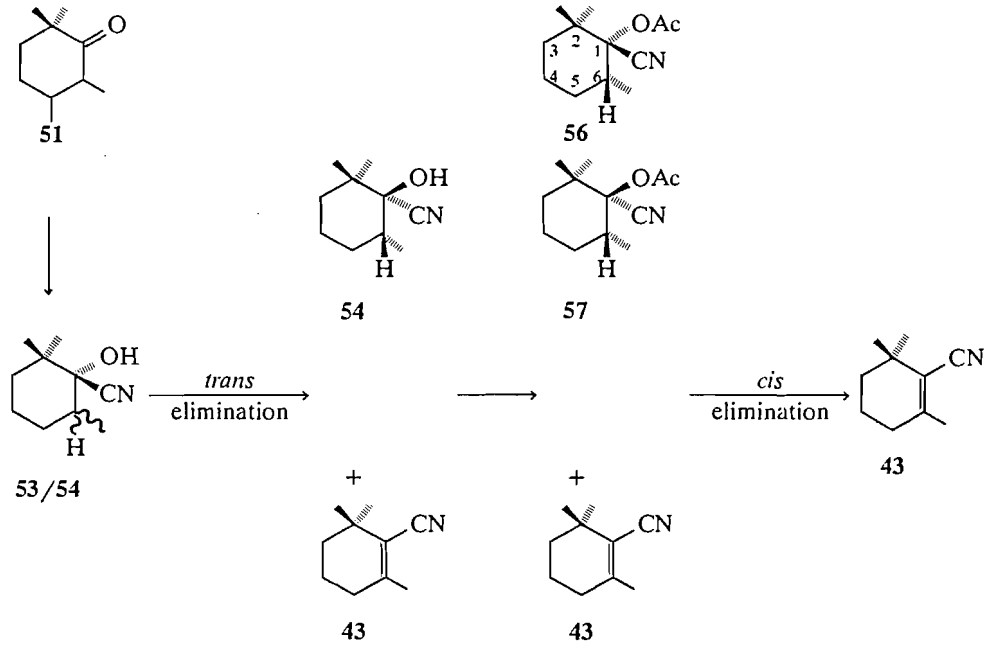

SCHEME 6. A highly efficient synthesis of β-cyclogeranotrile (**43**) from 2,2,6-trimethylcyclohexanone (**51**).

Can. J. Chem. Downloaded from www.nrcresearchpress.com by 217.78.4.112 on 09/08/12
For personal use only.

coupling constant, decoupling, and nOe difference data. The ^{13}C NMR spectra were recorded on Bruker AE-200 or Varian XL-300 spectrometers and the chemical shifts are reported on the delta (δ) scale in ppm relative to tetramethylsilane. The mass spectra were recorded on AEI-MS-9 or Kratos-MS-50 (using the electron impact ionization method for low and high-resolution analysis) or Delsi Nermag R10-10C (using the chemical ionization method) spectrometers. High-resolution mass measurements were obtained on samples that gave one peak on GC analysis or, in the case of mixtures of isomers, no unidentified peaks on GC analysis. Gas chromatography – mass spectroscopy (GC–MS) analyses were performed using a Varian 6000 chromatograph coupled to a Delsi Nermag R10-10C mass spectrometer. Elemental analyses were determined using a combustion technique by Mr. P. Borda, Microanalytical Laboratory, University of British Columbia. Gas chromatography (GC) was performed on a Hewlett–Packard 5890A gas chromatograph, using a flame ionization detector and a 25 m × 0.2 mm fused silica capillary column coated with cross-linked methyl silicone gum (HP1) or a 14.5 m × 0.252 mm fused silica capillary column coated with cyanopropylphenyl silicone gum (DP1701). Column chromatography was performed unless otherwise stated by modified "flash chromatography" (43) using columns of silica gel (230–400 mesh) with nitrogen gas pressure to obtain a suitable flow. Bulb-to-bulb distillation was performed using a Kugelrohr distillation apparatus obtained from Aldrich Chemical Co. with the air bath temperature at which distillation occurred given in parentheses.

All reactions were performed under a positive pressure of dry nitrogen at room temperature unless otherwise stated. Reactions performed at −78°C were cooled using a Dry Ice/acetone bath. All chromatography solvents were distilled prior to use. The term "petroleum ether" refers to commercially available hydrocarbons boiling in the 35–60°C range. "Active" manganese dioxide was prepared by the method of Attenburrow *et al.* (44) and tested by the method of Fatiadi (33). The source of "thujone" was redistilled Western red cedar leaf oil, which had a total thujone content ranging from 80 to 96%. Western red cedar leaf oil was obtained as a gift from Intrinsic Research and Development Incorporated.

Single crystal X-ray structure determinations were performed by Dr. S. Rettig with data obtained on a Rigaku AFC6S diffractometer (crystal structure data are available in the Appendix).

*(1S,5S) 4,4-Dimethyl-1-(1-methylethyl)-bicyclo[3.1.0]hexan-3-one (**8**) and (1S,2R,5S) 1-(1-methylethyl)-2,4,4-trimethylbicyclo[3.1.0]hexan-3-one (**9**)*

The source of "thujone" was redistilled cedar leaf oil, which had a total 3-(−)-isothujone/3-(+)-thujone content of 86%. Potassium *tert*-butoxide (157.6 g, 1.40 mol) was dissolved in *tert*-butanol (750 mL), diluted with anhydrous tetrahydrofuran (1500 mL), and the resulting solution heated to reflux. To this solution was added dropwise a solution of cedar leaf oil (158.6 g, 0.989 mol of thujone) in anhydrous tetrahydrofuran (750 mL) over 15 min. The reaction was stirred at reflux for a further 3 h, then cooled to room temperature. Iodomethane (88 mL, 1.4 mol) was added to the mixture, which was stirred for 85 min and then added to brine (2500 mL). The aqueous layer was extracted with petroleum ether (3 × 250 mL). The combined organic fractions were washed with brine (2 × 500 mL), dried (over $MgSO_4$), filtered, and evaporated *in vacuo* to give a yellow oil (164.2 g) that contained monomethylated thujone **8** (78.6%) and dimethylated thujone **9** (8.3%) by GC (1-menthol as internal standard). Based on the purity of the starting material, the yield for **8** is 86.4% and for **9** is 8.4%. It is possible to separate **8** from **9** either by repeated flash chromatography using diethyl ether/petroleum ether (1:19) as eluent, or by spinning band distillation.

Monomethylated thujone **8**: bp 68°C/8 Torr; (1 Torr = 133.3 Pa); $[\alpha]_D^{22}$ −22.2 ($CHCl_3$, *c* 0.144); IR ν_{max} (thin film): 2940, 2855, 1735 cm^{-1}; ^1H NMR (400 MHz, $CDCl_3$) δ: 0.01 (1H, dd, *J* = 6, 4 Hz, C6-H_{endo}), 0.64 (1H, ddd, *J* = 8, 6, 2.5 Hz, C6-H_{exo}), 0.96 (3H, d, *J* = 7 Hz, C7-CH_3), 1.02 (3H, d, *J* = 7 Hz, C7-CH_3), 1.03 (3H, s, C4-CH_3), 1.12 (3H, s, C4-CH_3), 1.17 (1H, dd, *J* = 8, 4 Hz, C5-H), 1.39 (1H, septet, *J* = 7 Hz, C7-H), 2.09 (1H, d, *J* = 19 Hz, C2-H_{endo}), 2.66 (1H, dd, *J* = 19, 2.5 Hz, C2-H_{exo}) ppm; MS *m/z*: 166 (M^+), 41 (100); high-resolution mass measurement calcd. for $C_{11}H_{18}O$: 166.1358; found: 166.1351. Anal. calcd. for $C_{11}H_{18}O$: C 79.47, H 10.91; found: C 79.53, H 10.90. ^1H NMR decoupling experiment: irradiation of the doublet of doublets resonating at δ 2.66 ppm collapsed the resonance at δ 2.09 ppm to a

Can. J. Chem. Downloaded from www.nrcresearchpress.com by 217.78.4.112 on 09/08/12
For personal use only.

singlet and simplified the doublet of doublet of doublets resonating at δ 0.64 ppm to a doublet of doublets (J = 8, 6 Hz).

Dimethylated thujone **9**: bp 68°C/8 Torr; $[\alpha]_D^{22}$ −49.2 ($CHCl_3$, c 3.282); IR ν_{max} (thin film): 2950, 2855, 1740 cm^{-1}; ^1H NMR (400 MHz, $CDCl_3$) δ: −0.16 (1H, dd, J = 6, 4 Hz, C6-H_{endo}), 0.54 (1H, ddd, J = 8, 6, 2 Hz, C6-H_{exo}), 0.98 (3H, d, J = 7 Hz, C7-CH_3), 0.99 (3H, s, C4-CH_3), 1.03 (3H, d, J = 7 Hz, C2-CH_{3endo}), 1.03 (3H, d, J = 7 Hz, C7-CH_3), 1.09 (3H, s, C4-CH_3), 1.12 (1H, m, C5-H), 1.51 (1H, septet, J = 7 Hz, C7-H), 2.80 (1H, qd, J = 7, 2 Hz, C2-H_{exo}) ppm; MS m/z: 180 (M^+), 165, 137, 123, 109, 83 (100); high-resolution mass measurement calcd. for $C_{12}H_{20}O$: 180.1514; found: 180.1510. Anal. calcd. for $C_{12}H_{20}O$: C 79.96, H 11.18; found: C 79.99, H 11.17. ^1H NMR decoupling experiment: irradiation of the quartet of doublets resonating at δ 2.80 ppm collapsed the doublet resonating at δ 1.03 ppm to a singlet and simplified the signal resonating at δ 0.54 ppm to a doublet of doublets (J = 8, 6 Hz).

*(1S,2R,5S) 1-(1-Methylethyl)-2,4,4-trimethylbicyclo[3.1.0] hexan-3-one (**9**), (1S,2S,5S) 1-(1-methylethyl)-2,4,4-trimethylbicyclo[3.1.0]hexan-3-one (**11**), and (1S,5S) 1-(1-methylethyl)-2,2,4,4-tetramethyl-bicyclo[3.1.0]hexan-3-one (**10**)*

To a solution of anhydrous diisopropylamine (0.93 mL, 6.6 mmol) in anhydrous tetrahydrofuran (50 mL) at −78°C was added *n*-butyllithium (1.55 M in hexanes, 4.25 mL, 6.58 mmol). The reaction was stirred for 50 min, then monomethylated thujone **8** (1.103 g, 6.64 mmol) in anhydrous tetrahydrofuran (20 mL) was added. The reaction was stirred at −78°C for 100 min, warmed to 10°C, and stirred for a further 60 min. Freshly purified iodomethane (1.23 mL, 19.8 mmol) was added and stirring continued for 40 min. The reaction was quenched by the addition of saturated ammonium chloride solution (30 mL) and extracted with diethyl ether (3 × 30 mL). The combined organic fractions were diluted with petroleum ether (150 mL), washed with brine (50 mL), dried (over $MgSO_4$), filtered, and evaporated *in vacuo* to give a yellow oil (1.132 g) that contained (by GC, 1-menthol as an internal standard) monomethylated thujone **8** (7.1%), dimethylated thujone **9** (24.9%), dimethylated thujone **11** (56.6%), and trimethylated thujone **10** (5.7%). Yield based on the calibration: **8** (7.3%); **9** (23.6%); **11** (53.6%); **10** (5.0%). To this oil (1.126 g) dissolved in ethanol (25 mL) was added potassium hydroxide (ca. 100 mg). The reaction was stirred for 7 h and the solvent evaporated *in vacuo*. The residue was diluted with diethyl ether (100 mL), washed with saturated ammonium chloride solution (3 × 50 mL), water (50 mL), dried (over $MgSO_4$), filtered, and evaporated *in vacuo* to give a yellow oil (0.9706 g) that contained (by GC, 1-menthol as an internal standard) **8** (7.2%), **9** (83.2%), **11** (1.5%), and **10** (6.0%).

In subsequent reactions a mixture of **8** and **9** was used. Thus, using the above procedure with **8**:**9** = 79:8 (54.405 g), 1.04 equivalents of lithium diisopropylamide, and 3 equivalents of iodomethane, an oil was obtained that was shown by GC (1-menthol as an internal standard) to contain **8** (24%), **9** (34%), **11** (25%), and **10** (10%). A solution of this oil and potassium hydroxide (4.20 g) in ethanol (400 mL) was stirred for 4.5 h. The reaction was quenched with saturated ammonium chloride solution (200 mL) and the organic solvent evaporated *in vacuo*. The residue was diluted with dichloromethane (200 mL) and the aqueous layer extracted with dichloromethane (2 × 200 mL). The combined organic layers were dried (over $MgSO_4$), filtered, and evaporated *in vacuo* to afford an oil (56.34 g) that was shown by GC (1-menthol as an internal standard) to contain **8** (22%), **9** (54%), **11** (1%), and **10** (11%).

Spinning band distillation followed by column chromatography on silica using diethyl ether/petroleum ether (1:19), followed by chromatography using diethyl ether/petroleum ether (2:98) gave pure samples of each of the four compounds. Dimethylated thujone **11**: mp 53–54°C; bp 67°C/8 Torr; $[\alpha]_D^{22}$ +15.6 ($CHCl_3$, c 0.63); IR ν_{max} ($CHCl_3$): 2960, 1740 cm^{-1}; ^1H NMR (400 MHz, $CDCl_3$) δ: −0.26 (1H, dd, J = 6, 5 Hz, C6-H_{endo}), 0.71 (3H, d, J = 7 Hz, C7-CH_3), 0.72 (1H, m, C6-H_{exo}), 0.98 (3H, d, J = 7 Hz, C7-CH_3), 1.03 (3H, s, C4-CH_3), 1.17 (3H, s, C4-CH_3), 1.26 (3H, d, J = 8 Hz, C2-CH_{3exo}), 1.40 (1H, dd, J = 9, 5 Hz, C5-H), 2.16 (1H, septet, J = 7 Hz, C7-H), 2.31 (1H, q, J = 8 Hz, C2-H_{endo}) ppm; MS m/z: 180 (M^+), 165, 152, 137, 83 (100); high-resolution mass measurement calcd. for $C_{12}H_{20}O$: 180.1514; found: 180.1511. Anal. calcd. for $C_{12}H_{20}O$: C 79.96, H 11.18; found: C 79.84, H 11.17. ^1H NMR decoupling experiments: irradiation of the signal resonating at δ −0.26 ppm affected the multiplet resonating at δ 0.72 ppm and simplified the doublet of doublets resonating at δ 1.40 ppm to a doublet (J = 9 Hz); irradiation of the doublet resonating at δ 1.26 ppm collapsed the quartet resonating at δ 2.31 ppm to a singlet.

Trimethylated thujone **10**: bp 68°C/8 Torr; $[\alpha]_D^{22}$ +15.7 ($CHCl_3$, c 0.70); IR ν_{max} ($CHCl_3$): 2975, 1735 cm^{-1}; ^1H NMR (400 MHz, $CDCl_3$) δ: −0.24 (1H, dd, J = 6.5, 4 Hz, C6-H_{endo}), 0.66 (1H, dd, J = 8.5, 4 Hz, C6-H_{exo}), 0.76 (3H, d, J = 7 Hz, C7-CH_3), 1.00 (3H, d, J = 7 Hz, C7-CH_3), 1.01 (3H, s), 1.07 (3H, s), 1.19 (3H, s), 1.22 (3H, s), 1.39 (1H, dd, J = 8.5, 6.5 Hz, C5-H), 2.20 (1H, septet, J = 7 Hz, C7-H) ppm; MS m/z: 194 (M^+), 179, 166, 123 (100); high-resolution mass measurement calcd. for $C_{13}H_{22}O$: 194.1671; found: 194.1666. Anal. calcd. for $C_{13}H_{22}O$: C 80.36, H 11.41; found: C 80.51, H 11.39. ^1H NMR decoupling experiments: irradiation of the doublet of doublets resonating at δ −0.24 ppm simplified the doublet of doublets resonating at δ 0.66 ppm to a doublet (J = 8.5 Hz) and simplified the doublet of doublets resonating at δ 1.39 ppm to a doublet (J = 8.5 Hz); irradiation of the septet resonating at δ 2.20 ppm collapsed the doublet resonating at δ 0.76 ppm to a singlet and collapsed the doublet resonating at δ 1.00 ppm to a singlet.

*Equilibration of **9** and **11***

A solution of dimethylthujone **11** (260.5 mg, 1.45 mmol) and potassium hydroxide (128 mg, 2.29 mmol) in ethanol (8 mL) was stirred for 4 h, then quenched with saturated ammonium chloride solution (20 mL). The organic solvent was evaporated *in vacuo* and the residue extracted with diethyl ether (3 × 30 mL). The combined organic fractions were dried (over $MgSO_4$), filtered, and evaporated *in vacuo* to leave a yellow oil (182.0 mg). Purification by flash chromatography using diethyl ether/petroleum ether (1:19) as eluent afforded a colourless oil (169.4 mg, 65% recovery) that was shown by GC (1-menthol as an internal standard) to contain **9** (98.6%) and **11** (1.4%).

A solution of dimethylthujone **9** (149.0 mg, 0.83 mmol) and potassium hydroxide (60 mg, 1.1 mmol) in ethanol (4 mL) was stirred for 4 h. The solvent was evaporated *in vacuo* and diethyl ether (30 mL) was added. The solution was washed with saturated ammonium chloride solution (10 mL), dried (over $MgSO_4$), filtered, and evaporated *in vacuo* to leave a yellow oil. Purification by flash chromatography using diethyl ether/petroleum ether (1:19) as eluent afforded a colourless oil (85.9 mg, 58% recovery) that was shown by GC (1-menthol as an internal standard) to contain **9** (98.8%) and **11** (1.2%).

*(1S,2R,3S,5S) 1-(1-Methylethyl)-2,4,4-trimethyl-3-trimethylsiloxybicyclo[3.1.0]hexane-3-carbonitrile (**12**) and (1S,2R,3R,5S) 1-(1-methylethyl)-2,4,4-trimethyl-3-trimethylsiloxybicyclo[3.1.0]hexane-3-carbonitrile (**13**)*

To a mixture of ketone **9** (906 mg, 5.03 mmol) and tetra-*n*-butylammonium cyanide (157 mg, 0.577 mmol) was added trimethylsilylcyanide (1.0 mL, 7.3 mmol). The solution was stirred at 75°C for 8 h, cooled, and added to pentane (50 mL) (the flask being washed with dichloromethane (3 mL)). The solution was filtered, evaporated *in vacuo*, and the residue dissolved in pentane (20 mL). Filtration through Celite followed by evaporation *in vacuo*

Can. J. Chem. Downloaded from www.nrcresearchpress.com by 217.78.4.112 on 09/08/12
For personal use only.

gave a yellow oil (1.379 g, 98%) that was shown by GC to contain trimethylsilyl enol ether **14** (2%), trimethylsilyl cyanohydrin **12** (70%), and trimethylsilyl cyanohydrin **13** (28%). The material was used in subsequent reactions without further purification.

Repeating the reaction on a larger scale followed by purification by flash chromatography using hexanes as eluent afforded a pure sample of trimethylsilyl enol ether **14**. Mixtures of **12** and **13** enriched in either **12** or **13** (up to 84%) were obtained.

Silyl cyanohydrins **12/13**: IR ν_{max} (thin film): 2955, 2220 (weak) cm^{-1}; ^1H NMR (400 MHz, $CDCl_3$) (signals corresponding to **12**) δ: 0.15 (1H, ddd, J = 8, 5, 1 Hz, C6-H_{exo}), 0.23 (9H, s, Si-$(CH_3)_3$), 0.85 (3H, d, J = 7 Hz, C7-CH_3), 0.87 (2H, m, C5-H, C6-H_{endo}), 0.95 (3H, d, J = 7 Hz, C7-CH_3), 1.06 (3H, s, C4-CH_3), 1.07 (3H, d, J = 7 Hz, C2-CH_3), 1.24 (3H, s, C4-CH_3), 1.50 (1H, septet, J = 7 Hz, C7-H), 2.72 (1H, qd, J = 7, 1 Hz, C2-H_{exo}) ppm; (signals corresponding to **13**) δ: 0.24 (9H, s, Si-$(CH_3)_3$), 0.25 (1H, m), 0.86 (3H, d, J = 7 Hz, C7-CH_3), 0.88 (1H, m), 0.96 (3H, d, J = 7 Hz, C7-CH_3), 1.00 (3H, s, C4-CH_3), 1.22 (3H, d, J = 7 Hz, C2-CH_3), 1.24 (3H, s, C4-CH_3), 1.26 (1H, m), 1.44 (1H, septet, J = 7 Hz, C7-H), 2.40 (1H, qd, J = 7, 1 Hz, C2-H_{exo}) ppm; MS m/z: 264 (M^+-15), 252, 237 (100); CI MS (NH_3): 297 ($M + NH_4^+$), 264; high-resolution mass measurement calcd. for $C_{15}H_{26}NSiO$: 264.1783; found: 264.1782. Anal. calcd. for $C_{16}H_{29}NSiO$: C 68.76, H 10.46, N 5.01; found: C 68.82, H 10.35, N 5.04.

*(1S,2R,5S) 1-(Methylethylene)-2,4,4-trimethyl-3-trimethylsiloxybicyclo[3.1.0]hexane-3-carbonitrile (**15/16**), (1S,2R,5S) 1-acetyl-2, 4, 4-trimethyl-3-trimethylsiloxybicyclo[3.1.0]hexane-3-carbo-nitrile (**17/18**) and (1S,2R,5S) 1-(1-hydroxy-1-methylethyl)-2,4,4-trimethyl-3-trimethylsiloxybicyclo[3.1.0]hexane-3-carbonitrile (**19/20**)*

Ozone was bubbled through a solution of trimethylsilyl cyanohydrins[7] (**12**:**13** = 28:70, 1.899 g, 6.79 mmol) and sodium bicarbonate (2.25 g) in ethyl acetate (400 mL) at 0°C for 8 h. The reaction was flushed with nitrogen, filtered, and evaporated *in vacuo* to give an oil (4.082 g). The residue was dissolved in dichloromethane (80 mL), washed with sodium bicarbonate solution (25 mL), dried (over $MgSO_4$), filtered, and evaporated *in vacuo* to give an oil (2.355 g). Purification of a portion of this oil (1.330 g) by flash chromatography using ethyl acetate/petroleum ether (1:39) as eluent gave a mixture of epimeric alkenes **15**:**16** (60:40) (16.1 mg, 1%) as a colourless oil. Further elution with ethyl acetate/petroleum ether (1:19) gave a mixture of epimeric ketones **17**:**18** (71:29) (486 mg, 45%) as a colourless oil. Further elution with ethyl acetate/petroleum ether (1:9) gave a mixture of epimeric alcohols **19**:**20** (66:34) (241 mg, 21%) as a white solid.

Alkenes **15/16**: ^1H NMR (400 MHz, $CDCl_3$) (signals corresponding to **15**) δ: 0.23 (9H, s, Si$(CH_3)_3$), 0.58 (1H, ddd, J = 8, 4.5, 1.5 Hz, C6-H_{exo}), 1.03 (3H, d, J = 7 Hz, C2-CH_3), 1.08 (3H, s, C4-CH_3), 1.08 (1H, m), 1.27 (1H, m), 1.28 (3H, s, C4-CH_3), 1.70 (3H, br s, $w_{h/2}$ = 3 Hz, C7-CH_3), 2.88 (1H, qd, J = 7, 1.5 Hz, C2-H), 4.78 (1H, br s, $w_{h/2}$ = 4 Hz, C8-H), 4.85 (1H, br s, $w_{h/2}$ = 5 Hz, C8-H) ppm; (signals corresponding to **16**) δ: 0.23 (9H, s, Si$(CH_3)_3$), 0.69 (1H, ddd, J = 8, 6.5, 1.5 Hz, C6-H_{exo}), 1.05 (3H, s, C4-CH_3), 1.08 (1H, m), 1.18 (3H, d, J = 7 Hz, C2-CH_3), 1.25 (3H, s, C4-CH_3), 1.27 (1H, m), 1.70 (3H, br s, $w_{h/2}$ = 3 Hz, C7-CH_3), 2.56 (1H, qd, J = 7, 1.5 Hz, C2-H), 4.78 (1H, br s, $w_{h/2}$ = 4 Hz, C8-H), 4.85 (1H, br s, $w_{h/2}$ = 5 Hz, C8-H) ppm; MS m/z: 277(M^+), 262, 250, 235, 107 (100); high-resolution mass measurement calcd. for $C_{16}H_{27}NOSi$: 277.1862; found: 277.1863.

Ketones **17/18**: IR ν_{max} (thin film): 2960, 1690 cm^{-1}; ^1H NMR (400 MHz, $CDCl_3$) (signals corresponding to **17**) δ: 0.24 (9H, s, Si$(CH_3)_3$), 1.12 (3H, s, C4-CH_3), 1.13 (3H, d, J = 7 Hz, C2-CH_3), 1.24 (3H, s, C4-CH_3), 1.25 (1H, m), 1.59 (1H, t, J = 6 Hz), 1.69 (1H, dd, J = 8, 6 Hz), 1.92 (3H, s, $COCH_3$), 3.37 (1H, qd, J = 7, 1 Hz, C2-H) ppm; (signals corresponding to **18**) δ: 0.23 (9H, s, Si$(CH_3)_3$, 1.02 (3H, s, C4-CH_3), 1.25 (1H, m), 1.29 (3H, d, J = 7 Hz, C2-CH_3), 1.29 (3H, s, C4-CH_3), 1.52 (1H, dd, J = 8, 6 Hz), 1.71 (1H, dd, J = 9, 6 Hz), 1.94 (3H, s, $COCH_3$), 2.95 (1H, qd, J = 7, 1 Hz, C2-H) ppm; MS m/z: 279(M^+), 264, 252; high-resolution mass measurement calcd. for $C_{15}H_{25}NO_2Si$: 279.1654; found: 279.1658. Anal. calcd. for $C_{15}H_{25}NO_2Si$: C64. 47, H 9.02, N 5.01; found: C 64.25, H 9.20, N 5.00.

Alcohols **19/20**: mp 35–37°C; IR ν_{max} ($CHCl_3$): 3601 (sharp), 2972 cm^{-1}; ^1H NMR (400 MHz, $CDCl_3$) (signals corresponding to **19**) δ: 0.23 (9H, s, Si$(CH_3)_3$), 0.45 (1H, ddd, J = 8.5, 5, 1.5 Hz, C6-H_{exo}), 0.95 (1H, t, J = 5 Hz), 1.06 (3H, s, C4-CH_3), 1.10 (1H, dd, J = 8.5, 5 Hz), 1.11 (1H, br s, $w_{h/2}$ = 8 Hz, exchangeable, OH), 1.15 (3H, d, J = 7 Hz, C2-CH_3), 1.16 (3H, s, C4-CH_3), 1.24 (3H, s, C7-CH_3), 1.26 (3H, s, C7-CH_3), 2.92 (1H, qd, J = 7, 1.5 Hz, C2-H) ppm; (signals corresponding to **20**) δ: 0.23 (9H, s, Si$(CH_3)_3$), 0.58 (1H, ddd, J = 8.5, 6.5, 1.5 Hz, C6-H_{exo}), 0.90 (1H, dd, J = 6.5, 4 Hz), 1.02 (3H, s, C4-CH_3), 1.11 (1H, br s, $w_{h/2}$ = 8 Hz, exchangeable, OH), 1.13 (1H, m), 1.19 (3H, s, C4-CH_3), 1.24 (3H, s, C7-CH_3), 1.26 (3H, s, C7-CH_3), 1.30 (3H, d, J = 7 Hz, C2-CH_3), 2.58 (1H, qd, J = 7, 1.5 Hz, C2-H) ppm; MS m/z: 295 (M^+), 280, 277, 262; high-resolution mass measurement calcd. for $C_{16}H_{29}NO_2Si$: 295.1968; found: 295.1966. Anal. calcd. for $C_{16}H_{29}NO_2Si$: C 65.04, H 9.89, N 4.74; found: C 64.81, H 9.93, N 4.87. ^1H NMR decoupling experiments: irradiation of the quartet of doublets resonating at δ 2.58 ppm collapsed the doublet resonating at δ 1.30 ppm to a singlet and simplified the doublet of doublet of doublets resonating at δ 0.58 ppm to a doublet of doublet (J = 8.5, 6.5 Hz); irradiation of the quartet of doublets resonating at δ 2.92 ppm collapsed the doublet resonating at δ 1.15 ppm to a singlet and simplified the doublet of doublet of doublets resonating at δ 0.45 ppm to a doublet of doublet (J = 8.5, 5 Hz).

*(1S,2R,5S) 1-(1-Chloro-1-methylethyl)-2,4,4-trimethyl-3-(trimethylsiloxy)bicyclo[3.1.0]hexane-3-carbonitrile (**23/24**)*

To a solution of alcohols **19**:**20** (60:40, 59.0 mg, 0.227 mmol) in dichloromethane (2 mL) at 0°C was added cold concentrated hydrochloric acid (2 mL). After vigorous stirring for 20 min, the organic fraction was separated, diluted with cold dichloromethane (10 mL), washed with cold brine (10 mL), dried (over $MgSO_4$), filtered, and evaporated *in vacuo* to give a red oil. GC analysis indicated a 60:40 mixture of the unstable chlorides **23/24**. Partial ^1H NMR (400 MHz, $CDCl_3$) (approximately 30% decomposition to alkenes) (signals corresponding to **23**) δ: 0.63 (1H, ddd, J = 8, 6, 1.5 Hz, C6-H_{exo}), 3.11 (1H, qd, J = 7, 1.5 Hz, C2-H) ppm; (signals corresponding to **24**) δ: 0.75 (1H, ddd, J = 9, 7, 1.5 Hz, C6-H_{exo}), 2.78 (1H, qd, J = 7, 1.5 Hz, C2-H) ppm; MS m/z: 315/313 (M^+), 300/298, 277.

*(2R,4S) 4-Chloromethyl-3-(1-methylethylidene)-2,5,5-trimethyl-1-(trimethylsiloxy)cyclopentane-1-carbonitrile (**21**)*

To a solution of alcohols **19**:**20** (60:40, 192.0 mg, 0.650 mmol) in dichloromethane (10 mL) was added concentrated hydrochloric acid (10 mL). The reaction was stirred vigorously for 88 h. The aqueous layer was extracted with dichloromethane (2 × 50 mL). The combined organic fractions were washed with sodium bicarbonate (50 mL), dried (over $MgSO_4$), filtered, and evaporated *in vacuo* to give a red oil. Purification by flash chromatography using ethyl acetate/petroleum ether (1:19) as eluent afforded a mixture of these three isomeric chlorides (105.4 mg, 52%), of which **21** is predominant (83%): IR ν_{max} (thin film): 2974, 2232, 1673 cm^{-1}. Anal. calcd. for $C_{16}H_{28}NOSiCl$: C 61.22, H 8.99, N 4.46; found: C 61.50, H 9.10, N 4.63.

Further repeated chromatography using diethyl ether/petroleum ether (3:97) as eluent gave a pure sample of chloride **21** as a colourless oil: ^1H NMR (400 MHz, $CDCl_3$) δ: 0.28 (9H, s, Si$(CH_3)_3$), 1.10 (3H, s, C5-CH_3), 1.15 (3H, d, J = 7 Hz, C2-CH_3), 1.25 (3H, s, C5-CH_3), 1.70 (3H, br s, $w_{h/2}$ = 3 Hz, C=C-CH_3), 1.75 (3H, br s, $w_{h/2}$ = 3 Hz, C=C-CH_3), 2.67 (1H, dd, J = 8, 5.5 Hz, C4-H), 3.16 (1H, br q, J = 7 Hz, C2-H), 3.47 (1H, dd, J = 11.5, 5.5 Hz, C4-C*H*Cl), 3.87 (1H, dd, J = 11.5, 8 Hz, C4-

[7]Contains 2% trimethylsilyl enol ether **14**.

Can. J. Chem. Downloaded from www.nrcresearchpress.com by 217.78.4.112 on 09/08/12
For personal use only.

CHCl) ppm; MS *m/z*: 315/313 (M^+), 300/298, 277, 262; high-resolution mass measurement calcd. for $C_{16}H_{28}NOSi^{35}Cl$: 313.1629; found: 313.1631.

(2R) 3-(1-Methylethylidene)-2,6,6-trimethyl-1-(trimethylsiloxy)-cyclohexane-1-carbonitrile (27/28)

A solution of the chlorides obtained in the preceeding section (314.0 mg, 1.00 mmol, containing **21** (83%)), 2,2 azobis(2-methylpropionitrile) (AIBN, 33.0 mg, 0.20 mmol), and tri-*n*-butyltin hydride (1.08 mL, 4.00 mmol) in anhydrous toluene (10 mL) was heated at reflux for 4 h. The solvent was evaporated *in vacuo* to leave an oil (>1 g). Purification by flash chromatography using petroleum ether as eluent removed the tin compound present. Further elution using diethyl ether/petroleum ether (1:199) gave a mixture of alkenes **27/28** (83:17, 193.0 mg, 69%). Further purification by flash chromatography using diethyl ether/petroleum ether (1:199) afforded a pure sample of **27**: ^{1}H NMR (400 MHz, $CDCl_3$) δ: 0.29 (9H, s, $Si(CH_3)_3$), 1.03 (3H, s, C6-CH_3), 1.07 (3H, d, J = 7 Hz, C2-CH_3), 1.09 (3H, s, C6-CH_3), 1.48 (2H, m, C5-H_2), 1.72 (6H, br s, $w_{h/2}$ = 4 Hz, C=C-$(CH_3)_2$), 2.03 (1H, m, C4-H), 2.44 (1H, dtd, J = 14, 3, 1 Hz, C4-H), 3.28 (1H, q, J = 7 Hz, C2-H) ppm.

(1S,2R,5S) 1-(1-Hydroxyethyl)-2,4,4-trimethyl-3-(trimethylsiloxy)bicyclo[3.1.0]hexane-3-carbonitrile (31, 32, 33, 34)

To a solution of ketones **17/18**[8] (504 mg, 1.80 mmol) in ethanol (20 mL) was added sodium borohydride (130 mg, 3.42 mmol). After stirring for 1.5 h at room temperature, the solvent was removed *in vacuo*. Diethyl ether (50 mL) and saturated ammonium chloride solution (50 mL) were added to the residue. The organic layer was washed with brine (20 mL), dried (over $MgSO_4$), filtered, and evaporated *in vacuo* to give an oil (554 mg). Purification by flash chromatography using ethyl acetate/petroleum ether (1:9) as eluent afforded a mixture of four isomeric alcohols **31, 32, 33, 34** (38:35:14:13) (411.6 mg, 92% based on purity of starting material) as a colourless oil: IR ν_{max} (thin film): 3475 (br), 2960, 2210 (weak) cm^{-1}; ^{1}H nmr (400 MHz, $CDCl_3$) (partial assignments for **31**) δ: 0.23 (9H, s, $Si(CH_3)_3$), 2.94 (1H, qd, J = 7, 1 Hz, C2-H), 3.60 (1H, q, J = 6.5 Hz, C7-H) ppm; (partial assignments for **32**) δ: 0.23 (9H, s, $Si(CH_3)_3$), 2.82 (1H, qd, J = 7, 1 Hz, C2-H), 3.70 (1H, q, J = 6.5 Hz, C7-H) ppm; (partial assignments for **33**) δ: 0.23 (9H, s, $Si(CH_3)_3$), 1.28 (3H, d, J = 7 Hz, C2-CH_3), 2.60 (1H, qd, J = 7, 1 Hz, C2-H), 3.56 (1H, q, J = 6.5 Hz, C7-H) ppm; (partial assignments for **34**) δ: 0.23 (9H, s, $Si(CH_3)_3$), 0.45 (1H, ddd, J = 7, 6, 1 Hz, C6-H_{exo}), 1.02 (3H, s, C4-CH_3), 1.27 (3H, d, J = 7 Hz, C2-CH_3), 2.50 (1H, qd, J = 7, 1 Hz, C2-H), 3.66 (1H, q, J = 6.5 Hz, C7-H) ppm; MS *m/z*: 281 (M^+), 279, 266, 263, 248, 239, 236; high-resolution mass measurement calcd. for $C_{15}H_{27}NO_2Si$: 281.1811; found: 281.1807. Anal. calcd. for $C_{15}H_{27}NO_2Si$: C 64.00, H 9.67, N 4.98; found: C 63.89, H 9.76, N 4.90.

(1S,2R,5S) 1-(1-Chloroethyl)-2,4,4-trimethyl-3-(trimethylsiloxy)bicyclo[3.1.0]hexane-3-carbonitrile (35/36)

To a solution of alcohols **31, 32, 33, 34** (38:35:14:13, 397.2 mg, 1.41 mmol) in dichloromethane (15 mL) was added concentrated hydrochloric acid (17 mL) and the reaction was stirred vigorously for 31 h. The aqueous layer was extracted with dichloromethane (10 mL). The combined organic layers were washed with water (25 mL), dried (over $MgSO_4$), filtered, and evaporated *in vacuo* to give a red oil (419.6 mg), which was shown by GC to contain no starting alcohols. Purification by flash chromatography using diethyl ether/petroleum ether (1:19) as eluent gave a mixture of chlorides **35/36** (63:37, 139.0 mg, 33%, 83% based on recovered starting material). Further elution afforded recovery of starting material (240.0 mg, 60%).

Chlorides **35/36**: IR ν_{max} (thin film): 2950, 2210, 1660 cm^{-1}; ^{1}H NMR (400 MHz, $CDCl_3$) (partial assignment of signals corresponding to **35**) δ: 0.23 (9H, s, $Si(CH_3)_3$), 0.47 (1H, ddd, J = 9, 7, 1.5 Hz, C6-H_{exo}), 1.08 (3H, s, C4-CH_3), 1.13 (3H, d, J = 7 Hz, C2-CH_3), 1.28 (3H, s, C4-CH_3), 1.40 (3H, d, J = 7 Hz, C7-CH_3), 3.03 (1H, qd, J = 7, 1.5 Hz, C2-H), 4.11 (1H, q, J = 7 Hz, C7-H) ppm; (partial assignment of signals corresponding to **36**) δ: 0.23 (9H, s, $Si(CH_3)_3$), 0.40 (1H, ddd, J = 9, 6, 1.5 Hz, C6-H_{exo}), 1.07 (3H, s, C4-CH_3), 1.17 (3H, d, J = 7 Hz, C2-CH_3), 1.29 (3H, s, C4-CH_3), 1.55 (3H, d, J = 7 Hz, C7-CH_3), 3.04 (1H, m, C2-H), 3.75 (1H, q, J = 7 Hz, C7-H) ppm; MS *m/z*: 301/299 (M^+), 286/284, 263; high-resolution mass measurement calcd. for $C_{15}H_{26}NOSi^{35}Cl$: 299.1472; found: 299.1471.

(2R) 3-(1-Ethylidene)-2,6,6-trimethyl-1-(trimethylsiloxy)cyclohexane-1-carbonitrile (37/38)

To a solution of chlorides **35/36** (63:37, 152.3 mg, 0.508 mmol) and AIBN (ca. 10 mg) in anhydrous toluene (4 mL) was added tri-*n*-butylin hydride (179 μl, 0.632 mmol). The reaction was heated at reflux for 2 h, cooled, and diluted with petroleum ether (50 mL). The reaction was washed with water (50 mL), dried (over $MgSO_4$), filtered, and evaporated *in vacuo* to give an oil (664.0 mg). Purification by flash chromatography using petroleum ether as eluent removed the tin by-products. Further elution with diethyl ether/petroleum ether (1:49) gave a mixture of predominantly two alkenes **37/38** (72:28) as a colourless oil (127.6 mg, 95%): IR ν_{max} (thin film): 2960, 1660 cm^{-1}; ^{1}H NMR (400 MHz, $CDCl_3$) (partial assignment of signals corresponding to **37**) δ: 0.21 (9H, s, $Si(CH_3)_3$), 1.05 (3H, s, C6-CH_3), 1.20 (3H, d, J = 7 Hz, C2-CH_3), 1.24 (3H, s, C6-CH_3), 1.62 (3H, br d, J = 7 Hz, C7-CH_3), 1.95 (1H, m), 2.48 (1H, dt, J = 14, 4 Hz, C4-H), 2.65 (1H, br q, J = 7 Hz, C2-H), 5.20 (1H, br q, J = 7 Hz, C7-H) ppm; (partial assignment of signals corresponding to **38**) δ: 0.29 (9H, s, $Si(CH_3)_3$), 1.04 (3H, s, C6-CH_3), 1.11 (3H, d, J = 7 Hz, C2-CH_3), 1.11 (3H, s, C6-CH_3), 1.65 (3H, dd, J = 7, 1 Hz, C7-CH_3), 1.93 (1H, m), 3.27 (1H, q, J = 7 Hz, C2-H), 5.41 (1H, qd, J = 7, 1.5 Hz, C7-H) ppm; MS *m/z*: 265 (M^+), 250, 238, 223.

(2R,3S*) 2,4,4-Trimethyl-3-trimethylsiloxycyclohexan-1-one-3-carbonitrile (29) and (2R*,3R*) 2,4,4-trimethyl-3-trimethylsiloxycyclohexan-1-one-3-carbonitrile (30)*

Method A

Ozone was bubbled through a solution of alkenes **37**:**38** (72:28) (80.3 mg, 0.303 mmol) in ethyl acetate (10 mL) at −78°C for 30 min. Dimethyl sulphide (0.5 mL) was then added and the reaction allowed to warm to room temperature. The reaction was diluted with diethyl ether (25 mL), washed with sodium bicarbonate solution (25 mL), dried (over $MgSO_4$), filtered, and evaporated *in vacuo* to give an oil (119.3 mg). Purification by flash chromatography using ethyl acetate/petroleum ether (1:9) as eluent gave ketone **29** (70.9 mg, 93%), slightly contaminated with its isomer **30** (5%). Further purification gave enriched purity to ketone **29** (purity 98.5%), and a sample enriched in **30** (17%).

Ketone **29**: $[\alpha]_D^{22}$ − 28.0 ($CHCl_3$, c = 0.3); IR ν_{max} (thin film): 2950, 1725 cm^{-1}; ^{1}H NMR (400 MHz, $CDCl_3$) δ: 0.23 (9H, s, $Si(CH_3)_3$), 1.17 (3H, s, C4-CH_3), 1.23 (3H, d, J = 7 Hz, C2-CH_3), 1.41 (3H, s, C4-CH_3), 1.60 (1H, ddd, J = 14, 6.5, 2 Hz, C5-H_{eq}), 2.01 (1H, td, J = 14, 5 Hz, C5-H_{ax}), 2.34 (1H, ddd, J = 14, 5, 2 Hz, C6-H_{eq}), 2.45 (1H, td, J = 14, 6.5 Hz, C6-H_{ax}), 2.89 (1H, q, J = 7 Hz, C2-H_{ax}) ppm; MS *m/z*: 253 (M^+), 238 (100); high-resolution mass measurement calcd. for $C_{13}H_{23}NO_2Si$: 253.1498; found: 253.1496. Anal. calcd. for $C_{13}H_{23}NO_2Si$: C 61.62, H 9.15, N 5.53; found: C 61.80, H 9.20, N 5.60. ^{1}H NMR decoupling experiment: irradiation of the quartet resonating at δ 2.89 ppm collapsed the doublet resonating at δ 1.23 ppm to a singlet. ^{1}H NMR nOe difference experiment: irradiation of the quartet resonating at δ 2.89 ppm led to enhancement of the signals resonating at δ 1.23, 1.41, and 2.45 ppm; irradiation of the singlet resonating at δ 0.23 ppm led to enhancement of the signals resonating at δ 1.17 and 1.23 ppm.

Ketone **30**: ^{1}H NMR (400 MHz, $CDCl_3$) (partial signals corre-

[8]Sample contained alcohols **19/20** (60.3 mg).

Can. J. Chem. Downloaded from www.nrcresearchpress.com by 217.78.4.112 on 09/08/12
For personal use only.

sponding to **30**) δ: 0.26 (9H, s, $Si(CH_3)_3$), 1.74 (1H, ddd, J = 14, 7, 3 Hz), 1.81 (1H, td, J = 14, 6 Hz), 2.74 (1H, q, J = 7 Hz) ppm. GC–MS of second isomer m/z: 253 (M^+), 238.

Method B

To a solution of cyanohydrins **12**:**13** (63:37) (5.6656 g, 20.27 mmol) in ethyl acetate (300 mL) was added solid sodium bicarbonate (2.0 g). The mixture was cooled to 0°C and ozone bubbled through for 9.5 h. The reaction was flushed with oxygen, diluted with ethyl acetate (400 mL), washed with saturated sodium bicarbonate solution (2 × 100 mL), water (100 mL), dried (over $MgSO_4$), filtered, and evaporated *in vacuo*. The residue was dissolved in ethanol (200 mL) and sodium borohydride (800 mg, 21.1 mmol) was added. After stirring for 30 min, the solvent was evaporated *in vacuo*. The residue was dissolved in diethyl ether (300 mL), washed with saturated ammonium chloride solution (2 × 100 mL), water (100 mL), dried (over $MgSO_4$), filtered, and evaporated *in vacuo* to give a colourless oil (6.50 g). This was dissolved in dichloromethane (300 mL) and concentrated hydrochloric acid (300 mL). After stirring vigorously for 78.5 h, the aqueous layer was separated and extracted with dichloromethane (100 mL). The combined organic fractions were washed with water (2 × 200 mL), dried (over $MgSO_4$), filtered, and evaporated *in vacuo* to give a yellow oil (5.00 g). To a solution of this oil in anhydrous toluene (165 mL) was added AIBN (400 mg, 2.8 mmol) and tri-*n*-butyltin hydride (8.0 mL, 30 mmol). The reaction was heated at reflux for 4.5 h, cooled, washed with water (100 mL), dried (over $MgSO_4$), filtered, and evaporated *in vacuo* to give an oil (12.11 g). Purification by flash chromatography using petroleum ether as eluent removed the tin compounds present. Further elution gave a mixture of alkenes (3.3427 g). This oil was dissolved in ethyl acetate (200 mL) and cooled to −78°C. Ozone was bubbled through the solution for 30 min until a blue colouration persists. Dimethyl sulphide (1 mL) was added and the reaction allowed to warm to room temperature. Most of the solvent was removed *in vacuo* and ethyl acetate (200 mL) was added. The solution was washed with saturated sodium bicarbonate solution (50 mL), water (50 mL), dried (over $MgSO_4$), filtered, and evaporated *in vacuo* to leave a colourless oil (3.21 g). Purification by flash chromatography using ethyl acetate/petroleum ether (1:9) as eluent gave ketone **30** contaminated with 5% of ketone **31** (1.8153 g, 35% for five steps).

*2,4,4-Trimethylcyclohex-2-en-1-one-3-carbonitrile (**39**)*

Thionyl chloride (2.1 mL, 29 mmol) was added slowly to a solution of cyanohydrin **29** (1.0000 g, 3.953 mmol) in methanol (55 mL) and the reaction was stirred for 2 h. The solvent was evaporated *in vacuo*, and diethyl ether (75 mL) was added to the residue. The organic solution was washed with saturated sodium bicarbonate solution (30 mL), brine (30 mL), dried (over $MgSO_4$), filtered, and evaporated *in vacuo* to leave an oil (820 mg). Purification by flash chromatography using diethyl ether/petroleum ether (1:9) as eluent gave an unidentified compound as an unstable oil (337.0 mg, 52%). Further elution gave ketone **39** as a colourless oil (306.1 mg, 48%).

Unidentified compound: IR ν_{max} (thin film): 3500 (br), 2950, 2195, 1645, 1580 cm^{-1}; UV λ_{max} (MeOH): 306 nm (ϵ = 4400), 217 nm (ϵ = 4550); ^1H NMR (400 MHz, $CDCl_3$) δ: 1.13 (6H, s, C6-$(CH_3)_2$), 2.05 (3H, s, C2-CH_3), 2.22 (2H, d, J = 6 Hz, C5-H_2), 4.88 (1H, t, J = 6 Hz, C4-H) ppm; MS m/z: 162 (M^+-1, 100).

Ketone **39**: IR ν_{max} (thin film): 2950, 2200, 1690, 1645 cm^{-1}; UV λ_{max} (MeOH): 248 nm (ϵ = 12 000); ^1H NMR (400 MHz, $CDCl_3$) δ: 1.22 (6H, s, C4-$(CH_3)_2$), 1.94 (2H, t, J = 7 Hz, C5-H_2), 2.06 (3H, s, C2-CH_3), 2.57 (2H, t, J = 7 Hz, C6-H_2) ppm; MS m/z: 163 (M^+), 148, 135, 121, 120 (100); high-resolution mass measurement calcd. for $C_{10}H_{13}NO$: 163.0997; found: 163.0994.

*2,4,4-Trimethylcyclohex-2-en-1-ol-3-carbonitrile (**40**)*

Method A

To a solution of enone **39** (163.0 mg, 1.00 mmol) in methanol (2.5 mL) was added cerium III chloride heptahydrate (372 mg, 1.00 mmol) followed by sodium borohydride (38.0 mg, 1.00 mmol). After stirring for 5 min, the reaction was quenched by addition of saturated ammonium chloride solution (30 mL), diluted with diethyl ether (30 mL), and the aqueous layer extracted with diethyl ether (10 mL). The combined organic extracts were washed with water (10 mL), dried (over $MgSO_4$), filtered, and evaporated *in vacuo* to give allylic alcohol **40** (163.3 mg, 99%) as a viscous oil that crystallized on cooling: mp 25–26°C; IR ν_{max} (thin film): 3400, 2950, 2220, 1645 cm^{-1}; UV λ_{max} (MeOH): 216 nm (ϵ = 8100); ^1H NMR (400 MHz, $CDCl_3$) δ: 1.11 (3H, s, C4-CH_3), 1.17 (3H, s, C4-CH_3), 1.48 (1H, ddd, J = 13.5, 9, 3 Hz) 1.68 (2H, m), 1.90 (1H, m), 2.08 (3H, s, C2-CH_3), 2.58 (1H, br s, $w_{h/2}$ = 28 Hz, exchangeable, OH), 4.03 (1H, t, J = 6 Hz, Cl-H) ppm; ^{13}C NMR (50 MHz, $CDCl_3$) δ: 19.8, 27.9, 28.0, 28.3, 33.0, 33.7, 68.3, 117.2, 119.9, 151.9 ppm; MS m/z: 165 (M^+), 150, 123, 109 (100); high-resolution mass measurement: calcd. for $C_{10}H_{15}NO$: 165.1154; found: 165.115. Anal. calcd. for $C_{10}H;1_5NO$: C 72.70, H 9.15, N 8.48; found: C 72.73, H 9.30, N 8.35.

Method B

Thionyl chloride (1.0 mL, 13 mmol) was added slowly to a solution of cyanohydrin **29** (1.659 g, 6.55 mmol) in methanol (65 mL) at −10°C. The reaction was warmed to room temperature, and stirred for 2.5 h. The solvent was evaporated *in vacuo* and diethyl ether (70 mL) was added to the residue. The organic solution was washed with saturated sodium bicarbonate solution (50 mL), water (50 mL), dried (over $MgSO_4$), filtered, and evaporated *in vacuo* to leave an oil (1.0033 g). This oil was dissolved in methanol (15.5 mL) and cerium III chloride heptahydrate (2.291 g, 6.15 mmol) was added. After cooling to −78°C, sodium borohydride (245.0 mg, 6.48 mmol) was added in small portions. The reaction was allowed immediately to warm to room temperature with stirring proceeding at this temperature for 30 min. The reaction was diluted with diethyl ether (100 mL) and saturated ammonium chloride solution (50 mL). The aqueous layer was extracted with diethyl ether (2 × 50 mL). The combined organic layers were washed with water (20 mL), dried (over $MgSO_4$), filtered, and evaporated *in vacuo* to leave a yellow oil (1.028 mg). Purification by flash chromatography using ethyl acetate/petroleum ether (3:7) as eluent gave alcohol **40** (990.5 mg, 92%) as a colourless oil that crystallized on cooling.

Method C

To a solution of unsaturated nitrile **43** (1.1254 g, 7.54 mmol) in carbon tetrachloride (25 mL) was added *N*-bromosuccinimide (1.520 g, 8.54 mmol) and benzoyl peroxide (40 mg, 1.7 × 10^{-1} mmol). The reaction was heated at reflux for 40 min, then cooled and filtered to give a crude sample of bromide **41** (1.8548 g) as a red oil. Water (55 mL) and calcium carbonate (1.07 g, 10 mmol) were added and the reaction heated at reflux for 19 h. The reaction was cooled, diluted with diethyl ether (75 mL), and the aqueous layer extracted with diethyl ether (2 × 75 mL). The combined organic layers were washed with water (50 mL), dried (over $MgSO_4$), filtered, and evaporated *in vacuo* to give a yellow oil. Purification by flash chromatography using ethyl acetate/petroleum ether (3:7) as eluent gave enone **39** (144.8 mg, 12%) as a colourless oil. Further elution afforded alcohol **40** (987.4 mg, 79%) as a colourless oil that crystallized on cooling.

*2,6,6-Trimethyl-3-bromocyclohex-1-ene-1-carbonitrile (**41**)*

To a solution of alcohol **40** (355.2 mg, 2.15 mmol) in petroleum ether (5 mL) at 0°C was added phosphorus tribromide (225 μL, 2.37 mmol). The reaction was stirred for 1 h at 0°C, then diluted with petroleum ether (25 mL), washed with sodium bicarbonate solution (2 × 20 mL), dried (over $MgSO_4$), filtered, and evaporated *in vacuo* to give bromide **41** (449.0 mg, 92%) as a colourless oil: IR ν_{max} (thin film): 2965, 2210, 1626 cm^{-1}; UV λ_{max} (MeOH): 229 nm (ϵ = 12 300); ^1H NMR (400 MHz, $CDCl_3$) δ: 1.11 (3H, s, C6-CH_3), 1.24 (3H, s, C6-CH_3), 1.57 (1H, dt, J = 13, 3.5 Hz, C5-H), 1.96 (1H, ddd, J = 13, 10, 6 Hz, C5-H), 2.10 (2H, m, C4-H_2), 2.13 (3H, s, C2-CH_3), 4.63 (1H, t, J = 3 Hz,

Can. J. Chem. Downloaded from www.nrcresearchpress.com by 217.78.4.112 on 09/08/12
For personal use only.

C3-H) ppm; MS *m/z*: 229/227 (M^+), 214/212, 148 (100); high-resolution mass measurement calcd. for $C_{10}H_{14}N^{81}Br$: 229.0291; found: 229.0288. Anal. calcd. for $C_{10}H_{14}NBr$: C 52.64, H 6.18, N 6.16; found: C 52.85, H 6.19, N 6.30.

*2,6,6-Trimethylcyclohex-1-ene-1-carbonitrile (**43**)*

A solution of bromide **41** (1.088 g, 4.77 mmol) and sodium iodide (980 mg, 6.54 mmol) in anhydrous dimethyl sulphoxide (100 mL) was stirred at room temperature for 15 min, at which time sodium borohydride (630 mg, 16.5 mmol) and methanol (600 μL, 14.8 mmol) were added. After stirring for a further 1.5 h, the reaction was quenched with water (50 mL) and extracted with diethyl ether (2 × 100 mL). The combined organic layers were dried (over $MgSO_4$), filtered, and evaporated *in vacuo* to give a colourless oil (932.6 mg). Purification by flash chromatography using diethyl ether/petroleum ether (1:49) as eluent afforded a mixture of nitriles **43** and **44** (22:3, 501.9 mg, 71%). Further elution afforded a pure sample of nitrile **43** (99.8 mg, 14%) as a colourless oil.

Nitrile **43**: IR ν_{max} (thin film): 2930, 2200, 1635 cm^{-1}; UV λ_{max} (MeOH): 214 nm (ϵ = 11 400); ^1H NMR (400 MHz, $CDCl_3$) δ: 1.16 (6H, s, C6-$(CH_3)_2$), 1.46 (2H, m, C5-H_2), 1.61 (2H, m, C4-H_2), 1.96 (3H, s, C2-CH_3), 2.07 (2H, t, J = 6 Hz, C3-H_2) ppm; ^{13}C NMR (50 MHz, $CDCl_3$) δ: 19, 24, 28, 32, 34, 37, 116, 118, 152 ppm; MS *m/z*: 149 (M^+), 134 (100); high-resolution mass measurement calcd. for $C_{10}H_{15}N$: 149.1204; found: 149.1204. Anal. calcd. for $C_{10}H_{15}N$: C 80.48, H 10.13, N 9.39; found: C 80.18, H 9.99, N 9.48. ^1H NMR decoupling experiment: irradiation of the triplet resonating at δ 2.07 ppm affected the multiplet resonating at δ 1.61 ppm.

Nitrile **44**: ^1H NMR (400 MHz, $CDCl_3$) (partial signals) δ: 1.82 (3H, br s, $w_{h/2}$ = 7 Hz, C2-CH_3), 2.75 (1H, s, C1-H), 5.65 (1H, br s, $w_{h/2}$ = 8 Hz, C3-H) ppm.

*2,6,6-Trimethylcyclohexa-1,3-diene-1-carbonitrile (**127**)*

Method A

A solution of alcohol **40** (24.6956 g, 149.5 mmol) and *para*-toluenesulphonic acid (5.00 g, 26.3 mmol) was heated at reflux with azeotropic removal of water for 30 h. The reaction was cooled, diluted with diethyl ether (1 L), washed with water (2 × 200 mL), dried (over $MgSO_4$), filtered, and evaporated *in vacuo* to leave a red oil (22.6472 g). Purification by distillation (100–120°C, 11 Torr) gave safronitrile (**42**) (16.4631 g, 75%) as a colourless liquid: IR ν_{max} (thin film): 2950, 2180, 1640, 1575 cm^{-1}; UV λ_{max} (MeOH): 285 nm (ϵ = 7200); ^1H NMR (400 MHz, $CDCl_3$) δ: 1.17 (6H, s, C6-CH_3), 2.08 (3H, s, C2-CH_3), 2.22 (2H, dd, J = 4, 2 Hz, C5-H_2), 5.93 (1H, dt, J = 9, 2 Hz, C3-H), 6.07 (1H, dt, J = 9, 4 Hz, C4-H) ppm; ^{13}C NMR (50 MHz, $CDCl_3$) δ: 21.8, 27.7, 32.5, 37.7, 114.5, 118.2, 127.2, 131.9, 146.3 ppm; MS *m/z*: 147(M^+), 132; high-resolution mass measurement cald. for $C_{10}H_{13}N$: 147.1048; found: 147.1046. Anal. calcd. for $C_{10}H_{13}N$: C81.59, H 8.90, N 9.51; found: C 81.76, H 8.83, N 9.49.

Method B

A solution of bromide **41** (151.6 mg, 0.664 mmol) and DBU (300 μL, 2.0 mmol) in benzene (10 mL) was heated at reflux for 4 h. After cooling, the reaction was diluted with diethyl ether (30 mL), washed with saturated ammonium chloride solution (10 mL), water (10 mL), dried (over $MgSO_4$), filtered, and evaporated *in vacuo* to leave an oil (153.2 mg). Purification by flash chromatography using diethyl ether/petroleum ether (1:9) as eluent gave **42** (26.5 mg, 27%) as a colourless oil.

*2,6,6-Trimethylcyclohexa-1,3-diene-1-carbaldehyde (**45**)*

To a solution of safronitrile **42** (580.0 mg, 3.94 mmol) in anhydrous benzene (3.5 mL) at 0°C was added DIBAL-H (1.5 M in toluene, 4.9 mL, 7.4 mmol). The reaction was stirred for 2.5 h at room temperature, then added to deoxygenated 5% sulphuric acid (30 mL) along with diethyl ether (20 mL). After stirring vigorously for 15 min, the aqueous layer was extracted with diethyl ether (3 × 50 mL). The combined organic layers were washed with water (50 mL), dried (over $MgSO_4$), filtered, and evaporated *in vacuo* to leave an orange oil (543 mg). Purification by bulb-to-bulb distillation (100–105°C, 11 Torr) afforded pure safronal (**45**) (371.6 mg, 63%) as a colourless oil: IR ν_{max} (thin film): 2960, 2930, 2870, 1665, 1635 cm^{-1}; UV λ_{max} (MeOH): 309 nm (ϵ = 7500); ^1H NMR (400 MHz, $CDCl_3$) δ 1.20 (6H, s, C6-CH_3), 2.16 (2H, dd, J = 4, 2 Hz, C5-H_2), 2.18 (3H, s, C2-CH_3), 5.93 (1H, dt, J = 10, 2 Hz, C3-H), 6.17 (1H, dt, J = 10, 4 Hz, C4-H), 10.15 (1H, s, CHO) ppm; MS *m/z*: 150 (M^+), 135, 121, 107 (100); high-resolution mass measurement calcd. for $C_{10}H_{14}O$: 150.1045; found: 150.1045. Anal. calcd. for $C_{10}H_{14}O$: C 79.96, H 9.39; found: C 80.18, H 9.42.

*(E)-1-(2,6,6-Trimethylcyclohexa-1,3-dienyl)-but-2-en-1-ol (**46**) and (Z)-1-(2,6,6-trimethylcyclohexa-1,3-dienyl)-but-2-en-1-ol (**47**)*

To a solution of safronal (**45**) (256.7 mg, 1.71 mmol) in anhydrous tetrahydrofuran (12 mL) at 0°C was added 1-propenylmagnesium bromide[9] (1.21 M in tetrahydrofuran, 2.0 mL, 2.4 mmol). The reaction was stirred at 0°C for 10 min, quenched with saturated ammonium chloride solution (15 mL), and extracted with diethyl ether (2 × 30 mL). The combined organic layers were washed with water (50 mL), dried (over $MgSO_4$), filtered, and evaporated *in vacuo* to leave a yellow oil (344.2 mg). Purification by bulb-to-bulb distillation (115–125°C, 11 Torr) afforded a mixture of alcohols **46** and **47** (49:51, 293.9 mg, 89%) as a colourless oil: IR ν_{max} (thin film): 3400 (br), 2960, 1680 (br) cm^{-1}; ^1H NMR (400 MHz, $CDCl_3$) (partial signals corresponding to **47**) δ: 1.06 (3H, s, C6′-CH_3), 1.11 (3H, s, C6′-CH_3), 1.40 (1H, br s, $w_{h/2}$ = 8 Hz, exchangeable, O-*H*), 1.74 (3H, dd, J = 8, 1 Hz, C4-H_3), 1.95 (3H, s, C2′-CH_3), 2.07 (2H, t, J = 3 Hz, C5′-H_2), 5.40 (1H, d, J = 9 Hz, C1-H), 5.58 (1H, dqd, J = 11, 8, 1 Hz, C3-H), 5.74 (2H, m, C3′-H, C4′-H), 5.83 (1H, ddq, J = 11, 9, 1 Hz, C2-H) ppm. Purification by flash chromatography of a portion of this oil using ethyl acetate/petroleum ether (1:19) as eluent afforded pure *trans*-alcohol **46** (79.2 mg, 43% overall) as a colourless oil: IR ν_{max} (thin film): 3400 (br), 2960, 1680 (br) cm^{-1}; UV λ_{max} (MeOH): 271 nm (ϵ = 9040); ^1H NMR (400 MHz, $CDCl_3$) δ: 1.04 (3H, s, C6′-CH_3), 1.10 (3H, s, C6′-CH_3), 1.53 (1H, br s, $w_{h/2}$ = 6 Hz, exchangeable, O-*H*), 1.72 (3H, dd, J = 7, 1 Hz, C4-H_3), 1.88 (3H, s, C2′-CH_3), 2.06 (2H, t, J = 4 Hz, C5′-H_2), 5.03 (1H, br d, J = 5 Hz, C1-H), 5.73 (4H, m, C3′-H, C4′-H, C2-H, C3-H) ppm; MS *m/z*: 192 (M^+), 177, 174, 159, 121 (100); high-resolution mass measurement calcd. for $C_{13}H_{20}O$: 192.1514; found: 192.1516. ^1H NMR decoupling experiments: irradiation of the doublet of doublets resonating at δ 1.74 ppm simplified the signal resonating at δ 5.58 ppm to a doublet of doublets (J = 11, 1 Hz) and simplified the signal resonating at δ 5.83 ppm to a doublet of doublets (J = 11, 9 Hz); irradiation of the doublet resonating at δ 5.40 ppm simplified the signal resonating at δ 5.83 ppm to a doublet of quartets (J = 11, 1 Hz) and affected the signal resonating at δ 5.58 ppm.

The *cis*-alcohol **47** decomposed on chromatography.

*(E)-1-(2,6,6-Trimethylcyclohexa-1,3-dienyl)-but-2-en-1-one (β-damascenone) (**48**)*

Method A

To a solution of *trans*-alcohol **46** (18.9 mg, 0.098 mmol) in petroleum ether (3 mL) was added "active" manganese dioxide (170 mg, 1.95 mmol). After stirring for 1 h the reaction was filtered and evaporated *in vacuo* to afford β-damascenone (**48**) (16.7 mg, 100%) as a colourless oil: IR ν_{max} (thin film): 2980, 2950, 1670, 1635, 1610 cm^{-1}; UV λ_{max} (MeOH): 305 nm (ϵ = 2220), 226 nm (ϵ = 13 800); ^1H NMR (400 MHz, $CDCl_3$) δ: 1.05 (6H , s, C6′-$(CH_3)_2$), 1.64 (3H, s, C2′-CH_3), 1.94 (3H, dd, J = 7, 2 Hz, C4-H_3), 2.12 (2H, dd, J = 5, 1 Hz, C5′-H_2), 5.84 (2H, m, C3′-H, C4′-H), 6.20 (1H, dq, J = 16, 2 Hz, C2-H), 6.85 (1H, dq, J = 16, 7 Hz, C3-H) ppm; MS *m/z*: 190 (M^+), 175, 159, 121, 69 (100); high-resolution mass measurement calcd. for $C_{13}H_{18}O$: 190.1357; found:

[9]Prepared as a mixture of isomers 49:51.

Can. J. Chem. Downloaded from www.nrcresearchpress.com by 217.78.4.112 on 09/08/12
For personal use only.

190.1355. ^{1}H NMR decoupling experiments: irradiation of the doublet of quartets resonating at δ 6.20 ppm simplified the signals resonating at δ 1.94 ppm to a doublet (J = 7 Hz) and simplified the signal resonating at δ 6.85 ppm; irradiation of the signal resonating at δ 6.85 ppm simplified the doublet of doublets resonating at δ 1.94 ppm to a doublet (J = 2 Hz) and affected the signal resonating at δ 6.20 ppm; irradiation of the doublet of doublets resonating at δ 2.12 ppm simplified the signal resonating at δ 5.84 ppm to an AB quartet; irradiation of the signal resonating at δ 1.94 ppm simplified the signal resonating at δ 6.20 ppm to a doublet (J = 16 Hz) and simplified the signal resonating at δ 6.85 ppm to a doublet (J = 16 Hz).

Method B

To a solution of alcohols **46** and **47** (49:51, 139.4 mg, 0.725 mmol) in petroleum ether (30 mL) was added "active" manganese dioxide (700 mg, 8.05 mmol). After stirring for 2 h, a further portion of manganese dioxide (700 mg, 8.05 mmol) was added. After stirring for 1.5 h, the reaction was filtered and evaporated *in vacuo* to afford a mixture of β-damascenone (**48**) and enone **49** (**48**:**49** = 49:51, 138.7 mg, 100%) as a colourless oil. ^{1}H NMR (400 MHz, $CDCl_3$) (signals corresponding to enone **49**) δ: 1.10 (6H, s, C6′-$(CH_3)_2$), 1.74 (3H, s, C2′-CH_3), 2.11 (2H, dd, J = 5, 1 Hz, C5′-H_2), 2.16 (3H, d, J = 7 Hz, C4-H_3), 5.84 (2H, m, C3′-H, C4′-H), 6.20 (2H, m, C2-H, C3-H) ppm. The mixture of ketones and *para*-toluenesulphonic acid (20 mg, 0.1 mmol) in anhydrous tetrahydrofuran was heated at reflux for 20 h. The reaction was cooled and diluted with diethyl ether (150 mL). The organic layer was washed with water (30 mL), saturated sodium bicarbonate solution (50 mL), water (30 mL), dried (over $MgSO_4$), filtered, and evaporated *in vacuo* to give a colourless oil (136.2 mg). Purification by flash chromatography using ethyl acetate/petroleum ether (1:19) as eluent afforded pure β-damascenone (**48**) (105.0 mg, 76%) as a colourless oil.

*2,2,6-Trimethylcyclohexanone (**51**)*

This procedure is a modification of that reported by Fitzer and Quabeck (**35**).

To a solution of diisopropylamine (90 mL, 640 mmol) in anhydrous tetrahydrofuran (2 L) at −78°C was added *n*-butyllithium (1.6 M in hexanes, 405 mL, 648 mmol) dropwise. After the addition was complete, the reaction was stirred for a further 45 min at −78°C and then 2,6-dimethylcyclohexanone[10] (75.00 g, 594.3 mmol) in anhydrous tetrahydrofuran (50 mL) was added over 5 min. The reaction was stirred at −78°C for 1 h, warmed to 0°C, and stirred at this temperature for a further 1 h. Iodomethane (120 mL, 1.93 mol) was added over 15 min, and the reaction was stirred for a further 20 min at 0°C. After quenching with saturated ammonium chloride solution (900 mL), the reaction was extracted with petroleum ether (3 × 600 mL). The combined organic extracts were washed with water (500 mL), dried (over $MgSO_4$), filtered, and evaporated *in vacuo* to leave a red oil. Purification by distillation at atmospheric pressure gave a fraction (70.85 g, 85%) that was shown by GC and ^{1}H NMR to contain 97% 2,2,6-trimethylcyclohexanone **51** and 3% 2,2,6,6-tetramethylcyclohexanone **52**.

(1R,6R*) 1-Hydroxy-2,2,6-trimethylcyclohexane-1-carbonitrile (**53**) and (1R*,6S*) 1-hydroxy-2,2,6-trimethylcyclohexane-1-carbonitrile (**54**)*

To a mixture of 2,2,6 trimethylcyclohexanone[11] (**51**) (12.6188 g, 89.94 mmol) and powdered sodium cyanide (9.166 g, 187.0 mmol) in water (23 mL) at 0°C,[12] was added a solution of sodium bisulphite (17.587 g) in water (40 mL). The reaction was stirred for 6 h at 0–15°C, then extracted with diethyl ether (4 × 100 mL). The combined organic layers were dried (over $MgSO_4$), filtered, and evaporated *in vacuo* to give an oil (15.0255 g, 100%) that solidified on standing. GC and ^{1}H NMR analysis indicated a mixture of cyanohydrins **54**:**53** = 77:23. Purification by column chromatography using either silica (230–400 mesh) or Florisil® resulted in partial reversion to 2,2,6-trimethylcyclohexanone: mp 38–40°C; IR ν_{max} ($CHCl_3$): 3580 (sharp), 3450 (br), 2930, 2250 (weak) cm^{-1}; ^{1}H NMR (400 MHz, $CDCl_3$) (signals corresponding to **53**) δ: 1.13 (3H, d, J = 7 Hz, C6-CH_3), 1.15 (3H, s, C2-CH_3), 1.17 (3H, s, C2-CH_3), 1.40–1.60 (6H, m), 2.06 (1H, m, C6-H), 2.35 (1H, br s, $w_{h/2}$ = 100 Hz, exchangeable, OH) ppm; (signals corresponding to **13**) δ: 1.01 (3H, s, C2-CH_3), 1.13 (3H, d, J = 7 Hz, C6-CH_3), 1.20 (3H, s, C2-CH_3), 1.33–1.62 (5H, m), 1.72 (1H, m), 1.91 (1H, m, C6-H), 2.35 (1H, br s, $w_{h/2}$ = 100 Hz, exchangeable, OH) ppm; ^{13}C nmr (50 MHz, $CDCl_3$) (signals corresponding to **53**) δ: 16.1, 17.1, 23.2, 26.2, 27.7, 32.6, 35.1, 38.0, 78.2, 121.0 ppm; (signals corresponding to **13**) δ: 16.4, 19.2, 20.6, 26.8, 32.2, 36.3, 37.6, 38.4, 81.4, 119.6 ppm; MS m/z: 167 (M^+), 166, 152, 140, 82 (100); high-resolution mass measurement calcd. for $C_{10}H_{17}NO$: 167.1310; found: 167.1306. Anal. calcd. for $C_{10}H_{17}NO$: C 71.80, H 10.25, N 8.41; found: C 71.60, H 10.24, N 8.31.

(1R,6R*) 1-Acetoxy-2,2,6-trimethylcyclohexane-1-carbonitrile (**56**) and (1R*,6S*) 1-acetoxy-2,2,6-trimethylcyclohexane-1-carbonitrile (**57**)*

Method A

A mixture of cyanohydrins **53** and **54** (30:70, 1.0332 g, 6.18 mmol), acetic anhydride (1.40 mL, 14.8 mmol), and acetyl bromide (100 μL, 1.35 mmol) was heated at 120°C for 6.5 h. The cooled reaction was poured into water (30 mL) and extracted with diethyl ether (100 mL). The organic layer was washed with water (50 mL), saturated sodium bicarbonate solution (2 × 50 mL), water (30 mL), dried (over $MgSO_4$), filtered, and evaporated *in vacuo* to leave a deep red oil (1.2004 g). Purification by flash chromatography using ethyl acetate/petroleum ether (1:9) as eluent afforded a mixture of cyanohydrin acetates **56** and **57** (28:72, 1.0200 g, 79%) as a white solid: IR ν_{max} ($CHCl_3$): 2950, 1750 cm^{-1}; ^{1}H NMR (400 MHz, $CDCl_3$) δ: 2.10 (0.72 × 3H, s), 2.12 (0.22 × 3H, s) ppm. Data on pure **57** is given below (Method B).

Method B

To a solution of cyanohydrins **53** and **54** (30:70, 328.5 mg, 1.96 mmol) and *N*,*N*-dimethylaminopyridine (DMAP, 72 mg, 0.59 mmol) in dichloromethane (25 mL) was added triethylamine (400 μL, 2.87 mmol) and acetic anhydride (300 μL, 3.18 mmol). After stirring for 78 h at room temperature, the reaction was added to iced water (100 mL). The aqueous layer was extracted with dichloromethane (50 mL). The combined organic layers were washed with water (30 mL), dried (over $MgSO_4$), filtered, and evaporated *in vacuo* to give a brown oil (540.8 mg). Purification by flash chromatography using ethyl acetate/petroleum ether (1:19) as eluent afforded in order of elution: 2,2,6-trimethylcyclohexanone (**51**) (135.1 mg, 51%), a pure sample of acetate **57** (56.3 mg, 14%) as a white solid, and a mixture of acetates **56** and **57** (14:86, 41.0 mg, 10%).

Acetate **57**: mp 67–68°C (ether/hexanes); IR ν_{max} ($CHCl_3$): 2950, 1750 cm^{-1}; ^{1}H NMR (400 MHz, $CDCl_3$) δ: 1.06 (3H, s, C2-CH_3), 1.07 (3H, d, J = 7 Hz, C6-CH_3), 1.16 (3H, s, C2-CH_3), 1.48 (4H, m), 1.74 (2H, m), 2.10 (3H, s, OCOCH_3), 2.12 (1H, m, C6-H) ppm; MS m/z: 209 (M^+), 194, 167 (100); high-resolution mass measurement calcd, for $C_{12}H_{19}NO_2$: 209.1416; found: 209.1414. Anal. calcd. for $C_{12}H_{19}NO_2$: C 68.87, H 9.15, N 6.69; found: C

[10]Obtained form Aldrich Chemical Co. as a 77:23 mixture of isomers.

[11]Contains 3% 2,2,6,6-tetramethylcyclohexanone. In this and subsequent reactions this impurity reacted in a similar manner to 2,2,6-trimethylcyclohexanone (except in elimination reactions). However, no compounds derived from this compound were isolated or even characterized in the various spectra. Crude yields reflect the presence of these derivatives, however.

[12]The reaction was repeated at various temperatures, 0°C, 20°C, 30°C, 80°C, with the ratio varying from 20:80 at 0°C up to 30:70 at 60°C.

Can. J. Chem. Downloaded from www.nrcresearchpress.com by 217.78.4.112 on 09/08/12
For personal use only.

69.05, H 9.09, N 6.69. Single crystal X-ray structure data is given in the Appendix.

Method C

A mixture of nitrile **43** and cyanohydrin **54** (30:70 by GC, derived as indicated below, Method B, 1.0077 g), acetic anhydride (1.0 mL, 10 mmol), and acetyl bromide (70 μL, 0.95 mmol) was heated at 120°C for 8 h. The cooled reaction was added to iced water (50 ml) and extracted with diethyl ether (3 × 70 mL). The combined organic layers were washed with water (50 mL), saturated sodium bicarbonate solution (50 mL), dried (over $MgSO_4$), filtered, and evaporated *in vacuo* to leave a red oil (1.4386 g). Purification by flash chromatography using ethyl acetate/petroleum ether (1:19) as eluent afforded pure nitrile **43** (289.3 mg, 29%) as a colourless oil. Further elution afforded pure "*cis*"-acetate **57** (807.6 mg, 63%) as a white solid.

*2,6,6-Trimethylcyclohex-1-ene-1-carbonitrile (**43**) and 2-methyl-1-(1-methylethylene)-cyclopentane-1-carbonitrile (**55**)*

Method A

To a solution of cyanohydrins **53** and **54** (23:77, 567.6 mg, 3.39 mmol) in anhydrous benzene (2.5 mL) at 0°C were added pyridine (700 μL, 8.65 mmol) and thionyl chloride (500 μL, 6.36 mmol). The reaction was heated at reflux for 1 h. The cooled reaction was poured into water (10 mL) and extracted with diethyl ether (4 × 30 mL). The combined organic layers were washed with 2 M hydrochloric acid (20 mL), saturated sodium bicarbonate solution (10 mL), water (20 mL), dried (over $MgSO_4$), filtered, and evaporated *in vacuo* to leave an oil (664.6 mg). Purification by flash chromatography using diethyl ether/petroleum ether (1:24) as eluent afforded pure nitrile **55** (82.9 mg, 16%), a mixture of nitriles **55** and **43** (81:19, 335.1 mg, 66%), and pure nitrile **43** (63.2 mg, 12%) as colourless oils.

Nitrile **55**: IR ν_{max} (thin film): 3000, 2910, 2260, 1650 cm^{-1}; ^1H NMR (400 MHz, $CDCl_3$) δ: 1.10 (3H, d, J = 7 Hz, C2-CH_3), 1.58 (1H, m), 1.75 (1H, m), 1.79 (3H, br s, $w_{h/2}$ = 3 Hz, Cl′-CH_3), 1.95 (3H, m), 2.13 (2H, m), 5.02 (1H, br s, $w_{h/2}$ = 4 Hz, Cl′-H), 5.24 (1H, s, Cl′-H) ppm; ^{13}C NMR (50 MHz, $CDCl_3$) δ: 15.0, 18.5, 21.7, 32.1, 37.2, 41.2, 55.4, 114.1, 121.6, 140.6 ppm; MS *m/z*: 149 (M^+), 148, 134, 121, 107, 94 (100); high-resolution mass measurement calcd. for $C_{10}H_{15}N$: 149.1204; found: 149.1206. Anal. calcd. for $C_{10}H_{15}N$: C 80.48, H 10.13, N 9.39; found: C 80.30, H 10.00, N 9.60. ^1H NMR decoupling experiment: irradiation of the doublet resonating at δ 1.10 ppm affected the multiplet resonating at δ 2.13 ppm.

Method B

To a solution of cyanohydrins **53** and **54** (20:80, 6.371 g, 38.08 mmol) in anhydrous toluene (30 mL) at 0°C was added pyridine (8.0 mL, 98 mmol) and thionyl chloride (5.6 mL, 71 mmol). The reaction was stirred at 4°C for 17 h. The reaction was poured into water (200 mL) and extracted with diethyl ether (4 × 200 mL). The combined organic layers were washed with 2 M hydrochloric acid (100 mL), water (100 mL), dried (over $MgSO_4$), filtered, and evaporated *in vacuo* to leave an oil. Purification by flash chromatography using ethyl acetate/petroleum ether (1:19) as eluent afforded a mixture of nitrile **43** and 2,2,6-trimethylcyclohexanone (**51**)(1.3677 g). Further elution gave a mixture of "*cis*"-cyanohydrin **54** and 2,2,6-trimethylcyclohexanone (**51**) (4.696 g).

Repetition of this experiment (using **53**:**54** = 30:70) without purification afforded a mixture of **43** and **54** (30:70, 97%).

Method C

A mixture of acetates **56** and **57** (23:77, 318.0 mg, 1.52 mmol) was vacuum pyrolyzed (furnace temperature 450°C, 11 Torr) to obtain a colourless oil that was dissolved in diethyl ether (100 mL), washed with water (50 mL), dried (over $MgSO_4$), filtered, and evaporated *in vacuo* to give a colourless oil (306.7 mg). Purification by flash chromatography using ethyl acetate/petroleum ether (1:19) as eluent afforded pure nitrile **43** (163.3 mg, 72%). Further elution afforded a mixture of acetates **56** and **57** (91:9, 89.1 mg, 28% recovery).

Method D

To a solution of 2,2,6-trimethylcyclohexanone (**51**) (60.00 g, 428.0 mmol) and powdered sodium cyanide (30.00 g, 612.0 mmol) in water (108 mL) was added a solution of sodium bisulphite (84 g, 800 mmol) in water (192 mL). The reaction was stirred for 48 h at room temperature, then diluted with water (500 mL) and diethyl ether (500 mL). The aqueous layer was extracted with diethyl ether (2 × 500 mL). The combined organic layers were dried (over $MgSO_4$), filtered, and evaporated *in vacuo* to give an oil (71.05 g, 99%) that solidified on standing. GC and ^1H NMR analysis indicated a mixture of cyanohydrins **53**:**54** = 20:80. This solid was dissolved in anhydrous toluene (300 mL), cooled to 0°C, and the pyridine (87 mL, 1.1 mol) and thionyl chloride (61 mL, 780 mmol) were added. The reaction was stirred at 4°C for 3 days. The reaction was poured into water (1 L) and extracted with diethyl ether (3 × 500 mL). The combined organic layers were washed with 2 M hydrochloric acid (300 mL), water (300 mL), dried (over $MgSO_4$), filtered, and evaporated *in vacuo* to leave a yellow oil (70.52 g). This oil was gently heated at reflux with acetic anhydride (75 mL, 790 mmol) and acetyl bromide (4.5 mL, 61 mmol) for 12 h. The cooled reaction was poured into water (1 L) and extracted with diethyl ether (3 × 500 mL). The combined organic layers were washed with water (300 mL), saturated sodium bicarbonate solution (300 mL), dried (over $MgSO_4$), filtered, and evaporated *in vacuo* to leave a deep red oil (110 mL). This oil was flash pyrolyzed (furnace temperature 525–550°C) in 20–25 mL batches. The fractions collected were combined, diluted with diethyl ether (1.5 L), washed with water (300 mL), saturated sodium bicarbonate solution (300 mL), dried (over $MgSO_4$), filtered, and evaporated *in vacuo* to leave a deep red oil (65.8 g). Purification by distillation afforded nitrile **43** (bp 99–102°C/11 Torr, 51.95 g, 81% for 4 steps).

(1R,2R*) 1-Acetyl-2-methyl-cyclopentane-1-carbonitrile (**56**)*

A stream of ozone was bubbled into a solution of nitrile **55** (68.9 mg, 0.46 mmol) in ethyl acetate (7 mL) at −78°C until a persistent blue coloration was present. Dimethyl sulphide (300 μL) was added stirring continued for a further 10 min. The reaction was diluted with ethyl acetate (30 mL), washed with saturated sodium bicarbonate solution (30 mL), dried (over $MgSO_4$), filtered, and evaporated *in vacuo* to give a colourless oil. Purification by flash chromatography using diethyl ether/petroleum ether (1:24) as eluent afforded ketone **56** (50.9 mg, 73%) as a colourless oil: IR ν_{max} (thin film):2980, 2260, 1725 cm^{-1}; ^1H NMR (400 MHz, $CDCl_3$) δ: 1.19 (3H, d, J = 8 Hz, C2-CH_3), 1.55 (1H, m, C2-H), 1.80 (1H, m), 1.98 (2H, m), 2.25 (2H, m), 2.40 (1H, m), 2.41 (3H, s, -COCH_3) ppm; ^{13}C NMR (50 MHz, $CDCl_3$) δ: 17, 23, 29, 34, 38, 43, 61, 120, 201 ppm; MS *m/z*: 151 (M^+), 136, 109, 94, 82, 43 (100); high-resolution mass measurement calcd. for $C_9H_{13}NO$: 151.0997; found: 151.0994. Anal. calcd. for $C_9H_{13}NO$: C71.49, H 8.66, N 9.26; found: C 71.30, H 8.68, N 9.10. ^1H NMR decoupling experiment: irradiation of the doublet resonating at δ 1.19 ppm affected the multiplet resonating at δ 1.55 ppm.

*2,6,6-Trimethylcyclohex-1-ene-1-carbaldehyde (**45**)*

This procedure is a modification of that reported by Picard *et. al.* (37).

To a solution of nitrile **43** (500 mg, 3.4 mmol) in anhydrous benzene (3 mL) at 0°C was added DIBAL-H (1.5 M in toluene, 3.2 mL, 4.8 mmol). The reaction was stirred for 1.5 h at 0°C after which a further portion of DIBAL-H (1.5 M, 1.0 mL, 1.5 mmol) was added. The reaction was stirred at 0°C for a further 30 min, then added to deoxygenated 5% sulphuric acid (25 mL) along with diethyl ether (20 mL). After stirring vigorously for 15 min, the aqueous layer was extracted with diethyl ether (3 × 50 mL). The combined organic layers were washed with water (40 mL), dried (over $MgSO_4$), filtered, and evaporated *in vacuo* to leave a yellow oil (546 mg). Purification by bulb-to-bulb distillation (100°C,

15 Torr) afforded pure β-cyclocitral (**45**) (461.1 mg, 90%) as a colourless oil: IR ν_{max} ($CHCl_3$): 2950, 1665, 1610 cm^{-1}; ^1H NMR (400 MHz, $CDCl_3$) δ: 1.20 (6H, s, C6-CH_3), 1.45 (2H, m), 1.64 (2H, m), 2.11 (3H, s, C2-CH_3), 2.21 (2H, t, J = 7 Hz, C3-H_2), 10.11 (1H, s, -*CH*O ppm; ^{13}C nmr (50 MHz, $CDCl_3$) δ: 18.6, 19.3, 21.4, 27.8, 33.0, 35.7, 40.5, 128.2, 129.0, 192.2 ppm; MS *m/z*: 152 (M^+), 137, (100).

Acknowledgements

Financial aid from the Natural Sciences and Engineering Research Council of Canada and the National Research Council of Canada is gratefully acknowledged. We are also grateful to Intrinsic Research and Development Inc. for generous samples of cedar leaf oil.

1. J. P. Kutney, K. Piotrowska, Y. H. Chen, K. P. N. Cheng, Z. Gao, and S. J. Rettig. Can. J. Chem. **68**, 1698 (1990).
2. E. T. Theimer Editor Fragrance Chemistry, The Science of the Sense of Smell, Academic Press, New York. 1982, and references cited therein.
3. E. Kovats, E. Demole, G. Ohloff, and M. Stoll. U.S. Patent 4,187,863 (1980), and references cited therein.
4. R. L. Snowden and S. M. Linder. Helv. Chim. Acta, **71**, 1587 (1988), and references cited therein.
5. C. Fehr and J. Galindo. J. Am. Chem. Soc. **110**, 6909 (1988), and references cited therein.
6. S. Torii, K. Uneyama, and H. Ichimura. J. Org. Chem. **44**, 2292 (1979).
7. G. Buchi and H. Wuest. Helv. Chim. Acta, **54**, 1767 (1971).
8. P. Gosselin. Tetrahedron, **44**, 1979 (1988).
9. Y. Nakatani, K. Kubota, R. Takara, and Y. Shigematsu. Agric. Biol. Chem. **38**, 1351 (1974).
10. R. Pelliciari, E. Sisani, and R. Fringuelli. Tetrahedron Lett. 4039 (1980).
11. H. J. Liu, H. K. Hung, G. L. Mhehe, and M. L. D. Weinberg. Can. J. Chem. **56**, 1368 (1978).
12. S. Isoe, S. Katsumura, and T. Sakan. Helv. Chim. Acta, **56**, 1514 (1973).
13. E. Azzari, C. Faggi, N. Gelsomini, and M. Taddei. J. Org. Chem. **55**, 1106 (1990).
14. R. H. Eastman and A. V. Winn. J. Am. Chem. Soc. **82**, 5908 (1960).
15. D. A. Evans, L. K. Truesdale, and G. L. Carroll. J. Chem. Soc. Chem. Commun. 55 (1973).
16. D. A. Evans and L. K. Truesdale. Tetrahedron Lett. 4929 (1973).
17. M. Oda, A. Yamamuro, and T. Watanabe. Chem. Lett. 1427 (1979).
18. D. A. Evans, G. L. Carroll, and L. K. Truesdale. J. Org. Chem. **39**, 914 (1974).
19. N. S. Nudelman, Z. Gatto, and L. Bohe. *J. Org. Chem.* **49**, 1540 (1984).
20. W. P. Neumann. Synthesis, 665 (1987).
21. M. Castaing, M. Pereyre, M. Ratier, P. M. Blum, and A. G. Davies. J. Chem. Soc. Perkin Trans. 2, 287 (1979).
22. D. S. Mariano and E. Bay. J. Org. Chem. **45**, 1763 (1980).
23. E. Winterfeldt. Synthesis, 617 (1975).
24. J. L. Luche. J. Am. Chem. Soc. **100**, 2226 (1978).
25. A. L. Gemal and J. L. Luche. J. Am. Chem. Soc. **103**, 5454 (1981).
26. H. M. Bell, C. W. Vanderslice, and A. Spehar. J. Org. Chem. **34**, 3923 (1969).
27. R. O. Hutchins, D. Hoke, J. Keogh, and D. Koharski. Tetrahedron Lett. 3495 (1969).
28. C. H. Eugster, L. Leichner, and E. Jenny. Helv. Chim. Acta, **46**, 543 (1963).
29. K. H. Schulte-Elte, H. Strickler, F. Gautschi, W. Pickenhagen, M. Gadola, J. Limacher, B. L. Muller, F. Wuffli, and G. Ohloff. Liebigs. Ann. Chem. 484 (1975).
30. E. Demole, P. Enggist, U. Sauberli, M. Stoll, and E. Kovats. Helv. Chim. Acta, **53**, 541 (1970).
31. J. P. Picard, G. Nzabamwita, F. Lacoste, R. Calas, and J. Dunogues. Synth. Commun. **19**, 135 (1989).
32. C. Fehr and J. Galindo. J. Org. Chem. **53**, 1828 (1988).
33. A. J. Fatiadi. Synthesis, 65 (1976).
34. R. L. Snowden, S. M. Linder, B. L. Muller, and K. H. Schulte-Elte. Helv. Chim. Acta. **70**, 1858 (1987).
35. L. Fitjer and U. Quabeck. Synth. Commun. **15**, 855 (1985).
36. E. W. Kuemmerle, T. A. Rettig, and J. K. Stille. J. Org. Chem. **40**, 3665 (1975).
37. J. P. Picard, G. Nzabamwita, F. Lacoste, R. Calas, and J. Dunogues. Synth. Commun. **19**, 135 (1989).
38. T. Holm. Acta Chem. Scand. **18**, 1577 (1964).
39. G. Buchi and J. D. White. J. Am. Chem. Soc. **86**, 2884 (1964).
40. M. Mousseron-Canet, J. C. Mani, and J. L. Olive. C. R. Acad. Sci. **262**, 1725 (1966).
41. E. Demole, P. Enggist, U. Sauberli, and M. Stoll. Helv. Chim. Acta, **53**, 541 (1970).
42. S. Danishefsky and K. Tsuzuki. J. Am. Chem. Soc. **102**, 689 (1980).
43. W. C. Still, M. Kahn, and A. Mitra. J. Org. Chem. **43**, 2923 (1978).
44. J. Attenburrow, A. F. B. Cameron, J. H. Chapman, R. M. Evans, B. A. Hems, A. B. A. Jansen, and T. Walker. J. Chem. Soc. 1094 (1952).
45. International tables for X-ray crystallography. Vol. IV. Kynoch Press: Birmingham, U.K. (present distributor Kluwer Academic Publishers, Dordrecht. The Netherlands). 1974. pp. 99–102 and 149.

Appendix: X-ray crystallographic analysis of compound 57

Experimental

Crystallographic data appear in Table A1. The final unit-cell parameters were obtained by least squares on the setting angles for 25 reflections with 2θ = 79.5–91.1°. The intensities of three standard reflections, measured every 200 reflections throughout the data collection, remained essentially constant. The data were processed[13] and corrected for Lorentz and polarization effects, and absorption (empirical, based on azimuthal scans for four reflections).

The structure was solved by direct methods, the coordinates of the non-hydrogen atoms being determined from an *E*-map and those of the hydrogen atoms from subsequent difference Fourier syntheses. The non-hydrogen atoms were refined with anisotropic thermal parameters and the hydrogen atoms were refined with isotropic thermal parameters. Neutral atom scattering factors and anomalous dispersion corrections for the non-hydrogen atoms were taken from the *International tables for X-ray crystallography* (45). Final atomic coordinates and equivalent isotropic thermal parameters, bond lengths, and bond angles appear in Tables A2–A4, respectively. Hydrogen atom parameters, anisotropic thermal parameters, bond lengths and angles involving hydrogen, torsion angles, packing diagram, and measured and

[13]TEXSAN/TEXRAY structure analysis package, which includes versions of the following: MITHRIL, integrated direct methods, by C. J. Gilmore; DIRDIF, direct methods for difference structures, by P. T. Beurskens; ORFLS, full-matrix least-squares, and ORFFE, function and errors, by W. R. Busing, K. O. Martin, and H. A. Levy; ORTEP II, illustrations, by C. K. Johnson.

Can. J. Chem. Downloaded from www.nrcresearchpress.com by 217.78.4.112 on 09/08/12
For personal use only.

Can. J. Chem. Downloaded from www.nrcresearchpress.com by 217.78.4.112 on 09/08/12
For personal use only.

TABLE A1. Crystallographic data[a]

Compound	**57**
Formula	$C_{12}H_{19}NO_2$
fw	209.29
Crystal system	Monoclinic
Space group	$P2_1/c$
a, Å	8.271(2)
b, Å	11.035(2)
c, Å	13.726(1)
β_o	105.102(9)
V, Å^3	1209.5(3)
Z	4
ρ_{calc}, g/cm^3	1.149
$F(000)$	456
μ(Cu-K_α), cm^{-1}	5.87
Crystal size, mm	0.30 × 0.30 × 0.40
Transmission factors	0.89–1.00
Scan type	ω–2θ
Scan range, deg in ω	1.21 + 0.20 tan θ
Scan speed, deg/min	32 (8 rescans)
Data collected	$+h$, $+k$, $\pm l$
$2\theta_{max}$, deg	155
Crystal decay	Negligible
Total reflections	2553
Total unique reflections	2361
R_{merge}	0.016
No. of reflections with $I \geq 3\sigma(I)$	1675
No. of variables	213
R	0.040
R_w	0.048
gof	3.07
Max Δ/σ (final cycle)	0.08
Residual density e/Å^3	−0.12 to +0.15

[a]Temperature 294 K, Rigaku AFC6S diffractometer, Cu-K_α radiation (λ = 1.54178 Å), graphite monochromator, takeoff angle 6.0°, aperture 6.0 × 6.0 mm at a distance of 285 mm from the crystal, stationary background counts at each end of the scan (scan/background time ratio 2:1, up to 8 rescans), $\sigma^2(F^2) = [S^2(C + 4B) + (0.01\,F^2)^2]/\mathrm{Lp}^2$ (S = scan rate, C = scan count, B = normalized background count), function minimized $\Sigma w(|F_o| - |F_c|)^2$ where $w = 4F_o^2/\sigma^2(F_o^2)$, $R = \Sigma||F_o| - |F_c||/\Sigma|F_o|$, $R_w = (\Sigma w(|F_o| - |F_c|)^2/\Sigma w|F_o|^2)^{1/2}$, and gof = $[\Sigma w(|F_o| - |F_c|)^2/m - n)]^{1/2}$. Values given for R, R_w, and gof are based on those reflections with $I \geq 3\sigma(I)$.

TABLE A2. Final atomic coordinates (fractional) and B_{eq} (Å^2)[a]

Atom	x	y	z	B_{eq}
O(1)	0.0566(2)	0.1412(1)	0.16273(8)	4.70(5)
O(2)	−0.0904(2)	−0.0294(1)	0.1135(1)	7.47(8)
N(1)	0.2309(2)	−0.1372(1)	0.2637(1)	6.14(8)
C(1)	0.1747(2)	0.0965(1)	0.2525(1)	3.82(6)
C(2)	0.3454(2)	0.1573(1)	0.2526(1)	4.14(7)
C(3)	0.4715(3)	0.1293(2)	0.3536(1)	5.01(8)
C(4)	0.4116(3)	0.1657(2)	0.4445(2)	5.8(1)
C(5)	0.2445(3)	0.1072(2)	0.4419(1)	5.6(1)
C(6)	0.1102(2)	0.1324(2)	0.3446(1)	4.39(7)
C(7)	0.3229(3)	0.2951(2)	0.2388(2)	5.6(1)
C(8)	0.4112(3)	0.1088(2)	0.1661(2)	5.4(1)
C(9)	0.1973(2)	−0.0371(2)	0.2525(1)	4.29(7)
C(10)	−0.0545(3)	0.0722(3)	0.3456(2)	6.0(1)
C(11)	−0.0691(2)	0.0761(2)	0.1038(1)	4.93(8)
C(12)	−0.1762(4)	0.1563(3)	0.0260(2)	6.9(1)

[a]$B_{eq} = (8/3)\pi^2\Sigma\Sigma U_{ij}a_i{\cdot}a_j{*}(a_i{*}a_j)$.

TABLE A3. Bond lengths (Å) with estimated standard deviations

Atom	Atom	Distance	Atom	Atom	Distance
O(1)	C(1)	1.445(2)	C(2)	C(7)	1.538(3)
O(1)	C(11)	1.346(2)	C(2)	C(8)	1.526(3)
O(2)	C(11)	1.190(2)	C(3)	C(4)	1.513(3)
N(1)	C(9)	1.140(2)	C(4)	C(5)	1.517(3)
C(1)	C(2)	1.563(2)	C(5)	C(6)	1.524(3)
C(1)	C(6)	1.546(2)	C(6)	C(40)	1.519(3)
C(1)	C(9)	1.486(2)	C(11)	C(12)	1.489(3)
C(2)	C(3)	1.533(2)			

calculated structure factor amplitudes are included as supplementary material.[14]

[14]Supplementary material mentioned in the text may be purchased from: The Depository of Unpublished Data, Document Delivery, CISTI, National Research Council of Canada, Ottawa, Canada K1A 0R6.

Tables of hydrogen atom coordinates, bond lengths and angles involving hydrogen, and a packing diagram have also been deposited with the Cambridge Crystallographic Data Centre and can be obtained on request from The Director, Cambridge Crystallographic Data Centre, University Chemical Laboratory, Lensfield Road, Cambridge, CB2 1EW, U.K.

TABLE A4. Bond angles (deg) with estimated standard deviations

Atom	Atom	Atom	Angle	Atom	Atom	Atom	Angle
C(1)	O(1)	C(11)	125.1(1)	C(7)	C(2)	C(8)	107.9(2)
O(1)	C(1)	C(2)	105.3(1)	C(2)	C(3)	C(4)	113.6(2)
O(1)	C(1)	C(6)	108.0(1)	C(3)	C(4)	C(5)	111.1(2)
O(1)	C(1)	C(9)	113.3(1)	C(4)	C(5)	C(6)	113.2(2)
C(2)	C(1)	C(6)	113.1(1)	C(1)	C(6)	C(5)	110.0(2)
C(2)	C(1)	C(9)	108.2(1)	C(1)	C(6)	C(10)	113.3(2)
C(6)	C(1)	C(9)	108.9(1)	C(5)	C(6)	C(10)	111.3(2)
C(1)	C(2)	C(3)	108.4(1)	N(1)	C(9)	C(1)	171.0(2)
C(1)	C(2)	C(7)	110.1(2)	O(1)	C(11)	O(2)	124.7(2)
C(1)	C(2)	C(8)	110.7(2)	O(1)	C(11)	C(12)	109.6(2)
C(3)	C(2)	C(7)	110.1(2)	O(2)	C(11)	C(12)	125.7(2)
C(3)	C(2)	C(8)	109.7(2)				

Discussion of crystal structure

The crystal structure of **57** consists of well-separated molecules, the shortest intermolecular distance between non-hydrogen atoms ($O(2)\cdots C(12)(-x, -y, -z) = 3.562(4)$ Å) corresponding to a normal van der Waals interaction. The cyclohexane ring has a relatively undistorted chair conformation with the bulky substituents occupying equatorial positions (e.g., at C(1): the -$OC(O)CH_3$ group is equatorial and the -CN group axial; at C(6): the methyl group is equatorial). The ester function is planar within experimental error. Bond lengths and angles (Tables A3 and A4) are generally as expected. The C(1)—C(2) bond, between two fully substituted ring carbon atoms, is lengthened to 1.563(2) Å. The cyano group shows a significant deviation from linearity, N(1)—C(9)—C(1) = 171.0(2)°, presumably as a result of packing forces ($N(1)\cdots H(8)(1 - x, -1/2 - y, 1/2 - z) = 2.76(3)$ Å).

Can. J. Chem. Downloaded from www.nrcresearchpress.com by 217.78.4.112 on 09/08/12
For personal use only.

Studies with plant cell cultures of *Catharanthus roseus*. Oxidative coupling of dibenzylbutanolides catalyzed by plant cell culture extracts

JAMES P. KUTNEY,[1] G. M. HEWITT, TERENCE C. JARVIS, JAN PALATY, AND STEVEN J. RETTIG
Department of Chemistry, University of British Columbia, 2036 Main Mall, Vancouver, B.C., Canada V6T 1Z1

Received November 3, 1991

JAMES P. KUTNEY, G. M. HEWITT, TERENCE C. JARVIS, JAN PALATY, and STEVEN J. RETTIG. Can. J. Chem. **70**, 2115 (1992).

Utilizing appropriate dibenzylbutanolides, for example **7**, obtained via an efficient synthetic route from readily available aldehydes, and cell-free extracts obtained from *Catharanthus roseus* cell cultures, it was possible to achieve enzyme-catalyzed oxidative coupling of **7** to picropodophyllotoxin analogues. Studies are presently underway to convert such compounds to intermediates employed in the synthesis of the commercially important anti-cancer drug, etoposide.

JAMES P. KUTNEY, G. M. HEWITT, TERENCE C. JARVIS, JAN PALATY et STEVEN J. RETTIG. Can. J. Chem. **70**, 2115 (1992).

Utilisant des buténolides appropriés, comme le composé **7**, obtenus par une méthode de synthèse efficace à partir d'aldéhydes facilement disponibles, et des extraits sans cellules obtenus à partir des cultures de cellules du *Catharanthus roseus*, on a pu réaliser un couplage oxydant, catalysé par les enzymes, du composé **7** conduisant à des analogues de la picropodophyllotoxine. Des études sont en cours pour transformer de tels composés en intermédiaires utilisés dans la synthèse de l'étoposide, une drogue anticancéreuse commercialement importante.

[Traduit par la rédaction]

Can. J. Chem. Downloaded from www.nrcresearchpress.com by 217.78.4.112 on 09/08/12
For personal use only.

The podophyllotoxin family of natural products exemplified by the structures **1**–**5** have received considerable attention over the years. Excellent reviews (1, 2) of the earlier investigations pertaining to their chemistry and pharmacology are available and the most recent interest due to the important anti-cancer activity of the clinical drug, etoposide (**6**), also extensively reviewed (3, 4), has stimulated continued pursuit of synthetic (5–23) and biosynthetic studies (24). The synthesis of **6** from podophyllotoxin (**1**) is also well established (25–27) and presently provides the commercial route to this clinical drug. However, the latter route requires the

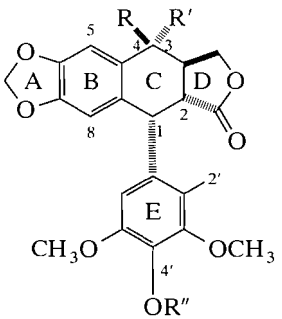

Podophyllotoxin **1**: R = H; R′ = OH; R″ = CH_3
Epipodophyllotoxin **2**: R = OH; R′ = H; R″ = CH_3
Deoxypodophyllotoxin **2**: R = OH; R′ = H; R″ = CH_3
Deoxypodophyllotoxin **3**: R = R′ = H; R″ = CH_3
4′-Demethylpodophyllotoxin **4**: R = H; R′ = OH; R″ = H
4′-Demethylepipodophyllotoxin **5**: R = OH; R′ = H; R″ = H
Etoposic **6**: R = CH_3 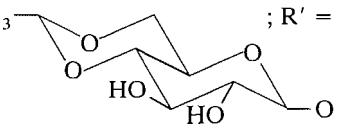 ; R′ = H; R″ = H

isolation of **1** via extraction of *Podophyllum peltatum* plants, followed by a two-step chemical process to 4′-demethylepipodophyllotoxin (**4**), the latter being the crucial intermediate for synthesis of **6**.

In our program concerning the combined utilization of synthetic chemistry and biotechnological methods, specifically plant cell culture, to develop efficient routes to complex natural products and related biologically active substances (28, 29), we focussed our attention on deriving an efficient route to **4**. In this study, the primary focus was eliminating the dependence on plant extraction and, hopefully, also eliminating some chemical conversions, so as to obtain a more direct synthesis of **4**. This publication presents some results of our studies in this direction.

Our general strategy in utilizing plant cell cultures or enzymes derived from within the cells as "reagents" in organic synthesis, requires initial consideration of "target" synthetic molecules that can subsequently be biotransformed into the desired end products. For this purpose, an understanding of the biosynthetic pathway leading to the podophyllotoxin family is required. It was clear from the detailed studies by Dewick and co-workers (24) that "appropriate" dibenzylbutanolides could act as substrates in enzyme-catalyzed oxidative cyclization reactions to the corresponding podophyllotoxins. In effect, this type of process (see **7** → **9**, Scheme 2) is expected to involve radical intermediates and, within living systems, the latter are usually generated by peroxidase enzymes (30, 31). Indeed such peroxidase enzymes had been produced within our plant cell culture line (coded as AC3) of *Catharanthus roseus* and their role evaluated in the biosynthesis of the clinical anti-cancer drugs vinblastine and vincristine (28). The question as to whether these enzymes could act as "reagents" in catalyzing the cyclization of dibenzylbutanolides to the podophyllotoxin system was of interest and required evaluation.

The first substrate to be studied in incubation experiments with enzymes derived from *C. roseus* plant cell cultures was the butanolide **7** prepared according to Scheme 1.

Isovanillin (**1**) was treated with benzyl chloride and potassium carbonate to give the benzyl ether **2** in quantitative yield and the latter was then subjected to a Stobbe condensation with dimethylsuccinate to afford the conjugated hemisuccinate **3** in 73% yield. Spectral data (see Experimental) indicated that only one geometrical isomer (probably *cis*) was

[1]Author to whom correspondence may be addressed.

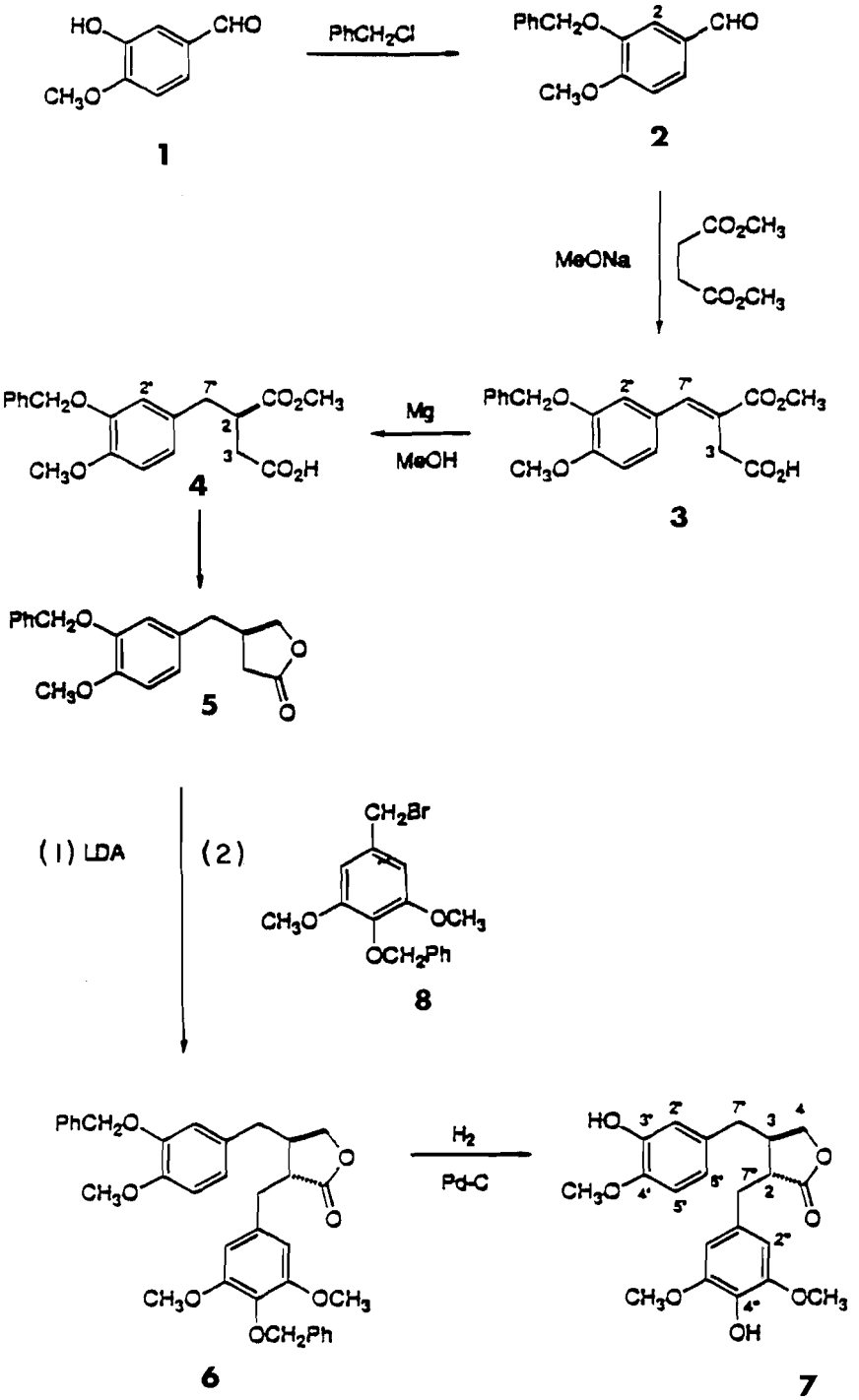

SCHEME 1. Synthesis of dibenzylbutanolide 7.

present, as expected, by comparison with the results reported for the analogous reaction with piperonal (32). The double bond of the hemiester **3** was reduced with magnesium in methanol (33) to give the unconjugated hemisuccinate **4** in 89% yield. The ^{1}H NMR spectrum of the product showed H(2), H(3), and H(7′) proton signals as either multiplets or doublets of doublets due to the creation of a chiral centre at C-2. The carbonyl frequency in the IR spectrum, in comparison with that of **3**, had increased to 1720 cm^{-1}, demonstrating the loss of conjugation of the ester group with the aromatic ring.

The reductive lactonization of the hemisuccinate **4** to the butanolide **5** was initially performed using the potassium salt of **4** and calcium borohydride prepared *in situ* (34). However, the crude reaction product was very complex and the yields of **5** were low, but by using the stronger reducing agent lithium borohydride (35) directly with the hemisuccinate **4**, satisfactory yields of pure **5** could be realized. The butanolide **5** was characterized by its ^{1}H NMR spectrum, which showed the two new methylene protons (H(4)) as doublets of doublets at δ 3.91 and δ 4.21, respectively. Formation of the lactone ring was demonstrated by the IR spectrum, which showed the carbonyl absorption at a frequency of 1770 cm^{-1}, well above the value observed for the hemisuccinate **4**.

Can. J. Chem. Downloaded from www.nrcresearchpress.com by 217.78.4.112 on 09/08/12
For personal use only.

Can. J. Chem. Downloaded from www.nrcresearchpress.com by 217.78.4.112 on 09/08/12
For personal use only.

Alkylation of **5** with the bromide **8** (prepared by the literature procedure (36)) gave the dibenzylbutanolide **6** in 80% yield. The ^{1}H NMR spectrum of the product, in comparison with that of **5**, showed the loss of one H(2) signal but the expected *trans* orientation of the two substituents with respect to the lactone ring could not be confirmed owing to the close proximity of the complex H(2) and H(3) signals.

Finally, the benzyl protecting groups of the butanolide **6** were quantitatively cleaved by hydrogenolysis using palladium-on-carbon as a catalyst, to afford the bis(hydroxybenzyl)butanolide **7** in 87% yield. The ^{1}H NMR spectrum of **7** showed the C(3′) and C(4″) phenolic hydroxyl group singlets, which disappeared with D_2O addition, at δ 5.42 and δ 5.58 respectively. The ^{13}C NMR spectrum showed two benzyl methylene carbon signals (C(7′) and C(7″)), which were identified by the attached proton test (APT). The EI mass spectrum of **7** clearly showed the molecular ion at *m/z* 388 and revealed a fragmentation pattern consistent with the structural assignment. In summary, the dibenzylbutanolide **7** was prepared from isovanillin in six steps in 40% overall yield.

With **7** on hand, studies concerning the biotransformation of this compound with an enzyme preparation (cell-free extract, CFE) previously obtained from our *C. roseus* cell line (AC3) (37–40) were initiated. A large number of experiments with **7** and CFE (prepared as indicated in the experimental section) were conducted. The reaction parameters (pH, H_2O_2 as cofactor, units of peroxidase enzyme per mmol substrate, reaction time) were evaluated in small-scale experiments (10–15 mg of **7**) in order to derive optimum conditions for the biotransformation of **7** to **9** (Scheme 2) and only a summary of the most pertinent features is provided here.

One of the important parameters was the pH (pH_h, the pH of the buffer used to prepare the CFE, Fig. 1) and its effect on the enzymatic activity. Figure 1 summarizes the changes in peroxidase activity and specific activity of the CFE with pH of buffer employed (see Experimental for procedures to measure these activities). A value of 6.3 appeared to be a good compromise between high peroxidase activity and specific activity, or the quotient of peroxidase activity and soluble protein concentration. The protein concentration was determined spectrophotometrically by complexing the dissolved protein with a commercial dye solution (41, 42).

The ideal ratio of peroxidase to substrate was determined using an arbitrary amount of 2.0 molar equivalents of hydrogen peroxide and conducting the reaction at pH 6.3. As shown in Fig. 2, **7** was very nearly consumed within 15 min when an amount of CFE corresponding to 400 units peroxidase per millimole of substrate was used. Increasing the peroxidase: substrate ratio or the reaction time (180 min, Fig. 3) failed to completely convert **7** to **9**: instead, the sole effect was to promote the reaction of aryltetralin **9** to **10** (Scheme 2), a species subsequently identified as the dimer of **9** (see later).

It was concluded that a peroxidase: substrate ratio of approximately 250 units per millimole of butanolide **7** would give optimum yields of the aryltetralin **9**. Higher values promoted dimerization while lower values resulted in incomplete conversion of substrate. The complete structure and stereochemistry of the desired cyclic analogue **9** was established by X-ray diffraction analysis (Fig. 4).

The dimer **10**, also obtained in the biotransformation of **7** was characterized by its ^{1}H NMR and mass spectra. The ^{1}H NMR spectrum of **10** strongly resembled that of the monomer **9** but there was a second signal of equal intensity for all protons shown by **9** except H(5), which is not present. This doubling represents the proton signals of the two diastereomers of the dimer molecules since the monomer units are racemic. The dimeric nature of the compound was demonstrated more clearly by the mass spectrum obtained using desorption chemical ionization (DCI) with ammonia, which showed a peak at *m/z* 788 corresponding to $(\mathbf{10} + NH_4)^+$. There was a very weak molecular ion peak in the EI mas spectrum at *m/z* 770, as well as peaks at *m/z* 784, 798, and 812 resulting from the intermolecular transfer of methyl radicals. In addition, the high degree of fragmentation and the low intensity of the monomer peak at *m/z* 386, in relation to the fragments at *m/z* 167 and 154, were in sharp contrast to the pattern observed in the EI spectrum of the monomer **9**. Unfortunately, neither the EI nor the DCI spectra showed any significant fragments in the region spanned by the molecular weights of the monomer and the dimer, suggesting that the bond between the monomer units is very weak.

In larger scale experiments, a third very minor component could be isolated and based on its spectral data was assigned structure **11**. Its EI mass spectrum was virtually identical to that of **9**. The ^{1}H NMR spectrum was also quite similar except for two *ortho*-coupled (J = 8 Hz) proton signals noted at δ 6.77 and 6.85, thereby suggesting that the ring B hydroxyl group is at C(8) of the aryltetralin rather than at C(6) as in **9**. Other significant features of the spectrum were the three separate methoxy proton signals at δ 3.59, 3.80, and 3.89 and the two *meta*-coupled (J = 2.5 Hz) doublets at δ 5.56 and 6.09, which implied nonequivalence of the two sides of ring E due to the loss of its ability to rotate about the C(1)—C(1′) bond. This was not surprising in view of the proximity of the C(8) hydroxyl to ring E. The low yield of this compound (0.53%) is readily explained by these major steric interactions of the C(8) hydroxyl with ring E.

The optimum hydrogen peroxide: substrate ratio was determined using 250 units peroxidase per millimole of **7** in buffer at pH 6.3. In the absence of hydrogen peroxide, no reaction occurred after 15 min (Fig. 5). A similar result was noted when the reaction was allowed to proceed for 180 min. The yield of **9** and **10** then increased with hydrogen peroxide concentration but remained approximately constant at about 80% when more than 2.0 molar equivalents (3.1 nM) were present. However, these results clearly did not represent the exclusive requirements of the oxidative coupling reactions of **7** and **9** in view of the ability of the CFE alone to consume hydrogen peroxide. This property was demonstrated when the CFE was stirred for 15 min with hydrogen peroxide *prior* to precursor addition. The yield of **9** was only 28% (vs. 64% for the control, where precursor **7**, hydrogen peroxide, and CFE were added simultaneously) after 1 h but had increased sharply to 50% 1 h after a further 2.0 equivalents of hydrogen peroxide were added. These competing processes may have involved the catalytic decomposition of hydrogen peroxide (catalyzed by peroxidase, catalase, or metal ions) or the oxidation of cell material.

It was concluded that 2.0 molar equivalents of hydrogen peroxide would give optimum yields of **9**. Lower values resulted in incomplete biotransformation of **7** while higher ratios promoted the dimerization of **9** to **10**. There appeared to be a distinct decrease in enzyme activity when more than 3 equivalents of hydrogen peroxide were used as cofactors.

Can. J. Chem. Downloaded from www.nrcresearchpress.com by 217.78.4.112 on 09/08/12
For personal use only.

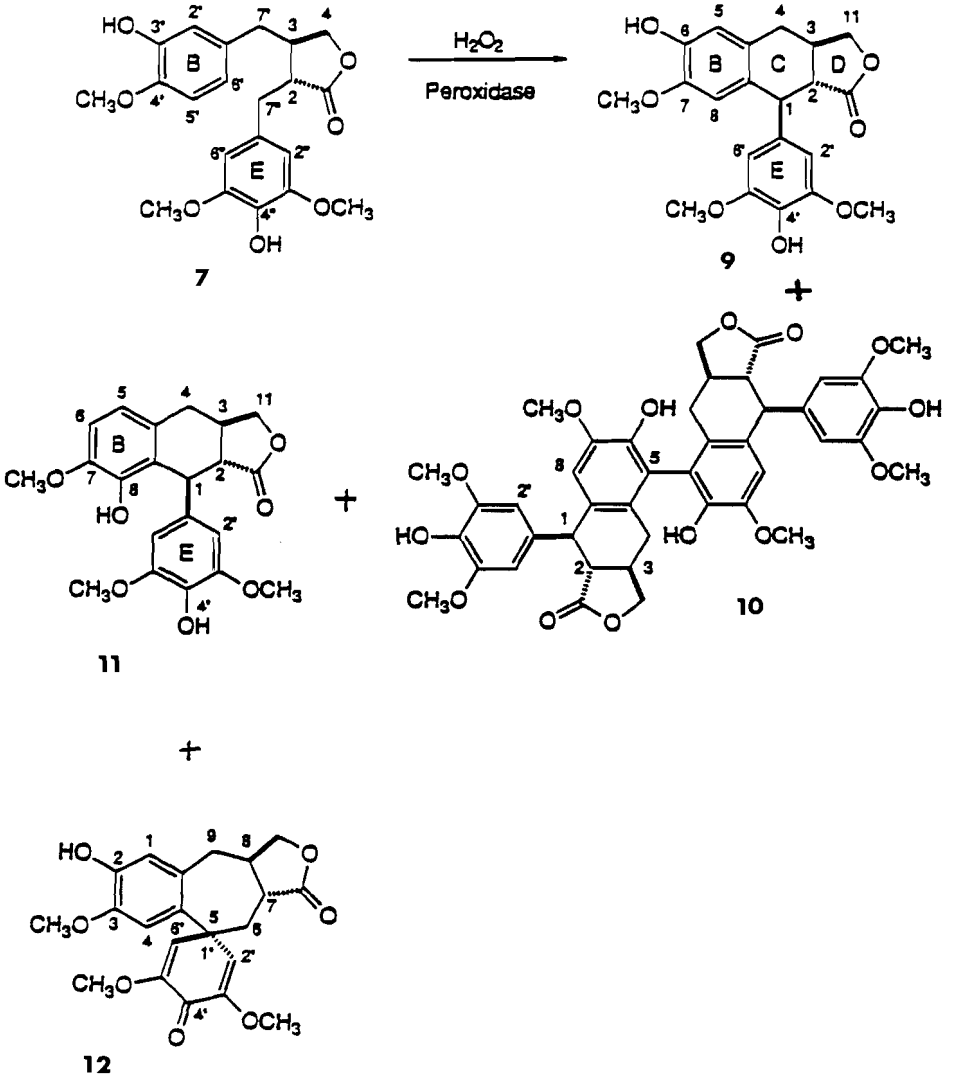

SCHEME 2. Biotransformation of dibenzylbutanolide **7** with cell free extracts of *Catharanthus roseus* cell cultures.

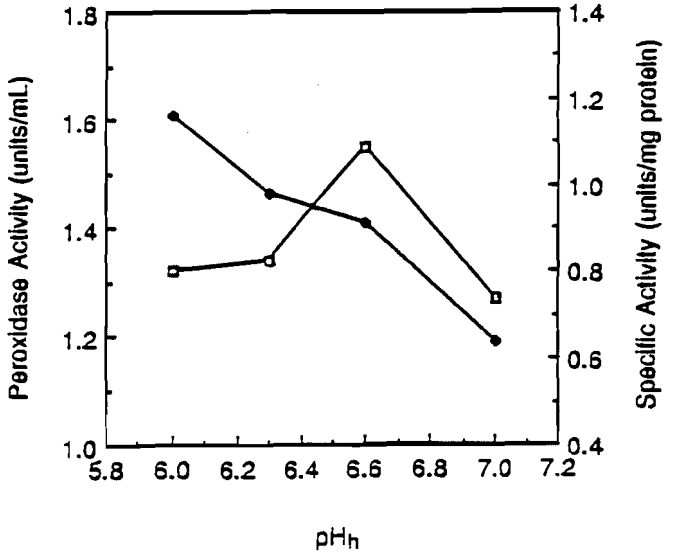

FIG. 1. Effect of pH_h on peroxidase activity and specific activity. □, Peroxidase activity, ◆, specific activity.

The optimum biotransformation pH (pH_r) for the cyclization of **7** to **9** could now be reliably determined, as the ideal peroxidase: substrate and peroxide: substrate ratios had been established. Up to this point, a value of pH 6.3 had been used and found to give good results but it was clearly desirable to identify the optimum value of pH_r more closely. This value (Fig. 6) was found to be about 6.3 based on the yield of **9**, using the optimum conditions established previously. The yield of **9** showed only minor variations over the pH range 6.0–6.6 but decreased markedly at more basic values.

Finally, it was determined that the CFE solution, when stored at 4°C, was quite stable with respect to both the oxidation of pyrogallol (peroxidase assay) and the biotransformation of **7**. The age of the CFE was thus not a significant factor in the reproducibility of individual experiments. In summary, it was found that the biotransformation of **7** to **9** could be accomplished most efficiently using the conditions described in Table 1. The yields of **9** were consistently 70% or higher in the subsequent larger scale experiments (generally 1 g of **7**) and the dimer **10** could be completely suppressed. In these latter studies, a further minor product (usually 1% yield) was isolated and shown to possess the spirodienone structure **12**. The latter was characterized by

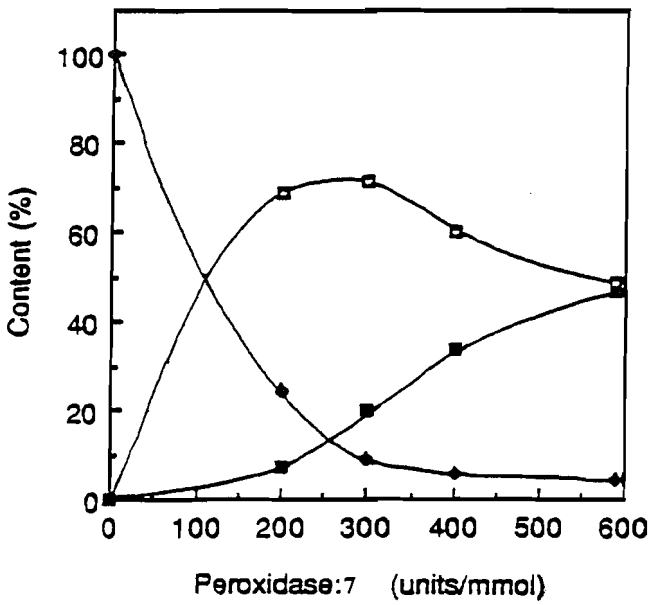

FIG. 2. Effect of peroxidase: substrate ratio on biotransformation of **7**. Reaction time = 15 min; ◆, **7**; □, **9**; ■, **10**.

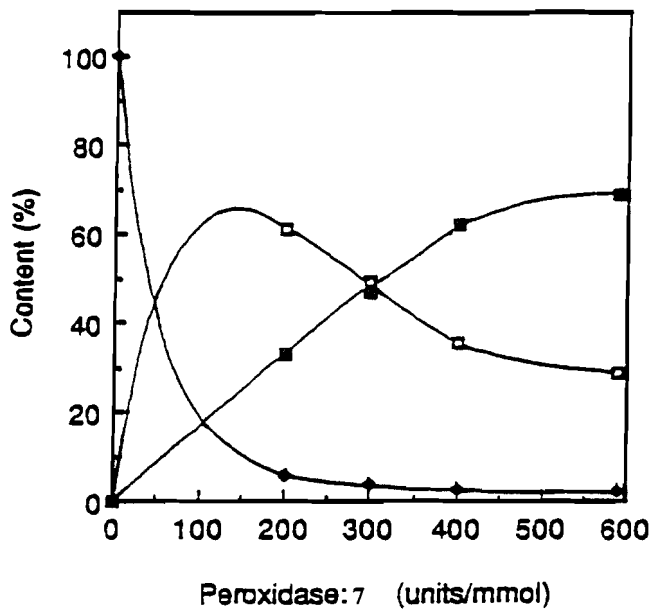

FIG. 3. Effect of peroxidase: substrate ratio on biotransformation of **7**. Reaction time = 180 min; ◆, **7**; □, **9**; ■, **10**.

IR, ^{1}H NMR, and mass spectroscopy. Its IR spectrum showed, in addition to the lactone carbonyl (1774 cm^{-1}), a second carbonyl band at 1673 cm^{-1} that was associated with the C(4′) dienone. The mass spectrum showed the molecular ion as the base peak at *m/z* 386 and virtually no fragmentation. The ^{1}H NMR spectrum showed three distinct methoxy proton signals, two H(6) proton signals (assigned by decoupling H(7)), and two sharp doublets (J = 2.8 Hz) at δ 6.13 and 6.25 that represent H(2′) and H (6′). The chemical shift and coupling constant values of H(2′) and H(6′) were very similar to those reported for a related compound (43).

In summary, it was now clear that the enzymes of *C. roseus* cell cultures, originally developed for the production of indole alkaloids, could tolerate "foreign" substrates of the dibenzylbutanolide family and afford high yields of the desired podophyllotoxin analogues.

It is of interest to note that for the sake of comparison, the biotransformation of **7** to **9** was investigated with commercial horseradish peroxidase. The reaction mixture was complex and the best yields of **9** were 15–19%, thereby revealing that the *C. roseus* derived enzymes are *far superior* for the present study.

In further studies involving enzyme-catalyzed cyclization of dibenzylbutanolides, it was of interest to ascertain whether functionality other than that present in **7** could be tolerated by the *C. roseus* derived enzymes. For this purpose, the butanolide **20** (Scheme 3) was selected as the next substrate to study.

An alternative, superior route to **20** was developed as shown in Scheme 3. The crucial step in the sequence involved a tandem conjugate addition method (44,45) in which the anion of **14** is reacted with butenolide **15** and the resulting intermediate **16**, without isolation, is reacted with **8** to afford **17**.

The dithioacetal **14** was obtained from piperonal (**13**), as shown in Scheme 3, in 98% yield (46). The dithioketal **17** was then prepared in overall 55% yield, as shown, using but-2-en-4-olide (**15**), the latter obtained by a standard procedure (47). The IR spectrum of **17** showed a strong carbonyl band at 1770 cm^{-1}, a frequency substantially higher than that observed for the butenolide (1740 cm^{-1}). The EI mass spectrum showed no significant peaks with *m/z* values greater than 584 ((M$^+$ − SPh) + H) but the fast atom bombardment ionization (FAB) mass spectrum revealed a weak molecular ion at *m/z* 693.

Considerable problems were encountered in the subsequent conversion of the dithioketal **17** to the ketone **18** (R = H or CH_2Ph). Treatment of **17** with perchloric acid (Method 1 in Experimental) (48) gave complex mixtures and poor yields of **18** (R = CH_2Ph) along with the hydroxy ketone **18** (R = H) as a minor product. Varying the reaction time and the amount of perchloric acid failed to improve these results. Treatment of **17** with sulfuryl chloride and wet silica gel (Method 2) (49) gave complex mixtures containing no readily identifiable products. Oxidation with iodine in methanol followed by acid hydrolysis (Method 3) (50), however, gave good yields of the ketone **18** (R = CH_2Ph), which was characterized by ^{1}H NMR, mass, and IR spectroscopy. The ^{1}H NMR spectrum, in comparison with that of the dithioketal **17**, showed a reduction in the number of aromatic protons to five and a considerable downfield shift of the H(3) signal to δ 4.01. The EI mass spectrum exhibited a molecular ion peak at *m/z* 490, and other characteristic fragments consistent with structure **17**.

Hydrogenation (H_2, Pd/C) of **18** (R = CH_2Ph) afforded a mixture of **18** (R = H, 46%) and the alcohol **19** (R = H, 30%), the latter occurring as a mixture of alcohols epimeric at C(7′) (approx. ratio of 3:1). The major isomer was tentatively identified as the alcohol with a β-orientation of the C(7′) hydroxyl for the depicted enantiomer, based on the relative accessibility of the faces of the C(7′) carbonyl group in the most favourable conformation of **18** (R = CH_2Ph) according to Dreiding models, and the results of reductions of closely related dibenzylbutanolides (48). The ^{1}H NMR spectrum of this alcohol mixture showed doublets at δ 1.94

Can. J. Chem. Downloaded from www.nrcresearchpress.com by 217.78.4.112 on 09/08/12
For personal use only.

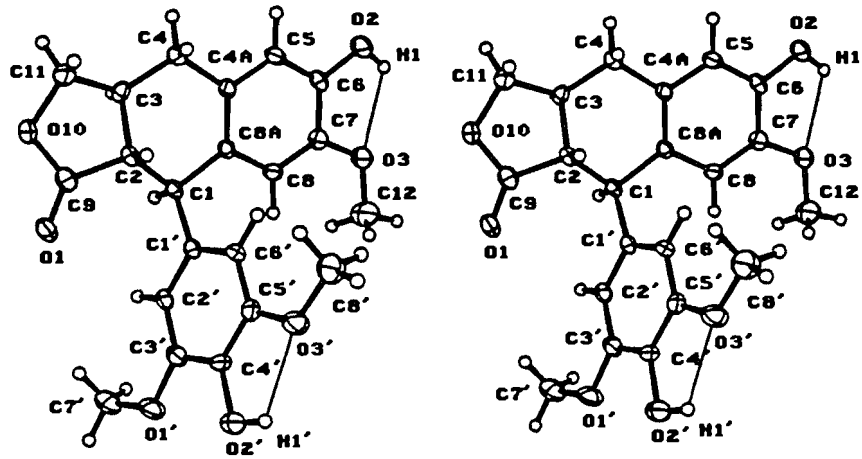

FIG. 4. Stereoview of **9**; 33% probability thermal ellipsoids are shown for the non-hydrogen atoms. Fine lines represent hydrogen bonds.

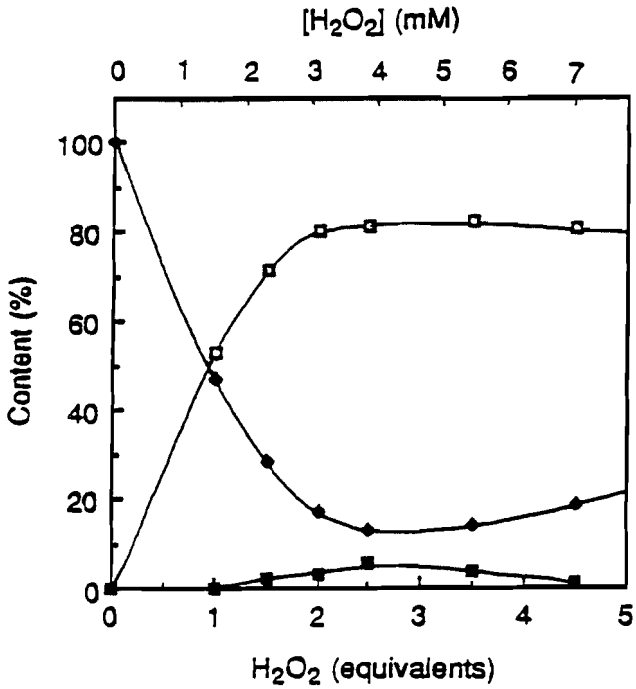

FIG. 5. Effect of hydrogen peroxide concentration on biotransformation of **7**. Reaction time = 15 min; ◆, **7**; □, **9**; ■, **10**.

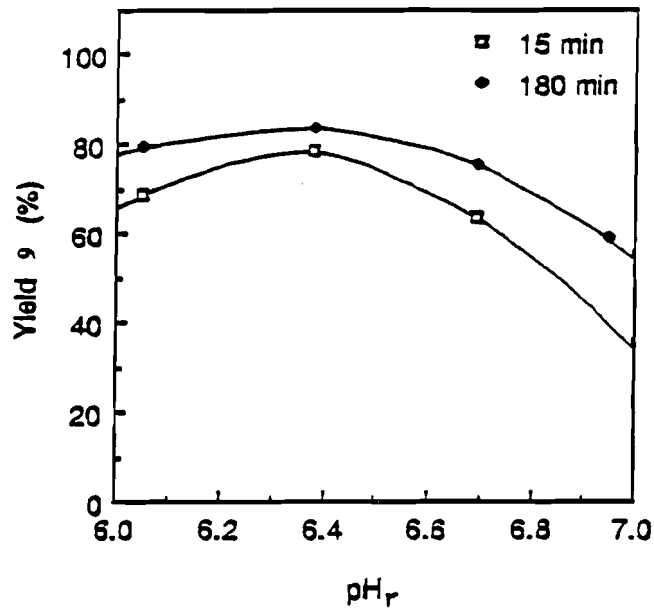

FIG. 6. Effect of pH_r in biotransformation of **7**. □, 15 min; ◆, 180 min.

TABLE 1. Optimum conditions for *C. roseus* CFE-catalyzed biotransformation of butanolide **7** to aryltetralin **9**

pH_h	6.3
pH_r	6.3
Hydrogen peroxide (equivalents)	2.0
CFE (units peroxidase per mmol 7)	250
Reaction time (min)	180

and 2.00 and a phenolic hydroxyl singlet at δ 5.40, all of which disappeared upon D_2O addition. The doublets correspond to the C(7′) α and β hydroxyl protons, respectively. The H(3)–H(7′) coupling constants of the two epimers (7.6 and 6.7 Hz for minor and major isomers, respectively) were too similar to be useful in assigning the C(7′) stereochemistry of the individual isomers.

A much preferable route to the alcohol **19** was achieved by low-temperature reduction with sodium borohydride to afford a quantitative yield of **19** (R = CH_2Ph) as an epimeric mixture (4.9:1 in favor of the C(7′) β-hydroxyl group). Studies with the sterically hindered reagent, lithium aluminum tri-tertbutoxy hydride at −78°C, improved the epimeric ratio (5.7:1) but the yields were substantially lower (60%).

When the above mixture of alcohol **19** (R = CH_2Ph) was treated under varying conditions with boron trichloride (4–6 equivalents and different time periods, 30–120 min), the desired dibenzylbutanolide **20** was obtained but only in low yield (generally 25%). Difficulties in chromatographic separation of this very polar compound (recovery of 50% on silica and 67% on Fluorosil) and compound instability are major factors influencing the yield of pure product.

In summary, **20** is available in 12% overall yield for the five-step conversion from piperonal (**13**).

Can. J. Chem. Downloaded from www.nrcresearchpress.com by 217.78.4.112 on 09/08/12
For personal use only.

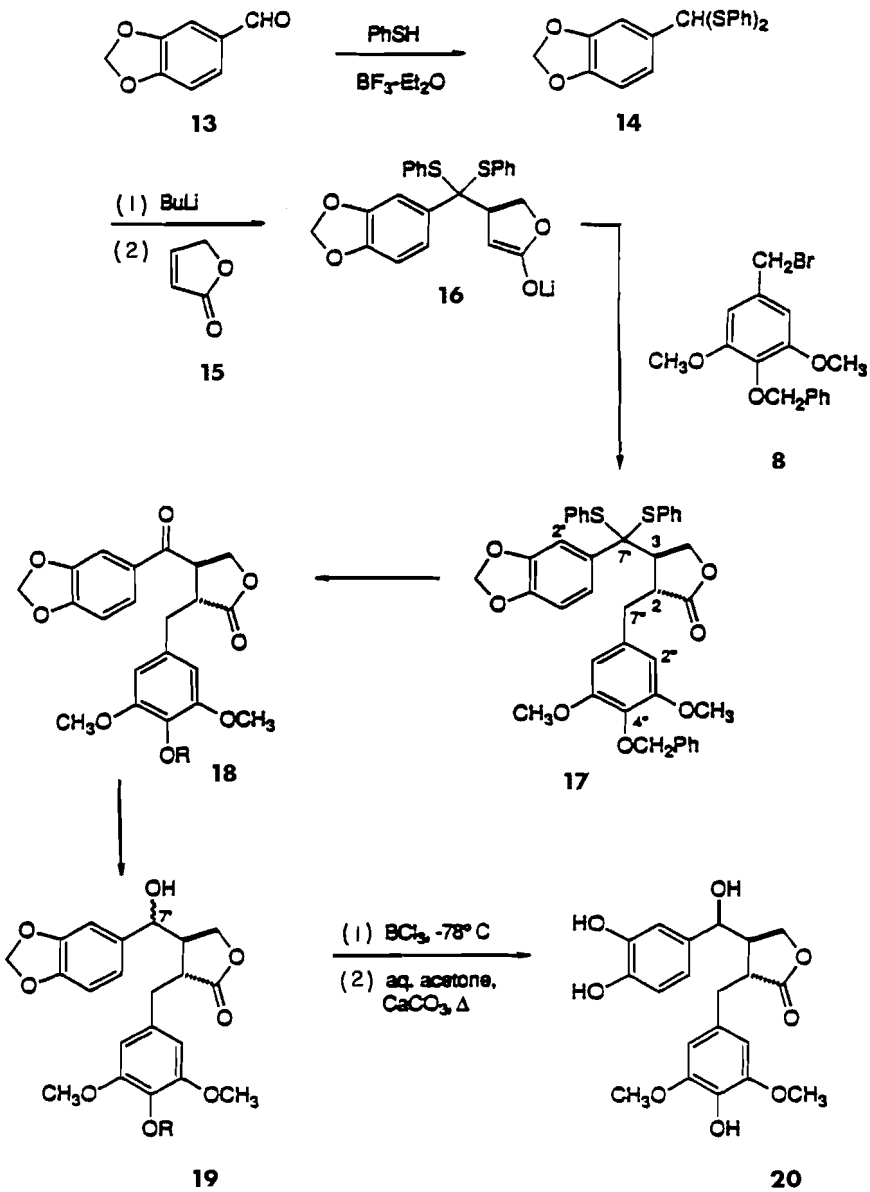

SCHEME 3. Synthesis of dibenzylbutanolide **20**.

We then proceeded to investigate the biotransformation of **20** by the *C. roseus* CFE with the intention of performing the oxidative coupling of **20** to the aryltetralin **21** and (or) the quinone (**22**) (Scheme 4) since both compounds could be converted readily to podophyllotoxin analogues bearing the desired methylene dioxy function in ring B as required for etoposide synthesis. Since catechols are known to react very readily with peroxidase to form *ortho*-quinones (51) and the corresponding diacids (52), the biotransformation of **20**, as described in Table 2, was conducted under oxidizing conditions considerably milder than those employed for **7**. In addition to lower peroxidase:substrate ratio, a higher pH was employed in order to achieve a lower peroxidase reactivity. Nevertheless, the color of the reaction mixture changed from an initial pale yellow to dark purple within 1 min, suggesting extensive oxidation of starting material to quinones. No such color change had been observed in the biotransformation of **7**. A control experiment was also performed in order to determine if hydrogen peroxide, in the absence of CFE, was able to oxidize **20** under the conditions used in the biotransformation. Extraction of the reaction mixture gave 96% recovery of a material consisting exclusively of **20**. No color change was observed. It was concluded that hydrogen peroxide alone was unable to oxidize **20** under the given conditions.

A great deal of difficulty was encountered in the isolation of identifiable products from the various biotransformation experiments with **20**. Recovery of material into organic extracts (ethyl acetate or methanol, for example) was poor and it was clear that extensive decomposition was occurring even in short time incubations (for example, 10 min, Table 2). After much effort, the extraction procedure summarized in Scheme 5 was developed in which sodium borohydride was employed to reduce any resulting unstable quinones and (or) diazomethane was used to convert highly polar and possibly water-soluble carboxylic acids to esters. Under these conditions recovery of identifiable products could be achieved (Table 3).

Can. J. Chem. Downloaded from www.nrcresearchpress.com by 217.78.4.112 on 09/08/12
For personal use only.

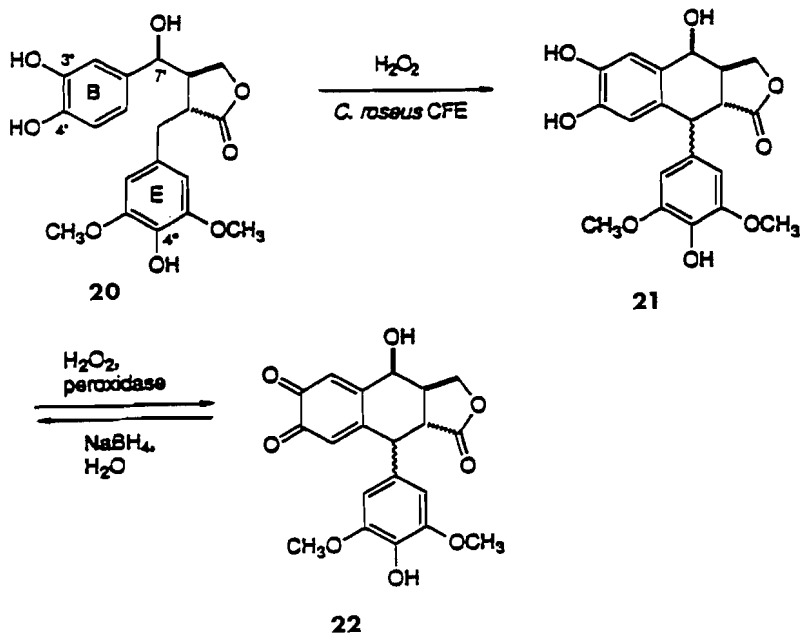

SCHEME 4. Proposed biotransformation of dibenzylbutanolide **20** with cell free extracts of *Catharanthus roseus* cell cultures.

TABLE 2. Catharanthus roseus CFE biotransformation of dibenzylbutanolide **20**

Substrate **20** (mg)	73
pH_h, pH_r	7.0
Hydrogen peroxide (equivalents)	2.0
CFE (units peroxidase per mmol **20**)	120
Reaction time (min)	10
Ethyl acetate extract (mg)	68
Methanol extract (mg)	205

Direct analysis of the ethyl acetate extract by TLC showed the presence of only **20** and very polar unidentified compounds. Addition of sodium borohydride (Table 3, Entry 1) gave a second major component, according to TLC, even prior to the reaction being quenched with dilute hydrochloric acid. The ^{1}H NMR spectrum and other spectral properties were identical with a product obtained in our earlier studies involving the reaction of boron trichloride with **19** (R = H) to which the "retro-lignan" type structure **26** (Scheme 6) had been assigned. The ^{1}H NMR spectrum of **26** showed singlets at δ 3.18 and 3.87 (methoxy protons), singlets at δ 7.12, 7.54, and 7.56 (hydroxyl protons) that disappeared upon D_2O addition, and a total of only four aromatic protons. The trisubstituted ring B aromatic signal pattern was present but the H(2″) signal appeared as only a single proton at δ 6.65. The EI mass spectrum of **26** in contrast to that of **20**, showed a very strong molecular ion peak at m/z 372 and a low degree of fragmentation. The proposed mechanism for the formation of **26** from **20** is shown in Scheme 6.

Only the substrate **20** and partially methylated **20** (**27**) were obtained when the ethyl acetate extract was treated with diazomethane (Entry 2, Table 3). The butanolide **27** was seen as a single spot on TLC analysis and spectroscopic data were consistent with the structural assignment. The ^{1}H NMR spectrum was nearly identical with that of **20** except for two additional methoxy proton signals and an apparent doubling

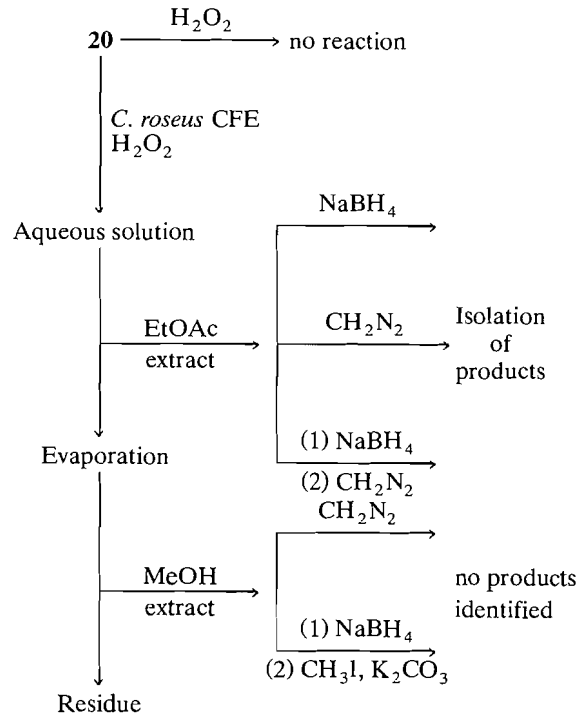

SCHEME 5. Extraction procedure for reaction mixture obtained in biotransformation of **20** with cell free extracts of *Catharanthus roseus* cell cultures.

of all signals that suggested two very similar compounds (**27***a*, **27***b*).

Successive treatments of the ethyl acetate extract with large excesses of sodium borohydride and freshly prepared diazomethane (Entry 3, Table 3) afforded two new products. One of these, assigned the structure **28**, was characterized by an ^{1}H NMR spectrum that showed a broad doublet at δ 4.22 (H(4)) and an aromatic signal pattern consistent with the trisubstituted aromatic ring at C(4), and the EI mass spectrum that clearly showed the molecular ion at m/z 414.

Can. J. Chem. Downloaded from www.nrcresearchpress.com by 217.78.4.112 on 09/08/12
For personal use only.

TABLE 3. Compounds isolated from ethyl acetate extract of biotransformation of butanolide **20**

Entry	Reagent(s)	Products	Yield (%)	Recovery[a] (%)
1	Sodium borohydride	**20**	12	39
		26	14	
2	Diazomethane	**20**	9	59
		27	15	
3	(1) Sodium Borohydride	**28**	20	82
	(2) Diazomethane	**29**	25	

[a] Total recovery of material from chromatographic column or preparative TLC plate.

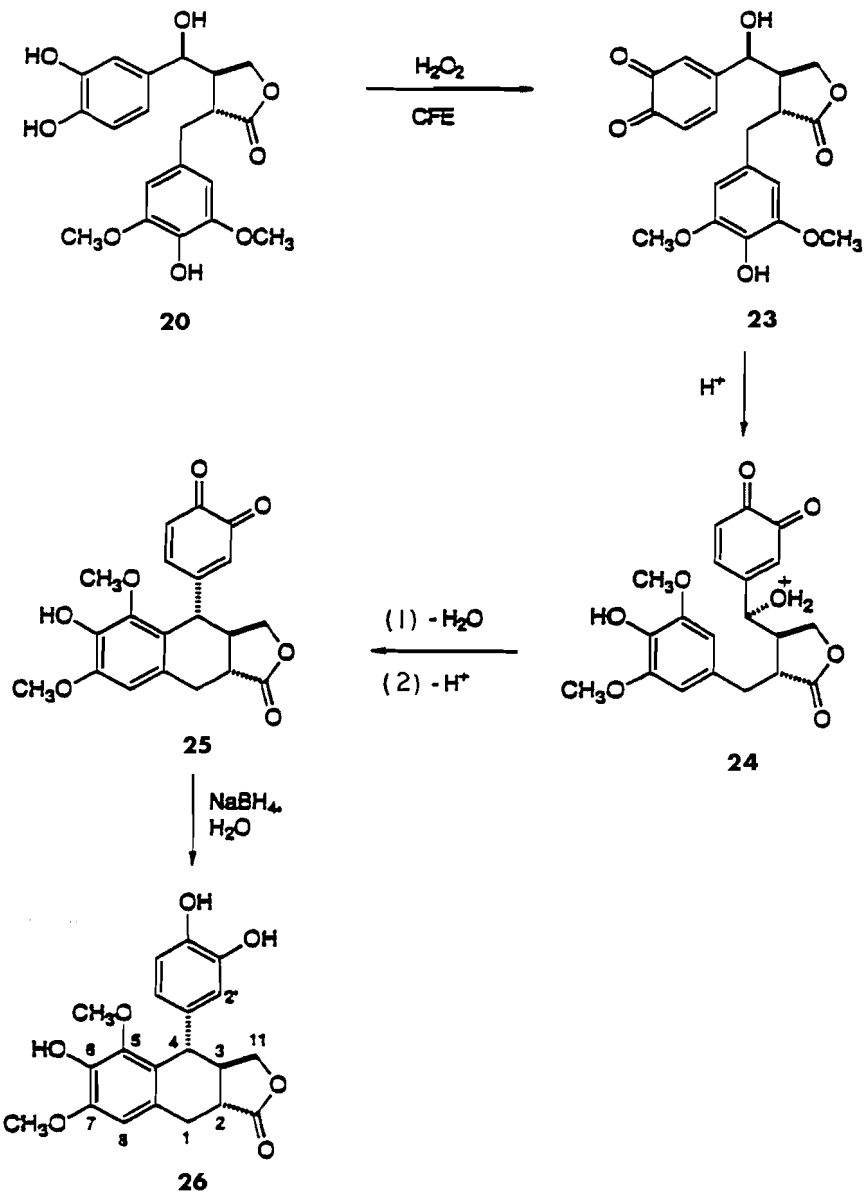

SCHEME 6. Biotransformation of dibenzylbutanolide **20** with cell free extracts of *Catharanthus roseus* cell cultures.

However, the ^{1}H NMR and mass spectral data for the other product, tentatively assigned structure **29**, did not permit an unambiguous structural assignment to be made. It is proposed that the large excess of sodium borohydride in an aqueous medium may have resulted in the hydrolysis of the lactone to the hydroxy acid **29**. Such a structure would be consistent with the polarity of this compound, as acetone was required to elute **29** from the chromatographic column of silica. Further support is provided by the presence of a broad O–H stretch at 3320 cm^{-1} and a carbonyl band at 1670 cm^{-1}

Can. J. Chem. Downloaded from www.nrcresearchpress.com by 217.78.4.112 on 09/08/12
For personal use only.

Can. J. Chem. Downloaded from www.nrcresearchpress.com by 217.78.4.112 on 09/08/12
For personal use only.

in the IR spectrum, both of which resemble the characteristic stretching frequencies of a carboxylic acid. Both the EI and DCI mass spectra of **29** exhibited a very high degree of fragmentation and peaks of low intensity, as expected for an acyclic compound. However, the acid moiety produced by saponification should have reacted with diazomethane in the subsequent step to afford an ester and this was clearly not the case. Due to its low yield and no direct relevance to

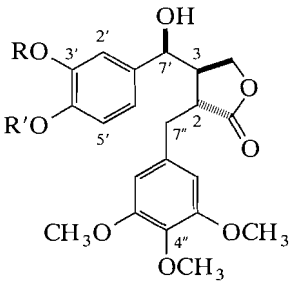

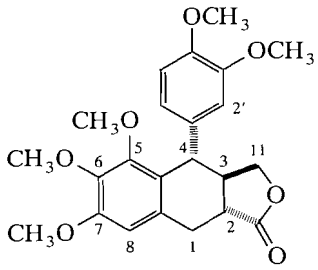

27*a*: R = H; R′ = CH_3
27*b*: R = CH_3; R′ = H

28

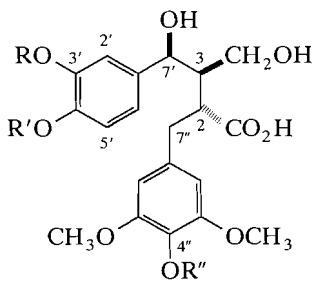

R, R′, R″ = H or CH_3

29

the objectives of this study, more detailed investigations to establish a more definitive structure for **29** were not pursued.

The nature of the unrecovered biotransformation products of **20** is not known. The total recovery of material from the chromatographic separation of the ethyl acetate extract, which had been subjected to reduction and methylation (Entry 3, Table 3), was 82% but only 30% of this material showed aromatic proton signals as determined by ^{1}H NMR spectroscopy. Consequently, the methanol extract of the biotransformation mixture was expected to contain a significant portion of the biotransformation products but TLC analysis showed only baseline (R_f 0) material after treatment with sodium borohydride or diazomethane. Treatment with excess sodium borohydride followed by methylation and isolation of material with an R_f value greater than zero by silica TLC analysis gave only minor amounts of an unidentified compound, assumed to be derived from the CFE.

Although the studies with **20** were not entirely conclusive because of the poor recovery of starting material and products, it gave no evidence of the formation of either the desired aryltetralin **21** or its *ortho*-quinone **22** (Scheme 4). It was thus concluded that the oxidation of ring B in **20** to some unidentified species was too rapid to permit the formation of the quinone methide intermediates required for cyclization to **21**. The low recovery values were probably also the result of a highly reactive substrate resulting from the presence of a catechol-like functionality in ring B.

In conclusion, these studies have thus far indicated that *C. roseus* cell culture derived enzymes, originally developed for production of indole alkaloids, are capable of biotransforming selected dibenzylbutanolides, via oxidative coupling, to compounds closely related to the podophyllotoxins. The process can be highly efficient *if* the substrate, as in the case of **7**, possesses a hydroxyl group at C(3′) of the dibenzylbutanolide system. On the other hand, further activation of the ring system, as in **20** where hydroxyl functionality is present at two adjacent centers (C(3′) and C(4′)), leads to competitive facile oxidation and ring closure reactions become of minimal significance. With these data in hand, further studies with various dibenzylbutanolides and cell cultures of *Podophyllum peltatum*, the plant from which the podophyllotoxins are isolated, will be presented in further publications.

Experimental

Melting points were determined using a Reichert melting point apparatus and are uncorrected. The recrystallization solvents are given in parentheses. Infrared spectra were recorded on Perkin Elmer 1710, 710, or 710B spectrometers, using sodium chloride cells, as a chloroform solution (0.1 mm path length), thin film, or Nujol mull. Band frequencies are reported relative to polystyrene (1601 cm^{-1}). Ultraviolet spectra were recorded as methanol solutions on a Cary 15 spectrometer using 1 cm quartz cells. ^{1}H NMR spectra were recorded on Bruker WH-400, Bruker AC 200, or Varian XL-300 spectrometers. Chemical shift values are reported in ppm relative to tetramethylsilane as an internal standard. ^{1}H COSY NMR spectra were recorded on a Bruker AC 200 spectrometer. ^{13}C NMR spectra were recorded on a Varian XL-300 spectrometer at 75.3 MHz or a Bruker AC-200 spectrometer at 50.2 MHz. Signals with a negative intensity in the attached proton test (APT) are indicated as such by "(−)" and imply the attachment of an odd number of protons. Mass spectra were recorded on AEI-MS-9 (low resolution) or Kratos-MS-50 (high resolution) spectrometers, employing electron impact, fast atom bombardment, or desorption chemical ionization methods. Elemental analyses were performed using combustion analysis by Mr. P. Borda, Microanalytical Laboratory, University of British Columbia. Determination of structures by X-ray crystallography was performed by the X-ray Crystallography Laboratory, University of British Columbia.

Cell suspension culture of the AC3 line of *C. roseus* was obtained from Biological Services of the Department of Chemistry, University of British Columbia. Column chromatography (referred to as "flash chromatography") (53) was performed using columns of silica gel (230–400 mesh, Merck art. 9385) or Florisil (60–100 mesh, Fisher F-100) with air or nitrogen gas pressure to obtain a rapid flow rate. Thin-layer chromatography was performed using commercial aluminum-backed silica gel plates (Merck art. 5554). Visualization was accomplished by spraying with 5% ammonium molybdate in 10% aqueous sulfuric acid followed by heating. High-pressure liquid chromatography was performed using a Waters C^{18} "Radial Pak" liquid chromatography cartridge, a Waters 440 absorbance detector set at 280 nm, and a methanol/water eluent. Circular dichroism analysis was performed using a Jasco J-20 automatic recording spectropolarimeter.

3-Benzyloxy-4-methoxybenzaldehyde (2)

A suspension of isovanillin (**1**, 24.9 g, 164 mmol), potassium carbonate (24.8 g, 179 mmol), benzyl chloride (24.8 g, 194 mmol), sodium iodide (1.0 g, 6.7 mmol), and ethanol (75 mL) was refluxed for 4.5 h while stirring with a mechanical stirrer. Water (50 mL) was added and the ethanol removed *in vacuo*. The slurry was poured into a mixture of 1 M sodium hydroxide (125 mL) and

Can. J. Chem. Downloaded from www.nrcresearchpress.com by 217.78.4.112 on 09/08/12
For personal use only.

ice (50 g). The solids were filtered off and washed with ice-cold water (3 × 25 mL). Drying *in vacuo* gave the benzyl ether **2** (40.2 g, 100%) as a tan solid. A sample was recrystallized from ethyl acetate/hexanes for analysis.

Physical properties of **2**: mp 60.0–60.5°C (ethyl acetate/hexanes), IR ν_{max} ($CHCl_3$): 1690 cm^{-1}; UV λ_{max} (log ϵ): 273 (4.03), 305 (3.91) nm; ^1H NMR δ: 3.97 (3H, s, $-OCH_3$), 5.20 (2H, s, $-OCH_2Ph$), 7.01 (1H, d, H(5), J = 8 Hz), 7.30–7.49 (7H, m, aromatic), 9.81 (1H, br s, $-CHO$); MS *m/z*: 242 (M^+), 214, 181, 168. High-resolution molecular weight determination calcd. for $C_{15}H_{14}O_3$: 242.0943; found: 242.0942. Anal. calcd. for $C_{15}H_{14}O_3$: C 74.36, H 5.82; found: C 74.25, H 5.82.

E-*2-(3-Benzyloxy-4-methoxybenzylidene)butanedioic acid 1-methyl ester (3)*

A solution of sodium methoxide was prepared by the careful addition of sodium (14.6 g, 633 mmol) to dry methanol (250 mL) under nitrogen. A solution of the benzyl ether **2** (95.7 g, 395 mmol) in dimethylsuccinate (81.6 g, 558 mmol) was added dropwise over 40 min at reflux. After an additional 70 min of stirring at reflux, the bulk of the solvent was removed *in vacuo*. The suspension was cooled to O°C and acidified with 6 M hydrochloric acid. The solids were removed by filtration and the filtrate extracted with dichloromethane (2 × 400 mL). The solids were added to the organic extract, washed with brine (400 mL), dried over magnesium sulfate, filtered, and evaporated *in vacuo* to yield an oily yellow solid, which was recrystallized from ethyl acetate/hexanes to give the hemisuccinate **3** (102.1 g, 73%) as a yellowish powder.

Physical properties of **3**: mp 123–125°C (ethyl acetate/hexanes); IR ν_{max} ($CHCl_3$): 1700 cm^{-1}; UV λ_{max} (log ϵ): 290 (4.03), 307 (4.03) nm; ^1H NMR δ: 3.51 (2H, s, H(2)), 3.86, 3.93 (3H each, s, s, $-CO_2CH_3$, Ar-OCH_3), 5.22 (2H, s, $-OCH_2Ph$), 6.94 (1H, d, H(5′), J = 8 Hz), 7.05 (1H, dd, H(6′), J = 8, 1 Hz), 7.10 (1H, d, H(2′), J = 1 Hz), 7.37–7.45 (5H, m, phenyl), 7.81 (1H, s, H(7′)). MS *m/z*: 356 (M^+), 324, 296. High-resolution molecular weight determination calcd. for $C_{20}H_{20}O_6$: 356.1260; found: 356.1268.

(±)-2-(3-Benzyloxy-4-methoxybenzyl)butanedioic acid 1-methyl ester (4)

Hemisuccinate **3** (96.4 g, 271 mmol) was added to a suspension of magnesium shavings (66.2 g, 2.72 mol) in dry methanol (750 mL) under nitrogen. After a few minutes stirring, the reaction vessel was immersed in an ice bath and stirred at 0°C for 5 h. The suspension was acidified with 6 M hydrochloric acid and the remaining solids were removed by filtration. The filtrate was extracted with dichloromethane (3 × 400 ml), washed with brine (500 mL), dried over magnesium sulfate, filtered, and evaporated *in vacuo* to give the hemisuccinate **4** (86.4 g, 89%) as an amber resin that solidified upon standing at 3°C.

Physical properties of **4**: mp 78–82°C; IR ν_{max} ($CHCl_3$): 1720 cm^{-1}; UV λ_{max} (log ϵ): 279 (3.49) nm; ^1H NMR δ: 2.34 (1H, dd, H(3), J = 18, 4.5 Hz), 2.58–2.72 (2H, m, H(3), H(2)), 2.90–3.10 (2H, m, H(7′)), 3.66 (3H, s, $-CO_2CH_3$), 3.88 (3H, s, Ar-OCH_3), 5.13 (2H, s, $-OCH_2Ph$), 6.70 (2H, m, H(2′), H(6′)), 6.82 (1H, d, H(5′), J = 7.8 Hz), 7.25–7.50 (5H, m, phenyl); MS *m/z*: 358 (M^+), 308, 281. High-resolution molecular weight determination calcd. for $C_{20}H_{22}O_6$: 358.1417; found: 358.1413.

(±)-3-(3-Benzyloxy-4-methoxybenzyl)butanolide (5)

Method 1

The hemisuccinate **4** (2.1 g, 5.7 mmol) was dissolved at 0°C in water (5 mL) with 2 M potassium hydroxide. The solution was neutralized and evaporated *in vacuo* to yield the potassium salt of **4**. A solution of calcium borohydride was prepared by adding a solution of calcium chloride (3.29 g, 28.5 mmol) in methanol (60 mL) to a solution of sodium borohydride (1.62 g, 40.7 mmol) in ethanol (60 mL) at −20°C. Potassium hydroxide (180 mg, 3.2 mmol) was added followed by the potassium salt of **4** dissolved in ethanol (50 mL). The solution was allowed to warm to room temperature and stirred for 4.5 days before being cooled to 0°C, and acidified with 6 M hydrochloric acid. The solution was concentrated *in vacuo*, extracted with dichloromethane (3 × 100 mL), dried over magnesium sulfate, filtered, and evaporated *in vacuo*. Purification by flash chromatography using ethyl acetate/petroleum ether (9:11, v/v) gave the β-benzylbutanolide **5** (1.16 g, 65%) as a yellowish oil that solidified upon standing.

Method 2

Lithium borohydride (0.91 g, 42 mmol) in dry THF (150 mL) was added carefully to a solution of the hemisuccinate **4** (14.7 g, 40.9 mmol) in THF (250 mL) at reflux under nitrogen. The solution was stirred for 2 h at reflux and then cooled to room temperature. Water (2 mL) and 6 M hydrochloric acid (9 mL) were added and the solution was stirred at room temperature for 2.5 h. The bulk of the solvent was removed by evaporation *in vacuo* and the resultant mixture extracted with ether (50 mL). The organic extract was washed with saturated sodium bicarbonate (3 × 25 mL) and water (25 mL) before being dried over magnesium sulfate, filtered, and evaporated *in vacuo* to give the pure β-butanolide **5** (11.4 g, 88%) as a clear oil that solidified upon standing.

Physical properties of **5**: mp 51–54°C; IR ν_{max} ($CHCl_3$): 1770 cm^{-1}; UV λ_{max} (log ϵ): 279 (3.48) nm; ^1H NMR δ: 2.19 (1H, dd, H(2), J = 17.6, 6.7 Hz), 2.50 (1H, dd, H(2), J = 17.6, 7.9 Hz), 2.61–2.80 (3H, m, H(3), H(7′)), 3.89 (3H, s, -OCH_3), 3.91 (1H, dd, H(4), J = 9.1, 6.0 Hz), 4.21 (1H, dd, H(4), J = 9.1, 7.0 Hz), 5.16 (2H, s, -OCH_2Ph), 6.65 (1H, d, H(2′), J = 1 Hz), 6.71 (1H, dd, H(6′), J = 8, 1Hz), 6.85 (1H, d, H(5′), J = 8 Hz); MS *m/z*: 312 (M^+), 222, 137. High-resolution molecular weight determination calcd. for $C_{19}H_{20}O_4$: 312.1362; found: 312.1371.

(±)-trans-*2-(4-Benzyloxy-3,5-dimethoxybenzyl)-3-(3-benzyloxy-4-methoxybenzyl)butanolide (6)*

To a solution of diisopropylamine (2.9 mL, 21 mmol) in dry THF (30 mL) at −78°C was added butyllithium (11 mL, 1.6 M solution, 17 mmol) and stirring continued for 15 min at −78°C and then for 30 min at 0°C. The clear solution was cooled to −78°C, β-butanolide **5** (4.3 g, 14 mmol) in THF (15 mL) was added, and the bright yellow solution stirred for 90 min prior to the addition of the bromide **8** (5.5 g, 16 mmol) in THF (15 mL) and stirring for 8 h at −78°C. The solution was warmed to 0°C, acidified with 1 M hydrochloric acid, and extracted with dichloromethane (2 × 150 mL). The combined organic extracts were washed with water (80 mL), dried over magnesium sulfate, filtered, and evaporated *in vacuo*. Flash chromatography using ethyl acetate/petroleum ether (9:11, v/v) gave the dibenzylbutanolide **6** (6.2 g, 80%) as a yellowish foam.

Physical properties of **6**: mp 35–37°C, IR ν_{max} ($CHCl_3$): 1770 cm^{-1}; UV λ_{max} (log ϵ): 278 (3.55) nm; ^1H NMR δ: 2.32 (1H, dd, H(7″), J = 14.4, 8.2 Hz), 2.45–2.70 (3H, m, H(7″), H(2), H(3)), 3.06 (1H, dd, H(7′), J = 14.0, 8.0 Hz), 3.32 (1H, dd, H(7′), J = 14.0, 5.4 Hz), 3.74 (1H, dd, H(4), J = 9, 8 Hz), 3.80 (6H, s, -OCH_3(3″, 5″)), 3.88 (3H, s, -OCH_3(4′)), 3.99 (1H, dd, H(4), J = 9.2, 7.0 Hz), 5.05, 5.13 (2H each, s, s, -OCH_2Ph), 6.52–6.58 (3H, m, H(2″), H(6′)), 6.69 (1H, s, H(2′)), 6.77 (1H, d, H(5′), J = 8.0 Hz), 7.25–7.49 (10H, m, phenyl); MS *m/z*: 568 (M^+), 402, 312, 167, 137, 91. High-resolution molecular weight determination calcd. for $C_{35}H_{36}O_7$: 568.2461; found: 568.2457.

(±)-trans-*2-(3,5,-Dimethoxy-4-hydroxybenzyl)-3-(3-hydroxy-4-methoxybenzyl)butanolide (7)*

Palladium-on-charcoal (5%, 1.05 g) was suspended in ethanol (40 mL) and stirred under hydrogen at atmospheric pressure for 1.5 h. The dibenzylbutanolide **6** (6.2 g, 11 mmol) was added as an ethyl acetate/ethanol solution (1:3, v/v, 40 mL) and the resultant suspension stirred for 5 h. The catalyst was filtered off and the solvent evaporated *in vacuo* to yield the bis(hydroxybenzyl)butanolide **7** (3.7 g, 87%) as an amorphous white solid after

Can. J. Chem. Downloaded from www.nrcresearchpress.com by 217.78.4.112 on 09/08/12
For personal use only.

flash chromatography using ethyl acetate/petroleum ether (11:9, v/v). Small samples were crystallized from diethyl ether/petroleum ether for melting point determination or distilled (240°C, 0.15 Torr; 1 Torr = 133.3 Pa) for microanalysis.

Physical properties of **7**: mp 68–69°C (diethyl ether/petroleum ether); IR ν_{max} ($CHCl_3$): 3540, 1770 cm^{-1}; UV λ_{max} (log ϵ): 279 (3.57) nm; ^1H NMR δ: 2.45–2.65 (4H, m, H(2), H(3), H(7″)), 2.88 (1H, dd, H(7′), J = 14.6, 5.7 Hz), 2.93 (1H, dd, H(7′), J = 14.6, 6.4 Hz), 3.87–3.89 (10 H, m, -OCH_3, H(4)), 4.15 (1H, dd, H(4), J = 7.5, 3.0 Hz), 5.42 (1H, s, -OH(4″)), 5.58 (1H, s, -OH(3′)), 6.49 (1H, dd, H(6′), J = 8.5, 2.1 Hz), 6.62 (1H, d, H(2′), J = 2.1 Hz), 6.73 (1H, d, H(5′), J = 8.5 Hz). All hydroxyl signals disappear upon addition of D_2O. ^{13}C NMR δ: 35.363 (C(7″), 38.147 (C(7′)), 41.891(−), 47.055(−), 56.175(−), 56.531(−) (-OCH_3(3″)), 71.756 (C(4)), 107.549(−) (C(2″)), 112.307(−), 116.348(−), 120.434(−), 129.383, 132.645, 135.354, 146.894, 147.280, 148.544, 179.051 (C(1)); MS *ms/z*: 388 (M^+), 167, 153, 137. High-resolution molecular weight determination calcd. for $C_{21}H_{24}O_7$: 388.1522; found: 388.1520. Anal. calcd. for $C_{21}H_{24}O_7$: C 64.94, H 6.23; calcd. for $C_{21}H_{26}O_8$ (58 + H_2O): C 62.06, H 6.45; found: C 62.31, H 6.25.

*1-Bis(phenylthio)methyl-3,4-methylenedioxybenzene (**14**)*

To a solution of piperonal **13** (1.0 g, 6,7 mmol) in dry chloroform (10 mL) at −40°C under argon was added thiophenol (1.4 mL, 14 mmol) and boron trifluoride etherate (4.6 mL, 45% solution, 17 mmol). The solution was stirred for 15 min at −40°C and then poured into ice-cold water (10 mL). The organic layer was drawn off and the aqueous layer extracted with chloroform (30 mL). The combined organic extracts were washed with 7% potassium hydroxide (2 × 25 mL), water (25 mL), and brine (25 mL) before being dried over potassium carbonate, filtered, and evaporated *in vacuo* to yield the pure dithioacetal **14** (2.3 g, 98%) as a yellowish oil. The physical properties of **14** were determined using a distilled (190°C, 0.15 Torr) sample.

Physical properties of **14**: iR ν_{max} (neat): 2890, 1490 cm^{-1}; UV λ_{max} (log ϵ): 248 (4.14), 282 (3.88) nm; ^1H NMR δ: 5.37 (1H, s, -CH ($SPh)_2$), 5.96 (2H, s, -OCH_2O-), 6.67 (1H, d, H(5), J = 4 Hz), 6.78 (1H, dd, H(6), J = 4, 2 Hz), 6.98 (1H, d, H(2), J = 2 Hz), 7.23–7.32 (6H, m, phenyl), 7.34–7.42 (4H, m, phenyl); MS *m/z*: 352 (M^+), 243. High-resolution molecular weight determination calcd. for $C_{20}H_{16}O_2S_2$: 352.0592; found: 352.0598. Anal. calcd. for $C_{20}H_{16}O_2S_2$: C 68.15, H 4.58; found: C 68.11, H 4.63.

*(±)-trans-2-(4-Benzyloxy-3,5-dimethoxybenzyl)-3-(3,4-methylenedioxy)-α,α-bis(phenylthio)benzyl)butanolide (**17**)*

Butyllithium (3.60 mL, 1.6 M solution, 5.76 mmol) was added to a solution of dithioacetal **14** (2.00 g, 5.69 mmol) in dry THF (10 mL) at −78°C and the purple solution was stirred for 2.5 h. But-2-en-4-olide (**15**, 0.481 g, 5.73 mmol) in THF (8 mL) was added and the solution stirred for 2.5 h at −78°C prior to the addition of the bromide **8** (2.06 g, 6.10 mmol) in THF (10 mL). The solution was allowed to warm slowly to room temperature overnight. Water (25 mL) was added and the mixture extracted with ethyl acetate (160 mL). The organic extract was washed with water (2 × 25 mL) before being dried over magnesium sulfate, filtered, and evaporated *in vacuo*. Purification by flash chromatography using dichloromethane gave the expected dithioketal **16** (replace OLi by carbonyl) (2.16 g. 55%) as an amorphous solid.

Physical properties of **17**: mp 55–57°C (acetone); IR ν_{max} ($CHCl_3$): 1770 cm^{-1}; UV λ_{max} (log ϵ): 279 (3.82), 286 (3.80) nm; ^1H NMR δ: 2.79 (1H, dd, H(7″), J = 14, 5 Hz), 2.85–2.90 (1H, m, H(2)), 3.12 (1H, dd, H(7″), J = 14, 4 Hz), 3.29–3.34 (1H, m, H(3)), 3.49 (1H, dd, H(4), J = 10, 8 Hz), 3.70 (6H, s, -OCH_3), 4.46 (1H, dd, H(4), J = 10, 3 Hz), 5.02 (2H, s, -OCH_2Ph), 6.00, 6.01 (2H total, d, d, -OCH_2O-, J = 1 Hz each), 6.18 (2H, s, H(2″)), 6.73 (1H, d, H(5′), J = 8 Hz), 7.13 (1H, dd, H(6′), J = 8, 2 Hz), 7.21–7.38 (14H, m, phenyl, H(2′)), 7.43–7.47 (2H, m, phenyl); FAB MS *m/z*: 693 (M^+), 584, 473, 383, 218, 185, 167, 154, 135; MS *m/z*: 584, 583, 383, 218, 185, 167, 154, 135. High-resolution molecular weight determination calcd. for $C_{34}H_{31}O_7S$ (M^+−SPh): 583.1790; found: 583.1792. Anal. calcd. for $C_{40}H_{36}O_7S_2$: C 69.34, H 5.24, S 9.25; found: C 69.18, H 5.42, S 9.23.

*(±)-trans-2-(4-Benzyloxy-3,5-dimethoxybenzyl)-3-(3,4-methylenedioxybenzoyl)butanolide (**18**, R = CH_2Ph) and (±)-trans-2-(3,5-dimethoxy-4-hydroxybenzyl)-3-(3,4-methylenedioxybenzoyl)butanolide (**18**, R = H)*

Method 1

Dithioketal **16** (replace OLi by carbonyl) (34.5 mg, 50.0 μmol) was dissolved in ethyl acetate (6 mL). Perchloric acid (70%, 1 drop) was added and the solution stirred for 4 h. Water (1 mL and ethyl acetate (10 mL) were added and the phases separated. The organic extract was washed with brine (2 mL) and saturated sodium bicarbonate (2 × 2 mL), dried over magnesium sulfate, filtered, and evaporated *in vacuo*. Flash chromatography using acetate/dichloromethane (1:19, v/v) gave the ketones **18** (R = CH_2Ph) (10.8 mg, 44%) and **18** (R = H) (2.0 mg, 10%).

Method 2

Sulfuryl chloride (11.8 mg, 87.4 μmol) in dichloromethane (0.4 mL) was added to a mixture of dithioketal **16** (replace OLi by carbonyl) (48.7 mg, 70.3 μmol), silica gel (230–400 mesh, 30 mg), and water (30 mg) in dichloromethane (0.35 mL). After stirring for 2 h, finely powdered anhydrous potassium carbonate was added and stirring continued for 0.5 h. The solids were filtered off and washed with dichloromethane. The filtrate was evaporated *in vacuo* and purified by flash chromatography using acetone/dichloromethane (1:49, v/v) but neither **18** (R = CH_2Ph) nor **18** (R = H) could be identified by ^1H NMR spectroscopy of the major fractions.

Method 3

Iodine (1.46 g, 11.5 mmol) was added to a solution of dithioketal **16** (replace OLi by carbonyl) (1.85 g, 2.68 mmol) in methanol (50 mL) and THF (5 mL). The solution was then stirred at reflux for 1.5 h prior to the addition of saturated sodium thiosulfate (10 mL), brine (10 mL), and water (20 mL). The mixture was extracted with ethyl acetate (100 mL), diluted with water (10 mL) and brine (10 mL), and re-extracted with ethyl acetate (100 mL). The organic extract was washed with water (20 mL), dried over magnesium sulfate, filtered, and evaporated *in vacuo*. THF (5 mL) and 3 M hydrochloric acid (6 mL) were added and the suspension stirred at room temperature for 1 h before being diluted with water (10 mL) and extracted with dichloromethane (2 × 50 mL). The organic extract was washed with water (2 × 20 mL), dried over magnesium sulfate, filtered, and evaporated *in vacuo*. Ether (25 mL) was added and the suspension sonicated for 5 min, stored at 3°C for 3 days, filtered, and washed with ice-cold ether (2 × 5 mL) to give the ketone **18** (R = CH_2Ph) as a white powder (0.920 g). The filtrate was evaporated and purified by flash chromatography using acetone/dichloromethane (0:1 to 1:49 gradient, v/v) to afford **18** (R = CH_2Ph) (134 mg) for a total yield of 80%.

Physical properties of **18** (R = CH_2Ph): mp 43–44°C (diethyl ether); IR ν_{max} ($CHCl_3$): 1770, 1670 cm^{-1}; UV λ_{max} (log ϵ): 275 (3.82), 314 (3.90) nm; ^1H NMR δ: 3.00 (1H, dd, H(7″), J = 14, 6 Hz), 3.09 (1H, dd, H(7″), J = 14, 5 Hz), 3.55–3.61 (1H, m, H(2)), 3.70 (6H, s, -OCH_3), 4.01 (1H, ddd, H(3) J = 8, 8, 8 Hz), 4.10 (1H, dd, H(4), J = 9, 8 Hz), 4.38 (1H, dd, H(4), J = 9, 8 Hz), 4.92 (2H s, -OCH_2Ph), 6.01, 6.04 (1H each, d, d, -OCH_2O-, J = 1 Hz each), 6.28 (2H, s, H(2″)), 6.80 (1H, d, H(5′), J = 8 Hz), 7.24–7.38 (5H, m, H(2′), H(6′), phenyl), 7.47 (2H, dd, phenyl, J = 7, 1 Hz); MS *m/z*: 490 (M^+), 399, 223, 149, 91. High-resolution molecular weight determination calcd. for $C_{28}H_{26}O_8$:

Can. J. Chem. Downloaded from www.nrcresearchpress.com by 217.78.4.112 on 09/08/12
For personal use only.

490.1627; found: 490.1627. Anal. calcd. for $C_{28}H_{26}O_8$: C 68.56, H 5.34; found: C 68.78, H 5.56.

Physical properties of **18** (R = H): mp 56–58°C; IR ν_{max} ($CHCl_3$): 3530, 1770, 1670 cm^{-1}; UV λ_{max} (log ϵ): 276 (3.80), 314 (3.86) nm; ^1H NMR δ: 3.01 (1H, d, H(7″), J = 14, 7 Hz), 3.07 (1H, dd, H(7″), J = 14, 6 Hz), 3.53–3.60 (1H, m, H(2)), 3.78 (6H, s, -OCH_3), 4.02 (1H, ddd, H(3), J = 9, 9, 9 Hz), 4.12 (1H, dd, H(4), J = 9, 9 Hz), 4.41 (1H, dd, H(4), J = 9, 9 Hz), 5.37 (1H, s, -OH, disappears with D_2O), 6.07 (2H, m, -OCH_2O-), 6.30 (2H, s, H(2″)), 6.81 (1H, d, H(5′), J = 8 Hz), 7.23 (1H, d, H(2′), J = 2 Hz), 7.27 (1H, dd, H(6′), J = 8, 2 Hz); MS m/z: 400 (M^+), 224, 167, 149. High-resolution molecular weight determination calcd. for $C_{21}H_{20}O_8$: 400.1158; found: 400.1164.

(±)-trans-*2-(3,5-Dimethoxy-4-hydroxybenzyl)-3-(α-hydroxy-3,4-methylenedioxybenzyl)butanolide (**19**, R = H)*

Method 1

Palladium-on-charcoal (10%, 1.676 g) was suspended in ethanol (100 mL) and stirred for 1 h under hydrogen at atmospheric pressure. A solution of the ketone **18** (R = CH_2Ph) (4.50 g, 9.16 mmol) in ethyl acetate (100 mL) was added and the resultant suspension stirred for 7 h. The catalyst was filtered off and the solution evaporated *in vacuo*. The residue was purified by column chromatography using acetone/dichloromethane (1:19 to 1:9 gradient, v/v) to give ketone **18** (R = Ch_2Ph) (0.685 g, 15%), ketone **18** (R = H) (1.686 g, 46%), and alcohol **19** (R = H) (1.113 g, 30%, 3.3:1 mixture of C(7′) epimers according to ^1H NMR spectroscopy).

Method 2

Sodium borohydride (47 mg, 1.2 mmol) was added to a suspension of the ketone **18** (R = H) (464 mg, 1.16 mmol) in dry methanol (50 mL) at 0°C under nitrogen. After stirring for 2.5 h at O°C, 1 M hydrochloric acid (2 mL) was added to the resultant clear solution, which was then concentrated *in vacuo*, diluted with water (5 mL) and brine (5 mL), and extracted with ethyl acetate (2 × 50 mL). The combined organic extracts were washed with water (15 mL), dried over magnesium sulfate, filtered, and evaporated *in vacuo* to give the alcohol **19** (R = H) (443 mg, 95%) as an amorphous white solid. ^1H NMR spectroscopy showed the product to be a 6:1 mixture of C(7′) epimers.

Properties of 3.3:1 mixture of **19** (R = H) (C(7′) β-hydroxyl epimer assumed as major): IR ν_{max} ($CHCl_3$): 3600, 3530, 1770 cm^{-1}; UV λ_{max} (log ϵ): 282 (3.60) nm; ^1H NMR (integrals relative to minor (α) epimer) δ: 1.94 (1H, d, -OH(7′, α), J = 3 Hz), 2.00 (3.3 H, d, -OH(7′, β), J = 3 Hz), 2.51–3.11 (17.2 H, m, H(7″), H(2), H(3)), 3.85 (6H, s, -OCH_3(α)), 3.87 (19.8 H, s, -OCH_3(β)), 3.92–3.96 (6.6 H, m, H(4, β)), 4.17 (1H, dd, H(4, α), J = 9.6, 7.6 Hz), 4.37 (1H, dd, H(7′, α), J = 8.0, 2.5 Hz), 4.40 (1H, dd, H(4, α), J = 9.6, 6.1 Hz), 4.62 (3.3 H, dd, H(7′, β), J = 6.7, 2.9 Hz), 5.40 (4.3 H, s, -OH(4″)), 5.97, 5.98 (3.3 H each, d, d, -OCH_2O-(β), J = 1 Hz), 5.99, 6.00 (1H each, d, d, -OCH_2O-(α), J = 1 Hz), 6.27 (2H, s, H(2″, α)), 6.40 (6.6 H, s, H(2″, β)), 6.61–6.76 (12.9 H, m, H(2′), H(5′), H(6′)). Upon addition of D_2O, all hydroxyl signals disappear and the H(7′) signals collapse to doublets. MS m/z: 402 (M^+), 384, 178, 167, 224, 151, 135, 123. High-resolution molecular weight determination calcd. for $C_{21}H_{20}O_8$: 402.1314; found: 402.1302. Anal. calcd. for $C_{21}H_{22}O_8$: C 62.28, H 5.51; found: C 62.33, H 5.80.

Physical properties of 6:1 mixture of **19** (R = H): mp 43–51°C.

(±)-trans-*2-(3,5-Dimethoxy-4-hydroxybenzyl)-3-(3,4-dihydroxy-α-hydroxybenzyl)butanolide (**20**) and (±)-4-(3,4-dihydroxyphenyl)-5,7-dimethoxy-6-hydroxy-2-hydroxymethyl-1,2,3,4-tetrahydro-2-naphthoic acid γ lactone (**26**)*

Method 1

Alcohol mixture **19** (R = H) (210 mg, 0.52 mmol) dissolved in dichloromethane (10 mL) was added to a solution of boron trichloride (3.1 mmol) in dichloromethane (23.5 mL) at −78°C. After stirring for 2 h at −78°C, saturated potassium bicarbonate (2 mL) was added and the suspension allowed to warm to room temperature. Water (5 mL) and brine (1 mL) were added and the mixture was extracted with ethyl acetate (2 × 50 mL). The organic extract was dried over magnesium sulfate, filtered, and evaporated *in vacuo*. Acetone (4 mL), water (5 mL), and calcium carbonate (330 mg) were added and the suspension stirred for 1.5 h at 65°C. The solids were dissolved by the addition of 6 M hydrochloric acid and the clear solution extracted with ethyl acetate (2 × 50 mL). The organic extract was washed with water (15 mL), dried over magnesium sulfate, filtered, and evaporated *in vacuo*. Flash chromatography using acetone/dichloromethane (2:8 to 3:8, v/v) gave the aryltetralin **26** (78 mg, 40%) and the catechol **20** (49 mg, 24%, single epimer by ^1H NMR spectroscopy) as amorphous white solids. A sample of **26** was recrystallized from methanol/chloroform for analysis.

Method 2

Alcohol **19** (R = CH_2Ph) (161 mg, 0.327 mmol) dissolved in dichloromethane (6.5 mL) was added to a stirred solution of boron trichloride (2.0 mmol) in dichloromethane (15.3 mL) at −78°C. After stirring for 2 h, water (3 mL), saturated potassium hydrogen carbonate (1 mL), and brine (1 mL) were added and the mixture allowed to warm to room temperature. The mixture was extracted with ethyl acetate (2 × 40 mL), dried over magnesium sulfate, filtered, and evaporated *in vacuo*. Acetone (3 mL), water (6.5 mL), and calcium carbonate (210 mg) were added and the suspension stirred for 1.5 h at 65°C. The solids were dissolved with 6 M hydrochloric acid and the solution extracted with ethyl acetate (2 × 40 mL). The organic extracts were washed with water (10 mL), dried over magnesium sulfate, filtered, and evaporated *in vacuo* to afford a yellowish foam. Flash chromatography using acetone/dichloromethane (1:4 to 3:2 gradient, v/v) afforded the alcohols **19** (R = H) (42 mg, 32%, 5:1 mixture of epimers by ^1H NMR spectroscopy) and **20** (33 mg, 26%).

Physical properties of **20**: mp 49–56°C; IR ν_{max} (Nujol): 3380, 1740 cm^{-1}; UV λ_{max} (log ϵ): 281 (3.57) nm; ^1H NMR δ: 2.64–2.77, 2.95–3.05 (4H total, m, m, H(7″), H(2), H(3)), 3.80 (6H, s, -OCH_3), 3.93 (1H, dd, H(4), J = 17, 9 Hz), 3.98 (1H, dd, H(4), J = 17, 8 Hz), 4.55 (1H, d, -OH(7′), J = 3.6 Hz), 4.68 (1H, dd, H(7′), J = 6.0, 3.6 Hz), 6.42 (2H, s, H(2″)), 6.68 (1H, dd, H(6′), J = 8, 2 Hz), 6.80 (1H, d, H(5′), J = 8 Hz), 6.88 (1H, d, H (2′), J = 2 Hz), 6.91 (1H, brs, -OH(4″)), 7.80 (2H, brs, -OH(3′), -OH(4′)). Upon addition of D_2O, all hydroxyl signals disappear and the H(7′) signal collapses to a doublet. ^{13}C NMR δ: 35.619 (C(7″)), 43.787(−), 45.709(−), 56.464(−) (-OCH_3), 68.892 (C(4)), 74.217(−) (C(7′)), 107.994(−) (C(2″)), 114.086(−), 115.787(−), 118.432(−), 129.114, 135.743; 145.227, 145.826, 148.339, 179.568 (C(1)); MS m/z: 390 (M^+), 372, 167, 154, 123, 110. High-resolution molecular weight calcd. for $C_{20}H_{22}O_8$: 390.1315; found: 390.1313.

Physical properties of **26**: mp 222–224°C (methanol/chloroform); IR ν_{max} (Nujol): 3400, 3250, 1730 cm^{-1}; UV λ_{max} (log ϵ): 283 (3.70) nm; ^1H NMR δ: 2.30–2.41 (1H, m, H(3)), 2.51 (1H, ddd, H(2), J = 13.6, 11.7, 4.5 Hz), 2.88–2.92 (1H, m, H(1)), 3.03 (1H, dd, H(1), J = 15.3, 4.5 Hz), 3.18 (3H, s, -OCH_3(5)), 3.87 (3H, s, OCH_3(7)), 4.04 (1H, brd, H(4), J = 10.8 Hz), 4.16–4.20 (2H, m, H(11)), 6.50 (1H, dd, H(6′), J = 8, 2 Hz), 6.55 (1H, d, H(2′), J = 2 Hz), 6.65 (1H, s, H(8)), 6.74 (1H, d, H(5′), J = 8 Hz), 7.12 (1H, s, -OH(6)), 7.54, 7.56 (1H each, s, s, -OH(3′), -OH(4′)). All hydroxyl signals disappear upon addition of D_2O. ^{13}C NMR δ: 41.595(−), 46.525(−), 50.499(−), 56.255(−), 58.614(−), 72.246, 101.389, 107.912(−), 114.565(−), 115(779(−), 118.991(−), 127.733, 139.071, 139.320, 143.913, 145.686, 177.2 (C(1)); MS m/z: 372 (M^+), 262. High-resolution molecular weight determination calcd. for $C_{20}H_{20}O_7$: 372.1219;

found: 372.1217. Anal. calcd. for $C_{20}H_{20}O_7$: C 64.51, H 5.41; found: C 63.58, H 5.57.

*(±)-*trans*-2-(4-Benzyloxy-3,5-dimethoxybenzyl)-3-(α-hydroxy-3,4-methylenedioxybenzyl)butanolide (**19**, R = CH_2Ph)*

Method 1

Sodium borohydride (19 mg, 0.51 mmol) was added to a suspension of ketone **18** (R = Ch_2Ph) (173 mg, 0.352 mmol) in dry methanol (25 mL) at 0°C under nitrogen. After stirring for 5 h at 0°C, 1 M hydrochloric acid (3 mL) was added to the resultant clear solution, which was then concentrated *in vacuo*, diluted with brine (2 mL), and extracted with dichloromethane (2 × 40 mL). The combined organic extracts were washed with water (8 mL), dried over magnesium sulfate, filtered, and evaporated *in vacuo* to give alcohol **19** (R = CH_2Ph) (172 mg, 99%) as an amorphous white solid. ^1H NMR spectroscopy indicated that the product was a 4.9:1 mixture of epimers.

Method 2

Lithium aluminum tri-*tert*-butoxy hydride (690 mg, 2.7 mmol) in THF (8 mL) was added to a stirred suspension of the ketone **18** (R = Ch_2Ph) (380 mg, 0.78 mmol) in dry ether (25 mL) and THF (5 mL) under nitrogen at −78°C. The mixture was stirred for 3 h and then acidified with 1 M hydrochloric acid (6 mL), diluted with water (15 mL), and extracted with ethyl acetate (2 × 50 mL). The organic extract was washed with saturated sodium bicarbonate (2 × 15 mL) and water (10 mL), dried over magnesium sulfate, filtered, and evaporated *in vacuo* to afford a foam (329 mg) that, by ^1H NMR spectroscopy, contained the alcohol **19** (R = CH_2Ph) (70%, 5.7:1 mixture of epimers) and the ketone **18** (R = CH_2Ph).

Physical properties of 4.9:1 mixture of **19** (R = CH_2Ph) (C(7′) β-hydroxyl epimer assumed as major): mp 46–49°C, IR ν_{max} ($CHCl_3$): 3450, 1770 cm^{-1}; UV λ_{max} (log ε): 284 (3.55) nm; ^1H NMR δ: 1.87 (1h, d, OH(7′, α), J = 3 Hz), 1.96 (4.9 H, d, -OH(7′, β), J = 2.8 Hz), 2.47–3.10 (23.6 H, m, H(2), H(3), H(7′)), 3.78–3.79 (35.4 H, m, $-OCH_3$), 3.89–3.96 (9.8 H, m, H(4, β)), 4.15–4.17 (1H, m, H(4, α)), 4.33 (1H, dd, H(7′, α), J = 7.1, 3 Hz), 4.37 (1H, dd, H(4, α), J = 9.3, 6.4 Hz), 4.60 (4.9 H, dd, H(7′, β), J = 7.1, 2.8 Hz), 5.00 (11.8 H, s, $-OCH_2Ph$), 5.93–6.01 (11.8 H, m, $-OCH_2O-$), 6.25 (2H, s, H(2″, α)), 6.38 (9.8 H, s, H(2″, β)), 6.57–6.78 (17.7 H, m, H(2′), H(5′), H(6′)), 7.22–7.50 (29.5 H, m, phenyl). Upon D_2O addition, both hydroxyl signals disappear and H(7′) signals collapse to doublets. MS m/z: 492 (M^+), 474, 161, 149, 131, 91. High-resolution molecular weight determination calcd. for $C_{28}H_{28}O_8$: 492.1784, found: 492.1784.

Preparation of C. roseus *cell-free extract (CFE)*

Catharanthus roseus (AC 3 line) cell suspension culture was grown in shake flasks in the dark in a 1B5 medium (54) (500 mL) containing agar (7–8 g) at pH 5.5. The cell line was subcultured every 10 days using a 12% (60 mL) inoculum and harvested at age 11 days. The whole cell suspension was filtered with Miracloth, drained thoroughly, washed with water (75 mL/flask), and drained again. The rest of the procedure was carried out at 0–4°C. Potassium phosphate buffer (0.100 M, pH_h, 0.50 mL/g fresh weight) was added and the suspension homogenized with an Ultra-Turrax blender at 20 000 rpm in four 30-s periods with 30-s intervals. The material was centrifuged, using a Sorvall RC-5B centrifuge and Sorvall GSA rotor, at 10 000 g for 30 min and the supernatant (CFE) analyzed for peroxidase activity (55) and protein concentration (41,42,56) using a Bausch and Lomb Spectronic 20 spectrophotometer.

Determination of hydrogen peroxide consumption by C. roseus *CFE*

An aliquot (3.00 mL) of a solution of **7** (15.3 mg, 39.3 μmol) in ethanol/water (8:17, v/v) was added to water (3.00 mL) and hydrogen peroxide (1.00 mL, 81.6 mM solution, 81.6 μmol). Potassium phosphate buffer (0.100 M, pH 6.3, 10.70 mL) and CFE (pH 6.3, specific activity 0.98 units/mg, 7.30 mL, 9.83 units) were added and the solution (Solution A) stirred for 3 h. An identical solution of water, hydrogen peroxide, buffer, and CFE was stirred for 15 min upon the addition of CFE: an aliquot of **7** was then added as before and the solution (solution B) stirred for an additional 3 h. After each solution had been stirred 1 h following addition of **7**, hydrogen peroxide (1.00 mL, 81.6 μmol) was added to Solution B and water (1.00 mL) to Solution A. HPLC analysis was then performed.

*(±)-1-(3,5-Dimethoxy-4-hydroxyphenyl)-6-hydroxy-3-hydroxymethyl-7-methoxy-1,2,3,4-tetrahydro-2-naphthoic acid γ lactone **9**; (±-5,5′-bis(1-(3,5-dimethoxy-4-hydroxyphenyl)-6-hydroxy-3-hydroxymethyl-7-methoxy-1,2,3,4-tetrahydro-2-naphthoic acid γ lactone (**10**), and (±)-1-(3,5-dimethoxy-4-hydroxyphenyl)-8-hydroxy-3-hydroxymethyl-7-methoxy-1,2,3,4-tetrahydro-2-naphthoic acid γ lactone (**11**)*

Catharanthus roseus CFE (pH 6.3, specific activity 1.5 units/mg, 215 mL, 330 units) was added to a solution containing butanolide **7** (1.860 g, 4.79 mmol) in ethanol (25 mL), water (100 mL), and hydrogen peroxide (20 mL, 0.17 M solution, 3.4 mmol). After stirring for 1 h, further hydrogen peroxide (10 mL, 1.7 mmol) was added and stirring continued for an additional 4.5 h. The reaction mixture was diluted with dichloromethane (500 mL), filtered through Celite, and the organic extract dried over anhydrous magnesium sulfate. The dichloromethane extract was purified by column chromatography using acetone/dichloromethane (1:4–1:0, v/v) to afford aryltetralin **9** (901 mg, 48%), dimer **10** (680 mg, 37%), and aryltetralin **11** (9.8 mg, 0.53%).

Physical properties of **9**: mp 240–241°C (chloroform); IR ν_{max} ($CHCl_3$): 3530, 1778 cm^{-1}; UV λ_{max} (log ε): 282 (3.53) nm; ^1H NMR δ: 2.47 (1H, dd, H(2), J = 14, 11 Hz), 2.59 (1H, m, H(3)), 2.90 (1H, br dd, H(4), J = 15, 11 Hz), 2.97 (1H, dd, H(4), J = 14, 5 Hz), 3.64 (3H, s, $-OCH_3$(7)), 3.85 (6H, s, $-OCH_3$(3″)), 3.98 (1H, dd, H(11), J = 11, 8 Hz), 4.07 (1H, br d, H(1), J = 11 Hz), 4.52 (1H, dd, H(11), J = 11, 7 Hz), 5.43, 5.51 (1H each, s, s, -OH(4′), -OH(6)), 6.34, 6.70 (1H each, s, s, H(5), H(8)), 6.45 2H, s, H(2′)). Both hydroxyl signals disappear upon addition of D_2O. ^{13}C NMR δ: 32.661 (C(4)), 40.68(−), 47.037(−), 48.544(−), 56.106(−), 56.558(−), ($-OCH_3$(3′)), 71.384 (C(11)), 107.810(−) C(2′)), 113.754(−), 115.696(−), 115.777(−), 176(C(1)). MS m/z: 386 (M^+), 232, 167, 154, 139. High-resolution molecular weight determination calcd. for $C_{21}H_{22}O_7$: 386.1366; found: 386.1366. Anal. calcd. for $C_{21}H_{22}O_7$: C 65.28, H 5.74; found: C 65.12, H 5.72. Circular dichroism analysis: no Cotton effect observed for 0.208 nM methanol solution (250–320 nm). A sample crystallized from chloroform/dichloromethane (1:1, v/v) by slow evaporation was submitted for X-ray analysis. The X-ray data are attached as an Appendix 1.

Physical properties of **10**: mp 156–168°C; IR ν_{max} ($CHCl_3$): 3540, 1780 cm^{-1}; ^1H NMR δ: 2.40–2.52 (3H, m, H(2) (twice), H(4)), 2.55–2.68 (2H, m, H(3)), 2.90 (1H, br dd, H(4), J = 14, 13 Hz), 2.98 (1H, dd, H(4), J = 14, 4 Hz), 3.48–3.55 (1H, m, H(4)), 3.61 (3H, s, OCH_3(7)), 3.67, 3.67 (3H total, s, s, $-OCH_3$(7)), 3.75 (6H, s, $-OCH_3$(3′)), 3.83, 3.83 (6H total, s, s, $-OCH_3$(3′)), 3.95–4.03 (2H, m, H(11)), 4.14 (2H, br d, H(1), J = 12 Hz), 4.48–4.56 (2H, m, H(11)), 5.44, 5.55, 6.02, 6.05 (4H total, s, s, s, s, -OH), 6.18 (1H, s, -OH(6)), 6.36, 6.36 (1H total, s, s, H(8)), 6.45 (2H, br s, H(2′)), 6.51 (2H, br s, H(2′)), 6.73 (1H, s, H(8)). All hydroxyl signals disappear upon addition of D_2O. DCI MS m/z: 788 (83 + $NH_4)^+$, 404. EI MS m/z: 770 (M^+), 400, 386, 167, 154.

Physical properties of **11**: ^1H NMR δ: 2.36 (1H, m, H(2)), 2.59–2.74 (2H, m, H(3), H(4)), 3.08 (1H, dd, H(4), J = 16, 2 Hz), 3.60 (3H, s, $-OCH_3$), 3.74 (1H, d, H(1), J = 11 Hz), 3.80, 3.89 (3H each, s, s, $-OCH_3$), 4.09 (1H, dd, H(11), J = 10, 9 Hz), 4.61 (1H, dd, H(11), J = 10, 7 Hz), 5.38, 5.43 (1 H each, s, s, -OH(6),

Can. J. Chem. Downloaded from www.nrcresearchpress.com by 217.78.4.112 on 09/08/12
For personal use only.

Can. J. Chem. Downloaded from www.nrcresearchpress.com by 217.78.4.112 on 09/08/12
For personal use only.

-OH(4′)), 5.56, 6.09 (1H each, d, d, H(2′), H(6′), J = 2.5 Hz each), 6.77, 6.85 (1H each, d, d, H(5), H(6), J = 8 Hz each); MS m/z: 386 (M^+), 154, 139. High-resolution molecular weight determination calcd. for $C_{21}H_{22}O_7$: 386.1366; found: 386.1373.

Attempted biotransformation of trans-*2-(3,5-dimethoxy-4-hydroxybenzyl)-3-(3-hydroxy-4-methoxybenzyl)butanolide (7) without hydrogen peroxide*

Catharanthus roseus CFE (ph 6.3, specific activity 2.5 units/mg, 30.4 mL, 47 units) was added to a solution containing butanolide **7** (61.0 mg, 2.32 mmol), ethanol (3.8 mL), potassium phosphate buffer (0.100 M, pH 6.3, 43.0 mL), and water (20.2 mL). The solution was stirred for 3 h and extracted by the above procedure to afford butanolide **7** (59.3 mg, 97% recovery), which was pure by ^{1}H NMR spectroscopy.

Attempted dimerization of 1-(3,5-dimethoxy-4-hydroxyphenyl)-6-hydroxy-3-hydroxymethyl-7-methoxy-1,2,3,4-tetrahydro-2-naphthoic acid γ lactone (9) without CFE

Aryltetralin **9** (15.2 mg, 39.3 μmol) was dissolved in a solution of ethanol (7.3 mL), water (6.7 mL), hydrogen peroxide (2.16 mL, 81.6 mM solution, 1.76 mmol), and potassium phosphate buffer (0.100 M, pH 6.3, 8.9 mL). The solution was stirred for 17 h and analyzed by HPLC; no products were detected.

(±)-2-Hydroxy-8-hydroxymethyl-6,7,8,9-tetrahydro-3,3′,5′-trimethoxyspiro [5H-benzocycloheptene-5,1′-cyclohexa-2′,5′-dien]-4′-one-7-oic acid γ lactone (12)

Catharanthus roseus CFE (pH 6.3, specific activity 2.5 units/mg, 450 mL, 690 units), was added to a solution containing butanolide **7** (900 mg, 2.32 mmol), ethanol (90 mL), water (150 mL), and hydrogen peroxide (30 mL, 0.17 M solution, 5.1 mmol). The solution was stirred for 3 h and extracted by the standard procedure. The dichloromethane extract was purified by column chromatography using ethyl acetate/chloroform (1:4–9:11, v/v) to afford aryltetralin **9** (633 mg, 71%), butanolide **7** (56 mg, 6%), and spirodienone **12** (9.7 mg, 1.1%).

Physical properties of 12: mp 225–230°C; IR ν_{max} ($CHCl_3$): 3539, 1774, 1673 cm^{-1}; UV λ_{max} (log ε): 272 (3.83) nm; ^{1}H NMR δ: 2.03 (1H, dd, H(6), J = 13.3, 12.8 Hz), 2.32 (1H, dd, H(6), J = 13.7, 2.6), 2.32–2.44 (1H, m, H(8)), 2.68 (1H, ddd, H(7), J = 12.6, 12.6, 2.6 Hz), 2.97 (1H, dd, H(9), J = 15, 2.3 Hz), 3.07 (1H, dd, H(9), J = 14, 10.9 Hz), 3.65 (3H, s, -OCH_3(3)), 3.79, 3.84 (3H each, s, s, -OCH_3(3′), -OCH_3(5′)), 3.98 (1H, dd, -CH_2OCO-, J = 9, 8.4 Hz), 4.51 (1H, dd, -CH_2OCO-, J = 9, 7.6 Hz), 5.55 (1H, br s, -OH(2), disappears upon addition of D_2O), 6.13, 6.25 (1H each, d, d, H(2′), H(6′), J = 2.8 Hz each), 6.78, 6.92 (1H each, s, s, H(1), H(4)). Irradiation of H(7) collapses H(6) signals to doublets (J = 13.6 Hz each) and simplifies H(8) multiplet. MS m/z: 386 (M^+). High-resolution molecular weight determination calcd. for $C_{21}H_{22}O_7$: 386.1366; found: 386.1362.

Control experiment with butanolide 20

Butanolide **20** (4.20 mg, 10.8 μmol) was dissolved in a solution of ethanol (0.28 mL), water (0.87 mL), and potassium phosphate buffer (0.100 M, pH 7.0, 5.16 mL). Hydrogen peroxide (0.28 mL, 81.6 mM solution, 23 μmol) was added and the solution was stirred for 10 min prior to being extracted with ethyl acetate (2 × 50 mL). The organic extract was dried over magnesium sulfate, filtered, and evaporated *in vacuo*. The product (4.01 mg, 95% recovery) was found to be pure butanolide **7** by ^{1}H NMR spectroscopy and TLC.

*Biotransformation of (±)-*trans-*2-(3,5-dimethoxy-4-hydroxybenzyl)-3-(3,4-dihydroxy-α-hydroxybenzyl)butanolide (20)*

Hydrogen peroxide (4.58 mL, 81.6 mM solution, 0.37 mmol) and *C. roseus* CFE (pH 7.0, specific activity 0.51 units/mg, 22.1 mL, 150 units) were added in rapid succession to a solution containing butanolide **20** (73.2 mg, 0.187 mmol), ethanol (4.6 mL), water (14.5 mL), and phosphate buffer (0.100 M, pH 7.00, 63.7 mL). The solution turned dark purple within 1 min. After 10 min of stirring, ethyl acetate (80 mL) and Celite were added and the suspension was stirred vigorously for an additional 5 min and then filtered. Additional ethyl acetate (320 mL) was added and the phases were separated. The organic extract was dried over magnesium sulfate, filtered, and evaporated *in vacuo* to yield a brown solid (60.3 mg). The aqueous residue was subjected to a continuous extraction with ethyl acetate for 2 days. The organic extract was dried over magnesium sulfate, filtered, and evaporated *in vacuo* to afford a brown solid (7.6 mg), which was combined with the previous ethyl acetate extract. The aqueous residue was evaporated *in vacuo* and stirred in refluxing methanol (100 mL) for 16 h. The suspension was filtered while hot and evaporated *in vacuo* to yield brown solids (205.1 mg).

Reduction of ethyl acetate extract (Entry 1, Table 3): (±)-4-(3,4-dihydroxyphenyl)-5,7-dimethoxy-6-hydroxy-2-hydroxymethyl-1,2,3,4-terahydro-2-naphthoic acid γ lactone (26)

A sample of the ethyl acetate extract from the above experiment (Scheme 5, Entry 1, Table 3) (15.47 mg) was dissolved in a mixture of methanol (5 mL) and water (1 mL). Sodium borohydride (1.6 mg, 42 μmol) was added, resulting in an instantaneous color change of the solution from reddish-brown to yellow. After stirring for 5 min, 2 M hydrochloric acid (2 drops) was added, followed by water (2 mL) and brine (1 mL). The mixture was extracted with ethyl acetate (30 mL) and the organic extract was dried over magnesium sulfate, filtered, and evaporated *in vacuo* to afford a brown oil (16.62 mg). Purification by preparative TLC using acetone/dichloromethane (2:3, v/v) gave the aryltetralin **26** (2.23 mg, 14.0%) and **20** (2.06 mg, 12.3%).

Methylation of ethyl acetate extract (Entry 2, Table 3): (±)-2-(3,5-dimethoxy-4-hydroxybenzyl)-3-(3-hydroxy-4-methoxybenzyl-α-hydroxy)butanolide (27a) and (±)-2-(3,5-dimethoxy-4-hydroxybenzyl)-3-(4-hydroxy-3-methoxybenzyl-α-hydroxy)butanolide (27b)

Diazomethane in ethereal solution (approximately 0.4 M) was added to a sample of the ethyl acetate extract from the above experiment (23.19 mg) dissolved in dry methanol (5 mL) until no further effervescence was observed. After stirring for 22 h, aqueous acetic acid (10%, 2 drops) was added and the solution evaporated *in vacuo*. The residue was purified by preparative TLC using acetone/dichloromethane (1:4, v/v) to yield **20** (3.66 mg, 15%) and **27***a* and **27***b* (2.38 mg, 9%, 1:1 mixture of isomers by ^{1}H NMR spectroscopy).

Physical properties of **27***a* and **27***b*: IR ν_{max} ($CHCl_3$): 3600, 3540, 1770 cm^{-1}; ^{1}H NMR δ: 2.64–2.85, 2.85–3.02 (8H total, m, m, H(2), H(3), H(7″)), 4.02–4.15 (4H, m, H(4)), 4.72 (1H, d, H(7′), J = 5.1 Hz), 4.76 (1H, d, H(7′), J = 5.1 Hz), 6.39 (2H, s, H(2″)), 6.40 (2H, s, H(2″)), 6.70–6.92 (6H, m, H(2′), H(5′), H(6′)); EI MS m/z: 418 (M^+), 400, 181, 167, 153. High-resolution molecular weight determination calcd. for $C_{22}H_{26}O_8$: 418.1628; found: 418.1633.

Reduction and methylation of ethyl acetate extract (Entry 3, Table 3): (±)-4-(3,4-dimethoxyphenyl)-3-hydroxymethyl-1,2,3,4-tetrahydro-5,6,7-trimethoxy-2-naphthoic acid γ lactone (28) and unidentified compound (29)

Sodium borohydride (42 mg, 1.1 mmol) was added to a sample of the ethyl acetate extract from the above experiment (26.94 mg) dissolved in a mixture of methanol (4.5 mL) and water (0.5 mL) and the bright yellow solution was stirred at room temperature for 1 h. The solution was acidified with 1 M hydrochloric acid, and water (5 mL) and brine (2 mL) were added. The solution was extracted with ethyl acetate (2 × 60 mL) and the extract was dried over magnesium sulfate, filtered, and evaporated *in vacuo* before

Can. J. Chem. Downloaded from www.nrcresearchpress.com by 217.78.4.112 on 09/08/12
For personal use only.

being redissolved in ethanol (5 mL). Freshly prepared ethereal diazomethane (approximately 0.3 g, 7 mmol) was added and the solution stirred for 15 h. Aqueous acetic acid (10%, 0.2 mL) was added and the solution evaporated *in vacuo* to afford a yellow oil (67.5 mg), which was separated by column chromatography using acetone/dichloromethane (1:19 to 1:0 gradient, v/v) to afford 42.92 mg (64%) of eluted products, including **29** (8.56 mg, 25%) and **28** (6.00 mg, 20%). The column packing was removed and stirred in a mixture of acetate (50 mL), water (30 mL), and calcium carbonate (700 mg) at 45°C for 1 h. The mixture was acidified with 2 M hydrochloric acid and the solids filtered and washed with warm acetone (2 × 30 mL). The filtrate was evaporated *in vacuo* and the final traces of silica removed to afford a yellow oil (12.27 mg, no identifiable material by ^{1}H NMR spectroscopy) for a total column recovery of 82%.

Physical properties of **28**: IR ν_{max} ($CHCl_3$): 1770 cm^{-1}; ^{1}H NMR δ: 2.29–2.74 (2H, m, H(2),H(3)), 2.97–3.09 (1H, m), 3.14 (3H, s, -OCH_3(5)), 3.37 (1H, dd, J = 7.0, 6.6 Hz), 3.5–3.6 (1H, m), 3.69–3.91 (12H, m, -OCH_3), 4.04–4.18 (1H, m), 4.22 (1H, br d, H(4), J = 8.0 Hz), 6.60 (1H, m, H(6')), 6.72–6.84 (2H, m, m H(2'), H(8)), 6.90 (1H, d, H(5'), J = 8 Hz); EI MS m/z: 414 (M^+), 400, 181, 151, 137. High-resolution molecular weight determination calcd. for $C_{23}H_{26}O_7$: 414.1679; found: 414.1678.

Physical properties of **29**: IR ν_{max} ($CHCl_3$): 3320, 2970, 2940, 2870, 1670 cm^{-1}; MS m/z: 432 ($M^+ - H_2O$?), 418, 282, 167.

Methylation of methanol extract (Scheme 5)

Diazomethane in ethereal solution (approximately 0.4 M) was added to a sample of the methanol extract obtained from the above experiment and, in accord with Scheme 5 (90.82 mg), dissolved in dry methanol (10 mL) until no further effervescence was observed. The yellow solution was stirred overnight. Analysis by silica TLC showed no new spots in comparison with the initial methanol extract. In both cases no spots with an R_f value greater than zero were observed using acetone/dichloromethane (1:4, v/v).

Reduction and methylation of methanol extract (Scheme 5)

Sodium borohydride (137 mg, 3.6 mmol) was added to a sample of the methanol extract obtained from the above experiment (108.65 mg) dissolved in a mixture of methanol (9 mL) and water (1 mL) and the solution was stirred at room temperature for 1 h. The solution was acidified with 1 M hydrochloric acid, and water (5 mL) and brine (2 mL) were added. The solution was extracted with ethyl acetate (3 × 60 mL) and the extract was dried over magnesium sulfate, filtered, and evaporated *in vacuo* before being redissolved in dry THF (10 mL). Potassium carbonate (180 mg, 1.3 mmol) and methyl iodide (0.5 mL, 8 mmol) were added and the solution stirred for 1 h. Water (2 mL) was added and the mixture acidified with 2 M hydrochloric acid before being extracted with ethyl acetate (2 × 20 mL). The organic extract was dried over magnesium sulfate, filtered, and evaporated *in vacuo* to afford brown solids (43.9 mg). Sonication in dichloromethane followed by filtration and evaporation *in vacuo* gave tan solids (5.35 mg), which exhibited no aromatic proton signals by ^{1}H NMR spectroscopy.

Acknowledgement

Financial aid from the Natural Sciences and Engineering Research Council of Canada is gratefully acknowledged.

1. R. S. Ward. Chem. Soc. Rev. **11**, 75 (1982), and references cited therein.
2. I. Jardine. In Anticancer agents based on natural product models. *Edited by* J. M. Cassady and J. D. Douros. Academic Press, New York. 1980, 319.
3. B. F. Issell. Cancer Chemother. Pharmacol. **7**, 73 (1982).
4. B. F. Issell, F. M. Muggia, and S. K. Carter. Etoposide (VP-16) — Current status and new developments. Academic Press, Orlando, Fla. 1984.
5. W. J. Gensler, C. M. Samour, S. Y. Wang, and F. Johnson. J. Am. Chem. Soc. **82**, 1714 (1960).
6. W. J. Gensler and C. D. Gatsonis. J. Org. Chem. **31**, 4004 (1966).
7. J. Renz, M. Kuhn, and A. von Warburg. Liebigs Ann. Chem. **681**, 207 (1965).
8. A. S. Kende, L. S. Liebeskind, J. E. Mills, P. S. Rutledge, and D. P. Curran. J. Am. Chem. Soc. **99**, 7082 (1977).
9. H. P. Plaumann, J. G. Smith, and R. Rodrigo. J. Chem. Soc. Chem. Commun. 354 (1980).
10. R. Rodrigo. J. Org. Chem. **45**, 4538 (1980).
11. A. S. Kende, M. L. King, and D. P. Curran. J. Org. Chem. **46**, 2826 (1981).
12. D. Rajapaksa and R. Rodrigo. J. Am. Chem. Soc. **103**, 6208 (1981).
13. W. S. Murphy and S. Wattanansin J. Chem. Soc. Perkin Trans. 1, 271 (1982).
14. D. I. Macdonald and T. Durst. J. Org. Chem. **51**, 4749 (1986).
15. D. M. Vyas, P. M. Skonezny, T. A. Jenks, and T. W. Doyle. Tetrahedron Lett. **27**, 3099 (1986).
16. J. Van der Eycken, P. De Clerq, and M. Vandewalle. Tetrahedron, **42**, 4297 (1986).
17. H. Yamaguchi, M. Arimoto, S. Nakajima, M. Tanoguchi, and Y. Fukada. Chem. Pharm. Bull. **34**, 2056 (1986).
18. T. Kaneko and H. Wong. Tetrahedron Lett. **28**, 517 (1987).
19. D. W. Jones and A. M. Thompson. J. Chem. Soc. Chem. Commun. 1797 (1987).
20. R. C. Andrews, S. J. Teague, and A. I. Meyers. J. Am. Chem. Soc. **110**, 7854 (1988).
21. D. W. Jones and A. M. Thompson. J. Chem. Soc. Chem. Commun. 1370 (1989).
22. T. Morimoto, M. Chiba, and K. Achiwa. Tetrahedron Lett. **31**, 261 (1990).
23. K. Kanematsu, M. Tsuruoka, Y. Takaoka, and T. Sasaki. Heterocycles, **32**, 859 (1991).
24. A. J. Broomhead, M. M. A. Rahman, P. M. Dewick, D. E. Jackson, and J. A. Lucas. Phytochemistry, **30**, 1489 (1991), and references cited therein.
25. M. Kuhn, A. von Wartburg, and C. Keller-Juslen. Helv. Chim. Acta, **52**, 944 (1969).
26. M. Kuhn and A. von Wartburg. Helv. Chim. Acta, **52**, 948 (1969).
27. C. Keller-Juslen, M. Kuhn, A. von Wartburg, and H. Stahelin. J. Med. Chem. **14**, 936 (1971).
28. J. P. Kutney. Nat. Prod. Rep. **7**, 85 (1990), and references cited therein.
29. J. P. Kutney. Synlett, **1**, 11 (1991), and references cited therein.
30. H. Kohler and H. Jenzer. Free Radical Biol. Med. **6**, 323 (1989).
31. W. D. Hewson and L. P. Hager. *In* The Porphyrins. Vol. 7. *Edited by* D. Dolphin. Academic Press, New York. p. 295.
32. L. S. El-Assal and S. A. M. El-Wahhab. J. Chem. Soc. 849 (1960).
33. R. Brettle and S. M. Shibib. J. Chem. Soc. Perkin Trans. **1**, 2912 (1982).
34. C. Kaneko, A. Sugimoto, Y. Eguchi, S. Yamada, M. Ishikawa, S. Sasaki, and T. Suda. Tetrahedron, **30**, 2701 (1974).
35. H. C. Brown, S. Narasimhan, and Y. M. Choi. J. Org. Chem. **47**, 4702 (1982).
36. E. Brown and A. Dougan. Heterocycles, **26**, 1169 (1987).
37. J. P. Kutney, L. S. L. Choi, T. Honda, N. G. Sato, K. L. Stuart, and B. R. Worth. Helv. Chim. Acta, **65**, 2088 (1982).
38. J. P. Kutney, C. A. Boulet, L. S. L. Choi, W. Gustowski, M.

McHugh, J. Nakano, T. Nikaido, H. Tsukamoto, G. M. Hewitt, and R. Suen. Heterocycles, **27**, 613 (1988).
39. J. P. Kutney, C. A. Boulet, L. S. L. Choi, W. Gustowski, M. McHugh, J. Nakano, T. Nikaido, H. Tsukamoto, G. M. Hewitt, and R. Suen. Heterocycles, **27**, 621 (1988).
40. J. P. Kutney, B. Botta, C. A. Boulet, C. A. Buschi, L. S. L. Choi, J. Golinski, M. Gumulka, G. M. Hewitt, G. Lee, M. McHugh, J. Nakano, T. Nikaido, J. Onodera, I. Perez, P. Salisbury, M. Singh, R. Suen, and H. Tsukamoto. Heterocycles, **27**, 629 (1988).
41. Bio-Rad Chemical Division Bio-Rad Protein Assay, Bio-Rad, Richmond, Calif.
42. B. C. Saunders, A. G. Holmes-Siedle, and B. P. Stark. *In* Peroxidase. Butterworth, London. 1964. p. 135.
43. B. F. Bowden, R. W. Read, and W. C. Taylor. Aust. J. Chem. **33**, 1823 (1980).
44. F. E. Ziegler and J. A. Schwartz. Tetrahedron Lett. **52**, 4643 (1975).
45. A. Pelter, R. S. Ward, P. Satyanarayana, and P. Collins. J. Chem. Soc. Perkin Trans. **1**, 643 (1983).
46. M. Tanoguchi, T. Kashima, H. Saika, T. Inoue, M. Arimoto, and H. Yamaguchi. Chem. Pharm. Bull. Jpn. **37**, 68 (1989).
47. C. C. Price and J. M. Judge. Org. Synth. Collect. Vol. 5, 255 (1973).
48. A. Pelter, R. S. Ward, M. C. Pritchard, and I. T. Kay. J. Chem. Soc. Perkin Trans. **1**, 1603 (1988).
49. M. Hojo and R. Masuda. Synthesis, **10**, 678 (1976).
50. B. M. Trost, T. N. Salzmann, and K. Hiroi. J. Am. Chem. Soc. **98**, 4887 (1976).
51. C. E. M. Pugh and H. S. Raper. Biochem. J. **21**, 1370 (1927).
52. H. W. Schmidt, S. D. Haemmerti, H. E. Shoemaker, and M. S. Leisola. Biochemistry, **28**, 1776 (1989).
53. W. C. Still, M. Kahn, and A. Mitra. J. Org. Chem. **43**, 2923 (1978).
54. O. L. Gamborg and D. E. Eveleigh. Can. J. Biochem. **46**, 417 (1968).
55. B. Chance and A. C. Maehly. *In* Methods in enzymology. Vol. 2. *Edited by* S. P. Colowick and N. O. Kaplan. Academic Press, New York. 1955, p. 773.
56. M. M. Bradford. Anal. Biochem. **72**, 248 (1976).
57. International tables for X-ray crystallography. Vol. IV. Kynoch Press, Birmingham, U.K. (present distributor: Kluwer Academic Publishers, Dordrecht, The Netherlands). 1974. pp. 99–102 and 149.

TABLE A1. Crystallographic data[a]

Compound	**9** · $CHCl_3$
Formula	$C_{21}H_{22}O_7 \cdot CHCl_3$ ·
fw	505.78
Crystal system	Monoclinic
Space group	$P2_1/a$
a, Å	27.957(1)
b, Å	7.427(2)
c, Å	11.204(1)
β°	99.129(5)
V, Å^3	2296.8(7)
Z	4
ρ_{calc}, g/cm^3	1.462
$F(000)$	1048
μ(Mo-K_α), cm^{-1}	4.39
Crystal size, mm	0.10 × 0.15 × 0.23
Transmission factors	0.92–1.00
Scan type	ω
Scan range, deg in ω	1.25 + 0.35 tan θ
Scan speed, deg/min	16 (9 rescans)
Data collected	$+h, +k, \pm l$
$2\theta_{max}$, deg	55
Crystal decay	Negligible
Total reflections	5544
Total unique reflections	5277
R_{merge}	0.43
No. of reflcns with $I \geq 3\sigma(I)$	1564
No. of variables	297
R	0.045
R_w	0.040
gof	1.89
Max Δ/σ (final cycle)	0.02
Residual density, e/Å^3	−0.28 to +0.27

[a]Temperature 294 K, Rigaku AFC6S diffractometer, Mo-K_α radiation (λ = 0.71069 Å), graphite monochromator, takeoff angle 6.0°, aperture 6.0 × 6.0 mm at a distance of 285 mm from the crystal, stationary background counts at each end of the scan (scan/background time ratio 2:1, up to 9 rescans), $\sigma^2(F^2) = [S^2(C + 4B) + (0.01F^2)^2]/Lp^2$ (S = scan rate, C = scan count, B = normalized background count), function minimized $\Sigma w(|F_o|-|F_c|)^2$ where $w = 4F_o^2/\sigma^2(F_o^2)$, $R = \Sigma||F_o|-|F_c||/\Sigma|F_o|$, $R_w = (\hbar w(|F_o|-|F_c|)^2/\Sigma w|F_o|^2)^{1/2}$, and gof = $[\Sigma w(|F_o|-|F_o|)^2/(m-n)]^{1/2}$. Values given for R, R_w, and gof are based on those reflections with $I \geq 3\sigma(I)$.

Appendix: X-ray crystallographic analysis of compound 9

Experimental

Crystallographic data appear in Table A1. The final unit-cell parameters were obtained by least squares on the setting angles for 25 reflections with 2θ = 79.5–91.1°. The intensities of three standard reflections, measured every 150 reflections throughout the data collection, remained essentially constant. The data were processed[2] and corrected for Lorentz and polarization effects, and absorption (empirical, based on azimuthal scans for four reflections).

The structure was solved by direct methods, the coordinates of the non-hydrogen atoms being determined from an E-map. There is one molecule of chloroform in the asymmetric unit along with the molecule of **9**. The non-hydrogen atoms were refined with anisotropic thermal parameters, the OH hydrogen atoms were refined with isotropic thermal parameters, and the remaining hydrogen atoms were fixed in calculated positions (C—H = 0.98 Å, $B_H = 1.2\ B_{bonded\ atom}$). Neutral atom scattering factors and anomalous dispersion corrections for the non-hydrogen atoms were taken from the *International tables for X-ray crystallography* (57). Final atomic coordinates and equivalent isotropic thermal parameters, bond lengths, bond angles, and hydrogen-bond data appear in Tables A2-A5, respectively. Hydrogen atom parameters, anisotropic thermal parameters, bond lengths and angles involving hydrogen, torsion angles, packing dia-

[2]TEXSAN/TEXRAY structure analysis package, which includes versions of the following: MITHRIL, integrated direct methods, by C. J. Gilmore; DIRDIF, direct methods for difference structures, by P. T. Beurskens; ORFLS, full-matrix least-squares, and ORFFE, function and errors, by W. R. Busing, K. O. Martin, and H. A. Levy; ORTEP II, illustrations, by C. K. Johnson.

Can. J. Chem. Downloaded from www.nrcresearchpress.com by 217.78.4.112 on 09/08/12
For personal use only.

Can. J. Chem. Downloaded from www.nrcresearchpress.com by 217.78.4.112 on 09/08/12
For personal use only.

TABLE A2. Final atomic coordinates (fractional) and B_{eq} (Å^2)[a]

Atom	x	y	z	B_{eq}
Cl(1)	0.22269(7)	0.3256(3)	0.7077(2)	7.2(1)
Cl(2)	0.23922(7)	0.6537(4)	0.5851(2)	9.2(1)
Cl(3)	0.31943(7)	0.4453(4)	0.6991(2)	11.4(2)
O(1)	0.5330(1)	0.1945(5)	1.0847(3)	4.0(2)
O(2)	0.4895(1)	0.2557(6)	0.2992(3)	3.7(2)
O(3)	0.5787(1)	0.1425(5)	0.3924(3)	3.8(2)
O(10)	0.4552(1)	0.2602(5)	1.0248(3)	3.4(2)
O(1′)	0.7000(1)	0.1819(6)	1.0868(3)	4.0(2)
O(2′)	0.7241(1)	0.4966(7)	1.0153(4)	4.7(2)
O(3′)	0.6664(1)	0.6896(6)	0.8494(3)	4.2(2)
C(1)	0.5420(2)	0.2039(7)	0.8114(4)	2.1(2)
C(2)	0.5034(2)	0.2901(7)	0.8754(4)	2.2(2)
C(3)	0.4518(2)	0.2510(7)	0.8153(4)	2.4(2)
C(4)	0.4422(2)	0.3411(8)	0.6925(4)	2.8(3)
C(4A)	0.4812(2)	0.2856(7)	0.6204(4)	2.2(2)
C(5)	0.4704(2)	0.2950(8)	0.4942(5)	2.7(3)
C(6)	0.5031(2)	0.2461(7)	0.4218(4)	2.6(3)
C(7)	0.5489(2)	0.1873(7)	0.4739(5)	2.5(2)
C(8)	0.5605(2)	0.1798(7)	0.5981(4)	2.4(2)
C(8A)	0.5272(2)	0.2274(7)	0.6737(4)	2.0(2)
C(9)	0.5014(2)	0.2402(7)	1.0046(5)	3.0(3)
C(11)	0.4245(2)	0.3137(8)	0.9130(5)	3.2(3)
C(12)	0.6266(2)	0.097(1)	0.4396(5)	6.5(4)
C(13)	0.2607(2)	0.511(1)	0.7039(5)	5.9(4)
C(1′)	0.5919(2)	0.2796(7)	0.8595(4)	2.1(2)
C(2′)	0.6230(2)	0.1856(7)	0.9464(4)	2.5(2)
C(3′)	0.6667(2)	0.2599(8)	0.9982(5)	2.9(3)
C(4′)	0.6801(2)	0.4270(8)	0.9613(5)	2.8(3)
C(5′)	0.6493(2)	0.5225(8)	0.8745(4)	2.7(3)
C(6′)	0.6053(2)	0.4481(8)	0.8237(4)	2.5(3)
C(7′)	0.6864(2)	0.017(1)	1.1344(5)	5.4(4)
C(8′)	0.6368(2)	0.7919(8)	0.7616(6)	4.7(3)

[a] $B_{eq} = (8/3)\pi^2\Sigma\Sigma U_{ij} a_i^* a_j^* (a_i \cdot a_j)$.

TABLE A3. Bond lengths (Å) with estimated standard deviations

Atom	Atom	Distance	Atom	Atom	Distance
Cl(1)	C(13)	1.742(7)	C(2)	C(3)	1.521(6)
Cl(2)	C(13)	1.734(7)	C(2)	C(9)	1.504(7)
Cl(3)	C(13)	1.722(6)	C(3)	C(4)	1.515(6)
O(1)	C(9)	1.205(6)	C(3)	C(11)	1.503(7)
O(2)	C(6)	1.368(5)	C(4)	C(4A)	1.513(6)
O(3)	C(7)	1.371(5)	C(4A)	C(5)	1.399(6)
O(3)	C(12)	1.401(6)	C(4A)	C(8A)	1.398(6)
O(10)	C(9)	1.354(6)	C(5)	C(6)	1.364(6)
O(10)	C(11)	1.456(5)	C(6)	C(7)	1.391(6)
O(1′)	C(3′)	1.377(6)	C(7)	C(8)	1.379(6)
O(1′)	C(7′)	1.412(7)	C(8)	C(8A)	1.400(6)
O(2′)	C(4′)	1.383(6)	C(1′)	C(2′)	1.386(6)
O(3′)	C(5′)	1.374(6)	C(1′)	C(6′)	1.383(7)
O(3′)	C(8′)	1.404(6)	C(2′)	C(3′)	1.381(6)
C(1)	C(2)	1.528(6)	C(3′)	C(4′)	1.379(7)
C(1)	C(8A)	1.543(6)	C(4′)	C(5′)	1.387(7)
C(1)	C(1′)	1.522(6)	C(5′)	C(6′)	1.386(6)

gram, and measured and calculated structure factor amplitudes are included as supplementary material.[3]

[3]Supplementary material mentioned in the text may be purchased from: The Depository of Unpublished Data, Document Delivery, CISTI, National Research Council Canada, Ottawa, Canada K1A 0R6.

Tables of hydrogen atom parameters, bond lengths and angles involving hydrogen, and the packing diagram have also been deposited with The Cambridge Crystallographic Data Centre and can be obtained on request from The Director, Cambridge Crystallographic Data Centre, University Chemical Laboratory, Lensfield Road, Cambridge, CB2 1EW, U.K.

TABLE A4. Bond angles (deg) with estimated standard deviations

Atom	Atom	Atom	Angle	Atom	Atom	Atom	Angle
C(7)	O(3)	C(12)	116.9(4)	C(1)	C(8A)	C(4A)	123.1(4)
C(9)	O(10)	C(11)	109.5(4)	C(1)	C(8A)	C(8)	118.5(4)
C(3′)	O(1′)	C(7′)	116.5(4)	C(4A)	C(8A)	C(8)	118.3(4)
C(5′)	O(3′)	C(8′)	116.6(4)	O(1)	C(9)	O(10)	120.9(5)
C(2)	C(1)	C(8A)	108.9(4)	O(1)	C(9)	C(2)	130.7(5)
C(2)	C(1)	C(1′)	110.8(4)	O(10)	C(9)	C(2)	108.4(5)
C(8A)	C(1)	C(1′)	113.5(4)	O(10)	C(11)	C(3)	104.2(4)
C(1)	C(2)	C(3)	113.8(4)	C(1)	C(13)	Cl(2)	11.3(3)
C(1)	C(2)	C(9)	119.0(4)	C(1)	C(13)	Cl(3)	111.5(4)
C(3)	C(2)	C(9)	101.6(4)	C(2)	C(13)	Cl(3)	111.4(4)
C(2)	C(3)	C(4)	109.6(4)	C(1)	C(1′)	C(2′)	120.0(5)
C(2)	C(3)	C(11)	100.0(4)	C(1)	C(1′)	C(6′)	120.4(5)
C(4)	C(3)	C(11)	119.2(4)	C(2′)	C(1′)	C(6′)	119.5(4)
C(3)	C(4)	C(4A)	109.1(4)	C(1′)	C(2′)	C(3′)	120.5(5)
C(4)	C(4A)	C(5)	117.9(4)	O(1′)	C(3′)	C(2′)	125.9(6)
C(4)	C(4A)	C(8A)	123.2(4)	O(1′)	C(3′)	C(4′)	114.2(5)
C(5)	C(4A)	C(8A)	118.9(5)	C(2′)	C(3′)	C(4′)	119.9(5)
C(4A)	C(5)	C(6)	122.0(5)	O(2′)	C(4′)	C(3′)	118.1(5)
O(2)	C(6)	C(5)	118.6(5)	O(2′)	C(4′)	C(5′)	121.7(6)
O(2)	C(6)	C(7)	121.8(5)	C(3′)	C(4′)	C(5′)	120.2(5)
C(5)	C(6)	C(7)	119.6(5)	O(3′)	C(5′)	C(4′)	114.1(5)
O(3)	C(7)	C(6)	114.4(4)	O(3′)	C(5′)	C(6′)	126.2(5)
O(3)	C(7)	C(8)	126.3(4)	C(4′)	C(5′)	C(6′)	119.7(5)
C(6)	C(7)	C(8)	119.3(5)	C(1′)	C(6′)	C(5′)	120.3(5)
C(7)	C(8)	C(8A)	121.9(4)				

TABLE A5. Hydrogen bond geometry

Interaction	O—H (Å)	H···O (Å)	O···O (Å)	O—H···Cl/O (°)
O(2)—H(1)···O(1)($x,y,z-1$)	0.84(5)	2.19(5)	2.896(5)	142(5)
O(2)—H(1)···O(3)	0.84(5)	2.23(5)	2.680(5)	114(5)
O(2′)—H(1′)···O(3′)	0.77(5)	2.23(5)	2.677(6)	118(5)
O(2′)—H(1′)···O(1′)($3/2-x$, $1/2+y$, $2-z$)	0.77(5)	2.34(5)	2.911(6)	132(5)
C(13)—H(14)···O(2′)($1-x$, $1-y$, $2-z$)	0.98	2.34	3.108(7)	134
C(13)—H(14)···O(1′)($1-x$, $1-y$, $2-z$)	0.98	2.47	3.332(8)	146

Discussion of crystal structure

The crystal structure of **9** · $CHCl_3$ is dominated by weak hydrogen bonding. The two hydroxyl hydrogen atoms (H(1) and H(1′)) and the chloroform hydrogen atom (H(14)) are each involved in bifurcated hydrogen bonding arrangements (see Table A5). H(1) is intramolecularly H-bonded to O(3) and intermolecularly H-bonded along the *c* axis to O(1). H(1′) is similarly hydrogen-bonded, intramolecularly to O(3′) and intermolecularly to O(1′) of a molecule related by the twofold screw axis along *b*. The chloroform solvate molecule is linked by a pair of C—H···O hydrogen bonds to O(1′) and O(2′) of the same molecule. The molecule **9** is shown in Fig. 1. The junction between the five-membered lactone ring and the central six-membered ring is *trans*. The lactone ring has a C(3)-envelope conformation and the central cyclohexene ring has C(2) and C(3) displaced in opposite directions from the plane defined by C(1), C(8a), C(4a), and C(4). The bulky 4-OH-3,5-$(OMe)_2$-C_6H_2 substituent at C(1) occupies a pseudo-equatorial position. The two aromatic rings are planar to within experimental error. Bond lengths and angles (Tables A3 and A4) are as expected.

Can. J. Chem. Downloaded from www.nrcresearchpress.com by 217.78.4.112 on 09/08/12
For personal use only.

Phosphonolipids. 3. Phosphonic acid analogues of phosphatidylinositol and related materials[1,2]

CLIFFORD PRATT, YUE-JIN LIU, TING-YI CHU, KARIN MELKONIAN, BURTON E. TROPP, AND ROBERT ENGEL[3]

Department of Chemistry and Biochemistry, Queens College of the City University of New York, Flushing, NY 11367, U.S.A.

Received February 6, 1992

CLIFFORD PRATT, YUE-JIN LIU, TING-YI CHU, KARIN MELKONIAN, BURTON E. TROPP, and ROBERT ENGEL. Can. J. Chem. **70**, 2135 (1992).

A convergent synthesis of an isosteric phosphonic acid analogue of phosphatidylinositol has been accomplished in which a non-hydrolyzable P—C—C linkage is present in place of the normal P—O—C esteric linkage joining the phosphate and diacylglycerol portions of the molecule. The synthetic route used provides the configuration at each stereogenic center to correspond to that present in the biologically generated phospholipid. In addition, the approach provides asymmetric introduction of acyl functions, placing saturated and unsaturated acyl groups in the terminal and internal positions respectively of the backbone portion of the analogue, corresponding to that present in the biologically generated phospholipid.

CLIFFORD PRATT, YUE-JIN LIU, TING-YI CHU, KARIN MELKONIAN, BURTON E. TROPP et ROBERT ENGEL. Can. J. Chem. **70**, 2135 (1992).

On a réalisé une synthèse convergente d'un acide phosphonique isostère analogue du phosphatidylinositol dans lequel on rencontre une liaison P—C—C à la place de la liaison normale P—O—C de l'ester qui relie les portions phosphate et diacylglycérol de la molécule. La voie de synthèse utilisée permet d'établir que la configuration de chacun des centres stéréogènes correspond à celle qui est présente dans la phospholipide généré d'une façon biologique. De plus, cette approche permet d'introduire des fonctions acyles d'une façon asymétrique, plaçant des groupes saturés et insaturés respectivement dans les positions terminales et internes du squelette de l'analogue, comme on les retrouve dans le phospholipide généré d'une façon biologique.

[Traduit par la rédaction]

Introduction

Phosphoinositides have been the subject of intensive investigation in recent years owing to the recognition of their role for intracellular signalling in response to extracellular stimuli (3). Following the recognition of this biological role for phosphoinositides have come efforts toward the laboratory synthesis of not only phosphatidylinositol (a phosphate diester) (4), but of a variety of analogues designed to probe details of the mechanism of signalling and the potential for regulation of the biochemical processes involved (1, 5).

In the continuing effort of our laboratory concerning the synthesis and investigation of isosteric phosphonic acid analogues of biological phosphates (2, 6), the preparation of an analogue of phosphatidylinositol (**1**) that incorporates all but one of the functional and stereochemical characteristics of the biological material has been undertaken. The structural variation of this analogue (**2**), which is of particular interest and described herein, involves the introduction of a P—C—C linkage in place of the normal P—O—C linkage connecting the phosphate with the diacylglycerol backbone of phosphatidylinositol. In **2** the entire remaining structural elements have been maintained in correspondence with the biological material. Specifically, the configuration at each stereogenic site in **2**, both in the inositol and modified diacylglycerol portions, matches that of the corresponding site of the biological material. Further, the analogue **2** is generated with regiospecific disposition of the acyl groups, saturated (R_s) at the terminal position and unsaturated (R_u) at the internal position. This disposition is in accord with phosphatidylinositol exhibiting preferential interaction with phosphatidylinositol-specific phospholipase C (7).

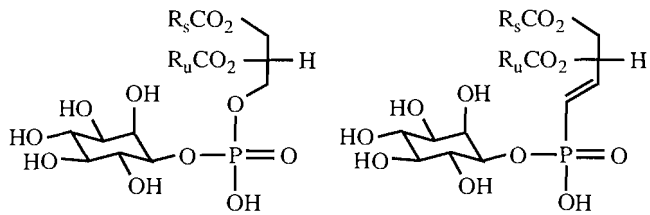

1 **2**

The route used for the preparation of **2** is a convergent one, separate syntheses of the protected inositol and lipid portions being performed, followed by a coupling and final deprotection sequence. Two approaches are described for the synthesis of the lipid portion, itself an analogue of phosphatidic acid, these being a classical protection/deprotection route and a regioselective epoxide-opening procedure. The latter general approach has also been used for the preparation of a phosphonic acid analogue of PAF.[4]

The analogue **2**, bearing a non-hydrolyzable ester linkage in the phospholipid portion of the molecule, is anticipated to be of use in the investigation of phospholipase C mediated processes of phosphatidylinositol.

Results and discussion

The synthesis of the lipid component of **2**, an isosteric phosphonic acid analogue of phosphatidic acid, has been

[1]For preliminary reports of this work see ref. 1.

[2]Paper 2 in this series is ref. 2.

[3]Author to whom correspondence may be addressed.

[4]Y.-j. Liu, B. E. Tropp, and R. Engel, unpublished results of this laboratory.

Can. J. Chem. Downloaded from www.nrcresearchpress.com by 109.225.110.28 on 09/08/12
For personal use only.

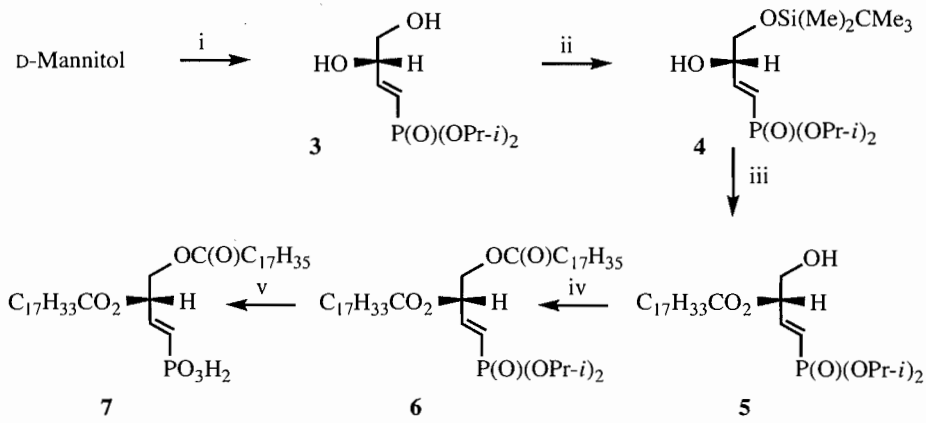

i. acetone, $ZnCl_2$; $Pb(OAc)_4$; tetraisopropyl methylenebisphosphonate/BuLi; aq. acid: ii. *tert*-butyldimethylsilyl chloride, imidazole, DMF (66% yield): iii. oleoyl chloride, pyridine, DMAP, 0°C; Bu_4NF, THF (36% yield): iv. stearic anhydride, pyridine, DMAP, 0°C–r.t. (68% yield): v. TMSBr, ether; water (75% yield)

SCHEME 1

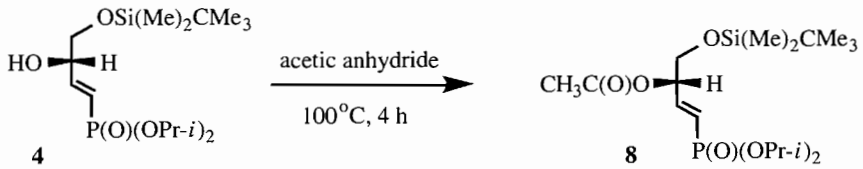

98.5% yield

SCHEME 2

accomplished by two routes. The first of these, involving a classical approach of protection/deprotection, is illustrated in Scheme 1.

Standard procedures were used for the conversion of D-mannitol to **3**, including the initial protection and cleavage to D-glyceraldehyde acetonide (8), the preparation of the tetraisopropyl methylenebisphosphonate (9), and its use for the synthesis of the diisopropyl (*R*)-(*E*)-3,4-dihydroxybut-1-enyl-1-phosphonate (10).

Selective protection of the terminal hydroxyl group of **3** was accomplished using a 3% excess of *tert*-butyldimethylsilyl chloride with imidazole. Small amounts of the internally silylated and disilylated product were removed easily using flash chromatography.

The verification of the position of silylation in **4** was accomplished by the preparation of a derivative and examination of its ^{1}H NMR spectrum. In the 200 MHz ^{1}H NMR spectrum of **3** the signals for the hydrogens attached to C-3 and C-4 were virtually indistinguishable, appearing as a multiplet at δ 3.7 and integrating for three hydrogens. A sample of the material **4** was acetylated using acetic anhydride to give **8** in nearly quantitative yield (Scheme 2).

The acetate **8** exhibited a downfield shift (to δ 5.3) for a one-hydrogen multiplet corresponding to the C-3 hydrogen while a two-hydrogen multiplet remained at δ 3.7. Differentiation of sites of acylation on a phosphonate lipid backbone have been noted previously by similar shifts for related systems, the differentiation having been confirmed by specific enzymatic action (11).

The material **4** was acylated using oleoyl chloride in pyridine with 4-(dimethylamino)pyridine (DMAP) at 0°C, conditions slightly modified from those known not to permit significant acyl migration (12). Deprotection of the terminal hydroxyl group was performed to generate **5** prior to complete structural and purity analysis. The ^{1}H NMR spectrum of **5** verified that no acyl migration had occurred during the work-up, exhibiting an upfield multiplet for the pair of hydrogens at C-4 and a downfield multiplet for the single hydrogen at C-3. Further acylation placing a saturated fatty-acyl function at the terminal hydroxyl position was accomplished, again using conditions known not to permit significant acyl migration, and cleavage of the phosphonate esters was accomplished using a standard procedure (13).

In light of the success demonstrated for the preparation of symmetric-chain glycerophospholipids starting with optically active glycidyl tosylate (14), an alternative synthesis of **6**, and subsequently **7**, was developed as illustrated in Scheme 3.

The generation of the epoxide **9** from the diol **3** was accomplished in a two-step procedure, the tosylate being formed first, followed by intramolecular displacement to effect ring closure. Although IR and NMR spectra could be obtained which were in accord with the proposed structures of the tosylate and epoxide **9** species, these compounds proved too reactive for storage or satisfactory elemental analysis and were used immediately upon isolation in continuing reactions. Regiospecific ring opening was accomplished using a modification of the previously reported technique (14) facilitated by boron trifluoride etherate. The ^{1}H NMR spectrum of **10** verified the introduction of the acyl function at the terminal position of the chain. (The regiospecificity of this type of reaction has been in-

Can. J. Chem. Downloaded from www.nrcresearchpress.com by 109.225.110.28 on 09/08/12
For personal use only.

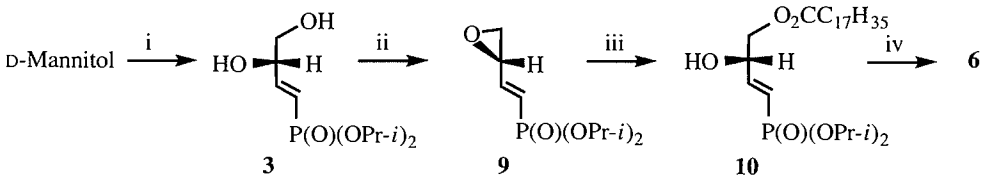

i. acetone, $ZnCl_2$; $Pb(OAc)_4$; tetraisopropyl methylenebisphosphonate/BuLi; aq. acid: ii. *p*-toluenesulfonyl chloride, pyridine; K_2CO_3, methanol (76% yield): iii. BF_3 etherate, stearic acid (70% yield): iv. oleic anhydride, DMF, pyridine, DMAP, 0°C–r.t. (84% yield)

SCHEME 3

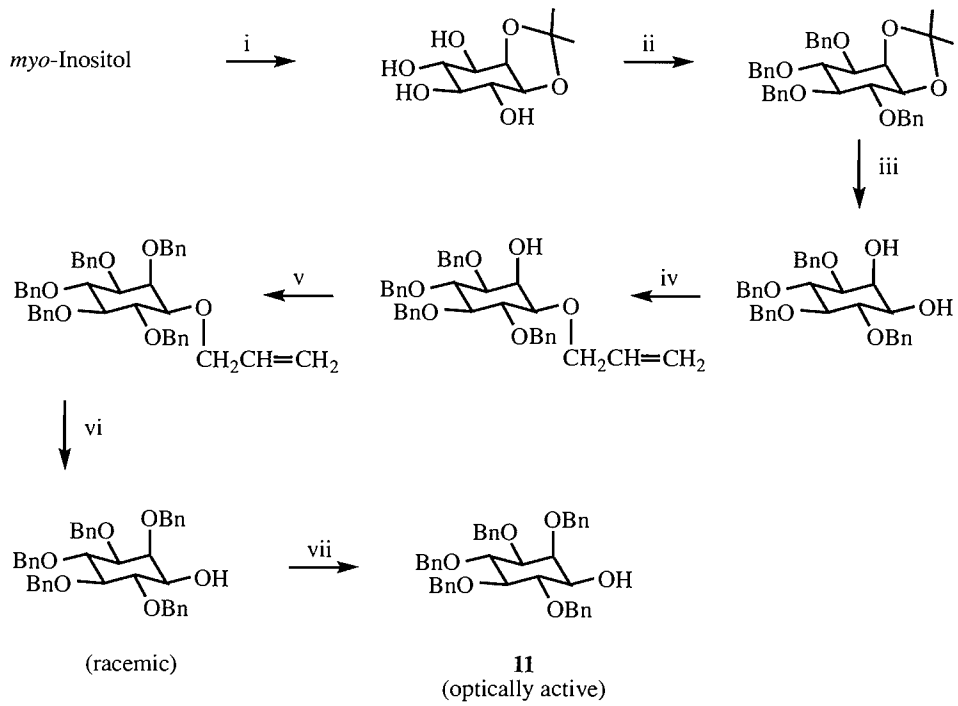

i. DMSO, 2,2-dimethoxypropane, *p*-TsOH (50% yield): ii. DMF, 97% NaH, benzyl bromide (70% yield): iii. 0.9 M HCl in methanol (75% yield): iv. benzene, NaOH, allyl bromide (58% yield): v. benzene, 97% NaH, benzyl bromide (90% yield): vi. aqueous methanol, *p*-TsOH, 10% Pd/C (38% yield): vii. methylene chloride, triethylamine, (*S*)-(−)-camphanic acid chloride (95% yield); HPLC separation of diastereoisomers, Lichrosorb Si-60, 1% diethyl ether in methylene chloride eluent; 0.1 M KOH in ethanol (98% yield).

SCHEME 4

vestigated and is to be published separately.[5]) Finally, **10** was acylated at the internal position using a procedure known not to involve acyl migration in structurally related systems (12). The materials **6** and **7** from the two approaches were identical.

Once prepared, the analogue **7** of phosphatidic acid was ready for coupling with a suitably protected, optically active derivative **11** of inositol for the generation of the target material **2**. The overall route for the preparation of the protected inositol **11** is one that involves modifications of inositol-related and allyl ether cleavage processes previously reported (15–17) and is outlined in Scheme 4.

Resolution of the pentabenzyl-*myo*-inositol is accomplished by the generation of a diastereoisomeric ester mixture using (*S*)-camphanic acid chloride followed by separation of the diastereoisomers using HPLC. The synthesis of **2** is completed by the coupling of **11** with the independently prepared **7** and deprotection as shown in Scheme 5.

[5]Y.-j. Liu and R. Engel, unpublished results of this laboratory.

The use of (*S*)-camphanic acid chloride for the resolution of 2,3,4,5,6-penta-*O*-benzyl-*myo*-inositol has been discussed recently (18). The coupling using trichloroacetonitrile is an adaptation of a procedure used previously in this laboratory and elsewhere (19). The deprotection using iodotrimethylsilane (20) rapidly cleaves benzyl ether linkages selectively compared to other ether linkages and ester linkages, liberating the target material without reduction of the olefinic linkages.

This procedure represents the first preparation of a nominally isosteric phosphonic acid analogue of phosphatidyl inositol in which the esteric oxygen of the normal diacylglycerol backbone has been replaced by a carbon–phosphorus linkage.

Experimental

General

All chemicals were of reagent quality and used without further purification with the following exceptions: chloroform was distilled over phosphorus pentoxide; pyridine was dried over calcium hydride and distilled; dimethylformamide (DMF) was dried over

Can. J. Chem. Downloaded from www.nrcresearchpress.com by 109.225.110.28 on 09/08/12
For personal use only.

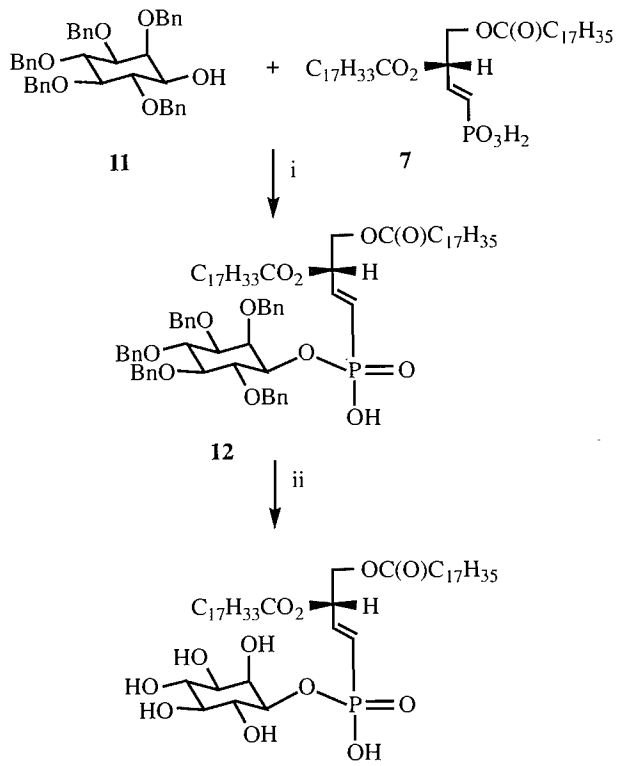

i. pyridine, trichloroacetonitrile, 50°C, 72 h (20% yield): ii. chloroform, iodotrimethylsilane, 20 min (85% yield).

SCHEME 5

molecular sieves 4A prior to use; oleoyl chloride (commercial source) was kept in the sealed ampoule until immediately prior to use; methanol for chromatographic purposes was distilled prior to use.

(*S*)-(*E*)-3,4-Dihydroxybut-1-enylphosphonic acid diisopropyl ester (**3**) and its precursors were prepared as previously described (10). Racemic 1-*O*-allyl-2,3,4,5,6-tetra-*O*-benzyl-*myo*-inositol and its precursors were prepared as previously described (15). Thin-layer chromatography (TLC) was performed using Polygram Sil N-HR sheets (Brinkmann)(PS) or Kodak Chromagram sheets (Eastman) (KC). Silica gel for flash chromatography was from EM Science (230–300 mesh). HPLC was performed using a Waters 6000A instrument with either a Lichrosorb Si60 (10 μm) column or a Bakerbond Chiral DNBPG (Coval) (5 μm) column. Infrared spectra were measured using a Perkin–Elmer 1600 FTIR instrument, and ^{1}H NMR spectra were measured using an IBM–Bruker WP200SY instrument. Optical rotations were measured using a JASCO DIP-140 digital polarimeter. Elemental analyses were performed by Desert Analytics of Tucson, Arizona, and by Schwarzkopf Microanalytical Laboratories of Woodside, New York.

Preparation of (S)-(E)-*4*-tert-*butyldimethylsiloxy-3-hydroxybut-1-enylphosphonic acid diisopropyl ester (4)*

The (*S*)-(*E*)-3,4-dihydroxybut-1-enylphosphonic acid diisopropyl ester (**3**)(16.14 g, 64 mmol) was dissolved in dry DMF (200 mL) and there was added to it with stirring at room temperature *tert*-butyldimethylsilyl chloride (9.96 g, 66 mmol) and imidazole (10.90 g, 160 mmol). The reaction mixture was stirred at room temperature for 72 h after which time the volatile materials were evaporated under reduced pressure. Water (150 mL) was added to the residue and the aqueous solution was extracted with ethyl acetate (3 × 200 mL). The extracts were combined, dried over calcium chloride, filtered, and volatile materials were evaporated under reduced pressure. The residue was subjected to flash chromatography on a silica gel column (120 g, 5 cm diameter) packed with methylene chloride. The elution of the column was performed with the following order of solvents: 525 mL methylene chloride; 375 mL 1:1 methylene chloride:chloroform; 75 mL chloroform; 150 mL chloroform:ethyl acetate; 775 mL ethyl acetate. Fractions from the ethyl acetate portion of the elution exhibiting a single spot of R_f = 0.67 on TLC (KC, ethyl acetate) as visualized with phosphomolybdate spray reagent were combined to give the pure desired material (15.48 g, 0.042 mol, 66%), which exhibited IR and NMR spectra in accord with the proposed structure (**4**). Specific rotation: $[\alpha]_D$ −34.0 (0.16 M, ethanol). The ^{1}H NMR ($CDCl_3$) exhibited the following signals: δ 0.1, singlet, 6H; δ 0.9, singlet, 9H; δ 1.4, doublet of doublets, 12H; δ 3.5–3.9, multiplet, 3H; δ 4.3, broad, 1H; δ 4.7, multiplet, 2H; δ 5.8–7.5, multiplet, 2H. Anal. calcd. for $C_{16}H_{35}O_5PSi$: C 52.43, H 9.62%; found: C 52.46, H 9.69%. A small amount of material eluted immediately prior to the desired material and exhibited ^{1}H NMR and IR spectra indicating it to be the result of silylation at both hydroxyl groups of the starting diol.

Preparation of (S)-(E)-*4*-tert-*butyldimethylsiloxy-3-acetoxybut-1-enylphosphonic acid diisopropyl ester (8)*

A sample of **4** (100 mg, 0.27 mmol) was dissolved in acetic anhydride (10 mL) and heated at 100°C for 4 h. After this time all volatile materials were removed under reduced pressure. The solid residue was found to exhibit a single spot of R_f = 0.15 on TLC (KC, chloroform) visualized with phosphomolybdate spray reagent. This material exhibited IR and ^{1}H NMR spectra in accord with the proposed structure (**8**) (112 mg, 98.5%). Specific rotation: $[\alpha]_D$ −1.1 (0.054 M, ethanol). The ^{1}H NMR ($CDCl_3$) spectrum exhibited the following signals: δ 0.1, singlet, 6H; δ 0.9, singlet, 9H; δ 1.4, doublet of doublets, 12H; δ 2.2, singlet, 3H; δ 3.7, multiplet, 2H; δ 4.4, multiplet, 2H; δ 4.7, multiplet, 1H; δ 5.8–7.5, multiplet, 2H. Anal. calcd. for $C_{18}H_{37}O_6PSi$: C 52.92, H 9.13%; found: C 53.22, H 9.19%.

Preparation of (S)-(E)-*4-hydroxy-3-oleoyloxybut-1-enylphosphonic acid diisopropyl ester (5)*

The material (**4**) (2.16 g, 5.89 mmol) was dissolved in chloroform (40 mL) and cooled to 0°C in an ice bath. There was then added to it pyridine (0.9 g, 11.38 mmol) and a catalytic amount of 4-dimethylaminopyridine (0.050 g) followed by a solution of oleoyl chloride (2.95 g, 9.8 mmol) in chloroform (5 mL). The reaction mixture was allowed to come to room temperature and was stirred for 4 days. The volatile materials were then removed under reduced pressure, the residue was dissolved in tetrahydrofuran (10 mL), and there was added tetrabutylammonium fluoride (0.7 g, 3.23 mmol) and the reaction mixture was stirred at room temperature for 12 h. Chloroform (100 mL) and water (50 mL) were then added and the mixture was stirred vigorously. The layers were separated and the aqueous layer was washed with chloroform (50 mL). The organic solutions were combined, dried over sodium sulfate, filtered, and volatile materials were removed under reduced pressure. The residue exhibited a single spot of R_f = 0.70 on TLC (KC, ethyl acetate) and IR and ^{1}H NMR spectra in accord with the proposed structure (**5**) (1.09 g, 36%). Specific rotation: $[\alpha]_D$ −1.6 (0.05 M, ethanol). The ^{1}H NMR ($CDCl_3$) spectrum exhibited the following signals: δ 0.9, broad triplet, 3H; δ 1.2–1.7, broad, 34H; δ 2.0, multiplet, 5H (including OH); δ 2.2, multiplet, 2H; δ 3.9, multiplet, 2H; δ 4.7, multiplet, 2H; δ 5.1, multiplet, 2H; δ 5.3, triplet, 1H; δ 5.8–7.5, multiplet, 2H. Anal. calcd. for $C_{28}H_{53}O_6P$: C 65.09, H 10.34%; found: C 64.89, H 10.51%.

Preparation of (S)-(E)-*3,4-epoxybut-1-enylphosphonic acid diisopropyl ester (9)*

The material (**3**) (2.0 g, 7.93 mmol) was dissolved in chloroform (7.8 mL) and cooled to 0°C with an ice bath. Pyridine (1.26 mL) was then added followed by *p*-toluenesulfonyl chloride

Can. J. Chem. Downloaded from www.nrcresearchpress.com by 109.225.110.28 on 09/08/12
For personal use only.

Can. J. Chem. Downloaded from www.nrcresearchpress.com by 109.225.110.28 on 09/08/12
For personal use only.

(2.22 g, 11.6 mmol) and the reaction mixture was stirred for 2 h. After this time ether (25 mL) and water (6 mL) were added to the reaction mixture. The organic layer was separated and washed with water (2 × 16 mL), dried over calcium chloride, filtered, and the volatile materials were removed under reduced pressure. The ^{1}H NMR ($CDCl_3$) of the crude material (2.2 g) indicated the desired material to be present, exhibiting the following signals: δ 1.4, doublet of doublets, 12H; δ 2.2, broad, 1H; δ 2.5, singlet, 3H; δ 3.5–3.9, multiplet, 3H; δ 4.8, multiplet, 2H; δ 5.8–7.5, multiplet, 2H; δ 7.8 AA′BB′, 4H. The material exhibited one major spot of R_f = 0.25 on TLC (KC, 1:15 ethyl acetate:hexane) as visualized with phosphomolybdate spray reagent and was used without further purification. The isolated tosylate (2.2 g) was dissolved in methanol (24 mL) under nitrogen and potassium carbonate (0.98 g, 7.08 mmol) was added. The reaction mixture was stirred for 2 h at −10°C. After this time ether (24 mL) was added and the mixture was filtered twice through a pad of silica gel. The crude material (1.41 g, 76%) exhibited one major spot of R_f = 0.59 on TLC (KC, ethyl acetate) visualized with phosphomolybdate spray reagent and IR and ^{1}H NMR spectra in accord with the proposed structure. The ^{1}H NMR ($CDCl_3$) spectrum exhibited the following signals: δ 1.4, doublet of doublets, 12H; δ 2.7, multiplet, 1H; δ 3.1, multiplet, 1H; δ 3.4, multiplet, 1H; δ 4.7, multiplet 2H; δ 6.0–7.8, multiplet, 2H. The material proved to be too reactive for storage or elemental analysis and was used immediately upon isolation.

Preparation of (S)-(E)-*3-hydroxy-4 stearoyloxybut-1-enylphosphonic acid diisopropyl ester (**10**)*

Stearic acid (0.34 g, 1.20 mmol), (*S*)-(*E*)-3,4-epoxybut-1-enylphosphonic acid diisopropyl ester (**9**) (0.28 g, 1.20 mmol), and boron trifluoride etherate (0.082 g, 1.20 mmol) in ether (total volume 11 mL) were stirred overnight at room temperature. Volatile materials were removed under reduced pressure and the residue was subjected to flash chromatography (20 g, 2 cm diameter) packed and eluted with chloroform. Fractions exhibiting a single spot of R_f = 0.18 on TLC (KC, chloroform) as visualized with phosphomolybdate spray reagent were combined to give the pure desired material (0.436 g, 70%) which exhibited IR and ^{1}H NMR spectra in accord with the proposed structure (**10**). The ^{1}H NMR ($CDCl_3$) exhibited the following signals: δ 0.9, triplet, 3H; δ 1.2, broad, 42H; δ 2.3, triplet, 2H; δ 3.3, broad, 1H; δ 3.7, multiplet, 1H; δ 4.1–4.9, multiplet, 4H; δ 5.8–7.6, multiplet, 2H. Analysis, $C_{28}C_{55}O_6P$ requires C 64.83%, H 10.69%; found: C 64.71%, H 10.82%. Specific rotation: $[\alpha]_D$ = 8.9 (0.176 M, chloroform).

Preparation of (S)-(E)-*3-oleoyloxy-4-stearoyloxybut-1-enylphosphonic acid diisopropyl ester (**6**)*

*Method A: from **5***

To (*S*)-(*E*)-4-hydroxy-3-oleoyloxybut-1-enylphosphonic acid diisopropyl ester (**5**)(1.66 g, 3.21 mmol) dissolved in chloroform (15 mL) cooled to 0°C with an ice bath was added pyridine (0.9 g, 11.38 mmol) with a catalytic amount of 4-dimethylaminopyridine (0.050 g). There was then added stearic anhydride (1.57 g, 5.52 mmol) under a nitrogen atmosphere and the reaction mixture was stirred for 3 days, being allowed to come to room temperature. The volatile materials were removed under reduced pressure and the residue was subjected to flash chromatography (20 g, 2 cm diameter) packed with chloroform and eluted with ethyl acetate. Fractions exhibiting a single spot of R_f = 0.33 on TLC (KC, ethyl acetate) as visualized with phosphomolybdate spray reagent were combined to give the pure desired material (1.71 g, 68%), which exhibited IR and NMR spectra in accord with the proposed structure (**5**). Specific rotation $[\alpha]_D$ 0.18 (0.2 M, ethyl acetate). The ^{1}H NMR ($CDCl_3$) exhibited the following signals: δ 0.9, broad, 6H; δ 1.3, broad, 64H; δ 1.8–2.5, multiplet, 8H; δ 4.1–5.1, multiplet, 5H; δ 5.3, triplet, 2H; δ 5.8–7.5 multiplet, 2H. Anal. calcd. for $C_{46}H_{87}O_7P$: C 70.55, H 11.20%; found: C 70.41, H 11.24%.

*Method B: from **10***

To (*S*)-(*E*)-3-hydroxy-4-stearoyloxybut-1-enylphosphonic acid diisopropyl ester (**10**) (160 mg, 0.305 mmol) in dry dimethyl formamide (2.5 mL) with pyridine (0.25 mL) and 4-dimethylaminopyridine (0.05 g) at 0°C was added oleic anhydride (0.2 g, 0.366 mmol). The reaction mixture was stirred and allowed to come to room temperature overnight. Volatile materials were removed under reduced pressure and the residue was subjected to flash chromatography (20 g, 2 cm diameter) packed with chloroform and eluted with ethyl acetate:chloroform 3:1. Fractions exhibiting a single spot of R_f = 0.33 on TLC (KC, ethyl acetate) as visualized with phosphomolybdate spray reagent were combined to give the pure desired material (201 mg, 84%), which exhibited IR and ^{1}H NMR spectra and optical rotations identical to those noted for **6** prepared in Method A as noted previously.

Preparation of (S)-(E)-*oleoyloxy-4-stearoyloxybut-1-enlyphosphonic acid (**7**)*

Under a nitrogen atmosphere (*S*)-(*E*)-3-oleoyloxy-4-stearoyloxybut-1-enylphosphonic acid diisopropyl ester (**6**) (0.70 g, 0.89 mmol) was added to diethyl ether (15 mL). To the solution was added dropwise bromotrimethylsilane (0.46 g, 3.0 mmol) and the resultant mixture was stirred at room temperature overnight. The reactant mixture was then washed with water (3 × 35 mL) and the organic layer was separated, dried over anhydrous sodium sulfate, filtered, and evaporated under reduced pressure. The resulting solid was recrystallized from a minimum volume of methanol and the precipitate was subjected to flash chromatography (20 g, 5 cm diameter) packed with chloroform and eluted with chloroform (200 mL) followed by ethyl acetate (4 × 200 mL). Fractions of the ethyl acetate eluent exhibiting a single spot of R_f = 0.14 on TLC (KC, chloroform) as visualized with phosphomolybdate spray reagent were combined to give the pure desired material (466 mg, 75%), which exhibited IR and ^{1}H NMR spectra in accord with the proposed structure (**7**). Specific rotation: $[\alpha]_D$ 1.42 (0.13 M, chloroform). The ^{1}H NMR ($CDCl_3$) exhibited the following signals: δ 0.9, broad triplet, 6H; δ 1.2, broad, 52H; δ 1.8–2.5, multiplet, 8H; 4.3–4.9, multiplet, 3H; δ 5.3, triplet, 2H; δ 5.8–7.5, multiplet, 2H; δ 11.5, singlet, 2H. Anal. calcd. for $C_{40}H_{75}O_7P$: C 68.73, H 10.82%; found: C 68.73, H 11.01%.

*Preparation of (±)-2,3,4,5,6-penta-*O*-benzyl-*myo*-inositol (±)-(**11**)*

The racemic 1-*O*-allyl-2,3,4,5,6-penta-*O*-benzyl-*myo*-inositol (4.38 g, 6.72 mmol) was dissolved in methanol (10 mL) to which water (10 mL) was added. There was then added 10% Pd/C (0.44 g) along with *p*-toluenesulfonic acid monohydrate (0.44 g) and the resulting mixture was heated at reflux for 24 h. Solid materials were removed by filtration and the volatile materials of the filtrate were removed under reduced pressure to leave an oily residue. This residue was partitioned between a water/ether mixture (80 mL of each) and the ether layer was collected, dried over anhydrous magnesium sulfate, filtered, and evaporated under reduced pressure. The oily residue was subjected to flash chromatography (40 g, 2 cm diameter) packed and eluted with chloroform:ether 50:1. Fractions exhibiting a single spot of R_f = 0.62 on TLC (PS, chloroform:ether 50:1) as visualized with iodine were combined to give the pure desired material (1.55 g, 38%) as a clear oil, which crystallized on standing to give white crystals that exhibited IR and ^{1}H NMR spectra in accord with the proposed structure and a melting point in agreement with that previously reported (15). The ^{1}H NMR ($CDCl_3$) exhibited the following signals: δ 2.05–2.46, broad singlet, 1H; δ 3.33–3.62, multiplet, 3H; δ 3.74–3.94, multiplet, 1H; δ 3.96–4.20 multiplet, 2H; δ 4.56–5.13, multiplet, 10H; δ 7.10–7.62, multiplet, 25H.

*Resolution of (±)-2,3,4,5,6-penta-*O*-benzyl-*myo*-inositol (±)-(**11**)*

The (±)-2,3,4,5,6-penta-*O*-benzyl-*myo*-inositol (1.55 g, 2.46 mmol) was dissolved in methylene chloride (37 mL) and to it was added DMAP (0.033 g, 0.27 mmol), triethylamine (0.75 g, 7.43 mmol), and (−)-camphanic acid chloride (0.64 g, 2.95 mmol). The reaction mixture was stirred at room temperature for 24 h, after which time it was washed with water (2 × 30 mL) and saturated

Can. J. Chem. Downloaded from www.nrcresearchpress.com by 109.225.110.28 on 09/08/12
For personal use only.

aqueous sodium chloride solution (20 mL). It was then dried over anhydrous magnesium sulfate, filtered, and the volatile materials were evaporated under reduced pressure. The residual solid was subjected to flash chromatography (40 g, 2 cm diameter) packed and eluted using methylene chloride:ether 99:1. Material exhibiting R_f between 0.5 and 0.75 on TLC (PS, methylene chloride:ether 99:1) as visualized using iodine was separated into two components using HPLC (Lichrosorb Si-60 10 μm) eluting with methylene chloride:ether 99:1. In this way two components (less polar ester, R_f = 0.73, 1.03 g, and more polar ester, R_f = 0.60, 0.99 g, using the above noted TLC conditions) were isolated as pure materials, which exhibited IR and ^{1}H NMR spectra in accord with their proposed structures and which were separately subjected to hydrolysis. The ^{1}H NMR ($CDCl_3$) exhibited the following signals: (less polar ester) δ 0.83–0.96, singlet, 3H; δ 0.96–1.05, singlet, 3H; δ 1.05–1.19, singlet, 3H; δ 1.48–2.02, multiplet, 3H; δ 2.15–2.43, multiplet, 1H; δ 3.50–3.73, multiplet, 2H; δ 4.01–4.32, multiplet, 3H; δ 4.50–5.17, multiplet, 11H; δ 6.90–7.54, multiplet, 25H; (more polar ester) δ 0.74–0.90, singlet, 3H; δ 0.90–1.03, singlet, 3H; δ 1.03–1.22, singlet, 3H; δ 1.43–2.10, multiplet; 3H; δ 2.15–2.46, multiplet, 1H; δ 3.43–3.80, multiplet, 2H; δ 3.90–4.40, multiplet, 3H; δ 4.44–5.70, multiplet, 11H; δ 6.93–7.68, multiplet, 25H.

The more polar and less polar esters were each separately hydrolyzed using the procedure as described here for the more polar ester. The more polar ester (0.99 g, 1.22 mmol) was added to a 0.1 M solution of potassium by hydroxide in ethanol (100 mL) and the mixture was stirred at room temperature for 24 h. After this time the volatile materials were evaporated under reduced pressure and the residue was partitioned between ether:water 10:7 (170 mL). The layers were separated and the aqueous layer was extracted with ether (35 mL). The organic layers were combined, dried over magnesium sulfate, filtered, and volatile materials were evaporated under reduced pressure. The oily residue was subjected to flash chromatography (20 g, 2 cm diameter) packed and eluted with hexane:ether 1:3. The fractions exhibiting a single spot of R_f = 0.81 (PS, hexane:ether 1:3) were combined to give the pure desired material (0.725 g, 94.2%), which exhibited IR and ^{1}H NMR spectra in accord with the proposed structure (−)-(**11**). Specific rotation: $[\alpha]_D$ −9.0 (0.11 M, ethanol). The ^{1}H NMR ($CDCl_3$) exhibited the following signals: δ 2.02–2.26, broad doublet, 1H; δ 3.25–3.60, multiplet, 3H; δ 3.60–3.87, multiplet, 1H; δ 3.87–4.14, multiplet, 2H; δ 4.46–5.08, multiplet, 10H; δ 6.94–7.55, multiplet, 25H.

The equivalent procedure was performed using the less polar ester (1.03 g, 1.27 mmol) leading to the isolation of (+)-(**11**) (0.726 g, 90.9%), which exhibited IR, TLC, and NMR data in accord with the proposed structure. Specific rotation: $[\alpha]_D$ +8.8 (0.11 M, ethanol). The ^{1}H NMR ($CDCl_3$) exhibited the following signals: δ 2.08–2.25, broad doublet, 1H; δ 3.22–3.53, multiplet, 3H; δ 3.60–3.84, multiplet, 1H; δ 3.86–4.08, multiplet, 2H: δ 4.40–5.04, multiplet, 10H; δ 6.88–7.47, multiplet, 25H.

The observed specific rotations were in accord with those previously reported (16).

Preparation of (S)-(E)*-3-oleoyloxy-4-stearoyloxybut-1-enyl-phosphonic acid 2,3,4,5,6-penta-*O*-benzyl-*myo*-inosit-1-yl ester (12)*

To (*S*)-(*E*)-3-oleoyloxy-4-stearoyloxybut-1-enylphosphonic acid (**7**) (70 mg, 0.10 mmol) dissolved in freshly distilled pyridine (0.5 mL) was added (−)-2,3,4,5,6-penta-*O*-benzyl-*myo*-inositol (−)-(**11**) (50 mg, 0.08 mmol), followed by an excess of trichloroacetonitrile (0.45 g). The reaction flask was stoppered under a nitrogen atmosphere and the reaction mixture was stirred for 3 days using a controlled temperature water bath at 51°C. After this time volatile materials were evaporated under reduced pressure and the residue was purified by flash chromatography (10 g, 2 cm diameter) packed and eluted using methylene chloride:ether 50:1. The fractions exhibiting R_f = 0.85 on TLC (PS, methylene chloride:ether 50:1) as visualized with phosphomolybdate spray reagent were combined to give the pure desired material (21 mg, 20%), which exhibited IR and ^{1}H NMR spectra in accord with the proposed structure (**12**). Specific rotation: $[\alpha]_D$ −2.47 (0.0014 M, CCl_4). The ^{1}H NMR ($CDCl_3$) exhibited the following signals: δ 0.9, broad multiplet, 6H; δ 1.1–1.4, broad multiplet, 52H; δ 1.9–2.5, multiplet, 8H; δ 3.3–3.6, multiplet, 3H; δ 3.8–4.0, multiplet, 2H; δ 4.0–5.0, multiplet, 13H; δ 5.2, multiplet, 1H; δ 5.4, triplet, 2H; δ 5.6–7.8, multiplet, 2H; δ 7.0–7.4, multiplet, 25H; δ 12.1, singlet, 1H. Anal. calcd. for $C_{81}H_{115}O_{12}P$: C 74.17, H 8.84%; found: C 73.91, H 9.14%.

Preparation of (S)-(E)*-3-oleoyloxy-4-stearoyloxybut-1-enylphosphonic acid* myo*-inosit-1-yl ester (2)*

The material (*S*)-(*E*)-3-oleoyloxy-4-stearoyloxybut-1-enylphosphonic acid 2,3,4,5,6-penta-*O*-benzyl-*myo*-inosit-1-yl ester (**12**) (7.3 mg, 0.0056 mmol) was dissolved in chloroform (0.5 mL), an excess of iodotrimethylsilane (0.25 mL) was added, and the reaction mixture was stirred at room temperature for 15 min. The reaction was quenched by the addition of methanol (0.75 mL). Volatile materials were removed under reduced pressure and diethyl ether (1 mL) was added to the residue. Saturated aqueous sodium bisulfite solution (2 drops) was added until the material became clear. Volatile materials were removed again under reduced pressure and the residue was subjected to flash chromatography (20 g, 2 cm diameter) packed and eluted with chloroform. Those fractions exhibiting a single spot of R_f = 0.31 (PS, chloroform) were combined to give the pure desired material (3.7 mg, 76.7%), which exhibited IR and ^{1}H NMR spectra in accord with the proposed structure (**2**). Specific rotation: $[\alpha]_D$ −6.38 (0.0021 M, $CHCl_3$). The ^{1}H NMR exhibited the following signals: δ 0.9, broad multiplet, 6H; δ 1.0–1.6, broad multiplet, 52H; δ 1.6–2.5, broad, 8H; δ 3.6, 6H, singlet; δ 3.7–4.5, broad multiplet, 9H; δ 5.4,, triplet, 2H; δ 5.7–7.8, multiplet, 2H. Anal. calcd. for $C_{46}H_{85}O_{12}P$: C 64.16, H 9.95%; found: C 63.90, H 10.10%.

Acknowledgement

This work was supported by grants from the National Institutes of Health (GM 40441) and the PSC-BHE Research Award Program (no. 668261).

1. (*a*) T.-y. Chu, B. E. Tropp, and R. Engel. Paper no. 35 Organic Division, 199th National Meeting of the American Chemical Society, Boston, Mass. April 1990; (*b*) C. Pratt, B. E. Tropp, and R. Engel. Paper no. 1 Organic Division, 200th National Meeting of the American Chemical Society, Washington, D.C., August 1990.
2. P. W. Schwartz, B. E. Tropp, and R. Engel. Chem. Phys. Lipids, **49**, 131 (1988).
3. M. J. Berridge. Annu. Rev. Biochem. **56**, 159 (1987), and references therein.
4. D. C. Billington. Chem. Soc. Rev. **18**, 83 (1989).
5. (*a*) V. N. Krylova, H. P. Gornaeva, V. I. Shvets, and R. P. Evstigneeva. Dokl. Akad. Nauk S.S.S.R. **246**, 339 (1979); (*b*) V. N. Krylova, A. I. Lyutik, N. P. Gornaeva, and V. I. Shvets. Zh. Obshch. Khim. S.S.S.R. **51**, 210 (1981); (*c*) S. S. Yang, T. R. Beattie, and T. Y. Shen. Tetrahedron Lett. **23**, 5517 (1982); (*d*) J. G. Ward and R. C. Young. Tetrahedron Lett. **29**, 6013 (1988); (*e*) C. E. Dreef, C. J. J. Elie, P. Hoogerhout, G. A. van der Marel, and J. H. van Boom. Tetrahedron Lett. **29**, 6513 (1988); (*f*) K. S. Ishaq, M. Capobianco, C. Piantadosi, A. Noseda, L. W. Daniel, and E. J. Modest. Pharm. Res. **6**, 216 (1989); (*g*) M. Jones, K. K. Rana, J. G. Ward, and R. C. Young. Tetrahedron Lett. **30**, 5353 (1989); (*h*) C. J. J. Elie, C. E. dreef, R. Verduyn, G. A. van der Marel, and J. H. van Boom, Tetrahedron, **45**, 3477 (1989); (*i*) R. C. Young, C. P. Downes, D. S. Eggleston, M. Jones, C. H. Macphee, K. K. Rana, and J. G. Ward. J. Med. Chem. **33**, 641 (1990); (*j*) C. E. Dreef, C. J. J. Elie, G. A.

van der Marel, and J. H. van Boom. Tetrahedron Lett. **32**, 955 (1991).
6. A. Mazur, B. E. Tropp, and R. Engel. Tetrahedron, **40**, 3949 (1984).
7. T. Takenawa and Y. Nagai. J. Biol. Chem. **256**, 6769 (1981).
8. E. Baer and H. O. L. Fischer. J. Biol. Chem. **128**, 463 (1939).
9. C. H. Roy. U.S. Patent 3, 251, 907 (17 May 1966); Chem. Abstr. **65**, 3908f (1966).
10. N. Lalinde, B. E. Tropp, and R. Engel. Tetrahedron, **39**, 2369 (1983).
11. J.-C. Tang, C.-T. Tang, B. E. Tropp, and R. Engel. Chem. Phys. Lipids, **19**, 99 (1977).
12. B. Perly, E. J. Dufourc, and H. C. Jarrell. J. Labelled Compd. Radiopharm. **21**, 1 (1984).
13. (*a*) R. Rabinowitz, J. Org. Chem., **28**, 2975 (1963); (*b*) C. E. McKenna, M. T. Higa, N. H. Cheung, and M.-C. McKenna. Tetrahedron Lett. 155 (1977).
14. S. Ali and R. Bittman. Chem. Phys. Lipids, **50**, 11 (1989).
15. R. Gigg and C. D. Warren. J. Chem. Soc. 2367 (1969).
16. D. C. Billington, R. Baker, J. J. Kulagowski, and I. W. Mawer. J. Chem. Soc. Chem. Commun. 314 (1987).
17. R. Boss and R. Scheffold. Angew. Chem. Int. Ed. Engl. **15**, 558 (1976).
18. C. E. Dreef, M. Douwes, C. J. J. Elie, G. A. van der Marel, and J. H. van Boom. Synthesis, 443 (1991).
19. P. W. Schwartz, B. E. Tropp, and R. Engel. Chem. Phys. Lipids, **48**, 1 (1988).
20. M. E. Jung and M. A. Lyster. J. Org. Chem. **42**, 3761 (1977).

Can. J. Chem. Downloaded from www.nrcresearchpress.com by 109.225.110.28 on 09/08/12
For personal use only.

Studies on novel carbacephem analogs: synthesis of 7-methoxy-homo-PS-5 and a 7-methoxy-8-epi-homothienamycin intermediate

S. R. SHAKYA AND T. DURST[1]

Chemistry Department, Ottawa–Carleton Chemistry Institute, University of Ottawa, Ottawa, Ont., Canada K1N 6N5

Received February 5, 1992

S. R. SHAKYA and T. DURST. Can. J. Chem. **70**, 2142 (1992).

The synthesis of two carbacephems bearing a 7-methoxy group and either an additional ethyl (PS-5) or hydroxyethyl (thienamycin) side chain has been completed. Rhodium carbenoid insertion methodology was used to generate the bicyclic ring systems.

S. R. SHAKYA et T. DURST. Can. J. Chem. **70**, 2142 (1992).

On a réussi la synthèse de deux carbacéphèmes portant un groupe 7-méthoxy ainsi que des chaînes latérales additionnelles éthyle (PS-5) ou hydroxyéthyle (thiénamycine). On a utilisé la méthodologie d'insertion d'un carbénoïde de rhodium pour générer les systèmes bicycliques.

[Traduit par la rédaction]

Introduction

As a part of program of synthesizing unusual bicyclic β-lactams bearing two substituents α to the β-lactam carbonyl group[2] we would like to report our work concerning the preparation of the carbacephem analogs **1** and **2**, which carry a 7β-methoxy group in addition to either an ethyl or hydroxyethyl group typical of PS-5 or thienamycin (2, for general reference) antibiotics, respectively. The most important methodology for the construction of the bicyclic ring system of both carbapenems and carba-cephems is the rhodium carbenoid insertion route developed by Cama[3] and co-workers at Merck (3).[4] Surprisingly, this cyclization procedure has not been applied to examples that carry a methoxy group at C-6 or C-7 in the final product (4). Success in such cases is by no means assured[5] since intramolecular trapping of carbenoids by ether oxygen (eq. [1]) has often been observed and studied in considerable detail (5).[6] Nitrogen substituents,[7] when present at these positions, were shown to interfere in the cyclization process as shown in eq. [2] (6).

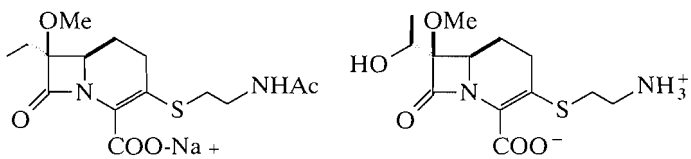

1 **2**

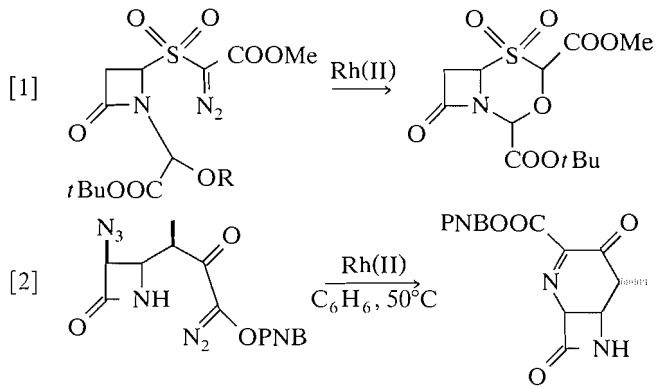

The combination of ring size and the 7,7-disubstitution pattern of **1** and **2** are also of interest for structure–activity studies. Carbacephems having a typical amide substituent at C-7 are chemically more stable than the analogous cephalosporins but tend to have comparable biological activity (7). The replacement of the amide nitrogen by an ester oxygen at the carbon α to the β-lactam carbonyl in penicillin and cephalosporin was found to diminish the activity (8). Homothienamycin is more stable than thienamycin, but inactive (9). Some activity has been reported in oxacephems bearing a hydroxyethyl substituent (10). These results indicate that the compounds may not have the high antimicrobial activity displayed by thienamycin. Thus compounds **1** and **2** were considered worthwhile targets, as model compounds, from the methodology point of view.

Results and discussion

Preparation of the β-ketoesters 7 and 11

Both 3,3-disubstituted azetidinones **3** and **8** were available in multigram quantity via reaction of the β-lactam

[1] Author to whom correspondence may be addressed.

[2] See ref. 1.

[3] This reaction was first developed by Cama and Christensen in oxapenam cyclization (17*b*) and extended to carbapenems by Ratcliffe *et al.* (3*a*).

[4] For rhodium carbenoid cyclizations to (1) carbapenems: ref. 3*a* and (2) carbacephems: ref. 9. For other cyclization methods, see refs. 3*b* and 3*c* for carbapenems 3*d*–3*r* and 7*c* for carbacephems. For other methods of preparing β-ketoester precursors for rhodium cyclization: refs. 3*s*–3*u*.

[5] Successful rhodium carbenoid cyclizations were reported in synthesis of 1-methoxy-carbapenem (16), 1-oxapena(e)m (17) and 1-oxacepham nuclei (18). In these examples the ethereal oxygen is one or two carbons removed from the carbenoid centre. These results do not undermine the importance of the present study since the distance and stereochemical relationship of methoxy groups to the carbenoid center are quite different in the problem at hand.

[6] For intramolecular insertion into ether yielding a six-membered ring, see ref. 5*g*.

[7] Successful annulations have been reported in the case of carbacephem (3*s*) and carbapenem (19) with an α-nitrogen substituent. It appears that the substituent and stereochemical relationship govern the product. Oxacephem having an α-nitrogen group has been prepared by this methodology (18*a*). These authors reported a small amount of product derived from the insertion of the carbenoid into the NH bond at C-7.

Can. J. Chem. Downloaded from www.nrcresearchpress.com by 109.225.110.28 on 09/08/12
For personal use only.

[3] 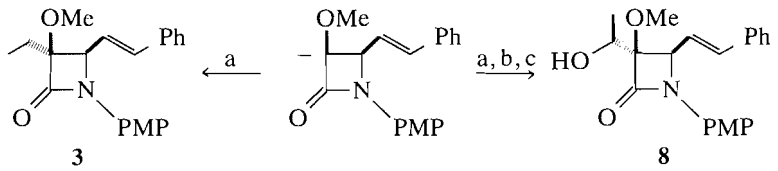

(a) LDA, THF, EtI, −78 to −30°C or CH_3CHO, −78°C; (b) PCC, CH_2Cl_2, NaOAc, 4 Å mol. sieves, 25°C; (c) L-Selectride, TMEDA, THF, −78°C

enolate derived from *N*-*p*-methoxyphenyl-4-cinnamyl-3-methoxyazetidin-2-one (11) with ethyl iodide and acetaldehyde, respectively (eq. [3]).

Diastereomerically pure **8** was obtained by oxidation of the initially produced mixture of 3-hydroxyethyl adducts to the 3-acetyl derivative followed by L-Selectride reduction under non-chelating conditions (11). The *p*-methoxyphenyl (PMP) group in **3** was cleaved using ceric ammonium nitrate (CAN) at −25 to −30°C (12). Ozonolysis of the N-TBDMS derivative (tert-butyldimethylsilyl triflate, TBDMSOTf (13)) **4** was carried out in dichloromethane with traces of methanol and molecular sieves to yield **5** (ir: 1755 and 1740 cm^{-1}; ^1H nmr: 9.61 ppm) in 43% overall yield from **3** (Scheme 1).

The two-carbon homologation to **6** was achieved in excellent yield and in a practical manner on a multigram scale using benzyl(triphenylphosphoranylidene)acetate;[8] both reduction of the double bond and the debenzylation occurred upon hydrogenation with 10% Pd on C. The further elaboration of **6** to β-ketoester was achieved by activation with carbonyldiimidazole and subsequent reaction with the magnesium salt of mono-*p*-nitrobenzylester of malonic acid following the Masamune protocol (14). Methanolic HCl treatment of the *N*-silyl β-ketoester gave the key desilylated compound **7**.

A similar sequence was used to obtain the intermediate **11** having both the 7-methoxy and epithienamycin type side chains at C-3. Thus compound **8** was silylated (TBDMSOTf and 2,6-lutidine) and cleaved with ozone to afford the aldehyde **9** in 81% overall yield from **8**.[9] Removal of the *p*-methoxyphenyl group with CAN afforded the expected aldehyde, which was rather unstable and difficult to handle compared to the *N*-silylated aldehyde **5**. Therefore the aldehyde was quickly purified by column chromatography to a usable state and subjected to the Wittig homologation sequence described above. The carboxylic acid **10** was obtained in 36% overall yield from **9**. The homologation of **10** to β-keto ester **11** was again achieved using Masamune's method (Scheme 2).

Annulation

Diazo transfer between **7** or **11** and 4-carboxybenezenesulfonazide was catalyzed by triethylamine (15). The resulting diazo compounds were refluxed in benzene with about 0.3 mol% of $Rh_2(OAc)_4$ to give **12** (60% from **7**) and **13** (32% from **11**), respectively. No other major products were evident by tlc, thus indicating that interference by the methoxy group in the carbenoid cyclization was not of major concern. The formation of the second ring in both products is evident from the ^1H nmr[10] and ir spectra. The appearance of an AB pattern for the benzylic protons (δ = 5.25 ppm (1H, d, J = 13.9 Hz) and 5.47 ppm (1H, d, J = 13.4 Hz)) and shift of the β-lactam carbonyl from 1740 (monocyclic precursor) to 1752 cm^{-1} (bicyclic ketoester) are expected changes in going from **7** to **12**. The conversion of **11** to **13** shows similar changes. The benzylic protons in **11** (δ = 5.23 ppm (s)) became a quartet in **13** (δ = 5.24 ppm (1H, d, J = 13.7 Hz) and 5.45 ppm (d, J = 13.4 Hz). A con-

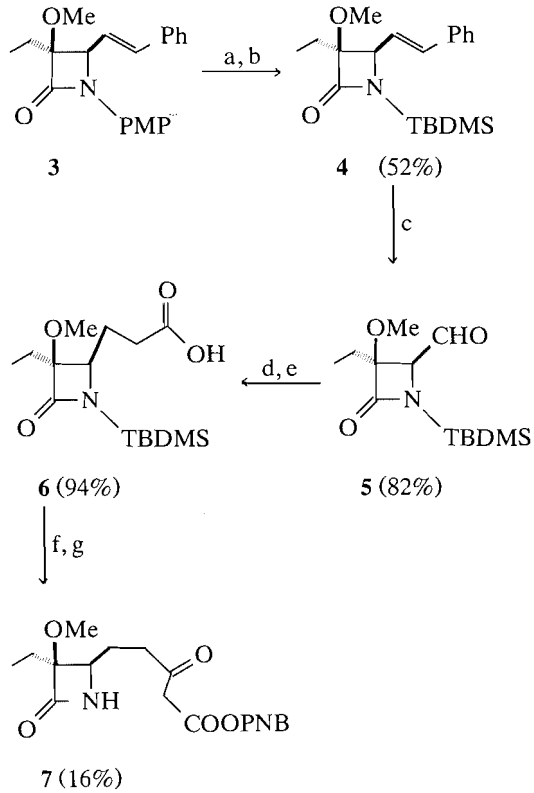

(a) CAN, MeCN, H_2O, −25 to −30°C; (b) TBDMSOTf, 2,6-lutidine, CH_2Cl_2, 0–25°C; (c) O_3, CH_2Cl_2 MeOH, −78°C, DMS, −78–25°C; (d) $Ph_3P{=}CHCOOBn$, toluene, reflux; (e) H_2, Pd–C, EtOH, 25°C; (f) CDI, THF, $Mg(OOCCH_2COOPNB)_2$, THF, 25°C; (g) 10% HCl, MeOH, 25°C

SCHEME 1

[8]Wittig reaction resulting in four-carbon homologations using (triphenylphosphoranylidene)-2,2,6-trimethyl-4*H*-1,3-dioxin-4-one has been reported (3*t*). This suggested an alternate route from **5** to **7**. However, in our hands this reagent proved to be difficult to prepare and purify especially on a multigram scale.

[9]See ref. 1 for experimental details of this conversion.

[10]Proton and ^{13}C nmr spectra for all key compounds have been deposited as Supplementary Material and may be purchased from: The Depository of Unpublished Data, Document Delivery, CISTI, National Research Council Canada, Ottawa, Canada KIA 0S2.

Can. J. Chem. Downloaded from www.nrcresearchpress.com by 109.225.110.28 on 09/08/12
For personal use only.

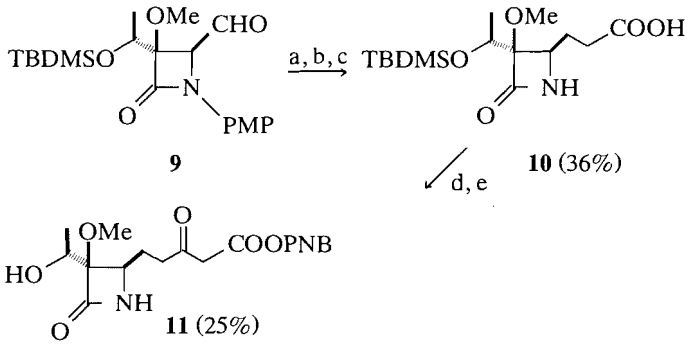

(a) CAN, MeCN, H_2O, −10°C; (b) $Ph_3P{=}CHCOOBn$, toluene, reflux; (c) H_2, Pd–C, EtOH, 25°C; (d) CDI, THF, $Mg(OOCCH_2COOPNB)_2$, THF, 25°C; (g) 6 N HCl, MeOH, 25°C

SCHEME 2

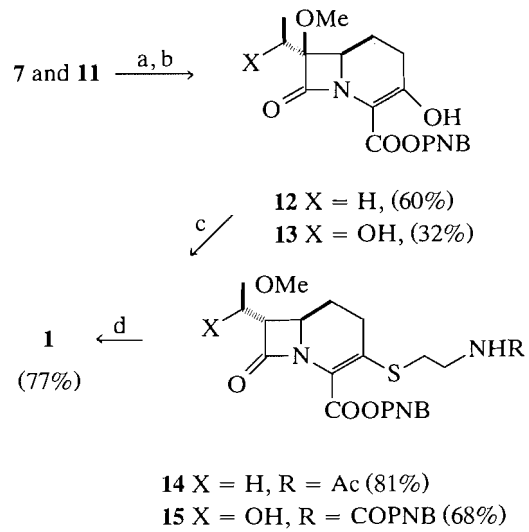

14 X = H, R = Ac (81%)
15 X = OH, R = COPNB (68%)

(a) 4-$HOOCPhSO_2N_3$, Et_3N, MeCN, 0°C; (b) $Rh_2(OAc)_4$, C_6H_6, reflux; (c) $(PhO)_2POCl$, DIPEA, MeCN, 0°C, $HSCH_2CH_2NHR$, DIPEA, 0°C; (d) H_2, Pd–C, THF: H_2O

SCHEME 3

comitant shift for the β-lactam carbonyl from 1740 to 1750 cm^{-1} was also observed.

The conversion of **12** to **14** involved the activation of the enol group with diphenylchlorophosphate followed by addition of *N*-acetylaminoethanethiol in the presence of diisopropylethylamine (DIPEA). The epi-homothienamycin analog **15** was obtained in similar manner using carbo-*p*-nitrobenzyloxyaminoethanethiol. Removal of the *p*-nitrobenzyl groups from **14** and **15** via catalytic hydrogenation afforded the crude carboxylic acids (Scheme 3). Reverse-phase column chromatography purification and lyophilization of the resultant aqueous solution gave the compound **1** as a white powder; mp: becomes translucent at 177–178°C and chars at or above 217°C; ir (KBr): 1742 (β-lactam C=O) cm^{-1}. In vitro antibacterial activity of **1** was determined by conventional microtiter dilution procedures. The MIC's were higher than 64 μg/mL for organisms such as *Streptococcus pneumoniae*, *Streptococcus pyogenes*, and *Haemophilus influenzae*, and 128 μg/mL for *Enterococcus faecalis*, *Enterococcus faecium*, *Staphylococcus aureus*, *Staphylococcus epidermidis*, *Staphylococcus haemolypticus*, *Escherichia coli*, *Klebsiella pneumoniae*, *Enterobacter cloacae*, *Proteus mirabilis*, *Proteus vulgaris*, *Morganella morganii*, *Proteus rettgeri*, *Serrafia marcescens*, *Pseudomonas aeruginosa*, *Pseudomonas cepacia*, and *Xanthomonas maltophilia*. The purification of carboxylic acid derived from **15** was unsuccessful on the first attempt. Due to lack of material and the discouraging results observed in the studies of antibacterial activity of **1**, purification of this compound was not repeated.

Conclusion

7-Methoxyhomo-PS-5, **1**, was found to be inactive as an antibacterial compound. From a methodology point of view, this study did indicate that the rhodium carbenoid annulation can be applied in β-lactams having a methoxy group α to the lactam carbonyl. We have successfully applied this methodology to the preparation of several 6-methoxy carbapenems including 6-methoxy-PS **5**. None of these examples display intervention by the α-methoxy group; which will be reported shortly.

Experimental

The analytical instruments used in spectral analysis are given in ref. 1. In addition to these, Bomem Michelson MB100 and Kratos concept 2H instruments were used for infrared and mass spectra, respectively. Solvent purification and chromatographic separation have also been described (1).

1-tert-Butyldimethylsilyl-4-cinnamyl-3-ethyl-3-methoxyazetidin-2-one (4)

A solution of the azetidinone **3** (6.50 g, 19.3 mmol) in 250 mL of MeCN was cooled to −25 to −30°C. (Some material precipitated out after 10 min but the procedure was continued without further addition of the solvent.) CAN (32 g, 58.4 mmol) in 60 mL of ice-cold water was added dropwise over 20 min. The initial greenish-black color turned yellow and at the end of the reaction time, the homogeneous solution was brown. Usual work-up using ethyl acetate for extraction gave a yellow solid, which on trituration with ether gave the free NH β-lactam as a white solid (2.30 g, 52%).

A solution of this intermediate in 50 mL of dry CH_2Cl_2 was cooled to 0°C and 2,6-lutidine (2.32 mL, 19.9 mmol) and TBDMSOTf (3.43 mL, 14.9 mmol) was added via syringe. The reaction mixture was stirred for 30 min at 0°C and 1.5 h at room temperature. Usual work-up and purification by column chromatography (1:15 EtOAc:hexanes) gave 3.40 g (99%) of a pale yellowish oil **4**; ir (film): 1744 (β-lactam C=O) cm^{-1}; ^1H nmr δ: 0.15 (3H, s, CH_3Si), 0.21 (3H, s, CH_3Si), 0.93 (9H, s, *t*BuSi), 0.97 (3H, t, J = 7.3 Hz, CH_3CH_2), 1.79–2.01 (2H, m, CH_2CH_3), 3.43 (3H, s, OCH_3), 3.98 (1H, d, J = 8.7 Hz, CHN), 6.22 (1H, dd, J = 16.0, 8.9 Hz, CH=CHPh), 6.54 (1H, d, J = 16.0 Hz, CH=CHPh), 7.10–7.30 (5H, m, Ph); ms (ei): 345 (M^+, 11), 330 (M^+ − 15, 18), 302 (M^+ − 15−28, 4), 288 (M^+ − 57, 3), 188 (M^+ − 157, 100). Exact Mass (HRMS) calcd. for $C_{20}H_{31}NO_2Si$: 345.2112; found: 345.2118.

1-tert-Butyldimethylsilyl-3-ethyl-4-formyl-3-methoxyazetidin-2-one (5)

Ozone was passed through a solution of **4** (3.40 g, 9.85 mmol) in 50 mL of dry CH_2Cl_2 and 5 mL of MeOH containing about 0.50 g of 4Å molecular sieves at −78°C till the solution was bluish. Excess ozone was removed by bubbling dry nitrogen through the reaction mixture and 3 mL of dimethyl sulfide was added. The re-

Can. J. Chem. Downloaded from www.nrcresearchpress.com by 109.225.110.28 on 09/08/12
For personal use only.

Can. J. Chem. Downloaded from www.nrcresearchpress.com by 109.225.110.28 on 09/08/12
For personal use only.

sulting reaction mixture was warmed slowly to 25°C and kept for 18 h. After removal of the solvent, the crude product was purified by column chromatography (1:10 EtOAc:hexanes) to yield 2.20 g (82%) of aldehyde **5** as a colorless oil; ir (film): 1740 (CHO), 1755 (β-lactam C=O) cm^{-1}; ^1H nmr δ: 0.10 (3H, s, CH_3Si), 0.29 (3H, s, CH_3Si), 0.94 (9H, s, *t*Bu), 1.01 (3H, t, J = 7.3 Hz, CH_3CH_2), 1.68–1.88 (1H, m, CH_2CH_3), 1.94–2.12 (1H, m, CH_2CH_3), 3.40 (3H, s, OCH_3), 3.81 (1H, d, J = 3.1 Hz, CHN), 9.61 (1H, d, J = 3.0 Hz, CHO); ms (ei): 272 (M^+ + 1, 3), 244 (M^+ + 1−28, 3), 214 (M^+ − 57, 29), 187 (M^+ +1−28−57, 87), 171 (M^+ − 100, 3).

1-tert-*Butyldimethylsilyl-4-(2-carboxyethyl)-3-ethyl-3-methoxyazetidin-2-one (**6**)*

The solution of benzyl(triphenylphosphoranylidene)acetate (3.99 g, 9.73 mmol) in 100 mL of toluene was stirred with the aldehyde **4** (2.20 g, 8.12 mmol) at 50–60°C for 18 h. Toluene was removed and the residue was triturated with 100 mL of hexanes. Triphenylphosphine oxide was filtered off and the filtrate was concentrated to a yellow oil, which on purification by column chromatography (1:10 EtOAc:hexanes) gave 3.10 g (95%) of a *cis–trans* (1:4) mixture of the corresponding α,β unsaturated ester as a colorless oil.

This ester (3.10 g, 7.69 mmol) was dissolved in 10 mL of EtOH and hydrogenated in the presence of 2 g of Pd–C (10%) at 20 psi (1 psi = 6.9 kPa) for 18 h. Usual work-up gave 2.40 g (99%) of acid **6** as a colorless oil; ir (film): 3127 (COOH), 1741 (C=O), 1676 (COOH) cm^{-1}; ^1H nmr δ: 0.18 (3H, s, CH_3Si), 0.21 (3H, s, CH_3Si), 0.87–0.94 (12H, t with overlapping s, CH_3CH_2, *t*Bu), 1.48–1.68 (1H, m, CH_2CH_3), 1.90–2.12 (3H, m, CH_2CH_3, CH_2), 2.21–2.61 (2H, m, CH_2CO), 3.37 (1H, dd, J = 4.8, 9.2 Hz, CHN), 3.47 (3H, s, OCH_3); ms (ei): 315 (M^+, 5), 300 (M^+ − 15, 14), 272 (M^+ − 15−28, 5), 258 (M^+ − 57, 12), 243 (258−15, 1). Exact Mass (HRMS) calcd. for $C_{15}H_{29}NO_4Si$: 315.1868; found: 315.1867.

3-tert-*Butyldimethylsilyloxyethyl-4-(2-carboxyethyl)-3-methoxyazetidin-2-one (**10**)*

The aldehyde **9** (7.10 g, 18 mmol) was reacted with CAN (29.59 g, 54 mmol) at −10°C to yield 3.50 g (66%) of *N*-deprotected aldehyde as a brown oil after column chromatography (1:4 EtOAc:hexanes). This compound showed the aldehyde proton at 9.61 ppm and was judged to be about 60% pure by ^1H nmr. It was used as such.

Reaction of the aldehyde (3.50 g, 12 mmol) with benzyl(triphenylphosphoranylidene)acetate (7.35 g, 17.9 mmol) gave 2.70 g (36% from **9**) of a brownish oil after column chromatography (1:4 EtOAc:hexanes). The resultant oil was hydrogenated to yield 2.10 g (99%) of **10** as a brown oil; ir (film): 3362 (COOH), 1740 (C=O) cm^{-1}; ^1H nmr δ: 0.02 (3H, s, CH_3Si), 0.04 (3H, s, CH_3Si), 0.84 (9H, s, *t*Bu), 1.21 (3H, d, J = 6.4 Hz, CH_3CH_2), 1.80–1.93 (2H, m, CH_2COO), 2.20–2.55 (2H, m, CH_2CH_2COO), 3.58 (3H, s, OCH_3), 3.59–3.72 (1H, m, overlaps with 3.58 of OCH_3, CHN), 4.10 (1H, q, J = 6.4 Hz, CHO), 6.73 (1H, br, NH); ms (ei): 316 (M^+ − 15, 2), 302 (M^+ − 29, 1), 287 (M^+ − 44, 3), 274 (M^+ − 57, 26), 230 (M^+ − 101, 21). Exact Mass (HRMS) calcd. for $C_{14}H_{26}NO_5Si$ (M^+ − 15): 316.1576; found: 316.1578.

3-Ethyl-3-methoxy-4-(4'-p-*nitrobenzyloxycarbonyl-3-oxobutyl)azetidin-2-one (**7**)*

Carbonyldiimidazole (CDI, 1.50 g, 9.52 mmol) was added to a solution of the acid **6** (2.00 g, 6.35 mmol) in 10 mL of THF and the mixture was stirred at 25°C for 3.75 h. The suspension of the magnesium salt of the mono-*p*-nitrobenzyl ester of malonic acid[11] (3.20 g, 6.39 mmol) was added by cannula and stirred vigorously for 16 h. The reaction mixture was diluted with EtOAc and washed with saturated NaCl solution. Column chromatography (1:4 EtOAc:hexanes) of the resulting crude product afforded 0.70 g (22%) of a colorless oil.

The β-ketoester thus obtained (0.70 g, 1.42 mmol) in 10 mL of MeOH was stirred overnight with 1 mL of 10% aqueous HCl. Excess of the acid was neutralized by adding solid $NaHCO_3$. The crude product obtained after work-up using EtOAc for extraction was purified by column chromatography (6:4 hexanes:EtOAc) to yield 0.39 g (73%) of **7** as a pale yellowish oil; ir (film): 3292 (NH), 1740 (C=O), 1720 (COOR), 1522 and 1348 (NO_2) cm^{-1}; ^1H nmr δ: 0.91 (3H, t, J = 7.4 Hz, CH_3CH_2); 1.62–1.69 (1H, m, CH_2CH_3), 1.86–2.03 (3H, m, CH_2CH_3, CH_2), 2.54–2.69 (2H, m, CH_2CO), 3.41–3.52 (6H, m, overlapping with s at 3.48, OCH_3, $COCH_2COOR$, CHN), 5.24 (2H, s, CH_2PNB), 5.90 (1H, br, NH), 7.50 (2H, d, J = 8.9 Hz, PNB), 8.21 (2H, d, J = 8.9 Hz, PNB); ms (ci): 379 (M^+ + 1, 9), 351 (M^+ + 1−28, 50), 333 (M^+ + 1−28−18, 12), 319 (M^+ + 1−60, 33), 301 (319−18, 1).

*3-Hydroxyethyl-3-methoxy-4-(4-*p-*nitrobenzyloxycarbonyl-3-oxobutyl)azetidin-2-one (**11**)*

The carboxylic acid **10** (2.13 g, 6.43 mmol) gave 1.2 g (37%) of β-ketoester as a yellow oil using the above homologation procedure.

O-Desilylation of the β-ketoester obtained above was effected by treating the methanolic solution of this ester (1.2 g, 2.36 mmol) with 2 mL of 6 N HCl dropwise at 0–25°C for 18 h to afford 630 mg (68%) of **11**, after passage of the crude product through a short silica gel column using EtOAc, as a yellow oil; ir (CH_2Cl_2): 3327 (NH), 1740 (broad C=O), 1523 and 1348 (NO_2) cm^{-1}; ^1H nmr δ: 1.20 (3H, overlapping with EtOAc, CH_3CH_2), 1.80–2.10 (2H, m, CH_2), 2.30–2.70 (2H, m, CH_2), 3.56–3.65 (6H, m with overlapping s due to OCH_3, CHN, CH_2), 4.12 (1H, overlapping with EtOAc), 5.23 (2H, s, CH_2PNB), 6.20 (1H, s, br, NH), 7.49 (2H, d, J = 8.2 Hz, PNB), 8.20 (2H, d, J = 8.8 Hz, PNB); ms (ci): 353 (M^+ + 1−42, 2), 279 (M^+ + 1−116, 2), 274 (M^+ +1−120, 20), 259 (M^+ +1−136, 1), 215 (M^+ + 1−180, 6). This compound was purified after conversion to the corresponding diazo compound.

p-*Nitrobenzyl(7-ethyl-7-methoxy)-3-hydroxyl-1-carba-1-dethia-3-cephemcarboxylate (**12**)*

4-Carboxybenzenesulfonazide (0.37 g, 1.63 mmol) was added to a solution of the compound **7** (0.38 g, 1.00 mmol) in 25 mL of dry MeCN at 0°C. The resulting suspension turned to a clear solution after addition of Et_3N (0.56 mL, 4.02 mmol) and was stirred for 6 h. The cloudy reaction mixture was diluted with EtOAc and washed successively with 5% $NaHCO_3$ and saturated NH_4Cl. Purification of the crude product by column chromatography (2:5 EtOAc:hexanes) gave 0.35 g (85%) of diazo compound as a colorless oil.

The diazo compound obtained above (0.35 g, 0.86 mmol) was dissolved in 30 mL of dry benzene and 15 mL of solvent was distilled off. After cooling to 25°C under N_2, about 1 mg of $Rh_2(OAc)_4$ was added and the solution was refluxed overnight. Purification of the crude product by column chromatography (2:5 EtOAc:hexanes) furnished 0.23 g (70%) of the product **12** as a white solid; mp 125–126°C; ir (KBr): 3435 (br OH), 1752 (C=O), 1518 and 1344 (NO_2) cm^{-1}; ^1H nmr δ: 1.00 (3H, t, J = 7.4 Hz, CH_3CH_2), 1.55 (1H, br, OH), 1.79–2.21 (4H, m, CH_2CH_3, CH_2), 2.47–2.54 (2H, m, CH_2CO), 3.40–3.48 (4H, dd, J = 10.3, 4.4 Hz, overlapping with s, CHN, OCH_3), 5.25 (1H, d, J = 13.9 Hz, CH_AH_BPNB), 5.47 (1H, d, J = 13.4 Hz, CH_BH_APNB), 7.66 (2H, d, J = 8.9 Hz, PNB), 8.21 (2H, d, J = 8.9 Hz, PNB); ms (ei): 376 (M^+, 2), 348 (M^+ − 28, 5), 318 (M^+ − 28−30, 2), 302 (318−16, 0.3), 240 (M^+ − 136, 2). Exact Mass (HRMS) calcd. for $C_{18}H_{20}N_2O_7$: 376.1268; found: 376.1256.

p-*Nitrobenzyl[3-hydroxy-7-1-(1-hydroxyethyl)-7-methoxy]-1-carba-1-dethia-3-cephemcarboxylate (**13**)*

Compound **11** (610 mg, 1.55 mmol) when subjected to the diazo transfer reaction yielded 520 mg (80%) of a yellowish semisolid

[11]See refs. 9 and 14.

Can. J. Chem. Downloaded from www.nrcresearchpress.com by 109.225.110.28 on 09/08/12
For personal use only.

(ir: 2120 cm^{-1}) after usual work-up and column chromatography (1:2, acetone:hexanes).

The rhodium carbenoid insertion reaction of the diazo compound (400 mg, 0.950 mmol) and purification by column chromatography (2:3, acetone:hexanes) gave 370 mg (40%) of **13** as a yellowish oil; ir (film): 1710–1780 (broad peak centered at 1750 C=O), 1520 and 1350 (NO_2) cm^{-1}; ^1H nmr δ: 1.26 (3H, d, J = 6.5 Hz, CH_3CH_2), 1.97–2.14 (2H, m, CH_2CO), 2.48–2.60 (2H, m, CH_2CH_2CO), 3.64 (4H, 2s due to OCH_3 overlapping with CHN), 3.83 (1H, s, COCHCOO), 4.38 (1H, q, J = 6.7 Hz, CHO), 5.24 (1H, d, J = 13.7 Hz, CH_AH_BPNB), 5.45 (1H, d, J = 13.4 Hz, CH_BH_APNB), 7.63 (2H, d, J = 8.3 Hz, PNB), 8.20 (2H, d, J = 9.8 Hz, PNB); nmr looks like a mixture of ketoenol tautomers based on the complexity of the spectrum and two methoxy peaks; ms (ei): 391 ($M^+ - 1$, 0.4), 277 ($M^+ - 115$, 100), 271 ($M^+ - 121$, 15), 256 ($M^+ - 136$, 2), 211 ($M^+ - 180$, 11).

p-*Nitrobenzyl(7-ethyl-7-methoxy)-3*-N-*acetylethanethio-1-carba-1-dethia-3-cephemcarboxylate* (***14***)

Compound **12** (0.20 g, 0.53 mmol) in 5 mL of dry MeCN was cooled to 0°C under N_2. Addition of DIPEA (0.12 mL, 0.69 mmol) gave a yellow-colored solution that disappeared when the reaction mixture was stirred for 1 h after addition of diphenylchlorophosphate (0.13 mL, 0.63 mmol). A solution of *N*-acetylaminoethanethiol (0.12 g, 1.01 mmol) in 2 mL of dry MeCN and DIPEA (0.12 mL, 0.69 mmol) was added and the reaction mixture was stirred for 1 h. After usual work-up using EtOAc as solvent, the column chromatography of the crude product was carried out using a gradient of solvents. EtOAc:hexanes (1:2) gave starting compound **12**; EtOAc:hexanes (3:1) gave *N*-acetylaminoethanethiol; and hexanes:EtOAc:MeCN (20:40:40) gave 0.20 g (81%) of the desired product **14** as a yellowish oil; ir ($CHCl_3$): 3329 (br, NH), 1755 (β-lactam C=O), 1713 (COOR), 1660 (CONH), 1530 and 1361 (NO_2) cm^{-1}; ^1H nmr δ: 0.98 (3H, t, J = 7.4 Hz, CH_3CH_2), 1.75–2.10 (7H, m with overlapping s at 1.90 due to CH_3CO, CH_2, CH_2CH_3), 2.43–2.76 (2H, m, CH_2), 2.79 (2H, t, J = 5.8 Hz, CH_2S), 3.25–3.46 (6H, m, with overlapping s at 3.35 due to OCH_3, CH_2N, CHN), 5.20 (1H, d, J = 13.6 Hz, CH_AH_BPNB), 5.30 (1H, d, J = 13.7 Hz, CH_BH_APNB), 6.76 (1H), br t, NH), 7.52 (2H, d, J = 8.9 Hz, PNB), 8.09 (2H, d, J = 8.9 Hz, PNB); ^{13}C nmr δ: 7.3 (CH_3), 21.3 (CH_2), 22.7 (CH_3), 22.8 (CH_2), 26.6 (CH_2), 30.1 (CH_2), 38.9 (CH_2), 52.7 (CH_3O), 56.7 (CH), 65.7 (CH_2PNB), 90.7 (C-7), 122.6 (C=C), 123.6 (CH of PNB), 128.4 (CH of PNB), 133.2 (C=C), 142.9 (C of PNB), 147.6 (C of PNB), 162.1 (C=O), 166.3 (C=O), 170.7 (C=O); ms : no M^+ ion in ei or ci, 356 ($M^+ - 121$, 1), 328 ($356-28^+$, 4).

p-*Nitrobenzyl(7-hydroxyethyl-7-methoxy-3*-N-*acetylethanethio)-1-carba-1-dethia-3-cephemcarboxylate* (***15***)

Purification solvent mixture (20:20:80 EtOAc:hexanes:MeCN); a yellow oil (68%); ir (film): 3400 (br, OH), 1700–1770 (broad, C=O), 1520 and 1350 (NO_2) cm^{-1}; ^1H nmr δ: 1.26 (3H, d, J = 6.4 Hz, CH_3CH_2), 1.80–2.60 (4H, m, CH_2CH_2), 2.88–2.94 (2H, m, CH_2N), 3.34–3.59 (2H, m, CH_2S), 3.60 (3H, s, CH_3O), 3.63–3.68 (1H, m, CHN), 4.38 (1H, q, J = 6.5 Hz, CHO), 5.16 (2H, s, CH_2PNB), 5.27 (1H, d, J = 13.5 Hz, CH_AH_BPNB), 5.39 (1H, d, J = 13.4 Hz, CH_BH_APNB), 5.59 (1H, br, NH), 7.48 (2H, d, J = 8.8 Hz, PNB), 7.58 (2H, d, J = 9.0 Hz, PNB), 8.19 (4H, d, J = 8.8 Hz, PNB); ms (ei): highest peak is 238 (MW = 630).

Sodium (7-ethyl-7-methoxy)-3-N-*acetylethanethio-1-carba-1-dethia-3-cephemcarboxylate* (***1***)

The PNB ester **14** (0.20 g, 0.42 mmol) in 20 mL of THF:H_2O (1:1) was hydrogenated in the presence of 0.12 g of Pd–C (10%) at 40 psi and 25°C for 7 h. After removal of the catalyst and THF, the suspension was treated with 36 mg of $NaHCO_3$. The resulting mixture was washed with EtOAc and the aqueous layer was lyophilized to give 0.14 g of crude product. Reverse phase column chromatography (10% MeCN in H_2O) yielded 0.13 g (77%) of **1** as a white solid; mp: becomes translucent at 177–178°C and chars at or above 217°C; ir (KBr): 3396 (br, NH), 1742 (β-lactam C=O), 1661 (CONH), 1610 (COO^-) cm^{-1}; ^1H nmr (D_2O) δ: 0.99 (3H, t, J = 7.4 Hz, CH_3CH_2), 1.79–1.91 (1H, m, CH_2CH_3), 1.98 (3H, s, CH_3CO), 2.00–2.17 (3H, m, CH_2CH_3, CH_2), 2.42–2.54 (2H, m, CH_2), 2.80–2.86 (2H, m, CH_2S), 3.31–3.42 (2H, m, CH_2N), 3.44 (3H, s, OCH_3), 3.68 (1H, dd, J = 11.7, 3.4 Hz, CHN); ^{13}C nmr (D_2O) δ: 9.6 (CH_3), 24.1 (CH_2), 24.6 (CH_3), 25.4 (CH_2), 28.8 (CH_2), 32.5 (CH_2), 42.1 (CH_2), 55.5 (CH_3O), 60.6 (CH), 94.2 (C-7), 120.4 (C=C), 134.7 (C=C), 169.7 (C=O), 172.8 (C=O), 177.2 (C=O); ms (ei) of free acid: 342 (M^+, 0.4), 341 ($M^+ - 1$, 2), 314 ($M^+ - 28$, 8), 270 ($M^+ - 72$, 5), 242 ($M^+ - 100$, 2). Exact Mass (HRMS) calcd. for $C_{15}H_{22}N_2O_5S$ (free acid); 342.1235; found: 342.1242.

Acknowledgements

The financial assistance of the Natural Sciences and Engineering Research Council of Canada (NSERC) is gratefully acknowledged. Thanks are due to Dr. Harold Mastalerz (Bristol–Myers Squibb) for arranging MIC determination experiments.

1. S. Shakya and T. Durst. Heterocycles, **34**, 67 (1992).
2. R. W. Ratcliffe and G. Albers-Schonberg. *In* Chemistry and biology of β-lactam Antibiotics. Vol. 2. Academic Press, New York. 1982. pp. 227–361.
3. (*a*) R. W. Ratcliffe, T. N. Salzmann, and B. G. Christensen. Tetrahedron Lett. **21**, 31 (1980); (*b*) T. Kametani. Heterocycles, **17**, 463 (1982); (*c*) T. Kametani and T. Nagahara. Heterocycles, **25**, 729, (1987); (*d*) J. Finkelstein, K. G. Holden, and C. D. Perchonock. Tetrahedron Lett. **19**, 1629, (1978); (*e*) R. N. Guthikonda, L. D. Cama, and B. G. Christensen. J. Am. Chem. Soc. **96**, 7584 (1974); (*f*) R. A. Firestone, J. L. Fahey, N. S. Maciejewiz, G. S. Patel, and B. G. Christensen. J. Med. Chem. **20**, 551 (1977); (*g*) J. A. S. Bremner, E. W. Colvin, G. Gallacher, and A. MacLeod. Tetrahedron Lett. **24**, 3783 (1983); (*h*) T. W. Doyle, T. T. Conway, M. Casey, and G. Lim. Can. J. Chem. **57**, 222 (1979); (*i*) T. W. Doyle, T. T. Conway, G. Lim, and B. Luh. Can. J. Chem. **57**, 227 (1979); (*j*) T. W. Doyle, A. Martel, and B. Luh. Can. J. Chem. **57**, 614 (1979); (*k*) T. W. Doyle, A. Martel, J. L. Douglas, B. Belleau, T. T. Conway, C. F. Ferrari, D. E. Harning, G. Lim, M. Menard, L. R. Morris, and B. Luh. Can. J. Chem. **58**, 2508 (1980); (*l*) M. Hatanaka and T. Ichimaru. Tetrahedron Lett. **24**, 4837 (1983); (*m*) H. Saito, H. Matsushima, C. Shiraki, and T. Hirata. Chem. Pharm. Bull. **37**, 275 (1989); (*n*) T. Ogasa, H. Saito, Y. Hashimoto, K. Saito, and T. Hirata. Chem. Pharm. Bull. **37**, 315 (1989); (*o*) H. Saito, F. Suzuki, and T. Hirata. Chem. Pharm. Bull. **37** 2298, (1989); (*p*) I. Matsukuma, S. Yoshiiye, K. Mochida, Y. Hashimoto, K. Sato, R. Okachi, and T. Hirata. Chem. Pharm. Bull. **37**, 1239 (1989); (*q*) B. G. Jackson, J. P. Gardner, and P. C. Heath. Tetrahedron Lett. **31**, 6317 (1990); (*r*) S. Uyeo and H. Ono. Chem. Pharm. Bull. **28**, 1563 (1980); (*s*) D. A. Evans and E. B. Sjorgen. Tetrahedron Lett. **27**, 3787 (1985); (*t*) C. Bodurow and M. A. Carr. Tetrahedron Lett. **30**, 4081 (1989); (*u*) C. C. Bodurow, B. D. Boyer, J. Brennan, C. A. Bunnell, J. E. Burks, M. A. Carr, C. W. Doeke, T. M. Eckrich, J. W. Fisher, J. P. Gardner, B. J. Graves, P. Hines, R. C. Hoying, B. G. Jackson, M. D. Kinnick, C. D. Kochert, J. S. Lewis, W. D. Luke, L. L. Moore, J. M. Morin, R. L. Nist, D. E. Prather, D. L. Sparks, and W. C. Vladuchick. Tetrahedron Lett. **30**, 2321 (1989).
4. (*a*) T. Yoshioka, A. Watanabe, K. Isshiki, and Y. Fukagawa. Tetrahedron Lett. **26**, 4335 (1986); (*b*) A. Watanabe, Y. Fukagawa, T. Ishikura, and T. Yoshioka. Bull. Chem. Soc. Jpn. **60**, 2091 (1987); (*c*) P. M. W. Foxton, R. C. Mearman, C. E. Newall, and P. Ward. Tetrahedron Lett. **22**, 2497 (1981); (*d*) D. T. W. Chu, J. E. Hengeveld, and D. Lester. Tetrahedron Lett. **24**, 139 (1983).

5. (*a*) K. G. Taylor. Tetrahedron, **38**, 2751 (1982); (*b*) S. D. Burke and P. A. Grieco. *In* Organic reactions. Vol. 26. John Wiley and Sons, New York. 1979. p. 361; (*c*) M. P. Doyle. Acc. Chem. Res. **19**, 348 (1986); (*d*) E. Wenkert, M. E. Alonso, B. L. Buckwaler, and E. L. Sanchez. J. Am. Chem. Soc. **105**, 2021 (1983); (*e*) A. Padwa, R. L. Chinn, S. F. Hornbuckle, and L. Zhi. Tetrahedron Lett. **30**, 301 (1989); (*f*) M. G. Martin and B. Ganem. Tetrahedron Lett. **25**, 251 (1984); (*g*) P. H. Crackett, P. Sayer, R. J. Stoodley, and C. W. Greengrass. J. Chem. Soc. Perkin Trans. 1, 1235 (1991).
6. T. N. Salzmann, F. P. Dininno, M. L. Greenlee, R. N. Guthikonda, M. L. Quesada, S. M. Schmitt, J. J. Herrmann, and M. F. Woods. *In* Recent advances in the chemistry of β-lactam antibiotics. *Edited by* A. G. Brown and S. M. Roberts. The Royal Society of Chemistry, London. 1985. p. 171.
7. (*a*) T. A. Crowell, B. D. Halliday, J. H. McDonald III, J. M. Indelicato, C. E. Pasini, and E. C. Y. Wu. J. Med. Chem. **32**, 2436 (1989); (*b*) G. K. Cook, J. H. McDonald III, W. Alborn Jr., D. B. Boyd, J. A. Eudaly, J. M. Indelicato, R. Johnson, J. S. Kasher, C. E. Pasini, D. A. Preston, and E. C. Y. Wu. J. Med. Chem. **32**, 2442 (1989); (*c*) J. A. Eudaly, W. J. Hornback, R. L. Johnson, C. L. Jordan, J. E. Munroe, W. E. Wright, and C. Y. E. Wu. *In* Recent advances in the chemistry of β-lactam antibiotics. *Edited by* P. H. Bentley and R. Southgate. The Royal Society of Chemistry, London. 1989. p. 333.
8. (*a*) J. C. Sheehan and Y. S. Lo. J. Am. Chem. Soc. **94**, 8253 (1972); (*b*) J. C. Sheehan. *In* Recent advances in the chemistry of β-lactam antibiotics. *Edited by* J. Elks. The Chemical Society, London. 1977. pp. 20–24.
9. T. N. Salzmann, R. W. Ratcliffe, and B. G. Christensen. Tetrahedron Lett. **21**, 1193 (1980).
10. (*a*) M. Murakami, T. Aoki, and W. Nagata. Heterocycles, **30**, 567 (1990); (*b*) S. Nishimura, H. Sasako, N. Yasuda, Y. Matsumoto, T. Kamimura, K. Sakane, and J. Takaya. J. Antibiot. **42**, 1124 (1989).
11. T. Durst, M. K. Sharma, E. J. Gabe, and F. L. Lee. J. Org. Chem. **55**, 5525 (1990).
12. D. R. Kronenthal, C. Y. Han, and M. K. Taylor. J. Org. Chem. **47**, 2765 (1982).
13. E. J. Corey, H. Cho, C. Rucker, and D. H. Hua. Tetrahedron Lett. **22**, 3455 (1981).
14. S. Masamune, D. W. Brooks, and L. D. L. Lu. Angew. Chem. Int. Ed. Engl. **18**, 72 (1978).
15. J. B. Hendrickson and W. A. Wolf. J. Org. Chem. **33**, 3610 (1968).
16. Y. Nagao, T. Abe, H. Shimizu, T. Kumagai, and Y. Inoue. J. Chem. Soc. Chem. Commun. 821 (1989).
17. (*a*) L. D. Cama, R. A. Firestone, and B. G. Christensen. Abstr. 10th Middle Atlantic regional meeting of ACS, Philadelphia, Pa. Feb. 23–26, 1976. Abstr. J-16; (*b*) L. D. Cama and B. G. Christensen. Tetrahedron Lett. **19**, 4233 (1978).
18. (*a*) S. Yamamoto, H. Itani, H. Takahashi, T. Tsuji, and W. Nagata. Tetrahedron Lett. *25*, 4545 (1984); (*b*) D. Habich and W. Hartwig. Tetrahedron, **40**, 3667 (1984).
19. K. Yamamoto, M. Nishio, and Y. Kato. Tetrahedron Lett. **23**, 5339 (1982).

Can. J. Chem. Downloaded from www.nrcresearchpress.com by 109.225.110.28 on 09/08/12
For personal use only.

Ascorbate: antioxidant activity determined in a hydrocarbon phase using quaternary ammonium salts as phase-transfer agents

L. Ross C. Barclay[1] and Kelly A. Dakin
Department of Chemistry, Mount Allison University, Sackville, N.B., Canada E0A 3C0

and

Hayder A. Zahalka
Polysar, Research and Development Department, Sarnia, Ont., Canada N7T 7M2

Received November 22, 1991

L. Ross C. Barclay, Kelly A. Dakin, and Hayder A. Zahalka. Can. J. Chem. **70**, 2148 (1992).

By shaking sodium ascorbate with tetra-*n*-butyl ammonium bromide in a two-phase system consisting of water and organic phases, such as 1,1,2,2-tetrachloroethane (TCE) or chlorobenzene, sufficient concentrations of the quaternary ammonium-ascorbate (quat-ascorbate) are transferred into the organic phase to be useful for antioxidant studies in nonpolar solvents. The antioxidant activity of the quat-ascorbate was determined by measurement of the (inhibition) rate constant, k_{inh}, for the inhibition of autoxidation of styrene initiated thermally by azobisisobutyrylnitrile (AIBN) at 30°C. The k_{inh} of ascorbate in styrene, found to be $(9.63 \pm 2.0) \times 10^4$ M^{-1} s^{-1}, is very much lower than that found for ascorbyl-6-palmitate, $k_{inh} = (110 \pm 11) \times 10^4$ M^{-1} s^{-1} under these conditions. The differences are discussed in terms of the relative effectiveness of hydrogen-atom transfer from the enolic hydroxyl at position 2 of the ascorbate ion compared with the more facile such transfer from position 3 of ascorbyl 6-palmitate in a nonpolar medium.

L. Ross C. Barclay, Kelly A. Dakin et Hayder A. Zahalka. Can. J. Chem. **70**, 2148 (1992).

Lorsqu'on agite de l'ascorbate de sodium avec du bromure de tetra-*n*-butyl-ammonium dans un système à deux phases formé des phases aqueuses et organiques comme le 1,1,2,2-tétrachloroéthane (TCE) ou le chlorobenzène, les concentrations du complexe d'ascorbate qui sont transférées vers la phase organique sont utiles pour des études d'anti-oxydant dans des solvants non-polaires. On a détermiré l'activité anti-oxydante d'ascorbate ainsi transféré en mesurant la constante de vitesse de l'inhibition, k_{inh}, de l'auto-oxydation du styrène initiée thermiquement par l'azobisisobutyronitrile (AIBN), à 30°C. La constante d'inhibition de l'ascorbate dans le styrène, $k_{inh} = (9{,}63 \pm 2{,}0) \times 10^4$ M^{-1} s^{-1}, est beaucoup plus faible que celle observée avec le palmitate du 6-ascorbyle pour lequel $k_{inh} = (110 \pm 11) \times 10^4$ M^{-1} s^{-1} dans les mêmes conditions. On discute des différences en fonction des efficacités relatives du transfert de l'atome d'hydrogène porté par l'hydroxyle énolique en position 2 de l'ion ascorbate par rapport à celui porté en position 3 du palmitate du 6-ascorbyle dans un milieu non-polaire.

[Traduit par la rédaction]

Introduction

The antioxidant property of ascorbic acid is widely recognized and several detailed reviews have appeared on this subject (1–5). The antioxidant action of ascorbate as well as the cooperative or synergistic antioxidant action between ascorbate and vitamin E has been reported in a wide variety of media including homogeneous solution (6, 7), in micelles (8), phospholipid bilayers (9–12), low density lipoproteins (13), and blood platelets (14), but there is recent evidence that vitamin C does not "spare" vitamin E "in vivo" (15, 16).

Several anomalies are reported for the antioxidant or prooxidant behaviour of ascorbic acid and derivatives and results obtained frequently depend on the phase selected for the study. Ascorbate alone is not an effective antioxidant when autoxidation is initiated in the lipid phase of bilayers, whereas it is an active antioxidant against peroxyls in the aqueous phase (11, 12); and it is reported to be the outstanding antioxidant in human blood plasma (17). Pryor *et al.* (18) found that, in a SDS micellar system, lipid-soluble (micellar) 6-ascorbyl palmitate has 65 times the activity of water-soluble ascorbate. However, ascorbic acid has about the same reactivity as 6-steryl ascorbate with a vitamin E radical in solution, whereas the ascorbic ester substituted at the 2 and 6 positions was only 0.01 times as reactive as ascorbic acid (19). Derivatives having an ester group at position 2 were reported by Niki and co-workers (20) to not act as antioxidants in homogeneous solution, suggesting that the enolic 2-OH is the hydrogen donor in inhibition reactions. However, others report that the 2-O-alkylascorbic acids (21) or 3-O-alkylascorbic acids (22) exhibit potent inhibition of lipid peroxidation in rat brain homogenates, indicating that both enolic OH groups can act as H-atom donors. Studies of the antioxidant properties of ascorbate are further complicated by its ease of oxidation (23–25) and its reported behaviour as a *prooxidant* under certain conditions, such as in aqueous solution containing heavy metal ions (26–28).

Considering the significance of vitamin C in biological systems and its potential for application as an inhibitor in other systems, such as inhibition of coloration of wood pulps,[2] it is very surprising that its *intrinsic antioxidant activity against peroxyl radicals is not yet known*. To address this problem properly, several basic requirements need be met:

1. It is necessary to generate peroxyl radicals in an appropriate system at a constant and known rate, the rate of chain initiation (R_i), and where the rate constant of chain propagation, k_p, is reliably known.
2. The antioxidant activity of the ascorbate ion, AH^-, should be determined in a nonpolar medium where polar solvation effects, known to strongly affect antioxidant activities (29), are absent.
3. The antioxidant activity of ascorbate, AH^-, should be

[1]Author to whom correspondence may be addressed.

[2]J. A. Schmidt and C. Heitner. Private communication, Pulp and Paper Research Institute of Canada, Pointe Claire, Quebec.

Can. J. Chem. Downloaded from www.nrcresearchpress.com by 109.225.110.28 on 09/08/12
For personal use only.

compared with an unionized derivative, such as a solvent-soluble derivative.

To meet requirement 1, we selected the inhibited autoxidation of styrene method (30) where the R_i can be controlled and measured and the k_p is known. The suppressed oxygen uptake with antioxidant present is given by eq. [1]:

$$[1] \quad -d[O_2]/dt = k_p/k_{inh}[RH] \times R_i/n[Inh]$$

where n, the stoichiometric factor, is the number of peroxyl radicals trapped per molecule of inhibitor, Inh, and can be determined when the R_i is known from measurement of the inhibition period, τ, using eq. [2]:

$$[2] \quad R_i = n \times [Inh]/\tau$$

Condition 2 is met by using a quaternary ammonium salt (Q^+X^-) to form the ion-pair quaternary ammonium ascorbate (AH^-Q^+) under solid–liquid phase transfer conditions (31) and transferring this into an organic solvent where the concentration of the salt is measured. The third condition is met by employing the organic solvent-soluble ester 6-ascorbyl palmitate as antioxidant. In addition, antioxidant activities of the ascorbate salt, AH^-, and the ester are compared with that of 2,2,5,7,8-pentamethyl-6-hydroxychroman (PMHC), which has a known activity, k_{inh}, under these conditions (30).

Results

Formation of quaternary ammonium ascorbate (AH^-Q^+)

Equilibration of sodium ascorbate with tetra-*n*-butyl ammonium bromide between water and a larger volume of organic solvent (chlorobenzene or 1,1,2,2-tetrachloroethane) (TCE) by stirring or shaking the mixture under argon gave organic solutions containing ascorbate concentrations suitable for inhibition studies. The procedure using a shaken sealed ampoule yielded more reproducible results and is the preferred method. With the TCE solvent, transferred-ascorbate concentrations were determined spectrophotometrically by reference to a calibration curve using sodium ascorbate in water: methanol (20:80) where ϵ(ascorbate) at 268 nm = 12 090 M^{-1} cm^{-1}. Under the conditions used, shaking in TCE in a sealed ampoule under argon at 30°C, the equilibration time to reach a constant ascorbate concentration (4.0×10^{-4} M) was approximately 2 h. Aliquots of this ascorbate concentration were used for studies of antioxidant activities.

Inhibition rate constants for ascorbate and ascorbyl palmitate compared with PMHC

The AIBN-initiated autoxidation of styrene has certain known advantages as a system to measure antioxidant activities and the inhibition rate constants for a variety of phenolic inhibitors are known in this medium (30). Typical experimental traces for the antioxidant action of phase-transferred ascorbate (AH^-Q^+) ascorbyl palmitate, and PMHC for the inhibited autoxidation of styrene are illustrated in Fig. 1. Experimental traces for AH^-Q^+ induction periods typically gave indistinct breaks and a slow return to the uninhibited rate (e.g., Fig. 1(IB)), a feature observed before with inefficient inhibitors (29).

Inhibition rate constants (k_{inh}) were obtained from measurements of oxygen uptake during the inhibition periods by using the integration expression, eq. [3], for the kinetics during inhibition as explained previously (18, 29, 30):

$$[3] \quad \Delta[O_2]_t = -k_p/k_{inh} \times [RH]\ln(1 - t/\tau)$$

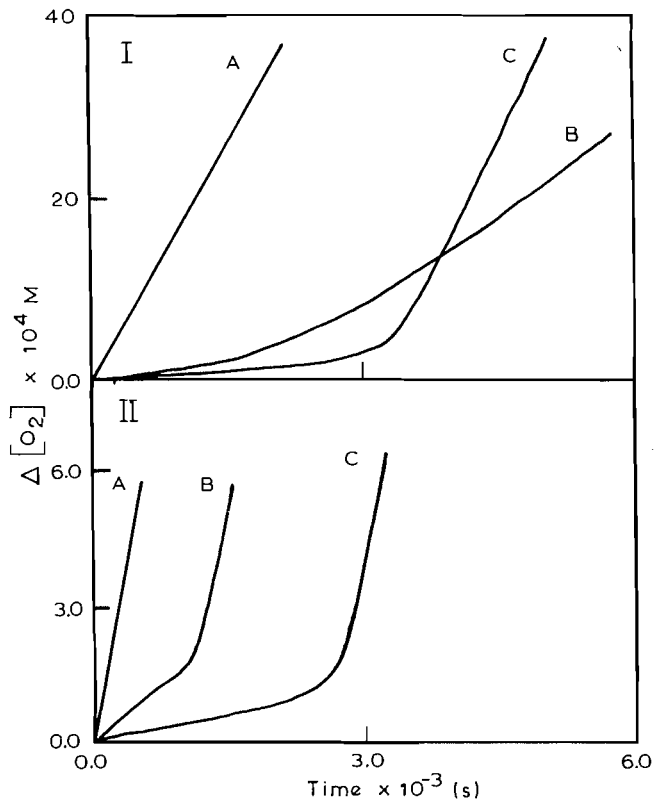

FIG. 1. Antioxidant action on peroxidation of styrene (2.00 mL) thermally initiated by AIBN at 30°C. (I) AIBN, 3.69×10^{-5} mol; (A) uninhibited reaction; (B) inhibited by ascorbate (AH^-Q^+), 3.23×10^{-8} mol; (C) inhibited by PMHC, 9.17×10^{-9} mol; $R_i = 2.62 \times 10^{-9}$ M s^{-1}. (II) AIBN, 3.66×10^{-5} mol; (A) uninhibited reaction; (B) inhibited by ascorbyl 6-palmitate, 1.01×10^{-8} mol; (C) inhibited by PMHC, 7.67×10^{-9} mol; $R_i = 2.74 \times 10^{-9}$ M s^{-1}.

where τ is the total inhibition period, and the oxygen uptake, $[O_2]_t$, is measured at various times, t, during the inhibition period. The rate of chain initiation (R_i) in each experiment was measured by injecting measured amounts of PMHC, known to be an efficient antioxidant which traps two peroxyl radicals per molecule, e.g., its stoichiometric factor, $n = 2$ (30). The k_{inh} for PMHC under these conditions was calculated for each run from the slopes of the plots of $\Delta[O_2]$ versus $-\ln(1 - t/\tau)$ and using the known k_p for styrene autoxidation, 41 M^{-1} s^{-1} (30). These plots were linear for PMHC inhibition at least 70% through the induction period (Fig. 2). The results are summarized in Table 1. The average k_{inh}, 354 ± 31 M^{-1} s^{-1}, agrees with the literature value (30) within experimental error.

The results for determination of k_{inh} for the ascorbate ion and ascorbyl 6-palmitate are summarized in Table 2. Linear plots were obtained for $\Delta[O_2]$ versus $-\ln(1 - t/\tau)$ through about 50% of the inhibition period (Fig. 2) but were nonlinear near the end of the induction period for ascorbate as the chain lengths increased. Concentrations of quat-ascorbate in chlorobenzene were not measured. Calculations of antioxidant activities by the slope method (eq. [3]) do not require the concentration of inhibitor nor the stoichiometric factor n. This factor has been reported to be less than integral values for ascorbate and derivatives due to the loss of inhibitor in other "wasting" reactions. For example, n is reported as 1.5 for ascorbyl palmitate in SDS micelles (18) and it is

Can. J. Chem. Downloaded from www.nrcresearchpress.com by 109.225.110.28 on 09/08/12
For personal use only.

Can. J. Chem. Downloaded from www.nrcresearchpress.com by 109.225.110.28 on 09/08/12
For personal use only.

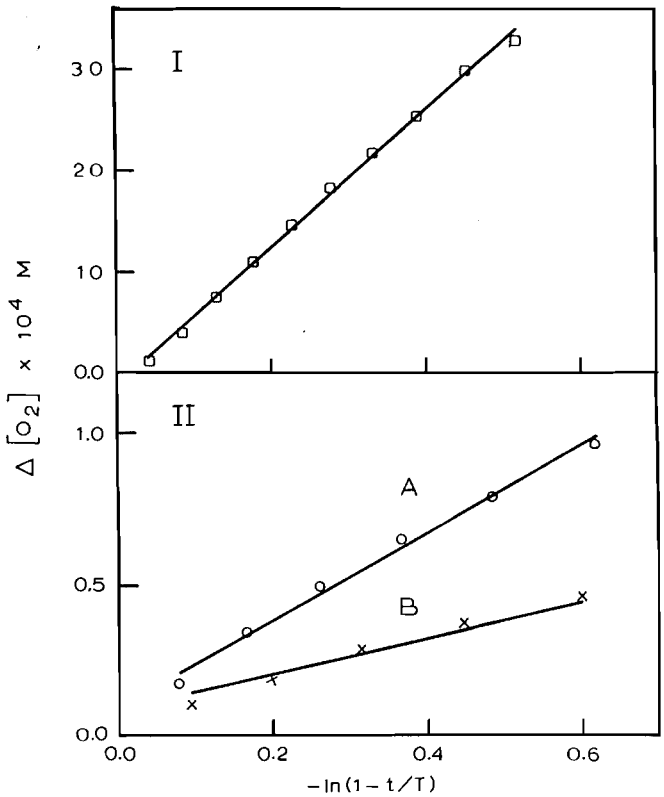

FIG. 2. Plots of oxygen uptake during inhibition periods versus $-\ln(1 - t/\tau)$ during autoxidation of styrene (2.00 mL) thermally initiated by AIBN (3.65×10^{-5} mol) at 30°C. (I) Inhibited by AH^-Q^+, 8.54×10^{-9} mol. (II) (A) Inhibited by ascorbyl 6-palmitate, 1.01×10^{-8} mol; (B) inhibited by PMHC, 7.71×10^{-9} mol.

known to be concentration dependent for vitamin C in aqueous solutions, varying from 2 at low initial concentrations (1 μM) to a low value at high concentrations (1 mM), due to its ease of autoxidation (32). Under our conditions (C = 5 μM), we determined the stoichiometric factor for ascorbyl 6-palmitate to be 0.7 by measurements of the induction period, τ, for this inhibitor under conditions where the R_i was determined by PMHC (e.g., eq. [2].

A few experiments were carried out to determine if ascorbate, (AH^-Q^+), and ascorbyl palmitate could act cooperatively with PMHC, a phenomenon observed before with vitamins C and E (6–12). Combinations of PMHC with AH^-Q^+ extend the efficient inhibition periods of PMHC as illustrated in a typical example in Fig. 3. Similar results were obtained for combinations of PMHC and ascorbyl palmitate (not shown). The extension of the efficient PMHC by AH^-Q^+ is indicative of reductive regeneration of PMHC from its phenoxyl radical. The product of the extension of the induction period of PMHC in each case and the R_i is a measure of the stoichiometric factor, e.g., eq. [4],

$$[4] \quad n = R_i [\tau_{(PMHC + C)} - \tau_{PMHC}]/C$$

The values of n, *under these conditions*, are 0.96 for AH^-Q^+ and 0.81 for ascorbyl palmitate.

A variation in the stoichiometric factor for ascorbate can cause quite large errors in determination of k_{inh} because of the loss of antioxidant by reactions other than inhibition during the measurement, especially at high initial inhibitor concentration. Therefore, inhibition rate constants for the ascorbate ion-pair were determined for a range of initial concentrations (1.7–16 μM) and the results are given in Table 2. Reasonably consistent k_{inh}'s are calculated within any given run as illustrated for the detailed results given in Run No. 1, but variations occur by as much as a factor of 2 between runs, probably due to the loss of ascorbate by autoxidation. A range of k_{inh} for ascorbate ion-pair is taken as $(8–12) \times 10^4$ M^{-1} s^{-1} or an average of $(9.63 \pm 2.0) \times 10^4$ M^{-1} s^{-1}. The value for ascorbyl palmitate determined under these conditions is significantly higher, $(110 \pm 11) \times 10^4$ M^{-1} s^{-1}.

Discussion

In the aprotic hydrocarbon medium in our studies, ascorbyl 6-palmitate is expected to be present as the nonionic form **1**, whereas the ascorbate ion-pair is represented by **2**. Structure **1** has two enolic hydrogens at positions 2 and 3 that might act as hydrogen-atom donors to peroxyl radicals. However, only the radical at position 3 can be stabilized by delocalization over the entire conjugated 5-atom system as represented by **3**. On the other hand, the ascorbate in ion-pair **2** can only donate an enolic hydrogen atom from position 2, resulting initially in a less favoured cross-conjugated enolic radical. Structure **2** can be regarded as a model for the usual form of ascorbate under physiological conditions (pH 7)

TABLE 1. Antioxidant activity of PMHC for AIBN[a] thermally initiated peroxidation of styrene at 30°C

No.	Antioxidant PMHC (mol × 10^9)	R_i[b] (M s^{-1} × 10^9)	ν[c] range	k_{inh}[d] (M^{-1} s^{-1} × 10^{-4})
1	7.67	2.74	18–25	393
2	7.49	3.22	13–39	332
3	7.71	3.86	16–43	362
4	7.31	3.27	12–39	314
				350 ± 35

[a]2.00 mL styrene and 3.65×10^{-5} mol AIBN were used.

[b]The R_i, rate of chain initiation, as measured by the inhibition period method, eq. [2] of text, by PMHC.

[c]The chain length, ν, calculated at points along the inhibition period from the equation:
$\nu_t = ([O_2]_t - [O]t=0)/n[AH]_0 (1 - t/\tau) \ln(1 - t/\tau)$ (refs. 29, 30)

[d]Calculated from the slope of the plot of $\Delta[O_2]$ versus $-\ln(1 - t/\tau)$, eq. [3], using k_p = 41 M^{-1} s^{-1} (30).

TABLE 2. Determination of k_{inh} of ascorbate (AH^-Q^+) and ascorbyl palmitate (asc-pal) for AIBN thermally initiated peroxidation of styrene at 30°C[a]

No.	Antioxidant (mol × 10^9)	R_i[b] (M s^{-1} × 10^9)	t/τ	$-\ln(1 - t/\tau)$	$[O_2]$ (M × 10^4)	ν[c]	k_{inh} (M^{-1} s^{-1} × 10^{-4})
1	14.6 (AH^-)	2.50	0.121	0.129	4.73	570	9.77
			0.151	0.164	6.62	650	8.88
			0.182	0.201	8.51	710	8.43
			0.212	0.238	10.6	772	8.06
			0.242	0.277	12.7	830	7.80
			0.273	0.318	14.8	876	7.70
			0.303	0.361	16.8	918	7.66
			0.333	0.405	19.3	976	7.53
			0.363	0.452	21.6	1028	7.49
			0.394	0.500	23.9	1080	7.49
			0.424	0.552	26.1	1126	7.55
			0.454	0.606	28.5	1182	7.59
			0.484	0.663	31.0	1244	7.64
							k_{avg} = 7.97[d] ± 0.68
2	19.1 (AH^-)	3.64				312–1162	11.9 ± 2.5
3	3.41 (AH^-)	2.62				[c]	8.82 ± 0.44
4	3.76 (AH^-)	2.61				[c]	12.4 ± 1.5
5	5.29 (AH^-)	2.81				[c]	8.06 ± 0.57
6	32.6 (AH^-)	2.63				142–552	8.63 ± 1.4
7	10.1 (asc-pal)	2.98				46–58	117 ± 15
8	23.5 (asc-pal)	3.54				22–28	102 ± 12

[a]Each run used 2.00 mL styrene and AIBN ($3.35 \times 10^{-5} - 3.70 \times 10^{-5}$ mol).
[b]R_i obtained with PMHC injected immediately before injection of AH^-Q^+ or asc-pal.
[c]See Table 1, footnote [c]; approximating $n = 1$, for AH^- and asc-pal (see text). The ranges of ν were: No. 2, 300–1100; No. 6, 140–500 to 3000 for Nos. 3–5.
[d]k_{inh} calcd. by the slope method = 7.38×10^4 M^{-1} s^{-1}.

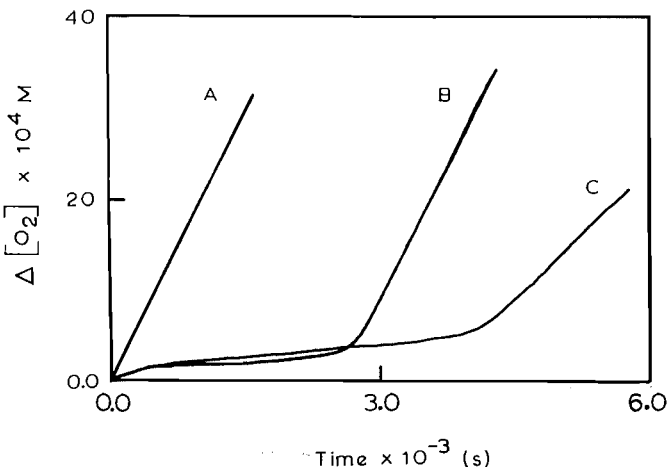

FIG. 3. Cooperative action of antioxidants on peroxidation of styrene thermally initiated by AIBN (3.69×10^{-5} mol) at 30°C. (A) Uninhibited reaction; (B) inhibited by PMHC, 5.99×10^{-9} mol; (C) inhibited by PMHC (5.99×10^{-9} mol) and AH^-Q^+ (2.29×10^{-8} mol).

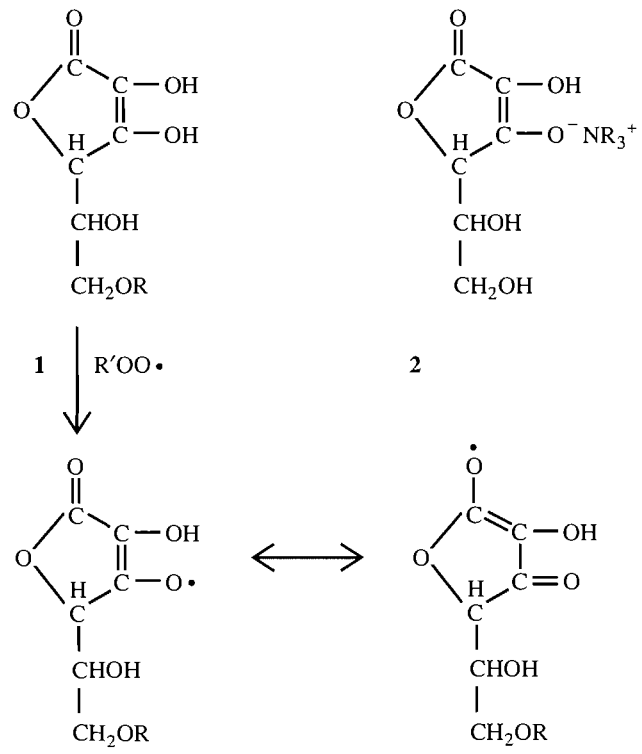

where it would be present in such an ionized form, since $pK_{a1} = 4.2$.

Some rate constants for the reaction of ascorbic acid and 6-ascorbyl palmitate with peroxyl radicals, reported by various researchers as illustrated in Table 3, indicate remarkable variations. There is no precedent for the determination of k_{inh} for ascorbic acid or ascorbate under the conditions we used. Various factors could account for such differences in rate constants including the reactivities of the peroxyls involved, the effect of the medium, since protic solvents are known to lower the k_{inh} values of phenolic antioxidants (29)

Can. J. Chem. Downloaded from www.nrcresearchpress.com by 109.225.110.28 on 09/08/12
For personal use only.

TABLE 3. Some absolute rate constants for the reaction of ascorbic acid with peroxyl radicals

No.	Radical[a]	Method[b]	Medium	k (M^{-1} s^{-1})	Reference
1	CH_3OO	pr	aq. alcohol (pH7)	2.2×10^6	34
2	$Cl_3COO\cdot$	pr	aq. alcohol (pH 7)	2.0×10^8	34
3	HOO·	pr	aq. (pH 0.3–1.0)	1.6×10^4	24
4	LinOO·	ia	TBA/CH_3OH	7.5×10^4	6
5	LinOO·	ia	SDS/micelles (pH 7)	3.2×10^3 asc	18
				2.10×10^5 asc-pal	18
6	Polystyryl OO·	ia	Styrene	9.6×10^4 AH^-Q^+	This work
6	Polystyryl OO·	ia	Styrene	1.10×10^6 asc-pal	This work

[a]LinOO· refers to the peroxyl radical formed during peroxidation of linoleate.
[b]pr, pulse radiolysis and ia, inhibition of autoxidation methods.

(and presumably of ascorbic acid), and the experimental method. We employed the method of inhibited autoxidation of styrene developed by Ingold and co-workers (30), because it is reproducible and their value for PMHC was obtained in the nonpolar medium of neat styrene. The reaction of HOO· with ascorbic acid would occur by hydrogen-atom donation (Table 3, No. 3) but hydrogen bonding in the aqueous medium is expected to lower the reactivity of the peroxyl radical (33) and reduce the H-atom donating ability of ascorbic acid. Similar solvation effects could account at least in part for lower rate constant values observed in alcohols (No. 4) and aqueous micelles (No. 5). We find the ratios of antioxidant activities of ascorbyl palmitate – ascorbate = 11.5 in styrene significantly different from that of 65.6 reported in SDS micelles (Table 3, Nos. 5 and 6). Solvation effects of the biphasic aqueous-micellar system probably results in differences in absolute and relative reactivities compared with homogenous solution in styrene.

The antioxidant activity of ascorbyl palmitate, **1**, (k_{inh} = 110×10^4 M^{-1} s^{-1}) compares favourably with that of phenolic antioxidants or even of the hydroxy chroman, Trolox (k_{inh} = 110×10^4 M^{-1} s^{-1}), where activities were determined under similar conditions (30). This relatively high activity is interpreted as arising by hydrogen-atom donation to peroxyl radicals from the enolic hydrogen at position 3 of **1**; that is, the k_{inh} is controlled by the stability of the resulting radical, **3**. On the other hand, the ion-pair, **2**, would donate a hydrogen from position 2 in the rate-controlling step resulting in a less stable radical. We realize that this is probably an oversimplification of the mechanism of antioxidant action of ascorbic acid and the ascorbate ion. Our results do not distinguish between other possibilities; for example, electron transfer from ascorbate, **2**, to peroxyls followed by hydrogen-ion transfer would be equivalent overall to hydrogen-atom abstraction from **2** by peroxyls. We also note that our interpretation does not account for the rather surprising finding that ascorbic acid with an ester group at the 2-position is reported not to act as an antioxidant in the oxidation of methyl linoleate in homogeneous solution (20). It is possible that a steric effect may be operating to inhibit the attack of linoleoyl peroxyl at the 3-position when position 2 is occupied by a fatty acid ester.

Our results do distinguish for the first time between the antioxidant action of ascorbic acid as its 6-ester, a remarkably effective antioxidant, and ascorbate ion, a relatively poor one, under *comparable conditions in an aprotic medium*. It is anticipated that these quantitative results will aid our understanding of the varying behaviour of ascorbic acid and ascorbate ion as antioxidants, including antioxidant activities under conditions in which it is either in the protic form or in the ionic form at pH ranges approaching physiological conditions.

Experimental

Chemicals and preparations

Common solvents used, methanol and water, were of HPLC quality. Chlorobenzene, Aldrich highest purity, was distilled from glass and 1,1,2,2-tetrachloroethane was obtained from Fisher Scientific. Styrene (Aldrich) was distilled under reduced pressure and passed through basic alumina to remove traces of peroxides just before use. The quaternary salt, tetrabutylammonium bromide (Aldrich) was dissolved in tetrachloroethane; 90–93 mM. Solutions of 2,2′-azobisisobutyronitrile (AIBN), Polysciences, Inc., were prepared in chlorobenzene and stored at −2°C. Solutions of the inhibitors ascorbyl 6-palmitate, ICN Nutritional Biochemicals, in chlorobenzene ((2.2–4.6) × 10^{-4} M) and 2,2,5,7,8-pentamethyl-6-hydroxychroman (PMHC), a gift from Dr. Graham Burton, National Research Council of Canada, Ottawa, in chlorobenzene ((3.6–4.6) × 10^{-4} M) were stored at −30°C in the dark. Sodium ascorbate (Aldrich) was used as received.

Procedures

Phase transfer and analysis of ascorbate

In a typical phase-transfer experiment, a mixture of solid sodium ascorbate (0.160 g), water (100 μL), tetrachloroethane (4 mL), followed by the addition of 4 mL of a solution of tetrabutylammonium bromide (93 mM) in tetrachloroethane, was either magnetically stirred under argon in a round-bottom flask or shaken in a sealed glass ampoule at 30°C. The latter gave the more consistent analytical results for ascorbate and was used in the inhibition experiments.

Measurement of the concentration of the quat-ascorbate, AH^-Q^+, in the organic phase required the determination of the λ_{max} and ϵ of ascorbate. For this purpose, a calibration plot was prepared for various known concentrations of sodium ascorbate in water:methanol (20:80) containing comparable amounts of tetrachloroethane. The ϵ for ascorbate under these conditions was 12 090 at 268 nm.

Determination of the quat-ascorbate concentration was carried out on the samples after centrifugation to remove possible traces of sodium ascorbate. Aliquots (100 μL) of the organic phase were diluted to 5.0 mL in water:methanol (20:80) and the absorbance measured at 268 nm with the same solvent containing tetrachloroethane as reference. These experiments were conducted after various mixing (or shaking) times to estimate the equilibrium concentration of quat-ascorbate in the organic phase.

Can. J. Chem. Downloaded from www.nrcresearchpress.com by 109.225.110.28 on 09/08/12
For personal use only.

Autoxidation and inhibition studies

Autoxidation was carried out on neat styrene (2.00 mL) at 30°C at an initial pressure of 760 Torr (1 Torr = 133.3 Pa) of oxygen using the calibrated dual-channel apparatus described previously (29). The rate of uninhibited oxygen uptake was measured. This was followed by determination of the rate of chain initiation (R_i) by injection of a known amount of PMHC and measurement of the resulting inhibition period. Then known amounts of quat-ascorbate ion-pair solutions, typically 20–30 μL of chlorobenzene or tetrachloroethane containing 4.0×10^{-4} AH^-Q^+, or ascorbyl palmitate, were injected and inhibition periods measured. Separate blank experiments were carried out by injections of similar amounts of these solvents mixed with water and tetra-*n*-butyl ammonium bromide (e.g., without ascorbate). There was no observed effect on the rate or induction period. Some measurements were also made with mixtures of PMHC and ascorbate or ascorbyl palmitate.

Acknowledgement

This research was carried out under the sponsorship of the Mechanical and Chemimechanical Wood-Pulps Network, part of Canada's Networks of Centres of Excellence. This support is gratefully acknowledged.

1. B. H. J. Bielski. Adv. Chem. Ser. **200** (1982). Chap. 4, pp. 81–99.
2. E. Niki. World Rev. Nutr. Diet. **64**, 1 (1991).
3. Y.-C. Liu, Z.-L. Liu, and Z.-X. Han. Rev. Chem. Intermed. **10**, 269 (1988).
4. A. Bendich, L. J. Machlin, O. Scandurra, G. W. Burton, and D. D. M. Wayner. Adv. Free Radical Biol. Med. **2**, 419 (1986).
5. P. B. McCay. Annu. Rev. Nutr. **5**, 323 (1985).
6. E. Niki, T. Saito, A. Kawakami, and Y. Kamiya. J. Biol. Chem. **259**, 4177 (1984).
7. C. Rousseau, C. Richard, and R. Martin. J. Chim. Phys. **81**, 137 (1984).
8. L. R. C. Barclay, S. J. Locke, and J. M. MacNeil. Can. J. Chem. **63**, 366 (1985).
9. H.-W. Leung, M. J. Vang, and R. D. Mavis. Biochim. Biophys. Acta, **664**, 266 (1981).
10. M. Scarpa, A. Rigo, M. Maiorino, F. Ursini, and C. Gregolin. Biochim. Biophys. Acta, **801**, 215 (1984).
11. T. Doba, G. W. Burton, and K. U. Ingold. Biochim. Biophys. Acta, **835**, 298 (1985).
12. E. Niki, A. Kawakami, Y. Yamamoto, and Y. Kamiya. Bull. Chem. Soc. Jpn. **58**, 1971 (1985).
13. K. Sato, E. Niki, and H. Shimasaki. Arch. Biochem. Biophys. **279**, 402 (1990).
14. G. T. Vatassery, W. E. Smith, and H. T. Quach. Lipids, **24**, 1043 (1989).
15. G. W. Burton, U. Wronska, L. Stone, D. O. Foster, and K. U. Ingold. Lipids, **25**, 199 (1990).
16. L.-H. Zeng, J. Wu, D. Carey, and T.-W. Wu. Biochem. Cell Biol. **69**, 198 (1991).
17. B. Frei, L. England, and B. N. Ames. Proc. Natl. Acad. Sci. **86**, 6377 (1989).
18. W. A. Pryor, M. J. Kaufman, and D. F. Church. J. Org. Chem. **50**, 281 (1985).
19. K. Mukai, K. Fukuda, K. Ishizu, and Y. Kitamura. Biochem. Biophys. Res. Commun. **146**, 134 (1987).
20. M. Takahashi, E. Niki, A. Kawakami, A. Kumasaka, Y. Yamamoto, Y. Kamiya, and K. Tanaka. Bull. Chem. Soc. Jpn. **59**, 3179 (1986).
21. K. Kato, S. Terao, N. Shimamoto, and H. Hirata. J. Med. Chem. **31**, 793 (1988).
22. Y. Nihro, H. Miyataka, T. Sudo, H. Matsumoto, and T. Satoh. J. Med. Chem. **34**, 2152 (1991).
23. D. T. Sawyer, G. Chiericato, and T. Tsuchiya. J. Am. Chem. Soc. **104**, 6273 (1982).
24. D. E. Cabell and B. H. J. Biekski. J. Phys. Chem. **87**, 1809 (1983).
25. D. B. Shin and M. S. Feather. J. Carbohydr. Chem. **9**, 461 (1990).
26. E. Niki, K. Yamamoto, and M. Takahashi. *In* The role of oxygen in chemistry and biochemistry: Studies in organic chemistry. Vol. **33**. *Edited by* W. Ando and Y. Moro-oka. Elsevier Publishers, Amsterdam. 1988. pp. 509–514.
27. A. W. Girotti, J. P. Thomas, and J. E. Jordan. Photochem. Photobiol. **41**, 267 (1985).
28. E. Shinar, T. Navok, and M. Chevion. J. Biol. Chem. **258**, 14778 (1983).
29. L. R. C. Barclay, K. A. Baskin, K. A. Dakin, S. J. Locke, and M. R. Vinqvist. Can. J. Chem. **68**, 2258 (1990).
30. G. W. Burton, T. Doba, E. J. Gabe, L. Hughes, F. L. Lee, L. Prasad, and K. U. Ingold. J. Am. Chem. Soc. **107**, 7053 (1985).
31. H. A. Zahalka and Y. Sasson. Can. J. Chem. **67**, 245 (1989).
32. D. D. M. Wayner, G. W. Burton, and K. U. Ingold. Biochim. Biophys. Acta, **884**, 119 (1986).
33. F. F. Rust and E. A. Youngman. J. Org. Chem. **27**, 3778 (1965).
34. J. E. Packer, R. L. Willson, D. Bahnemann, and K.-D. Asmus. J. Chem. Soc. Perkin Trans. 2, 296 (1980).

Can. J. Chem. Downloaded from www.nrcresearchpress.com by 109.225.110.28 on 09/08/12
For personal use only.

A study of computed rotational barriers of methyl groups and ^1H and ^{13}C spin-lattice relaxation rates in some steroids

LAWRENCE D. COLEBROOK[1] AND NING QING

Department of Chemistry and Biochemistry, Concordia University, 1455 de Maisonneuve Blvd. W., Montreal, Que., Canada H3G 1M8

Received November 5, 1990[2]

LAWRENCE D. COLEBROOK and NING QING. Can. J. Chem. **70**, 2154 (1992).

^1H and ^{13}C spin-lattice relaxation rates of the methyl groups of 15 steroids have been measured, and rotational barriers of the methyl groups have been calculated, using force field methods. Correlations between relaxation rates and computed rotational barriers have been investigated. ^1H and ^{13}C relaxation rates are consistent, and correlate with rotational barriers in simpler steroids. Steroids that are highly substituted with polar groups, and that must be investigated in polar solvents, tend to show poor correlations, an observation that is attributed to limitations in the computational model employed, which does not account for the effects of specific solvation or molecular association.

LAWRENCE D. COLEBROOK et NING QING. Can. J. Chem. **70**, 2154 (1992).

On a mesuré les vitesses de relaxation spin-réseau ^1H et ^{13}C des groupes méthyles de 15 stéroïdes et on a calculé les barrières rotationelles des groupes méthyles en utilisant des méthodes de champs de force. On a étudié les corrélations entre les vitesses de corrélation et les valeurs calculées pour les barrières à la rotation. Les constantes de relaxation ^1H et ^{13}C sont cohérentes et il existe une corrélation avec les barrières rotationnelles dans des stéroïdes plus simples. Les stéroïdes portant plusieurs groupements fortement polaires, qui doivent être étudiés dans des solvants polaires, ont tendance à présenter de mauvaises corrélations; cette observation est attribuée aux limitations dans la méthode de calcul utilisée qui ne tient pas compte des effets de solvatation spécifique ou d'associations moléculaires.

[Traduit par la rédaction]

In dilute solution (≤0.1 M in a deuteriated solvent) the spin-lattice relaxation of most ^1H and ^{13}C nuclei is dominated by the intramolecular dipole-dipole mechanism. For a molecule tumbling isotropically, the dipole-dipole contribution, $R_1(\mathrm{dd})$, to the overall relaxation rate is given by eq. [1] in terms of the relaxation contribution between two nonequivalent nuclei, i, j:

$$[1] \quad R_1(\mathrm{dd}) \propto \sum_i \frac{\gamma_i^2 \cdot \gamma_j^2}{r_{ij}^6} \cdot \tau_c(i, j)$$

where γ_i and γ_j are the magnetogyric ratios of the i and j nuclei, r_{ij} is their internuclear separation, and $\tau_c(i, j)$ is the motional correlation time of the vector between them. The net R_1 value for a nucleus is dependent on the overall tumbling rate of the molecule as a unit, plus the contribution from any additional motion of a substituent group that carries that particular nucleus. Because of the $1/r^6$ term in eq. [1], the influence of a relaxation pathway is attenuated very rapidly with increasing distance between nuclei, so that it is the near neighbours of a nucleus which dominate its relaxation.

A methyl proton relaxes largely to its neighbouring protons on the same carbon atom. The carbon atom of a methyl group is relaxed almost exclusively by the protons it carries. Differences between the ^1H relaxation rates of methyl groups in the same molecule arise, therefore, largely from differences in the correlation times for local rotational motion of the methyl groups, while differences between the ^{13}C relaxation rates of methyl groups in the same molecule arise almost exclusively from this origin (1). An *increase* in the rate of methyl group rotation *reduces* the efficiency of the dipole-dipole relaxation mechanism.

Relaxation in small molecules, which experience fast tumbling and fast methyl group rotation, may be complicated by contributions from the spin-rotation mechanism (2), which has an inverse dependence on the rotational rate of the methyl group (3). The effect of the spin-rotation contribution is to reduce the sensitivity of the overall relaxation rate, which is usually dominated by the dipole-dipole mechanism (1), to steric factors that influence the methyl group rotational rate.

The sensitivity of methyl group relaxation in steroids to steric factors was first systematically investigated by ApSimon *et al.* (4). They measured the ^{13}C relaxation times of the 18- and 19-methyl groups for a number of compounds, and proposed a model for methyl group rotation and relaxation based on the number and type of steric interactions experienced by each methyl group. It was assumed that the ground-state and transition-state conformations of these methyl groups in steroids approximate to those in ethane, the former being the usual staggered conformation and the latter the eclipsed. The model assumes that a decrease in steric hindrance from a neighbouring group will stabilize the ground state more than the transition state, thereby increasing the activation energy for rotation of the methyl group with respect to the rest of the molecule. The net effect of the resultant decrease in rotation rate will be an increase in the observed R_1 value. The relative rates of rotation of the 18- and 19-methyl groups of the *trans-anti-trans* androstane/cholestane system were rationalized in terms of the number of *syn*-clinal interactions with axial hydrogen atoms of rings A, B, and C, plus smaller interactions with hydrogen atoms of ring D. Provided that the transition states for rotation are closely similar, it follows from this analysis that the rate of rotation of the 18-methyl group of androstane should be lower, and hence its R_1 value should be greater than that of the 19-methyl group. In a later study, Colebrook and Hall (5) investigated ^1H spin-lattice relaxation in a similar group of steroids. The experimental data of both groups were consistent with this model. Introduction of a double bond at

[1]Author to whom correspondence may be addressed.

[2]Revision received January 14, 1992.

Can. J. Chem. Downloaded from www.nrcresearchpress.com by 109.225.110.28 on 09/08/12
For personal use only.

Can. J. Chem. Downloaded from www.nrcresearchpress.com by 109.225.110.28 on 09/08/12
For personal use only.

C-1(2), C-4(5), or C-5(6), with resultant reduction in the number of interactions involving the 19-methyl group, increases the relaxation rate of that group but leaves the 18-methyl group largely unaffected, in accord with the model.

A severe limitation of this qualitative model is the difficulty in predicting the magnitude of the steric interactions affecting a methyl group. The two studies quoted show that it can work well when the methyl group can adopt a staggered, ethane-like geometry, with easily visualized *syn*-clinal interactions, but the predictions become much more difficult when other interactions are involved (5). The net steric influence on the rotational barrier of a methyl group will be the sum of a number of interactions of varying magnitude, which may affect both the ground and the transition states for rotation. What is needed is a quantitative, nonsubjective method for estimating methyl group rotational barriers.

The increasing accessibility and simplicity of operation of molecular mechanics calculations make computation of the barriers to rotation of methyl groups feasible. This offers the possibility of using quantitative estimates of methyl group rotational barriers with experimentally determined R_1 values to interpret ^1H and ^{13}C relaxation rates. The calculations can readily be carried out using a suitably equipped personal computer or workstation. We have evaluated this procedure for a number of steroids containing two or more methyl groups.

A molecular dynamics study of methyl group rotation in some podocarpanes, using force field calculations and ^{13}C relaxation times, has been reported by Bernassau and co-workers (6). Agreement was found between methyl group rotational barriers computed from nmr relaxation measurements and from force field calculations.

Methyl group rotational barriers may be calculated using the "dihedral driver" option of the MM2 and MMP2 algorithms (7), following optimization of the molecular structure (8). In this procedure, the energy of the structure is minimized for each chosen dihedral angle of the group being rotated, so that the energy calculated for the transition state for rotation allows for conformational changes in the rest of the molecule to accommodate rotation. All rotational barriers reported here were calculated by the full dihedral driver procedure.

^1H methyl group relaxation is complicated by the presence of factors that can lead to bi-exponential decay in the relaxation recovery curve used to determine R_1 (9–11). However, by working with data in the initial slope region of the recovery curve (12), where the effects of dipolar cross-correlation have been shown to be negligible (9), the R_1 data can be accurately characterized by a single exponential.

Results and discussion

The steroids examined in this study were classified into four groups according to the effects of structural changes on the 18- and 19-methyl groups:

Series I: Compounds **1**–**5**. Double bonds were successively introduced into ring A, so that nonbonded interactions involving the 19-methyl group were affected, but the 18-methyl group remained essentially unaffected.

Series II: Compounds **6** and **7**. The configurations of substituents (H, CH_3) at C-16 were interchanged, with consequent changes in nonbonded interactions with the 18-methyl groups.

Series III: Compounds **8**–**11**. The configuration of a hydroxyl group at C-11 was inverted and it was replaced by an oxo group to study the influence on rotational barriers and relaxation rates of both the 18- and the 19-methyl groups.

Series IV: Compounds **12**–**14**. The configurations of hydroxyl groups and the oxidation state at C-11 were varied for another series of compounds with a different substitution pattern at C-17.

The influences of structural changes on the rotational barriers and relaxation rates of the 18- and 19-methyl groups were investigated using two types of comparisons. *Internal* comparison permitted direct study of ^1H and ^{13}C spin-lattice relaxation rates of the 18- and 19-methyl groups and their computed rotational barriers within a molecule as structural changes were introduced (Series I and II). Since the relaxation rates of the 18- and 19-methyl groups are being compared within a single molecule, both groups experience similar influences from overall molecular tumbling. Examination of the ^{13}C relaxation rates of the protonated ring carbon atoms of testosterone, **2**, showed no evidence for anisotropic motion of the ring backbone (13), and it is assumed that any effects of overall anisotropic motion on 18- and 19-methyl group relaxation are negligible in all of the compounds examined. *External* comparison was necessary when the effects of structural changes influence both the 18- and 19-methyl groups, requiring study of the relaxation rates and computed rotational barriers in different compounds (Series III and IV). Normalization of the relaxation rates to that of a nucleus remote from the site of structural change is essential when external comparisons are being made, since the effects of differing experimental conditions and molecular tumbling rates must be eliminated (1).

Chemical shift assignments

Reliable ^1H chemical shift assignments based on NOED measurements have been reported for progesterone acetate (14) and 1-dehydrotestosterone, **3** (15). The 18- and 19-methyl group chemical shifts in prednisolone, **9**, were also assigned using this technique. The remaining steroids in this study were assigned (Table 1) by comparing their chemical shifts with those of the models, or by correlation with previously assigned ^{13}C spectra.

Spin-lattice relaxation rates

Since Bernassau and co-workers (6) established that the dipole-dipole mechanism is the sole ^{13}C relaxation mechanism in their podocarpanes, which are similar in molecular weight and geometry to steroids, it was considered unlikely that spin-rotation would make a significant contribution to methyl group relaxation in the present group of compounds. This assumption was verified through ^{13}C-{^1H} heteronuclear NOED measurements on 11α-hydroxyprogesterone, **12**. No significant reduction in the intensities of the ^{13}C 18- and 19-methyl group signals that would be characteristic of a contribution from a nondipolar mechanism was seen (1). It is assumed that contributions to ^1H relaxation mechanisms will parallel those of the ^{13}C nucleus of the same methyl group.

^1H and ^{13}C 18- and 19-methyl group R_1 values are reported for 15 steroids (Tables 2–4). In Series I, androstanolone, **1**, testosterone, **2**, and dehydrotestosterone, **3**, double bonds are successively introduced into the A ring, the rest of the molecule remaining unchanged. Similarly, the pair of compounds, 5α-pregnane-3,20-dione, **4**, and progesterone, **5**, differ by the introduction of a Δ_4 double bond into the latter

Can. J. Chem. Downloaded from www.nrcresearchpress.com by 109.225.110.28 on 09/08/12
For personal use only.

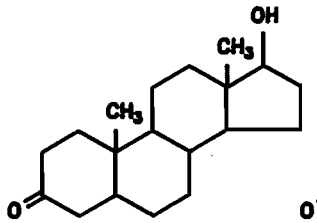

1

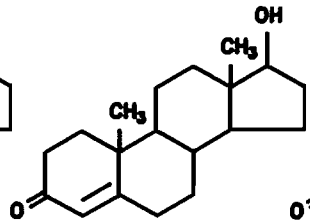

2

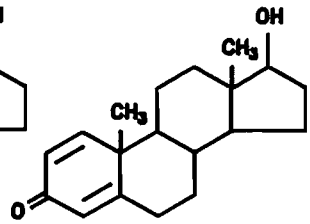

3

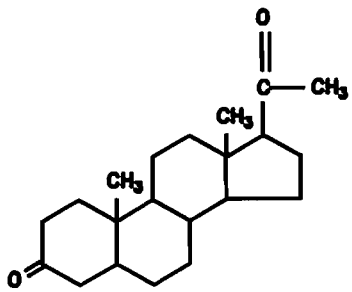

4

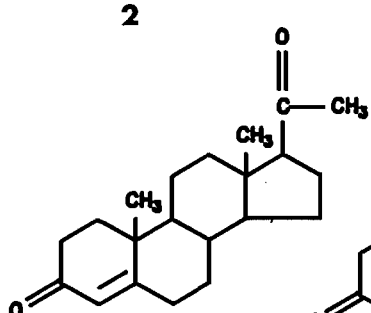

5

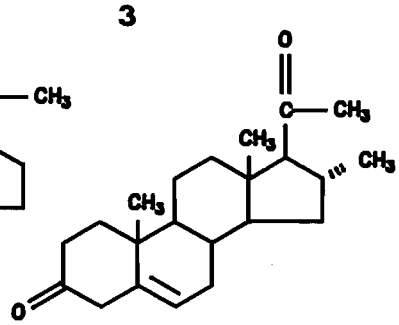

6

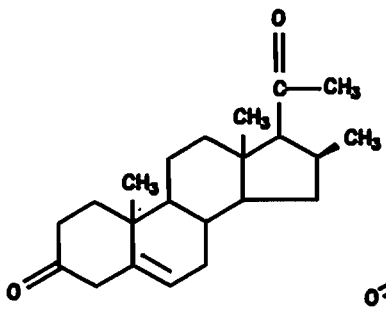

7

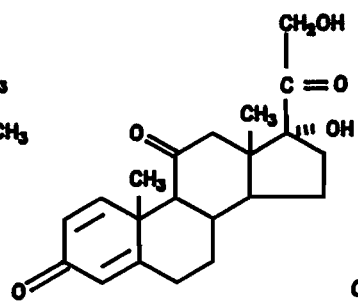

8

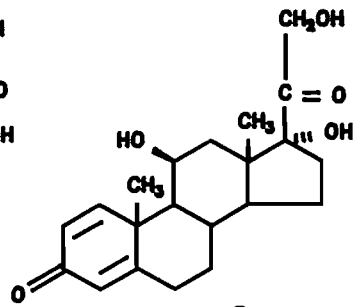

9

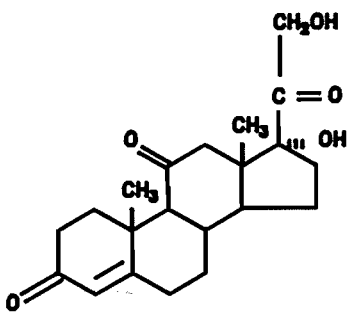

10

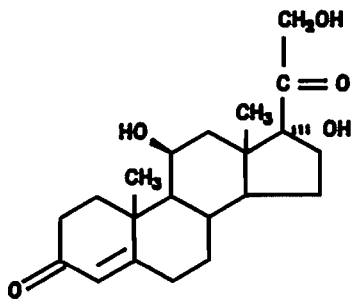

11

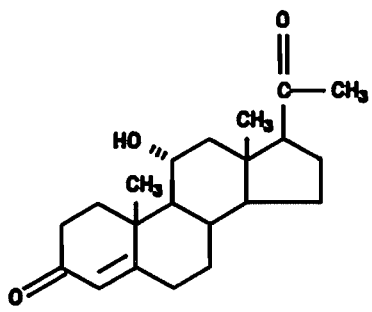

12

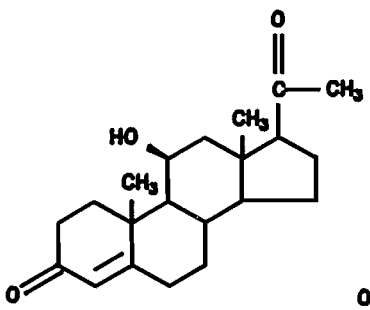

13

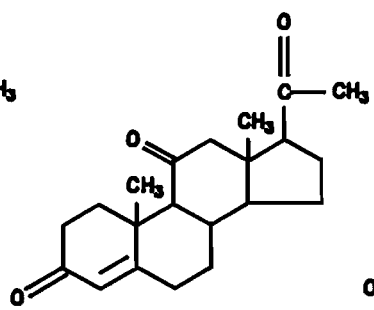

14

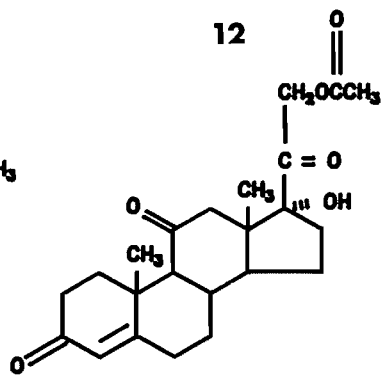

15

TABLE 1. Chemical shifts[a] of the 18- and 19-methyl groups of steroids

	Compound	^{1}H (ppm)		^{13}C (ppm)	
		18	19	18	19
1	Androstanolone	0.76	1.03	11.04[b]	11.37[b]
2	Testosterone	0.81	1.21	10.93	17.35
3	1-Dehydrotestosterone	0.82	1.25	11.04	18.59
4	Pregnanedione	0.60	1.00	11.63	13.57
5	Progesterone	0.65	1.18	13.44	17.63
6	16α-Methylpregnenolone	0.66	1.02		
7	16β-Methylpregnenolone	0.96	1.00		
8	Prednisone[c]	0.50	1.40	15.18	18.47
9	Prednisolone[c]	0.80	1.40	16.68	20.69
10	Cortisone[c]	0.46	1.30	15.25	16.78
11	Dihydrocortisone[c]	0.74	1.36	16.81	20.37
12	11α-Hydroxyprogesterone	0.70	1.32	14.06	17.92
13	11β-Hydroxyprogesterone	0.92[d]	1.46[d]		
14	11-Ketoprogesterone	0.62	1.40	13.74	16.79
15	Cortisone acetate	0.61	1.36		

[a]$CDCl_3$ solution, unless otherwise noted.
[b]Uncertain assignment.
[c]DMSO-d_6 solution.
[d]Assigned by comparison with progesterone, **5**.

(Table 2). It was demonstrated previously that removal of 1,3-nonbonded interactions between axial A-ring hydrogens and the 19-methyl group following the introduction of double bonds influences the ^{1}H and ^{13}C relaxation rates of this group (4, 5). Using qualitative arguments, this effect has been attributed to changes in the rate of rotation of the group resulting from changes in steric interference.

Removal of 1,3-nonbonded interactions is predicted to cause an *increase* in the rotational barrier of the methyl group. In androstanolone, **1**, the compound with the maximum number of nonbonded interactions, the methyl group has no energetically favorable conformation available — its rotational ground state energy is high. As nonbonded interactions are removed, available conformations become energetically more favorable, and the differences between rotational ground and transition state energies increase — the rotational barrier increases (4).

In Series I, the computed rotational barriers for the 18-methyl groups are essentially identical (Table 2), as expected. The computed barriers of the 19-methyl groups reflect the stabilization of the rotational ground state energies as double bonds are successively introduced (Table 2), increasing from 3.22 kcal/mol in androstanolone, **1**, to 5.07 kcal/mol in dehydrotestosterone, **3**. In androstanolone, the computed barrier for the 19-methyl group is smaller (89%) than that of the 18-methyl group; in the other compounds it is larger, 120% and 142% in testosterone and dehydrotestosterone, respectively. Thus, computation supports the qualitative model used previously (4,5).

The ^{13}C R_1 values in this series correlate well with the computed rotational barriers. Thus, in androstanolone, **1**, the 19-methyl group is predicted to have a lower barrier than the 18-methyl, and the observed ^{13}C relaxation rate is lower (85%). However, the ^{1}H relaxation rates of these groups are the same within experimental error in this compound. In the other two compounds, the 19-methyl group is predicted to have a higher barrier than the 18-methyl, and both the observed ^{1}H and ^{13}C R_1 rates are higher.

The dynamic range of ^{1}H R_1 values is much smaller than that of the ^{13}C R_1 values, and the correlation with predicted rotational barriers is not quite as good. In androstanolone, **1**, the 18- and 19-methyl relaxation rates are almost identical despite the predicted higher rate of the 18-methyl group. In the other two compounds, the 19-methyl group ^{1}H R_1 rates correlate well with prediction. Throughout the group, the *changes* in the 19-methyl group relaxation rates correlated well with the predicted changes in the rotational barriers.

Similarly, in the pregnanedione–progesterone pair, **4** and **5**, the predicted 18-methyl rotational barriers are identical, whereas the predicted 19-methyl group rotational barriers increase on the introduction of unsaturation to the A-ring. In both cases, the 19-methyl group is predicted to have a higher rotational barrier than the 18-methyl group. In both cases, the ^{13}C relaxation rates are significantly higher for the 19-methyl group, in accord with prediction. In pregnanedione, **4**, the ^{1}H R_1 values of the 18- and 19-methyl groups are almost identical, despite prediction, but the correlation is better in progesterone, with a higher predicted rotational barrier.

The 16α- (**6**) and 16β-methylpregnenolone (**7**) pair (Series II) differ through a configurational change at C-16, which should affect the 18- more than the 19-methyl group. Internal comparison shows a good correlation between rotational barriers and relaxation rates for both compounds, e.g., the rotational barrier of the 19-methyl group of **6** is higher than that of the 18-methyl group. (3.78 vs. 3.21 kcal/mol), and the ^{1}H R_1 value of the 19-methyl group is higher than that of the 18-methyl group (1.64 vs. 1.35 s^{-1}). Steroid **7** showed as good a correlation as **6**. The ^{1}H R_1 data show that epimerization at C-16 does affect the relaxation rate of the 18-methyl group, as predicted, but there is no detectable influence at the 19-methyl group.

The compounds in Series III provide a somewhat different comparison. Since the changes in the molecules at C-11 should affect both the 18- and the 19-methyl groups, external comparison was applied in this series by normalizing the methyl group R_1 values to those of ^{1}H-4 and ^{13}C-4. The calculated rotational barriers of the 18-and 19-methyl groups in **8** are lower than those of **9** (18-: 2.78 vs. 3.24 kcal/mol; 19-: 4.08 vs. 4.82 kcal/mol, respectively), thus the normalized ^{1}H relaxation rates of both methyl groups in **8** showed lower values than in **9** (18-: 3.67 vs. 4.30; 19-: 3.47 vs. 3.69) (Table 3). The normalized ^{13}C R_1 values, which show a small range, did not give as good correlations as the ^{1}H R_1 values (18-: 0.48 vs. 0.50; 19-: 0.46 vs. 0.42). Similarly, the rotational barriers of **10** and **11** correlated well with the R_1 values except that the ^{13}C R_1 values of both compounds are again similar. Internal comparisons in this series show anomalies that are discussed later.

Comparison of **8** and **10**, and **9** and **11**, shows that removal of 1,3 nonbonded interactions significantly increases the rotational barrier and the ^{1}H relaxation rates of the 19-methyl groups.

Series IV enables comparison of the effects of equatorial and axial hydroxyl and oxo groups in the 11-position of steroids. External comparison shows that both the 18- and the 19-methyl groups are affected by a change in stereochemistry or oxidation state at C-11. The 18-methyl group in 11β-hydroxyprogesterone, **13**, has the highest rotational barrier

Can. J. Chem. Downloaded from www.nrcresearchpress.com by 109.225.110.28 on 09/08/12
For personal use only.

TABLE 2. Calculated methyl group rotational barriers[a] and measured spin-lattice relaxation rates[b] of steroids

	18-Methyl			19-Methyl			Ratios		
	R_1 (s^{-1})			R_1 (s^{-1})			R_1 (19/18)		
Compound	^1H	^{13}C	RB[c]	^1H	^{13}C	RB[c]	^1H	^{13}C	RB
Series I									
1	1.01 0.92[d]	0.27	3.61	1.04 0.96[d]	0.23	3.22	1.03 1.04[d]	0.85	0.89
2	0.94 1.04[d]	0.29	3.59	1.17 1.20[d]	0.38	4.32	1.24 1.15[d]	1.31	1.20
3	1.13	0.33	3.58	1.58	0.75	5.07	1.40	2.27	1.42
4	0.96	0.22	2.58	0.95	0.27	3.47	0.99	1.23	1.34
5	0.98	0.32	2.58	1.12	0.43	4.35	1.14	1.34	1.69
Series II									
6[d]	1.35		3.21	1.64		3.79	1.21		1.18
7[d]	1.22		2.51	1.64		3.10	1.34		1.24

[a]Calculated using the dihedral driver option of MMX.
[b]Measured at 400 MHz (^1H, degassed 0.1 M $CDCl_3$ solutions) or 20.1 MHz (^{13}C, non-degassed $CDCl_3$ solutions), and calculated by nonlinear regression, unless otherwise noted.
[c]Calculated rotational barrier, kcal/mol.
[d]Measured at 270 MHz (non-degassed 0.1 M $CDCl_3$ solutions), and calculated using the null point method (from ref. 5).

TABLE 3. Calculated methyl group rotational barriers[a] and measured relative spin-lattice relaxation rates[b] of steroids

	18-Methyl			19-Methyl			Ratios		
	R_1			R_1			R_1 (19/18)		
Compound	^1H	^{13}C	RB[c]	^1H	^{13}C	RB[c]	^1H	^{13}C	RB
Series III (DMSO-d_6 solution)									
8	3.67	0.48	2.78	3.47	0.46	4.08	0.95	0.96	1.47
9	4.30	0.50	3.24	3.69	0.42	4.82	0.86	0.84	1.49
10	2.36	0.54	2.72	1.90	0.42	3.19	0.80	0.78	1.17
11	3.86	0.53	3.23	3.12	0.48	4.01	0.81	0.91	1.24
Series IV ($CDCl_3$ solution)									
12	2.09	0.48	2.47	2.45	0.66	4.35	1.17	1.38	1.76
13[d]	3.00		3.95	2.20		4.32	0.74		1.09
14	2.67	0.81	2.78	2.09	0.51	4.08	0.78	0.63	1.47

[a]Calculated using the dihedral driver option of MMX.
[b]Determined at 400 (^1H, degassed) or 20.1 (^{13}C, non-degassed) MHz, and calculated by nonlinear regression, unless otherwise noted. The R_1 values are normalized to the R_1 value of ^1H-4 or ^{13}C-4 (= 1.0).
[c]Calculated rotational barrier, kcal/mol.
[d]Determined at 270 MHz (0.1 M in $CDCl_3$, non-degassed), and calculated using the null point method (5).

(3.95 kcal/mol) and the highest normalized (3.00) ^1H R_1 value in the series, while its epimer, 11α-hydroxyprogesterone, **12**, has the lowest rotational barrier (2.47 kcal/mol) and the lowest normalized relaxation rate (2.09). The ketone, **14**, has an intermediate barrier (2.78 kcal/mol) and relative R_1 value (2.67). The 19-methyl groups in this series are less sensitive to the substituent at C-11. The rotational barrier of the 19-methyl group of **12** (4.35 kcal/mol) is slightly higher than that of **13** (4.32 kcal/mol), as is its normalized ^1H R_1 (2.45 vs. 2.20), whereas the ketone, **14**, has the lowest rotational barrier (4.08 kcal/mol) and relative relaxation rates (2.09). Thus, external correlations between rotational barriers and relaxation rates in Series IV are all in the expected sense.

In Series III and IV all 19-methyl groups are predicted to have higher rotational barriers than the 18-methyl groups. However, internal comparison shows that both the ^1H and ^{13}C relaxation rates of all of the 18-methyl groups are higher than those of the 19-methyl groups, with the exception of compound **12**. Since these compounds contain several carbonyl and hydroxyl groups, it is suggested that the methyl group rotational barriers are affected by strong solvation or association in solution.

Limited solubility in nonpolar solvents of steroids highly

Can. J. Chem. Downloaded from www.nrcresearchpress.com by 109.225.110.28 on 09/08/12
For personal use only.

TABLE 4. Calculated methyl group rotational barriers[a] and measured relative ^1H spin-lattice relaxation rates[b] of **12** and **15**

	18-Methyl		19-Methyl		Ratio, 19/18	
Solvent	R_1[c]	RB[d]	R_1[c]	RB[d]	R_1	RB
12 DMSO-d_6	2.90 (2.26)	2.47	3.53 (2.75)	4.35	1.22	1.76
12 $CDCl_3$	2.09 (1.44)	2.47	2.45 (1.69)	4.35	1.17	1.76
15 DMSO-d_6	2.76 (3.73)	3.71	2.00 (2.70)	3.79	0.72	1.02
15 $CDCl_3$	1.96 (2.48)	3.71	2.35 (2.97)	3.79	1.20	1.02

[a]Molecular mechanics calculations were carried out on an Olivetti M24 computer, using PCMODEL and MMX.

[b]^1H-R_1 values were determined at 400 MHz, 0.1 M solutions.

[c]R_1 values are relative to that of H-4, except experimental values are in parentheses.

[d]Calculated rotational barrier, kcal/mol.

functionalized with polar groups restricted investigation of solvent effects on methyl group relaxation. However, ^1H relaxation rates in both $CDCl_3$ and DMSO-d_6 solutions of 11α-hydroxyprogesterone, **12**, and cortisone acetate, **15**, could be measured. Average relaxation rates were higher in the more viscous solvent, DMSO-d_6, than in $CDCl_3$ solution in both compounds; e.g., the ^1H R_1 of H-4 in **15** is 1.35 s^{-1} in DMSO-d_6 and 0.79 s^{-1} in $CDCl_3$.

For compound **12**, the normalized (with respect to H-4) R_1 values in DMSO-d_6 of both the 18- and the 19-methyl groups are higher than those in $CDCl_3$, indicating that solvation affects the local motion of both methyl groups (Table 4). Since the molecule has polar functional groups adjacent to both methyl groups (a hydroxyl group centrally located and carbonyl groups flanking the methyl groups), solvation affects both methyl groups. Therefore, the experimental R_1 data for the two methyl groups are consistent with each other, and with the prediction.

For compound **15**, the density of polar functional groups is higher near ring D and, in DMSO-d_6 solution, the spin-lattice relaxation rate of the 18-methyl group is higher than that of the 19-methyl group (3.73 vs. 2.70, normalized), contrary to prediction (Table 4). The same discrepancy has been noted for compounds **8**–**13**. However, in $CDCl_3$ solution, the 18-methyl group of **15** relaxes more slowly than the 19-methyl group (2.48 vs. 2.97, normalized), in accord with prediction. These results indicate that there are differential solvent effects on the spin-lattice relaxation rates of the 18- and 19-methyl groups of **15**, and that the discrepancies from predictions based on molecular modelling occur when the more polar solvent is used.

Conclusions

Bernassau and co-workers (6) established a successful correlation between computed methyl group rotational barriers and experimentally determined barriers derived from ^{13}C relaxation times in five nonpolar podocarpane derivatives, measured in $CDCl_3$ solution. Our data also correlate well when the steroids have few polar substituents and are measured in a relatively nonpolar solvent ($CDCl_3$). However, when the steroid is heavily substituted with polar groups, and when the measurement must be taken in a polar solvent, the correlation between ^1H and ^{13}C spin-lattice relaxation rates and the computed rotational barriers may break down. The discrepancy is most likely attributable to an inadequate model for the force field calculations, which are gas phase, and do not take molecular interactions into account at the level at which the calculations were performed. There is evidence for preferential solvation effects, in which the methyl group adjacent to the polar substituents is more affected than the remote methyl group. Thus, force field calculations of this type may work well, but they should be applied with caution in predicting properties of polar molecules measured in polar solvents.

Experimental

The ^1H nmr spectra were determined (0.1 M in $CDCl_3$ or DMSO-d_6 solution) at 400 MHz using a Bruker WH-400 spectrometer located at the Montreal Regional High Field NMR Laboratory, with the exception of some 270 MHz spectra that were reported previously (5). ^{13}C spectra were determined at 20.1 MHz ($CDCl_3$ solutions) using a Bruker WP-80SY spectrometer fitted with a 10-mm broadband probe. ^1H-R_1 values were usually measured on degassed samples, since paramagnetic contributions from dissolved oxygen contribute to the overall relaxation rate. Samples for ^{13}C measurements were not degassed. The DEPT spectral editing sequence (16) was used as an aid to ^{13}C spectral assignments. The difference technique for measuring ^{13}C nOe enhancements has been described previously (1). R_1 values were measured using the standard inversion-recovery two-pulse sequence (17), followed by nonlinear regression analysis (performed on an Olivetti M24 microcomputer) of data down-loaded from a Bruker Aspect 2000 spectrometer computer. Data analysis was confined to the initial slope region (12), defined by a single exponential. The precision of the measurements was better than 2% or 5% for ^1H and ^{13}C R_1 values, respectively. Samples were used as received from Aldrich and Sigma Chemical Companies.

Molecular mechanics calculations were carried out with an Olivetti M24 microcomputer (with 640k memory, co-processor, hard disk, and Microsoft mouse) using the programs MMX and PCMODEL (18) (Serena Software, Bloomington, Ind., U.S.A.). MMX, a batch program lacking graphics output, is an implementation of the Allinger MMP2 algorithm (7), and includes π-calculations and the dihedral driver option. The version of PCMODEL used has graphics output but does not include π calculations or a dihedral driver (with optimization). It was used for structure input (for PCMODEL and MMX), using a mouse.

The structures of compounds containing conjugated π-systems were optimized using MMX. The structures of compounds without conjugated π-systems were initially optimized using PCMODEL. MMX was used for optimizations preceding dihedral driver calculations.

Acknowledgments

We thank the Natural Sciences and Engineering Research Council of Canada (NSERC) for an operating grant, for providing funding towards the purchase of the spectrometers, and for supporting the operation of the Montreal Regional High Field NMR Laboratory.

1. W. J. Chazin and L. D. Colebrook. Magn. Reson. Chem. **23**, 597 (1985).
2. E. Breitmaier and W. Voelter. Carbon-13 NMR spectroscopy. High-resolution methods and applications in organic chemistry and biochemistry. VCH Publishers, New York. 1987. p. 173.

Can. J. Chem. Downloaded from www.nrcresearchpress.com by 109.225.110.28 on 09/08/12
For personal use only.

3. R. K. Harris. Nuclear magnetic resonance spectroscopy. A physicochemical view. Pitman Publishing Inc., Marshfield, Mass. 1983. pp. 89–90.
4. J. W. ApSimon, H. Beierbeck, and J. K. Saunders. Can. J. Chem. **53**, 338 (1975).
5. L. D. Colebrook and L. D. Hall. Org. Magn. Reson. **21**, 532 (1983).
6. J. Bastard, J. M. Bernassau, Do Khac Duc, M. Fetizon, and E. Lesueur. J. Phys. Chem. **90**, 3936 (1986).
7. U. Burkert and N. L. Allinger. Molecular mechanics. ACS Monograph 177, American Chemical Society, Washington, D.C. 1982.
8. N. Qing, L. D. Colebrook, and F. Commodari. Magn. Reson. Chem. **29**, 459 (1991).
9. J. D. Cutnell and J. A. Glasel. J. Am. Chem. Soc. **98**, 264 (1976).
10. L. Werbelow. J. Magn. Reson. **34**, 439 (1979).
11. E. Haslinger and R. M. Lynden-Bell. J. Magn. Reson. **31**, 33 (1978).
12. R. Freeman, S. Wittekoek, and R. R. Ernst. J. Chem. Phys. **80**, 1529 (1970).
13. A. Allerhand, D. Doddrell, and R. Komoroski. J. Chem. Phys. **55**, 189 (1971).
14. J. K. M. Sanders and J. Mersh. Prog. Nucl. Magn. Reson. Spectrosc. **15**, 353 (1982).
15. L. D. Hall and J. K. M. Sanders. J. Am. Chem. Soc. **102**, 5703 (1980).
16. J. K. M. Sanders and B. K. Hunter. Modern NMR spectroscopy. A guide for chemists. Oxford University Press, Oxford. 1987. Chap. 8.
17. R. L. Vold, J. S. Waugh, M. P. Klein, and D. E. Phelps. J. Chem. Phys. **48**, 3831 (1968).
18. J. J. Gajewski, K. E. Gilbert, and J. McKelvey. Adv. Mol. Model. **2**, 65 (1990).

Can. J. Chem. Downloaded from www.nrcresearchpress.com by 109.225.110.28 on 09/08/12
For personal use only.

Polynuclear pyrazolate complexes of copper. Crystal and molecular structures of $[Cu(tmpz)]_3$, $[Cu(3\text{-}CO_2dmpz)(tmpzH)]_2Cu$, and $[Cu(4\text{-}Br\text{-}3\text{-}CO_2mepz)(4\text{-}Br\text{-}dmpzH)_2]_2$ (where mepz = methylpyrazolate, dmpz = dimethylpyrazolate, and tmpz = trimethylpyrazolate) and magnetic susceptibility studies on the dinuclear complex

MARTIN K. EHLERT, STEVEN J. RETTIG, ALAN STORR,[1] ROBERT C. THOMPSON,[1] AND JAMES TROTTER
Department of Chemistry, University of British Columbia, 2036 Main Mall, Vancouver, B.C., Canada V6T 1Z1

Received January 20, 1992

MARTIN K. EHLERT, STEVEN J. RETTIG, ALAN STORR, ROBERT C. THOMPSON, and JAMES TROTTER. Can. J. Chem. **70**, 2161 (1992).

The reaction of molten trimethylpyrazole (tmpzH) with copper metal shot in air yields a mixture of the trinuclear copper(I) complex $[Cu(tmpz)]_3$, **1**, and the trinuclear copper(I/II) complex $[Cu(3\text{-}CO_2dmpz)(tmpzH)]_2Cu$, **2** (where dmpz is dimethylpyrazolate). Crystals of **1** are monoclinic, $a = 8.403(3)$, $b = 22.453(2)$, $c = 11.362(2)$ Å, $\beta = 95.83(2)°$, $Z = 4$, space group $P2_1/c$. Crystals of **2** are triclinic, $a = 10.988(3)$, $b = 11.009(2)$, $c = 6.457(1)$ Å, $\alpha = 103.13(2)°$, $\beta = 103.02(2)°$, $\gamma = 108.70(2)°$, $Z = 1$, space group $P\bar{1}$. The reaction of molten 4-bromodimethylpyrazole (4-BrdmpzH) with copper metal shot in air gave the binuclear copper(II) complex $[Cu(4\text{-}Br\text{-}3\text{-}CO_2mepz)(4\text{-}BrdmpzH)_2]_2$, **3** (where mepz is methylpyrazolate). There are two crystalline forms of **3**: **3***a*, triclinic, $a = 10.152(3)$, $b = 13.068(3)$, $c = 10.033(3)$ Å, $\alpha = 112.38(2)°$, $\beta = 116.46(2)°$, $\gamma = 70.29(2)°$, $Z = 1$, space group $P\bar{1}$; and **3***b*, monoclinic, $a = 13.470(1)$, $b = 16.005(2)$, $c = 20.174(1)$ Å, $\beta = 98.142(6)°$, $Z = 4$, space group $C2/c$. Magnetic susceptibility studies on a bulk sample of **3** (2.0–300 K) revealed antiferromagnetic coupling between the double pyrazolate bridged copper centres and analysis of the data according to a Heisenberg model for coupled pairs of $S = 1/2$ metal ions gave -75.4 cm^{-1} for the value of the exchange coupling constant, J. The crystal structures of **1**, **2**, **3***a*, and **3***b* were solved by the Patterson method and were refined by full-matrix least-squares procedures to final R values of 0.036, 0.056, 0.042, and 0.042 for 2265, 1764, 2011, and 2575 reflections with $I \geq 3\sigma(I)$, respectively.

MARTIN K. EHLERT, STEVEN J. RETTIG, ALAN STORR, ROBERT C. THOMPSON et JAMES TROTTER. Can. J. Chem. **70**, 2161 (1992).

La réaction du triméthylpyrazole (tmpzH) fondu avec du cuivre métallique pulvérisé dans l'air fournit un mélange du complexe trinucléaire du cuivre(I) $[Cu(tmpz)]_3$, **1**, et le complexe trinucléaire de cuivre(I/II) $[Cu(3\text{-}CO_2dmpz)(tmpzH)]_2Cu$, **2** (dans lesquels dmpz est le diméthylpyrazolate). Les cristaux du produit **1** sont monocliniques, groupe d'espace $P2_1/c$ avec $a = 8{,}403(3)$, $b = 22{,}453(2)$ et $c = 11{,}362(2)$ Å, $\beta = 95{,}83°$ et $Z = 4$. Les cristaux du produit **2** sont tricliniques, groupe d'espace $P\bar{1}$ avec $a = 10{,}988(3)$, $b = 11{,}009(2)$ et $c = 6{,}457(1)$ Å, $\alpha = 103{,}13(2)$, $\beta = 103{,}02(2)$ et $\gamma = 108{,}70(2)°$ et $Z = 1$. La réaction du 4-bromodiméthylpyrazole (4-BrdmpzH) fondu avec du cuivre métallique pulvérisé dans l'air fournit le complexe dinucléaire du cuivre(II) $[Cu(4\text{-}Br\text{-}3\text{-}CO_2mepz)(4\text{-}BrdmpzH)_2]_2$, **3**, dans lequel mepz est le méthylpyrazolate. Il existe deux formes cristallines du produit **3** : **3***a*, triclinique, groupe d'espace $P\bar{1}$ avec $a = 10{,}152(3)$, $b = 13{,}068(3)$ et $c = 10{,}033(3)$ Å, $\alpha = 112{,}38(2)$, $\beta = 116{,}46(2)$ et $\gamma = 70{,}29(2)°$ et $Z = 1$; et **3***b*, monoclinique, groupe d'espace $C2/c$ avec $a = 13{,}470(1)$, $b = 16{,}005(2)$ et $c = 20{,}174(1)$ Å, $\beta = 98{,}142(6)°$ et $Z = 4$. Des études de susceptibilité magnétique sur un échantillon global du produit **3** (2,0–300 K) révèlent la présence d'un couplage antiferromagnétique entre les centres du cuivre doublement ponté au pyrazolate et une analyse des données, suivant le modèle de Heisenberg pour les paires couplées d'ions métalliques avec $S = 1/2$, conduit à une valeur de $-75{,}4$ cm^{-1}, pour la constante de couplage d'échange, J. Les structures cristallines des composés **1**, **2**, **3***a* et **3***b* ont été résolues par la méthode de Patterson et elles ont été affinées par la méthode des moindres carrés (matrice complète) jusqu'à des valeurs de R de 0,036, 0,056, 0,042 et 0,042 pour respectivement 2265, 1764, 2011 et 2575 réflexions avec $I \geq 3\sigma(I)$.

[Traduit par la rédaction]

Introduction

Reactions of copper metal shot with molten pyrazole and substituted pyrazoles in the presence of dioxygen have been successfully employed in the synthesis of the polymeric binary copper(II) pyrazolates, $[Cu(pz^*)_2]_x$ (where pz* = pyrazolate (1), 3-methylpyrazolate,[2] 4-methylpyrazolate (2), 3,5-dimethylpyrazolate (3), and indazolate[2]). By controlling the conditions in order to achieve slow polymer formation it has been possible to obtain the pyrazolate and 4-methylpyrazolate polymeric compounds in crystalline form suitable for single crystal X-ray diffraction studies (1, 2). In the current study, further investigation of this reaction with other substituted pyrazoles has revealed that products other than the binary copper(II) pyrazolates may form depending on conditions and particularly when the pyrazole involved contains methyl substituents in the 3- and 5-positions. In this paper we describe our studies with 3,4,5-trimethylpyrazole (tmpzH) and 4-bromo-3,5-dimethylpyrazole (4-BrdmpzH) in which, by isolation and X-ray structural characterization of the title compounds, we are able to identify an interesting reaction involving oxidation of a methyl substituent to carboxylate.

The trinuclear copper(I) and copper(I/II) complexes, $[Cu(tmpz)]_3$, **1**, and $[Cu(3\text{-}CO_2dmpz)(tmpzH)]_2Cu$, **2**, respectively were isolated from the reaction of molten tmpzH with copper metal shot in air. A similar reaction involving 4-BrdmpzH gave the binuclear copper(II) complex, $[Cu(4\text{-}Br\text{-}3\text{-}CO_2mepz)(4\text{-}BrdmpzH)_2]_2$, **3**. We report here single crystal X-ray diffraction studies on the three complexes and a variable temperature magnetic susceptibility study on the binuclear complex. Binuclear copper(II) complexes that have been structurally characterized, that contain bridging pyra-

[1]Authors to whom correspondence may be addressed.

[2]M. K. Ehlert, A. Storr, and R. C. Thompson, unpublished results.

Can. J. Chem. Downloaded from www.nrcresearchpress.com by 109.225.110.28 on 09/08/12
For personal use only.

Can. J. Chem. Downloaded from www.nrcresearchpress.com by 109.225.110.28 on 09/08/12
For personal use only.

zolate ligands, and that exhibit strong antiferromagnetic interactions have been reported previously (4–7). In this earlier work, however, the interpretation of the magnetic data was complicated by the presence, in the complexes, of other bridging ligands in addition to the bridging pyrazolates. The binuclear complex reported here is, to our knowledge, the first example of a structurally and magnetically characterized purely pyrazolate-bridged binuclear copper(II) species.

Experimental

Syntheses

3,4,5-Trimethylpyrazole and 4-bromo-3,5-dimethylpyrazole were prepared as described previously (3).

*[Cu(tmpz)]$_3$, **1**, and [Cu(3-CO$_2$dmpz)(tmpzH)]$_2$Cu, **2***

Copper metal shot (8.18 g, 129 mmol), cleaned by washing with 12 M HCl, water, and then acetone, was combined with tmpzH (4.73 g, 42.9 mmol) and the mixture was heated in air, without stirring, at 142°C for 40 h. After the first 18 h of heating, the neck of the reaction vessel had become plugged with sublimed tmpzH, which limited further contact of the reaction mixture with atmospheric dioxygen. At cessation of the reaction, the mixture was allowed to cool and solidify. The mixture was then extracted with 150 mL of dry THF and suction filtered. This yielded a brown filtrate and a filtercake (~0.08 g) that consisted of an approximately equal mixture of colourless crystals of **1** and pale purple crystals of **2**. Due to their insolubility in all solvents tested the compounds could not be separated by crystallization methods. A few crystals of each were separated by hand for X-ray diffraction studies. Because a bulk sample of **2** could not be isolated its characterization is limited to the X-ray study and an EPR study of a mixture of **1** and **2**. Bulk, microcrystalline **1** was prepared previously via a different route and this together with some characterization of the compound was described elsewhere (3).

*[Cu(4-Br-3-CO$_2$mepz)(4-BrdmpzH)$_2$]$_2$, **3***

Cleaned copper shot (*vide supra*) (~1 g) and 4-BrdmpzH (~2.5 g) were combined and the mixture was heated in air, without stirring, at 140°C for 3 days. After this time the reaction mixture was allowed to cool and solidify. The solid was extracted with CH_2Cl_2 and suction filtered, yielding a green filtrate and a filtercake that consisted of well-formed green crystals of **3**. The crystals were contaminated with small amounts of yellow and bluish-grey materials; the latter were removed by manual separation. The green crystals occur as a mixture of two different morphologies, a consequence of the fact that the molecule crystallizes in both triclinic, **3***a*, and monoclinic, **3***b*, forms. Most crystals were of the triclinic form. Anal. calcd. for $C_{30}H_{34}Br_6Cu_2N_{12}O_4$: Cu 10.30, C 29.22, H 2.78, N 13.63; found: Cu 10.30, C 29.45, H 2.75, N 13.87%.

Physical characterization

Differential scanning calorimetry (DSC) measurements were made with a Mettler DSC 20 standard cell and TC10 TA processor as described previously (8). Infrared spectra (450–4000 cm^{-1}) were obtained using a Perkin–Elmer model 598 spectrophotometer. The samples were mulled in Nujol and contained between KBr plates. A ^{1}H NMR spectrum of 4-BrdmpzH was recorded using a Bruker AC-200 FT NMR spectrometer equipped with a Bruker B-ACS 120 sample changer. The solvent used was $CDCl_3$. Electron paramagnetic resonance (EPR) measurements were made on powdered samples contained in 3 mm i.d. silica tubes employing a Varian E3 X-band spectrometer. The frequency was measured using an HP5255A frequency converter and the magnetic field was calibrated with a custom-built gaussmeter.

Magnetic susceptibilities were measured over the temperature range 2–300 K using a Quantum Design (MPMS) SQUID magnetometer (field = 10 000 Oe). Temperature measurement with this instrument was achieved using a combination of Ge and Pt resistance thermometers. Susceptibility calibration was performed using high-purity Ni and Bi standards. The sample was packed as a powder into a specially constructed sample holder made from PVC. The sample holder possessed a constant cross-sectional area, thus minimizing its contribution to the SQUID signal. Magnetic susceptibilities were corrected for sample holder background signal and diamagnetism: copper, −11; $C_5H_3BrN_2O_2$, −85; $C_5H_7BrN_2$, −90 (values in 10^{-6} cm^3 mol^{-1}). A correction of 60×10^{-6} cm^3 mol^{-1} was applied for temperature independent paramagnetism of the copper(II) ion.

C, H, and N analyses were performed by P. Borda of this department. Cu analysis was by iodometric titration.

X-ray crystallographic analyses

Crystallographic data for **1**, **2**, and two crystal forms of **3** appear in Table 1. The final unit-cell parameters were obtained by least squares on the setting angles for 25 reflections with 2Θ = 31.2–34.4° for **1**, 32.3–36.9° for **2**, 25.3–30.3° for triclinic **3** (**3***a*), and 33.9–70.4° for monoclinic **3** (**3***b*). The intensities of three standard reflections, measured every 200 reflections throughout the data collections, remained constant for all four data collections. The data were processed[3] and corrected for Lorentz and polarization effects, and absorption (empirical, based on azimuthal scans for three reflections).

The analyses of **2**, **3***a*, and **3***b* were initiated in the centrosymmetric space groups ($P\bar{1}$, $P\bar{1}$, and $C2/c$, respectively), these choices being confirmed by the subsequent successful solutions and refinements of the structures. The structures were all solved by the Patterson method, the coordinates of the Cu (and Br atoms for **3***a* and **3***b*) being determined from the Patterson functions and the coordinates of the remaining non-hydrogen atoms from subsequent difference Fourier syntheses. The non-hydrogen atoms were refined with anisotropic thermal parameters and hydrogen atoms were fixed in idealized positions (C—H = 0.98 Å, $B_H = 1.2\ B_{\text{bonded atom}}$). Neutral atom scattering factors for all atoms and anomalous dispersion corrections for the nonhydrogen atoms were taken from the *International tables for X-ray crystallography* (9). Final atomic coordinates and equivalent isotropic thermal parameters are given in Table 2 and bond lengths and angles appear in Tables 3 and 4. Anisotropic thermal parameters, bond lengths and angles involving hydrogen, general torsion angles, intermolecular distances, least-squares planes, and measured and calculated structure factor amplitudes for the four structures are included as supplementary material.[4]

Results and discussion

The 3,4,5-trimethylpyrazole reaction

Attempts to prepare the binary copper(II) trimethylpyrazolate polymer, $[Cu(tmpz)_2]_x$, by the reaction of copper metal shot with molten trimethylpyrazole in air or dioxygen under various conditions invariably resulted in the formation of a mixture of products. Under reaction conditions in which the mixture was kept stirring and freely exposed to air the prin-

[3]TEXSAN/TEXRAY structure analysis package, containing versions of the following: DIRDIF, direct methods for difference structures, by P. T. Beurskens; ORFLS, full-matrix least-squares, and ORFFE, function and errors, by W. R. Busing, K. O. Martin, and H. A. Levy; ORTEP II, illustrations, by C. K. Johnson.

[4]Supplementary material mentioned in the text may be purchased from: The Depository of Unpublished Data, Document Delivery, CISTI, National Research Council Canada, Ottawa, Canada K1A OR6.

Tables of atomic coordinates, bond lengths and angles involving hydrogen, and intermolecular distances have also been deposited with the Cambridge Crystallographic Data Centre and can be obtained on request from The Director, Cambridge Crystallographic Data Centre, University Chemical Laboratory, 12 Union Road, Cambridge CB2 1EZ, U.K.

TABLE 1. Crystallographic data[a]

Compound	**1**	**2**	**3***a*	**3***b*
Formula	$C_{18}H_{27}Cu_3N_6$	$C_{24}H_{32}Cu_3N_8O_4$	$C_{30}H_{34}Br_6Cu_2N_{12}O_4$	$C_{30}H_{34}Br_6Cu_2N_{12}O_4$
fw	518.09	687.21	1233.19	1233.19
Crystal system	Monoclinic	Triclinic	Triclinic	Monoclinic
Space group	$P2_1/c$	$P\bar{1}$	$P\bar{1}$	$C2/c$
a, Å	8.403(3)	10.988(3)	10.152(3)	13.470(1)
b, Å	22.453(2)	11.009(2)	13.068(3)	16.005(2)
c, Å	11.362(2)	6.457(1)	10.033(3)	20.174(1)
α,°	90	103.13(2)	112.38(2)	90
β,°	95.83(2)	103.02(2)	116.46(2)	98.142(6)
γ,°	90	108.70(2)	70.29(2)	90
V, Å^3	2132.7(9)	681.8(3)	1079.1(6)	4305.3(8)
Z	4	1	1	4
ρ_{calc}, g/cm^3	1.613	1.673	1.898	1.902
F(000)	1056	351	598	2392
Radiation	Mo	Mo	Mo	Cu
μ, cm^{-1}	29.89	23.70	65.37	82.19
Crystal size, mm	0.15 × 0.25 × 0.25	0.08 × 0.13 × 0.30	0.05 × 0.15 × 0.20	0.10 × 0.10 × 0.13
Transmission factors	0.69–1.00	0.83–1.00	0.75–1.00	0.87–1.00
Scan type	ω–2θ	ω–2θ	ω–2θ	ω–2θ
Scan range, deg in ω	1.10 + 0.35 tan θ	1.37 + 0.35 tan θ	0.94 + 0.35 tan θ	1.00 + 0.30 tan θ
Scan speed, deg/min	32	16	16	32
Data collected	$+h$, $+k$, $\pm l$	$+h$, $\pm k$, $\pm l$	$+h$, $\pm k$, $\pm l$	$+h$, $+k$, $\pm l$
$2\theta_{max}$, deg	60	60	55	155
Crystal decay	Negligible	Negligible	Negligible	Negligible
Total reflections	6763	4148	5235	4620
Unique reflections	6376	3930	4955	4485
R_{merge}	0.045	0.034	0.052	0.019
No. with $I \geq 3\sigma(I)$	2265	1764	2011	2575
No. of variables	245	178	244	244
R	0.036	0.056	0.042	0.042
R_w	0.042	0.067	0.044	0.049
gof	1.53	2.35	1.67	1.55
Max Δ/σ(final cycle)	0.05	0.04	0.004	0.05
Residual density e/Å^3	−0.31, +0.35	−0.50, +0.82	−0.68, +0.97	−0.86, +0.71

[a]Temperature 294 K, Rigaku AFC6S diffractometer, Mo-K_α radiation (λ = 0.71069 Å) or Cu-K_α (λ = 1.54178 Å), graphite monochromator, takeoff angle 6.0°, aperture 6.0 × 6.0 mm at a distance of 285 mm from the crystal, stationary background counts at each end of the scan (scan/background time ratio 2:1, up to 8 rescans), $\sigma^2(F^2) = [S^2(C + 4B) + (pF^2)^2]/\mathrm{Lp}^2$ (S = scan rate, C = scan count, B = normalized background count, p = 0.03 for **1**, **2**, and **3***b*, 0.025 for **3***a*). Function minimized $\Sigma w(|F_o| - |F_c|)^2$ where $w = 4F_o^2/\sigma^2(F_o^2)$, $R = \Sigma||F_o| - |F_c||/\Sigma|F_o|$, $R_w = (\Sigma w(|F_o| - |F_c|)^2/\Sigma w|F_o|^2)^{1/2}$, and gof = $[\Sigma w(|F_o| - |F_c|)^2/(m - n)]^{1/2}$. Values given for R, R_w, and gof are based on those reflections with $I \geq 3\sigma(I)$.

cipal product was the copper(II) polymer contaminated, however, by other unidentified products. The pure polymer was eventually successfully obtained from the reaction of copper(I) trimethylpyrazolate with dioxygen in molten trimethylpyrazole (3). Nevertheless, curiosity as to the course of the metal – molten tmpzH reaction and the possibility of identifying other products, as well as a desire to obtain the copper(II) polymer in crystalline form suitable for X-ray studies, prompted us to explore this reaction under other conditions. When the reaction is allowed to proceed very slowly, with no stirring and with limited access to air, as described in the experimental section, two copper-containing crystalline products are obtained (colourless prisms and light purple prisms). Examining the reaction mixture prior to separation of the products from the unreacted copper metal shot, we noted that the colourless prisms, identified by single crystal X-ray diffraction as the copper(I) trinuclear species $[Cu(tmpz)]_3$, **1**, formed a layer in contact with the metal shot. The other product, identified by X-ray studies as the copper(I/II) mixed oxidation state trinuclear species $[Cu(3\text{-}CO_2dmpz)(tmpzH)]_2Cu$, **2**, was found forming a second layer surrounding the layer of **1**. This observation as well as the presence of copper in both the +1 and +2 oxidation states in the products suggests a stepwise oxidation of copper metal and also that **1** may be a precursor of **2**. Conversion of copper(I) to copper(II) in such complexes has been verified by clean conversion of **1** to the copper(II) polymer, $[Cu(tmpz)_2]_x$ in molten tmpzH in the presence of dioxygen (3). If **1** is the precursor of **2**, and this is by no means certain, then the oxidation of the methyl groups seen under the conditions employed here presumably takes place on coordinated $tmpz^-$. We cannot rule out oxidation of tmpzH itself; however, we note that the presence of metallic copper, acting perhaps as a catalyst, does seem to be required since no carboxylate-containing products were observed in the reaction of **1** with dioxygen in molten tmpzH in the absence of metallic copper (3).

The structure of **1** is very similar to that recently reported and discussed in detail for $[Cu(3,5\text{-}dmpz)]_3$ (10), and consists of trinuclear molecules (Fig. 1) linked pairwise about crystallographic centres of symmetry by weak Cu ... Cu interactions (Fig. 2). The mean Cu—N and intramolecular Cu ... Cu distances and the mean N—Cu—N bond angle (1.853 Å, 3.212 Å, and 174.4°) for **1** are nearly identical to

Can. J. Chem. Downloaded from www.nrcresearchpress.com by 109.225.110.28 on 09/08/12
For personal use only.

Can. J. Chem. Downloaded from www.nrcresearchpress.com by 109.225.110.28 on 09/08/12
For personal use only.

TABLE 2. Final atomic coordinates (fractional) and B_{eq} (Å^2)[a]

Atom	x	y	z	B_{eq}
		[Cu(tmpz)]$_3$, **1**		
Cu(1)	0.50461(9)	0.62029(3)	0.33649(6)	3.80(3)
Cu(2)	0.54224(9)	0.48089(3)	0.31768(6)	3.74(3)
Cu(3)	0.7334(1)	0.55367(3)	0.53812(6)	3.89(3)
N(1)	0.4003(5)	0.5807(2)	0.2078(4)	3.5(2)
N(2)	0.4197(5)	0.5206(2)	0.1973(4)	3.5(2)
N(3)	0.6830(6)	0.4423(2)	0.4284(4)	3.5(2)
N(4)	0.7673(6)	0.4730(2)	0.5200(4)	3.4(2)
N(5)	0.7119(5)	0.6357(2)	0.5456(4)	3.6(2)
N(6)	0.6193(6)	0.6638(2)	0.4553(4)	3.6(2)
C(1)	0.3062(7)	0.5992(3)	0.1132(5)	3.6(3)
C(2)	0.2639(7)	0.5520(3)	0.0390(5)	3.6(3)
C(3)	0.3364(7)	0.5035(3)	0.0952(5)	3.2(3)
C(4)	0.7291(6)	0.3853(2)	0.4356(5)	3.2(2)
C(5)	0.8425(7)	0.3777(2)	0.5327(5)	3.3(3)
C(6)	0.8633(7)	0.4343(3)	0.5818(5)	3.5(3)
C(7)	0.7779(7)	0.6782(3)	0.6183(5)	3.4(3)
C(8)	0.7291(7)	0.7336(3)	0.5765(5)	3.7(3)
C(9)	0.6291(7)	0.7226(3)	0.4746(5)	3.5(3)
C(10)	0.2603(8)	0.6634(3)	0.0997(6)	5.4(4)
C(11)	0.1609(9)	0.5528(3)	−0.0777(5)	5.7(4)
C(12)	0.3348(8)	0.4401(3)	0.0550(6)	4.7(3)
C(13)	0.6614(7)	0.3406(2)	0.3474(5)	4.0(3)
C(14)	0.9220(8)	0.3210(3)	0.5752(5)	5.0(3)
C(15)	0.9716(7)	0.4539(3)	0.6866(5)	4.5(3)
C(16)	0.8912(8)	0.6615(3)	0.7236(5)	4.8(3)
C(17)	0.7758(8)	0.7930(3)	0.6292(6)	5.4(4)
C(18)	0.5420(8)	0.7657(3)	0.3890(5)	4.9(3)
		[Cu(3-CO$_2$dmpz)(tmpzH)]$_2$Cu, **2**		
Cu(1)	1/2	1/2	1/2	3.01(5)
Cu(2)	0.3957(1)	0.6033(1)	0.0291(2)	3.42(4)
O(1)	0.6240(5)	0.6002(5)	0.8115(9)	3.8(2)
O(2)	0.7749(6)	0.8076(5)	1.0233(9)	3.7(2)
N(1)	0.5533(6)	0.6747(6)	0.471(1)	3.1(2)
N(2)	0.5194(6)	0.7260(6)	0.303(1)	2.9(2)
N(3)	0.2620(7)	0.4930(6)	−0.246(1)	3.1(2)
N(4)	0.1963(6)	0.3571(6)	−0.300(1)	2.9(2)
C(1)	0.6415(8)	0.7750(7)	0.655(1)	2.8(2)
C(2)	0.6700(8)	0.8979(7)	0.613(1)	2.8(2)
C(3)	0.5927(8)	0.8636(7)	0.392(1)	2.9(2)
C(4)	0.2090(7)	0.5226(7)	−0.429(1)	3.0(2)
C(5)	0.1123(7)	0.4056(7)	−0.597(1)	2.9(2)
C(6)	0.1058(8)	0.3036(7)	−0.508(1)	3.1(2)
C(7)	0.6857(9)	0.7272(8)	0.848(1)	3.5(3)
C(8)	0.7650(9)	1.0390(8)	0.768(1)	4.0(3)
C(9)	0.5821(9)	0.9503(8)	0.245(1)	4.0(3)
C(10)	0.2511(9)	0.6643(8)	−0.430(2)	4.2(3)
C(11)	0.035(1)	0.3958(9)	−0.828(1)	4.3(3)
C(12)	0.0227(9)	0.1534(8)	−0.608(1)	4.1(3)
		[Cu(4-Br-3-CO$_2$mepz)(4-BrdmpzH)$_2$]$_2$, **3*a***		
Br(1)	−0.5578(1)	0.66395(8)	0.0350(1)	4.01(5)
Br(2)	0.3356(2)	−0.02740(9)	0.1548(1)	7.60(7)
Br(3)	0.2569(2)	0.9218(1)	0.6061(2)	8.74(9)
Cu(1)	0.0696(1)	0.46295(8)	0.1958(1)	2.75(5)
O(1)	−0.0552(6)	0.4779(4)	0.3118(6)	2.9(3)
O(2)	−0.2778(6)	0.5643(5)	0.3324(6)	3.5(3)
N(1)	−0.1283(7)	0.5323(5)	0.0595(7)	2.4(3)
N(2)	−0.1915(7)	0.5544(5)	−0.0811(7)	2.7(3)
N(3)	0.1706(8)	0.3081(5)	0.2324(7)	3.1(3)
N(4)	0.2308(8)	0.2954(5)	0.3772(7)	3.1(3)
N(5)	0.1575(8)	0.6119(6)	0.3929(8)	3.2(4)
N(6)	0.1139(8)	0.6466(6)	0.5150(7)	3.2(3)
C(1)	−0.235(1)	0.5620(6)	0.118(1)	2.4(3)
C(2)	−0.3688(9)	0.6054(7)	0.014(1)	2.8(4)
C(3)	−0.3408(9)	0.5982(7)	−0.1099(9)	2.8(4)
C(4)	−0.188(1)	0.5347(6)	0.2652(9)	2.4(4)
C(5)	−0.451(1)	0.6231(8)	−0.260(1)	4.1(5)
C(6)	0.294(1)	0.1872(7)	0.379(1)	3.7(4)
C(7)	0.272(1)	0.1280(7)	0.226(1)	4.1(4)
C(8)	0.195(1)	0.2047(7)	0.139(1)	3.8(4)
C(9)	0.364(1)	0.1499(8)	0.522(1)	5.9(5)
C(10)	0.142(1)	0.1844(8)	−0.032(1)	5.9(6)
C(11)	0.210(1)	0.6966(8)	0.404(1)	3.7(5)
C(12)	0.195(1)	0.7847(7)	0.533(1)	3.8(4)
C(13)	0.137(1)	0.7504(7)	0.602(1)	3.3(4)
C(14)	0.272(1)	0.6944(9)	0.293(1)	5.7(6)
C(15)	0.098(1)	0.8072(8)	0.745(1)	4.7(5)
		[Cu(4-Br-3-CO$_2$mepz)(4-BrdmpzH)$_2$]$_2$, **3*b***		
Br(1)	0.12087(5)	0.04038(7)	0.31126(4)	6.04(4)
Br(2)	0.15218(7)	−0.26714(6)	0.13097(5)	6.74(5)
Br(3)	0.35093(8)	0.36699(5)	0.04390(5)	6.76(5)
Cu(1)	0.45172(6)	0.01057(6)	0.15358(4)	2.90(3)
O(1)	0.4641(3)	−0.0130(2)	0.4172(2)	2.9(2)
O(2)	0.3085(3)	0.0049(3)	0.4401(2)	3.5(2)
N(1)	0.4128(3)	0.0186(3)	0.2903(2)	2.7(2)
N(2)	0.3725(3)	0.0321(3)	0.2255(2)	2.9(2)
N(3)	0.3553(4)	−0.0858(3)	0.1171(2)	3.5(2)
N(4)	0.2996(4)	−0.0821(3)	0.0562(2)	3.7(2)
N(5)	0.4200(4)	0.1292(3)	0.0969(2)	3.2(2)
N(6)	0.4307(4)	0.1295(3)	0.0308(2)	3.2(2)
C(1)	0.3402(4)	0.0189(4)	0.3286(3)	2.9(2)
C(2)	0.2495(4)	0.0322(4)	0.2882(3)	3.2(2)
C(3)	0.2721(4)	0.0408(4)	0.2235(3)	3.3(3)
C(4)	0.3163(5)	−0.1462(4)	0.1505(3)	3.7(3)
C(5)	0.2346(5)	−0.1799(4)	0.1088(3)	4.2(3)
C(6)	0.2246(5)	−0.1387(4)	0.0501(3)	3.8(3)
C(7)	0.3929(5)	0.2075(4)	0.1100(3)	3.4(3)
C(8)	0.3867(5)	0.2544(4)	0.0517(3)	3.9(3)
C(9)	0.4103(5)	0.2035(4)	0.0021(3)	3.4(3)
C(10)	0.3704(4)	0.0030(4)	0.4010(3)	2.7(2)
C(11)	0.2023(5)	0.0556(5)	0.1601(3)	4.4(3)
C(12)	0.3560(6)	−0.1724(5)	0.2198(4)	5.6(4)
C(13)	0.1507(6)	−0.1481(6)	−0.0119(4)	6.0(4)
C(14)	0.3769(6)	0.2346(5)	0.1781(4)	5.4(4)
C(15)	0.4145(6)	0.2190(5)	−0.0702(4)	5.2(4)

[a] $B_{eq} = (8/3)\pi^2\Sigma\Sigma U_{ij} a_i * a_j * (a_i \cdot a_j)$.

the corresponding values for [Cu(3,5-dmpz)]$_3$ (1.852 Å, 3.218 Å, and 174.6°). The intermolecular Cu ... Cu distance of 3.069(1) Å in **1** is significantly longer than the corresponding mean value of 2.946 Å observed for the 3,5-dimethylpyrazolate derivative (10). The copper atom not involved in the weak Cu ... Cu interactions (Cu(1)) lies 3.281 Å from the mean plane of the tmpz ring at the opposite end of the inversion-related trimer; the distance is only slightly longer than the corresponding mean distance of 3.272 Å in [Cu(3,5-dmpz)]$_3$. The difference between the weak metal–metal interactions in [Cu(3,5-dmpz)]$_3$ and **1**, as well as the slightly greater deviation of the central nine-membered Cu_3N_6 ring from planarity (0.129 vs. 0.07 Å) in the present structure, probably results from differences in the crystal packing. The mean N—N distance of

TABLE 3. Bond lengths (Å) with estimated standard deviations[a]

Atom	Atom	Distance	Atom	Atom	Distance
		[Cu(tmpz)]$_3$, **1**			
Cu(1)	N(1)	1.854(4)	C(1)	C(2)	1.379(8)
Cu(1)	N(6)	1.855(4)	C(1)	C(10)	1.496(8)
Cu(2)	N(2)	1.855(4)	C(2)	C(3)	1.373(7)
Cu(2)	N(3)	1.852(4)	C(2)	C(11)	1.508(8)
Cu(2)	Cu(3)*	3.069(1)	C(3)	C(12)	1.495(7)
Cu(3)	N(4)	1.848(4)	C(4)	C(5)	1.393(7)
Cu(3)	N(5)	1.853(5)	C(4)	C(13)	1.490(7)
N(1)	N(2)	1.367(6)	C(5)	C(6)	1.392(7)
N(1)	C(1)	1.335(7)	C(5)	C(14)	1.495(7)
N(2)	C(3)	1.348(6)	C(6)	C(15)	1.490(8)
N(3)	N(4)	1.382(6)	C(7)	C(8)	1.380(7)
N(3)	C(4)	1.338(6)	C(7)	C(16)	1.498(8)
N(4)	C(6)	1.336(6)	C(8)	C(9)	1.382(7)
N(5)	N(6)	1.377(6)	C(8)	C(17)	1.498(8)
N(5)	C(7)	1.344(6)	C(9)	C(18)	1.508(8)
N(6)	C(9)	1.339(6)			
		[Cu(3-CO_2dmpz)(tmpzH)]$_2$Cu, **2**			
Cu(1)	O(1)	1.978(5)	N(4)	C(6)	1.340(9)
Cu(1)	N(1)	1.889(5)	C(1)	C(2)	1.392(9)
Cu(2)	N(2)	1.860(6)	C(1)	C(7)	1.50(1)
Cu(2)	N(3)	1.869(6)	C(2)	C(3)	1.38(1)
Cu(2)	O(1)*	2.638(5)	C(2)	C(8)	1.51(1)
O(1)	C(7)	1.281(9)	C(3)	C(9)	1.50(1)
O(2)	C(7)	1.230(8)	C(4)	C(5)	1.39(1)
N(1)	N(2)	1.364(8)	C(4)	C(10)	1.48(1)
N(1)	C(1)	1.332(9)	C(5)	C(6)	1.36(1)
N(2)	C(3)	1.374(8)	C(5)	C(11)	1.50(1)
N(3)	N(4)	1.355(8)	C(6)	C(12)	1.51(1)
N(3)	C(4)	1.350(9)			
		[Cu(4-Br-3-CO_2mepz)(4-BrdmpzH)$_2$]$_2$, ***3a***			
Br(1)	C(2)	1.884(8)	N(5)	N(6)	1.352(8)
Br(2)	C(7)	1.864(8)	N(5)	C(11)	1.33(1)
Br(3)	C(12)	1.870(9)	N(6)	C(13)	1.34(1)
Cu(1)	O(1)	1.992(5)	C(1)	C(2)	1.39(1)
Cu(1)	N(1)	1.999(6)	C(1)	C(4)	1.48(1)
Cu(1)	N(2)*	1.947(6)	C(2)	C(3)	1.36(1)
Cu(1)	N(3)	2.027(6)	C(3)	C(5)	1.50(1)
Cu(1)	N(5)	2.273(7)	C(6)	C(7)	1.38(1)
O(1)	C(4)	1.271(9)	C(6)	C(9)	1.47(1)
O(2)	C(4)	1.244(9)	C(7)	C(8)	1.38(1)
N(1)	N(2)	1.365(8)	C(8)	C(10)	1.49(1)
N(1)	C(1)	1.34(1)	C(11)	C(12)	1.40(1)
N(2)	C(3)	1.36(1)	C(11)	C(14)	1.50(1)
N(3)	N(4)	1.355(8)	C(12)	C(13)	1.34(1)
N(3)	C(8)	1.34(1)	C(13)	C(15)	1.50(1)
N(4)	C(6)	1.35(1)			
		[Cu(4-Br-3-CO_2mepz)(4-BrdmpzH)$_2$]$_2$, ***3b***			
Br(1)	C(2)	1.861(6)	N(5)	N(6)	1.361(6)
Br(2)	C(5)	1.876(6)	N(5)	C(7)	1.342(7)
Br(3)	C(8)	1.866(7)	N(6)	C(9)	1.331(7)
Cu(1)	O(1)′	1.982(4)	C(1)	C(2)	1.386(7)
Cu(1)	N(1)′	2.011(4)	C(1)	C(10)	1.482(7)
Cu(1)	N(2)	1.949(5)	C(2)	C(3)	1.390(8)
Cu(1)	N(3)	2.083(5)	C(3)	C(11)	1.495(8)
Cu(1)	N(5)	2.226(5)	C(4)	C(5)	1.396(8)
O(1)	C(10)	1.283(6)	C(4)	C(12)	1.48(1)
O(2)	C(10)	1.226(7)	C(5)	C(6)	1.346(9)
N(1)	N(2)	1.360(6)	C(6)	C(13)	1.491(9)
N(1)	C(1)	1.331(7)	C(7)	C(8)	1.386(9)
N(2)	C(3)	1.354(7)	C(7)	C(14)	1.486(9)
N(3)	N(4)	1.347(6)	C(8)	C(9)	1.362(9)
N(3)	C(4)	1.330(8)	C(9)	C(15)	1.489(9)
N(4)	C(6)	1.350(7)			

[a]Here and elsewhere, * denotes symmetry operation $1 - x, 1 - y, 1 - z$ for **1** and **2**; $-x, 1 - y, -z$ for ***3a***; and ′ denotes symmetry operation $1 - x, y, 1/2 - z$ for ***3b***.

1.375 Å in **1** is shorter than the value of 1.383 Å reported for [Cu(3,5-dmpz)]$_3$, but longer than that of 1.355(8) Å found for the terminal tmpzH ligand in **2** (see Table 3). This may reflect significant Cu($d\pi$)–tmpz(π^*) interaction as discussed previously (10).

The centrosymmetric, trinuclear, mixed-valence Cu(I)/Cu(II) complex **2** is shown in Fig. 3. The entire molecule, apart from the hydrogen atoms, is planar to within 0.2 Å. The molecules stack in the solid state (Fig. 4), the shortest intermolecular distance being Cu(2) ... O(1)(x, y, $z - 1$) = 3.145(6) Å. The 3-CO_2dmpz ligands in **2** chelate the central copper(II) atom (Cu(1)) via the carboxylate oxygen atom O(1) and the adjacent ring nitrogen atom and also form bridges between Cu(1) and both of the copper(I) atoms (Cu(2) and Cu(2)*), one via a pyrazolate -N—N- bridge and the other via a single-atom bridge involving O(1). This latter bridge involves a very weak copper–oxygen interaction in which the distance involved (Cu(2)—O(1) = 2.638(5) Å) is long for a normal bond between copper(I) and oxygen but is significantly shorter than the sum of the van der Waals radii (2.95 Å (11)). The second oxygen atom of the carboxylate group, O(2), is not involved in coordination to the metal atoms but contributes to the stability of the complex by hydrogen-bonding to the NH proton of the terminal monodentate tmpzH ligand coordinated to Cu(2) (N(4)—H(1) ... O(2)*, H ... O = 1.88 Å, N ... O = 2.859(8) Å).

The central copper(II) atom, Cu(1), has *trans* square-planar coordination geometry with Cu—O = 1.978(5) Å, Cu—N = 1.889(5) Å, and the O–Cu–N bond angle within the five-membered chelate ring is 83.0(2)°. The copper(I) atom, Cu(2), has a T-shaped coordination geometry featuring a nearly linear N–Cu–N unit with strong Cu—N bonds (Cu—N = 1.860(6) and 1.869(6) Å, N–Cu–N = 173.8(3)°) perpendicular to the very weak Cu—O bond involving the asymmetrically bridging carboxylate oxygen atom, O(1) (Cu—O = 2.638(5) Å, N—Cu—O = 90.8(2) and 93.5(2)°). The mean Cu(2)—N bond distance of 1.865(5) Å in **2** is slightly longer than the corresponding mean copper(I)—N bond lengths of 1.853 Å in **1** and 1.852 Å in [Cu(3,5-dmpz)]$_3$ (10). The N—N distances in both of the pyrazole rings (N(1)—N(2) = 1.369(8) and N(3)—N(4) = 1.355(8) Å) are consistent with a weaker Cu–N interaction than is observed in the copper(I) trimers (mean N—N = 1.375 Å in **1**, 1.383 Å in [Cu(3,5-dmpz)]$_3$ (10)).

As described in the experimental section, while it was possible to isolate manually a few crystals of **2** from the mixture of **1** and **2**, the very small size of the crystals made it impractical to obtain a bulk sample of pure **2** by this means. Nonetheless, since **1** is EPR silent it was possible to obtain EPR spectra of **2** employing the mixture ground to a fine

Can. J. Chem. Downloaded from www.nrcresearchpress.com by 109.225.110.28 on 09/08/12
For personal use only.

Can. J. Chem. Downloaded from www.nrcresearchpress.com by 109.225.110.28 on 09/08/12
For personal use only.

TABLE 4. Bond angles (deg) with estimated standard deviations

Atom	Atom	Atom	Angle	Atom	Atom	Atom	Angle
			[Cu(tmpz)]$_3$, **1**				
N(1)	Cu(1)	N(6)	174.6(2)	N(1)	C(1)	C(10)	120.6(5)
N(2)	Cu(2)	N(3)	173.9(2)	C(2)	C(1)	C(10)	129.1(5)
N(2)	Cu(2)	Cu(3)*	97.0(1)	C(1)	C(2)	C(3)	104.5(5)
N(3)	Cu(2)	Cu(3)*	89.0(1)	C(1)	C(2)	C(11)	128.2(6)
N(4)	Cu(3)	N(5)	174.7(2)	C(3)	C(2)	C(11)	127.3(6)
N(4)	Cu(3)	Cu(2)*	86.9(1)	N(2)	C(3)	C(2)	110.0(5)
N(6)	Cu(3)	Cu(2)*	98.8(1)	N(2)	C(3)	C(12)	121.4(5)
Cu(1)	N(1)	N(2)	119.5(4)	C(2)	C(3)	C(12)	128.6(5)
Cu(1)	N(1)	C(1)	132.8(4)	N(3)	C(4)	C(5)	109.6(5)
N(2)	N(1)	C(1)	107.7(4)	N(3)	C(4)	C(13)	121.0(5)
Cu(2)	N(2)	N(1)	118.2(3)	C(5)	C(4)	C(13)	129.4(5)
Cu(2)	N(2)	C(3)	134.4(4)	C(4)	C(5)	C(6)	104.8(5)
N(1)	N(2)	C(3)	107.4(4)	C(4)	C(5)	C(14)	127.3(5)
Cu(2)	N(3)	N(4)	121.4(4)	C(6)	C(5)	C(14)	127.9(5)
Cu(2)	N(3)	C(4)	130.6(4)	N(4)	C(6)	C(5)	109.8(5)
N(4)	N(3)	C(4)	108.0(4)	N(4)	C(6)	C(15)	121.0(5)
Cu(3)	N(4)	N(3)	120.0(4)	C(5)	C(6)	C(15)	129.2(5)
Cu(3)	N(4)	C(6)	132.1(4)	N(5)	C(7)	C(8)	109.8(5)
N(3)	N(4)	C(6)	107.9(4)	N(5)	C(7)	C(16)	120.2(5)
Cu(3)	N(5)	N(6)	118.2(3)	C(8)	C(7)	C(16)	130.0(5)
Cu(3)	N(5)	C(7)	134.2(4)	C(7)	C(8)	C(9)	105.2(5)
N(6)	N(5)	C(7)	107.4(4)	C(7)	C(8)	C(17)	127.5(5)
Cu(1)	N(6)	N(5)	120.9(3)	C(9)	C(8)	C(17)	127.3(6)
Cu(1)	N(6)	C(9)	131.1(4)	N(6)	C(9)	C(8)	109.6(5)
N(5)	N(6)	C(9)	108.0(4)	N(6)	C(9)	C(18)	120.6(5)
N(1)	C(1)	C(2)	110.3(5)	C(8)	C(9)	C(18)	129.8(5)
			[Cu(3-CO_2dmpz)(tmpzH)]$_2$Cu, **2**				
O(1)	Cu(1)	O(1)*	180.00	N(1)	C(1)	C(7)	113.4(6)
O(1)	Cu(1)	N(1)	83.0(2)	C(2)	C(1)	C(7)	137.1(7)
O(1)	Cu(1)	N(1)*	97.0(2)	C(1)	C(2)	C(3)	104.6(6)
N(1)	Cu(1)	N(1)*	180.00	C(1)	C(2)	C(8)	129.2(7)
N(2)	Cu(2)	N(3)	173.8(3)	C(3)	C(2)	C(8)	126.2(6)
N(2)	Cu(2)	O(1)*	90.8(2)	N(2)	C(3)	C(2)	110.0(6)
N(3)	Cu(2)	O(1)*	93.5(2)	N(2)	C(3)	C(9)	119.4(7)
Cu(1)	O(1)	C(7)	113.5(5)	C(2)	C(3)	C(9)	130.6(7)
C(7)	O(1)	Cu(2)*	146.1(5)	N(3)	C(4)	C(5)	110.5(6)
Cu(1)	O(1)	Cu(2)*	100.0(2)	N(3)	C(4)	C(10)	121.1(7)
Cu(1)	N(1)	N(2)	134.9(5)	C(5)	C(4)	C(10)	128.3(7)
Cu(1)	N(1)	C(1)	115.2(5)	C(4)	C(5)	C(6)	105.3(6)
N(2)	N(1)	C(1)	109.8(6)	C(4)	C(5)	C(11)	126.5(7)
Cu(2)	N(2)	N(1)	117.2(4)	C(6)	C(5)	C(11)	128.2(7)
Cu(2)	N(2)	C(3)	136.8(5)	N(4)	C(6)	C(5)	108.0(6)
N(1)	N(2)	C(3)	106.0(6)	N(4)	C(6)	C(12)	120.9(7)
Cu(2)	N(3)	N(4)	123.8(5)	C(5)	C(6)	C(12)	131.0(7)
Cu(2)	N(3)	C(4)	131.3(5)	O(1)	C(7)	O(2)	125.0(8)
N(4)	N(3)	C(4)	104.9(6)	O(1)	C(7)	C(1)	114.6(7)
N(3)	N(4)	C(6)	111.2(6)	O(2)	C(7)	C(1)	120.4(7)
N(1)	C(1)	C(2)	109.5(6)				
			[Cu(4-Br-3-CO_2mepz)(4-BrdmpzH)$_2$]$_2$, **3***a*				
O(1)	Cu(1)	N(1)	81.6(2)	Br(1)	C(2)	C(1)	127.7(6)
O(1)	Cu(1)	N(2)*	179.0(3)	Br(1)	C(2)	C(3)	124.7(6)
O(1)	Cu(1)	N(3)	87.0(2)	C(1)	C(2)	C(3)	107.5(7)
O(1)	Cu(1)	N(5)	84.7(2)	N(2)	C(3)	C(2)	107.8(7)
N(1)	Cu(1)	N(2)*	98.6(2)	N(2)	C(3)	C(5)	123.9(7)
N(1)	Cu(1)	N(3)	136.5(3)	C(2)	C(3)	C(5)	128.2(8)
N(1)	Cu(1)	N(5)	104.5(2)	O(1)	C(4)	O(2)	124.3(7)
N(2)*	Cu(1)	N(3)	92.2(3)	O(1)	C(4)	C(1)	115.6(7)
N(2)*	Cu(1)	N(5)	96.2(3)	O(2)	C(4)	C(1)	120.0(8)
N(3)	Cu(1)	N(5)	116.2(3)	N(4)	C(6)	C(7)	104.8(7)
Cu(1)	O(1)	C(4)	114.4(5)	N(4)	C(6)	C(9)	123.3(8)

TABLE 4 (*concluded*)

Atom	Atom	Atom	Angle	Atom	Atom	Atom	Angle
Cu(1)	N(1)	N(2)	139.4(5)	C(7)	C(6)	C(9)	131.8(8)
Cu(1)	N(1)	C(1)	111.8(5)	Br(2)	C(7)	C(6)	125.1(7)
N(2)	N(1)	C(1)	108.6(6)	Br(2)	C(7)	C(8)	127.2(7)
Cu(1)*	N(2)	N(1)	121.5(5)	C(6)	C(7)	C(8)	107.7(7)
Cu(1)*	N(2)	C(3)	130.1(5)	N(3)	C(8)	C(7)	109.2(7)
N(1)	N(2)	C(3)	108.1(6)	N(3)	C(8)	C(10)	121.6(8)
Cu(1)	N(3)	N(4)	120.7(5)	C(7)	C(8)	C(10)	129.2(8)
Cu(1)	N(3)	C(8)	133.4(6)	N(5)	C(11)	C(12)	108.7(8)
N(4)	N(3)	C(8)	105.9(6)	N(5)	C(11)	C(14)	124.1(8)
N(3)	N(4)	C(6)	112.4(6)	C(12)	C(11)	C(14)	127.2(9)
Cu(1)	N(5)	N(6)	117.3(5)	Br(3)	C(12)	C(11)	126.5(7)
Cu(1)	N(5)	C(11)	134.1(6)	Br(3)	C(12)	C(13)	125.8(7)
N(6)	N(5)	C(11)	105.6(7)	C(11)	C(12)	C(13)	107.6(8)
N(5)	N(6)	C(13)	111.9(7)	N(6)	C(13)	C(12)	106.1(8)
N(1)	C(1)	C(2)	107.9(7)	N(6)	C(13)	C(15)	122.0(8)
N(1)	C(1)	C(4)	115.6(7)	C(12)	C(13)	C(15)	131.9(8)
C(2)	C(1)	C(4)	136.3(8)				
			[Cu(4-Br-3-CO_2mepz)(4-BrdmpzH)$_2$]$_2$, ***3b***				
O(1)′	Cu(1)	N(1)′	81.5(2)	Br(1)	C(2)	C(1)	129.7(5)
O(1)′	Cu(1)	N(2)	178.0(2)	Br(1)	C(2)	C(3)	124.3(4)
O(1)′	Cu(1)	N(3)	89.8(2)	C(1)	C(2)	C(3)	106.0(5)
O(1)′	Cu(1)	N(5)	83.1(2)	N(2)	C(3)	C(2)	108.2(5)
N(1)′	Cu(1)	N(2)	96.8(2)	N(2)	C(3)	C(11)	123.1(5)
N(1)′	Cu(1)	N(3)	135.8(2)	C(2)	C(3)	C(11)	128.6(5)
N(1)′	Cu(1)	N(5)	109.1(2)	N(3)	C(4)	C(5)	108.0(6)
N(2)	Cu(1)	N(3)	90.8(2)	N(3)	C(4)	C(12)	124.6(6)
N(2)	Cu(1)	N(5)	98.4(2)	C(5)	C(4)	C(12)	127.4(6)
N(3)	Cu(1)	N(5)	112.7(2)	Br(2)	C(5)	C(4)	125.9(5)
Cu(1)′	O(1)	C(10)	114.9(3)	Br(2)	C(5)	C(6)	125.8(5)
Cu(1)′	N(1)	N(2)	139.3(4)	C(4)	C(5)	C(6)	108.3(6)
Cu(1)′	N(1)	C(1)	110.9(4)	N(4)	C(6)	C(5)	105.6(5)
N(2)	N(1)	C(1)	109.4(4)	N(4)	C(6)	C(13)	123.1(6)
Cu(1)	N(2)	N(1)	120.1(3)	C(5)	C(6)	C(13)	131.3(6)
Cu(1)	N(2)	C(3)	130.2(4)	N(5)	C(7)	C(8)	109.0(6)
N(1)	N(2)	C(3)	107.8(4)	N(5)	C(7)	C(14)	122.2(6)
Cu(1)	N(3)	N(4)	121.9(4)	C(8)	C(7)	C(14)	128.8(6)
Cu(1)	N(3)	C(4)	129.1(4)	Br(3)	C(8)	C(7)	125.3(5)
N(4)	N(3)	C(4)	106.6(5)	Br(3)	C(8)	C(9)	126.8(5)
N(3)	N(4)	C(6)	111.5(5)	C(7)	C(8)	C(9)	107.9(6)
Cu(1)	N(5)	N(6)	117.8(4)	N(6)	C(9)	C(8)	105.5(6)
Cu(1)	N(5)	C(7)	137.2(4)	N(6)	C(9)	C(15)	122.7(6)
N(6)	N(5)	C(7)	104.9(5)	C(8)	C(9)	C(15)	131.8(6)
N(5)	N(6)	C(9)	112.7(5)	O(1)	C(10)	O(2)	125.1(5)
N(1)	C(1)	C(2)	108.6(5)	O(1)	C(10)	C(1)	114.1(5)
N(1)	C(1)	C(10)	116.7(5)	O(2)	C(10)	C(1)	120.8(5)
C(2)	C(1)	C(10)	134.7(6)				

powder. At room temperature, the spectrum shows two regions of absorption centred at $g_\parallel$ and $g_\perp$. Nuclear hyperfine splitting of $g_\parallel$ is observed with two of the four components resolved and the other two obscured by the $g_\perp$ absorption. There is no observable splitting of $g_\perp$. The EPR parameters, calculated to first order, are $g_\parallel = 2.202$, $g_\perp = 2.048$, and $|A_\parallel| = 132 \times 10^{-4}$ cm^{-1}. There is no significant change in the spectrum at 77 K. The two g-value spectrum is as expected for square-coplanar copper(II) with negligible exchange coupling (12). Exchange effects normally broaden the EPR spectra of copper(II) complexes in the solid state to an extent that hyperfine data are masked. The observation of hyperfine splitting of $g_\parallel$ in powdered samples is relatively rare; however, it has been observed previously, for example, in a number of tetrakis(pyridine) complexes of copper(II) (13).

4-Bromo-3,5-dimethylpyrazole reaction

Reaction of the copper metal shot with molten 4-BrdmpzH in air, with vigorous stirring, yields, over a 24 h period, a brown powder identified by elemental analysis to be largely [Cu(4-Brdmpz)$_2$]$_x$. One easily recognizable impurity in the brown powder is small amounts of a substance present as green prisms. By carrying out the reaction under conditions that lead to a slower rate of reaction (no stirring) the green crystals become the major product. The green crystals (two forms) were separated by hand from minor amounts of unidentified by-products. Subsequent characterization by X-ray diffraction revealed the crystals to have the dimeric

Can. J. Chem. Downloaded from www.nrcresearchpress.com by 109.225.110.28 on 09/08/12
For personal use only.

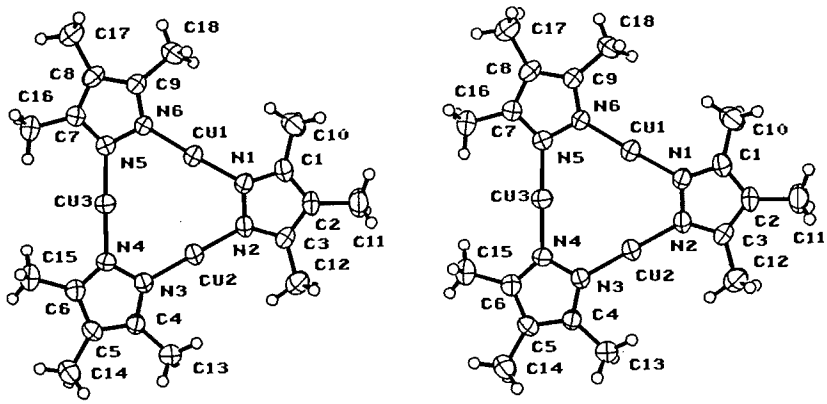

FIG. 1. Stereoview of **1**; 33% probability thermal ellipsoids are shown for the nonhydrogen atoms.

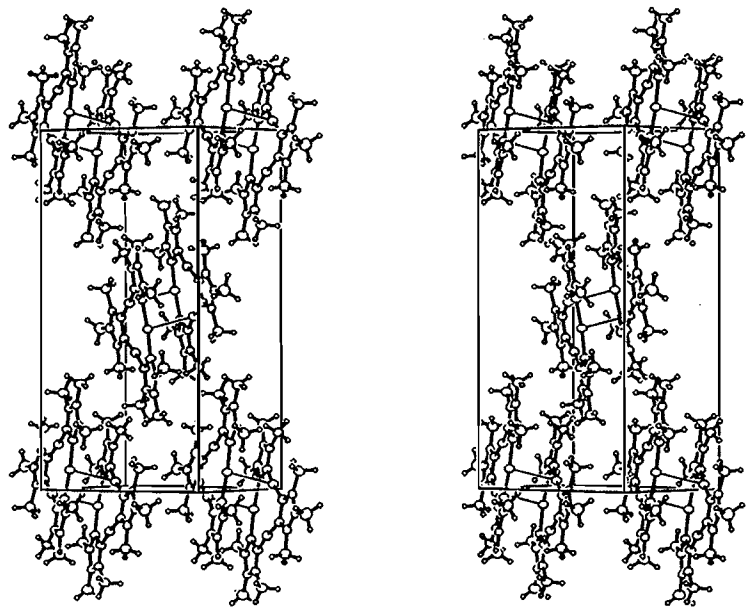

FIG. 2. Stereoview of the packing arrangement for **1**.

composition $[Cu(4\text{-Br-3-}CO_2\text{mepz})(4\text{-BrdmpzH})_2]_2$, **3**. Although the reaction conditions employed here were similar to those described above for the tmpzH reaction, no copper(I) species were seen to form in any significant amounts in this case.

Complex **3** (Fig. 5) is a binuclear copper(II) complex in which the 4-Br-3-CO_2mepz ligand is both bridging (Cu—N—N—Cu) and chelating (one carboxylate oxygen atom and the adjacent ring nitrogen atom). The molecule possesses crystallographic symmetry in both crystal forms: a centre of symmetry in the triclinic form **3***a* and a twofold axis in the monoclinic form **3***b*. The central Cu_2N_4 six-membered ring is exactly planar in **3***a* while in **3***b* it is nonplanar, having a N(2),N(2)′-boat conformation. The maximum deviation from the mean Cu_2N_4 plane in **3***b* is 0.330(5)Å for N(2).

The coordination geometry about the copper atoms in both **3***a* and **3***b* is axially compressed trigonal bipyramidal with the carboxylate oxygen atom and a nitrogen atom of the bridging 4-Br-3-CO_2mepz ligand occupying the axial positions. The equatorial ligand set comprises the chelating nitrogen atom of the 4-Br-3-CO_2mepz ligand and nitrogen atoms of the two terminal 4-BrdmpzH ligands. There is some distortion of the trigonal bipyramid towards a square-pyramidal geometry in which N(5) is apical. This may be responsible (along with steric factors) for the significant lengthening of the Cu—N(5) bond in both polymorphs of **3**. The axial bond lengths in **3***a* and **3***b* do not differ significantly (Cu—O = 1.992(5) and 1.982(4) Å, Cu—N = 1.947(6) and 1.949(5) Å, respectively for **3***a* and **3***b*). The three equatorial Cu—N distances in both **3***a* and **3***b* are significantly different from one another and, for the terminal 4-BrdmpzH ligands, the corresponding bond lengths in the two crystal forms also differ significantly (see Table 3). The average equatorial Cu—N distances in **3***a* and **3***b*, however, are nearly identical: 2.100 Å for **3***a* and 2.107 Å for **3***b*.

Even though the molecular symmetry is different in the two crystal forms of **3**, the hydrogen-bonding motifs are the same in **3***a* and **3***b*. In both crystalline modifications of this material the molecules are linked about crystallographic inversion centres by N—H ... O hydrogen bonds involving the N—H protons of the terminal 4-BrdmpzH ligands to form infinite chains extending along the crystallographic *c* axes

Can. J. Chem. Downloaded from www.nrcresearchpress.com by 109.225.110.28 on 09/08/12
For personal use only.

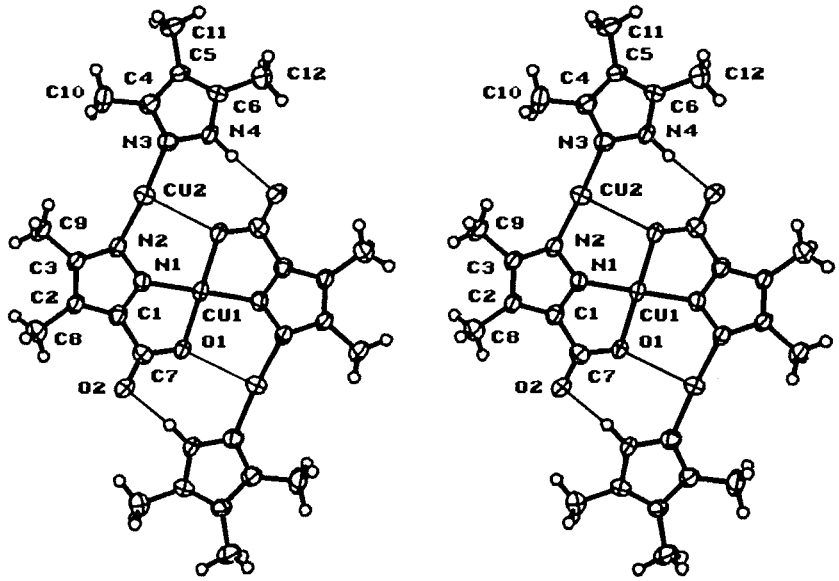

FIG. 3. Stereoview of **2**; 33% probability thermal ellipsoids are shown for the nonhydrogen atoms.

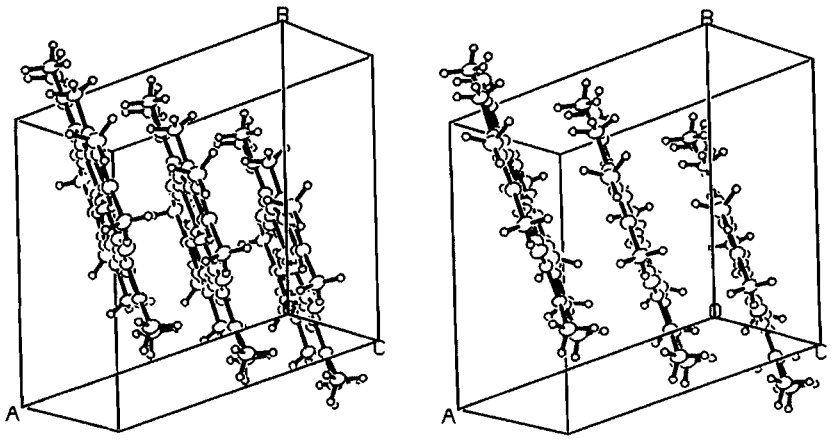

FIG. 4. Stereoview of the packing arrangement for **2**.

(Fig. 6). Each linkage involves two weak and two strong N—H ... O hydrogen bonds (Table 5). The strong hydrogen bonds involve the N(4) proton and the uncoordinated carboxylate oxygen atom, O(2). The weak hydrogen bonds are formed by the N(6) proton and the metal-coordinated oxygen atom, O(1), these atoms being involved in both intra- and intermolecular hydrogen bonds.

The physical characterization of **3**, including magnetic studies, was done on bulk samples composed mainly of crystals of the triclinic ***3a*** form but which contained small amounts, visually estimated at no more than 1%, of the monoclinic, ***3b***, form. The infrared spectrum of **3** was recorded and band frequencies have been deposited (see footnote 4). The compound exhibits thermochromism; it is bluish-green in color at 77 K.

DSC measurements on **3**, in air, show the onset of an endothermic event followed immediately by exothermic decomposition at ~250°C. To investigate the possibility that the endothermic event corresponds to loss of neutral 4-BrdmpzH, and to identify possible products of such a dissociation reaction, a sample of **3** was heated at 165°C under vacuum for 9 h. During the heating process, the compound changed color from green to olive-green and a white solid was seen to sublime from the sample. The white product was identified as 4-BrdmzH by melting point (117–118°C) and by ^{1}H NMR (δ 2.21 (s, 6, CH_3), 11.2 (br s, 1, NH)). The sample of **3** underwent a mass loss of 35% in the heating process, corresponding to the loss of 2.5 moles of 4-BrdmpzH per mole of compound. These observations are consistent with the formation of a compound of nominal composition Cu_4(4-Br-3-CO_2mepz)$_4$(4-BrdmpzH)$_3$. Anal. calcd. for $C_{35}H_{33}Br_7Cu_4N_{14}O_8$: C 26.42, H 2.09, N 12.32; found: C 26.11, H 2.28, N 12.41.

Magnetic susceptibility data for **3** over the temperature range 2–300 K have been deposited (footnote 4) and are shown as a plot versus temperature (20–300 K) in Fig. 7. The susceptibility passes through a broad maximum at 130 K, typical for two antiferromagnetically coupled copper centres. As is common in such systems the susceptibility rises with decreasing temperature at the lowest temperatures studied due to paramagnetic impurity. The magnetic susceptibilities (2–300 K) were fitted to the theoretical expression given by

Can. J. Chem. Downloaded from www.nrcresearchpress.com by 109.225.110.28 on 09/08/12
For personal use only.

Can. J. Chem. Downloaded from www.nrcresearchpress.com by 109.225.110.28 on 09/08/12
For personal use only.

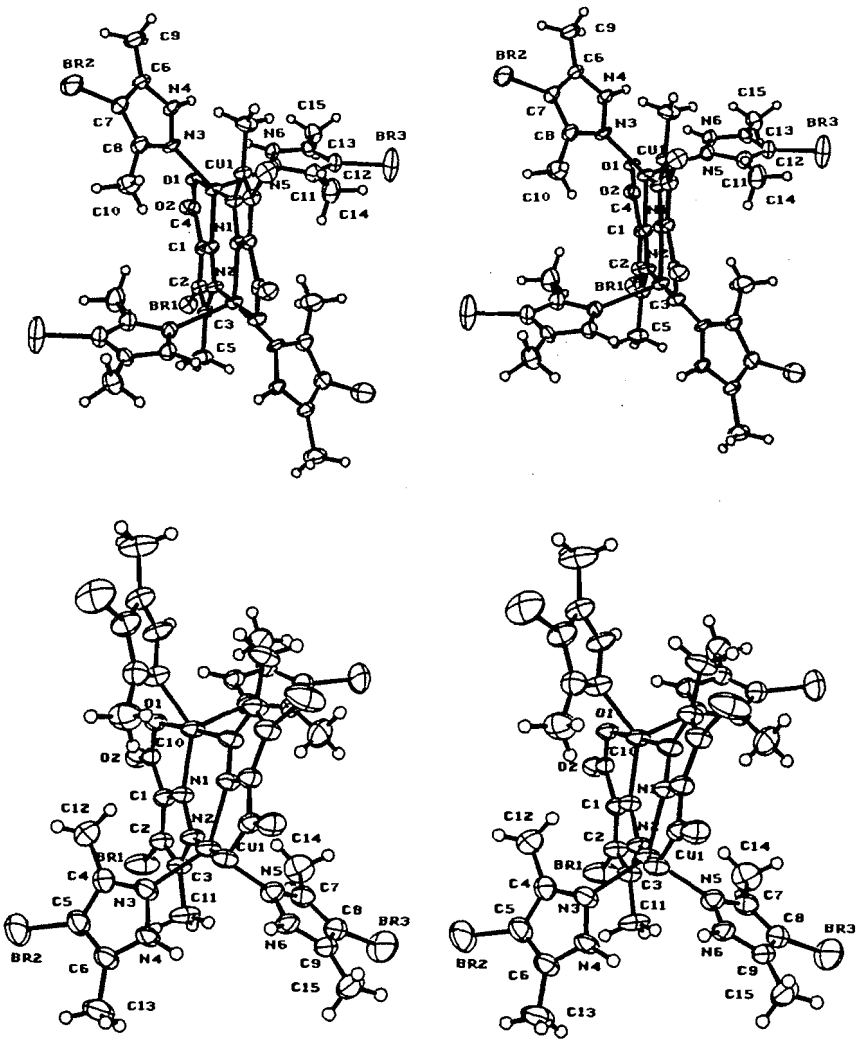

FIG. 5. Stereoviews of **3***a* (top) and **3***b* (bottom); 33% probability thermal ellipsoids are shown for the nonhydrogen atoms.

Bleaney and Bowers for antiferromagnetic dimeric copper(II) systems (14) with allowance made for a paramagnetic component. Allowing for the paramagnetic component, $\%P$, by modelling it as a Curie paramagnet with a g-value equal to that of the bulk sample gives the equation:

$$\chi = \frac{Ng^2\mu_B^2}{kT}\left[[1 - P]\left[\frac{e^{2J/kT}}{1 + 3e^{2J/kT}}\right] + \frac{P}{4}\right]$$

where J is the exchange coupling constant. This modelling procedure gives best fit values of J, g, and $\%P$ of $-74.0(6)$ cm^{-1}, 2.11(1), and 5.15(7) respectively with the fitting function $F = 0.029$. The function F:

$$F = \left[\frac{1}{n}\sum_{i=1}^{n}\frac{[\chi_i^{obs} - \chi_i^{calc}]^2}{[\chi_i^{obs}]^2}\right]^{1/2}$$

is minimized in the fitting procedure and provides a measure of the agreement between the experimental data and the model. A better fit is obtained if the paramagnetic component is modelled as a Curie–Weiss paramagnet. This fit, which is shown in Fig. 7, gives values of J, g, $\%P$, and Weiss constant, θ, of $-75.4(1)$ cm^{-1}, 2.123(2), 5.59(2), and $-0.46(2)$ K respectively ($F = 0.0061$). These parameters are considered valid for the triclinic form, **3***a*. Because of their similar molecular structures, particularly in terms of bond lengths and angles associated with the bridging atoms (Tables 3 and 4), **3***a* and **3***b* are unlikely to have very different magnetic properties. Hence, we would not expect the presence of ~1% **3***b* in the sample to result in experimental susceptibilities that are measurably different from those of pure **3***a*.

Previous studies on nine binary copper(II) pyrazolates that have extended chain structures and four-coordinate CuN_4 metal centres reveal antiferromagnetic exchange with values of $J = -58$ to -105 cm^{-1} (2, 3). Interestingly, in spite of the fact that **3** is dimeric and has five-coordinate metal centres, the magnitude of the exchange between the metal centres is not greatly different from that observed in the polymers. A more useful comparison might be made between **3** and other copper binuclear complexes containing the bridging pyrazolate moiety.

To our knowledge, except for the pyrazolate chain compounds (1, 2), there is no previous report of a structurally and magnetically characterized, purely pyrazolate-bridged polynuclear copper(II) complex. However, there are reports of copper(II) pyrazolate-bridged complexes that contain another bridging ligand. Mazurek *et al.* (4), Nishida and

Can. J. Chem. Downloaded from www.nrcresearchpress.com by 109.225.110.28 on 09/08/12
For personal use only.

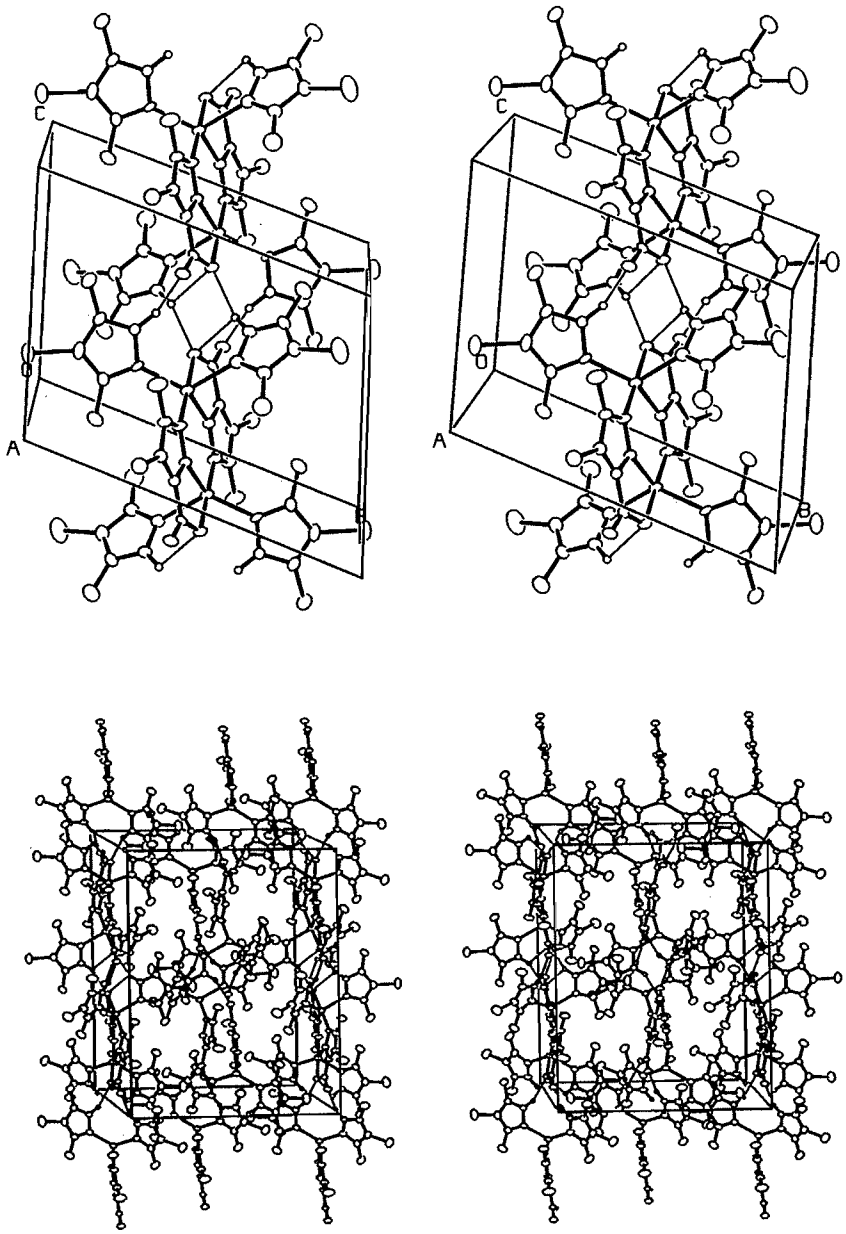

FIG. 6. Stereoviews of the packing arrangement for **3***a* (top) and **3***b* (bottom).

TABLE 5. Hydrogen bond geometry for compound **3**

Interaction	N—H, Å	H···O, Å	N···O, Å	N—H···O, °
		3*a*		
N(4)—H(1)···O(2)($-x$, $1-y$, $1-z$)	0.98	1.77	2.713(8)	160
N(6)—H(2)···O(1)($-x$, $1-y$, $1-z$)	0.98	2.21	3.124(8)	154
N(6)—H(2)···O(1)	0.98	2.32	2.824(9)	111
		3*b*		
N(4)—H(1)···O(2)(x, $-y$, $z-1/2$)	0.98	1.73	2.666(6)	158
N(6)—H(2)···O(1)(x, $-y$, $z-1/2$)	0.98	2.14	3.038(6)	152
N(6)—H(2)···O(1)	0.98	2.32	2.808(6)	110

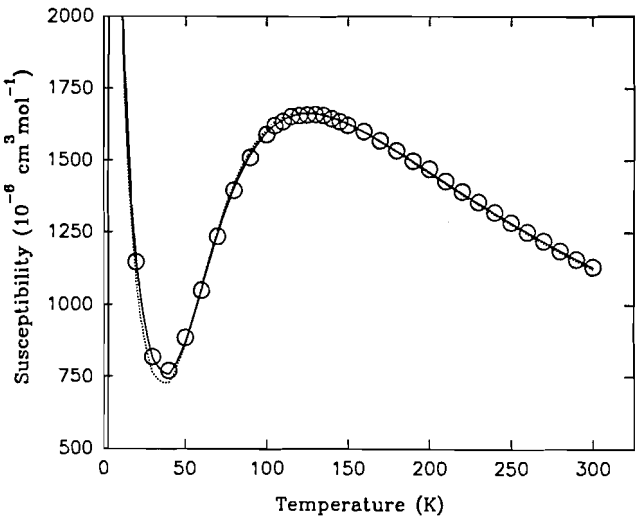

FIG. 7. Plot of magnetic susceptibility (per mole copper) versus temperature for **3**. Lines are calculated as described in the text employing the Bleany–Bowers equation with a Curie law paramagnetic impurity term (dotted line) and a Curie–Weiss law paramagnetic impurity term (solid line).

Kida (5), and Doman *et al.* (6) have reported on a series of pyrazolate-bridged, Schiff-base, square-planar copper(II) dinuclear species where the Schiff base is derived from a diamino straight-chain alcohol backbone and salicylaldehyde. In these complexes the copper(II) ions are also bridged by an alkoxide group. The *J*-values in these complexes range from -120 to -297.5 cm^{-1}. It must be recognized that the alkoxide bridge is very effective in propagating magnetic exchange and is likely to provide an important exchange pathway in these complexes making direct comparisons of their *J* values with that obtained for **3** inappropriate. The binuclear complex $[Cu(L\text{-}S)(pz)(CH_3OH)]_2$ (L-S = 2,6-bis-(4′-cyclohexyl-4′-hydroxy-2′,3′-diazabuta-1′,3′-dien-1′-yl)-4-methyl-thiophenolate) has been reported to be only weakly antiferromagnetic with $J = -1.8$ cm^{-1} (15). In addition to a pyrazolate bridge this compound has a bridging thiophenolate ligand and it seems likely that the latter is having a significant effect on the exchange.

Perhaps the most appropriate comparisons to made with **3** are with the binuclear complexes reported by Ajo, Bencini, and Mani (7) and by Prins *et al.* (16). The former authors reported magnetic studies on the species $[(H_2B(pz)_2)Cu(pz)_2(X)Cu(H_2B(pz)_2)]^-$ (pz = pyrazolate and X = Br, Cl) where square-pyramidally coordinated copper(II) ions are triply bridged by two pyrazolate ligands and one halide ion. *J*-values of -120.5 cm^{-1} and -122 cm^{-1} were found for the chloride and bromide complexes respectively.[5] The authors argue that because the exchange constants are insignificantly different for the bromide and chloride complexes the primary pathway for exchange must be the bridging pyrazolate ligands. Prins *et al.* reported studies on the related bis-triazolate-bridged $[Cu(bpt)(CF_3SO_3)(H_2O)]_2$ (bpt = bis-(pyridin-2-yl)−1,2,4-triazolate). In this complex, the copper(II) ions are present in distorted octahedral coordination environments and $J = -118$ cm^{-1}. The magnitude of the exchange coupling is virtually identical in these three complexes and is significantly greater that in **3**. Some or all of this difference in magnetic coupling may be accounted for by differences in the metal-ligand chromophores. In the previously studied complexes the coordination geometry is either square-pyramidal or tetragonally elongated octahedral with the $d_{x^2-y^2}$ orbital as the magnetic orbital and the bridging ligands bonded in the *xy* plane of each copper ion. In **3** the geometry is trigonal bipyramidal. The magnetic orbital is the d_{z^2} orbital and the pyrazolates bridge such that one nitrogen occupies an axial site on one copper while the other nitrogen occupies an equatorial site on the second copper. Since overlap of the magnetic d_{z^2} orbital with ligand orbitals in the *xy* plane is expected to be weaker than overlap with ligand orbitals on the *z* axis, the exchange pathway provided in this complex would not be expected to be very efficient and this could account for the weaker exchange coupling seen in **3**. Finally, it should be noted that several years ago Barraclough, Brookes, and Martin (17) reported the preparation and magnetic properties (92–280 K) of Cu(acac)(pz) (where acac = acetylacetonato). The compound was assumed to have a binuclear structure with square-coplanar copper ions, terminal acac ligands, and bridging pyrazolates. The exchange coupling was found to be significantly weaker ($J = -35$ cm^{-1}) than that reported here for **3**. The relatively weak exchange in the acac compound is somewhat surprising in view of the above discussion; however, the lack of a definitive structure for the compound and the lack of magnetic data to sufficiently low temperatures (no maximum in χ_m versus *T* was observed) prevents further analysis of these results other than to suggest that the previously proposed structure may be incorrect.

[5]The Hamiltonian used in ref. 7 has the form $-JS_1 \cdot S_2$ while the one here and in the other references quoted is of the form $-2JS_1 \cdot S_2$. Accordingly, for comparison purposes we have halved the *J* values reported in ref.7.

Acknowledgements

Funding for this project has been provided by the Natural Sciences and Engineering Research Council of Canada. We thank J. F. Carolan and W. N. Hardy, Department of Physics, U.B.C., for use of the SQUID magnetometer.

1. M. K. Ehlert, S. J. Rettig, A. Storr, R. C. Thompson, and J. Trotter. Can. J. Chem. **67**, 1970 (1989).
2. M. K. Ehlert, S. J. Rettig, A. Storr, R. C. Thompson, and J. Trotter. Can. J. Chem. **69**, 432 (1991).
3. M. K. Ehlert, A. Storr, and R. C. Thompson. Can. J. Chem. **70**, 1121 (1992).
4. W. Mazurek, B. J. Kennedy, K. S. Murray, M. J. O'Connor, J. R. Rogers, A. G. Wedd, and P. R. Zwack. Inorg. Chem. **24**, 3258 (1985).
5. Y. Nishida and S. Kida. Inorg. Chem. **27**, 447 (1988).
6. T. N. Doman, D. E. Williams, J. F. Banks, R. M. Buchanan, H. R. Chang, R. J. Webb, and D. N. Hendrickson. Inorg. Chem. **29**, 1058 (1990).
7. D. Ajo, A. Bencini, and F. Mani. Inorg. Chem. **27**, 2437 (1988).
8. J. S. Haynes, K. W. Oliver, and R. C. Thompson. Can. J. Chem. **63**, 1111 (1985).
9. International tables for X-ray crystallography, Vol. IV. Kynoch Press, Birmingham, U.K. (present distributor Kluwer Academic Publishers, Dordrecht, The Netherlands). 1974. pp. 99–102 and 149.
10. M. K. Ehlert, S. J. Rettig, A. Storr, R. C. Thompson and J. Trotter. Can. J. Chem. **68**, 1444 (1990).
11. A. Bondi. J. Phys. Chem. **68**, 441 (1964).

Can. J. Chem. Downloaded from www.nrcresearchpress.com by 109.225.110.28 on 09/08/12
For personal use only.

12. B. J. Hathaway and D. E. Billing. Coord. Chem. Rev. **5**, 143 (1970).
13. R. M. Morrison and R. C. Thompson. Can. J. Chem. **60**, 1048 (1982).
14. B. Bleaney and K. D. Bowers. Proc. R. Soc. London, A: **266**, 95 (1952).
15. P. Iliopoulos, K. S. Murray, R. Robson, J. Wilson, and G. A. Williams. J. Chem. Soc. Dalton Trans. 1585 (1987).
16. R. Prins, P. J. M. W. L. Birker, J. G. Haasnoot, G. C. Verschoor, and J. Reedijk. Inorg. Chem. **24**, 4128 (1985).
17. C. G. Barraclough, R. W. Brookes, and R. L. Martin. Aust. J. Chem. **27**, 1843 (1974).

Can. J. Chem. Downloaded from www.nrcresearchpress.com by 109.225.110.28 on 09/08/12
For personal use only.

Polyphenol interactions. The copigmentation case: thermodynamic data from temperature variation and relaxation kinetics. Medium effect

OLIVIER DANGLES AND RAYMOND BROUILLARD[1]

Laboratoire de chimie des polyphénols (Unité de recherche associée 31 du Centre national de la recherche scientifique), Université Louis Pasteur, Institut de chimie, 1, rue Blaise Pascal, 67008 Strasbourg, France

Received January 29, 1992

OLIVIER DANGLES and RAYMOND BROUILLARD. Can. J. Chem. **70**, 2174 (1992).

Copigmentation of malvin (a common anthocyanic pigment) with a series of naturally occurring colourless organic molecules (copigments) has been investigated by UV–visible absorption. The temperature-dependence of the visible spectrum of the copigmented solutions yields the copigmentation enthalpy and entropy changes. The experiments are carried out at pH 3.5 (malvin flavylium cation copigmentation) and pH 5.5 (copigmentation of the malvin quinonoidal bases). Copigmentation appears to be clearly enthalpically driven (exothermic process with unfavourable entropy change) in the case of chlorogenic acid and (+)-catechin. Concerning caffeine and tryptophan, favourable entropy changes, probably arising from solvation effects, have been recorded. Similar experiments in water–ethanol binary solvents have shown that the dramatic weakening of copigmentation on cosolvent addition is essentially entropic in origin. Salt effects on copigmentation have been investigated as well. Most of the results are discussed with a view to pointing out the major contributions to the magnitude of the copigmentation. Finally, relaxation kinetic measurements on the malvin–rutin system give striking evidence of the strong slowing down that a good copigment causes to the anthocyanin fading process (hydration). From the decrease in the apparent first-order rate constant of hydration on copigment addition, a general method for a quick determination of the copigmentation stability constants is proposed.

OLIVIER DANGLES et RAYMOND BROUILLARD. Can. J. Chem. **70**, 2174 (1992).

La copigmentation de la malvine (un pigment anthocyanique courant) par une série de molécules organiques naturelles incolores (copigments) a été étudiée par spectroscopie d'absorption UV–visible. Les modifications spectrales des solutions copigmentées, produites par variation de température, donnent accès aux variations d'enthalpie et d'entropie de copigmentation. Les expériences sont conduites à pH 3,5 (copigmentation du cation flavylium de la malvine) et à pH 5,5 (copigmentation des bases quinoniques de la malvine). La copigmentation est un phénomène sous contrôle enthalpique (processus exothermique accompagné d'une variation d'entropie défavorable) dans le cas de l'acide chlorogénique et de la (+)-catéchine. En ce qui concerne la caféine et le tryptophane, des variations d'entropie favorables, provenant probablement de phénomènes de solvatation, ont été mesurées. Des expériences similaires avec des solvants binaires eau–éthanol ont montré que l'affaiblissement considérable de la copigmentation, produit par l'addition de cosolvant, est essentiellement d'origine entropique. Des effets de sel sur la copigmentation ont également été étudiés. La plupart des résultats sont discutés en vue de mettre en évidence les principales contributions à l'interaction de copigmentation. Enfin, des mesures de cinétique de relaxation sur le système malvine–rutine illustrent de manière frappante le fort ralentissement produit par un bon copigment sur le processus de décoloration du pigment (hydratation). Une méthode générale de détermination des constantes de stabilité de copigmentation est proposée à partir des variations de la constante cinétique apparente d'hydratation (premier ordre) en fonction de la concentration de copigment.

Introduction

Anthocyanins are natural pigments that are responsible for most of the red, blue, and purple colours displayed in flowers and fruits (1–4). Their natural medium, the vacuolar cell sap of flower epidermal tissues, for instance, is essentially aqueous. In nature, anthocyanin molecules are frequently found in association with generally colourless molecules named copigments (4–8) (essentially, polyphenols and flavonoids), which exert a determining influence on the resulting colour (on both shade and intensity). In fact, the pigment–copigment molecular interaction (copigmentation) is certainly one of the key phenomena accounting for colour expression and variation in flowers. When monitored by UV–visible absorption spectrometry, the copigmentation reaction consists in an increase in the visible band intensity for the pigment (hyperchromic effect) and frequently in a shift of this very band toward longer wavelengths (bathochromic effect) (9–12). As previously demonstrated (13), the relative hyperchromic shift at a given wavelength (close to that of the absorption maximum) is the true parameter accounting for the magnitude of the copigmentation from which the thermodynamic parameters of the copigmentation reaction can be estimated (13–17). For a given anthocyanic pigment and at fixed pH and temperature, it depends essentially on the copigment chemical structure. Many quite different compounds (in particular, naturally occurring and biologically active molecules) have been shown to be anthocyanin copigments (9). Moreover, under suitable conditions, the hyperchromic shift produced by a good copigment on the anthocyanin visible band is not only exceptionally large (13, 14) (probably one of the largest reported) but also extremely sensitive to any modification of the medium. For instance, strong cosolvent effects on the copigmentation reaction have been already reported (15).

In this work, using visible absorption measurements, we compare the enthalpic and entropic contributions for diverse pigment–copigment systems to the overall free enthalpy change of copigmentation and show how a typical modification of the medium, such as salt or cosolvent addition, alters these thermodynamic parameters. From these results, we try to discern the most important factors sustaining the pigment–copigment molecular interaction in order to outline some structural features common to what may be called *good copigments*. Finally, we apply relaxation kinetics to the study of the influence of the copigment on the rate of the apparent hydration process for anthocyanin and we use

[1]Author to whom correspondence may be addressed.

Can. J. Chem. Downloaded from www.nrcresearchpress.com by 109.225.110.28 on 09/08/12
For personal use only.

such observations to devise a simple new method for the determination of the copigmentation equilibrium constants. The pigment chosen is malvin (**1**) (malvidin-3,5-diglucoside), a very common and readily available anthocyanin. Copigments have been selected from important families of natural compounds frequently encountered in the plant kingdom. These are chlorogenic acid (**2**), a polyphenol; caffeine (**3**), the well-known purine; and two members of the flavonoid family, (+)-catechin (**4**), a proanthocyanidin or condensed tannin, and rutin (**5**), a flavonol. Amino acids, which up to now have been little investigated for their ability to act as copigments (9), are taken into consideration as well.

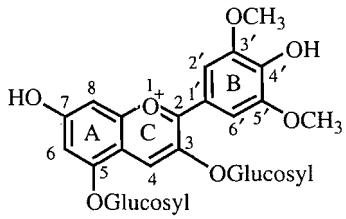

Malvin (**1**)

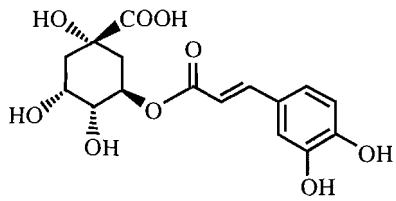

Chlorogenic acid (**2**)

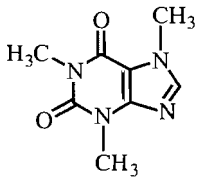

Caffeine (**3**)

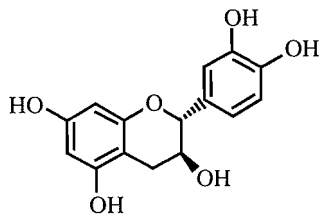

(+)-Catechin (**4**)

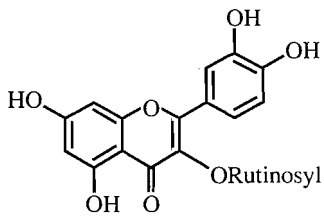

Rutin (**5**)

Experimental

Materials

Malvin chloride, chlorogenic acid, caffeine, (+)-catechin, and rutin were purchased from Roth. Their purity was checked by UV–vis and ^{1}H NMR spectroscopies. Tryptophan and its methylester (L-series) were provided by Fluka and used as such.

Absorption spectra

Spectra were recorded with a Hewlett–Packard diode-array spectrometer fitted with a quartz cell (d = 1 cm) equipped with a stirring magnet. A constant temperature in the cell was obtained by use of a Lauda water-thermostated bath; temperature measurements were made with a Comark thermocouple.

Thermodynamic measurements

Pigment and copigment titrated solutions are prepared by dissolving the compounds into a buffer (either 0.2 M acetic acid – 0.2 M sodium acetate or 0.1 M citric acid – 0.2 M Na_2HPO_4) whose pH has been adjusted to the desired value. In all experiments, the pigment concentration is held constant. The values of the copigmentation equilibrium constants K (at 25°C) are obtained by measuring the relative hyperchromic shift (at a given wavelength) either as a function of the overall concentration of the copigment, at a fixed pH, or as a function of pH at a fixed overall concentration of copigment. These procedures have already been published (13–15). ΔH^0 and ΔS^0 stem from a temperature variation on the pigment–copigment system at fixed pH and overall copigment concentration. Details are given in the discussion (see eq. [2]). In the study on cosolvent effects, the molar fraction of water in each binary solvent remains larger than 0.9 so that pH correction is not necessary.

Kinetic measurements

(i) Flavylium cation copigmentation

One millilitre of an equilibrated 4×10^{-4} M malvin solution in 0.025 M citric acid (pH about 2.3) is magnetically stirred in the spectrometer cell (T = 25°C); 1 mL of a freshly prepared rutin solution in 0.02 M NaOH at variable copigment concentration (usually ranging from 4×10^{-4} to 2×10^{-3} M) is quickly added to the cell and the visible spectra are immediately recorded, and again every 2 s. The final pH value is always close to 3.4.

(ii) Copigmentation of the quinonoidal bases

The above-described experiment is repeated starting with a 6×10^{-4} M malvin solution in 0.025 M citric acid. Rutin solutions are now prepared in 0.05 M NaOH. Visible spectra are recorded every 20 s just after adding the alkaline solution of rutin (concentrations from 6×10^{-4} to 3×10^{-3} M) to the cell. The final pH value is always close to 5.2.

In both types of experiment, the corresponding rate constant

Can. J. Chem. Downloaded from www.nrcresearchpress.com by 109.225.110.28 on 09/08/12
For personal use only.

Can. J. Chem. Downloaded from www.nrcresearchpress.com by 109.225.110.28 on 09/08/12
For personal use only.

reference values are gained by adding 1 mL of a NaOH solution without copigment to the initial malvin solution.

Results

Temperature variation experiments in water and binary solvents

Two typical temperature variation experiments on a malvin–copigment system are shown in Figs. 1 and 2. In both cases, the copigment is (+)-catechin. The visible spectra of the solution (at fixed pigment and copigment concentrations) are recorded for different temperatures at pH 3.5 (Fig. 1) and pH 5.5 (Fig. 2). At pH 3.5, a temperature increase from 10 to 30°C leads to a strong decrease in the malvin visible absorption in the presence of the copigment, whereas the corresponding changes in the absence of the copigment are negligible. Thus, the fading of the copigmented solution on increasing temperature is essentially attributable to the copigmentation process itself. Similar observations have already been reported on the malvin – chlorogenic acid and the cyanin – chlorogenic acid couples at pH close to 3.6 (13, 14). These observations remain valid at pH 5.5 (temperature range from 15 to 45°C), although the temperature-dependence of the visible absorption of malvin without copigment is no longer negligible in that case. Note, however, that a rise in temperature leads to opposite changes in the visible band of the pigment depending on whether or not the copigment is present. Thus, here again, copigmentation is responsible for the fading of the copigmented solution on increasing temperature. In fact, the increase in the pigment absorbance of the uncopigmented solution when the temperature is raised from 15 to 45°C is mainly due to thermal buffer effects that slightly alter the pH. However, the pH is the same for both copigmented and uncopigmented solutions at a given temperature, and the temperature-dependence of the pH is weak enough for the theoretical treatment to apply to this case (see eq. [1]). Similar experiments were carried out with other copigments, in particular, caffeine and tryptophan. Finally, some of the experiments were repeated after addition of given amounts of ethanol. Assuming the van't Hoff hypothesis, the temperature-independent ΔH^0 and ΔS^0 for the copigmentation reaction as well as the corresponding K value at 25°C were derived for the different copigments investigated. These parameters are listed in Tables 1 and 2. In Fig. 3 are shown the spectral changes in the visible range of a malvin copigmented solution on addition of increasing amounts of ethanol at fixed temperature and pH.

Salt effects

The influence on the visible spectrum of malvin of large additions of alkali halides to slightly acidic solutions of malvin without copigment are illustrated in Figs. 4 and 5. In Table 3 are listed the values at 25°C of the relative hyperchromic shift caused by caffeine addition to malvin under slightly acidic solutions at a given ionic strength fixed either by LiCl, KCl, or $MgCl_2$. In each case, the corresponding copigmentation equilibrium constant has been roughly estimated.

Relaxation kinetic measurements

Figures 6 and 7 show the time-dependence of the visible absorbance of malvin at a fixed wavelength just after mixing of the pigment and copigment solutions, for different copigment concentrations. The measurements reported in Fig. 6 deal with the flavylium cation (λ = 520 nm; final pH 3.4) whereas those reported in Fig. 7 deal with the quinonoidal bases (λ = 570 nm; final pH 5.2).

Discussion

Most of the results reported here must be discussed in the light of the structural transformations that anthocyanic pigments undergo in aqueous solution (18). First, depending on the pH of the medium, three distinct classes of visible light-absorbing species must be taken into consideration (see Scheme 1; Gl stands for glucosyl): these coloured forms are the flavylium cation AH^+ (usually red) and the forms deriving from successive deprotonations of AH^+ on increasing the pH, that is, the neutral quinonoidal bases A (two forms in tautomeric equilibrium, usually purple) and the ionized quinonoidal bases A^- (usually blue, not shown in the scheme). In the case of malvin, the corresponding pK_a values at 25°C (19) are about 4 for the AH^+/A acid–base couple and 7 for A/A^-. The pH values of the vacuolar cell sap from the coloured epidermal tissues of fresh flowers have been demon-

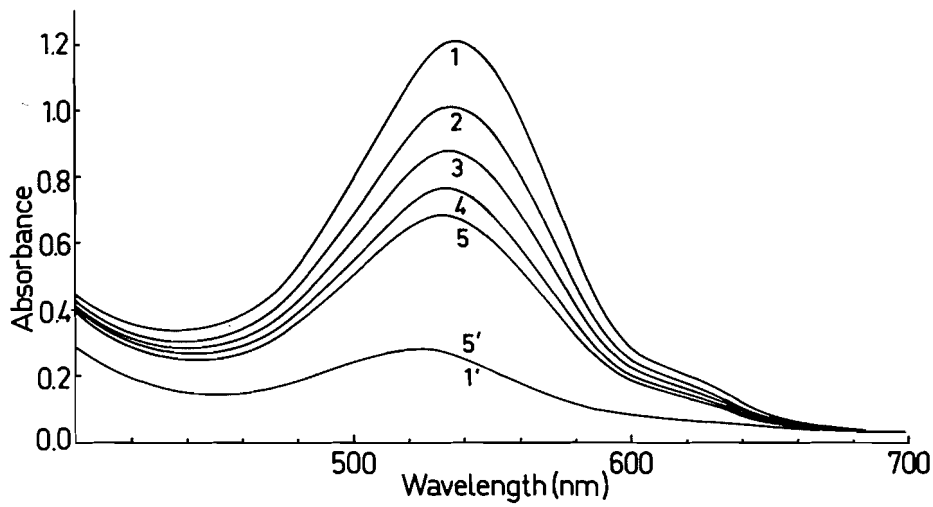

FIG. 1. Temperature-dependence of the visible absorption band of malvin for the malvin–(+)catechin system at pH 3.5 (0.2 M acetic acid – 0.2 M sodium acetate buffer). Malvin: 6×10^{-4} M. (+)-Catechin: 10^{-2} M. Temperature values are 10°C (1), 15°C (2), 20°C (3), 25°C (4), and 30°C (5). Spectra 1′ and 5′ concern malvin without copigment at 10°C (1′) and 30°C (5′).

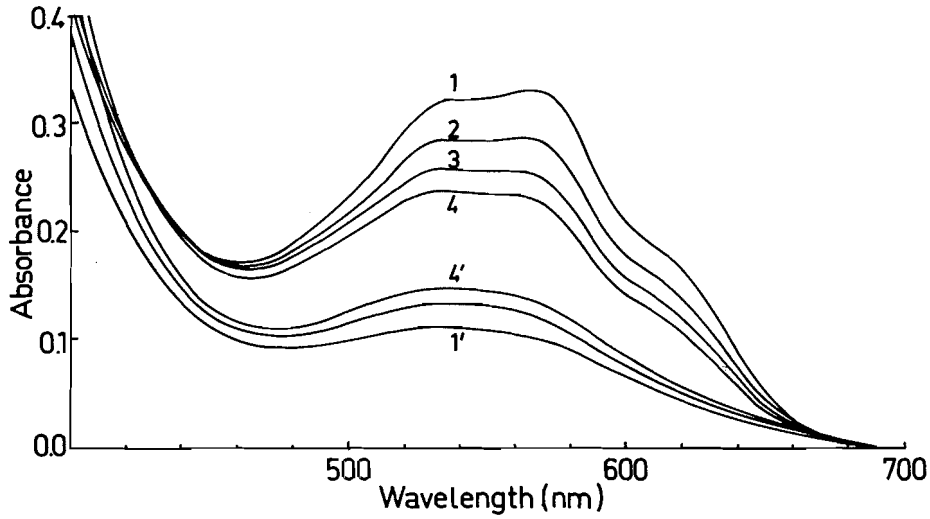

FIG. 2. Temperature-dependence of the visible absorption band of malvin for the malvin–(+)catechin system at pH 5.5 (0.1 M citric acid – 0.2 M Na_2HPO_4 buffer). Malvin: 6×10^{-4} M. (+)-Catechin: 6×10^{-3} M. Temperature values are 15°C (1), 25°C (2), 35°C (3), and 45°C (4). Spectra 1′–4′ concern malvin without copigment from 15°C (1′) to 45°C (4′).

TABLE 1. Copigmentation thermodynamic parameters for different malvin–copigment couples in water. $K = \exp(-\Delta G^0/RT)$ with $\Delta G^0 = \Delta H^0 - T\Delta S^0$ and $T = 25$°C. The K values in parentheses were computed from $(D - D_0)/D_0$ plots versus pH at 25°C. The standard deviation values for ΔS^0 were computed using $\Delta r = \pm 0.1$. Chlorog. acid: chlorogenic acid. Trp: (L)-tryptophan. Trp-OMe: (L)-tryptophan methylester.

Copigment	Malvin form	ΔH^0 (kJ mol^{-1})	ΔS^0 (J K^{-1} mol^{-1})	K (M^{-1})
Chlorog. acid	AH+	−24.1 (±1.2)	−36.1 (±5.2)	220 (300)
Chlorog. acid	A	−18.3 (±0.9)	−20.1 (±2.9)	140 (120)
Caffeine	AH+	−11.7 (±0.6)	+0.9 (±0.2)	125 (130)
Caffeine	A	−17.6 (±0.9)	−16.0 (±2.3)	180 (220)
(+)-Catechin	AH+	−30.4 (±1.5)	−58.6 (±8.4)	185
(+)-Catechin	A	−25.0 (±1.3)	−39.2 (±5.7)	215
Trp	AH+	−6.8 (±0.4)	+11.8 (±1.7)	64 (65)
Trp-OMe	AH+	−12.3 (±0.6)	−11.5 (±1.7)	36

TABLE 2. Copigmentation thermodynamic parameters for different malvin–copigment couples in water–ethanol mixtures. x stands for the molar fraction of ethanol. The standard deviation values for ΔS^0 were computed using $\Delta r = \pm 0.1$. Chlorog. acid: chlorogenic acid.

Copigment	Malvin form	x (%)	ΔH^0 (kJ mol^{-1})	ΔS^0 (J K^{-1} mol^{-1})	K (M^{-1}) at 25°C
Chlorog. ac.	AH+	5.4	−29.6 (±2.7)	−61.8 (±10.2)	90
Caffeine	AH+	4.4	−17.7 (±1.7)	−24.0 (±6.6)	70
Caffeine	A	5.4	−22.3 (±2.0)	−37.7 (±6.2)	85
(+)−Catechin	AH+	4.0	−33.1 (±3.2)	−75.1 (±20.2)	75

strated to range from about 2.5 to 7.5 (20); thus, the flavylium cation and the neutral quinonoidal bases are the main anthocyanic forms responsible for colour expression in flowers. However, a lot of blue flowers are displayed in nature and it is good evidence of the occurrence in plants of colour variation phenomena, the most important being copigmentation (4). In fact, copigmentation, which consists in molecular complex formation between the anthocyanin coloured forms and the copigment colourless molecules, leads to a bathochromic shift in the visible band of the pigment known as the *bluing effect* (9–12, 17).

Concerning the other spectral change characteristic of copigmentation, that is, the large hyperchromic shift in the visible band of slightly acidic anthocyanin solutions (see Figs. 1 and 2), it cannot be interpreted without taking into account all anthocyanin structural transformations (see Scheme 1), the more important being the relatively slow flavylium cation hydration (21, 22) giving rise to the colourless hemiacetal B. Since the consecutive opening of the hemiacetal B-ring leading to the pale yellow E-chalcone (C_E) is a very fast process (23) (equilibrium reached within a few milliseconds), the B and C_E forms can be written together in what is an overall hydration equilibrium. The very minor Z-chalcone (C_Z) arising from very slow C—C double-bond iso-

Can. J. Chem. Downloaded from www.nrcresearchpress.com by 109.225.110.28 on 09/08/12
For personal use only.

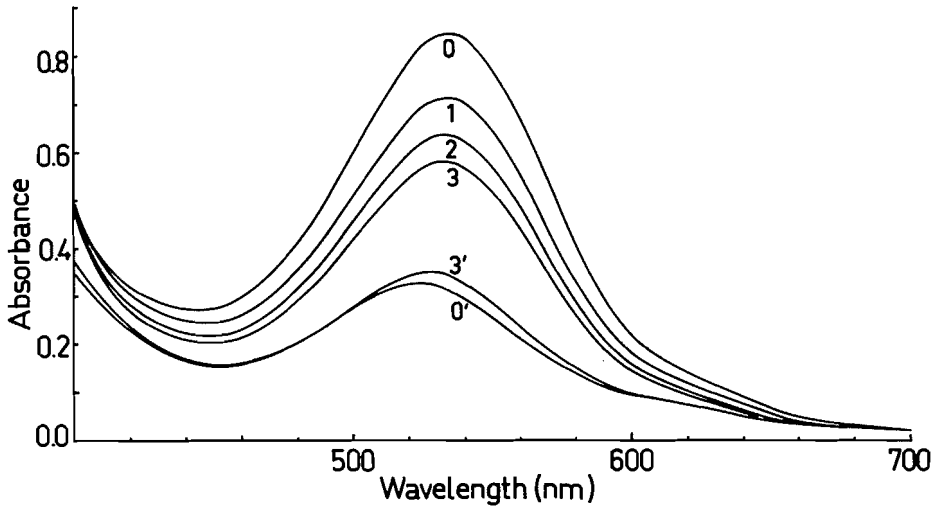

FIG. 3. Changes in the visible absorption of malvin on cosolvent addition to the malvin – chlorogenic acid system at pH 3.6 (0.2 M acetic acid – 0.2 M sodium acetate buffer). T = 20°C. Malvin: 6.7×10^{-4} M. Chlorogenic acid: 6.7×10^{-3} M. The cosolvent is ethanol. The molar fraction x of ethanol is 0 (0), 2.7% (1), 4.1% (2) and 5.4% (3). Spectra 0′ and 3′ concern malvin without copigment with x = 0 (0′) and x = 5.4 % (3′).

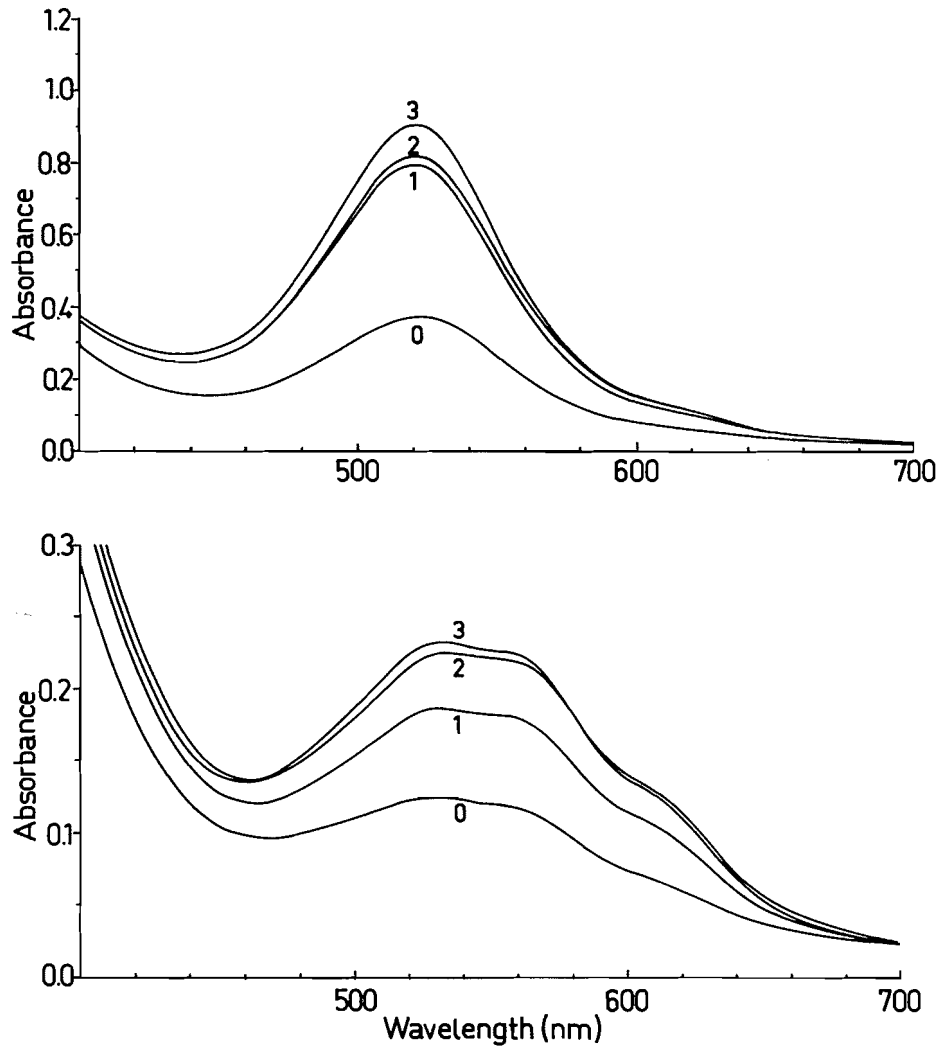

FIG. 4. Changes in the visible absorption of malvin on salt addition to the solution. T = 25°C. Malvin: 5×10^{-4} M. Salt: 2 M. Salts are NaCl (1), LiCl (2), and NaBr (3). Spectrum 0: no salt. Upper part: pH 3.25. Lower part: pH 5.0.

Can. J. Chem. Downloaded from www.nrcresearchpress.com by 109.225.110.28 on 09/08/12
For personal use only.

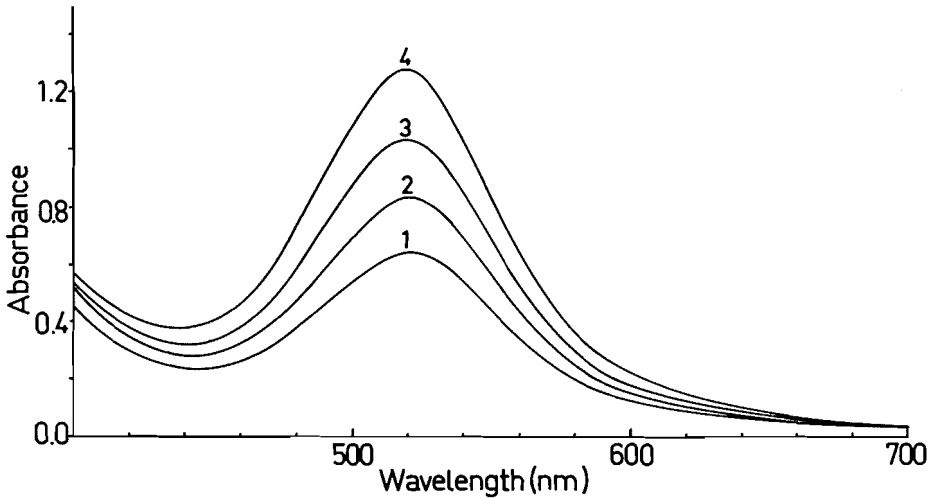

FIG. 5. Changes in the visible absorption of malvin on KCl addition to a malvin solution at pH 3.3. T = 25°C. Malvin: 5×10^{-4} M. Salt concentration is 1 M (1), 2 M (2), 3 M (3), and 4 M (4).

TABLE 3. Salt effects on the copigmentation of malvin (5×10^{-4} M) with caffeine (10^{-2} M) at pH 3.36 and 25°C. Salt concentration is 2 M for LiCl and KCl, 2/3 M for $MgCl_2$; I is 2 in each case. Reference: malvin (4.2×10^{-4} M) + caffeine (1.33×10^{-2} M) at pH 3.55 (T = 25°C; $I < 10^{-3}$). When necessary, pH values were adjusted by addition of a few μL of concentrated HCl or NaOH solutions. The K values were roughly estimated from $K = (D - D_0)/(rD_0L_t)$ Ref.: reference.

Salt	D_0	D	$(D - D_0)/D_0$	$K(M^{-1})$
LiCl	0.992	1.900	0.915	114
KCl	0.892	1.718	0.926	116
$MgCl_2$	0.753	1.460	0.939	117
Ref. (no salt)	0.245	0.615	1.510	142

merization in C_E can be neglected. The equilibrium constant of the overall hydration reaction (see Scheme 2) can be expressed as

$$K_h = a_{H^+}([B] + [C_E])/[AH^+]$$

where a_{H^+} is 10^{-pH}. In the case of malvin, pK_h is about 2 at 25°C (19) and typical values range from 2 to 3 for the simplest anthocyanins (18, 24). Consequently, in their natural medium (pH 2.5–7.5), most anthocyanins are essentially present in colourless forms. Thus, the presence in flowers of so many vivid colours cannot be simply due to anthocyanins dissolved in the vacuoles since the corresponding solutions would be very poorly coloured. Some colour-stabilizing effects must take place. In fact, the hydration equilibrium, which connects the highly coloured flavylium cation and the colourless hemiacetal and chalcone forms, is the true phenomenon accounting for colour changes occurring in anthocyanin solutions and any physical or chemical

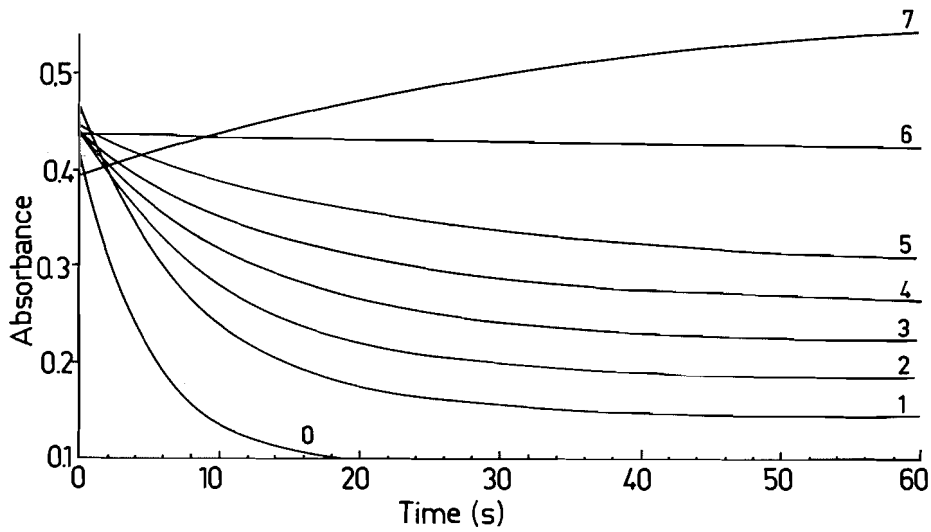

FIG. 6. Time-dependence of the malvin absorbance at 520 nm after mixing equal volumes of a 4×10^{-4} M malvin solution in 0.025 M citric acid and a rutin solution in 0.02 M NaOH. T = 25°C. Rutin concentration (before mixing) is 0 (0), 4×10^{-4} M (1), 8×10^{-4} M (2), 12×10^{-4} M (3), 16×10^{-4} M (4), 2×10^{-3} M (5), 3×10^{-3} M (6), and 6×10^{-3} M (7). Final pH 3.4. The total concentrations of pigment and copigment in the mixtures are half of the above-mentioned values.

Can. J. Chem. Downloaded from www.nrcresearchpress.com by 109.225.110.28 on 09/08/12
For personal use only.

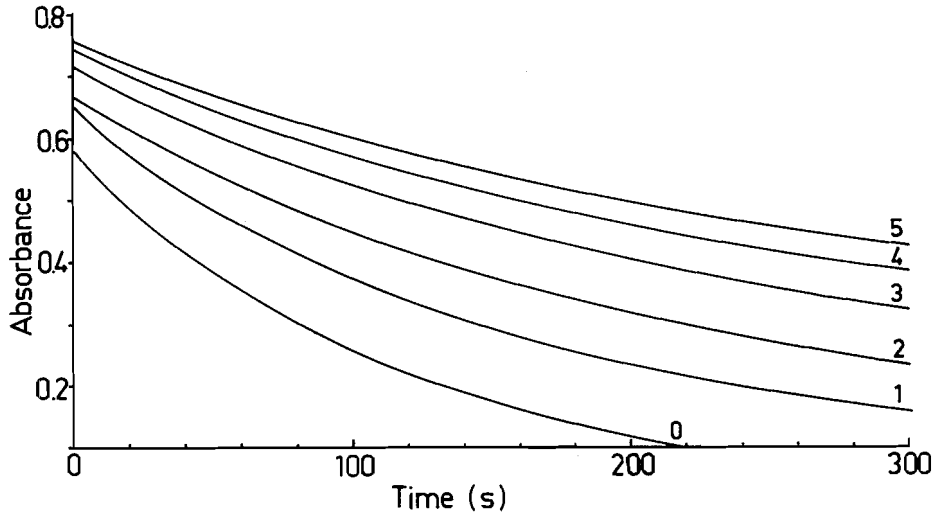

FIG. 7. Time-dependence of the malvin absorbance at 570 nm after mixing equal volumes of a 6×10^{-4} M malvin solution in 0.025 M citric acid and a rutin solution in 0.05 M NaOH. $T = 25°C$. Rutin concentration (before mixing) is 0 (0), 6×10^{-4} M (1), 12×10^{-4} M (2), 18×10^{-4} M (3), 24×10^{-4} M (4), and 30×10^{-4} M (5). Final pH 5.2. The total concentrations of pigment and copigment in the mixtures are half of the above-mentioned values.

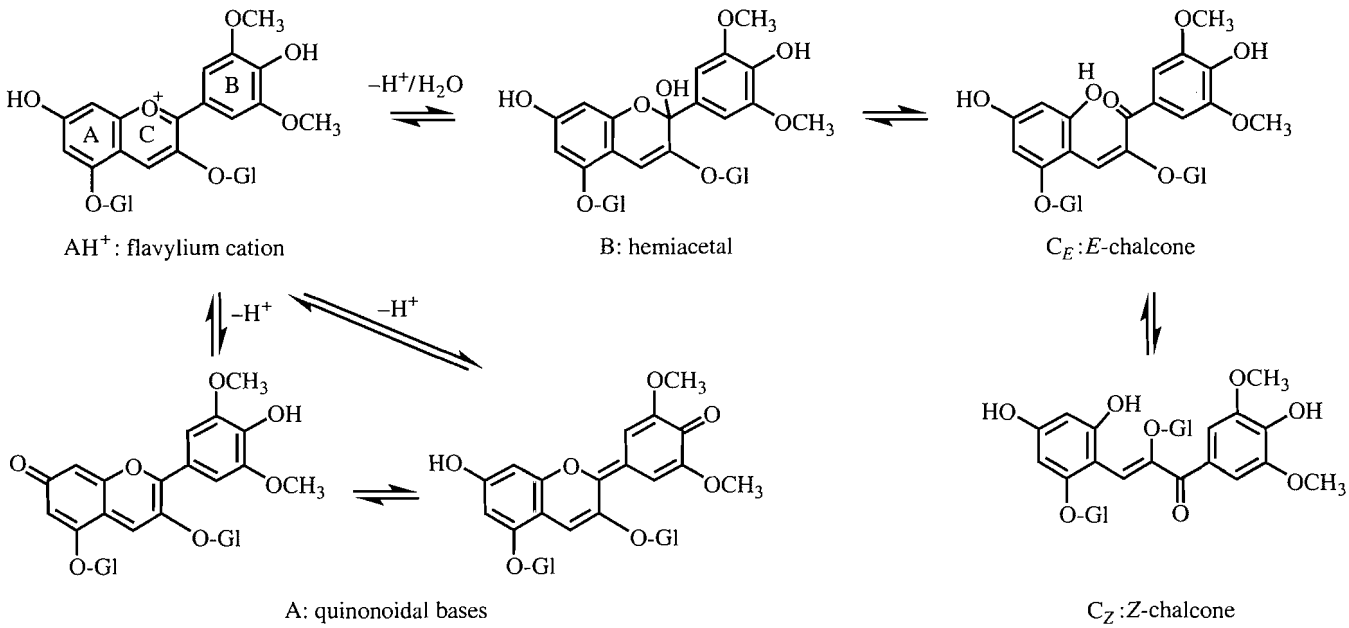

SCHEME 1

process tending to reverse this very equilibrium can be considered as colour stabilizing. Two examples are the reduction of water activity on addition of large amounts of ionic salts (25) and complexation selectively involving the anthocyanin coloured forms (13, 26). In both cases, the nucleophilic attack of water on the pyrylium ring of the flavylium cation is minimized because of a competing process: the hydration of ions produced by salt dissolution in the former case and the molecular association between the pyrylium ring and a copigment molecule in the latter case. Both phenomena cause a displacement of the hydration equilibrium toward the flavylium cation and are thus accompanied by large hyperchromic shifts in the anthocyanin visible band (Figs. 1, 2, 4, and 5). These spectacular gains of colour only occur when the colourless forms are predominant (15, 26), i.e., the pH of the medium must be larger than pK_h. For convenient investigation of colour-stabilizing processes involving anthocyanins, this general condition must be verified. On the contrary, in strongly acidic solutions where the hydration process can be neglected ($pH < pK_h$), copigmentation for instance reduces to a classical complexation of the flavylium cation and it is essentially characterized by a small bathochromic shift in the pigment visible band (15) (the molar absorption coefficients of the free flavylium cation and its complexed form have similar values for all copigments investigated). Whereas it is doubtful that ionic salts in large concentrations (larger than 1 M) should be present in the natural medium of anthocyanins, many in vivo investiga-

Can. J. Chem. Downloaded from www.nrcresearchpress.com by 109.225.110.28 on 09/08/12
For personal use only.

$$AH^+ \overset{K_a}{\rightleftharpoons} A + H^+$$

$$AH^+ + H_2O \overset{K_h}{\rightleftharpoons} (B + C_E) + H^+$$

$$AH^+ + L \overset{K_1}{\rightleftharpoons} AHL^+$$

$$A + L \overset{K_2}{\rightleftharpoons} AL$$

SCHEME 2

tions have shown that anthocyanins are often associated with copigments in flowers (4–8). Moreover, in contrast to copigmentation, the presence of ionic salts does not induce any bathochromic shift in the visible absorption of the pigment and so may not take part in the bluing of the colour. In fact, among the mechanism by which colour is produced and varied in plants, copigmentation deserves particular attention.

Copigmentation thermodynamic data

As mentioned in the previous section, a temperature increase in a slightly acidic solution of malvin without copigment is of weak influence on the visible spectrum of the pigment, a fact largely attributable to the small ΔH^0 value (19) (about 1 kcal mol^{-1}) for the hydration equilibrium. In contrast, a similar experiment performed in the presence of copigment leads to a remarkable weakening of the visible band of the pigment, which can be easily interpreted: the pigment–copigment interaction is exothermic and a temperature increase tends to dissociate the copigmentation complexes, giving more free coloured forms that, through the flavylium cation, are consecutively converted into colourless species, thus leading to a loss of colour (Figs. 1 and 2). In each experiment, the pH value was selected so that only one coloured form of anthocyanin was present in appreciable quantity. In the case of malvin, pH 3.5 was selected for investigating copigmentation involving the flavylium cation (Fig. 1) whereas similar experiments with the neutral quinonoidal bases were carried out at pH 5.5 (Fig. 2). At both pH values, however, the concentrations of the coloured forms of the pigment are not more than a few percent of the overall concentration of the pigment. In such conditions, the recently established general relation (15) giving the relative hyperchromic shift of copigmentation reduces to eq. [1],

$$[1] \quad (D - D_0)/D_0 = rK[L]$$

D_0 and D stand for the absorbances of the anthocyanic chromophore, at a fixed wavelength in the visible range, in the absence and in the presence of copigment, respectively. For good accuracy, the selected wavelength must be close to that of the absorption maximum. Throughout this work, L represents the copigment r is expressed by the following ratio of molar absorption coefficients: $\varepsilon_{AHL^+}/\varepsilon_{AH^+}$ at pH 3.5; $\varepsilon_{AL}/\varepsilon_A$ at pH 5.5. K stands for the copigmentation equilibrium constant and is expressed by $K_1 = [AHL^+]/([AH^+][L])$ for copigmentation involving the flavylium cation (pH 3.5) and by $K_2 = [AL]/([A][L])$ for copigmentation involving the neutral quinonoidal bases (pH 5.5). Typical values of the concentrations used in the present work are about 10^{-2} M for the copigment and 5×10^{-4} M for malvin. Under such conditions, the free copigment concentration [L] is much higher than the concentration of copigment associated with malvin, and thus it is approximately equal to the total concentration of copigment L_t. Moreover, the theoretical treatment does not need to take into account the formation of complexes whose stoichiometry is different than 1:1. The previous quantitative investigations on copigmentation (13, 14, 16, 17) are consistent with this assumption. Finally, any self-association process involving the coloured forms of the pigment (27, 28) (whose actual equilibrium concentrations are less than 10^{-5} M) can also be neglected. Assuming van't Hoff's hypothesis (temperature-independent ΔH^0), eq. [1] transforms into eq. [2]. Hence, a linear plot of $\ln[(D - D_0)/D_0]$ as a reciprocal of temperature gives the values of the copigmentation enthalpy and entropy changes (Table 1). For

$$[2] \quad \ln[(D - D_0)/D_0] = \ln(rL_t) + \Delta S^0/R - \Delta H^0/(RT)$$

each copigment, the r values generally derive from a comparison of the experimental and theoretical plots of $(D - D_0)/D_0$ versus pH (15). However, the $\varepsilon_{AHL^+}/\varepsilon_{AH^+}$ ratio can be directly estimated by measuring D_0 for a 0.2 M HCl malvin solution and then D after addition of a large excess of copigment so that the flavylium cation is entirely complexed (13). At 520 nm, whatever the copigment selected, $\varepsilon_{AHL^+}/\varepsilon_{AH^+}$ and $\varepsilon_{AL}/\varepsilon_A$ were found close to 0.8 and 0.9, respectively.

In all cases presented here, copigmentation appears as an exothermic process. Using a thermodynamic cycle, the copigmentation overall enthalpy change ΔH^0 can be artificially divided into two terms. The first one accounts for the pigment–copigment interaction in the gas phase. It is essentially composed of stabilizing contributions, the major one being the electrostatic and dispersion forces, including for instance π–π overlap between aromatic residues, dipole–dipole interactions, and possible hydrogen bonding. The second term is the sum of the enthalpy changes accompanying the transfer of the free-binding partners from the solvent (water) to the gas phase (desolvation) and of the solvation enthalpy of the molecular complex; it represents the solvent contribution to the overall enthalpy change. The association of the pigment and copigment molecules reduces their surfaces in contact with the solvent so that there is a net desolvation that brings some water molecules from the solvation shells to the bulk solvent. If this contribution is exothermic, it means that a water molecule interacts more strongly with its neighbours in the bulk (other water molecules) than with its neighbours in a solvation shell (the solute molecule and other water molecules). This is certainly true for at least two reasons: first, water is by far the solvent of lowest polarizability (α = 1.47 Å^3). Thus, dispersion interactions between water molecules and solute molecules (even their most apolar parts) must be very weak (29). Secondly, the solvation water molecules are higher in enthalpy than the water molecules within the liquid water network (bulk).

From their investigations on carbohydrate–protein interaction (particularly from Monte Carlo simulations of carbohydrate and protein hydration), Lemieux *et al.* (30) proposed a general model for the association of amphiphilic molecules in water. Since malvin and most copigments investigated in this work (particularly, chlorogenic acid, catechin, and rutin) are hydrophilic through their hydroxyl groups and hydrophobic particularly through their aromatic rings, such a model can be usefully applied to copigmentation. In

Can. J. Chem. Downloaded from www.nrcresearchpress.com by 109.225.110.28 on 09/08/12
For personal use only.

Can. J. Chem. Downloaded from www.nrcresearchpress.com by 109.225.110.28 on 09/08/12
For personal use only.

this model, hydrogen bonding between a water molecule and a hydroxyl group close to a hydrophobic region in the amphiphilic solute molecule places the water molecule farther from the solute surface, i.e., creates a cavity along the hydrophobic region. In these conditions, the colinear arrangement proper to strongest hydrogen bonding can be achieved. Such cavities have been formed at the cost of an increase in enthalpy so that their partial collapse on molecular association brings a favourable exothermic contribution to the overall copigmentation enthalpy change. In all cases investigated the pigment–copigment interaction was actually found to be exothermic, especially with catechin and chlorogenic acid (Table 1). Whatever the interacting coloured form of anthocyanin (AH^+ at pH close to 3.5, A at pH 5.5), the copigmentation exothermicity decreases in the catechin – chlorogenic acid – caffeine series. The attractive term in the dispersion interaction was pointed out to be one of the major components in the interaction energy between two molecules (29, 31). This seems particularly true in the case of the pigment–copigment interaction, as indicated by the high polarizabilities of the malvin chromophores (computed from atomic increments (32)): 32.8 $Å^3$ for the flavylium chromophore and 32.5 $Å^3$ for the quinonoidal chromophore (the glucosyl moieties have not been taken into account). Taking the copigment molecular polarizability as a rough measure of the copigment ability to establish attractive dispersion forces with the pigment molecule, we computed α values of 33.0, 28.9, and 18.9 $Å^3$ for chlorogenic acid, catechin, and caffeine, respectively. The large polarizabilities of chlorogenic acid and catechin certainly contribute to the strong exothermicity of their association, especially with the flavylium cation. However, in spite of its rather weak polarizability, caffeine interacts strongly with the quinonoidal bases. Some dipole–dipole and (or) inductive attractive forces between these highly polar species could take place, as well as possible hydrogen bonding between the hydroxyl groups of the pigment and caffeine. In the same way, Haslam and coworkers (33, 34) already pointed out remarkable interactions between caffeine and various polyphenols. Using X-ray crystallography and ^1H NMR data, these authors proposed that both hydrophobic interactions and hydrogen bonding should contribute to complex stability. Moreover, replacing malvin by synthetic anthocyanidins (anthocyanins without any sugar residue on their chromophore, such as the 7-hydroxy 3,4′-dimethoxyflavylium cation) in copigmentation experiments with chlorogenic acid and caffeine (35) results in similar copigment effects in the case of only chlorogenic acid. By contrast, whatever the pH, much smaller hyperchromic shifts have been detected in the case of caffeine. In addition, malvin and the 7-hydroxy 3,4′-dimethoxyflavylium cation possess similar abilities to hydrate (pK_h about 2 at 25°C in both cases). Thus, the presence of glycosyl residues on the anthocyanic chromophore appears to be determining for caffeine copigmentation. In fact, hydrogen bonding between the hydroxyl groups of the malvin glycosyl residues and the tertiary amide carbonyl groups of caffeine must be necessary to enforce vertical stacking (demonstrated by ^1H NMR investigations (17)) of the purine ring onto the pyrylium ring. Although tryptophan polarizability (21.6 $Å^3$) is higher than that of caffeine, the tryptophan–flavylium cation interaction is significantly less exothermic than the corresponding interaction involving caffeine. This could be due to particularly strong hydrogen bonds between water and the tryptophan NH_2 and COOH groups, making the desolvation contribution to the overall ΔH^0 less exothermic. Indeed, the replacement of the COOH group by the less solvated COOMe group leads to much more exothermic pigment–copigment interaction (in addition to the small increase in the overall polarizability: 23.5 $Å^3$ for Trp-OMe). The ability of tryptophan to act as a malvin copigment has been observed not only with the flavylium cation (K_1 about 65 M^{-1} at 25°C) but also with the quinonoidal bases. However, the effect is weaker (K_2 about 20 M^{-1} at 25°C). This behaviour seems unique in the amino acid series since the other amino acids investigated, even the most polarizable tyrosine and phenylalanine, do not exhibit appreciable copigment effects. Contrary to previous qualitative investigations (9), copigmentation involving the flavylium cation of cyanin (an anthocyanic pigment analogous to malvin but bearing a catechol group on its terminal B-ring) and proline appeared to be hardly significant (K of the order of unity at 25°C). This remains true for *N*-acetylproline and other small derivatives like the dipeptides Pro-Phe and Pro-Pro. The large hydrophilic character of the NH_2 and COOH groups probably makes the competition between molecular association and solvation of the free partners favour the latter phenomenon. However, for longer peptides, formation of hydrophobic pockets, involving for instance the apolar side chains of aromatic residues, probably allows much stronger interactions with polyphenols in general. Indeed, proanthocyanidins (condensed tannins), whose skeleton is close to that of anthocyanins, are well known for their ability to bind (and, ultimately, precipitate) proteins (33, 34, 36–38).

More than the overall molecular polarizabilities of both free partners, the area of π-overlap is a relevant measure of the interaction energy between aromatic molecules in the gas phase (39). Indeed, among the dispersion forces at work between the pigment and the copigment molecules, $\pi-\pi$ interactions must be of particular importance. For instance, up to now, no copigment has been found that does not possess at least one aromatic or pseudo-aromatic (caffeine-type) structure. Of course, the presence in a given molecule of one aromatic moiety does not necessarily imply that this molecule will act as a copigment (see the examples of tyrosine and phenylalanine). Similarly, tryptophan, which presents a large aromatic structure, is a weak copigment only. Solvation considerations must be taken into account. $\pi-\pi$ interactions between the pigment and copigment molecules have been demonstrated using ^1H NMR analysis (4, 17, 40): when pigment and copigment are mixed together, the chemical shifts of their aromatic protons are significantly displaced. Such displacements are the result of ring current diamagnetic anisotropy in neighbouring aromatic moieties and can be used to estimate the copigmentation equilibrium constant. The hypothesis of determining $\pi-\pi$ interactions in copigmentation permits us to explain why the copigment molecule essentially interacts with the coloured forms rather than with the colourless forms of the pigment. Whereas the coloured forms possess almost planar chromophores with electronic delocalization distributed on three aromatic rings, the colourless hemiacetal and chalcone forms bear only two isolated aromatic rings.

As evidenced by Table 1, the copigmentation entropy change is highly dependent on the copigment structure. Moreover, most of the ΔS^0 values reported here are negative. Indeed, the overall entropy change is composed of an

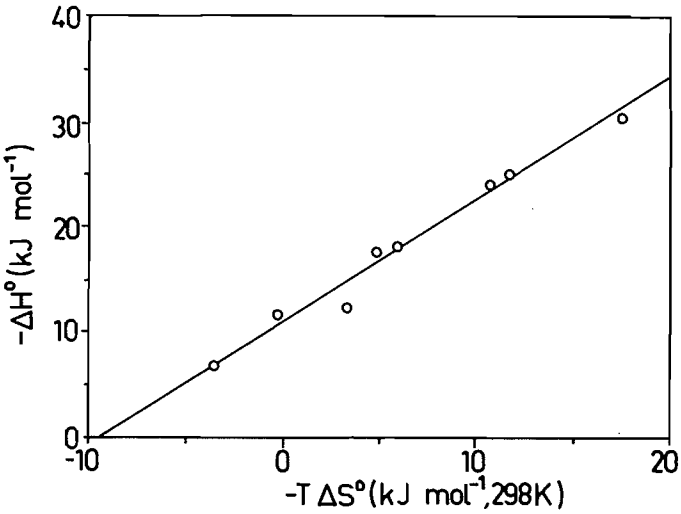

FIG. 8. Enthalpy–entropy compensation for eight pigment–copigment couples. The corresponding ΔH^0 and ΔS^0 values are from Table 1. T = 298 K ρ = 0.988; slope = 1.148 (±0.074); intercept = 11.057 (±0.661).

unfavourable (negative) term accounting for the reduction of the degrees of freedom of both partners when they associate (in the gas phase) and of a second term including the solvent contributions. Following Lemieux *et al.* (30), we may assume that water molecules have greater mobility at the surface of amphiphilic solute molecules, where cavities are present, than in the bulk where water molecules are tightly associated. Thus, an ordering is expected to occur in the water molecules taking part in the net desolvation process accompanying the molecular complexation so that the main contribution of the solvent to the overall entropy change would be an unfavourable (negative) term as well. The experimental entropy changes for most pigment–copigment systems (Table 1) are consistent with this view: copigmentation results in a loss of entropy except in the case of caffeine and tryptophan interacting with the malvin flavylium cation. In those cases, the large planar and rigid molecules of copigment probably allow the formation at their surfaces of well-ordered arrangements of water molecules, which partially collapse on association with the flavylium cation giving a positive net entropy change. Replacing the tryptophan COOH group by a COOMe group strongly alters ΔS^0. In fact, owing to its high ability to establish hydrogen bonds, the COOH group might be inserted in a more organized water cavity than that surrounding the COOMe group. Moreover, the enthalpy and entropy changes are expected to be correlated. For instance, the more intimate the contact between the pigment and copigment molecules, the stronger the reduction of their respective degrees of freedom. Similarly, the looser the contact between solvation water molecules and amphiphilic solute molecules, the stronger the ordering of these water molecules on their release in the bulk (30). Indeed, a plot of $-\Delta H^0$ versus $-T\Delta S^0$ is linear (Fig. 8) suggesting enthalpy–entropy compensation. The compensation temperature has been found equal to 342 (±23) K.

Cosolvent effects

In this paragraph, we consider only the problem of small additions of organic cosolvent (less than 6% molar) in the aqueous medium where copigmentation typically occurs. Indeed, the copigmentation phenomenon is closely connected to the pH-dependent chemical transformations that anthocyanins undergo in water (proton transfers and hemiacetal formation); large additions of cosolvent would pose the difficult problem of pH correction. In our conditions, pH correction is not necessary and cosolvent addition does not markedly affect the visible spectrum of the pigment in the absence of copigment. Thus, in the presence of copigment, the changes occurring in the visible absorption of anthocyanin when water is replaced by a binary solvent, water remaining the main component, are essentially due to cosolvent effect on copigmentation (see Fig. 3, the case of water–ethanol mixtures). These changes, which consist of a strong decrease in the hyperchromic shift characteristic of copigmentation, spectacularly illustrate the influence of the medium on the magnitude of the copigmentation.

Similar effects have been recently reported with a series of organic cosolvents (15). In that series, the less damaging effects were observed with methanol, ethanol, and ethylene glycol, probably because they are, as protic solvents, relatively close to water and are similarly characterized by a network of hydrogen-bonded molecules. Solvent effects in molecular complexation have been widely investigated. In their work dealing with inclusion of apolar solutes in cyclophane cavities, Smithrud and Diederich (29) found the corresponding inclusion complexes to be much more stable in water than in any other solvent. These authors interpreted this result by taking into account at the same time the strong cohesive forces between water molecules in the bulk and the extremely weak polarizability of water. Both factors explain why the water molecules interact much more strongly with themselves than with apolar solutes, thus providing a net driving force for molecular complexation. In this view, changing water into a more polarizable solvent must lead to more favourable solvent–solute dispersion interactions and weaker cohesive forces between solvent molecules in the bulk. Thus, the net desolvation process and finally the overall molecular complexation are expected to be less exothermic. Curiously, in our systems, whatever the copigment used, malvin copigmentation (involving either the flavylium cation or the quinonoidal bases) is significantly more exothermic in water–ethanol mixtures than in water (Table 2). Moreover, the pigment and copigment molecules must be more solvated in protic organic solvents such as ethanol, where they are freely soluble, than in water where their solubility is rather low.

So, how can species that are more solvated in their free state interact in a more exothermic way? A possible explanation would be that the pigment and copigment molecules are better solvated by the binary solvent when they are π-stacked in the complex, than when in their free state. This could be due to a microenvironment of ethanol molecules around the stacks. As has been suggested by Sigel *et al.* (41), the aromatic stacks originally present in water might act as "germs to attract the organic solvent molecules and to form a micelle-like hydrophobic environment." In spite of a more favourable ΔH^0 value, cosolvent effect on copigmentation consists in a strong weakening of the pigment–copigment interaction (whose magnitude is expressed by the K value). It is thus attributable to a more unfavourable entropy change (Table 2). Whereas copigmentation is an enthalpically driven phenomenon (large negative ΔH^0, ΔS^0 being generally unfavourable), cosolvent effect on copigmentation appears to

Can. J. Chem. Downloaded from www.nrcresearchpress.com by 109.225.110.28 on 09/08/12
For personal use only.

Can. J. Chem. Downloaded from www.nrcresearchpress.com by 109.225.110.28 on 09/08/12
For personal use only.

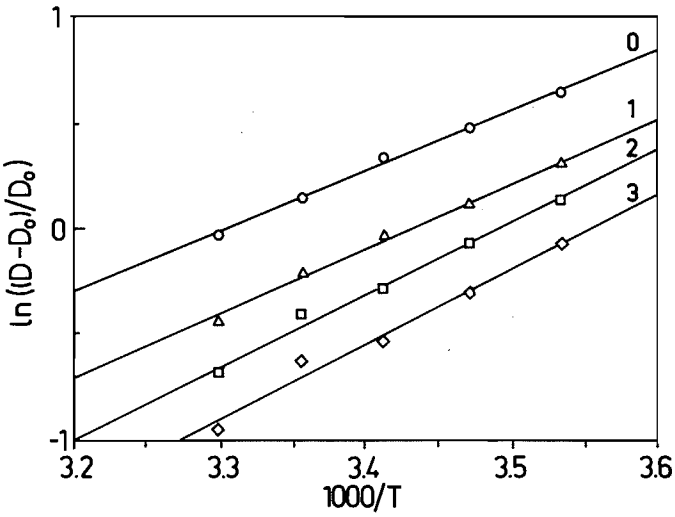

FIG. 9. Plots of $\ln[(D - D_0)/D_0]$ as a reciprocal of the temperature for the malvin – chlorogenic acid system at pH 3.6 in different water–ethanol mixtures. Malvin: 6.7×10^{-4} M. Chlorogenic acid: 6.7×10^{-3} M. D and D_0 are the malvin absorbances at 520 nm with and without chlorogenic acid, respectively. The molar fractions of ethanol are 0 (0), 2.7% (1), 4.1% (2), and 5.4% (3). ρ = 0.996 (0); 0.995 (1); 0.995(2); 0.988 (3). Slope = 2.896 (±0.145) (0); 3.078 (±0.171) (1); 3.429 (±0.197) (2); 3.565 (±0.321) (3). Intercept = −9.57 (±0.50) (0); −10.56 (±0.58) (1); −11.97 (±0.67) (2); −12.67 (±1.10) (3).

be controlled by ΔS^0. Cosolvent molecules in water are expected to partially disrupt the approximately tetrahedral network of water molecules in the bulk. Thus, the release of solvation molecules on molecular complexation should not be so entropically costly as it is in the absence of cosolvent. In fact, the origin of the net decrease in entropy on cosolvent addition is probably to be found in the preferential arrangement of cosolvent molecules around the stacks. The linear plots yielding ΔH^0 and ΔS^0 for the malvin – chlorogenic acid association (pH 3.6) are reported in Fig. 9 for different molar fractions (x) of ethanol. The variations of ΔH^0, ΔS^0, and ΔG^0 (25°C) versus x seem to be roughly linear in the x range investigated (Fig. 10).

Salt effects

Large additions of alkali halides to weakly acidic solutions of malvin without copigment give rise to strong hyperchromic shifts in the visible band of the pigment (Figs. 4 and 5), a phenomenon already pointed out with other anthocyanic pigments (25). Unlike copigmentation, this phenomenon is not accompanied by any shift in the wavelength of the absorption maximum. However, just as with copigmentation, remarkable salt effects in anthocyanin solutions take place only when the pigment is mainly hydrated ($pH > pK_h$), the minor coloured forms being either the flavylium cation or the quinonoidal bases according to the pH of the medium (Fig. 4). This can be interpreted by the decrease in water activity due to ion solvation that, in turn, induces a displacement of the hydration equilibrium toward the flavylium cation. Note that these salt effects are highly dependent on the nature of both the metallic cation and the halide anion. Indeed, the degree of solvation of an ion is a function of its size and its charge density. For instance, the small Li^+ cation is very solvated and is thus expected to produce a stronger

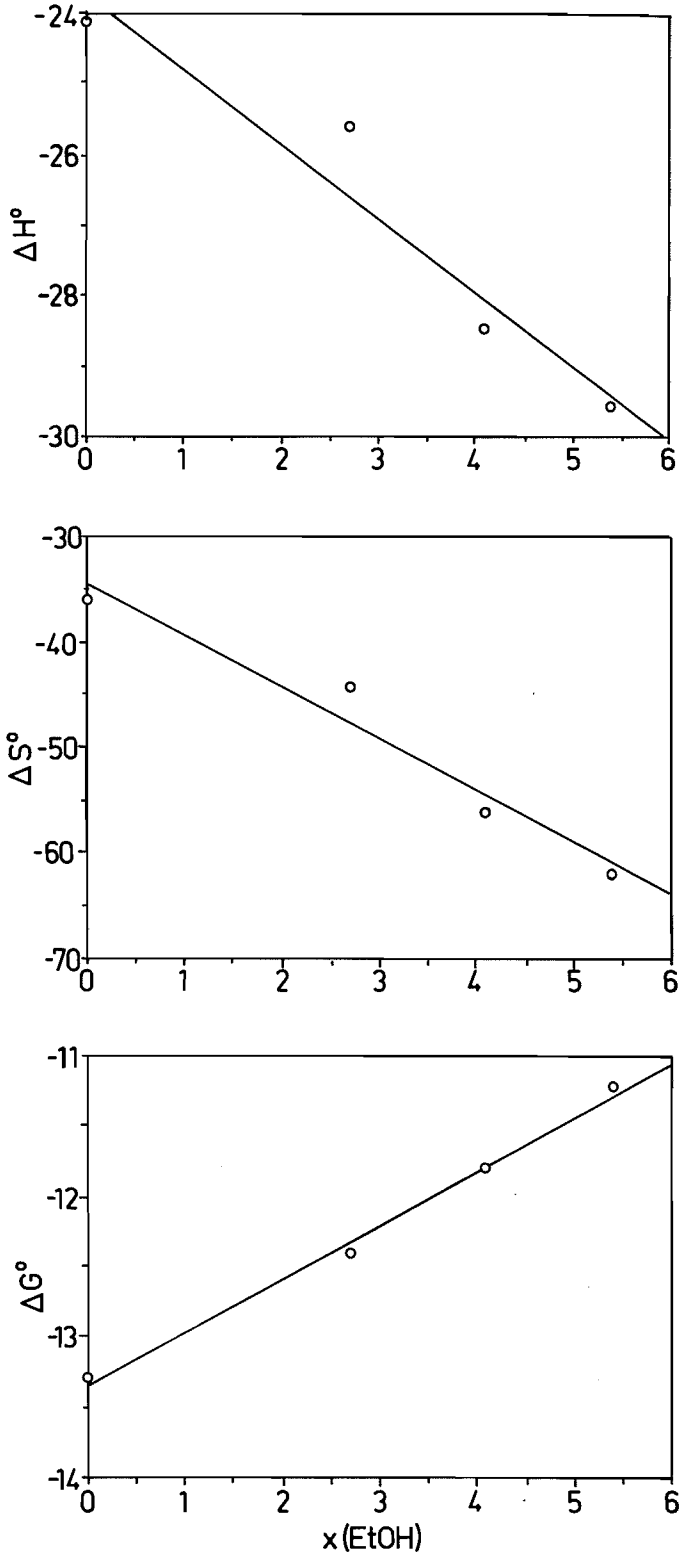

FIG. 10. Molecular association of the malvin flavylium cation with chlorogenic acid in different water–ethanol mixtures. Variations of thermodynamic parameters versus molar fraction of ethanol. Upper part: ΔH^0 (ρ = 0.965). Middle part: ΔS^0 (ρ = 0.979). Lower part: ΔG^0 at 25°C (ρ = 0.997).

hyperchromic effect in the visible band of malvin than the larger Na^+ and K^+ cations (for a given counteranion). Experiment confirms this view (Fig. 4).

Can. J. Chem. Downloaded from www.nrcresearchpress.com by 109.225.110.28 on 09/08/12
For personal use only.

For anions, this simple explanation seems no longer valid. For example, although the bromine anion is larger (and probably less solvated) than the chlorine anion, the stabilizing effect of NaBr on both the flavylium cation and the quinonoidal bases is stronger than that of NaCl. Now, how do these salt effects alter copigmentation? The experiment, whose results are reported in Table 3, consists of measuring the relative hyperchromic shift produced by a given amount of caffeine when added to a malvin solution (pH 3.36) containing a large salt concentration. The salt concentration is 2 M for LiCl and KCl and 2/3 M for $MgCl_2$ so that the ionic strength is about 2 in each case. Whatever the salt, the relative hyperchromic shifts are very close and notably lower than that recorded in the absence of salt (ionic strength about 10^{-3}). Whereas salt addition results in large specific effects on the pigment hydration process, its influence on the magnitude of the intrinsic copigmentation is relatively small and almost non-specific. In fact, the small weakening of copigmentation on large salt additions probably consists only of an ionic strength effect.

Relaxation kinetic measurements as an efficient method for the determination of copigmentation equilibrium constants

Among all the equilibria displayed in Scheme 2, proton transfer and copigmentation equilibria are extremely fast reactions. In contrast, the hydration of the flavylium cation into the colourless hemiacetal B (followed by instantaneous tautomerization into C_E) is a rather slow process. Its rate is highly dependent on the acidity of the medium (21). Typically, the hydration equilibrium is reached within a few tens of seconds in slightly acidic solutions (pH 3–4) but requires several minutes at pH values near neutrality. In the experiments whose results are presented in Figs. 6 and 7, a copigment alkaline solution is quickly added to a malvin acidic solution. In that way, the hydration process is perturbed by both pH-jump and flavylium cation complexation. The change in the visible absorbance, D of the pigment from its initial value just after mixing, D_0, toward its value in the final equilibrium state, D^*, has been recorded as a function of time. D is measured at a given wavelength near that of the absorption maximum, for instance, 520 nm when the coloured form of the pigment present in the medium is the flavylium cation (final pH 3–4) and 570 nm when the quinonoidal bases are largely predominant (final pH 5–6). The copigment selected for this study is rutin (**5**), a member of the flavonol family, among which are found the strongest anthocyanin copigments reported up to now (9, 12). Figure 6 shows the influence of copigmentation on the visible absorption of malvin just after the pH of the pigment solution was quickly raised from 2.3 to 3.4. It points out the remarkable slowing down of the flavylium cation hydration due to flavylium cation – rutin complexation. Raising the pH of an equilibrated acidic solution of malvin without copigment results in a shift of the hydration equilibrium toward the colourless forms of the pigment so that the visible absorbance decreases. When the pH increase is accompanied by the simultaneous addition of the rutin copigment, the instantaneous complexation of the coloured forms (copigmentation) is opposed to the former shift. When the pH-jump effect is predominant, we get $D_0 > D^*$ (positive relaxation amplitude defined as $D_0 - D^*$), i.e., the visible absorbance decreases during the relaxation process. When the copigment concentration is large enough for the copigment effect to prevail, we get $D^* > D_0$ (negative relaxation amplitude), i.e., the visible absorbance increases upon the relaxation process. Both situations can be seen in Fig. 6. Note that pH-jump and copigment effects cancel each other (amplitude zero) at a rutin to malvin molar ratio close to 7.5. The qualitative observations about the influence of copigmentation on the flavylium cation hydration kinetics remain valid for the apparent hydration of the quinonoidal base (through the flavylium cation) when pH goes from 2.3 to 5.2 (Fig. 7): again the hydration process is much slower in the presence of the copigment. In that case, however, no change in the sign of the signal amplitude occurs in the investigated concentration range of the copigment. For good sensitivity of method, it is important to start from an acidic solution of malvin (pH about 2) giving an intense absorption band in the visible range. Under such conditions, signals of large amplitudes can be recorded. When the total concentration of copigment is raised, the differences in the D_0 absorbance values just after mixing of the pigment and copigment solutions (i.e., when the hydration process is still negligible) essentially reflect the differences in the molar absorption coefficients of the free and complexed forms at the selected wavelength. In the case of rutin, ε_{AHL^+} appears to be close to ε_{AH^+} at 520 nm (small differences in the D_0 values in Fig. 6) whereas ε_{AL} must be larger than ε_A at 570 nm (increasing D_0 values on increasing the total concentration of copigment as shown in Fig. 7).

Interestingly, our kinetic results can be applied to the determination of copigmentation equilibrium constants (the theoretical treatment is detailed in the Appendix): the apparent first-order rate constant of hydration k (reciprocal of the relaxation time), is computed at different copigment concentrations from the slope of the linear plot of $\ln|D - D^*|$ versus time. k can be related to k_0, the apparent rate constant of hydration in the absence of copigment, by eqs. [3] and [4]:

$$[3] \qquad \frac{1}{k_0 - k} = \frac{1}{k_1} + \frac{1}{k_1 K_1}\frac{1}{L_t}$$

$$[4] \qquad \frac{1}{k_0 - k} = \frac{K_a 10^{pH}}{k_1} + \frac{K_a 10^{pH}}{k_1 K_2}\frac{1}{L_t}$$

k_1 stands for the elementary rate constant of the flavylium cation hydration process. Equation [3] is valid at a final pH of about 3.5 and a plot of $1/(k_0 - k)$ as a reciprocal of L_t yields the copigmentation constant of the flavylium cation K_1. Equation [4] is valid at final pH 5–6 and the same type of plot yields the quinonoidal base copigmentation constant K_2. Equations [3] and [4] can be used with any copigment provided that its total concentration is much larger than the concentration of the coloured form of the pigment (L_t is approximately equal to [L]).

The considerable advantage of this method over the equilibrium procedure (13, 15) is that the new plot is independent of spectral parameters such as the molar absorption coefficient ratio r, which requires a previous time-consuming (although not so accurate) determination. The corresponding plots with rutin as copigment are reported in Figs. 11 and 12. The following values for K_1 and K_2 have been estimated at 25°C: K_1 = 3370 (±550) M^{-1}, K_2 = 1030

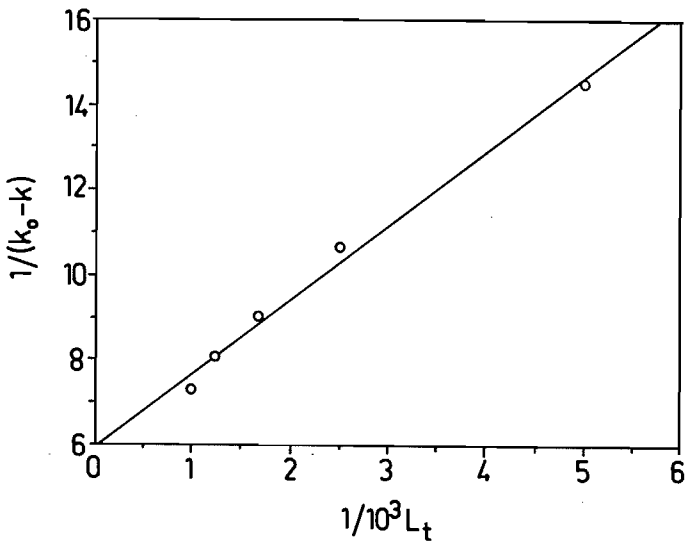

FIG. 11. Molecular association of the malvin flavylium cation and rutin. Double-reciprocal plot of $k_0 - k$ versus L_t. k and k_0 are the apparent first-order rate constants of hydration at pH 3.4 in the presence and in the absence of copigment, respectively. L_t is the total concentration of copigment. T = 25°C. ρ = 0.995; slope = 1.757 (±0.057); intercept = 5.915 (±0.590).

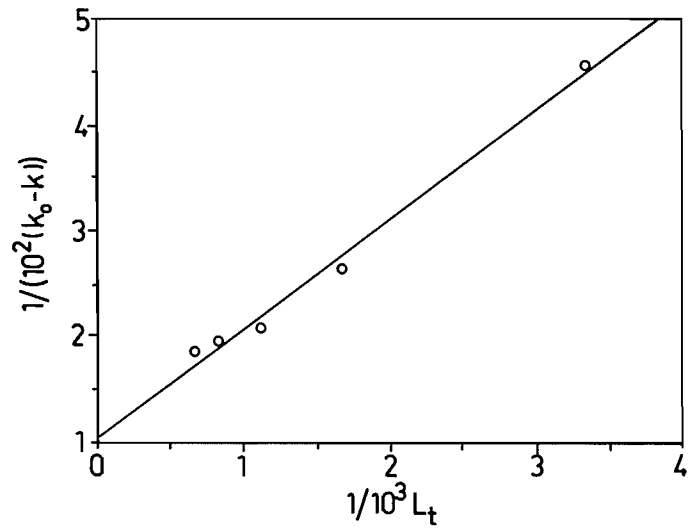

FIG. 12. Molecular association of the malvin quinonoidal bases and rutin. Double-reciprocal plot of $k_0 - k$ versus L_t. k and k_0 are the apparent rate constants of hydration at pH 5.2 with and without copigment, respectively. L_t is the total concentration of copigment. T = 25°C. ρ = 0.995; slope = 1.032 (±0.062); intercept = 1.059, (±0.112).

(±170) M^{-1}. In both cases, consistent k_1 values have been found, 0.169 (±0.017) s^{-1} from the first plot (pH 3.4) and 0.150 (±0.050) s^{-1} from the second plot (pH 5.2). Both values are in good agreement with previously reported values (19). K_1 deduced from relaxation kinetic measurements is slightly lower than that computed from Sadlowski's static experiments (19) on rutin (K_1 about 4000 M^{-1} at 25°C (13)). In comparison, let us mention that Haslam and co-workers (17), using the $\ln[(D) - D_0)/D_0]$ versus $\ln L_t$ plot, recently measured a constant of about 1686 (±58) M^{-1} for the copigmentation of the malvin flavylium cation (T = 22°C) with quercetin-3-β-D-galactoside, another flavonol differing from rutin only by the diosyl residue but markedly more soluble in water. In fact, the water solubility of rutin is very poor (of the order of 10^{-4} M) whereas its solubility in alkaline solutions (where deprotonation of the phenolic OH groups takes place) is quite good (more than 10^{-2} M).

Now, mixing the acidic malvin solution and the alkaline rutin solution yields a slightly acidic solution in which rutin is in a thermodynamically unstable state of supersaturation. This unusual phenomenon may persist for a few minutes before precipitation occurs (19). In classical copigmentation experiments on equilibrated solutions, such a delay is generally not sufficient to be sure that the hydration equilibrium state is entirely established, particularly in the case of experiments dealing with quinonoidal base copigmentation (pH 5–6). Thus, in the case of rutin, our kinetic method for the determination of the copigmentation equilibrium constants seems to be by far more accurate. Since K_1 is much higher than K_2, rutin enters the class of copigments better stabilizing the flavylium cation than the quinonoidal bases. Interestingly, the overall affinity of rutin for malvin is much greater than that of (+)-catechin although the carbon skeletons of these two copigments are similar. In fact, by contrast with catechin, the rutin central ring is unsaturated and quite planar. Hence, the three unsaturated rings in rutin must be almost coplanar, a conformation strongly favouring π–π stacking. Moreover, the very unfavourable entropic terms in the malvin–catechin association (Table 1) might partly reflect the distortion occurring in the catechin central ring for both aromatic side rings to reach the coplanar conformation proper to strongest interaction in the complex. Such a distortion is probably absent in the case of rutin since coplanarity is already achieved in the copigment free state. In addition, for rutin as well as for tryptophan and caffeine, the solvent water might provide a positive contribution to ΔS^0. Thus, more favourable entropy changes are expected. Preliminary results from temperature variation on the flavylium cation – rutin system (ΔS^0 close to zero) seem to confirm that view.

Acknowledgments

The authors thank the Hewlett Packard France Company for the gift of a HP 8452 diode-array spectrophotometer, and the Conseil Régional d'Alsace for financial support.

1. R. Brouillard. *In* The flavonoids. Advances in Research. *Edited by* J. B. Harborne. Chapman and Hall, London. 1988. p. 525.
2. G. Mazza and R. Brouillard. Food Chem. **25**, 207 (1987).
3. Y. Osawa. *In* Anthocyanins as food colors. *Edited by* P. Markakis. Academic Press, New York. 1982. p. 41.
4. T. Goto and T. Kondo. Angew. Chem. Int. Ed. Engl. **30**, 17 (1991).
5. S. Asen, R. N. Stewart, and K. H. Norris. Phytochemistry, **14**, 2677 (1975).
6. S. Asen, Phytochemistry, **23**, 2523 (1984).
7. S. Asen and R. J. Griesbach. J. Am. Soc. Hortic. Sci. **108**, 845 (1983).
8. C. F. Van Sumere, K. Vande Casteele, R. De Loose, and J. Heursel. *In* The biochemistry of plant phenolics. *Edited by* C. F. Van Sumere and P. J. Lea. Clarendon Press, Oxford. 1985. p. 17.
9. S. Asen, R. N. Stewart, and K. H. Norris. Phytochemistry, **11**, 1139 (1972).
10. M. Williams and G. Hrazdina. Food Sci. **44**, 66 (1979).

Can. J. Chem. Downloaded from www.nrcresearchpress.com by 109.225.110.28 on 09/08/12
For personal use only.

11. J. G. Sweeny, M. M. Wilkinson, and G. A. Iacobucci. J. Agric. Food Chem. **29**, 563 (1981).
12. L. J. Chen and G. Hrazdina. Phytochemistry, **20**, 297 (1981).
13. R. Brouillard, G. Mazza, Z. Saad, A. M. Albrecht-Gary and A. Cheminat. J. Am. Chem. Soc. **111**, 2604 (1989).
14. G. Mazza and R. Brouillard. Phytochemistry, **29**, 1097 (1990).
15. R. Brouillard, M. C. Wigand, O. Dangles, and A. Cheminat. J. Chem. Soc. Perkin Trans. 2, 1235 (1991).
16. P. Rüedi and B. Hutter-Beda. Bull. Liaison Groupe Polyphénols, **15**, 332 (1990).
17. T. V. Mistry, Y. Cai, T. H. Lilley, and E. Haslam. J. Chem. Soc. Perkin Trans. 2, 1287 (1991).
18. R. Brouillard and B. Delaporte. J. Am. Chem. Soc. **99**, 8461 (1977).
19. E. S. Sadlowski. Ph. D. Thesis, Colorado State University, Fort Collins, Colo. 1985.
20. R. N. Stewart, K. H. Norris, and S. Asen. Phytochemistry, **14**, 937 (1975).
21. R. Brouillard and J. E. Dubois. J. Am. Chem. Soc. **99**, 1359 (1977).
22. R. Brouillard, B. Delaporte, and J. E. Dubois. J. Am. Chem. Soc. **100**, 6202 (1978).
23. R. Brouillard and J. Lang. Can. J. Chem. **68**, 755 (1990).
24. E. Sondheimer. J. Am. Chem. Soc. **75** 1507 (1953).
25. T. Goto, T. Hoshino, and M. Ohba. Agr. Biol. Chem. **40**, 1593 (1976).
26. R. Brouillard, M. C. Wigand, and A. Cheminat. Phytochemistry, **29**, 3457 (1990).
27. T. Hoshino and T. Goto. Tetrahedron Lett. **31**, 1593 (1990).
28. T. Hoshino. Phytochemistry, **30**, 2049 (1991).
29. D. B. Smithrud and F. Diederich. J. Am. Chem. Soc. **112**, 339 (1990).
30. R. U. Lemieux, L. T. J. Delbaere, H. Beierbeck, and U. Spohr. *In* Host–guest molecular interactions: from chemistry to biology. Ciba Foundation Symposium. J. Wiley and Sons, Chichester. 1991. p. 231.
31. S. L. Price and A. J. Stone. J. Chem. Phys., **86**, 2859 (1987).
32. K. J. Miller and J. A. Savchik. J. Am. Chem. Soc. **101**, 7206 (1979).
33. C. M. Spencer, Y. Cai, R. Martin, S. H. Gaffney, P. N. Goulding, D. Magnolato, T. H. Lilley, and E. Haslam. Phytochemistry, **27**, 2397 (1988).
34. Y. Cai, S. H. Gaffney, T. H. Lilley, D. Magnolato, R. Martin, C. M. Spencer, and E. Haslam. J. Chem. Soc. Perkin Trans. 2, 2197 (1990).
35. M. C. Wigand. Thèse de Doctorat, Université Louis Pasteur, Strasbourg. 1991.
36. J. E. Beart, T. H. Lilley, and E. Haslam. Phytochemistry, **24**, 33 (1985).
37. J. P. McManus, K. G. Davis, J. E. Beart, S. H. Gaffney, T. H. Lilley, and E. Haslam. J. Chem. Soc. Perkin Trans. 2, 1429 (1985).
38. T. Okuda, K. Mori, and T. Hatano. Chem. Pharm. Bull. **33**, 1424 (1985).
39. C. A. Hunter and J. K. M. Sanders. J. Am. Chem. Soc. **112**, 5525 (1990).
40. Y. Cai, T. H. Lilley, and E. Haslam. J. Chem. Soc. Chem. Commun. 380 (1990).
41. H. Sigel. R. Malini-Balakrishnan, and U. K. Häring. J. Am. Chem. Soc. **107**, 5137 (1985).

Appendix: how to derive the copigmentation equilibrium constants from relaxation kinetic measurements

(i) Flavylium cation copigmentation

We must take into account the slow hydration equilibrium and the instantaneous copigmentation equilibrium involving the flavylium cation (Scheme 3). For the purpose of clarity, the fast equilibrating B and C_E ring-chain tautomers are represented by B only. The general rate equation can be written as eq. [5]:

$$[5] \quad dc_B/dt = k_1 c_{AH} - k_2 c_B c_H$$

c_i stands for the time-dependent concentration of species i and can be expressed as follows: $c_i = c_i^* + \Delta c_i$ where c_i^* is the c_i value in the final equilibrium state (reached after perturbation) and Δc_i is the time-dependent deviation from this value. At the final equilibrium, eq. [5] becomes eq. [6]:

$$[6] \quad 0 = k_1 c_{AH}^* - k_2 c_B^* c_H^*$$

Thus, substituting the expressions for c_i in eq. [5] and using eq. [6] leads to eq. [7]:

$$[7] \quad d\Delta c_B/dt = k_1 \Delta c_{AH} - k_2 (c_H^* \Delta c_B + c_B^* \Delta c_H + \Delta c_B \Delta c_H)$$

Now, in the buffered citric solution, the final pH value is reached just after mixing the pigment and copigment solutions, i.e., it is not changed by the consecutive relaxation process of the hydration equilibrium. Hence, we get $\Delta c_H << \Delta c_B$. In addition, Δc_B and c_B^* are smaller than the pigment total concentration M_t, which in turn, is of the order of c_H^* (pH = 3.4; $M_t = 2 \times 10^{-4}$ M). Thus, in eq. [7] the sum $c_B^* \Delta c_H + \Delta c_B \Delta c_H$ can be neglected and eq. [7] reduces to eq. [8]:

$$[8] \quad d\Delta c_B/dt = k_1 \Delta c_{AH} - k_2 c_H^* \Delta c_B$$

According to the principle of mass conservation, we have for pigment and copigment, respectively (eqs. [9] and [10]):

$$[9] \quad \Delta c_{AH} + \Delta c_B + \Delta c_{AHL} = 0$$

$$[10] \quad \Delta c_L + \Delta c_{AHL} = 0$$

Since the fast copigmentation equilibrium remains established throughout the relaxation process, the mass law expression gives: $K_1 = c_{AHL}/(c_{AH} c_L) = c_{AHL}^*/(c_{AH}^* c_L^*)$. Substituting the expressions for c_i in this equation leads to eq. [11]:

$$[11] \quad K_1 (c_L^* \Delta c_{AH} + c_{AH}^* \Delta c_L + \Delta c_{AH} \Delta c_L) = \Delta c_{AHL}$$

The principle of mass conservation for pigment in the final equilibrium state gives: $M_t = c_{AH}^* + c_B^* + c_{AHL}^* = c_{AH}^* (1 + K_h/c_H^* + K_1 c_L^*)$. Thus, the total concentration of the coloured forms of the pigment is expressed by: $c_{AH}^* + c_{AHL}^* = c_{AH}^* (1 + K_1 c_L^*) = M_t (1 + K_1 c_L^*)/(1 + K_h/c_H^* + K_1 c_L^*)$. Except in the case of exceptionally stable copigmentation complexes ($K_1 > 10^4$), we have: $1 + K_1 c_L^* << K_h/c_H^*$ (about 25 with $K_h = 10^{-2}$ at 25°C). Thus, $c_{AH}^* + c_{AHL}^*$ is much smaller than M_t, which, consequently, is approximately equal to c_B^*. Moreover, the total concentration of copigment L_t is markedly larger than M_t and, thus, much larger than c_{AHL}^*. We may write: $L_t = c_L^*$. Assuming c_L to remain almost constant throughout the relaxation process ($\Delta c_L << c_L^*$), eq. [11] reduces to eq. [12]:

$$[12] \quad K_1 (L_t \Delta c_{AH} + c_{AH}^* \Delta c_L) = \Delta c_{AHL}$$

Combining eqs. [10] and [12], we get: $K_1 L_t \Delta c_{AH} + (1 + K_1 c_{AH}^*) \Delta c_L = 0$. Assuming $K_1 < 10^4$, we have: $K_1 c_{AH}^* =$

Can. J. Chem. Downloaded from www.nrcresearchpress.com by 109.225.110.28 on 09/08/12
For personal use only.

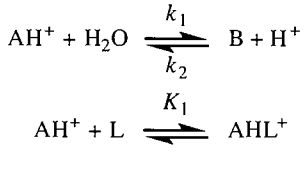

SCHEME 3

$K_1M_tc_H^*/K_h << 1$. Thus, Δc_{AH} and Δc_L are related simply by eq. [13]:

[13] $K_1L_t\Delta c_{AH} + \Delta c_L = 0$

Combining eqs. [9] and [10] leads to eq. [14]:

[14] $\Delta c_{AH} + \Delta c_B = \Delta c_L$

Finally, from eqs. [13] and [14], Δc_{AH} is related to Δc_B according to eq. [15]:

[15] $(1 + K_1L_t)\Delta c_{AH} + \Delta c_B = 0$

Equations [8] and [15] are combined to express the apparent first-order rate constant k for change in B defined by: $d\Delta c_B/dt = -k\Delta c_B$. We get eq. [16]:

[16] $k = k_2c_H^* + k_1/(1 + K_1L_t)$

In the absence of copigment ($L_t = 0$), k becomes k_0, which is expressed by eq. [17]:

[17] $k_0 = k_2\, c_H^* + k_1$

The difference $k_0 - k$ reduces to $k_1K_1L_t/(1 + K_1L_t)$ so that a double-reciprocal plot of $k_0 - k$ versus L_t is linear and yields k_1 and K_1 (see eq. [3]). For each copigment concentration, the k value can be estimated from the time-dependence of the pigment absorption at a fixed wavelength (520 nm for the flavylium cation). Indeed, the visible absorbance D can be written as: $D = \varepsilon_{AH}dc_{AH} + \varepsilon_{AHL}dc_{AHL}$ where d is the optical pathlength. Thus, the absorbance deviation from the equilibrium value D^* is $\Delta D = D - D^* = \varepsilon_{AH}d\Delta c_{AH} + \varepsilon_{AHL}d\Delta c_{AHL}$. The free copigment concentration remains almost constant during the relaxation process ($c_L = c_L^* = L_t$) and c_{AH}^* is much smaller than c_L^*. Thus, eq. [12] can be approximately written as: $K_1L_t\Delta c_{AH} = \Delta c_{AHL}$. Thus, the absorbance deviation becomes $\Delta D = D - D^* = \varepsilon_{AH}d\Delta c_{AH} \times (1 + r_1K_1L_t)$ with $r_1 = \varepsilon_{AHL}/\varepsilon_{AH}$. Finally, using eq. [15], the following expression for ΔD is derived (eq. [18]):

[18] $\Delta D = -\varepsilon_{AH}d\Delta c_B(1 + r_1K_1L_t)/(1 + K_1L_t)$

ΔD is time-dependent in the same way as Δc_B, i.e., $d\Delta D/dt = -k\Delta D$. Thus, the visible absorbance of the pigment varies with time according to $-dD/dt = k(D - D^*)$. On integration, we get $\ln|D - D^*| = \ln|D_0 - D^*| - kt$ where D_0 stands for the initial absorbance just after mixing of the pigment and copigment solutions. Thus, a plot of $\ln|D - D^*|$ versus time must be linear with a slope equal to $-k$. Repeating the experiment at different copigment concentrations gives a series of k values that can be used according to eq. [3] to determine the flavylium cation copigmentation constant K_1.

(ii) Copigmentation of the quinonoidal bases

The equilibria that must be taken into account are summed up in Scheme 4. AH^+ is now a very minor component and its complexation with L has been neglected. The theoretical

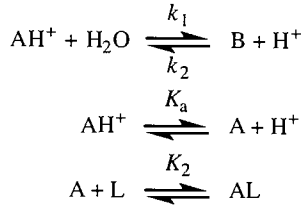

SCHEME 4

treatment presented above can be easily transposed to that case. The equations of mass conservation are now eqs. [19] and [20]:

[19] $\Delta c_{AH} + \Delta c_B + \Delta c_A + \Delta c_{AL} = 0$

[20] $\Delta c_L + \Delta c_{AL} = 0$

For the fast copigmentation and acid–base equilibria, the mass law is expressed as eqs. [21] and [22]:

[21] $K_2\,(c_L^*\Delta c_A + c_A^*\Delta c_L + \Delta c_A\Delta c_L) = \Delta c_{AL}$

[22] $c_A^*\Delta c_H + c_H^*\Delta c_A + \Delta c_H\Delta c_A = K_a\Delta c_{AH}$

Assuming $\Delta c_L << c_L^*$, eq. [21] becomes eq. [23]:

[23] $K_2(c_L^*\Delta c_A + c_A^*\Delta c_L) = \Delta c_{AL}$

The apparent hydration equilibrium constant can be written as: $K_h/K_a = c_B^*/c_A^*$. Here again, c_B^* is approximately equal to M_t and we have: $c_A^* = M_tK_a/K_h = M_t/100$ ($K_h = 10^{-2}$; $K_a = 10^{-4}$ at 25°C). Thus, c_H^* and c_A^* are of the same order of magnitude (pH = 5.2; $M_t = 3 \times 10^{-4}$ M). Assuming $\Delta c_H << \Delta c_A$ and $\Delta c_H << c_H^*$, eq. [22] simplifies to eq. [24]:

[24] $c_H^*\Delta c_A = K_a\Delta c_{AH}$

Combining eqs. [20] and [23], we get eq. [25]:

[25] $(1 + K_2c_A^*)\Delta c_L + K_2c_L^*\Delta c_A = 0$

Assuming $K_2 < 10^4$, we have $K_2c_A^* << 1$. Thus, eq. [25] simplifies to eq. [26]:

[26] $\Delta c_L + K_2c_L^*\Delta c_A = 0$

From eqs. [19] and [20], we get eq. [27]:

[27] $\Delta c_{AH} + \Delta c_B + \Delta c_A = \Delta c_L$

Equations [24], [26], and [27] are combined to give eq. [28]:

[28] $\Delta c_{AH}(1 + (1 + K_2c_L^*)K_a/c_H^*) + \Delta c_B = 0$

$(1 + K_2c_L^*)K_a/c_H^*$ is much larger than 1 and eq. [28] finally reduces to eq. [29] (here again, we may take $c_L^* = L_t$):

[29] $\Delta c_{AH}(1 + K_2L_t)K_a/c_H^* + \Delta c_B = 0$

Assuming eq. [8] to remain valid, we combine it with eq. [29] to get the expression for the apparent first-order rate constant k for change in B (eq. [30]):

[30] $$k = k_2c_H^* + \frac{c_H^*}{K_a}\frac{k_1}{1 + K_2L_t}$$

In the absence of copigment, k becomes k_0 (eq. [31]):

[31] $k_0 = k_2\, c_H^* + k_1\, c_H^*/K_a$

Here again, the double-reciprocal plot of $k_0 - k$ versus L_t is linear and yields k_1/K_a and K_2 (see eq. [4]). k_0 and k are de-

Can. J. Chem. Downloaded from www.nrcresearchpress.com by 109.225.110.28 on 09/08/12
For personal use only.

termined from linear plots of $\ln|D - D^*|$ versus time. However, at pH about 5 in the presence of rutin the hydration process is generally too slow for the equilibrium state to be reached before rutin precipitation occurs. Thus, a direct experimental determination of D^* is not possible. We get a first D^* value from a rough extrapolation of the curve expressing D versus time. Then, a more accurate estimation is achieved by plotting $\ln|D - D^*|$ versus time for different D^* values close to the extrapolated value and by selecting the one giving the best linear plot.

Can. J. Chem. Downloaded from www.nrcresearchpress.com by 109.225.110.28 on 09/08/12
For personal use only.

Hydroxythioéthers éthyléniques : synthèse et réarrangement spontané

GHISLAINE MARTIN, JEAN SAULEAU, MICHÈLE DAVID ET ARMELLE SAULEAU[1]
Laboratoire de chimie pharamaceutique, Faculté de pharmacie, Université de Rennes I, Avenue du Professeur Léon Bernard, 35043 Rennes CEDEX, France

ET

SOURISAK SINBANDHIT
Centre régional de mesures physiques de l'ouest, Faculté des sciences, Université de Rennes I, 35042 Rennes CEDEX, France

Reçu le 29 juillet 1991

GHISLAINE MARTIN, JEAN SAULEAU, MICHÈLE DAVID, ARMELLE SAULEAU et SOURISAK SINBANDHIT. Can. J. Chem. **70**, 2190 (1992).

On étudie la réaction entre des époxydes α éthyléniques et des thiophénols ou le phénylthiotriméthylsilane avec ZnI_2 ou *n*BuLi à température ambiante. Ces réactions qui peuvent être régio et stéréospécifiques, conduisent avec de bons rendements à trois types d'hydroxythioéthers éthyléniques isomères de position. La stéréochimie, le degré de substitution des oxiranes et les conditions réactionnelles, gouvernent les sites d'attaques. Durant la réaction de condensation, il peut se produire une migration 1,3 du reste thiophényle. Sous l'action de la lumière, les hydroxythioéthers allyliques subissent, par un mécanisme radicalaire, la rupture de la liaison ArS – reste allylique. On détermine les constantes de vitesse, les conditions du réarrangement ainsi que les composés formés.

GHISLAINE MARTIN, JEAN SAULEAU, MICHÈLE DAVID, ARMELLE SAULEAU, and SOURISAK SINBANDHIT. Can. J. Chem. **70**, 2190 (1992).

Reactions of vinyloxiranes and thiophenols or phenylthiotrimethyl silane with ZnI_2 or *n*BuLi, at room temperature, were studied. These condensations proceed regio and stereospecifically to afford, in good yields, three families of hydroxy aryl ethylenic sulfides. The regiochemistry is determined by the stereochemistry, the substitution of the oxiranes, and the reaction conditions. During the condensation, 1,3 phenylthio migration occurs. Light initiates the rearrangement by bringing about cleavage of the allyl sulfur bond — a radical chain mechanism — of the hydroxy allylphenyl sulfides. Scope, rate constants, and product composition of the rearrangement were studied.

Introduction

Si la littérature relate souvent l'ouverture d'époxydes saturés par des thiols (1), la place réservée aux oxiranes monoéthyléniques est plus restreinte. En effet, seuls les cas des oxydes commerciaux (de butadiène ou d'isoprène) semblent avoir été rapportés (2–4).

Dans cette étude nous étendons la réaction à toute une gamme d'époxydes α éthyléniques notamment à des structures diastéréoisomères *R*R**, *R*S**. La recherche de conditions expérimentales précises a permis d'atteindre des réactions régio et stéréospécifiques.

Il nous a ainsi été possible de synthétiser une série d'hydroxythioéthers insaturés nouveaux où l'hydroxyle et le groupe soufré sont en position allylique ou homoallylique.

Le réarrangement spontané de certains de ces composés, nous a amené à étudier la cinétique et l'influence des substituants sur leur facilité d'isomérisation.

Résultats des condensations époxydes/thiols : voies I, II, III et IV

Les époxydes utilisés ici, synthétisés selon une méthode mise au point par l'un d'entre nous (5), sont soit primaires–tertiaires **1** et **2**, soit secondaires–tertiaires **3** et **4**, de stéréochimie connue.

Le mélange thiophénols/Na/trifluoroéthanol (TFE) ou le phénylthiotriméthylsilane dans le 1,2-dichloroéthane (DCE) conduit à trois types d'hydroxythioéthers **I**, **II** et **III** selon les voies I, II et III.

La voie IV correspond à l'isomérisation des hydroxythioéthers de structure **II** en composés type **III**, lorsque le milieu réactionnel est, à température ambiante, abondonné à la lumière du jour ou à celle d'une lampe à incandescence.

Compte-tenu des deux origines possibles de **III**, nous avons dû éviter ce réarrangement pour déterminer les pourcentages relatifs exacts des produits types **II** et **III** résultant d'une attaque nucléophile sur les époxydes; cela a été possible en ajoutant des quantités catalytiques d'hydroquinone dans le milieu de condensation.

Les résultats des condensations, reportés tableau 1, appellent plusieurs remarques.

Les voies I et II traduisent l'attaque nucléophile de chacun des carbones hétérocycliques de l'oxirane.

1. *En présence de thiophénols* la voie I est préférentielle (hydroxythioéthers type **I** majoritaires) avec les époxydes primaires–tertiaires (**1** et **2**) où le site d'attaque nucléophile est dépourvu de gêne stérique. Dans ces réactions, l'influence de la nature du solvant de condensation (benzène, dioxane) susceptible d'assister l'ouverture de l'oxirane, n'apparaît pas déterminante; en effet, on obtient des résultats très voisins de ceux indiqués, tableau 1, pour le TFE.

La réaction selon la voie II ne se produit qu'avec les époxydes encombrés **3** et **4**. Leur stéréochimie est essentielle puisqu'elle gouverne une éventuelle conjugaison entre le cycle oxygéné et le système éthylénique (6). Celle-ci a pour effet d'orienter l'ouverture du cycle sur le carbone le plus substitué. Ainsi, avec les époxydes **3** *R*R**, **3** *R*S**, **4** *R*R**, cette activation jour pleinement; on obtient 80–95% de composés type **II**.

Avec ces époxydes trisubstitués, si l'on veut favoriser la formation des hydroxythioéthers type **I** au détriment du type **II**, il est nécessaire qu'il y ait empêchement à la conjugai-

[1]Auteur à qui toute correspondance doit être adressée.

Can. J. Chem. Downloaded from www.nrcresearchpress.com by 109.225.110.28 on 09/08/12
For personal use only.

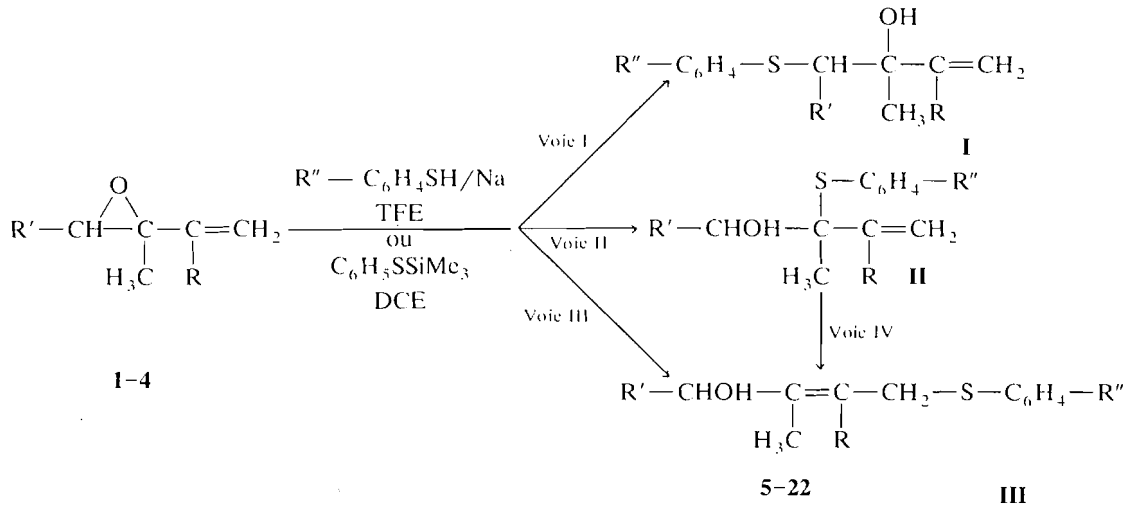

		I	II	III	
1	R = R′ = H	**5**	—	**7**	(R″ = H)
2	R′ = H, R = CH_3	**6**	—	**8**	(R″ = H)
3*R*S**	R = H, R′ = CH_3	**9**	**10**	**11**	(R″ = H)
		—	**12**	**13**	(R″ = CH_3)
3*R*R**	R = H, R′ = CH_3	**14**	**15**	**11**	(R″ = H)
		16	**17**	**13**	(R″ = CH_3)
4*R*R**	R = R′ = CH_3	**18**	**19**	**20**	(R″ = H)
		—	**21**	**22**	(R″ = CH_3)
4*R*S**	R = R′ = CH_3	**23**	—	**20**	(R″ = H)
		24	—	**22**	(R″ = CH_3)

SCHÉMA 1

son. C'est ce qui se produit avec l'époxyde **4** *R*S** où le reste méthyle et le groupe éthylénique volumineux (isopropényle) sont tous deux en position *cis*; on explique ainsi le taux de 95% en composé de type **I**.

2. Les hydroxythioéthers de structure **III** sont majoritaires voire uniques dans les mélanges réactionnels, à condition d'employer le *phénylthiotriméthylsilane* en présence de traces de ZnI_2. C'est la complexation de l'oxygène époxydique avec formation d'un intermédiaire cationique, délocalisable jusqu'aux carbones sp_2, qui privilégie la voie III. Le remplacement de ZnI_2 par des quantités catalytiques de *n*BuLi, entraîne des résultats différents. En effet, dans quatre exemples sur six, l'ouverture des époxydes **1–4** est régiospécifique, la voie I est unique, mais les rendements sont parfois faibles.

Par ailleurs, il faut souligner que toutes ces réactions sont stéréospécifiques et procèdent, comme il est couramment admis, avec d'autres nucléophiles (5), par une *trans* addition. Nous avons par exemple vérifié en RMN 300 MHz, que les hydroxythioéthers **9** et **14** (ou **10** et **15**) issus des époxydes **3** *R*S** et **3** *R*R**, sont chacun de stéréochimie différente et unique. Par contre, une vérification par voie chimique a échoué : la transformation **10** (ou **15**) en époxydes **3** (sous l'action du fluoroborate de triméthyloxonium) n'est pas ici stéréospécifique.

L'étude des spectres RMN a permis de différencier aisément les composés de structure **I**, **II** et **III**, dans les mélanges bruts débarrassés du solvant. Par exemple, il nous a été possible de distinguer des signaux à déplacements chimiques voisins : ceux d'un reste méthylène à 3,55 ppm (composé **11**) ne peuvent être confondus avec le proton du reste C*H*OH (3,71 ppm) de **10** ou du reste C*H*-CH_3 (3,27 ppm) dans **9** (tableaux 2 et 3).

La géométrie *Z* ou *E* de la double liaison dans les structures **III** a été déterminée en RMN ^{13}C. Pour les produits où R = H, l'effet γ-*gauche* est concluant : pour **11** par exemple, le déplacement chimique du reste CH_3 (11,50 ppm) porté par un carbone sp_2 est significatif d'une géométrie *E* (pour l'isomère *Z* on trouve 17,20 ppm) (tableau 3). Par contre, dans le cas des composés où R = CH_3, l'attribution de la géométrie est plus délicate; nous nous sommes référés à des éthers phénoliques de structure voisine, préparés par nous (5*c*) ainsi qu'à des données de la littérature (7).

Étude de la transformation spontanée des hydroxythioéthers de type II (voie IV)

Le milieu réactionnel brut — thiophénols/époxydes — en l'absence d'hydroquinone, est étudié après élimination du solvant.[2]

La RMN haute résolution du ^1H et du ^{13}C a permis en particulier :

(*i*) de suivre le réarrangement des composés type **II** en type **III** : par exemple pour le produit **10**, on note la disparition progressive des signaux correspondants au groupe vinyle entre 4,8 et 5,8 ppm (ou 114,1 et 140,3 ppm) et l'apparition simultanée du produit **11** où le reste CH_2, fixé au substi-

[2]Lorsque les condensations sont menées dans le phénylthiotriméthylsilane, aucune isomérisation **II** vers **III** n'est constatée.

Can. J. Chem. Downloaded from www.nrcresearchpress.com by 109.225.110.28 on 09/08/12
For personal use only.

TABLEAU 1. Bilan de la réaction thiols/époxydes en présence d'hydroquinone

Époxyde	Réactif		Temps (h)	Rdt (%)	Type d'hydroxythioéthers	
					% relatifs	% *Z*/*E* de **III**
1	C_6H_5SH/Na		5	90	**I** : **III** (90 : 10)	10/90
	$C_6H_5SSiMe_3$	ZnI_2	24	90	**III** (100)	50/50
		*n*BuLi	5	80	**I** (100)	
2	C_6H_5SH/Na		7,5	85	**I** : **III** (70 : 30)	60/40
	$C_6H_5SSiMe_3$	ZnI_2	20	90	**III** (100)	52/48
		*n*BuLi	5	80	**I** (100)	
3 *R*S**	C_6H_5SH/Na		12	85	**I** : **II** : **III** (6 : 86 : 8)	5/95
	$pCH_3C_6H_4SH$/Na		12	100	**II** : **III** (95 : 5)	[a]
	$C_6H_5SSiMe_3$	ZnI_2	26	82	**II** : **III** (20 : 80)	10/90
		*n*BuLi	22	36	**I** (100)	
3 *R*R**	C_6H_5SH/Na		33	100	**I** : **II** : **III** (5 : 90 : 5)	[a]
	$pCH_3C_6H_4SH$/Na		24	90	**I** : **II** : **III** (5 : 90 : 5)	[a]
	$C_6H_5SSiMe_3$	ZnI_2	24	88	**II** : **III** (16 : 84)	40/60
		*n*BuLi	24	40	**I** : **II** : **III** (35 : 32 : 33)	30/70
4 *R*R**	C_6H_5SH/Na		2,5	90	**I** : **II** : **III** (5 : 87 : 8)	60/40
	$pCH_3C_6H_4SH$/Na		6	88	**II** : **III** (80 : 20)	60/40
	$C_6H_5SSiMe_3$	ZnI_2	2	100	**II** : **III** (33 : 67)	60/40
		*n*BuLi	48	47	**I** : **II** (56 : 44)	
4 *R*S**	C_6H_5SH/Na		16	85	**I** : **III** (95 : 5)	[a]
	$pCH_3C_6H_4SH$/Na		24	87	**I** : **III** (95 : 5)	[a]
	$C_6H_5SSiMe_3$	ZnI_2	18	90	**III** (100)	70/30
		*n*BuLi	28	53	**I** (100)	

[a]L'isomère *E* des hydroxyéthers type **III** est majoritaire (pourcentages difficiles à déterminer à la précision de la RMN $\simeq$ 5%).

tuant thiophényle, est à 3,55 ppm (31,7 ppm) (tableaux 2 et 3).

(*ii*) de déterminer les demi-vies de la transformation en notant la disparition du proton (ou du système protonique) le mieux résolu, en fonction du temps.

Pour chaque composé type **II**, on porte en fonction du temps, le rapport de sa concentration (instant *t*) à sa concentration initiale. Dans tous les cas, l'obtention d'une droite, pour un avancement de la réaction allant au-delà de 95%, indique que la réaction est du premier ordre par rapport aux produits **II** (dans nos conditions). Les résultats inscrits dans le tableau 4 permettent quelques remarques qualitatives : (*i*) les vitesses de conversion diffèrent d'un composé à l'autre : on remarque qu'un méthyle fixé au reste éthylénique des produits type **II**, accélère l'isomérisation (comparer **10** à **19** ou **12** à **21**); (*ii*) la vitesse est liée à la nature du reste migrant; il suffit de comparer **10** à **12**, le temps de demi-vie varie d'un facteur deux.

Enfin, nous avons constaté que les produits type **II** sont stables, même en l'absence d'hydroquinone, à partir du moment où ils sont débarrassés de toutes traces de thiophénols ou de diphényldisulfures (après plusieurs passages sur colonne de gel de silice). Mais, si au produit ainsi stabilisé on ajoute une très faible quantité (M/100) d'un arylthiophénol, son réarrangement réapparaît.

Des études en spectrographie de masse ont confirmé qu'il s'agit d'une transformation radicalaire, avec migration 1,3 d'un radical thiyle.

Deux réactions croisées ont été effectuées et analysées par cette méthode au départ de **10**. Si on ajoute à **10** du *para*-méthylthiophénol ou du *para*-tertiobutylthiophénol, on peut déceler la présence simultanée des ions moléculaires des composés de réarrangement, respectivement **11** et **13** d'une part, **11** et **25** d'autre part (les pourcentages de quelques ions les plus significatifs sont précisés dans le schéma 2).

De plus, si le diphényl disulfure est toujours présent ($\simeq$ 4%), la décomposition de **11** ($M - H_2O^{\ddagger}$: 190) est totalement différente de celle de **13** ou de **25**, composés issus du croisement, où l'on décèle ($M - CH_3 - CHO^{\ddagger}$: 178 ou 220).

Le réarrangement observé pour les composés type **II**, où les groupes thioéther et hydroxyle sont réunis dans la même molécule, constitue à notre connaissance, le premier exemple de la littérature.[3]

Pour expliquer cette isomérisation, nous pouvons nous référer à des arylthioéthers allyliques de structure voisine de

[3]Le réarrangement d'un phénylthiopropényle cyclohexanol, uniquement en présence d'un initiateur radicalaire (azobisisobutyronitrile) vient d'être rapporté (10).

Can. J. Chem. Downloaded from www.nrcresearchpress.com by 109.225.110.28 on 09/08/12
For personal use only.

Can. J. Chem. Downloaded from www.nrcresearchpress.com by 109.225.110.28 on 09/08/12
For personal use only.

TABLEAU 2. Caractéristiques RMN et spectrométrie de masse des composés de types **I** et **II**

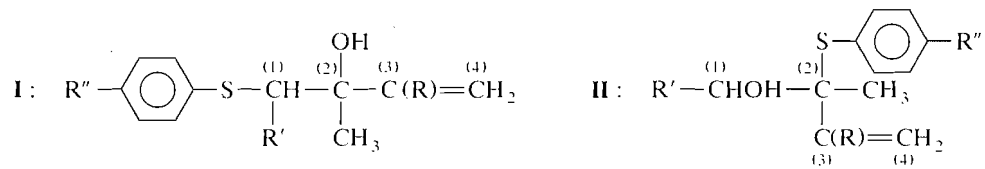

	RMN ^{1}H (δ ppm, J en Hz)						RMN ^{13}C (δ ppm, J en Hz)											
N°	-CH-	R′	CH_3	R	$=CH_2$	H arom (R″)	C(1)	C(2)	C(3)	C(4)	C(1′)	C(2′)	C(3′)	C(4′)	CH_3 (1)	CH_3 (2)	CH_3 (3)	R″
5	3,08–3,25 J = 3,1 (AB)		1,36(s)		5,07–5,95(m)	7,10–7,50(m)	47,6	72,7	143,2	113,2	136,8	129,8	128,9	126,4	—	27,1	—	—
6	3,08–3,40 J = 12,9 (AB)		1,40(s)	1,75(s)	4,90–5,10(m)	7,20–7,60(m)	46,4	74,5	148,8	111,1	136,6	130,0	128,8	126,3	—	26,7	19,3	—
9	3,27(q) J = 7,0	1,33(d) J = 7,0	1,35(s)		5,14–6,00(m)	7,25–7,50(m)	54,0 J = 140,3	76,8	142,6	112,2		[a]			17,6	23,9	—	—
14	3,27(q) J = 7,0	1,29(d) J = 7,0	1,38(s)		5,08–5,75(m)	7,20–7,50(m)	57,4 J = 141,3	75,0	141,0	114,1	135,6	131,8	129,0	127,0	18,2	25,8	—	—
23	3,45(q) J = 7,0	1,28(d) J = 7,0	1,36(s)	1,78(s)	4,93–5,01(m)	7,20–7,50(m)	53,9	77,0	148,5	112,2	135,4	132,4	128,9	127,5	17,4	23,5	18,9	—
18	3,41(q)	1,29(d)	1,38(s)	1,79(s)	4,90–5,12(m)	7,20–7,50(m)	53,4 J = 139,0	77,2	148,2	111,1		[a]			17,3	27,0	19,6	—
16	3,19(q) J = 7,1	1,37(d) J = 7,1	1,37(s)		5,16–6,40(m)	7,00–7,40(m)	58,0 J = 141,0	77,2	141,0	114,0		[a]			18,2	25,8	—	21,2
24	3,37(q) J = 6,3	1,26(d) J = 7,0	1,35(s)	1,78(s)	4,93–5,08(m)	7,00–7,40(m)	54,4	76,8	148,5	112,1	137,4	133,0	129,7	137,4	17,3	23,4	18,9	21,0
10	3,71(q) J = 6,3	1,12(d) J = 6,3	1,29(s)		4,87–5,73(m)	7,20–7,50(m)	70,0 J = 145,0	59,8	140,3	114,1	129,1	137,5	128,7	129,3	15,6	16,3	—	—
15	3,66(s) J = 6,3	1,16(d) J = 6,3	1,27(s)		5,06–6,12(m)	7,20–7,50(m)	71,2 J = 146,0	59,8	138,3	116,5	129,0	137,4	129,0	129,1	20,6	16,7	—	—
19	3,95(s) J = 6,3	1,32(d) J = 6,3	1,26(s)	2,01(s)	4,76–4,99(m)	7,20–7,50(m)	70,1 J = 145,4	61,4	145,2	115,3	129,0	136,6	128,5	128,7	19,7	17,0	20,8	—
12	3,68(s) J = 6,3	1,11(d) J = 6,3	1,28(s)		4,87–5,72(m)	7,10–7,40(m) (2,36)	69,7	59,7	140,5	113,7	126,5	137,4	129,4	139,4	16,2	16,7	21,2	21,2
17	3,63(s) J = 6,3	1,15(d) J = 6,3	1,25(s)		5,07–5,25(m)	7,00–7,40(m) (2,35)	71,2 J = 145,4	59,6	138,5	116,3	126,9	137,4	129,5	139,3	20,7	16,7	—	21,2
21	3,91(s) J = 6,3	1,30(d) J = 6,3	1,24(s)	2,00(s)	4,75–4,98(m)	7,08–7,39(m) (2,33)	70,0 J = 145,5	61,3	145,2	115,2	127,8	136,7	129,3	138,9	19,7	17,0	20.9	21,2

[a] Attributions difficiles : **9**, **16** et **18** en faible proportion dans respectivement **10**, **17** et **19**.

SM M^+ (%) : **5** 194(15,24), 124(100), 110(16,99), 71(53,25), 43(17,83); **6** 208(8,09), 124(100), 110(10,47), 85(33,57); **15** 208(1,17), 164(33,27), 110(72,33), 98(10,07), 65(14,10), 43(100); **23** 222(9,05), 137(100), 113(34,13), 110(32,17), 85(32,02), 43(29,9).

Can. J. Chem. Downloaded from www.nrcresearchpress.com by 109.225.110.28 on 09/08/12
For personal use only.

TABLEAU 3. Caractéristiques RMN et spectrométrie de masse des composés de type **III**

III : 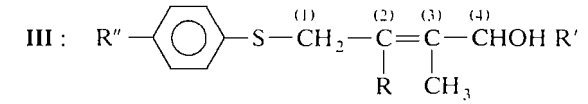

N°		R′	-CHOH	CH_3	R	CH_2	H arom (R″)	C(1)	C(2)	C(3)	C(4)	C(1′)	C(2′)	C(3′)	C(4′)	CH_3 (2)	CH_3 (3)	CH_3 (4)	R″
			RMN ^{1}H (δ ppm, *J* en Hz)					RMN ^{13}C (δ ppm, *J* en Hz)											
7	*E*		3,97(s)	1,60(s)	5,57(t) *J* = 8,0	3,57(d) *J* = 8,0	7,10–7,60(m)	32,2	120,1	138,9	68,1	136,2	130,1	128,8	126,3	—	13,5	—	—
	Z		3,97(s)	1,70(s)	5,46(t) *J* = 7,7	3,56(d) *J* = 7,7	7,10–7,60(m)	32,2	122,7	138,9	61,2	135,7	131,3	128,8	126,9	—	22,2	—	—
8	*E*		4,19(s)	1,63(s)	1,86(s)	3,57(s)	7,20–7,50(m)	39,0	127,7	135,8	63,1	133,2	132,0	128,8	127,2	18,6	16,9	—	—
	Z		3,84(s)	1,73(s)	1,83(s)	3,39(s)	7,20–7,50(m)	39,3	127,7	136,4	63,8	132,6	131,0	128,7	126,6	17,5	16,1	—	—
11	*E*	1,20(d) *J* = 6,4	4,18(q) *J* = 6,4	1,55(s)	5,56(t) *J* = 7,6	3,55(s)	7,20–7,90(m)	31,7	119,6	142,7	72,7	136,1,	130,4	128,7	126,3	—	11,5	21,4	—
	Z	1,14(d) *J* = 6,5	4,57(q) *J* = 6,5	1,70(s)	5,36(t) *J* = 7,7	3,55(s)	7,20–7,90(m)	31,7	121,0	142,4	65,2	135,8	131,4	128,8	126,1	—	17,2	20,8	—
20	*E*	1,06(d) *J* = 6,4	4,46(q) *J* = 6,4	1,50(s)	1,82(s)	3,45–3,71 AB *J* = 11,9	7,20–7,50(m)	38,6	125,3	136,6	66,4	136,3	131,9	128,8	127,1	18,9	11,9	20,7	—
	Z	1,15(d) *J* = 6,5	4,79(q) *J* = 6,5	1,60(s)	1,80(s)	3,47–3,60 AB *J* = 11,8	7,20–7,50(m)	39,7	124,9	136,5	67,0	136,2	131,3	128,7	126,7	17,5	11,4	20,7	—
13	*E*	1,20(d) *J* = 6,4	4,17(q) *J* = 6,4	1,52(s)	5,54(t) *J* = 7,8	3,55(s)	7,07–7,40(m) (2,31)	32,4	119,9	142,5	72,7	132,2	131,3	129,5	136,1	—	11,4	21,4	21,0
	Z	1,11(d) *J* = 6,4	4,50(q) *J* = 6,4	1,69(s)	5,34(t) *J* = 7,8	3,55(s)	7,07–7,40(m) (2,31)	31,8	119,6	142,7	72,8	132,2	132,2	130,4	136,6	—	11,5	21,4	21,0
22	*E*	1,03(d) *J* = 6,3	4,48(q) *J* = 6,3	1,60(s)	1,80(s)	3,34–3,70 AB *J* = 12,2	7,08–7,40(m) (2,32)	39,1	125,4	136,9	66,3	132,0	132,9	129,6	137,5	18,9	11,8	20,6	21,0
	Z	1,14(d) *J* = 6,3	4,76(q) *J* = 6,3	1,46(s)	1,80(s)	3,42–3,55 AB *J* = 11,8	7,08–7,40(m) (2,32)	40,3	125,2	137,5	67,0	132,4	132,1	129,4	136,9	17,2	11,1	20,7	21,0

SM M^+ (%) : **11** 208(9,89), 164(5,10), 110(83,15), 98(31,06), 65(19,65), 43(100); **13** 222(5,82), 178(1,66), 124(25,76), 109(14,26), 84(100); **8***Z* 208(4,69), 110(100), 98(66,27), 65(6,59), 43(40,28); **8***E* 208(1,22), 110(62,17), 98(100), 65(6,19), 43(33,95).

TABLEAU 4. Réarrangement d'hydroxythioéthers type **II** : pourcentages des composés type **III**, constantes de vitesse

Produits type **II**				Pourcentages relatifs en composés **III** après le temps t					Constante de vitesse ($k\ s^{-1}$)	Demi-vie (s)
N°	R	R′	R″	N°	t (h)	%	Z	E		
10 *R*R**	H	CH_3	H	**11**	214,25	96,3	8	92	$3{,}62 \times 10^{-6}$	$191{,}47 \times 10^{3}$
12 *R*R**	H	CH_3	CH_3	**13**	143,9	96	8	92	$7{,}94 \times 10^{-6}$	$87{,}29 \times 10^{3}$
15 *R*S**	H	CH_3	H	**11**	221,6	96,4	15	85	$2{,}84 \times 10^{-6}$	$244{,}06 \times 10^{3}$
17 *R*S**	H	CH_3	CH_3	**13**	115	97,4	15	85	$1{,}53 \times 10^{-5}$	$45{,}30 \times 10^{3}$
19 *R*S**	CH_3	CH_3	H	**20**	32,25	99	56	44	$3{,}33 \times 10^{-4}$	$2{,}08 \times 10^{3}$
21 *R*S**	CH_3	CH_3	CH_3	**22**	2,25	100	47	53	$2{,}70 \times 10^{-5}$	$25{,}67 \times 10^{3}$

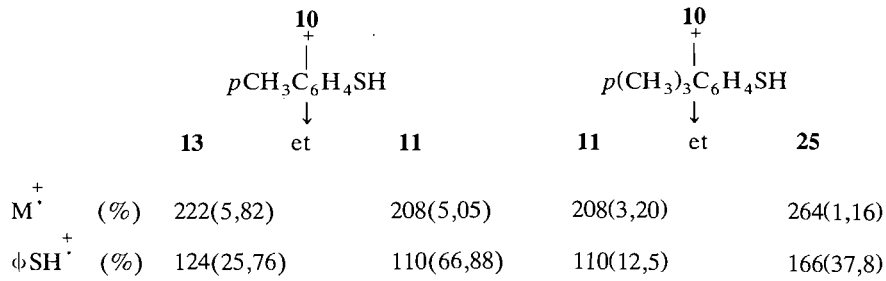

SCHÉMA 2

nos composés type **II**, mais non hydroxylés; il est connu que ceux-ci s'isomérisent soit par un intermédiaire ouvert (8) (chaine radicalaire et entité phénylthiyle) soit par un mécanisme cyclique (9). Dans notre cas, il est probable que la transformation observée procède plutôt par l'intervention d'un système ouvert puisque nous n'avons constaté aucune influence de la stéréochimie *R*S** ou *R*R** des composés type **II**, sur la nature de leurs produits de réarrangement type **III**.

Conclusion

La stéréochimie *R*R** ou *R*S** des époxydes, le choix du réactif soufré, sont des facteurs essentiels réglant la régiosélectivité des réactions étudiées : l'accès à un seul hydroxythioéther de structure définie est alors rendu possible.

Des informations sur la migration 1,3 du groupe aryl thioéther sont apportées : de nature radicalaire, allant jusqu'à modifier les résultats des condensations, elle peut être inhibée dans des conditions qui sont précisées.

Partie expérimentale

Appareillage

RMN Bruker AM 300 WB : 300 MHz (^1H), 75,469 MHz (^{13}C). Les pourcentages figurés dans les tableaux, sont déterminés en RMN ^1H à partir de l'intégration des signaux les mieux résolus; les déplacements chimiques, dans $CDCl_3$, sont exprimés en ppm par rapport au TMS, les constantes de couplage J en hertz (tableaux 2 et 3).

Spectrométrie de Masse (SM) : Varian Matt 311 avec procédé M.I.K.E.; les rapports m/z des principales fragmentations sont suivis, entre parenthèses, des pourcentages par rapport au pic de base. Les ruptures des composés de structure **I**, **II** et **III** indiquées tableaux 2 et 3, sont valables pour tous les autres produits de même type.

Chromatographie phase gazeuse : Fractovap Carlo Erba 4160, colonne capillaire SE 52 de 25 m. Fractovap GT Carlo Erba détecteur à ionisation de flamme, gaz porteur N_2, colonne SE 30 à 10% sur Chromosorb W 60/80 lavé aux acides.

Chromatographie sur colonne gel de silice 60 Merck (70–230 mesh). Eluant : $C_6H_6/CH_3COOC_2H_5$ 95 : 5 pour la séparation des composés **5** et **7**; $C_6H_6/CH_3COOC_2H_5$, 92 : 8 pour la séparation des isomères *E*, *Z* de **7** et de **8**; CH_2Cl_2 dans tous les autres cas.

Pour l'élimination de l'excès de thiophénols et des disulfures dans le milieu réactionnel, on utilise le toluène.

Un contrôle de pureté est réalisé sur chacun des produits, par chromatographie phase vapeur et spectrométrie de masse.

Mode opératoire général

Les réactions sont toutes conduites sous atmosphère inerte d'azote. Eventuellement une quantité d'hydroquinone (nombre de mole d'époxyde $\times 10^{-2}$) est ajoutée au milieu réactionnel.

Utilisation du mélange thiophénols/sodium

À 10.2 mmol de thiophénol (ou de *para*-méthylthiophénol), préalablement purifié sous azote, dissous dans 12 mL de solvant, on ajoute 0,23 g de sodium. Après disparition du sodium et refroidissement, on ajoute sous agitation en une seule fois, 5.1 mmol d'époxyde et éventuellement, 0.05 mmol d'hydroquinone. Tout en maintenant l'agitation à température ordinaire, le terme de la réaction (disparition de l'époxyde) est déterminé par chromatographie en phase gazeuse (colonne SE 30). Le mélange est ensuite versé sur 10 mL d'eau, extrait plusieurs fois à l'éther. Les phases éthérées sont séchées sur Na_2SO_4 et évaporées.

Utilisation du phénylthiotriméthylsilane (3)

Au départ de 8.1 mmol d'époxyde et de 8.3 mmol, de phénylthiotriméthylsilane, on ajoute soit une solution de 0.42 mmol de *n*BuLi dans 12 mL de THF soit une solution de 0.8 mmol de ZnI_2 dissous dans 12 mL de 1,2-dichloroéthane. Après agitation à température ordinaire et contrôle chromatographique (pour le terme de la réaction), le milieu réactionnel est traité par 8 mL de méthanol puis 1.2 mmol d'acide acétique suivi de deux lavages par une solution aqueuse à 10% d'hydroxyde de baryum. Le composé isolé contient parfois un faible pourcentage de son dérivé *O*-silylé. Nous donnons les caractéristiques spectrales RMN et spectrographie de masse des composés silylés **5** et **6**.

Can. J. Chem. Downloaded from www.nrcresearchpress.com by 109.225.110.28 on 09/08/12
For personal use only.

Quel que soit le mode opératoire utilisé, le mélange brut réactionnel est toujours purifié sur colonne de gel de silice.

*Traitement de **10** ou **15** par le tétrafluoroborate de triméthyloxonium*

À une solution de 4.2 mmol de **10** *R*R** (ou **15** *R*S**), dans 30 mL de CH_2Cl_2, maintenue à 0°C et sous azote, on introduit en une seule fois 4.5 mmol de fluoroborate de triméthyloxonium. La solution devient limpide en 1,5 h. On ajoute alors goutte à goutte tout en maintenant à 0°C, 8.5 mL de NaOH 10%. Une fois l'addition terminée, le mélange réactionnel est analysé en chromatographie phase gazeuse (colonne SE 30). La formation de l'époxyde **3** est pratiquement immédiate (10 min). Il se trouve sous forme d'un mélange des diastéréoisomères **3** *R*R** / **3** *R*S** (40 : 60) identifié directement au moyen d'échantillons témoins de stéréochimie pure. Cette réaction n'est donc pas stéréospécifique, dans notre cas, contrairement à ce que Pirkle et Rinaldi (11) ont observé au départ d'hydroxysulfures à restes saturés.

Détermination des constantes de vitesse

Les réactions de transformation ont été suivies en tube RMN scellé; les composés **II** sont en solution dans $CDCl_3$: le signal du trichloro-1,1,1-éthane, constant dans le temps, sert de référence aux intégrales des signaux. La variation de l'aire d'un signal décroissant, mesurée par référence à celle de l'étalon interne a permis de doser les produits type **II** décroissants. Les spectres, à 300 MHz, sont enregistrés à la température de l'aimant.

Les produits **II** sont à concentration moyenne de 8×10^{-5} M, la référence interne de 10^{-5} M. Pour la reproductibilité des résultats, le tube scellé est soumis à la lumière d'une lampe à incandescence de 150 W située à 38 cm de l'échantillon (cas de **17**) tandis que 60 W pour 12 cm sont utilisés pour tous les autres produits type **II**.

Nous avons vérifié que, dans chacun des cas, les pentes expérimentales et les pentes calculées (droites de tendance, méthode des moindres carrés) ont en valeur, un écart inférieur aux erreurs expérimentales (considérées voisines de 5%). Les résultats sont indiqués tableau 4.

Données spectroscopiques complémentaires

Composé **5** silylé : RMN ^1H : 0,10 (s, 9H); 1,45 (s, 3H); 3,04–3,14 (2H, AB, J = 12,62); 5,07–5,27 et 5,94–6,03 (3H, ABX, J_{AB} = 10,59, J_{BX} = 10,66, J_{AX} = 17,03); 7,12–7,37 (m, 5H). ^{13}C : 2,39 ($Si(CH_3)_3$); 26,32 (CH_3); 47,66 (CH_2); 75,9 (C-OSi); 113,32 (=CH_2); 125,55 (C4′); 128,69 (C3′); 128,98 (C2′); 128,07 (C1′); 144,04 (=CH). SM, $C_{14}H_{22}OSSi$: masse calculée : 266,1160; trouvée : 266,1146. $M^{\ddagger}$: 266 (6,05), 251 (2,98), 143 (100), 75 (26,12), 73 (81,83).

Composé **6** silylé : RMN ^1H : 0,11 (s, 9H); 1,52 (s, 3H); 1,76 (m, 3H); 3,07–3,19 (2H, AB, J = 12,95); 4,90 et 5,04 (m, 2H); 7,20–7,50 (m, 5H). ^{13}C : 2,17 ($Si(CH_3)_3$); 18,99 (CH_3); 26,05 (CH_3); 46,10 (CH_2); 74,59 (C-OSi); 111,15 (=CH_2); 125,52 (C4′); 128,67 (C3′); 128,96 (C2′); 138,07 (C1′); 149,12 (=CH). SM, $C_{15}H_{24}OSSi$: masse calculée : 280,1317; trouvée : 280,1336. $M^{\ddagger}$: 280 (4,30), 157 (91,95), 124 (41,07), 75 (26,10), 73 (100).

1. (*a*) J. Gorzynski Smith. Synthesis, **8**, 629 (1984), et références citées; (*b*) B. A. Marples, C. G. Saint et J. R. Traynor. J. Chem. Soc. Perkin Trans. 1, 567 (1986); (*c*) A. E. Vougioukas et H. B. Kagan. Tetrahedron Lett. **28**, 6065 (1987).
2. E. V. Nekhorosheva et V. M. Al'Bitskaya. Zh. Org. Khim. **5**, 1002 (1969); Chem. Abstr. **71**, 70413b (1969).
3. Y. Guindon, R. N. Young et R. Frenette. Synth. Commun. **11**, 391 (1981).
4. A. Yasuda, M. Takahashi et H. Takaya. Tetrahedron Lett. **22**, 2419 (1981).
5. (*a*) J. Huet, H. Bouget et J. Sauleau. C. R. Acad. Sci. Ser. C, **271** 430 (1970); (*b*) J. Sauleau. Thèse de Doctorat ès-Sciences Physiques, Rennes N° 250. 1976; (*c*) M. David, J. Sauleau et A. Sauleau. Can. J. Chem. **63**, 2449 (1985).
6. A. Sauleau, J. Sauleau. J. P. Monti et R. Faure. Org. Magn. Reson. **24**, 15 (1986).
7. U. Vogeli et W. Von Philips Born. Org. Magn. Reson. **7**, 617 (1975).
8. (*a*) P. Brownbridge et S. Warren. J. Chem. Soc. Perkin Trans. 1, 2125 (1976); (*b*) 1131 (1977); (*c*) 2272 (1977); (*d*) M. Hannaby et S. Warren. J. Chem. Soc. Perkin Trans. 1, 303 (1989); (*e*) I. Fleming, I. Paterson et A. Pearce. J. Chem. Soc. Perkin Trans. 1, 256 (1981), et réferences citées; (*f*) P. Brownbridge, I. Fleming, A. Pearce et S. Warren. J. Chem. Soc. Chem. Commun. 751 (1976).
9. (*a*) H. Kwart et N. A. Johnson. J. Org. Chem. **42**, 2855 (1977); (*b*) H. Kwart et T. J. George. J. Am. Chem. Soc. **99**, 5214 (1977); (*c*) A. P. Kozikowski et E. Huie. J. Am. Chem. Soc. **104**, 2059 (1982).
10. E. Schaumann, A. Kirschning et F. Narjes. J. Org. Chem. **56**, 717 (1991).
11. W. H. Pirkle et P. L. Rinaldi. J. Org. Chem. **43**, 3803 (1978), et réf. 8 citée.

Can. J. Chem. Downloaded from www.nrcresearchpress.com by 109.225.110.28 on 09/08/12
For personal use only.

Isothermes 75°C, des systèmes ternaires limitant le système quaternaire réciproque : H^+, K^+, PO_4^{3-}, SO_4^{2-}, H_2O

NÉJI BOURGUIBA[1] ET TAHAR JOUINI

Département de chimie, faculté des sciences de Tunis, Campus universitaire, 1060 Tunis, Tunisie

Reçu le 18 octobre 1991

NÉJI BOURGUIBA et TAHAR JOUINI. Can. J. Chem. **70**, 2197 (1992).

Les cinq isothermes ternaires limitant le système quaternaire indiqué au titre ont été établies comme première étape de l'étude de ce système à 75°C et 1 atm (101,3 kPa). Cette température a été choisie en vue d'appliquer les résultats à la fabrication industrielle d'engrais phosphopotassiques par attaque sulfurique du minerai phosphaté, dont la température optimale est de 70–80°C. (*i*) Système ternaire réciproque anhydre H_2SO_4–H_3PO_4–K_2SO_4–K_3PO_4. Phases solides : $KHSO_4$, $KH_2PO_4 \cdot KHSO_4$, $KH_5(PO_4)_2$ et une solution solide de substitution $K_8(H_2PO_4)_{1+x}(HSO_4)_{7-x}$, $0 \leq x \leq 1$, continue entre les deux compositions limites $KH_2PO_4 \cdot 7KHSO_4$ et $KH_2PO_4 \cdot 3KHSO_4$ dont les diagrammes de poudre indéxés sont donnés. (*ii*) Système ternaire K_3PO_4–H_3PO_4–H_2O. Phases solides : $KH_5(PO_4)_2$, KH_2PO_4, $3K_2HPO_4 \cdot KH_2PO_4 \cdot 2H_2O$, K_2HPO_4 et $K_3PO_4 \cdot 3H_2O$. (*iii*) Système ternaire K_2SO_4–H_2SO_4–H_2O. Phases solides : K_2SO_4, $K_2SO_4 \cdot KHSO_4$, $K_2SO_4 \cdot 7KHSO_4 \cdot H_2O$ et $KHSO_4$. Un phénomène de solubilité rétrograde en fonction de la teneur en eau y est mis en évidence. (*iv*) Système ternaire K_2SO_4–K_3PO_4–H_2O. Phases solides : K_2SO_4 et $K_3PO_4 \cdot 3H_2O$. (*v*) Le système ternaire H_3PO_4–H_2SO_4–H_2O est constitué d'un seul domaine liquide à 75°C.

NÉJI BOURGUIBA and TAHAR JOUINI. Can. J. Chem. **70**, 2197 (1992).

The five ternary isotherms limiting the quaternary system mentioned in the title have been established as a first step toward the study of this system at 75°C and 1 atm (101.3 kPa). This temperature has been chosen in order to be able to apply the results to the industrial preparation of phosphopotassium fertilizers through a sulphuric treatment of a phosphate ore for which the optimum temperature is 70–80°C. (*i*) Anhydrous reciprocal ternary system : H_2SO_4–H_3PO_4–K_2SO_4–K_3PO_4. Solid phases : $KHSO_4$, $KH_2PO_4 \cdot KHSO_4$, $KH_5(PO_4)_2$, and a solid substituting solution $K_8(H_2PO_4)_{1+x}(HSO_4)_{7-x}$, $0 \leq x \leq 1$, continuous between the two limiting compositions $KH_2PO_4 \cdot 7KHSO_4$ and $KH_2PO_4 \cdot 3KHSO_4$ for which the indexed powder diagrams are given. (*ii*) Ternary system K_3PO_4–H_3PO_4–H_2O. Solid phases: $KH_5(PO_4)_2$, KH_2PO_4, $3K_2HPO_4 \cdot KH_2PO_4 \cdot 2H_2O$, K_2HPO_4, and $K_3PO_4 \cdot 3H_2O$. (*iii*) Ternary system K_2SO_4–H_2SO_4–H_2O. Solid phases: K_2SO_4, $K_2SO_4 \cdot KHSO_4$, $K_2SO_4 \cdot 7KHSO_4 \cdot H_2O$, and $KHSO_4$. A phenomenon of retrosolubility as a function of the water content has been observed. (*iv*) Ternary system K_2SO_4–K_3PO_4–H_2O. Solid phases: K_2SO_4 and $K_3PO_4 \cdot 3H_2O$. (*v*) The ternary system H_3PO_4–H_2SO_4–H_2O is formed by only one liquid phase at 75°C.

[Journal translation]

Introduction

Les techniques de préparation industrielle des engrais sont actuellement orientées vers la fabrication, utilisant des matériaux disponibles, d'engrais combinés les plus riches en éléments fertilisants.

Dans ce cadre figure la fabrication d'engrais phosphopotassiques à partir de minerai phosphaté (apatite) et de sulfate acide de potassium $KHSO_4$ provenant du procédé Pennzoil (1–4)

$$H_2SO_4 + KCl \rightarrow KHSO_4 + HCl$$

L'attaque par $KHSO_4$ de l'apatite produit un mélange hétérogène. Aprés dégagement des composés volatils (HF, SiF_4, CO_2 . . .) et séparation de l'insoluble constitué essentiellement de phosphogypse, la solution aqueuse résultante contient les ions H^+, K^+, PO_4^{3-} et SO_4^{2-}.

On est donc amené à étudier le quaternaire K_2O–SO_3–P_2O_5–H_2O. Il est commode de considérer, à l'intérieur de ce système, celui faisant intervenir les composés présents en milieu aqueux : H_3PO_4, K_2SO_4, H_2SO_4, K_3PO_4. Il s'agit d'un système quaternaire réciproque caractérisé par la réaction de double décomposition:

$$2H_3PO_4 + 3K_2SO_4 \overset{H_2O}{\rightleftharpoons} 3H_2SO_4 + 2K_3PO_4$$

Toute application industrielle devra se baser sur la connaissance de ce diagramme d'équilibre. De plus cette fabrication constitue, en particulier, l'un des objectifs de l'industrie tunisienne.

Nous avons choisi d'établir l'isotherme 75°C. En effet la température optimale de l'attaque sulfurique de l'apatite est de 70–80°C. En s'en écartant trop on risque un blocage de la réaction ou la formation du monohydrogénophosphate $CaHPO_4 \cdot 2H_2O$ qui syncristallise avec le gypse provoquant une perte de phosphate. De plus ce diagramme n'a fait l'objet d'aucune étude dans cet intervalle de température.

Nous présentons en une première étape, dans ce mémoire, les diagrammes limitant cette isotherme.

Partie expérimentale

A. Techniques expérimentales

Les solubilités ont été essentiellement mesurées par analyse chimique des solutions à l'équilibre, saturées par une ou deux phases solides. Quelques déterminations de solubilité ont été effectuées par conductimétrie (5–7). Les résistances ont été mesurées au moyen d'un pont de marque Général-Radio de type impédance bridge B-1650.

L'évolution des mélanges est contrôlée d'une part en examinant les phases solides par diffraction des rayons X sur poudre et au microscope polarisant, d'autre part en mesurant la résistance de la solution. Lorsque l'équilibre est atteint la résistance du liquide prend une valeur constante. Cela nécessite en général quelques jours. Les mélanges visqueux, trés riches en acides, nécessitent une agitation énergique de plusieurs semaines. De plus pour nous assurer de la reproductibilité de nos résultats, la composition de chaque point invariant a fait l'objet de mesures indépendantes sur au moins deux mélanges différents.

Lors de ces analyses répétitives nous avons constaté que pour une

[1]Auteur à qui adresser toute correspondance.

Can. J. Chem. Downloaded from www.nrcresearchpress.com by 109.225.110.28 on 09/08/12
For personal use only.

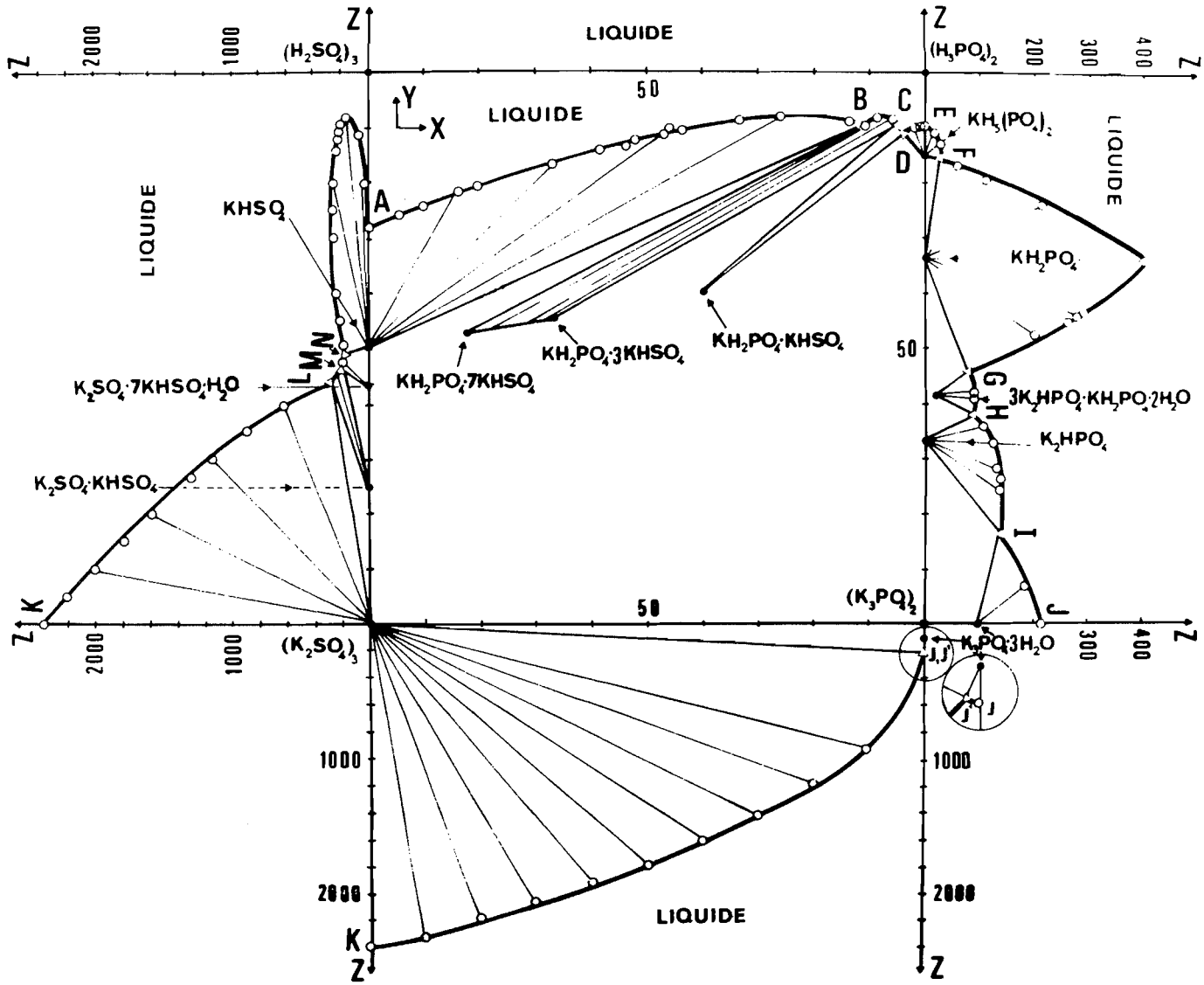

FIG. 1. Isothermes 75°C, des systèmes ternaires limitant le système quaternaire réciproque : H_2SO_4–H_3PO_4–K_2SO_4–K_3PO_4–H_2O, rabattus dans le carré de base.

même composition les coordonnées X et Y fluctuent de 0,5 à 1% et les coordonnées Z de 1 à 2%. Cela conduit à un nombre de chiffres significatifs de 3 à 4, comme c'est en général le cas dans les publications relatives aux digrammes de solubilité. Par exemple dans celles compilées dans l'ouvrage de Linke (8).

Les phases solides connues ont été identifiées par leurs diagrammes de diffraction des rayons X sur poudre effectués sur une chambre de type Guinier–Dewolf de marque Enraf–Nonius permettant le travail en atmosphère contrôlée, dans le cas présent sous air sec pour les sels hygroscopiques. Les phases solides pour lesquelles nous ne disposons pas d'une liste des distances réticulaires ont été au préalable identifiées par les méthodes des restes (9) et des ensembles (10). Les phases solides sont également observées au microscope polarisant et pour les plus caractéristiques d'entre elles identifiées.

B. Produits utilisés

1. Produit du commerce

Nous avons utilisé les produits Merck pour analyse et Prolabo R.P. suivants : l'acide sulfurique à 95%, $\rho = 1{,}83$ g cm^{-3}, l'acide phosphorique à 85%, $\rho = 1{,}7$ g cm^{-3}, l'acide de Nordhausen à 20% d'anhydride sulfurique, le sulfate acide de potassium, le sulfate de potassium, le phosphate diacide de potassium, le phosphate monoacide de potassium et le phosphate tri-potassique dihydraté.

2. Produits préparés au laboratoire

Acide sulfurique anhydre : Il a été préparé par addition, à la burette, d'une quantité calculée d'eau à de l'acide de Nordhausen à 20% d'anhydride sulfurique. L'opération est effectuée dans un récipient plongé dans un mélange de glace et de chlorure de sodium, en évitant toute projection.

$KH_5(PO_4)_2$: Ce produit est utilisé pour préparer les mélanges très riches en H_3PO_4. Sa préparation est basée sur la connaissance du système ternaire K_3PO_4–H_3PO_4–H_2O à 75°C établie au cours de cette étude.

C. Mode de represéntation

Le mode de représentation choisi pour le système quaternaire est celui du prisme droit à base carré de Le Chatelier (11)–Janecke (12).

Les sommets du carré de base représentent les composés de départ. Les arêtes du prisme correspondent aux systèmes binaires limites faisant intervenir l'eau. Les parois verticales du prisme sont des systèmes ternaires limites simples et la base est un système ternaire limite réciproque anhydre.

Un mélange quelconque sera caractérisé par trois coordonnées

Can. J. Chem. Downloaded from www.nrcresearchpress.com by 109.225.110.28 on 09/08/12
For personal use only.

TABLEAU 1. Coordonnées des points représentatifs des invariants ternaires dans les isothermes 75°C, des systèmes ternaires limitant le système quaternaire réciproque : H^+, K^+, PO_4^{3-}, SO_4^{2-}, H_2O

(*a*) Système : H_2SO_4–H_3PO_4–K_2SO_4–K_3PO_4

Points invariants	Composition pondérale % K_2O	% P_2O_5	% SO_3	% H_2O	Janecke *X*	*Y*	Phases solides en équilibre
B	12,19	54,42	12,26	21,13	88,24	90,07	$KHSO_4 + KH_2PO_4 \cdot 7KHSO_4$
C	12,09	61,27	04,61	22,03	95,74	90,51	$KH_2PO_4 \cdot 3KHSO_4 + KH_2PO_4 \cdot KHSO_4$
D	13,53	61,07	03,89	21,51	96,37	89,27	$KH_2PO_4 \cdot KHSO_4 + KH_5(PO_4)_2$

(*b*) Système : K_3PO_4–H_3PO_4–H_2O

Points invariants	Composition pondérale % K_2O	% P_2O_5	% H_2O	Janecke *Y*	*Z*	Phases solides en équilibre
F	17,12	53,88	29,00	84,00	28,76	$KH_5(PO_4)_2 + KH_2PO_4$
G	36,90	34,20	28,90	45,67	88,27	$KH_2PO_4 + 3K_2HPO_4 \cdot KH_2PO_4 \cdot 2H_2O$
H	39,87	32,51	27,60	38,21	92,51	$3K_2HPO_4 \cdot KH_2PO_4 \cdot 2H_2O + K_2HPO_4$
I	43,93	26,49	29,58	16,49	138,57	$K_2HPO_4 + K_3PO_4 \cdot 3H_2O$

(*c*) Système : K_2SO_4–H_2SO_4–H_2O

Points invariants	Composition pondérale % K_2O	% SO_3	% H_2O	Janecke *Y*	*Z*	Phases solides en équilibre
N	24,50	40,61	34,89	48,78	166,5	$KHSO_4 + K_2SO_4 \cdot 7KHSO_4 \cdot H_2O$
M	25,24	39,87	34,89	46,25	171,4	$K_2SO_4 \cdot 7KHSO_4 \cdot H_2O + K_2SO_4 \cdot KHSO_4$
L	22,52	34,15	43,33	44,00	260,0	$K_2SO_4 \cdot KHSO_4 + K_2SO_4$

(*d*) Système : K_2SO_4–K_3PO_4–H_2O

Points invariants	Composition pondérale % K_2O	% P_2O_5	% H_2O	Janecke *X*	*Z*	Phases solides en équilibre
J	43,17	21,69	35,14	100	213,0	$K_3PO_4 \cdot 3H_2O + K_2SO_4$

TABLEAU 2. Paramètres affinés des solutions solides limites $K_8(H_2PO_4)_{1+x}(HSO_4)_{7-x}$, $x = 0$ et $x = 1$

Composés limites	*a*(Å)	*b*(Å)	*c*(Å)	α(°)	β(°)	γ(°)
$KH_2PO_4 \cdot 7KHSO_4$	7,201(3)	7,503(3)	7,582(3)	108,57(4)	88,29(4)	93,70(3)
$KH_2PO_4 \cdot 3KHSO_4$	7,180(4)	7,497(5)	7,599(6)	108,52(6)	88,51(7)	93,77(5)

X, *Y* et *Z*. *X* et *Y* sont respectivement les pourcentages ou fractions molaires d'ions phosphates et de protons :

$$X = 3 \times 10^2 [PO_4^{3-}]/D$$

$$Y = 10^2 [H^+]/D$$

où *D* est la relation qui traduit la neutralité électrique du milieu.

$$D = [H^+] + [K^+] = 2[SO_4^{2-}] + 3[PO_4^{3-}]$$

Les variables entre crochets représentent des nombres de moles. La composition en eau, portée par les arêtes verticales du prisme, s'exprime par :

$$Z = 10^2 [H_2O]/D$$

Il en résulte que le point représentatif de l'eau pure (*D* tendant vers 0) est rejeté à l'infini.

Pour l'une des isothermes ternaires nous avons aussi utilisé le mode de représentation plus classique en triangle équilatéral.

Résultats expérimentaux

Les systèmes ternaires limites étudiés sont représentés à la figure 1. Les compositions des points représentatifs des invariants ternaires isothermes et les phases en équilibre correspondantes sont consignées au tableau 1.

1. Isotherme 75°C du système ternaire réciproque anhydre : H_2SO_4–H_3PO_4–K_2SO_4–K_3PO_4

Ce diagramme n'a à notre connaissance fait l'objet d'aucune étude antérieure. Il est représenté à l'intérieur du carré de la figure 1. Cette étude fait intervenir $KH_5(PO_4)_2$ et H_2SO_4 anhydres. Il en résulte des mélanges très visqueux et hygroscopiques nécessitant des précautions particulières : agitation mécanique très énergique et prolongée (quelques heures à plusieurs jours) et une parfaite étanchéité des tubes laboratoires, assurée par des joints en mercure. Les prélèvements effectués au moyen de pipettes à bout filtrant, des solutions à analyser, sont également rendus difficiles par la viscosité.

Can. J. Chem. Downloaded from www.nrcresearchpress.com by 109.225.110.28 on 09/08/12
For personal use only.

TABLEAU 3. Diagramme de poudre indexé de $KH_2PO_4 \cdot 7KHSO_4$

h	k	l	d_{obs}	d_{calc}	I/I_0	h	k	l	d_{obs}	d_{calc}	I/I_0
1	−1	1	4,795	4,796	18	2	−2	2	2,397	2,398	13
−1	−1	1	4,520	4,528	10	0	0	3		2,396	
1	1	1	3,707	3,704	46	0	3	0	2,367	2,367	9
2	0	0	3,590	3,593	94	0	−2	3		2,364	
0	2	0	3,553	3,550	100	−1	−1	3	2,356	2,360	12
1	−2	1	3,368	3,366	10	−1	−3	1	2,313	2,312	6
2	−1	0	3,286	3,284	14	3	−1	0		2,311	
1	0	2	3,229	3,227	57	1	0	3	2,2793	2,2795	10
−1	−2	1	3,194	3,192	80	3	0	1		2,2791	
2	1	0	3,134	3,133	5	−3	−1	1	2,1878	2,1873	7
0	−2	2	3,052	3,057	47	2	−1	3	2,097	2,097	22
−2	−1	1	3,019	3,022	31	2	−3	0	2,029	2,031	13
0	1	2	2,860	2,861	24	−2	−3	1	1,988	1,990	6
2	1	1	2,744	2,743	16	−2	0	3		1,984	
−1	1	2	2,670	2,673	5	−3	0	2	1,984	1,984	10
1	2	1	2,605	2,607	28	−1	−3	3	1,929	1,931	14
−2	−2	1	2,490	2,491	15	2	3	0		1,926	
2	2	0	2,4554	2,4551	6	−2	2	2	1,9026	1,9021	11
1	−1	3	2,4062	2,4062	5	0	−4	1	1,867	1,867	4
1	−3	1		2,4062		3	1	2	1,8220	1,8228	8

TABLEAU 4. Diagramme de poudre indexé de $KH_2PO_4 \cdot 3KHSO_4$

h	k	l	d_{obs}	d_{calc}	I/I_0	h	k	l	d_{obs}	d_{calc}	I/I_0
1	−1	1	4,792	4,788	19	−2	2	0	2,597	2,600	27
−1	−1	1	4,517	4,526	10	−2	−2	0	2,484	2,486	14
1	1	1	3,696	3,697	42	2	2	0	2,446	2,447	7
2	0	0	3,578	3,582	98	3	0	0	2,389	2,388	14
0	2	0	3,545	3,548	100	0	−3	0	2,351	2,347	15
1	−2	1	3,363	3,363	12	−1	0	3	2,271	2,273	9
−2	1	0	3,278	3,279	22	3	0	1		2,270	
−1	0	2	3,207	3,212	53	2	2	1	2,175	2,179	5
−2	0	1		3,200		1	2	2	2,087	2,086	20
2	−1	1	3,177	3,170	54	2	−3	2	2,023	2,023	8
2	1	0	3,121	3,122	4	−3	−1	2	1,979	1,977	15
0	−2	2	3,049	3,058	50	3	2	0	1,925	1,928	12
−2	−1	1	3,014	3,017	21	2	3	0		1,921	
0	2	1	2,844	2,845	27	0	−1	4	1,895	1,895	12
2	1	1	2,731	2,734	12	−2	1	3	1,812	1,811	13
						1	−4	2		1,810	

Dans ce système on observe en particulier un domaine limité par la courbe de solubilité BC où se manifeste une solution solide continue $K_8(H_2PO_4)_{1+x}(HSO_4)_{7-x}$ avec $0 \leq x \leq 1$. Les compositions limites $KH_2PO_4 \cdot 7KHSO_4$ et $KH_2PO_4 \cdot 3KHSO_4$ (abréviations P.7S et P.3S) ont été déterminées par analyse chimique de cristaux obtenus de la façon décrite ci-aprés. Deux mélanges ont été préparés respectivement dans les deux triangles d'invariance ternaire isotherme situés de part et d'autre du domaine de la solution solide. Ces mélanges sont triphasés : dans chacun d'eux coexistent l'une des solutions solides limites avec le sel appartenant au domaine voisin, en présence de solution. Nous avons fait croître des cristaux de ces phases solides par sursaturation. Les cristaux des solutions solides limites reconnaissables à leur forme de baguettes, sont séparés par triage pour analyse chimique et aux rayons X. Les paramètres de leurs mailles ont été déterminés par étude des cristaux sur chambre de Weissenberg puis affinés par moindres carrés en utilisant les raies des diagrammes de poudre mesurées au moyen d'un diffractomètre automatique à deux cercles «STOE/css». Les paramètres, des deux composés limites, reportés au tableau 2 diffèrent peu malgré l'importante différence stoechiométrique. Cela s'explique par la similitude des dimensions des tétraèdres PO_4^{3-} et SO_4^{2-}. Les dia-

Can. J. Chem. Downloaded from www.nrcresearchpress.com by 109.225.110.28 on 09/08/12
For personal use only.

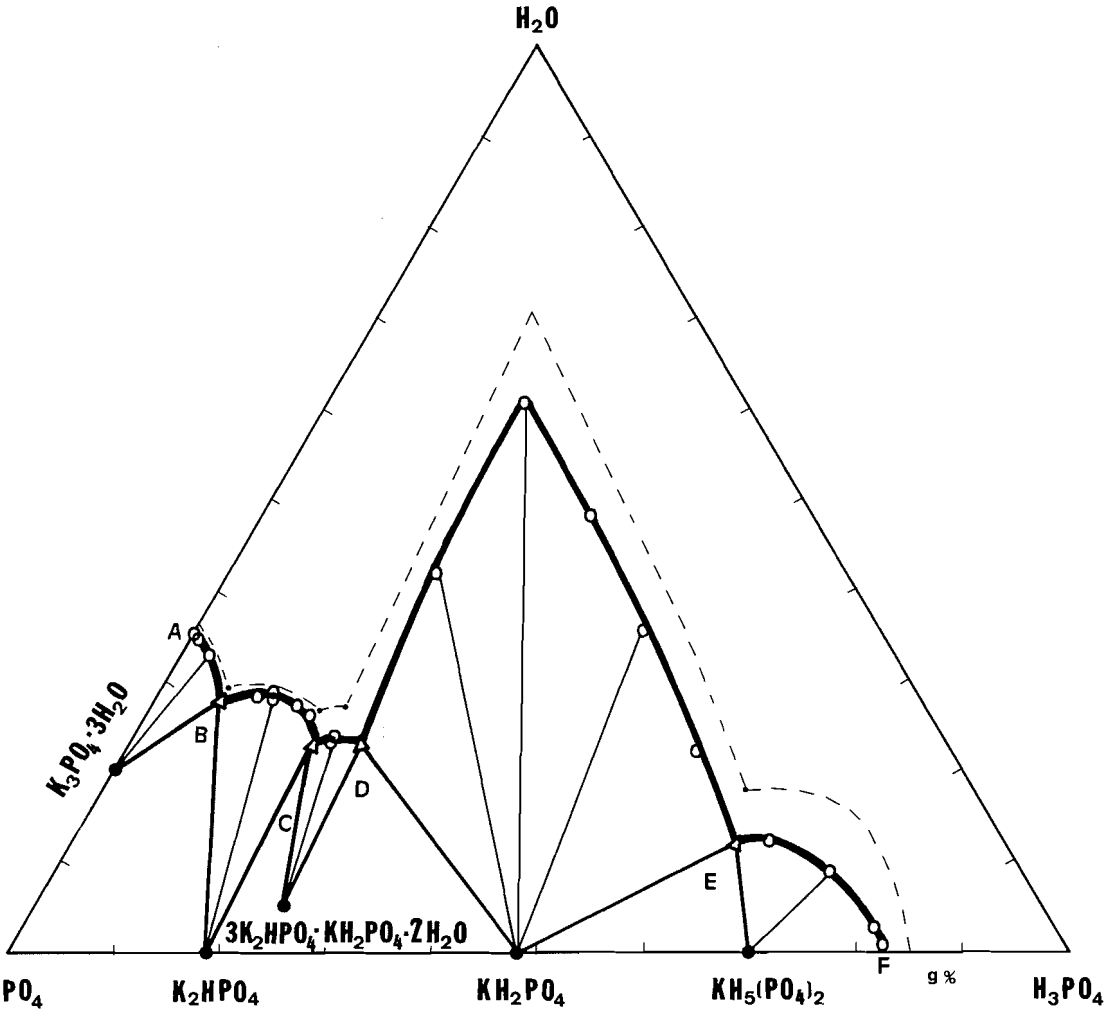

FIG. 2. (——) Isotherme 75°C du système ternaire : K_3PO_4–H_3PO_4–H_2O. (------) Isotherme 50°C du même système (Wendrow et Kobe (21)).

grammes de poudre indéxés de P.7S et P.3S sont donnés dans les tableaux 3 et 4.

On relève dans la littérature que lors d'une étude du système KH_2PO_4–$KHSO_4$ (13) les limites du domaine d'existence de cette solution solide n'ont pu être déterminées avec précision et les diagrammes de poudre, non indexés, fournis comportaient des raies parasites que nous avons attribuées à $KHSO_4$. D'autre part les structures de $KH_2PO_4 \cdot KHSO_4$ (14) et celle de $KHSO_4$ (15) ont été décrites.

2. Système ternaire K_3PO_4–H_3PO_4–H_2O–isotherme 75°C

Les phases solides caractérisées au cours de cette étude sont : $KH_5(PO_4)_2$, KH_2PO_4 (39,29), $3K_2HPO_4 \cdot KH_2PO_4 \cdot 2H_2O$ (76,57), K_2HPO_4(72,74) et $K_3PO_4 \cdot 3H_2O$ (81,15). Les nombres indiqués entre parenthèses représentent pour les sels à solubilité congruente la solubilité dans l'eau à 75°C en grammes de sel pour 100 g de solution saturée. Notons que les mélanges riches en H_3PO_4 donnent lieu à des solutions très visqueuses, nécessitant une agitation prolongée (un à plusieurs jours).

Ce système ayant fait l'objet de nombreux travaux à d'autres températures (16–22), utilisant la représentation en triangle rectangle isocèle ou en triangle équilatéral, nous l'avons également traduit dans ce dernier mode de représentation (figure 2). La comparaison avec l'isotherme 50°C établie par Wendrow et Kobe (21), montre que les mêmes phases solides se manifestent dans les deux diagrammes et que les courbes de solubilité présentent des allures semblables. On observe un très faible écart entre ces dernières dans la région basique. Nous avons vérifié dans la bibliographie (8, 23) qu'effectivement les solubilités relatives à K_2HPO_4 et $K_3PO_4 \cdot 3H_2O$ dans d'autres diagrammes évoluent peu en fonction de la température. On relève également dans la littérature une étude critique sur la solubilité de KH_2PO_4, K_2HPO_4 et K_3PO_4 dans des solutions aqueuses et non aqueuses (24–26).

La structure de KH_2PO_4 a fait l'objet de nombreux travaux dont les plus récents (27–31) sont justifiés par les propriétés optiques et ferroélectriques de cette phase.

3. Système ternaire K_2SO_4–H_2SO_4–H_2O–isotherme 75°C

De nombreuses études ont été consacrées à ce système (32–41). Elles sont justifiées par l'interêt qu'il présente dans la fabrication d'engrais. On relève cependant dans tous ces travaux un désaccord sur la stoechiométrie de l'une des phases solides qui se manifeste dans ce système. Nous avons montré dans un travail antérieur (42), par une détermination structurale aux rayons X, effectuée sur des cristaux que nous avons

Can. J. Chem. Downloaded from www.nrcresearchpress.com by 109.225.110.28 on 09/08/12
For personal use only.

fait croître, que la formule exacte est : $K_2SO_4 \cdot 7KHSO_4 \cdot H_2O$. Notons que l'allure «tournante» de la courbe de solubilité relative à $KHSO_4$ traduit l'existence d'un phénomène de solubilité rétrograde en fonction de la teneur en eau : des mélanges liquides binaires K_2SO_4–H_2SO_4 tels que $75 < Y < 90$ (figure 1) commencent par précipiter $KHSO_4$ par addition d'eau. Des ajouts supplémentaires d'eau permettent d'obtenir de nouveau un mélange liquide. En effet les points représentatifs de ces mélanges traversent successivement un domaine liquide, un domaine biphasé (solide–liquide) et de nouveau un domaine liquide.

La solubilité de K_2SO_4 à 75°C est de 16,90 g de sel pour 100 g de solution saturée.

La structure de $K_2SO_4 \cdot KHSO_4$ à été récemmment publiée (43).

4. Système ternaire K_2SO_4–K_3PO_4–K_2O–isotherme 75°C

Deux phases solides sont observées : K_2SO_4 et $K_3PO_4 \cdot 3H_2O$. La solubilité de $K_3PO_4 \cdot 3H_2O$ à 75°C est 81,15 g de sel pour 100 g de solution saturée. Le domaine de K_2SO_4 englobe la presque totalité du diagramme. Il en résulte que la courbe de solubilité de $K_3PO_4 \cdot 3H_2O$ se réduit pratiquement au point J du système binaire K_3PO_4–H_2O (figure 1). Ce diagramme ne semble pas avoir été étudié précédemment.

5. L'isotherme : H_2SO_4–H_3PO_4–H_2O est constitué d'un seul domaine liquide puisque les acides H_3PO_4 et H_2SO_4 sont eux-même liquides à 75°C.

1. Pennzoil. Phosphorus Potassium, **68** 44 (1973).
2. H. Gabriel, L. Kacalski, U. Glabisz et Z. Trojanowski. Pr. Nauk. Akad. Ekon. im. Oskara Langego Wroclawiu, **267**, 305 (1984).
3. L. Huanwei. Faming Zhuanli Shenqing Gongkai Shuomingshu, CN 1,045,388 (Cl.C05F17/00), 19 Sep. 1990; Appl. 89,101,314, 10 Mar. 1989; 5 pp.
4. V. A. Khusnutdinov, T. G. Akhmetov, V. V. Shestakov et R. Kh. Khuziakhmetov. Pr. Nauk. Akad. Ekon. im. Oskara Langego Wroclawiu, **526**, 122 (1990).
5. O. Sackur et E. Fritzman. Z. Electrochem. **15**, 842 (1909).
6. J. Nyvlt. Solid–liquid phase equilibria. Elsevier Scientific Publishing Company, Amsterdam. 1977. p. 98.
7. M. Bouchacourt, M.-T. Saugier et R. Cohen-Adad. Bull. Soc. Chim. Fr. **9–10**, 842 (1977).
8. W. F. Linke. *Dans* Solubilities of inorganic and metal organic compounds. Vol. 2. American Chemical Society. 1965. pp. 284–285.
9. F. A. H. Schreinemakers. Z. Phys. Chem. **11**, 76 (1893).
10. A. Chretien. Ann. Chim. **12**, 26 (1919).
11. Le Chatelier. C. R. Hebd. Seances Acad. Sci. **118**, 415 (1894); **172**, 345 (1921).
12. E. Janecke. Z. Anorg. Chim. **51**, 132 (1906); **71**, 1 (1911).
13. F. d' Yvoire, R. Diament, M. Mariée et J. Martin. C.R. Acad. Sci. Paris, **257**, 1094 (1963).
14. M. T. Averbuch–Pouchot et A. Durif. Mater. Res. Bull. **15**, 427 (1980).
15. J. Baran. J. Mol. Struct. **172**, 1 (1988).
16. E. Janecke. Z. Phys. Chim. **71**, 127 (1927).
17. J. D'ans et O. Schreiner. Z. Phys. Chem. **75**, 101 (1910).
18. E. G. Parker. J. Phys. Chem. **18**, 653 (1914).
19. L. G. Berg. Izv. Akad. Nauk SSSR, Otd. Mat. Estestv. Nauk, 1, (1938).
20. M. I. Ravich. Kabit U.R.S.S. **10**, 33 (1936).
21. B. Wendrow et K. A. Kobe. Chem. Rev. **54**, 891 (1954).
22. J. Eysseltova. Solubility Data Ser. **31**, 168 (1988).
23. M. Mazghouni et N. Kbir-Ariguib. Thermochim. Acta, **47**, 125 (1981).
24. J. Eysseltova. Solubility Data Ser. **31**, 206 (1988).
25. J. Eysseltova. Solubility Data Ser. **31**, 278 (1988).
26. J. Eysseltova. Solubility Data Ser. **31**, 297 (1988).
27. E. Shoichi et K. Kichiro. Nippon Butsuri Gakkaishi, **45**, 575 (1990).
28. J. West. Ferroelectrics, **71**(1–4), 1 (1987).
29. R. J. Nelmes. Ferroelectrics, **71**(1–4), 87 (1987).
30. R. J. Nelmes, Z. Tun et W. F. Kuhs. Ferroelectrics, **71**(1–4), 125 (1987).
31. R. J. Nelmes, W. F. Kuhs, C. J. Howard, J. E. Tibballs et T. W. Ryan. J. Phys. C: Solid State Phys. **18**, 711 (1985).
32. M. W. Stortenbeker. J. Recl. Trav. Chim. Pays-Bas, **21**, 399 (1902).
33. P. Silber et C. Avinens. C. R. Acad. Sci. Paris, **257**, 3923 (1963).
34. C. Avinens. C. R. Acad. Sci. Paris, Sér. C, **262**, 1872 (1966).
35. J. Balej et A. Regner. Collect. Czech. Chem. Commun. 34, 2161 (1969).
36. V. A. Storozhenko et V. G. Shevchuk. Zh. Neorg. Khim. **6**, 235 (1971).
37. A. W. Frazier. J. Agric. Food Chem. **28**, 461 (1980).
38. S. Bursa, M. Olzak-Humienik et D. Mozejko-Silewicz. Pr. Nauk. Politech. Szczecin. **183**, 89 (1982).
39. S. V. Buksha, I. D. Sokolov, B. A. Kopylev et Yu. V. Buksha. Zh. Prikl. Khim. **59**, 2255 (1986).
40. V. T. Orlova, E. A. Konstantinova, Ya. S. Shenkin and I. N. Lepeshkov. Zh. Neorg. Khim. **31**, 3155 (1986).
41. E. M. Nalivaiko, V. A. Storozhenko et M. K. Prikhod'ko. Zh. Neorg. Khim. **33**, 2158 (1988).
42. N. Bourguiba et T. Jouini. C. R. Acad. Sci. Paris, Sér. II, **309**, 1643 (1989).
43. N. Yukio et K. Hirofimi. J. Phys. Soc. Jpn. **60**, 13 (1991).

Can. J. Chem. Downloaded from www.nrcresearchpress.com by 109.225.110.28 on 09/08/12
For personal use only.

Basicité de liaison hydrogène de formamidines substituées sur l'azote imino

EWA D. RACZYŃSKA
Institut de chimie générale, Université d'Agriculture, 02–528 Varsovie, Pologne

ET

CHRISTIAN LAURENCE[1] ET MICHEL BERTHELOT
Laboratoire de spectrochimie, Faculté des sciences et des techniques, Université de Nantes, 44072 Nantes CEDEX 03, France

Reçu le 6 janvier 1992

EWA D. RACZYŃSKA, CHRISTIAN LAURENCE et MICHEL BERTHELOT. Can. J. Chem. **70**, 2203 (1992).

La basicité de liaison hydrogène des formamidines **1–19** a été mesurée à partir de la constante de formation K_{HB} de leurs complexes avec le *p*-fluorophénol et du déplacement de fréquence $\Delta\nu$(OH) des complexes du méthanol. L'étude de la bande ν(C=N) montre que la liaison hydrogène s'effectue sur l'azote imino. Sur l'échelle de basicité de liaison hydrogène les formamidines se placent au même niveau que les imidazoles et au-dessus des amides et des pyridines correspondantes. L'effet de champ de substituants électroattracteurs et l'effet stérique de groupes alkyles volumineux, fixés sur l'azote imino, diminuent sensiblement la basicité de liaison hydrogène de ce dernier.

EWA D. RACZYŃSKA, CHRISTIAN LAURENCE, and MICHEL BERTHELOT. Can J. Chem. **70**, 2203 (1992).

The basicity of the hydrogen bonds of formamidines **1–19** was measured by means of the formation constant K_{HB} of their complexes with *p*-fluorophenol and the frequency shift $\Delta\nu$(OH) of methanol hydrogen-bonded to **1–19**. The study of the ν(C=N) band shows that hydrogen bonding takes place with the imino nitrogen atom. On the hydrogen-bonding basicity scale, the formamidines appear to be more basic than the corresponding amides and pyridines, and as basic as the imidazoles. The field effect of electron-withdrawing substituents and the steric effect of bulky alkyl groups on the imino nitrogen atom markedly decrease the hydrogen-bonding basicity.

Can. J. Chem. Downloaded from www.nrcresearchpress.com by 109.225.110.28 on 09/08/12
For personal use only.

Introduction

Les travaux de Taft et coll. (1–3) ont montré l'intérêt de mesurer la basicité de liaison hydrogène des molécules organiques. En effet la basicité de liaison hydrogène se différencie de la basicité de Brønsted en solution aqueuse (4) et en phase gazeuse (5). L'échelle de basicité de liaison hydrogène initialement construite par Taft et coll. (6, 7) a été développée par Abraham *et al.* (8). Elle repose sur la constante de l'équilibre [1] de *partage de proton* entre la base B et un donneur de liaison hydrogène de référence, le *p*-fluorophénol, dans des conditions standard de solvant (CCl_4) et de température (298 K),

[1] $B(CCl_4) + p\text{-}FC_6H_4OH\ (CCl_4) \leftrightarrows p\text{-}FC_6H_4OH \ldots B\ (CCl_4)$

$$K_{HB} = [\text{complexe}]/[B]\ [p\text{-}FC_6H_4OH]$$

de la même manière que la basicité de Brønsted repose sur la constante de l'équilibre [2] de *transfert de proton* en solution aqueuse

[2] $B(aq) + H_2O \leftrightarrows BH^+(aq) + OH^-(aq)$

Pour les molécules neutres, l'échelle $pK_{HB} = \log K_{HB}$ s'étend de −1,1 point «magique» de l'échelle d'Abraham *et al.* (8) à +3,66 pour l'oxyde de triphénylarsine.

La famille très importante des amidines

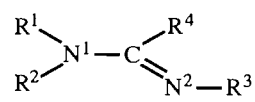

n'est représentée dans cette échelle que par la tétraméthylguanidine ($R^1 = R^2 = Me$, $R^4 = NMe_2$, $R^3 = H$) dont le pK_{HB} vaut 3,14. Des résultats complémentaires ont par la suite été établis par Vaes *et al.* pour quelques formamidines ($R^4 = H$) (9). Malheureusement ces résultats se rapportent soit à l'éthanol (dans CCl_4, à 298 K) soit à des phénols substitués autres que le *p*-fluorophénol (dans le cyclohexane, à 303 K). Ils ne permettent donc pas de placer directement ces formamidines sur l'échelle de basicité de liaison hydrogène déjà construite. Au contraire les résultats de Raczyńska *et al.* pour d'autres formamidines (10), des acétamidines ($R^4 = Ph$) (11) et des benzamidines ($R^4 = Ph$) (11) permettent d'établir une échelle pK_{HB} d'amidines.

Ces travaux suggèrent, mais n'établissent pas formellement, que le site de fixation de la liaison hydrogène est l'azote imino N^2 plutôt que l'azote amino N^1. De ce point de vue il est important de diversifier les effets stériques et électriques des substituants sur l'azote imino N^2. Puisque les travaux précédents ont été limités aux substituants C_6H_5 (et *o*-, *m*- ou *p*-XC_6H_4), $C_6H_5CH_2$ (et *m*- ou *p*-$XC_6H_4CH_2$), *n*-Pr et i-Bu, nous les étendons maintenant à une nouvelle série de N^1,N^1-diméthylformamidines N^2-substituées **1–19**. Les substituants **1–6** diffèrent principalement par leur effet stérique, les substituants **7–13** par leur effet de champ et les substituants **14–19** par leurs effets de résonance et de champ.

Nous nous proposons de placer ces bases **1–19** sur l'échelle pK_{HB} par la mesure de la constante de l'équilibre [1]. Outre cette échelle thermodynamique, une échelle spectroscopique de basicité de liaison hydrogène (*vide infra*) sera aussi obtenue pour ces composés. Nous pensons de plus mettre en évidence le site de fixation de la liaison hydrogène par l'étude de la vibration de valence ν(C=N). Enfin les corrélations de pK_{HB} avec les paramètres électriques σ_F de Taft et Topsom (12) et stérique υ de Charton (13) doivent permettre de déterminer les effets structuraux majeurs dont dépend la basicité de liaison hydrogène des formamidines substituées sur l'azote imino.

[1]Auteur à qui adresser toute correspondance.

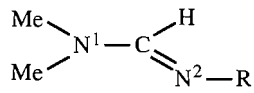

1	R = Me (méthyl)	**7**	R = $CH_2CH{=}CH_2$	**14**	R = NMe_2
2	R = i-Pr (isopropyl)	**8**	R = CH_2CH_2OMe	**15**	R = 4-$Me_2NC_6H_4$
3	R = c-Pr (cyclopropyl)	**9**	R = $CH_2C{\equiv}CH$	**16**	R = 4-$MeOC_6H_4$
4	R = c-Hex (cyclohexyl)	**10**	R = $CH_2CH_2C{\equiv}N$	**17**	R = 4-FC_6H_4
5	R = 1-Adam (adamantyl)	**11**	R = CH_2CF_3	**18**	R = 4-$CF_3C_6H_4$
6	R = *t*-Pen (tertiopentyl)	**12**	R = 3-$CF_3C_6H_4CH_2$	**19**	R = 3,5-$(NO_2)_2C_6H_3$
		13	R = 3-$MeOC_6H_4CH_2$		

Partie Expérimentale

Produits

La synthèse et la purification des formamidines **1–19** ont déjà été décrites (14). Le tétrachlorure de carbone et le méthanol sont des produits de qualité spectroscopique séchés sur tamis moléculaire respectivement 4 et 3 Å. Le *p*-fluorophénol est purifié par sublimation.

Spectres

Ils sont enregistrés sur un spectromètre IR-TF Bruker IFS 45 WHR à la résolution de 1 cm^{-1} et avec 256 accumulations.

Cellules

Une cellule en quartz de 1 cm et en KBr de 1 mm sont utilisées pour étudier respectivement les régions ν(OH) et ν(C=N). Elles sont thermorégulées à 25°C par effet thermoélectrique.

Constantes d'équilibre

Pour l'équilibre [1] dans CCl_4, C^0_B, la concentration initiale de formamidine et C^0_A, la concentration initiale de *p*-fluorophénol, sont déterminées par pesées. La concentration C_c de complexe à l'équilibre est calculée à partir de l'absorbance de la bande libre ν(OH) du *p*-fluorophénol à 3614 cm^{-1}. La constante K_{HB} de l'équilibre [1] se calcule alors par l'expression : $K_{HB} = C_c/[(C^0_B - C_c)(C^0_A - C_c)]$.

Résultats

pK_{HB}

Le logarithme décimal de la constante de formation (en L mol^{-1}) des complexes du *p*-fluorophénol avec les formamidines **1–19** dans CCl_4 à 298 K est reporté dans le tableau 1. La précision sur les constantes est estimée à ±7% soit une erreur d'environ ±0,03 unité de p*K*.

Δν(OH)

Par complexation, la vibration ν(OH) du *p*-fluorophénol se déplace vers les basses fréquences d'autant plus que les formamidines sont plus basiques. Ce déplacement $\Delta\nu$(OH) = 3614 − ν(OH...) ne peut être mesuré avec précision car la bande ν(OH...) du complexe se recouvre avec le massif ν(CH). C'est pourquoi nous mesurons le déplacement $\Delta\nu$(OH) = 3644 − ν(OH...) de la vibration ν(OH) du méthanol, pour lequel ce recouvrement ne se produit pas car c'est un donneur de liaison hydrogène moins fort que le *p*-fluorophénol. Ces déplacements, donnés dans le tableau 1, constituent une échelle spectroscopique de basicité de liaison hydrogène des formamidines **1–19**.

Cette échelle spectroscopique $\Delta\nu$(OH) est cohérente avec l'échelle thermodynamique pK_{HB}, et valide donc les délicates mesures de constantes d'équilibre, à condition de prendre en compte les caractères spécifiques de chaque échelle. Ainsi une très bonne corrélation est observée sur la figure 1 entre pK_{HB} et $\Delta\nu$(OH) à condition de séparer le sous-ensemble des N^2-phénylformamidines **15–19** de celui des N^2-alkylformamidines **1–13** et, dans ce dernier sous-ensemble, d'éliminer de la corrélation les substituants les plus encombrants (*t*-Pen et 1-Adam). L'origine de ces spécificités, déjà envisagée dans un travail antérieur (10), sera étudiée ultérieurement lors d'une comparaison pK_{HB}/$\Delta\nu$(OH) pour un large ensemble de bases azotées.

Pour les formamidines **8** (R = CH_2CH_2OMe) et **10** (R = $CH_2CH_2C{\equiv}N$) on observe (figure 2) deux bandes de complexe ν(OH...). Pour la formamidine **14** (R = NMe_2) on observe une bande ν(OH...) de complexe anormalement large: la largeur de bande à mi-hauteur vaut 295 cm^{-1} alors qu'elle est comprise entre 200 et 220 cm^{-1} pour les autres formamidines de ce travail.

Fréquence ν(C=N)

La bande très intense (coefficient d'extinction molaire voisin de 1680 L mol^{-1} cm^{-1} pour le composé **4**) ν(C=N) des formamidines **1–19** en solution dans CCl_4 se situe entre 1629 cm^{-1} (**14**, NMe_2) et 1661 cm^{-1} (**1**, Me). La figure 3 montre que par addition de *p*-fluorophénol à une solution tétrachlorocarbonique de formamidine, cette bande diminue d'intensité, et qu'il apparaît une nouvelle bande plus large aux fréquences plus basses. L'abaissement du nombre d'onde varie selon les formamidines de 6 à 10 cm^{-1}. Seule la formamidine **14** (NMe_2) fait exception à ce comportement.

Discussion

Site de fixation de la liaison hydrogène

Les concentrations très diluées de *p*-fluorophénol (~3 × 10^{-3} M) et de formamidines (de 5 × 10^{-4} M à 10^{-2} M) utilisées dans ce travail impliquent la formation exclusive de complexe(s) 1 : 1. Par ailleurs la présence d'une seule bande ν(OH...) de complexe (à l'exception des formamidines **8** et **10**, *vide infra*) implique la formation d'un seul complexe 1 : 1. La question se pose de déterminer si le site de fixation de la liaison hydrogène est l'azote amino ou l'azote imino. Des études antérieures (9, 10) ont suggéré qu'il s'agissait du site imino.

L'étude de la région ν(C=N) confirme cette attribution. La nouvelle bande observée (*vide supra*) dans la région ν(C=N) ne peut être attribuée qu'à la vibration ν(C=N) du complexe, puisqu'elle se forme au détriment de la bande ν(C=N) de la formamidine libre, et que son intensité augmente quand on déplace l'équilibre [1] par addition croissante de *p*-fluorophénol. De plus la liaison hydrogène ne peut se former que sur l'azote imino N^2 car la bande ν(C=N) des formamidines complexées est plus basse que celle des for-

Can. J. Chem. Downloaded from www.nrcresearchpress.com by 109.225.110.28 on 09/08/12
For personal use only.

TABLEAU 1. Basicité de liaison hydrogène de formamidines $Me_2N—CH=N—R$

N°	R	$\Delta\nu$(OH)[a]	pK_{HB}[b]	N°	R	$\Delta\nu$(OH)[a]	pK_{HB}[b]
1	Me	386	2,70	**10**	$CH_2CH_2C{\equiv}N$	364[g]	2,15[h]
c	*n*-Pr	395[c]	2,59[c]	**11**	CH_2CF_3	302	1,60
2	i-Pr	389	2,60	**12**	$3\text{-}CF_3C_6H_4CH_2$	355	1,99
3	c-Pr	368	2,36	**13**	$3\text{-}MeOC_6H_4CH_2$	376	2,40
4	c-Hex	395	2,59	**14**	NMe_2	381	2,43
c	i-Bu	390[c]	2,52[c]	**15**	$4\text{-}Me_2NC_6H_4$	334	2,32
5	1-Adam	399	2,52	**16**	$4\text{-}MeOC_6H_4$	327	2,08
6	*t*-Am	392	2,26	c	Ph	316[c]	1,90[c]
7	$CH_2CH{=}CH_2$	376	2,48	**17**	$4\text{-}FC_6H_4$	309	1,80
c	CH_2Ph	371[c]	2,35[c]	**18**	$4\text{-}CF_3C_6H_4$	287	1,43
8	CH_2CH_2OMe	396[d]	2,75[e]	**19**	$3,5\text{-}(NO_2)_2C_6H_3$	~230[i]	~0,60[i]
9	$CH_2C{\equiv}CH$	[f]	~2,30				

[a]Abaissement en cm^{-1} de la vibration ν(OH) du méthanol.
[b]$pK_{HB} = \log K_{HB}$, avec K_{HB} en L mol^{-1}.
[c]Valeurs tirées de la référence 10.
[d]Une deuxième bande associée est observée avec un déplacement de 159 cm^{-1}.
[e]Correspond à la constante totale; pour le seul site imino pK_{HB} = 2,74.
[f]Impossible à mesurer à cause de l'absorption $\nu(\equiv CH)$.
[g]Une deuxième bande associée est observée avec un déplacement de 86 cm^{-1}.
[h]Correspond à la constante totale; pour le seul site imino pK_{HB} = 2,12.
[i]Imprécis à cause de la trop faible solubilité dans CCl_4.

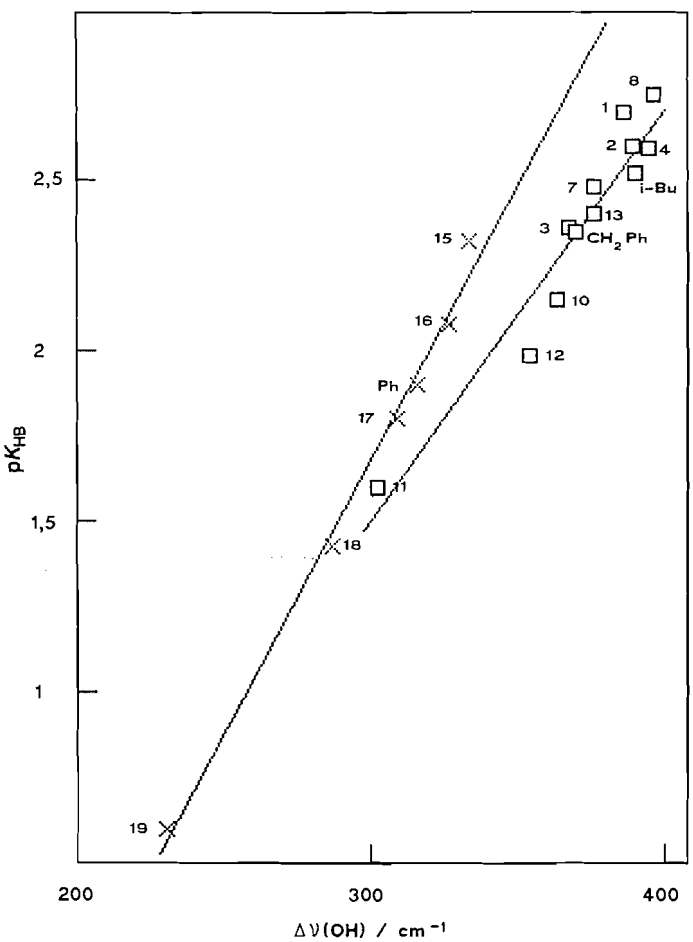

FIG. 1. Corrélation entre échelle thermodynamique (pK_{HB}) et échelle spectroscopique ($\Delta\nu$ OH). Les N^2-phénylformamidines (X) se différencient des N^2-alkylformamidines (□).

mamidines libres. En effet une fixation sur l'azote amino aurait pour effet de diminuer la conjugaison $n-\pi$ des amidines (15) et donc d'augmenter l'indice de liaison C=N et la constante de force et donc la fréquence de vibration.

Le comportement du motif

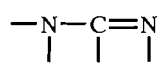

des complexes amidines-phénols est donc identique à celui du motif

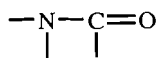

des complexes amides-phénols dans lesquels la bande ν(C=O) est élargie et abaissée (de 17 cm^{-1} pour le complexe phénol–diméthylformamide) par raport à l'amide libre, ce qui démontre que la liaison hydrogène se forme sur l'oxygène et non sur l'azote (16, 17).

Pour les composés **8** $Me_2N\text{-}CH{=}N\text{-}CH_2CH_2OMe$ et **10** $Me_2N\text{-}CH{=}N\text{-}CH_2CH_2C{\equiv}N$ qui contiennent un site O et $C{\equiv}N$ accepteur de liaison hydrogène, la deuxième bande ν(OH...) observée (figure 2) respectivement à 3485 et 3565 cm^{-1} est proche de celle des complexes méthanol $\text{-}Et_2O$ à 3494 et méthanol -EtC≡N à 3565 cm^{-1} et est donc attribuée respectivement à ν(OH... O) et ν(OH... N≡C). Des constantes (en L mol^{-1}) totales K = 562 pour **8** et K = 141 pour **10** il convient donc de soustraire respectivement les valeurs 10 du complexe *p*-fluorophénol–Et_2O (6) et 8 du complexe *p*-fluorophénol–EtC≡N pour obtenir la contribution propre de basicité de liaison hydrogène de l'azote imino, soit pK_{HB} (imino) = 2,12 au lieu de pK_{HB} (total) = 2,15 pour **10** et 2,74 au lieu de 2,75 pour **8**.

Pour le composé **14** $Me_2N^1\text{-}CH{=}N^2\text{-}N^3Me_2$, on observe une bande ν(OH...) unique et grossièrement symétrique, mais cela ne constitue pas la preuve d'un site unique de fixation, car cette bande est anormalement large et pourrait donc correspondre à la superposition de plusieurs bandes, par exemple ν(OH... N^2) et ν(OH... N^3).

Can. J. Chem. Downloaded from www.nrcresearchpress.com by 109.225.110.28 on 09/08/12
For personal use only.

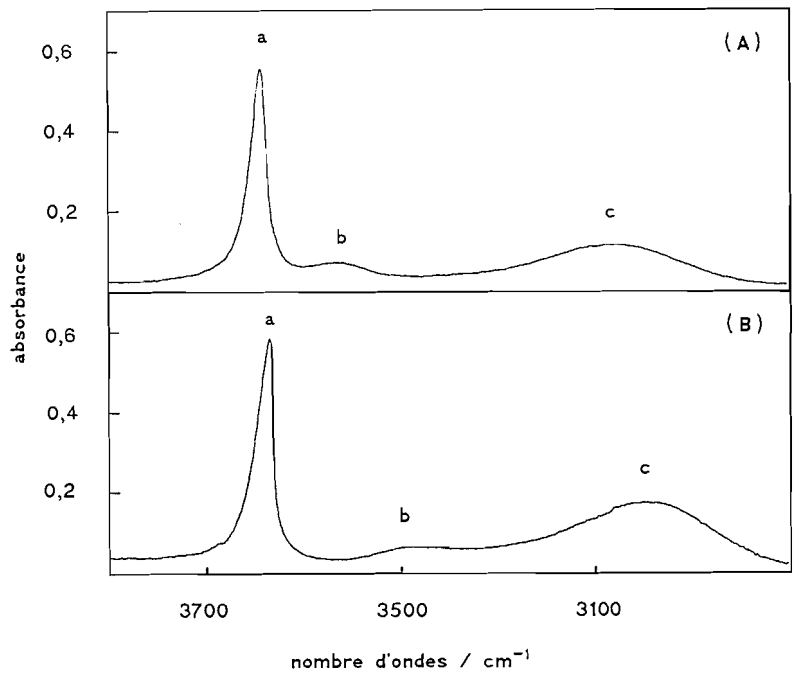

FIG. 2. Spectres IR d'une solution tétrachlorocarbonique de méthanol après addition de la formamidine **10** (*A*) et de la formamidine **8** (*B*). On observe dans chaque cas trois bandes ν(OH) : (a) celle du méthanol libre à 3644 cm^{-1}; (b) celle du complexe OH · · · N≡C (A) ou OH · · · OMe(B); (c) celle du complexe OH · · · N^2.

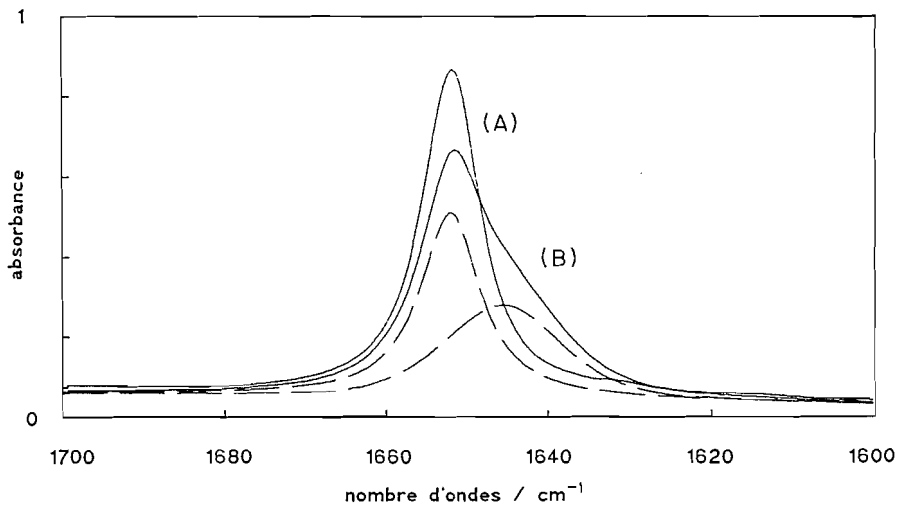

FIG. 3. (*A*) Spectre IR d'une solution tétrachlorocarbonique 5×10^{-3} M de N^1,N^1-diméthyl-N^2-cyclohexylformamidine, (*B*) Même spectre après addition de 4×10^{-3} M de *p*-fluorophénol. La décomposition de ce massif en ses bandes composantes met en évidence la bande ν(C=N) de la formamidine libre à 1653 cm^{-1} et la bande ν(C=N) élargie du complexe formamidine–*p*-fluorophénol à 1646 cm^{-1}.

Position des formamidines dans l'échelle de basicité de liaison hydrogène

Le tableau 2 compare les valeurs de pK_{HB} de la triméthylformamidine **1** et d'autres bases oxygénées et azotées. On observe que la formamidine est plus basique que l'amide et la pyridine correspondante et aussi plus basique que les amines. Elle a la même basicité que le *N*-méthylimidazole alors que dans ce dernier les azotes amino et imino sont substitués par des carbones sp^2 plus électronégatifs que les carbones sp^3 de la triméthylformamidine. L'handicap provoqué par les substituants électronégatifs sur le motif amidine du *N*-méthylimidazole est en fait compensé par la configuration *Z* de ce dernier. Au contraire la triméthylformamidine **1** a la configuration *E*, comme toutes les N^1,N^1-diméthylformamidines (18), et la paire libre de l'azote imino, tournée vers le substituant encombrant Me_2N, est moins accessible au *p*-fluorophénol.

Influence de l'effet de champ des substituants sur l'azote imino

Un effet de champ électroattracteur des substituants sur N^2 diminue la basicité de liaison hydrogène comme l'illustre le substituant CH_2CF_3 (pK_{HB} = 1,60 au lieu de 2,70 pour Me). Si on mesure cet effet de champ par le paramètre σ_F de Taft (12), on obtient la relation approchée [2] pour les substi-

Can. J. Chem. Downloaded from www.nrcresearchpress.com by 109.225.110.28 on 09/08/12
For personal use only.

TABLEAU 2. Comparaison des valeurs pK_{HB} de quelques bases de liaison hydrogène

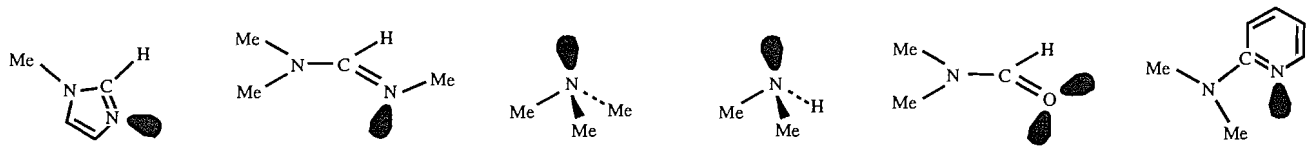

2,71	2,70	2,27	2,15	2,10	1,61

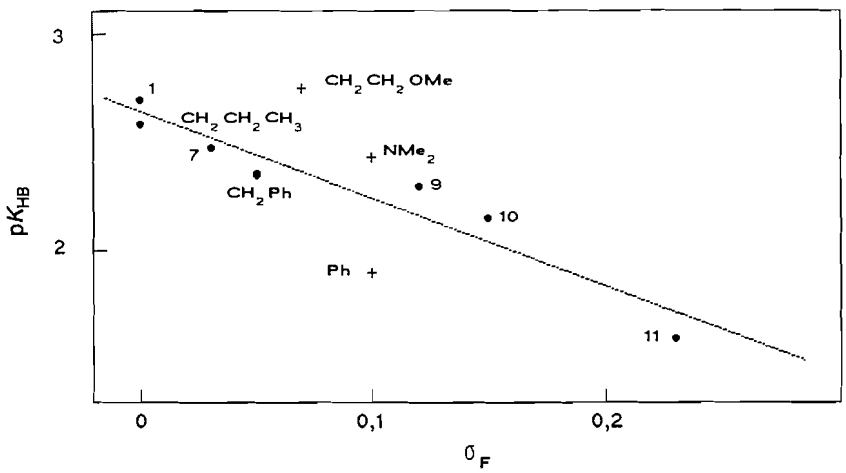

FIG. 4. Corrélation entre le pK_{HB} des composés $Me_2NCH{=}N\text{-}R$ et la constante de substituant σ_F mesurant l'effet de champ du substituant R. Les substituants CH_2CH_2OMe, Ph et NMe_2 n'ont pas été utilisés pour calculer l'équation de la droite de régression.

tuants Me et *n*-Pr ($\sigma_F = 0$), $CH_2CH{=}CH_2$ (0,03), CH_2Ph (0,05), $CH_2C{\equiv}CH$ (0,12), $CH_2CH_2C{\equiv}N$ (0,15) et CH_2CF_3 (0,23) (fig. 4).

[3] $pK_{HB} = -4{,}06\sigma_F + 2{,}64$

(coefficient de corrélation $r = 0{,}965$;
écart-type = 0,11; nombre de points $n = 7$)

La relation [3] permet d'estimer la basicité de liaison hydrogène de l'azote imino de composés particuliers comme $Me_2N\text{-}CH{=}N\text{-}C{\equiv}N$ ou $Me_2N\text{-}CH{=}N\text{-}SO_2Ph$. Si on suppose que les substituants $C{\equiv}N$ ($\sigma_F = 0{,}60$) et SO_2Ph ($\sigma_F = 0{,}63$) agissent uniquement par effet de champ, on calcule respectivement $K_{HB} = 1{,}6$ et 1,2 L mol^{-1} pour les composés correspondants, ce qui représente respectivement 1,3% et 1,6% des constantes totales mesurées pour ces composés dans un travail antérieur (19), soit déjà une contribution négligeable. Cette contribution s'approche de zéro si l'on tient compte de l'effet de résonance électroattracteur de $C{\equiv}N$ ($\sigma^-_R = 0{,}10$) et de SO_2Ph ($\sigma^-_R = 0{,}14$). La relation [3] confirme donc que le site unique de fixation de liaison hydrogène de ces systèmes «push–pull» est l'azote du groupe nitrile ou les oxygènes du groupe sulfonyle.

La figure 4 montre que les substituants NMe_2, Ph et CH_2CH_2OMe n'obéissent pas à la relation [3]. La déviation du substituant Ph peut s'expliquer par son effet de résonance qui n'est pas pris en compte par σ_F. Celle du substituant NMe_2 peut s'expliquer par son effet de résonance et (ou) la possibilité déjà envisagée qu'il constitue un deuxiéme site de fixation de la liaison hydrogène. Celle du substituant CH_2CH_2OMe, pour lequel la correction du deuxième site de fixation de la liaison hydrogène a été effectuée (*vide supra*), reste pour l'instant inexpliquée.

Influence de l'effet stérique des substituants alkyles sur l'azote imino

L'effet stérique des substituant alkyles sur N^2 diminue la basicité de liaison hydrogène comme l'illustre le substituant tert-pentyl ($pK_{HB} = 2{,}26$ au lieu de 2,70 pour Me). Si on mesure cet effet stérique par le paramètre υ de Charton (13), on obtient la relation [4] pour les substituants Me($\upsilon = 0{,}52$), *n*-Pr(0,68), i-Pr(0,76), c-Hex(0,87), i-Bu(0,98), 1-Adam-(1,33) et *t*-Pen(1,63).

[4] $pK_{HB} = -0{,}33\,\upsilon + 2{,}86$

$r = 0{,}925$, $s = 0{,}06$, $n = 7$

Le comportement des substituants alkyles volumineux R est donc tout à fait différent dans les formamidines $Me_2N\text{-}CH{=}N\text{-}R$ où ils diminuent la basicité de celui dans les alcools R-OH (20) où ils augmentent la basicité de liaison hydrogène (par un mécanisme à préciser : polarisabilité, hyperconjugaison et (ou) électronégativité).

1. R. W. Taft, J. L. M. Abboud, M. J. Kamlet et M. H. Abraham. J. Solution Chem. **14**, 153 (1985).
2. R. W. Taft, T. Gramstad et M. J. Kamlet. J. Org. Chem. **47**, 4557 (1982).
3. M. H. Abraham, R. M. Doherty, M. J. Kamlet et R. W. Taft. Chem. Br. 551 (1986).
4. M. J. Kamlet, J. F. Gal, P. C. Maria et R. W. Taft. J. Chem. Soc. Perkin Trans. 2, 1583 (1985).

Can. J. Chem. Downloaded from www.nrcresearchpress.com by 109.225.110.28 on 09/08/12
For personal use only.

5. M. J. Kamlet, R. M. Doherty, J. L. M. Abboud, M. H. Abraham et R. W. Taft. Chemtech, 566 (1986).
6. D. Gurka et R. W. Taft. J. Am. Chem. Soc. **91**, 4794 (1969).
7. R. W. Taft, D. Gurka, L. Joris, P. v. R. Schleyer et J. W. Rakshys. J. Am. Chem. Soc. **91**, 4801 (1969).
8. M. H. Abraham, P. L. Grellier, D. V. Prior, J. J. Morris et P. J. Taylor. J. Chem. Soc. Perkin Trans. 2, 521 (1990).
9. J. Vaes, F. Foubert et Th. Zeegers-Huyskens. Can. J. Chem. **53**, 604 (1975).
10. E. D. Raczyńska, C. Laurence et P. Nicolet. J. Chem. Soc. Perkin Trans. 2, 1491 (1988).
11. E. D. Raczyńska et C. Laurence. J. Chem. Res. (S), 148 (1989).
12. R. W. Taft et R. D. Topsom. Prog. Phys. Org. Chem. **16**, 1 (1987).
13. M. Charton. J. Am. Chem. Soc. **97**, 1552 (1975).
14. (*a*) M. Decouzon, J. F. Gal, P. C. Maria et E. D. Raczyńska. J. Org. Chem. **56**, 3669 (1991); (*b*) M. Decouzon, J. F. Gal, P. C. Maria et E. D. Raczyńska. Org. Mass. Spectrom. Sous presse.
15. O. Exner, M. Budesinsky, D. Hnyk, V. Vsetecka et E. D. Raczyńska. J. Mol. Struct. **178**, 147 (1988).
16. T. Gramstad et W. J. Fuglevik. Acta Chem. Scand. **16**, 1369 (1962).
17. C. Dorval et Th. Zeegers-Huyskens. Spectrochim. Acta, **29A**, 1805 (1973).
18. B. Tinant, J. Dupont-Fenfau, J. P. Declercq, J. Podlaha et O. Exner. Collect. Czech. Chem. Commun. **54**, 3245 (1989).
19. C. Laurence, M. Berthelot, E. D. Raczyńska, J. Y. Le Questel, G. Duguay et P. Hudhomme. J. Chem. Res. (S), 250 (1990).
20. C. Laurence, M. Berthelot, M. Helbert et K. Sraïdi. J. Phys. Chem. **93**, 3799 (1989).

Can. J. Chem. Downloaded from www.nrcresearchpress.com by 109.225.110.28 on 09/08/12
For personal use only.

Calculated electrostatic potentials and local surface ionization energies of *para*-substituted anilines as measures of substituent effects

MARKUS HAEBERLEIN, JANE S. MURRAY, TORE BRINCK, AND PETER POLITZER[1]
Department of Chemistry, University of New Orleans, New Orleans, LA 70148, U.S.A.

Received February 29, 1992

MARKUS HAEBERLEIN, JANE S. MURRAY, TORE BRINCK, and PETER POLITZER. Can. J. Chem. **70**, 2209 (1992).

Using an *ab initio* self-consistent-field molecular orbital approach, we computed 3-21G//STO-3G* and STO-5G//STO-3G* electrostatic potentials and average local ionization energies for 17 *para*-substituted anilines. Our results demonstrate that the most negative potentials (V_{min}) and the local surface ionization energy minima ($\bar{I}_{S,min}$) associated with the amine nitrogen lone pairs are highly sensitive indicators of the electron-donating and electron-attracting tendencies of the *para* substituents. We find excellent linear relationships between the 3-21G//STO-3G* amine nitrogen V_{min} and $\bar{I}_{S,min}$ and the σ_p^0 Hammett constants of the substituent X; the correlation coefficients are 0.99. Correlations of slightly lesser quality are shown to exist between V_{min}, $\bar{I}_{S,min}$, and σ_p^-, σ_p, and pK_a. Estimates of previously unknown σ_p^0 and pK_a values are given. The presence of ring carbon $\bar{I}_{S,min}$ *meta* to the substituent X also provides a predictive capability for determining σ_m values.

MARKUS HAEBERLEIN, JANE S. MURRAY, TORE BRINCK et PETER POLITZER. Can. J. Chem. **70**, 2209 (1992).

Utilisant une approche de calculs *ab initio* d'orbitales moléculaires en champ auto-cohérent, on a calculé les potentiels électrostatiques ainsi que les énergies moyennes d'ionisation locale de 17 anilines *para*-substituées, aux niveaux 3-21G//STO-3G* et STO-5G//STO-3G*. Nos résultats démontrent que les potentiels les plus négatifs (V_{min}) et les minima de l'énergie d'ionisation de la surface locale ($\bar{I}_{S,min}$) associés avec les paires libres de l'azote de l'amine sont des indicateurs sensibles des tendances des substituants *para* à agir comme électro-donneurs ou électro-accepteurs. On a obtenu une excellente relation linéaire entre les valeurs de V_{min} et $\bar{I}_{S,min}$ de l'azote de l'amine au niveau 3-21G//STO-3G* et les constantes σ_p^0 de Hammett du substituant X; les coefficients de corrélation sont égaux à 0,99. On rapporte des évaluations des valeurs de σ_p^0 et de pK_a qui étaient jusqu'à présent inconnues. La présence de $\bar{I}_{S,min}$ pour le carbone du cycle en *méta* du substituant X fournit aussi une possibilité de prédire les valeurs de σ_m.

[Traduit par la rédaction]

Background

A continuing focus of our computational studies is the interpretation and prediction of chemical reactive behavior (1–7). We recently demonstrated that good correlations exist between two calculated gaseous phase properties (the electrostatic potential $V(\boldsymbol{r})$ and the average local ionization energy $\bar{I}(\boldsymbol{r})$) and several experimentally based indices of reactivity derived from solution studies (5–14), including the Hammett and Taft substituent constants. These are well-established measures of the electron-donating and -attracting tendencies of substituent groups (15–19).[2] The properties $V(\boldsymbol{r})$ and $\bar{I}(\boldsymbol{r})$ are discussed briefly below as background to the present work.

The electrostatic potential $V(\boldsymbol{r})$ has emerged as an effective tool for studying the reactive behavior of molecules in both electrophilic and nucleophilic processes, and also in molecular recognition interactions (1–4, 6, 24, 25). $V(\boldsymbol{r})$ is a real physical property that expresses the net electrical effect of the nuclei and electrons of a molecule, at any point $\boldsymbol{r}$, and is given rigorously by eq. [1].

$$[1] \quad V(\boldsymbol{r}) = \sum_A \frac{Z_A}{|\boldsymbol{R}_A - \boldsymbol{r}|} - \int \frac{\rho(\boldsymbol{r}')d\boldsymbol{r}'}{|\boldsymbol{r}' - \boldsymbol{r}|}$$

Z_A is the charge on nucleus A, located at $\boldsymbol{R}_A$, and $\rho(\boldsymbol{r})$ is the electronic density function of the molecule. The sign of $V(\boldsymbol{r})$ in any particular region depends upon whether the effects of the nuclei or electrons are dominant there. Sites reactive toward electrophiles can be identified and ranked by means of the local minima (most negative values) of $V(\boldsymbol{r})$ (1–4, 6, 10, 13, 14, 24, 25) while the maxima of $V(\boldsymbol{r})$ on the molecular surface serve the same purpose for nucleophilic attack (6, 12–14).

We recently introduced another property, the average local ionization energy $\bar{I}(\boldsymbol{r})$ (5), which is defined by eq. [2].

$$[2] \quad \bar{I}(\boldsymbol{r}) = \sum_i \frac{\rho_i(\boldsymbol{r})\,|\varepsilon_i|}{\rho(\boldsymbol{r})}$$

$\rho(\boldsymbol{r})$ is the electronic density of the ith molecular orbital at the point $\boldsymbol{r}$ and ε_i is the orbital energy. We interpret $\bar{I}(\boldsymbol{r})$ as the average energy required to remove an electron from any point $\boldsymbol{r}$ in the space of an atom or molecule. In a series of studies, we have demonstrated that $\bar{I}(\boldsymbol{r})$ plotted on molecular surfaces is an effective indicator of reactivity toward electrophiles, even in aqueous solution (5, 7, 9, 11). For example, we have shown for a series of monosubstituted benzenes that surface $\bar{I}(\boldsymbol{r})$ minima ($\bar{I}_{S,min}$) provide a quantitative measure of the activating/deactivating and the directing tendencies of the various substituents, and also correlate well with the Hammett constants σ_p and (or) σ_m (5, 7). For several families of acids, we found that the calculated $\bar{I}_{S,min}$ of the conjugate bases correlate well with the respective pK_a values, which can be viewed as reflecting reactivity toward the electrophile H^+ (9, 11).

Present objectives

In an earlier study involving a group of 24 NH_2-X molecules, we demonstrated a good correlation between the electrostatic potential minimum (V_{min}) of the amine nitrogen and the total electron-attracting tendency of X, as measured by the σ_I and σ_R substituent constants (8). More recently, we showed that the nitrogen $\bar{I}_{S,min}$ can also be used for this pur-

[1]Author to whom correspondence may be addressed.

[2]For some earlier investigations of relationships between substituent constants and calculated atomic charges, see refs. 20–23.

Can. J. Chem. Downloaded from www.nrcresearchpress.com by 109.225.110.28 on 09/08/12
For personal use only.

TABLE 1. Calculated V_{min} and $\bar{I}_{S,min}$ of the amine nitrogens in some *para*-substituted anilines, and experimentally derived substituent constant (σ_p, σ_p^0, and σ_p^-) and pK_a values

para-Substituent	V_{min}(kcal/mol)		$\bar{I}_{S,min}$(eV)		Substituent constants[a]			Conjugate acid pK_a
	STO-5G	3–21G	STO-5G	3–21G	σ_p	σ_p^0	σ_p^-	
$N(CH_3)_2$	−92.5	−93.9	12.35	11.86	−0.63	−0.32	−0.32	(6.2)[c] (6.2)[d]
NH_2	−91.0	−92.7	12.42	11.91	−0.57	−0.30	−0.30	6.11[f]
OH	−89.7	−90.2	12.51	12.06	−0.38	−0.22	−0.22	5.48[f]
CH_3	−89.6	−90.7	12.50	12.00	−0.14	−0.14	−0.14	5.08[e]
OCH_3	−90.2	−91.0	12.48	12.01	−0.28	−0.12	−0.12	5.34[g]
H	−88.1	−89.0	12.57	12.08	0.00	0.00	0.00	4.63[e]
SH	−89.7	−86.3	12.50	12.23	0.15	0.06	0.06	(4.6)[c] (4.5)[d]
CH_2Cl	−83.1	−83.7	12.82	12.32	0.12	0.12	0.12	(4.0)[c] (4.0)[d]
F	−86.3	−85.2	12.66	12.27	0.06	0.15	0.15	4.65[e]
Cl	−80.7	−80.7	12.97	12.43	0.22	0.24	0.24	4.15[e]
NF_2	—	−78.5	—	12.57	(0.49)[b]	(0.47)[c] (0.44)[d]	—	(3.0)[c] (2.8)[d]
COOH	−80.8	−78.1	12.93	12.57	0.44	0.47	0.78	2.50[e]
CHO	−81.5	−78.2	12.89	12.57	0.44	0.47	0.94	(2.9)[c] (2.8)[d]
CF_3	−79.8	−76.4	12.97	12.65	0.53	0.53	0.62	2.75[g]
CN	−74.9	−73.6	13.20	12.75	0.71	0.71	0.99	1.71[f]
$N(NO_2)_2$	—	−71.7	—	12.84	(0.73)[h]	(0.74)[c] (0.74)[d]	—	(1.6)[c] (1.6)[d]
NO_2	−71.6	−68.0	13.36	13.00	0.81	0.81	1.25	1.00[e]

[a]Reference 17.
[b]Estimated value, taken from ref. 5.
[c]Estimated value, using 3–21G amine nitrogen V_{min} correlations.
[d]Estimated value, using 3–21G amine nitrogen $\bar{I}_{S,min}$ correlations.
[e]Reference 36.
[f]Reference 37.
[g]Reference 38.
[h]Estimated value, taken from ref. 35.

Can. J. Chem. Downloaded from www.nrcresearchpress.com by 109.225.110.28 on 09/08/12
For personal use only.

pose (13). However, while the NH_2-X framework is effective for studying the electron-attracting power of X, it does not provide an opportunity to assess any tendency for resonance donation of charge by the substituent (8, 13).

For this reason, we have now investigated the use of a different framework, *para*-substituted aniline (**1**), as a tool for studying substituent effects. It was anticipated that this system might allow some degree of resonance donation of

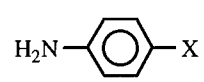

X = H, F, Cl, CH_3, CF_3, NH_2, OH, OCH_3, CN, NO_2, CHO, COOH, $N(CH_3)_2$, SH, CH_2Cl, NF_2, $N(NO_2)_2$

1

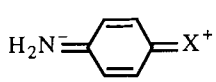

1*a*

charge by X, which would be reflected in the V_{min} and $\bar{I}_{S,min}$ of the amine group, due to the contribution of structure **1***a*.

We have accordingly computed these properties for a series of 17 *para*-substituted anilines.

Methods and procedure

We have used an *ab initio* self-consistent-field molecular orbital (SCF-MO) procedure (GAUSSIAN 88 (26)) to compute optimized geometries for 17 *para*-substituted aniline derivatives. Due to the sizes of the molecules, the STO-3G* basis set was selected for this purpose. While it is known to exaggerate the pyramidal character of amine nitrogens, past experience suggests that the structures should be generally satisfactory (27). For example, our calculated STO-3G* geometry for aniline is in reasonable agreement with gas phase experimental data (28). The largest discrepancy in bond lengths is in the C—N distance, which we overestimate by 0.042 Å; however, the errors for the other bonds are 0.008 Å (average) for the C—C, 0.028 Å for the N—H, and essentially zero for the C—H. (The STO-3G* basis is identical to the STO-3G for atoms H–Ne; for Na–Xe, the STO-3G* includes a set of polarization functions (27).)

TABLE 2. Correlations between some calculated and experimentally derived properties

Calculated property, y	Experimentally determined quantity, x	Least-squares equation	Correlation coefficient
3–21G amine nitrogen $\bar{I}_{S,min}$	σ_p^0	$y = 0.920x + 12.163$	0.99
3–21G amine nitrogen V_{min}	σ_p^0	$y = 21.013x - 87.293$	0.99
STO-5G amine nitrogen $\bar{I}_{S,min}$	σ_p^0	$y = 0.799x + 12.611$	0.96
STO-5G amine nitrogen V_{min}	σ_p^0	$y = 16.618x - 87.359$	0.96
3–21G amine nitrogen $\bar{I}_{S,min}$	σ_p^-	$y = 0.637x + 12.142$	0.97
3–21G amine nitrogen V_{min}	σ_p^-	$y = 14.566x - 87.780$	0.97
STO-5G amine nitrogen $\bar{I}_{S,min}$	σ_p^-	$y = 0.549x + 12.594$	0.93
STO-5G amine nitrogen V_{min}	σ_p^-	$y = 11.448x - 87.724$	0.93
3–21G amine nitrogen $\bar{I}_{S,min}$	σ_p	$y = 0.739x + 12.241$	0.96
3–21G amine nitrogen V_{min}	σ_p	$y = 16.849x - 85.509$	0.96
STO-5G amine nitrogen $\bar{I}_{S,min}$	σ_p	$y = 0.636x + 12.679$	0.92
STO-5G amine nitrogen V_{min}	σ_p	$y = 13.179x - 85.934$	0.93
3–21G amine nitrogen $\bar{I}_{S,min}$	pK_a	$y = -0.210x + 13.168$	0.97
3–21G amine nitrogen V_{min}	pK_a	$y = -4.820x - 64.216$	0.98
STO-5G amine nitrogen $\bar{I}_{S,min}$	pK_a	$y = -0.183x + 13.501$	0.96
STO-5G amine nitrogen V_{min}	pK_a	$y = -3.837x - 68.740$	0.97
3–21G ring carbon $\bar{I}_{S,min}$	σ_m	$y = 1.131x + 12.905$	0.97

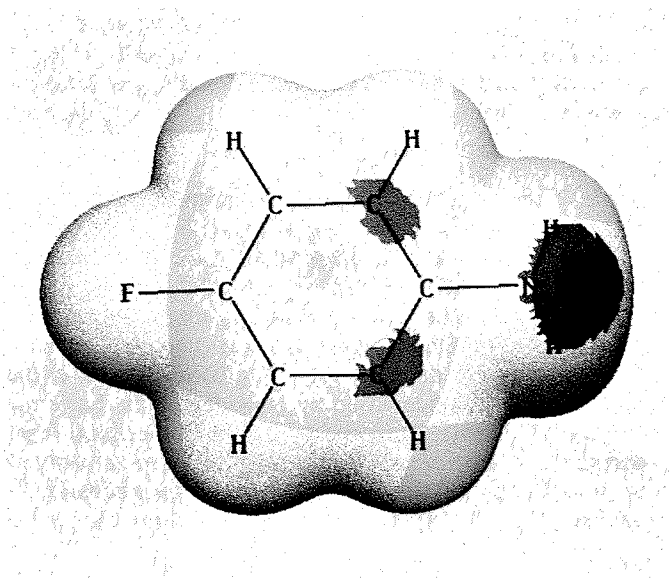

FIG. 1. Calculated $\bar{I}(r)$ on the molecular surface of *para*-fluoroaniline. Three ranges of $\bar{I}(r)$ are depicted, in eV. Black: $\bar{I}(r) < 12.52$; gray: $12.52 < \bar{I}(r) < 13.47$; white: $\bar{I}(r) > 13.47$.

As anticipated, the STO-3G* basis set consistently yields a pyramidal amine group for these aniline derivatives; the variation in the H—N—H angle is only over the range 107°–109°. For comparison, the experimentally determined value for aniline is 113 ± 2° (28). From the standpoint of this study, in which we plan to use the amine V_{min} as a probe, the near constancy of the H—N—H angle is useful, because it means that changes in the magnitude of V_{min} can be attributed to electronic factors rather than structural ones; we showed earlier that amine V_{min}'s are strongly dependent upon the H—N—H angle (6, 8, 29).

Using these structures, we computed $V(r)$ (via eq. [1], using GAUSSIAN 88) and surface $\bar{I}(r)$ (via eq. [2]). The molecular surfaces were defined, following the approach of Bader *et al.* (30), by the 0.002 electrons/bohr^3 contour of the electronic density. The calculations were carried out at

TABLE 3. Calculated *meta* carbon $\bar{I}_{S,min}$ and Hammett constants σ_m

para-substituent	$\bar{I}_{S,min}$ (eV)[a] [3–21G] C_2, C_6	Hammett constant, σ_m, for *para*-substituent[b]
$N(CH_3)_2$	12.84	−0.10
NH_2	12.94	−0.09
CH_3	12.80	−0.06
H	12.82	0.00
OCH_3[c]	12.86, 13.06	0.10
CH_2Cl	13.10	0.11
OH[c]	13.02, 13.15	0.13
F	13.32	0.34
Cl	13.33	0.37
CF_3	13.45	0.46
NF_2	13.52	(0.54)[d] (0.54)[e]
CN	13.54	0.62
NO_2	13.77	0.71
$N(NO_2)_2$	13.89	(0.87)[d] (0.87)[f]

[a]The $\bar{I}_{S,min}$ are above the C_2 and C_6 positions, on the same side of the ring as the amine nitrogen lone pair.
[b]Reference 17.
[c]For OX substituents, the lowest $\bar{I}_{S,min}$ is located on the same half of the ring as X.
[d]Estimated value, using ring carbon $\bar{I}_{S,min}$ vs. σ_m correlation.
[e]Estimated value, taken from ref. 5.
[f]Estimated value, taken from ref. 35.

Can. J. Chem. Downloaded from www.nrcresearchpress.com by 109.225.110.28 on 09/08/12
For personal use only.

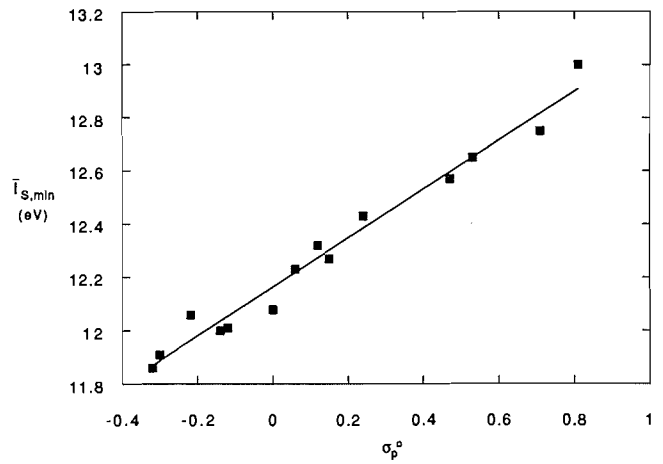

FIG. 2. Correlation between 3–21G//STO-3G* amine nitrogen $\bar{I}_{S,min}$ and σ_p^0 for 15 *para*-substituted anilines. The correlation coefficient is 0.99.

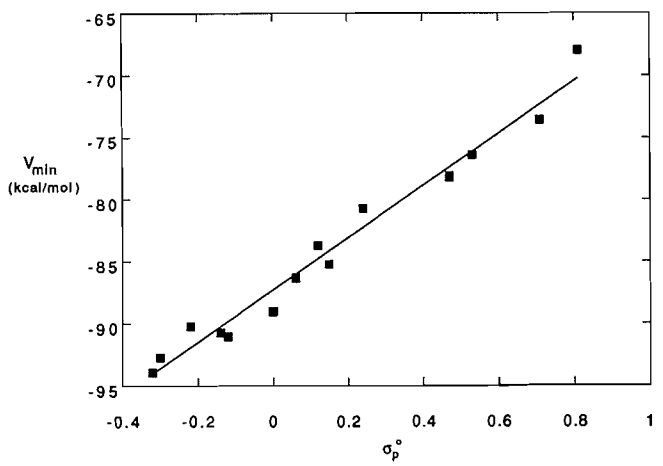

FIG. 3. Correlation between 3–21G//STO-3G* amine nitrogen V_{min} and σ_p^0 for 15 *para*-substituted anilines. The correlation coefficient is 0.99.

both the HF/STO-5G and HF/3-21G levels. We found these basis sets to be satisfactory for $V(\boldsymbol{r})$ and $\bar{I}(\boldsymbol{r})$ (1, 3, 4, 6–10, 12–14).

Results

The electrostatic potential of aniline, presented earlier (31), is positive everywhere in the plane of the ring, with large negative regions above and below this plane that are attributed to the π electrons. The most negative V_{min} is found in the lone pair region of the nitrogen, and is indicative of the basic nature of aniline. This nitrogen is indeed a highly favorable site for protonation (32, 33). The surface $\bar{I}(\boldsymbol{r})$ of aniline is characterized by $\bar{I}_{S,min}$ found in the vicinity of the amine nitrogen and above the *ortho* and *para* carbon positions (5), consistent with these all being favorable sites for electrophilic attack (33, 34).

The calculated amine nitrogen V_{min} and $\bar{I}_{S,min}$ of the 17 *para*-substituted anilines **1** are listed in Table 1, along with the Hammett constants σ_p, σ_p^0, and σ_p^- of the substituents X and the experimentally determined pK_a values of some of these molecules. Positive values of σ_p, σ_p^0, and σ_p^- are interpreted as indicating the degree of electron attraction by a *para* substituent, while negative values measure electron donation. The general trend in Table 1 is that the V_{min} become less negative and the $\bar{I}_{S,min}$ higher as the Hammett constants increase and pK_a decreases. Molecules for which the overall effect of X is electron attraction (σ_p, σ_p^0, $\sigma_p^- > 0$) have V_{min} less negative and $\bar{I}_{S,min}$ higher than those of aniline (X = H), while molecules with electron-donor substituents (σ_p, σ_p^0, $\sigma_p^- < 0$) show V_{min} more negative and $\bar{I}_{S,min}$ lower than aniline. Thus, we find that the computed V_{min} and $\bar{I}_{S,min}$ of the amine nitrogen in the *para*-H_2N-C_6H_4-X framework can indeed reflect either overall electron-donating or electron-attracting tendencies of *para* substituents on aromatic rings.

The sensitivities of the amine nitrogen V_{min} and $\bar{I}_{S,min}$ to substituent effects are confirmed by Table 2, which summarizes the correlations with σ_p, σ_p^0, σ_p^-, and pK_a. These relationships will be discussed in detail in the next section.

An interesting feature of the surface $\bar{I}(\boldsymbol{r})$ of the *para*-substituted anilines is that $\bar{I}_{S,min}$ are found above the ring carbons that are *meta* to the substituent X, even if X is an *ortho*/*para* director. For example, the surface $\bar{I}(\boldsymbol{r})$ of *para*-fluoroaniline (Fig. 1) shows $\bar{I}_{S,min}$ above the positions *meta* to the fluorine in addition to the one associated with the amine nitrogen. This presumably reflects the strong *ortho*/*para* directing tendencies of the NH_2 group. (For substituents that are strong resonance donors, there are also $\bar{I}_{S,min}$ *ortho* to X.) The 3-21G $\bar{I}_{S,min}$ values of the *meta* carbons (relative to X) are listed in Table 3 along with the σ_m values of X. There is a linear relationship between these $\bar{I}_{S,min}$ and σ_m, with a correlation coefficient of 0.97 (see Table 2).

Discussion

Table 2 shows that the best correlations with Hammett constants for both $\bar{I}_{S,min}$ and V_{min} are with σ_p^0 at the 3-21G level (correlation coefficients = 0.99; see Figs. 2 and 3), followed by those with σ_p^- and σ_p, also 3-21G. The trends in the STO-5G results follow the same pattern but the relationships are not quite as closely obeyed.

The superiority of the $\sigma_p^0 - \bar{I}_{S,min}$, V_{min} correlations over the σ_p and σ_p^- can be understood by considering the basis for each set of constants. The original σ_p's were obtained from experimental data for the ionizations of *para*-substituted benzoic acids (**2**) and rates of hydrolysis of *para*-substituted benzoates, e.g., **3** (15). However, as seen in Fig. 4*a*, these

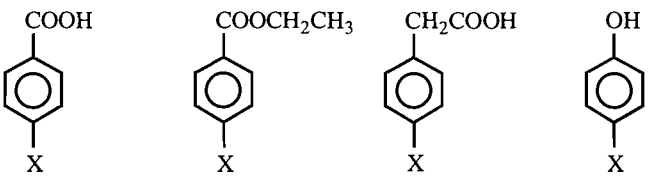

systems allow significant "through-resonance" that affects σ_p for resonance donors such as NH_2, OH, and OCH_3, but not for attractors such as CHO, CN, and NO_2 (17). Thus σ_p for a donor substituent is meaningful for systems in which such through-resonance is possible, but it is less applicable when this opportunity is not present.

To develop a set of constants appropriate for systems in which no through-resonance can occur, the effects of substituents X upon the ionization of **4** were determined and used to establish the σ_p^0 scale (17, 18). The absence of through-

Can. J. Chem. Downloaded from www.nrcresearchpress.com by 109.225.110.28 on 09/08/12
For personal use only.

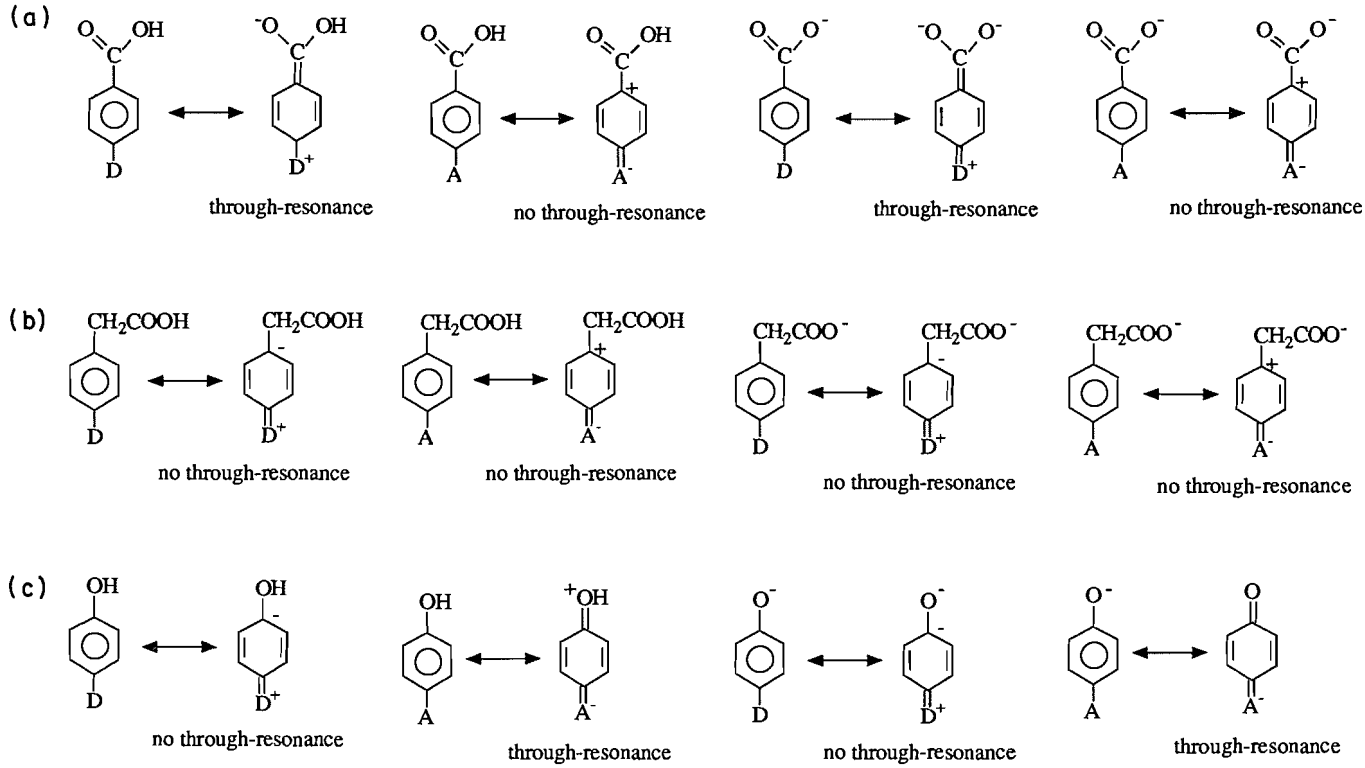

FIG. 4. Resonance structures relevant to Hammett constants σ_p, σ_p^0, and σ_p^-. Both the neutral and the ionized forms of each molecule are included. D and A refer to resonance-donor and -acceptor substituents, respectively.

resonance in this framework can be seen in Fig. 4*b*. The σ_p^0 constants of resonance donors such as NH_2, OH, and OCH_3 are also applicable to reactions, such as the ionization of phenol, which are not expected to be affected by through-resonance with donors (17). (See, e.g., Fig. 4*c*.)

The σ_p^- constants are designed for systems in which substituents that are electron attractors by resonance (e.g., CHO, CN, and NO_2) have the opportunity to participate in through-resonance. The ionizations of *para*-substituted phenols (**5**) (Fig. 4*c*) and anilines (**1**) were used to obtain the σ_p^- values (17). In systems such as these, through-resonance does not occur to any significant degree for donors.

On the basis of the preceding discussion, it can be anticipated that σ_p^0 and σ_p^- should be very similar for resonance donor substituents, while σ_p is more negative. For resonance-attracting groups, on the other hand, σ_p and σ_p^0 should be similar, and σ_p^- more positive. All of these expectations are borne out by the data in Table 1.

Since our analyses use the calculated $\bar{I}_{S,min}$ and V_{min} of the amine nitrogens of *para*-substituted anilines as probes of substituent effects, it would seem that the most successful correlations should be with σ_p^-, however, they are actually found to be with σ_p^0. We believe that this is because the STO-3G basis set, used to optimize geometries, is unable to fully account for the through-resonance interactions with the amine group. This interpretation is consistent with the known limitations of this basis set in describing conjugation (27), which is reflected in the overestimated C—NH_2 bond length in aniline, mentioned earlier.

Our results clearly provide a predictive capability for obtaining σ_p^0 values for substituents for which these are not known, and these should in turn be good estimates of σ_p for resonance attractors and of σ_p^- for resonance donors. Our predicted σ_p^0 for NF_2 and $N(NO_2)_2$ are given in Table 1. It is gratifying that the $\bar{I}_{S,min}$ and V_{min} correlations yield values that are in such close agreement, since the two properties are quite different. It is also pleasing that these σ_p^0 are very similar to estimates of σ_p obtained earlier from an $\bar{I}_{S,min}$ relationship for monosubstituted benzenes (5, 35).

Proceeding to the correlations of $\bar{I}_{S,min}$ and V_{min} with pK_a (Table 2), we again find our 3-21G results to be successful (correlation coefficients of 0.97 and 0.98). (It is noteworthy that the 3-21G $\bar{I}_{S,min}$ and pK_a values fit well into a relationship between these quantities that we recently found for a group of azines and azoles (9); the overall correlation coefficient is 0.95.) Table 1 includes some predicted pK_a values, calculated using the 3-21G equations in Table 2. The results obtained from $\bar{I}_{S,min}$ and V_{min} are again remarkably similar.

The relationship between *meta* carbon $\bar{I}_{S,min}$ and σ_m (Table 2) allows us to estimate the σ_m values for NF_2 and $N(NO_2)_2$ to be 0.54 and 0.87, respectively (Table 3). These are in excellent agreement with earlier predictions (5, 35).

Summary

We have shown that the calculated $\bar{I}_{S,min}$ and V_{min} of the amine nitrogen lone pair regions in *para*-substituted anilines reflect the general electron-donating and electron-attracting tendencies of substituents on aromatic rings. Our 3-21G//STO-3G* amine nitrogen $\bar{I}_{S,min}$ and V_{min} are found to be highly sensitive indicators of substituents effects described by the Hammett constant σ_p^0 and also of pK_a. The very good agreement that is found between predicted σ_p^0 and pK_a obtained from $\bar{I}_{S,min}$ and those based on V_{min} is particu-

Can. J. Chem. Downloaded from www.nrcresearchpress.com by 109.225.110.28 on 09/08/12
For personal use only.

larly significant because the latter two properties are so different in nature. The presence of ring carbon $\bar{I}_{S,min}$ *meta* to the substituent X in the *para*-substituted anilines provides a means of estimating σ_m constants.

Acknowledgements

We thank Professor Corwin Hansch for suggesting this study. We greatly appreciate the support of this work by the Office of Naval Research through contract no. N00014-91-J-4057. A portion of this research was conducted using the Cornell National Supercomputer Facility, a resource of the Center for Theory and Simulations in Science and Engineering (Cornell Theory Center), which receives major funding from the National Science Foundation and IBM Corporation, with additional support from New York State and members of the Corporate Research Institute.

1. P. Politzer and K. C. Daiker. *In* The force concept in chemistry. *Edited by* B. M. Deb. Van Nostrand Reinhold Co., New York. 1981. Chap. 6.
2. P. Politzer and D. G. Truhlar (*Editors*). Chemical applications of atomic and molecular electrostatic potentials. Plenum Press, New York. 1981.
3. P. Politzer and J. S. Murray. *In* Molecular structure and energetics. Vol. 7. *Edited by* J. F. Liebman and A. Greenberg. VCH Publishers, New York. 1988. Chap. 1.
4. P. Politzer and J. S. Murray. *In* Theoretical biochemistry and molecular biophysics. Vol. 2. Proteins. *Edited by* D. L. Beveridge and R. Lavery. Adenine Press, Schenectady, N.Y. 1991. Chap. 13.
5. P. Sjoberg, J. S. Murray, T. Brinck, and P. Politzer. Can. J. Chem. **68**, 1440 (1990).
6. P. Politzer and J. S. Murray. *In* Reviews of computational chemistry. *Edited by* K. B. Lipkowitz and D. B. Boyd. VCH Publishers, New York. 1991. Chap. 7.
7. J. S. Murray, T. Brinck, and P. Politzer. J. Mol. Struct. (Theochem). In press.
8. J. S. Murray and P. Politzer. Chem. Phys. Lett. **152**, 364 (1988).
9. T. Brinck, J. S. Murray, P. Politzer, and R. E. Carter. J. Org. Chem. **56**, 2934 (1991).
10. J. S. Murray, S. Ranganathan, and P. Politzer. J. Org. Chem. **56**, 3734 (1991).
11. T. Brinck, J. S. Murray, and P. Politzer. J. Org. Chem. **56**, 5012 (1991).
12. J. S. Murray and P. Politzer. J. Org. Chem. **56**, 6715 (1991).
13. J. S. Murray, T. Brinck, M. E. Grice, and P. Politzer. J. Mol. Struct. (Theochem), **256**, 29 (1992).
14. J. S. Murray and P. Politzer. J. Chem. Res. S, 110 (1992).
15. L. P. Hammett. Trans Faraday Soc. **34**, 156 (1938).
16. R. W. Taft. J. Am. Chem. Soc. **79**, 1045 (1957).
17. L. P. Hammett. Physical organic chemistry. McGraw–Hill, New York. 1970.
18. O. Exner. Correlation analysis of chemical data. Plenum Press, Czechoslavakia. 1988.
19. C. Hansch, A. Leo, and R. W. Taft. Chem. Rev. **91**, 165 (1991).
20. R. T. C. Brownlee and R. W. Taft. J. Am. Chem. Soc. **90**, 6537 (1968).
21. R. T. C. Brownlee and R. W. Taft. J. Am. Chem. Soc. **92**, 7007 (1970).
22. W. J. Hehre, R. W. Taft, and R. D. Topsom. Prog. Phys. Org. Chem. **12**, 159 (1976).
23. R. D. Topsom. Prog. Phys. Org. Chem. **16**, 125 (1987).
24. E. Scrocco and J. Tomasi. Top. Curr. Chem. **42**, 95 (1973).
25. E. Scrocco and J. Tomasi. Adv. Quantum Chem. **11**, 115 (1978).
26. M. J. Frisch, M. Head-Gordon, H. B. Schlegel, *et al.* GAUSSIAN 88. Gaussian Inc., Pittsburgh, Pa. 1988.
27. W. J. Hehre, L. Radom, P. v. R. Schleyer, and J. A. Pople. Ab initio molecular orbital theory. John Wiley and Sons, New York. 1986.
28. D. G. Lister, J. K. Tyler, J. H. Høg, and N. W. Larsen. J. Mol. Struct. **23**, 253 (1974).
29. J. S. Murray and P. Politzer. Chem. Phys. Lett. **136**, 283 (1987).
30. R. F. W. Bader, M. T. Carroll, J. R. Cheeseman, and C. Chang. J. Am. Chem. Soc. **109**, 7968 (1987).
31. P. Politzer, L. Abrahmsen, and P. Sjoberg. J. Am. Chem. Soc. **106**, 855 (1984).
32. I. Dzidic. J. Am. Chem. Soc. **94**, 8333 (1972).
33. S. K. Pollack, J. L. Devlin III, K. D. Summerhays, R. W. Taft, and W. J. Hehre. J. Am. Chem. Soc. **99**, 4583 (1977).
34. J. March. Advanced organic chemistry. John Wiley & Sons, New York. 1985.
35. P. Politzer, J. S. Murray, J. M. Seminario, and R. S. Miller. J. Mol. Struct. (Theochem). In press.
36. R. C. Weast (*Editor*). CRC handbook of chemistry and physics. 63rd ed. CRC Press, Boca Raton, Fla. 1982.
37. J. Buckingham (*Editor*). Dictionary of organic compounds. 5th ed. Chapman and Hall, New York. 1982.
38. A. Streitwieser, Jr. and C. H. Heathcock. Introduction to organic chemistry. 3rd ed. MacMillan Publishing Co., New York. 1989.

Can. J. Chem. Downloaded from www.nrcresearchpress.com by 109.225.110.28 on 09/08/12
For personal use only.

Crystal and molecular structures of two triosmium carbonyl cluster complexes containing *ortho*-metalated phenylphosphines (μ-H)$Os_3(CO)_8L[PFcPh(C_6H_4)]$ (L = $PFcPh_2$ or CO)

WILLIAM R. CULLEN,[1] STEVEN J. RETTIG, AND TU CAI ZHENG
Chemistry Department, University of British Columbia, Vancouver, B. C., Canada V6T 1Z1

Received March 5, 1992

WILLIAM R. CULLEN, STEVEN J. RETTIG, and TU CAI ZHENG. Can. J. Chem. **70**, 2215 (1992).

Pyrolysis of $Os_3(CO)_{11}(PFcPh_2)$, **7**, and $Os_3(CO)_{10}(PFcPh_2)_2$, **8**, (FcH = $(Fe(\eta\text{-}C_5H_5)_2$ affords (μ-H)$Os_3(CO)_9$-[$PFcPh(C_6H_4)$], **5**, and (μ-H)$Os_3(CO)_8(FcPPh_2)$[$PFcPh(C_6H_4)$], **6**, respectively. The structures of **5** and **6** are analogous; they both contain a bridging hydride and a μ_3-$PFcPh(C_6H_4)$ moiety resulting from the *ortho*-metalation of one phenyl group and subsequent formation of a η^2-bond from that metalated phenyl to the third osmium atom. Crystals of **5**, are triclinic, a = 11.380(2), b = 15.930(3), c = 9.467(1) Å, α = 92.82(1)°, β = 100.32(1)°, γ = 71.55(1)°, Z = 2, space group $P\bar{1}$, and those of **6** · CH_2Cl_2, are also triclinic, a = 13.151(3), b = 17.177(4), c = 12.619(3) Å, α = 91.98(2)°, β = 104.18(2)°, γ = 67.72(2)°, Z = 2, space group $P\bar{1}$. The structures were solved by heavy atom methods and were refined by full-matrix least-squares procedures to R = 0.028 and 0.026 by using 8080 and 9336 reflections with $I \geq 3\sigma(I)$, respectively.

WILLIAM R. CULLEN, STEVEN J. RETTIG et TU CAI ZHENG. Can. J. Chem. **70**, 2215 (1992).

La pyrolyse du $Os_3(CO)_{11}(PFcPh_2)$, **7**, et du $Os_3(CO)_{10}(PFcPh_2)_2$, **8**, fournit respectivement le (μ-H)$Os_3(CO)_9$-[$PFcPh(C_6H_4)$], **5** et (μ-H)$Os_3(CO)_8(FcPPh_2)$[$PFcPh(C_6H_4)$], **6**. Les structures des composés **5** et **6** sont analogues; elles contiennent toutes les deux un pont hydrure et une portion μ_3-$PFcPh(C_6H_4)$ qui résulte de l'*ortho*-métallation d'une groupe phényle et de la formation subséquente d'une liaison η^2 reliant le phényle métallé au troisième atome d'osmium. Les cristaux du composé **5** sont tricliniques, groupe d'espace $P\bar{1}$ avec a = 11,380(2), b = 15,930(3) et c = 9,467(1) Å, α = 98,82(1)°, β = 100,32(1)° et γ = 71,55(1)° et Z = 2 alors que ceux du composé **6** · CH_2Cl_2 sont aussi tricliniques, groupe d'espace $P\bar{1}$ avec a = 13,151(3), b = 17,177(4) et c = 12,619(3) Å, α = 91,98(2)°, β = 104,18(2)° et γ = 67,72(2)° et Z = 2. On a résolu les structures par le méthode des atomes lourds et on les a affinées par la méthode des moindres carrés (matrice entière) jusqu à des valeurs de R de 0,028 et 0,026 respectivement pour 8080 et 9336 réflexions avec $I \geq 3\sigma(I)$.

[Traduit par la rédaction]

Introduction

Heating $Os_3(CO)_{11}L$ or $Os_3(CO)_{10}L_2$, where L is a tertiary phosphine, usually results in bond cleavage within the ligand L accompanied by loss of CO (1–8). Both C—H and P—C bond cleavage are common and are known for both alkyl and aryl phosphines. For example, $Os_3(CO)_{11}(PEt_3)$ in refluxing nonane undergoes two C—H cleavages to form $H_2Os_3(Et_2PCCH_3)(CO)_9$ (2, 3), and pyrolysis of $Os_3(CO)_{10}$-$(PPh_3)_2$ in refluxing xylene affords six products, all of which involve at least one C—H cleavage, and four of which involve at least one P—C cleavage (4, 5). Mixed alkylarylphosphine complexes also undergo similar reactions (6–8). For example, thermolysis of $Os_3(CO)_{11}(PMePh_2)$ leads to one aryl C—H and two aryl C—P cleavages to give the benzyne derivative $Os_3(\mu_3\text{-}C_6H_4)(\mu_3\text{-}PMe)(CO)_9$, **1**, R = Me (1, 8). Many other phenyl phosphine complexes form benzyne complexes under extensive pyrolysis, and two of the ways in which the benzyne moiety is bound are shown in **1** and **2** (1, 8, 9).

These cluster transformations seem to take place in steps, and some intermediates can be isolated by using a lower reaction temperature or shorter reaction time or a combination of the two. Deeming *et al.* were able to isolate and structurally characterize two intermediates in the transformation of $Os_3(CO)_{11}(PMePh_2)$ to $Os_3(CO)_9(\mu_3\text{-}PMe)(\mu\text{-}C_6H_4)$ (1). One of the intermediates is $HOs_3(CO)_9(\mu_3\text{-}C_6H_4PMePh)$, **3**, containing an *ortho*-metalated phenyl group which is also η^2-bound to the third osmium atom. An analogous intermediate $HOs_3(CO)_9(\mu_3\text{-}C_6H_4PPh_2)$ was also isolated although not structurally characterized (1). We have been interested in studying ferrocenyl phosphines with the objective of obtaining *ortho*-metalated ferrocenyl moieties and from the pyrolysis of $Os_3(CO)_{10}(PFcPh_2)_2$ we were able

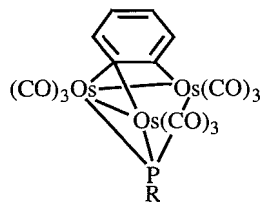

1

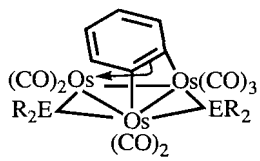

2

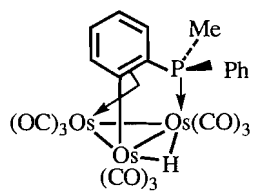

3

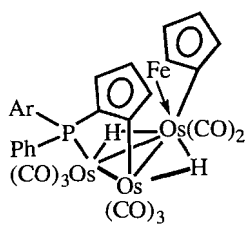

4

to isolate $H_2Os_3(CO)_8[(PPh_2(C_5H_3)Fe(C_5H_4)]$, **4**, in which double metalation has occurred (10). However, given the choice between a Fc- or Ph-group on the same ligand, it seems that *ortho*-metalation is more likely to take place within the phenyl group as judged by the product distributions. Here we report the preparation and structural characterization of

[1]Author to whom correspondence may be addressed.

Can. J. Chem. Downloaded from www.nrcresearchpress.com by 109.225.110.28 on 09/08/12
For personal use only.

TABLE 1. Spectroscopic data of the compounds **5**, **6**, and **8**[a]

Compound no.	$^{31}P\{^1H\}$ nmr ($CDCl_3$)	^1H nmr ($CDCl_3$)		Mass spectra (*m/e*)
		Ferrocenyl protons	Phenyl protons	
8[c]	−12.0 (broad, $W_{1/2}$ −85 Hz)[b]	4.05(s,10H) 4.30(m,4H) 4.65(m,4H)	7.2–7.5(m,20H)	1593(M^+, base peak), 1565, 1537, 1509, 1481, 1453, 1424, 1405, 1387, 1370, 1359, 1346, 1316, 1291, 1165, 1087, 1025, 968, 940, 862, 749
5	−6.1	4.37 (s,5H) 3.26 (m,1H) 4.48(m,1H) 4.78(m,1H) 5.16(m,1H) hydride −17.82(d,1H) J = 17.5	7.2–7.5(m,5H) 6.5–6.6(m,2H) 6.6–6.75 (m,2H)	1194(M^+, base peak), 1166, 1138, 1110, 1082, 1060, 1054, 1032, 1026, 998, 970, 942, 920, 892
6	0.09(d) −2.55(d) J_{P-P} = 15.1	3.28(m,1H) 3.88(s + m, 5 + 1H) 4.18(s,5H) 4.38(m,1H) 4.42(m,2H) 4.49(m,1H) 4.67(m,1H) 5.14(m,1H) hydride −17.42(dd,1H) J_1 = 18, J_2 = 9	6.11(m,1H) 6.41(m,1H) 6.52(bm,4H) 6.74(m,1H) 6.82–6.93(m,3H) 7.01(m,1H) 7.07–7.17(m,3H) 7.25–7.43(m,5H)	1536(M^+, base peak), 1508, 1480, 1451, 1423, 1218, 1144, 1070

[a] *J* values are in Hz.
[b] The broadness is due to the presence of both symmetrical and unsymmetrical isomers, ref. 14.
[c] $^{13}C\{^1H\}$ nmr: 69.9(s), 71.1(d, J = 8), 73.8(d, J = 11.5), 82.0(d, J = 58.8), 127.7(d, J = 10.5), 130.0(d, J = 2.1), 132.8(d, J = 11), 137.7(d, J = 53.7).

two such complexes, $(\mu\text{-H})Os_3(CO)_9[PFcPh(C_6H_4)]$, **5**, and $(\mu\text{-H})Os_3(CO)_8[PFcPh(C_6H_4)](PFcPh_2)$, **6**.

Experimental

All reactions were carried out under an argon atmosphere. Solvents were predried and distilled prior to use. $^{31}P\{^1H\}$ and ^1H nmr chemical shifts are given in ppm from TMS, and 85% H_3PO_4, respectively, and the spectra were recorded by using Bruker AC-200 or WH-400, or Varian XL-300 spectrometers. FAB mass spectra were recorded by using an AEI MS-9 spectrometer. The exciting gas was argon and the matrix was nitrobenzyl alcohol. Elemental analyses were performed by Mr. Peter Borda of this department. Some spectroscopic data are given in Table 1. Analytical and spectroscopic data for **7** have been published (9).

Preparation of $Os_3(CO)_{11}(PFcPh_2)$, 7, and $Os_3(CO)_{10}(PFcPh_2)_2$, 8

To a stirred solution of triosmium dodecacarbonyl (272 mg, 0.3 mmol) in dichloromethane (20 mL) in a Schlenk tube was added acetonitrile (5 mL, excess) and trimethylamine oxide (23 mg, 0.3 mmol). The reaction mixture was stirred for 2 h at room temperature and the ligand $PFcPh_2$ (112 mg, 0.3 mmol) was added. After a further 2 h the solvent was removed under reduced pressure, and the residue was applied to a silica chromatographic column. By using 3:1 petroleum ether/CH_2Cl_2 as eluent, pure orange product **7** was obtained in 65% isolated yield (240 mg) after solvent evaporation.

Compound **8** was prepared similarly except that 2 molar equivalents of trimethylamine oxide (48 mg, 0.63 mmol) and ferrocenyldiphenylphosphine (230 mg, 0.61 mmol) were used. Pure **8** was obtained in about 60% yield, following chromatography, as yellow crystals. Anal. calcd. for $C_{54}H_{38}Fe_2O_{10}Os_3P_2$: C 40.76, H 2.41; found: C 41.10, H 2.65.

Pyrolysis of $Os_3(CO)_{11}(PFcPh_2)$, 7, and preparation of 5

Pyrolysis of **7** in refluxing octane for 3 h produces mainly **1** (R = Fc) (9). Compound **7** (110 mg) in heptane (20 mL) was refluxed for 5 h. The solution was cooled and the solvent removed under reduced pressure. The orange-red residue was applied to a silica chromatographic column and eluted with 4:1 petroleum ether/CH_2Cl_2. The second band to elute proved to contain **5** and a pure sample was obtained in ~20% yield. Suitable crystals for X-ray structure analysis were grown by slow evaporation of the solvent from the collected fraction. Anal. calcd. for $C_{31}H_{19}FeO_9Os_3P$: C 31.21, H 1.61; found: C 31.35, H 1.58.

Pyrolysis of $Os_3(CO)_{10}(PFcPh_2)_2$, 8, and the preparation of 6

The pyrolysis of **8** has been described previously (10). Compound **6** was eluted as the sixth band in ~15% yield. Suitable crystals for X-ray structure analysis were grown from a 3:1 petroleum ether/CH_2Cl_2 mixture. Anal. calcd. for $C_{53}H_{40}Cl_2Fe_2O_8Os_3P_2$, **6** · CH_2Cl_2: C 39.29, H 2.49; found: C 39.45, H 2.65.

X-ray crystallographic analyses

Crystallographic data for $\{[(\eta^5\text{-}C_5H_5)Fe(\eta^5\text{-}C_5H_4)](C_6H_5)P(\mu{:}\eta^3\text{-}C_6H_4)\}(\mu\text{-H})Os_3(CO)_9$, **5**, and $\{[(\eta^5\text{-}C_5H_5)Fe(\eta^5\text{-}C_5H_4)](C_6H_5)P(\mu{:}\eta^3\text{-}C_6H_4)\}\{[(\eta^5\text{-}C_5H_5)Fe(\eta^5\text{-}C_5H_4)]P(C_6H_5)_2\}(\mu\text{-H})Os_3(CO)_8 \cdot CH_2Cl_2$, **6** · CH_2Cl_2, appear in Table 2. The final unit-cell parameters were obtained by least squares on the setting angles for 25 reflections with 2θ = 53.2–54.9° for **5** and 32.6–36.4° for **6** · CH_2Cl_2. The intensities of three standard reflections, measured every 200 reflections throughout the data collections, remained

Can. J. Chem. Downloaded from www.nrcresearchpress.com by 109.225.110.28 on 09/08/12
For personal use only.

TABLE 2. Crystallographic data[a]

Compound	**5**	**6** · CH_2Cl_2
Formula	$C_{31}H_{19}FeO_9Os_3P$	$C_{53}H_{40}Cl_2Fe_2O_8Os_3P_2$
fw	1192.91	1620.04
Color, habit	Orange, prism	Orange, prism
Crystal size, mm	0.25 × 0.35 × 0.35	0.18 × 0.28 × 0.32
Crystal system	Triclinic	Triclinic
Space group	$P\bar{1}$	$P\bar{1}$
a, Å	11.380(2)	13.151(3)
b, Å	15.930(3)	17.177(4)
c, Å	9.467(1)	12.619(3)
α,°	92.82(1)	91.98(2)
β,°	100.32(1)	104.18(2)
γ,°	71.55(1)	67.72(2)
V, Å^3	1601.8(5)	2552(1)
Z	2	2
ρ_{calc}, g/cm^3	2.473	2.108
$F(000)$	1092	1532
μ(Mo-K_α), cm^{-1}	124.18	82.24
Transmission factors	0.72–1.00	0.46–1.00
Scan type	ω–2θ	ω–2θ
Scan range, deg in ω	1.21 + 0.35 tan θ	1.10 + 0.35 tan θ
Scan rate, deg/min	32	32
Data collected	$+h, \pm k, \pm l$	$+h, \pm k, \pm l$
$2\theta_{max}$, deg	65	60
Crystal decay	Negligible	Negligible
Total no. of reflections	12033	15470
No. of unique reflections	11526	14867
R_{merge}	0.032	0.031
Reflcns. with $I \geq 3\sigma(I)$	8080	9336
No. of variables	407	647
R	0.028	0.026
R_w	0.030	0.027
gof	1.66	1.22
Max Δ/σ (final cycle)	0.04	0.14
Residual density e/Å^3	−1.17 to +1.24 (near Os)	−0.80 to +0.78

[a]Temperature 294 K, Rigaku AFC6S diffractometer, Mo-K_α radiation (λ = 0.71069 Å), graphite monochromator, takeoff angle 6.0°, aperture 6.0 × 6.0 mm at a distance of 285 mm from the crystal, stationary background counts at each end of the scan (scan/background time ratio 2:1, up to 8 rescans), $\sigma^2(F^2) = [S^2(C + 4B) + (pF^2)^2]/Lp^2$($S$ = scan rate, C = scan count, B = normalized background count, p = 0.01 for **5**, 0.02 for **6**), function minimized $\Sigma w(|F_o| - |F_c|)^2$ where $w = 4F_o^2/\sigma^2(F_o^2)$, $R = \Sigma||F_o| - |F_c||/\Sigma|F_o|$, $R_w = (\Sigma w(|F_o| - |F_c|)^2/\Sigma w|F_o|^2)^{1/2}$, and gof = $[\Sigma w(|F_o| - |F_c|)^2/(m - n)]^{1/2}$. Values given for R, R_w, and gof are based on those reflections with $I \geq 3\ \sigma(I)$.

constant for both compounds. The data were processed[2] and corrected for Lorentz and polarization effects, and absorption (empirical, based on azimuthal scans for four reflections).

Both structures were solved by heavy atom methods, the coordinates of the Os and Fe atoms being determined from the Patterson functions and those of the remaining non-hydrogen atoms from subsequent difference Fourier syntheses. Both structure analyses were initiated in the centrosymmetric space group $P\bar{1}$, these choices being confirmed by the subsequent successful solution and refinement of the structures. There is one molecule of dichloromethane in the asymmetric unit of **6**. All non-hydrogen atoms of both complexes were refined with anisotropic thermal parameters. The metal hydride atoms in both complexes were included in difference map positions but were not refined. All other hydrogen atoms in both structures were fixed in idealized positions (C—H = 0.98 Å, $B_H = 1.2\ B_{bonded\ atom}$). Corrections for secondary extinction were applied for both structures, the final values of the extinction coefficient being 3.14×10^{-7} for **5** and 1.58×10^{-7} for **6** · CH_2Cl_2.

[2]TEXSAN/TEXRAY structure analysis package which includes versions of the following: DIRDIF, direct methods for difference structures, by P. T. Beurskens, ORFLS, full-matrix least-squares, and ORFFE, function and errors, by W. R. Busing, K. O. Martin, and H. A. Levy, ORTEPII, illustrations, by C. K. Johnson. Neutral atom scattering factors and anomalous dispersion corrections for the non-hydrogen atoms were taken from the *International tables for X-ray crystallography* (11). Final atomic coordinates and equivalent isotropic thermal parameters, selected bond lengths, and selected bond angles appear in Tables 3–8, respectively. Hydrogen atom parameters, anisotropic thermal parameters, complete tables of bond lengths and bond angles, torsion angles, intermolecular contacts, least-squares planes, and measured and calculated structure factor amplitudes are included as supplementary material.[3]

[3]Hydrogen atom parameters, anisotropic thermal parameters, complete tables of bond lengths and bond angles, torsion angles, intermolecular contacts, least-squares planes, and measured and calculated structure factor amplitudes for **5** and **6** · CH_2Cl_2 may be purchased from: The Depository of Unpublished Data, Document Delivery, CISTI, National Research Council Canada, Ottawa, Canada KIA 0S2.

The tables of hydrogen atom parameters have also been deposited with the Cambridge Crystallographic Data Centre and can be obtained on request from The Director, Cambridge Crystallographic Data Centre, University Chemical Laboratory, 12 Union Road, Cambridge, CB2 IEZ, U.K.

Can. J. Chem. Downloaded from www.nrcresearchpress.com by 109.225.110.28 on 09/08/12
For personal use only.

TABLE 3. Final atomic coordinates (fractional) and B_{eq} (Å^2) for **5**[a]

Atom	x	y	z	B_{eq}
Os(1)	0.34925(2)	0.13712(1)	0.23759(2)	1.850(8)
Os(2)	0.44950(2)	0.26495(1)	0.43098(2)	1.834(9)
Os(3)	0.49420(2)	0.23784(1)	0.15292(2)	1.978(9)
Fe(1)	−0.00405(8)	0.20853(6)	−0.1539(1)	3.25(4)
P(1)	0.2018(1)	0.26738(8)	0.1293(1)	1.85(5)
O(1)	0.3406(5)	0.0248(3)	−0.0312(5)	5.2(3)
O(2)	0.1703(4)	0.0703(3)	0.3728(6)	5.1(3)
O(3)	0.5874(4)	−0.0132(3)	0.3618(5)	3.9(2)
O(4)	0.6491(4)	0.3553(3)	0.5190(5)	4.7(3)
O(5)	0.2904(5)	0.3591(4)	0.6523(6)	6.0(3)
O(6)	0.6195(4)	0.1058(3)	0.6189(5)	3.8(2)
O(7)	0.6253(6)	0.3641(4)	0.0787(8)	7.5(4)
O(8)	0.4779(5)	0.1612(4)	−0.1474(5)	5.9(4)
O(9)	0.7423(4)	0.1063(3)	0.2786(6)	5.1(3)
C(1)	0.1195(5)	0.2699(3)	−0.0523(6)	2.5(2)
C(2)	0.1629(6)	0.2229(4)	−0.1745(6)	3.2(3)
C(3)	0.0715(7)	0.2580(5)	−0.2973(7)	4.2(4)
C(4)	−0.0270(7)	0.3256(5)	−0.2549(7)	4.3(4)
C(5)	−0.0012(6)	0.3335(4)	−0.1037(6)	3.2(3)
C(6)	−0.009(1)	0.1078(6)	−0.035(1)	6.6(6)
C(7)	0.0121(9)	0.0769(5)	−0.169(1)	6.6(6)
C(8)	−0.095(1)	0.1294(7)	−0.269(1)	7.3(7)
C(9)	−0.1749(8)	0.1881(7)	−0.187(1)	6.5(6)
C(10)	−0.1235(8)	0.1744(7)	−0.047(1)	6.3(6)
C(11)	0.2897(4)	0.3443(3)	0.1276(5)	2.0(2)
C(12)	0.3618(5)	0.3599(3)	0.2619(5)	2.2(2)
C(13)	0.3801(6)	0.4457(4)	0.2726(6)	3.0(3)
C(14)	0.3381(6)	0.5058(4)	0.1629(8)	3.8(3)
C(15)	0.2798(6)	0.4853(4)	0.0274(7)	3.7(3)
C(16)	0.2528(5)	0.4078(4)	0.0115(6)	2.7(3)
C(17)	0.0745(5)	0.3272(3)	0.2253(6)	2.3(2)
C(18)	−0.0036(5)	0.2836(4)	0.2665(6)	2.9(3)
C(19)	−0.1022(6)	0.3284(5)	0.3331(8)	3.9(3)
C(20)	−0.1252(6)	0.4159(5)	0.3638(7)	4.2(4)
C(21)	−0.0501(6)	0.4610(4)	0.3257(7)	3.8(3)
C(22)	0.0505(5)	0.4162(4)	0.2565(7)	3.0(3)
C(23)	0.3436(5)	0.0681(4)	0.0682(7)	3.0(3)
C(24)	0.2366(5)	0.0960(4)	0.3245(7)	3.1(3)
C(25)	0.4997(5)	0.0445(3)	0.3193(6)	2.5(3)
C(26)	0.5730(5)	0.3214(4)	0.4848(6)	2.9(3)
C(27)	0.3495(6)	0.3212(4)	0.5713(6)	3.3(3)
C(28)	0.5544(5)	0.1640(3)	0.5490(6)	2.4(2)
C(29)	0.5757(6)	0.3188(4)	0.1097(7)	3.5(3)
C(30)	0.4801(6)	0.1907(4)	−0.0356(6)	3.3(3)
C(31)	0.6476(6)	0.1553(4)	0.2318(7)	3.3(3)

[a] $B_{eq} = (8/3)\pi^2\Sigma\Sigma U_{ij} a_i * a_j * (a_i \cdot a_j)$.

Results and discussion

When compound **7** is refluxed in octane for 3 h it undergoes two P—C cleavages and one C—H cleavage to form **1** (R = Fc) in high yield (>70%) (9). Both the ^{1}H and ^{31}P nmr spectra show no sign of the formation of the alternative ferrocyne compound, but they do show the formation of intermediates. To optimize isolation of these intermediates, the reaction was carried out in refluxing heptane. Thin-layer chromatographic monitoring showed that one intermediate was at a maximum concentration after 5 h. This compound, **5**, was isolated and the spectroscopic data suggest that it should be formulated as $Os_3(CO)_9(\mu\text{-}H)[PFcPh(C_6H_4)]$. Thus the ^{31}P resonance at ~6.1 ppm ($\Delta\delta$ = 4.6 ppm from **7**) is consistent with the presence of a phosphine ligand on the cluster. The ^{1}H nmr spectrum (Table 1) clearly suggests one ferrocenyl, one phenyl, and one metalated phenyl group on the phosphine ligand. One bridging hydride is also present. The parent peak from the FAB mass spectrum indicates the loss of two carbonyls from the parent compound **7**. These data, however, do not distinguish between two possible structures, one electron deficient, e.g., **9** (12), the other electron precise, e.g., **3** (1) and **10** (13) so a single crystal X-ray analysis was carried out. The electron-precise structure is shown in Fig. 1.

The products of the pyrolysis of $Os_3(CO)_{10}(PFcPh_2)_2$, **8**, are much more numerous. Refluxing in octane for 7 h affords at least eight compounds. One product, **4**, which results from metalation of each of the cyclopentadienyl rings

Can. J. Chem. Downloaded from www.nrcresearchpress.com by 109.225.110.28 on 09/08/12
For personal use only.

Can. J. Chem. Downloaded from www.nrcresearchpress.com by 109.225.110.28 on 09/08/12
For personal use only.

TABLE 4. Bond lengths (Å) with estimated standard deviations

Atom	Atom	Distance	Atom	Atom	Distance
Os(1)	Os(2)	3.0259(6)	Fe(1)	C(9)	2.038(8)
Os(1)	Os(3)	2.8659(5)	Fe(1)	C(10)	2.044(9)
Os(1)	P(1)	2.359(1)	Fe(1)	Cp(1)	1.644(3)
Os(1)	C(23)	1.902(6)	Fe(1)	Cp(2)	1.659(5)
Os(1)	C(24)	1.927(6)	P(1)	C(1)	1.801(5)
Os(1)	C(25)	1.936(5)	P(1)	C(11)	1.813(5)
Os(1)	H(1)	1.87	P(1)	C(17)	1.829(5)
Os(2)	Os(3)	2.7576(5)	O(1)	C(23)	1.142(7)
Os(2)	C(12)	2.135(5)	O(2)	C(24)	1.134(7)
Os(2)	C(26)	1.882(6)	O(3)	C(25)	1.147(6)
Os(2)	C(27)	1.908(6)	O(4)	C(26)	1.152(7)
Os(2)	C(28)	1.935(5)	O(5)	C(27)	1.134(7)
Os(2)	H(1)	1.84	O(6)	C(28)	1.139(6)
Os(3)	C(11)	2.386(5)	O(7)	C(29)	1.125(7)
Os(3)	C(12)	2.371(5)	O(8)	C(30)	1.136(7)
Os(3)	C(29)	1.906(6)	O(9)	C(31)	1.139(7)
Os(3)	C(30)	1.902(6)	C(1)	C(2)	1.424(8)
Os(3)	C(31)	1.873(6)	C(1)	C(5)	1.441(7)
Fe(1)	C(1)	2.037(5)	C(2)	C(3)	1.417(9)
Fe(1)	C(2)	2.028(6)	C(3)	C(4)	1.39(1)
Fe(1)	C(3)	2.039(7)	C(4)	C(5)	1.417(9)
Fe(1)	C(4)	2.058(7)	C(6)	C(7)	1.37(1)
Fe(1)	C(5)	2.033(6)	C(6)	C(10)	1.39(1)
Fe(1)	C(6)	2.022(8)	C(7)	C(8)	1.45(1)
Fe(1)	C(7)	2.047(8)	C(8)	C(9)	1.39(1)
Fe(1)	C(8)	2.035(7)	C(9)	C(10)	1.35(1)
C(11)	C(12)	1.441(7)			
C(11)	C(16)	1.443(7)			
C(12)	C(13)	1.441(7)			
C(13)	C(14)	1.362(8)			
C(14)	C(15)	1.408(9)			
C(15)	C(16)	1.358(8)			
C(17)	C(18)	1.403(7)			
C(17)	C(22)	1.384(8)			
C(18)	C(19)	1.366(8)			
C(19)	C(20)	1.36(1)			
C(20)	C(21)	1.38(1)			
C(21)	C(22)	1.399(8)			

and formation of an Fe—Os bond, has been fully characterized and was described previously (10). A second product, **6**, has now been isolated in moderate yield. The spectroscopic results show that **6** is very similar to **5**, as is borne out by the X-ray crystallographic study. The structure of **6** is shown in Fig. 2.

In both **5** and **6** the metalated phenyl moiety adopts the unsymmetrical electron-precise structure as in **3** and **10** (1, 13). Both **5** and **6** apparently result from the metalation of one P-C_6 ring and subsequent formation of a π-bond. The C_6H_4PFcPh bridge acts as a five-electron donor to the cluster, two electrons via the P atom, one via the ortho-metalated C, and two via the η^2-bond from the metalated ring. The metrical details for the two structures are very similar so detailed comments will be confined to **6** because the presence of the phosphine ligand at Os(1) adds additional interest.

The three Os—Os bonds of **6** show considerable variation in length ranging from 3.0259(6) Å for the hydrogen-bridged Os(1)—Os(3) through 2.8661(9) Å for Os(3)—Os(2), to 2.7746(8) Å for Os(2)—Os(1). The shortest bond in **6** is *trans* to the tertiary phosphine ligand; it is longer than the corresponding bond in **5** (Os(2)—Os(3) = 2.7576(5) Å). These Os—Os bond lengths are not unusual, the average for

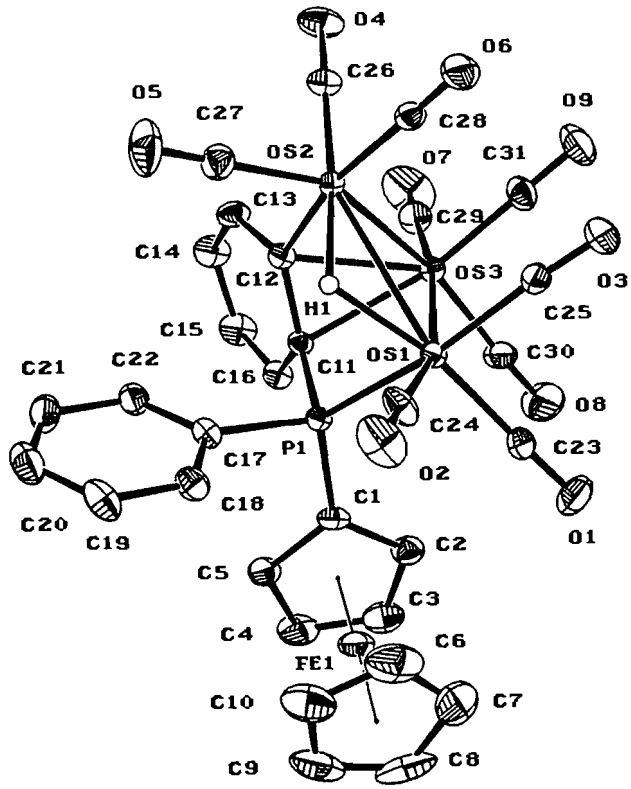

FIG. 1. ORTEP diagram for **5**. 50% probability thermal ellipsoids are shown for the non-hydrogen atoms.

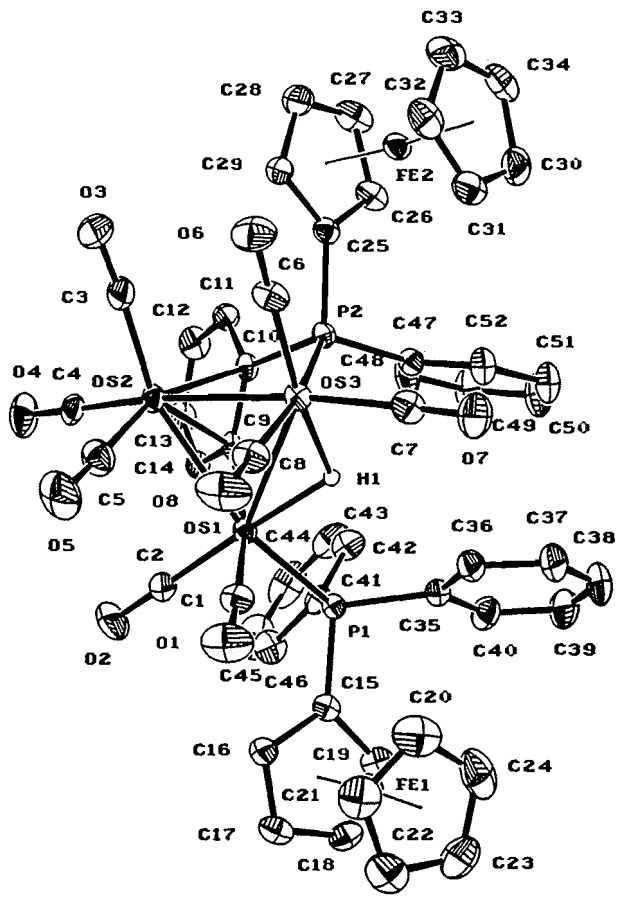

FIG. 2. ORTEP diagram for **6**. 50% probability thermal ellipsoids are shown for the non-hydrogen atoms.

TABLE 5. Bond angles (deg) with estimated standard deviations

Atom	Atom	Atom	Angle	Atom	Atom	Atom	Angle
Os(2)	Os(1)	Os(3)	55.73(1)	Os(1)	Os(2)	H(1)	36
Os(2)	Os(1)	P(1)	83.74(3)	Os(3)	Os(2)	C(12)	56.3(1)
Os(2)	Os(1)	C(23)	151.9(2)	Os(3)	Os(2)	C(26)	93.5(2)
Os(2)	Os(1)	C(24)	111.4(2)	Os(3)	Os(2)	C(27)	152.7(2)
Os(2)	Os(1)	C(25)	87.4(2)	Os(3)	Os(2)	C(28)	109.5(2)
Os(2)	Os(1)	H(1)	35	Os(3)	Os(2)	H(1)	91
Os(3)	Os(1)	P(1)	74.21(3)	C(12)	Os(2)	C(26)	89.2(2)
Os(3)	Os(1)	C(23)	96.8(2)	C(12)	Os(2)	C(27)	98.2(2)
Os(3)	Os(1)	C(24)	165.1(2)	C(12)	Os(2)	C(28)	165.6(2)
Os(3)	Os(1)	C(25)	91.7(2)	C(12)	Os(2)	H(1)	91
Os(3)	Os(1)	H(1)	87	C(26)	Os(2)	C(27)	95.6(3)
P(1)	Os(1)	C(23)	94.8(2)	C(26)	Os(2)	C(28)	89.6(2)
P(1)	Os(1)	C(24)	98.2(2)	C(26)	Os(2)	H(1)	175
P(1)	Os(1)	C(25)	165.9(2)	C(27)	Os(2)	C(28)	96.2(2)
P(1)	Os(1)	H(1)	76	C(27)	Os(2)	H(1)	79
C(23)	Os(1)	C(24)	96.6(3)	C(28)	Os(2)	H(1)	91
C(23)	Os(1)	C(25)	87.9(2)	Os(1)	Os(3)	Os(2)	65.07(1)
C(23)	Os(1)	H(1)	169	Os(1)	Os(3)	C(11)	78.2(1)
C(24)	Os(1)	C(25)	95.2(2)	Os(1)	Os(3)	C(12)	86.1(1)
C(24)	Os(1)	H(1)	79	Os(1)	Os(3)	C(29)	171.8(2)
C(25)	Os(1)	H(1)	102	Os(1)	Os(3)	C(30)	91.1(2)
Os(1)	Os(2)	Os(3)	59.19(1)	Os(1)	Os(3)	C(31)	93.1(2)
Os(1)	Os(2)	C(12)	86.4(1)	Os(2)	Os(3)	C(11)	76.3(1)
Os(1)	Os(2)	C(26)	149.4(2)	Os(2)	Os(3)	C(12)	48.5(1)
Os(1)	Os(2)	C(27)	115.0(2)	Os(2)	Os(3)	C(29)	108.9(2)
Os(1)	Os(2)	C(28)	87.4(1)	Os(2)	Os(3)	C(30)	156.1(2)
Os(2)	Os(3)	C(31)	86.0(2)	C(6)	C(7)	C(8)	105.9(9)
C(11)	Os(3)	C(12)	35.3(2)	C(7)	C(8)	C(9)	106.8(9)
C(11)	Os(3)	C(29)	95.1(2)	C(8)	C(9)	C(10)	109.0(9)
C(11)	Os(3)	C(30)	97.8(2)	C(6)	C(10)	C(9)	109(1)
C(11)	Os(3)	C(31)	162.3(2)	Os(3)	C(11)	P(1)	97.4(2)
C(12)	Os(3)	C(29)	85.7(2)	Os(3)	C(11)	C(12)	71.8(3)
C(12)	Os(3)	C(30)	132.5(2)	Os(3)	C(11)	C(16)	117.9(4)
C(12)	Os(3)	C(31)	129.8(2)	P(1)	C(11)	C(12)	117.4(4)
C(29)	Os(3)	C(30)	94.6(3)	P(1)	C(11)	C(16)	118.7(4)
C(29)	Os(3)	C(31)	92.0(3)	C(12)	C(11)	C(16)	120.5(4)
C(30)	Os(3)	C(31)	97.8(3)	Os(2)	C(12)	Os(3)	75.3(2)
Cp(1)	Fe(1)	Cp(2)	176.5(2)	Os(2)	C(12)	C(11)	125.3(3)
Os(1)	P(1)	C(1)	122.3(2)	Os(2)	C(12)	C(13)	120.1(4)
Os(1)	P(1)	C(11)	105.3(2)	Os(3)	C(12)	C(11)	72.9(3)
Os(1)	P(1)	C(17)	117.3(2)	Os(3)	C(12)	C(13)	122.5(4)
C(1)	P(1)	C(11)	104.2(2)	C(11)	C(12)	C(13)	114.5(4)
C(1)	P(1)	C(17)	102.0(3)	C(12)	C(13)	C(14)	123.1(5)
C(11)	P(1)	C(17)	103.5(2)	C(13)	C(14)	C(15)	121.3(5)
P(1)	C(1)	C(2)	129.2(4)	C(14)	C(15)	C(16)	118.9(5)
P(1)	C(1)	C(5)	123.3(4)	C(11)	C(16)	C(15)	121.3(5)
C(2)	C(1)	C(5)	106.8(5)	P(1)	C(17)	C(18)	120.2(4)
C(1)	C(2)	C(3)	108.0(6)	P(1)	C(17)	C(22)	121.6(4)
C(2)	C(3)	C(4)	109.0(6)	C(18)	C(17)	C(22)	118.2(5)
C(3)	C(4)	C(5)	108.5(5)	C(17)	C(18)	C(19)	120.7(6)
C(1)	C(5)	C(4)	107.7(6)	C(18)	C(19)	C(20)	120.9(6)
C(7)	C(6)	C(10)	109.4(9)	C(19)	C(20)	C(21)	120.2(6)
C(20)	C(21)	C(22)	119.7(6)				
C(17)	C(22)	C(21)	120.4(6)				
Os(1)	C(23)	O(1)	178.1(6)				
Os(1)	C(24)	O(2)	178.2(6)				
Os(1)	C(25)	O(3)	176.4(5)				
Os(2)	C(26)	O(4)	179.2(5)				
Os(2)	C(27)	O(5)	176.1(6)				
Os(2)	C(28)	O(6)	177.6(5)				
Os(3)	C(29)	O(7)	176.7(7)				
Os(3)	C(30)	O(8)	176.7(6)				
Os(3)	C(31)	O(9)	178.4(6)				
Os(1)	H(1)	Os(2)	109				

Can. J. Chem. Downloaded from www.nrcresearchpress.com by 109.225.110.28 on 09/08/12
For personal use only.

TABLE 6. Final atomic coordinates (fractional) and B_{eq} (Å^2) for **6**[a]

Atom	x	y	z	B_{eq}
Os(1)	0.28505(2)	0.21454(1)	0.08436(2)	2.24(1)
Os(2)	0.47300(2)	0.24312(1)	0.20526(2)	2.59(1)
Os(3)	0.25830(2)	0.37301(1)	0.20777(2)	2.38(1)
Fe(1)	−0.03809(7)	0.21569(5)	−0.20602(6)	3.35(4)
Fe(2)	0.31481(6)	0.40864(4)	0.59024(6)	2.83(4)
Cl(1)[b]	0	0	1/2	10.1(3)
Cl(2)[b]	−0.1953(5)	0.1340(4)	0.4719(5)	10.1(5)
Cl(3)	0.5433(4)	0.4758(3)	−0.0954(3)	15.2(4)
P(1)	0.1490(1)	0.15403(7)	0.0580(1)	2.33(6)
P(2)	0.3120(1)	0.28267(7)	0.3660(1)	2.26(6)
O(1)	0.1825(4)	0.3255(3)	−0.1295(4)	5.9(3)
O(2)	0.4225(4)	0.0858(3)	−0.0478(4)	5.4(3)
O(3)	0.6142(4)	0.3301(4)	0.3497(4)	7.1(4)
O(4)	0.6820(4)	0.0870(3)	0.1985(4)	5.8(3)
O(5)	0.4657(5)	0.3131(3)	−0.0141(4)	6.7(4)
O(6)	0.3623(4)	0.4954(3)	0.3195(4)	5.0(3)
O(7)	0.0138(4)	0.4838(3)	0.2065(4)	5.1(3)
O(8)	0.2326(5)	0.4635(3)	−0.0084(3)	6.0(3)
C(1)	0.2171(5)	0.2845(3)	−0.0479(4)	3.3(3)
C(2)	0.3707(4)	0.1326(3)	0.0046(4)	3.4(3)
C(3)	0.5585(5)	0.2976(4)	0.2992(5)	4.4(4)
C(4)	0.6025(4)	0.1445(3)	0.2015(5)	3.4(3)
C(5)	0.4661(5)	0.2879(4)	0.0685(5)	4.3(4)
C(6)	0.3242(5)	0.4478(3)	0.2793(4)	3.4(3)
C(7)	0.1054(5)	0.4415(3)	0.2098(4)	3.5(3)
C(8)	0.2432(5)	0.4272(3)	0.0702(5)	3.8(3)
C(9)	0.3919(4)	0.1475(3)	0.2363(4)	2.3(2)
C(10)	0.4185(4)	0.1845(3)	0.3385(4)	2.3(2)
C(11)	0.5051(4)	0.1339(3)	0.4325(4)	2.9(3)
C(12)	0.5616(5)	0.0499(3)	0.4272(5)	3.9(3)
C(13)	0.5343(5)	0.0115(3)	0.3290(5)	3.5(3)
C(14)	0.4561(4)	0.0576(3)	0.2395(4)	2.9(3)
C(15)	0.0891(4)	0.1389(3)	−0.0821(4)	2.8(3)
C(16)	0.1307(4)	0.1419(3)	−0.1760(4)	3.1(3)
C(17)	0.0692(5)	0.1134(3)	−0.2654(4)	3.9(3)
C(18)	−0.0113(5)	0.0914(4)	−0.2304(5)	4.1(4)
C(19)	−0.0006(5)	0.1071(3)	−0.1170(4)	3.3(3)
C(20)	−0.0919(7)	0.3388(4)	−0.1656(6)	6.1(5)
C(21)	−0.0670(6)	0.3320(4)	−0.2690(6)	5.1(4)
C(22)	−0.1372(6)	0.2976(4)	−0.3382(5)	5.3(4)
C(23)	−0.2053(6)	0.2811(4)	−0.2781(7)	5.8(4)
C(24)	−0.1773(7)	0.3072(5)	−0.1717(7)	6.5(5)
C(25)	0.3751(4)	0.3085(3)	0.4999(4)	2.7(2)
C(26)	0.3626(5)	0.2807(3)	0.6012(4)	3.5(3)
C(27)	0.4325(5)	0.3069(3)	0.6888(4)	4.5(3)
C(28)	0.4862(5)	0.3497(4)	0.6434(5)	4.4(3)
C(29)	0.4526(4)	0.3506(3)	0.5291(4)	3.4(3)
C(30)	0.1470(5)	0.4636(4)	0.5898(6)	4.9(4)
C(31)	0.1681(5)	0.4985(4)	0.5019(5)	4.4(3)
C(32)	0.2478(5)	0.5341(3)	0.5447(5)	4.4(3)
C(33)	0.2778(6)	0.5214(3)	0.6588(5)	4.6(4)
C(34)	0.2165(6)	0.4778(4)	0.6887(5)	4.6(4)
C(35)	0.0213(4)	0.2006(3)	0.1100(4)	3.0(3)
C(36)	−0.0245(5)	0.2879(3)	0.1174(5)	3.6(3)
C(37)	−0.1276(5)	0.3263(4)	0.1442(6)	5.2(4)
C(38)	−0.1851(6)	0.2795(5)	0.1653(6)	6.0(5)
C(39)	−0.1405(6)	0.1935(5)	0.1592(6)	5.5(5)
C(40)	−0.0378(5)	0.1530(4)	0.1314(5)	4.1(3)
C(41)	0.2119(4)	0.0443(3)	0.1146(4)	2.9(3)
C(42)	0.2218(5)	0.0257(4)	0.2240(5)	4.0(3)
C(43)	0.2763(6)	−0.0576(5)	0.2664(6)	5.5(5)
C(44)	0.3207(6)	−0.1202(4)	0.2041(8)	6.6(5)
C(45)	0.3115(6)	−0.1019(4)	0.0956(7)	6.4(5)
C(46)	0.2567(5)	−0.0201(3)	0.0494(5)	4.2(3)
C(47)	0.2035(4)	0.2522(3)	0.3984(4)	2.5(2)
C(48)	0.2298(5)	0.1692(3)	0.4322(5)	3.9(3)
C(49)	0.1505(6)	0.1458(4)	0.4626(6)	5.2(4)
C(50)	0.0444(5)	0.2056(4)	0.4580(6)	5.0(4)
C(51)	0.0171(5)	0.2872(4)	0.4256(5)	4.3(4)
C(52)	0.0968(5)	0.3107(3)	0.3953(5)	3.6(3)
C(53)[b]	−0.105(2)	0.064(1)	0.412(1)	11(2)
C(54)[b]	0.556(1)	0.477(1)	0.031(2)	8(1)

[a] $B_{eq} = (8/3)\pi^2\Sigma\Sigma U_{ij} a_i * a_j * (a_i \cdot a_j)$.
[b] Occupancy factor 0.50.

TABLE 7. Bond lengths (Å) with estimated standard deviations for **6**

Atom	Atom	Distance	Atom	Atom	Distance
Os(1)	Os(2)	2.7746(8)	Fe(1)	C(23)	2.035(6)
Os(1)	Os(3)	3.0344(8)	Fe(1)	C(24)	2.042(6)
Os(1)	P(1)	2.342(1)	Fe(1)	Cp(1)	1.645(3)
Os(1)	C(1)	1.903(5)	Fe(1)	Cp(2)	1.654(3)
Os(1)	C(2)	1.876(5)	Fe(2)	C(25)	2.040(5)
Os(1)	C(9)	2.141(5)	Fe(2)	C(26)	2.043(5)
Os(1)	H(1)	1.86	Fe(2)	C(27)	2.038(5)
Os(2)	Os(3)	2.8661(9)	Fe(2)	C(28)	2.033(6)
Os(2)	C(3)	1.901(6)	Fe(2)	C(29)	2.034(5)
Os(2)	C(4)	1.903(5)	Fe(2)	C(30)	2.043(6)
Os(2)	C(5)	1.881(6)	Fe(2)	C(31)	2.038(5)
Os(2)	C(9)	2.359(5)	Fe(2)	C(32)	2.037(6)
Os(2)	C(10)	2.369(4)	Fe(2)	C(33)	2.027(5)
Os(3)	P(2)	2.363(1)	Fe(2)	C(34)	2.036(5)
Os(3)	C(6)	1.896(6)	Fe(2)	Cp(3)	1.638(3)
Os(3)	C(7)	1.913(6)	Fe(2)	Cp(4)	1.647(3)
Os(3)	C(8)	1.930(6)	Cl(1)	C(53)	1.59(2)
Os(3)	H(1)	1.87	Cl(2)	C(53)	1.65(2)
Fe(1)	C(15)	2.043(5)	Cl(3)	C(54)	1.56(2)
Fe(1)	C(16)	2.041(5)	Cl(3)′	C(54)	1.64(2)
Fe(1)	C(17)	2.047(5)	P(1)	C(15)	1.804(5)
Fe(1)	C(18)	2.052(6)	P(1)	C(35)	1.837(5)
Fe(1)	C(19)	2.039(5)	P(1)	C(41)	1.835(5)
Fe(1)	C(20)	2.050(6)	P(2)	C(10)	1.825(4)
Fe(1)	C(21)	2.039(6)	P(2)	C(25)	1.811(5)
Fe(1)	C(22)	2.042(6)	P(2)	C(47)	1.828(5)
O(1)	C(1)	1.158(6)	C(26)	C(27)	1.432(8)
O(2)	C(2)	1.147(6)	C(27)	C(28)	1.410(9)
O(3)	C(3)	1.145(7)	C(28)	C(29)	1.401(8)
O(4)	C(4)	1.142(6)	C(30)	C(31)	1.409(9)
O(5)	C(5)	1.140(7)	C(30)	C(34)	1.429(9)
O(6)	C(6)	1.156(6)	C(31)	C(32)	1.397(9)
O(7)	C(7)	1.138(6)	C(32)	C(33)	1.398(8)
O(8)	C(8)	1.141(6)	C(33)	C(34)	1.405(9)
C(9)	C(10)	1.442(6)	C(35)	C(36)	1.398(7)
C(9)	C(14)	1.448(6)	C(35)	C(40)	1.395(7)
C(10)	C(11)	1.455(6)	C(36)	C(37)	1.386(7)
C(11)	C(12)	1.358(7)	C(37)	C(38)	1.37(1)
C(12)	C(13)	1.416(8)	C(38)	C(39)	1.37(1)
C(13)	C(14)	1.355(7)	C(39)	C(40)	1.390(8)
C(15)	C(16)	1.433(7)	C(41)	C(42)	1.392(7)
C(15)	C(19)	1.449(7)	C(41)	C(46)	1.389(7)
C(16)	C(17)	1.408(7)	C(42)	C(43)	1.391(8)
C(17)	C(18)	1.415(8)	C(43)	C(44)	1.34(1)
C(18)	C(19)	1.429(8)	C(44)	C(45)	1.38(1)
C(20)	C(21)	1.41(1)	C(45)	C(46)	1.384(8)
C(20)	C(24)	1.41(1)	C(47)	C(48)	1.391(7)

Can. J. Chem. Downloaded from www.nrcresearchpress.com by 109.225.110.28 on 09/08/12
For personal use only.

TABLE 7 (*concluded*)

Atom	Atom	Distance	Atom	Atom	Distance
C(21)	C(22)	1.40(1)	C(47)	C(52)	1.374(7)
C(22)	C(23)	1.41(1)	C(48)	C(49)	1.386(8)
C(23)	C(24)	1.41(1)	C(49)	C(50)	1.373(8)
C(25)	C(26)	1.447(7)	C(50)	C(51)	1.360(8)
C(25)	C(29)	1.434(7)	C(51)	C(52)	1.391(7)

Primes denote symmetry operation: $1 - x$, $1 - y$, $-z$. Cp (1–4) are the centroids of the C(15–19, 20–24, 25–29, 30–34) rings.

$Os_3(CO)_{12}$ being 2.877(3) Å. The Os(1)—P(1) bond (2.342(1) Å) is shorter than Os(3)—P(2) (2.363(1) Å).

The P—Fc bonds in **6** are shorter than the P—Ph bonds and if data from both **5** and **6** are used the two distances are avg. 1.805 Å and avg. 1.828 Å. P—Fc distances in another molecule $Os_3(CO)_8(H)_2[\eta\text{-}C_5H_3PFcPh)Fe(\eta\text{-}C_5H_4)]$ reflect this trend with P—Ph = 1.833(5) Å and P—Fc = 1.801(6) Å (10).

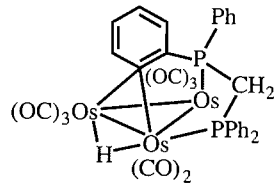

9

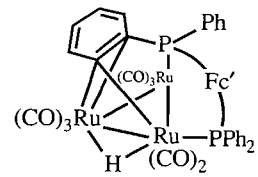

10

The Os(2)—C distances in **6** are essentially the same (avg. 2.364 Å). (In **3** the equivalent bonds are of length 2.319(22) and 2.417(18) Å). The Os(1)—C(9) interaction in **6** is shorter (2.141(5) Å) (in **3** it is 2.154(19) Å) and these data support the η^1, η^2-interaction between the C_6-ring and the Os_3 cluster. The metalated C_6-ring in **6** is tilted 45° with respect to the Os_3 plane. Neither P(2) nor Os(1) are coplanar with the C_6-ring, the former is 0.66 Å from the plane and the latter 0.26 Å but on the opposite side. This effect may account for the lengthening of Os(3)—P(2) relative to Os(1)—P(1) mentioned above. The μ_2-bonding involving C(9) and C(10)

TABLE 8. Bond angles (deg) with estimated standard deviations

Atom	Atom	Atom	Angle	Atom	Atom	Atom	Angle
Os(2)	Os(1)	Os(3)	58.92(2)	Os(1)	Os(2)	C(10)	76.8(1)
Os(2)	Os(1)	P(1)	153.50(3)	Os(3)	Os(2)	C(3)	94.0(2)
Os(2)	Os(1)	C(1)	111.1(2)	Os(3)	Os(2)	C(4)	170.5(2)
Os(2)	Os(1)	C(2)	93.0(2)	Os(3)	Os(2)	C(5)	90.5(2)
Os(2)	Os(1)	C(9)	55.6(1)	Os(3)	Os(2)	C(9)	86.1(1)
Os(2)	Os(1)	H(1)	90	Os(3)	Os(2)	C(10)	78.6(1)
Os(3)	Os(1)	P(1)	121.22(3)	C(3)	Os(2)	C(4)	94.0(2)
Os(3)	Os(1)	C(1)	88.1(2)	C(3)	Os(2)	C(5)	99.8(3)
Os(3)	Os(1)	C(2)	147.3(2)	C(3)	Os(2)	C(9)	133.6(2)
Os(3)	Os(1)	C(9)	85.8(1)	C(3)	Os(2)	C(10)	99.0(2)
Os(3)	Os(1)	H(1)	36	C(4)	Os(2)	C(5)	93.2(2)
P(1)	Os(1)	C(1)	95.2(2)	C(4)	Os(2)	C(9)	84.7(2)
P(1)	Os(1)	C(2)	91.4(2)	C(4)	Os(2)	C(10)	95.1(2)
P(1)	Os(1)	C(9)	98.2(1)	C(5)	Os(2)	C(9)	126.6(2)
P(1)	Os(1)	H(1)	86	C(5)	Os(2)	C(10)	158.8(2)
C(1)	Os(1)	C(2)	87.2(2)	C(9)	Os(2)	C(10)	35.5(2)
C(1)	Os(1)	C(9)	166.5(2)	Os(1)	Os(3)	Os(2)	56.01(2)
C(1)	Os(1)	H(1)	93	Os(1)	Os(3)	P(2)	84.96(4)
C(2)	Os(1)	C(9)	91.4(2)	Os(1)	Os(3)	C(6)	148.6(2)
C(2)	Os(1)	H(1)	177	Os(1)	Os(3)	C(7)	114.6(2)
C(9)	Os(1)	H(1)	89	Os(1)	Os(3)	C(8)	86.2(2)
Os(1)	Os(2)	Os(3)	65.06(2)	Os(1)	Os(3)	H(1)	35
Os(1)	Os(2)	C(3)	159.1(2)	Os(2)	Os(3)	P(2)	73.59(4)
Os(1)	Os(2)	C(4)	106.7(2)	Os(2)	Os(3)	C(6)	93.7(2)
Os(1)	Os(2)	C(5)	82.2(2)	Os(2)	Os(3)	C(7)	168.6(2)
Os(1)	Os(2)	C(9)	48.5(1)	Os(2)	Os(3)	C(8)	93.6(2)
Os(2)	Os(3)	H(1)	87	Os(1)	C(2)	O(2)	176.4(5)
P(2)	Os(3)	C(6)	94.7(2)	Os(2)	C(3)	O(3)	174.8(5)
P(2)	Os(3)	C(7)	100.2(2)	Os(2)	C(4)	O(4)	177.7(5)
P(2)	Os(3)	C(8)	167.1(2)	Os(2)	C(5)	O(5)	177.6(6)
P(2)	Os(3)	H(1)	76	Os(3)	C(6)	O(6)	177.4(5)
C(6)	Os(3)	C(7)	96.4(2)	Os(3)	C(7)	O(7)	176.9(5)
C(6)	Os(3)	C(8)	88.0(2)	Os(3)	C(8)	O(8)	176.1(5)
C(6)	Os(3)	H(1)	170	Os(1)	C(9)	Os(2)	76.0(1)
C(7)	Os(3)	C(8)	92.1(2)	Os(1)	C(9)	C(10)	126.1(3)
C(7)	Os(3)	H(1)	83	Os(1)	C(9)	C(14)	119.8(3)
C(8)	Os(3)	H(1)	102	Os(2)	C(9)	C(10)	72.6(3)
Cp(1)	Fe(1)	Cp(2)	176.7(2)	Os(2)	C(9)	C(14)	119.9(3)
Cp(3)	Fe(2)	Cp(4)	176.1(1)	C(10)	C(9)	C(14)	113.6(4)
Os(1)	P(1)	C(15)	116.0(2)	Os(2)	C(10)	P(2)	96.8(2)

Can. J. Chem. Downloaded from www.nrcresearchpress.com by 109.225.110.28 on 09/08/12
For personal use only.

TABLE 8 (*concluded*)

Atom	Atom	Atom	Angle	Atom	Atom	Atom	Angle
Os(1)	P(1)	C(35)	121.7(2)	Os(2)	C(10)	C(9)	71.9(2)
Os(1)	P(1)	C(41)	111.6(2)	Os(2)	C(10)	C(11)	119.2(3)
C(15)	P(1)	C(35)	101.5(2)	P(2)	C(10)	C(9)	118.2(3)
C(15)	P(1)	C(41)	99.7(2)	P(2)	C(10)	C(11)	117.1(3)
C(35)	P(1)	C(41)	103.6(2)	C(9)	C(10)	C(11)	121.2(4)
Os(3)	P(2)	C(10)	105.0(1)	C(10)	C(11)	C(12)	120.8(5)
Os(3)	P(2)	C(25)	122.0(2)	C(11)	C(12)	C(13)	119.1(5)
Os(3)	P(2)	C(47)	117.6(2)	C(12)	C(13)	C(14)	121.1(5)
C(10)	P(2)	C(25)	105.3(2)	C(9)	C(14)	C(13)	124.1(5)
C(10)	P(2)	C(47)	105.0(2)	P(1)	C(15)	C(16)	127.7(4)
C(25)	P(2)	C(47)	100.4(2)	P(1)	C(15)	C(19)	124.9(4)
Os(1)	C(1)	O(1)	175.7(5)	C(16)	C(15)	C(19)	106.6(4)
C(15)	C(16)	C(17)	108.8(5)	C(37)	C(38)	C(39)	119.6(6)
C(16)	C(17)	C(18)	108.8(5)	C(38)	C(39)	C(40)	121.3(6)
C(17)	C(18)	C(19)	108.0(5)	C(35)	C(40)	C(39)	119.3(6)
C(15)	C(19)	C(18)	107.8(5)	P(1)	C(41)	C(42)	120.6(4)
C(21)	C(20)	C(24)	107.6(7)	P(1)	C(41)	C(46)	119.5(4)
C(20)	C(21)	C(22)	108.3(7)	C(42)	C(41)	C(46)	119.7(5)
C(21)	C(22)	C(23)	108.3(6)	C(41)	C(42)	C(43)	119.3(6)
C(22)	C(23)	C(24)	107.4(7)	C(42)	C(43)	C(44)	121.3(6)
C(20)	C(24)	C(23)	108.4(7)	C(43)	C(44)	C(45)	119.6(6)
P(2)	C(25)	C(26)	123.7(4)	C(44)	C(45)	C(46)	121.2(7)
P(2)	C(25)	C(29)	129.2(4)	C(41)	C(46)	C(45)	118.9(6)
C(26)	C(25)	C(29)	106.8(5)	P(2)	C(47)	C(48)	120.1(4)
C(25)	C(26)	C(27)	107.1(5)	P(2)	C(47)	C(52)	121.4(4)
C(26)	C(27)	C(28)	108.5(5)	C(48)	C(47)	C(52)	118.4(5)
C(27)	C(28)	C(29)	108.6(5)	C(47)	C(48)	C(49)	120.9(5)
C(25)	C(29)	C(28)	108.9(5)	C(48)	C(49)	C(50)	119.2(5)
C(31)	C(30)	C(34)	107.5(6)	C(49)	C(50)	C(51)	120.8(5)
C(30)	C(31)	C(32)	108.4(6)	C(50)	C(51)	C(52)	119.9(5)
C(31)	C(32)	C(33)	108.3(6)	C(47)	C(52)	C(51)	120.7(5)
C(32)	C(33)	C(34)	108.8(6)	Cl(1)	C(53)	Cl(2)	111(1)
C(30)	C(34)	C(33)	107.1(6)	Cl(3)	C(54)	Cl(3)′	127(1)
P(1)	C(35)	C(36)	118.7(4)				
P(1)	C(35)	C(40)	122.1(4)				
C(36)	C(35)	C(40)	118.8(5)				
C(35)	C(36)	C(37)	120.4(6)				
C(36)	C(37)	C(38)	120.6(6)				

of the C_6-ring appears to result in electron localization in the ring. C(9)—C(10) is lengthened to 1.442(6) Å whereas C(13)—C(14) and C(11)—C(12) are shortened to 1.355(7) and 1.358(17) Å respectively. The C—C—C angle at C(9) (113.6(4)°), the metalated carbon atom, is different from the others in the ring that are close to the usual 120°.

The other bond angles and distances in **6** (and **5**) are as expected.

Acknowledgement

We are grateful to the Natural Sciences and Engineering Research Council of Canada for financial support (W.R.C.) and the University of British Columbia for a Graduate Fellowship (T.C.Z.).

1. A. J. Deeming, S. E. Kabir, N. I. Powell, P. A. Bates, and M. B. Hursthouse. J. Chem. Soc. Dalton Trans. 1529 (1987).
2. A. J. Deeming and M. Underhill. J. Chem. Soc. Dalton Trans. 2727 (1973).
3. A. J. Deeming. J. Organomet. Chem. **128**, 63 (1977).
4. C. W. Bradford, R. S. Nyholm, G. J. Gainsford, J. M. Guss, P. R. Ireland, and R. Mason. J. Chem. Soc. Chem. Commun. 87 (1972).
5. G. J. Gainsford, J. M. Guss, P. R. Ireland, R. Mason, C. W. Bradford, and R. S. Nyholm. J. Organomet. Chem. **40**, C70 (1972).
6. A. J. Deeming, S. E. Kabir, and M. Underhill. J. Chem. Soc. Dalton Trans. 2589 (1973).
7. A. J. Deeming, I. P. Rothwell, M. B. Hursthouse, and J. D. J. Backer-Dirks. J. Chem. Soc. Dalton Trans. 1879 (1981).
8. S. C. Brown, J. Evans, and L. E. Smart. J. Chem. Soc. Chem. Commun. 1021 (1980).
9. W. R. Cullen, S. J. Rettig, and T. C. Zheng. Organometallics. In press.
10. W. R. Cullen, S. J. Rettig, and T. C. Zheng. Organometallics, **11**, 277 (1992).
11. International tables for X-ray crystallography. Vol. IV. Kynoch Press, Birmingham, U.K. (present distributor Kluwer Academic Publishers, Dordrecht, The Netherlands). 1974. pp. 99–102 and 149.
12. J. A. Clucas, D. F. Forester, M. M. Harding, and A. K. Smith. J. Chem. Soc. Chem. Commun. 949 (1984).
13. M. I. Bruce, P. A. Humphrey, O bin Shawkataly, M. R. Snow, E. R. T. Tiekink, and W. R. Cullen. Organometallics, **9**, 2910 (1990).
14. W. R. Cullen, S. J. Rettig, and T. C. Zheng. Can. J. Chem. In press.

Can. J. Chem. Downloaded from www.nrcresearchpress.com by 109.225.110.28 on 09/08/12
For personal use only.

Open-chain nitrogen compounds. Part XV.[1] A kinetic study of the hydrolysis of 1-aryl-3-aryloxymethyl-3-methyltriazenes and related triazenes

KEITH VAUGHAN[2]
Saint Mary's University, Halifax, N.S., Canada B3H 3C3

AND

DONALD L. HOOPER AND MARCUS P. MERRIN
Dalhousie University, Halifax, N.S., Canada B3H 4J3

Received December 20, 1991

KEITH VAUGHAN, DONALD L. HOOPER, and MARCUS P. MERRIN. Can. J. Chem. **70**, 2224 (1992).

The kinetics of hydyrolysis of a series of 1-aryl-3-aryloxymethyl-3-methyltriazenes, Ar-N=N-NMe-CH_2OAr', was studied over the pH range 2–7.5. Reactions were followed by the change in UV absorbance spectra of the triazenes. The aryloxymethyltriazenes decompose more slowly at pH 7.5 than the hydroxymethyltriazenes, Ar-N=NMe-CH_2OH; the hydrolysis is favoured by the presence of an electron-withdrawing group in Ar'. A mixed isopropanol/buffer system was developed in order to improve solubility of the aryloxymethyl triazenes. Lowering the pH caused an increase in the rate of hydrolysis and under strongly acidic conditions an electron-withdrawing group in Ar' actually slows down the reaction. A Hammett plot of the pseudo-first-order rate constant, k_{obs}, is curved, indicating that two or more mechanisms operate simultaneously and that the contribution of each mechanism is substituent-dependent. A plot of k_{obs} vs. [buffer] is linear; the slope of the plot affords the rate constant, k_b, for the buffer-catalyzed reaction for each substituent. A Hammett plot of k_b vs. σ is linear with $\rho = +0.55$, suggesting that the buffer-catalyzed reaction involves nucleophilic displacement of the phenoxy group by the buffer anion. Further analysis afforded the specific acid-catalyzed rate constants, k_{H^+}, for each substituent; this component of the reaction has a negative ρ, consistent with a mechanism involving protonation at the ether oxygen. The postulation that specific acid catalysis is a component of the reaction mechanism was confirmed by the observation of a solvent deuterium isotope effect, $2.28 > k_H/k_D > 1.60$. Only the *p*-NO_2 and *p*-CN phenyloxymethyltriazenes showed any spontaneous decomposition.

KEITH VAUGHAN, DONALD L. HOOPER et MARCUS P. MERRIN. Can. J. Chem. **70**, 2224 (1992).

On a déterminé la cinétique de l'hydrolyse d'une série de 1-aryl-3-aryloxyméthyl-3-méthyltriazènes, Ar-N=N-NMe-CH_2OAr', à des pH allant de 2 à 7,5. On a suivi les réactions par le changement du spectre d'absorbance UV des triazènes. À un pH de 7,5, les aryloxyméthyltriazènes se décomposent plus lentement que les hydroxyméthyltriazènes, Ar-N=N-NMe-CH_2OH; l'hydrolyse est favorisée par la présence d'un groupe électro-attracteur dans la portion Ar'. On a développé un système mixte isopropanol/tampon pour améliorer la solubilité des aryloxyméthyltriazènes. Un abaissement du pH provoque une augmentation de la vitesse d'hydrolyse et, dans des conditions fortement acides, un groupe électro-attracteur dans la portion Ar' inhibe complètement la réaction. La courbe de Hammett de la constante de vitesse du pseudo-premier ordre, k_{obs}, n'est pas rectiligne; ceci indique que deux ou plusieurs mécanismes opèrent simultanément et que la contribution de chacun dépend du substituant. Une courbe de k_{obs} vs. [tampon] est linéaire; la pente de la courbe fournit la constante de vitesse, k_b, pour la réaction catalysée par le tampon pour chaque substituant. Une courbe de Hammett de k_b vs. σ est linéaire et $\rho = +0{,}55$, suggérant que la réaction catalysée par le tampon implique une substitution nucléophile du groupe phénoxyle par l'anion du tampon. Une analyse plus approfondie fournit les constantes de vitesse des réactions soumises à une catalyse acide spécifique, k_{H^+}, pour chaque substituant; la valeur de ρ pour cette composante de la réaction est négative et cette valeur est en accord avec un mécanisme impliquant une protonation de l'oxygène de l'éther. Le postulat à l'effet que la catalyse acide spécifique est une composante du mécanisme de la réaction a été confirmé par l'observation d'un effet isotopique du deutérium du solvant, $2{,}28 > k_H/k_D > 1{,}60$. Les seuls phényloxyméthyltriazènes à se décomposer spontanément sont les dérivés *p*-NO_2 et *p*-CN.

[Traduit par la rédaction]

Introduction

1-Aryl-3,3-dimethyltriazenes (**1***a*) have been known for many years (1) to have antitumour activity against murine tumours and one such triazene, DTIC (Dacarbazine, NSC 45388), has found clinical use against human malignant melanoma (2). The presumed mode of action of DTIC involves enzymatic oxidation to a hydroxymethyltriazene (**1***b*), followed by loss of formaldehyde to give the monomethyltriazene, Ar-N=N-NHMe, the putative cytotoxic metabolite. It has been suggested that one of the limitations to DTIC efficacy is the apparent inefficiency of oxidative metabolism in the human liver (3). Thus it would seem to be a worthwhile exercise to search for a triazene derivative of DTIC that would act as a prodrug and not require oxidative metabolism.

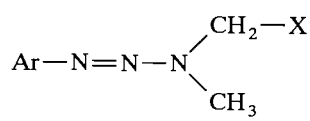

1 *a* X = H
b X = OH
c X = OMe
d X = OAc
e X = SAr'

The hydroxymethyltriazene (**1***b*) ("HMT") would seem to be an ideal candidate as a pro-drug, but all of the biological

[1]For Part XIV in ths series, see ref. 8.
[2]Author to whom correspondence may be addressed.

Can. J. Chem. Downloaded from www.nrcresearchpress.com by 109.225.110.28 on 09/08/12
For personal use only.

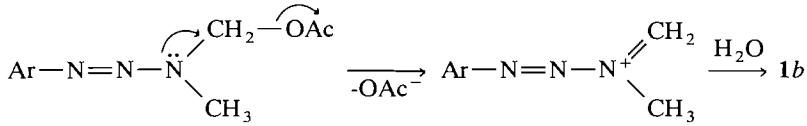

FIG. 1

studies suggest that the hydroxymethyltriazene is a very transient species in vivo. Nevertheless, we were successful in achieving the synthesis of the first stable hydroxymethyltriazene (4), and although these compounds are stable in the crystalline state, they do indeed decompose rapidly in solution under physiological conditions (5). In developing the chemistry of these novel *N*-hydroxymethyl compounds, we were aware of the desirability of preparing a further derivative of HMT with appropriate stability for pro-drug use.

Thus we synthesized the methyl ether derivatives (**1***c*) and the acetoxymethyltriazenes (**1***d*) (6); the difference in chemical behavior of these two apparently similar derivatives is quite striking but can be rationalized by the difference in the facility of the leaving group X. The ether derivatives (**1***c*) with a poor leaving group, OMe, are comparable in stability at pH 7.5 to the dimethyltriazene (**1***a*), whereas the acetoxymethyltriazene (**1***d*) decomposes in solution as rapidly as the hydroxymethyltriazene (**1***b*). Apparently the relatively good leaving group, OAc, is displaced rapidly to afford an iminium ion, which hydrolyses to the HMT (See Fig. 1).

We previously extended the range of hydroxymethyltriazene derivatives to the 1-aryl-3-arylthiomethyl-3-methyltriazenes (**1***e*) (7) and more recently to the 1-aryl-3-aryloxymethyl-3-methyltriazenes (**2***a–h*) (8). The isolation of these compounds is an exciting development in the search for the ultimate triazene pro-drug, since the aryloxy group would be expected to fall in between the methoxy and acetoxy groups in leaving group ability. Furthermore, the extensive variation of the Y-group in **2** should provide for a "tailor-made" leaving group with the appropriate reactivity required in the pro-drug. Accordingly we have undertaken a thorough study of the solution behavior of these new aryloxymethyltriazenes in order to assess their potential as triazene pro-drugs.

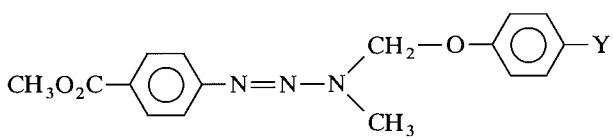

2 *a* Y = OCH_3
b Y = CH_3
c Y = H
d Y = Cl
e Y = Br
f Y = CO_2CH_3
g Y = CN
h Y = NO_2

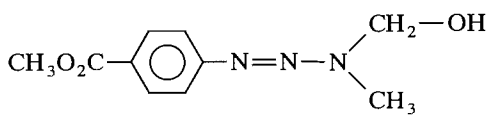

3

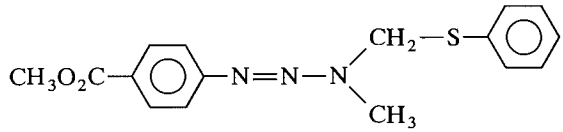

4

Experimental

The compounds used in this study were prepared by established procedures from the literature (5, 6) with the exception of the 3-aryloxymethyl-3-methyltriazenes (**2***a–h*) whose synthesis and characterization are reported in the previous paper in this series (8). All compounds used were recrystallized to constant melting point. Approximately 1.5 mg of each test compound was dissolved in 1 mL of dried, distilled dimethyl sulfoxide. These solutions were stored under refrigeration (−10°C) and thawed for use as required. Buffers were prepared as follows.

MES buffer

2(*N*-Morpholino)ethanesulfonic acid (Sigma M8250) (4.88 g) was dissolved in 250 mL distilled water to give a 0.1 M solution. This was adjusted to pH 5.5 using 0.2 M sodium hydroxide.

Formate buffers (pH 3.3)

0.1 M: 88% formic acid solution (3.206 g) and sodium formate (2.630 g) made up to 1 L. 0.5 M: 88% formic acid solution (16.03 g) and sodium formate (13.17 g) made up to 1 L. 0.01 M: 88% formic acid solution (0.321 g) and sodium formate (0.236 g) made up to 1 L.

HCl pH 2.0 (not a true buffer)

0.2 M Hydrochloric acid (6.5 mL) and 0.2 M potassium chloride (43.5 mL) made up to 100 mL.

NaOH pH 12.0 (not a true buffer)

0.2 M Sodium hydroxide (6.0 mL) and 0.2 M potassium chloride (44 mL) made up to 100 mL.

Phosphate pH 7.5

0.2 M monobasic sodium phosphate (16 mL) and 0.2 M dibasic sodium phosphate (84 mL) made up to 200 mL.

The pH of the buffer solutions was checked periodically using an Accumet model 810 pH meter (Fisher Scientific) standardized with commercial standard buffers at pH 7.00 and 4.00 (Fisher Scientific). The pH measurements were carried out with solutions thermostatted at 38 ± 1°C, but there was no attempt to control the ionic strength of the medium.

UV analysis

UV–visible absorption measurements were made using a Cary 219 spectrophotometer (Varian) with repeat scan and timed delay facilities. The cell chamber was thermostatted at 38 ± 1°C. These measurements were made in one of three modes. For fast hydrolyses ($t_{1/2} < 10$ min) the spectrophotometer was operated at fixed wavelength (320 nm, close to the triazene maximum) with the chart set for time drive to give a continuous trace of decay with time at this wavelength. For intermediate rates (10 min $< t_{1/2} <$ 60 min), the spectrophotometer was set to scan from 450 to 230 nm at 2 nm s^{-1} repeatedly with a 4 min cycle time in overlay mode so that isosbestic points could be observed as a check on spectrophotometer stability. Very slow hydrolyses ($t_{1/2} > 60$ min) were measured at a fixed wavelength (320 nm) with a timed delay so that a measurement was made for 10 sec every hour or every 90 min as appropriate.

Hydrolyses were carried out in stoppered Spectrosil quartz cells (Fisher Scientific) in neat buffer (3 mL) or in a 2:1 buffer–isopro-

Can. J. Chem. Downloaded from www.nrcresearchpress.com by 109.225.110.28 on 09/08/12
For personal use only.

TABLE 1. Kinetic data for the hydrolysis of aryloxymethyltriazenes at pH 2.0 in 0.066 M isopropanol/chloride buffer mixture

Compound	Intercept	Slope	$k_{obs}/10^{-3}$ (s^{-1})	Log k	$t_{1/2}$ (min)	r
2*a*	−0.329	−0.367	6.12	−2.213	1.9	0.983
2*b*	0.264	−0.365	6.08	−2.216	1.2	0.988
2*c*	0.016	−0.356	5.95	−2.226	2.0	0.998
2*d*	−0.054	−0.288	4.80	−2.318	2.2	0.999
2*e*	−0.234	−0.268	4.47	−2.349	1.7	0.999
2*f*	0.083	−0.195	3.25	−2.213	1.9	0.999
2*g*	0.071	−0.177	2.95	−2.530	4.3	0.999
2*h*	0.114	−0.237	3.96	−2.403	3.4	0.999
3	−0.082	−1.093	0.018	−0.174	0.56	0.998

TABLE 2. Kinetic data for the hydrolysis of aryloxymethyltriazenes at pH 3.3 in isopropanol/formate buffer mixture of differing buffer concentration

	0.33 M[a]			0.066 M[a]			0.0066 M[a]		
Compound	$k_{obs}/10^{-3}$ (s^{-1})	Log k	$t_{1/2}$ (min)	$k_{obs}/10^{-3}$ (s^{-1})	Log k	$t_{1/2}$ (min)	$k_{obs}/10^{-3}$ (s^{-1})	Log k	$t_{1/2}$ (min)
2*a*	1.313	−2.882	8.99	0.567	−3.246	20.6	0.379	−3.421	30.6
2*b*	1.211	−2.917	9.42	0.387	−3.413	26.1	0.286	−3.543	36
2*c*	0.940	−3.027	12.6	0.291	−3.536	40.6	0.182	−3.741	63.8
2*d*	1.101	−2.958	10.6	0.298	−3.525	36.0	0.167	−3.776	54.1
2*e*	1.422	−2.847	8.37	0.325	−3.487	35.2	0.162	−3.788	68.7
2*f*	1.694	−2.771	6.86	0.342	−3.466	33.8	0.155	−3.81	75
2*g*	2.456	−2.609	4.8	0.491	−3.309	22.5	0.249	−3.603	45.4
2*h*	5.010	−2.299	2.6	2.25	−2.648	4.24	1.498	−2.825	7.4
3	—	—	—	19.54	−1.709	0.66	—	—	—

[a]Buffer concentration.

TABLE 3. Kinetic data for the hydrolysis of aryloxymethyltriazenes at pH 5.5 in 0.066 M isopropanol/MES buffer mixture

Compound	Intercept	Slope/10^{-3}	$k_{obs}/10^{-5}$ (s^{-1})	Log k	$t_{1/2}$ (h)	r
2*a*	−0.029	−1.122	1.869	−4.728	10.7	0.999
2*b*	0.022	−1.065	1.776	−4.753	11.2	0.999
2*c*	0.012	−0.448	0.746	−5.127	26.2	0.999
2*d*	0.028	−0.575	0.958	−5.018	20.9	0.992
2*e*	0.0008	−0.557	0.928	−5.032	20.8	0.999
2*f*	−0.046	−2.170	3.620	−4.441	4.97	0.999
2*g*	0.029	−7.127	10.87	−3.925	1.69	0.999
2*h*	0.359	−87.60	146.0	−2.836	0.20	0.999
3	0.023	−0.108	179.0	−2.745	0.11	0.999

panol mixture (2 mL buffer:1 mL isopropanol). An aliquot (50 μL) of the DMSO solution of the compound under investigation was added to the cell, which was then quickly stoppered, inverted once to mix, inserted in the spectrophotometer, and the appropriate program started. Volumes were measured with Eppendorf pipettes.

After each run, absorbances were measured manually and values for ln A calculated according to:

$$[1] \quad \ln A = \ln (A_t - A_\infty)/(A_\infty - A_0)$$

where A_t is the absorbance after time t, A_∞ is the absorbance after complete hydrolysis, and A_0 is the initial absorbance. All experiments were carried out in duplicate. If the corresponding values of ln A for the two runs differed by more than 0.05, then the data were discarded and the experiment repeated. A simple linear least-squares fit program was used to generate plots of these results. The slope of each plot represents the rate constant k_{obs} (s^{-1}). Half-lives were calculated using:

$$[2] \quad t_{1/2} = 60\{(\ln 0.5) - A\}/B$$

where A is the y-intercept and B the slope in min^{-1}. The results of this kinetic analysis are presented in Tables 1–3.

Changes in rate constant k_{obs} with buffer concentration at constant pH were examined by measuring the hydrolysis rate for each compound in formate buffer (pH 3.3) at three concentrations. The original buffers were 0.1, 0.01, and 0.5 M, which on dilution with isopropanol became 0.06, 0.006, and 0.33 M. These rates are shown in Fig. 8 plotted against Hammett σ_p values.

Can. J. Chem. Downloaded from www.nrcresearchpress.com by 109.225.110.28 on 09/08/12
For personal use only.

TABLE 4. Retention times and response factors for reference standards

Compound	Retention time (min)	Response factor ($mg^{-1}/10^7$)[a]	Molar response ($mmol^{-1}/10^9$)
2e	2.41 ± 0.05	1.16 ± 0.02	4.38 ± 0.08
M4HB	4.71 ± 0.02	9.1 ± 0.3	13.83 ± 0.5
M4AB	2.86 ± 0.02	2.351 ± 0.002	3.555 ± 0.003
HOC_4H_4Br	3.18 ± 0.02	0.272 ± 0.009	0.471 ± 0.002

[a]Response in integrator units.

HPLC analyses

HPLC analyses were performed on a Varian model 5000 liquid chromatograph equipped with a microprocessor-controlled binary solvent delivery system. Data were collected with a Varian model 4290 integrator. A 250 × 4 mm, 10 μm Lichrosorb NH_2 (Hibar) column was used with a 3 mm amino guard column (Brownlee Labs). Isocratic elution with isopropanol/*n*-hexane (60:40) at a flow of 1.5 mL min^{-1} gave the best separations. External standards were prepared by dissolving a weighed mass of the desired compound in 25 mL isopropanol as follows.

Compound **2e**	4.9 mg
4-Bromophenol (HOC_4H_4Br)	14.7 mg
Methyl-4-aminobenzoate (M4AB)	2.2 mg
Methyl-4-hydroxybenzoate (M4HB)	0.74 mg

Standards, with the exception of compound **2e**, were reagent grade (Aldrich) used without further purification and were found to be of acceptable purity (>98%). The standards were run in triplicate and their retention times and response factors are given in Table 4.

Hydrolysis of the 4-bromophenyloxymethyltriazene (**2e**) was carried out as follows. Formate buffer (pH 3.3, 25 mL) and isopropanol (12.5 mL) were equilibrated in a water bath. The triazene was dissolved in the isopropanol, which was then added to the buffer. Immediately, and then at ca. 30 min intervals, a 5 mL aliquot was pipetted into a separatory funnel. This aqueous phase was extracted with dichloromethane (3 × 10 mL), and the organic layers were combined, dried with anhydrous sodium sulphate, filtered, and evaporated under vacuum. This material was then dissolved in isopropanol, filtered through a 0.2 μm membrane (Metricel GA-8), and made up to 10 mL.

A test mixture containing suitable amounts of the three likely products was prepared and subjected to the extraction procedure outlined above. The analysis of this extract was compared with the standards to establish the efficiency of the extraction process for each component. For the starting material, the t_0 concentration was established by comparison with the standard and this value then related to the known amount of substrate in the system. The recoveries were as follows: compound **2e**, 76%; M4HB, 97.8%; M4AB, 61.4%; HOC_4H_4Br, 78.5%.

The chromatograms for the hydrolysis experiment are shown in Fig. 2. The results of this analysis are given in Table 5, and the assay of the hydrolysis in Table 6.

Solvent deuterium isotope effect

The *p*-bromophenyloxymethyltriazene (**2e**) was dissolved in dimethyl sulfoxide (1.5 mg/mL) and 50 μL of this solution was added to the buffer/isopropanol mixture (0.1 M, pH/pD 3.07, 40 ± 1°C) in a cuvette. In one experiment, the buffer was made up in H_2O to give the rate constant (k_H); in a second experiment, the buffer was made up in D_2O to give the deuterium isotope rate constant (k_D). The observed k_H/k_D value was 1.60. Since the isopropanol was not deuterated, an exchange can take place, i.e.,

$$i\text{-PrOH} + D_3O^+ \rightleftharpoons i\text{-PrOD} + HD_2O^+$$

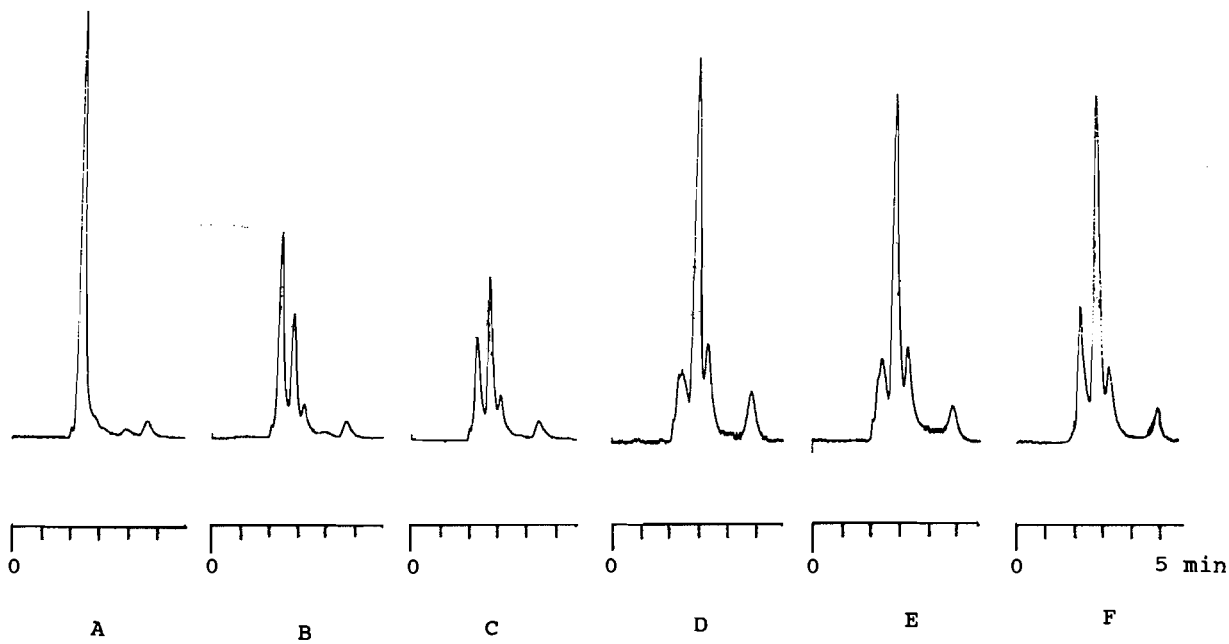

FIG. 2. Hydrolysis of 1-(4-carbomethoxyphenyl)-3-(4-bromophenyloxymethyl)-3-methyltriazene (**2e**) followed by HPLC. A, 0 min; B, 32 min; C, 56 min; D, 92 min; E, 18 h; F, 6 days.

Can. J. Chem. Downloaded from www.nrcresearchpress.com by 109.225.110.28 on 09/08/12
For personal use only.

TABLE 5. Results of HPLC analysis of the hydrolysis of compound **2e** measured by disappearance of substrate

Time (min)	Amount in sample ($g/10^{-3}$)	Corrected for recovery ($g/10^{-3}$)	Moles/10^{-5}	ln C^a
0	11.7	15.4	4.08	0
32	6.17	8.11	2.15	−0.641
65	3.49	4.59	1.22	−1.210
92	1.88	2.47	0.654	−1.830
1080	1.03	1.35	0.358	−2.433

[a] ln (M_t/M_0) where M_t is the number of moles present at time t and M_0 is the number of moles present at the start of the experiment.

TABLE 6. Assay of products of HPLC hydrolysis experiment

Time (min)	Assay in moles/10^{-5}		
	M4AB	Bromophenol	M4HB
0		—	—
32	2.19	2.13	0.051
65	2.55	2.86	0.057
92	3.13	3.43	0.055
1080	3.17	3.58	0.053

which implies that k_D(obs) could be expressed as:

$$1/3\ k_H + 2/3\ k_D\ (\text{true}) = k_D\ (\text{obs}) = 5.15 \times 10^{-4}\ s^{-1}$$

(since the reaction solvent is composed of 2/3 buffer and 1/3 isopropanol).

Thus the true k_D could be as low as $3.61 \times 10^{-4}\ s^{-1}$ and the upper limit of k_H/k_D would equal 2.28 (if all the isopropanol was deuterated). The conclusion of the experiment is that there is definitely a solvent deuterium isotope effect in the range $1.60 < k_H/k_D < 2.28$.

Results and discussion

The most reactive compound of the series of aryloxymethyl triazenes (**2a–h**) at physiological pH was predictably the *p*-nitrophenyloxymethyltriazene (**2h**), which decomposed in neat pH 7.5 phosphate buffer in almost exactly the same manner as its parent hydroxymethyltriazene (**3**). A close examination of the UV absorbance decay of the hydrolysis of **2h** (Fig. 3) reveals some subtle differences from the hydrolysis of **3**. Firstly, there is a short induction period at the start of the reaction during which the triazene absorbance at 320 nm does not decay; after this induction period, the UV absorbance decays in a first-order manner to give a pseudo-first-order rate constant, k_2, equal to $1.05 \times 10^{-3}\ s^{-1}$ corresponding to a half-life ($t_{1/2}$) of 11 min. This value is equal, within experimental error, to the half-life of the parent hydroxymethyltriazene (5).

The second feature of Fig. 3 is the observation of a second absorbance at ca. 400 nm that *grows in* during the early stage of reaction. This absorbance can be attributed to the

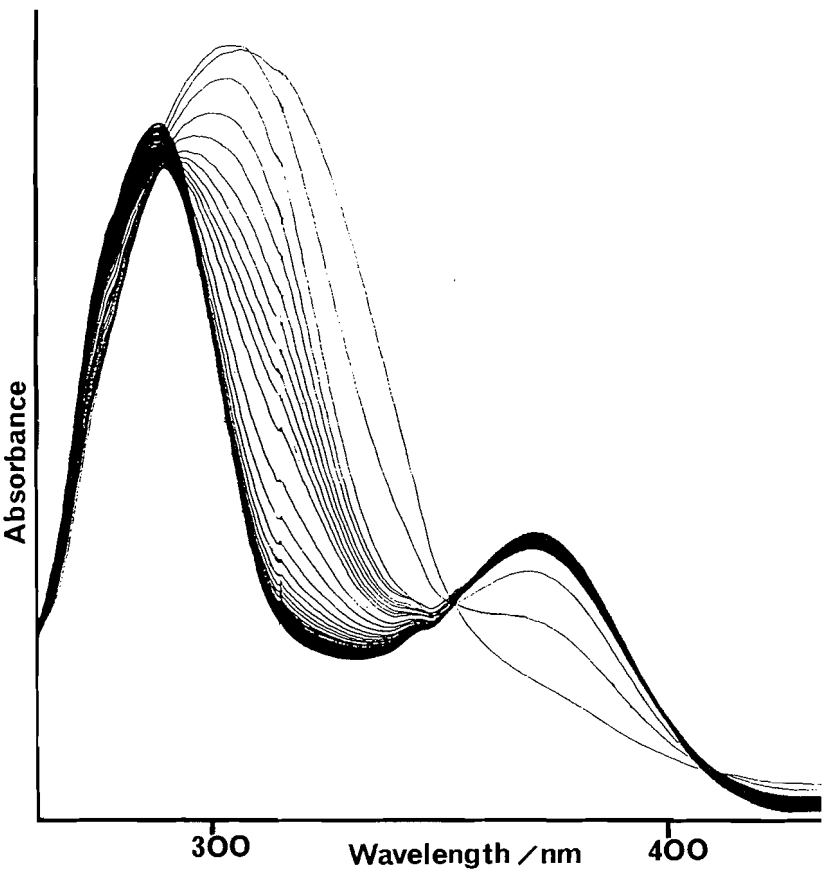

FIG. 3. Repeat-scan (cycle time 1 min) UV spectrum for 1-(4-carbomethoxyphenyl)-3-(4-nitrophenyloxymethyl)-3-methyl triazene (**2h**) in pH 7.5 phosphate buffer.

Can. J. Chem. Downloaded from www.nrcresearchpress.com by 109.225.110.28 on 09/08/12
For personal use only.

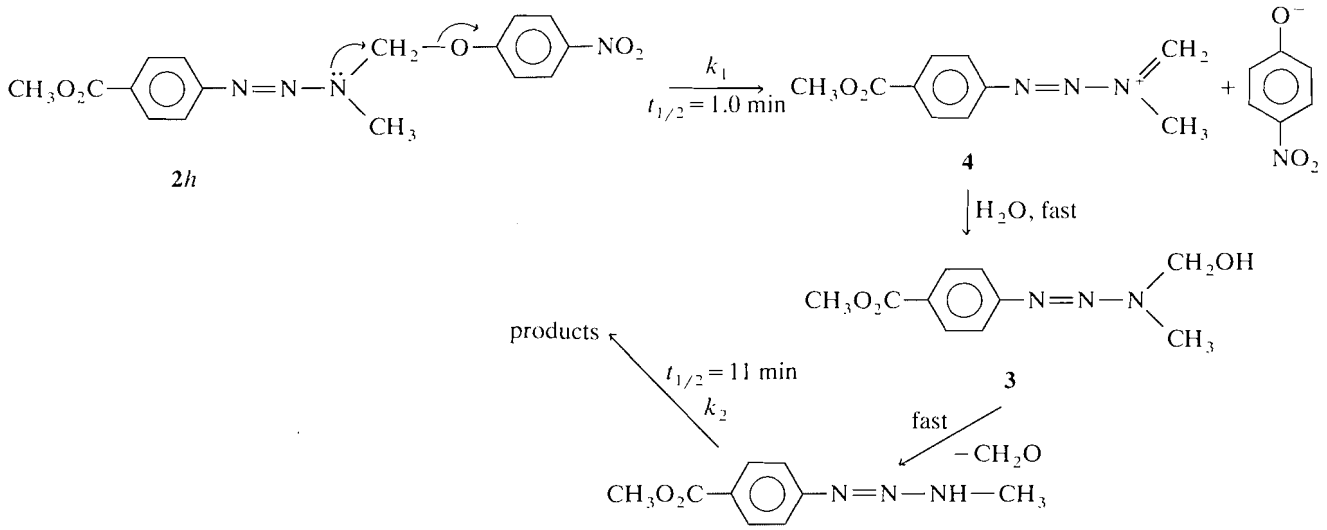

FIG. 4

formation and release of the *p*-nitrophenolate ion during the initial, rapid decomposition of the aryloxymethyltriazene (**2***h*). Kinetic analysis of the growth of the 400-nm peak gives a second pseudo-first-order rate constant, k_1, equal to 1.15×10^{-2} s^{-1}, which converts into a half-life of 1.0 min.

This result can be explained logically by the mechanism shown in Fig. 4, in which the triazene (**2***h*) undergoes spontaneous ionization (k_1) to afford the iminium ion intermediate (**4**) and the *p*-nitrophenolate ion. Fast hydrolysis of the iminium ion by water affords the hydroxymethyltriazene (**3**), followed by rapid loss of formaldehyde to afford the monomethyltriazene, Ar-N=N-NHMe, which then decomposes with the observed half-life (k_2) of 11 min (5). The decomposition of the *p*-nitrophenoxymethyltriazene (**2***h*) under these conditions is unique in our experience in that it represents the first absolute measurement of the fast rate of the initial decomposition of a hydroxymethyltriazene derivative.

The success of the hydrolysis experiment with the *p*-nitrophenoxymethyltriazene (**2***h*) in neat aqueous buffer was not, unfortunately, carried over to the other compounds in this series. With the exception of **2***h*, the solubility of the aryloxymethyltriazenes in the buffer was too low to give concentrations suitable for UV spectrophotometric analysis. The triazene simply precipitated out of solution before any measurable reaction occurred. For this reason, it was deemed desirable to develop a mixed buffer/isopropanol system. An important consideration of using such a system is the establishment of a pH scale for such a mixture. It has been shown that the presence of alcohols in aqueous systems leads to disruption of hydrogen bonding, which in turn leads to a greater number of free water molecules being available to solvate protons and hence a lowering of the effective hydrogen ion concentration (9). The pH values quoted are those obtained from a normal laboratory pH meter and are thus only an approximate indication of acidity.

To compare the reactivity of the new aryloxymethyltriazenes (**2**) with the parent hydroxymethytriazene (**3**) it was necessary to establish the kinetic parameters of **3** at different pH values and in the mixed buffer/isopropanol solvent system.

The decomposition of compound **3** was examined over the pH range 3.3–12.0 and was found to follow first-order behavior in all cases. The kinetic data from these experiments are shown in Table 7. Thus in an alkaline medium at pH 12.0 the hydroxymethyltriazene is surprisingly stable, with a half-life of 14.7 h. In phosphate buffer at pH 7.5, the rate of hydrolysis is 43 times faster, and at acid pH 5.5 the rate of hydrolysis of the HMT (**3**) is increased by a further factor of 23. Lowering the pH further to pH 3.3 has a much smaller effect on the very fast rate of hydrolysis.

TABLE 7. Kinetic data for the hydrolysis of the hydroxymethyltriazene (**3**) for various buffers and pH values

	Neat buffer		Buffer–isopropanol	
pH	$t_{1/2}$	$k_{obs}/10^{-3}$ (s^{-1})	$t_{1/2}$	$k_{obs}/10^{-3}$ (s^{-1})
3.3	18.2 s	44.2	40 s	19.5
5.5	1.59 min	11.9	6.7 min	1.78
7.5	9.81 min	0.52	4.2 h	0.046
12.0	14.7 h	0.012	—	—

Adding isopropanol to the buffer system slows the hydrolysis of the HMT (**3**) by a factor of 11.3 at pH 7.5 and by a factor of 6.7 at pH 5.5. The rate of hydrolysis of **3** at pH 3.3 is much less affected by the presence of the alcohol. These observations are consistent with the presence of isopropanol causing a decrease in the effective hydrogen ion concentration. Furthermore, it can be adduced from this evidence that protonation plays a significant role in the acid-catalyzed decomposition of the hydroxymethyltriazenes.

Tables 1, 2, and 3 show the results for the measurement of kinetic parameters of the aryloxymethyltriazenes (**2**) in isopropanol/buffer systems of pH 2.0, 3.3, and 5.5 obtained from the plots of ln *A* versus time for the loss of the triazene UV absorbance. In all cases the aryloxymethyltriazenes decompose at a significantly lower rate than the parent hydroxymethyltriazene (**3**). For example, the *p*-bromophenyloxymethyltriazene (**2***e*) decomposes from 3 to 190 times more slowly than **3**, depending upon the pH. All sets of data show varying half-life values for the decomposition of the aryloxymethyltriazenes (**2***a*–*h*) as a function of the substituent X in the aryl moiety. It is logical therefore to

Can. J. Chem. Downloaded from www.nrcresearchpress.com by 109.225.110.28 on 09/08/12
For personal use only.

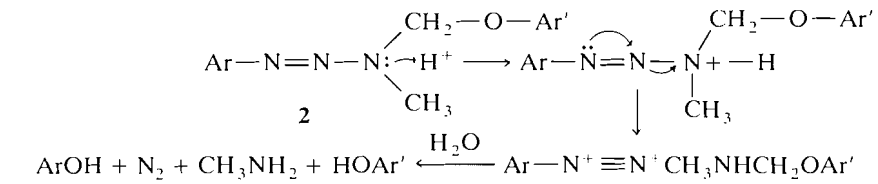

FIG. 5

look for a Hammett correlation for these various substituents.

A general observation from the data in Tables 1–3 is that, for each compound, the lower the pH the faster the reaction. This observation suggests that protonation of the ether oxygen is important in the rate-determining step.

However, at pH 3.3, it is evident that both strongly electron-donating (OCH_3) and electron-withdrawing (NO_2) groups promote the hydrolysis, whereas at pH 5.5 a simpler pattern emerges where the electron-withdrawing ability favours the hydrolysis.

A possible site of protonation in the aryloxymethyltriazenes (**2**) is the N-3 nitrogen, which would ultimately lead to fragmentation of the triazene at the N2—N3 bond as shown in Fig. 5. Subsequent decomposition of the arenediazonium ion leads to a phenol (methyl-4-hydroxybenzoate in the compounds studied) in addition to the phenol produced by the decomposition of the phenoxymethylamine fragment. The HPLC study of the decompositton of the *p*-bromophenoxymethyltriazene (**2*e***) provided evidence that the mechanism depicted in Fig. 5 is *not* operative. Although traces of methyl-4-hydroxybenzoate were detected in the hydrolysis mixture, its level was low (<2 mol%) and constant. This compound was subsequently found to be a ubiquitous contaminant of α-hydroxymethyltriazenes and their derivatives. The $t_{1/2}$ value obtained for compound **2*e*** was 36.4 min by HPLC compared to 35.2 min by UV spectrophotometry.

The HPLC method did have one shortcoming in that over long periods of time a degree of transesterification took place between the solvent isopropanol and the methyl 4-aminobenzoate product. This ester had a retention time almost identical with that of the substrate and was not resolvable by the method in use. This transesterification was slow compared with the hydrolysis of interest, isopropyl 4-aminobenzoate only being detectable after 18 h of hydrolysis.

The actual products of hydrolysis of **2*e*** are principally methyl-4-aminobenzoate and *p*-bromophenol, which is consistent with a fragmentation of **2*e*** at the ether linkage to give *p*-bromophenol and the hydroxymethyltriazene (Fig. 6 and Tables 5 and 6). However, the ultimate question is how does this fragmentation occur, and to find an answer we turn our attention to a Hammett analysis.

Figure 7 is a Hammett plot for the hydrolysis rate constants, k_{obs}, of the aryloxymethyltriazenes (**2**) at the pH values 2.0, 3.3, and 5.5 using the data for k_{obs} in Tables 1, 2, and 3. The curved nature of the Hammett plots at all pH's suggests strongly that there is more than one pathway of decomposition. In addition to a spontaneous decomposition, there is clearly an acid-catalyzed component to the overall reaction, since for every substituent the rate of reaction goes up as the pH is lowered.

A second revealing Hammett plot is that shown in Fig. 8, which shows the effect of changing the buffer concentration while holding the pH constant at 3.3. It is clear from Fig. 8 that the rate of reaction increases for each substituent as the buffer concentration is increased, suggesting that there is a third, buffer-catalyzed component to the overall decomposition of **2**.

Thus it appears that the rate of decomposition of the aryloxymethyltriazenes (**2*a–h*)** is the sum of the rates of three distinct processes: (*i*) the spontaneous decomposition (k_{sp}); (*ii*) an acid-catalyzed reaction (k_{H^+}); and (*iii*) a buffer-catalyzed reaction (k_B). The measured rate constant, k_{obs}, must itself have three components and may be expressed as follows:

$$[3] \quad k_{obs} = k_{sp} + k_{H^+}[H^+] + k_B[B]$$

The only uncertain quantity in this expression is [B], which could be assumed to be either the buffer anion concentration [A^-], or the buffer acid concentration [HA], or the total buffer concentration {[A^+] + [HA]}. As a first step we used the total buffer concentration, which was plotted against the k_{obs} at pH 3.3 for each substituent. The slope of each line affords k_B for the respective substituent and these values are shown in Table 8. A Hammett plot of log k_B versus σ_p gives a good straight line fit with $\rho = +0.55$. Since the ρ-value for

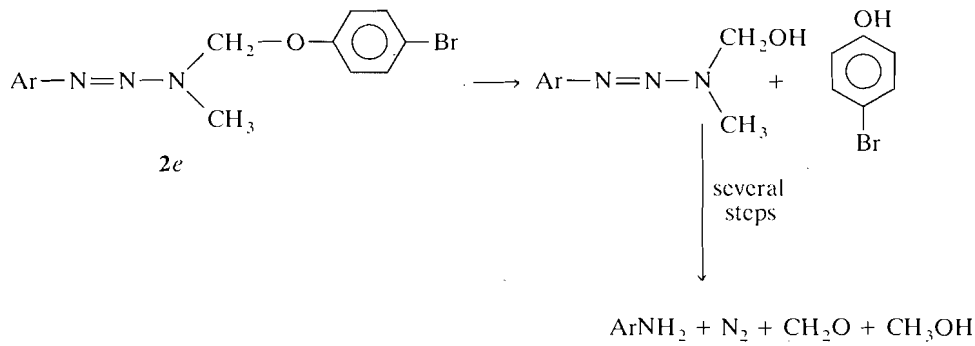

FIG. 6

Can. J. Chem. Downloaded from www.nrcresearchpress.com by 109.225.110.28 on 09/08/12
For personal use only.

Can. J. Chem. Downloaded from www.nrcresearchpress.com by 109.225.110.28 on 09/08/12
For personal use only.

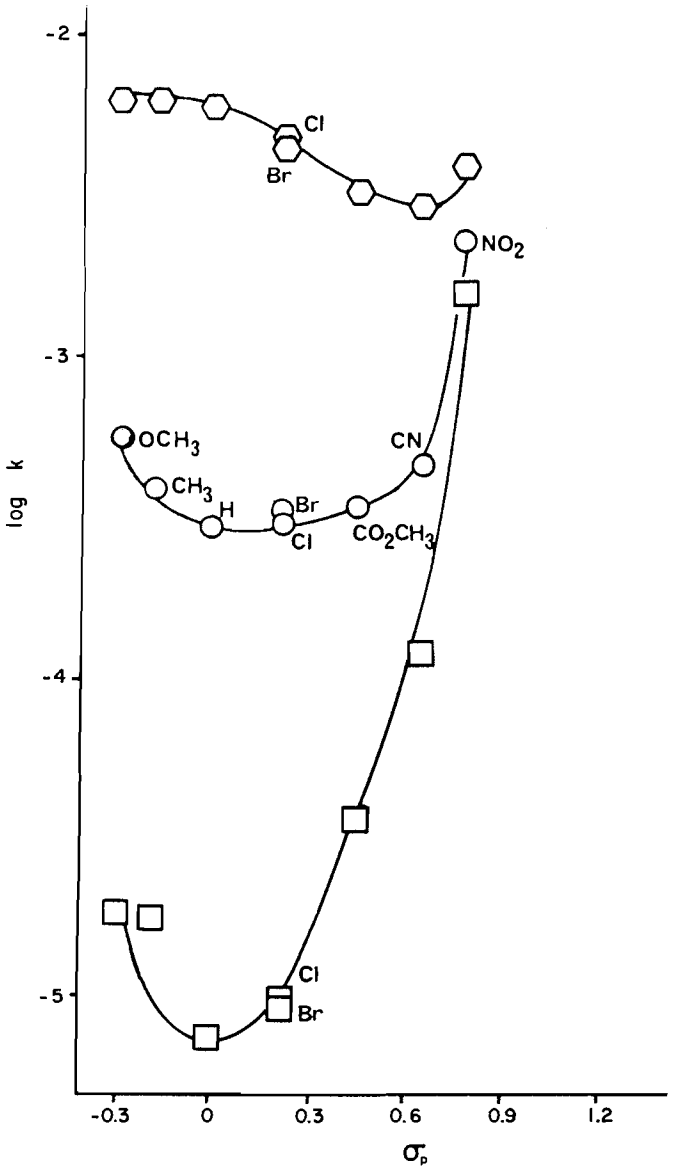

FIG. 7. Hammett plots for the hydrolysis of the aryloxy methyltriazenes (*2a–h*) at various pH values: -O-O- pH 2.0; -○-○- pH 3.3; -□-□- pH 5.5.

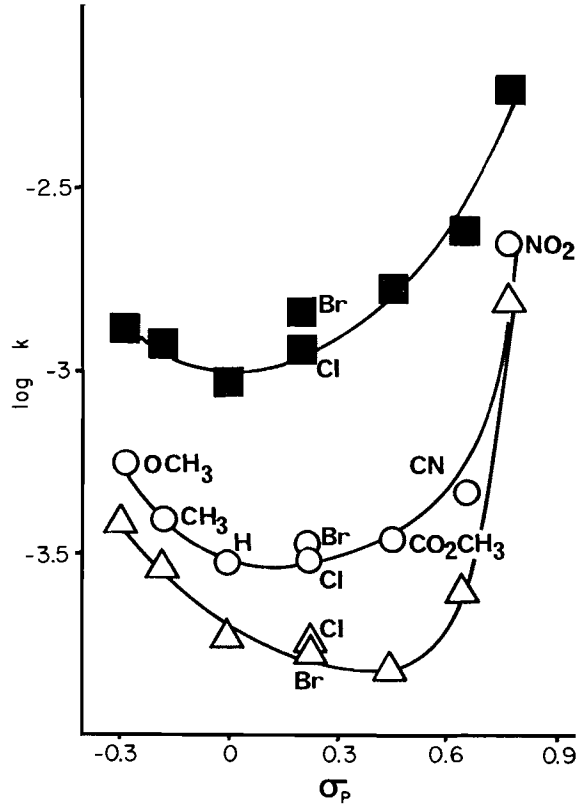

FIG. 8. Hammett plots for hydrolysis of aryloxymethyl triazenes (*2a–h*) at pH 3.3 with various buffer concentrations: -■-■- 0.33 M; -○-○- 0.066 M; -△-△- 0.0066 M.

the specific acid-catalyzed reaction has a negative value (see below), this observation is more consistent with a buffer anion catalyzed S_N2 displacement of the leaving group.

Using the k_B from the analysis above, the next step was to plot, for each substituent, the term $\{k_{obs} - k_B[B]\}$ versus $[H^+]$. The slope of this line gives the k_{H^+} for each substituent, and the intercept at $[H^+] = 0$ gives k_{sp}. The results are tabulated in Table 8, but it should be noted that these values represent an approximation due to the uncertainty in the pH value of the mixed solvent system and also because of the difficulty of relating one buffer system to another with respect to the k_B term in eq. [3].

The kinetic analysis in Table 8 is consistent with the three mechanisms shown in Fig. 9. The spontaneous rate constant turns out to be essentially zero for all but the nitro and cyano substituted compounds (**2***g* and **2***h*), which is consistent with a spontaneous dissociation mechanism, Fig. 9 (*i*), affording the iminium ion and the free phenolate ion. This

TABLE 8. Kinetic parameters calculated for the hydrolysis of 1-aryl-3-aryloxymethyl-3-methyltriazenes in aqueous buffer according to

$$k_{obs} = k_{Sp} + k_{H^+}[H^+] + k_B[B]$$

where [B] is defined as [HA] + [NaA]

Substituent	σ	$k_B{}^a \times 10^4$ (s^{-1} mol^{-1})	$k_{H^+}{}^b$ (s^{-1} mol^{-1})	$k_{Sp}{}^c \times 10^4$ (s^{-1})
OCH_3	−0.27	18.9	0.58	0.778
CH_3	−0.17	19.4	0.60	−1.11
H	0.00	15.7	0.60	−2.05
Cl	0.23	19.4	0.50	−1.57
Br	0.23	26.2	0.44	−0.911
CO_2CH_3	0.32	32.1	0.31	−0.279
CN	0.66	46.3	0.26	1.64
NO_2	0.78	70.9	0.18	19.6
ρ-values		+0.55	−0.49	+8.98

[a]From plot of k_{obs} vs. [B] extrapolated to [B] = 0 pH 3.3.
[b]Slope of plots of $k_{obs} - k_B[B]$ vs. $[H^+]$.
[c]Intercept of $k_{obs} - k_B[B]$ vs. $[H^+]$.

pathway is evidently facilitated by the presence of a strongly electron-withdrawing substituent (X), which improves the leaving group character of the aryloxy group beyond the apparent threshold for reactivity.

The Hammett plot of k_{H^+} versus σ_p gives a negative value, consistent with the proton-catalyzed mechanism, Fig. 9 (*ii*). Protonation of the ether oxygen precedes the dissociation step so that this pathway is favoured by an increase in electron

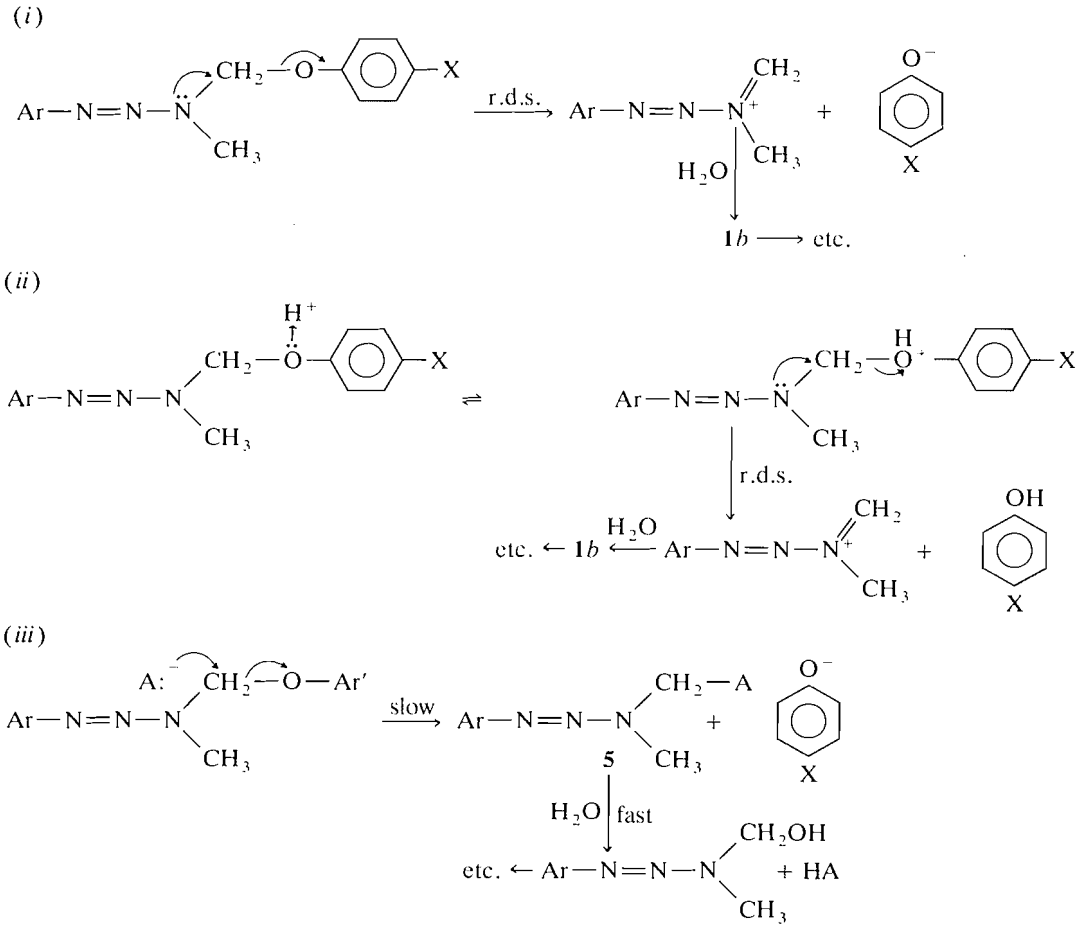

FIG. 9

density at the ether oxygen when an electron-releasing substituent is present at X.

The surprising result of this analysis is the positive ρ-value obtained from the Hammett plot for the buffer-catalyzed reaction. Significantly, the slope of this Hammett plot was still positive when we carried out the analysis using buffer acid concentration [HA] in place of [B] in eq. [4]. If the buffer catalysis was due to general acid catalysis by the buffer acid, HA, then the slope of the Hammett plot should be negative in the same manner as the specific acid catalysis. The positive ρ for the buffer-catalyzyed reaction is consistent with the nucleophilic catalysis mechanism, Fig. 9 (*iii*), in which the anion A^- causes a slow displacement of the aryloxy leaving group followed by fast displacement of A^- by water. When A^- is formate, the intermediate **5** is similar in structure to an acetoxymethyltriazene (**1***d*), which is known to hydrolyse rapidly in buffer solution (6).

If the hypothesis of Fig. 9 (*iii*) is correct, then there should be a similar or possibly better fit of the data to eq. [3] using the buffer anion concentration $[A^-]$ in place of total buffer concentration. The results of such an analysis are shown in Table 9; k_A replaces k_B. The results are essentially the same as those in Table 8; the slope of the specific acid-catalysis Hammett plot turns out to be more negative, indicating a greater sensitivity to the electronic character of X. Thus the analysis presented in Table 9 provides added support to the mechanistic hypothesis in Fig. 9. However, an alternative mechanism involving the displacement of ArOH by S_N2 attack of the buffer anion on the protonated substrate, i.e.,

TABLE 9. Kinetic parameters calculated for the hydrolysis of 1-aryl-3-aryloxymethyl-3-methyltriazenes in aqueous buffer according to:

$$k_{obs} = k_{Sp} + k_{H^+}[H^+] + k_A[A^-]$$

Substituent	σ	k_A[a] × 10^4 (s^{-1} mol^{-1})	k_{H^+}[b] (s^{-1} mol^{-1})	k_{Sp}[c] × 10^4 (s^{-1})
OCH_3	−0.27	0.49	0.56	0.478
CH_3	−0.17	0.50	0.56	−0.429
H	0.00	0.41	0.56	−0.768
Cl	0.23	0.50	0.47	−0.221
Br	0.23	0.68	0.38	−0.209
CO_2CH_3	0.32	0.83	0.23	1.362
CN	0.66	1.20	0.17	0.246
NO_2	0.78	1.83	0.06	14.830
ρ-values		+0.55	−0.82	—

[a]From plot of k_{obs} vs. $[A^-]$ extrapolated to $[A^-] = 0$ at pH 3.3.
[b]Slope of plots of $k_{obs} - k_A[A^-]$ vs. $[H^+]$.
[c]Intercept of $k_{obs} - k_A[A^-]$ vs. $[H^+]$.

Can. J. Chem. Downloaded from www.nrcresearchpress.com by 109.225.110.28 on 09/08/12
For personal use only.

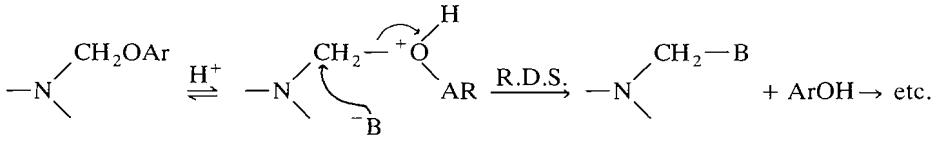

cannot entirely be ruled out.

To verify that there is specific acid catalysis in the hydrolysis of the aryloxymethyltriazenes, a solvent deuterium isotope experiment was performed with the *p*-bromophenyloxymethyltriazene (**2***e*). The rate of hydrolysis of **2***e* at pH 3.07 in buffer/D_2O (k_D) was compared with the rate of hydrolysis in buffer/H_2O (k_H) at 40°C, using nondeuterated isopropanol as the cosolvent. The observed ratio, k_H/k_D = 1.60, may only be an appparent value due to the possible exchange of deuterium with the solvent; the true value of k_H/k_D could be as high as 2.28. Nevertheless, it can be said categorically that there is a solvent deuterium isotope effect in the hydrolysis of **2***e* at pH 3.07, which supports the prior argument that the hydrolysis is subject to specific acid catalysis.

Conclusion

In conclusion, it is interesting to compare the results of this study with similar work of Iley *et al.* (10)[3] on the kinetics of hydrolysis of the 1-aryl-3-alkoxymethyl-3-methyl triazenes (**1***c*). These compounds hydrolyse in acidic solutions to give the corresponding anilines, and the kinetic study, over the pH range 1–5, showed that the reaction suffers specific acid catalysis. Apparently, the alkoxymethyltriazenes do not decompose spontaneously and do not react by an anion-catalyzed mechanism analogous to that shown in Fig. 9 (*iii*) for the aryloxymethyltriazenes. This behaviour is entirely consistent with the subtle, but significant, difference in structure between the alkoxy- and aryloxy-methyltriazenes, in particular with respect to the leaving group ability. Evidently, the methoxide ion, MeO^-, is not able to dissociate spontaneously, nor is it readily displaced by weak anions, whereas the aryloxide ion can suffer both types of reaction in addition to the specific acid-catalyzed reaction shared by both classes of compound.

Finally, is there any point in considering these aryloxy methyltriazenes as candidates for drug screening? The results reported in this paper clearly show that the stability of these compounds in aqueous media is exquisitely sensitive to the electronic character of the X substituent in the aryloxy moiety; the half-lives range from 1 min to several days! Thus, it is highly probably that a suitable aryloxymethyl triazene can be tailor-made with the perfect chemical stability and slow-release characteristics for use as a pro-drug. Preliminary investigations of the biological activity of these new compounds shows that some members of the series demonstrate stastically significant differential toxicity to several cell lines of the NCI tumour panel.

Acknowledgements

The authors wish to express their gratitude to the Natural Sciences and Engineering Research Council of Canada, to Dalhousie University Faculty of Graduate Studies, and to the Senate Research Committee of Saint Mary's University for financial support. We are also extremely grateful to Dr. Jim Iley of the Open University, Milton Keynes, U.K., for helpful discussions.

1. D. A. Clarke, R. K. Barklay, C. C. Stock, J. O'Loughlin, and P. Hagan. Proc. Soc. Exper. Biol. Med. **90**, 484 (1955).
2. V. S. Lucas, Jr. and A. T. Huang. Chemotherapy of melanoma. *In* Developments in oncology. Vol. 5. Clinical management of melanoma. *Edited by* H. F. Siegler. Martinus Nijhoff, The Hague, The Netherlands. 1982. p. 382; H. Breithaupt, A. Damman, and K. Aigner. Cancer Chemother. Pharmacol. **9**, 103 (1982).
3. C. J. Rutty, D. R. Newell, R. B. Vincent, G. Abel, P. M. Goddard, S. J. Harland, and A. H. Calvert. Br. J. Cancer, **48**, 140 (1983).
4. A. Gescher, J. A. Hickman, R. J. Simmonds, M. F. G. Stevens, and K. Vaughan. Tetrahedron Lett. 5041 (1978).
5. K. Vaughan, Y. Tang, G. Llanos, J. K. Horton, R. J. Simmonds, J. A. Hickman, and M. F. G. Stevens. J. Med. Chem. **27**, 357 (1984).
6. C. M. Hemens, H. W. Manning, K. Vaughan, R. J. LaFrance, and Y. Tang. Can. J. Chem. **62**, 741 (1984).
7. K. Vaughan, H. W. Manning, M. P. Merrin, and D. L. Hooper. Can. J. Chem. **66**, 2487 (1988).
8. M. P. Merrin, D. L. Hooper, R. J. LaFrance, R. Snooks, and K. Vaughan. Can. J. Chem. **70**, 144 (1992).
9. J. P. Boyer, R. J. P. Corrin, R. J. M. Perz, and C. G. Reye. Tetrahedron, **31**, 2075 (1975).
10. J. Iley, A. Nunes, and E. Rosa. Abstr. 11th Annu. Meet. Port. Soc. Chem., Lisbon, December, 1988. OR-P42.

[3]And personal communication with Jim Iley.

Can. J. Chem. Downloaded from www.nrcresearchpress.com by 109.225.110.28 on 09/08/12
For personal use only.

The acidity of polyhalogenated silanes and silyl radicals

C. F. RODRIQUEZ AND A. C. HOPKINSON[1]
Department of Chemistry, York University, North York, Ont., Canada M3J 1P3

Received January 13, 1992

C. F. RODRIQUEZ and A. C. HOPKINSON. Can. J. Chem. **70**, 2234 (1992).

The results of *ab initio* molecular orbital calculations at the MP4SDTQ/6-31++G(*d*,*p*)//HF/6-31++G(*d*,*p*) level have been used to calculate acidities of fluoro- and chloro-substituted silanes and silyl radicals. The radicals are more acidic than the silanes and substituent effects are also slightly larger in the radicals. For the gas phase deprotonation of fluorosilanes at 298 K, ΔH_r (kcal/mol) values are SiH_4, 378.5; SiH_3F, 374.5; SiH_2F_2 366.7, and $SiHF_3$, 351.0, i.e., interaction between fluorine atoms leads to increased enhancement of acidity. For chlorosilanes substituent effects are larger but strictly additive (13 kcal/mol for each Cl atom) with ΔH_r values SiH_3Cl, 365.4; SiH_2Cl_2 352.5, and $SiHCl_3$ 339.4. The electron affinities of silyl radicals calculated using isogyric reactions at the MP4SDTQ/6-31++G(*d*,*p*) level are too low by ~0.3 eV, but at the MP4SDTQ/6-311++G(*2df*,*p*) level the calculated electron affinity of SiH_3 is 1.39 eV, compared with an experimental value of 1.44 ± 0.03 eV. This higher level of theory gives calculated electron affinities of 1.53 eV for SiH_2F and 1.92 eV for SiH_2Cl. Heats of formation obtained by using isogyric reactions to calculate atomization energies at the MP4SDTQ/6-311++G(*2df*,*p*) level are within 3 kcal/mol of experimental values except for SiH_2F (where the "experimental" value was obtained from linear interpolation between SiH_3 and SiF_3). ΔH_f^0 (298 K) (kcal/mol) calculated for the anions are SiH_3^-, 14.4; SiH_2F^-, −78.0; and SiH_2Cl^-, −37.6.

C. F. RODRIQUEZ et A. C. HOPKINSON. Can. J. Chem. **70**, 2234 (1992).

On a utilisé les résultats de calculs d'orbitales moléculaires *ab initio* au niveau MP4SDTQ/6-31++G(*d*,*p*)//HF/6-31++G(*d*,*p*) pour calculer les acidités de silanes et de radicaux silyles substitués par un chlore ou un fluor. Les radicaux sont plus acides que les silanes et les effets des substituants sont aussi un peu plus prononcés dans les radicaux. Pour la déprotonation en phase gazeuse des fluorosilanes à 298 K, les valeurs du ΔH_r (kcal/mol) sont SiH_4, 378,5; SiH_3F, 374,5; SiH_2F_2, 366,7 et $SiHF_3$, 351,0 ce qui signifie que les interactions entres les atomes de fluor provoquent une plus grande augmentation de l'acidité. Pour les chlorosilanes, les effets des substituants sont plus importants, mais strictement additifs (13 kcal/mol pour chaque atome de Cl) avec des valeurs de ΔH_r de SiH_3Cl, 365,4; SiH_2Cl_2, 352,5 et $SiHCl_3$, 339,4. Les affinités électroniques des radicaux silyles calculées en faisant appel aux réactions isogyriques au niveau MP4SDTQ/6-31++G(*d*,*p*) sont trop basses par ~0,3 eV, mais au niveau MP4SDTQ/6-311++G(*2df*,*p*), l'affinité électronique calculée pour le SiH_3 est égale à 1,39 eV comparée à une valeur expérimentale de 1,44 ± 0,03 eV. Le niveau de théorie plus élevée conduit à des valeurs calculées pour les affinités électroniques de SiH_2F et de SiH_2Cl de 1,53 et 1,92 eV. Les chaleurs de formation obtenues en utilisant les réactions isogyriques pour calculer les énergies d'atomisation au niveau MP4SDTQ/6-311++G(*2df*,*p*) ne different que par 3 kcal/mol des valeurs expérimentales, à l'exception de SiH_2F (alors que la valeur «expérimentale» a été obtenue par interpolation linéaire entre le SiH_3 et le SiF_3). Les valeurs des ΔH_r^0 (298 K) (kcal/mol) calculées pour les anions sont SiH_3^-, 14,4; SiH_2F^-, −78,0 et SiH_2Cl^-, −37,6.

[Traduit par la rédaction]

Introduction

Electron-withdrawing substituents assist in delocalizing negative charge and are strongly stabilizing in carbanions (1–3). By contrast, substituent effects in methanes are relatively small and consequently electron-withdrawing substituents greatly enhance the acidity of methane. Silicon accommodates a negative charge more easily than carbon and silane is more acidic than methane (experimental acidities (4) are 376 and 417 kcal/mol respectively). Stabilization of the anion by substituents then is less of a factor in determining the acidity of silanes, and first-row substituents NH_2 and OH, which both enhance the acidity of methane, actually decrease the acidity of silane (5–7). A fluorine substituent also increases the acidity of methane, but its effect on the acidity of silane is less clear. Hartree–Fock calculations with (DZ + *d*) (5) and 6-31G** (6) basis sets have shown fluorine to increase the acidity of silane by small amounts while the most recent calculations (7), which include correlation energy, show a fluorine substituent to decrease the acidity. Second-row substituents SiH_3, PH_2, SH, and Cl are more polarizable than their first-row counterparts, and all greatly enhance the acidities of both methanes (3) and silanes (7).

Recently, there has been considerable interest in the geminal interactions between fluorine atoms (8) and between oxygen atoms (9). Negative hyperconjugation as illustrated for SiH_2F_2 (structure **1**) involves donation from the lone pair on one fluorine atom F_a to the σ* orbital of the other Si—F bond. The reciprocal interaction, donation from F_b to σ* for Si—F_a, makes an equivalent contribution. The stabilization resulting from these interactions can be estimated from eq. 1. Using this approach, Schleyer has shown the geminal interactions in SiH_2F_2 to be 7.7 kcal/mol and in $SiHF_3$ to be 17.5 kcal/mol (8)

[1] $$SiH_mF_n + (n-1)SiH_4 \rightarrow nSiH_3F$$

In anions, halogen substituents carry a large fraction of the excess negative charge and this enhances their ability to function as π-donors. Also, in anions the molecular orbitals are more weakly bound and, more importantly as regards negative hyperconjugation, the antibonding molecular orbitals are lower in energy and more available for the type of interaction outlined in structure **1**. Both conditions necessary for a strong negative hyperconjugative interaction, namely the presence of a powerful π-donor and a readily available σ* orbital, then are present in geminally substituted anions and the interaction is expected to be larger than in neutral molecules. Any such increased interaction should lead to an increased stabilization of the anions, which in turn

[1]Author to whom correspondence may be addressed.

Can. J. Chem. Downloaded from www.nrcresearchpress.com by 109.225.110.28 on 09/08/12
For personal use only.

Can. J. Chem. Downloaded from www.nrcresearchpress.com by 109.225.110.28 on 09/08/12
For personal use only.

should be reflected in an increase in acidity. The objective of this study, then, is to examine the synergistic effect, if any, of halogen substituents on the acidities of silanes and silyl radicals. We have used all possible combinations of fluorine and chlorine substituents. Our calculations on silyl radicals and silyl anions also permit us, in principle, to make estimates of the electron affinities of radicals. We report calculated electron affinities for several silyl radicals but for the larger radicals they must be considered to be lower estimates as accurate calculation of electron affinities requires extremely high levels of calculation (10–12), higher than is computationally feasible for the larger radicals studied here.

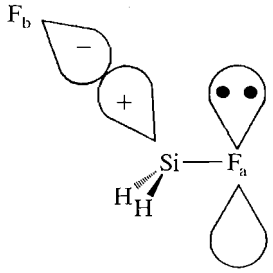

1

Theoretical details

Ab initio molecular orbital calculations were performed with GAUSSIAN 82 (13) and GAUSSIAN 86 (14). Molecular geometries were optimized at the HF/6-31++G(*d*,*p*) level (3, 15–17) employing analytical gradients (18, 19), and structural details, including some already published data on anions (20), are given in Table 1. Vibrational frequency calculations computed at HF/6-31++G(*d*,*p*) showed all the structures to be minima (i.e., no imaginary frequencies) and yielded the zero-point energies given in Table 2. Electron correlation energies were calculated by single-point calculations with frozen core Møller–Plesset perturbation theory (21, 22) including single, double, triple, and quadruple excitations. Electronic energies from three levels of theory, the HF optimization, MP2(full), and MP4SDTQ (frozen core), are given in Table 2. Electronic energies from MP4/6-311++G(2*df*,*p*) (23) calculations on some of the smaller molecules are given in Table 3.

We use the proton affinities of anions as a measure of the acidity of silanes and silyl radicals. The difference in electronic energies of SiH_mX_n and $SiH_{(m-1)}X_n^-$, when corrected for the difference in zero-point energies, gives ΔH(0 K) for the reaction in eq. [2]. Relatively small corrections, the last four terms in eq. [3], are then needed to calculate ΔH(298 K).

[2] $$SiH_mX_n \rightarrow SiH_{(m-1)}X_n^- + H^+$$

[3] $$\Delta H(298\text{ K}) = \Delta E^{elec} + \Delta E^{vib}_{zero\text{-}point} + \Delta E^{vib}_{0-298} + \Delta E^{rot}_{298} + \Delta E^{trans}_{298} + \Delta(PV)_{298}$$

ΔE^{vib}_{0-298} was obtained from standard statistical formulas (24), translational and rotational energies were calculated classically, and a pressure–volume term for the formation of two molecules from one, *RT*, was added. Values of ΔH(298 K) for reaction [2] are given in Table 4.

Calculation of electron affinities using eq. [4] presents a problem since the product silyl anion has one more pair of electrons than the reactants, i.e., there is a difference in correlation energy. Using eq. [4] with calculations in which correlation energy is omitted (i.e., HF level calculations) produces electron affinities that are too small (and often negative). Even medium-sized basis set calculations that include correlation energy often yield unacceptably low values of electron affinities (10, 11).

[4] $$SiH_mX_n^- \rightarrow SiH_mX_n + e$$

A better method, which minimizes problems due to correlation effects, is to use a reaction in which there is an equal number of unpaired electrons in both reactants and products. For silyl radicals the appropriate isogyric reaction is given in eq. [5].

[5] $$SiH_2X^- + 2H \rightarrow SiH_2X + H_2 + e$$

The electron affinity of the radical SiH_nX_m is obtained by first calculating ΔE^{elec} for eq. [5] using energies from *ab initio* molecular orbital calculations, then adding D_e, the dissociation energy of H_2 (0.17447 hartrees), to yield ΔE^{elec} for eq. [4]. Finally, correction for the difference in zero-point energies of SiH_nX_m and $SiH_nX_m^-$ gives the calculated electron affinity. Values obtained with various levels of theory are given in Table 6.

Results and discussion

Structures

The optimized geometries of the fluorosilanes (Table 1) are in excellent agreement with experimental values. Previously reported structural parameters for the fluorosilanes optimised at the Hartree–Fock level with the slightly smaller 6-31G(*d*) basis set are also in excellent agreement (25). Increasing the number of fluorine atoms results in a systematic shortening of the Si—F bond distances by ~0.016 Å per fluorine atom. This same trend, with approximately the same shortening, occurs in the silyl radicals and also in both series of fluorinated anions. Multiple substitution by chlorine atoms also leads to a shortening of Si—Cl bond distances and this is particularly pronounced in the anions (the distance in $SiCl_2^-$ is 0.044 Å shorter than in $SiHCl^-$). Similar systematic changes in the fluoromethanes have been rationalized in terms of electrostatic effects (8, 25–28). Following this argument, increasing the number of fluorine atoms increases the positive charge on the central silicon atom and decreases the covalent radius of the silicon, thereby making the Si—F bond shorter.

The geometries of the silyl anions and radicals in Table 1 differ very slightly from those reported in our previous work (20) because we have now included polarization functions on the hydrogen atoms. Comparison of the structures of Brønsted acid/base pairs show some major differences in geometries. Removal of a proton from silicon results in elongation of the remaining Si—H bonds by 0.06–0.07 Å. The Si—F bonds increase by 0.09 Å and Si—Cl by over 0.2 Å, with the largest change 0.224 Å, in the deprotonation of SiH_2Cl. The Si—Cl bond is weak, particularly in anions where there is a tendency to dissociate into SiH_n and Cl^-, and we were concerned that such ions were not adequately described at the HF/6-31++G(*d*,*p*) level. We therefore optimized SiH_2Cl^- at the MP2(full)/6-31++G(*d*,*p*) level and the result was a somewhat shortened Si—Cl bond (2.247 Å compared with 2.284 Å) but the Si—Cl distance was still 0.178 Å longer than in SiH_3Cl.

TABLE 1. Geometries as optimized at 6-31++G(*d*,*p*)[a,b]

Molecule	Point group	Si—F	Si—Cl	Si—H	HSiX	XSiX	XSiY	α[c]
SiH_4	T_d			1.476 (1.481)		109.5 (109.5)		
SiH_3F	C_{3v}	1.605 (1.593)		1.469 (1.468)	108.1 (108.5)	HSiH = 110.8 (110.4)		
SiH_2F_2	C_{2v}	1.589 (1.577)		1.460 (1.471)	HSiH = 114.5 (112.0)	FSiF = 107.3 (107.9)		
$SiHF_3$	C_{3v}	1.574 (1.562)		1.447 (1.447)	110.9 (110.6)	108.0 (108.3)		
SiH_3Cl	C_{3v}		2.069 (2.049)	1.468 (1.486)	108.2 (108.5)	HSiH = 110.8 (110.4)		
SiH_2Cl_2	C_{2v}		2.051 (2.033)	1.460 (1.480)	HSiH = 113.2 (111.3)	ClSiCl = 110.1 (109.7)		
$SiHCl_3$	C_{3v}		2.038 (2.012)	1.454 (1.465)	109.4 (108.3)	109.5 (110.6)		
SiH_2ClF	C_s	1.577	2.025	1.449	HSiF = 108.5	HSiCl = 108.9	HSiH = 113.7	
$SiHCl_2F$	C_s	1.581	2.031	1.453	HSiF = 109.7	HSiCl = 110.4	ClSiCl = 110.6	
$SiHClF_2$	C_s	1.577	2.025	1.449	HSiF = 110.2	HSiCl = 111.5	FSiF = 107.4	
SiH_3	C_{3v}			1.476		111.0		50.7
SiH_2F	C_s	1.609		1.474	108.2	111.6		56.3
$SiHF_2$	C_s	1.593		1.471	108.5	106.7		57.9
SiH_2Cl	C_s		2.071	1.472	108.6	111.5		55.1
$SiHCl_2$	C_s		2.057	1.468	108.4	110.4		56.3
SiHClF	C_1	1.596	2.054	1.470	HSiCl = 109.1	HSiF = 108.3	FSiCl = 108.0	
SiH_3^-	C_{3v}			1.536	96.7			79.8
SiH_2F^-[d]	C_s	1.700		1.541	98.1	HSiH = 94.5		78.0
$SiHF_2^-$	C_s	1.682		1.541	96.3	97.2		80.5
SiF_3^-	C_{3v}	1.668				96.5		80.3
SiH_2Cl^-[e]	C_s		2.284	1.525	95.2	HSiH = 94.7		81.7
$SiHCl_2^-$	C_s		2.242	1.513	93.5	99.7		84.6
$SiCl_3^-$	C_{3v}		2.210			100.5		77.9
$SiHClF^-$	C_1	1.672	2.276	1.529	HSiF = 96.5	HSiCl = 93.1	FSiCl = 97.5	
$SiCl_2F^-$	C_s	1.641	2.236			98.3	96.1	80.7
$SiClF_2^-$	C_s	1.655	2.277			96.6	96.1	80.8
SiH_2^-	C_{2v}			1.542		94.0		
$SiHF^-$	C_s	1.701		1.547		96.2		
SiF_2^-	C_{2v}	1.682				96.1		
$SiHCl^-$	C_s		2.295	1.531	93.3			
$SiCl_2^-$	C_{2v}		2.251			98.5		
$SiClF^-$	C_s	1.674	2.289				96.4	

[a]Distances in angstroms, angles in degrees.
[b]Experimental geometries are in parentheses. These were taken from ref. 4.
[c]The out-of-plane angle, α, in SiX_2Y is defined as the supplement of the angle between the SiY bond and the line bisecting the SiX_2 angle.
[d]Optimization at MP2/6-31++G(*d*,*p*) gave SiF 1.738; SiH 1.536; HSiH 94.3; FSiH 97.5; and α 78.9. The total energy was −389.84718 a.u., which is 0.3 kcal/mol better than obtained in the MP2(full)/6-31++G(*d*,*p*)//SCF/6-31++G(*d*,*p*) calculation.
[e]Optimization at MP2/6-31++G(*d*,*p*) gave SiCl 2.247; SiH 1.523; HSiH 94.4; ClSiH 95.6; and α 81.7. The total energy was −749.84843 a.u., which is 0.1 kcal/mol better than obtained in the MP2(full)/6-31++G(*d*,*p*)//SCF/6-31++G(*d*,*p*) calculation.

Bond distances in silylene anions, $SiHX^-$, are considerably longer than in silyl radicals, SiH_2X, and also are slightly longer than in the silyl anions. The parent silylene anion, SiH_2^-, has a bond angle of 94.0°, close to the angle of 93.3° calculated for SiH_2 (29, 30). These structures are consistent with the lone pair on silicon being essentially in the 3*s* atomic orbital with only the 3*p* orbitals being involved in bonding. The halide-substituted silylene anions have slightly larger bond angles, with the largest being 98.5° in $SiCl_2^-$.

Acidities

As outlined above, we use ΔH_r for the loss of a proton (eq. [2]) to assess acidities. A low ΔH_r value indicates a high acidity and, applying this criterion to the data in Table 4, $SiHCl_2$ is the most acidic molecule and SiH_4 is the least.

Equation [2] contains the same number of electron pairs in both the reactant molecule and the product ions and the calculated ΔH_r is therefore expected to show little dependence on correlation energy. Inclusion of correlation energy at the MP2(full) and more extensive MP4SDTQ levels results in the same relative order of acidities with the MP4 calculations always giving the lower ΔH_r values, but the difference in calculated ΔH_r values for any molecule is never greater than 1.4 kcal/mol. However, comparison of the SCF and Møller–Plesset results in Table 4 reveal some systematic variations. For the fluorosilanes, comparing the calculated ΔH_r at the SCF level with the MP4 values, there is an incremental decrease of about 2.8 kcal/mol per fluorine atom. For the chlorosilanes the inclusion of correlation energy has the opposite effect and the calculated ΔH_r increases by 1–2 kcal/mol.

Inspection of Table 4 reveals several trends. The parent silyl radical is more acidic than silane ($\Delta\Delta H_r$ is 14.9 kcal/mol), and substituent effects are larger in the radicals. In the 6-31++G(*d*,*p*) calculations, fluorosilane is more acidic than silane, as in earlier relatively low-level calculations, but with the larger 6-311++G(2*df*,*p*) basis set both molecules have essentially the same acidity. Chlorine is a larger, more polarizable atom than fluorine and, as in methane (3, 31), it enhances the acidity of silane. Further chlorine substituents

Can. J. Chem. Downloaded from www.nrcresearchpress.com by 109.225.110.28 on 09/08/12
For personal use only.

TABLE 2. Total energies (hartrees) at HF/6-31++G(d,p) geometries

Silicon	SCF	MP2(full)	MP4SDTQ	ZPE[a]	THERMAL
Neutrals					
SiH_4	−291.23203	−291.35309	−291.36780	18.6	1.9
SiH_3F	−390.15974	−390.45372	−390.46479	16.4	2.0
SiH_2F_2	−489.09552	−489.56282	−489.57005	13.7	2.2
$SiHF_3$	−588.03348	−588.67359	−588.67673	10.7	2.6
SiH_3Cl	−750.18902	−750.43951	−750.45318	15.7	2.1
SiH_2Cl_2	−1209.14513	−1209.52836	−1209.54095	12.3	2.5
$SiHCl_3$	−1668.09874	−1668.61756	−1668.62904	8.5	3.2
SiH_2ClF	−849.11969	−849.54532	−849.55546	13.0	2.4
$SiHCl_2F$	−1308.07622	−1308.63633	−1308.64551	9.3	3.0
$SiHClF_2$	−948.05445	−948.65478	−948.66121	10.0	2.8
SiH_3	−290.61171	−290.71165	−290.72295	12.7	1.9
SiH_2F	−389.53492	−389.80839	−389.81615	10.5	1.9
$SiHF_2$	−488.46687	−488.91409	−488.91795	7.9	2.2
SiH_2Cl	−749.56759	−749.79749	−749.80800	10.0	2.0
$SiHCl_2$	−1208.52317	−1208.88607	−1208.89572	6.7	2.5
SiHClF	−848.49427	−848.89961	−848.90659	7.3	2.3
Anions					
SiH_3^-	−290.61959	−290.74075	−290.75548	11.5	1.8
SiH_2F^-	−389.54947	−389.84666	−389.85898	9.3	2.0
$SiHF_2^-$	−488.49373	−488.96788	−488.97715	6.9	2.2
SiF_3^-	−587.45258	−588.10404	−588.10933	4.2	2.6
SiH_2Cl^-	−749.60020	−749.84824	−749.86262	9.0	2.1
$SiHCl_2^-$	−1208.57913	−1208.95813	−1208.97183	6.0	2.7
$SiCl_3^-$	−1667.55501	−1668.06920	−1668.08193	2.2	3.5
$SiHClF^-$	−848.53742	−848.96359	−848.97525	6.4	2.5
$SiCl_2F^-$	−1307.52294	−1308.08233	−1308.09304	2.8	3.2
$SiClF_2^-$	−947.48930	−948.09394	−948.10217	3.5	3.0
SiH_2^-	−290.02445	−290.12408	−290.13557	6.3	1.8
$SiHF^-$	−388.95434	−389.23122	−389.24044	4.5	1.9
SiF_2^-	−487.89947	−488.35427	−488.36055	2.2	2.2
$SiHCl^-$	−749.00627	−749.23292	−749.24412	4.0	2.1
$SiCl_2^-$	−1207.98720	−1208.34498	−1208.35554	1.2	2.6
$SiClF^-$	−847.94412	−848.34987	−848.35843	1.7	1.9

[a]Zero-point energies scaled by a factor of 0.89.

TABLE 3. Total energies (hartrees) from single-point calculations with the 6-311++G(2*df*,*p*) basis set

	SCF	MP2(valence)	MP4SDTQ
SiH_4	−291.25808	−291.38930	−291.42225
SiH_3F	−390.21943	−390.59242	−390.62619
SiH_3	−290.63733	−290.74464	−290.77291
SiH_2F	−389.59416	−389.94363	−389.97264
SiH_2Cl	−749.62705	−749.90873	−749.95370
SiH_3^-	−290.64308	−290.78252	−290.81576
SiH_2F^-	−389.60367	−389.98544	−390.02042
SiH_2Cl^-	−749.65362	−749.96615	−750.01615

have the systematic effect of increasing the acidity by ~13 kcal/mol per chlorine, i.e., the effect of chlorine substituents is roughly additive. The same trend occurs in the chlorosilyl radicals. With fluorosilanes and fluorosilyl radicals the situation is dramatically different. With the 6-31++G(*d*,*p*) basis set, monofluorosilane is only slightly more acidic than silane (the difference in ΔH_r is 4.0 kcal/mol), a second fluorine substituent increases the acidity by another 7.8 kcal/mol, and a third fluorine results in a further increase of 15.7 kcal/mol. The same trend, slightly more pronounced, occurs in the fluoro-substituted silyl radicals. These results then clearly demonstrate that fluorine–fluorine interactions have a synergistic effect on the acidity of silanes, but that similar interactions in chlorosilanes do not.

We have used eq. [1] to calculate the stabilization energies resulting from interaction between halogen atoms. The results in Table 5 show modest stabilization in the fluorosilanes, slightly smaller but comparable with values previously reported (8). In the fluorine-substituted silyl anions the stabilization is much larger and this difference in stabilization between an acid and its conjugate base is the origin of the increased acidity. For the deprotonation of fluorosilanes then, the decrease in ΔH_r consists of an increment of ~4 kcal/mol per fluorine atom, attributable to the ability of fluorine to accommodate negative charge by σ-withdrawal, plus a contribution from the increased hyperconjugation in the anion relative to the fluorosilane. For example, $\Delta\Delta H_r$, the difference in acidities between difluorosilane and silane, consists of a term (2 × 4 = 8 kcal/mol) for the inductive stabilization by the two fluorine atoms and a term (4 kcal/mol) for

Can. J. Chem. Downloaded from www.nrcresearchpress.com by 109.225.110.28 on 09/08/12
For personal use only.

TABLE 4. ΔH_r (298) for the reaction $SiH_mX_n \rightarrow SiH_{(m-1)}X_n^- + H^+$[a]

SiH_mX_n	SCF	MP2(full)	MP4SDTQ	Expt.[b]
6-31++G(*d*,*p*)				
SiH_4	378.6	378.5	378.5	372.4
SiH_3F	377.3	375.3	374.5	
SiH_2F_2	372.3	368.0	366.7	
$SiHF_3$	359.3	352.4	351.0	346.0
SiH_3Cl	364.3	366.8	365.4	
SiH_2Cl_2	350.5	353.2	352.5	
$SiHCl_3$	337.3	340.2	339.4	
$SiHCl_2F$	342.4	342.8	341.9	
$SiHClF_2$	349.8	347.1	346.0	
SiH_3	363.5	363.7	363.6	
SiH_2F	359.8	357.7	356.7	
$SiHF_2$	351.8	347.1	345.8	
SiH_2Cl	347.8	349.8	349.4	
$SiHCl_2$	332.4	335.6	335.0	
SiHClF	340.7	340.4	339.5	
6-311++G(2*df*,*p*)				
SiH_4	380.2	(375.0)[c]	374.9	372.4
SiH_3F	380.8	(375.3)[c]	374.5	

[a]Energies in kcal/mol.
[b]JANAF Thermochemical Tables, Third Edition, Vol 14. 1985, Supplement No. 1.
[c]Values in parentheses are at MP2 (valence) level.

TABLE 5. Stabilization energies[a,b] as calculated using eq. [1]

Species	SCF	MP2(full)	MP4SDTQ	Literature
SiH_2F_2	5.1	5.3	5.2	7.8,[c] 6.4[d]
$SiHF_3$	11.5	11.7	11.3	17.5,[c] 14.7[d]
$SiHF_2$	5.5	5.6	5.4	
SiH_2Cl_2	−0.6	1.5	1.5	
$SiHCl_3$	3.3	3.3	3.2	
$SiHCl_2$	−0.2	1.7	1.7	
$SiHF_2^-$	9.0	9.6	9.2	
SiF_3^-	27.2	28.6	25.5	
SiF_2^-	9.6	10.0	9.6	
$SiHCl_2^-$	−1.1	1.5	1.3	
$SiCl_3^-$	−4.0	3.8	3.1	
$SiCl_2^-$	−0.6	2.0	1.8	

[a]Energies are in kcal/mol.
[b]Differences in electronic energies, i.e., not corrected for zero point and thermal energies.
[c]From MP2 (valence)/6-31G(*d*) calculations in ref. 8.
[d]Reference 40.

the difference in hyperconjugative stabilization of $SiHF_2^-$ (9.2 kcal/mol) and SiH_2F_2(5.25 kcal/mol). $\Delta\Delta H_r$ calculated by this method is 12.0 kcal/mol, and this compares with a value of 11.8 kcal/mol from Table 4. A similar calculation for $SiHF_3$ gives $\Delta\Delta H_r = (3 \times 4) + 14.2 = 26.2$ kcal/mol and this compares with a value of 27.5 kcal/mol from Table 4.[2]

There is little or no geminal interaction between chlorine atoms in both neutral molecules and in the anions (Table 5). One chlorine atom increases the acidity of silane by 13.0 kcal/mol and, in the absence of contributions from negative hyperconjugation, the effect of additional chlorine atoms is for each to increase the acidity by a further 13 kcal/mol. The silyl radicals are slightly more sensitive to substituent effects but here again there are negligible contributions from negative hyperconjugation and each chlorine atom increases the acidity by ~14.0 kcal/mol.

[2]Note the energies in Tables 4 and 5 are not strictly comparable. Table 4 contains ΔH_r values at 298 K and Table 5 contains ΔE^{elec}.

TABLE 6. Electron affinities[a]

Silyl radical	Using $SiH_mX_n^- \rightarrow SiH_mX_n + e$ SCF	MP4	Using $SiH_2X^- + 2H \rightarrow SiH_2X + H_2 + e$[b] SCF	MP4	Experimental[c]
(*a*) 6-31++G(*d*,*p*)					
SiH_3	0.27	0.94	1.34	1.11	1.44 ± 0.03
SiH_2F	0.45	1.22	1.52	1.39	
SiH_2Cl	0.93	1.53	2.01	1.70	
$SiHF_2$	0.77	1.65	1.85	1.82	
$SiHCl_2$	1.55	2.10	2.63	2.27	
SiHClF	1.21	1.91	2.29	2.08	
(*b*) 6-311++G(2*df*,*p*)					
SiH_3	0.21	1.22	1.34	1.39	1.44 ± 0.03
SiH_2F	0.31	1.35	1.44	1.53	
SiH_2Cl	0.77	1.74	1.90	1.92	

[a]Energies in eV.
[b]Electronic energies (in a.u.) for H at 6-31++*G*(*d*,*p*) −0.49823 and at 6-311++*G*(2*df*,*p*) −0.49981; for H_2 at HF/6-31++*G*(*d*,*p*) −1.13140, at MP4/6-31++G(*d*,*p*) −1.16468, at HF/6-311++G(2*df*,*p*) −1.13250, and at MP4/6-311++G(2*df*,*p*) −1.16772.
[c]Reference 32.

Electron affinities

We have calculated electron affinities by both the direct method in eq. [4] and by the more accurate isogyric reaction in eq. [5]. The results are in Table 6. Electron affinities at the SCF level using eq. [4] are the lowest and least reliable due to the neglect of correlation energy in a reaction where the number of electron pairs in the reactant and products differ. Comparison of electron affinities from the MP4 calculations shows the isogyric reaction to consistently give higher calculated values. Unfortunately there is only one experimental value for comparison, but our largest calculation (MP4/6-311++G(2*df*,*p*) on SiH_3 gives a calculated electron affinity of 1.39 eV, within 0.05 eV of the experimental value of 1.44 ± 0.03 eV (32) and within 0.03 eV of Pople's G2 level calculation of 1.42 eV (33). Previous work (12) has shown that molecular orbital calculations at this level consistently give electron affinities within 0.1 eV of the experimental values. We are therefore confident that the calculated electron affinities of 1.53 eV for SiH_2F and of 1.92 eV for SiH_2Cl should be accurate within 0.1 eV.

The MP4/6-31++G(*d*,*p*) calculations using the isogyric reaction clearly underestimate the electron affinities, probably by 0.2–0.3 eV. For the disubstituted radicals it was not computationally feasible to use a higher level of theory and the calculated electron affinities of 1.82 eV for $SiHF_2$, 2.27 eV for $SiHCl_2$, and 2.08 eV for SiHClF should be taken

Can. J. Chem. Downloaded from www.nrcresearchpress.com by 109.225.110.28 on 09/08/12
For personal use only.

TABLE 7. Heats of formation (kcal/mol) calculated from isogyric reactions at MP4SDTQ/6-311++G(2*df*,*p*)

Molecule	ΔH_f^0 (0 K)	ΔH_f^0 (298 K)	Previous calculations	Experimental[a,b]
SiH_4	7.6	5.3	6.3,[c] 6.3[d]	8.2 ± 0.5
SiH_3F	−84.4	−86.7	−85.8,[c] −85.6,[e] −85.5[j]	−90 ± 5.0
SiH_3	47.9	46.6	47.3,[d] 47.7,[c] 47.4[j]	46.6 ± 1.5,[f] 48.5 ± 1.6[g]
SiH_2F	−41.5	−42.8	−44.9,[c] −42.2[j]	−49 ± 5[h]
SiH_2Cl	7.8	6.5	7.8[i]	
SiH_3^-	15.8	14.4		15.1 ± 2.4
SiH_2F^-	−76.7	−77.9		
SiH_2Cl^-	−36.4	−37.6		

[a] ΔH_f^0 (298 K).
[b] Unless otherwise noted, experimental values taken from JANAF Thermochemical Tables, Third Edition, Vol. 14, 1985. Supplement No. 1.
[c] Reference 35*b*.
[d] Reference 29.
[e] Reference 40.
[f] Reference 41.
[g] Reference 42.
[h] Obtained by linear interpolation, JANAF Thermochemical Tables (footnote *b* above).
[i] Reference 38.
[j] Reference 37.

only as lower estimates, with the correct electron affinity probably being about 0.3 eV higher.

Heats of formation

Recently *ab initio* molecular orbital calculations were used to calculate heats of formation of SiH_n (29, 34–36), SiH_nF_m (35, 37), and SiH_nCl_m (38). When large basis sets are used, and correlation energy is calculated at the MP4 level it is possible to calculate ΔH_f^0(298 K) to at least within 3 kcal/mol (38). Two approaches have been used, one including experimental heats of formation for SiH_n and SiF_4 in isodesmic reactions (35), and the other calculating heats of atomization. We have used the latter procedure with our MP4SDTQ/6-311++G(2*df*,*p*) calculations to obtain the ΔH_f^0 values in Table 7.

We illustrate our method, essentially that introduced by Pople *et al.* (29, 34), by using the example of SiH_2Cl^-. Our initial objective was to obtain ΣD_0, the heat of atomization, for the reaction in eq. [6].

[6] $SiH_2Cl^- \rightarrow Si + 2H + Cl^-$

This reaction is not isogyric and, in an attempt to minimize the difference in correlation energy, we calculated the ΔE^{elec} for eq. [7] and then used a correction of 0.17447 a.u. per hydrogen molecule to obtain ΣD_e = 201.8 kcal/mol for eq. [6].

[7] $4H + SiH_2Cl^- \rightarrow Si + 2H + Cl^- + 2H_2$

Subtraction of the zero-point energy of SiH_2Cl^- gave ΣD_0 = 192.8 kcal/mol. Addition of the electron affinity of chlorine (calculated to be 82.1 kcal/mol at MP4SDTQ/6-311++G(2*df*,*p*)) gave ΣD_0 for eq. [8] to be 274.9 kcal/mol.

[8] $SiH_2Cl^- \rightarrow Si + 2H + Cl + e$

From standard thermochemical tables (39) $\Sigma\Delta H_f^0$ (0 K) for the product atoms in eq. [8] is 238.5 kcal/mol and, combining this with ΣD_0, gives ΔH_f^0 (0 K) = −36.4 kcal/mol. Using standard heat capacities for Si(c), H_2(g), and Cl_2(g) (39) and calculated thermal energy and work terms for SiH_2Cl^- to correct to 298 K gives ΔH_f^0 (298 K) = −37.6 kcal/mol.

For the limited number of molecules for which experimental heats of formation are available, the theoretical ΔH_f^0 (298 K) in Table 7 are mainly within 3 kcal/mol. The one exception is SiH_2F and in this instance the "experimental" value was obtained by interpolation between experimental values for SiH_3 and SiF_3. The other theoretical ΔH_f^0 (298 K) for SiH_2F in the literature (35) is close to our value and, noting that agreement between experiment and theory at this level is usually within 3 kcal/mol, we conclude that the "experimental" value is probably in error by about 4 kcal/mol.

Conclusions

Substitution of one fluorine into silane has little effect on the acidity but when a second is introduced negative hyperconjugation between the two fluorine atoms stabilizes the anion more than the silane and the energy for deprotonation decreases. A third fluorine substituent results in even greater stabilization by negative hyperconjugation and a much larger increase in acidity. By contrast, one chlorine atom enhances the acidity of silane by ~13 kcal/mol, but negative hyperconjugation between chlorine atoms is insignificant and further substitution results in incremental increases of ~13 kcal/mol for each additional chlorine atom. Silyl radicals are more acidic than silanes, but the same trends in substituent effects occur.

To calculate electron affinities it is essential to include correlation energy and from the limited data here it is obvious that a larger basis set than 6-31++G(*d*,*p*) is required. Extensive calculations at MP4SDTQ/6-311++G(2*df*,*p*) have been shown to consistently give electron affinities within 0.1 eV of experimental values and our calculated value for SiH_3 is within this limit (0.05 eV below the experimental value). We therefore believe the calculated electron affinities of SiH_2F (1.53 eV) and of SiH_2Cl(1.92 eV) should be reliable.

Can. J. Chem. Downloaded from www.nrcresearchpress.com by 109.225.110.28 on 09/08/12
For personal use only.

Heats of formation can be calculated within ±3 kcal/mol of experimental values only if very high levels of theory are used. From our MP4SDTQ/6-311++G(2*df*,*p*) calculations we find good agreement both with previous theoretical and experimental ΔH_f^0 (298 K) values. For SiH_2F the "experimental" ΔH_f^0 (298 K) of −49 ± 5 kcal/mol is lower than both the previous (−44.9 kcal/mol) and our (−42.8 kcal/mol) theoretical values. We therefore suggest that the "experimental" value is too low by about 5 kcal/mol.

Acknowledgement

We thank the Natural Sciences and Engineering Research Council of Canada for continued financial support, and Steve Quan for technical assistance.

1. A. C. Hopkinson and M. H. Lien. Int. J. Quantum Chem. **18**, 1371 (1980).
2. A. Pross, D. J. DeFrees, B. A. Levi, S. K. Pollack, L. Radom, and W. J. Hehre. J. Org. Chem. **46**, 1693 (1981).
3. G. W. Spitznagel, T. Clark, J. Chandrasekhar, and P. v. R. Schleyer. J. Comput. Chem. **3**, 363 (1982).
4. S. G. Lias, J. E. Bartmess, J. F. Liebman, R. D. Levin, and W. G. Mallard. J. Phys. Chem. Ref. Data, Supplement 1 (1988).
5. A. C. Hopkinson and M. H. Lien. Tetrahedron, **37**, 1105 (1981).
6. E. Magnusson. Tetrahedron, **41**, 2945 (1985).
7. M. S. Gordon, D. E. Volk, and D. R. Gano. J. Am. Chem. Soc. **111**, 9273 (1989).
8. A. E. Reed and P. v. R. Schleyer. J. Am. Chem. Soc. **109**, 7362 (1987).
9. A. E. Reed, C. Schade, P. v. R. Schleyer, P. V. Kamath, and J. Chandrasekhar. J. Chem. Soc. Chem. Commun. **67**, (1988).
10. D. J. De Frees and A. D. McLean. J. Comput. Chem. **7**, 321 (1986).
11. J. Baker, R. H. Nobes, and L. Radom. J. Comput. Chem. **7**, 349 (1986).
12. J. A. Pople, P. v. R. Schleyer, J. Kaneti, and G. W. Spitznagel. Chem. Phys. Lett. **145**, 359 (1988).
13. J. S. Binkley, M. J. Frisch, D. J. DeFrees, K. Raghavachari, R. A. Whiteside, H. B. Schlegel, E. M. Fluder, and J. A. Pople. GAUSSIAN 82, Carnegie-Mellon University, Pittsburgh, Pa. 1982.
14. M. J. Frisch, J. S. Binkley, H. B. Schlegel, K. Raghavachari, C. F. Melius, R. L. Martin, J. J. P. Stewart, F. W. Bobrowicz, C. M. Rohlfing, L. R. Kahn, D. J. DeFrees, R. Seeger, R. A. Whiteside, D. J. Fox, E. M. Fluder, and J. A. Pople. GAUSSIAN 86, Carnegie-Mellon University, Quantum Chemistry Publishing Unit, Pittsburgh, Pa. 1984.
15. P. C. Hariharan and J. A. Pople. Theor. Chem. Acta, **28**, 213 (1973).
16. M. J. Frisch, J. A. Pople, and J. S. Binkley. J. Chem. Phys. **80**, 3265 (1984).
17. J. Chandrasekhar, J. G. Andrade, and P. v. R. Schleyer. J. Am. Chem. Soc. **103**, 5609 (1981).
18. P. Pulay. Mol. Phys. **17**, 197 (1969).
19. (*a*) H. B. Schlegel, S. Wolfe, and F. Bernardi. J. Chem. Phys. **63**, 3632 (1975), (*b*) H. B. Schlegel. J. Comput. Chem. **3**, 214 (1982).
20. A. C. Hopkinson, C. F. Rodriquez, and M. H. Lien. Can. J. Chem. **68**, 1309 (1990).
21. C. Møller and M. S. Plesset. Phys. Rev. **46**, 618 (1934).
22. J. A. Pople, J. S. Binkley, and R. Seeger. Int. J. Quantum Chem. Symp. **10**, 1, (1976).
23. R. Krishnan, J. S. Binkley, R. Seeger, and J. A. Pople. J. Chem. Phys. **72**, 650 (1980).
24. K. S. Pitzer. Quantum chemistry. Prentice Hall, Englewood Cliffs, N. J. 1961.
25. H. B. Schlegel. J. Phys. Chem. **88**, 6255 (1984).
26. H. A. Bent. Chem. Rev. **61**, 275 (1961).
27. D. Peters. J. Chem. Phys. **38**, 561 (1963).
28. E. Shustorovich. J. Am. Chem. Soc. **100**, 7513 (1978).
29. J. A. Pople, B. T. Luke, M. J. Frisch, and J. S. Binkley. J. Phys. Chem. **89**, 2198 (1985).
30. A. C. Hopkinson and M. H. Lien. Can. J. Chem. **67**, 991 (1989).
31. W. J. Hehre, L. Radom, P. v. R. Schleyer, and J. A. Pople. *Ab initio* molecular orbital theory. Wiley–Interscience, New York. 1985.
32. R. D. Mead, A. E. Stevens, and W. C. Lineberger. *In* Gas phase ion chemistry. Vol. 3. *Edited by* M. T. Bowers. Academic Press, New York. 1984 Chap. 22. p. 213.
33. L. A. Curtis, K. Raghavachari, G. W. Trucks, and J. A. Pople. J. Chem. Phys. **94**, 7221 (1991).
34. L. A. Curtiss and J. A. Pople. Chem. Phys. Lett. **144**, 38 (1988).
35. (*a*) H. B. Schlegel. J. Phys. Chem. **88**, 6254 (1984); (*b*) I. W. Ignacio and H. B. Schlegel. J. Chem. Phys. **92**, 5404 (1990).
36. A. F. Sax and J. Kalcher. J. Phys. Chem. **95**, 1768 (1991).
37. P. Ho and C. F. Melius. J. Phys. Chem. **94**, 5120 (1990).
38. P. Ho, M. E. Coltrin, J. S. Binkley, and C. F. Melius. J. Phys. Chem. **89**, 4647 (1985).
39. Report of the CODATA task group. J. Chem. Thermodyn. **10**, 903 (1978).
40. D. A. Dixon. J. Phys. Chem. **92**, 86 (1988).
41. A. M. Doncaster and R. Walsh. Int. J. Chem. Kinet. **13**, 503 (1981).
42. B. H. Boo and P. B. Armentrout. J. Am. Chem. Soc. **109**, 3549 (1987).

Can. J. Chem. Downloaded from www.nrcresearchpress.com by 109.225.110.28 on 09/08/12
For personal use only.

Synthesis of a series of 3-aryl-1-methyltriazene 1-oxides with substituents in the *ortho* or *para* position in the aryl group

LYNN M. CAMERON AND KEITH VAUGHAN[1]
Department of Chemistry, Saint Mary's University, Halifax, N. S., Canada B3H 4J3

AND

DONALD L. HOOPER
Dalhousie University, Halifax, N. S., Canada B3H 4J3

Received January 2, 1992

LYNN M. CAMERON, KEITH VAUGHAN, and DONALD L. HOOPER. Can. J. Chem. **70**, 2241 (1992).

A series of 3-aryl-1-methyltriazene 1-oxides, with a variety of substituents in the *ortho* or *para* position, have been prepared by coupling of the appropriate diazonium salt with *N*-methylhydroxylamine. The substituents range from electron withdrawing, i.e., CO_2Et, NO_2, CN, $COCH_3$, Br, and CF_3, to electron releasing, i.e., OCH_3. In all cases studied, the triazenes exist as the 1-oxide tautomer; there is no evidence for the presence of a 3-hydroxy tautomer in any of these cases. The 1-oxide structures have been confirmed by IR and NMR spectroscopy and by elemental analysis of new compounds. In the case of the -CO_2Et and -CN substituents, a significant change to lower frequency is seen in the N—H vibration frequency in the IR spectra when the substituent is moved from the *para* to the *ortho* position. This change can be readily explained by the presence of intramolecular H-bonding, which is confirmed by the NMR spectra. The presence of an ortho substituent with H-bonding potential (i.e., CO_2Et, -$COCH_3$, or NO_2) causes a downfield shift of the N—H proton resonance.

LYNN M. CAMERON, KEITH VAUGHAN et DONALD L. HOOPER. Can. J. Chem. **70**, 2241 (1992).

Utilisant le couplage d'un sel de diazonium approprié avec la *N*-méthylhydroxylamine, on a préparé une série de 1-oxydes de 3-aryl-1-méthyltriazènes portant divers substituants dans les positions *ortho* et *para*. Les substituants comportent des groupes électro-attracteurs comme CO_2Et, NO_2, CN, $COCH_3$, Br et CF_3 et des groupes électro-donneurs comme OCH_3. Dans tous les cas étudiés, les triazènes existent sous la forme du tautomère 1-oxyde; dans aucun de ces cas, on n'a pu mettre en évidence la présence du tautomère 3-hydroxy. Les structures 1-oxydes ont été confirmées par les spectroscopies IR et RMN et par des analyses élémentaires des nouveaux composés. Dans le cas des composés portant les substituants -CO_2Et et -CN, on observe un déplacement important de la fréquence de vibration du N—H dans l'IR lorsqu'on déplace le substituant de la position *para* vers la position *ortho*. On peut facilement expliquer ce changement par la présence de liaisons hydrogènes intramoléculaires que l'on a pu confirmer par les spectres RMN. La présence d'un substituant en *ortho* pouvant former une liaison hydrogène (comme -CO_2Et, -$COCH_3$ ou NO_2) provoque un déplacement de la résonance du proton du N—H vers les bas champs.

[Traduit par la rédaction]

Can. J. Chem. Downloaded from www.nrcresearchpress.com by 109.225.110.28 on 09/08/12
For personal use only.

Introduction

3-Aryl-1-alkyltriazene 1-oxides (**I***a*) are commonly synthesized by the reaction of an aryldiazonium salt with *N*-methylhydroxylamine (1) and were originally described as 1-aryl-3-hydroxy-3-methyltriazenes (**I***b*).

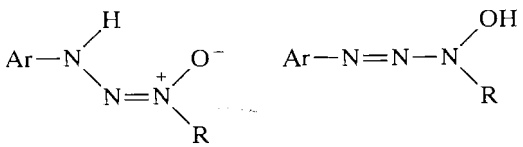

I*a*

I*b*

Spectroscopic studies using IR (2) and NMR (3) data suggested that the structure was better described as the 1-oxide (**I***a*), which has been confirmed by the X-ray crystallographic analysis of 3-(4-carbamoylphenyl)-1-methyltriazene 1-oxide (4).

Additional interest in these triazene 1-oxides stems from their observed anti-tumour activity against certain tumours in rodents (5) and from the recent suggestion that a triazene 1-oxide may be implicated in the metabolism of the anti-tumour 1-aryl-3,3-dimethyltriazenes (6).

The tautomerism of **I***a* and **I***b* bears some resemblance to the tautomerism exhibited by 1-aryl-3-alkyltriazenes, Ar·N=N—NHR ⇌ Ar·NH—N=NR ("mono-methyltriazenes"). The monomethyltriazene tautomerism has been shown to be strongly influenced by the presence of electron-withdrawing groups in the *ortho* and *para* positions of the aryl group (7). It is possible that the tautomerism of **I***a* and **I***b* might similarly be affected by the nature and position of substituents in the aryl group, so we have undertaken to synthesize a series of *ortho*- and *para*-substituted 3-aryl-1-methyltriazene 1-oxides and to investigate their structures by spectroscopic analysis.

Experimental

Infrared spectra were recorded with a Perkin Elmer model 299 spectrophotometer. NMR spectra were obtained with Varian EM360 (60 MHZ) and Nicolet 360NB (360 MHZ) spectrometers. Elemental analysis was carried out by the Canadian Microanalytical Service, Vancouver, B.C., Canada.

*3-Aryl-1-methyltriazene 1-oxides (**1–16**)*

The appropriately substituted aniline (0.01 mol) was dissolved in 2 N hydrochloric acid (15 mL, 0.03 mol) and heated if necessary. Once the solution became clear, it was cooled to 0–5°C. A solution of sodium nitrite (0.011 mol) in a minimum amount of water was added slowly to the cold anilinium hydrochloride solution and the resulting mixture was stirred cold for 0.5 h. The cold

[1]Author to whom correspondence may be addressed.

TABLE 1. Yields and physical data of the 3-aryl-1-methyltriazene 1-oxides.

No.	Subst.	Yield (%)	Melting point (°C)	Recrystallizing solvent	IR(cm^{-1})
1	H	30	64[a]	EtOH	3276
2	*p*-CO_2Et	80	149–152	EtOAc	1706, 3275
3	*o*-CO_2Et	56	121–122	Toluene	1689, 3229
4	*p*-NO_2	66	228–230[b]	CH_2Cl_2	3272
5	*o*-NO_2	44	145[c]	Toluene	3271
6	*p*-CN	50	195[d]	EtOAC/hexane	2224, 3273
7	*o*-CN	53	94–95	Toluene/hexane	2223, 3252
8	*p*-$COCH_3$	53	170–172	Toluene	1672, 3274
9	*o*-$COCH_3$	61	150–151	Toluene	1652, 3190
10	*p*-CF_3	50	149–152	Toluene	3110
11	*o*-CF_3	72	60–62	Et_2O/hexane	3285
12	*m*-CF_3	67	88–90	Et_2O	3274
13	*p*-OCH_3	27	97–98[e]	Et_2O/toluene	3272
14	*o*-OCH_3	30	72–73[e]	Toluene	3298
15	*p*-Br	15	148–150[f]	Et_2O/toluene	3273
16	*o*-Br	95	68–69	Et_2O/toluene	3265

[a]Literature mp 72–73°C (ref. 9).
[b]Literature mp 231°C (ref. 10).
[c]Compound **5** has been reported but no melting point was given (ref. 11).
[d]Literature mp 197–198°C (dec) (ref. 6).
[e]Compounds **13** and **14** were reported but no melting points given (ref. 12).
[f]Literature mp 149°C (ref. 13).

Can. J. Chem. Downloaded from www.nrcresearchpress.com by 109.225.110.28 on 09/08/12
For personal use only.

diazonium salt solution was filtered, if necessary, to remove any insoluble impurities, and then treated with a solution of *N*-methylhydroxylamine hydrochloride (0.015 mol) in a minimum volume of water. After stirring the mixture for 15 min., a saturated solution of sodium bicarbonate was added until the solution was neutral, whereupon the triazene 1-oxide precipitated and was collected by vacuum filtration. The dry 1-oxide was recrystallized from an appropriate solvent. Yields, melting points, and IR data of the triazene 1-oxides are given in Table 1.

Results and discussion

The diazonium coupling reaction with *N*-methylhydroxylamine gave good yields of all 16 of the 3-aryl-1-methyltriazene 1-oxides and the yield does not appear to be affected by the location of the substituent, i.e., *ortho* or *para*. However, the yield was statistically lower when the electron-releasing methoxyl group was present. Several of the triazene 1-oxides studied here are known compounds; literature mp's and references are footnoted in Table 1. All new compounds were analyzed for the principal elements and the elemental analyses for these nine compounds and known compound **6** are given in Table 2.

All of the compounds prepared in this study showed spectral characteristics of the triazene 1-oxide tautomer (**I***a*) and not the 3-hydroxytriazene (**I***b*). These spectral properties, IR and NMR, are discussed separately in the following sections.

Infrared spectra

The infrared spectra of all the 3-aryl-1-methyltriazene 1-oxides (**1**–**16**) display distinct N—H stretching vibration bands in the range 3190–3298 cm^{-1}, with no evidence of an O—H stretching vibration band. This observation confirms that these compounds exist in the preferred 1-oxide tautomeric form (**I***a*) and not the *N*-hydroxytriazene form (**I***b*). A closer look at the variation of the N—H stretching frequency with the substituent reveals an interesting observation as the substituent is moved from the *para* to the *ortho* position.

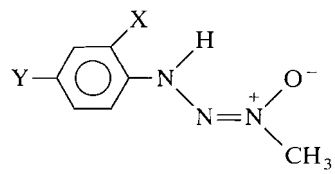

1	X = Y = H	**9**	X = $COCH_3$, Y = H
2	X = H, Y = CO_2Et	**10**	X = H, Y = CF_3
3	X = CO_2Et, Y = H	**11**	X = CF_3, Y = H
4	X = H, Y = NO_2	**12**	X = H, Y = m-CF_3
5	X = NO_2, Y = H	**13**	X = H, Y = OCH_3
6	X = H, Y = CN	**14**	X = OCH_3, Y = H
7	X = CN, Y = H	**15**	X = H, Y = Br
8	X = H, Y = $COCH_3$	**16**	X = Br, Y = H

In the case of the nitro, trifluoromethyl, and bromo substituents, the change of position from *para* to *ortho* causes negligible change in the N—H frequency. When the substituent is cyano, a small but significant change of frequency occurs with a slight shift of 21 cm^{-1}. The most significant difference is observed in the case of the acetyl substituent (3274 cm^{-1} for **8** (*para*-$COCH_3$) and 3190 cm^{-1} for **9** (*ortho*-$COCH_3$)) and the ester group (3275 cm^{-1} for **2** (*para*-CO_2Et) and 3229 cm^{-1} for **3** (*ortho*-CO_2Et)). This change is consistent with the presence of an intramolecular H-bond, which causes a slight weakening of the N—H bonding interaction and, hence, a shift to lower vibration frequency. The intramolecular H-bond has a similar effect on the carbonyl stretching vibration band in **3** and **9**.

It may be significant that the electron-releasing methoxy

TABLE 2. Elemental analysis of new triazene 1-oxides

No.	Subst.	Formula		C	H	N	Other
2	*p*-CO_2Et	$C_{10}H_{13}N_3O_3$	Found	53.27	5.68	18.36	
			Calcd.	53.81	5.83	18.83	
3	*o*-CO_2Et	$C_{10}H_{13}N_3O_3$	Found	53.93	5.70	18.80	
			Calcd.	53.81	5.83	18.83	
6	*p*-CN	$C_8H_8N_4O$	Found	54.57	4.50	32.15	
			Calcd.	54.55	4.55	31.82	
7	*o*-CN	$C_8H_8N_4O$	Found	54.53	4.54	31.97	
			Cacld.	54.55	4.55	31.82	
8	*p*-$COCH_3$	$C_9H_{11}N_3O_2$	Found	55.96	5.65	21.51	
			Calcd.	55.96	5.70	21.76	
9	*o*-$COCH_3$	$C_9H_{11}N_3O_2$	Found	56.13	5.70	21.75	
			Calcd.	55.96	5.70	21.76	
12	*m*-CF_3	$C_8H_8N_3OF_3$	Found	43.86	3.60	19.24	F = 25.05
			Calcd.	43.84	3.65	19.18	26.03
11	*o*-CF_3	$C_8H_8N_3OF_3$	Found	43.92	3.67	19.28	F = 25.47
			Calcd.	43.84	3.65	19.18	26.03
10	*p*-CF_3	$C_8H_8N_3OF_3$	Found	43.81	3.64	19.25	
			Calcd.	43.84	3.65	19.18	
16	*o*-Br	$C_7H_8N_3OBr$	Found	36.55	3.51	18.28	
			Calcd.	36.52	3.48	18.26	

TABLE 3. NMR data of the 3-aryl-1-methyltriazene 1-oxides

		^{1}H NMR data (ppm)				C-13 NMR data (ppm)							
No.	Subst.	N-H	N-CH_3	Aromatic	Subst.	Subst.	C-1	C-2	C-3	C-4	C-5	C-6	C-7
1	H	10.14	3.96	6.98–7.33	—	—	49.94	139.76	129.36	114.26	122.58	114.26	129.36
2	*p*-CO_2Et	10.28	3.99	$H_A + H_A'$, 7.14	1.38 (CH_3)	14.38 (CH_3)							
				$H_B + H_B'$, 8.01	4.35 (CH_2)	60.73 (CH_2)	50.32	143.31	131.34	113.50	124.36	113.50	131.34
						166.12 (C=O)							
3	*o*-CO_2ET	12.60	4.01	6.96–8.00	1.41 (CH_3)	14.26 (CH_3)							
					4.41 (CH_2)	61.26 (CH_2)	50.39	142.18	134.21	120.59	114.24	131.20	112.53
						166.93 (C=O)							
4	*p*-NO_2	10.99	4.03	7.16–8.21	—	—	50.99	135.86	126.11	116.34	120.98	116.34	126.11
5	*o*-NO_2	12.40	4.07	7.03–8.24	—	—	50.99	136.66	135.86	116.34	126.11	132.88	120.99
6	*p*-CN	10.32	4.01	$H_A + H_A'$, 7.18	—	105.2 (CN)	50.55	143.14	133.74	114.31	119.05	114.31	133.74
				$H_B + H_B'$, 7.59									
7	*o*-CN	10.53	4.03	7.03–7.54	—	97.30 (CN)	50.62	142.18	134.19	114.68	122.09	132.76	115.85
8	*p*-CO · CH_3	10.33	4.00	$H_A + H_A'$, 7.16	2.56 (CH_3)	26.32 (CH_3)							
				$H_B + H_B'$, 7.94		196.48 (C=O)	50.39	143.52	130.36	113.59	131.50	113.59	130.36
9	*o*-CO · CH_3	13.18	4.01	6.98–7.85	2.64 (CH_3)	28.02 (CH_3)							
						200.39 (C=O)	50.52	141.96	134.64	114.51	120.26	131.72	119.01
10	*p*-CF_3	10.29	4.00	7.18–7.57	—	—	50.31	142.45	126.75	113.89	—	113.89	126.75
11	*o*-CF_3	10.62	4.00	7.04–7.59	—	—	50.34	137.50	133.16	126.50	121.75	133.50	115.66
12	*m*-CF_3	10.28	3.99	7.24–7.43	—	—	50.23	140.32	118.99	110.98	117.29	—	129.93
13	*p*-OCH_3	10.06	3.94	6.90–7.08	3.78 (CH_3)	55.63 (CH_3)	49.66	133.73	115.84	114.89	129.27	114.89	115.84
14	*o*-OCH_3	10.27	3.97	6.87–7.38	3.88 (CH_3)	55.62 (CH_3)	50.01	129.54	122.23	110.78	113.72	121.21	146.32
15	*p*-Br	10.13	3.96	6.99–7.42	—	—	50.07	114.99	115.94	132.36	139.07	132.36	115.94
16	*o*-Br	10.44	4.00	6.85–7.51	—	—	50.31	108.86	132.76	115.31	123.14	128.47	137.62

substituent gives a reverse effect. The N—H frequency is significantly higher in the *ortho*-substituted compound (**14**) than in the *para*-substituted isomer (**13**). However, there is no immediately obvious explanation for this phenomena.

NMR spectra

The most significant feature of the ^{1}H NMR data of the triazene 1-oxides (Table 2) is the variation of the N—H chemical shift as the substituent is moved from the *para* to the *ortho* position. The pattern is consistent with the hypothesis of an intramolecular H-bond derived from the IR spectral data.

In molecules that do not present the possibility of intramolecular H-bonding, the N—H chemical shift is consistent in the range 10.14–10.99 ppm. The presence of an *ortho* substituent with H-bonding potential (i.e., -CO_2Et, -Ac, or -NO_2) causes a downfield shift of the N—H proton to the range 12.40–13.18 ppm. This observation is consistent with the intramolecular H-bonding typified by structure II; interaction of the N—H proton with the electronegative oxygen

Can. J. Chem. Downloaded from www.nrcresearchpress.com by 109.225.110.28 on 09/08/12
For personal use only.

of the carbonyl (or nitro) group causes a decrease in electron density around the proton.

The NMR data also reveals more subtle effects on N—H chemical shift by electron-withdrawing and -donating groups in the *para* position. An electron-donating group (OMe) (**13**) in the *para* position causes an upfield shift of the N—H resonance compared to the unsubstituted compound (**1**), whereas the electron-withdrawing groups in **2**, **4**, **6**, **8**, and **10** shift the N—H resonance slightly downfield from that in **1**.

Other features of the ^{1}H NMR spectra are very predictable and show little variation with the nature or placement of the substituent.

The ^{13}C NMR spectra of the 3-aryl-1-methyltriazene 1-oxides (Table 3) confirm the assigned structures, but do not offer any particularly profound information concerning the **I***a* ⇌ **I***b* tautomerism question. The *N*-methyl ^{13}C resonance is consistently in the range 49.66–50.99 ppm and shows little sensitivity to the electron-releasing/withdrawing character or *ortho/para* location of the substituent (X or Y). The ring carbon atom closest to the region of potential tautomeric change, i.e., C-2, shows a little variation in ^{13}C resonance but the variation does not appear to correlate with the nature or position of the substituent. There are significant differences in the ^{13}C resonance of the ring carbons at C-5 and C-7 in the respective *ortho/para* isomeric pairs, but these changes are entirely predictable by consideration of the substituent location and do not indicate any influence from a tautomeric equilibrium.

The IR and NMR spectra of the series of 1-methyl-3-aryltriazene 1-oxides reported here show that these molecules prefer the 1-oxide tautomer (**I***a*) to the still unknown 3-hydroxytriazene structure (**I***b*). The preference for the 1-oxide tautomer may be further enhanced by the presence of a potentially H-bonding substituent in the *ortho* position of the aryl moiety.

Conclusion

The IR and NMR spectra of the series of 1-methyl-3-aryltriazene 1-oxides reported here, show that these molecules prefer the 1-oxide tautomer (**I***a*) to the still unknown 3-hydroxytriazene structure (**I***b*). The preference for the

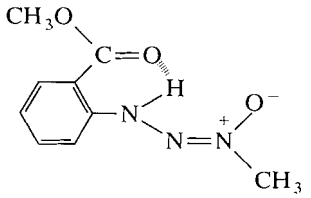

II

1-oxide tautomer may be further enhanced by the presence of a potentially H-bonding substituent in the ortho position of the aryl moiety as illustrated by structure **II**. These observations have been corroborated by an X-ray crystal structure examination of two of the compounds in this series, namely **2** and **3** (8). The ortho isomer **3** shows definite evidence for the intramolecular hydrogen bond shown in structure **II**.

1. J. L. Miesel. U.S. Patent No. 3,962,434 (1976).
2. T. Mitsuhashi, Y. Osamura, and O. Shimamura. Tetrahedron Lett. **30**, 2593 (1965).
3. A. G. Guimanini, L. Lassiani, C. Nisi, A. Petric, and B. Stanovnik. Bull. Chem. Soc. Jpn. **56** 1887 (1983).
4. R. Kuroda and D. E. V. Wilman. Acta. Crystallogr. Sect. C: Cryst. Struct. Commun. **C41**, 1543 (1985).
5. D. E. V. Wilman. Triazene *N*-oxides. *In* Proc. 3rd Int. Symp. on the Biological Oxidation of Nitrogen in Organic Molecules. *Edited by* J. W. Gorrod and L. A. Damani. Ellis Horwood, Chichester. 1985 pp. 297–302.
6. K. Vaughan and D. E. V. Wilman. J. Chem. Res. (S), 249 (1991).
7. D. L. Hooper and K. Vaughan. J. Chem. Soc. Perkin Trans. 2, 1161 (1981); K. Vaughan. J. Chem. Soc. Perkin Trans. 2, 17 (1977).
8. K. Vaughan, L. M. Cameron, S. Christie, and M. J. Zaworotko. Acta Crystallogr. Sect. C. In press.
9. M. Elkins and L. Hunter. J. Chem. Soc. 1346(1938).
10. E. Bamberger and E. Renault. Chem. Ber. **30**, 2278 (1897).
11. D. N. Purohit. J. Indian Chem. Soc. **61**, 710 (1984).
12. D. N. Purohit. Cienc. Cult. (Sao Paulo), **38**, 1059 (1986).
13. D. N. Purohit and Nizamuddin. J. Indian Chem. Soc. **60**, 712 (1983).

Can. J. Chem. Downloaded from www.nrcresearchpress.com by 109.225.110.28 on 09/08/12
For personal use only.

Synthesis and physico-chemical studies of newer mono and diperoxo heteroligand complexes of vanadium

MANISH BHATTACHARJEE,[1] MIHIR K. CHAUDHURI,[2] AND PRADIP C. PAUL
Department of Chemistry, North-Eastern Hill University, Shillong-793003, India

Received July 9, 1991[3]

MANISH BHATTACHARJEE, MIHIR K. CHAUDHURI, and PRADIP C. PAUL. Can. J. Chem. **70**, 2245 (1992).

The synthesis of monoperoxo-vanadium(V) complexes, $[VO(O_2)QL]$ (Q = 8-quinolinolate and L = EtOH, DMF, DMSO, or THF), and diperoxovanadates(V), $A_3[VO(O_2)_2(HPO_4)] \cdot 2H_2O$ (A = K or NH_4) are described. While the $[VO(O_2)QL]$ complexes have been synthesized from the reaction of V_2O_5 with H_2O_2 and a solution of 8-quinolinol in different donor solvents (L) at pH ca. 2, the oxodiperoxo(hydrophosphato) vanadate(V) dihydrates, $A_3[VO(O_2)_2(HPO_4)] \cdot 2H_2O$, have been prepared from the reaction of V_2O_5 with H_2O_2 and phosphoric acid at pH 6 of the reaction medium. The compounds have been characterized by chemical analyses, magnetic susceptibility, and molar conductance measurements, and by IR, laser Raman, ^1H NMR, and electronic spectroscopic studies. Evidence has been provided for triangularly bonded peroxide (O_2^{2-}) and coordinated heteroligands. The existence and stability of the complex $[VO(O_2)_2(HPO_4)]^{3-}$ in solution have been ascertained from solution Raman spectroscopy and conductance measurements.

MANISH BHATTACHARJEE, MIHIR K. CHAUDHURI et PRADIP C. PAUL. Can. J. Chem. **70**, 2245 (1992).

On décrit la synthèse des complexes monoperoxo–vanadium(V), $[VO(O_2)QL]$ (Q = 8-quinoléinolate et L = EtOH, DMF, DMSO ou THF) et diperoxovanadates(V), $A_3[VO(O_2)_2(HPO_4)] \cdot 2H_2O$ (A = K ou NH_4). Alors que les complexes $[VO(O_2)QL]$ ont été synthétisés par la réaction du V_2O_5 avec du H_2O_2 et une solution du 8-quinoléinol dans divers solvants donneurs (L), à un pH d'environ 2, les dihydrates de l'oxodiperoxy(hydrophosphato)vanadate $A_3[VO(O_2)_2(HPO_4)] \cdot 2H_2O$ ont été préparés par la réaction du V_2O_5 avec le H_2O_2 et de l'acide phosphorique, au pH de 6 du milieu réactionnel. On a caractérisé les produits par des analyses chimiques, par des mesures de susceptibilité magnétique et de conductivité molaire et par des études spectroscopiques IR, Raman au laser, RMN du ^1H et électroniques. On a obtenu des données relatives au peroxyde (O_2^{2-}) lié d'une façon triangulaire et aux hétéroligands qui sont coordonnés. Sur la base de la spectroscopie Raman et des mesures de conductivité, on a établi l'existence et la stabilité du complexe $[VO(O_2)_2(HPO_4)]^{3-}$ en solution.

[Traduit par la rédaction]

Introduction

Peroxo-vanadium systems are important for a variety of reasons including their role in oxidation catalysis (1,2) and biochemical relevance (3–9). Suitable heteroligands are known to bring about stability to such systems enabling isolation in the solid state, for instance, $NH_4[VO(O_2)_2(C_{10}H_8N_2)]$, which was synthesized by Vuletic and Djordjevic (10) and crystallographically characterized by Szentivanyi and Stomberg (11). In addition, the synthesis and structural assessment of several NO-donor–peroxo-vanadium(V) complexes with pyridine-2-carboxylate (1, 12), pyrazine-2-carboxylate (1), pyridine-2,6-dicarboxylate (13), iminodiacetate (14), and *N*-(2-oxidophenyl)salicylidinaminate (2) as the heteroligands are notable contributions to the domain of peroxo-chemistry of the metal. Over the past few years, we have been working in this area (15, 16) and our major emphasis has been on the development of newer synthetic methodologies as well as to synthesize new compounds. The selection of heteroligands is important and the coligands chosen for the present studies include 8-quinolinol and phosphate. While the importance of 8-quinolinol as a ligand has already been emphasized (17, 18), our concern with phosphate was to ascertain if it would form a peroxo(phosphato)vanadium(V) species. Such a complex is expected to be of considerable interest in the context of the vanadate–phosphate antagonism in physiology and the use of phosphate buffers in the reconstitution of vanadium bromoperoxidase. Since a citrate/phosphate buffer was used in the purification process of bromoperoxidases (3, 4, 19) containing vanadium(V), the possibility of phosphate coordination with a peroxovanadate(V) cannot be ruled out. Indeed, there has been definite evidence to support the formation of a mononuclear monophosphato–vanadium complex in aqueous solutions (20, 21).

In this paper, the synthesis and physico-chemical characterization of complexes of the type $[VO(O_2)QL]$ (Q = 8-quinolinolate and L = EtOH, DMSO, DMF, or THF) and $A_3[VO(O_2)_2(HPO_4)] \cdot 2H_2O$ (A = NH_4 or K) are presented. Also reported here are the results of solution Raman and conductance experiments in support of the existence and stability of the complex $[VO(O_2)_2(HPO_4)]^{3-}$ ion in solution.

Experimental

The chemicals used were all reagent grade products. The IR spectra were recorded on a Perkin Elmer model 983 spectrophotometer. The laser Raman (LR) spectra were recorded at ambient temperatures on a SPEX Ramalog model 1403 spectrometer using the line at 6471 Å of a Krypton laser from a Coherent model Innova 90-K(UV) as the excitation source. The UV–visible spectra were recorded in water or DMF solutions on a Hitachi model 330 spectrophotometer. Molar conductances were measured either in conductivity grade water or in DMF using a Systronics type 304 digital direct-reading conductivity bridge. The pH values of the reaction solutions were measured with a Systronics type 335 digital pH meter and also with pH indicator paper (BDH). The ^1H NMR spectra were recorded in deuterated DMSO using a Varian 390 90-MHz spectrometer. Tetramethyl silane (TMS) was used as the internal standard. Carbon, hydrogen, and nitrogen were determined by microanalytical methods (Micro-Analysis Lab., Depart-

[1]Present address: Department of Chemistry, Indian Institute of Technology, Kharagpur 721 302, India.

[2]Author to whom correspondence may be addressed.

[3]Revision received February 25, 1991.

Can. J. Chem. Downloaded from www.nrcresearchpress.com by 109.225.110.28 on 09/08/12
For personal use only.

Can. J. Chem. Downloaded from www.nrcresearchpress.com by 109.225.110.28 on 09/08/12
For personal use only.

ment of Chemistry, NEHU, Shillong-793003). Vanadium, peroxide, and phosphate were estimated by the methods given in our earlier papers (15, 22).

Synthesis of oxoperoxo-8-quinolinolatovanadium(V) complexes, [VO(O$_2$)QL] (Q = 8-quinolinolate, L = EtOH, DMSO, DMF, or THF)

As the methods of synthesis of [VO(O$_2$)QL] compounds are similar, only a representative procedure is described.

V_2O_5 (1 g, 5.49 mmol) was first dissolved in 30% hydrogen peroxide (15 cm^3, 132.36 mmol) to obtain a red solution with liberation of heat. To this was added a solution of 8-quinolinol (1.6 g, 11.02 mmol), made up separately in each of the following donor solvents (100 cm^3), EtOH, DMSO, DMF, or THF, with continuous stirring. The concentration ratio of V:8-quinolinol: H_2O_2 was 1:2:24.1. No colour change or heat liberation was apparent. The reaction mixture was stirred for ca. 30 min in an ice-bath, whereupon a brick-red microcrystalline solid separated out. The pH value of the solution was recorded to be ca. 2. The solid oxoperoxo-8-quinolinolato-vanadium(V) complex [VO(O$_2$)QL] (Q = 8-quinolinolate, L = EtOH, DMSO, DMF, or THF) was filtered off, washed three or four times with ethanol, and finally dried *in vacuo* over concentrated H_2SO_4. The yields of [VO(O$_2$)Q(EtOH)], [VO(O$_2$)Q(DMSO)], [VO(O$_2$)Q(DMF)], and [VO(O$_2$)Q(THF)] were 2.6 g (82%), 2.8 g (80%), 2.9 g (85%), and 2.7 g (78%), respectively.

Anal. calcd. for [VO(O$_2$)Q(EtOH)]: V 17.62, O_2^{2-} 11.07, C 45.7, N 4.84, H 4.15; found: V 17.28, O_2^{2-} 10.85, C 45.56, N 4.96, H 4.2. ^{1}H NMR (DMSO-d_6) δ: 8.85 (d,H), 8.7 (d,H), 7.8(d,H), 7.6(d,H), 7.4(d,H), 7.15(d,H), 3.43(q,2H), 2.5(s,H), 1.06(t,3H).

Anal. calcd. for [VO(O$_2$)Q(DMF)]: V 16.11, O_2^{2-} 10.12, C 45.59, N 8.85, H 4.11; found: V 15.98, O_2^{2-} 10.2, C 45.92, N 9.03, H 4.12. ^{1}H NMR (DMSO-d_6) δ: 8.82(d,H), 8.65(d,H), 7.76(d,H), 7.59(d,H), 7.35(d,H), 7.13(d,H), 7.93(s,H), 2.83(s,3H), 2.7(s,3H).

Anal. calcd. for [VO(O$_2$)Q(DMSO)]: V 15.86, O_2^{2-} 9.96, C 41.14, N 4.35, H 3.73; found: V 15.62, O_2^{2-} 9.81, C 42.10, N 4.42, H 3.78. ^{1}H NMR (DMSO-d_6) δ: 8.86(d,H), 8.7(d,H), 7.85(d,H), 7.68(d,H), 7.38(d,H), 7.10(d,H), 2.3(s,6H).

Anal. calcd. for [VO(O$_2$)Q(THF)]: V 16.16, O_2^{2-} 10.15, C 49.55, N 4.44, H 4.44; found: V 15.94, O_2^{2-} 9.85, C 50.11, N 4.54, H 4.38. ^{1}H NMR (DMSO-d_6) δ: 8.82(d,H), 8.65(d,H), 7.79(d,H), 7.58(d,H), 7.25(d,H), 7.11(d,H), 3.60(m,4H), 1.73(m,4H).

Synthesis of ammonium and potassium oxodiperoxo-(hydrophosphato)vanadate(V) dihydrates, $A_3[VO(O_2)_2(HPO_4)]\cdot 2H_2O$ (A = NH$_4$ or K)

In a typical procedure, a mixture of vanadium pentoxide (1 g, 5.49 mmol) and 88% phosphoric acid (1 cm^3, 17.85 mmol, density 1.75 g cm^{-3}) was reacted with 30% hydrogen peroxide (15 cm^3, 132.36 mmol) in an ice-bath with stirring. A clear red solution thus obtained was stirred for ca.15 min followed by the addition of aqueous ammonia (specific gravity 0.9) or 20% KOH solution until the reaction medium attained a pH value of 6 with its colour turning to yellow. An addition of ethanol to this precipitated out a yellow microcrystalline product. The compound was filtered off, washed two or three times with ethanol, and finally dried *in vacuo* over concentrated H_2SO_4. The yield of $(NH_4)_3[VO(O_2)_2(HPO_4)]\cdot 2H_2O$ was 2.82 g (81%) and that of $K_3[VO(O_2)_2(HPO_4)]\cdot 2H_2O$ was 3.17 g (76%). Anal. calcd. for $(NH_4)_3[VO(O_2)_2(HPO_4)]\cdot 2H_2O$: V 16.07, O_2^{2-} 20.19, PO_4^{3-}, 29.96, N 13.25, H 5.36; found: V 15.92, O_2^{2-} 20.1, PO_4^{3-} 29.21, N 13.11, H 5.32. Anal. calcd. for $K_3[VO(O_2)_2(HPO_4)]\cdot 2H_2O$: V 13.39, O_2^{2-} 16.83, PO_4^{3-} 24.97, H 1.31; found: V 13.13, O_2^{2-} 16.3, PO_4^{3-}, 25.25, H 1.38.

Results and discussion

Vanadium has a strong affinity for peroxide (O_2^{2-}) and the composition of a peroxo-vanadium species is pH dependent (15, 16, 23–26). The number of coordinated O_2^{2-} generally increases as the solution pH value is raised. In one of the present reactions, the interaction of V_2O_5 with hydrogen peroxide and a solution of 8-quinolinol (QH) in each of the donor solvents (L) (L = EtOH, DMSO, DMF, or THF) was conducted at pH 2. This led to the synthesis of new heteroligand monoperoxovanadium(V) compounds of the type [VO(O$_2$)QL] in very high yields. QH was dissolved in the chosen organic solvents (L) so that an option for the formation of quaternary complexes existed. Since monoperoxo complexes of the metal are far less frequently encountered, it was one of our concerns to improvise a route to such species. Accordingly, the pH value of ca. 2 attained spontaneously was not raised so that the goal could be achieved. In contrast, the successful synthesis of complex peroxovanadates(V) containing HPO_4^{2-} as the heteroligand was possible from the reaction of V_2O_5 with phosphoric acid (H_3PO_4) and H_2O_2, only when the pH value was raised to 6. The products isolated at pH values < 6, though containing both peroxide and phosphate, were inconsistent in regard to their compositions. A comparatively higher pH value is believed to have directed the formation of the ternary diperoxovanadate(V), $[VO(O_2)_2(HPO_4)]^{3-}$. The complex was isolated as $A_3[VO(O_2)_2(HPO_4)]\cdot 2H_2O$ (A = K or NH_4) by the addition of ethanol, which facilitated the precipitation. The alkali used to raise the pH of the solution served also as a source of the counter-cation NH_4^+ or K^+ (A^+). The occurrence of an acid phosphate, HPO_4^{2-}, can be rationalized in terms of the pH value maintained in the synthesis.

Both the brick-red [VO(O$_2$)QL] and the yellow $A_3[VO(O_2)_2(HPO_4)]\cdot 2H_2O$ were obtained as microcrystalline products. They are insoluble in nonpolar organic solvents. While the former is insoluble in water, but soluble in polar organic solvents like DMF and DMSO, the latter is soluble only in water. The compounds are stable for a prolonged period and are capable of being stored in closed sample containers. Both the mono- and the diperoxo compounds reported herein are diamagnetic in nature in conformity with the oxidation state of the metal. The molar conductances of [VO(O$_2$)QL] recorded in DMF and those of $A_3[VO(O_2)_2(HPO_4)]\cdot 2H_2O$ recorded in water were found to lie in the ranges 5–10 Ω^{-1} cm^2 mol^{-1}, and 370–380 Ω^{-1} cm^2 mol^{-1}, respectively, in agreement with their formulae. Furthermore, the results of conductance measurements, obtained over a period of 10 days at an interval of 24 h each, were practically similar to those recorded on freshly prepared solutions. This clearly attests to the stability of the compounds in the respective solutions.

Each of the monoperoxo-vanadium(V) and diperoxovanadate(V) complexes exhibited a characteristic spectral pattern in the infrared region. The significant general features are the absorptions at ca. 950, ca. 855, ca. 620, and ca. 580 cm^{-1} assigned to ν(V═O), ν(O—O) (ν_1), ν(V—O$_2$)(ν_2), and ν(V—O$_2$)(ν_3), respectively (15, 16, 27). The occurrence of bands at ca. 855 cm^{-1}, ca. 620, and ca. 580 cm^{-1} clearly indicates the presence of triangularly bonded (C_{2v}) peroxide (15, 16, 27). In addition to the features originating from VO^{3+} and coordinated peroxide, the monoperoxo complexes [VO(O$_2$)QL] show bands due to the coordinated 8-quinolinolate ligand(Q) with the pattern comparing very well with that reported (17, 28) for the 8-quinolinolato coordinated systems. Moreover, the IR spectra of [VO(O$_2$)Q(DMSO)] and [VO(O$_2$)Q(DMF)] exhibit strong bands at 940 cm^{-1} (ν(S═O)) (29) and at 1650 cm^{-1} (ν(C═O)) (30),

TABLE 1. Comparison of peroxo stretching frequencies [ν(O—O)] for the complexes to those of previously reported compounds from this laboratory

Compound	ν(O—O) (cm^{-1}) IR	Raman	Reference
$K_2[V(O_2)_3F]$	855s		15*a*)
$K_2[VO(O_2)_2F]$	870s, 890s		32
$K_2[V(O_2)_3Cl]$	855s		15*b*)
$K_2[VO(O_2)_2Cl]$	875s, 890s		15*b*)
$K_3[VO(O_2)_2CO_3] \cdot 3H_2O$	865s	865s	33
$K[VO(O_2)_2en]$	870s	880	34
$K[VO(O_2)_2(H_2O)]$	860s	870	16*a*)
$K[VO(O_2)_2GlyH]$	850s		16*b*)
$K_2[V_2O_2(O_2)_3(cysH)_2] \cdot H_2O$	851s, 818m		35
$[VO(O_2)Q(EtOH)]$	855s		This work
$[VO(O_2)Q(DMF)]$	850s		
$[VO(O_2)Q(DMSO)]$	850s		
$[VO(O_2)Q(THF)]$	855s		
$K_3[VO(O_2)_2(HPO_4)] \cdot 2H_2O$	865s	857	
$(NH_4)_3[VO(O_2)_2(HPO_4)] \cdot 2H_2O$	860s	860	

Abbreviations: en = ethylenediamine, Q = 8-quinolinolate, GlyH = glycine, cysH = cysteinate, EtOH = ethyl alcohol, DMF = dimethylformamide, DMSO = dimethyl sulphoxide, THF = tetrahydrofuran.

respectively. The presence of distinct bands at 940 and 1650 cm^{-1} suggests that the DMSO and DMF are bonded to the metal centre through their O-atoms in the respective cases (29, 30). The bands due to the coordinated EtOH and THF in the complexes [$VO(O_2)QL$] (L = EtOH or THF) could not be identified because of their overlap with those of the 8-quinolinolato ligand.

In addition to the bands due to V=O and coordinated O_2^{2-}, the IR spectra of $A_3[VO(O_2)_2(HPO_4)] \cdot 2H_2O$(A = NH_4 or K) display a strong but broad absorption in the region 1010–1160 cm^{-1} and a medium intensity broad absorption at 2800–2900 cm^{-1}. These resemble, in their shapes and positions, those observed for the coordinated hydrophosphate group (HPO_4^{2-}) (31) and lend support to the contention. The signals at ca. 960, ca. 860, ca. 630, and ca. 580 cm^{-1} due to the ν(V=O), ν(O—O)(ν_1), ν(V—O_2)(ν_2), and ν(V—O_2)(ν_3) modes, respectively, observed in the laser Raman spectra of the compounds, complement the corresponding IR modes. The additional bands at ca. 1640 s, and ca. 3500 s, br cm^{-1} in the IR spectra of the complexes represented the δ(H—O—H) and ν(O—H) modes of uncoordinated water (ref. 29, p. 228). A comparison of the vibrational spectra of the newly synthesized compounds with those of some of our previously reported peroxo-vanadium(V) complexes (15, 16, 32–35) causes us to state that the most significant band [ν(O—O)], characteristic of the bound peroxides, does not appear to show any remarkable variation in its position with changes in the metal coordination sphere (Table 1). The ν(O—O) bands lie in the region 850–890 cm^{-1} in the IR spectra, while similar modes occur between 855 and 880 cm^{-1} in the Raman spectra of the compounds so far investigated by us. In other words, the vibrational spectra of the coordinated peroxide seem to be independent of the nature of the heteroligands present in the complex peroxo-vanadium(V) species.

From the biochemical point of view, the peroxo(hydrophosphato)-vanadate(V) complex, $[VO(O_2)_2(HPO_4)]^{3-}$, is of considerable interest. To furnish evidence for its existence in solution, we sought to show that the use of laser Raman (LR) spectroscopy provided very valuable information in this regard. The LR spectrum of the yellow solution of V_2O_5, phosphoric acid, and H_2O_2 at pH 6 adjusted by the addition of KOH solution (*vide* Experimental) was recorded before isolating the compound. The spectrum exhibited polarized bands at 972, 865, and at 565 cm^{-1} due to ν(V=O), ν(O—O)(ν_1), ν_s(V—O_2)(ν_3), respectively, and a depolarized band at 630 cm^{-1} assigned to ν_{as}(V—O_2)(ν_2). The LR spectral pattern of the corresponding solid $K_3[VO(O_2)_2(HPO_4)]$, including the positions of the Raman signals, was similar to the above with its ν(V=O), ν(O—O)(ν_1), ν_s(V—O_2)(ν_3), and ν_{as}(V—O_2)(ν_2) occurring at 970, 857, 575, and 630 cm^{-1}, respectively. Furthermore, the LR spectrum of a freshly prepared solution of $K_3[VO(O_2)_2(HPO_4)]$ exhibited these bands at positions very close in wave numbers to the LR bands observed for the solution prior to isolating the complex, as well as to bands for the solid $K_3[VO(O_2)_2(HPO_4)]$ as discussed above. Equally significant is the consistent appearance of a very strong but broad signal with its peak at ca. 1065 cm^{-1} in each of the three spectra recorded for the complex under consideration. The band, in terms of its shape and position, compares very well to the corresponding IR band of the coordinated HPO_4^{2-} observed for the solid $K_3[VO(O_2)_2(HPO_4)]$, thereby lending further credence to the contention. These results attest not only to the existence but also to the stability of the complex $[VO(O_2)_2(HPO_4)]^{3-}$ species in solution, at least under the present experimental conditions.

The electronic spectra of [$VO(O_2)QL$] complexes in DMF showed two bands, one each at ca. 268 ($\varepsilon = 1.525 \times 10^4$ L mol^{-1} cm^{-1}) and at 360–410 (broad) nm ($\varepsilon = 2 \times 10^3$ L

Can. J. Chem. Downloaded from www.nrcresearchpress.com by 109.225.110.28 on 09/08/12
For personal use only.

mol^{-1} cm^{-1}). While the former has been assigned to the internal transition ($\pi-\pi^*$) of the 8-quinolinolate ligand (28), the latter probably owes its origin to a combination of a peroxo (LMCT) and the internal ($\pi-\pi^*$) transition of the 8-quinolinolato ligand. The UV–visible spectra of the diperoxo compounds $A_3[VO(O_2)_2(HPO_4)] \cdot 2H_2O$ (A = NH_4 or K), recorded in water, exhibited only one (LMCT) band at 320 nm. The transition at 320 nm is similar to that of the other diperoxovanadium compounds containing triangularly bonded peroxide (36).

The ^1H NMR spectra of the monoperoxovanadium(V) complexes, $[VO(O_2)QL]$, were recorded in DMSO-d_6 solvent. The significant features of the NMR spectra are the signals due to the coordinated 8-quinolinolato ligand and the coordinated L (L = EtOH, DMF, or THF). The signals due to coordinated 8-quinolinolato ligands, observed at δ values ca. 8.9, ca. 8.7, ca. 7.8, ca. 7.6, ca. 7.4, and ca. 7.2, are similar to those previously reported for the 8-quinolinolatovanadium complexes (17, 37, 38). Apart from these, the signals due to the coordinated ethanol appear at δ 1.06(t), 2.5(s), and 3.43(q) originating from $-CH_3$, O-H and, $-CH_2-$, respectively (39). The DMF signals, for L = DMF, were observed at δ 7.93(s), 2.83(s), and 2.7(s) assigned to HCO-, $-CH_3$, and $-CH_3$, respectively (ref. 39, p. 344). The THF signals of the corresponding complex appear at δ 1.73(m) and 3.6(m) due to $-CH_2-CH_2-$ and $-CH_2-O-CH_2-$, respectively (ref. 39, p. 348). Thus, the ^1H NMR results show conclusively that the 8-quinolinolato ligand is bonded to the metal center. The results are consistent with the presence of a metal–oxygen covalent bond and a long labile V—N bond (17). The chemical shifts agree with this proposition. The NMR spectroscopic studies also suggest that each of the L molecules, i.e., EtOH, DMF, and THF, is bonded to the metal center.

Can. J. Chem. Downloaded from www.nrcresearchpress.com by 109.225.110.28 on 09/08/12
For personal use only.

Acknowledgements

The authors thank the Council of Scientific and Industrial Research, New Delhi, for the award of fellowships to M.B and P.C.P, and the Department of Atomic Energy for financial support. We also thank the reviewers for valuable comments.

1. H. Mimoun, L. Saussine, E. Daire, M. Postel, J. Fischer, and R. Weiss. J. Am. Chem. Soc. **105**, 3101 (1983).
2. H. Mimoun, M. Mignard, P. Brechot, and L. Saussine. J. Am. Chem. Soc. **108**, 3711 (1986).
3. H. Vilter. Phytochemistry, **23**, 1387 (1984).
4. E. de Boer, M. G. M. Tromp, H. Plat, B. E. Krenn, and R. Wever. Biochim. Biophys. Acta, **872**, 104 (1986).
5. B. J. Hales, J. E. Morningstar, and E. E. Case. Recl. Trav. Chim. Pays-Bas, **106**, 410 (1987).
6. R. L. Richards. Chem. Ber. **24**, 133 (1988).
7. S. G. Brand, C. J. Hawkins, and D. L. Parry. Inorg. Chem. **26**, 629 (1987).
8. K. Kustin, G. C. McLeod, T. R. Gilbert, and Le B. R. Briggs. Struct. Bonding (Berlin), **53**, 139 (1983).
9. N. D. Chasteen. Struct. Bonding (Berlin), **53**, 105 (1983).
10. N. Vuletic and C. Djordjevic. J. Chem. Soc. 1137 (1973).
11. H. Szentivanyi and R. Stomberg. Acta Chem. Scand. Ser. A: **A37**, 553 (1983).
12. R. E. Drew and F. W. B. Einstein. Inorg. Chem. **12**, 829 (1973).
13. K. Wieghardt. Inorg. Chem. **17**, 57 (1978).
14. C. Djordjevic, S. A. Craig, and E. Sinn. Inorg. Chem. **24**, 1281 (1985).
15. (*a*) M. K. Chaudhuri and S. K. Ghosh. Inorg. Chem. **21**, 4020 (1982); (*b*) Inorg. Chem. **23**, 534 (1984); (*c*) J. Chem. Soc. Dalton Trans. 507 (1984).
16. (*a*) M. N. Bhattacharjee, M. K. Chaudhuri, and N. S. Islam. Inorg. Chem. **28**, 2420 (1989); (*b*) M. Bhattacharjee, M. K. Chaudhuri, N. S. Islam, and P. C. Paul. Inorg. Chim. Acta, **169**, 97 (1990).
17. L. W. Amos and D. T. Sawyer. Inorg. Chem. **13**, 78 (1974).
18. T. L. Riechel and D. T. Sawyer. Inorg. Chem. **14**, 1869 (1975).
19. B. E. Krenn, Y. Izumi, H. Yamada, and R. Wever. Biochim. Biophys. Acta, **63**, 998 (1989).
20. A. A. Ivakin, Z. M. Voronova, and L. D. Koorbatova. Zh. Neorg. Khim. **20**, 1246 (1975).
21. M. J. Gresser, A. S. Tracey, and K. M. Parkinson. J. Am. Chem. Soc. **108**, 6229 (1986).
22. M. Bhattacharjee and M. K. Chaudhuri. J. Chem. Soc. Dalton Trans. 477 (1987).
23. O. W. Howarth and J. R. Hunt. J. Chem. Soc. Dalton Trans. 1388 (1979).
24. O. W. Howarth and A. T. Harrison. J. Chem. Soc. Dalton Trans. 1173 (1985).
25. N. J. Campbell, A. C. Dengel, and W. P. Griffith. Polyhedron, **8**, 1379 (1989).
26. J. S. Jaswal and A. S. Tracey. Inorg. Chem. **30**, 3718 (1991).
27. W. P. Griffith and T. D. Wickins. J. Chem. Soc. A: 397 (1968).
28. R. P. Henry, P. C. H. Mitchell, and J. E. Prue. Inorg. Chim. Acta. **7**, 150 (1973).
29. K. Nakamoto. Infrared and Raman spectra of inorganic and coordination compounds. 4th ed. Wiley, New York. 1986. p. 270.
30. R. C. Paul, A. K. Moudgil, S. L. Chadha, and S. K. Vasisht. Indian J. Chem. **8**, 1017 (1970).
31. D. E. C. Corbridge and E. J. Lowe. J. Chem. Soc. 493 (1954).
32. M. K. Chaudhuri and S. K. Ghosh. Polyhedron, **1**, 553 (1982).
33. J. K. Basumatary, M. K. Chaudhuri, R. N. Dutta Purkayastha, and Z. Hiese. J. Chem. Soc. Dalton Trans. 709 (1986).
34. J. K. Basumatary, M. K. Chaudhuri, and Z. Hiese. Synth. React. Inorg. Met. Org. Chem. **17**, 35 (1987).
35. M. K. Chaudhuri and P. C. Paul. Indian J. Chem. **31A**, 466 (1992).
36. C. Djordjevic, B. C. Puryear, N. Vuletic, C. J. Abelt, and S. J. Sheffield. Inorg. Chem. **27**, 2926 (1988).
37. B. C. Baker and D. T. Sawyer. Anal. Chem. **40**, 1945 (1968).
38. B. C. Baker and D. T. Sawyer. Inorg. Chem. **8**, 1160 (1969).
39. J. G. Grasselli and W. M. Ritchey. *In* CRC atlas of spectral data and physical constants for organic compounds. Vol. 3. CRC Press, Ohio. 1975. p. 266.

Short syntheses of rigid acyclic or macrocyclic poly-imine ligands and their use in Ru(II), Fe(III), and alkali metal complexation

ROBERT DASH AND PIERRE G. POTVIN[1]

Department of Chemistry, York University, 4700 Keele Street, North York, Ont., Canada M3J 1P3

Received July 16, 1991

ROBERT DASH and PIERRE G. POTVIN. Can. J. Chem. **70**, 2249 (1992).

Lipophilic derivatives of 2,6-bis(3-pyrazolyl)pyridine and 1,3-bis (3-pyrazolyl)benzene were obtained in acceptable yields by Stork reactions and transformed by *N*-alkylations into three pentadentates, three bis(bidentates), and one macrocyclic octadentate ligand. The parent bis(pyrazolyl) pyridine constituted a terpyridine analogue and readily formed a Ru(II) complex. By comparison of ^{1}H nuclear magnetic resonance patterns, it was found that the alkylations in the bis(pyrazolyl)pyridine series conferred an *anti,anti* conformation of the imino nitrogens. The pentadentates were then able to extract alkali metal ions into $CHCl_3$ with only modest strength and selectivity, but the preferred extraction of Li^+ by one of these was notable. By variation of the reaction conditions, a tri-iron(III) and a di-iron(III) complex were obtained from a bis(bidentate).

ROBERT DASH et PIERRE G. POTVIN. Can. J. Chem. **70**, 2249 (1992).

Des dérivés lipophiles de la 2,6-bis(3-pyrazolyle)pyridine et du 1,3-bis(3-pyrazolyle)benzène furent préparés en rendements acceptables par des réactions de Stork, puis *N*-alkylés pour fournir trois pentadentates, trois bis(bidentate) et un octadentate macrocyclique. En tant qu'analogue de la terpyridine, la bis(pyrazolyle)pyridine forma aisément un complexe au Ru(II). D'après la résonance magnétique nucléaire, les alkylations de la bis(pyrazolyle)pyridine ont forcé l'adoption de conformations *anti,anti* et les pentadentates étaient donc de modestes récepteurs pour les cations alkalins et ont démontré une faible sélectivité en extraction dans le chloroforme. Néanmoins, on souligne l'extraction préferentielle du Li^+ par l'un d'eux. Un bis(bidentate) forma, selon les conditions employées, des complexes bi- et tri-nucléaires avec le Fe(III).

Can. J. Chem. Downloaded from www.nrcresearchpress.com by 109.225.110.28 on 09/08/12
For personal use only.

Introduction

Rigid, poly-heterocyclic multidentate ligands/receptors offer a high degree of preorganization for the binding of metal ions and neutral organic molecules (for some recent examples, see ref. 1). For a variety of purposes, we sought rapid access to such molecules and chose the general architecture and the synthetic path illustrated in Scheme 1. Largely for reasons of synthetic simplicity, pyrazoles were chosen as binding sites to flank a central aromatic ring, in spite of the weaker basicity (2) and metal-binding ability (3) of pyrazole itself, relative to pyridine. Although several *N*-linked 2,6-bis(1-pyrazolyl)pyridines were recently prepared by facile reactions of pyrazolate ions with pyridyl halides (4), the linkage in Scheme 1 (*i.e.*, at the pyrazole 3-position) was dictated by a desire to apply the same methodology to develop both monotopic (X = N) and ditopic (X = CH) varieties of ligands. The parent 2,6-bis(3-pyrazolyl)pyridine has been prepared by a Mannich-type condensation (5). However, we additionally required substituents at the pyrazole 4- and 5-positions to ensure good liposolubility and poor solubility in water, and the Mannich reaction was not amenable to this. Claisen condensations involving methyl ketones had been used to prepare two 5-substituted analogues via bis(β-diketones) (6) but, in our hands, a similar condensation with cyclohexanone failed completely. We instead used Stork reactions (7) to form the bis(β-diketone) precursors that we required, and herein present short (two- or three-step) syntheses of a family of poly-heterocyclic ligands derived therefrom. We also report on our explorations of the complexing abilities of some of these and on the implications for future ligand design.

Results and discussion

In a model one-pot reaction, *N*-cyclohexen-1-yl-morpholine and Et_3N (1 equiv.) were treated with benzoyl chloride (1 equiv./0°C/THF) and hydrazine hydrate (1 equiv.). Extraction, chromatography, and recrystallization provided a 64% yield of **1**. However, the analogous one-pot reaction with 2, 6-di (chlorocarbonyl) pyridine (0.5 equiv.) provided only a 29% yield of **2***a* after chromatography and recrystallization, along with a 17% yield of **3** (identified only by nmr). Reasoning that **3** arose from *mono*-reacted material that had reacted further with the morpholine liberated during the hydrazine quench, $AlCl_3$ (0.5 equiv.) was added to the reaction mixture after the acid chloride and the mixture stood overnight before quenching and work-up. This provided a 40% yield of **2***a* and only a trace of **3**.

If the quench was carried out with H_2O, tetraketone **4***a* was obtained in 44% yield after chromatography and recrystallization, and this was quantitatively converted to **2***a* in a second step (2 equiv. $N_2H_4 \cdot H_2O/CH_2Cl_2$/room temp./15 min) with no need for a second chromatographic purification. Thus, the two-step process provided a modest increase in overall yield over the one-pot reaction. In entirely analogous fashion, isophthaloyl chloride was used to produce tetraketone **4***b* in 51% isolated yield, and bis-pyrazole **2***b* in quantitative yield thereafter.

Tetraketones **4***a* and **4***b* are interesting molecules in their own right. In entire analogy with 2,6-bis(3-oxobutanoyl)-pyridine (8) and 1,3-bis(3-oxobutanoyl)benzene (9), **4***b* was actually in the bis-enol form while **4***a* was a mixture of tautomers in $CDCl_3$ solution, and few useful nmr assignments could be made (there were at least three keto isomers present). Attempts to symmetrize its spectra by conversion to the dianion were hampered by its insolubility in purely aqueous solutions of base and by a tendency to undergo base-catalyzed ring-opening reactions in alcoholic solution. In the mass spectrometer (EI) both **4***a* and **4***b* showed molecular ions as well as loss of CO and 2-oxocyclohexyl radical. This, along with elemental analyses and conversions to the bis-pyrazoles, confirmed their structures. Unfortunately, attempts to produce 2:2 complexes (8) of either one with Zn^{2+}, Ni^{2+}, or

[1]Author to whom correspondence may be addressed.

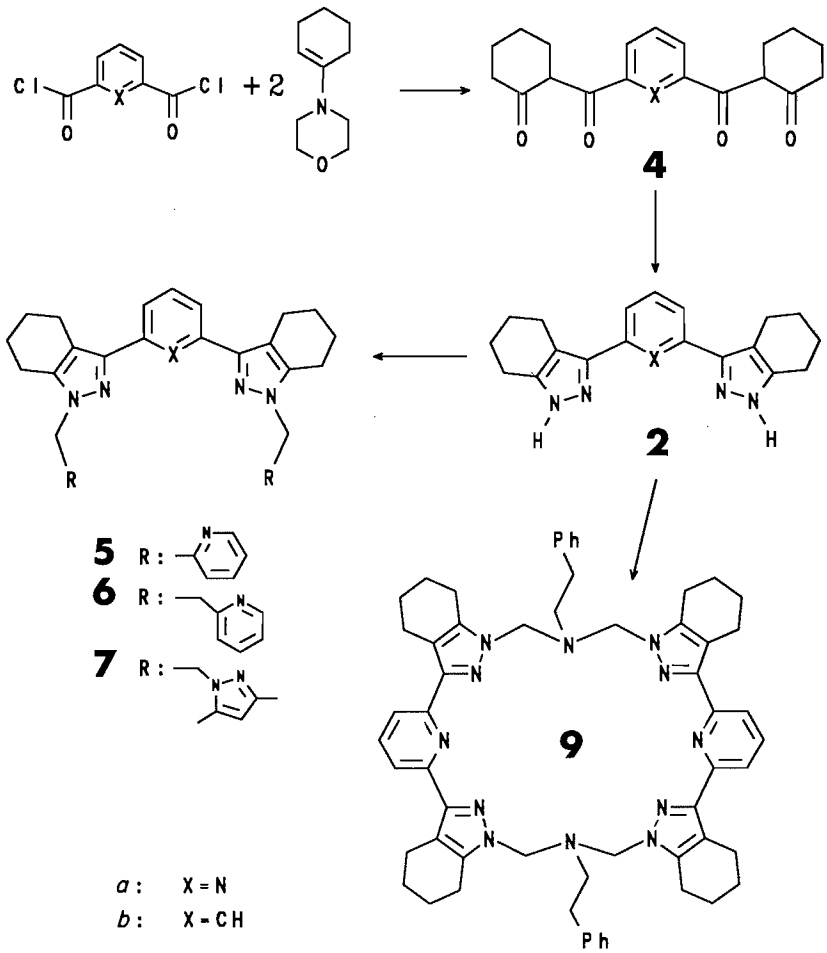

SCHEME 1

$Ti(O^iPr)_4$ met with failure. The bis-pyrazoles **2***a* and **2***b* gave symmetric nmr spectra and were further characterized by mass spectrometry (both showed molecular ions and loss of N_2) and elemental analyses.

As a fairly rigid tridentate, **2***a* readily formed a purple-red Ru(II) complex by reaction with $Ru(DMSO)_4Cl_2$ (10) (0.5 equiv./EtOH/reflux/1 day), followed by precipitation and recrystallization (72% yield). The nmr spectra were symmetric, showing downfield displacements of the signals due to the pyridine nuclei, and the electronic spectrum included a band at 432 nm (ϵ 4.7 mM^{-1} cm^{-1}) more reminiscent of the MLCT bands of the complexes of terpyridine (473 nm, ϵ 16.2 mM^{-1} cm^{-1}) and bipyridine (452 nm, ϵ 14.6 mM^{-1} cm^{-1}) (11) than was that at 377 nm obtained with the *N*-linked analogue, 2,6-bis(1-pyrazolyl)pyridine (12). Its redox chemistry will be reported elsewhere.

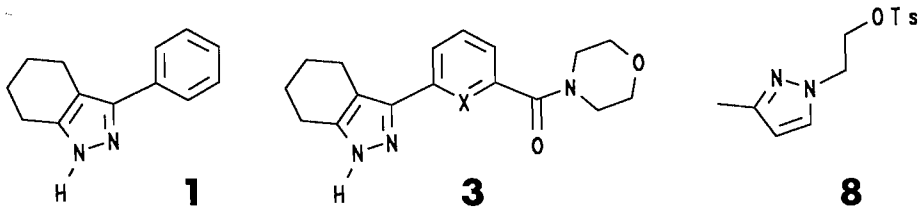

In a procedure borrowed from the literature (13), the successive treatment of bis(pyrazolyl)pyridine **2***a* with NaH (2.4 equiv./THF/room temp./2 h) and picolyl chloride (2.3 equiv./THF/room temp./overnight), followed by dilution with H_2O, extraction into CH_2Cl_2, chromatography, and recrystallization provided **5***a* in 69% isolated yield. An entirely similar alkylation with 2-(2-pyridyl)ethyl tosylate afforded **6***a* in 51% yield. Our first attempt to prepare the tetrapyrazole analogue **7***a* involved the condensation of tetraketone **4***a* with 2-hydroxyethylhydrazine. This, unfortunately, gave a mixture of *in/out* isomers, as revealed by ^1H nmr, that were poorly resolved by chromatography. Instead, hydroxyethylhydrazine was converted to **8** by condensation with acetylacetone and tosylation (72% overall yield). When **8** was used in the alkylation of **2***a* as before, **7***a* was obtained in 58% yield.

Can. J. Chem. Downloaded from www.nrcresearchpress.com by 109.225.110.28 on 09/08/12
For personal use only.

Can. J. Chem. Downloaded from www.nrcresearchpress.com by 109.225.110.28 on 09/08/12
For personal use only.

In entirely similar reactions, bis(pyrazolyl)benzene **2***b* was transformed into **5***b*, **5***b*, and **7***b* in 65, 49, and 59% isolated yields, respectively.

All of these materials were crystalline and H_2O-insoluble. In the mass spectrometer, all fragmented in the same way with loss of their appendages: **5***a*/*b* and **6***a*/*b* lost pyridinyl, pyridinylmethyl and (or) pyridinylethyl radicals, while **7***a*/*b* lost the corresponding dimethylpyrazole-containing radicals. The ^1H and ^{13}C nmr spectra showed symmetry and were entirely as expected, except that the pairs of CH_2 groups in **7***a* and **7***b* coincidentally overlapped in their ^1H nmr spectra, appearing as singlets in each case. Although these alkylations might have produced *in,in* and *in,out* isomers as well as the *out,out* form depicted, a single symmetric isomer was isolated in each case, and the exclusive production of *in,in* isomers would be discountable on steric grounds. Certainly, an *out,out*-directing effect could be expected in the alkylations of **2***a* if its dianion was able to complex Na^+. Moreover, the ability of the resulting series of ligands to complex alkali metal ions (*vide infra*) support this assignment.

Several attempts were made to convert **2***a* to a macrocyclic ligand. The literature reports several pyrazole-containing macrocycles (6, 14, 15). Of special interest to us were a bicyclic cryptand from a 3+2 alkylation of ammonia with a doubly electrophilic 2,2′-bipyrazole (15) and a macromonocycle obtained by 2+2 alkylation of 2,6-bis(5-methylpyrazol-3-yl)pyridine with bis(chloromethyl) ether (6). However, this latter reaction proceeded in only 2% yield and was accompanied by more substantial amounts of the 1+1 product. Several reactions of **2***a* with KBH_4 were carried out with a view to produce macrocyclic (2+2) and macrobicyclic (3+2) pyrazolyl hydridoborates (16), but these were slow and gave only insoluble materials. Reactions with base and coupling with CH_2Cl_2 or CH_2I_2 failed to provide identifiable products. However, reaction with aqueous HCHO[2] was instantaneous and produced an unstable, symmetric bis(*N*-hydroxymethyl) derivative (identified only by nmr). This was condensed with 2-phenylethylamine *in situ* and macrocycle **9** precipitated over a period of several weeks. Filtration, chromatography, and recrystallization provided an 18% yield. That this was indeed a 2+2 condensation product was shown by mass spectrometry: although no molecular (or heavier) ions were seen by either EI or FAB techniques, the heaviest fragments observed (up to *m*/*z* 918) well exceeded the molecular weight of a 1+1 product. Further, **9** in $CDCl_3$ was able to dissolve solid sodium picrate with colour entrainment, severely broadened ligand nmr signals, and the appearance of a singlet due to picrate ion. (Ligands **2***a* and **5***a* gave the same results.) A 1+1 product, arising from *in,in* alkylation, would not be expected to bind metal ions. This also confirmed that alkylation proceeded to give *out,out* products. Complexation studies with **9** and both cations and anions are planned and will be reported in due course. Unfortunately, the analogous condensations with histamine (to furnish pendant imidazole ligating groups) or ammonia (to provide a bicyclic analogue) did not proceed to completion.

With such floppy terminal pyridine and dimethylpyrazole groups, the pyridine series of acyclic ligands could not be expected to be ideally pre-organized for the binding of metal ions in their cavities. An examination of the aromatic regions in the ^1H nmr spectra was instructive in that regard. In Table 1 are reproduced the chemical shifts of the singlet (H-2 in the *b* series), doublet (H-3/5 in the *a* series, H-4/6 in the *b* series), and triplet signals (H-4 in the *a* series, H-5 in the *b* series) from this family of molecules. In the *a* series, the doublet was upfield of the triplet in **2***a* but moved downfield of the triplet upon alkylation. The triplet was less affected, but was shifted slightly upfield, probably a reflection of the electron-donating character of the *N*-CH_2 groups. In the *b* series, the doublet was consistently downfield of the triplet but shifted further downfield in the *N*-alkylated molecules, as did the singlet. The position of the triplet changed little. (The nmr data for the 2,6-bis(5-alkylpyrazol-3-yl)-pyridine (6) were reported in insufficient detail to allow comparisons.) Given that the doublets would normally be expected to appear downfield of the triplet in both pyridine and benzene series on purely electronic grounds (as was the case with the diacid chlorides), our interpretations of the pattern changes are as follows.

(*a*) The bis(pyrazolyl)pyridine **2***a* is in a planar conformation with the nitrogens held *syn* to one another (as must also be true of **2***a* in the Ru complex) by virtue of hydrogen bonds between *in*-NH and pyridine N. (Molecular mechanics calculations suggested that the *anti,anti* and *syn,anti* forms of **2***a* were in fact the most stable, but these calculations could not take hydrogen bonding into account and mostly reflect steric effects.) This would give rise to a shielding of the pyridine H-3/5 by the cyclohexene CH_2 groups.

(*b*) *N*-Alkylation of **2***a* caused a reversion to *anti* forms, analogous to that adopted by 2,2′-bipyridine (17), and a loss of that shielding. (Similarly, "tetraketone" **4***a* probably also preferred *anti* forms.) Complexation with metal ions would be expected to force a *syn,syn* arrangment with the operation of the shielding effect. This appeared to be the case with Ru(II), but could not be confirmed with Na^+ due to signal broadening and overlap (*vide supra*).

(*c*) In the benzene series, the conformational preferences are weaker, and H-2 and H-4/6 were about equally affected by *N*-alkylation.

Therefore, even the bis(pyrazolyl)pyridine cores of **5***a*–**7***a* were not well pre-organized for binding and only moderate binding strengths could then be expected, although this could be offset somewhat by the strongly dipolar nature of the imino sites. However, this and the rapid complex formation and dissociation rates afforded by acyclic ligands such as these are beneficial and necessary characteristics for efficient passive ion transport (18).

To test this, the association constants in $CHCl_3$ between these ligands and a series of picrate salts were measured by Cram's uv method (19), assuming 1:1 complexes. These are displayed in Fig. 1 As expected, the binding was only moderate throughout. It would appear that **5***a* preferred Li^+ and that **6***a* preferred Na^+. However, all three bound K^+ about equally well and Na^+ was bound equally well by **5***a* and **6***a*. Thus, Li^+ rejected **6***a* and **7***a*, and Na^+ rejected **7***a*, likely due to intra-ligand repulsions and distortions induced by these smaller ions. Nevertheless, the extraction of Li^+ by a polyaza acyclic ligand is notable and comparable in efficiency to extractions with rigid, acyclic oligo(tetrahydropyrans) (20). None of the ligands bound well to the large Cs^+ nor to NH_4^+, which ideally requires a tetrahedral array of H-bond acceptors. Clearly, a greater degree of pre-organization would be

[2]J. de Mendoza, personal communication.

TABLE 1. The ^{1}H nmr chemical shifts (in ppm) of singlet (s), doublet (d), and triplet (t) patterns in the aromatic regions

Pyridine (*a*) series			Benzene (*b*) series			
Compound	d	t	Compound	s	d	t
2,6-Diacid chloride	8.40	8.22	1,3-Diacid chloride	8.82	8.44	7.77
4*a*[a]	8.20	8.00	**4***b*	7.70	7.62	7.49
2*a*	7.46	7.81	**2***b*	7.87	7.60	7.47
(**2***a*)$_2$RuCl$_2$	7.93	8.08	**5***b*	8.08	7.73	7.44
5*a*	7.88	7.71	**6***b*	8.00	7.71	7.46
6*a*	7.85	7.72	**7***b*	7.97	7.68	7.44
7*a*	7.81	7.71				
9	7.89	7.70				

[a]Peak positions of the major product.

required for stronger binding of alkali metal ions. A second covalent linkage between pyridine and pyrazole rings would impose the required *syn,syn* conformation but this would be synthetically difficult to achieve. At least, replacement of the fused cyclohexanes with long alkyl chains at the pyrazole 5-positions would help to reduce the steric hindrance to the adoption of the *syn,syn* conformation in the triaromatic cores.

Ligands **5***b*, **6***b*, and **7***b* are ditopic bisbidentates and should be suitable for two small transition metals ions. We were particularly interested in a biomimetic (21) μ-oxo-bis(μ-carboxylato)di-iron(III) complex. In our first attempt, $FeCl_3 \cdot 6H_2O$ (2.0 equiv./EtOH/room temp.) was added to a solution of **5***b* in EtOH and a red-brown solid, analyzing for (**5***b*)$_2$Fe$_3$Cl$_9$, immediately precipitated in 49% yield, based on ligand. A possible structure is **10**, where the central ligand is in an *anti* conformation, although a *syn* form with possible chloride bridging cannot be excluded. Its visible light spectrum included absorption bands at 330 nm (ε 5043 M^{-1} cm^{-1}) and at 450 nm (ε 744 M^{-1} cm^{-1}), reminiscent of bands by the μ-oxo bis(μ-carboxylato)chlorobipyridine iron(III) dimer of Vincent *et al.* (22) at 329 nm (ε 6060 M^{-1} cm^{-1}) and at 464 nm (ε 387 M^{-1} cm^{-1}). It appeared that the assembly of this trimetallic array was initiated by the rapid binding of one metal to sites from two separate ligands followed by reaction with the pendant sites, leaving unreacted $FeCl_3$ (eq. [1]). This could be used to advantage to prepare hetero-trimetallic complexes and perhaps higher oligomeric materials in a controlled manner by repeated and alternating additions of ligand and metal.

[1] $2\ L + 4\ FeCl_3 \rightarrow L_2Fe_3Cl_9 + FeCl_3$

However, to circumvent this in a second attempt, slow, inverse addition and heat were employed and little precipitation occurred. After treatment with Et_3N and HOAc, and prolonged heating, the solution changed from red to green, the colour typical of μ-oxo-bis(μ-carboxylato)diiron(III) cores (22–24). Filtration and trituration provided light green crystals that analyzed for (**5***b*)$_3$Fe$_2$(OAc)Cl$_5$, for which a symmetric μ-carboxylato structure with unused ligand sites can be drawn (**11**). The yield, based on ligand, was only 27%. Its visible light spectrum consisted of a similar MLCT band at 369 nm (ε 1469 M^{-1} cm^{-1}) and a much broader *d–d* transition centred near 631 nm (ε 127 M^{-1} cm^{-1}), similar to that shown by met-chloro hemerythrin (656 nm, ε 180 M^{-1} cm^{-1}) (25). Though this was not the exclusive product (there was an insoluble brown material produced here as well), the tendency for the metal to bind two ligands was a problem here again.

A third attempt made use of the pre-formed μ-oxo dimer (Et$_4$N)$_2$Fe$_2$OCl$_6$(26) and the more hindered ligand **7***b* in the prescribed manner (23), but this resulted in the recovery of unreacted ligand.

We ascribe our difficulties in forming a μ-oxo complex to the inability of the bidentate units in these ligands to twist

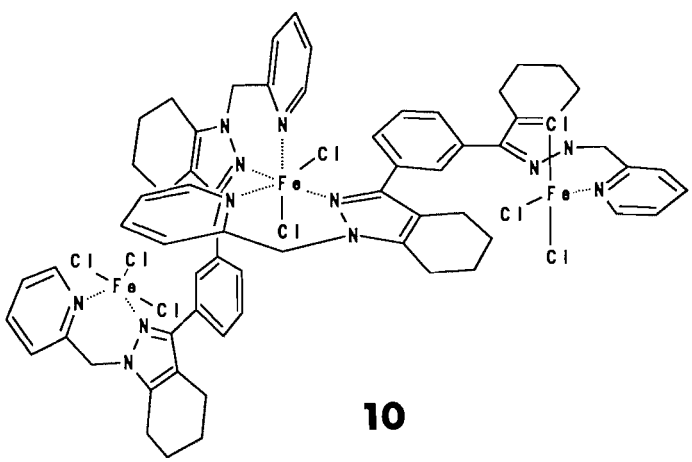

10

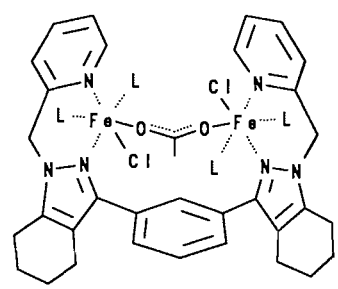

11

Can. J. Chem. Downloaded from www.nrcresearchpress.com by 109.225.110.28 on 09/08/12
For personal use only.

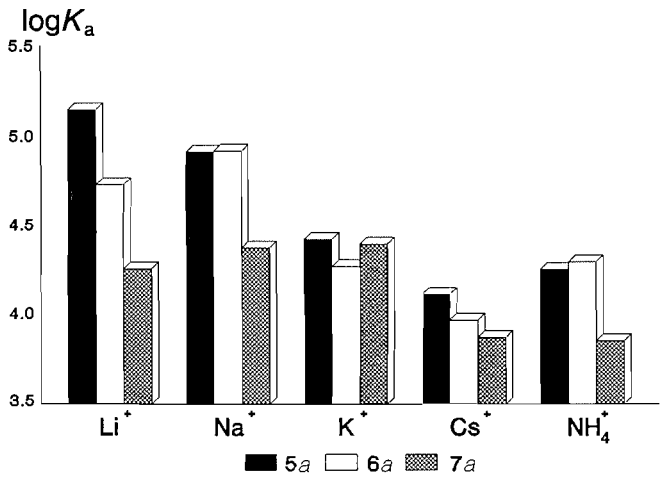

FIG. 1

into sufficient proximity to wrap around a μ-oxo dimer core without hindrance from the benzene H-2 and (or) between the terminal pyridines, although molecular modelling suggested that this should have been possible. One might use a more flexible polymethylene linkage between the metal binding sites but Stork reactions with flexible diacid chlorides are known to not proceed in the required manner (27) and loosely linked ditopic ligands have a tendency to form plynuclear Fe(III) complexes (21). One could instead use phenoxo bridges (28), with ligands based on 2,6-bis(3-pyrazol)phenol. Work on this problem is underway.

Experimental section

All solvents used were reagent grade and used without drying or purification, except for THF, which was distilled over K and benzophenone. The petroleum ether used was the light fraction (bp 30–60°C). *N*-(Cyclohexen-1-yl)morpholine was prepared according to Hünig *et al.* (29). 2-(2-Pyridinyl)-ethyl tosylate was prepared by tosylation in the usual manner of the commercial alcohol. All melting points were determined on a Fisher–Johns apparatus. Nuclear magnetic resonance spectra were measured on a Bruker AM-300 spectrometer, operating at 300.13 MHz (^{1}H) or 75.1 MHz (^{13}C), run either in $CDCl_3$, with TMS as internal reference (at 0.00 ppm in ^{1}H spectra, and at 77.00 ppm for ^{13}C), or in $CDCl_3$/CD_3OD, with TMS or CD_2HOD (3.30 ppm in ^{1}H spectra, and at 49.00 ppm in ^{13}C) as the internal references. Ultraviolet and visible spectra were obtained on a Hewlett–Packard 8451A diode array spectrophotometer. Microanalyses were performed by Canadian Microanalytical Services, Burnaby, B.C., and Guelph Laboratories Ltd., Guelph, Ont.. Molecular modelling was performed using PC-MODEL (Serena Software, Bloomington, Indiana).

1H-3-Phenyl-4,5,6,7-tetrahydrobenzopyrazole, 1

Benzoyl chloride (1.00 mL, 8.54 mmol) was added dropwise to a stirring solution of 1-(cyclohexen-1-yl)morpholine (1.44 mL, 8.60 mmol) and triethylamine (1.20 mL, 8.60 mmol) in THF (25 mL) under nitrogen while cooling in an ice-water bath. A white precipitate (Et_3NHCl) formed immediately. The mixture was stirred for several hours, then treated with hydrazine hydrate (0.42 mL, 8.60 mmol). The mixture was washed with water (10 mL) and the crude product was isolated by extraction with CH_2Cl_2. Purification was carried out by column chromatography on alumina using 2:98 MeOH:CH_2Cl_2 as eluent. The pyrazole was recrystallized from EtOH (1.08 g, 64% yield), mp 123–125°C; ^{1}H nmr ($CDCl_3$) δ: 1.80 (m, 4H), 2.63 (m, 2H), 2.72 (m, 2H), 7.30 (m, 1H), 7.38 (m, 2H), 7.64 (d, 2H, J = 7.3 Hz) ppm, ^{13}C nmr ($CDCl_3$) δ: 22.08, 22.22, 22.66, 23.58, 112.93, 126.58, 127.24, 127.67, 128.50, 132.96, 144.31 ppm; ms, m/z(%) = 198 ($M^{+\cdot}$, 90), 170 (100), 95 (20), 77 (20), 49 (20). Anal. calcd. for $C_{13}H_{14}N_2$: C 78.75, H 7.12, N 14.13; found: C 78.61, H 7.03, N 14.14.

*2,6-Di(2-oxocyclohexanecarbonyl)pyridine, 4*a

A solution of 1-(cyclohexen-1-yl)morpholine (9.08 mL, 54.0 mmol) and Et_3N (7.53 mL, 54.0 mmol) in THF (50 mL) was slowly added to a stirring solution of 2,6-pyridinedicarboxylic acid chloride (5.0 g, 24.5 mmol) in THF (100 mL) under Ar while cooling in an ice-water bath. Et_3NHCl immediately precipitated. Then $AlCl_3$ (1.63 g, 12.2 mmol) was carefully added and the resulting mixture was allowed to stand overnight. After the addition of water (30 mL), the mixture was stirred vigorously for 1 h. The crude product was isolated by extraction with CH_2Cl_2. Purification was carried out by column chromatography on silica gel using 30:70 EtOAc:petroleum ether as eluent. The product was recrystallized from Et_2O to give white crystals (3.52 g, 44% yield), mp 112–114°C. Overlap of ^{1}H nmr signals made assignments impossible; ^{13}C nmr ($CDCl_3$) δ: 21.62, 23.10, 23.26, 23.61, 24.06, 25.34, 25.73, 27.67, 27.79, 29.03, 29.27, 29.40, 33.29, 42.44, 42.65, 42.69, 57.27, 57.70, 58.10, 108.03, 122.93, 124.55, 125.29, 125.44, 127.39, 138.01, 138.35, 138.39, 151.12, 151.54, 154.62, 184.60, 192.06, 197.87, 198.74, 208.09, 208.71, 208.83 ppm; ms, m/z(%): 327 ($M^{+\cdot}$, 100), 299 (35), 271 (50), 243 (16), 230 (10), 202 (23), 176 (77). Anal. calcd. for $C_{19}H_{21}NO_4$: C 69.71; H 6.47, N 4.28; found: C 69.47, H 6.41, N 4.31.

*1,3-Di(2-oxocyclohexanecarbonyl)benzene, 4*b

Following the procedure described above for **4***a*, isophthaloyl dichloride (5.0 g, 24.6 mmol) was used instead. The product was recrystallized from CCl_4 to give white crystals (4.01 g, 51% yield), mp 125–127°C; ^{1}H nmr ($CDCl_3$) δ: 1.63 (m, 4H), 1.78 (m, 4H), 2.41 (m, 4H), 2.50 (m, 4H), 7.49 (t, 1H, J = 7.7 Hz), 7.62 (d, 2H, J = 7.7 Hz), 7.70 (s, 1H), 13.14 (s, 2H) ppm; ^{13}C nmr ($CDCl_3$) δ: 21.71, 23.32, 26.31, 32.64, 107.04, 126.72, 127.98, 129.37, 137.32, 189.92, 190.11 ppm; ms, m/z(%): 326 ($M^{+\cdot}$, 30), 298 (5), 270 (5), 229 (100), 200 (60), 185 (10). Anal. calcd. for $C_{20}H_{22}O_4$: C 73.60, H 6.79; found: C 73.22, H 6.83.

*2,6-Di(1H-4,5,6,7-tetrahydrobenzopyrazol-3-yl)pyridine, 2*a

Hydrazine hydrate (1.10 mL, 22.6 mmol) was added to a solution of tetraketone **4***a* (3.52 g, 10.8 mmol) in CH_2Cl_2 (25 mL) at room temperature. Precipitation occurred and the reaction was complete in 15 min. The product was collected by vacuum filtration, with a second crop obtained after evaporation of the solvent. The product was recrystallized from MeOH to give white crystals (3.43 g, >99% yield), mp 275–277°C; ^{1}H nmr ($CDCl_3$/CD_3OD) δ: 1.88 (br, 8H), 2.73 (br, 4H), 2.85 (br, 4H), 7.46 (d, 2H, J = 7.9 Hz), 7.81 (t, 1H, J = 7.9 Hz ppm; ^{13}C nmr ($CDCl_3$/CD_3OD) δ: 22.19, 22.55, 22.90, 23.20, 113.73, 118.05, 137.33, 148.83 ppm. MS, m/z(%): 319 ($M^{+\cdot}$, 100), 290 (20), 265 (10), 205 (10), 149 (10), 95 (8). Anal. calcd. for $C_{19}H_{21}N_5 \cdot 1/2H_2O$: C 70.45, H 6.69, N 21.62; found: C 70.09, H 6.58, N 21.85.

(2a)$_2$ RuCl$_2$

Bispyrazole **2***a* (0.100 g, 0.31 mmol) and $RuCl_2(DMSO)_4$ (0.080 g, 0.16 mmol) were dissolved in EtOH (5 mL) and the mixture heated to reflux for 1 day. The solution turned pink after 15 min and was a dark purple after overnight reaction. The solution was cooled and most of the solvent was removed. Addition of ether precipitated the purple complex. This was filtered and washed with ether. Recrystallization from CH_3CN/H_2O gave purple crystals (0.090 g, 72%), mp > 350°C; uv–vis (EtOH): 432 nm (ε = 4736 M^{-1} cm^{-1}), 536 nm (ε = 1513 M^{-1} cm^{-1}); ^{1}H nmr ($CDCl_3$/CD_3OD) δ: 1.77 (br, 4H), 1.82 (br, 4H), 2.50 (br, 4H), 2.95 (br, 4H), 7.93 (d, 2H, J = 7.8 Hz), 8.08 (t, 1H, J = 7.8 Hz) ppm; ^{13}C nmr ($CDCl_3$/CD_3OD) δ: 20.17, 20.52, 21.23, 21.99, 115.77, 117.70, 135.22, 142.41, 149.36, 154.01 ppm. Anal. calcd. for $C_{38}H_{42}N_{10}RuCl_2 \cdot 4H_2O$: C 51.72, H 5.70, N 15.87; found: C 51.38, H 5.16, N 16.00.

*1,3-Di(1H-4,5,6,7-tetrahydrobenzopyrazol-3-yl)benzene, 2*b

Following the procedure described above for **2***a*, the tetraketone **4***b* (3.00 g, 9.4 mmol) was treated with hydrazine hydrate

Can. J. Chem. Downloaded from www.nrcresearchpress.com by 109.225.110.28 on 09/08/12
For personal use only.

Can. J. Chem. Downloaded from www.nrcresearchpress.com by 109.225.110.28 on 09/08/12
For personal use only.

(0.95 mL, 19.5 mmol). The product was recrystallized from MeOH to give light brown crystals (2.93 g, >99% yield), mp 164–166°C; ^{1}H nmr ($CDCl_3/CD_3OD$) δ: 1.86 (br, 8H), 2.73 (br, 8H), 7.47 (t, 1H, J = 7.5 Hz), 7.60 (d, 2H, J = 7.5 Hz), 7.87 (s, 1H) ppm; ^{13}C nmr ($CDCl_3/CD_3OD$) δ: 21.94, 22.17, 22.53, 23.45, 112.74, 124.52, 125.25, 128.57, 132.70, 143.49, 144.78 ppm; ms, m/z(%): 318 ($M^{+\cdot}$, 100), 290 (37), 242 (16), 225 (31), 214 (16), 197 (10), 131 (10), 95 (30). Anal. calcd. for $C_{20}H_{22}N_4 \cdot CH_3OH$: C 71.97, H 7.48; N 15.99; found: C 72.29, H 7.32, N 16.12.

2,6-Di(1-(pyridin-2-yl)methyl-4,5,6,7-tetrahydrobenzopyrazol-3-yl)pyridine **5**a

Bispyrazole **2***a* (0.50 g, 1.57 mmol) was dissolved in THF (15 mL) and slowly added to a stirring suspension of NaH (0.181 g 50% oil dispersion, 3.76 mmol) in THF (15 mL). There was an immediate release of H_2 gas and formation of a white precipitate (sodium pyrazolide salt). The resulting mixture was kept under Ar and stirred for 2 h at room temperature. Picolyl chloride (0.460 g, 3.61 mmol) was added to this solution and the mixture allowed to stand overnight. This solution was then washed with water and the crude product was isolated by extraction with CH_2Cl_2. Purification was carried out by column chromatography on alumina using 80:20 EtOAc:petroleum ether as eluent, and recrystallization from CH_3CN to give light brown crystals (0.540 g, 69% yield), mp 167–168°C; ^{1}H nmr ($CDCl_3$) δ: 1.81 (m, 8H), 2.54 (m, 4H), 3.01 (m, 4H), 5.45 (s, 4H), 6.90 (d, 2H, J = 7.8 Hz), 7.17 (m, 2H), 7.61 (m, 2H), 7.71 (t, 1H, J = 7.7 Hz), 7.88 (d, 2H, J = 7.7 Hz), 8.56 (d, 2H, J = 4.3 Hz) ppm; ^{13}C nmr ($CDCl_3$) δ: 21.58, 22.33, 22.93, 23.18, 54.59, 116.30, 119.36, 121.20, 122.36, 136.41, 137.09, 140.19, 148.07, 149.00, 153.23, 157.21 ppm; ms, m/z(%): 501 ($M^{+\cdot}$, 100), 424 (20), 409 (45), 316 (6), 251 (5), 92 (11). Anal. calcd. for $C_{31}H_{31}N_7$: C 74.22, H 6.23, N 19.55; found: C 73.99, H 6.26, N 19.52.

2,6-Di(1-(2-pyridin-2-yl)ethyl-4,5,6,7-tetrahydrobenzopyrazol-3-yl)pyridine **6**a

Following the procedure described above for **5***a*, bispyrazole **2***a* (0.49 g, 1.54 mmol) was treated with 2-(2-pyridinyl)ethyl tosylate (1.08 g, 3.90 mmol). Recrystallization from CH_3CN gave light brown crystals (0.415 g, 51% yield), mp 138–140°C; ^{1}H nmr ($CDCl_3$) δ: 1.67 (m, 8H), 2.26 (m, 4H), 2.91 (m, 4H), 3.35 (t, 4H, J = 6.9 Hz), 4.42 (t, 4H, J = 6.9 Hz), 6.94 (d, 2H, J = 7.8 Hz), 7.14 (m, 2H), 7.51 (m, 2H), 7.72 (t, 1H, J = 7.7 Hz), 7.85 (d, 2H, J = 7.7 Hz), 8.57 (d, 2H, J = 4.9 Hz) ppm; ^{13}C nmr ($CDCl_3$) δ: 21.45, 22.47, 22.90, 23.32, 38.96, 48.32, 115.09, 119.04, 121.53, 123.77, 136.24, 139.70, 147.74, 149.36, 153.54, 158.66 ppm; ms, m/z(%): 529 ($M^{+\cdot}$, 100), 437 (7), 424 (10), 332 (10), 318 (8), 106 (50). Anal. calcd. for $C_{33}H_{35}N_7$: C 74.83, H 6.66, N 18.51; found: C 74.43, H 6.70, N 18.53.

2.6-Di(1-(2-(3,5-dimethylpyrazol-1-yl))ethyl-4,5,6,7-tetrahydrobenzopyrazol-3-yl)pyridine **7**a

Following the procedure described above for **5***a*, bispyrazole **2***a* (0.51 g, 1.60 mmol) was treated with tosylate **8** (1.13 g, 3.85 mmol). Purification was carried out by column chromatography on alumina using 2:98 MeOH:CH_2Cl_2 as eluent and recrystallization from CH_3CN to give white crystals (0.522 g, 58% yield), mp 140–142°C; ^{1}H nmr ($CDCl_3$) δ: 1.63 (br, 8H), 1.67 (s, 6H), 1.94 (br, 4H), 2.22 (s, 6H), 2.85 (br, 4H), 4.39 (s, 8H), 5.67 (s, 2H), 7.71 (t, 1H, J = 7.7 Hz), 7.81 (d, 2H, J = 7.7 Hz) ppm; ^{13}C nmr ($CDCl_3$) δ: 9.71, 13.37, 20.48, 22.37, 22.72, 23.22, 48.72, 48.92, 104.74, 115.32, 119.06, 136.25, 140.37, 140.88, 148.05, 148.28, 153.31 ppm; ms, m/z(%): 563 ($M^{+\cdot}$, 100), 467 (18), 454 (16), 441 (18), 345 (24), 319 (21), 229 (27), 200 (25), 123 (40). Anal. calcd. for $C_{33}H_{41}N_9$: C 70.31, H 7.33; N 22.36; found: C 70.28, H 7.38, N 22.40.

2-(3,5-Dimethylpyrazol-1-yl) ethyl tosylate **8**

2-Hydroxyethylhydrazine (1.64 mL, 24.2 mmol) was added to 2,4-pentanedione (2.50 mL, 24.2 mmol) in THF (50 mL) and stirred at room temperature for 1 h before the addition of *p*-toluenesulfonyl chloride (5.70 g, 30.0 mmol) and triethylamine (4.18 mL, 30.0 mmol). The resulting mixture was allowed to reflux overnight. This solution was then stirred vigorously for 1 h after the addition of water (30 mL). The crude product was isolated by extraction with CH_2Cl_2. Purification was carried out by column chromatography on alumina gel using 30:70 EtOAc:petroleum ether as eluent and recrystallization from ether/petroleum ether to give white crystals (5.15 g, 72% yield); ^{1}H nmr ($CDCl_3$) δ: 2.11 (s, 3H, CH_3), 2.23 (s, 3H, CH_3), 2.44 (s, 3H, CH_3), 4.19 (t, 2H, J = 5.1 Hz, CH_2), 4.31 (t, 2H, J = 5.1 Hz, CH_2), 5.72 (s, 1H, pyrazole H), 7.28 (d, 2H, J = 8.2 Hz, tosyl H), 7.62 (d, 2H, J = 8.2 Hz, tosyl H) ppm; ^{13}C nmr ($CDCl_3$) δ: 10.87 (pyrazole CH_3), 13.28 (pyrazole CH_3), 21.55 (tosyl CH_3), 47.03 (CH_3), 68.56 (CH_2), 105.18 (pyrazole CH), 127.79 (tosyl CH), 129.76 (tosyl CH), 132.27 (tosyl C), 140.05 (pyrazole C), 144.81 (tosyl C), 148.08 (pyrazole C) ppm.

1,3-Di(1-(pyridin-2-yl)methyl-4,5,6,7-tetrahydrobenzopyrazol-3-yl)benzene **5**b

Following the procedure described above for **5***a*, bispyrazole **2***b* (0.25 g, 0.79 mmol) was treated with picolyl chloride (0.24 g, 1.90 mmol). Recrystallization from CH_3CN gave light brown crystals (0.255 g, 65% yield), mp 154–156°C; ^{1}H nmr ($CDCl_3$) δ: 1.87 (m, 8H), 2.53 (m, 4H), 2.78 (m, 4H), 5.42 (s, 4H), 6.89 (d, 2H, J = 7.8 Hz), 7.16 (m, 2H), 7.44 (t, 1H, J = 7.7 Hz), 7.60 (m, 2H), 7.73 (d, 2H, J = 7.7 Hz), 8.08 (s, 1H), 8.55 (d, 2H, J = 4.6 Hz) ppm; ^{13}C nmr ($CDCl_3$) δ: 21.61, 22.32, 22.51, 23.32, 54.60, 114.42, 121.24, 122.31, 125.24, 125.58, 128.63, 134.44, 137.02, 140.04, 148.15, 149.10, 157.53 ppm; ms, m/z(%): 500 ($M^{+\cdot}$, 100), 408 (95), 315 (20), 250 (7), 93 (32). Anal. calcd. for $C_{32}H_{32}N_6$: C 76.77, H 6.44, N 16.79; found: C 76.31, H 6.36, N 16.64.

(5b)$_2$Fe$_3$Cl$_9$

To a solution of **5***b* (0.125 g, 0.25 mmol) in EtOH (2 mL) was added a solution of $FeCl_3 \cdot 6H_2O$ (0.135 g, 0.50 mmol) in EtOH (3 mL). The immediate red-brown precipitate was collected by filtration, mp 294–302°C. Yield 91 mg (49%). Anal. calcd. for $C_{62}H_{62}Cl_9Fe_3N_{12}$: C 51.66, H 4.34; N 11.30, Cl 21.44; found: C 51.45; H 4.63, N 11.09, Cl 21.31.

(5b)$_3$Fe$_2$(OAc)Cl$_5$

To a stirring solution of $FeCl_3 \cdot 6H_2O$ (0.108 g, 0.40 mmol) in EtOH (10 mL) was slowly added a solution of **5***b* (0.100 g, 0.20 mmol) in EtOH (15 mL). A small amount of white precipitate formed when half of the ligand had been added. The remaining ligand was added at 60°C, whereupon the white precipitate redissolved. After refluxing for 2 h, HOAc (23 μL, 0.40 mmol) and Et_3N (56 μL, 0.40 mmol) were added. The reaction mixture was refluxed for 6-days, during which the colour changed from red to green, and a brown precipitate formed. This was removed by filtration (yield 25 mg) and found to be insoluble in all solvents tested except hot DMF. The filtrate was rid of solvents and the green oily residue was triturated with CH_3CN and recrystallized from that solvent to give light green crystals (33 mg, 27% yield), mp 181–183°C. Anal. calcd. for $C_{98}H_{99}Cl_5Fe_2N_{18}O_2 \cdot H_2O$:C 63.01; H 5.45, N 13.50, Cl 9.49; found: C 62.79; H 5.48, N 13.79, Cl 9.57.

1,3-Di(1-(2-pyridin-2-yl)ethyl-4,5,6,7-tetrahydrobenzopyrazol-3-yl)benzene **6**b

Following the procedure described above for **5***a*, bispyrazole **2***b* (0.11 g, 0.34 mmol) was treated with 2-(2-pyridine)-ethyl tosylate (0.25 g, 0.92 mmol). Recrystallization from CH_3CN/H_2O gave light brown crystals (0.090 g, 49% yield), mp 124–126°C; ^{1}H nmr ($CDCl_3$) δ: 1.68 (m, 8H), 2.25 (m, 4H), 2.69 (m, 4H), 3.35 (t, 4H, J = 7.0 Hz), 4.41 (t, 4H, J = 7.0 Hz), 6.92 (d, 2H, J = 7.8 Hz), 7.13 (m, 2H), 7.46 (t, 1H, J = 7.7 Hz), 7.52 (m, 2H), 7.71 (d, 2H, J = 7.7 Hz), 8.00 (s, 1H), 8.57 (d, 2H, J = 4.7 Hz) ppm; ^{13}C nmr ($CDCl_3$) δ: 21.35, 22.33, 22.38, 23.35, 39.03, 48.25, 113.07, 121.57, 123.86, 125.10, 125.36, 128.59, 134.56, 136.29, 139.64, 147,73, 149.32, 158.67 ppm. Anal. calcd. for $C_{34}H_{36}N_6 \cdot 1/2H_2O$: C 75.95, H 6.94, N. 15.63; found: C 75.65, H 6.51, N 15.63.

1,3-Di(1-(2-(3,5-dimethylpyrazol-1-yl))ethyl-4,5,6,7-tetrahydrobenzopyrazol-3-yl)benzene 7b

Following the procedure described above for **5***a*, bispyrazole **2***b* (0.34 g, 107 mmol) was treated with tosylate **8** (0.73 g, 2.48 mmol). Purification was carried out by column chromatography on alumina using 2:98 MeOH:CH_2Cl_2 as eluent and recrystallization from CH_3CN to give white crystals (0.355 g, 59% yield), mp 158–159°C; ^{1}H nmr ($CDCl_3$) δ: 1.63 (br, 8H), 1.64 (s, 6H), 1.91 (br, 4H), 2.22 (s, 6H), 2.66 (br, 4H), 4.38 (s, 8H), 5.66 (s, 2H), 7.44 (t, 1H, J = 7.7 Hz), 7.68 (d, 2H, J = 7.7 Hz), 7.97 (s, 1H) ppm; ^{13}C nmr ($CDCl_3$) δ: 9.72, 13.45, 20.48, 22.35, 23.38, 48.85, 48.92, 104.75, 113.41, 125.12, 125.50, 128.67, 134.52, 140.47, 140.87, 148.12, 148.38 ppm; ms, m/z(%): 562 ($M^{+\cdot}$, 100), 466 (30), 453 (7), 440 (10), 370 (95), 344 (50), 281 (10), 233 (12), 185 (11), 123 (40). Anal. calcd. for $C_{34}H_{42}N_8$: C 72.57, H 7.52, N 19.91; found: C 72.76, H 7.58, N 19.86.

Macrocycle **9**

Bispyrazole **2***a* (0.42 g, 1.32 mmol) and aqueous formaldehyde (0.20 mL, 2.67 mmol) were stirred for 2 h at room temperature in MeOH (25 mL), before the addition of phenylethylamine (0.17 mL, 1.32 mmol). Although a deposit soon appeared, the reaction mixture was left for several months, which resulted in the slow precipitation of a thick semisolid. The crude product was obtained by decanting off the supernatant. Purification was carried out by column chromatography on alumina using $CHCl_3$ as eluent, and recrystallization from CCl_4/EtOH to give light brown crystals (0.12 g, 18%), mp 144–147°C; ^{1}H nmr ($CDCl_3$) δ: 1.77 (br, 16H), 2.55 (br, 8H), 2.83 (br, 8H), 2.74 (br, 4H), 3.10 (br, 4H), 5.09 (br, 8H), 7.04 (m, 4H), 7.16 (m, 6H), 7.70 (t, 2H, J = 7.6 Hz), 7.89 (d, 4H, J = 7.6 Hz) ppm; ^{13}C nmr ($CDCl_3$) δ: 21.70, 22.51, 23.01, 23.28, 33.71, 51.12, 65.90, 125.86, 128.19, 128.66, 136.24, 116.11, 119.87, 139.18, 140.02, 147.66, 153.41 ppm. Anal. calcd. for $C_{58}H_{64}N_{12} \cdot H_2O$: C 73.54, H 7.02, N 17.74; found: C 73.51, H 6.63, N 18.18.

Extraction experiments

All operations were conducted at room temperature. Absorbances were determined at 380 nm with an Aminco DW-2a UV/VIS spectrophotometer. The picrate salts were dried under high vacuum before use. Aqueous solutions of the picrate salts were prepared in the 0.0118–0.029 M concentration range. Aliquots (0.4 mL) of the appropriate picrate solution were transferred with a Hamilton Gastight syringe into 1 mL Eppendorf tubes. To these tubes, 0.4 mL of 0.004–0.005 M $CDCl_3$ solutions of the hosts was added by syringe. The tubes were covered immediately to prevent evaporation, and shaken thoroughly using a Vortex Genie mixer for 2 min. The tubes were then placed in a centrifuge for 3 min at high speeds. Aliquots of 0.200 mL of the organic phase were carefully removed by syringe and transferred to 5-mL volumetric flasks, which were then brought to the mark with CH_3CN. The absorbance of each sample was then determined and the R and K_a values were calculated according to Cram's equations (19).

Acknowledgements

The authors thank the Natural Sciences and Engineering Research Council of Canada for financial support and a referee for useful suggestions concerning our conformational analysis.

1. T. W. Bell and F. Guzzo. J. Am. Chem. Soc. **106**, 6111 (1984); S.-K. Chang and A. D. Hamilton. J. Am. Chem. Soc. **110**, 1318 (1988); T. W. Bell and J. Liu. J. Am. Chem. Soc. **110**, 3673 (1988); T. R. Kelly and M. P. Maguire. J. Am. Chem. Soc. **109**, 6549 (1987); T. R. Kelly, C. Zhao, and G. J. Bridges. J. Am. Chem. Soc. **111**, 3744 (1989); V. Hegde, P. Madhukar, J. D. Madura, and R. P. Thummell. J. Am. Chem. Soc. **112**, 4549 (1990); T. W. Bell, A. Firestone, and R. Ludwig. J. Chem. Soc. Chem. Commun. 1902 (1989).
2. A. Alberty. *In* Physical methods in heterocyclic chemistry. Vol. 1. *Edited by* A. R. Katritzky. Academic Press, New York. 1963. p. 44.
3. L. G. Sillen and A. E. Martell. Chem. Soc. Spec. Publ. No. 25, 280 (1971); 369 (1971).
4. D. L. Jameson and K. A. Goldsby. J. Org. Chem. **55**, 4992 (1990); A. A. Watson, D. A. House, and P. J. Steel. J. Org. Chem. **56**, 4072 (1991).
5. Y. Lin and S. A. Lang, Jr. J. Heterocycl. Chem. **14**, 345 (1977).
6. M. Gal, G. Tarrago, P. Steel, and C. Marzin. Nouv. J. Chim. **9**, 617 (1985).
7. G. Stork, A. Brizzolara, H. Landesman, J. Szmuszkovicz, and R. Terrell. J. Am. Chem. Soc. **85**, 207 (1963).
8. D. E. Fenton, J. R. Tate, U. Casellato, S. Tamburini, P. A. Vigato, and M. Vidali. Inorg. Chim. Acta, **83**, 23 (1984).
9. D. E. Fenton, C. M. Regan, U. Casellato, and P. A. Vigato. Inorg. Chim. Acta, **58**, 83 (1982).
10. I. P. Evans, A. Spencer, and G. Wilkinson. J. Chem. Soc. Dalton Trans. 204 (1973).
11. S. T. Lin, W. Bottcher, M. Chou, C. Creutz, and N. Sutin. J. Am. Chem. Soc. **98**, 6536 (1976).
12. D. L. Jameson, J. K. Blaho, K. T. Kruger, and K. A. Goldsby. Inorg. Chem. **28**, 4312 (1989).
13. P. Steel and E. C. Constable. J. Chem. Res. Miniprint, 1601 (1989).
14. J. Elguero, P. Navarro, and M. I. Rodriguez-Franco. Chem. Lett. 425 (1984); J. Elguero, P. Navarro, M. I. Rodriguez-Franco, F. H. Cano, C. Foces-Foces, and A. Samat. J. Chem. Res. Synop. 312 (1985); A. Ramdani and G. Tarrago. Tetrahedron, **37**, 991 (1981); B. Lupo, M. Gal, and G. Tarrago. Bull. Soc. Chim. Fr. 464 (1984); B. Lupo and G. Tarrago. Bull. Soc. Chim. Fr. 464 (1984); G. Tarrago, I. Zidane, C. Marzin, and A. Tep. Tetrahedron, **44**, 91 (1988); J. C. Cuevas, J. de Mendoza, and P. Prados. J. Org. Chem. **53**, 2055 (1988).
15. O. Juanes, J. de Mendoza, and J.-C. Rodriguez-Ubis. J. Chem. Soc. Chem. Commun. 1765 (1985).
16. S. Trofimenko. Chem. Rev. **72**, 497 (1972).
17. L. L. Merritt, Jr. and E. D. Schröder. Acta Crystallogr. **9**, 801 (1956).
18. J.-P. Behr, M. Kirch, and J.-M. Lehn. J. Am. Chem. Soc. **107**, 241 (1985).
19. S. Moore, T. Tarnowski, M. Newcomb, and D. J. Cram. J. Am. Chem. Soc. **99**, 6398 (1977).
20. T. Iimori, A. Rheingold, D. Staley, and W. C. Still. J. Am. Chem. Soc. **111**, 3439 (1989).
21. S. J. Lippard. Angew. Chem. Int. Ed. Engl. **27**, 344 (1988).
22. J. B. Vincent, J. C. Huffman, G. Christou, Q. Li, M. A. Nanny, D. N. Hendrickson, R. H. Fong, and R. H. Fish. J. Am. Chem. Soc. **110**, 6898 (1988).
23. W. H. Armstrong, A. Spool, G. C. Papaefthymiou, R. B. Frankel, and S. J. Lippard. J. Am. Chem. Soc. **106**, 3653 (1984).
24. P. Gomez-Romero, N. Casan-Pastor, A. Ben-Hussein, and G. B. Jameson. J. Am. Chem. Soc. **110**, 1988 (1988).
25. K. Garbett, D. W. Darnall, I. M. Klotz, and R. J. P. Williams. Arch. Biochem. Biophys. **135**, 419 (1969).
26. W. H. Armstrong and S. J. Lippard. Inorg. Chem. **24**, 981 (1985).
27. S. Hünig and E. Lücke. Adv. Org. Chem. **4**, 1 (1963).
28. K. D. Karlin, R. W. Cruse, Y. Gultneh, J. C. Hayes, and J. Zubieta. J. Am. Chem. Soc. **106**, 3372 (1984); A. Borovik, L. Que, Jr., V. Papaefthymiou, E. Münck, L. F. Taylor, and O. P. Anderson. J. Am. Chem. Soc. **110**, 1986 (1988).
29. S. Hünig, E. Lücke and W. Brenninger. Org. Synth. Collect. Vol. **5**, 808 (1973).

Can. J. Chem. Downloaded from www.nrcresearchpress.com by 109.225.110.28 on 09/08/12
For personal use only.

The solution structures of chiral Ti^{4+} alkoxides. II. The roles of diolate basicity and side-chain binding group polarity

STEPHEN BIANCHET AND PIERRE G. POTVIN[1]

Department of Chemistry, York University, 4700 Keele Street, North York, Ont., Canada M3J 1P3

Received July 16, 1991[2]

STEPHEN BIANCHET and PIERRE G. POTVIN. Can. J. Chem. **70**, 2256 (1992).

With a view to reproduce the structure in solution of the Katsuki–Sharpless catalyst (the dimeric complex formed by homochiral diisopropyl tartrate with $Ti(O^iPr)_4$), five C_2-symmetric chiral 2,3-butanediols, related to L-threitol but bearing *N*-, S-, and P-containing groups at the 1- and 4-positions, were prepared and their reactions with $Ti(O^iPr)_4$ were examined by nuclear magnetic resonance spectroscopy. The 1,4-dithioether formed a non-fluxional 2:2 tricyclic complex entirely analogous to those formed by alkylated sugar derivatives. The related disulfone formed a similar complex, but only at low temperatures, probably because of oligomerization at higher temperatures. A symmetric 2:1 complex also formed with excess $Ti(O^iPr)_4$, but incompletely and in equilibrium with the 2:2 species. No well-defined complexes were formed with pyrazole or phosphine oxide functionalities. However, in the presence of trifluoroacetic acid (TFA), a 1:2:2 L:Ti:TFA complex was identified with the dimethylpyrazole-containing diol and this resembled the 2:3 complexes formed by tartramides. Generally, the degree of spectral asymmetry and the coupling constant between diolate protons were instrumental in assigning structures and were used to classify all chiral diolate complexes into two groups according to whether or not they exhibited metal chelation and diolate bridging. By comparison of the effects of complexation on the diolate nuclei, a correlation was found between ^{13}C and ^1H nmr signal positions and between the pairs of signals in the spectra of asymmetric complexes, except in four cases where metal-bound side-chain groups induced a shielding of the bridging diolate proton. This could serve as an additional indication of metal chelation and diolate bridging and confirmed that nuclei at bridging positions appeared upfield of terminal ones. Noting that all the diols that readily chelated and bridged possessed electron-releasing side chains, while tartrates and tartramides that did not chelate possessed electron-withdrawing side chains, the basicity of the diolate oxygens is considered the most important determinant of structure. Side-chain polarity was instead found to influence whether or not a well-defined complex could form.

STEPHEN BIANCHET et PIERRE G. POTVIN. Can. J. Chem. **70**, 2256 (1992).

Afin de copier la structure en solution du catalyseur de Katsuki et Sharpless (le dimère formé par un tartrate homochiral avec le $Ti(O^iPr)_4$), cinq 2,3-butanediols homochiraux et C_2-symétriques, apparentés au L-thréitol mais possédant des groupements azotés, sulfurés ou phosphorés aux positions 1 et 4, furent préparés et leurs réactions avec le $Ti(O^iPr)_4$ furent étudiées par la résonance magnétique nucléaire. Comme l'avaient fait trois glycitols alkylés, le diol 1,4-di(thiophényle) forma un complexe 2 : 2 rigide et tricyclique. La 1,4-disulfone correspondante fit de même, mais seulement à basses températures, probablement par tendance à oligomeriser à températures plus élevées. Un complexe symétrique 2 : 1 s'est incomplètement formé en présence d'excès de $Ti(O^iPr)_4$ et était en équilibre avec l'espèce 2 : 2. Les trois autres diols, par contre, n'ont formé aucun complexe distinct sauf, avec un 1,4-dipyrazole, en présence d'acide trifluoroacétique (TFA). Ceci donna un complexe à rapport 1 : 2 : 2 en diol, titane et acide qui ressemblait aux complexes 2 : 3 formés par deux tartramides. En général, la structure d'un complexe pouvait être déduite en examinant le degré d'asymmétrie spectrale et la constante de couplage entre protons, et ces critères pouvaient servir à classer tous les complexes de diols-1,2 chiraux en deux groupes, selon qu'ils chélatent le titane et pontent les deux métaux d'un dimère ou non. En comparant l'effet d'une complexation sur les positions des raies de rmn dues aux noyaux du groupement diol, on a trouvé, qu'en général, le déplacement chimique d'un proton est relié à celui du carbone-13 auquel il est lié et que, dans les complexes asymétriques où les raies sont doublées, la position d'une raie est reliée à la position de son double. Cependant, quatre exceptions à ces règles étaient dues à un blindage du proton du pont par certains groupements terminaux fixés au titane. Ce phénomène révéla que les raies dus aux noyaux des groupements OCH en position pontante sont à champs plus élevés que ceux dus à la position terminale, et peut aussi servir comme indicateur de chélation et de pontage. Comme il est devenu apparent que tous les diols relativement acides forment des ponts alors que les tartrates et les tartramides, qui sont relativement peu acides, ne pontent pas, c'est l'acidité du diol qui, plus que tout autre facteur, détermine la structure du complexe qu'il pourrait former, alors que les groupements terminaux à polarité élevée peuvent nuire à une complexation nette.

Introduction

The epoxidation of allylic alcohols by ^{t}BuOOH catalyzed by complexes of Ti^{4+} with tartrate esters (e.g., H_2**1**) or tartramides, the Katsuki–Sharpless epoxidation (1), is a rare example of a general and catalytic chiral induction system (2, 3). We had found that analogous complexes of three non-tartrate diol ligands, destined for use in reactions where tartrates would not be compatible (e.g., in enolate chemistry), were poorly enantioselective epoxidation catalysts.[3] Similarly, the Sharpless group (3) explored complexes of some 50 related ligands and also failed to duplicate the success with tartrates. We suspected that this difference in enantioselectivity was due to differences in the structures of the complexes in solution. This was confirmed upon examination of the nmr and mass spectra of the complexes of several ligands (H_2**1**–H_2**9**) with $Ti(O^iPr)_4$ (4). Thus, ligands H_2**2**–H_2**4** gave non-fluxional and strongly asymmetric 2:2 complexes showing little coupling between diolate OC*H* units, little temperature dependence, little concentration dependence, and a reluctance to form 2:1 Ti:ligand species in the presence of excess $Ti(O^iPr)_4$. They were therefore assigned generic structure **A**, essentially that found for Ti_2**5**$_2(O^iPr)_4$ in the solid

[1]Author to whom correspondence may be addressed.

[2]Revision received January 28, 1992.

[3]P. G. Potvin and P. C. C. Kwong, unpublished results.

Can. J. Chem. Downloaded from www.nrcresearchpress.com by 109.225.110.28 on 09/08/12
For personal use only.

state (5). On the other hand, $Ti_2\mathbf{1}_2(O^iPr)_4$ was fluxional, with rapid equilibration between free and metal-bound ester groups and with rapid TiO^iPr–HO^iPr exchange. At temperatures low enough to arrest these exchanges, the spectra showed only slight asymmetry but strong coupling between skeletal OC*H*. Further, additional $Ti(O^iPr)_4$ produced a mixture of $Ti_2\mathbf{1}_2(O^iPr)_4$ and $Ti_2\mathbf{1}(O^iPr)_6$, which was also fluxional. Upon cooling, the latter dominated and the fluxionality disappeared, giving rise to strongly differentiated but weakly coupled OC*H* groups, as had the non-tartrate complexes at room temperature. With this and other evidence, $Ti_2\mathbf{1}(O^iPr)_6$ at low temperature was assigned structure **B**, the bicyclic analogue of **A**. The *meso* analogue, $Ti_2\mathbf{9}(O^iPr)_6$, behaved in the same way and was assigned an analogous structure. The Katsuki–Sharpless catalyst, $Ti_2\mathbf{1}_2(O^iPr)_4$, was instead assigned a more open structure lacking the diolate bridges (and the metal chelation), **C**, the same structure that had been originally assigned (2) in analogy to the crystal structures of the tartrate salts of transition metal ions (6). With the tartramides $H_2\mathbf{5}$–$H_2\mathbf{8}$, no well-defined species formed at 1:1 stoichiometry, i.e., there was no evidence of the solid-state structure **A** in solution, and we suspected that oligomers had formed. Tartramides had been used in epoxidation with limited success at 2:1 Ti:tartramide ratio (7) but, in our hands, this ratio produced equal amounts of $Ti_3(tartramide)_2(O^iPr)_8$ and free $Ti(O^iPr)_4$ and one cannot explain how such a mixture can produce >75% e.e. without some redistribution in the presence of substrate and (or) product alcohols.

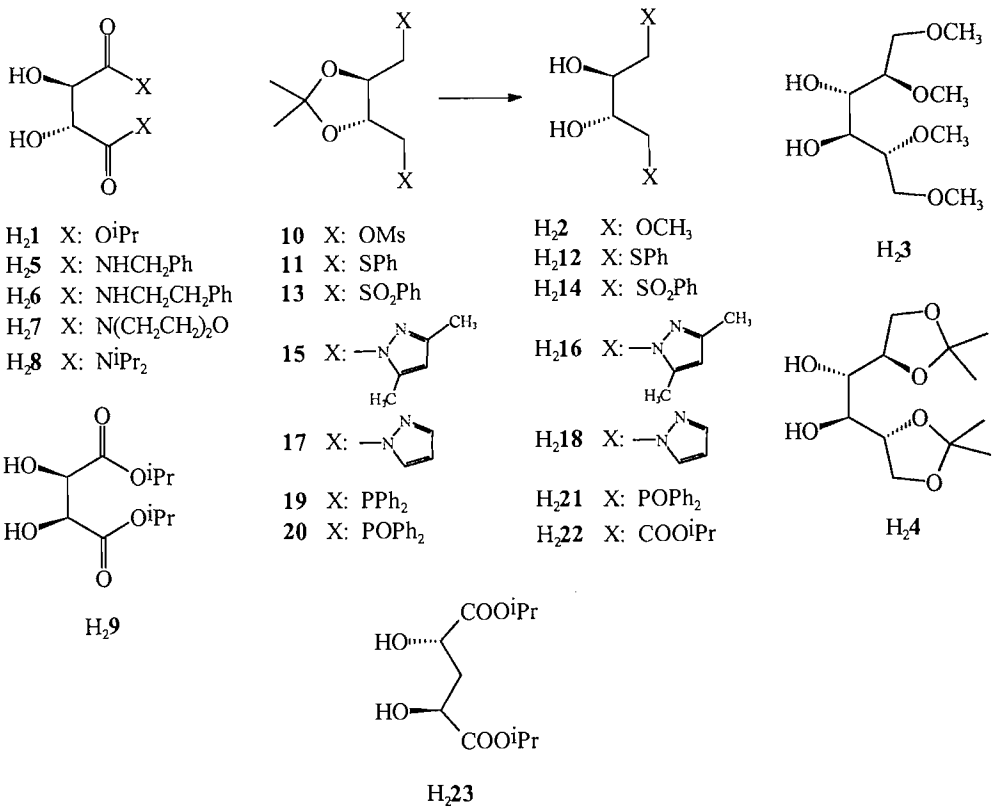

More recently, Finn and Sharpless (8) reported extensive nmr and ir data for tartrate complexes (and only tartrate complexes) and these were interpreted as supporting their assignment of structure **A** to $Ti_2\mathbf{1}_2(O^iPr)_4$. Their ^1H and ^{13}C nmr data matched ours, but these alone are insufficient to differentiate between **A** and **C**. We disagree, however, with some of their interpretations of the ir and ^{17}O nmr data. In particular, the metal-bound C=O stretching frequency assigned to $Ti_2\mathbf{1}(O^iPr)_6$ was higher (1684 cm^{-1}) than that assigned to $Ti_2\mathbf{1}_2(O^iPr)_4$ (1638 cm^{-1}), indicating a *weaker bond in the former*. We think this is due to [2.2.1] bicyclic strain in **B** that is absent in structure **C**. Complexes from tartrate enriched in ^{17}O at the hydroxyls gave rise to two broad ^{17}O nmr peaks some 64–150 ppm apart. This was believed to arise from one terminal and one bridging diolate (as in **A**). The possibility that these peaks arose from two terminal positions in different coordination sites (as in **C**) was dismissed as unlikely, but this was premature as there were no examples of signals from bona fide bridging diolates (in fact, oligomeric $Ti(OEt)_4$, $Ti(O^nBu)_4$, and $Ti(OCH_2Ph)_4$ all showed a single peak in the same region) and because the range of ^{17}O signals was very wide (about 560 ppm), even for simple hydroxyl ^{17}O signals (about 65 ppm).

We attribute the success of $Ti_2\mathbf{1}_2(O^iPr)_4$ to fast reactions on the pentacoordinate template **C** and believe that **A**-like templates are unsuccessful because they react slowly and allow a poorly enantioselective bimetallic mechanism to operate (8). The Sharpless group have discounted a bimetallic mechanism and rather believe that the success of $Ti_2\mathbf{1}_2(O^iPr)_4$ is due to rapid on–off rates for carbonyl binding on an **A**-like template, owing to [2.2.1] bicyclic strain, while all other complexes react more slowly than the trace

Can. J. Chem. Downloaded from www.nrcresearchpress.com by 109.225.110.28 on 09/08/12
For personal use only.

amounts of non-enantioselective $Ti(O^iPr)_4$ that may accompany them (8). In any event, it remains that the one really useful complex was also the only one showing its particular nmr spectral features. We believe that one could obtain useful catalysts for other templated reactions if one could reproduce those features with other ligands and we reasoned that the more dipolar side-chains in tartrates and tartramides and the negatively charged side chains of tartrate anion were able to stabilize pentacoordination. Consequently, we have prepared and examined ligands H_2**14**, H_2**16**, H_2**18**, and H_2**21** to test this hypothesis. These ligands bear strongly dipolar secondary binding sites one atom further removed from the alkoxide oxygen than in H_2**1**–H_2**9** and this was expected to also relieve some of the [2.2.1] bicyclic ring strain inherent in tricyclic 2:2 structures like **A** (6). We also examined complexation with the precursor to H_2**14**, the bis-sulfide H_2**12**, with the expectation that it would behave as had the ethers H_2**2**–H_2**4**. In the end, the results support our structural views but our hypothesis was wrong. An examination of the body of available data reveals some common trends that lead to a predictive rationale for the structures formed by chiral diols in general, one formulated in consideration of the basicities of the diolate oxygens as well as the polarities of the side-chain binding groups.

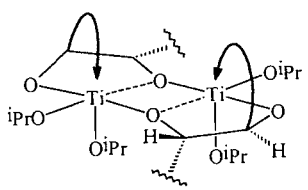

A

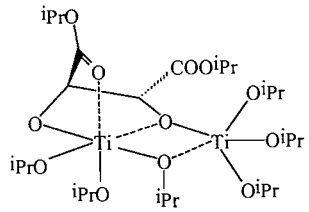

B

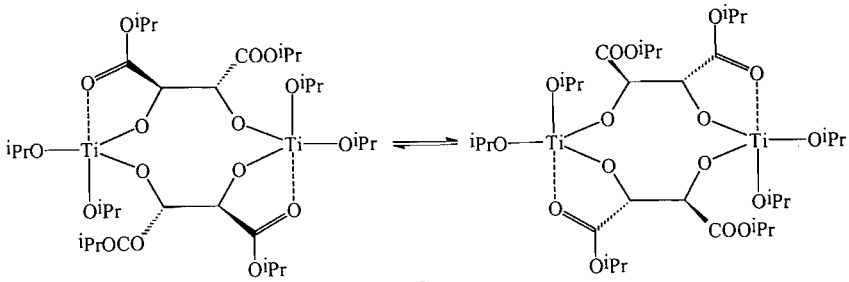

C

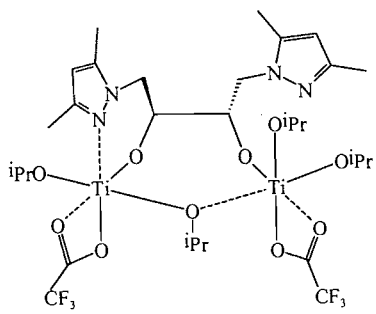

D

Experimental section

General

THF (dried with K and benzophenone), CH_3CN (CaH_2), CH_2Cl_2 (P_2O_5), TFA (P_2O_5), and $Ti(O^iPr)_4$ were freshly distilled prior to use. $CDCl_3$ was dried over $Mg(ClO_4)_2$. Melting points were obtained on a Reichert apparatus and are uncorrected. The ir spectra were obtained either with neat films on NaCl discs or with mulls in KBr on a Perkin–Elmer 1310 spectrometer. Nuclear magnetic resonance spectroscopy in $CDCl_3$ and spectral simulation, to confirm the chemical shifts and coupling constants in ABX systems, were performed as before (4*b*). The EI and FAB mass spectra were obtained on a ZAB-80 instrument at the McMaster Regional Centre for Mass Spectroscopy, McMaster University. 1,4-Di-*O*-methanesulfonyl-2,3-*O*-isopropylidene-L-threitol (**10**) was prepared by the method of Feit (9), using 2 equivalents of Et_3N in THF rather than pyridine solvent.

(2R,3R)-1,4-Bis(phenylthio)-2,3-dihydroxy-2,3-O-isopropylidenebutane ***11***

Dimesylate **10** (1.437 g, 4.52 mmol) and KBH_4 (1.022 g, 18.95 mmol) were dissolved in dry HO^iPr (20 mL) in a round-bottomed flask, flushed with Ar, and sealed with a septum. While stirring at room temperature, Ph_2S_2 (0.986 g, 4.52 mmol) dissolved in a small amount of HO^iPr was introduced via syringe. After stirring for 48 h, the HO^iPr was removed *in vacuo* and replaced with

Can. J. Chem. Downloaded from www.nrcresearchpress.com by 109.225.110.28 on 09/08/12
For personal use only.

Can. J. Chem. Downloaded from www.nrcresearchpress.com by 109.225.110.28 on 09/08/12
For personal use only.

EtOAc. This was washed with H_2O, then evaporated to dryness to produce a quantitative yield of an orange oil. This was suitable for the hydrolysis or oxidation steps. A portion (0.384 g) was chromatographed on Silica Gel 60, using 10% EtOAc in hexanes as eluant, to afford 0.330 g of a clear oil (corresponding to an overall 86% yield); ^{1}H nmr δ: 7.38–7.16 (m, 10H, Ph), 4.07 (m, 2H, X part of ABX system, OC*H*), 3.27–3.18 (m, 4H, AB part of ABX system, CH_2), 1.41 (s, 6H, CH_3) ppm; ^{13}C nmr δ: 135.66, 129.41, 128.99, 126.31 (Ph), 109.74 (*C*Me$_2$), 79.01 (OCH), 37.01 (CH_2), 27.30 (CH_3) ppm. Anal. calcd. for $C_{19}H_{22}O_2S_2$: C 65.86, H 6.40, S 18.50; found: C 66.04, H 6.40, S 18.39.

*(2R,3R)-1,4-Bis(phenylthio)-2,3-dihydroxybutane H_2**12***

Crude **11** (0.688 g, 1.96 mmol) was dissolved in MeOH (3 mL) containing CF_3COOH (5 drops) and the mixture heated to reflux for 5 days. After removal of the volatiles *in vacuo*, the pale yellow solid remaining was triturated with hexanes and recrystallized from Et_2O to afford 0.426 g (71% yield) of a flocculent white solid, mp 114.5–115.5°C; ^{1}H nmr δ: 7.37–7.20 (m, 10H, Ph), 3.73 (X part of ABX system, 2H, OC*H*), 3.115 (AB part of ABX system, 4H, Δδ = 0.05 ppm, CH_2), 2.63 (d, 2H, OH) ppm; J_{AB} = 14.2, J_{AX} = 9.14, J_{BX} = 2.68 Hz; ^{13}C nmr δ: 134.82, 130.08, 129.09, 126.73 (Ph), 70.25 (OCH), 38.31 (CH_2) ppm. Anal. calcd. for $C_{16}H_{18}O_2S_2$: C 62.71, H 5.92, S 20.92; found: C 62.47, H. 5.53, S 21.80. For complexation at 1:1 ratio, 81.0 mg of H_2**12** in 2.0 mL of $CDCl_3$ was treated with 79 μL of Ti(O^{i}Pr)$_4$ (total [**12**] = 132 mM). At 2:1 ratio, 42.0 mg of H_2**12** and 82 μL of Ti(O^{i}Pr)$_4$ were used in 1.5 mL of $CDCl_3$ (total [**12**] = 91.4 mM). Aliquots of 0.5 mL were examined by nmr.

Ti$_2$**12**$_2$(O^{i}Pr)$_4$: ^{1}H nmr δ: 7.42–7.15 (m, 20H, Ph), 4.81 (X part of ABX system, 2H, diolate OC*H*), 4.72 (bm, 4H, O^{i}Pr OC*H*), 4.56 (X′ part of A′B′X′ system, 2H, diolate OC*H*), 3.31 (AB part of ABX system, 4H, Δδ = 0.22 ppm, CH_2), 3.18 (A′B′ part of A′B′X′ system, 4H, Δδ = 0.15 ppm, CH_2), 1.20 (d, 24H, O^{i}Pr CH_3) ppm; J_{AB} = 13.52, J_{AX} = 3.29, J_{BX} = 9.91, $J_{XX'}$ = 0, $J_{A'B'}$ = 12.88, $J_{A'X'}$ = 4.30, $J_{B'X'}$ = 8.40 Hz; ^{13}C nmr δ: 136.36, 135.95 (Ar *i*-C), 126.10, 125.95 (Ar *p*-C), 129.41, 128.91, 128.78 (Ar *o*-and *m*-C), 88.41, 83.77 (diolate OCH), 79.28 (O^{i}Pr OCH), 40.44, 37.38 (CH_2), 25.78 (CH_3) ppm.

*(2R,3R)-1,4-Bis(phenylsulfonyl)-2,3-dihydroxy-2,3-*O*-isopropylidenebutane **13***

Crude **11** (0.682 g, 1.97 mmol) in CH_2Cl_2 (10 mL) was treated with 80–85% *meta*-chloroperbenzoic acid (2.02 g) in CH_2Cl_2 (50 mL) via a dropping funnel over the course of 4 h at room temperature. After stirring for 3 days the solvent was removed *in vacuo* and the resulting solid was taken up in saturated $NaHCO_3$, then extracted several times with $CHCl_3$. The combined extracts were dried ($MgSO_4$), filtered, and evaporated. The white solid residue was recrystallized from 1:1 CH_2Cl_2–MeOH to provide 0.655 g, in 2 crops, of a white solid (81% yield); ^{1}H nmr δ: 8.07–7.93 (m, 4H, Ph), 7.69–7.54 (m, 6H, Ph), 4.33 (m, 2H, X part of ABX system, OC*H*), 3.57–3.41 (m, 4H, AB part of ABX system, CH_2), 1.22 (s, 6H, CH_3) ppm; ^{13}C nmr δ: 139.47, 133.97, 129.20, 128.18 (Ph), 110.66 (*C*Me$_2$), 74.49 (OCH), 58.71 (CH_2), 26.69 (CH_3) ppm.

*(2R,3R)-1,4-Bis(phenylsulfonyl)-2,3-dihydroxybutane H_2**14***

Crude **13** was hydrolyzed as was **11**. Recrystallization from $CHCl_3$ afforded an 84% overall yield of a white solid, mp 142.5–143°C; ^{1}H nmr δ: 7.92 (d, 4H, *o*-Ph), 7.70 (t, 2H, *p*-Ph), 7.60 (dd, 4H, *m*-Ph), 4.17 (m, 2H, X part of ABX system, OC*H*), 3.36 (m, 4H, AB part of ABX system, CH_2), 1.57 (bs, 2H, OH) ppm; ^{13}C nmr δ: 138.93 (Ar *i*-C), 134.29 (Ar *p*-C), 129.56 (Ar *o*-C), 127.94 (Ar *m*-C), 67.79 (OCH), 58.73 (CH_2) ppm. Anal. calcd. for $C_{16}H_{18}O_6S_2$: C 51.88, H 4.90, S 17.31; found: C 51.52, H 4.88, S 17.95.

For complexation at 1:1 ratio, 68.4 mg of H_2 **14** in 1.75 mL of $CDCl_3$ was treated with 55 μL of Ti(O^{i}Pr)$_4$ (total [**14**] = 106 mM). At 2:1 ratio, 47.3 mg of H_2**14** and 76 μL of Ti(O^{i}Pr)$_4$ were used in 3.0 mL of $CDCl_3$ (total [**14**] = 42.6 mM). Aliquots of 0.5 mL were examined by nmr.

Ti$_2$**14**$_2$(O^{i}Pr)$_4$: ^{1}H nmr (−23°C) δ: 7.99, 7.93 (2d, 8H, Ph *o*-H), 7.7–7.3 (m, 12H, Ph), 5.22 (X part of ABX system, 2H, diolate OC*H*), 4.81 (X′ part of A′B′X′ system, 2H, diolate OC*H*), 4.12 (bm, 4H, O^{i}Pr OC*H*), 3.66 (AB part of ABX system, 4H, Δδ = 0.35 ppm, CH_2), 3.52 (A′B′ part of A′B′X′ system, 4H, Δδ = 0.45 ppm, CH_2), 1.15 (d, 24H, O^{i}Pr CH_3) ppm; J_{AB} = 14.18, J_{AX} = 9.35, J_{BX} = 0, $J_{X'X'}$ = 0, $J_{A'B'}$ = 14.26, $J_{A'X'}$ = 8.47, $J_{B'X'}$ = 0 Hz; ^{13}C nmr (−53°C) δ: 138.76, 138.55 (Ar *i*-C), 134.22, 133.90 (Ar *p*-C), 129.35, 129.20 (Ar *o*-C), 127.91, 127.78 (Ar *m*-C), 81.82, 79.47 (diolate OCH), 77.20 (O^{i}Pr OCH), 58.85, 57.71 (CH_2), 25.06 (CH_3) ppm. Ti$_2$**14**(O^{i}Pr)$_6$: ^{1}H nmr (−10°C) δ: 7.99, 7.93 (2d, 4H, Ph *o*-H), 7.7–7.3 (m, 6H, Ph), 5.08 (X part of ABX system, 2H, diolate OC*H*), 4.66 (bm, 6H, O^{i}Pr OC*H*), 3.62 (AB part of ABX system, 4H, Δδ = 0.17 ppm, CH_2), 1.25, 1.20 (2d, 18H, O^{i}Pr CH_3) ppm; J_{AB} = 14.23, J_{AX} = 9.14, J_{BX} = 2.68 Hz; ^{13}C nmr δ: 139.97 (Ar *i*-C), 133.50 (Ar *p*-C), 129.17 (Ar *o*-C), 128.45 (Ar *m*-C), 81.13 (diolate OCH), 78.05, 76.2 (O^{i}Pr OCH), 59.92 (CH_2), 26.50, 25.41 (CH_3) ppm.

*(2S,3S)-1,4-Bis(3,5-dimethylpyrazol-1-yl)-2,3-dihydroxy-2,3-*O*-isopropylidenebutane **15***

In a flame-dried flask capped with a septum and under an Ar atmosphere, a suspension of NaH (0.236 g of a 50% oil dispersion freed of oil by petroleum ether triturations, 4.92 mmol) in CH_3CN (12 mL) was treated with 3,5-dimethylpyrazole (0.379 g, 3.94 mmol). After the effervescence had subsided, a solution of **10** (0.625 g, 1.96 mmol) in CH_3CN (6 mL) was added via syringe through the septum. A condenser and drying tube were attached to the flask and the contents were heated to 50°C. After 61 h, the solvent was removed *in vacuo* and the residue was dissolved in CH_2Cl_2 (50 mL). After washing with H_2O (2 × 50 mL) and back-extracting the aqueous phases with fresh CH_2Cl_2 (50 mL), the combined organic layers were dried ($MgSO_4$), filtered, and evaporated to dryness, leaving a viscous yellow oil (0.534 g, 85% yield) that was quite pure and used as such in the hydrolysis step; ^{1}H nmr δ: 5.78 (s, 2H, Ar *H*), 4.31 (m, 2H, X part of ABX system, OC*H*), 4.16–4.01 (m, 4H, AB part of ABX system, CH_2), 2.28, 2.19 (2s, 2 × 6H, Ar CH_3), 1.23 (s, 6H, C(CH_3)$_2$) ppm; ^{13}C nmr δ: 147.54 (Ar *C*CH$_3$), 140.34 (Ar *C*CH$_3$), 109.69 (*C*Me$_2$), 105.24 (Ar *C*H), 77.39 (OCH), 49.73 (CH_2), 26.78 (C(CH_3)$_2$), 13.36 (Ar CH_3), 11.14 (Ar CH_3) ppm.

*(2S,3S)-1,4,-Bis(3,5-dimethylpyrazol-1-yl)-2,3-dihydroxybutane H_2**16***

Crude **15** (0.406 g, 1.28 mmol) was hydrolyzed in 1:1 MeOH–H_2O (40 mL) containing 0.5 mL concentrated HCl at 65°C for 2 days. Cooling, neutralization with excess Et_3N, extraction into $CHCl_3$, and removal of solvent produced a white solid (81% crude yield) that was recrystallized from 20% MeOH in H_2O. This afforded 0.212 g (60% yield) of flocculent white material, mp 137–138°C; ^{1}H nmr δ: 5.78 (s, 2H, Ar *H*), 4.10 (AB part of ABX system, 4H, Δδ = 0.08 ppm, CH_2), 3.92 (X part of ABX system, 2H, OC*H*), 2.23, 2.18 (2s, 2 × 6H, CH_3) ppm; J_{AB} = 14.02, J_{AX} = 6.57, J_{BX} = 5.07 Hz; ^{13}C nmr δ: 148.02 (Ar *C*CH$_3$), 140.24 (Ar *C*CH$_3$), 105.03 (Ar *C*H), 70.66 (OCH), 50.15 (CH_2), 13.36 (CH_3), 11.00 (CH_3) ppm. Anal. calcd. for $C_{14}H_{22}N_4O_2$: C 60.41, H 7.97, N 20.13; found: C 60.43, H 8.03, N 20.04.

*Titration reactions involving H_2**16***

(*a*) With addition of H_2**16** last: At fixed 1:1 TFA:H_2**16** ratios, 0.5 mL aliquots of a $CDCl_3$ solution 134 mM in each of Ti(O^{i}Pr)$_4$ and TFA in an nmr tube were treated with 100 μL (0.25 equiv.) increments of a 168 mM $CDCl_3$ solution of H_2**16**. For 2:1 TFA:H_2**16** ratios, a stock solution that was 134 mM in Ti(O^{i}Pr)$_4$ and 268 mM in TFA was used instead.

(*b*) With addition of Ti(O^{i}Pr)$_4$ last: At fixed 1:1 TFA:H_2**16** ratios, a 400 μL aliquot of a 48.3 mM $CDCl_3$ solution of H_2**16** in an nmr tube was treated with 100 μL of a 195 mM stock solution of TFA in $CDCl_3$, then with 25 μL (0.5 equiv.) increments of a 390 mM stock solution of Ti(O^{i}Pr)$_4$ in $CDCl_3$. Appropriate aliquots of the TFA solution were used to explore 1.5:1, 2:1, 3:1, and 4:1 ratios.

Can. J. Chem. Downloaded from www.nrcresearchpress.com by 109.225.110.28 on 09/08/12
For personal use only.

Ti_2**16**$(OCOCF_3)_2(O^iPr)_4$: Solid diol H_2**16** (22.3 mg) was treated with 0.4 mL aliquots of 403 mM TFA and 402 mM $Ti(O^iPr)_4$ solutions in $CDCl_3$. A 0.5 mL aliquot of the mixture was used for nmr spectroscopy; ^{1}H nmr δ: 5.94, 5.79 (2s, 2 × 1H, Ar*H*), 4.99 (h, 1H, O^{i}Pr OC*H*), 4.89 (3h, 3H, O^{i}Pr OC*H*), 4.77 (M part of ABMM′A′B′ system, 1H, diolate OC*H*), 4.68 (M′ part of ABMM′A′B′ system, 1H, diolate OC*H*) 4.24 (AB part of ABMM′A′B′ system, 2H, Δδ = 0.067 ppm, CH_2), 3.81 (A′B′ part of ABMM′A′B′ system, 2H, Δδ = 0.233 ppm, CH_2), 2.63, 2.29, 2.22, 2.19 (4s, 4 × 3H, ArCH_3), 1.41–1.33 (m, 9H, O^{i}Pr CH_3), 1.03, 0.78 (2d, 3H, O^{i}Pr CH_3) ppm; J_{AB} = 14.0, J_{AM} = 6.7, J_{BM} = 5.6, $J_{MM'}$ = 7.15, $J_{A'M'}$ = 1.9; $J_{B'M'}$ = 10.6, $J_{A'B'}$ = 14.2 Hz; ^{13}C nmr δ: 151.39, 147.13, 141.83, 141.60 (Ar *C*CH_3), 116.18, 115.49 (2q, *C*F_3, J_{CF} = 289 Hz), 106.46, 105.24 (Ar *C*H), 87.58, 85.62 (diolate O*C*H), 81.74, 81.07, 79.59, 79.12 (O^{i}Pr O*C*H), 52.17, 50.48 (*C*H_2), 24.61, 24.49, 24.29, 24.21, 24.18 (O^{i}Pr *C*H_3), 15.23, 13.05, 11.23, 10.96 (Ar *C*H_3) ppm.

*(2S,3S)-1,4-Bis-(pyrazol-1-yl)-2,3-dihydroxy-2,-3-*O*-isopropylidenebutane* ***17***

In a procedure entirely analogous to the preparation of **15**, an 81% yield of crude **17** was obtained as a pale yellow oil and used as such in the hydrolysis step; ^{1}H nmr δ: 7.51 (d, 2H, J = 1.7 Hz, H-3′ or H-5′), 7.47 (d, 2H, J = 2.2 Hz, H-5′ or H-3′), 6.26 (t, 2H, J = 2.1 Hz, H-4′), 4.32–4.19 (m, 4H, AB part of ABX system, CH_2), 4.09 (m, 2H, X part of ABX system, OC*H*), 1.24 (s, 6H, C(CH_3)$_2$) ppm; ^{13}C nmr δ: 139.57 (C-3′ or C-5′), 130.67 (C-5′ or C-3′), 109.94 (*C*Me_2), 105.85 (C-4′), 76.78 (O*C*H), 52.59 (*C*H_2), 26.81 (C(*C*H_3)$_2$) ppm.

(2S,3S)-1,4-Bis(pyrazol-1-yl)-2,3-dihydroxybutane H_2***18***

Crude **17** was hydrolyzed as was **15**, and the product was recrystallized from hot EtOAc to provide an 18% (unoptimized) overall yield of colourless plates, mp 144–145°C; ^{1}H nmr δ: 7.51 (d, 2H, J = 1.6 Hz, H-3′ or H-5′), 7.44 (d, 2H, J = 2.1 Hz, H-5′ or H-3′), 6.26 (t, 2H, J = 2.1 Hz, H-4′), 4.30 (m, 4H, AB portion of ABX system, CH_2), 3.92 (X portion of ABX system, 2H, J_{app} = 2.5, 5.0 Hz, OC*H*), 3.67 (bs, 2H, OH) ppm; ^{13}C nmr δ: 139.84 (C-3′ or C-5′), 130.81 (C-5′ or C-3′), 105.69 (C-4′), 70.74 (O*C*H), 54.01 (*C*H_2) ppm. Anal. calcd. for $C_{10}H_{14}N_4O_2$; C 54.04, H 6.35, N 25.21; found: C 53.88, H 6.16, N 25.30.

*(2*R*,3*R*)-1,4-Bis(diphenylphosphino)-2,3-dihydroxy-2,3-*O*-isopropylidenebutane* P,P′*-dioxide* ***20***

R,R-DIOP (Aldrich, 0.8641 g, 1.73 mmol) in acetone (25 mL) was treated with 30 w/w % H_2O_2 (0.49 mL). While stirring for 30 min, a white precipitate formed. The mixture was then evaporated to dryness and the residue was recrystallized from acetone to provide two crops of white needles, mp 218–220°C, amounting to 86% yield; ir (KBr): 2980, 1435, 1375, 1187, 1120, 895, 695 cm^{-1}; ^{1}H nmr δ: 7.81–7.74 (m, 8H, Ph), 7.52–7.42 (m, 12H, Ph), 4.16 (m, 2H, X part of ABX system, OC*H*), 2.86–2.75 (m, 2H, A part of ABX system, C*H*H), 2.67–2.56 (m, 2H, B part of ABX system, CH*H*), 1.17 (s, 6H, CH_3) ppm; ^{13}C nmr δ: 133.73 (d, Ar *i*-C, J_{PC} = 43.5 Hz), 132.40 (d, Ar *i*-C, J_{PC} = 43.2 Hz), 131.75 (d, Ar *p*-C, J_{PC} = 2.7 Hz), 131.65 (d, Ar *p*-C, J_{PC} = 2.7 Hz), 131.00 (d, Ar *o*-C, J_{PC} = 23.5 Hz), 130.87 (d, Ar *o*-C, J_{PC} = 23.5 Hz), 128.59 (d, Ar *m*-C, J_{PC} ≈ 12.1 Hz), 128.42 (d, Ar *m*-C, J_{PC} ≈ 12.8 Hz), 109.20 (*C*CH_3), 76.43 (d, J_{PC} = 3.0 Hz, O*C*H), 33.05 (d, J_{PC} = 70.5 Hz, *C*H_2), 26.74 (*C*H_3) ppm.

*(2*R*,3*R*)-1,4-Bis(diphenylphosphino)-2,3-dihydroxybutane* P,P′*-dioxide* H_2***21***

Compound **20** was hydrolyzed as was **11**. Recrystallization from CH_3CN containing 10% MeOH provide a 76% yield of white needles, mp 226–228°C; ir (KBr): 3320, 3070, 1435, 1185, 1150, 830, 725, 695 cm^{-1}; ^{1}H nmr δ: 7.72, 7.45 (AB system + m, 20H, Ph), 4.61 (bs, 2H, O*H*), 4.11 (m, 2H, OC*H*), 2.75–2.54 (m, 4H, CH_2) ppm; ^{13}C nmr δ: 133.00 (d, Ar *i*-C, J_{PC} = 60.5 Hz), 132.04 (d, Ar *p*-C, J_{PC} ≈ 2.8 Hz), 132.00 (d, Ar *p*-C, J_{PC} ≈ 2.7 Hz), 131.67 (d, Ar *i*-C, J_{PC} ≈ 60.5 Hz), 130.73 (d, Ar *o*-C, J_{PC} = 22.7 Hz), 130.60 (d, Ar *o*-C, J_{PC} = 22.8 Hz), 128.79 (d, Ar *m*-C, J_{PC} = 12.0 Hz), 128.73 (d, Ar *m*-C, J_{PC} = 11.8 Hz), 69.41 (dd, J_{PC} = 3.2, 10.1 Hz, O*C*H), 32.08 (d, J_{PC} = 70.4 Hz, *C*H_2) ppm.

Results

The ligands H_2**12**, H_2**14**, H_2**16**, H_2**18** and H_2**21** were prepared from **10** in straightforward reactions. Compound H_2**21** is apparently not new (3, 10) but, to our knowledge, no details of its preparation have appeared. We found that the bisphosphine analogue of H_2**21** spontaneously oxidized in air and was always contaminated with H_2**21**; it was therefore not studied in complexation experiments.

The bis-sulfide H_2**12** behaved exactly as had the sugar derivatives H_2**2**–H_2**4** in complexation. In a 1:1 mixture with $Ti(O^iPr)_4$, HO^{i}Pr was liberated and a single asymmetric complex formed. It revealed well-resolved and strongly differentiated ligand ^{1}H and ^{13}C nmr signals, even in the phenyl regions. In particular, the diolate O*CH* signals appeared as the uncoupled X portions of separate and overlapping ABX systems downfield of free ligand positions. This was entirely consistent with generic structure **A**. (Unfortunately, both EI and FAB mass spectrometry were totally uninformative.) However, the TiO^{i}Pr and HO^{i}Pr O*CH* signals were unusually broad, indicating rapid TiO^{i}Pr–HO^{i}Pr exchange on an otherwise rigid framework, but these sharpened considerably upon adding excess $Ti(O^iPr)_4$. (No new species had formed with this treatment. Ligands H_2**2**–H_2**4** had shown a similar reluctance to form 2:1 species.) We believe that fast TiO^{i}Pr–HO^{i}Pr exchange in Ti_2**12**$_2(O^iPr)_4$ is due to rapid on–off rates for weaker side-chain binding than in complexed **2**–**4** owing to [2.2.1] bicyclic strain and perhaps to the size and softness of the SPh group, and that extra $Ti(O^iPr)_4$ successfully competes with Ti_2**12**$_2(O^iPr)_4$ in that exchange.

The bis-sulfone H_2**14**, however, behaved very differently. Mixing 1 equivalent of each of H_2**14** and $Ti(O^iPr)_4$ at room temperature (RT) resulted in very broad, indistinguishable ^{1}H and ^{13}C resonances, much as had occurred with tartramides H_2**5** and H_2**6**. However, mixing these while cooling in a $CHCl_3$/Dry Ice bath, and monitoring the spectra while still cold, resulted in a single set of much sharper signals readily attributable to an asymmetric 2:2 **A**-like species. After warming to RT, these signals slowly broadened and overlapped over a few hours, but there was no sign of coalescence during this time, in accord with the formation of a fairly rigid **A**-like structure under conditions of kinetic control while other, perhaps linear and (or) oligomeric species formed under thermodynamic control. The spectral asymmetry was pronounced here also, yet no TiO^{i}Pr signal was visible. Instead, a single, broad O^{i}Pr O*CH* band at 4.12 ppm, accounting for all O^{i}Pr groups, and a single CH_3 doublet appeared. Similarly, a single strong OCH resonance at 77.2 ppm was observed, along with a broad band for HO^{i}Pr O*C*H and a single *C*H_3 signal. Again, excess $Ti(O^iPr)_4$ resolved the one O*CH* resonance into two broad heptets at more normal positions, and this seemed to indicate rapid TiO^{i}Pr–HO^{i}Pr exchanges here too. However, unlike with H_2**12**, treatment with a full second equivalent of $Ti(O^iPr)_4$ also transformed the broad, featureless RT spectrum to reveal a mixture containing the same asymmetric ligand signals, this time showing no tendency to broaden at RT, and a new, symmetric **14**-containing species, presumably Ti_2**14**$(O^iPr)_6$ and accounting for about half the total ligand, along with a corresponding amount of unreacted

Can. J. Chem. Downloaded from www.nrcresearchpress.com by 109.225.110.28 on 09/08/12
For personal use only.

$Ti(O^iPr)_4$. The new diolate OC*H* resonance, part of a single ABX system, appeared at a position between the two resonances due to the putative 2:2 species. Single, albeit somewhat broad, signals were also found in the ^{13}C spectrum. In analogy with H_2**1**, the following equilibrium could then be postulated, with $K \approx 2.9$ (with 0.085 M Ti at RT):

$$Ti_2\mathbf{14}_2(O^iPr)_4 + 2\ Ti(O^iPr)_4 \rightleftharpoons 2\ Ti_2\mathbf{14}(O^iPr)_6$$

Tartrate H_2**1** had more readily formed its 2:1 species at RT ($K \approx 240$), and that equilibrium had shifted in favour of Ti_2**1**$(O^iPr)_6$ upon cooling. Several subtle changes occurred upon cooling the 2:1 mixture of H_2**14**, however, and the situation was much less clear than with H_2**1**. The proportion of free $Ti(O^iPr)_4$ was not readily quantified due to signal overlap and raised baselines. The *ortho* phenyl doublets and, to a lesser extent, the OC*H* signals were helpful in following the equilibrium shifts and coalescence/de-coalescence phenomena during warming or cooling and revealed that the equilibrium shifted toward the right upon cooling with asymmetrization of the 2:1 signals (a new, smaller pair of *o*-Ph doublets also appeared and signaled a third species) and to the left upon heating with coalescence of the 2:2 signals. Similarly, the CH_3 doublet due to free $Ti(O^iPr)_4$ decreased upon cooling and increased upon heating. Apart from the appearance of a third species at low temperature, these changes qualitatively matched the changes seen with H_2**1** in that the putative 2:1 species was symmetric at RT, became asymmetric and more dominant at lower temperatures, and merged with the putative 2:2 species at higher temperatures. However, there was a greater reluctance to form the 2:1 species and the low-temperature OC*H* signals from both 2:1 and 2:2 species overlapped, which we take to indicate that the two have similar ligand environments at low temperature, unlike what was observed with the corresponding 2:1 Ti:H_2**1** mixture (4). Thus, if we assign a **B**-like structure to Ti_2**14**$(O^iPr)_6$ at low temperature (undergoing rapid equilibration at RT), then a non-equilibrating **A**-like structure for Ti_2**14**$_2(O^iPr)_4$ is reasonable, and vice versa. Mass spectrometry (EI, FAB) was attempted with the more stable 2:1 Ti:H_2**14** mixture, but the sample nevertheless decomposed during the process and the spectra were uninformative.

To explain the puzzling, rapid TiO^iPr–HO^iPr exchange and the signal broadening observed only at 1:1 Ti:H_2**14** ratio, both of which were suppressed or slowed with extra $Ti(O^iPr)_4$, we propose the following equilibria, much like those proposed to arise with the tartramides (4*b*), between closed dimeric, linear oligomeric, and 2:1 species, and involving a small amount of open monomer:

$$Ti_2\mathbf{14}_2(O^iPr)_4 + 2\ HO^iPr \rightleftharpoons 2\ Ti(H\mathbf{14})(O^iPr)_3$$

$$n\ Ti(H\mathbf{14})(O^iPr)_3 \rightleftharpoons (Ti\mathbf{14}(O^iPr)_2)_n\ O^iPr + (n-1)\ HO^iPr$$

$$Ti(H\mathbf{14})(O^iPr)_3 + Ti(O^iPr)_4 \rightleftharpoons Ti_2\mathbf{14}(O^iPr)_6 + HO^iPr$$

Since a well-defined 2:2 species could be obtained with H_2**14** by forming the complex at low temperature, a similar strategy was attempted with the tartramides, since only unresolved spectra had previously been obtained at 1:1 stoichiometry (4*b*). Unfortunately, ligands H_2**5**–H_2**7** were too insoluble to form complexes in cold $CDCl_3$ (the complex of H_2**8** precipitated from solution). Inverse addition (ligand to metal) also failed. The dissolution of $CDCl_3$-insoluble H_2**5** in the presence of $Ti(O^iPr)_4$ constitutes an inverse addition, but this required several hours and also resulted in unresolved spectra. The addition of aliquots of H_2**6** to $Ti(O^iPr)_4$, confirmed the 2:3 stoichiometry of the only well-defined species (4*b*).

The bis-pyrazole H_2**16** apparently did not form well-defined complexes at RT at either 1:1 or 2:1 stoichiometries, though liberation of HO^iPr clearly took place, producing a multiplicity of overlapping signals. Cooling or heating failed to clarify the situation and no useful assignments could be made. We surmised that H_2**16** was too bulky and we therefore examined the unsubstituted analogue H_2**18**, but with similar discouraging results. Bulk was therefore not the sole factor. However, a well-defined complex was serendipitously obtained with material that was later determined to be the di-trifluoroacetate salt of H_2**16**, formed when the base treatment was accidentally omitted from the work-up of the TFA-catalyzed hydrolysis of **15**. The preparation of this salt was not entirely reproducible as its melting point, and the shapes and the positions of its ^1H nmr signals were variable, depending on the drying time and upon the age of the material, and this may have been due to varying amounts of trapped TFA. Therefore, this ternary system was instead examined by titration of 1:1–4 ligand–TFA mixtures in $CDCl_3$ with up to 4 equivalents of $Ti(O^iPr)_4$ or, equivalently, of ligand–$Ti(O^iPr)_4$ mixtures with TFA at the same ratios. These experiments revealed two distinct species giving rise to well-resolved spectra.

At a 2:1:2 Ti–H_2**16**–TFA ratio, by either mode of mixing, clear spectra of a single asymmetric **16**-containing species were obtained, with no sign of unreacted H_2**16** or $Ti(O^iPr)_4$ and no detectable broad signals due to binary $Ti(O^iPr)_4$–TFA complexes (examined in control experiments). We presumed, therefore, that this stoichiometry also represented the molecularity of a ternary complex. Mass spectrometry (EI) confirmed this, with fragments at *m/z* 775, 725, 721, and 716, among others, corresponding to loss of $\cdot O^iPr$, cleavage of a side-chain ($C_6H_9N_2\cdot$), loss of $CF_3COO\cdot$ and of two $\cdot O^iPr$, respectively. The signals due to **16** included two aromatic H singlets, one of which was downfield of the corresponding position in the spectrum of free H_2**16**, and four CH_3 singlets with one quite downfield of the other three, as expected for the binding of one side chain per ligand unit. There were also two closely spaced skeletal OC*H* multiplets that were strongly coupled to one another (J = 7.15 Hz) and to separate sets of CH_2 multiplets in an overall ABMM′A′B′ pattern. One CH_2 set was relatively narrow with nearly equal couplings to the attached OC*H* but the other, shifted upfield, was much wider and showed unequal couplings to its attached methine. This coupling pattern, especially the strong coupling between skeletal methines, was very different from those exhibited by the complexes of the other threitol derivatives H_2**2**, H_2**12**, and H_2**14**. This, along with the closely spaced OC*H* signals, indicated the formation here of a different type of complex. Because the same spectra were obtained whether TFA was added last or whether H_2**16** was added to preformed Ti–TFA complexes, because four equally intense TiO^iPr OCH were found, as expected for a 2:1:2 molecularity (the corresponding OC*H* heptets overlapped), and because of the mass spectral data, the TFA was exclusively Ti-bound and not protonating any pyrazole groups. One O^iPr group gave rise to a pair of diastereotopic

TABLE 1. Complexation-induced displacements in ppm of downfield ($\delta_d - \delta_f$) and upfield ($\delta_u - \delta_f$) skeletal OCH signals, and OC*H*–OC*H* coupling constants (J) in Hz

Entry	Complex	$\delta_d^H - \delta_f^H$	$\delta_u^H - \delta_f^H$	$\delta_d^C - \delta_f^C$	$\delta_u^C - \delta_f^C$	J
1	$Ti_2\mathbf{1}_2(O^iPr)_4$[a]	0.635	0.585	13.55	13.35	7.0
2	$Ti_3\mathbf{5}_2(O^iPr)_8$[a]	[b]	[b]	[b]	[b]	7.2
3	$Ti_3\mathbf{6}_2(O^iPr)_8$[a]	0.70	0.64	15.6	14.4	6.8
4	$Ti_2\mathbf{16}(OCOCF_3)_2(O^iPr)_4$	0.86	0.76	16.81	15.15	7.15
5	$Ti_2\mathbf{1}(O^iPr)_6$[a]	0.71	0.27	14.12	10.69	≈0
6	$Ti_2\mathbf{9}(O^iPr)_6$[a]	0.85	0.67	11.52	8.63	4.6
7	$Ti_2\mathbf{12}_2(O^iPr)_4$	1.07	0.82	18.16	13.52	0
8	$Ti_2\mathbf{14}_2(O^iPr)_4$	1.06	0.69	15.38	12.81	0
9	$Ti_2\mathbf{2}_2(O^iPr)_4$[a]	0.86	0.55	17.30	11.30	2.25
10	$Ti_2\mathbf{3}_2(O^iPr)_4$[a]	0.73	0.45	18.48	12.19	1.1
11	$Ti_2\mathbf{4}_2(O^iPr)_4$[a]	0.91	0.50	19.37	15.87	≈0
12	$Ti_2\mathbf{22}_2(O^iPr)_4$[c]	0.81	0.44	18.2	13.3	[d]

[a] From ref. 4*b*.
[b] Free $H_2\mathbf{5}$ is insoluble in $CDCl_3$ and δ_f values are not available. $\Delta\delta^H = 0.02$ ppm. $\Delta\delta^C = 1.44$ ppm.
[c] From data in ref. 10.
[d] Not reported.

CH_3 doublets that were strongly shielded, probably by a neighbouring bidentate TFA unit.

The modest chemical shift differences for the methine nuclei and the substantial J value were more reminiscent of the 2:2 Ti–tartrate and 3:2 Ti–tartramide complexes (4*b*) than of the complexes of $H_2\mathbf{2}$–$H_2\mathbf{4}$, $H_2\mathbf{12}$, or $H_2\mathbf{14}$, and were consistent with a non-chelating, non-bridging mode of ligation. That only one side chain per ligand was metal-bound without fast exchange implied a certain rigidity that can be rendered by a cyclic structure involving either O^{i}Pr or TFA bridges. Of the several such structures that can be drawn, **D** provides two hexacoordinate metals with an even distribution of TFA units, although no direct evidence of a bridging O^{i}Pr was available and other **D**-like arrangements cannot be ruled out. Similar 7-membered ring structures had been proposed to occur in the 3:2 tartramide complexes, also showing little fluxionality, weak $\Delta\delta$ and large J (entries 2 and 3) (4*b*). They were also found in a crystalline 4:4 tartrate complex (11).

With additional $Ti(O^iPr)_4$ in the mixture (i.e., at 3:1:2 and 4:1:2 Ti–$H_2\mathbf{16}$–TFA stoichiometries) or with more TFA present (i.e., at 3:1:3, 4:1:3, 3:1:4, or 4:1:4 stoichiometries) a new species formed and became dominant. Its spectral features were very similar to those of the putative 2:1:2 species, with only small changes in the positions of the side-chain signals. Broad resonances owing to binary Ti–TFA species were also present. Mass spectrometry of a 4:1:4 sample showed fragments attributable to a mixture of 2:1:4, 2:1:3, and 2:1:2 species at *m/z* 888 ($Ti_2\mathbf{16}(TFA)_4O^iPr$), 829 ($Ti_2\mathbf{16}(TFA)_3(O^iPr)_2$), 775 ($Ti_2\mathbf{16}(TFA)_2(O^iPr)_3$), and 725 ($Ti_2\mathbf{16}(TFA)_2(O^iPr)_4$–$C_6H_9N_2^{\bullet}$, i.e., cleavage of a side chain), among others. Such a mixture could arise by substitution during solvent evaporation. At this time, we cannot fully account for the new species' spectra but they do show that **16** adopts a very similar binding mode (i.e., non-chelating and non-bridging), as in the putative 2:1:2 species.

Unfortunately, the bis-phosphine oxide $H_2\mathbf{21}$ produced unresolved spectra when it was added to either 2 or 1 equivalents of $Ti(O^iPr)_4$ at room temperature or in the cold. Standing, heating, or further cooling failed to improve the resolution. We verified that the P=O group was able to bind by mixing the protected form **20** with $Ti(O^iPr)_4$: the CH_2 multiplet and an *ortho* Ar*H* signal were alone affected. The inability of $H_2\mathbf{21}$ to form a single, well-defined species at least helps explain the complete inability of the Ti–$H_2\mathbf{21}$ mixture to induce enantioselective epoxidation (3, 10).

Discussion

The premise of our structural assignments, essentially whether a diolate moiety is chelating, as in **A** or **B**, or not, as in **C** or *D*, has been based on four criteria: (*a*) rigidity, i.e., slow or fast intra-ligand and TiO^{i}Pr–HO^{i}Pr exchanges (on the nmr timescale), whereby slow exchanges indicate chelation and hexacoordination, and fast exchanges indicate non-chelation and more reactive pentacoordinate metals; (*b*) asymmetry in the signals from the diolate moiety ($\Delta\delta$), whereby strong asymmetry indicates one terminal and one bridging OCH unit per diolate moiety while weak asymmetry indicates a pair of terminal OCH units; (*c*) asymmetry in side-chain signals, whereby strong asymmetry indicates one metal-bound and one free side chain per ligand unit; and (*d*) skeletal conformation, whereby for ligands with one Ti-bound side chain, a weak OC*H*–OC*H* coupling constant (J) is expected from a chelating ligand and a larger J from a non-chelating one. Thus, **A**-like complexes were identified with both $H_2\mathbf{12}$ and $H_2\mathbf{14}$, as previously with $H_2\mathbf{2}$–$H_2\mathbf{4}$ (4), and species lacking chelation were formed from $H_2\mathbf{16}$ and TFA, as previously found with $H_2\mathbf{1}$, $H_2\mathbf{5}$, and $H_2\mathbf{6}$ (4*b*). The complexation behaviour of $H_2\mathbf{14}$, $H_2\mathbf{16}$, and $H_2\mathbf{18}$, and $H_2\mathbf{21}$ certainly did not fit our expectation that their side chains might stabilize pentacoordinate Ti and so give complexes resembling $Ti_2\mathbf{1}_2(O^iPr)_4$. Instead, the side-chain polarity seemed to affect the ease of formation and the stability of well-defined 2:2 or 1:2 complexes.

Upon examination of the entire body of available nmr data, an additional criterion becomes available to further substantiate our view. Table 1 groups the complexes according to the displacements of each of the paired diolate signals in the complexes from their positions in the free ligands ($\delta_d - \delta_f$ and $\delta_u - \delta_f$) and according to measured J values. As described above, two broad groups are apparent: cases with large $\Delta\delta$ ($=\delta_d - \delta_u$) and small J have been associated with

Can. J. Chem. Downloaded from www.nrcresearchpress.com by 109.225.110.28 on 09/08/12
For personal use only.

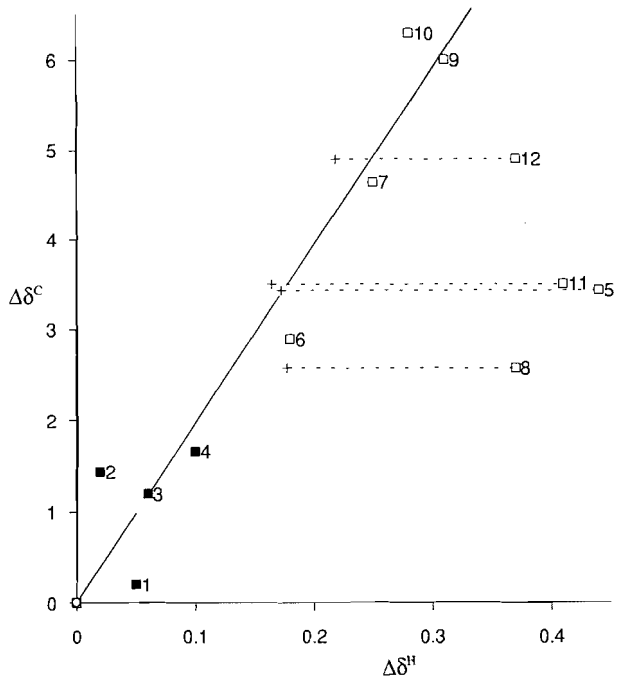

FIG. 1. Plot of $\Delta\delta^C$ vs. $\Delta\delta^H$ for complexes with J = 6.8–7.2 Hz (■) or with $J \leq 2.25$ Hz (□). The least-squares line that excludes the four outliers and that passes through the origin has r = 0.95 and slope 19.6 ± 1.1. If the outliers are "corrected" using interpolated values from Fig. 2 (+), the regression line has r = 0.93 and slope 19.7 ± 0.8 (see text). Numbers on the graph are the entry numbers of Table 1.

metal chelation and diolate bridging whereas those exhibiting small $\Delta\delta$ and large J have been associated with non-chelating and non-bridging modes of ligation. (The *meso* case, entry 6, belongs in the former group even though its *cis* stereochemistry dictates a dissimilar J.) Included in Table 1 is the 2:2 complex of the homotartrate H_2**22** reported (without a value for J) by the Sharpless group (10). It fits into the large $\Delta\delta$-small J group and we thereby agree with the **A**-like structure assigned to it. (It is also noteworthy that Ti_2**22**$_2(O^iPr)_4$ was also a poorly enantioselective epoxidation catalyst.)

It is reasonable to expect that the ^{13}C signal from an OCH grouping be related to its ^1H signal in the degree of downfield displacement resulting from complexation. Consequently, the dissimilarity in ^{13}C chemical shifts between non-equivalent OCH units in a complexed ligand ($\Delta\delta^C$) should correlate with the dissimilarity in the ^1H positions ($\Delta\delta^H$). Figure 1 shows that relation: with the exception of 4 outliers (entries 5, 8, 11, and 12), one can write $\Delta\delta^C \approx 20\Delta\delta^H$ and $(\delta^C - \delta_f^C) \approx 20(\delta^H - \delta_f^H)$. In the four exceptional cases, $\Delta\delta^C$ is unusually small or $\Delta\delta^H$ is unusually large, or both are unusual. Remarkably, one can calculate from Table 1 that $(\delta_u^C - \delta_f^H) = (0.99 \pm 0.06)(\delta_u^C - \delta_f^C)/(\delta_u^H - \delta_f^H)$ for all but the exceptional cases, where $(\delta_u^C - \delta_f^C)/(\delta_u^H - \delta_f^H)$ values are unusually large. In other words, though the ratios of ^{13}C to ^1H displacements vary somewhat from complex to complex, they are usually very much the same within a complex and the downfield positions are correlated to the upfield ones. In fact, a plot of $(\delta^C - \delta_f^C)$ vs. $(\delta^H - \delta_f^C)$ values (Fig. 2) reveals that upfield and downfield partners are connected in a straight line to the origin except in those same four cases where $(\delta^H - \delta_f^H)$ values are unusually small (i.e., their upfield OC*H* signals lie unusually far upfield), leading to the large $\Delta\delta^H$ values in Fig. 1. (If the upfield ^1H displacements are "corrected" in the four exceptional cases by interpolation to the line joining the downfield partners with the origin, then these cases fit the expected correlation of Fig. 1.)

There seems to operate a shielding of the upfield OC*H* in only these four cases. According to Marsi and Roe (12), bridging alkoxide signals are upfield of terminal ones. As well, Grindley and Thangarasa (13) recently found that the bridging OCH nuclei in diols were less affected by complexation to Sn than were terminal ones. Such probably also applies to these Ti–diolate complexes. In one of the exceptional cases, Ti_2**1**$(O^iPr)_6$, we had earlier ascribed the far upfield position of one of the pair of OC*H* signals to a shielding of the bridging OC*H* in **B** by the nearby inward-oriented and metal-bound carbonyl (4*b*) (Fig. 3), an effect not expected in the *meso* analogue of **B** and not apparent from the spectra of Ti_2**9**$(O^iPr)_6$, nor is it expected in complexes lacking chelation. Similar shielding effects appear to be exerted by the sulfonyl group of complexed **14**, by the dimethyldioxolane group of **4**, and by the ester carbonyl of **22**, and assignments of **A**-like structures are therefore fitting. The pyrazole groups of complexed **16** (or **18**) might also be expected to exert this effect; that none was apparent with the ternary complex of H_2**16** further supports the assignment of a non-chelating and non-bridging mode of complexation as in **D**. A similar argument also applies to the parent Katsuki–Sharpless catalyst, Ti_2**1**$_2(O^iPr)_4$: a shielding effect operating in **B** would also be expected in an **A**-like structure; that none was apparent argues against it.

We have thus far been unable to reproduce the spectral behaviour of this catalyst by simply incorporating strongly dipolar groups on a threitol skeleton. Similarly, Burns *et al.* found that Ti_2**22**$_2(O^iPr)_4$ did not resemble nor behave like Ti_2**1**$_2(O^iPr)_4$, but the 2:2 complex of H_2**23** did show ir and nmr similarities to that of **1** and was an enantioselective epoxidation catalyst for primary allylic alcohols (10). The two complexes should therefore have similar structures. Unlike Ti_2**1**$_2(O^iPr)_4$, however, Ti_2**23**$_2(O^iPr)_4$ was poor at kinetic selection between secondary allylic alcohol enantiomers. That observation was arduously rationalized on an **A**-like template (10) but is readily understood in terms of the increased but detrimental flexibility in a **C**-like complex with two extra methylenes. As these authors have pointed out, the major difference between H_2**22** and H_2**23** (or H_2**1**) is *the basicity of the diolate oxygens*: the sp^2 carbons attached to the diol moieties in H_2**1** and H_2**23** render their diolate oxygens less basic than do the sp^3 carbons in H_2**22**. Indeed, this is the major difference between tartrates, tartramides, or H_2**23**, which have electron-withdrawing side–chains and which give small $\Delta\delta$ – large J complexes, on the one hand, and all of the other ligands giving large $\Delta\delta$ – small J complexes with electron-releasing side – chains, on the other. The added basicity in the latter group stabilizes diolate bridges (chelation).

Other effects might conceivably be at play. For instance, the choice of chelation by H_2**14** and H_2**22** might have been influenced by a reduction in bicyclic strain (to [3.2.1]) that the extra methylenes in these ligands afford, but this cannot be the dominant influence since chelation was apparently also obtained with H_2**2**–H_2**4** and H_2**12**. In fact, the difference in C=O chemical shifts between bound and free ester groups

Can. J. Chem. Downloaded from www.nrcresearchpress.com by 109.225.110.28 on 09/08/12
For personal use only.

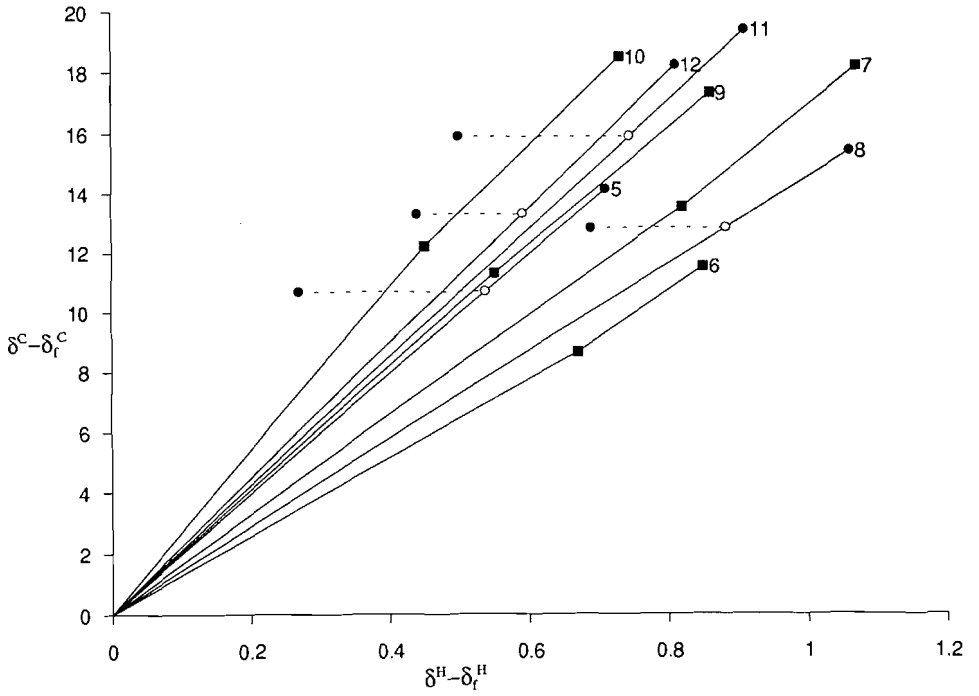

FIG. 2. Plots of $\delta^C - \delta_f^C$ vs. $\delta^H - \delta_f^H$ for strongly asymmetric complexes (i.e., with $J \leq 2.25$ Hz), including outliers (●) and interpolated values (○) (see text). Numbers on the graph are the entry numbers of Table 1.

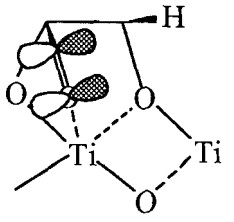

FIG. 3

in $Ti_2\mathbf{22}_2(O^iPr)_4$ was smaller than in $Ti_2\mathbf{1}_2(O^iPr)_4$ (2.1 (10) vs. ≈5 ppm (4*b*) at −10°C) and ν_{CO} for the Ti-bound ester group from **22** was higher (1688 (10) vs. 1635 (8) cm^{-1}) than that from **1**. Both observations indicate *stronger metal–carbonyl bonds* in $Ti_2\mathbf{1}_2(O^iPr)_4$. This is inconsistent with **A**-like structures for both $Ti_2\mathbf{1}_2(O^iPr)_4$ and $Ti_2\mathbf{22}_2(O^iPr)_4$ but is consistent with a **C**-like structure for $Ti_2\mathbf{1}_2(O^iPr)_4$. Therefore, instead of side-chain polarity or bicyclic strain, we now believe that diolate basicity is the most important determinant of complex structure and, by association, of catalyst enantioselectivity.

The lack of diolate bridging and hexacoordination in $Ti_2\mathbf{1}_2(O^iPr)_4$ must be due to bicyclic strain: Consider the fragments of the crystal structures (5) of $Ti_2\mathbf{5}_2(O^iPr)_4$ and $Ti_2det_2(ONPhBz)_2(OEt)_2$ (H_2det = diethyl tartrate) reproduced in Fig. 4. The main effects of the [2.2.1] bicyclic strain in the former are a long bridge (2.173 Å)[4] and a long bond to the carbonyl (2.206 Å)[4], compared to a bridge of normal (14) length (averaging 2.008 Å)[4] and a shorter bond to the carbonyl (averaging 2.084Å)[4] in the latter structure lacking such strain. Overall, the tricyclic core of crystalline $Ti_2\mathbf{5}_2(O^iPr)_4$ appears incompletely formed and "spring-loaded" (3, 10), at a delicate compromise in the tug of war between bridge formation with a poorly basic oxygen and binding to the polar carbonyl, a compromise that could not be guaranteed to persist in solution (it appears not to (4*b*)) and that $Ti_2\mathbf{1}_2(O^iPr)_4$, with less dipolar side–chains, evidently cannot easily reach on its own. In the absence of added univalent bidentates like HONPhBz, the 2:2 tartrate complex appears to make do with pentacoordination, preferring to altogether forego the bridge to, instead, strongly bind the carbonyl uninhibited by bicyclic strain. The pentacoordination can ex-

[4]From atomic positional parameters (supplementary material, ref. 5).

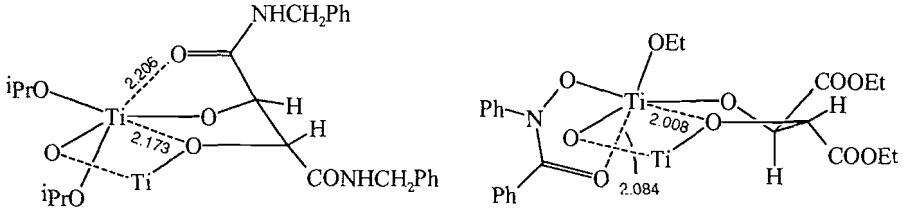

FIG. 4. Partial crystal structures of $Ti_2\mathbf{5}_2(O^iPr)_4$ (left) and $Ti_2det_2(ONPhBz)_2(OEt)_2$ (right).

Can. J. Chem. Downloaded from www.nrcresearchpress.com by 109.225.110.28 on 09/08/12
For personal use only.

plain the observed high exchange and epoxidation rates. Generally, however, the more basic diolates in non-tartrate complexes favour bridging at the expense of side-chain binding, leading to lower rates, with two qualifications: too polar a side–chain seems to allow complex, ill-resolved mixtures (probably of oligomers) to develop, and the presence of bidentate TFA ligands obviated the need for H_2**16** to form diolate bridges.

With respect to the design of chiral Lewis acids for use in reactions under strongly nucleophilic or basic conditions, we have yet to achieve our goal. However, we are currently endeavouring to prepare ligands with base- and nucleophile-stable, but electron-withdrawing, side-chain groups that reduce the diolate basicity and favour **C**-like structures.

Acknowledgements

The authors wish to thank the Natural Sciences and Engineering Research Council of Canada for financial support of this work and for a University Research Fellowship to P.G.P.

1. T. Katsuki and K. B. Sharpless, J. Am. Chem. Soc. **102**, 5974 (1980).
2. K. B. Sharpless, S. S. Woodard, and M. G. Finn. Pure Appl. Chem. **55**, 1823 (1983).
3. M. G. Finn and K. B. Sharpless. *In* Asymmetric synthesis. Vol. 5. *Edited by* J. D. Morrison. Academic Press, New York. 1985. p. 247.
4. (*a*) P. G. Potvin, P. C. C. Kwong, and M. A. Brook. J. Chem. Soc. Chem. Commun. 773 (1988); (*b*) P. G. Potvin, R. Gau, P. C. C. Kwong, and S. Bianchet. Can. J. Chem. **67**, 1523 (1989).
5. I. D. Williams, S. F. Pedersen, K. B. Sharpless, and S. J. Lippard. J. Am. Chem. Soc. **106**, 6430 (1984).
6. G. L. Robbins and R. E. Tapscott. Inorg. Chem. **15**, 154 (1976); R. E. Tapscott, R. L. Belford, and I. C. Paul. Coord. Chem. Rev. **4**, 323 (1969).
7. L. D. L. Lu, R. A. Johnson, M. G. Finn, and K. B. Sharpless. J. Org. Chem. **49**, 728 (1984).
8. M. G. Finn and K. B. Sharpless. J. Am. Chem. Soc. **113**, 113 (1990).
9. P. W. Feit. J. Med. Chem. **7**, 14 (1964).
10. C. J. Burns, C. A. Martin, and K. B. Sharpless. J. Org. Chem. **54**, 2826 (1989).
11. S. F. Pedersen, J. C. Dewan, R. R. Eckman, and K. B. Sharpless. J. Am. Chem. Soc. **109**, 1279 (1987).
12. M. Marsi and D. C. Roe. Presented at the ACS National Meeting, Los Angeles, Sept. 1988.
13. T. B. Grindley and R. Thangarasa. Can. J. Chem. **68**, 1007 (1990).
14. R. J. H. Clark. *In* Comprehensive inorganic chemistry. Vol. 3. *Edited by* J. C. Bailar, Jr., H. J. Emeléus, R. Nyholm, and A. F. Trotman-Dickenson. Pergamon Press, Oxford. 1973. p. 355.

Can. J. Chem. Downloaded from www.nrcresearchpress.com by 109.225.110.28 on 09/08/12
For personal use only.

Réduction électrochimique régiosélective d'aroyl-2- ou d'acetyl-2 chromones en milieu non aqueux

PATRICK BOUTOUTE ET GUY MOUSSET[1]

Laboratoire d'électrochimie organique unité associée au centre national de la recherche scientifique n° 434, Thermodynamique et électrochimie en solution, Université Blaise Pascal, 24, Avenue des Landais, 63177 Aubière CEDEX, France

Reçu le 22 janvier 1992

PATRICK BOUTOUTE et GUY MOUSSET. Can. J. Chem. **70**, 2266 (1992).

Le comportement électrochimique de chromones substituées en position 2 par des groupements benzoyle et acétyle a été étudié par voltammétrie cyclique en milieu non aqueux (DMF). La présence d'une fonction phénol sur le groupement benzoyle entraine un phénomène d'auto-protonation. Des macroélectrolyses réalisées en présence d'un donneur de proton ont mis en évidence une réduction régiosélective de la fonction carbonyle du groupement benzoyle avec la benzoyl-2 chromone et de la double liaison pour l'acétyl-2 chromone. L'électrochimie permet, par un choix judicieux du potentiel, de réaliser un second transfert électronique sur les produits de réduction avec formation de structures dimères thermiquement instables conduisant à des radicaux libres par coupure homolytique d'une liaison carbone–carbone.

PATRICK BOUTOUTE and GUY MOUSSET. Can. J. Chem. **70**, 2266 (1992).

The electrochemical behaviour of chromones substituted in position 2 by benzoyl or acetyl groups was studied by cyclic voltammetry in a nonaqueous solvent. Self-protonation reactions were observed with compounds possessing a phenol function on the benzoyl group. Macroelectrolyses achieved in the presence of a proton donor afford a regioselective reduction of the carbonyl function in position 2 of the benzoyl-2 chromone and of the double bond for the acetyl-2 chromone. Moreover the further reduction leads to the formation of thermally unstable dimers, which may give homolytic cleavage to free radicals.

Can. J. Chem. Downloaded from www.nrcresearchpress.com by 109.225.110.28 on 09/08/12
For personal use only.

Introduction

Les chromones et leurs dérivés sont des molécules rencontrées fréquemment dans certains médicaments dont le métabolisme fait intervenir une forme réduite (1–4). Notre travail est consacré à l'étude de la réduction électrochimique d'aroyl-2 ou d'acétyl-2 chromones du type :

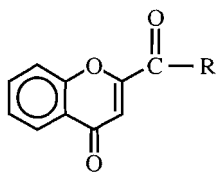

R = C_6H_5 **1**; CH_3 **2**; *o*-C_6H_4OH **3**; *p*-C_6H_4OH **4**

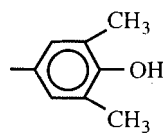

5

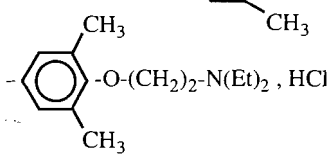

6

Chacun de ces composés possède, en position 2 du cycle chromone, un substituant comprenant une fonction carbonyle aromatique ou non, conjuguée avec la fonction cétone α,β-éthylénique du cycle de la chromone. La réduction chimique régiosélective de l'une ou l'autre des fonctions carbonyles ou de la double liaison est délicate et fournit souvent des mélanges de produits (5, 6). Le comportement électrochimique des cétones aromatiques ou α,β-éthyléniques aromatiques a donné lieu à de nombreuses études (7–13) et les mécanismes de leur réduction sont maintenant bien établis. Dans ce travail, nous avons étudié la réduction des chromones substituées **1**–**6** en milieu aprotique (DMF) ou en présence d'un donneur de proton essentiellement dans le but de réaliser des réductions sélectives des diverses fonctions présentes dans ces molécules. Ainsi, le choix du potentiel imposé peut permettre de réduire uniquement une fonction de la chromone. Le produit de la réaction étant lui-même électroactif, un nouveau transfert électronique peut être réalisé à un potentiel plus négatif que celui du substrat de départ, avec formation d'un second produit de réduction. Une complémentarité entre les méthodes chimiques et électrochimiques a déjà été mentionnée dans le cas de thiazines substituées (14).

[1]Auteur à qui adresser toute correspondance.

Résultats et discussion

*Cas de la benzoyl-2 chromone **1***

Étude en milieu aprotique

En milieu aprotique (fig. 1), la benzoyl-2 chromone (BC, R = C_6H_5) se réduit en deux étapes monoélectroniques dont les potentiels de pics sont E_{pc1} = −0,63 V et E_{pc2} = −1,16 V. La différence de potentiel entre les pics anodiques et cathodiques est δE_p = 80 mV pour chaque étape considérée donc comme quasi réversible. Le premier transfert correspond à la formation du radical anion et le second au dianion :

$$BC + 1e^- \underset{}{\overset{E_{pc1}}{\rightleftharpoons}} BC^{\cdot -}$$

$$BC^{\cdot -} + 1e^- \underset{}{\overset{E_{pc2}}{\rightleftharpoons}} BC^{2-}$$

La réversibilité du second transfert montre que le dianion n'est pas une base très forte en raison de la délocalisation importante de la charge. Une électrolyse au potentiel de la première étape de réduction, conduite *in situ* dans l'entrefer d'un appareil de RPE a permis d'obtenir le spectre du radical-anion $BC^{\cdot -}$ (fig. 2).

Une structure hyperfine est ainsi observée : elle correspond aux couplages avec l'atome d'hydrogène porté par la double liaison et avec ceux des noyaux aromatiques. Seule

Can. J. Chem. Downloaded from www.nrcresearchpress.com by 109.225.110.28 on 09/08/12
For personal use only.

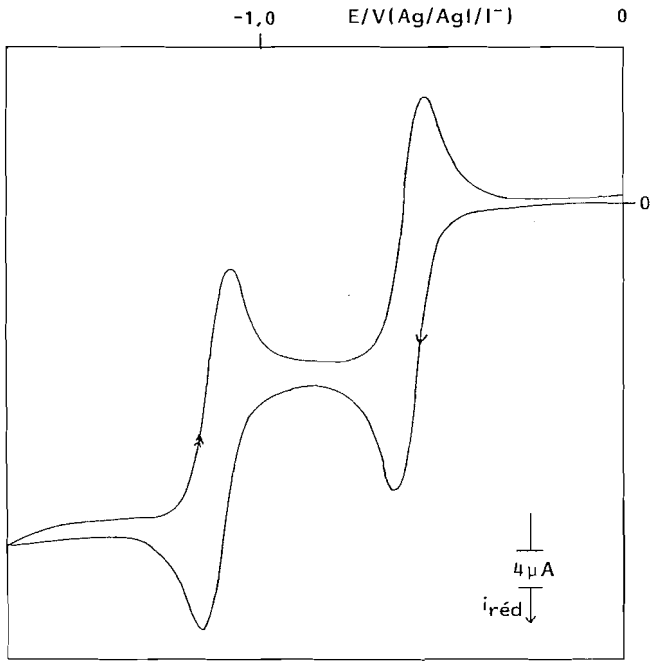

FIG. 1. Voltammogramme de la benzoyl-2 chromone **1** en solution dans le DMF ($C = 5 \times 10^{-3}$ M). Electrolyte support Bu_4NBF_4 (0,1 M). Electrode de carbone vitreux $v = 0{,}02$ V s^{-1}.

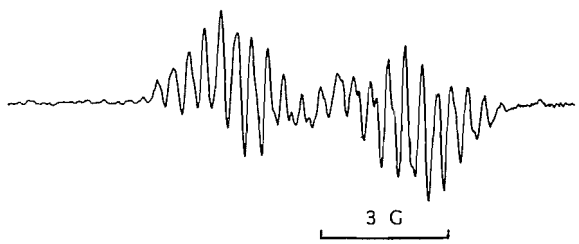

FIG. 2. Spectre de RPE enregistré en cours d'électrolyse sur cathode de Cu/Hg ($A \simeq 1{,}5$ cm^2) de la benzoyl-2 chromone ($c = 5 \times 10^{-3}$ M). Electrolyte support Bu_4NBF_4 (0,1 M). Gain $2{,}5 \times 10^5$. Modulation $1{,}6 \times 10^{-1}$ G. Champ 3270 G. $i = 150$ µA.

la constante de couplage de l'électron avec l'hydrogène éthylénique a été mesurée. Sa valeur $a_{Heth} = 4{,}36$ G permet de déterminer, par la formule de MacConnell et Chesnut (15), une densité de spin assez faible sur ce carbone ($\rho = 0{,}180$). Une microcoulométrie réalisée au potentiel de la première étape fournit la valeur $n = 0{,}84$ F mol^{-1}.

Etude en milieu protique

Nous avons utilisé comme donneur de proton le phénol (PhOH), l'hydrogénosulfate de tétrabutyl ammonium (Bu_4NHSO_4) ou l'acide acétique (AcOH), ce dernier présentant l'inconvénient de donner, pour des quantités importantes d'acide, une étape de réduction du proton.

Des additions successives de phénol (ou de Bu_4NHSO_4) entrainent une augmentation de l'intensité de la première étape de réduction de la benzoyl-2 chromone sans modifier son potentiel (fig. 3). Pour un rapport de concentrations m = [donneur de proton]/[chromone] = 6 l'intensité a presque doublé ce qui indique que le système évolue vers un stade biélectronique. Une coulométrie réalisée dans ces conditions (phénol, $m = 6$) indique une consommation d'électricité correspondant à 1,6 F mol^{-1}. Parallèlement à

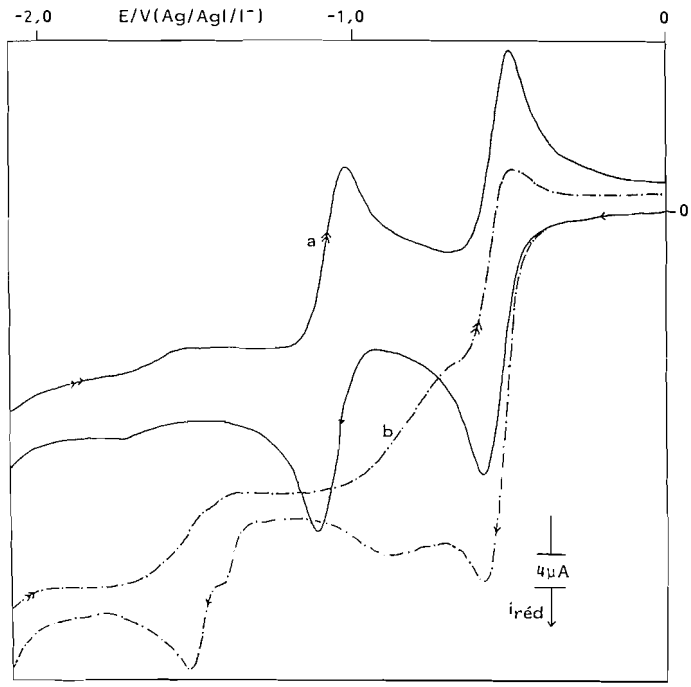

FIG. 3. Voltammogrammes de la benzoyl-2 chromone **1** ($c = 5 \times 10^{-3}$ M) dans le DMF. Electrolyte support Bu_4NBF_4 (0, 1 M). Concentration en phénol (*a*) $c' = 0$; (*b*) $c' = 10^{-2}$ M. Electrode de carbone vitreux $v = 0{,}02$ V s^{-1}.

cette évolution, on note la disparition progressive de la réversibilité de cette étape. Les premières additions de phénol entrainent une diminution de l'intensité de la seconde étape et l'apparition progressive de deux nouveaux pics de réduction à des potentiels plus négatifs ($E_{pc3} = -1{,}42$ V et $E_{pc4} = -1{,}52$ V). Ceux-ci peuvent être liés à la réduction du (ou des) produit(s) formés à la première étape en milieu protique. Nous sommes en présence d'un mécanisme de type biélectronique avec protonation du radical-anion intermédiaire selon :

$$BC \underset{}{\overset{1e^-}{\rightleftharpoons}} BC^{\cdot-} \xrightarrow{PhOH} BCH^{\cdot} \xrightarrow[(\text{ou } BC^{\cdot-})]{1e^-} BCH^- \xrightarrow{PhOH} BCH_2$$

Des additions d'acide acétique entrainent la disparition progressive de la seconde étape de réduction de la chromone et une modification de la première par formation d'une prévague dont l'intensité croit avec la concentration en acide jusqu'à correspondre à un échange biélectronique. Une coulométrie réalisée en présence d'acide dans le rapport m = [acide]/[chromone] = 5 conduit à une consommation d'électricité égale à $n = 1{,}65$ F mol^{-1}. La présence d'un prédstade traduit la formation d'une espèce plus électroactive que la chromone elle-même.

$$BC \overset{AcOH}{\rightleftharpoons} [BC\text{–}HOAc] \xrightarrow[E'_{pc1}]{1e^-} BCH^{\cdot} \xrightarrow[E'_{pc1}]{1e^-} BCH^- \xrightarrow{AcOH} BCH_2$$

Comme dans le cas du phénol, la première étape de réduction

devient irréversible et son intensité augmente aux dépens de la seconde jusqu'a correspondre à un système biélectronique.

Une macroélectrolyse réalisée en présence de deux équivalents d'acide acétique au potentiel de −0,55 V conduit après consommation de 1,69 F mol^{-1} à l'(hydroxy-1 benzyl)-2 chromone 7

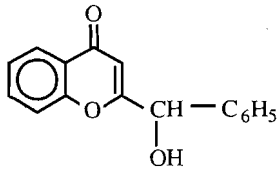

L'effet attracteur du groupement benzoyle a entraîné une localisation préférentielle de l'électron célibataire sur la partie

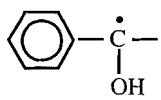

de la molécule conduisant à la réduction de la fonction carbonyle, le carbanion issu du second transfert étant vraisemblablement protoné plus rapidement que la forme énolate. La structure du produit est confirmée par comparaison avec un échantillon authentique obtenu par réduction chimique avec $NaBH_4$.

Réduction de l'acétyl-2 chromone 2

En milieu aprotique, l'acétyl-2 chromone (AC) **2** se réduit en trois étapes dont les deux premières sont faiblement réversibles (fig. 4(*a*)).

Les potentiels des pics sont respectivement $E_{pc1} = -0,70$ V, $E_{pc2} = -1,15$ V et $E_{pc3} = -1,46$ V. La première étape conduit par un transfert monoélectronique à un radical anion relativement instable.

$$AC + 1e^- \rightleftarrows AC^{\cdot -}$$

La faible réversibilité de cette étape peut provenir d'une protonation partielle du radical anion par des impuretés acides du solvant (SH) ou par le substrat lui-même qui possède des atomes d'hydrogène en α d'une fonction carbonyle (16).

$$AC^{\cdot -} + SH \text{ (ou } AC) \rightarrow ACH^{\cdot} + S^- \text{ (ou } AC^-)$$

La seconde étape qui disparait en présence d'un donneur de proton est attribuée à la réduction du radical-anion en dianion

$$AC^{\cdot -} + 1e^- \rightarrow AC^{2-}$$

La troisième étape dont l'intensité est augmentée par addition d'un donneur de proton peut correspondre à la réduction d'une forme dihydro ACH_2 résultant de la protonation du dianion par un mécanisme ECEC. Il faut cependant noter que l'acétyl-2 chromone donne lieu à d'importants phénomènes de maxima sur électrode de mercure en particulier en présence d'un donneur de proton (fig. 4(*b*)). L'interprétation des voltammogrammes est de ce fait rendue difficile.

Une macroélectrolyse réalisée au potentiel de −0,6 V en présence de deux équivalents d'acide acétique conduit ici à la réduction de la double liaison du cycle chromone avec formation de l'acétyl-2 chromanone

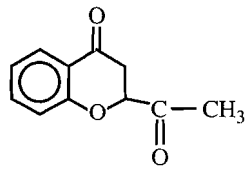

8

Réduction des aroyl-2 chromones substituées ***3–6***

Ces composés pourront jouer le rôle de donneur de proton par l'intermédiaire de leur fonction phénol ou chlorhydrate d'amine. Les anions électrogénérés en milieu de faible acidité seront protonés par le substrat selon un processus d'auto-protonation (17–20). Ainsi, les voltammogrammes des chromones substituées **3–6** présentent tous une étape de

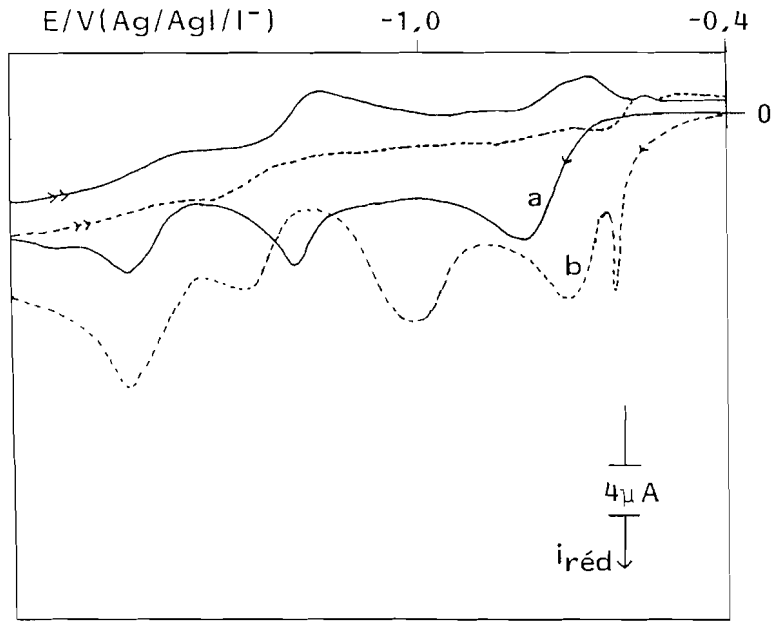

FIG. 4. Voltammogrammes de l'acétyl-2 chromone **2** ($c = 5 \times 10^{-3}$ M) dans le DMF. Electrolyte support Bu_4NBF_4 (0,1 M). Electrode de mercure stationnaire. $v = 0,1$ V s^{-1}. Concentration en CH_3COOH (*a*) $c' = 0$; (*b*) $c' = 10^{-2}$ M.

Can. J. Chem. Downloaded from www.nrcresearchpress.com by 109.225.110.28 on 09/08/12
For personal use only.

Can. J. Chem. Downloaded from www.nrcresearchpress.com by 109.225.110.28 on 09/08/12
For personal use only.

réduction irréversible C_1 située à un potentiel moins négatif que celui observé pour la benzoyl-2 chromone **1**. Nous étudierons à titre d'exemple (fig. 5) la (diméthyl-3',5' hydroxy-4' benzoyl)-2 chromone ainsi que les *ortho* et *para* hydroxybenzoyl-2 chromones. Les valeurs des potentiels des diverses étapes sont réunies dans le tableau 1. Nous pouvons observer que la première étape de réduction de l'isomère *ortho*-hydroxylé **3** se situe à un potentiel moins négatif que celle de l'isomère *para* **4** (tableau 1). Ce phénomène déjà observé dans le cas de céto-alcools (21) est relié à l'établissement pour l'isomère *ortho* d'une liaison hydrogène entre les fonctions phénol et carbonyle rendant cette dernière plus facilement réductible que pour l'isomère *para* où une telle interaction est impossible. L'étape de réduction irréversible C_1 dont le courant limite est supprimé par addition d'un équivalent de base (Bu_4NOH) correspond logiquement à la réduction du substrat sous sa forme phénolique (BCOH). Le radical-anion formé :

$$BCOH + 1e^- \xrightarrow{C_1} BC^{\cdot}OH$$

est ici protoné par le dépolarisant avec formation du radical neutre $HBC^{\cdot}OH$ plus facilement réductible. L'absence de réversibilité pour le pic C_1 peut se justifier par l'existence d'un deuxième transfert à l'électrode (processus ECE) ou par une dismutation (DISP) (20, 22).

$$BC^{\cdot}OH + BCOH \leftrightarrows HBC^{\cdot}OH + BCO^-$$

$$HBC^{\cdot}OH + 1e^- \xrightarrow[\text{rapide}]{} HBC^-OH$$

ou

$$HBC^{\cdot}OH + BC^{\cdot}OH \rightarrow HBC^-OH + BCOH$$

Afin de déterminer la nature du mécanisme, nous avons réalisé une étude des variations du potentiel de pic E_{pc1} en fonction de la vitesse de balayage ou de la concentration. Aucune réversibilité pour le pic C_1 n'est observée jusqu'à la vitesse de 150 V s^{-1} qui est le maximum que nous puissions obtenir. Pour le composé **4**, la fonction $E_p = f(\log c_o/v)$ est représentée par une droite de pente $dE_p/d(\log c_o/v) = 29{,}9$ mV. La variation du potentiel de pic en fonction de c_o pour une vitesse $v = 0{,}1$ V s^{-1} conduit également à une droite de pente $dE_p/d(\log c_o) = 29{,}6$ mV par décade de concentration. La mesure de la largeur de pic pour différentes vitesses de balayage (0,1–25 V s^{-1}) fournit une valeur moyenne $E_{p/2} - E_p = 58$ mV. L'ensemble de ces résultats est en accord avec un processus de type ECE_{irr} ou DISP 1 (17). L'absence de réversibilité ne permettant pas de définir la valeur de E_o pour le système $BCOH/BCOH^{\cdot-}$, il est difficile de préciser lequel des deux mécanismes intervient dans ce cas. Une coulométrie réalisée au potentiel de l'étape C_1 a fourni une valeur $n = 0{,}82$ F mol^{-1}.

L'étape réversible C_2 prépondérante en milieu basique, correspond à la réduction de l'ion phénate :

$$BCO^- + 1e^- \underset{E_{pA_2}}{\overset{E_{pC_2}}{\rightleftharpoons}} BC^{\cdot}O^-$$

En présence de base, l'intensité du pic cathodique C_2 augmente au détriment de l'étape C_1 qui le précède et sa réversibilité est améliorée. Une électrolyse *in situ* dans la cavité d'un spectromètre de RPE a permis d'enregistrer le spectre du radical dianion en présence d'un équivalent de base (fig. 6).

Le troisième pic C_3 faiblement réversible, dont l'intensité augmente en présence d'un équivalent de base correspond à la réduction de derivés carbonylés formés par destruction de la chromone en milieu fortement basique (6).

La dernière étape C_4 située à potentiel très réducteur rend compte de la réduction de l'espèce formée en C_2 :

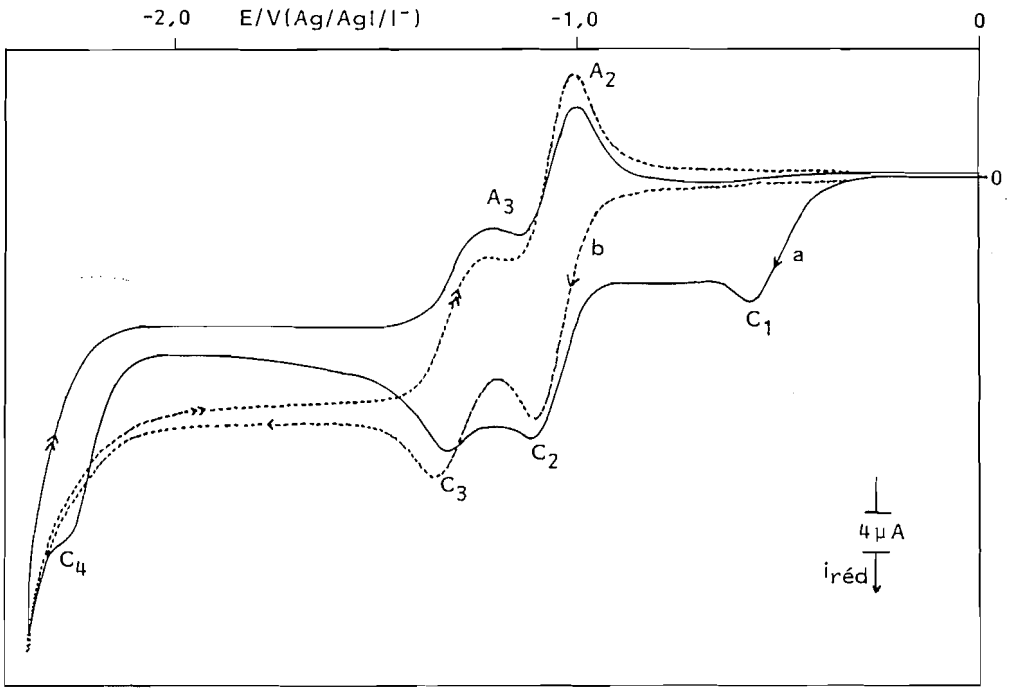

FIG. 5. Voltammogramme de la (diméthyl-3',5' hydroxy-4' benzoyl)-2 chromone **5** ($c = 5 \times 10^{-3}$ M) dans le DMF. Electrolyte support Bu_4NBF_4 (0,1 M). Electrode de carbone vitreux $v = 0{,}02$ V s^{-1}. Concentration en base (Me_4NOH) : (*a*) 0; (*b*) 5×10^{-3} M.

Can. J. Chem. Downloaded from www.nrcresearchpress.com by 109.225.110.28 on 09/08/12
For personal use only.

TABLEAU 1. Valeurs des potentiels de pic obtenues pour les chromones **3–6** ($c = 5 \times 10^{-3}$ M) en milieu organique aprotique (DMF). Electrode de carbone vitreux ($A = 7$ mm^2), vitesse de balayage $v = 0{,}02$ V s^{-1}. Les potentiels sont donnés par rapport à l'électrode Ag/AgI/I$^-$ (Bu_4NI 0,1 M DMF).

Chromone	E_{pc1} (V)	E_{pc2} (V)	E_{pc3} (V)	E_{pc4} (V)
3	−0,40	−0,98	−1,13	−2,19
4	−0,62	−1,03	−1,4	−2,25
5	−0,57	−1,11	−1,32	−2,27
6[a]	−0,40	−0,62	−1,12	−2,25

[a]Des phénomènes de maxima perturbent le voltammogramme de ce composé.

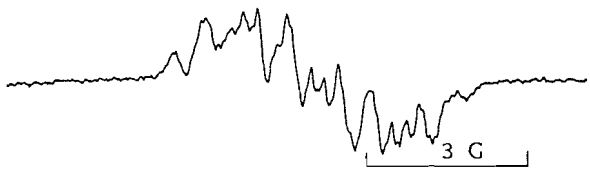

FIG. 6. Spectre de RPE enregistré en cours d'électrolyse sur cathode de Cu/Hg ($A \simeq 2{,}5$ cm^2) de la (diméthyl-3′,5′ hydroxy-4′ benzoyl)-2 chromone **5** ($c = 5 \times 10^{-3}$ M) en présence d'un équivalent de base (Me_4NOH). Electrolyte support Bu_4NBF_4 0,1 M. Champ 3270 G. Gain $1{,}6 \times 10^5$ et modulation $1{,}6 \times 10^{-1}$ G. $i = 40$ μA.

$$BC^{\cdot}O^- + le^- \rightarrow BC^{2-}O^- \xrightarrow[\text{rapide}]{\text{solvant}} BCOH^{2-}$$

Le trianion qui est une base très forte est protoné rapidement par les impuretés acides du milieu de telle sorte que sa réoxydation ne peut être observée. Des additions de base qui suppriment sa protonation déplacent son potential vers des valeurs plus négatives et ne permettent plus de l'observer de manière nette en raison de la proximité de la vague de réduction de l'électrolyte.

En présence d'un donneur de proton (AcOH), l'étape C_2 disparait au profit de la première C_1 dont l'intensité augmente jusqu'à correspondre à un échange biélectronique. Lorsque l'addition d'acide est réalisée en présence d'un mélange d'(hydroxy-2′-) et d'(hydroxy-4′ benzoyl)-2 chromones **3** et **4**, on constate que la protonation a lieu en premier avec l'(hydroxy-4′ benzoyl)-2 chromone **4**, cette dernière ne possédant pas de liaison hydrogène avec la fonction carbonyle susceptible de rendre la protonation plus difficile (fig. 7).

Étude électrochimique des produits obtenus par électroréduction en milieu protique de la benzoyl-2 et de l'acétyl-2 chromone

L'(hydroxy-1 benzyl)-2 chromone **7** et l'acétyl-2 chromanone **8** obtenues lors des macroélectrolyses réalisées avec les chromones **1** et **2** en présence d'acide acétique possèdent encore une fonction carbonyle électroréductible. Le voltammogramme de l'(hydroxy-1 benzyl)-2 chromone obtenu sans addition d'un donneur de proton est constitué de deux pics cathodiques situés aux potentiels $E_{pc'1} = -1{,}38$ V et $E_{pc'2} = -1{,}64$ V et d'un pic anodique dont le potentiel est $E_{pA} = -0{,}50$ V (fig. 8). Le premier pic cathodique est irréversible alors que le second d'intensité moindre possède une faible réversibilité. Une électrolyse au potentiel de la première étape n'entraîne pas la disparition de la seconde dont l'intensité augmente. Des additions d'un donneur de proton (AcOH ou Bu_4NHSO_4) provoquent la disparition de cette seconde étape avec formation d'une vague unique irréversible au potentiel de −1,25 V. Une étude du premier pic de réduction en fonction de la vitesse de balayage montre une irréversibilité totale jusqu'à 150 V s^{-1}. Lorsque la concentration en dépolarisant est augmentée, on constate un déplacement du potentiel de pic vers des valeurs plus positives ($\Delta E_p = 12$ mV lorsque la concentration varie entre $2{,}5 \times 10^{-4}$ M et $2{,}5 \times 10^{-3}$ M). L'ensemble de ces résultats ainsi que la consommation de 1 F mol^{-1} par électrolyse en présence d'acide acétique au potentiel de −1,25 V suggère une dimérisation rapide des radicaux neutres formés.

La molécule de substrat possède une fonction alcool en position benzylique d'une part et allylique d'autre part avec des atomes fortement attracteurs. Celle-ci peut jouer le rôle de donneur de proton vis à vis des anions électrogénérés :

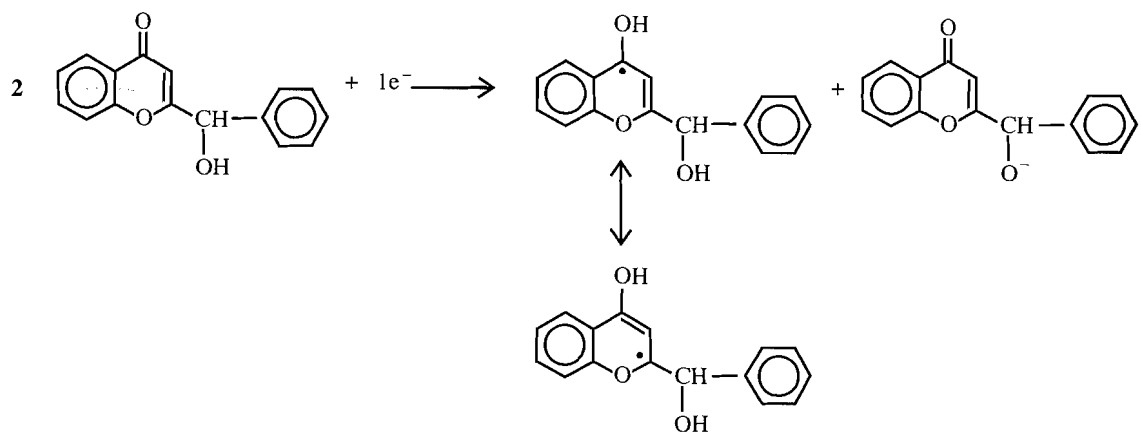

La présence d'une faible réversibilité pour la seconde étape et le fait qu'un donneur de proton entraine sa disparition au profit de la première permet d'envisager à ce stade une réduction monoélectronique de la forme anionique :

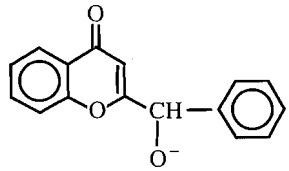

Des macroélectrolyses ont été réalisées au potentiel de $-1{,}25$ V en présence de quatre équivalents de donneur de proton (acide acétique ou Bu_4NHSO_4). Le produit de réduction isolé présente une grande instabilité en solution. Les extraits éthérés doivent être séchés sur sulfate de sodium et non sur sulfate de magnésium, ce dernier provoquant l'apparition d'une intense coloration rouge. La présence de traces d'acide entraine immédiatement l'apparition de cette même coloration. Le spectre UV réalisé avec une solution dans $CHCl_3$ en présence d'acide chlorhydrique présente trois nouvelles bandes d'absorption à $\lambda_1 = 265$ nm, $\lambda_2 = 410$ nm et $\lambda_3 = 525$ nm (fig. 9).

Le produit est également sensible à la température et subit une décomposition dès 30°C. Les spectres de RMN ont fourni avec tous les solvants usuels un ensemble de signaux très élargis qu'il est impossible d'interpréter en termes de couplages. Ce phénomène suggère la présence possible dans la solution, d'espèces paramagnétiques formées par rupture d'une liaison dès que la température s'élève pour atteindre celle de la sonde RMN (environ 34°C). Afin de vérifier cette hypothèse, nous avons réalisé par RPE une étude de l'influence de la température sur le produit solide (fig. 10).

Nous avons pu constater la présence d'espèces paramagnétiques dès la température ambiante, l'intensité du signal augmentant rapidement lorsque la température s'élève. Un spectre infrarouge réalisé en pastille de KBr montre la présence de fonctions alcool et l'absence de groupement carbonyle. Ce résultat est en accord avec une dimérisation des radicaux de manière préférentielle avec l'atome de carbone de la fonction carbonyle pour former le pinacol :

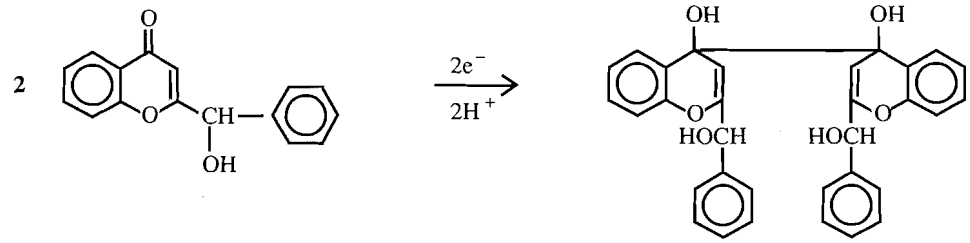

9

Les analyses élémentaires ont fourni des résultats en accord avec cette formule (calc. % C : 75,88; % H : 5,13; % O : 18,97; trouvé % C : 75,35; % H : 5,81; % O : 17,02) et le spectre de masse montre la présence d'un pic important à $m/e = 253$ qui correspond au fragment :

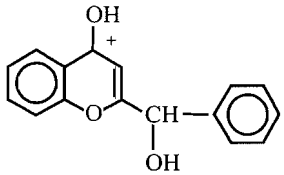

La faible stabilité thermique d'un tel dimère laisse présager une réversibilité pour la réaction de couplage en raison de la rupture homolytique d'une liaison carbone–carbone entraînant la formation de deux radicaux **10**. La molécule de dimère possède également des fonctions alcool en position allyliques et benzyliques susceptibles d'entrainer, en présence de traces d'acide, l'apparition de carbocations d'où l'évolution du spectre UV–visible.

Le voltammogramme de l'(hydroxy-1 benzyl)-2 chromone **7** obtenu avec une électrode de carbone vitreux (fig. 8) montre un croisement des traces cathodiques et anodiques ainsi que la présence d'un pic anodique. Un tel comportement déjà observé dans le cas de dérivés halogénés (23) peut être lié à la formation, dès le début du balayage retour, d'une espèce radicalaire plus facilement réductible. Le pic anodique situé à $E_{pa} = -0{,}50$ V correspond à l'oxydation de l'anion formé après réduction du radical. Un second balayage cathodique réalisé immédiatement après la réoxydation (fig. 8) montre l'apparition d'un nouveau pic cathodique correspondant à la réduction du radical libre formé par oxydation du carbanion. Avec une électrode de mercure stationnaire, l'étape anodique est très fortement perturbée par des phénomènes d'adsorption. Dans les deux cas, la présence d'un donneur de proton entraîne sa disparition.

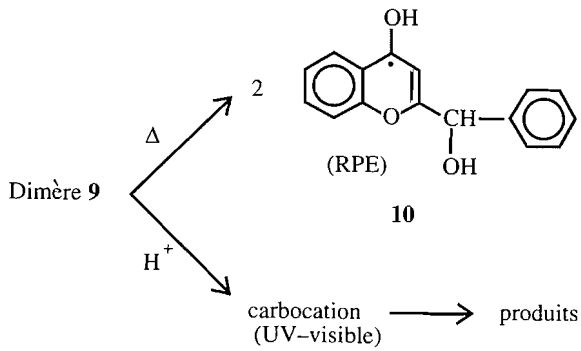

L'acétyl-2 chromanone **8** présente, en voltammétrie cyclique, un seul pic de réduction $E_{pc} = -1{,}21$ V (fig. 11) et un croisement des traces cathodiques et anodiques encore plus marqué que dans le cas précédent.

Aucun pic anodique n'est par contre observé dans ce cas en raison vraisemblablement d'une protonation rapide de l'anion moins conjugué. La forme très aigüe du pic cathodique laisse présager une désactivation rapide du substrat par les bases électrogénérées. Le produit isolé à partir de macroélectrolyses en présence d'acide acétique a présenté également des caractéristiques d'instabilité comme dans le cas précédent.

En conclusion, la benzoyl-2 et l'acétyl-2 chromone ont

Can. J. Chem. Downloaded from www.nrcresearchpress.com by 109.225.110.28 on 09/08/12
For personal use only.

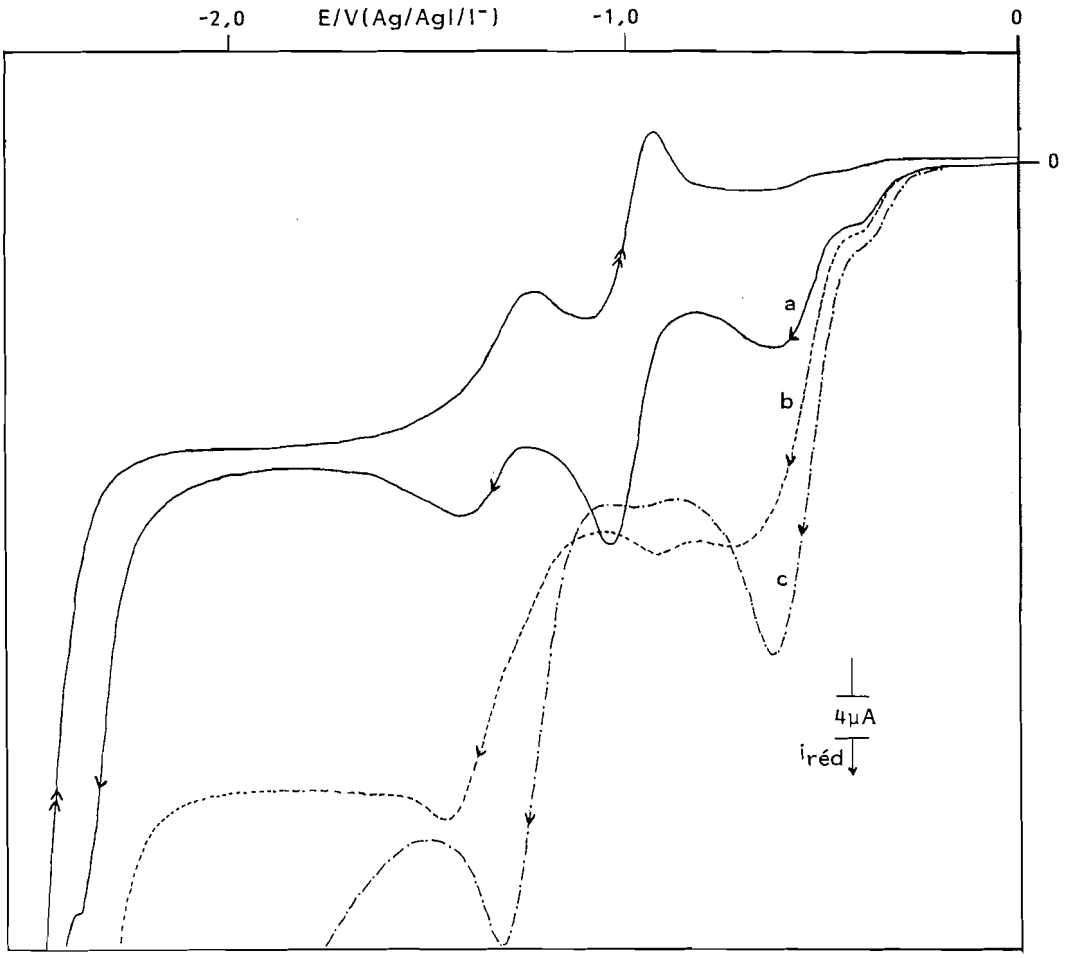

FIG. 7. Voltammogrammes d'un mélange (hydroxy-4′ benzoyl)-2 chromone (70%) – (hydroxy-2′ benzoyl)-2 chromone (30%) dans le DMF ($c = 5 \times 10^{-3}$ M). Electrolyte support Bu_4NBF_4 (0,1 M). Evolution en fonction de la concentration en CH_3COOH (*a*) 0; (*b*) 5×10^{-3}; (*c*) $2,5 \times 10^{-2}$ M. Electrode de carbone vitreux $v = 0,02$ V s^{-1}.

montré des comportements électrochimiques différents. Si la première conduit, en milieu protique, à la réduction de la fonction carbonyle du groupement benzoyle, la seconde permet d'isoler un produit unique correspondant à la réduction de la double liaison du cycle chromone. Les réducteurs chimiques ($NaBH_4$) réduisent seulement la fonction carbonyle en position 2 sur le cycle chromone alors que l'action de l'hydrogène en présence de métaux divisés (6) entraîne des réactions non sélectives affectant les deux fonctions carbonyles et la double liaison du cycle.

Partie expérimentale

Techniques électrochimiques

Le diméthylformamide (DMF) est distillé sous préssion réduite après avoir été séché sur carbonate de sodium. L'électrolyte indifférent est le tétrafluoroborate de tétrabutylammonium à la concentration de 0,1 M. Les tensions sont indiquées par rapport à l'électrode de référence $Ag/AgI/I^-$ (Bu_4NI 0,1 M dans le DMF). L'électrode de travail est constituée soit d'un disque de carbone vitreux, soit d'une goutte de mercure stationnaire. Toutes les mesures ont été réalisées à température ambiante après désaération par un courant d'azote ou d'argon. Les voltammogrammes ont été enregistrés à l'aide d'un ensemble Tacussel comprenant un potentiostat type PRT-20X équipé d'un générateur de signaux triangulaires et d'un amplificateur de type ADTP. Les différentes coulométries ont été réalisées dans une cellule contenant une nappe de mercure agitée pendant toute la durée de l'électrolyse. L'installation comprend un potentiostat PRT 100 et un intégrateur Tacussel IG5N. Chaque essai porte sur environ 25 mg de produit correspondant à une concentration initiale de 5×10^{-3} M.

Synthèse des substrats

La benzoyl-2 chromone a été obtenue par réaction de Friedel et Crafts entre le benzène et le chlorure de l'acide chromone carboxylique-2 (1), ce dernier résultant de la réaction du pentachlorure de phosphore PCl_5 sur l'acide (24). Dans un réacteur muni d'un agitateur, d'un réfrigérant, d'une ampoule à brome, on introduit 4,8 g de chlorure d'aluminum dans 100 cm^3 de benzène. Après avoir refroidi l'ensemble vers 5°C on ajoute très lentement 3,7 g de chlorure d'acide chromone carboxylique-2 en solution dans 40 cm^3 de benzène. L'addition terminée, on agite pendant 24 h. Le milieu réactionnel est versé sur un mélange de 150 cm^3 d'acide chlorhydrique et 300 g de glace. La couche benzénique est décantée, lavée à l'eau, séchée sur sulfate de sodium et évaporée. Le produit obtenu est recristallisé dans l'éthanol après traitement au noir animal. Les composés **3**, **4** et **5** sont obtenus également par une réaction de Friedel et Crafts à partir du chlorure d'acide et des phénols correspondants en présence de $AlCl_3$ selon le mode opératoire décrit par M. Besson (1). Le composé **6** est préparé à partir de **5** par action de K_2CO_3 en présence de *N*,*N*-diéthylamino-2 bromo-1 éthane (1). Un échantillon d'acétyl-2 chromone nous a été fourni par le Professeur M. Paillard (Laboratoire de chimie organique, Faculté des sciences pharmaceutiques de Toulouse) que nous remercions. L'(hydroxy-1 benzyl)-2 chromone a pu être également obtenu par réduction de la benzoyl-2 chromone par le borohydrure de sodium (2).

Can. J. Chem. Downloaded from www.nrcresearchpress.com by 109.225.110.28 on 09/08/12
For personal use only.

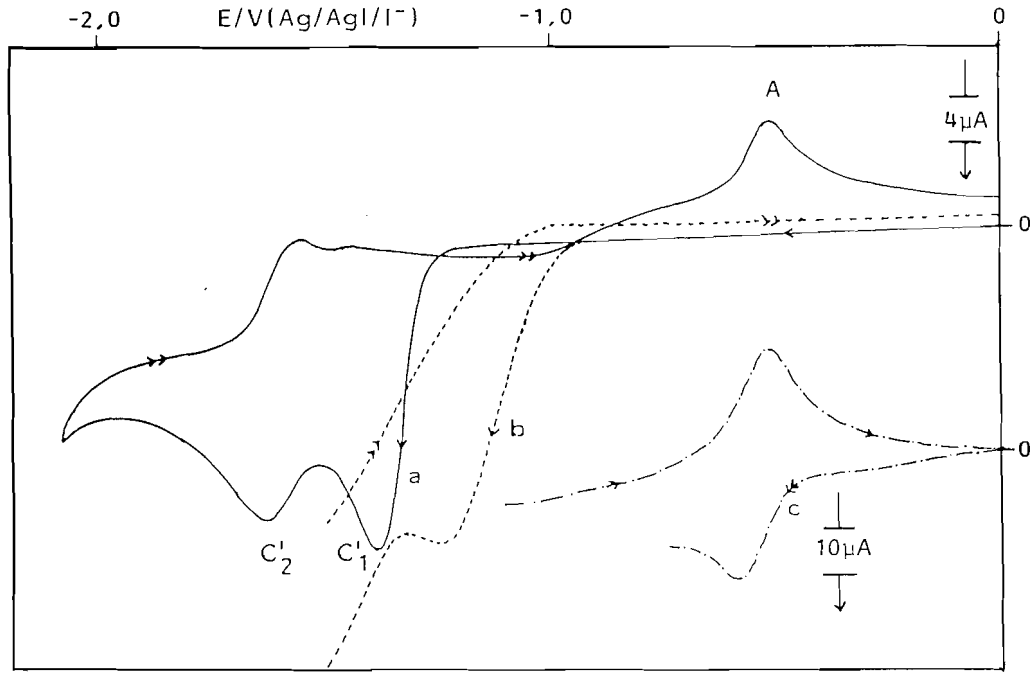

FIG. 8. Voltammogramme de l'(hydroxy-1 benzyl)-2 chromone **7** ($c = 5 \times 10^{-3}$ M) dans le DMF. Electrolyte support Bu_4NBF_4 (0,1 M). Electrode de carbone vitreux $v = 0{,}02$ V s^{-1}, (*a*) $[CH_3COOH] = 0$ et (*b*) 10^{-2} M. Courbe (*c*) : second balayage cathodique après oxydation à −0,50 V, $v = 0{,}10$ V^{-1}.

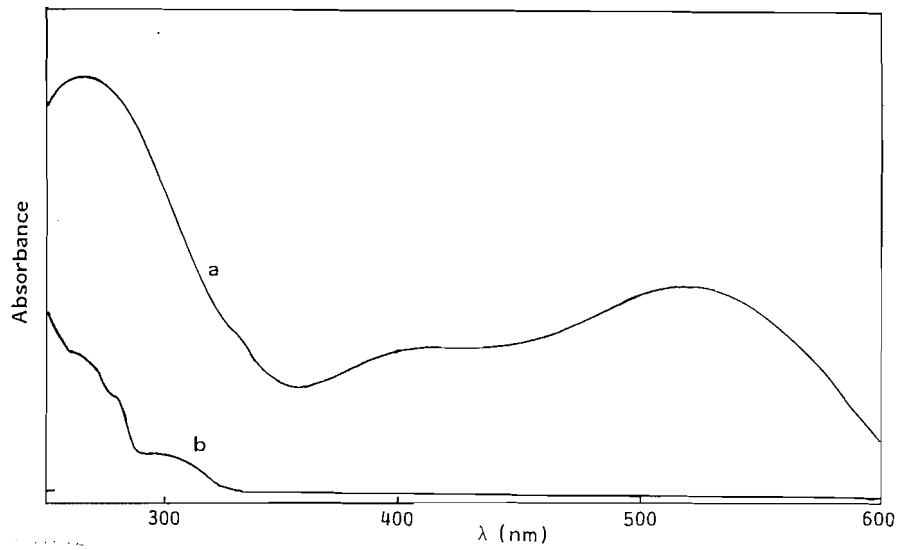

FIG. 9. Spectre UV–visible du produit de réduction de **7**. (*a*) Solution dans $CHCl_3$ $c = 2{,}5 \times 10^{-4}$ M + 1 goutte de HCl; (*b*) solution dans $CHCl_3$ $c = 2{,}5 \times 10^{-4}$ M.

Electrolyses préparatives

Toutes les électrolyses préparatives ont été effectuées dans une cellule à trois compartiments dont la cathode est une nappe de mercure et l'électrode auxiliaire une plaque de graphite. Après électrolyse, le catholyte est repris par 500 cm^3 d'eau, neutralisé si besoin par l'hydrogénocarbonate de sodium et les produits de réduction sont extraits à l'éther. La phase éthérée est ensuite lavée à l'eau, séchée sur sulfate de magnésium sauf indication contraire, et évaporée sous vide.

Techniques d'analyses des produits

Les spectres de RMN ^1H et ^{13}C ont été réalisés sur les appareils Bruker MSL 300, Varian T60 et Jeol FX60 (RMN ^{13}C).

Les spectres IR ont été enregistrés sur un ensemble Beckmann type Acculab 2.

Les spectres UV–visible ont été obtenus avec un spectrophotomètre UV–visible Beckmann type DU-8.

L'(hydroxy-1 benzyl)-2 chromone **7** et l'acétyl-2 chromanone **8** ont été purifiées sur une colonne de silice Merck Kieselgel 60 avec comme éluant un mélange acétate d'éthyle – hexane dans les proportions 50/50 et 25/75 respectivement pour les composés **7** et **8**.

(Hydroxy-1 benzyl)-2 chromone **7** : $F = 106$°C (litt. $F = 111$°C (2)); Rdt : 75% (après purification). Infrarouge (solvant $CHCl_3$) : 3360 (OH), 1700 (C=O), 1620 (C=C), 1580 cm^{-1} (aromatiques). RMN ^1H (δ_{ppm}/TMS solvant $CDCl_3$) : 4,35 (OH), 5,60 (HC—O), 6,60 (=C—H), 7,1 – 8,1 (H aromatiques). RMN C^{13}

Can. J. Chem. Downloaded from www.nrcresearchpress.com by 109.225.110.28 on 09/08/12
For personal use only.

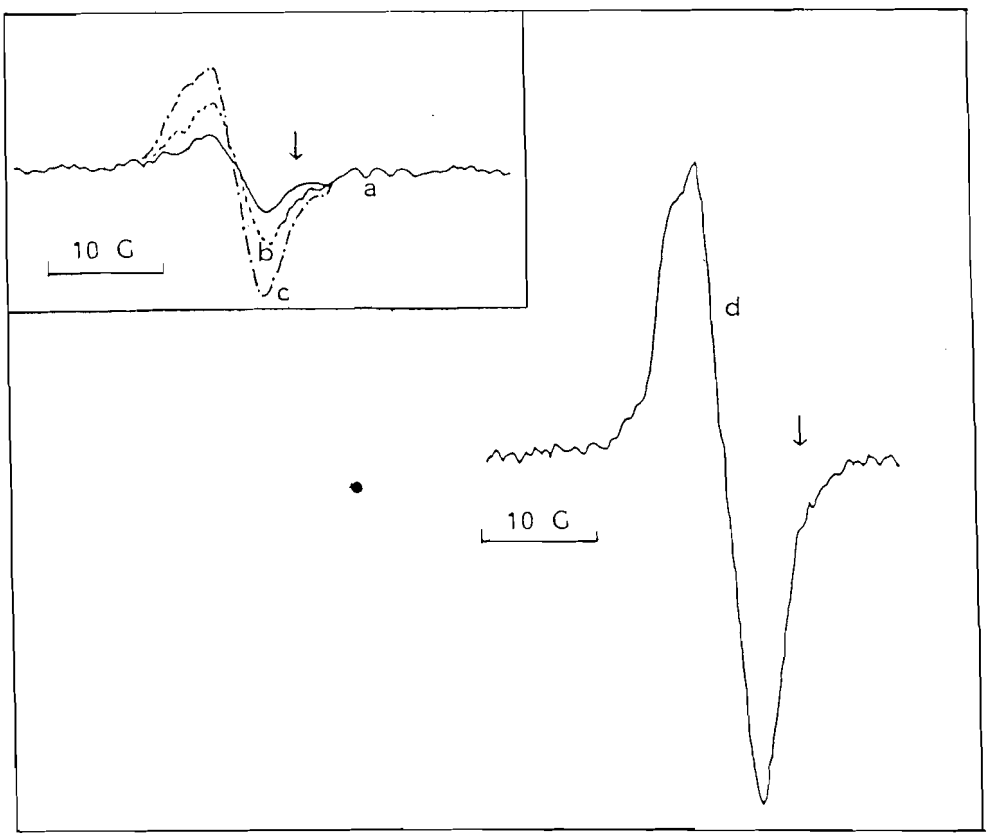

FIG. 10. Spectre de RPE du solide obtenu par réduction de **7**. Champ 3340 G (↓). Evolution en fonction de la température : (*a*) T = 290 K; (*b*) T = 310 K; (*c*) T = 340 K avec gain 2,5 × 10^5 et modulation 2,5 × 10^{-1} G; (*d*) T = 380 K avec gain 4 × 10^5 et modulation 1,25 × 10^{-1} G.

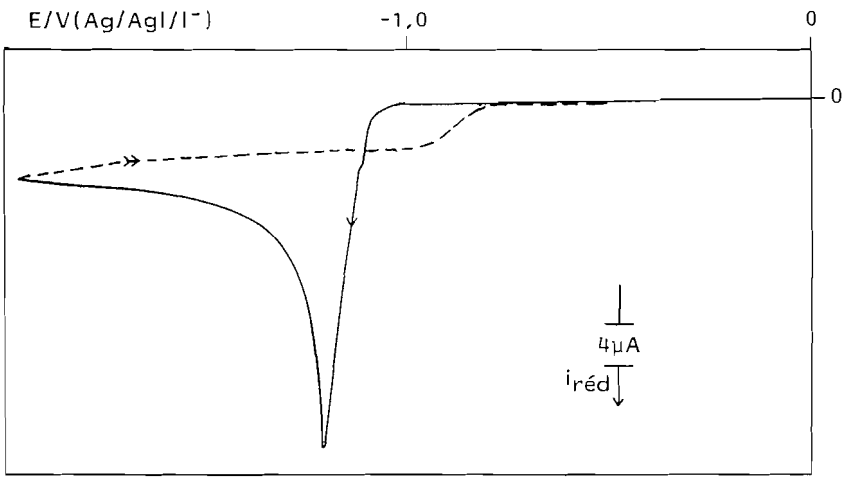

FIG. 11. Voltammogramme de l'acétyl-2 chromanone en solution dans le DMF c = 5 × 10^{-3} M. Electrolyte support Bu_4NBF_4 (0,1 M). Electrode de mercure stationnaire v = 0,1 V s^{-1}.

(δ_{ppm}/TMS solvant $CDCl_3$) : 71 (—C—OH), 105 – 168 (carbones aromatiques et éthyléniques), 176 (C=O).

Acétyl-2 chromanone **8** : F = 64°C; Rdt : 55% (après purification). Son spectre de RMN ^1H présente en particulier un massif ABX caractéristique. Les déplacements chimiques de chaque atome d'hydrogène ont fourni les valeurs suivantes (δ_{ppm}/TMS solvant $CDCl_3$) : 2,23 $\left(\begin{matrix}CH_3—C— \\ \| \\ O\end{matrix}\right)$, 2,90 $\left(\begin{matrix}H_B \\ | \\ —C—H_A\end{matrix}\right)$, 4,85

Can. J. Chem. Downloaded from www.nrcresearchpress.com by 109.225.110.28 on 09/08/12
For personal use only.

$\left(\begin{array}{c} | \\ O-C-H_X \\ | \end{array}\right)$, 6,90 – 7,20 (4H aromatiques). La RMN du ^{13}C off-résonance confirme cette structure (δ_{ppm}/TMS solvant $CDCl_3$) : 25,9 (q, CH_3), 38,6 (t, CH_2), 81,0 $\left(\begin{array}{c} | \\ \text{d, } H-C-O \\ | \end{array}\right)$, 118, 122, 127, 136 (d, C aromatiques) 160 (s, C aromatiques), 190 et 205 (s, C=O). Le spectre IR montre des bandes d'absorption à 1710 (CH_3—C=O) et 1680 cm^{-1} (C=O conjugué).

Remerciements

Nous remercions Monsieur le Professeur J. Simonet (Université de Rennes I) pour d'utiles conseils ainsi que Monsieur le Professeur M. Paillard (Université de Toulouse) et la Société Transphyto qui nous ont fourni des échantilions de chromones substituées.

1. M. Besson. Thèse Clermont Fd (1980).
2. M. Payard, G. Mouysset, P. Tronche et J. Bastide. Eur. J. Med. Chem. **20**, 117 (1985).
3. J. Castaner. (*a*) Drugs Future, **3**, 236 (1978); (*b*) **3**, 841 (1978).
4. M. Payard. Thèse Clermont Fd (1974).
5. M. Payard et J. Couquelet. Synthesis, 889 (1979).
6. G. Mouysset. Thèse Toulouse (1988).
7. P. H. Given, M. E. Peover et J. Schoen. J. Chem. Soc. 2674 (1958).
8. S. Wawzonek et A. Gundersen. (*a*) J. Electrochem. Soc. **103**, 456 (1956); (*b*) **107**, 537 (1960).
9. J. Simonet. Bull. Soc. Chim. Fr. 1533 (1970).
10. L. G. Feokistov et H. Lund. *Dans* Organic electrochemistry. *Edité par* M. M. Baizer. M. Dekker, New York. 1973. Chap. VIII. p. 347.
11. P. Martinet et J. Simonet. Bull. Soc. Chim. Fr. 3533 (1967).
12. E. Lamy, L. Nadjo et J. M. Savéant. J. Electroanal. Chem. **50**, 141 (1974).
13. C. P. Andrieux et J. M. Savéant. Bull. Soc. Chim. Fr. 2090 (1973).
14. M. Jubault, A. Tallec, B. Bujoli, J. C. Roze et J. P. Pradère. Tetrahedron Lett. **26**, 745 (1988).
15. S. H. M. MacConnell et D. B. Chesnut. J. Chem. Phys. **28**, 107 (1958).
16. M. A. Michel, G. Mousset et J. Simonet. J. Electroanal. Chem. **98**, 319 (1979).
17. C. Amatore, C. Capobianco, G. Farnia, G. Sandona, J. M. Savéant, M. G. Severin et E. Vianello. J. Am. Chem. Soc. **107**, 1815 (1985).
18. E. Brillas, G. Farnia, M. C. Severin et E. Vianello. Electrochim. Acta, **31**, 759 (1986).
19. J. Sarrazin, J. Simonet et A. Tallec. Electrochim. Acta, **27**, 1763 (1982).
20. S. Roffia, V. Concialini, C. Paradisi, F. Maran et E. Vianello. J. Electroanal. Chem. **302**, 115 (1991).
21. J. Simonet et A. Albisson. Bull. Soc. Chim. Fr. 1125 (1971).
22. C. Amatore et J. M. Savéant. J. Electroanal. Chem. **86**, 227 (1978).
23. C. P. Andrieux, A. Merz et J. M. Savéant. J. Am. Chem. Soc. **107**, 6097 (1985).
24. M. Paillard. Bull. Soc. Chim. Fr. 2392 (1973).

Can. J. Chem. Downloaded from www.nrcresearchpress.com by 109.225.110.28 on 09/08/12
For personal use only.

Phytotoxic metabolites of *Phomopsis convolvulus*, a host-specific pathogen of field bindweed

YOULA S. TSANTRIZOS[1] AND KELVIN K. OGILVIE[2]
Department of Chemistry, McGill University, Montréal, P. Q., Canada H3A 2K6

AND

ALAN K. WATSON
Department of Plant Science, Macdonald College of McGill University, Ste-Anne-de-Bellevue, P. Q., Canada H9X 1C0

Received December 17, 1991

YOULA S. TSANTRIZOS, KELVIN K. OGILVIE, and ALAN K. WATSON. Can. J. Chem. **70**, 2276 (1992).

Phomopsis convolvulus is a host-specific pathogen which causes leaf spots and anthracnose lesions in the important perennial weed *Convolvulus arvensis* (field bindweed). Investigation of the metabolites produced by the fungus led to the isolation of the known fungal metabolites ergosterol (**1**) and ergosterol peroxide (**2**), in addition to four novel phytotoxins: the phthalides convolvulanic acid A (**3**), convolvulanic acid B (**4**), convolvulol (**5**), and the α-pyrone convolvulopyrone (**6**). The latter compounds were assigned the structures of 4-carboxy-3-hydroxy-7-methoxy-6-methyl-1(3*H*)-isobenzofuranone (**3**), 4-carboxy-7-methoxy-6-methyl-1(3*H*)-isobenzofuranone (**4**), 4-(hydroxymethyl)-7-methoxy-6-methyl-1(3*H*)-isobenzofuranone (**5**), and 3-[4-methoxy-3-methyl-α-pyron-6-yl]-2-methyl-2-butenoic acid (**6**) respectively. Strong herbicidal activity against *C. arvensis* was observed with compounds **3** and **4** at concentrations of $3–5 \times 10^{-4}$ M.

YOULA S. TSANTRIZOS, KELVIN K. OGILVIE et ALAN K. WATSON. Can. J. Chem. **70**, 2276 (1992).

Le *Phomopsis convolvulus* est un pathogène spécifique pour un hôte qui provoque des taches sur les feuilles et des lésions anthracnoses de l'importante herbe persistante *Convolvulus arvensis* (liseron des champs). Une étude des métabolites produits par le champignon a permis d'isoler l'ergostérol (**1**) et le peroxyde d'ergostérol (**2**), des métabolites fongiques connus, en plus de quatre nouvelles phytotoxines : les phtalides de l'acide convolvulanique A (**3**) et B (**4**), le convolvulol (**5**) et l'α-pyrone, convolvulopyrone (**6**), auxquels on a attribué les structures respectives suivantes : 4-carboxy-3-hydroxy-7-méthoxy-6-méthyl-1(3*H*)-isobenzofuranone (**3**), 4-carboxy-7-méthoxy-6-méthyl-1(3*H*)-isobenzofuranone (**4**), 4-(hydroxyméthyl)-7-méthoxy-6-méthyl-1(3*H*)-isobenzofuranone (**5**) et l'acide 3-[4-méthoxy-3-méthyl-α-pyron-6-yl]-2-méthylbut-2-ènoïque (**6**). Avec les composés **3** et **4**, on a observé de fortes activités herbicides contre le *C. arvensis* à des concentrations de 3 à 5×10^{-4} M.

[Traduit par la rédaction]

Introduction

The perennial plant field bindweed (also known as wild morning glory) is a serious agricultural problem around the world with the exception of the tropics. Field bindweed infestations are encountered along roadsides and in city green spaces and cultivated lands throughout most of Canada (1) and it has been classified as one of the most important weeds worldwide (2). Phenoxy herbicides (3, 4) that are presently used for the control of this pest are generally costly and ineffective in suppressing its spread (5).

In the early 1970's, a number of independent studies on the biological control of field bindweed were initiated. Among them, insects and gall mites were considered (6, 7) but were found to be inadequately host-specific causing damage to crop plants in addition to the weed. Fungi which are pathogenic to field bindweed present an alternate possibility for its biological control. The fungus *Phomopsis convolvulus* is a pathogen that was recently isolated and classified (8) and that infects field bindweed causing nectrotic lesions surrounded by yellow haloes, characteristic of phytotoxin production (9). Leaf-puncture bioassays (10) on bindweed using cell-free extracts of *P. convolvulus*, further supported the existence of phytotoxic compounds leading to the formation of necrotic spots in the tissue of young leaf cuttings. The subsequent investigation into the metabolites produced by *P. convolvulus* led to the isolation of the two known steroids **1** and **2**,[3] the phytotoxic phthalides **3**, **4**, **5** and the novel α-pyrone **6**.

Results and discussion

Phomopsis convolvulus cultures were grown on moist barley grains at room temperature for periods of 28–30 days. The extracellular metabolites were initially extracted by washing the grains with methanol and then partitioned between ethyl acetate and dilute aqueous HCl (pH ~3). Biological activity was found only in the organic layer and its mixture of metabolites was further partitioned between CH_2Cl_2 and aqueous $NaHCO_3$. Phytotoxicity against both *Lemna* plants and field bindweed cuttings was observed with both extracts, but the aqueous extract was significantly more potent.

Analysis of the metabolites dissolved in the CH_2Cl_2 layer revealed the presence of two major compounds, metabolites **1** and **2**, which were purified by flash column chromatography (11) and preparative thin-layer chromatography. The remaining minor components of this extract were void of biological activity.

[1]Present address: Department of Chemistry & Biochemistry, Concordia University, Montreal, Que., Canada H3G 1M8.

[2]Author to whom correspondence should be addressed, Vice President Academic, Acadia University, Wolfville, N.S., Canada B0P 1X0.

[3]Special precautions to avoid exposure of the *P. convolvulus* metabolites to air and ordinary light were not taken.

Can. J. Chem. Downloaded from www.nrcresearchpress.com by 109.225.110.28 on 09/08/12
For personal use only.

TABLE 1. Nuclear Overhauser enhancement (^{1}H NMR, 300 MHz, acetone-d_6)

Compound **3**		Compound **5**	
δ (irradiated H)	NOE (%)	δ (irradiated H)	NOE (%)
6.91 (H-3)	None	5.22 (H-3)	H-4′, 7-OMe (<2%)
—	—	4.66 (H-4′)	H-5 (12%), H-3 (3%)
8.09 (H-5)	6-Me (14%)	7.31 (H-5)	6-Me (5%), H-4′ (2%)
2.35 (6-Me)	7-OMe (10%), H-5 (4%)	2.26 (6-Me)	H-5 (6%), 7-OMe (2%)
4.14 (7-OMe)	6-Me (14%)	3.90 (7-OMe)	6-Me (<2%), H-5 (<2%)

The structural assignment of metabolite **1** was based primarily on its spectral data, which was identical to that of ergosterol (12, 13). The NMR data and high resolution MS of metabolite **2** led to its identification as ergosta-6,22-dien-5a,8a-epidioxy-3-ol, better known as ergosterol peroxide (**2**). Biological testing of this compound on *Lemna* plants and bindweed leaf-cuttings showed weak toxicity to both, indicating that it may play a role in the disease symptoms observed on bindweed when infected with *P. convolvulus* (14).

Purification of the phytotoxins dissolved in the aqueous $NaHCO_3$ solution proved to be unsuccessful using either silica gel or cellulose chromatography. However, flash column chromatography on C18 reverse phase silica, prepared using Evans' procedure (15) led to a moderate separation of its components. Fractions found to have activity against both *Lemna* and bindweed plants (fractions 18–21, 40–60% MeOH in H_2O) were further purified by HPLC, yielding metabolites **3**–**6**.

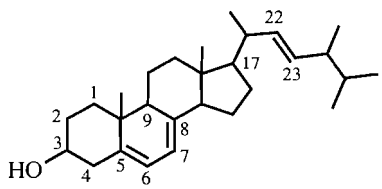

1

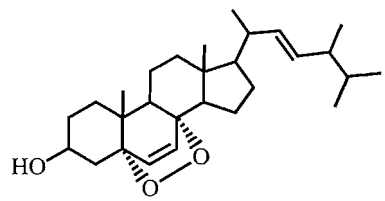

2

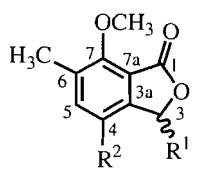

3, R^1 = OH, R^2 = COOH
4, R^1 = H, R^2 = COOH
5, R^1 = H, R^2 = CH_2OH

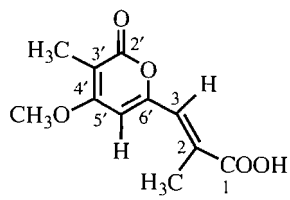

6

Based on the ^{1}H, NOE (Table 1), ^{13}C NMR (Table 2), APT, and DEPT NMR data of metabolite **3** both structures **3** and **7** or their tautomeric mixture were considered possible. The IR spectrum of metabolite **3** showed an OH absorption at 3381 cm^{-1}, —C=C— absorption at 1613 cm^{-1}, and carbonyl absorptions at 1728 and 1773 cm^{-1} due to a carboxylic acid and a phthalide-type lactone. In addition, (NH_3)CI MS was consistent with an elemental composition of $C_{11}H_{10}O_6$ for this compound. Final proof in support of structure **3** was obtained through low temperature ^{1}H–^{13}C coupled NMR experiments and literature ^{13}C NMR values of related compounds.

Most of the ^{13}C NMR experiments were conducted at very low temperatures (−45 to −55°C). At higher temperatures the signals at δ 165.7 and 121.9 were either very broad or non-observable (16). In the fully coupled spectrum of **3** the expected ^1J and ^3J coupling constants were observed for C-5 (δ 139.3), C-3 (δ 97.4), 7-OMe (δ 62.6), and 6-Me (δ 15.7). The signal of C-5 appeared as a doublet of quartets due to additional long-range coupling with the protons of the 6-Me (^1J = 162 Hz, ^3J = 5 Hz). Similarly, 6-Me (δ 15.7) appeared as a quartet of doublets (^1J = 128 Hz, ^3J = 5 Hz) which collapsed to a simple quartet upon decoupling of H-5. The C-3 carbon appeared as a doublet (^1J = 179 Hz) which collapsed to a singlet upon irradiation of the proton at δ 6.91 (H-3). The quaternary carbons at δ 121.9 and 118.3 were singlets in all spectra and they were assigned to C-4 and C-7a respectively. The multiplets of the quaternary carbons at δ 134.2 and 160.5 were assigned to C-6 and C-7 respectively in structure **3** or C-6 and C-5 in structure **7**, since both of them showed long-range coupling with the methyl and methoxy protons.

Both carbonyl carbons (C-1: δ 166.4, ^3J = 4 Hz; C-4′: δ 165.7, ^3J = ~2.5 Hz) and the C-3a signal (δ 149.4, ^3J =

Can. J. Chem. Downloaded from www.nrcresearchpress.com by 109.225.110.28 on 09/08/12
For personal use only.

TABLE 2. ^{13}C NMR (300 MHz, −52°C, acetone-d_6) of convolvulanic acid A (**3**)

C	Decoupled δ	Calculated δ	H–C coupled	H-3[a]	H-5[a]
1	166.4	~167	d; $^3J_{C\text{-}H3}$ = 4 Hz	s	d
4′[b]	165.7[b]	—	d; ^3J = ~2.5 Hz	s(br)[c]	s(sh)
7	160.5	161.6	m	m	m
3*a*	149.4	152.5	d; $^3J_{C\text{-}H5}$ = 7.7 Hz	d	s
5	139.3	139.3	d, q; ^1J = 162 Hz d; $^3J_{C\text{-}Me}$ = 5 Hz	d, q	q
6	134.2	133.6	q; $^2J_{C\text{-}Me}$ = 6 Hz	q	q
4[b]	122.0[b]	119–124	s	s	s
7a	118.3	117.7	s	s	s
3	96.0	96.0	d; ^1J = 179 Hz	s	d
7-OMe	62.7	63.1	q; ^1J = 146 Hz	q	q
6-Me	15.7	—	d, q; ^1J = 128 Hz $^3J_{C\text{-}H5}$ = 5 Hz	d, q	q

[a]Decoupled proton.
[b]Broad signals at room temperature.
[c]Broad signal due to ^4J coupling between C-4′ and H-3 of ~1–2 Hz.

7.7 Hz) appeared as doublets in the fully coupled spectrum. Selective decoupling of the aromatic proton (^1H: δ 8.09) led to the collapse of the doublet of the C-3a and of the carboxylic acid doublet, but had no affect on the doublet of the lactone, as would be expected for structure **3**. However, these results would be unlikely if tautomer **7** was the correct structure; ^3J coupling between the aromatic proton and the lactone carbonyl of compound **7** should be observed, whereas ^5J coupling with the carboxylic acid should be insignificant. In addition, selective decoupling of H-3 (δ 6.91) led to the collapse of the lactone carbonyl doublet to a sharp singlet, leaving the carboxylic acid signal as a doublet, further supporting **3** as the correct structure.

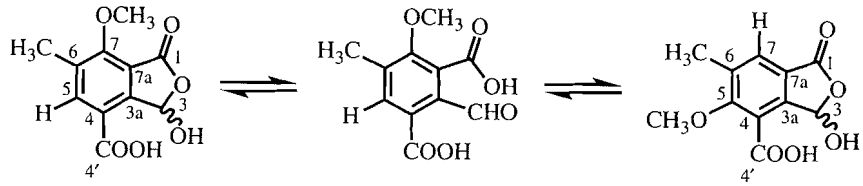

3 **7**

Metabolite **3** did not exhibit any optical activity due to spontaneous racemization via its aldehyde – carboxylic acid tautomer. However, since only one set of NMR signals was observed (even at −55°C), the lactone **3** must be by far the most predominant structure. A literature search for structurally related compounds revealed, among others, the natural product 4-formyl-3,5-dihydroxy-7-methoxy-6-methyl-1(3*H*)-isobenzofuranone (**8**), an antibacterial metabolite of *Aspergillus duricaulis* (16). Considering the structural similarities between metabolites **3** and **8**, it was expected that approximate chemical shifts for the ^{13}C NMR of **3** could be calculated from those of **8** using empirical parameters for substituted benzene rings (17). In fact, all calculated values were found to be within 0–3 ppm from the experimental shifts of **3** and they are shown in Table 2. The ^{13}C NMR data of several other naturally occurring (18) and synthetic phthalides (19) were also considered. On the bases of all the evidence, the structure of **3** was assigned to 4-carboxy-3-hydroxy-7-methoxy-6-methyl-1(3*H*)-isobenzofuranone and it was given the trivial name convolvulanic acid A.

Compound **4** was the second water-soluble toxin of *P. convolvulus* to be isolated. Its ^1H, ^{13}C (Table 3), APT, and DEPT NMR spectra were almost identical to those of **3** except for one signal, whose change suggested that the C-3 hydroxyl substituent of **3** had been replaced by a proton in **4**. The IR data was also consistent with structure **4** and high resolution $(NH_3)CI$ MS gave a molecular ion of mass 223.0621 (M^+ + 1), supporting the elemental composition of $C_{11}H_{10}O_5$ (calculated mass for M^+ + 1 is 223.0606). Hence, the chemical structure of 4-carboxy-7-methoxy-6-methyl-1(3*H*)-isobenzofuranone (**4**) and the trivial name of convolvulanic acid B were proposed for this compound. In addition, ^1H–^{13}C fully coupled and selectively decoupled NMR experiments were carried out and all of the data obtained were in complete agreement with the proposed structure (Table 3). The ^{13}C chemical shifts of the known compound 4-formyl-5-hydroxy-7-methoxy-6-methyl-1(3*H*)-isobenzofuranone (**9**) (20) were used to calculate "theoreti-

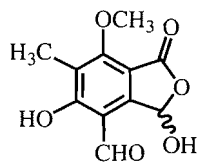

8

Can. J. Chem. Downloaded from www.nrcresearchpress.com by 109.225.110.28 on 09/08/12
For personal use only.

TABLE 3. ^{13}C NMR (300 MHz, −52°C, acetone-d_6) of convolvulanic acid B (**4**)

C	Decoupled δ	Calculated δ	H–C coupled	H-3[a]	H-5[a]
1	168.4	~168	s(br)	s(sh)[c]	s(br)
4'[b]	166.4[b]	—	s(br)	s(br)	s(sh)[c]
7	161.2	162.0	m	m	m
3a	150.7	153.1	m	d; $^3J_{C\text{-}H5}$ = 7.8 Hz	s(br)
5	138.8	140.3	d, q; ^1J = 162 Hz	d, q	q; $^3J_{C\text{-}H9} < 5$ Hz
6	132.2	131.8	q; $^2J_{C\text{-}OME}$ = 6 Hz	q	q
4[b]	120.5[b]	118.0	s	s	s
7a	117.6	116.7	s	s	s
3	70.9	~68	t; ^1J = 159 Hz	s	t
7-OMe	62.6	62.2	q; ^1J = 146 Hz	q	q
6-Me	15.6	—	d; q; ^1J = 128 Hz $^3J_{C\text{-}H5}$ = ~4.5 Hz	d, q	q

[a]Decoupled proton.
[b]Broad signals at room temperature.
[c]Sharpening of signal indicates the removal of coupling having a very small J value.

TABLE 4. ^{13}C NMR (300 MHz, −52°C, acetone-d_6) of convolvulol (**5**)

C	Decoupled δ	Calculated δ	H–C coupled	H-8[a]	H-5[a]
1	171.2	~170	s	s	s
7	157.7	155.4	m	m	m
3a	146.7	144.6	m	d; $^3J_{C\text{-}H5}$ = 8.4 Hz	s(br)
5	137.2	134.8	d, m; ^1J = 156 Hz	d, q; $^3J_{C\text{-}H9}$ = 5 Hz	m
6	132.7	132.1	q; $^2J_{C\text{-}H9}$ = 6 Hz	q	q
4	131.2	128.1	s	s	s
7a	117.8	116.3	s	s	s
3	70.1	68.4	t; ^1J = 155 Hz	t	t
7-OMe	62.5	62.2	q, ^1J = 145 Hz	q	q
4'	62.1	59.8	t, d; ^1J = 139 Hz	d; $^3J_{C\text{-}H4'}$ = 12 Hz	t
6-Me	15.4	—	d, q; ^1J = 128 Hz $^3J_{C\text{-}H5}$ = 5 Hz	d, q	q

[a]Decoupled proton.

cal" shifts for metabolite **4** and the results obtained were in close agreement with the experimental values (Table 3).

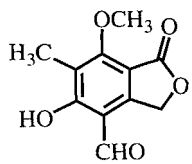

9

The third pthalide (metabolite **5**) was sufficiently soluble in $CDCl_3$ to permit a complete proton spectrum to be observed (Table 1). Close similarities between **4** and **5** were observed in the ^1H, NOE (Table 1), ^{13}C (Table 4), DEPT, and APT NMR spectra. One extra methylene carbon (δ 62.2) was observed in the ^{13}C NMR spectrum and of the six quaternary carbons only one had the appropriate chemical shift for a carboxylic acid or lactone (δ 171.2); the remaining quaternary signals had the chemical shifts very close to those of C-3a, C-6, C-7, and C-7a of metabolite **4** and one was approximately 10 ppm downfield from the C-4 carbon of **4**. The room temperature ^{13}C NMR spectra of **5** did not show any broad signals nor did it show any changes when recorded at low temperatures. These observations, coupled with the fact that a carbonyl carbon was lost and a —CH_2—OH had appeared, suggested that metabolite **5** was a reduced analogue of **4**. NMR data obtained from ^1H–^{13}C fully coupled and selectively decoupled experiments were in complete agreement with the proposed structure (Table 4).

In addition, the IR ($CHCl_3$) of metabolite **5** showed absorptions for only one carbonyl, a lactone at 1762 cm^{-1}. High resolution (NH_3)CI MS gave a molecular ion of 209.0814 ($M^+ + 1$), suggesting an elemental composition of $C_{11}H_{12}O_4$ (calculated mass: 209.0814). Taking into consideration all of these data the structure of 4-(hydroxymethyl)-7-methoxy-6-methyl-1(3*H*)-isobenzofuranone and the trivial name of convolvulol were proposed for **5**. The ^{13}C NMR chemical shifts of the literature compound 5-hydroxy-4-(hydroxymethyl)-7-methoxy-6-methyl-1(3*H*)-isobenzofuranone (**10**) (16) were used in order to calculate "theoretical" chemical shifts for **5**. All of the calculated shifts were within 2 ppm of the experimental values (Table 4).

The last compound (**6**) isolated from the aqueous phytotoxic extract of *P. convolvulus* shared many spectral similarities with the previous metabolites. Its ^1H NMR showed two methyls (δ 1.87 and 2.42), a methoxy (δ 4.04), and two single olefinic protons (δ 6.62 and 6.91) without coupling between any of the signals. The proton at δ 6.91 exhibited positive NOE effects with both the methyl at δ 2.42 and the methoxy at δ 4.04 (Table 5).

The ^{13}C NMR of **6** showed a total of 11 carbons as in all

Can. J. Chem. Downloaded from www.nrcresearchpress.com by 109.225.110.28 on 09/08/12
For personal use only.

TABLE 5. NMR data of convolvulopyrone (**6**)

^{1}H	(δ)	NOE[a]	COSY[b]	^{13}C	(δ)	HETCOR[b]
				C-1	(169.4 (br))	
				C-2	(143.2)	
H-3	(6.62)		2-Me, H-5′	C-3	(121.8)	
				C-2′	(167.9)	
				C-3′	(105.3)	
				C-4′	(166.4)	
H-5′	(6.91)	4′-OMe (4%), and 2-Me (3%)	3′-Me, H-3, and 4′-OMe	C-5′	(98.4)	H-5′ (δ 6.91)
				C-6′	(159.2)	
2-Me	(2.42)	H-5′ (10%)		2-Me	(13.6)	
3′-Me	(1.87)			3′-Me	(8.8)	
4′-OMe	(4.04)	H 5′ (12%)	H 5′	4′-OMe	(57.5)	

[a]Resonance in ^{1}H column irradiated.
[b]Correlations with signal in ^{1}H column (COSY) or ^{13}C column (HETCOR).

previous cases. A broad carboxylic acid signal (δ 169.4), a lactone (δ 167.9), an olefinic carbon to which the methoxy group was attached (δ 166.4 ppm), a methoxy (δ 57.5), and two methyls (δ 13.6, 8.8) were observed. The differences between **6** and the three phthalides were much more evident in the APT NMR spectrum. Three quaternary carbons at δ 159.2, 143.2, and 105.3 were observed, all of which had a shift difference of at least 10 ppm from the possibly equivalent carbons of compounds **3**, **4**, and **5** (C-3a, C-6, C-7a, respectively). In addition, there were two tertiary carbons at δ 98.4 and 121.8, of which the latter was broad in the normal ^{13}C NMR and almost nonobservable in the APT spectra.

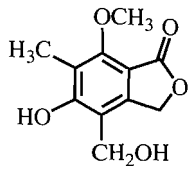

10

The IR spectrum showed absorptions characteristic of conjugated carboxylic acids and α-pyrones (1717 and 1707 cm^{-1}) and high resolution $(NH_3)CI$ MS of **6** gave an intense molecular ion at 225.0739 ($M^+ + 1$), suggesting a molecular composition of $C_{11}H_{12}O_5$ (calculated mass of $M^+ + 1$ is 225.0763). Thus the general structure of the α-pyrone **11** was at first proposed.

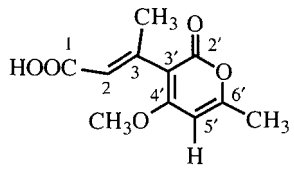

11

Assuming that the chemical shift of 6′-Me was at δ 2.42 and H-5′ at δ6.91, the structure of **11** was in reasonable agreement with the ^{1}H, ^{13}C, and NOE NMR data. However, when the ^{1}H NMR spectrum of metabolite **6** was observed in acetone-d_6 containing a few drops of D_2O, the signals at δ 6.62 (1H) and δ 2.42 (CH_3) changed from broad singlets to doublets (J = 1.3 Hz). This coupling was confirmed by COSY NMR (in the same solvent mixture) and additional coupling was observed between the proton at δ 6.91 and the methyl at δ 1.87, the two olefinic protons (δ 6.62 and 6.91), and between the proton at δ 6.91 and the methoxy group (δ 4.04). These results could not support the structure of **11** and the alternate structure of 3-(4-methoxy-3-methyl-α-pyron-6-yl)-2-methyl-2-butenoic acid (**6**) was proposed.

The HETCOR NMR spectrum of metabolite **6** showed the expected coupling for the methoxy and methyl signals and between C-5′ and H-5′ (^{13}C δ 98.4 to ^{1}H δ 6.91), but failed to show a cross-peak resonance for C-3 to H-3 (the existence of a cross-peak resonance between ^{13}C δ 121.8 and ^{1}H δ 6.62 was assumed). Although the carbonyl signals of α-pyrones are more frequently observed at δ ~162, there are many compounds known (including the fungal metabolites nectriapyrone (21) and aurovertin (22)) where the resonance of their carbonyls is at δ ~168–169. In structure **6**, coupling between H-5′ and 3′Me could reasonably be expected as well as between H-5′ and H-3. The latter proton (H-3) would also be coupled to the C-2 methyl.

In considering the NOE effects observed for compound **6**, the energies involved for the two most likely conformers of this molecule were examined. The positive NOE effect observed between H-5′ and 2-Me and the absence of an NOE effect between H-5′ and H-3, strongly suggest that conformer **6** is more stable than **6′**. Molecular modeling calculations[4] for both of these structures gave an energy difference of 3.2 kcal in favor of **6** (Fig. 1), implying an equilibrium ratio of about 99/1 for the two conformers.[5]

A number of different bioassays were initially evaluated for their ability to detect the presence of phytotoxins in crude metabolite mixtures of *P. convolvulus*. The small aquatic plant *Lemna paucicostata* was found to be highly sensitive to these compounds and suitable for measuring inhibition of

[4]A PCMODEL program was used that was obtained from Serena Software, P.O. Box 3076, Bloomington, Indiana, U.S.A.

[5]The energies of several other conformers were also calculated and they were all found to have energy levels higher than that of **6** (−105.4 kcal). However, the existence of these other minimum energies indicated the limitations of these calculations and the possibility that even the −105.4 kcal value may represent a local minimum and not the absolute minimum energy of the compound.

Can. J. Chem. Downloaded from www.nrcresearchpress.com by 109.225.110.28 on 09/08/12
For personal use only.

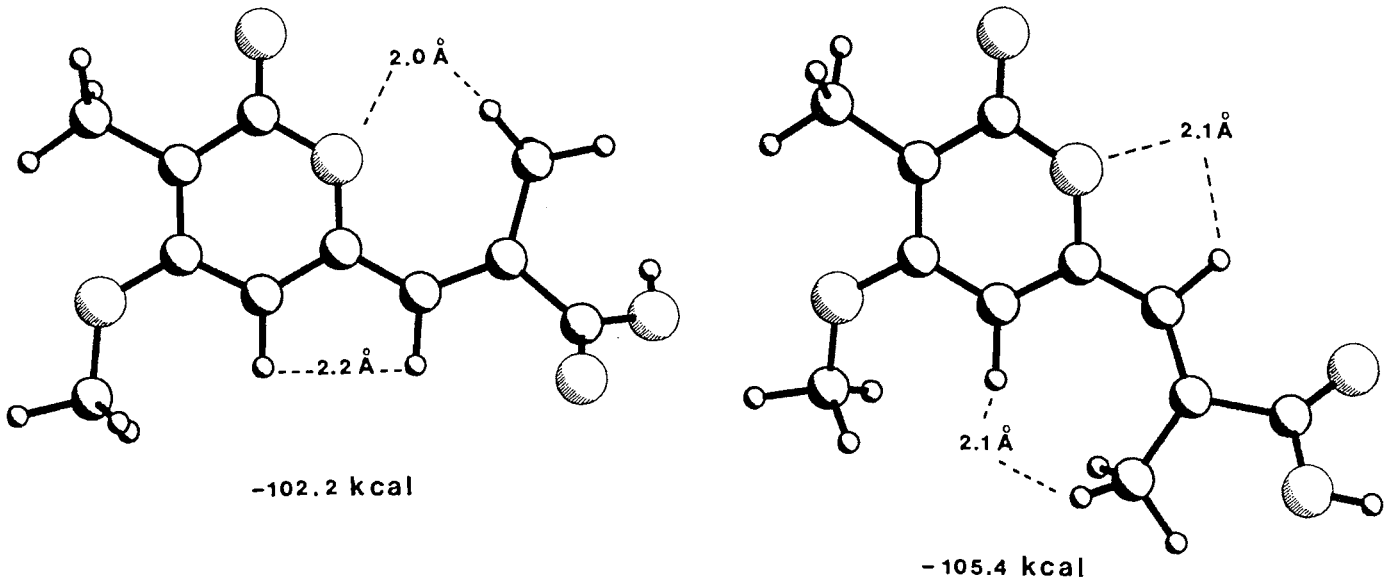

FIG. 1. Computer-generated molecular models of conformers 6 and 6′.

Can. J. Chem. Downloaded from www.nrcresearchpress.com by 109.225.110.28 on 09/08/12
For personal use only.

growth and chlorophyll biosynthesis (23), when used under standardized assay conditions (24).

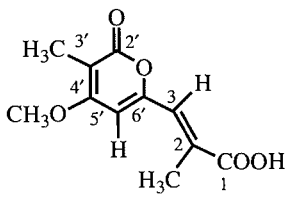

6

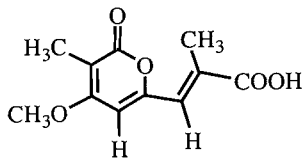

6′

Metabolites **3**, **4**, **5**, and **6** were tested at five different concentrations and in each case a 1% ethanol solution in *Lemna* medium was used as the control. Metabolite **4** was found to be the most potent phytotoxin, causing total inhibition of growth and 100% chlorosis of the *Lemna* plants within 12 h at concentrations of 5.9×10^{-4} M and within 24 h at concentrations of 3.5×10^{-4} M. At concentration of 5.9×10^{-4} M, metabolites **3** and **5** were also found to inhibit the growth of *Lemna* plants by approximately 80 and 50% respectively, whereas the effects of metabolite **6** were very minor in comparison with those of the three phthalides.

The principal objective was to isolate active metabolites of *P. convolvulus* that could potentially be used as herbicides for the effective control of field bindweed. Thus, the phytotoxic effects of all isolated compounds were also examined on leaf-cuttings of this weed. Minor effects were observed with metabolites **5** and **6**, whereas intense toxicity symptoms were observed with both **3** and **4**. Metabolite **4** caused wilting and browning of plant tissues after only 4 h at concentrations of 3.5×10^{-4} M. Twelve hours later, the same symptoms appeared on the leaves exposed to metabolite **3** at a 5×10^{-4} M concentration. When several young bindweed shoots (~2 in. long) were placed in a solution of the less potent phytotoxic metabolite **3**, at a concentration of $\sim 1 \times 10^{-3}$ M, the systemic absorption and toxicity of **3** was clearly observed; after 40–48 h the plants exposed to the toxin displayed obvious signs of wilting and at the end of the observation period (~5–6 days later) the leaves of the treated plants were almost completely wilted and brown, whereas the plants in the control solution did not show any signs of deterioration. It is interesting to note that in spite of the strong structural similarities between the metabolites of *P. convolvulus* and those of *A. duricaulis* (e.g., metabolites **3** and **8** respectively), there is no analogous similarity in their biological activity. For example, 0.1 μg of metabolite **8** was shown to exhibit strong antibiotic activity against *Bacillus subtilis* causing an 8-mm inhibition zone on a paper-disk diffusion assay. Under similar bioassay conditions, metabolite **3** failed to inhibit *B. subtilis* even when a 50 μg sample was used.

In conclusion, the metabolites produced by *Phomopsis convolvulus*, a host-specific pathogen of field bindweed (*Convolvulus arvensis*), were investigated. Four phytotoxic compounds (**3**–**6**), believed to be chemical mediators of the disease symptoms inflicted by *P. convolvulus* on its host plant, were isolated and characterized. Metabolites **3**–**6** were shown to be novel fungal metabolites.[6]

Experimental

General

Ultraviolet spectra were recorded on a Hewlett Packard 8451A DIODE ARRAY spectrophotometer. Nuclear magnetic resonance spectra were obtained at 20–22°C (unless otherwise indicated) using Varian XL-200 and XL-300 MHz instruments. ^{1}H and ^{13}C NMR chemical shifts are quoted in ppm and are referenced to the internal deuterated solvent downfield from tetramethylsilane (TMS). All mass spectra were performed at the Biomedical Mass Spectrometry Unit, McGill University. The low resolution $(NH_3)Cl$ MS spectra were obtained using a HP 5980A spectrometer. FAB and high resolution $(NH_3)Cl$ MS spectra were obtained using a ZAB 2F HS instrument.

[6]The synthesis of compounds **4** and **5** were reported in 1953 by Brown and Newbold (25); unfortunately, the amount of spectral data available from that report (i.e., mp and uv) was of limited help in the structural assignment of the natural products.

Can. J. Chem. Downloaded from www.nrcresearchpress.com by 109.225.110.28 on 09/08/12
For personal use only.

Chromatography

Silica gel chromatography was performed on Merck Kieselgel 60 (230–400 mesh, #9385) using flash chromatography. Reverse phase flash column chromatography was carried out on silica gel (Merck Kieselgel 60, 230–400 mesh, #9385) reacted with *n*-octadecyltrichlorosilane. All chromatographic solvents were fractionally distilled prior to use with the exception of HOAc.

HPLC

Doubly distilled H_2O and HPLC grade MeOH were filtered through a 0.45 μ filter membrane (Millipore Corp., Bedford, MA) before they were used in HPLC. Analysis and purification was carried out on a reverse phase, C18 column, CSC-S ODS2 (25 cm × 9.4 mm ID, 5 μm particles, Chromatography Science Company Inc., Montreal, Que.) using a Waters instrument (pump model 501, variable wavelength detector model 450, U6K injector). All retention times were recorded after the void volume.

General extraction of active metabolites from P. convolvulus

Stock cultures of *P. convolvulus* (conidia) were maintained at 4°C in slant tubes containing potato carrot agar, covered with mineral oil. An aqueous suspension of conidia was used to inoculate potato dextrose agar (PDA) plates which were then incubated at room temperature for a period of 2–4 weeks. The new conidia were isolated by washing the surface of the agar plates with a small volume (5–10 mL/plate) of sterile water. Large scale cultures were subsequently initiated by inoculating moist barley grains in Erlenmeyer flasks (150 × 250 mL flasks, 20 g of grain plus 30 mL of H_2O in each) under aseptic conditions. The cultures were stored at room temperature, with only occasional shaking. After an incubation period of 28–30 days, 100 mL of H_2O were added to each flask and they were placed overnight on a rotary shaker. Filtration through several layers of cheese cloth and centrifugation at 5,000 rpm for 8 min led to the removal of barley grains and mycelia, separation of conidia, and isolation of a biologically active aqueous mixture of metabolites (Pc1).

The volume of Pc1 (~15 L) was reduced (~3 L) under high vacuum at 30°C and then freeze-dried to obtain ~27 g of a very fine powder. This powder was extracted twice with MeOH (2 × 1.5 L), the first time at 40°C for 3 h and the second time at room temperature overnight. The methanolic solution (Pc2) was filtered through several layers of cheese cloth and centrifuged to remove the undissolved material, which was biologically inactive. The MeOH was then evaporated and the crude metabolite mixture was redissolved in ~100 mL of water to obtain a cloudy suspension that was acidified to pH 2.5–3 with 0.1 M HCl. EtOAc extraction (3 × 150 mL, plus overnight with 300 mL) led to the isolation of a biologically active mixture in the organic layer (Pc3) and a mixture void of biological activity in the aqueous layer. The yields of the combined EtOAc extracts varied greatly (0.25–7.5 mg/g of barley) giving an average of 2.5 mg of a light brown gum (Pc3) per gram of infected barley grains.

The residue Pc3 was suspended in CH_2Cl_2 (100 mL) and extracted with a saturated solution of $NaHCO_3$ (3 × 100 mL) to partition the mixture into Pc4 and Pc5. The organic layer (Pc4) contained mostly steroidal metabolites exhibiting very weak phytotoxicity, whereas the aqueous layer was strongly phytotoxic. The aqueous layer was subsequently acidified to pH ~2.5–3 with 0.1 M HCl, reduced in volume under high vacuum at 30°C and extracted with EtOAc (3 × 100 mL) to recover the phytotoxic mixture of metabolites from Pc5.

Isolation of ergosterol (1) and ergosterol peroxide (2)

Flash column chromatography of residue Pc4 using a solvent mixture of petroleum ether – EtOAc (1:1) led to the isolation of ergosterol (**1**, R_f 0.55) and ergosterol peroxide (**2**, R_f 0.28). Pure, crystalline ergosterol was obtained after a second flash column, eluted with (5:1) petroleum ether – EtOAc (R_f 0.16), followed by recrystallization from EtOH. The crude ergosterol peroxide (**2**) was purified on preparative TLC plates, developed twice with a mixture of petroleum ether – EtOAc (1:1). Since this compound is not UV active, the TLC plates were examined over a light table. The high density band visualized at R_f 0.4–0.5 corresponded to ergosterol peroxide. The silica gel was extracted with EtOAc and pure ergosterol peroxide crystallized from CH_2Cl_2 or EtOH. Both compounds were also present in the mycelia of *P. convolvulus*, and they could be isolated from their dry mass via soxhlet extraction with methylene chloride or acetone.

Preparation of C18 reverse-phase silica gel

Silica gel (40 g, Merck Kieselgel 60, 230–400 mesh) was added to 300 mL of dry CCl_4 (distilled from P_2O_5) in a septum-capped round-bottom flask under a N_2 atmosphere. *n*-Octadecyltrichlorosilane (4 mL) was added and the suspension was stirred at room temperature for 2 h. The product was filtered into a dry seinter-glass funnel and washed free of unreacted silane with dry CCl_4 (3 × 100 mL). Any residual chloride substituents were converted to methoxy groups by washing the silica with dry MeOH (2 × 100 mL, distilled over Mg metal). The product was then quickly washed with dry CH_2Cl_2 (2 × 100 mL, distilled from P_2O_5) and dried briefly under vacuum. A fresh 300 mL volume of dry CCl_4 was added to the bonded silica along with 4 mL of trimethylchlorosilane. The mixture was stirred at room temperature for an additional 2 h, then filtered and washed with dry CH_2Cl_2 (3 × 100 mL). The bonded silica was dried at 40°C overnight and then under high vacuum at room temperature for 24 h.

Reverse-phase flash column chromatography of phytotoxic residue Pc5

A reverse phase silica gel column (1.2 × 32 cm) was packed as a methanolic slurry (~12 g C18 bonded silica) and then *very* slowly equilibrated with H_2O.

The residue Pc5 (~1.3 g) was dissolved in a mixture of H_2O–CH_3OH–CH_2Cl_2 and absorbed onto a small amount of C18 bonded silica gel (1–2 g) by evaporating off the organic solvents. The aqueous slurry obtained (5–10 mL) was added to the top of the reverse-phase column and eluted with a gradient of solvents from 100% H_2O to 100% methanol, at a flow rate of ~1 mL/min. All fractions (8 mL each) were tested for biological activity and phytotoxicity was observed only in fractions 18–21 (40–60% MeOH in H_2O) Metabolites **3** and **5** were isolated from fractions 18 and 19 after HPLC chromatography on a C18 reverse-phase column, using an eluent mixture of 59.8% H_2O, 40% MeOH, and 0.2% HOAc at a flow rate of 2 mL/min. The retention time of **3** was 22–23 min while that of **5** was 16–17 min. Metabolite **5** was rechromatographed on the same HPLC column using a solvent mixture of 54.1% H_2O, 45.8% MeOH, and 0.1% HOAc. At a flow rate of 2 mL/min, its elution time was 10–11 min. HPLC chromatography of fractions 20 and 21, on the same C18 reverse-phase column using 54.4% H_2O, 45.4% MeOH, and 0.2% HOAc as the eluting solvent, led to the isolation of metabolites **4** and **6**. At a flow rate of 2 mL/min, the retention times were 20–22 min for **6** and 27–29 min for **4**.

Ergosterol (1): TLC: petroleum ether – EtOAc (1:1), R_f 0.55, CH_2Cl_2, R_f 0.21; mp: 163–164°C (lit. value 165°C) (13); IR ($CDCl_3$): 3650 (OH), 2960, 2872 (CH), 1601 (C=H) cm^{-1}; UV (CH_3CH_2OH, nm): max 274, 284, min 294 (shd); ^1H NMR (200 MHz, $CDCl_3$): δ 0.61 (s, 3H, 18-CH_3), 0.79–0.88 (2d, J = 6.8 Hz, 6H, 26-CH_3, and 27-CH_3), 0.90 (*d*, J = 6.8 Hz, 3H, 28-CH_3), 0.93 (s, 3H, 19-CH_3), 1.02 (d, J = 6.6 Hz, 3H, 21-CH_3), 1.22–2.03 (m, 19H), 2.26–2.27 (tm, 1H, H-4a), 2.41–2.49 (ddd, 1H, H-4b), 3.60–3.66 (m, 1H, H-3), 5.16–5.20 (2dd, 2 × 1H, H-2 and H-23), 5.35–5.38 (m, 1H, H-7) and 5.54–5.56 (dd, 1H, H-6); ^{13}C NMR (300 MHz, $CDCl_3$): δ 12.09 (C-18), 16.31 (C-19), 17.64 (C-28), 19.65 (C-26), 19.98 (C-27), 21.15 (C-21 and C-11), 23.03 (C-15), 28.26 (C-16), 32.06 (C-2), 33.14 (C-25), 37.10 (C-10), 38.43 (C-1), 39.15 (C-12), 40.41 (C-20), 40.87 (C-4), 42.88 (C-24 and C-13), 46.33 (C-9), 54.61 (C-14), 55.84 (C-17), 70.46 (C-3), 116.36 (C-7), 119.65 (C-6), 132.06 (C-23), 135.60 (C-22), 139.77 (C-5), and 141.37 (C-8); DEPT NMR (300 MHz, $CDCl_3$): 6-CH_3 (δ 12.1, 16.3, 17.6, 19.7, 20.0, 21.1), 7-CH_2 (δ 21.2, 23.0, 28.3,

Can. J. Chem. Downloaded from www.nrcresearchpress.com by 109.225.110.28 on 09/08/12
For personal use only.

32.1, 38.4, 39.2, 40.9), 11-CH (δ 33.1, 40.4, 42.9, 46.3, 54.6, 55.8, 70.5, 116.4, 119.7, 132.1, 135.6); APT (D2 = 4 ms) NMR (300 MHz, $CDCl_3$): δ 37.1, 42.9, 139.8, 141.4; MS ($(NH_3)CI$, direct inlet, 220°C), *m/z* (% relative intensity, assignment): 414 (2, $M^+ + NH_3$), 397 (40, $M^+ + 1$), 396 (7, M^+), 379 (100, 397-H_2O).

Ergosterol peroxide (2): TLC: petroleum ether – EtOAc, R_f 0.28; mp: 176–177°C (lit. value 178°C) (13); ^1H NMR (200 MHz, $CDCl_3$): δ 0.82 (s, 3H, 18-CH_3), 0.80–0.85 (2d, 6H, 26-CH_3 and 27-CH_3), 0.89 (s, 3H, 19-CH_3), 0.91 (d, 3H, 28-CH_3), 1.00 (s, 3H, 21-CH_3), 1.2–2.2 (m, 21H, steroid skeleton), ~4 (m br, 1H, H-3), 5.15–5.21 (2dd, 2 × 1H, H-22 and H-23), 6.25 (d, *J* = 8.5 Hz, 1H, H-7), 6.51 (d, *J* = 8.5 Hz, 1H, H-6); DEPT NMR (300 MHz, $CDCl_3$): 6-CH_3 (δ 13.0, 17.7, 18.3, 19.8, 20.1, 21.0), 7-CH_2 (δ 20.8, 23.5, 28.8, 30.2, 34.8, 37.0, 39.4) 11-CH (δ 33.2, 39.9, 42.9, 51.1, 51.8, 56.3, 66.5, 130.7, 132.2, 135.2, 135.4); APT (D2 = 4 ms) NMR (300 MHz, $CDCl_3$): δ 37.1 (C-10), 44.7 (C-13), 79.5 (C-5), 82.2 (C-8); MS (high resolution, (*i*-but) CI, direct inlet, 220°C): *m/z* calculated ($M^+ + 1$) ion 429.33685, found 429.33687.

4-Carboxy-3-hydroxy-7-methoxy-6-methyl-1(3H)-isobenzofuranone (convolvulanic acid A. 3): TLC: CH_2Cl_2–EtOAc–CH_3COOH (5:5:0.2), R_f 0.24; IR (CH_3CN): 3381, 3226 (OH), 1773 (C=O, lactone), 1728 (C=O, carboxylic acid), 1613 (C=C) cm^{-1}; UV (CH_3CH_2OH, nm): max 220, 250 (shd), min 300; ^1H NMR (200 MHz, acetone-d_6): δ 2.35 (s, 3H, 6-CH_3), 4.14 (s, 3H, 7-OCH_3), 6.91 (s, 1H, H-3), and 8.09 (s, 1H, H-5); NOE: data given in Table 1; ^{13}C NMR (300 MHz, acetone-d_6, *T* −46.5°C): δ 15.7 (6-CH_3), 62.6 (7-OCH_3), 97.4 (C-3), 118.3 (C-7*a*), 121.9 (C-4), 134.3 (C-6), 139.3 (C-5), 149.4 (C-3a), 160.5 (C-7), 165.7 (C-4′), and 166.4 (C-1); coupled ^1H–^{13}C NMR: data given in Table 2; APT (D2 = 4 ms) NMR (300 MHz, acetone-d_6, *T* −46.5°C): δ 118.3, 121.9, 134.3, 149.4, 160.5, 165.7, and 166.4 (97.4, 139.3 tertiary carbons); MS ($(NH_3)CI$, direct inlet, 260°C): *m/z* (% relative intensity, assignment): 256 (100, $M^+ + NH_4^+$), 239 (53, $M^+ + 1$), 227 (56, $M^+ + NH_4$ + -CHO), 209 (15, M^+ -CHO).

4-Carboxy-7-methoxy-6-methyl-1(3H)-isobenzofuranone (convolvulanic acid B. 4): TLC: CH_2Cl_2–EtOAc–CH_3COOH (5:5:0.2), R_f 0.45; IR (CH_3CN): 3629, 3542 (OH), 1764 (C=O, lactone), 1725 (sh), 1717 (C=O, carboxylic acid), 1630 (C=C) cm^{-1}; UV (CH_3CH_2OH, nm): max 216, 246 (shd), min 300; ^1H NMR (200 MHz, acetone-d_6): δ 2.34 (s, 3H, 6-CH_3), 4.15 (s, 3H, 7-OCH_3), 5.49 (s, 2H, H-3), and 8.13 (s, 1H, H-5); ^{13}C NMR (acetone-d_6, 300 MHz, *T* −46.5°C): δ 15.6 (6-CH_3), 62.6 (-OCH_3), 70.9 (C-3), 117.6 (C-7a), 120.5 (C-4), 132.2 (C-6), 138.8 (C-5), 150.7 (C-3a), 161.2 (C-7), 166.4 (C-4′), and 168.4 (C-1); coupled ^1H–^{13}C NMR: data given in Table 3; APT (D2 = 4 ms) NMR (acetone-d_6, 300 MHz, *T* −46.5°C): δ 117.6, 120.5, 132.6, 150.7, 161.2, 166.4, and 168.4 (138.8 tertiary carbon); MS (high resolution, $(NH_3)CI$, direct inlet, 250°C): *m/z* for ($M^+ + 1$) ion: calculated 223.0606, found 223.0621.

4-(Hydroxymethyl)-7-methoxy-6-methyl-1(3H)-isobenzofuranone (convolvulol, 5): TLC: CH_2Cl_2–EtOAc–CH_3COOH (5:5:0.2), R_f = 0.38; IR (CH_3CN): 3630, 3540 (OH), 1762 (C=O, lactone), 1600 (C=C) cm^{-1}; UV (CH_3CH_2OH, nm): max 212, 238 (shd), min 300. ^1H NMR (300 MHz, $CDCl_3$, *T* −51.5°C): δ 2.26 (s, 3H, 6-CH_3), 2.6–2.7 (br, 1H, 4′-OH), 3.90 (s, 3H, 7-OCH_3), 4.66 (*d*, *J* = 6 Hz, 2H, H-4′), 5.22 (s, 2H, H-3), and 7.31 (s, 1H, H-5). D_2O exchange causes the disappearance of the signal at δ 2.6–2.7, as expected, and the collapsing of the doublet at δ 4.66 to a singlet. Decoupling of H-5 led to the change of the OH signal from a broad multiplet to a broad triplet ($J_{H8\text{-}OH}$ = ~6 Hz), indicating the presence of long range coupling between H-5 and OH. NOE: data given in Table 1; ^{13}C NMR (300 MHz, CD_3OD): δ 15.4 (6-CH_3), 62.2 (C-4′), 62.5 (7-OCH_3), 70.1 (C-3), 117.9 (C-7a), 132.2 (C-4), 132.7 (C-6), 137.2 (C-5), 146.7 (C-3a), 157.7 (C-7), and 171.2 (C-1); coupled ^1H–^{13}C NMR: data given in Table 4; DEPT NMR (CD_3OD, 300 MHz): 2-CH_3 (δ 15.4, 62.5), 2-CH_2 (δ 62.2, 70.1), 1-CH (δ 137.2); MS (high resolution, $(NH_3)Cl$, direct inlet, 250°C): *m/z* for ($M^+ + 1$) on: calculated 209.0814, found 209.0814.

3-(4-Methoxy-3-methyl-α-pyron-6-yl)-2-methyl-2-butenoic acid (convolvulopyrone, 6): TLC: CH_2Cl_2–EtOAc–CH_3COOH (5:5:0.2), R_f 0.33; IR (CH_3CN): 3628, 3618 (OH), 1717 (C=O, α-pyrone), 1707, 1702 (sh) (C=O, carboxylic acid) cm^{-1}; UV (CH_3CH_2OH, nm): max 238, min 340; ^1H NMR (200 MHz, acetone-d_6): δ 1.87 (s, 3H, 3′-CH_3), 2.42 (s, 3H, 2-CH_3), 4.04 (s, 3H, 4′-OCH_3), 6.62 (s, 1H, H-3) and 6.91 (s, 1H, H-5′); NOE NMR: data given in Table 5; ^{13}C NMR (300 MHz, CD_3OD): δ 8.8 (3′-CH_3), 13.6 (2-CH_3), 57.5 (4′-OCH_3), 98.4 (C-5′), 105.3 (C-3′), 121.8 (C-3), 143.2 (C-2), 159.2 (C-6′), 166.4 (C-4′), 167.9 (C-2′), and 169.4 (br, C-1); Coupled ^1H–^{13}C NMR (400 MHz, CD_3OD): δ 8.8 (m, 3′-CH_3), 13.6 (q, *J* = 129 Hz, 2-CH_3), 57.5 (q, *J* = 147 Hz, 4′-OCH_3), 98.4 (d, *J* = 170 Hz, C-5′), and 121.8 (d, *J* = 165 Hz, C-3); APT (D2 = 4 ms) NMR (300 MHz, CD_3OD): δ 105.3, 143.2, 159.9, 166.4, 167.9, and 169.4 (98.4, 121.8, tertiary carbons); MS (high resolution, $(NH_3)Cl$, direct inlet, 250°C): *m/z* calculated for the ($M^+ + 1$) ion 225.0763, found 225.0739.

Lemna *medium*: *Lemna paucicostata* plants were grown at room temperature, under a growth-lamp (cool-white fluorescent plus incandescent light), in autoclaved Erlenmeyer flasks (250 mL) containing 100 mL of sterile nutrient medium. The nutrient medium was a solution of $Ca(NO_3)_2 \cdot 4H_2O$ (1.4 mM), KNO_3 (1.0 mM), KH_2PO_4 (0.4 mM), NH_4Cl (1.2 mM), $MgSO_4 \cdot 7H_2O$ (0.4 mM), $Na_2MoO_4 \cdot 2H_2O$ (6.1 μM), H_3BO_3 (69.0 μM), K_2H_2EDTA (30.0 μM), $FeCl_3 \cdot 6H_2O$ (56.6 μM), FeNaEDTA (56.7 μM), $MnNa_2EDTA$ (13.8 μM), $ZnNa_2EDTA$ (2.8 μM), $CuNa_2EDTA$ (3.3 μM), and $CoNa_2EDTA$ (4.8 μM). To prevent precipitation of the salts, all EDTA-containing components were added before the $FeCl_3 \cdot 6H_2O$. Finally, the pH of the solution was adjusted to 5.85 using 1.0 M KOH.

Lemna *bioassays*

All tested metabolites (or metabolite mixtures obtained during the initial stages of chromatography) were dissolved in absolute ethanol, aliquots of which (50–5 μl) were added to *Lemna* nutrient broth to make the final test samples. The toxicity of ethanol to *L. paucicostata* was initially evaluated and growth inhibition or chlorosis was only observed when the concentrations of ethanol was greater than 1% (v/v) of the total nutrient medium; thus bioassays were performed with test solutions containing less than 1% ethanol in *Lemna* nutrient medium. In all cases, the observations made with the *Lemna* bioassays were consistent with the results obtained by the leaf-puncture bioassays on field bindweed.

Field bindweed plant production and phytotoxicity assay

A commercial sample of bindweed seeds was used for the production of seedlings. Seeds were scarified with concentrated H_2SO_4 for 30 min, rinsed with distilled H_2O, dried at 21°C, and stored in the dark for approximately 2 months at 4°C. Germinated seeds (3–4) were sown in 10-cm pots in moist potting soil at a depth of 1 cm. Pots were placed in growth cabinets adjusted to a day/night temperature of 25/20°C, with a photoperiod of 15 h (300 μE m^{-2} s^{-1}, cool-white fluorescent plus incandescent light). Relative humidity was maintained at 50–55% until the plants were used for the bioassays. The phytotoxic effects of all metabolites on field bindweed were also evaluated using leaf cuttings, from plants 3–4 weeks old. For each assay, an average of 5–8 leaves were used, which were cut at the base of the stem and placed on a moist piece of filter paper (0.5 mL H_2O) in a covered Petri dish. Only the top two leaves of young shoots were used and they were cut using a sharp scalpel while submerged under water. Half of the leafs were then punctured with the tip of a fine needle and all of them were soaked with the test solution, covered and placed under a growth-lamp for a period of 5 days. The test samples were prepared by dissolving each metabolite in absolute ethanol, and then diluting the samples with doubly distilled water to a total volume of 2 mL. The most concentrated sample of each assay had an ethanol content of 1%; hence, the control solution was also a 1% ethanol solution in water. In leaf-puncture bioassays of field bindweed with aqueous solu-

tions of ethanol, toxicity was not observed at concentrations of up to 2%.

Acknowledgements

The Natural Sciences and Engineering Research Council (NSERC) of Canada and Fonds pour la formation de chercheurs et l'aide à la recherche (FCAR) of Québec are gratefully acknowledged for financial support.

1. J. F. Alex. *In* Biology and ecology of weeds. *Edited by* W. Holzner and M. Numata. W. Junk Publishers, The Hague. 1982. p. 309.
2. L. G. Holm, D. L. Plunknett, J. V. Pancho, and J. P. Herberger. *In* The World's worst weeds. University Press of Hawaii, Honolulu, Hawaii. 1977. Chap. 12.
3. W. P. Anderson. *In* Weed science: Principles. 2nd ed. West Publishing Co., St. Paul. 1983.
4. Herbicide handbook. 5th ed. Weed Science Society of America, Champaign. 1983.
5. S. S. Rosenthal. Calif. Agric. **37**, 16 (1983).
6. S. S. Rosenthal and J. Carter. J. Environ. Entomol. **6**, 155 (1977).
7. S. S. Rosenthal. Entomophaga, **23**, 367 (1978).
8. J. Ormeno-Nunez, R. D. Reeleder, and A. K. Watson. Can. J. Bot. **66**, 2228 (1988).
9. L. Morin, A. K. Watson, and R. D. Reeleder. Weed Sci. **37**, 830 (1989).
10. F. Sugawara, G. Strobel, R. N. Strange, J. N. Siedow, G. D. Van Duyne, and J. Clardy. Proc. Natl. Acad. Sci. U.S.A. **84**, 3081 (1987).
11. W. C. Still, M. Kahn, and A. Mitra. J. Org. Chem. **43**, 2923 (1978).
12. W. B. Smith. Org. Magn. Reson. **9**, 644 (1977).
13. L. F. Fieser and M. Fieser. *In* Steroids. Reinhold Publishing Corporation, New York. 1959.
14. N. Otomo, H. Sato, and S. Sakamura. Agric. Biol. Chem. **47**, 1115 (1983).
15. M. B. Evans, A. D. Dale, and C. J. Little. Chromatographia, **13**, 5 (1980).
16. H. Achenbach, A. Muhlenfeld, B. Weber, W. Kohl, and G.-U. Brillinger. Z. Naturforsch. **37B**, 1091 (1982).
17. F. W. Wehrli and T. Wirthlin. *In* Interpretation of carbon-13 NMR spectra. Wiley Heyden, New York. 1978.
18. F. C. Fischer, and M. J. M. Gijbels. Planta medica, 77 (1987); M. Fujita, M. Yamada, S. Nakajima, K.-I. Kawai, and M. Nagai. Chem. Pharm. Bull. **32**, 2622 (1984).
19. E. Solcaniova, P. Hrnciar, and T. Liptaj. Collect. Czech. Chem. Commun. **45**, 2772 (1980).
20. H. Achenbach, A. Muhlenfeld, and G. U. Brillinger. Liebigs Ann. Chem. 1596 (1985). .
21. M. S. R. Nair and S. T. Carey. Tetrahedron Lett. 1655 (1975).
22. L. J. Mulheirn, R. B. Beechey, D. P. Leworthy, and M. D. Osselton. J. Chem. Soc. Chem. Commun. 874 (1974).
23. F. A. Einhellig, G. R. Leather, and L. L. Hobbs. J. Chem. Ecol. **11**, 65 (1985).
24. A. H. Datko, S. H. Mudd, and J. Giovanelli. Plant Physiol. **65**, 906 (1980).
25. J. J. Brown and G. T. Newbold. J. Chem. Soc. 1285 (1953).

Can. J. Chem. Downloaded from www.nrcresearchpress.com by 109.225.110.28 on 09/08/12
For personal use only.

Catalysis of the deprotonation of β-diketones during formation of the 1:1 metal complexes

CARLOS A. BLANCO[1]
Departamento de Química Física, Facultad de Ciencias, Universidad de Valladolid, 47005 Valladolid, Spain
AND
MICHAEL J. HYNES
Department of Chemistry, University College, Galway, Ireland

Received December 9, 1991

CARLOS A. BLANCO and MICHAEL J. HYNES. Can J. Chem. **70**, 2285 (1992).

Catalytic effects on the deprotonation rate constants of β-diketones were observed during kinetic studies of the formation reactions of the 1:1 complexes of these ligands. When vanadium(IV), chromium(III), iron(III), cobalt(II), nickel(II), copper(II), and uranium(VI) react with pentane-2,4-dione, heptane-3,5-dione, 1,1,1-trifluoropentane-2,4-dione, 4,4,4-trifluoro-1-(2-thienyl)-butane-1,3-dione, 1-phenylbutane-1,3-dione, and 2-acetylcyclohexanone a significant catalytic effect on the rate of ionization of the keto tautomer of the ligand was observed. A considerable enhancement of the rate of ionization of the enol tautomers of these ligands was observed during the complex formation reactions with Cu^{2+}. A mechanism is proposed that accounts for these catalytic effects. In the case of Cu^{2+} the increased rate of proton removal from the ligands may be rationalized in terms of the relatively large reduction potential of this metal ion.

CARLOS A. BLANCO et MICHAEL J. HYNES. Can. J. Chem. **70**, 2285 (1992).

On a observé des effets catalytiques sur les constantes de vitesse de déprotonation des β-dicétones au cours d'études cinétiques sur les réactions de formation des complexes 1 : 1 de ces coordinats. Lorsqu'on fait réaction du vanadium(IV), du chrome(III), du fer(III), du cobalt(II), du nickel(II), du cuivre(II) et de l'uranium(VI) avec la pentane-2,4-dione, l'heptane-3,5-dione, la 1,1,1-trifluoropentane-2,4-dione, la 4,4,4-trifluoro-1-(2-thiényl)-butane-1,3-dione, la 1-phénylbutane-1,3-dione et la 2-acétylcyclohexanone, on observe un effet catalytique important sur la vitesse d'ionisation du tautomère cétonique du coordinat. On a observé une augmentation considérable de la vitesse d'ionisation des tautoméres énoliques de ces coordinats au cours des réactions de formation de complexes avec le Cu^{2+}. On propose un mécanisme qui explique ces effets catalytiques. Dans le cas du Cu^{2+}, on peut rationaliser l'accélération de la vitesse d'enlèvement du proton des coordinats en fonction d'un relativement grand potentiel de réduction de cet ion métallique.
[Traduit par la rédaction]

Introduction

During the last number of years, the kinetics and mechanisms of the complex formation reactions of β-diketones with a variety of metal and oxo-metal ions have been the focus of considerable attention (1–18). In view of the fact that β-diketones can exist in solution as keto and enol tautomers and as the enolate ion, their complex formation reactions have considerable potential for mechanistic variation. Apart from their intrinsic interest, the reactions of these ligands with metal ions are of interest because of the considerable practical applications of the metal complexes in analytical chemistry, as catalysts for polymerization reactions, as insecticides, for the control of soil-borne fungi, and in laser technology (19).

Metal complexes were first classified as either labile or inert on the basis of the electronic configuration of the metal ion (20). In general, complexes of metal ions with d^3 and low-spin configurations were classified as inert (20). However, the substantial body of kinetic results obtained since Taube's review demonstrate that other properties of metal ions, such as charge and ionic radius, as well as the electronic and structural character of the ligands also have a considerable effect on the rates and mechanisms of ligand substitution processes (21–27).

To evaluate the inherent kinetic nature of metal ions, it has been essential to compare rate constants for complex formation of various metal ions with structurally similar ligands having a range of substituent groups that exert a variety of electronic effect. In the case of the complex formation reactions of β-diketones, some of the kinetic investigations were concerned with the influence of both electron-releasing and electron-withdrawing groups on the reaction mechanisms, others have investigated the effect of the chain length on the reactivity of β-diketones towards metal ions, while more recent investigations have concentrated on medium effects (18). In addition, the nature of the metallic centres (such as their acid–base properties, lability, and hardness) have also been considered. Recent results have highlighted the catalytic effect of Cu^{2+} on the ionization of the keto and enol tautomers of 2-acetylcyclohexanone (28).

As part of our continuing interest in the reactions of metal ions with β-dicarbonylic compounds we now report a comparative study of the catalytic effects of a range of metal ions on the complex formation reactions of metal β-diketonates.

Experimental

$VOSO_4 + H_2O$ (B.D.H.), $Cr(NO_3)_3 \cdot 9H_2O$ (Aldrich), $Fe(NO_3)_3 \cdot 9H_2O$ (AnalaR), $Co(ClO_4)_2 \cdot 6H_2O$ (Johnson Matthey), $Ni(ClO_4)_2 \cdot 6H_2O$ (Johnson Matthey), $Cu(NO_3)_2 \cdot 3H_2O$ (B.D.H.), and $(UO_2)(NO_3)_2 \cdot 6H_2O$ (AnalaR) were used as the source of metal ions. Stock solutions were standardized using recognised procedures (29).

4,4,4-Trifluoro-1-(2-thienyl)-butane-1,3-dione, Htftbd (Koch–Light), and 1-phenylbutane-1,3-dione, Hpbd (Fluka), were used as purchased. Pentane-2,4-dione, Hpd (B.D.H.); heptane-3,5-dione, Hhptd (Kodak); 1,1,1-trifluoropentane-2,4-dione, Htfpd (Koch–Light); 2-acetylcyclohexanone, Hachx (Fluka), were freshly dis-

[1]Author to whom correspondence may be addressed.

Can. J. Chem. Downloaded from www.nrcresearchpress.com by 109.225.110.28 on 09/08/12
For personal use only.

Can. J. Chem. Downloaded from www.nrcresearchpress.com by 109.225.110.28 on 09/08/12
For personal use only.

tilled under reduced pressure prior to use. Stock solutions were standardized by titration with standard sodium hydroxide.

Perchloric acid (B.D.H.) was used as the source of hydrogen ions and all solutions were adjusted to an ionic strength of 0.5 mol dm^{-3} using $NaClO_4$ (Riedel–de Haën) as the inert electrolyte. Unless otherwise indicated, all materials were of analytical reagent grade and were used without further purification.

UV/visible spectra were recorded on a Shimadzu UV-260 spectrophotometer equipped with a chart recorder and a thermostatted cell compartment. pH measurements were made with a PTI6 pH-meter equipped with a Russell combination electrode. From spectrophotometric and potentiometric data a quantitative evaluation of the ligand and complex equilibria was carried out using published procedures (30, 31).

The kinetic data were obtained either on the Shimadzu UV-260 spectrophotometer or on a Hi-Tech SF-20 stopped-flow spectrophotometer that was interfaced to a BBC microcomputer via a Datalab DL901 transient recorder. The pseudo-first-order rate constants were the average of at least three determinations. Data for from three to four half-lives were utilized in these calculations. The standard deviation in individual runs was usually less than one percent.

All measurements were carried out at 25.0 ± 0.01°C.

Results and discussion

The keto–enol equilibrium of β-diketones is usually represented as in eq. [1], where k_e is the rate of enolization

$$[1]\quad HK \underset{k_f}{\overset{k_e}{\rightleftharpoons}} HE$$

and k_f is the rate of ketonization. However, the enolization of β-diketones does not proceed by direct transfer of a proton from carbon to oxygen. Instead, the enolate ion is formed as an intermediate and eq. [2] is a more complete description of the actual mechanism.

$$[2]\quad HK \underset{k_b}{\overset{k_a}{\rightleftharpoons}} H^+ + E^- \underset{k_d}{\overset{k_c}{\rightleftharpoons}} HE$$

In eq. [2] $k_c > k_b > k_d > k_a$ and k_c is diffusion controlled ($\approx 3 \times 10^{10}$ dm^3 mol^{-1} s^{-1}) (32). In terms of the ionization scheme, $k_e = k_a$ and $k_f = K_{HE}k_b$ where K_{HE} is the dissociation constant of the enol tautomer of the ligand.

For many complex formation reactions, the rate constant for loss of a proton by the ligand is considerably greater than the rate of complex formation with the deprotonated form of the ligand. For example, the rate of proton loss from acetic acid is 8.2×10^5 s^{-1} (33) while the rate of reaction of Ni^{2+} with CH_3COO^- is 1.5×10^5 dm^3 mol^{-1} s^{-1} (27). However, in the case of β-diketones it has been found that the rates of proton loss from either the keto or enol tautomer are frequently less than, or of a similar order of magnitude to, the rates of complex formation. Table 1 contains a list of the rates of ionization of the keto and enol tautomers of the β-diketones discussed here. The values of $k_a = k_c$ were determined by a bromination procedure (14, 16). The values of k_d were calculated from the known values of K_{HE} and k_c, assuming that the k_c pathway is diffusion controlled. Relevant kinetic data for the reactions of vanadium(IV), chromium(III), iron(III), cobalt(II), nickel(II), copper(II), and uranium(VI) with β-diketones from our previous published and unpublished work and from the literature (1–18, 28) are summarized in Table 2. The values given include those that are derived on the basis of the previously established mechanisms (18). In Table 2 the rate constants for reaction of the metal species with the keto (k_{HK}) and enol tautomers (k_{HE}) of the β-diketone are compared with the rate of proton loss from both the keto (k_a) and enol tautomers (k_d) respectively. Since the vast majority of these reactions were carried out in neutral or acidic medium where the pH is considerably less than the pK of the ligand, the fraction of the ligand present as the enolate ion is very small indeed. A number of deductions can be made from the data in Table 2. Firstly, it is apparent that the enol tautomer of all the β-diketones studied is considerably more reactive than the keto tautomer. It would appear also that direct reaction with the keto tautomer is restricted to those metal ions which are either very labile or which form relatively stable complexes, e.g., Fe^{3+}, Cu^{2+}, $[UO_2]^{2+}$, and that metal ions such Ni^{2+}, which form complexes of relatively low stability and which are relatively inert, react exclusively with the enol tautomer.

TABLE 1. Rates of ionization of the keto and enol tautomers of β-diketones

β-Diketone	k_a (s^{-1})	k_d (s^{-1})	Reference
(Hpd)	1.52×10^{-2}	167.	2
(Hhptd)	5.78×10^{-3}	26.5	16
(Htfpd)	3.46×10^{-3}	3.54×10^6	7
(Htftbd)	8.40×10^{-3}	2.88×10^6	3
(Hpbd)[a]	9.00×10^{-3}	172.	14
(Hachx)[a]	3.25×10^{-4}	0.408	Unpublished results

[a]In methanol:water (70:30 v/v).

The second important deduction that can be made from the data in Table 2 is that, with the exception of chromium(III), the rate constants for reaction of metal and oxo-metal ions with either the keto or enol tautomers of all β-diketones are considerably less than would be predicted on the basis of the Eigen–Wilkins mechanism. This retardation has been quantified in terms of the non-dimensional parameter R (34) (eq. [3]).

$$[3]\quad R = (4/3)k_{cf}/k_sK_o$$

In eq. [3] k_{cf} is the rate of complex formation, k_s is the rate of solvent exchange, and K_o is the outer sphere association constant, while the (4/3) is a statistical factor that accounts for the fact that not every solvent exchange leads to complex formation. In the present investigation, in view of the fact that the keto and enol tautomers of β-diketones are uncharged, the Rorabacher modification (35) of the Eigen–Fuoss equation (36, 37) was used to calculate K_o. A value of 0.3 was used throughout.

In the case of chromium(III) the exceptionally slow rate of water exchange together with the fact that it is believed to react by an I_a mechanism (26) make it extremely unlikely that retardation effects such as those exhibited by labile metal ions such as Ni^{2+} and Cu^{2+} would be apparent.

The presence of some catalytic effects on the ionization reactions of β-diketone are indicated by the data in Table 2. Although reversible base-catalyzed transformation of β-diketones into their tautomeric forms (38–40) is well established, such a mechanism would not be operative in the acidic conditions under which the work described here was carried out. The enolization of β-diketones is not an acid-catalyzed

TABLE 2. Rate constants for formation of 1:1 complexes of β-diketones. Comparative values with ligand ionization rate constants, k_a (keto) and k_d (enol)

Ligand	Metal	k_{HE} ($dm^3\ mol^{-1}\ s^{-1}$)	R^a	k_{HE}/k_d ($dm^3\ mol^{-1}$)	k_{HK} ($dm^3\ mol^{-1}\ s^{-1}$)	R^b	k_{HK}/k_a ($dm^3\ mol^{-1}$)	Reference
Hpd	$[VO]^{2+}$				4.4	3.9×10^{-2}	293.	6
Hpd	Cr^{3+}	1.05×10^{-2}	1.9×10^{4}	6.28×10^{-5}				12
Hpd	$Cr(OH)^{2+}$	0.278	6.8×10^{3}	1.66×10^{-3}				12
Hpd	Fe^{3+}	5.2	0.14	3.11×10^{-2}	0.29	7.1×10^{-6}	19.3	2
Hpd	$Fe(OH)^{2+}$	4.4×10^{3}	0.16	26.3	5.4	2.0×10^{-3}	360.	2
Hpd	Co^{2+}	1.36×10^{2}	2.3×10^{-4}	0.813	0.84	1.2×10^{-6}	56.	10
Hpd	Ni^{2+}	19.3	2.7×10^{-3}	0.115				5
Hpd	Cu^{2+}	2.0×10^{4}	1.8×10^{-4}	119.	12.	8.1×10^{-3}	800.	1
Hpd	$[UO_2]^{2+}$	5.33×10^{3}		31.9	3.85		238.	4
Hhptd	$[VO]^{2+}$	5.35	4.8×10^{-2}	0.20	0.91	8.1×10^{-3}	157.	17
Hhptd	Co^{2+}	67.1	9.3×10^{-5}	2.52	0.96	1.3×10^{-6}	16.6	16
Hhptd	Ni^{2+}	10.0	1.4×10^{-3}	0.37				15
Hhptd	Cu^{2+}	1.14×10^{4}	1.0×10^{-4}	429.	8.89	7.9×10^{-8}	1539.	17
Htfpd	$[VO]^{2+}$	3.5	3.1×10^{-2}	9.87×10^{-7}				6
Htfpd	Fe^{3+}	19.6	0.54	5.53×10^{-6}				9
Htfpd	Co^{2+}	>76.	$>1.1 \times 10^{-4}$	$>2.14. \times 10^{-5}$				9
Htfpd	Ni^{2+}	1.7	2.4×10^{-4}	4.80×10^{-7}				9
Htfpd	$[UO_2]^{2+}$	$>1.0 \times 10^{3}$		$>2.82 \times 10^{-4}$				7
Htftbd	$[VO]^{2+}$	7.6	6.8×10^{-2}	2.6×10^{-6}				6
Htftbd	Fe^{3+}	1.4	3.8×10^{-2}	4.9×10^{-7}				3
Htftbd	$Fe(OH)^{2+}$	1.3×10^{3}	4.8×10^{-2}	4.5×10^{-4}				3
Htftbd	Ni^{2+}	2.3	3.2×10^{-4}	8.0×10^{-7}				*d*
Htftbd	$[UO_2]^{2+}$	$>1.0 \times 10^{3}$		$>2.8 \times 10^{-4}$				7
Hpbd[c]	Ni^{2+}	3.21	4.5×10^{-4}	0.019				14
Hpbd[c]	Cu^{2+}	5.03×10^{3}	4.5×10^{-5}	29.3				14
Hachx[c]	Ni^{2+}	0.114	1.6×10^{-5}	0.28				*d*
Hachx[c]	Cu^{2+}	1.27×10^{3}	1.1×10^{-5}	3.10×10^{3}	0.93	8.3×10^{-9}	2.86×10^{3}	*d*

[a] $R = k_{HE}/(3/4)k_aK_o$.
[b] $R = k_{HK}/(3/4)k_aK_o$.
[c] Methanol:water (70:30 v/v).
[d] Unpublished results.

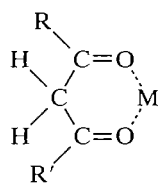

FIG. 1

process (41, 42). The catalytic effects observed during metal complex formation may be explained with reference to the intimate mechanism involved in the reactions of metal ions with β-diketones. The idea that these reactions proceed via a precursor complex was first proposed by Pearson and Anderson during their investigation of the reactions of Cu^{2+} with the keto tautomer of pentane-2,4-dione (1). A possible structure for such a precursor complex is shown in Fig. 1 in which the metal ion is symmetrically bonded to the two oxygens of the keto tautomer. Support for this idea stems from the fact that a number of such complexes have actually been isolated and characterized (43, 44). A similar type of precursor complex could be envisaged for the enol tautomer. The stability of this precursor complex would be an important element in determining the rate of reaction of metal ions with both the keto and enol tautomers of β-diketones. The complex formation in this instance could best be described as a metal-ion-catalyzed proton release from this precursor complex. Undoubtedly, the metal ion does catalyze proton release in those cases where pseudo-first-order rate constants are considerably greater than rates of ligand ionization (see Table 2). The copper(II) ion obviously acts as a catalyst in this step as the overall complex formation reactions are at least 100 times more rapid than loss of proton from the uncoordinated ligand.

Considering the data in Table 2, the formation of $[Cu(acxh)]^+$ is a case where the catalytic effect appears to be particularly high, the rates of complex formation being increased by about 3×10^3 compared to the rate of ionization. This may be related to the relatively slow rate of proton release from this ligand. In this particular case the rate constant for ionization of the keto tautomer of Hachx (k_a) is the smallest by more than one order of magnitude while the rate constant for loss of a proton from the enol tautomer (k_d) is almost two orders of magnitude less than the next smallest value in Table 1. The slow rate of loss of proton from the keto tautomer can be ascribed to the fact that the 2-carbon on Hachx has only one proton attached compared to two on the methine carbon in linear β-diketones. In addition, the acidic

Can. J. Chem. Downloaded from www.nrcresearchpress.com by 109.225.110.28 on 09/08/12
For personal use only.

TABLE 3. Limiting Eigen–Wilkins (k_{E-W}) complex formation rate constants and standard reduction potentials of the ions

Metal	d^n	k_{E-W}[a] ($dm^3\ mol^{-1}\ s^{-1}$)	Reduction potential $E°$ (V)
$[VO]^{2+}$	(d^1)	1.1×10^2	
Cr^{3+}	(d^3)	5.4×10^{-7}	−0.71
Fe^{3+}	(d^5)	3.6×10^1	−0.04
Co^{2+}	(d^7)	7.2×10^5	−0.28
Ni^{2+}	(d^8)	7.2×10^3	−0.25
Cu^{2+}	(d^9)	1.0×10^9	+0.35

[a] $k_{E-W} = (3/4)k_s K_o$.

proton is attached to a tertiary ring carbon and this may hinder the process of proton removal.

This large catalytic effect is not reproduced in the reaction of any other metal ion with the enol tautomer of a β-diketone. It has been proposed that the ability to accept transferred charge should be related to the standard electrode potential of the metal in aqueous solution (45). The electrode reduction potential of Cu^{2+} (+0.35 V) is considerably greater than the reduction potential of any other 3-*d* transition metal ion, reflecting its greater ability to accept charge (Table 3). This higher tendency for Cu^{2+} to capture electrons may be reflected in its greater ability to stabilize precursor complexes of the type shown in Fig. 1 compared to other transition metal ions. This increased stability will in turn be reflected in an increased rate of proton loss from the precursor complex, leading to increased rate of complex formation.

The catalytic effect is greater when the metal ion reacts with the keto rather than with the enol tautomer of the ligand. There may be two reasons for this. Firstly, the keto tautomer is more inert than the enol tautomer and consequently has a greater potential to exhibit a catalytic effect. Secondly, it may be related to the more facile approach of the metal to the keto tautomer; such an approach would indeed in all probability be hindered by the extensive intramolecular hydrogen bonding present in the enol tautomer. The only exceptions to this are the reactions of copper(II) with 2-acetylcyclohexanone where $k_{HE}/k_d > k_{HK}/k_a$ (Table 2). This may be attributed to the cyclic structure of Hachx.

The arguments presented here give a plausible explanation of the ability of many metal ions to catalyze the ionization of the keto tautomers of β-diketones. Even those metal ions with negative reduction potentials such as Co^{2+} (−0.28 V) and Fe^{3+} (−0.04 V) are able to catalyze proton loss during the complex formation process through electrostatic interaction with oxygen centres. Most striking in this respect is the ability of $Fe(OH)^{2+}$ to catalyze proton loss from the enol tautomer of pentane-2,4-dione. Although it is known that hydroxide complexes of Cr(III), Fe(III), Co(III), and Cu(II) usually give larger rate constants than the aquometal ions (27) for many substitution reactions, the reactivity of $Fe(OH)^{2+}$ towards Hpd is considerably greater than would be predicted for a doubly charged metal. This is similar to the internal conjugate base mechanism proposed by Rorabacher (46) but, in this instance, the hydrogen bonding occurs between the acidic proton on the diketone and the oxygen of the coordinated hydroxide group. Such effects are believed to operate largely via an enhancement of the outer-sphere association constant (47).

The ability of some metal ions to catalyze the ionization of both the keto and enol tautomers of β-diketones has been demonstrated. The effects of the various metal ions have been rationalized in terms of their reduction potentials, their ability to stabilize the proposed precursor complexes, and their ability to increase the outer-sphere association constant via hydrogen bonding.

Acknowledgements

One of us (C.A.B.) thanks the Vicerrectorado de Investigación of the University of Valladolid for financial support.

1. R. G. Pearson and O. P. Anderson. Inorg. Chem. **9**, 39 (1970).
2. D. P. Fay, A. R. Nichols, and N. Sutin. Inorg. Chem. **10**, 2096 (1971).
3. M. R. Jaffe, D. P. Fay, M. Cefola, and N. Sutin. J. Am. Chem. Soc. **93**, 2878 (1971).
4. M. J. Hynes and B. D. O'Regan. Proc. R. Irish Acad. **77B**, 285 (1977).
5. M. J. Hynes and B. D. O'Regan. J. Chem. Soc. Dalton Trans. 162 (1979).
6. M. J. Hynes and B. D. O'Regan. J. Chem. Soc. Dalton Trans. 7 (1980).
7. M. J. Hynes and B. D. O'Regan. J. Chem. Soc. Dalton Trans. 1502 (1980).
8. I. Ando, K. Yoshizumi, K. Ito, K. Ujimoto, and H. Kurihara. Bull. Chem. Soc. Jpn. **56**, 1368 (1983).
9. M. J. Hynes and M. T. O'Shea. J. Chem. Soc. Dalton Trans. 2, 331 (1983).
10. M. J. Hynes and M. T. O'Shea. Inorg. Chim. Acta, **73**, 201 (1983).
11. M. Harada, M. Mori, M. Adachi, and W. Eguchi. J. Chem. Eng. Jpn. **16**, 187 (1983).
12. M. J. Hynes, C. O'Mara, and D. F. Kelly. Inorg. Chim. Acta, **120**, 131 (1986).
13. J. M. Hernando, C. Blanco, and T. Prieto. Bull. Soc. Chim. Fr. **5**, 775 (1987).
14. M. J. Hynes and M. T. Mooney. Proc. R. Irish Acad. **89B**, 441 (1989).
15. C. Blanco and M. J. Hynes. Bull. Soc. Chim. Fr. **5**, 611 (1989).
16. C. Blanco and M. J. Hynes. J. Chim. Phys. **86**, 1989 (1989).
17. C. Blanco and M. J. Hynes. Inorg. Chim. Acta, **173**, 115 (1990).
18. M. J. Hynes. Rev. Inorg. Chem. **11**, 21 (1991).
19. M. A. Ribeiro Da Silva. NATO ASI Ser., Ser. C. **119**, 317 (1984).
20. H. Taube. Chem. Rev. **50**, 69 (1952).
21. C. H. Langford and H. B. Gray. Ligand substitution processes. Benjamin, New York. 1965.
22. R. G. Wilkins and M. Eigen. Adv. Chem. Ser. **49**, 55 (1964).
23. J. O. Edwards, F. Monacelli, and G. Ortaggi. Inorg. Chim. Acta. **11**, 47 (1974).
24. A. E. Merbach. Pure Appl. Chem. **54**, 1479 (1982).
25. T. W. Swaddle. Adv. Inorg. Bioinorg. Mech. **2**, 96 (1983).
26. R. Van Eldik (*Editor*). Inorganic high pressure chemistry: kinetics and mechanisms. Elsevier, Amsterdam. 1986.
27. D. W. Margerum. G. R. Cayley, D. C. Weatherburn, and G. K. Pagenkopf. *In* Coordination chemistry. Vol. 2. *Edited by* A. E. Martell. American Chemical Society Monograph 174, Washington D.C. 1978. Chap. 1.
28. M. J. Hynes, C. A. Blanco, and M. T. Mooney. J. Chem. Soc. Perkin Trans. Submitted.
29. A. I. Vogel. Textbook of quantitative chemical analysis. 5th ed. *Revised by* G. H. Jeffrey, J. Bassett, J. Mendham, and R. C. Dempsey. Longman Scientific and Technical Publishers, London. 1989.
30. P. Gans, A. Sabatini, and A. Vacca. J. Chem. Soc. Dalton Trans. 1195 (1985).

Can. J. Chem. Downloaded from www.nrcresearchpress.com by 109.225.110.28 on 09/08/12
For personal use only.

31. D. A. Leggett and W. A. E. McBryde. Anal. Chem. **47**, 1065 (1975).
32. M. Eigen and L. C. de Maeyer. *In* Technique of organic chemistry. Vol VIII. Part. II. *Edited by* S. L. Friess, E. S. Lewis, and A. Weissberger. Interscience, New York. 1963. p. 1037.
33. M. Eigen. Angew. Chem. **3**, 1 (1964).
34. P. K. Chattopadhyay and J. F. Coetzee. Inorg. Chem. **12**, 113 (1973).
35. D. B. Rorabacher. Inorg. Chem. **5**, 1891 (1966).
36. M. Eigen. Z. Phys. Chem. (Frankfurt am Main) NF, **1**, 176 (1954).
37. R. M. Fuoss. J. Am. Chem. Soc. **80**, 5059 (1958).
38. H. M. Dawson, C. R. Hoskins, and J. E. Smith. J. Chem. Soc. 1884 (1929).
39. K. J. Pederson. J. Phys. Chem. **38**, 999 (1934).
40. R. P. Bell and J. Hansson. Proc. R. Soc. (London), **A255**, 214 (1960).
41. R. P. Bell and O. M. Lidwell. Proc. R. Soc. (London), **A176**, 88 (1940).
42. R. G. Pearson and J. M. Mills. J. Am. Chem. Soc. **72**, 1692 (1950).
43. P. W. N. M. Van Leeuwen. Recl. Trav. Chim. Pays-Bas, **87**, 396 (1968).
44. A. L. Allred and D. W. Thompson. Inorg. Chem. **7**, 1196,
45. D. P. Graddon. An introduction to coordination chemistry. 2nd ed. Pergamon Press, Oxford. 1968.
46. D. B. Rorabacher. Inorg. Chem. **5**, 1891 (1966).
47. W. W. Taylor, H. K. Stepien, and D. B. Rorabacher. Inorg. Chem. **2**, 1282 (1974).

Can. J. Chem. Downloaded from www.nrcresearchpress.com by 109.225.110.28 on 09/08/12
For personal use only.

Transient 1,3-dipoles containing sulfur: a novel example of rearrangement from ethyl-1-oxo-1-(2,3-dichloro-4-phenoxyacetic acid)-2-[3-thio-5-(4-chlorophenyl)-1,2-dithiolium] bromide

MARTINE VARACHE-LEMBEGE, ALAIN NUHRICH, AND GUY DEVAUX[1]

Laboratoire de pharmacie chimique et chimie thérapeutique. Faculté des Sciences pharmaceutiques, Université de Bordeaux II, 3, place de la Victoire, 33076 Bordeaux CEDEX, France

AND

FRANÇOISE DUBOUDIN

Laboratoire de chimie organique et organométallique (Unité associée 35), Université de Bordeaux I, 351, cours de la Libération, 33405 Talence CEDEX, France

Received October 24, 1991

MARTINE VARACHE-LEMBEGE, ALAIN NUHRICH, GUY DEVAUX, and FRANÇOISE DUBOUDIN. Can. J. Chem. **70**, 2290 (1992).

During the basic treatment of the compound named in the title the expected ketone was not obtained. The Fast Atom Bombardment (FAB) mass spectrum of the new product formed was reported in this paper: the fragmentation pattern shows an S—S bridge sequence in a dimeric compound. This structure was also investigated by ^{1}H and ^{13}C nuclear magnetic resonance spectroscopy, the results of which were in accordance with the mass spectral data. The formation of this compound was explained by the hypothesis of a thiirane intermediate structure that could spontaneously isomerize to the enethiol form and undergo oxidation to the disulfide.

MARTINE VARACHE-LEMBEGE, ALAIN NUHRICH, GUY DEVAUX et FRANÇOISE DUBOUDIN. Can. J. Chem. **70**, 2290(1992).

Lors du traitement basique du composé mentionné dans le titre, il ne se forme pas la cétone attendue mais un nouveau produit dont la structure est élucidée dans cette publication. Les modes de fragmentation déduits du spectre de masse FAB de ce dérivé mettent en évidence l'existence d'un pont disulfure dans un dimère. L'étude des spectres de RMN du ^{1}H et du ^{13}C permet de confirmer les données de la spectrométrie de masse. La formation de ce composé s'expliquerait par une structure thiirane intermédiaire pouvant s'isomériser en une forme ènethiol qui s'oxyderait ensuite en disulfure.

Introduction

To extend our earlier work on a new diuretic thiopyranylidene phenoxyacetic ketone (1), we attempted to synthesize 2,3-dichloro-(1-oxo{5-(4-chlorophenyl)-1,2-dithiol-3-ylidene}-2-ethyl)-4-phenoxyacetic acid **2** (Fig. 1). A method similar to those of Sauvé and Lozac'h (2) was followed. A solution containing the bromide **1** in dry pyridine was refluxed for 1.5 h. The IR spectrum was in agreement with the structure of the expected ketone **2**: in particular, two strong bands at 1590 cm^{-1} and 1540 cm^{-1} were observed, as reported in the 1500–1610 cm^{-1} range for different 5-aryl-1,2-dithiol-3-ylidene acetophenones by Lozac'h (3). However the elemental analysis (Table 1) was in disagreement with

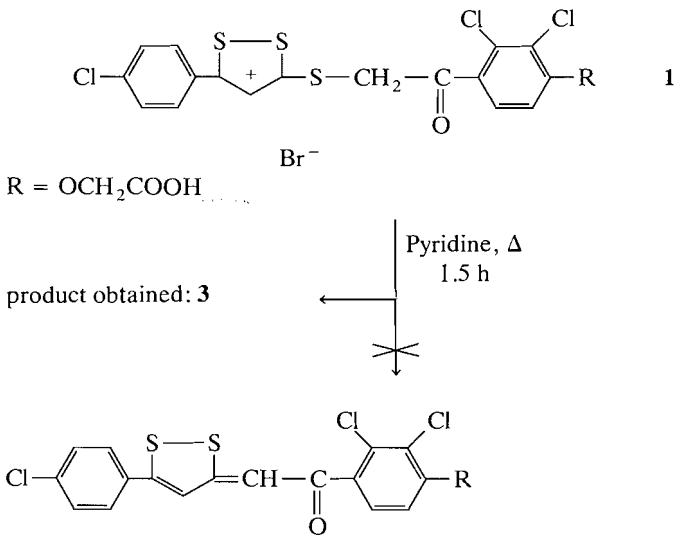

FIG. 1

TABLE 1. Elemental analysis percentage expected for a ketone compound

Element	Found for product **3**	Calculated for the expected ketone $C_{19}H_{11}Cl_3O_4S_2$
C	45.02	48.17
H	1.98	2.34
S	18.66	13.53
Cl	20.91	22.45

TABLE 2. Elemental analysis percentage for the proposed structure $C_{38}H_{20}Cl_6O_8S_6$

Element	Found for product **3**	Calculated for the disulfide $C_{38}H_{20}Cl_6O_8S_6$
C	45.02	45.20
H	1.98	1.99
S	18.66	19.05
Cl	20.91	21.06

[1]Author to whom correspondence may be addressed.

Can. J. Chem. Downloaded from www.nrcresearchpress.com by 109.225.110.28 on 09/08/12
For personal use only.

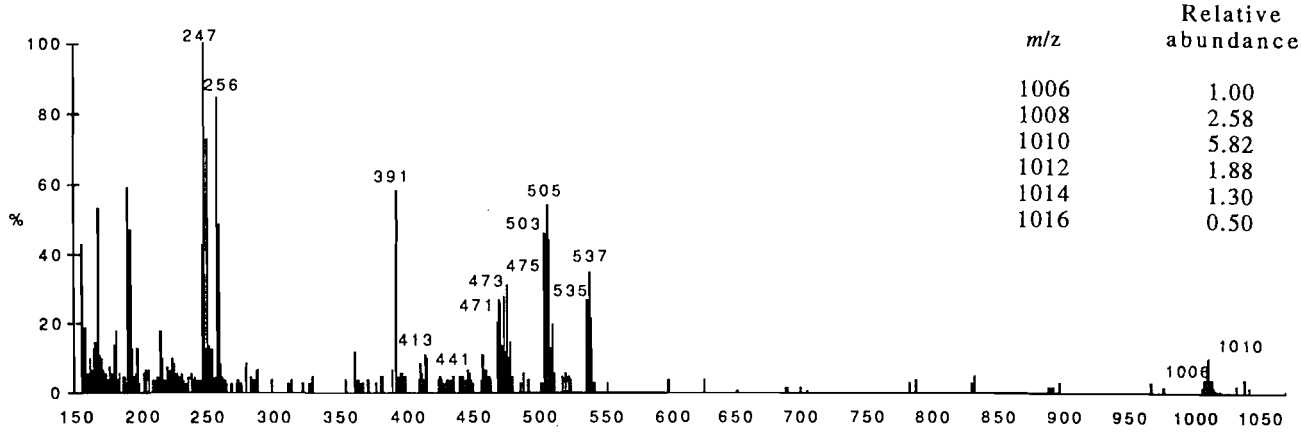

FIG. 2. FAB mass spectrum (positive ion detection) of **3**.

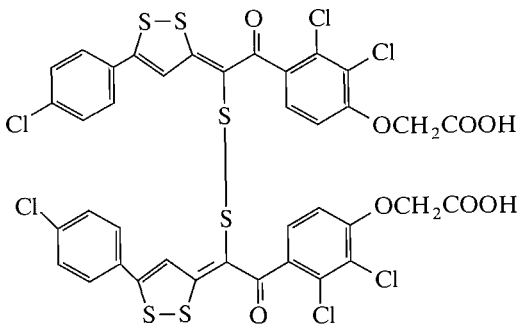

3

FIG. 3. Condensed structural formula of disulfide $C_{38}H_{20}Cl_6O_8S_6$.

an α-ethylenic ketone structure. The study of the ^1H NMR spectrum of the product obtained, **3**, did not allow us to establish its structure, but it confirmed the presence of a phenoxyacetic group, and aromatic and thiophene rings. This paper reports the structural study of the product **3**.

Results and discussion

Mass spectrum

A dimeric structure was identified by its FAB mass spectrum (Fig. 2). It exhibited a small molecular ion M^+ 1006 and the isotopic figure 6-Cl,6-S. Thus the experimental relative abundances of the isotopic molecular peaks were in excellent agreement with those calculated according to Beynon's method (4).

Fragment ions at *m/z* 535 and 471, which contained respectively (3-Cl,4-S) and (3-Cl,2-S), showed the presence of a disulfide bond. Thus a structure could be proposed (Fig. 3) and was in agreement with the elemental analysis percentage for sulfur and hydrogen (Table 2).

The major fragmentation of the molecular ion followed four pathways: (A) from $[M]^{+\cdot}$ to *m/z* ($M^+ - 503$), 503 (Scheme 1); (B) from $[M]^{+\cdot}$ to *m/z* ($M^+ - R$), 535 and 471 (Scheme 2); (C) from $[M]^{+\cdot}$ to *m/z* (base peak) 247 (Scheme 3); (D) from $[M]^{+\cdot}$ to *m/z* ($M^+ - R$), 256 (Scheme 4).

Pathway A: The presence of a fragment ion at *m/z* 503 and its isotopic figure 3-Cl,3-S showed the cleavage of the di-

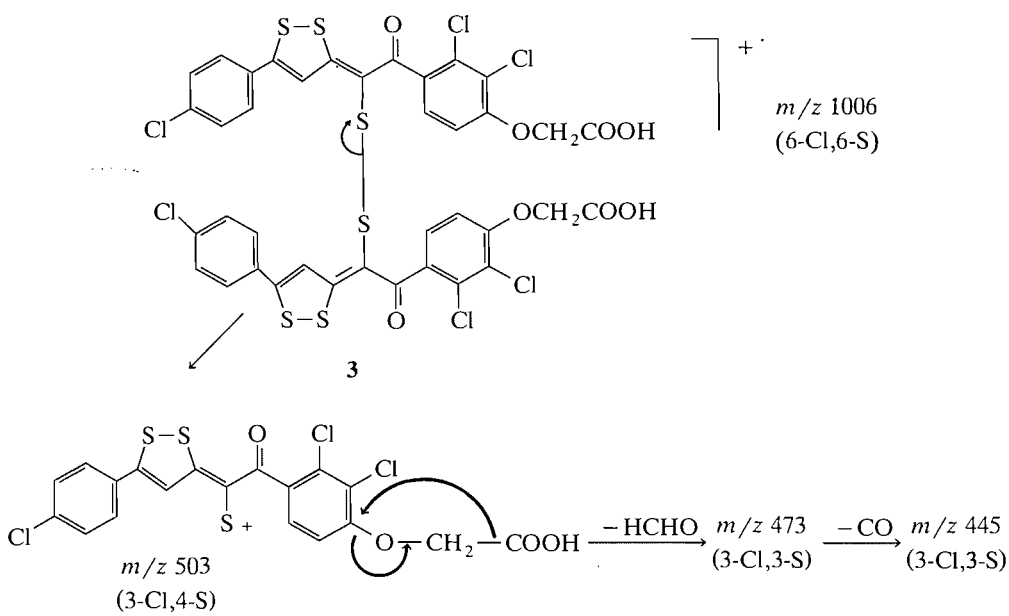

SCHEME 1. Cleavage of the S—S bond.

Can. J. Chem. Downloaded from www.nrcresearchpress.com by 109.225.110.28 on 09/08/12
For personal use only.

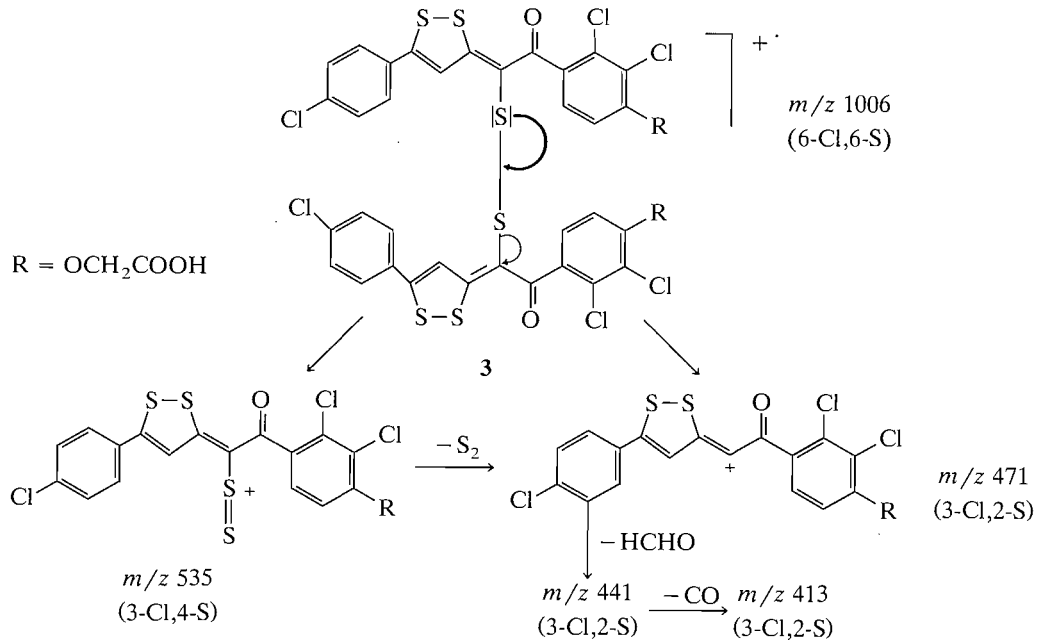

SCHEME 2. Simple S—S bridge α-cleavage.

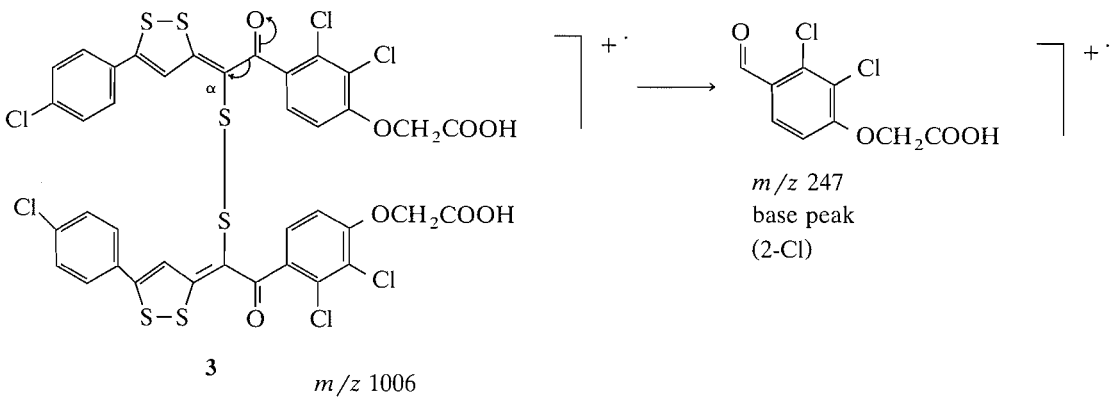

SCHEME 3. Simple carbonyl group α-cleavage.

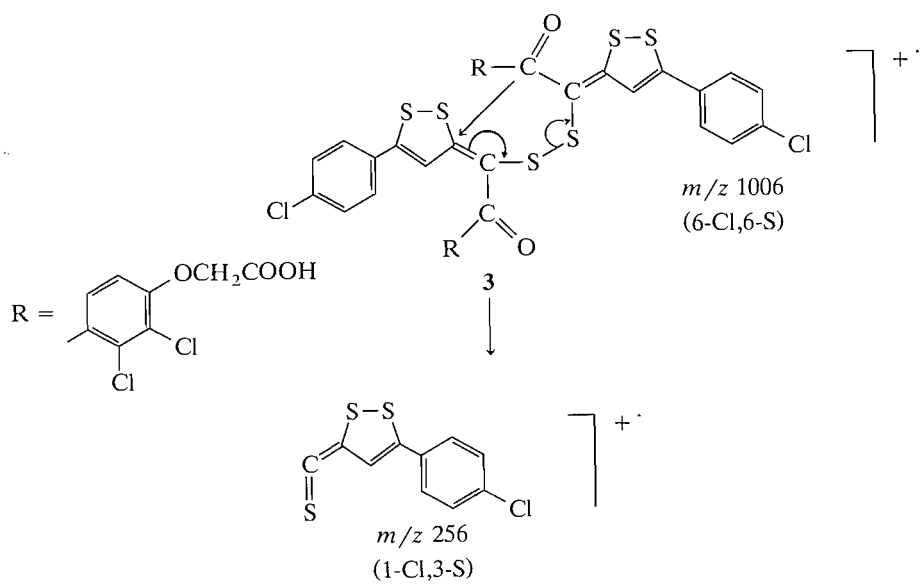

SCHEME 4. Cyclic process (MacLafferty) rearrangement.

Can. J. Chem. Downloaded from www.nrcresearchpress.com by 109.225.110.28 on 09/08/12
For personal use only.

TABLE 3. ^{1}H NMR spectral data of compound **3**

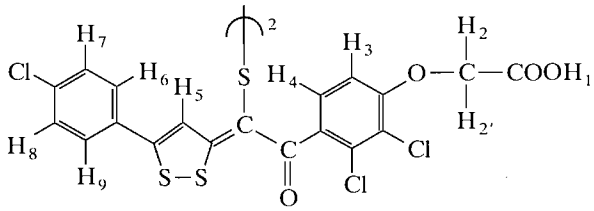

	Chemical shifts in ppm
H2–H2′	4.86 (s, 2H)
H3–H4	AM system (2H) J = 7.65 Hz δ = 7.00–7.76
H1[a]	7.27 (s, 30% bound hydroxyl) 7.89 (s, 70% free hydroxyl)
H5	7.60 (s, 1H)
H6–H7–H8–H9	AA′BB′ system at 7.67 (m, 4H)

[a]This appeared as two singlets: one was fine at 7.89 ppm and the other was broad at 7.27 ppm. The sum of the intensities of these two peaks corresponded to only one proton.

TABLE 4. ^{13}C NMR chemical shifts in δ (ppm) and assignments for quaternary carbons of compound **3**

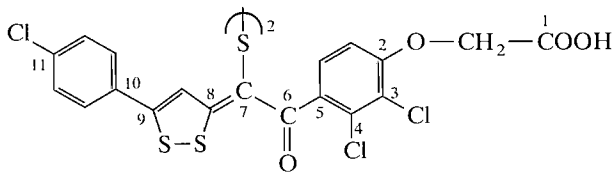

Position	Measured	Predicted[a]
1	178.80	
2	165.70	164.9
3	120.19	120.7
4	136.34[c]	137.6
5	130.75[b]	131.0
10	136.34[c]	139.8
11	131.06[b]	134.2
6	187.46	
7	154.50	148.0
8	169.19[c]	
9	169.19[c]	

[a]δ calculated using the increment rule (7).
[b]May be permuted.
[c]According to peak intensity.

TABLE 5. Base treatment of various thiocarbonyl ylides

Initial product	Base used	Hypothetical intermediate thiirane	% Final product
[a] 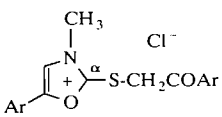	NaH in DMSO	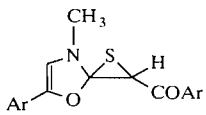	100% ketone
[b] 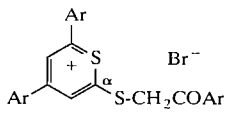	Pyridine	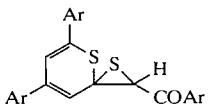	70–75% ketone
[c] 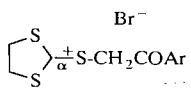	Et_3N in acetonitrile	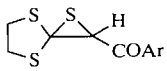	49% ketone + 40% enethiol
[c] 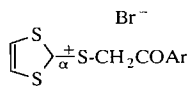	Et_3N in acetonitrile	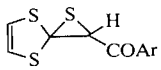	17% ketone + 71% disulfide
[d] 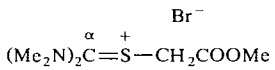	NaH in THF	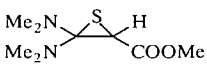	100% disulfide
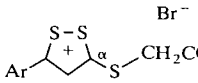	Et_3N in acetic acid[e] Pyridine[f]	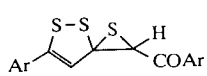	100% disulfide

[a]See ref. 12.
[b]See ref. 2.
[c]See ref. 13.
[d]See ref. 5.
[e]See ref. 14.
[f]This work.

Can. J. Chem. Downloaded from www.nrcresearchpress.com by 109.225.110.28 on 09/08/12
For personal use only.

sulfide bond in **3** as formulated for the analogous compound (5). The peaks at m/z 473 and 445 are respectively attributed to the loss of a formaldehyde molecule and a carbonyl group, from the fragment ion m/z 503.

Pathway B: Fragment ions at m/z 535 and 471 are explained by a simple S—S bridge α-cleavage from the molecular ion (5). Also, fragment ions at m/z 441 and 413 resulted from the expulsion of a formaldehyde molecule and the expulsion of a carbonyl group from the fragment ion m/z 471, respectively.

Pathway C: The base peak (m/z 247) is formed by a simple carbonyl group α-cleavage as shown in Scheme 3.

Pathway D: A cyclic process may lead to the formation of a radical ion (m/z 256).

The study of these fragment peaks and their isotopic structures allowed us to propose a dimeric structure (**3**) containing an S—S bridge for the product.

NMR spectra

^{1}H and ^{13}C NMR yielded spectra that confirm the structure of each symmetrical part of **3**.

The ^{1}H chemical shift data of the various protons in compound **3** are given in Table 3.

The ^{13}C spectrum of **3** shows both the resonance at δ_C 65.25, and resonances at δ_C 111.16, 125.39, 127.26, 129.15, and 129.43. Using a DEPT experiment, these were shown to be one CH_2 group and five different CH groups, respectively. It follows that the resonances reported in Table 4 can be assigned to 11 quaternary carbons. The chemical shift of C1 at 178.80 ppm indicated the presence of a carboxylic acid function while the chemical shift of C6 at 187.46 ppm indicated the presence of a carbonyl group. The last value is in agreement with those reported by McKinnon and Abouzeid (6). Calculations using the increment rule (7) allowed us to attribute most of the chemical

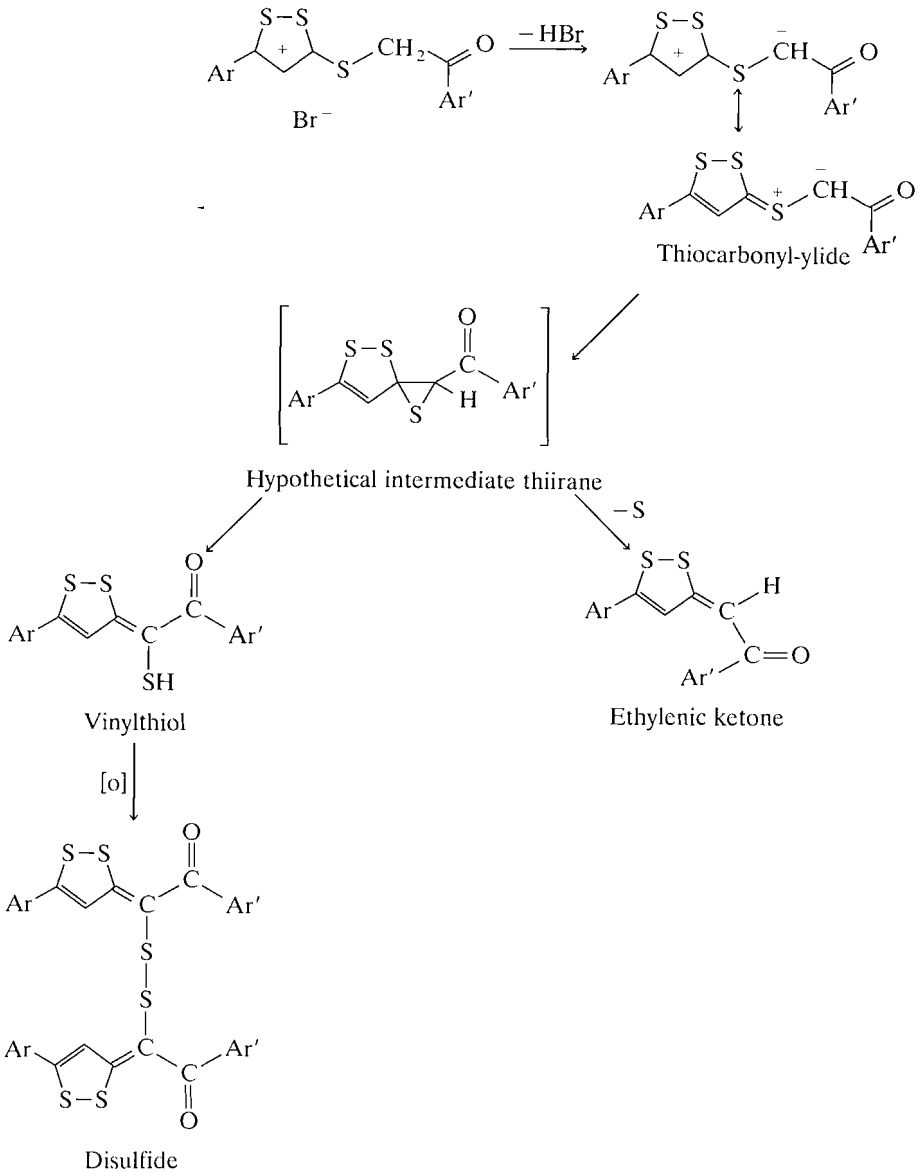

SCHEME 5. Hypothetical mechanism.

Can. J. Chem. Downloaded from www.nrcresearchpress.com by 109.225.110.28 on 09/08/12
For personal use only.

shifts to the other quaternary carbons. C8 and C9 were identified at 169.19 ppm.

Thus the total number of carbons and the division between the secondary, tertiary, and quaternary carbons were in agreement with the disulfide structure **3**.

Hypothetical mechanism

During the last decade, relatively few papers investigating the chemistry of thiocarbonyl ylides have been published (8–11). Some studies on bis(dimethylamino methylene) sulfonium bromides (5) showed that by deprotonation with a base these compounds produce a thiocarbonyl ylide that could cyclize into unstable non-isolated thiirane. The latter undergoes a very quick isomerization to give an enethiol whose air oxidation leads to the final disulfide product.

On the other hand, other works on thiocarbonyl ylides treated with various bases state that the reaction proceeded either to the formation of a disulfide or to an ethylenic ketone by decomposition of the hypothetical intermediate thiirane with release of elemental sulfur (Table 5).

We hypothesized that the title compound might be formed as indicated in Scheme 5. The rearrangement of the hypothetical intermediate thiirane could be in accordance with that previously reported (15) for unimolecular isomerization of thiirane to vinylthiol through the following intermediate state:

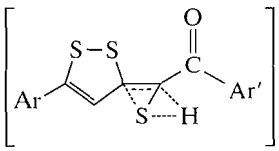

We have never found an ethylenic ketone.

We cannot yet explain the influence of the structure of α-carbon substituents in the initial product on the nature and proportions of the products obtained.

Experimental

The positive ion Fast Atom Bombardment (FAB) mass spectrum was obtained on a VG-ZAB-ZEQ spectrometer. The sample, dissolved in thioglycerol/$HClO_4$, using dioctylphthalate as the internal reference, was analyzed by a direct insertion probe with a source temperature of 0°C.

Nuclear magnetic resonance spectra were measured at 250 MHz (^1H) and 62.9 MHz (^{13}C) with a Bruker AC 250 spectrometer, in acetone as a solvent. Off-resonance and DEPT spectra were recorded. Chemical shifts were measured in ppm (δ) using tetramethylsilane as the internal reference.

Acknowledgements

We would like to thank Mrs. A. Lagardère and M. S. Larrouture for their technical assistance.

1. A. Nuhrich, M. Varache-Béranger, G. Devaux, J. Cambar, C. Dorian, and A. Carpy. Eur. J. Med. Chem. **21**, 49 (1986).
2. J.-P. Sauvé and N. Lozac'h. Bull. Soc. Chim. Fr. II, 427 (1980).
3. N. Lozac'h. *In* A. R. Katritzky and A. J. Boulton. Adv. Heterocycl. Chem. **13**, 161 (1971); cf. p. 219.
4. J.-H. Beynon. Mass spectrometry and its applications to organic chemistry. Elsevier, Amsterdam. 1964. pp. 298 and 301.
5. M. Takaku, S. Mitamura, and H. Nozaki. Tetrahedron Lett. **41**, 3651 (1969).
6. D. M. McKinnon and A. A. Abouzeid. J. Heterocycl. Chem. **28**, 749 (1991).
7. E. Breitmaier and W. Voelter. Carbon-13 NMR spectroscopy. VCH Publishers, Weinheim. 1987. pp. 319 and 320.
8. R. Huisgen, C. Fulka, I. Kalwinsch, L. Xingya, G. Mloston, J. R. Moran, and A. Probstl. Bull. Soc. Chim. Belg. **93**, 511 (1984).
9. Y. Terao, M. Tanaka, N. Imai, and K. Achiwa. Tetrahedron Lett. **26**, 3011 (1985).
10. Y. Terao, M. Aono, I. Takamashi, and K. Achiwa. Chem. Lett. 2089 (1986).
11. Y. Terao, M. Aono, N. Imai, and K. Achiwa. Chem. Pharm. Bull. **35**, 1734 (1987).
12. Y. Ueno and M. Okawara. Bull. Chem. Soc. Jpn. **45**, 1797 (1972).
13. J. Nakayama, T. Takemasa, and M. Hoshino. Bull. Chem. Soc. Jpn. **53**, 2281 (1980).
14. E. I. G. Brown, D. Leaver, and D. M. McKinnon. J. Chem. Soc. (C), 1202 (1970).
15. U. Zoller. *In* A. Hassner. Heterocycl. Compd. **42**, 398 (1983).

Can. J. Chem. Downloaded from www.nrcresearchpress.com by 109.225.110.28 on 09/08/12
For personal use only.

Modeling the effect of Zn(II) on the hydrogen transfer in inhibition processes

ISABEL ROZAS[1] AND GUSTAVO A. ARTECA[2]

Department of Chemistry, University of Saskatchewan, Saskatoon, Sask., Canada S7N 0W0

Received July 24, 1991[3]

ISABEL ROZAS and GUSTAVO A. ARTECA. Can. J. Chem. **70**, 2296 (1992).

We present in this work the results of a rather simplified theoretical approach to some of the processes involved in the inhibition of Zn-containing active sites. Our aim is to calibrate a model in which Zn is replaced by Be. The motivation for this strategy is to provide a qualitatively correct, but fast, approach that can be used in the simulation of many inhibitors interacting with a Zn site. The use of Be allows us to retain some of the essential features of the inhibitor–Zn interaction, while involving much less computation time. It should be noted that we are *not* modeling a Be-containing active site, but processes occurring in a Zn-containing one. We design a scaling transformation that permits us to relate the electronic properties associated with a given Be–ligand distance to the same electronic properties associated with a desired Zn–ligand distance. The results provided by the Be-containing model are comparable to those corresponding to the actual Zn-containing model. One of the processes we are interested in describing here is the effect that the presence of a Zn(II) cation has on the ability of an inhibitor to donate a proton to an acceptor. This process is of importance in the inhibition of Zn-containing enzymes, such as liver alcohol dehydrogenase (LADH). The inhibitory mechanism of LADH seems to involve first the interaction of a ligand with the Zn cation, followed by the transfer of a proton to an acceptor, and finally the binding of the deprotonated ligand to the nicotinamide adenine dinucleotide (NAD^+) coenzyme. In this work, we considered the molecule of formaldehydehydrazone as a model of an inhibitor (e.g., pyrazole). This simplified model contains the strict essentials needed to study proton transfer mediated by a metallic cation. We found a parallelism between the roles of the two metals in the H transfer from this model of inhibitor that allows us to make some qualitative predictions for other processes in Zn from the results obtained exclusively in the presence of Be.

ISABEL ROZAS et GUSTAVO A. ARTECA. Can. J. Chem. **70**, 2296 (1992).

Dans ce travail, on présente les résultats d'une étude théorique assez simplifiée de quelques processus impliqués dans l'inhibition de sites actifs contenant du Zn. Le but du travail est de calibrer un modèle dans lequel le Zn est remplacé par du Be. La motivation de cette stratégie est de fournir une approche qualitativement correcte, mais rapide, qui pourrait être utilisée dans la simulation de plusieurs inhibiteurs qui interagissent avec un site de Zn. L'utilisation du Be permet de retenir quelques-unes des caractéristiques essentielles de l'interaction inhibiteur–Zn tout en demandant moins de temps de calcul. On doit noter que l'on n'examine *pas* un modèle d'un site actif contenant du Be, mais bien les processus se produisant dans un site qui contient du Zn. On a mis au point une transformation scalaire qui permet de relier les propriétés spectroscopiques associées à une distance Be–ligand donnée avec les mêmes propriétés électroniques associées avec une distance donnée Zn–ligand désirée. Les résultats fournis par le modèle contenant du Be sont comparables à ceux correspondants au modèle contenant du Zn. L'un des processus que nous étions intéressés à décrire ici est l'effet de la présence d'un cation Zn(II) sur l'habilité d'un inhibiteur à donner un proton à un accepteur. Ce processus est important dans l'inhibition des enzymes contenant du Zn, comme la déshydrogénase de l'alcool du foie (LADH). Le mécanisme d'inhibition de la LADH semble impliquer au départ une interaction d'un ligand avec un cation Zn, puis le transfert d'un proton vers un accepteur et finalement l'association du ligand déprotoné au coenzyme du dinucléotide de l'adénine nicotinamide (NAD^+). Dans ce travail, on a considéré la molécule d'hydrazone du formaldéhyde comme un modèle d'un inhibiteur (p. ex., pyrazole). Ce modèle simplifié contient le strict minimum requis pour une étude de transfert de proton initié par un cation métallique. On a trouvé un parallélisme entre les rôles des deux métaux sur le transfert d'hydrogène à partir de ce modèle de l'inhibiteur qui nous permet, en se basant uniquement sur des résultats obtenus en présence de Be, de faire quelques prédictions qualitatives pour d'autres processus impliquant du Zn.

[Traduit par la rédaction]

Introduction

In this work we study the interaction between a rather simplified model of pyrazole with Zn(II) and Be(II) cations. The aim is to seek a possible parallelism between the interactions Zn(II)–N and Be(II)–N in order to describe approximately the electronic properties associated with a given Zn(II)–ligand distance from the properties corresponding to a different distance in the computationally more accessible Be(II)–ligand model. The goal is to provide a transformation from the calibrated Be(II) system to the Zn(II) system in which one is actually interested. The motivation for this approach is the appreciable saving of computing time achieved when replacing Zn by Be, especially if the computations are repeated when simulating the behavior of a large number of inhibitors. This approach can be viewed as *a first step* towards the construction of a more detailed (but simplified) model of an actual active site, where the actual ligands at the site are added at a second step.

An application of interest for this Be-calibrated system is found when modeling the more complicated processes occurring in the inhibition of Zn-containing enzymatic active sites. One example of these active sites is found in liver alcohol dehydrogenase (LADH). Essential processes involved in the inhibition of LADH are (*i*) the interaction of a ligand with the metal cation; (*ii*) the transfer of a proton from this ligand to an acceptor, mediated by the presence of the metal. Finally, the binding of the deprotonated ligand to the nicotinamide adenine dinucleotide (NAD^+) coenzyme completes the process (1). Our study of ligand–metal interactions can be relevant to the understanding of the first two processes.

[1]Permanent address: Instituto de Química Médica, C.S.I.C., Juan de la Cierva 3, 28006-Madrid, Spain.

[2]Present address: Département de chimie et biochimie, Université Laurentienne, Chemin du Lac Ramsey, Sudbury, Ont., Canada P3E 2C6.

[3]Revision received February 25, 1992.

Can. J. Chem. Downloaded from www.nrcresearchpress.com by 109.225.110.28 on 09/08/12
For personal use only.

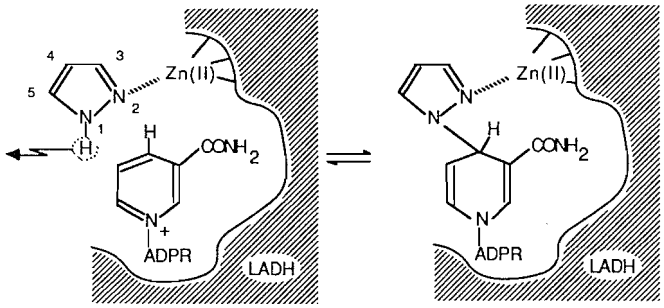

FIG. 1. Scheme of the interaction between LADH, one of its inhibitors (the pyrazole molecule), and the coenzyme NAD^+.

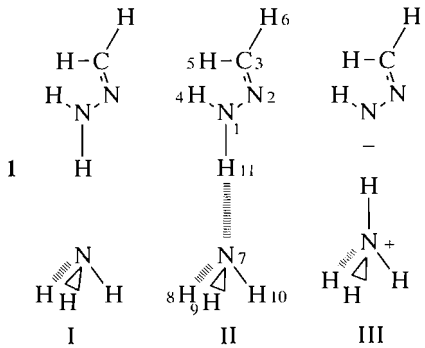

FIG. 2. Proton transfer process between formaldehydehydrazone (1) and ammonia. Structures I, II, and III correspond to the initial arrangement, H-bonded minimum, and final arrangement, respectively.

It has long been known that LADH catalyzes the first step in alcohol metabolism (1*a*). There have been several studies on the structure of the complex LADH–NAD^+ and various inhibitors (2), as well as on their activity. Pyrazole and its derivatives are the strongest inhibitors known for this enzyme (3). They form a strong ternary complex with LADH and NAD^+ (2*a*, 4) (see Fig. 1).

To analyze the effect of the metal cation in the proton transfer process we also studied this step in the absence of the metal. As a model reaction, we considered the molecule of formaldehydehydrazone (a simplified model for pyrazole) as proton donor and ammonia as proton acceptor. The two limiting cases for the proton transfer are given, on the one hand, by the structure where the H is attached to the terminal amine group of formaldehydehydrazone and, on the other hand, by the arrangement involving the NH_4^+ cation (see Fig. 2).

In this approximation to the inhibitor–metal – proton acceptor complex, we look for a relationship between properties that are involved directly in the inhibitor–receptor interaction. These include: N–metal bond order, number of bonding electrons per atom (valency), and atomic charge (5). In a following section we discuss the reaction surface and reaction path for the hydrogen donation. The information obtained from this study is then used to calibrate the Be(II)-containing model that mimics the actual Zn(II)–ligand interaction.

Role of a metal in the proton transfer between formaldehydehydrazone and ammonia

Properties of the system without metals

Formaldehydehydrazone (compound **1**, as shown in Fig. 2) represents a formal "half" of pyrazole (cf. pyrazole in Fig. 1 with compound **1** in Fig. 2). This molecule does not have the aromatic character of pyrazole, but the nature of the interaction with the metal and the geometry for the proton donation can still be described adequately. This is, the intrinsic properties of the inhibitor will be poorly described (due to the absence of a five-membered ring), but this model inhibitor contains all the features needed to describe the N—H···N proton transfer process, which is our aim in this work. To this end, we considered the formaldehydehydrazone molecule as planar, forcing the N(1) atom to adopt an sp^2 hybridization and a geometrical configuration similar to that in pyrazole. All other internal coordinates were optimized.

The calculations were carried out at the *ab initio* level, using the GAUSSIAN 88 series of programs (DEC version) (6), and with the minimal basis set (with polarization functions) STO-3G* (7). This rather small basis set was chosen since we shall later incorporate Zn, and no larger basis set for this system was affordable to us. A more accurate (but costly) description would probably require mixed basis sets (8). To avoid some of the intrinsic problems of the minimal basis set (such as the wrong prediction of single-well reaction barriers for proton transfers (8)), PM3 semiempirical calculations (9) were carried out. For the exploratory analysis performed in this work, these levels of calculation may suffice to indicate the correct qualitative trends in the results.

As a first step, we studied the proton-transfer reaction in this system. A cross section of the reaction surface for this process was calculated at the *ab initio* level, with the STO-3G* minimal basis set (7). This cross section was obtained by calculating the total energy of the system for various placements of the central proton along the N–N internuclear axis. The N(1)—N(7) and N(1)—H(11) distances (Fig. 2) were chosen as the variables defining the cross section. Steps of 0.2 Å were used to compute the cross section. The remaining internal coordinates were optimized, retaining the planarity of the formaldehydehydrazone molecule and orienting the ammonia molecule for a linear transfer of the proton H(11) as shown in Fig. 2.

The linearity in the N—H···N moiety was preserved, since previous calculations in related systems (pyrazole–ammonia (10), ammonium–ammonia (11), pyridine–pyrrole (11*b*)) showed it to be almost or totally linear, a result consistently obtained with basis sets of various qualities.

The cross section obtained for this proton-transfer reaction is represented in Fig. 3. There are two minima corresponding to the limiting states, one when the proton is attached to the formaldehydehydrazone molecule (case I in Fig. 2) and the other when the proton is forming the ammonium cation (case III in Fig. 2). The difference in energy between these two minima is approximately 153.78 kcal mol^{-1} (0.24507 au), at the STO-3G* level of optimization.

Between these two minima, and along the reaction path, we found another shallow minimum, structure II, corresponding to a system type I, in which the interaction between the amine terminal group and the ammonia molecule seems to occur through a hydrogen bond.

This critical point II was localized at the MP2 level of

Can. J. Chem. Downloaded from www.nrcresearchpress.com by 109.225.110.28 on 09/08/12
For personal use only.

Can. J. Chem. Downloaded from www.nrcresearchpress.com by 109.225.110.28 on 09/08/12
For personal use only.

TABLE 1. Geometrical parameters for the minimum II (H-bonded structure) at MP2/STO-3G* and PM3 levels and second minimum found at PM3 level (the "2nd Minimum" refers to the *second* well of the double-well potential for the H-bonded structures, which appears at the PM3 level (minimum II is the *first* well)

	Minimum II(MP2)	Minimum II (PM3)	2nd Minimum (PM3)
Distances (Å)			
C(3)—H(4)	1.101	1.090	1.087
C(3)—H(5)	1.101	1.090	1.087
C(3)—N(2)	1.338	1.298	1.305
N(2)—N(1)	1.402	1.341	1.314
N(1)—H(6)	1.039	0.993	0.999
N(1)—H(11)	1.052	1.011	1.660
N(1)—N(7)	2.785	2.838	2.728
H(11)—N(7)	1.733	1.827	1.068
N(7)—H(8)	1.054	1.000	0.999
N(7)—H(9)	1.054	1.000	0.999
N(7)—H(10)	1.054	1.000	0.999
Angles (degrees)			
H(4)—C(3)—N(2)	117.35	116.99	117.60
H(5)—C(3)—N(2)	124.18	125.90	125.51
C(3)—N(2)—N(1)	114.07	122.74	124.57
N(2)—N(1)—H(6)	120.00	120.00	120.00
N(2)—N(1)—H(11)	120.00	120.00	120.00
N(1)—H(11)—N(7)	180.00	180.00	180.00
H(11)—N(7)—H(8)	110.85	106.33	109.87
H(11)—N(7)—H(9)	117.94	112.32	110.27
H(11)—N(7)—H(10)	117.99	114.05	110.28

TABLE 2. N—N, N—H, and H···N distances in H-bonded systems at different levels of computation

System	N—N	N—H	H···N	Θ(N—H···N)	Basis set
$H_2CNHNH\cdots NH_3$	2.785	1.052	1.733	180.0	MP2/STO-3G*[a]
Pyridine–pyrrole	2.000	—	—	179.0	MINI-1[b]
$H_3CH_2NH^+\cdots NH_2CH_3$	2.51	1.25	1.26	180.0	STO-3G[c]
$H_3CH_2NH^+\cdots NH_2CH_3$	2.75	1.07	1.68	180.0	STO-3G(ABH:6-31G)[c]
$H_3CH_2NH^+\cdots NH_2CH_3$	2.75	1.07	1.68	180.0	6-31G[c]
$H_3NH^+\cdots NH_3$	2.816	1.060	1.756	—	MP4/6-31+G[d]
$H_3NH^+\cdots NH_3$	2.731	1.086	1.645	—	4-31G[e]
$H_3NH^+\cdots NH_3$	2.761	1.074	1.687	—	4-31+G[e]
$H_3NH^+\cdots NH_3$	2.816	1.060	1.756	—	6-31G*[e]
$H_3NH^+\cdots NH_3$	2.716	1.100	1.616	180.0	4-31G[f]
$H_3NH^+\cdots NH_3$	2.817	1.060	1.757	180.0	6-31G[g]
$H_3NH^+\cdots NH_3$	2.846	1.054	1.792	180.0	6-31+G[g]
$H_3NH^+\cdots NH_3$	2.731	1.087	1.644	—	4-31G[h]
$H_2CHNH^+\cdots NH_3$	2.823	1.047	1.776	180.0	4-31G*[i]

[a]This work.
[b]Reference 11*b*.
[c]Reference 8.
[d]Reference 11*a*.
[e]Reference 11*c*.
[f]Reference 11*d*.
[g]Reference 11*e*.
[h]Reference 12.
[i]Reference 11*f*.

calculation. This level of correlation is appropriate to describe H-bonded complexes (11*a*), though in our case the description will be modest due to the use of a minimum basis set. The geometrical parameters characterizing minimum II are shown in Table 1. The results are in good agreement with the values obtained for related systems at different levels of calculation (see Table 2). Moreover, our geometrical parameters are quite close to those of Pardo *et al.* (8) obtained when using a STO-3G (ABH:6-31G) mixed basis set (cf. Table 2). The agreement suggests that a minimal STO-3G* basis set may suffice to extract the essential qualitative features of our system, in spite of its known inadequacy to compare H-transfer reaction barriers (8).

At minimum II, the proton is attached mostly to the ni-

Can. J. Chem. Downloaded from www.nrcresearchpress.com by 109.225.110.28 on 09/08/12
For personal use only.

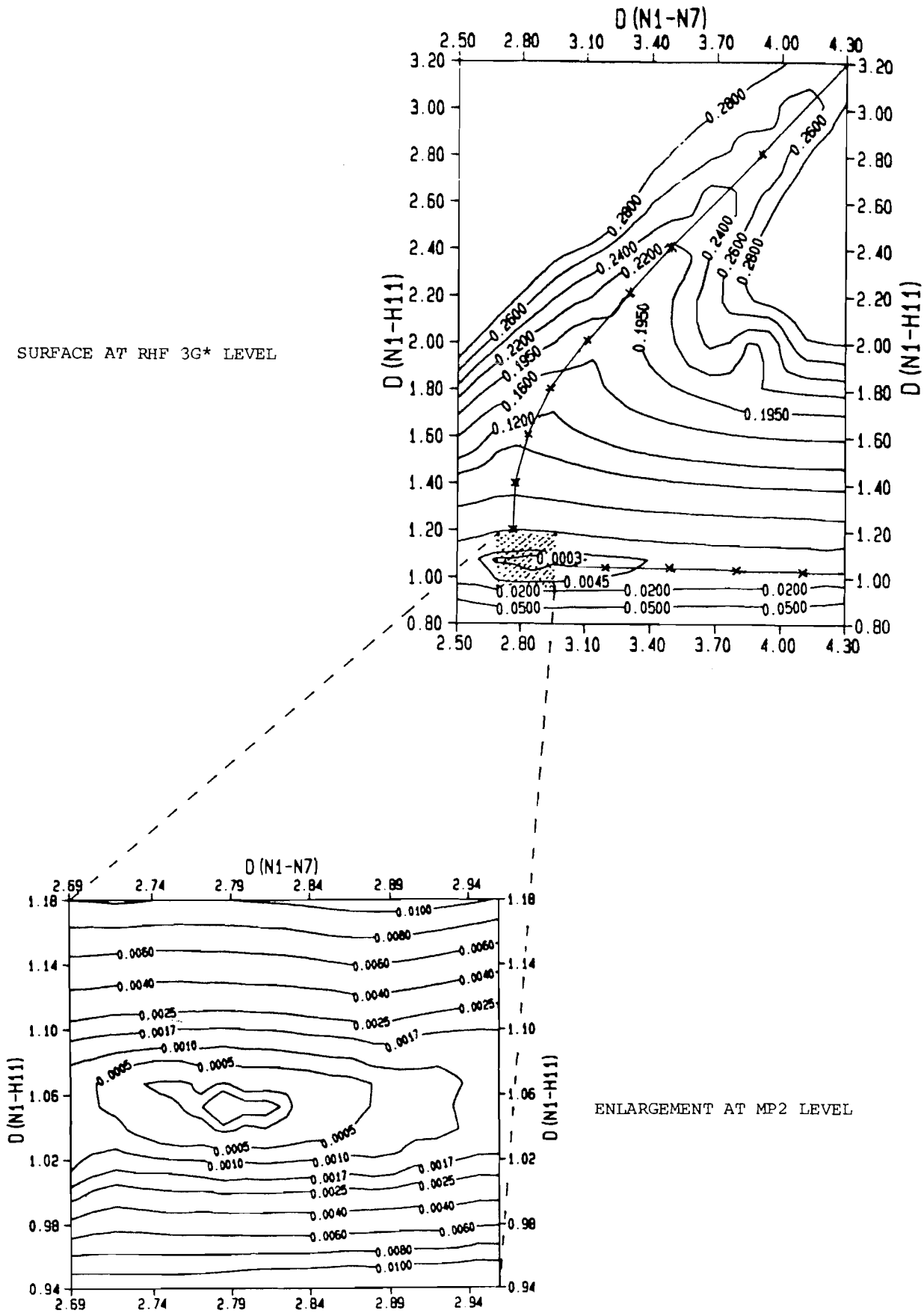

FIG. 3. Cross section of the proton transfer reaction surface at the STO-3G* *ab initio* level of calculation. The reaction path is represented over the cross section. An enlargement at the MP2 level of the area corresponding to the H-bonded minimum (II) is displayed in the graph at the bottom.

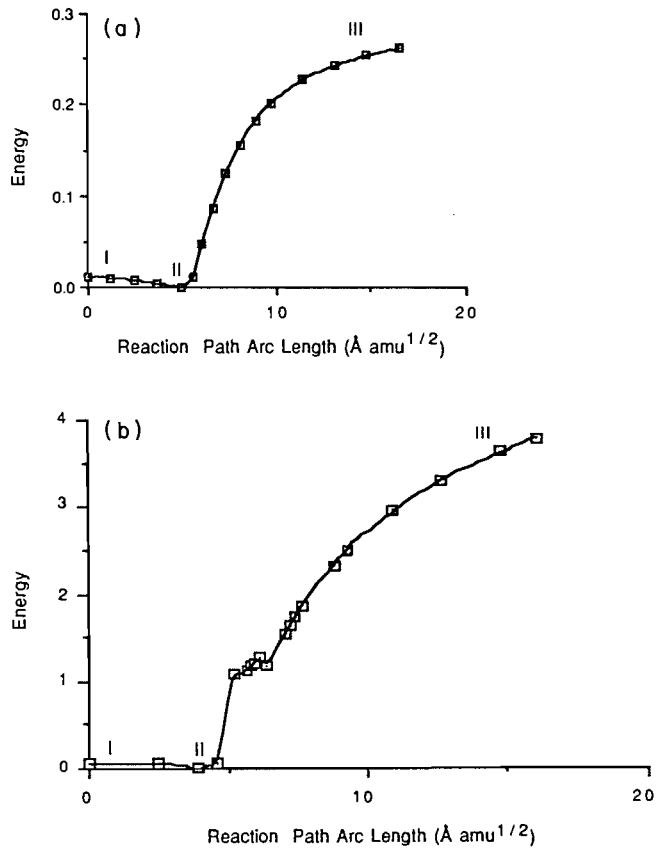

FIG. 4. Energy profiles of the reaction path: (*a*) at the STO-3G* level of calculation; (*b*) at the PM3 level of calculation.

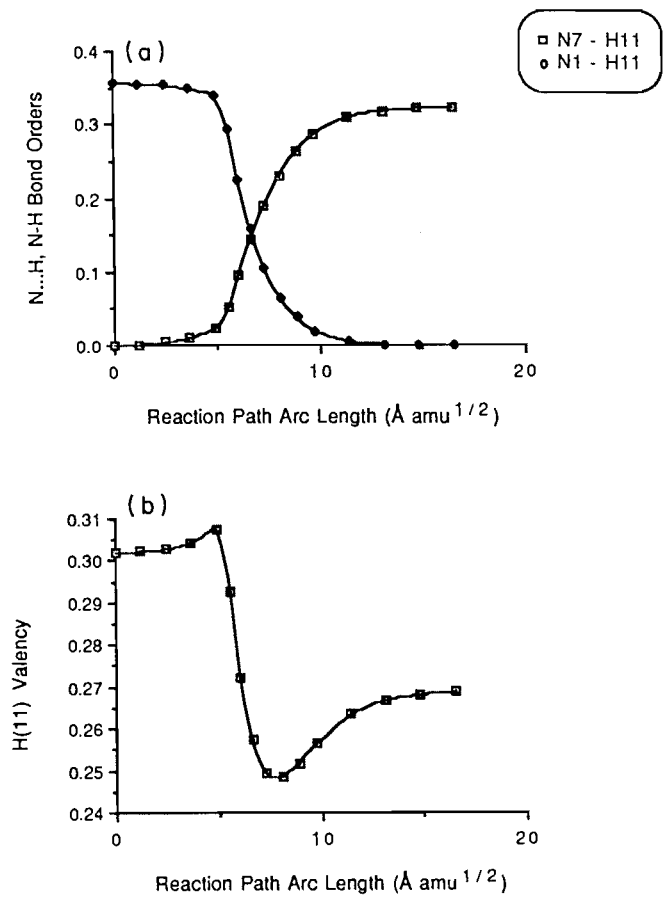

FIG. 5. Variation of (*a*) the N(1)—H(11) and N(7)—H(11) bond orders along the reaction path, and (*b*) the valency. Both properties are calculated at the *ab initio* level.

trogen atom of molecule **1**. This result is in agreement with the fact that hydrogen bridges longer than 2.65 Å are asymmetric (12). The occurrence of an H-bonded minimum in this proton-transfer reaction is not unexpected, since the formation of such a bond is a necessary condition for all proton-transfer processes of the type: $AH\cdots B = A^-\cdots H^+B$, according to Zundel (13).

The most dramatic changes in the electron density (corresponding to N(1) and N(7)) occur along the direction in space defined by the H bond. The electron distribution is distorted differently for each N. The region between N(1) and H(11) increases its electron population, whereas the region between N(7) and H(11) becomes depleted in electron density. This is consistent with the findings of Scheiner (14), and seems to indicate that the presence of an H bond permits the delocalization of the π system from one molecule to the other, a fact that stabilizes the overall system. Our results indicate a stabilization of about 7.15 kcal mol^{-1} (0.0114 au).

Using the cross section of the reaction surface as a starting point, we calculated the corresponding reaction path (Fig. 3), optimizing each point of the path at the MP2 level (*vide supra*). An energy profile is displayed in Fig. 4(*a*).

As was pointed out before, the main failures of the STO-3G* basis set for describing a proton transfer are known to be in the shape of the reaction barrier (8). For a better description of the reaction barrier, we recalculated the reaction path, optimizing each point with the semiempirical program PM3 as implemented in the MOPAC package (9).

At this level of calculation, a double-minima barrier is obtained. The lowest energy minimum is the same structure as minimum II, obtained before using *ab initio* calculations with the minimal basis set. The other minimum corresponds to a complex where H(11) is almost bonded to the ammonia moiety, at 1.99 Å from the N(5) of the formaldehydehydrazone. The interaction between this H(11) atom and the N(5) seems to be more electrostatic than H-bonding. The geometrical parameters of both minima at the PM3 level are shown in Table 1, and the energy profile obtained is displayed in Fig. 4(*b*). It is worth remembering that our main objective is to analyze the role of the metal cations in the proton transfer, and thus only the proton-bonded minimum II is of interest. This structure II appears to have the same geometry at the *ab initio* as well as at the PM3 level. In both cases, structure II is the lowest-lying minimum.

One can gain a deeper insight into the behavior of the model by analyzing other molecular properties along the reaction path. The formation of the N(7)—H(11) bond and the breaking of the N(1)—H(11) bond appear to be simultaneous (see Fig. 5(*a*)) at the *ab initio* level. This last bond seems to be stronger than the N(7)—H(11) bond according to the respective bond order values (0.356 vs. 0.321). This can be explained by the fact that in formaldehydehydrazone there exists a conjugation with a double bond, resulting in a stronger bond to H(11) than to the ammonium cation.

The valency (number of bonding electrons) of H(11) along the reaction path (Fig. 5(*b*)) shows that, at the minimum II, this atom exhibits the maximum bonding to atoms N(1) (by

Can. J. Chem. Downloaded from www.nrcresearchpress.com by 109.225.110.28 on 09/08/12
For personal use only.

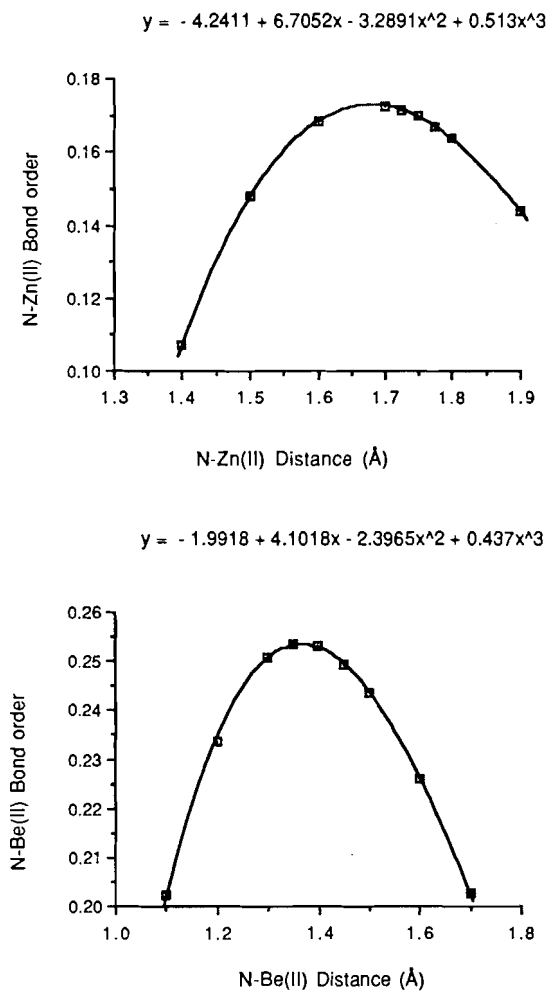

FIG. 6. Curves for Zn(II)—N and Be(II)—N bond orders (obtained by using *ab initio* calculations) as functions of cation–N distances, fitted by least-squares third-degree polynomials for the systems with ammonia as proton acceptor.

a covalent bond) and N(7) (by a hydrogen bond), simultaneously.

Figure 5(*b*) shows a minimum at about 8.0 units of arc length from the reactants. This minimum in valency corresponds to the same structure found to be the second minimum in energy in the PM3 reaction path profile (cf. Fig. 4(*b*)). This fact suggests that in this complex the H(11) atom is the least attached to the rest of the system.

Properties of the systems with Zn(II) and Be(II)

As mentioned before, the inhibition process of LADH by pyrazole is thought to involve first a binding of the N(2) atom of the inhibitor to the Zn(II) cation. After a proton is released from N(1), the unprotonated N(1) atom binds to the nicotinamide ring of the coenzyme (15). Accordingly, the minimum II found above could serve as a model for the interaction of pyrazole with the metal cation, *at the moment of transferring the proton to an acceptor, a separate step that takes place before the binding of the pyrazole anion to the* NAD^+.

It is known that LADH still maintains a catalytic activity if the Zn(II) cation is substituted by Co(II), Cd(II), Ni(II), and Fe(II) (16, and refs. therein). Reconstruction of the enzyme was also possible with Cu(II), Fe(III), and Pb(II), but in these cases the activity is lost (16). One could argue whether our Be(II) model would simulate a Zn(II)- or Be(II)-containing enzyme. A real Be(II)-containing LADH would be inactive. Our aim is not to approximate this latter enzyme, but to construct a simple, "artificial" model with Be(II) that deviates from an actual Be-containing system, but whose behavior would be similar to the natural Zn(II) in the active site.

The simulation of a Zn(II) cation in the active site of an enzyme by a Be(II) cation has been used before. In MO studies of the enzymatic activity of carboxypeptidase A (17), the $[Be(OH)(NH_3)_2]^+$ complex was used to simulate the catalytic Zn(II) coordinated with two histidines and one glutamate. Scheiner and Lipscomb (17) concluded that these electrophiles may serve as an adequate model for the Zn(II) and its ligands in carboxypeptidase A. Moreover, the authors suggested that the *d*-orbitals of Zn might not be fully involved in forming a complex with the substrate. However, Osman and Weinstein (18) carried out a comparative study of Zn(II)- and Be(II)-containing complexes (in order to study the active center of metalloenzymes, as carboxypeptidase and carbonic anhydrase), and concluded that the transition metals seem to play a special role in these biological systems.

In our present case, the metallic cations (Zn(II) or Be(II)) were situated on the same plane as the formaldehydehydrazone. This approach is suggested by results in the literature. For example, the interaction between Zn(II) and imidazole (related to pyrazole) occurs in an energetically favoured planar geometry (19). Consequently, the metal atom was located along the lone pair of N(2) of formaldehydehydrazone.

We studied the systems with Zn(II) and Be(II) at both *ab initio* (using the STO-3G* basis set) and semiempirical (using the program PM3) levels. In these systems, we used the optimized parameters of minimum II, keeping the planarity of the formaldehydehydrazone moiety and the linearity of the H bond. The rest of the internal coordinates were optimized, including those describing the shifting hydrogen. This analysis was repeated for various N(2)–metal distances.

The effect of the N(2)–metal interaction on various properties (bond order, valency, and atomic charge of N(2), Zn(II), and Be(II)) was studied using the STO-3G*. Third-degree polynomials were fitted to each set of data. Results are shown in Figs. 6–8.

The maximum values of bond order (Fig. 7) obtained for N(2)–metal cations are collected in Table 3. An important feature appears in these complexes: *the interaction N(2) – metal cations produces the H transfer from the N(1) of the formaldehydehydrazone to the ammonia molecule.* Thus, starting from the geometrical arrangement of minimum II (neutral molecules linked by an H bond) the interaction with Zn(II) and Be(II) ions generates complexes where the central H(11) forms part of the ammonium cation (see the N—N and N—H distances in Table 4).

Using the N–metal(II) distances obtained for the maximum bond order at the *ab initio* level we calculated the cationic complex using the program PM3. The same H transfer is observed from the formaldehydehydrazone to the ammonia molecule. In addition, the ammonium cation is shifted away from the formaldehydehydrazone–metal(II) complex (see the obtained geometrical parameters in Table 4).

The fact that the approach of a cation can facilitate a pro-

Can. J. Chem. Downloaded from www.nrcresearchpress.com by 109.225.110.28 on 09/08/12
For personal use only.

Can. J. Chem. Downloaded from www.nrcresearchpress.com by 109.225.110.28 on 09/08/12
For personal use only.

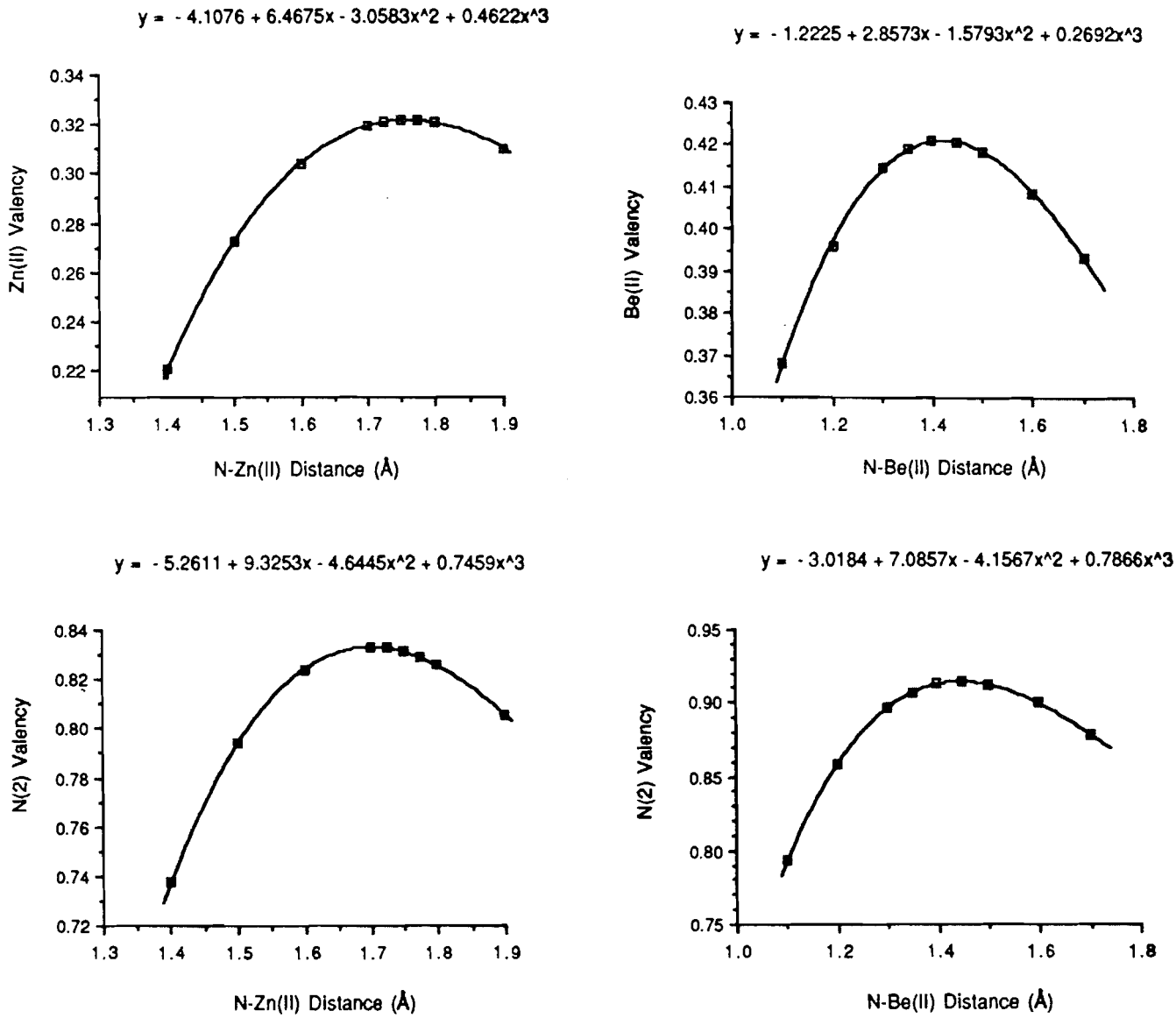

FIG. 7. Curves for N(2), Zn(II), and Be(II) valencies (obtained by using *ab initio* calculations) as functions of cation–N distances, fitted by least-squares third-degree polynomials for the systems with ammonia as proton acceptor.

ton transfer has been observed before for systems other than N—H···N (20). In refs. 20, it was noted that the interaction of Li^+ and Na^+ with an N or an O atom causes the release of an H directly bonded to these atoms. In our case, doubly charged cations of a very different nature, such as Zn(II) and Be(II), induce the transfer of an N-bonded H atom to the proton acceptor.

The effect of Zn(II) in facilitating deprotonation has been observed in imidazole and also in water (21). On the other hand, studies carried out on the role of zinc in LADH show that Zn(II) could be essential for the catalytic action of this enzyme but only in the H-transfer step (22). The results obtained in our calculations are in agreement with this model.

This effect of the metal interaction was observed for both cations and at different levels of calculation, which gives support to the use of Be(II) instead of Zn(II) for subsequent computations.

The maxima of valency (Fig. 7) obtained for Zn(II) and Be(II), using the STO-3G* basis set, are displayed in Table 3 together with the maximum valency for the N(2) atom when interacting with the cations. As expected, larger values are obtained for N(2) due to the multiple bonding of this atom.

The change in the atomic charges as a function of N(2)–metal distances is shown in Fig. 8. The values corresponding to the maxima appear in Table 3.

We conclude that the presence of a proton acceptor makes the whole system more conjugated, and the presence of cations facilitates the H-transfer process to the acceptor (ammonia).

Quantitative relationships between the systems with different metal cations

From the results discussed in the previous sections, it is clear that, to a certain extent, our system with Be(II) behaves similarly to that with Zn(II). In this section we establish a quantitative relationship between the two systems that

Can. J. Chem. Downloaded from www.nrcresearchpress.com by 109.225.110.28 on 09/08/12
For personal use only.

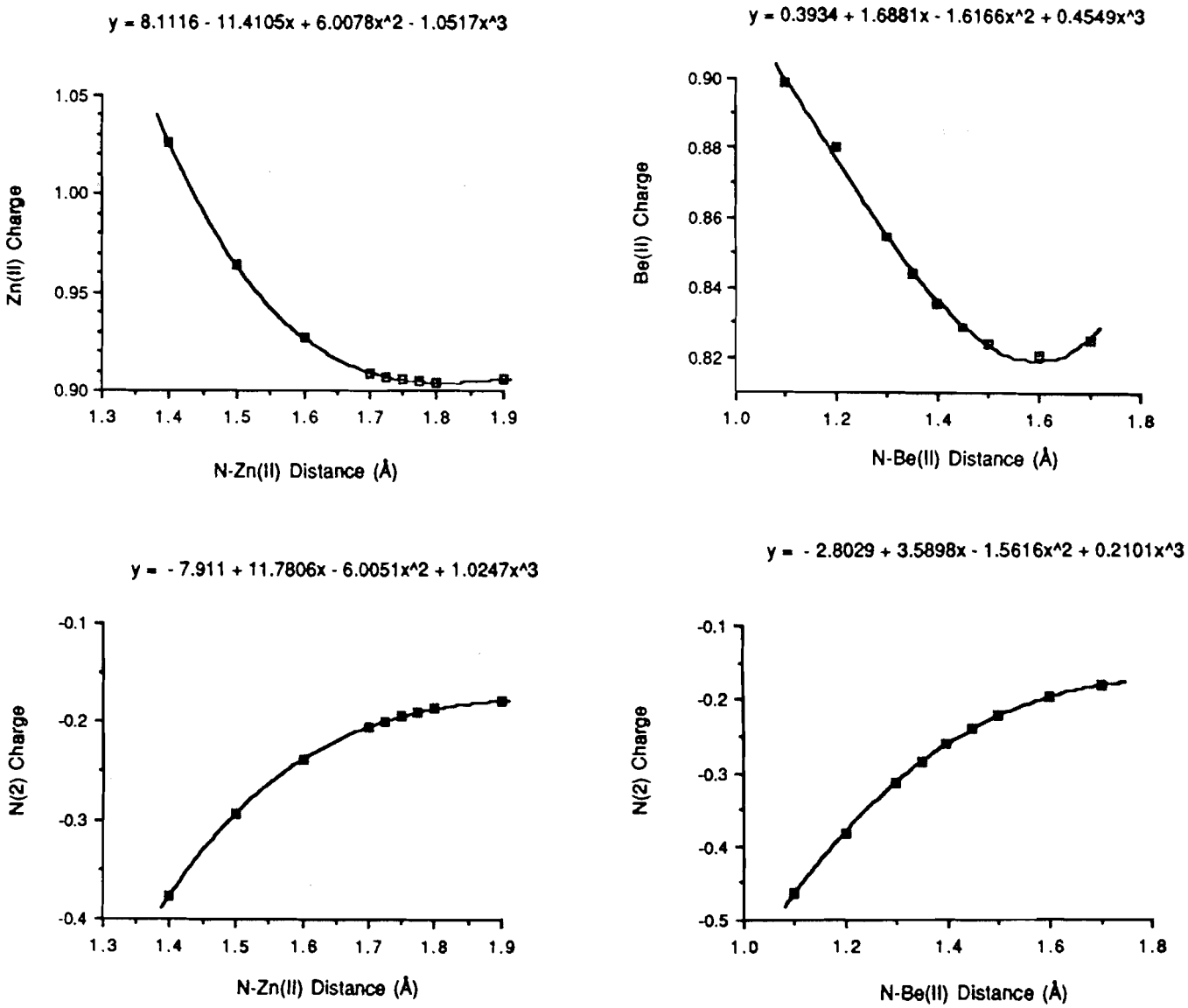

FIG. 8. Curves for N(2), Zn(II), and Be(II) atomic charges (obtained by using *ab initio* calculations) as functions of cation–N distances, fitted by least-squares third-degree polynomials for the systems with ammonia as proton acceptor.

allows us to calibrate a Be(II)-containing model to predict the results in the more costly Zn(II) system.

The approach we follow here is suggested by the fact that the properties of the systems with Zn(II) and Be(II) ions are similar and approximately derivable from one another by appropriate scaling. Thus, starting from a known N—Zn(II) distance (x_1) (the one for the enzyme–inhibitor system), and by taking a scaling factor β, we obtain the corresponding N—Be(II) distance (x_2). With this value x_2, we can determine the approximate property value (y_2) for the Be(II) system and use this to obtain the approximate property value (y_1) for Zn(II) system as follows:

$$x_2 = x_1\,\beta; \qquad y_1(x_1) = \alpha\, y_2(\beta\, x_1)$$

The numerical computation of the α and β parameters is discussed in the Appendix. Taking the bond order as the property y_2, the correlation between the Zn(II) and the Be(II) systems is satisfactory ($J = 3.59 \times 10^{-2}$). The α and β values obtained (2.0817 and 0.7984, respectively) give a good description of this property for Zn(II) by using only Be(II) results. The correlations obtained for the valency are not so good (J\{Zn(II),Be(II)\} = 0.2360 and J\{N[Zn(II)],N[Be(II)]\} = 0.1106). In contrast, the values obtained for the charge of N(2) correlate quite well ($J = 7.75 \times 10^{-3}$). The α and β values in this latter case are 2.8142 and 1.1685, respectively.

According to these results, both the bond order between the cations and the N(2) atom of pyrazole, as well as the atomic charge of N(2), are adequate properties to correlate the effects of Zn(II) and Be(II).

Conclusions

According to the results, the following conclusions are reached:

1. A minimum corresponding to an H-bonded formaldehydehydrazone – proton acceptor model in the cross section

Can. J. Chem. Downloaded from www.nrcresearchpress.com by 109.225.110.28 on 09/08/12
For personal use only.

TABLE 3. Bond orders, valencies, and atomic charges as a function of the N(2)—metal distance for the system with ammonia as proton acceptor. The results correspond to *ab initio* calculations. In the case of atomic charges, only the ranges are provided since the charge does not exhibit an extremum over the range of distances studied

	Maximum bond order	N(2)–metal distance (Å)
N(2)—Zn(II)	0.1725	1.700
N(2)—Be(II)	0.2537	1.350

	Maximum valency	N(2)–metal distance (Å)
Zn(II)	0.3218	1.750
Be(II)	0.4212	1.400
N(2)···(Zn(II))	0.8332	1.700
N(2)···(Be(II))	0.9140	1.450

	Range of atomic charges	Range of N(2)–metal distance
Zn(II)	1.0262– 0.9058	1.400–1.900
Be(II)	0.8986– 0.8252	1.100–1.700
N(2)···(Zn(II))	−0.3765–−0.1781	1.400–1.900
N(2)···(Be(II))	−0.4635–−0.1807	1.100–1.700

TABLE 4. N—N and N—H distances (in Å) between the three atoms characterizing the linear H-transfer complex, in the case of ammonia interacting with the Zn(II) and Be(II) cations (minimum II). The STO-3G* basis set and PM3 program were used

d{N(2)–**Zn**(II)}	*d*{N(1)–N(7)}	*d*{N(1)–H(11)}	*d*{N(7)–H(11)}
1.400	2.603	1.475	1.128
1.500	2.608	1.481	1.127
1.600	2.614	1.489	1.125
1.700	2.633	1.516	1.118
1.725	2.623	1.501	1.121
1.750	2.625	1.503	1.121
1.775	2.627	1.506	1.121
1.800	2.629	1.509	1.120
1.900	2.640	1.524	1.116
1.700 (PM3)	6.469	5.468	1.001
d{N(2)–**Be**(II)}	*d*{N(1)–N(7)}	*d*{N(1)–H(11)}	*d*{N(7)–H(11)}
1.100	2.847	1.778	1.069
1.200	2.811	1.737	1.074
1.300	2.812	1.738	1.075
1.350	2.816	1.742	1.074
1.400	2.822	1.748	1.074
1.450	2.830	1.756	1.074
1.500	2.838	1.765	1.073
1.600	2.854	1.782	1.072
1.700	2.875	1.805	1.070
1.350 (PM3)	17.797	16.798	0.999
Minimum II	2.785	1.052	1.733

of the corresponding reaction surface was found at the STO-3G* level and characterized. As stated before, formaldehydehydrazone simulates pyrazole as an inhibitor.

2. By using the semiempirical program PM3, a double-well energy profile is obtained. The minimum of lowest energy corresponds with the H-bonded structure obtained at the *ab initio* level. The other minimum obtained shows a non-symmetrical ammonium cation electrostatically attracted to the formaldehydehydrazone anion.

3. Whereas a single minimum was found for the proton transfer at the STO-3G* level, the geometrical description we obtained for the N—H···N hydrogen bond is satisfactory. This result is comparable with those obtained in the literature for other related systems with larger basis sets. In this work we were mostly interested in the effect of a metal on this H-bonded structure. We believe that the minimal basis set STO-3G* should be sufficient to extract these qualitative features correctly.

4. The main result that we found, at both *ab initio* and semiempirical levels, is the effect of the Zn(II) and Be(II) cations on the model inhibitor – ammonia complex. Our results suggest that the presence of these cations causes the transfer of a proton, covalently bonded to the inhibitor (and hydrogen-bonded to ammonia), to the proton acceptor. A similar mechanism was postulated to take place in the natural inhibition of LADH by pyrazole and related compounds. It is remarkable that this crucial feature is already present in a model as simplified as the present one.

5. The results obtained for Zn(II) and Be(II) show a close parallelism of their effect on the model inhibitor – proton acceptor system. A quantitative expression of this effect has been given in terms of the properties of the interacting metal and nitrogen atoms. We have shown how to interrelate the functional dependences on the N(2)–metal distance for two properties (N(2) – metal bond order and charge on N(2)) for the two metallic systems. We developed a scaling procedure that allows us to find the distance at which a Be(II) cation produces an effect similar to the effect exhibited by the Zn(II) ion. This relationship opens the possibility of replacing the more computationally demanding Zn metal by Be in studies of larger molecular systems, and still retain the correct qualitative behavior.

Acknowledgments

The authors would like to thank Prof. Paul G. Mezey for helpful discussions. This work has been supported by both operating and strategic research grants from the Natural Sciences and Engineering Research Council (NSERC) of Canada. One of us (I.R.) would like to acknowledge financial support of the Consejería de Educación of the Comunidad de Madrid, Spain, and the World University Service of Canada (WUSC).

1. (*a*) R. W. Fries, D. P. Bohlken, and B. V. Plapp. J. Med. Chem. **22**, 356 (1979); (*b*) H. Eklund, B. Nordström, E. Zeppezauer, G. Söderlund, I. Ohlsson, T. Boiwe, B. Söderberg, O. Tapia, C.-I. Brändén, and Å Åkeson. J. Mol. Biol. **102**, 27 (1976); (*c*) C.-I. Brändén and H. Jörvall. *In* Dehydrogenases requiring nicotinamide coenzyme. *Edited by* J. Jeffery. Birkhäuser Verlag, Basel. 1980. pp. 40–84; (*d*) O. Tapia, R. Cárdenas, J. Andrés, J. Krechl, M. Campillo, and F. Colonna-Cesari. Int. J. Quantum Chem. **39**, 767 (1991).
2. (*a*) H. Eklund, J.-P. Samana, and L. Wallén. Biochemistry, **21**, 4858 (1982), and references therein; (*b*) E. Horjales, H. Eklund, and C.-I. Brändén. J. Mol. Biol. **197**, 685 (1987).
3. B.-R. Tolf, R. Dahlbom, H. Theorell, and Å. Åkeson. Acta Chem. Scand. Ser. B: **B36**, 101 (1982).
4. (*a*) H. Theorell, T. Yonetani, and B. Sjöberg. Acta Chem. Scand. **23**, 255 (1969); (*b*) H. Theorell and T. Yonetani. Biochem. Z. **338**, 537 (1963); (*c*) B.-R. Tolf, T. Siddiqui, R.

Dahlbom, Å. Åkeson, and H. Theorell. Eur. J. Med. Chem. **17**, 395 (1982); (*d*) B.-R. Tolf, R. Dahlbom, Å. Åkeson, and H. Theorell. Acta Pharm. Suec. **22**, 147 (1985).
5. (*a*) D. R. Armstrong, P. G. Perkins, and J. J. Stewart. J. Chem. Soc. **833**, 2273 (1973); (*b*) M. S. Gopinathan and K. Jug. Theor. Chim. Acta, **63**, 497 (1983).
6. M. J. Frisch, M. Head-Gordon, H. B. Schlegel, *et al.* GAUSSIAN 88. Gaussian, Inc., Pittsburgh, Pa. 1986.
7. J. B. Collins, P.v.R. Schleyer, J. S. Binkley, and J. A. Pople. J. Chem. Phys. **64**, 5142 (1976).
8. L. Pardo, A. P. Mazurek, and P. Osman. Int. J. Quantum Chem. **37**, 701 (1990).
9. MOPAC (6.0): QCPE program 455, Department of Chemistry, Indiana University, Bloomington, Indiana. PM3 parameters: J. J. P. Stewart. J. Comput. Chem. **12**, 320 (1991).
10. O. Mó, M. Yáñez, and J. Elguero. J. Org. Chem. **52**, 1713 (1987).
11. (*a*) J. E. Del Bene. J. Comput. Chem. **10**, 603 (1989); (*b*) M. Foucrault, P. Hobza, and C. Sandorfy. J. Mol. Struct. (Theochem), **152**, 11 (1987); (*c*) H. Z. Cao, M. Allavena, O. Tapia, and E. M. Evleth. J. Phys. Chem. **89**, 1581 (1985); (*d*) P. J. Desmeules and L. C. Allen. J. Chem. Phys. **72**, 4731 (1980); (*e*) J. E. Del Bene, M. J. Frisch, and J. A. Pople. J. Phys. Chem. **89**, 3669 (1985); (*f*) E. A. Hillenbrand and S. Scheiner. J. Am. Chem. Soc. **107**, 7690 (1985).
12. Z. Malarski and K. L. Sobczy. J. Mol. Struct. **177**, 339 (1988).
13. G. Zundel. J. Mol. Struct. **177**, 43 (1988).
14. S. Scheiner. J. Phys. Chem. **86**, 376 (1982).
15. (*a*) O. Tapia, C.-I. Brändén, and A.-M. Armbruster. *In* Quantum theory of chemical reactions. Vol III. *Edited by* R. Daudel, A. Pullman, L. Salem, and A. Viellard. D. Reidel Publishing Co., Dordrecht. 1982. pp. 97–123; (*b*) O. Tapia. J. Mol. Catal. **47**, 199 (1988).
16. M. Zeppezauer. *In* The coordination chemistry of metalloenzymes. *Edited by* I. Bertini, R. S. Drago, and C. Luchinat. D. Reidel Publishing Co., Dordrecht. 1983. pp. 99–122.
17. S. Scheiner and N. Lipscomb. J. Am. Chem. Soc. **99**, 3466 (1977).
18. R. Osman and H. Weinstein. Isr. J. Chem. **19**, 149 (1980).
19. D. Demoulin and A. Pullman. Theor. Chem. Acta, **49**, 161 (1978).
20. (*a*) B. M. Rode. Theor. Chim. Acta, **56**, 245 (1980); (*b*) B. M. Rode and K. P. Sagarik. Chem. Phys. Lett. **88**, 337 (1982); (*c*) S. Scheiner, P. Redfern, and M. M Szczesniak. J. Phys. Chem. **89**, 262 (1985); (*d*) J. Parra-Mouchet, W. H. Fink, and C. P. Nash. J. Phys. Chem. **89**, 524 (1985).
21. D. Demoulin, A. Pullman, and B. Sarkar. J. Am. Chem. Soc. **99**, 8498 (1977).
22. I. Iweibo and H. Weiner. Biochemistry, **11**, 1003 (1972).

Appendix

Consider two comparable molecular systems, which we shall label as 1 and 2. In our case, these systems will be the inhibitor – proton acceptor complexes in the presence of Zn(II) and Be(II) cations, respectively. The properties of these systems have been studied in the text as functions of the distance between the N(2) of the model inhibitor and the metal ions. In this appendix we discuss how to establish and characterize a quantitative relationship between the two systems.

Let x_1 and x_2 be the N(2)—Zn(II) and N(2)—Be(II) distances, respectively. Consider now a given molecular property in both systems. As discussed in the text, the N(2)–metal bond order and the charge on the N(2) atom appear to be relevant properties to compare the two systems, since they have similar qualitative behavior with the changes in the metal–ligand distances. Let $y_1(x_1)$ and $y_2(x_2)$ be any of these molecular properties, for systems 1 and 2, respectively. For simplicity, we shall represent these properties as polynomials,

$$[1] \quad y_1 = \sum_{s=0}^{N} c_s x_1^s, \qquad y_2 = \sum_{s=0}^{N} a_s x_2^s$$

an approximation that holds reasonably well within a large range of interatomic distances x_1 and x_2. The form of the relation we intend to use is given as:

$$[2] \quad y_1(x_1) \approx \alpha\, y_2(\beta\, x_1)$$

Our goal is to determine a set of two constants α and β, that would allow us to approximate a function value for one polynomial by knowing only a function value for the other one. In other words, if a property y_2 is known for the beryllium system at a N(2)–Be(II) distance x_2, then the same property will have an approximate value $\alpha y_2(x_2)$ for the zinc system at an N(2)–Zn(II) distance equal to x_2/β.

We proceed by least-squares fitting to obtain the best α and β values for eq. [2]. From eqs. [1] and [2], we minimize the following function:

$$[3] \quad J(\alpha,\beta) = \sum_{s=0}^{N} (\alpha\, a_s\, \beta^s - c_s)^2$$

over changes in the variables α and β. Solving for $\partial J/\partial\alpha = 0$, we obtain an expression for α as a function of β. Introducing this result into the equation $\partial J/\partial\beta = 0$, we obtain an algebraic equation for β:

$$[4] \quad \sum_{k=0}^{3N-1} \beta^k\, b_k = 0$$

with the coefficients b_k given as:

$$[5] \quad b_k = \sum_{i=0}^{\mathrm{int}((k+1)/2)} (k + 1 - 3i)\, a_i^2\, a_{k+1-2i}\, c_{k+1-2i}$$

The upper limit in the sum in eq. [5] stands for the integer part of $(k + 1)/2$. It is easily proven that $b_{3N-1} = 0$.

In the actual application we obtained numerically all the positive real roots of eq. [5] for $N = 3$ and selected the one leading to the smallest $J(\alpha,\beta)$. With this β value we immediately calculate the corresponding α value. The results obtained and the quality of the description of the Zn(II) system in terms of the analogous Be(II) system are discussed in the text.

Can. J. Chem. Downloaded from www.nrcresearchpress.com by 109.225.110.28 on 09/08/12
For personal use only.

Étude des conditions de la réaction de condensation de Claisen–Schmidt de la furylméthylcétone sur le 2,5-furanedicarboxaldehyde

CARMEN DOMINGUEZ ET JOAQUÍN PLUMET

Departamento de Química Orgánica I, Facultad de Ciencias Químicas, Universidad Complutense de Madrid, 28040 Madrid, Spain

ET

ANTOINE GASET ET LUC RIGAL[1]

Laboratoire de chimie des agroressources, École nationale supérieure de chimie, 118, route de Narbonne, 31077 Toulouse CÉDEX, France

Reçu le 3 décembre 1991

CARMEN DOMINGUEZ, JOAQUÍN PLUMET, ANTOINE GASET et LUC RIGAL. Can. J. Chem. **70**, 2306 (1992).

La réction de condensation de Claisen–Schmidt du 2,5-furanedicarboxaldéhyde (FDC) sur la furylméthylcétone (FMC) conduit à trois produits différents en fonction des conditions opératoires. L'influence de cinq facteurs sur l'orientation de cette réaction est étudiée grâce à la réalisation d'un plan factoriel fractionnaire à deux niveaux.

CARMEN DOMINGUEZ, JOAQUÍN PLUMET, ANTOINE GASET, and LUC RIGAL. Can. J. Chem. **70**, 2306 (1992).

The Claisen–Schmidt reaction of 2,5-furandicarboxaldehyde (FDC) with 2-acetylfuran allows for the synthesis of three products as a function of the reaction conditions. The main effects of five factors and their interaction effects on seven responses have been quantified by means of a fractional factorial design.

Introduction

La réaction de Claisen–Schmidt permet une conversion aisée des composés carbonylés en alcools et doubles liaisons éthyléniques dans des conditions, en général, très douces (1). Cette caractéristique est particulièrement intéressante dans le cas de certains aldéhydes issus de la biomasse, à cause de l'instabilité et du craactère polyfonctionnel de ces dérivés. C'est le cas du 2,5-furanedicarboxaldéhyde (FDC), synthétisé directement à partir du D-fructose (2). Celui-ci, grâce à la combinaison de deux fonctions aldéhyde sur un cycle furanique, apparaît comme un intermédiaire très important pour la synthèse d'un grand nombre de dérivés furaniques bifonctionnalisés en positions 2 et 5, qui trouvent des applications dans des domaines aussi variés que la pharmacie ou les macromolécules (3). Par ailleurs, la possibilité de fonctionnalisation non symétrique de cette molécule (fonctionnalisation sélective d'une seule fonction aldéhyde) élargit encore les possibilités de synthèse (4).

Pour notre part, nous avons étudié la réaction de condensation de Claisen–Schmidt du FDC avec plusieurs cétones aromatiques et hétéroaromatiques (5), en milieu basique, conduisant à des dérivés symétriques ou dissymétriques, selon les conditions de réaction mises en oeuvre :

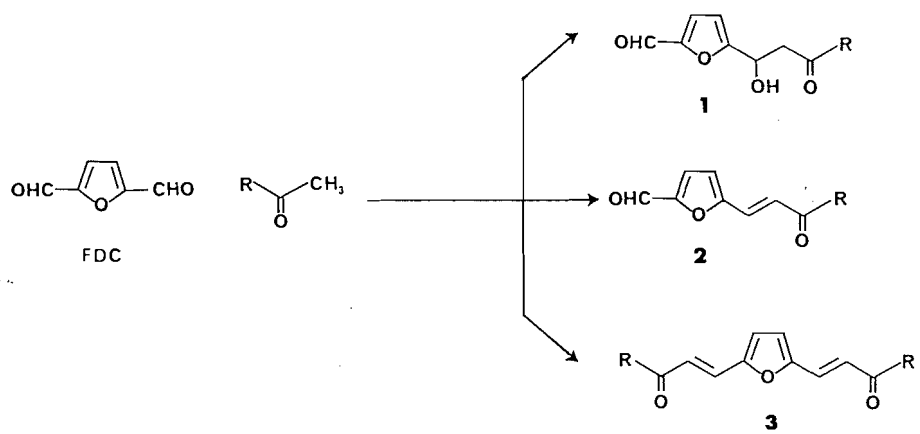

a, R = C_6H_4; *b*, R = *p*-MeO-C_6H_4; *c*, R = *p*-NO_2-C_6H_4; *d*, R = 2-thienyl; *e*, R = 2-furyl

SCHÉMA 1

Les résultats obtenus lors des essais préliminaires ont permis d'envisager l'influence de cinq facteurs sur l'orientation de la réaction : A, rapport molaire FDC/cétone; B, concentration de NaOH dans le milieu réctionnel: C, concentration du FDC dans le milieu réactionnel; D, rapport $EtOH/H_2O$ (solvant); E, température.

L'objectif de ce travail est d'étudier l'influence des différents facteurs sur la réaction du FDC avec la furylméthylcétone (FMC) afin de déterminer les conditions d'obtention de chacun des produits **1***e*, **2***e* et **3***e* avec le meilleur rendement et la plus haute sélectivité. Le choix de la furylméthylcétone (FMC) (5) se justifie par l'intérêt des

[1]Auteur à qui adresser toute correspondance.

Can. J. Chem. Downloaded from www.nrcresearchpress.com by 109.225.110.28 on 09/08/12
For personal use only.

Can. J. Chem. Downloaded from www.nrcresearchpress.com by 109.225.110.28 on 09/08/12
For personal use only.

dérivés obtenus en tant que molécules à activité biologique et comme intermédiaires de synthèse furaniques.

Partie expérimentale

Les points de fusion ont été mesurés à l'aide d'un appareil Büchi-510 et ils ne sont pas corrigés. Les spectres infra-rouges ont été réalisés sur un spectrophotomètre Perkin–Elmer 298. Les spectres RMN du ^1H ont été enregistrés au moyen d'un appareil Varian T60 A à 60 MHz avec le tétraméthylsilane comme référence interne. Les spectres RMN du ^{13}C ont été réalisés sur un appareil Varian FT 80A.

Le FDC a été synthétisé selon un procédé original mis au point au laboratoire (2).

Synthèse des produits **1***e*, **2***e et* **3***e*

Dans un ballon de 25 mL muni d'une agitation magnétique, et thermostaté à 0°C, on dissout le FDC (250 mg, 2 mmol) dans l'éthanol (8 mL), on ajoute la furylméthylcétone (220 mg, 2 mmol) et une solution de NaOH à 10% (0.5 mL). Après 1 h de réaction à 0°C, on neutralise avec une solution de H_2SO_4 à 10%. Le milieu réactionnel est ensuite extrait trois fois avec du chlorure de méthylène. Après évaporation des solvants organiques, on sépare les différents constituants par chromatographie sur colonne de silicagel 60 (Merck) comme phase stationnaire et un mélange acétate d'éthyle/hexane (1 : 2) comme éluant.

5-[2-(2-Furoyl)-1-hydroxyéthyl]-2-furanecarboxaldéhyde **1***e* : IR(CCl_4). ν : 3400, 1690 cm^{-1}. RMN du ^1H ($CDCl_3$)[1]. δ : 9.51 (s, 1H, CHO), 7.52(d, 1H, J = 2.0 Hz H12), 7.12–7.10(m, 2H, H3, H10), 6.54–6.41(m, 2H, H4, H11), 5.32(t, 1H, J = 5.9 Hz, H6), 3.42(d, 2H, J = 5.9 Hz, H7) ppm.

(E)-5-(2-Furoylvinyl)-2furanecarboxaldehyde **2**e : P_f : 140–142°C (AcOEt) IR(KBr), ν : 1690, 1660 cm^{-1}. RMN du $^1H(CDCl_3)$[2] δ : 9.90(s, 1H, CHO), 7.71(d, 1H, J = 1.9 Hz, H12), 7.62(s, 2H, H6, H7), 7.42(d, 1H, J = 4.1 Hz, H3), 7.31(d, 1H, J = 4.1 Hz, H10), 6.90(d, 1H, J = 4.1 Hz, H4), 6.70(dd, 1H, $J_{10,11}$ = 4.1 Hz, $J_{11,12}$ = 1.9 Hz, H11) ppm. Anal. calc. pour $C_{12}H_8O_4$: C 66.67, H 3.74; tr. : C 66.96, H 3.59.

(E, E)-2,5-Di-[2-(2-furoly)vinyl]furane **3**e : P_f : 170–171°C (EtOH) IR(KBr), ν : 1590, 1645 cm^{-1}. RMN du $^1H(CDCl_3)$, δ : 7.66(d, 2H, J = 2.2 Hz, H9), 7.56, 7.44(AB_q, 4H, J = 14.9 Hz, CH=CH−CO), 7.35(d, 2H, J = 3.5 Hz, H7), 6.78(s, 2H, H1), 6.59(dd, 2H, $J_{8,9}$ = 2.2 Hz, $J_{7,8}$ = 3.5 Hz, H8) ppm.

RMN du ^{13}C ($CDCl_3$), δ: 177.39(C5), 153.67(C6), 153.49(C2), 146.82(C9), 128.98(C4), 120.95(C3), 118.61(C1), 117.87(C7), 112.74(C8) ppm. Anal. calc. pour $C_{18}H_{12}O_5$: C 70.13, H 3.93; tr. : C 70.06, H 3.87.

Analyses quantitatives des milieux réactionnels

Le milieu réactionnel est dosé par chromatographie liquide haute performance (CLHP) dans les conditions suivantes :

Appareil : Perkin–Elmer series 2 avec détecteur UV (λ : 296 nm)
Colonne : LCD 24051 Milton Roy, Spherisorb 5CN (longueur : 25 cm, diamètre interne : 4.6 mm)
Eluant : Acétate de méthyle/hexane (2 : 3)
Débit d'éluant : 0.4 mL/min.

La courbe d'étalonnage est établie pour le FDC, la furylméthylcétone et les produits **1***e*, **2***e* et **3***e* grâce à la méthode de l'étalon interne. L'étalon choisi est le naphtaléne (1 g/L).

Protocole d'un essai type

L'ensemble des 16 essais du plan d'expériences ainsi que les dosages du milieu réctionnel ont été effectués selon le protocole opératoire général suivant : dans un ballon de 50 mL thermostaté et muni d'un agitateur magnétique, on dissout du FDC (200 mg, 1.61 mmol) dans la quantité correspondante de mélange $EtOH/H_2O$. La furylméthylcétone est ensuite ajoutée au milieu. La quantité choisie d'une solution de NaOH est ensuite ajoutée, goutte à goutte.

[2]Le système est numéroté arbitrairement, en considérant les dérivés **1***e* et **2***e* comme des chaines linéaires et en prenant comme carbone 1 le carbone du groupe aldéhyde.

TABLEAU 1. Domaine expérimental pour l'étude des l'influence des différents facteurs

Facteurs	Unité	Niveau inférieur (−)	Niveau supérieur (+)
A : FDC/FMC	—	1/1	1/4
B : [NaOH]	g/L	0.1	2.0
C : [FDC]	g/L	6.0	16.0
D : $EtOH/H_2O$	—	60/40	95/5
E : Température	°C	0	25

TABLEAU 2. Matrice d'expériences du plan factoriel 2^{5-1}

Essais (n°)[a]	A	B	C	D	E
1	−	−	−	−	+
2	+	−	−	−	−
3	−	+	−	−	−
4	+	+	−	−	+
5	−	−	+	−	−
6	+	−	+	−	+
7	−	+	+	−	+
8	+	+	+	−	−
9	−	−	−	+	−
10	+	−	−	+	+
11	−	+	−	+	+
12	+	+	−	+	−
13	−	−	+	+	+
14	+	−	+	+	−
15	−	+	+	+	−
16	+	+	+	+	+

[a]L'ordre des expériences a été tiré au hasard.

Apres 1 h de réction, le milieu est neutralisé avec une solution de H_2SO_4 à 10%. Un millilitre de cette solution est prélevé et mélangé avec 1 mL de solution d'étalon interne. Les différents produits du milieu sont dosés.

Résultats et discussion

La réalisation d'un plan factoriel fractionnaire à deux niveaux permet d'estimer les effets principaux et d'interactions de tous les facteurs étudiés avec la meilleure précision et une bonne efficacité (6–8). En ne retenant que les interactions entre facteurs pris deux à deux (interactions du premier ordre), un plan factoriel fractionnaire 2^{5-1} avec le générateur indépendant défini par la relation : E = ABCD (16 essais) permet de calculer tous les effets principaux et d'interactions de premier ordre.

Le domaine expérimental est défini par les niveaux inférieurs et supérieurs des différents facteurs adoptées dans les essais préliminaires (Tableau 1). Les réponses étudiées sont :

(*i*) rendement en produits **1***e*, **2***e* et **3***e*, défini par les rapports molaires :

$$R_1 = \mathbf{1}e \cdot 100/FDC_i; \qquad R_2 = \mathbf{2}e \cdot 100/FDC_i;$$

$$R_3 = \mathbf{3}e \cdot 100/FDC_i$$

1*e*, **2***e* et **3***e* représentent la quantité des produits **1***e*, **2***e* et **3***e* formée (mol) et FDC_i représente la quantité de FDC introduit (mol).

TABLEAU 3. Conditions experimentates et resultats obtenus

Essais	A	B (g/L)	C (g/L)	D	E (°C)	Rendement (%) R_1	R_2	R_3	Sélectivité (%) S_1	S_2	S_3	Perte FDC (%) PE
1	1/1	0.1	6	60/40	25	42	22	0	58	31	0	7
2	1/4	0.1	6	60/40	0	14	0	0	100	0	0	0
3	1/1	2.0	6	60/40	0	18	28	0	32	49	0	10
4	1/4	2.0	6	60/40	25	0	69	31	0	69	31	0
5	1/1	0.1	16	60/40	0	0	0	0	0	0	0	3
6	1/4	0.1	16	60/40	25	0	0	0	0	0	0	12
7	1/1	2.0	16	60/40	25	0	62	22	0	73	26	0
8	1/4	2.0	16	60/40	0	2	42	56	2	42	56	0
9	1/1	0.1	6	95/5	0	3	0	0	100	0	0	0
10	1/4	0.1	6	95/5	25	74	4	0	93	5	0	1
11	1/1	2.0	6	95/5	25	0	59	18	0	76	24	0
12	1/4	2.0	6	95/5	0	7	31	51	7	31	51	11
13	1/1	0.1	16	95/5	25	18	0	0	100	0	0	0
14	1/4	0.1	16	95/5	0	0	0	0	0	0	0	5
15	1/1	2.0	16	95/5	0	8	30	17	9	36	21	27
16	1/4	2.0	16	95/5	25	0	54	46	0	54	46	0

TABLEAU 4. Répétabilité des résultats expérimentaux. Essais au centre du domaine expérimental

Essai[a]	Rendement (%) 1	2	3	Sélectivité (%) 1	2	3	Perte FDC (%)
17	0	58	42	0	58	42	0
18	0	64	36	0	64	36	0
19	0	63	37	0	63	37	0
20	0	61	38	0	61	38	0
Moyenne	—	61.5	38.2	—	61.5	38.2	—
σ	—	2.64	2.63	—	2.64	2.63	—

[a]Conditions expérimentales : A = 1/2.5; B = 1.01 g/L; C = 10 g/L; D 76/24; E = 12°C.

(*ii*) Sélectivité en produits **1***e*, **2***e* et **3***e*, définie par les rapports molaires :

$$S_1 = \mathbf{1}e \cdot 100/\mathrm{FDC_c}; \qquad S_2 = \mathbf{2}e \cdot 100/\mathrm{FDC_c};$$

$$S_3 = \mathbf{3}e \cdot 100/\mathrm{FDC_c}$$

$\mathrm{FDC_c}$ représente la quantité de FDC consommée.

(*iii*) Perte en FDC, définie par la relation :

$$\mathrm{PE} = [\mathrm{FDC_c} - (\mathbf{1}e + \mathbf{2}e + \mathbf{3}e)/\mathrm{FDC_i}]$$

La matrice d'expériences du plan factoriel fractionnaire 2^{5-1} est rapportée dans le Tableau 2. Chaque ligne de la matrice définit un essai par la combinaison des niveaux de chacun des cinq facteurs. L'ensemble des conditions opératoires et des résultats expérimentaux correspondants sont rassemblés dans le Tableau 3. Le dosage des différents constituants des milieux réactionnels a été effectué par chromatographie liquide haute performance (CLHP). La signification des effets calculés par rapport à l'erreur expérimentale est obtenue à partir de l'étude de la répétabilité des résultats expérimentaux (Tableau 4). L'ensemble des calculs concernant les effets principaux et les effets d'interactions a été effectué à l'aide du programme «fraction» inclus dans l'ensemble de programmes NEMROD (9). Les valeurs des effets sont rassemblées dans le Tableau 5.

Dans le domaine expérimental considéré, l'analyse des effets significatifs par rapport à l'erreur expérimentale nous conduit à choisir la combinaison de niveaux A (+) B (−) C (−) D (+) E (+) ou E (−) afin d'obtenir le rendement maximum en produit **1***e*. La réalisation de l'essai correspondant à la combinaison A (−) B (−) C (−) D (+) E (+) nous a permis d'obtenir le produit **1***e* avec une sélectivité de 100% et un rendement de 41% après 9 h de réaction. Ceci confirme l'orientation choisie.

Egalement, l'analyse des effets permet de choisir la combinaison de niveaux A (−) B (+) C (−) D (−) E (+) comme la plus favorable pour obtenir le produit **2***e* avec le maximum de rendement et de sélectivité. La réalisation de l'essai correspondant à cette combinaison nous a permis d'obtenir le produit **2***e* avec 87% de rendement et 100% de sélectivité. Néanmoins, l'essai correspondant à la combinaison de niveaux la plus favorable pour l'obtention de **3***e*, A (+) B (+) C (+) D (−) E (−), permet de l'obtenir avec un rendement de 56%, mais une faible sélectivité (56%).

Ces orientations soulignent l'intérêt de la méthode des plans d'expériences pour l'étude de l'influence de plusieurs facteurs sur les conditions d'une réaction. En effet, en première approche, la conversion de **1***e* en **2***e* qui est une réaction de déshydratation devrait être favorisée par une augmentation de la concentration en soude [B(+)] du rapport $\mathrm{EtO/H_2O}$ [D(+)] et de la température [E(+)]. Or l'analyse des effets principaux et d'interaction montre que la formation de **2***e* est favorisée par la combinaison B(+) D(−) E(+), c'est-à-dire effectivement par une augmentation de la concentration en soude et de la température mais à l'inverse par une diminution du rapport $\mathrm{EtOH/H_2O}$, et donc une augmentation de la quantité d'eau. Ce résultat met en évidence le rôle de stabilisation du produit **1***e* joué par l'éthanol. Ceci pourrait étayer l'hypothèse d'une liaison hydrogène intra-moléculaire dans l'aldol. La présence d'une plus grande proportion d'eau défavoriserait cette liaison, augmentant ainsi la réactivité de l'aldol.

Conclusion

L'influence des cinq facteurs sur les sept réponses ont été évalués grâce à la réalisation d'un plan factoriel fraction-

Can. J. Chem. Downloaded from www.nrcresearchpress.com by 109.225.110.28 on 09/08/12
For personal use only.

TABLEAU 5. Effets principaux et d'interaction des facteurs[a]

CODE	R_1	R_2	R_3	S_1	S_2	S_3	PE
A	+0.50	−0.06	+7.93	−6.06	−4.00	+7.06	−1.12
B	+7.25	+21.81	+15.06	−25.06	+24.62	+15.93	+1.25
C	−8.12	−1.56	+2.56	−17.43	−3.50	+2.68	+1.12
D	+2.12	−2.81	+1.43	+7.31	−3.87	+1.81	0.75
E	+5.12	+8.68	−0.43	+0.06	+9.37	−0.06	−2.25
AB	−2.62	+2.18	+7.93	+2.06	+0.75	+7.06	−2.12
AC	−3.50	+0.56	−0.06	−7.31	+2.37	−0.18	−0.50
AD	+6.00	+0.06	−0.18	−7.56	+1.25	−0.56	−0.12
AE	+1.25	−1.94	−3.31	−2.06	−2.50	−3.68	+1.87
BC	+6.25	+1.68	+2.56	+13.93	+1.00	+2.68	−0.37
BD	−2.75	−0.56	+1.43	−9.56	−0.62	+1.81	+2.75
BE	−9.50	+5.43	−0.43	−6.31	+4.87	−0.06	−3.75
CD	+0.87	+0.31	−3.31	+6.06	+0.75	−3.68	+1.37
CE	−4.12	−3.18	−0.18	+11.06	−3.25	−0.56	−0.62
DE	+4.12	−1.68	−0.06	+9.56	−0.87	−0.18	−3.00

[a]Les valeurs soulignées sont les valeurs significatives par rapport à l'erreur expérimentale. Chaque effet est calculé en effectuant la moyenne arithmetique des 16 résultats, affectés du signe correspondant au facteur ou à l'interaction entre facteur. Par exemple :

Niveau de A : − + − + − + − + − + − + − + − +
Niveau de B : − − + + − − + + − − + + − − + +
Niveau de AB : + − − + + − − + + − − + + − − +
Résultats : $Y_1\ Y_2\ Y_3\ Y_4\ Y_5\ Y_6\ Y_7\ Y_8\ Y_9\ Y_{10}\ Y_{11}\ Y_{12}\ Y_{13}\ Y_{14}\ Y_{15}\ Y_{16}$

$$\text{Effet de A} = \frac{1}{16}[-Y_1 + Y_2 - Y_3 + Y_4 - Y_5 + Y_6 - Y_7 + Y_8 - Y_9 + Y_{10} - Y_{11} + Y_{12} - Y_{13} + Y_{14} - Y_{15} + Y_{16}]$$

$$\text{Effet de AB} = \frac{1}{16}[+Y_1 - Y_2 - Y_3 + Y_4 + Y_5 - Y_6 - Y_7 + Y_8 + Y_9 - Y_{10} - Y_{11} + Y_{12} + Y_{13} - Y_{14} - Y_{15} + Y_{16}]$$

naire 2^{5-1} en seulement 16 essais, ceci constitue un avantage sur la méthode traditionnelle «facteur pour facteur». Grâce à cette approche, on a pu orienter le choix des conditions expérimentales vers la direction la plus favorable pour l'obtention des produits **1***e* et **2***e* avec de bons rendements et une sélectivité totale. Dans le cas du produit **3***e*, le rendement et la sélectivité sont moyennes. Cette étude ouvre de nouvelles perspectives pour le développement de cette réaction à plus grande échelle du fait de la simplicité du protocole opératoire.

1. J. March. Advanced organic chemistry. Wiley, New York. 1985. pp. 829–834.
2. S. Hariaty, L. Rigal et A. Gaset. Brevet français n° 90 14833, 22 novembre 1990.
3. (*a*) R. G. Johnston et D. Kidd. J. Chem. Soc. 4730 (1964); (*b*) J. P. Majoral, M. Badri, A. M. Caminade, M. Delmas et A. Gaset. Inorg. Chem. **27**, 3873 (1988); (*c*) J. P. Majoral, M. Badri, G. Garrigues, L. Rigal, M. Delmas et A. Gaset. Brevet français n° 97 03610, 13 mars 1987.
4. (*a*) W. F. Cooper et W. H. Nutall. J. Chem. Soc. **101**, 1074 (1912); (*b*) T. M. Cresp, M. V. Sargent et P. Vogel. J. Chem. Soc. Perkin Trans. 1, **1**, 37 (1974); (*c*) C. Dominguez, G. Escobar, J. Plumet, L. Rigal et. A. Gaset. An. Quim. **82**(C), 241 (1986). (*d*) C. Dominguez, A. G. Csaky, J. Magano et J. Plumet. Synthesis, 172 (1989).
5. I. Hernandez-Fuentes, C. Abradelo, C. Dominguez, A. G. Csaky, J. Plumet, C. Cativiela, J. A. Mayoral, A. Gaset et L. Rigal. Heterocycles, **29**, 657 (1989).
6. R. Phan Tan Luu, D. Mathieu et D. Feneuille. Méthodologie de la recherche experimentale : Introduction. Laboratoire de Prospective Réactionnel et d'Analyse de l'Information, Aix en Provence, France. 1977.
7. G. E. P. Box, W. G. Hunter, J. S. Hunter. Statistics for experimenters. An introduction to design, data analysis and model building. Wiley, New York. 1978.
8. J. Goupy. La méthode des plans d'expériences. Optimisation du choix des essais et de l'interprétation des résultats. Dunod–Bordas, Paris. 1988.
9. D. Mathieu et R. Phan Tan Luu. New efficient methodology for research of optimal design. Laboratoire de Prospective Réactionnelle et d'Analyse de l'Information, Université d'Aix-Marseille, Marseille. 1982.

Can. J. Chem. Downloaded from www.nrcresearchpress.com by 109.225.110.28 on 09/08/12
For personal use only.

Influence of temperature on the liquid-to-liquid extraction of ethanol from (water + ethanol + 1,2-dichloroethane)

HORACIO N. SÓLIMO[1] AND JOSÉ L. ZURITA

Instituto de Fisica, Facultad de Ciencias Exactas y Tecnologia, Universidad Nacional de Tucumán, Avda. Independencia 1800, 4000 San Miguel de Tucuman, Argentina

Received November 19, 1991

HORACIO N. SÓLIMO and JOSÉ L. ZURITA. Can. J. Chem. **70**, 2310 (1992).

To evaluate the influence of temperature on the extraction of ethanol from aqueous solutions with 1,2-dichloroethane, liquid–liquid equilibrium data for the system water + ethanol + 1,2-dichloroethane were obtained at 298.15, 308.15, and 318.15 K. The binodal curves were determined by the cloud-point method, and conjugate points on the tie-lines were obtained by correlating the refractive index of these curves as a function of composition. The tie-line data at each temperature were satisfactorily correlated using the method of Othmer and Tobias, and the plait-point coordinates were estimated. The experimental data were also compared to values calculated by the UNIFAC group contribution method for the activity coefficients using the isoactivity conditions as restraint equations, and with the NRTL and UNIQUAC models. The UNIFAC method proved to be more accurate than the NRTL and UNIQUAC equations fitted to the experimental data. Under the experimental conditions used, ethanol extraction by 1,2-dichloroethane appears to be independent of the temperature.

HORACIO N. SÓLIMO et JOSÉ L. ZURITA. Can. J. Chem. **70**, 2310 (1992).

Dans le but d'évaluer l'influence de la température sur l'extraction d'éthanol des mélanges aqueux, les données d'équilibre liquide–liquide pour le systeme eau + éthanol + 1,2-dichloroéthane ont été determinés operant à des températures de 298,15, 308,15 et 318,15 K. On a determiné les données des courbes binodales à l'aide de la méthode du point de rosée et on a obtenu les points conjugués de la ligne de jonction pour chacune des températures. Faisant appel à la méthode d'Othmer et de Tobias on a pu établir une bonne corrélation entre les données relatives aux lignes de jonction pour chacune des températures et on a evalué les coordonnées des points plissement. Les données expérimentales ont été comparées avec les valeurs calculées par la méthode de contribution du groupe UNIFAC, et par les modèles NRTL et UNIQUAC, en utilisant les conditions d'isoactivité comme équations limites. Le modèle UNIFAC montre un meilleur accord avec les valeurs expérimentales que les modèles NRTL et UNIQUAC. Nos résultats expérimentaux montrent que l'extraction de l'éthanol avec le 1,2-dichloroéthane ne dépend pas de la température.

Introduction

In recent years, liquid–liquid equilibria (LLE) studies have become increasingly important in chemical technology. The rising cost of energy has made new separation processes based on extraction more attractive than before. Liquid–liquid extraction provides an important alternative to distillation for the recovery of ethanol from dilute aqueous solutions using a nonmiscible solvent.

The aim of this work was to evaluate the potential of 1,2-dichloroethane (DE) for the recovery of ethanol from aqueous solutions. We report the experimental results of LLE studies of ternary mixtures water + ethanol + DE at 298.15, 308.15, and 318.15 K. Several tie-lines were determined for each temperature and the correlation of mutual solubility with tie-line data (Othmer and Tobias' method) permitted the estimation of the plait-point coordinates.

The results were also used to test the validity of the NRTL and UNIQUAC equations and the UNIFAC group contribution method.

Experimental

Anhydrous ethanol (Merck, reagent grade) was dried with magnesium activated with iodine under reflux. The product was then fractionally distilled and the middle fraction collected. The last traces of water were removed by circulating the ethanol through a glass column (0.03 × 2 m) packed with 0.3-nm molecular sieves.

1,2-Dichloroethane (Fisher Scientific Co., certified) was used without further purification.

Water was bidistilled in an all-glass apparatus.

All purified organic chemicals were stored over activated molecular sieves to prevent water absorption.

The binodal curves were determined by the cloud-point method (1), as described earlier (2), in a cell equipped with a magnetic stirrer and a jacket for circulating the isothermal water at the desired temperatures (±0.05 K). Compositions at the ends of the tie-lines were determined in the same cell. Mixtures with compositions within the heterogeneous region were shaken vigorously for at least 2 h at constant temperature for the tie-line determinations, and allowed to settle for 3 h. The compositions of samples taken from both layers were determined by measuring their refractive indices at each temperature with a Jena Abbé refractometer with an accuracy of ±0.0001.

Results and discussion

Figure 1 shows the LLE diagram at 298.15 K for the water + ethanol + DE system. LLE data predicted by the UNIFAC method are also shown. The smoothing curves connecting the experimental data points are hand-drawn, since no attempt to fit the data by an empirical equation was made. Similar plots were obtained for the other two temperatures.[2]

The tie-line data at all the temperatures are satisfactorily correlated by the method of Othmer and Tobias (3). An empirical equation:

$$[1] \quad \log[(1 - W_{11})/W_{11}] = m \log[(1 - W_{33})/W_{33}] + b$$

can represent all the tie-line data with adequate precision.

[1]Author to whom correspondence may be addressed.

[2]Tables of experimental binodal curves, tie-lines data, plait-point coordinates, parameters of eq. [1], residuals, and parameters of the NRTL and UNIQUAC equations at the three temperatures may be purchased from: The Depository of Unpublished Data, Document Delivery, CISTI, National Research Council Canada, Ottawa, Canada K1A 0S2.

Can. J. Chem. Downloaded from www.nrcresearchpress.com by 109.225.110.28 on 09/08/12
For personal use only.

Can. J. Chem. Downloaded from www.nrcresearchpress.com by 109.225.110.28 on 09/08/12
For personal use only.

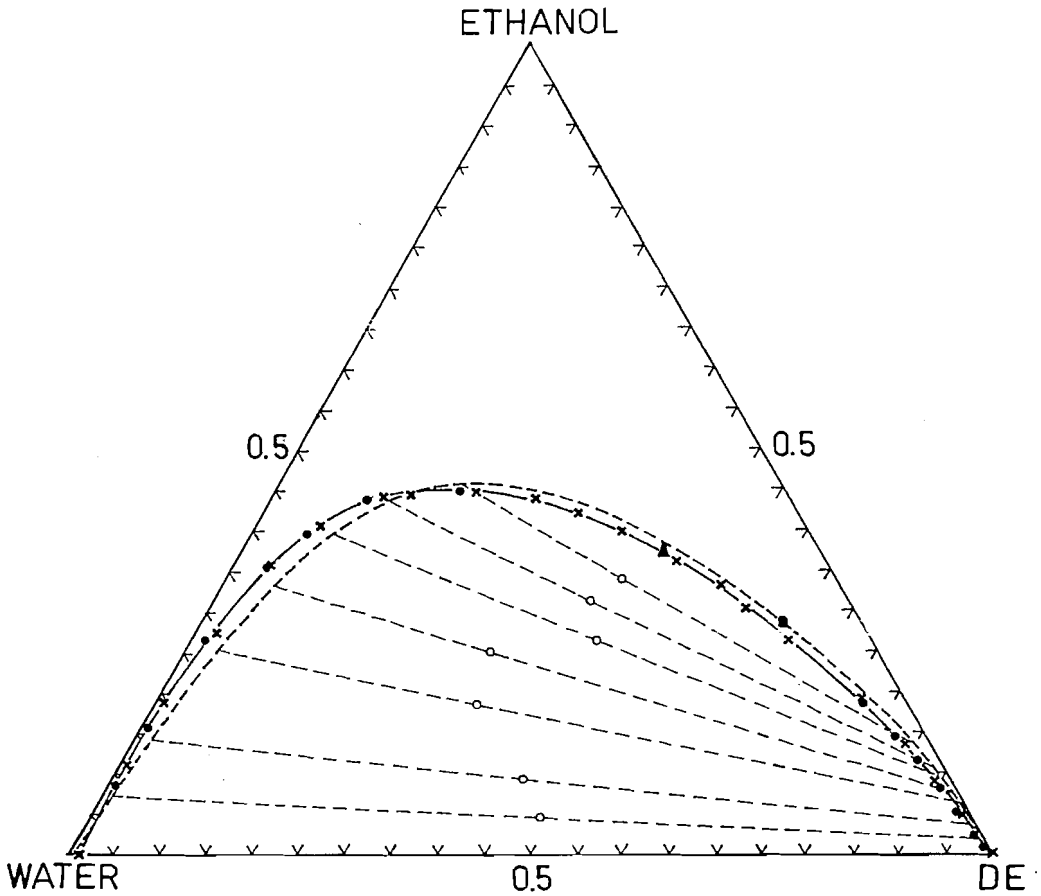

FIG. 1. Liquid–liquid equilibria for the system water(1) + ethanol(2) + DE(3) at 298.15 K. ×, Experimental binodal points. ●, Experimental compositions for tie-lines. Dashed line, LLE, and tie-lines predicted by UNIFAC method. PP = Plait point, o, overall compositions for tie-lines, ▲, experimental PP; ■, UNIFAC PP.

TABLE 1. Ethanol extraction properties of DE

D_e	D_w	S_w^{EtOH}	W_{23}
	298.15 K		
0.094	0.002	47	0.008
0.141	0.004	35	0.022
0.198	0.011	18	0.052
0.225	0.013	17	0.080
0.289	0.020	14	0.114
0.331	0.029	11	0.145
0.413	0.043	10	0.185
	308.15 K		
0.281	0.003	94	0.025
0.256	0.007	37	0.042
0.279	0.011	25	0.058
0.263	0.012	22	0.075
0.333	0.021	16	0.115
0.358	0.025	14	0.125
0.488	0.057	9	0.205
	318.15 K		
0.141	0.005	28	0.012
0.336	0.013	25	0.045
0.360	0.017	21	0.090
0.395	0.022	18	0.115
0.400	0.025	16	0.130
0.500	0.042	12	0.180
0.540	0.054	10	0.200
0.586	0.075	8	0.232

$D_e = W_{23}/W_{21}$; $D_w = W_{13}$; $S_w^{EtOH} = D_e/D_w$.

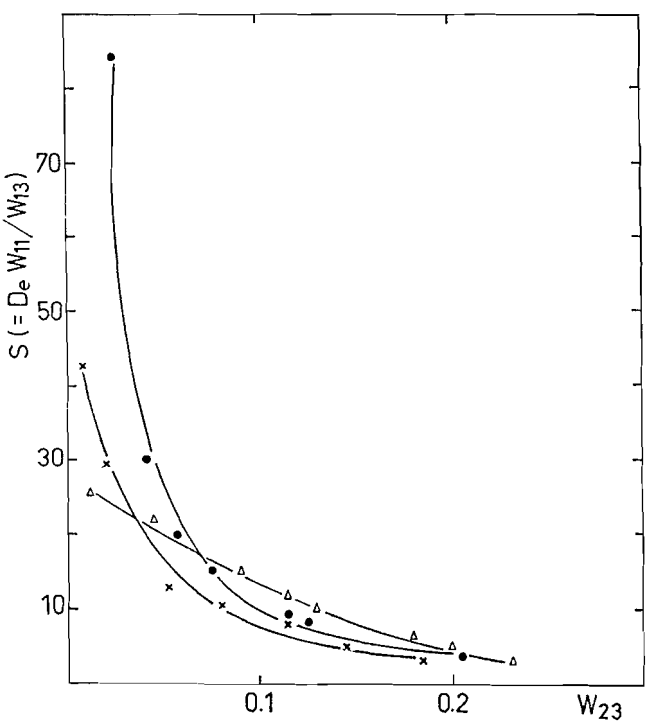

FIG. 2. Selectivity diagram for the system water(1) + ethanol(2) + DE(3) at several temperatures. ×, 298.15 K; ●, 308.15 K; △, 318.15 K.

Can. J. Chem. Downloaded from www.nrcresearchpress.com by 109.225.110.28 on 09/08/12
For personal use only.

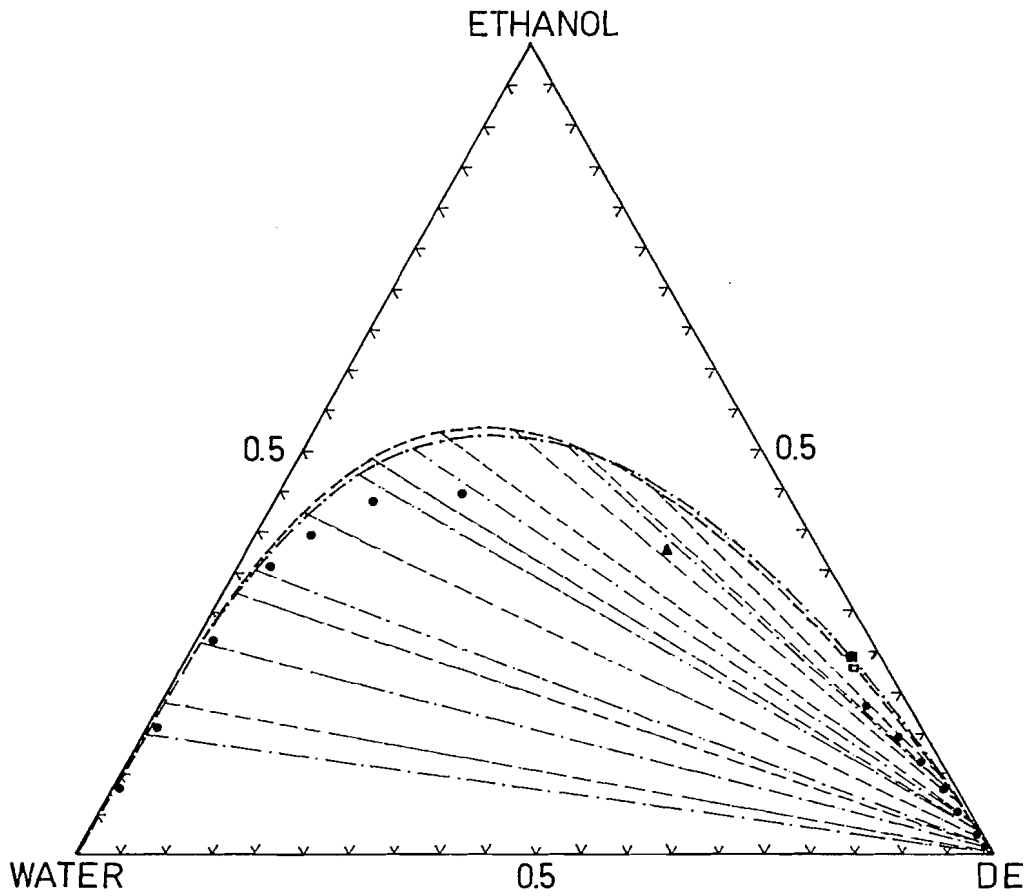

FIG. 3. Binodal curves and tie-lines calculated for the system water(1) + ethanol(2) + DE(3) at 298.15 K using the equations (----, NRTL and (–·–·–) UNIQUAC, together with the corresponding experimental compositions for tie-lines (●). ▲, Experimental PP; ■, UNIQUAC PP; □, NRTL PP.

As shown in Table 1, the ethanol distribution coefficients D_c (defined as the ratio of the ethanol concentration (wt.%) in the organic phase to that in the aqueous phase) are not constant, and have a tendency to increase as the ethanol concentration is increased. A similar conclusion can be derived from the distribution coefficient for water D_w (defined as the equilibrium water content in the solvent phase). The ratio of the ethanol distribution coefficient to the water distribution coefficient yields the separation factor S_w^{EtOH} shown in Table 1. As can be seen, the extraction properties of DE for ethanol do not depend on the temperature, except for the lowest ethanol concentration range.

Zane Egan *et al.* (4) conclude that solvents with experimental distribution coefficients for ethanol greater than 0.15, and a separation factor greater than 10, are potential candidates for extraction processes. These properties are largely exceeded by DE, making it a useful alternative for ethanol extraction. However, at the three temperatures considered, the aqueous layer is richer in ethanol than the organic layer (see Fig. 1). As expected, the size of the two-phase region decreases with an increase in temperature.

Figure 2 shows a selectivity (S) diagram (5) for the three temperatures, considering ethanol as the distributed substance. It shows that the selectivity at 318.15 K is greater than at the other temperatures in the range $0 \leq W_{23} \leq 0.05$, but has approximately the same value for $0.05 \leq W_{23} \leq 0.15$ at all temperatures. This last range of concentration is the most important region for ethanol extraction from fermentation broth. Therefore, ethanol extraction could be carried out at room temperature, thus saving energy while preserving a fairly important heterogeneous zone.

Thermodynamic models, such as the NRTL (6) and UNIQUAC (7), were used to estimate the LLE for this system, with the help of an iterative computer program developed by Sørensen (8). To minimize the values of the two objective functions in terms of activity and molar fractions, a penalty term, designed to reduce the risk of multiple solutions associated with high parameter values, was included. Figure 3 shows the LLE predictions using these models.

The structural parameters of water and ethanol necessary for the UNIQUAC equation were obtained from Anderson and Prausnitz (9). For DE they were calculated from UNIFAC parameters (10).

The nonrandomness of the liquid mixture, which is represented by the third parameter in the NRTL equation (α_{ij}), was set at a value of 0.2 in the present study.

The UNIFAC group contribution method (10) was employed by using the group interaction parameters obtained by Magnussen *et al.* (11).

As can be seen from Figs. 1 and 3, the UNIFAC method is more accurate than both the NRTL and the UNIQUAC equations fitted to the experimental data for this system because the calculated residuals are smaller.

Acknowledgment

The authors are indebted to the Consejo Nacional de Investigaciones Cientificas y Técnicas of Argentina for financial support under Grant PID 3-141900/88.

1. D. F. Othmer, R. E. White, and E. Trueger. Ind. Eng. Chem. **33**, 1240 (1941).
2. H. N. Sólimo, H. E. Martinez, and R. Riggio. J. Chem. Eng. Data, **34**, 176. (1989).
3. D. F. Othmer and P. E. Tobias. Ind. Eng. Chem. **34**, 690 (1942).
4. B. Zane Egan, D. D. Lee, and D. A. McWhirter. Ind. Eng. Chem. Res. **27**, 1330 (1988).
5. R. E. Treybal. Liquid extraction. McGraw–Hill, New York, San Francisco, Toronto, and London. 1963. p. 122.
6. H. Renon and J. M. Prausnitz. AIChE J. **14**, 135 (1968).
7. D. S. Abrams and J. M. Prausnitz. AIChE J. **21**, 116 (1975).
8. J. M. Sørensen. Phase equilibria and separation processes. MAN 8106. ESTM: Estimation of UNIQUAC and NRTL parameters from ternary LLE data. Instituttet for Kemiteknik, Lyngby, Denmark. 1980.
9. T. F. Anderson and J. M. Prausnitz. Ind. Eng. Chem. Process Des. Dev. **17**, 552 (1978).
10. Aa. Fredenslund, J. Gmehling, and P. Rasmussen. Vapor–liquid equilibria using UNIFAC. Elsevier, Amsterdam. 1977.
11. T. Magnussen, P. Rasmussen, and Aa. Fredenslund. Ind. Eng. Chem. Process Des. Dev. **20**, 331 (1981).

Can. J. Chem. Downloaded from www.nrcresearchpress.com by 109.225.110.28 on 09/08/12
For personal use only.

Iron porphyrin catalyzed oxidation of lignin model compounds: the oxidation of veratryl alcohol and veratryl acetate

FUTONG CUI AND DAVID DOLPHIN

The University of British Columbia, Department of Chemistry, 2036 Main Mall, Vancouver, B.C., Canada V6T 1Y6

Received September 13, 1991

FUTONG CUI and DAVID DOLPHIN. Can. J. Chem. **70**, 2314 (1992).

meso-Tetra(2,6-dichloro-3-sulfonatophenyl)porphyrin iron chloride catalyzes the oxidation of 3,4-dimethoxybenzyl alcohol (veratryl alcohol) in aqueous solution to give veratraldehyde along with demethoxylation and ring-cleavage products. The isolation of a direct ring-cleavage product from the oxidation of veratryl acetate in aqueous solution supports the previously proposed ring-cleavage mechanisms. The oxidation in methanol, however, does not lead to ring-cleavage products. When veratryl alcohol was oxidized in methanol, solvent was found to be incorporated into the 3-position of veratryl alcohol, giving new insight into the mechanism of oxidation.

FUTONG CUI et DAVID DOLPHIN. Can. J. Chem. **70**, 2314 (1992).

Le chlorure du *méso*-tétra(2,6-dichloro-3-sulfonatophényl)porphyrine fer catalyse l'oxydation de l'alcool 3,4-diméthoxybenzylique (alcool vératrylique), en solution aqueuse, qui conduit à la formation de vératraldéhyde et des produits de déméthoxylation et de clivage de cycle. Le fait que l'on a pu isoler un produit de clivage direct du cycle au cours de l'oxydation de l'acétate de vératryle, en solution aqueuse, supportent les mécanismes proposés antérieurement pour le clivage de cycle. Toutefois, l'oxydation dans le méthanol ne conduit pas à des produits de clivage de cycle. Lorsqu'on oxyde l'alcool vératrylique dans le méthanol, on a trouvé que le solvant s'incorpore en position 3 de l'alcool; ce résultat jette de la lumière sur le mécanisme de l'oxydation.

[Traduit par la rédaction]

Introduction

Lignin is a three-dimensional, irregular, aromatic biopolymer occurring widely in vascular plants. It is the second most abundant organic compound on Earth and comprises about 15–25% of the land-produced biomass. The biodegradation of this highly resistant polymer has interested researchers in many disciplines. Since the first discovery of lignin-degrading enzymes from the white-rot fungus *Phanerochaete chrysosporium Burds* in 1983 (1, 2), rapid progress has been made in understanding the mechanism of lignin biodegradation. The lignin-degrading enzymes, the lignin peroxidases (1–7) (ligninases) and the manganese-dependent peroxidases (3, 5, 8–10), are all hemeproteins and contain one heme (iron protoporphyrin IX) per molecule. Lignin peroxidase when oxidized by a two-electron oxidant (hydrogen peroxide) subsequently oxidizes lignin model compounds by two one-electron transfer processes (11, 12). The manganese-dependent peroxidase requires a Mn(II) cofactor to accomplish a similar cycle (13). One of the unique properties of the lignin-degrading enzymes is their low substrate specificity; substrates varying from polymeric lignin to oligomeric, dimeric, and monomeric lignin model compounds, to polycyclic aromatic hydrocarbons (14) and polychlorinated phenols have been shown to be oxidized (15). It is unlikely that a lignin peroxidase could have an active site to bind this great diversity of substrates. It is assumed, therefore, that the function of the protein of the lignin-degrading enzymes is to protect the highly reactive intermediates of the prosthetic group, the protohemin iron (IV) cation radical (12) and thus simple iron porphyrins could be good models for the enzymes. As both lignin and lignin-degrading enzymes are large molecules, a simple biomimetic porphyrin might be advantageous in degrading lignin in that the interaction of lignin and a small molecular reactant, such as a porphyrin, could be much easier than that between lignin and a large enzymic molecule.

Commercially available iron porphyrins have been used as lignin peroxidase models by Shimada and coworkers (16–19). These porphyrins, however, suffer two major disadvantages. The porphyrins are very unstable and a catalyst to substrate ratio of 1:10 had to be used. In addition, the reactions have to be carried out in organic solvents, conditions quite different from that of the enzymatic reactions. Furthermore, these porphyrins do not closely mimic the enzyme in every case (18). A number of sterically protected, water-soluble porphyrins have been synthesized and used as lignin peroxidase models in our laboratory (20, 21). We report here on the oxidation of veratryl alcohol and veratryl acetate by *meso*-tetra (2,6-dichloro-3-sulfonatophenyl) porphyrin iron chloride (TDCSPPFeCl, **1**) using *m*-chloroperbenzoic acid (*m*CPBA) as oxidant in both aqueous and organic solvents.

Results

Oxidation of veratryl alcohol in methanol

When veratryl alcohol was oxidized by TDCSPPFeCl and *m*CPBA in methanol, vetraldehyde, 2-hydroxymethyl-5-methoxy-2,5-cyclohexadien-1,4-dione (**7**), 4,5-dimethoxy-3,5-cyclohexadien-1,2-dione (**8**), 2-hydroxymethyl-4,4,5-trimethoxy-2,5-cyclohexadien-1-one (**13**), and 2-dimethoxymethyl-4,4,5-trimethoxy-2,5-cyclohexadien-1-one (**14**) were found as products. The yields of the products were found to be dependent on the reaction condition. When the reaction was carried out open to the air with moderate stirring, veratraldehyde and **13** were produced in 49 and 42% yield, respectively, and compound **14** was not isolated. Under highly aerobic condition (open to the air, vigorous stirring), the yields of veratraldehyde, **13**, and **14** were 51, 11, and 32%, respectively; compounds **7** and **8** were produced in very small amounts. Under anaerobic condition, compound **14** was found in trace amounts.

When the reaction was carried out in ethanol (containing a small amount of DMF to increase the solubility of TDCSPPFeCl), **16** was obtained in addition to other prod-

Can. J. Chem. Downloaded from www.nrcresearchpress.com by 109.225.110.28 on 09/08/12
For personal use only.

ucts. Treatment of **13** with tetrahydrofuran (THF)/water/concentrated HCl (1:1:0.1) at room temperature for 2 min gave **7** as the sole product. When 4-ethoxy-3-methoxybenzyl alcohol was used as the substrate instead of veratryl alcohol, **15** was the product corresponding to **13**.

Oxidation of veratryl acetate in methanol

In addition to small amounts of veratraldehyde, veratryl acetate, and **10**, oxidation of veratryl acetate with TDCSPPFeCl and *m*CPBA in air gave **17** as the major product (82%). Under anaerobic condition, **17** was also found as a product.

Oxidation of veratryl alcohol in pH 3 phosphate buffer

Oxidation of veratryl alcohol in aqueous solution gave veratraldehyde as the major product (>80%) along with small amounts of **2**, **4**, **5**, and **7**. When 4-ethoxy-3-methoxybenzyl alcohol was used as the substrate, **4** and **5** were also isolated.

Oxidation of veratryl acetate in pH 3 buffer

Although not soluble in aqueous solution, veratryl acetate was successfully oxidized by TDCSPPFeCl and *m*CPBA to give **10**, 3,4-dimethoxyphenol (**11**), and the aromatic ring cleaved product **12**.

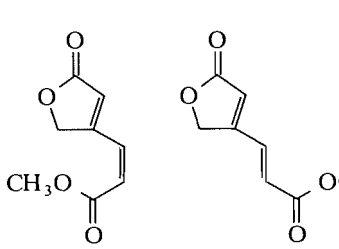

2

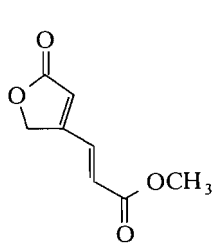

3

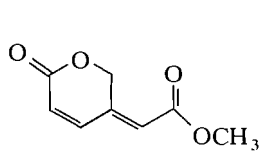

4

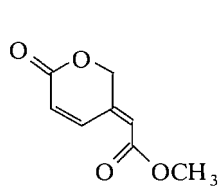

5

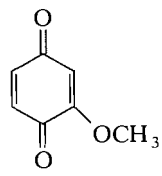

6

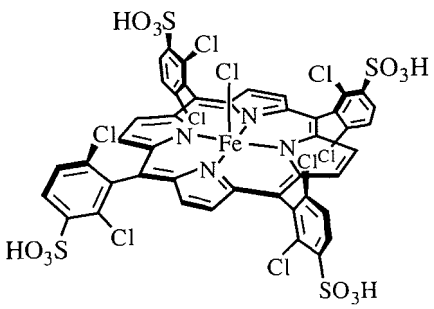

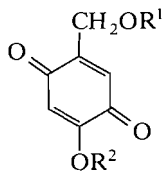

7 $R^1 = H, R^2 = CH_3$
10 $R^1 = COCH_3, R^2 = CH_3$
18 $R^1 = H, R^2 = C_2H_5$

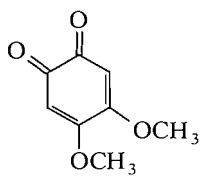

8

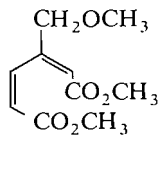

9

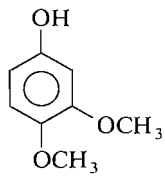

11

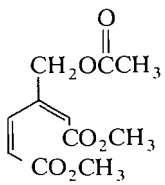

12

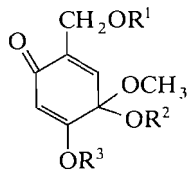

13 $R^1 = H, R^2 = R^3 = CH_3$
15 $R^1 = H, R^2 = CH_3, R^3 = C_2H_5$
16 $R^1 = H, R^2 = C_2H_5, R^3 = CH_3$
17 $R^1 = COCH_3, R^2 = R^3 = CH_3$

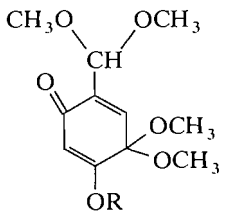

14 $R = CH_3$
19 $R = C_2H_5$

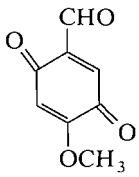

20

Discussion

Veratryl alcohol, a secondary metabolite (22, 23) of lignin degradation by *Phanerochaete chrysosporium*, plays a unique role in lignin biodegradation (24). It has been reported to be able to stimulate lignin degradation (25, 26) and benzo (*a*) pyrene oxidation (27) by lignin peroxidase. It was found later that veratryl alcohol could induce the biosynthesis of lignin peroxidase (28) and protect the enzyme from deactivation by excess oxidant (29–31). In addition, veratryl alcohol has been widely used as a simple lignin model compound. As a secondary metabolite and also a substrate of lignin peroxidase, veratryl alcohol is readily oxidized to veratraldehyde, which in turn is also readily reduced back to veratryl alcohol and accumulates in the ligninolytic culture of *P. chrysosporium* (23). This cyclic redox process, unlike metabolism to carbon dioxide, is energetically wasteful and results in oxidizing power being expended on veratryl alcohol instead of lignin. Leisola and co-workers (32) recently reported that veratryl alcohol was rapidly metabolized to carbon dioxide in carbon-limited cultures of *P. chrysosporium*, compared with the slow and incomplete degradation in nitrogen-limited culture. They also showed that veratraldehyde, the major oxidation product of veratryl alcohol by lignin peroxidase, cannot be metabolized directly by the fungus. It is reduced back quantitatively to

Can. J. Chem. Downloaded from www.nrcresearchpress.com by 109.225.110.28 on 09/08/12
For personal use only.

Can. J. Chem. Downloaded from www.nrcresearchpress.com by 109.225.110.28 on 09/08/12
For personal use only.

veratryl alcohol by the fungus and then degraded via quinones and ring-cleavage products.

Leisola *et al.* (33) first found aromatic ring-cleavage products, two δ-lactones, of veratryl alcohol in 1985. These reactions have been extensively studied and since then additional products have been isolated and their mechanism of formation proposed (32, 34, 35–38). It now seems clear that an initial one-electron oxidation of veratryl alcohol gives a cation radical; reaction with water then gives a carbon-centered radical. Coupling of the radical with molecular oxygen leads to aromatic ring cleavage, whereas further one-electron oxidation of the radical followed by reaction with water leads to demethoxylation products, i.e., quinones.

Oxidation of veratryl alcohol by TDCSPPFeCl and *m*CPBA at room temperature in air using aqueous pH 3 buffer as solvent gave veratraldehyde as the major product along with small amounts of **2**, **4**, **5**, and **7**. The δ-lactone structure of **4** and **5** was confirmed, in addition to NMR and MS data, by the fact that **4** and **5** were formed when 4-ethoxy-3-methoxybenzyl alcohol was oxidized under the same conditions. Compounds **4** and **5** are δ-lactones, since the ethoxy group was lost during their formation from 4-ethoxy-3-methoxybenzyl alcohol. Compounds **3** and **8**, found in the oxidation of veratryl alcohol by lignin peroxidase and hydrogen peroxide, were not found in our experiments using aqueous buffer as solvent. However, compound **8** was found as a product when using methanol as solvent under otherwise the same conditions.

When veratryl acetate was oxidized in aqueous buffer, **10** (the acetate derivative of **7**), 3,4-dimethoxyphenol, and a direct ring-cleavage product (**12**) were isolated. Quinones **6** and **8** have been previously found as phenyl–alkyl cleavage products of veratryl alcohol (32, 35, 38). To our knowledge, this is the first time a phenol (**11**) has been found as a side-chain cleavage product of a veratryl alcohol derivative. The isolation of the direct ring–cleavage product **12** supports the ring-cleavage mechanism previously proposed (35–38). We learned while preparing this manuscript that Schmidt *et al.* (34) used veratryl alcohol methyl ether as a substrate and found a similar product (**9**). Schmidt *et al.* (34) found veratraldehyde was the major product of the oxidation of veratryl alcohol methyl ether. In the oxidation of veratryl acetate by TDCSPPFeCl and *m*CPBA, however, veratraldehyde was only a minor product and **10** and **12** were the major products. The cleavage of a C_α-ether bond through C_α oxidation has been demonstrated (34, 39). The isolation of veratraldehyde from the oxidation of veratryl acetate, though in low yield, suggests that the C_α-ester bond can also be cleaved in a similar way.

Shimada *et al.* (18) studied the degradation of β-1, β-O-4, and β-5 dimeric lignin model compounds by protohemin (iron protoporphyrin IX chloride) and *t*-BuOOH in chloroform. Though β-1 and β-5 model compounds were oxidatively degraded, the oxidation of the β-O-4 model compound, 4-ethoxy-3-methoxyphenylglycerol-β-guaiacyl ether, did not give the same products as that of the lignin peroxidase catalyzed reaction. The same β-O-4 dimer, however, was oxidatively cleaved by TDCSPPFeCl and *m*CPBA in aqueous solution in the same manner as the ligninase-catalyzed reaction (21). Dordick *et al.* (40) reported that both natural and synthetic lignin were vigorously depolymerized by horseradish peroxidase and other peroxidases in organic solvents but not in water. Their results, however, were later questioned (41).

As TDCSPPFeCl is soluble in both water and polar organic solvents, we have studied solvent effects on the oxidation of veratryl alcohol and veratryl acetate. In addition to veratraldehyde, **7**, and **8**, the solvent-incorporated products **13** and **14** were isolated when veratryl alcohol was oxidized in methanol. A mechanism for the formation of **13** is proposed in Fig. 1. When veratryl acetate was the substrate, compound **10** and veratraldehyde were found as minor products with **17** as the major product. It is interesting to note that when veratryl alcohol was oxidized in ethanol, **16** was isolated and the 3-methoxy group of **16** did not exchange with solvent under the reaction conditions. Another interesting observation was that no ring-cleavage product was found in the reaction using methanol as solvent.

Compound **13**, formed in methanol, is the analog of **7** formed in aqueous solution; however, the analog of **14**, 2-formyl-5-methoxy-2,5-cyclohexedine-1-one (**20**), was not found during the oxidation of veratryl alcohol in aqueous solution.

Shimada *et al.* (35) proposed two possible pathways for aromatic ring-cleavage of veratryl alcohol and suggested that the pathway in which water specifically attacks the C_3 position of the substrate cation radical is more plausible. Although no ring-cleavage products were found when either veratryl alcohol or veratryl acetate was oxidized in methanol, the specific incorporation of methanol into the 3-position to give **13** and **14** clearly supports Shimada's earlier suggestion.

In conclusion, TDCSPPFeCl/*m*CPBA closely mimics the enzymic lignin peroxidase/hydrogen peroxide system in the oxidation of veratryl alcohol in aqueous solution. The isolation of a direct ring-cleavage product of veratryl acetate supports the previously proposed mechanism for ring cleavage. The results of the oxidation of veratryl alcohol and veratryl acetate in aqueous buffer and in methanol clearly demonstrated solvent effects on lignin model compound oxidations.

Experimental

NMR spectra were recorded on Varian XL 300 or Bruker WH 400 spectrometers using tetramethylsilane as internal standard. Low-resolution and high-resolution mass spectra were recorded on an AE1 MS 9 and Cratos MS 50 spectrometers. Preparative thin-layer chromatography (TLC) was carried out on a Model 7924T Chromatotron (Harrison Research) using Silica Gel 60 PF_{254} as absorbent. Merck pre-coated Silica Gel 60 PF_{254} (0.2 mm) was used for analytical purposes. Veratryl alcohol and veratraldehyde were purchased from Aldrich. Veratryl acetate was prepared by acetylation of veratryl alcohol with excess 1:1 acetic anhydride/pyridine at room temperature for 24 h. 4-Ethoxy-3-methoxybenzyl alcohol was prepared as previously reported (42).

Oxidation of veratryl alcohol and veratryl acetate

Substrate (0.3 mmol) and TDCSPPFeCl (0.5 μmol in 0.5 mL water) were dissolved in either pH 3 aqueous buffer or methanol (20 mL) and *m*CPBA (0.6 mmol) was added as a powder and the solution stirred at room temperature for 2 h. The solution was partitioned between saturated sodium bicarbonate (20 mL) and ethyl acetate (20 mL). The aqueous layer was further extracted twice with ethyl acetate (10 mL). The organic extracts were combined and dried over sodium sulphate, evaporated and separated on a Chromatotron using either methanol/methylene chloride (0–1% methanol) or ethyl acetate/hexane (10–30% ethyl acetate) as eluent. When veratryl alcohol was the substrate, the residue was acety-

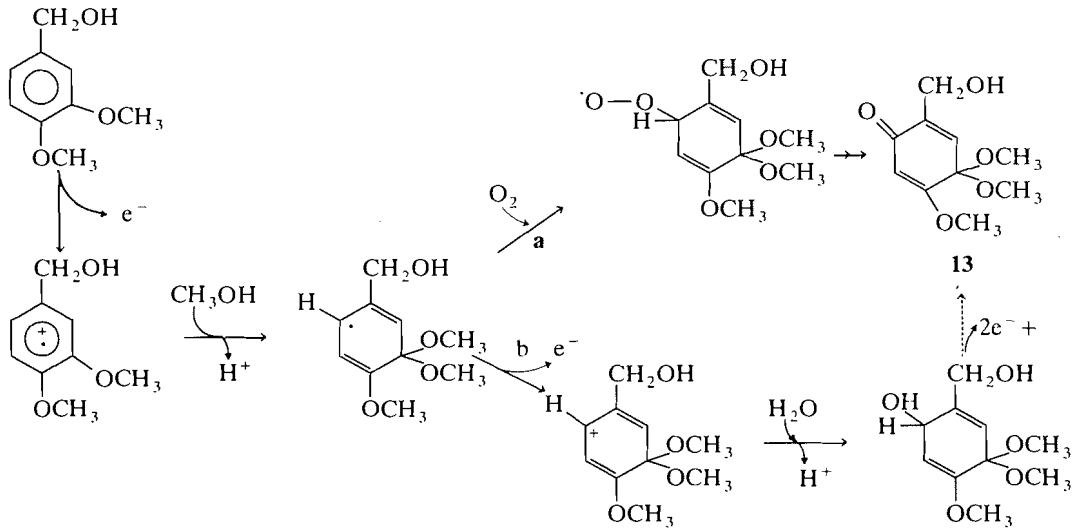

FIG. 1. Possible mechanism for the formation of the methanol-incorporated product **13**.

lated with excess 1:1 acetic anhydride/pyridine at room temperature for 24 h before separation. The purity of each component was checked by analytical TLC using methanol/methylene chloride (1:99) and hexane/ethyl acetate (1:4) as solvents. Impure components were further separated on the Chromatotron. The yields were based on the substrates and estimated by GC.

All the products were characterized by MS and ^{1}H NMR and compared with those reported in the literature. The structure of **12** was confirmed by comparing its NMR spectrum with that of **9**. Compound **13** was characterized by MS, ^{1}H NMR, ^{13}C NMR, and elemental analysis. The structure of **14** was elucidated by comparing its MS and ^{1}H NMR with that of **13**.

Methyl (Z)-furan-5(2H)-one-3-butenoate (33) (2): ^{1}H NMR ($CDCl_3$) δ: 3.78 (3H, S), 5.25 (2H, m), 6.13 (1H, d, J = 12 Hz), 6.30 (1H, m), 6.77 (1H, dd, J_1 = 12 Hz, J_2 = 1–2 Hz); MS *m/z* (%): 168 (12.6, M), 137 (19.4), 136 (48.2), 124 (35.2), 111 (26.0), 109 (33.4), 108 (21.6), 81 (49.2), 80 (28.6), 79 (60.5), 59 (22.5), 53 (94.8), 52 (45.5), 51 (100.0), 50 (46.6).

Methyl (Z)-6-oxo-2H-pyran-3(6H)-ylideneacetate (34) (4): ^{1}H NMR ($CDCl_3$) δ: 3.78 (S, 3H), 5.69 (2H, d, *J* = 3 Hz), 5.99 (1H, m), 6.19 (1H, d, *J* = 10 Hz), 7.01 (1H, dd, J_1 = 1 Hz, J_2 = 10 Hz); MS *m/z* (%): 168 (14.0), 137 (16.7) 136 (100), 111 (13.5), 109 (25.2), 108 (37.3), 97 (11.2), 83 (10.5), 81 (42.3), 80 (31.8), 79 (29.1), 53 (61.0), 52 (20.1), 51 (37.2).

Methyl (E)-6-oxo-2H-pyran-3(6H)-ylideneacetate (34) (5): ^{1}H NMR ($CDCl_2$) δ: 3.80 (3H, S), 5.03 (2H, d, *J* = 2 Hz), 5.94 (1H, m), 6.21 (1H, dd, J_1 = 10 Hz, J_2 = 2 Hz), 8.35 (1H, dd, J_1 = 1 Hz, J_2 = 10 Hz); MS *m/z* (%): 168 (13.0), 136 (17.9), 124 (14.8), 112 (10.7), 109 (33.0), 108 (14.0), 81 (36.5), 80 (10.7), 79 (10.9), 59 (12.6), 53 (100.0), 52 (23.3), 51 (37.0), 50 (19.0).

2-Hydroxymethyl-5-methoxy-2,5-cyclohexadien-1,4-dione (35) (7): ^{1}H NMR ($CDCl_3$) δ: 3.85 (3H, S), 4.57 (2H, *J* = 1 Hz), 5.92 (1H, S), 6.72 (1H, t, *J* = 1 Hz); ^{13}C NMR (CD_3OD) δ: 188.798, 183.500, 160.461, 150.891, 129.456, 108.426, 58.959, 56.959; MS *m/z* (%): 170 (M, 1.2), 169 (16.5), 168 (100.0), 167 (64.9), 153 (16.9), 150 (12.2), 140 (10.2), 139 (55.4), 122 (15.6), 111 (31.9), 83 (14.4). Exact Mass calcd. for $C_8H_{10}O_4$: 170.0579; found (HRMS): 170.0588.

4,5-Dimethoxy-3,5-cyclohexadien-1,2-dione (34) (8): ^{1}H NMR ($CDCl_3$) δ: 3.90 (6H, S), 5.78 (2H, S); MS *m/z* (%): 170 (5.74), 168 (3.38), 167 (7.28), 155 (4.12), 149 (24.44), 140 (100.0), 125 (27.94), 69 (18.34). Exact Mass calcd. for $C_8H_8O_4$: 168.0420; found (HRMS): 168.0403.

2-Acetylhydroxymethyl-5-methoxy-2,5-cyclohexadien-1,4-dione (10): ^{1}H NMR ($CDCl_3$) δ: 2.17 (3H, S), 3.85 (3H, S), 5.02 (2H, d, *J* = 1–2 Hz), 5.95 (1H, S), 6.62 (1H, t, *J* = 1–2 Hz); ^{13}C NMR ($CDCl_3$) δ: 185.947, 181.402, 169.860, 158.628, 143.815, 129.264, 107.495, 59.642, 56.468, 20.774; MS *m/z* (%); 210 (2.41), 168 (100.0), 167 (25.23), 153 (10.16), 139 (13.23), 69 (22.9), 43 (78.0). Exact Mass calcd. for $C_{10}H_{10}O_5$: 210.0528; found (HRMS): 210.0535.

3,4-Dimethyoxyphenol (43) (11): ^{1}H NMR ($CDCl_3$) δ: 3.84 (3H, S), 3.86 (3H, S), 4.56 (1H, broad), 6.36 (1H, dd, J_1 = 9 Hz, J_2 = 2 Hz), 6.50 (1H, d, *J* = 2 Hz), 6.75 (1H, d, *J* = 9 Hz); MS *m/z* (%): 154 (100.0), 139 (94.8), 111 (62.7), 96 (10.6), 93 (40.8), 81 (11.0), 69 (21.5), 68 (11.1), 65 (25.4), 55 (12.7).

Dimethyl 3-acetylhydroxymethyl-2,4-hexadienoate (12): ^{1}H NMR ($CDCl_3$) δ: 2.12 (3H, S), 3.705 (3H, S), 3.710 (3H, S), 4.85 (2H, m), 6.00 (1H, d, *J* = 12 Hz), 6.00 (1H, d, *J* = 1–2 Hz), 7.06 (1H, dd, J_1 = 12 Hz, J_2=1–2 Hz); MS *m/z* (%): 242 (0.1), 184 (9.8), 183 (100.0), 169 (28.4), 141 (22.7), 136 (10.5), 109 (43.8), 43 (55.5). Exact Mass calcd. for $C_{11}H_{14}O_6$: 242.0786; found (HRMS): 242.0782.

2-Hydroxymethyl-4,4,5-trimethoxy-2,5-cyclohexadien-1-one (13) (identified as its acetate 17): ^{1}H NMR ($CDCl_3$) δ: 2.14 (3H, S), 3.34 (6H, S), 3.84 (3H, S), 4.92 (2H, d, *J* = 1–2 Hz), 5.67 (1H, S), 6.53 (1H, t, *J* = 1–2 Hz); ^{13}C NMR ($CDCl_3$) δ: 184.449, 170.076, 169.097, 136.119, 136.057, 103.832, 94.349, 60.314, 56.252, 51.534, 20.898; MS *m/z* (%): 256 (2.2), 241 (25.9), 199 (33.2), 183 (100.0), 182 (25.9), 167 (29.0), 155 (50.8), 139 (29.7), 124 (23.4), 123 (61.5), 95 (28.4), 69 (32.9), 43 (85.9). Anal. calcd. for $C_{12}H_{16}O_6$: C 56.25, H 6.29; found: C 56.37, H 6.37. Exact Mass calcd. for $C_{12}H_{16}O_6$: 256.0948; found: 256.0948.

2-Dimethoxymethyl-4,4,5-trimethoxy-2,5-cyclohexadien-1-one (14): ^{1}H NMR ($CDCl_3$) δ: 3.35 (6H, S), 3.39 (6H, S), 3.82 (3H, S), 5.34 (1H, S), 5.65 (1H, S), 6.81 (1H, S); ^{13}C NMR ($CDCl_3$) δ: 184.744, 168.959, 137.144, 104.092, 97.798, 94.454, 56.222, 54.032, 51.540, 29.679; MS (EI) *m/z* (%): 243 (0.3), 227 (100.0), 212 (19.8), 180 (37.3), 153 (10.8), 75 (31.5), 69 (12.1); MS (DCI + NH_3) *m/z* (%): 259 (29.6, M + 1), 227 (58.4), 213 (13.6), 212 (100.0).

5-Ethoxy-2-hydroxymethyl-4,4-dimethoxy-2,5-cyclohexadien-1-one (15) (identified as its acetate): ^{1}H NMR ($CDCl_3$) δ: 1.47 (3H, t, *J* = 8Hz), 2.13 (3H, S), 3.33 (6H, S), 4.05 (2H, q, *J* = 8 Hz), 4.92 (2H, d, *J* = 1 Hz), 5.63 (1H, S), 6.51 (1H, t, *J* = 1–Hz); MS *m/z* (%): 270 (1.8), 199 (23.8), 197 (100.0), 182 (32.9), 169 (37.2), 153 (24.6), 141 (35.7), 139 (34.3), 123 (14.8), 109 (43.9), 69 (27.1), 43 (76.0).

4-Ethoxy-2-hydroxymethyl-4,5-dimethoxy-2,5-cyclohexadien-1-one (16) (isolated as its acetate): ^{1}H NMR ($CDCl_3$) δ: 1.23 (3H,

Can. J. Chem. Downloaded from www.nrcresearchpress.com by 109.225.110.28 on 09/08/12
For personal use only.

t, J = 7 Hz), 2.13 (3H, S), 3.31 (3H, S), 3.40–3.60 (2H, m, when decoupling at 1.23, pattern close to an AB quartet), 4.91 (2H, d, J = 1 Hz), 5.66 (1H, S), 6.52 (1H, t, J = 1 Hz); MS m/z (%): 270 (1.5), 241 (29.7), 199 (35.8), 197 (87.2), 183 (100.0), 182 (26.1), 169 (45.2), 167 (43.8), 155 (32.4), 153 (26.7), 141 (31.0), 139 (25.6), 123 (51.3), 109 (57.4), 95 (24.2), 69 (28.6), 43 (88.5).

2-Ethoxy-5-hydroxymethyl-2,5-cyclohexadien-1,4,-dione ***(18)*** *(isolated as its acetate):* ^{1}H NMR ($CDCl_3$) δ: 1.50 (3H, t, J = 8 Hz), 2.17 (3H, S), 4.03 (2H, q, J = 8 Hz), 5.02 (2H, d, J = 1–2 Hz), 5.93 (1H, S), 6.62 (1H, t, J = 1–2 Hz); MS m/z (%): 224 (8.6), 182 (26.0), 166 (14.0), 154 (28.9), 153 (25.7), 151 (12.7), 138 (13.5), 120 (17.2), 69 (67.5), 60 (20.9), 53 (27.7), 45 (52.0), 43 (100.0), 42 (21.6), 41 (20.1).

2-Dimethoxymethyl-5-ethoxy-3,4-dimethoxy-2,5-cyclohexadien-1-one ***(19)****:* ^{1}H NMR ($CDCl_3$) δ: 1.46 (3H, t, J = 8 Hz), 3.35 (6H, S), 3.39 (6H, S), 4.03 (2H, q, J = 8 Hz), 5.34 (1H, S), 5.61 (1H, S), 6.79 (1H, S); MS m/z (%): 242 (13.3), 241 (100.0), 226 (28.4), 194 (44.9), 181 (17.4), 167 (10.8), 153 (16.2), 75 (24.1), 69 (13.6).

Acknowledgements

This work was supported by the Natural Sciences and Engineering Research Council of Canada, the Institute for Chemical Science and Technology, and the Industrially Oriented Research Grant.

1. M. Tien and T. K. Kirk. Science, **221**, 661 (1983).
2. J. K. Glenn, M. A. Morgan, M. B. Mayfield, M. Kuwahara, and M. H. Gold. Biochem. Biophys. Res. Commun. **114**, 1077 (1983).
3. M. S. A. Leisola, B. Kozalic, F. Menssdoerffer, and A. Fiechter. J. Biol. Chem. **262**, 419 (1987).
4. M. Tien and T. K. Kirk. Proc. Natl. Acad. Sci. U.S.A. **81**, 2280 (1984).
5. M. Kuwahara, J. K. Glenn, M. A. Morgan, and M. H. Gold. FEBS Lett. **169**, 247 (1984).
6. M. H. Gold, M. Kuwahara, A. A. Chiu, and J. K. Glenn. Arch. Biochem. Biophys. **234**, 353 (1984).
7. V. Renganathan, K. Miki, and M. H. Gold. Arch. Biochem. Biophys. **241**, 304 (1985).
8. J. K. Glenn and M. H. Gold. Arch. Biochem. Biophys. **242**, 329 (1985).
9. A. Paszczynski, Van-Ba Huynh, and R. Crawford. Arch. Biochem. Biophys. **244**, 750 (1986).
10. H. Wariishi, L. Akileswaran, and M. H. Gold. Biochemistry, **27**, 5365 (1988).
11. P. J. Kersten, M. Tien, B. Kalyanaraman, and T. K. Kirk. J. Biol. Chem. **260**, 2609 (1985).
12. V. Renganathan and M. H. Gold. Biochemistry, **25**, 1626 (1986).
13. M. H. Gold, H. Wariishi, L. Akileswaran, Y. Mino, and T. M. Loehr. Colloq. INRA (Lignin Enzymic Microb. Degrad.), **40**, 113 (1987).
14. D. Sanglard, M. S. A. Leisola, and A. Fiechter. Enzyme Microb. Technol. **8**, 209 (1986).
15. K. E. Hammel, B. Kalyanaraman, and T. K. Kirk. Colloq. INRA (Lignin Enzymic Micorb. Degrad.), **40**, 45 (1987).
16. M. Shimada, T. Habe, T. Umezawa, T. Higuchi, and T. Okamoto. Biochem. Biophys. Res. Commun. **122**, 1247 (1984).
17. T. Habe, M. Shimada, and T. Higuchi. Mokuzai Gakkaishi, **31**, 54 (1985).
18. M. Shimada, T. Habe, T. Higuchi, T. Okamoto, and B. Panijpan. Holzforschung, **41**, 277 (1987).
19. M. Shimada, T. Hattori, T. Umezawa, T. Higuchi, and T. Okamoto. Colloq. INRA (Lignin Enzymic Microb. Degrad.), **40**, 151 (1987).
20. D. Dolphin, T. Nakano, T. E. Maione, T. K. Kirk, and R. Farrell. Colloq. INRA (Lignin Enzymic Microb. Degrad.), **40**, 157 (1987).
21. F. Cui and D. Dolphin. *In* Biogenesis and biodegradation of plant cell wall polymers. *Edited by* N. G. Lewis and M. G. Paice. ACS Symp. Ser. **399**, Chap. 37, (1989).
22. K. Lundquist and T. K. Kirk. Phytochemistry, **17**, 1676 (1978).
23. M. Shimada, F. Nakatsubo, T. K. Kirk, and T. Higuchi. Arch. Microbiol. **129**, 321 (1981).
24. T. K. Kirk and R. L. Farrell. Annu. Rev. Microbiol. **41**, 465 (1987).
25. M. S. A. Leisola, D. C. Ulmer, R. Waldner, and A. Fiechter. J. Biotechnol. **1**, 331 (1984).
26. D. C. Ulmer, M. S. A. Leisola, and A. Fiechter. J. Biotechnol. **1**, 13 (1984).
27. S. D. Haemmerli, M. S. A. Leisola, D. Sanglard, and A. Fiechter. J. Biol. Chem. **261**, 6900 (1986).
28. B. D. Faison, T. K. Kirk, and R. L. Farrell. Appl. Environ. Microbiol. **52**, 251 (1986).
29. T. Tonon and E. Odier. Appl. Environ. Microbiol. **54**, 466 (1988).
30. P. J. Harvey, H. E. Schoemaker, and J. M. Palmer. Colloq. INRA (Lignin Enzymic Microb. Degrad.), **40**, 145 (1987).
31. H. Wariishi and M. H. Gold. FEBS Lett. **243**, 165 (1989).
32. S. D. Haemmorli, H. E. Schoemaker, H. W. H. Schmidt, and M. S. A. Leisola. FEBS Lett. **220**, 149 (1987).
33. M. S. A. Leisola, B. Schmidt, U. Thanei-wyss, and A. Fiechter. FEBS Lett. **189**, 267 (1985).
34. H. W. H. Schmidt, S. D. Haemmerli, R. E. Schoemaker, and M. S. A. Leisola. Biochemistry, **28**, 1776 (1989).
35. M. Shimada, T. Hattori, T. Umezawa, T. Higuchi, and K. Uzura. FEBS Lett. **221**, 327 (1987).
36. M. S. A. Leisola, S. D. Haemmerli, J. D. G. Smit, J. Troller, R. Waldner, H. E. Schoemaker, and H. Schmidt. Colloq. INRA (Lignin Enzymic Microb. Degrad.) **40**, 81 (1987).
37. M. S. A. Leisola, S. D. Haemmerli, R. Waldner, H. E. Schoemaker, H. W. H. Schmidt, and A. Fiechter. Cellul. Chem. Technol. **22**, 267 (1988).
38. T. Hattori, M. Shimada, T. Umezawa, T. Higuchi, M. S. A. Leisola, and A. Fiechter. Agric. Biol. Chem. **52**, 879 (1988).
39. T. K. Kirk, M. Tien, P. J. Kersten, M. D. Mozuch, and B. Kalyanaraman. Biochem. J. **236**, 279 (1986).
40. J. S. Dordick, M. A. Marletta, and A. M. Klibanov. Proc. Natl. Acad. Sci. U.S.A. **83**, 6255 (1986).
41. N. G. Lewis, R. A. Razal, and E. Yamamoto. Proc. Natl. Acad. Sci. U.S.A. **84**, 7925 (1987).
42. T. Umezawa, F. Nakatsubo, and T. Higuchi. Agric. Biol. Chem. **47**, 2677 (1983).
43. R. I. Meltzer and J. Doczi. J. Am. Chem. Soc. **72**, 4986 (1950).

Can. J. Chem. Downloaded from www.nrcresearchpress.com by 109.225.110.28 on 09/08/12
For personal use only.

Synthesis and characterization of chemical intermediates of acyl or alkyl phospholipids

BOUBKER NASSER

Laboratoire de chimie organique and Laboratoire de biochimie et biologie moléculaire (Unité associée au Centre national de la recherche scientifique, no 531), Université de Franche-Comté, 16 route de Gray, 25030 Besançon CEDEX, France

CLAUDE MORPAIN AND BERNARD LAUDE

Laboratoire de chimie organique, Université de Franche-Comté, 16 route de Gray, 25030 Besançon CEDEX, France

AND

NORBERT LATRUFFE[1]

Laboratoire de biologie moléculaire et cellulaire, Université de Bourgogne, Faculté des sciences de la vie, Mirande, BP 138, Dijon, France

Received July 24, 1991

BOUBKER NASSER, CLAUDE MORPAIN, BERNARD LAUDE, and NORBERT LATRUFFE. Can. J. Chem. **70**, 2319 (1992).

Precursors of phospholipids or ether lipids were synthesized from D-mannitol, i.e., 1-*O*-myristoyl-2-*O*-benzyl-*sn*-glycerol **11** and 1-*O*-hexadecyl-2-*O*-benzyl-*sn*-glycerol **13**. The chemical pathways involved sequential protection reactions using allyl, triphenylmethyl, or benzyl groups via 3-*O*-allyl-*sn*-glycerol. Eleven intermediates were isolated and for the first time characterized with their spectrometric (especially ^{1}H nmr) and physical parameters and yield. This work allowed preparation of chemically defined membrane phospholipids from compound **11** as well as ether lipids from compound **13** with cell mediator activities bearing different probes such as photoactivatable, fluorescent, or radioactive groups.

BOUBKER NASSER, CLAUDE MORPAIN, BERNARD LAUDE et NORBERT LATRUFFE. Can. J. Chem. **70**, 2319 (1992).

Divers précurseurs de phospholipides et d'éthers lipidiques, comme le 1-*O*-myristoyl-2-*O*-benzyl-*ns*-glycerol **11** et le 1-*O*-hexadecyl-2-*O*-benzyl-*ns*-glycerol **13**, ont été synthétisés à partir de D-mannitol. Cette méthode implique une séquence de réactions de protections à l'aide des groupes allyle, triphénylméthyle ou benzyle via le 3-*O*-allyl-*ns*-glycérol. Onze intermédiaires ont été isolés et pour la première fois leurs paramètres spectroscopiques (^{1}H rmn) et physiques ont été précisés. Ce travail permet d'accéder à partir du composé **11** à des phospholipides membranaires chimiquement définis ou à partir du compose **13** à des éthers lipidiques médiateurs cellulaires porteurs de diverses sondes (photoactivable, fluorescente ou radioactive).

Introduction

Lipids, especially phospholipids and derivatives, have numerous and essential functions in cell life. For instance, biomembranes are involved in transport, transduction signalling, or enzyme activation through lipid–protein and lipid–lipid interactions. On the other hand, some lipids can exhibit mediator functions such as ether-lipids including PAF acether (1, 2).

Since natural phospholipids are largely heterogenous and generally weakly chemically reactive, advances in knowledge in these fields are largely beneficial to the use of synthetic phospholipids or analogues, chemically defined or eventually modified by the coupling of different probes (photoactivatable, fluorescent, or radioactive groups).

To have access to these tools it is absolutely essential to find the best synthetic pathway and to master all the chemical steps including intermediate isolation and characterization.

For instance, the understanding of the lipid function in the catalytic properties of mitochondrial membrane bound R-3-hydroxybutyrate dehydrogenase was greatly improved by the use of phospholipid analogues (3, 4).

In this paper we report the chemical synthesis that allows the preparation of phospholipid or ether lipid precursors. Indeed, the compound **11** (1-*O*-myristoyl-2-*O*-benzyl-*sn*-glycerol) is a key intermediary in the phospholipid (or analogue) preparation and compound **13** (1-*O*-hexadecyl-2-*O*-benzyl-*sn*-glycerol) leads to the preparation of ether phospholipids, such as PAF and analogues (5–7).

Whereas Eibl and Woolley (8) previously described a similar pathway, we put forward the characterization of all of the intermediary, including physicochemical and spectroscopic parameters, which has not been done before. The principle of this synthesis sequence is summarized in Scheme 1. Traditionally it involved the use of well-known protecting agents such as the *allyl* moiety, which can be easily transposed in a propenyl group that is then eliminated by bromine in buffer medium (8); the *triphenylmethyl* group, which only reacts with primary alcohols and is easily displaced with diluted acids; and *benzyl*, which is generally used to block the (C_2) of glycerol in the PAF acether synthesis (6, 7, 9).

To our knowledge compounds **6–12** have never been described. Compound **13** alone has previously been isolated by other procedures (5–7).

Phospholipids (or analogues) or ether lipids (i.e., PAF acether) can be prepared from compounds **11** and **13**, as has been described (6, 9, 10).

Experimental

Materials and methods

Dimethylformamide, dimethyl sulfoxide, allyl bromide, and benzyl chloride were purchased from Aldrich and distilled prior to use. Triethylamine and pyridine were dried over 4Å molecular

[1]Author to whom correspondence may be addressed.

Can. J. Chem. Downloaded from www.nrcresearchpress.com by 109.225.110.28 on 09/08/12
For personal use only.

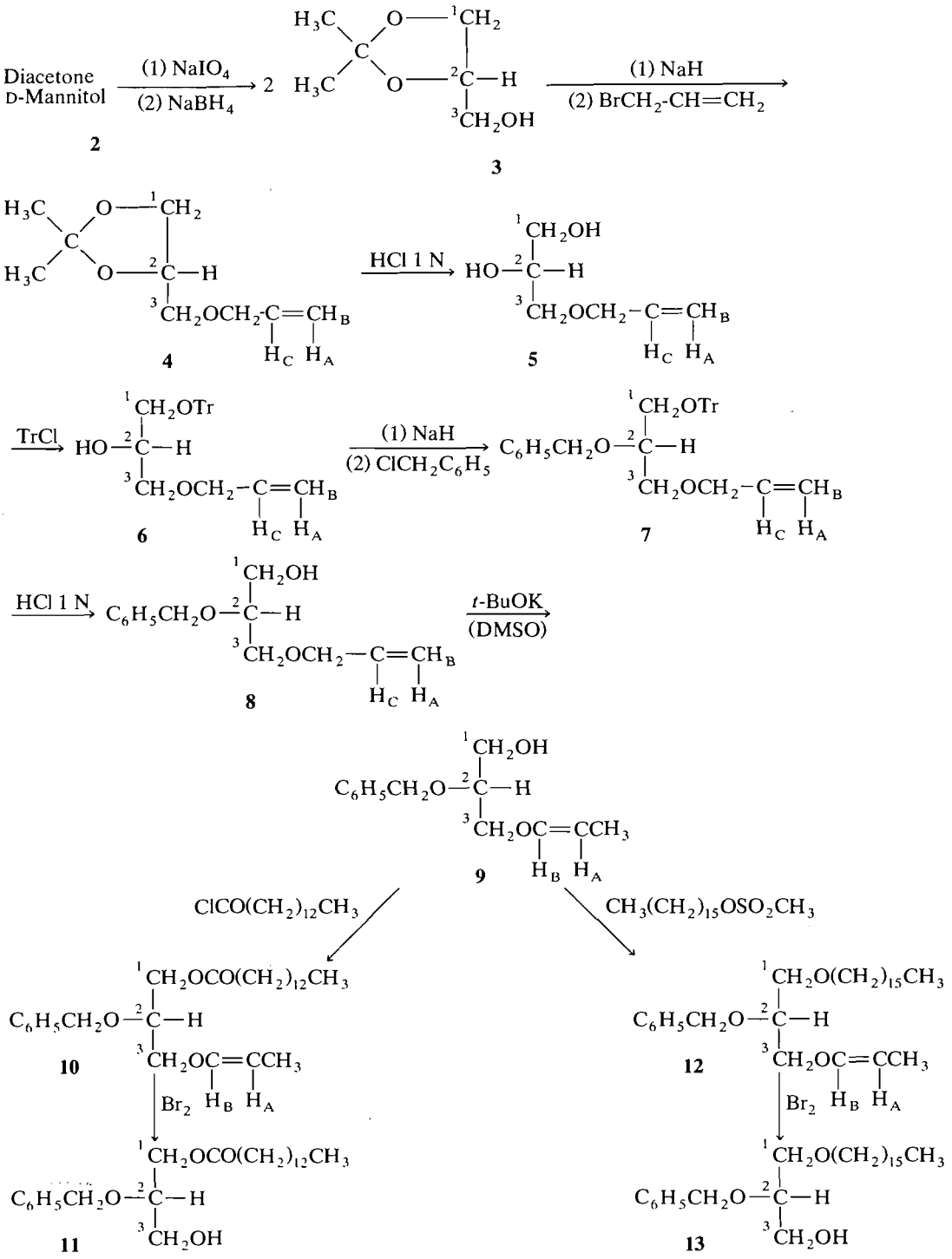

SCHEME 1. Reaction pathway for the synthesis of intermediates of acyl or alkyl phospholipids.

sieves (Merck). Hexadecylmethane sulfonate and hexadecanoyl chloride were prepared according to refs. 11 and 12 respectively. All solvents and reagents were of reagent grade and used as obtained. Thin-layer chromatography (tlc) was carried out by using silica gel (Merck, precoated sheets, 60 F 254). Compound spots in tlc were visualized under uv light or by iodine vapor. Column chromatography was carried out by using silica gel 60 (70–230 mesh, Merck). Melting points were measured with a Kofler hot-stage apparatus and uncorrected. Optical rotations were recorded by means of a Roussel-Jouan 71 micropolarimeter. The ^{1}H nmr spectra were measured on a Bruker Spectrospin AC 200 (200 MHz) using a solution in $CDCl_3$ with tetramethylsilane as internal standard. Infrared spectra were recorded on a Beckman I.R. 33.

Results

*1,2-O-Isopropylidene-*sn*-glycerol (3)*

Di-*O*-acetone-D-mannitol (**2**) (65.5 g, 0.25 mol) was suspended in 600 mL of water by stirring. The sodium metaperiodate (53.5 g, 0.25 mol) was slowly added in several fractions (45 min total time); the temperature had to remain below 30°C. The pH was maintained neutral (pH = 6–7) by

Can. J. Chem. Downloaded from www.nrcresearchpress.com by 109.225.110.28 on 09/08/12
For personal use only.

Can. J. Chem. Downloaded from www.nrcresearchpress.com by 109.225.110.28 on 09/08/12
For personal use only.

addition of sodium hydroxide pellets. Stirring was maintained for 1.5 h more at room temperature. Methanol (300 mL) was added to precipitate iodate. The mixture was left for 2 h at 20°C. The precipitate was separated, then washed with a solution (200 mL) of methanol–water (1:1). The solution was cooled in an ice-water bath. The sodium tetrahydridoborate (9.5 g, 0.25 mol) was added in portions by stirring. Stirring was continued for 1 h more at 15–20°C. The mixture was neutralized with 2 N hydrochloric acid to pH 7–8. Sodium chloride (200 g) was added. The organic phase was extracted with 250 mL of chloroform (3 times), then dried over sodium sulfate. After removal of solvent under vacuum, the resulting oil was distilled under vacuum: bp 84°C/15 Torr (1 Torr = 133.3 Pa); weight 46.2 g (70%); $[\alpha]_{589}$ +11.5, $[\alpha]_{578}$ +12.2, $[\alpha]_{546}$ +14.1, $[\alpha]_{436}$ +29.6 (*c* 0.024, methanol) (lit. (13)$[\alpha]_{589}$ +11.57, $[\alpha]_{578}$ +12.16, $[\alpha]_{546}$ +14.00, $[\alpha]_{436}$ +25.5° (methanol)).

1,2-O-Isopropylidene-3-O-allyl-sn-*glycerol* (**4**)

This was prepared according to ref 14: bp 85°C/14 Torr; yield 82%; $[\alpha]_{589}$ +16.2, $[\alpha]_{578}$ +16.9, $[\alpha]_{546}$ +19.7, $[\alpha]_{436}$ +33.7 (*c* 0.026, $CHCl_3$); ir: 3090, 1630 (-CH = CH_2), 1370, and 1385 cm^{-1} ($C(CH_3)_2$); ^1H nmr δ ppm: 1.40 (s, 3H, CH_3), 1.45 (s, 3H, CH_3), 3.40–3.60 (AB part of an ABX system located at 3.50 ppm with ^2J = 9.85 Hz; each transition was split with ^3J = 5.75 Hz, 2H, C^1H_2O or C^3H_2O), 3.72 (dd, $^2J_{AB}$ = 8.20 Hz, ^3J = 6.40 Hz, 1H of C^1H_2O or C^3H_2O), 4.0–4.10 (m, 3H, OCH_2-CH = CH_2 and 1H of C^1H_2O or C^3H_2O), 4.20–4.40 (tt, 1H, J = 5.75 Hz and J = 6.40 Hz, C^2HO), 5.20 (ddt, 1H, J_{gem} = 1.80 Hz; J_{cis} = 10.30 Hz; ^4J = 1.25 Hz, H^A), 5.30 (ddt, 1H, J_{gem} = 1.80 Hz; J_{trans} = 17.20 Hz; ^4J = 1.60 Hz, H^B), 5.90 (ddt, 1H, J_{cis} = 10.30 Hz; J_{trans} = 17.20 Hz and ^3J = 4.90 Hz, H^C).

3-O-Allyl-sn-*glycerol* (**5**)

Hydrochloric acid (1 N, 4.5 mL) was added to compound **4** (18 g, 0.18 mol) in methanol (140 mL). The mixture was heated at reflux for 1 h. After cooling, the solution was neutralized with 10% sodium hydrogen carbonate. The solvents were removed under vacuum and the solid phase dried by azeotropic distillation with anhydrous benzene. Vacuum distillation, gave 3-*O*-allyl-*sn*-glycerol (26 g): bp 104–106°C/0.1 Torr; yield 86%; $[\alpha]_{589}$ +0.6, $[\alpha]_{578}$ +0.7, $[\alpha]_{546}$ +1, $[\alpha]_{436}$ +1.3 (*c* 0.017, pyridine); ir: 3400 (υOH), 3080, 3015, 1640 cm^{-1} (CH = CH_2); ^1H nmr ($CDCl_3$) δ ppm: 3.40–3.95 (m, 7H, C^1H_2OH, C^2HOH, and C^3H_2O); 4.05 (dt, ^3J = 5.50 Hz; ^4J = 1.30 Hz, 2H, OCH_2-CH = CH_2), 5.18 (ddt, 1H, J_{gem} = 1.60 Hz; J_{cis} = 10.3 Hz; ^4J = 1.30 Hz, H^A), 5.30 (ddt, 1H, J_{gem} = 1.6 Hz, J_{trans} = 17.20 Hz; ^4J = 1.30 Hz, H^B), 5.90 (ddt, 1H, J_t = 17.20 Hz, J_c = 10.30 Hz, ^3J = 5.5 Hz, H^C).

1-O-Trityl-3-O-allyl-sn-*glycerol* (**6**)

Compound **5** (8.8 g, 0.066 mol) was dissolved in 140 mL of *tert*-butanol. After addition of trityl chloride (23.3 g, 0.084 mol) and triethylamine (9.89 g, 0.098 mol), the mixture was heated to reflux for 1 h. After cooling, 70 mL of diisopropyl ether and 70 mL of water were added. After decantation the aqueous phase was extracted twice with 70 mL of diisopropyl ether. The organic phases were combined and dried over sodium sulfate. After solvent evaporation, the oil was chromatographed on a column (100 g of silica gel) (gradient hexane – ethyl ether). The trityl derivative was eluted with hexane – ether mixtures 90:10 and 80:20. It crystallized from 40 mL of hexane in the presence of a few drops of ether: weight 23.4 g; yield 94%; mp 58°C; R_f: 0.24 (hexane–ether 1/4); $[\alpha]_{589}$ −4.4; $[\alpha]_{578}$ −4.7; $[\alpha]_{546}$ −5; $[\alpha]_{436}$ −9.5° (*c* 0.013, $CHCl_3$); ir: 3480 (υOH), 3030–3100 cm^{-1} (C_6H_5, CH = CH_2); ^1H nmr ($CDCl_3$) δ ppm: 2.50 (d, 1H, J = 4.70 Hz, O*H*), 3.20 (AB part of a system ABX with ^2J = 9.40 Hz; each transition was split with ^3J = 5.50 Hz, 2H, C^1H_2O or C^3H_2O), 3.53 (AB part of a system ABX with $^2J_{AB}$ = 9.70 Hz, $^3J_{AX}$ = 4.40 Hz, $^3J_{BX}$ = 6.30 Hz, 2H, C^1H_2O or C^3H_2O), 3.90–4.05 (dt, located at 3.98 ppm, ^3J = 5.60 Hz, ^4J = 1.40 Hz, OCH_2-CH=CH_2, overlapped at a multiplet 1H, HC_2O), 5.20 (ddt, 1H, J_{gem} = 1.65 Hz; J_{cis} = 10.30 Hz, ^4J = 1.40 Hz, H^A), 5.25 (ddt, 1H, J_{gem} = 1.65 Hz, J_{trans} = 17.20 Hz, ^4J = 1.40 Hz, H^B), 5.90 (ddt, 1H, J_{cis} = 10.30 Hz, J_{trans} = 17.20 Hz, ^3J = 5.60 Hz, H^C), 7.15–7.50 (m, 15H aromatic).

1-O-Trityl-2-O-benzyl-3-O-allyl-sn-*glycerol* (**7**)

The previous compound (8 g, 0.021 mol) was dissolved in 40 mL of anhydrous DMF. Sodium hydride (0.026 mol) was slowly added with magnetic stirring and under dry nitrogen. Benzyl chloride (2.8 g, 0.022 mol) was then added dropwise. After 21 h stirring at room temperature the mixture was poured over ice. The organic phase was extracted 3 times with 100 mL of chloroform, washed with water, and then dried over sodium sulfate. After removal of solvent under vacum, the oil was chromatographed (200 g of silica gel, gradient hexane–ether). The compound was eluted with a hexane–ether mixture 90:10; weight 9.4 g; yield 95%; R_f 0.44 (hexane–ether 4:1); $[\alpha]_{589}$ −10.7, $[\alpha]_{578}$ −11.3, $[\alpha]_{546}$ −13.2, $[\alpha]_{436}$ −22.7 (*c* 0.021, $CHCl_3$); ^1H nmr δ ppm: 3.25 (d, ^3J = 5 Hz, C^1H_2O or C^3H_2O), 3.50–3.70 (AB part of a ABX system, J_{AB} = 10.20 Hz, J_{AX} = 5.95 ppm, J_{BX} = 4.25 Hz, 2H, C^1H_2O or C^3H_2O), 3.75 (ddt, J = 5.95 Hz, J = 4.25 Hz and J = 5 Hz, 1H, C^2HO), 3.96 (ddd, ^3J = 5.45 Hz, ^4J = 1.65 Hz, ^4J = 1.30 Hz, 2H, O-CH_2-CH=CH_2), 4.66 (syst. AB, J_{AB} = 12.35 Hz, 2H, O-CH_2-Ph), 5.15 (ddt, J_{cis} = 10.30 Hz, J_{gem} = 1.85 Hz, ^4J = 1.30 Hz, H^B), 5.23 (ddt, J_{trans} = 17.30 Hz, J_{cis} = 10.30 Hz, ^4J = 1.65 Hz, H^A), 5.86 (ddt, J_{trans} = 17.30 Hz, J_{cis} = 10.30 Hz, ^3J = 5.45 Hz, H^C), 7.15–7.50 (m, 20H aromatic).

2-O-Benzyl-3-O-allyl-sn-*glycerol* (**8**)

The trityl derivative (6 g, 0.013 mol) was dissolved in methanol (35 mL) and acidified with 1 N hydrochloric acid (3.5 mL). The solution was heated at reflux for 1 h with stirring. After cooling, the mixture was diluted with 100 mL of water. The organic phase was extracted 3 times with 50 mL of diisopropyl ether. The ether phase was washed with 20 mL of 1 N sodium hydroxide, and then with water. The organic phase was dried over magnesium sulfate. The solvent was removed and the oil was chromatographed (35 g of silica gel; eluent gradient hexane–ether). The product was eluted with a hexane–ether mixture 75:25; weight 2.33 g; yield 81%; R_f 0.56 (diisopropyl ether); $[\alpha]_{589}$ +26.1, $[\alpha]_{578}$ +27.3, $[\alpha]_{546}$ +31.3, $[\alpha]_{436}$ +53.4 (*c* 0.02, $CHCl_3$); ir: 3420 (υOH), 1670 cm^{-1} (υCH=CH_2) (allyl); ^1H nmr ($CDCl_3$) δ ppm: 2.50 (s, 1H, O*H*), 3.50–3.80 (m, 5H, C^1H_2O + C^2HO + C^3H_2O), 3.98 (dt, 2H, ^3J = 5.50 Hz, ^4J = 1.3 Hz, OCH_2-CH = CH_2), 4.57–4.73 (AB system located at 4.65 ppm with J_{AB} = 11.80 Hz, 2H, $C_6H_5CH_2O$), 5.18 (ddt, 1H, J_{cis} = 10.30 Hz, J_{gem} = 1.75 Hz, ^4J = 1.30 Hz, H^A), 5.28 (ddt, 1H, J_{trans} = 17.50 Hz, J_{gem} = 1.75 Hz, ^4J = 1.30 Hz, H^B), 5.90 (ddt, 1H, J_{trans} = 17.5 Hz, J_{cis} = 10.30 Hz, ^3J = 5.50 Hz, H^C), 7.30 (m, 5H aromatic).

Can. J. Chem. Downloaded from www.nrcresearchpress.com by 109.225.110.28 on 09/08/12
For personal use only.

2-O-Benzyl-3-propenyl-sn-*glycerol* (**9**)

Compound **8** was dried by azeotropic distillation with anhydrous benzene (50 mL) (twice) and dissolved in anhydrous and distilled DMSO (30 mL). Dry potassium *tert*-butylate (3 g) was added. The mixture was stirred and heated at 100°C. After 15 min, the reaction was complete (controlled by thin-layer chromatography (tlc); solvent diisopropyl ether: **8**, R_f 0.56, **9**, R_f 0.69). After cooling, the reaction mixture was diluted with chilled water (100 mL). The organic phase was extracted twice with diisopropyl ether then washed 4 times with water (50 mL). After drying over sodium sulfate, the solvent was eliminated under vacuum. The oil was used directly; weight 3.85 g; yield 95%; R_f 0.59 (diisopropyl ether); $[\alpha]_{589}$ +4.3, $[\alpha]_{576}$ +4.6, $[\alpha]_{546}$ +5.20, $[\alpha]_{436}$ +6.9 (*c* 0.014, $CHCl_3$); ir: 3400 (υOH), 1670 cm^{-1} (υCH=CH_2); ^1H nmr ($CDCl_3$) δ ppm: 1.59 (dd, 3H, ^3J = 6.85 Hz, ^4J = 1.70 Hz, CH=CH-CH_3), 2.30 (s, 1H, O*H*), 3.55–3.90 (m, 5H, C^1H_2O + C^2HO + C^3H_2O), 4.42 (dq, 1H, J_{cis} = 6.20 Hz, ^3J = 6.85 Hz, H^A), 4.57–4.75 (AB system located at 4.66 ppm with J_{AB} = 11.70 Hz, 2H, C_6H_5-CH_2O), 5.94 ppm (dq, 1H, J_{cis} = 6.20 Hz, ^4J = 1.70 Hz, H^B), 7.35 ppm (m, 5H, aromatic).

1-O-Hexadecyl-2-O-benzyl-3-O-propenyl-sn-*glycerol* (**12**)

Sodium hydride (0.307 g, 12.8 mmol) was added to a solution of compound **9** (1.42 g, 6.4 mmol) in anhydrous benzene (10 mL). After 30 min a solution of hexadecyl methanesulfonate (2.81 g, 8 mmol) in benzene (10 mL) was added dropwise. The mixture was then heated at 80–90°C for 5 h with stirring. After cooling, methanol (2 mL) was added. The mixture was diluted with water (50 mL). The organic phase was extracted twice with a mixture of chloroform–methanol (2:1) (75 mL), washed with water, then dried over sodium sulfate. The solvent was removed and oil chromatographed (40 g of silica gel, eluent gradient hexane–ether). The product was eluted with a mixture of hexane–ether 95:5; weight 2.27 g; yield 77%; R_f 0.85 (hexane – diisopropyl ether, 1:1); $[\alpha]_{589}$ −5.3, $[\alpha]_{578}$ −5.5, $[\alpha]_{546}$ −6.2, $[\alpha]_{436}$ −11 (*c* 0.026, $CHCl_3$); ir: 1670 cm^{-1} (υCH=CH_2); ^1H nmr ($CDCl_3$) δ ppm: 0.88 (t, 3H, *J* = 6.70 Hz, CH_3, hexadecyl), 1.25 (s, 26H, $(CH_2)_{13}$), 1.59 (dt, 3H, ^3J = 6.85 Hz, ^4J = 1.70 Hz, CH=CH-CH_3 and m, 2H, OCH_2CH_2), 3.43 (t, 3H, *J* = 6.55 Hz, OCH_2CH_2), 3.52 (d, 2H, *J* = 5 Hz, C^1H_2O or C^3H_2O), 3.70–3.95 (m, 3H, C^1H_2O or C^3H_2O and C^2HO), 4.39 (dq, 1H, J_{cis} = 6.20 Hz, ^3J = 6.85 Hz, H^A), 4.70 (s, 2H, $C_6H_5CH_2$), 5.98 (dq, 1H, J_{cis} = 6.20 Hz, ^4J = 1.70 Hz, H^B), 7.35–7.40 (m, 5H aromatic).

1-O-Myristoyl-2-O-benzyl-3-O-propenyl-sn-*glycerol* (**10**)

Myristoyl chloride (1.58 g, 7 mmol) in chloroform (5 mL) was added to a solution of compound **9** (1.42 g, 6.4 mmol) in anhydrous pyridine (3 mL) with stirring. The mixture was allowed to stand at room temperature for 36 h. The excess of acid chloride was destroyed with ice. The organic phase was extracted 3 times with chloroform (75 mL), washed successively with 2 N sulfuric acid, 10% sodium hydrogen carbonate, and water. The organic phase was dried (Na_2SO_4). After removal of solvent, the oil was chromatographed (40 g of silica gel; eluent gradient hexane – diethyl ether). The product was eluted with a mixture of hexane–ether 95:5; weight 2 g; yield 72%; R_f 0.62 (hexane – diisopropyl ether 5:1); $[\alpha]_{589}$ −1.7, $[\alpha]_{578}$ −1.7, $[\alpha]_{546}$ −1.9, $[\alpha]_{436}$ −3.8 (*c* 0.020, $CHCl_3$); ^1H nmr ($CDCl_3$) δ ppm: 0.88 (t, 3H, *J* = 6.70 Hz, CH_3, myristoyl), 1.25 (s, 20H, $(CH_2)_{10}$), 1.60 (dd, 3H, ^3J = 6.85 Hz, ^4J = 1.65 Hz, CH=CH-CH_3 and m, 2H, $COCH_2$-CH_2), 2.32 (t, 2H, *J* = 7.10 Hz, $COCH_2$), 3.70–3.90 (m, 3H, C^2HO + C^1H_2O or C^3H_2O), 4.05–4.35 (m, 2H, C^1H_2O or C^3H_2O), 4.41 (dq, 1H, J_{cis} = 6.20 Hz, ^3J = 6.85 Hz, H^A), 4.70 (s, 2H, $C_6H_5CH_2$), 5.95 (dq, 1H, J_{cis} = 6.20 Hz, ^4J = 1.65 Hz, H^B), 7.35 ppm (m, 5H aromatic).

1-O-Hexadecyl-2-O-benzyl-sn-*glycerol* (**13**)

The previous compound **12** (1.21 g, 2.6 mmol) was dissolved in tetrahydrofuran (5 mL); 0.2 M sodium phosphate buffer (pH 5) (5 mL) was added. Bromine (20 mmol) in tetrahydrofuran (10 mL) was then added dropwise with stirring to obtain a permanent yellow colour (about 1.5 mL). After 15 min, the solution was diluted with water (50 mL). The organic phase was extracted with chloroform (twice), neutralized with 10% sodium hydrogen carbonate (25 mL), washed with water, and dried over Na_2SO_4. The solvent was removed and the oil was chromatographed (40 g of silica gel, gradient hexane–ether). The compound was eluted with a mixture of hexane–ether 75:25 and 70:30; weight 0.66 g; yield 60%; R_f 0.24 (hexane – diisopropyl ether 1:1); $[\alpha]_{589}$ −12.5, $[\alpha]_{578}$ −13, $[\alpha]_{546}$ −14.8, $[\alpha]_{436}$ −25.4 (*c* 0.0189, $CHCl_3$), $[\alpha]_{589}$ −1.14, $[\alpha]_{578}$ −1.14, $[\alpha]_{546}$ −1.26, $[\alpha]_{436}$ −2.14 (*c* 0.016, methanol) (lit. (6) $[\alpha]_D$ −1.15 (methanol); and (7) $[\alpha]_D$ −1.21 (methanol); ir: 3400 cm^{-1} (υOH); ^1H nmr ($CDCl_3$) δ ppm: 0.88 (t, 3H, *J* = 6.7 Hz, CH_3 hexadecyl), 1.25 (s, 26H, $(CH_2)_{13}$), 1.57 (m, 2H, OCH_2CH_2), 2.17 (s broad, 1H, O*H*), 3.44 (t, 3H, *J* = 6.55 Hz, OCH_2CH_2), 3.47–3.85 (m, 5H, C^1H_2O + C^2HO + C^3H_2O), 4.59–4.75 (AB system located at 4.67 ppm with J_{AB} = 11.80 Hz, 2H, $C_6H_5CH_2$-O), 7.35 ppm (m, 5H aromatic).

1-O-Myristoyl-2-O-benzyl-sn-*glycerol* (**11**)

Compound **11** was prepared from compound **10** using the same procedure as for compound **13**; yield 62%; R_f 0.17 (hexane – diisopropyl ether 1:1); $[\alpha]_{589}$ −1.1, $[\alpha]_{578}$ −1.15, $[\alpha]_{546}$ −1.20, $[\alpha]_{436}$ −2.2 (*c* 0.018, $CHCl_3$); ir: 3440 cm^{-1} (υOH); ^1H nmr ($CDCl_3$) δ ppm: 0.88 (t, 3H, *J* = 6.70 Hz, CH_3, myristoyl), 1.25 (s, 20H, $(CH_2)_{10}$), 1.62 (m, 2H, $COCH_2$-CH_2), 2.06 (s broad, 1H, O*H*), 2.32 (t, 2H, *J* = 7.10 Hz, $COCH_2$), 3.55–3.80 (m, 3H, C^1H_2O + C^2HO or C^3H_2O), 4.24 (d, 2H, ^3J = 4.60 Hz, C^1H_2O or C^3H_2O), 4.57–4.75 (AB system located at 4.66 ppm with J_{AB} = 11.70 Hz, 2H, $C_6H_5CH_2$-O), 7.35 (m, 5H aromatic).

Discussion

Compounds **11** and **13** were obtained from D-mannitol with good yield. The removal of the trityl group by acid hydrolysis is easy. The transposition of the allyl double bond in propenyl is fast and complete after 15 min in the presence of dry potassium terbutylate in anhydrous dimethyl sulfoxide. The reaction is stereospecific since it leads to the *cis* isomer only, as checked by ^1H nmr.

Compound **9** is quite unstable; nevertheless we succeeded in purifying it by column chromatography. In some experiments, another compound appeared through the column, indicating a chemical reaction in the column. Compounds **10** and **12** are also unstable and it is advisable to remove the propenyl group rapidly. Once after 2 months storage, we observed the conversion of compounds **10** and **12** into compounds **11** and **13** respectively. After column chromatography, these compounds were isolated with the same physical characteristics. The ^1H nmr patterns were obtained by a selective spin–spin decoupling technique. The

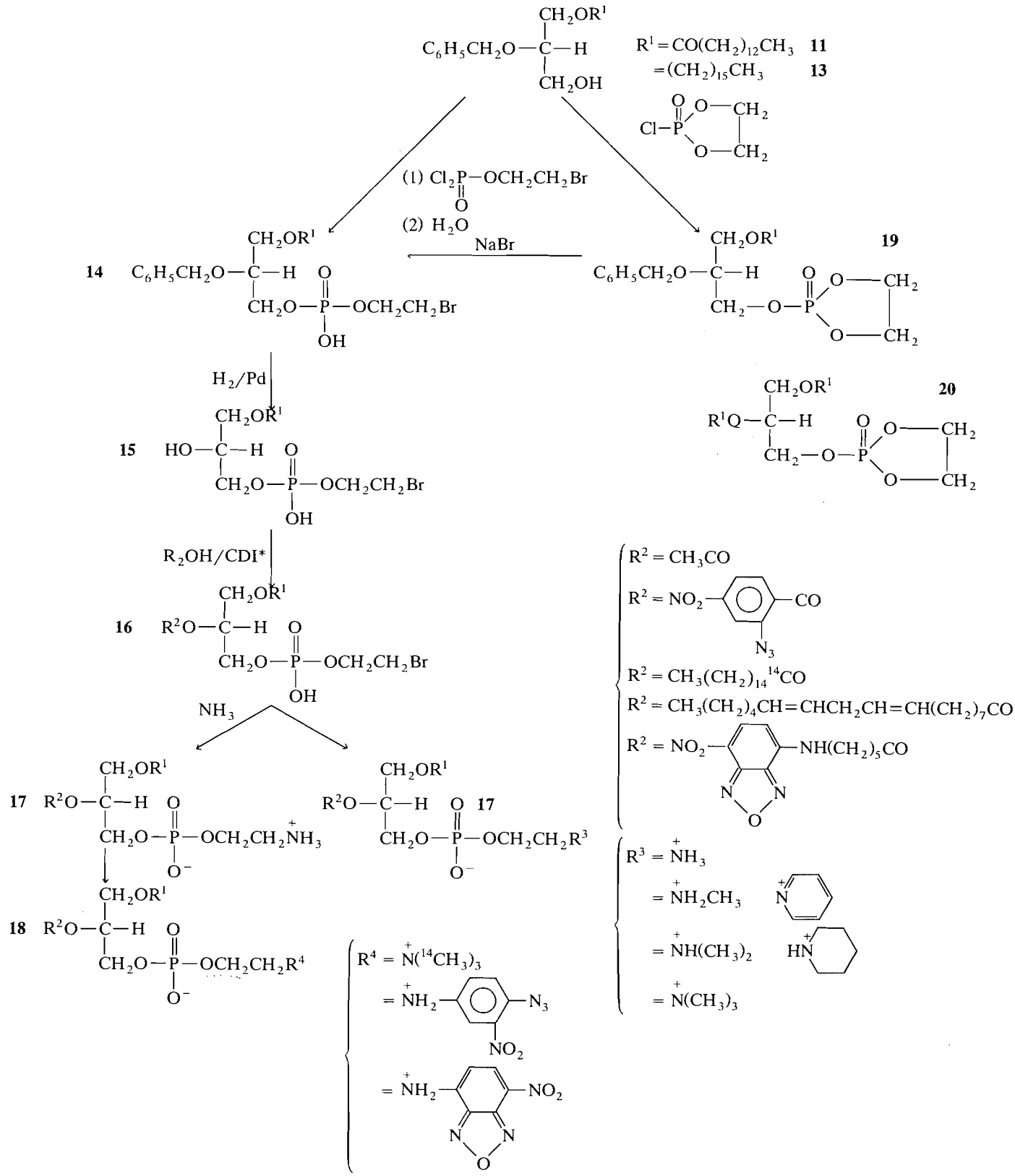

* CDI: Carbonyldiimidazole

SCHEME 2. Pathway for the synthesis of phospholipids analogues.

Can. J. Chem. Downloaded from www.nrcresearchpress.com by 109.225.110.28 on 09/08/12
For personal use only.

^{1}H nmr assignments of compound **13** are in agreement with literature (6, 9).

Optical rotations of all the compounds are specified. Enantiomeric purity of the isopropylidene-*sn*-glycerol, raw material of all the other intermediates, is the same as that obtained by Hirth and Walther (13). These authors had established by gas phase chromatography of an acetone-glycerol derivative that the optical purity of acetone-glycerol was better than 99.4%.

The optical rotation of compound **13** is very close to that given in the literature (6, 7).

We did not verify the enantiomeric purity or the eventual extent of contamination of each intermediate by a chromatographic study either with a chiral phase, as done by Takagi *et al.* (15–17), or with a normal phase for diastereoisomeric derivatives, as done by Laakso and Christie (18). However, comparison of the optical rotations of our compound **13** with those given in the literature (6, 7) allowed us to believe that the quality of the substances obtained here is sufficient to enter into other reaction sequences.

Thus, different fatty acids can be introduced on carbon-2 of compound **14** (Scheme 2). These acids can vary in fatty acid length, unsaturation, and can be either brominated and then used as fluorescent quenching agents (19) or anchored to different probe positions of fluorescent, photoactivable, or radiolabelled groups (20–25).

The polar head can be also modified from compound **16** (26–30). We synthesized the following compounds from compound **16**: 1,2-di-*O*-myristoyl-*sn*-glycero-3-phosphoryl *N*-pyridinio-2-ethanol (**17**, $R^1 = R^2 = CO(CH_2)_{12}CH_3$, $R^3 = N^+(C_5H_5)$) and 1,2-di-*O*-myristoyl-*sn*-glycero-3-phosphoryl *N*-piperidino-2 ethanol (**17**, $R^1 = R^2 = CO(CH_2)_{12}CH_3$, $R^3 = NC_5H_{10}$). We also studied the influence of an uncharged phospholipid (1,2-di-*O*-myristoyl-*sn*-glycero-3-phosphoryl-2-oxo-1,3,2-dioxaphospholane) (**20**) and of compound **16** ($R^1 = R^2 = CO(CH_2)_{12}CH_3$) on BDH reactivation (30, 31). Fluorescent, photoactivatable, or radiolabelled probes can be added to the polar head (20, 22, 32, 33, 35).

Compounds **15** ($R^1 = CO(CH_2)_{12}CH_3$ and $R^1 = (CH_2)_{15}CH_3$) allow the production of both photoactivatable groups and fluorescent probes either on the glycerol carbon-2 or on the polar head. Such molecules have recently been used in our laboratory to estimate the labelling of R-3-hydroxybutyrate dehydrogenase with phospholipids without the use of radioisotopes (35).

Acknowledgements

This work was supported by a grant from ARC, CNRS URA 040541, and INSERM CRE 877005. We thank Professor Y. Gaudemer for his encouragement.

1. M. Aglietta, W. Piacibello, F. Sanavio, and F. Gavosto. In 3rd. Int. Symp. Therapy Acute Leukemias, abstracts, Rome, December 11–14, 1982. p. 175.
2. R. Andreesen, H. Neumann, I. Dulicsch, and W. G. Lohr. Blut, **51**, 194 (1985).
3. N. Latruffe, J. M. Berrez, and M. S. El Kebbaj. Biochimie, **68**, 481 (1986).
4. B. Nasser, C. Morpain, B. Laude, and N. Latruffe. J. Lipid Mediators, **4**, 225 (1991).
5. N. Nakamura, H. Miyazaki, N. Ohkawa, H. Koike, T. Sada, F. Asai, and S. Kobayashi. Chem. Pharm. Bull. **32**, 2452 (1984).
6. M. Ohno, K. Fujita, H. Nakai, S. Kobayashi, K. Inoue, and S. Nojima. Chem. Pharm. Bull. **33**, 572 (1985).
7. T. Tsuri and S. Kamata. Tetrahedron Lett. **26**, 5195 (1985).
8. H. Eibl and P. Woolley. Chem. Phys. Lipids, **41**, 53 (1986).
9. F. Heymans, E. Michel, M. C. Borrel, B. Wichrowski, J. J. Godfroid, O. Convert, E. Coeffier, M. Tence, and J. Benveniste. Biochim. Biophys. Acta, **666**, 230 (1981).
10. S. K. Bhatia and J. Hajdu. Tetrahedron Lett. **28**, 271 (1987).
11. P. Bette-Bobillo, A. Bienvenue, C. Broquet, and L. Maurin. Chem. Phys. Lipids, **37**, 215 (1985).
12. R. G. Jensen and R. E. Pitas. Adv. Lipid Res. **14**, 213 (1976).
13. G. Hirth and W. Walther. Helv. Chim. Acta, **68**, 1863 (1985).
14. J. Cunningham and R. Gigg. J. Chem. Soc. 2968 (1965).
15. T. Takagi and Y. Itabashi. Lipids, **22**, 596 (1987).
16. T. Takagi and T. Suzuki. J. Chromatogr. **519**, 237 (1990).
17. Y. Itabashi, A. Kukis, L. Marai, and T. Takagi. J. Lipid Res. **31**, 1711 (1990).
18. P. Laakso and W. W. Christie. Lipids, **25**, 349 (1990).
19. N. Latruffe, B. Nasser, C. Morpain, J. Zirkel, M. Seiter, B. Laude, and W. Trommer. Bioelectrochem. Bioenerg. In press.
20. R. Bisson and C. Montecucco. Biochem. J. **193**, 757 (1981).
21. M. S. El Kebbaj, J. M. Berrez, T. Lakhlifi, C. Morpain, and N. Latruffe. FEBS Lett. **182**, 176 (1985).
22. C. Montecucco and G. Schiavo. Biochem. J. **237**, 309 (1986).
23. K. J. Longmuir, O. C. Martin, and R. E. Pagano. Chem. Phys. Lipids, **36**, 197 (1985).
24. P. Chakrabarti and H. G. Khorana. Biochemistry, **14**, 5021 (1975).
25. B. Wichrowski, E. Michel, F. Heymans, J. Roy, J. L. Morgat, and J. J. Godfroid. J. Labelled Compd. **20**, 991 (1983).
26. H. Eibl and A. Nicksch. Chem. Phys. Lipids, **22**, 1 (1978).
27. S. Tsushima, Y. Yoshioka, S. Tanida, H. Nomura, S. Nojima, and M. Hozumi. Chem. Pharm. Bull. **30**, 3260 (1982).
28. S. Tsushima, Y. Yoshioka, S. Tanida, H. Nomura, S. Nojima, and M. Hozumi. Chem. Pharm. Bull. **32**, 2700 (1984).
29. E. Coeffier, M. C. Borrel, J. Lefort, M. Chignard, C. Broquet, F. Heymans, J. J. Godfroid, and B. B. Vargaftig. Eur. J. Pharmacol. **131**, 179 (1986).
30. B. Nasser, C. Morpain, B. Laude, and N. Latruffe. C.R. Soc. Biol. **182**, 565 (1988).
31. B. Nasser. Thesis, University of Franche-Comte, Besançon. December, 1990.
32. A. H. Ross, R. Radhaskrishnan, R. J. Robson, and H. G. Khorana. J. Biol. Chem. **257**, 4152 (1982).
33. B. K. Burnett, R. J. Robson, Y. Takagaki, R. Radhakrishnan, and H. G. Khorana. Biochim. Biophys. Acta, **815**, 57 (1985).
34. D. K. Struck, D. Hoekstra, and R. E. Pagano. Biochemistry. **20**, 4093 (1981).
35. N. Latruffe, B. Nasser, C. Morpain, and B. Laude. Submitted.

Can. J. Chem. Downloaded from www.nrcresearchpress.com by 109.225.110.28 on 09/08/12
For personal use only.

Chiral 2-acetamidoacrylates in conjugate addition – asymmetric enolate trapping reactions. Asymmetric synthesis of phenylalanine

CARLOS CATIVIELA,[1] MARIA DOLORES DIAZ-DE-VILLEGAS, AND JOSÉ ANTONIO GALVEZ
Instituto de Ciencia de Materiales de Aragón, Departamento de Quimica Orgánica, Universidad de Zaragoza-C.S.I.C., 50009 Zaragoza, Spain

Received December 10, 1991

CARLOS CATIVIELA, MARIA DOLORES DIAZ-DE-VILLEGAS, and JOSÉ ANTONIO GALVEZ. Can. J. Chem. **70**, 2325 (1992).

A new route to the asymmetric synthesis of α-amino acids based on the reactivity of chiral 2-acetamidoacrylates with nucleophiles through a conjugate addition followed by diastereoselective protonation of the enolate is described. Phenylalanine precursors are obtained in excellent chemical yields (80–95%) with moderate diastereomeric excess (0–44%) through the reaction of chiral 2-acetamidoacrylates with phenylmagnesium bromide in the presence of CuI followed by diastereoselective enolate protonation.

CARLOS CATIVIELA, MARIA DOLORES DIAZ-DE-VILLEGAS et JOSÉ ANTONIO GALVEZ. Can. J. Chem. **70**, 2325 (1992).

On décrit une nouvelle méthode de synthèse asymétrique des acides α-aminés qui est basée sur l'addition conjuguée de nucléophiles sur des 2-acétamidoacrylates chiraux, suivie d'une protonation diastéréosélective de l'énolate. Faisant appel à une réaction des 2-acétamidoacrylates chiraux avec du bromure de phénylmagnésium en présence de CuI, suivie d'une protonation diastéréosélective de l'énolate, on a obtenu des précurseurs de la phénylalanine avec d'excellents rendements (80–95%) et des excès diastéréoisomériques modérés (0–44%).

[Traduit par la rédaction]

Introduction

Numerous new and useful approaches to the asymmetric synthesis of α-amino acids have appeared in recent years (1), most of them involving the asymmetric hydrogenation of prochiral didehydroamino acids derivatives (2) or the highly stereoselective hydrogenation of chiral, nonracemic, didehydroamino acid derivatives (3). The most recent advances in this field have concentrated on the development of chiral, optically pure, amino acid enolate equivalents (4) and amino acid cation equivalents (5). The attraction of these asymmetric amino acid equivalents is their inherent versatility in the preparation of a diverse array of amino acids from a few common precursors with the appropriate C—C bond-forming technology.

Enantioselective protonation (6) of prochiral substrates has been applied to deracemization and has been used to prepare optically active α-amino acids (7). This procedure is based on deprotonation, with a suitable base, of an asymmetric centre with an attached hydrogen activated by the electron-attracting effect of at least one substituent to afford a nucleophilic prochiral centre. Protonation of the enolate by an optically active proton carrier gives the product in optically active form.

A different methodology would be the diastereoselective protonation of chiral enolates obtained by conjugate addition of nucleophilic reagents on chiral α,β-didehydroamino acid derivatives, which would make it possible to obtain a diverse array of amino acids from a single precursor. This strategy is similar to the one developed by Opplozer and Kingma (8) to obtain chiral compounds from the corresponding α,β-unsaturated compound.

Although it was previously reported (9) that methyl 2-acetamidoacrylate can act as an acceptor in conjugate additions, to the best of our knowledge this synthetic approach has not been used to obtain amino acid derivatives stereoselectively. Therefore, we have studied the behaviour of chiral 2-acetamidoacrylates in conjugate addition – diastereoselective enolate protonation to afford phenylalanine derivatives.

Results and discussion

Chiral 2-acetamidoacrylates **1**, which can be obtained from methyl 2-acetamidoacrylate and the corresponding dimethylaluminum – chiral alcohol complex (10), can be conveniently β-functionalized by Michael addition of phenylmagnesium bromide promoted by copper(I) iodide (11). Diastereoselective protonation of the intermediate enolate in the *E*-configuration favoured by the presence of a coordinating group in the α position using saturated aqueous ammonium chloride solution provides the corresponding *N*-acetylphenylalanine esters in high chemical yields.

To understand the influence of the chiral auxiliary on the diastereofacial differentiation, this reaction was tested on a variety of chiral 2-acetamidoacrylates.

In some cases the nucleophilic prochiral centre and the chiral matrix in the enolate system are not ordered enough to restrict single-bond rotation and chirality transfer during the neutralization process is low (12). However, there are some rationally designed chiral auxiliaries that exhibit excellent reaction diastereoselection as they can incorporate non-bonding interactions to restrict rotation and have a large group that provides an effective barrier to electrophilic approach to one diastereoface of the enolate. Examples are the concave chiral auxiliaries according to Helchem's concept (13).

Conventional chiral auxiliaries (1*R*,2*S*,5*R*-(−)-menthol, 1*S*,2*R*,5*S*-(+)-menthol, and [(1*S*)-*endo*]-borneol) and concave chiral alcohols (1*R*,2*S*,5*R*-(−)-8-phenylmenthol and 1*R*,2*S*,3*R*,4*S*-(−)-*cis*-hydroxyisobornyl neopentyl ether) were used to probe the relationship between the extent of extraannular chirality transfer and the morphological aspect of the chiral alcohol (Table 1). Surprisingly, the best diastereoselectivity was obtained when menthyl esters, whose architectural features are not thought to be optimal, were used (runs 1 and 2).

From these results it can be assumed that β-functionalization of α-acetamidoacrilates provides an intermediate *E*-

[1]Author whom correspondence may be addressed.

Can. J. Chem. Downloaded from www.nrcresearchpress.com by 109.225.110.28 on 09/08/12
For personal use only.

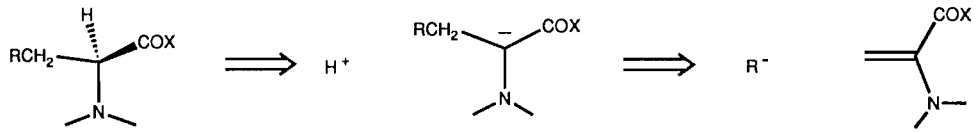

FIG. 1. Disconnection analyses for the synthesis of phenylalanine.

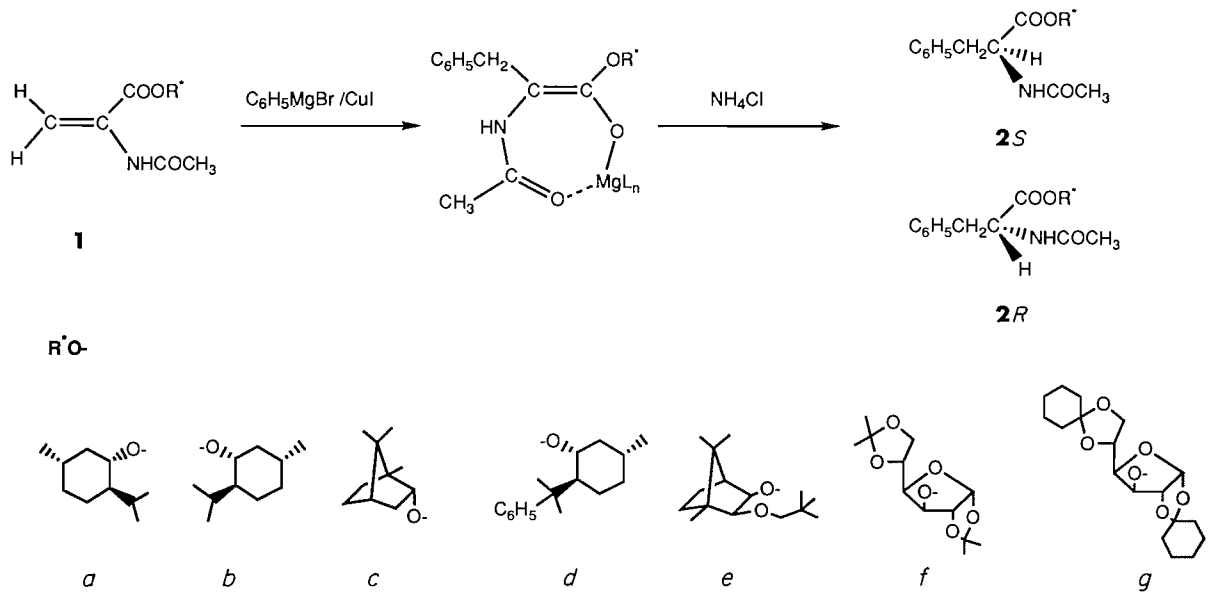

SCHEME 1

TABLE 1. Results of asymmetric conjugate addition

Run	Substrate	Yield (%)	d.e. (%)	δCH_3CONH (ppm)[a]
1	**1***a*	82	27 (*S*)	1.96, 1.99
2	**1***b*	80	28 (*R*)	1.96, 1.99
3	**1***c*	90	6[b]	1.86, 1.88
4	**1***d*	95	0	1.80, 1.83
5	**1***e*	95	10[b]	1.91 1.94
6	**1***f*	80	44 (*S*)	1.96, 2.00
7	**1***g*	83	14[b]	1.97, 2.00

[a]The underlined value corresponds to the major diastereoisomer.
[b]Absolute configuration was not determined due to the low diastereoselectivity.

enolate that possesses a large group in the α-position, which forces the chiral matrix as far as possible from the alkene moiety. As a consequence, diastereoselective protonation does not depend on the morphological aspect of the chiral alcohol since non-bonding interactions are restricted.

As previously described (14) carbohydrate ester enolates have peculiar properties because they have a marked complexing ability towards cations. D-Glucofuranose derivatives, which should provide the enolate in a more ordered geometry by intramolecular complexation of the cation, were used to improve diastereoselectivity. However, when the carbohydrate derivative 1,2:5,6-diisopropylidene-D-glucofuranose was used as a chiral auxiliary (run 6), diastereoselectivity was only slightly increased.

To understand the role of the acetamido group in the protonation of the intermediate enolate, methyl 2-acetamidoacrylate was reacted with phenylmagnesium bromide in the presence of CuI followed by protonation with saturated aqueous ammonium chloride solution, deuteration with deuterated water, or methylation with methyl iodide to afford *N*-acetylphenylalanine methyl ester, α-deutero-*N*-acetylphenylalanine methyl ester, and α-methyl-*N*-acetylphenylalanine methyl ester respectively.

From these results it can be concluded that (*a*) the unprotected -NH- group is not acidic enough to react with the organometallic reagent and (*b*) the poor level of diastereoface differentiation is not due to the presence of the -NH- acidic group competing with the electrophile since the -NH- group does not neutralize the enolate but an external proton (or electrophile) source does.

Diastereomeric excess (% d.e.) was determined by ^1H NMR integration of the acetamido singlet of each diastereomer in the crude reaction spectrum. Comparison of the sign of optical rotation at 589 nm of the methyl ester obtained by transesterification with the reported data (15), indicated the absolute configuration of each product.

Experimental

General

All reactions were carried out under Ar with magnetic stirring. Diethyl ether was distilled from sodium/benzophenone ketyl over 4 Å molecular sieves prior to use. Chiral 2-acetamidoacrylates **1***a*–**1***g* were prepared according to the previously described procedure (10). Phenylmagnesium bromide 3.0 M solution in diethyl ether and copper(I) iodide were purchased from Aldrich and were used from freshly opened bottles without purification. "Work-up" denotes extraction with diethyl ether, washing of the organic phase with water, drying with $MgSO_4$, and evaporation (rotatory evaporator).

Can. J. Chem. Downloaded from www.nrcresearchpress.com by 109.225.110.28 on 09/08/12
For personal use only.

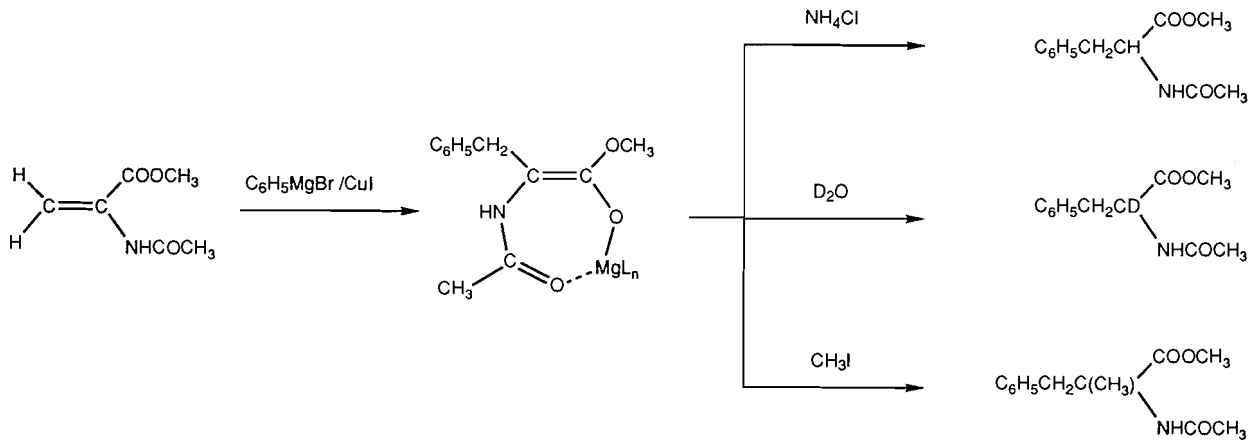

SCHEME 2

Thin-layer chromatography (TLC) was performed on Merck precoated silica gel plates. TLC plates were visualized using UV light and anisaldehyde/sulphuric acid/ethanol (2:1:100). Flash chromatography was performed using 230–400 mesh (Merck) silica gel. NMR spectra were recorded on a Varian Unity 300 MHz spectrometer. Optical rotations were measured on a Perkin–Elmer 241-C polarimeter. For polarimetric determination the measured optical rotations were compared to that of (*S*)-*N*-acetylphenylalanine methyl ester (589 nm), $[\alpha]^{25}$ +103.3 (*c* 1.2, $CHCl_3$).

Conjugate addition of phenylmagnesium bromide and subsequent diastereoselective enolate protonation

A stirred slurry of 0.027 g (0.14 mmol) of CuI in 10 mL of dry diethyl ether under an argon atmosphere was cooled to 0°C in an ice bath. A solution of 0.93 mL (2.8 mmol) of 3.0 M phenylmagnesium bromide in diethyl ether was added and, after 10 min, 1.4 mmol of the corresponding 2-acetamidoacrylate **1** dissolved in 15 mL of diethyl ether was added dropwise and stirring was continued for an additional hour at 0°C. The reaction mixture was then cooled to −80°C and quenched with saturated aqueous NH_4Cl solution. The cold bath was removed after 5 min and the mixture was allowed to warm to room temperature.

(1S,2R,5S)-Menthyl 2-acetamido-3-phenylpropanoate **2**a

Work-up afforded 0.396 g (82%) of a mixture of diastereoisomers (d.e. 27%) as a crude oil that was chromatographed on a silica gel column (230–400 mesh) eluting with methylene chloride/diethyl ether (2:1). ^{1}H NMR of the major diastereoisomer, δ: 0.72 (d, 3H), 0.87 (d, 3H), 0.90 (d, 3H), 0.96–2.10 (m, 9H), 1.96 (s, 3H), 3.00–3.49 (m, 2H), 4.67 (dt, 1H), 4.85 (dd, 1H), 5.84 (d, 1H), 7.11–7.15 (m, 2H), 7.23–7.32 (m, 3H). ^{13}C NMR of the major diastereoisomer, δ: 15.8, 20.8, 21.9, 23.1, 25.8, 31.3, 34.0, 37.9, 40.5, 46.7, 53.3, 76.0, 127.0, 128.5, 129.3, 135.9, 169.5, 171.5. Anal. calcd. for $C_{21}H_{31}NO_3$: C 73.01, H 9.04, N 4.05; found: C 72.98, H, 9.19, N 3.87.

(1R,2S,5R)-Menthyl 2-acetamido-3-phenylpropanoate **2**b

Work-up afforded 0.386 g (80%) of a mixture of diastereoisomers (d.e. 28%) as a crude oil that was chromatographed on a silica gel column (230–400 mesh) eluting with methylene chloride/diethyl ether (2:1). ^{1}H NMR of the major diastereoisomer, δ: 0.72 (d, 3H), 0.87 (d, 3H), 0.90 (d, 3H), 0.96–2.10 (m, 9H), 1.96 (s, 3H), 3.00–3.49 (m, 2H), 4.67 (dt, 1H), 4.85 (dd, 1H), 5.84 (d, 1H), 7.11–7.15 (m, 2H), 7.23–7.32 (m, 3H). ^{13}C NMR of the major diastereoisomer, δ: 15.8, 20.8, 21.9, 23.1, 25.8, 31.3, 34.0, 37.9, 40.5, 46.7, 53.3, 76.0, 127.0, 128.5, 129.3, 135.9, 169.5, 171.5. Anal. calcd. for $C_{21}H_{31}NO_3$: C 73.01, H 9.04, N 4.05; found: C 73.12, H, 9.13, N 4.17.

[(1S)-endo]-Bornyl 2-acetamido-3-phenylpropanoate **2**c

Work-up afforded 0.432 g (90%) of a mixture of diastereoisomers (d.e. 6%) as a crude oil that was chromatographed on a silica gel column (230–400 mesh) eluting with methylene chloride/diethyl ether (2:1). ^{1}H NMR of the major diastereoisomer, δ: 0.69 (s, 3H), 0.76 (s, 3H), 0.79 (s, 3H), 0.84–1.36 (m, 3H), 1.48–1.80 (m, 3H), 1.86 (s, 3H), 2.10–2.29 (m, 1H), 2.92–3.08 (m, 2H), 4.69–4.87 (m, 2H), 6.47 (d, 1H), 7.02–7.24 (m, 5H). ^{13}C NMR of the major diastereoisomer, δ: 13.2, 18.5, 19.3, 22.6, 26.7, 27.5, 35.9, 37.8, 44.4, 47.5, 48.4, 53.0, 81.1, 126.7, 128.2, 129.0, 135.8, 169.5, 171.9. Anal. calcd. for $C_{21}H_{29}NO_3$: C 73.44, H 8.51, N 4.08; found: C 73.32, H, 8.38, N 4.23.

(1R,2S,5R)-8-Phenylmenthyl 2-acetamido-3-phenylpropanoate **2**d

Work-up afforded 0.559 g (95%) of a mixture of diastereoisomers (d.e. 0%) as a crude oil that was chromatographed on a silica gel column (230–400 mesh) eluting with hexane/diethyl ether (1:3). ^{1}H NMR of the mixture of diastereoisomers, δ: (0.79 d, 0.82 d) 3H; (1.12 s, 1.13 s) 3H; (1.21 s, 1.23 s) 3H; (0.88–2.08 m) 8H; (1.80 s, 1.83 s) 3H; (2.61–2.97 m) 2H; (4.16 dd, 4.34 dd) 1H; (4.75 dt, 4.81 dt) 1H; (5.61 d, 5.75 d) 1H; (7.15–7.32 m) 10H. ^{13}C NMR of the mixture of diastereoisomers, δ: (21.4, 21.5); (22.7, 22.8); (26.1, 26.5); 27.0; 28.8; (30.9, 31.0); (34.1, 34.2); (36.6, 36.9); (39.1, 39.5); (41.0, 41.1); (49.7, 49.9); (52.7, 53.6); (75.8, 76.0); 125.0; 125.1; 126.5; (127.7, 127.8); (128.0, 128.1); 129.2; (136.1, 136.2); (150.9, 151.6); 169.1; (170.1, 170.5). Anal. calcd. for $C_{27}H_{35}NO_3$: C 76.93, H 8.37, N 3.32; found: C 74.12, H, 8.21, N 3.11.

*(1R,2S,3R,4S)-*cis*-3-Hydroxyisobornyl neopentyl ether 2-acetamido-3-phenylpropanoate* **2**e

Work-up afforded 0.570 g (95%) of a mixture of diastereoisomers (d.e. 10%) as a crude oil that was chromatographed on a silica gel column (230–400 mesh) eluting with hexane/diethyl ether (2:1). ^{1}H NMR of the major diastereoisomer, δ: 0.78 (s, 3H), 0.83 (s, 9H), 0.90 (s, 3H), 1.05 (s, 3H), 0.98–1.08 (m, 2H), 1.40–1.54 (m, 1H), 1.61–1.76 (m, 2H), 1.94 (s, 3H), 2.99 (s, 2H), 3.01–3.22 (m, 2H), 3.24 (d, 1H), 4.68 (t, 1H), 4.81–4.91 (m, 1H), 6.43 (d, 1H), 7.08–7.15 (m, 2H), 7.17–7.33 (m, 3H). ^{13}C NMR of the major diastereoisomer, δ: 11.1, 18.0, 20.3, 20.6, 22.6, 23.7, 26.4, 26.5, 32.0, 32.9, 37.7, 46.6, 49.1, 49.5, 53.1, 79.1, 83.0, 87.1, 126.6, 128.1, 129.1, 136.0, 169.3, 170.8. Anal. calcd. for $C_{26}H_{39}NO_4$: C 72.69, H 9.15, N 3.26; found: C 72.92, H, 8.91, N 3.32.

1,2:5,6-Di-O-Isopropylidene-D-glucofuranosyl 2-acetamido-3-phenylpropanoate **2**f

Work-up afforded 0.502 g (80%) of a mixture of diastereoisomers (d.e. 44%) as a crude oil that was chromatographed on a sil-

Can. J. Chem. Downloaded from www.nrcresearchpress.com by 109.225.110.28 on 09/08/12
For personal use only.

ica gel column (230–400 mesh) eluting with methylene chloride/diethyl ether (3:1). ^{1}H NMR of the major diastereoisomer, δ: 1.28 (s, 3H), 1.29 (s, 3H), 1.40 (s, 3H), 1.51 (s, 3H), 1.96 (s, 3H), 3.03–3.29 (m, 2H), 4.01–4.42 (m, 4H), 4.55 (d, 1H), 4.83–5.03 (m, 1H), 5.31 (d, 1H), 5.88 (d, 1H), 5.91 (d, 1H), 7.17–7.25 (m, 2H), 7.28–7.36 (m, 3H). ^{13}C NMR of the major diastereoisomer, δ: 22.9, 24.2, 24.3, 24.8, 25.6, 37.5, 52.8, 67.2, 71.9, 77.1, 79.8, 82.5, 104.7, 110.2, 113.1, 127.1, 128.4, 129.4, 135.7, 169.7, 170.6. Anal. calcd. for $C_{23}H_{31}NO_8$: C 61.46, H 6.95, N 3.12; found: C 61.22, H, 6.91, N 2.98.

1,2:5,6-Di-O-cyclohexylidene-D-glucofuranosyl 2-acetamido-3-phenylpropanoate **2**g

Work-up afforded 0.614 g (83%) of a mixture of diastereoisomers (d.e. 14%) as a crude oil that was chromatographed on a silica gel column (230–400 mesh) eluting with methylene chloride/diethyl ether (3:1). ^{1}H NMR of the major diastereoisomer, δ: 1.25–1.76 (m, 20H), 1.97 (s, 3H), 3.01–3.24 (m, 2H), 3.91–4.39 (m, 4H), 4.50 (d, 1H), 4.83–4.95 (m, 1H), 5.27 (d, 1H), 5.88 (d, 1H), 5.91 (d, 1H), 7.15–7.22 (m, 2H), 7.25–7.35 (m, 3H). ^{13}C NMR of the major diastereoisomer, δ: 22.9, 23.5, 23.7, 23.9, 24.7, 25.0, 34.6, 35.5, 36.2, 36.6, 37.4, 38.1, 52.8, 67.2, 71.9, 77.0, 79.8, 82.6, 104.7, 110.1, 113.0, 127.2, 128.5, 129.4, 135.7, 169.7, 170.7. Anal. calcd. for $C_{29}H_{39}NO_8$: C 65.77, H 7.42, N 2.64; found: C 65.52, H, 7.45, N 2.38.

Transesterification to methyl 2-acetamido-3-phenyl-propanoate

A mixture of diastereoisomers (27% d.e.) of purified (−)-menthyl 2-acetamido-3-phenylpropanoate **1***a* (0.5 g, 1.4 mmol) and absolute methanol saturated with dry HCl gas (30 mL) were placed in a glass pressure tube and the mixture was heated at 75°C for 2 h. Upon cooling, the reaction mixture was evaporated to dryness and the residue was chromatographed on a silica gel column (230–400 mesh) using diethyl ether/hexane (1:1) as eluent to afford the corresponding methyl 2-acetamido-3-phenylpropanoate in 30% optical purity mixture of enantiomers; $[\alpha]^{25}$ +31.7 (*c* 1.2, $CHCl_3$).

Acknowledgment

This work was supported by the Dirección General de Investigación Cientifica y Técnica, project number PB 88-0038. J. A. G. would like to express his gratitude to the Ministerio de Educacion y Ciencia for a grant.

1. (*a*) M. J. O'Donnell (*Editor*). α-Amino acid synthesis. Tetrahedron Symposia-in-Print Number 33, Pergamon Press, Oxford. 1988. p. 5253; (*b*) R. M. Williams. Synthesis of optically active α-amino acids. Pergamon Press, Oxford. 1989.
2. J. D. Morrison (*Editor*). Asymmetric synthesis, chiral catalysis. Vol. **5**. Academic Press, Orlando, Fla. 1985.
3. (*a*) J. P. Vigneron, H. Kagan, and A. Horeau. Tetrahedron Lett. 5681 (1968); (*b*) E. J. Corey, R. J. McCaully, and H. S. Sachdev. J. Am. Chem. Soc. **92**, 2476 (1970); (*c*) E. J. Corey, H. S. Sachdev, J. Z. Gougoutas, and W. Saenger. J. Am. Chem. Soc. **92**, 2488 (1970).
4. (*a*) U. Schollkopf, T. Tiller, and J. Bardenhagen. Tetrahedron, **44**, 5293 (1988); (*b*) A. El Achqar, M. Boumzebra, M. L. Roumestant, and P. Viallefont. Tetrahedron, **44**, 5319 (1988); (*c*) R. M. Williams and M. N. Im. Tetrahedron Lett. **29**, 6075 (1988); (*d*) J. M. McIntosh, R. K. Leavitt, P. Mishra, K. C. Cassidy, J. E. Drake, and R. Chadha. J. Org. Chem. **53**, 1947 (1988); (*e*) W. Oppolzer, R. Moretti, and S. Thomi. Tetrahedron Lett. **30**, 6009 (1989); (*f*) A. Solladie-Cavallo and M. C. Simon. Tetrahedron Lett. **30**, 6011 (1989); (*g*) R. Polt and D. Seebach. J. Am. Chem. Soc. **111**, 2622 (1989); (*h*) J. F. Dellaria and B. D. Santarsiero. J. Org. Chem. **54**, 391 (1989); (*i*) I. Ojima, T. Komata, and X. Qiu. J. Am. Chem. Soc. **112**, 770 (1990); (*j*) L. Casella, M. Gullotti, G. Jommi, R. Pagliarin, and M. Sisti. J. Chem. Soc. Perkin Trans. 2, 771, (1990); (*k*) M. Ihara, M. Takahashi, N. Taniguchi, K. Yasui, H. Niitsuma, and K. Fukumoto. J. Chem. Soc. Perkin Trans. 1, 525 (1991).
5. (*a*) U. Schollkopf, S. Gruttner, R. Anderskewitz, E. Egert, and M. Dyrbusch. Angew. Chem. Int. Ed. Engl. **26**, 683 (1987); (*b*) Y. Yamamoto and W. Ito. Tetrahedron, **44**, 5415 (1988); (*c*) P. Ermert, J. Meyer, C. Stucki, J. Schneebeli, and J. P. Obrecht. Tetrahedron Lett. **29**, 1265 (1988); (*d*) K. E. Harding and C. S. Davis. Tetrahedron Lett. **29**, 1891 (1988); (*e*) R. M. Williams, J. P. Sinclair, D. Zhai, and D. Chen. J. Am. Chem. Soc. **110**, 1547 (1988); (*f*) R. M. Williams and J. A. Hendrix. J. Org. Chem. **55**, 3723 (1990); (*g*) C. Agami, F. Couty, J. C. Daran, B. Prince, and C. Puchot. Tetrahedron Lett. **31**, 2889 (1990); (*h*) A. Papadopoulos, B. Lewall, E. Steckhan, K. D. Ginzel, F. Knoch, and M. Nieger. Tetrahedron, **47**, 563 (1991).
6. (*a*) L. Duhamel, P. Duhamel, J. C. Launay, and J. C. Plaquevent. Bull. Soc. Chim. Fr. 1984, 421; (*b*) U. Gerlach and S. Hunig. Angew. Chem. Int. Ed. Engl. **26**, 1283 (1987); (*c*) C. Fehr and J. Galindo. J. Am. Chem. Soc. **110**, 6909 (1988); (*d*) D. Potin, K. Williams, and J. Rebek. Angew. Chem. Int. Ed. Engl. **29**, 1420 (1990).
7. (*a*) L. Duhamel and J. C. Plaquevent. Tetrahedron Lett. **21**, 2521 (1980); (*b*) Bull. Soc. Chim. Fr. 75 (1982); (*c*) L. Duhamel, S. Fouquay, and J. C. Plaquevent. Tetrahedron Lett. **27**, 4975 (1986); (*d*) L. Duhamel, P. Duhamel, S. Fouquay, J. J. Eddine, O. Peschard, J. C. Plaquevent, A. Ravard, R. Solliard, J. Y. Valnot, and H. Vincens. Tetrahedron, **44**, 5495 (1988).
8. W. Oppolzer and A. J. Kingma. Helv. Chim. Acta, **72**, 1337 (1989).
9. C. Cardellicchio, V. Fiandanese, G. Marchese, F. Naso, and L. Ronzini. Tetrahedron Lett. **26**, 4387 (1985).
10. C. Cativiela, M. D. Diaz de Villegas, and J. A. Galvez. Synthesis, 198 (1990).
11. G. H. Posner. Org. React. **19**, 1 (1972).
12. D. A. Evans. Asymmetric synthesis, stereodifferenciating addition reactions. Vol. **5**. *Edited by* J. D. Morrison. Academic Press, Orlando, Fla. 1985. pp. 93–100, and references therein.
13. (*a*) G. Helmchen and R. Schmierer. Angew. Chem. Int. Ed. Engl. **20**, 205 (1981); (*b*) R. Schmierer, G. Grotemeier, G. Helmchen, and A. Selim. Angew. Chem. Int. Ed. Engl. **20**, 207 (1981).
14. H. Kunz and J. Mohr. J. Chem. Soc. Chem. Commun. 1315 (1988).
15. R. Glaser, S. Geresh, J. Blumenfeld, B. Vainas, and M. Twaik. Isr. J. Chem. **15**, 17 (1976).

Can. J. Chem. Downloaded from www.nrcresearchpress.com by 109.225.110.28 on 09/08/12
For personal use only.

Crystal and molecular structure of an unusual unsymmetrical isomer of 1,2-$Os_3(CO)_{10}\{P(C_6H_5)[(\eta\text{-}C_5H_4)Fe(\eta\text{-}C_5H_5)]_2\}_2$

WILLIAM R. CULLEN,[1] STEVEN J. RETTIG, AND TU CAI ZHENG
Chemistry Department, University of British Columbia, 2036 Main Mall, Vancouver, B.C., Canada V6T 1Z1

Received March 3, 1992

WILLIAM R. CULLEN, STEVEN J. RETTIG, and TU CAI ZHENG. Can. J. Chem. **70**, 2329 (1992).

The reaction of $Os_3(CO)_{10}(MeCN)_2$ with PFc_2Ph (Fc = $(\eta\text{-}C_5H_4)Fe(\eta\text{-}C_5H_5)$) affords the unsymmetrical isomer of 1,2-$Os_3(CO)_{10}(PFc_2Ph)_2$, **2**. Crystals of **2** are monoclinic, a = 27.846(4), b = 11.253(4), c = 38.520(3) Å, β = 107.813(9)°, Z = 8, space group $C2/c$. The structure was solved by heavy atom methods and was refined by full-matrix least-squares procedures to R = 0.030 and R_w = 0.027 for 5073 reflections with $I \geq 3\sigma(I)$.

WILLIAM R. CULLEN, STEVEN J. RETTIG et TU CAI ZHENG. Can. J. Chem. **70**, 2329 (1992).

La réaction du $Os_3(CO)_{10}(MeCN)_2$ avec le PFc_2Ph (Fc = $(\eta\text{-}C_5H_4)Fe(\eta\text{-}C_5H_5)$) conduit à l'isomère dissymétrique du composé $Os_3(CO)_{10}$-1,2-$(PFc_2Ph)_2$, **2**. Les cristaux du composé **2** appartiennent au groupe d'espace monoclinique $C2/c$ avec a = 27,846(4), b = 11,253(4), c = 38,520(3) Å, β = 107,813(9)°, Z = 8. On a résolu la structure par la méthode des atomes lourds et on l'a affinée par la méthode des moindres carrés, matrice complète, jusqu'à des valeurs de R = 0,030 et de R_w = 0,027 pour 5073 réflexions avec $I \geq 3\sigma(I)$.

[Traduit par la rédaction]

Introduction

Tertiary phosphine substituted triosmium carbonyl cluster compounds of the type $Os_3(CO)_{10}L_2$ (L = monodentate phosphine) can be synthesized by using a number of procedures (1, 2). Because thermal and photochemical reactions of the phosphines L with $Os_3(CO)_{12}$ usually give a mixture of mono-, di-, and tri-substituted products, $Os_3(CO)_{10}$-$(MeCN)_2$ or $Os_3(CO)_{10}(C_8H_{14})_2$ (C_8H_{14} = cyclooctene) have been widely used as precursors for high-yield syntheses of $Os_3(CO)_{10}L_2$ compounds (1–11). Many compounds of this type have been isolated and some were subjected to structure analyses in order to better understand the bonding in these complexes (1, 2). Phosphines are always found to occupy the equatorial sites due to their bulkiness, but three structural isomers for $Os_3(CO)_{10}L_2$, **1***a*–**1***c*, are possible (10).

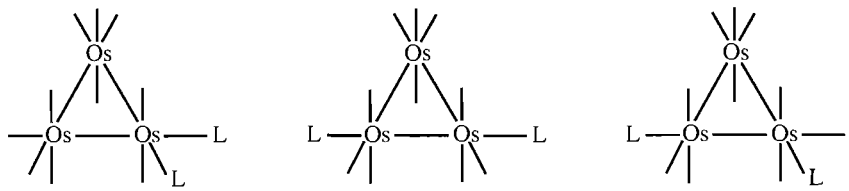

1*a* **1***b* **1***c*

The 1,1-isomers **1***a* have to be synthesized by using Os_3 $(CO)_{10}(\eta^4\text{-}C_4H_6)$ (C_4H_6 = *cis*-buta-1,3-diene) as precursor because the diene is coordinated at an axial and an equatorial site at one osmium atom (9, 10, 12). The 1,2-isomers are easily synthesized from the reaction of phosphines with either $Os_3(CO)_{10}(MeCN)_2$ or $Os_3(CO)_{10}(C_8H_{14})_2$ or $Os_3(CO)_{10}(\eta^4$-$C_4H_6)$ (here C_4H_6 = *trans*-buta-1,3-diene) (7, 10). Usually only the symmetrical 1,2-isomers **1***b* are obtained even if different reaction procedures are employed. This has been attributed to the bulkiness of the ligands that tend to react with the cluster so as to be as far away from each other as possible. On this basis smaller phosphines such as PMe_2Ph or PEt_3, of cone angles 122° and 132° respectively (13, 14), might be expected to afford a mixture of **1***b* and **1***c*, or even pure **1***c*. In fact nmr spectroscopic studies show that 1,2-$Os_3(CO)_{10}(PMe_2Ph)_2$ exists as a rapidly interconverting mixture of both isomers **1***b* and **1***c* (7, 10), but 1,2-$Os_3(CO)_{10}(PEt_3)_2$ is reported to exist only as the unsymmetrical isomer **1***c* (15). These results suggest that electronic effects also play a part in determining the molecular geometry.

In this report, we describe the reaction of $Os_3(CO)_{10}$-$(MeCN)_2$ with PFc_2Ph, which affords the unsymmetrical isomer of 1,2-$Os_3(CO)_{10}(PFc_2Ph)_2$, **2**, exclusively. This is a surprising result in view of the fact that PFc_2Ph is a very bulky ligand with a cone angle of 178° (16). The unusual electronic effect of the PFc_2Ph ligand is discussed together with a description of the crystal structure of **2**.

Experimental

Reactions were carried out under an argon atmosphere. The ^1H and ^{31}P nmr chemical shifts are given in ppm from TMS and 85% H_3PO_4, respectively, and were recorded by using a Bruker AC-200 spectrometer. Elemental analysis was performed by Mr. Peter Borda of this department. PFc_2Ph was prepared as previously described (16). The fast atom bombardment (FAB) mass spectrum was obtained by using an AEI MS-9 spectrometer and 3-nitrobenzyl alcohol as matrix.

[1]Author to whom correspondence may be addressed.

Can. J. Chem. Downloaded from www.nrcresearchpress.com by 109.225.110.28 on 09/08/12
For personal use only.

Can. J. Chem. Downloaded from www.nrcresearchpress.com by 109.225.110.28 on 09/08/12
For personal use only.

Preparation of $Os_3(CO)_{10}(PFc_2Ph)_2$, 2

To a stirred solution of triosmium dodecacarbonyl (365 mg, 0.4 mmol) in dichloromethane (50 mL) was added acetonitrile (5 mL, excess) and trimethylamine oxide (67 mg, 0.9 mmol) (6). After 2 h, PFc_2Ph (385 mg, 0.8 mmol) was added to the above mixture and after another 2 h the solvent was removed under reduced pressure. The residue was applied to a silica chromatographic column and eluted with 4:1 petroleum ether/CH_2Cl_2. Some very small bands were not collected. The only major product **2** (75%) eluted as the fourth (orange) band; $^{31}P\{^1H\}$ nmr σ: −25.4, −29.8; ^1H nmr σ: 7.76(m, 2H), 7.28(bm, 8H), 4.54(m, 4H), 4.46(m, 4H), 4.40(m, 2H), 4.24(m, 14H), 4.14(s, 10H), 4.04(m, 2H). Mass spectrum (FAB) *m/z*: 1809 (base peak), 1781, 1753, 1725, 1697, 1669, 1648, 1641, 1620, 1613, 1596, 1585. Anal. calcd. for $C_{62}H_{46}Fe_4O_{10}Os_3P_2$: C 41.21, H 2.57; found: C 41.21, H 2.62.

X-ray crystallographic analysis of 2

X-ray quality crystals of **2** were obtained by slow evaporation of the eluting solvent following chromatographic separation. An orange crystal ca. 0.07 × 0.27 × 0.35 mm in size was mounted on a glass fiber. Unit-cell parameters were refined by least squares on setting angles for 25 reflections (2θ = 28.0–30.6°) measured on a diffractometer with Mo-K_α radiation (λ = 0.71069 Å). Crystal data at 21°C are as follows:

$C_{62}H_{46}Fe_4O_{10}Os_3P_2$ f.w. = 1806.97

Monoclinic, a = 27.846(4), b = 11.253(4), c = 38.520(3) Å, β = 107.813(9)°, V = 11492(5) Å^3, Z = 8, ρ_c = 2.089 Mg m^{-3}, $F(000)$ = 6880, μ(Mo-K_α) = 77.09 cm^{-1}. Absent reflections: *hkl*, *h+k* odd, and *h01*, *l* odd, space group $C2/c$ (No. 15) from structure analysis.

Intensities were measured with graphite-monochromated Mo-K_α radiation on a Rigaku AFC6S diffractometer. An ω scan at 32° min^{-1} over a range of (0.85 + 0.35 tan θ)° in ω (with up to 8 rescans, background/scan time ratio = 0.5) was employed. Data were measured to 2θ = 50°. The intensities of three check reflections, measured every 200 reflections throughout the data collection, showed only small random variations. After data reduction[2] an empirical absorption correction, based on azimuthal scans for three reflections, was applied. Transmission factors range from 0.42 to 1.00. Of the 10 914 reflections measured, 10 662 were unique (R_{merge} = 0.037) and 5073 had intensities greater than or equal to $3\sigma(F^2)$ above background where $\sigma^2(F^2) = [S^2(C + 4B) + (0.01F^2)^2]/Lp^2$ with S = scan speed, C = scan count, B = total background count, and Lp = Lorentz–polarization factor.

The structure was solved by heavy atom methods, the Os and Fe coordinates being determined from the Patterson function. The analysis was initiated in the centrosymmetric space group $C2/c$ on the basis of the Patterson function, this choice being confirmed by the successful solution and refinement of the structure. The remaining non-hydrogen atoms were positioned from subsequent difference Fourier syntheses. The non-hydrogen atoms were refined with anisotropic thermal parameters and the hydrogen atoms were fixed in calculated positions (C—H = 0.98 Å, B_H = 1.2 $B_{bonded\ atom}$). Scattering factors for all atoms and anomalous dispersion corrections for the non-hydrogen atoms were taken from ref. (17). The weighting scheme $w = 4F_o/\sigma^2(F_o^2)$ gave uniform average values of $w(|F_o|-|F_c|)^2$ over ranges of both $|F_o|$ and sin θ/λ and was employed in the final stages of full matrix least-squares refinement of 730 variables. Reflections with $I < 3\sigma(F^2)$ were not included in the refinement. Convergence was reached at R = 0.030 and R_w = 0.027 for 5073 reflections with $I \geq 3\sigma(I)$. The function minimized was $\Sigma w(|F_o|-|F_c|)^2$, $R = \Sigma||F_o|-|F_c||/\Sigma|F_o|$, $R_w = (\Sigma w(|F_o|-|F_c|)^2/\Sigma w|F_o|^2)^{1/2}$.

[2]TEXSAN/TEXRAY structure analysis package, which includes versions of the following: MITHRIL, integrated direct methods, by C. J. Gilmore, DIRDIF, direct methods for difference structures, by P. T. Beurskens, ORFLS, full-matrix least-squares and ORFFE, function and errors, by W. R. Busing, K. O. Martin, and H. A. Levy, ORTGPII, illustrations, by C. K. Johnson.

TABLE 1. Final atomic coordinates (fractional) and B_{eq} (Å^2)[a]

Atom	x	y	z	B_{eq}
Os(1)	0.38378(1)	0.12059(4)	0.11053(1)	2.94(2)
Os(2)	0.28821(1)	0.10866(4)	0.12711(1)	3.43(2)
Os(3)	0.33150(2)	0.33778(4)	0.12016(1)	3.42(2)
Fe(1)	0.45822(5)	0.2944(1)	0.2118(3)	3.44(6)
Fe(2)	0.55100(6)	−0.0416(1)	0.13542(4)	4.44(7)
Fe(3)	0.19805(5)	−0.2191(1)	0.05551(4)	3.90(7)
Fe(4)	0.20666(6)	−0.0703(1)	0.20456(4)	4.33(7)
P(1)	0.46150(9)	0.2029(2)	0.11066(6)	2.7(1)
P(2)	0.2762(1)	−0.0932(2)	0.13877(6)	3.2(1)
O(1)	0.4010(3)	−0.1316(7)	0.0891(2)	6.9(5)
O(2)	0.4262(3)	0.0581(7)	0.1921(2)	5.4(4)
O(3)	0.3343(3)	0.161(1)	0.0285(2)	7.6(5)
O(4)	0.1886(3)	0.2153(9)	0.1275(3)	9.0(6)
O(5)	0.3368(3)	0.1563(8)	0.2090(2)	6.4(4)
O(6)	0.2438(3)	0.0862(8)	0.0437(2)	7.7(5)
O(7)	0.2547(3)	0.4562(8)	0.1507(2)	7.4(5)
O(8)	0.3807(3)	0.5576(7)	0.0996(2)	6.0(4)
O(9)	0.4092(3)	0.3375(7)	0.1961(2)	5.6(4)
O(10)	0.2610(4)	0.3415(8)	0.0408(2)	8.6(5)
C(1)	0.4636(4)	0.3096(8)	0.0754(2)	3.0(4)
C(2)	0.5094(3)	0.3448(9)	0.0692(2)	3.4(4)
C(3)	0.4993(4)	0.440(1)	0.0445(3)	4.1(5)
C(4)	0.4472(4)	0.4649(9)	0.0349(2)	3.8(5)
C(5)	0.4247(4)	0.384(1)	0.0532(2)	3.6(4)
C(6)	0.4363(4)	0.130(1)	0.0022(2)	4.1(5)
C(7)	0.4856(4)	0.149(1)	0.0016(3)	4.3(5)
C(8)	0.4846(4)	0.248(1)	−0.0210(3)	4.8(6)
C(9)	0.4333(5)	0.286(1)	−0.0345(2)	4.6(5)
C(10)	0.4032(4)	0.214(1)	−0.0202(3)	4.7(5)
C(11)	0.5123(3)	0.1036(9)	0.1090(2)	3.1(4)
C(12)	0.5652(4)	0.128(1)	0.1248(2)	4.3(5)
C(13)	0.5927(4)	0.049(1)	0.1101(3)	4.7(5)
C(14)	0.5593(4)	−0.023(1)	0.0855(3)	4.0(5)
C(15)	0.5094(4)	0.007(1)	0.0846(2)	3.6(5)
C(16)	0.5249(9)	−0.108(2)	0.1753(6)	10(1)
C(17)	0.575(1)	−0.068(2)	0.1902(4)	10(1)
C(18)	0.6039(7)	−0.133(2)	0.1743(5)	9(1)
C(19)	0.5730(8)	−0.211(1)	0.1492(5)	8(1)
C(20)	0.5238(7)	−0.195(2)	0.1491(6)	10(1)
C(21)	0.2588(3)	−0.198(1)	0.1011(2)	3.3(4)
C(22)	0.2742(4)	−0.198(1)	0.0685(3)	4.1(5)
C(23)	0.2590(4)	−0.305(1)	0.0500(3)	5.2(6)
C(24)	0.2358(5)	−0.375(1)	0.0701(3)	5.4(6)
C(25)	0.2356(4)	−0.308(1)	0.1013(3)	4.7(6)
C(26)	0.1517(4)	−0.076(1)	0.0486(3)	5.4(6)
C(27)	0.1604(4)	−0.107(1)	0.0155(3)	5.2(6)
C(28)	0.1438(4)	−0.222(1)	0.0052(3)	6.2(7)
C(29)	0.1246(4)	−0.267(1)	0.0319(4)	7.0(8)
C(30)	0.1295(4)	−0.177(2)	0.0587(3)	6.8(8)
C(31)	0.2272(4)	−0.1244(9)	0.1597(2)	3.4(4)
C(32)	0.1778(4)	−0.072(1)	0.1491(2)	4.0(5)
C(33)	0.1477(4)	−0.139(1)	0.1651(3)	4.6(5)
C(34)	0.1767(4)	−0.231(1)	0.1863(3)	5.0(6)
C(35)	0.2259(4)	−0.224(1)	0.1831(3)	4.5(5)
C(36)	0.2582(6)	0.028(2)	0.2439(5)	7(1)
C(37)	0.218(1)	0.096(1)	0.2240(4)	8(1)
C(38)	0.1751(7)	0.053(2)	0.2293(6)	9(1)
C(39)	0.1864(9)	−0.045(2)	0.2502(5)	9(1)
C(40)	0.2386(8)	−0.059(1)	0.2595(3)	7.1(8)
C(41)	0.4934(3)	0.2918(9)	0.1513(2)	2.8(4)
C(42)	0.4952(4)	0.415(1)	0.1509(3)	3.8(5)
C(43)	0.5177(4)	0.478(1)	0.1829(3)	4.3(5)
C(44)	0.5378(4)	0.418(1)	0.2151(3)	4.8(6)
C(45)	0.5372(4)	0.297(1)	0.2158(2)	4.4(5)
C(46)	0.5150(4)	0.235(1)	0.1847(3)	4.1(5)

TABLE 1 (*concluded*)

Atom	*x*	*y*	*z*	B_{eq}
C(47)	0.3316(3)	−0.1707(9)	0.1690(2)	3.3(4)
C(48)	0.3468(4)	−0.155(1)	0.2066(3)	5.0(6)
C(49)	0.3884(5)	−0.210(1)	0.2287(3)	6.0(6)
C(50)	0.4158(4)	−0.284(1)	0.2143(3)	5.5(6)
C(51)	0.4023(4)	−0.298(1)	0.1778(3)	6.1(6)
C(52)	0.3601(4)	−0.245(1)	0.1543(3)	4.2(5)
C(53)	0.3948(4)	−0.036(1)	0.0986(3)	4.1(5)
C(54)	0.4095(4)	0.084(1)	0.1623(3)	3.6(5)
C(55)	0.3516(4)	0.152(1)	0.0592(3)	4.5(5)
C(56)	0.2265(4)	0.171(1)	0.1287(3)	6.0(6)
C(57)	0.3195(4)	0.136(1)	0.1784(3)	4.7(6)
C(58)	0.2621(4)	0.092(1)	0.0740(3)	5.8(6)
C(59)	0.2827(4)	0.414(1)	0.1384(3)	4.8(6)
C(60)	0.3648(4)	0.476(1)	0.1082(3)	4.1(5)
C(61)	0.3808(4)	0.332(1)	0.1674(3)	3.9(5)
C(62)	0.2873(5)	0.335(1)	0.0702(3)	5.4(6)

[a] $B_{eq} = (8/3)\pi^2\Sigma\Sigma U_{ij}a_i^*a_j^*(a_i \cdot a_j)$.

TABLE 2. Bond lengths (Å) with estimated standard deviations[a]

Atom	Atom	Distance	Atom	Atom	Distance
Os(1)	Os(2)	2.9237(6)	Fe(1)	Cp(2)	1.652(5)
Os(1)	Os(3)	2.9259(9)	Fe(2)	C(11)	2.05(1)
Os(1)	P(1)	2.353(2)	Fe(2)	C(12)	2.02(1)
Os(1)	C(53)	1.87(1)	Fe(2)	C(13)	2.01(1)
Os(1)	C(54)	1.95(1)	Fe(2)	C(14)	2.02(1)
Os(1)	C(55)	1.94(1)	Fe(2)	C(15)	2.023(9)
Os(2)	Os(3)	2.893(1)	Fe(2)	C(16)	2.03(1)
Os(2)	P(2)	2.359(3)	Fe(2)	C(17)	2.03(1)
Os(2)	C(56)	1.88(1)	Fe(2)	C(18)	2.03(1)
Os(2)	C(57)	1.93(1)	Fe(2)	C(19)	2.02(1)
Os(2)	C(58)	1.96(1)	Fe(2)	C(20)	2.02(1)
Os(3)	C(59)	1.91(1)	Fe(2)	Cp(3)	1.629(5)
Os(3)	C(60)	1.93(1)	Fe(2)	Cp(4)	1.65(1)
Os(3)	C(61)	1.92(1)	Fe(3)	C(21)	2.045(9)
Os(3)	C(62)	1.94(1)	Fe(3)	C(22)	2.04(1)
Fe(1)	C(1)	2.055(8)	Fe(3)	C(23)	2.02(1)
Fe(1)	C(2)	2.04(1)	Fe(3)	C(24)	2.03(1)
Fe(1)	C(3)	2.04(1)	Fe(3)	C(25)	2.02(1)
Fe(1)	C(4)	2.04(1)	Fe(3)	C(26)	2.03(1)
Fe(1)	C(5)	2.027(9)	Fe(3)	C(27)	2.02(1)
Fe(1)	C(6)	2.02(1)	Fe(3)	C(28)	2.06(1)
Fe(1)	C(7)	2.04(1)	Fe(3)	C(29)	2.04(1)
Fe(1)	C(8)	2.045(9)	Fe(3)	C(30)	2.00(1)
Fe(1)	C(9)	2.043(9)	Fe(3)	Cp(5)	1.639(5)
Fe(1)	C(10)	2.05(1)	Fe(3)	Cp(6)	1.643(6)
Fe(1)	Cp(1)	1.648(4)	Fe(4)	C(31)	2.070(8)
Fe(4)	C(32)	2.040(9)	O(10)	C(62)	1.15(1)
Fe(4)	C(33)	2.02(1)	C(1)	C(2)	1.43(1)
Fe(4)	C(34)	2.03(1)	C(1)	C(5)	1.43(1)
Fe(4)	C(35)	2.06(1)	C(2)	C(3)	1.40(1)
Fe(4)	C(36)	2.06(1)	C(3)	C(4)	1.41(1)
Fe(4)	C(37)	2.01(1)	C(4)	C(5)	1.41(1)
Fe(4)	C(38)	2.02(1)	C(6)	C(7)	1.40(1)
Fe(4)	C(39)	2.02(1)	C(6)	C(10)	1.42(1)
Fe(4)	C(40)	2.03(1)	C(7)	C(8)	1.41(1)
Fe(4)	Cp(7)	1.646(5)	C(8)	C(9)	1.43(1)
Fe(4)	Cp(8)	1.664(8)	C(9)	C(10)	1.39(1)
P(1)	C(1)	1.827(8)	C(11)	C(12)	1.44(1)
P(1)	C(11)	1.82(1)	C(11)	C(15)	1.42(1)
P(1)	C(41)	1.840(9)	C(12)	C(13)	1.40(1)
P(2)	C(21)	1.82(1)	C(13)	C(14)	1.37(1)
P(2)	C(31)	1.820(9)	C(14)	C(15)	1.42(1)
P(2)	C(47)	1.84(1)	C(16)	C(17)	1.41(2)
O(1)	C(53)	1.17(1)	C(16)	C(20)	1.40(2)
O(2)	C(54)	1.14(1)	C(17)	C(18)	1.37(2)
O(3)	C(55)	1.14(1)	C(18)	C(19)	1.39(2)
O(4)	C(56)	1.15(1)	C(19)	C(20)	1.38(2)
O(5)	C(57)	1.15(1)	C(21)	C(22)	1.44(1)
O(6)	C(58)	1.13(1)	C(21)	C(25)	1.40(1)
O(7)	C(59)	1.13(1)	C(22)	C(23)	1.40(1)
O(8)	C(60)	1.12(1)	C(23)	C(24)	1.39(1)
O(9)	C(61)	1.15(1)	C(24)	C(25)	1.42(1)
C(26)	C(27)	1.41(1)	C(51)	C(52)	1.38(1)
C(26)	C(30)	1.41(2)			
C(27)	C(28)	1.39(2)			
C(28)	C(29)	1.39(2)			
C(29)	C(30)	1.42(2)			
C(31)	C(32)	1.43(1)			
C(31)	C(35)	1.45(1)			
C(32)	C(33)	1.41(1)			
C(33)	C(34)	1.41(1)			
C(34)	C(35)	1.42(1)			
C(36)	C(37)	1.38(2)			
C(36)	C(40)	1.35(2)			
C(37)	C(38)	1.36(2)			
C(38)	C(39)	1.34(2)			
C(39)	C(40)	1.39(2)			
C(41)	C(42)	1.39(1)			
C(41)	C(46)	1.40(1)			
C(42)	C(43)	1.39(1)			
C(43)	C(44)	1.37(1)			
C(44)	C(45)	1.36(1)			
C(45)	C(46)	1.36(1)			
C(47)	C(48)	1.39(1)			
C(47)	C(52)	1.39(1)			
C(48)	C(49)	1.36(1)			
C(49)	C(50)	1.36(1)			
C(50)	C(51)	1.35(1)			

[a] Cp(1–8) refer to the unweighted centroids of the C(1–5, 6–10, . . ., 36–40) cyclopentadienyl rings, respectively.

On the final cycle of refinement the maximum parameter shift corresponded to 0.16σ. The mean error in an observation of unit weight was 1.22. The final difference map showed maximum fluctuations of −0.64 to +0.50 e Å^{-3}. The final positional and (equivalent) isotropic thermal parameters for the non-hydrogen atoms appear in Table 1. Selected bond lengths and angles are given in Tables 2 and 3. Complete tables of hydrogen atom parameters, anisotropic thermal parameters, torsion angles, intermolecular contacts, least-squares planes, and structure factors have been deposited.[3]

Results and discussion

The reaction of $Os_3(CO)_{10}(MeCN)_2$ with PFc_2Ph gives a good yield of the expected product 1,2-$Os_3(CO)_{10}(PFc_2Ph)_2$,

[3] Supplementary material mentioned in the text may be purchased from the Depository of Unpublished Data, Document Delivery, CISTI, National Research Council Canada, Ottawa, Canada K1A 0R6.

Table S1 (hydrogen atom coordinates) and the ORTEP stereoview of **2** have also been deposited with the Cambridge Crystallographic Data Centre and can be obtained on request from The Director, Cambridge Crystallographic Data Centre, University Chemical Laboratory, 12 Union Road, Cambridge, CB2 1EZ, U.K.

Can. J. Chem. Downloaded from www.nrcresearchpress.com by 109.225.110.28 on 09/08/12
For personal use only.

Can. J. Chem. Downloaded from www.nrcresearchpress.com by 109.225.110.28 on 09/08/12
For personal use only.

TABLE 3. Bond angles (deg) with estimated standard deviations

Atom	Atom	Atom	Angle	Atom	Atom	Atom	Angle
Os(2)	Os(1)	Os(3)	59.28(2)	P(2)	Os(2)	C(58)	94.4(4)
Os(2)	Os(1)	P(1)	156.31(6)	C(56)	Os(2)	C(57)	92.1(5)
Os(2)	Os(1)	C(53)	103.9(3)	C(56)	Os(2)	C(58)	91.1(5)
Os(2)	Os(1)	C(54)	80.8(3)	C(57)	Os(2)	C(58)	173.7(4)
Os(2)	Os(1)	C(55)	93.6(3)	Os(1)	Os(3)	Os(2)	60.32(2)
Os(3)	Os(1)	P(1)	99.43(7)	Os(1)	Os(3)	C(59)	149.1(3)
Os(3)	Os(1)	C(53)	160.7(3)	Os(1)	Os(3)	C(60)	110.3(3)
Os(3)	Os(1)	C(54)	95.0(3)	Os(1)	Os(3)	C(61)	81.4(3)
Os(3)	Os(1)	C(55)	83.4(3)	Os(1)	Os(3)	C(62)	92.8(3)
P(1)	Os(1)	C(53)	98.7(3)	Os(2)	Os(3)	C(59)	90.1(3)
P(1)	Os(1)	C(54)	91.8(3)	Os(2)	Os(3)	C(60)	168.7(3)
P(1)	Os(1)	C(55)	94.0(3)	Os(2)	Os(3)	C(61)	94.6(3)
C(53)	Os(1)	C(54)	91.1(4)	Os(2)	Os(3)	C(62)	85.5(3)
C(53)	Os(1)	C(55)	88.8(5)	C(59)	Os(3)	C(60)	100.0(5)
C(54)	Os(1)	C(55)	174.2(4)	C(59)	Os(3)	C(61)	92.9(4)
Os(1)	Os(2)	Os(3)	60.40(2)	C(59)	Os(3)	C(62)	93.8(5)
Os(1)	Os(2)	P(2)	106.09(6)	C(60)	Os(3)	C(61)	89.8(4)
Os(1)	Os(2)	C(56)	153.4(4)	C(60)	Os(3)	C(62)	89.0(5)
Os(1)	Os(2)	C(57)	93.4(3)	C(61)	Os(3)	C(62)	173.3(4)
Os(1)	Os(2)	C(58)	81.3(3)	Cp(1)	Fe(1)	Cp(2)	177.0(2)
Os(3)	Os(2)	P(2)	164.37(6)	Cp(3)	Fe(2)	Cp(4)	173.5(4)
Os(3)	Os(2)	C(56)	94.5(4)	Cp(5)	Fe(3)	Cp(6)	176.4(3)
Os(3)	Os(2)	C(57)	83.1(3)	Cp(7)	Fe(4)	Cp(8)	172.7(4)
Os(3)	Os(2)	C(58)	91.3(4)	Os(1)	P(1)	C(1)	119.7(3)
P(2)	Os(2)	C(56)	99.9(4)	Os(1)	P(1)	C(11)	118.8(3)
P(2)	Os(2)	C(57)	90.3(3)	Os(1)	P(1)	C(41)	114.9(3)
C(1)	P(1)	C(11)	100.2(4)	C(13)	C(14)	C(15)	108.9(9)
C(1)	P(1)	C(41)	99.1(4)	C(11)	C(15)	C(14)	108.2(9)
C(11)	P(1)	C(41)	100.7(4)	C(17)	C(16)	C(20)	109(2)
Os(2)	P(2)	C(21)	119.4(3)	C(16)	C(17)	C(18)	107(2)
Os(2)	P(2)	C(31)	116.0(3)	C(17)	C(18)	C(19)	109(2)
Os(2)	P(2)	C(47)	115.9(3)	C(18)	C(19)	C(20)	109(2)
C(21)	P(2)	C(31)	100.2(4)	C(16)	C(20)	C(19)	107(2)
C(21)	P(2)	C(47)	99.5(4)	P(2)	C(21)	C(22)	128.2(8)
C(31)	P(2)	C(47)	103.0(4)	P(2)	C(21)	C(25)	125.4(7)
P(1)	C(1)	C(2)	122.7(7)	C(22)	C(21)	C(25)	105.3(9)
P(1)	C(1)	C(5)	129.8(7)	C(21)	C(22)	C(23)	109(1)
C(2)	C(1)	C(5)	107.0(7)	C(22)	C(23)	C(24)	109(1)
C(1)	C(2)	C(3)	108.7(8)	C(23)	C(24)	C(25)	107(1)
C(2)	C(3)	C(4)	107.9(8)	C(21)	C(25)	C(24)	110(1)
C(3)	C(4)	C(5)	108.6(8)	C(27)	C(26)	C(30)	105(1)
C(1)	C(5)	C(4)	107.7(8)	C(26)	C(27)	C(28)	111(1)
C(7)	C(6)	C(10)	110(1)	C(27)	C(28)	C(29)	107(1)
C(6)	C(7)	C(8)	107(1)	C(28)	C(29)	C(30)	108(1)
C(7)	C(8)	C(9)	107(1)	C(26)	C(30)	C(29)	109(1)
C(8)	C(9)	C(10)	110(1)	P(2)	C(31)	C(32)	125.3(7)
C(6)	C(10)	C(9)	106(1)	P(2)	C(31)	C(35)	126.2(8)
P(1)	C(11)	C(12)	124.9(8)	C(32)	C(31)	C(35)	107.0(8)
P(1)	C(11)	C(15)	127.2(7)	C(31)	C(32)	C(33)	107.5(9)
C(12)	C(11)	C(15)	105.7(8)	C(32)	C(33)	C(34)	110(1)
C(11)	C(12)	C(13)	108.7(9)	C(33)	C(34)	C(35)	108(1)
C(12)	C(13)	C(14)	108.6(9)	C(31)	C(35)	C(34)	108(1)
C(37)	C(36)	C(40)	106(1)	Os(2)	C(58)	O(6)	175(1)
C(36)	C(37)	C(38)	108(2)	Os(3)	C(59)	O(7)	177(1)
C(37)	C(38)	C(39)	109(2)	Os(3)	C(60)	O(8)	175(1)
C(38)	C(39)	C(40)	106(2)	Os(3)	C(61)	O(9)	174(1)
C(36)	C(40)	C(39)	110(1)	Os(3)	C(62)	O(10)	175(1)
P(1)	C(41)	C(42)	123.0(7)				
P(1)	C(41)	C(46)	119.8(8)				
C(42)	C(41)	C(46)	117.1(9)				
C(41)	C(42)	C(43)	120(1)				
C(42)	C(43)	C(44)	120(1)				
C(43)	C(44)	C(45)	120(1)				
C(44)	C(45)	C(46)	120(1)				

TABLE 3 (*concluded*)

Atom	Atom	Atom	Angle	Atom	Atom	Atom	Angle
C(41)	C(46)	C(45)	122(1)				
P(2)	C(47)	C(48)	121.9(8)				
P(2)	C(47)	C(52)	120.0(7)				
C(48)	C(47)	C(52)	118(1)				
C(47)	C(48)	C(49)	122(1)				
C(48)	C(49)	C(50)	120(1)				
C(49)	C(50)	C(51)	119(1)				
C(50)	C(51)	C(52)	123(1)				
C(47)	C(52)	C(51)	118(1)				
Os(1)	C(53)	O(1)	176(1)				
Os(1)	C(54)	O(2)	176(1)				
Os(1)	C(55)	O(3)	174(1)				
Os(2)	C(56)	O(4)	175(1)				
Os(2)	C(57)	O(5)	177(1)				

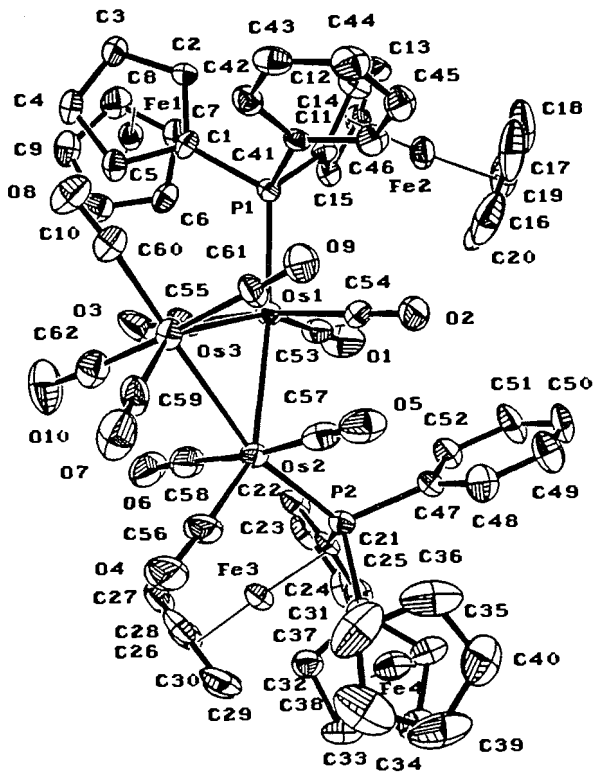

FIG. 1. Stereoview of the $\{[(\eta^5-C_5H_5)Fe(\eta^5-C_5H_4)]_2(C_6H_5)P\}_2Os_3(CO)_{10}$ molecule, **2**; 33% probability thermal ellipsoids are shown for the non-hydrogen atoms.

2. The $^{31}P\{^1H\}$ nmr spectra of **2** run in a range of solvents including $CDCl_3$, CD_3CN, DMSO-d_6, C_6D_6, and C_7D_8 show two sharp signals of equal intensity clearly showing it to be the isomer of structure **1***c*. No evidence for the presence of other isomers was found. This conclusion was confirmed by an X-ray diffraction study.

The molecular structure of **2** is shown in Fig. 1. Like $Os_3(CO)_{12}$ it is a closed Os_3 cluster but one carbonyl group on Os(1) and Os(2) is replaced by the phosphine ligand PFc_2Ph. The Os—Os distances are as usual with Os(2)—Os(3) (2.893(1) Å) being slightly shorter than the other two (2.9237(6) and 2.9259(9) Å). The two bulky phosphines adopt the **1***c* unsymmetrical arrangement. The osmium centers have distorted octahedral geometry, and although the two phosphines are situated on one side of the Os_3 plane (0.4491 Å for P(1) and 0.3369 Å for P(2)), these ligands clearly occupy two equatorial coordination sites. One equatorial carbonyl (C(59)) also lies on the same side of the Os_3 plane (by 0.3213 Å), while the other three alternating equatorial carbonyls (C(53), C(56), and C(60)) are situated on the other side (0.3227, 0.3106, and 0.2167 Å, respectively). As a consequence the six axial carbonyls are distorted from their idealized positions. On the P(1), P(2), C(59) side of the Os_3 plane, C(54), C(57), and C(61) have moved towards Os(2), Os(3), and Os(1), respectively (C(54)—Os(1)—Os(2) 80.8(3)°, C(57)—Os(2)—Os(3) 83.1(3)°, C(61)—Os(3)—Os(1) 81.4(3)°). On the other side of the Os_3 plane, a compensating motion of C(55), C(58), and C(62) occurs towards Os(3), Os(1), and Os(2), respectively (C(55)—Os(1)—Os(3) 83.4(3)°, C(58)—Os(2)—Os(1) 81.3(3)°, C(62)—Os(3)—Os(2) 85.5(3)°).

The Os(1)—C(53) and Os(2)—C(56) bond distances (1.87(1) and 1.88 (1) Å) are probably shorter than the other Os—C distances, while all C—O distances are the same and normal (average 1.14(1) Å) and all Os—C—O bonds linear (average 175(1)°). Both Os—P distances are the same and normal (2.353(2) and 2.359(3) Å). All Fe—C distances are the same and so are the Fe—Cp distances. The Cp rings are parallel with small dihedral angles (2.48° for Fc(1), 3.27° for Fc(3)), but the values for Fc(2) and Fc(4) are larger than usual (6.75° and 9.06°, respectively). This is also indicated by the Cp—Fe—Cp bond angles (Cp(3)—Fe(2)—Cp(4) = 173.5(4)° and Cp(7)—Fe(4)—Cp(8) = 172.7(4)°, while Cp(1)—Fe(1)—Cp(2) = 177.0(2)° and Cp(5)—Fe(3)—Cp(6) = 176.4(3)° are usual).

Many phosphine complexes of the class $M_3(CO)_{10}L_2$ are known but, as discussed in the Introduction, few are reported to be of structures other than **1***b*. Compound **2** is the first molecule of structure **1***c* to be characterized in the solid state. Our recent work with ligands such as $PFcPh_2$, PFc_2Ph, and $PFcPr^i_2$ shows that **2** is not unique and that mixtures of isomers **1***b* and **1***c* can be obtained for both osmium and ruthenium complexes.[4] In view of the considerable steric bulk of these ligands (16) this phenomenon must be somewhat attributable to the electronic effects of these ferrocenyl-

[4]W. R. Cullen and T. C. Zheng, unpublished results.

Can. J. Chem. Downloaded from www.nrcresearchpress.com by 109.225.110.28 on 09/08/12
For personal use only.

phosphine ligands. The stereospecificity of the product **2** can be attributed to the strong electron-donating ability of the PFc_2Ph ligand. In contrast to phenyl, which is weakly electron withdrawing, ferrocenyl groups are strongly electron releasing. Strongly electron-donating ligands will have a high *trans* influence and this will cause the molecule to adopt the **1***c* geometry where the two phosphines are not *trans* to each other via the Os—Os bond. Electronic effects must also come into play in the case of the PMe_2Ph and PEt_3 complexes described above (both these ligands are less bulky than PFc_2Ph).

Acknowledgement

We are grateful to the Natural Sciences and Engineering Research Council of Canada for financial support (W. R. Cullen) and the University of British Columbia for a graduate fellowship (T. C. Zheng).

1. A. J. Deeming. *In* Advances in organometallic chemistry. Vol. 26. 1986. pp. 1–96 and references therein.
2. R. D. Adams and J. P. Selegue. *In* Comprehensive organometallic chemistry. Vol. 3. *Edited by* G. Wilkinson, F. G. A. Stone, and E. W. Abel. Pergamon, New York. 1982. pp. 967–1064, and references therein.
3. V. Shvo and E. Hazum. J. Chem. Soc. Chem. Commun. 336(1974).
4. H. Alper and J. T. Edward. Can. J. Chem. **48**, 1543(1970).
5. R. J. Lawson and J. R. Shapley. J. Am. Chem. Soc. **98**, 7433(1976).
6. B. F. G. Johnson, J. Lewis, and D. A. Pippard. J. Chem. Soc. Dalton Trans. 407 (1981).
7. M. Tachikawa and J. R. Shapley. J. Organomet. Chem. **124**, C19(1977).
8. B. F. G. Johnson, J. Lewis, and D. A. Pippard. J. Organomet. Chem. **145**, C4(1978).
9. M. Tachikawa, J. R. Shapley, R. C. Haltiwanger, and C. G. Pierpont. J. Am. Chem. Soc. **98**, 4651(1976).
10. A. J. Deeming, S. Donovan-Mtzunki, S. E. Kabir, and P. J. Manning. J. Chem. Soc. Dalton Trans. 1039(1985).
11. S. C. Tripathi, S. C. Srivastava, R. P. Mani, and A. K. Shrimal. Inorg. Chim. Acta, **15**, 249(1975).
12. C. G. Pierpont. Inorg. Chem. **17**, 1976(1978).
13. J. P. Collman, L. S. Hegedus, J. R. Norton, and R. G. Finke. Principles and applications of organotransition metal chemistry. 2nd ed. University Science Books, Mill Valley, Calif. 1987. pp. 67–71.
14. C. A. Tolman. Chem. Rev. **77**, 313(1977).
15. B. F. G. Johnson, J. Lewis, B. E. Reicher, and K. T. Schorpp. J. Chem. Soc. Dalton Trans. 1403(1976).
16. S. T. Chacon, W. R. Cullen, M. I. Bruce, O. B. Shawkataly, F. W. B. Einstein, R. H. Johnes, and A. C. Willis. Can. J. Chem. **68**, 2001(1990).
17. International Tables for X-Ray Crystallography. Vol. IV. Kynoch Press, Birmingham, U. K. (present distributor Kluwer Academic Publishers, Dordrecht, The Netherlands). 1924. pp. 99–102 and 149.

Can. J. Chem. Downloaded from www.nrcresearchpress.com by 109.225.110.28 on 09/08/12
For personal use only.

Transannular Diels–Alder cyclization of a substituted 13-membered macrocyclic triene. An approach to the A.B.C.[6.6.5] rings of the *Veratrum* alkaloids

MIGUEL QUIMPÈRE, LUC RUEST, AND PIERRE DESLONGCHAMPS[1]

Laboratoire de synthèse organique, Département de chimie, Faculté des sciences, Université de Sherbrooke, Sherbrooke (Québec), Canada J1K 2R1

Received February 24, 1992

MIGUEL QUIMPÈRE, LUC RUEST, and PIERRE DESLONGCHAMPS. Can. J. Chem. **70**, 2335 (1992).

The synthesis and Diels–Alder cyclization of a substituted macrocyclic 13-membered triene **45** is described. Tricyclic compound A.B.C.[6.6.5] **46** having ring junctions of *cis-anti-cis* (CAC) stereochemistry was used to investigate the possibility of introducing a hemiketal oxygen bridge between positions 9 and 4 of the *Veratrum* alkaloid skeleton.

MIGUEL QUIMPÈRE, LUC RUEST et PIERRE DESLONGCHAMPS. Can. J. Chem. **70**, 2335 (1992).

On décrit la synthèse et la cyclisation Diels–Alder d'un macrocycle substitué à 13 chaînons **45**. Le composé tricyclique A.B.C.[6.6.5] **46** de stéréochimie *cis-anti-cis* (CAC) en jonction de cycle a été utilisé pour étudier la possibilité d'introduire un pont d'oxygène hémicétalique entre les positions 9 et 4 des alkaloïdes *Veratrum*.

Can. J. Chem. Downloaded from www.nrcresearchpress.com by 109.225.110.28 on 09/08/12
For personal use only.

Veratrum alkaloids are an important category of natural compounds (1) obtained from the *Liliaceae* family, from *Veratrum album* in Europa and from *Veratrum viride* in North America. These alkaloids have been known since the early 1800's (2) for their sternutatory properties, but it was only in the late 1940's that their isolation and identification was undertaken systematically (3). At least 40 compounds from this family are now known and they all have the main hexacyclic skeleton presented in Fig. 1. There are four major types, differing in the hydroxylation pattern: germine (**1**) (4), veracevine (**2**) (5), protoverine (**3**) (4*a*, 6), and zygadenine (**4**) (7) and its 3-epimer cevine (**5**). These compounds are found in nature as esters of different carboxylic acids. The biological activity (8) of these steroidal alkaloids, particularly their ability to lower blood pressure (9), was studied in the 1950's.

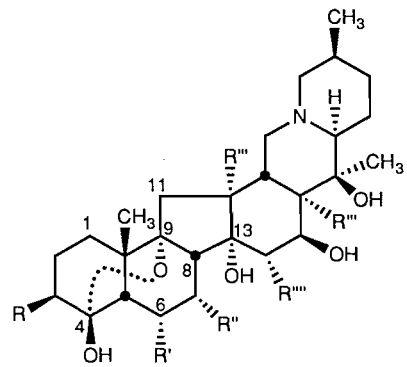

1 Germine R = β-OH, R' = R''' = H, R'' = R'''' = OH
2 Veracevine R = β-OH, R' = R'' = R'''' = H, R''' = OH
3 Protoverine R = β-OH, R' = R'' = R'''' = OH, R''' = H
4 Zygadenine R = β-OH, R' = R'' = R''' = H, R'''' = OH
5 Cevine R = α-OH, R' = R'' = R'''' = H, R''' = OH

FIG. 1. Ceveratrum major isometric alkamines.

In spite of the large pharmacological potential of these compounds, to our knowledge no group has attempted to devise a total synthesis of a *Veratrum* alkaloid. No doubt the presence of several asymmetric centers (17 in protoverine (**3**)) and an unusual presence of a tertiary hydroxyl group at position 9 (steroid numbering) could account for this situation. A synthetic strategy with a high degree of control on chemo-, regio-, and stereoselectivity has to be used in order to synthesize efficiently molecules of such complexity. Intramolecular processes (10–12) usually give excellent control on these factors. In recent years, our group has shown (13, 14) that the transannular Diels–Alder cyclization of macrocyclic trienes (see general formulation in Scheme 1, i → ii) is an efficient tool to synthesize functionalized 14-membered tricyclic A.B.C.[6.6.6] compounds with a high level of stereoselectivity.

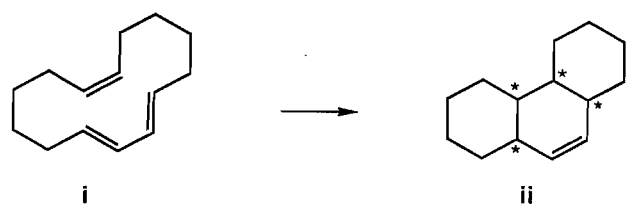

i ii

SCHEME 1. Transannular Diels–Alder cyclization.

Moreover, this strategy was also been applied in a model study by Bérubé and Deslongchamp (15) from our group to synthesize a tricyclic homolog **8** (Scheme 2), namely an A.B.C.[6.6.5] skeleton, starting with a 13-membered macrocyclic *trans-trans-cis* (TTC) triene **7**, which was formed by the internal cyclization of an acyclic malonate chloride **6**. The use of an oxygen substituent on the dienophilic part of the macrocyclic triene showed the interesting possibility of introducing such a substituent at position 9 (steroid numbering) of the resulting tricyclic product. It was shown that the reaction of a *trans-trans-cis* (TTC) macrocyclic triene **7** leads to a mixture of tricyclic compounds **8** having *trans-syn-trans* (TST) and *cis-syn-cis* (CSC) geometries (2:1, respectively) at the ring junctions.

These preliminary results were used to devise a synthetic strategy leading to the A.B.C. rings of the *Veratrum* alkaloids. Indeed, in a recent model study (16) we showed (Scheme 3*a*) that the same strategy could be applied to the synthesis of an A.B.C.[6.6.5] tricyclic compound (see **11**) having the *cis-anti-cis* (CAC) geometry at the ring junctions. In this work and as shown in previous series (14*b*), it

[1]Author to whom correspondence may be addressed.

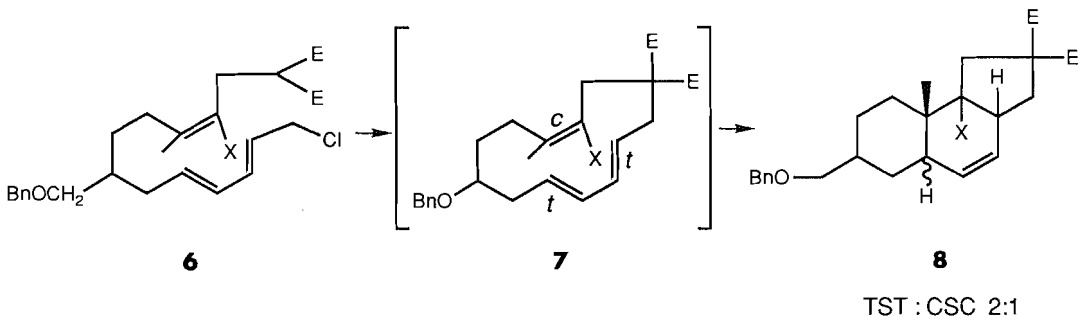

SCHEME 2. E = CO_2CH_3; X = OMOM; TST: *trans-syn-trans*; CSC: *cis-syn-cis*.

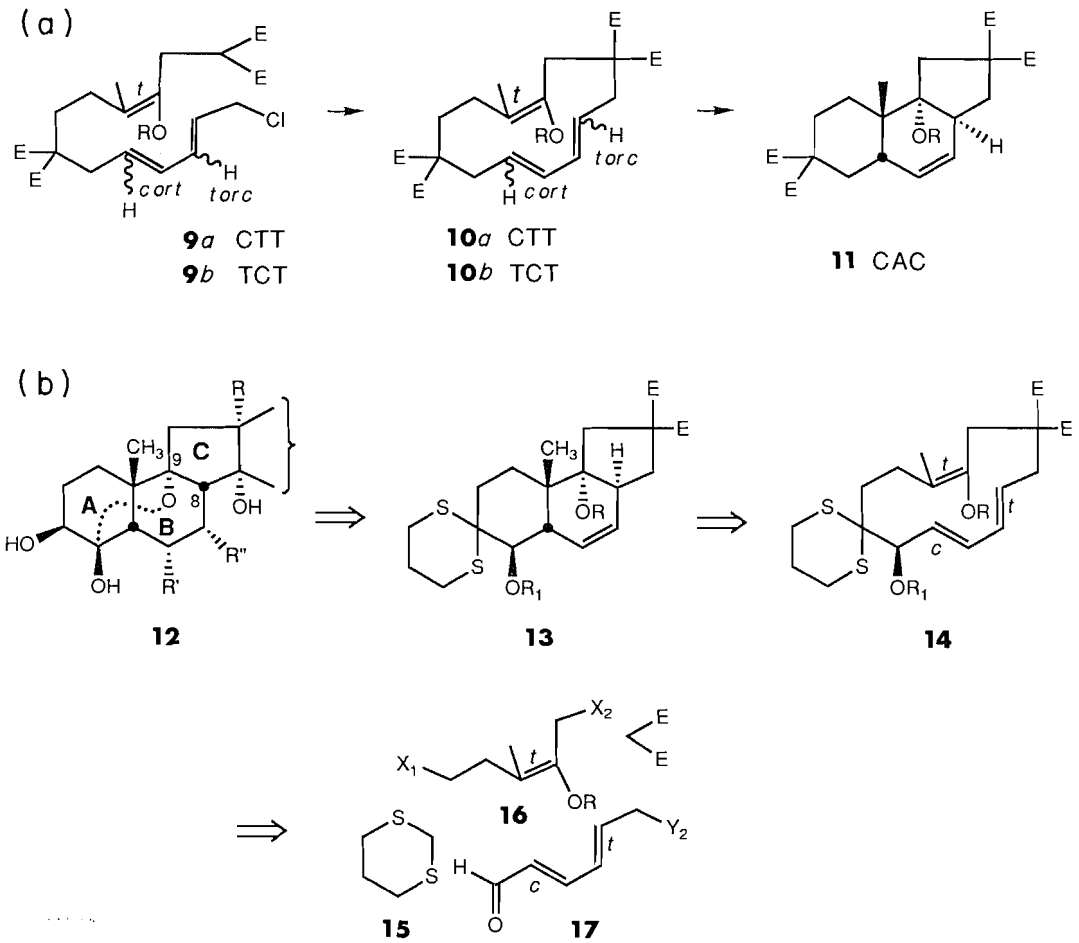

SCHEME 3

was found that both macrocyclic trienes **10***a* (CIT) and **10***b* (TCT) can give access to tricycle **11** (CAC).

The results of the first two model studies led us to devise a new route affording tricyclic intermediates that are more similar to the A.B.C.[6.6.5] portion of the general *Veratrum* skeleton. The retrosynthetic analysis shown in Scheme 3*b* indicates that the A.B.C. system (see **12**) might be formed from a tricyclic compound **13** itself obtained by a transannular Diels–Alder cyclization of macrocycle **14**. This macrocyclic triene might come from the assemblage of 1,3-dithiane (**15**), dienophile **16**, diene **17**, and dimethylmalonate in a highly convergent synthetic sequence. The use of 1,3-dithiane as a connector between dienophile **16** and diene **17** will insure the right oxidation level in the future ring A. The CT geometry in the diene **17** should give a CAC geometry in the final tricycle. The stereochemistry at position 8 will therefore have to be corrected with the help of functionalities left in ring C or B.

We will discuss now the synthesis of dienophile **16** and diene **17** as well as their assemblage to macrocycle **13**. We will then present the results of its Diels–Alder cyclization and we will report chemical transformations carried out on tricycle **13** to set the hemiketal bridge between positions 9 and 4.

Can. J. Chem. Downloaded from www.nrcresearchpress.com by 109.225.110.28 on 09/08/12
For personal use only.

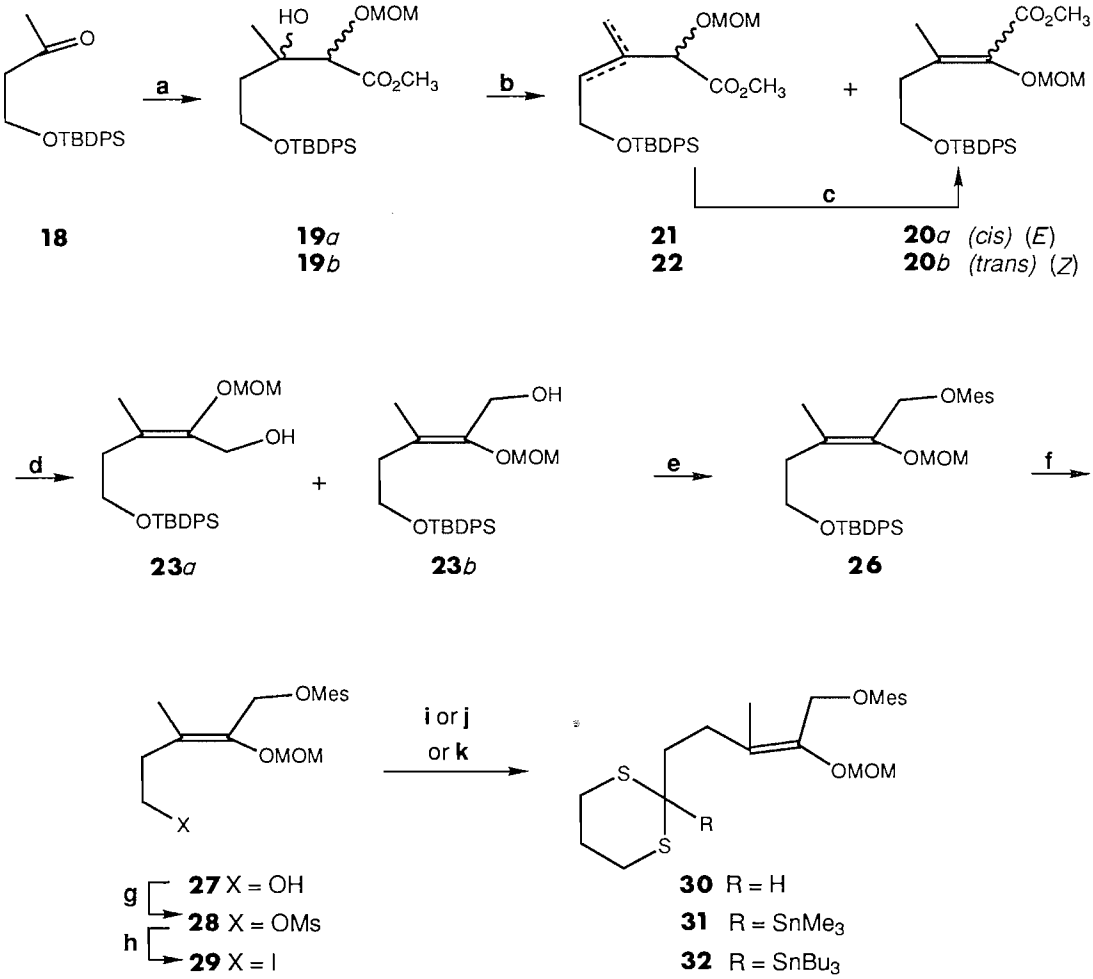

(**a**) $MOMOCHLiCO_2CH_3$, THF, -78°C, 97%; (**b**) pyridine, $SOCl_2$, -60 → -20°C, 85%;
(**c**) CH_3OK, CH_3OH, reflux, 71%; (**d**) DIBAL, CH_2Cl_2, -78°C;
(**e**) Mesitoic acid, DCC, DMAP, CH_2Cl_2, 25°C, 91%; (**f**) $n$$Bu_4NF$, THF (99%);
(**g**) MsCl, Et_3N, CH_2Cl_2, 0°C (quant.); (**h**) NaI, acetone, refl. (91%);
(**i**) $(CH_2)_3S_2CHLi$, -78°C, THF, 12%; (**j**) $(CH_2)_3S_2C((CH_3)_3Sn)Li$, THF, -78°C, 38%;
(**k**) $(CH_2)_3S_2C((C_4H_9)_3Sn)Li$, -78°C, THF, 87%

SCHEME 4

Dienophile 32

Following the methodology used previously (16), ketone **18** (Scheme 4) was alkylated in good yield with the lithium derivative of methyl methoxymethyloxyacetate (MOMO acetate) to afford a separable mixture of alcohols **19***a* and **19***b*. These, as a mixture, were dehydrated by thionyl chloride (17) in pyridine to α,β-unsaturated esters **20***a* and **20***b* (unseparable mixture) and unconjugated esters **21** and **22** in a ratio of (approximately) 1:1:2:2, respectively. Compounds **20***a* and **20***b* are the *cis* and *trans* isomers, respectively, and the double bond geometry was established by the following observations: a careful separation of diastereoisomers **19***a* and **19***b* provided an opportunity to obtain the pure α,β-unsaturated esters **20***a* and **20***b*, respectively, after dehydration (Scheme 5). These pure conjugated esters **20***a* and **20***b* were separately desilylated to the corresponding alcohols **24***a* and **24***b*. During this transformation, compound **24***a* was partly cyclized to lactone **25**, which was characterized. This cyclization proved that compound **24***a* was the *cis* (*E*) isomer. The two unconjugated esters **21** and **22** (Scheme 4) were converted to esters **20***a* and **20***b* by isomerization of the double bond with potassium methoxide in methanol.

The mixture of *E* and *Z* isomers **20** was reduced to easily separable alcohols **23***a* (*E* isomer) and **23***b* (*Z* isomer) with diisobutylaluminum hydride (DIBAL). Alcohol **23***b*, the *trans* isomer, was acylated with mesitoic acid (18) in the presence of dicyclohexylcarbodiimide (DCC) and *N*,*N*-dimethylaminopyridine (DMAP) to give mesitoate **26**, a hindered ester that is inert to butyllithium and to 1,3-dithiane anion used subsequently (*vide infra*). Desilylation of ether **26** with fluoride ion (19) and mesylation (20) of the resulting alcohol **27** led to mesylate **28**, which was transformed to iodide **29** by sodium iodide in refluxing acetone.

At this point, three 1,3-dithiane connectors were tested in the form of their anions: 1,3-dithiane, 2-trimethylstannyl-1,3-dithiane (21), and 2-tributylstannyl-1,3-dithiane (22). In our

Can. J. Chem. Downloaded from www.nrcresearchpress.com by 109.225.110.28 on 09/08/12
For personal use only.

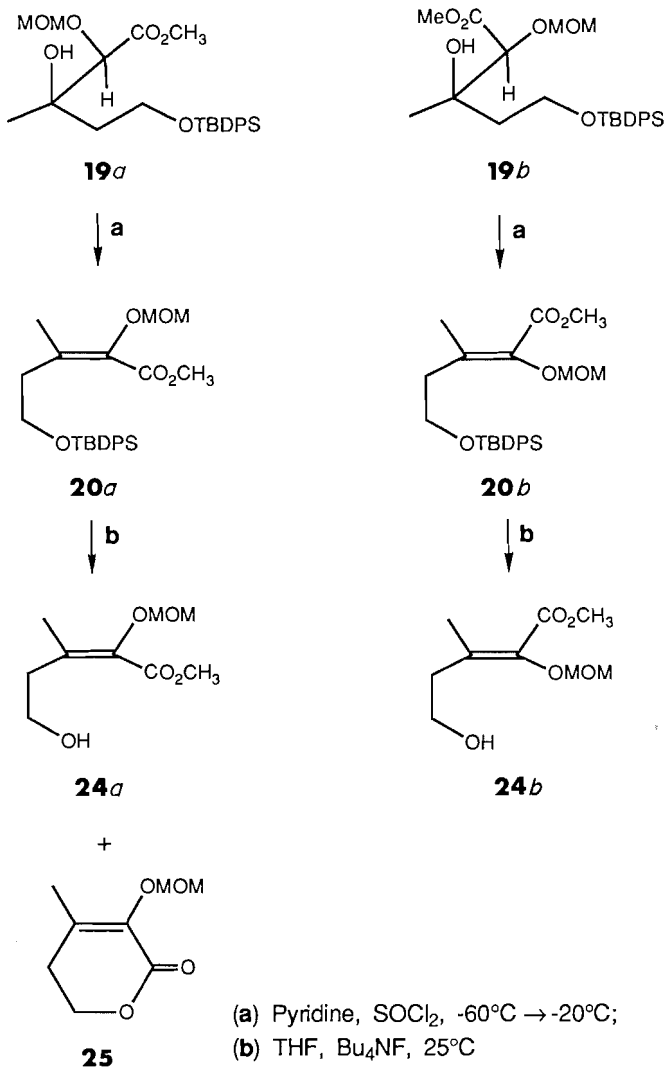

SCHEME 5

hands, following a Seebach procedure (21, 22), the reaction of iodide **29** with 2-lithio-1,3-dithiane gave a low yield for adduct **30** (12%); with 2-lithio-2-trimethylstannyl-1,3-dithiane the yield for compound **31** was only 38%. Nevertheless, the use of 2-lithio-2-tributylstannyl-1,3-dithiane increased the yield to 87% for adduct **32**, the dienophilic synthon that has still to be alkylated with dienic synthon **36** to give the acyclic triene **44**.

Diene 36 and acyclic triene 44

Synthesis of diene **36** began with *cis-trans* diene **33** easily obtained from *cis*-but-2-ene-1,4-diol (14*a*, 16). Following previous work in our group, silylation of alcohol **33** (Scheme 6) with *tert*-butoxydiphenylsilyl chloride (23) led to diene **34** whose tetrahydropyranyl protecting group was then cleaved in *tert*-butanol in the presence of pyridinium *para*-toluenesulfonate (24) to obtain *cis-trans* allylic alcohol **35**. The use of *tert*-butanol instead of *i*-propanol (see ref. 16) eliminated an otherwise extensive exchange of the alkoxy group on the silyl ether moiety. Oxidation of alcohol **35** at low temperature (Swern conditions) (25) furnished aldehyde **36**.

The coupling reaction between dienophile **32** and aldehyde **36** was performed in good yield (86%) at low temperature (−93°C). We observed that the temperature of the reaction mixture has a critical influence on the yields. The *trans*-metallation of stannyl derivative **32** to the lithio derivative was first performed at −93°C by a fast addition of a precooled (−90°C) solution of butyllithium. A cooled (−90°C) solution of aldehyde **36** was then rapidly added to the mixture. Without these specific experimental conditions, several side reactions occurred, such as the formation of adduct **38** which comes from anionic attack on aldehyde **36** by the *para*-methyl group of the mesitoate moiety after its deprotonation by either butyllithium or internally by the 2-lithio-1,3-dithiane anion.

The alcohol function of **37** was silylated with *tert*-butyldimethylsilyl triflate and the resulting protected ester **39** was reduced to alcohol **40** with lithium aluminum hydride. Chloride **41**, obtained (26) from alcohol **40**, was converted to malonate **42** by substitution with methyl sodiomalonate. After selective cleavage of the terminal *tert*-butoxydiphenylsilyl ether of compound **42** with fluoride ion in methylene chloride (23), allylic alcohol **43** was converted to the desired acyclic triene, allylic chloride **44**.

Macrocyclization and transannular Diels–Alder reaction

Slow addition of trienic malonate chloride **44** to a warm (78°C) solution of cesium carbonate and 18-crown-6 ether in acetonitrile led to the formation of macrocyclic triene **45** in 75% yield. Subsequent heating of this compound in toluene (220°C, 7 h) resulted in the smooth formation of a single tricycle **46** (76%) together with a secondary compound (16%) to which structure **47** has been assigned on the basis of its spectroscopic data. At a slightly higher temperature and a shorter reaction time (240°C, 1.5 h) the yield was somewhat lowered (**46** (69%) and **47** (15%)).

The assignment of stereochemistry for tricycle **46** was done on the basis of its nmr data, which show a very small coupling constant (1.8 Hz) between the allylic proton at position 5 (steroid numbering) and the proton at position 4 bearing the *O*-silyl group. This would be consistent with an equatorial–equatorial or an equatorial–axial coupling. The latter possibility has been discarded after the following considerations and analysis of molecular models.

Thus, on the basis of our previous results (14), macrocyclic triene CTT **45** should react to give only tricycle CAC. In the present instance (see Scheme 7), two stereoisomers **46***a* and **46***b*, which are different only in the relative configuration of the silyloxy group (as enantiomeric structures), are possible. Indeed, macrocyclic triene **45** can react through conformation **45**i or **45**ii to produce either tricycle **46***a* or **46***b* in their conformations **46***a*i and **46***b*i, respectively. The process **45**ii → **46***b*i must be disfavored due to the important steric hindrance from the silyloxy substituent, which has to take a pseudo-axial orientation. That steric interaction is absent in the process **45**i → **46***a*i in which the silyloxy substituent is in a pseudo-equatorial orientation. Thus, the favored process should lead to stereoisomer **46***a* in which both protons at positions 4 and 5 are equatorial (see the more stable conformation, **46***a*ii and **46***b*ii of **46***a* and **46***b*). This conclusion was later firmly secured by X-ray diffraction analysis of a crystalline derivative **62** (*vide infra*).

Compound **47** shows three olefinic protons (5.23, 5.45, and 5.60 ppm) and a methyl group attached to a double bond (1.45 ppm) in its nmr spectrum. By 2D nmr experiments it was possible to propose a bicyclic structure **47** for this compound, which could result from a transannular ene-type reaction (see **45**iii or **45**iv → **47**) (Scheme 8), examples of

Can. J. Chem. Downloaded from www.nrcresearchpress.com by 109.225.110.28 on 09/08/12
For personal use only.

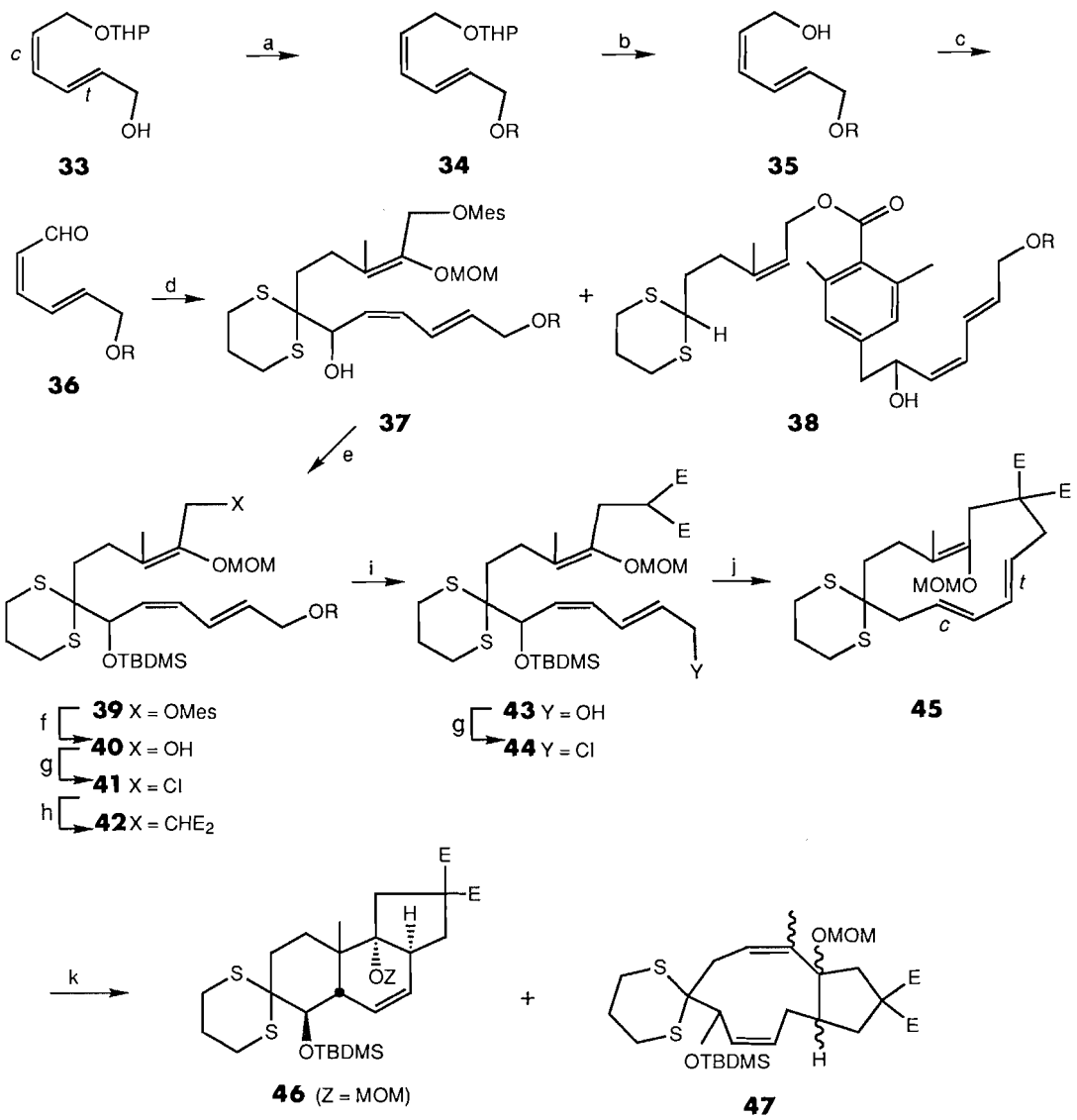

(a) *t*-Butoxydiphenylsilylchloride (TBODPSCl), Et_3N, CH_2Cl_2, 99%; (b) *t*-BuOH, PPTS, 60°C, 51%; (c) DMSO, $(COCl)_2$, DIPEA, -78°C, 76%; (d) i): **32**, *n*-BuLi, -93°C, 15 s then **36**, THF, -90°C, 86%; (e) TBDMSTf, Et_3N, CH_2Cl_2, 0°C, 85%; (f) $LiAlH_4$, ether, 25°C, 82%; (g) MsCl, LiCl, collidine, DMF, 25°C (**41**, 90%; **44**, 82%); (h) E_2CHNa, THF:DMF (1:1), KI, 25°C, 81%; (i) Bu_4NF, CH_2Cl_2, 25°C, 88%; (j) Cs_2CO_3, 18-crown-6, CH_3CN, 78°C, 75%; (k) toluene, 220°C, 7 h, **46** (76%), **47** (16%).

SCHEME 6. E = CO_2CH_3; R = TBODPS.

which were observed and reported previously (14*a*). The geometry of the newly formed double bond and the stereochemistry at the ring junction are still unknown. Molecular models show that this ene reaction may involve either proton H_A (**45**iii) or H_B (**45**iv), leading to different geometries for the trisubstituted olefin.

Towards the A.B.C. rings of Veratrum *alkaloids*

To test the validity of the present model series in an eventual sequence towards the A.B.C. rings of *Veratrum* alkaloids, we investigated the introduction of the oxygen bridge between positions 9 and 4.

The thioketal moiety of tricycle **46** (Scheme 9) was cleaved with mercuric chloride on calcium carbonate (27) in aqueous acetonitrile, and then the obtained ketone **54** was reduced with methanolic sodium borohydride to epimeric separable alcohols **55** and **56**, both useful for this preliminary investigation. The epimers were identified through their benzoate derivatives **57** and **58**, which showed that the proton at C_3 is axial in **57** (and therefore in **55**) (one coupling constant is 12.5 Hz) and equatorial in **58** (and therefore in **56**) (all the coupling constants are smaller than 3 Hz). Cleavage of the MOM protecting group of **57** and **58** in acid medium gave alcohols **59** and **60** selectively and in quantitative yield, leaving the *tert*-butyldimethylsilyl ether moiety unaffected. Subsequent treatment of silyl ether benzoate **59** with tetrabutylammonium fluoride led to hydroxybenzoate lactone **61** (19%) and diol lactone **62** (61%). The basicity of the reaction medium (presence of a catalytic amount of tetrabutyl ammonium hydroxide) was presumably sufficient to promote lactonization of the free 9-hydroxyl group with the adjacent methyl ester of the malonate moiety and to induce

Can. J. Chem. Downloaded from www.nrcresearchpress.com by 109.225.110.28 on 09/08/12
For personal use only.

Can. J. Chem. Downloaded from www.nrcresearchpress.com by 109.225.110.28 on 09/08/12
For personal use only.

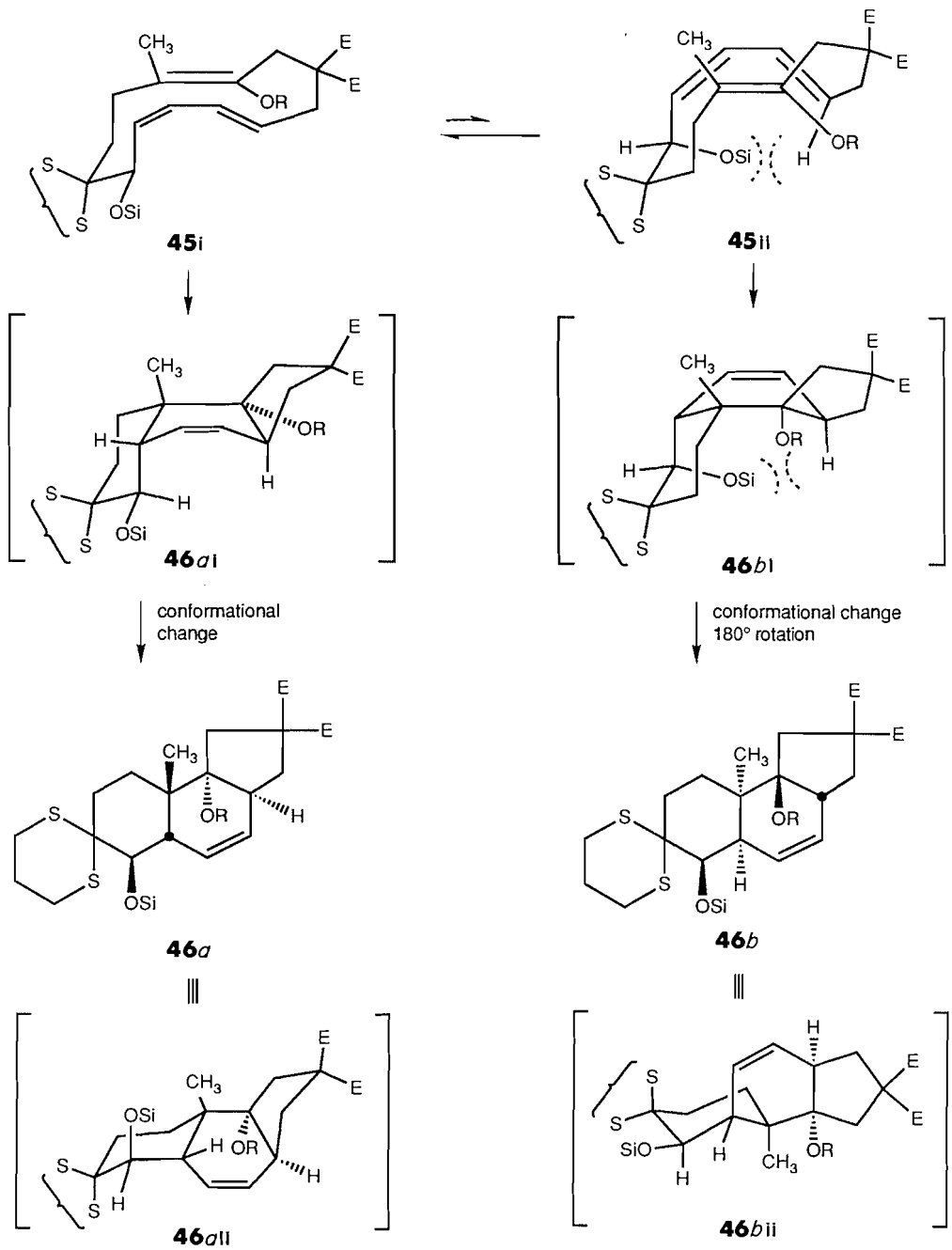

SCHEME 7. R = MOM; E = CO_2CH_3.

transesterification of the equatorial benzoate at position 3. X-ray diffraction analysis (see Fig. 2) of crystalline diol **62** (28) confirmed the α and axial orientation of the proton at C_3, as well as the predicted stereochemistry of all the asymmetric centers of the molecule, in particular the ones that had been formed during the transannular Diels–Alder reaction.

On the other hand, cleavage of silyl benzoate **58** with fluoride ion led to benzoate alcohol lactone **63** in good yield (81%). Even though compound **61** has its 9-hydroxyl inserted into a lactone bridge, and therefore not immediately available for a hemiketal bridging with position 4, we tested the oxidation of the axial β-hydroxyl at position 4 of that compound with PCC and obtained ketone **64** as the only product. We did not investigate any further reaction at this point, having learned that the oxidation of the 4-OH group should be performed before the MOM cleavage. On the other hand the presence of the lactone bridge gives the opportunity of differentiating the two ester moieties of the malonate connector, which is a lead for further studies.

In conclusion, we have shown that it is possible to synthesize in good yield a specifically functionalized tricyclic A.B.C.[6.6.5] skeleton, having a *cis-anti-cis* (CAC) stereochemistry at the ring junction, by a transannular Diels–Alder reaction of a macrocyclic triene. Very recently, Dory (29) from our group showed that the use of a sulfone connector (besides a malonate) and a *trans-trans* diene in a similar general strategy has given access to a CAT tricyclic skeleton. Applied to our problem, this modification should

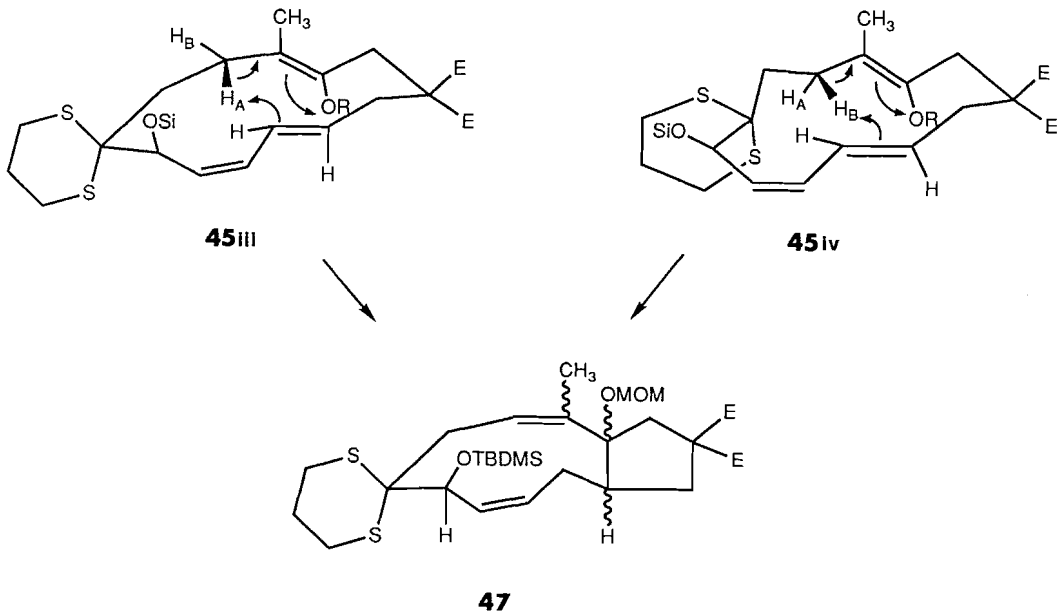

SCHEME 8

lead to a CAT A.B.C.[6.6.5] skeleton having the desired stereochemistry at the position 8 ring junction. Further studies are in progress in order to use this method and complete the synthesis of the first three rings of the *Veratrum* alkaloid skeleton.

Experimental

All reactions were carried out under an argon or anhydrous nitrogen atmosphere. All solvents were dried before use. Chromatographic separations were made using Merck Kieselgel 60 (230–400 mesh ASTM). The infrared spectra (ir) were taken on a Perkin–Elmer 681 spectrophotometer or on a FT-IR Bomem MB-102. Proton nmr spectra were recorded on a Bruker WP-80 or Bruker WM-250 instrument. Carbon nmr spectra were recorded on a Bruker WM-250 instrument. Chemical shifts are reported in δ values relative to tetramethylsilane or chloroform. Abbreviations used are m: multiplet, s: singlet, d: doublet, t: triplet, dd: double doublets, etc. Mass spectral assays (ms *m/e*) and peak matching were obtained using a VG Micromass ZAB-1F spectrometer.

*Methyl 5-*tert*-butyldiphenylsilyloxy-3-hydroxy-2-methoxymethyloxy-3-methylpentanoate (**19**a and **19**b)*

To a cold (−78°C) solution of lithium diisopropyl amide (LDA), obtained from diisopropylamine (DIPA) (20.5 mL, 146 mmol) and BuLi (1.6 mL in hexane) (90 mL, 144 mmol) in tetrahydrofuran (500 mL) at −20°C, was added dropwise (3.5 h) a solution of methyl methoxymethyloxyacetate (19.43 g, 145 mmol) in tetrahydrofuran (150 mL). The mixture was stirred at −78°C for 15 min and a solution of ketone **18** (23.2 g, 71.17 mmol) in tetrahydrofuran (150 mL) was added dropwise (1 h). After an additional 60 min at −78°C and treatment with a saturated solution of ammonium chloride the mixture was extracted with methylene chloride; the organic layer was dried over sodium sulfate and evaporated. The residue was purified by flash chromatography using hexane:ethyl acetate (19:1–7:3) as the eluent to afford alcohols **19***a* and **19***b* (31.9 g, 97.4%). These two diastereoisomers were separated on a small scale for their characterization.

Isomer **19**a (less polar): ir ($CHCl_3$): 3500, 1740 cm^{-1}; ^1H nmr ($CDCl_3$, δ ppm): 1.05 (9H, s, $-C(CH_3)_3$), 1.30 (3H, s, $-CH_3$), 1.90 (2H, m, $-CH_2-CH_2OTBDPS$), 3.33 (3H, s, $-OCH_3$), 3.77 (3H, s, $-CO_2CH_3$), 3.92 (2H, m, $-CH_2-OTBDPS$), 4.09 (1H, s, $-CH(CO_2CH_3)-$), 4.64 (2H, s, $-OCH_2O-$), 7.42 and 7.67 (10H, m, Ph_2).

Isomer **19**b (more polar): ir ($CHCl_3$): 3500, 1740 cm^{-1}; ^1H nmr ($CDCl_3$, δ ppm): 1.04 (9H, s, $-C(CH_3)_3$), 1.30 (3H, s, $-CH_3$), 1.80 (1H, dt, J = 6 and 15 Hz, $-CHH-CH_2OTBDPS$), 2.03 (1H, dt, J = 6 and 15 Hz, $-CHH-CH_2OTBDPS$), 3.38 (3H, s, $-OCH_3$), 3.75 (3H, s, $-CO_2CH_3$), 3.92 (2H, dd, J = 5.4 and 7 Hz, $-CH_2-OTBDPS$), 4.06 (1H, s, $-CH(CO_2CH_3)-$), 4.69 (2H, m, $-OCH_2O-$), 7.42 and 7.67 (10H, m, Ph_2).

*Methyl (2*E*) and (2*Z*)-5-*tert*-butyldiphenylsilyloxy-2-methoxymethyloxy-3-methylpent-2-enoate (**20**a and **20**b)*

Starting from alcohols **19***a* and **19***b* separately or a mixture of both:

To a solution of mixed alcohols **19***a* and **19***b* (29.5 g, 64.1 mmol) in pyridine (400 mL), at −60°C, thionyl chloride (25 mL, 343 mmol) was added all at once. The mixture was stirred at −60°C 15 min, at −30°C for 30 min, and at −20°C for 100 min. A saturated solution of sodium bicarbonate was added and the mixture was extracted with methylene chloride. The organic layer was dried over magnesium sulfate and evaporated. The residue was purified by flash chromatography using hexane:ethyl acetate (19:1–7:3) as the eluent to afford a mixture of unseparable α,β-unsaturated esters **20***a* and **20***b* and the two separable isomers **21** and **22** (**20***a* and **20***b* (7.65 g, 27%); **21** and **22** (16.4 g, 58%)).

Starting from isomers **21** and **22**:

To a solution of isomers **21** and **22** (16 g, 36.2 mmol) in anhydrous methanol (250 mL) was added potassium methoxide obtained from potassium (3 g, 77 mmol) dissolved in methanol (250 mL). The mixture was refluxed for 3 h, cooled, and poured into a saturated solution of ammonium chloride. The mixture was acidified to pH 6 with hydrochloric acid and extracted with methylene chloride. The organic layer was dried over sodium sulfate, evaporated, and the residue was purified by flash chromatography using hexane:ethyl acetate (19:1–7:3) as the eluent to afford pure α,β-unsatured esters **20***a* and **20***b* (11.3 g, 71%).

Isomer (E)-**20**a (obtained pure from pure **19***a*): ^1H nmr ($CDCl_3$, δ ppm): 1.03 (9H, s, $-C(CH_3)_3$), 1.90 (3H, s, $-CH_3$), 2.75 (2H, t, J = 7 Hz, $-CH_2-CH_2OTBDPS$), 3.50 (3H, s, $-OCH_3$), 3.71 (3H, s, $-CO_2CH_3$), 3.78 (2H, t, J = 7 Hz, $-CH_2-OTBDPS$), 4.80 (2H, s, $-OCH_2O-$), 7.41 and 7.67 (10H, m, Ph_2).

*Isomer (Z)-**20*** (obtained pure from pure **19***b*): ^1H nmr ($CDCl_3$, δ ppm): 1.04 (9H, s, $-C(CH_3)_3$), 1.98 (3H, s, $-CH_3$), 2.57 (2H, t, J = 7 Hz, $-CH_2-CH_2OTBDPS$), 3.44 (3H, s, $-OCH_3$), 3.77 (3H,

Can. J. Chem. Downloaded from www.nrcresearchpress.com by 109.225.110.28 on 09/08/12
For personal use only.

Can. J. Chem. Downloaded from www.nrcresearchpress.com by 109.225.110.28 on 09/08/12
For personal use only.

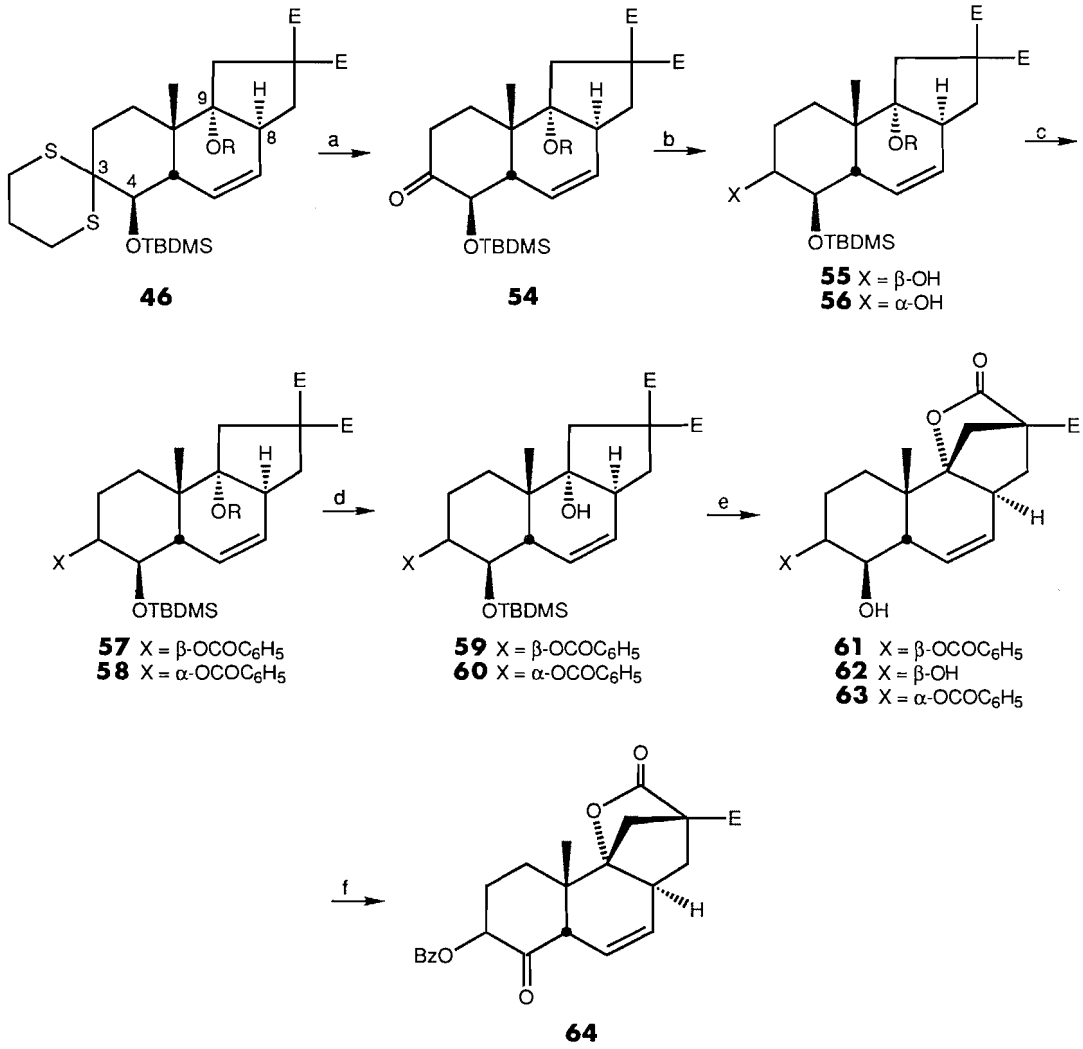

46 **54** **55** X = β-OH **56** X = α-OH

57 X = β-$OCOC_6H_5$ **58** X = α-$OCOC_6H_5$ **59** X = β-$OCOC_6H_5$ **60** X = α-$OCOC_6H_5$ **61** X = β-$OCOC_6H_5$ **62** X = β-OH **63** X = α-$OCOC_6H_5$

64

(a) $HgCl_2$, $CaCO_3$, aq. CH_3CN, 25°C, 70%;
(b) $NaBH_4$, MeOH, 94%;
(c) C_6H_5COCl, Et_3N, DMAP, CH_2Cl_2, 25°C (**57**, 89%; **58**, 86%);
(d) HCl 6N, THF aq. 25°C, 98%;
(e) Bu_4NF, THF, 25°C (**61**, 19% and **62**, 61%; **63**, 81%);
(f) PCC, CH_2Cl_2, 25°C, 98%

SCHEME 9. E = CO_2CH_3; R = MOM.

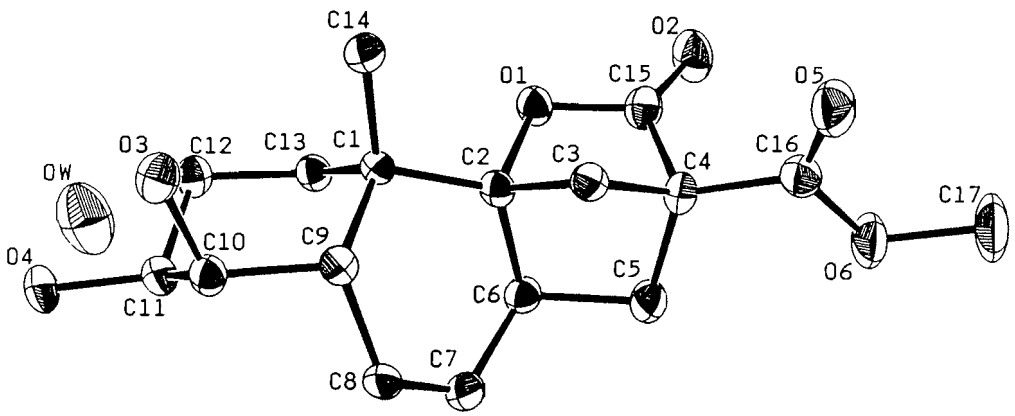

FIG. 2. Stereoview of crystalline **62**; 50% probability thermal ellipsoids are shown for the non-hydrogen atoms.

Can. J. Chem. Downloaded from www.nrcresearchpress.com by 109.225.110.28 on 09/08/12
For personal use only.

s, -CO_2CH_3), 3.78 (2H, t, J = 7 Hz, -CH_2-OTBDPS), 4.74 (2H, s, -OCH_2O-), 7.41 and 7.67 (10H, m, Ph_2).

Isomer ***21*** (less polar than **22**): ^{1}H nmr ($CDCl_3$, δ ppm): 1.04 (9H, s, -$C(CH_3)_3$), 2.37 (2H, q, J = 6.6 Hz, -CH_2-CH_2OTBDPS), 3.35 (3H, s, -OCH_3), 3.70 (3H, s, -CO_2CH_3), 3.79 (2H, dt, J = 6.8 Hz and 1.0 Hz, -CH_2-OTBDPS), 4.61 (1H, d J = 6.8 Hz, -OCHHO-), 4.66 (1H, d, J = 6.8 Hz, -OCHHO-), 4.62 (1H, s, -$CH(CO_2CH_3)$-), 5.13 (1H, s, CHH=), 5.26 (1H, s, CHH=), 7.40 and 7.66 (10H, m, Ph_2).

Isomer 22: ^{1}H nmr ($CDCl_3$, δ ppm): 1.04 (9H, s, -$C(CH_3)_3$), 1.46 (3H, d, J = 1.1 Hz, -CH_3), 3.38 (3H, s, -OCH_3), 3.74 (3H, s, -CO_2CH_3), 4.27 (2H, d, J = 6 Hz, -CH_2-OTBDPS), 4.56 (1H, s, -$CH(CO_2CH_3)$-), 4.65 (2H, s, -OCH_2O-), 5.82 (1H, t, J = 6 Hz, -CH=), 7.40 and 7.67 (10H, m, Ph_2).

*Methyl (2*E*)-5-hydroxy-2-methoxymethyloxy-3-methylpent-2-enoate (**24**a) and its conversion to 2-methoxymethyloxy-3-methylpent-2-en-5-olide (**25**)*

To a solution of pure **20***a* (22 mg, 0.05 mmol) in tetrahydrofuran (2 mL) was added at 0°C a solution of tetrabutylammonium fluoride (100 μL, 0.1 mmol). The mixture was stirred at room temperature for 2.5 h and the solvent was evaporated. The residue was purified by flash chromatography using hexane:ethyl acetate (4:1–3:2) as the eluent to afford pure lactone **25** (2 mg, 23%) and **24** (2.5 mg, 25%) (on silica gel, alcohol **24***a* partly forms lactone **25**). Lactone **25**: ir ($CHCl_3$, ν cm^{-1}): 1720, 1655; ^{1}H nmr ($CDCl_3$, δ ppm): 1.99 (3H, s, -CH_3), 2.50 (2H, t, J = 6.3 Hz, -CH_2CH_2-OCO-), 3.53 (3H, s, -OCH_3), 4.34 (2H, t, J = 6.2 Hz, -CH_2-CH_2-OCO-), 5.00 (2H, s, -OCH_2O-).

*Methyl (2*Z*)-5-hydroxy-2-methoxymethyloxy-3-methylpent-2-enoate (**24**b)*

To a solution of **20***b* (75 mg, 0.17 mmol) in tetrahydrofuran (6.0 mL), was added at 0°C a solution of tetrabutylammonium fluoride (340 μL, 0.34 mmol). The mixture was stirred at room temperature for 2 h and the solvent was evaporated. The residue was purified by flash chromatography using hexane:ethyl acetate (3:2) as the eluent to afford pure alcohol **24***b* (25 mg, 72%); ir ($CHCl_3$, ν cm^{-1}): 3600, 3460, 3030, 3010, 2950, 1720, 1640; ^{1}H nmr ($CDCl_3$, δ ppm): 2.09 (3H, s, -CH_3), 2.60 (2H, t, J = 6.3 Hz, -CH_2-CH_2OH), 3.53 (3H, s, -OCH_3), 3.79 (3H, s, -CO_2CH_3), 3.80 (2H, t, J = 6.3 Hz, -CH_2OH), 4.84 (2H, s, -OCH_2O-). Exact Mass calcd. for $C_9H_{16}O_5$: 172.0736 (M^+ − CH_3OH); found: 172.0734 ± 0.0005.

*(2*E*) and (2*Z*)-5-*tert*-Butyldiphenylsilyloxy-2-methoxymethyloxy-3-methylpent-2-en-1-ol (**23**a and **23**b)*

To a cold solution (−78°C) of esters **20** (8.55 g, 19.3 mmol) in methylene chloride (1 L) was added a solution of DIBAL (26 mL, 1.5 M, 39 mmol). The mixture was stirred vigourously for 2 h, then treated with decahydrated sodium sulfate (8 g). The mixture was warmed to room temperature, diluted with acetone (1 L), and stirred overnight. The mixture was dried over anhydrous sodium sulfate, filtered, and the residue on filter washed five times with acetone. Evaporation of the solvent left a residue, which was purified by flash chromatography using hexane:ethyl acetate (4:1–3:2) as the eluent to afford pure alcohols **23***a* (1.28 g, 16%) and **23***b* (6.60 g, 83%); ir (CH_2Cl_2, ν cm^{-1}): 3600, 3480, 3060, 2960, 2940, 2860, 1680. Exact Mass calcd. for $C_{24}H_{34}O_4Si$: 414.2226 (M^+); found: 414.2234 ± 0.0012.

*(*E*) Isomer **23**a* (less polar): ^{1}H nmr ($CDCl_3$, δ ppm): 1.04 (9H, s, -$C(CH_3)_3$), 1.64 (3H, s, -CH_3), 2.34 (2H, t, J = 6.5 Hz, -CH_2-CH_2OTBDPS), 2.93 (1H, t, J = 6 Hz, -OH), 3.50 (3H, s, -OCH_3), 3.66 (2H, t, J = 6.5 Hz, -CH_2OTBDPS), 4.12 (2H, d, J = 6 Hz, -CH_2OH), 4.87 (2H, s, -OCH_2O-), 7.41 and 7.66 (10H, m, Ph_2); ^{13}C nmr ($CDCl_3$, δ ppm): 15.4 (=C-CH_3), 19.0 (-$C(CH_3)_3$), 26.8 (-$C(CH_3)_3$), 35.8 (-CH_2-C=), 56.3 (OCH_3), 58.4 (CH_2-OTBDPS), 62.2 (CH_2-OH), 96.2 (OCH_2O), 119.7 (CH_3-C=C-), 127.7, 129.7, 133.5, 135.6 (C, aromatic), and 149.8 (C=C-OMOM).

*(Z) Isomer **23**b* (more polar): ^{1}H nmr ($CDCl_3$, δ ppm): 1.04 (9H, s, -$C(CH_3)_3$), 1.67 (3H, s, -CH_3), 2.39 (2H, t, J = 7 Hz, -CH_2-CH_2OTBDPS), 2.95 (1H, t, J = 6.4 Hz, -OH), 3.43 (3H, s, -OCH_3), 3.71 (2H, t, J = 7 Hz, -CH_2OTBDPS), 4.13 (2H, d, J = 6.4 Hz, -CH_2OH), 4.72 (2H, s, -OCH_2O-), 7.40 and 7.66 (10H, m, Ph_2); ^{13}C nmr ($CDCl_3$, δ ppm): 16.9 (=C-CH_3), 19.1 (-$C(CH_3)_3$), 26.8 (-$C(CH_3)_3$), 34.6 (-CH_2-C=), 56.2 (OCH_3), 58.5 (CH_2-OTBDPS), 62.3 (CH_2-OH), 96.7 (OCH_2O), 120.2 (CH_3-C=C-), 127.6, 129.6, 133.9, 135.6 (C, aromatic), and 148.9 (C=C-OMOM).

*(2Z)-5-*tert*-Butyldiphenylsilyloxy-2-methoxymethyloxy-3-methyl-1-(2,4,6-trimethylbenzoyloxy)pent-2-ene (**26**)*

To a solution of 2,4,6-trimethylbenzoic acid (mesitoic acid) (784 mg, 4.78 mmol), dicyclohexylcarbodiimide (1.39 g, 6.74 mmol), and 4-dimethylaminopyridine (400 mg, 3.28 mmol) in methylene chloride (8.8 mL) was added a solution of alcohol **23***b* (1.5 g, 3.62 mmol) in methylene chloride (3.7 mL). The mixture was stirred at room temperature for 7 days and a saturated solution of sodium bicarbonate was added. The mixture was extracted with methylene chloride, and the organic layer was dried over magnesium sulfate and evaporated. The residue was purified by flash chromatography using hexane:ethyl acetate (9:1–4:1) as the eluent to afford pure ester **26** (1.9 g, 94%); ir (CH_2Cl_2, ν cm^{-1}): 3060, 2960, 2940, 2860, 1720, 1610; ^{1}H nmr ($CDCl_3$, δ ppm): 1.03 (9H, s, -$C(CH_3)_3$), 1.75 (3H, s, -CH_3), 2.24 (6H, s, *ortho*-CH_3 of OMes), 2.27 (3H, s, *para*-CH_3 of OMes), 2.46 (2H, t, J = 7 Hz, -CH_2-CH_2OTBDPS), 3.37 (3H, s, -OCH_3), 3.72 (2H, t, J = 7 Hz, -CH_2-OTBDPS), 4.79 (2H, s, -OCH_2O-), 4.97 (2H, s, -CH_2-OMes), 6.82 (2H, s, CH aromatic), 7.38 and 7.66 (10H, m, Ph_2). Exact Mass calcd. for $C_{34}H_{44}O_5Si$: 503.2254 (M^+ − *tert*-butyl); found: 503.2250 ± 0.0015.

*(2Z)-2-Methoxymethyloxy-3-methyl-1-(2,4,6-trimethylbenzoyloxy)pent-2-en-5-ol (**27**)*

To a cold (0°C) solution of ester **26** (5.15 g, 9.2 mmol) in tetrahydrofuran (225 mL) was added a solution of tetrabutylammonium fluoride (18.4 mL, 18.4 mmol). The mixture was stirred at room temperature for 1.5 h and the solvent was evaporated. The residue was purified by flash chromatography using hexane:ethyl acetate (3:2) as the eluent to afford pure alcohol **27** (2.95 g, 99%); ir (CH_2Cl_2, ν cm^{-1}): 3620, 3500, 3060, 2990, 2960, 2930, 1720, 1610; ^{1}H nmr ($CDCl_3$, δ ppm): 1.84 (3H, s, -CH_3), 2.27 and 2.28 (9H, 2s, -CH_3 aromatic), 2.48 (2H, t, J = 6.4 Hz, -CH_2-CH_2OH), 3.46 (3H, s, -OCH_3), 3.73 (2H, t, J = 6.4 Hz, -CH_2-OH), 4.90 (2H, s, -OCH_2O-), 5.01 (2H, s, -CH_2-OMes), 6.84 (2H, s, CH aromatic). Exact Mass calcd. for $C_{18}H_{26}O_5$: 322.1780 (M^+); found: 322.1786 ± 0.0012.

*(2Z)-5-Mesyloxy-2-methoxymethyloxy-3-methyl-1-(2,4,6-trimethylbenzoyloxy)pent-2-ene (**28**)*

To a cold (0°C) solution of alcohol **27** (2.49 g, 7.73 mmol) and triethylamine (4.3 mL, 30.9 mmol) in methylene chloride (100 mL) was added mesyl chloride (950 μL, 12.3 mmol). The mixture was stirred at 0°C for 30 min and a saturated solution of sodium bicarbonate was added. The mixture was extracted with methylene chloride, and the organic layer was dried over sodium sulfate and evaporated. The residue was purified by flash chromatography with hexane:ethyl acetate (3:2) as the eluent to afford pure mesylate **28** (3.09 g, 98%); ir (CH_2Cl_2, ν cm^{-1}): 3060, 2990, 2960, 2930, 1725, 1360; ^{1}H nmr ($CDCl_3$, δ ppm): 1.86 (3H, s, -CH_3), 2.27 (9H, s, -CH_3 aromatic), 2.64 (2H, t, J = 7 Hz, -CH_2-CH_2OMs), 2.97 (3H, s, -SO_2-CH_3), 3.44 (3H, s, -OCH_3), 4.29 (2H, t, J = 7 Hz, -CH_2-OMs), 4.91 (2H, s, -OCH_2O-), 5.01 (2H, s, -CH_2-OMes), 6.84 (2H, s, CH aromatic). Exact Mass calcd. for $C_{19}H_{28}O_7S$: 400.1556 (M^+); found: 400.1563 ± 0.0014.

*(2Z)-5-Iodo-2-methoxymethyloxy-3-methyl-1-(2,4,6-trimethylbenzoyloxy)pent-2-ene (**29**)*

To a solution of mesylate **28** (2.25 g, 5.63 mmol) in acetone (340 mL) was added sodium iodide (38 g, 253 mmol). The mix-

Can. J. Chem. Downloaded from www.nrcresearchpress.com by 109.225.110.28 on 09/08/12
For personal use only.

ture was heated at 56°C for 5.5 h and then acetone was evaporated. The residue was dissolved in ether (500 mL) and filtered. The solvent was evaporated and the residue was purified by flash chromatography using hexane:ethyl acetate (7:3) as the eluent to afford pure iodide **29** (2.2 g, 91%); ir (CH_2Cl_2, ν cm^{-1}): 3060, 2990, 1725, 1610; ^1H nmr ($CDCl_3$, δ ppm): 1.83 (3H, s, $-CH_3$), 2.28 (9H, s, $-CH_3$ aromatic), 2.77 (2H, t, J = 7.5 Hz, $-CH_2-CH_2I$), 3.18 (2H, t, J = 7.5 Hz, $-CH_2I$), 3.46 (3H, s, $-OCH_3$), 4.91 (2H, s, $-OCH_2O-$), 4.99 (2H, s, $-CH_2$-OMes, 6.84 (2H, s, CH aromatic). Exact Mass calcd. for $C_{18}H_{25}O_4I$: 432.0799 (M^+); found: 432.0817 ± 0.0013.

*(2Z)-2-Methoxymethyloxy-3-methyl-6,6-(propylenedithio)-1-(2,4,6-trimethylbenzoyloxy)hex-2-ene (**30**)*

A solution of butyllithium (1.6 M in hexane) (285 μL, 0.46 mmol) was added to a cold (−30°C) solution of 1,3-dithiane (55.7 mg, 0.46 mmol) in tetrahydrofuran (0.6 mL). The mixture was stirred between −35°C and −25°C for 100 min. Then it was cooled to −78°C and a solution of iodide **29** (150 mg, 0.347 mmol) in tetrahydrofuran (0.6 mL) was added. The mixture was stirred at −78°C for 3 h and at −45°C for 1 h. Water was then added and the mixture was extracted with methylene chloride. The organic layer was dried over sodium sulfate and evaporated. The residue was purified by flash chromatography using hexane:ethyl acetate (9:1–3:2) as the eluent to afford pure **30** (17 mg, 12%) and iodide **29** (100 mg, 66%). ^1H nmr ($CDCl_3$, δ ppm): 1.79 (3H, s, $-CH_3$), 1.86 (2H, m, $-SCH_2CH_2CH_2S-$), 1.89 and 2.13 (2H, m, $-CH_2-CHS_2$), 2.27 (9H, s, $-CH_3$ aromatic), 2.38 (2H, m, $=C(CH_3)-CH_2CH_2-$), 2.85 (4H, m, $-SCH_2CH_2CH_2S-$), 3.46 (3H, s, $-OCH_3$), 4.02 (1H, t, J = 7 Hz, -S-CH-S-), 4.88 (2H, s, $-OCH_2O-$), 4.99 (2H, s, $-CH_2$-OMes), 6.83 (2H, s, CH aromatic).

*(2Z)-2-Methoxymethyloxy-3-methyl-6,6-(propylenedithio)-6-trimethylstannyl-1-(2,4,6-trimethylbenzoyloxy)hex-2-ene (**31**)*

To a cold (−78°C) solution of 2-trimethylstannyl-1,3-dithiane (864 mg, 3.06 mmol) in tetrahydrofuran (4.3 mL), was added a solution of LDA obtained at 0°C from DIPA (421 μL, 3.01 mmol) and BuLi (1.6 M in hexane) (1.9 mL, 3.04 mmol) in tetrahydrofuran (4.3 mL). The mixture was stirred at −30°C for 3 h and at −78°C for 30 min. Then a solution of iodide **29** (632 mg, 1.46 mmol) in tetrahydrofuran (3 mL) was added. The mixture was stirred at this temperature for an additional 1.5 h, treated with water, and warmed to room temperature. The mixture was extracted with methylene chloride; the organic layer was dried over sodium sulfate, evaporated, and the residue was purified by flash chromatography using hexane:ethyl acetate (19:1–7:3) as the eluent to afford pure **31** (325 mg, 38%) and **30** (111 mg, 18%); ^1H nmr ($CDCl_3$, δ ppm): 0.28 (9H, t, $J_{Sn(119)-H}$ = 27.2 Hz, $J_{Sn(117)-H}$ = 26.1 Hz, $-Sn-(CH_3)_3$), 1.85 (3H, s, $-CH_3$), 2.05 (2H, m, $-SCH_2CH_2CH_2S-$), 2.27 and 2.30 (9H, s, CH_3 aromatic), 2.31 (4H, m, $=C(CH_3)-CH_2-CH_2-$), 2.40 (2H, m, -SCHH-CH_2-CHH-S-), 3.15 (2H, m, -SCHH-CH_2-CHH-S-), 3.45 (3H, s, $-OCH_3$), 4.90 (2H, s, $-OCH_2O-$), 5.02 (2H, s, $-CH_2$-OMes), 6.85 (2H, s, CH aromatic).

*(2Z)-2-Methoxymethyloxy-3-methyl-6,6-(propylenedithio)-6-tributylstannyl-1-(2,4,6-trimethylbenzoyloxy)hex-2-ene (**32**)*

To a solution of 2-tributylstannyl-1,3-dithiane (2 g, 4.9 mmol) in tetrahydrofuran (7 mL) at −78°C, was added a solution of LDA obtained at 0°C from DIPA (690 μL, 4.9 mmol) and BuLi (1.6 M in hexane) (2.9 mL, 4.6 mmol) in tetrahydrofuran (7 mL). The mixture was stirred at −30°C for 3 h and at −78°C for 30 min. Then a solution of iodide **29** (967 mg, 2.24 mmol) maintained in tetrahydrofuran (6 mL) at −30°C was added. The mixture was stirred at this temperature for an additional 75 min and water was added. The solution was warmed to room temperature. The mixture was extracted with methylene chloride and the organic layer was dried with sodium sulfate and evaporated. The residue was purified by flash chromatography using hexane:ethyl acetate (19:1–9:1) as the eluent to afford pure **32** (1.383 g, 87%); ir (CH_2Cl_2, ν cm^{-1}): 3060, 2960, 2920, 2860, 1720, 1610; ^1H nmr ($CDCl_3$, δ ppm): 0.90 (9H, t, J = 7.2 Hz, $-(CH_2)_3-CH_3$), 1.08 (6H, m, $-Sn-CH_2-$), 1.34 (6H, m, J = 7 Hz, $-CH_2-CH_2-CH_3$), 1.55 (6H, m, $-Sn-CH_2-CH_2-$), 1.86 (3H, s, $-CH_3$), 2.05 (2H, m, $-SCH_2CH_2CH_2S-$), 2.21 and 2.33 (4H, m, $=C(CH_3)-CH_2-CH_2-$), 2.27 and 2.30 (9H, s, $-CH_3$ aromatic), 2.43 (2H, m, -SCHH-CH_2-CHH-S-), 3.15 (2H, m, SCHH-CH_2-CHH-S-), 3.45 (3H, s, $-OCH_3$), 4.90 (2H, s, $-OCH_2O-$), 5.03 (2H, s, $-CH_2$-OMes), 6.84 (2H, s, CH aromatic). Exact Mass calcd. for $C_{34}H_{58}O_4S_2Sn$: 657.2094 (M^+ − *tert*-butyl); found: 657.2105 ± 0.0018.

*(2Z,4E)-6-*tert*-Butoxydiphenylsilyloxy-1-tetrahydropyranyloxyhexa-2,4-diene (**34**)*

To a solution of alcohol **33** (2.32 g, 11.7 mmol) and triethylamine (2.5 mL, 17.8 mmol) in methylene chloride (50 mL) was added *tert*-butoxydiphenylsilyl chloride (3.2 mL, 12.2 mmol) at 0°C. The mixture was stirred at room temperature for 40 min and a saturated solution of ammonium chloride was added. The mixture was extracted with hexane:ether (4:1); the organic layer was dried with sodium sulfate and evaporated. The residue was purified by flash chromatography using hexane:ether (4:1) as the eluent to afford pure **34** (5.25 g, 99%); ir (CH_2Cl_2, ν cm^{-1}): 3050, 2980, 2940, 2860, 1430; ^1H nmr ($CDCl_3$, δ ppm): 1.31 (9H, s, $-OC-(CH_3)_3$), 1.47–1.86 (6H, m, $-OCH_2-(CH_2)_3-$), 3.49 and 3.87 (2H, m, $-OCH_2-(CH_2)_3-$), 4.20 (1H, dd, J = 7.5 and 12.5 Hz, THPO-CHH-CH=CH-), 4.35 (1H, dd, J = 7.5 and 12.5 Hz, THPO-CHH-CH=CH-), 4.34 (2H, d, J = 4.6 Hz, $-CH_2$-OTBODPS), 4.65 (1H, t, J = 3.5 Hz, -O-CH(O-)-), 5.57 (1H, dt, J = 7 and 10.9 Hz, THPO-CH_2-CH=CH-), 5.83 (1H, dt, J = 5.2 and 15 Hz, $-CH=CH-CH_2$OTBODPS), 6.16 (1H, dd, J = 11.1 and 11.1 Hz, THPO-CH_2-CH=CH-), 6.60 (1H, dd, J = 11.5 and 15 Hz, CH=CH-CH_2OTBODPS), 7.37 and 7.67 (10H, m, Ph_2). Exact Mass calcd. for $C_{27}H_{36}O_4Si$: 395.1679 (M^+ − *tert*-butyl); found: 395.1674 ± 0.0011.

*(2Z,4E)-6-*tert*-Butoxydiphenylsilyloxyhexa-2,4-dien-1-ol (**35**)*

To a solution of **34** (16.7 g, 36.9 mmol) in *tert*-butanol (270 mL) was added pyridinium *para*-toluenesulfonate (1.68 g, 6.7 mmol). The mixture was heated to 60°C for 10 h and then a saturated solution of sodium bicarbonate was added. The mixture was extracted with hexane:ether (4:1), and the organic layer was dried with sodium sulfate and evaporated. The residue was purified by flash chromatography using hexane:ethyl acetate (9:1–3:2) as the eluent to afford pure alcohol **35** (6.89 g, 51%) and starting **34** (6.2 g, 37%); ir (CH_2Cl_2, ν cm^{-1}): 3600, 3060, 2980, 2940, 2880; ^1H nmr ($CDCl_3$, δ ppm): 1.31 (9H, s, $-OC(CH_3)_3$), 4.30 (2H, dd, J = 5.7 and 5.7 Hz, $-CH_2OH$), 4.35 (2H, d, J = 5.2 Hz, $-CH_2$-OTBODPS), 5.59 (1H, ddd, J = 7.5, 7.5, and 10.9 Hz, HO-CH_2-CH=CH-), 5.84 (1H, ddd, J = 5, 5, and 15 Hz, $-CH=CH-CH_2$OTBODPS), 6.10 (1H, dd, J = 11.5 and 11.5 Hz, HO-CH_2-CH=CH-), 6.54 (1H, dd, J = 12 and 15 Hz, $-CH=CH-CH_2$OTBODPS), 7.37 and 7.67 (10H, m, Ph_2). Exact Mass calcd. for $C_{22}H_{28}O_3Si$: 311.1103 (M^+ − *tert*-butyl); found: 311.1082 ± 0.0009.

*(2Z,4E)-6-*tert*-Butoxydiphenylsilyloxyhexa-2,4-dien-1-al (**36**)*

To a solution of oxalyl chloride (1.7 mL, 19.5 mmol) in methylene chloride (52 mL) at −78°C was added dimethyl sulfoxide (2.8 mL, 39.5 mmol). The mixture was stirred at −78°C for 10 min and a solution of alcohol **35** (5.5 g, 15.0 mmol) in methylene chloride (42 mL) was added. The mixture was stirred for 50 min at −78°C, and diisopropylethylamine (DIPEA) (10.5 mL, 60.4 mmol) was added. The mixture was stirred for 15 min at −78°C and for 25 min at 0°C, water was added, and the mixture was extracted with methylene chloride. The organic layer was dried over sodium sulfate and evaporated. The residue was purified by flash chromatography using hexane:ethyl acetate (9:1) as the eluent to afford pure aldehyde **36** (4.15 g, 76%); ^1H nmr ($CDCl_3$, δ ppm): 1.31 (9H, s, $-OC(CH_3)_3$), 4.45 (2H, d, J = 4 Hz, $-CH_2$-OTBODPS), 5.84 (1H, dd, J = 8 and 11 Hz, HCO-CH=CH-), 6.21 (1H, dt, J = 5 and 15 Hz, $-CH=CH-CH_2$OTBODPS), 6.98 (1H, dd, J = 11.5 and

Can. J. Chem. Downloaded from www.nrcresearchpress.com by 109.225.110.28 on 09/08/12
For personal use only.

11.5 Hz, HCO-CH=CH-), 7.38 and 7.66 (11H, m, Ph_2 and -CH=CH-CH_2OTBODPS), 10.17 (1H, d, J = 8 Hz, HCO-).

*(2Z,8Z,10E)-12-*tert*-Butoxydiphenylsilyloxy-7-hydroxy-2-methoxymethyloxy-3-methyl-6,6-(propylenedithio)-1-(2,4,6-trimethylbenzoyloxy)dodeca-2,8,10-triene (**37**)*

To a cold (−93°C) solution of **32** (485 mg, 0.68 mmol) in tetrahydrofuran (7.6 mL) was added rapidly a cold (−90°C) solution of BuLi (1.6 M in hexane) (850 μL, 1.36 mmol) and, 15 s later, a cold (−93°C) solution of aldehyde **36** (790 mg, 2.16 mmol) in tetrahydrofuran (11 mL) was added. The mixture was stirred at −93°C for 35 min and a saturated solution of ammonium chloride was added. The mixture was warmed to room temperature and extracted with methylene chloride. The organic layer was dried over sodium sulfate and evaporated. The residue was purified by flash chromatography using hexane:ethyl acetate (9:1–4:1) as the eluent to afford pure alcohol **37** (462 mg, 86%), and a small amount of **38** (15 mg, 3%).

Compound 37: ir (CH_2Cl_2, ν cm^{-1}): 3050, 2980, 1720; ^{1}H nmr ($CDCl_3$, δ ppm): 1.30 (9H, s, -OC$(CH_3)_3$), 1.77 (3H, s, -CH_3), 1.78 (3H, m, -$SCH_2CH_2CH_2S$- and =C(CH_3)-CH_2-CHH-), 2.01 (1H, ddd, J = 5, 11.7, and 14.5 Hz, =C(CH_3)-CH_2-CHH-), 2.27 (9H, s, -CH_3 aromatic), 2.38 (1H, ddd, J = 4.9, 12.2, and 12.2 Hz, =C(CH_3)-CHH-CH_2-), 2.48 (1H, ddd, J = 5.3, 12.4, and 12.4 Hz, =C(CH_3)-CHH-CH_2-), 2.60 (2H, m, -SCHH-CH_2-CHH-S-), 2.76 (1H, d, J = 2.2 Hz, -CH-OH), 2.92 (2H, m, -SCHH-CH_2-CHH-S-), 3.45 (3H, s, -OCH_3), 4.38 (2H, d, J = 4.1 Hz, -CH_2-OTBODPS), 4.85 (1H, d, J = 6.6 Hz, -OCHHO-), 4.88 (1H, d, J = 6.6 Hz, -OCHHO-), 4.92 (1H, d, J = 10 Hz, -CH-OH), 4.97 (2H, s, -CH_2-OMes), 5.56 (1H, dd, J = 10 and 10.5 Hz, -CH(OH)-CH=CH-), 5.90 (1H, dt, J = 5 and 15 Hz, -CH=CH-CH_2OTBODPS), 6.31 (1H, dd, J = 11.3 and 11.3 Hz, -CH(OH)-CH=CH-), 6.78 (1H, dd, J = 12.5 and 15 Hz, -CH=CH-CH_2OTBODPS), 6.83 (2H, s, CH aromatic), 7.35 and 7.66 (10H, m, Ph_2). Exact Mass calcd. for $C_{44}H_{58}O_7S_2Si$: 790.3393 (M^+); found: 790.3387 ± 0.0023.

Compound 38: ^{1}H nmr ($CDCl_3$, δ ppm): 1.31 (9H, s, -OC$(CH_3)_3$), 1.80 (3H, s, -CH_3), 1.85 (2H, m, -$SCH_2CH_2CH_2S$-), 1.90 (1H, m, =C(CH_3)-CH_2-CHH-), 2.10 (1H, m, =C(CH_3)-CH_2-CHH), 2.27 (6H, s, -CH_3 aromatic), 2.40 (2H, m, =C(CH_3)-CH_2-), 2.75 (2H, m, Ar-CH_2-CH(OH)-), 2.84 (4H, m, -SCH_2-CH_2-CH_2-S-), 3.46 (3H, s, -OCH_3), 4.02 (1H, t, J = 7 Hz, -CH-S_2), 4.35 (2H, d, J = 5 Hz, -CH_2-OTBODPS), 4.78 (1H, m, -CH(OH)-), 4.88 (2H, s, -OCH_2O-), 5.00 (2H, s, -CH_2-OMes), 5.44 (1H, dd, J = 10 and 10.5 Hz, -CH(OH)-CH=CH-), 5.85 (1H, dt, J = 5 and 15 Hz, -CH=CH-CH_2OTBODPS), 6.07 (1H, dd, J = 11 and 11 Hz, -CH(OH)-CH=CH-), 6.60 (1H, dd, J = 12 and 15 Hz, -CH=CH-CH_2OTBODPS), 6.88 (2H, s, CH aromatic), 7.36 and 7.66 (10H, m, Ph_2).

*(2Z,8Z,10E)-12-*tert*-Butoxydiphenylsilyloxy-7-*tert*-butyldimethylsilyloxy-2-methoxymethyloxy-3-methyl-6,6-(propylenedithio)-1-(2,4,6-trimethylbenzoyloxy)dodeca-2,8,10-triene (**39**)*

To a solution of alcohol **37** (1.115 g, 1.41 mmol) and triethylamine (980 μL, 7.04 mmol) in methylene chloride (26 mL) was added at 0°C, *tert*-butyldimethylsilyl triflate (500 μL, 2.2 mmol). The mixture was stirred at 0°C for 80 min and a saturated solution of sodium bicarbonate was added. The mixture was extracted with methylene chloride, and the organic layer was dried over sodium sulfate and evaporated. The residue was purified by flash chromatography with hexane:ethyl acetate (9:1) as the eluent to afford pure **39** (1.09 g, 85%); ir (CH_2Cl_2, ν cm^{-1}): 3060, 3050, 2980, 2960, 2930, 2860, 1720, 1610; ^{1}H nmr ($CDCl_3$, δ ppm): 0.02 and 0.10 (6H, 2s, -OSi$(CH_3)_2$C$(CH_3)_3$), 0.89 (9H, s, -OSi$(CH_3)_2$C$(CH_3)_3$), 1.30 (9H, s, -OC$(CH_3)_3$), 1.80 (3H, s, -CH_3), 1.82–2.12 (4H, m, -$SCH_2CH_2CH_2S$- and =C(CH_3)-CH_2-CH_2-), 2.28 (9H, s, -CH_3 aromatic), 2.47 (2H, m, =C(CH_3)-CH_2-), 2.76 (4H, m, -SCH_2-CH_2-CH_2-S-), 3.43 (3H, s, -OCH_3), 4.37 (2H, d, J = 4.3 Hz, -CH_2-OTBODPS), 4.84 (1H, d, J = 6.6 Hz, -OCHHO-), 4.88 (1H, d, J = 6.6 Hz, -OCHHO-), 4.88 (1H, d, J = 10 Hz, -CH(OTBDMS)-), 4.99 (2H, s, -CH_2-OMes), 5.55 (1H, dd, J = 10.4 and 10.5 Hz, -CH(OTBDMS)-CH=CH-), 5.88 (1H, dt, J = 4.4 and 14.9 Hz, -CH=CH-CH_2OTBODPS), 6.19 (1H, dd, J = 11.3 and 11.3 Hz, -CH(OTBDMS)-CH=CH-), 6.77 (1H, dd, J = 12.4 and 14.8 Hz, -CH=CH-CH_2OTBODPS), 6.83 (2H, s, CH aromatic), 7.35 and 7.67 (10H, m, Ph_2). Exact Mass calcd. for $C_{50}H_{72}O_7S_2Si_2$: 904.4258 (M^+); found: 904.4232 ± 0.0026.

*(2Z,8Z,10E)-12-*tert*-Butoxydiphenylsilyloxy-7-*tert*-butyldimethylsilyloxy-2-methoxymethyloxy-3-methyl-6,6-(propylenedithio)dodeca-2,8,10-trien-1-ol (**40**)*

To a solution of mesitoate **39** (2.16 g, 2.39 mmol) in ether (80 mL) was added, at 0°C, lithium aluminum hydride (136 mg, 3.6 mmol). The mixture was stirred at 0°C for 30 min and at room temperature for 90 min. A saturated solution of ammonium chloride and ice were added and the mixture was extracted with methylene chloride. The organic layer was dried over sodium sulfate and evaporated. The residue was purified by flash chromatography using hexane:ethyl acetate (9:1–3:2) as the eluent to afford pure alcohol **40** (1.478 g, 82%); ir (CH_2Cl_2, ν cm^{-1}): 3500, 3060, 2980, 2960, 2940, 2860; ^{1}H nmr ($CDCl_3$, δ ppm): 0.03 and 0.11 (6H, 2s, -OSi$(CH_3)_2$C$(CH_3)_3$), 0.90 (9H, s, -OSi$(CH_3)_2$C$(CH_3)_3$), 1.31 (9H, s, -OC$(CH_3)_3$), 1.73 (3H, s, -CH_3), 1.75–2.12 (4H, m, -$SCH_2CH_2CH_2S$- and =C(CH_3)-CH_2-CH_2-), 2.40 (2H, m, =C(CH_3)-CH_2-), 2.77 (4H, m, -SCH_2-CH_2-CH_2-S-), 3.02 (1H, t, J = 6.3 Hz, -OH), 3.48 (3H, s, -OCH_3), 4.14 (2H, d, J = 6.3 Hz, -CH_2-OH), 4.38 (2H, d, J = 4.3 Hz, -CH_2-OTBODPS), 4.80 (2H, s, -OCH_2O-), 4.88 (1H, d, J = 10 Hz, -CH(OTBDMS)-), 5.55 (1H, dd, J = 10.3 and 10.4 Hz, -CH(OTBDMS)-CH=CH-), 5.88 (1H, dt, J = 4.5 and 14.9 Hz, -CH=CH-CH_2OTBODPS), 6.20 (1H, dd, J = 11.3 and 11.3 Hz, -CH(OTBDMS)-CH=CH-), 6.77 (1H, dd, J = 12.3 and 14.2 Hz, -CH=CH-CH_2OTBODPS), 7.36 and 7.67 (10H, m, Ph_2). Exact Mass calcd. for $C_{40}H_{62}O_6S_2Si_2$: 758.3526 (M^+); found: 758.3508 ± 0.0022.

*(2Z,8Z,10E)-12-*tert*-Butoxydiphenylsilyloxy-7-*tert*-butyldimethylsilyloxy-1-chloro-2-methoxymethyloxy-3-methyl-6,6-(propylenedithio)dodeca-2,8,10-triene (**41**)*

To a cold (0°C) solution of alcohol **40** (1.47 g, 1.94 mmol), lithium chloride (742 mg, 17.5 mmol), and collidine (1.25 mL, 9.46 mmol) in dimethylformamide (10 mL) was added mesyl chloride (475 μL, 6.14 mmol). The mixture was stirred at 0°C for 15 min, then at room temperature for 1 h, and a saturated solution of ammonium chloride was then added together with a saturated solution of sodium bicarbonate. The mixture was extracted with hexane:ether (1:1) and the organic layer was dried over sodium sulfate and evaporated. The residue was purified by flash chromatography using hexane:ethyl acetate (4:1) as the eluent to afford pure chloride **41** (1.357 g, 90%); ir (CH_2Cl_2, ν cm^{-1}): 3060, 2980, 2960, 2940, 2860, 1660; ^{1}H nmr ($CDCl_3$, δ ppm): 0.02 and 0.10 (6H, 2s, -OSi$(CH_3)_2$C$(CH_3)_3$), 0.89 (9H, s, -OSi$(CH_3)_2$C$(CH_3)_3$), 1.30 (9H, s, -OC$(CH_3)_3$), 1.74 (3H, s, -CH_3), 1.70–2.13 (4H, m, -$SCH_2CH_2CH_2S$- and =C(CH_3)-CH_2-CH_2-), 2.44 (2H, m, =C(CH_3)-CH_2), 2.77 (4H, m, -SCH_2-CH_2-CH_2-S-), 3.47 (3H, s, -OCH_3), 4.27 (2H, s, -CH_2Cl), 4.37 (2H, d, J = 4.4 Hz, -CH_2-OTBODPS), 4.88 (2H, s, -OCH_2O-), 4.87 (1H, d, J = 10 Hz, -CH(OTBDMS)-), 5.55 (1H, dd, J = 10.5 and 10.5 Hz, -CH(OTBDMS)-CH=CH-), 5.88 (1H, dt, J = 4.5 and 14.8 Hz, -CH=CH-CH_2OTBODPS), 6.20 (1H, dd, J = 11.3 and 11.3 Hz, -CH(OTBDMS)-CH=CH-), 6.77 (1H, dd, J = 12.5 and 14.5 Hz, -CH=CH-CH_2OTBODPS), 7.37 and 7.67 (10H, m, Ph_2); ms m/e: 740 (M^+ − HCl).

*(3Z,9Z,11E)-13-*tert*-Butoxydiphenylsilyloxy-8-*tert*-butyldimethylsilyloxy-1,1-*bis*-methoxycarbonyl-3-methoxymethyloxy-4-methyl-7,7-(propylenedithio)trideca-3,9,11-triene (**42**)*

Dimethyl malonate (200 μL, 1.75 mmol) was added at 0°C to a suspension of NaH (60% in oil) (64 mg, 1.6 mmol) in tetrahydro-

Can. J. Chem. Downloaded from www.nrcresearchpress.com by 109.225.110.28 on 09/08/12
For personal use only.

furan:dimethylformamide (1:1) (4 mL). The mixture was stirred at room temperature for 15 min and a solution of chloride **41** (201 mg, 0.259 mmol) in tetrahydrofuran:dimethylformamide (1:1) (2 mL) was added at 0°C together with a small quantity (5 mg) of potassium iodide. The mixture was stirred at room temperature for 3 h and a saturated solution of ammonium chloride was added to the solution. The mixture was extracted with hexane:ether (1:1), and the organic layer was dried over sodium sulfate and evaporated. The residue was purified by flash chromatography using hexane:ethyl acetate (4:1) as the eluent to afford pure **42** (183 mg, 81%); ir (CH_2Cl_2, ν cm^{-1}): 3060, 2980, 2960, 2935, 1735; ^1H nmr ($CDCl_3$, δ ppm): 0.01 and 0.09 (6H, 2s, $-OSi(CH_3)_2C(CH_3)_3$), 0.89 (9H, s, $-OSi(CH_3)_2C(CH_3)_3$), 1.30 (9H, s, $-OC(CH_3)_3$), 1.64 (3H, s, $-CH_3$), 1.75–2.00 (4H, m, $-SCH_2CH_2CH_2S-$ and $=C(CH_3)-CH_2-CH_2-$), 2.36 (2H, m, $=C(CH_3)-CH_2-$), 2.76 (4H, m, $-SCH_2-CH_2-CH_2-S-$), 2.85 (2H, d, J = 7.6 Hz, $-CH_2-CH(CO_2CH_3)_2$), 3.44 (3H, s, $-OCH_3$), 3.71 (6H, s, $(CO_2CH_3)_2$), 3.71 (1H, t, J = 7.6 Hz, $CH(CO_2CH_3)_2$), 4.37 (2H, d, J = 4.2 Hz, $-CH_2$-OTBODPS), 4.74 (2H, s, $-OCH_2O-$), 4.86 (1H, d, J = 10 Hz, -CH(OTBDMS)-), 5.54 (1H, dd, J = 10.5 and 10.5 Hz, -CH(OTBDMS)-CH=CH-), 5.87 (1H, dt, J = 4.2 and 14.6 Hz, $-CH=CH-CH_2$OTBODPS), 6.19 (1H, dd, J = 11.4 and 11.4 Hz, -CH(OTBDMS)-CH=CH-), 6.76 (1H, dd, J = 12 and 14.9 Hz, $-CH=CH-CH_2$OTBODPS), 7.36 and 7.67 (10H, m, Ph_2). Exact Mass calcd. for $C_{45}H_{68}O_9S_2Si_2$: 872.3843 (M^+); found: 872.3827 ± 0.0026.

*(3Z,9Z,11E)-8-*tert*-Butyldimethylsilyloxy-1,1-bis-methoxycarbonyl-3-methoxymethyloxy-4-methyl-7,7-(propylenedithio)trideca-3,9,11-trien-13-ol (**43**)*

A solution of tetrabutylammonium fluoride (1.0 M in THF, 2.4 mL, 2.4 mmol) was added at 0°C to a solution of **42** (865 mg, 0.99 mmol) in methylene chloride (17 mL). The mixture was stirred at 0°C for 15 min and at room temperature for 3.5 h, then diluted with water. The mixture was extracted with ether and the organic layer was dried over sodium sulfate. Then the solution was filtered on a silica gel pad and the solvent was evaporated. The residue was purified by flash chromatography using hexane:ethyl acetate (3:2) as the eluent to afford pure alcohol **43** (539 mg, 88%); ir (CH_2Cl_2, ν cm^{-1}): 3060, 2990, 2960, 2860, 1735; ^1H nmr ($CDCl_3$, δ ppm): 0.01 and 0.10 (6H, 2s, $-OSi(CH_3)_2C(CH_3)_3$), 0.89 (9H, s, $-OSi(CH_3)_2C(CH_3)_3$), 1.64 (3H, s, $-CH_3$), 1.91 (4H, m, $-SCH_2CH_2CH_2S-$ and $=C(CH_3)-CH_2-CH_2-$), 2.38 (2H, m, $=C(CH_3)-CH_2-$), 2.84 (4H, m, $-SCH_2-CH_2-CH_2-S-$), 2.85 (2H, d, J = 7.9 Hz, $-CH_2-CH(CO_2CH_3)_2$), 3.47 (3H, s, $-OCH_3$), 3.71 and 3.72 (6H, 2s, $(CO_2CH_3)_2$), 3.71 (1H, t, J = 7.6 Hz, $-CH(CO_2CH_3)_2$), 4.24 (2H, s large, $-CH_2-OH$), 4.77 (2H, s, $-OCH_2O-$), 4.79 (1H, d, J = 10 Hz, -CH(OTBDMS)-), 5.60 (1H, dd, J = 10.5 and 10.5 Hz, -CH(OTBDMS)-CH=CH-), 5.92 (1H, dt, J = 5 and 15 Hz, $-CH=CH-CH_2OH$), 6.17 (1H, dd, J = 11.2 and 11.2 Hz, -CH(OTBDMS)-CH=CH-), 6.59 (1H, dd, J = 12 and 15 Hz, $-CH=CH-CH_2OH$). Exact Mass calcd. for $C_{29}H_{50}O_8S_2Si$: 618.2716 (M^+); found: 618.2710 ± 0.0018.

*(3Z,9Z,11E)-8-*tert*-Butyldimethylsilyloxy-13-chloro-1,1-bis-methoxycarbonyl-3-methoxymethyloxy-4-methyl-7,7-(propylenedithio)trideca-3,9,11-triene (**44**)*

Mesyl chloride (230 μL, 2.97 mmol) was added to a cold (0°C) solution of alcohol **43** (540 mg, 0.874 mmol), lithium chloride (634 mg, 14.9 mmol), and collidine (660 μL, 5.0 mmol) in dimethylformamide (6 mL). The mixture was stirred at 0°C for 15 min and at room temperature for 4 h and then a saturated solution of ammonium chloride was added. The mixture was extracted with hexane:ether (1:1), and the organic layer was dried over sodium sulfate and evaporated. The residue was purified by flash chromatography using hexane:ethyl acetate (7:3) as the eluent to afford pure chloride **44** (484 mg, 87%); ^1H nmr ($CDCl_3$, δ ppm): 0.00 and 0.10 (6H, 2s, $-OSi(CH_3)_2C(CH_3)_3$), 0.88 (9H, s, $-OSi(CH_3)_2C(CH_3)_3$), 1.64 (3H, s, $-CH_3$), 1.95 (4H, m, $-SCH_2CH_2CH_2S-$ and $=C(CH_3)-CH_2-CH_2-$), 2.35 (2H, m, $=C(CH_3)-CH_2-$), 2.81 (6H, m, $-SCH_2-CH_2-CH_2-S-$ and $-CH_2-CH(CO_2CH_3)_2$), 3.47 (3H, s, $-OCH_3$), 3.72 (6H, s, $(CO_2CH_3)_2$), 3.73 (1H, t, J = 7 Hz, $-CH(CO_2CH_3)_2$), 4.15 (2H, d, J = 7 Hz, $-CH_2-Cl$), 4.77 (2H, s, $-OCH_2O-$), 4.76 (1H, d, J = 10 Hz, -CH(OTBDMS)-), 5.65 (1H, dd, J = 10.3 and 10.3 Hz, -CH(OTBDMS)-CH=CH-), 5.88 (1H, dt, J = 7.5 and 15 Hz, $-CH=CH-CH_2Cl$), 6.16 (1H, dd, J = 11.2 and 11.2 Hz, -CH(OTBDMS)-CH=CH-), 6.63 (1H, dd, J = 11.3 and 14.8 Hz, $-CH=CH-CH_2Cl$).

*(3Z,9Z,11E)-8-*tert*-Butyldimethylsilyloxy-1,1-bis-methoxycarbonyl-3-methoxymethyloxy-4-methyl-7,7-(propylenedithio)cyclotrideca-3,9,11-triene (**45**)*

To a warm (78°C) solution of cesium carbonate (1.025 g, 3.14 mmol) and 18-crown-6 (870 mg, 3.29 mmol) in acetonitrile (350 mL) was added dropwise a solution of chloride **44** (390 mg, 0.613 mmol) in acetonitrile (26 mL). The addition was done at a rate of 12 mL in 2 h, 6.5 mL in 2.5 h, and 7.5 mL in 3.5 h. The mixture was heated at 78°C for an additional 8 h, then cooled, filtered, and the solvents were evaporated. The residue was purified by flash chromatography using hexane:ethyl acetate (9:1–4:1) as the eluent to afford pure macrocycle **45** (276 mg, 75%); ir (CH_2Cl_2, ν cm^{-1}): 3060, 2990, 2960, 2930, 1735; ^1H nmr ($CDCl_3$, δ ppm): 0.08 and 0.15 (6H, 2s, $-OSi(CH_3)_2C(CH_3)_3$), 0.94 (9H, s, $-OSi(CH_3)_2C(CH_3)_3$), 1.36 (1H, dd, J = 9.6 and 13.5 Hz, $=C(CH_3)-CH_2-CHH-$), 1.58 (3H, s, $-CH_3$), 1.80–2.21 (4H, m, $-SCH_2CH_2CH_2S-$ and $=C(CH_3)-CHH-CHH-$), 2.49 (1H, d, J = 15 Hz, =C(OMOM)-CHH-), 2.59–2.83 (4H, m, $-SCHH-CH_2-CHH-S-$, $=C(CH_3)-CHH-$ and $-CH=CH-CHH-$), 3.19–3.35 (4H, m, $-SCHH-CH_2-CHH-S-$, =C(OMOM)-CHH- and $-CH=CH-CHH-$), 3.52 (3H, s, $-OCH_3$), 3.72 and 3.73 (6H, 2s, $(CO_2CH_3)_2$), 4.67 (1H, d, J = 6.2 Hz, -OCHHO-), 4.82 (1H, d, J = 6.2 Hz, -OCHHO-), 4.94 (1H, d, J = 9.3 Hz, -CH(OTBDMS)-), 5.45 (1H, ddd, J = 5, 11, and 15 Hz, $-CH=CH-CH_2-$), 5.59 (1H, dd, J = 10.5 and 10.5 Hz, -CH(OTBDMS)-CH=CH-), 6.00 (1H, dd, J = 11 and 11 Hz, -CH(OTBDMS)-CH=CH-), 6.55 (1H, dd, J = 10.8 and 15 Hz, $-CH=CH-CH_2-$); ^1H nmr (C_6D_6, δ ppm): 0.21 and 0.29 (6H, 2s, $-OSi(CH_3)_2C(CH_3)_3$), 1.07 (9H, s, $-OSi(CH:i3)_2C(CH_3)_3$), 1.60 (3H, s, $-CH_3$), 1.67 (3H, m, $-SCH_2CH_2CH_2S-$ and $=C(CH_3)-CH_2-CHH-$), 2.05 (1H, m, $=C(CH_3)-CH_2-CHH-$), 2.40 (3H, m, $-SCHH-CH_2-CHH-S-$ and $=C(CH_3)-CHH-$), 2.74 (1H, d, J = 15.3 Hz, =C(OMOM)-CHH-), 2.94–3.18 (4H, m, $-SCHH-CH_2-CHH-S-$, $=C(CH_3)-CHH-$, and $-CH=CH-CHH-$), 3.27 and 3.30 (6H, 2s, $(CO_2CH_3)_2$), 3.38 (3H, s, $-OCH_3$), 3.53 (1H, d, J = 15.3 Hz, =C(OMOM)-CHH-), 3.59 (1H, dd, J = 11.2 and 13.6 Hz, $-CH=CH-CHH-$), 4.59 (1H, d, J = 6.1 Hz, -OCHHO-), 4.72 (1H, d, J = 6.1 Hz, -OCHHO-), 5.23 (1H, d, J = 8.4 Hz, -CH(OTBDMS)-), 5.60 (1H, ddd, J = 5, 11, and 15 Hz, $-CH=CH-CH_2-$), 5.94 (2H, dd, J = 11 Hz, -CH(OTBDMS)-CH=CH-), 6.89 (1H, dd, J = 10 and 14.9 Hz, $-CH=CH-CH_2-$); ^{13}C nmr ($CDCl_3$, δ ppm): −4.4 ($-Si(CH_3)_2-$), 15.5 ($C=C-CH_3$), 18.4 ($-C(CH_3)_3$), 24.1, 25.1, 27.1, 27.6, 32.8, 34.4, 35.3 ($7 \times CH_2$), 26.1 ($-C(CH_3)_3$), 52.5, 52.7 ($-CO_2CH_3$), 55.4, 57.1 ($-C(S_2-$ and $-C(CO_2CH_3)_2-$), 57.0 ($-OCH_3$), 76.7 (-CH(OTBDMS)-), 97.7 ($-OCH_2O-$), 124.9 ($-C=C-CH_3$), 129.6, 130.0, 130.1, 131.1 ($-CH=CH-CH=CH-$), 142.6 (=C-OMOM). Exact Mass calcd. for $C_{29}H_{48}O_7S_2Si$: 600.2611 (M^+); found: 600.2599 ± 0.0017.

*rel(1S,2R,6S,9S,10R)-10-*tert*-Butyldimethylsilyloxy-4,4-bis-methoxycarbonyl-2-methoxymethyloxy-1-methyl-11,11-(propylenedithio)tricyclo[7.4.0.$0^{2,6}$]tridec-7-ene (**46**)*

Macrocycle **45** (48 mg) was dissolved in toluene (1.2 mL) and heated, in a sealed quartz tube at 240°C for 1.5 h. The solvent was evaporated and the residue was purified by flash chromatography using hexane:ethyl acetate (4:1) as the eluent to afford pure tricycle **46** (33 mg, 69%) and bicycle **47** (7 mg, 15%).

The same reaction was done with macrocycle **45** (45 mg) in toluene (0.9 mL) at 220°C for 7 h to give tricycle **46** (34 mg, 76%) and bicycle **47** (7 mg, 16%).

*Tricyclic compound **46**:* ir (CH_2Cl_2, ν cm^{-1}): 3050, 2980, 2960, 2930, 1735; ^1H nmr ($CDCl_3$, δ ppm): 0.13 and 0.19 (6H, 2s, $-OSi(CH_3)_2C(CH_3)_3$), 0.94 (9H, s, $-OSi(CH_3)_2C(CH_3)_3$), 1.25 (3H,

Can. J. Chem. Downloaded from www.nrcresearchpress.com by 109.225.110.28 on 09/08/12
For personal use only.

s, $-CH_3$), 1.45–3.0 (16H, m, $-S(CH_2)_3S-$, $-C(CH_3)-CH_2-CH_2-$, $-CH_2-C(CO_2CH_3)_2-CH_2-$, and -CH-CH=CH-CH-), 3.33 (3H, s, $-OCH_3$), 3.67 and 3.70 (6H, 2s, $(CO_2CH_3)_2$), 3.99 (1H, d, J = 1.8 Hz, -CH(OTBDMS)-), 4.70 (1H, d, J = 7.4 Hz, -OCHHO-), 4.76 (1H, d, J = 7.4 Hz, -OCHHO-), 5.18 (1H, d, J = 10 Hz, -CH=CH-), 5.41 (1H, d, J = 10 Hz, -CH=CH-). Exact Mass calcd. for $C_{29}H_{48}O_7S_2Si$: 600.2611 (M^+); found: 600.2605 ± 0.0017.

Bicyclic compound ***47***: ir (CH_2Cl_2, ν cm^{-1}): 3060, 2990, 2960, 2930, 2860, 1735; ^1H nmr ($CDCl_3$, δ ppm): 0.01 and 0.11 (6H, 2s, $-OSi(CH_3)_2C(CH_3)_3$), 0.90 (9H, s, $-OSi(CH_3)_2C(CH_3)_3$), 1.45 (3H, s, $-CH_3$), 1.61 (1H, d, J = 15 Hz, -CH(OTBDMS)-CH=CH-CHH-), 1.84–2.07, 2.48–3.09, and 3.26 (11H, m, $-S(CH_2)_3S-$ and $-CH_2-C(CO_2CH_3)_2-CH_2-CH-$), 2.30 (1H, dd, J = 10.5 and 15.5 Hz, $-C(CH_3)$=CH-CHH-), 2.55 (1H, dd, J = 12.5 and 15 Hz, -CH(OTBDMS)-CH=CH-CHH-), 2.86 (1H, d, J = 15 Hz, $-C(CH_3)$=CH-CHH-), 3.34 (3H, s, $-OCH_3$), 3.72 and 3.74 (6H, 2s, $(CO_2CH_3)_2$), 4.63 (1H, d, J = 7 Hz, -OCHHO-), 4.66 (1H, d, J = 7 Hz, -OCHHO-), 4.68 (1H, d, J = 10 Hz, -CH(OTBDMS)-), 5.23 (1H, ddd, J = 5, 12.5, and 12.5 Hz, -CH(OTBDMS)-CH=CH-CH_2-), 5.45 (1H, dd, J = 10 and 12 Hz, -CH(OTBDMS)-CH=CH-), 5.60 (1H, d, J = 10 Hz, $-C(CH_3)$=CH-CH_2-). Exact Mass calcd. for $C_{29}H_{48}O_7S_2Si$: 600.2611 (M^+); found: 600.2605 ± 0.0017.

*rel(1S,2R,6S,9S,10R)-10-*tert*-Butyldimethylsilyloxy-4,4-bis-methoxycarbonyl-2-methoxymethyloxy-1-methyltricyclo[7.4.0.0^{2,6}]tridec-7-en-11-one (**54**)*

Mercuric chloride (103 mg, 0.38 mmol) was added to a mixture of **46** (57 mg, 0.095 mmol) and calcium carbonate (43 mg, 0.43 mmol) in acetonitrile:water (4:1) (8 mL). The mixture was stirred at room temperature for 21 h and water was added. The mixture was extracted with hexane:ether (1:1); the organic layer was washed with water, dried over sodium sulfate, and evaporated. The residue was purified by flash chromatography using hexane:ethyl acetate (4:1) as the eluent to afford pure ketone **54** (34 mg, 70%); ^1H nmr ($CDCl_3$, δ ppm): 0.02 and 0.07 (6H, 2s, $-OSi(CH_3)_2C(CH_3)_3$), 0.88 (9H, s, $-OSi(CH_3)_2C(CH_3)_3$), 1.40 (3H, s, $-CH_3$), 1.68–2.13 (3H, m, $-CH_2-CH_2CO-$ and -CH-CH=), 2.20 (1H, d, J = 13.6 Hz, -C(OMOM)-CHH- or $-C(CO_2CH_3)_2-CHH-$), 2.55 (1H, d, J = 15.8 Hz, -C(OMOM)-CHH-or $-C(CO_2CH_3)_2-CHH-$), 2.58 (1H, s, -CH-CH=), 2.75 (1H, d, J = 15.6 Hz, -C(OMOM)-CHH- or $-C(CO_2CH_3)_2-CHH-$), 2.83 (1H, d, J = 13.3 Hz, -C(OMOM)-CHH- or $-C(CO_2CH_3)_2-CHH-$), 2.80 (2H, m, $-CH_2-CH_2-CO-$), 3.32 (3H, s, $-OCH_3$), 3.68 and 3.70 (6H, 2s, $(CO_2CH_3)_2$), 3.80 (1H, m, -CH(OTBDMS)-), 4.66 (1H, d, J = 7.6 Hz, -OCHHO-), 4.78 (1H, d, J = 7.6 Hz, -OCHHO-), 5.25 and 5.36 (2H, m, -CH=CH-).

*rel(1S,2R,6S,9S,10R,11R) and rel(1S,2R,6S,9S,10R,11S)-10-*tert*-Butyldimethylsilyloxy-4,4-bis-methoxycarbonyl-2-methoxymethyloxy-1-methyltricyclo[7.4.0.0^{2,6}]tridec-7-en-11-ol (**56** and **55** respectively)*

To a cold (0°C) solution of ketone **54** (34 mg, 67 μmol) in methanol (10 mL) was added sodium borohydride (70 mg). The mixture was stirred at room temperature for 1 h and a saturated solution of ammonium chloride was added. The mixture was extracted with methylene chloride, and the organic layer was dried over sodium sulfate and evaporated. The residue was purified by flash chromatography using hexane:ethyl acetate (3:1) as the eluent to afford pure alcohols **55** (16 mg, 47%) and **56** (16 mg, 47%).

Compound ***55*** (less polar): ^1H nmr ($CDCl_3$, δ ppm): 0.13 and 0.15 (6H, 2s, $-OSi(CH_3)_2C(CH_3)_3$), 0.94 (9H, s, $-OSi(CH_3)_2C(CH_3)_3$), 1.22 (3H, s, $-CH_3$). 1.46–1.80 (4H, m, $-CH_2-CH_2-$CH(OH)-), 2.22 (1H, d, J = 13.5 Hz, $-C(CO_2CH_3)_2-CHH-$), 2.41 (1H, s, -CH-CH=), 2.49 (1H, d, J = 15.6 Hz, -C(OMOM)-CHH-), 2.70 (1H, d, J = 15.6 Hz, -C(OMOM)-CHH-), 2.77 (1H, m, -CH-CH=), 2.89 (1H, dd, J = 7.5 and 13.5 Hz, $-C(CO_2CH_3)_2-$CHH-), 3.33 (3H, s, $-OCH_3$), 3.68 and 3.71 (6H, 2s, $(CO_2CH_3)_2$), 3.66 (1H, m, -CH(OH)-), 3.90 (1H, dd, J = 3 and 3 Hz, -CH(OTBDMS)-), 4.68 (1H, d, J = 7.5 Hz, -OCHHO-), 4.76 (1H, d, J = 7.5 Hz, -OCHHO-), 5.20 (1H, d, J = 10 Hz, -CH=CH-), 5.33 (1H, d, J = 10 Hz, -CH=CH-).

Compound ***56*** (more polar): ^1H nmr ($CDCl_3$, δ ppm): 0.07 and 0.08 (6H, 2s, $-OSi(CH_3)_2C(CH_3)_3$), 0.89 (9H, s, $-OSi(CH_3)_2C(CH_3)_3$), 1.23 (3H, s, $-CH_3$), 1.45–1.70 (3H, m, $-CH_2-$CHH-CH(OH)-), 2.02 (1H, m, $-CH_2-$CHH-CH(OH)-), 2.22 (1H, d, J = 13 Hz, $-C(CO_2CH_3)_2-CHH-$), 2.25 (1H, s, -CH-CH=), 2.51 (1H, d, J = 15.5 Hz, -C(OMOM)-CHH-), 2.66 (1H, d, J = 15.5 Hz, -C(OMOM)-CHH-), 2.89 (1H, d, J = 13 Hz, $-C(CO_2CH_3)_2-CHH-$), 2.90 (1H, m, -CH-CH=), 3.34 (3H, s, $-OCH_3$), 3.69 and 3.71 (7H, 2s, $(CO_2CH_3)_2$ and -CH(OH)-), 3.89 (1H, dd, J = 2.3 and 2.3 Hz, -CH(OTBDMS)-), 4.70 (1H, d, J = 7.4 Hz, -OCHHO-), 4.77 (1H, d, J = 7.5 Hz, -OCHHO-), 5.34 (1H, d, J = 10 Hz, -CH=CH-), 5.45 (1H, d, J = 10 Hz, -CH=CH-).

*rel(1S,2R,6S,9S,10R,11S)-11-Benzoyloxy-10-*tert*-butyldimethylsilyloxy-4,4-bis-methoxycarbonyl-2-methoxymethyloxy-1-methyltricyclo[7.4.0.0^{2,6}]tridec-7-ene (**57**)*

Procedure A

To a solution of alcohol **55** (16 mg, 31.3 μmol) and triethylamine (150 μL, 1.08 mmol) in methylene chloride (5 mL) were added at 0°C benzoyl chloride (40 μL, 0.34 mmol) and a few milligrams of DMAP. The mixture was stirred at room temperature for 24 h and a saturated solution of sodium bicarbonate was added. The mixture was extracted with methylene chloride, and the organic layer was dried over sodium sulfate and evaporated. The residue was purified by flash chromatography using hexane:ethyl acetate (4:1) as the eluent to afford pure **57** (17 mg, 89%); ^1H nmr ($CDCl_3$, δ ppm): −0.07 and 0.04 (6H, 2s, $-OSi(CH_3)_2C(CH_3)_3$), 0.91 (9H, s, $-OSi(CH_3)_2C(CH_3)_3$), 1.32 (3H, s, $-CH_3$), 1.56–1.75 (3H, m, $-CH_2-$CHH-CH(OBz)-), 2.15 (1H, ddd, J = 3, 12, and 12 Hz, $-CH_2-CHH_{ax}-$CH(OBz)-), 2.25 (1H, d, J = 13.4 Hz, $-C(CO_2CH_3)_2-$CHH-), 2.43 (1H, s, -CH-CH=), 2.50 (1H, d, J = 15.5 Hz, -C(OMOM)-CHH-), 2.72 (1H, d, J = 15.5 Hz, -C(OMOM)-CHH-), 2.82 (1H, m, -CH-CH=), 2.91 (1H, dd, J = 7.5 and 13.5 Hz, $-C(CO_2CH_3)_2-CHH-$), 3.35 (3H, s, $-OCH_3$), 3.69 and 3.72 (6H, 2s, $(CO_2CH_3)_2$), 4.19 (1H, dd, J = 2.5 Hz and 2.5 Hz, -CH(OTBDMS)-), 4.71 (1H, d, J = 7.4 Hz, -OCHHO-), 4.79 (1H, d, J = 7.4 Hz, -OCHHO-), 4.90 (1H, ddd, J = 3, 5, and 12.5 Hz, $-CH_{ax}$(OBz)-), 5.38 (2H, s, -CH=CH-), 7.42 (2H, m, *meta*-H of OBz), 7.55 (1H, m, *para*-H of OBz), 8.04 (2H, m, *ortho*-H of OBz).

*rel(1S,2R,6S,9S,10R,11R)-11-Benzoyloxy-10-*tert*-butyldimethylsilyloxy-4,4-bis-methoxycarbonyl-2-methoxymethyloxy-1-methyltricyclo[7.4.0.0^{2,6}]tridec-7-ene (**58**)*

Using procedure A described above, compound **56** (16 mg, 31.3 μmol) afforded, after flash chromatography, compound **58** (16.5 mg, 86%); ir (CH_2Cl_2, ν cm^{-1}): 3050, 2980, 1730; ^1H nmr ($CDCl_3$, δ ppm): 0.12 and 0.16 (6H, 2s, $-OSi(CH_3)_2C(CH_3)_3$), 0.92 (9H, s, $-OSi(CH_3)_2C(CH_3)_3$), 1.29 (3H, s, $-CH_3$), 1.48–1.92 (3H, m, $-CH_2-$CHH-CH(OBz)-), 2.12 (1H, m, $-CH_2-CHH_{eq}-$CH(OBz)-), 2.28 (1H, d, J = 13.3 Hz, $-C(CO_2CH_3)_2-CHH-$), 2.31 (1H, m, -CH-CH=), 2.53 (1H, d, J = 15.6 Hz, -C(OMOM)-CHH-), 2.72 (1H, d, J = 15.6 Hz, -C(OMOM)-CHH-), 2.92 (1H, d, J = 13 Hz, $-C(CO_2CH_3)_2-CHH-$), 2.93 (1H, m, -CH-CH=), 3.36 (3H, s, $-OCH_3$), 3.66 and 3.72 (6H, 2s, $(CO_2CH_3)_2$), 4.00 (1H, s, -CH(OTBDMS)-), 4.74 (1H, d, J = 7.4 Hz, -OCHHO-), 4.80 (1H, d, J = 7.5 Hz, -OCHHO-), 4.99 (1H, d, J = 2.6 Hz, $-CH_{eq}$(OBz)-), 5.20 (1H, d, J = 10 Hz, -CH=CH-), 5.28 (1H, d, J = 10 Hz, -CH=CH-), 7.42 (2H, dd, J = 7.5 and 7.5 Hz, *meta*-H of OBz), 7.55 (1H, m, *para*-H of OBz), 7.99 (2H, m, *ortho*-H of OBz). Exact Mass calcd. for $C_{33}H_{48}O_9Si$: 585.2883 (M^+ − OMe); found: 585.2876 ± 0.0017.

*rel(1S,2R,6S,9S,10R,11S)-11-Benzoyloxy-10-*tert*-butyldimethylsilyloxy-4,4-bis-methoxycarbonyl-1-methyltricyclo[7.4.0.0^{2,6}]tridec-7-en-2-ol (**59**)*

Procedure B

To a solution of **57** (17 mg, 0.028 mmol) in tetrahydrofuran:water (4:1) (5.5 mL) was added a solution of 6 M hydro.chloric acid (15 drops). The mixture was stirred at room temperature for 15 h and a saturated solution of sodium bicarbon-

Can. J. Chem. Downloaded from www.nrcresearchpress.com by 109.225.110.28 on 09/08/12
For personal use only.

ate was added. The mixture was extracted with methylene chloride; the organic layer was dried over sodium sulfate and evaporated. The residue was purified by flash chromatography using hexane:ethyl acetate (7:3) as the eluent to afford pure alcohol **59** (16 mg, quantitative); ^{1}H nmr ($CDCl_3$, δ ppm): -0.08 and 0.03 (6H, 2s, $-OSi(CH_3)_2$-$C(CH_3)_3$), 0.91 (9H, s, $-OSi(CH_3)_2C(CH_3)_3$), 1.32 (3H, s, $-CH_3$), 1.55–1.80 (3H, m, $-CH_2$-CHH-CH(OBz)-), 2.1–2.35 (2H, m, $-CH_2$-CHH-CH(OBz)- and -CH-CH=), 2.13 (1H, s, -C(OH)-CHH-), 2.31 (1H, s, -C(OH)-CHH-), 2.39 (1H, d, J = 14.3 Hz, $-C(CO_2CH_3)_2$-CHH-), 2.64 (1H, m, -CH-CH=), 2.76 (1H, dd, J = 7.5 and 14.3 Hz, $-C(CO_2CH_3)_2$-CHH-), 3.72 and 3.76 (6H, 2s, $(CO_2CH_3)_2$), 4.19 (1H, dd, J = 2 and 2 Hz, -CH(OTBDMS)-), 4.91 (1H, ddd, J = 3, 3, and 12 Hz, -CH(OBz)-), 5.41 (1H, d, J = 10 Hz, -CH=CH-), 5.49 (1H, d, J = 10 Hz, -CH=CH-), 7.42 (2H, m, *meta*-H of OBz), 7.55 (1H, m, *para*-H of OBz), 8.04 (2H, m, *ortho*-H of OBz).

*rel(1S,2R,6S,9S,10R,11R)-11-Benzoyloxy-10-tert-butyldimethylsilyloxy-4,4-bis-methoxycarbonyl-1-methyltricyclo[7.4.0.0^{2,6}]tridec-7-en-2-ol (**60**)*

Using procedure B, compound **58** (16 mg, 0.026 mmol) afforded, after flash chromatography, compound **60** (14.5 mg, 98%); ir (CH_2Cl_2, ν cm^{-1}): 3600, 3050, 2960, 2930, 2860, 1720; ^{1}H nmr ($CDCl_3$, δ ppm): 0.11 and 0.17 (6H, 2s, $-OSi(CH_3)_2C(CH_3)_3$), 0.93 (9H, s, $-OSi(CH_3)_2C(CH_3)_3$), 1.30 (3H, s, $-CH_3$), 1.53–1.90 (3H, m, $-CH_2$-CHH-CH(OBz)-), 2.07–2.17 (1H, m, $-CH_2$-CHH-CH(OBz)-), 2.15 (1H, s, -C(OH)-CHH-), 2.23 (1H, s, -CH-CH=), 2.34 (1H, s, -C(OH)-CHH-), 2.38–2.47 (1H, m, $-C(CO_2CH_3)_2$-CHH-), 2.74 (1H, s, -CH-CH=), 2.75 (1H, m, $-C(CO_2CH_3)_2$-CHH-), 3.71 and 3.76 (6H, 2s, $(CO_2CH_3)_2$), 4.00 (1H, m, -CH(OTBDMS)-), 5.01 (1H, d, J = 3 Hz, -CH(OBz)-), 5.25 (1H, dm, J = 10 Hz, -CH=CH-), 5.37 (1H, dm, J = 10 Hz, -CH=CH-), 7.42 (2H, m, *meta*-H of OBz), 7.55 (1H, m, *para*-H of OBz), 8.00 (2H, m, *ortho*-H of OBz). Exact Mass calcd. for $C_{31}H_{44}O_8Si$: 555.2778 (M^+ − OH); found: 555.2760 ± 0.0016.

*rel(1S,2R,4R,6S,9S,10R,11S)-11-Benzoyloxy-4-methoxycarbonyl-1-methyltricyclo[7.4.0.0^{2,6}]tridec-7-en-10-ol-4,2-carbolactone (**61**)*

Procedure C

To a solution of **59** (16 mg, 0.028 mmol) in tetrahydrofuran (10 mL) was added a solution of tetrabutylammonium fluoride (56 μL, 0.056 mmol). The mixture was stirred at room temperature for 90 min and the solvent was evaporated. The residue was purified by flash chromatography using hexane:ethyl acetate (3:2) as the eluent to afford pure **61** (2.5 mg, 19%) and **62** (6 mg, 61%).

*Compound **61*** (less polar): ir (CH_2Cl_2, ν cm^{-1}): 3600, 3050, 2980, 1780, 1735, 1715; ^{1}H nmr ($CDCl_3$, δ ppm): 1.42 (3H, s, $-CH_3$), 150–2.22 and 2.35–2.55 (9H, m, 4 × $-CH_2$- and -CH-CH=), 2.80 (1H, m, -CH-CH=), 3.82 (3H, s, CO_2CH_3), 4.23 (1H, dd, J = 2 and 2 Hz, -CH(OH)-), 5.02 (1H, ddd, J = 2.5, 3.5, and 12 Hz, -CH(OBz)-), 5.42 (1H, ddd, J = 2, 2, and 10 Hz, -CH=CH-), 5.73 (1H, ddd, J = 2.5, 2.5 ,and 10 Hz, -CH=CH-), 7.47 (2H, m, *meta*-H of OBz), 7.60 (1H, m, *para*-H of OBz), 8.04 (2H, m, *ortho*-H of OBz). Exact Mass calcd. for $C_{24}H_{26}O_7$: 426.1678 (M^+); found: 426.1675 ± 0.0013.

*Compound **62*** (more polar): ir (CH_2Cl_2, ν cm^{-1}): 3600, 3050, 2980, 1785, 1735; ^{1}H nmr (CD_2Cl_2, δ ppm): 1.32 (3H, s, $-CH_3$), 1.53–2.00 and 2.28–2.46 (9H, m, 4 × $-CH_2$- and -CH-CH=), 2.73 (1H, m, -CH-CH=), 3.60 (1H, ddd, J = 2.5, 3.5, and 12 Hz, -CH(OH)-CH_2-), 3.77 (3H, s, CO_2CH_3), 3.95 (1H, dd, J = 2.8 and 2.8 Hz, $-CH_2$-CH(OH)-CH(OH)-), 5.33 (1H, ddd, J = 2.2, 2.2, and 10.1 Hz, -CH=CH-), 5.64 (1H, ddd, J = 2.7, 2.7, and 10.2 Hz, -CH=CH-). Exact Mass calcd. for $C_{17}H_{22}O_6$: 322.1416 (M^+); found: 322.1413 ± 0.0009.

*rel(1S,2R,4R,6S,9S,10R,11R)-11-Benzoyloxy-4-methoxycarbonyl-1-methyltricyclo[7.4.0.0^{2,6}]tridec-7-en-10-ol-4,2-carbolactone (**63**)*

Using procedure C, compound **60** (7.5 mg, 0.013 mmol) afforded, after flash chromatography, compound **63** (4.5 mg, 81%); ir (CH_2Cl_2, ν cm^{-1}): 3600, 3050, 2980, 1785, 1735, 1710: ^{1}H nmr ($CDCl_3$, δ ppm): 1.42 (3H, s, $-CH_3$), 1.54–2.62 (9H, m, 4 × $-CH_2$- and -CH-CH=), 2.94 (1H, m, -CH-CH=), 3.82 (3H, s, CO_2CH_3), 4.17 (1H, s, -CH(OH)-), 5.17 (1H, d, J = 2.8 Hz, -CH(OBz)-), 5.33 (1H, ddd, J = 2.2, 2.2, and 10.1 Hz, -CH=CH-), 5.60 (1H, ddd, J = 2.7, 2.7, and 10.1 Hz, -CH=CH-), 7.44 (2H, m, *meta*-H of OBz), 7.58 (1H, m, *para*-H of OBz), 7.99 (2H, m, *ortho*-H of OBz). Exact Mass calcd. for $C_{24}H_{26}O_7$: 426.1678 (M^+); found: 426.1688 ± 0.0013.

*rel(1S,2R,4R,6S,9S,11S)-11-Benzoyloxy-4-methoxycarbonyl-1-methyltricyclo[7.4.0.0^{2,6}]tridec-7-en-10-one-4,2-carbolactone (**64**)*

To a solution of **61** (1 mg, 2.2 μmol) in methylene chloride (1 mL) was added pyridinium chlorochromate (5 mg, 23.2 μmol). The mixture was stirred at room temperature for 3 h and was filtered on Florisil using ethyl acetate as a solvent. The solvent was evaporated and the residue was purified by flash chromatography using hexane:ethyl acetate (3:2) as the eluent to afford pure ketone **64** as the only product; ir (CH_2Cl_2, ν cm^{-1}): 3030, 2960, 2930, 2860, 1790, 1740; ^{1}H nmr ($CDCl_3$, δ ppm): 1.30 (3H, s, $-CH_3$), 1.50–2.55 (8H, m, 4 × $-CH_2$-), 3.00 (2H, m, -CH-CH=CH-CH-), 3.83 (3H, s, CO_2CH_3), 5.52 (1H, dd, J = 7.5 and 7.5 Hz, -CH(OBz)-), 5.58 (1H, dm, J = 10 Hz, -CH=CH-), 5.92 (1H, ddd, J = 2.5, 2.5, and 10 Hz, -CH=CH-), 7.5 (3H, m, *meta*-H and *para*-H of OBz), 8.09 (2H, m, *ortho*-H of OBz). Exact Mass calcd. for $C_{24}H_{24}O_7$: 424.1514 (M^+); found: 424.1514 ± 0.0012.

Acknowledgements

This research was supported by the Natural Sciences and Engineering Research Council of Canada (NSERCC, Ottawa) and by the "Ministère de l'Éducation" (FCAR, Québec).

1. K. J. Morgan and J. A. Barltrop. Q. Rev. **12**, 34 (1958).
2. P. J. Pelletier and J. B. Caventou. Ann. Chim. Phys. **14**, 69 (1820).
3. (*a*) J. A. Henry. The plant alkaloids. J. and A. Churchill. London. 1949; (*b*) L. F. Fieser and M. Fieser. The natural products related to phenanthrene. Reinhold Publ. Corp., New York 1949; (*c*) O. Jeger and V. Prelog. *In* The alkaloids. Vol 3. *Edited by* R. H. F. Manske and H. L. Holmes Academic Press Inc., New York. 1953. p. 247; (*d*) J. McKenna. Q. Rev. **7**, 231 (1953); (*e*) A. Stoll. Gazzetta, **84**, 1190 (1954); (*f*) V. Prelog and O. Jeger. *In* The alkaloids. Vol. 7. *Edited by* R. H. F. Manske Academic Press Inc., New York. 1960. p. 363; (*g*) S. M. Kupchan and W. A. Arnold. *In* The alkaloids. Vol. 10. *Edited by* R. H. F. Manske Academic Press Inc., New York. 1968. p. 193; (*h*) K. Nakanishi. *In* Natural products chemistry. Vol. 2. Kodansha Ltd. and Academic Press Inc., New York. 1975. pp. 278–282; (*i*) L. F. Fieser and M. Fieser. Steroids. Reinhold Publ. Co., New York. 1959. pp. 879–894.
4. (*a*) W. Poethke. Arch. Pharm. **275**, 357 (1937); **275**, 571 (1937); (*b*) L. C. Craig and W. A. Jacobs. J. Biol. Chem. **148**, 57 (1943); **149**, 451 (1943); (*c*) W. A. Jacobs and S. W. Pelletier. J. Org. Chem. **18**, 765 (1953); (*d*) S. M. Kupchan and C. R. Narayanan. J. Am. Chem. Soc. **81**, 1913 (1959); (*e*) S. M. Kupchan. J. Am. Chem. Soc. **81**, 1921 (1959).
5. (*a*) W. A. Jacobs and L. C. Craig. J. Biol. Chem. **119**, 141 (1937); **120**, 447 (1937); **124**, 659 (1938); (*b*) L. C. Craig and W. A. Jacobs. J. Biol. Chem. **148**, 57 (1943); (*c*) J. Am. Chem. Soc. **61**, 2252 (1939); (*d*) S. W. Pelletier and W. A. Jacobs. J. Am. Chem. Soc. **75**, 3248 (1953); (*e*) S. M. Kupchan, D. LaVie, C. V. Deliwala, and B. Y. A. Andoh. J. Am. Chem. Soc. **75**, 5519 (1953); (*f*) S. M. Kupchan, W. S. Johnson, and S. Rajagopalan. Tetrahedron, **7**, 47 (1959); (*g*) W. T. Eeles. Tetrahedron Lett. 24 (1960).
6. S. M. Kupchan, C. I. Ayres, M. Neeman, R. H. Hensler, T. Masamune, and S. Rajagopalan. J. Am. Chem. Soc. **82**, 2242 (1960).
7. (*a*) F. W. Heyl, F. E. Hepner, and S. K. Loy. J. Am. Chem.

Soc. **35**, 258 (1913); (*b*) F. W. Heyl and M. E. Herr. J. Am. Chem. Soc. **71**, 1751 (1949); (*c*) S. M. Kupchan. J. Am. Chem. Soc. **81**, 1925 (1959).
8. (*a*) E. D. Fries, J. R. Stanton, and F. C. Moister. J. Pharmacol. Exp. Ther. **98**, 166 (1950); (*b*) G. L. Maison, E. Gotz, and J. W. Stutzman. J. Pharmacol. Exp. Ther. **103**, 74 (1951); (*c*) O. Krayer and G. A. Acheson. Physiol. Rev. **26**, 383 (1946); (*d*) R. Hunt. Am. J. Physiol. **6**, 414 (1902).
9. (*a*) L. S. Goodman and A. Gilman. *In* The pharmacological basis of therapeutics. The Macmillan Co., New York. 1955. pp. 747–754; (*b*) O. Krayer and V. A. Drill. *In* Pharmacology in medicine. McGraw–Hill Book, New York. 1958. pp. 515–524; (*c*) E. Meilman and O. Krayer. Circulation, **1**, 204 (1950).
10. H. Gan, J. L. King, and N. C. Yang. Tetrahedron Lett. **30**, 1205 (1989).
11. (*a*) D. Craig. Chem. Soc. Rev. **16**, 187 (1987); (*b*) A. G. Fallis. Can. J. Chem. **62**, 183 (1984); (*c*) G. Brieger and J. N. Bennett. Chem. Rev. **80**, 63 (1980); (*d*) W. Oppolzer. Angew. Chem. Int. Ed. Engl. **16**, 10 (1977).
12. (*a*) G. Stork and N. A. Saccomano. Tetrahedron Lett. **28**, 2087 (1987); (*b*) T. Kametani, H. Matsumoto, H. Nemoto, and K. Fukumoto. J. Am. Chem. Soc. **100**, 6218 (1978).
13. (*a*) P. Deslongchamps, S. Lamothe, et H. S. Lin. Can. J. Chem. **65**, 1298 (1987); (*b*) D. Brillon and P. Deslongchamps. Can. J. Chem. **65**, 43 (1987); **65**, 56 (1987).
14. (*a*) A. Ndibwami. Thèse de doctorat, Université de Sherbrooke, Sherbrooke, Québec (1988); (*b*) S. Lamothe, A. Ndibwami, and P. Deslongchamps. Tetrahedron Lett. **29**, 1639, 1641 (1988); (*c*) K. Baettig, C. Dallaire, R. Pitteloud, and P. Deslongchamps. Tetrahedron Lett. **28**, 5249 (1987); (*d*) K. Baettig, A. Marinier, R. Pitteloud, and P. Deslongchamps. Tetrahedron Lett. **28**, 5253 (1987).
15. G. Bérubé and P. Deslongchamps. Tetrahedron Lett. **28**, 5255 (1987).
16. M. Quimpère, L. Ruest, and P. Deslongchamps. Synthesis, 132 (1992).
17. (*a*) W. S. Allen and S. Bernstein. J. Am. Chem. Soc. **77**, 1028 (1955); (*b*) S. Berstein, R. H. Lenhard, W. S. Allen, M. Heller, R. Littell, S. M. Stotar, L. I. Feldman, and R. H. Blank. J. Am. Chem. Soc. **78**, 5693 (1956).
18. (*a*) B. Neises and W. Steglick. Angew. Chem. Int. Ed. Engl. **17**, 522 (1978); (*b*) I. J. Bolton, R. G. Harrison, B. Lythgse, and R. S. Manwaring. J. Chem. Soc. (C), 2944 (1971).
19. S. Hanessian and P. Lavallée. Can. J. Chem. **53**, 2975 (1975); **55**, 562 (1977).
20. R. K. Grossland and K. L. Servis. J. Org. Chem. **35**, 3195 (1970).
21. (*a*) P. C. B. Page, M. B. Van Neil, and J. C. Prodger. Tetrahedron, **45**, 7643 (1989); (*b*) P. Blatcher and S. Warren. J. Chem. Soc. Perkin Trans. 1, 1074 (1979); (*c*) D. Seebach and E. J. Corey. J. Org. Chem. **40**, 231 (1975); (*d*) D. Seebach. Synthesis, 17 (1969); (*e*) D. Seebach, N. R. Jones, and E. J. Corey. J. Org. Chem. **33**, 300 (1968); (*f*) E. J. Corey and D. Grouse. J. Org. Chem. **33**, 298 (1968).
22. D. Seebach, I. Willert, A. K. Beck, and B. T. Gröbel. Helv. Chim. Acta, **61**, 2510 (1978).
23. J. N. Gillard, R. Fortin, H. E. Morton, C. Yoakim, C. A. Quesnelle, S. Daignault, and Y. Guindon. J. Org. Chem. **53**, 2602 (1988).
24. M. Miyashita, A. Yoshikoshi, and P. A. Grieco. J. Org. Chem. **42**, 3772 (1977).
25. K. Omura and D. Swern. Tetrahedron, **34**, 1651 (1978).
26. E. W. Collington and A. I. Meyers. J. Org. Chem. **36**, 3044 (1971).
27. (*a*) E. J. Corey and B. W. Erickson. J. Org. Chem. **36**, 3553 (1971); (*b*) A. J. Meyers, D. L. Comins, D. M. Roland, R. Henning, and K. Shimizu. J. Am. Chem. Soc. **101**, 7104 (1979); (*c*) T. Hylton and V. Boekelheide. J. Am. Chem. Soc. **90**, 6887 (1968).
28. M. Drouin, A. G. Michel, M. Quimpère, and P. Deslongchamps. Acta Crystallogr. Submitted.
29. Y. Dory and P. Deslongchamps. Research report, Université de Sherbrooke. 1990.

Can. J. Chem. Downloaded from www.nrcresearchpress.com by 109.225.110.28 on 09/08/12
For personal use only.

Stereocontrolled chiral synthesis of a *trans-anti-trans* tricycle by a transannular Diels–Alder reaction

ANNE MARINIER[1] AND PIERRE DESLONGCHAMPS[2]

Laboratoire de synthèse organique, Département de chimie, Faculté des sciences, Université de Sherbrooke, Sherbrooke (Québec), Canada J1K 2R1

Received March 2, 1992

ANNE MARINIER and PIERRE DESLONGCHAMPS. Can. J. Chem. **70**, 2350 (1992).

The racemic and chiral synthesis of *trans-cis-cis* macrocyclic triene **5** is described. Heating this compound at 262°C leads via a transannular Diels–Alder reaction to the tricyclic structure **6**, which can be further transformed into tricyclic compound **7**. This work constitutes a preliminary study for the synthesis of corticoids.

ANNE MARINIER et PIERRE DESLONGCHAMPS. Can. J. Chem. **70**, 2350 (1992).

On décrit la synthèse racémique et chirale du triène macrocyclique *trans-cis-cis* **5**. En chauffant à 262°C, ce composé subit une reaction de Diels–Alder transannulaire et conduit à l'adduit tricyclique **6** qui peut être transformé dans le composé **7**. Ce travail constitue une étude préliminaire en vue de la synthèse de corticostéroïdes.

Can. J. Chem. Downloaded from www.nrcresearchpress.com by 109.225.110.28 on 09/08/12
For personal use only.

Introduction

Recent interest in organic synthesis focused on macrocyclic compounds. Indeed many naturally occurring molecules containing medium and large rings have been isolated and progress in their synthesis led to the development of good methods of cyclization (1, 2). These investigations also revealed that *intermolecular* reactions of such macrocyclic structures might occur with high chemo, regio, and stereoselectivity (3, 4).

Very recently we pointed out the enormous synthetic potential residing in *intramolecular* reactions of macrocyclics, particularly transannular processes of such systems (5, 6). These transformations occur with high regio and stereoselectivity due to conformational restriction and proximity effects that become operative, increasing the rate of one reaction at the expense of others normally competing. Thus transannular processes on macrocarbocyclics are powerful tools for the synthesis of complex polycyclic skeletons (6*c*). For example, the Diels–Alder reaction of 14- or 13-membered macrocycles (**1** → **2** or **3** → **4**) (Scheme 1) should represent a good synthetic approach to polycyclic systems such as diterpenes, triterpenes, steroids, etc. Recent papers from our laboratory (7) and by Takahashi *et al.* (8) confirmed this prediction and showed the great potential of the transannular Diels–Alder reaction for the synthesis of natural products. We now wish to report our work on a new approach to the synthesis of corticosteroids.

Most of the natural corticosteroids have the *trans-anti-trans* (TAT) ring junction for the A, B, and C rings of the carbon skeleton. However, in recent communications, (7*e*, *d*) we demonstrated that the transannular Diels–Alder strategy is not appropriate for the direct construction of the TAT ring junction. On the contrary, the *trans-syn-cis* (TSC) ring junction is directly and easily accessible by the Diels–Alder reaction of a *trans-cis-cis* (TCC) macrocyclic triene (5). The hydroxyl or the keto group at position 11 in corticosteroids not only provides a route for a subsequent epimerization at C9, thereby delivering systems having TAT stereochemistry, but can also be exploited to induce chirality.

We report herein, as a preliminary study for the synthesis of corticoids, the racemic and chiral syntheses of macrocyclic compound **5** as well as its transformation into tricyclic compound **7** via compound **6** (Scheme 1).

Results and discussion

Racemic synthesis of macrocyclic triene 5

As previously described (7*f*), the synthesis of macrocyclic triene **5** was based on our original convergent approach (7*c*, *e*). Scheme 2 summarizes the preparation of the *Z* dienophile moiety. Thus alcohol **8** (9) was first benzylated, followed by removal of the benzylidene protecting group in acidic medium (85%). Diol **10** was then monosilylated (10) (51%) to afford alcohol **11**, which was oxidized (11) to aldehyde **12**. Without further purification, this crude aldehyde was used in a Wittig reaction with the ylide derived from the phosphonium salt **14**. The latter was prepared by condensing the THP derivative (12) of 2-bromoethanol **13** with ethyltriphenylphosphonium bromide (13*a*). The Wittig reaction provided a 55:45 mixture of *Z* and *E* olefins in a 63% yield from **11**. The geometry of these isomers was easily established by ^{13}C nmr spectroscopy. The C4-methyl in the *E* isomer, which is *cis*-disposed to the chain, displays a higher field chemical shift (17.1) than the corresponding *trans*-disposed methyl in the *Z* isomer (23.8). On the contrary the C5-methylene displays a higher field chemical shift (32.8) in the *Z* isomer than the corresponding C5-methylene in the *E* isomer (39.7). These findings are in complete agreement with assignments for *Z* and *E* olefins (13*b*). Furthermore, the stereochemistry of our olefin was firmly secured by a chemical proof (*vide infra*).

After chromatographic separation, the pure *Z* olefin **15***a* was desilylated (14) to give alcohol **16***a*, which was smoothly converted into the corresponding mesylate **17***a* (92%) followed by conversion into mesylate **20***a* facilitated its intramolecular cyclization to **21**, demonstrating ipso-facto the presence of the *Z* geometry. The same sequence of reactions was effected with the *E* isomer. The *E* compound **20***b* was, however, unable to cyclize in the same conditions used for the *Z* isomer **20***a*.

Dienophile **20***a* and the *trans-cis* diene **22** (7*c*) were coupled in dimethylformamide and tetrahydrofuran (1:1), producing triene **23** in 84% yield (Scheme 3). Subsequent alkylation with the anion of dimethyl malonate at 80°C gave

[1]NSERCC and FCAR predoctoral fellowships, 1988–1990.

[2]Author to whom correspondence may be addressed.

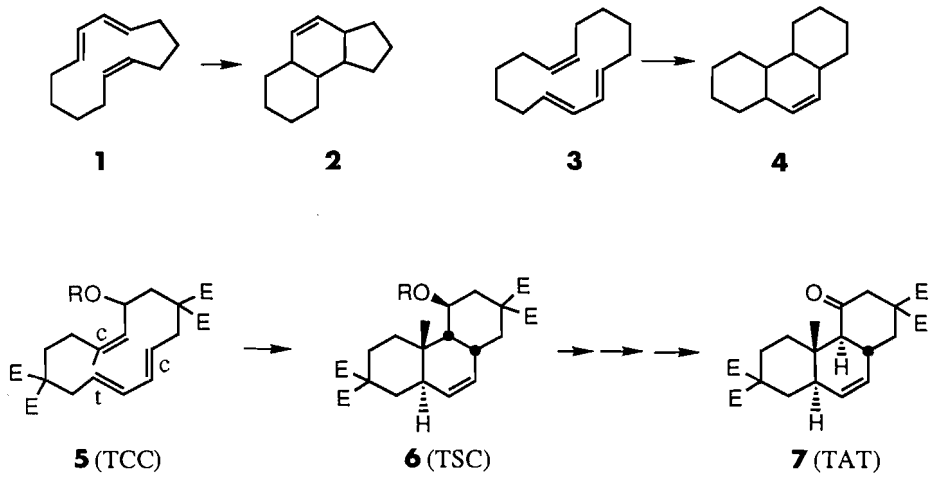

E = CO_2CH_3, R = $CH_2C_6H_5$ or $CH_2C_6H_4OCH_3$

SCHEME 1

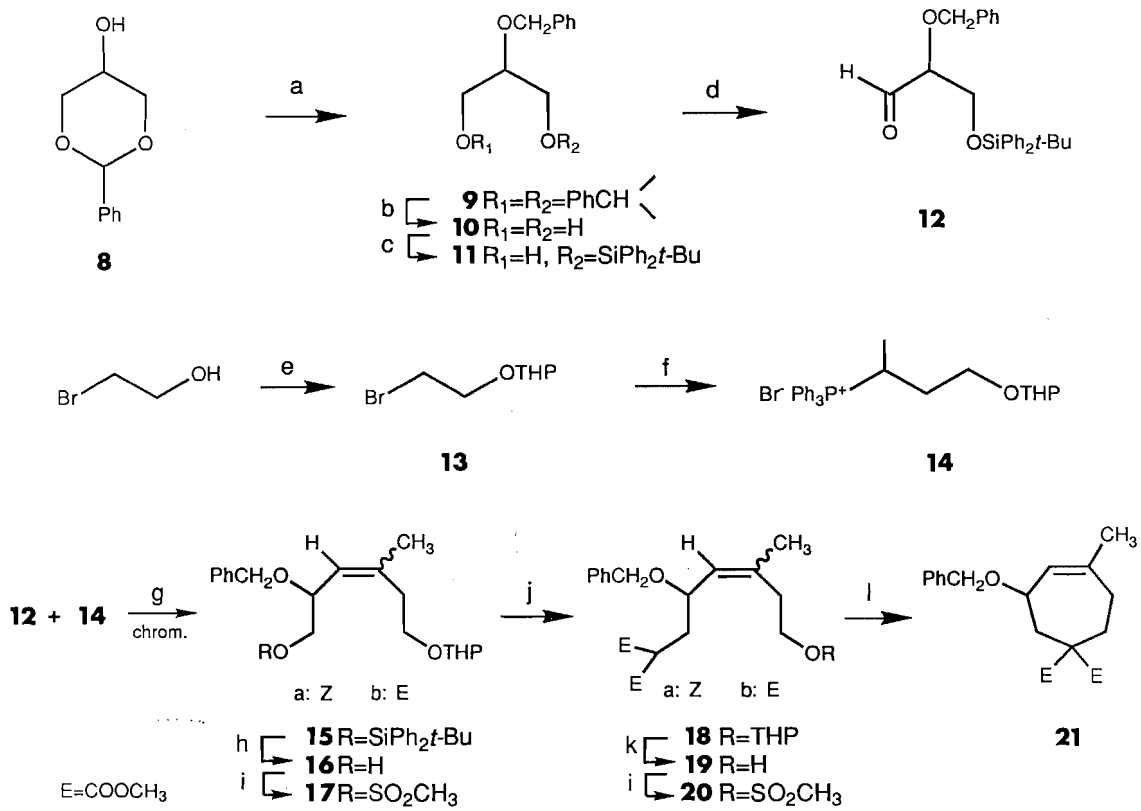

(a) $PhCH_2Br$, NaH, THF, 0°C to r.t. (b) HCl 10%, H_2O (85%) (c) *t*-$BuPh_2SiCl$, imidazole, THF, r.t. (51%) (d) $(COCl)_2$, DMSO, Et_3N, CH_2Cl_2, -78°C to r.t. (e) DHP, PPTS, CH_2Cl_2, r.t. (82%) (f) (i) $Br^-Ph_3P^+CH_2CH_3$, HMDSK, toluene, THF, 0°C (ii) **13**, THF, 48 h, r.t. (81%) (g) (i) **14**, BuLi, hexane, THF, -78°C to 0°C (ii) **12**, THF, chromatography (*cis* = 36%, *trans* = 27% from alcohol **11**) (h) *n*-Bu_4NF, THF, 0°C to r.t. (93%) (i) CH_3SO_2Cl, Et_3N, CH_2Cl_2, 0°C (j) $CH_2(CO_2CH_3)_2$, NaH, THF/DMF 1:1, KI, 85°C (84%) (k) CH_3OH, PPTS, reflux (92%) (l) HMDSNa, THF/DMF 1:1, 80°C, 4.5 x 10^{-3} M (77%)

SCHEME 2

compound **24** (80%), which, after desilylation (14) (91%), led to alcohol **25**. The latter was then converted to the corresponding allylic chloride **26** by the procedure of Collington and Meyers (15). Finally, the crude chloride **26** was allowed to cyclize under high-dilution conditions (Cs_2CO_3, THF/DMF 1:1, 70°C, 10 h, 2.5 × 10^{-3} M, slow addition) to afford macrocyclic compound **5** (R = CH_2Ph) (75% from alcohol **25**).

Can. J. Chem. Downloaded from www.nrcresearchpress.com by 109.225.110.28 on 09/08/12
For personal use only.

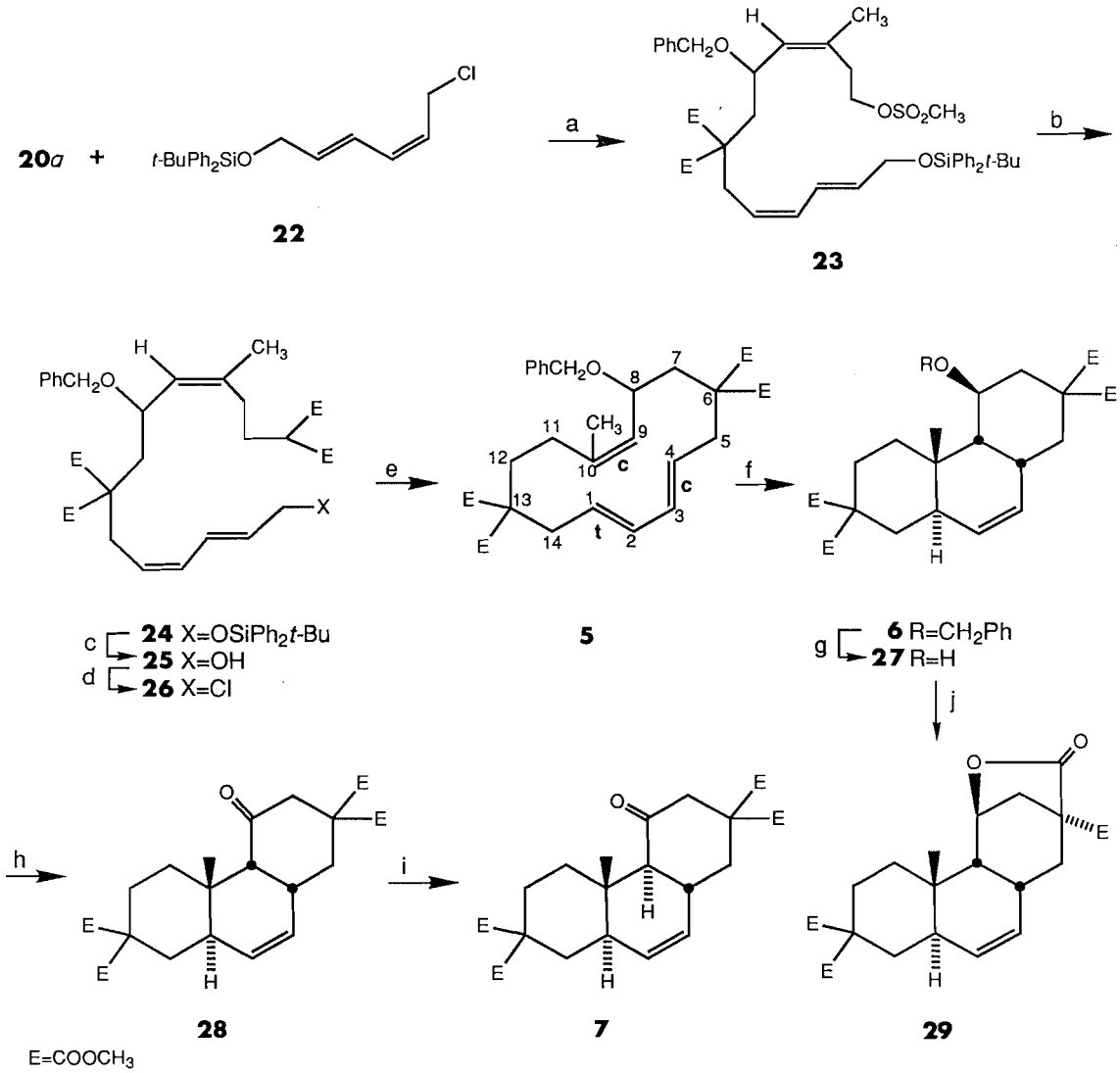

(a) (i) **20a**, NaH, THF/DMF 1:1, 0°C to r.t. (ii) **22**, THF/DMF 1:1, r.t. (84%) (b) (i) $CH_2(CO_2CH_3)_2$, NaH, THF/DMF 1:1 (ii) **23**, THF/DMF, 80°C (80%) (c) *n*-Bu_4NF, THF, 0°C to r.t. (91%) (d) CH_3SO_2Cl, s-collidine, LiCl, DMF, r.t. (e) Cs_2CO_3, DMF/THF 1:1, 2.5 x 10^{-3} M, 75°C, slow addition (75% from alcohol **25**) (f) sealed tube, toluene, 270°C, 2.75 h (84%) (g) $SnCl_4$, CH_2Cl_2, r.t. (87%) (h) PCC, CH_2Cl_2, r.t. (87%) (i) Na_2CO_3, CH_3OH, 50°C, 9h (94%) (j) PTSA, C_6H_6, reflux (86%)

SCHEME 3

Chiral synthesis of macrocyclic triene 5

The chiral dienophile moiety was synthesized as indicated in Scheme 4. Thus 3-bromobutyric acid **30** was first treated with triphenylphosphine to give the corresponding phosphonium salt **31** (94%). Without further purification, the acid function of the phosphonium salt was esterified to its methyl ester **32** in 81% yield after crystallization. Reduction of ester **32** with diisobutylaluminum hydride produced alcohol **33***a* in 62% yield. The corresponding phosphonium bromide **33***b* was also prepared by methanolysis of the phosphonium salt **14** in the presence of pyridinium *p*-toluenesulfonate (83%).

A Wittig reaction with aldehyde **34** (16) in tetrahydrofuran led to a *Z* and *E* mixture (5:1) of olefins **35** in 60% yield. The respective geometries were assigned by ^{13}C nuclear magnetic resonance as described above. The optical purity of the separated *Z* olefin **35***a* was verified in the following manner. The hydroxyl functionality was protected as a silyl ether (10) leading to **36** (79%), which, after hydrolysis, provided diol **37** in 55% yield. Subsequent monotosylation of diol **37** to alcohol **38** (72%) allowed esterification with the chiral acid **40** and gave Mosher ester **39** (90%). This compound proved to be one single diastereomer by ^1H nmr spectroscopy. The same sequence of reactions was carried out with the *S* enantiomer of silyl ether **36**, already synthesized in our laboratory (7*g*). In this case, a different isomer of compound **39** (99%) was obtained, also homogenous by ^1H nmr spectroscopy.

The *Z* isomer of olefin **35**, purified by column chromatography, was benzoylated (89%) (Scheme 5) and then hydrolyzed to afford diol **42** (87%). After monotosylating diol **42**, the remaining free hydroxyl group was protected via treatment with *p*-methoxybenzyltrichloroacetimidate (17) (73%). Alkylation of benzyl ether **44** with dimethyl malon-

Can. J. Chem. Downloaded from www.nrcresearchpress.com by 109.225.110.28 on 09/08/12
For personal use only.

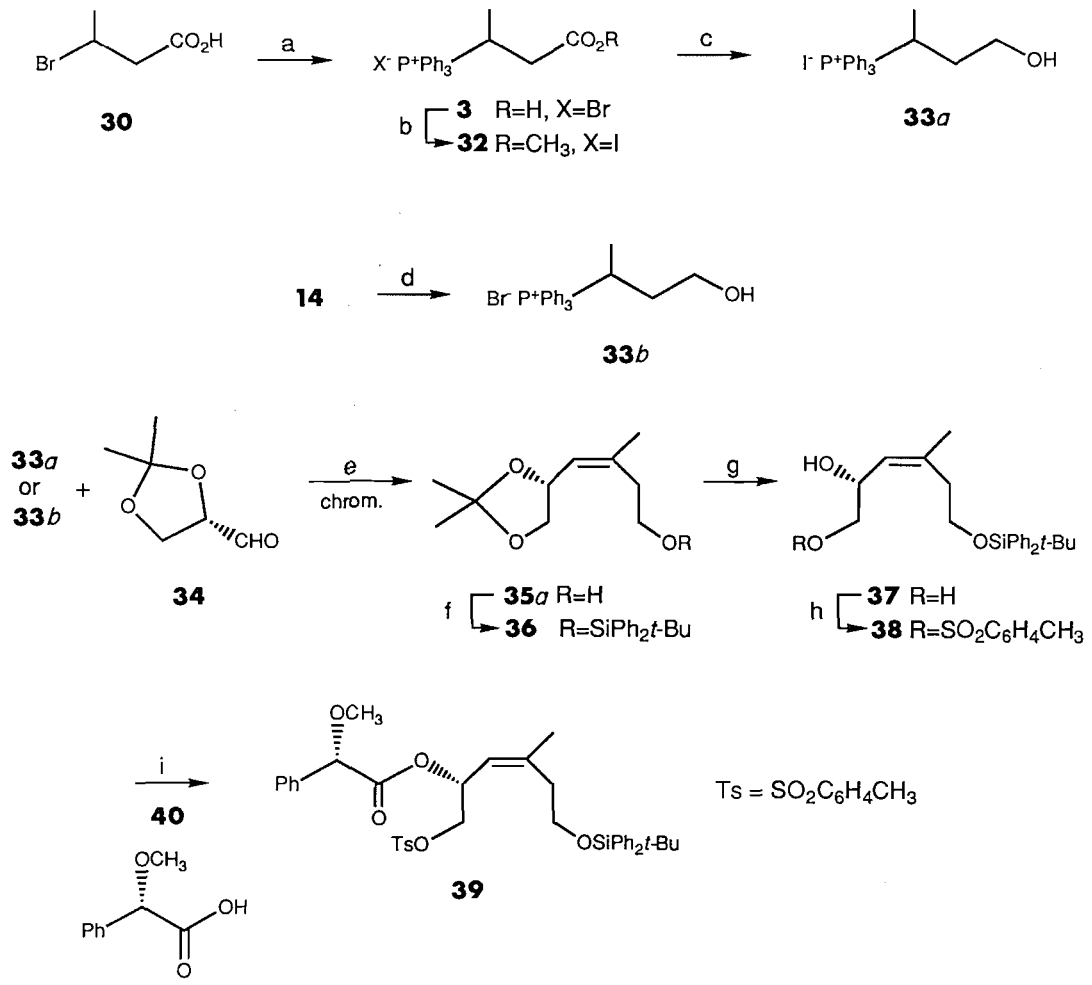

(a) PPh_3, toluene, reflux, 48 h (b) CH_3I, Na_2CO_3, NaI, acetone, reflux, 12 h (81%)
(c) DIBAL,CH_2Cl_2, -78°C, 2 h (62%) (d) *p*-PTS, CH_3OH, 50°C, 18 h (83%)
(e) (i) **33**, BuLi, hexane, THF, -78°C to 0°C; (ii) **34**, THF, chromatography (*cis*=50%, *trans*=10%) (f) *t*-$BuPh_2SiCl$, imidazole, DMF, 4 h (79%)
(g) PPTS, CH_3OH, r.t., 4 h (55%) (h) TsCl, NEt_3, DMAP, CH_2Cl_2, r.t., 3 h (60%)
(i) $Ph(OCH_3)CHCOOH$ (**40**), DCC, DMAP, CH_2Cl_2, r.t., 0.5 h (99%)

SCHEME 4

ate furnished compound **46** (72%). This adduct was then submitted to the coupling conditions previously described, yielding triene **47** in 87% yield. Alkylation with dimethyl malonate carried out on iodide **45** instead of tosylate **44** gave about the same yield (77%).

Hydrolysis of benzoate **47** in methanol afforded alcohol **48** (94%), which was transformed into mesylate **49** in 97% yield. The same strategy as described above was then applied to mesylate **49**. Thus condensation with the anion originating from dimethyl malonate (84%) followed by a treatment with fluoride ions gave alcohol **51** (94%) via compound **50**. Conversion of this alcohol into the corresponding allylic chloride **52** then allowed the cyclization leading to macrocyclic triene (−)**5** (R = $CH_2C_6H_4OCH_3$) obtained in 78% yield for the last two steps.

Transannular Diels–Alder reaction of macrocyclic trienes 5

When heated at 270°C for 2.75 h, racemic macrocyclic triene **5** (R = CH_2Ph) underwent transannular Diels–Alder reaction to give, in 84% yield, tricyclic compound **6** (R = CH_2Ph) and a mixture of two minor compounds, which were not separable by column chromatography (Scheme 3). The stereochemistry of the five asymmetric centers in the major compound can be predicted by an analysis of the possible transition states (see Scheme 6). Thus, the relative stereochemistry TSC at the ring junctions becomes apparent after examination of such transition states; only transition states 2 and 3 are structurally allowed. Approach 1 is not possible because it is sterically impossible to get the boat form of the central ring with a 1,2-diaxial disposition of ring C. Also, despite the equatorial disposition of the benzyl ether in approach 3 and the 1,3-diaxial interaction between one of the esters E and the benzyl ether in approach 2, the latter will be favored since the benzyl ether is sterically less encumbered and therefore energetically favored. Consequently, the major compound should be compound **6***a* with an equatorial benzyl ether after conformational change. This orientation was confirmed by nmr spectroscopy of the proton adjacent to the

Can. J. Chem. Downloaded from www.nrcresearchpress.com by 109.225.110.28 on 09/08/12
For personal use only.

Can. J. Chem. Downloaded from www.nrcresearchpress.com by 109.225.110.28 on 09/08/12
For personal use only.

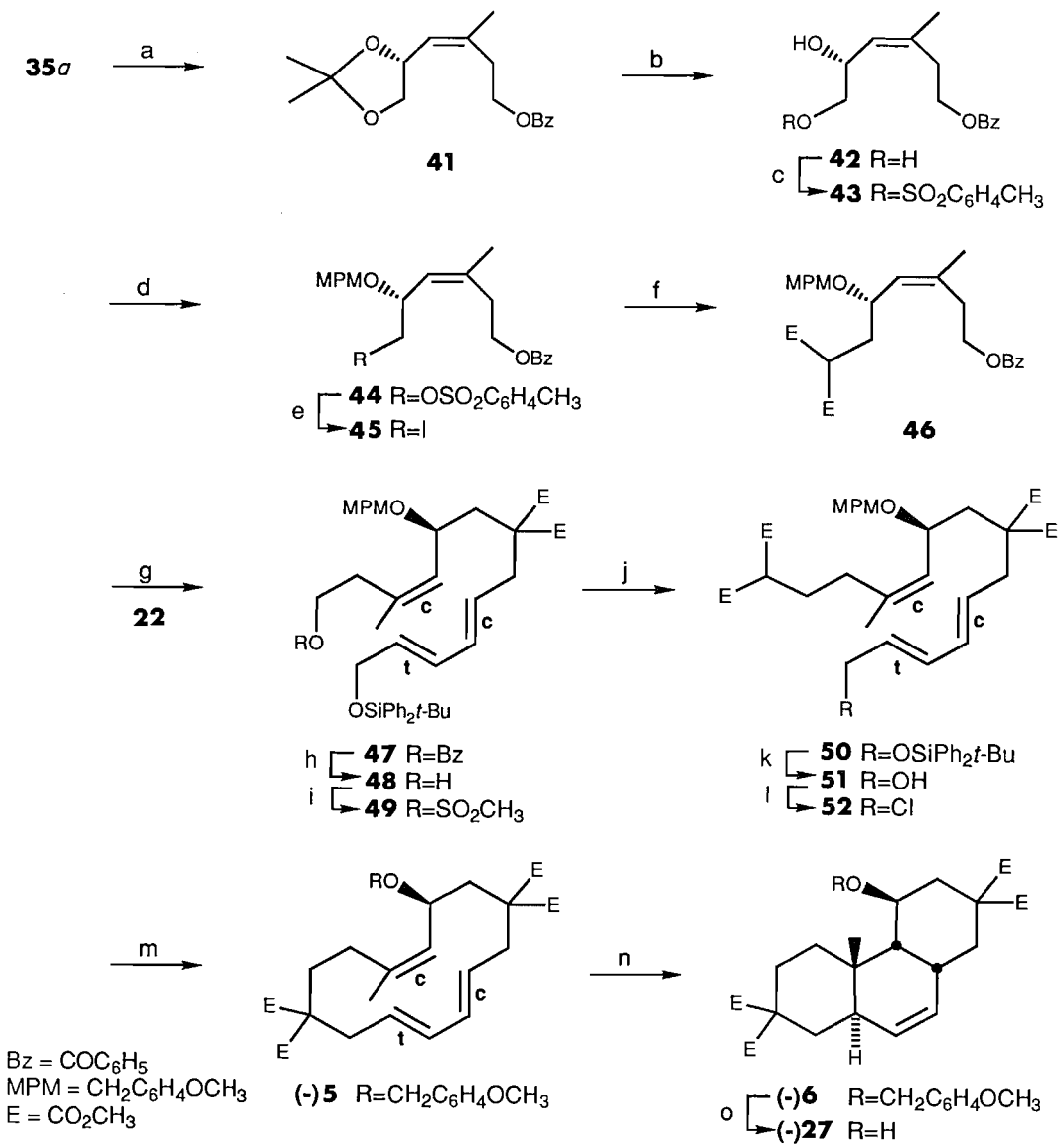

(a) BzCl, NEt_3, DMAP, CH_2Cl_2, r.t., 1.5 h (89%) (b) *p*-TSA, CH_3OH, r.t., 1.5 h (87%) (c) TsCl, NEt_3, DMAP, CH_2Cl_2, 0°C, 1.5 h (72%) (d) $Cl_3CC(NH)OCH_2C_6H_4OCH_3$, TfOH, Et_2O, 0°C, 3 h (73%) (e) NaI, nBu_4NI, acetone, 50°C, 70 h (99%) (f) $CH_2(CO_2CH_3)_2$, NaH, THF/DMF 1:1, KI, 85°C (77%) (g) (i) NaH, THF/DMF 1:1, 0°C to r.t.; (ii) **22**, THF/DMF 1:1, r.t. (87%) (h) K_2CO_3, CH_3OH, 65°C, 4 h (94%) (i) CH_3SO_2Cl, NEt_3,CH_2Cl_2, 0°C, 0.5 h (97%) (j) $CH_2(CO_2CH_3)_2$, NaH, THF/DMF 1:1, KI, 80°C (84%) (k) nBu_4NF, THF, 0°C to r.t. (94%) (l) CH_3SO_2Cl, NEt_3, *s*-collidine, LiCl, DMF, r.t. (m) Cs_2CO_3, DMF/THF 1:1, 2.5×10^{-3} M, 75°C, slow addition (78% from **51**) (n) sealed tube, toluene, 262°C, 3 h (82%) (o) DDQ, H_2O, CH_2Cl_2 (76%)

SCHEME 5

benzyl ether (3.76 ppm, doublet of doublets of doublets, 9.9, 9.9, and 4.4 Hz). Two larger coupling constants indicate an axial hydrogen and therefore an equatorial benzyl ether. It can also be predicted that one of the minor compounds should have an axial benzyl ether by virtue of the signal observed at 4.01 ppm (doublet of doublets of doublets, $J = 2.7$ Hz), which corresponds to the proton adjacent to the benzyl ether. Moreover, the TSC stereochemistry of the ring junctions could be established following an unequivocal chemical transformation in the chiral series (*vide infra*).

Diels–Alder reaction of the chiral macrocyclic triene was performed at 262°C in a sealed tube for 3 h (Scheme 5). As for the racemic compound, a major tricyclic compound was isolated in 84% yield along with a mixture of two minor compounds in 15% yield. The ^1H nmr spectrum of the major compound shows the same characteristic peaks observed in

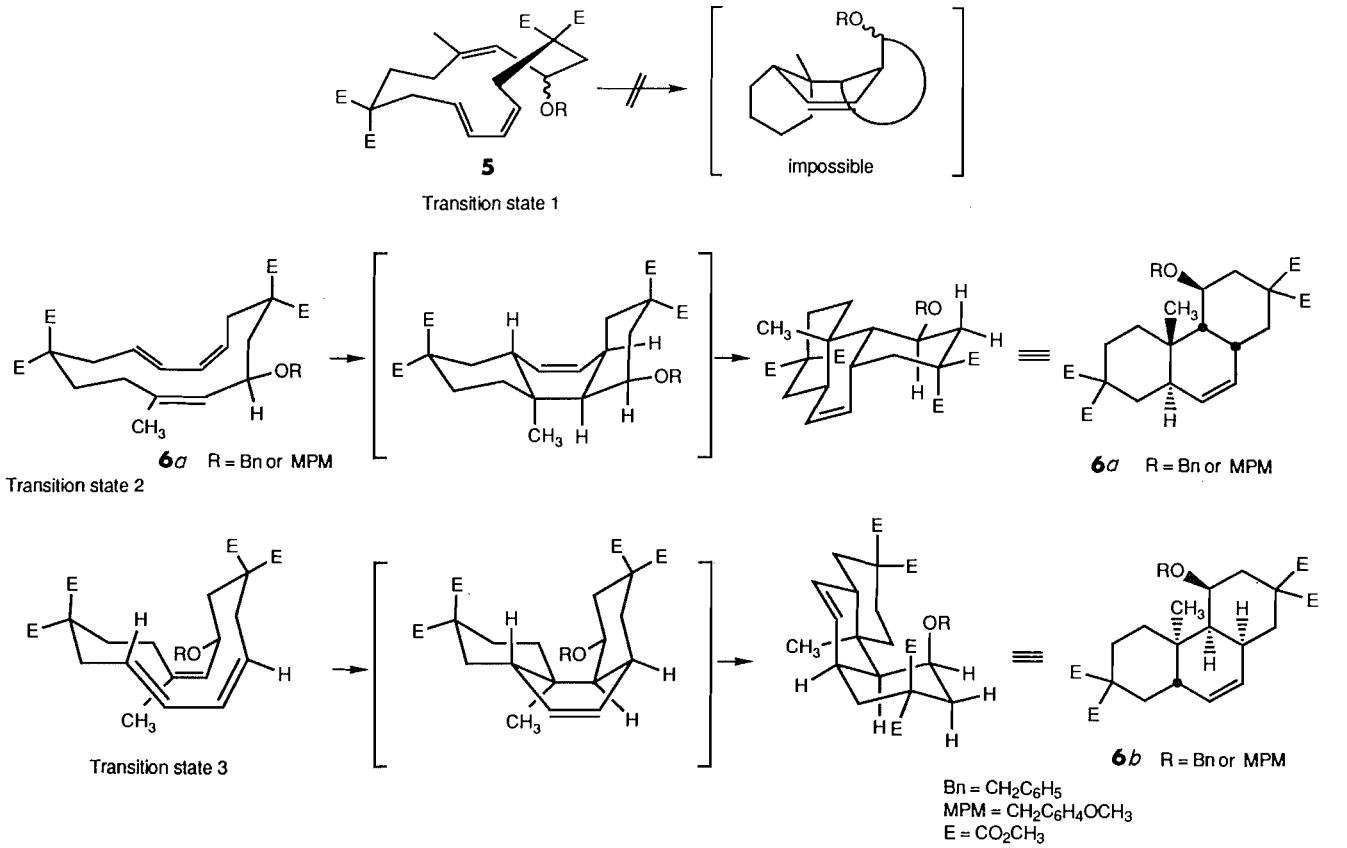

SCHEME 6

the ^1H nmr spectrum of the major racemic tricyclic compound.

Synthesis of the trans-anti-trans *tricyclic compounds 7*

Removal of the benzyl protecting group in the racemic series was achieved with tin tetrachloride in dichloromethane (18) (87%) (Scheme 3) and with 2,3-dichloro-5,6-dicyano-1,4-benzoquinone for the chiral series (76%) (Scheme 5). The resulting alcohol **27** was then oxidized by pyridinium chlorochromate to afford ketone **28** (Scheme 3) in 87% yield. The TSC relative stereochemistry of this ketone was confirmed by a single crystal X-ray diffraction analysis (19).

When these two reactions were performed on the two-compound mixture isolated from the chiral sequence, the same ketone **28** was obtained, thus proving the TSC stereochemistry and hence the structure ***6b*** proposed for one of the compounds in the mixture.[3] Finally, treatment with sodium carbonate in methanol at 65°C over 2.5 h converted ketone **28** into another ketone **7** (94%), which was spectroscopically and chemically different from the former (Scheme 3). This ketone **7** must obviously have the desired TAT stereochemistry obtained by isomerization at position C9. It must finally be noted that acidic treatment of alcohol **27** provided lactone **29** in 86% yield.

Conclusion

The formation of one major diastereomer in the Diels–Alder reaction points out the excellent control of stereochemistry at position C11. This has also been proven by the chiral synthesis of a tricyclic compound starting from an optically active precursor that had the appropriate absolute configuration for the C11 secondary benzyl ether. Moreover, the synthesis of lactone **29** allows a good differentiation of the two esters of a malonate. The carbonyl carbon of this lactone moiety could represent a precursor for the C18 hemiacetal function of aldosterone or other corticoids of this type.

Hence, this preliminary work demonstrates that a transannular Diels–Alder reaction on a suitable macrocycle followed by epimerization gives ready access to a tricyclic compound having a TAT stereochemistry. In addition, this method could be very promising for the synthesis of optically active corticosteroids. Work in this direction is currently underway in our laboratory.

Experimental

Infrared spectra were recorded on a Perkin–Elmer 681 spectrophotometer. The ^1H nmr and ^{13}C nmr spectra were taken on a Bruker WM-250 spectrometer. The following abbreviations are used in the text: s, singlet; d, doublet; t, triplet, q, quadruplet; m, multiplet. Mass spectra (ms) were recorded on a VG-Micromass ZAB-1F mass spectrometer. Melting points (mp) were measured on a Büchi apparatus and were not corrected. Thin-layer chromatography (tlc) was performed using silica gel 60 F-250. For flash chromatography Merck Kiesel gel (no. 9385) was used. Acetonitrile, amines, dimethylformamide (DMF), hexamethylphosphoramide (HMPA), and dichloromethane (CH_2Cl_2) were distilled from calcium hydride; methanol from magnesium and iodine; acetone and ethyl acetate from potassium carbonate; benzene, toluene, diethyl

[3]The second minor product in the mixture was not identified.

Can. J. Chem. Downloaded from www.nrcresearchpress.com by 109.225.110.28 on 09/08/12
For personal use only.

Can. J. Chem. Downloaded from www.nrcresearchpress.com by 109.225.110.28 on 09/08/12
For personal use only.

ether, and tetrahydrofuran (THF) from sodium and benzophenone ketyl. Unless otherwise specified, all reactions were carried out in a dry apparatus under argon or nitrogen.

*1-Bromo-2-[(2-tetrahydropyranyl)oxy]-ethane (**13**)*

To a stirred solution of 2-bromoethanol (74.93 g, 599.6 mmol) in dichloromethane (35 mL) were added, at 0°C, pyridinium *p*-toluenesulfonate (755 mg, 3.0 mmol) and dihydropyran (3.70 g, 44.0 mmol). The mixture was stirred for 1 h at room temperature. Potassium carbonate was then added and the mixture was filtered. After concentration, the residual oil was purified by column chromatography (5% to 10% of ethyl acetate in hexane) to yield bromide **13** (107.97 g, 86%); bp 70–75°C at 20 Torr (1 Torr = 133.3 Pa); ir ($CHCl_3$) ν: 3010, 2945, 2875, 2850, 1205, 1132, 1122, 1090, 1032 cm^{-1}; ^1H nmr ($CDCl_3$) δ: 4.68 (1H, t, J = 3.3 Hz, -O-C*H*-O-), 4.02 (1H, dt, J = 11.2, 6.2 Hz, -CH_2OTHP), 3.94–3.85 (1H, m, -CH_2-O-CH-O-), 3.77 (1H, dt, J = 11.4, 6.3 Hz, -CH_2OTHP), 3.57–3.48 (3H, m, -CH_2-O-CH-O- and -CH_2Br), 1.88–1.50 (6H, m, -O-CH_2-(CH_2)$_3$-); ms m/e (70 eV): 207 (M^+ − H). Exact Mass (M^+) calcd: 207.0021; found: 207.0020.

*3-[(2-Tetrahydropyranyl)oxy]-1-methylpropyltriphenylphosphonium bromide (**14**)*

Potassium bis(trimethylsilyl)amide (122.4 mL, 0.5 M in toluene) was added to a suspension of ethyltriphenylphosphonium bromide (22.70 g, 61.2 mmol) in tetrahydrofuran (100 mL) at −78°C. The mixture was stirred at room temperature for 1 h and bromide **13** (19.18 g, 91.8 mmol) was then added at 0°C. The mixture was stirred at room temperature for 48 h. The white solid formed was filtered and dissolved in dichloromethane. After evaporation of dichloromethane, the solid was recrystallized from dichloromethane and hexane to yield the phosphonium salt **14** (24.74 g, 81%); mb 197–198°C; ir ($CHCl_3$) ν: 3010, 2940, 1440, 1240, 1115, 1080, 1035 cm^{-1}; ^1H nmr ($CDCl_3$) δ: 8.03–7.66 (15H, m, 3 × -C_6H_5), 5.09–4.99 (1H, m, $Br^-P^+Ph_3$-C*H*(CH_3)-), 4.60–4.58 (1H, m, -O-C*H*-O-), 4.19–4.09 (1H, m, -O-CH-O-CH_2-), 3.91–3.80 (2H, m, -CH_2OTHP), 3.55–3.46 (1H, m, -O-CH-O-CH_2-), 2.35–2.17 (1H, m, -CH(CH_3)-CH_2-), 1.86–1.36 (7H, m, -CH(CH_3)-CH_2- and -O-CH_2-(CH_2)$_3$-), 1.44 (3H, dd, J = 19.8, 6.9 Hz, -CH(CH_3)-).

*2-Benzyloxy-1,3-propanediol (**10**)*

5-Hydroxy-2-phenyl-1,3-dioxane **8** (4.98 g, 27.7 mmol) (9) was added at 0°C to a stirred suspension of sodium hydride (1.23 g, 60% in oil, 30.7 mmol) in tetrahydrofuran (120 mL). The mixture was stirred at room temperature for 10 min. The temperature was reduced to 0°C and then benzyl bromide (3.62 mL, 30.4 mmol) was added. After stirring the solution at room temperature for 3 h, half of the tetrahydrofuran was evaporated followed by addition of water (36 mL) and 10% aqueous hydrochloric acid (84 mL). The mixture was heated to reflux for 1.5 h, then poured into a saturated solution of sodium carbonate and extracted with ethyl acetate. The organic layers were combined, dried over anhydrous magnesium sulfate, filtered, and concentrated. The residual oil was purified by column chromatography (50% to 100% of ethyl acetate in hexane) to afford diol **10** (4.30 g, 85%); ir ($CHCl_3$) ν: 3600, 3580, 3050, 2930, 2880, 1260, 1110, 1060 cm^{-1}; ^1H nmr ($CDCl_3$) δ: 7.42–7.29 (5H, m, -CH_2-C_6H_5), 4.67 (2H, s, -C$H_2C_6H_5$), 3.84–3.69 (4H, m, -CH_2-CH(OBn)-CH_2-), 3.61 (1H, q, J = 4.6 Hz, -C*H*-(OCH_2-C_6H_5)), 2.05 (2H, s, -CH_2O*H*); ms m/e (70 eV): 182 (M^+), 151 (M^+ − CH_2OH). Exact Mass (M^+) calcd: 182.0943; found: 182.0945.

*3-Benzyloxy-3-[(*tert*-butyldiphenylsilyl)oxy]-propan-1-ol (**11**)*

Imidazole (344.0 mg, 5.05 mmol) and *tert*- butyldiphenylsilyl chloride (1.26 g, 4.57 mmol) were added at 0°C to a stirred solution of diol **10** (0.832 g, 4.57 mmol) in tetrahydrofuran (20 mL). The solution was stirred at room temperature for 3.5 h, after which tetrahydrofuran was evaporated. The residual oil was purified by column chromatography (25% to 100% of ethyl acetate in hexane) to afford alcohol **11** (1.06 g, 55%), doubly protected diol (0.874 g, 29%), and starting material **10** (0.137 g, 16%); ir ($CHCl_3$) ν: 3580, 3070, 3010, 2960, 2930, 2860, 1470, 1430, 1100 cm^{-1}; ^1H nmr ($CDCl_3$) δ: 7.69–7.66 and 7.45–7.28 (15H, m, -$OCH_2C_6H_5$ and -OSi-(C_6H_5)$_2$*t*Bu), 4.64 (1H, d, J_{AB} = 11.7 Hz, -OCH_2Ph), 4.52 (1H, d, J_{AB} = 11.7 Hz, -OCH_2Ph), 3.84–3.71 (4H, m, -CH_2OH and -CH_2OSiPh$_2$*t*Bu), 3.67–3.60 (1H, m, -C*H*(OBn)-), 2.08 (1H, s, -CH_2O*H*), 1.06 (9H, s, -OSiPh$_2$C(CH_3)$_3$); ms m/e (70 eV): 285 (M^+ − *t*Bu − Ph − H). Exact Mass (M^+ − *t*Bu − Ph − H) calcd: 285.0947; found: 285.0955.

*2-Benzyloxy-3-[(*tert*-butyldiphenylsilyl)oxy]-propanal (**12**)*

Dimethyl sulfoxide (1.64 mL, 23.11 mmol) was added slowly at −78°C to a stirred solution of oxalyl chloride (1.01 mL, 11.56 mmol) in dichloromethane (28 mL). The solution was stirred for 10 mins and a solution of alcohol **11** (1.93 g, 4.60 mmol) in dichloromethane (14 mL) was added at −78°C. The mixture was stirred for 0.75 h and triethylamine (6.44 mL, 46.22 mmol) was then added at −78°C. The temperature of the mixture was raised to −10°C and the solution was stirred for 0.5 h. After addition of water, the mixture was extracted with dichloromethane and the organic layer was dried over magnesium sulfate and concentrated. The residual oil (1.81 g, 94% crude) was used for the next step without any purification; ir ($CHCl_3$) ν: 3070, 3010, 2930, 2860, 1738, 1730, 1430, 1115 cm^{-1}; ^1H nmr ($CDCl_3$) δ: 9.76 (1H, d, J = 1.4 Hz, -C*H*O), 7.69–7.64 and 7.44–7.30 (15H, m, -OSi(C_6H_5)$_2$*t*Bu and -O-$CH_2C_6H_5$), 4.69 (1H, d, J_{AB} = 12.4 Hz, -OCH_2Ph), 4.65 (1H, d, J_{AB} = 12.4 Hz, -OCH_2Ph), 3.98–3.96 (2H, m, -CH_2OSiPh$_2$*t*Bu), 3.91 (1H, dd, J = 4.0 and 1.4 Hz, OHC-C*H*(OBn)-), 1.04 (9H, s, -OSiPh$_2$C(CH_3)$_3$); ms m/e (70 eV): 361 (M^+ − *t*Bu). Exact Mass (M^+ − *t*Bu) calcd: 361.1260; found: 361.1266.

*2-Benzyloxy-1-[(*tert*-butyldiphenylsilyl)oxy]-6-[(2-tetrahydropyranyl)oxy]-4-methylhex-3-ene (**15**)*

Butyllithium (185 μL, 1.6 M in hexane, 0.296 mmol) was added at −78°C to a stirred suspension of phosphonium bromide **14** (0.162 g, 0.325 mmol, dried under vacuum at 115–120°C for 12 h) in tetrahydrofuran (1.5 mL). The mixture was brought to 0°C and stirred until the solution became dark red (≈ 0.5 h). A solution of aldehyde **12** (0.100 g crude, 0.277 mmol) in tetrahydrofuran (1.5 mL) was then added at 0°C. After 10 min, the mixture was poured into a saturated solution of ammonium chloride and was extracted with ethyl ether. The combined organic layers were dried over anhydrous magnesium sulfate, filtered, and concentrated. The residual oil was purified by column chromatography (5% ethyl acetate in hexane) to afford *Z* olefin **15***a* (45.2 mg, 43%) and *E* olefin **15***b* (33.8 mg, 32%); ir ($CHCl_3$) ν, *Z* and *E* isomers: 2950, 2855, 1112 cm^{-1}; ^1H nmr ($CDCl_3$) *Z* isomer, δ: 7.71–7.65 and 7.41–7.25 (15H, m, -$OCH_2C_6H_5$ and -OSi(C_6H_5)$_2$*t*Bu), 5.16 (1H, d, J = 10.0 Hz, -C*H*=C(CH_3)-), 4.62 (1H, d, J_{AB} = 12.0 Hz, -OCH_2Ph), 4.48 (1H, m, -O-C*H*-O-), 4.46 (1H, d, J_{AB} = 12.0 Hz, -OCH_2-Ph), 4.29 (1H, m, -C*H*(OBn)-), 3.85–3.68 (2H, m, -CH_2OTHP and -O-CH-O-CH_2-), 3.79 (1H, dd, J_{AB} = 10.5 Hz, J_{AX} = 6.8 Hz, -CH_2OSiPh$_2$*t*Bu), 3.60 (1H, dd, J_{AB} = 11.5 Hz, J_{BX} = 4.6 Hz, -CH_2OSiPh$_2$*t*Bu), 3.50–3.40 (1H, m, -O-CH-O-CH_2-), 3.39–3.28 (1H, m, -CH_2OTHP), 2.36–2.17 (2H, m, =C(CH_3)-CH_2-CH_2-), 1.78 (3H, s, -CH=C(CH_3)-), 1.76–1.42 (6H, m, -O-CH_2(CH_2)$_3$-), 1.05 (9H, s, -OSiPh$_2$C(CH_3)$_3$); ^{13}C nmr ($CDCl_3$) *Z* isomer, δ: 19.6, 23.8, 25.4, 26.9, 30.6, 32.8, 62.2, 65.7, 67.0, 70.2, 76.2, 98.8, 125.5, 127.2, 127.6, 128.2, 129.5, 133.8, 135.7, 138.2, 139.1; ^1H nmr ($CDCl_3$) *E* isomer, δ: 7.74–7.63 and 7.44–7.25 (15H, m, -O-CH_2-C_6H_5 and -OSi(C_6H_5)$_2$*t*Bu), 5.12 (1H, dm, J = 9.0 Hz, -C*H*=C(CH_3)-), 4.62 (1H, d, J_{AB} = 12.1 Hz, -OCH_2Ph), 4.60–4.56 (1H, m, -O-C*H*-O-), 4.43 (1H, d, J_{AB} = 12.1 Hz, -OCH_2Ph), 4.25–4.17 (1H, m, -C*H*(OBn)-), 3.85–3.76 (3H, m, -CH_2OSiPh$_2$-*t*Bu), 3.50–3.43 (2H, m, -CH_2OTHP and -O-CH-O-CH_2-), 2.30 (2H, t, J = 7.0 Hz, =C(CH_3)-CH_2-), 1.84–1.40 (6H, m, -O-CH_2-(CH_2)$_3$-), 1.54 (3H, d, J = 1.6 Hz, -CH=C(CH_3)-), 1.04 (9H, s, -OSiPh$_2$C(CH_3)$_3$); ^{13}C nmr ($CDCl_3$)

Can. J. Chem. Downloaded from www.nrcresearchpress.com by 109.225.110.28 on 09/08/12
For personal use only.

E isomer, δ: 17.1, 19.4, 25.4, 26.8, 30.7, 39.7, 62.1, 65.9, 66.8, 70.0, 76.1, 98.8, 124.7, 127.2, 127.6, 128.2, 129.5, 133.8, 135.7, 138.1, 139.1; ms *m/e* (70 eV): 501 ($M^+ - t$Bu). Exact Mass ($M^+ - t$Bu) calcd: 501.9711; found: 501.9711.

*(3Z)-2-Benzyloxy-6-[(2-tetrahydropyranyl)oxy]-4-methylhex-3-en-1-ol (**16**a)*

A solution of tetrabutylammonium fluoride in tetrahydrofuran (1M, 860 μL, 0.860 mmol) was added at 0°C to a stirred solution of silyl ether **15***a* (0.417 g, 0.748 mmol) in tetrahydrofuran (8.5 mL). The mixture was stirred at room temperature for 2 h and then poured into water and extracted with ethyl acetate. The combined organic layers were dried over magnesium sulfate, filtered, and concentrated. The residual oil obtained was purified by column chromatography (25% to 50% of ethyl acetate in hexane) to yield alcohol **16***a* (0.228 g, 95%); ir ($CHCl_3$) *ν*: 3580, 3470, 3010, 2945, 2875, 1452, 1212, 1120, 1060, 1030 cm^{-1}; ^1H nmr ($CDCl_3$) δ: 7.36–7.26 (5H, m, -OCH$_2$C$_6$*H*$_5$), 5.22 (1H, d, *J* = 9.4 Hz, -C*H*=C(CH$_3$)-), 4.63 (d, 1H, J_{AB} = 11.6 Hz, -OC*H*$_2$Ph), 4.58–4.54 (1H, m, -O-C*H*-O-), 4.38 (1H, dd, J_{AB} = 11.6 Hz, J_{BX} = 0.9 Hz, -OC*H*$_2$Ph), 4.34–4.24 (1H, m, C*H*(OBn)-), 3.89–3.78 (2H, m, -C*H*$_2$OH and -O-CH-O-C*H*$_2$-), 3.68–3.39 (4H, m, -C*H*$_2$OTHP, -C*H*$_2$OH, and O-CH-O-C*H*$_2$-), 2.57–2.45 (1H, m, -CH$_2$O*H*), 2.34–2.23 (2H, m, =C(CH$_3$)-C*H*$_2$-CH$_2$OTHP), 1.83 (3H, dd, *J* = 1.3 Hz, -CH=C(C*H*$_3$)-), 1.82–1.49 (6H, m, -O-CH$_2$-(C*H*$_2$)$_3$-); ms *m/e* (70 eV): 280 ($M^+ - CH_2OH$). Exact Mass ($M^+ - CH_2OH$) calcd: 289.1804; found: 289.1801.

*(3E)-2-Benzyloxy-6-[(2'-tetrahydropyranyl)oxy]-4-methylhex-3-en-1-ol (**16**b)*

The preceding procedure was applied, using silyl ether **15***b* (99.2 mg, 0.178 mmol), tetrabutylammonium fluoride (1M in tetrahydrofuran, 215 μL, 0.215 mmol), and tetrahydrofuran (2.5 mL), and afforded alcohol **16***b* (50.0 mg, 88%); ^1H nmr ($CDCl_3$) δ: 7.35–7.28 (5H, m, -OCH$_2$C$_6$*H*$_5$), 5.16 (1H, dq, *J* = 9.2, 1.2 Hz, -C*H*=C(CH$_3$)-), 4.62 (1H, d, J_{AB} = 11.6 Hz, -OC*H*$_2$Ph), 4.59 (1H, t, *J* = 3.6 Hz, -O-C*H*-O-), 4.37 (1H, d, J_{AB} = 11.6 Hz, -OC*H*$_2$Ph), 4.31–4.22 (1H, m, -C*H*(OBn)-), 3.90–3.79 (2H, m, -C*H*$_2$OH and -O-CH-O-C*H*$_2$-), 3.64–3.44 (4H, m, -C*H*$_2$OTHP, -C*H*$_2$OH, and -O-CH-O-C*H*$_2$-), 2.36 (2H, t, *J* = 7.0 Hz, =C(CH$_3$)-C*H*$_2$-), 2.20–2.10 (1H, m, -CH$_2$O*H*), 1.83–1.46 (6H, m, -O-CH$_2$-(C*H*$_2$)$_3$-), 1.71 (3H, d, *J* = 1.2 Hz, -CH=C(C*H*$_3$)-).

*(3Z)-2-Benzyloxy-1-methanesulfonyloxy-6-[(2'-tetrahydropyranyl)oxy]-4-methylhex-3-ene (**17**a)*

Triethylamine (520 μL, 3.73 mmol) and methanesulfonyl chloride (160 μL, 2.07 mmol) were added at 0°C to a stirred solution of alcohol **16***a* (0.594 g, 1.86 mmol) in dichloromethane (11 mL). The mixture was stirred for 0.5 h and then poured into water and extracted with dichloromethane. The organic layers were dried over magnesium sulfate, filtered, and concentrated. The residual oil was used for the next reaction without any purification; ir ($CHCl_3$) *ν*: 3010, 3000, 2940, 2870, 1455, 1445, 1170 cm^{-1}; ^1H nmr ($CDCl_3$) δ: 7.34–7.26 (5H, m, -OCH$_2$C$_6$*H*$_5$), 5.20 (1H, d, *J* = 9.1 Hz, -C*H*=C(CH$_3$)-), 4.62 (1H, d, J_{AB} = 11.7 Hz, -OC*H*$_2$Ph), 4.54–4.44 (2H, m, -O-C*H*-O- and -C*H*(OBn)-), 4.40 (1H, dd, J_{AB} = 11.7 Hz, J_{BX} = 1.1 Hz, -OC*H*$_2$Ph), 4.25–4.17 (2H, m, -C*H*$_2$OSO$_2$CH$_3$), 3.88–3.76 (2H, m, -O-CH-O-C*H*$_2$ and -C*H*$_2$-OTHP), 3.66–3.35 (2H, m, -O-CH-O-C*H*$_2$- and -C*H*$_2$OTHP), 2.98 (3H, s, -SO$_2$C*H*$_3$), 2.49–2.22 (2H, m, =C(CH$_3$)-C*H*$_2$-), 1.83 (3H, d, *J* = 1.4 Hz, -CH=C(C*H*$_3$)-), 1.82–1.46 (6H, m, -O-CH$_2$-(C*H*$_2$)$_3$-), 1.82–1.46 (6H, m, -O-CH$_2$-(C*H*$_2$)$_3$-); ms *m/e* (70 eV): 313 (M^+ − OTHP). Exact Mass (M^+ − OTHP) calcd: 313.1110; found: 313.1106.

*(3E)-2-Benzyloxy-1-methanesulfoxy-6-[(2'-tetrahydropyranyl)oxy]-4-methylhex-3-ene (**17**b)*

The preceding procedure was applied, using alcohol **16***b* (42.1 mg, 0.132 mmol), methanesulfonyl chloride (11 μL, 0.142 mmol), and triethylamine (37 μL, 0.265 mmol), yielding mesylate **17***b* (53.2 mg, 100% crude); ^1H nmr ($CDCl_3$) δ: 7.34–7.28 (5H, m, -OCH$_2$C$_6$*H*$_5$), 5.16 (1H, d, *J* = 9.4 Hz, -C*H*=C(CH$_3$)-), 4.62 (1H, d, J_{AB} = 11.8 Hz, -OC*H*$_2$Ph), 4.62–4.58 (1H, m, -O-C*H*-O-), 4.48–4.37 (1H, m, -C*H*OBn-), 4.40 (1H, d, J_{AB} = 11.8 Hz, -OC*H*$_2$Ph), 4.26–4.13 (2H, m, -C*H*$_2$OSO$_2$CH$_3$), 3.91–3.81 (2H, m, -O-CH-O-CH$_2$- and -CH$_2$OTHP), 3.56–3.45 (2H, m, -O-CH-O-C*H*$_2$- and -C*H*$_2$OTHP), 2.99 (3H, s, -SO$_2$C*H*$_3$), 2.36 (2H, t, *J* = 6.9 Hz, =C(CH$_3$)-C*H*$_2$-), 1.88–1.47 (6H, m, -O-CH$_2$-(C*H*$_2$)$_3$-), 1.70 (3H, d, *J* = 1.3 Hz, -CH=C(C*H*$_3$)-).

*Methyl (5Z)-4-benzyloxy-8-[(2-tetrahydropyranyl)oxy]-2-methoxycarbonyl-6-methyloct-5-enoate (**18**a)*

Dimethyl malonate (1.12 mL, 9.84 mmol) was added at 0°C to a stirred suspension of sodium hydride (0.383 g, 60% in oil, 9.58 mmol) in tetrahydrofuran (5 mL) and dimethylformamide (5 mL). The mixture was stirred at room temperature for 0.5 h and a solution of mesylate **17***a* (0.739 g, 1.86 mmol) in tetrahydrofuran (2.5 mL) and dimethylformamide (2.5 mL) was then added followed by potassium iodide (0.462 g, 2.79 mmol). The mixture was heated at reflux (≈ 80°C) for 48 h, poured into a saturated solution of ammonium chloride, and extracted with a mixture of hexane and ether (2:1). The combined organic layers were dried over magnesium sulfate, filtered, and concentrated. The residual oil was purified by column chromatography (20% ethyl acetate in hexane) to afford malonate **18***a* (0.717 g, 89%); ir ($CHCl_3$) *ν*: 3000, 2945, 2865, 1745, 1730, 1450, 1437, 1205 cm^{-1}; ^1H nmr ($CDCl_3$) δ: 7.32–7.25 (5H, m, -OCH$_2$C$_6$*H*$_5$), 5.21 (1H, dq, *J* = 8.9, 1.2 Hz, -C*H*=C(CH$_3$)-), 4.57 (1H, t, *J* = 3.5 Hz, -O-C*H*-O-), 4.52 (1H, d, J_{AB} = 11.6 Hz, -OC*H*$_2$Ph), 4.25 (1H, d, J_{AB} = 11.6 Hz, -OC*H*$_2$Ph), 4.16 (1H, ddd, $J_1 = J_2$ = 8.9 Hz, J_3 = 4.5 Hz, -C*H*OBn-), 3.88–3.75 (2H, m, -O-CH-O-C*H*$_2$- and -C*H*$_2$OTHP), 3.66 and 3.65 (6H, 2s, -CH(CO$_2$C*H*$_3$)$_2$), 3.54–3.38 (3H, m, -C*H*(CO$_2$CH$_3$)$_2$, -O-CH-O-C*H*$_2$-, and -C*H*$_2$OTHP), 2.34 (2H, t, *J* = 7.2 Hz, =C(CH$_3$)-C*H*$_2$-), 2.24–2.09 (2H, m, -CH(OBn)-C*H*$_2$-), 1.80 (3H, br s, -CH=C(C*H*$_3$)-), 1.79–1.47 (6H, m, -O-CH$_2$-(C*H*$_2$)$_3$-); ms *m/e* (70 eV): 349 (M^+ − OTHP). Exact Mass (M^+ − OTHP) calcd: 349.1651; found: 349.1649.

*Methyl (5E)-4-benzyloxy-8-[(2-tetrahydropyranyl)oxy]-2-methoxycarbonyl-6-methyloct-5-enoate (**18**b)*

Sodium iodide (0.383 g, 2.55 mmol) was added to a solution of mesylate **17***b* (22.5 mg, 0.057 mmol) in acetone (3 mL). The mixture was heated at reflux for 3 h. After dilution with ethyl ether, the mixture was poured into a saturated solution of sodium thiosulfate and extracted with ethyl ether. The combined organic layers were dried over magnesium sulfate, filtered, and concentrated. The residual oil was quickly purified by column chromatography (10% to 25% ethyl acetate in hexane) to afford the corresponding iodide (11.8 mg, 49%), which was used immediately for the next reaction.

The preceding procedure was applied, using iodide (11.8 mg, 0.027 mmol) instead of mesylate, sodium hydride (6.4 mg, 60% in oil, 0.160 mmol), dimethyl malonate (19 μL, 0.165 mmol), tetrahydrofuran (0.2 mL), and dimethylformamide (0.2 mL), yielding malonate **18***b* (7.1 mg, 60%); ^1H nmr ($CDCl_3$) δ: 7.32–7.25 (5H, m, -OCH$_2$C$_6$*H*$_5$), 5.18 (1H, d, *J* = 8.9 Hz, -C*H*=C(CH$_3$)-), 4.62–4.58 (1H, m, -O-C*H*-O-), 4.52 (1H, d, J_{AB} = 11.7 Hz, -OC*H*$_2$Ph), 4.25 (1H, d, J_{AB} = 11.7 Hz, -OC*H*$_2$Ph), 4.10 (1H, ddd, $J_1 = J_2$ = 8.9 Hz, J_3 = 4.8 Hz, -C*H*OBn-), 3.89–3.79 (2H, m, -O-C*H*-O-CH$_2$- and -C*H*$_2$OTHP), 3.66 and 3.66 (6H, 2s, -CH(CO$_2$C*H*$_3$)$_2$), 3.64 (1H, dd, *J* = 8.2, 7.2 Hz, -C*H*(CO$_2$CH$_3$)$_2$), 3.54–3.44 (2H, m, -O-CH-O-C*H*$_2$- and -C*H*$_2$OTHP), 2.34 (2H, t, *J* = 6.9 Hz, =C(CH$_3$)-C*H*$_2$-), 2.24–2.00 (2H, m, -CH(OBn)-C*H*$_2$-), 1.90–1.50 (6H, m, -O-CH$_2$-(C*H*$_2$)$_3$-), 1.65 (3H, d, *J* = 1.3 Hz, -CH=C(C*H*$_3$)-).

*Methyl (5Z)-4-benzyloxy-8-hydroxy-2-methoxycarbonyl-5-methyloct-5-enoate (**19**a)*

Pyridinium *para*-toluenesulfonate (34.0 mg, 0.135 mmol) was added to a solution of ether **18***a* (74.6 mg, 0.172 mmol) in methanol (10 mL, 95%). The mixture was heated at reflux for 1.5 h, then the solvent was evaporated. The residual oil was purified by

Can. J. Chem. Downloaded from www.nrcresearchpress.com by 109.225.110.28 on 09/08/12
For personal use only.

column chromatography (25% to 50% ethyl acetate in hexane) to afford alcohol **19***a* (53.2 mg, 88%); ir (CH_2Cl_2) ν: 3600, 3490, 3060, 2950, 2880, 1750, 1730, 1437, 1215, 1157, 1055 cm^{-1}; ^1H nmr ($CDCl_3$) δ: 7.33–7.26 (5H, m, -$OCH_2C_6H_5$), 5.27 (1H, d, J = 8.7 Hz, -CH=$C(CH_3)$-), 4.53 (1H, d, J_{AB} = 11.7 Hz, -OCH_2Ph), 4.27 (1H, d, J_{AB} = 11.7 Hz, -OCH_2Ph), 4.12 (1H, ddd, $J_1 = J_2$ = 8.8 Hz, J_3 = 5.0 Hz, -CHOBn-), 3.78–3.61 (3H, m, -$CH(CO_2CH_3)_2$ and -CH_2OH), 3.68 and 3.66 (6H, 2s, -$CH(CO_2CH_3)_2$), 2.42–2.05 (4H, m, =$C(CH_3)$-CH_2- and -CH_2-$CH(CO_2CH_3)_2$), 1.78 (3H, d, J = 1.4 Hz, -CH=$C(CH_3)$-), 1.64 (1H, s, -CH_2OH); ms m/e (70 eV): 351 (MH^+). Exact Mass (MH^+) calcd: 351.1807; found: 351.1805.

*Methyl-(5E)-4-benzyloxy-8-hydroxy-2-methoxycarbonyl-6-methyloct-5-enoate (**19**b)*

The preceding procedure was applied, using ether **18***b* (7.4 mg, 0.017 mmol), pyridinium *para*-toluenesulfonate (4.0 mg, 0.016 mmol), and methanol (10 mL, 95%), yielding alcohol **19***b* (5.9 mg, 99%); ^1H nmr ($CDCl_3$) δ: 7.33–7.27 (5H, m, -$OCH_2C_6H_5$), 5.20 (1H, dq, J = 8.9, 1.3 Hz, -CH=$C(CH_3)$-), 4.52 (1H, d, J_{AB} = 11.7 Hz, -OCH_2Ph), 4.28 (1H, d, J_{AB} = 11.7 Hz, -OCH_2Ph), 4.13 (1H, ddd, $J_1 = J_2$ = 8.8 Hz, J_3 = 4.8 Hz, -CHOBn-), 3.79–3.61 (3H, m, -$CH(CO_2CH_3)_2$ and -CH_2OH), 3.68 and 3.67 (6H, 2s, -$CH(CO_2CH_3)_2$), 2.30 (2H, t, J = 6.3 Hz, =$C(CH_3)$-CH_2-), 2.28–2.03 (2H, m, -CH_2-$CH(CO_2CH_3)_2$), 1.65 (3H, d, J = 1.3 Hz, -CH=$C(CH_3)$-), 1.58 (1H, s, -CH_2OH).

*Methyl (5Z)-4-benzyloxy-2-methoxycarbonyl-6-methyloct-5-enoate (**20**a)*

The same procedure as that used for **17***a* was applied: alcohol **19***a* (53.2 mg, 0.152 mmol), triethylamine (42 μL, 0.304 mmol), methanesulfonyl chloride (13 μL, 0.167 mmol), and dichloromethane (3 mL) yielding mesylate **20***a* (65.8 mg, 100% crude); ir ($CHCl_3$) ν: 3020, 2950, 1745, 1730, 1457, 1360, 1337, 1215, 1175 cm^{-1}; ^1H nmr ($CDCl_3$) δ: 7.34–7.26 (5H, m, $OCH_2C_6H_5$), 5.32 (1H, d, J = 9.1 Hz, -CH=$C(CH_3)$-), 4.53 (1H, d, J_{AB} = 11.7 Hz, -OCH_2Ph), 4.26 (1H, d, J_{AB} = 11.7 Hz, -OCH_2Ph), 4.24 (2H, t, J = 6.9 Hz, -CH_2OMs), 4.08 (1H, ddd, $J_1 = J_2$ = 9.0 Hz, J_3 = 4.2 Hz, -CH(OBn)-), 3.68 (1H, dd, J = 6.2 Hz, -$CH(CO_2CH_3)_2$), 3.67 and 3.66 (6H, 2s, -$CH(CO_2CH_3)_2$), 3.01 (3H, s, -OSO_2CH_3), 2.58–2.48 and 2.22–2.00 (4H, 2m, =$C(CH_3)$-CH_2- and -CH_2-$CH(CO_2CH_3)_2$), 1.82 (3H, d, J = 1.4 Hz, -CH=$C(CH_3)$-).

*Methyl (5E)-4-benzyloxy-8-methanesulfonyloxy-2-methoxycarbonyl-6-methyloct-5-enoate (**20**b)*

The preceding procedure was applied, using alcohol **19***b* (10.3 mg, 0.029 mmol), triethylamine (8.2 μL, 0.059 mmol), methanesulfonyl chloride (2.5 μL, 0.032 mmol), and dichloromethane (0.5 mL), yielding mesylate **20***b* (10.1 mg, 80% crude); ^1H nmr ($CDCl_3$) δ: 7.33–7.27 (5H, m, -$OCH_2C_6H_5$), 5.23 (1H, dq, J = 8.8, 1.2 Hz, -CH=$C(CH_3)$-), 4.52 (1H, d, J_{AB} = 11.7 Hz, -OCH_2Ph), 4.30 (2H, t, J = 6.7 Hz, -CH_2OMs), 4.27 (1H, d, J_{AB} = 11.7 Hz, -OCH_2Ph), 4.11 (1H, ddd, $J_1 = J_2$ = 8.8 Hz, J_3 = 4.7 Hz, -CHOBn-), 3.68 and 3.67 (6H, 2s, -$CH(CO_2CH_3)_2$), 3.64 (1H, dd, J = 8.2, 8.8 Hz, -$CH(CO_2CH_3)_2$), 3.00 (3H, s, -OSO_2CH_3), 2.48 (2H, t, J = 6.6 Hz, =$C(CH_3)$-CH_2-), 2.24–2.01 (2H, m, -CH_2-$CH(CO_2CH_3)_2$), 1.67 (3H, d, J = 1.2 Hz, -CH=$C(CH_3)$-).

*(4Z)-7-Benzyloxy-5,5-dimethoxycarbonyl-2-methylcyclohept-1-ene (**21**)*

Sodium bis(trimethylsilyl)amide (45 μL, 1 M in tetrahydrofuran, 0.045 mmol) was added at −78°C to a stirred solution of mesylate **20***a* (19.2 mg, 0.045 mmol) in tetrahydrofuran (5 mL) and dimethylformamide (5 mL). The temperature of the mixture was allowed to reach room temperature and then potassium iodide was added to the solution. The resulting mixture was stirred at 80°C for 4.5 h. After evaporation of the solvents under vacuum, the residual oil was purified by column chromatography (10% ethyl acetate in hexane) to yield cycloheptene **21** (11.5 mg, 77%); ir ($CHCl_3$) ν: 3020, 3010, 2950, 2855, 1728, 1455, 1435, 1245, 1215, 1090 cm^{-1}; ^1H nmr ($CDCl_3$) δ: 7.35–7.24 (5H, m, -$OCH_2C_6H_5$), 5.54 (1H, m, -CH=$C(CH_3)$-), 4.59 (1H, d, J_{AB} = 12.0 Hz, -OCH_2Ph), 4.55 (1H, d, J_{AB} = 12.0 Hz, -OCH_2Ph), 4.16 (1H, d, J = 11.0 Hz, -CHOBn-), 3.71 and 3.69 (6H, 2s, -$C(CO_2CH_3)_2$-), 2.63 (1H, ddd, J_{AB} = 13.8 Hz, $J_{AX1} = J_{AX2}$ = 1.5 Hz, -CH(OBn)-CH_2-), 2.26 (1H, dd, J_{AB} = 13.8 Hz, J_{BX} = 10.4 Hz, -CH(OBn)-CH_2-), 2.18–2.13 (4H, m, =$C(CH_3)$-CH_2-CH_2-), 1.72 (3H, dd, $J_1 = J_2$ = 1.6 Hz, -CH=$C(CH_3)$-), ms m/e (70 eV): 332 (M^+), 241 (M^+ − CH_2Ph). Exact Mass (M^+) calcd: 332.1624; found: 332.1619.

*(3Z,9Z,11E)-5-Benzyloxy-13-[(tert-butyldiphenylsilyl)oxy]-1-methanesulfonyloxy-7,7-dimethoxycarbonyl-3-methyltrideca-3,9,11-triene (**23**)*

A solution of crude malonate **20***a* (65.8 mg, 0.154 mmol) in tetrahydrofuran (0.5 mL) and dimethylformamide (0.5 mL) was added at 0°C to a stirred suspension of sodium hydride (7.7 mg, 60% in oil, 0.193 mmol) in tetrahydrofuran (0.5 mL) and dimethylformamide (0.5 mL). After stirring for 0.5 h at room temperature the solution was cooled again to 0°C and then a solution of chloride **22** (7*e*) (86.4 mg, 0.232 mmol) in tetrahydrofuran (0.5 mL) and dimethylformamide (0.5 mL) was added at 0°C. The mixture was stirred for 10 h at room temperature and was then poured into a saturated solution of ammonium chloride and extracted with a mixture of hexane and ethyl ether (2:1). The combined organic layers were dried over magnesium sulfate, filtered, and concentrated. The residual oil was purified by column chromatography (25% to 50% of ethyl acetate in hexane) to afford the triene **23** (99.4 mg, 86%); ir (CH_2Cl_2) ν: 3070, 3010, 2945, 2855, 1732, 1425, 1360, 1265, 1110 cm^{-1}; ^1H nmr ($CDCl_3$) δ: 7.70–7.66, 7.46–7.34, and 7.28–7.16 (15H, 3m, -$OSi(C_6H_5)_2t$Bu, -O-$CH_2C_6H_5$), 6.48 (1H, dd, J = 15.7, 11.1 Hz, -CH=CH-CH=CH-CH_2OSiPh_2tBu), 6.11 (1H, dd, $J_1 = J_2$ = 11.1 Hz, -CH=CH-CH=CH-CH_2OSiPh_2tBu), 5.80 (1H, dt, J = 15.7, 5.1 Hz, -CH=CH-CH_2OSiPh_2tBu), 5.30 (1H, d, J = 9.4 Hz, -CH=$C(CH_3)$-), 5.25–5.14 (1H, m, -CH=CH-CH=CH-CH_2OSiPh_2tBu), 4.40 (1H, d, J_{AB} = 11.1 Hz, -OCH_2Ph), 4.27–4.12 (5H, m, -CH_2OSiPh_2tBu, -$CH_2OSO_2CH_3$, -CHOBn-), 4.16 (1H, d, J_{AB} = 11.1 Hz, -OCH_2Ph), 3.56 and 3.53 (6H, 2s, -$C(CO_2CH_3)_2$-), 2.97 (3H, s, -OSO_2CH_3), 2.87 (2H, d, J = 7.9 Hz, -$C(CO_2CH_3)_2$-CH_2-CH=), 2.55–2.35 (2H, m, =$C(CH_3)CH_2$-), 2.23 (1H, dd, J_{AB} = 14.8 Hz, J_{AX} = 10.3 Hz, -$C(CO_2CH_3)_2$-CH_2-CHOBn-), 2.01 (1H, dd, J_{AB} = 14.8 Hz, J_{BX} = 2.6 Hz, -$C(CO_2CH_3)_2$-CH_2-CHOBn-), 1.79 (3H, d, J = 1.3 Hz, -CH=$C(CH_3)$-), 1.06 (9H, s, -$OSiPh_2C(CH_3)_3$); ms m/e (70 eV): 705 (M^+ − tBu). Exact Mass (M^+ − tBu) calcd: 705.2553; found: 705.2558.

*Methyl (5Z,11Z,13E)-7-benzyloxy-15-[(tert-butyldiphenylsilyl)-oxy]-5-methyl-2,9,9-trimethoxycarbonylpentadeca-5,11,13-trienoate (**24**)*

Dimethyl malonate (100 μL, 0.875 mmol) was added at 0°C to a stirred suspension of sodium hydride (32.4 mg, 60% in oil, 0.810 mmol) in tetrahydrofuran (1 mL) and dimethylformamide (1 mL). The mixture was stirred at room temperature for 0.5 h and a solution of mesylate **23** (131.1 mg, 0.171 mmol) in tetrahydrofuran (1 mL) and dimethylformamide (1 mL) was added at 0°C. Potassium iodide (14 mg, 0.085 mmol) was then added and the mixture was heated at 85°C for 6 h, poured into a saturated solution of ammonium chloride, and extracted with a mixture of hexane and ethyl ether (2:1). The combined organic layers were dried over magnesium sulfate, filtered, and concentrated. The residual oil was purified by column chromatography (10% of ethyl acetate in hexane) to yield malonate **24** (112.9 mg, 83%); ir ($CHCl_3$) ν: 3020, 3000, 2950, 2940, 1730, 1432, 1205, 1110, 1075 cm^{-1}; ^1H nmr ($CDCl_3$) δ: 7.69–7.66, 7.46–7.35, and 7.28–7.09 (15H, m, -$OSi(C_6H_5)_2t$Bu and -$OCH_2C_6H_5$), 6.50 (1H, ddd, J = 15.0, 11.1, 1.0 Hz, -CH=CH-CH=CH-CH_2OSiPh_2tBu), 6.09 (1H, dd, $J_1 = J_2$ = 11.1 Hz, -CH=CH-CH=CH-CH_2OSiPh_2tBu), 5.79 (1H, dt, J = 15.0, 5.0 Hz, -CH=CH-CH_2SiPh_2tBu), 5.30–5.18 (1H, m,

Can. J. Chem. Downloaded from www.nrcresearchpress.com by 109.225.110.28 on 09/08/12
For personal use only.

-C*H*=CH-CH=CH-CH_2OSiPh_2tBu), 5.16 (1H, dq, J = 9.0, 1.2 Hz, -C*H*=C(CH_3)-), 4.38 (1H, d, J_{AB} = 11.0 Hz, -OCH_2Ph), 4.24 (2H, dd, J = 5.0, 0.9 Hz, -CH_2OSiPh_2tBu), 4.15 (1H, d, J_{AB} = 11.0 Hz, -OCH_2Ph), 4.11–4.22 (1H, m, -C*H*OBn-), 3.72, 3.71, 3.56, and 3.50 (12H, 4s, 4 × -CO_2CH_3), 3.32 (1H, t, J = 6.9 Hz, -C*H*(CO_2CH_3)$_2$), 2.99–2.77 (2H, m, -C(CO_2CH_3)$_2$-CH_2-CH=), 2.33–2.21 and 2.17–1.92 (6H, 2m, -CH_2-CH(CO_2CH_3)$_2$, -CHO-Bn-CH_2-, and =C(CH_3)-CH_2-), 1.75 (3H, d, J = 1.2 Hz, -CH=C(CH_3)-), 1.06 (9H, s, -OSiPh_2C(CH_3)$_3$); ms *m/e* (70 eV): 741 (M^+ − *t*Bu). Exact Mass (M^+ − *t*Bu) calcd: 741.3095; found: 741.3087.

*Methyl (5Z,11Z,13*E*)-7-benzyloxy-15-hydroxy-5-methyl-2,9,9-trimethoxycarbonylpentadeca-5,11,13-trienoate (25)*

Tetrabutylammonium fluoride (170 μL, 1 M in tetrahydrofuran, 0.170 mmol) was added at 0°C to a stirred solution of silyl ether **24** (112.4 mg, 0.141 mmol) in tetrahydrofuran (3.5 mL). The mixture was stirred at room temperature for 1.75 h and then the solvent was evaporated. The residual oil was purified by column chromatography (25% to 50% ethyl acetate in hexane) to afford alcohol **25** (67.7 mg, 87%); ir ($CHCl_3$) ν: 3600, 3010, 2950, 1730, 1435, 1230, 1070 cm^{-1}; ^{1}H nmr ($CDCl_3$) δ: 7.33–7.25 (5H, m, -O$CH_2C_6H_5$), 6.46 (1H, ddd, J = 15.2, 11.2, 1.2 Hz, -CH=CH-C*H*=CH-CH_2OH), 6.08 (1H, dd, J_1 = J_2 = 11.2 Hz, -CH=C*H*-CH=C*H*-CH_2OH), 5.85 (1H, dt, J = 15.2, 5.3 Hz, -CH=CH-CH_2OH), 5.28–5.18 (1H, m, -C*H*=CH-CH=CH-CH_2OH), 5.15 (1H, dq, J = 9.2, 1.3 Hz, -C*H*=C(CH_3)-), 4.40 (1H, d, J_{AB} = 11.1 Hz, -OCH_2Ph), 4.18 (2H, d, J = 5.3 Hz, -CH_2OH), 4.16 (1H, d, J = 11.1 Hz, -OCH_2Ph), 4.11 (1H, ddd, J_1 = J_2 = 9.7 Hz, J_3 = 2.7 Hz, -CHOBn-), 3.74, 3.73, 3.61 and 3.50 (12H, 4s, 4 × -CO_2CH_3), 3.32 (1H, t, J = 6.6 Hz, -CH(CO_2CH_3)$_2$), 2.89 (2H, d, J = 7.8 Hz, -C(CO_2CH_3)$_2$-CH_2-CH=), 2.35–2.22 and 2.06–1.92 (6H, 2m, -CH_2-CH(CO_2CH_3)$_2$, -CHOBn-CH_2, and =C(CH_3)-CH_2-), 1.75 (3H, d, J = 1.3 Hz, -CH=C(CH_3)-), 1.72 (1H, s, -CH_2OH); ms *m/e* (70 eV): 545 (M^+ − CH_3), 542 (M^+ − H_2O). Exact Mass (M^+ − CH_3) calcd: 545.2387; found: 545.2396.

*Methyl (5Z,11Z,13*E*)-7-benzyloxy-15-chloro-2,9,9-trimethoxycarbonyl-5-methylpentadeca-5,11,13-trienoate (26)*

s-Collidine (32 μL, 0.242 mmol) and methanesulfonyl chloride (19 μL, 0.242 mmol) were added at 0°C to a stirred solution of alcohol **25** (67.7 mg, 0.121 mmol) and lithium chloride (15.4 mg, 0.363 mmol) in dimethylformamide (1 mL). The mixture was stirred at 0°C for 2 h, was poured into water, and then extracted with a mixture of hexane and ethyl ether (2:1). The combined organic layers were washed with an aqueous solution of copper nitrate and with water, dried over magnesium sulfate, filtered, and concentrated. The crude chloride **26** (67.5 mg, 97%) residual oil was used immediately for the next reaction; ir ($CHCl_3$) ν: 2950, 2922, 2855, 1732, 1438, 1235, 1200, 1075 cm^{-1}; ^{1}H nmr ($CDCl_3$) δ: 7.33–7.26 (5H, m, -O$CH_2C_6H_5$), 6.47 (1H, ddd, J = 14.9, 11.2, 1.0 Hz, -CH=CH-C*H*=CH-CH_2Cl), 6.07 (1H, dd, J_1 = J_2 = 11.2 Hz, -CH=C*H*-CH=CH-CH_2Cl), 5.80 (1H, dt, J = 14.9, 7.4 Hz, -CH=C*H*-CH_2Cl), 5.40–5.30 (1H, m, -C*H*=CH-CH=CH-CH_2Cl), 5.16 (1H, dq, J = 9.8, 1.2 Hz, -C*H*=C(CH_3)-), 4.41 (1H, d, J_{AB} = 11.1 Hz, -OCH_2Ph), 4.17 (1H, d, J_{AB} = 11.1 Hz, -OCH_2Ph), 4.19–4.06 (1H, m, -C*H*OBn-), 4.07 (2H, d, J = 7.4 Hz, -CH_2Cl), 3.74, 3.73, 3.61, and 3.53 (12H, 4s, 4x -CO_2CH_3), 3.31 (1H, t, J = 7.0 Hz, -C*H*(CO_2CH_3)$_2$), 2.99–2.78 (2H, m, -C(CO_2CH_3)$_2$-CH_2-CH=), 2.28, 2.07–1.92, and 1.84 (6H, dd, J = 14.8, 10.4 Hz, m and s, -CH_2-CH(CO_2CH_3)$_2$, -CHOBn-CH_2, and =C(CH_3)-CH_2-), 1.76 (3H, d, J = 1.2 Hz, -CH=C(CH_3)-).

*(1*E*,3Z,9Z)-8-Benzyloxy-10-methyl-6,6,13,13-tetramethoxycarbonylcyclotetradeca-1,3,9-triene (5)*

To a stirred suspension of cesium carbonate (190.2 mg, 0.584 mmol) in tetrahydrofuran (12 mL) and dimethylformamide (12 mL) at 75°C, was added during 10 hs a solution of chloride **26** (67.5 mg, crude, 0.117 mmol) in tetrahydrofuran (12 mL) and dimethylformamide (12 mL). The mixture was stirred for 10 more hours, then was cooled at room temperature, filtered, and evaporated under vacuum. The residual oil was purified by column chromatography (hexane/ethyl/acetate/dichloromethane, 7.5:0.5:2–7:1:2) yielding carbocycle **5** (48.5 mg, 74%); mp 161–162°C; uv (hexane) λ_{max}: 232, 266 nm; ir ($CHCl_3$) ν: 3010, 2950, 1760, 1437, 1205, 1215, 1175 cm^{-1}; ^{1}H nmr ($CDCl_3$) δ: 7.40–7.31 (5H, m, -O$CH_2C_6H_5$), 6.08–5.94 (2H, m, -CH=C*H*-C*H*=CH-), 5.23–5.03 and 4.99–4.86 (2H, 2m, -C*H*=CH-CH=C*H*-), 5.02 (1H, d, J = 9.5 Hz, -C*H*=C(CH_3)), 4.44 (1H, d J_{AB} = 11.6 Hz, -OCH_2Ph), 4.05 (1H, d, J_{AB} = 11.6 Hz, -OCH_2Ph), 4.08–3.99 (1H, m, -C*H*OBn-), 3.77, 3.73, 3.71, and 3.49 (12H, 4s, 4x -CO_2CH_3), 2.98–2.74 (3H, m, -CH_2-CH=CH-CH=CH-CH_2-), 2.41 (1H, dd, J = 14.3, 11.9 Hz, -CH_2-CH=CH-), 2.33 (1H, dd, J = 14.6, 11.6 Hz, -CH(OBn)-CH_2-), 2.17–2.13 (2H m, -CH_2-C(CH_3)=), 1.74 (3H, d, J = 1.3 Hz, -CH=C(CH_3)-), 1.68 (1H, dd, J = 14.6, 2.6 Hz, -CHOBn-CH_2-), 1.42–1.23 (2H, m, -CH_2-CH_2-C(CH_3)=); ms *m/e* (70 eV): 542 (M^+). Exact Mass (M^+) calcd: 542.2516; found: 542.2517.

3β-Benzyloxy-1β-methyl-5,5,12,12-tetramethoxycarbonyl-trans-cisoid-cis-*tricyclo[8.4.0.0^{2,7}]tetradec-8-ene (6)*

A solution of macrocyclic triene **5** (R = CH_2Ph) (16.8 mg, 0.031 mmol) in toluene (0.2 mL) was heated in a sealed tube at 270°C for 2.75 h. The solvent was then evaporated and the residual oil was purified by column chromatography (10% to 25% ethyl acetate in hexane) to afford the tricyclic compound **6** (R = CH_2Ph) (14.2 mg, 85%) and a mixture of two other compounds (2.6 mg, 15%); mp 104–106°C; ir ($CHCl_3$) ν: 3020, 3030, 2955, 1730, 1435, 1455, 1220, 1250, 1265 cm^{-1}; ^{1}H nmr ($CDCl_3$) δ: 7.38–7.25 (5H, m, -O$CH_2C_6H_5$), 5.27 (2H, s, H-C8 and H-C9), 4.61 (1H, d, J_{AB} = 10.8 Hz, -OCH_2Ph), 4.43 (1H, d, J_{AB} = 10.8 Hz, -OCH_2Ph), 3.76 (1H, ddd, J_1 = J_2 = 9.9 Hz, J_3 = 4.4 Hz, -C*H*OBn-), 3.70, 3.69, 3.69, and 3.65 (12H, 4s, 4x -CO_2CH_3), 2.93–2.73 and 2.46–1.27 (13H, m H-C2, H-C4, H-C6, H-C7, H-C10, H-C11, H-C13, H-C14), 0.92 (3H, s, -CH_3-C1); ms *m/e* (70 eV): 542 (M^+), 511 (M^+ − OCH_3). Exact Mass (M^+ − OCH_3) calcd: 511.2332; found: 511.2319.

3β-Hydroxy-1β-methyl-5,5,12,12-tetramethoxycarbonyl-trans-cisoid-cis-*tricyclo[8.4.0.0^{2,7}]tetradec-8-ene and (1S,3S)-3-hydroxy-1-methyl-5,5,12,12-tetramethoxycarbonyl*-trans-cisoid-cis-*tricyclo[8.4.0.0^{2,7}]tetradec-8-ene (27)*

Tin tetrachloride (21 μL, 0.179 mmol) was added to a stirred solution of benzyl ether **6** (R = CH_2Ph) (5.4 mg, 0.010 mmol) in dichloromethane (1 mL). The mixture was stirred at room temperature for about 19 h,[4] poured into water, and extracted with dichloromethane. The combined organic layers were washed with brine, dried over magnesium sulfate, filtered, and concentrated. The residual oil was purified by column chromatography (40% of ethyl acetate in hexane) to afford alcohol **27** (3.9 mg, 87%).

2,3-Dichloro-5,6-dicyano-1,4-benzoquinone was added to a stirred solution of *para*-methoxybenzyl ether **6** (R = CH_2-$C_6H_4OCH_3$) (8.0 mg, 0.014 mmol) in dichloromethane (8 mL) and water (100 μL). The mixture was stirred at room temperature for 1.5 h, then was poured into water and extracted with dichloromethane. The residual oil was purified by column chromatography (25% to 50% ethyl acetate in hexane) to yield alcohol **27** (4.7 mg, 76%); $[\alpha]_D^{25}$ −88.5 (*c* 0.72, CH_2Cl_2); ir ($CHCl_3$) ν: 3600, 3020, 3010, 2950, 2920, 2850, 1727, 1455, 1450, 1435, 1255, 1245, 1205 cm^{-1}; ^{1}H nmr ($CDCl_3$) δ: 5.26–5.20 (2H, m, H-C8 and H-C9), 4.03 (1H, ddd, J_1 = J_2 = 9.5 Hz, J_3 = 4.8 Hz, -C*H*OH-) 3.78, 3.70, 3.69, 3.67 (12H, 4s, 4x -CO_2CH_3), 2.88–2.83 and 2.49–1.47 (13H, m, H-C2, H-C4, H-C6, H-C7, H-C10, H-C11, H-C13, and H-C14), 0.92 (3H, s, -CH_3-C1); ms *m/e* (70 eV): 434 (M^+ − H_2O). Exact Mass (M^+ − H_2O) calcd: 434.1941; found: 434.1937.

[4]Variable reaction times. In some cases lactone **29** was also isolated.

Can. J. Chem. Downloaded from www.nrcresearchpress.com by 109.225.110.28 on 09/08/12
For personal use only.

1β-Methyl-5,5,12,12-tetramethoxycarbonyl-trans-cisoid-cis-*tricyclo[8.4.0.0^{2,7}]tetradec-8-en-3-one and (1S)-1-methyl-5,5,12,12-tetramethoxycarbonyl*-trans-cisoid-cis-*tricyclo[8.4.0.0^{2,7}]tetradec-8-en-3-one (28)*

Pyridinium chlorochromate (10.4 mg, 0.048 mmol) was added to a stirred solution of alcohol **27** (7.3 mg, 0.016 mmol) in dichloromethane (1 mL). The mixture was stirred for 1.5 h at room temperature, poured into water, and extracted with dichloromethane. The combined organic layers were washed with water, dried over magnesium sulfate, filtered, and concentrated. The residual oil was purified by column chromatography (25% to 40% ethyl acetate in hexane) to yield ketone **28** (6.3 mg, 87%); mp 150–151°C (racemix mixture); $[\alpha]_D^{25}$ −93.2 (*c* 0.63, CH_2Cl_2); ir ($CHCl_3$) ν: 3020, 2955, 1730, 1435, 1260, 1220 cm^{-1}; ^{1}H nmr ($CDCl_3$) δ: 5.33–5.47 (2H, m, H-C8 and H-C9), 3.82, 3.74, 3.70, and 3.69 (12H, 4s, 4x -CO_2CH_3), 2.86 (1H, dd, J_{AB} = 14.7 Hz, J_W = 1.0 Hz, H-C4), 2.64 (1H, d, J_{AB} = 14.7 Hz, H-C4), 3.17–3.05 and 2.55–1.33 (11H, m, H-C2, H-C6, H-C7, H-C10, H-C11, H-C13, and H-C14), 0.90 (3H, s, -CH_3-C1); ms *m/e* (70 eV): 450 (M^+). Exact Mass (M^+) calcd: 450.1890; found: 450.1884.

1β-Methyl-5,5,12,12-tetramethoxycarbonyl-trans-transoid-trans-*tricyclo[8.4.0.0^{2,7}]tetradec-8-en-3-one and (1S)-methyl-5,5,12,12-tetramethoxycarbonyl*-trans-transoid-trans-*tricyclo[8.4.0.0^{2,7}]tetradec-8-en-3-one (7)*

Sodium carbonate (1.0 mg, 0.009 mmol) was added to a stirred solution of ketone **28** (3.1 mg, 0.007 mmol) in methanol (1 mL) and tetrahydrofuran (minimum amount necessary to solubilize ketone **28**). The mixture was heated at 65°C for 2.5 h, then poured into a saturated solution of ammonium chloride and extracted with dichloromethane. The combined organic layers were dried over magnesium sulfate, filtered, and concentrated. The residual oil was purified by column chromatography (25% of ethyl acetate in hexane) to afford ketone **7** (2.9 mg, 94%); mp 114–115°C (racemix mixture); $[\alpha]_D^{25}$ +14.4 (*c* 0.30, CH_2Cl_2); ir ($CHCl_3$) ν: 2955, 2920, 2850, 1730, 1435, 1455, 1465, 1250, 1220 cm^{-1}; ^{1}H nmr ($CDCl_3$) δ: 5.47 (1H, ddd, J_{AB} = 10.2 Hz, J_{BX1} = J_{BX2} = 2.2 Hz, H-C8 or H-C9), 5.37 (1H, dm, J_{AB} = 10.2 Hz, H-C8 or H-C9), 3.75, 3.74, 3.73, and 3.70 (12H, 4s, 4x -CO_2CH_3), 2.91 (1H, dd, J_{AB} = 14.0 Hz, J_W = 2.2 Hz, H-C4), 2.62 (1H, dd, J_{AB} = 14.0 Hz, J_W = 1.1 Hz, H-C4), 2.61–1.05 (11H, m, H-C2, H-C6, H-C7, H-C10, H-C11, H-C13, and H-C14), 0.95 (3H, s, -CH_3-C1); ms *m/e* (70 eV): 450 (M^+). Exact Mass (M^+) calcd: 450.1890, found: 450.1884.

1β-Methyl-5,12,12-trimethoxycarbonyl-trans-cisoid-cis-*tricyclo[8.4.0.0^{2,7}]tetradec-8-ene-5,3β-carbolactone (29)*

para-Toluenesulfonic acid (1.0 mg, 0.005 mmol) was added to a stirred solution of alcohol **27** (1.0 mg, 0.002 mmol) in benzene (0.5 mL). The mixture was heated at 65°C for 1.5 h, poured into a solution of sodium bicarbonate (5%), and extracted with dichloromethane. The combined organic layers were dried over magnesium sulfate, filtered, and concentrated. The residual oil was purified by column chromatography (25% of ethyl acetate in hexane) to yield lactone **29** (0.8 mg, 86%); ir ($CHCl_3$) ν: 3015, 2950, 2920, 1780, 1730, 1450, 1435, 1255, 1220 cm^{-1}; ^{1}H nmr ($CDCl_3$) δ: 5.58 (1H, ddd, J_{AB} = 9.8 Hz, J_{BX1} = J_{BX2} = 2.3 Hz, H-C8 or H-C9), 5.35 (1H, dm, J_{AB} = 9.8 Hz, H-C9 or H-C8), 4.82 (1H, d, *J* = 4.3 Hz, H-C3), 3.78, 3.77, 3.72 (9H, 3s, 3x -CO_2CH_3), 2.81–1.28 (13H, m, H-C2, H-C4, H-C6, H-C7, H-C10, H-C11, H-C13, and H-C14), 0.94 (3H, s, -CH_3-C1); ms *m/e* (70 eV): 420 (M^+). Exact Mass (M^+) calcd: 420.1784; found: 420.1781.

2-Carboxy-1-methylethyltriphenylphosphonium bromide (31)

A stirred mixture of triphenylphosphine (28.88 g, 0.110 mmol) and 3-bromobutanoic acid **30** (18.39 g, 0.110 mmol) in toluene (250 mL) was heated at reflux for 24 h. The solid was filtered and washed with toluene to afford phosphonium salt **31** (44.48 g, 94% crude); ir ($CHCl_3$) ν: 3500–2400, 3030, 3010, 2955, 1730, 1440, 1215 cm^{-1}; ^{1}H nmr ($CDCl_3$) δ: 8.30 (1H, s, -COO*H*), 7.86–7.69 (15H, m, aromatic protons), 4.61–4.40 (1H, m, $Br^-P^+Ph_3$-$CH(CH_3)$-), 3.18–2.87 (2H, m, -CH_2-CO_2H), 1.41 (3H, dd, *J* = 18.8, 6.9 Hz, $Br^-P^+Ph_3CH(CH_3)$-).

2-Methoxycarbonyl-1-methyltriphenylphosphonium iodide (32)

Sodium iodide (22.54 g, 0.150 mmol), sodium carbonate (10.62 g, 0.100 mmol), and iodomethane (12.5 mL, 0.2 mol) were added to a stirred solution of phosphonium bromide **31** (43.00 g, 0.100 mol) in acetone (1 L). The mixture was heated at reflux for 12 h. The solvent was then evaporated and the residue was dissolved in dichloromethane. After filtration and evaporation of the solvent, the residue was purified by recrystallization from dichloromethane and hexane to afford phosphonium salt **32** (39.85 g, 81%); mp 163–165°C; ir ($CHCl_3$) ν: 3010, 2935, 1735, 1588, 1485, 1455, 1440, 1230, 1215, 1105 cm^{-1}; ^{1}H nmr ($CDCl_3$) δ: 7.93–7.71 (15H, m, aromatic protons), 4.90–4.73 (1H, m, $I^-P^+Ph_3$-$CH(CH_3)$-) 3.71 (3H, s, -CO_2CH_3), 2.92 (1H, ddd, J_1 = J_2 = 15.6 Hz, J_3 = 2.9 Hz, -$CH_2CO_2CH_3$), 2.40 (1H, m, -$CH_2CO_2CH_3$), 1.50 (3H, dd, *J* = 18.6, 7.0 Hz, $I^-P^+Ph_3$-$CH(CH_3)$-).

3-Hydroxy-1-methylpropyltriphenylphosphonium iodide (33a)

Diisobutylaluminium hydride (5.0 mL, 7.52 mmol) was added at −78°C to a stirred solution of ester **32** (1.229 g, 2.51 mmol) in dichloromethane (20 mL). The mixture was stirred at −78°C for 2 h. Decahydrated sodium sulfate (775 mg, 2.41 mmol) was then added at −78°C and the mixture was allowed to warm up slowly to room temperature. After stirring for 12 h, anhydrous sodium sulfate was added and the salts were filtered and washed with acetone. The filtrate was concentrated and the residual solid was recrystallized from hexane and dichloromethane to yield phosphonium salt **33** (0.717 g, 62%); mp 219–221°C, ir ($CHCl_3$) ν: 3350, 3020, 2950, 1440, 1215, 1112 cm^{-1}; ^{1}H nmr ($CDCl_3$) δ: 7.95–7.86 and 7.78–7.65 (15H, m, aromatic protons), 5.12–4.96 (1H, m, $I^-P^+Ph_3$-$CH(CH_3)$-), 4.48 (1H, dd, *J* = 7.7, 6.6 Hz, -CH_2OH), 4.04–3.92 and 3.80–3.71 (2H, 2m, -CH_2OH), 2.28–2.13 (1H, m, -CH_2-CH_2OH), 1.40 (3H, dd, *J* = 19.5, 6.8 Hz, $I^-P^+Ph_3$-$CH(CH_3)$-), 1.03–1.12 (-CH_2-CH_2OH).

3-Hydroxy-1-methylpropyltriphenylphosphonium bromide (33b)

Pyridinium *para*-toluenesulfonate (861 mg, 3.43 mmol) was added to a stirred solution of phosphonium bromide **14** (17.10 g, 34.27 mmol) in methanol (250 mL). The solution was heated at 50°C for 18 h and then sodium bicarbonate (0.864 g, 10.29 mmol) was added. The mixture was filtered and the filtrate was evaporated. The residual solid was dissolved in dichloromethane and the mixture was again filtered. After evaporation of the filtrate, the residual solid was recrystallized from dichloromethane and hexane to yield phosphonium salt **33***b* (11.81 g, 83%).[5]

(2R)-1,2-O-Isopropylidene-4-methylhex-3-en-1,2,6-triol (35)

Butyllithium (30.2 mL, 1.6 M in hexane, 48.3 mmol) was added at −78°C to a stirred suspension of phosphonium bromide **33** (10.06 g, 24.2 mmol, dried under vacuum at 115–120°C for 48 h) in tetrahydrofuran (62 mL). The temperature was allowed to reach 0°C and the solution was stirred until it became dark red (≈0.5 h). A solution of aldehyde **34** (5.43 g, 41.8 mmol) in tetrahydrofuran (62 mL) was then added at 0°C. After 10 min, the mixture was poured into a saturated solution of ammonium chloride and extracted with dichloromethane and with ethyl acetate. The combined organic layers were dried over magnesium sulfate, filtered, and concentrated. The residual oil was purified by column chromatography (25% ethyl acetate in hexane) to afford *Z* olefin **35***a*[6] (2.23 g, 50%)[7] and *E* olefin **35***b*[6] (0.443 g, 10%)[7]; $[\alpha]_D^{25}$, *E* isomer −12.2 (*c* 4.20, $CHCl_3$); ir ($CHCl_3$) ν, *Z* isomer: 3610, 3480, 3005, 2980, 2930, 2870, 1445, 1370, 1380, 1215, 1155, 1050 cm^{-1}; ir ($CHCl_3$) ν, *E* isomer: 3610, 3480, 3005, 2985, 2935, 2870, 1450, 1320, 1330, 1235, 1228, 1155, 1150 cm^{-1}; ^{1}H nmr ($CDCl_3$) δ, *Z* isomer: 5.39 (1H, d, *J* = 8.5 Hz, -C*H*=C(CH_3)-), 4.78 (1H,

[5]Spectral data are identical with those obtained for **33***a*.

[6]Volatile compounds.

[7]Yield calculated from phophonium salt **33**.

Can. J. Chem. Downloaded from www.nrcresearchpress.com by 109.225.110.28 on 09/08/12
For personal use only.

ddd, $J_1 = J_2 = 8.2$ Hz, $J_3 = 5.9$ Hz, -OCH$_2$-C*H*-O-), 4.06 (1H, dd, $J_{AB} = 8.0$ Hz, $J_{AX} = 5.9$ Hz, -OC*H*$_2$-CH-O-), 3.69 (2H, t, $J = 6.2$ Hz, -C*H*$_2$OH), 3.56 (1H, dd, $J_{AB} = 8.0$ Hz, $J_{BX} = 8.0$ Hz, -OC*H*$_2$-CH-O-), 2.52–2.30 (2H, m, -C*H*$_2$-CH$_2$OH), 1.79 (3H, d, $J = 1.4$ Hz, -CH=C(C*H*$_3$)-), 1.41 and 1.38 (6H, 2s, -O-C(C*H*$_3$)$_2$-O-), 1.96 (1H, s, -CH$_2$O*H*); ^{13}C nmr (CDCl$_3$) δ, *Z* isomer: 23.6, 25.8, 26.6, 35.5, 60.0, 69.4, 72.3, 108.8, 124.9, 139.3; ^{1}H nmr (CDCl$_3$) δ, *E* isomer: 5.28 (1H, dq, $J = 8.6$, 1.3 Hz, -C*H*=C(CH$_3$)-), 4.80 (1H, ddd, $J_1 = J_2 = 8.3$ Hz, $J_3 = 5.9$ Hz, -OCH$_2$-C*H*-O-), 4.06 (1H, dd, $J_{AB} = 8.1$ Hz, $J_{AX} = 5.9$ Hz, -OC*H*$_2$-CH-O-), 3.70 (2H, t, $J = 6.4$ Hz, -C*H*$_2$OH), 3.50 (1H, dd, $J_{AB} = 8.1$ Hz, $J_{BX} = 8.1$ Hz, -OC*H*$_2$-CH-O-), 2.29 (2H, td, $J = 6.4$, 1.1 Hz, -C*H*$_2$-CH$_2$OH), 1.74 (3H, d, $J = 1.4$ Hz, -CH=C(C*H*$_3$)-), 1.41 and 1.38 (6H, 2s, -O-C(C*H*$_3$)$_2$-O-); ^{13}C nmr (CDCl$_3$) δ, *E* isomer: 16.6, 25.9, 26.9, 42.5, 60.2, 69.4, 72.7, 108.9, 124.6, 138.4; ms *m/e* (70 eV): 186 (M$^+$), 171 (M+ − CH$_3$). Exact Mass (M$^+$) calcd: 186.1256; found: 186.1254.

*(2R)-(3Z)-6-Benzoyloxy-1,2-O-isopropylidene-4-methylhex-3-ene-1,2-diol (**41**)*

Triethylamine (225 μL, 1.62 mmol), benzoyl chloride (150 μL, 1.30 mmol), and dimethylaminopyridine (26 mg, 0.22 mmol) were added at 0°C to a stirred solution of alcohol **35***a* (0.201 g, 1.08 mmol) in dichloromethane (11 mL). The mixture was stirred at 0°C for 1.5 h, then poured into a saturated solution of ammonium chloride and extracted with dichloromethane. The combined organic layers were dried with magnesium sulfate, filtered, and concentrated. The residual oil was purified by column chromatography (40% ethyl acetate in hexane) to yield benzoate **41** (0.280 g, 89%); $[\alpha]_D^{25}$ −0.9 (*c* 1.30, CHCl$_3$), ir (CHCl$_3$) *ν*: 3020, 2990, 2940, 1718, 1455, 1280, 1250, 1220, 1115, 1058 cm^{-1}; ^{1}H nmr (CDCl$_3$) δ: 8.05–8.01, 7.59–7.53, and 7.46–7.40 (5H, 3m, -OCOC$_6$*H*$_5$), 5.34 (1H, d, $J = 8.9$ Hz, -C*H*=C(CH$_3$)-), 4.82 (1H, ddd, $J_1 = J_2 = 8.1$ Hz, $J_3 = 6.0$ Hz, -OCH$_2$-C*H*-O-), 4.39 (2H, td, $J = 6.6$, 1.2 Hz, -C*H*$_2$OBz), 3.96 (1H, dd, $J_{AB} = 8.1$ Hz, $J_{AX} = 6.0$ Hz, -OC*H*$_2$-CH-O-), 3.46 (1H, dd, $J_{AB} = 8.1$ Hz, $J_{BX} = 8.1$ Hz, -OC*H*$_2$-CH-O-), 2.72–2.47 (2H, m, -C*H*$_2$OBz), 1.86 (3H, d, $J = 1.5$ Hz, -CH=C(C*H*$_3$)-), 1.40 and 1.36 (6H, 2s, -O-C(C*H*$_3$)$_2$-O-); ms *m/e* (70 eV): 290 (M$^+$), 275 (M$^+$ − CH$_3$). Exact Mass (M$^+$) calcd: 290.1518; found: 290.1524.

*(2R)-(3Z)-6-Benzoyloxy-4-methylhex-3-en-1,2-diol (**42**)*

para-Toluenesulfonic acid monohydrate (55 mg, 0.29 mmol) was added at 0°C to a stirred solution of acetonide **41** (0.280 g, 0.96 mmol) in methanol (23 mL). The mixture was stirred at room temperature for 1.5 h, then poured into a saturated solution of sodium chloride and extracted with dichloromethane. The combined organic layers were dried with magnesium sulfate, filtered, and concentrated. The residual oil was purified by column chromatography (80% of ethyl acetate in hexane then pure ethyl acetate) to afford diol **42** (0.212 g, 87%); mp 47–48°C; $[\alpha]_D^{25}$ −8.9 (*c* 1.06, CHCl$_3$); ir (CHCl$_3$) *ν*: 3600, 3010, 2965, 2935, 1718, 1450, 1275, 1215, 1118 cm^{-1}; ^{1}H nmr (CDCl$_3$) δ: 8.05–8.01, 7.60–7.54, 7.48–7.42 (5H, 3m, -OCOC$_6$*H*$_5$), 5.34 (1H, d, $J = 9.5$ Hz, -C*H*=C(CH$_3$)-), 4.57–4.47 (1H, m, -C*H*OH-), 4.42 (2H, t, $J = 6.8$ Hz, -C*H*$_2$OCOPh), 3.62–3.42 (2H, m, -C*H*$_2$OH), 2.61 (2H, t, $J = 6.8$ Hz, -C*H*$_2$CH$_2$OBz), 2.07 (1H, d, $J = 3.1$ Hz, -CHO*H*-), 1.94 (1H, t, $J = 5.7$ Hz, -CH$_2$O*H*), 1.84 (3H, d, $J = 1.1$ Hz, -CH=C(C*H*$_3$)-); ms *m/e* (70 eV): 219 (M$^+$ −CH$_2$OH).

*(2R)-(3Z)-6-Benzoyloxy-1-[(para-toluenesulfonyl)oxy]-4-methylhex-3-en-2-ol (**43**)*

Triethylamine (110 μL, 0.79 mmol), *para*-toluenesulfonyl chloride (0.179 g, 0.94 mmol), and dimethylaminopyridine (70 mg, 0.58 mmol) were added at 0°C to a stirred solution of diol **42** (0.180 g, 0.72 mmol) in dichloromethane (18 mL). The mixture was stirred at 0°C for 1.5 h, then poured into a saturated solution of ammonium chloride and extracted with dichloromethane. The combined organic layers were dried over magnesium sulfate, filtered, and concentrated. The residual oil was purified by column chromatography (25% to 50% ethyl acetate in hexane, then pure ethyl acetate) to give tosylate **43** (0.210 g, 72%) and diol **42** (25.3 mg, 14%); $[\alpha]_D^{25}$ −33.8 (*c* 1.71, CHCl$_3$); ir (CHCl$_3$) *ν*: 3590, 3020, 2950, 1717, 1600, 1452, 1365, 1275, 1220, 1190, 1175, 1120, 1100 cm^{-1}; ^{1}H nmr (CDCl$_3$) δ: 8.02–7.98, 7.79–7.76, 7.61–7.54, 7.47–7.41, and 7.34–7.31 (9H, 5m, -OCOC$_6$*H*$_5$, -CH$_2$OSO$_2$-C$_6$*H*$_4$CH$_3$), 5.23 (1H, d, $J = 9.0$ Hz, -C*H*=C(CH$_3$)-), 4.72–4.62 (1H, m, -C*H*OH-), 4.37 (2H, t, $J = 6.8$ Hz, -C*H*$_2$OCOPh), 4.01–3.86 (2H, m, -C*H*$_2$OTs), 2.53 (2H, td, $J = 6.8$, 2.2 Hz, -C*H*$_2$CH$_2$OCOPh), 2.43 (3H, s, -OSO$_2$C$_6$H$_4$C*H*$_3$), 2.11 (1H, d, $J = 3.6$ Hz, -CHO*H*-), 1.80 (3H, d, $J = 1.4$ Hz, -CH=C(C*H*$_3$)-).

*(2R)-(3Z)-6-Benzoyloxy-2-[(para-methoxybenzyl)oxy]-1-[(para-toluenesulfonyl)oxy]-4-methylhex-3-ene (**44**)*

A solution of trichloro-*para*-methoxybenzylacetimidate (0.569 g, 2.01 mmol) in ethyl ether (1 mL) was added to a solution of alcohol **43** (0.204 g, 0.50 mmol) in ethyl ether (20 mL). The mixture was cooled to 0°C and trifluoromethanesulfonic acid (40 μL, solution 1 μL in 1 mL of ethyl ether, 0.0005 mmol) was added. The mixture was stirred at 0°C for 3 h, then poured into a saturated solution of sodium carbonate and extracted with dichloromethane. The combined organic layers were dried over magnesium sulfate, filtered, and concentrated. The residual oil was purified by column chromatography (25% of ethyl acetate in hexane and 2% acetone in toluene) to afford ether **44** (0.214 g, 73%); $[\alpha]_D^{25}$ −8.5 (*c* 1.30, CHCl$_3$); ir (CHCl$_3$) *ν*: 3020, 2930, 1718, 1612, 1600, 1515, 1450, 1360, 1275, 1250, 1212, 1178 cm^{-1}; ^{1}H nmr (CDCl$_3$) δ: 8.02–7.99, 7.76–7.73, 7.59–7.53, 7.46–7.40, 7.28–7.25, 7.14–7.11, and 6.84–6.80 (13H, 7m, -OCOC$_6$*H*$_5$, -OSO$_2$C$_6$*H*$_4$CH$_3$, -OCH$_2$C$_6$*H*$_4$OCH$_3$), 5.14 (1H, d, $J = 9.1$ Hz, -C*H*=C(CH$_3$)-), 4.42 (1H, d, $J_{AB} = 11.3$ Hz, -OC*H*$_2$C$_6$H$_4$OCH$_3$), 4.38–4.30 (1H, m, -C*H*(OMPM)-), 4.32 (2H, t, $J = 7.0$ Hz, -C*H*$_2$OCOPh), 4.24 (1H, d, $J_{AB} = 11.3$ Hz, -OC*H*$_2$C$_6$H$_4$OCH$_3$), 4.03–3.92 (2H, m, -C*H*$_2$OTs), 3.78 (3H, s, -OCH$_2$C$_6$H$_4$OC*H*$_3$), 2.46 (2H, t, $J = 7.0$ Hz, -C*H*$_2$-CH$_2$OBz), 2.40 (3H, s, -OSO$_2$C$_6$H$_4$C*H*$_3$), 1.83 (3H, d, $J = 1.2$ Hz, -CH=C(C*H*$_3$)-).

*(2R)-(3Z)-6-Benzoyloxy-1-iodo-2-[(para-methoxybenzyl)oxy]-4-methylhex-3-ene (**45**)*

Sodium iodide (183 mg, 1.221 mmol) and tetrabutylammonium iodide (680 mg, 1.854 mmol) were added to a stirred solution of tosylate **44** (32.0 mg, 0.061 mmol) in acetone (5 mL) and the mixture stirred for 70 h at 50°C. The solvent was then evaporated and the residual solid was purified by column chromatography (25% of ethyl acetate in hexane) to yield iodide **45** (28.9 mg, 99%); $[\alpha]_D^{25}$ +10.1 (*c* 1.34, CHCl$_3$); ir (CHCl$_3$) *ν*: 3010, 1718, 1515, 1278, 1215 cm^{-1}; ^{1}H nmr (CDCl$_3$) δ: 8.03–8.00, 7.59–7.52, 7.46–7.40, 7.27–7.22, and 6.87–6.83 (9H, 5m, -OCOC$_6$*H*$_5$ and -OCH$_2$C$_6$*H*$_4$OCH$_3$), 5.25 (1H, d, $J = 9.0$ Hz, -C*H*=C(CH$_3$)-), 4.49 (1H, d, $J_{AB} = 11.3$ Hz, -OC*H*$_2$C$_6$H$_4$OCH$_3$), 4.40 (2H, dt, $J_1 = J_2 = 6.9$ Hz, -C*H*$_2$OCOPh), 4.34 (1H, d, $J_{AB} = 11.3$ Hz, -OC*H*$_2$C$_6$H$_4$OCH$_3$), 4.22–4.14 (1H, m, -C*H*(OMPM)-), 3.78 (3H, s, -OCH$_2$C$_6$H$_4$OC*H*$_3$), 3.24–3.09 (2H, m, -CH$_2$I), 2.53 (2H, td, $J = 6.9$, 3.8 Hz, -C*H*$_2$-CH$_2$OBz), 1.89 (3H, d, $J = 1.4$ Hz, -CH=C(C*H*$_3$)-); ms *m/e* (70 eV): 480 (M$^+$), 449 (M$^+$−OCH$_3$), 342 (M$^+$−I). Exact Mass (M$^+$) calcd: 480.0799; found: 480.0788.

*Methyl (4S)-(5Z)-8-benzoyloxy-4-[(para-methoxybenzyl)oxy]-2-methoxycarbonyl-6-methyloct-5-enoate (**46**)*

The same procedure as used for **18***a* was applied using the following quantities: sodium hydride (0.133 g, 50% in oil, 2.76 mmol), dimethyl malonate (335 μL, 2.93 mmol), tosylate **44** (0.270 g, 0.51 mmol), potassium iodide (111 mg, 0.67 mmol), tetrahydrofuran (15 mL), dimethylformamide (15 mL), and afforded malonate **46** (0.179 g, 72%) and unreacted tosylate (28.3 mg, 10%).

Similarly, the above procedure was applied using iodide **45** and the following quantities: sodium hydride (16 mg, 60% in oil, 0.400 mmol), dimethyl malonate (48 μL, 0.42 mmol), iodide (28.9 mg, 0.060 mmol), tetrahydrofuran (1.5 mL), dimethylformamide (1.5 mL). Malonate **46** (22.3 mg, 77%) and unreacted iodide (3.3 mg, 11%) were obtained; $[\alpha]_D^{25}$ −16.8 (*c* 1.20, CHCl$_3$);

Can. J. Chem. Downloaded from www.nrcresearchpress.com by 109.225.110.28 on 09/08/12
For personal use only.

ir ($CHCl_3$) ν: 3020, 2958, 2858, 1730, 1715, 1610, 1512, 1450, 1440, 1272, 1248, 1215 cm^{-1}; ^1H nmr ($CDCl_3$) δ: 8.04–8.00, 7.57–7.51, 7.44–7.38, 7.18–7.15, and 6.85–6.81 (9H, 5m, -OCO-C_6H_5, -$OCH_2C_6H_4OCH_3$), 5.27 (1H, dq, J = 9.0, 1.2 Hz, -CH=$C(CH_3)$-), 4.41 (1H, d, J_{AB} = 11.3 Hz, -$OCH_2C_6H_4OCH_3$), 4.39 (2H, td, J = 6.9, 2.0 Hz, -CH_2OBz), 4.15 (1H, d, J_{AB} = 11.3 Hz, -$OCH_2C_6H_4OCH_3$), 4.20–4.11 (1H, m, -CH(OMPM)-), 3.77 (3H, s, -$OCH_2C_6H_4OCH_3$), 3.67 and 3.64 (6H, 2s, -CO_2CH_3), 3.62 (1H, t, J = 6.2 Hz, -$CH(CO_2CH_3)_2$), 2.52 (2H, t J = 6.9 Hz, -CH_2-CH_2OBz), 2.22–2.00 (2H, m, -CH_2-$CH(CO_2CH_3)_2$), 1.87 (3H, d, J = 1.2 Hz, -CH=$C(CH_3)$-); ms m/e (70 eV): 484 (M^+), 469 (M^+-CH_3), 453 (M^+-OCH_3). Exact Mass (M^+) calcd: 484.2097; found: 484.2082.

*(5S)-(3Z,9Z,11E)-1-Benzoyloxy-13-[(*tert-*butyldiphenylsilyl)oxy]-5-[(*para-*methoxybenzyl)oxy]-7,7-dimethoxycarbonyl-3-methyltrideca-3,9,11-triene (**47**)*

The procedure employed for **23** was applied using the following quantities: malonate **46** (0.295 g, 0.61 mmol), sodium hydride (35 mg, 50% in oil, 0.73 mmol), chloride **22** (7*e*) (0.207 g, 0.73 mmol), tetrahydrofuran (2 × 3.5 mL), dimethylformamide (2 × 3.5 mL), and afforded triene **47** (0.432 g, 87%); $[\alpha]_D^{25}$ +23.4 (*c* 1.15, $CHCl_3$); ir ($CHCl_3$) ν: 3025, 2955, 2940, 2860, 1735, 1518, 1440, 1280, 1250, 1205, 1115 cm^{-1}; ^1H nmr ($CDCl_3$) δ: 8.03–7.99 (2H, m, -$OCOC_6H_5$), 7.69–7.63 (4H, m, -$OSi(C_6H_5)_2tBu$), 7.55–7.48 (1H, m, -$OCOC_6H_5$), 7.42–7.33 (8H, m, -$OSi(C_6H_5)_2tBu$ and -$OCOC_6H_5$), 7.18–7.12 and 6.83–6.77 (4H, 2m, -OC_6H_4-OCH_3), 6.53 (1H, ddd, J = 15.0, 11.0, 0.9 Hz, -CH=CH-CH=CH_2OSiPh_2tBu), 6.04 (1H, dd, J_1 = J_2 = 11.1 Hz, -CH=CH-CH=CH-CH_2OSiPh_2tBu), 5.75 (1H, dt, J = 15.0, 5.0 Hz, -CH=CH-CH=CH_2OSiPh_2tBu), 5.27 (1H, dq, J = 8.0, 1.1 Hz, -CH=$C(CH_3)$-), 5.25–5.16 (1H, m, -CH=CH-CH=CH-CH_2OSiPh_2tBu), 4.38–4.04 (7H, m, -CH(OMPM)-, -CH_2OSiPh_2tBu, -$OCH_2C_6H_4OCH_3$, and -CH_2OBz), 3.75 (3H, s, -$OCH_2C_6H_4OCH_3$), 3.57 and 3.48 (6H, 2s, 2 × -CO_2CH_3), 2.89 (2H, d, J = 7.6 Hz, -$C(CO_2CH_3)_2$-CH_2-CH=CH-), 2.52 (2H, t, J = 6.9 Hz, -CH_2-CH_2OBz), 2.29 (1H, dd, J_{AB} = 14.8 Hz, J_{AX} = 10.4 Hz, -CH(OMPM)-CH_2-), 2.03 (1H, dd, J_{AB} = 14.8 Hz, J_{BX} = 2.6 Hz, -CH(OMPM)-CH_2-), 1.85 (3H, d, J = 1.1 Hz, -CH=$C(CH_3)$-), 1.05 (9H, s, -$OSiPh_2C(CH_3)_3$); ms m/e (70 eV): 818 (M^+), 761 (M^+-tBu). Exact Mass (M^+-tBu) calcd: 761.3146; found: 761.3140.

*(5S)-(3Z,9Z,11E)-13-[(*tert-*Butyldiphenylsilyl)oxy]-5-[(*para-*methoxybenzyl)oxy]-7,7-dimethoxycarbonyl-3-methyltrideca-3,9,11-trien-1-ol (**48**)*

Potassium carbonate (73 mg, 0.53 mmol) was added to a stirred solution of benzoate **47** (0.432 g, 0.53 mmol) in methanol (35 mL), the stirring being continued at 65°C for 4 h. After dilution in dichloromethane, the solution was poured into a saturated solution of ammonium chloride and extracted with dichloromethane. The combined organic layers were dried over magnesium sulfate, filtered, and concentrated. The residual oil was purified by column chromatography (25% to 50% of ethyl acetate in hexane) to afford alcohol **48** (0.352 g, 94%); $[\alpha]_D^{25}$ +33.0 (*c* 1.84, $CHCl_3$); ir ($CHCl_3$) ν: 3600, 3020, 2960, 2935, 2860, 1730, 1518, 1440, 1430, 1250, 1220, 1115 cm^{-1}; ^1H nmr ($CDCl_3$) δ: 7.70–7.66 and 7.42–7.35 (10H, 2m, -$OSi(C_6H_5)_2tBu$), 7.24–7.19 and 6.84–6.79 (4H, 2m, -$OCH_2C_6H_4$-OCH_3), 6.51 (1H, dd, J = 15.1, 11.1 Hz, -CH=CH-CH_2OSiPh_2tBu), 6.10 (1H, dd, J_1 = J_2 = 11.1 Hz, -CH=CH-CH=CH-CH_2OSiPh_2tBu), 5.80 (1H, dt, J = 15.1, 5.2 Hz, -CH=CH-CH_2OSiPh_2tBu), 5.17 (2H, m, -CH=C-(CH_3)-, -CH=CH-CH=CH-CH_2OSiPh_2tBu), 4.35 (1H, d, J_{AB} = 10.7 Hz, -$OCH_2C_6H_4OCH_3$), 4.24–4.14 (3H, m, -CH(OMPM)-, -CH_2OSiPh_2tBu), 4.10 (1H, d, J_{AB} = 10.7 Hz, -$OCH_2C_6H_4OCH_3$), 3.75 (3H, s, -$OCH_2C_6H_4OCH_3$), 3.69–3.60 (2H, m, -CH_2OH), 3.58 and 3.52 (6H, 2s, 2 × -CO_2CH_3), 2.97–2.78 (2H, m, -$C(CO_2CH_3)_2$-CH_2-CH=CH-), 1.99–1.48 (4H, m, -CH(OMPM)-CH_2- and =$C(CH_3)$-CH_2), 1.78 (3H, d, J = 1.2 Hz, -CH=$C(CH_3)$-), 1.07 (9H, s, -$OSiPh_2C(CH_3)_3$); ms m/e (70 eV): 657 (M^+-tBu).

*(5S)-(3Z,9Z,11E)-13-[(*tert-*Butyldiphenylsilyl)oxy]-1-methanesulfonyloxy-5-[(*para-*methoxybenzyl)oxy]-7,7-dimethoxycarbonyl-3-methyltrideca-3,9,11-triene (**49**)*

The procedure described for **17***a* was applied using the following quantities: alcohol **48** (0.352 g, 0.49 mmol), methanesulfonyl chloride (46 μL, 0.59 mmol), triethylamine (103 μL, 0.74 mmol), dichloromethane (10 mL), and yielded mesylate **49** (0.379 g, 97%); $[\alpha]_D^{25}$ +25.4 (*c* 1.12, $CHCl_3$); ir ($CHCl_3$) ν: 3015, 2955, 2930, 2860, 1730, 1612, 1515, 1428, 1438, 1250, 1205, 1175 cm^{-1}; ^1H nmr ($CDCl_3$) δ: 7.70–7.64 and 7.43–7.34 (10H, m, -$OSi(C_6H_5)_2tBu$), 7.22–7.17 and 6.85–6.80 (4H, m, -$OCH_2C_6H_4OCH_3$), 6.53 (1H, dd, J = 15.0, 11.4 Hz, -CH=CH-CH_2OSiPh_2tBu), 6.11 (1H, dd, J_1 = J_2 = 11.4 Hz, -CH=CH-CH=CH-CH_2OSiPh_2tBu), 5.80 (1H, dt, J = 15.0, 5.0 Hz, -CH=CH-CH_2-$OSiPh_2tBu$), 5.30 (1H, d, J = 8.6 Hz, -CH=$C(CH_3)$-), 5.26–5.17 (1H, m, -CH=CH-CH=CH-CH_2OSiPh_2tBu), 4.33 (1H, d, J_{AB} = 10.7 Hz, -$OCH_2C_6H_4OCH_3$), 4.26–4.15 (5H, m, -CH_2OMs, -CH_2OSiPh_2tBu, and -CH(OMPM)-), 4.10 (1H, d, J_{AB} = 10.7 Hz, -$OCH_2C_6H_4OCH_3$), 3.76 (3H, s, -$OCH_2C_6H_4OCH_3$), 3.56 and 3.52 (6H, 2s, 2 × -CO_2CH_3), 2.97 (3H, s, -OSO_2CH_3), 2.87 (2H, d, J = 8.3 Hz, -$C(CO_2CH_3)_2$-CH_2-CH=CH-), 2.60–2.37 (2H, m, =$C(CH_3)$-CH_2-), 2.22 (1H, dd, J_{AB} = 14.8 Hz, J_{AX} = 10.2 Hz, -CH(OMPM)-CH_2-), 2.00 (1H, dd, J_{AB} = 14.8 Hz, J_{BX} = 2.7 Hz, -CH(OMPM)-CH_2-), 1.80 (3H, d, J = 1.2 Hz, -CH=$C(CH_3)$-), 1.06 (9H, s, -$OSiPh_2C(CH_3)_3$); ms m/e (70 eV): 735 (M^+-tBu).

*Methyl (7S)-(5Z,11Z,13E)-15-[(*tert-*butyldiphenylsilyl)oxy]-7-[(*para-*methoxybenzyl)oxy]-5-methyl-2,9,9-trimethoxycarbonylpentadeca-5,11,13-trienoate (**50**)*

The procedure described for **24** was applied: mesylate **49** (0.378 g, 0.48 mmol), dimethyl malonate (305 μL, 2.67 mmol), sodium hydride (121 mg, 50% in oil, 2.53 mmol), potassium iodide (40 mg, 0.24 mmol), tetrahydrofuran (7.5 mL), dimethylformamide (7.5 mL) afforded malonate **50** (0.330 g, 84%); $[\alpha]_D^{25}$+14.4 (*c* 1.02, $CHCl_3$); ir ($CHCl_3$) ν: 3010, 2950, 2860, 1732, 1512, 1435, 1220, 1200, 1110 cm^{-1}; ^1H nmr ($CDCl_3$) δ: 7.70–7.64 and 7.43–7.34 (10H, m, -$OSi(C_6H_5)_2tBu$), 7.25–7.18 and 6.87–6.80 (4H, 2m, -$OCH_2C_6H_4OCH_3$), 6.54 (1H, dd, J = 15.0, 11.0 Hz, -CH=CH-CH_2OSiPh_2tBu), 6.09 (1H, dd, J_1 = J_2 = 11.0 Hz, -CH=CH-CH=CH-CH_2OSiPh_2tBu), 5.79 (1H, dt, J = 15.0, 5.0 Hz, -CH=CH-CH_2OSiPh_2tBu), 5.30–5.19 (1H, m, -CH=CH-CH=CH-CH_2OSiPh_2tBu), 5.16 (1H, d, J = 8.9 Hz, -CH=$C(CH_3)$-), 4.31 (1H, d, J_{AB} = 10.6 Hz, -$OCH_2C_6H_4OCH_3$), 4.25 (2H, d, J = 4.7 Hz, -CH_2OSiPh_2tBu), 4.19–4.08 (1H, m, -CH(OMPM)-), 4.08 (1H, d, J_{AB} = 10.6 Hz, -$OCH_2C_6H_4OCH_3$), 3.76 (3H, s, -$OCH_2C_6H_4OCH_3$), 3.72, 3.71, 3.56, and 3.48 (12H, 4s, 4 × -CO_2CH_3), 3.33 (1H, t, J = 6.8 Hz, -$CH(CO_2CH_3)_2$), 2.99–2.77 (2H, m, -$C(CO_2CH_3)_2$-CH_2-CH=CH-), 2.25 (1H, dd, J = 14.8, 10.3 Hz, -CH(OMPM)-CH_2-), 2.00–1.91 (5H, m, -CH-(OMPM)-CH_2-, =$C(CH_3)$-CH_2-CH_2-), 1.76 (3H, d, J = 1.1 Hz, -CH=$C(CH_3)$-), 1.06 (9H, s, -$OSiPh_2C(CH_3)_3$); ms m/e (70 eV): 828 (M^+), 785 (M^+-CH_3OH + H), 771 (M^+-tBu). Exact Mass (M^+-tBu): 771.3200; found: 771.3192.

*Methyl (7S)-(5Z,11Z,13E)-15-hydroxy-7-[(*para-*methoxybenzyl)oxy]-5-methyl-2,9,9-trimethoxycarbonylpentadeca-5,11,13-trienoate (**51**)*

The procedure used for **25** was applied: silyl ether **50** (0.133 g, 0.161 mmol), tetrabutylammonium fluoride (175 μL, 1 M in tetrahydrofuran, 0.175 mmol, 1.1 equiv.), tetrahydrofuran (4 mL) gave alcohol **51** (89.6 mg, 94%); $[\alpha]_D^{25}$ +12.4 (*c* 1.01, $CHCl_3$); ir ($CHCl_3$) ν: 3600, 3050, 2955, 2880, 1730, 1512, 1435, 1440, 1250, 1200, 1177, 1075 cm^{-1}; ^1H nmr ($CDCl_3$) δ: 7.27–7.20 and 6.89–6.84 (4H, 2m, -$OCH_2C_6H_4OCH_3$), 6.45 (1H, dd, J = 15.2, 11.5 Hz, -CH=CH-CH_2OH), 6.08 (1H, dd, J_1 = J_2 = 11.5 Hz, -CH=CH-CH=CH-CH_2OH), 5.85 (1H, dt, J = 15.2, 5.0 Hz, -CH=CH-CH_2OH), 5.24–5.17 (1H, m, -CH=CH-CH=CH-CH_2OH), 5.15 (1H, d, J = 9.1 Hz, -CH=$C(CH_3)$-), 4.33 (1H, d, J_{AB} = 10.7 Hz, -$OCH_2C_6H_4OCH_3$), 4.18 (2H, d, J = 6.0 Hz,

Can. J. Chem. Downloaded from www.nrcresearchpress.com by 109.225.110.28 on 09/08/12
For personal use only.

-CH_2OH), 4.14–4.04 -(1H, m, -CH(OMPM)-), 3.91 (1H, d, J_{AB} = 10.7 Hz, -OCH_2C$_6$H$_4$OCH$_3$), 3.80 (3H, s, -OCH$_2$-C$_6$H$_4$OCH_3), 3.74, 3.73, 3.62, and 3.51 (12H, 4s, 4 × -CO$_2$CH$_3$), 3.31 (1H, t, J = 6.4 Hz, -CH(CO$_2$CH$_3$)$_2$), 2.88 (2H, d, J = 6.8 Hz, -C(CO$_2$CH$_3$)$_2$-CH_2-), 2.29 (1H, dd, J = 14.8 Hz, 10.4 Hz, -CH(OMPM)-CH_2-) 2.03, 1.92 (5H, m, -CH(OMPM)-CH_2-, =C(CH$_3$)-CH_2-CH_2-), 1.75 (3H, d, J = 1.3 Hz, -CH=C(CH_3)-); ms m/e (70 eV): 591 (MH$^+$), 572 (M$^+$−H$_2$O), 558 (M$^+$−CH$_3$OH).

*Methyl (7*S*)-(5*Z*,11*Z*,13*E*)-15-chloro-7-[(para-methoxybenzyl)oxy]-5-methyl-2,9,9-trimethoxycarbonylpentadeca-5,11,13-trienoate (**52**)*

The procedure used for **26** was applied: alcohol **51** (87.2 mg, 0.148 mmol), *s*-collidine (43 μL, 0.325 mmol), methanesulfonyl chloride (23 μL, 0.296 mmol), dimethylformamide (2.5 mL), lithium chloride (19 mg, 0.443 mmol) yielded chloride **52** (89.4 mg, 99% crude); ir (CHCl$_3$) ν: 3010, 2950, 2930, 2850, 1730, 1512, 1435, 1212, 1205 cm^{-1}; ^{1}H nmr (CDCl$_3$) δ: 7.25–7.20 and 6.89–6.84 (4H, 2m, -OCH$_2$C$_6$$H_4OCH_3$), 6.45 (1H, dd, J = 15.0, 11.2 Hz, -CH=CH-CH$_2$Cl), 6.06 (1H, dd, J_1 = J_2 = 11.2 Hz, -CH=CH-CH=CH-CH$_2$Cl), 5.79 (1H, dt, J = 15.0, 7.4 Hz, -CH=CH-CH$_2$Cl), 5.39–5.28 (1H, m, -CH=CH-CH=CH-CH$_2$Cl), 5.37 (1H, dq, J = 8.8, 1.2 Hz, -CH=C(CH$_3$)-), 4.34 (1H, d, J_{AB} = 10.8 Hz, -OCH_2C$_6$H$_4$OCH$_3$), 4.09 (1H, d, J_{AB} = 10.8 Hz, -OCH_2C$_6$H$_4$OCH$_3$), 4.07 (2H, d, J = 7.4 Hz, -CH_2Cl), 4.13–4.03 (1H, m, -CH(OMPM)-), 3.80 (3H, s, -OCH$_2$-C$_6$H$_4$OCH_3), 3.74, 3.73, 3.61, and 3.54 (12H, 4s, 4 × -CO$_2$CH_3), 3.31 (1H, t, J = 6.9 Hz, -CH(CO$_2$CH$_3$)$_2$), 3.01–2.75 (2H, m, -(CO$_2$CH$_3$)$_2$-CH_2-CH=CH), 2.27 (1H, dd, J = 14.9, 10.5 Hz, -CH(OMPM)-CH_2), 2.06–1.92 (5H, m, -CH(OMPM)-CH_2-, =C(CH$_3$)-CH_2-CH_2-), 1.76 (3H, d, J = 1.2 Hz, -CH=C(CH_3)-); ms m/e (70 eV): 608 (M$^+$), 573 (M$^+$−Cl).

*(3*S*)-(4*Z*,10*E*,12*Z*)-3-[(para-Methoxybenzyl)oxy]-5-methyl-1,1,8,8-tetramethoxycarbonylcyclotetradeca-4,10,12-triene ((−)**5**)*

The procedure used for racemic **5** (R=Bn) was applied: chloride **52** (87.4 mg, 0.144 mmol crude), cesium carbonate (258 mg, 0.731 mmol), tetrahydrofuran (30 mL), dimethylformamide (30 mL) led to cyclic triene **5** (R=CH$_2$C$_6$H$_4$OCH$_3$) (66.1 mg, 78% for 2 steps); mp 184–186°C;[α]$_D^{25}$ −54.5 (*c* 1.01, CHCl$_3$); ir (CHCl$_3$) ν: 3010, 2950, 1730, 1512, 1435, 1205 cm^{-1}; ^{1}H nmr (CDCl$_3$) δ: 7.31–7.27 and 6.93–6.90 (4H, 2m, -OCH$_2$C$_6$$H_4OCH_3$), 6.08–5.97 (2H, m, -CH=CH-CH=CH-), 5.34–5.19 and 4.99–4.86 (2H, 2m, -CH=CH-CH=CH-), 5.01 (1H, d, J = 9.6 Hz, -CH=C(CH$_3$)-), 4.38 (1H, d, J_{AB} = 11.4 Hz, -OCH_2C$_6$H$_4$OCH$_3$), 4.06–3.97 (1H, m, -CH(OMPM)-), 3.83 (3H, s, -OCH$_2$C$_6$H$_4$OCH_3), 3.77, 3.73, 3.70, and 3.50 (12H, 4s, 4 × -CO$_2$CH_3), 2.96–2.72 (3H, m, -CH_2-CH=CH-CH=CH-CH_2-), 2.44 (1H, dd, J = 14.3, 12.0 Hz, -CH_2-CH=CH-), 2.30 (1H, dd, J = 14.8, 11.4 Hz, -CH(OMPM)-CH_2-), 2.17–2.13 (2H, m, =C(CH$_3$)-CH_2-), 1.74 (3H, d, J = 0.8 Hz, -CH=C(CH_3)-), 1.66 (1H, dd, J = 14.8, 2.6 Hz, -CH(OMPM)-CH_2-), 1.42–1.23 (2H, m, =C(CH$_3$)-CH$_2$-CH_2); ms m/e (70 eV): 572 (M$^+$). Exact Mass (M$^+$) calcd: 572.2621; found: 572.2627.

*(3*S*,1*S*)-3-[para-Methoxybenzyl)oxy]-1-methyl-5,5,12,12-tetramethoxycarbonyl-*trans*-cisoid-cis-tricyclo[8.4.0^{2,7}]tetradec-8-ene ((-)**6**)*

A solution of macrocyclic triene **5** (R = CH$_2$C$_6$H$_4$OCH$_3$) (8.8 mg, 0.015 mmol) in toluene (0.5 mL) was heated in a sealed tube at 262°C for 3 h. The solvent was evaporated and the residual oil was purified by column chromatography (10% to 25% of ethyl acetate in hexane) to afford tricyclic compound **6** (R = CH$_2$C$_6$H$_4$OCH$_3$) (7.2 mg, 82%) and a mixture of two compounds (1.5 mg, 17%); [α]$_D^{25}$ −49.3 (*c* 0.98, CHCl$_3$); ir (CH$_2$Cl$_2$) ν: 3060, 2990, 2960, 1730, 1615, 1515, 1440, 1270, 1250 cm^{-1}; ^{1}H nmr (CDCl$_3$) δ: 7.32–7.28 and 6.89–6.84 (4H, 2m, -OCH$_2$C$_6$$H_4OCH_3$), 5.27 (2H, s, -C$H$=C$H$-), 4.53 (1H, d, J_{AB} = 10.2 Hz, -OCH_2C$_6$H$_4$OCH$_3$), 4.36 (1H, d, J_{AB} = 10.2 Hz, -OCH_2C$_6$H$_4$OCH$_3$), 3.83–3.63 (1H, m, -CH(OMPM)-), 3.79 (3H, s, -OCH$_2$C$_6$H$_4$OCH_3), 3.71, 3.71, 3.70, 3.69 (12H, 4s, 4x -CO$_2$CH_3), 2.95–1.21 (13H, m, H-C2, H-C4, H-C6, H-C7, H-C10, H-C11, H-C13, and H-C14), 0.91 (3H, s, -CH_3-C1); ms m/e (70 eV): 572 (M$^+$), 554 (M$^+$ − H$_2$O). Exact Mass (M$^+$) calcd: 572.2621; found: 572.2630.

*(2*R*)-(3*Z*)-6-[(tert-Butyldiphenylsilyl)-oxy]-1,2-O-isopropylidene-4-methylhex-3-ene-1,2-diol (**36**)*

Imidazole (23 mg, 0.336 mmol) and *tert*-butyldiphenylsilyl chloride (73 μL, 0.284 mmol) were added to a stirred solution of alcohol **35***a* (48.1 mg, 0.259 mmol) in dimethylformamide (1.5 mL). The mixture was stirred at room temperature for 4 hs, then poured into a saturated solution of ammonium chloride and extracted with ethyl ether. The combined organic layers were dried over magnesium sulfate, filtered, and concentrated. The residual oil was purified by column chromatography (5% to 50% ethyl acetate in hexane) to yield silyl ether **36** (86.1 mg, 79%); [α]$_D^{25}$ (*R*): +3.6 (*c* 1.22, CHCl$_3$); (*S*): −4.5 (*c* 1.49 (CHCl$_3$); ir (CHCl$_3$) ν: 3020, 2930, 2860, 1430, 1215, 1110, 1055 cm^{-1}; ^{1}H nmr (CDCl$_3$)δ: 7.68–7.64 and 7.44–7.35 (10H, 2m, -OSi(C$_6$$H_5$)$_2$*t*Bu), 5.22 (1H, d, J = 8.8 Hz, -CH=C(CH$_3$)-), 4.63 (1H, ddd, J_1 = J_2 = 8.6 Hz, J_3 = 6.0 Hz, -OCH$_2$-CH-O-), 3.84 (1H, dd, J_{AB} = 8.0 Hz, J_{AX} = 6.0 Hz, -OCH_2-CH-O-), 3.74–3.56 (2H, m, -CH_2-OSiPh$_2$*t*Bu), 3.40 (1H, dd, app t, J_{AB} = J_{BX} = 8.0 Hz, -OCH_2-CH-O-), 2.58–2.18 (2H, m, -CH_2-CH$_2$OSiPh$_2$*t*Bu), 1.69 (3H, d, J = 1.4 Hz, -CH=C(CH_3)-), 1.39 and 1.36 (6H, 2s, -O-C(CH_3)$_2$-O-), 1.04 (9H, s, -OSiPh$_2$C(CH_3)$_3$); ms m/e (70 eV): 424 (M$^+$), 409 (M$^+$ − CH$_3$), 367 (M$^+$ − *t*Bu).

*(2*R*)-(3*Z*)-6-[(tert-Butyldiphenylsilyl)oxy]-4-methylhex-3-en-1,2-diol (**37**)*

Pyridinium *para*-toluenesulfonate (10.2 mg, 0.041 mmol) was added at 0°C to a stirred solution of acetonide **36** (86.1 mg, 0.203 mmol) in methanol (2 mL). The mixture was stirred for 4 h at room temperature (until the appearance of triol by TLC). The mixture was poured into a saturated solution of sodium chloride and extracted with dichloromethane. The combined organic layers were dried over magnesium sulfate, filtered, and concentrated. The residual oil was purified by column chromatography (50% ethyl acetate in hexane) to yield diol **37** (42.8 mg, 55%) and starting material **36** (40.1 mg, 45%). The starting material was then recycled twice to afford diol **37** (67.5 mg, 87% total); [α]$_D^{25}$ (*R*): −10.2 (*c* 1.54, CHCl$_3$); (S): +10.8 (*c* 1.59, CHCl$_3$); ir (CHCl$_3$) ν: 3580, 3450, 3015, 2960, 2930, 2860, 1430, 1215, 1110 cm^{-1}; ^{1}H nmr (CDCl$_3$) δ: 7.69–7.64 and 7.45–7.36 (10H, 2m, -OSi(C$_6$$H_5$)$_2$*t*Bu), 5.40 (1H, d, J = 7.8 Hz, -CH=C(CH$_3$)-), 4.35 (1H, ddd, J_1 = J_2 = 7.6 Hz, J_3 = 3.8 Hz, -CHOH-), 3.71–3.44 (4H, m, -CH_2OH and -CH_2OSiPh$_2$*t*Bu), 2.61–2.19 (2H, m, -CH_2-CH$_2$OSiPh$_2$*t*Bu), 1.68 (3H, d, J = 1.3 Hz, -CH=C(CH_3)-), 1.05 (9H, s, -OSiPh$_2$C(CH_3)$_3$); ms m/e (70 eV): 353 (M$^+$ − OCH$_3$). Exact Mass (M$^+$ − OCH$_3$) calcd: 353.1937; found: 353.1935.

*(2*R*)-(3*Z*)-6-[(tert-Butyldiphenylsilyl)oxy]-1-[(para-toluenesulfonyl)-oxy]4-methylhex-3-en2-ol (**38**)*

The procedure used for **43** was applied: diol **37** (31.3 mg, 0.082 mmol), *para*-toluenesulfonyl chloride (17.0 mg, 0.090 mmol), triethylamine (12.5 μL, 0.090 mmol), dimethylaminopyridine (10.0 mg, 0.082 mmol), and dichloromethane (1 mL) yielded tosylate **38** (25.9 mg, 60%) and starting material **37** (8.5 mg, 27%). The starting material was then recycled to afford tosylate **38** (33.2 mg, 76% total); [α]$_D^{25}$ (*R*): − 24.3 (*c* 1.42, CHCl$_3$); (*S*): +25.6 (*c* 1.37, CHCl$_3$); ir (CHCl$_3$) ν: 3450, 3020, 2950, 2930, 2860, 1430, 1362, 1230, 1190, 1175, 1110 cm^{-1}; ^{1}H nmr (CDCl$_3$) δ: 7.80–7.76, 7.66–7.61, 7.47–7.30 (14H, 3m, -OSi(C$_6$$H_5$)$_2$*t*Bu and -OSO$_2$-C$_6$$H_4CH_3$), 5.26 (1H, dq, J = 8.0, 1.2 Hz, -CH=C(CH$_3$)-), 4.49–4.41 (1H, m, -CHOH-), 3.97–3.85 and 3.67–3.59 (4H, 2m, -CH_2OSiPh$_2$*t*Bu and -CH_2OTs), 2.49–2.31 and 2.24–2.14 (2H, 2m, -CH_2-CH$_2$OSiPh$_2$*t*Bu), 2.43 (3H, s, -OSO$_2$C$_6$H$_4$CH_3), 2.09–1.96 (1H, s, -CHOH-), 1.64 (3H, d, J = 1.3 Hz, -CH=C(CH_3), 1.02 (9H, s, -OSiPh$_2$C(CH_3)$_3$.

*(2R)-(3Z)-6-[(*tert*-Butyldiphenylsilyl)oxy]-2-[(2S)-2-methoxy-2-phenylacetoxy]-1[(*para*-toluenesulfonyl)-oxy]4-methylhex-3-ene (**39**)*

(2*S*)-2-Phenyl-2-methoxyacetic acid (**40**) (20) (11.3 mg, 0.068 mmol), dicyclohexylcarbodiimide (14.1 mg, 0.068 mmol), and dimethylaminopyridine (4.0 mg, 0.034 mmol) were added at 0°C to a stirred solution of (*R*) alcohol **38** (18.5 mg, 0.034 mmol) in dichloromethane (1 mL). The mixture was stirred for 0.75 h at 0°C and then filtered on Celite. After evaporation of the solvent, the residual solid was purified by column chromatography (25% ethyl acetate in hexane) to afford ester **39** (24.3 mg, 99%); $[\alpha]_D^{25}$ +48.2 (*c* 1.17, $CHCl_3$); ir ($CHCl_3$) *ν*: 3020, 2930, 2855, 1748, 1430, 1365, 1172, 1110 cm^{-1}; ^1H nmr ($CHCl_3$) δ: 7.70–7.59 and 7.42–7.25 (19H, -OSi(C_6H_5)$_2$*t*Bu, -$OSO_2C_6H_4CH_3$, and -OCOCH(OCH_3)C_6H_5), 5.56–5.48 (1H, m, -*CH*(OCOCH(OCH_3)Ph)-), 4.90 (1H, d, *J* = 9.2 Hz, -*CH*=C(CH_3)-), 4.66 (1H, s, -OCOC*H*(OCH_3)Ph), 3.94–3.92 and 3.65–3.44 (4H, 2m, -CH_2-$OSO_2C_6H_4CH_3$ and -CH_2OSiPh_2*t*Bu), 3.37 (3H, s, -OCOCH-(OCH_3)Ph), 2.47–2.35 and 2.06–1.96 (2H, 2m, -CH_2-CH_2-OSiPh_2*t*Bu), 2.40 (2H, s, -$OSO_2C_6H_4CH_3$), 1.55 (3H, d, *J* = 1.3 Hz, -CH=C(CH_3)-), 0.99 (9H, s, -OSiPh_2C(CH_3)$_3$).

*(2S)-(3Z)-6-[(*tert*-Butyldiphenylsilyl)oxy]-2-[(2S)-2-methoxy-2-phenylacetoxy]-1-[(*para*-toluenesulfonyl)oxy]-4-methylhex-3-ene (**39**)*

The previous procedure was applied: (2*S*)-2-phenyl-2-methoxyacetic acid (**40**) (20) (9.0 mg, 0.055 mmol), dicyclohexylcarbodiimide (11.0 mg, 0.055 mmol), (*S*) alcohol **38** (14.7 mg, 0.027 mmol), dimethylaminopyridine (3.3 mg, 0.027 mmol), and dichloromethane (1 mL) yielded ester **39** (16.8 mg, 90%); $[\alpha]_D^{25}$ +0.9 (*c* 1.13, $CHCl_3$); ^1H nmr ($CDCl_3$) δ: 7.64–7.59, 7.54–7.51, 7.43–7.31, and 7.23–7.19 (19H, 4m, -OSi(C_6H_5)$_2$*t*Bu, -OSO_2-$C_6H_4CH_3$, and -OCOCH(OCH_3)C_6H_5), 5.48–5.39 (1H, m, -*CH*-(OCOCH(OCH_3)Ph),-), 5.07 (1H, d, *J* = 9.4 Hz, -*CH*=C(CH_3)-), 4.69 (1H, s, -OCOC*H*(OCH_3)Ph), 3.81 (2H, d, *J* = 5.2 Hz, -CH_2O-$SO_2C_6H_4CH_3$), 3.69–3.49 (2H, m, -CH_2OSi-Ph_2*t*Bu), 3.36 (3H, s, -OCOCH(O*CH*$_3$)Ph), 3.56–3.45 (1H, m, -*CH*$_2$-CH_2OSiPh_2*t*Bu), 2.39 (3H, s, -$OSO_2C_6H_4CH_3$), 2.17–2.06 (1H, m, -CH_2-CH_2OSi-Ph_2*t*Bu), 1.64 (3H, d, *J* = 1.4 Hz, -CH=C(*CH*$_3$)-), 1.00 (9H, s, -OSiPh_2C(*CH*$_3$)$_3$).

Acknowledgements

This research was supported by the Natural Sciences and Engineering Research Council of Canada (NSERCC, Ottawa) and by the "Ministère de l'Enseignement supérieur et de la Science" (Fonds FCAR, Québec). We acknowledge the help of Dr. Solo Goldstein in writing this manuscript.

1. (*a*) J. Tsuji, T. Yamada, M. Kaito, and T. Mandai. Tetrahedron Lett. 2257 (1979); (*b*) J. Tsuji and T. Mandai. Tetrahedron Lett. 3285 (1977); (*c*) J. Tsuji and S. Hashiguchi. Tetrahedron Lett. **21**, 2955 (1980); (*d*) J. P. Schaeffer and J. J. Bloomfield. Org. React. **15**, 1 (1967); (*e*) G. Stork and E. Nakamura. J. Org. Chem. **44**, 4010 (1979); (*f*) K. C. Nicolaou, S. P. Seitz, M. R. Pavia, and N. A. Petasis. J. Org. Chem. **44**, 4011 (1979); (*g*) J. W. McMurry, K. L. Kees, M. P. Flemming, and L. R. Krebski. J. Org. Chem. **43**, 3255 (1978); (*h*) B. M. Trost and T. R. Verhoeven. J. Am. Chem. Soc. **102**, 4743 (1980); (*i*) T. Takahaski, H. Nemoto, and J. Tsuji. Tetrahedron Lett. **24**, 2005 (1983); **24**, 3485 (1983); (*j*) T. Takahashi, K. Kitamura, and J. Tsuji. Tetrahedron Lett. **24**, 4695 (1983); (*k*) M. A. Casadei, C. Galli, and L. Mandolini. J. Org. Chem. **46**, 3127 (1983); (*l*) M. Kodama, S.-I. Yokoo, H. Yamada, and S. Itô. Tetrahedron Lett. **34**, 3121 (1978); (*m*) W. C. Still and D. Mobilio. J. Org. Chem. **48**, 4786 (1983); (*n*) J. A. Marshall and D. G. Cleary. J. Org. Chem. **51**, 858 (1986); (*o*) T. Kitahara and K. Mori. J. Org. Chem. **49**, 3281 (1984).
2. (*a*) P. Deslongchamps, S. Lamothe, and H.-S. Lin. Can. J. Chem. **65**, 1298 (1987); (*b*) D. Brillon and P. Deslongchamps. Can. J. Chem. **65**, 43 (1987); **65**, 56 (1987).
3. W. C. Still and I. Galynker. Tetrahedron, **37**, 3981 (1981).
4. E. Neeland, J. P. Ounsworth, R. J. Sims, and L. Weiler. Tetrahedron Lett. **28**, 35 (1987), and references quoted therein.
5. (*a*) J. Gauthier and P. Deslongchamps. Can. J. Chem. **45**, 297 (1967); (*b*) A. Belanger, J. Poupart, and P. Deslongchamps. Tetrahedron Lett. **17**, 2127 (1968); (*c*) P. Deslongchamps, A. Belanger, D. J. F. Berney, H.-J. Borschberg, R. Brousseau, A. Douteau, R. Durand, H. Katayama, R. Lapalme, D. M. Leturc, C.-C. Liao, F. N. MacLachlan, J.-P. Maffrand, F. Marazza, R. Martino, C. Moreau, L. St-Laurent, R. Saintonge, P. Soucy, and L. Ruest. Can. J. Chem. **57**, 3348 (1979); **68**, 115 (1990); **68**, 127 (1990); **68**, 153 (1990); **68**, 186 (1990); (*d*) E. G. Baggiolini, H. L. Lee, G. Pizzolato, and M. R. Uskokovik. J. Am. Chem. Soc. **104**, 6460 (1982); (*e*) J. A. Marshall, T. M. Jenson, and B. S. Dehoff. J. Org. Chem. **51**, 4316 (1986); (*f*) J. A. Marshall, J. Lebreton, B. S. Dehoff, and T. M. Jenson. J. Org. Chem. **52**, 3883 (1987); (*g*) J. A. Marshall and J. Lebreton. Tetrahedron Lett. **28**, 3323 (1987); (*h*) J. Am. Chem. Soc. **110**, 2925 (1988); (*i*) J. Org. Chem. **53**, 4108 (1988); (*j*) J. A. Marshall, E. D. Robinson, and J. Lebreton. J. Org. Chem. **55**, 227 (1990); (*k*) G. Kim, M. Y. Chu-Moyer, and S. J. Danishefsky. J. Am. Chem. Soc. **112**, 2003 (1990).
6. (*a*) P. Deslongchamps. Aldrichimica Acta, **17**, 59 (1984); (*b*) Bull. Soc. Chim. Fr. II, **9–10**, 349 (1984); (*c*) Aldrichimica Acta, **24**, 43 (1991).
7. (*a*) K. Baettig, C. Dallaire, R. Pitteloud, and P. Deslongchamps. Tetrahedron Lett. **28**, 5249 (1987); (*b*) K. Baettig, A. Marinier, R. Pitteloud, and P. Deslongchamps. Tetrahedron Lett. **28**, 5253 (1987); (*c*) G. Bérubé and P. Deslongchamps. Tetrahedron Lett. **28**, 5255 (1987); (*d*) S. Lamothe, A. Ndibwami, and P. Deslongchamps. Tetrahedron Lett. **29**, 1639 (1988); (*e*) Tetrahedron Lett. **29**, 1641 (1988); (*f*) A. Marinier and P. Deslongchamps. Tetrahedron Lett. **29**, 6215 (1988); (*g*) F. Grimley. Post-doctoral report, University of Sherbrooke, Sherbrooke, Quebec, 1989; (*h*) Y.-C. Xu, M. Cantin, and P. Deslongchamps. Can. J. Chem. **68**, 2137 (1990).
8. T. Takahashi, K. Shimizu, T. Doi, and J. Tsuji. J. Am. Chem. Soc. **110**, 2674 (1988).
9. C. Piatandosi, C. E. Anderson, A. E. Brecht, and C. L. Yarbro. J. Am. Chem. Soc. **80**, 6613 (1958).
10. S. Hanessian and P. Lavallée. Can. J. Chem. **53**, 2975 (1975).
11. K. Omura and D. Swern. Tetrahedron, **34**, 1651 (1978).
12. N. Miyashita, A. Yoshikoshi, and P. A. Grieco. J. Org. Chem. **42**, 3772 (1977).
13. (*a*) A. Maercker. Org. React. **14**, 293 (1965); (*b*) R. M. Silverstein, G. C. Bassler, and T. C. Morrill. Spectrometric identification of organic compounds. 4th ed. John Wiley & Sons, New York. 1981.
14. E. J. Corey and A. Venkateswarlu. J. Am. Chem. Soc. **94**, 6190 (1972).
15. E. W. Collington and A. I. Meyers. J. Org. Chem. **36**, 3044 (1971).
16. (*a*) K. E. Maloneyhuss. Synth. Commun. **15**, 273 (1985); (*b*) M. E. Jung and T. J. Shaw. J. Am. Chem. Soc. **102**, 6304 (1980); (*c*) S. Takano, H. Numata, and K. Ogasawara. Heterocycles, **19**, 327 (1982); (*d*) C. Hubschwerlen. Synthesis, 962 (1986).
17. N. Nakajima, K. Horita, R. Abe, and O. Yonemitsu. Tetrahedron Lett. **29**, 4139 (1988).
18. M. H. Park, R. Takeda, and K. Nakanishi. Tetrahedron Lett. **28**, 3823 (1987).
19. A. G. Michel, G. Boulay, and A. Marinier. Acta Crystallogr. Sect. C: Cryst. Struct. Commun. **C45**, 325 (1989).
20. J. A. Dale and H. S. Mosher. J. Am. Chem. Soc. **95**, 512 (1973).

Can. J. Chem. Downloaded from www.nrcresearchpress.com by 109.225.110.28 on 09/08/12
For personal use only.

^{1}H nuclear magnetic resonance and molecular orbital estimates of the internal rotational barrier in phenylpropynal in solution and in the vapor

TED SCHAEFER, RUDY SEBASTIAN, AND ROBERT W. SCHURKO[1]
Department of Chemistry, University of Manitoba, Winnipeg, Man., Canada R3T 2N2

Received January 24, 1992

TED SCHAEFER, RUDY SEBASTIAN, and ROBERT W. SCHURKO. Can. J. Chem. **70**, 2365 (1992).

The ^{1}H nuclear magnetic resonance spectra of phenylpropynal and 1-phenylpropyne are analyzed for CS_2/C_6D_{12} and acetone-d_6 solutions. The ensuing spin–spin coupling constants over eight formal bonds are used in assessing the conformational dependence of the one in the propynal derivative, as compared to the one over six bonds in benzaldehyde. The eight-bond coupling constant in phenylpropynal implies, via a hindered rotor model, that the twofold barrier to internal rotation is 5.9 ± 1.6 kJ/mol in both solutions. This number is much smaller than that for the internal barrier in benzaldehyde, reflecting the reduced π electron conjugation in phenylpropynal. Molecular orbital computations, with geometry optimization, confirm the essentially purely twofold internal barrier in the free propynal. The theoretical magnitudes are given for AM1 calculations, as well as for *ab initio* computations with STO-3G, 3-21G, 6-31G, and 6-31G* bases. To within experimental error, the barrier magnitudes from the split-valence basis sets agree with those obtained in solution.

TED SCHAEFER, RUDY SEBASTIAN et ROBERT W. SCHURKO. Can. J. Chem. **70**, 2365 (1992).

On a analysé les spectres de résonance magnétique nucléaire du ^{1}H du phénylpropynal et du 1-phénylpropyne en solutions dans le CS_2/C_6D_{12} et dans l'acétone-d_6. On a utilisé les constantes de couplage spin–spin à travers huit liaisons formelles pour déterminer la dépendance conformationnelle de la constante de couplage dans le propynal par comparaison avec celle à travers six liaisons dans le benzaldéhyde. La constante de couplage à travers huit liaisons dans le phénylpropynal implique, en se basant sur un modèle à rotor empêché, que la barrière binaire à la rotation interne est de 5,9 ± 1,6 kJ/mol dans chacune des solutions. Cette valeur est beaucoup plus faible que celle pour la barrière interne dans le benzaldéhyde et elle est le reflet d'une conjugaison π réduite dans le phénylpropynal. Des calculs d'orbitales moléculaires, avec optimisation de géométrie, confirment le caractère essentiellement binaire pur de la barrière interne dans le propynal libre. On rapporte les amplitudes théoriques obtenus par calculs AM1 ainsi que par calculs *ab initio* avec des bases STO-3G, 3-21G, 6-31G et 6-31G*. Aux erreurs expérimentales près, les amplitudes des barrières calculées avec les ensembles à valence partagée sont en bon accord avec celles obtenues en solution.

[Traduit par la rédaction]

Introduction

The use of motionally averaged long-range spin–spin coupling constants in conformational analysis has had some success. For example, for benzyl fluoride (1) the barrier to rotation about the exocyclic C—C bond is comparable in magnitude to thermal energies at ambient temperatures and is significantly dependent on the solvent, so much so that the minimum in the internal rotational dependence apparently shifts by 90° in going from polar solvents to the free molecule. Experiments of this kind are feasible for relatively small internal barriers, say those in which their magnitude is less than $6kT$, because otherwise the bonds carrying the coupled nuclei do not sample a satisfactory portion of the rotational potential surface. However, it is just such barriers that are hard to ascertain by lifetime measurements such as in dynamic nmr; also, the latter need a chemical shift marker, unnecessary in the application of motionally averaged coupling constants.

If follows that, while dynamic nmr is successful in assessing the barrier height (free energy of activation) for benzaldehyde in solution, which is likely greater than 30 kJ/mol (ref. 2, a review giving a collection of data and a discussion), ^6J(H, CHO) should be very small, presumably being proportional to sin $^2\theta$, whose expectation value at 300 K is then only about 0.045, where θ is the internal torsion angle. Yet INDO MO FPT computations (3) yield (4, 5) $^6J_{90}$ (θ = 90°) as near −1.0 Hz, so that a measurable value of about −0.05 Hz should appear in a reasonably high-resolution ^{1}H nmr spectrum of benzaldehyde in solution. The formal analysis of the ^{1}H nmr spectra implies ^6J as about −0.015 Hz (5, 6), not yet detected as a splitting in the spectrum. In the presence of two *ortho* chlorine substituents, ^6J is −0.135(3) Hz (7). Combined with STO-3G MO computations (the minimal basis set, of all those employed (8), being in best agreement with experiment for benzaldehyde), this number leads to a $^6J_{90}$ of -0.3_3 Hz (7). A different approach (5), based on ^6J in 2-chlorobenzaldehyde, yields a $^6J_{90}$ of −0.4 Hz. If $^6J_{90}$ lies between −0.3 and −0.4 Hz in benzaldehyde and if the positive component of ^6J is indeed negligible in the absence of ring substituents, then a barrier (9, 10) of 30.5–33.0 kJ/mol entails a ^6J of 0.042 (−0.35 ± 0.05) or −0.015 ± 0.002 Hz in benzaldehyde in solution; this number is consistent with the spectral analyses (5, 6).

Now, consider phenylpropynal, **1**. The π electron conjugation between the formyl and phenyl groups, mediated

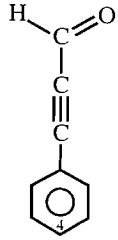

1

by the triple bond, will be weaker than in benzaldehyde; its absence would imply essentially free internal rotation, while its presence would favour a planar molecule. The triple bond may reduce the σ–π contribution to ^6J in **1**. If the barrier to

[1]Undergraduate research participant, 1991.

Can. J. Chem. Downloaded from www.nrcresearchpress.com by 109.225.110.28 on 09/08/12
For personal use only.

TABLE 1. The ^{1}H nmr spectral parameters of **1** and **2** at 300 K

Parameter	1-Phenylpropyne		Phenylpropynal	
	CS_2/C_6D_{12}[a]	Acetone-d_6[b]	CS_2/C_6D_{12}[a]	Acetone-d_6[b]
ν(CHO/CH_3)	589.361[c,d]	600.618	2796.495	2843.114
ν_2	2170.333	2210.920	2249.616	2299.945
ν_3	2142.423	2191.807	2196.984	2249.617
ν_4	2139.007	2187.191	2219.797	2273.081
$^3J_{23}$	7.751	7.766	7.766	7.786
$^3J_{34}$	7.526	7.553	7.586	7.608
$^4J_{24}$	1.282	1.269	1.284	1.269
$^4J_{26}$	1.752	1.784	1.754	1.788
$^4J_{35}$	1.402	1.405	1.329	1.327
$^5J_{25}$	0.621	0.637	0.637	0.649
$^6J_{2X}$[e]	−0.295	−0.298	−0.065	−0.065
$^7J_{3X}$	0.137	0.145	0.047	0.048
$^8J_{4X}$	−0.251	−0.254	−0.035	−0.038
Transitions calcd.	540	551	164	164
Transitions assigned	445	440	143	143
Peaks observed	185	221	114	121
Largest difference	0.022	0.016	0.009	0.007
Root-mean-square deviation	0.007	0.006	0.003	0.003

[a]5.0 mol% in CS_2, containing also 10.0 mol% of C_6D_{12} and 0.5 mol% of TMS.
[b]5.0 mol% in acetone-d_6, containing also 0.5 mol% of TMS.
[c]In Hz at 300.135$_2$ MHz to high frequency of internal TMS.
[d]For all spectral parameters, the standard deviation in the last significant figure is 0.001 Hz, or less, except for $^3J_{23}$ in column 2, for which it is 0.002 Hz.
[e]X is a methyl proton in 1-phenylpropyne or the formyl proton in phenylpropynal.

internal rotation is small enough, however, then a precise measurement of ^8J may still lead to an estimate of its magnitude.

In this report, the ^{1}H nmr spectra of **1** and **2**, 1-phenylpropyne, are obtained and analyzed for polar and nonpolar

2

solutions. The ensuing ^8J values yield an estimate of the internal barrier in **1**, which is also calculated for the free molecule at various levels of molecular orbital theory.

Experimental

The compounds, 1-phenylpropyne and phenylpropynal, from Aldrich, were prepared as 5.0 mol% solutions in CS_2/C_6D_{12}/TMS and acetone-d_6/TMS solvent mixtures (see the tables for details). The solutions were filtered into 5 mm o.d. nmr sample tubes, which were degassed by at least four cycles of the freeze–pump–thaw procedure. Careful flame-sealing produced fairly symmetrical tops on the sample tubes.

The ^{1}H nmr spectra were obtained on an AM 300 Bruker spectrometer using acquisition times of 50 s or more, digital resolution of 0.002–0.005 Hz/point, and some resolution enhancement procedures (see figures). Weak irradiation experiments (11–14) established the signs of the long-range coupling constants in the aldehyde and the strongly second-order spectrum of the methyl compound was determined by the signs of its long-range coupling constants, which were already known (15) for its 2,5-dichloro derivative.

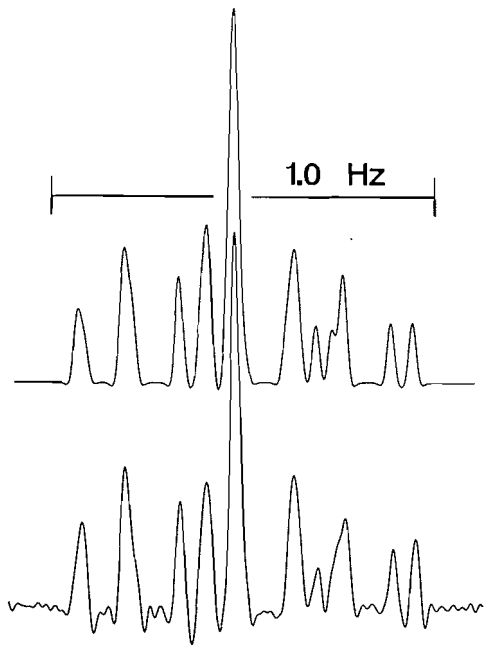

FIG. 1. The ^{1}H nmr spectrum at 300 MHz of the methyl protons of 1-phenylpropyne, as a 5 mol% solution in acetone-d_6 at 300 K, has a linewidth at half height of somewhat less than 0.03 Hz. The acquisition time is 50.0 s and some resolution enhancement is employed. The theoretical spectrum takes the enhancement into account, uses the spectral parameters from Table 1, and assumes a linewidth of 0.025 Hz. The relative signs of the coupling constants to the ring protons follow from the observed pattern in this figure.

Can. J. Chem. Downloaded from www.nrcresearchpress.com by 109.225.110.28 on 09/08/12
For personal use only.

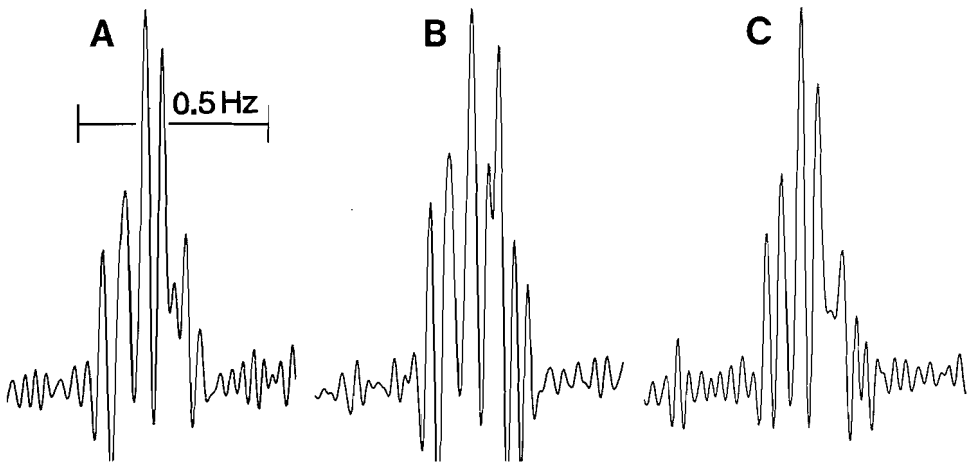

FIG. 2. In A is shown the ^{1}H nmr spectrum at 300 MHz and 300 K of the formyl proton in phenylpropynal as a 5 mol% solution in acetone-d_6. The digital resolution is 0.002 Hz/point, the acquisition time is 51.2 s, and rather severe resolution enhancement, a LB of −0.120 and a GB of 0.600, is applied. In B a weak second radiofrequency field is applied to the doublet (splitting of ca. 0.06 Hz due to the formyl proton) at highest frequency in the spectrum of the *ortho* protons. The spectral pattern is consistent with expectation if ^7J(H, CHO)/$^3J_{23} > 0$ and ^8J(H, CHO)/$^4J_{24} < 0$. In C the peak (split by about 0.04 Hz) near 2280.20 Hz in the *para* proton region is being irradiated. This peak corresponds to opposite spin states for the *meta* and *para* protons, say negative and positive, respectively. If ^6J(H, CHO)/$^4J_{24} < 0$ and ^7J(H, CHO)/$^3J_{34} > 0$, then, with the correct amplitude of the second field, the right-hand peak in the formyl proton spectrum should split (tickling conditions (11)), as observed. Six sets of experiments were performed to confirm the sign relationships given in Table 1 and simulations of the double resonance experiments used the program DOR (13).

Can. J. Chem. Downloaded from www.nrcresearchpress.com by 109.225.110.28 on 09/08/12
For personal use only.

Molecular orbital computations utilized the program GAUSSIAN 86 (16), with various basis sets (17). INDO MO FPT (3) calculations of long-range coupling constants employed the geometries obtained from the optimizations in the molecular orbital iterations.

Results and discussions

Spectral analyses

The spectral parameters, obtained with the program NUMARIT (18), extensively reworked by R. Sebastian, appear in Table 1. Figure 1 displays the ^{1}H nmr spectrum of the methyl group in 1-phenylpropyne and Fig. 2 illustrates one of a series of experiments designed to determine the signs of the coupling constants involving the formyl proton in phenylpropynal.

*^{8}J in 1-phenylpropyne, **1**, and phenylpropynal, **2**, and the internal barrier in **1***

In toluene, ^6J(H, CH_3) is −0.602(2) Hz, is a pure σ−π coupling constant (19–22) and hence is proportional to sin $^2\theta$. ^8J in **2** is −0.252(3) Hz (the mean of −0.251(1) and −0.254(1) Hz) and is most likely also a pure σ−π parameter. Therefore the triple bond reduces the σ−π interactions by a factor of 0.42, confirming a previous conclusion (15). $^8J_{90}$ in **2** is thus 0.504(6)Hz, that is, when the C—H bond of the methyl group lies in a plane perpendicular to the molecular plane; the internal barrier is essentially zero, so that ⟨sin $^2\theta$⟩ is 0.5.

The analogous procedure for the aldehyde, **1**, then implies that $^8J_{90}$ is (-0.35 ± 0.05) 0.42 or $-0.14_7 \pm 0.02_1$ Hz. The measured value (Table 1) of ^8J is $-0.036_5 \pm 0.001_5$ Hz. Therefore ⟨sin $^2\theta$⟩ is 0.248 ± 0.047 at 300 K. If the internal barrier is purely twofold, then its magnitude follows as 5.9 ± 1.6 kJ/mol, considerably lower than in benzaldehyde in the vapor, where the internal barrier is predominantly twofold and very near 20 kJ/mol (23–26), or in solution, where the free energy of activation to internal ro-

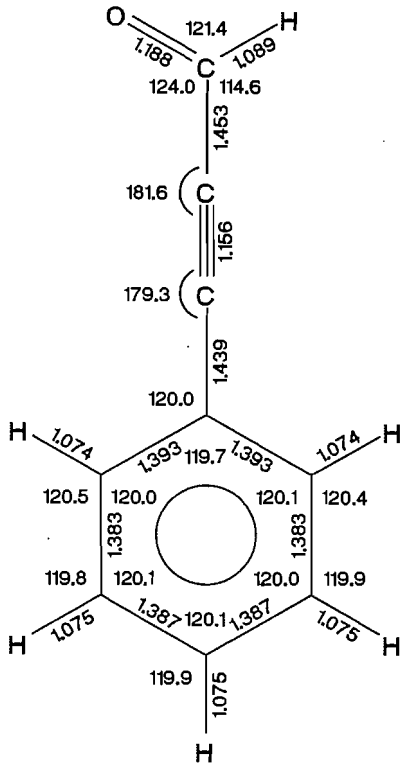

FIG. 3. The 6-31G* structure of planar phenylpropynal is displayed. Calculations with this basis set give C—C and C—H equilibrium bond lengths in a phenyl group longer and shorter, respectively, by very near 0.01 Å than, for example, r_0 values from microwave spectroscopy (35).

TABLE 2. Relative computed energies of various conformers of phenylpropynal, **1**

θ/deg	Relative energy/kJ mol^{-1}				
	AM1	STO-3G	3-21G	6-31G	6-31G*
0[a]	0.000	0.000[c]	0.000[d]	0.000[e]	0.000[f]
15	0.105	0.126	0.357	0.362	0.536[g]
30	0.388	1.472	1.334	1.356	1.202
45	0.784	0.944	2.671	2.719	2.495[g]
60	1.170	1.410	4.016	4.093	3.628
75	1.462	1.751	5.005	5.106	4.524[g]
90[b]	1.560	1.876	5.367	5.479	4.853

[a]For the planar molecule.
[b]For an angle of 90° between the planes of the formyl and phenyl groups.
[c]The total energy is −413.853 823 au.
[d]The total energy is −416.758 514 au.
[e]The total energy is −418.943 554 au.
[f]The total energy is −419.104 150 au.
[g]For this conformation the energy is computed for a geometry that is the average of those for the encompassing values of θ.

tation is nearer 30 kJ/mol. The smaller value in **1** can be understood qualitatively as a consequence of reduced conjugation of the π electron systems in question.

Molecular orbital computations

The results of the calculations with various bases (27–31) of the conformational energies for **1** are summarized in Table 2. During the SCF cycles, the nuclei of the phenyl group were constrained to a plane, but all other bond angles and lengths were optimized. The relative energies in Table 2 are reproducible by an almost purely twofold internal potential, any fourfold component having a magnitude of 0.02 kJ/mol or less. The split-valence basis sets agree with the magnitude of the barrier deduced from ^8J to within experimental error. The perturbation of the barrier by the solvent is not known.[2] It would be of interest to have an experimental value of the internal barrier for the molecule in the gas phase. Figure 3 shows the 6-31G* (polarization functions on the heavy atoms) structure of **1**, probably of use in such studies.

The INDO MO FPT computations confirm that ^8J in **1** varies as sin $^2\theta$, the magnitude depending, as expected, on the geometry. In view of the quantitative discrepancies between theory and experiment for $^6J_{90}$ in benzaldehyde (4, 5, 7), it cannot be said that the computations of $^8J_{90}$ sin $^2\theta$ in **1** necessarily bear out the discussion in the previous section, where $^8J_{90}$ is estimated as −0.15Hz, although the theoretical coefficient of sin $^2\theta$ ranges from −0.15 Hz for the STO-3G to −0.20 Hz for the 6-31G* geometries.

Turning to 1-phenylpropyne, **2**, the computations confirm intuition, even under tight optimization conditions, that the internal rotational barrier vanishes to within the significance of the computed energies. The INDO MO FPT computations of ^8J confirm its dependence on sin$^2\theta$, where θ is the angle by which the C—H bond of the methyl group twists away from the plane containing the phenyl group.

[2]The computed dipole moments of the planar conformers of **1** vary from 1.40 D with AM1 to 4.87 D with the 6-31G basis. For the split-valence bases, the dipole moments decrease by 0.3 D in the perpendicular conformers, so that some solvent stabilization of the planar conformer is possible. The dipole moment of **1** is 3.39 D in benzene solution at 298 K (32), midway between 4.35 D (6-31G*) and 2.33 D (STO-3G).

The other spectral parameters

It may be noted that the ratios of $^{(n+2)}J$(H, CH_3) in 1-phenylpropyne (Table 1) to the corresponding ^nJ(H, CH_3) in toluene (19) range from 0.42_2 to 0.42_9. Because ^4J(H, CH_3) and ^5J(H, CH_3) in toluene contain also σ electron contributions, in addition to the σ−π components (19–22), it appears that the triple bond reduces any σ components of ^6J(H, CH_3) and ^7J(H, CH_3) in 1-phenylpropyne by the same factor with which it reduces the σ−π components. Such a result is not borne out by our INDO MO FPT computations in 1-phenylpropyne. Because, however, such computations are also unsatisfactory for ^5J(H, CH_3) and ^4J(H, CH_3) in toluene (19, 33, 34), more discussion is unwarranted here. Further study of the coupling mechanisms is required.

Turning to the intraring coupling constants, it is interesting that $^3J_{23}$, $^3J_{34}$, $^4J_{26}$, and $^5J_{25}$ are larger in the polar than in the relatively nonpolar solution; the opposite is true for $^4J_{24}$, while $^4J_{35}$ is unchanged by a change in solvent. The solvent perturbations are an order of magnitude larger than the standard deviations in the coupling constants. Exactly the same pattern has now been established (unpublished data) for phenylethyne and cyanobenzene.

Acknowledgments

We are grateful to the Natural Sciences and Engineering Research Council of Canada for a grant-in-aid of research.

1. T. Schaefer, C. Beaulieu, R. Sebastian, and G. H. Penner. Can. J. Chem. **65**, 581 (1990).
2. K. Unemoto and K. Ouchi. Proc. Indian Acad. Sci. (Chem. Sci.), **94**, 1 (1985).
3. J. A. Pople, J. W. McIver, Jr., and N. S. Ostlund. J. Chem. Phys. **49**, 2960 (1968); **49**, 2965 (1968).
4. R. Wasylishen and T. Schaefer. Can. J. Chem. **49**, 3216 (1971).
5. R. Laatikainen, K. Tuppurainen, Y. Hiltunen, and S. Lotjonen. Magn. Reson. Chem. **28**, 939 (1990).
6. T. Schaefer and C. S. Takeuchi. Can. J. Chem. **67**, 827 (1989).
7. T. Schaefer, J. Peeling, G. H. Penner, and A. Lemire, and R. Laatikainen. Can. J. Chem. **64**, 1859 (1986).
8. G. H. Penner, P. George, and C. W. Bock. J. Mol. Struct. (Theochem.), **152**, 201 (1987).
9. F. A. L. Anet and M. Ahmad. J. Am. Chem. Soc. **86**, 119 (1964).
10. D. M. Doddrell, M. R. Bendall, P. F. Barron, and T. D. Pegg. J. Chem. Soc. Chem. Commun. 77 (1979).
11. R. Freeman and W. A. Anderson. J. Chem. Phys. **37**, 2053 (1962).
12. R. Kaiser. J. Chem. Phys. **39**, 2435 (1963).
13. G. Govil and D. H. Whiffen. Mol. Phys. **12**, 449 (1967).
14. R. R. Ernst, G. Bodenhausen, and A. Wokaun. Principles of nuclear magnetic resonance in one and two dimensions. Oxford University Press, London. 1987. p. 230.
15. C. J. Macdonald, G. K. Hamer, I. R. Peat, and W. F. Reynolds. Can. J. Chem. **50**, 2035 (1972).
16. M. J. Frisch, J. S. Binkley, H. B. Schlegel, K. Raghavachari, C. F. Melius, R. L. Martin, J. J. P. Steward, F. W. Bobrowicz, D. F. Rohlfing, L. R. Kahn, D. J. Defrees, R. Seeger, R. A. Whiteside, D. J. Fox, E. M. Fluder, and J. A. Pople. Carnegie–Mellon Quantum Publishing Unit, Pittsburgh, Pa. 1984.
17. W. J. Hehre, L. Radom, P. v. R. Schleyer, and J. A. Pople. Ab initio molecular orbital theory. Wiley–Interscience, New York. 1986.
18. J. S. Martin, A. R. Quirt, and K. E. Worvill. The NMR program library, Daresbury Laboratory, Daresbury, U.K.

Can. J. Chem. Downloaded from www.nrcresearchpress.com by 109.225.110.28 on 09/08/12
For personal use only.

19. T. Schaefer, R. Sebastian, and G. H. Penner. Can. J. Chem. **63**, 2597 (1985).
20. C. J. Macdonald and W. F. Reynolds. Can. J. Chem. **48**, 1002 (1970).
21. R. Wasylishen and T. Schaefer. Can. J. Chem. **50**, 1852 (1972).
22. T. Schaefer and C. A. Takeuchi. Can. J. Chem. **67**, 1022 (1989).
23. R. K. Kakar, E. A. Rinehart, C. R. Quade, and T. Kojima. J. Chem. Phys. **52**, 3803 (1970).
24. F. A. Miller, W. G. Fateley, and R. E. Witkowski. Spectrochim. Acta, Part A, **23**, 891 (1967).
25. L. A. Glebova, Y. A. Pentin, and V. I. Tyulin. Vestn. Mosk. Univ. Ser. 2, Khim. 21, (1980).
26. J. R. Durig, D. H. Bist, K. Furic, J. Qui, and T. S. Little. J. Mol. Struct. **129**, 45 (1985).
27. M. J. S. Dewar, E. J. Zoebisch, E. F. Healy, and J. J. P. Stewart. J. Am. Chem. Soc. **107**, 3902 (1985).
28. W. J. Hehre, R. Ditchfield, R. F. Stewart, and J. A. Pople. J. Chem. Phys. **52**, 2769 (1970).
29. M. S. Gordon, J. S. Binkley, J. A. Pople, W. J. Pietro, and W. J. Hehre. J. Am. Chem. Soc. **104**, 2797 (1982).
30. M. M. France, W. J. Pietro, W. J. Hehre, J. S. Binkley, M. S. Gordon, D. J. DeFrees, and J. A. Pople. J. Chem. Phys. **77**, 3654 (1982).
31. P. C. Hariharan and J. A. Pople. J. Am. Chem. Soc. **59**, 2301 (1937).
32. H. L. Goebel and H. H. Wenske. J. Am. Chem. Soc. **59**, 2301 (1937).
33. M. Barfield, C. J. Fallick, K. Hata, S. Sternhell, and P. W. Westerman. J. Am. Chem. Soc. **105**, 2178 (1983).
34. T. Schaefer and R. Laatikainen. Can. J. Chem. **61**, 2785 (1983).
35. C. W. Bock, M. Trachtman, and P. George. J. Comput. Chem. **6**, 592 (1985).

Can. J. Chem. Downloaded from www.nrcresearchpress.com by 109.225.110.28 on 09/08/12
For personal use only.

The conformational behavior of isobutylbenzene in CS_2/C_6D_{12} solution at 300 K

TED SCHAEFER AND LINA B.-L. LEE
Department of Chemistry, University of Manitoba, Winnipeg, Man., Canada R3T 2N2

Received February 24, 1992

TED SCHAEFER and LINA B.-L. LEE. Can. J. Chem. **70**, 2370 (1992).

The ^1H nuclear magnetic resonance spectrum of isobutylbenzene as a dilute solution in CS_2/C_6D_{12} at 300 K is analyzed. The *gauche* conformer (statistical weight 2) predominates, as was previously shown for a jet-cooled stream of this compound. The apparent twofold barrier to rotation about the Csp^2—Csp^3 bond is 10.5 ± 0.5 kJ/mol, as must be the case for the analogous *gauche* conformer of *n*-propylbenzene. The internal barriers are compared for ethylbenzene, *gauche* isobutylbenzene, and neopentylbenzene. AM1 and STO-3G MO computations of the conformer stabilities and barriers are reported, the latter being in better agreement with experiment.

TED SCHAEFER et LINA B.-L. LEE. Can. J. Chem. **70**, 2370 (1992).

On a analysé le spectre de résonance magnétique nucléaire du ^1H de l'isobutylbenzène, en solution diluée dans le CS_2/C_6H_{12}, à 300 K. Comme il a été démontré antérieurement pour un échantillon de ce composé existant sous la forme d'un écoulement refroidi par un jet, le conformère *gauche* (poids statistique de 2) prédomine. La barrière binaire apparente à la rotation autour de la liaison Csp^2—Csp^3 est de 10,5 ± 0,5 kJ/mol, comme ce doit être le cas pour le conformère *gauche* analogue du *n*-propylbenzène. On a comparé les barrières internes avec celles de l'éthylbenzène, de l'isobutylbenzène *gauche* et du néopentylbenzène. On rapporte les résultats obtenus par calculs d'OM AM1 et STO-3G des stabilités et des barrières; l'accord avec les résultats expérimentaux est meilleur dans le dernier cas.

[Traduit par la rédaction]

Can. J. Chem. Downloaded from www.nrcresearchpress.com by 109.225.110.28 on 09/08/12
For personal use only.

Introduction

Apart from their intrinsic interest, the potentials retarding the motion about the Csp^2—Csp^3 bond in alkylbenzenes are important in the study of liquid crystals (1, 2), many of whose molecules contain such fragments, and for the concept of 1,3-benzylic strain (3), used in the discussion of the stereoselectivity of attack by nucleophiles or electrophiles.

Apart from toluene, in which the internal rotational barrier is almost negligibly small (4), the alkylbenzene most investigated in this respect is ethylbenzene, **1**. Supersonic molecular, jet laser spectroscopy (5) and low- (6) and high- (7) resolution microwave spectra for the vapor show that **4** is the conformation of lowest energy; the latter spectra

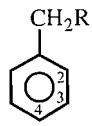

1, R = CH_3

2, R = $CH(CH_3)_2$

3, R = $C(CH_3)_3$

(7) are consistent with an internal barrier ranging from 4.9 to 7.8 kJ/mol, in rough agreement with various (7, 8) *ab initio* molecular orbital computations at the Hartree–Fock or post-Hartree–Fock level of theory, as well as with heat capacity data (9). In solution (8), the long-range coupling

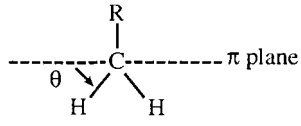

4, perpendicular

constant over six bonds between the methylene and *para* ring protons suggests that the conformational behaviour of ethylbenzene is the same in various solvents and that, if the barrier is purely twofold, its magnitude is $5.3_5 \pm 0.3_5$ kJ/mol.

At low temperatures in a molecular jet (10), the two-color time-of-flight mass spectra of **2**, isobutylbenzene, and its derivatives prove that **4** is the stable conformer, as expected on steric grounds, and further that, at low temperatures at least, the *gauche* conformer, **5**, is present to the exclusion of **6**. Molecular mechanics calculations (10) have **5** as

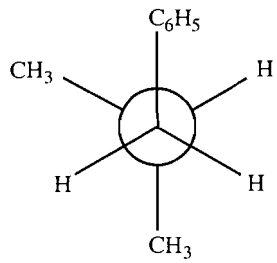

5

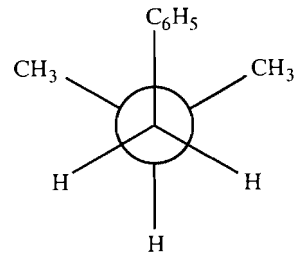

6

2.9 kJ/mol more stable than **6**, which is also disfavored by an entropy of $R \ln 2$. The barrier to rotation about the Csp^2—Csp^3 bond is not known.

In solution, the long-range coupling constant, $^6J(H, CH_2)$, will yield an estimate of the sp^2–sp^3 barrier and $^3J(CH, CH_2)$ in the side chain should confirm the predominant presence of **5**. If the barrier is predominantly of steric origin, that is, caused by repulsions between the group R and the *ortho* C—H bonds, then it should be larger in isobutylbenzene than in ethylbenzene, even if only **5** exists (models). This paper reports the analysis of the ^1H nmr spectrum of isobutylbenzene in a CS_2/C_6D_{12} solvent mixture and discusses the conformational information available from the coupling constants. Apparently the molecule has not been conformationally characterized in solution. The results of the present investigation allow a comparison of the barriers to rotation about the Csp^2—Csp^3 bonds as ethylbenzene is transformed, by successive substitution by methyl groups, into *n*-propyl, isobutyl, and neopentyl benzenes.

Experimental

A 4.0 mol% solution of isobutylbenzene (Aldrich) in a standard CS_2/C_6D_{12}/TMS/C_6F_6 solvent mixture (see Table 1) was filtered into a 5 mm o.d. nmr sample tube. The solution was degassed by five cycles of the freeze–pump–thaw procedure and was flame-sealed under vacuum. At a probe temperature of 300 K, ^1H nmr

TABLE 1. The ^{1}H nmr spectral parameters for isobutylbenzene as a 4.0 mol% solution in CS_2/C_6D_{12}[a] at 300 K

Parameter	Value	Parameter	Value
$\nu(CH_3)$	264.654(o)[b,c]	$^4J_{26}$	1.902(1)
$\nu(CH)$	543.179(2)	$^4J_{35}$	1.452(1)
$\nu(CH_2)$	724.2[d]	^5J(CH, H-2)[f]	0.038(2), 0.015(2)
ν_2	2101.218(1)	$^5J(CH_2, H-3)$	0.272(1)
ν_3	2136.725(1)	$^5J_{25}$	0.596(0)
ν_4	2109.823(1)	$^6J(CH_3, H-2)$	−0.001(1)
$^3J(CH, CH_3)$	6.613(1)[c]	^6J(CH, H-3)	0.001(1)
$^3J(CH, CH_2)$	7.154(1)	$^6J(CH_2, H-4)$	−0.374(1)
$^3J_{23}$	7.644(2)	^7J(CH, H-4)	−0.001(2)
$^3J_{34}$	7.431(1)	Calculated transitions	864[g] 539[h]
$^4J(CH_2, CH_3)$	−0.009(1)[e]	Assigned transitions	215 349
$^4J(CH_2, H-2)$	−0.538(1)	Observed peaks	190 total
$^4J_{24}$	1.271(1)	Largest difference	0.016 0.019
		Root-mean-square deviation	0.006 0.007

[a]4.0 mol% in CS_2, containing also 10 mol% of C_6D_{12} and 0.25 mol% each of tetramethylsilane (TMS) and C_6F_6.

[b]In Hz at 300.135$_2$ MHz to high frequency of internal TMS.

[c]Numbers in parentheses are standard deviations in the last significant figure.

[d]No transitions assigned, very small but finite coupling constants with the six methyl protons causing broadening of a strongly second-order pattern and exacerbated by the tightly coupled ring protons, all of which couple to these methylene protons.

[e]No direct evidence exists for this coupling constant, indirect evidence coming from the assigned transitions of the methyl protons and from the apparent broadening of the methylene proton peaks.

[f]The value of 0.038(2) Hz originates in the iterative analysis of the ^{1}H nmr spectrum of the side-chain protons as part of an A_6BC_2DD' spin system (D and D′ are the *ortho* ring protons) and unfortunately correlates by 0.87 with the chemical shift of the methine proton. The value of 0.015(2) Hz comes from the analysis of the spectrum of the ring protons as part of an $AB_2CC'DD'E$ spin system, that is, ignoring the methyl protons.

[g]Number of transitions calculated for the side-chain protons, there being many, essentially degenerate, transitions.

[h]Number of transitions calculated for the ring protons, again with many degenerate ones; note the essentially zero coupling constants, ^7J(CH, H-4) and ^6J(CH, H-3).

Can. J. Chem. Downloaded from www.nrcresearchpress.com by 109.225.110.28 on 09/08/12
For personal use only.

spectra were obtained on an AM 300 Bruker spectrometer, they employed digital resolution of 0.024 Hz/point, an acquisition time of 41 s per free induction decay; the latter were zero-filled twice or four times before transformation to the frequency domain.

Molecular orbital computations used the program GAUSSIAN 86 (11) on an Amdahl 5870 system. Geometry optimization procedures allowed bond angles and lengths to vary, with the constraint that the nuclei of the phenyl group remained in a plane. The AM1 parameterization (12) as well as the *ab initio* minimal basis set, STO-3G (13), were utilized. The latter basis set yields relative conformational energies for ethylbenzene very similar to those obtained from basis sets as large as 6-31G and 6-31G* (7, 8).

Results and discussion

Spectral analysis

The 14 protons of isobutylbenzene constitute an inconveniently large spin system. Fortunately, the methyl protons do not couple significantly to the ring protons, so that a composite analysis proved successful. The ^{1}H nmr spectrum of the side-chain protons was amenable to an analysis based on the spin system, A_6BC_2DD' (two magnetically nonequivalent *ortho* ring protons are included), while that of the ring protons yielded to an analysis based on $AB_2CC'DD'E$. The methine proton couples significantly to the *ortho* protons but its magnitude is somewhat imprecise, as seen in the collection of the spectral parameters in Table 1. The computer program NUMARIT (14), substantially modified by R. Sebastian in this laboratory, was used in the analytical procedures.

Figure 1 and its caption illustrate the spectral quality obtainable for the ring protons.

The apparent twofold barrier

Because $^6J(H, CH_2)$ is a pure σ–π coupling constant (15–20) and is therefore proportional to $\sin^2\theta$, where θ is the angle by which the α C-H twists away from the benzene plane (see **4**), a knowledge of $^6J_{90}$ yields the expectation value of $\sin^2\theta$. This quantity is related to the barrier to rotation about the Csp^2—Csp^3 via a hindered rotor model (21, 22) or a classical averaging procedure; the foldedness of the internal rotational potential enters into this relationship. $^6J_{90}$ depends on the electronegativity of the substituent, R; it is −1.204(4) Hz in toluene (19), R = H, and has been shown to be −0.941(4) Hz in benzyl fluoride, R = F (23). For R = OCH_3, $^6J_{90}$ is −1.02 Hz (24, 25). A linear interpolation implies $^6J_{90}$ as −1.16 Hz for the present molecule, as for ethylbenzene (8).

$^6J(H, CH_2)$ is −0.374(1) Hz for isobutylbenzene (Table 1). Hence $\langle\sin^2\theta\rangle$ at 300 K is 0.322(4), assuming an uncertainty of 0.01 Hz in $^6J_{90}$. Because a rigid **4** has $\langle\sin^2\theta\rangle$ as 0.25, and because a vanishing barrier implies a value of 0.5, it appears that **4** is also the stable conformation in solution. The apparent twofold barrier is 10.5 ± 0.5 kJ/mol, roughly twice that for ethylbenzene (8).

Although *ab initio* molecular orbital computations with geometry optimization would be very time-consuming with higher level basis sets, those with the minimal basis set,

Can. J. Chem. Downloaded from www.nrcresearchpress.com by 109.225.110.28 on 09/08/12
For personal use only.

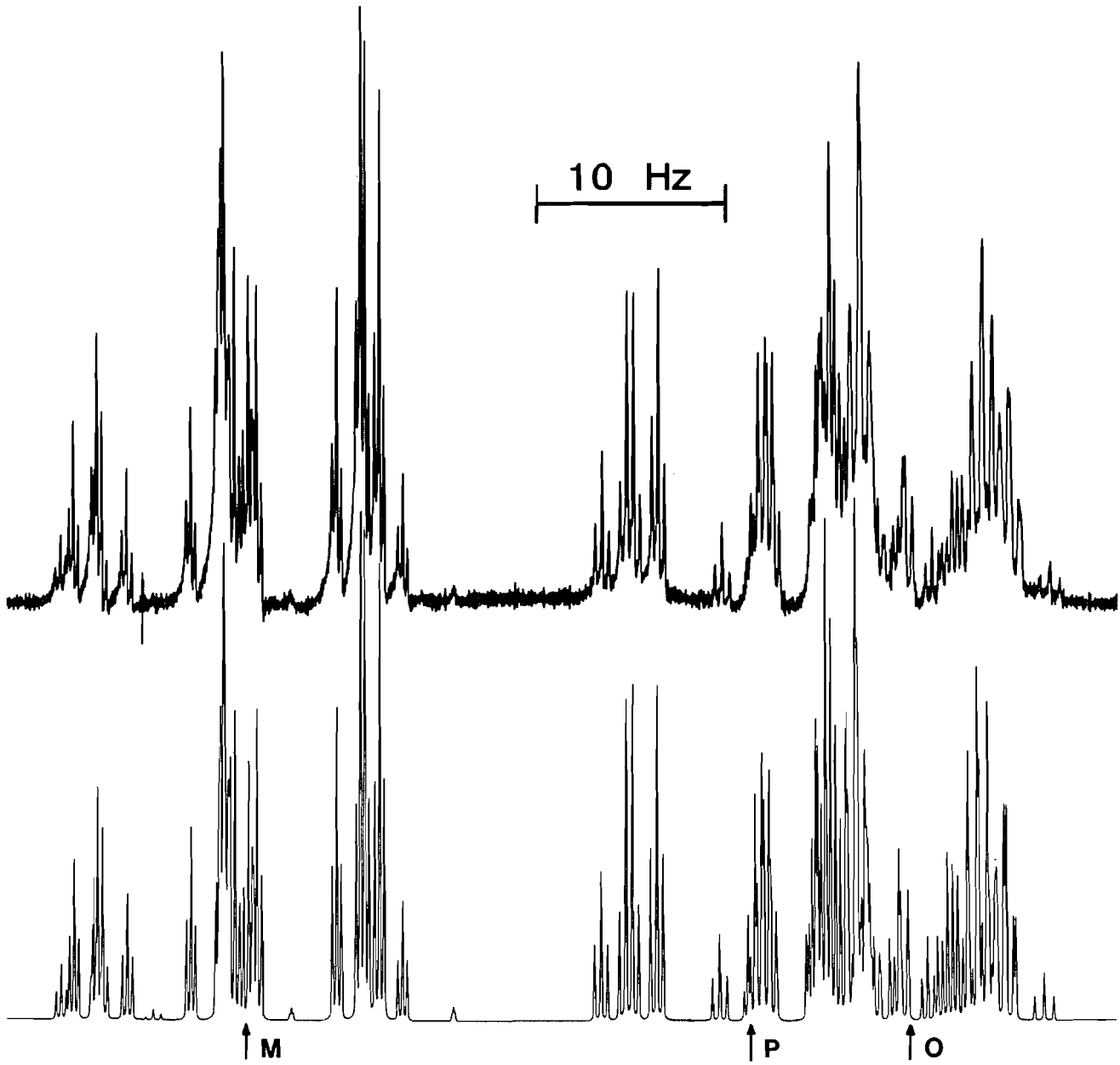

FIG. 1. The ^{1}H nmr spectrum at 300 MHz and 300 K of the ring protons of isobutylbenzene, as a 4.0 mol% solution in CS_2/C_6D_{12}, is displayed. The simulated spectrum employs the parameters in Table 1. The spacings in the triplets from the *meta* protons, when apparent, are about 0.25 Hz in magnitude. Some broadening of the peaks comes from small coupling interactions with the methine and methyl protons in the side chain (see the text and Table 1).

STO-3G, gave **4** as 11.1 kJ/mol more stable than the conformer in which the C(α)—C(β) bond lies in the benzene plane.[1] However, optimization for a range of twist angles gave a minimum energy for a conformation in which the C(α)—C(β) bond lies about 15° from the perpendicular, that is, from **4**. A fit to a Fourier series showed that this minimum must be attributed in the main to a strikingly large eightfold component of the barrier, 2.5 kJ/mol. This somewhat unexpected result can hardly be ruled out by the experimental value of 0.32_2 for $\langle \sin^2\theta \rangle$, the STO-3G data yielding 0.33_1 at 300 K.

[1]AM1 optimizations have this stability as 4.3 kJ/mol, very likely too low; such optimizations yield a barrier height of 2.3 kJ/mol for ethylbenzene, too low by at least a factor of two.

In this connection, the only other available computations (26) for the free molecule are those based on molecular mechanics (MM2 and CAMSEQ) in a comparative study of alkylbenzenes and some arylalkylamines of biological interest. The MM2 computations do indeed have a deviation of 8° from the perpendicular orientation in **4**, but also find **5** and **6** as isoenergetic, an unlikely result (see below). The CAMSEQ parameterization predicts no deviation from perpendicularity in **4**, but favors **5** by 8.4 kJ/mol over **6**, qualitatively correct. The MOMM numbers are 2.9 kJ/mol (10), agreeing with the present STO-3G result of 3.0 kJ/mol.

A rationalization of a small deviation from perpendicularity in the stable conformer, **4**, goes as follows. In **6**, both methyl groups are situated over the phenyl group and, by symmetry, the conformer is perpendicular (make models).

Can. J. Chem. Downloaded from www.nrcresearchpress.com by 109.225.110.28 on 09/08/12
For personal use only.

Now, **6** is certainly less stable than **5**. Apart from an entropy term (see below), attribution of the instability to repulsion between the methyl groups and the phenyl group implies that such a repulsion for a single methyl group in **5** is relieved by a small twist from the perpendicular, increasing the distance between the methyl and phenyl electron clouds. That is indeed the direction of twist predicted by the STO-3G MO computations. Such a rationalization needs support from high-level molecular orbital calculations, which are costly. They would be of real interest, however, because of recent discussions of the nature, attractive or repulsive, of the forces between the π system of the phenyl group and the alkyl group (27).

In this connection, it is of interest that, in CS_2 solution, the enthalpy difference favoring the *trans* conformer of *n*-propyl-3,5-dibromobenzene is 1.9 kJ/mol at 305 K (28). The *gauche* conformer has an additional entropy of R ln 2, so that in solution at this temperature, the *gauche* and *trans* conformers are of roughly equal abundance. In the gas phase at low temperatures, both conformers exist (10) and MOMM computations imply a steric destabilization energy of 1.6 kJ/mol in the *gauche* form. Furthermore, it was predicted that $^6J(H, CH_2)$ in the *gauche* form would be -0.38 Hz (28), very close to the -0.37 Hz now measured for isobutylbenzene, which in solution exists predominantly in the *gauche* form (see below). In that case, rotations about the Csp^2—Csp^3 bonds in the *gauche* forms of *n*-propylbenzene and of isobutylbenzene involve the close approach of one methyl group to the *ortho* C—H bonds; hence they should have very similar barriers and $^6J(H, CH_2)$ values.

In summary, STO 3G MO optimizations predict a barrier height of 6.6 and 12.5 kJ/mol for ethyl (8) and isobutylbenzene, respectively, whereas the apparent twofold barriers in solution are $5.3_5 + 0.3_5$ and 10.5 ± 0.5 kJ/mol. The substitution by one more methyl group, to give neopentylbenzene, **3**, causes at least a second doubling of the experimental internal barrier (29, 30), presumably because of the greater difficulty experienced by the methyl groups in avoiding close H,H contacts with the *ortho* C—H bonds at the height of the barrier.

*The equilibrium between **5** and **6** in solution*

The symmetrical conformer, **6**, is not detectable at low temperatures in a jet-cooled stream (10). In the CS_2 solution at 300 K, $^3J(CH, CH_2)$ is 7.15_4 Hz and is a population weighted average of $(^3J_g + {}^3J_t)/2$ in **5** and $^3J'_g$ in **6**, the two *gauche* coupling constants, ^3J_g and $^3J'_g$, not necessarily being equal. If the barrier to interconversion of **5** and **6** is large compared to thermal energies, as is probably true (31), then the implied assumption of a two-site equilibrium is reasonably reliable.[2] The vicinal coupling constants, in addition to their dihedral angle dependence, are also sensitive to substituent electronegativity and other perturbations. Fortunately, a thorough study of 2-methylbutane (replace the phenyl by a methyl group) exists. Here the equivalent $(^3J_g + {}^3J_t)/2$ and ^3J_g are determined as 7.06 ± 0.01 and 3.52 ± 0.13 Hz, respectively. It is assumed that R ln 2 represents the entropy difference between the conformers analogous to **5** and **6** (32). The application of the parameters for the butane derivative to isobutylbenzene, yields the fractional population of **5** as 1.02 ± 0.01, apparently absurd.

Of course, the electronegativities of phenyl and methyl groups are not identical and the relevant torsion angles may well deviate from regular tetrahedral values by different amounts in **5** and **6** as compared to the analogous conformers of the butane derivative. Another estimate of the population of **5** can be had from the estimates of 12.5 and 2.5 Hz for ^3J_t and ^3J_g in 2,4-diphenylpentane, in which a phenyl group, a methyl group, and an sp^3 carbon centre are bonded to the coupling fragment (33). These numbers, applied to isobutylbenzene, yield the fractional population of **5** as 0.93, using now the relationship $7.15 = P_5\ (12.5 + 2.5)/2 + (1 - P_5)\ 2.5$. It appears that **5** does indeed predominate in CS_2 solution at 300 K. A population of 0.93 would correspond to a free energy difference of 6.4 kJ/mol and an enthalpy difference of 4.7 kJ/mol, favoring **5**.

(i) Absence of $^4J(CH_2, CH_3)$

The iterative analysis of the ^{1}H nmr spectrum gave $^4J(CH_2, CH_3)$ as $-0.009(1)$ Hz; actual splittings assignable to this coupling constant were not detected, although the methyl doublet does display some fine structure, but due to second-order perturbations. Using the theoretical values in column D of ref. 34, $^4J(CH_2, CH_3)$ is calculated as -0.04 Hz in **5** and 0.14 Hz in **6**. These numbers are based on regular tetrahedral geometries and the theoretical values for various dihedral angles are also somewhat uncertain (34), so that this comparison can only be said to indicate consistency with a preponderance of **5** in solution.

(ii) Ring proton, methine proton coupling, $^5J(CH, H\text{-}2)$

Two values for the coupling constant between the methine and *ortho* ring protons came from the separate analyses of the side-chain and ring proton spectra. The A_6BC_2DD' system gave ^5J as 0.038(2) Hz while that of $AB_2CC'DD'E$ yielded 0.015(2) Hz. The larger value correlates by 0.87 with the chemical shift of the methine proton and is very likely not as reliable as the smaller value. The finite value of ^5J quite possibly arises from a close approach of the two C—H bonds carrying the coupled nuclei. As the molecule twists about the Csp^2—Csp^3 bond in the predominant *gauche* conformer (models), the hydrogen atoms of the two bonds could come within 1.8 Å of each other at the extremes of the motion, leading to proximate coupling interactions. In the minor conformer, **6**, this situation does not obtain. The absence of significant coupling between the methyl and ring protons may well be a consequence of the fact that, in the *gauche* conformer, the protons in the distant methyl group remain far from the *ortho* C—H bonds; any coupling interactions are averaged over *all* methyl protons, of course. It seems highly probable that significant coupling constants would be observed in **6** between methyl and *ortho* ring protons (through-space interactions).

(iii) $^4J_o(H\text{-}2, CH_2)$ and $^5J_m(H\text{-}3, CH_2)$

J_o (H-2, CH_2) $\equiv {}^4J_o$ is $-0.538(1)$ Hz and contains a σ in addition to the σ–π component. For toluene, the theoretical expression is $^4J/\text{Hz} = -1.08\ \langle\sin^2\theta\rangle - 0.32\ \langle\cos^2\theta\rangle$, the first term representing the σ–π contribution (35), and predicts -0.70 Hz for $^4J(H,CH_3)$, precisely as measured (19). Just as for $^6J_{90}$, the coefficient of $\langle\sin^2\theta\rangle$ should be reduced by a factor of 1.16/1.20, to yield -1.04 Hz. Based on a $\langle\sin^2\theta\rangle$ of 0.322, obtained from $^6J(H, CH_2)$ above, one has ^4J_o as -0.552 Hz; the $\langle\sin^2\theta\rangle$ from the STO-3G potential, 0.332, entails a ^4J_o of -0.559 Hz. However, a reduction of the

[2]Of course, if the interconversion barrier is not large compared to kT, then the dihedral angle takes on many values other than 60° (^3J_g) or 180° (^3J_t) with high probabilities, and a procedure similar to that described above for ^6J would become essential.

magnitude of the coefficient of $\langle\cos^2\theta\rangle$, from 0.32 to 0.30 Hz, would produce exact agreement with experiment. It is reasonable to conclude that ^4J_o is compatible with the STO-3G potential as well as with an apparent twofold barrier of 10.5 ± 0.5 kJ/mol.

Again, ^5J_m (H-3, CH_2) ≡ ^5J_m is a function of $\langle\sin^2\theta\rangle$ and $\langle\sin^2(\theta/2)\rangle$. The equation suggested for toluene (19) yields ^5J_m in isobutylbenzene as 0.266 and 0.269 Hz, respectively, according to the $\langle\sin^2\theta\rangle$ values from ^6J(H, CH_2) or from the STO-3G potential. The measured ^5J_m is 0.272(1) Hz.

Conclusion

The apparent twofold barrier to rotation about the Csp^2—Csp^3 bond in isobutylbenzene, existing predominantly as the *gauche* conformer at 300 K, is 10.5 ± 0.5 kJ/mol, very close to that in the *gauche* conformer of *n*-propylbenzene (28), and roughly twice that in ethylbenzene (7, 8) and the *trans* conformer of *n*-propylbenzene (28). Substitution by another methyl group at the β carbon atom of isobutylbenzene, to produce neopentylbenzene, raises this barrier to greater than 20 kJ/mol (29, 30); the methyl groups are now unable easily to avoid the *ortho* C—H bonds of the benzene moiety. All these statements refer to experimental results in solution.

Acknowledgments

We thank the Natural Sciences and Engineering Research Council of Canada for financial, and R. Sebastian for other, assistance. We thank the referees for helpful criticism.

1. D. J. Photimes, E. T. Samulski, and H. Toriumi. J. Chem. Phys. **94**, 2758 (1991).
2. A. Ferrarini, G. J. Moro, and P. L. Nordio. Liquid Cryst. **8**, 593 (1990).
3. J. L. Broeker, R. W. Hoffmann, and K. N. Houk. J. Am. Chem. Soc. **113**, 5006 (1991).
4. H. D. Rudolph, H. Dreizler, A. Jaeschke, and P. Wendling. Z. Naturforsch. A: Astrophys. Phys., Phys. Chem. **22**, 940 (1967).
5. P. J. Breen, E. R. Bernstein, and J. I. Seeman. J. Chem. Phys. **87**, 3269 (1987).
6. N. S. True, M. S. Farag, R. K. Bohn, M. A. McGregor, and J. Rahdakrishnan. J. Phys. Chem. **87**, 4622 (1983).
7. W. Caminati, D. Damiani, G. Corbelli, B. Velino, and C. W. Bock. Mol. Phys. **74**, 885 (1991).
8. T. Schaefer, G. H. Penner, and R. Sebastian. Can. J. Chem. **65**, 873 (1987).
9. A. Miller and D. W. Scott. J. Chem. Phys. **68**, 1317 (1978).
10. J. I. Seeman, H. V. Secor, P. J. Breen, V. H. Grassian, and E. R. Bernstein. J. Am. Chem. Soc. **111**, 3140 (1989).
11. M. J. Frisch, J. S. Binkley, H. B. Schlegel, K. Raghavachari, C. F. Melius, R. L. Martin, J. J. P. Steward, F. W. Bobrowicz, D. F. Rohlfing, L. R. Kahn, D. J. Defrees, R. Seeger, R. A. Whiteside, D. J. Fox, E. M. Fluder, and J. A. Pople. Carnegie–Mellon Quantum Publishing Unit, Pittsburgh, Pa. 1984.
12. M. J. S. Dewar, E. J. Zoebisch, E. F. Healy, and J. J. P. Stewart. J. Am. Chem. Soc. **107**, 3902 (1985).
13. W. J. Hehre, R. Stewart, and J. A. Pople. J. Chem. Phys. **51**, 2657 (1969).
14. J. S. Martin, A. R. Quirt, and K. E. Worvill. The NMR program library, Daresbury, Laboratory, Daresbury, U.K.
15. C. J. Macdonald and W. F. Reynolds. Can. J. Chem. **49**, 94 (1971).
16. M. Barfield and B. Chakrabarti. J. Am. Chem. Soc. **91**, 4346 (1969).
17. R. Wasylishen and T. Schaefer. Can. J. Chem. **50**, 1852 (1972).
18. J. B. Rowbotham and T. Schaefer. Can. J. Chem. **52**, 496 (1974).
19. T. Schaefer, R. Sebastian, and G. H. Penner. Can. J. Chem. **63**, 2597 (1985).
20. T. Schaefer and C. S. Takeuchi. Can. J. Chem. **67**, 1022 (1989).
21. P. B. Ayscough, M. S. Brice, and R. E. D. McClung. Mol. Phys. **20**, 41 (1971).
22. W. J. E. Parr and T. Schaefer. Acc. Chem. Res. **13**, 400 (1980).
23. T. Schaefer, C. Beaulieu, R. Sebastian, and G. H. Penner. Can. J. Chem. **68**, 591 (1990).
24. R. Laatikainen. Magn. Reson. Chem. **24**, 588 (1986).
25. R. Laatikainen and K. Tuppurainen. J. Chem. Soc. Perkin Trans. 2, 121 (1987).
26. G. L. Grunewald, M. W. Creese, and H. J. R. Weintraub. J. Comput. Chem. **9**, 315 (1988).
27. M. Nishio and M. Hirota. Tetrahedron, **45**, 7201 (1989), and references therein.
28. T. Schaefer, L. J. Kruczynski, B. Krawchuk, R. Sebastian, J. L. Charlton, and D. M. McKinnon. Can. J. Chem. **58**, 2452 (1980).
29. S. Andersson and T. Drakenberg. Org. Magn. Reson. **21**, 730 (1983), and references therein.
30. T. Schaefer, G. H. Penner, C. S. Takeuchi, and C. Beaulieu. Can. J. Chem. **67**, 1283 (1989).
31. K. W. Wiberg and M. A. Murcko. J. Am. Chem. Soc. **110**, 8029 (1988).
32. R. L. Lipnick and E. W. Garbisch, Jr. J. Am. Chem. Soc. **95**, 6375 (1973).
33. F. A. Bovey, F. P. Hood, E. W. Anderson, and L. C. Synder. J. Chem. Phys. **42**, 3900 (1965).
34. M. Barfield, A. M. Dean, C. J. Fallick, R. J. Spear, S. Sternhell, and P. W. Westerman. J. Am. Chem. Soc. **97**, 1482 (1975).
35. M. Barfield, C. J. Fallick, K. Hata, S. Sternhell, and P. W. Westerman. J. Am. Chem. Soc. **105**, 2178 (1983).

Can. J. Chem. Downloaded from www.nrcresearchpress.com by 109.225.110.28 on 09/08/12
For personal use only.

Nonbonded C=O · · · S and C—H · · · S interactions in 2-(4-chlorophenylthio) benzaldehyde in solution. An average skew conformation

TED SCHAEFER, LINA B.-L. LEE, AND RUDY SEBASTIAN
Department of Chemistry, University of Manitoba, Winnipeg, Man., Canada R3T 2N2

Received March 16, 1992

TED SCHAEFER, LINA B.-L. LEE, and RUDY SEBASTIAN. Can. J. Chem. **70**, 2375 (1992).

The ^{1}H nuclear magnetic resonance spectral parameters are reported for 4.0 mol% solutions of 2-(4-chlorophenylthio) benzaldehyde in CS_2/C_6D_{12} and acetone-d_6 at 300 K. In CS_2 the *O-syn* conformer is 36% abundant, rising to 50% in acetone-d_6. These abundances are compared to those of the *O-syn* and *O-trans* conformers of 2-(alkylthio) benzaldehydes in CCl_4 solution. On the basis of coupling constants and chemical shifts it is concluded that the skew conformer of the title compound is very likely the one of minimum energy in both solutions. In the skew conformer the plane of the 4-chlorophenyl group lies perpendicular to the CSC plane and also to that of the other aromatic moiety. It is suggested that the S · · · O interaction is rather weak and that the population of the *O-syn* conformer is controlled by the orientation of the mainly 3*p* lone-pair orbital on sulfur. At best, the S · · · O interaction is attractive only when the 3*p* orbital lies perpendicular to the plane of the formyl group. The skew conformation of the title compound is contrasted to the skew conformation of 2-hydroxyphenyl phenyl sulfide in which, however, the role of the two aromatic planes is reversed; the 3*p* orbital now lies in or near the plane of the phenyl group COH due to an attractive O—H · · · 3*p* interaction.

TED SCHAEFER, LINA B.-L. LEE et RUDY SEBASTIAN. Can. J. Chem. **70**, 2375 (1992).

Opérant à 300 K, on a déterminé les paramètres spectraux en résonance magnétique nucléaire du ^{1}H du 2-(4-chlorophénylthio) benzaldéhyde en solution à 4 mol% dans le CS_2/C_6D_{12} et dans l'acétone-d_6. L'abondance du conformère *O-syn* est de 36% dans le CS_2 et elle atteint 56% dans l'acétone-d_6. On a comparé ces abondances à celles des conformères *O-syn* et *O-trans* des 2-(alkylthio) benzaldéhydes en solution dans le CCl_4. En se basant sur les constantes de couplage et sur les déplacements chimiques, on arrive à la conclusion que le conformère *gauche* du composé mentionné dans le titre est très probablement celui qui possède l'énergie minimale dans les deux solutions. Dans le conformère *gauche*, le plan du groupe 2-chlorophényle se trouve dans un plan perpendiculaire à celui du CSC et également au plan de l'unité aromatique. On suggère que l'interaction S · · · O est plutôt faible et que la population du conformère *O-syn* est principalement contrôlée par l'orientation du doublet libre de l'orbitale 3*p* du soufre. Cette interaction S · · · O n'est optimale que lorsque le plan des orbitales 3*p* est perpendiculaire à celui du groupe formyle. La conformation *gauche* du composé mentionné dans le titre est à l'opposé de la conformation *gauche* du sulfure de phényle et de 2-hydroxyphényle dans lequel, cependant, le rôle des deux plans de la portion aromatique est inversé; l'orbitale 3*p* se trouve maintenant dans le plan ou près du plan du groupe phényle COH à cause d'une interaction attractive OH · · · 3*p*.

[Traduit par la rédaction]

Can. J. Chem. Downloaded from www.nrcresearchpress.com by 109.225.110.28 on 09/08/12
For personal use only.

Introduction

A recent review (1) discusses extensive investigations of nonbonded sulfur–oxygen interactions, those in the so-called donor–acceptor region. The S · · · O distances span 2.3–3.2 Å, less than the sum of the van der Waals distances but greater than covalent bond lengths. Semi-quantitative interpretations of these phenomena have been given in terms of valence bond and molecular orbital models (2).

For divalent sulfur, an electrostatic model has some predictive power (3, 4). This model recognizes the relatively large difference in energy between the 3*s* and 3*p* orbitals on sulfur and the concomitant tendency to keep the 3*s* orbital fully occupied during bond formation (5, 6). In addition, for sulfur the 3*p* orbital extends significantly farther from the atomic centre than does the 3*s* orbital (7), in contrast to the situation in oxygen, for example. Hence a qualitative model, in which the two pairs of lone electrons on sulfur are distinguished by their mainly 3*s* and 3*p* characters, rationalizes the fact, pertaining to crystal structures, that electrophiles favor an approach perpendicular to the X—S—Y plane, in line with the directional 3*p* lone-pair. Nucleophiles orient preferentially in the X—S—Y plane, away from the X—S and X—Y bonds (8, 9). Such a model also allows an easy interpretation of the observation that 2-hydroxythiophenol adopts the conformation **2**, and not **1**, in solution (3). The polar O^-—H^+ bond overcomes the 3*p* · · · π conjugative stabilization of **1**

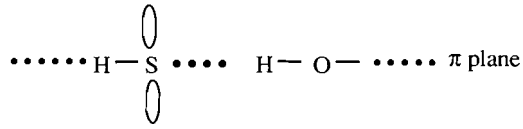

1

2

and twists the mainly 3*p* orbital into the aromatic plane, to produce **2**. Again, the structure of the H_2S,HF and H_2S,HCl complexes in the gas phase, in which the HX direction lies roughly perpendicular to the HSH plane, is in line with such a model (10, 11).

More particularly, in the crystal, methyl 2-(methylthio) benzoate, **3**, is planar, the SCH_3 conjugating with the aryl

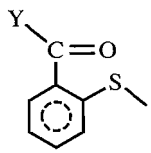

3 Y = OCH_3, R = CH_3

4 Y = OCH_3, R = 4-NO_2-C_6H_4

ring. The C=O bond is strongly ionic (12, 13), qualitatively accounting for the observed structure (electrostatics).

Can. J. Chem. Downloaded from www.nrcresearchpress.com by 109.225.110.28 on 09/08/12
For personal use only.

If Y = OCH_3 and R = 4-NO_2-C_6H_4, then the conformation is skew, that is, the 4-nitrophenyl group lies nearly perpendicular to the plane of the page in **4** (14). This conformation is taken (14) to mean that the S · · · O interaction dominates the conjugative interaction between the 3*p* lone-pair and the 4-nitrophenyl moiety; in **4** the 3*p* orbital lies effectively in the plane of the latter (low conjugation). Presumably this conclusion depends also on the assumption that the *ortho* ester and the *para* nitro groups are roughly equally strong π-electron acceptors.

While it appears likely that the S · · · O interaction in **3** and **4** is attractive, sulfur being relatively easily polarized by the $\overset{+}{C}\text{---}\overset{-}{O}$ bond, the argument might well be stronger were Y = H in **3** and **4**. For, it is known (15) that for 2-(methylthio) benzaldehyde, in CCl_4 solution at 305 K, the *O-syn* is less abundant than the *O-trans* conformer, being present to the extent of 40% only. Furthermore, as the methyl group is successively replaced by ethyl, isopropyl, and *tert*-butyl groups, the proportion of the *O-syn* conformer decreases monotonically and is not detectable for the *tert*-butyl derivative. In the latter, the 3*p* lone pair lies mainly in the ring plane and repels the C=O bond. On the basis of ^{13}C nmr chemical shifts and spin–spin coupling constants (16) it is estimated that the perpendicular conformer of *tert*-butyl phenyl sulfide is about 18 kJ/mol more stable than the planar. Consequently the S · · · O interaction is attractive by less than 18 kJ/mol in 2-(*tert*-butylthio) benzaldehyde.

Here we report ^1H nmr spectra of 2-(4-chlorophenylthio) benzaldehyde in CS_2 and acetone-d_6 solutions. If, by analogy to **4** in the crystal, a strong S · · · O attraction dominates the conformational properties, then **5** will predominate. Yet, the skew conformer may be a consequence of the cross-conjugation between the π donor and acceptor (17), in which case the *O-syn* orientation need not be dominant. The stereospecific coupling constant over five formal bonds, ^5J(H, CHO), is a good measure of the *O-syn/O-trans* equilibrium. In **5**, for example, ^5J(H-5, CHO) will be very small or undetectable (15, 18), whereas ^5J(H-3, CHO) will be 0.8 Hz or larger. Again, if the skew conformation is strongly stabilized, then H-3, for example, lies in the shielding cone of the C_6H_4Cl groups and should undergo a characteristic shift to low frequency. Any shift in the *O-syn/O-trans* equilibrium between nonpolar and polar solutions would provide evidence for the importance of intermolecular perturbations of S · · · O interactions.

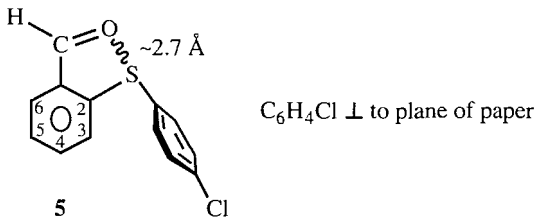

C_6H_4Cl ⊥ to plane of paper

5

In **5**, the 3*p* orbital is situated in the plane of the C_6H_4Cl group, so that delocalization into the other π-electron system is favored, as expected from cross-conjugation with the π-electron acceptor, the formyl group. The mobile bond order of the S—C_6H_4Cl bond is reduced relative to the other C—S bond, allowing the chlorophenyl plane to orient so as to reduce steric repulsions from the H-3 bond in **5**. On the other hand, a gable (butterfly) conformation also minimizes such repulsions, but places the 3*p* orbital into both aromatic planes. Then only the *O-trans* conformer is expected, together with very little screening of ring protons from delocalization of 3*p* density into the π orbitals of the aromatic moieties.

The chlorine substituent, while providing a polar C—X bond, is not a strong π-electron acceptor or donor, perturbs the shielding of *ortho* and *para* protons relatively little (19), and hence makes possible the disentanglement of spectral peaks arising from the protons in the two aromatic rings.

Experimental

The title compound, from Maybridge Chemicals, was dissolved in CS_2/C_6D_{12}/TMS and acetone-d_6/TMS solvent mixtures (see Table 1 for details). The solutions were filtered into 5 mm o.d. nmr sample tubes. These were degassed by five cycles of the freeze–pump–thaw procedure and were then flame-sealed to produce reasonably symmetric tops.

The ^1H nmr spectra were obtained from a Bruker AM 300 spectrometer at a probe temperature of 300 K. Final shimming was done manually on the free induction decay of tetramethylsilane, the internal reference. Using an acquisition time of 41 s and a digital resolution of 0.006 and 0.012 Hz/point, 64 decays were coadded. Zero-filling to twice the original data, followed by a small amount of resolution enhancement (see Fig. 1) produced peak widths at half height of as little as 0.05 Hz.

Results and discussion

Spectral analyses

The computer program NUMARIT (20), extensively modified by R. Sebastian, was employed to extract the spectral parameters displayed in Table 1. Fortunately, the chemical shift between the protons of the S-C_6H_4-Cl fragment was small, causing a few intense peaks that did not obscure any peaks from the protons in the other fragment of the molecule. Simulation of the AA′BB′ spectra, assuming additivity of substituent perturbations of the coupling constants in benzene (21, 22), demonstrated that the internal chemical shift was ≤0.003 ppm in CS_2 solution and 0.013(1) ppm in acetone-d_6 solution. The sign of the first value could not be determined reliably, but, for the acetone-d_6 solution, small interring, through-space, coupling constants involving H-3 in **5** showed that the protons *meta* to chlorine were more shielded than those placed *ortho* to this substituent.

The O-syn/O-trans *equilibrium*

Previous discussions (15, 18, 23) of the stereospecificity of ^5J(H, CHO) show that ^5J(H-3, CHO)/^5J(H-5, CHO) is a reasonably accurate measure of the ratio of the *O-syn* to *O-trans* populations in benzaldehyde derivatives. The data in Table 1 therefore imply that the *O-syn* fractional population is 0.36 in the CS_2/C_6D_{12} solution at 300 K and is 0.50 in acetone-d_6 solution, corresponding to an increase in stabilization by 1.4 kJ/mol in free energy in the polar solvent. The *O-syn* population in the nonpolar solvent is very similar to that of 0.41 deduced for 2-(methylthio) benzaldehyde (15) as a 4 mol% solution in CCl_4 at 305 K (a 4.0 mol% solution of 2-(4-chlorophenylthio) benzaldehyde in CCl_4 solution gave an ^1H nmr spectrum for the formyl proton that was almost identical to that in CS_2 solution, implying a negligible difference of *O-syn* populations in the two solutions).

In this connection, it is of interest that a recent study of the torsional motion of the thiomethyl group in the thiomethyl compound deduces an average twist angle, actually arc cos $\langle\cos^4\theta\rangle^{1/4}$, of 19(2)°, roughly 7(3)° lower than for thioanisole (24). This result is in qualitative agreement with

TABLE 1. The ^{1}H nmr spectral parameters for dilute solutions of 2-(4-chlorophenylthio) benzaldehyde in CS_2/C_6D_{12} and acetone-d_6 solutions at 300 K

Parameter	Solvent		Parameter	Solvent	
	CS_2/C_6D_{12}[a]	Acetone-d_6		CS_2/C_6D_{12}[a]	Acetone-d_6[b]
ν(CHO)	3083.436[c,d]	3104.522	$^5J_{36}$	0.472	0.468
ν_3	2121.646	2142.160	^4J(H-6, CHO)	−0.157	−0.182
ν_4	2202.474	2261.692	^5J(H-3, CHO)	0.305	0.406
ν_5	2183.562	2235.015	^5J(H-5, CHO)	0.534	0.412
ν_6	2331.018	2382.648	^6J(H-4, CHO)	−0.023	−0.009
$^3J_{34}$	7.977	8.025	Transitions calculated	83[e]	80[e]
$^3J_{45}$	7.313	7.350	Transitions assigned	76	74
$^3J_{56}$	7.676	7.673	Peaks observed	61	59
$^4J_{35}$	1.127	1.091	Largest difference	0.020	0.006
$^4J_{46}$	1.614	1.603	Root-mean-square deviation	0.006	0.002

[a]As a 4.0 mol% solution in CS_2, containing also 10.0 mol% of C_6D_{12} and 0.5 mol% of TMS.
[b]As a 4.0 mol% solution in acetone-d_6, containing also 0.5 mol% of TMS.
[c]In Hz at 300.135$_2$ MHz to high frequency of internal TMS.
[d]In the CS_2 solution, the standard deviations in the last significant figures are all 0.002 Hz while in acetone-d_6 solution they are 0.001 Hz or less.
[e]For the benzaldehyde ring. For the C_6H_4Cl group, the chemical shifts of the *ortho* and *meta* protons are 7.244 ± 0.006 ppm in the CS_2 solution; in acetone-d_6 solution, the protons *ortho* to chlorine resonate at 7.465(1) ppm, those *meta* at 7.451(1) ppm relative to TMS.

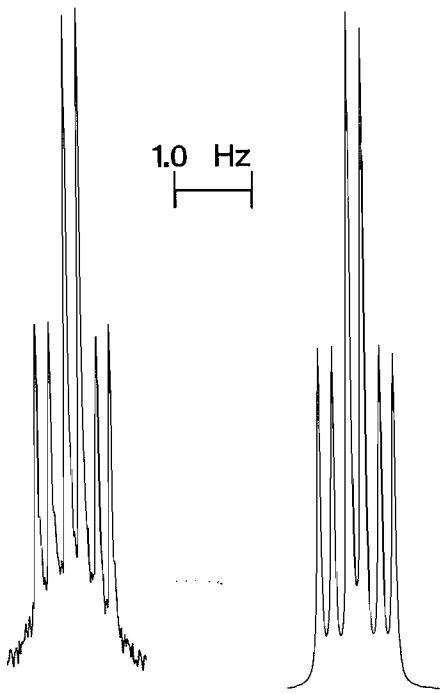

FIG. 1. The ^{1}H nmr spectrum at 300 MHz of the formyl proton is shown for a 4.0 mol% solution of 2-(4-chlorophenylthio) benzaldehyde in acetone-d_6 at 300 K. The computed spectrum assumes the spectral parameters in Table 1. ^5J(H-3, CHO) and ^5J(H-5, CHO) differ by 0.006(2) Hz, according to the full analysis, causing the 1:2:1 appearance of spectrum, the line widths being 0.05 Hz. The small splittings arise from ^4J(H-6, CHO), which is −0.182(1) Hz.

the small increased shielding of the proton placed *para* to the thiomethyl group in this compound, a lower average twist angle allowing more effective $3p \cdots \pi$ conjugation (25).

Treating 2-(methylthio) benzaldehyde as planar allows a comparison with a recent molecular orbital computation (2) of the relative energies of the model conformers **6** and **7**. The energy of **6** is computed as lower than that of **7** by 0.54, 3.72, and 12.0 kJ/mol with the basis sets STO-3G, 3-21G,

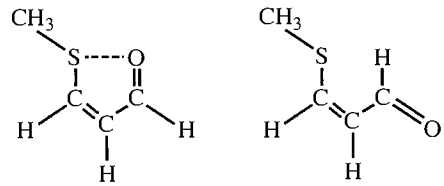

6 **7**

and 3-21G augmented with sulfur *d* orbitals, respectively. Insofar as **6** and **7** model 2-(methylthio) benzaldehyde and insofar as differences in the entropies and zero-point energies of the two conformers are small, none of the computations agree with the experimental free energy difference of 0.9 kJ/mol favoring the *O-trans* conformer in CCl_4 solution at 305 K. Accordingly, geometry-optimized STO-3G MO computations on the planar *O-syn* and *O-trans* conformers of 2-(methylthio) benzaldehyde were performed, with the result that the *O-syn* was calculated as *less* stable than the *O-trans* conformer by 1.88 kJ/mol. If this energy difference is equated to a difference in free energy, then the *O-syn* abundance is 32% at 300 K. The measured value is 41% in CCl_4 solution.

Experimentally, it appears that the *O-syn* population is controlled by the extent to which the 3*p* orbital twists into the benzene plane. The arc sin $\langle \sin^2\theta \rangle^{1/2}$ values, rough measures of average torsion angles, for C_6H_5—S—R in solution are 31, 40, 49, and 74° for R = CH_3, CH_2CH_3, $CH(CH_3)_2$, and $C(CH_3)_3$, respectively (16). For the corresponding 2-(S—R) benzaldehydes, the *O-syn* populations in CCl_4 solutions are 0.41, 0.23, 0.09, and 0.0, implying that no significant *O-syn* population occurs for an average twist

Can. J. Chem. Downloaded from www.nrcresearchpress.com by 109.225.110.28 on 09/08/12
For personal use only.

Can. J. Chem. Downloaded from www.nrcresearchpress.com by 109.225.110.28 on 09/08/12
For personal use only.

angle of as low as 60°. If, however, arc cos $\langle \cos {}^4\theta \rangle^{1/4}$ values are used for thioanisole and 2-(methylthio) benzaldehyde, which are 26° and 19°, respectively (25), and the additional assumption is made that similar differences exist for the other alkyl groups, then this limiting twist angle becomes about 50°, approximately half way to coplanarity of the 3*p* orbital with the aromatic ring.

The barriers to rotation about the Csp^2—S bond of C_6H_5SR in solution are 5.4, 1.9, −1.4, and 18.8 kJ/mol, respectively (16), for the sequence R = CH_3 to $C(CH_3)_3$, a negative number indicating that the planar conformation is least stable, whereas the free energy differences favoring the *O-trans* conformer are 0.9, 3.1, and 5.9 kJ/mol in the sequence R = CH_3, CH_2CH_3, $CH(CH_3)_2$. Allowance of, say, a 5–10% error in all these numbers (18, 26) emphasizes the similarity in the range of the two energy sequences and, by implication, the relatively weak S · · · O interaction.

Now, in 2-(4-chlorophenylthio) benzaldehyde the *O-syn* population is nearly that for the 2-methylthio derivative. Hence the skew conformation, **5**, analogous to **4** in the crystal, appears likely in solution; a twisted conformation, as in diphenyl sulfide (17, 27, 28), would display a substantial twist about the Csp^2—S bond of the benzaldehyde ring and therefore a lower *O-syn* population.

The average conformation of 2-(4-chlorophenythio) benzaldehyde

(i) Ring proton shifts

Relative to those in benzaldehyde, at the same concentrations in the same solvent mixtures (29), the chemical shifts are shown in **8**. Those in parentheses are for the acetone-d_6 solution, given in ppm, positive values indicating an increase in shielding relative to benzaldehyde. In the putative skew conformation, oscillations of significant amplitude will occur about the C—S bonds because the barrier to rotation about these bonds is not very large compared to thermal energies. Thus, the barrier in thioanisole is 5.4 kJ/mol (26) in solution, only about twice as large as *RT* at 300 K. In **8**, the barrier to rotation near the minima (a planar conformer would, of course, experience large steric repulsions be-

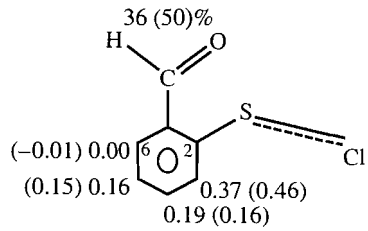

8

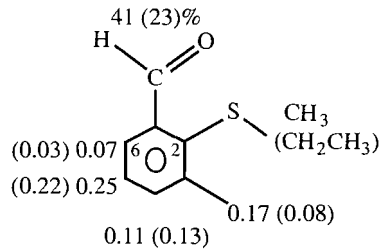

9

tween the *ortho* C—H bonds, the interhydrogen distance then being only about 0.5 Å) will likely be less than in thioanisole because the 3*p* lone pair, whose partial delocalization is associated with a partial double bond character of the C—S bonds and hence with a barrier to rotation about these bonds, is to some extent at least shared with both aromatic moieties. Nevertheless, on the assumption that **8** represents an energy minimum in both solvents, the numbers in **8** can be examined as to their consistency with such an assumption.

First, the *para* protons in both phenyl vinyl sulfide (unpublished data from this laboratory) and in diphenyl sulfide (30) in CS_2 and CCl_4 solutions are shielded by 0.08–0.09 ppm relative to benzene. In both molecules this is attributed to partial delocalization of the 3*p* lone pair into the two π systems present in each molecule. In diphenyl sulfide, the *para* proton is 7 Å, or somewhat more, distant from the centre of the neighbouring phenyl, so that shielding perturbations from the diamagnetic anisotropy of the latter (ring currents) are small (31) and, in view of the datum for phenyl vinyl sulfide, are here taken as negligible. Then, for ethyl phenyl sulfide (unpublished work) and thioanisole (32), the *para* protons are shielded by 0.20(1) ppm relative to benzene in CS_2 and CCl_4 solutions. In **8**, the excess shielding at H-5, *para* to sulfur, is 0.16 ppm, suggesting that more of the 3*p* lone pair is delocalized into this aromatic moiety than into the C_6H_4Cl group. In a rigid **8** this bias would be complete, the second ring lying in the plane of the 3*p* orbital.

Second, in **9**, the excess shielding at H-5 is 0.25 ppm in CCl_4 solution for R = CH_3 and 0.22 ppm for R = CH_2CH_3 (15), again implying that, in **8**, the delocalization into the benzaldehyde moiety is greater than that into the C_6H_4Cl group.

Third, in a rigid skew conformation, H-3 lies in the shielding cone of the chlorophenyl ring. Whatever the actual magnitude of the induced magnetic dipole, the shielding of H-3 is here estimated to be larger than that of H-4 by a factor of 2.3; this factor rises to 22 for H-5. Of course, the C_6H_4Cl group undergoes torsion about the C—S bond, so that such shielding due to its diamagnetic anisotropy will decrease due to the torsion (deshielding of H-3 and H-4 occurs for coplanar rings, naturally). Comparison of excess shifts in **8** and **9** implies consistency with **8** as the conformer of minimum energy. In **8**, H-6 lies in the deshielding cone of the second aromatic ring; however, it is so distant from this ring that its vanishing excess shift can hardly be attributed to ring currents.

Fourth, in CS_2 solution the internal chemical shift in the C_6H_4Cl group is ≤0.003 ppm, the deshielding, relative to benzene, being 0.02 ppm. In a rigid **8** the vector from the proton situated *ortho* to sulfur in C_6H_4Cl intersects the induced magnetic moment vector of the other ring at about 55°, the anisotropic shift therefore being near zero ($3\cos^2 55 - 1 = 0.01$). At the *meta* position a chlorine substituent shields a proton by 0.05 ppm (33) in the presence of a *para* SCH_3 group. Hence the *ortho* protons are deshielded by 0.07 ppm, relative to expectations. In fact, it is known that protons

Can. J. Chem. Downloaded from www.nrcresearchpress.com by 109.225.110.28 on 09/08/12
For personal use only.

placed *ortho* to a 3*p* orbital lying in the aromatic plane are deshielded (4, 15). In particular, in 2-(*tert*-butylthio) benzaldehyde, in which such an orientation of the 3*p* orbital roughly obtains, the deshielding amounts to 0.11 ppm (15). Attribution of the 0.07 ppm in **8** to such a cause is once more consistent with the putative skew conformation as that of lowest energy. Similarly, the *meta* protons in thioanisole, at 7.14 ppm, and those in 4-chlorothioanisole, at 7.19 ppm (32), when compared to the 7.24 ppm in **8** and 7.22 ppm for benzene in CS_2, imply that the increased screening caused by $3p\cdots\pi$ conjugation has been reduced in **8**. While these protons, *ortho* to chlorine, lie in the deshielding cone of the other ring, they are at least 6.2 Å removed from its centre. Hence their chemical shift is again consistent with a bias towards the skew conformation.

(ii) The shift of the formyl proton

In the 2-(alkylthio) benzaldehydes, the chemical shift of the formyl proton is dependent on the proximity of the 3*p* orbital on sulfur. As this orbital twists into the benzene plane, the proton is deshielded, being 10.697 ppm in the *tert*-butyl, and 10.267 ppm in the methyl, derivative (15). In **8**, the value of 10.273 ppm in CS_2 solution is consistent, first, with the very similar proportions of the *O-syn* conformers of **8** and **9** and, second, with similar degrees of twisting about the Csp^2—S bonds in these molecules.

(iii) Coupling constants

In the 2-(alkylthio) benzaldehydes many of the coupling constants between the aromatic protons are sensitive to the out-of-plane twist of the alkyl group (15). Those for the ethyl and methyl derivatives are in best agreement with the coupling constants in Table 1 (CS_2 solution); the average deviations between sets of six coupling constants are 0.02 Hz, whereas for the *tert*-butyl derivative the average rises to 0.09 Hz. These comparisons are consistent with the above conclusions concerning the preferred skew conformation of the diphenyl sulfide derivative.

Evidence for the anticipated substantial oscillational amplitudes of the C_6H_4Cl plane about its C—S bond comes from the extra broadening of 0.1 Hz observed for the H-3 peaks in both solvents. A twist of about 30° about this bond brings the *ortho* protons of the C_6H_4Cl group to within 2.3 Å of the midpoint of the C—H (−3) bond of the other ring. Under such conditions, substantial through-space interring coupling could occur (33, 34). The coupling magnitude is an average of those to the two *ortho* protons; that to the distant proton vanishes. The through-space mechanism depends crucially on the interproton distance but very likely also on the relative arrangement of the C—H bonds (35). Hence an average torsion angle cannot be deduced here.

The shifts and coupling constants in acetone-d_6 *solution*

The decrease in screening of protons of polar molecules dissolved in polar solvents is often attributed to the reaction in field induced in the dielectric continuum of the solvent; this field increases the polarity of the solute molecule. Be that as it may, it is observed in this laboratory that those protons in the solute that are protected from a close approach of acetone-d_6 molecules are deshielded rather less than those on the periphery. It is interesting, therefore, that H-3 in **8** is deshielded by only 0.07 ppm in passing from CS_2 to acetone-d_6 solution. By way of contrast, the protons *ortho* to sulfur in the C_6H_4Cl group are deshielded by 0.22 ppm, those *meta* to sulfur by 0.21 ppm. These three numbers emphasize the distinctions between the positions on the molecular topology occupied on average by these protons and are again consistent with a low-energy skew conformation. The somewhat larger excess shift, 0.46 ppm, see **8**, of H-3 in acetone-d_6 solution is most likely a consequence of the lower solvent effect on this "hidden" site of the molecule and not of a greater rigidity of the skew conformer. True, the population of the *O-syn* conformer has risen to 50% in acetone-d_6 solution and, in terms of the previous arguments, would imply a lower twist away from perpendicularity of the 3*p* orbital in **8**. However, the excess shifts of the other protons are not very different in the two solutions. This may be caused by differential solvent shifts of the protons on the "exposed" sites, so that the above explanation appears sensible.

The solvent dependence of intraring coupling constants (Table 1) is not unique to the present compound, similar patterns being observed in this laboratory for many aromatic derivatives. These patterns will be discussed in due course.

Conclusion

The S···O interaction in 2-alkylthio- and 2-phenylthiobenzaldehydes is relatively weak in solution. The *O-syn* population appears to be controlled by the orientation of the 3*p* lone pair on sulfur and not vice versa. A rather flexible skew conformation of 2-(4-chlorophenylthio) benzaldehyde is very likely the one of lowest energy in polar and nonpolar solvents, the *O-syn* population being 36% in the former and 50% abundant in the latter. The compound is a solid at room temperature; it would be interesting to ascertain its conformation in the crystal, particularly with regard to the orientation of the formyl group. It is interesting that 2-hydroxyphenyl phenyl sulfide also adopts a skew conformation (4) with the distinction that the conformational roles of the two aromatic rings are now reversed (see **2**). Here an attractive O—H···3*p* interaction occurs.

Acknowledgements

We thank the Natural Sciences and Engineering Research Council of Canada for a grant-in-aid of research.

1. Á. Kucsman and I. Kapovits. *In* Organic sulfur chemistry: theoretical and experimental advances. *Edited by* I. G. Csizmadia, A. Mangini, and F. Bernardi. Elsevier, Amsterdam. 1985. pp. 191–245.
2. J. G. Ángyán, R. A. Poirier, Á. Kucsman, and I. G. Csizmadia. J. Am. Chem. Soc. **109**, 2237 (1987) and references therein.
3. T. Schaefer, T. A. Wildman, and S. R. Salman. J. Am. Chem. Soc. **102**, 107 (1980).
4. T. Schaefer, S. R. Salman, T. A. Wildman, and P. D. Clark. Can. J. Chem. **60**, 342 (1982).
5. M. B. Hall. J. Am. Chem. Soc. **100**, 6333 (1978).
6. E. Magnusson. J. Am. Chem. Soc. **106**, 1177 (1984).
7. W. Kutzelnigg. Angew. Chem. Int. Ed. Engl. **23**, 272 (1984).
8. D. Britton and J. D. Dunitz. Helv. Chim. Acta, **63**, 1068 (1980).
9. T. N. Guro Row and R. Parthasarathy. J. Am. Chem. Soc. **103**, 477 (1981).
10. R. Viswanathan and T. R. Dyke. J. Chem. Phys. **77**, 1166 (1982).
11. E. J. Goodwin and A. C. Legon. J. Chem. Soc. Faraday Trans. 2, **80**, 51 (1984).

12. T. Slee, A. Larouche, and R. F. W. Bader. J. Phys. Chem. **92**, 6219 (1988).
13. K. B. Wiberg and C. M. Breneman. J. Am. Chem. Soc. **114**, 831 (1992).
14. Á. Kucsman, I. Kapovits, L. Párkányi, and A. Kálmán. J. Mol. Struct. **140**, 141 (1986).
15. T. Schaefer, G. H. Penner, K. J. Davie, and R. Sebastian. Can. J. Chem. **63**, 777 (1985).
16. T. Schaefer and G. H. Penner. Can. J. Chem. **66**, 1641 (1988).
17. N. Goodhand and T. A. Manor. J. Fluorine Chem. **48**, 45 (1990), and references therein.
18. T. Schaefer and C. S. Takeuchi. Can. J. Chem. **68**, 339 (1990), and references therein.
19. K. Hayamizu and O. Yamamoto. J. Mol. Spectrosc. **28**, 89 (1968), and references therein.
20. J. S. Martin, A. R. Quirt, and K. E. Worvill. The NMR program library. Daresbury Laboratory, Daresbury, U.K.
21. K. Hayamizu and O. Yamamoto. J. Mol. Spectrosc. **25**, 422 (1968), and references therein.
22. V. A. Chertkov and N. M. Sergeyev. J. Magn. Reson. **52**, 400 (1983).
23. R. Laatikainen, K. Tuppurainen, Y. Hiltunen, and S. Lotjonen. Magn. Reson. Chem. **28**, 939 (1990).
24. T. Schaefer, R. Sebastian, S. R. Salman, J. D. Baleja, G. H. Penner, and D. M. McKinnon. Can. J. Chem. **69**, 620 (1991).
25. T. Schaefer, R. Sebastian, and S. R. Salman. J. Magn. Reson. **46**, 325 (1982).
26. T. Schaefer and J. D. Baleja. Can. J. Chem. **64**, 1376 (1986).
27. B. Rozsondai, J. H. Moore, D. C. Gregory, and I. Hargittai. Acta Chim. (Budapest), **94**, 321 (1977).
28. J. P. Canselier and P. Cassoux. J. Mol. Struct. **39**, 301 (1977).
29. T. Schaefer and C. S. Takeuchi. Can. J. Chem. **67**, 827 (1989).
30. G. Llabrès, M. Baiwar, L. Christiaens, and J-L. Piette. Can. J. Chem. **57**, 2967 (1979).
31. C. W. Haigh and R. B. Mallion. Org. Magn. Reson. **4**, 203 (1972).
32. G. Llabrès, M. Baiwar, L. Christiaens, J. Denoel, L. Laitem, and J-L. Piette. Can. J. Chem. **56**, 2008 (1978).
33. T. Schaefer and K. Chum. Can. J. Chem. **54**, 2231 (1976).
34. R. H. Contreras, M. A. Natiello, and G. E. Scuseria. Magn. Reson. Rev. **9**, 239 (1985).
35. M. Barfield, A. M. Dean, C. J. Fállick, R. J. Spear, S. Sternhell, and P. W. Westerman. J. Am. Chem. Soc. **97**, 1482 (1975).

Can. J. Chem. Downloaded from www.nrcresearchpress.com by 109.225.110.28 on 09/08/12
For personal use only.

Reactions of nitriles with binuclear rhodium hydrides. The stepwise reduction of a carbon–nitrogen triple bond at two metal centres

MICHAEL D. FRYZUK,[1] WARREN E. PIERS,[2] AND STEVEN J. RETTIG[3]

Department of Chemistry, University of British Columbia, 2036 Main Mall, Vancouver, B.C., Canada V6T 1Z1

Received April 28, 1992

MICHAEL D. FRYZUK, WARREN E. PIERS, and STEVEN J. RETTIG. Can. J. Chem. **70**, 2381 (1992).

The reaction of simple nitriles, R′CN (R′ = CH_3, Ph, *o*-tol) with the electron-rich binuclear rhodium hydride derivatives $[(R_2PCH_2CH_2PR_2)Rh]_2(\mu\text{-}H)_2$ (R = Pr^i: [(dippe) $Rh]_2(\mu\text{-}H)_2$; R = OPr^i: [(dipope)$Rh]_2(\mu\text{-}H)_2$) results in the formation of alkylideneimido derivatives $[(R_2PCH_2CH_2PR_2)Rh]_2(\mu\text{-}H)(\mu\text{-}N{=}CHR')$, apparently by insertion of the nitrile moiety into a bridging hydride bond; this was confirmed by the reaction of nitriles with the dideuteride [(dippe)$Rh]_2(\mu\text{-}D)_2$, which resulted in the formation of [(dippe)$Rh]_2(\mu\text{-}D)(\mu\text{-}N{=}CHR')$. Further reduction can take place by addition of H_2 to generate the corresponding amide hydride derivatives [(dippe)$Rh]_2(\mu\text{-}H)(\mu\text{-}NHCH_2R')$; this represents an overall stoichiometric reduction of a nitrile to a coordinated amide at a binuclear centre. These same amido-hydride complexes can be accessed by addition of amine to the starting binuclear rhodium hydride derivatives. The X-ray structure of $[(Pr^i_2PCH_2CH_2PPr^i_2)Rh]_2(\mu\text{-}H)(\mu\text{-}N{=}CHCH_3)$ was undertaken to confirm the structure of these particular intermediates. Crystals of this material are monoclinic, a = 19.036(2), b = 15.139(1), c = 13.604(1) Å, β = 104.119(7)°, Z = 4, space group $P2_1/c$. The structure was solved by heavy atom methods and was refined by full-matrix least-squares procedures to R = 0.038 and R_w = 0.041 for 5814 reflections with $I \geq 3\sigma(I)$.

MICHAEL D. FRYZUK, WARREN E. PIERS et STEVEN J. RETTIG. Can. J. Chem. **70**, 2381 (1992).

La réaction des nitriles simples, R′CN (R′ = CH_3, Ph, *o*-tol) avec les dérivés d'hydrures du rhodium riches en électrons $[(R_2PCH_2CH_2PR_2)Rh]_2(\mu\text{-}H)_2$ (R = Pr^i: [(dippe)$Rh]_2(\mu\text{-}H)_2$; R = OPr^i: [(dipope)$Rh]_2(\mu\text{-}H)_2$) conduisent à la formation de dérivés alkylidèneimido $[(R_2PCH_2CH_2PR_2)Rh]_2(\mu\text{-}H)(\mu\text{-}N{=}CHR')$ apparemment par simple insertion de l'unité nitrile dans l'hydrure ponté; cette conclusion a été confirmée par la réaction des nitriles avec le dideutérure [(dippe)$Rh]_2(\mu\text{-}D)_2$ qui conduit à la formation du [(dippe)$Rh]_2(\mu\text{-}D)$ $(\mu\text{-}N{=}CHR')$. On peut obtenir une réduction plus poussée en ajoutant du H_2 pour générer les dérivés hydrures amides correspondants [(dippe)$Rh]_2(\mu\text{-}H)(\mu\text{-}NHCH_2R')$; ceci représente une réduction stoechiométrique globale d'un nitrile en un amide coordonnée à un centre binucléaire. On peut accéder à ces mêmes complexes amido-hydrures en ajoutant une amine aux dérivés d'hydrure de rhodium binucléaire de départ. Dans le but d'établir la structure de ces intermédiaires particuliers, on a étudié la structure du dérivé $[Pr^i_2PCH_2CH_2PPr^i_2)Rh]_2$-$(\mu\text{-}H)$ $(\mu\text{-}N{=}CHCH_3)$ par diffraction de rayons X. Les cristaux de ce composé appartiennent au groupe d'espace monoclinique $P2_1/c$, avec a = 19,036(2), b = 15,139(1) et c = 13,604(1) Å, β = 104,119(7)° et Z = 4. On a résolu la structure par des méthodes des atomes lourds et on l'a affinée par la méthode des moindres carrés (matrice complète) jusqu'à des valeurs de R = 0,038 et de R_w = 0,041 pour 5814 réflexions avec $I \geq 3\sigma$ (I).

[Traduit par la rédaction]

Introduction

A possible reason for the paucity (1–4) of homogeneous systems for the catalytic hydrogenation of nitriles (R—C≡N) may be due to a fundamental preference for binding to a metal centre via the nitrogen lone pair rather than the carbon–nitrogen triple bond (C≡N) π system. Although some examples of side-bonded nitrile ligands are known (5–8), insertion of a carbon–nitrogen triple bond into a late transition metal – hydride bond is relatively rare (9–11). On the other hand, heterogeneous catalysts such as Pd/C or Raney nickel are effective in the hydrogenation of nitriles (12), suggesting that multiple metal bonding sites may be necessary for the success of the reduction process. This notion is supported by the observed *stoichiometric* hydrogenation of RC≡N on the face of a trinuclear iron carbonyl species (13–16). The complete characterization of intermediates en route to the fully hydrogenated μ_3-NCH_2R product showed that all three metal centres were apparently involved in the hydrogenation process. Unfortunately, desorption of the product amine from this cluster was not facile under conditions required to maintain cluster stability and thus the reaction is not catalytic.

Although the above example involved a trinuclear complex, in principle the stepwise reduction process could be carried out by only two metal centres since the effect and importance of a third metal centre is debatable. The coordinatively unsaturated binuclear rhodium hydrides **1***a* (17) and **1***b* (18) react rapidly with simple organic nitriles R′—C≡N (R′ = CH_3, C_6H_5, *o*-$CH_3C_6H_5$) to provide binuclear μ-alkylideneimido-hydride derivatives apparently resulting from the insertion of the nitrile C≡N bond into a Rh—H bond.

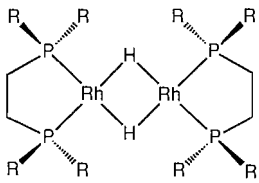

1*a* : R = Pr^i ⟹ [(dippe)$Rh]_2(\mu\text{-}H)_2$

1*b* : R = OPr^i ⟹ [(dipope)$Rh]_2(\mu\text{-}H)_2$

These compounds react further with dihydrogen to yield binuclear μ-amido-hydride complexes in which the nitrile moiety has been fully hydrogenated. We report here the details of these studies, along with the X-ray crystallographic characterization of one of the μ-alkylideneimido hydride compounds. Unlike the reactions of **1***a* and **1***b* with imines (19), intermediates in these reactions could not be observed spectroscopically; however, a reasonable mechanism may be proposed, based on analogy to the results of the imine reactions.

[1]E. W. R. Steacie Fellow (1990–1992).
[2]NSERC Postgraduate Scholar (1984–1988).
[3]Experimental Officer: UBC Crystallographic Service.

Can. J. Chem. Downloaded from www.nrcresearchpress.com by 109.225.110.28 on 09/08/12
For personal use only.

Can. J. Chem. Downloaded from www.nrcresearchpress.com by 109.225.110.28 on 09/08/12
For personal use only.

Experimental

General procedures

General laboratory procedures have been reported elsewhere (20). Benzonitrile, *ortho*-tolynitrile, and benzylamine were purchased from the Aldrich Chemical Company and distilled prior to use. Spectrograde acetonitrile (BDH) was dried either by refluxing over calcium hydride under argon for 12 h (large quantities) or by letting sit over activated 3Å molecular sieves for 8 h (small quantities). In the latter case, the acetonitrile was then degassed by vacuum transferring away from the molecular sieves followed by two freeze–pump–thaw cycles. Ethylamine was obtained from Matheson Gas Products and condensed prior to use; it was then vacuum transferred from a −10°C bath to minimize transfer of any water present. Literature procedures were used to prepare [(dippe)Rh]$_2$(μ-H)$_2$ (**1***a*), [(dippe)Rh]$_2$(μ-D)$_2$ (d_2-**1***a*), (17), and [(dipope)Rh]$_2$(μ-H)$_2$ (**1***b*) (18).

*X-ray crystallographic analysis of [(dippe)Rh]$_2$[μ-N=C(H)CH$_3$]-(μ-H), 2*a

A crystal ca. 0.16 × 0.23 × 0.37 mm in size was mounted in a Lindemann glass capillary. Unit-cell parameters were refined by least squares on setting angles for 25 reflections (2θ = 40.0–47.2°) measured on a diffractometer with Mo-K$_\alpha$ radiation ($\lambda_{K\alpha1}$ = 0.70930, $\lambda_{K\alpha2}$ = 0.71359 Å). Crystal data at 21°C are as follows: $C_{30}H_{69}NP_4Rh_2$ f.w. = 773.59 Monoclinic, a = 19.036(2), b = 15.139(1), c = 13.604(1) Å, β = 104.119(7)°, V = 3801.9(6) Å^3, Z = 4, ρ_c = 1.351 Mg m^{-3}, F(000) = 1624, μ(Mo-K$_\alpha$) = 10.39 cm^{-1}. Absent reflections: *h*0*l*, odd, and 0*k*0, *k* odd, uniquely indicate the space group $P2_1/c$ (No. 14).

Intensities were measured with graphite-monochromated Mo-K$_\alpha$ radiation on an Enraf–Nonius CAD4-F diffractometer. An ω–2θ scan at 1.6–10.1° min^{-1} over a range of (0.90 + 0.35 tan θ)° in ω (scan extended by 25% on each side for background measurement) was employed. Data were measured to 2θ = 55°. The intensities of three check reflections, measured every hour of X-ray exposure time throughout the data collection, showed only small random variations. The data were processed[4] and corrected for Lorentz and polarization effects and absorption (analytical method). Transmission factors range from 0.674 to 0.876. Of the 8710 independent reflections measured, 5814 (66.8%) had intensities greater than or equal to 3σ(I) above background where $\sigma^2(I) = [C + 2B + (0.04(C - B))^2]$ with C = scan count, B = normalized total background count.

The structure was solved by heavy atom methods, the coordinates of the rhodium and phosphorus atoms being determined from the Patterson function. The non-hydrogen atoms were refined with anisotropic thermal parameters and the carbon-bound hydrogen atoms were fixed in idealized positions (C(sp^2)—H = 0.97, C(sp^3)—H = 0.98 Å, $U_H \propto U_{\text{bonded atom}}$). The metal hydride was refined with an isotropic thermal parameter. Scattering factors for all atoms and anomalous dispersion corrections for the non-hydrogen atoms were taken from ref. 21. The weighting scheme $w = 1/\sigma^2(F)$ gave uniform average values of $w(|F_o| - |F_c|)^2$ over ranges of both $|F_o|$ and sin θ/λ and was employed in the final stages of full-matrix least-squares refinement of 338 variables. Reflections with $I < 3\sigma(I)$ were not included in the refinement. Convergence was reached at R = 0.038 and R_w = 0.041 for 5814 reflections with $I \geq 3\sigma(I)$. The function minimized was $\Sigma w(|F_o| - |F_c|)^2$, $R = \Sigma||F_o| - |F_c||/\Sigma|F_o|$, $R_w = (\Sigma w(|F_o| - |F_c|)^2/\Sigma w|F_o|^2)^{1/2}$. On the final cycle of refinement the maximum parameter shift corresponded to 0.14σ. The mean error in an observation of unit weight was 1.59. The largest peak on the final difference map, 1.72 e Å^{-3}, is near Rh(2).

TABLE 1. Final positional (fractional × 10^4, Rh and P × 10^5, H × 10^3) and isotropic thermal parameters (U × 10^3 Å^2) with estimated standard deviations in parentheses[a]

Atom	x	y	z	U_{eq}/U_{iso}
Rh(1)	23226(2)	43676(2)	36508(2)	30
Rh(2)	28827(2)	53936(2)	23083(2)	32
P(1)	11615(5)	40863(7)	35360(8)	34
P(2)	25204(6)	38243(7)	52178(8)	35
P(3)	21472(6)	61878(8)	11281(8)	42
P(4)	37663(6)	62318(7)	19888(7)	36
N	3343(2)	4592(2)	3501(2)	38
C(1)	1003(2)	3792(3)	4791(3)	42
C(2)	1676(2)	3364(3)	5460(3)	46
C(3)	2618(3)	7143(3)	716(3)	51
C(4)	3415(3)	6948(3)	863(3)	51
C(5)	467(2)	4958(3)	3108(3)	44
C(6)	752(2)	3131(3)	2747(3)	46
C(7)	3170(3)	2903(3)	5653(4)	53
C(8)	2820(3)	4631(3)	6266(3)	52
C(9)	1380(3)	6736(4)	1499(4)	59
C(10)	1702(3)	5665(4)	−102(4)	62
C(11)	4576(2)	5747(3)	1644(3)	49
C(12)	4198(3)	7045(3)	2972(3)	54
C(13)	668(3)	5790(4)	3735(4)	63
C(14)	−317(3)	4695(4)	3040(5)	66
C(15)	1172(3)	2292(4)	3093(4)	68
C(16)	703(3)	3291(4)	1638(4)	65
C(17)	3104(3)	2200(4)	4835(5)	74
C(18)	3132(3)	2473(4)	6662(5)	84
C(19)	2254(3)	5337(4)	6235(5)	78
C(20)	3528(3)	5058(5)	6227(6)	89
C(21)	1644(3)	7242(4)	2497(5)	75
C(22)	904(3)	7323(5)	685(5)	98
C(23)	2268(4)	5314(5)	−623(4)	88
C(24)	1179(4)	4936(5)	32(5)	94
C(25)	4349(3)	4994(4)	901(4)	69
C(26)	5065(3)	6392(4)	1256(4)	70
C(27)	3663(4)	7716(4)	3169(4)	82
C(28)	4565(3)	6590(4)	3952(4)	81
C(29)	3910(2)	4161(3)	3862(3)	46
C(30)	4590(3)	4133(4)	3504(4)	60
H(Rh)	204(2)	489(3)	248(3)	54(13)

[a] U_{eq} = 1/3 trace (diagonalized U).

The final positional and (equivalent) isotropic thermal parameters for the non-hydrogen atoms appear in Table 1. Bond lengths and angles are given in Tables 2 and 3. Hydrogen atom parameters, anisotropic thermal parameters, general torsion angles, and structure factors have been deposited.[5]

*Synthesis of [(dippe)Rh]$_2$[μ-N=C(H)CH$_3$](μ-H), 2*a

To a stirred solution of [(dippe)Rh]$_2$(μ-H)$_2$, **1***a* (0.100 g, 0.14 mmol), in toluene (5 mL) was added an excess of acetoni-

[4] Computer programs used include locally written programs for data processing and locally modified versions of the following: MULTAN80, multisolution program by P. Main, S. J. Fiske, S. E. Hull, L. Lessinger, G. Germain, J. P. Declercq, and M. M. Woolfson; ORFLS, full-matrix least-squares, and ORFFE, function and errors, by W. R. Busing, K. O. Martin, and H. A. Levy; FORDAP, Patterson and Fourier syntheses, by A. Zalkin; ORTEP II, illustrations, by C. K. Johnson.

[5] Supplementary material mentioned in the text may be purchased from the Depository of Unpublished Data, CISTI, National Research Council Canada, Ottawa, Canada K1A 0R6.

The table of hydrogen atom parameters has also been deposited with the Cambridge Crystallographic Data Centre and can be obtained on request from the Director, Cambridge Crystallographic Data Centre, University Chemical Laboratory, 12 Union Road, Cambridge, CB2 1EZ, U.K.

Can. J. Chem. Downloaded from www.nrcresearchpress.com by 109.225.110.28 on 09/08/12
For personal use only.

TABLE 2. Bond lengths (Å) with estimated standard deviations in parentheses

Bond	Length (Å)	Bond	Length (Å)
Rh(1)—P(1)	2.2186(10)	N—C(29)	1.255(5)
Rh(1)—P(2)	2.2297(10)	C(1)—C(2)	1.524(6)
Rh(1)—N	2.030(3)	C(3)—C(4)	1.510(6)
Rh(1)—H(Rh)	1.74(5)	C(5)—C(13)	1.517(7)
Rh(2)—P(3)	2.2106(11)	C(5)—C(14)	1.526(6)
Rh(2)—P(4)	2.2327(10)	C(6)—C(15)	1.513(7)
Rh(2)—N	2.044(3)	C(6)—C(16)	1.508(7)
Rh(2)—H(Rh)	1.84(4)	C(7)—C(17)	1.523(8)
P(1)—C(1)	1.860(4)	C(7)—C(18)	1.537(7)
P(1)—C(5)	1.858(4)	C(8)—C(19)	1.511(8)
P(1)—C(6)	1.856(4)	C(8)—C(20)	1.507(7)
P(2)—C(2)	1.853(4)	C(9)—C(21)	1.533(8)
P(2)—C(7)	1.862(5)	C(9)—C(22)	1.532(7)
P(2)—C(8)	1.858(5)	C(10)—C(23)	1.521(9)
P(3)—C(3)	1.858(5)	C(10)—C(24)	1.526(8)
P(3)—C(9)	1.854(5)	C(11)—C(25)	1.514(7)
P(3)—C(10)	1.858(5)	C(11)—C(26)	1.530(6)
P(4)—C(4)	1.863(4)	C(12)—C(27)	1.509(7)
P(4)—C(11)	1.867(4)	C(12)—C(28)	1.512(7)
P(4)—C(12)	1.856(5)	C(29)—C(30)	1.490(6)

trile (2–3 drops). The deep green to orange-red colour change accompanying the reaction was instantaneous. The toluene and excess acetonitrile were removed *in vacuo* and the residues recrystallized from toluene/hexanes (1:1). After washing with cold hexanes, the yield of red crystals was 0.089 g (84%). ^{1}H NMR (C_6D_6, ppm): N=C*H*CH$_3$, 8.75 (m, 1H, ^3J_H = 4.4 Hz, ^4J_P couplings of 15.6, 8.8, and 4.8 Hz); C*H*(CH$_3$)$_2$, 2.23, 2.04–2.20 (overlapping dsp, 8H, ^2J_P = 2.0–4.0 Hz, ^3J_H = 6.4–7.6 Hz); N=CHC*H*$_3$, 2.06 (d, 3H); CH(C*H*$_3$)$_2$, 1.43, 1.40, 1.32, 1.31, 1.20, 1.15, 1.14, 1.11 (overlapping dd, 48H, ^3J_P = 12.4–13.4 Hz); PC*H*$_2$C*H*$_2$P, signals buried underneath methyl resonances; Rh-*H*-Rh, −7.54 (m, $^1J_{Rh}$ = 20.8–21.7 Hz). ^{31}P{^{1}H} NMR (C_6D_6, ppm): $P_{trans(N)}$, 104.0 (dd, $^1J_{Rh}$ = 153.4 Hz, ^2J_P = 26 Hz); $P_{trans(N)}$, 102.6 (dd, $^1J_{Rh}$ = 153.0 Hz, ^2J_P = 24 Hz); $P_{cis(N)}$, 87.0 (br dm, $^1J_{Rh}$ = 195.6 Hz, $^4J_P \approx$ 32 Hz); $P_{cis(N)}$, 83.3 (br dm, $^1J_{Rh}$ = 193.2 Hz). ^{13}C{^{1}H} NMR(C_6D_6, ppm): N=*C*HCH$_3$, 159.1 (s); N=CH*C*H$_3$, obscured by ligand resonances between 19 and 30 (overlapping signals). Anal. calcd. for $C_{30}H_{69}P_4Rh_2N$: C 46.58, H 8.99, N 1.81%; found: C 46.80, H 9.11, N 1.71%.

Reaction of [(dippe)Rh]$_2$(μ-D)$_2$, d$_2$-***1a****, with CH$_3$CN*

An identical procedure to that described above was followed using *d*$_2$-**1***a* (0.033 g, 0.04 mmol). In the ^{1}H NMR spectrum of the product the signals due to the ethylideneimido proton and the bridging hydride ligand were absent; ^{2}H NMR spectroscopy confirmed the presence of the label in these positions.

Synthesis of [(dippe)Rh]$_2$[μ-N=C(H)C$_6$H$_5$](μ-H), ***3****a*

To a stirred solution of [(dippe)Rh]$_2$(μ-H)$_2$, **1***a* (0.185 g, 0.25 mmol), in toluene (5 mL) was added a solution of distilled benzonitrile (0.029 g, 0.27 mmol) in toluene (1 mL). The solution changed colour instantly from deep green to dark red. The toluene was removed *in vacuo* and the residues recrystallized from toluene/hexanes (1:1) at −20°C. After washing with cold hexanes, 0.173 g (82%) of dark red-purple crystals was isolated. ^{1}H NMR (C_7D_8, ppm): N=C*H*C$_6$H$_5$, 9.00 (br m, 1H, coupled to four phosphorus nuclei); H_{ortho}, 7.97 (d, 2H, $^3J_{H_{meta}}$ = 7.2 Hz); H_{meta}, 7.15 (m, 2H, $^3J_{H_{para}}$ = 7.2 H); H_{para}, 7.09 (m, 1H); C*H*(CH$_3$)$_2$, 2.05–2.25 (br overlapping dsp, 8H, ^3J_H = 6.6–7.6 Hz); CH(C*H*$_3$)$_2$, 1.34, 1.33, 1.30, 1.21, 1.05, 0.97, 0.96, 0.95 (overlapping dd, 48H, ^2J_P = 12.0–14.0 Hz); PC*H*$_2$C*H*$_2$P, 1.1 (br m, 8H); Rh-*H*-Rh, −7.82 (m, $^1J_{Rh}$ = 21.4–22.0 Hz): ^{31}P{^{1}H} NMR (C_6D_6, ppm): $P_{trans(N)}$, 108.9 (dd, $^1J_{Rh}$ = 153.7 Hz, ^2J_P = 27 Hz); $P_{trans(N)}$, 108.3 (dd, $^1J_{Rh}$ = 153.9 Hz, ^2J_P = 28 Hz); $P_{cis(N)}$, 94.4 (br dm, $^1J_{Rh}$ = 195.9 Hz, $^4J_P \approx$ 32 Hz); $P_{cis(N)}$, 87.5 (br dm, $^1J_{Rh}$ = 193.9 Hz). ^{13}C{^{1}H} NMR (C_6D_6, ppm): N=*C*HC$_6$H$_5$, 159.9 (s, ^1J_H = 163.6 Hz); C_{ipso}, 143.9; other aromatic carbons, 129.1, 127.6, 127.1; ligand resonances, 19–28. Anal. calcd. for $C_{35}H_{71}P_4Rh_2N$: C 50.31, H 8.56, N 1.68%; found: C 50.00, H 8.40, N 1.50%.

Synthesis of [(dippe)Rh]$_2$[μ-N=C(H)-o-CH$_3$-C$_6$H$_4$](μ-H), ***4****a*

To a stirred solution of [(dippe)Rh]$_2$(μ-H)$_2$, **1***a* (0.100 g, 0.14 mmol), in toluene (5 mL) was added to a solution of distilled *o*-tolylnitrile (0.018 g, 0.15 mmol) in toluene (1 mL). The solution changed colour instantly from deep green to dark red. The toluene was removed *in vacuo* and the residues recrystallized from toluene/hexanes (1:1) at −20°C. After washing with cold hexanes, 0.105 g (88%) of dark red-purple crystals was isolated. ^{1}H

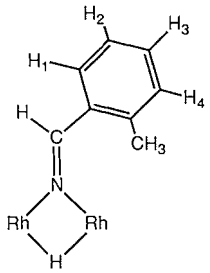

NMR (C_6D_6, ppm): N=C*H*, 10.09 (br m, coupled to 4 phosphorus nuclei); C-*H*$_1$, 8.18 (dd, 1H, ^3J_H = 5.6 Hz, ^4J_H = 3.9 Hz); C-*H*$_2$ and C-*H*$_3$, 7.06 (m, 2H); C-*H*$_4$, 6.93 (m, 1H); C-C*H*$_3$, 2.41 (s, 3H); C*H*(CH$_3$)$_2$, 2.18 (8H, overlapping dsp); CH(C*H*$_3$)$_2$, PC*H*$_2$C*H*$_2$P, 0.9–1.4 (56H, br overlapping signals); Rh-*H*-Rh, −8.92 (ttt, $^2J_{P_{trans}}$ = 60.4 Hz, $^2J_{P_{cis}}$ = 11.6 Hz, $^1J_{Rh}$ = 21.6 Hz). ^{31}P{^{1}H} NMR (C_6D_6, ppm): $P_{trans(N)}$, 107.9 (dd, $^1J_{Rh}$ = 152.6 Hz, ^2J_P = 26.9 Hz); $P_{trans(N)}$, 107.8 (dd, $^1J_{Rh}$ = 152.5 Hz, ^2J_P = 26.8 Hz); $P_{cis(N)}$, 94.1 (br dm, $^1J_{Rh}$ = 193.9 Hz) $^4J_P \approx$ 32 Hz); $P_{cis(N)}$, 82.9 (br dm, $^1J_{Rh}$ = 193.8 Hz). ^{13}C{^{1}H} NMR (C_6D_6, ppm): N=*C*H, 159.8 (s); $C_{ipso(N)}$, 143.5; $C_{ipso(CH3)}$, 135.3; other aromatic carbons, 130.2, 129.1, 127.1, 125.7; C-*C*H$_3$, obscured by ligand resonances in region 19–29. Anal. calcd. for $C_{36}H_{73}P_4Rh_2N$: C 50.89, H 8.66, N 1.65%; found: C 51.22, H 8.59, N 1.74%.

Reaction of [(dippe)Rh]$_2$(μ-D)$_2$, d$_2$-***4****a, with* o-*CH$_3$-C$_6$H$_4$CN*

An identical procedure to that described above was followed using *d*$_2$-**1***a* (0.036 g, 0.05 mmol). In the ^{1}H NMR spectrum of the product the signals due to the *o*-tolylideneimido proton and the bridging hydride ligand were absent; ^{2}H NMR spectroscopy confirmed the presence of the label in these positions.

Synthesis of [(dipope)Rh]$_2$[μ-N=C(H)CH$_3$](μ-H), ***2****b*

To a stirred solution of [(dipope)Rh]$_2$(μ-H)$_2$, **1***b* (0.152 g, 0.18 mmol), in toluene (5 mL) was added two drops of acetonitrile. The reaction was allowed to stir for a further 30 min at which time the toluene was removed *in vacuo*. The orange residue was recrystallized from hexanes, yielding 0.122 g (77%) of **2***b*. ^{1}H NMR (C_6D_6, ppm): N=C*H*CH$_3$, 9.24 (m, 1H, ^3J_H = 4.9 Hz, and couplings of 20.0, 13.6, 6.4, and 1.8 Hz to phosphorus); OC*H*(CH$_3$)$_2$, 5.17, 5.01, 4.75, 4.66 (dsp, 2H each, ^3J_H = 5.6–6.4 Hz, ^2J_P = 2.0–3.0 Hz); N=CHC*H*$_3$, 2.47 (d, 3H); PC*H*$_2$C*H*$_2$P, 1.73 (m, 8H); OCH(C*H*$_3$)$_2$, 1.42, 1.35, 1.34, 1.33, 1.21, 1.20, 1.20, 1.19 (d, 48H); Rh-*H*-Rh, −6.42 (ttt, $^2J_{P_{trans}}$ = 76.0 Hz, $^2J_{P_{cis}}$ = 4–5 Hz, $^1J_{Rh}$ = 21.2 Hz). ^{31}P{^{1}H} NMR (C_6D_6): simulation of the spectrum

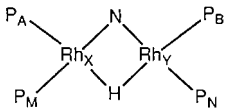

of **2***b* was performed using the following parameters: δ_A = 5220.0 Hz (actual chemical shift 189.3 ppm); δ_B = 4945.4 Hz (actual chemical shift 186.9 ppm); δ_M = 7640.0 Hz (actual chemical shift 209.1 ppm); δ_N = 7500.8 Hz (actual chemical shift 207.8

Can. J. Chem. Downloaded from www.nrcresearchpress.com by 109.225.110.28 on 09/08/12
For personal use only.

TABLE 3. Bond angles (deg) with estimated standard deviations in parentheses

Bonds	Angle(deg)	Bonds	Angle(deg)
P(1)—Rh(1)—P(2)	85.96(4)	C(11)—P(4)—C(12)	101.2(2)
P(1)—Rh(1)—N	170.39(10)	Rh(1)—N—Rh(2)	86.78(12)
P(1)—Rh(1)—H(Rh)	86.8(14)	Rh(1)—N—C(29)	128.8(3)
P(2)—Rh(1)—N	102.43(9)	Rh(2)—N—C(29)	141.3(3)
P(2)—Rh(1)—H(Rh)	170.1(14)	P(1)—C(1)—C(2)	110.4(3)
N—Rh(1)—H(Rh)	85.4(14)	P(2)—C(2)—C(1)	112.0(3)
P(3)—Rh(2)—P(4)	85.60(4)	P(3)—C(3)—C(4)	110.5(3)
P(3)—Rh(2)—N	166.45(9)	P(4)—C(4)—C(3)	111.7(3)
P(3)—Rh(2)—H(Rh)	84(1)	P(1)—C(5)—C(13)	110.5(3)
P(4)—Rh(2)—N	107.13(9)	P(1)—C(5)—C(14)	116.4(3)
P(4)—Rh(2)—H(Rh)	169(1)	C(13)—C(5)—C(14)	111.0(4)
N—Rh(2)—H(Rh)	83(1)	P(1)—C(6)—C(15)	111.0(3)
Rh(1)—P(1)—C(1)	111.33(14)	P(1)—C(6)—C(16)	111.6(3)
Rh(1)—P(1)—C(5)	120.4(1)	C(15)—C(6)—C(16)	110.2(4)
Rh(1)—P(1)—C(6)	117.44(14)	P(2)—C(7)—C(17)	111.2(3)
C(1)—P(1)—C(5)	101.3(2)	P(2)—C(7)—C(18)	115.4(4)
C(1)—P(1)—C(6)	101.9(2)	C(17)—C(7)—C(18)	110.0(5)
C(5)—P(1)—C(6)	101.9(2)	P(2)—C(8)—C(19)	111.1(4)
Rh(1)—P(2)—C(2)	110.9(1)	P(2)—C(8)—C(20)	111.4(4)
Rh(1)—P(2)—C(7)	121.6(2)	C(19)—C(8)—C(20)	109.5(5)
Rh(1)—P(2)—C(8)	116.1(2)	P(3)—C(9)—C(21)	110.7(4)
C(2)—P(2)—C(7)	101.5(2)	P(3)—C(9)—C(22)	115.4(4)
C(2)—P(2)—C(8)	103.2(2)	C(21)—C(9)—C(22)	111.0(5)
C(7)—P(2)—C(8)	101.1(2)	P(3)—C(10)—C(23)	110.4(4)
Rh(2)—P(3)—C(3)	112.1(2)	P(3)—C(10)—C(24)	111.6(4)
Rh(2)—P(3)—C(9)	116.6(2)	C(23)—C(10)—C(24)	111.0(5)
Rh(2)—P(3)—C(10)	119.4(2)	P(4)—C(11)—C(25)	110.2(3)
C(3)—P(3)—C(9)	101.7(2)	P(4)—C(11)—C(26)	116.4(4)
C(3)—P(3)—C(10)	102.0(2)	C(25)—C(11)—C(26)	110.4(4)
C(9)—P(3)—C(10)	102.7(3)	P(4)—C(12)—C(27)	112.0(4)
Rh(2)—P(4)—C(4)	110.7(2)	P(4)—C(12)—C(28)	111.2(4)
Rh(2)—P(4)—C(11)	122.2(2)	C(27)—C(12)—C(28)	109.7(4)
Rh(2)—P(4)—C(12)	117.3(1)	N—C(29)—C(30)	128.3(4)
C(4)—P(4)—C(11)	100.1(2)	Rh(1)—H(Rh)—Rh(2)	103(2)
C(4)—P(4)—C(12)	102.4(2)		

ppm). J_{AB} = 68.3 Hz; J_{AM} = 30.2 Hz; J_{AN} = 8.3 Hz. J_{AX} = 250.3 Hz; J_{AY} = 12.2 Hz; J_{BM} = 10.5 Hz; J_{BN} = 29.8 Hz; J_{BX} = 11.3 Hz; J_{BY} = 245.9 Hz; J_{MN} = 0.0 Hz; J_{MX} = 199.3 Hz; J_{MY} = 5.6 Hz; J_{NX} = 4.4 Hz; J_{NY} = 200.1 Hz; J_{XY} = 3.8 Hz. $^{13}C\{^1H\}$ NMR (C_6D_6, ppm): N=*C*H, 168.9; O*C*H(CH_3)$_2$, 4 signals 69.2–69.9; P*C*H$_2$*C*H$_2$P, 32.1–33.4 (m); N=CH*C*H$_3$, 31.9; OCH(*C*H$_3$)$_2$, 8 signals 24.4–25.5. Anal. calcd. for $C_{30}H_{69}O_8P_4Rh_2N$: C 39.97, H 7.71, N 1.55%; found: C 40.10, H 7.81, N 1.49%.

*Synthesis of [(dipope)Rh]$_2$[μ-N=C(H)C$_6$H$_5$](μ-H), 3*b

To a stirred solution of [(dipope)Rh]$_2$(μ-H)$_2$, **1***b* (0.157 g, 0.19 mmol), in toluene (5 mL) was added a solution of distilled benzonitrile (0.022 g, 0.21 mmol) in toluene (1 mL). The reaction was stirred for 30 min to ensure completion; the colour change accompanying the reaction was slight. The toluene was removed *in vacuo* and the remaining red solid recrystallized from hexanes. After washing with cold hexanes, 0.137 g (73%) of crystals of **3***b* was obtained. ^1H NMR (C_6D_6, ppm): N=C*H*C$_6$H$_5$, 10.34 (br m, 1H, coupled to three phosphorus nuclei, $J_P \approx 16$, 16, and 4 Hz); H_{ortho}, 8.17 (d, 2H, $^3J_{H_{meta}}$ = 7.2 Hz); H_{meta}, 7.29 (m, 2H, $^3J_{H_{para}}$ = 7.3 Hz); H_{para}, 7.20 (m, 1H); O*C*H(CH_3)$_2$, 5.18, 5.17, 4.95, 4.50 (dsp, 8H, ^3J_H = 6.8–7.6 Hz, ^2J_P = 2.0–3.0 Hz); P*C*H$_2$*C*H$_2$P, 1.76, 1.70, (m, 8H); OCH(*C*H$_3$)$_2$, 0.95–1.5 (br signals, 48H); Rh-*H*-Rh, −6.80 (ttt, $^2J_{Ptrans}$ = 75.2 Hz, $^2J_{Pcis} \approx 4$ Hz, $^1J_{Rh}$ = 20.4 Hz). $^{31}P\{^1H\}$ NMR (C_6D_6, ppm): $P_{trans(N)}$, 204.7 (dd, $^1J_{Rh}$ = 198.7 Hz, ^2J_P = 27.3 Hz); $P_{trans(N)}$, 201.0 (dd, $^1J_{Rh}$ = 203.6 Hz, ^2J_P = 36.1 Hz); $P_{cis(N)}$, 187.0 (br ddd, $^1J_{Rh}$ = 257.1 Hz, ^2J_P = 27.3 Hz, ^4J_P = 59.3 Hz); $P_{cis(N)}$, 175.0 (br ddd, $^1J_{Rh}$ = 263.3 Hz), $^{13}C\{^1H\}$ NMR (C_6D_6, ppm): N=*C*H, 168.0 (^1J_H = 169.3 Hz); C_{ipso}, 140.7; other aromatic carbons, 129.3, 128.9, 127.7; O*C*H(CH_3)$_2$, 70.0 (2), 69.8, 69.1; P*C*H$_2$*C*H$_2$P, 31–34; OCH(*C*H$_3$)$_2$, 24.9–25.6. Anal calcd. for $C_{35}H_{71}O_8P_4Rh_2N$: C 43.60, H 7.47, N 1.45%; found: C 43.43, H 7.60, N 1.40%.

*Synthesis of [(dipope)Rh]$_2$[μ-N=C(H)-o-CH$_3$-C$_6$H$_4$](μ-H), 4*b

To a stirred solution of [(dipope)Rh]$_2$(μ-H)$_2$, **1***b* (0.102 g, 0.12 mmol), in toluene (5 mL) was added a solution of distilled *o*-tolylnitrile (0.015 g, 0.13 mmol) in toluene (1 mL). The reaction was stirred for 45 min to insure completion. The toluene was removed *in vacuo* and the remaining red solid recrystallized from hexanes; after washing the crystals with cold hexanes, 0.088 g (76%) of **4***b* was isolated. ^1H NMR (C_6D_6, ppm): N=C*H*, 10.40 (br m, 1H, coupled to three phosphorous nuclei, $J_P \approx 16$, 16, and 4 Hz); C-H_1, 8.36 (dd, 1H, ^3J_H = 7.2 Hz, ^4J_H = 1.8 Hz); C-H_2 and C-H_3, 7.16 (m, 2H); C-H_4, 7.01 (d, 1H, ^3J_H = 6.8 Hz); O*C*H(CH_3)$_2$, 5.22, 5.16, 4.93, 4.46 (dsp, 8H, ^3J_H = 6.4–7.6 Hz, ^2J_P = 2.0–3.0 Hz); C-C*H*$_3$, 2.55 (s, 3H); P*C*H$_2$*C*H$_2$P, 1.78, 1.73 (m, 8H); OCH(*C*H$_3$)$_2$, 1.45, 1.40, 1.36, 1.35, 1.27, 1.20, 0.97, 0.93 (d, 48H); Rh-*H*-Rh, −6.80 (br ttt, $^2J_{Ptrans}$ = 73.6 Hz, $^2J_{Pcis}$ = 4.8 Hz, $^1J_{Rh}$ = 20.8 Hz). $^{31}P\{^1H\}$ NMR (C_6D_6, ppm): $P_{trans(N)}$, 207.8 (dd, $^1J_{Rh}$ = 200.0 Hz, ^2J_P = 29.0); $P_{trans(N)}$, 201.2 (dd, $^1J_{Rh}$ = 203.6 Hz, ^2J_P = 34.6 Hz); $P_{cis(N)}$, 186.5 (br dm, $^1J_{Rh}$ = 256.2 Hz, $^4J_P \approx$ 55 Hz); $P_{cis(N)}$, 175.0 (br dm, $^1J_{Rh}$ = 262.7 Hz), $^{13}C\{^1H\}$ NMR (C_6D_6, ppm): N=*C*H, 167.4 (s); $C_{ipso(N)}$, 136.0; $C_{ipso(CH_3)}$, 131.9; other aromatic carbons, 128.9, 128.7, 126.5, 126.4; O*C*H(CH_3)$_2$, 70.1(2), 69.8, 68.9; P*C*H$_2$*C*H$_2$P, 32.1–33.5 (m); OCH(*C*H$_3$)$_2$,

Can. J. Chem. Downloaded from www.nrcresearchpress.com by 109.225.110.28 on 09/08/12
For personal use only.

24.6–25.6; C-CH_3, obscured in methyl region. Anal. calcd. for $C_{36}H_{71}O_8P_4Rh_2N$: C 44.23, H 7.53, N 1.43%; found: C 43.99, H 7.56, N 1.39%.

Synthesis of [(dippe)Rh]$_2$[μ-(H)N(CH_2CH_3)](μ-H), 5a

Method A

Solid [(dippe)Rh]$_2$[μ-N=C(H)CH_3](μ-H), **2***a* (0.072 g, 0.09 mmol), was loaded into a small reactor bomb along with toluene (5 mL) and a magnetic stir bar. The solution was degassed on a vacuum line and cooled to −196°C. Dihydrogen was admitted to 1 atm (101.3 kPa) of pressure and the solution was allowed to warm to room temperature. Vigorous stirring was continued for 6–7 h during which time a red to yellow-orange colour change occurred. The toluene was removed *in vacuo* and the residues recrystallized from toluene/hexanes (1:1) yielding 0.059 g (78%) of oily yellow crystals. ^{1}H NMR (C_6D_6, ppm): N-*H*, 3.97 (br s, 1H); H-NCH_2, 3.69 (br m, 2H); C*H*(CH_3)$_2$, 2.40, 2.28, 2.06, 1.92 (dsp, 8H, ^2J_P = 2.0–4.0 Hz, ^3J_H = 7.3–8.0 Hz); CH(CH_3)$_2$, 1.50, 1.33, 1.31, 1.20, 1.17, 1.13, 1.12, 1.01 (dd, 48H, ^3J_P = 12.0–14.4 Hz); NCH_2CH_3, PCH_2CH_2P, obscured under methyl resonances; Rh-*H*-Rh, −7.30 (ttt, $^2J_{Ptrans}$ = 61.2 Hz, $^2J_{Pcis}$ = 13.2 Hz, $^1J_{Rh}$ = 21.2 Hz). ^{31}P{^{1}H} NMR (C_6D_6, ppm): $P_{trans(N)}$, 104.2 (dm, $^1J_{Rh} \approx$ 154 Hz); $P_{cis(N)}$, 87.1 (dm, $^1J_{Rh} \approx$ 193 Hz). ^{13}C{^{1}H} NMR (C_6D_6, ppm): H-NCH_2, 52.7; NCH_2CH_3, ligand resonances 17–28. Anal. calcd. for $C_{30}H_{71}P_4Rh_2N$: C 46.46, H 9.23, N 1.81%; found: C 46.09, H 9.27, N 1.81%.

Method B

A solution of [(dippe)Rh]$_2$(μ-H)$_2$, **1***a* (0.103 g, 0.14 mmol), in toluene (5 mL) was loaded into a small reactor bomb equipped with a magnetic stir bar. The solution was degassed on a vacuum line and dihydrogen admitted to a pressure of 1 atm. To this solution of the tetrahydride was added acetonitrile (0.1 mL) via syringe under a strong flow of dihydrogen. The reaction mixture was cooled to −196°C and the Kontes valve port sealed completely. Stirring was continued for 16 h during which time a slow brown to yellow-orange colour change ensued. The toluene, excess dihydrogen, and excess acetonitrile were removed *in vacuo* and the residues recrystallized from toluene/hexanes (1:1) yielding 0.070 g (64%) of crystals of **5***a*. The product was found to be spectroscopically identical to that obtained in the reaction of **2***a* and dihydrogen.

Method C

A solution of [(dippe)Rh]$_2$(μ-H)$_2$, **1***a* (0.092 g, 0.12 mmol), in toluene (5 mL) was loaded into a small reactor bomb equipped with a magnetic stir bar. The solution was degassed on a vacuum line. A moderate excess of ethylamine was then vacuum transferred into the vessel from a −10°C bath. The reaction was stirred until the green to yellow colour change was complete (8–12 h). The toluene and excess ethylamine were removed under reduced pressure and the residues recrystallized from toluene/hexanes (1:1) yielding 0.082 g (84%) of crystals of **5***a*. The product was spectroscopically identical to samples of **5***a* and obtained via the routes described above.

Synthesis of [(dippe)Rh]$_2$[μ-(H)N($CH_2C_6H_5$)](μ-H), 6a

Method A

An identical procedure to method A described above was employed using **3***a* (0.093 g, 0.11 mmol). Yellow crystals of the μ-benzylamido hydride complex **6***a* were obtained (0.086 g, 81%). ^{1}H NMR (C_6D_6, ppm): H_{ortho}, 8.01 (d, 2H, $^3J_{H_{meta}}$ = 7.6 Hz); H_{meta}, 7.24 (m, 2H, $^3J_{H_{para}}$ = 7.5 Hz); H_{para}, 7.14 (t, 1H); H-NCH_2, 5.17 (br m, 2H, $J_P \approx$ 3.0 Hz); N-*H*, 4.10 (br s, 1H); C*H*(CH_3)$_2$, 2.45, 2.16, 2.13, 1.95 (dsp, 8H, ^2J_P = 2.0–4.0 Hz, ^3J_H = 7.2–8.2 Hz); CH(CH_3)$_2$, 1.56, 1.45, 1.34, 1.18, 1.09, 1.07, 1.01, 0.78 (dd, 48H, ^3J_P = 11.4–15.2 Hz; PCH_2CH_2P, 1.26 (m, 8H); Rh-*H*-Rh, −7.44 (ttt, $^2J_{Ptrans}$ = 60.2 Hz, $^2J_{Pcis}$ = 12.6 Hz, $^1J_{Rh}$ = 21.6 Hz). ^{31}P{^{1}H} NMR (C_6D_6, ppm): $P_{trans(N)}$, 103.7 (dm, $^1J_{Rh} \approx$ 152 Hz); $P_{cis(N)}$, 85.8 (dm, $^1J_{Rh} \approx$ 193 Hz). Anal. calcd. for $C_{35}H_{73}P_4Rh_2N$: C 50.18, H 8.78, N 1.67%; found: C 49.96, H 8.73, N 1.80%.

Method B

An identical procedure to method B described above was employed using **1***a* (0.103 g, 0.14 mmol) and benzonitrile (0.72 g in 0.5 mL toluene, 5 equivalents). The product, **6***a*, was isolated in 75% yield (0.088 g) and was spectroscopically identical to the product obtained in the reaction of **3***a* with dihydrogen.

Method C

To a stirred solution of [(dippe)Rh]$_2$(μ-H)$_2$, **1***a* (0.087 g, 0.11 mmol), in toluene (5 mL) was added pure benzylamine (0.064 g, 5 equivalents). The reaction was stirred for 2 h while a green to yellow-orange colour change occurred. Removal of the toluene, followed by recrystallization, yielded 0.087 g (88%) of yellow-orange crystals of **6***a*. This product was spectroscopically identical to samples of **6***a* obtained via the routes described above.

Synthesis of [(dippb)Rh]$_2$[μ-(H)N(CH_2CH_3)](μ-H), 6d

A solution of the tetrahydride [(dippb)Rh]$_2$(H)(μ-H)$_3$, **5***c* (18) (0.098 g, 0.12 mmol), in toluene (5 mL) was loaded into a small reactor bomb equipped with a magnetic stir bar. Acetonitrile (1 mL) was added and the reaction mixture degassed on a vacuum line via two freeze–pump–thaw cycles; the vessel was back-filled with pure dinitrogen. The reaction was stirred at 70°C for 3 days, at which time a colour change from brown-green to yellow was complete. Toluene and excess acetonitrile were removed *in vacuo* and the residues analyzed by ^{1}H and ^{31}P{^{1}H} NMR spectroscopy. ^{1}H NMR (C_6D_6, ppm): N-*H*, 3.41 (br s, 1H); H-NCH_2, 3.27 (br m, 2H); C*H*(CH_3)$_2$, 2.35, 2.18, 2.15, 1.96 (dsp, 8H, ^2J_P = 2.0–4.0 Hz, ^3J_H = 7.4–8.0 Hz); NCH_2CH_3, 1.70 (t, 3H, ^3J_H = 7.6 Hz); CH(CH_3)$_2$, 1.58, 1.55, 1.46, 1.32, 1.30, 1.21, 1.19, 1.17 (dd, 48H, ^3J_P = 12.0–14.0 Hz); P(CH_2)$_4$P, resonances obscured by methyl signals; Rh-*H*-Rh, −10.87 (ttt, $^2J_{Ptrans}$ = 57.2 Hz, $^2J_{Pcis}$ = 13.2 Hz, $^1J_{Rh}$ = 21.6 Hz). ^{31}P{^{1}H} NMR (C_6D_6, ppm): $P_{trans(N)}$, 61.2 (dm, $^1J_{Rh} \approx$ 154 Hz); $P_{cis(N)}$, 33.7 (dm, $^1J_{Rh} \approx$ 195 Hz).

Results and discussion

The observed reactivity between the dihydrides [(dippe)-Rh]$_2$(μ-H)$_2$, **1***a*, and [(dipope)Rh]$_2$(μ-H)$_2$, **1***b*, and the carbon–nitrogen double bonds of imines (19) led us to explore the behaviour of these dimers towards the carbon–nitrogen triple bonds of simple nitrile substrates. The dihydrides were found to react smoothly with one or more equivalents of R′CN (R′ = CH_3, C_6H_5, *o*-CH_3-C_6H_4) at room temperature to produce the red or red-purple, air-sensitive μ-alkylideneimido hydride complexes **2**–**4***a* and **2**–**4***b* (eq. [1]). The reactions were spectroscopically clean, producing the product in >95% yield by ^{1}H and ^{31}P{^{1}H} NMR spectroscopy; isolated yields for **2**–**4***a* were 82–88%, whereas the more soluble compounds of the dipope series, **2***b*–**4***b*, were isolated in 72–78% yield. Similar to the trends in the reactions with imines (19), the dippe dimer **1***a* reacted instantly with the nitriles employed, while the dipope dihydride required about 30 min to undergo the same transformations.

The related binuclear hydride, [(dippp)Rh]$_2$(μ-H)$_2$, where dippp is 1,3-bis(diisopropylphosphino)propane ($Pr^i_2PCH_2CH_2CH_2PPr^i_2$) (20), undergoes a slow reaction with acetonitrile at elevated temperatures, but fails to react with either benzonitrile or *o*-tolynitrile. The presence of the μ-ethylideneimido dippp product was noted spectroscopically, but the prohibitively slow rate of this transformation discouraged complete characterization of this complex.

The ^{1}H, ^{13}C{^{1}H}, and ^{31}P{^{1}H} NMR spectral data collected for these complexes were consistent with the proposed structure for these molecules; in addition, a single crystal X-ray analysis on **2***a* confirmed the structural assignment (*vide infra*). In the ^{1}H NMR spectra of these compounds, the signals of interest are those for alkylideneimido

[1]

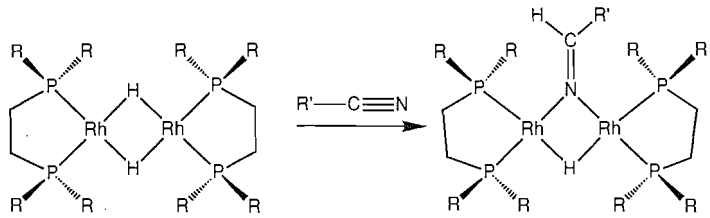

1a R = Pr^i
1b R = OPr^i

R = Pr^i	R' = Me	**2a**
R = Pr^i	R' = Ph	**3a**
R = Pr^i	R' = o-tol	**4a**
R = OPr^i	R' = Me	**2b**
R = OPr^i	R' = Ph	**3b**
R = OPr^i	R' = o-tol	**4b**

proton and the bridging hydride ligand. The alkylideneimido protons resonate downfield in the region 8.75–10.5 ppm, and give rise to a complex signal with coupling to four inequivalent phosphorus nuclei present (no Rh–H coupling was observed; therefore this coupling is <2.5 Hz). The μ-hydrido ligands also show coupling to four inequivalent phosphorus atoms; one-bond rhodium coupling constants of ≈20–22 Hz are also observed.

In the $^{13}C\{^1H\}$ NMR spectra, the μ-alkylideneimido carbon atom resonates at ≈159 ppm for the dippe *a* series of compounds and ≈168 ppm in the complexes of the dipope *b* series. Little ^{13}C NMR data has been reported for μ-alkylideneimido complexes, but these chemical shifts do fall in the range in which the imine carbon in free imines usually resonate (≈160 ppm) (22).

As expected, the $^{31}P\{^1H\}$ NMR spectra for these compounds are complex, particularly in the dippe series. Four inequivalent phosphine environments and the long-range P–P and Rh–P couplings between opposite sides of the dimer generate an ABMNXY spin system, which we have successfully simulated for the dipope derivative **2***b*; see experimental section. A large four-bond coupling between the two phosphorus nuclei *cis* to the ethylideneimido ligand is observed ($^4J_{P-P}$ = 68.3 Hz) and substantial three-bond couplings of 11.3 and 12.2 Hz from the *cis* phosphorus nuclei to the distal rhodiums are also present. In general, the spectra of the dippe compounds **2–4***a* are broader with less well-defined couplings.

*The solid state structure of [(dippe)Rh]$_2$[μ-N=C(H)CH$_3$] (μ-H), 2*a

Characterization of this family of compounds was completed via a single crystal X-ray analysis of the dippe ethylideneimido hydride complex **2***a*; two views of the ORTEP diagram of the binuclear complex are shown in Figure 1, while Tables 2 and 3 give bond distances and angles, respectively. Each rhodium centre in the dimer is of a distorted square planar geometry. When viewed looking down the Rh–Rh vector, the two square planes are slightly bent with respect to each other. The angle between the mean-square planes containing a rhodium atom and the four ligand atoms is 25.5°. The parameters associated with the chelating phosphine ligands are unremarkable; Rh—P bond lengths and the P—Rh—P angles of 86.44° and 85.89° are nearly identical to analogous values found in other structurally characterized rhodium complexes containing the dippe ligand (17, 20, 23–25). The angles P(2)—Rh(1)—Rh(2) and P(4)—Rh(2)—Rh(1) are 145.1° and 148.6°, respectively, and partially account for the large four-bond coupling between P(2) and P(4) (*vide supra*). The bridging hydride ligand was located and refined isotropically and was found to symmetrically bridge the two metal centres. The Rh—H bond lengths of 1.74(5)Å are about 0.1 Å shorter than those in other [(dippe)Rh]$_2$(μ-X)(μ-H) (17, 23, 24) complexes, which average ≈1.84 Å in length, but are comparable to the 1.70 Å distances found in the parent dihydride **1***a* (20). The "tighter" molecular core is also reflected by a slightly shorter than normal (≈2.86 Å) Rh—Rh separation of 2.7992(4) Å.

Bond and angle parameters in the μ-ethylideneimido ligand are typical of a bridging bonding mode with no π-donation from the C=N bond to either of the metal centres. The C=N bond length of 1.255(5) Å is slightly shorter than an average carbon–nitrogen double bond (1.28 Å) (26), but coincides well with other known C=N distances in complexes incorporating the μ-alkylideneimido ligand (9–11, 14, 27, 28).

The N—C(29)—C(30) bond angle of 128.3° suggests sp^2 hybridization about C(29) (the other two angles, i.e., N—C(29)—H and C(30)—C(29)—H, are idealized since the ethylideneimido proton was not refined). This is also supported by large $^1J_{C-H}$ coupling constants of ≈168 Hz in the alkylideneimido C—H bonds (22).

The discrepancy between Rh(1)—N—C(29) (128.8°) and Rh(2)—N—C(29) (141.3°) indicates that the μ-ethylideneimido ligand is slightly tilted such that the methyl group, C(30), is moved away from the isopropyl groups on P(4). Presumably, with the larger phenyl and *o*-tolyl substituents on C(29), this steric interaction would be exacerbated. It also provides a possible rationale for why the bulkier nitriles Bu^tCN and Pr^iCN do not react with **1***a* or **1***b* to produce the corresponding μ-alkylideneimido hydride complexes.

Mechanistic considerations

The reaction of d_2-**1***a* with acetonitrile or *o*-tolynitrile yielded d_2-**2***a* and d_2-**4***a*, respectively (eq. [2]), in which the deuterium label appears in the μ-alkylideneimido and μ-hydrido positions. Unlike the reactions involving **1***a* and imines (19), intermediates in the reactions with nitriles were not observed when the reactions were monitored at low temperatures; at −80°C, only peaks for the dihydride and the final product **4***a* were observed in the $^{31}P(^1H)$ NMR spectrum of the reaction between **1***a* and *o*-tolylnitrile. Nonetheless, it

Can. J. Chem. Downloaded from www.nrcresearchpress.com by 109.225.110.28 on 09/08/12
For personal use only.

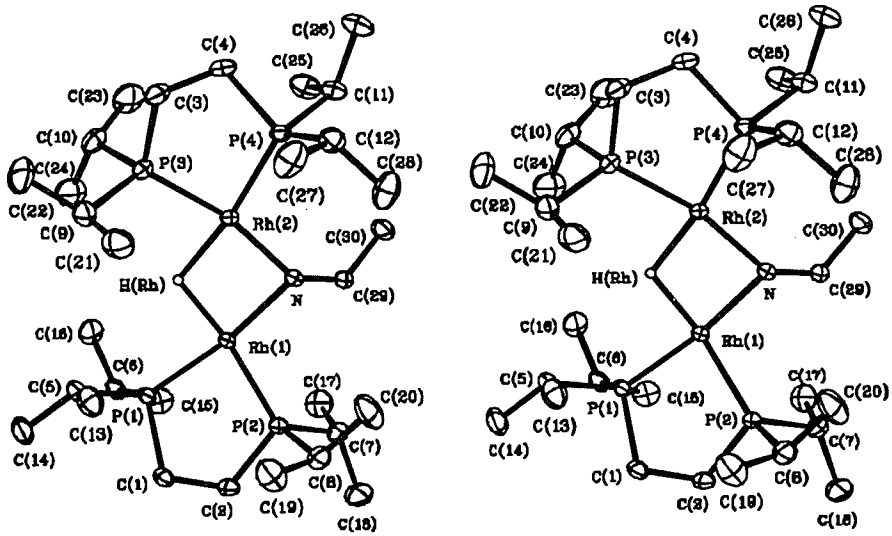

FIG. 1. Stereoview and numbering scheme for **2***a*; 50% probability thermal ellipsoids are shown for the non-hydrogen atoms.

seems reasonable to postulate a similar reaction course to the one proposed for the reactions of **1***a* and **1***b* with imines, i.e., activation of substrate via σ–π donation to adjacent coordinatively unsaturated metal centres, followed by Rh—H bond cleavage and finally insertion of the C≡N into the newly formed Rh—H terminal linkage. If such a mechanism is operative here, it is probable that the greater π-donating ability of C≡N compared to C=N is responsible for accelerating the rate-limiting migration of a bridging hydride into a terminal position, such that observation of intermediates is precluded in this system. The results of the labelling experiment are consistent with an insertion of the C≡N triple bond into a rhodium hydride bond, but based on the imine/dihydride study we consider it likely that both metal centres are involved in the formation of the alkylideneimido products.

The reactions of μ-alkylideneimido complexes with dihydrogen and related processes

The complete stoichiometric reduction of the nitrile C≡N bond is accomplished via the reaction of the alkylideneimido complexes with excess dihydrogen (eq. [3]). The reactions proceed nearly quantitatively, yielding primary amido hydride products akin to those produced in the reactions of the dihydrides with imines (19). Like their secondary analogs, the amido-hydrides **5***a* and **6***a* (R′ = CH_3 and C_6H_5, respectively) were relatively inert to further reaction with dihydrogen and were thus isolated in 85–92% yield. The overall sequence from **1***a* and R′C≡N to the amido hydrides represents a stoichiometric reduction of the nitrile to an amine mediated by two metal centres. Although stepwise reduction of R′C≡N on trinuclear clusters has been observed previously (M_3 = Fe_3 (13–16), Os_3 (9, 28)), this is the first example of this transformation occurring on a binuclear cluster. The amido hydrides also obtain when the tetrahydride hydrogen adduct of **1***a* (formed *in situ* from **1***a* and dihydrogen (20)) is treated with the nitriles. A related transformation is the reaction of the thermally stable tetrahydride [(dippb)Rh]$_2$(μ-H)$_3$(H) (20) [dippb = $Pr^i_2PCH_2CH_2$-$CH_2CH_2PPr^i_2$] with acetonitrile to generate the μ-ethylamido product (eq. [4]). Although no intermediates could be observed in these last two reactions, presumably alkylideneimido-type intermediates are involved but with additional hydride ligands present.

Mechanistically, the reaction in eq. [3] likely proceeds through an intermediate incorporating a μ–η^2–σ iminyl ligand, similar in nature to an intermediate observed in the **1***a*/imine reactions. Whether the reaction proceeds via hydrogenolysis of the Rh—N bond, or by H_2 oxidative-addition/N-H reductive-elimination sequence, the intermediate formed is probably similar to species **A**, shown below, which subsequently proceeds very rapidly to generate the amido-hydride products.

[2]

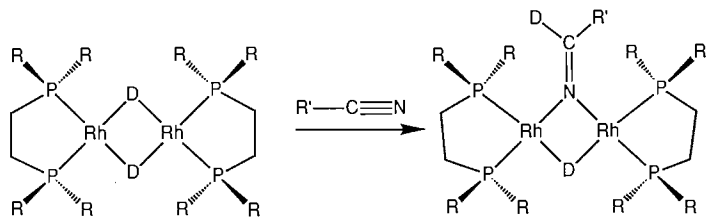

d*$_2$-1*a R = Pr^i

R = Pr^i R′ = Me ***d*$_2$-2*a***

R = Pr^i R′ = o-tol ***d*$_2$-4*a***

Can. J. Chem. Downloaded from www.nrcresearchpress.com by 109.225.110.28 on 09/08/12
For personal use only.

Can. J. Chem. Downloaded from www.nrcresearchpress.com by 109.225.110.28 on 09/08/12
For personal use only.

[3]

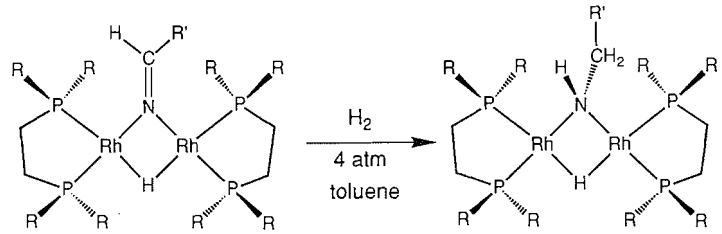

R = Pr^i R' = Me **2***a*
R = Pr^i R' = Ph **3***a*

R = Pr^i R' = Me **5***a*
R = Pr^i R' = Ph **6***a*

[4]

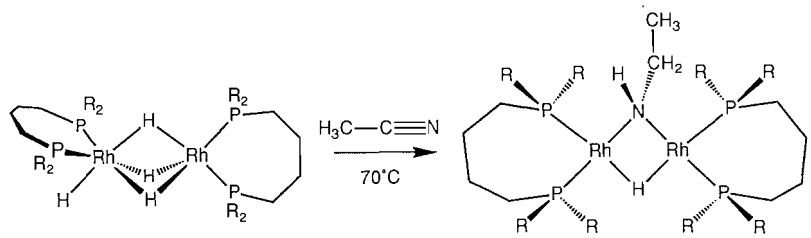

R = Pr^i **7**

R = Pr^i **5***c*

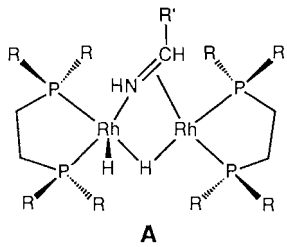

A

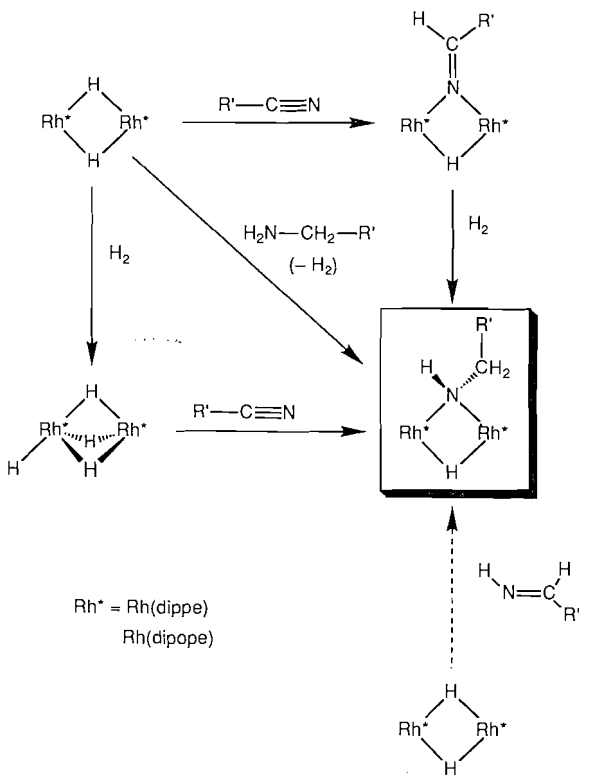

SCHEME 1

The thermodynamic stability of the amido-hydride derivatives is apparent from the number of routes to these complexes (Scheme 1). In addition to the reactions of **1***a* and **1***b* with imines and nitriles/H_2 (or H_2/nitriles), the stoichiometric reduction of isonitriles with the dihydride $\{[(Pr^iO)_3P]_2Rh\}_2(\mu\text{-}H)_2$ and dihydrogen produces related amido-hydride products (29). Another route is the reaction of primary amines with the dihydrides; this reaction, the reverse of which would be the last step in a catalytic cycle, proceeds smoothly with elimination of dihydrogen.

While the reactions of **1***a* with the amines were slowly reversible in the presence of excess dihydrogen at normal temperatures and pressures, obviously the presence of a four-electron donor in the bridging position is preferred over a two-electron donor hydride ligand. The thermodynamic stability of the amido-hydride functionality in these complexes is undoubtedly the reason homogeneous hydrogenation of both imines and nitriles fails for these systems.

1. T. Yoshida, T. Okano, and S. Otsuka. J. Chem. Soc. Chem. Commun. 870 (1979).
2. E. Band, W. R. Pretzer, M. G. Thomas, and E. L. Muetterties. J. Am. Chem. Soc. **99**, 7380 (1977).
3. R. A. Grey, G. P. Pez, and A. Wallo. J. Am. Chem. Soc. **103**, 7536 (1981).
4. T. Suarez and B. Fontal. J. Mol. Catal. **45**, 335 (1988).
5. B. N. Storhoff and H. C. Lewis, Jr. Coord. Chem. Rev. **23**, 1 (1977).
6. M. Kilner. Adv. Organomet. Chem. **10**, 115 (1972).
7. P. A. Chetcuti, C. B. Knobler, and M. F. Hawthorne. Organometallics, **7**, 650 (1988).
8. T. C. Wright, G. Wilkinson, M. Motevalli, and M. B. Hursthouse. J. Chem. Soc. Dalton Trans. 2017 (1986).
9. R. D. Adams, D. A. Katahira, and L.-W. Yang. J. Organomet. Chem. **219**, 85 (1981).
10. D. W. Prest, M. J. Mays, and P. R. Raithby. J. Chem. Soc. Dalton Trans. 2021 (1982).
11. Z. He, D. Neibecker, N. Lugan, and R. Mathieu. Organometallics, **11**, 817 (1992).

12. E. L. Muetterties and M. J. Krause. Angew. Chem. Int. Ed. Engl. **22**, 135 (1983).
13. M. A. Andrews and H. D. Kaesz. J. Am. Chem. Soc. **101**, 7238 (1979).
14. M. A. Andrews, G. van Buskirk, C. B. Knobler, and H. D. Kaesz. J. Am. Chem. Soc. **101**, 7245 (1979).
15. M. A. Andrews and H. D. Kaesz. J. Am. Chem. Soc. **101**, 7255 (1979).
16. M. A. Andrews, C. B. Knobler, and H. D. Kaesz. J. Am. Chem. Soc. **101**, 7260 (1979).
17. M. D. Fryzuk, T. Jones, and F. W. B. Einstein. Organometallics, **3**, 1556 (1984).
18. M. D. Fryzuk. Can. J. Chem. **61**, 1347 (1983).
19. M. D. Fryzuk and W. E. Piers. Organometallics, **9**, 986 (1990).
20. M. D. Fryzuk, W. E. Piers, F. W. B. Einstein, and T. Jones. Can. J. Chem. **67**, 883 (1989).
21. International tables for X-ray crystallography. Vol. IV. Kynoch Press, Birmingham, U.K. (present distributor D. Reidel, Dordrecht, The Netherlands). 1974. pp. 99–102 and 149.
22. G. C. Levy, R. L. Lichter, and G. L. Nelson. Carbon-13 nuclear magnetic resonance spectroscopy. Wiley, New York. 1980.
23. M. D. Fryzuk, M. L. Jang, T. Jones, and F. W. B. Einstein. Can. J. Chem. **64**, 174 (1986).
24. M. D. Fryzuk, W. E. Piers, S. J. Rettig, T. Jones, F. W. B. Einstein, and T. S. Albright. J. Am. Chem. Soc. **111**, 5709 (1989).
25. M. D. Fryzuk, L. Rosenberg, and S. J. Rettig. Organometallics **10**, 2537 (1991).
26. L. E. Sutton. Tables of interatomic distances and configuration in molecules and ions. Chemical Society Special Publication No. 11, Chemical Society, London. 1958.
27. Z. Dawoodi, M. J. Mays, and A. G. Orpen. J. Organomet. Chem. **219**, 251 (1981).
28. Z. Dawoodi, M. J. Mays, and K. Henrick. J. Chem. Soc. Dalton Trans. 433, (1984).
29. S. T. McKenna, R. A. Andersen, and E. L. Muetterties. Organometallics, **5**, 2233 (1986).

Can. J. Chem. Downloaded from www.nrcresearchpress.com by 109.225.110.28 on 09/08/12
For personal use only.

Tetramethylguanidino-substituted pyrylium and thiopyrylium salts

WLODZIMIERZ GALEZOWSKI,[1] KENNETH T. LEFFEK, AND PRZEMYSLAW PRUSZYNSKI[2]
Department of Chemistry, Dalhousie University, Halifax, N. S., Canada B3H 4J3

Received March 2, 1992

WLODZIMIERZ GALEZOWSKI, KENNETH T. LEFFEK, and PRZEMYSLAW PRUSZYNSKI. Can. J. Chem. **70**, 2390 (1992).

Four new tetramethylguanidino-substituted pyrylium and thiopyrylium salt dyes have been prepared and their absorption maxima in the visible region measured. The positions of the absorption maxima are similar to those observed for thiopyrylium salt dyes used in photoconductive film compositions. The λ_{max} values for the new dyes, when compared to those of other pyrylium and thiopyrylium dyes in the literature, yield a σ_p value of -0.86 ± 0.04 and a σ^+ value of -1.8 ± 0.1 for the tetramethylguanidino group, in good agreement with previous determinations.

WLODZIMIERZ GALEZOWSKI, KENNETH T. LEFFEK et PRZEMYSLAW PRUSZYNSKI. Can. J. Chem. **70**, 2390 (1992).

On a préparé quatre colorants de la famille des sels de pyrylium et de thiopyrylium substitués par un groupe tétraméthylguanidino et on a mesuré leurs maxima d'absorption dans le région visible. Les positions des maxima d'absorption sont semblables à celles observées avec les colorants des sels de thiopyrylium utilisés dans des compositions de films photoconducteurs. Les valeurs des λ_{max} des nouveaux colorants, lorsqu'elles sont comparées à celles d'autres colorants du pyrylium et du thiopyrylium rapportées dans la littérature, permettent de déterminer une valeur de σ_p de $-0{,}86 \pm 0{,}04$ et une valeur de σ^+ de $-1{,}8 \pm 0{,}1$ pour le groupe tétraméthylguanidino, ce qui est en bon accord avec les valeurs déterminées antérieurement.

[Traduit par la rédaction]

Introduction

Pyrylium and thiopyrylium dye salts have been used for a number of years in photoconductive film compositions in electrophotographic technology (1) and the structure and properties of such photoconductive films have been reviewed by Perlstein (2). The typical structure of these dye salts is shown in **1** where X is O or S and R^1, R^2, and R^3 are aromatic groups with one or more of the groups, usually a

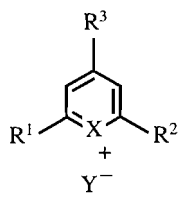

1

phenyl ring, substituted with a dimethylamino group (3, 4). Other similar thiopyrylium salts have also been prepared for the same purpose (5, 6). Our previous work on substituted phenyltetramethylguanidines (7, 8) showed that the tetramethylguanidino group (TMG) has a very large electron-donating power with a $\sigma_p = -0.8$ to -0.88. This suggested that dye salts of structure **1** with one of the phenyl rings *para*-substituted with the tetramethylguanidino group might provide new photosensitizing dyes additional to those already available.

Results and discussion

Since thiopyrylium salts of structure **1** are easily obtained from their pyrylium analogues by reaction with Na_2S (9), the synthesis focused on the pyrylium salts themselves. The direct reaction of 2,6-diphenylpyrylium perchlorate with 2-*N*-phenyl-1,1,3,3-*N*-tetramethylguanidine in acetic anhydride, by analogy with the method used by Kröhnke and Dickoré (10) to prepare the 4-(*p*-aminophenyl) flavylium perchlorate, failed in this case. This method was used by Katritzky *et al.* (4) in ethanol solvent to prepare *p*-dimethylamino derivatives, among others, of thiopyrylium salts of structure **1**. The method of Wizinger, Grüne, and Jacobi (11) of heating dialkyl anilines with diphenylpyrones in the presence of $POCl_3$ was also tried, using 2-*N*-phenyl-1,1,3,3-*N*-tetramethylguanidine, but this failed to give the desired product.

The pyrylium and thiopyrylium dyes with a TMG group *para*-substituted on the 4-phenyl ring were successfully synthesized in the form of guanidinium diperchlorates using the series of reactions shown in Scheme 1.

Solutions of 1,1,3,3-*N*-tetramethyl-2*N*-[4-(2,6-diphenyl-4-thiopyrylio)phenyl]guanidinium diperchlorate **9** in DMSO turn from dark yellow to blue upon dilution to a concentration of about 2×10^{-5} M. The visible spectrum of **9** itself was obtained in the presence of perchloric acid, which prevented the loss of a proton from the nitrogen atom, and shows a strong absorption band at $\lambda_{max} = 428$ nm ($\epsilon = 34\,000$). The spectrum of 2.5×10^{-5} M **9** in DMSO without the addition of $HClO_4$ shows only one absorption at $\lambda_{max} = 596$ nm ($\epsilon = 42\,000$). This band is ascribed to the structure **1** with $R^1 = R^2 = C_6H_5$, $R^3 = C_6H_4N{=}C(N(CH_3)_2)_2$, X = S, and $Y = ClO_4$. The corresponding compound with $R^3 = C_6H_4N(CH_3)_2$ was reported by Wizinger and Ulrich (9) to have a $\lambda_{max} = 583$ nm, a bathochromic shift of 13 nm. A plot of λ_{max} for the three thiopyrylium salts with *para* substituents H, $-OCH_3$, and $-N(CH_3)_2$, studied by Wizinger and Ulrich (9), against the Hammett substituent constant σ_p (correlation coefficient 0.9978) and the λ_{max} of the deprotonated form of **9** may be used to determine σ_p for the TMG group. This procedure gives a σ_p value for TMG of -0.89.

For deprotonated **9** it would be expected that a considerable amount of through conjugation would exist between the N—C double bond and positively charged pyrylium ring so that Hammett σ^+ values would be appropriate. When these are plotted against the λ_{max} values of Wizinger and Ulrich (9) for their three dyes, a linear relationship is obtained but with a relatively poor correlation coefficient of 0.9763. This relationship yields a σ^+ for the TMG group of -1.90. These

[1]Postdoctoral Fellow 1990.
[2]Research Associate 1986–1989.

Can. J. Chem. Downloaded from www.nrcresearchpress.com by 109.225.110.28 on 09/08/12
For personal use only.

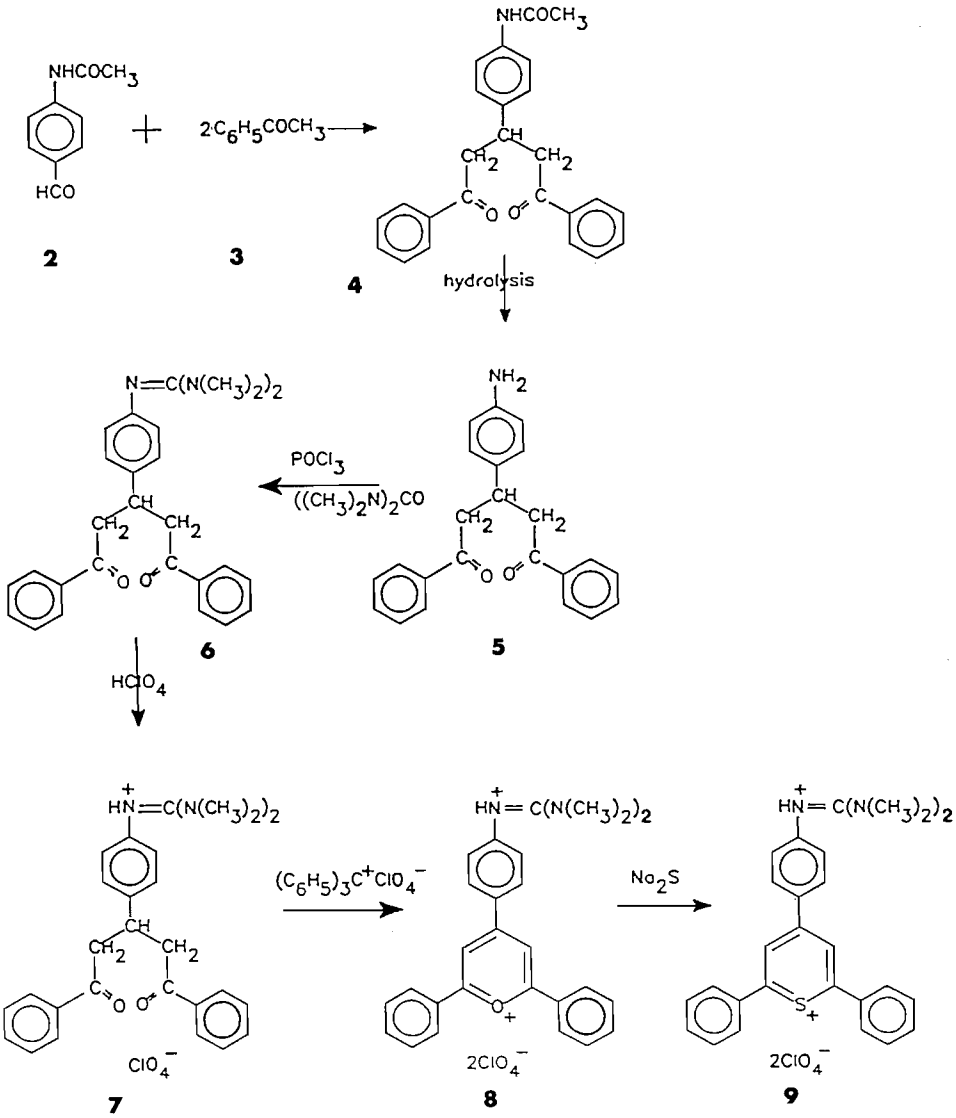

SCHEME 1

σ determinations may contain considerable error since they are based on only three measurements from the literature. However, we do have four different dyes, the absorption maxima of which can be used to obtain four separate estimates of σ.

The visible absorption peak for solutions of 1,1,3,3,-*N*-tetramethyl-2-*N*-[4-(2,6-diphenyl-4-pyrylio)phenyl]guanidinium diperchlorate **8** in DMSO has a λ_{max} = 422 nm (ε = 42 000) in the presence of $HClO_4$. The deprotonated compound showed λ_{max} = 555 nm (ε = 45 000). This latter peak combined with the data of Wizinger and Ulrich gives σ_p = −0.90 and σ^+ = −1.9. Again the correlation coefficients are better with σ_p (0.9999) than with σ^+ (0.9880).

The diperchlorate dyes with the TMG group substituted at the *para* position of the R^2 phenyl group of structure **1** were prepared by a series of reactions summarized in Scheme 2. The spectrum of the thiopyrylium dication **16** in DMSO with $HClO_4$ gave a peak, λ_{max} = 454 nm (ε = 14 000). A dilute solution in DMSO in the absence of acid gave the spectrum of the thiopyrylium salt dye and showed a λ_{max} = 610 nm (ε = 14 000). The pyrylium diperchlorate **15** gave a peak λ_{max} = 452 nm (ε = 12 000) in DMSO with acid, and λ_{max} = 565 nm (ε = 12 000) in the absence of acid. When these absorption maxima were compared to Hammett plots generated from absorption maxima reported by Wizinger and Ulrich (9), the thiopyrylium salt gave σ_p = −0.82 and σ^+ = −1.75 and the pyrylium salt gave σ_p = −0.815 and σ^+ = −1.7.

A possible source of error in these determinations is the difference in the solvents used in determining the visible spectra. Wizinger and Ulrich used glacial acetic acid, whereas ours were determined in DMSO. However, the λ_{max} values are not sensitive to this solvent change. Wizinger and Ulrich reported λ_{max} = 540 nm for the dimethylamino analogue of deprotonated **8** in glacial acetic acid. A sample of this compound prepared by us gave λ_{max} = 544 nm (ε = 53 000) in DMSO, so that the average σ values quoted below for the TMG group are probably reliable to within the stated standard deviations. The average σ values for the four determinations given above are σ_p = −0.86 ± 0.04 and σ^+ = −1.8 ± 0.1. There are now three determinations of σ_p for the TMG group, from nqr spectra (7) giving −0.88, from pK_a

Can. J. Chem. Downloaded from www.nrcresearchpress.com by 109.225.110.28 on 09/08/12
For personal use only.

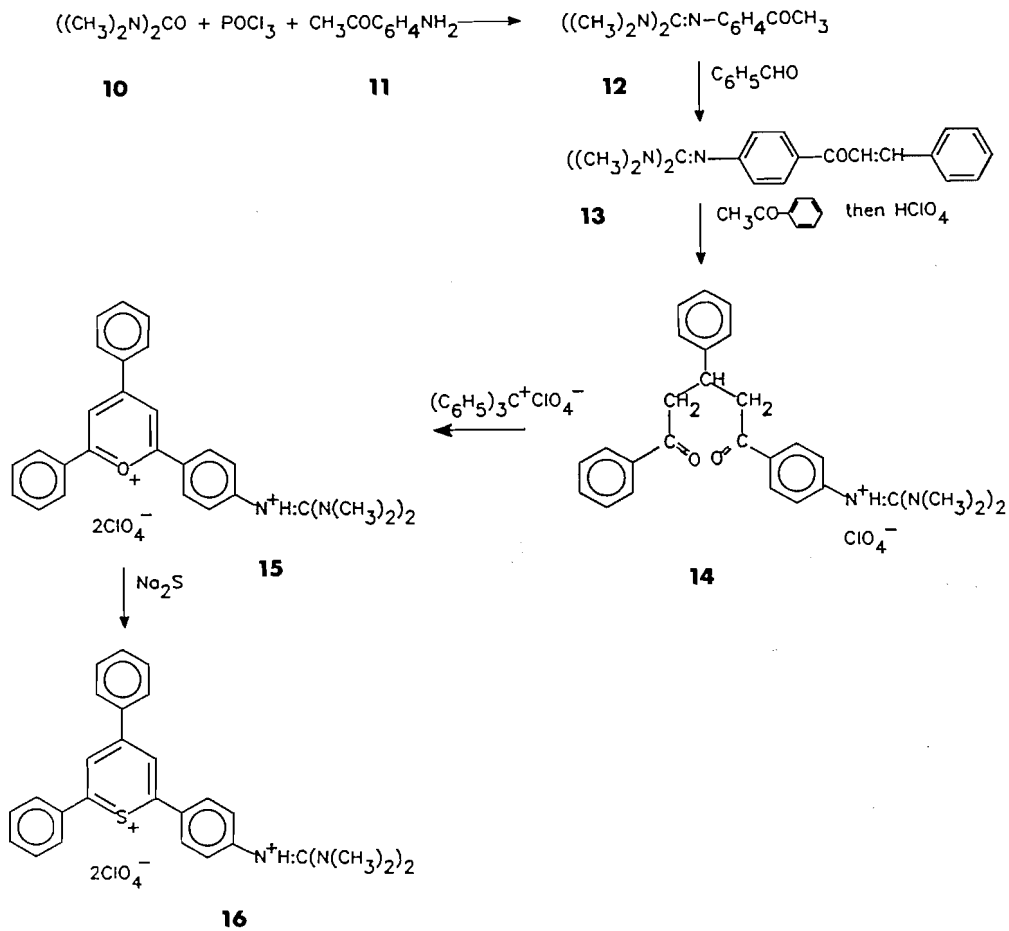

SCHEME 2

measurements (8) giving −0.80, and the present work from visible spectra giving −0.86. Thus the electron-releasing capacity of the TMG group is well established and is shown to be slightly greater than that of the dimethylamino group, which has a σ_p value of −0.83 (12).

The tetramethylguanidino-substituted pyrylio and thiopyrylio dyes are most readily prepared and stored as the diperchlorates because of the high basicity of the TMG group. However, the proton is lost in dilute DMSO solutions, giving dyes with visible absorption maxima very similar to those of the dimethylamino-substituted analogues. Thus the TMG dyes might be suitable sensitizing dyes in electrophotographic processes.

Experimental

*Preparation of 1,1,3,3-*N*-tetramethyl-2*N*-[4-(2,6-diphenyl-4-thiopyrylio)phenyl]guanidinium diperchlorate*

A mixture of 4-acetamidobenzaldehyde **2** (Aldrich) (8.16 g, 0.05 mol) and acetophenone **3** (12 g, 0.1 mol), in 150 mL ethanol in which NaOH (2 g, 0.05 mol) had been dissolved, was heated under reflux for 2 h, during which time the solution turned red-brown. A standard work-up yielded the white 3-(4-aminophenyl)-1,5-diphenyl-1,5-pentadione **5**; 2.7 g (16% yield); mp 120–122°C; ^{1}H nmr δ: 3.26 (2H, dd, −16.4, 7.1 Hz), 3.45 (2H, dd, −16.4, 7.0 Hz), 3.55 (2H, br s), 3.95 (1H, q, 7.0 Hz), 6.58–7.06 (4H), 7.41–7.56 (6H, m), 7.93–7.97 (4H, m). Anal. calcd. for $C_{23}H_{21}NO_2$: C 80.44, H 6.16, N 4.08%; found: C 80.2, H 6.46 N 4.04%. The main product was 3-(4-acetylaminophenyl)-1,5-diphenyl-1,5-pentadione **4** (42% yield).

The amine **5** was reacted with tetramethylurea using the method of Bredereck and Bredereck (13) but with a large excess of the reagent. The substituted phenylguanidine **6** was obtained as a resinous material; ^{1}H nmr δ: 2.7 (12H, s), 3.25–3.45 (4H, m), 3.8–4.2 (1H, m), 7.3–7.65 (6H), 7.9–8.05 (4H).

The product **6** was dissolved in a small amount of ethanol, then treated with excess 60% $HClO_4$, dropwise, and finally with H_2O dropwise until the solution became cloudy. Crystallization of the perchlorate salt **7** took place overnight and a recrystallization was made from a dichloromethane/hexane mixture, mp 168–169°C; ^{1}H nmr δ: 2.9 (12H, s), 3.2–3.6 (4H, m), 3.8–4.2 (1H, m), 6.8–7.6 (10H, m), 7.8–8.1 (4H, m), 8.5 (1H, s).

A mixture of **7** (0.325 g, 6×10^{-4} mol), triphenylmethyl perchlorate (0.217 g, 6.6×10^{-4} mol), and 2.0 mL glacial acetic acid was refluxed (14) with stirring for 5 min with the reaction mixture protected from atmospheric moisture. The resulting yellow solid 1,1,3,3-*N*-tetramethyl-2*N*-[4-(2,6-diphenyl-4-pyrylio)phenyl]-guanidinium diperchlorate **8** was filtered, washed with glacial acetic acid and ether, and dried under vacuum, 0.33 g (yield 88%). Recrystallization was made from glacial acetic acid even though the solubility is very low, since this gave fine yellow crystals that melted, with decomposition at about 315°C; ^{1}H nmr δ: 3.02 (12H, s), 7.33 and 8.73 (4H), 7.81 (4H, t), 7.88 (2H, t), 8.59 (4H, d) 9.11 (2H, s). Anal. calcd. for $C_{28}H_{29}Cl_2N_3O_9$: C 54.03, H 4.69, Cl 11.39, N 6.75%; found: 53.8, H 4.7, Cl 11.7, N 6.6%.

The pyrylio function was converted to thiopyrylio by the method

Can. J. Chem. Downloaded from www.nrcresearchpress.com by 109.225.110.28 on 09/08/12
For personal use only.

of Wizinger and Ulrich (9), except that some DMSO was added to the solvent to improve the solubility of **8**.

A solution of **8** (0.781 g, 1.25×10^{-3} mol) in DMSO (5.0 mL) was diluted with acetone (25 mL) and treated with $Na_2S \cdot 9H_2O$ (0.63 g in 6.0 mL H_2O). The resulting red-brown solution was acidified with $HClO_4$ (7 mL 20% $HClO_4$ in 25 mL H_2O) and shiny golden crystals of 1,1,3,3,-tetramethyl-2*N*-[4-(2,6-diphenyl-4-thiopyrylio)phenyl]guanidine diperchlorate **9** formed, 0.78 g (97%). Recrystallization from acetic acid gave dark yellow needles, mp 318–320°C with decomposition; ^{1}H nmr δ: 3.01 (12H, s), 7.31 and 8.56 (4H), 7.78–7.84 (6H, m), 8.30 (4H, d), 9.24 (2H, s). Anal. calcd. for $C_{28}H_{29}Cl_2N_3O_8S$: C 52.67, H 4.58, Cl 11.10, N 6.58, S 5.02%; found: C 52.1, H 4.5, Cl 11.9, N 6.4, S 4.8%.

Preparation of 1,1,3,3,-N-*tetramethyl-2*-N-*[4-(4,6-diphenyl-2-thiopyrylio)phenyl]guanidinium diperchlorate*

2-*N*-(4-Acetophenyl) tetramethylguanidine **12** was prepared by the method of Bredereck and Bredereck (13) as white crystals, after recrystallization from hexane, mp 57–59°C (lit. (15) mp 59°C), yield 31%.

A mixture of **12** (4.7 g, 0.02 mol), benzaldehyde (2.0 g, 0.02 mol), NaOH (0.4 g, 0.01 mol) in ethanol (30 mL) was refluxed for 3 h. A standard work-up yielded a thick yellow oil of 1,1,3,3 -*N*-tetramethyl-2*N*-[4-(1-oxo-3-phenyl -2-propenyl)phenyl]-guanidine **13**, yield 6.0 g (97%); ^{1}H nmr δ: 2.75 (12H, s), 6.7 and 8.0 (4H), 7.3–7.8 (7H, m).

A mixture of **13** (3.2 g, 0.01 mol), acetophenone (4.8 g, 0.04 mol), and NaOH (1.0 g, 0.025 mol) in ethanol (100 mL) was refluxed for 3.5 h. Acid work-up with 20% $HClO_4$ yielded an oil that was triturated with ether to give solid 1,1,3,3-*N*-tetramethyl-2*N*-[4-(1,5-dioxo-3,5-diphenylpentyl)phenyl]guanidinium perchlorate **14**, yield 2.5 g (46%); ^{1}H nmr δ: 3.0 (12H, s), 3.2–3.6 (4H, m), 3.8–4.2 (1H, m) 6.9–8.1 (14H, m), 9.0 (1H, s). Anal. calcd. for $C_{28}H_{32}ClN_3O_6$: C 62.05, H 5.94, Cl 6.54, N 7.75%; found: C 60.9, H 5.8, Cl 7.0, N 7.4%.

Treatment of **14** (0.75 g, 1.7×10^{-3} mol) with triphenylmethyl perchlorate (0.6 g, 1.75×10^{-3} mol) in glacial acetic acid (10 mL) gave dark yellow crystals of 1,1,3,3-*N*-tetramethyl-2-*N*-[4-(4,6-diphenyl-2-pyrylio)phenyl]guanidinium diperchlorate **15**, yield 0.68 g (79%). After recrystallization from a DMSO/acetone/acetic acid mixture, mp 306–310°C with decomposition; ^{1}H nmr δ: 3.02 (12H, s), 7.34 and 8.65 (4H), 7.78–7.89 (6H, m), 8.57–8.60 (4H, m), 9.10 (2H, s). Anal. calcd. for $C_{28}H_{29}Cl_2N_3O_9$: C 54.03, H 4.69, Cl 11.39, N 6.74%; found: C 52.4, H 4.9, Cl 10.5, N 6.2%.

A solution of **15** (0.31 g, 5×10^{-4} mol) in acetone (10 mL) and DMSO (1 mL) was treated with $Na_2S \cdot 9H_2O$ (0.25 g, 1×10^{-3} mol) dissolved in water (2.5 mL) (9). The reaction mixture was acidified with 20% $HClO_4$ (2.5 mL) and dark orange crystals of crude 1,1,3,3-*N*-tetramethyl-2-*N*-[4-(4,6-diphenyl-2-thiopyrylio)phenyl]guanidinium diperchlorate **16** were obtained, yield 0.27 g (81%). After recrystallization from acetic acid, orange crystals were obtained, mp 305–307°C with decomposition; ^{1}H nmr δ: 3.00 (12H, s), 7.33 and 8.39 (4H), 7.7–7.8 (6H, m), 8.3 (2H, d), 8.42 (2H, d), 9.22 (2H, s). Anal. calcd. for $C_{28}H_{29}Cl_2N_3O_8S$: C 52.69, H 4.58, Cl 11.10, N 6.58, S 5.02%; found: C 51.7, H 4.4, Cl 11.5, N 6.4, S 4.9%.

Acknowledgment

The authors are grateful for financial support from the Natural Sciences and Engineering Research Council of Canada.

1. W. J. Dulmage, W. A. Light, S. J. Marino, C. D. Salzburg, D. L. Smith, and W. J. Staudenmayer. J. Appl. Phys. **49**, 5543 (1978).
2. J. H. Perlstein. *In* Electrical properties of polymers. *Edited by* D. A. Seanor. Academic Press, New York. 1982. Chap. 2.
3. M. T. Regan, G. A. Reynolds, D. P. Specht, and J. A. Van Allan. Can. Patent No. 1077955 (1980).
4. A. R. Katritzky, B. J. Graphakos, G. A. F. Lhommet, and K. Reynolds. U.S. Patent No. 4,368,329 (1983).
5. K. Kawamura, H. Katsuyama, and H. Sato. U.S. Patent No. 4,343,948 (1982).
6. K. Kawamura, H. Sato, and H. Katsuyama. U.S. Patent No. 4,469,864 (1984).
7. B. Nogaj and P. Pruszynski. Magn. Reson. Chem. **25**, 301 (1987).
8. K. T. Leffek, P. Pruszynski, and K. Thanapaalasingham Can. J. Chem. **67**, 590 (1989).
9. R. Wizinger and P. Ulrich. Helv. Chim. Acta, **39**, 207 (1956).
10. F. Kröhnke and K. Dickoré. Chem. Ber. **92**, 46 (1959).
11. R. Wizinger, A. Grüne, and E. Jacobi. Helv. Chim. Acta, **39**, 1 (1956).
12. D. D. Perrin, B. Dempsey, and E. P. Serjeant. *In* pK_a prediction for organic acids and bases. Chapman and Hall, London. 1981. App.A.1.
13. H. Bredereck and K. Bredereck. Chem. Ber. **94**, 2278 (1961).
14. M. Siemiatycki and R. Fugnitto. Bull. Soc. Chim. Fr. **28**, 538 (1961).
15. H. Kessler and D. Leibfritz. Tetrahedron, **26**, 1805 (1970).

Can. J. Chem. Downloaded from www.nrcresearchpress.com by 109.225.110.28 on 09/08/12
For personal use only.

Ionic dissociation in complexes of iodine with triphenylphosphine and triphenylamine

YING RU ZHANG, SEYMOUR ARONSON,[1] AND P. GARY MENNITT

Department of Chemistry, City University of New York, Brooklyn College, Brooklyn, NY, U.S.A. 11210

Received August 28, 1991[2]

YING RU ZHANG, SEYMOUR ARONSON, and P. GARY MENNITT. Can. J. Chem. **70**, 2394 (1992).

An electrochemical technique has been employed to study the ionization of the iodine complexes of $(C_6H_5)_3N$ and $(C_6H_5)_3P$. Comparison of the results with a previous study indicates that, at high iodine concentrations, the phosphorus compound behaves like $(C_6H_5)_3As$ and $(C_6H_5)_3Sb$ with the formation of a doubly charged ionic species, $(C_6H_5)_3PI_2^{2+}$. The nitrogen compound resembles pyridine in its behavior. Chemical shift data on the $(C_6H_5)_3P$–I_2 system using ^{31}P NMR indicates the presence of additional equilibrium processes.

YING RU ZHANG, SEYMOUR ARONSON and P. GARY MENNITT. Can. J. Chem. **70**, 2394 (1992).

On a utilisé une technique électrochimique pour étudier l'ionisation des complexes de l'iode avec le $(C_6H_5)_3N$ et le $(C_6H_5)_3P$. Une comparaison de nos résultats avec ceux obtenus au cours d'une étude antérieure indique que, à des concentrations élevées d'iode, le composé du phosphore se comporte comme le $(C_6H_5)_3As$ et le $(C_6H_5)_3Sb$ et il conduit à la formation d'espèces ioniques doublement ionisées, $(C_6H_5)_3PI_2^{2+}$. Le comportement du composé de l'azote ressemble à celui de la pyridine. Les données relatives aux déplacements chimiques observés avec le système $(C_6H_5)_3P$–I_2, en faisant appel à la RMN du ^{31}P, indiquent qu'il existe d'autres processus d'équilibre.

[Traduit par la rédaction]

Introduction

The triphenyl compounds, Ph_3M, of nitrogen, phosphorus, arsenic, and antimony form complexes with iodine in organic solution (1–3). In a recent study (4), we presented data on the ionization of the iodine complexes of Ph_3As, Ph_3Sb, and pyridine (Py) in the polar organic solvent 1,2-dichloroethane. At high iodine concentrations, we observed that pyridine produced only the ionic species PyI^+, whereas the ionic species, Ph_3MI^+ and $Ph_3MI_2^{2+}$, were produced from Ph_3As and Ph_3Sb.

Ph_3N and Ph_3P are isostructural with Ph_3As and Ph_3Sb. The question arises as to whether the behavior of Ph_3N and Ph_3P in their interaction with iodine is more similar to the behavior of Ph_3As and Ph_3Sb or to that of pyridine. Nitrogen and phosphorus are essentially covalent in their chemistry, whereas arsenic and antimony show increasing tendencies towards cationic behavior (5). All four Group VA elements have available electron pairs and can act as donors. Only phosphorus, arsenic, and antimony, however, have empty *d* orbitals of fairly low energy which have the potential to interact with electrons from an acceptor atom to create additional bonding (5). It is, therefore, possible that Ph_3N may behave like pyridine and that Ph_3P may behave like Ph_3As and Ph_3Sb.

In the present study, we have utilized an electrochemical technique previously used to investigate the interaction of iodine with Ph_3As, Ph_3Sb, and pyridine to obtain information on the ionization of the iodine complexes of Ph_3N and Ph_3P. We have also used ^{31}P NMR to obtain chemical shift information on the iodine complexes of Ph_3P in an effort to further elucidate equilibrium processes in the system.

Experimental

Triphenylamine (Ph_3N), triphenylphosphine (Ph_3P), and tetraethylammonium iodide (TEAI) were obtained in the highest commercial grades available from Aldrich Chemical Co. Spectrophotometric grades of 1,2-dichloroethane (DCE) and $CHCl_3$ and reagent grade iodine were also obtained from Aldrich.

Details of the electrochemical technique using cells of the type Pt|R, I_2‖R, I_2, TEAI|Pt, where R represents the organic molecule, have been discussed previously (4).

^{31}P NMR measurements were made with a Bruker 250 MHz high-resolution Fourier transform nuclear magnetic resonance spectrometer. Triphenylphosphine–iodine complexes in 1,2-dichloroethane were contained in 10 mm cylindrical Pyrex tubes. A lock signal was obtained by using a capillary tube containing D_2O inserted into the sample tube. Eighty-five percent orthophosphoric acid in a sealed 10 mm tube, obtained from Wilmad Glass Co. Inc., Buena N.J., was used as an external reference standard.

Results and discussion

The reaction schemes used to analyze the data for Ph_3As, Ph_3Sb, and pyridine are applicable to Ph_3P and Ph_3N. Readers are referred to the previous paper (4) for details of the mathematical treatment of the electrochemical data. The numbers assigned to identify the various reactions in Sects. A and B of this paper are the same as those used in the previous paper.

A. High iodine concentrations

The following reaction scheme is used for high concentration ratios of iodine to organic molecule in DCE.

$$[1] \quad R + I_2 \rightarrow RI_2$$

$$[2] \quad RI_2 + I_2 \rightleftharpoons RI^+ + I_3^-$$

$$[3] \quad RI^+ + 2I_2 \rightleftharpoons RI_2^{2+} + I_3^-$$

$$[4] \quad I_2 + TEAI \rightarrow I_3^- + TEA^+$$

R represents the organic molecule. The same assumptions used previously apply here.

The electrochemical data obtained on the Ph_3N and Ph_3P compounds are shown in Tables 1 and 2 respectively. The equilibrium reaction represented by reaction [2] was used to interpret the emf data in Table 1. The only ionic complex of Ph_3N which forms is Ph_3NI^+. The value of the equilibrium constant, K_2, which best fits the data, 4.8×10^{-3}, is close

[1]Author to whom correspondence may be addressed.

[2]Revision received May 1, 1992.

Can. J. Chem. Downloaded from www.nrcresearchpress.com by 109.225.110.28 on 09/08/12
For personal use only.

Can. J. Chem. Downloaded from www.nrcresearchpress.com by 109.225.110.28 on 09/08/12
For personal use only.

TABLE 1. The emf values for triphenylamine–iodine solutions at high iodine concentrations

$c(I_2)^a$ (M × 10)	c(TEAI) (M × 10^3)	Emf (mV)^b Experimental	Calculated
1.50	0.455	9.5	9.3
1.50	0.833	16.0	15.5
1.50	1.15	19.6	20.1
1.50	1.43	23.0	23.6
2.25	1.50	20.4	22.5
2.25	3.00	31.7	35.5

[a]The symbol *c* represents the "total concentration". It is the number of moles of I_2, TEAI, or Ph_3N added to a liter of DCE solution. Dissociation and interaction in solution are not considered. The total Ph_3N concentration in all these measurements was 1.50×10^{-3} M.

[b]The equilibrium constant, K_2, used to calculate the emf values was 4.8×10^{-3}.

TABLE 2. The emf values for triphenylphosphine–iodine solutions at high iodine concentrations

$c(I_2)^a$ (M × 10)	c(TEAI) (M × 10^3)	Emf (mV)^b Experimental	Calculated
1.13	0.500	7.0	6.6
1.13	0.750	8.6	9.3
1.13	1.50	17.0	16.3
1.13	3.00	26.5	26.4
0.750	0.500	6.8	7.0
0.750	0.750	9.4	9.9
0.750	1.50	16.4	17.0
0.750	3.00	27.6	27.3
0.375	0.500	8.4	7.3
0.375	0.750	11.0	10.3
0.375	1.50	19.3	17.6
0.375	3.00	33.1	27.9

[a]See the footnote in Table 1 for the definition of *c*, the "total concentration." The total Ph_3P concentration in all these measurements was 1.50×10^{-3} M.

[b]The equilibrium constant, K_3, used to calculate the emf values was 1.2×10^{-2} M^{-1}.

to the equilibrium constant for the pyridine reaction, 3.9×10^{-3} (4).

The data in Table 2 on Ph_3P is best fitted by assuming that reaction [2] has proceeded all the way to the right and that the equilibrium shown in reaction [3] is operative. The equilibrium constant, K_3, used to calculate the emf values, 1.2×10^{-3} M^{-1}, is reasonably close to the values of 2.9×10^{-2} M^{-1} and 3.8×10^{-2} M^{-1} obtained for Ph_3As and Ph_3Sb respectively (4).

It will be noted that there is some discrepancy in the bottom set of data in each table between the calculated and experimental emf values. The calculated values in Table 1 are higher than the experimental values. The reverse is true for the data in Table 2. A suggested reason for the discrepancy in Table 1 is that reaction [3] begins to be operative at the high I_2/Ph_3N concentration ratio of 150. This would result in lower than expected experimental values for the emf. In the case of Ph_3P in Table 2, at the low I_2/Ph_3P concentration ratio of 25, reaction [2] may not go to completion, resulting in higher than expected experimental values of the emf.

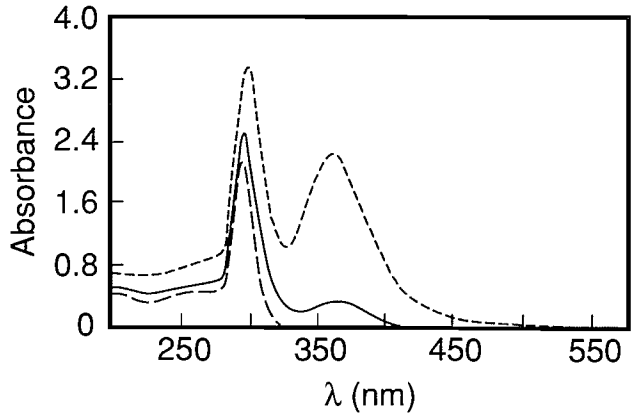

FIG. 1. UV–visible spectra of Ph_3P–I_2 solutions in DCE: (———)$c(Ph_3P)$ 2×10^{-3} M, $c(I_2)$ 2×10^{-4} M;(——)$c(Ph_3P)$ 1×10^{-3} M, $c(I_2)$ 2×10^{-4} M;(-----)$c(Ph_3P)$ 2×10^{-4} M, $c(I_2)$ 2×10^{-4} M;

The above results indicate that Ph_3P, in its interaction with iodine, behaves like Ph_3As and Ph_3Sb, whereas Ph_3N resembles pyridine in its behavior. Whether or not the lack of low energy *d* orbitals in nitrogen is responsible for this difference in behavior requires further theoretical consideration.

B. High Ph_3P concentrations

The behavior of the triphenyl compounds at high organic concentrations is less consistent than at high iodine concentrations. In the previous paper (4), the electrochemical data for Ph_3Sb could not be interpreted on the basis of a simple mechanism. In the case of Ph_3As, analysis could only be made at a Ph_3As/I_2 concentration ratio above 500. In the present investigation, the data on Ph_3N could not be easily interpreted. The Ph_3P data can be analyzed using the same mechanism which was applied to Ph_3As.

The reaction scheme is

[1] $R + I_2 \rightarrow RI_2$

[11] $RI_2 \rightleftharpoons RI^+ + I^-$

In Fig. 1 is shown the UV–visible spectroscopic changes which occur as the Ph_3P/I_2 concentration ratio changes from 1 to 10. It is observed that the I_3^- signal at 360 nm decreases as the Ph_3P/I_2 ratio increases and is absent at a ratio of 10. We assume that reaction [11] is operative at that ratio and above.

The data for Ph_3P at ratios of 10 and 20 are shown in Table 3. An equilibrium constant, K_{11}, equal to 2.24×10^{-4} M, gave good agreement between the calculated and experimental emf values. The corresponding equilibrium constant for Ph_3As at a Ph_3As/I_2 concentration ratio of 500 was 2.4×10^{-5} M.

C. ^{31}P NMR spectra

P-31 has a significant NMR signal, which can be used to further investigate complex formation and ionization in the Ph_3P–I_2 system. The sensitivity of the NMR technique is such that concentrations of iodine complex in the range of 0.01 M and above are required. Concentrations of complex in the range of 0.001 M were used in the electrochemical mea-

Can. J. Chem. Downloaded from www.nrcresearchpress.com by 109.225.110.28 on 09/08/12
For personal use only.

TABLE 3. The emf values for triphenylphosphine–iodine solutions at high concentrations of Ph_3P

$c(Ph_3P)^a$ ($M \times 10^2$)	$c(I_2)$ ($M \times 10^3$)	c(TEAI) ($M \times 10^3$)	Emf (mV)[b]	
			Experimental	Calculated
1.00	1.00	0.100	3.4	3.3
1.00	1.00	0.400	12.0	12.1
1.00	1.00	0.700	19.1	19.3
1.00	1.00	1.00	24.6	25.2
2.00	1.00	0.182	6.1	5.9
2.00	1.00	0.462	13.3	13.7
2.00	1.00	0.571	16.2	16.4
2.00	1.00	0.750	21.2	20.4

[a]See the footnote in Table 1 for the definition of c.
[b]The equilibrium constant, K_{11}, used to calculate the emf values was 2.24×10^{-4} M.

TABLE 4. ^{31}P chemical shifts in mixtures of triphenylphosphine and iodine in chloroform and in 1,2-dichlorethane

Solvent	$c(Ph_3P)$ (M)	$c(I_2)$ (M)	Chemical shift[a] (ppm)		
			Signal 1	Signal 2	Signal 3
$CHCl_3$	0.200	0.0200	35.3		−3.6
	0.0400	0.0200	40.8		
	0.0040	0.200	48.6		
$C_2H_4Cl_2$	0.100				−3.2
	0.100	0.0100	36.6		−3.9
	0.0500	0.0100	38.0		−4.5
	0.100	0.0200	39.1		−4.9
	0.100	0.0300	40.3		−6.4
	0.100	0.0800	46.6		
	0.0500	0.0800	51.4	11.2	
	0.0500	0.100	51.6	11.3	
	0.0500	0.250	55.0	15.0	
	0.0500[b]	0.250	55.7	14.8	
	0.0500[b,c]	0.250	55.9	15.1	

[a]Orthophosphoric acid (85%) was used as an external standard.
[b]See Fig. 2.
[c]This sample also contained 0.0500 M TEAI.

surements. The low sensitivity of the NMR method and the limited solubilities of I_2 and Ph_3P in organic solvent limited the concentration ratios of Ph_3P/I_2 for which good data could be obtained to the range between 0.1 and 10. At these concentration ratios, reactions [2] and [11] and not reaction [3] would be operative.

NMR spectra were obtained in two solvents, $CHCl_3$ and DCE. Significant ionization of the I_2 complex of Ph_3P does not occur in $CHCl_3$ because of its low dielectric constant. By comparing the spectra in $CHCl_3$ and DCE, the effects of ionization could be investigated.

Spectra obtained in $CHCl_3$ are summarized in Table 4. The high-field signal at −3.6 ppm is attributable to Ph_3P. Muller *et al.* (6) reported a value of −5.9 ppm for Ph_3P in an unidentified solvent. The down-field signal at 35.3 ppm is presumably that for the unionized complex. As the concentration ratio of I_2/Ph_3P increased, the Ph_3P signal disappeared and the down-field signal was observed to shift to 40.8 ppm and 48.6 ppm.

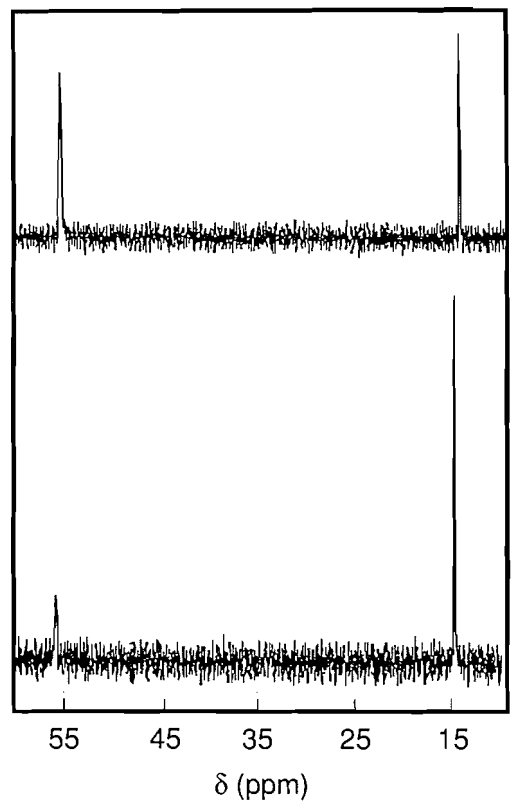

FIG. 2. Lower spectrum: ^{31}P NMR spectrum of $Ph_3P–I_2$ in DCE: $c(Ph_3P)$ 0.05 M, $c(I_2)$ 0.25 M. Upper spectrum: ^{31}P NMR spectrum of $Ph_3P–I_2$ in DCE: $c(Ph_3P)$ 0.05 M, $c(I_2)$ 0.25 M, c(TEAI) 0.05 M.

We suggest a reason for this movement of the signal with change in concentration. We postulate that at high concentration ratios of Ph_3P/I_2 the complex formed is $(Ph_3P)_2I_2$, whereas at low ratios the complex formed is Ph_3PI_2. The equilibrium reaction involved in the case of excess Ph_3P is

$$[5] \quad Ph_3PI_2 + Ph_3P \rightleftharpoons (Ph_3P)_2I_2$$

and in the case of excess I_2 is

$$[6] \quad (Ph_3P)_2I_2 + I_2 \rightleftharpoons 2Ph_3PI_2$$

We further postulate a rapid exchange of Ph_3P between the equilibrium concentrations of $(Ph_3P)_2I_2$ and Ph_3PI_2 in the solution which results in an averaging effect on the position of the merged signals. At high concentration ratios of Ph_3P/I_2, only the $(Ph_3P)_2I_2$ complex is present with a signal at about 35 ppm. At low ratios, only the Ph_3PI_2 complex is present with a signal at about 49 ppm. At ratios in between, both complexes are present, resulting in signals appearing at intermediate positions.

NMR data obtained on $Ph_3P–I_2$ samples in DCE are summarized in Table 4. We identify signal 3 with the compound Ph_3P. Signals 1 and 2 are attributed to the unionized complex and the ionized complex respectively. The signal for the unionized complex gradually moves from a value of 36 ppm for $(Ph_3P)_2I_2$ to a value of 57 ppm for Ph_3PI_2, with intermediate values corresponding to equilibrium mixtures of the two complexes. A plot of the chemical shift as a function of $\log[c(I_2)/c(Ph_3P)]$ is shown in Fig. 3. The reasons for the small changes in the positions of signals 2 and

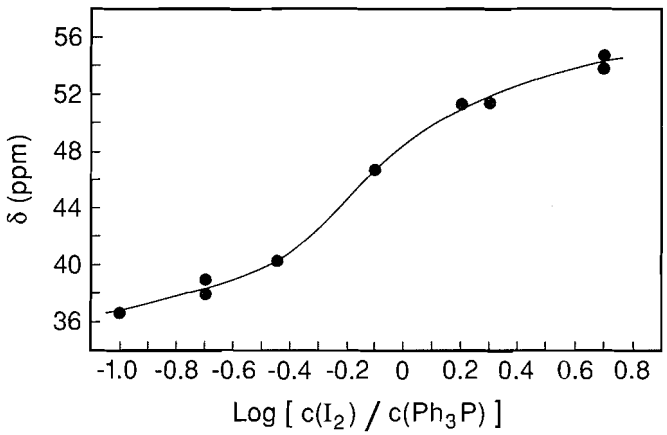

FIG. 3. ^{31}P chemical shift as a function of the $c(I_2)/c(Ph_3P)$ ratio.

3 in Table 4 are not known but may involve experimental factors or effects of concentration.

A comparison of the spectra in Fig. 2, corresponding to the last two columns in Table 4, shows the effect of adding TEAI to the system. The addition of TEAI shifts the equilibrium in reaction [2] to the left. The addition of TEAI suppresses the concentration of the unionized complex. This results in an increase in the magnitude of signal 1 at the expense of signal 2.

If the equilibria described by reactions [5] and [6] are operative, reactions [1] and [11], at high concentration ratios of Ph_3P/I_2, cannot be correct. We would have to invoke reactions of the type

[7] $2R + I_2 \rightarrow R_2I_2$

[8] $R_2I_2 \rightleftharpoons R_2I^+ + I^-$

[8′] $R_2I_2 \rightleftharpoons RI^+ + I^- + R$

The application of reaction [8] instead of reaction [11] would not effect the mathematical treatment used above and would yield the same value, 2.24×10^{-4} M, for K_8 as was used for K_{11}. The application of reaction [8′] would, however, require some modification of the mathematical treatment. Additional spectroscopic and electrochemical data are required to further elucidate the equilibrium processes in the concentration range in which neither Ph_3P nor I_2 is present in large excess.

1. K. R. Bhaskar, S. N. Bhat, S. Singh, and C. N. R. Rao. J. Inorg. Nucl. Chem. **28**, 2060 (1966).
2. A. D. Beveridge, G. S. Harris, and F. Inglis. J. Chem. Soc. 520 (1966).
3. R. Sahai, P. C. Pande, and V. Singh. Indian J. Chem. **18A**, 217 (1979).
4. Y. R. Zhang, I. Solomon, and S. Aronson. Can. J. Chem. **69**, 606 (1991).
5. F. A. Cotton and G. Wilkinson. *In* Advanced inorganic chemistry 4th ed. John Wiley and Sons, New York, N.Y. 1980. pp. 438–440.
6. N. Muller, P. C. Lauterbur, and J. Goldenson. J. Am. Chem. Soc. **78**, 3557 (1956).

Can. J. Chem. Downloaded from www.nrcresearchpress.com by 109.225.110.28 on 09/08/12
For personal use only.

FT-IR and ^{29}Si, ^{27}Al, and ^{19}F MAS NMR studies of the adsorption of CdF_2, ZnF_2, and CuF_2 onto montmorillonite K10; activity towards Friedel–Crafts alkylation[1]

FATHI M. ASSEID AND JACK M. MILLER[2]
Department of Chemistry, Brock University, St. Catharines, Ont., Canada L2S 3A1

AND

JAMES H. CLARK
Department of Chemistry, University of York, Heslington, York, YO1 5DD, England

Received January 21, 1992

FATHI M. ASSEID, JACK M. MILLER, and JAMES H. CLARK. Can. J. Chem. **70**, 2398 (1992).

ZnF_2, CdF_2, and CuF_2 have been adsorbed onto the surface of montmorillonite K10, and the infrared and ^{19}F, ^{27}Al, and ^{29}Si MAS NMR spectra of the resulting reagents over a range of loadings and activation temperatures have been obtained. CuF_2 was observed to attack the SiO_2 layer and form the complex $CuSiF_6$, ZnF_2 tends to attack the aluminium oxide layer, in which Zn isomorphously replaces Al, and forms AlF_3 and AlF_4^- complexes. The spectroscopic evidence rules out the formation of any Al–F and (or) Si–F species as CdF_2 is adsorbed on the surface of montmorillonite K10. The reactivity of MF_2–K10 reagents towards the Friedel–Crafts reaction of benzene with benzyl chloride varies from one reagent to another. ZnF_2–K10 was observed to be the most reactive and CuF_2 was the least reactive.

FATHI M. ASSEID, JACK M. MILLER et JAMES H. CLARK. Can. J. Chem. **70**, 2398 (1992).

On a adsorbé du ZnF_2, du CdF_2 et du CuF_2 sur la surface de la montmorillonite K10 et on a déterminé les spectres infrarouges et RMN MAS du ^{19}F, du ^{27}Al et du ^{29}Si des réactifs ainsi obtenus dans un large intervalle de charge et de température. On a observé que le CuF_2 attaque la couche de SiO_2 pour former un complexe de $CuSiF_6$ alors que le ZnF_2, quant à lui, tend à s'attaquer à la couche d'oxyde d'aluminium dans laquelle le zinc isomorphe remplace l'aluminium et forme des complexes de AlF_3 et de AlF_4^-. Les preuves spectroscopiques éliminent la formation de toute espèce Al–F et (ou) Si–F lorsque le CdF_2 est adsorbé sur la surface de la montmorillonite K10. La réactivité des réactifs de MF_2–K10 par rapport à la réaction de Friedel et Crafts du benzène avec le chlorure de benzyle varie d'un réactif à l'autre. On a observé que le ZnF_2–K10 est le plus réactif et que le moins réactif est le CuF_2.

[Traduit par la rédaction]

Introduction

The fluorination of metal oxide catalysts causes changes in catalytic activity. The catalytic activity, surface structure, and the nature of active centres of fluorinated alumina and silica–alumina have been studied extensively. Fluorination of silica–alumina generally leads to generation of new Lewis acid sites (1). Fluorination of alumina results in a strong Lewis acid centre (2), and the strength of this acidity is highly dependent on the content of F^- and on the activation temperature. The prime technique used for studying fluorinated metal oxides is infrared spectroscopy (3). Solid state ^{19}F NMR spectroscopy is the most recent technique to be used for studying fluorinated silica and aluminosilicates (4, 5). Miller and co-workers recently combined both IR and ^{19}F MAS NMR spectroscopy to study the adsorption of alkali metal fluorides on the surface of silica gel (6), alumina (7), and montmorillonite K10 (8).

Interest has been growing in recent years in transition metal exchanged montmorillonite K10 (9). Given their importance in the catalysis of organic reactions such as Friedel–Crafts alkylations, a number of approaches have been developed to obtain optimum results. Laszlo and Mathy have doped montmorillonite K10 with a series of transition metal cations (10), to obtain reasonably effective catalysts for Friedel–Crafts reaction with halides, alcohols, and olefins. Montmorillonite K10 supported transition metal chlorides were also studied (11), and the Friedel–Crafts activity and selectivity of these reagents improved over unsupported MCl_2 and the standard Lewis acids such as $AlCl_3$ and BF_3. The final approach is the acid treatment of montmorillonite K10 as support for MCl_2 (12), which also becomes an effective catalyst for Friedel–Crafts alkylation. These types of reagents have been analyzed using ^{29}Si and ^{27}Al MAS NMR spectroscopy (13), to monitor possible changes that may occur within the SiO_2 tetrahedral layer or the octahedral aluminium layer.

Magic Angle Spinning (MAS) is one of the line-narrowing techniques available, which significantly improves the resolution of peaks in the NMR spectrum of a solid, and allows direct determination of the isotropic chemical shift. ^{29}Si and ^{27}Al MAS NMR have been extensively used to analyze aluminosilicates such as zeolites and clays. Since silicon has a low chemical shift anistropy (CSA), the line broadening can be removed at easily achievable spinning rates, whereas ^{27}Al requires high field and high spinning rates to overcome the quadrupolar interactions. ^{19}F MAS NMR has received much less attention, however; two recently described applications are in the analysis of fluorinated polymers (14), and of fluorohydroxyapatite (15). We are now studying the adsorption of ZnF_2, CdF_2, and CuF_2 onto the surface of montmorillonite K10 using FT-IR and ^{19}F, ^{27}Al, and ^{29}Si MAS NMR spectroscopy, and the activity of these reagents towards Friedel–Crafts alkylation.

Experimental

ZnF_2 (Aldrich) 99%, CdF_2 (Aldrich) 98%, and CuF_2 (Aldrich) 98% were used without further purification. Montmorillonite K10 clay (surface area 220–270 m^2/g) was obtained from Fluka. K10 is a commercial support material prepared by acid washing. Our samples have an extractable iron content of between 0.3 and 1.3%.

[1]Abstracted in part from the Brock M.Sc. Thesis of F. M. Asseid, 1991.

[2]Author to whom correspondence may be addressed.

Can. J. Chem. Downloaded from www.nrcresearchpress.com by 109.225.110.28 on 09/08/12
For personal use only.

Can. J. Chem. Downloaded from www.nrcresearchpress.com by 109.225.110.28 on 09/08/12
For personal use only.

On removing iron by five successive extractions with 50 mL of 3 M HNO_3, we extracted a total of 1.3% iron, after which no significant iron could be removed (this material contained about 3.0% iron according to Fluka spec. sheets; the difference is presumably tightly bonded iron). We could not detect changes in either our IR or ^{19}F NMR, with the additional extraction. Sodium, potassium, and calcium are all below 0.1% extractable, with any additional being found in the lattice sites. The silica gel was Merck Kieselgel 100, 70–230 mesh. The alumina was Merck 90 neutral, 70–230 mesh, activity 1, for chromatography.

The MF_2–K10 regents were prepared at loadings of 0.5, 1.0, 3.5, and 5.0 mmol/g by dissolving the appropriate quantity of MF_2 in water and adding the solution to K10 clay to form a slurry. The water was then removed on a rotary evaporator until the reagent had caked to the wall of the flask, and the reagents were then dried in air at various temperatures, usually overnight. MF_2–silica reagents were also prepared at a loading of 6.5 mmol/g.

Infrared spectra were obtained on an Analect FX6260 Fourier Transform spectrometer, attached to a MAP-66 data system. Samples were prepared as KBr discs, using a KBr/reagent ratio of about 20:1 by weight.

^{19}F and ^{29}Si MAS NMR spectra were obtained on a Bruker AC200 instrument at 188.3 and 39.74 MHz, respectively, using our home-built MAS probes. Samples were spun in Derlin rotors at about 3300 Hz. Since the spinning rate is considerably less than the CSA of fluorine (the CSA of KF is 323 ppm, which is equivalent to 65 KHz in a 200-MHz field, for example (16)), spinning side bands are seen in most of the spectra. Peaks of the ^{19}F spectra were referenced to external $CFCl_3$, and the ^{29}Si spectra were referenced to external tetramethylsialane (TMS). The ^{27}Al MAS NMR spectra were recorded on a Bruker AM-500 at the NMR facility at McMaster University, at a frequency of 130.32 MHz, line broadening of 100 Hz, and a relaxation of 1.0 s. The samples were spun at 8.0 KHz. ^{27}Al chemical shifts are reported in ppm with respect to standard aluminium nitrate, $Al(NO_3)_3\alpha H_2O$, in aqueous medium.

The reaction of benzyl chloride with benzene were carried out with 0.05 mol of benzyl chloride and 0.8 mol of benzene warmed to 70°C, then 4.0 g of the MF_2–K10 catalyst to be tested was added. After refluxing and stirring for 30 min the reaction was stopped, the catalyst was filtered off, and the unreacted benzene was removed by a rotary evaporator. The reaction of paraformaldehyde with benzene used 0.025 mol of paraformaldehyde and 0.5 mol of benzene. The mixture was warmed up to 80°C, then 10 g of 1.0 mmol/g of MF_2–K10 was added. After refluxing and stirring for 4 h the catalyst was filtered off and the unreacted benzene was removed by a rotary evaporator, resulting in the isolated product, diphenylmethane. The diphenylmethane yield was determined by GC analysis and confirmed with ^1H NMR and GC–MS.

Results

Infrared analysis

Each of ZnF_2–, CdF_2–, and CuF_2–K10 reagents was prepared at several loadings and dried over a range of temperatures. IR spectra of ZnF_2–K10 reagents dried at 573 K, shown in Fig. 1, reveal certain changes from the spectrum of the parent clay as the loading of ZnF_2 increases from 1.0 to 5.0 mmol/g. One of the changes is the gradual diminishing of the band at 802 cm^{-1} (lit. value 799 cm^{-1} (17)), which corresponds to tetrahedral SiO_4 groups, and the other is the development of a new band at 663 cm^{-1} that is presumably due to AlF_3 (lit. value 668 cm^{-1} (18)). To insure that these significant changes were really taking place, an additional loading of 6.5 mmol/g was prepared and analyzed. A sample dried at low temperature (373 K) shows an additional band at 755 cm^{-1} corresponding to AlF_4^- (lit. value 760 cm^{-1} (19)). The spectrum of the high-temperature

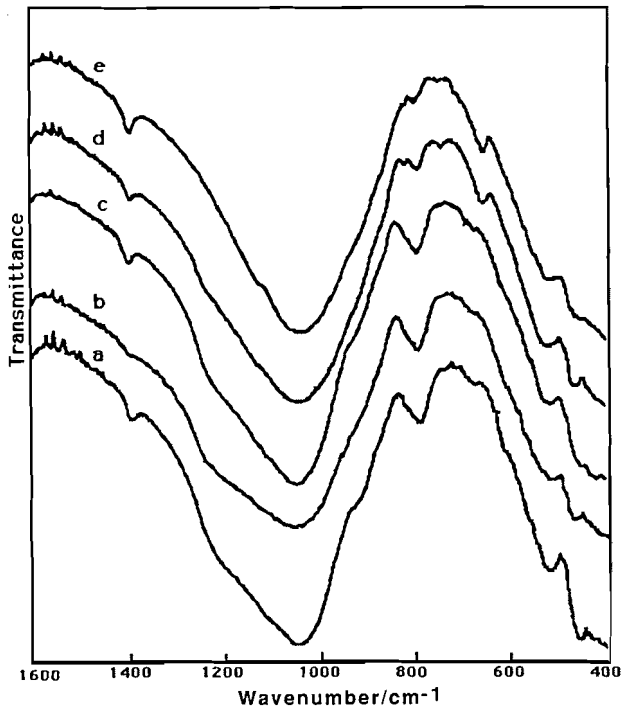

FIG. 1. Infrared spectra of ZnF_2–K10 reagents dried at 573 K; (*a*) montmorillonite K10, (*b*) 0.5 mmol/g, (*c*) 1.0 mmol/g, (*d*) 3.5 mmol/g, (*e*) 5.0 mmol/g.

(873 K) dried sample shows a new band at 570 cm^{-1} that is presumably due to skeletal ZnO_4 species (lit. value 570 cm^{-1} (19)).

IR spectra of CdF_2–K10 reagents show no obvious changes as content of CdF_2 increases. The band corresponding to layer SiO_4 groups at 802 cm^{-1} remains unchanged for all reagents. On the other hand, spectra of CuF_2–K10 appear rather different from those of the above reagents (Fig. 2). As the loading of CuF_2 increases, the band at 802 cm^{-1} gradually disappears, and consequently a new band at 743 cm^{-1} and an AlF_3 band at 665 cm^{-1} appears. The band at 743 cm^{-1} corresponds to the SiF_6^{2-} complex (lit. value 740 cm^{-1} (19)). The band at 743 cm^{-1} diminishes as calcining temperature increases (not shown). This is due to decomposition of SiF_6^{2-} to gaseous SiF_4 and free F^-.

Infrared spectra of 5.0 mmol/g of ZnF_2–silica, CdF_2–silica, and CuF_2–silica reagents dried at 373 K are shown in Fig. 3. These spectra clearly indicate that CuF_2–silica is the only reagent that results in a band at 743 cm^{-1}, which corresponds to the SiF_6^{2-}complex. The ZnF_2–silica reagents show a shoulder on the side of the band at 802 cm^{-1}, which is probably due to distortion to the SiO_2 tetrahedral structure or the presence of surface Si–F species. The infrared spectrum of CdF_2–silica (not shown) showed no clear absorption that may indicate presence of surface Si–F species.

^{19}F MAS NMR analysis

^{19}F MAS NMR spectra of MF_2–K10 reagents show significant differences at high loadings and high drying temperatures. All reagents at the low loading of 1.0 mmol/g (which represents monolayer coverage) show spectra of similar line shape, i.e., a central peak appears at −151 ppm and is surrounded by a set of asymmetric spinning side bands

Can. J. Chem. Downloaded from www.nrcresearchpress.com by 109.225.110.28 on 09/08/12
For personal use only.

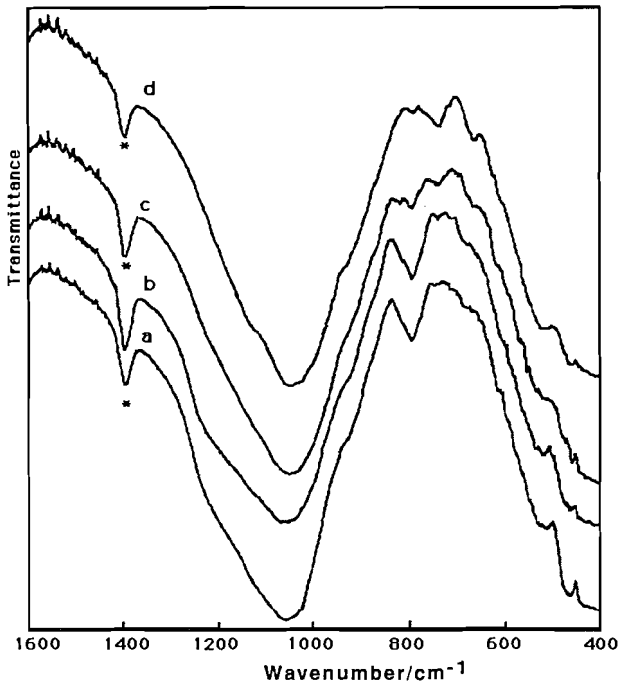

FIG. 2. Infrared spectra of CuF_2–K10 reagents dried at 573 K; (*a*) 0.5 mmol/g, (*b*) 1.0 mmol/g, (*c*) 3.5 mmol/g, (*d*) 5.0 mmol/g (* indicates impurities).

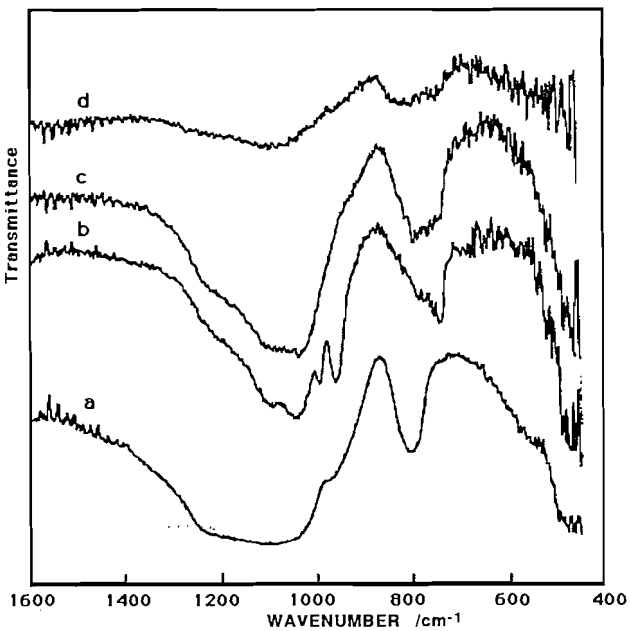

FIG. 3. Infrared spectra of MF_2–silica reagents dried at 373 K; (*a*) silica gel, (*b*) CuF_2–K10, (*c*) ZnF_2–K10, (*d*) CdF_2–K10.

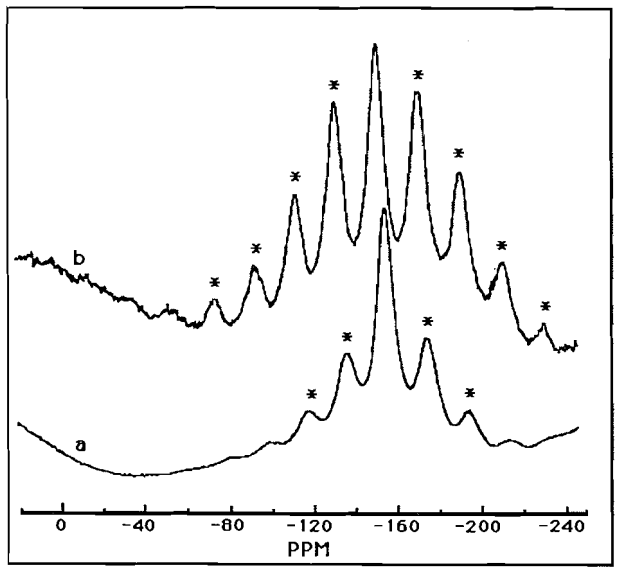

FIG. 4. ^{19}F MAS NMR spectrum of ZnF_2–K10 reagent compared to spectrum of mixed AlF_6^{3-} and AlF_4^-; (*a*) mixed AlF_6^{3-} and AlF_4^-, (*b*) 3.5 mmol/g of ZnF_2–K10 dried at 573 K, (* spinning side bands).

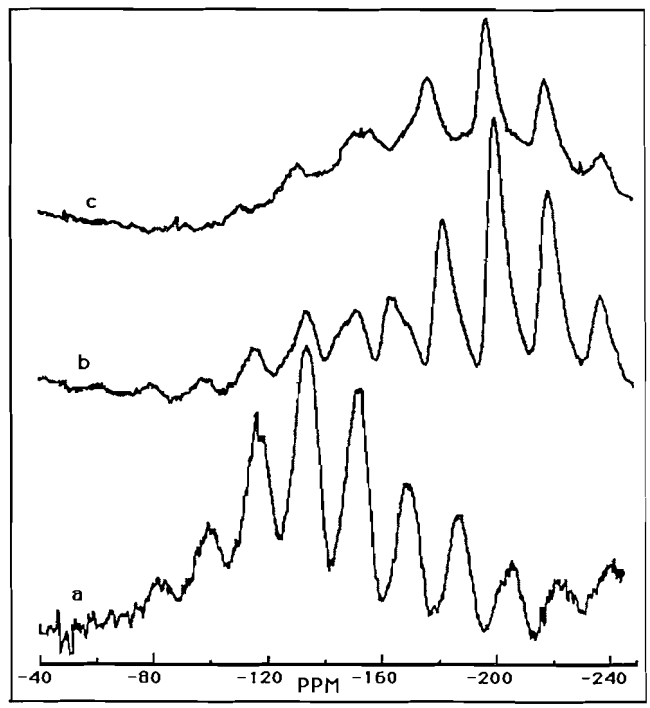

FIG. 5. ^{19}F MAS NMR spectra of CdF_2–K10 reagents dried at 873 K; (*a*) 1.0 mmol/g, (*b*) 3.5 mmol/g, (*c*) 5.0 mmol/g.

that presumably correspond to chemisorption of F^- on the surface the clay. These groups can be either surface Al–F and (or) Si–F groups. As the loading increases to 5.0 mmol/g dried at 573 K, ZnF_2–K10 reagent tends to show symmetrical spinning side bands around the central peak positioned at −153 ppm that closely approximate the spectrum of the AlF_4^- and AlF_6^{3-} mixture (Fig. 4). As the drying temperature increases to 873 K the line shape of the spectrum tends to broaden, which can be an indication of formation of AlF_3 (which usually results in a broad line, due to high dipole–dipole interactions (5)) from decomposed AlF_4^- or AlF_6^{3-}.

^{19}F MAS NMR spectra of CdF_2–K10 of the high-loading reagent dried at 573 K did not change significantly from those of the spectra of the low-loading reagents. However, as the calcining temperature increased to 873 K (Fig. 5), a sharp peak appeared at −197 ppm, which corresponds to CdF_2 (lit. value −197 ppm (20)) and, by a comparison of the spectrum of CdF_2, to that of highly loaded, highly dried CdF_2–K10 reagent. The reformation of CdF_2 is probably due to the

Can. J. Chem. Downloaded from www.nrcresearchpress.com by 109.225.110.28 on 09/08/12
For personal use only.

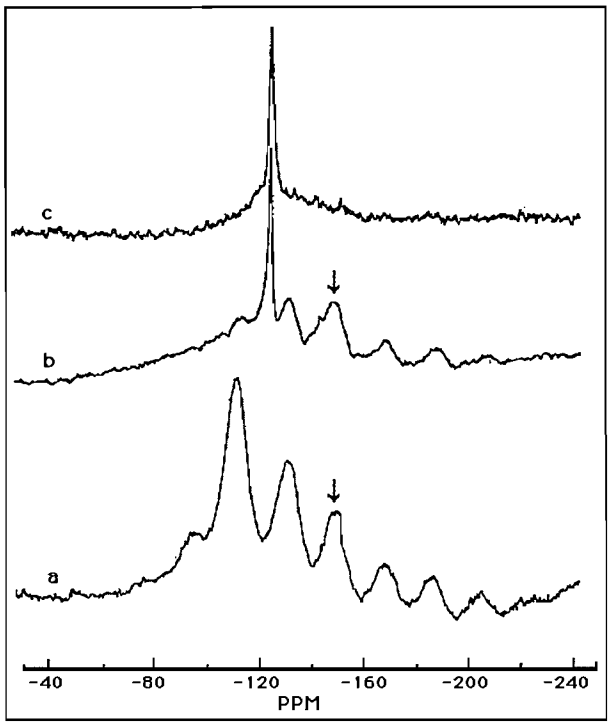

FIG. 6. ^{19}F MAS NMR spectra of MF_2–silica reagents dried at 373 K; (*a*) CuF_2–silica, (*b*) ZnF_2–silica, (*c*) CdF_2–silica.

high affinity of the ligand F^- for Cd^{2+}. Spectra of the high loading of CuF_2–K10 reagents also produced spectra with the central peak slightly shifted to −149 ppm. ^{19}F MAS NMR (Fig. 6) experiments on MF_2–silica gel to examine the reactivity of MF_2 towards the SiO_2 tetrahedral layer were performed, and appear to be quite consistent with the IR results. CuF_2–silica resulted in a peak at −149 ppm surrounded by asymmetrical spinning side bands, which presumably indicate physisorption of SiF_6^{2-} on the silica surface. ZnF_2–silica resulted in a sharp and intense peak at −124 ppm, which corresponds to free F^- ion or probably $F^-H_3O^+$ species (lit. value −125 ppm (21)). In addition it resulted in a weak peak at −149 ppm, which also indicates presence of physisorbed SiF_6^{2-} complex on the silica surface. CdF_2 proved to be unreactive towards the silica layer, since ^{19}F NMR spectra of CdF_2–silica resulted in no evidence of any Si–F species. The only ^{19}F NMR signal observed is located at −124 ppm, which corresponds to free F^-, or probably $F^-H_3O^+$.

^{29}Si MAS NMR analysis

The effect of MF_2 content on the structure of montmorillonite K10 can be monitored clearly by ^{29}Si MAS NMR spectroscopy. Spectra of ZnF_2–K10 reagents dried at 573 K (Fig. 7) show gradual changes to the original peak of the parent clay as content of ZnF_2 increases. At low ZnF_2 loadings, the signal position did not change from that of the parent peak at −107 ppm. Then as concentration of ZnF_2 increases to an intermediate level (3.5 mmol/g), a new peak at −97 ppm results. At the maximum ZnF_2 concentration (5.0 mmol/g) the original peak at −107 ppm is removed and the new peak at −95 ppm dominates the spectrum. We believe that as content of ZnF_2 increases, Zn replaces Al isomorphously and, consequently, Al replaces Si atoms in the SiO_2 tetrahedral layer resulting in a new ^{29}Si environment responsible for the new peak at −95 ppm.

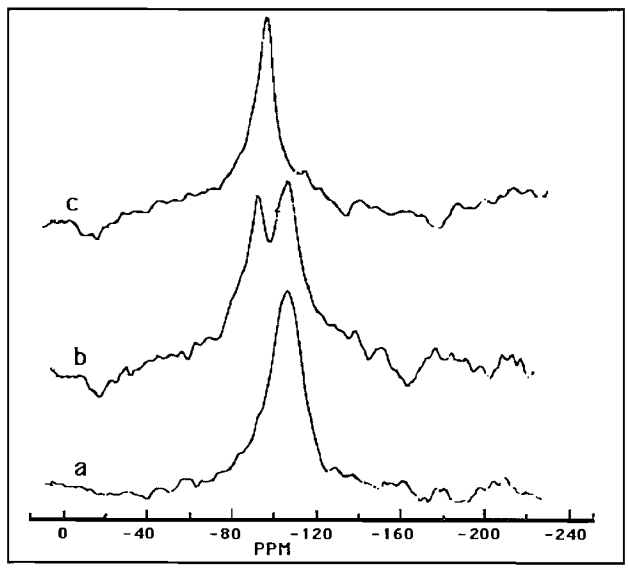

FIG. 7. ^{29}Si MAS NMR spectra of ZnF_2–K10 reagents dried at 573 K; (*a*) 1.0 mmol/g, (*b*) 3.5 mmol/g, (*c*) 5.0 mmol/g.

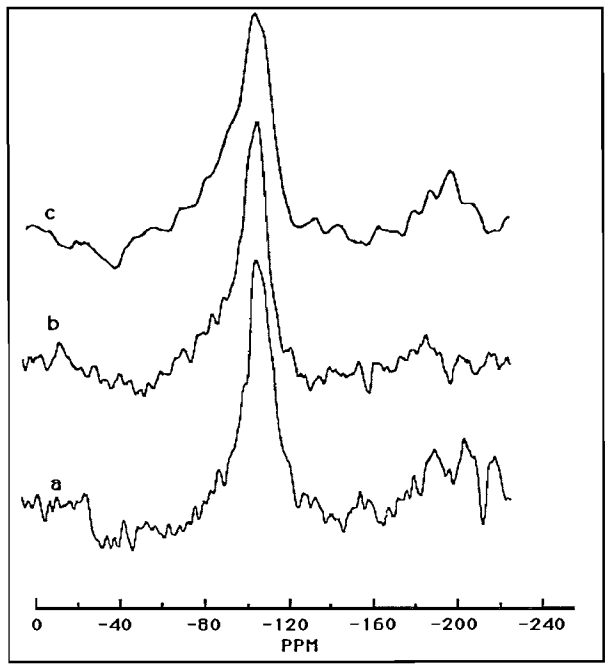

FIG. 8. ^{29}Si MAS NMR spectra of CuF_2–K10 reagents dried at 573 K; (*a*) montmorillonite K10, (*b*) 1.0 mmol/g, (*c*) 3.5 mmol/g.

^{29}Si MAS NMR spectra of CuF_2–K10 reagents (Fig. 8) also show changes as loading increases, but rather different from those observed for ZnF_2–K10. At the maximum concentration of CuF_2 (5.0 mmol/g) the spectrum (not reproduced here) still shows a peak at −107 ppm but with an observable shoulder at −95 ppm, which could indicate partial substitution of Si by Al atoms in the SiO_2 tetrahedral layer. Spectra of CdF_2–K10 reagents, on the other hand, show no changes from the parent clay spectrum as concentration of CdF_2 is maximized, which presumably indicates less isomorphous replacement of Al by Cd due to the large size of the divalent Cd^{2+} ion compared to size of Al^{3+}.

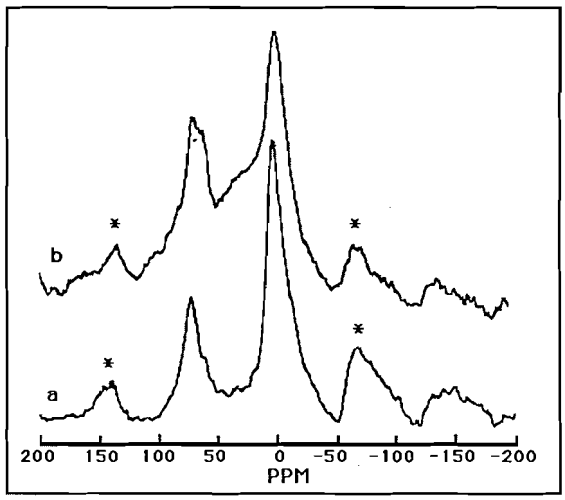

FIG. 9. ^{27}Al MAS NMR spectra of 5.0 mmol/g of CuF_2–K10 dried at (*a*) 573 K, (*b*) 873 K (* spinning side bands).

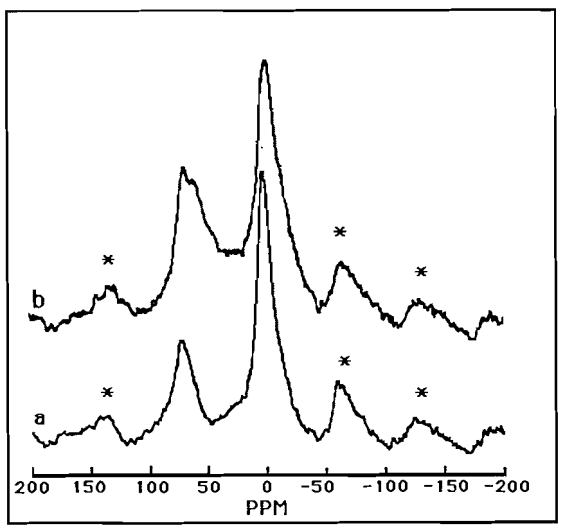

FIG. 10. ^{27}Al MAS NMR spectra of 5.0 mmol/g of CdF_2–K10 reagents dried at (*a*) 573 K, (*b*) 873 K (* spinning side bands).

^{27}Al MAS NMR analysis

^{27}Al MAS NMR spectra of MF_2–K10 reagents revealed certain information about the aluminium coordination for the different reagents at different calcining temperatures. Spectra of all reagents show two signals centred at 0 and 61–70 ppm, which generally correspond to octahedral and tetrahedral coordinated aluminium, respectively. Spectra of low loading (1.0 mmol/g) and high loading (5.0 mmol/g) of ZnF_2–K10 reagents show no observable differences in their peak positions or intensities. As activation temperature is increased to 873 K the spectra show an increase in the intensity in tetrahedral signal accompanied by a slight shift in position from 69 ppm at low activation temperature to 61 ppm at the activation temperature of 873 K. In addition, this shows a hint of a peak at 30 ppm, which is presumably due to five-coordinated aluminium (Fig. 9).

The most important feature of the ^{27}Al MAS NMR spectra for the CdF_2–K10 high loading, high-temperature-dried, reagent (Fig. 10) is the observation of two types of Al tetrahedral environments at 61 and 70 ppm. No significant shift

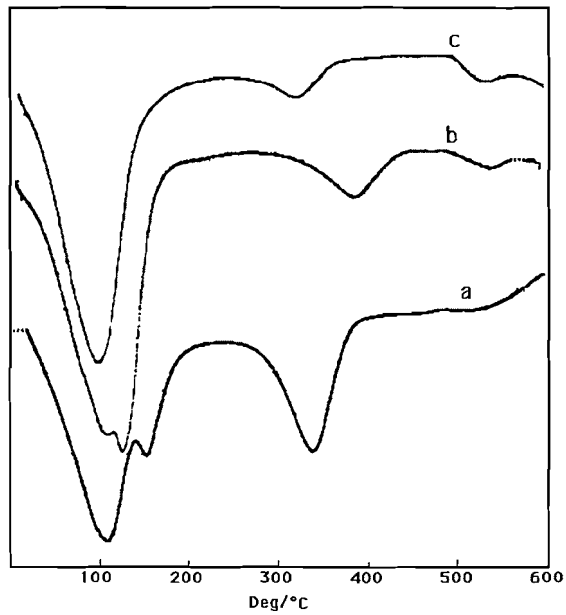

FIG. 11. Differential Scanning Calorimetry (DSC) spectra of 5.0 mmol/g MF_2–K10 reagents (*a*) CuF_2–K10, (*b*) ZnF_2–K10, (*c*) CdF_2–K10.

is observed for the octahedrally coordinated aluminium positioned at 3 ppm, but there has been, however, a noticeable decrease in the intensity of this signal as calcining temperature increased to 873 K. Spectra of CuF_2–K10 did not vary much from those of the CdF_2–K10 reagents. A noticeable shoulder at 30 ppm can be clearly seen for the highly dried samples. This shoulder again indicates the presence of penta-coordinated aluminium.

Thermal analysis

Differential scanning calorimetry (DSC) results for the high loading 5.0 mmol/g MF_2–K10 reagents indicate certain changes taking place as activation temperature increases. The DSC data for this series of reagents (Fig. 11) show a characteristic endotherm at 100–110°C, which is associated with dehydration of the interlayer within montmorillonite K10. A notable difference can be seen for the additional endotherms, at 340°C for CuF_2–K10, at 300°C for CdF_2–K10, and at 400°C for ZnF_2–K10. We believe that the endotherm at 340°C for CuF_2–K10 is associated with the thermal decomposition of the species SiF_6^{2-} to gaseous SiF_4 and possibly CuF_2 or HF (24), and the endotherm at 400°C for ZnF_2–K10 is possibly due to generation of the gaseous $HAlF_4$ component resulting from the reaction of solid AlF_3 and HF gas.

$$AlF_3\,(s) + HF\,(g) \xrightarrow{400°C} AlF_4H\,(g)$$

Reaction studies

The reactivity of the above reagents towards Friedel–Crafts alkylation varied from one reagent to another. We have successfully employed all of the different loadings of MF_2–K10 reagents dried at different temperatures in the Friedel–Crafts reaction of benzene with benzyl chloride and reaction with paraformaldehyde. The reactivity of the reagents was observed to be highly dependent on the reagent loading and the activation temperature employed. The reactivity of the low-loading reagents (1.0 mmol/g) seems to decrease as the activation temperature increases. This is deduced from

Can. J. Chem. Downloaded from www.nrcresearchpress.com by 109.225.110.28 on 09/08/12
For personal use only.

TABLE 1. Friedel–Crafts benzylation of benzene using MF_2–K10 reagents[a]

Reagent	Alkylator	Loading (mmol/g)	Activation temp (K)	Benzyl chloride conversion	Diphenylmethane yield (%)[b]
ZnF_2–K10	$PhCH_2Cl$	1.0	573	100	90
			873	40	70
	$(CH_2O)_n$	1.0	573	—	75
	$PhCH_2Cl$	5.0	573	80	60
			873	90	82
CdF_2–K10	$PhCH_2Cl$	1.0	573	90	80
			873	60	40
	$(CH_2O)_n$		573	—	60
	$PhCH_2Cl$	5.0	573	50	60
			873	60	80
CuF_2–K10	$PhCH_2Cl$	1.0	573	82	70
			873	40	25
	$(CH_2O)_n$	1.0	573	—	65
	$PhCH_2Cl$	5.0	573	70	60
			873	70	65

[a]M = Zn, Cd, and Cu.
[b]Yield determined by GC analysis, and confirmed by GC–MS and ^1H NMR.

the poor conversion of benzyl chloride, and the low yield of diphenylmethane obtained. The high activation temperature had no significant effect on the highly loaded reagents. In fact, highly loaded and high-temperature-calcined reagents seem to be more active than highly loaded and moderately dried reagents.

Table 1 shows the conversion of benzyl chloride and the calculated yield of diphenylmethane. ZnF_2–K10 was observed to be the most reactive of the series, and CuF_2–K10 showed significantly lower reactivity in the series. To further evaluate the catalysts, another Friedel–Crafts reaction was selected, which involves the alkylation of benzene with paraformaldehyde. This reaction presumably involves the solid acid depolymerizing the polymer $-(CH_2O)_n-$ to provide a source of CH_2O, as well as a Friedel–Crafts reaction. ZnF_2–K10 was again observed to be the most reactive.

Discussion

The results of infrared, and ^{19}F, ^{29}Si, ^{27}Al MAS NMR spectroscopic studies indicate significant changes taking place on the surface and within the structure of montmorillonite K10 when treated with MF_2. Evidence from infrared spectroscopy studies of the different reagent loadings clearly indicates structural rearrangement within the silica framework, since the IR band at 802 cm^{-1}, corresponding to the free silica layer SiO_2, diminishes as ZnF_2 and CuF_2 loadings increase. This rearrangement presumably involves the isomorphous replacement of Si by Al in the SiO_2 framework. The IR spectra of ZnF_2–K10 reagents showed bands at 755 and 663 cm^{-1}, which suggest the formation of AlF_4^- and AlF_3, respectively, and spectra of CdF_2–K10 remained nearly unchanged from the original spectrum of montmorillonite K10. IR spectra of CuF_2–K10 showed a band at 743 cm^{-1}, which suggests the formation of the SiF_6^{2-} complex. We obtained similar results for MF_2–silica reagents, which led to the conclusion that only CuF_2 has the tendency to attack the SiO_2 layer. Thus ZnF_2 is like PbF_2 and seems only to affect the Al part of the structure.

^{19}F NMR spectra of low-loading ZnF_2–K10 reagent resulted in a line shape of asymmetrical spinning side bands with the central peak at −151 ppm, which corresponds to either surface Si–F or Al–F groups. The high-loading samples showed symmetrical spinning side bands with the centre peak at −153 ppm, and the highly dried samples resulted in a very broad line suggesting the formation of AlF_3. ^{19}F NMR results of CdF_2–K10 were similar to those of ZnF_2–K10, except for the highly loaded reagents dried at high temperature, which resulted in a signal at −197 ppm suggesting the reformation of CdF_2. Spectra of CuF_2–K10 reagents also showed a signal at −151 ppm corresponding to either surface Si–F or Al–F groups.

^{29}Si MAS NMR spectra of ZnF_2–K10 reagents suggest that as the loading of ZnF_2 increases, further replacement of Si by Al takes place, which is indicated by the change in the ^{29}Si environment from $^{29}Si(OSi)_3(OAl)$ to $^{29}Si(OSi)_2(OAl)_2$. Spectra of CuF_2–K10 indicated only partial replacement of Si by Al, whereas spectra of CdF_2–K10 gave no indication of any changes regarding the ^{29}Si environment. ^{27}Al NMR spectra of the high-loading, highly dried samples of MF_2–K10 reagents show some differences, which appear mainly around the tetrahedral Al signal at 61–69 ppm. ZnF_2–K10 reagent showed an intense peak at 61 ppm, whereas CdF_2–K10 and CuF_2–K10 showed an additional signal at 69 ppm. The signal observed at 61 ppm presumably corresponds to the dehydroxylated tetrahedral aluminium in the SiO_2 tetrahedral layer, and the signal at 69 ppm corresponds to hydroxylated tetrahedral aluminium.

Upon combining the results of IR and DSC for high-loading (5.0 mmol/g) CuF_2–K10 reagent, we can clearly observe the thermal decomposition of the species SiF_6^{2-}. As was discussed earlier, the IR spectrum of the high-loading low-temperature-dried CuF_2–K10 reagent showed a band at 740 cm^{-1} due to the SiF_6^{2-} complex; then, as it is calcined to 600°C, this band diminished. A number of attempts were made to trap the gaseous species SiF_4, but the rapid hydrolysis of the gas by HF and (or) residual H_2O to H_2SiF_6 acid prevented the monitoring of pure SiF_4. IR spectra of the gas trapped in the cell gave very strong bands at 741 and 480 cm^{-1}, which are presumably due to SiF_6^{2-} of H_2SiF_6 (lit. values 740 and 483 cm^{-1}, respectively (19)) (pH analysis of

Can. J. Chem. Downloaded from www.nrcresearchpress.com by 109.225.110.28 on 09/08/12
For personal use only.

TABLE 2. Electronegativities and atomic radii of Zn, Al, Cu, and Cd

Element	Electronegativity[a]	Atomic radii[b] (Å)
Al	1.61	1.25
Zn	1.65	1.35
Cd	1.69	1.55
Cu	1.90	1.35

[a]Electronegativity values from Pauling (1967).
[b]Atomic radii from Slater (1964, 1972).

the condensed matter in the cell indicated strong acidity). An additional weak band at 1072 cm^{-1} corresponds to SiF_4 (lit. value 1070 cm^{-1} (25))

$$2SiF_4\,(g) + 2H_2O(g) \rightarrow H_2SiF_6 + SiO_2 + 2HF$$

$$SiF_4\,(g) + 2HF\,(g) \rightarrow H_2SiF_6$$

The reactivity of MF_2–K10 reagents in the catalysis of Friedel–Crafts benzylation of benzene with benzyl chloride is considerably greater than that of cation exchanged M(II)–K10 (10) and MCl_2–K10 reagents (11). ZnF_2–K10 was observed to be the most reactive of the series, and CuF_2–K10 showed significantly low reactivity compared to the other MF_2–K10 reagents. The cause of the difference in the strength of the observed Lewis acidity is not fully understood. The only valid possibility is the newly formed surface Al–F groups, which have been reported to contribute to Lewis acidity (3, 22). At low loadings and high calcining temperatures, the metal fluorides were totally lost with a resultant decrease in activity. The other possibility, which cannot ruled out, is the formation of the strongly acidic species HF_2^-, but there is no definite spectroscopic evidence that shows the presence of such species. Recent ^{19}F NMR studies (23) reported different values of HF_2^- chemical shifts (ranging from −167 to −146 ppm), which fall in the range obtained for some of the MF_2–K10 reagents. Table 2 compares the values of electronegativities and atomic radii of Al to those of Zn, Cd, and Cu. The Zn atom, whose size and electronegativity appear to be very close to those of the Al atom, replaces Al quite extensively. The size of the Cu atom is also comparable to that of Al, but its electronegativity is high; as a result Cu did not replace Al as extensively. The large size of Cd is probably the only factor inhibiting the replacement of Al by Cd.

In conclusion, we believe the above study has demonstrated the complexity of what really goes on as a transition metal fluoride is adsorbed onto montmorillonite K10, and can be of good use to those who are studying fluorinated or transition-metal-supported clay. The reagents we have presented show a significant improvement in the catalysis of Friedel–Crafts benzylation of benzene over commonly used standard Lewis-acid catalysts. We consider these reagents to be new, environmentally friendly, catalysts, and reasonably safe to handle at any possible scale needed.

Acknowledgements

We would like to thank the Natural Sciences and Engineering Research Council of Canada (NSERC) for operating and equipment grants (to J. M. Miller), the Science and Engineering Research Council (SERC) (U.K.) for an equipment grant (to Dr. J. H. Clark), and Dr. A. P. Kybett for his advice. We are also grateful to Mr. T. R. B. Jones for technical assistance with the NMR instrument and Mr. P. Elliot for assistance with the thermal analysis work.

1. V. R. Choudhavy. Ind. Eng. Chem. Prod. Res. Dev. **16**, 12 (1977).
2. A. K. Ghosh and R. A. Kydd. J. Catal. **103**, 399 (1987).
3. P. O. Scokart, S. A. Selim, J. P. Damon, and P. C. Rouxhet. J. Colloid Interface Sci. **70**, 209 (1979).
4. J. R. Schlup and R. W. Vaughan. J. Catal. **85**, 311 (1984).
5. J. R. Schlup and R. W. Vaughan. J. Catal. **99**, 304 (1986).
6. J. M. Miller, C. V. A. Duke, J. H. Clark, and A. P. Kybett. Spectrochim. Acta. **64A**, 1381 (1990).
7. J. M. Miller, C. V. A. Duke, J. H. Clark, and A. P. Kybett. J. Mol. Catal. **62**, 233 (1990).
8. F. M. Asseid, C. V. A. Duke, and J. M. Miller. Can. J. Chem. **68**, 1420 (1990).
9. P. Laszlo. Preparative chemistry using supporting reagents, Academic Press, New York. 1987. pp. 288–312, 151–162.
10. P. Laszlo and A. Mathy. Helv. Chim. Acta. **70**, 577, (1987).
11. J. H. Clark, A. P. Kybett, D. J. Macquarrir, S. J. Barlow, and P. Landon. J. Chem. Soc. Chem. Commun. 1353 (1989).
12. C. N. Rhodes, M. Franks, G. M. B. Parkes, and D. R. Brown. J. Chem. Soc. Chem. Commun. 804 (1991).
13. P. Laszlo. La Recherche, **219**, 314 (1990).
14. S. F. Dec, R. A. Wind, and G. E. Maciel. Macromolecules, **20**, 2754 (1987).
15. M. J. Mobley and J. P. Yesinowski. J. Am. Chem. Soc. **105**, 6191 (1983).
16. J. C. Miller and M. Majda. J. Am. Chem. Soc. **107**, 1419 (1985).
17. D. T. B. Tennakoon, J. M. Thomas, W. Jones, T. A. Carpenter, and S. Ramdas. J. Chem. Soc. Faraday Trans. 1, **82**, 545 (1986).
18. D. B. Shin, D. S. Crocket, and H. M. Haendler. Inorg. Chem. **5**, 1927 (1966).
19. K. Nakamoto. Infrared spectra of inorganic and coordination compounds. Wiley–Interscience, New York. 1986.
20. R. W. Vaughan, D. D. Elleman, W. K. Rhim, and L. M. Satcey. J. Phys. Chem. **57**, 5383 (1972).
21. C. H. Duncan and J. R. VanWozer. Compilation of reported ^{19}F NMR chemical shifts. Wiley–Interscience, New York. 1970.
22. V. C. Farmer and J. D. Russell. Spectrochim. Acta, **20**, 1149 (1964).
23. K. O. Christe and W. W. Wilson. J. Fluorine Chem. **46**, 339 (1990).
24. E. S. Freeman and V. D. Hogan. Anal. Chem. **36**, 120 (1964).
25. J. P. Guertin and M. Onyszchuk. Can. J. Chem. **41**, 1477 (1963).

Can. J. Chem. Downloaded from www.nrcresearchpress.com by 109.225.110.28 on 09/08/12
For personal use only.

Thermal and photochemical reactions of steroidal α-azido ketones[1,2]

O. E. EDWARDS, J. L. DOUGLAS,[3] D. C. HORWELL,[3] W. RANK,[3] AND T. SANO[3]
Department of Chemistry, Carleton University, Ottawa, Ont., Canada K1S 5B6

Received March 5, 1992

O. E. EDWARDS, J. L. DOUGLAS, D. C. HORWELL, W. RANK, and T. SANO. Can. J. Chem. **70**, 2405 (1992).

Photolysis of 9α-azido-3β,20β-diacetoxy-5α-pregnan-11-one in methanol gave the *N*-acyl imine 11-aza-3β,20β-diacetoxy-C-homo-5α-pregn-9,11-en-12-one **4** and the aminoketone 9a-aza-3β,20β-diacetoxy-9-methoxy-B-homo-5α-pregnan-11-one **7**. In dichloromethane containing triethylamine the irradiation of this azide gave the *N*-acyl imine **4** and the α,β-unsaturated amino ketone 9a-aza-3β,20β-diacetoxy-B-homo-5α-pregn-8-en-11-one **8**. Thermolysis or photolysis of 12α-azido-3α,20β-diacetoxy-5β-pregnan-11-one gave the *N*-acyl imine 12-aza-3α,20β-diacetoxy-C-homo-5β-pregn-12-en-11-one **10** as major product. Photolysis of 20β-acetoxy-12α-azido-3α-hydroxy-5β-pregnan-11-one gave the 3-hydroxy analogue of **10**. Transformation products of the *N*-acyl imines are described.

O. E. EDWARDS, J. L. DOUGLAS, D. C. HORWELL, W. RANK et T. SANO. Can. J. Chem. **70**, 2405 (1992).

La photolyse de la 9α-azido-3β,20β-diacétoxy-5α-pregnan-11-one, en solution dans le méthanol, conduit à la *N*-acyl imine, 11-aza-3β,20β-diacétoxy-C-homo-5α-pregn-9,11-èn-12-one, **4**, et à l'aminocétone, 9a-aza-3β,20β-diacétoxy-9-méthoxy-B-homo-5α-pregnan-11-one, **7**. Dans du dichlorométhane contenant de la triéthylamine, l'irradiation de cet azoture fournit la *N*-acyl imine **4** et la cétone aminée α,β-insaturée, 9a-aza-3β,20β-diacétoxy-B-homo-5α-pregn-8-èn-11-one **8**. La thermolyse ou la photolyse de la 12α-azido-3α,20β-diacétoxy-5β-pregnan-11-one fournit la *N*-acyl imine, 12-aza-3α,20β-diacétoxy-C-homo-5β-pregn-12-èn-11-one **10** comme produit principal. La photolyse de la 20β-acétoxy-12α-azido-3α-hydroxy-5β-pregnan-11-one conduit à l'analogue 3-hydroxy, **10**. On décrit les produits de transformation des *N*-acyl imines.

[Traduit par la rédaction]

Can. J. Chem. Downloaded from www.nrcresearchpress.com by 109.225.110.28 on 09/08/12
For personal use only.

The discovery (1) that photolysis[4] of two steroidal α-azido ketones gave moderate yields of isolable *N*-acyl imines led to much interest, in our laboratories, in this class of compound. This was reinforced by the possibility that many biologically active natural products could have *N*-acylimines as precursors (2). Furthermore we were attracted by the possibility that azasteroids with strategically located *N*-acyl imine functions would act as hormone mimics, irreversibly binding to receptor sites in hormone-dependent tumor cells (3; see also reviews cited in ref. 16).

We now present a full account of the photolysis of three steroidal azido ketones, thermolysis of one of these, and reactions of the products.

Results

The preparation of 9α-azido-3β,20β-diacetoxy-5α-pregnan-11-one (**3**) from 11-ketoprogesterone (**1**) (5) was improved by use of lithium in ammonia reduction of the conjugated ketone, and Sarett (6) or pyridinium chlorochromate (7) oxidation of the intermediate hydroxy azide **2**.

Photolysis of **3** in dry methanol gave two major products. The most abundant one was the *N*-acyl imine **4**. The characteristic identifying features were the carbonyl (ν_{max} 1698 cm^{-1}) and imine (ν_{max} 1668 cm^{-1}) infrared frequencies and the ^{13}C nmr singlets at 186 (C=O) and 180 (C=N) ppm. The action of dry *p*-toluenesulfonic acid in benzene on **4** converted it into the enamide **5**. The amide carbonyl of **5** had $\nu_{max}(CCl_4)$ 1660 cm^{-1} and a ^{13}C nmr signal at 176 ppm. The double bond carbons resonated at 137.8 and 124.6 ppm, and **5** had λ_{max} 232 nm (ε 6200).

The second important product from the photolysis in methanol was a very weak base (pK_a 3.8 in 95% ethanol). It had a ketone carbonyl ($\nu_{max}(CCl_4)$ 1715 cm^{-1}; 209.4 ppm) and a methoxyl group. When a benzene solution of this base was treated with a catalytic amount of *p*-toluenesulfonic acid on silica gel, methanol was eliminated giving an α,β-unsaturated amino ketone ($\nu_{max}(CH_2Cl_2)$ 1682 cm^{-1}; λ_{max} 236 nm (ε 4500) and 297.5 nm (ε 2400)). The double bond gave two ^{13}C nmr singlets at 140 and 115.5 ppm. These data, analysis, and complete spectra were consistent with structure **7** for the methoxy-keto base and **8** for the conjugated unsaturated amino-ketone.

Irradiation of **3** in dichloromethane gave enamide **5** as a readily crystallized product (30%). If, however, a small amount of triethylamine was present the *N*-acyl imine **4** (40%) and the α,β-unsaturated amino-ketone **8** (ca. 45%) were the major products.

Photolysis of 12α-azido-3α,20β-diacetoxy-5β-pregnan-11-one **9** on a one-gram scale in dichloromethane gave a good yield (47.5%) of *N*-acyl imine **10**. The unusual amide carbonyl (ν_{max} 1715 cm^{-1}; ^{13}C nmr signal at 190 ppm) and the imine ^{13}C nmr doublet at 169 ppm with the proton on the imine carbon resonating at δ7.94 indicated the type-structure. Its reactions confirmed this. Acidic methanol converted **10** into a carbinolamide ether **11**. This was now a normal secondary amide (ν_{max} 3230 and 1670 cm^{-1}; ^{13}C nmr for the carbonyl 179.9 ppm), while exposure of an aqueous dioxane solution of **10** to a sulfonic acid resin gave carbinolamide **12**. Acidic methanol converted **12** to **11**. Hydrogenation of **10** produced a saturated lactam **13** (ν_{max} 3230 and 1670 cm^{-1}), which was also produced when **11** was partially reduced by lithium aluminum hydride, followed by

[1]Dedicated to Prof. G. Fodor on the occasion of his 75th birthday, and in recognition of his notable contributions to teaching and natural products research.

[2]Much of this work was performed in the Division of Chemistry and Division of Biological Sciences, National Research Council of Canada, Ottawa. It was presented in part at the Symposium on Heterocyclic Chemistry, Poznan, July 24–26, 1972.

[3]Research Associates, National Research Council of Canada.

[4]The photolysis was proposed by Dr. N. F. Elmore as a method of preparing 12-imino 11-ketones from the azido ketones following Barton and Starratt (4), and he did preliminary studies on **9**. We gratefully acknowledge this contribution.

reacetylation. Finally, an X-ray crystallographic analysis (8) confirmed the structure and gave bond lengths and angles for **10**.

More-polar fractions from the large-scale photolysis of **9** contained much carbinolamide **12** since treatment with acidic methanol gave a 14% yield (based on starting material) of ether **11**. Thus the overall yield of products resulting from acyl migration onto nitrogen was 61%.

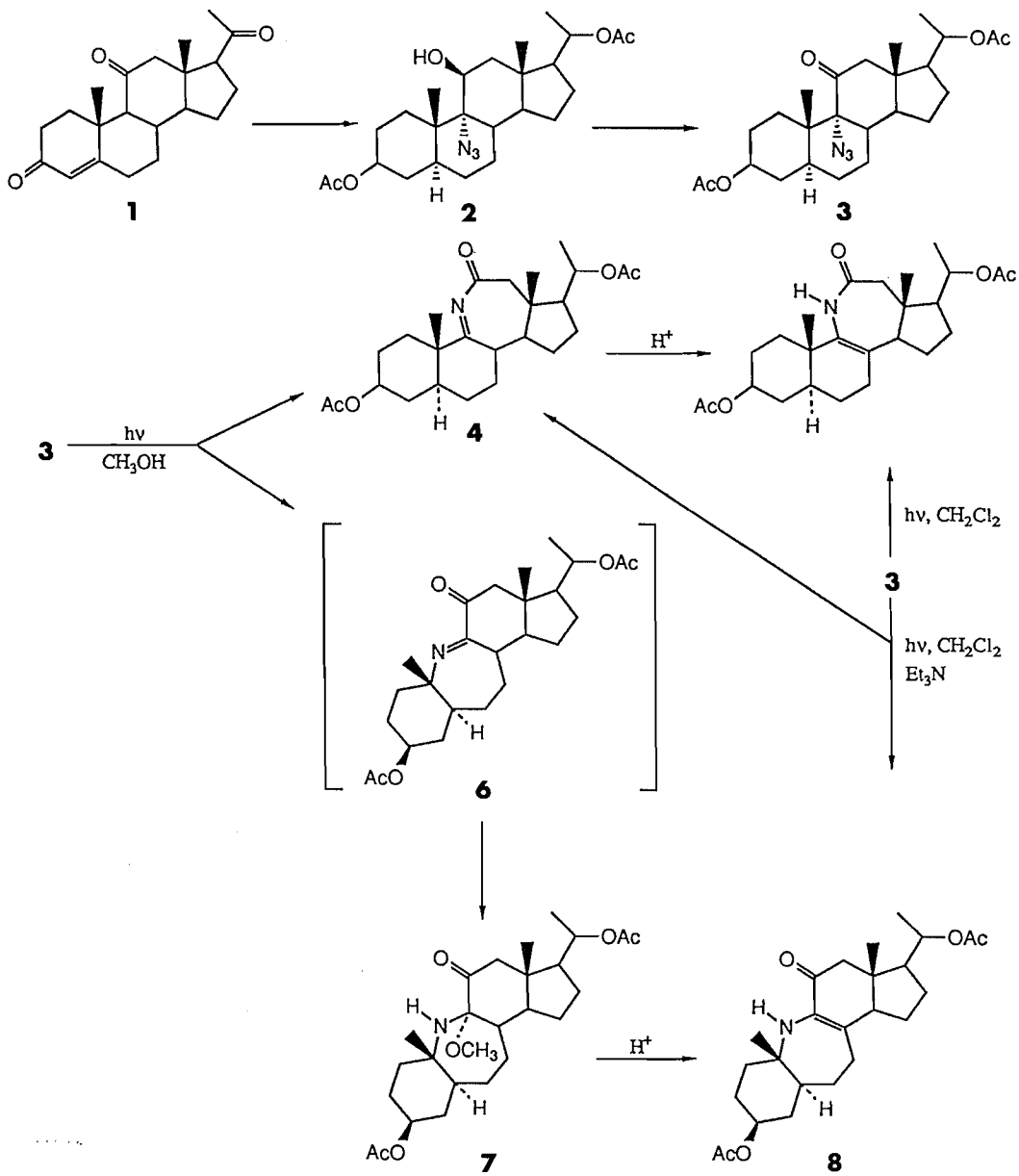

Attempts to reproduce the photolysis of **9** on a smaller scale, or carry it out using a Vycor flask and a Rayonet photoreactor with lamps giving peak radiation at 300 nm on a 100–200 mg scale, gave low yields of **10**. This was eventually attributed to traces of acid formed from the dichloromethane and traces of water carried into the reaction. Addition of dry triethylamine prior to the photolysis eliminated the problem, and isolated yields of around 60% of **10** were consistently obtained. We were unable to isolate the imine **14** (R^1 = Ac) or products derived from it. However the total ether-soluble products from these photolyses gave a ^1H nmr signal at δ7.56 in addition to the major one at δ7.95(*N*-acyl imine), suggestive of its presence. Subsequent handling of the noncrystalline products after removal of most of **10** led to fractions containing aldehyde hydrogens (δ10.0 and 9.7) and new carbonyl groups (207.3 and 206.4 ppm). Thus products formed by opening of ring C of **10** and **14** (R^1 = Ac) seemed to be present.

Photolysis of **9** in dry methanol using Pyrex-filtered ultraviolet light gave a 56% yield of pure **11** ($R^1 = R^2$ = Ac).

The observation of slow nitrogen loss from **9** above its melting point prompted a study of its thermolysis. Because of the evident sensitivity of **10** to acid we chose to do the thermolysis in dry dimethylaniline, thus providing an adequately high boiling point and a weakly basic medium. Heating at ca. 200°C in this solvent for 13.5 h did indeed

Can. J. Chem. Downloaded from www.nrcresearchpress.com by 109.225.110.28 on 09/08/12
For personal use only.

convert **9** into products, from which **10** was isolated in a yield of 51%.

Stepwise hydrolysis of the acetoxy groups of the carbinolamide ether lactam **11** ($R^1 = R^2 = Ac$) was possible using sodium methoxide in methanol. The 3-acetoxy group was much more reactive, so that the 3-hydroxy-20-acetoxy ether **11** ($R^1 = H$, $R^2 = Ac$) and the dihydroxy ether **11** ($R^1 = R^2 = H$) could be prepared. After two days in 1 M sodium methoxide in methanol, the diacetoxy *N*-acyl imine **10** gave an 87% yield of the dihydroxy ether **11** ($R^1 = R^2 = H$).

Similar hydrolysis of the diacetoxy azide **9** gave the 3-hydroxy-20-acetoxy azide **15** ($R^1 = H$, $R^2 = Ac$) and the corresponding diol **15** ($R^1 = R^2 = H$).

Photolysis of the 3-hydroxy-20-acetoxy azide **15** ($R^1 = H$, $R^2 = Ac$) in dichloromethane containing triethylamine gave a 60% isolated yield of the *N*-acyl imine **16** ($R^1 = H$, $R^2 = Ac$) after chromatography on neutral alumina. Evidence was obtained for the presence of the keto imine **14** ($R^1 = H$) (δ7.5; 206.7 and 160.9 ppm) in the products, but no pure **14** could be isolated on the small scale used. The *N*-acyl imine **16** ($R^1 = H$) survived, in part, quick chromatography on "flash" silica gel and elution with 1% methanol in dichloromethane. Its melting point in an evacuated capillary was 185°C with slight bubbling, but the melt didn't really liquefy until above 220°C, indicating probable intermolecular solvation of the imine in the melt.

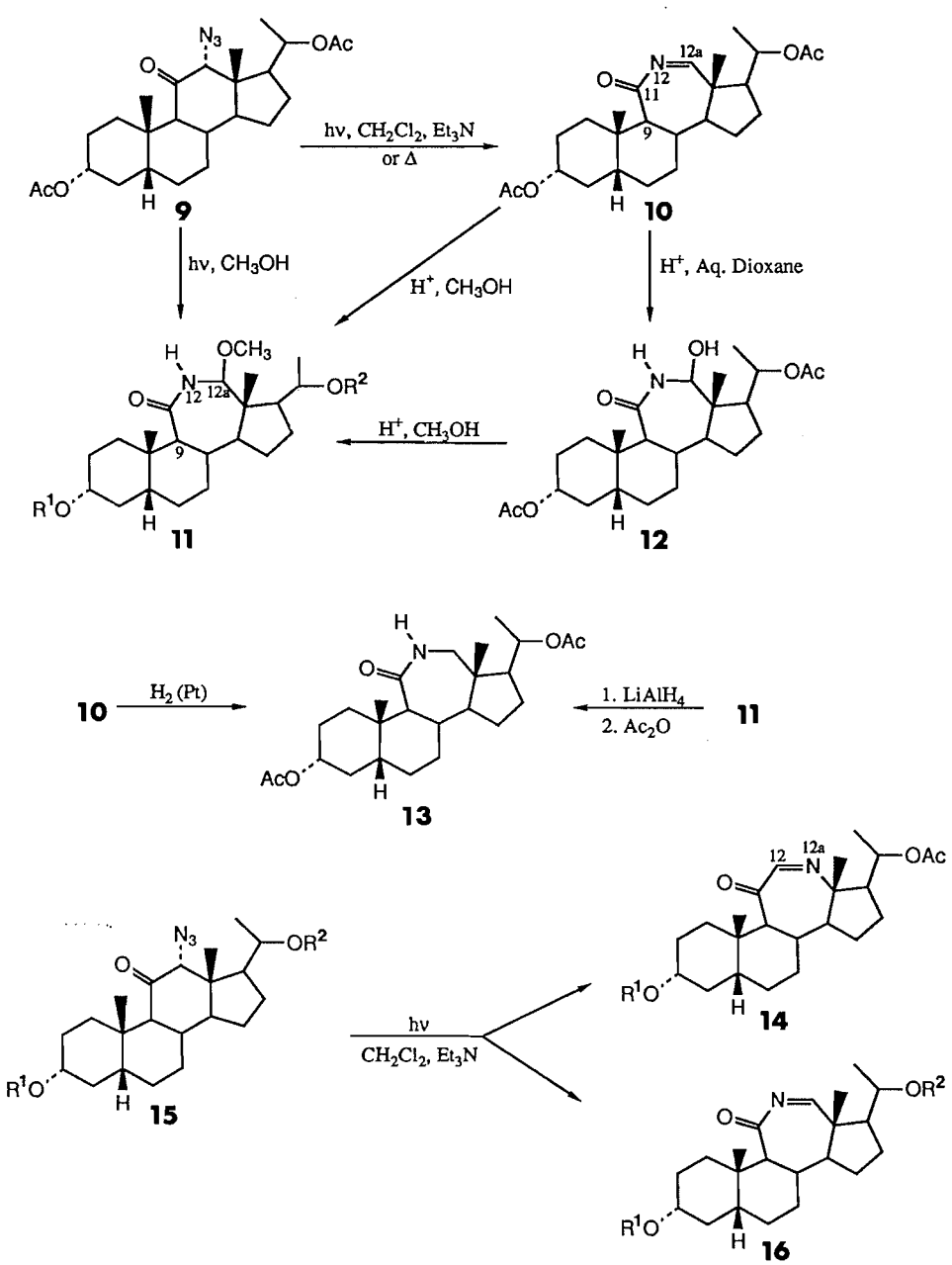

In contrast, photolysis of the dihydroxy azide **15** ($R^1 = R^2 = H$) as for the monoacetate gave no detectable *N*-acyl imine (nmr). However, a keto imine (δ7.53; 205.1 and 160.8 ppm) appeared to be present, but could not be isolated. When **15** ($R^1 = R^2 = H$) was irradiated in dichloromethane–triethylamine at −25°C, then the product treated with metha-

Can. J. Chem. Downloaded from www.nrcresearchpress.com by 109.225.110.28 on 09/08/12
For personal use only.

nol and a sulfonic acid resin, a 56% yield of the dihydroxy methyl ether **11** ($R^1 = R^2 = H$) was obtained.

Discussion

The mechanism of the photolysis of α-azido ketones, esters, and amides has been discussed (9). Transient formation of a singlet nitrene seems probable, with a zwitterion **17** as a likely intermediate between this and the rearranged prod-

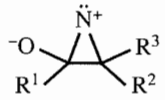

17

ucts. The axial orientation of the azide groups in **3** and **9** would make formation of such intermediates very favorable.

The competition between alkyl and acyl migration onto electron-deficient nitrogen in the photolysis of our examples of α-azido ketones slightly favors the latter (see also ref. 9).

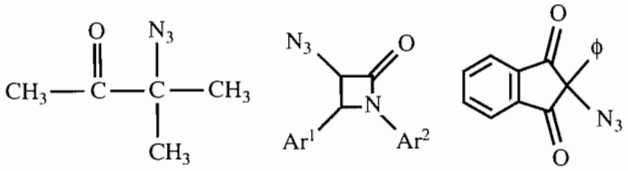

18 **19** **20**

However, Margaretha and Steffen (10) only observed alkyl migration when **18** was photolyzed. Thus the only other observation of photochemical acyl migration onto nitrene-like nitrogen appears to be that of Moriarty *et al.* (11) on dimethyl diazidomalonate. Pyrolytic acyl migration onto the nitrogen of a decomposing azide was observed by Moriarty and Serridge for methyl diazidomalonate (12), Millership and Suschitzky (13) for **19**, Moore and co-workers (14) for **20**, and Ogilvie and Rank (15) for ethyl 2,2-diazido-3-keto-butyrate.

The near coplanarity of the carbonyl and the lone pair on nitrogen in the cyclic *N*-acyl imines means that amide resonance does not exist. This is reflected in their high infrared stretching frequency (1698 and 1715 cm^{-1} for **4** and **10** respectively) and the ^{13}C nmr shifts (186 and 190 ppm) of the carbonyl groups. The restoration of the amide resonance in solvation products such as **11** may provide a 15–20 kcal/mol driving force for the reaction, resulting in the sensitivity of the *N*-acyl imines to alcohols or water. Since this sensitivity should extend to sulfhydryl and amine groups, this suggested the possibility of preparing analogues of the steroid hormones containing *N*-acyl imine functions with biological alkylating potential. These could act as very specific chemotherapeutic agents for hormone-sensitive tumors (3). Our studies show that the *N*-acyl imine function in a steroid skeleton can be resistant enough at physiological pH to enable delivery to target sites in the body.

Unfortunately we have been unable to prepare steroidal *N*-acyl imines with *normal ring sizes* and nitrogen in rings A or D for biological studies[5] (see also the work of Back *et al.*, ref. 16). Only one other steroidal *N*-acyl imine **21** seems to have been isolated (17).

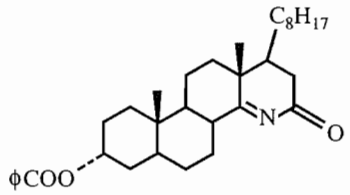

21

Experimental

Ultraviolet spectra were taken in 95% ethanol; infrared spectra on a Perkin–Elmer model 683 grating spectrometer were taken of dichloromethane solutions unless otherwise stated. The ^1H nmr and ^{13}C nmr spectra were taken of deuteriochloroform solutions on EM-360 Varian CW, Varian Gemini 200 FT, or Bruker AMX 400 FT spectrometers as indicated in the text. Melting points were in Pyrex capillaries.

5α-Pregnan-3,11,20-trione

A solution of 20 g of 11-ketoprogesterone in 250 mL of dry tetrahydrofuran was added slowly with stirring to a solution of 3 g of lithium in 1 L of anhydrous ammonia. Five minutes after completion of the addition, *tert*-butyl alcohol was added slowly until the blue color disappeared (ca. 40 mL), then 23 g of ammonium chloride was added slowly with stirring. The ammonia was evaporated in a stream of argon, then the tetrahydrofuran was removed on a rotating evaporator. The products were distributed between water and chloroform. The mixture was acidified (pH 2), then the chloroform extract and washings dried and distilled. The residual brown oil was dissolved in 200 mL of acetone, the solution cooled in ice, then 47 mL of Jones reagent (18) was added slowly. After 5 min the excess reagent was reduced using isopropyl alcohol. The supernatant liquid and acetone washings of the precipitate were evaporated, then the residue distributed between water and chloroform. The latter yielded a yellowish-brown solid on evaporation. This was dissolved in a minimum amount of 9:1 (v/v) benzene–chloroform, then adsorbed onto 400 g of neutral alumina (Act. III). The same solvent eluted 11 g of the desired 5α-pregnan-3,11,20-trione, mp 214–218°C. The catalytic reduction previously used (5) gave a mixture of 5α and 5β isomers.

9α-Azido-3β,20β-diacetoxy-5α-pregnan-11-one ***3***

The oxidation of 9α-azido-3,20-diacetoxy-11β-hydroxy-5α-pregnane (**2**) was improved from the previous report (5) by using either Sarett oxidation (6) or pyridinium chlorochromate (7).

(*a*) A solution of 590 mg of azido alcohol (**2**) in 6 mL of dry pyridine was added to a solution of 590 mg of chromium trioxide in 7 mL of pyridine. The mixture was stirred at room temperature for 17 h. It was then diluted with 60 mL of water and the products extracted into ether. The ether was washed with 5% aqueous acetic acid, water, then 10% sodium carbonate solution, dried, and evaporated. The residue gave 500 mg of **3**, mp 205–207°C after crystallization from acetone–hexane.

(*b*) A solution of 730 mg of **2** in 10 mL of dry dichloromethane was added to a suspension of 700 mg of pyridinium chlorochromate (7) in 20 mL of the same solvent. The mixture was stirred at room temperature for 3.3 h, then poured into 100 mL of dry ether. The precipitate was removed by filtration through Celite, then the filtrate passed through a 4 cm × 2.5 cm column of Florisil. The filtrate and ether washings were evaporated, then the residue crystallized from ethyl acetate – hexane. The prisms of **3** (670 mg) had mp 198–201°C.

Irradiation of 9α-azido-3β,20β-diacetoxy-5α-pregnan-11-one (***3***)

(a) In methanol

A solution of 305 mg of azide **3** in 70 mL of dry methanol was irradiated in a Vycor vessel at 15°C using a Rayonet photoreactor

[5]Unpublished work with T. G. Back, J. L. Douglas, C. Grieco, and G. Grue-Sorensen.

Can. J. Chem. Downloaded from www.nrcresearchpress.com by 109.225.110.28 on 09/08/12
For personal use only.

Can. J. Chem. Downloaded from www.nrcresearchpress.com by 109.225.110.28 on 09/08/12
For personal use only.

with lamps giving peak emission at 300 nm. After 1 h the azide had been destroyed (ir). The solution was evaporated below room temperature, the residue dissolved in dichloromethane, then this solution washed with water. The organic layer was dried and distilled giving a residue that crystallized from acetone, giving 85 mg of crude methoxy base **7**. Separation of the main product on 1.5 mm alumina plates using dichloromethane gave more **7** (total 95 mg; 31%; R_f 0.7) and 82 mg of the *N*-acyl imine **4** (29%; R_f 0.5).

Irradiation of azide **3** in methanol using a 100-W Hanovia high-pressure mercury lamp and Pyrex filter took 3 h for completion. The yield of methoxy base **7** was 33% and of *N*-acyl imine **4** was 41%.

(b) In dichloromethane

A solution of 249 mg of azide **3** in 35 mL of dichloromethane was irradiated using a 100-W high-pressure Hanovia mercury lamp in a quartz vessel. The photolysis was complete in 3 h. The products were adsorbed from benzene onto 2 g of neutral alumina, Activity IV. Benzene eluted 125 mg, rich in enamide **5**. After crystallization from hexane, and recrystallization from acetone–hexane, this gave 70 mg (30%) of **5** as needles, mp 205–207°C.

(c) In dichloromethane–triethylamine

A solution of 80 mg of azide **3** in 15 mL of dry dichloromethane containing 39 mg of triethylamine was irradiated in a Vycor vessel at 10°C using 300 nm lamps in a Rayonet apparatus for 1 h. The yellow solution was evaporated below room temperature, then the residue taken up in dry ether. The undissolved solid (ca. 2 mg of triethylamine hydrochloride) was removed by filtration. When concentrated the filtrate yielded 30 mg (40%) of crystalline *N*-acyl imine **4**. The mother liquor was evaporated and the residue dried under 0.5 Torr (1 Torr = 133.3 Pa). Its ^{13}C nmr spectrum showed that it contained approximately 30% of *N*-acyl imine but that the major component was the α,β-unsaturated amino-ketone **8** (estimated yield 45%) (23 major signals coincident with those for pure **8**). An attempt to purify this on a 1 mm alumina plate using dichloromethane gave only 14 mg (19%) of **8** (R_f 0.6). The major components (20 mg) now had low R_f, corresponding to hydrated products.

11-Aza-3β,20β-diacetoxy-C-homo-5α-pregn-9(11)-en-12-one **4**

The *N*-acyl imine **4** upon recrystallization from ether–hexane formed needles with mp 220–223°C and $[\alpha]_D$ 30.6 (*c* 1.08, in 95% ethanol). It had ν_{max} (CH_2Cl_2) 1728, 1686, and 1660 cm^{-1}; and λ_{max} 278 nm (ε 500). It gave ^1H nmr signals at δ 4.8(2H, br m), 3.0(1H, d, J = 14 Hz), 2.6(1H, d, J = 14 Hz), 2.05(6H, s), 1.22(3H, s), 1.15(3H, d, J = 6 Hz), and 0.82(3H, s) and ^{13}C nmr signals at 185.7 (s), 179.9(s), 170.4(s), 170.2(s) 72.6(d), 72.2(d), 56.4(d), 50.6(t), 48.6(d), 46.9(d), 44.9(d), 43.5(s), 41.1(s), 33.3(t), 32.6(t), 28.3(t), 27.4(t), 27.0(t), 24.9(t), 21.3(q) (double intensity), 19.9(q), 17.1(q), and 15.9(q) ppm. Anal. calcd. for $C_{25}H_{37}NO_5$: C 69.57, H 8.64, N 3.25; found: C 69.30, H 8.84, N 3.42.

11-Aza-3β,20β-diacetoxy-C-homo-5α-pregn-8-en-12-one **5**

The *N*-acyl imine **4** (46 mg) was added to a solution of 10 mg of *p*-toluenesulfonic acid hydrate, 50 mg of acetic acid, and 50 mg of acetic anhydride in 3 mL of dry benzene. The mixture was heated under gentle reflux for 2 h. The benzene was evaporated *in vacuo*, the residue dissolved in dichloromethane, then this solution stirred for 0.5 h with 5% aqueous sodium carbonate. The organic layer yielded 47 mg of product, which crystallized from acetone as stout needles mp 204–209°C. Recrystallization from acetone gave 29 mg (mp 205–210°C) of enamide **5**. This had ν_{max}(CCl_4) 3200, 1740, 1660, and 1250 cm^{-1} and λ_{max} 232 nm(ε 6200). It gave ^1H nmr signals at δ6.39 (1H, s), 4.73(2H, m), 2.89(1H, d, J = 14 Hz), 2.66(1H, t, J = 10 Hz), 2.07(3H, s) and 2.05(3H, s), 1.19(2H, d, J = 6 Hz), 1.09 (3H, s), and 0.72(3H, s). Its ^{13}C nmr spectrum had signals at 176.0, 170.8, 170.7, 137.8, 124.6, 73.4, 73.0, 56.1, 50.7, 49.5, 45.3, 40.5, 37.0, 33.33, 32.0, 27.6, 26.9, 26.3, 24.7, 21.7, 21.6, 19.9, 18.5, and 17.0 ppm. Its EI mass spectrum gave M^+ 431.26604; calcd. for $C_{25}H_{37}NO_5$: 431.26716.

9a-Aza-3β,20β-diacetoxy-9α-methoxy-B-homo-5α-pregnan-11-one **7**

After crystallization from acetone–hexane this had mp 189–191°C. In an evacuated capillary it had mp 232–235°C. It had ν_{max}(CCl_4) 1740, 1715, and 1250 cm^{-1} and ν_{max}(nujol) 3380(NH), 1742, and 1702 cm^{-1}. It had λ_{max} 255 nm(ε 58) and 315 nm(ε 58) and pK_a 3.8 in 95% ethanol. It gave ^1H nmr signals δ4.8(2H, m), 3.42(3H, s), 3.1(1H, m), 2.82 and 2.70(pair of 1H doublets, J = 12.3 Hz), 2.03(3H, s), 2.02(3H, s), 1.17(3H, d, J = 6.1 Hz), 1.02(3H, s), and 1.00(3H, s). Its ^{13}C nmr (100.6 MHz) spectrum had signals at 209.4 s, 170.5 s, 170.3 s, 91.9 s, 73.3d, 72.7 d, 54.1 d, 53.7 d, 52.3 t, 51.6 q, 48.7d, 47.2 s, 44.2 s, 38.0 t, 35.3 d, 33.5 t, 31.1 t, 29.4 t, 27.9 t, 26.6 t, 25.8 t, 21.5 q, 19.9 q, 15.6 q, and 14.4 q ppm. Anal. calcd. for $C_{26}H_{41}NO_6$: C 67.36, H 8.91, N 3.20; found: C 67.54, H 9.10, N 3.19. Its EI mass spectrum gave a weak peak at m/z 463 but a strong one at m/z 431 (M − 32).

9a-Aza-3β,20β-diacetoxy-B-homo-5α-pregn-8-en-11-one **8**

A suspension of 57 mg of methoxy base **7** and 49 mg of dry *p*-toluenesulfonic acid on silica gel (3% acid) in 3 mL of dry benzene was stirred under argon for 21 h. The mixture was filtered and the solid washed with benzene. The benzene solution yielded 52 mg of residue, which crystallized as fine needles from acetone–hexane. The silica gel was suspended in benzene containing 10% of pyridine. The solvent extracted 9 mg, which also crystallized. This and the mother liquor from the main crop of crystals was put on a 30 cm × 20 cm, 0.25 mm alumina plate and separated using chloroform (3/4% ethanol). The main zone (R_f 0.56) gave 7 mg of crystalline base. The combined crystals (45 mg, 85%) had mp 119–125°C. Recrystallization from aqueous methanol gave **8** as stout needles, mp 182–187°C. This had ν_{max} 3410, 1724, and 1682 cm^{-1} and λ_{max} 235.8 (ε 4500) and 297.5(ε 2400). Its ^1H nmr spectrum gave signals at δ5.40(1H, s), 4.87(1H, m), 4.60(1H, m), 3.21(1H, t, J = 9 Hz), 2.034 (3H, s), 2.026 (3H, s), 1.22(3H, s), 1.20(3H, d, J = 5 Hz), 0.94(3H, s) and its ^{13}C nmr spectrum gave signals at 208.4, 170.8, 170.7, 139.9, 115.5, 72.95, 72.56, 59.26, 53.24, 51.68, 50.37, 44.19, 37.96, 36.82, 36.46, 34.0, 30.83, 26.66, 26.0, 25.37, 21.58, 21.45, 19.79, 14.83, and 9.39 ppm. Its EI mass spectrum had M^+ 431.26516; calcd. for $C_{25}H_{37}NO_5$: 431.26716.

Photolysis of 12α-azido-3α,20β-diacetoxy-5β-pregnan-11-one **9**

(*a*) A solution of 1.44 g of azido ketone **9** (5) in 100 mL of dry dichloromethane was irradiated for 7 h using a 100 W high-pressure Hanovia mercury lamp in a water-cooled Pyrex well. By this time all the azide had been transformed. The solvent was removed on a rotating evaporator, the residue dissolved in benzene, then this solution passed through a column of 40 g of neutral alumina (Act. IV). Benzene (ca. 300 mL) eluted 1.0 g, rich in *N*-acyl imine **10**. This crystallized from ether–hexane mixtures giving **10** as prisms, (645 mg, 49.5%). Dichloromethane eluted 124 mg of yellow gum. A 1% solution of methanol in dichloromethane eluted 347 mg of amorphous solid. Its reactions (see below) showed it to contain much (ca. 14% yield) carbinolamide **12** or equivalent amido-aldehyde and polymer. Attempts to repeat this on a smaller scale gave much reduced yields of *N*-acyl imine **10**, apparently due to traces of water and traces of acid produced from the dichloromethane.

In a comparable experiment on 272 mg of azide **9** in 70 mL of dichloromethane but containing 1 mL of dry triethylamine the photolysis was complete in 2 h. After work-up as above, 153 mg (60%) of crystalline *N*-acyl imine **10** was obtained.

(*b*) When a solution of 100 mg of azide **9** in 17 mL of dry dichloromethane containing 69 mg of dry triethylamine (5A molecular sieve) was irradiated in a Vycor flask at 10°C using a Rayonet reactor with 300 nm lamps the photolysis was complete in 1 h. The pale yellow solution was evaporated to dryness. Dry ether (10 mL) was added, then the solution filtered to remove 9 mg of solid. The ether was evaporated, and the residue dried briefly at 90°C, 0.5 Torr. The ^1H nmr spectrum of this mixture showed it to be mainly *N*-acyl imine **10** (δ7.94) but to contain a component (ca.

Can. J. Chem. Downloaded from www.nrcresearchpress.com by 109.225.110.28 on 09/08/12
For personal use only.

25%) giving a signal at δ7.56. This corresponds to the expectation for the C-12 of keto imine **14** (R^1 = Ac). The ^{13}C nmr spectrum was mainly that of **10**, but again a signal at 160.74 ppm corresponded to the C-12 of **14** (22% of the height of the signal for C-12a of **10**). Chromatography of the ether-soluble products on Activity IV neutral alumina as in (*a*) partially decomposed the compounds. The yield of crystalline *N*-acyl imine **10** was 54 mg (58%). The ^1H nmr spectrum of the mother liquor from crystallization of **10** showed the presence of **10** and at least two aldehydes (δ9.7 and 10.0), probably the products of hydrolytic opening of ring C of **10** and **14**. Chloroform eluates from the column (17 mg) gave 5 mg of prisms from ether–hexane. These gave ^1H nmr signals at δ6.73(1H, s), 4.9(1H, m), 4.7(1H, m), 4.55(1H, d, J = 3 Hz), 2.10(3H, s), 2.02(3H, s), 1.30(3H, s), 1.18(3H, d, J = 6 Hz), and 1.07(3H, s) corresponding to those expected for carbinolamide **12**.

(*c*) A comparable photolysis to that described in (*b*), but using 3500 Å lamps in a Rayonet apparatus took longer for completion (5 h). A 58% yield of **10** was again obtained.

(*d*) A solution of 740 mg of azide **9** in 60 mL of dry methanol was irradiated at 0°C for 16.5 h through Pyrex using a 100-W high-pressure Hanovia lamp. Evaporation of the methanol left a gum. This was adsorbed from benzene on 15 g of neutral alumina (Act. IV). Elution with benzene gave 650 mg, rich in carbinolamide ether **11**. This crystallized from acetone–hexane, giving 420 mg (56%) of pure **11**.

Thermolysis of azido ketone ***9***

Two millilitres of dry dimethylaniline (4A molecular sieve) was added to 201 mg of azido ketone **9** in a dry flask. This was placed in a bath at 210°C, and allowed to reflux gently for 13.5 h. A small amount of azide persisted. The bulk of the dimethylaniline was removed at 110°C, 0.5 Torr, leaving a yellow gum. This was adsorbed from benzene onto 2 g of Activity IV neutral alumina. Benzene eluted 198 mg, which crystallized from ether–hexane giving 96 mg (51%) of crystalline *N*-acyl imine **10**.

12-Aza-3α,20β-diacetoxy-C-homo-5β-pregn-12-en-11-one ***10***

This had mp 190–192°C, $[\alpha]_D$ 184 (*c* 0.13, in 95% ethanol); $\nu_{max}(CCl_4)$ 1742, 1715, 1662, and 1245 cm^{-1}; and λ_{max} 288 nm(ε 1080). Its ^1H nmr spectrum had signals at δ 7.94 (1H, s), 4.77(2H, m), 2.02 (6H, s), 1.38(3H, s), 1.21(3H, d, J = 6 Hz), and 0.90(3H, s). Its ^{13}C nmr (100.6 MHz) spectrum had signals at 189.9 s, 170.5 s, 170.0 s, 168.9 d, 73.7d, 72.3 d, 52.8 d, 52.1 d, 50.4 s, 46.5 d, 42.2 d, 38.4 d, 35.0 t, 34.2 s, 31.8 t, 27.6 t, 27.5 t, 27.1 t, 26.0 t, 24.3q, 23.2t, 21.4 q, 21.2 q, 19.5 q, and 12.1 q ppm. Anal. calcd. for $C_{25}H_{37}NO_5$: C 69.57, H 8.64, N 3.25; found: C 69.43, H 8.82, N 3.19.

12-Aza-3α,20β-diacetoxy-12a-methoxy-C-homo-5β-pregnan-11-one ***11***

This formed prisms from acetone–hexane with mp 208–209°C, $[\alpha]_D$ 144 (*c* 0.286, in 95% ethanol), and ν_{max} 3230, 1740, 1670, and 1250 cm^{-1}. Its ^1H nmr spectrum (200 MHz) had signals at δ6.65(NH), 4.75(2H, m), 4.21(1H, d, J = 6 Hz), 3.40(3H, s), 2.04(6H, s), 1.29(3H, s), 1.16(3H, d, J = 6 Hz), and 0.63(3H, s). Its ^{13}C nmr spectrum (125.7 MHz) had signals at 179.9 s, 170.7 s, 170.0 s, 87.3 d, 74.1 d, 72.8 d, 55.5 q, 52.2 d, 49.2 s, 48.4 d, 44.6 d, 43.3 d, 35.4 t, 34.7 s, 32.8 d, 31.6 t, 27.5 t, 26.4 t, 26.0 q, 25.1 t, 23.7 t, 21.7 q, 21.5 q, 19.8 q, and 12.3 q ppm. Anal. calcd. for $C_{26}H_{41}NO_6$: C 67.36, H 8.91, N 3.02; found: C 67.18, H 9.03, N 3.16.

12-Aza-3α,20β-diacetoxy-12a-hydroxy-C-homo-5β-pregnan-11-one ***12***

Polar eluate from alumina of the products of photolysis of **9** in dichloromethane crystallized in part from ether as prisms. These melted partly around 140°C, resolidified, and melted at 207°C. The crystals had ν_{max} 3520, 3405, 1730, and 1680 cm^{-1} and gave ^1H nmr signals (400 MHz) at δ6.73(NH), 4.92 (1H, m), 4.75 (1H, m), 4.55 (1H, d, J = 3 Hz), 2.60(1H, d, J = 4 Hz, OH), 2.10(3H, s), 2.02(3H, s), 1.30(3H, s), 1.18(3H, d, J = 6 Hz), and 1.07(3H, s). Its ^{13}C nmr spectrum gave signals at 176.3, 170.6, 169.8, 74.8, 74.0, 72.7, 60.9, 59.6, 55.5, 42.6, 41.4, 35.9, 35.7, 32.0, 31.5, 26.7, 26.67, 26.3, 26.1, 23.2, 21.42, 21.41, 19.5, and 15.9 ppm (24 signals; 25 expected).

Acid-catalysed reactions of N-acyl imine ***10***

(*a*) A solution of 21 mg of **10** in 15 mL of dry methanol, containing 5 mg of *p*-toluenesulfonic acid hydrate, was left at room temperature for 1 h. The mixture was neutralized using sodium bicarbonate, then the solvent removed *in vacuo*. The residue was extracted with dichloromethane, the organic layer washed with water, dried, then distilled. The crystalline residue was recrystallized from acetone–hexane giving 18 mg of prisms, mp 206–208°C. This was identical (mixture mp, spectra) to carbinolamide ether **11**.

(*b*) A suspension of 0.5 mL of Rexyn 101 (H^+) beads in 5 mL of methanol containing 10 mg of *N*-acyl imine **10** was stirred at room temperature for 5 min. The resin was removed by filtration, then the methanol evaporated, giving 9.5 mg of carbinolamide ether **11**, pure by ir and tlc.

(*c*) Eighty-six milligrams of *N*-acyl imine **10** was dissolved in 5 mL of dioxane and 1 mL of water. After addition of ca. 0.3 mL of Rexyn 101(H^+) beads the mixture was stirred for 20 min, the Rexyn was removed by filtration, then the solvents removed under reduced pressure. The residue showed one spot on tlc and had ν_{max} 3520, 3405, 1730, and 1680 cm^{-1} consistent with carbinolamide structure **12**. This was converted to carbinolamide ether **11** by stirring overnight with Rexyn 101 (H^+) in methanol.

Action of acidic methanol on crude carbinolamide ***12***

The amorphous polar product from photolysis (*a*) above (347 mg) was dissolved in anhydrous methanol (30 mL) containing 15 mg of *p*-toluenesulfonic acid. After 1 h the mixture was worked up as for experiment (*a*). The product gave 195 mg of crystalline carbinolamide ether **11** after chromatography on Activity IV alumina and crystallization from acetone–hexane (14% yield based on azide photolyzed).

12-Aza-3α,20β-diacetoxy-C-homo-5β-pregnan-11-one ***13***

(*a*) Lithium aluminum hydride (300 mg) was added to a solution of 93 mg of carbinolamide ether **11** (R^1 = R^2 = Ac) in 20 mL of dry ether. The mixture was heated under gentle reflux for 20 h, then the excess hydride destroyed using wet ether. The crude product recovered from the ether (80 mg) was acetylated overnight in 1:1 pyridine – acetic anhydride. The product was adsorbed from benzene onto 2 g of neutral alumina (Act. IV). Benzene (25 mL) eluted a mixture of four products, followed (100 mL) by 40 mg of homogeneous product. This did not crystallize readily, so was distilled at 180°C under 1×10^{-4} Torr. The colorless glass had $[\alpha]_D$ 49 (*c* 0.25, in 95% ethanol) and ν_{max} 3230, 1740, 1670, and 1250 cm^{-1}. Its ^1H nmr spectrum had signals at δ6.16(NH), 4.75(2H multiplet), 3.7–2.9(2H broad), 2.03(6H, s), 1.37(3H, s), 1.17(3H, d, J = 6 Hz), and 0.61(3H, s). The broad bands between 3.7 and 2.9 collapsed to a pair of doublets centered at δ3.3 with ΔAB = 27 Hz, J_{AB} = 15 Hz after treatment with a trace of *p*-toluenesulfonic acid in D_2O. Anal. calcd. for $C_{25}H_{39}NO_5$: C 69.25, H 9.07, N 3.23; found: C 69.39, H 9.16, N 3.30.

(*b*) Ninety-five milligrams of *N*-acyl imine **10** in 10 mL of 95% ethanol containing 111 mg of 5% palladium-on-charcoal was stirred in a hydrogen atmosphere for 4 h. The catalyst was removed and the solvent evaporated. Purification as in (*a*) gave 80 mg of a glass identical by ir and tlc with the product from the lithium aluminum hydride reduction of **11** followed by acetylation.

*Deacetylation of 12-aza-3α,20β-diacetoxy-12a-methoxy-C-homo-5β-pregnan-11-one (***11***) (R^1 = R^2 = Ac)*

To a solution of 30 mg of diacetoxy-methoxy lactam **11** in 1 mL of methanol was added a solution of sodium methoxide (from 25 mg of sodium) in 2 mL of dry methanol. The mixture was stirred at room temperature for 30 min, then the solvent evaporated *in vacuo* below room temperature. The products were distributed between water and chloroform. The dried chloroform layer was

Can. J. Chem. Downloaded from www.nrcresearchpress.com by 109.225.110.28 on 09/08/12
For personal use only.

distilled then the residue allowed to crystallize from an ethyl acetate – hexane mixture. The material in the mother liquor was separated on a 0.5 mm silica gel plate using 10% methanol in chloroform. The zone with R_f 0.7 proved identical to the above crystals, and was identified as the 3-hydroxy-20-acetoxy-12a-methoxy lactam **11** (R^1 = H, R^2 = Ac) (22 mg total, 80%). The other major zone (R_f 0.3) contained the dihydroxy-methoxy lactam **11** (R^1 = R^2 = H) (5 mg, 20%). Comparable conditions, but 24 h reaction, effected complete hydrolysis to the diol **11** (R^1 = R^2 = H).

*Action of sodium methoxide in methanol on N-acyl imine **10***

N-Acyl imine **10** was dissolved in 10 mL of methanol and 1 mL of 1 M sodium methoxide in methanol. After 48 h tlc showed the reaction to be complete. Evaporation of the solvent and extraction of the residue with dichloromethane gave 73 mg of organic product. Trituration of this with ether left 66 mg (87%) of dihydroxy-methoxy lactam identical to the diol **11** (R^1 = R^2 = H) produced from deacetylation of **11** (R^1 = R^2 = Ac).

*20-Acetoxy-12-aza-3α-hydroxy-12a-methoxy-C-homo-5β-pregnan-11-one **11** (R^1 = H, R^2 = Ac)*

This crystallized from ethyl acetate – hexane as needles, mp 134–137 or 175–180°C. It had ν_{max} 3595, 3385, 1726, and 1665 cm^{-1}. Its ^1H nmr spectrum (500 MHz) had signals at δ5.82(1H, d, J = 6.1 Hz), 4.76(1H, m), 4.13(1H, d, J = 6.2 Hz), 3.63(1H, m), 3.40(3H, s), 2.92(1H, d, J = 11.4 Hz), 2.22(1H, q, J_1 = 20 Hz, J_2 = 10 Hz), 2.00(3H, s), 1.28(3H, s), 1.13(3H, d, J = 6.0 Hz), and 0.63(3H, s). A ^1H–^1H COSY spectrum showed the proton at δ4.76 to be coupled to the methyl doublet at δ1.13 and the proton (H-17) at δ2.22. A second weak set of signals indicated the presence of another isomer, presumably the 12aβ-methoxy compound. (see ref. 5 for evidence on the stereochemistry.)

*12-Aza-3α,20β-dihydroxy-12a-methoxy-C-homo-5β-pregnan-11-one (**11**, R^1 = R^2 = H)*

This was not obtained crystalline. It had ν_{max} ($CHCl_3$) 3600, 3400, and 1660 cm^{-1} and gave ^1H nmr signals at δ5.9(1H, d, J = 6 Hz) (NH), 4.8(1H, d, J = 6 Hz), 3.7(2H, m), 3.45(3H, s), 3.01(1H, d, J = 11 Hz), 1.33(3H, s), 1.15(3H, d, J = 6 Hz), and 0.75(3H, s).

*Hydrolysis of 12α-azido-3α,20β-diacetoxy-5β-pregnan-11-one (**9**)*

A solution of sodium methoxide prepared from 60 mg of sodium and 2 mL of dry methanol was added to a stirred suspension of 194 mg of diacetoxy azide **9** (R^1 = R^2 = Ac) in 4 mL of methanol. The azide dissolved within 5 min at room temperature. After 2 h the solution was concentrated to a syrup *in vacuo* below room temperature. Water and chloroform were added. The dried chloroform extracts yielded 190 mg of froth, which according to its ^1H nmr spectrum was mainly the monoacetate **15** (R^1 = H, R^2 = Ac). This was adsorbed from benzene onto 6 g of neutral alumina (Act. IV). Benzene and dichloromethane eluted the monoacetate (110 mg, 62%). The azido diol **15** (R^1 = R^2 = H) (60 mg, 41%) and minor polar impurities were eluted with 10% methanol in chloroform. Hydrolysis of **9** as above, but for 20 h, gave complete conversion to **15** (R^1 = R^2 = H).

*20β-Acetoxy-12α-azido-3α-hydroxy-5β-pregnan-11-one (**15**, R^1 = H, R^2 = Ac)*

The monoacetate crystallized from acetone–hexane as prisms, mp 163–164°C. It gave ν_{max} 3590, 2100, and 1727 cm^{-1} and ^1H nmr signals (500 MHz) at δ4.74(1H, br m), 3.61(1H, m), 3.58(1H, s), 2.84(1H, d, J = 11.2 Hz), 2.37(1H, dt, J_1 = 14.4, J_2 = 3.4 Hz), 2.22(1H, q, J_1 = 20, J_2 = 10 Hz), 2.03(3H, s), 1.17(3H, d, J = 6 Hz), 1.13(3H, s), and 0.60(3H, s). Irradiation at δ4.74 decoupled the methyl doublet at δ1.17 and partially collapsed the signals at δ2.22.

*12α-Azido-3α,20β-dihydroxy-5β-pregnan-11-one (**15**, R^1 = R^2 = H)*

An ethyl acetate – hexane solution of the diol (160 mg) deposited 25 mg of fine needles, mp 196–225°C. The remainder eventually crystallized from solvent mixtures richer in hexane as prisms, or as short rods, mp 167–169°C. This had ν_{max} 3590, 3450, 2100, and 1709 cm^{-1} and gave ^1H nmr signals (200 MHz) at δ4.05(1H, s), 3.67(2H, m), 2.87(1H, d, J = 11 Hz), 2.43(1H, dt, J_1 = 14.2, J_2 = 3.1 Hz), 1.19(3H, d, J = 6.2 Hz), 1.17(3H, s), and 0.72(3H, s).

The minor higher-melting product was shown by its ^1H nmr spectrum to be a mixture of the major azido diol with an isomer. The mixture had ν_{max} 3590, 3400, 2100, and 1707 cm^{-1} and its ^1H nmr spectrum had signals at δ4.50(s) and 0.89(s) in addition to those for the 169° azidodiol.

*Irradiation of 20β-acetoxy-12α-azido-3α-hydroxy-5β-pregnan-11-one **15** (R^1 = H, R^2 = Ac)*

A solution of 53 mg of the 12-azido monoacetate **15** (R^1 = H, R^2 = Ac) and 0.1 mL of triethylamine in dry dichloromethane was irradiated in a Vycor vessel at 10°C using Rayonet 300 nm lamps for 1 h. An infrared spectrum showed that all the azide had been transformed. The solvent and amine were removed *in vacuo*, finally under 0.1 Torr. The residue was suspended in dry ether, then filtered. Approximately 8 mg of triethylamine hydrochloride was removed. The yellow filtrate was evaporated and the residue freed of volatile material at 60°C under 0.1 Torr. Its nmr spectra (500 MHz) showed that a major component was the *N*-acyl imine **16** (R^1 = H, R^2 = Ac) (δ7.93; 190.1, 168.8 ppm), and a minor one had signals consistent with it being the keto imine **14** (R^1 = H) (δ7.53; 207.6 or 206.7, 160.9 ppm) (ratio 5:1). Traces of aldehydes (δ9.64 and 9.63) were present. The product was adsorbed from benzene onto a 20-fold ratio of neutral alumina (Act. IV). Benzene, then dichloromethane eluted 37 mg, which crystallized from ether–hexane mixtures, giving 30 mg of nearly pure *N*-acyl imine **16** (R^1 = H, R^2 = Ac) (56%).

*20β-Acetoxy-12-aza-3α-hydroxy-C-homo-5β-pregn-12-en-11-one **16** (R^1 = H, R^2 = Ac)*

Crystals of **16** (R^1 = H, R^2 = Ac) melted at 185°C in an evacuated capillary (immersed at 170°C) but did not become completely liquid until 220°C. It had ν_{max} 3595, 1730, 1702, and 1695 cm^{-1} and ^1H nmr (400 MHz) signals at δ7.93(1H, s), 4.78(1H, m), 3.64(1H, m), 2.03(3H, s), 1.37(3H, s), 1.22(3H, d, J = 6.05 Hz), and 0.90(3H, s). Its ^{13}C nmr spectrum (100.6 MHz) had signals at 190.1, 170.1, 168.8, 72.3, 72.1, 52.8, 52.0, 50.4, 46.6, 42.3, 38.4, 35.7, 35.3, 34.2, 31.1, 27.7, 27.5, 26.2, 24.4, 23.2, 21.2, 19.5, and 12.1 ppm. Its EI mass spectrum had m/z 389.2559 (M^+); calcd. for $C_{25}H_{35}NO_4$: m/z 389.2566.

*Irradiation of 12α-azido-3α,20β-dihydroxy-5β-pregnan-11-one **15** (R^1 = R^2 = H)*

(*a*) A solution of 79 mg of **15** (R^1, = R^2, = H) in 30 mL of dry dichloromethane was irradiated at 5°C in a Vycor vessel using a Rayonet photoreactor with light peaked at 300 nm. After 1 h no azide was left. The solution was evaporated below room temperature, leaving a white solid residue. This gave a milky suspension in acid-free deuteriochloroform. This was filtered through sintered glass under pressure. The fairly clear filtrate gave a ^1H nmr singlet at δ7.52. Its ^{13}C nmr spectrum had signals at 208.0, 205.1, 176.0, and 160.8. Thus no *N*-acyl imine seems to have survived (expected δ7.9 and 190 ppm). The signals are consistent with the presence of **14** (R^1 = H, 20-hydroxy).

(*b*) Irradiation of 132 mg of **15** (R^1 = R^2 = H) in 100 mL of dichloromethane containing 0.1 mL of triethylamine using a 100-W high-pressure Hanovia mercury lamp in a Pyrex well at −20 to −30°C required 7 h for complete reaction of the azide. After evaporation of solvent the residue was treated with Rexyn 101 (H^+) in methanol for 25 min. From the products a 56% yield of pure methyl ether **11** (R^1 = R^2 = H) was obtained after purification on

a silica gel plate (1:1 chloroform–acetone). It was identical (tlc and ^{1}H nmr to that produced by hydrolysis of **11** ($R^1 = R^2 = Ac$).

Acknowledgements

We thank H. Seguin for analyses, Dr. I. C. P. Smith and associates, Dr. B. Blackwell and K. Bourque, for nmr spectra, the Ottawa–Carleton Mass Spectrometry Center for the mass spectra, and K. Denike for the drawings. We are grateful to Prof. J. W. ApSimon for the opportunity to finish this work at Carleton University.

1. W. A. Court, O. E. Edwards, C. Grieco, W. Rank, and T. Sano. Can. J. Chem. **53**, 463 (1975).
2. B. W. Bycroft. Nature, **224**, 595 (1969); *In* Comprehensive organic chemistry. Vol. 5. *Edited by* D. H. R. Barton and W. D. Ollis. Pergamon Press, New York. 1979. pp. 241–287; J. D. M. Herscheid, R. J. Nivard, M. W. Tijhaus, and H. C. J. Ottenheijm. J. Org. Chem. **45**, 1885 (1980).
3. A. Lupulescu. Hormonal treatment of cancer. C.R.C. Press, Inc., Boca Raton, Fla. 1990; I.M.C. Niculescu-Duvaz, I. Baracu, and A. T. Balaban. *In* Chemistry of antitumor agents. *Edited by* D. E. Wilman. Blackie, London. 1989. pp. 63–123; M. Colvin and B. A. Chabner. *In* Cancer chemotherapy. *Edited by* B. A. Chabner and J. M. Collins. J. B. Lippencott, Philadelphia, Pa. 1990. pp. 276–313.
4. D. H. R. Barton and A. N. Starratt. J. Chem. Soc. 2444 (1965).
5. O. E. Edwards and T. Sano. Can. J. Chem. **47**, 3489 (1969).
6. G. I. Poos, C. E. Arth, and L. H. Sarett. J. Am. Chem. Soc. **75**, 422 (1953).
7. E. J. Corey and J. W. Suggs. Tetrahedron. Lett. 2647 (1975).
8. R. J. Baker, L. M. Trefonas, and R. J. Majeste. Cryst. Struct. Commun. **11**, 485 (1982).
9. O. E. Edwards and W. Rank. Can. J. Chem. **68**, 1425 (1990).
10. P. Margaretha and H. Steffen. Chimia, **27**, 479 (1973).
11. R. M. Moriarty, J. M. Kliegman, and C. Shovlin. J. Am. Chem. Soc. **89**, 5958 (1967).
12. R. M. Moriarty and P. Serridge. J. Am. Chem. Soc. **93**, 1534 (1971).
13. J. S. Millership and H. Suschitzky. Chem. Commun. 1496 (1971).
14. H. W. Moore and D. S. Pearce. Tetrahedron Lett. 1621 (1971); G. Landen and H. W. Moore. Tetrahedron Lett. 2513 (1976).
15. W. Ogilvie and W. Rank. Can. J. Chem. **65**, 166 (1987).
16. T. G. Back and K. Brunner. J. Org. Chem. **54**, 1904 (1989); T. G. Back, N. Ibrahim, and D. J. McPhee. J. Org. Chem. **47**, 3283 (1983); T. G. Back, J. H.-L. Chau, B. P. Dyck, and P. L. Gladstone. Can. J. Chem. **69**, 1482 (1991).
17. K. Tsuda and R. Hayatsu. J. Am. Chem. Soc. **78**, 4107 (1956).
18. K. Bowden, I. M. Heilbron, E. R. H. Jones, and B. C. L. Weedon. J. Chem. Soc. 39 (1946).

Can. J. Chem. Downloaded from www.nrcresearchpress.com by 109.225.110.28 on 09/08/12
For personal use only.

Identification of the tautomeric structure of H_2TMpyP4–DNA complexes from resonance Raman excitation profiles

LIU YIXIAN[1] AND J. A. KONINGSTEIN[2]

Department of Chemistry, The Ottawa–Carleton Chemistry Institute, Carleton University, Ottawa, Ont., Canada K1S 5B6

AND

Y. YEVDOKIMOV

Institute of Molecular Biology, Academy of Sciences of the U.S.S.R., Ul. Vavilov 32, Moscow, Russia

Received March 16, 1992

LIU YIXIAN, J. A. KONINGSTEIN, and Y. YEVDOKIMOV. Can. J. Chem. **70**, 2413 (1992).

Aspects of the electronic structure of tautomers of tetrakis(*N*-methyl-4-pyridyl)porphyrin (H_2TMpyP4) complexed to DNA have been determined from a study of the resonance Raman excitation profiles of normal modes of H_2TMpyP4 in buffer solutions containing monomeric and aggregated molecules and of a H_2TMpyP4/DNA complex with $r(c) \sim 25$. Maxima of the excitation profiles of the complex have been assigned to electronic origins for transitions between the ground state and states in the Soret absorption region of intercalated and externally groove-bound tautomers of H_2TMpyP4. The positions of the electronic origins support the assignment of the CD spectrum of the complex. From the shift of the C_β—H bending mode of the selectively excited resonance Raman spectra of tautomers of the porphyrin molecules it can be concluded that the pyridyl rings of externally bound H_2TMpyP4 molecules are twisted to a lesser degree than those rings for intercalated H_2TMpyP4. Raman intensity studies also reveal that the resonance-enhanced Raman intensity of modes of aggregated H_2TMpyP4 is greater than those of the monomer.

LIU YIXIAN, J. A. KONINGSTEIN et Y. YEVDOKIMOV. Can. J. Chem. **70**, 2413 (1992).

En se basant sur une étude des profils d'excitation de la résonance Raman des modes normaux du H_2TMpyP4, dans des solutions tamponnées contenant des molécules monomères et agrégées, et d'un complexe H_2TMpyP4/ADN avec $r(c) \sim 25$, on a déterminé les aspects de la structure électronique des tautomères de la tétrakis(*N*-méthyl-4-pyridyl)porphyrine (H_2TMpyP4) complexée avec l'ADN. On a attribué les maxima des profils d'excitation du complexe aux origines électroniques de la transition entre l'état fondamental et les états de la région d'absorption de Soret des tautomères de la H_2TMpyP4 intercalés et liés d'une façon externe. Les positions des origines électroniques sont en accord avec l'attribution du spectre CD du complexe. En se basant sur le déplacement du mode de déformation de la liaison C_β—H du spectre d'excitation de la résonance Raman des molécules de porphyrine, on peut conclure que les cycles pyridyles des molécules de H_2TMpyP4 liées d'une façon externe sont moins déformés que ceux des cycles correspondants des molécules de H_2TMpyP4 intercalées. Les études menées sur les intensités du spectre Raman révèlent aussi que l'intensité des spectres Raman rehaussés par la résonance est plus grande pour les modes des molécules de H_2TMpyP4 agrégées que pour ceux des monomères.

[Traduit par la rédaction]

Introduction

It is well known that the two inner hydrogen atoms (the NH protons) in free-base porphyrins exhibit tautomerization that results in protons being attached to different pairs of nitrogen atoms of the core. In symmetrical as opposed to asymmetrical porphyrins (1–4), the NH tautomers cannot be distinguished and have identical electronic spectra (1). The rate of tautomerization depends mainly on temperature and (or) whether the molecule resides in the ground state or an electronically excited state (1–3).

In this work we discuss the results of a resonance Raman study of the compound tetrakis(*N*-methyl-4-pyridyl)porphyrin (H_2TMpyP4). The structure of this symmetrical porphyrin molecule is different from the free-base porphyrin molecule in that four methylpyridyl groups are attached to diagonally opposed pyrrole rings, see Fig. 1. If dissolved in buffer solutions that contain DNA, complexes can be formed between the H_2TMpyP4 molecule and the large biological molecule. Depending on the concentration, porphyrin molecules intercalate and also become externally groove-bound to the double helix. The intercalated and groove-bound complexes have been extensively studied using various spectroscopic methods such as fluorescence (5, 6), circular dichroism (7, 8), linear dichroism (9), NMR (10), and resonance Raman spectroscopy (11–13). The H_2TMpyP4/DNA complexes are described by the $r(c)$ number, i.e., the concentration of base pairs of DNA relative to the total concentration of H_2TMpyP4.

According to the literature (6), the porphyrin molecule intercalates with DNA for $r(c) > 7000$; with a decrease in $r(c)$, porphyrins become externally groove-bound instead and an equilibrium distribution over the two sites occurs for $r(c) < 200$. Resonance Raman excitation profiles (RRP) of Raman bands in the electronic ground state give valuable information on the excited states of molecules. We have obtained RRP's of modes of H_2TMpyP4/DNA complexes that enable us to comment on the electronic states of tautomers for intercalated and externally bound porphyrin molecules.

Experimental

Instrumental

RRP's at a resolution of 1 nm were recorded using a Jobin–Yvon double monochromator for buffer solutions of H_2TMpyP4 and of H_2TMpyP4 with B-form DNA. The Raman spectra were excited with 7-ns pulses from a tunable dye laser (Lumonics model

[1]Visiting Scientist.

[2]Author to whom correspondence may be addressed.

Can. J. Chem. Downloaded from www.nrcresearchpress.com by 109.225.110.28 on 09/08/12
For personal use only.

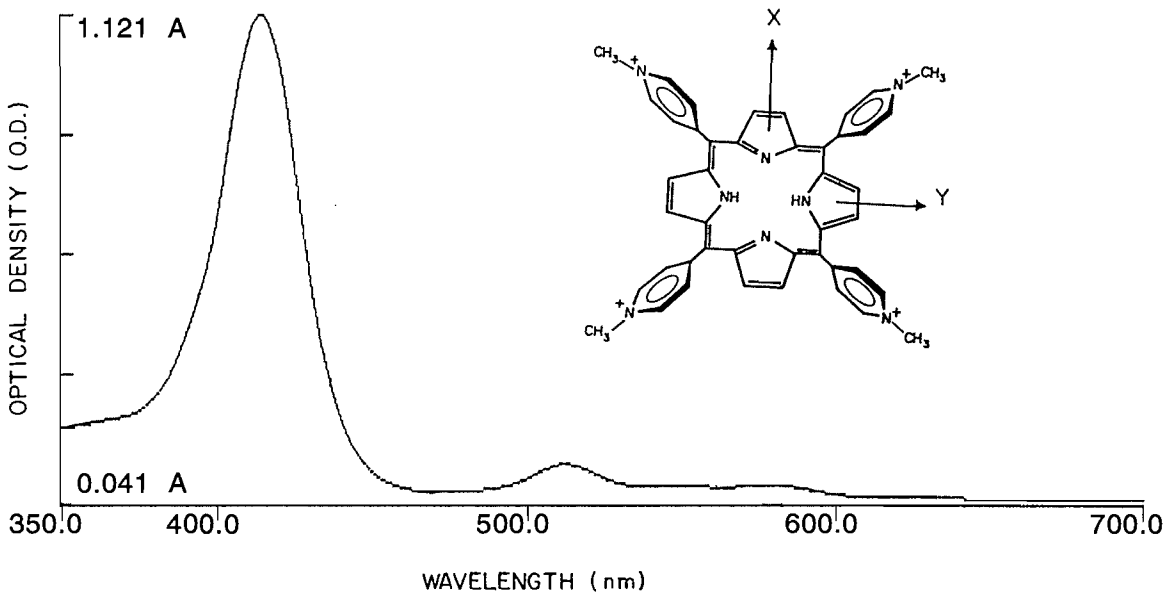

FIG. 1. Visible absorption spectrum of $H_2TMpyP4$ ($c = 1.5 \times 10^{-5}$ M) in buffer solution, and its chemical structure.

HYperDYE-300), which was pumped by an excimer laser (Lumonics model TE-430) operating at 25 Hz with a typical output of 4–7 mW. This radiation was used both focussed and unfocussed on the sample cell and the scattered light was observed at a 90° angle (4–7 cm^{-1} slit widths). Signals emerging from the exit slit of the monochromator were detected with a cooled RCA 31034 A photomultiplier tube (PMT). The output of the PMT was processed by a boxcar operating with a 3-ns gate (Stanford Research Associates models SR 250, 235, 275, and 245) and spectra were either recorded or stored in a computer.

Sample handling

Raman spectra were obtained from solutions that were prepared from a stock buffer solution containing $H_2TMpyP4$ and another stock solution of B-form DNA isolated from chicken blood erythrocytes (OD = 1.0 at 256 nm). The buffer solution (pH = 7) contained 0.01 M sodium phosphate, 0.3 M NaCl, and 1.47×10^{-3} M $H_2TMpyP4$. Fresh samples were prepared for each measurement and spectra were taken from solutions in air-tight cells. Spectroscopic data were obtained from monomeric as well as aggregated $H_2TMpyP4$ in solution and of $H_2TMpyP4$/DNA complexes with $r(c) \sim 25$. Earlier experiments (6)[3] for complexes in solutions with $r(c) \sim 25$ indicate that in addition to being intercalated or externally bound, a small amount of porphyrin remains in solution. However, the concentration of these free molecules is too small to be detected in the Raman spectra discussed below. All of the experiments were carried out at room temperature (20°C).

Results and discussion

Spectral aspects of $H_2TMpyP4$ in solution

The chemical structure and the absorption spectrum of $H_2TMpyP4$ in the visible spectral region is shown in Fig. 1. The molecule has D_{2h} symmetry and the planar aromatic structure enables the molecule to intercalate between adjacent base pairs of double-stranded nucleic acids without inducing major distortions to the B-form DNA. The principal absorption bands (9) of $H_2TMpyP4$ in the buffer solution are at 420 nm (Soret), 520 nm ($Q(y)$), and 580 nm ($Q(x)$). The fluorescence spectrum of the compound shows a rather broad band centered around 690 nm. The fluorescence lifetime $\tau(f)$ for $H_2TMpyP4$ in a buffer solution is ~5 ns and the rotational correlation time, $\tau(r)$, equals ~300 ps.[3] If excited with radiation of a laser tuned to the wavelength of the Soret band, the Raman spectrum of water as well as that of the porphyrin with shifts <1700 cm^{-1} is free from interference of the red fluorescence. The intensity of the Raman shift of water at ~3500 cm^{-1} is used as an internal standard to obtain the RRP of the porphyrin molecule in the ground state. Part of the Raman spectrum between 950 and 1700 cm^{-1} is shown in Fig. 2 while the assignment of the bands (13) is given in Table 1.

In our experiments, Raman spectra are obtained from 10^{-5} M solutions using pulsed radiation (7 ns duration, 25 Hz) from an excimer-pumped dye laser tuned to the Soret band. For a power level of 3 mW, the light source delivers 10^{13} photons/pulse to 10^{15} molecules in the irradiated volume (diameter of laser is 4 mm, length L of laser path is 1 cm). Thus, for an unfocussed laser beam, there are more molecules than photons. However, the number of molecules decreases to 3×10^{11} if the laser is focussed with a 10-cm lens and we find that the number of photons per pulse of 7 ns exceeds the number of molecules by a factor of 30. Therefore, once these photons are absorbed, then effective population saturation (via ground-state bleaching) of an excited state with a lifetime of >230 ps could take place. The effect of ground-state bleaching is to reduce the intensity of ground-state Raman scattering and as a result changes are expected in the contour of the RRP. These changes are expected to be most pronounced if the laser is tuned to the maximum of the Soret absorption band.

Figure 3*a* shows the RRP (unfocussed radiation) for a Raman band of $H_2TMpyP4$ at 1251 cm^{-1} together with the contour of the Soret absorption band. The Raman intensities are linear in laser intensity, yet if the laser beam is focussed in the solution with a 10-cm cylinder lens, a decrease is observed, see Fig. 3*b*, in the intensity of the Raman band for exciting radiation tuned to the region of 421–425 nm. The decrease is caused by the onset of ground-state bleaching.

[3]Shen Yizhong, P. Myslinski, Teresa Treszczanowicz, Liu Yixian, and J. A. Koningstein. Manuscript in preparation.

Can. J. Chem. Downloaded from www.nrcresearchpress.com by 109.225.110.28 on 09/08/12
For personal use only.

Can. J. Chem. Downloaded from www.nrcresearchpress.com by 109.225.110.28 on 09/08/12
For personal use only.

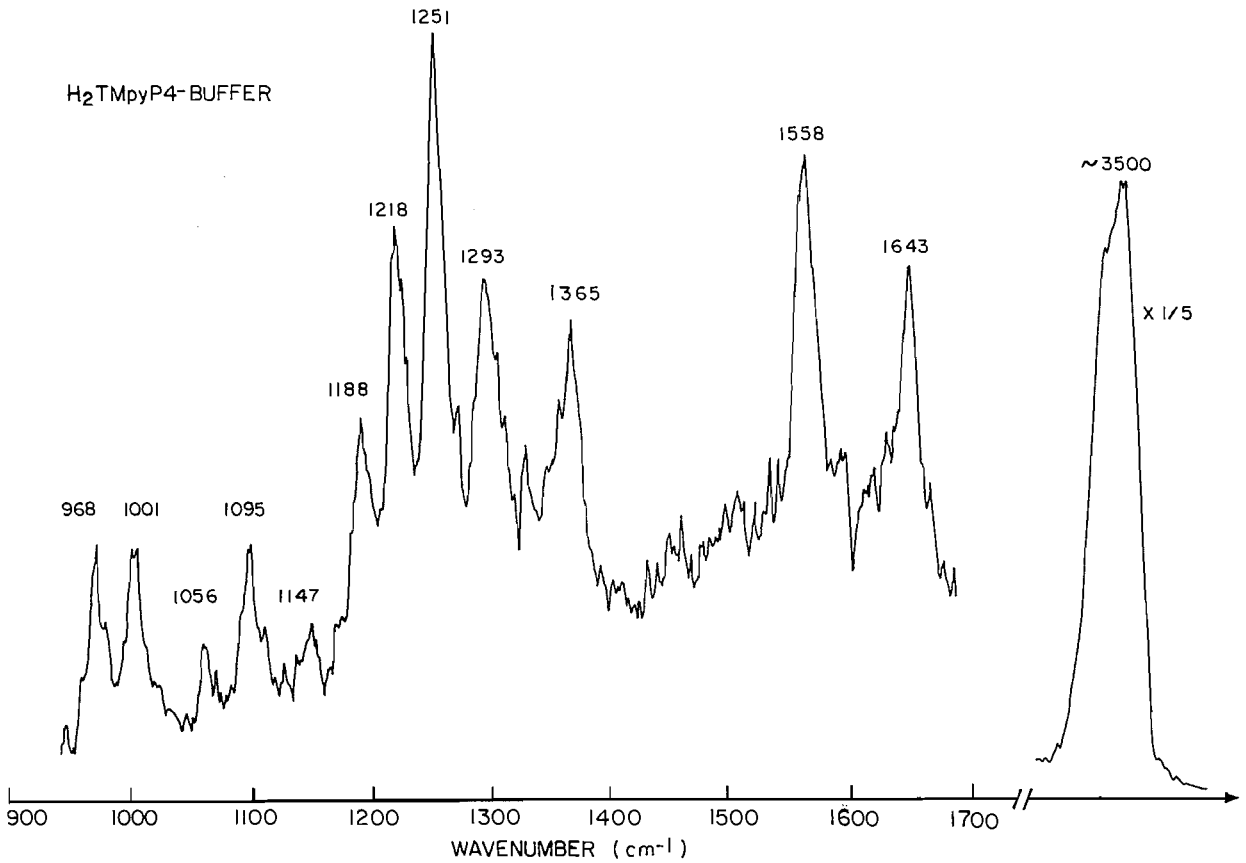

FIG. 2. Resonance Raman spectra of $H_2TMpyP4$ in buffer solution with concentration of 1.5×10^{-5} M, excitation wavelength 420 nm. Also shown is the intensity of the internal standard (water).

TABLE 1. Assignment[a] of part of the Raman spectrum of H_2TMpyP_4

Shift (cm^{-1})	Assignment
968 m	A_{1g} (in D_{4h})
1001 m	ν_2 (C_α—C_m), A_{1g}
1056 w	pyr δ (C—H), A_{1g}
1095 m	δ_2 (C_β—H), A_{1g}
1188 m	δ (pyr), ν (N^+—CH_3), A_{1g}
1218 s	δ (pyr), A_{1g}
1251 vs	δ (C_m—pyr), A_{1g}
1293 s	δ (pyr), A_{1g}
1365 s	ν_s (C_α—N), A_{1g}
1558 vs	ν (C_β—C_β), A_{1g}
1643 vs	δ (pyr), A_{1g}

[a]See ref. 13.

If unfocussed laser radiation is used, bleaching does not occur and the contour of the RRP follows that of the Soret absorption band. With an increase in the concentration of the porphyrin molecule in the buffer solution, aggregates are formed (6). This is seen by comparing the absorption spectrum of the 3×10^{-5} M solution shown in Fig. 4 with that of the less concentrated solution in Fig. 3. The Soret band is broader and the center of the band is shifted from 415 to 420 nm. The RRP (unfocussed laser radiation) between 420 and 440 nm for the more concentrated solution is shown in Fig. 4. When Fig. 4 is compared to Fig. 3 for monomeric porphyrin, the

TABLE 2. Assignment of part of the fluorescence spectrum, RRP, and absorption spectrum of $H_2TMpyP4$/DNA

Absorptions (nm)	Fluorescence (nm)	Assignment[a]
419	—	0–0 tautomer 1
423		Soret ext
427	—	0–0 tautomer 2
434	—	0–0 tautomer 1
437		Soret int
441	—	0–0 tautomer 2
523		Q_y : 0–2 both tautomers int and ext
565		Q_y : 0–1 both tautomers int and ext
600		Q_x : 0–2 both tautomers int and ext
635		Q_x : 0–1 both tautomers int and ext
	654	Q_x : 1–0 both tautomers int
	667	Q_x : 1–0 both tautomers ext
	715	Q_x : 2–0 both tautomers int
	725	Q_x : 2–0 both tautomers ext

[a]Abbreviations: int = intercalated; ext = external bound $H_2TMpyP4$.

Can. J. Chem. Downloaded from www.nrcresearchpress.com by 109.225.110.28 on 09/08/12
For personal use only.

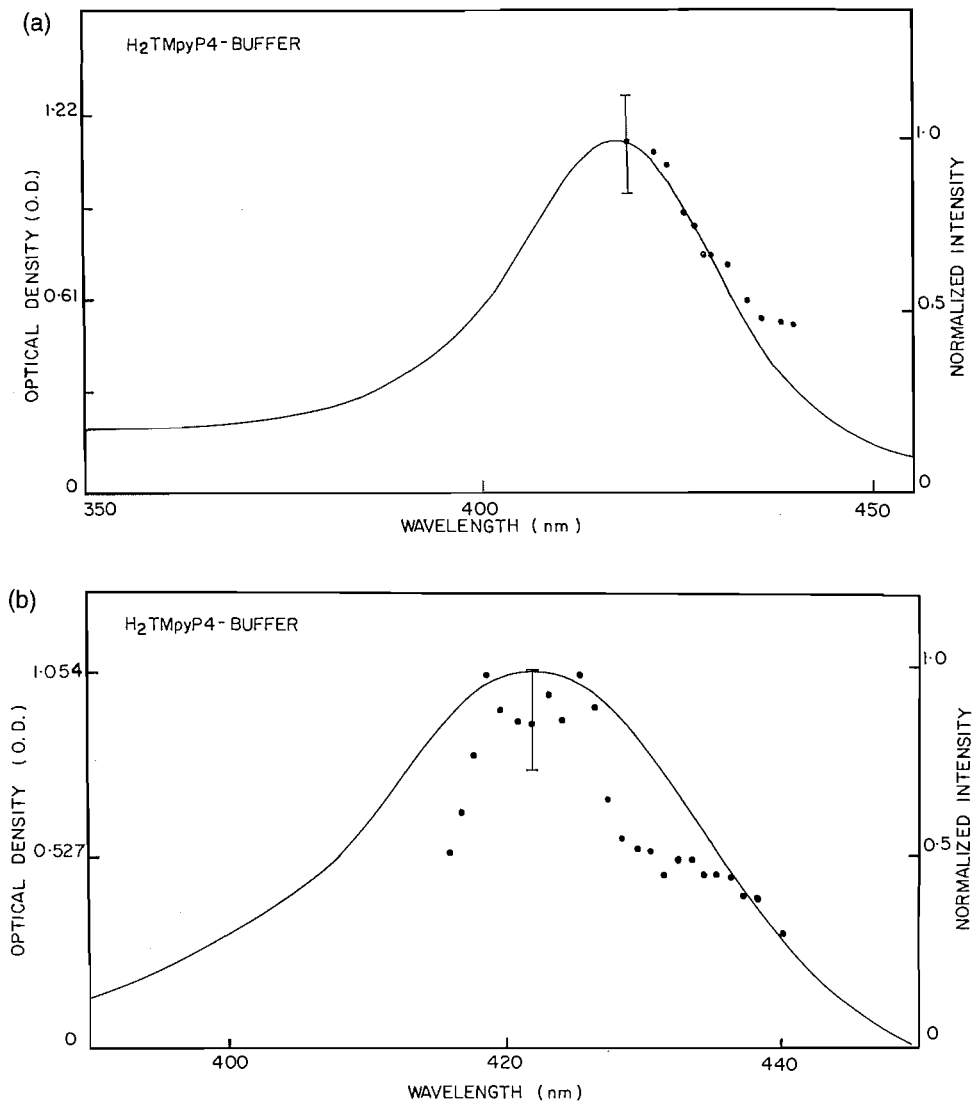

FIG. 3. (*a*) The resonance Raman excitation profile (dots) for the intensity of the shift at 1251 cm^{-1} for monomeric $H_2TMpyP4$ in buffer solution with concentration of 1.5×10^{-5} M in comparison to that of the contour of the Soret band. The data points are normalized at 420 nm, laser beam not focussed. (*b*) RRP for the intensity of the 1251 cm^{-1} band of monomeric $H_2TMpyP4$ in buffer solution with concentration of 1.5×10^{-5} M. Also shown is the absorption spectrum in the Soret band. A cylinder lens with $f = 10$ cm is used to excite the Raman spectra.

RRP is seen to be shifted to 431 nm. Within the spectral interval over which the RRP could be determined, no evidence is found for a maximum in the profile at 415 nm (for monomeric $H_2TMpyP4$). Thus we assign the enhancement of the intensity for excitation between 420 and 440 nm to resonance Raman scattering of aggregated porphyrin molecules in the buffer solution and conclude that the intrinsic intensity of Raman bands of the aggregate is greater than that of the monomeric $H_2TMpyP4$. The RRP does not indicate the presence of multiple maxima in case of a different electronic structure of the $H_2TMpyP4$ tautomers of the aggregate.

RRP and tautomeric structure of $H_2TMpyP4$/DNA complexes

The CD spectrum of a $H_2TMpyP4$/DNA complex with $r(c) \sim 10$ is shown in Fig. 5. As is well known (7, 8), the positive signal, which peaks at ~425 nm, is caused by porphyrin molecules that are externally groove-bound and the negative signal at ~431 nm is associated with the intercalated molecule. Figure 5 shows that the positive as well as the negative CD signals have side bands at 426 and 445 nm respectively. Compared to monomeric porphyrins, the broadened Soret band of the $H_2TMpyP4$/DNA complex is centered around 431 nm.

If excited with blue light, fluorescence from the complex is observed between 600 and 780 nm (5, 6). Time-resolved spectroscopy reveals (6, and footnote 3) that the emission is composed of contributions from both intercalated porphyrins peaking at 654 and 718 nm and externally bound porphyrins with bands at 667 and 725 nm for $r(c) > 50$, the fluorescence decay times being 10.0 ± 0.5 ns and 1.7 ± 0.2 ns, respectively. Preferential excitation of the fluorescence spectrum of intercalated porphyrins occurs if the laser radiation is tuned to 440 nm, while the emission of externally bound $H_2TMpyP4$ is stronger for radiation tuned to 415 nm.

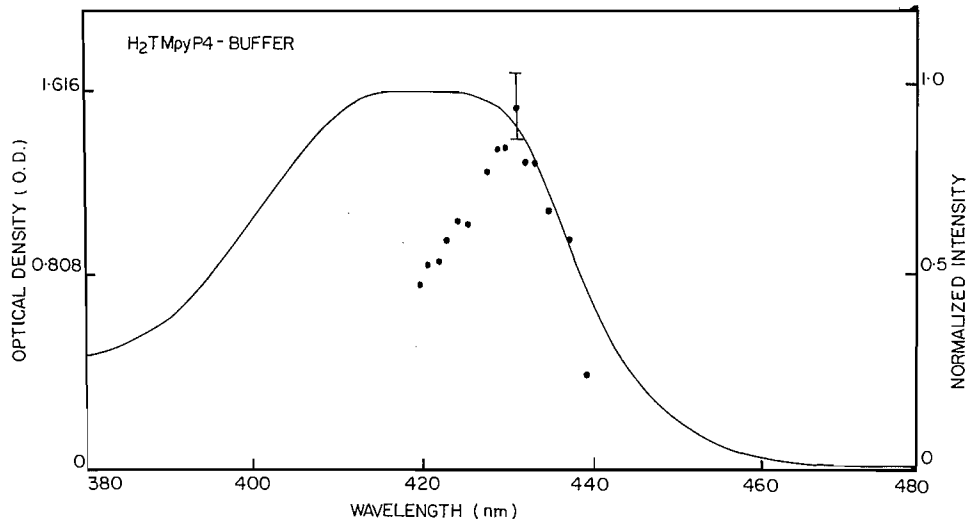

FIG. 4. RRP (dots) for a solution of $H_2TMpyP4$ ($c = 3 \times 10^{-5}$ M), which contains monomer as well as aggregates. The Soret band (see Fig. 3) is broadened towards longer wavelength and the dotted points are those for the intensity of the mode at 1251 cm^{-1} of an aggregate.

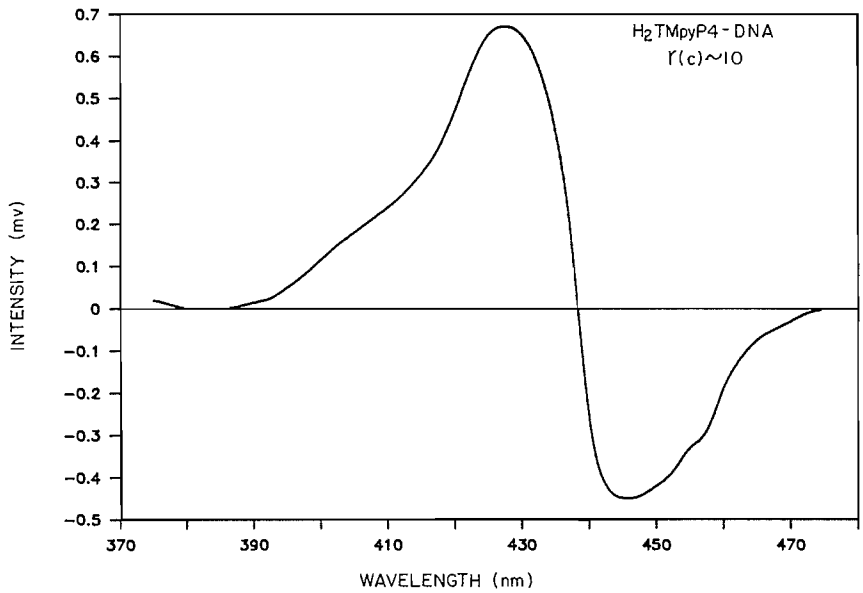

FIG. 5. The CD spectrum of a $H_2TMpyP4$/DNA complex in a buffer solution with $r(c) \sim 10$.

Although the absorption, CD, and time-resolved fluorescence spectra permit the assignment of transitions that originate in externally bound or intercalated porphyrin molecules, information on the spectroscopic signature of tautomeric structures of porphyrin of the $H_2TMpyP4$/DNA complex is not available. Resonance Raman excitation profiles for the intensity of normal modes of the ground state contain more information on the structure of the resonating electronic state than can be obtained from the contour of the absorption band, which is composed of transitions between the electronic surfaces of ground and (resonating) electronic states. The RRP of Fig. 6 for the intensity of the Raman band at 1251 cm^{-1} of the $H_2TMpyP4$ complex in comparison with the contour of the Soret absorption band is clearly no exception. As compared to the absorption band, the RRP shows maxima at four wavelengths. Table 1 shows the assignments of modes with shifts between 900 and 1650 cm^{-1} and, with the exception of the RRP of the band at 1100 cm^{-1}, all other modes follow the contour of the RRP of Fig. 6. Based on the interpretation of absorption spectra, CD spectra, and other information, we assign the maxima at 419 and 427 nm to electronic origins (which are hidden in the Soret band) for externally bound porphyrin molecules and the maxima of the profile at 433.5 and 441 nm to electronic origins of intercalated porphyrin molecules.

Molecular modelling (14) for porphyrin molecules that intercalate with DNA reveals that a rotation of the methylpyridyl (PYR) groups is required such that the rings become more parallel to the plane of the central core. For the free molecule, the two independent PYR rings of each half-

Can. J. Chem. Downloaded from www.nrcresearchpress.com by 109.225.110.28 on 09/08/12
For personal use only.

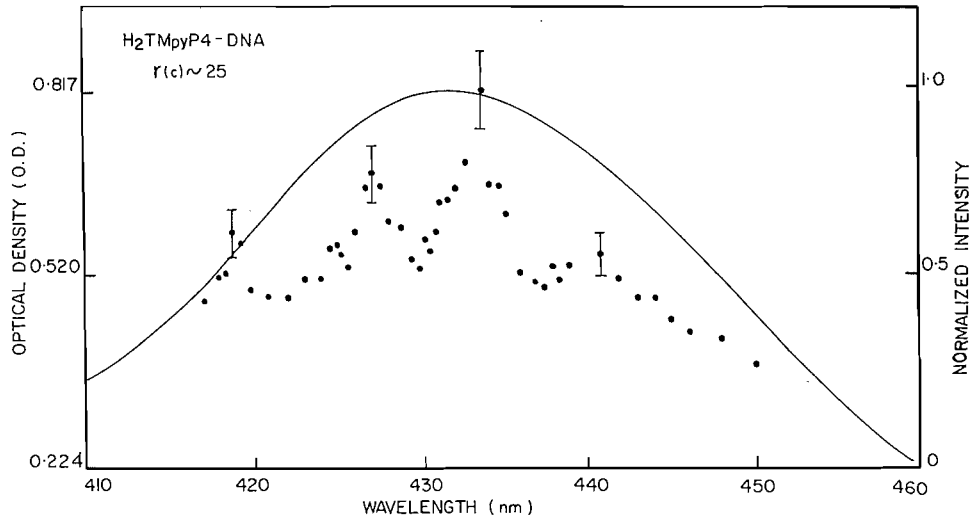

FIG. 6. The resonance Raman excitation profile for the intensity of the Raman band at 1251 cm^{-1} for a $H_2TMpyP4/DNA$ $r(c) \sim 25$ complex. Also shown is the contour of the Soret band of the complex.

molecule are inclined at 65.7° and 71.5° respectively with respect to the core (14). This suggests that the electronic structure for tautomers is identical because the protons are attached to nonadjacent core N atoms, resulting in a symmetrical configuration. Conversely, for intercalated porphyrins, the degree of rotation of the PYR rings does not have to be equivalent. In other words, the interaction of π-electrons of the core may not be symmetric about the pseudo fourfold rotation axis of the $H_2TMpyP4$ molecule, resulting in different electronic structures for the tautomers due to asymmetric configurations. The assignment is partially based on the discussion above and on results presented below but also on the fact that the maxima are at the same wavelength for a number of modes, which excludes the possibility that peaks in the profile at 427 and 419 nm are due to 1–0 vibronic side band resonances.

The existence of an asymmetric configuration for intercalated porphyrin becomes clear if the Raman spectra of Fig. 7 are compared with that of $H_2TMpyP4$ in the buffer solution. If excited with radiation at 441 and 434 nm, the positions of the shift of the C_β—H bending vibration of porphyrin (13) are at 1115 and 1135 cm^{-1} respectively. The corresponding and narrower Raman band of porphyrin in the buffer solution is at 1095 cm^{-1}. Rotation of the PYR rings towards the plane of the core, required for intercalation, results in larger shifts for the bending vibration. The shift of this mode for the tautomers does not have to be at the same position because nonequivalent force fields can exist for C_β—H bending modes in the asymmetric tautomeric half-molecules. It is relevant that the RRP of the mode is different from that of the other modes.

The RRP for the bending mode of externally bound porphyrin follows that of the other modes (Fig. 6) and the position of the Raman band of the tautomers does not change. The inclination of the PYR rings has not changed although the broadened Raman band suggests that small changes of the angles of inclination may exist among the externally bound porphyrin molecules.

The position of the maxima of the RRP's and the intensity of the C_α—C_m and C_α—N stretches at 1003 and 1365 cm^{-1}, respectively, yield information on the interaction of the π-electrons of the core with the different parts of the DNA molecule. In addition to the different positions of electronic origins (and thus different interaction for the π-electrons of the core), the RRP's reveal that the energy gap of the maxima for externally bound porphyrins is 447 cm^{-1}, in contrast to 392 cm^{-1} for intercalated $H_2TMpyP4$. These results may be correlated with data on intensity measurements where (within the experimental error) we find that the sum of the above-mentioned intensities of the modes with

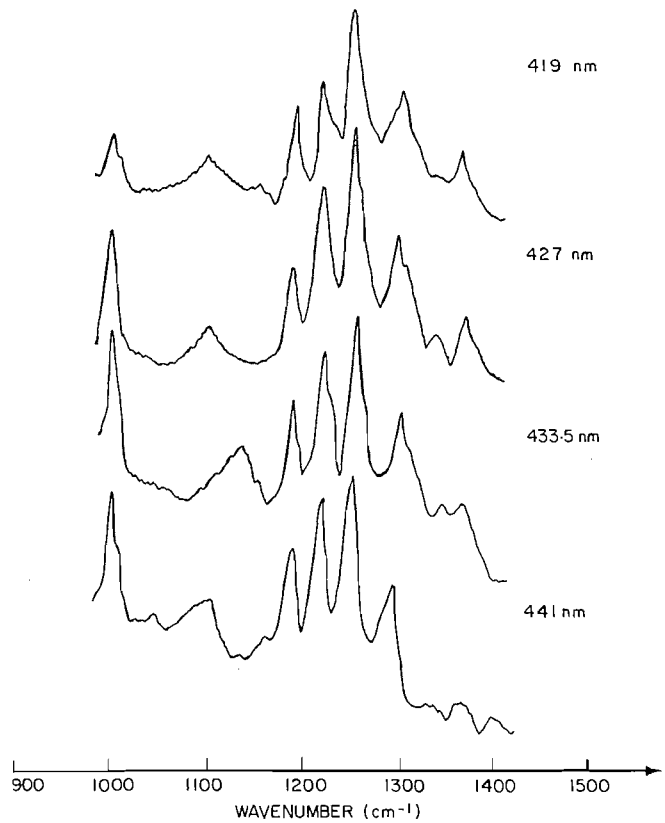

FIG. 7. Selectively excited resonance Raman spectra of the tautomers of intercalated (433.5 and 441 nm) and externally bound porphyrins (419 and 427 nm).

Can. J. Chem. Downloaded from www.nrcresearchpress.com by 109.225.110.28 on 09/08/12
For personal use only.

displacements along the conjugated path of the core is the same as that of the tautomers for intercalated, externally bound, and porphyrin in solution without DNA. However, the ratio R of these intensities for intercalated tautomers ($R = 5$) > externally bound tautomers ($R = 1.5$) > porphyrin in solution ($R = 0.66$).

Conclusions

Resonance Raman excitation profiles are reported for the intensity of normal modes of tetrakis(*N*-methyl-4-pyridyl)porphyrin in solution with and without B-form DNA. The RRP's of porphyrin/DNA complexes provide information on the position of electronic excited states of the tautomers of H_2TMpyP4 that are intercalated or externally bound to DNA. Part of the electronic structure of the tautomers has been discussed by comparing the resonance Raman studies with earlier data on fluorescence and CD absorption spectra.

From the position of a Raman shift of the C_β—H bending mode it is concluded that the pyridyl rings of the tautomers of intercalated H_2TMpyP4 are twisted to a larger degree than the rings of externally bound porphyrin.

Acknowledgement

This research was supported by the Natural Sciences and Engineering Research Council of Canada.

1. G. P. Gurinovich, E. I. Zenkevich, and A. M. Shulga. Porphyrins: excited state and dynamics. Vol. **321**. *Edited by* M. Gouterman, P. M. Rentzepis, and K. D. Straub. American Chemical Society, Washington, D.C. 1986. pp. 74–93.
2. E. I. Zenkevich, A. M. Shulga, I. V. Filatov, A. V. Chernook, and G. P. Gurinovich. Chem. Phys. Lett. **120**, 63 (1985).
3. E. I. Zenkevich, A. M. Shulga, A. V. Chernook, and G. P. Gurinovich. Chem. Phys. Lett. **109**, 306 (1984).
4. J. G. Radziszewski, J. Waluk, and J. Michl. Chem. Phys. **136**, 165 (1989).
5. J. M. Kelly, M. J. Murphy, D. J. McConnel, and V. OhUigin. Nucleic Acids Res. **13**, 167 (1985).
6. Liu Yixian, J. A. Koningstein, and Y. Yevdokimov. Can. J. Chem. **69**, 1791 (1991).
7. R. F. Pasternack, E. J. Gibbs, and J. J. Villafrance. Biochemistry, **22**, 2406 (1983).
8. M. J. Carvlin and R. J. Fiel. Nucleic Acids Res. **11**, 6212 (1983).
9. N. E. Geacintov, V. Ibanez, M. Rougee, and R. V. Bensasson. Biochemistry, **26**, 3087 (1987).
10. J. A. Strickland, D. L. Banville, W. D. Wilson, and L. G. Marzilli. Inorg. Chem. **26**, 3398 (1987).
11. K. Butje, J. H. Schneider, J. P. Kim, Y. Wang, S. Ikuta, and K. Nakamoto. J. Inorg. Biochem. **37**, 119 (1989).
12. J. H. Schneider, J. Odo, and K. Nakamoto. Nucleic Acids Res. **16**, 10323 (1988).
13. N. Blom, J. Odo, K. Nakamoto, and D. P. Strommen. J. Phys. Chem. **90**, 2847 (1986).
14. K. G. Ford, L. H. Pearl, and S. Neidle. Nucleic Acids Res. **15**, 6553 (1987).

Can. J. Chem. Downloaded from www.nrcresearchpress.com by 109.225.110.28 on 09/08/12
For personal use only.

Boron-11, boron-10, and nitrogen-14 NMR relaxation rates and quadrupole coupling constants in BH_3NH_3

GLENN H. PENNER,[1] STEPHEN I. DALEMAN,[2] AND ANGELA R. CUSTODIO

Department of Chemistry and Biochemistry, Guelph-Waterloo Centre for Graduate Work in Chemistry, University of Guelph, Guelph, Ont., Canada N1G 2W1

Received July 18, 1991[3]

GLENN H. PENNER, STEPHEN I. DALEMAN, and ANGELA R. CUSTODIO. Can. J. Chem. **70**, 2420 (1992).

The ^{11}B, ^{10}B, and ^{14}N spin–lattice relaxation times (T_1) for aqueous solutions of BH_3NH_3 were measured by NMR spectroscopy. The results of this investigation are consistent with the nuclear quadrupolar coupling constants reported in previous nuclear quadrupolar resonance and microwave studies. The activation energy associated with rotational reorientation of BH_3NH_3 in aqueous solution is 11.7 ± 0.6 kJ/mol. Electric field gradients were calculated at various levels of *ab initio* molecular orbital theory, in order to obtain theoretical ^{14}N and ^{11}B quadrupolar coupling constants. At the highest level of calculation (CI(SD)/6-31G**//MP2/6-31G**), these are in agreement with recently reported microwave results but not with previously reported NQR experiments.

GLENN H. PENNER, STEPHEN I. DALEMAN et ANGELA R. CUSTODIO. Can. J. Chem. **70**, 2420 (1992).

Faisant appel à la RMN, on a mesuré les temps (T_1) de relaxation spin–réseau du ^{11}B, du ^{10}B et du ^{14}N de solutions aqueuses de BH_3NH_3. Les résultats de nos travaux sont en accord avec les constantes de couplage quadripolaire nucléaire obtenues lors d'études de résonance quadripolaire nucléaire et de micro-ondes antérieures. L'énergie d'activation associée à la réorientation rotationnelle du BH_3NH_3 en solutions aqueuses est de 11,7 ± 0,6 kJ/mol. Dans le but de déterminer les constantes théoriques du couplage quadripolaire du ^{14}N et du ^{11}B, on a calculé les gradients de champs électriques à divers niveaux *ab initio* de la théorie des orbitales moléculaires. Les valeurs obtenues au niveau de calcul le plus élevé (CI(SD)6-31G**//MP2/6-31G**), sont en bon accord avec les valeurs rapportées récemment et basées sur les résultats de micro-onde; elles ne sont toutefois pas en accord avec les résultats antérieurs de RQN.

[Traduit par la rédaction]

Introduction

Since it was first synthesized and isolated by Shore and Parry (1, 2), the physical properties of borane ammoniate, BH_3NH_3 (amminetrihydroboron), have been investigated by many workers. The microwave spectra of nine isotopomers of BH_3NH_3 (substitution with ^2H, ^{10}B, and ^{15}N) have been measured. Analyses of these spectra have yielded the gas-phase geometry, dipole moment, and barrier to internal rotation (3, 4). Three crystal structure investigations have been reported (5–7). The most recent (7) suggests that there is an order–disorder phase transition in solid BH_3NH_3 at 225 K. Solution dipole moments have been studied (8) and the vibrational modes of BH_3NH_3 have been assigned (9). There is also an NQR study of BH_3NH_3 in which the ^{11}B and ^{14}N nuclear electric quadrupolar coupling constants have been reported (10). There have been numerous theoretical investigations of the molecular structure and the physical properties of BH_3NH_3, including studies of geometry (11–19), dipole moment (19–21), electric fields, electric field gradients, diamagnetic shielding and susceptibility (20), B—N bond dissociation energy (15–17), torsional barrier (14, 19), and vibrational frequencies (21).

The ^{11}B, ^{14}N, ^{15}N, and ^1H chemical shifts and spin–spin coupling constants in BH_3NH_3 have been measured in a number of solvents (22–27). The coupling constants have been compared with those calculated using the SOS–CI method (28). The only reported NMR relaxation study is a ^1H and ^{11}B T_1 investigation of the rotation of the BH_3 and NH_3 moieties about the B—N bond in solid BH_3NH_3 (29). In light of the fact that no ^{11}B, ^{10}B, or ^{14}N T_1 investigation of solvated BH_3NH_3 has been reported and that the quadrupolar coupling constants are now available for both the condensed phase (NQR) (10) and gas phase (microwave) (30), we have undertaken a ^{11}B, ^{10}B, and ^{14}N T_1 study of BH_3NH_3 in aqueous solution, together with high level *ab initio* molecular orbital calculations of the electric field gradients.

Theory

Boron-11, boron-10, and nitrogen-14 are quadrupolar nuclei with spins, I, of 3/2, 3, and 1, respectively. All three nuclei are expected to relax entirely by the quadrupolar mechanism (31). Under conditions of extreme narrowing the relaxation rate for a quadrupolar nucleus of spin I is given by [1], where

$$[1] \qquad R_1 = \frac{1}{T_1} = \frac{3\pi^2(2I+3)}{10I^2(2I-1)}\left(1+\frac{\eta^2}{3}\right)\chi^2\tau_c$$

τ_c is the integral of the reorientational correlation function, η is the asymmetry parameter, and χ is the quadrupolar coupling constant. The quadrupolar coupling constant is proportional to the quadrupolar moment, Q, which is a nuclear property, and the electric field gradient, q_{zz}, at the nucleus, which is a molecular property. Boron and nitrogen nuclei are expected to be in axially (cylindrically) symmetric environments in BH_3NH_3, thus η is zero. Substitution of the appropriate I values into eq. [1] yields eqs. [3]–[5] for ^{11}B, ^{10}B, and ^{14}N, respectively.

$$[2] \qquad \chi = \frac{e^2 q_{zz} Q}{h}$$

$$[3] \qquad R_1(^{11}B) = \frac{1}{T_1}(^{11}B) = \frac{2}{5}\pi^2\chi^2\tau_c$$

[1]Author to whom correspondence may be addressed.
[2]Undergraduate Research Participant, 1990–1991.
[3]Revision received May 14, 1992.

Can. J. Chem. Downloaded from www.nrcresearchpress.com by 109.225.110.28 on 09/08/12
For personal use only.

$$[4] \quad R_1(^{10}B) = \frac{1}{T_1}(^{10}B) = \frac{3}{50}\pi^2\chi^2\tau_c$$

$$[5] \quad R_1(^{14}N) = \frac{1}{T_1}(^{14}N) = \frac{3}{2}\pi^2\chi^2\tau_c$$

Although quadrupolar coupling constants cannot be obtained from T_1 measurements without explicit knowledge of τ_c, the ratios of χ^2 can be obtained if the two quadrupolar nuclei share the same reorientational correlation time, τ_c. The situation in which two or more nuclei lie on the molecular symmetry axis, and hence share the same reorientational correlation time, has been frequently exploited as an aid to analysis of T_1 data (32–38). This is the case for BH_3NH_3, where both boron and nitrogen nuclei lie on the molecular symmetry axis. The T_1 values can be related to the χ values through eq. [6].

$$[6] \quad \frac{T_1(^{14}N)}{T_1(^{11}B)} = \frac{4\chi^2(^{11}B)}{15\chi^2(^{14}N)}$$

Experimental

Samples of BH_3NH_3 were of commercial origin (Aldrich). These samples were of technical grade (~90%). Fortunately the impurities were insoluble in water and the spectra showed only the presence of BH_3NH_3. Because of this, concentrations of the prepared samples were only approximate. Approximately 1 M samples were prepared in D_2O and a 1:1 (by volume) mixture for ethylene glycol:methanol.

Spectra were obtained using a Varian UNITY-400 (B_0 = 9.4 T) NMR spectrometer. The T_1 measurements employed the inversion–recovery pulse sequence (39). The $\pi/2$ pulse widths were as follows: 8.4 μs for ^{11}B, 24.0 μs for ^{10}B (both using a 5 mm probe), and 78 μs for ^{14}N (using a 10 mm probe). Typically 8 scans at each variable delay, $d2$, in the inversion–recovery experiment were carried out. All T_1 values were calculated using between 9 and 15 different delay ($d2$) values. All experiments were performed in duplicate or triplicate.

Molecular orbital calculations were performed using GAUSSIAN 90 (40) on a Silicon Graphics Power Series 8 computer.

Results and discussion

Boron-11 relaxation

The ^{11}B spin–lattice relaxation times for a 1 M solution of BH_3NH_3 in D_2O at several temperatures are given in Table 1. The temperature dependence of the ^{11}B spin–lattice relaxation time is given by eq. [7],

$$[7] \quad \ln T_1 = \frac{-1439(37)}{T} + 1.53(61)$$

where the numbers in parentheses are standard deviations obtained from a linear regression analysis. The slope corresponds to an activation energy for molecular reorientation of 12.0 ± 0.3 kJ/mol. This can be compared to a value of 10.6 ± 0.9 kJ/mol for an aqueous solution of the isoelectronic species $CH_3NH_3^+$ (41).

To calculate τ_c values from T_1 data, a value for the ^{11}B quadrupolar coupling constant is required. Nuclear quadrupolar coupling constants are often strongly dependent on the intermolecular interactions present. In the gas phase the value for $\chi(^{11}B)$ is 2.584 MHz (30), whereas the solid state value is 1.504 MHz (9). These probably represent the upper and lower limits to $\chi(^{11}B)$. The corresponding τ_c values are given in Table 1. Boron-11 T_1 values at several concentrations are given in Table 2. Reducing the concentration of BH_3NH_3 in D_2O to 0.1 M yields essentially no change in T_1 (39.5 ms) and increasing the concentration to 4 M caused a small decrease in T_1 of only 1.9 ms. A very slow evolution of gas, presumably hydrogen due to molecular decomposition, was observed at the highest temperature and at concentrations above 4 M. As a result these were the upper limits for temperature and concentration.

TABLE 1. Boron-11 T_1 and τ_c values for BH_3NH_3.

Temperature[a] (K)	T_1 (ms)[b]	τ_c (ps)[c] NQR	τ_c (ps)[c] MW
302	39.7	2.82	0.955
314	47.9	2.34	0.793
325	56.5	1.98	0.671
337	64.9	1.73	0.586
349	73.9	1.52	0.515
360	86.0	1.30	0.440

[a]Estimated error is ±1 K.
[b]Estimated error is less than 5%.
[c]Calculated with NQR value of $\chi(^{11}B)$ = 1.504 MHz (10) or MW value of $\chi(^{11}B)$ = 2.59 MHz (30).

TABLE 2. Boron-11 T_1 values at various temperatures

Concentration (M)	T_1 (ms)	Number of T_1 values used for average
1	39.2 (0.6)	12
2	39.1 (1.5)	12
3	37.6 (1.3)	14
4	37.8 (0.1)	8

[a]Numbers in parentheses are standard deviations.

TABLE 3. Boron-10 T_1's and $\chi(^{10}B)$ values for BH_3NH_3.

Temperature[a] (K)	T_1 (ms)[b]	χ(MHz)[c]
302	60.3	3.15
314	74.9	3.10
325	88.6	3.10
337	105.1	3.05
349	116.4	3.09
360	130.0	3.16

[a]Estimated error is ±1 K.
[b]Estimated error is less than 5%.
[c]Calculated using ^{10}B T_1 values, τ_c (NQR values from Table 1), and eq. [4].

Boron-10 relaxation

The ^{10}B spin–lattice relaxation times for a 1 M solution of BH_3NH_3 in D_2O at several temperatures are given in Table 3. The temperature dependence of the ^{10}B T_1 is given by eq. [8].

$$[8] \quad \ln T_1 = \frac{-1458(65)}{T} + 2.04(20)$$

The corresponding activation energy for molecular rota-

Can. J. Chem. Downloaded from www.nrcresearchpress.com by 109.225.110.28 on 09/08/12
For personal use only.

TABLE 4. Nitrogen-14 T_1's and $\chi(^{14}N)$ values for BH_3NH_3.

Temperature[a] (K)	T_1 (ms)[b]	χ (MHz)[c] A	B
304	15.8	1.23	2.10
314	19.5	1.22	2.14
324	22.1	1.24	2.12
334	25.0		
345	28.0		
356	30.0		

[a]Estimated error is ±1 K.
[b]Estimated error is less than 5%.
[c]Columns A and B calculated using the $\chi(^{11}B)$ value from NQR and MW experiments, respectively.

tional reorientation is 12.1(5) kJ/mol, in excellent agreement with the value obtained from the temperature dependence of the ^{11}B T_1 values.

Using the τ_c values from the ^{11}B NQR and $^{11}BT_1$ measurements (Table 1) and the T_1 values for ^{10}B (Table 3) yields a χ value for ^{10}B of 3.11 ± 0.04 MHz (the average of 6 values). The quadrupolar coupling constants for different isotopes of the same nucleus are related through their quadrupole moments, Q, according to eq. [9] (42–46).

$$[9] \quad \frac{\chi(^{10}B)}{\chi(^{11}B)} = \frac{Q(^{10}B)}{Q(^{11}B)}$$

The quadrupole moments of ^{10}B and ^{11}B are 0.085×10^{-28} m^2 and 0.041×10^{-28} m^2, respectively (47). Using the NQR value of $\chi(^{11}B)$ the ratio of quadrupole moments predicts a $\chi(^{10}B)$ value of 3.118 ± 0.021 MHz, in excellent agreement with that obtained from our ^{10}B T_1 measurements. Equation [9] predicts a $\chi(^{10}B)$ value of 5.34 MHz for BH_3NH_3 in the gas phase.

Nitrogen-14 relaxation

The ^{14}N T_1 values for 1 M BH_3NH_3 in D_2O at several temperatures are given in Table 4. The nitrogen-14 quadrupolar coupling constants are calculated for the three lowest temperatures, where ^{14}N and ^{11}B experiments were performed at the same temperature (within probe temperature error limits). The $\chi(^{11}B)$ values, as obtained from NQR and MW experiments, were used together with ^{11}B and ^{14}N T_1 measurements to calculate $\chi(^{14}N)$. The values of $\chi(^{14}N)$ using the MW data and NQR $\chi(^{11}B)$ values are well within experimental error of those directly measured by MW and NQR. The ratio of $\chi^2(^{11}B)$ to $\chi^2(^{14}N)$ predicted by our T_1 measurements is 1.49. This is in excellent agreement with the ratios of 1.44 and 1.48 obtained from NQR and MW experiments. Therefore our T_1 results are consistent with both nuclear quadrupolar resonance and microwave spectroscopic results. For a molecule such as BH_3NH_3 T_1 measurements in the high temperature extreme narrowing regime allow only the determination of the ratio of nuclear quadrupolar coupling constants. The absolute values of the quadrupolar coupling constants can be obtained from the T_1 minimum. Unfortunately the samples of BH_3NH_3 in D_2O froze before the T_1 minimum was reached. Nitrogen-14 T_1 measurements were also performed on a 1 M sample for BH_3NH_3 in 1:1 ethylene glycol:methanol but the T_1 values fell below the limits of our spectrometer (100 μs) before a T_1 minimum was reached. In aqueous solution the NH_3 hydrogens undergo rapid exchange with the solvent, as shown by the lack of NH_3 proton coupling to ^{14}N, ^{11}B, or ^{10}B and by the lack of a ^3J(BH, NH) coupling in the proton spectrum. Exchange of the NH protons may affect the ^{14}N relaxation via the scalar coupling mechanism of the first kind (31, 39). It is much more common for scalar relaxation to affect T_2 (and hence the linewidth) than T_1. The dominance of the ^{14}N spin–lattice relaxation by the quadrupolar interaction is confirmed by the excellent agreement of ^{11}B and ^{14}N T_1 measurements with eq. [6]. The results presented here suggest that, at the temperatures studied, molecular reorientation is the dominant pathway for ^{14}N relaxation.

TABLE 5. *Ab initio* MO calculations of the electric field gradients at the boron and nitrogen nuclei of BH_3NH_3 and boron-11 and nitrogen-14 quadrupolar coupling constants.

Basis set	EFG (au)	χ (MHz)[a]
STO-3G	B: −0.327	3.18
	N: 0.762	−3.49
6-31G**	B: −0.291	2.89
	N: 0.552	−2.52
MP2/6-31G**	B: −0.277	2.69
	N: 0.463	−2.12
CISD/6-31G**	B: −0.277	2.67
//MP2/6-31G**	B: −0.500	−2.29
Expt. (MW)[b]	B:	2.59
	N:	−2.13
Expt. (NQR)[c]	B:	1.50
	N:	1.25

[a]Calculated using eq. [11] and Q values of 0.041×10^{-28} m^2 for ^{11}B and 0.0193×10^{-28} m^2 for ^{14}N (47).
[b]From ref. 30.
[c]Taken from ref. 10; only absolute values are available.

A plot of ln T_1 as a function of inverse temperature is best fit by the linear equation [10].

$$[10] \quad \ln T_1 = \frac{-1335(97)}{T} + 0.29(30)$$

The corresponding activation energy is 11.0 ± 0.8 kJ/mol, in good agreement with the values obtained from the ^{11}B and ^{10}B data.

Electric field gradient calculations

Electric field gradients (EFG's) at the boron and nitrogen of BH_3NH_3, calculated at the STO-3G, 6-31G**, MP2/6-31G**, and CI(SD)/6-31G** //MP2/6-31G** levels are given in Table 5. The quadrupolar coupling constant, χ (in MHz), can be related to the nuclear quadrupole moment, Q (in units of 10^{-28} m^2), and the electric field gradient, q_{zz}, at the nucleus (in atomic units) by eq. [11] (49).

$$[11] \quad \chi = -237Qq_{zz}$$

We have chosen the most recent experimental Q value for ^{14}N (48), which agrees closely with the latest molecular orbital calculations (49, 50). The χ values calculated from the molecular orbital generated q_{zz} values (the largest EFG) are also given in Table 5.

The χ values calculated at the MP2/6-31G** level are in

Can. J. Chem. Downloaded from www.nrcresearchpress.com by 109.225.110.28 on 09/08/12
For personal use only.

very good agreement with the gas-phase experimental values but are a factor of about 1.7–1.8 larger in magnitude than the solid state values. A single point calculation at the CI(SD)/6-31G** level yielded little change in $\chi(^{11}B)$ but increased the magnitude of $\chi(^{14}N)$ slightly. Our calculations and the gas-phase microwave results are also in very good agreement with previous *ab initio* calculations of $\chi(^{11}B)$ and $\chi(^{14}N)$ (52). Molecular orbital calculations of nuclear quadrupolar coupling constants are usually in good agreement with gas-phase experimental values if the calculations are performed with second-order correlation effects taken into account (49, 50, 52).

Conclusions

The spin–lattice relaxation times for ^{14}N, ^{11}B, and ^{10}B in aqueous solutions of BH_3NH_3 are completely dominated by the quadrupolar mechanism. Measurements of T_1 as a function of temperature for ^{14}N, ^{11}B, and ^{10}B yield a set of results that are consistent with both NQR and MW experiments and predict an effective activation energy for reorientation of the B—N bond of 11.7 ± 0.6 kJ/mol. It is interesting to note that although the T_1 measurements provide only the ratios of the ^{14}N and ^{11}B quadrupolar coupling constants these values are in excellent agreement with the ratios for *both* the gas phase (microwave) and solid state (NQR) quadrupolar coupling constants. Unfortunately, T_1 minima and hence absolute values of $\chi(^{11}B)$, $\chi(^{10}B)$, or $\chi(^{14}N)$, could not be obtained. *Ab initio* molecular orbital calculations yield nuclear quadrupole coupling constants that are in excellent agreement with the values obtained from microwave spectroscopy experiments. The NQR values of $\chi(^{11}B)$ and $\chi(^{14}N)$ are about a factor of 1.8 smaller.

Acknowledgements

We are grateful to the Natural Science and Engineering Research Council of Canada for financial support. A. R. Custodio thanks the Fundação de Amparo a Pesquisa do Estado de São Paulo for a postdoctoral fellowship. We wish to thank H. Dreizler and K. Varman for a preprint of ref. 30.

1. S. G. Shore and R. W. Parry. J. Am. Chem. Soc. **77**, 6084 (1955).
2. S. G. Shore and R. W. Parry. J. Am. Chem. Soc. **80**, 8 (1958).
3. R. D. Suenram and L. R. Thorne. Chem. Phys. Lett. **78**, 157 (1981).
4. L. R. Thorne, R. D. Suenrum, and F. J. Lovas. J. Chem. Phys. **78**, 167 (1983).
5. E. W. Hughes. J. Am. Chem. Soc. **78**, 502 (1956).
6. E. L. Lippert and W. N. Lipscomb. J. Am. Chem. Soc. **78**, 503 (1956).
7. C. F. Hoon and E. C. Reynhardt. J. Phys. C, **16**, 6129 (1983).
8. J. R. Weaver, S. G. Shore, and R. W. Parry. J. Chem. Phys. **29**, 1 (1958).
9. J. Smith, K. S. Seshadri, and D. White. J. Mol. Spectrosc. **15**, 327, (1993).
10. A. Lötz and J. Voitländer. J. Magn. Reson. **48**, 1 (1982).
11. D. R. Armstrong and P. G. Perkins. Inorg. Chem. Acta, **10**, 77 (1974).
12. S. D. Peyerimhoff and R. J. Buenker. J. Chem. Phys. **49**, 312 (1968).
13. A. Veillard. Chem. Phys. Lett. **3**, 128 (1969).
14. H. Umeyama and K. Morokuma. J. Am. Chem. Soc. **98**, 7208 (1976).
15. C. Zirz and R. Ahlrichs. J. Chem. Phys. **75**, 4980 (1981).
16. R. Ahlrichs and W. Koch. Chem. Phys. Lett. **53**, 341 (1978).
17. L. T. Redman, G. D. Purvis III, and R. J. Bartlett. J. Am. Chem. Soc. **101**, 2856 (1979).
18. J. D. Dill, P. v. R. Schleyer, and J. A. Pople. J. Am. Chem. Soc. **97**, 3402 (1975).
19. J. S. Binkley and L. R. Thorne. J. Chem. Phys. **79**, 2932 (1983).
20. M. Dixon and W. E. Palke. J. Chem. Phys. **61**, 2250 (1974).
21. P. Brint, B. Sangchakr, and P. W. Fowler. J. Chem. Soc. Faraday Trans. 2, **85**, 29 (1989).
22. D. F. Gaines and R. Schaeffer. J. Am. Chem. Soc. **86**, 1505 (1964).
23. R. Schaeffer, F. Tebbe, and C. Phillips. Inorg. Chem. **3**, 1475 (1964).
24. C. W. Heitsch. Inorg. Chem. **4**, 1019 (1974).
25. H. Nöth and B. Wrackmeyer. Chem. Ber. **109**, 3070 (1974).
26. M. G. Hu, J. M. Van Paasschen, and R. A. Geanangel. Inorg. Nucl. Chem. **34**, 2147 (1977).
27. B. Wrackmeyer. J. Magn. Reson. **66**, 172 (1986).
28. V. Galasso. J. Chem. Phys. **80**, 365 (1984).
29. E. C. Reynhardt and C. F. Hoon. J. Phys. C, **16**, 6137 (1983).
30. K. Vorman and H. Dreizler. Z. Naturforsch. A: Phys. Sci. **46**, 1060 (1991).
31. A. Abragam. The principles of nuclear magnetism. Oxford University Press, New York. 1961.
32. N. M. Szeverenyi, R. R. Vold, and R. L. Vold. Chem. Phys. **18**, 23 (1976).
33. R. R. Vold, R. L. Vold, and N. M. Szeverenyi. J. Chem. Phys. **70**, 5213 (1979).
34. S. P. Wang, P. Yuan, and M. Schwartz. Inorg. Chem. **29**, 484 (1990).
35. R. R. Vold, S. W. Sparks, and R. L. Vold. J. Magn. Reson. **30**, 497 (1978).
36. A. Pulkkinen, J. Jokisaari, and J. Kowalewski. J. Magn. Reson. **51**, 388 (1989).
37. R. E. Wasylishen. Can. J. Chem. **65**, 2077 (1987).
38. G. H. Penner. Can. J. Chem. **69**, 1054 (1991).
39. T. C. Farrar and E. D. Becker. Pulse and Fourier transform NMR — introduction to theory and methods. Academic Press, New York. 1971.
40. M. J. Frisch, M. Head-Gordon, G. W. Trucks, J. B. Foresman, H. B. Schlegel, K. Raghavachari, M. A. Robb, J. S. Binkley, C. Gonzalez, D. J. DeFrees, D. J. Fox, R. A. Whiteside, R. Seeger, C. F. Melins, J. Baker, R. L. Martin, L. R. Kahn, J. J. P. Stewart, S. Topiol, and J. A. Pople. GAUSSIAN 90, Revision F. Gaussian, Inc., Pittsburgh, PA. 1990.
41. J. D. Halliday, P. E. Binder, and S. Padamshi. Can. J. Chem. **63**, 2975 (1985).
42. T. C. Ng and E. Tward. J. Magn. Reson. **51**, 361 (1983).
43. N. Hao, B. G. Sayer, G. Denes, D. G. Bickley, C. Detellier, and M. J. McGlinchey. J. Magn. Reson. **50**, 50 (1982).
44. R. R. Vold and R. L. Vold. J. Magn. Reson. **19**, 365 (1975).
45. R. T. Brownlee, M. J. O'Connor, B. P. Shehan, and A. G. Wedd. J. Magn. Reson. **61**, 516 (1985).
46. R. G. Kidd. J. Magn. Reson. **45**, 88 (1981).
47. G. H. Fuller. J. Phys. Chem. Ref. Data, **5**, 835 (1976).
48. H. Winter and H. J. Andrä. Phys. Rev. A, Gen. Phys. **21**, 581 (1980).
49. T.-K. Ha. Chem. Phys. Lett. **107**, 117 (1984).
50. P. W. Fowler and V. Spirko. J. Chem. Soc. Faraday Trans. 2, **86**, 1991 (1990).
51. T.-K. Ha. Z. Naturforsch. A: Phys. Sci. **41**, 163 (1986).
52. M. H. Palmer. Z. Naturforsch. A: Phys. Sci. **45**, 357 (1990).

Can. J. Chem. Downloaded from www.nrcresearchpress.com by 109.225.110.28 on 09/08/12
For personal use only.

Spectroscopic and reactivity studies of diastereomeric iridium(III) hydride complexes of the chelating tritertiary phosphine ligand Cyttp

STEVEN M. SOCOL,[1,2] CHIHAE YANG,[3] AND DEVON W. MEEK[4]
Department of Chemistry, The Ohio State University, Columbus, OH 43210, U.S.A.

AND

ROBERT GLASER[1]
Department of Chemistry, Ben-Gurion University of the Negev, Beersheva 84105, Israel

Received February 10, 1992

STEVEN M. SOCOL, CHIHAE YANG, DEVON W. MEEK, and ROBERT GLASER. Can. J. Chem. **70**, 2424 (1992).

The chelating tritertiary phosphine $C_6H_5P(CH_2CH_2CH_2P(C_6H_{11})_2)_2$ (Cyttp) in octahedral six-coordinate iridium(III) complexes $[IrH_2Z(Cyttp)]^{(0\text{ or }1+)}$ (Z = Cl, CO, CH_3CN, and related ligands) is meridionally bound. The conformation of the Cyttp ligand is such that the phenyl group of the central phosphorus lies out of the meridional plane. This leads to diastereomers in which the Z group is *syn* or *anti* to the phenyl group in question. These diastereomers were readily characterized by a general nuclear Overhauser effect difference NMR technique involving an intensity change to the apical-hydrido absorbance *syn*-to-phenyl upon irradiation of phenyl-*ortho* protons. A single diastereomer, *cis-anti-mer*-[IrH_2Cl(Cyttp)] (**6***a*), was prepared by (*a*) refluxing $[IrCl(COD)]_2$ and Cyttp in ethanol or (*b*) treatment of [IrCl(COD)(Cyttp)] in benzene with excess dihydrogen. The stereochemical course for ligand substitution reactions on **6***a* was determined using the Cyttp phenyl group as a stereochemical label. Of six chloro-ligand metathesis reactions performed on *cis-anti-mer*-[IrH_2Cl(Cyttp)] (**6***a*), four gave mixtures of the two *cis-syn-mer-/cis-anti-mer*-$[IrH_2Z(Cyttp)]^{(0\text{ or }1+)}$ diastereomers (Z = CH_3CN, CN, PMe_2Ph, and $P(OCH_2)_3CEt$), one gave inversion only (the *cis-syn-mer* compound (Z = CO)), and only one gave retention (*cis-anti-mer*-[IrH_2I(Cyttp)]. A dissociative mechanism is proposed for the substitution reactions. Loss of stereochemical integrity in **6***a* was also observed in other reactions. Insertions of CS_2 into the iridium–meridonal-hydride bond and $SnCl_2$ into the iridium–chlorine bond produced mixtures of *cis-syn-mer/cis-anti-mer* diastereomers. Electrophiles ($C_7H_7^+$ in the presence of CH_3CN, I_2, HCl, and HOAc in the presence of Tl^+) attack only the meridonal hydride to yield various ratios of geometric and (or) *syn/anti* isomers. Trends in the relative chemical shifts of the hydride protons and ^{31}P nuclei in *syn* versus *anti* isomers are noted and rationalized.

STEVEN M. SOCOL, CHIHAE YANG, DEVON W. MEEK et ROBERT GLASER. Can. J. Chem. **70**, 2424 (1992).

La phosphine chélatante tritertiaire $C_6H_5P(CH_2CH_2CH_2P(C_6H_{11})_2)_2$ (Cyttp) présente dans les complexes hexa-coordonnés octaédriques de l'iridium(III) $[IrH_2Z(Cyttp)]^{(0\text{ ou }1+)}$ (Z = Cl, CO, CH_3CN et autres ligands apparentés) est liée d'une façon méridionale. La conformation du ligand Cyttp est telle que le groupe phényle du phosphore central ne se trouve pas dans le plan méridional. Cette situation conduit à l'existence de diastéréoisomères dans lesquels le groupe Z est soit *syn* ou *anti* par rapport à ce phényle. La RMN permet de caractériser facilement ces diastéréoisomères grâce à une différence générale d'effet Overhauser nucléaire impliquant un changement d'intensité d'absorption de l'hydrure apical *syn* par rapport au phényle lorsqu'on irradie les protons *ortho* du phényle. Nous avons préparé un diastéréoisomère spécifique, le *cis-anti-mer*-[IrH_2Cl(Cyttp)] (**6***a*), (*a*) par chauffage au reflux du $[IrCl(COD)]_2$ avec du Cyttp dans l'éthanol ou (*b*) par traitement du [IrCl(COD)(Cyttp)] en solution dans le benzène avec un excès de dihydrogène. Nous avons déterminé la stéréochimie des réactions de substitution du ligand sur le composé **6***a* en utilisant le groupe phényle comme sonde stéréochimique. Parmi les six réactions de métathèse réalisées sur le *cis-anti-mer*-[IrH_2Cl(Cyttp)] (**6***a*), quatre ont conduit à des mélanges des deux diastéréoisomères *cis-syn-mer-/cis-anti-mer*-$[IrH_2Z(Cyttp)]^{(0\text{ ou }1+)}$ (Z = CH_3CN, CN, PMe_2Ph et $P(OCH_2)_3CEt$. Une autre n'a conduit qu'à une inversion (conduisant au produit *cis-syn-mer* (Z = CO)) et une seule a donné lieu à une rétention de configuration *cis-anti-mer*-[IrH_2I(Cyttp)]. On propose un mécanisme dissociatif pour les réactions de substitution. Nous avons également observé une perte d'intégrité stéréochimique de **6***a* dans d'autres réactions. Les insertions de CS_2 dans la liaison iridium–hydrure méridional et de $SnCl_2$ dans la liaison iridium–chlore conduisent à des mélanges des diastéréoisomères *cis-syn-mer/cis-anti-mer*. Les électrophiles ($C_7H_7^+$ en présence de CH_3CN, I_2, HCl et HOAc en présence de Tl^+) n'attaquent que l'hydrure méridional et fournissent des rapports variés d'isomères géométriques et (ou) *syn/anti*. Nous avons noté et rationalisé des differences des déplacements chimiques entre les protons des hydrures et des noyaux de ^{31}P dans divers isomères *syn* vs. *anti*.

[Traduit par la rédaction]

Previously we (1) and others (2) have reported the syntheses of some iridium(III) dihydride complexes of Cyttp, $C_6H_5P(CH_2CH_2CH_2P(C_6H_{11})_2)_2$, **1** (3), and ttp = $C_6H_5P(CH_2CH_2CH_2P(C_6H_5)_2)_2$, **2** (4, 5), (bis((3-di(cyclohexyl or phenyl)-phosphino)propyl) phosphine). The tridentate Cyttp ligand **1** was found to be meridonally bound in the octahedral iridium(III) complexes by NMR spectroscopic and single crystal X-ray diffraction techniques (1*a*, 6). Similar results were obtained for ttp **2** (2, 7). Two isomers are possible for octahedral complexes of ttp-type ligands which have the formula *apical* (*H*,*Z*)-[MHYZ(L-L-L)]. These isomers are described as being *syn* or *anti*, and are defined by analogy to the procedure used for olefinic *E*,*Z* diastereomers (8). In this method, the Cahn–Ingold-Prelog sequence rule (9) is used to classify the relative priority of the two *apical* ligands. The *syn* diastereomer is defined as that in which the highest priority *apical* ligand and the phenyl group are both

[1]Authors to whom correspondence may be addressed.
[2]Present address: Southern Utah University, Department of Physical Sciences, Cedar City, UT 84720.
[3]Present address: Denison University, Department of Chemistry, Granville, OH 43023.
[4]Deceased.

Can. J. Chem. Downloaded from www.nrcresearchpress.com by 109.225.110.28 on 09/08/12
For personal use only.

on the same side of the three-phosphorus reference plane. The *anti*-diastereomer is defined as that in which these moieties are located on opposite sides of the reference plane. By this definition, **3** is a *syn* diastereomer, whereas **4** is an *anti* diastereomer.

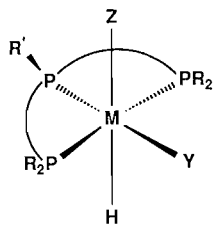

3

Syn **diastereomer**

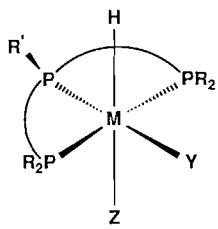

4

Anti **diastereomer**

Triphosphine ligand = $R_2P(CH_2)_3PR'(CH_2)_3PR_2$

This type of isomerism was first noted in a series of six-coordinate ruthenium(II) complexes of ttp: *cis-syn-mer-/cis-anti-mer-/trans-mer*-[RuH($P(OMe)_3)_2$(ttp)][BF_4], **5** (7). Configurational assignments for **5** were made on the basis of ^1H and ^{31}P {^1H} NMR spectroscopy (*cis* vs. *trans*), and single crystal X-ray diffraction analysis of one of the *cis*-diastereomers (*syn* vs. *anti*) (7). This type of isomerism has also been proposed for some octahedral iridium(III) and rhodium(III) complexes which contain the triphosphine ligand *t*-BuP($CH_2CH_2CH_2PPh_2)_2$ and some ruthenium(II) hydride complexes which contain Cyttp (10). We have previously shown that the *syn/anti* configuration in octahedral metal complexes of Cyttp can be determined via a relatively facile and general nuclear Overhauser effect (difference NOE (11)) technique (1*a*, 10*c*).

This paper reports the syntheses of iridium(III) complexes **6***a–i*, **7***a–c*, **8***a–c* and their ^1H and ^{31}P NMR spectral parameters. It will be shown that a number of ligand substitution and insertion reactions on *cis-syn-mer*-[IrH_2Cl(Cyttp)] **6***a* proceed with a loss of configurational integrity of the starting material. In addition, this paper demonstrates that some of the NMR parameters of the diastereomeric products of these reactions show correlations with their *syn/anti* configurations.

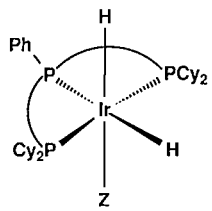

6 or $[6]^+[X]^-$

6*a*	Z = Cl
6*b*	Z = H
6*c*	Z = CH_3CN; X = BF_4
6*d*	Z = CO; X = BF_4
6*e*	Z = I
6*f*	Z = CN
6*g*	Z = $P(OCH_2)_3CEt$; X = BF_4
6*h*	Z= PMe_2Ph; X = BF_4
6*i*	Z = $SnCl_3$

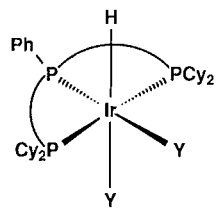

7 or $[7]^+[X]^-$

7*a*	Y = Cl
7*b*	Y = η^2-S_2CH; X = AsF_6
7*c*	Y = η^2-O_2CCH_3; X = AsF_6

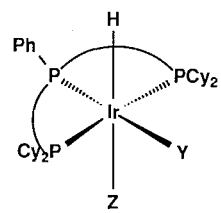

8 or $[8]^+[X]^-$

8*a*	Y = CO; Z = CH_3; X = BPh_4
8*b*	Y = Cl (or I); Z= I (or Cl)
8*c*	Y = CH_3CN (or Cl); Z = Cl (or CH_3CN)

Experimental

Elemental analyses were preformed by MHW Laboratories, Phoenix, AZ. Infrared spectra were recorded on a Perkin–Elmer 283B spectrophotometer. Proton NMR spectra (11.7 T) were recorded in acetone-d_6 solution (except when noted otherwise) at 500 MHz on a Bruker AM-500 Fourier transform spectrometer (equipped with an Aspect 3000 data system) at The Ohio State University Chemical Instrument Center. ^{13}C NMR spectra (11.7 T) were recorded in dichloromethane-d_2 solution at 125 MHz on the above-mentioned Bruker AM-500 spectrometer. Deuterated solvents were used for internal lock and the carbon or residual protio-solvent resonances were used as internal secondary references (relative to tetramethylsilane). ^{31}P NMR spectra (2.1 T) were recorded in acetone solution (except when noted otherwise) at 36.43 MHz on a Bruker HX-90 Fourier transform spectrometer. For ^{31}P NMR spectra, an acetone-d_6 solution of trimethyl phosphate [$(CH_3O)_3P{=}O$] in a coaxial tube was used for deuterium lock and a secondary ^{31}P reference (1.549 ppm relative to 85% H_3PO_4), respectively. The ^{31}P NMR spectra of isomer mixtures were assigned by comparing signal intensity ratios with the ^1H NMR. In **6***g,h* the assignments of the ^{31}P NMR spectra were made by means of ^1H {sel ^{31}P} NMR techniques. For all NMR spectra, negative chemical shifts are upfield from the respective reference standards. Protons were decoupled from the carbon and phosphorous nuclei by broad-band irradiation. NOE experiments were performed in the difference NOE mode. Iteration calculations and simulated NMR spectra were calculated with the use of the PANIC program (12). PANIC is a microcomputer version of the LAOCOON (13) program. All reactions were carried out under an atmosphere of high purity nitrogen by using standard Schlenk techniques. Solutions of air-sensitive reagents were transferred between reaction vessels with syringes flushed with nitrogen, stainless steel needles, or a glass transfer tube equipped with a

Can. J. Chem. Downloaded from www.nrcresearchpress.com by 109.225.110.28 on 09/08/12
For personal use only.

Can. J. Chem. Downloaded from www.nrcresearchpress.com by 109.225.110.28 on 09/08/12
For personal use only.

Teflon stopcock. Solvents were purged with nitrogen for 30 min prior to use. Iridium trichloride trihydrate (Matthey Bishop Inc. or Englehard Industries, Inc.), ethereal tetrafluoroboric acid (Cationics Inc.), dimethylphenylphosphine (Aldrich Chemical Co.), and 1,5-cyclooctadiene (Aldrich Chemical Co.) were purchased from commercial sources and used as received. Bis((3-di(cyclohexyl)-phosphino)propyl)phenylphosphine (Cyttp, **1**) was prepared as previously described (3). $[IrCl(COD)]_2$ (14) and $P(OCH_2)_3CEt$ (15) were prepared by literature methods.

*[IrCl(COD)(Cyttp)], **12***

To a solution of $[IrCl(COD)]_2$ (300 mg, 0.45 mmol) in benzene was added a 0.25 M benzene solution of **1** (3.6 mL, 0.90 mmol). The solution changed color from red to yellow upon stirring for 0.5 h. After removal of the solvent *in vacuo*, the residual yellow solid was suspended in hexane, collected on a frit, washed with hexane, and dried *in vacuo* to yield 531 mg (64%) of **12**; ^1H NMR (C_6D_6) δ: 8.0–7.0 (m, 5H, aromatic H), 3.9 (m, 4H, olefinic H), 3.0–0.7 (m, 64H, aliphatic H); $^{31}P\{^1H\}$ NMR (C_6D_6) δ: −7.8 (s, free Cy_2P), −23.1 (d, bound Cy_2P, J_{PP} 42 Hz), −27.5 (d, bound Ph*P*, J_{PP} 42 Hz). Anal. calcd. for $C_{44}H_{73}ClIrP_3$: C 57.28, H 7.98, Cl 3.84; found: C 56.88, H 8.28, Cl 4.05.

cis-anti-mer-*[IrH_2Cl(Cyttp)]*, **6**a

*Method A (1*a*)*

To a solution of $[IrCl(COD)]_2$ (500 mg, 0.74 mmol) in absolute ethanol (50 mL) was added a 0.25 M benzene solution of **1** (6.0 mL, 1.5 mmol). Upon heating to reflux 2 h, the solution changed color from red to yellow. After removal of the solvent *in vacuo*, the residue was dissolved in dichloromethane (30 mL), and absolute ethanol (30 mL) was added. A solid separated upon removal of most of the dichloromethane under reduced pressure. The solid was collected on a frit, washed with ether, and dried *in vacuo* to yield 490 mg (40%) of **6***a*.

Method B

A benzene solution of **12** (1.62 mmol) was prepared *in situ* by the method described above and stirred for 0.5 h. Hydrogen gas was bubbled into the reaction mixture over a period of 2 h. After removal of the solvent *in vacuo*, the residue was dissolved in tetrahydofuran (30 mL). A solid separated upon repeated treatments consisting of addition of absolute ethanol (30 mL), followed by removal of half the solvent under reduced pressure. The solid was collected on a Schlenk frit, and dried *in vacuo* to yield 529 mg (40%) of **6***a*. Infrared, ^1H, and $^{31}P\{^1H\}$ NMR spectral analysis showed this material to be identical in all respects to that produced by method A. Anal. calcd. for $C_{36}H_{63}ClIrP_3$: C 52.94, H 7.78, Cl 4.34; found: C 53.13, H 7.67, Cl 4.07.

cis-anti-mer-*[IrD_2Cl(Cyttp)]*

The reaction vessel and a syringe were rinsed with deuterium oxide and baked in an oven at 100°C for several hours. After evaporation *in vacuo* of a 0.25 M benzene solution of **1** (2.00 mL, 0.50 mmol) for 12 h, the oily residue was dissolved in ethanol-d_6 (2 ML), combined with $[IrCl(COD)]_2$ (167 mg, 0.25 mmol), and stirred for 1 day. The solvent was evaporated *in vacuo* and the residue was washed with acetone-d_6 and dried *in vacuo* to yield 162 mg (40%) of the title compound; ^2H NMR (C_6H_6) δ: −8.9 (d, *mer*-D, $^2J_{PD}$ 19 Hz), −22.0 (s, *apical*-D).

mer-*[IrH_3(Cyttp)]·C_2H_5OH, **6**b·*EtOH*

Method A

To a solution of $[IrCl(COD)]_2$ (206 mg, 0.31 mmol) in absolute ethanol (20 mL) was added a 0.25 M benzene solution of **1** (2.5 mL, 0.62 mmol), followed by a solution of KOH (50 mg, 0.89 mmol) dissolved in absolute ethanol (20 mL). The solution gradually changed color from red to cream. After stirring overnight, the white precipitate was filtered on a frit, and recrystallized (tetrahydrofuran/absolute ethanol) to give 224 mg (44%) of **6***b* as monoethanolate solvate.

Method B

To a solution of **6***c* (15 mg, 0.018 mmol) in tetrahydrofuran (20 mL) was added $NaBH_4$ (30 mg, 0.27 mmol). The mixture was allowed to stir for 20 min after which ethanol (10 mL) was added and the mixture allowed to stir for an additional 1 h. The solvent was removed under reduced pressure. Tetrahydrofuran (10 mL) was added to dissolve the product. After filtration, a ^{31}P NMR spectrum of the crude product showed complete conversion to **6***b*. Anal. calcd. for $C_{36}H_{64}IrP_3 \cdot C_2H_5OH$: C 55.10, H 8.52, Cl 0.00; found: C 54.52, H 8.76, Cl trace.

Mixture of cis-syn-mer- *and* cis-anti-mer-*[$IrH_2(CH_3CN)$(Cyttp)] [BF_4]*, **6**c

To a suspension of **6***a* (332 mg, 0.400 mmol) in CH_3CN (10 mL) was added $TlBF_4 \cdot 6H_2O$ (166 mg, 0.421 mmol). The reaction was allowed to stir for 2 h, during which time **6***a* reacted and went into solution and TlCl precipitated. The mixture was then filtered. The filtrate was evaporated *in vacuo* and the residue was washed with water and then dried *in vacuo* to yield 234 mg (63%) of **6***c*. The ^1H NMR spectrum revealed the presence of *cis-syn-mer* and *cis-anti-mer* isomers in 3:2 ratios, respectively. Anal. calcd. for $C_{38}H_{66}BF_4IrNP_3$: C 50.22, H 7.32, N 1.54; found: C 50.07, H 7.41, N 1.76.

cis-syn-mer-*[$IrH_2(CO)$(Cyttp)][BF_4]*, **6**d

To a solution of **6***a* (0.26 g, 0.32 mmol) and $TlBF_4 \cdot 6H_2O$ (0.12 g, 0.30 mmol) in tetrahydrofuran (30 mL) a slow stream of CO bubbles was introduced for a period of 3 h. The solution was then purged with N_2 for 15 min. The TlCl was removed by filtration, after which the solvent was removed under reduced pressure. The product, **6***d*, was separated from the starting material **6***a* by extraction of **6***d* with acetone. The acetone was removed under reduced pressure and the product was washed with water and recrystallized from acetone/ether to yield 0.10 g (35%) of **6***d*. Anal. calcd. for $C_{37}H_{63}BF_4IrOP_3$: C 49.61, H 7.09, P 10.37; found: C 49.78, H 7.29, P 10.10.

cis-anti-mer-*[IrH_2I(Cyttp)]*, **6**e

Method A

To a solution of **6***a* (152 mg, 0.19 mmol) in tetrahydrofuran (50 mL) was added solid NaI (1.30 g, 8.67 mmol). After stirring 4 h, the solvent was removed *in vacuo* and the residue was dissolved in benzene (30 mL). After filtering on a frit, absolute ethanol (60 mL) was added and a solid separated. Evaporation of the solvent *in vacuo* gave 144 mg (85%) of **6***e*.

Method B

To a solution of $[IrCl(COD)]_2$ (200 mg, 0.30 mmol) in acetone (15 mL) was added a solution of NaI (90 mg, 0.60 mmol) in acetone (10 mL). The resulting deep-purple slurry was stirred for 2 h, the solvent was removed *in vacuo*, and the residue was dissolved in benzene (10 mL). After filtering on a frit, half the solvent was removed *in vacuo*, and a solid separated upon addition of excess ether. The solid was collected on a frit, washed with acetone and then ether, and then dried *in vacuo* (0.1 Torr (1 Torr = 133.3 Pa)) to afford 133 mg (52%) of $[IrI(COD)]_2$ as an intermediate product. Starting with $[IrI(COD)]_2$, the same method B as for **6***a* yielded 40% of the title compound. Infrared, ^1H, and $^{31}P\{^1H\}$ NMR spectral analysis showed this material to be identical in all respects to that produced by method A. Anal. calcd. for $C_{36}H_{63}IIrP_3$: C 47.62, H 7.01, I 13.98; found: C 47.55, H 7.08, I 13.76.

Mixture of cis-syn-mer- *and* cis-anti-mer-*[$IrH_2(CN)$(Cyttp)]*, **6**f

To a solution of **6***a* (266 mg, 0.28 mmol) in a mixture of tetrahydrofuran (30 mL) and 95% ethanol (30 mL) was added KCN (602 mg, 0.24 mmol). After stirring for 12 h, the solvent was removed *in vacuo*, the residue was dissolved in benzene, and the solution was filtered. Upon addition of a 1:1 mixture of 95% ethanol/water, a solid separated. The solid was collected on a frit and dried *in vacuo* to give 154 mg (69%) of **6***f*. The ^1H NMR spectrum revealed the presence of *cis-syn-mer* and *cis-anti-mer* isomers in 1:9 ratio respectively. Anal. calcd. for $C_{37}H_{63}IrNP_3$: C 55.07, H 7.87, N 1.74; found: C 54.91, H 7.89, N 1.77.

Can. J. Chem. Downloaded from www.nrcresearchpress.com by 109.225.110.28 on 09/08/12
For personal use only.

Mixture of cis-syn-mer- *and* cis-anti-mer-*[$IrH_2(P(OCH_2)_3CEt)(Cyttp)$][$BF_4$]*, **6**g*

To a solution of **6***a* (300 mg, 0.37 mmol) in tetrahydrofuran (25 mL) was added $TlBF_4 \cdot 6H_2O$ (150 mg, 0.38 mmol) followed by $P(OCH_2)_3CEt$ (75 mg, 0.46 mmol). After stirring for 3 h, during which time TlCl precipitated, acetone (25 mL) was added and the mixture was filtered. The filtrate was evaporated *in vacuo* and the residue was washed with water and then recrystallized (acetone/ether) to give 299 mg (79%) of **6***g*. The ^{1}H NMR spectrum revealed the presence of *cis-syn-mer* and *cis-anti-mer* isomers in 2:1 ratio, respectively. Anal. calcd. for $C_{42}H_{74}BF_4IrO_3P_4$: C 52.53, H 7.43, P 12.32; found: C 52.46, H 7.45, P 12.09.

Mixture of cis-syn-mer- *and* cis-anti-mer-*[$IrH_2(SnCl_3)(Cyttp)$]*, **6**i*

To a solution of **6***a* (100 mg, 0.12 mmol) in dichloromethane (40 mL) was added anhydrous $SnCl_2$ (24 mg, 0.13 mmol). After stirring for 3 h, the mixture was filtered and the solvent was removed *in vacuo*. The solid was suspended in hexane, collected on a frit, washed with hexane, and dried *in vacuo* to yield 80 mg (65%) of **6***i*. The ^{1}H NMR spectrum revealed the presence of *cis-syn-mer* and *cis-anti-mer* isomers in 3:2 ratio, respectively. Anal. calcd. for $C_{36}H_{63}Cl_3IrP_3Sn$: C 42.98, H 6.31, Cl 10.57; found: C 42.88, H 6.10, Cl 10.80.

cis-anti-mer-*[$IrHCl_2(Cyttp)$]*, 7*a

To a solution of **6***a* (100 mg, 0.122 mmol) in tetrahydrofuran (20 mL) was added 1 mL of 6 M aqueous HCl. The solution was allowed to stir for 3 h. After removing the solvent under reduced pressure and washing with hexanes, 85 mg (81%) of 7*a* was obtained. Anal. calcd. for $C_{36}H_{62}Cl_2IrP_3$: C 50.82, H 7.34, Cl 8.33; found: C 51.00, H 7.42, Cl 8.19.

Mixture of cis-syn-mer- *and* cis-anti-mer-*[$IrH(CS_2H)(Cyttp)$][AsF_6]*, 7b

To a solution of **6***a* (184 mg, 0.23 mmol) in tetrahydrofuran (25 mL) was added $TlAsF_6 \cdot 6H_2O$ (120 mg, 0.24 mmol) followed by CS_2 (5 mL). The solution immediately became yellow in color as TlCl precipitated. After stirring for 20 min, most of the solvent was removed under a stream of nitrogen and the remainder was removed *in vacuo*. Acetone (25 mL) was added to the residue, the mixture was filtered, and the solvent was removed *in vacuo*. The residue was washed with water, dried *in vacuo*, and recrystallized (acetone/ether) to give 179 mg (76%) of 7*b*. The ^{1}H NMR spectrum revealed the presence of *cis-syn-mer-* and *cis-anti-mer* isomers in 7:3 ratio, respectively. Anal. calcd. for $C_{37}H_{63}AsF_6IrP_3S_2$: C 42.48, H 6.07, S 6.13; found: C 42.29, H 6.10, S 6.00.

cis-syn-mer-*[$IrH(O_2CCH_3)(Cyttp)$][AsF_6]*, 7c

To a solution of **6***a* (85 mg, 0.10 mmol) in tetrahydrofuran (30 mL) was added $TlAsF_6 \cdot 6H_2O$ (53 mg, 0.11 mmol) followed by glacial acetic acid (0.50 mL, 8.7 mmol). After stirring for 0.5 h, the solvent was removed *in vacuo*, the residue was extracted with acetone (30 mL), and the solvent volume was reduced to about 10 mL under a stream of nitrogen. A solid separated upon addition of excess ether. The solid was filtered, washed with water, and dried *in vacuo* to give 71 mg (66%) of 7*c*. Anal. calcd. for $C_{38}H_{65}AsF_6IrO_2P_3$: C 44.36, H 6.38, F 11.08; found: C 45.14, H 6.42, F 11.41.

apical(H,CH_3)-anti-mer-*[$IrH(CH_3)(CO)(Cyttp)$][BPh_4]*, **8**a

A solution of $[IrCl(COD)]_2$ (541 mg, 0.81 mmol) and $AgBF_4$ (378 mg, 1.94 mmol) in absolute ethanol (25 mL) was heated gently for 5 min and the precipitated AgCl was removed by filtration. A 0.25 M benzene solution of **1** (6.5 mL, 1.63 mmol) was added to the filtrate and the solution was refluxed for 1 h. The solution changed color from red to pale yellow. The solid which separated upon addition of excess $NaBPh_4$ (750 mg, 2.19 mmol) was collected on a frit, washed with absolute ethanol, recrystallized from CH_2Cl_2/ethanol, and dried *in vacuo* to give 600 mg (32%) of **8***a*. Anal. calcd. for $C_{62}H_{85}BIrOP_3$: C 65.19, H 7.50, P 8.13; found: C 64.68, H 7.49, P 7.79.

Mixture of apical(H,Cl)-syn-mer-, *and* apical(H,I)-syn-mer-, apical(H,Cl)-anti-mer-, *and* apical(H,I)-anti-mer-*[$IrHCl(Cyttp)$]*, **8**b*

A solution of **6***a* (100 mg, 0.12 mmol) and iodine (40 mg, 0.16 mmol) in tetrahydrofuran (20 mL) was stirred for 1 h. The resultant precipitate was collected on a frit, washed with acetone, and dried *in vacuo* to yield 88 mg (76%) of **8***b*. The ^{1}H NMR spectrum revealed the presence of two *apical(H,X)-syn-mer* and two *apical(H,X)-anti-mer* isomers in (1:1):(7:11) ratio, respectively. Anal. calcd. for $C_{36}H_{62}ClIIrP_3$: C 45.88, H 6.63, I 13.47; found: C 45.76, H 6.55, I 13.29.

Mixture of apical(H,Cl)-syn-mer, *and* apical(H,CH_3CN)-anti-mer-*[$IrHCl(CH_3CN)(Cyttp)$][BF_4]*, **8**c*

A solution of $C_7H_7BF_4$ (35 mg, 0.20 mmol) in CH_3CN (20 ml) was added to a solution of **6***a* (150 mg, 0.18 mmol) via a stainless steel needle. The resulting mixture was stirred for 5 h after which the solvent was evaporated *in vacuo*. The product was redissolved in methylene chloride and filtered. The solution volume was reduced to 5 mL and the product was precipitated upon the addition of Et_2O to yield 112 mg (64%) of **8***c*. Anal. calcd. for $C_{38}H_{65}BClF_4IrNP_3$: C 48.38, H 6.95, N 1.48; found: C 48.23, H 6.68, N 1.31.

Results and discussion

Determination of syn-/anti *configuration*[5]

The configurational assignment of complexes **6**–**8** was based on ^{1}H NMR spectroscopic analysis of the heteronuclear AMRX$_2$ five-spin system (diagram **9**). The *apical-* and *mer*-hydrido protons (nuclei 3 and 4, respectively) are readily differentiated on the basis of their respective geminal heteronuclear coupling constants to phosphorus. For the *apical*-hydrido proton, the two heteronuclear coupling constants ($^2J_{13}$ and $^2J_{23}$) are with *cis*-coupled nuclei. For the *mer*-hydrido proton, this relationship is true for only one coupling constant ($^2J_{24}$), whereas the other ($^2J_{14}$) arises from a *trans* internuclear relationship and, as such, is expected to be considerably larger in magnitude (16). The *syn-/anti*-configurational orientation of nucleus 3 vis-a-vis the phenyl group was determined by nuclear Overhauser effect (difference NOE) experiments involving irradiation of the phenyl-ring *ortho* protons (nuclei 5 and 6), see diagrams **10** and **11**. Typical NOE intensity enhancements for nucleus 3 were ca. 5–7% (5, 6).

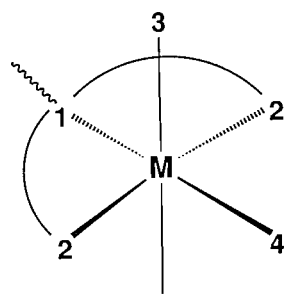

9

[5]The *cis* and *mer* descriptors will be eliminated for simplicity and only the *syn/anti* descriptors for Ir-Cyttp complexes **6**, **7** will be used from now on in the text. All the six-coordinate iridium(III) Cyttp complexes discussed in this paper have *cis* stereochemistry. Since all the complexes **6**–**8** discussed in this paper have *mer*-coordinated Cyttp ligands, the *mer* descriptors will also be eliminated for simplicity in the case of complexes **6**–**8**.

Can. J. Chem. Downloaded from www.nrcresearchpress.com by 109.225.110.28 on 09/08/12
For personal use only.

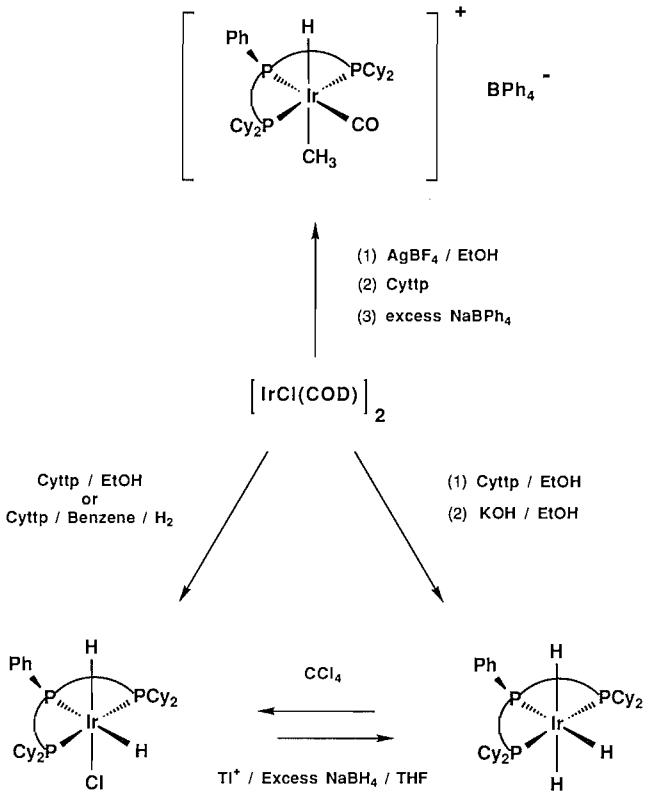

SCHEME 1

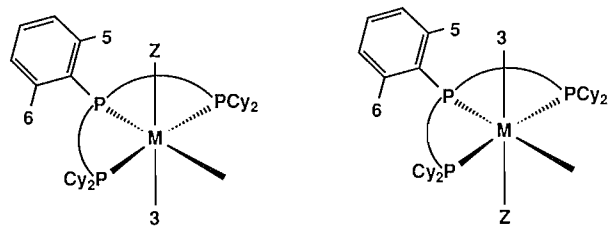

10 11

The two signals at δ ca. 8.1 and δ ca. 7.6 (ratio 2:3, respectively) in 500 MHz ^{1}H NMR spectra of complexes **6–8** were assigned to the *ortho* and *meta/para* aromatic protons, respectively. Only for the *anti* configuration (diastereomer **11**) is a NOE expected for nucleus 3 upon irradiation of nuclei 5 and 6 (11). It is noted that the analogous ttp complexes are not amenable to NOE {Ph–H} determination of *syn/anti* configuration, since ttp has phenyl groups on both sides of the meridional plane.

Preparation of complexes

Scheme 1 illustrates syntheses routes for *anti*-[IrH_2Cl(Cyttp)], ***6a***. We have previously reported that ***6a*** can be prepared directly by treating $[IrCl(COD)]_2$ with Cyttp in boiling ethanol (1*a*). The dideuteride analogue can be prepared by reacting $[IrCl(COD)]_2$ with Cyttp in ethanol-d_6. We have also found that ***6a*** can be synthesized by a two-step procedure in which the five-coordinate complex [IrCl(COD)(Cyttp)], **12**, is prepared as an intermediate by the reaction of $[IrCl(COD)]_2$ with Cyttp in benzene. This compound can be isolated as a yellow solid. The ^{31}P NMR of **12** shows only two of the three phosphorus atoms of the ligand are bound to iridium. An analogous five-coordinate iridium(I) complex, [IrCl(COD)$(PMe_3)_2$] has previously been reported (17). One of the two terminal phosphorus atoms in **12** is unbound (−7.8 ppm) and shows the value as the corresponding unbound phosphorus in [$PtMe_2$(Cyttp)] (18). Treatment of **12**, generated *in situ*, with H_2 gas also produced only one dihydride complex, *anti*-[IrH_2Cl(Cyttp)] ***6a***.

It was previously reported by Dahlenburg and co-workers (2) that treatment of $[IrCl(C_8H_{14})_2]_2$ with ttp in toluene resulted in complete displacement of the monodentate olefin ligand to yield the four-coordinate iridium(I) complex [IrCl(ttp)]. Introduction of hydrogen gas into a toluene solution of [IrCl(ttp)] produced an unspecified isomer of *cis-mer*-[IrH_2Cl(ttp)] (2). We found that [IrCl(Cyttp)] prepared in an analogous manner was somewhat unstable and forms a compound which we have so far been unable to characterize.[6,7] Preliminary results indicate, however, that the addition of H_2 to benzene solutions of [IrCl(Cyttp)] produced both *syn*- and *anti*-[IrH_2Cl(Cyttp)].[7]

Reaction of $[IrCl(COD)]_2$ with an ethanolic solution of $AgBF_4$, filtration of the AgCl precipitate, followed by addition of the Cyttp ligand resulted in the isolation of one diastereomer of the [$IrH(CH_3)$(CO)(Cyttp)][BPh_4] complex, ***8a***, upon treatment of the reaction mixture with $NaBPh_4$. The configuration of this diastereomer was determined by multinuclear NMR spectroscopy to be *apical(H,CH_3)-antimer*. The hydrido proton was found to be in an *apical* orientation on the same side of the three-phosphorus atom reference plane as the phenyl ring by ^{1}H NMR difference NOE spectroscopy. The carbonyl group, which is seen both in IR and ^{13}C NMR spectra, is *trans* to phosphorus on the basis of the large $^2J_{PC}$ coupling constant. The sixth ligand site (*trans* to the hydride) is occupied by a methyl group as evidenced by ^{13}C NMR DEPT (19) experiments (positive intensity versus ca. null in 135° versus 90° pulse-width spectra). The very high-field (−33.61 ppm) methyl carbon signal is consistent with CH_3 bound to a platinum metal (20). Abstraction of carbon monoxide from boiling alcoholic solvents by phosphine complexes of platinum metals has been well documented (21). The removal of chloride from iridium apparently opens up a site for decarbonylation to take place. The facility of the reaction in this case is most unusual.

The trihydride complex *mer*-[IrH_3(Cyttp)], ***6b***, was prepared by reaction of ligand with $[IrCl(COD)]_2$ followed by treatment with ethanolic KOH. Single crystal X-ray diffraction studies of ***6b*** · EtOH confirm the presence of three hydrides in a *mer* configuration (6). Structural constraints imposed by a chelating ligand can be an important factor in promoting isomer stability, as shown by the fact that only ^{1}H NMR resonances attributable to the *mer*-isomer ***6b*** were noted in C_6D_6 solution (*vide infra*) as opposed to [$IrH_3(PPh_3)_3$] which shows *mer/fac* isomerization in the same solvent (22).

Iridium–hydride reactivity

The reaction conditions and product stereochemistry of complexes discussed in this and in the following section are summarized in Table 1. Early workers in iridium(III) hydride chemistry found that hydrido ligands *trans* to phosphorus ligands are labile to attack by mineral acids, whereas hydride ligands *trans* to chloro ligands are stable (22, 23). For example, it was noted that *cis-mer*-[$IrH_2Cl(PEt_2Ph)_3$]

[6] C. Yang, S. M. Socol, and D. W. Meek. Unpublished results.
[7] C. Prengel, E. H. K. Zeiher, and D. W. Meek. Unpublished results.

TABLE 1. Reactions of *cis-anti-mer*-[IrH_2Cl(Cyttp)] (**6***a*) discussed in this paper[a]

Reagents	Products
Excess $TlBF_4$, excess $NaBH_4$	**6***b*, [IrH_3(Cyttp)]
Excess $TlBF_4$, excess CH_3CN[b]	**6***c*, *syn-/anti*-[$IrH_2(CH_3CN)$(Cyttp)][BF_4] 3:2
Excess $TlBF_4$, excess CO	**6***d*, *syn*-[IrH_2(CO)(Cyttp)][BF_4]
Excess NaI	**6***e*, *syn*-[IrH_2I(Cyttp)]
Excess KCN[c]	**6***f*, *syn-/anti*-[IrH_2(CN)(Cyttp)] 1:9
1 equiv. $TlBF_4$, 1.25 equiv. $P(OCH_2)_3CEt$	**6***g*, *syn-/anti*-[$IrH_2(P(OCH_2)_3CEt)$(Cyttp)][BF_4] 2:1
1 equiv. $TlBF_4$, 1.25 equiv. PMe_2Ph	**6***h*, *syn-/anti*-[$IrH_2(PMe_2Ph)$(Cyttp)][BF_4] 3:4
1 equiv. anh. $SnCl_2$[d]	**6***i*, *syn-/anti*-[$IrH_2(SnCl_3)$(Cyttp)] 3:2
Excess aq. HCl	**7***a*, *anti*-[$IrHCl_2$(Cyttp)]
1 equiv. $TlAsF_6$, excess CS_2	**7***b*, *syn-/anti*-[$IrH(S_2CH)$(Cyttp)][AsF_6] 7:3
1 equiv. $TlAsF_6$, excess glacial HOAc	**7***c*, *syn*-[$IrH(O_2CCH_3)$(Cyttp)][AsF_6]
1.3 equiv. I_2	**8***b*, *apical(H,X)-syn/apical(H,X)-anti*-[IrHClI(Cyttp)] (1:1):(7:11)[e]
1 equiv. $C_7H_7BF_4$, excess CH_3CN[b]	**8***c*, *apical(H,Cl)-syn*-and *apical(H,CH_3CN)-anti*-[$IrHCl(CH_3CN)$(Cyttp)][BF_4]

[a]All reactions were performed in THF, unless noted otherwise, and at ambient temperature.
[b]Solvent = CH_3CN.
[c]Solvent blend = 95% EtOH/THF (1:1).
[d]Solvent = CH_2Cl_2.
[e]X = Cl or I.

reacted with HCl in ethanol to yield *cis-mer*-[$IrHCl_2(PEt_2Ph)_3$] (22). Likewise, we have found that the addition of aqueous HCl to THF solutions of *anti*-[IrH_2Cl(Cyttp)] (**6***a*) produced only one diastereomer, *anti*-[$IrHCl_2$(Cyttp)], **7***a*, in a stereoselective manner.

On the other hand, the reaction of *anti*-[IrH_2Cl(Cyttp)], **6***a*, with an electrophilic reagent, I_2, afforded four products. Partial configurational assignments of the two major *apical(H,Cl)/apical(H,I)-anti* isomers (54%, 34%) and of the two minor *apical(H,Cl)/apical(H,I)-syn* isomers (7%, 5%) of [IrHClI(Cyttp)], **8***b*, were made on the basis of ^{1}H NMR spectroscopy. In a mixed sample containing all four species, the single hydrido signal from each of the four diastereomers exhibited only *cis* $^2J_{HP}$ coupling constants characteristic of *apical*-hydrido ligands, whereas only the apical protons in the two major species showed NOE intensity enhancement (5 (6)).

The reaction of *anti*-[IrH_2Cl(Cyttp)] **6***a* with the electrophile $C_7H_7^+$ in CH_3CN solution forms two products of the formulation *mer*-[$IrHCl(CH_3CN)$(Cyttp)][BF_4] **8***c*. The major (>80%, $\delta_{H(3)} = -20.30$) and minor ($\delta_{H(3)} = -20.40$) products both show an NOE intensity enhancement for the *apical* hydride {$H_{phenyl\text{-}ortho}$} in solution. These isomers are thus assigned as geometric isomers in which either Cl or CH_3CN is *trans* to the hydride. Since it has been shown here and elsewhere (22, 23) that hydride ligands *trans* to phosphorus ligands tend to be inert, it is most likely that the hydride ligand attacked is the hydride ligand which is initially *trans* to chlorine, and the two geometric isomers are formed via a five-coordinate intermediate. Ciani and co-workers (24) have previously proposed that the substitution of metal hydrides with $C_7H_7^+$ in the presence of donor species takes place by a two-step mechanism in which the first step is the abstraction of the H^- ligand.

Transition-metal complexes which contain labile ligands are known to insert CS_2 (25). For example, the reaction of $IrH_3(PPh_3)_3$ with CS_2 in benzene produced $IrH_2(S_2CH)(PPh_3)_2$ (26). It was found that *anti*-[IrH_2Cl(Cyttp)] (**6***a*) did not react with refluxing CS_2, most likely due to the tendency of the chelating triphosphine ligand not to dissociate (26). However, introduction of $TlAsF_6$ to a solution of **6***a* and CS_2 in THF at ambient temperature resulted in the formation of 2:1 *syn-/anti*-[$IrH(S_2CH)$(Cyttp)][AsF_6], **7***b*. The existence of the dithiofomate moiety was confirmed by signals in the ^{1}H NMR spectrum (acetone-d_6) at δ 13.9 and δ 14.2 for the dithioformyl proton in the *syn* and *anti* diastereomer, respectively (25).

Lack of an NOE suggested the *syn* configuration for the single [$IrH(O_2CCH_3)$(Cyttp)][AsF_6] diastereomer, **7***c*, stereoselectively formed from the reaction of *anti*-[IrH_2Cl(Cyttp)] **6***a*, $TlAsF_6$, and acetic acid in THF. Configurational inversion in the product was confirmed by single-crystal X-ray diffraction analysis which indicated that the acetato ligand was bound to both the *mer* position and to an *apical* site on the same side as the phenyl moiety vis-a-vis the three-phosphorus atom reference plane.[8]

The monohydrido products **7** and **8** discussed above all share a common structural feature; the hydrido ligand is always found in an *apical* binding site. The *syn/anti* configurations, however, varied. In the single diastereomeric product [$IrHCl_2$(Cyttp)] (**7***a*) the *anti* geometry was retained. On the other hand, in the single diastereomeric product [$IrH(O_2CCH_3)$(Cyttp)][AsF_6] **7***c*, an inversion to the *syn* configuration was noted. Finally, in the case of [IrHClI(Cyttp)] **8***b* and [$IrH(HCS_2)$(Cyttp)][AsF_6] **7***b* products, stereochemical integrity was lost as evidenced by the appearance of both *syn* and *anti* species.

Metal hydride complexes are also known to react with halogenated solvents to form the corresponding metal chlorides (27). When [IrH_3(Cyttp)] **6***b* was dissolved in CCl_4 in an NMR tube at ambient temperature, *anti*-[IrH_2Cl(Cyttp)] **6***a* and *anti*-[$IrHCl_2$(Cyttp)] **7***a* were formed in a 4:1 ratio as shown by the $^{31}P\{^1H\}$ NMR spectrum recorded after 15 min. At room temperature *anti*-[IrH_2Cl(Cyttp)] **6***a* was found to be surprisingly stable in CCl_4, although it was found that refluxing for four h resulted in ca. 20% conversion to *anti*-[$IrHCl_2$(Cyttp)] **7***a*. It is significant that syntheses by multiple routes (three for **6***a* and two for **7***a*) afforded the same chloro ligand containing iridium(III) complexes only in the *anti* configuration. In light of the generally observed loss of

[8]C. Yang, S. M. Socol, R. Glaser, J. C. Gallucci, and D. W. Meek. Unpublished results.

Can. J. Chem. Downloaded from www.nrcresearchpress.com by 109.225.110.28 on 09/08/12
For personal use only.

Can. J. Chem. Downloaded from www.nrcresearchpress.com by 109.225.110.28 on 09/08/12
For personal use only.

starting material configurational integrity (e.g., **7***b*,*c* and **8***b*), this apparent stereoselectivity for **6***a* and **7***a* is likely to reflect a thermodynamic bias.

Iridium–chloride bond reactivity

Previously we have reported that the iridium–chloride bond in *anti*-[IrH_2Cl(Cyttp)] **6***a* can be metathesized by CO, CH_3CN (both in the presence of $TlBF_4$), and I^- in THF solution to form products with differing stereochemical configurations (the single *syn* diastereomer of [IrH_2(CO)(Cyttp)][BF_4] (**6***d*); a 3:2 mixture of *syn*/*anti* diastereomers of [IrH_2(CH_3CN)(Cyttp)][BF_4] (**6***c*); and only the single *anti* diastereomer of [IrH_2I(Cyttp)] (**6***e*) (1*a*)). Other metathesis reactions were investigated in which the chloro ligand was replaced by cyanide, $P(OCH_2)_3CEt$, or PMe_2Ph.

In contrast to the metathesis of *anti*-[IrH_2Cl(Cyttp)] (**6***a*) by iodide in THF, reaction with cyanide (in THF/95% EtOH (1:1)) afforded a mixture of *syn*-/*anti*-[IrH_2(CN)(Cyttp)] diastereomers, **6***f*, in a ratio of ca. 1:9, respectively. Diastereomeric product mixtures were also observed when $P(OCH_2)_3CEt$ or PMe_2Ph were reacted with THF solutions of **6***a* in the presence of $TlBF_4$. In the case of the [IrH_2($P(OCH_2)_3CEt$)(Cyttp)][BF_4] (**6***g*) reaction product, the *syn*/*anti* ratio was ca. 2:1, respectively, whereas for [IrH_2(PMe_2Ph)(Cyttp)][BF_4] (**6***h*) the ratio was ca. 3:4, respectively.

Acetonitrile coordinated to iridium(III) has been shown to be somewhat labile (28, 29) and replaceable by stronger ligands (30). Accordingly it was found that the addition of $P(OCH_2)_3CEt$ to a THF solution of a ratio 3:2 of *syn*-/*anti*-[IrH_2(CH_3CN)(Cyttp)][BF_4] (**6***c*) resulted in the displacement of CH_3CN to form the corresponding **6***g* complex (*syn*-*anti* ratio ca. 2:1). The mixture of *syn*-/*anti*-[IrH_2($P(OCH_2)_3CEt$)(Cyttp)][BF_4] diastereomers (**6***g*) was found to be stable overnight in CH_3CN. The CH_3CN ligand in the diastereomeric mixture of **6***c* did not exchange noticeably overnight in acetone, THF, or ethanol solutions. This is in accordance with reports by Moore and co-workers (28) that coordinated acetone is 10^5 times more labile than coordinated acetonitrile in complexes of the $[IrH_2(PPh_3)_2(solvent)_2]^+$ type and the work of Crabtree *et al.* (29) which showed that CH_3CN is more strongly bound in these complexes than is acetone, THF, ethanol, or water.

We have previously shown that the acetonitrile ligand in both diastereomers of [IrH_2(CH_3CN)(Cyttp)][BF_4] (**6***c*), *syn*/*anti* ratio of 1:2, can be metathesized by bubbling CO gas into the THF solution to yield only the *syn* diastereomer of [IrH_2(CO)(Cyttp)][BF_4] (**6***d*) (1*a*). The same single *syn* isomer of **6***d* is also formed by the direct treatment of *anti*-[IrH_2Cl(Cyttp)] with $TlBF_4$ and CO bubbled into the THF solvent (1*a*). The configurational characterization of the *syn* diastereomer **6***d* was made on the basis of the lack of an NOE between hydride and phenyl and subsequently confirmed by single crystal X-ray diffraction analysis.[8] The presence of only the single *syn* diastereomer **6***d* suggests that a common intermediate arises from both the *syn*- and the *anti*-[IrH_2(CH_3CN)(Cyttp)][BF_4] **6***c* starting materials.

In contrast to the reactions of RuH_4(Cyttp) with neutral monodentate ligands, where steric factors seem to determine the stereochemistry of the initial complexes formed (10*c*), the factors which determine the stereochemical outcome of the substitution reactions reported herein are not obvious, although the fact that inversion does sometime take place is indicative of a dissociative mechanism in which the configurational integrity of the starting material is lost. The fact that the addition of Tl^+ facilitates these reactions supports this conclusion. A dissociative mechanism has previously been proposed for solvent exchange with $[Ir(PR_3)_2(solvent)_2H_2]^+$ (28). Although the fact that *syn*-[IrH_2CO(Cyttp)]$^+$ is synthesized stereospecifically by two routes suggests a thermodynamic bias, the relative importance of thermodynamic and kinetic factors in the remainder of the substitution reactions is unclear.

The iridium–chlorine bond in *anti*-[IrH_2Cl(Cyttp)] (**6***a*) can be reduced with $NaBH_4$ to produce [IrH_3(Cyttp)] **6***b*. The trihydride complex, **6***b*, is also produced by the reaction of [IrH_2(CH_3CN)(Cyttp)][BF_4] **6***c* diastereomers and $NaBH_4$, with the latter reaction being much faster. The **6***c* diastereomeric mixture was quantitatively converted to *mer*-[IrH_3(Cyttp)] (**6***b*) after 20 min at ambient temperature. On the other hand, no reaction was observed for the case of **6***a* under the same conditions, whereas refluxing the reaction mixture for 2 h afforded an 80% conversion to **6***b*. The $NaBH_4$ reaction with **6***a* became more facile upon the addition of excess Tl^+, and a 95% conversion to **6***b* was noted after 15 min at room temperature (during which time Tl(I) was reduced to Tl(0)).

Iridium(III) chloride complexes have also been known to insert $SnCl_2$ (31). The addition of $SnCl_2$ to CH_2Cl_2 solutions of *anti*-[IrH_2Cl(Cyttp)] **6***a* produced a *syn*/*anti* mixture of [IrH_2SnCl_3(Cyttp)] diastereomers, **6***i*, in the ratio of 3:2, respectively. The ^1H NMR parameters of the **6***i* diastereomers are consistent with those observed for *cis*-*mer*-[$IrH_2SnCl_3(PPh_3)_3$], **13** (32). Single crystal X-ray diffraction analysis of **13** confirmed the *mer* arrangement of the three phosphine ligands and the *cis* relationship of the two hydrido protons (32).

Spectroscopic studies

It is well established that the position of the hydrido proton resonance in ^1H NMR spectra of iridium(III) hydride complexes is a function of the nature of the *trans* ligand (33, 34). Ligands which have high *trans* influence in square planar platinum(II) complexes induce downfield shifts in the resonance of *trans* hydrido nuclei in iridium(III) complexes. In addition, Olgemoller and Beck (35) found that a linear relationship exists between the $\nu_{Ir\text{-}H}$ stretching frequency and the $\delta_{H(hydride)}$ value in ^1H NMR spectra of [IrHCl(CO)L-$(PPh_3)_2$]$^{(0\text{ or }1+)}$, where L is a neutral or anionic ligand (r = 0.98). We found only a moderately good correlation of this plot in our system [r = 0.75 (r = 0.91 if the data for **6***b* are excluded)].[9] Part of the deviation from linearity of this plot may be due to vibrational interaction between the iridium hydride stretch and the *trans* moiety (36).

The chemical shift of the hydrido protons correlated with the *syn*/*anti* stereochemistry of complexes **6**–**8**. In all eight *syn*/*anti* pairs of diastereomers (**6***c*,*f*–*i*; **7***b*; **8***b*,*b*′) prepared in this study, the hydrido protons in the *anti* diastereomer always resonated at lower field than the protons in the corresponding *syn* diastereomer. The same behavior was also noted for the two *apical*-hydrido protons in *mer*-[IrH_3(Cyttp)] (**6***b*) in that the apical proton *syn*-to-phenyl resonated at a

[9]The hydride chemical shifts of mixtures **6***c*, **6***f*, **6***g*, **6***h*, **6***i*, **7***b*, **8***b*, and **8***c* were estimated by calculating a weighted average of the hydride shifts based on relative abundancies.

TABLE 2. NMR and infrared spectral parameters of Ir(III) complexes **6–8**[a]

Compound	δ_{P1}[b]	δ_{P2}[c]	δ_{H3}[d]	δ_{H4}[e]	$^2J_{12}$	$^2J_{13}$	$^2J_{14}$	$^2J_{23}$	$^2J_{24}$	$^2J_{34}$	ν(IrH3)[d]	ν(IrH4)[e]
6a[f]	−25.14[g]	−0.50[g]	−22.38[h]	−9.09[h]	26	7	130	14	17	6	2238	1995
6b[i]	−22.16[g]	9.97[g]	−12.30[h,j]	−12.53[h]	27	9	113	15	19	6	1720	1998
6c[k]	−38.16	−0.55	−21.79	−11.10	24	15	121	15	17	3	2242[l]	1995[l]
6c[f,m]	−30.74	−4.47	−20.97	−10.30	24	9	121	14	16	5	2242[l]	1995[l]
6d[k,n]	−37.48[g]	−0.89[g]	−12.01[o]	−11.81[o]	22	18	107	18	16	<1	2103	ca.2000
6e[f]	−35.52[g]	−7.80[g]	−20.09[h]	−10.38[h]	26	7	126	13	16	6	2225	2000
6f[k,p]	−41.06[g]	−1.20[g]	−15.34[o]	−12.66[o]	26	17	120	17	17	<2	2075[l]	2015[l,q]
6f[f,p]	−31.38[g]	−3.35[g]	−14.51[o]	−11.92[o]	26	10	118	16	16	5	2075[l]	2015[l,q]
6g[k,r]	−42.89	−3.05	−13.00	−13.37	23	18	109	18	15	<1	2090[l]	2050[l]
6g[f,s]	−35.17	−9.96	−11.56	−11.57	24	14	107	14	14	<2	2090[l]	2050[l]
6h[k,t]	−55.17	−9.24	−14.56	−13.71	31	18	108	18	19	2	2065[l]	2031[l]
6h[f,u]	−48.78	−21.61	−13.10	−11.40	33	14	109	14	15	2	2065[l]	2031[l]
6i[k,v]	−35.03[w]	−8.77[w]	−17.43[o]	−13.26[o]	25	14	106	14	16	<1	2110[l]	2050[l]
6i[f,x]	−33.86[w]	−0.15[w]	−15.18[o]	−11.41[o]	28	11	100	11	13	2	2110[l]	2050[l]
7a[f]	−35.00[w]	−20.44[w]	−21.21[o]	—	21	12	—	12	—	—	2247	—
7b[k,y]	−35.52	−13.38	−18.91	—	22	16	—	16	—	—	[z]	—
7b[f,aa]	−21.32	−17.69	−18.13	—	23	13	—	13	—	—	[z]	—
7c[k]	−27.17	−2.91	−27.33	—	20	29	—	12	—	—	2260	—
8a[f,bb]	−34.74	−24.71	−10.81[o]	173.89[o,cc]	34	14	108	14	11	<1	2027	—
8b[k]	[z]	[z]	−21.80	—	[z]	10	—	12	—	—	2235[l,dd]	—
	[z]	[z]	−21.21	—	[z]	12	—	12	—	—	2235[l,dd]	—
8b[f]	−25.05	−37.46	−18.94	—	24	8	—	12	—	—	2235[l,dd]	—
	−19.55	−26.91	−18.34	—	24	12	—	12	—	—	2235[l,dd]	—
8c[f]	[ee]	[ee]	−20.30	—	23	12	—	12	—	—	2258	—
	[ee]	[ee]	−20.40	—	23	12	—	12	—	—	2258	—

[a] ^{1}H and ^{31}P{^{1}H} NMR spectra measured in acetone-d_6 and acetone, respectively, unless noted otherwise; δ_P and δ_H/δ_C values given in ppm from 85% H_3PO_4 and tetramethylsilane, respectively; indirect coupling constants (J) are in Hz; infrared data given in cm^{-1} and were measured in KBr pellets, unless noted otherwise.

[b] Cyttp internal P.

[c] Cyttp terminal P.

[d] *Apical* H.

[e] *Mer*-H nucleus, unless noted otherwise.

[f] *Anti* isomer.

[g] In THF.

[h] In C_6D_6.

[i] *Anti*-to-Ph *apical*-H nucleus 5: δ_5 −12,61, $^2J_{15}$ 18 Hz, $^2J_{25}$ 18 Hz, $^2J_{35}$ <1 Hz, $^2J_{45}$ 5 Hz.

[j] *Syn*-to-Ph *apical* H.

[k] *Syn* isomer.

[l] Value for mixture of diastereomers.

[m] Diastereotopic methylene-H nucleus 5: δ_5 2.48, $^4J_{45}$ 2.2 Hz.

[n] ν(CO) 1990 cm^{-1}.

[o] In CD_2Cl_2.

[p] ν(CN) 2115 cm^{-1}.

[q] 2025 cm^{-1} (shoulder).

[r] *Syn*-to-Ph *apical* phoshito-P nucleus 5: δ_5 81.0, $^2J_{15}$ 23 Hz, $^2J_{25}$ 23 Hz, $^2J_{35}$ 190 Hz, $^2J_{45}$ 25 Hz.

[s] *Anti*-to-Ph *apical* phosphito-P nucleus 5: δ_5 83.28. $^2J_{15}$ 12 Hz, $^2J_{25}$ 24 Hz, $^2J_{35}$ 199 Hz, $^2J_{45}$ 14 Hz.

[t] *Syn*-to-Ph *apical* monophosphino-P nucleus 5: δ_5 −64.58, $^2J_{15}$ 23 Hz, $^2J_{25}$ 20 Hz, $^2J_{35}$ 110 Hz, $^2J_{45}$ 19 Hz.

[u] *Anti*-to-Ph *apical* monophosphino-P nucleus 5: δ_5 −66.69, $^2J_{15}$ 16 Hz, $^2J_{25}$ 20 Hz, $^2J_{35}$ 119 Hz, $^2J_{45}$ 15 Hz.

[v] *Syn*-to-Ph *apical*-Sn nucleus 5: $^2J_{25}$ 149 Hz, $^2J_{35}$ 1177 Hz, $^2J_{45}$ 207 Hz.

[w] In CH_2Cl_2.

[x] *Anti*-to-Ph *apical*-Sn nucleus 5: $^2J_{25}$ 154 Hz, $^2J_{35}$ 1267 Hz, $^2J_{45}$ 122 Hz.

[y] Dithioformate-H nucleus 5: δ_5 13.90, $^4J_{15}$ 4 Hz, $^4J_{25}$ 4 Hz, $^4J_{35}$ <1 Hz.

[z] Not assigned.

[aa] Dithioformate-H nucleus 5: δ_5 14.19, $^4J_{15}$ 7 Hz, $^4J_{25}$ 7 Hz, $^2J_{35}$ <1 Hz.

[bb] *Anti*-to-Ph *apical* methyl-C nucleus 5: δ_5 −33.61, $^2J_{15}$ 8 Hz, $^2J_{25}$ 5 Hz; methyl-H nuclei 6: δ_6 0.06, $^3J_{16}$ 6 Hz, $^3J_{26}$ 4 Hz, $^3J_{36}$ <1 Hz; ν(CO) 2010 cm^{-1}.

[cc] *Mer* carbonyl-C nucleus.

[dd] 2240 cm^{-1} (shoulder).

[ee] Not assigned, chemical shifts of the four signals are all within a range of 20.5 ± 1.0 ppm.

lower field as compared with the apical proton which is *anti*-to-phenyl. Moreover, this correlation is also found in ^{1}H NMR spectra of diastereomeric ruthenium hydride compounds containing polyphosphine ligands that were reported earlier (7, 10*c*).

It is tempting to rationalize the upfield chemical shifts of the *apical* hydrides of the *syn* isomers as compared with the *anti* as being due to the *apical* hydrido being located in the deshielding region of the arene ring in the *anti* isomers (37). It is seen, however, that the *mer* hydrides, which have the same arrangement vis-a-vis the phenyl ring in both isomers, show a parallel trend (Table 2).

The relatively upfield chemical shifts of the *syn* isomer hydrides may be due, in part, to differences in metal–li-

Can. J. Chem. Downloaded from www.nrcresearchpress.com by 109.225.110.28 on 09/08/12
For personal use only.

Can. J. Chem. Downloaded from www.nrcresearchpress.com by 109.225.110.28 on 09/08/12
For personal use only.

gand bond lengths and shielding by metal *d*-electrons. The high-field shifts in the ^{1}H NMR of metal hydrides have been partially rationalized in terms of shielding by incomplete metal *d*-shells (38). This effect is dependent on the inverse cube of the distance from the hydride to the *d*-electrons and will thus be a function of the metal–hydride bond length (38). It would seem reasonable that metal – *apical* ligand *Z* distances would be shorter in *anti*-isomers **4** as opposed to *syn*-isomers **3** due to the less steric interactions involving the phenyl group attached to the Cyttp central phosphorus and the *syn*-to-phenyl *apical* ligand. A shorter metal–ligand bond will most likely increase the effective *cis* and *trans* influence of the ligand, lengthen the metal–hydride bonds, and thus mitigate the shielding effect of the metal *d*-orbitals. The observation that the difference in the chemical shift of H(3) in *syn* vs. *anti* isomers increases with increasing steric size of the *trans* ligand supports this explanation. For example, the difference in chemical shifts of the two mutually-*trans* hydrides in **6***b* is 0.22 ppm, as compared with 0.82 ppm and 0.83 ppm in **6***c* and **6***f* (where the *trans* ligands are the relatively small CH_3CN and CN), and 1.44, 1.46, 2.25 ppm in **6***g*, **6***h*, and **6***i*, respectively (where the *trans* ligands are larger). An analysis of the H(4) resonances yields the same result.

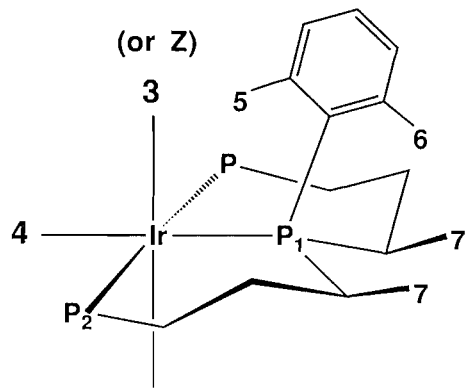

14

Of all the complexes **6**–**8** studied by ^{1}H NMR in this investigation, only one of them, *anti*-[$IrH_2(CH_3CN)$(Cyttp)]-[BF_4] (**6***c*) exhibited a long-range homonuclear coupling constant, $^4J_{47}$ 2.2 Hz, between the *mer*-hydrido proton and two chemical shift equivalent spin-1/2 nuclei. Selective homonuclear decoupling experiments showed the two nuclei to be the aliphatic protons H(7) giving rise to a signal at δ 2.48, see diagram **14**. Irradiation of the *ortho* aromatic protons resulted in a ca. 5% NOE enhancement for the δ 2.48 protons. The most likely candidates for H(7) are the pair of enantiotopic methylene protons adjacent (on both sides) to the central phosphorus nucleus. Using the X-ray diffraction structure of crystalline *anti*-[IrH_2Cl(Cyttp)] (**6***a*) as a model, these protons (which are not symmetry related in the solid state) are 2.30 and 2.52 Å away from one of the two *ortho* protons, and thus their positions are consistent with the observed NOE phenomenon. These chelating ring protons are favored candidates since long-range coupling constants of such a magnitude (2.2 Hz) are usually associated with relatively rigid arrangements in which the nuclei involved are disposed in a planar zig-zag path (39). It is presently unclear why only the *anti*-**6***c* diastereomer showed this long-range phenomenon.

In five of the six diastereomeric pairs reported herein (**6***c,f,g,h,i* and **7***b*) the P(1) nuclei in the *syn* diastereomer were found at higher field than in those of the corresponding *anti* diastereomers, whereas the P(2) nuclei in the *syn* diastereomers were found at relatively lower field. This relationship was also seen in the previously reported diastereomeric pairs of ruthenium hydride complexes which contain chelating triphosphines (7, 10*c*). The diastereomeric pairs of **6***i* do not follow this trend in that whereas the P(1) nucleus of the *syn* isomer was found upfield of the *anti* diastereomer, the P(2) nuclei of the *syn* diastereomer was also found at higher field than that of the corresponding *anti* isomer.

Conclusions

NMR spectroscopic techniques have been used to characterize the configuration of six-coordinate [IrH_2L(Cyttp)] diastereomeric pairs and to follow the stereochemical course of their reactions. Most of the reactions noted in this investigation proceed with a loss of the stereochemical integrity of the starting complex, which is suggestive of dissociative mechanisms. The relatively upfield chemical shifts of the hydride ligands in *syn* vs. *anti* isomers is rationalized in terms of expected shorter metal–hydride bond distances and, hence, greater shielding by metal *d*-orbitals.

Acknowledgements

The authors would like to thank Dr. Charles Cottrell for performing the NOE experiments and Mr. Carl Engleman for his assistance in producing some of the ^{1}H NMR spectra. Gratitude is also expressed to Prof. Robert Crabtree, Mr. Daniel Perreault, Ms. Heather Heywood, Dr. Michael DiPierro, and Dr. William C. Stevens for their assistance in the preparation of the manuscript. FT-NMR spectra at 11.75 T (500 MHz) were obtained at the Ohio State University Chemical Instrument Center using equipment funded in part by NIH grant no. 1 S10 RR01458-01A1. This study was partially supported by Proctor and Gamble Company's University Exploratory Research Program and by a grant from SOHIO.

1. (*a*) C. Yang, S. M. Socol, R. Glaser, D. J. Kountz, and D. W. Meek. Inorg. Chem. Acta, **114**, 119 (1986); (*b*) S. M. Socol, D. W. Meek, and R. Glaser. Polyhedron, **8**, 1903 (1989).
2. E. Arpac and L. Z. Dahlenburg. Z. Naturforsch. B, **36**, 672 (1981).
3. (*a*) J. B. Letts. Ph.D. Dissertation, The Ohio State University, Columbus, Ohio. 1982; (*b*) R. Uriarte, T. J. Mazanec, K. D. Tau, and D. W. Meek. Inorg. Chem. **19**, 79 (1980).
4. T. E. Nappier, Jr., D. W. Meek, R. M. Kirchner, and J. A. Ibers. J. Am. Chem. Soc. **95**, 4194 (1973).
5. K. D. Tau. Ph.D. Dissertation, The Ohio State University, Columbus, Ohio. 1978.
6. D. J. Kountz. Ph.D. Dissertation, The Ohio State University, Columbus, Ohio. 1984.
7. J. B. Letts, T. J. Mazanec, and D. W. Meek. J. Am. Chem. Soc. **104**, 3898 (1982).
8. J. E. Blackwood, C. L. Gladys, K. L. Loening, A. E. Petrarca, and J. E. Rush. J. Am. Chem. Soc. **90**, 509 (1968).
9. (*a*) R. S. Cahn, C. Ingold, and V. Prelog. Angew. Chem. Int. Ed. Engl. **5**, 385 (1966); (*b*) V. Prelog and G. Helmchen. Angew. Chem. Int. Ed. Engl. **21**, 567 (1982).
10. (*a*) L. Dahlenburg and C. Prengel. Inorg. Chim. Acta, **122**, 55 (1986); (*b*) L. Dahlenburg, N. Hock, and H. Berke. Chem.

Ber. **121**, 2083 (1988); (*c*) G. Jia, D. W. Meek, and J. C. Gallucci. Inorg. Chem. **30**, 403 (1991).
11. J. H. Noggle and R. E. Schirmer. The nuclear Overhauser effect–chemical applications. Academic Press, New York. 1971.
12. PANIC. Parameter adjustment in NMR by interaction calculation program. Bruker Analytische Messtichnik, Karlsruhe. 1982.
13. S. Castellano and A. A. Bothner-By. J. Chem. Phys. **41**, 3863 (1962).
14. R. H. Crabtree, J. M. Quirk, H. Felkin, and T. Fillebeen-Kahn. Synth. React. Inorg. Met. Org. Chem. **12**, 407 (1982).
15. T. J. Huttemann, B. M. Foxman, C. R. Sperati, and J. G. Verkade. Inorg. Chem. **4**, 950 (1965).
16. H. D. Kaesz and R. B. Saillant. Chem. Rev. **72**, 231 (1972).
17. M. J. Burk and R. H. Crabtree. Inorg. Chem. **25**, 931 (1986).
18. K. D. Tau, R. Uriarte, T. J. Mazanec, and D. W. Meek. J. Am. Chem. Soc. **101**, 6614 (1979).
19. D. M. Doddrell, D. T. Pegg, and M. R. Bendall, J. Magn. Reson. **48**, 323 (1982).
20. B. E. Mann. Adv. Organometal. Chem. **12**, 135 (1974).
21. (*a*) J. J. Levison and S. D. Robinson. J. Chem. Soc. A, 2947 (1970); (*b*) D. Evans, J. A. Osborn, and G. Wilkinson. Inorg. Synth. **11**, 99 (1968); (*c*) J. Chatt and B. L. Shaw. Chem. Ind. 931 (1960).
22. J. Chatt, R. S. Coffey, and B. L. Shaw. J. Chem. Soc. 7391 (1965).
23. L. Vaska. J. Am. Chem. Soc. **83**, 756 (1961).
24. T. Beringhelli, G. Ciani, G. D'Alfonso, P. Romiti, A. Sironi, and M. Freni. Inorg. Chem. **23**, 2849 (1984).
25. (*a*) S. Gopinathan, I. R. Unni, C. Gopinathan, V. G. Puranik, S. S. Tavale, and T. N. G. Row. Polyhedron, **6**, 1859 (1987); (*b*) S. D. Robinson and A. Sahajpal. Inorg. Chem. **16**, 2718 (1977); (*c*) M. Freni, D. Giusto, and P. Romiti. J. Inorg. Nucl. Chem. **33**, 75 (1971); (*d*) V. G. Albano, P. L. Bellon, and G. Ciani. J. Organomet. Chem. **31**, 75 (1971).
26. (*a*) T. E. Nappier, D. W. Meek, R. M. Kirchner, and J. A. Ibers. J. Am. Chem. Soc. **95**, 4194 (1973); (*b*) J. Niewahner and D. W. Meek. *In* Catalytic aspects of metal phosphine compounds. Vol. 196. *Edited by* E. C. Alyea and D. W. Meek. Advances in Chemistry Series, American Chemical Society, Washington. 1982. pp. 257–272.
27. R. A. Schurr. *In* Transition metal hydrides. *Edited by* E. L. Muetterties. Marcell Dekker, New York. 1971. pp. 203–270.
28. O. W. Howarth, C. H. McAteer, P. Moore, and G. E. Morris. J. Chem. Soc. Dalton Trans. 1171 (1984).
29. R. H. Crabtree, P. C. Demou, D. Eden, J. M. Mihelcic, C. A. Parnell, J. M. Quirk, and G. E. Morris. J. Am. Chem. Soc. **104**, 6994 (1982).
30. T. R. Greene and W. R. Roper. J. Organomet. Chem. **299**, 245 (1986).
31. R. G. Taylor, J. F. Young, and G. Wilkinson. Inorg. Chem. **5**, 20 (1966).
32. M. Kretschmer, P. S. Pregosin, A. Albinati, and A. Togni. J. Organomet. Chem. **281**, 365 (1985).
33. T. G. Appleton, H. C. Clark, and L. E. Manzer. Coord. Chem. Rev. **10**, 355 (1973).
34. D. S. Moore and S. D. Robinson. Chem. Soc. Rev. 415 (1983).
35. B. Olgemoller and W. Beck. Inorg. Chem. **22**, 997 (1983).
36. L. Vaska. J. Am. Chem. Soc. **88**, 4100 (1966).
37. E. D. Becker. High resolution MNR: theory and chemical applications. 2nd ed. Academic Press, New York. 1980. pp. 73–74.
38. A. D. Buckingham and P. J. Stephens. J. Chem. Soc. 4583 (1964).
39. R. K. Harris. Nuclear magnetic resonance spectroscopy. Pitman, London. 1983. p 223.

Can. J. Chem. Downloaded from www.nrcresearchpress.com by 109.225.110.28 on 09/08/12
For personal use only.

Differential reactivity of carbohydrate hydroxyls in glycosylations. I. Intramolecular interaction of the 5′-hydroxyl group with the heteroaromatic base in a model compound of 2′-deoxycytidine

TING-HUA TANG,[1] DENNIS M. WHITFIELD,[2] STEPHEN P. DOUGLAS,[2] AND JIRI J. KREPINSKY[2,3]

Protein Engineering Network of Centres of Excellence. Departments of Molecular and Medical Genetics, Medical Biophysics, and Chemistry, and Carbohydrate Research Centre, University of Toronto, Toronto, Ont., Canada M5S 1A8

AND

IMRE G. CSIZMADIA[3]

Lash Miller Laboratories, Department of Chemistry, University of Toronto, Toronto, Ont., Canada M5S 1A1

Received February 17, 1992

TING-HUA TANG, DENNIS M. WHITFIELD, STEPHEN P. DOUGLAS, JIRI J. KREPINSKY, and IMRE G. CSIZMADIA. Can. J. Chem. **70**, 2434 (1992).

It is a well-recognized conjecture that the unusual reactivity of certain carbohydrate hydroxyls in glycosylation reactions is due to non-covalent intramolecular bonding interactions involving that hydroxyl. A model compound 1-[β-D-2′,3′-dideoxyribofuranosyl]-2-(1*H*)-pyrimidinone, which is related to the poor glycosyl acceptor 2′-deoxy-3′-*O*,4-*N*-diacetylcytidine (**1**), has been studied in order to assess the effects of hydrogen bonding involving O5′—H and the heteroaromatic system present in the molecule. The conformational potential energy surfaces of the model compound (lacking only the acetoxy at C3′ and the acetamido at C4) were calculated, using semiempirical (PM3) and *ab initio* (STO-3G) methods. The O5′—H···O2 intramolecular hydrogen-bonded *syn* conformation of the model compound is the global minimum at the *ab initio* level of theory. The existence of this intramolecular hydrogen bonding was confirmed, theoretically, by Bader-type topological analysis of charge distribution at the 3-21G**//STO-3G level of theory. Such a conformation of the model compound strongly resembles that found for **1** by NMR in CD_2Cl_2 solution. The complex formation between this model compound and BF_3 was also studied at the STO-3G, 3-21G**//STO-3G, and 6-31G**//STO-3G levels of theory. The results explain why glycosylation of hydrogen-bonded substrates succeeds when promoted by Lewis acids.

TING-HUA TANG, DENNIS M. WHITFIELD, STEPHEN P. DOUGLAS, JIRI J. KREPINSKY et IMRE G. CSIZMADIA. Can. J. Chem. **70**, 2434 (1992).

Il est bien connu que la réactivité de groupes hydroxyles de certains hydrates de carbone dans les réactions de glycosylation est due aux liaisons intermoléculaires non covalentes impliquant ces groupes hydroxyles. Afin de déterminer les effets des liaisons hydrogènes O5′—H et le système hétéroaromatique présent dans la molécule, on a étudié la 1-[β-D-2′,3′-didéoxyribofuranosyl]-2(1*H*)-pyrimidinone, un modèle moléculaire apparenté à la 2′-déoxy-3′-*O*,4,*N*-diacétylcytidine (**1**), un faible accepteur de glycosyle. Faisant appel aux méthodes semi-empiriques (PM3) et *ab initio* (STO-3G), on a calculé l'énergie potentielle des surfaces d'énergie du composé modèle (dans lequel il ne manque que le groupe acétoxy en C3′ et le groupe acétamido en C4). Au niveau théorique *ab initio*, l'énergie de la conformation *syn* de la liaison hydrogène intramoléculaire O5′—H···O2 du composé modèle correspond à un minimum global. On a théoriquement confirmé l'existence de cette liaison hydrogène par une analyse topologique, du type Bader, de la distribution de charges au niveau théorique 3-21G**//STO-3G. Une telle conformation du modèle ressemble fortement à celle trouvée pour **1** par RMN en solution dans le CD_2Cl_2. On a également étudié la formation du complexe entre le composé modèle et le BF, aux niveaux théoriques STO-3G, 3-21G**//STO-3G et 6-31G**//STO-3G. Les résultats expliquent pourquoi les réactions de glycosylation des substrats ayant des liaisons hydrogènes se font avec succès lorsqu'on utilise des acides de Lewis comme catalyseurs.

[Traduit par la rédaction]

Introduction

It is a known phenomenon in carbohydrate chemistry that certain hydroxyl groups do not undergo glycosylation under standard conditions for the formation of glycosidic bonds (1). This is particularly surprising in the case of primary hydroxyl groups of aldohexopyranosides (C6) and aldopentofuranosides (C5) (2). In some cases the glycosylating agent glycosylates exclusively at the secondary hydroxyl[4] instead of the usually more reactive primary one (3). This happens in spite of the fact that in most cases one would expect that the primary hydroxyls should experience lesser steric hindrance. This puzzling situation negatively affects the planning and execution of multistep oligosaccharide syntheses. Since the efficient synthesis of oligosaccharides is of increasing importance for the application of biologically active glycopeptides and glycolipids in biomedical sciences and biotechnology industries (4), understanding and overcoming this unusual reactivity is essential for the rational development of oligosaccharide syntheses.

Closer examination of molecular models of substances with such unreactive hydroxyls does not suggest unusual steric problems. However, all observed cases contain a π-electron system, either aromatic or heteraromatic, or just double bonds. The π-electron systems are mostly in such

[1]Postal address: Department of Chemistry, University of Toronto.
[2]Postal address: Department of Molecular and Medical Genetics, University of Toronto.
[3]Authors to whom correspondence may be addressed.
[4]P. Sinay. Private communication.

Can. J. Chem. Downloaded from www.nrcresearchpress.com by 109.225.110.28 on 09/08/12
For personal use only.

Can. J. Chem. Downloaded from www.nrcresearchpress.com by 109.225.110.28 on 09/08/12
For personal use only.

protecting groups as benzyl or allyl (2), or in the heterocyclic base in the case of nucleosides.[5] In certain conformations these π-electron systems can be oriented to interact with the unreactive hydroxyl groups. A simplified case involving water and benzene molecules was investigated, and quantum chemical calculations showed that H_2O can interact with benzene in two different ways. In one, the O—H bond of water is perpendicular to the benzene ring and a hydrogen-bond-like interaction is present between the proton of water and the π-electron of benzene (approximately 2 kcal/mol). In the other, an electron lone pair of the oxygen is hydrogen-bonded to one of the aromatic C—H protons in an edge-on geometry (5, 6). Such interactions have been shown to be important for the structure of globular proteins (7). The question arises whether analogous intramolecular interactions could be responsible for the low reactivity (or unreactivity) in glycosylation reactions.

Such an interaction essentially involves a hydrogen bond (5, 8), and intramolecular hydrogen bonding in molecules containing hydroxyls as the proton donor (in systems such as O—H···O) has been used as an explanation of unusual reactivities on numerous occasions (3, 9–11). Since it appears that the oxygen of the hydroxyl experiences an increase in electron density (by the partial "removal" of the counterbalancing proton), the rates of reactions in which this oxygen acts as a nucleophile should be enhanced. This has indeed been observed in a large number of examples (3, 9–11). A decreased reactivity, or unreactivity, of hydrogen-bonded hydroxyls in certain apparently nucleophilic reactions is not satisfactorily explained. The reaction of diazomethane with hydroxyls resembles glycosylations in that proton dissociation is a necessary step. Certain hydrogen-bonded phenolic hydroxyls are unreactive with diazomethane and its derivatives (11). It may be postulated that proton loss is rate limiting in these cases.

Recently, during the syntheses of a series of 5′-*O*-galactosylated nucleosides in this laboratory, a low-reactivity problem involving the primary O5′—H was encountered.[5] This is surprising since the 5′-hydroxyl in nucleosides is the most reactive hydroxyl in the sugar portion of the molecule (3) and this fact has been utilized for differential protection in many synthetic strategies. Glycosylation reactions are normally described as nucleophilic attack of a hydroxyl of an aglycon at the anomeric carbon of a glycosylating agent. Considering 3′-*O*-,4-*N*-diacetyl-2′-deoxyribocytosine (**1**, cf. Fig. 1) (12) as an example, it seems obvious that access to the 5′-hydroxyl should not be hindered in any possible conformation. NMR studies have shown that in dichloromethane, a solvent typically used for glycosylation, the molecule adopted one predominant conformation that was suitable for formation of a hydrogen bond. This compound is small enough so that quantum chemical calculations might feasibly be carried out to confirm the presence or the absence of hydrogen bonding. Moreover, if no hydrogen bond exists, then such calculations could conceivably indicate whether any unusual electronic properties exist that could explain the low reactivity. Such rationalization by theoretical means is very desirable since it has recently become possible in our laboratory to overcome the unreactivity of such nucleosides

[5]D. M. Whitfield, S. P. Douglas, F. H. Moolten, T.-H. Tang, I. G. Csizmadia, and J. J. Krepinsky. Manuscript in preparation.

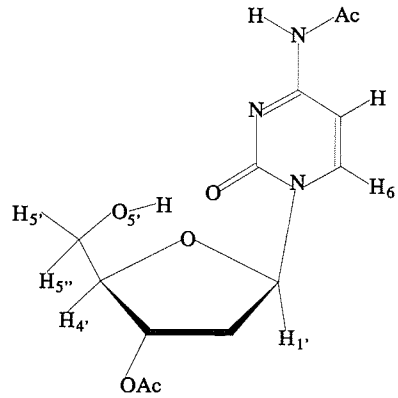

FIG. 1. *syn* Conformation of a 2′-deoxycytidine derivative (**1**).

using Lewis acid-catalyzed glycosylation conditions. It is, of course, a possibility that a stereoelectronic preference for glycosylation exists in a transition state that would not be available for hydrogen-bonded systems (13, 14).

The existence of intramolecular hydrogen bonding in nucleosides, including **1**, is well documented (15). For example, crystallographic data have shown that an intramolecular O5′—H···O2 bond associated with the sugar ring puckering can be observed in the *syn* conformation for pyrimidine nucleosides (16). Such a type of intramolecular hydrogen bonding was also observed (17) for uridine derivatives in $CHCl_3$ solution by combined used of NMR, CD, and IR spectroscopy. The conformations of nucleoside antibiotics such as formycin and showdomycin were studied (18*a*) theoretically using a semiempirical method of calculations (PCILO). It was reported that the *syn* conformation is stabilized by intramolecular hydrogen bonding between O5′—H of the sugar and N3 of the base for formycin and there is also an intramolecular hydrogen bond between O5′—H of the sugar and O2 of the base for showdomycin. Only a few *ab initio* studies have been published about nucleosides and these dealt with adenosine (18*b*, *c*) at the STO-3G level of theory. However, even in these MO studies no attention was paid to intramolecular hydrogen bonding that may exist between the 5′-hydroxyl group of the sugar and the heteroaromatic base. On the other hand, intramolecular hydrogen bonds involving the hydroxymethyl group and the tetrahydrofuran ring oxygen and thymine's C2 carbonyl oxygen in 3′-azido-3′-deoxythymidine (AZT) have been suggested recently, using molecular mechanics and NMR techniques (19). For this reason, it seemed that a theoretical study of the conformational analysis of a 2′-deoxycytidine derivative was needed in order to gain some understanding of the conformational dependence of the various attractive and repulsive interactions that may exist between such hydroxyl groups and the heteroaromatic system in the nucleoside. Obviously the understanding of the detailed nature of such intramolecular interactions at the level of electron density redistribution was also desirable.

Since, as mentioned above, Lewis acids have been shown to help overcome the unreactivity of such nucleosides during glycosylation reactions, the Lewis complex formation between BF_3 and the selected cytidine model compound was also studied.

Although the NMR study was performed on 2′-deoxy-3′-

Can. J. Chem. Downloaded from www.nrcresearchpress.com by 109.225.110.28 on 09/08/12
For personal use only.

O,4-*N*-diacetylcytidine (**1**), to simplify the calculations they were done on a model substance 1-[β-D-2′,3′-dideoxyribofuranosyl]-2-(1*H*)-pyrimidinone (**2**).

Experimental and computational methods

NMR spectrometry

2′-Deoxy-3′-*O*,4-*N*-diacetylcytidine (compound **1**) was prepared as described (12). ^{1}H NMR spectra of **1** were obtained with a Bruker AM 500 spectrometer in the NMR Laboratory, Carbohydrate Research Centre, University of Toronto, at 19 ± 2°C in CD_2Cl_2 (Merk, Sharpe and Dohme) using the residual $CHDCl_2$ resonance (5.32 ppm) as reference signal. A small amount of activated powdered 4Å molecular sieves was added directly to the NMR tube to remove any residual H_2O. For D_2O exchange one drop of D_2O was added to the sample and then mixed vigorously. The spectrum was recorded after equilibration and removal of residual D_2O (HDO) by the molecular sieves. Steady-state ^{1}H–^{1}H NOE data were obtained in the difference mode using stationary samples, a 90° monitor pulse, and a frequency cycling method for low-power preirradiations. Individual irradiation periods at a given frequency value were set equal to the 90° decoupler pulse at the chosen decoupler power level; the total preirradiation period was determined experimentally by monitoring enhancements of resonances due to spatially distant protons with low NOE buildup rates.

Computational methods

Parametric Method 3 (PM3) type molecular orbital calculations (20) were carried out using the MOPAC program (21) on an Apollo DN 10000 minicomputer at the Department of Chemistry, University of Toronto. The PM3 method is a new semiempirical method that has been developed to improve the modified neglect of diatomic overlap (MNDO) method (22, 23).

All *ab initio* computations were conducted on the Cray X-MP/24 supercomputer at the Ontario Centre for Large Scale Computation (OCLSC) using the GAUSSIAN 90 program (24). The *ab initio* geometrical optimizations were performed at the STO-3G basis set level (25) for each of the conformers obtained previously by semiempirical PM3 SCF computations. Thus the starting or input geometries for the *ab initio* computation were the final geometries obtained previously by the PM3 calculations. *Ab initio* energies reported in this paper are, therefore, for the fully optimized geometries obtained by energy gradient optimization. Each conformation at the present basis set level took more than 3 h CPU time on the Cray supercomputer; therefore it seemed impractical to carry out calculations at a higher basis set level of theory.

On going from a lower level to a higher level of theory, local minima on the potential energy surface (PES) very often (26, 27) disappear. However, to ensure that it is indeed the case here, a careful search was carried out in those cases where a conformation obtained by the PM3 method was annihilated on going to the *ab initio* level of theory.

For Bader-type topological analysis of charge density (28), the 3-21G** and 6-31G** polarized basis set (29) was used on the STO-3G optimized geometries. The topological properties of the electronic density were determined by the atoms in molecules theory (28) using the AIMPAC program.[6]

Results and discussion

Conformational analysis

Conformational potential energy surfaces of a simplified model compound were generated to establish the nature of possible interactions between the 5′-hydroxyl and the heteroaromatic base. The model compound **2** and its atomic labels of interest are specified in Fig. 2. Compound **2** lacks the 4-acetamido and 3′-*O*-acetate of the parent compound **1**.

[6]Available from Professor R. F. W. Bader's laboratory, McMaster University, Hamilton, Ont., Canada L85 4M1.

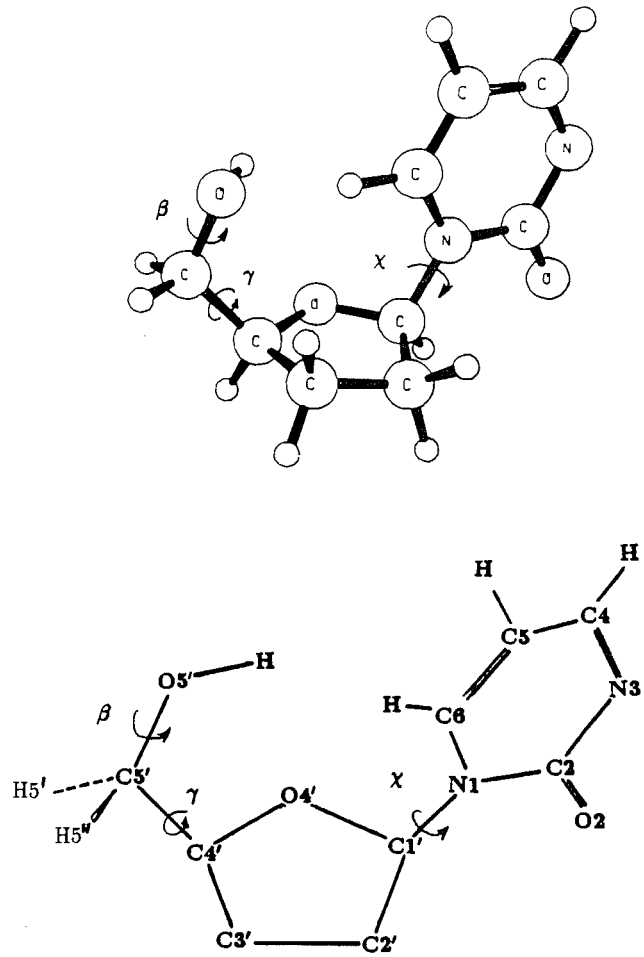

FIG. 2. Model compound (**2**) mimicking 2′-deoxycytidine derivative and the atomic labels of interest.

Neither of these groups should significantly affect the conformational degrees of freedom studied here. The conformation about the aromatic base – carbohydrate linkage N1—C1′ is described by the torsional angle χ. The orientations of the hydroxymethyl group and hydroxyl group are described by the torsion angles γ and β, respectively.

[1] $\chi = \theta(O4'—C1'—N1—C2)$

[2] $\gamma = \theta(O5'—C5'—C4'—C3')$

[3] $\beta = \theta(H—O5'—C5'—C4')$

The sign of the torsion angles is defined and labelled[7] in agreement with the recommendations of the IUPAC–IUB commission of Biochemical Nomenclature (30). For each optimal γ, corresponding to the nominal 60°, 180°, and 300° values, representing the $-sc$, ap, and $+sc$ conformations, respectively, potential energy surfaces $E = E(\beta, \chi)$ were

[7]

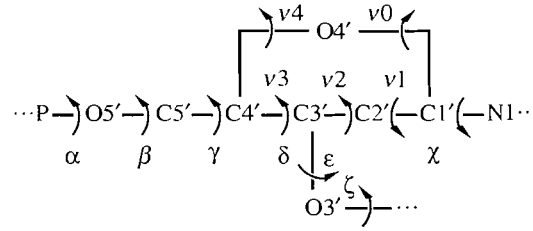

Can. J. Chem. Downloaded from www.nrcresearchpress.com by 109.225.110.28 on 09/08/12
For personal use only.

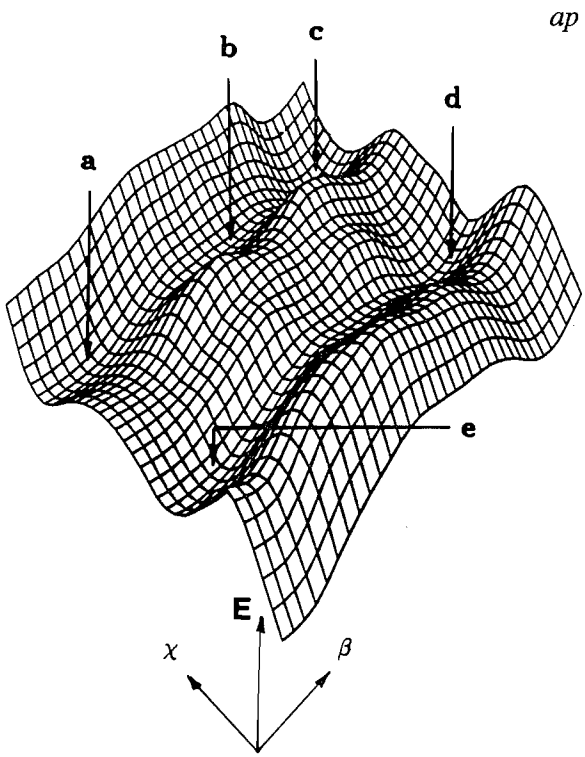

FIG. 3. The PM3 potential energy surface related to the *ap* conformation about the C5′—C4′ bond.

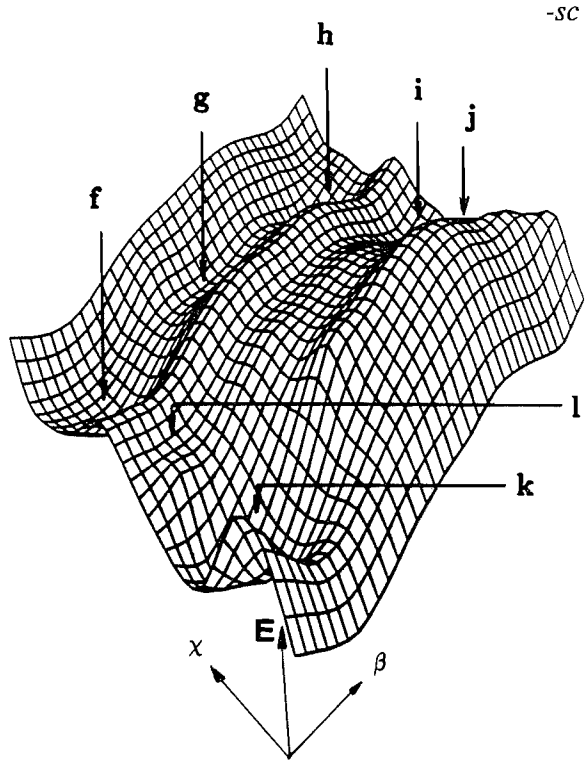

FIG. 4. The PM3 potential energy surface related to the $-sc$ conformation about the C5′—C4′ bond.

generated at 30° increments along the β and χ torsional angles.

In the first phase of this study, the SCF energy values of the model compound were calculated by the PM3 method. Three potential energy surfaces (PES), shown in Figs. 3, 4, and 5 were found to relate to *ap*, $-sc$, and $+sc$ conformations respectively. On the first PES (Fig. 3) associated with *ap*, five minima were found corresponding to conformers **a**, **b**, **c**, **d**, and **e**. Seven conformers (**f**–**l**) were located on the second PES (Fig. 4) associated with $-sc(\gamma \approx 60°)$ and again five conformers (**m**–**q**) were identified on the third PES (Fig. 5) associated with $+sc$ ($\gamma \approx 300°$). The geometries of these 17 conformers (**a**–**q**) are illustrated in Fig. 6. For conformer **k**, the O5′—H and O2 atom of the carbonyl group of the heteroaromatic base are almost colinear and the distance between the H of the hydroxyl group and O2 is 1.82 Å (with the O5′···O2 distance being 2.76 Å). This corresponds to a computed bond order of 2.9% of a single bond. The PM3 bond order using the MOPAC program was computed as the sum of squares of the density matrix elements connecting any two atoms. In spite of the above, as may be judged from the PM3 SCF energy value, conformation **k** is not the global minimum. The global minimum on the three PM3 PES is an *anti* conformation **c**.

In the second phase of this study, the geometries of the 17 conformers (**a**–**q**) related to the 17 local energy minima on the three PM3 PES (Figs. 3–5) were reoptimized by the *ab initio* method using a standard STO-3G basis set. The SCF energies, both PM3 and *ab initio* results, as functions of the β, γ, and χ torsional angles are summarized in Table 1. Instead of 17, only 14 minima were found on the *ab initio* PES. The *ab initio* geometries (**a′**–**q′**), as illustrated in Fig. 7, are related to the semiempirical conformers (**a**–**q**) with **i′**, **j′**, and

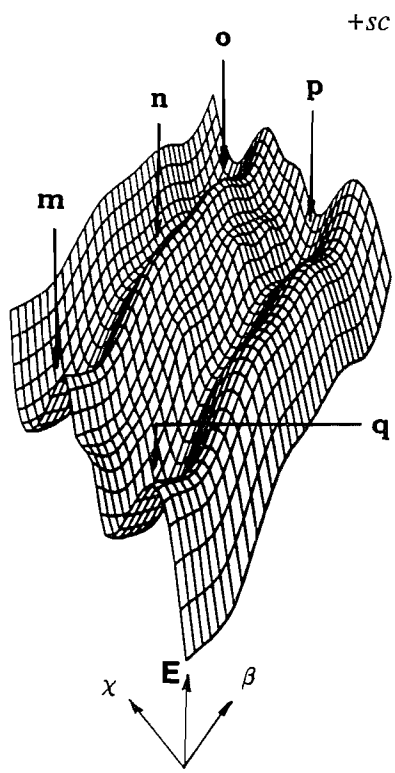

FIG. 5. The PM3 potential energy surface related to the $+sc$ conformation about the C5′—C4′ bond.

Can. J. Chem. Downloaded from www.nrcresearchpress.com by 109.225.110.28 on 09/08/12
For personal use only.

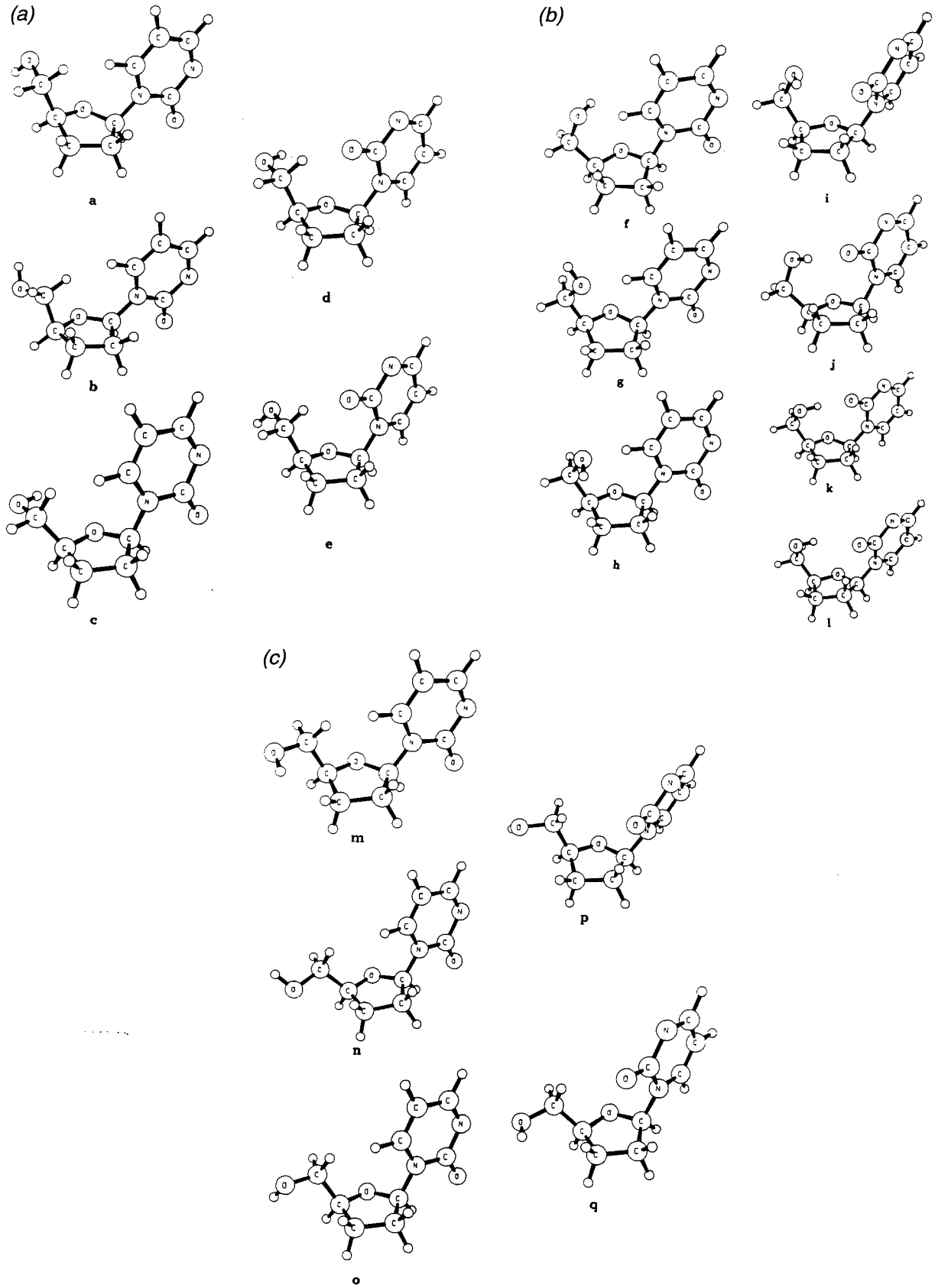

FIG. 6. (*a*) The geometries of conformers **a**–**e** from PM3 calculations. (*b*) The geometries of conformers **f**–**l** from PM3 calculations. (*c*) The geometries of conformers **m**–**q** from PM3 calculations.

TABLE 1. The SCF energies from PM3 and *ab initio STO-3G* calculation versus b, t and x torsion angles

Conformation		PM3				*Ab initio*(STO-3G)					
According to γ	According to β and χ	β	γ	χ	*E* (eV)	β	γ	χ	*E*(au)	Relative energies (kcal/mol)	Dipole moments (Debye)
	a or **a′**	49.80	179.94	235.44	−2456.75694	57.19	174.87	237.01	−672.6368211	4.03	5.50
	b or **b′**	164.69	162.05	254.40	−2456.66455	181.45	186.94	244.57	−672.6363918	4.30	4.65
ap	**c** or **c′**	301.41	179.94	235.56	−2456.80611	310.41	175.45	232.35	−672.6400099	2.03	6.42
	d or **d′**	290.72	191.83	66.22	−2456.68687	303.34	179.29	73.74	−672.6410995	1.34	5.03
	e or **e′**	57.90	182.67	68.76	−2456.59739	60.04	181.55	71.68	−672.6376456	3.51	5.00
	f or **f′**	78.25	68.20	227.53	−2456.73303	71.26	72.00	283.53	−672.6397365	2.20	4.41
	g or **g′**	167.91	50.46	235.39	−2456.65707	176.18	52.09	242.31	−672.6430013	0.15	6.59
	h or **h′**	299.91	43.79	231.65	−2456.72747	281.13	57.37	240.02	−672.6402135	1.90	6.59
−*sc*	**i**	306.26	64.48	105.99	−2456.60410	—	—	—	—	—	—
	j	320.28	76.51	72.27	−2456.65280	—	—	—	—	—	—
	k or **k′**	56.41	36.49	63.95	−2456.69645	58.91	27.83	62.69	−672.6432464	0.00	5.73
	l	53.15	35.32	90.73	−2456.59643	—	—	—	—	—	—
	m or **m′**	54.05	300.71	237.84	−2456.75628	64.59	288.13	237.53	−672.6364590	4.26	4.92
	n or **n′**	232.34	294.24	242.20	−2456.69432	182.86	297.81	242.80	−672.6383427	3.08	4.16
+*sc*	**o** or **o′**	295.86	294.17	242.00	−2456.76976	294.05	299.94	243.44	−672.6379595	3.32	5.16
	p or **p′**	294.80	281.14	96.68	−2456.62855	294.15	298.10	104.42	−672.6382768	3.12	5.17
	q or **q′**	68.49	286.22	72.83	−2456.65132	70.70	291.83	81.78	−672.6381310	3.21	4.73

l′ being annihilated. The geometry of each of the *ab initio* conformers seems to show no substantial change when compared with the PM3 geometries (see Table 1).

Recognizing that β, just like all torsional angles, are periodic, the minima labelled as **i**, **j**, **k**, **l** are next to one another and similarly **i′**, **j′**, **k′**, **l′** would also represent nearest neighbours. On going from PM3 to *ab initio* these four PM3 minima collapsed to a single minimum, annihilating three minima (**i′**, **j′**, and **l′**) retaining only one minimum that corresponded to **k′**.

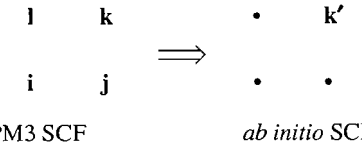

PM3 SCF *ab initio* SCF

It should be noted that during the collapse of these four minima into a single minimum not only β and χ were altered but γ as well: **k** (γ = 36.49°) → **k′** (γ = 27.83°). Nevertheless, the hydrogen-bonded *syn* conformation is **k′** at the *ab initio* level of theory. This **k′** conformer (χ = 62.69°, β = 58.91°, and γ = 27.83°) is in fact the global (i.e., the lowest energy) minimum among these 14 minima on the *ab initio* potential energy hypersurfaces. The next conformer is an *anti* conformer **g′**. For conformer **k′**, the O5′—H and O2 atom are also close to being colinear. The distance between the hydroxyl group H and O2 is 1.77 Å (O5′···O2 distance being 2.74 Å). For this intramolecular hydrogen-bonded system, the optimized geometrical parameters, obtained at the STO-3G basis set level of theory, are summarized in Table 2.

Multidimensional conformational analysis (MDCA) (31) predicts $3^3 = 27$ minima for a triple rotor with threefold topological multiplicity. In the case of saturated hydrocarbons this is indeed the case and all 27 legitimate minima may be obtained by gradient optimization (32, 33). These represent ideal conformational systems. However, heteroatom-containing molecules have extensive interactions that result in the annihilation of some of the legitimate minima, leading to nonideal conformational PES (34). Simple peptides, for example, have been shown to exhibit such behaviour (27). The present model compound **2** therefore corresponds to a nonideal system both in terms of PM3 and *ab initio* SCF calculations, since out of the 27 legitimate minima only 17 and 14 minima, respectively, were found on these PES. There is reason to believe that all minima on both the PM3 and *ab initio* PES have been located.

The topological representation of three conformational PES obtained at the PM3 and *ab initio* level of theory is shown in Fig. 8. The topology for the *ab initio* surfaces at γ ≈ 180° and γ ≈ 300° are analogous, as shown in Fig. 8. However, the two γ ≈ 60° surfaces show a marked difference with respect to each other and with respect to the surfaces generated at γ ≈ 180° and 300°. This dramatic difference is due to the fact that the O5′—H···O2 hydrogen bonding occurs at the γ ≈ 60° (i.e., −*sc*) surfaces.

NMR determinations

Figure 9 shows the 500 MHz ^{1}H NMR anomeric proton (H1′) irradiated NOE spectrum of deoxycytidine derivative **1** in CD_2Cl_2 solution. Surprisingly, a large NOE to the base proton H6 is observed. This result indicates that this derivative is predominantly in the *syn* conformation, χ ≈ 60° (cf. $\chi_{calc.}$ = 62.69° for **k′** and H1′···H6 is 2.116 Å). Most deoxycytidine derivatives investigated to date are found in the *anti* conformation (35).

Figure 10*a* shows the 500 MHz ^{1}H NMR spectrum of the H4′, H5′, H5″, H2′, H2″, and O5′-H protons of the same deoxycytidine derivative (**1**). The coupling patterns of the H2′ and H2″ are indicative of an approximately 50:50 mixture of the two common 2-*endo* and 3-*endo* conformations of the furanoside ring. Figure 10*b* shows the spectrum of the same sample after exchange with D_2O. The O5′-H disappears and one coupling is removed from each of the H5′ and H5″ res-

Can. J. Chem. Downloaded from www.nrcresearchpress.com by 109.225.110.28 on 09/08/12
For personal use only.

Can. J. Chem. Downloaded from www.nrcresearchpress.com by 109.225.110.28 on 09/08/12
For personal use only.

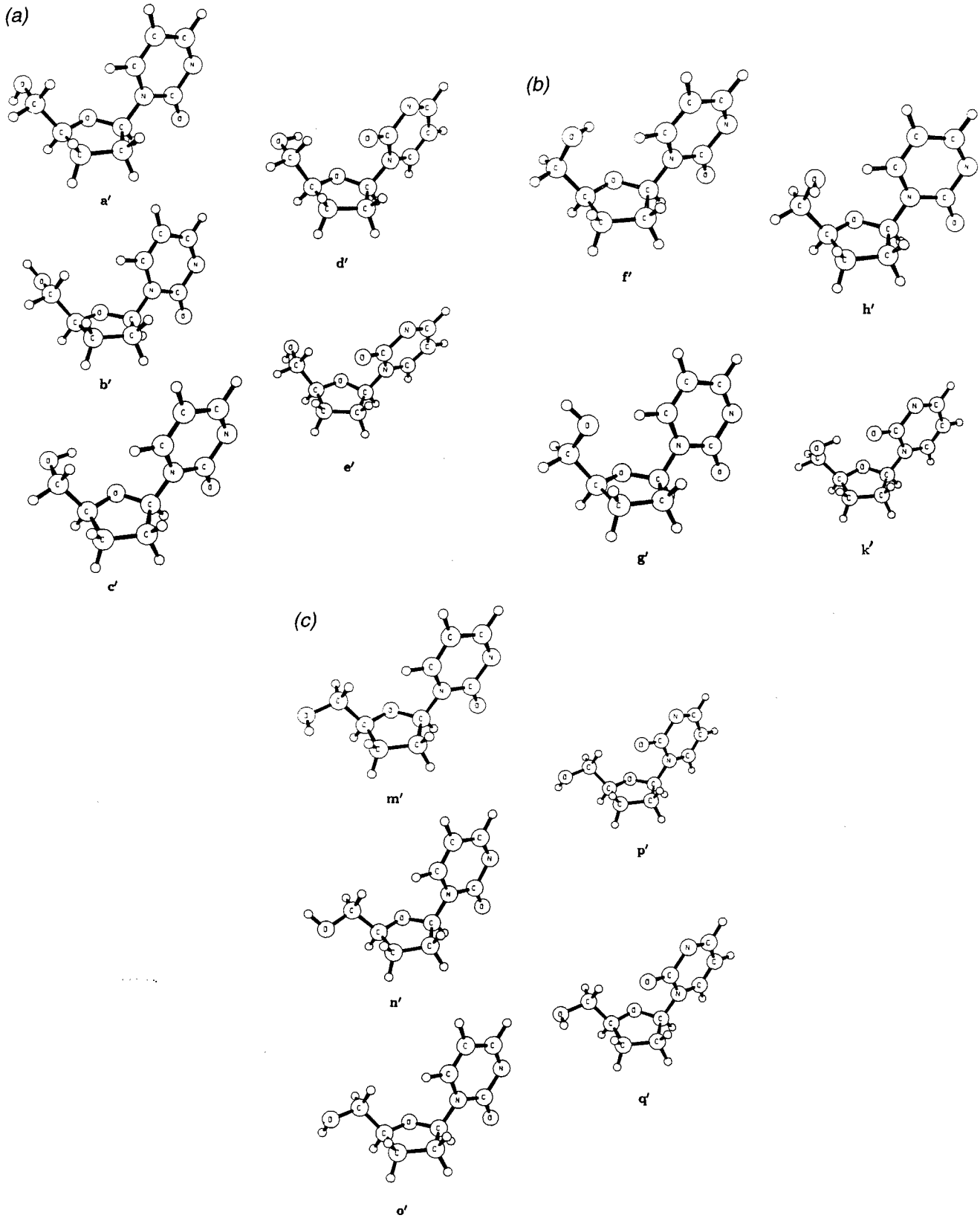

FIG. 7. (*a*) The geometries of conformers **a′**–**e′** from STO-3G calculations. (*b*) The geometries of conformers **f′**–**k′** from STO-3G calculations. (*c*) The geometries of conformers **m′**–**q′** from STO-3G calculations.

Can. J. Chem. Downloaded from www.nrcresearchpress.com by 109.225.110.28 on 09/08/12
For personal use only.

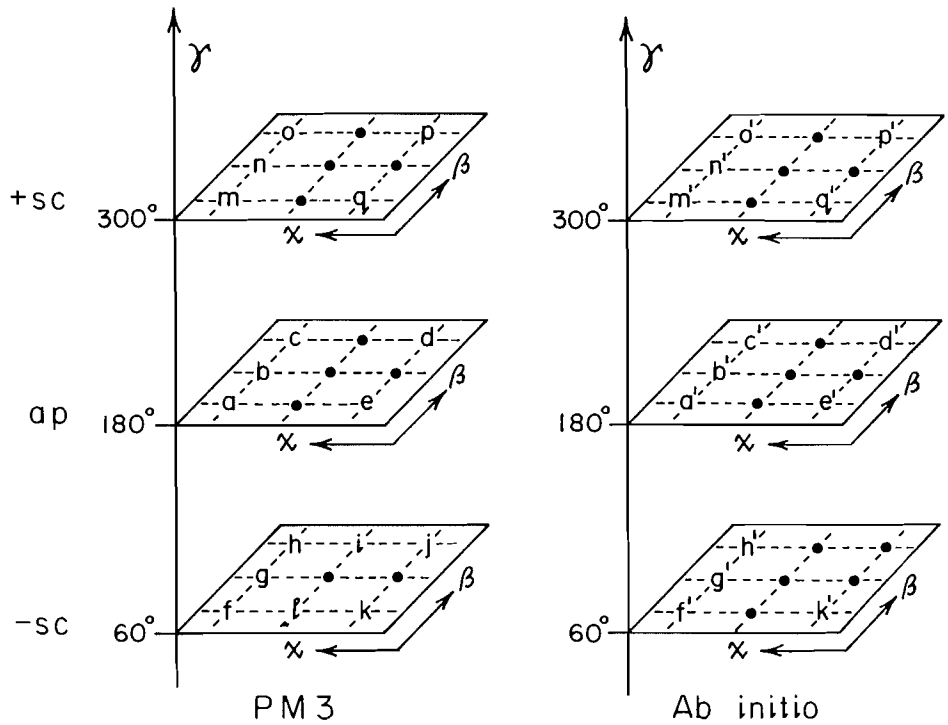

FIG. 8. Topological representation of minima associated with the $E = E(\chi, \beta, \gamma)$ conformational potential energy hypersurfaces computed at the PM3 and *ab initio* level of theory for model compound **2**.

TABLE 2. STO-3G optimized geometrical parameters of conformer **k**′

	Bond lengths (Å)		
N1—C2	1.4385	C1′—C2′	1.5614
C2—N3	1.4579	C2′—C3′	1.5460
N3—C4	1.2952	C3′—C4′	1.5530
C4—C5	1.4567	C1′—O4	1.4316
C5—C6	1.3313	C4′—O4′	1.4446
N1—C6	1.3984	C4′—C5′	1.5707
C2—O2	1.2225	C5′—O5′	1.4244
N1—C1′	1.4890	O5′—H	0.9889
H···O2	1.7732	C5′—H5′	1.0977
		C5′—H5″	1.0938
	Bond angles (deg)		
N1C1′O4′	109.89	C1′C2′C3′	104.91
C1′N1C6	119.78	C2′C3′C4′	105.60
N1C6C5	121.13	C2′C1′O4′	109.50
C4C5C6	117.43	C3′C4′C5′	113.46
N3C4C5	125.81	C4′C5′O5′	115.03
C2N3C4	117.22	C5′O5′H	104.58
O2C2N3	121.20	C4′C5′H5′	107.24
		C4′C5′H5″	107.78
	Dihedral angles (deg)		
C1′C2′C3′—C4′	−0.02	C2′C1′N1—C6	125.07
O4′C1′C2′—C3′	3.02	C5C6N1—C1′	177.29
C2′C3′C4′—C5′	−125.72	C4C5C6—N1	−0.69
C3′C4′C5′—O5′	27.83	N3C4C5—C6	−1.04
C4′C5′O5′—H	59.91	C5C4N3—C2	−0.25
C3′C2′C1′—N1	127.10	C4N3C2—O2	−178.14
C3′C4′C5′—H5′	153.51	O4′C1′N1—C2	62.69
C3′C4′C5′—H5″	−91.13		

onances as expected. The residual H4′–H5′ and H4′–H5″ couplings are both small and are nearly identical to those before D_2O exchange (2.7 and 2.9, Hz respectively, cf. Figs. 10*a* and 10*b*). Such couplings are only consistent with O5′ being *anti*-periplanar to H4′, i.e., $\gamma \approx 60°$ (36) (cf. $\gamma_{calc.} = 27.83°$ for **k**′).

If the C5′—C4′ bond is constrained to one minimum as suggested by the coupling constants, then it is possible to stereospecifically assign the prochiral protons by NOE spectroscopy. Indeed, irradiation of the most upfield H5″ proton produces NOE's to H3′ and H4′ whereas irradiation of H5′ produces only NOE's to H4′. Thus H5″ can be assigned as the pro*R* and H5′ as the pro*S* proton. This assignment agrees with previous assignments based on stereospecific deuteration of other deoxynucleosides (38). If conformation **k**′ is populated in solution, then O5′—H should be *anti*-periplanar to H5″ (calcd. 178.43°) and therefore the corresponding coupling constant should be about 12.1 Hz and $J_{O5'—H,H5'}$ about 1.5 Hz (O5′—H-O5′—C5′—H5′ = −64.11° in **k**′) (37). These calculated values compare to experimental values of 5.9 and 3.0 Hz, suggesting preferential but not exclusive population of conformers like **k**′. If the hydroxyl were freely equilibrating in solution, then the two couplings to H5′ and H5″ would be equivalent and the signal for O5′—H would be a broad triplet and not the observed doublet of doublets (see Fig. 10*a*). The NMR spectral parameters of compound **1** were sensitive to concentration, solvent, and the amounts of residual water in the sample. All these factors should affect any intramolecular hydrogen bonding. It can be concluded that conformers like **k**′ are the predominant conformers in dry CH_2Cl_2 solutions in which glycosylations are typically performed.

Can. J. Chem. Downloaded from www.nrcresearchpress.com by 109.225.110.28 on 09/08/12
For personal use only.

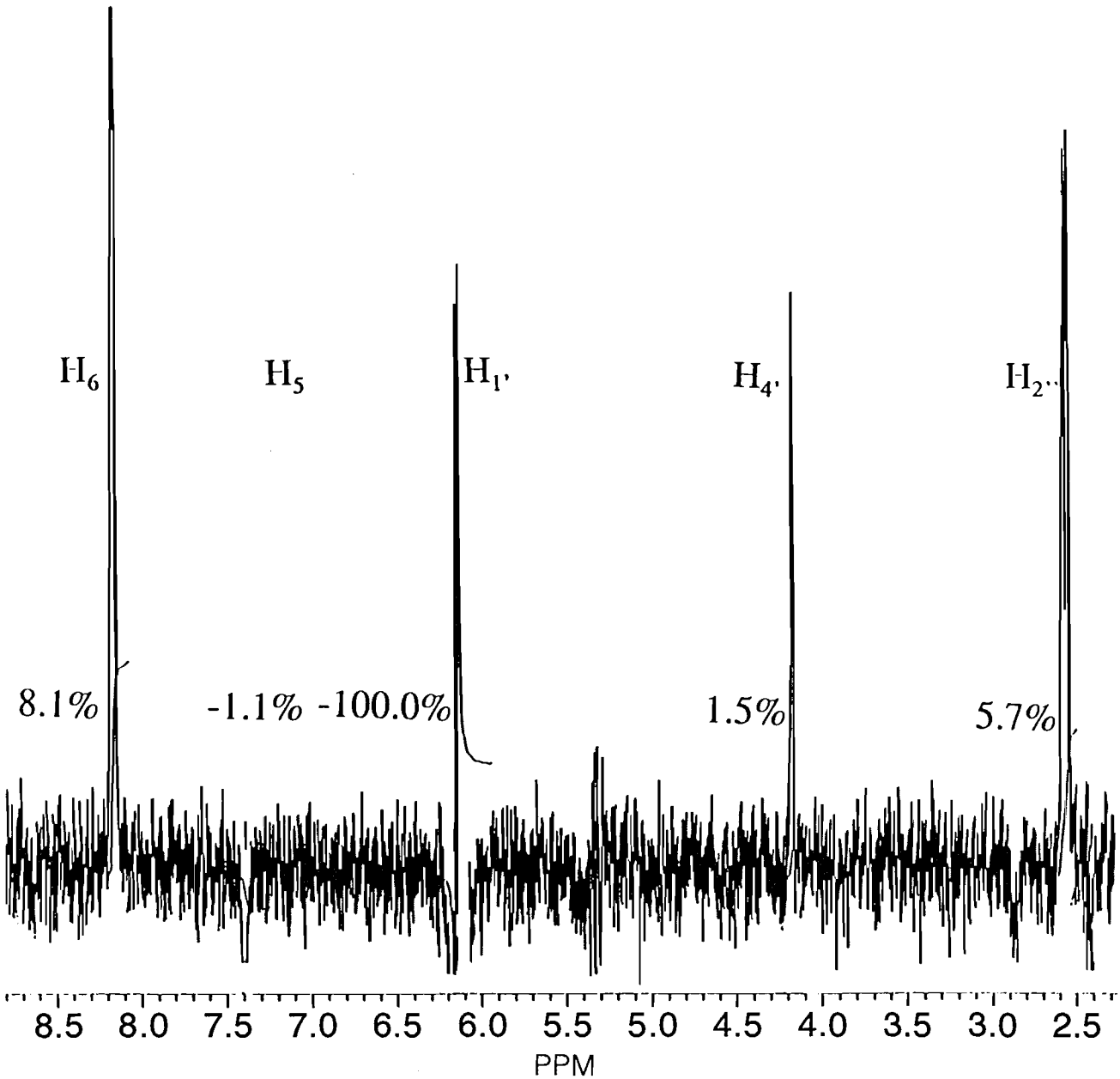

FIG. 9. Nuclear Overhauser Effect spectrum of **1** measured at 500 MHz after irradiation of H1′ showing a strong NOE on H6 of the base.

Lewis acid (BF_3) complexes with the model compound

Lewis acids, such as BF_3 supplied in the form of $BF_3 \cdot Et_2O$, are frequently used as promoters in glycosylation reactions. In fact such promoters have been shown to overcome the unreactivity of compound **1** in glycosylation reaction. In the present paper, we only examine the possible complex formation between the model compound **2** (that mimics the 2-deoxycytidine derivative) and a Lewis acid. In the simplified model compound **2**, three heteroatoms could be attacked by the Lewis acid; these are O5′, O2, and N3. Due to the lack of parameters for the element boron (21) in the PM3 program, the CH_3^+ cation was used instead of BF_3 in the initial part of the present study. Because the PM3 method was used systematically in the present work, it did not seem prudent to switch to another semiempirical method since CH_3^+ is as suitable a Lewis acid as BF_3. The five PM3 geometries of CH_3^+ complexes labelled from **K**(O5′)1 to **K**(O2)2 are shown in Fig. 11. Since each oxygen atom (O5′ and O2) has two lone electron pairs, it is possible to have two sites where CH_3^+ might be attached leading to four geometries **K**(O5′)1, **K**(O5′)2, **K**(O2)1, and **K**(O2)2. Of course, BF_3 could attach in one mode only to N3, forming one geometry labelled **K**(N3). The distances between the H atom of the 5′-hydroxyl group and O2 of the carbonyl group ($d_{H\cdots O2}$), for the **K**(N3), **K**(O2)1, and **K**(O2)2 conformers, are 2.7054, 3.3011, and 4.4471 Å respectively. These values are too large to be intramolecular hydrogen-bonded systems. However, the values of $d_{H\cdots O2}$ are 1.6540 and 1.6310 Å for the first two CH_3^+ complexes (**K**(O5′)1 and **K**(O5′)2), still indicating hydrogen bonding. Complex

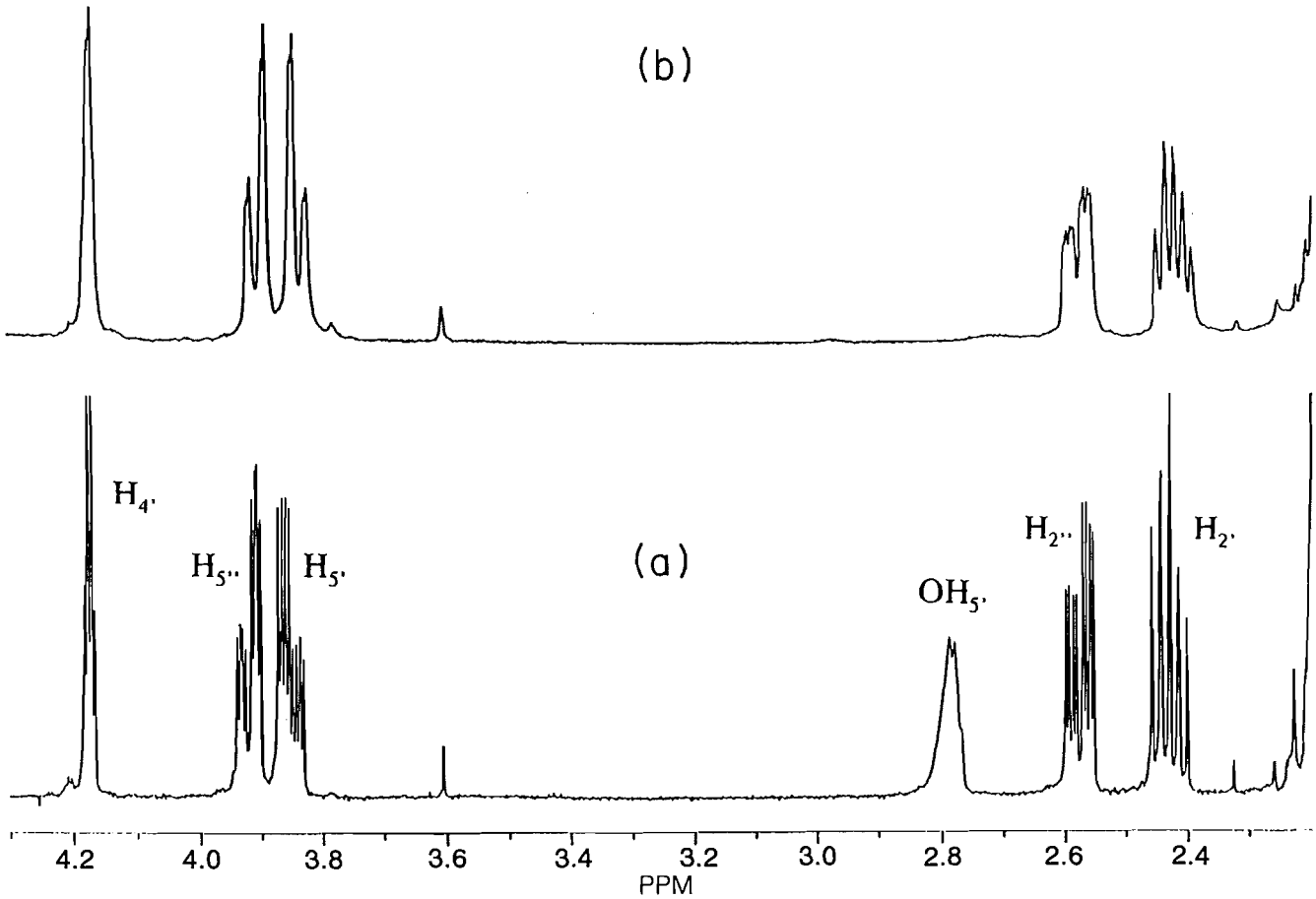

FIG. 10. 500 MHz NMR spectrum of **1**: (*a*: lower tracing) the spectrum in CD_2Cl_2 solution; (*b*: upper tracing) as above after exchange with D_2O.

Can. J. Chem. Downloaded from www.nrcresearchpress.com by 109.225.110.28 on 09/08/12
For personal use only.

energies (in kcal/mol) are all exothermic at all possible attachment sites: **K**(N3), −104.08; **K**(O2)1, −93.68; **K**(O2)2, −84.65; **K**(O5′)1, −74.80; and **K**(O5′)2, −73.90. The two last complexes involved in hydrogen bonding are of higher energy content than the remaining ones. The lower energy complexes, including the lowest one **K**(N3), thus can be the possible reactive intermediates in the glycosylation reaction. This observation would explain why some glycosylations do not proceed unless Lewis acids are present.

The complex formation between BF_3 and model compound (**2**) was studied by *ab initio* MO. The BF_3 was attached to one site of the O5′ atom of **k**′, forming a BF_3 complex labeled **K**′(O5′)1. This geometry is analogous to that of **K**(O5′)1. The conformer **K**′(O5′)1 was of course optimized using a standard STO-3G basis set in the *ab initio* calculation. Its geometry is shown in Fig. 12 and its geometrical parameters are summarized in Table 3. The energetics of such Lewis complex formation, as computed with different basis sets, are shown in Fig. 13. The reaction is computed to be strongly exothermic at all three basis set levels.

Charge density distribution analysis

In addition to the energetic considerations mentioned above, there is an alternative method to analyze hydrogen bonding. This involves the topological analysis of the electronic density distribution, which can be used to analyze intramolecular hydrogen bonding between the hydroxyl group with the oxygen atom of the carbonyl group of model compound **2** to gain some insight into the reactivity of 5′-OH. Although the topic of intramolecular hydrogen bonding has been widely studied (5) experimentally and theoretically, it has only recently been analyzed by using Bader-type topological analysis of charge density distribution (28, 40). The topological properties of the electronic density distribution are based on the gradient vector field of the electronic density $\nabla\rho(\boldsymbol{r})$, and on the Laplacian of the electronic density $\nabla^2\rho(\boldsymbol{r})$. Several excellent reviews have been published (28) on this subject, therefore only a brief description of selected topological parameters, pertinent to the present work, is discussed here. The electronic charge distribution of a molecule is described by $\rho(\boldsymbol{r}, \boldsymbol{X})$ where $\boldsymbol{r}$ is a variable position vector in ordinary three-dimensional space with r_1, r_2, and r_3 components and $\boldsymbol{X}$ represents a particular set of nuclear coordinates in the space corresponding to the nuclear configurations of the molecule in question. An atom in a molecule is defined (28) as a region of real three-dimensional space bounded by a zero-flux surface of the gradient vector field of $\rho(\boldsymbol{r})$, that is, a surface for which all points on this surface satisfy the equation

$$[4] \quad \nabla\rho(\boldsymbol{r}) \cdot \mathrm{n}(\boldsymbol{r}) = 0$$

where $n(\boldsymbol{r})$ is the unit vector normal to the surface at $\boldsymbol{r}$. Two

Can. J. Chem. Downloaded from www.nrcresearchpress.com by 109.225.110.28 on 09/08/12
For personal use only.

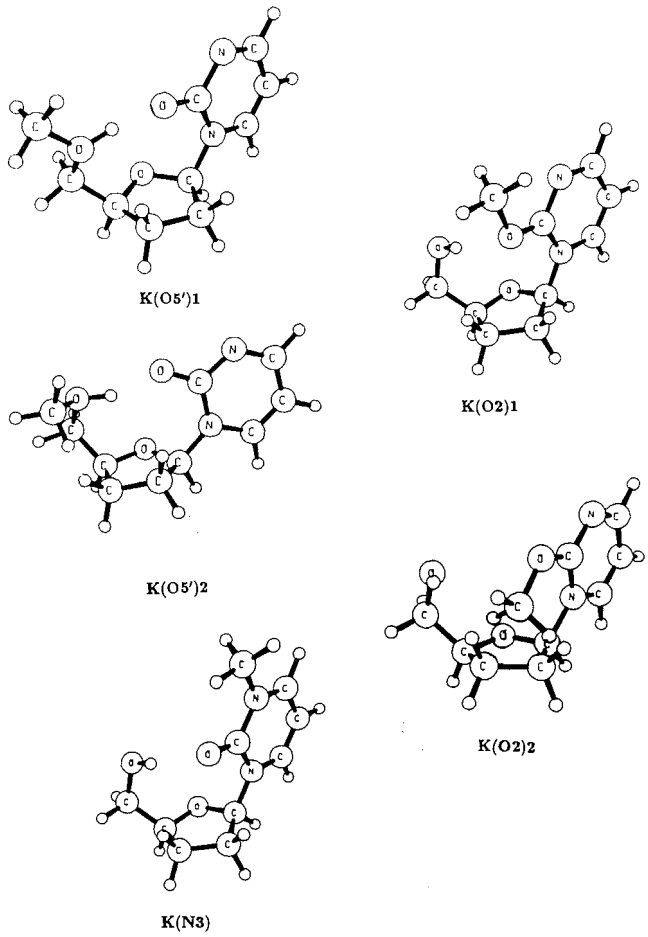

FIG. 11. Five geometries of CH_3^+ complexes with the model compound from **K**(O5′)1 to **K**(O2)2 from PM3 calculations.

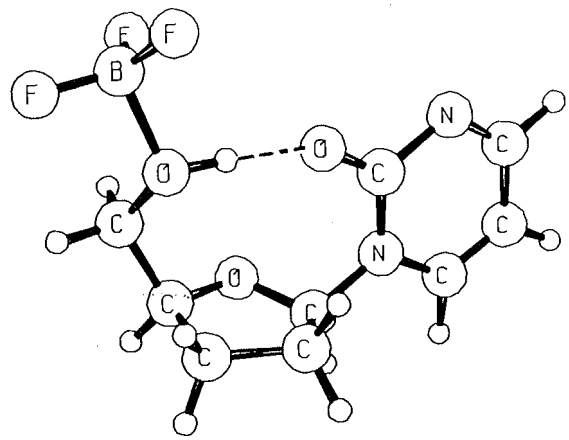

FIG. 12. The geometry of BF_3 complex with the model compound labeled as **K′** (O5′)1 from *ab initio* STO-3G calculation.

interacting atoms in a molecule form a critical point in the electronic density called a bond critical point (BCP), where

[5] $\nabla\rho(\boldsymbol{r}) = 0$

The pairs of gradient paths, which originate at a BCP and terminate at neighbouring nuclei ("attractor" in the gradient field of $\rho(\boldsymbol{r})$) define a line through electronic charge distribution along which $\rho(\boldsymbol{r})$ is a maximum with respect to any lateral displacement called an atomic interaction line. The presence of such a line linking two nuclei in a molecule that exists in a minimum energy geometry implies that the two atoms are bonded to one another, and in this instance this line is called a bond path. The necessary and sufficient condition for two atoms to be bonded to one another is that their nuclei be linked by a bond path. The network of bond paths for a molecule in a given nuclear configuration $\boldsymbol{X}$ defines the molecular graph, which essentially is the union of the closures of the bond paths. As a topological structure the molecular graph usually corresponds to the commonly drawn chemical bond network. For a molecule AB, the bond path, the BCP, and the zero-flux surface between these two atoms can be portrayed as follows:

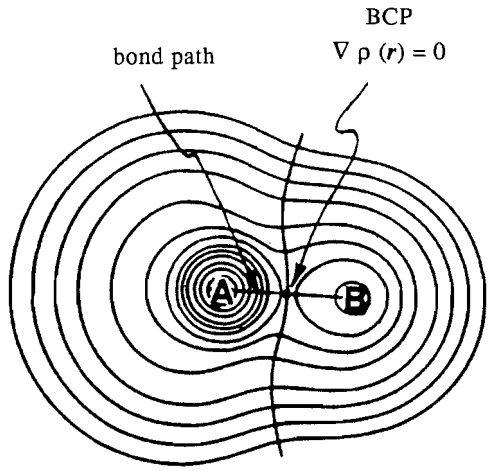

$\nabla\rho(\boldsymbol{r}) \cdot n(\boldsymbol{r}) = 0$
zero-flux surface

The Laplacian of electronic charge density, the quantity

[6] $\nabla^2\rho(\boldsymbol{r}) = \Sigma_{j=1,3}\partial^2\rho(\boldsymbol{r})/\partial x_j^2$

determines the regions of space wherein electronic charge is locally concentrated or depleted. From the definition of a second derivative, one finds that $\rho(\boldsymbol{r})$ is greater than the average of its values over an infinitesimal sphere centered on $\boldsymbol{r}$ when $\nabla^2\rho(\boldsymbol{r}) < 0$, and $\rho(\boldsymbol{r})$ is less than this average when $\nabla^2\rho(\boldsymbol{r}) > 0$. Thus a local maximum (or minimum) in $-\nabla^2\rho(\boldsymbol{r})$ signifies a local concentration (or depletion) of electronic charge. The numbers, location, and relative sizes of the bonded and nonbonded concentration of charge in the valence shell of a bonded atom as determined by the Laplacian of $\rho(\boldsymbol{r})$ are found to be in generally good agreement with the corresponding properties that are ascribed to bonded and nonbonded pairs in Gillespie's VSEPR model of molecular geometry (39).

The theory of atoms in molecules has been widely applied to many chemical problems including the description of hydrogen-bonded systems (see for example refs. 28*a* and 41).

For conformer **k′**, there is a bond path linking the H of the 5′-hydroxyl group and O2 of the carbonyl group for the intramolecular hydrogen-bonded system of model compound (**2**) (Fig. 14). Thus, at this point, one can say unambiguously that hydrogen bonding does exist in this system. The electronic density $\rho(\boldsymbol{r})$ at the bond critical point is called $\rho_b(\boldsymbol{r})$,

Can. J. Chem. Downloaded from www.nrcresearchpress.com by 109.225.110.28 on 09/08/12
For personal use only.

TABLE 3. STO-3G optimized geometrical parameters of BF3 complex with model compound

Bond lengths (Å)			
N1—C2	1.4334	C1′—C2′	1.5627
C2—N3	1.4535	C2′—C3′	1.5420
N3—C4	1.2972	C3′—C4′	1.5540
C4—C5	1.4553	C1′—O4′	1.4315
C5—C6	1.3314	C4′—O4′	1.4446
N1—C6	1.3995	C4′—C5′	1.5562
C2—O2	1.2264	C5′—O5′	1.4289
N1—C1′	1.4885	O5′—H	0.9985
H···O2	1.5460	O5′—B	1.6974
		B—F1	1.3424
		B—F2	1.3453
		B—F3	1.3458
Bond angles (deg)			
N1C1′O4′	108.47	C1′C2′C3′	105.02
C1′N1C6	119.52	C2′C3′C4′	104.62
N1C6C5	120.98	C2′C1′O4′	109.01
C4C5C6	117.41	C3′C4′C5′	113.74
N3C4C5	125.75	C4′C5′O5′	111.26
C2N3C4	117.28	C5′O5′H	109.85
O2C2N3	120.36	C5′O5′B	120.36
		O5′BF1	100.70
		O5′BF2	101.20
		O5′BF3	102.63
Dihedral angles (deg)			
C1′C2′C3′—C4′	10.31	C2′C1′N1—C6	112.16
O4′C1′C2′—C3′	−0.37	C5C6N1—C1′	179.72
C2′C3′C4′—C5′	−135.85	C4C5C6—N1	−0.13
C3′C4′C5′—O5′	38.88	N3C4C5—C6	−1.03
C4′C5′O5′—H	49.20	C5C4N3—C2	0.00
C3′C2′C1′—N1	121.31	C4N3C2—O2	−179.11
C4′C5′O5′—B	194.91	O4′C1′N1—C2	51.64
C5′O5′B—F1	181.17		
C5′O5′B—F2	60.87		
C5′O5′B—F3	−58.45		

the magnitude of which is a measure of bond strength (28*b*). From the 3–21G**//STO-3G calculation, for O5′—H the $\rho_b(\mathbf{r})$ is 0.3456 au and for H···O2 the $\rho_b(\mathbf{r})$ is 0.0322 au, respectively. Moreover, the value of $\nabla^2\rho(r_c)$ at the bond critical point for O5′—H is −2.4521 au and for H···O2 is +0.1229 au. Thus, this is a typical intramolecular hydrogen bond in which a hydrogen atom is bound to the heteroatom contained in the acid fragment (O5′) by a shared interaction and to the heteroatom of the base (O2) by a closed-shell interaction (28*b*).

The Laplacian "relief plot" generated according to Bader's method (28*b*) for the fragment plane of the O5′—H···O2 system is displayed in Fig. 15. Two nonbonded regions of charge concentration are seen in the oxygen of the carbonyl group of the heterocyclic base and this is in agreement with the VSEPR model. The region of charge depletion in the valence shell of O5′—H, which is located away from the position of the proton on the O5′—H bond axis, is directed at one of the nonbonded charge concentrations of O2, thereby yielding a stable hydrogen-bonded structure (see arrows in Fig. 15).

The Bader-type topological analysis of charge density was also performed on the BF_3 complex, labeled as **K**′(O5′)1, at the 3–21G**//STO-3G level of theory. Contrary to expectation, it is found that only one bond critical point (BCP) exists between the H of the 5′-hydroxyl group and O2 (Fig. 16) at this level of theory. Using the more flexible basis set (6–31G**) two BCP were found, as expected, along the nearly colinear bond paths (O5′—H···O2).[8] Again, this confirms intramolecular hydrogen bonding. Moreover, based on the value of $\rho_b(\mathbf{r})$, which equals 0.0574 au (3–21G**), it seems that the hydrogen bonding in the BF_3–**2** complex, labeled as **K**′(O5′)1, is strengthened compared with conformer **k**′ of the uncomplexed model compound **2**. The topological properties of the charge density of **k**′ and **K**′(O5′)1 are summarized in Table 4.

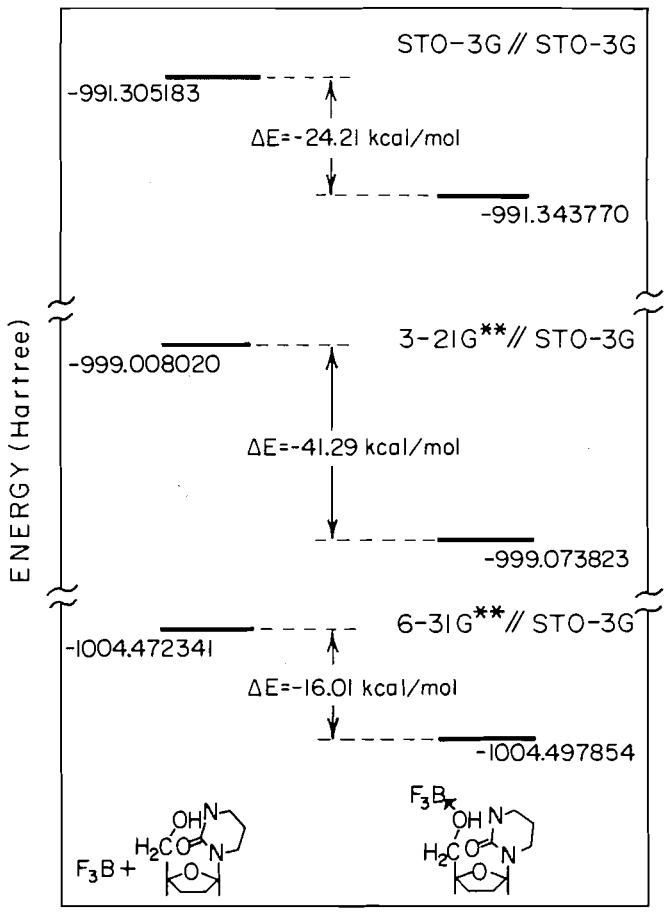

FIG. 13. Energetics of Lewis complex formation involving BF_3 and model compound **2**.

Conclusion

It has been shown at both semiempirical and *ab initio* levels of calculation that hydrogen bonding between O5′—H and O2 is a stabilizing factor for the predominant conformation **k**′ of model compound **2**. This result has been confirmed by solution NMR measurements on the parent compound **1**. The *ab initio* calculations gave the best fit to the NMR data, re-

[8]The use of Bader-type topological analysis of electron density to detect hydrogen bonding is rigorously correct for the exact density. Moreover, it is usually valid for electron density computed from sophisticated wave functions. However, at a lower level of theory the analysis might be unable to detect the existence of hydrogen bonding and in that case one must use a larger basis set to determine if a hydrogen bond does or does not exist.

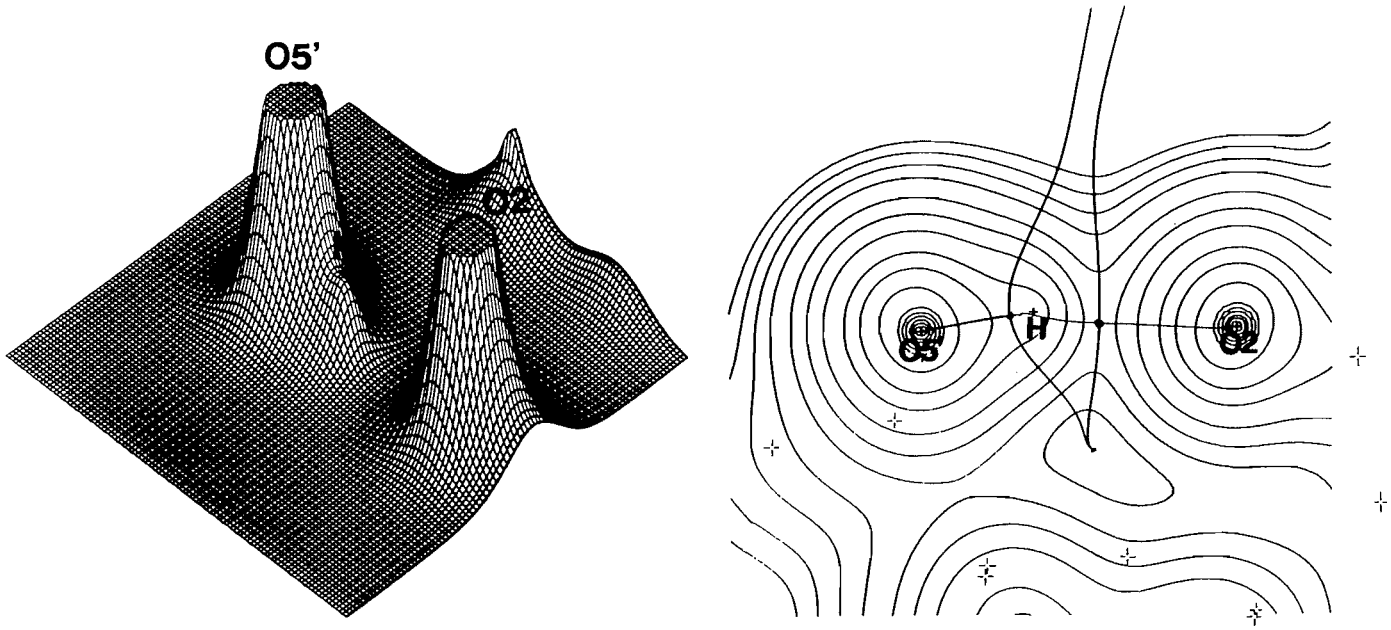

FIG. 14. (*a*) Three-dimensional plot of $\rho(\mathbf{r})$ for a plane containing O5′—H···O2 nuclei in conformer **k**′. The plot was made using a 3-21G**//STO-3G basis set. (*b*) Contour map of the charge density for a plane containing O5—H···O2 nuclei in conformer **k**′. The bond critical points are denoted by black dots. The bond paths, a line linking the nuclei along which the charge density is a maximum with respect to any neighboring line, and the intersection of the interatomic surface, which are defined by the lines of steepest descent through the three-dimensional charge distribution starting from the bond critical point, are also shown. The projected positions of out-of-plane nuclei are indicated by open crosses. The plot was made using a 3-21G**//STO-3G basis set.

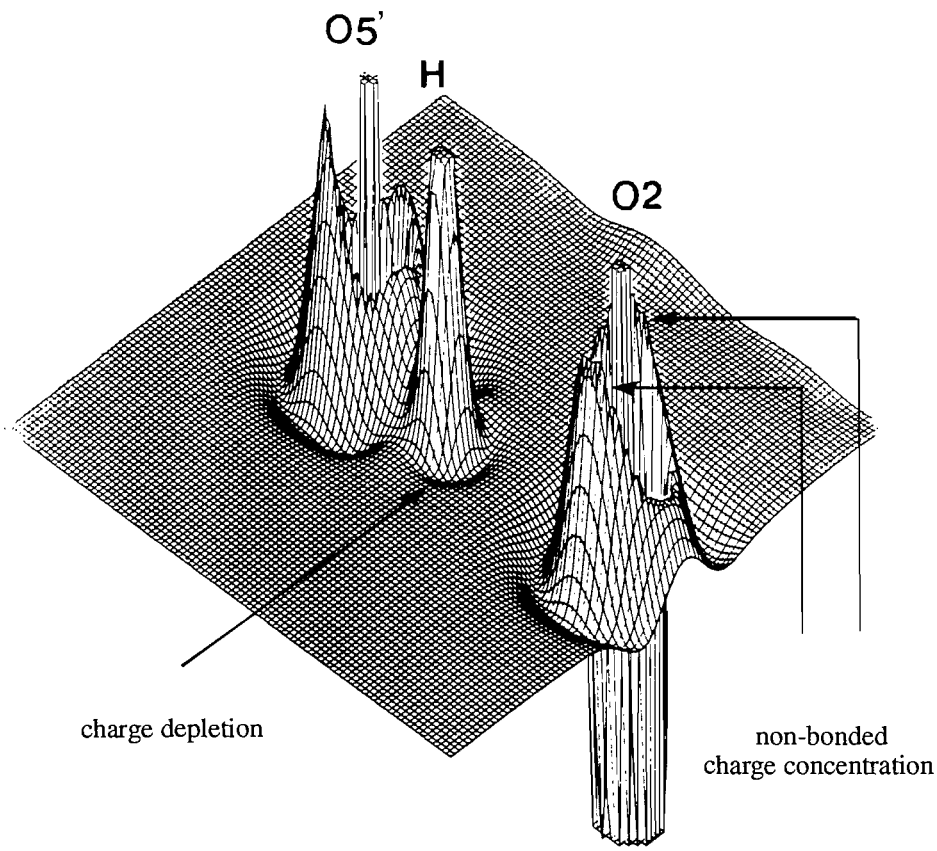

FIG. 15. A relief map of $-\nabla^2\rho$ for a plane containing O5′—H···O2 nuclei in conformer **k**′. A maximum in the relief map is a maximum in charge concentration. The plot was made using a 3-21G**//STO-3G basis set.

Can. J. Chem. Downloaded from www.nrcresearchpress.com by 109.225.110.28 on 09/08/12
For personal use only.

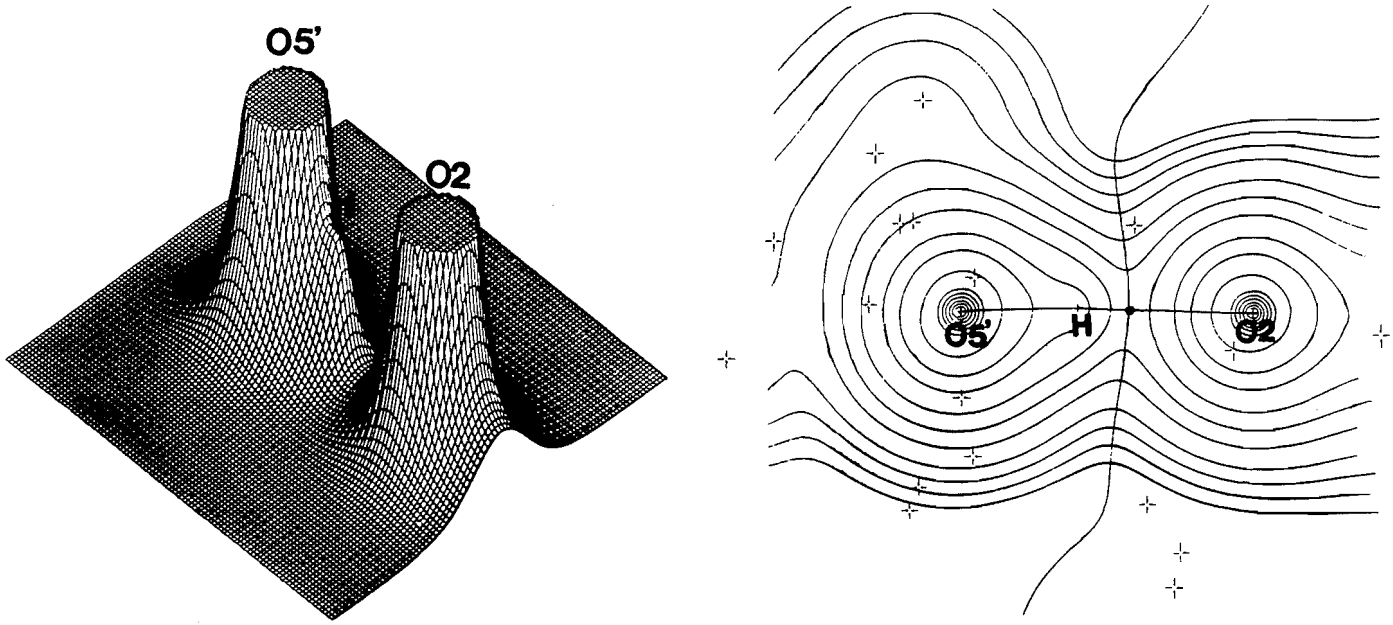

FIG. 16. (*a*) Three-dimensional plot of $\rho(\mathbf{r})$ for a plane containing O5′—H···O2 nuclei in BF_3 complex related to **K**′(O5′)1. The plot was made using a 3-21G**//STO-3G basis set. (*b*) Contour map of charge density for a plane containing O5—H···O2 nuclei in BF_3 complex related to **K**′(O5′)1. The bond critical points are denoted by black dots. The bond paths and the intersection of the interatomic surface are also shown. The projected positions of out-of-plane nuclei are indicated by open crosses. The plot was made using a 3-21G**// STO-3G basis set.

TABLE 4. Values of $\rho_b(r)$ and $\nabla^2\rho(r_c)$ at the bond critical points of O5′—H···O2 in conformers **k**′ and **K**′ (O5′)1

		O5′—H		H···O2	
Conformer	Basis set	$\rho_b(r)$	$\nabla^2\rho(r_c)$	$\rho_b(r)$	$\nabla^2\rho(r_c)$
k′	3-21G**//STO-3G	0.3456	−2.4521	0.0322	+0.1229
K′ (O5′)1	3-21G**//STO-3G	—	—	0.0572	+0.1875
	6-31G**//STO-3G	0.3127	−2.1390	0.0582	+0.2096

affirming the utility of this level of calculation to investigate organic reactions. These calculations permitted the use of Bader's charge density topological approach to model the hydrogen bond. Furthermore, it has been found that Lewis acids can form strongly exothermic complexes with O5′ of **2** that enhance the hydrogen bridge between O5′—H and O2. Other Lewis acid complexes are of lower energy and, more importantly, are not involved in hydrogen bonding. These results explain why glycosylation reactions involving hydrogen-bonded substances occur in the presence of Lewis acids, although they do not advance under other conditions. Clearly, several examples containing a variety of OH groups reacting differently need to be examined at this level of calculation, so that the importance of non-covalent interactions in the mechanism of the glycosylation reaction can be assessed. The utility of such approaches, in this direction, is currently being investigated.

Acknowledgements

One of us (T.H.T.) wishes to express his gratitude to Professor R. F. W. Bader for permission to use his computational facilities. Thanks are also due to Mr. J. R. Cheeseman for his assistance.

The continued financial support of the Natural Sciences and Engineering Research Council (NSERC) of Canada and the Protein Engineering Network of Centres of Excellence is gratefully acknowledged. The Carbohydrate Research Centre is partially supported by the Medical Research Council (MRC) of Canada. The access to the Cray X-MP/24 supercomputer was made possible by an allocation from the Ontario Centre for Large Scale Computation (OSLSC), which is gratefully acknowledged.

1. H. Paulsen. Angew. Chem. Int. Ed. Engl. **21**, 155 (1982); **29**, 823 (1990).
2. S. P. Douglas, D. M. Whitfield, and J. J. Krepinsky. Abstracts, Fuji '90 Post-Symposium: Recent Progress of Synthetic Methods in Carbohydrates and Their Applications to Synthetic Chemistry. Susono City, Shizuoka, Japan. 1990; The Fuji Training Institute, Shizuoka.
3. A. H. Haines. Adv. Carbohydr. Chem. Biochem. **33**, 11 (1976).
4. R. A. Dwek and F. A. Quiocho. Curr. Opin. Struct. Biol. **1**, 709 (1990), and following articles.
5. F. Hilbbert and J. Emsley. Adv. Phys. Org. Chem. **26**, 255 (1991).

Can. J. Chem. Downloaded from www.nrcresearchpress.com by 109.225.110.28 on 09/08/12
For personal use only.

Can. J. Chem. Downloaded from www.nrcresearchpress.com by 109.225.110.28 on 09/08/12
For personal use only.

6. G. Karmstrom, P. Linse, A. Wallquist, and B. Jonsson. J. Am. Chem. Soc. **105**, 3777 (1983).
7. S. K. Burley and G. A. Petsko. Adv. Protein Chem. **39**, 125 (1988).
8. P. A. Kollman and L. C. Allen. Chem. Rev. **72**, 283 (1972).
9. H. Honig and H. Weidman. Carbohydr. Res. **73**, 260 (1979).
10. K. Kefurt, J. Stanek, Jr., Z. Kefurtova, and J. Jary. Collect. Czech. Chem. Commun. **40**, 300 (1975).
11. I. D. Sadekov, V. I. Minkin, and A. E. Lutskii. Russ. Chem. Rev. **39**, 179 (1970).
12. A. M. Michelson and A. R. Todd. J. Chem. Soc. 34 (1954).
13. P. Delongchamps. Stereoelectronic effects in organic chemistry. Pergamon Press, Oxford. 1985.
14. I. Tvaroska and T. Bleha. Adv. Carbohydr. Chem. Biochem. **47**, 45 (1989).
15. G. I. Birnbaum and D. Shugar. *In* Topics in molecular and structural biology. *Edited by* S. Neidle and W. Fuller. MacMillan Press, New York, N.Y. 1987. Vol. 9. pp. 1–77, and references therein.
16. G. I. Birnbaum, F. E. Hruska, and W. P. Niemczura. J. Am. Chem. Soc. **102**, 5586 (1980).
17. D. Plochocka, A. Rabczenko, and D. B. Davies. J. Chem. Soc. Perkin Trans. 2, 82 (1981).
18. (*a*) A. Saran, C. K. Mitra, and B. B. Pullman. Int. J. Quantum Chem. Quantum Biol. Symp. **4**, 43 (1977); (*b*) J. S. Kwiatkowski and B. Pullman. Int. J. Quantum Chem. **15**, 499 (1979); (*c*) G. A. Walker, S. C. Bhatia, and J. H. Hall, Jr. J. Am. Chem. Soc. **109**, 7629 (1987).
19. G. R. Painter, J. P. Schockcor, and C. W. Andrews. Adv. Mol. Model. **2**, 135 (1990).
20. (*a*) J. J. P. Stewart, J. Comput. Chem **10**, 209 (1989); **10** 221 (1989); (*b*) J. Comput. Chem. **12**, 320 (1991).
21. J. J. P. Stewart. MOPAC (Version 6), QCPE Program No. 455 (1990).
22. M. J. S. Dewer and W. Thiel. J. Am. Chem. Soc. **99**, 4899 (1977).
23. M. J. S. Dewar and H. S. Rzepa. J. Comput. Chem. **4**, 158 (1983).
24. M. Frisch, M. Head-Gordon, G. W. Trucks, J. B. Foresman, H. B. Schlegel, K. Raghavachari, M. A. Robb, J. S. Binkley, C. Gonzalez, D. J. Defrees, D. J. Fox, J. J. P. Stewart, S. Topiol, and J. A. Pople. GAUSSIAN 90 (Revision F Version), Gaussian Inc., Pittsburgh, Pa. (1990).
25. W. J. Hehre, R. F. Stewart, and J. A. Pople. J. Chem. Phys. **51**, 2657 (1969).
26. T. Head-Gordon, M. Head-Gordon, M. J. Frisch, C. Brooks II, and J. A. Pople. J. Am. Chem. Soc. **113**, 5989 (1991).
27. A. Perczel, J. G. Angyan, M. Kajtar, W. Viviani, J.-L. Rivail, J. F. Marcoccia, and I. G. Csizmadia. J. Am. Chem. Soc. **113**, 6256 (1991).
28. (*a*) R. F. W. Bader. Chem. Rev. **91**, 893 (1991); (*b*) Atoms in molecules: a quantum theory. Oxford University Press, Oxford. 1990; (*c*) Acc. Chem. Res. **18**, 9 (1985).
29. (*a*) P. C. Hariharan and J. A. Pople. Chem. Phys. Lett. **66**, 217 (1972); (*b*) J. S. Binkley, J. A. Pople, and W. J. Hehre. J. Am. Chem. Soc. **102**, 939 (1980); (*c*) M. S. Gordon, J. S. Binkley, J. A. Pople, W. J. Pietro, and W. J. Hehre J. Am. Chem. Soc. **104**, 2997 (1982); (*d*) W. J. Pietro, M. M. Francl, W. J. Hehre, D. J. Defrees, J. A. Pople, and J. S. Binkley. J. Am. Chem. Soc. **104**, 5039 (1982).
30. IUPAC–IUB, Commission on Biochemical Nomenclature, Arch. Biochem. Biophys. **145**, 405 (1971), J. Mol. Biol. **52**, 1 (1970), Biochemistry, **9**, 3471 (1970).
31. I. G. Csizmadia. *In* New theoretical concepts for understanding organic reactions. *Edited by* J. Bertran and I. G. Csizmadia. Kluwer Academic Publisher, The Netherlands. 1989. pp. 1–31.
32. (*a*) M. R. Peterson and I. G. Csizmadia. J. Am. Chem. Soc. **100**, 6911 (1978); (*b*) Prog. Theor. Org. Chem. **3**, 190 (1982).
33. (*a*) J. B. Lagowski, I. G. Csizmadia, and G. J. Vansco. J. Mol. Struct. (Theochem). In press; (*b*) Int. J. Quantum Chem. In press.
34. J. G. Angyan, R. Daudel, A. Kucsman, and I. G. Csizmadia. Chem. Phys. Lett. **136**, 1 (1987).
35. D. B. Davies, P. Rajani, and H. Sadikot. J. Chem. Soc. Perkin Trans. 2, 279 (1985).
36. F. E. Hruska, D. J. Wood, T. N. McCaig, A. A. Smith, and A. Holy. Can. J. Chem., **52**, 497 (1974).
37. R. R. Fraser, M. Kaufman, P. Morand, and G. Govil. Can. J. Chem. **47**, 403 (1969).
38. P. C. Kline and A. S. Serianni. Magn. Reson. Chem. **28**, 324 (1990).
39. R. J. Gillespie. Molecular geometry. Van Nostrand–Reinhold, London. 1972.
40. S. C. Choi and R. J. Boyd. Can. J. Chem. **64**, 2042 (1986).
41. (*a*) R. F. W. Bader, T.-H. Tang, Y. Tal, and F. W. Biegler-Konig. J. Am. Chem. Soc. **104**, 940 (1982); **104**, 946 (1982); (*b*) T.-H. Tang and X.-Y. Fu. Int. J. Quantum. Chem. **24**, 317 (1983); (*c*) R. F. W. Bader, T. S. Slee, D. Cremer, and E. Kraka. J. Am. Chem. Soc. **105**, 5061 (1983); (*d*) C. Gatti, M. Barzaghi, and M. Simonetta. J. Am. Chem. Soc. **107**, 887 (1985); (*e*) R. F. W. Bader and P. J. MacDougall. J. Am. Chem. Soc. **107**, 6788 (1985); (*f*) R. F. W. Bader, R. J. Gillespie, and P. J. MacDougall. J. Am. Chem. Soc. **110**, 7329 (1987); (*g*) R. J. Boyd. Stud. Org. Chem. (Amsterdam), **31**, 485 (1987); (*h*) O. Knop, R. J. Boyd, and S. C. Choi. J. Am. Chem. Soc. **110**, 7299 (1988); (*i*) J. R. Cheeseman, M. T. Carroll, and R. F. W. Bader. Chem. Phys. Lett. **143**, 450 (1988); (*j*) M. T. Carroll, C. Chang, and R. F. W. Bader. Mol. Phys. **63**, 387 (1988); (*k*) M. T. Carroll and R. F. W. Bader. Mol. Phys. **65**, 695 (1988); (*l*) R. F. W. Bader and C. Chang, J. Phys. Chem. **93**, 2946 (1989); **93**, 5095 (1989); (*m*) T.-H. Tang, W.-J. Hu, D.-Y. Yan and Y.-P. Cui, J. Mol. Struct. (Theochem), **207**, 319 (1990); **207**, 327 (1990); (*n*) W. Zhou, Y.-P. Cui, and T.-H. Tang. J. Mol. Struct. (Theochem), **230**, 401 (1991).

Theoretical studies applicable to the design of novel anticonvulsants: an AM1 molecular orbital structure–activity study of dihydropyridine calcium channel antagonists

JACK ANDREW BIKKER
Department of Chemistry, Queen's University at Kingston, Kingston, Ont., Canada K7L 3N6

AND

DONALD FREDRIC WEAVER[1]
Departments of Chemistry and Medicine (Neurology), Queen's University at Kingston, Kingston, Ont., Canada K7L 3N6

Received March 17, 1992

Can. J. Chem. Downloaded from www.nrcresearchpress.com by 109.225.110.28 on 09/08/12
For personal use only.

JACK ANDREW BIKKER and DONALD FREDRIC WEAVER. Can. J. Chem. **70**, 2449 (1992).

The development and synthesis of anticonvulsant new chemical entities that are distinct from the cyclic ureides in current clinical use is a continuing neuropharmacologic priority. The design of neuronal specific dihydropyridines active at the L-type calcium channel protein represents a rational approach to this design problem. To provide the structural data required for the design of anticonvulsant dihydropyridines, an AM1 semi-empirical molecular orbital study has been undertaken. Forty-six dihydropyridine calcium channel antagonists have been fully optimized at the AM1 level. Each of the 46 analogues was considered in six conformations to provide a systematic evaluation of changes in ester and phenyl ring orientation. The calculational validity of the AM1 Hamiltonian when applied to dihydropyridines was demonstrated by comparing AM1-optimized structures to experimental (X-ray crystallographic) and *ab initio* molecular orbital (STO 3G basis set) geometries. For each dihydropyridine, 79 AM1-derived geometric and electronic descriptors were obtained. The resulting descriptor matrix comparing structural descriptors with biological activity was statistically reduced to provide regression and discriminant structure–activity models for dihydropyridine calcium channel antagonism.

JACK ANDREW BIKKER et DONALD FREDRIC WEAVER. Can. J. Chem. **70**, 2449 (1992).

Le développement et la synthèse de nouvelles entités chimiques anticonvulsives distinctes des uréides cycliques actuellement en usage clinique sont des priorités neuropharmacologiques permanentes. La conception de dihydropyridines de spécificité neuronale, actives au niveau de la protéine de type L du canal du calcium, représente une approche rationnelle à ce problème. Afin d'obtenir les données structurales nécessaires pour la conception de dihydropyridines anticonvulsives, on a entrepris une étude d'orbitales moléculaires semi-empiriques AM1. Opérant au niveau AM1, on a optimisé 46 dihydropyridines antagonistes du canal du calcium. Afin d'obtenir une évaluation systématique des changements dans l'orientation de l'ester et du noyau phényle, on a considéré chacun de ces 46 analogues dans six conformations. On a démontré que l'hamiltonien AM1 appliqué aux dihydropyridines est valide pour les calculs en procédant à une comparaison des structures optimisées par AM1 avec celles obtenues expérimentalement (diffraction des rayons X) et avec les géométries obtenues par des calculs d'orbitales moléculaires *ab initio* (base STO 3G). Pour chaque dihydropyridine, on a obtenu 79 descripteurs géométriques et électroniques dérivés du AM1. On a réduit statistiquement la matrice résultante de descripteurs comparant les descripteurs structuraux avec l'activité biologique afin d'obtenir des modèles de régression et d'activité–structure discriminatoires pour la dihydropyridine antagoniste du canal du calcium.
[Traduit par la rédaction]

1. Introduction

Of the more than 50 million people worldwide suffering from epilepsy, approximately 35% are either unable to tolerate conventional drugs or simply do not respond to these medications (1). Therefore, there is a need to devise new approaches in the rational design of antiepileptic drugs, thus developing novel compounds distinct from the cyclic ureides in current clinical use. Modulation of the neuronal calcium currents involved in the propagation of seizure-related aberrant electrical activity within the brain represents such an approach. Dihydropyridine (DHP) calcium channel antagonists are an important class of pharmacotherapeutic compounds (2, 3). Although initially used for cardiovascular indications, recent studies have investigated DHPs as a potential treatment for neurologic disorders such as epilepsy (4–9). These studies suggest that, while the DHPs possess significant anticonvulsant activity, they are not as potent as currently available anticonvulsants, such as 5,5-diphenylhydantoin (9). The reason for these limitations is that the currently available DHPs were designed primarily for cardiovascular indications, not neurologic indications.

Recently, the need to design neuronal-specific DHPs for the treatment of seizures has been suggested (10). The design problem may be conceptualized as twofold: (*i*) the DHP must bind strongly with its receptor site on the transmembrane voltage-activated calcium channel protein and (*ii*) the DHP must have the capacity to cross the blood–brain barrier and be delivered to the microenvironment of the receptor site. The first is a pharmacodynamic consideration; the latter is a pharmacokinetic consideration. If the molecular fragment of the DHP that interacts with the receptor can be identified, the rest of the molecule can be engineered to improve site-specific delivery to the brain.

To provide the structural data necessary for the design of anticonvulsant dihydropyridines, a semi-empirical quantum mechanical study has been undertaken. The goals of this study are threefold: (*i*) to evaluate the utility of the AM1 Hamiltonian in the optimization of DHP geometries and conformation, (*ii*) to perform a rigorous search of the con-

[1]Author to whom correspondence may be addressed.

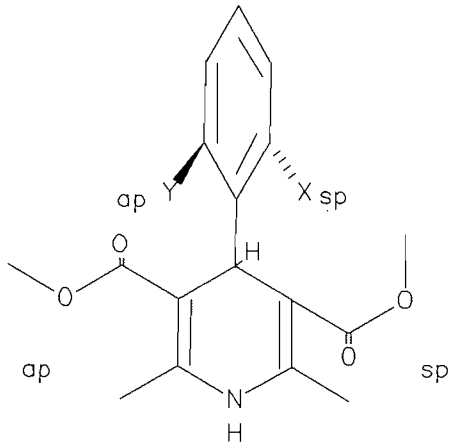

FIG. 1. Conformational nomenclature of ester groups and phenyl ring.

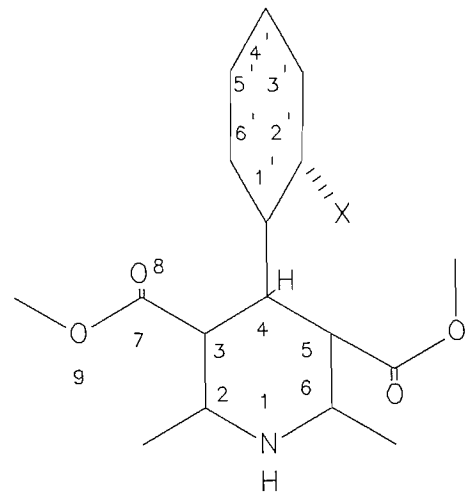

FIG. 2. Basic dihydropyridine calcium antagonist structure with numbering scheme.

formations available to the DHPs, and (*iii*) to preliminarily evaluate the correlation of AM1-derived properties with biological activities in an attempt to deduce the bioactive structural and electronic congeners. To achieve these goals, 46 DHPs have been fully optimized using AM1. Six conformers of each of the DHPs were fully optimized, providing the heats of formation of the various conformations and assisting in the prediction of the putative bioactive conformation. AM1 geometries were then compared to their corresponding crystal structures and *ab initio* conformations to assess the usefulness of the semi-empirical calculational approach. To permit this comparison, seven DHPs were fully optimized at the STO-3G *ab initio* level. Finally, AM1-derived geometric and electronic properties were statistically correlated with pharmacologic data for 34 mono-substituted DHPs for which comparable biological data was available.

2. Calculations

2.1. AM1 conformational optimization calculations

The first phase of this study ascertained the utility of AM1 calculations in representing DHP geometries. Conformational calculations were performed on an IBM RS/6000 550 RISC computer operating under AIX. For semi-empirical molecular orbital calculations, the AM1 (11) Hamiltonian implemented in MOPAC 5.01 was used (12). For *ab initio* molecular orbital calculations, STO-3G basis set calculations were performed using the HONDO (13) program within the MOTECC-90 family of programs (14).

The conformations of the DHPs are labelled according to the convention shown in Fig. 1; the numbering system about the rings and side chains of the DHP is shown in Fig. 2. An ester is considered to be *synperiplanar* (*sp*) if its carbonyl group eclipses the adjacent double bond of the dihydropyridine ring and *ap* if the carbonyl group is oriented *anti* to the adjacent double bond. The *synperiplanar* conformation can also be considered to be *cis* or *Z*, and the *antiperiplanar* (*ap*) to be *trans* or *E*. The conformation of the phenyl ring is classified according to the orientation of the phenyl substituent with the C(4)—H bond of the dihydropyridine ring. Thus, a conformation in which the phenyl substituent lies above the dihydropyridine ring is *ap*; that in which it is oriented away from the ring and eclipses the C(4)—H bond is *sp*. The esters are distinguished as "left" and "right" with respect to the dihydropyridine ring viewed with the phenyl group oriented forward and up above the C(2)—C(3)—C(5)—C(6) plane. (In all cases, the acronym DHP represents the entire dihydropyridine calcium channel blocker; where only the six-membered dihydropyridine ring is indicated, the entire word is used.)

Initial geometries of the dihydropyridine calcium channel blockers were taken from crystal structures of the 2-nitro (15) and 3-nitro (16) substituted DHPs obtained from the Cambridge Crystallographic Database (17). Templates were constructed based upon the AM1-optimized conformations of these structures. Using these templates, the KGNMOL molecular graphics package (18) was used to generate starting conformations for the balance of the compounds. For each of the 46 DHPs, six starting conformations were examined (*phenyl:left ester/right ester*): *sp:sp/sp*; *sp:sp/ap*; *sp:ap/ap*; *ap:sp/sp*; *ap:sp/ap*; and *ap:ap/ap* (see Fig. 3). These conformations were chosen to evaluate the six most probable conformers available to the DHPs; they represent systematic rotations about the three bonds that significantly affect DHP conformation. The side chains were set so that the torsional angle between the carbonyl of the ester and the adjacent double bond of the ring deviated by less than 5° from either 0 or 180 degrees. Similarly, the phenyl ring was rotated so that it eclipsed the C(4)—H bond. In the subsequent optimizations, the ester groups and the phenyl ring were free to rotate.

Root-mean-square comparisons of geometries were performed using the Comp routine in the KGNGRAF program (14). To compare AM1 with experimental conformations, crystal structures were obtained from the Cambridge Crystallographic Database (17).

To compare AM1 with *ab initio* conformations, seven DHPs were fully optimized using *ab initio* calculations at the STO-3G basis set level. Starting conformations were obtained from the AM1-optimized conformations. The convergence threshold on the maximum gradient component was set at 10^{-6}. Convergence was achieved in all cases.

2.2. Statistical structure–activity relationship calculations

In the second phase of this study, AM1-derived structural and electronic properties were statistically correlated with biological activity. Statistical calculations were per-

Can. J. Chem. Downloaded from www.nrcresearchpress.com by 109.225.110.28 on 09/08/12
For personal use only.

Can. J. Chem. Downloaded from www.nrcresearchpress.com by 109.225.110.28 on 09/08/12
For personal use only.

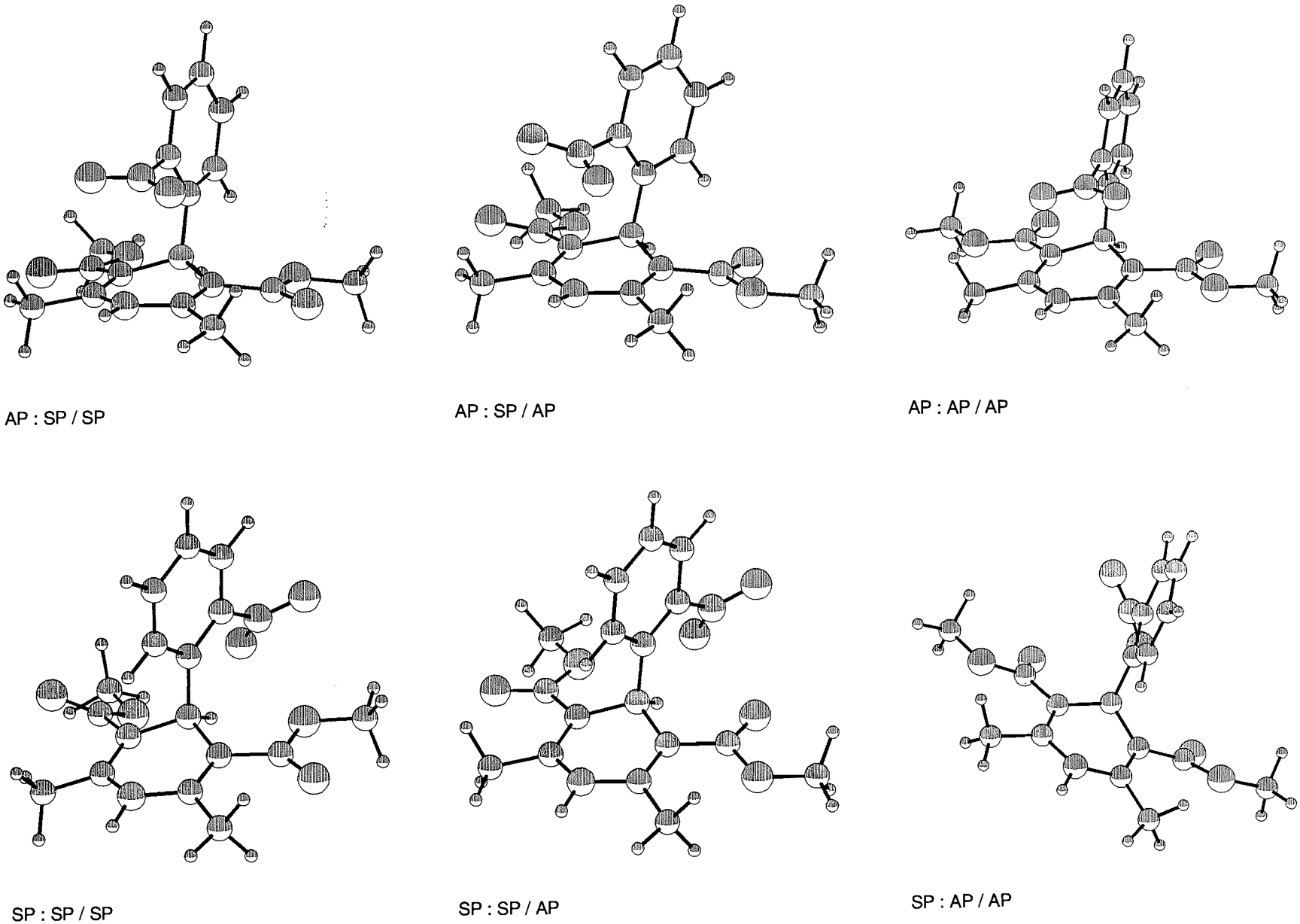

FIG. 3. AM1-optimized conformations of 2′-NO_2 DHP (nifedipine). Conformations, clockwise from upper left, are *ap:sp/sp*, *ap:sp/ap*, *ap:ap/ap*, *sp:ap/ap*, *sp:sp/ap*, and *sp:sp/sp*.

Can. J. Chem. Downloaded from www.nrcresearchpress.com by 109.225.110.28 on 09/08/12
For personal use only.

formed on an IBM ES/9129 mainframe computer operating under VM/CMS. Regression and discriminant analyses were performed using the SAS package of programs (19), version 6.06.

To describe DHP molecular properties, a series of geometric and electronic descriptors were obtained from the AM1 optimizations for each DHP analogue. All descriptors were obtained from the optimized geometry having the phenyl substituent oriented *sp* and the ester side chains oriented *sp*/*sp*. Each analogue was described by 79 descriptors. These descriptors may be classified into the following 11 groups. (*i*) bond lengths about the dihydropyridine and phenyl rings, (*ii*) bond angles about the dihydropyridine rings, (*iii*) torsional angles about the dihydropyridine ring, (*iv*) torsional angles about the C(3)—C(7) and C(4)—C(1′) bonds, (*v*) interatomic distance between the distal atomic centre of the phenyl substituent and its point of attachment to the phenyl ring, (*vi*) atomic charges about the dihydropyridine and phenyl rings, as well as the sum of atomic charges of the substituent, (*vii*) bond orders about the dihydropyridine and phenyl rings, (*viii*) energies of the HOMO and LUMO, (*ix*) magnitude of the molecular dipole, (*x*) molecular weight, and (*xi*) ring puckering parameters.

Biological data for calcium channel blocking activity were obtained from Coburn *et al.* (20). These data were acquired using a standard protocol that measured the inhibition of smooth muscle contraction by calcium channel blockade. As calcium channel antagonism is believed to be the mechanism of the DHP's anticonvulsant action, these data serve as an indirect, rather than a direct, measure of anticonvulsant activity. Complementary data for a number of compounds were obtained from Rovnyak *et al.* (21, 22).

A total of 34 compounds of differing biological activity were used in the analysis. Each compound was described by its biological activity and 79 geometric and electronic descriptors, giving rise to a 34 × 79 descriptor matrix. A principal goal of the study was to identify a restricted number of descriptors that correlated well with the biological activity and could therefore be used to predict compound activity. Stepwise regression analysis and stepwise discriminant analysis were used to identify subgroups of descriptors that were correlated with the biological data. These subsets of descriptors were then incorporated into regression and discriminant models, which provided complementary methods of estimating compound activity.

The regression models were constructed using the following procedure. A subset of descriptors that correlated well with activity was selected from the full descriptor matrix using stepwise and forward selective regression procedures at the 95% confidence level. These descriptors were then fit to pharmacologic activity (obtained from ref. 20 as -log EC_{50}) using linear regression. This procedure was applied to subgroups of compounds substituted at the 2′, the 3′, and the 4′ positions of the phenyl ring, to those substituted at either the 2′ or 3′ positions on the phenyl ring, and to the entire data set of 34 compounds.

For the discriminant analysis, DHPs were classified as more active (MA) if their biological activity was greater than 7.00 or less active (LA) if less than 7.00. Stepwise discriminant analysis at the 95% confidence level was used on the entire data set to identify a subset of descriptors with discriminatory ability. Discriminant analysis using this smaller group of descriptors was then performed on the entire data set.

To critically evaluate this discriminatory model, a balanced subset of DHPs consisting of the 14 most active and 14 least active DHPs was created. The remaining compounds were those at the border between classes (and thus somewhat ambiguously classified) and the 3′-N_3 and 4′-Me for which no comparable biological data was available. Thirty trials of the discriminant model were performed using the smaller test set. In each trial, 10 randomly chosen compounds (5 more active, 5 less active) were used as a test set and the remaining 18 (9 active, 9 less active) were used as the training set. The performance of the discriminant model could be evaluated for each trial by its ability to correctly classify the molecules in the training set itself, the randomly determined test set, and the molecules at the class border. The error for each trial was estimated by the misclassified compounds as a fraction of all classified compounds in both the training and test data sets. The error in the discriminant function was then estimated by calculating the percentage misclassified for all trials.

TABLE 1. Comparison of AM1 results with crystal geometries: root-mean-square fit and ring pucker

DHP	RMS	Crystal $\Sigma\|\tau\|$	AM1 $\Sigma\|\tau\|$	Crystal Q	AM1 Q
2′-CF_3	0.568	62.7	78.4	0.179	0.242
2′-Cl	0.297	63.7	72.5	0.187	0.170
2′-NO_2	0.200	85.8	65.2	0.207	0.198
2′-NH_2	0.207	82.9	79.9	0.238	0.236
3′-NO_2	0.358	90.6	66.7	0.325	0.200
3′-CN	0.316	112.5	70.5	0.325	0.232
3′-Me	0.392	93.5	80.3	0.270	0.242
4′-NMe_2	0.320	104.5	68.2	0.304	0.204
2′-Cl, 5′-NO_2	0.334	92.2	74.0	0.293	0.218
F_5	0.270	57.7	55.2	0.147	0.246

NOTE: Torsional angles reported are for AM1 compounds in the *sp*/*ap* ester conformation. $\Sigma|\tau|$ is the sum of the absolute values of the torsional angles and Q is the total puckering amplitude of the ring as determined the method of Cremer and Pople (25).

3. Results

3.1. Comparison between AM1 conformations and crystal structures

AM1-optimized structures were compared with experimental crystallographic data for 10 DHPs (Table 1). Root-mean-square values ranged from 0.200 to 0.568. Distances and angles about the DHP ring are better conserved among AM1-optimized geometries than among their corresponding crystal structures (15, 16, 21, 23, 24). As shown in Table 2, AM1-optimized geometries have longer bonds between the ring nitrogen and the adjacent C_{sp^2} carbon, but shorter carbon double bonds within the dihydropyridine ring. In addition, the intra-annular angles at N(1) and C(4) of the AM1-optimized geometries are smaller than those in the crystal structures. In the case of the ester group, AM1 predicts carbon–oxygen bonds that are longer than those experimentally observed. However, AM1 also predicts that the C3—C7 bond is shorter than that in the crystal structures. This is also true of the C4—C1′ single bond.

The pucker of the dihydropyridine ring of AM1-optimized geometries and crystal geometries was also compared. Two measures of ring pucker were employed: a simple sum of the absolute values of the torsional angles about the dihydropyridine ring and the total puckering amplitude as defined by Cremer and Pople (25). The latter is a measure of deviation from a mean plane fit to the coordinates of the

TABLE 2. Comparison of AM1 results with crystal structures: bond lengths and angles

DHP	N(1)—C(2)	C(2)—C(3)	C(3)—C(4)	C(3)—C(7)	C(7)—O(8)	C(7)—O(9)	C(4)—C(1′)	216	123	234	345
2′-CF_3	1.394	1.374	1.502	1.462	1.239	1.368	1.513	119.4	120.4	121.6	110.8
crystal	1.378	1.357	1.527	1.468	1.211	1.346	1.540	123.9	119.8	121.2	111.2
2′-Cl	1.394	1.372	1.500	1.462	1.239	1.371	1.508	120.1	120.2	122.1	110.7
crystal	1.426	1.363	1.584	1.485	1.222	1.405	1.567	126.3	116.7	121.5	114.2
2′-NO_2	1.393	1.371	1.501	1.464	1.239	1.368	1.511	120.8	120.3	121.7	111.5
crystal	1.374	1.355	1.524	1.447	1.206	1.355	1.528	123.8	120.2	120.7	111.0
2′-NH_2	1.394	1.370	1.502	1.464	1.239	1.371	1.508	120.5	120.1	121.9	110.5
crystal	1.441	1.354	1.615	1.528	1.304	1.351	1.537	126.9	117.3	120.1	113.9
3′-NO_2	1.393	1.373	1.497	1.461	1.239	1.371	1.508	120.8	120.3	121.6	111.7
crystal	1.386	1.347	1.519	1.491	1.202	1.355	1.524	122.5	119.4	121.2	110.4
3′-CN	1.395	1.372	1.496	1.462	1.239	1.371	1.508	121.0	120.1	121.7	111.4
crystal	1.383	1.345	1.512	1.472	1.199	1.336	1.529	123.6	118.3	120.2	110.3
3′-CH_3	1.394	1.372	1.499	1.461	1.239	1.372	1.506	120.5	120.2	121.4	111.0
crystal	1.385	1.360	1.519	1.471	1.217	1.355	1.519	123.4	119.0	120.6	110.7
4′-NO_2	1.392	1.373	1.499	1.461	1.238	1.372	1.508	121.0	120.1	121.6	111.6
crystal	1.382	1.362	1.520	1.470	1.219	1.354	1.532	124.0	119.2	120.3	111.4
4′-$N(Me)_2$	1.393	1.371	1.501	1.464	1.239	1.368	1.511	120.8	120.2	121.9	111.5
crystal	1.371	1.367	1.545	1.479	1.190	1.377	1.529	123.7	118.5	121.4	109.9
H	1.393	1.372	1.499	1.461	1.239	1.372	1.507	120.3	120.2	121.9	110.7
crystal	1.409	1.389	1.503	1.493	1.199	1.382	—	125.0	116.7	120.9	111.5
2-Cl, 5-NO_2	1.390	1.375	1.500	1.466	1.236	1.372	1.512	120.9	120.3	121.2	111.6
crystal	1.382	1.361	1.517	1.471	1.190	1.321	1.525	121.4	119.8	120.6	110.1
P_5	1.388	1.373	1.499	1.461	1.239	1.372	1.509	121.2	120.2	121.6	111.4
crystal	1.368	1.360	1.517	1.462	1.206	1.339	1.529	124.8	118.9	120.9	112.5

NOTE: All bond lengths are given in angstroms. Crystal geometries were obtained from the Cambridge Crystallographic Database and have been published (15, 16, 21–23). AM1 bond lengths and angles are taken from the conformation corresponding to that of the crystal structure.

Can. J. Chem. Downloaded from www.nrcresearchpress.com by 109.225.110.28 on 09/08/12
For personal use only.

ring atoms. Results are reported in Table 1. No correlation between crystal and calculated pucker was found.

3.2. Comparison of AM1 and STO-3G conformations

The AM1 results were compared to seven DHPs fully optimized using the *ab initio* molecular orbital at the STO-3G basis set level. All were optimized in the *sp:sp/sp* conformation. The results reported in Tables 3 and 4 show that AM1 calculations closely match those obtained using the *ab initio* approach.

The AM1-optimized bond lengths match those of the corresponding STO-3G optimized bond lengths to within 0.06 Å. Within the dihydropyridine ring, AM1-optimized geometries have double bond lengths 0.06 Å longer than their corresponding STO-3G geometries and N—C_{sp^2} and C_{sp^2}—C_{sp^3} bond lengths, which are respectively 0.04 and 0.03 Å shorter. The dihydropyridine–phenyl bond is also shorter, by approximately 0.04 Å. In the case of the ester substituents, both the single bond from the carbonyl carbon to the C_{sp^2} carbon of the dihydropyridine ring and the single bond to the methoxy oxygen are calculated to be shorter in AM1 geometries than in STO-3G optimized structures. Conversely, the carbonyl double bond is calculated to be longer by AM1. Overall, the root-mean-square fit of non-hydrogen atoms ranged from 0.088 to 0.277.

Using both calculational methods, bond lengths and angles determined for different DHPs were conserved. Where there were changes, AM1 appears to reproduce the trends in bond lengths observed in STO-3G geometries.

Bond angles about the dihydropyridine ring calculated by AM1 and STO-3G are in close agreement, differing by less than 3°. The torsional angles differ somewhat more; the dihedral angles of the nitrogen–C_{sp^2} bond are calculated to be approximately 8° less than those calculated by STO-3G. However, the torsional angles of the ring double bonds are about 4° larger. Generally, the ester side chains as calculated by AM1 deviate from a conformation coplanar with the dihydropyridine ring more than those calculated by STO-3G. Similarly, the phenyl ring is less constrained to lie in the N(1)—C(4)—C(1′) plane. Overall, there is good correspondence between STO-3G and AM1 geometries.[2]

3.3. Energies of conformers

The heats of formation of the six optimized conformers of each compound are given in Table 5. Overall, the energy differences among conformers were not large; differences less than 5 kcal/mol between the highest and lowest energy conformer for each compound were typical. In all cases, a

[2]Tables of AM1 geometries: bond lengths, and bond angles and torsional angles about the DHP ring have been deposited as supplementary material and may be purchased from: The Depository of Unpublished Data, Document Delivery, CISTI, National Research Council Canada, Ottawa, Canada K1A 0S2.

These tables have also been deposited with the Cambridge Crystallographic Data Centre and can be obtained on request from The Director, Cambridge Crystallographic Data Centre, University Chemical Laboratory, 12 Union Road, Cambridge, CB2 1EZ, U.K.

TABLE 3. Comparison of AM1 and STO-3G geometries: bond lengths

Compound	N(1)—C(2)	C(2)—C(3)	C(3)—C(4)	C(3)—C(7)	C(7)—C(8)	C(7)—C(9)	C(4)—C(1′)	C(4)—H	N(1)—H
H:									
STO 3G	1.428	1.330	1.534	1.512	1.222	1.397	1.547	1.089	1.023
AM1	1.391	1.372	1.503	1.463	1.238	1.375	1.510	1.134	0.994
2′-CF_3:									
STO 3G	1.428	1.330	1.535	1.514	1.221	1.396	1.553	1.086	1.023
AM1	1.391	1.374	1.504	1.464	1.238	1.371	1.512	1.133	0.995
F_5:									
STO 3G	1.422	1.332	1.533	1.512	1.221	1.397	1.548	1.090	1.022
AM1	1.388	1.375	1.498	1.465	1.237	1.372	1.511	1.137	0.994
2′-Cl:									
STO 3G	1.429	1.330	1.533	1.516	1.220	1.395	1.550	1.088	1.024
AM1	1.392	1.374	1.501	1.467	1.236	1.371	1.510	1.134	0.993
2′-NH_2:									
STO 3G	1.430	1.328	1.533	1.511	1.220	1.405	1.550	1.087	1.023
AM1	1.392	1.371	1.500	1.463	1.237	1.378	1.507	1.132	0.994
2′-NO_2:									
STO 3G	1.428	1.331	1.534	1.516	1.220	1.394	1.553	1.089	1.024
AM1	1.391	1.373	1.502	1.468	1.236	1.367	1.512	1.134	0.994
2′-CH_3:									
STO 3G	1.428	1.330	1.535	1.514	1.221	1.398	1.552	1.087	1.023
AM1	1.391	1.372	1.500	1.466	1.237	1.374	1.510	1.133	0.995

NOTE: All results reported are for DHPs in the *sp:sp/sp* conformation. Bond lengths are reported in angstroms.

TABLE 4. Comparison of AM1 and STO-3G geometries: bond angles and torsional angles

Compound	123	234	345	612	1234	3456	6123	Left ester	Right ester	Phenyl	RMS Fit
H:											
STO 3G	119.9	121.7	110.7	119.1	0.9	20.1	21.5	−1.1	−3.8	3.2	0.277
AM1	120.0	121.2	111.7	120.9	4.4	20.0	13.6	23.7	−16.5	21.5	
2′-CF_3:											
STO 3G	119.9	121.6	110.5	118.8	0.5	21.8	22.7	13.3	−4.6	4.1	0.143
AM1	120.0	121.3	111.6	121.0	3.4	20.5	14.4	23.3	−13.4	0.9	
F_5:											
STO 3G	120.0	121.6	111.0	119.9	1.5	19.8	19.3	20.7	−6.9	1.2	0.089
AM1	120.2	121.1	111.7	121.5	8.3	19.2	8.7	33.2	−10.3	1.3	
2′-Cl:											
STO 3G	120.0	121.5	110.5	118.6	0.5	22.3	22.6	33.1	−8.5	5.9	0.101
AM1	121.1	120.5	111.8	120.4	3.4	19.7	14.1	43.2	−15.1	6.1	
2′-NH_2:											
STO 3G	119.8	121.8	110.6	119.1	1.4	21.8	21.1	20.7	−6.9	1.2	0.994
AM1	120.7	120.9	111.9	120.8	4.1	18.9	13.1	25.7	−18.6	9.1	
2′-NO_2:											
STO 3G	120.1	121.5	110.5	118.6	0.6	21.6	22.4	35.9	−1.5	11.3	0.091
AM1	120.5	121.2	111.7	120.6	3.8	17.4	14.2	45.1	−7.3	−11.5	
2′-CH_3:											
STO 3G	120.0	121.7	110.4	118.9	1.0	21.3	21.5	24.6	−11.0	2.8	0.093
AM1	120.7	121.3	111.4	120.5	4.6	18.6	12.9	34.4	−18.0	2.4	

NOTE: All DHPs were calculated in the *sp:sp/sp* conformation.

conformation with both ester ester groups *ap* was the least energetically favourable. The lowest energy conformation was generally one in which the ester groups were oriented *sp* and the phenyl ring was oriented either *ap* or *sp*. The energy differences between phenyl conformations were most pronounced with *ortho* substitution at the phenyl ring. In

Can. J. Chem. Downloaded from www.nrcresearchpress.com by 109.225.110.28 on 09/08/12
For personal use only.

TABLE 5. Enthalpies of formation of AM1-optimized conformations (kcal/mol)

	Ester					
	Phenyl *sp*			Phenyl *ap*		
Molecule	*apsp*	*spsp*	*apap*	*apsp*	*spsp*	*apap*
2-NO_2	−110.7*	−112.4	−108.6	−110.8	−111.3	−111.4
3-NO_2	−117.0*	−117.5	−115.6	−117.2	−117.7	−117.3
4-NO_2	−117.8*	−117.3	−116.8			
2-NH_2	−121.3*	−119.9	−120.1	−116.9	−119.0	−117.1
3-NH_2	−121.0	−121.0	−120.1	−120.7	−121.0	−119.9
2-F	−162.9	−163.4	−164.0	−164.8	−166.1	−164.4
3-F	−165.3	−164.5	−164.0	−161.7	−162.2	−161.5
4-F	−165.5	−165.6	−164.6			
2-Cl	−123.8*	−124.1	−122.6	−123.4	−124.2	−122.9*
3-Cl	−127.1	−127.1	−126.0	−127.0	−127.4	−126.5
4-Cl	−127.5	−128.0	−126.3			
2-Br	−110.6	−111.1	−109.6	−110.8	−111.3	−110.4
3-Br	−115.2	−115.4	−114.1	−114.9	−115.6	−114.6
4-Br	−115.5	−115.8	−114.5			
2-I	−98.0	−98.4	−97.1	−96.6	−98.1	−97.2
3-I	−103.2	−104.0	−102.8	−103.8	−104.2	−103.0
4-I	−104.3	−104.1	−103.1			
2-CF_3	−269.6*	−269.8	−267.3	−266.3	−265.8	−265.4
3-CF_3	−276.6	−276.7	−275.1	−276.6	−277.0	−276.2
2-CH_3	−126.4	−126.4	−122.9	−121.7	−123.2	−121.3
3-CH_3	−127.5*	−127.2	−126.0	−126.8	−127.2	−126.2
4-CH_3	−127.6*	−127.0	−126.3			
H	−119.9*	−120.0	−118.5			
2-CN	−85.3	−85.8	−83.7	−86.0	−86.3	−85.7
3-CN	−88.9	−90.0	−87.6	−88.7*	−89.2	−88.3
4-CN	−89.3	−89.0	−88.1			
3-NMe_2	−110.1	−110.4	−109.8	−109.4	−110.0	−109.0
4-NMe_2	−110.5*	−110.0	−109.6			
2-OCH_3	−154.5	−154.4	−153.1	−152.7	−153.4	−152.1
3-OCH_3	−157.1	−157.6	−155.7	−156.9	−157.3	−155.2
2-$CH{=}CH_2$	−100.5	−97.8	−98.8	−97.4	−100.5	−96.5
2-Et	−126.4	−126.4	−122.9	−121.7	−123.2	−121.3
2-OEt	−158.3	−160.1	−158.2	−156.9	−159.4	−155.8
3-OH	−163.5	−164.2	−163.5	−163.4	−163.4	−163.1
3-OAc	−196.2	−193.6	−193.6	−192.4	−194.3	−191.1
3-OCOPh	−155.2	−156.5	−154.5	−155.3	−156.4	−155.0
3-N_3	−32.8	−33.9	−33.1	−33.6	−34.0	−19.9
2,6-Cl_2	−126.1	−126.3	−125.3			
2,3-Cl_2	−129.3	−129.6	−127.9	−128.9	−129.5	−128.5
3,5-Cl_2	−134.1	−134.2	−133.0			
2,4-Cl_2	−130.7	−131.1	−129.4	−130.1	−130.8	−130.0
2-F, 6-Cl	−165.9	−166.3	−164.3	−164.1	−165.1	−163.6
2-Cl, 5-NO_2	−120.7	−121.0*	−119.7	−119.4	−120.6	−118.7
2-OH, 5-NO_2	−164.1	−159.7	−163.2	−157.0	−158.4	−157.3
3,5-Me_2	−131.7	−134.0	−130.7			
F_5	−329.5	−329.6*	−327.8			

NOTE: Crystal conformations are marked with an asterisk (*).

these cases, the *sp* phenyl conformation was often preferred. Those conformations with ester carbonyl groups in opposite orientations (i.e., *sp/ap*) generally had associated energies close to that of the *sp/sp* orientations. The 2′-NH2 and 3′-OAc substituted DHP both showed a notable preference for the *sp:sp/ap* conformation.

3.4. Correlation of AM1 properties with biological activity

The geometric and electronic information obtained from the AM1-optimized conformations was analyzed for structure–activity relationships. A set of 34 monosubstituted compounds for which comparable biological testing exists was used for this investigation. All data was obtained from the *sp:sp/sp* conformation. For each compound, 79 electronic, geometric, and *ad hoc* descriptors were generated. The dimensionality of this data set was reduced using statistical routines contained in the SAS (19) family of programs.

The forward and stepwise regression procedures within SAS that selected descriptors correlated with activity were employed. The confidence level for entry and removal from the model was set at 95%. These models were then tested using standard linear regression procedures. The statistical

Can. J. Chem. Downloaded from www.nrcresearchpress.com by 109.225.110.28 on 09/08/12
For personal use only.

Can. J. Chem. Downloaded from www.nrcresearchpress.com by 109.225.110.28 on 09/08/12
For personal use only.

models obtained are given below for the DHPs substituted at the *ortho* position (eq. [1]), for the data without *para*-substituted compounds (eq. [2]), and for the entire data set of mono-substituted DHPs (eq. [3]). The order of the descriptors in a model is the same order in which they were entered into the model by the stepwise regression procedure.

$$[1]\quad \text{Act} = -61.4 - 4.01\,(E_{\text{HOMO}}) + 24.84\,(\text{bo}_{2'3'})$$
$$R^2 = 0.84, \qquad F = 24.8, \qquad n = 13$$

where E_{HOMO} = energy of HOMO in kcal/mol; $\text{bo}_{2'3'}$ = bond order of the C(2′)—C(3′) bond of the phenyl ring; Act = pharmacologic activity (-log(EC_{50})).

$$[2]\quad \text{Act} = 79.4 - 0.54\,(\text{L}_{3'}) - 1.44\,(E_{\text{HOMO}}) - 105\,(\text{bo}_{34}) - 1.38\,(A_{345}) + 142\,(\text{bo}_{56}) + 0.92\,(A_{165})$$
$$R^2 = 0.89, \qquad F = 26.9, \qquad n = 27$$

where $\text{L}_{3'}$ = distance from point of attachment to distant atom on substituent at *meta* (3′) position of phenyl ring; E_{HOMO} = energy of HOMO in kcal/mol; bo_{34} = bond order of the C(3)—C(4) bond of the dihydropyridine ring; bo_{56} = bond order of the C(5)—C(6) bond of the dihydropyridine ring; A_{345} = C(3)—C(4)—C(5) bond angle; A_{165} = N(1)—C(6)—C(5) bond angle; Act = pharmacologic activity (-log(EC_{50})).

$$[3]\quad \text{Act} = -3.17 - 2.05\,(l_{4'}) - 0.47\,(\text{L}_{3'}) - 2.88\,(E_{\text{HOMO}}) + 567\,(\text{Q}_5)$$
$$R^2 = 0.73, \qquad F = 20.5, \qquad n = 35$$

where $l_{4'}$ = axial length of *para* substituent on phenyl ring; $L_{3'}$ = distance from point of attachment to distant atom on substituent at *meta* (3′) position of phenyl ring; E_{HOMO} = energy of HOMO in kcal/mol; Q_5 = charge at C(5) of dihydropyridine ring; Act = pharmacologic activity (-log(EC_{50})).

No significant correlations with R^2 greater than 0.70 were obtained from the series of *para*- and *meta*-substituted compounds.

A discriminant model was also developed to distinguish active from less active compounds. The DHPs in the full data set were divided into two categories, more active and less active. The somewhat arbitrary criterion used for this assignment was that all compounds with activity (-log EC_{50}) of 7.00 or greater were assigned as more active; the rest as less active. Stepwise discriminant analysis at the 95% confidence level yielded four descriptors which could be used to assign the class of a molecule. These descriptors were

$\text{bo}_{3'4'}$ = bond order of C(3′)—C(4′) bond of phenyl ring

$\text{bo}_{4'5'}$ = bond order of C(4′)—C(5′) bond of phenyl ring

E_{HOMO} = energy of HOMO

$l_{3'4'}$ = length of C(3′)—C(4′) bond

The discriminant model using these descriptors was evaluated using smaller subsets of data as training and test sets. Overall, the four-descriptor model using subsets of 18 compounds (9 active, 9 less active) as training sets and 10 randomly chosen compounds (5 more active, 5 less active) as a test set correctly classified both the training and test sets in 97% of all cases. The misclassified compounds were 4′-I, 3′-NMe_2, and 2′-NH_2. Of the remaining data, the 3′-Me and 2′-OEt DHPs were consistently classified as more active by all models, and the 3′-N_3 DHP was classified as more active in 10 of 30 cases.

Table 6 provides a summary of experimental activities and predicted activities of the DHPs determined using the regression model for the full data set, the classes assigned initially and predicted by the discriminant model, and the values of descriptors used in generating the discriminant model.

4. Discussion

4.1. Comparison of AM1 and crystal geometries

The AM1 Hamiltonian (11) has emerged as a dominant molecular orbital method for the structural optimization of biomolecules. Previously, DHPs were not extensively analysed using this technique. Rovnyak *et al.* (21, 22) used AM1 calculations in conjunction with NMR experiments in the analysis of 13 DHPs. The current study, optimizing 237 conformations, provides a thorough examination of the viability of AM1 for the calculational study of DHPs. Moreover, since some authors (26) have identified weaknesses in the AM1 treatment of biomolecules, the AM1 geometries have been critically evaluated by comparison to crystallographic data.

The AM1-optimized geometries closely match those of the crystal structures. Both the low root-mean-square fitting values and the close agreement of bond lengths and angles indicate that the calculations closely reproduce the experimentally observed structures. The AM1 Hamiltonian therefore appears to be a reasonable method for calculating the structure of DHPs.

The variations in geometry that are observed are noteworthy. Bond lengths, angles, and torsional angles are better conserved among AM1 optimizations than among their corresponding crystal structures. This conservation of geometry with differing substitution is also seen in the series of compounds optimized at the *ab initio* level. Thus, some of the deviation in DHP conformation observed in crystal structures may be an artefact of the crystal packing forces, and not an intrinsic property of the molecule. This is emphasized by the ring pucker of AM1-optimized geometries. No correlation could be generated between the pucker of the calculated structures and those of the crystal structures.

The AM1-optimized conformations of the ester groups and the phenyl ring were less well conserved. Although in both the crystal structure and the STO-3G geometries the ester carbonyls eclipsed the dihydropyridine ring double bond, this was less the case with the AM1 results. AM1 optimizations produced ester conformations deviating by up to 50° from planarity. Similarly, the phenyl ring, constrained to lie in the N(1)—C(4)—C(1′) plane in both crystal and *ab initio* geometries, also deviated by as much as 30°. AM1 seemingly overpredicts the conformational flexibility about these bonds.

4.2. Comparison of AM1 and STO-3G geometries

In addition to reproducing experimental (X-ray) conformational data, an effective semi-empirical molecular orbital method must also reproduce *ab initio* geometries. Prior to this study, no *ab initio* studies were reported on full DHPs. Limited *ab initio* geometries obtained at the STO-3G level

TABLE 6. Statistical correlations and discriminant analysis

Compound	Act.[a]	Predicted act.[b]	Act.[c]	Class	Predicted class	$bo_{3'4'}$	$bo_{4'5'}$	E_{HOMO}	$l_{3'4'}$
3′-Br	8.89	7.41		MA	MA	1.39	1.42	−8.87	1.398
2′-CF_3	8.82	7.52		MA	MA	1.44	1.39	−8.90	1.390
2′-Cl	8.66	8.14	8.51	MA	MA	1.43	1.40	−8.76	1.392
3′-NO_2	8.40	7.78	8.40	MA	MA	1.36	1.43	−9.11	1.405
2′-CH=CH_2	8.35	6.98		MA	MA	1.43	1.40	−8.71	1.392
2′-NO_2	8.29	8.55	9.30	MA	MA	1.44	1.39	−8.98	1.398
2′-Me	8.22	7.74		MA	MA	1.43	1.41	−8.70	1.392
2′-Et	8.19	7.62		MA	MA	1.42	1.41	−8.70	1.392
2′-Br	8.12	8.34	9.40	MA	MA	1.43	1.40	−8.77	1.392
2′-CN	7.80	7.89		MA	MA	1.39	1.42	−8.93	1.392
3′-Cl	7.80	7.38		MA	MA	1.43	1.40	−8.85	1.398
3′-F	7.68	7.40		MA	MA	1.37	1.42	−8.88	1.405
H	7.55	7.43		MA	MA	1.41	1.42	−8.73	1.394
3′-CN	7.46	7.66	7.95	MA	MA	1.37	1.43	−8.95	1.403
3′-I	7.38	7.34		MA	MA	1.40	1.42	−8.85	1.396
2′-F	7.37	7.89	8.17	MA	MA	1.43	1.40	−8.77	1.390
2′-I	7.33	8.25	9.30	MA	MA	1.43	1.40	−8.78	1.392
2′-OMe	7.24	7.71		MA	MA	1.41	1.42	−8.63	1.394
3′-CF_3	7.13	7.34		MA	MA	1.38	1.43	−8.98	1.398
3′-CH_3	6.96	6.84		LA	MA	1.39	1.42	−8.72	1.400
2′-OEt	6.96	7.35		LA	MA	1.41	1.42	−8.62	1.394
4′-F	6.89	7.17		LA	LA	1.36	1.36	−8.86	1.406
3′-Ome	6.72	6.37		LA	LA	1.37	1.41	−8.72	1.401
3′-NMe_2	5.24	6.05		LA	LA	1.35	1.44	−8.30	1.417
3′-OH	6.00	6.93		LA	LA	1.36	1.41	−8.75	1.401
3′-NH_2	5.70	5.84		LA	LA	1.34	1.43	−8.33	1.416
4′-NO_2	5.50	3.24	5.52	LA	LA	1.36	1.37	−9.17	1.403
4′-CN	5.46	4.76		LA	LA	1.37	1.37	−8.98	1.402
4′-Br	5.40	5.87		LA	LA	1.39	1.39	−8.88	1.398
3′-OAc	5.22	6.39		LA	LA	1.36	1.42	−8.97	1.401
3′-OCOPh	5.20	5.16		LA	LA	1.37	1.41	−8.88	1.399
4′-Cl	5.09	5.69		LA	LA	1.38	1.39	−8.83	1.399
4′-I	4.64	5.83		LA	LA	1.40	1.40	−8.87	1.395
2′-NH_2	4.40	5.59		LA	LA	1.45	1.39	−8.23	1.387
4′-NMe_2	4.00	3.24		LA	LA	1.37	1.37	−8.65	1.411
3′-N_3	—			—	LA	1.36	1.42	−8.62	1.411
4′-Me	—			—	LA	1.39	1.39	−8.72	1.401

[a]Data from ref. 20, values reported as -log(EC_{50}). The 3′-NMe_3 substituted DHP was not included as it represents a departure from the uncharged nature of the balance of the DHPs examined.
[b]Predicted using model based on entire data set.
[c]Data from refs. 21 and 22, values given as -log(IC_{50}).
[d]Class assigned as follows: MA (more active) if activity > 7.00, LA (less active) if activity < 7.00.

for smaller model compounds related to the DHPs have been reported (27, 28). However, in this study, *ab initio* geometries of full DHPs were judged to provide a better comparison to the AM1 geometries. The seven DHPs were calculated in the *sp:sp/sp* conformation; this conformation was selected as it was considered to be of potential biological interest (29) and because it conformed to previous calculations (28).

The STO-3G optimized geometries reported above produce consistent bond lengths and angles for the DHPs. They suggest a strong preference for a conformation in which the ester groups lie coplanar with the dihydropyridine ring and in which the phenyl ring is constrained to a plane perpendicular to the dihydropyridine ring and passing through N(1) and C(4). The dihydropyridine ring has a flattened boat conformation and is significantly puckered. The boat conformation is due to the bond angles at N(1) and C(4), which cause these atoms to lie above the plane generated by the two double bonds. Each double bond, however, constrains its attached atoms to be coplanar, with little deviation observed. The conformation of the dihydropyridine ring is conserved among different DHPs. The conformations reported by Hofmann and Cimiraglia for model DHPs are also in agreement with these results. The methyl groups at the C(2) and C(6) positions of the dihydropyridine ring produce longer C(2)—C(3) and C(5)—C(6) double bonds than those reported for the model compounds.

The AM1-optimized geometries closely reproduce STO-3G geometries, as is evidenced by the low deviations calculated by the root-mean-square fitting procedure. Generally, AM1 geometries have slightly shorter single bonds and somewhat longer double bonds than STO-3G geometries. The AM1 geometries also have conformations in which the ester carbonyls are less likely to be coplanar with the dihydropyridine ring, and in which the phenyl ring is allowed greater axial rotation. Minor variations in bond lengths, angles, and

Can. J. Chem. Downloaded from www.nrcresearchpress.com by 109.225.110.28 on 09/08/12
For personal use only.

Can. J. Chem. Downloaded from www.nrcresearchpress.com by 109.225.110.28 on 09/08/12
For personal use only.

torsional angles in the STO-3G geometries are also reproduced in the AM1 geometries and follow similar trends among compounds. AM1 results therefore appear to provide a representation of DHP conformation that closely follows the *ab initio* results.

4.3. Energies of conformers

Differences in the AM1-calculated heats of formation of the various conformers of a DHP were shown to be generally less than 5 kcal/mol. Although the differences were not substantial, most compounds had clearly identifiable preferred conformations. In all cases, the conformations with both esters oriented *ap* were energetically disfavoured. Most also had a minimum energy conformer in which both esters were oriented *sp*; if not, such a conformation was not appreciably disfavoured. The *sp/ap* ester conformations were also generally accessible, which is expected as almost all known crystal structures have geometries with the esters in either the *sp/sp* or *sp/ap* orientation (29). *ortho*-Substituted compounds generally favour an *sp* phenyl orientation, with *meta*- and *para*-substituted compounds showing less preference for a particular phenyl orientation.

These conclusions are supported by NMR analyses of isoxazolidine DHPs (30) and by studies from Rovnyak *et al.* on solution-phase DHP conformation (21, 22). These studies examined the populations of *sp* and *ap* phenyl rotamers in solution; the significance of the *ap* rotamer to solution conformation was noted.

These data may also support the recent binding model by Langs *et al.* (29, 31), which postulates that the active conformer of a DHP has *sp/sp* ester orientation. Provided binding transition state energies are not large, the populations of various conformers may influence their binding and thus pharmacologic activity. In such a case, *a priori* preference for *sp/sp* ester orientation may predispose the DHPs to bind at their receptor. Notably, the 2′-amino and 3′-acetyl substituted DHPs had *sp/ap* ester orientation in their energetically favoured conformation; they are both weakly active DHPs (20).

Other modelling studies have also been employed to explain compound activity. These have sought to identify differences between DHPs that are calcium channel blockers and DHPs of similar structure that have been shown to be calcium channel activators (32). Mahmoudian and Richards (33) proposed a model that postulates that patterns of hydrogen bonding are responsible for either activator or antagonist activity. Using pseudo-receptor modelling, Höltje and coworkers (34–36) developed a model that employed differing regions of molecular electrostatic potential. In both cases, ester conformation has been explicitly or implicitly related to the molecule's active conformation. Identification of the most probable conformer and its relative contribution is therefore of some importance to the eventual usefulness of these models.

This information is also of practical utility in the rational design of a neurologically active DHP. To be effective, such a compound must be able to cross the blood–brain barrier and enter the receptor microenvironment; considerable functional group engineering may be necessary to produce a DHP with these desired pharmacokinetic properties. The criterion developed above suggests that modifications that result in a DHP that has significantly disfavoured *sp/sp* ester orientation will probably lead to a pharmacodynamically less active compound. This is therefore a potentially useful structural consideration in the design process.

4.4. Correlation of AM1 properties with biological activity

DHPs probably exert anticonvulsant effects by the blockade of post-synaptic L-type calcium channels in the neuron (7, 9). This blockade would reduce neuronal excitability and hence suppress seizures. An understanding of the DHP properties that contribute to the blockade of L-type calcium channels is therefore of considerable interest to rational antiepileptic drug design. The recent identification of the putative DHP binding site in a region of conserved sequence homology within the calcium channel protein suggests that the features of the DHP that interact with its receptor are similar in skeletal, cardiac, and neurologic calcium channels (37). Earlier structure–activity studies using empirical descriptors (20, 38–40) have attempted to define these features; typically these have used successively larger numbers of DHPs to improve the statistical treatment. The following attributes have been correlated to DHP bioactivity: (*i*) a hydrogen available for hydrogen bonding on the ring nitrogen (38); (*ii*) decreasing activity with increasing bulk (sterimol B1) on *para*-substituted compounds and with increasing length (sterimol L) on *meta*-substituted compounds (20); (*iii*) lipophilicity effect of substituents on the phenyl ring (20, 39, 40); (*iv*) a related inductive effect of phenyl ring substituents (20); and (*v*) decreasing activity with increasing ester side-chain bulk (39).

Furthermore, in studies relating crystallographic structure to activity, it was suggested that increasing pucker of the dihydropyridine ring increases activity (16, 41). However, this observation is not general to all dihydropyridines for which a crystal structure has been determined (42). It is also not supported by the calculations reported both here and by Rovnyak *et al.* (21, 22).

The optimized geometries produced by AM1 yielded a large number of descriptors for use in quantitative structure–activity relationship (QSAR) analysis. Conceptually, AM1 results provide descriptors for electronic and geometric properties; lipophilicity and steric bulk descriptors, which are also useful in describing activity, are not obtained using AM1. Hence, the principal goals of the AM1-derived QSAR study were to refine the electronic and geometric facets of the bioactive portion ("pharmacophore") of the DHP molecule.

For the *ortho*-substituted series of compounds, the activity is well correlated with a model containing the energy of the HOMO and a bond order within the phenyl ring. For these compounds, the energy of the HOMO was most important to the model, indicating that frontier molecular orbital considerations may be important to DHP activity. The effect of the substituent on adjacent bond strength was also important, and was entered into the model as the bond order adjacent to the point of attachment of the substituent. However, the size of the substituent was not correlated with activity.

The model that was developed to describe both *ortho*- and *meta*-substituted DHPs includes the length of the *meta* substituent, the energy of the HOMO, and bond angles and bond orders within the dihydropyridine ring. The length of the *meta* substituent is the distance from the point of attachment of the phenyl ring to the most distant atom; it is therefore a direct

Can. J. Chem. Downloaded from www.nrcresearchpress.com by 109.225.110.28 on 09/08/12
For personal use only.

measurement that corresponds to the sterimol L descriptor used in previous studies (20, 40). The energy of the HOMO also appears in the model developed for *ortho* substituents. Angles and bond orders in the dihydropyridine ring are likewise shown to be important. This suggests that either subtle changes in the bonding and conformation of the dihydropyridine ring affect activity or, more likely, that the electronic effects of the substitution on the phenyl ring cause subtle changes in the dihydropyridine ring.

The model for the entire data merits examination. The introduction of a substituent at the 4′ position of the phenyl ring reduces the activity of the DHP. This appears in the model as the projected axial length of the 4′ substituent and is expected from previous QSAR studies (20, 38–40). The length of the *meta* substituent and the energy of the HOMO are also included in the model. The inclusion of the charge on C(5) of the dihydropyridine ring most probably is due to an inductive effect of the substituent on the phenyl ring.

Table 6 shows the predicted results based on the model for the entire data set compared to experimental data. The model has a tendency to underpredict the activity of the most active compounds and overpredict the activity of the least active compounds. This is probably due to lipophilic and steric factors, which AM1 calculations do not address. Notably, however, the model overpredicts the activity of the 2′-Br and 2′-I DHPs. Complementary pharmacological results obtained using guinea pig myocardial tissue (21, 22) are also included in Table 6. According to these results, the 2′-Br and 2′-I DHPs are the most active, in line with the predictions of the model.

The discriminant analysis yielded a model that is very effective at distinguishing more active from less active compounds using four descriptors. Again, the ubiquitous energy of the HOMO is included. The bond orders and lengths included are adjacent to the points of attachment of the substituents on the phenyl ring. These reflect the location of attachment and subsequent bond strengthening and weakening due to the ring substituents. The effectiveness of the model is indicated by its 97% success rate at classifying DHPs when using random training and test data sets.

These QSAR results have implications for the design of a neuronally active DHP. To be active in the central nervous system, DHP lipophilicity must be tailored so that the drug can cross the blood–brain barrier. Changing the phenyl substituent is a potentially effective way of doing this. In conjunction with previous QSAR studies (20, 38–40), the unfavourable effect of substitution at the 4′ position of the phenyl ring and of large substituents at the 3′ position is underlined. The energy of the HOMO has been shown to be important. DHPs with large *meta* and *para* substituents and with low ionization potentials are thus predicted to be weakly active. The development of an efficient discriminant model based solely on the results of semi-empirical calculations is also potentially useful. In conjunction with the regression models, it can be used to screen out unfavourable substitutions on the phenyl ring of the DHP. These QSAR correlations are therefore of utility in the rational design process.

5. Conclusions

The results reported in this study have shown that AM1-optimized structures closely match both crystal structures and geometries optimized at the *ab initio* level of calculation. There are only slight differences between the AM1 geometries and those obtained experimentally. However, in the case of ring pucker, both *ab initio* and AM1 calculations failed to reproduce the pucker observed in the crystal structures.

Various conformers were examined for each DHP; the preferred conformation had both ester groups oriented *syn-periplanar* to the double bond of the dihydropyridine ring. There was no consistent preference for an *sp* or *ap* phenyl conformation.

Correlation of biological data with AM1-calculated electronic and geometric descriptors yielded meaningful correlations for mono-substituted DHPs. A discriminant model was also developed that successfully distinguished between strongly and weakly active DHPs. The energy of the HOMO (negative energy of ionization potential) was shown to be the electronic descriptor that was most useful in evaluating DHP activity. This represents a refinement of previous QSAR investigation of the DHPs.

The information obtained from this study can also be used toward the rational design of novel antiepileptic DHPs. The tailoring of functionality can be constrained both by the requirement for a comparatively low energy *sp/sp* ester conformation and by the QSAR correlations. In this way, changes in DHP structure that improve its pharmacokinetic properties can be evaluated to ensure that its pharmacodynamic behaviour is not sacrificed.

6. Acknowledgements

J. A. B. gratefully acknowledges the support of a Savoy Foundation Studentship. D. F. W. acknowledges an Ontario Ministry of Health Career Scientist Award. This research was funded in part by the Medical Research Council of Canada.

1. R. J. Porter. *In* New anticonvulsant drugs. *Edited by* B. S. Meldrum and R. J. Porter. John Libbey, London. 1986. pp. 3–17.
2. D. J. Triggle, D. A. Langs, and R. A. Janis. Med. Res. Rev. **9**, 123 (1989).
3. R. A. Janis, P. Silver, and D. J. Triggle. Adv. Drug Res. **16**, 309 (1987).
4. C. Morocutti, F. Pierelli, L. Sanarelli, E. Stefano, A. Peppe, and G. L. Mattioli. Epilepsia, **27**, 498 (1986).
5. S. J. Dolin, A. B. Hunter, M. J. Halsey, and H. J. Little. Eur. J. Pharmacol. **152**, 19 (1988).
6. G. Gandalfo, C. Gottesman, J.-N. Bidard, and M. Lazdunski. Eur. J. Pharmacol. **160**, 173 (1989).
7. M. A. Moron, C. W. Stevens, and T. L. Yaksh. J. Pharmacol. Exp. Ther. **252**, 1150 (1990).
8. S. K. O'Neill and G. T. Bolger. Brain Res. Bull. **25**, 211 (1990).
9. F. B. Meyer, R. E. Anderson, and T. M. Sundt, Jr. Epilepsia, **31**, 68 (1990).
10. J. M. Littleton. *In* Alcohol and seizures. *Edited by* R. J. Porter, R. H. Mattson, J. A. Cramer, and I. Diamond. F. A. Davis, Philadelphia. 1990. pp. 51–63.
11. M. J. S. Dewar, E. G. Zoebisch, E. F. Healy, and J. J. P. Stewart. J. Am. Chem. Soc. **107**, 3902 (1985).
12. J. J. P. Stewart. Quantum Chem. Prog. Exchange Bull. **9**, 99 (1989). QCPE Program No. 581.
13. M. Dupuis. *In* MOTECC-90: Modern techniques in computational chemistry. *Edited by* E. Clementi. ESCOM Science Publishers, Leiden. 1990. pp. 277–324.
14. E. Clementi. *In* MOTECC-90: Modern techniques in com-

putational chemistry. *Edited by* E. Clementi. ESCOM Science Publishers, Leiden. 1990. pp. 1–39.
15. A. M. Triggle, E. Shefter, and D. J. Triggle. J. Med. Chem. **23**, 1442 (1980).
16. R. Fossheim, K. Svarteng, A. Mostad, C. Romming, E. Shefter, and D. J. Triggle. J. Med. Chem. **25**, 126 (1982).
17. Cambridge Crystallographic Database. Cambridge University, U.K.
18. S. Chin, R. Tagliavani, J. P. Prost, and M. Martins-Costa. *In* MOTECC-90: Modern techniques in computational chemistry. *Edited by* E. Clementi. ESCOM Science Publishers, Leiden. 1990. pp. 1021–1053.
19. SAS Institute Inc., version 6.06, Cary, North Carolina. 1991.
20. R. A. Coburn, M. Wierzba, M. J. Suto, A. J. Solo, A. M. Triggle, and D. J. Triggle. J. Med. Chem. **31**, 2103 (1988).
21. G. Rovnyak, N. Andersen, J. Gougoutas, A. Hedberg, S. D. Kimball, M. Malley, S. Moreland, M. Porubcan, and A. Pudzianowski. J. Med. Chem. **31**, 936 (1988).
22. G. Rovnyak, N. Andersen, J. Gougoutas, A. Hedberg, S. D. Kimball, M. Malley, S. Moreland, M. Porubcan, and A. Pudzianowski. J. Med. Chem. **34**, 2521 (1991).
23. R. Fossheim. Acta Chem. Scand. Ser. B, **39**, 785 (1985).
24. R. Fossheim. Acta Chem. Scand. Ser. B, **40**, 776 (1986).
25. D. Cremer and J. A. Pople. J. Am. Chem. Soc. **97**, 1354 (1975).
26. M. Khalil, R. J. Woods, D. F. Weaver, and V. H. Smith. J. Comput. Chem. **12**, 584 (1991).
27. H.-J. Hofmann and R. Cimiraglia. FEBS Lett. **241**, 38 (1988).
28. H.-J. Hofmann and R. Cimiraglia. J. Mol. Struct. (Theochem), **205**, 1 (1990).
29. D. A. Langs, P. D. Strong, and D. J. Triggle. J. Comput.-Aided Mol. Des. **4**, 215 (1990).
30. N. R. Natale, D. J. Triggle, R. B. Palmer, B. J. Lefler, and W. D. Edwards. J. Med. Chem. **33**, 2255 (1990).
31. D. A. Langs, Y. W. Kwon, P. D. Strong, and D. J. Triggle. J. Comput.-Aided Mol. Des. **5**, 95 (1991).
32. D. A. Langs and D. J. Triggle. Mol. Pharmacol. **27**, 544 (1985).
33. M. Mahmoudian and G. W. Richards. J. Chem. Soc. Chem. Commun. 739 (1986).
34. S. Marrer and H.-D. Höltje. J. Protein Chem. **8**, 420 (1989).
35. H.-D. Höltje. *In* QSAR: Quantitative structure–activity relationships in drug design. Vol. 29. Alan. R. Liss, New York. 1989. p. 237.
36. H.-D. Höltje and S. Marrer. J. Comput.-Aided Mol. Des. **1**, 23 (1987).
37. R. W. Tsien, P. T. Ellinor, and W. A. Horne. Trends Pharmacol. Sci. **12**, 349 (1991).
38. B. Loev, M. M. Goodman, K. M. Snader, T. Tedeschi, and E. Macko. J. Med. Chem. **17**, 956 (1974).
39. R. Rodenkirchen, R. Bayer, R. Steiner, F. Bossert, H. Meyer, and E. Möller. Naunyn-Schmeideberg's Arch. Pharmacol. **310**, 69 (1979).
40. M. Mahmoudian and W. G. Richards. J. Pharm. Pharmacol. **38**, 272 (1986).
41. R. Fossheim, A. Joslyn, A. J. Solo, E. Luchowski, A. Rutledge, and D. J. Triggle. J. Med. Chem. **31**, 300 (1988).
42. A. Miyamae, S. Koda, and Y. Morimoto. Chem. Pharm. Bull. **34**, 3071 (1986).

Can. J. Chem. Downloaded from www.nrcresearchpress.com by 109.225.110.28 on 09/08/12
For personal use only.

Cyano-bridged heterodinuclear complexes of nickel(II) and palladium(II). A disordered structure for the linkage isomer [LPd-CN-NiL](ClO_4)[1]

PARIMAL PAUL, RAMPRASAD DAS, AND KAMALAKSHA NAG[2]
Department of Inorganic Chemistry, Indian Association for the Cultivation of Science, Calcutta, India 700032

AND

ERIC J. GABE AND JEAN-PIERRE CHARLAND[3]
Division of Chemistry, National Research Council, Ottawa, Ont., Canada K1A 0R6

Received February 21, 1992

PARIMAL PAUL, RAMPRASAD DAS, KAMALAKSHA NAG, ERIC J. GABE, and JEAN-PIERRE CHARLAND. Can. J. Chem. **70**, 2461 (1992).

The homodinuclear [$M_2L_2\mu$(CN)](ClO_4) complexes and the heterodinuclear [LPd-CN-NiL](ClO_4) and [LNi-CN-PdL](ClO_4) complexes of nickel(II) and palladium(II) have been synthesized with a tridentate ligand HL (methyl 2-[(2′-aminoethyl)amino]cyclopent-1-enedithiocarboxylate). In solution both the isomers dissociate, $[LNi\text{-}CN\text{-}PdL]^+$ much more rapidly than $[LPd\text{-}CN\text{-}NiL]^+$, and a steady state equilibrium between the $[LPd\text{-}CN\text{-}NiL]^+$, $[Pd_2L_2\mu\text{-}(CN)]^+$, and $[Ni_2L_2\mu\text{-}(CN)]^+$ species is established. The isomer $[LPd\text{-}CN\text{-}NiL]^+$ exhibits a band at 555 nm that is absent in the other isomer and homodinuclear complexes. The X-ray structure of [LPd-CN-NiL](ClO_4) has been studied. Crystals of the compound are monoclinic, a = 8.964(2), b = 23.852(2), c = 14.096(2) Å, β = 105.92(1)°, Z = 4, space group $P2_1/a$. The structure was solved by direct methods and was refined by full-matrix least-squares procedures to R = 0.054 and R_w = 0.034 for 4426 reflections with $I \geq 2.5\sigma(I)$. The two metal centres are in a square-planar environment provided by the N_2S donor set of the ligand and cyanide bridge, but the metal atoms as well as C and N atoms of μ-CN could not be distinguished due to disorder. An alternate stacking of Pd-CN-Ni and Ni-NC-Pd units has been proposed to explain the 1:1 occupancy of the atoms concerned.

PARIMAL PAUL, RAMPRASAD DAS, KAMALAKSHA NAG, ERIC J. GABE et JEAN-PIERRE CHARLAND. Can. J. Chem. **70**, 2461 (1992).

On a synthétisé les complexes homodinucléaires [$M_2L_2\mu$(CN)](ClO_4) et les complexes hétérodinucléaires [LPd-CN-NiL] et [LNi-CN-PdL](ClO_4) du nickel(II) et du palladium(II) incluant le ligand tridentate HL (2-[(2′-aminoéthyl)-amino]cyclopent-1-ènedithiocarboxylate de méthyle). En solution, les deux isomères se dissocient, le $[LNi\text{-}CN\text{-}PdL]^+$ beaucoup plus rapidement que le $[LPd\text{-}CN\text{-}NiL]^+$, et il s'établit un état stationnaire entre les espèces $[LPd\text{-}CN\text{-}NiL]^+$, $[Pd_2L_2\mu\text{-}(CN)]^+$ et $[Ni_2L_2\mu\text{-}(CN)]^+$. L'isomère $[LPd\text{-}CN\text{-}NiL]^+$ présente une bande à 555 nm qui est absente dans l'autre isomère et dans les complexes homodinucléaires. On a déterminé la structure par diffraction des rayons X. Les cristaux sont monocliniques, groupe d'espace $P2_1/a$, avec a = 8,964(2), b = 23,852(2) et c = 14,096(2) Å, β = 105,92(1)° et Z = 4. On a résolu la structure par des méthodes directes et on l'a affinée par le méthode des moindres carrés (matrice entière) jusqu'à des valeurs de R = 0,054 et R_w = 0,034 pour 4426 réflexions avec $I \geq 2{,}5\sigma(I)$. Les deux centres métalliques sont dans un environnement plan carré formé par l'ensemble donneur N_2S du ligand et le pont cyanure; toutefois, à cause du désordre, on ne peut distinguer ni les atomes métalliques ni les atomes de C et de N du μ-CN. On a proposé un empilement alternatif des unités Pd-CN-Ni et Ni-NC-Pd pour expliquer la présence 1 : 1 des atomes concernés.

[Traduit par la rédaction]

Introduction

The bridging ability of cyanide ion has been used to synthesize a large variety of dinuclear M-CN-M (1–6) or M-CN-M′ (7–12) complexes as well as trinuclear M-CN-M′-CN-M (13–15) complexes. Magnetic (16, 17), electrochemical (18, 19), spectroscopic (20), and intramolecular electron transfer (13, 14, 21–25) properties of these complexes have received considerable attention. Quite recently a novel -CN- linked molecular material whose structure resembles scaffolding was reported (26). Although linkage isomerism in homodinuclear or heterodinuclear cyano complexes could be expected to be a common phenomenon, surprisingly only a few such systems have been reported so far. These include $[(NH_3)_5Co\text{-}CN\text{-}Co(CN)_5]$ and $[(NH_3)_5Co\text{-}NC\text{-}Co(CN)_5]$ (12*a*, 12*b*), $[(H_2O)_5Cr\text{-}CN\text{-}Co(CN)_5]$ and $[(H_2O)_5Cr\text{-}NC\text{-}Co(CN)_5]$ (12*c*), *cis*-$(C_6F_5)_2Pd[(\mu\text{-}NC)$*trans*-$Pd(C_6F_5)(PPh_3)_2]$ and *cis*-$(C_6F_5)_2Pd[(\mu\text{-}CN)$*trans*-$Pd(C_6F_5)(PPh_3)_2]$ (1), and [CN(dpe)Ni-CN-Co$(dmgH)_2$Cl] and [CN-$(dmgH)_2$Co-CN-Ni(dpe)Cl] (7) (dpe = bis(diphenylphosphino)ethane; $dmgH_2$ = dimethylglyoxime); of which the first pair has been characterized by X-ray crystallography (27). While the heterodinuclear μ-CN complexes derived from kinetically inert metal ions can be expected to be thermodynamically stable in solution, the behaviour of similar complexes of labile metal ions may, however, be quite intriguing. The purpose of this study was to examine the stability of the linkage isomers obtained from labile metal ions

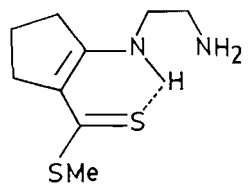

HL

[1]NRCC No. 34196.

[2]Author to whom correspondence may be addressed.

[3]Present address: Energy Research Laboratories, CANMET, 555 Booth Street, Ottawa, Ont., Canada K1A 0R6.

Can. J. Chem. Downloaded from www.nrcresearchpress.com by 109.225.110.28 on 09/08/12
For personal use only.

Can. J. Chem. Downloaded from www.nrcresearchpress.com by 109.225.110.28 on 09/08/12
For personal use only.

like nickel(II) and palladium(II). To this end, we synthesized the square-planar complexes [LPd-CN-NiL][ClO_4] and [LNi-CN-PdL](ClO_4)(HL = methyl 2-[(2′-aminoethyl)-amino]cyclopent-1-enedithiocarboxylate) and structurally characterized the isomer Pd-CN-Ni.

Experimental

Materials

Reagents were those available commercially and were used as received. The complexes [PdL(MeCN)][ClO_4] (28) and [NiL(MeCN)][ClO_4] (29) were prepared according to the previously published procedures.

Synthesis

*[MLCN] (M = Ni, Pd) **1**, **2***

To an acetonitrile solution (25 mL) of [ML(MeCN)](ClO_4) (5 mmol), an aqueous solution (5 mL) of NaCN (0.25 g, 5 mmol) was added in small portions with stirring. After additional stirring for 0.5 h the product was collected by filtration and washed successively with water, MeCN, and MeOH. The compound was recrystallized from boiling MeCN. Anal. calcd. for $C_{10}H_{15}N_3NiS_2$: C 40.04, H 5.00, N 14.01, Ni 19.59; found: C 40.18, H 5.14, N 13.92, Ni 19.45. Anal. calcd. for $C_{10}H_{15}N_3S_2Pd$: C 34.54, H 4.32, N 12.09, Pd 30.63; found: C 34.38, H 4.26, N 12.18, Pd 30.43.

*[LM-CN-ML](ClO_4)(M = Ni, Pd) **3**, **4***

To a suspension of [MLCN] (2 mmol) in MeCN (30 mL) was added an MeCN solution (20 mL) of [ML(MeCN)](ClO_4) (2 mmol). The mixture was stirred and heated at 80°C for 0.5 h, during which time a clear solution was obtained. After filtration, the solution was concentrated and cooled to deposit the crystalline product. The compound was recrystallized from MeCN. Anal. calcd. for $C_{19}H_{30}N_5O_4S_4ClNi_2$: C 33.88, H 4.46, N 10.40, Ni 17.45; found: C 33.88, H 4.55, N 10.58, Ni 17.58. Anal calcd. for $C_{19}H_{30}N_5O_4S_4ClPd_2$: C 29.67, H 3.90, N 9.11, Pd 27.70; found: C 29.52, H 4.12, N 9.25, Pd 27.52.

*[LPd-CN-NiL](ClO_4) **5***

To a vigorously stirred solution of [PdLCN] (0.35 g, 1 mmol) in MeCN (40 mL) was added rapidly a solution of [NiL(MeCN)][ClO_4] (0.41 g, 1 mmol) in MeCN (10 mL). The solution was filtered and immediately reduced to ca. 20 mL under reduced pressure. The crystalline product that was obtained on ice cooling was collected by filtration and washed with acetone. Anal. calcd. for $C_{19}H_{30}N_5O_4S_4ClNiPd$: C 31.64, H 4.16, N 9.71, Ni 8.15, Pd 14.76; found: C 31.48, H 4.25, N 9.85, Ni 8.22, Pd 14.58.

*[LNi-CN-PdL](ClO_4) **6***

To a cold solution (10°C) of [PdL(MeCN)](ClO_4) (0.46 g, 1 mmol) in MeCN (20 mL) was added solid [NiLCN] (0.3 g, 1 mmol) with vigorous stirring. The suspension momentarily became clear, but the product was immediately precipitated. This was collected by filtration and washed with cold MeCN and acetone. Anal. calcd. for $C_{19}H_{30}N_5O_4S_4ClNiPd$: C 31.64, H 4.16, N 9.71, Ni 8.15, Pd 14.76; found: C 32.08, H 4.11, N 9.93, Ni 7.97, Pd 14.97.

Caution ! Although the perchlorate salts reported here were found to be indefinitely stable at room temperature, they should be considered potentially explosive at elevated temperatures.

Physical measurements

IR spectra were recorded on a Perkin–Elmer model 783 spectrophotometer using KBr discs. Electronic spectra were recorded on a Jasco 7850 spectrophotometer. Room temperature magnetic susceptibility was measured on an EG & G PAR 155 vibrating sample magnetometer. C, H, N analyses were performed on a Perkin–Elmer 240C elemental analyzer.

Ni and Pd were estimated gravimetrically as their dimethylglyoximates.

*X-ray crystallographic analysis of [LPd-CN-NiL](ClO_4) **5***

Crystals suitable for X-ray diffraction were obtained by recrystallizing **5** from MeCN. A deep purple rod-shaped crystal of dimensions 0.104 × 0.038 × 0.041 mm was mounted on a glass fiber. Unit-cell parameters were refined by least squares on setting angles for 30 reflections (2θ = 100–115dg) measured on a diffractometer with CuK_α radiation (λ = 1.54178 Å). Crystal data are as follows:

$C_{19}H_{30}N_5O_4S_4ClPdNi$ f.w. 721.28

Monoclinic, a = 8.964(2), b = 23.852(2), c = 14.096(2) Å, β = 105.92(1)°, V = 2898.3(8) Å^3, Z = 4, ρ_c = 1.653 Mg m^{-3}, μ ($CuK\alpha$) = 97.62 cm^{-1}; space group $P2_1/a$ (alt. $P2_1/c$) was determined by systematic absences.

Diffraction intensities were measured on an Enraf–Nonius CAD4 diffractometer at 295 K using CuK_α radiation (λ = 1.54178Å). An ω–2θ scan mode at a scan speed of 2°/min was employed. Three standards were measured after every 100 reflections and no significant crystal decay was detected. Data were collected to 2θ = 156° (hkl, $\bar{h}kl$, $h\bar{k}l$). Lorentz and polarization factors were applied and absorption correction was made. Transmission factors ranged from 0.401 to 0.137. Of the 10 131 reflections measured, 6077 were unique (R_{merge} = 0.031) and 4426 having $I \geq 2.5\sigma(I)$ were used for structure analysis.

Direct methods (MULTAN)(30) were used to locate heavier atoms (Pd, Ni, S, Cl) followed by normal difference Fourier map for lighter atoms, including H atoms. The peak heights of the two highest peaks in the E-map were unexpectedly very similar. Other solutions were investigated and showed the same anomalous peak height results. Isotropic refinement of all non-hydrogen atoms except those of the μ-CN group, which were defined as carbons and refined on occupancy, was carried out by full-matrix least squares. The resulting occupancies of the -CN- atoms were such that it was impossible to distinguish between the C and N atoms. Furthermore, the two metal atoms had unusually low and high thermal parameters. This implied that the Pd site has a lower electron density than presumed and the opposite for the Ni site. Additional refinement of these occupancies established identical electron density midway between the number of electrons expected for Ni(II) and Pd(II), respectively, i.e., their occupancy of each site is 0.50 with a small uncertainty. Clearly, the structure of **5** is disordered in that the Pd and Ni, and C and N, atoms are statistically scrambled. A possible explanation would be the presence of equal amounts of superimposed -Pd-CN-Ni- and -Ni-NC-Pd- fragments (see later). Additional scattering curves were generated to take into account this 1:1 distribution for Pd/Ni and C/N. Anisotropic full-matrix refinement (H atoms isotropic) using the weighting scheme $w = 1/[\sigma^2(F_o) + 0.0009F_o^2]$ with (F_o) from counting statistics, gave satisfactory agreement factors R and R' of 0.054 and 0.034, where $R = \Sigma||F_o| - |F_c||/\Sigma|F_o|$ and $R_w = (\Sigma\, w(|F_o| - |F_c|)^2/w|F_o|^2)^{1/2}$. All calculations were performed with the NRCVAX crystal structure programs (31). Scattering factors were taken from the *International tables for X-ray crystallography* (32). The final atomic positional parameters and equivalent isotropic temperature factors are listed in Table 2. Anisotropic thermal parameters, calculated hydrogen parameters, and calculated structure factors are available as supplementary data.[4]

[4]Tables of observed and calculated structure factor amplitudes, of temperature factors, of hydrogen parameters, and of detailed bond distances and angles may be purchased from: The Depository of Unpublished Data, Document Delivery, CISTI, National Research Council Canada, Ottawa, Canada K1A 0S2.

Tables of hydrogen atom parameters and of bond lengths and angles have also been deposited with the Cambridge Crystallograph Data Centre and can be obtained on request from The Director, Cambridge Crystallographic Data Centre, University Chemical Laboratory, 12 Union Road, Cambridge, CB2 IEZ, U.K.

TABLE 1. UV–vis and IR spectral data for the complexes

Complex	λ_{max}/nm(ϵ/mol dm^3 cm^{-1})[a]	νCN	νNH
[NiLCN] **1**	490sh(180), 395(6000), 300(8500)	2120	3230, 3200
[PdLCN] **2**	385(5500), 370(5600)	2125	3230, 3200
[Ni_2L_2-(CN)](ClO_4) **3**	395(11 500), 375sh(9700) 300(19 800)	2160	3280, 3240
[Pd_2L_2-(CN)](ClO_4) **4**	385(11 800), 295(17 700)	2165	3280, 3235
[LPd-CN-NiL](ClO_4) **5**	555(90), 395(10 000), 375sh(8900) 300(15 000)	2175	3280, 3235
[LNi-CN-PdL](ClO_4) **6**	390(10 500), 300(14 600)	2160	3290, 3245

[a]In DMF.

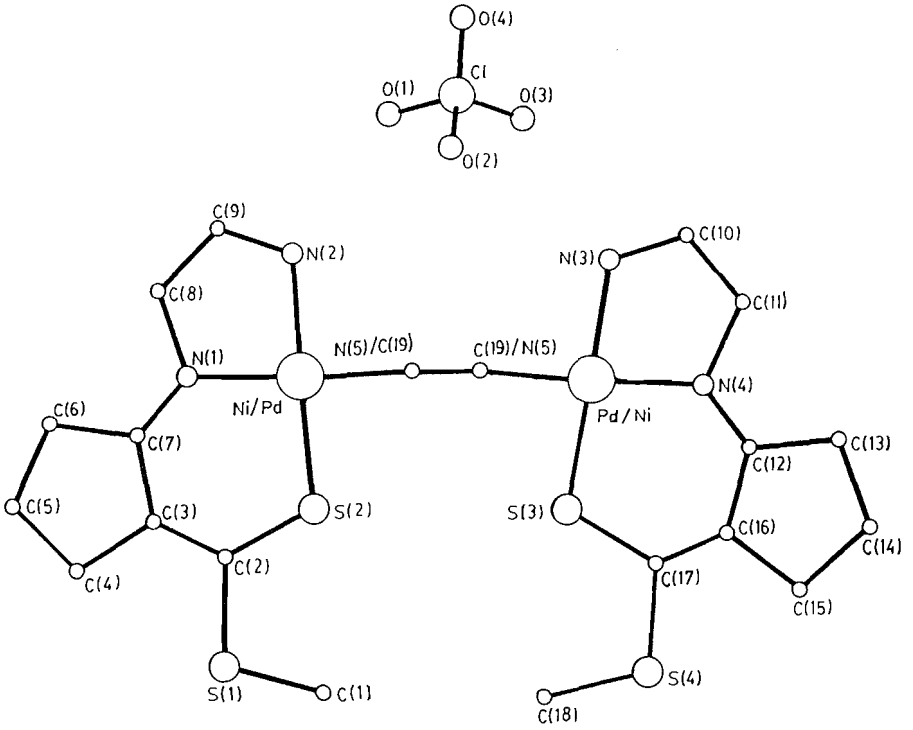

FIG. 1. Molecular structure of [LPd-CN-NiL] (ClO_4) with the atom labelling scheme.

Results and discussion

The cyano-bridged complexes were synthesized by reacting stoichiometric amounts of two different complementary mononuclear complexes, one containing the terminal cyano group and the other a weakly coordinating ligand. Thus, while for the preparation of the homodinuclear complexes [LM-CN-ML][ClO_4] (M = Ni, Pd) the reactants used were [MLCN] and [ML(MeCN)][ClO_4], the heterodinuclear [LM-CN-ML][ClO_4] complexes were obtained by reacting [MLCN] (M = Pd, Ni) with [ML(MeCN)][ClO_4] (M = Ni, Pd). We previously demonstrated (28, 29, 33) that HL is a potentially tridentate ligand with N_2S donors, and the fourth coordinating group (X) in the square-planar nickel(II) and palladium complexes $[MLX]^{n+}$ (n = 0 or 1) undergoes interesting chemical transformations. All the dinuclear complexes are soluble in polar solvents such as Me_2SO, *N*,*N*-dimethylformamide (DMF), and MeCN, less so in $MeNO_2$ and Me_2CO, but practically insoluble in MeOH or CH_2Cl_2. They are diamagnetic compounds and their salient IR and UV–vis spectral data are given in Table 1. The terminal νCN^- vibrations for the mononuclear complexes, which are observed at 2120 (**1**) and 2125 (**2**) cm^{-1}, are shifted to higher frequencies by ca. 40 cm^{-1} in the dinuclear complexes. This shift is also accompanied by similar changes in the NH stretching frequencies of the ligand. Thus, while for complexes **1** and **2** the νNH bands are observed at 3200 and 3230 cm^{-1}, they appear at about 3240 and 3285 cm^{-1} in complexes **3–6**. Clearly, this difference in νNH arises because of the stronger electron-withdrawing ability of the terminal cyanide. The dinuclear complexes in addition exhibit characteristic bands due to the ionic perchlorate at ca. 1100 and 630 cm^{-1}.

In the UV region all the complexes exhibit absorption bands more or less in the same positions indicating their origin belongs primarily to internal ligand transitions. Complex **1** shows a shoulder at 490 nm, which probably can be associated with its square-planar geometry. The isomer $[LPd\text{-}CN\text{-}NiL]^+$ also exhibits a fairly strong band in the visible region with the peak at 555 nm (ϵ = 90 dm^{3}mol^{-1}cm^{-1}). By contrast, the absorption of $[LNi\text{-}CN\text{-}NiL]^+$ and $[LNi\text{-}CN\text{-}PdL]^+$ continually goes on decreasing in the range 400–

Can. J. Chem. Downloaded from www.nrcresearchpress.com by 109.225.110.28 on 09/08/12
For personal use only.

Can. J. Chem. Downloaded from www.nrcresearchpress.com by 109.225.110.28 on 09/08/12
For personal use only.

TABLE 2. Final atomic positional parameters and equivalent isotropic Debye–Waller temperature factors (esd's) for [LPd-CN-NiL](ClO_4)

Atom	x	y	z	B_{iso}[a]
Ni/Pd*	0.34636(7)	0.042449(23)	0.07240(4)	3.46(3)
Pd/Ni*	0.14947(7)	−0.082012(25)	0.28965(4)	4.04(3)
Cl	0.3622 (3)	0.11660 (10)	0.41968(15)	6.44(12)
S1	−0.15017(23)	−0.22170 (7)	0.06741(15)	5.95(10)
S2	0.04665(19)	−0.12564 (6)	0.15182(11)	4.37(8)
S3	0.19707(18)	−0.01177 (6)	−0.04020(10)	4.20(7)
S4	0.12460(20)	−0.03783 (7)	−0.25305(11)	5.12(9)
O1	0.2314 (7)	0.0949 (3)	0.4408 (4)	11.8 (5)
O2	0.4379 (8)	0.0693 (3)	0.3967 (5)	13.3 (6)
O3	0.3264 (8)	0.1499 (3)	0.3403 (5)	16.1 (6)
O4	0.4455 (9)	0.1459 (3)	0.4942 (5)	17.0 (6)
N1	0.0628 (5)	−0.1289 (2)	0.3734 (3)	3.68(24)
N2	0.2540 (8)	−0.0411 (3)	0.4141 (4)	5.3 (3)
N3	0.4842 (8)	0.0900 (3)	0.1774 (4)	4.9 (3)
N4	0.4176 (5)	0.0899 (2)	−0.0149 (3)	3.46(22)
C19/N5*	0.2807 (6)	−0.0025 (2)	0.1633 (4)	3.58(25)
C1	−0.0789 (13)	−0.1937 (4)	−0.0274 (8)	7.2 (5)
C2	−0.0570 (6)	−0.1809 (2)	0.1729 (4)	3.7 (3)
C3	−0.0804 (7)	−0.1990 (2)	0.2580 (5)	3.9 (3)
C4	−0.1731 (11)	−0.2497 (3)	0.2692 (8)	6.0 (5)
C5	−0.1750 (15)	−0.2528 (4)	0.3737 (8)	8.3 (6)
C6	−0.0650 (10)	−0.2091 (3)	0.4297 (6)	5.3 (4)
C7	−0.0209 (7)	−0.1741 (2)	0.3531 (4)	3.9 (3)
C8	0.1187 (11)	−0.1117 (4)	0.4774 (5)	5.4 (4)
C9	0.1641 (10)	−0.0516 (3)	0.4845 (6)	5.7 (5)
C10	0.5026 (9)	0.1442 (3)	0.1365 (5)	4.9 (4)
C11	0.5300 (9)	0.1342 (3)	0.0377 (5)	4.7 (4)
C12	0.4014 (7)	0.857 (2)	−0.1099 (4)	3.8 (3)
C13	0.4790 (9)	0.1257 (3)	−0.1668 (6)	4.5 (4)
C14	0.4131 (9)	0.1098 (3)	−0.2759 (5)	4.9 (4)
C15	0.3260 (9)	0.0548 (3)	−0.2793 (5)	4.5 (4)
C16	0.3096 (7)	0.0448 (2)	−0.1760 (4)	3.7 (3)
C17	0.2242 (6)	0.0051 (2)	−0.1528 (4)	3.5 (3)
C18	0.0270 (13)	−0.0909 (4)	−0.2019 (9)	6.5 (5)
N5/C19*	0.2334 (6)	−0.0321 (2)	0.2134 (4)	3.58(24)

[a] B_{iso} is the mean of the principal axes of the thermal ellipsoid.
*Disordered position.

TABLE 3. Selected bond lengths (Å) and angles (°) in [LPd-CN-NiL](ClO_4)

Pd/Ni—S(3)	2.1948(15)	Ni/Pd—S(2)	2.1736(16)
Pd/Ni—N(3)	1.999(5)	Ni/Pd—N(2)	2.002(5)
Pd/Ni—N(4)	1.908(4)	Ni/Pd—N(1)	1.936(4)
Pd/Ni—C(19)/N(5)	1.885	Ni/Pd—N(5)/C(19)	1.892(5)
C(19)/N(5)—N(5)/C(19)	1.58(8)		
S(3)—Pd/Ni—N(3)	178.39(19)	S(2)—Ni/Pd—N(2)	177.00(21)
S(3)—Pd/Ni—N(4)	97.41(14)	S(2)—Ni/Pd—N(1)	97.23(15)
S(3)—Pd/Ni—C(19)/N(5)	85.09(15)	S(2)—Ni/Pd—N(5)/C(19)	86.01(15)
N(3)—Pd/Ni—N(4)	83.84(24)	N(1)—Ni/Pd—N(2)	85.22(23)
N(3)—Pd/Ni—C(19)/N(5)	93.67(24)	N(2)—Ni/Pd—N(5)/C(15)	91.60(23)
N(4)—Pd/Ni—C(19)/N(5)	177.50(20)	N(1)—Ni/Pd—N(5)/C(19)	176.17(21)
Pd/Ni—S(3)—C(17)	108.52(20)	Ni/Pd—S(2)—C(2)	109.64(22)
Pd/Ni—N(3)—C(10)	109.1(4)	Ni/Pd—N(2)—C(9)	107.4(5)
Pd/Ni—N(4)—C(12)	130.6(4)	Ni/Pd—N(1)—C(7)	130.5(4)
Pd/Ni—N(4)—C(11)	113.3(4)	Ni/Pd—N(1)—C(8)	111.3(4)
Pd/Ni—C(19)/N(5)—N(5)/C(19)	177.2(4)		
Ni/Pd—N(5)/C(19)—C(19)/N(5)	175.0(4)		

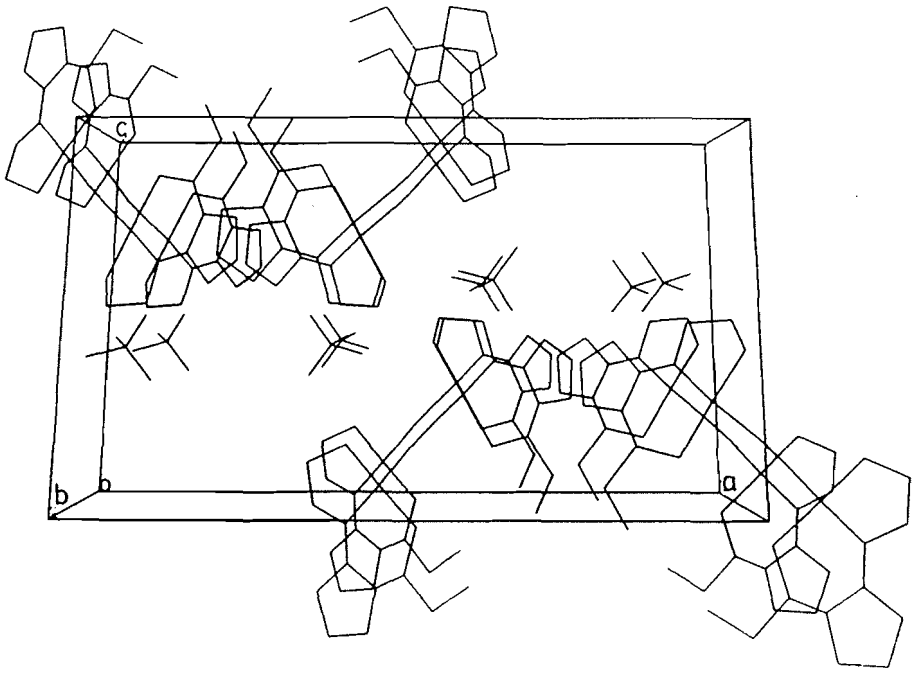

FIG. 2. Packing diagram of [LPd-CN-NiL] (ClO_4) in the unit cell.

TABLE 4. Hydrogen bond interactions for [LPd-CN-NiL](ClO_4)

O(1)—N(2)	3.278(9)	O(3)—N(3)	3.331(11)
O(2)—N(2)	3.151(9)	O(2)—N(3)	3.268(10)
O(2)′—N(2)	3.338(9)		
Cl—O(3)—N(3)	105.8(4)	Cl—O(1)—N(2)	105.2(4)
Cl—O(2)—N(3)	107.0(4)	Cl—O(2)—N(2)	111.0(4)
Cl—O(2)—N(2)′	109.0(3)	N(3)—O(2)—N(2)	113.88(24)
N(3)—O(2)—N(2)′	119.6(3)	N(2)—O(2)—N(2)′	96.06(24)
O(1)—N(2)—O(2)′	99.85(21)	O(2)—N(2)—O(2)′	83.94(22)

′$1 - x, -y, 1 - z$

700 nm. Evidently, the band at 555 nm cannot be attributed to a nickel(II)-centered *d–d* transition; in that case complexes **3** and **6** would have exhibited a band or a shoulder in the visible region. While we are not sure about the exact nature of this band, it nevertheless appears to be a charge transfer transition involving the chromophore Pd-CN-Ni.

To find the stability of the dinuclear cyano complexes in solution, the time-dependent spectral changes that occurred in the DMF solutions for $[LPd\text{-}CN\text{-}NiL]^+$, $[LNi\text{-}CN\text{-}PdL]^+$, and a 1:1 mixture of $[Ni_2L_2\mu\text{-}(CN)]^+$ and $[Pd_2L_2\mu\text{-}(CN)]^+$ in the range 500–700 nm were recorded. The absorption spectrum of the Pd-CN-Ni isomer changed very slowly with time by the gradual transformation of the peak at 555 nm to a shoulder. It was noted that the spectral changes for complex **5** occurred very slowly before 0.5 h and after 20 h, but more quickly in the mid-period. In contrast, the spectrum of the Ni-CN-Pd isomer (**6**) began to change rapidly from the beginning and reached completion in about 10 h. In this case the successive absorption curves passed through an isosbestic point at 540 nm. The spectral change that occurred for the mixture of the two homodinuclear species is similar to that of complex **6**. The final spectrums for all three cases were identical, clearly indicating the establishment of the same steady state equilibrium. The greater stability of Pd-CN-Ni species relative to Ni-CN-Pd species is understandably due to the stronger Pd—C bond and lesser lability of Pd^{2+} ion. The gross reaction leading to the steady state equilibrium can be given by eq. [1]:

$$[1]\quad 2\text{Ni-CN-Pd} \xrightarrow{k_1} \text{Ni-CN-Ni} + \text{Pd-CN-Pd} \underset{k_3}{\overset{k_2}{\rightleftharpoons}} 2\text{Pd-CN-Ni}$$

Crystal structure analysis

A PLUTO (34) diagram of $[LPd\text{-}CN\text{-}NiL][ClO_4]$ **5** is shown in Fig. 1 together with the atom labelling scheme. As already noted, due to crystallographic disorder the two metal atoms as well as the C and N atoms of μ-CN could not be distinguished. Accordingly, they are alternately designated as Pd/Ni, Ni/Pd, C(19)/N(5), and N(5)/C(19). Final atomic coordinates for the non-hydrogen atoms and selected bond lengths and angles are given in Tables 2 and 3.

The structure for the cation of **5** consists of two ML (M = Pd, Ni) fragments linked by a cyanide ion. The metal atoms in the ML fragments are in distorted square-planar environments provided by the N_2S donor set of the ligand and the C or N atom of the cyanide. The two ligand moieties in

Can. J. Chem. Downloaded from www.nrcresearchpress.com by 109.225.110.28 on 09/08/12
For personal use only.

Can. J. Chem. Downloaded from www.nrcresearchpress.com by 109.225.110.28 on 09/08/12
For personal use only.

the complex are in *cisoid* conformation. In the two ML fragments corresponding metal–donor bond lengths are quite similar. There are two sets of M—N distances in each ML fragment, of which the M—N(2) or M—N(3) distances are about 0.18 Å longer than the M—N(1) or M—N(4) distances. This difference is expected because M—N bonds to a 4-coordinate nitrogen (terminal) should be longer than to a 3-coordinate one (middle). Moreover, the M—N(terminal) bond is further elongated by the *trans* directing influence of S. The M—N(1) or M—N(4) distances are normal for square-planar nickel(II) and palladium(II) complexes. The two M—S distances in **5** differ by ca. 0.02 Å and the average distance 2.184(2) Å may be compared with the reported low-spin Ni—S distances ranging between 2.10 and 2.20 Å (35, 36) and the Pd—S distance of 2.24 Å observed in a closely related complex (33*c*). The M—C/N distance (avg. 1.89 Å) and the C—N distance (1.158(8) Å) are similar to the other cyano-bridged complexes (27). The *cis* angles in the ML fragments deviate to some extent from 90°. For example, the angles S(3)—M—N(4) (97.41(14)°) and N(3)—M—C/N (93.67(24)°) are wider compared with S(3)—M—C/N (85.09(15)°) and N(3)—M—N(4) (83.84(24)°). The *trans* angles N(3)—M—S(3) (178.39(19)°) and N(4)—M—C/N (177.50(20)°), however, are almost linear. It may be noted that the MCNM bridge angles (177.2(4)° and 175.0(4)°) are not perfectly linear. The displacements (Å) of the constituent atoms from the mean planes of N(2), N(1), S(2), C/N (plane 1) and N(3), N(4), S(3), C/N (plane 2) are: N(2)[−0.067(9)], N(1)[0.026(6)], S(2)[−0.003(2)], C/N[0.034(7)]; N(3)[−0.022(9)], N(4)[0.008(6)], S(3)[−0.001(2)], C/N[0.010(7)]. While in plane (2) the metal atom is displaced above the least-squares plane by 0.046(9) Å, in plane (1) this displacement (0.157(10) Å) is even more significant. It might appear that the two metal atoms are square-pyramidally distorted in the same direction, albeit to a different extent. However, for square-pyramidal d^8 metal ion complexes the basal angles (that is, the angles produced by atoms in the diagonal positions) should be less than 170° (37) as compared with 176–178° observed in the present case. The displacement of the two metal atoms from the mean planes may therefore be attributed to crystal packing forces. It may also be noted that the two ML fragments in the complex are not perfectly parallel; the dihedral angle between planes (1) and (2) is 5.85(12)°.

The packing diagram of **5** (Fig. 2) shows that stacking of the complex cations occurs roughly along the *a* axis of the unit cell. To account for 1:1 Pd:Ni and C:N occupancy, the presence of equal amounts of superimposed Pd-C-N-Ni and Ni-N-C-Pd fragments in the unit cell has already been considered. There are other possibilities also for disordering. For example, one may consider the superposition of Ni-C-N-Pd and Pd-N-C-Ni fragments. However, it has already been demonstrated that the $[Ni\text{-}CN\text{-}Pd]^+$ species is thermodynamically less stable than the $[Pd\text{-}CN\text{-}Ni]^+$ species. The possibility for the co-crystallization of the homodinuclear $[Pd\text{-}CN\text{-}Pd]^+$ and $[Ni\text{-}CN\text{-}Ni]^+$ species, according to eq. [1], may also be considered. However, the solubilities of these two homodinuclear complexes and the precursor complex **5** in MeCN, the solvent from which crystals were grown, are not identical. The decreased order of solubility is $[Ni_2L\ \mu\text{-}CN](ClO_4) > [Pd_2L\ \mu\text{-}CN](ClO_4) > [LPd\text{-}CN\text{-}NiL](ClO_4)$. In a situation like this the species which crystallizes is usually controlled by solubilities, not solution equilibria (38). Thus, stacking of Pd-CN-Ni, Ni-NC-Pd, and so on appears to provide a reasonable basis for the crystallographic observation.

The ClO_4^- ion in **5** is not disordered. From the molecular structure (Fig. 1) it is apparent that the O(1), O(2), and O(3) atoms of the ClO_4^- ion are amenable to H-bonding with the protons of the N(2) and N(3) atoms. The interatomic distances and angles involved in H-bonding are listed in Table 4.

1. R. Uson, J. Fornies, M. A. Uson, and M. L. Mas. Inorg. Chim. Acta, **168**, 59 (1990).
2. J. Casabo, T. Flor, F. Teixdor, and J. Ribas. Inorg. Chem. **25**, 3166 (1986).
3. G. J. Baird, S. G. Davies, S. D. Moon, S. J. Simpson, and R. H. Jones. J. Chem. Soc. Dalton Trans. 1479 (1985).
4. J. A. Davies, F. R. Hartley, and S. G. Murray. Inorg. Chim. Acta, **41**, 249 (1980).
5. P. L. Gaus and A. L. Crumbliss. Inorg. Chem. **15**, 739 (1976); **15**, 2080 (1976).
6. D. Dodd, M. D. Johnson, and C. W. Fong. J. Chem. Soc. Dalton Trans. 58 (1974).
7. M. J. Bermejo and S. Alvarez. Inorg. Chim. Acta, **82**, L23 (1984).
8. C. A. Josephson and J. E. House. J. Inorg. Nucl. Chem. **43**, 953 (1981).
9. J. Ribas, M. Serra, A. Escuer, and J. M. Coronas. J. Inorg. Nucl. Chem. **43**, 3113 (1981).
10. M. L. Alvarez and J. M. Coronas. J. Inorg. Nucl. Chem. **42**, 707 (1980).
11. J. Ribas, J. Casabo, M. Serra, and J. M. Coronas. Inorg. Chim. Acta, **36**, 41 (1970).
12. (*a*) R. A. de Castello, C. P. MacColl, N. B. Egen, and A. Haim. Inorg. Chem. **8**, 699 (1969); (*b*) R. A. de Castello, C. P. MacColl, and A. Haim. Inorg. Chem. **10**, 203 (1971); (*c*) D. Gaswick and A. Haim. J. Inorg. Nucl. Chem. **40**, 437 (1978).
13. M. Shou, B. W. Pfennig, J. Steiger, D. Van Engen, and A. B. Bocarsly. Inorg. Chem. **29**, 2456 (1990).
14. A. Gogler and H. Kunkley. Inorg. Chim. Acta, **150**, 1 (1988).
15. S. Alvarex and C. Lopez. Inorg. Chim. Acta, **63**, 57 (1982).
16. (*a*) D. S. Bieksza and D. N. Hendrickson. Inorg. Chem. **16**, 924 (1977); (*b*) K. R. Mann, D. M. Duggan, and D. N. Hendrickson. Inorg. Chem. **14** 2577 (1975); (*c*) D. M. Duggan, R. G. Jungst, K. R. Mann, G. D. Stucky, and D. N. Hendrickson. J. Am. Chem. Soc. **96**, 3443 (1974).
17. C. P. Landee, M. Wicholas, R. D. Willet, and T. Woldford. Inorg. Chem. **18**, 2317 (1979).
18. (*a*) G. Barrado, G. A. Carriedo, C. Diaz-Valenzuela, and V. Riera. Inorg. Chem. **30**, 4416 (1991); (*b*) G. A. Carriedo, N. G. Connelly, M. C. Crespo, I. C. Quarmby, V. Riera, and G. H. Worth. J. Chem. Soc. Dalton Trans. 315 (1991).
19. P. Paul, R. Das, S. K. Mandal, and K. Nag. Indian J. Chem. **29A**, 335 (1990).
20. R. E. Hester and E. M. Nour. J. Chem. Soc. Dalton Trans. 339 (1981).
21. B. T. Reagor, D. F. Kolley, D. H. Huchital, and P. M. Rentzepis. J. Am. Chem. Soc. **104**, 7400 (1982).
22. M. Nishizawa and P. C. Ford. Inorg. Chem. **20**, 2016 (1981).
23. (*a*) A. Vogler and H. Kunkley. Ber. Bunsen-ges. Phys. Chem. **79**, 83 (1975); (*b*) A. Vogler, A. H. Osman, and H. Kunkley. Inorg. Chem. **26**, 2337 (1987); (*c*) A. Vogler and J. Kisinger. J. Am. Chem. Soc. **104**, 2311 (1982).
24. L. Rosenheim, D. Spencer, and A. Haim. Inorg. Chem. **13**, 1951 (1974).
25. D. H. Huchital and J. Lepore. Inorg. Chem. **17**, 1134 (1978).

26. B. F. Hoskins and R. Robson. J. Am. Chem. Soc. **112**, 1546 (1990).
27. (*a*) B. Wang, W. P. Schaefer, and R. E. Marsh. Inorg. Chem. **10**, 1492 (1971); (*b*) F. R. Fronczek and W. P. Schaefer. Inorg. Chem. **13**, 727 (1974).
28. R. Roy, S. K. Mondal, and K. Nag. J. Chem. Soc. Dalton Trans. 1935 (1983).
29. R. Roy, M. Chaudhury, S. K. Mondal, and K. Nag. J. Chem. Soc. Dalton Trans. 1681 (1984).
30. G. Germain, P. Main, and M. M. Woolfson. Acta Crystallogr. Sect. A: Cryst. Phys. Diffr. Theor. Gen. Crystallogr. **A27**, 368 (1971).
31. E. J. Gabe, F. L. Lee, and Y. Le Page. *In* Crystallographic computing III. *Edited by* G. M. Sheldrick, C. Kruger, and R. Goddard. Clarendon, Oxford, England. 1985. p. 167.
32. International tables for X-ray crystallography. Vol. IV. Kynoch Press, Birmingham, England. 1974.
33. (*a*) P. Paul and K. Nag. Inorg. Chem. **26**, 1586 (1987); (*b*) **26**, 2969 (1987); (*c*) J. Chem. Soc. Dalton Trans. 2373 (1988); (*d*) P. Paul, S. Chakladar, and K. Nag. Inorg. Chim. Acta, **170**, 27 (1990); (*e*) R. Das, P. Paul, K. Nag, and K. Venkatsubramanian. Inorg. Chim. Acta, **185**, 221 (1991).
34. S. Motherwell and W. Clegg. PLUTO 78, Program for drawing crystal and molecular structures. University of Cambridge, Cambridge, England. 1978.
35. C. H. Wei and L. F. Dahl. Inorg. Chem. **9**, 1978 (1970), and references therein.
36. M. J. M. Campbell. Coord. Chem. Rev. **15**, 279 (1975).
37. A. R. Rossi and R. Hoffmann. Inorg. Chem. **14**, 365 (1975).
38. J. P. Collman. Acc. Chem. Res. **10**, 265 (1977).

Can. J. Chem. Downloaded from www.nrcresearchpress.com by 109.225.110.28 on 09/08/12
For personal use only.

A kinetic study of the thermal dehydration of calcium sulphite hemihydrate

CARL ANDERSON AND ANDREW K. GALWEY[1]

School of Chemistry and Questor Centre, The Queen's University of Belfast, Belfast BT9 5AG, Northern Ireland

Received February 20, 1992

CARL ANDERSON and ANDREW K. GALWEY. Can. J. Chem. **70**, 2468 (1992).

An isothermal kinetic study of the dehydration of orthorhombic calcium sulphite hemihydrate is reported:

$$CaSO_3 \cdot 1/2H_2O(s) \rightarrow CaSO_3(s) + 1/2H_2O(g)$$

Fractional reaction (α)–time curves exhibit the sigmoid shape characteristic of nucleation and growth reactions proceeding in the solid state. Yield–time data exhibit a very satisfactory obedience to the Avrami–Erofe'ev ($n = 2$) equation

$$[-\ln(1 - \alpha)]^{1/2} = kt$$

Rate studies were concerned with the temperature interval 573–673 K and the calculated activation energy was 173 ± 8 kJ mol^{-1}, showing the hydrate to be thermally relatively stable. The mechanism of dehydration is discussed and reference is made to the dehydration of calcium hydroxide with which it shows close similarities.

CARL ANDERSON et ANDREW K. GALWEY. Can. J. Chem. **70**, 2468 (1992).

On rapporte une étude cinétique isotherme de la déshydratation de l'hémihydrate du sulfite de calcium orthorhombique :

$$CaSO_3 \cdot 1/2H_2O(s) \rightarrow CaSO_3(s) + 1/2H_2O(g)$$

Les courbes de la réaction fractionnaire (α)–temps présentent la forme sigmoïde caractéristique des réactions de nucléation et de croissance se produisant dans l'état solide. Les données relatives au rendement–temps obéissent bien à l'équation de Avrami–Erofe'ev ($n = 2$) :

$$[-\ln(1 - \alpha)]^{1/2} = kt$$

On a réalisé des études de vitesses entre 573 et 673 K et l'énergie d'activation calculée, égale à 173 ± 8 kJ mol^{-1}, démontre que l'hydrate est thermiquement relativement stable. On discute du mécanisme de déshydratation et on fait référence à la déshydratation de l'hydroxyde de calcium avec laquelle il existe d'importantes similarités.

[Traduit par la rédaction]

Introduction

The present study is a further contribution to an extensive, systematic investigation of the kinetics and mechanisms of diverse solid state dehydration reactions. Previous work has been concerned with the release of water from alums (1, 2), lithium potassium tartrate monohydrate (3), lithium sulphate monohydrate (4), magnesium chloride dihydrate (5), and lignite (brown coal) (6). Conclusions based on dehydration studies have contributed significantly to our theoretical understanding of solid state reactions generally (7–10) and the reaction models developed have been applied to diverse chemical changes proceeding in varied crystalline reactants (7). In extending this approach we now report a study of the dehydration of $CaSO_3 \cdot 1/2H_2O$. This complements our previous investigations (1–6) by including the mechanism of a reaction that occurs within a relatively high-temperature interval, 570–670 K. Thus, in this process the participation of water, condensed within the reaction interface, can be excluded from consideration of the mechanism. This reaction feature contrasts with the chemical steps proposed for the low-temperature dehydration of alums (1, 2) where temporary retention of water at the reactant/product interface is believed to promote the difficult solid product recrystallization process.

It was also of interest to compare $CaSO_3 \cdot 1/2H_2O$ dehydration with the extensively studied dehydrations of $CaSO_4 \cdot 2H_2O$ and $CaSO_4 \cdot 1/2H_2O$, investigated in various temperature intervals within the overall range 341–425 K, and which are controlled both by phase boundary and diffusion processes, Ball *et al.* (11, 12) and Okhotnikov *et al.* (13). The present work shows that $CaSO_3 \cdot 1/2H_2O$ on decomposition yields water vapour, in contrast with the chemical changes that occur in a similar temperature interval (623–803 K) for $MgCl_2 \cdot 2H_2O$ where the water of crystallization interacts with the anion to yield hydrogen chloride as the principal product.

We are aware of no previous isothermal kinetic study of $CaSO_3 \cdot 1/2H_2O$ dehydration, though the reaction temperature (ca. 620 K) has been mentioned (14). To characterize the factors controlling the reaction rate, the present observations are discussed in the context of mechanistic proposals for water evolution from other crystalline solids.

$CaSO_3 \cdot 1/2H_2O$ exists in three crystallographic structures (14, 15); the present work was concerned with the α (orthorhombic) form. The dehydrated material undergoes dissociation ($CaSO_3 \Leftrightarrow CaO + SO_2$) and (or) decomposition ($4CaSO_3 \rightarrow 3CaSO_4 + CaS$) at temperatures well above (800 K) those of the present reaction (15–17). However, these subsequent reactions did not overlap with dehydration.

Experimental

Calcium sulphite hemihydrate

Reagent grade (Pfaltz and Bauer) $CaSO_3 \cdot 1/2H_2O$ in the form of a fine powder was used throughout the present study. Analytical results for the reactant supplied were as follows: Ca, 30.0, SO_3^{2-}, 56.2; and H_2O, 6.9% (theoretical $CaSO_3 \cdot 1/2H_2O$: Ca, 31.01; SO_3^{2-}, 62.01; and H_2O, 6.98%). Calcium was determined by complexometric titration, sulphite was determined by back titration with standard $Na_2S_2O_3$ after addition of excess standard iodine solution. Water was calculated from the hydrogen content of

[1]Author to whom correspondence may be addressed.

Can. J. Chem. Downloaded from www.nrcresearchpress.com by 109.225.110.28 on 09/08/12
For personal use only.

Can. J. Chem. Downloaded from www.nrcresearchpress.com by 109.225.110.28 on 09/08/12
For personal use only.

the sample measured by combustion analysis. Powder X-ray diffraction confirmed the identity of the reactant as $CaSO_3 \cdot 1/2H_2O$ (orthorhombic) (14).

Isothermal kinetic studies

$CaSO_3 \cdot 1/2H_2O$ dehydration kinetics were measured from the water vapour pressure evolved at known times in an initially evacuated conventional glass apparatus using an absolute pressure diaphragm gauge. This Baratron MKS 222B gauge worked in the range 0–10 Torr (1 Torr = 133.3 Pa) and was read to ± 0.001 Torr. The output from this gauge, and that from a thermocouple junction positioned beside the heated reactant sample, was interfaced with a computer that automatically recorded (time, pressure, temperature) values at a preset time interval for subsequent kinetic analyses. New data were recorded only if a prespecified extent of reaction had occurred. The frequency of data collection was, therefore, related to reaction rate. The computer programme also included facilities for graphical testing of obedience of data to rate expressions applicable to solid state reactions and to print both plots and tabulated results. The apparatus has been described previously (18).

Each reactant sample, ca. 50 mg (weighed to ±0.2 mg), was retained in a small glass reactant tube by a loose glass-wool plug and placed in the vacuum apparatus before evacuation at <0.05 Torr for at least 1 h at ambient temperature. After isolation of the constant volume system from the pumps the reactant was introduced into the constant temperature (±1 K) heated zone.

Scanning electron microscopy

Samples of the unreacted salt, the fully reacted product, and material partially dehydrated to measured extents were observed and examined using a Jeol 35 CF scanning electron microscope. Each specimen was rendered conducting before examination by coating with a light evaporated film of Au/Pd.

Results and discussion

Electron microscopic examinations

Reactant

Figures 1*a–c* show representative textures of the reactant studied. The powder is composed of rectangular crystallites, the longest dimension being 5–10 μm, together with a small proportion of much finer particles. Approximately half of the material was in the form of crystal aggregates up to 100 μm diameter, Figs. 1*a* and *b*, and the remainder was composed of separate crystals of similar size. Most of the crystals exhibited flat surfaces but a small proportion had rounded faces: some are seen in Fig. 1*c* to left of centre.

Product

Representative textures of the dehydrated salt are shown in Figs. 2*a* and *b*. The sizes and shapes of the component crystallites are not perceptibly different from those of the original hydrate (compare with Figs. 1*a–c*). Large crystal aggregates remained together with a similar proportion of dispersed individual particles. There was no evidence that the salt melted during dehydration. Detailed examinations of reacted salt surfaces (Figs. 3*a* and *b*) showed that dehydration was accompanied by some surface roughening and an increase in the number of pores. Internal textures, exposed by crushing after reaction, Fig. 4, show the generation of an extensive internal pore structure permeating each crystallite. Such channels arise through reactant contraction after water loss and provide pathways for water loss.

Partially dehydrated salt

The textures of salt samples partially decomposed to various known extents were indistinguishable from appearances shown in Figs. 2–4. No systematic changes of texture with extent of reaction was discerned.

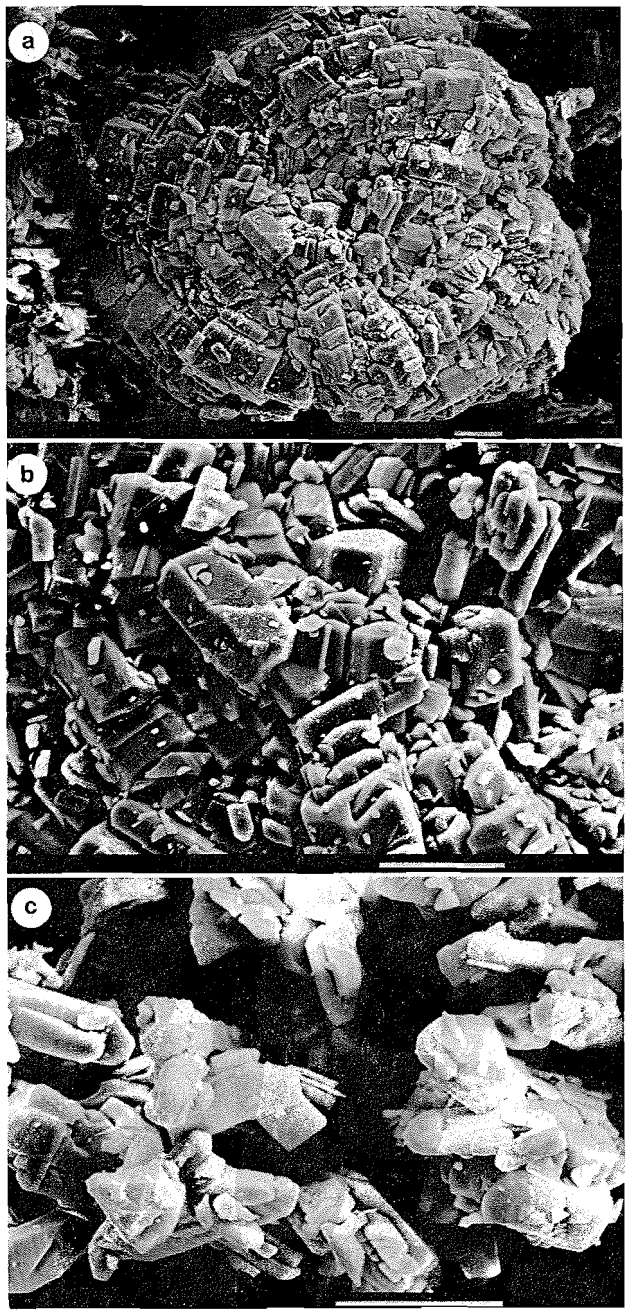

FIG. 1. Calcium sulphite hemihydrate reactant is composed of rectangular crystallites, longest edge 5–10 μm. About half of the reactant was agglomerates, diameters up to 100 μm (Figs. 1*a* and *b*) while a similar amount is dispersed, Fig. 1*c*. The latter also shows atypical rounded particles present in small proportion only. (Scale bars: all 10 μm.)

Comment

The most important microscopic observations were that dehydration was not accompanied by melting and that no structures identifiable as nuclei could be discerned. Dehydration resulted in surface roughening and pore development but textural features expected to be useful in elucidating

Can. J. Chem. Downloaded from www.nrcresearchpress.com by 109.225.110.28 on 09/08/12
For personal use only.

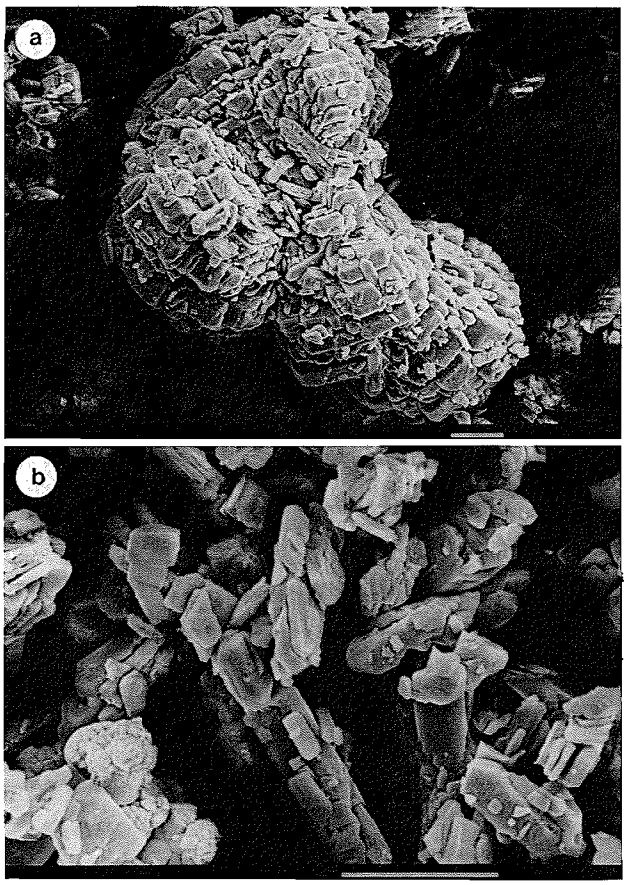

FIG. 2. Crystallites of calcium sulphite dehydrated in vacuum at 618 K. The sizes and shapes of product crystals are indistinguishable from those of the reactant: see Figs. 1*a–c*. (Scale bars: both 10 μm.)

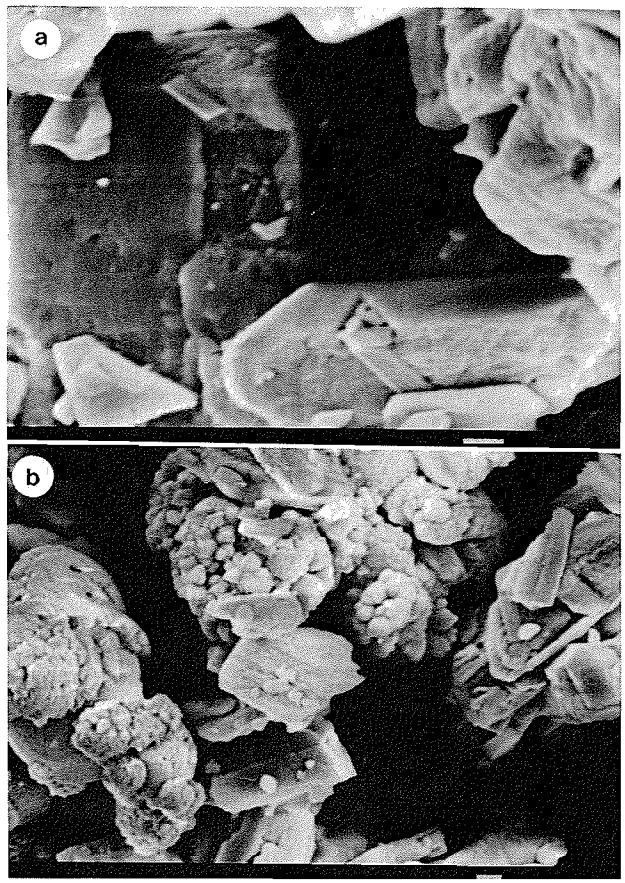

FIG. 3. Surface textures of salt dehydrated at 618 K were roughened and contained pores and (*b*) some rounded particles were generated. (Scale bars: both 1.0 μm.)

the reaction mechanism or kinetic controls were below the limits of resolution in these small crystallites.

Reaction stoichiometry

The reactant weight loss on dehydration (mean 7.1%, theoretical 6.98%) and product pressure measured in the calibrated volume of the apparatus agreed, within the limits of experimental error, with that expected for

$$CaSO_3 \cdot 1/2H_2O(s) \rightarrow CaSO_3(s) + 1/2H_2O(g)$$

It was confirmed by powder X-ray diffraction that the solid product was the orthorhombic form of $CaSO_3$ (14). Refrigerant traps (78 and 178 K) condensed the product water vapour and residual pressures corresponded to ca. 1% of the water pressure yield.

Kinetic measurements

The initial reaction

The main dehydration process was preceded by the rapid evolution of 2.0–2.5% of the constituent water during the heating of the sample to reaction temperature. (There was some evidence that an additional amount of water may have been lost during initial sample evacuation, before isolation from the pumps and heating.) Thereafter the rate of water evolution diminished and became approximately constant between $0.025 < \alpha < 0.05$ (α is the fractional reaction). The activation energy for the zero-order process was 130 ± 15 kJ mol^{-1}, at 570–650 K.

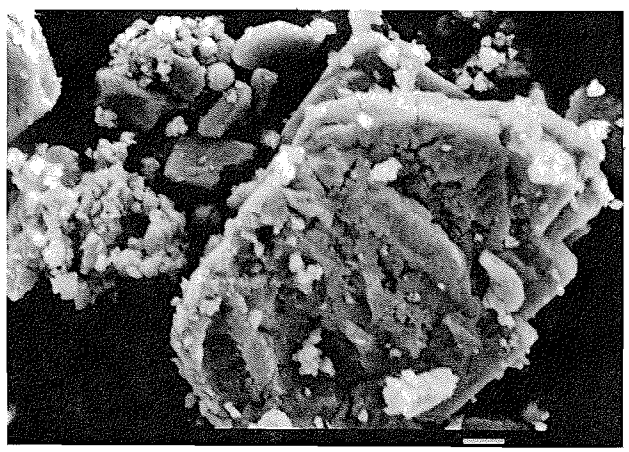

FIG. 4. A crystallite interior, exposed by crushing after dehydration at 618 K, shows evidence of irregular internal pore development during reaction. (Scale bar: 1.0 μm.)

The extent of this initial reaction was estimated to correspond to the superficial dehydration of crystal surfaces to a thickness of 10–20 nm. The approximately zero-order behaviour is ascribed to overlap between the deceleratory completion of the initial process and the acceleratory onset of the main reaction.

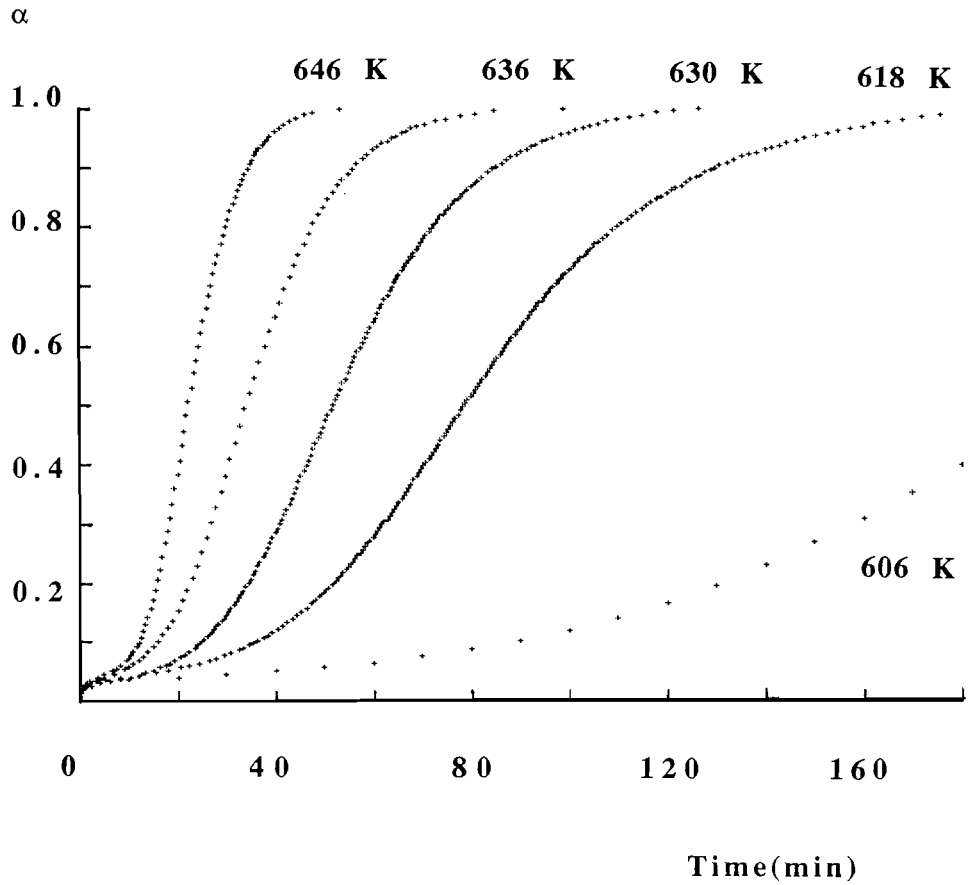

FIG. 5. Representative α–time plots for the isothermal dehydration of calcium sulphite hemihydrate at five temperatures 606–646 K. The characteristic sigmoid shaped curves are ascribed to a nucleation and growth reaction mechanism.

Can. J. Chem. Downloaded from www.nrcresearchpress.com by 109.225.110.28 on 09/08/12
For personal use only.

The main reaction

Representative α–time plots for $CaSO_3 \cdot 1/2H_2O$ dehydrations are shown in Fig. 5. Following a short induction period the reaction exhibited the sigmoid shape yield–time relationship that is characteristic (7) of nucleation and growth processes. After subtracting the contribution from the initial reaction (α_i = ca. 0.04), the most satisfactory kinetic obedience was found for the Avrami–Erofe'ev (n = 2) equation (7):

$$[1] \quad [-\ln(1 - \alpha)]^{1/2} = kt$$

This equation was obeyed for $0.09 < \alpha < 0.96$; the fits of data from Fig. 5 are shown in Fig. 6. Rate constants from 17 experiments gave a calculated activation energy of 173 ± 8 kJ mol^{-1}, at 573–673 K.

Interruption of reaction

Dehydration reactions were interrupted at various α values and the salt cooled to ambient temperature before restoring conditions prevailing previously. Such interruption caused no appreciable change in the kinetic characteristics of the resumed reaction.

Reactant packing

The dehydration kinetics of salt loosely dispersed on glass wool (19) were identical with the behaviour of powder packed more densely in the reaction vessel. This is consistent with the expectation that the reverse reaction would not exert perceptible influence on rate characteristics at this relatively high reaction temperature.

Incorporation of a small proportion (10%) of previously dehydrated salt caused no change in dehydration behaviour. The onset of water loss was not promoted by the presence of the anhydrous product.

Crushed salt

The effect of reactant crushing with pestle and mortar on the rate of subsequent dehydration is shown in Fig. 7. In comparative experiments it was shown that this mechanical pretreatment significantly accelerated the onset of reaction, the induction period was reduced by about 50%, and the acceleratory period was subsequently completed at a lower α value (ca. 0.2). Plots of $[-\ln(1 - \alpha)]^{1/2}$ against time showed two linear regions. The first ($0.09 < \alpha < 0.62$) gave rate constants that were 1.5× values for the uncrushed powder and the second, following a short curved transition region, represented a rate similar to that of the uncrushed powder ($0.07 < \alpha < 0.97$). A more satisfactory kinetic obedience was given by the contracting cube equation (7), $[1 - (1 - \alpha)^{1/3}] = kt$, which fitted the data after completion of the acceleratory process, $0.20 > \alpha > 0.94$. This may be due to the initial establishment of the reactant interface during abrasion. The overall effect of crushing, a rate increase of about 50% during the early stages, was, however, relatively small.

Dehydration of rehydrated salt

Water uptake by the dehydrated salt was slow and strongly deceleratory. Preliminary experiments, in 5 Torr water vapour at 300, 400, and 500 K, identified no conditions under which a kinetic study of the rehydration proceeded at a rate

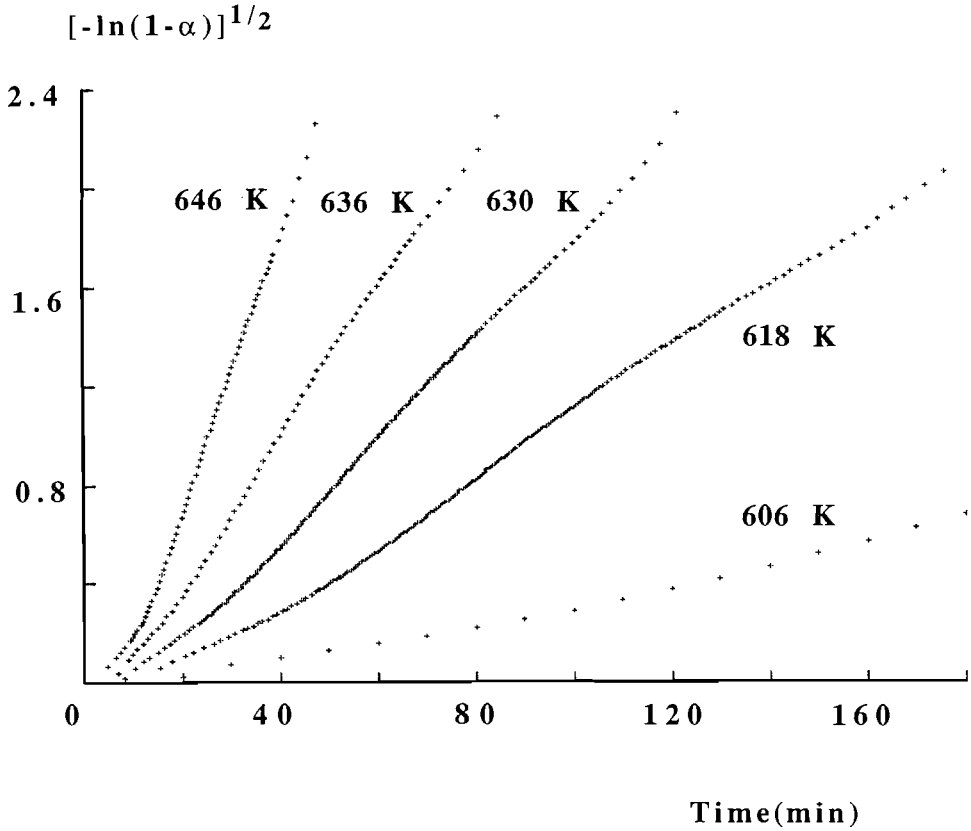

FIG. 6. Linear plots of $[-\ln(1 - \alpha)]^{1/2}$ against time for the data in Fig. 5 confirming kinetic obedience of the reaction to the Avrami–Erofe'ev equation ($n = 2$) (7).

suitable for kinetic measurements. Exposure of the dehydrated salt to saturated water vapour (ca. 14 Torr at 290 K) for 24 h resulted in a weight gain corresponding to the water uptake required for $CaSO_3 \cdot 1/2H_2O$. Water yields from successive (2nd, 3rd, and 4th) dehydrations were below theoretical expectation (75–80%), indicating losses during initial evacuation.

Figure 7 includes a typical α–time plot for a second dehydration (the most rapid of the three reactions shown) and can be compared with the curve for the first dehydration of the same reactant sample (the slowest of the curves shown) at 625 K. The following pattern of kinetic behaviour was identified in a series of comparative experiments (580–630 K) for rehydrated salt. An initial evolution of water was rapid to $\alpha = 0.20$ but kinetic studies were impracticable because this slightly deceleratory process overlapped with the reactant heating stage. The subsequent reaction obeyed eq. [1] for α between 0.2 and 0.7, rate constants were larger (×5–7) than those for the prepared salt, and this dehydration was completed in the approximate time required to initiate reaction in the original salt at the same temperature (see Fig. 7). Further kinetic analyses showed that the dehydration of rehydrated reactant fitted the contracting cube equation $0.4 < \alpha < 0.9$, with relatively slow completion of the last stages of dehydration. Precrushing the original reactant resulted in no detectable influence on the rate of water loss in second and subsequent dehydrations.

The relatively greater rate of water loss from the rehydrated salt may be explained by a reduction in effective crystallite size to ca. one sixth those of the original reactant. The contracting cube equation, $[1 - (1 - \alpha)^{1/3}] = 2\,kt/a$, includes the particle size dimension, a. This reaction model is consistent with the crack development found in the dehydrated product (Fig. 4). The increase in surface area ×6 is also consistent with the observed rise in extent of initial reaction, 2.5% in the original salt to 20% for a second reaction, though this ratio is somewhat greater, ×8.

Other experiments

Dehydration enthalpy

DSC studies, using a Perkin–Elmer DSC-7, detected only a single response at ca. 670 K, identified as dehydration, and no other thermal event between 300 and 800 K. From this peak the $CaSO_3 \cdot 1/2H_2O$ dehydration enthalpy was measured as 52 ± 5 kJ mol^{-1}.

Surface area measurements

Surface areas were measured by the BET method from nitrogen adsorption at 78 K. The surface area of the reactant was determined as 3 ± 1 m^2 g^{-1} and product 5 ± 2 m^2 g^{-1}. These correspond to assemblages of particles having an edge of ca. 1 μm, indicating the absence of extensive pore structures within the crystallites observed by electron microscopy.

Calcium sulphite and sodium metabisulphite

The dehydration kinetics of crushed mixtures ($CaSO_3 \cdot 1/2H_2O + Na_2S_2O_5$: 3:1 molar ratio) were identical with the reaction of $CaSO_3 \cdot 1/2H_2O$ alone. There was no evidence of fusion and the additive exerted no detectable influence on the dehydration.

Can. J. Chem. Downloaded from www.nrcresearchpress.com by 109.225.110.28 on 09/08/12
For personal use only.

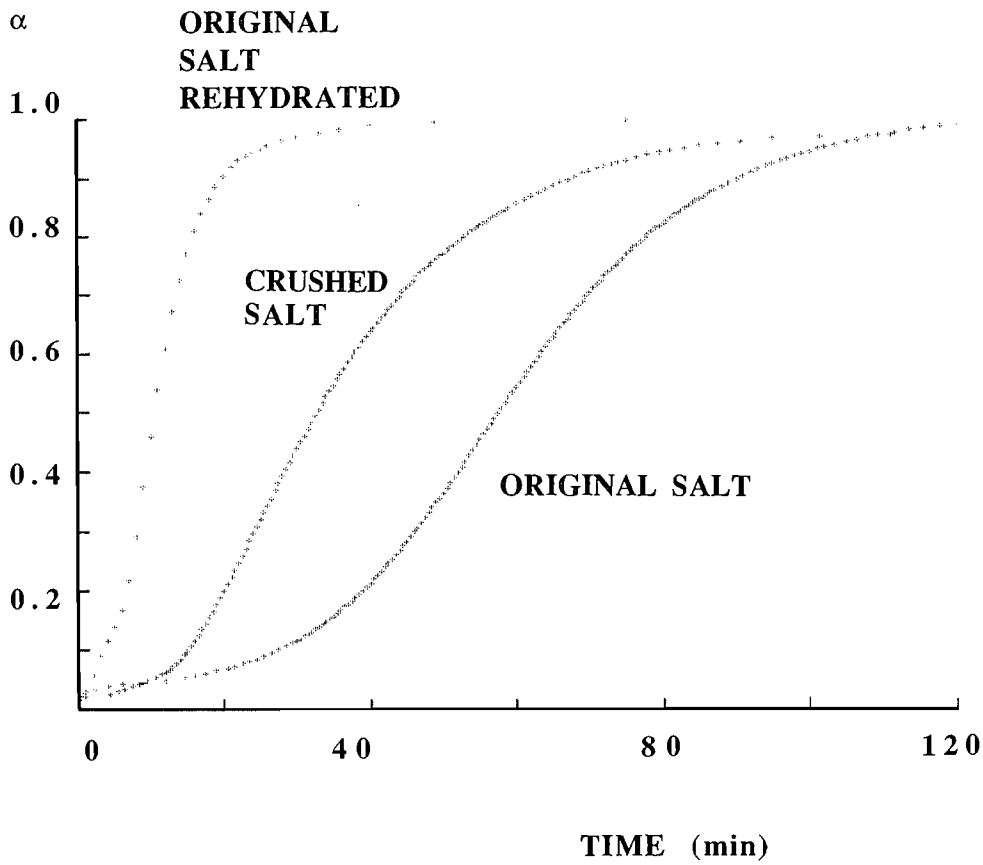

FIG. 7. Dehydration rates were increased by crushing and after rehydration following a previous dehydration. The α–time plots were sigmoid shaped for all three reactant samples dehydrated at 625 ± 1 K.

Can. J. Chem. Downloaded from www.nrcresearchpress.com by 109.225.110.28 on 09/08/12
For personal use only.

The mechanism of reaction

The dehydration of calcium sulphite hemihydrate

$$CaSO_3 \cdot 1/2H_2O \rightarrow CaSO_3 + 1/2H_2O$$

is accompanied by recrystallization (14) and we conclude, therefore, that the sigmoid shaped α–time curves result from a nucleation and growth reaction (7). Confirmation of this interpretation by microscopic observations was not possible because of the small size of the reactant crystallites and the absence of textural features that enabled the reactant and product phases to be distinguished.

The initial reaction (yielding 4% of the water from the prepared salt or 20% from the rehydrated salt) is ascribed to the facile loss of water from the less perfect crystallite surfaces. The calculated activation energy for this process was relatively low.

Onset of the main reaction is ascribed to the appearance of stable growth nuclei of product $CaSO_3$ in the reactant crystals. The promotion of nucleation by crushing is ascribed to (*i*) an increase in the surface area upon which nucleation can occur and (*ii*) increased ease with which the new phase can be formed within the damaged and imperfect crystal peripheries. The continued growth of the established reaction interface was not inhibited by interruption of the reaction by cooling. Water loss results in a contraction of the reactant (estimated to be 12% from crystallographic data (14)), thus accounting for the development of the extensive crack system within the anhydrous product particles that are pseudomorphic with the reactant crystallites (Fig. 4). This particle division also explains the more rapid dehydration rate observed in the finely divided crystallites for reactant samples of rehydrated salt.

The kinetic behaviour for $CaSO_3 \cdot 1/2H_2O$ dehydration was most satisfactorily expressed as obedience to eq. [1] with $n = 2$ and the fit with $n = 3$ was almost as good. Thus the rate characteristics are ascribed (7) to instantaneous nucleation followed by the growth of compact nuclei (three-dimensional growth) in the asymmetric reactant crystallites (one dimension longer than the other two). Unfortunately this geometric interpretation (10) of the kinetic characteristics could not be confirmed microscopically.

The considerable stability of $CaSO_3 \cdot 1/2H_2O$ is a consequence of the strong bonding of the oxygen atom in the water molecule to two (7 coordinated) Ca^{2+} ions: the Ca^{2+}—Ow bond length is 2.499 Å (16). (This structure may be contrasted with the linkage of water to a single Ca^{2+} in gypsum (16).) Dehydration is accompanied by recrystallization and the activation energy associated with the necessary bond reorganization is relatively large (173 kJ mol^{-1}), significantly greater than the dehydration enthalpy (52 kJ mol^{-1}). The activation energy clearly did not include a contribution from the nucleation step, which was rapidly completed at the onset of reaction ($n = 2$ or 3 for growth of nuclei, extrapolations of data in Fig. 6 are close to times required for sample heating). Although the lattice adopted by the anhydrous product may be influenced by the presence of a low relative vapour pressure of water (20), $CaSO_3 \cdot 1/2H_2O$ dehydration

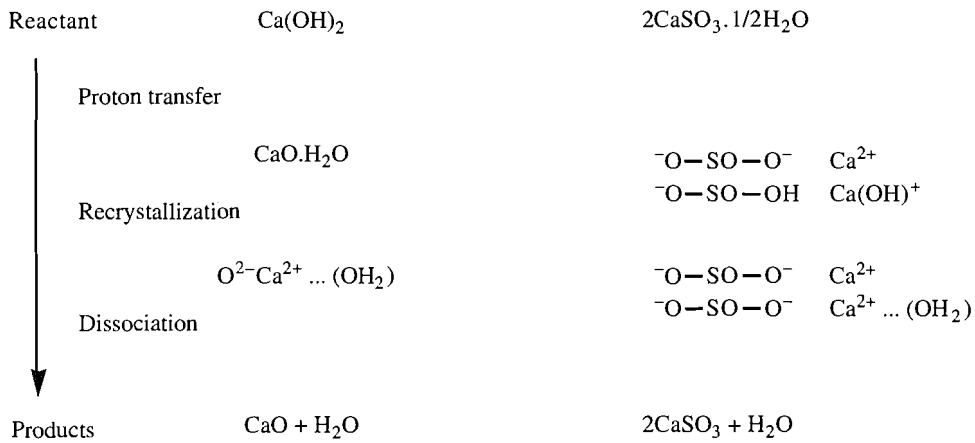

SCHEME 1. Mechanisms of dehydrations of calcium hydroxide and of calcium sulphite hemihydrate

was certainly irreversible at these reaction temperatures. There was no evidence that water reacted with the anion, in contrast with the high-temperature dehydration of $MgCl_2 \cdot 2H_2O$ (5).

The rate of $CaSO_3 \cdot 1/2H_2O$ dehydration was closely similar to that of $Ca(OH)_2$ dehydration; at the same temperatures reaction velocities, measured from slopes of α–time plots across the median region of both reactions, usually agreed within $\times 2$. The α–time curves for the two systems showed a significant difference in that the calcium hydroxide reaction was predominantly deceleratory. Studies in this laboratory using the same apparatus and identical reaction conditions showed that for $Ca(OH)_2 \rightarrow CaO + H_2O$ the activation energy was 174 ± 20 kJ mol^{-1} (633–683 K) (21), which is in remarkably close agreement with the value calculated for the present reaction, 173 ± 8 kJ mol^{-1} (573–673 K). Various other studies of calcium hydroxide dehydration have given comparable values: 143–180 kJ mol^{-1} (22) and 161–188 kJ mol^{-1} (23), as well as lower values (24).

In considering this close coincidence of absolute reactivity, including activation energy, between these two reactants, we assessed the possibility that $Ca(OH)_2$ was formed as an intermediate during $CaSO_3 \cdot 1/2H_2O$ dehydration. Mechanisms such as

$$2CaSO_3 \cdot 1/2H_2O \rightarrow CaS_2O_5 + Ca(OH)_2$$

were discounted because the metabisulphite would be expected to decompose at lower temperatures, by comparison with the known (25) stabilities of $Na_2S_2O_5$ (decomposed at 500 K) and $K_2S_2O_5$ (decomposed at 550 K). $CaSO_3 \cdot 1/2H_2O$ dehydration was not accompanied by SO_2 evolution, which is the expected product of $S_2O_5^{2-}$ anion breakdown (SO_2 yields here were always $< 2\%$ of the evolved gases). The dehydration rate was not influenced by added $Na_2S_2O_5$ and no anion other than SO_3^{2-} was detected by infrared spectroscopic examination of the anhydrous $CaSO_3$ product.

The close reactivity similarities apparent between the dehydrations of $CaSO_3 \cdot 1/2H_2O$ and $Ca(OH)_2$ are, therefore, ascribed to common mechanistic features in the water elimination and recrystallization processes. The steps contributing to the overall chemical changes are proton transfer and the dissociation of a strong calcium to water (oxygen) bond. It is not known which of these is rate limiting for the dehydration reaction, but the essential steps in both reactions are compared in Scheme 1. We suggest that a proton transfer step in the dehydration of $CaSO_3 \cdot 1/2H_2O$ permits reorganization of the coordination shell around the Ca^{2+} ion, here represented as involving the temporary formation of a $^-O—SO—OH$ ion. Because the activation energy (173 kJ mol^{-1}) is much larger than the dehydration enthalpy (52 kJ mol^{-1}) we conclude that the water elimination mechanism is more complicated than a single bond rupture step. Thus the onset of dehydration occurs at the common temperature at which proton transfer becomes possible in both salts. This is one possible explanation of the similarity of reactivity. Alternatively, if the rupture of similar strong Ca^{2+} ---- (OH_2) bonds in both salts controls the dehydration rate, then again the similarities of behaviour are explained. We conclude, therefore, that the dehydration of $CaSO_3 \cdot 1/2H_2O$ is rate controlled by the recrystallization (reactant $\rightarrow$ product), which may be promoted by proton transfer or the Ca^{2+}—OH_2 bond rupture step.

Acknowledgements

We thank Miss C. Nolan for DSC measurements of the dehydration enthalpy and Dr. M. E. Brady for helpful discussions of the reaction mechanism. We also thank the staff of the Electron Microscope Unit, QUB, for help and advice in obtaining the electron micrographs. One of us (C. A.) thanks the Department of Education for Northern Ireland for the Award of a Postgraduate Scholarship held during the period of this work.

1. A. K. Galwey, R. Spinicci, and G. G. T. Guarini. Proc. R. Soc. (London), **A378**, 477 (1981).
2. A. K. Galwey and M. A. Mohamed. Thermochim. Acta, **121**, 97 (1987).
3. A. K. Galwey and V. B. Okhotnikov. J. Therm. Anal. **33**, 441 (1988).
4. A. K. Galwey, N. Koga, and H. Tanaka. J. Chem. Soc. Faraday Trans. 1, **86**, 531 (1990).
5. A. K. Galwey and G. M. Laverty. Thermochim. Acta, **138**, 115 (1989).
6. M. E. Brady, M. G. Burnett, and A. K. Galwey. J. Chem. Soc. Faraday Trans. 1, **86**, 1573 (1990).
7. M. E. Brown, D. Dollimore, and A. K. Galwey. *In* Comprehensive chemical kinetics. Vol. 22. *Edited by* C. H. Bamford and C. F. H. Tipper. Elsevier, Amsterdam. 1980.
8. A. K. Galwey and G. M. Laverty. Solid State Ionics, **38**, 155 (1990).
9. A. K. Galwey and G. M. Laverty. J. Chim. Phys. **87**, 1207 (1990).

Can. J. Chem. Downloaded from www.nrcresearchpress.com by 109.225.110.28 on 09/08/12
For personal use only.

10. A. K. Galwey. React. Solids, **8**, 211 (1990).
11. M. C. Ball and L. S. Norwood. J. Chem. Soc. (A), 1633 (1969).
12. M. C. Ball and R. G. Urie. J. Chem. Soc. (A), 528 (1970).
13. V. B. Okhotnikov, S. E. Petrov, B. I. Yakobson, and N. Z. Lyakhov. React. Solids, **2**, 359 (1987).
14. Y. Arai, T. Yasue, N. Nagata, and H. Shiino. Bull. Chem. Soc. Jpn. **55**, 738 (1982).
15. R. Matsuzaki, H. Masumizu, N. Murakami, and Y. Saeki. Bull. Chem. Soc. Jpn. **51**, 121 (1978).
16. L. Schröpfer. Z. Anorg. Allgem. Chem. **401**, 1 (1973).
17. G. Van Houte and B. Delmon. J. Chem. Soc. Faraday Trans. 1, **75**, 1593 (1979).
18. N. J. Carr and A. K. Galwey. Proc. R. Soc. (London), **A404**, 101 (1986).
19. A. K. Galwey and M. E. Brown. J. Chem. Soc. Faraday Trans. 1, **78**, 411 (1982).
20. A. Cohen and M. Zangen. Thermochim. Acta, **133**, 251 (1988).
21. G. M. Laverty. Ph.D. Thesis. The Queen's University of Belfast (1989).
22. Z. D. Zivkovic. Rud.-Metal. Zb. **4**, 359 (1977).
23. N. G. Dave and S. K. Chopra. J. Am. Ceram. Soc. **49**, 575 (1966).
24. I. Lindquist and M. Morsell. Acta Crystallogr. **10**, 406 (1957).
25. E. G. Janzen. J. Phys. Chem. **76**, 157 (1972).

Can. J. Chem. Downloaded from www.nrcresearchpress.com by 109.225.110.28 on 09/08/12
For personal use only.

Study of the aqueous reactions of K[Pt(DMSO)Cl_3] with nitrile ligands and crystal structures of Cl(DMSO)Pt(μ-$C_4H_8NO)_2$Pt(DMSO)Cl and Cl(DMSO)Pt(μ-$C_5H_{10}NO)_2$Pt(DMSO)Cl

FERNANDE D. ROCHON,[1] RADIA BOUGHZALA, AND ROBERT MELANSON

Département de chimie, Université du Québec à Montréal, C. P. 8888, Succ. A, Montréal (Québec), Canada H3C 3P8

Received February 18, 1992

FERNANDE D. ROCHON, RADIA BOUGHZALA, and ROBERT MELANSON. Can. J. Chem. **70**, 2476 (1992).

The aqueous reactions of K[Pt(DMSO)Cl_3] with nitriles were studied in different conditions of pH. At normal pH (≈2.4), the ligands RCN, where R is an alkyl group, produced the yellow complexes Pt(DMSO)(R-CN)Cl_2. Infrared spectroscopy suggested *cis* isomers. The ^{195}Pt NMR spectra of the compounds show a resonance around −3000 ppm. The same reactions in neutral medium (pH adjusted to ~7 with NaOH) produced acetamido-bridged dimers (DMSO)ClPt(μ-RCONH)$_2$Pt(DMSO)Cl with all the ligands studied: propionitrile, butyronitrile, dimethylacetonitrile, trimethylacetonitrile, fluoroacetonitrile, chloroacetonitrile, bromoacetonitrile, and dibromoacetonitrile. The results of ^{195}Pt NMR spectroscopy show a head-to-tail isomer, since only one signal around −2750 ppm is observed for each complex. These dimeric compounds are all blue or green depending on the ligand. The same dimers are obtained with all the haloacetonitrile ligands when the pH is not adjusted (≈2.4). The crystal structures of Cl(DMSO)Pt(μ-$C_4H_8NO)_2$Pt(DMSO)Cl (**1**) and Cl(DMSO)Pt(μ-$C_5H_{10}NO)_2$Pt(DMSO)Cl (**2**) were determined. The results confirm that the dimers are head-to-tail isomers with the DMSO ligands located in *trans* position to the *O*-acetamido atoms. The two crystals belong to the $Pna2_1$ space group with a = 11.112(4), b = 20.414(9), c = 10.161(4) Å for **1** and a = 11.607(6), b = 20.113(11), and c = 10.641(5) Å for **2**. The structures were refined to R = 0.054 for **1** and R = 0.056 for **2**. The Pt—Cl bond lengths are 2.328(10), 2.293(10) Å for **1** and 2.317(9), 2.317(10) Å for **2**, while the Pt—S bond lengths are 2.173(10), 2.193(10) for **1** and 2.180(9), 2.176(9) Å for **2**. The Pt—O bonds vary from 1.91(2) to 2.08(2) and the Pt—N from 1.88(2) to 2.03(2) Å. The dihedral angle between the two Pt(II) planes is 36°.

FERNANDE D. ROCHON, RADIA BOUGHZALA et ROBERT MELANSON. Can. J. Chem. **70**, 2476 (1992).

On a étudié les réactions aqueuses du K[Pt(DMSO)Cl_3] avec les nitriles à divers pH. À pH normal (pH ≈ 2,4) les ligands RCN, ou R est un groupe alkyle, donnent des complexes jaunes Pt(DMSO)(R-CN)Cl_2. La spectroscopie infrarouge révèle qu'il s'agit d'isomères *cis*. Les spectres RMN du ^{195}Pt présentent une résonance à environ −3000 ppm. Avec tous les ligands étudiés (propionitrile, butyronitrile, diméthylacétonitrile, triméthylacétonitrile, fluoroacétonitrile, chloroacétonitrile, bromoacétonitrile et dibromoacétonitrile) ces réactions, réalisées en milieu neutre (le pH est ajusté à 7 avec du NaOH), conduisent à des dimères avec le groupe acétamido en position de pont (DMSO)ClPt(μ-RCONH)$_2$(DMSO)Cl. Les résultats de la RMN du ^{195}Pt indiquent un isomère avec une structure tête-à-queue puisqu'on ne retrouve qu'un seul signal à environ −2750 ppm pour chacun de ces complexes. Tous ces dimères sont bleus ou verts dépendant du ligand. Tous les ligands haloacétonitriles donnent les mêmes dimères à pH normal (pH ≈2,4). On a déterminé la structure cristalline du Cl(DMSO)Pt(μ-$C_4H_8NO)_2$Pt(DMSO)Cl (**1**) et du Cl(DMSO)Pt(μ-$C_5H_{10}NO)_2$Pt(DMSO)Cl (**2**). Les résultats confirment que les dimères sont des isomères comportant une structure tête-à-queue dans laquelle le ligand DMSO est en position *trans* par rapport à l'atome d'oxygène du groupe acétamido. Les deux cristaux appartiennent au groupe d'espace $Pna2_1$ avec a = 11,112(4), b = 20,414(9), c = 10,161(4) Å pour le composé **1** et a = 11,607(6), b = 20,113(11) et c = 10,641(5) Å pour le composé **2**. On a affiné les structures jusqu'à des valeurs de R = 0,054 pour le composé **1** et de R = 0,056 pour le composé **2**. Les longueurs de liaison Pt—Cl sont de 2,328(10) et 2,293(10) Å pour le composé **1** et de 2,317(9), 2,317(10) Å pour le composé **2** tandis que la liaison Pt—S est de 2,173(10) et 2,193(10) Å pour le composé **1** et de 2,180(9) et 2,176(9) Å pour le composé **2**. La liaison Pt—O varie de 1,91(2) à 2,08(2) Å et la liaison Pt—N de 1,88(2) à 2,03(2) Å. L'angle dièdre entre les plans des deux Pt(II) est de 36°.

[Traduit par la rédaction]

Introduction

Recently, we started a study on the reactions of K[Pt(DMSO)Cl_3] with nitriles in aqueous medium. When K[Pt(DMSO)Cl_3] is dissolved in water, the pH of the solution is 2.35 (0.025 M), indicating some hydrolysis reactions. Its reaction with CH_3CN produced *cis*-Pt(DMSO)-(CH_3CN)Cl_2, which was studied by X-ray diffraction (1, 2). When the solution was neutralized with NaOH before adding CH_3CN, a dimer with acetamido bridges {Pt(DMSO)-Cl(μ-C_2H_4NO)}$_2$ (head-to-tail isomer) was isolated and characterized. The acetamido ligand was formed from the hydrolysis of CH_3CN. In this reaction, a blue solution was observed. The acetamido-bridged dimers can also be formed without adjusting the pH. If the reacting mixture (pH ~ 2.4) is left at room temperature for several weeks, a blue solution gradually forms and acetamido-bridged dimers can be eventually obtained. We also obtained the same dimers from the aqueous reaction of K[Pt(DMSO)Cl_3] with diacetamide.

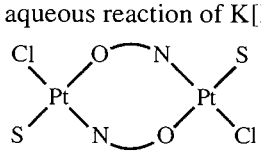

head-to-tail isomer

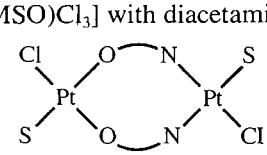

head-to-head isomer

A similar study with no adjustment of pH (~2.4) with trichloroacetonitrile showed only the presence of *cis*-Pt-(DMSO)(H_2O)Cl_2 and its crystal structure has been reported (3). The presence of three chlorine atoms on the ligand lowers the donor properties of the N atom. At neutral pH, a monomer Pt(DMSO)Cl($C_4NO_2Cl_6$) containing a bidentate

[1]Author to whom correspondence may be addressed.

Can. J. Chem. Downloaded from www.nrcresearchpress.com by 109.225.110.28 on 09/08/12
For personal use only.

Can. J. Chem. Downloaded from www.nrcresearchpress.com by 109.225.110.28 on 09/08/12
For personal use only.

deprotonated imide ligand, formed from the dimerization and hydrolysis of trichloroacetonitrile, was characterized by X-ray diffraction methods. No acetamido-bridged dimers were detected with this ligand.

When these reactions are done at neutral pH, a blue color is always observed after a few days. This blue compound, which is very soluble in water, is probably an analogue of *platinblau* reported in 1907 (4) and whose exact structure is still unknown. It was suggested that it contains deprotonated acetamido ligands bound to platinum(II), the acetamide being produced from the reaction of water with coordinated acetonitrile (5–7). But attempts to obtain *platinblau* by direct combination of platinum(II) with acetamide were not successful.

A systematic study of the aqueous reaction of K[Pt(DMSO)Cl_3] with no adjustment of pH(~2.4), and at neutral pH, was made with several alkyl and halo acetonitrile derivatives. Since trichloroacetonitrile is not a good ligand for Pt(II), we were interested to know if the monohaloacetonitriles would coordinate to Pt(II). The products of these reactions were analyzed by IR and by ^{195}Pt and ^{1}H NMR spectroscopy. The results of this study are described below.

Experimental section

The decomposition points were measured on a Fisher–Johns instrument. The pH values were measured on a Radiometre pHM 28 pH-meter with a Graphic-Controls microelectrode (13-620-253). The IR spectra were recorded in the solid state (KBr pellets) on a Perkin–Elmer 783 spectrometer. The ^{1}H NMR spectra were measured on a Bruker W-H 400 (400 MHz) with external TMS as reference. The ^{195}Pt NMR spectra were recorded on the same instrument (85.83 MHz), the external reference being K_2PtCl_4 adjusted to $\delta = -1628$ ppm from Na_2PtCl_6 ($\delta = 0$). The NMR spectra were measured in DMF-d_7 (^{1}H), in a mixture of DMF-d_7 and normal DMF (^{195}Pt), and occasionally in acetone-d_6. K_2PtCl_4 was bought from Johnson Matthey Inc. and was purified by crystallization from water before use. The nitrile ligands were obtained from Aldrich and the deuterated solvents from Cambridge Isotopes.

K[Pt(DMSO)Cl_3] was prepared by the published method (8). Yield: 90%; IR (cm^{-1}): ν(S=O) 1101, ν(Pt—Cl) 349m, 310m, 332s; NMR (ppm in D_2O): 3.50 (s + d), ^{3}J(Pt–H) = 24 Hz, δ(Pt) −2998; (ppm in DMF): 3.33 (s + d), ^{3}J(Pt–H) = 22 Hz, δ(Pt) −2965 (lit. (9) −2969 ppm in DMSO).

cis-Pt(DMSO)(CH_3CN)Cl_2 and Cl(DMSO)Pt(μ-$C_2H_4NO)_2$Pt(DMSO)Cl were prepared as already reported (1). *cis*-Pt(DMSO)(CH_3-CN)Cl_2: NMR (δ, ppm in DMF): CH_3 (DMSO) 3.50 s + d, $^{3}J(^{195}Pt-^{1}H)$ = 18 Hz, CH_3 2.79s, δ(Pt) −3010. Cl(DMSO)Pt(μ-$C_2H_4NO)_2$Pt(DMSO)Cl: δ(Pt) −2753 ppm in DMF.

The reactions of K[Pt(DMSO)Cl_3] with different nitriles were studied in water by two differents methods.

1. With no adjustment of pH

K[Pt (DMSO)Cl_3] (~0.5 mmol) was dissolved in a minimum quantity of distilled water, an excess of ligand (Pt:ligand = 1:4) was added to the solution, and the mixture was agitated and left at room temperature until a yellow precipitate was observed. The precipitate was then filtered, washed with water, and dried in vacuum. For the haloacetonitrile ligands, the isolated compounds were identical to those obtained at pH ~7 as described below. For the other ligands, the products were identified as Pt(DMSO)(RCN)Cl_2.

Pt(DMSO)(C_2H_5CN)Cl_2: Yield 50%; dec. 118–220°C; IR (cm^{-1}): 2318m, 1462w, 1428w, 1407m, 1378w, 1318w, 1305w, 1170s, 1155s, 1074m, 1030s, 987m, 928w, 918w, 776w, 737m, 692m, 447s, 381w, 360w, 340m, 322 sh.; NMR (δ, ppm in acetone-d_6): CH_3 (DMSO) 3.53s + d, $^{3}J(^{195}Pt-^{1}H)$ = 21Hz, CH_3 1.40t, ^{3}J = 7.5Hz, CH_2 3.05q, δ(Pt) −2997, δ(Pt) −3006 ppm in DMF.

Pt(DMSO)(n-C_3H_7CN)Cl_2: Yield 45%; dec. 115–220°C; IR (cm^{-1}): 2318w, 2310m, 1458m, 1408m, 1382w, 1315m, 1295m, 1147s, 1020s, 980m, 940m, 911m, 735s, 695w, 448s, 382m, 363m, 340s, 320w; NMR (δ, ppm in acetone-d_6): CH_3 (DMSO) 3.53s + d, $^{3}J(^{195}Pt-^{1}H)$ = 22Hz, CH_3 1.14t, ^{3}J = 7Hz, CH_2 3.04t, ^{3}J = 7Hz, CH_2 1.83m, δ(Pt) −2999 ppm in DMF.

Pt(DMSO)($CH(CH_3)_2CN$)Cl_2: Yield 73%; dec. 170–225°C; IR (cm^{-1}): 2190w, 1403m, 1316s, 1100vs, 1028s, 976m, 942m, 926m, 732m, 691m, 447m, 382m, 348m, 310m.

Pt(DMSO)($C(CH_3)_3CN$)Cl_2: Yield 18%; dec. 115–225°C; IR (cm^{-1}): 2308w, 2299w, 1477m, 1455m, 1414m, 1362m, 1240m, 1162s, 1147s, 1031s, 1018s, 982m, 938m, 928w, 913w, 734m, 692m, 442s, 378w, 362s, 320s, 312sh; NMR, δ(Pt) −3010 ppm in DMF.

2. With adjustment of pH

K[Pt(DMSO)Cl_3] (~0.7 mmol) was dissolved in 15 mL of distilled water and the pH of the solution was adjusted to about 7 with 0.1 M NaOH. The nitrile ligand (0.3–0.5 mL) was then added slowly with mixing and the solution was left at room temperature until a precipitate formed (1 day to 3 weeks). The precipitate, which proved to be the acetamido-bridged dimer, was either yellow, green, or blue depending on the ligand and on the time of standing. The precipitate was filtered, washed with water, and dried in vacuum.

{Cl(DMSO)Pt(μ-C_3H_6NO)}$_2$: Yield 20%; dec. 190–207°C; IR (cm^{-1}): 3317w, 3300s, 1590vs, 1495w, 1465w, 1420w, 1320w, 1258s, 1220s, 1148s, 1120s, 1022s, 920w, 900w, 735w, 697m, 608m, 450s, 380m, 340m; NMR (δ, ppm in DMF): CH_3 (DMSO) 3.33s, 3.47s, CH_3 0.85t, ^{3}J = 8Hz, CH_2 2.13q, NH 6.8, δ(Pt) −2763.

{Cl(DMSO)Pt(μ-nC_4H_8NO)}$_2$: Yield 15%; dec. 198–202°C; IR (cm^{-1}): 3318s, 1585vs, 1482m, 1430w, 1297m, 1237s, 1142vs, 1020s, 980w, 930w, 696m, 610w, 450s, 382m, 340m; ^{195}Pt NMR: −2752 ppm in DMF.

{Cl(DMSO)Pt(μ-C_2H_3NOF)}$_2$: Yield 30%; dec. 180–220°C; IR (cm^{-1}): 3330l 1625sh, 1610s, 1482m, 1438m, 1352m, 1215m, 1152s, 1142s, 1053s, 1038s, 935w, 722m, 699w, 602m, 458s, 385m, 342m; NMR (δ, ppm in acetone-d_6): CH_3 (DMSO) 3.63s, 3.62s, CH_2 4.88d, $^{2}J(^{19}F-^{1}H)$ = 48 Hz, NH 6.7, δ(Pt) −2715; (δ, ppm in DMF): CH_3 (DMSO) 3.64s, 3.60s, CH_2 4.94d, $^{2}J(^{19}F-^{1}H)$ = 44 Hz, NH 7.3, δ(Pt) −2723.

{Cl(DMSO)Pt(μ-C_2H_3NOCl)}$_2$: Yield 20%; dec. 182–240°C; IR (cm^{-1}): 3315l, 3000s, 1632w, 1612m, 1465w, 1420w, 1402m, 1315m, 1297w, 1210m, 1140vs, 1130sh, 1028s, 977w, 960w, 928w, 790m, 740m, 698m, 577m, 452s, 380m, 340s; NMR (δ, ppm in acetone-d_6): CH_3 (DMSO) 3.62s, 3.58s, CH_2 4.21s, NH 6.8, δ(Pt) −2725; (δ, ppm in DMF): CH_3 (DMSO) 3.65s, 3.58s, CH_2 4.26s, NH 7.5, δ(Pt) −2750.

{Cl(DMSO)Pt(μ-C_2H_3NOBr)}$_2$: Yield 35%; dec. 180–195°C; IR (cm^{-1}): 3315l, 1630w, 1608m, 1416m, 1392w, 1318m, 1297m, 1205m, 1156s, 1142vs, 1028s, 923m, 856w, 738w, 690w, 642w, 582w, 446m, 382w, 362m 332s; NMR (δ, ppm in acetone-d_6): CH_3 (DMSO) 3.57s, 3.64s, CH_2 4.86s, NH 6.9, δ(Pt) −2748; δ(Pt) −2762 ppm in DMF.

{Cl(DMSO)Pt(μ-$C_2H_2NOBr_2$)}$_2$: Yield 10%; dec. 172–240°C; IR (cm^{-1}): 3345m, 3280l, 1612s, 1582m, 1465m, 1270m, 1142s, 1128m, 1027m, 772m, 700w, 600m, 452m, 386w, 350m; NMR (δ, ppm in acetone-d_6): CH_3 (DMSO) 3.62s, 3.67s, CH 6.42s, NH 6.8, δ(Pt) −2766; δ(Pt) −2773 ppm in DMF.

Crystallographic measurements and structure resolution

The two blue crystals (synthesized by adjusting the pH at ~7) were selected after examination for homogeneity under a polarizing microscope. They were obtained directly from the reacting medium. The unit cell parameters were obtained by least-squares refinement of the angles 2θ (11–25°), ω, and χ for 15 well-centered reflections on a Syntex P1 diffractometer using graphite-monochromatized MoKα radiation. Crystal data and other information are summarized in Table 1. Scan rates and data treatment have already been described (10). Crystal (**1**) gradually decomposed during the data collection, as shown by a gradual decrease of the intensity of the three standard reflections. At the end of the collection, the intensity was reduced by about 20%. Scaling on the standard reflections was made as usual. Corrections were made for absorption and Lorentz–polarization effects. The anom-

Can. J. Chem. Downloaded from www.nrcresearchpress.com by 109.225.110.28 on 09/08/12
For personal use only.

TABLE 1. Experimental details of the X-ray studies of Cl(DMSO)Pt(μ-$C_4H_8NO)_2$Pt(DMSO)Cl (**1**) and Cl(DMSO)Pt(μ-$C_5H_{10}NO)_2$Pt(DMSO)Cl (**2**)

	1	**2**
Compound	$C_{12}H_{28}N_2O_4S_2Cl_2Pt_2$	$C_{14}H_{32}N_2O_4S_2Cl_2Pt_2$
fw	789.57	817.62
Space group	$Pna2_1$	$Pna2_1$
a (Å)	11.112(4)	11.607(6)
b (Å)	20.414(9)	20.113(11)
c (Å)	10.161(4)	10.641(5)
Volume (Å^3)	2305(2)	2484(2)
Z	4	4
F(000)	1472	1536
ρ_{calcd}(Mg m^{-3})	2.275	2.186
λ(MoKα) (Å)	0.71069	0.71069
μ(MoKα) (mm)	12.68	11.77
Crystal faces and distance from center (mm)	(01$\bar{1}$), (0$\bar{1}$1) (0.036) (11$\bar{0}$), ($\bar{1}$1$\bar{0}$) (0.030) (10$\bar{1}$), ($\bar{1}$0$\bar{1}$) (0.030)	(01$\bar{1}$), (0$\bar{1}$1) (0.022) (110), ($\bar{1}\bar{1}$0) (0.096) (151), ($\bar{1}$5$\bar{1}$) (0.091)
Transmission factor range	0.357–0.544	0.094–0.567
2θ max (°)	52	50
Octants	h, k, l	h, k, l
h, k, l	0→13, 0→25, 0→12	0→13, 0→23, 0→12
Scan technique and rate (°/min.)	2θ/θ, 0.8–24	2θ/θ, 1.0–24
Std reflcns (var.)	064, 351, 131 (20% decrease)	140, 002, 21-3 (<2%)
Temp (K)	295	295
No. of independent reflcns.	2615	2522
No. of obsd reflcns ($I > 2.75\sigma(I)$)	1189	1711
Avg. shift/esd (max.)	0.07 (0.3)	0.06 (0.3)
R	0.054	0.056
wR	0.046	0.050
S	1.78	1.90

alous dispersion terms of Pt, S, and Cl were included in the calculations (11).

The coordinates of the Pt atoms for the two crystals were determined from a three-dimensional Patterson map and the positions of all the other non-hydrogen atoms were found by the usual Fourier methods. The refinements of the two structures were done by using full-matrix least-squares calculations minimizing $\Sigma w(|F_o| - |F_c|)^2$. Interchanging the positions of the O and N atoms of the bidentate ligands resulted in abnormal thermal factors. The proposed positions are the most probable based on the size of the thermal factors. The H atoms could not be located (as often encountered for platinum complexes), and they were fixed at their calculated positions with $U_{eq} = 1.2 \times U_{eq}$ of the C to which they are bonded. Isotropic secondary-extinction corrections (12) were included in the calculations. Individual weights $w = 1/\sigma^2(F)$ were applied. The refinement of the scale factor, coordinates, and anisotropic temperature factors of all atoms converged to $R = 0.054$ and $wR = 0.046$ for **1** and to $R = 0.056$ and $wR = 0.050$ for **2**. Refinement of the enantiomorphic structures resulted in significantly higher R factors. There were a few residual peaks (<1.2e Å^{-3} for **1** and <1.3e Å^{-3} for **2**) in the close environment of the Pt atoms.[2]

[2]The following tables are available as supplementary material: anisotropic temperature factors (Table S1), coordinates of the H atoms (Table S2), weighted least-squares planes (Table S3), torsion angles (Table S4) (9 pages), observed and calculated structure factor amplitutes (Table S5) (17 pages). These tables may be purchased from: The Depository of Unpublished Data, Document Delivery, CISTI, National Research Council Canada, Ottawa, Canada K1A 052.

Table S2 has also been deposited with the Cambridge Crystallographic Data Centre and can be obtained on request from the Director, Cambridge Crystallographic Data Centre, University Chemical Laboratory, 12 Union Road, Cambridge, CB2 1EZ, U.K.

The scattering curves of Cromer and Waber (13) were used. Most of the calculations were done on a SHELXTL system and the others on a Cyber 830 with programs already described (10).

Results and discussion

The aqueous reactions of K[Pt(DMSO)Cl_3] with several nitriles were studied without adjusting the pH (~2.4) and at neutral pH (adjusted to ~7 with 1 M NaOH). The results were compared with those obtained with CH_3CN where *cis*-Pt(CH_3CN)(DMSO)Cl_2 (pH ~2.4) and Cl(DMSO)Pt(μ-$C_2H_4NO)_2$Pt(DMSO)Cl (pH ~7 or at pH ~2.4 after several weeks) were characterized (1) and with CCl_3CN where only *cis*-Pt(DMSO)(H_2O)Cl_2 (pH ~2.4) and Pt(DMSO)($C_4NO_2Cl_6$)Cl (pH ~7) were detected (3). In the present study, the nitriles propionitrile, butyronitrile, isobutyronitrile, trimethylacetonitrile, fluoroacetonitrile, chloroacetonitrile, bromoacetonitrile, and dibromoacetonitrile were used. Most of the products were characterized by IR and by ^{1}H and ^{195}Pt NMR spectroscopy.

Pt(RCN)(DMSO)Cl_2

The reaction of K[Pt(DMSO)Cl_3] with RCN, where R is an alkyl group, gave the yellow compound Pt(RCN)(DMSO)Cl_2.

$$K[Pt(DMSO)Cl_3] + RCN \xrightarrow[pH\sim2.4]{H_2O} Pt(DMSO)(RCN)Cl_2$$

This reaction is similar to the reactions with CH_3CN (1, 2) and $PhCH_2CN$ (14) where *cis*-Pt(DMSO)(RCN)Cl_2 was obtained. Under the same conditions, reactions with the haloacetonitriles (FCH_2CN, $ClCH_2CN$, $BrCH_2CN$, and Br_2CHCN) did not produce the nitrile complex as observed

Can. J. Chem. Downloaded from www.nrcresearchpress.com by 109.225.110.28 on 09/08/12
For personal use only.

for CCl_3CN (3). These ligands all contain electron-attracting atoms, which decrease the donor properties of the molecule.

The IR spectra of the synthesized compounds Pt(DMSO)(RCN)Cl_2, where R = an alkyl group, were compared to that of *cis*-Pt(DMSO)(CH_3CN)Cl_2. The approximate skeleton symmetry of the complexes PtL_2X_2 is C_{2v} for the *cis* isomer and D_{2h} for the *trans* isomer. From group theory, two ν(Pt—Cl) vibrations are expected for *cis* isomers and only one for *trans* compounds (15). The IR spectrum of all the compounds showed two ν(Pt—Cl) bands between 310 and 348 cm^{-1}. We suggest, therefore, that the compounds Pt(DMSO)(RCN)Cl_2 are *cis* isomers like *cis*-Pt(DMSO)(CH_3CN)Cl_2, which also showed two ν(Pt—Cl) vibrations (1).

The formation of *cis* isomers might seem surprising because of the large *trans* effect of DMSO. The multiple nature of the Pt—S bond is probably an important factor. Besides the σ bond (S → Pt), there is a back-donation of electrons into a vacant $d\pi$-type orbital of the ligand (Pt → S). This π bond could be partially responsible for the large *trans* effect of DMSO, which is almost as large as that of C_2H_4 (16). The complexes Pt(DMSO)$_2Cl_2$ and Pt(CH_3CN)$_2Cl_2$ that are obtained in aqueous solution are also *cis* isomers (17, 18). For DMSO, it is now known that the first compound formed is *trans*-Pt(DMSO)$_2Cl_2$, which rapidly isomerizes to the *cis* compound. It was suggested that the enhanced $\pi(d$–$d)$ bonding is more efficient in the *cis* isomer than in the *trans* compound (19). Similarly, the reaction of K[Pt(DMSO)Cl_3] with the nitrile ligand could first produce the *trans* isomer, which would then isomerize to the more stable *cis* compound. For the compound *cis*-Pt(CH_3CN)$_2Cl_2$, the formation of a *cis* isomer can be explained by the same reasoning, but the nature of the π bond between platinum and CH_3CN is slightly different. The back-donation is made into a π^* molecular orbital of CH_3CN since N cannot use its high-energy *d* orbitals. Similarly, the formation of π bonds in the Pt—N and Pt—S bonds in Pt(DMSO)(RCN)Cl_2 would be more efficient in the *cis* configuration. We therefore suggest that the aqueous reaction of K[Pt(DMSO)Cl_3] with nitriles first produces the *trans* isomer, which then isomerizes to the *cis* compound. We intend to verify this hypothesis in the near future by changing the two ligands to more crowded ones, such as diphenyl sulfoxide and trimethylacetonitrile. With these ligands, the isomerization should be much slower and it should be possible to isolate the *trans* isomers. In a preliminary work, we studied the reaction of K[Pt(Ph_2SO)Cl_3] with CH_3CN. The ^{195}Pt NMR spectrum of the product showed the presence of several different Pt compounds, which have not yet all been identified. This project is being continued.

Some of the nitrile ligands show two bands in the infrared region at ~2250 cm^{-1}. There is a stretching vibration ν(C≡N) and a combination band $\partial(CH_3) + \partial$(C—C). These bands are observed for free CH_3CN at 2254 and 2290 cm^{-1}, respectively (20). Coordination of nitriles through the lone pair of electrons on the N atom increases the ν(C≡N) frequency because of kinematic coupling (with ν(Pt—N)) and the increased ionic character of the C—N bond (18). The ν(C≡N) vibrations in the complexes Pt(DMSO)(RCN)Cl_2 were observed around 2310 cm^{-1}, an increase in energy of about 55 cm^{-1}.

The ν(S=O) band in DMSO is observed at 1055 cm^{-1}. Upon coordination, the vibration is expected at higher energy since the binding site is the S atom. In K[Pt(DMSO)Cl_3], the band is observed at 1101 cm^{-1} while in the complexes *cis*-Pt(DMSO)(RCN)Cl_2 the vibration absorbs around 1150 cm^{-1}.

The ^{195}Pt NMR spectra of the four complexes *cis*-Pt(RCN)(DMSO)Cl_2, with R = CH_3, C_2H_5, *n*-C_3H_7, and $C(CH_3)_3$ measured in DMF, show signals at −3010, −3006, −2999, and −3010 ppm, respectively. These values are close to those reported for *cis*-Pt(DMSO)(RCN)Cl_2 where R = PhCN (−2994 ppm) and $PhCH_2CN$ (−3007 ppm) (14). The inductive repulsive effect follows the order $C(CH_3)_3$ > C_3H_7CN > C_2H_5CN > CH_3CN. The σ donating bond (N → Pt) bond should be stronger when R increases. We have observed that all complexes have almost the same chemical shifts (−3010 to −2999 ppm). The presence of π bonds in Pt–DMSO and Pt–NC-R complexes should not be neglected, but it is difficult to predict how the chemical shift will vary as R increases. An increase in the multiple nature of the Pt—N bond would decrease the electron density on Pt and therefore would produce a chemical shift towards lower field. The ^{195}Pt NMR spectrum of the compound *cis*-Pt(DMSO)(C_2H_5CN)Cl_2 was also measured in acetone-d_6. The resonance was observed at −2997 ppm, very close to the value (−3006 ppm) measured in DMF.

The ^{195}Pt NMR spectra of fresh DMF solutions of the complexes showed only one resonance, confirming the purity of the compounds. This is different from the synthesis of *cis*-Pt(DMSO)($PhCH_2CN$)Cl_2, which contained about 10% of an impurity assigned by the authors to the *trans* isomer (14). We believed that the signal observed at −2965 ppm in DMF might be caused by the presence of the starting material K[Pt(DMSO)Cl_3], which we observed at −2968 ppm in the same solvent. After about 1 h in DMF solution, the *cis*-Pt(DMSO)(RCN)Cl_2 compounds were shown to decompose slowly. A new peak was observed in the ^{195}Pt NMR spectrum at −2876 ppm. This signal is believed to be caused by the presence of Pt(DMSO)(DMF)Cl_2 as suggested for the decomposition of Pt(DMSO)($PhCH_2CN$)Cl_2 in DMF where the DMF species was observed at −2872 ppm (14).

The high-field ^{1}H NMR spectra were measured. The coupling constants $^3J(^{195}Pt$–$^1H)$ of DMSO and $^3J(^1H$–$^1H)$ were calculated when possible. These values are ~20 Hz and ~7 Hz respectively. The protons located on the carbon atom in the α position are more affected upon coordination than are the other protons. From the literature, the signals of the protons in DMSO in *cis*-Pt(CH_3CN)(DMSO)Cl_2 were observed at 3.41 ppm in acetonitrile-d_3 with a coupling constant ^3J(Pt–H) of 22.8 Hz (21). In our study, this resonance was observed around 3.50 ppm in DMF or acetone, with coupling constants between 18 and 22 Hz. A deshielding of about 0.9 ppm was observed for these protons upon coordination to platinum (pure DMSO, δ = 2.60 ppm).

Cl(DMSO) Pt(μ-RCONH)$_2$Pt(DMSO)Cl

The reaction of K[Pt(DMSO)Cl_3] in neutral solution (pH adjusted to ~7 with NaOH) with all the nitriles (R = alkyl or haloalkyl group) produced an acetamido-bridged dimer, similar to the reaction with CH_3CN, where in the same conditions Cl(DMSO)Pt(μ-$CH_3CONH)_2$Pt(DMSO)Cl was isolated and characterized by X-ray diffraction (1). We also determined the crystal structures of the compounds obtained with dimethylacetonitrile and trimethylacetonitrile. These results are discussed later in this publication.

$$K[(DMSO)Cl_3] + RCN \xrightarrow{pH\sim7} Cl(DMSO)Pt(\mu\text{-}RCONH)_2Pt(DMSO)Cl$$

Can. J. Chem. Downloaded from www.nrcresearchpress.com by 109.225.110.28 on 09/08/12
For personal use only.

The same compound was isolated without adjusting the pH (pH ~ 2.4) with the halonitriles, i.e., fluoroacetonitrile, bromoacetonitrile, chloroacetonitrile, and dibromoacetonitrile. These ligands do not form the compound *cis*-Pt(DMSO)(nitrile)Cl_2, as already mentioned. The formation of dimers with the halonitriles is faster at neutral pH than in acidic solution.

In organic chemistry, nitriles are known to hydrolyze but their conversion into amido ions usually requires acidic or basic conditions (22). In the presence of platinum, the reaction can be activated without the presence of acids or bases. The reaction is favored at neutral pH. With the ligands R-C≡N where R is an alkyl group, the hydrolysis reaction is quite slow in acidic medium (pH ~ 2.4) and *cis*-Pt(DMSO)(nitrile)Cl_2 is rapidly formed. This product is very insoluble and will precipitate immediately. If the mixture is not filtered and is left to stand at room temperature, acetamido-bridged dimers can be isolated after 1–2 months. In neutral solution, the dimers are formed more rapidly. For the nitrile ligands R-C≡N where R is a haloalkyl group like FCH_2CN, $ClCH_2CN$, $BrCH_2CN$, or Br_2CHCN, the compound *cis*-Pt(DMSO)(nitrile)Cl_2 is not stable and the dimer is isolated in acid or neutral solution, but the reaction is faster at neutral pH. Furthermore, for the halonitriles, the fastest reaction was with fluoroacetonitrile. The large electronegativity of fluorine drastically weakens the Pt—N (nitrile) bond, and the nitrile compound is the least stable. The hydrolysis of nitriles in the coordination sphere of metal ions has been known for several decades. It was first shown in 1967 that hydrolysis of 2-cyano-1,10-phenanthroline to the corresponding amide is strongly promoted by metal ions such as Cu^{2+}, Ni^{2+}, and Zn^{2+} (23). The rate acceleration was attributed to an entropy effect. A number of subsequent studies were reported and rate enhancements of 2×10^6 were observed in these reactions (24), including a report on hydration of nitriles to carboxamides catalyzed by platinum (25).

The structural analyses of Cl(DMSO)Pt(μ-C_2H_4NO)Pt(DMSO)Cl (1) and the two dimers described later show that the compounds are head-to-tail isomers, with the DMSO molecules in *trans* position to the *O*-acetamido atoms. The ^{195}Pt NMR signals of the synthesized compounds were observed between −2723 and −2773 ppm in DMF, very close to the value observed for the head-to-tail isomer obtained from CH_3CN (−2753 ppm in DMF). We suggest therefore that all the dimers synthesized in this project have the same configuration. The ^{195}Pt NMR spectrum of a head-to-head isomer would show two different signals of equal intensity around −2600 ppm for a Pt environment S Cl O O and around −3130 ppm for an environment S Cl N N similar to *cis* and *trans*-Pt(DMSO)$(NH_3)_2$Cl (δ = −3147 and −3126 ppm) (26). No ^{195}Pt NMR spectrum has yet been reported for this type of compound, but our values are close to that (δ = −2747 ppm) reported for Pt(DMSO)Cl($NH_2CH_2CO_2$) (26), which contains the same four donor atoms.

For the halonitriles, the chemical shifts follow the order of electronegativity of the halides. The observed values for the ligands FCH_2CN, $ClCH_2CN$, $BrCH_2CN$, and Br_2CHCN are −2723, −2750, −2762, and −2773 ppm, respectively, and the shielding increases with increase of the donor properties Br > Cl > F, covering a region of 50 ppm. For the ligands that do not contain any halogens, the δ(Pt) are constant (−2753, −2763, −2752, and −2756 ppm) for the complexes containing the hydrolyzed ligands of CH_3CN, C_2H_5CN, *n*-C_3H_7CN, and $C(CH_3)CN$, respectively. It was not possible to measure the ^{195}Pt NMR spectrum of the dimer with $CH(CH_3)_2CN$. The product obtained was deeply colored (green) and probably contains a small quantity of paramagnetic species. Nevertheless, a structure determination of one of the crystals showed it to be a head-to-tail acetamido-bridged dimer as described later in the text.

Fresh solutions of all the compounds except the product from trimethylacetonitrile (which showed a small signal at −2928 ppm) have shown only one resonance in ^{195}Pt NMR. But on standing in DMF, all the compounds decompose slowly. Figure 1 shows the ^{195}Pt spectrum of the dimer prepared with the ligand chloroacetonitrile at pH ~ 7, after 1 week in DMF. Nine peaks are observed. The signals at −2995, −2967, and at −2750 ppm can be assigned to *cis*-Pt(DMSO)(RCN)Cl_2 (~1%), $[Pt(DMSO)Cl_3]^-$ (~4%), and to the head-to-tail dimer Cl(DMSO)Pt(μ-$CH_2ClCNO)_2$Pt(DMSO)Cl (~18%), respectively. The other peaks observed at lower field (−2440, ~7%; −2426, ~7%; −2370, ~24%; −2312, ~2%; −2018, ~16%; and −1940 ppm, ~21%) are assigned to decomposed products containing DMF as ligand. DMF is a good O-donor ligand for platinum, producing species that would appear at lower field than species containing S- or N-donor ligands. These species have not yet been identified and the project is being continued.

The ^{1}H NMR spectra of these compounds have been measured and are listed in the experimental section. As ex-

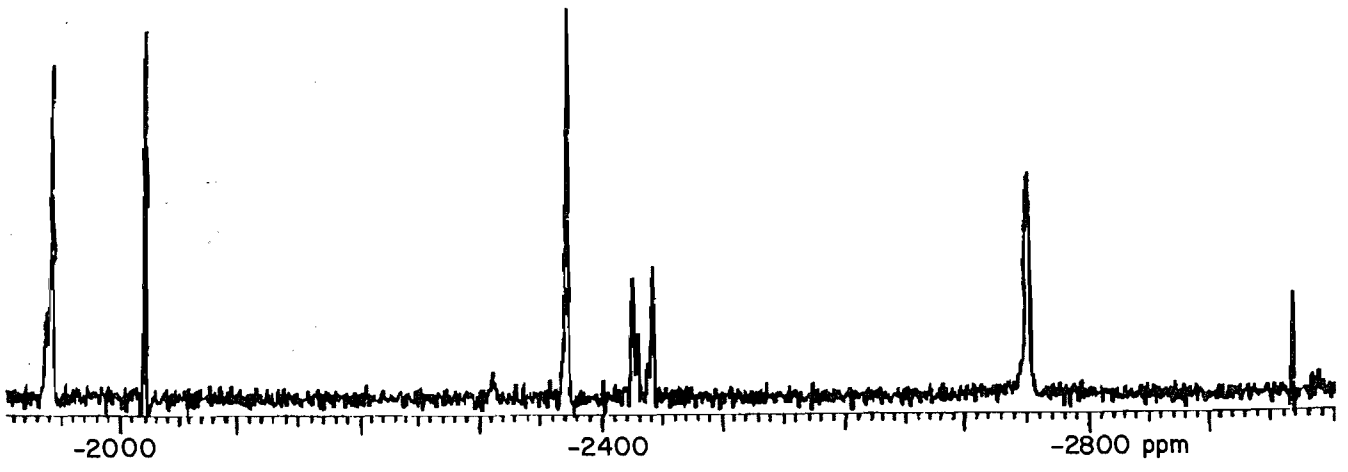

FIG. 1. ^{195}Pt NMR spectrum of Cl(DMSO)Pt(μ-$C_2H_3ClNO)_2$Pt(DMSO)Cl after 1 week in DMF.

Can. J. Chem. Downloaded from www.nrcresearchpress.com by 109.225.110.28 on 09/08/12
For personal use only.

TABLE 2. Positional parameters with their esd's and temperature factors ($\times 10^3$ except Pt, Cl, S: $\times 10^4$). $U_{eq} = 1/3\ \Sigma_i\Sigma_j U_{ij} a_i^* a_j^* a_i \cdot a_j$

Atom	x	y	z	U_{eq}
Cl(DMSO)Pt(μ-$C_4H_8NO)_2$Pt(DMSO)Cl (**1**)				
Pt(1)	719(1)	4133.7(6)	2000	555(4)
Pt(2)	2521(1)	3284.5(6)	636(2)	550(4)
Cl(1)	−1102(10)	3581(4)	1774(11)	893(26)
Cl(2)	2857(9)	3835(5)	−1297(11)	819(26)
S(1)	134(9)	4817(4)	490(10)	592(24)
S(2)	1494(8)	2554(5)	−478(10)	579(24)
O(1)	129(2)	353(1)	353(2)	85(3)
O(2)	363(2)	387(1)	147(2)	79(3)
O(3)	−21(2)	457(1)	−72(2)	67(3)
O(4)	224(2)	217(1)	−143(2)	74(3)
N(1)	218(2)	457(1)	234(2)	60(3)
N(2)	238(2)	285(1)	236(2)	56(3)
C(1)	337(3)	445(2)	206(3)	72(3)
C(2)	194(3)	301(2)	344(3)	67(3)
C(3)	212(3)	272(1)	471(3)	85(3)
C(4)	323(3)	283(2)	598(4)	156(3)
C(5)	182(4)	199(2)	458(4)	177(3)
C(6)	438(3)	487(2)	254(4)	67(3)
C(7)	549(3)	442(2)	280(4)	141(3)
C(8)	462(4)	539(2)	153(4)	164(3)
C(9)	29(3)	285(1)	−128(3)	77(3)
C(10)	91(3)	206(2)	63(3)	99(3)
C(11)	126(3)	546(2)	9(3)	110(3)
C(12)	−106(3)	533(2)	114(3)	90(3)
Cl(DMSO)Pt(μ-$C_5H_{10}NO)_2$Pt(DMSO)Cl (**2**)				
Pt(1)	4171(1)	9142.9(5)	8000	329(3)
Pt(2)	2389(1)	8270.8(5)	6833(2)	317(3)
Cl(1)	5876(7)	8551(4)	7827(11)	612(22)
Cl(2)	2004(8)	8811(5)	4956(10)	659(24)
S(1)	4748(8)	9780(4)	6466(9)	494(22)
S(2)	3338(7)	7520(5)	5785(8)	381(19)
O(1)	369(2)	858(1)	949(2)	50(3)
O(2)	131(1)	890(1)	766(2)	33(3)
O(3)	515(2)	943(1)	536(2)	90(3)
O(4)	270(2)	712(1)	485(2)	69(3)
N(1)	275(2)	967(1)	831(2)	45(3)
N(2)	261(2)	783(1)	854(2)	39(3)
C(1)	169(3)	951(1)	827(3)	56(3)
C(2)	312(2)	804(1)	953(3)	36(3)
C(3)	298(2)	771(1)	1077(3)	38(3)
C(4)	216(3)	815(2)	1158(3)	101(3)
C(5)	232(3)	704(2)	1069(3)	86(3)
C(6)	71(2)	994(1)	874(3)	50(3)
C(7)	413(3)	768(2)	1143(3)	103(3)
C(8)	−40(2)	958(1)	867(3)	60(3)
C(9)	66(2)	1058(1)	789(3)	60(3)
C(10)	104(3)	1017(2)	1013(3)	71(3)
C(11)	591(2)	1031(2)	703(3)	76(3)
C(12)	377(3)	1046(2)	601(3)	87(3)
C(13)	405(2)	700(1)	672(3)	56(3)
C(14)	458(2)	785(2)	500(3)	54(3)

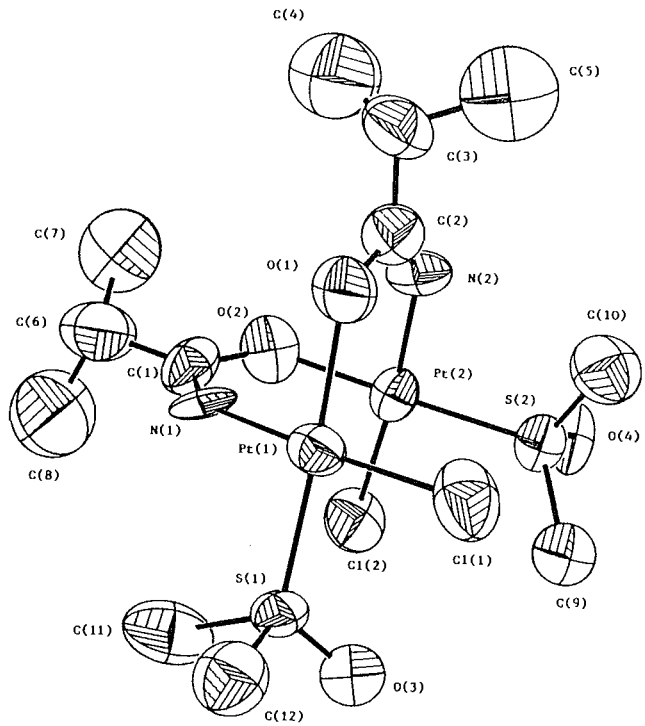

FIG. 2. Labeled diagram of Cl(DMSO)Pt(μ-$C_4H_8NO)_2$Pt-(DMSO)Cl (**1**).

pected, the protons located on a carbon atom in the α position of the acetamido ligands are the most affected upon coordination ($\Delta\delta \approx 0.6$ ppm). The protons in the β position are less deshielded ($\Delta\delta = 0.1$–0.2 ppm), while those in the γ position are not affected. All the dimeric species have shown two signals around 3.6 ppm for the protons of the DMSO ligands, indicating different environments for the two methyl groups, which differs from the compounds *cis*-Pt(DMSO)(nitrile)Cl_2 and $[Pt(DMSO)Cl_3]^-$ where only one signal was observed. Nevertheless, no $^3J(^{195}Pt-^1H)$ coupling was observed for the dimers, contrary to the two above monomers. The signal of the amide proton was observed around 7 ppm. Because of its width and its low intensity, it was not possible to observe a coupling with ^{195}Pt. The coupling constant $^2J(^{19}F-^1H)$ for the complex obtained from FCH_2CN is 46 Hz and agrees with similar reported values (44–81 Hz) (27).

The IR spectra of the dimers showed the absence of vibrations in the ν(C≡N) region, around 2300 cm^{-1}. One or two new bands around 1600 cm^{-1} were observed. These were assigned to the amido groups ν(C=O) and ∂(N—H). These complexes all show only one ν(Pt—Cl) band between 332 and 350 cm^{-1}. The ν(S—O) vibrations were observed between 1140 and 1156 cm^{-1}. An increase in the frequency of the vibration (S=O) of 85 cm^{-1} upon coordination confirmed that the binding site is the S atom. These values are close to those observed for the compounds *cis*-Pt(DMSO)(nitrile)Cl_2.

Most of the dimeric complexes obtained after adjusting the pH (~7) are green or blue. The same dimers obtained without adjusting the pH are usually yellow. The color is probably caused by the presence of a small quantity of a blue amorphous compound, not only on the surface (since it cannot be washed out) as suggested for the acetamido-bridged compound (1). The blue complex is believed to be an analogue of platinblau, which is probably an acetamido-bridged oligomer. A few research groups, especially those of Lippard and Lippert, have prepared several blue complexes with α-pyridone, uracil, and thymine derivatives (28–30). Several platinum blues were characterized crystallographically. These were found to be multinuclear species containing Pt in a fractional oxidation state (>2) with bridging α-pyridonate, uracilate, or thyminato ligands. It was suggested that the blue

Can. J. Chem. Downloaded from www.nrcresearchpress.com by 109.225.110.28 on 09/08/12
For personal use only.

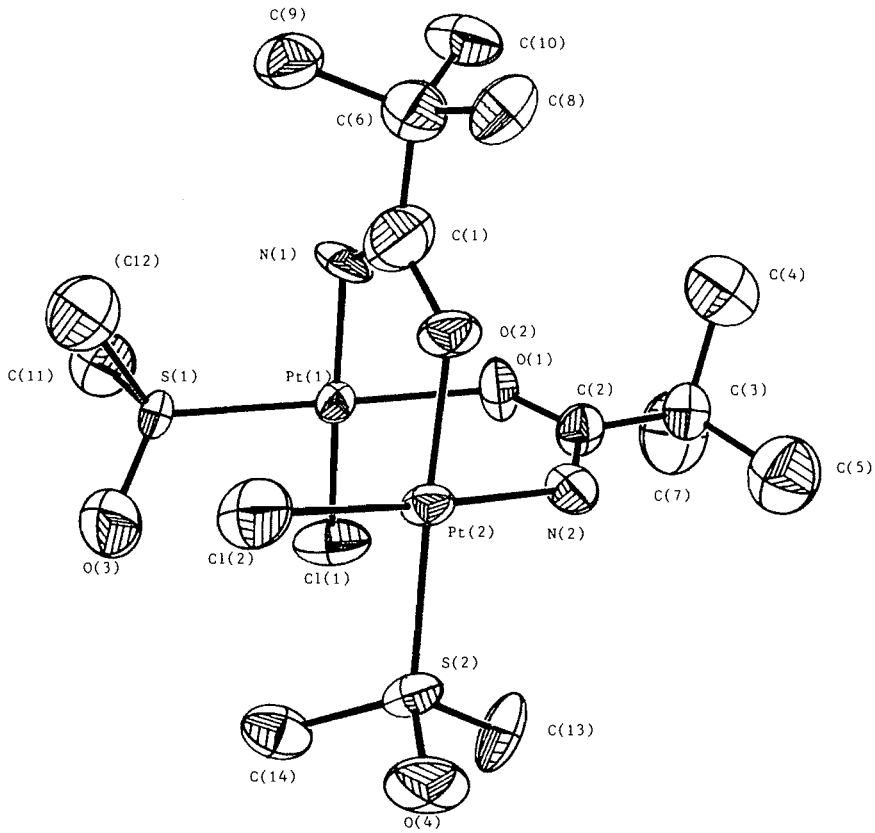

FIG. 3. Labeled diagram of Cl(DMSO)Pt(μ-$C_5H_{10}NO)_2$Pt(DMSO)Cl (**2**).

TABLE 3. Bond distances (Å) and angles (deg)

	1	**2**		**1**	**2**
Pt(1)—Cl(1)	2.328(10)	2.317(9)	Pt(2)—Cl(2)	2.293(10)	2.317(10)
Pt(1)—S(1)	2.173(10)	2.180(9)	Pt(2)—S(2)	2.193(10)	2.176(9)
Pt(1)—N(1)	1.88(2)	1.99(2)	Pt(2)—N(2)	1.97(2)	2.03(2)
Pt(1)—O(1)	2.08(2)	2.03(2)	Pt(2)—O(2)	1.91(2)	1.99(2)
S(1)—O(3)	1.39(2)	1.44(3)	S(2)—O(4)	1.49(2)	1.48(2)
S(1)—C(avg)	1.83(3)	1.83(3)	S(2)—C(avg)	1.67(3)	1.74(3)
O(1)—C(2)	1.28(4)	1.27(3)	O(2)—C(1)	1.36(4)	1.34(3)
N(1)—C(1)	1.38(4)	1.27(4)	N(2)—C(2)	1.25(4)	1.28(4)
C(1)—C(6)	1.49(5)	1.52(4)	C(2)—C(3)	1.44(5)	1.49(4)
C—C terminal avg	1.48(5)	1.54(4)	Pt(1)---Pt(2)	2.989(2)	2.983(2)
Cl(1)—Pt(1)—S(1)	88.9(4)	88.8(4)	Cl(2)—Pt(2)—S(2)	88.6(4)	88.9(4)
Cl(1)—Pt(1)—O(1)	92.8(7)	90.5(6)	Cl(2)—Pt(2)—O(2)	88.2(8)	87.7(6)
Cl(1)—Pt(1)—N(1)	175.0(8)	174.7(7)	Cl(2)—Pt(2)—N(2)	174.3(7)	175.4(6)
S(1)—Pt(1)—O(1)	176.6(7)	176.9(6)	S(2)—Pt(2)—O(2)	171.2(8)	171.3(6)
S(1)—Pt(1)—N(1)	94.8(8)	94.0(8)	S(2)—Pt(2)—N(2)	96.5(7)	95.2(7)
O(1)—Pt(1)—N(1)	83.3(10)	86.5(9)	O(2)—Pt(2)—N(2)	86.4(10)	87.9(8)
Pt(1)—S(1)—O(3)	118(1)	115(1)	Pt(2)—S(2)—O(4)	114(1)	118(1)
Pt(1)—S(1)—C avg	112(1)	113(1)	Pt(2)—S(2)—C avg	110(1)	113(1)
O(3)—S(1)—C avg	107(1)	109(1)	O(4)—S(2)—C avg	109(1)	107(1)
C—S(1)—C	99(1)	96(1)	C—S(2)—C	104(2)	96(1)
Pt(1)—O(1)—C(2)	127(2)	130(2)	Pt(2)—O(2)—C(1)	128(2)	123(2)
Pt(1)—N(1)—C(1)	135(2)	131(2)	Pt(2)—N(2)—C(2)	134(2)	130(2)
O(1)—C(2)—C(3)	111(3)	118(2)	O(2)—C(1)—C(6)	119(3)	114(2)
N(1)—C(1)—C(6)	124(3)	125(2)	N(2)—C(2)—C(3)	129(3)	122(2)
O(1)—C(2)—N(2)	120(3)	120(2)	O(2)—C(1)—N(1)	116(3)	122(2)
C—C—C avg	110(3)	109(2)			

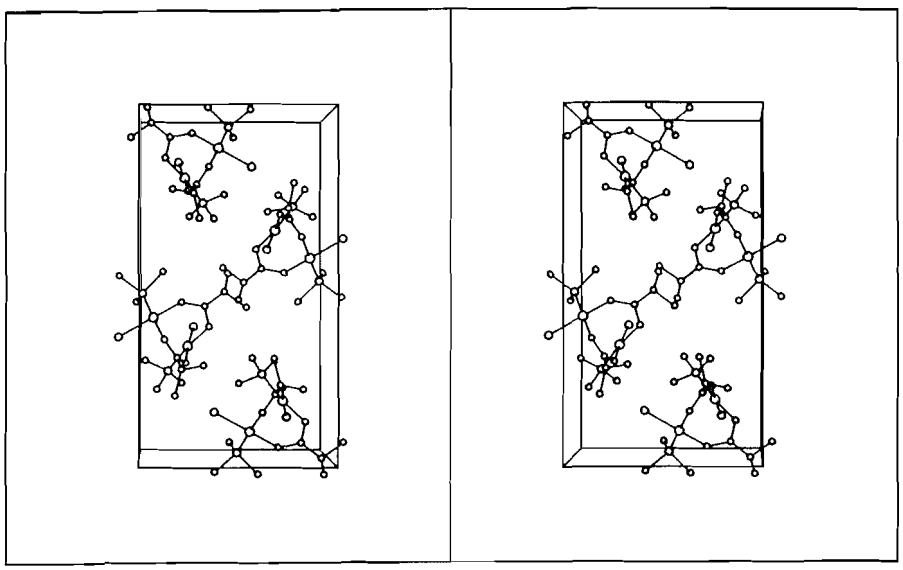

FIG. 4. Stereoscopic view of the unit cell in the crystal Cl(DMSO)Pt(μ-$C_3H_8NO)_2$Pt(DMSO)Cl (**1**) (*b* axis vertical, *a* axis horizontal).

color results from metal–metal charge transfer transitions (29, 30).

*Crystal structures of Cl(DMSO)Pt(μ-$C_3H_8NO)_2$Pt-(DMSO)Cl (**1**) and Cl(DMSO)Pt(μ-$C_5H_{10}NO)_2$Pt-(DMSO)Cl (**2**)*

The dimers obtained with dimethylacetonitrile and trimethylacetonitrile gave crystals suitable for diffraction methods. The two analyzed crystals are isostructural. The refined atomic parameters are shown in Table 2. The structures of the two compounds are similar to that of the acetamido-bridged dimer synthesized from CH_3CN. Labeled diagrams of the two molecules are shown in Figs. 2 and 3. The bond distances and angles are reported in Table 3. The two compounds are acetamido-bridged dimers with a head-to-tail configuration. The DMSO ligands, which are S-bonded to Pt, are in *trans* position to the acetamido oxygen atoms. The relatively short Pt···Pt distances (2.989(2) Å for **1** and 2.983(2) Å for **2**) are produced by the geometric requirements imposed by the two bridging ligands.

The coordination around each platinum atom is square-planar, but there are some slight square-pyramidal distortions. For each crystal, the Pt atoms are out of the plane formed by the four coordinating atoms by −0.056 and −0.096 Å in crystal **1** and by −0.068 and 0.092 Å in crystal **2**. The tilt angles between the two Pt planes are 36° (**1**) and 35° (**2**).

The Pt—Cl bonds (2.328(10), 2.293(10) Å for **1** and 2.317(9), 2.317(10) Å for **2**) are normal. The Pt—S bonds (2.173(10)–2.193(10) Å) are slightly shorter than the average value (2.21 Å) reported for Pt–DMSO complexes (17, 32), but similar to those reported for Cl(DMSO)Pt(μ-$C_2H_4NO)_2$Pt(DMSO)Cl (2.185(2) and 2.198(2) Å) (1). The results on these dimers are different from those observed in α-pyridonate-bridged platinum complexes where the Pt—N (ammine or ethylenediamine) distances *trans* to pyridonate oxygen atoms were significantly longer than those *trans* to pyridonate nitrogen atoms, revealing a larger *trans* influence of the O atom. Lippard and co-workers suggested that this *trans* influence originated in more extensive σ-overlap of the Pt—N (pyridonate) bond relative to the Pt—O (amidate) bond (29, 31). For our compounds, the Pt—S bonds that are located in *trans* position to the Pt—O (acetamido) bonds are slightly shorter than normal, probably indicating a greater π-character of the Pt—S bond. The S atoms in the DMSO ligands are in an approximate tetrahedral environment.

The Pt—O (1.91(2)–2.08(2) Å) and Pt—N (1.88(2)–2.03(2) Å) bonds seem normal and agree well with values found in ref. 1 and in the pyridonate and uracilate complexes mentioned above. The bond lengths and angles in the two bridging acetamido ligands are also normal. The N—C bond distances are 1.25(4)–1.38(4) Å while the O—C bond lengths are 1.27(4)–1.36(4) Å. The angles around C(1) and C(2) are in the range 111(2)–129(2)°, indicating a sp^2 hybrid. The internal angles at N(1), N(2), O(1), and O(2) are similar, varying from 123(2)° to 135(2)°. The moieties N—C(C)—O are planar with the two amido planes almost perpendicular to each other. The thermal factors of the methyl groups are quite high, resulting in high standard deviations. The torsion angles have been calculated and the table is part of the supplementary material (see footnote 2).

The packing of the molecules for crystal **1** is shown in Fig. 4. The environment of the acetamide N atoms was closely examined for the presence of hydrogen bonds. There might be such an intermolecular interaction with N(2)···Cl(1) distance = 3.39(1) Å and angles Pt(2)—N(2)···Cl(1) = 102(1)° and C(2)—N(1)···Cl(1) = 123(2)°. The closest such contact around N(1) is O(3) with a distance of 3.38(2) Å (**1**). Therefore hydrogen bonding does not seem a very important stabilizing factor in these crystal structures.

Acknowledgment

The authors are grateful to the Natural Sciences and Engineering Research Council of Canada for financial support of the project.

1. F. D. Rochon, P. C. Kong, and R. Melanson. Inorg. Chem. **29**, 1352 (1990).

Can. J. Chem. Downloaded from www.nrcresearchpress.com by 109.225.110.28 on 09/08/12
For personal use only.

2. V. K. Belsky, V. E. Konovalov, V. K. Kukushkin, and A. I. Moiseev. Inorg. Chim. Acta, **169**, 101 (1990).
3. F. D. Rochon, P. C. Kong, and R. Melanson. Inorg. Chem. **29**, 2708 (1990).
4. K. A. Hoffman and G. Bugge. Ber. **40**, 1772 (1907); Ber. **41**, 312 (1908).
5. I. I. Chernyaev and L. A. Nazarova. Izv. Sekt. Platiny Drugikh Blagorodn. Met. Inst. Obshch. Neorg. Khim. Akad. Nauk SSSR, **26**, 101 (1951); V. F. Barkovskii and L. M. Kul'berg. Izv. Sekt. Platiny Drugikh Blagorodn. Met. Inst. Obshch. Neorg. Khim. Akad. Nauk SSSR, **28**, 235 (1954).
6. R. D. Gillard and G. Wilkinson. J. Chem. Soc. 2835 (1964).
7. D. B. Brown, R. D. Burbank, and M. B. Robin. J. Am. Chem. Soc. **91**, 2895 (1969).
8. Y. N. Kukushkin, Y. E. Vyazmenskii, and L. I. Zorina. Russ. J. Inorg. Chem. **13**, 1573 (1968).
9. S. J. S. Kerrison and P. J. Sadler. Inorg. Chim. Acta, **104**, 197 (1985).
10. R. Melanson and F. D. Rochon. Can. J. Chem. **53**, 2371 (1975).
11. D. T. Cromer. Acta Crystallogr. **18**, 17 (1965).
12. P. Coppens and W. C. Hamilton. Acta Crystallogr. Sect. A: Cryst. Phys. Diffr. Theor. Gen. Crystallogr. **A26**, 71 (1970).
13. D. T. Cromer and J. T. Waber. Acta Crystallogr. **18**, 104 (1965).
14. V. Yu. Kukushkin, V. K. Belsky, V. E. Konovalov, G. A. Kirakosyan, L. V. Konovalov, A. I. Moiseev, and V. M. Tkachuk. Inorg. Chim. Acta, **185**, 143 (1991).
15. K. Nakamato. Infrared spectra of inorganic and coordination compounds. 2nd ed. John Wiley & Sons, New York. 1970.
16. Yu. N. Kukuskin. Inorg. Chim. Acta, **9**, 117 (1974).
17. R. Melanson and F. D. Rochon. Can. J. Chem. **53**, 2371 (1975).
18. F. D. Rochon, R. Melanson, H. E. Howard-Lock, C. J. L. Lock, and G. Turner. Can. J. Chem. **62**, 860 (1984).
19. J. H. Price, A. N. Williamson, R. F. Schramm, and B. B. Wayland. Inorg. Chem. **11**, 1280 (1972).
20. P. Venkatesuvarlu. J. Chem. Phys. **19**, 293 (1951).
21. Yu. N. Kukuskin, V. Igor, and G. Zenkevich. Inorg. Chim. Acta, **166**, 79 (1989).
22. K. Peter and C. Vollhardt. Organic chemistry. W. H. Freeman, New York. 1987.
23. R. Breslow, R. Fairther, and J. Keana. J. Am. Chem. Soc. **89**, 2135 (1967).
24. C. R. Clark and R. W. Hay. J. Chem. Soc. Dalton Trans. 2148 (1974).
25. M. A. Bennett and T. Yoshida. J. Am. Chem. Soc. **95**, 3030 (1973).
26. S. J. S. Kerrison and P. J. Sadler. J. Chem. Soc. Chem. Commun. 861 (1977).
27. D. L. Pavia, G. M. Lampman, and G. S. Kriz. Introduction to spectroscopy. W. B. Saunders Company, Philadelphia. 1979. p. 170.
28. J. K. Barton, H. N. Rabinowitz, D. J. Szalda, and S. J. Lippard. J. Am. Chem. Soc. **99**, 2827 (1977).
29. T. V. O'Halloran, P. K. Mascharak, I. D. Willams, M. M. Roberts, and S. J. Lippard. Inorg. Chem. **26**, 1261 (1987).
30. B. Lippert. Prog. Inorg. Chem. **37**, 1 (1989).
31. A. P. Ginsberg, T. V. O'Halloran, P. Fanwick, L. S. Hollis, and S. J. Lippard. J. Am. Chem. Soc. **106**, 5430 (1984).
32. (*a*) L. I. Elding and A. Oskarsson. Inorg. Chim. Acta, **130**, 209 (1987); (*b*) R. Melanson, J. Hubert, and F. D. Rochon. Acta Crystallogr. Sect. B: Struct. Crystallogr. Cryst. Chem. **B32**, 1914 (1976); (*c*) F. D. Rochon, P. C. Kong, and R. Melanson. Acta Crystallogr. Sect. C: Cryst. Struct. Commun. **C41**, 1602 (1985); (*d*) R. Melanson and F. D. Rochon. Inorg. Chem. **17**, 679 (1978); (*e*) R. Melanson and F. D. Rochon. Acta Crystallogr. Sect. B: Struct. Crystallogr. Cryst. Chem. **B33**, 3571 (1978); **B34**, 1125 (1978); **B34**, 941 (1978); Sect. C: Cryst. Struct. Commun. **C40**, 793 (1984).

Can. J. Chem. Downloaded from www.nrcresearchpress.com by 109.225.110.28 on 09/08/12
For personal use only.

Electrode-mediated Wacker oxidation of cyclic and internal olefins[1]

D. G. MILLER[2] AND D. D. M. WAYNER[3]

Steacie Institute for Molecular Sciences, National Research Council of Canada, Ottawa, Ont., Canada K1A 0R6

Received February 18, 1992

D. G. MILLER and D. D. M. WAYNER. Can. J. Chem. **70**, 2485 (1992).

An improved method for the electrode-mediated oxidations of olefins by palladium(II) is described. Current efficiencies from 80% to 95% were obtained in oxidations of 1-decene, styrene, *trans*-2-octene, and cyclohexene in which perchloric acid was added to a chloride-free solution of a palladium(II) acetate catalyst. The palladium(0) was reoxidized to palladium(II) by reaction with catalytic amounts of benzoquinone, which was, in turn, regenerated by anodic oxidation. Addition of varying amounts of perchloric acid did not affect the current efficiency but accelerated the oxidation reaction, up to a concentration of approximately 0.15 M. The current efficiency remained high (>80%) over the course of the electrode-mediated oxidations of 1-decene, *trans*-2-octene, and cyclohexene. At the end of the reactions, when the substrate was depleted, a drastic decrease in the current was observed, indicating that the catalytic cycle leading to product was primarily responsible for the electrochemical reaction. It also was shown that the rates of the electrochemical reactions were generally slower than those of homogeneous reactions in which a stoichiometric amount of benzoquinone was used, indicating that the electrochemical regeneration of benzoquinone was mass transport limited at the highest concentrations of perchloric acid. This is in contrast to other reports in the literature that suggested that the homogeneous (non-electrochemical) reactions were actually slower. Reasons for the discrepancy between these results are discussed.

D. G. MILLER et D. D. M. WAYNER. Can. J. Chem. **70**, 2485 (1992).

On décrit une méthode améliorée d'oxydation des oléfines par le palladium(II), assistée par une électrode. On a obtenu des efficacités de courant allant de 80 à 95% lors d'oxydations du déc-1-ène, du styrène, du *trans*-oct-2-ène et du cyclohexène au cours desquelles on avait ajouté de l'acide perchlorique à une solution sans chlorure d'un catalyseur d'acétate de palladium(II). Le palladium(0) est ré-oxydé en palladium(II) par une réaction impliquant des quantités catalytiques de benzoquinone qui est, à son tour, régénéré par oxydation anodique. L'addition de quantités variables d'acide perchlorique n'affecte pas l'efficacité de courant; toutefois, la réaction d'oxydation est accélérée jusqu'à une concentration d'environ 0,15 M. Avec le déc-1-ène, le *trans*-oct-2-ene et le cyclohexène, l'efficacité du courant demeure élevée (>80%) pour l'ensemble des oxydations assistées par une électrode. À la fin de réactions, lorsqu'il ne reste plus de substrat, on observe une dramatique diminution du courant qui indique que le cycle catalytique conduisant au produit est le principal responsable de la réaction électrochimique. On a montré que la vitesse des réactions électrochimiques est généralement plus lente que les réactions homogènes dans lesquelles on utilise une quantité stoechiométrique de benzoquinone; ceci indique que, à des concentrations élevées d'acide perchlorique, la régénération électrochimique de la benzoquinone est limitée par un transport de masse. Cette situation est en opposition avec d'autres rapports parus dans la littérature qui suggéraient que les réactions homogènes (non-électrochimiques) sont de fait plus lentes. On discute des raisons pouvant expliquer ces différences.

[Traduit par la rédaction]

Introduction

The oxidation of olefins to ketones by Pd(II) salts, the Wacker oxidation (eq. [1]), is important from both an industrial and synthetic chemistry perspective. This process has been used in the industrial production of low molecular weight aldehydes and ketones (1), as well as in the selective oxidation of unsaturates in organic synthesis (2–4). The reaction itself is not catalytic in palladium so a secondary oxidation system that regenerates Pd(II) from Pd(0) is required (eq. [2]). Chemical oxidants (Ox) such as Cu(II), Fe(III), MnO_2, heteropolyacids, or quinones have been used for this purpose (4–11).

[1] $RCH{=}CH_2 + H_2O + Pd(II) \rightarrow RC(O)CH_3 + 2H^+ + Pd(0)$

[2] $Pd(0) + Ox \rightarrow Pd(II) + Red$

The commercial Wacker process originally used $CuCl_2$ to recycle the Pd(II) (eq. [3]), and molecular oxygen to regenerate Cu(II) from Cu(I) (eq. [4]). The process fell into disfavour in the 1970's as a result of corrosion problems caused by the copper chloride salts as well as the safety hazards associated with the use of high pressures of molecular oxygen. Alternative processes that are less corrosive and do not require molecular oxygen may lead to the reemergence of the Wacker oxidation as an efficient route to oxygenate production. One possibility is to replace one of the homogeneous oxidation reactions with an electrochemical reaction. Direct electro-oxidation of Pd(0) is not practical since the metal forms a mirror over the apparatus (12, 13). However, it is

[3] $Pd(0) + 2CuCl_2 \rightarrow PdCl_2 + Cu_2Cl_2$

[4] $CuCl_2 + 2HCl + 1/2O_2 \rightarrow 2CuCl_2 + H_2O$

feasible to consider using only catalytic amounts of a homogeneous chemical oxidant to recycle the palladium and to regenerate the chemical oxidant from its reduced form electrochemically (eq. [5]).

[5] $Red \xrightarrow{anode} Ox + ne^-$

Tsuji and Minato have reported the electrode-mediated oxidation of olefins using $Pd(OAc)_2$ and benzoquinone under galvanostatic conditions (10). While that study focused on the oxidation of terminal olefins, it was noted that the oxi-

[1]Issued as NRCC No. 33317.

[2]Present address: Atomic Energy of Canada Ltd., Chalk River Laboratories, Chalk River, Ont., Canada K0J 1P0.

[3]Author to whom correspondence may be addressed.

Can. J. Chem. Downloaded from www.nrcresearchpress.com by 109.225.110.28 on 09/08/12
For personal use only.

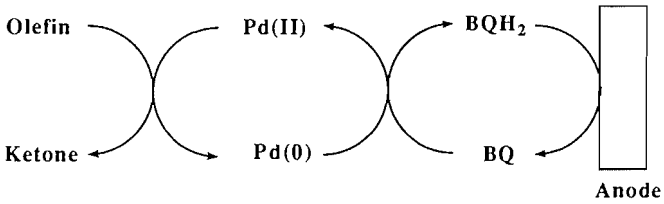

SCHEME 1

dation of cyclohexene and cyclopentene was possible even though no reaction occurred with these substrates in the absence of electrolysis. No explanation of this effect was offered.

In a similar study Horowitz (11) reported electrode-mediated olefin oxidations using $FeCl_3$ as the chemical oxidant. However, it is well known that chloride significantly inhibits the reaction (1, 6). Recent work in our laboratory (12) demonstrated that the homogeneous olefin oxidation was accelerated by as much as a factor of 40 by the addition of acid and the exclusion of chloride. Hence, we expected that improvements in the electrode-mediated oxidation process could be attained by using a completely chloride-free system in which a non-complexing (i.e., strong) acid was added.

In this paper, we have examined the controlled potential electrode-mediated oxidation of terminal, internal, and cyclic olefins, using this acid-enhanced, chloride-free method (12). Benzoquinone (BQ) has been used to reoxidize the Pd(0) (eq. [2]) since hydroquinone (BQH_2), the reduced form of benzoquinone (BQ), is easily oxidized to benzoquinone at the anode (Scheme 1). These data may have an impact on strategies for the large-scale production of cyclohexanone, an important intermediate for the production of caprolactam (one of the Nylon® monomers). In addition, Tsuji and Minato (10) reported that the palladium-catalysed oxidation of cyclic olefins was faster using electrode-mediated catalysis than it was in simple homogeneous reactions. Comparisons in this study of reaction with and without electrolysis will provide some insight into the reasons for those differences.

Results

Oxidations were carried out in solutions of acetonitrile/water (7:1v/v), containing benzoquinone (0.022 M, 20 mol% based on olefin), palladium acetate (0.0011 M, 1 mol% based on olefin), olefin (0.11 M), and perchloric acid (0.015–0.24 M). 1-Decene, styrene, *trans*-2-octene, and cyclohexene were oxidized to their corresponding ketones with current efficiencies consistently in the 75–90% range (Tables 1, 2).

The current efficiency (CE) is a measure of the fraction of the total number of moles of electrons used that result in the formation of the desired product (usually expressed as a percentage). The current efficiencies were calculated using eqs. [6]–[8].

$$[6] \quad CE = \frac{([\text{oxygenates}] - [\text{oxygenates}]_{\text{hom}}) \times 100}{[\text{oxygentates}]_{\text{theor}}}$$

where

$$[7] \quad [\text{oxygenates}]_{\text{theor}} = \frac{Q \times 100}{2FV[\text{olefin}]}$$

$$[8] \quad [\text{oxygenates}]_{\text{hom}} = \frac{[\text{Pd(II)}] + [\text{BQ}]}{[\text{olefin}]}$$

Q is the accumulated charge, V is the volume, and F is the faraday (96 487 coulombs/equiv.). The factor of 2 is necessary since the oxidation is an overall two-electron process (eqs. [1], [2], and [5]). Some of the product will form as a result of the homogeneous reaction (i.e., Pd(II) + benzoquinone) so the yield of product from the electrochemical reaction must be corrected for this contribution (eq. [8]).

High current efficiencies were obtained in electrode-mediated oxidations of 1-decene (Table 1, entries 1–3). Although the current efficiencies were about the same, the oxidation of 1-decene to 2-decanone was about ten times slower when $Cu(OAc)_2$ was the chemical oxidant compared to BQ (Table 1, entry 3). The homogeneous Wacker oxidations using a stoichiometric amount of $Cu(OAc)_2$ also were significantly slower than the oxidations using BQ.

Comparison of 1-decene oxidations in 0.015 M $HClO_4$ (Table 1, entry 1) and 0.12 M $HClO_4$ (Table 1, entry 2) confirmed, as was found for the homogeneous reaction (12), that the reaction rate increased as the concentration of perchloric acid increased. Once a steady state has been achieved the measured current is proportional to the overall rate. An average current of 220 mA was established during the reaction with the low $HClO_4$ concentration, whereas an average current of 415 mA was attained in the oxidation containing 0.12 M $HClO_4$. This rate enhancement of a factor of ca. 2 is less than that found in the homogeneous reaction using a stoichiometric amount of BQ (about a factor of 5) (12).

Data for the oxidation of styrene are shown in Table 1, entries 4–6. A decline in current efficiency from 83% at 700 C to 62% at 1400 C was observed, indicating that the conversion of the styrene had reached a maximum at ca. 60% (ca. 1000 C). After this point, continued electrolysis only served to decrease the current efficiency. The maximum conversion for the homogeneous reaction performed under the same conditions (12) was only 66%, demonstrating that the electrode-mediated oxidation is subject to limitations imposed upon it by the homogeneous reaction in this case.

trans-2-Octene was smoothly oxidized to a mixture of 4-, 3-, and 2-octanones (Table 1, entries 7–10). A small decrease in current efficiency (from 89 to 80%) was observed when the benzoquinone concentration was halved from 20 mol% (Table 1, entry 8) to 10 mol% (Table 1, entry 7); however, the average current remained relatively constant (ca. 190 mA). It is possible to use benzoquinone at concentrations even less than 10 mol% and still maintain high current efficiencies in electrode-mediated oxidations (this would ultimately simplify the isolation and purification of the products).

Rate enhancements with the addition of perchloric acid also were obtained in the *trans*-2-octene oxidations (Table 1, entries 8, 9). As was the case with 1-decene, the reaction was accelerated by about a factor of 2 when the concentration of acid was increased from 0.015 M to 0.12 M. The choice of electrolyte also influenced the rate. Comparison of *trans*-2-octene oxidations using 0.1 M tetrabutylammonium perchlorate (TBAP) as the supporting electrolyte (Table 1, entry 9) with that using 0.1 M sodium perchlorate (Table 1, entry 10) indicated that high current efficiencies could be

Can. J. Chem. Downloaded from www.nrcresearchpress.com by 109.225.110.28 on 09/08/12
For personal use only.

TABLE 1. Electrode-mediated olefin oxidations[a]

Entry	Substrate	$[HClO_4]$ (M)	Q^b (C)	Time (min)	Oxygenate yield (%)[c,d]	Current efficiency (%)[e]
1	1-Decene	0.015	1000	76	68(88)	90
2	1-Decene	0.12	1000	45	69(86)	92
3	1-Decene[f]	0.12	800	420	46(85)	82
4	Styrene	0.03	700	100	51(85)	83
5	Styrene	0.03	1020	82	59(81)	79
6	Styrene	0.03	1400	140	61(79)	62
7	*trans*-2-Octene[g]	0.015	1000	85	51(79)[i]	80
8	*trans*-2-Octene	0.015	1000	90	68(83)[i]	89
9	*trans*-2-Octene	0.12	1000	38	67(83)[i]	89
10	*trans*-2-Octene[h]	0.12	1097	75	76(90)[i]	96

[a]20 mol% benzoquinone, 1 mol% $Pd(OAc)_2$, 7:1 CH_3CN/H_2O, 25°C, 0.90 V vs. SCE, 0.1 M TBAP at a platinum mesh working electrode.
[b]Accumulated charge passed in coulombs.
[c]GC yield based on starting material.
[d]Material balance based on starting material in parentheses.
[e]Calculated using eq. [6].
[f]1.7 V vs. SCE, 0.1 M tetraethylammonium perchlorate, 20 mol% $Cu(OAc)_2$, 2 mol% $Pd(OAc)_2$, 22°C, 7:1 CH_3CN/H_2O.
[g]10 mol% benzoquinone, 1 mol% $Pd(OAc)_2$, 7:1 CH_3CN/H_2O, 22°C, 0.90 V vs. SCE, 0.1 M TBAP.
[h]0.1 M $NaClO_4$ as supporting electrolyte.
[i]Mixture of 2-, 3-, and 4-octanone in the ratio ca. 60:30:10. The ratio did not vary with $[HClO_4]$ or [BQ] and was the same as the ratio observed in the homogeneous (non-electrochemical) reaction [12].

TABLE 2. Electrode-mediated oxidation of cyclohexene versus $[HClO_4]$[a]

Entry	$[HClO_4]$ (M)	i^b (mA)	Cyclohexanone[c] yield (%)	Current[d] efficiency (%)
1	0.03	167	69(87)[e]	100
2	0.06	238	60(73)[e]	76
3	0.12	278	56(83)[e]	80
4	0.24	333	63(85)[e]	84
5	0.36	362	77(94)[e]	100

[a]10 mmol olefin, 20 mol% benzoquinone, 1 mol% $Pd(OAc)_2$, 0.1 M tetrabutylammonium perchlorate, 25°C, 1000 C accumulated at 0.90 V vs. SCE.
[b]Average current over duration of reaction.
[c]GC yield, based on starting materials.
[d]Calculated from: (cyclohexanone yield−homogeneous conversion)/theoretical electrochemical yield.
[e]Material balance, based on moles of starting material.

attained using either electrolyte. However, the reaction rate (i.e., average current) was significantly lower when $NaClO_4$ was used; 440 mA in the reaction with 0.1 M TBAP as the supporting electrolyte, versus 245 mA was observed in the reaction with 0.1 M $NaClO_4$ (the latter has a higher solution resistance).

Electrode-mediated oxidations of cyclohexene also were investigated (Table 2). In general, the yields and current efficiencies were very good. Again, it was found that the rates (i.e., average currents) but not the current efficiencies depended on the concentration of perchloric acid. It is interesting to note that the oxidation of cyclohexene using $Cu(OAc)_2$ in the electrochemical experiment was unsuccessful. In addition, the twofold increase in the rate of the electrochemically mediated cyclohexene oxidations over the concentration range of perchloric acid was less than that found for the homogeneous reaction (12) using $Pd(OAc)_2$, $Pd(NO_2)_2$, or $PdSO_4$ (ca. a factor of 5).

Discussion

The unique ability of BQ to oxidize Pd(0) to Pd(II), compared to other chemical oxidants such as Cu(II) or MnO_2, also was observed for the catalyzed acetoxylation of olefins by Bäckvall *et al.* (14, 15). In that work the experimental evidence suggested that BQ was actually coordinated to the Pd(II). In addition, Hiramatsu et al. (16) prepared and characterized stable Pd(0)/quinone complexes in solution. In that study it was found that the oxidation potential of the Pd(0) depended on the electron demand of the quinone. It is likely that the regeneration of Pd(II) proceeds via an efficient inner-sphere electron transfer mechanism that is promoted by protonation of a Pd(0)/BQ complex. This explanation also is consistent with the acid catalysis that we have observed.

While the effect of acid concentration on the average rates is similar for the homogeneous and the electrode-mediated reactions, it is not identical. The average currents for the oxidation of 1-decene and *trans*-2-octene as a function of acid concentration were found to be about the same, reaching a plateau near 0.1 M (Fig. 1). The maximum current (ca. 420 mA) represents an average turnover rate of 0.025 s^{-1} (i.e., moles of ketone per mole of catalyst per second). For cyclohexene, the average currents were slightly smaller than those for 1-decene or *trans*-2-octene. In this case, the maximum current represents a turnover rate of 0.020 s^{-1}. The effect of acid concentration on the rates of oxidation of 1-decene and cyclohexene under the same conditions using a stoichimetric amount of BQ are shown in Fig. 2. For these reactions, the maximum average turnover rates (at 0.12 M $HClO_4$) for the oxidation of 1-decene and cyclohexene are 0.14 and 0.055 s^{-1} respectively.

Some comment on the nature of the acid catalysis is jus-

Can. J. Chem. Downloaded from www.nrcresearchpress.com by 109.225.110.28 on 09/08/12
For personal use only.

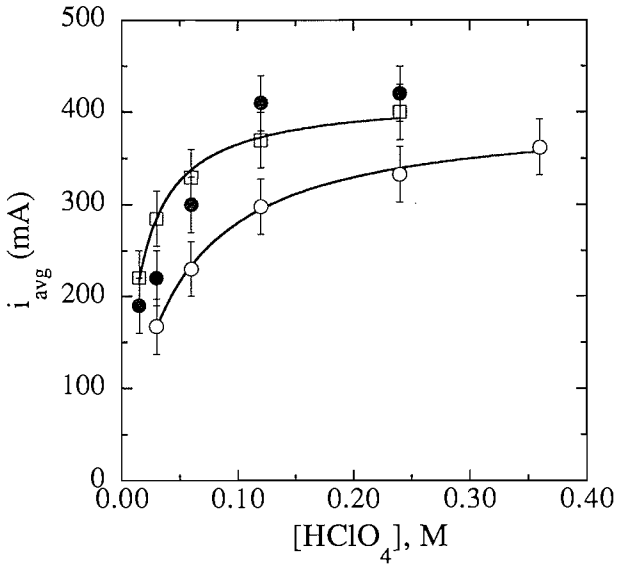

FIG. 1. Average current (i_{avg}) after 1000 C versus [$HClO_4$] for the electrode-mediated Wacker oxidation of 1-decene (□), *trans*-2-octene (●), and cyclohexene (○) in acetonitrile/water (7:1, v/v) with 1 mol% $Pd(OAc)_2$, 20 mol% benzoquinone at 0.9 V vs. SCE at 25°C.

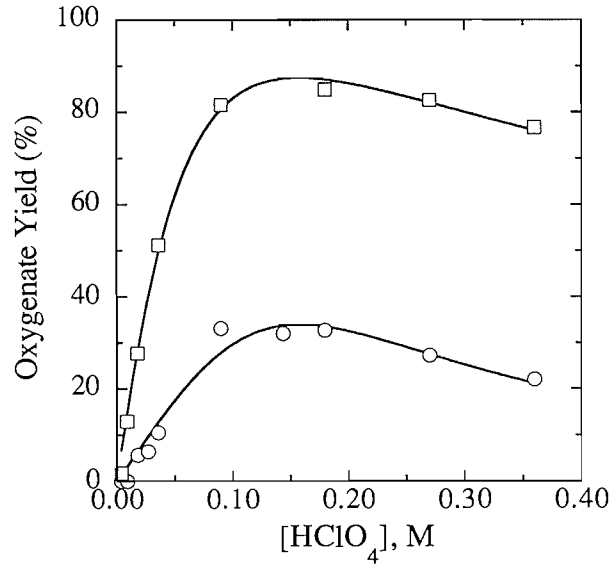

FIG. 2. Oxygenate yield versus [$HClO_4$] for the homogeneous Wacker oxidation of 1-decene (□) and cyclohexene (○) in acetonitrile/water (7:1, v/v) with 1 mol% $Pd(OAc)_2$, 100 mol% benzoquinone after 10 min at 25°C.

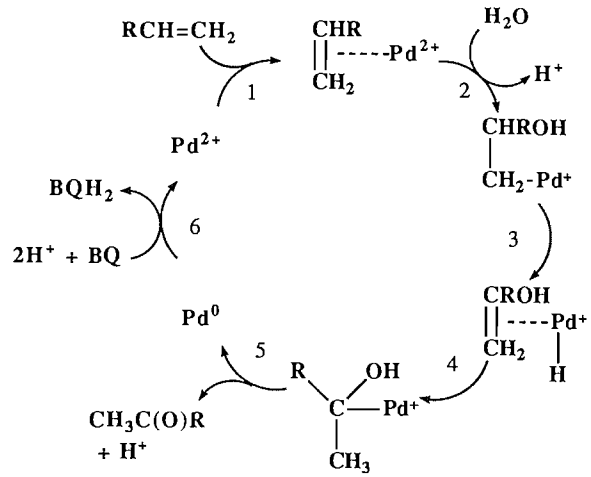

SCHEME 2

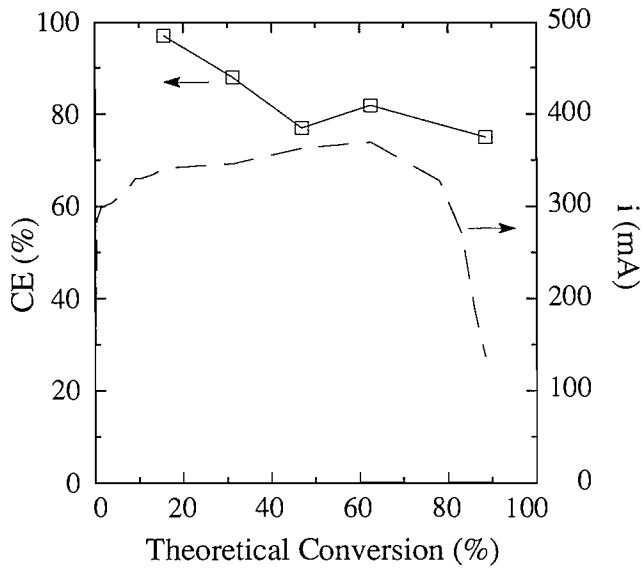

FIG. 3. Current (——) and current efficiency (□) as a function of the theoretical electrochemical conversion for the electrode-mediated oxidation of 1-decene in acetonitrile/water (7:1, v/v) with 1 mol% $Pd(OAc)_2$, 20 mol% benzoquinone at 0.9 V vs. SCE at 25°C.

tified. The Wacker oxidation is catalyzed by low concentration of acid. However, at higher concentrations some inhibition of the rate is evident (Fig. 2). We have suggested that the increased rate of ligand exchange is at least partly responsible for the acid catalysis (12). The rate of ligand exchange is acid catalysed at low acid concentration but approaches a limiting value at high acid concentration (17). Alternatively, the acceleration by low concentrations of acid may be a result of protonation of the ligand, which would increase the electrophilicity of the Pd(II) and increase its reactivity towards the olefin (18–20). The inhibition at high acid concentration can be understood from the simplified mechanism outlined in Scheme 2. In this scheme there are two reactions that result in the loss of a proton. At low acid concentration, the increased ligand exchange rate and the acid-catalysed decomposition of the Pd(0)/BQ complex are expected to control the overall kinetics. At higher concentrations, inhibition of reactions 2 and 4 in Scheme 2 become kinetically important, so the observed rates decrease.

It is clear that the oxidations are faster in the stoichiometric reactions by a factor of about six for 1-decene and about three for cyclohexene (the maximum currents for all three olefins at the highest acid concentration are about the same within the experimental uncertainty). The only obvious difference between the reactions (besides the electrode) is the concentration of BQ; 0.2 equivalents in the electrochemical reactions and 1.0 equivalent in the homo-

Can. J. Chem. Downloaded from www.nrcresearchpress.com by 109.225.110.28 on 09/08/12
For personal use only.

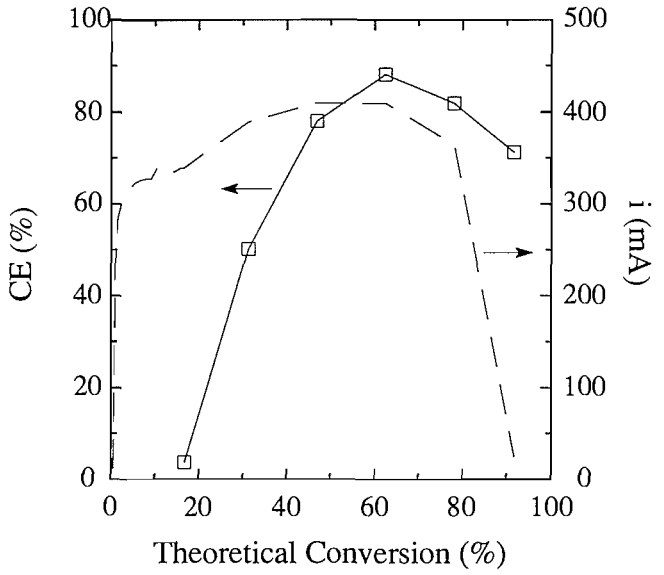

FIG. 4. Current (——) and current efficiency (□) as a function of the theoretical electrochemical conversion for the electrode-mediated oxidation of *trans*-2-octene in acetonitrile/water (7:1, v/v) with 1 mol% $Pd(OAc)_2$, 20 mol% benzoquinone at 0.9 V vs. SCE at 25°C.

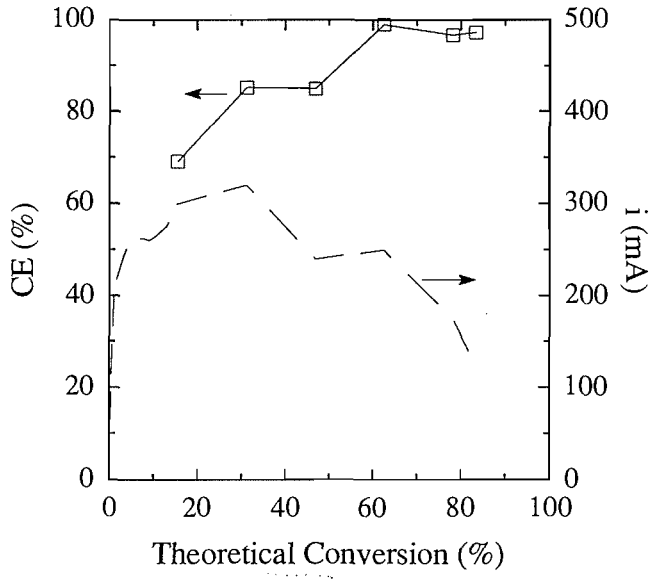

FIG. 5. Current (——) and current efficiency (□) as a function of the theoretical electrochemical conversion for the electrode-mediated oxidation of cyclohexene in acetonitrile/water (7:1, v/v) with 1 mol% $Pd(OAc)_2$, 20 mol% benzoquinone at 0.9 V vs. SCE at 25°C.

geneous reactions. It is tempting to attribute the difference in rates to the difference in concentration of BQ. However, this cannot be the case since the average current using only 0.1 equivalents of BQ (Table 1, entry 7) was the same as that using 0.2 equivalents (Table 1, entry 8). In this case, the evidence suggests that the reactions are limited by the rate of the electrochemical regeneration of BQ from BQH_2 (Scheme 1). This is clearly seen in Fig. 3–5 in which the cell current and current efficiencies for the oxidation of 1-decene, *trans*-2-octene, and cyclohexene have been plotted as a function of the theoretical electrochemical conversion. In general, a relatively constant plateau current was quickly established. A decrease in current only was observed near the end of the reaction when all of the olefin had been consumed (after about 80% of the olefin is consumed). At this point, the reaction can be restarted simply by adding more substrate. These figures also demonstrate the advantage of controlled potential electrolysis (as opposed to controlled current) since the reaction simply turns itself off when the substrate is depleted.

For *trans*-2-octene and cyclohexene induction periods for product formation were observed even though the currents had reached the limiting values (Figs. 4, 5). These induction periods are consistent with the work reported by Smidt *et al.* (1, 20) who demonstrated that the uptake of internal and branched olefins by Pd(II) salts is significantly slower than that of terminal olefins.

The use of potentiostatic (controlled potential) conditions is primarily responsible for the consistently high current efficiencies observed in the electro-oxidations. Under controlled potential conditions, the electrochemical oxidation is much more selective towards BQH_2; i.e., the current is determined by the concentration of BQH_2 only. Preliminary experiments performed under galvanostatic conditions were much less efficient, with current efficiencies <30%. Tsuji and Minato (10) also carried out controlled current oxidations and obtained current efficiencies only on the order of 50–60%. Under galvanostatic conditions, reasonable current efficiencies can only be attained when the rate of olefin oxidation (homogeneous) and the rate of the electrochemical regeneration of BQ (heterogeneous) are comparable. If the homogeneous reaction is too fast then the steady state concentration of BQ will be too low to prevent Pd(0) from precipitating. On the other hand, if the current is too high then the homogeneous oxidation rate is rate limiting and undesirable side reactions that sustain the high current result in a lowering of the overall current efficiency.

Tsuji and Minato (10) noted that cyclohexene and cyclopentene were oxidized readily under the electro-oxidation conditions (cyclohexanone yield 75%, current efficiency 59%; cyclopentanone yield 83%, current efficiency 53%), but almost no reaction occurred when a stoichiometric quantity of benzoquinone was added in lieu of electrochemical regeneration of benzoquinone. In contrast, we have found that the homogeneous reactions are actually faster than the electrochemically mediated reactions (*vide supra*). The discrepancy between the two sets of data is now easily explained. In the homogeneous oxidations carried out by Tsuji a suitable acid was not added. It is likely that under the galvanostatic conditions used in that work, the primary (perhaps the only) reaction at the initial stages of the reaction was the electrolysis of water, thus generating acid, since the Wacker oxidation is known to be slow. This electro-generated acid would then promote the homogeneous reaction and, consequently, appear to drive the reaction that was sluggish in the absence of electrolysis.

These data may have important implications in the large-scale synthesis of cyclohexanone, an important intermediate in the commercial caprolactam process (the monomer of Nylon 6®, Scheme 3). Virtually all industrial approaches to caprolactam go through cyclohexanone as an intermediate.

Can. J. Chem. Downloaded from www.nrcresearchpress.com by 109.225.110.28 on 09/08/12
For personal use only.

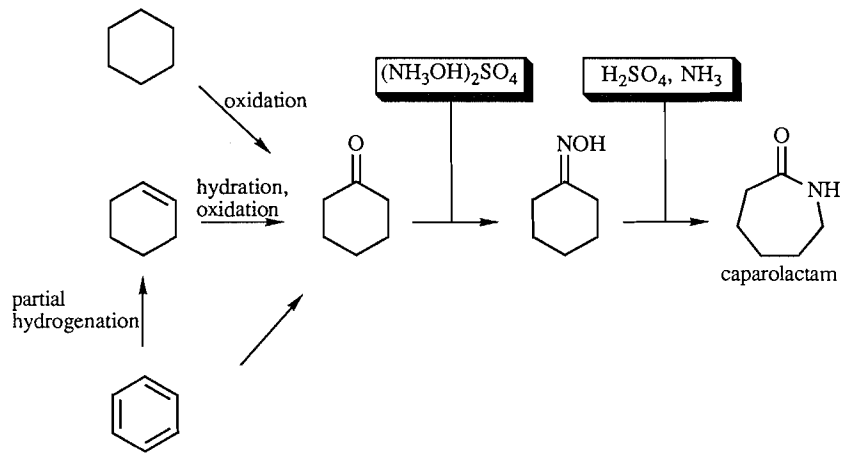

SCHEME 3

Most oxidation routes require high temperatures and pressures and generally give poor yields (21). The data presented in this work show, for the first time, that the oxidation of cyclohexene to cyclohexanone can occur at room temperature at commercially viable rates. Electrode-mediated catalysis is an attractive alternative if the high current efficiencies can be maintained in a scaled-up reactor. In addition, the catalytic amounts of quinone and Pd(II) would simplify the isolation and purification of products.

Experimental

All solutions were of spectroscopic quality. Olefins and palladium catalysts were commercially available (Aldrich) and were used as received. Tetrabutylammonium perchlorate (TBAP, Eastman) was recrystallized twice from ethylacetate/hexanes (9:1, v/v) and dried for 12 h in a vacuum oven (50°C, 5 Torr; 1 Torr = 133.3 Pa). Benzoquinone was passed through a silica gel column (chloroform as eluant) and recrystallized twice from hexane/ethyl acetate (10:1 v/v). A standard H-cell was used in all electro-oxidations (three-electrode configuration). An aqueous saturated calomel reference electrode was used for potential measurements. The potentiostat was a PAR model 173 equipped with a PAR model 176 digital coulometer. In all experiments both the working electrode and counter electrode were a platinum mesh (6 × 6 cm). All potentials are versus the saturated calomel electrode (SCE).

Olefin electro-oxidations

Palladium(II) acetate (0.1 mmol), benzoquinone (2 mmol), and perchloric acid (0.015–0.36 M) were dissolved in acetonitrite/water (7:1 v/v, 85 mL containing 0.1 M TBAP) in the anode compartment. Benzoquinone (3 mmol) and perchloric acid (0.015–0.36 M) were dissolved in 85 mL of the solvent/electrolyte, in the cathode compartment (the quinone in the cathodic compartment reduces the evolution of gases at the cathode). The electrochemical cell was deoxygenated by purging with argon for 30 min and stirred vigorously until the $Pd(OAc)_2$ was dissolved. The olefin (10 mmol) was added to the anode compartment (by syringe) and a potential of 0.9 V vs. SCE was applied until 1000 C had accumulated. After the reaction the contents of the anode compartment were removed (by pipette). Products were separated from the catalyst by extraction into diethyl ether, washed, and then analyzed by a capillary GC–internal standard method. *n*-Decane was the internal standard in the cylohexene reactions and *n*-tridecane was used in the internal standard in all other reactions.

Current efficiency versus theoretical conversion

The reactions were carried out as above, except that 2.0-mL samples were withdrawn (by syringe) periodically and were analyzed by the method described above. The reactions proceeded until the current decreased to a negligible value, after approximately 1700–1800 C had been accumulated.

1. J. Smidt, R. Hafner, R. Jira, R. Sieber, R. Sedlmeier, and A. Sabel. Angew. Chem. Int. Ed. Engl. **1**, 80 (1962).
2. J. Tsuji. Synthesis, 369 (1984).
3. P. A. Chaloner. Handbook of co-ordination catalysis in organic chemistry. Butterworths, London. 1985.
4. J. Tsuji. Organic synthesis with palladium compounds. Springer-Verlag, New York. 1980.
5. H. Agawa, H. Fujinami, K. Taya, and S. Tertani. Bull. Chem. Soc. Jpn. **57**, 1908 (1980).
6. R. Jira and W. Friesleben. Organomet. React. **3**, 5 (1972).
7. M. Kolb, E. Bratz, and K. Dialer. J. Mol. Catal. **2**, 399 (1977).
8. W. H. Clement and C. M. Selwitz. J. Org. Chem. **29**, 241 (1964).
9. I. I. Moiseev, M. N. Vargaftik, and Y. K. Syrkin. Dokl. Akad. Nauk SSSR, **130**, 820 (1960).
10. J. Tsuji and M. Minato. Tetrahedron Lett. 3683 (1987).
11. H. H. Horowitz. J. Appl. Electrochem. **14**, 779 (1984).
12. D. G. Miller and D. D. M. Wayner. J. Org. Chem. **55**, 2924 (1990).
13. D. D. M. Wayner and F. W. Hartstock. J. Mol. Catal. **48**, 15 (1988).
14. J. Bäckvall and A. Gogoll. J. Chem. Soc. Chem. Commun. 236 (1987).
15. J. Bäckvall, S. E. Byström, and R. E. Nordberg. J. Org. Chem. **49**, 4619 (1984).
16. M. Hiramatsu, K. Shiozaki, T. Fujinami, and S. Sakai. J. Organomet. Chem. **246**, 203 (1983).
17. A. Sen. Acc. Chem. Res. **21**, 421 (1988).
18. E. W. Stern. Catal. Rev. **1**, 73 (1967).
19. R. H. Crabtree. The organometallic chemistry of the transition metals. J. Wiley & Sons, New York. 1987.
20. J. Smidt, R. Sedlmeier, and R. Jira. Angew. Chem. **71**, 176 (1959).
21. J. M. Tedder, A. Nechvatal, and A. H. Jubb. Basic organic chemistry. Part 5: Industrial products. J. Wiley and Sons, New York. 1979.

Can. J. Chem. Downloaded from www.nrcresearchpress.com by 109.225.110.28 on 09/08/12
For personal use only.

Rearrangements in the acid-catalyzed formation of lactones from 2-hydroxynorbornane-2-acetic acid derivatives and related compounds

PETER YATES[1] AND MAGDY KALDAS
Lash Miller Chemical Laboratories, University of Toronto, Toronto, Ont., Canada M5S 1A1

Received February 20, 1992

PETER YATES and MAGDY KALDAS. Can. J. Chem. **70**, 2491 (1992).

A mixture of the epimeric ethyl 2-hydroxynorbornane-2-acetates (**1**) on treatment with concentrated sulfuric acid is converted in turn to the lactones of *exo*-2-hydroxynorbornane-1-acetic acid (**4**), *endo*-6-hydroxynorbornane-*endo*-2-acetic acid (**5**), and *exo*-3-hydroxynorbornane-*exo*-2-acetic acid (**6**). With trifluoroacetic acid or 50% sulfuric acid, **1** gives **4**, but this does not react further. In concentrated sulfuric acid the parent acids of **1** (**7**) and (*E*)- and (*Z*)-(norborn-2-ylidene)acetic acids (**8** and **9**) and their ethyl esters (**10** and **11**) give **6** as the infinity product. A mixture of 5-norbornene-*endo*- and *exo*-2-acetic acid (**30** and **31**) on treatment with 50% sulfuric acid gives **4**, **5**, **6**, and *exo*-2-hydroxynorbornane-*syn*-7-acetic acid lactone (**33**). Routes are proposed for the formation of the lactones that involve protonation and carbocation formation followed by rearrangement via Wagner–Meerwein, *endo*-6,2-hydride, and *exo*-3,2-hydride shifts in decreasing order of preference. It is postulated that the usual inhibition of the rearrangement of tertiary to secondary norbornyl carbocations is not operative when the third substituent is a carboxymethyl group or its derivatives because of the electron-withdrawing properties of such groups relative to simple alkyl groups. A preliminary study has shown that *exo*-5-acetyloxy-*endo*-2-hydroxynorbornane-*exo*-2-acetic acid (**35**) with 50% sulfuric acid gives four products that are considered to be the γ-lactones of *endo*-5-acetyloxy- and *endo*-5-hydroxynorbornane-1-acetic acid (**38** and **39**) and *exo*-2-acetyloxy-1-hydroxy- and 1,2-dihydroxynorbornane-*syn*-7-acetic acid (**40** and **41**). Protonation of either the hydroxyl or acetyloxyl group is postulated, giving two carbocations that undergo rearrangements as in the case of **1**, together with 3,2-hydroxyl shifts. The structures of the lactones are assigned on the basis of spectroscopy, reactivity, and analogy. The reactions of the lactones, which lead to a variety of hydroxy- and oxonorbornaneacetic acids, illustrate their synthetic potential.

PETER YATES et MAGDY KALDAS. Can. J. Chem. **70**, 2491 (1992).

Un mélange d'épimères de 2-hydoxynorbornane-2-acétates d'éthyle (**1**) traité par de l'acide sulfurique concentré conduit aux lactones des acides *exo*-2-hydroxynorbornane-1-acétique (**4**), *endo*-6-hydroxynorbornane-*endo*-2-acétique (**5**) et *exo*-3-hydroxynorbornane-*exo*-2-acétique (**6**). Par traitement avec de l'acide trifluorbacetique ou de l'acide sulfurique à 50%, le composé **1** conduit au composé **4**, mais la réaction ne va pas plus loin. En milieu acide sulfurique concentré, les acides parents du composé **1**, soit les composés (**7**), les acides (*E*)- et (*Z*)-(norborn-2-ylidène) acétiques (**8** et **9**) ainsi que leurs esters éthyliques (**10** et **11**) ne conduisent qu'au composé **6** comme produit obtenu après un temps infini. Un mélange des acides 5-norbornène-*endo*- et *exo*-2-acétique (**30** et **31**) traité par de l'acide sulfurique à 50% permet d'obtenir les composés **4**, **5**, **6** ainsi que la lactone de l'acide *exo*-2-hydroxynorbornane-*syn*-7-acétique (**33**). On propose une voie d'accès à cette lactone qui implique une protonation et la formation d'un carbocation suivie d'une transposition de Wagner–Meerwein, des déplacements d'hydrures *endo*-6,2 et *exo*-3,2 dans cet ordre décroissant d'importance. On suggère que, en raison de leurs propriétés électroattractives relatives à celles des groupes alkyles simples, l'inhibition habituelle de la transposition des carbocations norbornyles tertiaire et secondaire disparait lorsque le troisième substituant est un groupe carboxyméthyle ou un de ses dérivés. Une étude préliminaire indique que, sous l'influence de l'acide sulfurique à 50%, l'acide *exo*-5-acétyloxy-*endo*-2-hydroxynorbornane-*exo*-2-acetique (**35**) conduit à quatre produits que l'on considère être les γ-lactones des acides *endo*-5-acétyloxy- et *endo*-5-hydroxynorbornane-1-acétique (**38** et **39**) et des acides *exo*-2-acétyloxy-1-hydroxy- et 1,2-dihydroxynorbornane-*syn*-7-acétique (**40** et **41**). On suggère que les protonations soit du groupe hydroxyle soit du groupe acétyloxyle conduisent à deux carbocations qui se transposent tous les deux, comme dans le cas du composé **1**, par le biais de déplacements 3,2 d'hydroxyle. On a établi les structures de ces lactones sur la base d'analogies des études spectroscopiques et d'études de réactivité. Les réactions des lactones, qui conduisent à divers acides hydroxy- et oxonorbornaneacétiques, illustrent leur potentiel en synthèse.

[Traduit par la rédaction]

The structures and rearrangements of 2-norbornyl cations have been the subjects of countless investigations during the past 50 years (1, 2). Many questions have been answered and these species are no longer the cynosures they were. However, the study of their chemistry still provides results of synthetic and mechanistic interest. We describe here one such study, which followed up observations we had made during the course of our synthetic work on norbornanes with functionalized carbon substituents at a bridgehead (3).

Reaction of 2-hydroxynorbornane-2-acetic acid derivatives with acids

In our earlier work we found that the epimeric mixture of ethyl 2-hydroxynorbornane-2-acetates (**1**), formed by the Reformatsky reaction of 2-norbornanone with ethyl bromoacetate (4),[2] gives on treatment with 32% hydrogen bromide in acetic acid at room temperature a mixture of the rearrangement product *exo*-2-bromonorbornane-1-acetic acid (**2**) and its ethyl ester **3** (3).[3] We have subsequently found that with 48% hydrobromic acid at room temperature **1** gives solely the lactone of *exo*-2-hydroxynorbornane-1-acetic acid

[1]Author to whom correspondence may be addressed.

[2]Lauria *et al.* (4) report that a single diastereomer is formed; however, their product may have undergone fractionation during purification since they hydrolyzed the crude ester, crystallized the resulting acid, and then re-esterified.

[3]All compounds prepared in our present and previous studies in this area are racemic, but are structurally represented as single enantiomers.

Can. J. Chem. Downloaded from www.nrcresearchpress.com by 109.225.110.28 on 09/08/12
For personal use only.

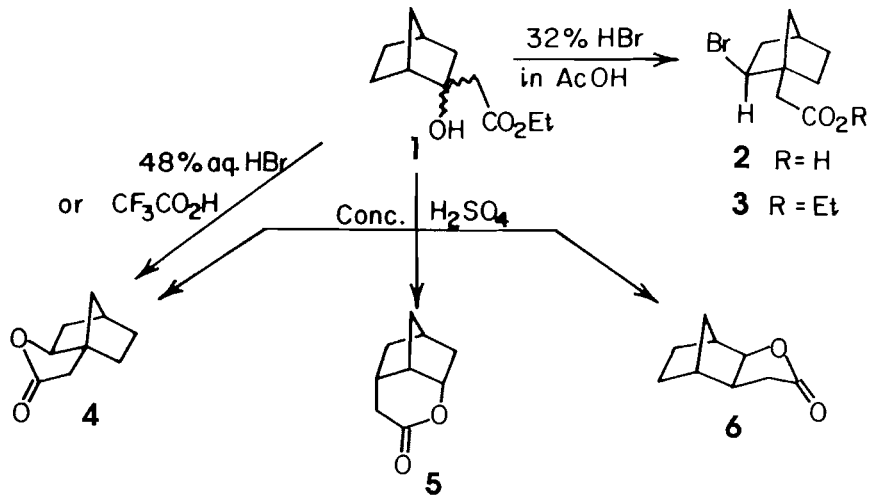

SCHEME 1

(**4**), as it does with trifluoroacetic acid (Scheme 1). Treatment of **1** with concentrated sulfuric acid at room temperature gives **4** and two isomeric lactones, **5** and **6**, derived from *endo*-6-hydroxynorbornane-*endo*-2-acetic and **exo**-3-hydroxynorbornane-*exo*-2-acetic acid, respectively, whose relative yields are time dependent (Table 1). Lactone **4** is formed first and is converted to lactones **5** and **6**; on longer standing **5** is converted to **6**, the infinity product. In accord with this, treatment of lactone **4** with concentrated sulfuric acid gives a mixture of **5** and **6**; after 10 min their ratio is 5:3 and after an extended reaction time **6** is the sole product. Treatment with weaker acids, e.g., 50% sulfuric acid returns **4** unchanged. We have also found that treatment of acids **7–9**[4] and esters **10** and **11** with concentrated sulfuric acid ultimately gives lactone **6**.

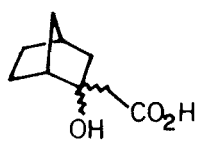

7

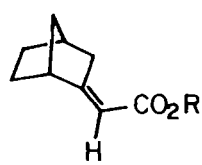

8 R = H
10 R = Et

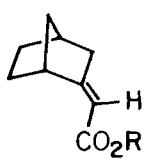

9 R = H
11 R = Et

It is clear that **1** and compounds **7–11** all react in acids via a common carbocationic intermediate of type **12** (Scheme 2).[5] Simple secondary 2-norbornyl cations are well known to undergo rearrangement via three different pathways, which are, in order of decreasing preference: (*i*) Wagner–Meerwein shifts, (*ii*) *endo*-6,2 hydride shifts, and (*iii*) *exo*-3,2-hydride shifts (1, 2). In general these involve the conversion of a secondary cation to another secondary cation or to a tertiary cation. In the case of simple tertiary 2-norbornyl cations, such as the 2-methyl-2-norbornyl cation, rearrangement is disfavored because it would entail the conversion of a tertiary to a secondary cation (1). The case of the tertiary 2-norbornyl cation **12** is exceptional, however, since the presence of the carboxymethyl substituent, CH_2CO_2H, or its equivalent, at C-2 may be expected to destabilize the ion relative to the methyl-substituted ion owing to the electron-withdrawing inductive effect of such substituents (6). Thus the reversible rearrangement of the tertiary cation can be accounted for and the pathways for the formation of the lactones **4**, **5**, and **6** from **12** shown in Scheme 2[6] can be proposed.

The cation **12** is postulated first to undergo reversible

TABLE 1. Relative yields of lactones **4–6** from the reaction of **1** with concentrated sulfuric acid

Reaction time	Relative yield (%)		
	4	**5**	**6**
6 min	25	50	25
30 min	5	52	43
1 h	Trace	55	45
2 h	0	41	59
10 h	0	0	100

[4]Vaughan *et al.* (5) have reported that **8** (or **9**) is converted to lactone **4** by treatment with trifluoroacetic acid at room temperature.

[5]It is highly probable that both the secondary and tertiary norbornyl cations invoked in this work are at least partially bridged (1). However, the work of itself makes no contribution to the nonclassical – classical ion controversy, and we choose to represent the intermediates as classical ions to facilitate visualization of the rearrangements involved.

[6]WM, 6,2, and 3,2 represent Wagner–Meerwein, *endo*-6,2-hydride, and *exo*-3,2-hydride shifts, respectively.

Can. J. Chem. Downloaded from www.nrcresearchpress.com by 109.225.110.28 on 09/08/12
For personal use only.

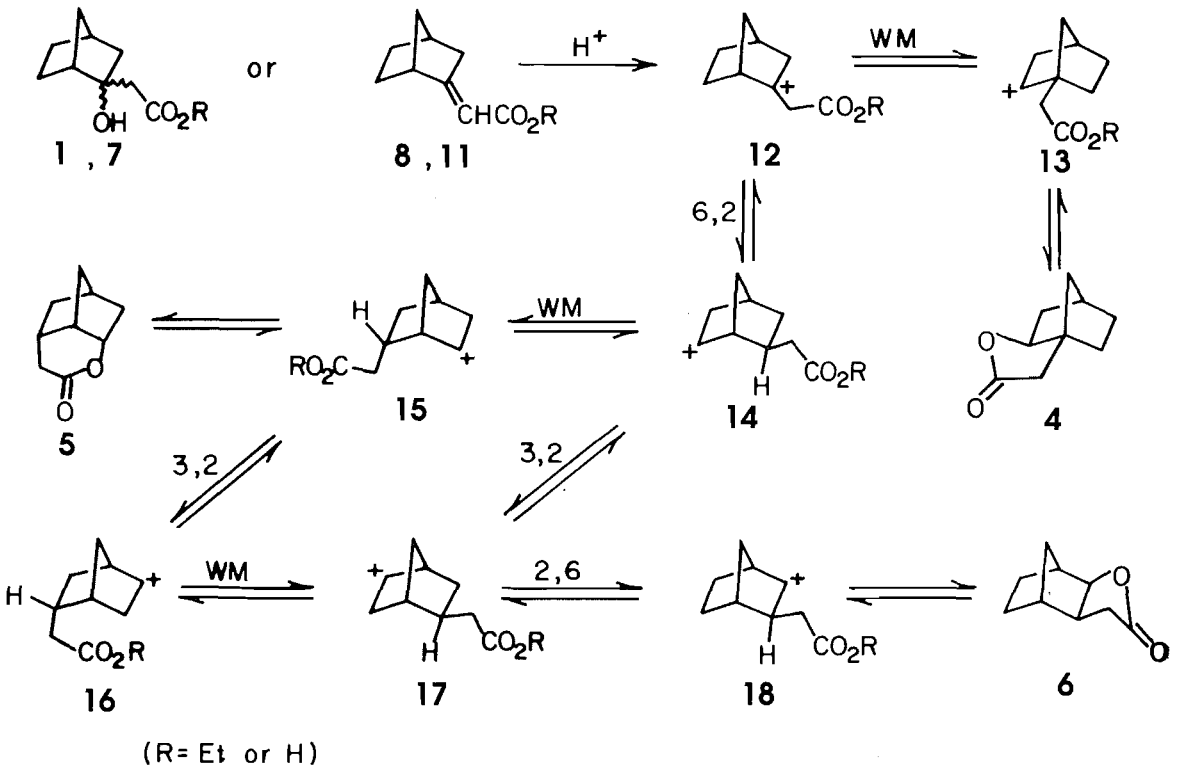

SCHEME 2

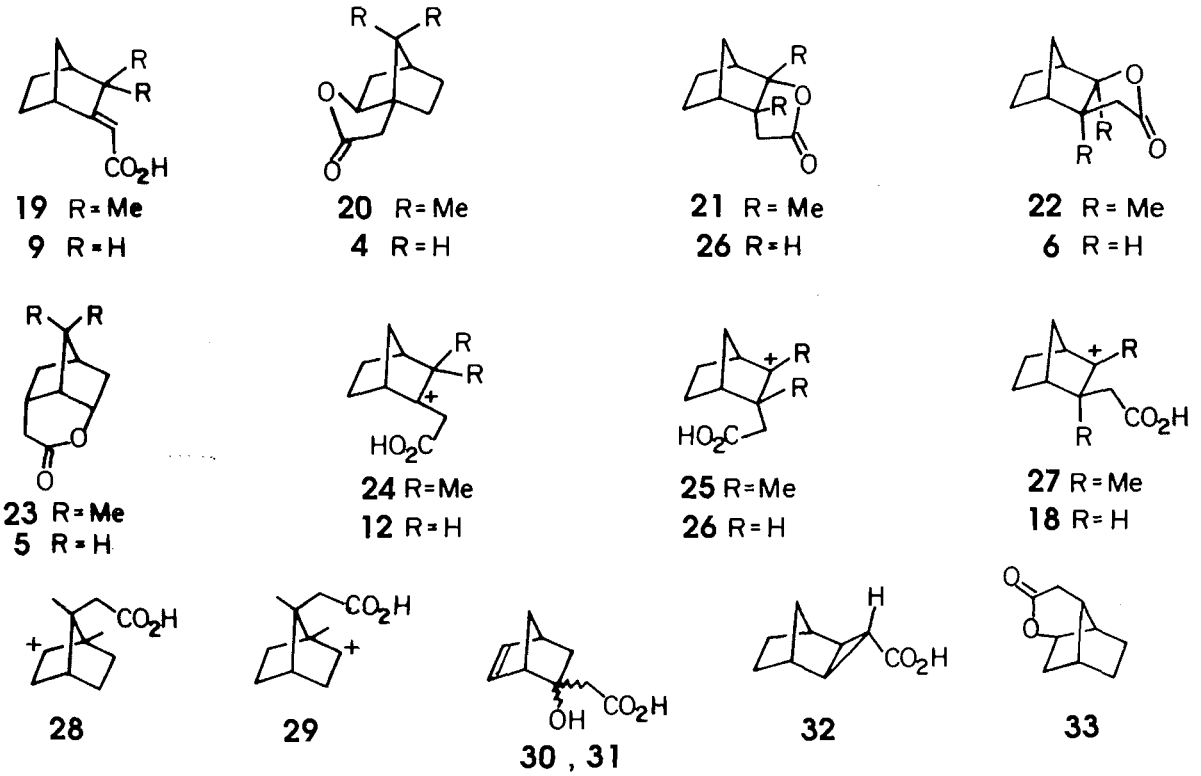

Wagner–Meerwein rearrangement to the cation **13** and lactone closure to **4** (in the cases where R = Et, the question of the timing of the loss of the ethyl group remains moot). The cation **12** is considered to undergo a slower, *endo*-6,2-hydride shift giving the cation **14**, followed by a Wagner–Meerwein shift to give the cation **15**, which closes to the lactone **5**; all of these steps are considered to be reversible. Finally, it is proposed that **15** and **14** undergo yet slower,

Can. J. Chem. Downloaded from www.nrcresearchpress.com by 109.225.110.28 on 09/08/12
For personal use only.

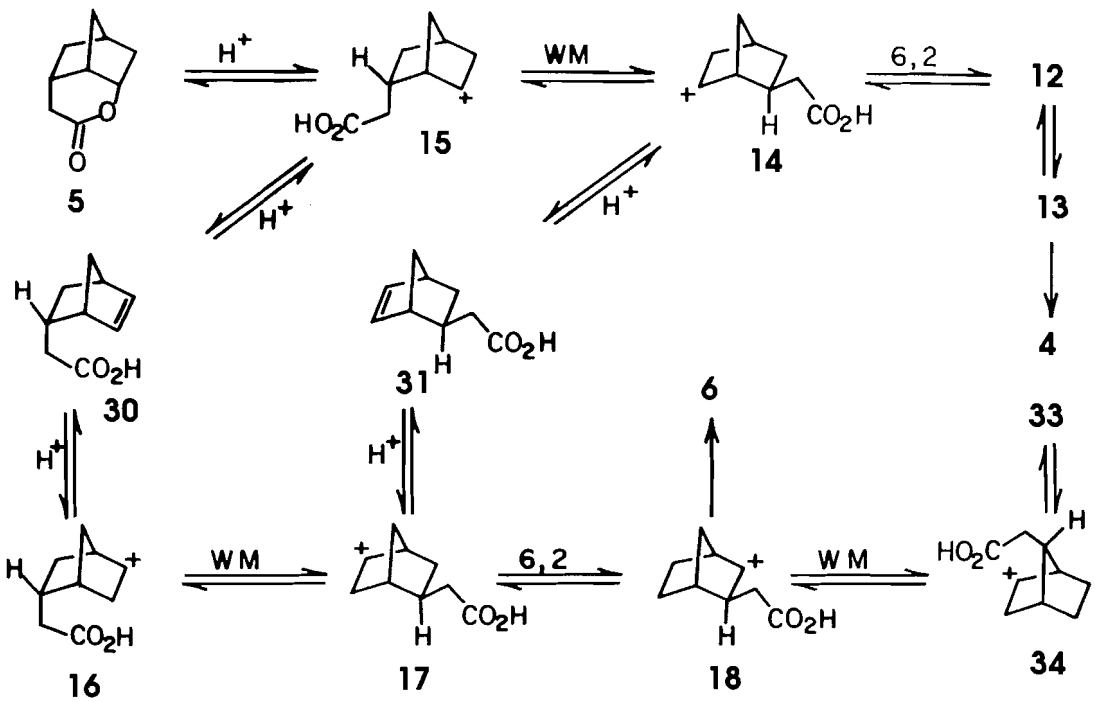

SCHEME 3

reversible, *exo*-3,2-hydride shifts to give **16** and **17**, respectively, which are interconvertible by Wagner–Meerwein shifts, and that **17** undergoes an *endo*-6,2-hydride shift to form the cation **18**, which closes to lactone **6**. The formation of **6** as the infinity product is attributed either to irreversible lactonization or to its being greatly favored at equilibrium. This interpretation may be oversimplified and additional pathways may well be involved (*vide infra*). However, it appears to us to be the most plausible one based on our postulates that rearrangement of tertiary cations of type **12** to secondary cations can occur, and that the commonly observed order of preference among the three types of shift is followed.

Vaughan and Wolinsky *et al.* (7) earlier examined the products formed by (*E*)-camphene-8-carboxylic acid (**19**), an analogue of **9**, under a variety of acid conditions. They found that lactone **20**, an analogue of **4**, is formed initially and that this can be converted in turn to lactone **21** and lactone **22**, the analogue of lactone **6**. In strong acids **22**, like **6**, is the infinity product. Their results differ from our own in the non-methyl series in the observation of the formation of the endo lactone **21** and the failure to observe the δ-lactone **23**, analogous to the δ-lactone **5**. The first difference can be accounted for in terms of an *exo*-3,2-methyl shift (Nametkin rearrangement (8)) in **24** leading to the formation of the stabilized, tertiary carbocation **25**; the formation of the corresponding series would require an *exo*-3,2-hydride shift in **12** to give the secondary carbocation **26**, a less energetically favored process. The second difference may be associated with the general circumstance that in multireaction manifolds the relative rates of the reactions are dependent on the nature of the substrate and that in a particular case an intermediate may be present in such low concentration that it fails to undergo detection. The same consideration can be invoked as a supplementary or alternative explanation of the failure to observe the formation of **23** from **12**. A further point of interest arises from this report (7). It concerns the origin of **22**, for which the authors propose ring closure of **27**, which arises from **25** by a Wagner–Meerwein shift to **28**, followed by an *endo*-6,2-hydride shift to **29** and another Wagner–Meerwein rearrangement to **27**. They note that the simplest pathway for the formation of **27** would be an *endo*-3,2-methyl shift in **24**, but disfavor this route because of the absence of established precedent for an *endo*-Nametkin rearrangement. However, there are difficulties with the lengthier route proposed, since the conversion of **25** to **28** involves an unfavorable Wagner–Meerwein rearrangement of a stabilized tertiary to a secondary carbocation (*vide supra*), and Haseltine and Sorensen (9) later reported that the *endo*-3,2-methyl shift occurs in related systems, albeit much more slowly than the corresponding *exo* shift. Thus the possibility of the formation of **27** by an *endo*-Nametkin rearrangement remains.

Reaction of 5-norbornene-2-acetic acids with acids

Sauers and Sonnet (10) were the first to examine the reaction of a mixture of racemic 5-norbornene-*endo*- and *exo*-2-acetic acids (**30** and **31**) with acids; in 75% sulfuric acid at 0°C for 22 h it gave the lactone **6** as the major product together with a second, unidentified lactone. They obtained the same major product from treatment of the isomeric tricyclic acid **32** with concentrated sulfuric acid for 18 days, accompanied by two other, unidentified lactones. Davies and Dowle (11) later investigated in greater detail the reaction of **30** and **31** with acids. They reported that in 50% sulfuric acid the *endo* isomer **30** or a mixture of this and the *exo* isomer **31** gave lactone **6** and the δ-lactone **33**; they did not observe the formation of lactones **4** and **5** and proposed a mechanistic scheme that took this into account. Since their results differed from ours with **1**, albeit in concentrated sulfuric acid,

Can. J. Chem. Downloaded from www.nrcresearchpress.com by 109.225.110.28 on 09/08/12
For personal use only.

we have repeated the reaction of a mixture of **30** and **31** with 50% sulfuric acid, and now find that in addition to lactones **6** and **33**, lactones **4** and **5** are also formed under these conditions. Proposed routes for the formation of the various lactones are given in Scheme 3, which corresponds with Scheme 2, but differs in (*i*) the point of entry to the reaction manifold, (*ii*) the inclusion of lactone **33**, and (*iii*) the irreversible formation of lactone **4**, which we have shown does not react in 50% sulfuric acid. Our failure to observe the formation of **33** from **1** could again be attributable to the fact that it is present in such low concentration under the conditions we used as to be unobservable (cf. the δ-lactone **5**, above). The limiting case would be irreversible formation of lactone **6** from the carbocation **18** in concentrated sulfuric acid, but not in 50% sulfuric acid, inhibiting the conversion of **18** to **33** via **34**.

Reaction of exo-5-acetyloxy-2-hydroxynorbornane-2-acetic acids with acid

We discussed above lactone formation from 2-hydroxynorbornane-2-acetic acids via the carbocation **12**. We also carried out a preliminary investigation of lactone formation from *exo*-5-acetyloxy-2-hydroxynorbornane-2-acetic acids (**35**), which may be expected to give products via carbocation **36** that are analogous to those formed via **12**, and via carbocation **37**. In addition to a synthetic role (cf. ref. 3), the acetyloxyl group in **35** can serve as a marker and aid in mechanistic interpretations. Furthermore, the stereochemistry at the carbon atom bearing the acetyloxyl group in the products can provide information since a Wagner–Meerwein rearrangement of **35** will result in inversion in the relative configuration at this carbon (**35**–**37**, Scheme 4).

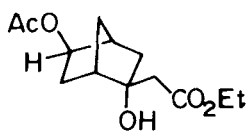

35

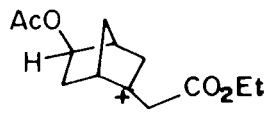

36

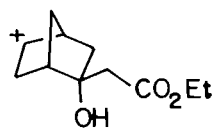

37

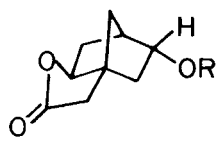

38 R = Ac
39 R = H

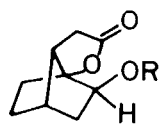

40 R = Ac
41 R = H

In the event, treatment of **35** with 50% sulfuric acid gave a mixture of four lactones. Two, the acetyloxy lactone **38** and hydroxy lactone **39**, had been obtained by us previously by a different route (3). The other two products are considered to be **40** and **41**, although the former was isolated only in admixture with **38**. We propose (Scheme 4) that lactone **38** is formed via **36** and **42** by a route analogous to that postulated for the formation of **4**, giving the *endo* acetyloxy lactone because of the involvement of a Wagner–Meerwein rearrangement in the formation of **42** (*vide supra*). Hydrolysis of **38** would lead to the hydroxy lactone **39**.

The other products from **35** are considered to arise via protonation of the acetyloxyl group and loss of acetic acid to give **37**,[7] which undergoes Wagner–Meerwein rearrangement to the carbocation **43**, which in turn undergoes an *endo*-6,2-hydride shift to give the cation **44**. An *exo*-3,2-hydroxyl shift to cation **45**, perhaps via a protonated epoxide, followed by an *endo*-3,2-hydride shift would then lead to the carbocation **46**. The occurrence of such an *endo* shift should be facilitated by electron donation from an unshared electron pair on the oxygen atom of the hydroxyl group. Cation **46** can give the protonated lactol **47**, which on loss of water followed by a Wagner–Meerwein rearrangement would give the carbocation **48** and thence the lactones **40** and **41** by *exo* nucleophilic attack (1). A closely related route for their formation could involve an *endo*-6,2-hydride shift in **37** to give the carbocation **49**,[8] and conversion of this by a series of steps analogous to the sequence **44** → **48** to **50**, the enantiomeric form of **48**.

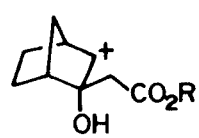

49

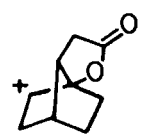

50

Structural assignments and synthetic utilization and potential

Here we discuss the assignments of structure to the lactones **4**, **5**, **6**, **33**, **38**, **39**, **40**, and **41**. These were based on infrared and ^{1}H nmr spectroscopy[9] (see experimental sec-

[7]The *exo* acetyloxyl group in **35** is expected to be lost much faster than an *endo* acetyloxyl group (1), accounting for the fact that no products were observed that derived from loss of the *endo* acetyloxyl group in **38** (cf. the slow conversion of ethyl *endo*-3-acetyloxy-*exo*-6-bromo-norbornane-1-acetate to its *exo*-3-acetyloxy epimer by hydrogen bromide in acetic acid (3)).

[8]This would give **44** on Wagner–Meerwein rearrangement.

[9]The ^{13}C nmr spectra, which are also in accord with the assignments, will be discussed elsewhere.

Can. J. Chem. Downloaded from www.nrcresearchpress.com by 109.225.110.28 on 09/08/12
For personal use only.

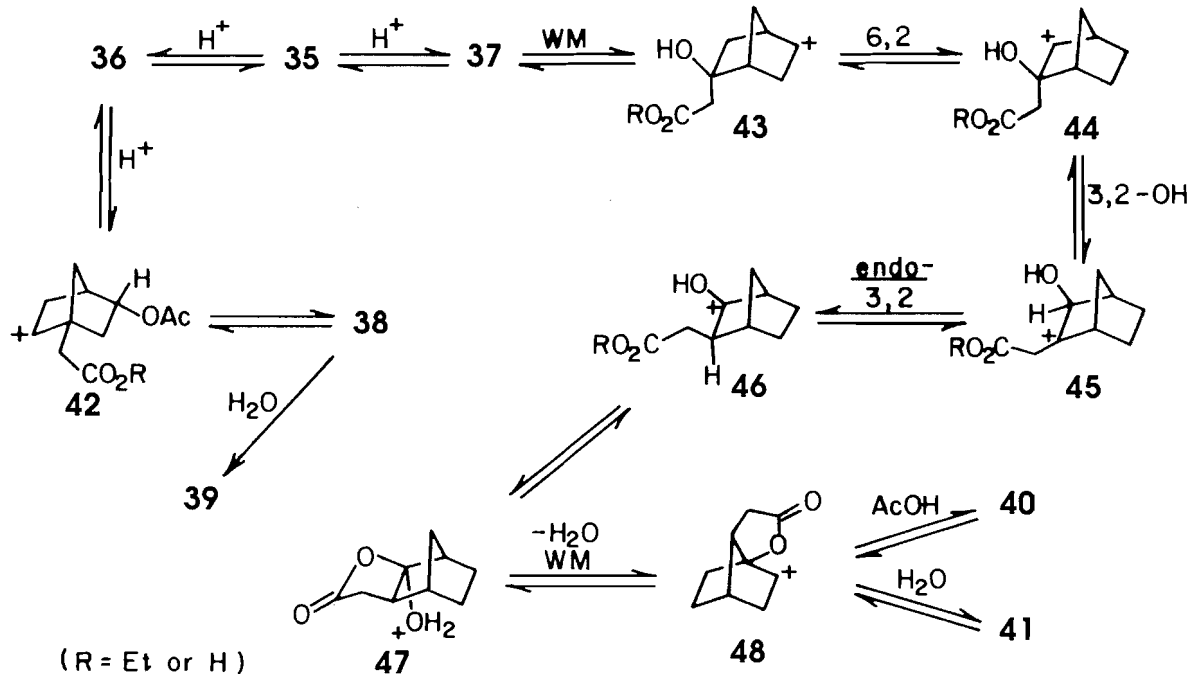

SCHEME 4

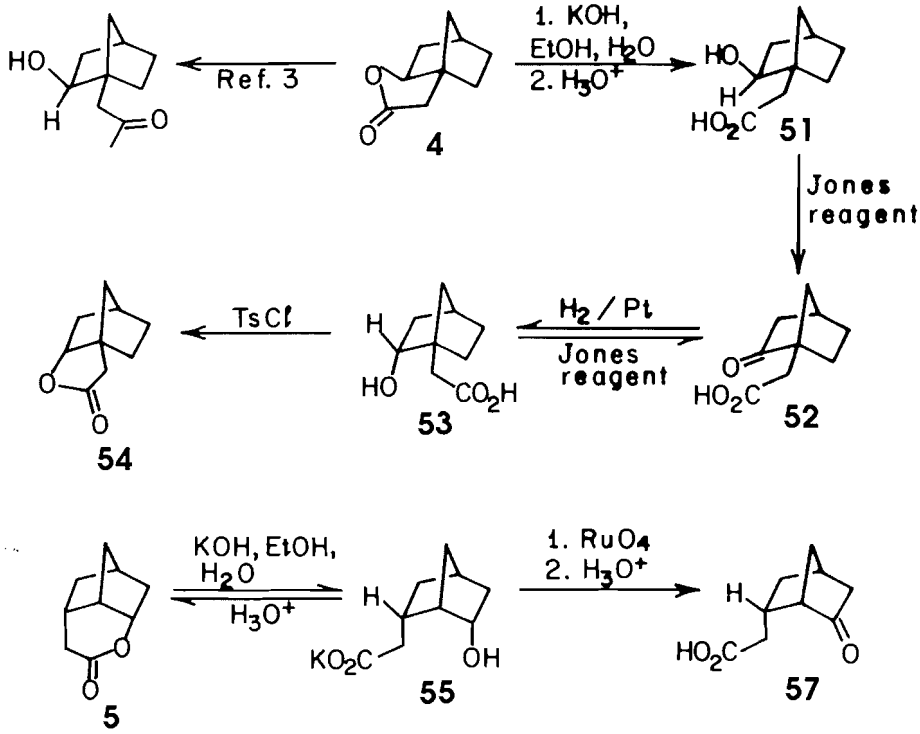

tion), on the reactions of the lactones, and on analogy with previous observations (2). The formation of the first four compounds has been reported by others, but in some cases their structures had not been rigorously established at the time much of the presently reported work was done. We refer briefly to some of their reactions here, both to confirm the structural assignments and to illustrate the synthetic potential of the lactones.

The structural assignments for the first six lactones were straightforward and we limit their discussion here to the schematic summary of their reactions below.

The assignments of structures **40** and **41** were less simple and we discuss these in more detail. Although **40** was obtained only as a mixture with **38**, it was possible to analyze its ir and ^{1}H nmr spectra because of the availability of the spectrum of pure **38**. The former showed it to be an acetyl-

Can. J. Chem. Downloaded from www.nrcresearchpress.com by 109.225.110.28 on 09/08/12
For personal use only.

oxy δ-lactone and the latter indicated that it contained only one proton on a carbon bearing an oxygen atom. Thus it must be either the δ-lactone of a tertiary alcohol and the acetate of a secondary alcohol or the δ-lactone of a secondary alcohol and acetate of a tertiary alcohol. Comparison of its ^{1}H nmr spectrum with that of **41** (*vide infra*) showed that the latter is the acetate of the former. Since **41** on oxidation with Jones reagent gives a keto δ-lactone, its hydroxyl group and the acetyloxyl group of **40** must be secondary. It follows that the lactone groups in **40** and **41** are tertiary. The ir spectrum of the oxidation product from **41** shows that the ketonic group is in a five-membered ring, strongly suggesting that the norbornane system is retained. Consideration of possible formulations in terms of these conclusions and the origin of the compounds leads to the assignment of structures **40** and **41**, with **64** as the structure of the oxidation product of the latter.

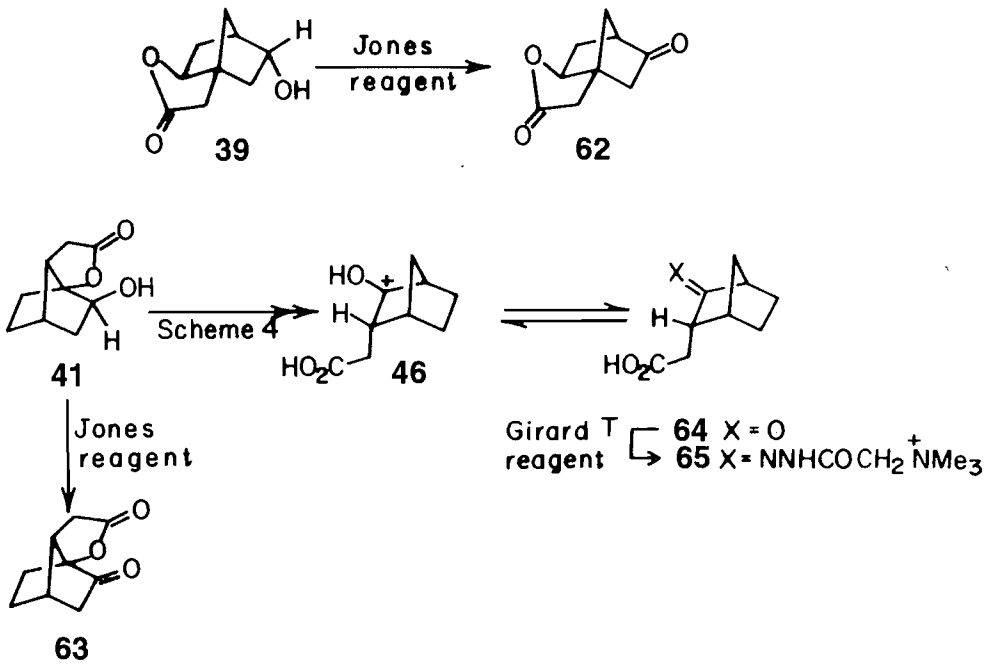

Compound **41** was obtained initially in a ca. 50:50 mixture with **39**; however, treatment of the mixture with Girard reagent T in the usual manner (12) resulted in removal of most of **41** from the organic layer and the isolation of a much enriched sample of **39** (85%). Acid hydrolysis of the aqueous layer gave a pure sample of **41**. It was thus possible to analyze the spectra of both **39** and **41**. Girard reagent T is normally used for the removal of aldehydes or ketones; since no such function is present in **41**, it must be generated from **41** under the conditions of the reaction. This is readily explicable in terms of structure **41** and the origin proposed for it in Scheme 4. Cation **46** could well be in equilibrium with a small amount of its parent ketone **65**, which could form the hydrazone **66** irreversibly with Girard reagent T; hydrolysis of this with acid would regenerate **46** and thence **41**.

These several transformations of the lactones illustrate their versatility, both observed and potential, in the synthesis of a variety of norbornane derivatives from 2-hydroxynorbornane-2-acetic acid and 5-norbornene-2-acetic acid derivatives. This potential is enhanced by the fact that the relative yields of the lactones can be controlled by variation of the reaction conditions for their formation.

Insofar as the routes for the formation of the lactones are concerned, definitive answers will require considerable further experimentation. In particular it will be of interest to determine the reactivities of all of the lactones under the several conditions of their formation, to observe the ionic intermediates by nmr spectroscopy, to undertake isotopic labeling studies, and to explore further the effect of CH_2CO_2R and related substituents on the stability of tertiary norbornyl cations relative to secondary and alkyl-substituted tertiary norbornyl cations.

Experimental

Melting points are uncorrected. Unless otherwise indicated infrared (ir) spectra were taken in chloroform solution and proton magnetic resonance (^{1}H nmr) spectra in deuteriochloroform solution. The ir peaks are strong unless otherwise described. Thin-layer chromatographic (tlc) analyses were carried out on Quanta/Gram precoated 20 × 20 cm silica plates (thickness 2 mm), activated for 30 min at 130°C. Organic solutions were dried with anhydrous magnesium sulfate unless otherwise stated.

exo-*2-Hydroxynorbornane-1-acetic acid lactone (4)*

(a) From treatment of 1 with hydrobromic acid

A solution of **1** (3.00 g, 15.00 mmol) in 48% hydrobromic acid (20 mL) was stirred at room temperature for 56 h, and the reaction mixture was extracted with dichloromethane (4 × 30 mL). The combined extracts were washed with aqueous 5% sodium bicarbonate (50 mL) and water (2 × 50 mL), and dried. The solvent was removed to give a yellow oil (2.20 g). This was subjected to molecular distillation (100–102°C/0.05 Torr; 1 Torr = 133.3 Pa) and the distillate was allowed to stand at 5°C for 2 weeks, by which time it had completely solidified. Sublimation gave lactone **4** (2.10 g, 92%) as plates, mp 69–70°C (lit. (5) mp 75–76°C)[10] ir (OCL_4) ν_{max}:

[10]The sample had $[\alpha]_D$ −0.72; it was possibly a single enantiomer (cf. ref. 5).

Can. J. Chem. Downloaded from www.nrcresearchpress.com by 109.225.110.28 on 09/08/12
For personal use only.

Can. J. Chem. Downloaded from www.nrcresearchpress.com by 109.225.110.28 on 09/08/12
For personal use only.

1773 cm^{-1}; ^1H nmr δ: 1.10–1.93 (m, 8H), 2.34 (m, 1H), 2.60 (s, 2H), 4.16 (t, J = 4 Hz; 1H); m/z: 152 (2) (M^+). Anal. calcd. for $C_9H_{12}O_2$: C 71.02, H 7.95; found: C 71.02, H 8.03.

(b) From treatment of ***1*** *with trifluoroacetic acid*

A solution of **1** (396 mg, 2.00 mmol) in freshly distilled trifluoroacetic acid (10 mL) was stirred at room temperature for 21 h. The reaction mixture was poured into ice-water (50 g) with stirring and extracted with chloroform (3 × 50 mL), and the combined extracts were dried (K_2CO_3–Na_2SO_4). The solvent was removed to give **4** (246 mg, 81%) as a colorless oil that solidified on cooling and had ir, ^1H nmr, and mass spectra and tlc behavior identical with those of the lactone **4** obtained from treatment of **1** with hydrobromic acid.

Treatment of ***1*** *with concentrated sulfuric acid. Formation of* ***4****,* endo*-6-hydroxynorbornane-*endo*-2-acetic acid lactone (****5****), and* exo*-3-hydroxynorbornane-*exo*-2-acetic acid lactone (****6****)*

(*i*) A solution of **1** (1.00 g) in concentrated sulfuric acid (15 mL) was stirred without external heating for 26 h. The reaction mixture was added slowly with stirring to a large amount of ice-water (ca. 300 g), and the mixture was extracted with dichloromethane (3 × 100 mL). The combined extracts were dried (K_2CO_3–Na_2SO_4), and the solvent was removed to give a brown oil (707 mg, 93%), which was purified by molecular distillation at 96°C/0.025 Torr onto a Dry Ice – acetone-cooled finger, giving **6** (10, 11, 13) (509 mg, 67%) as a colorless oil; ir ν_{max}: 1770 cm^{-1}; ^1H nmr δ: 1.08–1.65 (m, 6H), 1.88–2.84 (s, 5H), 4.46 (d of m, J = 4 Hz; 1H); m/z: 152 (27) (M^+).

(*ii*) In another run the reaction was followed by taking aliquots at intervals of 6 min, 30 min, 1 h, 2 h, and 10 h with work-up as above. Analysis by ^1H nmr spectroscopy showed the formation of lactones **4**, **5** (*vide infra*), and **6**; **4** and **5** in turn gave **6** irreversibly. The 6-min aliquot consisted of a mixture of **4**, **5**, and **6** in a ratio of 1:2:1, the 30-min aliquot showed a ratio of 1:11:9, the 1-h aliquot showed a ratio of **5** and **6** of 6:5 with only a trace of **4**, the 2-h aliquot showed a ratio of **5** and **6** of 7:10, and the 10-h aliquot showed only the lactone **6**. A column of silica gel that was packed in and eluted with dichloromethane was used in separating lactones **4**, **5**, and **6** from each other, lactone **4** being eluted first, followed by **5**, and finally **6**.

*Treatment of 2-hydroxynorbornane-2-acetic acid (****7****), (*E*)- and (*Z*)-(norborn-2-ylidene (****8*** *and* ***9****), and the ethyl esters of the latter (****10*** *and* ***11****) with concentrated sulfuric acid. Formation of* ***6***

Individual 5% solutions of **7** and mixtures of **8** and **9** and of **10** and **11** (3, 4) in concentrated sulfuric acid were stirred without external heating for 5, 10h, and 6 h, respectively. The reaction mixtures were quenched with large amounts of ice-water and extracted several times with dichloromethane. The combined extracts from each reaction mixture were dried (K_2CO_3–Na_2SO_4), and the solvent was removed giving brown oils, which were purified by molecular distillation to give almost quantitative yields (98, 94, and 99%, respectively) of lactone **6** as a colorless oil. Identifications were made by tlc and ir and ^1H nmr spectroscopic comparison with an authentic sample.

Treatment of ***4*** *with acids*

(a) Trifluoroacetic acid

(*i*) A solution of **4** (152 mg, 1.00 mmol) in freshly distilled trifluoroacetic acid (10 mL) was stirred at room temperature. After 10 days the reaction mixture was poured into ice-water (ca. 60 g) with stirring, and extracted with dichloromethane (3 × 50 mL). The combined extracts were dried (K_2CO_3–Na_2SO_4), and the solvent was removed to give a yellow oil (139 mg) that had ir and ^1H nmr spectra and tlc behavior identical with those of the starting material.

(*ii*) A solution of **4** (the material recovered from the treatment with trifluoroacetic acid above; 139 mg) in freshly distilled trifluoroacetic acid (10 mL) was boiled under reflux under nitrogen for 20 h. Work-up in the usual manner gave an oil that had ir and ^1H nmr spectra identical with those of the starting material.

(b) Formic acid – sulfuric acid

A solution of **4** in formic acid – sulfuric acid (9:1) was stirred at room temperature for 14 h. Work-up in the usual manner gave an oil that had ir and nmr spectra identical with those of the starting material.

(c) Sulfuric acid

(*i*) A solution of **4** (152 mg, 1.00 mmol) in 10% sulfuric acid (50 mL) was stirred at room temperature. After 36 h the reaction mixture was extracted with dichloromethane (3 × 50 mL). The combined extracts were dried (K_2CO_3–Na_2SO_4) and the solvent was removed to give a colorless oil (146 mg) that had ir and ^1H nmr spectra and tlc behavior identical with those of the starting material.

(*ii*) A solution of **4** in 50% sulfuric acid was found to return **4** unchanged after 6 days at room temperature.

(*iii*) A solution of **4** (760 mg, 5.00 mmol) in concentrated sulfuric acid (10 mL) was stirred at room temperature for ca. 24 h. Work-up in the usual manner gave a brown oil, which was purified by molecular distillation to give a colorless oil (48 mg, 67%) that had ir, ^1H nmr, and mass spectra and tlc behavior identical with those of lactone **6**.

(*iv*) A solution of **4** (1.52 g, 10.00 mmol) in concentrated sulfuric acid (20 mL) was stirred at room temperature for 10 min. Work-up in the usual manner gave a yellow oil which was dissolved in dichloromethane; the solution was washed with aqueous 5% sodium carbonate (5 × 50 mL), dried, and concentrated under reduced pressure to give a yellowish oil (1.31 g, 86%) that consisted of a mixture of **5** and **6** in a ratio of 5:3 with only a trace of **4**. The mixture was chromatographed on a column of silica gel that had been packed in dichloromethane. Lactone **5** was recovered and sublimed to give **5** (14) as plates, mp 68–69°C; ir ν_{max}: 1721 cm^{-1}; ^1H nmr δ: 0.84–1.60 (m, 4H), 1.74–2.60 (m, with a prominent s at 2.53; 7H), 4.79 (m, 1H). Exact Mass calcd. for $C_9H_{12}O_2$ (m/z): 152.0837; found: 152.0836. Anal. calcd. for $C_9H_{12}O_2$: C 71.02, H 7.95; found: C 71.04, H 7.95.

*Treatment of norborn-5-ene-endo-2-acetic acid (****30****) and norborn-5-ene-*exo*-2-acetic acid (****31****) with sulfuric acid. Formation of* ***4****,* ***5****,* ***6****, and* exo*-2-hydroxynorbornane-*syn*-7-acetic acid (****33****)*

A solution of a mixture of **30** and **31** (3, 11) (760 mg, 5.00 mmol) in 50% aqueous sulfuric acid (20 mL) was stirred at room temperature. After 2.5 h the reaction mixture was poured onto ice and extracted with dichloromethane (5 × 50 mL). The combined extracts were dried (K_2CO_3–Na_2SO_4) and the solvent was removed under reduced pressure to give the crude product as a yellow oil (729 mg). The crude product was chromatographed on a column of silica gel that had been packed in dichloromethane. Upon elution with dichloromethane four fractions were collected.

Concentration of the first fraction under reduced pressure and sublimation of the resulting oil afforded lactone **4** (121 mg, 16% as plates), mp 69–70°C. Mixture with an authentic sample of **4** did not depress the mp. Its ^1H nmr and ir spectra were identical to those of this sample.

The second fraction was concentrated under reduced pressure and the residue was molecularly distilled (94–97°C/0.02 Torr) to give **33** (11) (175 mg, 23%) as a colorless oil; ir ν_{max}: 1727 cm^{-1}; ^1H nmr δ: 1.10–2.73 (m, 11H), 4.38 (m, 1H); m/z: 152 (11) (M^+).

The third fraction was concentrated under reduced pressure. Thin-layer chromatography (silica gel/dichlormethane–benzene, 1:1) revealed it to be a mixture of **5** and **33**. This mixture was separated on a plate of silica gel eluted with dichloromethane–benzene (1:1) to give **5** (38 mg, 5%) as a colorless oil, which matched an authentic sample of **5** in every respect.

The last fraction was concentrated under reduced pressure. Distillation of the residue (97–98°C/0.025 Torr) afforded lactone **6** (220 mg, 29%) as a colorless oil, which was identified by ir, ^1H nmr, and tlc comparison with an authentic sample of **6**.

Can. J. Chem. Downloaded from www.nrcresearchpress.com by 109.225.110.28 on 09/08/12
For personal use only.

Treatment of ethyl exo-*5-acetyloxy*-endo-*2-hydroxynorbornane*-exo-*2-acetate (35) with sulfuric acid. Formation of* endo-*5-acetyloxy*-exo-*2-hydroxy- and* exo-*2*,endo-*5-dihydroxynorbornane-1-acetic acid γ-lactones (38 and 39) and* exo-*2-acetyloxy-1-hydroxy- and 1*,exo-*2-dihydroxynorbornane*-syn-*7-acetic acid γ-lactones (40 and 41)*

A solution of **35** (3) (2.56 g, 10.00 mmol) in 50% sulfuric acid (100 mL) was stirred at room temperature. After 60 h the reaction mixture was poured into ice-water (200 g) with stirring and extracted with dichloromethane (2 × 200 mL). The combined extracts were dried (K_2CO_3–Na_2SO_4), and the solvent was removed to give a yellow oil (1.99 g), which was chromatographed on a column of silica gel (ca. 60 g) that was packed in and eluted with dichloromethane. Two major fractions were collected. The first fraction was concentrated under reduced pressure and molecularly distilled (89–93°C/0.025 Torr) to give a colorless oil (630 mg, 30%). Thin-layer chromatography (silica gel/dichloromethane) revealed two unresolved spots. Further attempts to separate this mixture by tlc were unsuccessful. This mixture was identified as a 1:1 mixture of **38** and **40** (3); ir ν_{max}: 1770, 1736 cm^{-1}; ^1H nmr δ: 1.00–2.70 (m, with prominent s's at 2.03 and 2.56; 12H), 4.20 (d of m, 0.5H), 4.76 (m, 0.5H), 5.10 (m, 0.5H).

The second fraction (822 mg, 49%) was found to be a mixture of approximately equal amounts of **39** and **41**. To the mixture (822 mg, 4.90 mmol) Girard reagent T (12) (1.00 g) and acetic acid (1 mL) in 95% ethanol (10 mL) were added and the solution was boiled under reflux for 45 min, and then cooled. Ether (20 mL), water (20 mL), and saturated aqueous sodium chloride (10 mL) were added. The ether layer was separated, dried (K_2CO_3–$MgSO_4$), and concentrated under reduced pressure to give a yellowish oil (415 mg, 51%), shown by ^1H nmr spectroscopy to be an 85:15 mixture of **39** and **41**; ir ν_{max}: 3510 (w), 3355 (w), 1770, 1742 (w) cm^{-1}; ^1H nmr δ: 0.92–2.55 (m, with prominent ABq at 2.51, J = 16 Hz; 11H), 3.13 (s, 1.15H; absent after D_2O treatment), 4.04 (d of m, J_{app} = 3 Hz; 0.15H), 4.25 (d of d, J = 3 and 7 Hz; 1H), 4.35 (m, 1H).

The aqueous layer was separated, treated with concentrated hydrochloric acid (1 mL), and heated on a steam bath for 1 h. Additional ether (40 mL) was added and the ether extract was removed, dried (K_2CO_3–$MgSO_4$), and concentrated under reduced pressure. The residue was subjected to molecular distillation (103–104°C/0.025 Torr) to give **41** (271 mg, 33%) as a colorless, viscous oil; ir ν_{max}: 3510 (w), 3400 (w), 1776 cm^{-1}; ^1H nmr δ: 1.50–2.22 (m, 7H), 2.57, (m, 3H), 2.74 (br s, 1H; absent after D_2O treatment), 4.04 (d of m, J_{app} = 3 Hz; 1H). Anal. calcd. for $C_9H_{12}O_3$: C 64.27, H 7.19; found: C 64.38, H 7.15.

Hydrolysis of 4. Formation of exo-*2-hydroxynorbornane-1-acetic acid (51)*

To a solution of **4** (1.52 g, 10.0 mmol) in ethanol (30 mL) was added potassium hydroxide (5.60 g) with continuous swirling. The mixture was heated on a steam bath for 30 min followed by stirring without external heating for 3 h. Water (100 mL) was added, and the total volume was reduced on a rotary evaporator to ca. 75 mL. The concentrate was acidified to pH 4 with 6 N sulfuric acid while the temperature was maintained at 0–5°C. The solution was immediately extracted with dichloromethane (5 × 50 mL), and the combined extracts were washed with water (50 mL), and dried. The solvent was removed to give a white solid (1.50 g), which was crystallized from ether followed by sublimation at 67°C/0.125 Torr to give **51** (1.20 g, 70%), mp 93–94.5°C; ir ν_{max}: 3610–2410, 1706 cm^{-1}; ^1H nmr δ: 1.00–2.08 (m, 8H), 2.10–2.30 (m, 1H), 2.67 (ABq, J = 14 Hz; 2H), 3.66–3.92 (d of m, 1H), 6.50 (s, 2H; absent after D_2O treatment); m/z: 170 (2) (M^+). Anal. calcd. for $C_9H_{14}O_3$: C 63.51, H 8.28; found: C 63.41, H 8.25.

Oxidation of 51. Formation of 2-oxonorbornane-1-acetic acid (52)

A solution of **51** (170 mg, 1.00 mmol) in acetone was cooled to 5–10°C, stirred, and titrated with a freshly prepared solution of Jones reagent[11] until the orange color persisted for 1 h. The excess oxidant was destroyed by the dropwise addition of methanol. The solution was concentrated under reduced pressure and the residue was dissolved in chloroform. The solution was dried, and the solvent was removed. Molecular distillation (115–117°C/0.125 Torr) of the residue afforded **52** (166 mg, 99%) as a colorless oil that solidified on cooling to give **52** as needles, mp 57–59°C; ir ν_{max}: 3570–2440, 1739, 1706 cm^{-1}; ^1H nmr δ: 1.10–2.32 (m, 8H), 2.36–3.00 (m, with prominent ABq at 2.73, J = 17 Hz; 3H), 11.15 (s, 1H); m/z: 168 (M^+). Anal. calcd. for $C_9H_{12}O_3$: C 64.27, H 7.19; found: C 64.13, H 7.21.

Hydrogenation of 52. Formation of endo-*2-hydroxynorbornane-1-acetic acid (53)*

To a solution of **52** (210 mg, 1.20 mmol) in acetic acid (25 mL) was added platinum oxide (20 mg), and the mixture was shaken under hydrogen (3.5 atm; 1 atm = 101.3 kPa) at room temperature for 6 h. The reaction mixture was filtered and stripped of acetic acid by distillation under reduced pressure to give a yellow oil, which was crystallized from chloroform to give **53** (64 mg, 92%) as plates, mp 205–207°C (dec.), mixture mp with its *exo* isomer **51**, 39–68°C; ir ν_{max}: 3510–2325, 1704 cm^{-1}; ^1H nmr δ: 0.80–2.30 (m, 9H), 2.65 (s, 2H), 3.88–4.32 (d of m, 1H), 6.66 (br s, 2H; absent after D_2O treatment); m/z: 170 (4) (M^+). Anal. calcd. for $C_9H_{14}O_3$: C 63.51, H 8.28; found: C 63.69, H 8.23.

Reduction of 52 with sodium borohydride. Formation of 51 and 53

To a solution of **52** (183 mg, 1.10 mmol) in ethanol (10 mL) was added sodium borohydride (6.7 mg) portionwise over 5 min and the mixture was then poured into ice-water (ca. 50 g). The solution was saturated with sodium chloride and extracted with ether (4 × 50 mL). Evaporation of the ether under reduced pressure afforded a yellow oil (160 mg) that was shown to be a mixture of lactone **4** and the epimeric acids **53** and **51** in a 5:2 ratio by ir and ^1H nmr spectroscopic and tlc comparison with authentic samples.

Oxidation of 53. Regeneration of 52

A solution of **53** (50 mg) in acetone (25 mL) was cooled to 5–10°C, stirred, and titrated with a freshly prepared solution of Jones reagent[11] until the orange color persisted for 1 h. The excess oxidant was destroyed by dropwise addition of methanol. The acetone layer was separated and concentrated under reduced pressure. The residue was dissolved in chloroform, the solution was dried, and the solvent was removed to give **52** as a colorless oil, identified by ir and ^1H nmr spectroscopic comparison with an authentic sample.

Lactonization of 53. Formation of endo-*2-hydroxynorbornane-1-acetic acid lactone (54)*

To a solution of **53** (170 mg, 1.00) in dry pyridine (10 mL) was added benzenesulfonyl chloride (700 mg, 4.00 mmol), and the mixture was boiled under reflux under nitrogen for 15 min. The reaction mixture was cooled to room temperature and poured into ice-water (ca. 30.00 g). The mixture was extracted with chloroform (3 × 25 mL), and the combined extracts were washed with cold 10% hydrochloric acid (2 × 50 mL) to remove pyridine and then with water, dried (K_2CO_3–Na_2SO_4), and concentrated under reduced pressure to a viscous, pale yellow oil. Thin-layer chromatography (silica gel – dichloromethane) revealed one new spot in addition to that which corresponded to **53**. Analysis of the ^1H nmr and ir spectra indicated that this new compound is the *endo* lactone **54**, ir ν_{max}: 1776 cm^{-1}; ^1H nmr δ: 4.82 (m).

Hydrolysis of 5. Formation of endo-*6-hydroxynorbornane*-endo-*2-acetic acid and its potassium salt 56*

(*i*) To a solution of **5** (152 mg, 1.00 mmol) in ethanol (25 mL) was added potassium hydroxide (3.00 g) with continuous swirling. The mixture was heated on a steam bath for 30 min followed by stirring without external heating for ca. 5 h. Water (100 mL) was added and the total volume was reduced under reduced pressure to

[11]Reference 12, pp. 142–143.

Can. J. Chem. Downloaded from www.nrcresearchpress.com by 109.225.110.28 on 09/08/12
For personal use only.

ca. 20 mL. The concentrate was acidified to pH 6 with concentrated hydrochloric acid while the temperature was maintained below 5°C. Solid sodium chloride was added to saturate the solution, which was immediately extracted with ethyl acetate (2 × 25 mL), and the combined extracts were dried. The solvent was removed under reduced pressure to give a pale yellow oil that was identified as **5** by ir, ^{1}H nmr, and tlc comparison.

(*ii*) The hydrolysis was repeated as in (*i*). The aqueous ethanolic solution was treated with ether (250 mL) and the precipitate was collected, washed with dry ether, and air-dried to give potassium *endo*-6-hydroxynorbornane-*endo*-2-acetate (**56**) as a white solid (186 mg, 97%); ir (KBr) ν_{max}: 1575, 1414 cm^{-1}; ^{1}H nmr δ(D_2O): 0.8–2.7 (m, 11H), 4.12–4.51 (m, 1H).

*Oxidation of **56**. Formation of 6-oxonorbornane-*endo*-2-acetic acid (**57**)*

To an aqueous solution of **56** (186 mg, 0.97 mmol, in 10 mL of water) ruthenium dioxide (6 mg) was added. The mixture was cooled to ca. 15°C and vigorously stirred while a solution containing ca. 10% of the stoichiometric amount of sodium periodate was added. The solution developed a yellow color indicating the presence of ruthenium tetroxide. Upon the precipitation of the black ruthenium dioxide another aliquot of sodium periodate was added. Each successive addition required more time for the disappearance of the yellow color of the tetroxide. After the addition of a slight excess of periodate the remaining ruthenium tetroxide was destroyed with isopropyl alcohol. The solution was acidified with 6 N hydrochloric acid to ca. pH 4 and extracted with ethyl acetate (5 × 20 mL). The combined extracts were dried, and the solvent removed under reduced pressure. The residue was crystallized from ether – ethyl acetate followed by sublimation to give **57** (125 mg, 77%), mp. 97–99°C (lit. (15) mp 96–97°C); ir ν_{max}: 3450–2355, 1742, 1715 cm^{-1}; ^{1}H nmr δ: 0.83–2.67 (m, 11H), 10.04 (br s, 1H; absent after D_2O treatment).

*Hydrolysis of **33**. Formation of* exo-*2-hydroxynorbornane*-syn-*7-acetic acid (**58**)*

To a solution of **33** (304 mg, 2.00 mmol) in ethanol (40 mL) was added potassium hydroxide (4.00 g) with continuous stirring. The mixture was heated on a steam bath for 30 min followed by stirring without external heating for 2 h. Water (100 mL) was added and the total volume was reduced under reduced pressure to ca. 15 mL. The concentrate was acidified to pH 4 with concentrated hydrochloric acid while the temperature was maintained below 5°C. The solution was saturated with sodium chloride and extracted with dichloromethane (3 × 50 mL). The combined extracts were dried and stripped of solvent under reduced pressure to give a pale yellow oil. Molecular distillation (106–109°C/0.02 Torr) afforded **58** (282 mg, 83%) as a colorless, viscous oil; ir ν_{max}: 3570–2380, 1695 cm^{-1}; ^{1}H nmrδ: 0:90–2.48 (m, 11H), 3.74 (d of d, J = 3 and 6 Hz; 1H), 7.10 (br s, 2H; absent after D_2O treatment). Anal. calcd. for $C_9H_{14}O_3$: C 63.51, H 8.28; found: C 63.45, H 8.21.

*Oxidation of **58**. Formation of 2-oxonorbornane-*syn-*7-acetic acid (**59**)*

A solution of **58** (255 mg, 1.50 mmol) in acetone was cooled in an ice-bath, stirred, and titrated with Jones reagent[11] until the orange color persisted for 10 min. The excess oxidant was destroyed by dropwise addition of methanol until the solution became colorless. The solution was concentrated under reduced pressure, and the residue was dissolved in dichloromethane (50 mL). The solution was dried, and the solvent was removed. Molecular distillation (117–119°C/0.025 Torr) of the residue gave **59** (232 mg, 92%) as a colorless oil; ir ν_{max}: 3579–2410, 1754, 1724 cm^{-1}; ^{1}H nmr δ: 0.92–2.60 (m, 11H), 11.67 (s, 1H; absent after D_2O treatment). Anal. calcd. for $C_9H_{12}O_3$: C 64.26, H 7.19; found: C 63.86, H 7.35.

*Hydrogenation of **59** in acetic acid. Formation of* endo-*2-acetyloxynorbornane*-syn-*7-acetic acid (**60**)*

To a solution of **59** (168 mg, 1.00 mmol) in acetic acid (15 mL) was added platinum oxide (10.00 mg), and the mixture was shaken under hydrogen (3.5 atm) at room temperature for 61 h. The reaction mixture was filtered, diluted with water (30 mL), and stripped of solvent by distillation under reduced pressure to give a yellow oil, which was molecularly distilled (85–88°C/0.02 Torr) to give **60** (201 mg, 95%) as a colorless oil; ir ν_{max}: 3570–2485, 1727 cm^{-1}; ^{1}H nmr δ: 0.85–2.54 (m, with a prominent s at 2.07; 14H), 4.76–5.15 (m, 1H), 10.32 (br s, 1H; absent after D_2O treatment). Exact Mass calcd. for $C_{11}H_{16}O_4$: 212.1049; found: 212.1068.

*Hydrolysis of **60**. Formation of* endo-*2-hydroxynorbornane*-syn-*7-acetic acid (**61**)*

To a solution of **60** (106 mg, 0.50 mmol) in ethanol (15 mL) was added potassium hydroxide (2.00 g) with continuous swirling. The mixture was heated on a steam bath for 30 min followed by stirring without external heating for 3 h. Water (30 mL) was added, and the total volume was reduced on a rotary evaporator to ca. 10 mL. The concentrate was acidified to pH 4 with 6 N sulfuric acid while the temperature was maintained at 0–5°C. The solution was immediately extracted with dichloromethane (5 × 10 mL), and the combined extracts were washed with water (2 × 10 mL) and dried. The solvent was removed under reduced pressure to give a colorless, viscous oil, which was molecularly distilled (64–68°C/0.005 Torr) to give **61** (51 mg, 60%) as a colorless, viscous oil; ir ν_{max}: 3570–2380, 1695 cm^{-1}; ^{1}H nmr δ: 0.77–2.48 (m, 11H), 4.06 (m, 1H), 7.30 (br s, 2H; absent after D_2O treatment). Exact Mass calcd. for $C_9H_{14}O_3$: 170.0947; found: 170.0943.

*Oxidation of **39**. Formation of* exo-*2-hydroxy-5-oxo-norbornane-1-acetic acid lactone (**62**)*

A solution of **39** (86% purity) (400 mg, 2.38 mmol) in acetone was cooled to 5–10°C, stirred, and titrated with a freshly prepared solution of Jones reagent[11] until the orange color persisted for 2 min. The excess oxidant was destroyed by dropwise addition of methanol. The acetone layer was concentrated under reduced pressure, and the residue was dissolved in dichloromethane. The solution was dried and the solvent was removed. Sublimation (65–67°C, 0.005 Torr) of the residue afforded **62** (291 mg, 73%) as white plates, mp 137–139°C; ir ν_{max}: 1776, 1751 cm^{-1}; ^{1}H nmr δ: 1.84 (s, 2H), 2.07 (m, 2H), 2.20 (ABq, J = 18 Hz; 2H), 2.73 (m, with sharp s at 2.73; 3H), 4.34 (t, J = 5 Hz; 1H). Exact Mass calcd. for $C_9H_{10}O_3$: 166.0629; found: 166.0634. Anal. calcd. for $C_9H_{10}O_3$: C 65.05, H 6.07; found: C 64.54, H 6.11.

*Oxidation of **41**. Formation of 1-hydroxy-2-oxonorbornane-*syn-*7-acetic acid lactone (**63**)*

A solution of **41** (168 mg, 1.00 mmol) in acetone was cooled to 0–5°C, stirred, and titrated with a freshly prepared solution of Jones reagent[11] until the orange color persisted for 2 min. The excess oxidant was destroyed by dropwise addition of methanol. The acetone layer was concentrated under reduced pressure, and the residue was dissolved in dichloromethane. The solution was dried and the solvent was removed. The oily residue was molecularly distilled (70–71°C, 0.005 Torr) to give **63** (118 mg, 71%) as a colorless oil; ir ν_{max}: 1772, 1751 cm^{-1}; ^{1}H nmr δ: 1.8–2.3 (m, 7H), 2.65 (m, 1H), 2.94 (m, 2H). Exact Mass calcd. for $C_9H_{10}O_3$: 166.0630); found: 166.0627.

Acknowledgment

We thank the Natural Sciences and Engineering Research Council of Canada for support of this work.

1. D. Lenoir, Y. Peloig, D. Arad, and P. von R. Schleyer. J. Org. Chem. **53**, 661 (1988).
2. C. K. Johnson and C. J. Collins. J. Am. Chem. Soc. **96**, 2514 (1974); C. J. Collins, C. K. Johnson, and V. F. Raaen. J. Am. Chem. Soc. **96**, 2524 (1974).

3. P. Yates and M. Kaldas. Can. J. Chem. **70**, 1492 (1992).
4. F. Lauria, V. Vecchietti, W. Logemann, G. Tosolini, and E. Dradi. Tetrahedron, **25**, 3989 (1969).
5. W. R. Vaughan, B. A. Gross, S. F. Burkle, M. A. Langell, R. Caple, and D. B. Oakes. J. Org. Chem. **48**, 4792 (1983); P. C. Moes, J. R. Knox, and W. R. Vaughan. J. Am. Chem. Soc. **100**, 1978 (1978).
6. J. March. Advanced organic chemistry. 3rd ed. Wiley, New York. 1985. p. 247.
7. W. R. Vaughan, J. Wolinsky, R. R. Deultgen, S. Greey, and F. S. Seichter. J. Org. Chem. **35**, 400 (1970).
8. W. F. Erman. Chemistry of the monoterpenes. Marcel Dekker, Inc., New York. 1985. pp. 1120–1124.
9. R. P. Haseltine and T. S. Sorensen. Can. J. Chem. **53**, 1067 (1975).
10. R. R. Sauers and P. E. Sonnet. Tetrahedron, **20**, 1029 (1964).
11. D. I. Davies and M. D. Dowle. J. Chem. Soc. Perkin Trans. 1, 227 (1978).
12. L. F. Fieser and M. Fieser. Reagents for organic synthesis. Vol. 1. Wiley. 1867. pp. 410–411.
13. S. Torii, T. Inokuchi, and K. Kondo. J. Org. Chem. **50**, 4980 (1982); E. J. Corey and A. W. Gross. Tetrahedron Lett. **25**, 4291 (1985); W. E. Fristad and J. R. Peterson. J. Org. Chem. **50**, 10 (1985).
14. A. Nickon, H. R. Kwasnik, C. T. Mathew, T. D. Swartz, R. O. Williams, and J. B. Digiorgio. J. Org. Chem. **43**, 3904 (1978).
15. K. Naemura and M. Kakazaki. Bull. Soc. Chem. Jpn. **46**, 888 (1983).

Can. J. Chem. Downloaded from www.nrcresearchpress.com by 109.225.110.28 on 09/08/12
For personal use only.

Photodissolution of iron oxides. IV. A comparative study on the photodissolution of hematite, magnetite, and maghemite in EDTA media

MARTA I. LITTER AND MIGUEL A. BLESA[1]

Departamento Quimica de Reactores, Comision Nacional de Energia Atomica, Av. del Libertador 8250, 1429 Buenos Aires, Argentina

Received July 15, 1991[2]

MARTA I. LITTER and MIGUEL A. BLESA. Can. J. Chem. **70**, 2502 (1992).

The thermal and 254-nm photochemical dissolution reactions of magnetite (Fe_3O_4), maghemite (γ-Fe_2O_3), and hematite (α-Fe_2O_3) suspended in EDTA aqueous solutions were compared. γ-Fe_2O_3 and Fe_3O_4 are thermally and photochemically more reactive than α-Fe_2O_3. Both thermal and photochemical dissolution reactions are governed by an initiation step, which involves the production of Fe^{II}_{aq}, and a subsequent thermal reaction of these ions with the solid, to produce Fe^{III}_{aq}. The initiation step under UV irradiation involves the photoreduction of surface $>Fe^{III}$ – EDTA complexes to yield Fe^{II}_{aq} and the photooxidation of adsorbed EDTA to yield CH_2O and other oxidation products. After Fe^{III} – EDTA complexes build up in solution through the following step, homogeneous photolysis is the main source of Fe^{II} and CH_2O. Oxides with spinel type structure are characterized by faster rates in the two processes, and O_2 may inhibit the dissolution processes by changing the stoichiometry of the initiation step to that of the autooxidation of EDTA. The relative importance of autooxidation and photodissolution depends on the nature of the oxide and the experimental conditions. Photooxidation reaction rates parallel those of the photodissolution initiation steps, and long-term stability towards photocorrosion (dissolution) implies low photocatalytic activity for the oxidation of EDTA. The set of differential equations describing all the reaction rates is discussed and applied to the different cases.

MARTA I. LITTER et MIGUEL A. BLESA. Can. J. Chem. **70**, 2502 (1992).

On a comparé les réactions de dissolutions thermiques et photochimiques, à 254 nm, de la magnétite (Fe_3O_4), de la maghemite (γ-Fe_2O_3) et de l'hématite (α-Fe_2O_3) suspendues dans des solutions aqueuses d'EDTA. Le γ-Fe_2O_3 et le Fe_3O_4 sont thermiquement et photochimiquement plus réactifs que l'α-Fe_2O_3. Les réactions de dissolutions tant thermiques que photochimiques sont régies par une étape d'initiation, impliquant la production de Fe^{II}_{aq}, et une réaction thermique subséquente de ces ions avec le solide, conduisant à la formation de Fe^{III}_{aq}. L'étape d'initiation sous irradiation UV implique la photoréduction des complexes superficiels $>Fe^{III}$ – EDTA en Fe^{II}_{aq} et la photo-oxydation de l'EDTA adsorbé en CH_2O et en d'autres produits d'oxydation. Les oxydes dont la structure ressemble à celle de la spinnelle sont caractérisés par des vitesses de réactions des deux processus qui sont plus rapides, et l'O_2 peut inhiber les processus de dissolution en changeant la stoechiométrie de l'étape d'initiation vers celle de l'auto-oxydation de l'EDTA. L'importance relative de l'auto-oxydation et de la photo-dissolution dépend de la nature de l'oxyde et des conditions expérimentales. Les vitesses des réactions de photo-oxydation sont parallèles à celles des étapes de l'initiation de la photo-dissolution, et la stabilité à long terme vis-à-vis de la photocorrosion (dissolution) implique une faible activité photocatalytique pour l'oxydation de l'EDTA. On discute de l'ensemble des équations différentielles décrivant toutes les vitesses de réaction et on les applique aux differents cas.

[Traduit par la rédaction]

Introduction

The main kinetic features of the dissolution of magnetite in aqueous solutions have been established in a series of previous papers (see ref. 1 and references therein; see also refs. 2–9); analogous data for other iron oxides and oxohydroxides are less abundant (1, 5, 9–14). From the existing data it seems safe to conclude that the basic mechanisms are of general application to all iron oxides, but the actual rates of dissolution may span various orders of magnitude.

It is well known (15) that corrosion of semiconducting oxides may imply transfer of holes (h^+) from the valence band to the reductant and of electrons (e^-) from the conduction band, in the case of iron(III) oxides, as Fe^{II}. Because of this fact, photochemical dissolution is possible, and has been studied in a series of papers by others (13, 14, 16–25) and by us (26–28). It is well established that electron transfer reactions take place through localized sites of the semiconductor; the formation of surface complexes by adsorption of adequate ligands is equivalent in semiconductor terminology to the formation of extrinsic surface states. These surface complexes may trap e^- and (or) h^+ very efficiently (29), thus enhancing photodissolution and photocatalytic rates. The participation of individual Fe^{III} centers in the photochemical reactions of iron oxides has been considered (22, 30). Indeed, the usage of the surface complexation formalism leads to an adequate description of photocatalytic activity and photocorrosion, irrespective of whether primary light absorption involves the particle or the surface complex (25, 26). Spinel type oxides, such as γ-Fe_2O_3 or Fe_3O_4, are known to be more easily photocorroded than α-Fe_2O_3; it has been proved that this corundum structure is characterized by a fast surface recombination of the generated e^-/h^+ pairs (31, 32). Moreover, it has been shown that the existence of spinel phase inclusions in the α-Fe_2O_3 corundum structure enhances its photocatalytic reactivity for H_2 production (33). Hematite is called "photostable" because the optical transition that generates the electron-hole pairs is metal-ion centered (*d–d*) and does not affect Fe—O bonds (34). Consequently, because of the narrowness of *d*-bands and the consequent low mobility of holes, it has very poor photocatalytic properties. In this paper we show that the higher photocatalytic activity expected for spinel-type oxides derives easily in photodissolution, thus making these materials less promising for the photooxidation of organic matter.

Because of the electrochemical nature of the thermal dissolution of iron oxides, much can be learnt about these open circuit processes by studying the influence of light; in a pre-

[1]Author to whom correspondence may be addressed.

[2]Revision received April 14, 1992.

Can. J. Chem. Downloaded from www.nrcresearchpress.com by 109.225.110.28 on 09/08/12
For personal use only.

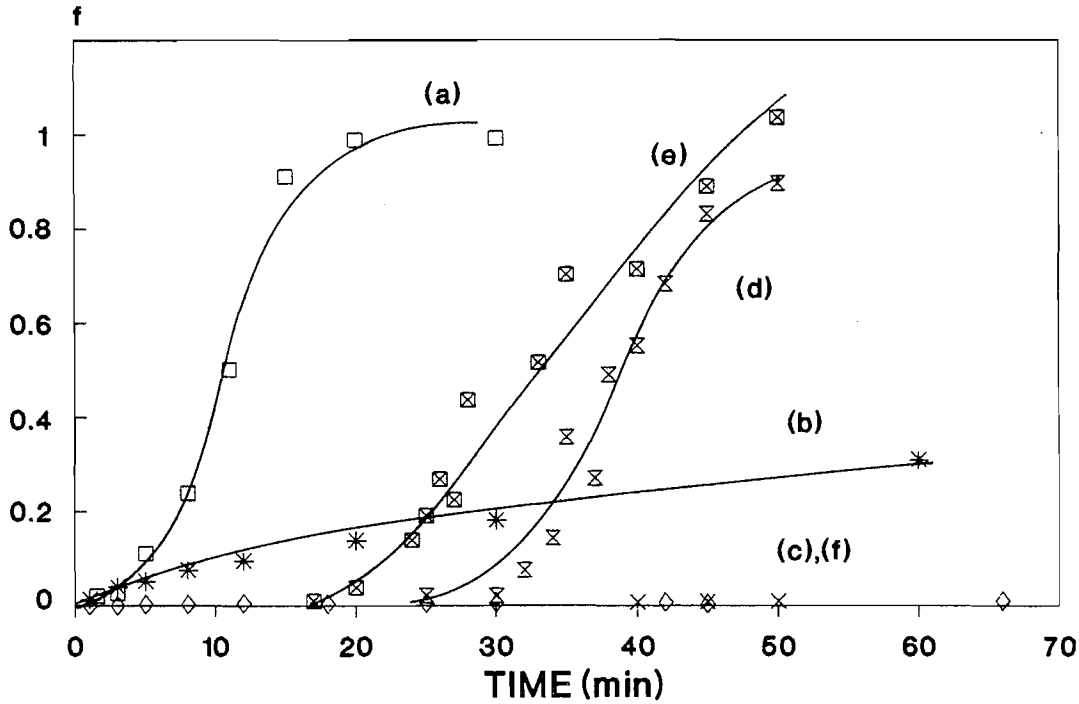

FIG. 1. Iron fraction dissolved from iron oxides by EDTA at 30°C and pH 3 as a function of time. [Oxide] = 1 g dm^{-3} in the thermal experiments and 0.5 g dm^{-3} in the photochemical experiments; [EDTA] = 2×10^{-2} mol dm^{-3}. (*a*): Fe_3O_4, thermal, $[Fe^{2+}]_0 = 5.6 \times 10^{-5}$ mol dm^{-3} (□); (*b*): γ-Fe_2O_3, thermal, $[Fe^{2+}]_0 = 5.1 \times 10^{-5}$ mol dm^{-3} (*); (*c*): α-Fe_2O_3, thermal, $[Fe^{2+}]_0 = 6.1 \times 10^{-5}$ mol dm^{-3} (◇); (*d*): Fe_3O_4, λ = 254 nm, $[Fe^{2+}] = 0$ (⧖); (*e*) γ-Fe_2O_3, λ = 254 nm, $[Fe^{2+}] = 0$ (⊠); (*f*) α-Fe_2O_3, λ = 254 nm, $[Fe^{2+}] = 0$ (×).

vious paper (28), we discussed the interrelationship between thermal and light-promoted maghemite dissolution in the presence of reductive ligands. This approach is extended in this paper to include other iron oxides; the results of a comparative study of the thermal and photochemical dissolution of α-Fe_2O_3, γ-Fe_2O_3, and Fe_3O_4 in aqueous solutions containing EDTA are presented here, and used to derive values of rate constants for the individual stages of the mechanism: the initial slow photochemical dissolution of reductive stoichiometry, and the following fast thermal dissolution by electron exchange between surface $>Fe^{III}$ centers and adsorbed Fe^{II} complexes.

The widespread interest in iron oxide dissolution reflects the relevance of these processes in fields such as transport of contaminants in waters, metal corrosion, decontamination of nuclear reactors, and mobilization of metals in aquatic systems (35–38).

Experimental

Maghemite (γ-Fe_2O_3) was a commercial sample and was the same as used in previous studies (26–28); its specific surface area was 25 m^2 g^{-1}. Hematite (α-Fe_2O_3) was a commercial sample (Mallinckrodt); its specific surface area was 9.8 m^2 g^{-1}. Magnetite (Fe_3O_4) was prepared as previously described (39); it was composed of cubo-octahedral particles of 0.26 μm average edge length, and its specific surface area was 5.5 m^2 g^{-1}.

The three oxides were characterized by chemical analyses, X-ray diffractometry, SEM, and BET surface area measurements.

Reagents were of analytical purity or better and were used without further purification. Water was bidistilled in a quartz apparatus. Dilute H_2SO_4 or NaOH were used for pH adjustment.

Thermal and photochemical experiments were carried out as in ref. 28. Thermal reactions were carried out under N_2 atmosphere; in the photochemical experiments, air-saturated suspensions were used in an effort to prevent formaldehyde losses from the system due to N_2 stripping. Furthermore, the effect of dissolved O_2 was of interest.

Total iron was determined by the thioglycolate method (40) and formaldehyde by the chromotropic acid technique (41).

Actinometry at 254 nm was performed by the ferrioxalate method (42), the total incident light intensity per unit solution volume (I_0) being 1.1×10^{-5} einstein s^{-1} dm^{-3}.

The reflectance spectra were obtained on a Shimadzu 210 A spectrophotometer equipped with an integrating sphere. Absorbances were measured in a Metrolab 2500 spectrophotometer.

Results

Spectral characteristics

The reflectance spectral features of α-Fe_2O_3, γ-Fe_2O_3, and Fe_3O_4 are in agreement with those reported previously in the literature (43–47). The three iron oxides present bands assigned to charge-transfer (260–390 nm), spin-flip (420–530 nm), and ligand-field (580–780 nm) transitions.

The principal difference between the reflectance spectra of Fe_3O_4 and the ferric oxides is the lack of the band edge in the visible region. For hematite and maghemite, a sharp increase of the absorptivity is observed below 600 nm, corresponding to a band gap of 2.0 eV, while for magnetite, the band edge is beyond 800 nm. Muret (46) reported a sharp increase in the absorption coefficient at 826 nm (1.5 eV).

Dissolution reactions

The dissolution profiles of Fe_3O_4, γ-Fe_2O_3, and α-Fe_2O_3 in EDTA at pH 3, brought about thermally by added ferrous ions and photochemically by irradiation at 254 nm, are shown in Fig. 1. The extent of dissolution under both experimental conditions is extremely low for hematite (curves *c* and *f*), but the two other iron oxides dissolve faster. In agreement with the results of previous studies of the thermal dissolution in EDTA and oxalic acid media (2, 4, 6), magnetite is

Can. J. Chem. Downloaded from www.nrcresearchpress.com by 109.225.110.28 on 09/08/12
For personal use only.

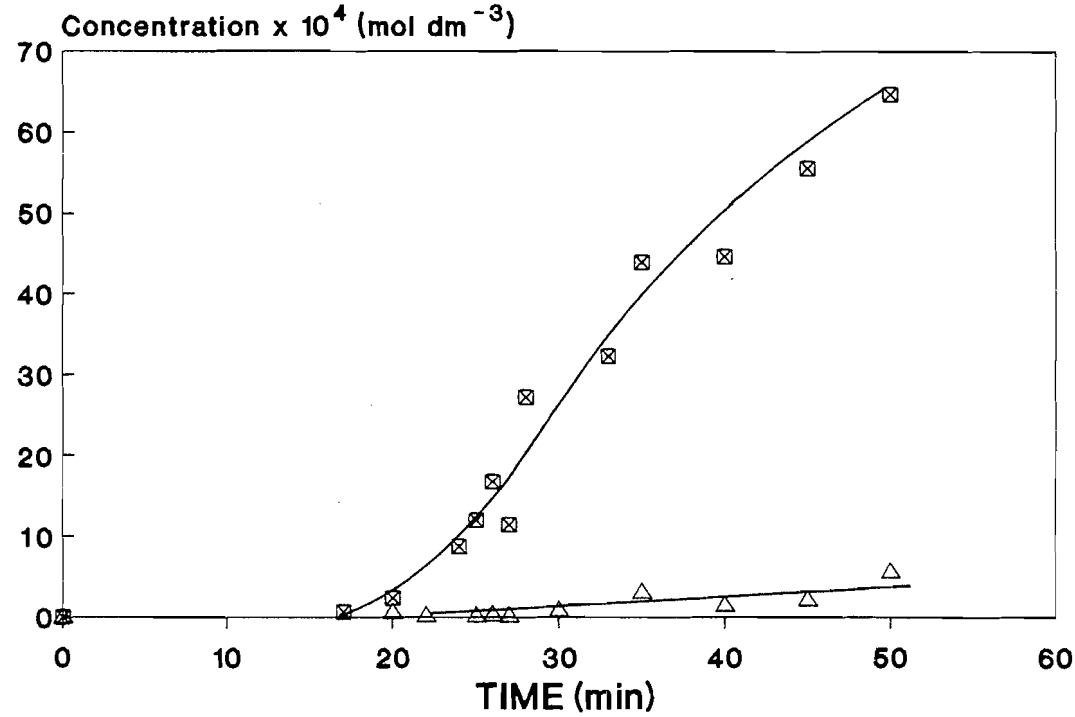

FIG. 2. Comparison of the production rates of iron (⊠) and formaldehyde (△) in the 254-nm photodissolution of γ-Fe_2O_3 (0.5 g dm^{-3}) in EDTA (2×10^{-2} mol dm^{-3}) at pH 3 and 30°C.

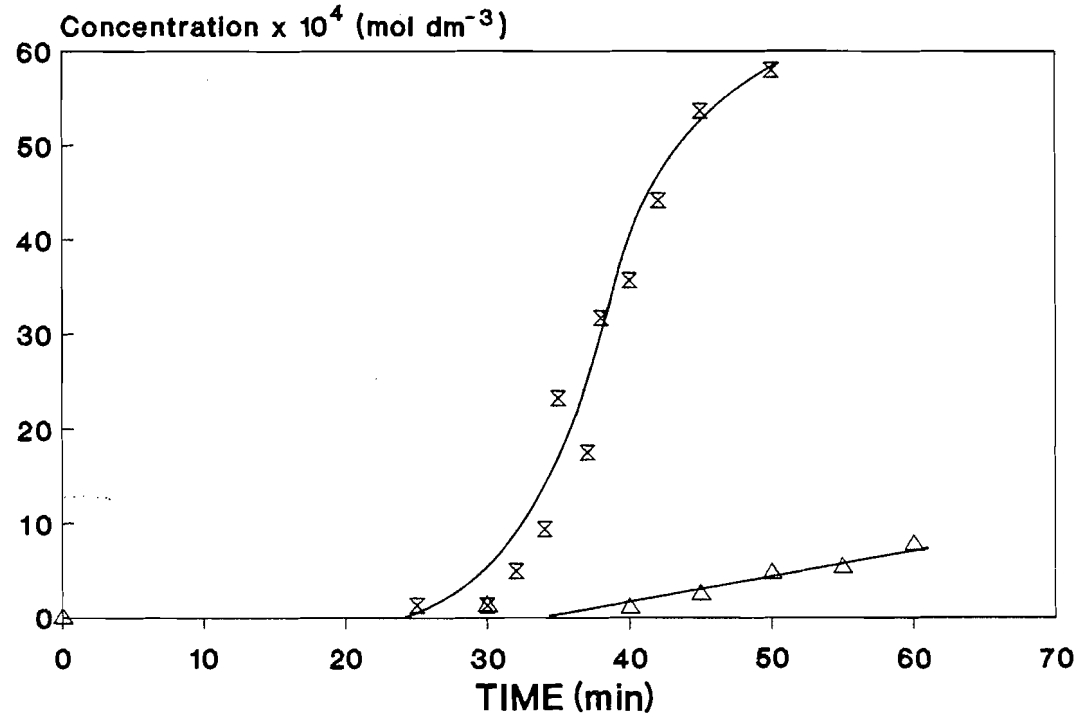

FIG. 3. Comparison of the production rates of iron (⧖) and formaldehyde (△) in the 254-nm photodissolution of Fe_3O_4 (0.5 g dm^{-3}) in EDTA (2×10^{-2} mol dm^{-3}) at pH 3 and 30°C.

characterized by sigmoidal f/t profiles (where $f = (m_0 - m)/m_0$ is the dissolved fraction of total iron and m_0 and m are the initial and instantaneous mass of the iron oxide; t is the reaction time). Practically no induction time is observed in the presence of Fe^{2+} under N_2 atmosphere (curve *a*), but under 254-nm irradiation, in O_2 atmosphere and with no added Fe^{2+} (curve *d*), the reaction presents an induction period. In the case of maghemite, the photodissolution (curve *e*) shows similar behavior to that observed with magnetite. The thermal (dark) dissolution profiles are similar only in the very

Can. J. Chem. Downloaded from www.nrcresearchpress.com by 109.225.110.28 on 09/08/12
For personal use only.

Can. J. Chem. Downloaded from www.nrcresearchpress.com by 109.225.110.28 on 09/08/12
For personal use only.

early stages: whereas magnetite dissolution is acceleratory, the maghemite dissolution rate decreases steadily with reaction time and, furthermore, total dissolution is not observed in the dark (see curve *b*). The dark reaction requires added Fe^{2+}; otherwise negligible dissolution is observed in time span of our experiments.

The formation of formaldehyde was observed only in the photolysis of γ-Fe_2O_3 and Fe_3O_4 suspensions at long reaction times (Figs. 2 and 3).

Discussion

Thermal dissolution

The mechanism of dissolution of iron oxides by reducing ligands in acid media can be described by the following steps (3–6):

(*a*) A fast preequilibrium adsorption step in which surface complexes are formed:

$$[1] \quad >Fe^{III} + L^{n-} \xrightarrow{H^+} >Fe^{III}\text{–}(L^{n-})(H^+)$$

where $>$ denotes the lattice surface of the oxide.

(*b*) Slow dissolution of $>Fe^{III}$–L surface complexes through acid (b_1) or reductive dissolution (b_2) parallel paths:

$$[2] \quad >Fe^{III}\text{–}(L^{n-})(H^+) \xrightarrow{k_1} (Fe^{III}\text{–}L)^{3-n}{}_{aq} (+ H^+) \qquad (b_1)$$

$$[3] \quad >Fe^{III}\text{–}(L^{n-})(H^+) \xrightarrow{k_2} >Fe^{II} + L^{(n-1)-} (+ H^+) \qquad (b_2)$$

$$\text{fast} \downarrow L^{n-}$$

$$(Fe^{II}\text{–}L)^{2-n}{}_{aq}$$

(*c*) A fast reductive reaction between Fe^{II} – L complexes and $>Fe^{III}$ surface centers:

$$[4] \quad >Fe^{III}\text{–}(L^{n-}) + (Fe^{II}\text{–}L)^{2-n}{}_{aq} \xrightarrow[H^+]{k_{Th}} >Fe^{II}\text{–}(L^{n-})(H^+) + (Fe^{III}\text{–}L)^{3-n}{}_{aq}$$

$$\downarrow$$

$$(Fe^{II}\text{–}L)^{2-n}{}_{aq}$$

The overall rate of dissolution can be expressed by the contribution of steps (*b*) and (*c*) by the following expression:

$$[5] \quad \frac{df}{dt} = R_0 + k\,[Fe^{II}]S$$

where $R_0 = (k_1 + k_2)\,[>Fe^{III}\text{–}(L^{n-})(H^+)]$ is a composite reaction rate term independent of $[Fe^{2+}]$, corresponding to the reaction steps mediated by Fe^{III} – L complexes (eqs. [2] and [3]), and the second term accounts for the reductive dissolution process promoted by aqueous Fe^{II} – L complexes[3] (eq. [4]); S is the instantaneous surface area, and k is related to k_{Th} (see below).

When no Fe^{II} is added to α-Fe_2O_3 or γ-Fe_2O_3 suspensions, the second term on the right-hand side of eq. [5] reflects essentially the buildup of Fe^{II} through b_2 (eq. [3]). In the case of magnetite, Fe^{II} is put in solution through b_1, b_2, and *c*; assuming congruent dissolution, pathway *c* produces 0.5 Fe^{II} for each dissolved Fe^{III}.

In the presence of added Fe^{2+}, the first term in eq. [5] is negligible and the expression becomes:

$$[6] \quad \frac{df}{dt} = k\,[Fe^{II}]\,S$$

For magnetite, $[Fe^{II}] = [Fe^{II}]_0 + [Fe^{II}]_{diss}$, where $[Fe^{II}]_0$ is the concentration of added ferrous salt, and $[Fe^{II}]_{diss}$ is the concentration of Fe^{II} arising from the dissolution of magnetite. As the main source of dissolved ions is pathway *c*,

$$[7] \quad [Fe^{II}]_{diss} = 1/3\,[Fe_T] = (m_0/3VM)f$$

where $[Fe_T]$ refers to dissolved Fe, exclusive of added Fe^{II} salts. In eq. [7], V is the suspension volume, and M the mass of oxide FeO_x, magnetite in this case, per mole of iron atoms. Therefore, eq. [6] can be changed to:

$$[8] \quad \frac{df}{dt} = k\,([Fe_T]/3 + [Fe^{II}]_0)\,S$$

$$= 3/2\,k_{Th}\,\{f/3 + (VM/m_0)\,[Fe^{II}]_0\}\,S$$

where $k_{Th} = 2/3\,(m_0/VM)\,k$. The 2/3 coefficient arises from the difference between the stoichiometry of the reaction and the rate-determining step, eq. [4].

Our sample of magnetite is composed of cubo-octahedral particles; the instantaneous surface area is therefore $S = S_0(1 - f)^{2/3}$ (contracting volume kinetic regime) (2*a*), and eq. [9] results:

$$[9] \quad \frac{df}{dt} = k_a f\,(1 - f)^{2/3} + k_b\,(1 - f)^{2/3}$$

where $k_a = k_{Th}\,S_0/2$ and $k_b = 3/2\,(VM/m_0)\,[Fe^{II}]_0\,k_{Th}\,S_0$.

Equation [9] can be easily integrated by casting it in the form [10]:

$$[10] \quad \frac{3dx}{dt'} = x^3 - c^3$$

where $t' = k_a t$, $x = (1 - f)^{1/3}$, and $c = (1 + k_b/k_a)^{1/3}$.

Integration of eq. [10] leads to the following expression:

$$[11] \quad t' = \frac{1}{c^2}\left\{\frac{1}{2}\ln\left[\frac{(x-c)^2}{(x^2+cx+c^2)}\right] - \sqrt{3}\tan^{-1}\left(\frac{2x+c}{\sqrt{3}c}\right) - \frac{1}{2}\ln\left[\frac{(1-c)^2}{(1+c+c^2)}\right] + \sqrt{3}\tan^{-1}\left(\frac{2+c}{\sqrt{3}c}\right)\right\}$$

Equation [11] fits the experimental values reasonably well (see Fig. 4, curve *a*), and the calculated value of k_{Th} for our sample of magnetite, derived from the fitting, is $2.3 \times 10^{-7}\ s^{-1}\ cm^{-2}$.

In the cases of maghemite and hematite, for $[Fe^{II}]_0 = 0$,

[3] Strictly, the rate should be first order on the surface concentration of Fe^{II} – L complexes adsorbed onto the oxide surface; this surface concentration is related to the concentration in the solution through some form of an adsorption isotherm, the simplest being the Langmuir expression:

$$[Fe^{II}]_{ads} = \frac{N_s\,K\,[Fe^{II}]_{sol}}{1 + K\,[Fe^{II}]_{sol}}$$

where N_s is the number of active surface sites on the oxide and K is the corresponding Langmuir constant for the adsorption of Fe^{II} – L complex. As the value of K reported (4*a*) for Fe^{II} – EDTA complexes in ca. 1200 $mol^{-1}\ dm^3$, and the concentration of Fe^{2+} added to the solution at the initial time of the reaction is ca. 10^{-5} mol dm^{-3}, in the early stages of dissolution $1 \gg K\,[Fe^{II}]_{sol}$, justifying the approximation $[Fe^{II}]_{ads} \cong N_s\,K\,[Fe^{II}]_{sol}$; the rate constant k (eq. [5]) embodies $N_s\,K$. Analogously, the rate terms for b_1 and b_2 can be written in the form $k_1\,S$ and $k_2\,S$.

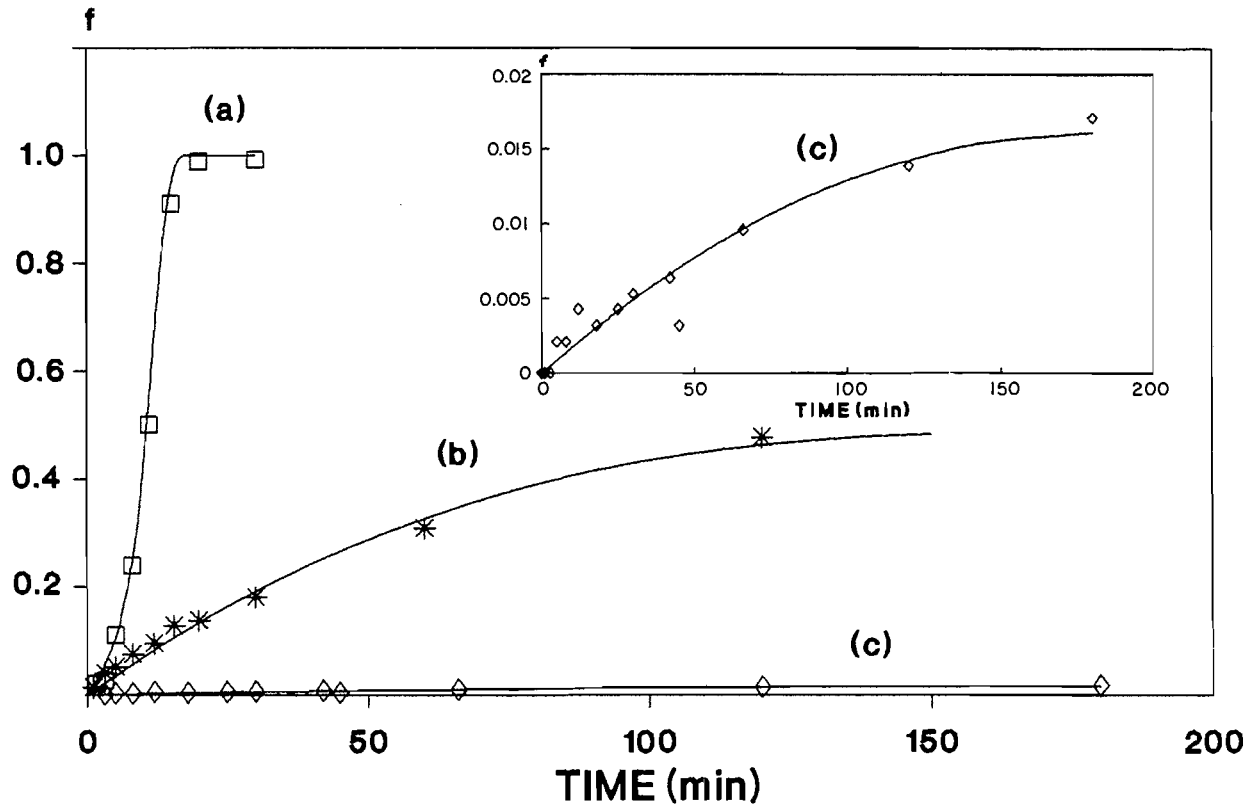

FIG. 4. Fitting of thermal dissolution curves for iron oxides in EDTA at 30°C and pH 3. Experimental data are those of Fig. 1. Calculated curve (*a*) for Fe_3O_4 was obtained through eq. [11]; calculated curve (*b*) for γ-Fe_2O_3, through integrated eq. [13], and calculated curve (*c*) for α-Fe_2O_3, through eq. [14]. Insert: enlargement of curve (*c*).

the lack of structural Fe^{II} makes dissolution slow at room temperature (6, 11, 28); the only source of Fe^{II} is reaction *b*. This reaction is very slow at low temperatures, and dissolution is observed at appreciable rates only when Fe^{II} is added to the suspension. For $[Fe^{II}] = [Fe^{II}]_0$, eq. [6] predicts a rate law of the form:

$$[12] \quad \frac{df}{dt} = k\,[Fe^{II}]_0\,S_0\,(1-f)^{1/n}$$

where n depends on the particle shape (see below). Equation [12] is the typical contracting geometry kinetic expression with a constant penetration rate (48). For low $[Fe^{II}]_0$ values, under our experimental conditions, the initial added Fe^{2+} is slowly consumed by the fast reaction with traces of oxygen that enter into the system. Assuming zero-order kinetics, eq. [6] takes the form [13]; note that the maghemite particles are acicular, the instantaneous surface area being therefore proportional to $(1-f)^{1/2}$ (49). In this case, $k_{Th} = (m_0/VM)\,k$.

$$[13] \quad \frac{df}{dt} = (VM/m_0)\,k_{Th}\,S_0\,(1-f)^{1/2}\,[Fe^{II}]_0\,(1-t/\tau)$$

In eq. [13], M is here the mass of maghemite (γ-Fe_2O_3) per mole of iron atoms, and $\tau = [Fe^{II}]_0/4\,R$ is the time required to consume the initial added Fe^{2+}, R being the rate of O_2 ingress into the system. Equation [13] is easily integrated, and the experimental points can be fitted reasonably well with a value of $\tau = 150$ min (curve *b*, Fig. 4). The slow dissolution regime in such a situation accounts for the arrest of dissolution at rather low values of f. This fitting procedure leads to $k_{Th} = 1.2 \times 10^{-7}\ s^{-1}\ cm^{-2}$.

For hematite, assuming spherical particles,[4] expression [14] applies:

$$[14] \quad \frac{df}{dt} = (VM/m_0)\,k_{Th}\,S_0\,(1-f)^{2/3}\,[Fe^{II}]_0\,(1-t/\tau)$$

Taking $\tau = 180$ min, the value of k_{Th} that fits the experimental results is $6.3 \times 10^{-9}\ s^{-1}\ cm^{-2}$ (curve *c*, insert of Fig. 4). The value of τ is better considered as a lower limit, due to the low measured amounts of iron.

From these results, we conclude that our sample of magnetite is twice as reactive as our sample of maghemite. The appreciably higher reactivity of these two spinel type oxides compared with the corundum type hematite can be related to the electronic and structural properties of the spinel octahedral iron sublattice, characterized by a fast electron-hopping (51).

Photochemical dissolution

Anaerobic systems

In ref. 28 we proposed a mechanism for the UV light promoted dissolution of maghemite in the presence of reductive ligands. Light provides an alternative initiation step (b_3) to the reaction sequence [2]–[4]:

[4]Although the sample of hematite is polydisperse, this assumption does not affect the f/t profiles, except in the latter stages of dissolution ($f > 0.6$) (50).

Can. J. Chem. Downloaded from www.nrcresearchpress.com by 109.225.110.28 on 09/08/12
For personal use only.

Can. J. Chem. Downloaded from www.nrcresearchpress.com by 109.225.110.28 on 09/08/12
For personal use only.

[15] $>Fe^{III}-(L)^{n-}(H^+) \xrightarrow{h\nu} >Fe^{II} + L^{(n-1)-}(+H^+) \quad (b_3)$
$\downarrow$
$(Fe^{II}-L)^{2-n}_{aq}$

Equation [15] is in fact the result of a series of events that include the creation of e^-, h^+ pairs, the trapping of e^- by surface $>Fe^{III}$ complexes, and the reaction of photoholes with adsorbed EDTA. As discussed below, the apparent quantum yield $\phi_1 = (d[Fe^{II}]/dt)/I_0$ for reaction [15] is very low, below 10^{-5} mol einstein $^{-1}$ (28). By itself, this quantum yield is too low to give rise to fast dissolution; the role of I_0 is therefore that of increasing the value of R_0 in eq. [5], thereby becoming the main source of $[Fe^{II}]$.

When aqueous Fe^{III} – L builds up in solution, its photolysis, either as a dissolved or adsorbed species, may provide an alternative to eq. [15] as the initiation step. If adsorption of Fe^{III} is large, the photodecomposition of $(Fe^{III} - L)_{aq}$ may be subjected to heterogeneous catalysis. No evidence for this phenomenon was found in this study. On the other hand, the photolysis of dissolved Fe^{III} – EDTA complexes, eq. [16], is the main photochemical reaction after a large fraction of dissolution is achieved, and accounts for the time dephasing observed between CH_2O production and iron oxide dissolution.

[16] $(Fe^{III}-L)_{aq} \xrightarrow{I_0\phi_2} Fe^{2+}$ + oxidation products of L

In the course of thermal dissolution, iron is put in solution essentially with negligible change in the oxidation state (except during the induction period). In the illuminated systems, it is better to write individual rate equations for Fe^{II} and Fe^{III}. These equations for hematite and maghemite are

$$[17] \quad \frac{d[Fe^{II}]}{dt} = k_1' S + k_2' [Fe^{III}]$$

$$[18] \quad \frac{d[Fe^{III}]}{dt} = -k_2'[Fe^{III}] + k_{Th} S [Fe^{II}]$$

In writing eqs. [17] and [18], the following assumptions were made: the amount of thermally produced Fe^{II} from the oxide, k_2S (eq. [3]), is negligible compared with the photochemical production, $k_1' S = I_0\phi_1$ (eq. [15]); the photochemical production (eq. [15]) is assumed to be proportional to the surface area, even though its contribution to $[Fe^{II}]$ is proportional to the surface area, even though its contribution to $[Fe^{II}]$ is important only at low conversions, and therefore the actual dependence on particle surface area is not important; at longer times, homogeneous photolysis dominates, with $I_0\phi_2 = k_2' [Fe^{III}]$ (i.e., the fraction of the total incident light absorbed by dissolved Fe^{III} is proportional to its concentration); $k_1S < k_{Th}S [Fe^{II}]$ (i.e., the amount of Fe^{III} produced by dissolution through reaction [2] is negligible in comparison to that produced by reaction [4]; this assumption breaks down only in the induction period, during which the extent of dissolution is below the detection limit in the short time interval required to trigger reaction [4]).

For magnetite, a factor 1.5 (due to the stoichiometry) must multiply the first term in eq. [17], and an additional term must be added to describe the contribution of Fe^{II} from the lattice, which goes into solution together with Fe^{III}:

$$[19] \quad \frac{d[Fe^{II}]}{dt} = 1.5\, k_1' S + k_2' [Fe^{III}] + 0.5\, k_{Th} S [Fe^{II}]$$

In general, for an oxide $Fe^{II}_n Fe^{III}_m O_p$,

$$[20] \quad \frac{d[Fe^{II}]}{dt} = \left(\frac{n+m}{2}\right) k_1' S + k_2' [Fe^{III}] + \left(\frac{n}{m}\right) k_{Th} S [Fe^{II}]$$

For Fe_2O_3, $\left(\frac{n+m}{2}\right) = 1$ and $(n/m) = 0$, and for Fe_3O_4, $\left(\frac{n+m}{2}\right) = 1.5$ and $(n/m) = 0.5$.

The equation for Fe^{III} production is the same for all the oxides.

The low extent of photodissolution of α-Fe_2O_3 in EDTA prevents the evaluation of the kinetic parameters corresponding to this oxide. The value of k_{Th} for hematite, obtained in the thermal experiments (6.3×10^{-9} s^{-1} cm^{-2}), is similar to the value calculated by us (28) to describe the photochemical dissolution of α-Fe_2O_3 by oxalic acid (25) (9.7×10^{-10} s^{-1} cm^{-2}). The following discussion refers to Fe_3O_4 and γ-Fe_2O_3.

In our previous paper we obtained the analytical solution of the set of kinetic equations [17] and [18] and the parameters $k_1' S_0$, k_2', and $k_{Th} S_0$ that fitted reasonably well the experimental data of the maghemite/EDTA system. In this paper, we have improved the analysis by introducing into the equations the thermal constant per unit area k_{Th} obtained from the thermal experiments described in the previous section, and we also sort out the two contributions lumped together in the empirical triggering kinetic parameter: the true photochemical initiation rate constant, called $k_1'S_0$ here, and the arresting effect of oxygen. As before, the requirement $S \cong S_0$ is maintained to simplify the mathematical treatment.

The influence of oxygen

In the presence of oxygen, eqs. [17], [18], and [19] must be modified:

$$[21] \quad \frac{d[Fe^{II}]}{dt} = k_1' S_0 - k_{ox} [O] [Fe^{II}] + k_2' [Fe^{III}]$$

$$[22] \quad \frac{d[Fe^{III}]}{dt} = -k_2' [Fe^{III}] + \{k_{ox} [O] + k_{Th} S_0\} [Fe^{II}]$$

$$[23] \quad \frac{d[Fe^{II}]}{dt} = 1.5\, k_1' S_0 - k_{ox} [O] [Fe^{II}] + k_2' [Fe^{III}] + 0.5\, k_{Th} S [Fe^{II}]$$

The simplest case corresponds to a fast scavenging of Fe^{II} by O_2; in such a case, an induction period ensues, corresponding to the time τ' required to generate enough Fe^{II} to suppress all oxidant.[5] The amount of Fe^{II} released through

[5]Note that τ' is given by $4\,[O_2]_0/k_1' S_o$, whereas the parameter τ used in the discussion of the thermal dissolution of γ-Fe_2O_3 is given by $[Fe^{II}]_0/4\,R$, (see eq. [13]). In both cases, the chemical reaction of Fe^{II} – EDTA and O_2 is fast, as expected (52).

TABLE 1. Comparison of the kinetic parameters for Fe_3O_4, γ-Fe_2O_3, and α-Fe_2O_3

Parameter	Fe_3O_4	γ-Fe_2O_3	α-Fe_2O_3
k_1'/mol dm^{-3} s^{-1} cm^{-2}	8.5×10^{-12}	3.5×10^{-12}	(Very low)
k_2'/s^{-1}	3.2×10^{-6}	3.2×10^{-6}	3.2×10^{-6}
k_{Th}/s^{-1} cm^{-2}	2.3×10^{-7}	1.2×10^{-7}	6.3×10^{-9}

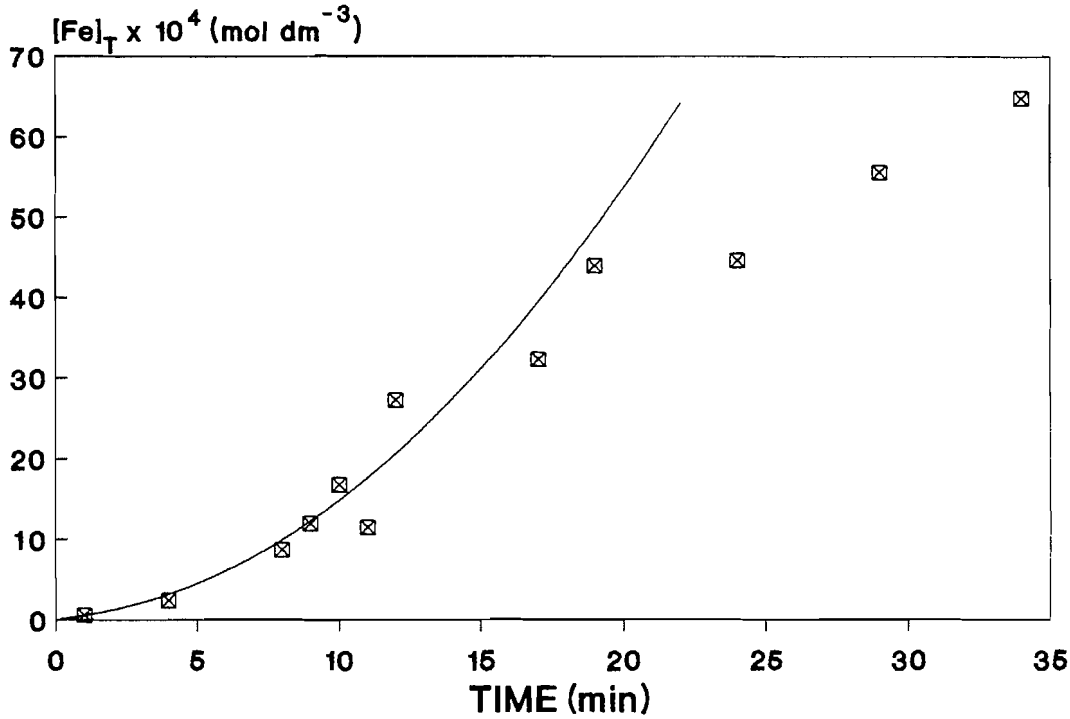

FIG. 5. Fitting of the 254-nm photodissolution curve for γ-Fe_2O_3 in EDTA at 30°C and pH 3. Experimental data (⊠) are those of Fig. 1. Solid curve was obtained through the analytical solution of eqs. [21] and [22], taking $\tau' = 16$ min.

the path defined by k_1' and required to scavenge all oxidant present is given by $k_1' S_0 \tau'$ in the case of maghemite and by $1.5\, k_1' S_0 \tau'$ in the case of magnetite. From our data, by setting τ' at approximately the beginning of the ascendant part of the curves *d* and *e* of Fig. 1, the values 26 min for magnetite and 16 min for maghemite are obtained. Combining these figures with the values of k_{Th} determined in the dark, and the value of k_2' found previously (28) (3.2×10^{-6} s^{-1}), the values $k_1' = 3.5 \times 10^{-12}$ mol dm^{-3} s^{-1} cm^{-2} (γ-Fe_2O_3), and $k_1' = 8.5 \times 10^{-12}$ mol dm^{-3} s^{-1} cm^{-2} (Fe_3O_4) are derived; Figs. 5 and 6 show the results of the fitting of the experimental points from Fig. 1 (converting f to [Fe_T]). The lower value of k_1' for γ-Fe_2O_3 indicates a somewhat lower photoreactivity, which may be explained by a faster recombination of the electron-hole pairs, facilitated by defects or vacancies in the oxide structure (29). Table 1 shows the comparison of the kinetic parameters for the three iron oxides.

This treatment implies that the low quantum yields for photodissolution also apply to heterogeneous photoassisted autooxidation, a result well in line with those described by Hoffmann and co-workers (30). Thus hematite, although more stable towards photocorrosion, is also less effective to photoinduce the degradation of organic matter. In agreement, Leland and Bard (53) reported that the rate of photoassisted autooxidation of oxalate on γ-Fe_2O_3 is ca. 14 times higher than on α-Fe_2O_3; EDTA shares with oxalate its ability to form surface complexes and thus it is also autooxidized in a photoassisted process at a rate that depends on the nature of the oxide; being less easily oxidizable, the low quantum yields seem reasonable. The differences in rates on γ-Fe_2O_3 and α-Fe_2O_3 are known to become much less marked in the case of relatively fast autooxidation reactions, such as that of SO_3^{2-}, which proceeds even in the dark (53). In this case, the quantum yield is appreciably higher, of the order of 0.1 (54). The low quantum yields may imply little importance of iron oxides as photocatalysts in the environmental degradation of organic matter; the mobilization of iron may, however, be strongly influenced.

Formaldehyde photoproduction

As indicated in ref. 28, formaldehyde is detected only after a sizeable fraction of the solid has dissolved (i.e. ≅20% for maghemite). This experimental result stresses the fact that the oxide dissolves essentially through pathway *c*, as Fe^{III} (eq. [4]), Fe^{II} being mainly produced at longer times by homogeneous photolysis.

The slopes of the curves for formaldehyde production (ca. 5×10^{-7} mol dm^{-3} s^{-1}) in both systems γ-Fe_2O_3 and Fe_3O_4 (Figs. 2 and 3), are in reasonable agreement with the calculated value of $\phi_2 I_0 = 1.8 \times 10^{-6}$ mol dm^{-3} s^{-1} (see eq. [16]), where ϕ_2 is the literature quantum yield of Fe^{2+} pro-

Can. J. Chem. Downloaded from www.nrcresearchpress.com by 109.225.110.28 on 09/08/12
For personal use only.

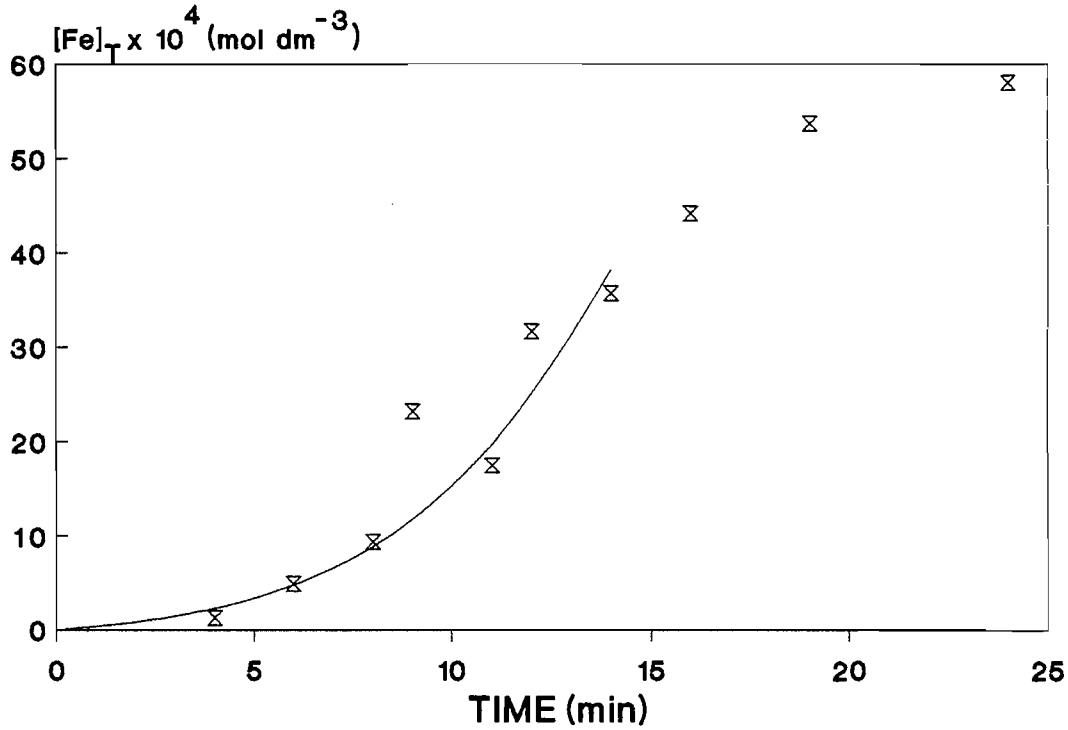

FIG. 6. Fitting of the 254-nm photodissolution curve for Fe_3O_4 in EDTA at 30°C and pH 3. Experimental data (⧖) are those of Fig. 1. Solid curve was obtained through the analytical solution of eqs. [22] and [23], taking $\tau' = 26$ min.

duction by homogeneous photolysis of Fe^{III} – EDTA (ca. 0.2 (55)); in agreement, k_2' is the same for all iron oxides.

Conclusions

1. The profiles f/t for the thermal and photochemical dissolution by carboxylic acids of the iron oxides studied in this paper exhibit different shapes, depending on the particular system. However, only one general mechanism is required to describe the dissolution of all the oxides, and the influence of dissolved ferrous ions and oxygen.

2. Oxygen inhibits the photodissolution in certain conditions: low rate of Fe^{II} production or any other case that warrants a high ratio of O_2/Fe^{II}. Conversely, a kinetic regime characterized by the fast production of high-surface Fe^{II} concentrations cannot be quenched by oxygen.

3. Spinel-type oxides are more reactive than α-Fe_2O_3, both in the direct reductive photodissolution and in the thermal dissolution by Fe^{II} complexes.

Acknowledgments

To the Consejo Nacional de Investigaciones Científicas y Técnicas (CONICET), of which M.I.L. and M.A.B. are members.

1. M. A. Blesa, A. E. Regazzoni, and A. J. G. Maroto. Mater. Sci. Forum, **29**, 31 (1988).
2. (*a*) E. Baumgartner, M. A. Blesa, H. A. Marinovich, and A. J. G. Maroto. Inorg. Chem. **22**, 2224 (1983); (*b*) M. A. Blesa, H. A. Marinovich, E. C. Baumgartner, and A. J. G. Maroto. Inorg. Chem. **26**, 3713 (1987).
3. E. Baumgartner, M. A. Blesa, and A. J. G. Maroto. J. Chem. Soc. Dalton Trans. 1649 (1982).
4. (*a*) E. B. Borghi, A. E. Regazzoni, A. J. G. Maroto, and M. A. Blesa. J. Colloid Interface Sci. **130**, 299 (1989); (*b*) M. A. Blesa, E. B. Borghi, A. J. G. Maroto, and A. E. Regazzoni. J. Colloid Interface Sci. **98**, 295 (1984).
5. E. B. Borghi, P. J. Morando, and M. A. Blesa. Langmuir, **7**, 1652 (1991).
6. R. Torres, M. A. Blesa, and E. Matijević. J. Colloid Interface Sci. **134**, 475 (1990).
7. M. del V. Hidalgo, N. E. Katz, A. J. G. Maroto, and M. A. Blesa. J. Chem. Soc. Faraday Trans. 1, **84**, 9 (1988).
8. R. M. Sellers and W. J. Williams. Faraday Discuss. Chem. Soc. **77**, 265 (1984).
9. M. Dos Santos Afonso, P. J. Morando, M. A. Blesa, S. Banwart, and W. Stumm. J. Colloid Interface Sci. **138**, 74 (1990).
10. P. S. Sidhu, R. J. Gilkes, R. M. Cornell, A. M. Posner, and J. P. Quirk. Clays Clay Miner. **29**, 269 (1981).
11. R. Torres, M. A. Blesa, and E. Matijević. J. Colloid Interface Sci. **131**, 567 (1989).
12. D. Suter, C. Siffert, B. Sulzberger, and W. Stumm. Naturwissenschaften, **75**, 571 (1988).
13. B. Wehrli, B. Sulzberger, and W. Stumm. Chem. Geol. **78**, 167 (1989).
14. B. Sulzberger, D. Suter, C. Siffert, S. Banwart, and W. Stumm. Mar. Chem. **28**, 127 (1989).
15. R. L. Segall, R. St. C. Smart, and P. S. Turner. *In* Surface and near surface chemistry of oxide materials. *Edited by* J. Nowotny and L.-C. Dufour. Elsevier Science Publishers B. V., Amsterdam. 1987. Chap. 13.
16. R. M. Cornell and P. W. Schindler. Clays Clay Miner. **35**, 347 (1987).
17. K. M. Cunningham, M. C. Goldberg, and E. R. Weiner. Photochem. Photobiol. **41**, 409 (1985).
18. R. D. Stramel and J. K. Thomas. J. Colloid Interface Sci. **110**, 121 (1986).
19. T. D. Waite and F. M. M. Morel. J. Colloid Interface Sci. **102**, 121 (1984).
20. T. D. Waite and F. M. M. Morel. Environ. Sci. Technol. **18**, 860 (1984).

Can. J. Chem. Downloaded from www.nrcresearchpress.com by 109.225.110.28 on 09/08/12
For personal use only.

21. T. D. Waite, A. Torikov, and J. David Smith. J. Colloid Interface Sci. **112**, 412 (1986).
22. B. C. Faust and M. R. Hoffmann. Environ. Sci. Technol. **20**, 943 (1986).
23. T. D. Waite and A. Torikov. J. Colloid Interface Sci. **119**, 228 (1987).
24. K. M. Cunningham, M. C. Goldberg, and E. R. Weiner. Environ. Sci. Technol. **22**, 1090 (1988).
25. (*a*) C. Siffert. Doctoral Thesis. ETH, Zurich, Switzerland, 1989; (*b*) B. Sulzberger. *In* Aquatic chemical kinetics — Reaction rates of processes in natural waters. *Edited by* W. Stumm. Wiley Interscience, New York, N.Y. 1990.; (*c*) C. Siffert and B. Sulzberger. Langmuir, **7**, 1627 (1991).
26. M. I. Litter and M. A. Blesa. J. Colloid Interface Sci. **125**, 679 (1988).
27. M. I. Litter and M. A. Blesa. Can. J. Chem. **68**, 728 (1990).
28. M. I. Litter, E. C. Baumgartner, G. Urrutia, and M. A. Blesa. Environ. Sci. Technol. **25**, 1907 (1991).
29. T. D. Waite. Rev. Mineral **23**, 554 (1990).
30. C. Kormann, D. W. Bahnemann, and M. R. Hoffman. J. Photochem. Photobiol. A: **48**, 161 (1989).
31. L. G. J. De Haart and G. Blasse. J. Electrochem. Soc. **132**, 2933 (1985).
32. K. L. Hardee and A. J. Bard, J. Electrochem. Soc. **124**, 215 (1977).
33. H. Nakanishi, C. Sánchez, M. Hendewerk, and G. A. Somorjai, Mater. Res. Bull. **21**, 137 (1986).
34. L. C. Schumacher, S. Mamiche-Afara, M. F. Weber, and M. J. Dignam. J. Electrochem. Soc. **132**, 2945 (1985).
35. A. T. Stone and J. J. Morgan. *In* Aquatic surface chemistry. *Edited by* W. Stumm. John Wiley & Sons Inc., New York, N.Y. 1987. pp. 221–254.
36. M. A. Blesa and A. J. G. Maroto. Proc. Int. Joint Meeting ANS–CNA on Decontamination of Nuclear Facilities (Keynote Addresses). Niagara Falls, Canada, 1982.
37. J. G. Hering and W. Stumm. Rev. Mineral. **23**, 427 (1990).
38. M. G. Segal and R. M. Sellers. *In* Advances in inorganic and bioinorganic mechanisms. Vol. 3. *Edited by* A. G. Sykes. Academic Press, London. 1984. pp. 97–129.
39. A. E. Regazzoni, G. A. Urrutia, M. A. Blesa, and A. J. G. Maroto. J. Inorg. Nucl. Chem. **43**, 1489 (1981).
40. (*a*) D. L. Leussing and I. M. Kolthoff. J. Am. Chem. Soc. **75**, 3904 (1953); (*b*) D. L. Leussing and L. Newman. J. Am. Chem. Soc. **78**, 552 (1956).
41. C. E. Bricker and H. R. Johnson. Ind. Eng. Chem. Anal. *Ed.* **17**, 400 (1945).
42. C. G. Hatchard and C. A. Parker. Proc. R. Soc. London, A: **235**, 518 (1956).
43. L. A. Marusak, R. Messier, and W. B. White. J. Phys. Chem. Solids, **41**, 981 (1980).
44. D. M. Sherman, R. G. Burns, and V. Mee Burns. J. Geophys. Res. **87**, 10169 (1982).
45. H. Boppart, A. Schlegel, and P. Wachter. Philos. Mag. B: **42**, 431 (1980).
46. P. Muret. Solid State Commun. **14**, 1119 (1974).
47. R. G. J. Strens and B. J. Wood. Mineral. Mag. **43**, 347 (1979).
48. W. E. Brown, D. Dollimore, and A. K. Galwey. *In* Comprehensive chemical kinetics. Vol. **22**. *Edited by* C. H. Bamford and C. F. H. Tipper. Elsevier Scientific Publishing Company, New York. 1980.
49. E. H. Rueda. Doctoral Thesis, Universidad Nacional del Sur, Bahía Blanca, Argentina. 1988. p. 225.
50. G. A. Urrutia and M. A. Blesa. React. Solids, **6**, 281 (1988).
51. M. A. Blesa, A. G. J. Maroto, and P. J. Morando. J. Chem. Soc. Faraday Trans. 1, **82**, 2345 (1986).
52. Y. Kurimura, R. Ochiai, and N. Matsuura. Bull. Chem. Soc. Jpn. **41**, 2234 (1968).
53. J. K. Leland and A. J. Bard. J. Phys. Chem. **91**, 5076 (1987).
54. B. C. Faust, M. R. Hoffmann, and D. W. Bahnemann. J. Phys. Chem. **93**, 6371 (1989).
55. P. Natarajan and J. F. Endicott. J. Phys. Chem. **77**, 2049 (1973).

Appendix. List of symbols

c	dimensionless rate constant: $c = (1 + k_b/k_a)^{1/3}$ (eq. [10])
f	dissolved fraction of total iron (dimensionless); $f = (m_0 - m)/m_0$
I_0	total incident light intensity per unit solution volume (einstein s^{-1} dm^{-3})
k	rate constant (eq. [6]) (mol^{-1} dm^3 s^{-1} cm^{-2}); $k = \alpha\ (VM/m_0)\ k_{Th}$, where α is the adequate stoichiometric coefficient
k_a	(eq. [9]) (s^{-1}); $k_a = k_{Th}\ S_0/2$
k_b	(eq. [9]) (s^{-1}); $k_b = 3/2\ (VM/m_0)\ [Fe^{II}]_0\ k_{Th}\ S_0$
k_1	rate constant of Fe^{III}_{aq} production by phase transfer of Fe^{III} surface complexes (eq. [2]) (mol dm^{-3} s^{-1} cm^{-2})
k_2	rate constant of Fe^{II}_{aq} production by reduction and phase transfer of Fe^{III} surface complexes (eq. [3]) (mol dm^{-3} s^{-1} cm^{-2})
k_1'	photochemical initiation rate constant (eq. [15]) (mol dm^{-3} s^{-1} cm^{-2}); $k_1' = I_0\phi_1/S$
k_2'	homogeneous photolysis rate constant (eq. [16]) (s^{-1}); $k_2' = I_0\phi_2/[Fe^{III}]$
k_{ox}	second-order rate constant for the oxidation of Fe^{II} (eqs. [21], [22], and [23]) (mol^{-1} dm^3 s^{-1})
k_{Th}	rate constant of Fe^{III}_{aq} production by eq. [4] (s^{-1} cm^{-2})
K	Langmuir constant for the adsorption of Fe^{II} – EDTA complex (mol^{-1} dm^3)
m	instantaneous mass of the iron oxide (g)
m_0	initial oxide mass (g)
M	mass of oxide FeO_x per mole of iron atoms (g mol^{-1})
n	geometric parameter related to the shape of oxide particles (dimensionless)
N_s	total number of active sites per unit area (mol cm^{-2})
R	rate of O_2 ingress into the thermal system (mol dm^{-3} s^{-1})
R_0	dissolution rate (df/dt) independent of $[Fe^{II}]$ (eq. [5]) (s^{-1})
S	instantaneous surface area (cm^2)
S_0	initial surface area (cm^2)
t	reaction time (s)
t'	dimensionless time (eq. [10]); $t' = k_a\ t$
V	volume (dm^3)
x	(eq. [10]); $x = (1 - f)^{1/3}$ (dimensionless)
ϕ_1	apparent quantum yield for reaction [15] (mol $einstein^{-1}$); $\phi_1 = (d[Fe^{II}]/dt)/I_0$
ϕ_2	quantum yield of Fe^{II} production by homogeneous photolysis of Fe^{III}–EDTA (eq. [16]) (mol $einstein^{-1}$)
τ	time required to consume the initial added Fe^{2+} (eq. [13]) (s); $\tau = [Fe^{II}]_0/4R$
τ'	time required to generate enough Fe^{II} to suppress all oxidant (s); $\tau' = 4\ [O_2]_0/k_1'S_0$

Can. J. Chem. Downloaded from www.nrcresearchpress.com by 109.225.110.28 on 09/08/12
For personal use only.

4457

1992 CIC Medal Award Address
50 years a spectroscopist — some personal reminiscences[1]

D. A. RAMSAY
Herzberg Institute of Astrophysics, National Research Council of Canada, Ottawa, Ont., Canada K1A 0R6

Received May 21, 1992

Can. J. Chem. Downloaded from www.nrcresearchpress.com by 109.225.110.28 on 09/08/12
For personal use only.

CIC Medal address 1992[2]

It is nearly 50 years since I started a career in molecular spectroscopy as a graduate student with Dr. G. B. B. M. Sutherland at the University of Cambridge, England. I was given a Hilger D209 infrared spectrometer equipped with a rock salt prism and a Schwartz thermocouple. The output from the latter was fed into a galvanometer and amplified by means of an optical system consisting of a lamp, two mechanical grids, the galvanometer mirror, and a phototube. As the galvanometer mirror moved, the image of the first grid moved across the second grid and changed the current in the phototube. Several years later I saw a similar system in the laboratory of Professor R. V. Jones at Aberdeen who used it to measure the tilt of Scotland with the tides. Considerable work was going on at Cambridge (and Oxford) during the wartime years on the infrared spectra of hydrocarbons as a means for identifying the sources of fuel for enemy aircraft but I was asked to work on polymers. Finding the infrared spectra of substances like cellulose acetate difficult to interpret, I subsequently studied the spectra of a series of pyranose and furanose sugars. To simplify matters further I then studied the series cyclohexane (1), tetrahydropyran, 1:4 dioxane (2), and trioxane (3) in an attempt to understand the ring frequencies. There was also interest in whether the molecules exist in a chair or boat structure, which belonged to different symmetry groups with different numbers of infrared and Raman active fundamentals.

In July 1947 I commenced as a Junior Research Officer in the Organic Spectrochemistry group of the Division of Chemistry of the National Research Council. Dr. R. Norman Jones had compiled a catalogue of infrared spectra of a large number of ketosteroids and was working in collaboration with Dr. Konrad Dobriner of the Memorial Hospital in New York in an attempt to find a clue as to the origin of cancer. One interesting spectroscopic result was that the carbonyl frequency could be used as a fairly reliable diagnostic for the position of the carbonyl group in the ketosteroid framework (4). I decided to see if intensities could add any useful information. I made a study of methods which could be used to obtain accurate intensity measurements (to 1 or 2%) with infrared spectrometers of limited resolving power and produced a paper on the *Intensities and shapes of infrared absorption bands of substances in the liquid phase* (5), which later became a Citation Classic. We also published a paper on the intensities of carbonyl bands in the infrared spectra of steroids (6).

Two years later in July 1949, I transferred to the Division of Physics to work with Dr. G. Herzberg on the electronic spectra of free radicals. Dr. Herzberg was very keen to obtain a spectrum of CH_2 and suggested producing the radical by the photolysis of ketene or diazomethane and photographing the spectrum in absorption with a Lyman flash lamp. The importance of high resolution was also discussed since sensitive detection of absorption features requires a spectrograph with a resolving power similar to the widths of the lines being studied. So I built a flash photolysis apparatus and started looking for the spectra of free radicals using a 21 ft concave grating spectrograph. The first polyatomic free radical which we found was NH_2. Lines in the absorption spectrum matched features found in the emission spectrum of an oxy-ammonia flame. A Letter was promptly sent to the Journal of Chemical Physics (7) with a diagram and instructions that the spectral lines should show quite clearly in the final publication. Fortunately I received a proof, for I found that the spectral lines had been enhanced by hand without due regard for the relative intensities. In the meantime I had obtained stronger spectra and the journal agreed to accept a substitute diagram. In the final publication the lines appeared with about the same intensity as in the original diagram.

The next polyatomic free radical to be found was HCO, which has an extensive absorption system throughout the visible region (8, 9), a system quite different from the well-known hydrocarbon flame bands. Later, spectra of other polyatomic free radicals, e.g., PH_2 (10), NCO and NCS (11), CCO (12), HCCS (13), and C_5H_5 (14) were found as well as the spectra of several diatomic species. The technique has proved to be quite prolific and spectra of about 40 free radicals have been found over the years by workers in the Spectroscopy Group at Ottawa (15, 16).

The analysis of the NH_2 spectrum presented quite a challenge. The assignment of the spectrum to NH_2 was established by isotopic substitution using ^{15}N and D. The $^{14}N-^{15}N$ isotope shifts indicated that the angle in the upper state is approximately 160° (17) but in view of the alternation of band types in the spectrum the molecule was assumed to be linear. Subsequent work has now confirmed that the excited state is quasilinear with an equilibrium angle of 144° (18). By studying bands with similar rotational structures I was able to establish ground state combination differences and determine ground state rotational constants (19). The ground state of NH_2 has a structure very similar to the ground state of water. The spectrum consists of a very long progression of bands involving successive quanta of the bending vibration in the excited state. The rotational structures alternate, successive bands showing Σ and Π sub-bands respectively. The

[1]This article is based on the CIC Medal address delivered by Dr. Ramsay on June 1, 1992, at the 75th Annual Conference of the Canadian Society for Chemistry, Edmonton, Alberta.

[2]I wish to thank the CIC for awarding me this medal for 1992. I have been asked to record my address for posterity and do so in part here. The live address focussed more on recent research work which will appear in future publications; here I give an overview of my past activities, highlighting matters which I find particularly interesting, and filling in some of the details about what goes on behind the scenes.

Can. J. Chem. Downloaded from www.nrcresearchpress.com by 109.225.110.28 on 09/08/12
For personal use only.

question remains, where are the other sub-bands which are expected? Eventually some Δ sub-bands were found by means of ground state combination differences but were found to lie about 110 cm^{-1} below the corresponding Σ sub-bands. Why this large separation? The clue was found in a comment in one of Mulliken's papers (20) which stated that "If $\Lambda = 1$, the Renner effect should, in general, cause relatively large energy differences between the different levels for a given v_2'." The two combining states of NH_2 are derived from a common $^2\Pi$ state in the linear configuration and large interactions may be expected between electronic and vibrational motions. Hence NH_2 was the first molecule in which the Renner effect was established (21, 22) although the magnitude of the effect was much larger than that considered by Renner (23). Work still continues on the spectrum of NH_2 and will do so for many years since there are numerous interactions between the rovibronic levels of the excited state and the high-lying levels of the ground state.

The HCO free radical provides another example of the Renner effect since the ground and excited states are derived from a common $^2\Pi$ state. All of the sub-bands, except for the Σ sub-bands, are diffuse, but by contour analysis of the latter the presence of the Renner effect has been established (24). One of the consequences is that bands with Σ sub-bands correspond to bands with *odd* values of the bending vibrational quantum number v_2'. In 1975 I had a 45 day visit from John Brown with the intention of finishing some work on magnetic rotation spectroscopy. On the third day we were discussing the HCO molecule and decided that we should try to confirm the vibrational numbering by attempting to observe the $H^{13}CO$ species in natural abundance. With our improved flash photolysis apparatus and path lengths up to 80 meters we did indeed observe the weak $H^{13}CO$ lines but in addition we found some weak lines of similar strength on the high-frequency side of the band head. These weak lines were produced by "axis-switching" (25) and enabled the determination of the *A*-rotational constant for the ground state for the first time. The work was completed within the 45 days and a paper submitted to the Herzberg issue of the Canadian Journal of Physics (26). Perhaps this illustrates the importance of allowing scientists the freedom to change course at short notice as ideas evolve.

I have had a number of summer students over the years with beneficial results. One of these was Ed Ballik who operated a King furnace and high-resolution infrared spectrometer with great skill. Our initial intention was to flow gases through the furnace rapidly and to look for transient species. We found a rich spectrum even when the furnace was evacuated and this turned out to be a new infrared band system of the C_2 molecule. One day Ed came to me with about a mile of chart paper and said that there was one line out of position. I confirmed his diagnosis and some time later was able to show that it was caused by a weak singlet–triplet perturbation. The outcome of this work was that it established that the ground state of the molecule is the lowest singlet state and not the lowest triplet state. This result was at first regarded as heresy since the Swan bands (a triplet system) are prominent in the spectra of comets. However the analysis of six singlet–triplet perturbations yielded the same result, namely, that the lowest singlet state lies below the lowest triplet state by 610 ± 5 cm^{-1} (27). The question remains, why are the Swan bands so prominent in the spectra of comets?

Another summer student was Maurice Clement. We decided to look for emission from the reaction of H atoms with NO. An apparatus was assembled in 2 days and the first exposure taken on a prism spectrograph showed a rich spectrum and a series of line-like features. Measurement of these features established them to be *R*-heads of sub-bands of the $\tilde{A}^1A'' - \tilde{X}^1A'$ system of HNO. The sub-bands involve much higher values of K' than seen in the absorption spectrum of HNO (28) and come to an abrupt halt after $K' = 13$ for the 000 level. This phenomenon is reminiscent of the well-known breaking-off in the rotational structures of diatomic molecules (29) and is caused by predissociation in the upper state. Breaking-off in the *K*-structures was observed at different K' values for two bands of HNO and three bands of DNO and gave consistent values for the upper limit for the dissociation energy of the molecule (30). This was the first example of breaking-off in the rotational structure of a polyatomic molecule and 30 years later is still the only example. Clement decided that experimental work was too easy and became a theoretician.

In 1962 I had the good fortune to meet Fraser Birss at the University of Alberta, Edmonton, and we forged a collaboration which lasted 25 years. He developed computer programmes for analysing singlet–singlet and triplet–singlet transitions of asymmetric top molecules of which only the former has been published (31). This programme was used initially for analysing many bands of the 4550 Å band system of *trans*-glyoxal and its isotopic derivatives (32–35). During these studies some weaker bands were found which gave the first evidence for the existence of the *cis* isomer (36). These results have had extensive applications in the field of photochemistry and the study of collisional processes (37).

The triplet–singlet programme has been used for obtaining rotational constants and spin constants of formaldehyde (38, 39), propynal (40), and glyoxal (41). By the application of electric fields, dipole moments were determined for formaldehyde (42) and propynal (43) in their triplet states as well as for CS_2 (44).

In 1970 we constructed a magnetic rotation apparatus and used it initially to detect triplet–singlet bands (45). However, we found that it also provided a sensitive method for detecting singlet–triplet perturbations in molecules and extensive studies were carried out on formaldehyde and its isotopic derivatives (46–50). These results were of direct interest to several groups of photochemists who at that time were carrying out lifetime measurements and fluorescence yields of single rovibronic levels of the $\tilde{A}^1A_2$ state (51). Further work on thioformaldehyde (H_2CS) led to the elucidation of the mechanism for the singlet–triplet perturbations observed in the zeroth level of the $\tilde{A}^1A_2$ excited state. The perturbations are caused by a vibronic spin-orbit interaction with a level of the $\tilde{a}^3A_2$ state and matrix elements have been evaluated (52).

The thioformaldehyde molecule has proved to be a valuable test molecule for many experiments. Advantages are that rotational analyses of bands of the $\tilde{a}^3A_2$–$\tilde{X}^1A_1$ and $\tilde{A}^1A_2$–$\tilde{X}^1A_1$ systems are available and that the bands lie in convenient regions for excitation with rhodamine dyes. Hang Fung carried out intermodulated fluorescence studies of some *K*-doublets and found that the measured splittings did not agree with the values calculated from the rotational constants. The discrepancies were in the range 10–300 MHz. We concluded that the excited state levels were perturbed by high

Can. J. Chem. Downloaded from www.nrcresearchpress.com by 109.225.110.28 on 09/08/12
For personal use only.

rovibronic levels of the ground state (53). This result was confirmed by microwave–optical double resonance experiments (54). Similar results were obtained from microwave–optical double resonance measurements on HNO and DNO (55, 56). Two other interesting results emerged from the double resonance experiments. First, a large number of microwave lines were observed which could not be assigned to transitions in either the excited state or the ground state. These lines have been assigned to transitions from rovibronic levels of the $\tilde{A}^1A_2$ excited state to high rovibronic levels of the ground state (57, 58). Second, the technique has been found to provide a very powerful method for studying rotational "selection rules" in molecular collisions. A specific level in the electronically excited state can be monitored by means of a strong microwave transition to a high rovibronic level of the ground state. The optical laser can then be scanned to excite various rovibronic levels in the excited state and the efficiency by which these levels are converted by collisions to the level being monitored is measured by the intensity of the microwave signal. This technique provides a rapid coverage of a wide range of rotational levels (59).

I have had a continuing interest for many years in astrophysical problems. With Werner Goetz a 33 meter absorption tube was constructed and equipped with multiple reflection mirrors. By filling the tube with methane at pressures up to 1.6 atmospheres (1 atm = 101.3 kPa) and using path lengths up to 5 km it was possible to match some of the bands observed in the spectrum of the atmosphere of Uranus (60). Also by filling a similar tube of smaller volume with HD the 3–0, 4–0, 5–0, and 6–0 vibrational bands were observed and from the measured frequencies and intensities it was possible to determine a value for the D/H ratio in Jupiter (61). The larger tube was also filled with oxygen and several new bands of the Herzberg I, II, and III systems were found (62–64). I have also been able to record high-resolution spectra of the comets Halley and Wilson on the Anglo-Australian telescope; these data are still being evaluated.

Recently I entered into a fruitful collaboration with Professor Ewald Fink of the University of Wuppertal, Germany. Fink has shown that near-infrared emissions can be excited by energy exchange between $^1\Delta_g$ oxygen molecules and other species with low-lying excited states. So far the b–X systems of all the Group VI – Group VI diatomic molecules, and also some bands of the a–X systems, have been recorded at high resolution with a Fourier-transform spectrometer. Some of these results are already published (65–69). The spectrum of SeS was particularly strong, and weak magnetic dipole transitions were observed in the same band as the strong electric dipole transitions. In addition, the weak electric quadrupole transition of oxygen, $b^1\Delta_g$–$a^1\Sigma_g^+$, has been recorded at high resolution and the O and S branches observed in addition to the P, Q, and R branches (70). At higher pressures (up to 10 Torr; 1 Torr = 133.3 Pa) and with added gases a continuous absorption is seen underneath the discrete structure and is attributed to collision-induced emission (71). Other diatomic molecules which have been excited are those with a large spin-orbit splitting in the ground state. Examples are TeH (72) and BiH (73), which have $^2\Pi$ and $^3\Sigma$ ground states respectively. Also the series HO_2, HS_2, HSe_2, and HTe_2 has given extensive spectra.

In conclusion I wish to thank many persons who have had a beneficial influence on my career. My parents, though not scientists, always encouraged me follow my own inclinations as long as I considered that I was making progress. My chemistry master at school, Mr. G. F. Fowles, spent many hours giving me private tuition when I was in the Sixth Form. My undergraduate supervisor at University, Dr. F. S. Dainton (now Lord Dainton of Hallam Moors), worked me hard and effectively. My research supervisors, Dr. G. B. B. M. Sutherland and Professor E. K. Rideal, were always helpful and inspiring. At the National Research Council I have benefitted from the philosophies of Drs. E. W. R. Steacie and G. Herzberg, who believed that one should select persons carefully and give them the freedom and support to follow their own ideas. I have enjoyed the collaboration with numerous Postdoctoral Fellows, Research Associates, Summer Students, and Visiting Research Scientists. Finally I wish to acknowledge the highly professional and loyal support of two Technical Officers, Werner Goetz and Mike Barnett, each of whom has assisted me for more than 25 years.

1. D. A. Ramsay and G. B. B. M. Sutherland. Proc. R. Soc. (London), **A190**, 245 (1947).
2. D. A. Ramsay. Proc. R. Soc. (London), **A190**, 562 (1947).
3. D. A. Ramsay. Trans. Faraday Soc. **44**, 289 (1948).
4. R. Norman Jones and Konrad Dobriner. Vitam. Horm. (N.Y.), **7**, 294 (1949).
5. D. A. Ramsay. J. Am. Chem. Soc. **74**, 72 (1952).
6. R. N. Jones, D. A. Ramsay, D. S. Keir, and K. Dobriner. J. Am. Chem. Soc. **74**, 80 (1952).
7. G. Herzberg and D. A. Ramsay. J. Chem. Phys. **20**, 347 (1952).
8. D. A. Ramsay. J. Chem. Phys. **21**, 960 (1953).
9. G. Herzberg and D. A. Ramsay. Proc. R. Soc. (London), **A233**, 34 (1955).
10. D. A. Ramsay. Nature, **178**, 374 (1956).
11. R. Holland, D. W. G. Style, R. N. Dixon, and D. A. Ramsay. Nature, **182**, 336 (1958).
12. C. Devillers and D. A. Ramsay. Can. J. Phys. **49**, 2839 (1971).
13. S. L. N. G. Krishnamachari and D. A. Ramsay. Discuss Faraday Soc. **71**, 205 (1981).
14. R. Engleman, Jr. and D. A. Ramsay. Can. J. Phys. **48**, 964 (1970).
15. G. Herzberg. Electronic spectra of polyatomic molecules. D. Van Nostrand Co. Inc., Princeton, N.J. 1967.
16. D. A. Ramsay. Electronic spectra of polyatomic free radicals. *In* Vibrational spectra and structure; a series of advances. *Edited by* J. R. Durig. Elsevier, Amsterdam. 1985. pp. 69–124.
17. G. Herzberg and D. A. Ramsay. Discuss. Faraday Soc. **14**, 11 (1953).
18. R. N. Dixon. Mol. Phys. **9**, 357 (1965).
19. D. A. Ramsay. J. Chem. Phys. **25**, 188 (1956).
20. R. S. Mulliken. Phys. Rev. **60**, 506 (1941).
21. K. Dressler and D. A. Ramsay. J. Chem. Phys. **27**, 971 (1957).
22. K. Dressler and D. A. Ramsay. Phil. Trans. R. Soc. (London), **A251**, 553 (1959).
23. R. Renner. Z. Phys. **92**, 172 (1934).
24. J. W. C. Johns, S. H. Priddle, and D. A. Ramsay. Discuss. Faraday Soc. **35**, 90 (1963).
25. J. T. Hougen and J. K. G. Watson. Can. J. Phys. **43**, 298 (1965).
26. J. M. Brown and D. A. Ramsay. Can. J. Phys. **53**, 2232 (1975).
27. E. A. Ballik and D. A. Ramsay. Astrophys. J. **137**, 84 (1963).
28. F. W. Dalby. Can. J. Phys. **36**, 1336 (1958).
29. G. Herzberg. Spectra of diatomic molecules. D. Van Nostrand Co. Inc., New York. 1950.

30. M. J. Y. Clement and D. A. Ramsay. Can. J. Phys. **39**, 205 (1961).
31. F. W. Birss and D. A. Ramsay. Comput. Phys. Commun. **38**, 83 (1985).
32. J. Paldus and D. A. Ramsay. Can. J. Phys. **45**, 1389 (1967).
33. F. W. Birss, J. M. Brown, A. R. H. Cole, A. Lofthus, S. L. N. G. Krishnamachari, G. A. Osborne, J. Paldus, D. A. Ramsay, and L. Watmann. Can. J. Phys. **48**, 1230 (1970).
34. D. M. Agar, E. J. Bair, F. W. Birss, P. Borrell, P. C. Chen, G. N. Currie, A. J. McHugh, B. J. Orr, D. A. Ramsay, and J.-Y. Roncin. Can. J. Phys. **49**, 323 (1972).
35. F. W. Birss, D. B. Braund, A. R. H. Cole, R. Engleman, Jr., A. A. Green, S. M. Japar, R. Nanes, B. J. Orr, D. A. Ramsay, and J. Szyszka. Can. J. Phys. **55**, 390 (1977).
36. G. N. Currie and D. A. Ramsay. Can. J. Phys. **49**, 317 (1971).
37. K. K. Butz, H. Du, D. J. Krajnovich, and C. S. Parmenter. J. Chem. Phys. **89**, 4680 (1988).
38. F. W. Birss, R. Y. Dong, and D. A. Ramsay. Chem. Phys. Lett. **18**, 11 (1973).
39. F. W. Birss, D. A. Ramsay, and S. M. Till. Can. J. Phys. **56**, 781 (1978).
40. F. W. Birss, R. Y. Dong, and D. A. Ramsay. Can. J. Phys. **51**, 1810 (1973).
41. D. A. Ramsay, M. Vervloet, F. Vanhorenbeke, M. Godefroid, and M. Herman. J. Mol. Spectrosc. **149**, 348 (1991).
42. A. D. Buckingham, D. A. Ramsay, and J. Tyrrell. Can. J. Phys. **48**, 1242 (1970).
43. R. Y. Dong and D. A. Ramsay. Can. J. Phys. **51**, 2444 (1973).
44. M. Larzillière and D. A. Ramsay. Can. J. Phys. **53**, 1579 (1975).
45. W. Goetz, A. J. McHugh, and D. A. Ramsay. Can. J. Phys. **48**, 1 (1970).
46. F. W. Birss, D. A. Ramsay, and S. M. Till. Chem. Phys. Lett. **53**, 14 (1978).
47. D. A. Ramsay and S. M. Till. Can. J. Phys. **57**, 1224 (1979).
48. M. Barnett, D. A. Ramsay, and S. M. Till. Chem. Phys. Lett. **65**, 440 (1979).
49. C. M. L. Kerr, D. C. Moule, and D. A. Ramsay. Can. J. Phys. **61**, 6 (1983).
50. D. J. Clouthier, A. M. Craig, and D. A. Ramsay. Can. J. Phys. **61**, 1073 (1983).
51. C. B. Moore and J. C. Weisshaar. Annu. Rev. Phys. Chem. **34**, 525 (1983).
52. D. J. Clouthier, D. A. Ramsay, and F. W. Birss. J. Chem. Phys. **79**, 5851 (1983).
53. K. Fung and D. A. Ramsay. J. Phys. Chem. **88**, 395 (1984).
54. J. C. Petersen, D. A. Ramsay, and T. Amano. Chem. Phys. Lett. **103**, 266 (1984).
55. J. C. Petersen, S. Saito, T. Amano, and D. A. Ramsay. Can. J. Phys. **62**, 1731 (1984).
56. J. C. Petersen, T. Amano, and D. A. Ramsay. J. Chem. Phys. **81**, 5449 (1984).
57. J. C. Petersen and D. A. Ramsay. Chem. Phys. Lett. **118**, 31 (1985).
58. J. C. Petersen and D. A. Ramsay. Chem. Phys. Lett. **124**, 406 (1986).
59. J. C. Petersen and D. A. Ramsay. Chem. Phys. Lett. **118**, 34 (1985).
60. B. L. Lutz and D. A. Ramsay. Astrophys. J. **176**, 521 (1972).
61. A. R. W. McKellar, W. Goetz, and D. A. Ramsay. Astrophys. J. **207**, 663 (1976).
62. D. A. Ramsay. Can. J. Phys. **64**, 717 (1986).
63. P. M. Borrell, P. Borrell, and D. A. Ramsay. Can. J. Phys. **64**, 721 (1986).
64. B. Coquart and D. A. Ramsay. Can. J. Phys. **64**, 726 (1986).
65. E. H. Fink, H. Kruse, and D. A. Ramsay. J. Mol. Spectrosc. **119**, 377 (1986).
66. E. H. Fink, H. Kruse, D. A. Ramsay, and D.-C. Wang. Mol. Phys. **60**, 277 (1987).
67. E. H. Fink, K. D. Setzer, D. A. Ramsay, and M. Vervloet. J. Mol. Spectrosc. **125**, 66 (1987).
68. E. H. Fink, K. D. Setzer, U. Kottsieper, D. A. Ramsay, and M. Vervloet. J. Mol. Spectrosc. **131**, 127 (1988).
69. E. H. Fink, K. D. Setzer, D. A. Ramsay, M. Vervloet, and G. Z. Xu. J. Mol. Spectrosc. **136**, 218 (1989).
70. E. H. Fink, H. Kruse, D. A. Ramsay, and M. Vervloet. Can. J. Phys. **64**, 242 (1986).
71. E. H. Fink, K. D. Setzer, J. Wildt, D. A. Ramsay, and M. Vervloet. Int. J. Quantum Chem. **39**, 287 (1991).
72. E. H. Fink, K. D. Setzer, D. A. Ramsay, and M. Vervloet. J. Mol. Spectrosc. **138**, 19 (1989).
73. E. H. Fink, K. D. Setzer, D. A. Ramsay, M. Vervloet, and J. M. Brown. J. Mol. Spectrosc. **142**, 108 (1990).

Can. J. Chem. Downloaded from www.nrcresearchpress.com by 109.225.110.28 on 09/08/12
For personal use only.

Kinetics and mechanism of aminolysis of (*Z*)-4-arylidene-2-phenyl-5(4*H*)oxazolones

SHARIFA S. ALKAABI AND AHMAD S. SHAWALI[1]
Department of Chemistry, Faculty of Science, University of Qatar, Douha, P.O. Box 2713, State of Qatar

Received March 6, 1992

SHARIFA S. ALKAABI and AHMAD S. SHAWALI Can. J. Chem. **70**, 2515 (1992).

The kinetics of the reactions of a series of (*Z*)-4-arylidene-2-phenyl-5(4*H*)oxazolones **1** with *n*-butylamine and piperidine were studied spectrophotometrically in dioxane, ethanol, and cyclohexane under pseudo-first-order conditions and at different temperatures. The relation $k_1(\text{obs}) = k_2[\text{amine}] + k_3[\text{amine}]^2$ was found applicable for all reactions studied in either dioxane or ethanol. However, in cyclohexane the *n*-butylaminolysis of **1** followed only third-order kinetics $k_1(\text{obs}) = k_3[n\text{-BuNH}_2]^2$. The kinetics of the reaction of **1** with *n*-butylamine in the presence of catalytic amounts of triethylamine in dioxane followed the equation: $k_1(\text{obs}) = k_2[n\text{-BuNH}_2] + k_3[n\text{-BuNH}_2]^2 + k_3'[n\text{-BuNH}_2]\,[\text{Et}_3\text{N}]$. The rate constants k_2 and k_3 correlated well with the Hammett equation and the corresponding activation parameters were determined. The results were interpreted in terms of a mechanism involving solvent- and amine-catalyzed processes.

SHARIFA S. ALKAABI et AHMAD S. SHAWALI. Can. J. Chem. **70**, 2515 (1992).

Faisant appel à des méthodes spectrophotométriques et opérant dans le dioxanne, l'éthanol et le cyclohexane, à différentes températures, dans des conditions de pseudo-premier-ordre, on a déterminé la cinétique des réactions d'une série de (*Z*)-4-arylidène-2-phényl-5(4*H*)oxazolones (**1**) avec la *n*-butylamine et la pipéridine. On a trouvé que la relation $k_1(\text{obs}) = k_2[\text{amine}] + k_3[\text{amine}]^2$ peut s'appliquer à toutes les réactions étudiées, soit dans le dioxanne ou l'éthanol. Toutefois, dans le cyclohexane, la *n*-butylaminolyse du produit **1** ne suit qu'une cinétique du troisième ordre, $k_1(\text{obs}) = k_3[n\text{-BuNH}_2]^2$. La cinétique de la réaction du produit **1** avec la *n*-butylamine en présence d'une quantité catalytique de triéthylamine dans le dioxanne suit l'équation : $k_1(\text{obs}) = k_2[n\text{-BuNH}_2] + k_3[n\text{-BuNH}_2]^2 + k_3'[n\text{-BuNH}_2]\,[\text{Et}_3\text{N}]$. Il existe une bonne corrélation entre les constantes de vitesse k_2 et k_3 et l'équation de Hammett et on a déterminé les paramètres d'activation. On interprète les résultats en fonction d'un mécanisme impliquant des processus catalysés par le solvant et l'amine.

[Traduit par la rédaction]

Although 4-arylidene-2-phenyl-5(4H)-oxazolones **1** were reported more than a century ago (1) and their reactions with various nucleophilic reagents have been extensively studied (2–9), the kinetics and mechanism of their ring cleavage by nitrogen nucleophiles have received little, if any, attention. Recently, in a study designed to determine the steric effect of remote substituents on peptide bond formation, it was reported that the reaction of (*Z*)-4-benzylidene-2-phenyl-5(4*H*)-oxazolone with benzylamine in acetonitrile followed second-order kinetics (10). This result seems surprising since the reaction of compounds **1**, being cyclic esters, with nitrogen nucleophiles in aprotic solvent would be expected to exhibit a kinetic pattern similar to that reported for aminolysis of acyclic esters. Extensive kinetic studies, in our laboratory and others, on the aminolysis of acyclic esters in aprotic solvents established that such reactions are subject to general base catalysis (11–23). Thus, under pseudo-first-order conditions the reactions of esters with primary amine (A) and in the presence of a tertiary amine (B) were found to follow the rate law: $k_1(\text{obs}) = k_2[\text{A}] + k_3[\text{A}]^2 + k_3'[\text{A}][\text{B}]$. In a few cases the k_2 term was not observed (16, 21, 22).

Since compounds **1** are versatile intermediates in the syntheses of peptides and didehydroamino acids (24), it was thought important to investigate in some detail the kinetics of their aminolysis to shed light on the mechanism of their ring cleavage by amines in both aprotic and protic solvents. For this purpose we studied the kinetics of the reactions of a series of (*Z*)-4-arylidene-2-phenyl-5-(4*H*)-oxazolones **1***a–i* with *n*-butylamine in dioxane, ethanol, and cyclohexane at different temperatures under pseudo-first-order conditions. The other objective of the present study was to determine both solvent and substituent effects on the aminolytic reactivity of **1**.

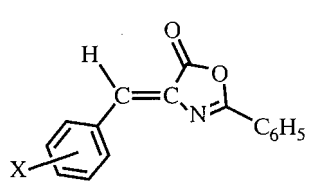

1 (*Z*)

	X
a	*p*-CH_3O
b	*p*-CH_3
c	*m*-CH_3
d	H
e	*m*-CH_3O

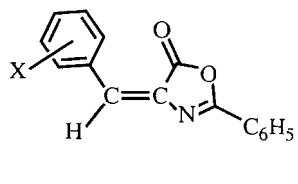

1 (*E*)

	X
f	*p*-Cl
g	*m*-Cl
h	*m*-NO_2
i	*p*-NO_2

Results and discussion

(*Z*)-4-Arylidene-2-phenyl-5(4*H*)-oxazolones **1***a–i* were prepared from hippuric acid and the appropriate substituted benzaldehyde in the presence of acetic anhydride and anhydrous sodium acetate according to the Erlenmeyer method (25). The *Z* configuration indicated was based on the fact that the latter method of synthesis of **1** was reported to give the thermodynamically more stable *Z* isomer (6, 26–28). The *E* isomer of **1** is obtained by isomerization of the *Z* isomer with hydrobromic acid (6, 25).

The reaction of **1***d*, taken as a typical example of the **1***a–i* series studied, with *n*-butylamine in dioxane at 31°C takes place quantitatively according to eq. [1].

[1]Author to whom correspondence may be addressed. Present address: Department of Chemistry, Faculty of Science, University of Cairo, Giza, Egypt.

Can. J. Chem. Downloaded from www.nrcresearchpress.com by 109.225.110.28 on 09/08/12
For personal use only.

Can. J. Chem. Downloaded from www.nrcresearchpress.com by 109.225.110.28 on 09/08/12
For personal use only.

[1] n-$C_4H_9NH_2$ + 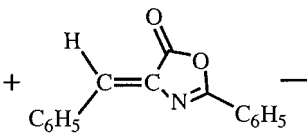 → 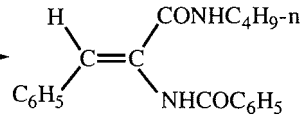

1*d* **2**

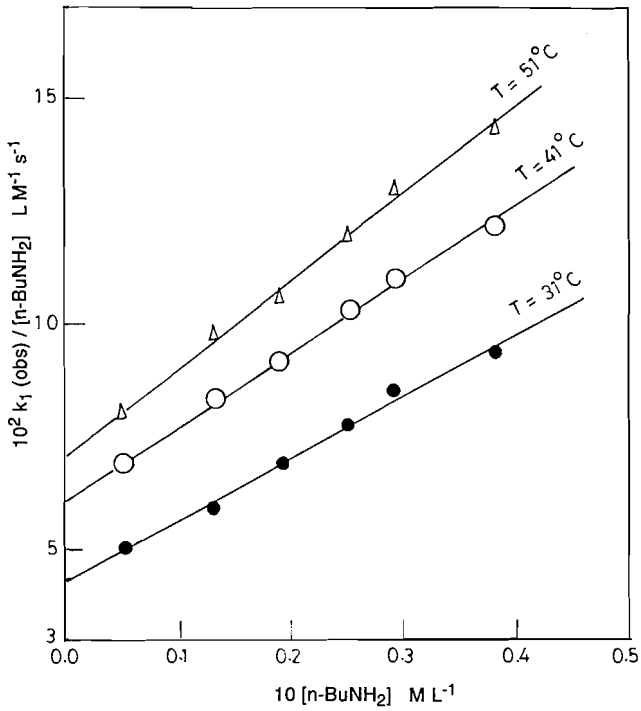

FIG. 1. Plots of k_1(obs)/[amine] against amine concentration for the reaction of azalactone **1***d* with n-butylamine in dioxane at different temperatures.

The reaction product was proved to be *N*-*n*-butyl-2-benzoylaminocinnamamide **2**. In anhydrous dioxane the reaction kinetics of each of **1***a–i* with tenfold excess or more of n-butylamine in the temperature range 31–51°C is pseudo-first-order with respect to **1** to at least 95% completion. The plot of the pseudo-first-order rate constant, k_1(obs), vs. n-butylamine concentration was not linear. However, the plot of k_1(obs)/[amine] against [amine] was, in each case, linear as shown in Fig. 1. Such plots indicate that the n-butylaminolysis of **1** in dioxane in the temperature range 31–51°C follows the rate equation [2]:

[2] $k_1(\text{obs}) = k_2[n\text{-BuNH}_2] + k_3[n\text{-BuNH}_2]^2$

Values of constants k_2 and k_3 were calculated, using the least-squares method, from the slopes and intercepts, respectively, of plots like those shown in Fig. 1. The data are summarized in Table 1. The correlation coefficients of such plots were in the range 0.986–0.990.

In ethanol the reaction of **1***a* with n-butylamine at 31°C followed eq. [2] as shown in Fig. 2. However, simple third-order kinetics were found for the reaction of **1***a* with n-butylamine in cyclohexane at 31°C (Fig. 2). In this case the reaction kinetics followed the rate equation [3].

[3] $k_1(\text{obs}) = k_3[n\text{-BuNH}_2]^2$

TABLE 1. Second- and third-order rate constants of the reactions of (*Z*)-4-arylidene-2-phenyl-5(4*H*)oxazolones **1***a–i* with n-butylamine in dioxane at 31°C

Oxazolone	$10\,k_2$ (L mol^{-1} s^{-1})	k_3 (L^2 mol^{-2} $^{-1}$)	k_3/k_2 (L mol^{-1})
1*a*	0.12	0.40	32.9
1*b*	0.22	0.61	28.4
1*c*	0.32	0.92	28.4
1*d*	0.43	1.36	31.4
1*e*	0.50	1.52	30.5
1*f*	0.90	2.75	30.5
1*g*	1.56	5.00	32.1
1*h*	5.45	17.70	32.5
1*i*	9.47	24.54	25.9

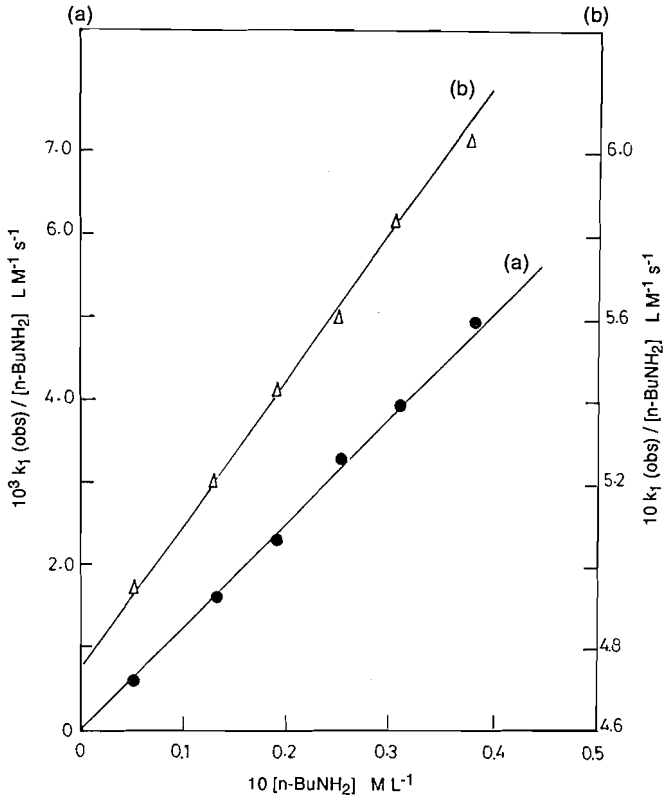

FIG. 2. Plots of k_1(obs)/[amine] against amine concentration for the reaction of azalactone **1***d* with n-butylamine at 31°C in cyclohexane (*a*) and ethanol (*b*).

The aminolysis of **1***d* with piperidine in dioxane at 31°C was correlated by eq. [2]. The corresponding values of constants k_2 and k_3 are given in Table 2.

Reaction of **1***d* with n-butylamine in the presence of triethylamine in dioxane at 31°C followed the rate equation [4].

TABLE 2. Rate constants for aminolysis of oxazolone **1***d* in different solvents at 31°C

Amine	Solvent	$10\,k_2$ (L mol^{-1} s^{-1})	k_3 (L^2 mol^{-2} s^{-1})	k_3' (L^2 mol^{-1} s^{-1})
n-$BuNH_2$	Dioxane	0.43	1.36	
n-$BuNH_2$	Ethanol	4.74	3.35	
n-$BuNH_2$	Cyclohexane		0.13	
Piperidine	Dioxane	0.28	5.06	
n-$BuNH_2$ + Et_3N	Dioxane			0.22

TABLE 3. Summary of the kinetic data for *n*-butylaminolysis of oxazolones **1** in dioxane at different temperatures[a]

	T = 31°C		T = 41°C		T = 51°C	
Oxazolone	$10\,k_2$	k_3	$10\,k_2$	k_3	$10\,k_2$	k_3
1*b*	0.22	0.61	0.29	0.79	0.38	0.86
1*d*	0.43	1.36	0.60	1.48	0.74	1.64
1*f*	0.90	2.75	1.13	2.00	1.40	3.18

[a] k_2, L mol^{-1} s^{-1}; k_3, L^2 mol^{-2} s^{-1}; ±0.06–0.25 and ±0.09, respectively.

$$[4]\quad k_1(\text{obs}) = k_2[n\text{-BuNH}_2] + k_3[n\text{-BuNH}_2]^2 + k_3'[n\text{-BuNH}_2][\text{Et}_3\text{N}]$$

The value of constant k_3' is given in Table 2.

The activation parameters, E_a and ΔS^*, were calculated from the least-squares fit of the data at different temperatures (Table 3) using eqs. [5] and [6], respectively, and the values are given in Table 4.

$$[5]\quad \ln k_1 = \ln A - (E_a/RT)$$

$$[6]\quad \ln A = \ln (RT/Nh) + (\Delta S^*/R)$$

The value of the term ln (RT/Nh) equals 29.53 at 314 K.

The present kinetic data obtained in dioxane or ethanol suggest that the *n*-butylaminolysis of **1** proceeds via concurrent second-order and third-order processes. The former process corresponds to a solvent-catalyzed reaction, whereas the latter represents an amine-catalyzed process. Another possibility for the quadratic third-order term in eq. [2] or [3] is that it may represent a reaction between **1** and an amine dimer. However, the present results exclude the involvement of such amine dimers in the aminolysis of **1**. This is because, if the amine dimer is catalytically active, it would be expected that as the amine concentration increases, the monomeric species would decrease and, in turn, the second-order term would disappear at high amine concentration. On the other hand, if the amine dimer were inactive a falloff in rate would be expected at high amine concentration. Neither expectation was observed experimentally.

The simplest stepwise mechanism that seems compatible with the present kinetic data is outlined in Scheme 1. Consistent with this mechanism are the following observations: (*i*) the disappearance of the k_2 term for the reaction of **1***d* with *n*-butylamine in cyclohexane; (*ii*) the rate acceleration observed when triethylamine is added to the reaction mixture; and (*iii*) the higher value of k_2 for the reaction of **1***d* with *n*-butylamine in ethanol as compared to that obtained for the same reaction in dioxane (Table 2).

The overall second-order and third-order rate constants (k_2 and k_3, respectively) were correlated with the Hammett substituent constant σ (29). The results of such correlations are summarized in Table 5. The ρ values indicate that both solvent- and amine-catalyzed reactions exhibit similar sensitivities towards substituent and that both are favoured by electron-withdrawing groups in the benzylidene moiety. The sensitivity is, however, small. This is because the ρ values for aminolysis comprise contributions from both steps of the indicated mechanism (Scheme 1). An electron-withdrawing substituent in the benzylidene moiety, while having a favorable effect on the first step, inhibits the ring opening. The net ρ value should be small, and this is what is observed experimentally. Furthermore, the similarity between the ρ values for the k_2 and k_3 processes indicates that both processes have a common intermediate whose collapse to products, by the help of either solvent or amine molecules, is rate determining. This is substantiated by the observation that the rate constant ratios (k_3/k_2) are approximately constant (Table 1). This finding is also consistent with the suggested mechanism outlined in Scheme 1.

The observed higher rate of aminolysis of **1***d* in ethanol as compared to that in dioxane may be viewed as a general acid catalysis. This rationalization is consistent with the re-

TABLE 4. Activation parameters for the second- and third-order processes of *n*-butylaminolysis of oxazolones **1** in dioxane[a]

	Second-order process			Third-order process		
Oxazolone	E_a	ΔS^*	ΔH^*	E_a	ΔS^*	ΔH^*
1*b*	5.660	−48.110	5.032	3.386	−48.844	2.658
1*d*	4.96	−48.920	4.335	2.216	−51.226	1.588
1*f*	4.362	−49.522	3.734	1.429	−52.326	0.801

[a] E_a, kcal mol^{-1}; ΔS^*, cal deg^{-1} mol^{-1}; $\Delta H^* = (E_a - RT)$, kcal mol^{-1}.

Can. J. Chem. Downloaded from www.nrcresearchpress.com by 109.225.110.28 on 09/08/12
For personal use only.

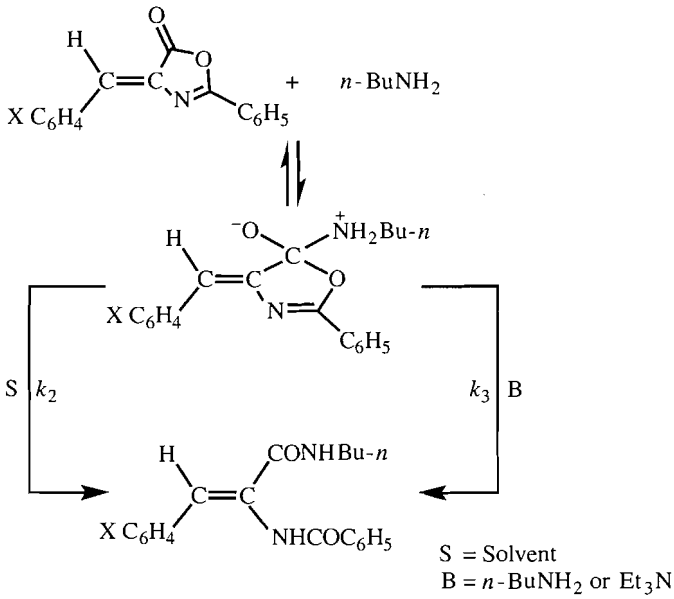

SCHEME 1

TABLE 5. Results of linear free energy correlations of rate constants of *n*-butylaminolysis of **1***a–i* in dioxane at 31°C[a]

$\log k_i = \rho\sigma + \log k_0$	r	s_{est}	s_ρ	n
$\log k_2 = 1.69\sigma - 1.41$	0.994	0.074	0.035	9
$\log k_3 = 1.68\sigma + 0.075$	0.998	0.041	0.035	9

[a]r = correlation coefficient; s_{est} = deviation; s_ρ = error estimate for ρ; n = number of points.

ported rate acceleration by the hydroxyl group in the aminolysis of salicylate in nonhydroxylic solvents (19).

Table 4 lists Arrhenius activation energies and entropies of activation for the second- and third-order processes of *n*-butylaminolysis of three representative compounds of the series studied. As expected, the energy of activation of the amine-catalyzed process is lower than that of the corresponding solvent-catalyzed process. In addition, the data show that the energy of activation for both the second- and third-order processes exhibits a regular variation with the substituent in the benzylidene moiety: an electron-withdrawing group decreases the energy of activation and in turn increases the reaction rate, while the reverse is true for an electron-donating group.

The large negative entropies of activation are as expected for bimolecular and termolecular reactions (30). The small differences between the entropies of activation for the second-order and third-order processes probably reflect small variations in solvation of the corresponding transition states.

Experimental section

Melting points were determined on an Electrothermal capillary apparatus and are uncorrected. Infrared spectra were measured with a Pye–Unicam SP3-100 spectrophotometer. A Beckman DJ-70 spectrophotometer with electrically thermostated jacketed cell compartment was used for recording the electronic absorption spectra and kinetic measurements. The solvents, dioxane, ethanol, and cyclohexane, were BDH AnalaR grade and were used without further purification. *n*-Butylamine and piperidine were BDH reagents and purified before use as previously described (16). (*Z*)-4-Benzylidene-2-phenyl-5(4*H*)-oxazolone **1***d* and its substituted derivatives were prepared from *N*-benzoylglycine and the appropriate benzaldehyde in the presence of acetic anhydride and anhydrous sodium acetate according to the Erlenmeyer method (31). The compounds were crystallized from ethanol to constant melting points, which agreed with those previously reported (32).

TABLE 6. Characteristic ultraviolet maxima for (*Z*)-4-benzylidene-2-phenyl-5(4*H*) oxazolone and its substituted derivatives in dioxane

Oxazolone	λ_{max}, nm	Oxazolone	λ_{max}, nm
1*a*	382	**1***f*	366
1*b*	368	**1***g*	362
1*c*	364	**1***h*	360
1*d*	360	**1***i*	378
1*e*	368		

Kinetics

The reactions were carried out in a 1-cm ground-glass stoppered, fused silica, absorption cell. The reference solution was that of the solvent used containing an amine concentration equal to that being used in the particular kinetic run. The reactions were followed by rate of disappearance of 4-arylidene-2-phenyl-5(4*H*)oxazolone absorption maximum (Table 6). The reaction products showed no absorption in the region of maximum absorption of **1***a–i*. For example, the complete spectrum of each kinetic run for the reaction of **1***d* with *n*-butylamine corresponded to the spectrum of *N*-*n*-butyl-2-benzoylaminocinnamamide solution of the same concentration. Beer's law was found to be obeyed within the concentration and wavelength ranges employed.

Stock solutions of **1***a–i*, usually about 10^{-2} M, were prepared. Stock amine solutions were prepared and the concentration determined by titration. Appropriate concentrations of amine and azalactone **1** were prepared by dilution of the stock solutions with the appropriate solvent. All azalactone concentrations were 5×10^{-4} M.

Reactions were followed up to 95% completion under pseudo-first-order conditions in which at least a tenfold excess of amine over azalactone was used. Duplicate or triplicate runs were performed for each concentration and readings taken in any kinetic run covered a range of 90% transmittance. The pseudo-first-order rate constants, k_1(obs), were calculated from log $(A_t - A_\infty)$ against time, t, data using the least-squares method. A_t and A_∞ are the absorbances of the reaction mixture at time t and infinite time, respectively. The average deviation from the mean value of the rate constant in duplicate or triplicate experiments was ±5% or less.

Identification of the reaction product

n-Butylamine (0.73 g, 0.01 mol) was added to a solution of **1***d* (0.002 mol) in dioxane (20 mL). The reaction mixture was immersed in a constant temperature water bath at 31 ± 0.1°C. After 24 h, the white solid that separated out was filtered. Crystallization from ethanol gave *N*-*n*-butyl-2-benzoylaminocinnamamide **2** in 85% yield, mp 190–191°C (lit. (33) mp 190°C); IR (KBr): 3265 (NH), 1640, 1667 (CO), 1520 (C=C) cm^{-1}; UV (dioxane), λ_{max} (log ε): 220 (4.292), 276 (4.218) nm; ^{1}H NMR ($CDCl_3$) δ: 0.72 (3H), 1.16 (2H), 1.34 (2H), 3.12 (2H), 6.85 (1H), 7.0–7.45 (5H), 7.78 (5H), 7.82 (1H), 9.10 (1H) ppm. Anal. found: calcd. for $C_{20}H_{22}N_2O_2$: C 74.51, H 6.88, N 8.69%; found: C 74.45, H 6.90, N 8.63%.

1. J. Plochl. Ber. Dtsch. Chem. Ges. **16**, 2815 (1883).
2. H. E. Carter. Org. React. **3**, 198 (1946).
3. A. K. Mukerjee. Heterocycles, **26**, 1077 (1987).
4. R. Filler. Adv. Heterocycl. Chem. **4**, 75 (1965).
5. Y. S. Rao and R. Filler. Synthesis, 749 (1975).

Can. J. Chem. Downloaded from www.nrcresearchpress.com by 109.225.110.28 on 09/08/12
For personal use only.

6. R. Filler and Y. S. Rao. Adv. Heterocycl. Chem. **21**, 175 (1977).
7. A. K. Mukerjee and P. Kumar. Heterocycles, **16**, 1995 (1985).
8. Y. S. Rao and R. Filler. Chemistry of heterocyclic compounds. Vol. 45. *Edited by* I. G. Turchi. John Wiley and Sons, New York. 1986.
9. J. W. Cornforth. Heterocyclic compounds. Vol. 5. *Edited by* R. C. Elderfield. John Wiley and Sons, New York. 1957.
10. D. J. Phelps, P. V. Gordreau, and E. S. Nicholas. J. Chem. Soc. Perkin Trans. 2, 140 (1981).
11. F. M. Menger. J. Am. Chem. Soc. **88**, 3081 (1966).
12. N. Nakamizo. Bull. Chem. Soc. Jpn. **42**, 1071 (1969).
13. H. Anderson, C. Su, and J. W. Watson. J. Am. Chem. Soc. **91**, 482 (1969).
14. P. R. Rony. J. Am. Chem. Soc. **91**, 6090 (1969).
15. D. P. N. Satchell and I. I. Secemski. J. Chem. Soc. B, 130 (1969).
16. A. S. Shawali and S. S. Biechler. J. Am. Chem. Soc. **89**, 3020 (1967).
17. D. P. N. Satchell and I. I. Secemski. J. Chem. Soc. B, 1013 (1970).
18. F. M. Menger and J. H. Smith. J. Am. Chem. Soc. **91**, 5346 (1969).
19. R. L. Snell, W. Kwok, and Y. Kim. J. Am. Chem. Soc. **89**, 6728 (1967).
20. F. M. Menger and J. H. Smith. Tetrahedron Lett. 4163 (1970).
21. F. M. Menger and J. H. Smith. J. Am. Chem. Soc. **94**, 3828 (1972).
22. F. M. Menger and A. C. Vitale. J. Am. Chem. Soc. **95**, 4931 (1973).
23. A. S. Shawali, A. Harhash, M. Sidky, H. M. Hassaneen, and S. S. Alkaabi. J. Org. Chem. **51**, 3498 (1986).
24. J. P. Greenstein and M. Winitz. Chemistry of amino acids. Vol. 2. Wiley, New York. 1961. pp. 823–843.
25. S. W. King, J. M. Riordan, E. M. Holt, and J. M. Stammer. J. Org. Chem. **37**, 3270 (1982).
26. K. Kumar, D. J. Phelps, and P. R. Careg. Can. J. Chem. **56**, 232 (1978).
27. E. P. Prokofev and E. I. Kapeiskaya. Tetrahedron Lett. 737 (1979).
28. A. W. Hanson. Acta Crystallogr. Sect. B: Struct. Crystallogr. Cryst. Chem. **B33**, 593 (1977).
29. C. Hansch and A. J. Leo. Substituent constants for correlation analysis in chemistry. Wiley, New York. 1979.
30. A. Frost and R. G. Pearson. Kinetics and mechanism. 2nd. ed. Wiley, New York. 1961. Chap. 7.
31. E. Erlenmeyer. Ber. Dtsch. Chem. Ges. **33**, 2036 (1900).
32. I. Arenal, M. Bernabe, and E. F. Alvarez. An. Quim. **77C**, 56 (1981).
33. P. K. Tripathy and A. K. Mukerjee. Synthesis, 285 (1985).

Can. J. Chem. Downloaded from www.nrcresearchpress.com by 109.225.110.28 on 09/08/12
For personal use only.

The reaction of boron trichloride – tertiary amine adducts with pseudohalide salts under phase transfer catalysis conditions

JEAN ATCHEKZAÏ, BERNARD BONNETOT, HENRI MONGEOT, SAMI BOUFI, AND BERNARD FRANGE[1]
Laboratoire de physicochimie minérale 1, 43 boulevard du 11 novembre 1918, 69622 Villeurbanne CEDEX, France

Received January 29, 1992

JEAN ATCHEKZAÏ, BERNARD BONNETOT, HENRI MONGEOT, SAMI BOUFI, and BERNARD FRANGE. Can. J. Chem. **70**, 2520 (1992).

The reaction of boron trichloride – tertiary amine adducts $D \cdot BCl_3$ with pseudohalide salts MX was investigated in a homogeneous medium or in two-phase systems under liquid/liquid or solid/liquid phase transfer catalysis conditions (PTC) as a potential route to the adducts $D \cdot BX_3$ (X = NCS, NCO). Best results were obtained with solid/liquid PTC with tetraglyme as catalyst. By suitable choice of the tertiary amine, solvent, and stoichiometry, the symmetric compounds $D \cdot BX_3$ were thus prepared with good yields, the same reaction leading either to mixed species $D \cdot BX_{3-n}Cl_n$ (n = 1, 2; X = NCS, NCO) or to the tetrapseudohaloborate anions BX_4^- (X = NCS, NCO). The mixed tetrahaloborates $BX_{4-n}Y_n^-$ could be obtained by exchange reaction from $BX_4^- + BY_4^-$ (X = NCS, Y = F, Cl, Br) or from BY_3 + Bu_4NX (X = NCS; Y = F, Cl, Br; X = NCO; Y = F). All these compounds were characterized by ^{11}B and, in one case, by ^1H and ^{13}C NMR. Pairwise additivity is observed for the ^{11}B NMR chemical shifts.

JEAN ATCHEKZAÏ, BERNARD BONNETOT, HENRI MONGEOT, SAMI BOUFI et BERNARD FRANGE. Can. J. Chem. **70**, 2520 (1992).

Nous avons étudié la réaction des complexes amine tertiaire – chlorure de bore $D \cdot BCl_3$ sur différents composés pseudohalogénés MX en opérant en milieu homogène ou hétérogène dans les conditions de la catalyse par transfert de phase (CTP) liquide/liquide ou solide/liquide. Les meilleurs résultats ont été obtenus par CTP solide/liquide avec le tetraglyme comme catalyseur. Les complexes symètriques $D \cdot BX_3$ (X = NCS, NCO) ont ainsi été préparés avec de bons rendements alors qu'en modifiant les conditions opératoires (solvant et stoechiomètrie), on obtient soit les dérivés mixtes $D \cdot BX_nCl_{3-n}$ (n = 1, 2; X = NCS, NCO) soit les ions tétrapseudohaloborates BX_4^- (X = NCS, NCO). Nous avons également obtenu les ions mixtes $BX_{4-n}Y_n^-$ par réaction d'échange entre BX_4^- et BY_4^- (X = NCS; Y = F, Cl, Br) ou BY_3 et Bu_4NX (X = NCS; Y = F, Cl, Br; X = NCO; Y = F). Tous ces dérivés ont été caractèrisés par RMN du ^{11}B et, dans un cas, par RMN du ^1H et du ^{13}C. Nous avons constaté que les déplacements chimiques du ^{11}B obéissent aux règles d'additivité.

Can. J. Chem. Downloaded from www.nrcresearchpress.com by 109.225.110.28 on 09/08/12
For personal use only.

Introduction

In a previous note (1), we reported our preliminary results concerning the reaction of KSCN with the adducts $C_6H_5CH_2NMe_2 \cdot BCl_3$, $BDMA \cdot BCl_3$, in an aromatic solvent with tetraglyme added as catalyst. In this paper, the scope of this new approach is investigated in a systematic way, aimed at preparing new adducts, mixed species, or tetrahaloborates anions by means of very simple methods. Thus, we were led to study the reaction of tertiary amine – boron trichloride adducts $D \cdot BCl_3$ (D = *N*,*N*-dimethylbenzylamine BDMA, *N*,*N*-dimethyloctylamine ODMA, and *N*,*N*-dilaurylamine LDMA) with thiocyanate and cyanate salts under various conditions, the relevant adducts being quite difficult (or impossible) to prepare by direct synthesis. The reaction was carried out in a refluxing aromatic solvent with a tetrabutylammonium salt, in two-phase liquid/liquid systems H_2O(NaOH)/organic solvent or in solid/liquid medium, a potassium (or sodium) salt being used in the latter case. The tertiary amines used are those whose adducts with boron halides are potential latent catalysts in the polymerization of epoxy resins (2). Further, these adducts are quite stable to moisture and could be kept in air for long periods of time without any degradation, at odds with the behaviour of related adducts that usually fume in air.

Experimental part

Physical measurements

NMR spectra were obtained with a Bruker AM 300 spectrometer at 96.28 MHz for ^{11}B with $BF_3 \cdot Et_2O$ as external reference (positive values downfield), and at 300 MHz for ^1H and 75 MHz for ^{13}C with TMS as reference in both cases. To obtain accurate values for the coupling constants, zero filling and Gaussian multiplication were applied prior to Fourier transformation, as reported earlier (3, 4). Typical ^{11}B NMR spectra were run with a spectral width of 20 000 Hz and 16 K data points. A least-squares fitting routine was used for the calculation of pairwise parameters $n_{i,j}$. Melting points were determined by differential scanning calorimetry (DSC). Elemental analyses were carried out by standard combustion at 1050°C for C, H, and N, the nitrogen oxides being reduced to nitrogen; S analysis was by combustion at 1400°C.

Materials

All reactions were performed under an atmosphere of dry argon. Tetraglyme was freshly distilled from sodium benzophenone; aromatic solvents were distilled over phosphorus pentachloride and stored over molecular sieves. Tetrabutylammonium cyanate was a commercial product (Fluka) and used as received. All reactions with the latter and with air-sensitive compounds were performed in an efficient dry-box.

Preparation of $D \cdot BX_3$ adducts

These were obtained by reaction of BX_3 with the suitable amine in hexane while stirring and cooling the mixture. The creamy slurry obtained was filtered, washed with several portions of hexane, and air dried. It was then thoroughly washed with cold water, dried again under vacuum at 100°C, and dissolved in dichloromethane. The solution was finally poured on a Florisil column (SiO_2/MgO 85:15) to remove any ionic impurity, providing analytical samples after recrystallization (CH_2Cl_2/hexane 1:1). The reaction was applied to $BDMA \cdot BX_3$ (X = F, Cl, Br, I), $ODMA \cdot BCl_3$, and $LDMA \cdot BCl_3$. The values reported for the ^1H, ^{13}C, and ^{11}B chemical shifts and coupling constants of $BDMA \cdot BX_3$ (X = F, Cl, Br, I, NCS) are summarized in Table 1.

[1]Author to whom correspondence may be addressed.

TABLE 1. NMR data for BDMA · BX_3 (X = F, Cl, Br, I, NCS)

(*a*) ^{1}H NMR

X	Solvent	δ CH_2	δ $(NCH_3)_2$	δ Har	$^3J(^{11}BH)^a$
None	$CDCl_3$	3.34 (s)	2.17 (s)	7.26 (m) 5p	
F	CD_2Cl_2	4.05 (s)	2.46 (q)	7.46 (m) 3p 7.36 (m) 2p	Unresolved
Cl	CD_2Cl_2	4.53 (s)	2.79 (q)	7.50 (m) 3p 7.40 (m) 2p	2.9
Br	CD_2Cl_2	4.73 (s)	2.94 (q)	7.50 (m) 3p 7.40 (m) 2p	3.2
I	C_6D_6	4.92 (s)	3.07 (q)	7.42 (m) 3p 7.35 (m) 2p	3.6
NCS	CD_2Cl_2	4.07 (s)	2.53 (q)	7.51 (m) 3p 7.37 (m) 2p	2.4

(*b*) ^{13}C NMR

X	Solvent	δ CH_2	δ $N(CH_3)_2$	δ C_1	δ $C_{2,6}$	δ $C_{3,5}$	δ C_4	$^3J(^{11}BC)^b$
None	$CDCl_3$	63.9	44.9	138.5	127.7	128.5	126.5	
F	CD_2Cl_2	60.6	42.6	129.4	129.1	133.0	129.9	1.1
Cl	$CDCl_3$	61.8	44.4	128.7	129.0	133.0	130.1	2.2
Br	CD_2Cl_2	63.2	45.8	129.2	129.4	133.5	130.5	2.3
	$CDCl_3$	62.8	45.5	128.7	129.1	133.1	130.2	2.3
I	C_6D_6	63.2	45.8	129.2	128.8	133.0	129.8	2.3
NCS	CD_2Cl_2	61.9	43.7	127.7	129.6	133.2	130.8	2.1
	$CDCl_3$	61.5	43.2	127.1	129.3	132.7	130.5	2.1

(*c*) ^{11}B NMR

X	Solvent	δ ^{11}B	δ ^{11}B BX_3	solvent
F	CH_2Cl_2	−18.1	10.0[c]	Methylcyclohexane
Cl	CH_2Cl_2	−7.7	46.5[c]	Methylcyclohexane
Br	CH_2Cl_2	−22.0	38.7[c]	Methylcyclohexane
I	C_6H_6	−71.9	−7.9[c]	Methylcyclohexane
NCS	CH_2Cl_2	−28.6	5.0[d]	CH_2Cl_2

[a]This long-range proton–boron coupling constant involves the methyl protons, consistent with earlier observations on $Me_3N \cdot BX_3$ adducts (5). In every case, the benzyl protons display an unresolved singlet.

[b]No $^2J(^{11}BC)$ could be detected with any of these compounds. Such behaviour is not uncommon with boron tetrahedral derivatives. Thus, in $B(C_6H_5)_4^-$, the $^2J(^{11}BC)$ is significantly smaller than the relevant ^3J, 1.5 vs. 2.7 Hz (6). For mixed tetraalkylborates, no $^2J(^{11}BC)$ has been found whereas a ^3J of about 4.0 Hz was measured (7). Further, similar trends are observed in organic chemistry, where $^2J(CH) << {}^3J(CH)$ for aromatic compounds.

[c]From ref. 8.

[d]From ref. 9.

Preparation of BDMA · B(NCS)$_3$

This preparation was reported earlier (1). Anal. calcd. for $C_{12}H_{13}N_4S_3B$: C 45.00, H 4.09, N 17.50, S 30.03, found: C 44.87, H 4.11, N 17.73, S 29.35.

Preparation of LDMA · B(NCS)$_3$

The reaction was carried out for 4 h in refluxing chlorobenzene with the molar ratio D · BCl_3/KNCS/TTG 1:9:0.2. After filtration, the clear solution was poured through a short column of Florisil, giving 60% of pure LDMA · $B(NCS)_3$, δ ^{11}B = −9.9 ppm (CH_2Cl_2), F = 30°C (DSC). Anal. calcd. for $C_{17}H_{31}N_4S_3B$: C 51.24, H 7.84; found: C 51.02, H 7.75.

Preparation of B(NCO)$_3$ adducts

The reaction was carried out in refluxing chlorobenzene for 8 h with a molar ratio D · BCl_3/NaNCO/TTG 1:9:0.2. After the same work-up as above, 80% of pure LDMA · $B(NCO)_3$ was obtained; δ ^{11}B = −6.1 ppm, F = 45°C. Anal. calcd. for $C_{17}H_{31}N_4O_3B$: C 58.29, H 8.92; found: C 57.92, H 8.75. ΔH_f = 90 J/g (DSC). The same reaction was applied to ODMA · BCl_3 in refluxing chlorobenzene for 5 h giving, after chromatographic treatment and recrystallization from CH_2Cl_2/hexane, 50% of pure ODMA · $B(NCO)_3$. Anal. calcd. for $C_{13}H_{23}N_4O_3B$: C 53.07, H 7.88; found: C 52.84, H 7.82. Finally, after refluxing BDMA · BCl_3 with NaNCO in chlorobenzene for 8 h, 95% BDMA · $B(NCO)_3$ was obtained together with 5% $B(NCO)_4^-$ (−6.0 and −11.6 ppm according to ^{11}B NMR). After the same work-up, 70% of pure BDMA · $B(NCO)_3$ was obtained. Anal. calcd. for $C_{12}H_{13}N_4O_3B$: C 52.97, H 4.81; found: C 52.72, H 4.67.

Preparation of NBu_4NCS

This was obtained according to a classical method (10) starting from NBu_4Br and KNCS in acetone, at room temperature for 12 h. After filtration of KBr (97%), the solution was evaporated to dryness and the solid residue twice recrystallized from hexane/

Can. J. Chem. Downloaded from www.nrcresearchpress.com by 109.225.110.28 on 09/08/12
For personal use only.

ethyl acetate 1:1 to give 60% of slightly yellow needles (F = 126–127°C (lit. (10) 123–125°C).

Preparation of tetrahaloborate anions

These were prepared by classical methods according to the reaction $BX_3 + NBu_4X$ (X = Cl, Br, I) performed in a dry-box with a suitable solvent. BF_4NBu_4 was obtained in the two-phase system $NaOH/CH_2Cl_2$ as already reported (3).

Reaction of $BF_3 \cdot Et_2O$ with NBu_4NCO

Mixing equimolar amounts of $BF_3 \cdot Et_2O$ and NBu_4NCO in dichloromethane, inside the dry-box, resulted in a slight precipitate with a broad signal in ^{11}B NMR spectroscopy ($\delta\ ^{11}B = -1.4$ ppm, $h_{1/2}$ = 150 Hz). After a few minutes, the signal became asymmetric and, after heating for short periods of time, a sharp signal appeared at −1.4 ppm, followed by broad, decreasing intensity signals at −2.4, −4.0, −7.4, and −11.5 ppm, consistent with the presence of the expected mixed species $BF_n(NCO)_{4-n}^-$. However, broad, unaccounted-for signals were also present downfield at −0.4 and +0.2 ppm. The compounds so obtained were quite stable in solution and could be recovered unchanged after several weeks.

Reaction of BCl_3 with NBu_4NCO

When bubbling BCl_3 in slight excess through a solution of NBu_4NCO in CH_2Cl_2, a slight precipitate was first observed, whereas a clear solution resulted if using the reverse order. The ^{11}B NMR spectrum of the fresh solution, besides the very sharp signal of BCl_4^- (7.2 ppm, $h_{1/2}$ about 4 Hz), contains two major signals at 30.4 and 22.4 ppm indicative of a substitution of BCl_3. With a larger excess of boron trichloride (6:1), the signal of free BCl_3 was also observed near 40 ppm, this latter signal being quite sensitive to concentration effects. Additional very small signals were also detected between 7.2 and 1.5 ppm in the ^{11}B NMR spectra but none could be attributed to $BCl_n(NCO)_{4-n}^-$ except for the one at 1.5 ppm (probably BCl_3NCO^-), still present in solution after several weeks.

Reaction of BBr_3 with NBu_4NCO

With boron tribromide and NBu_4NCO in CH_2Br_2, results obtained are still more complex. Adding the reactants in a 1:1 ratio, signals at 28.0 and 20.7 ppm denote the substitution reaction of BBr_3, whereas a very broad signal whose chemical shift ranges from −10 ppm to −14 ppm corresponds to an exchange reaction. Further, signals at −1.9, −7.6, and −9.2 ppm, still observed after several weeks, are clearly indicative of a reaction of BBr_3 on the NCO moiety. Adding BBr_3 in excess to NBu_4NCO in the same solvent resulted in a quite different ^{11}B NMR spectrum: a sharp signal (−25.4 ppm, $h_{1/2}$ = 6 Hz) pertains to BBr_4^- whereas a broad one (−19.7, $h_{1/2}$ = 29 Hz) is likely to belong to $BBr_2(NCO)_2^-$ originating from the disproportionation of BBr_3NCO^-, as deduced from the areas under the signals.

Results and discussion

Homogeneous vs. phase transfer reactions

Homogeneous medium

In this case, NBu_4NCS reacted with $LDMA \cdot BCl_3$ in xylene at different temperatures. Thus, in a typical run at 100°C, after 2 h a complex mixture was observed containing, according to ^{11}B NMR integration, $D \cdot BCl_3$ (27.6%), $D \cdot BCl_2NCS$ (23.0%), BCl_3NCS^- (9.4%), $BCl(NCS)_2^-$ (16.5%), $BCl_2(NCS)_2^-$ (10.4%), $D \cdot B(NCS)_3$ (4.7%), and $B(NCS)_4^-$ (8.3%) for a starting molar ratio $NBu_4NCS/LDMA \cdot BCl_3$ 1:1.3. Interestingly, the amounts of compounds deduced from ^{11}B NMR data point to a nucleophilic substitution of chlorine, followed by a breaking of the amine–boron bond, and thus leading to anionic species in a second step. Therefore, heating for longer periods (or at higher temperatures) results in increased yields of $B(NCS)_4^-$ and other anionic species while, conversely, the amount of substituted materials decreases. Although the "naked" NCS^- anion turns out to be a strong nucleophilic species, this reaction is of limited interest from a synthetic point of view.

Liquid/liquid PTC

The above reaction was also carried out in H_2O/organic solvent ($CHCl_3$ or CH_2Cl_2) under different conditions. In any case, at refluxing temperatures with such different catalysts as Aliquat 336 or TTG (see Table 2), no reaction at all could be detected. Similar reactions were performed with $BDMA \cdot BCl_3$ and several potassium salts in a slightly modified procedure using 10 N NaOH (instead of water) and benzene or toluene at refluxing temperatures with benzyltriethylammonium chloride as catalyst. The presence of concentrated aqueous NaOH is indeed quite attractive since it precludes further hydrolysis of the adducts. However, in refluxing benzene, no reaction was observed with $BDMA \cdot BCl_3$ and KNCS, whereas, with refluxing toluene, most of the adduct was destroyed. In one case, with $BDMA \cdot BCl_3$ and KBr, $BDMA \cdot BBr_3$ could be detected in very small amounts by ^{11}B NMR. This could be a way to perform the reverse reaction (11):

$$D \cdot BCl_3 + 3Y^- \rightarrow D \cdot BY_3 + 3X^-$$

Y standing for a heavier halogen than Cl, provided a suitable catalyst is found. Let us add that this order of reactivity is opposite to the ranking previously observed in solid/liquid PTC, that is to say, F > NCS > NCO, Cl > Br(1).

Solid/liquid PTC

Consistent with our earlier studies, the best results were obtained with solid/liquid PTC. To find the best catalyst the reaction $LDMA \cdot BCl_3/KNCS/$catalyst with molar ratios 1:9:0.25 was carried out for 4 h in refluxing benzene with different catalysts. The results are summarized in Table 2, the best results for the conversion being obtained with tetraglyme, which appeared as an even better catalyst than 18-crown-6. Interestingly, despite the formation of $B(NCS)_4^-$ in every case, no substituted derivative of the latter such as $BCl_n(NCS)_{4-n}^-$ could be observed by ^{11}B NMR, at variance with the above behaviour in a homogeneous medium. Similar yields were obtained with NaNCS (instead of KNCS). Thus it turned out that, by a suitable choice of the tertiary amine, stoichiometry, solvent, temperature, and reflux time, it was possible to direct the reaction towards the formation of any desired species. The relevant data with $D \cdot BCl_3/KNCO/TTG$ in molar ratios 1:9:0.15 are given in Table 3, enabling the synthesis of $LDMA \cdot B(NCO)_3$ in good yields with chlorobenzene as solvent. The adduct $LDMA \cdot B(NCS)_3$ could also be obtained in pure form (see experimental part).

Tetrapseudohaloborate anions and mixed species

The reaction of the previously prepared $B(NCS)_4^-\ K^+$ nTTG (n about 2.5) with BX_4^- (X = F, Cl, Br), NR_4^+ (R = Et, nBu) was carried out as a general route to the mixed anionic species $BX_{4-n}(NCS)_n^-$, the exchange, monitored by ^{11}B NMR, being rather slow (on the NMR time scale) and requiring previous heating of the solutions in CH_2Cl_2 or C_6H_5Cl. With BI_4^-, no exchange could be detected by ^{11}B NMR spectroscopy. However, such a reaction was difficult to perform for reasons of solubility. Hence, we were led to carry out the reaction of BX_3 with NCS^-, NBu_4^+ as an easier route to the same species. Thus, with $BF_3 \cdot Et_2O$ and $NCSNBu_4$ in a molar ratio 1:1 in CH_2Cl_2, the major compound was indeed $BF_3 \cdot NCS^-$ together with smaller amounts of BF_4^- and $BF_2(NCS)_2^-$. With $BF_3 \cdot Et_2O$ in excess (1.5:1 or 3:1) no

Can. J. Chem. Downloaded from www.nrcresearchpress.com by 109.225.110.28 on 09/08/12
For personal use only.

TABLE 2. Products of reaction of LDMA · BCl_3 + KNCS + catalyst (1:9:0.25 mol) for 4 h in refluxing benzene (percent of total boron species present)

Catalyst	D · BCl_3	D · BCl_2NCS	D · $BCl(NCS)_2$	D · $B(NCS)_3$	$B(NCS)_4^-$
TTG	19.5	16.5	11.5	38	14.5
18-Crown-6	30	25	16	19	10
A 336	48	12.5	15	9	15.5
NBu_4HSO_4	67	14.5	9	3	6.5
TPB	100	0	0	0	0

Abbreviations: TTG = tetraethyleneglycol dimethylether or tetraglyme. A336 = Aliquat 336, trioctylmethylammonium chloride $(C_8H_{17})_3NMeCl$. TPB = tributylhexadecylphosphonium bromide $(C_4H_9)_3C_{12}H_{25}PBr$. The amount of different compounds was deduced from the ^{11}B NMR spectra.

TABLE 3. Solid/liquid PTC reaction D · BCl_3 + KNCO + TTG (1:9:0.15 mol) in refluxing aromatic solvent

D	Solvent	t (h)	D · BCl_3	D · BCl_2NCO	D · $BCl(NCO)_2$	D · $B(NCO)_3$	$B(NCO)_4^-$
BDMA	tol.	4	67.8	32.2	0	0	0
BDMA	tol.	24	9.2	72.0	18.8	0	0[a]
ODMA	ben.	24	5.5	33.1	40.6	15.1	5.6
LDMA	chl.	5	48	42	0	0	0[b]
LDMA	chl.	8	0	0	2	98	0
LDMA	chl.	12	0	0	0	97	3[c]

Solvent: tol. = toluene, ben. = benzene, chl. = chlorobenzene. t = time of reflux (hours). The amounts of compounds (mol.%) were deduced from ^{11}B NMR spectra (ref. $BF_3 \cdot Et_2O$).

[a]Reaction carried out at 100°C.

[b]Important hydrolysis denoted by two broad signals in ^{11}B NMR spectra within the range 17–21 ppm belonging to unidentified three-coordinate species.

[c]The amount of $B(NCO)_4^-$ could be increased by use of diglyme as solvent at 140–150°C but additional unexplained ^{11}B NMR signals were also observed. Some of these signals could arise from cationic species $D_2BX_2^+$ and D_2BXY^+ as recently reported (12). However, the expected signal pertaining to $D_2BCl_2^+$, slightly downfield from D · BCl_3, could not be detected.

additional signals could be identified by ^{11}B NMR except for the 0 ppm signal pertaining to $BF_3 \cdot Et_2O$. Similar results could be observed with BCl_3 in the same solvent or BBr_3 in CH_2Br_2 to prevent a possible exchange reaction with CH_2Cl_2 (13). In the last example, with BBr_3/NCS^- in a molar ratio 1:1, an accurate measure of the areas under the broad ^{11}B NMR signals observed leads to the figures 1.7:1:0.91 for $BBr_3 \cdot NCS^-$, $BBr_2 \cdot (NCS)_2^-$, and BBr_4^-, respectively. Quite noteworthy is the fact that the amounts of $BBr_2(NCS)_2^-$ and BBr_4^- are identical within experimental error, giving strong support to the disproportionation reaction already observed with the fluoroanions BF_3A^- (14).

$$2\ BBr_3NCS^- \rightarrow BBr_2(NCS)_2^- + BBr_4^-$$

Similar results were observed with $BF_3 \cdot Et_2O$ and BCl_3. However, no exchange at all was observed when heating together mixtures of BX_4^- (X = F, Cl) and $NCSNBu_4$.

$B(NCO)_4^-$ was indeed detected by ^{11}B NMR, when the reaction of D · BCl_3 with NCO^- was carried out in homogeneous medium or solid/liquid systems ($\delta\ ^{11}B = -10.4$ to -11.5 ppm according to the solvent),[2] in any case but the overall yield of the latter in the mixture remains small although diglyme as solvent was instrumental in raising it, probably by formation of a solvate. Thus, the only possible route to mixed species was to carry out the reaction:

$$BX_3 + NCONBu_4 \rightarrow BX_3NCO^-,NBu_4^+$$

[2]Although few examples are available, the replacement of NCS by NCO in boron compounds appears to result in a shielding of the boron nucleus in ^{11}B NMR spectroscopy (15, 16).

However, the obtained results so far are quite different from those observed with NCS salts. Despite the literature data concerning the adducts $AlCl_3NCS^-$ and $AlCl_3NCO^-$, for which a $^1J(^{27}Al^{14}N)$ value of about 40 Hz was reported in both cases (17, 18), no coupling constant $^1J(^{11}B^{14}N)$ could be resolved in any of the three examples, at variance with our own results with the related adducts $BX_n(NCS)_{4-n}^-$ (X = F, Cl; n = 1, 2, 3) (3). Likewise, no $^1J(^{11}BF)$ could be resolved with the fluoro adducts $BF_n(NCO)_{4-n}^-$, consistent with earlier studies of $BF_3 \cdot NCO^-$ by ^{19}F NMR spectroscopy (14). In conclusion, the cyanate group has a behaviour quite different from the thiocyanate group. Besides the already quoted differences, the two nucleophilic sites of the ambidente cyanate ion do not have as large a difference in nucleophilicity as in the thiocyanate ion, the nitrogen atom being simultaneously the center of highest electron density and the most polarizable center (19), thus allowing the formation of cyanate compounds B-OCN as well as isocyanate compound B-NCO.

NMR data

^1H NMR data

The ^1H NMR spectra of the compounds BDMA · BX_3 (together with the ^{13}C and ^{11}B NMR spectra) are reported in Table 1. From the many ^1H NMR studies carried out with boron trihalide–amine adducts, the ^1H complexation shifts, i.e., the difference between the observed shift for the free amine and for the adduct, increase in the order $BF_3 < BCl_3 < BBr_3 < BI_3$, these complexation shifts being approximatively proportional to the heats of complexation (20). It is widely accepted that inductive effects explain this ranking although other factors can have an effect; for instance,

Can. J. Chem. Downloaded from www.nrcresearchpress.com by 109.225.110.28 on 09/08/12
For personal use only.

TABLE 4. ^{11}B NMR data for $BX_n(NCS)_{4-n}^-$ (X = F,Cl,Br; n = 0, 1, 2, 3)[a]

X = F	δ exp.	δ calcd.	X = Cl	δ exp.	δ calcd.	X = Br	δ exp.	δ calcd.
BF_4^-	−1.4	−1.4	BCl_4^-	+7.1	+7.1	BBr_4^-	−24.1	−24.1
BF_3NCS^-	−3.1	−3.2	BCl_3NCS^-	−0.7	−0.7	BBr_3NCS^-	−20.7	−20.8
$BF_2(NCS)_2^-$	−6.3	−6.3	$BCl_2(NCS)_2^-$	−7.2	−7.2	$BBr_2(NCS)_2^-$	−18.4	−18.4
$BF(NCS)_3^-$	−10.9	−10.8	$BCl(NCS)_3^-$	−12.7	−12.6	$BBr(NCS)_3^-$	−17.3	−17.1
$B(NCS)_4^-$	−16.7	−16.7	$B(NCS)_4^-$	−16.7	−16.7	$B(NCS)_4^-$	−16.7	−16.7

[a]From the reported data, the following set of parameters was obtained.: $h_{F,F} = -0.23$, $h_{NCS,NCS} = -2.78$, $h_{F,NCS} = -0.83$, $h_{Cl,Cl} = 1.18$, $h_{Cl,NCS} = 1.41$, $h_{Br,Br} = -4.02$, $h_{Br,NCS} = -2.91$.

TABLE 5. ^{11}B NMR chemical shifts of $D \cdot BCl_nY_{3-n}$ (Y = NCS, NCO; n = 1, 2, 3)[a]

Y = NCS	δ exp.	δ calcd.	Y=NCO	δ exp.	δ calcd.
$D \cdot BCl_3$	10.4	10.4	$D \cdot BCl_3$	10.4	10.4
$D \cdot BCl_2NCS$	2.4	2.5	$D \cdot BCl_2NCO$	4.3	4.3
$D \cdot BCl(NCS)_2$	−4.2	−4.2	$D \cdot BCl(NCO)_2$	−1.2	−1.2
$D \cdot B(NCS)_3$	−9.7	−9.7	$D \cdot B(NCO)_3$	−6.1	−6.0
$B(NCS)_4^-$	−16.7	−16.7	$B(NCO)_4^-$	−11.5	−11.5

[a]D = BDMA as tertiary amine although no significant change was observed with other amines. The following set of parameters were deduced: $\eta_{D,Cl} = 2.29$, $\eta_{D,NCS} = -0.45$, $\eta_{NCO,NCO} = -1.92$, $\eta_{D,NCO} = -0.08$, $\eta_{NCO,Cl} = -0.69$.

changes in long-range shielding are likely to be important with heavier halogens (21) as well as steric interactions in some well-defined examples (22). Further, the chemical shifts measured for the NCS group are quite significant. Thus, whereas from a steric point of view NCS^- can be compared with I^-, as exemplified by the dissociation constant for NBu_4X in dichloroethane, which takes the values 0.8×10^{-4}, 10^{-4}, 1.4×10^{-4}, and 1.45×10^{-4} for X = Cl^-, Br^-, NCS^-, and I^-, respectively (23), the position of the complexation shift of the thiocyanate group, between that of F^- and Cl^-, brings strong support to the predominant influence of the electronegativity of the NCS^- group on the observed shift. It may be considered as an additional proof of the fact that NCS is bonded to boron through nitrogen.[3] Similar trends are observed for the coupling constants $^3J(^{11}BH)$ of the relevant adducts, in line with the data reported for the $^3J(^{11}BH)$ (28) and $^1J(^{11}B^{15}N)$ (29, 30) of the $Me_3N \cdot BX_3$ adducts (X = F, Cl, Br, I).

^{13}C NMR data

Once the amines are complexed to the boron trihalides the carbon shifts are consistently to lower fields as the Lewis acid becomes stronger, in accord with electron withdrawal from the amine by the stronger Lewis acid ($BF_3 < BCl_3 < BBr_3 < BI_3$). Therefore, the shift to high field of many amine ^{13}C resonances on complexation has features in common with protonation shifts of amines (31). Such trends are indeed observed for the CH_2 and $N(CH_3)_2$ of the series $BDMA \cdot BX_3$ (Table 1) but, for the aromatic carbons, these effects are small and negligible in the presence of solvent effects. The most striking feature of these ^{13}C NMR spectra lies in the presence of the previously reported $^3J(^{11}BC)$ (3), which remains constant or slightly increases with the heavier halogens. Furthermore, such coupling results in a significant broadening of the signal of the relevant carbon atom, thus enabling a ready assignment of the latter. With the compounds $ODMA \cdot BX_3$ and $LDMA \cdot BX_3$, although ^{13}C NMR spectroscopy is a good purity test, the correct assignment of the different carbon atoms is impossible unless sophisticated NMR techniques, such as $^{13}C-^{13}C$ correlated spectroscopy using the INADEQUATE sequence, are used or, possibly, T_1 measurements. Also, the ^{13}C chemical shifts so far reported for the long-chain aliphatic amines are unreliable (32, 33) as soon as more than four carbons are involved.

^{11}B NMR data

Although an upfield shift of the ^{11}B resonance is generally observed when the coordination number of boron increases from 3 to 4, this cannot be used as a criterion of the Lewis acid strength of the boron trihalide; one reason is that the ^{11}B chemical shift of trivalent boranes is controlled primarily by the π electron density at boron, while in tetracoordinated boron compounds the overall electron density has to be considered (34). Thus, from the values reported in Table 1, there is no obvious relationship between the adducts and the uncomplexed boron trihalides. Further, the δ ^{11}B value for the NCS derivative probably reflects the strong diamagnetic anisotropic shielding effect of the NCS group. The X-ray structure determination of related compounds (35, 36) proved a nearly linear B-NCS unit supporting this argument. It is a well-documented point that the ^{11}B chemical shifts for the adducts are determined primarily by the number and type of heavy halogens present, amine substituents having only small effects (37). In several types of compounds, chemical shifts of nuclei (38–40) were shown to be additive pairwise with respect to the substituent groups, the same kind of correlation being obeyed by the coupling constants between directly bonded atoms. Thus, the chemical shift (or spin–spin coupling) can be expressed as $\delta = \Sigma\eta_{i,j}$ where $\eta_{i,j}$ is a parameter associated with substituents i and j and independent of all other substituents. The sum is taken over all substituents about a central atom, excluding the nucleus observed in the NMR experiment. Such a correlation

[3]In most examples, boron gives rise to isothiocyanato compounds, B-NCS. The so-called thiocyanato derivatives, B-SCN, whose structure was deduced from IR data (24, 25) appear as doubtful, except for $(C_6H_5)_2BSCN$ for which two isomers were characterized (26, 27).

Can. J. Chem. Downloaded from www.nrcresearchpress.com by 109.225.110.28 on 09/08/12
For personal use only.

Can. J. Chem. Downloaded from www.nrcresearchpress.com by 109.225.110.28 on 09/08/12
For personal use only.

has been extensively applied to boron trihalide adducts (30, 41, 42) and mixed tetrahaloborate ions (13). We shall try to extend such correlations to the pseudohalogen compounds reported in this work, assuming for NCS and NCO groups a behaviour identical to the classical halogens X (X = F, Cl, Br, I). Thus, in the case of a complex such as $D \cdot BCl_2(NCS)$

$$\delta\,^{11}B = \eta_{Cl,Cl} + 2\eta_{Cl,NCS} + 2\eta_{Cl,D} + \eta_{D,NCS}$$

$$^1J(^{11}B\text{–}^{14}N) = \eta'_{Cl,Cl} + 2\eta'_{Cl,NCS}$$

where η is different in each of the above equations, D standing for the tertiary amine involved. Let us add that the set of parameters are the same for tertiary amine adducts or tetrapseudohaloborate ions and mixed species. The results of such calculations for the tetrapseudohaloborate ions $BX_n(NCS)_{4-n}^-$ (X = F, Cl, Br, n = 0, 1, 2, 3, 4) are summarized in Table 4, those for $D \cdot BCl_nY_{3-n}$ (D = BDMA, Y = NCS, NCO, n = 0, 1, 2, 3) in Table 5. The agreement between observed and calculated shifts is quite good, thus giving strong support to the validity of the hypothesis involved for the pseudohalogen group. Because of the paucity, and lack of accuracy, of data related to coupling constants $^1J(^{11}BF)$ and $^1J(^{11}B^{14}N)$ no correlations have been attempted. Furthermore, the above data are of interest from an heuristic point of view: thus, the extrapolated ^{11}B chemical shift for the compound BCl_3NCO^- is 1.47 ppm, in good agreement with the signal observed near 1.5 ppm. Using the same set of parameters and assuming $\eta_{F,NCO} = -0.54$, the calculated ^{11}B chemical shifts for $BF_n(NCO)_{4-n}^-$ are −2.3, −4.3, and −7.4 ppm for n = 3, 2, 1, respectively, instead of the observed values −2.4, −4.0, and −7.4 ppm.

1. J. Atchekzaï, A. Ouassas, C. R'Kha, B. Bonnetot, H. Mongeot, and B. Frange. Synth. Inorg. Met.-Org. Chem. **21**, 1133 (1991).
2. J. Atchekzaî, B. Bonnetot, B. Frange, H. Mongeot, A. Anton, A. Dubuisson, and P. Chastagner. Polym. Bull. (Berlin), **27**, 47 (1991), and references herein.
3. A. Ouassas, J. C. Duplan, B. Fenet, and B. Frange. Magn. Reson. Chem. **28**, 693 (1990).
4. J. Atchekzaî, B. Bonnetot, J. C. Duplan, B. Fenet, B. Frange, and H. Mongeot. Magn. Reson. Chem. **27**, 699 (1989).
5. J. S. Hartman and J. M. Miller. Inorg. Nucl. Chem. Lett. **5**, 831 (1969).
6. D. J. Hart and W. T. Ford. J. Org. Chem. **39**, 363 (1974).
7. P. E. Hausen, O. K. Poulson, and A. Berg. Org. Magn. Reson. **8**, 632 (1976).
8. M. F. Lappert, M. R. Litzow, J. B. Pedley, and A. Tweedale. J. Chem. Soc. (A), 2426 (1971).
9. J. Dazord, H. Mongeot, H. Atchekzaî, et J. P. Tuchagues. Can. J. Chem. **54**, 2135 (1976).
10. H. Kobler, R. Munz, G. Al Gasser, and G. Simchen. Liebigs Ann. Chem. 1937 (1978).
11. A. Brandström. *In* Preparative ion pair extraction. 2nd ed. Apotekarsocieteten, Hässle Lakenmedel, Stockolm. 1976. pp. 127–129.
12. M. J. Farquharson and J. S. Hartman. Can. J. Chem. **67**, 1711 (1989).
13. J. S. Hartman and G. J. Schrobilgen. Inorg. Chem. **11**, 940 (1971).
14. S. Brownstein and G. Latremouille. Can. J. Chem. **56**, 2764 (1978).
15. R. Jefferson. Ph. D. Thesis, University of Sussex, England. 1967.
16. B. Wrackmeyer and H. Nöth. Chem. Ber. **109**, 3480 (1976).
17. V. P. Tarasov, S. P. Petrosyants, G. A. Kirakosyan, and Y. A. Buslaev. Dokl. Akad. Nauk SSSR, **242**, 156 (1978); V. P. Tarasov, V. I. Privalov, G. A. Kirakosyan, and Y. A. Buslaev. Koord. Khim. **6**, 52 (1980).
18. J. W. Akitt. Prog. Nucl. Magn. Reson. Spectrosc. **21**, 64 (1989).
19. O. A. Reutov, I. P. Beletskaya, and A. L. Kurts. *In* Ambident anions. *Edited by* Consultants Bureau. Translated by J. P. Michael. New York. 1983. p. 231.
20. J. M. Miller and M. Onyszchuk. Can. J. Chem. **42**, 1518 (1964); **44**, 899 (1966).
21. J. S. Hartman and J. M. Miller. Adv. Inorg. Chem. Radiochem. **21**, 147 (1978).
22. W. H. Myers, G. E. Ryschkewitsch, M. A. Mathur, and R. W. King. Inorg. Chem. **14**, 2874 (1975).
23. J. P. Antoine, I. de Aguirre, F. Janssens, and F. Thyrion. Bull. Soc. Chim. Fr. II, 207 (1980).
24. B. C. Hui. Inorg. Chem. **19**, 3185 (1980).
25. H. G. Srebny and W. Preetz. Z. Anorg. Allg. Chem. **513**, 7 (1984).
26. T. Wizemann, H. Mueller, D. Seybold, and K. Dehnicke. J. Organomet. Chem. **20**, 211 (1969).
27. M. F. Lappert, H. Pyszora, and M. Rieber. J. Chem. Soc. 4256 (1965); M. F. Lappert and H. Pyszora. J. Chem. Soc. A. 854 (1967).
28. B. Benton-Jones, M. E. A. Davidson, J. S. Hartman, J. J. Klassen, and J. M. Miller. J. Chem. Soc. Dalton Trans. 2603 (1972).
29. B. Wrackmeyer. J. Magn. Reson. **66**, 172 (1986).
30. J. M. Miller. Inorg. Chem. **22**, 2384 (1983).
31. J. B. Stothers. Carbon-13 NMR spectroscopy. Academic Press, New York 1972.
32. E. Breitmaier and W. Voelter. ^{13}C NMR spectroscopy. 2nd ed. Verlag Chemie, New York. 1978. p. 178.
33. H. Eggert and C. Djerassi. J. Am. Chem. Soc. **95**, 3710 (1973).
34. H. Nöth and B. Wrackmeyer. NMR: Basic Princ. Prog. **14**, 89 (1978).
35. P. T. Clarke and H. M. Powell. J. Chem. Soc. B, 1172 (1966).
36. D. S. Kendall and W. N. Lipscomb. Inorg. Chem. **12**, 2920 (1973).
37. A. Fox, J. S. Hartman, and R. E. Humphries. J. Chem. Soc. Dalton Trans. 1275 (1982).
38. E. R. Malinowski, T. Vladimiroff, and R. F. Tavares. J. Phys. Chem. **70**, 2046 (1966).
39. T. Vladimiroff and E. R. Malinowski. J. Chem. Phys. **46**, 1830 (1967).
40. E. R. Malinowski. J. Am. Chem. Soc. **91**, 4701 (1969).
41. J. S. Hartman and J. M. Miller. Inorg. Chem. **13**, 1467 (1974).
42. J. M. Miller and T. R. B. Jones. Inorg. Chem. **15**, 284 (1976).

The metabolites of *Trichoderma longibrachiatum*. Part 1. Isolation of the metabolites and the structure of trichodimerol[1]

ROMANO ANDRADE, WILLIAM A. AYER,[2] AND PAUL P. MEBE
Department of Chemistry, University of Alberta, Edmonton, Alta., Canada T6G 2G2

Received March 31, 1992

ROMANO ANDRADE, WILLIAM A. AYER, and PAUL P. MEBE. Can. J. Chem. **70**, 2526 (1992).

Trichoderma longibrachiatum Rifai aggr. is a fungus reported to be antagonistic to the fungus *Mycena citricolor*, the causative agent of the American leaf spot disease of coffee. We have investigated the metabolites produced when *T. longibrachiatum* is grown in liquid culture and have isolated the known compounds sorbicillin (**2**), bisvertinol (**3**), and bisvertinolone (**4**) as well as several new compounds including trichodimerol (**1**), an interesting new natural product possessing a proper axis of symmetry. The structure of trichodimerol (**1**) was determined by a combination of spectroscopic techniques, including ^{1}H and ^{13}C nuclear magnetic resonance, infrared, ultraviolet, circular dichroism, optical rotatory dispersion, and mass spectrometry, and by transformation to octahydrotrichodimerol (**6**) and symmetrical and unsymmetrical derivatives thereof. The relative stereochemistry of bisvertinol (**3**) and bisvertinolone (**4**) has been revised. The metabolites described are not biologically active against *Mycena citricolor*.

ROMANO ANDRADE, WILLIAM A. AYER et PAUL P. MEBE. Can. J. Chem. **70**, 2526 (1992).

Le *Trichoderma longibrachiatum* Rifai aggr. est un champignon qui serait antagoniste du champignon *Mycena citricolor*, l'agent causant des taches sur les feuilles de café américain. On a examiné les métabolites produits par culture liquide du *T. longibrachiatum* et on a identifié la sorbicilline (**2**), le bisvertinol (**3**) et la bisvertinolone (**4**), des composés connus, ainsi que plusieurs nouveaux composés, dont le trichodiméral (**1**), un nouveau produit naturel intéressant possédant un axe de symétrie propre. On a déterminé la structure du trichodiméral (**1**) par une combinaison de techniques spectroscopiques, dont la résonance magnétique nucléaire du ^{1}H et du ^{13}C, l'infrarouge, l'ultraviolet, le dichroïsme circulaire, la dispersion rotatoire optique et la spectrométrie de masse ainsi que par la transformation de **1** en octahydrotrichodiméral (**6**) et en des dérivés symétriques et asymétriques de ce dernier. On a révisé la stéréochimie relative du bisvertinol (**3**) et de la bisvertinolone (**4**). Les métabolites décrits ne sont pas biologiquement actifs contre la *Mycena citricolor*.

[Traduit par la rédaction]

Introduction

Fungi of the genus *Trichoderma* Persoon are widespread and their taxonomical classification is difficult. This has led to the development of a *species aggregate* system of classification (1), which groups together several "species". It has been noted, for example, that under the name *Trichoderma hamatum* (Bon.) Bain aggr. there may be two or three or more different but morphologically very similar species, and "that isolates considered to belong to this species aggregate may behave quite differently under different conditions" (1). It is not surprising, then, that there is no clear pattern among the wide variety of secondary metabolites produced by *Trichoderma* strains (2, 3). In recent years considerable interest has been shown in the use of *Trichoderma* species as biological control agents (4). In spite of the importance of the genus, there are no studies reported of the metabolites of strains of *Trichoderma longibrachiatum* Rifai aggr., or of other "yellow" *Trichoderma* strains, although Rifai (1) has documented the existence of yellow pigments in *Trichoderma* strains of the species aggregates *T. aureoviride* Rifai aggr., *T. longibrachiatum*, and *T. harzianum*.

Our interest in the chemistry of the metabolites produced by *T. longibrachiatum* was stimulated by its potential use as a biocontrol agent for the American leaf spot disease of coffee (ojo de gallo), caused by the fungus *Mycena citricolor* (5). When grown in agar plate co-cultures, *T. longibrachiatum* caused lysis of the hyphae of *M. citricolor*.[3]

Unfortunately the antagonistic activity sometimes observed with *T. longibrachiatum* against *M. citricolor* was not observed with the extracts obtained when *T. longibrachiatum* was grown on liquid still or shake culture. However, the isolation of some colorful and apparently structurally unique compounds from these extracts prompted us to examine the compounds in more detail.

We describe herein the isolation of several new natural products, trichodimerol (**1**), trichodermolide, sorbiquinol, bislongiquinolide, and 5-hydroxyvertinolide, along with the known compounds sorbicillin (**2**), bisvertinol (**3**), and bisvertinolone (**4**). The details for the determination of the structure of trichodimerol, a unique natural product, are described and evidence for the revision of the structures of bisvertinol and bisvertinolone is presented.

Results and discussion

Trichoderma longibrachiatum was grown in both liquid shake and liquid still culture on a medium, developed by our collaborators in Costa Rica, containing yeast extract, malt extract, glucose (or lactose), peptone, and trace elements. Extraction of either the mycelium ($CHCl_3$:CH_2Cl_2) or the broth ($CHCl_3$) provided a similar mixture of metabolites in approximately equal amounts. Attempted separation by

[1]This paper is dedicated to the memory of Prof. José Calzada, our collaborator and friend at the Universidad de Costa Rica, who first interested us in this problem.

[2]Author to whom correspondence may be addressed.

[3]Prof. E. Vargas, Facultad de Agronomia, Universidad de Costa Rica, personal communication.

Can. J. Chem. Downloaded from www.nrcresearchpress.com by 109.225.110.28 on 09/08/12
For personal use only.

chromatography over silica gel led to large losses of material and some metabolites were denatured as indicated by comparison of the ^{1}H nmr spectra of the fractions obtained using polar eluants with the ^{1}H nmr spectra of the initial mixtures. Sephadex LH20 chromatography proved to be a very useful tool in handling these silica-sensitive compounds. Sephadex LH20 chromatography of the extracts, followed by silica gel chromatography when possible, led to the isolation of the three known compounds, sorbicillin (**2**), bisvertinol (**3**), and bisvertinolone (**4**), and the five new polyketides trichodimerol (**1**), trichodermolide, sorbiquinol, bislongiquinolide, and 5-hydroxyvertinolide.

Sorbicillin (**2**), an orange crystalline compound, was first isolated as an impurity in penicillin by Cram and Tishler in 1948 (6) and chemical methods were used to determine its structure (7). It has also been isolated from *Verticillium intertextum* (8, 9) and has been synthesized (10). Compound **2** was converted by catalytic hydrogenation to tetrahydrosorbicillin, similar in all respects to the product described by Dreiding and co-workers (9).

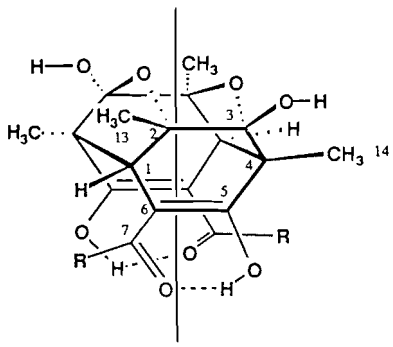

C2

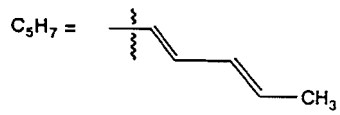

1 R = C_5H_7

6 R = *n*-C_5H_{11}

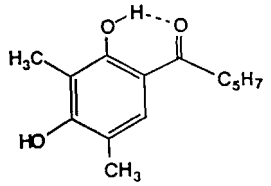

2

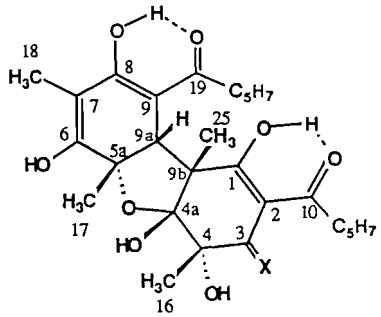

3 X = H_2

4 X = O

Trichodimerol (**1**) is a pale yellow, optically active, crystalline compound. Its molecular formula, $C_{28}H_{32}O_8$, was obtained from the high-resolution electron impact mass spectrum (hreims) and the molecular ion was confirmed by fast atom bombardment mass spectrometry (fabms: *m/z* 497, $M^+ + 1$, 35%). Its ^{13}C nmr spectrum shows 14 signals, indicating an element of symmetry in trichodimerol.[4] The compound gives a positive ferric chloride test and its uv maximum (λ_{max} 362 nm) shows a bathochromic shift upon addition of base (λ_{max} 378 nm), showing the acidic character of the chromophore. The presence of an enolized β-diketone is suggested by the ir (hydroxyl 3420 cm^{-1} and strongly chelated carbonyl 1613 cm^{-1}) and ^{1}H nmr spectra (enolized β-diketone hydrogen at δ 16.33 ppm).

[4]The element of symmetry present in trichodimerol must be a proper axis of symmetry, not a plane or point of symmetry, since the compound is optically active.

The ^{1}H nmr spectrum of trichodimerol (Table 1) also displays methyl singlets (δ 1.43 and 1.46 ppm), a methine singlet (δ 3.00 ppm), a hydroxyl hydrogen (δ 3.20 ppm), and signals characteristic of a sorbyl chain (δ 1.89 (d, 6.5 Hz, 3H), 6.11–6.34 (m, 3H), 7.32 (dd, 10, 15 Hz, 1H)). Further evidence of the presence of the sorbyl chain is given by the hreims, which shows a base peak at *m/z* 95 (C_6H_7O, 100%). The stereochemistry of this unsaturated chain was assigned as *E,E* on the basis of the magnitude of the ^{1}H nmr coupling constants measured in benzene solution (J = 15 Hz between δ 5.55 and 5.88 and between δ 6.25 and 7.38).

The ^{13}C nmr spectrum (Table 2) of trichodimerol shows 14 signals: carbons of the sorbyl chain, the methyls, a methine (δ 57.6), and a series of quaternary carbons (δ 58.9, 78.9, 102.8, 104.1, and 176.0). The quaternary carbon signals are assigned as follows: δ 102.8 and δ 176.0 to oxygenated carbons of the enolized β-diketone, δ 58.9 to an

Can. J. Chem. Downloaded from www.nrcresearchpress.com by 109.225.110.28 on 09/08/12
For personal use only.

TABLE 1. The ^{1}H nmr data[a] of trichodimerol (**1**), octahydrotrichodimerol (**6**), monoacetyl derivative (**7**), monoacetyloctahydrotrichodimerol (**8**), diacetyloctahydrotrichodimerol (**9**), triacetyloctahydrotrichodimerol (**10**), and tetraacetyloctahydrotrichodimerol (**11**) ($CDCl_3$, 360 MHz)

	Chemical shifts in δ (ppm)[b], multiplicity, *J* in Hz						
H	**1**	**6**	**7**	**8**	**9**	**10**	**11**[d]
1	3.00, s	3.00, s	2.98, s[c]	3.00, s[c]	3.03, s	3.11, s	3.09, s
1′	—	—	3.19, s[c]	2.96, s[c]	—	3.02, s	—
3 (OH)	3.20, s	3.28, s	6.12, s	2.98, s	—	—	—
5 (OH)	16.33, s	16.66, s	16.23, s[d]	16.40, s	16.41, s	—	—
5′ (OH)	—	—	15.94, s[d]	16.69, s	—	16.51, s	—
8	6.11–6.34, m	2.44–2.52 m	2.25–2.40 m	2.25–2.40, m	2.25–2.40, m	3.40, ddd[c]	3.11, m, 2.40, m
8′	—	—	2.25–2.40, m	2.25–2.40, m	—	2.25–2.40, m	—
9	7.32, dd, 15.5, 10	1.6, m	1.6, m	1.6, m	1.6, m	1.6, m	1.6, m
10	6.11–6.34, m	1.3, m	1.3, m	1.3, m	1.3, m	1.3, m	1.3, m
11	6.11–6.34, m	1.3, m	1.3, m	1.3, m	1.3, m	1.3, m	1.3, m
12 and 12′	1.89, d, 6.5	0.92, t, 7	0.85, m	0.85, t, 7	0.88, t, 7	0.85, m	0.86, t, 7
13	1.43, s[a]	1.46, s	1.44, s[a]	1.43, s[a]	1.49, s[a]	1.46, s[a]	1.45, s[a]
13′	—	—	1.47, s[b]	1.48, s[b]	—	1.48, s[b]	—
14	1.46, s[a]	1.46, s	1.47, s[b]	1.36, s[b]	1.33, s[a]	1.314, s[b]	1.31, s[a]
14′	—	—	1.51, s[a]	1.41, s[a]	—	1.35, s[a]	—
$COCH_3$	—	—	2.03, s	2.11, s	2.12, s	2.12, s	2.11, s
$COCH_{3'}$	—	—	—	—	—	2.12, s	—
$COCH_{3''}$	—	—	—	—	—	2.24, s	2.23, s

[a]Signals with the same superscript in the same column are interchangeable.
[b]Relative to the residual solvent signal (7.262 for chloroform).
[c]ddd, *J* = 13.5, 8.5, 5 Hz. The other H-8 signal is in the multiplet at 2.40 ppm.
[d]Preparation to be described in Part 2.

aliphatic carbon, δ 78.9 to a monooxygenated aliphatic carbon, and δ 104.1 to a dioxygenated carbon. Since there are only two oxygen-bearing sp^2 carbons, we may conclude that the carbonyl of the sorbyl chain is part of the enolized β-diketone system. These data are consistent with the presence of fragment **5**, an enol-sorbyl system, in trichodimerol.

The molecular formula of trichodimerol indicates it has 13 unsaturations. Since trichodimerol is dimeric, eight unsaturations may be attributed to two enol-sorbyl systems (**5**), leaving five unassigned unsaturations and indicating that trichodimerol is pentacyclic. There are eight oxygen atoms present in trichodimerol, four forming part of the enol-sorbyl systems. Since the ^{13}C nmr spectrum of trichodimerol displays two other signals attributed to oxygen-bearing carbons (the monooxygenated and dioxygenated carbons at δ 78.9 and 104.1), the remaining four oxygens must be present as two hemiacetals.

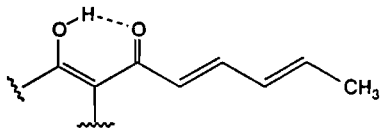

5

To obtain information about the relative position of the groups further ^{1}H nmr experiments were carried out. Nuclear Overhauser effect (nOe) difference experiments (Table 3) show that there is a large nOe enhancement between the δ 3.00 methine, the sorbyl hydrogen at δ 6.12, and the methyl groups at δ 1.43 and 1.46, which suggests that the methine is in close proximity to these functionalities. In solvent studies with pyridine, the ^{1}H nmr spectrum of trichodimerol shows that the methyls, the methine, and the hydroxyl group are significantly shifted (by 0.44, 0.57, 0.64, and 1.87 ppm, respectively). These shifts are considerably larger than those observed when benzene is used as solvent, suggesting that the methyl groups are vicinal, 1,3-, or in some other way close to the hemiacetal hydroxyl (11).

Of the various "dimeric" structures that can account for the structural features outlined above, only one, structure **1**, has a proper axis of symmetry and can account for the observed optical activity of trichodimerol. The absolute stereochemistry of trichodimerol was determined to be as depicted in **1** by use of the exciton chirality method (12). The cd spectrum of trichodimerol shows a split Cotton effect (amplitude) (A) = $\Delta\varepsilon_1 - \delta\varepsilon_2 = -25$) with a negative first Cotton effect, corresponding to a negative chirality.

Trichodimerol is unstable, decomposing to an insoluble brittle solid upon standing. It may be transformed to a stable derivative, octahydrotrichodimerol (**6**), by hydrogenation over palladium on carbon. The molecular formula of compound **6**, $C_{28}H_{40}O_8$, was confirmed by hreims. Its uv spectrum, λ_{max} 340 (ε = 390) and 294 (14 000) nm, is consistent with the presence of a enolized β-diketone chromophore (13). In addition to the signals expected for a five-carbon saturated chain, the ^{1}H nmr spectrum of **6** (Table 1) shows signals for a methine hydrogen at δ 3.00 (s), a hydroxyl hydrogen at δ 3.28 (br s), a six-hydrogen singlet at δ 1.46 (which may be resolved into two singlets when either pyridine or benzene is used as solvent), an enolized β-diketone hydrogen at δ 16.66, and no olefinic absorptions. The product retained its symmetry as shown by its ^{13}C nmr spectrum (Table 2, only 14 signals).

Octahydrotrichodimerol (**6**) is much more stable than trichodimerol (**1**) and remains unchanged after long periods of time. As in trichodimerol the methyl groups and the methine hydrogen of octahydrotrichodimerol (**6**) display large

Can. J. Chem. Downloaded from www.nrcresearchpress.com by 109.225.110.28 on 09/08/12
For personal use only.

TABLE 2. The ^{13}C nmr data of trichodimerol (**1**), octahydrotrichodimerol (**6**), monoacetyl derivative (**7**), monoacetyloctahydrotrichodimerol (**8**), diacetyloctahydrotrichodimerol (**9**), triacetyloctahydrotrichodimerol (**10**), and tetraacetyloctahydrotrichodimerol (**11**) ($CDCl_3$, 75.5 MHz)

	Chemical shift in δ (ppm)[a,b]						
C	**1**[c,d]	**6**[c,d]	**7**[c]	**8**[d]	**9**[c,d]	**10**[c,d]	**11**[e]
1	57.6	57.3	53.3[a]	58.0[a]	57.7	56.7	56.7
1′	—	—	56.8[a]	57.5[a]	—	57.5	—
2	78.9	78.8	89.0	78.9[e]	78.9	79.1[d]	79.1
2′	—	—	78.4	78.6[e]	—	78.7[d]	—
3	104.1	103.9	104.4	109.5	109.2	108.7	108.9
3′	—	—	202.2	103.5	—	109.1	—
4	58.9	58.0	60.8[b]	58.6	58.6	60.8	57.8
4′	—	—	63.8[b]	58.0	—	58.5	—
5	197.9	193.4	196.5[c]	187.3	187.5	167.4[e]	167.5
5′	—	—	195.1[c]	193.5[b]	—	188.6	—
6	102.8	103.3	106.0[g]	102.0[c]	101.4	117.5	117.2
6′	—	—	106.4[g]	102.7[c]	—	101.0	—
7	176.0	191.9	188.4[c]	196.5[b]	196.3	194.5[a]	193.6
7′	—	—	188.4[c]	191.8[b]	—	194.7[a]	—
8	118.6	34.7	33.6	33.3	33.4	33.7	33.3
8′	—	—	33.7	34.7	—	32.9	—
9	143.6	25.2	25.0[d]	25.8	25.8	26.8	26.6
9′	—	—	25.9[d]	25.1	—	25.3	—
10	131.0	31.5	31.6	31.6	31.6	31.4	31.8
10′	—	—	31.7	31.5	—	31.6	—
11	140.3	22.4	22.4[e]	22.4	22.4	22.4	22.4
11′	—	—	23.8[e]	22.4	—	22.4	—
12	18.7	13.9	13.9	13.9	13.9	13.9	13.9
12′	—	—	13.9	13.9	—	13.9	—
13	21.3	21.2	23.8[f]	21.5[d]	21.4[a]	21.3[b]	21.3[a]
13′	—	—	22.4[f]	21.1[d]	—	21.4[b]	—
14	18.9	18.8	21.4[f]	20.3[d]	20.2[a]	20.4[b]	20.2[a]
14′	—	—	20.0[f]	18.6[d]	—	20.2[b]	—
CO	—	—	173.3	169.0	169.0	169.2	169.1
Me	—	—	20.3[f]	?	20.7[a]	20.6[b]	20.7[a]
CO	—	—	—	—	—	167.2[e]	167.1[b]
Me	—	—	—	—	—	21.0[b]	20.9[a]
CO	—	—	—	—	—	167.4[e]	—
Me	—	—	—	—	—	21.1[b]	—

[a]Signals with the same superscript in the same column are interchangeable.
[b]Relative to the carbon of the solvent (77.0 for chloroform).
[c]APT obtained.
[d]Also obtained from [1-^{13}C]acetate incorporated trichodimerol.
[e]Only obtained from [1-^{13}C]acetate incorporated trichodimerol (see Part 2).

shifts in the ^1H nmr spectrum when pyridine is added. The methyl groups and the methine gave mutual nOe[5] enhancements, which are summarized in Table 3, together with the other observed enhancements. Because of its stability, compound **6** was used for additional spectroscopic studies and for the preparation of several derivatives.

Further evidence supporting the proposed structure of trichodimerol (**1**) was obtained from a $^{13}C[^1H]$ nOe enhancement experiment and a natural abundance ^{13}C INADEQUATE experiment on octahydrotrichodimerol (**6**). The location of the methine observed in the ^1H nmr spectrum relative to the non-hydrogen bearing carbons was investigated by the use of a $^{13}C[^1H]$ nOe difference experiment. Selective irradiation of H-1 of octahydrotrichodimerol gave enhancements to C-6, C-2, C-4, C-8, and a negative enhancement to C-3. The negative nOe must arise from an homonuclear nOe between H-1 and the two adjacent methyls (Me-13 and Me-14) followed by a heteronuclear nOe onto the carbons adjacent to the methyls. As well, the homonuclear nOe between the methine and the methyls is observed in the $^1H[^1H]$ nOe experiments. Indirect nOe enhancements of this type have been observed previously (14).

The abundant sample of octahydrotrichodimerol (**6**) justified a natural abundance ^{13}C two-dimensional INADEQUATE-type experiment (15). An INADSYM (16) spectrum was obtained and showed connectivities between C-3 and C-4, C-1 and C-6 and C-2, and between C-2 and C-3. These connectivities confirm that the structure of trichodimerol is as shown in **1**.

The formation of the different acetyl derivatives of octahydrotrichodimerol (**6**) demonstrates its interesting symmetry properties and confirms the presence of two

[5]Verified in benzene-d_6 where the two methyls give separate signals.

Can. J. Chem. Downloaded from www.nrcresearchpress.com by 109.225.110.28 on 09/08/12
For personal use only.

TABLE 3. The ^{1}H nmr nOe experiments with trichodimerol (**1**), octahydrotrichodimerol (**6**), monoacetyl derivative (**7**), monoacetyloctahydrotrichodimerol (**8**), diacetyloctahydrotrichodimerol (**9**), and triacetyloctahydrotrichodimerol (**10**) ($CDCl_3$, 360 MHz)

Signal saturated	Signal enhanced (%nOe)[a]	Signal saturated	Signal enhanced (%nOe)[a]
1		**8**	
1.43 (H-13)	3.00 (H-1) (2.8)	1.36 (H-14)	2.96 (H-1′) (4)
1.46 (H-14)	3.00 (H-1) (3.2)	1.41 (H-14′)	3.00 (H-1) (6.2)
	6.12 (H-8) (1.0)	1.43 (H-13)	3.00 (H-1) (3.4)
3.00 (H-1)	1.43 (H-13) (5)	1.48 (H-13′)	2.96 (H-1′) (2.5)
	1.46 (H-14) (7.8)		
	6.12 (H-8) (16)	**9**	
		1.33 (H-14)	3.03 (H-1) (9.6)
6		1.49 (H-13)	3.03 (H-1) (11)
1.46 (H′s-13, 14)	2.44–2.52 (H-8′s) (0.6)	3.03 (H-1)	1.33 (H-14) (5.3)
	3.00 (H-1) (3.9)		1.49 (H-13) (3.3)
	3.28 (OH-3) (1.6)		2.35 (H-8) (27)
2.44 (H-8a)	3.00 (H-1) (5.1)		
2.52 (H-8b)	3.00 (H-1) (5.7)		
3.00 (H-1)	2.44–2.52 (H-8′s) (12)	**10**	
	1.46 (H-13 and 14) (10)	1.32 (H-14)	3.02 (H-1′) (1.2)
3.28 (OH-3)	1.46 (H-13 and 14) (7.4)		2.30 (H-8) (2)
		1.35 (H-14′)	3.11 (H-1) (2.2)
7		1.46 (H-13)	3.11 (H-1) (5.7)
1.44 (H-13)	2.98 (H-1) (3.7)	1.48 (H-13′)	3.02 (H-1′) (3.7)
	6.12 (OH-3) (12)	3.02 (H-1′)	1.32 (H-14) (6)
1.47 (H-14, H-13′)	3.19 (H-1′) (4.5)		1.48 (H-13′) (5)
	6.12 (OH-3) (1.3)		2.30 (H-8) (17)
1.51 (H-14′)	2.38 (H-8′s) (0.9)	3.11 (H-1)	1.35 (H-14′) (7.6)
	2.98 (H-1) (5.2)		1.46 (H-13) (4)
2.98 (H-1)	1.44 (H-13) (6.4)		2.30 (3)
	1.51 (H-14′) (5.3)	3.40 (H-8a)	2.30 (H-8b) (24)
	2.38 (H-8′s) (10.6)		
	1.469 and 1.474 (H-13′		
3.19 (H-1′)	and H-14) (11.1)		
	2.31 (H-8′) (11.6)		
6.12 (OH-3)	1.44 (H-13) (9.3)		

[a]Ratio of the enhanced area over the irradiated signal's area in the difference spectra.

Can. J. Chem. Downloaded from www.nrcresearchpress.com by 109.225.110.28 on 09/08/12
For personal use only.

hemiacetals in trichodimerol. Treatment of octahydrotrichodimerol (**6**) with acetic anhydride in refluxing toluene or with acetic anhydride under reflux produced very complex product mixtures with at least 12 components as judged by tlc. When acetic anhydride, pyridine, and 4-*N*,*N*-dimethylaminopyridine (DMAP) in dichloromethane were used for acetylation of **6**, five acetylated products were isolated from the complex mixture formed.

Two different monoacetyl derivatives were obtained. The ir spectrum of monoacetate **7** shows the presence of a hydroxyl group (3400 cm^{-1}), a strongly chelated carbonyl (1605 cm^{-1}), and an acetoxyl carbonyl group (1728 cm^{-1}). The uv spectrum of monoacetate **7** is similar to that observed for octahydrotrichodimerol (**6**), indicating that the enolized β-diketone observed in **6** is unchanged in compound **7**.

The ^{1}H nmr spectrum of monoacetate **7** (Table 1) displays four methyl groups, enolized β-diketone hydrogens (δ 15.94 and 16.23), a hydroxyl hydrogen (δ 6.12 ppm), and methine hydrogens (δ 2.98 and 3.19), all as sharp singlets, indicating that compound **7** is not symmetrical. Accordingly, the ^{13}C nmr spectrum of **7** displays 29 signals, corresponding to 30 carbons. Five carbonyl-like absorptions are observed in the ^{13}C nmr spectrum (Table 2). It is apparent, however, from the integration of the signals that the signal at δ 188.4 corresponds to two carbons. One of the carbonyls can be assigned to the newly introduced acetyl group (δ 173.3), another four arise from the two enolized β-diketone systems (δ 188.4 × 2, 195.1, and 196.5), and the sixth may be assigned to a ketone (δ 202.2). The presence of only three signals in the region δ 100–110 indicates that compound **7** has a single hemiacetal group. Nuclear Overhauser experiments showed that there is a large nOe enhancement (12%) between the methyl hydrogens at δ 1.44 and the hydroxyl hydrogen at δ 6.12. Also, the chemical shift of the hydroxyl hydrogen occurs at unusually low field, suggesting it is chelated. The low-frequency absorption of the acetate carbonyl observed in the ir spectrum of **7** is consistent with this internal hydrogen bonding. These observations, together with the isolation of another monoacetate (**8**) (described below), lead us to conclude that one of the hemiacetals of octahydrotrichodimerol opens to the hydroxy ketone. The tertiary alcohol thus released is then acetylated to produce **7**. The acetyl carbonyl is conveniently located to allow hydrogen bonding with the hydroxyl group. This hydrogen bond explains the acetoxyl carbonyl absorption in the ir spectrum and the large nOe enhancement mentioned above.

The ^{13}C nmr chemical shifts of monoacetate **7** were compared with those of octahydrotrichodimerol (Table 2). A large

downfield shift for C-2 from δ 78.8 to 89.0 (10.2 ppm) is observed due to the acetylation of the tertiary alcohol. Other shifts observed are a downfield shift for C-4′ from δ 58.0 to 63.8 (5.8 ppm), and an upfield shift of C-1 and C-1′ from δ 57.3 to 53.3 and 56.8 (4.0 and 0.5 ppm, respectively) when **7** is compared with **6**. These downfield and upfield shifts are as expected for the change of a hemiacetal (in **6**) into a ketone (in **7**) (17). Furthermore, the nOe experiments (Table 3) allow the assignment of the methines and all the methyl hydrogen signals present in the ^{1}H nmr spectrum of monoacetate **7**.

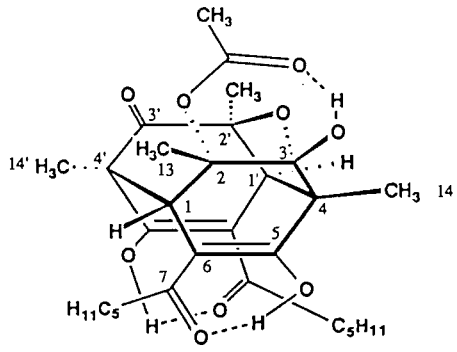

7

A second product obtained from the acetylation of octahydrotrichodimerol is monoacetyloctahydrotrichodimerol (**8**), $C_{30}H_{42}O_9$, which shows absorptions for a strongly chelated carbonyl (1600 cm^{-1}), hydroxyl (3440 cm^{-1}), and acetoxyl carbonyl (1752 cm^{-1}) in its ir spectrum. The ^{1}H nmr spectrum of **8** (Table 1) displays four methyl signals, (δ 1.36, 1.41, 1.43, and 1.48), methines (δ 2.96 and 3.00), acetyl methyl (δ 2.11), enolized β-diketone hydrogens (δ 16.40 and 16.69), and a hydroxyl hydrogen (δ 2.97). These signals indicate that compound **8** is not a symmetrical molecule.

Twenty-nine carbon signals were observed in the ^{13}C nmr spectrum of **8** (Table 2). There are five carbonyl-like carbon absorptions. One is attributed to the newly introduced acetyl carbonyl (δ 169.0) and four to the enolized β-diketone systems (δ 187.3, 191.8, 193.5, and 196.5). Furthermore, there are four carbon signals in the region 100–110 ppm, suggesting that compound **8** has two hemiacetals. Comparison of the ^{13}C nmr spectrum of **8** with that of **6** reveals that in **8** a hemiacetal carbon shifts from δ 103.9 to 109.5 (5.6 ppm). This shift is best explained if one hemiacetal hydroxyl of **6** has been acetylated to give the unsymmetrical acetate **8**.

A diacetate **9**, $C_{32}H_{44}O_{10}$, was also obtained upon acetylation of octahydrotrichodimerol. Its ir spectrum shows acetoxyl carbonyl (1753 cm^{-1}), a strongly chelated carbonyl (1599 cm^{-1}), but no free OH stretching absorption. The ^{1}H nmr spectrum of **9** (Table 1) displays the signals for hydrogens of methyls (δ 1.33 and 1.49), an enolized β-diketone hydrogen (δ 16.41), an acetyl methyl (δ 2.12), and a methine (δ 3.03), all as singlets. The ^{13}C nmr spectrum displays 16 signals, corroborating that compound **9** has an element of symmetry. Three carbon absorptions are carbonyl-like (Table 2): one is assigned to the acetate carbonyl (δ 169.0) and the other two to the enolized β-diketone system (δ 187.5 and 196.3). The hemiacetal carbon (δ 109.2) of **12** is shifted with respect to that observed in the ^{13}C nmr spectrum of octahydrotrichodimerol (**6**). From these data, the structure of the diacetate is assigned as the symmetrical hemiacetal diacetate **9**.

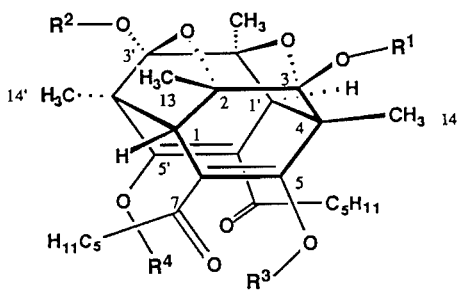

8 R^1 = Ac, R^2 = R^3 = R^4 = H
9 R^1 = R^2 = Ac, R^3 = R^4 = H
10 R^1 = R^2 = R^3 = Ac, R^4 = H
11 R^1 = R^2 = R^3 = R^4 = Ac

A fourth product isolated from the acetylation mixture is triacetate **10**, $C_{34}H_{46}O_{11}$, whose ir spectrum shows absorptions for acetoxyl carbonyl (1752 cm^{-1}), a conjugated ketone carbonyl (1699 cm^{-1}), a strongly chelated carbonyl (1612 cm^{-1}), but no free OH stretching. The uv spectrum of **10** differs from the uv spectrum of octahydrotrichodimerol (**6**) and the other acetates (**7**, **8**, **9**), suggesting that one of the enolized β-diketone systems of **6** has been acetylated.

The ^{1}H nmr spectrum of **10** (Table 1) shows signals for the acetate methyls (δ 2.11, 2.12, and 2.24), the quaternary methyls (δ 1.32, 1.35, 1.46, and 1.48), the methines (δ 3.02 and 3.11), and an enolized β-diketone hydrogen (δ 16.51) as singlets, as well as a one-hydrogen doublet of doublet of doublets at δ 3.40 (*J* 13, 8.5, 5 Hz) (Table 1) attributed to one of the side-chain H-8 hydrogens. Interestingly, in the ^{1}H nmr spectra of acetates **7**, **8**, and **9** the signal for the C-8 methylene hydrogens appears as a multiplet of two diastereotopic hydrogens. Although the chemical shift of the C-8 hydrogens is similar in the ^{1}H nmr spectra of compounds **7**, **8**, and **9**, one of the C-8 hydrogens has shifted more than 1 ppm in the ^{1}H nmr spectrum of **10**. This shift demonstrates that an enol system has been acetylated and suggests that the acetylated enol is endocyclic. If compound **10** had an exocyclic enol acetate, the side chain would retain its rigidity around the C-6, C-7 bond, and no significant change in any of the ^{1}H nmr signals of the C-8 hydrogens would be expected. The ^{13}C nmr spectrum of **10** (Table 2) is in agreement with the structure assigned.

A fifth acetate derivative was isolated from the acetylation of [1-^{13}C]acetate labelled octahydrotrichodimerol prepared during biosynthetic studies.[6] The ^{1}H and ^{13}C nmr

[6]Details of the biosynthetic studies will be presented in a subsequent paper.

Can. J. Chem. Downloaded from www.nrcresearchpress.com by 109.225.110.28 on 09/08/12
For personal use only.

Can. J. Chem. Downloaded from www.nrcresearchpress.com by 109.225.110.28 on 09/08/12
For personal use only.

spectra indicate it possesses structure **11**. The ir spectrum shows absorption for acetoxyl carbonyl (1751 cm^{-1}), conjugated carbonyl (1700 cm^{-1}), and double bond (1611 cm^{-1}) consistent with an enol acetate – ketone system.

The ^1H nmr spectrum of **11** (Table 1) shows absorptions corresponding to acetyl methyl hydrogens (δ 2.11 and 2.23), methyl hydrogens (δ 1.30 and 1.45), a methine hydrogen (δ 3.09), and a hexanoyl chain (δ 3.10 (m, 1H), 2.50 (m, 1H), 1.45 (m, 2H), 1.28 (m, 4H), and 0.88 (m, 3H). These characteristics indicate that tetraacetate **11** is symmetrical and that the enol acetates are endocyclic since, as indicated for triacetyloctahydrotrichodimerol (**10**), the chemical shift of the H-8 hydrogens changes to δ 3.11 and δ 2.50 in the ^1H nmr spectrum of tetraacetyloctahydrotrichodimerol (**11**). The ^{13}C nmr spectrum of **11** (Table 2) shows 18 signals and the assignment of these signals is in agreement with the proposed structure.

Octahydrotrichodimerol (**6**) is symmetrical and the progressive introduction of acetyl groups upon acetylation gives the following results. Introduction of one acetyl group, as in monoacetyloctahydrotrichodimerol (**7**) and monoacetyloctahydrotrichodimerol (**8**), destroys the symmetry present in octahydrotrichodimerol (**6**). Introduction of two acetyl groups, as in diacetyloctahydrotrichodimerol (**9**) yields a symmetrical product, while introduction of three acetyl groups, as in triacetyloctahydrotrichodimerol (**10**), destroys the symmetry again. The introduction of four acetyl groups restores the symmetry and gives tetraacetyloctahydrotrichodimerol (**11**).

As mentioned above, bisvertinol (**3**) and bisvertinolone (**4**), previously isolated by Dreiding and co-workers from *Verticillium intertextum* (18), were also obtained from *T. longibrachiatum*.[7] The previous workers favored a *trans* C-5a, C-9a ring junction and did not make a stereochemical assignment at the other ring junction (C-4a, C-9b).

We have investigated the stereochemistry of bisvertinol by nOe experiments with the following results: H-9a (δ 3.63) gave nOe enhancement to Me-17 and Me-25 (δ 1.26 (4%) and 1.42 (4%)), and to H-20 (δ 6.49 (18%)). H-3 (δ 2.44) gave an nOe enhancement to H-11 (δ 6.39 (7%)), to H-3′ (δ 2.71 (12%)), and to Me-16 (δ 1.19 (2%)). Furthermore, Me-16 gave enhancement to H-3 (1.4%) and Me-25 to H-20 (1.4%). Me-18 (δ 1.40 ppm) did not give rise to any nOe enhancement. These results allow us to assign the ^1H nmr signals of the quaternary methyls of bisvertinol.

The results of our nOe experiments and the cd spectrum (extrema of opposite sign at 410 and 353 nm (A = 75)) of bisvertinol indicate that the relative stereochemistry of Me-17, H-9a, and Me-25 in bisvertinol should be revised to an all-*cis* stereochemistry. The stereochemistry of the C-4a hydroxyl should then be *cis* on the basis of the enhanced stability of a *cis* 5–6 ring junction over a *trans* 5–6 ring junction, while the stereochemistry at C-4 should remain the same as proposed on biogenetic arguments (18). The stereochemistry of bisvertinol is thus as depicted in **3**. Application of the exciton chirality theory to the cd spectrum of bisvertinol indicates that its absolute stereochemistry is as shown in **3**.

Nuclear Overhauser enhancement experiments with bisvertinolone (**4**) showed similar results to the ones obtained for bisvertinol (**3**) and therefore the stereochemistry of bisvertinolone should also be revised from that proposed by Dreiding and co-workers (18).

The structures of the other new metabolites isolated from *T. longibrachiatum* will be described in Part 2 of this series.

[7]Identity was established by comparison of ^1H and ^{13}H nmr spectra with published values (9).

Experimental

General

High-resolution electron impact mass spectra (hreims) were recorded on an AEI MS-50 mass spectrometer coupled to a DS-50 computer. The hreims data are reported as m/z (relative intensity) except for the molecular ion, which is reported as m/z found (m/z calculated, relative intensity). Unless diagnostically significant, peaks with intensity less than 20% of the base peak are omitted. Chemical ionization mass spectra (cims) were recorded on an AEI MS-12 mass spectrometer with ammonia as the reagent gas. The data were processed using DS-55 software and a Nova-4 computer. The cims data are reported as m/z (assignment, relative intensity). Fourier transform infrared (ftir) spectra were recorded (as a cast from $CHCl_3$ solution unless otherwise noted) on a Nicolet FTIR 7199 interferometer. Ultraviolet (uv) spectra were recorded on a Hewlett Packard 8450A diode array spectrophotometer. Optical rotations were recorded on a Perkin Elmer 141 polarimeter. ^1H and ^{13}C nuclear magnetic resonance (nmr) spectra were measured (in $CDCl_3$ unless noted) on Brucker WM-360 and WH-300 (operating at 75.5 MHz for ^{13}C nmr) spectrometers, coupled to Aspect 2000 and Aspect 3000 computer systems, respectively. The multiplicity of the ^{13}C nmr signals was verified by APT experiments when possible. Chemical shifts are reported in parts per million (d value from tetramethylsilane (TMS)). The residual solvent signal was used as the internal standard, $CDCl_3$: ^1H: δ 7.262 ppm; ^{13}C: δ 77.00 ppm; acetone-d_6: ^1H: δ 2.04 ppm, ^{13}C: δ 29.0 ppm; MeOH-d_4: ^1H: δ 3.30 (methyl) ppm, ^{13}C: δ 49.00 ppm; C_6D_6: δ ^1H: 7.15 ppm, ^{13}C: δ 128.00 ppm relative to TMS.

Growth of Trichoderma longibrachiatum and isolation of the metabolites

Trichoderma longibrachiatum (UAMH 5068) was obtained from Professor Edgar Vargas of the University of Costa Rica and is deposited at the University of Alberta Microfungus Herbarium (UAMH 5068).

Trichoderma longibrachiatum (strain UAMH 4159) was obtained from the University of Alberta Mold Herbarium. It was originally deposited as *Trichoderma reesei* Simmons, mutant of ATCC 24449 (QM 9123). This strain (UAMH 4159) was previously deposited at the American Type Culture Collection (ATCC) as ATCC 26921, at the Commonwealth Mycological Institute (CMI) as CMI 192656, and at the Quatermaster Research and Development Center (QM) as QM 9414. *Trichoderma reesei* ATCC 24449 is a mutant of *T. reesei* ATCC 13631 (*T. viride* QM 6a) (CMI 45548), which was isolated from a "cotton duck shelter" by D. I. Fennell (19).

Slant cultures (PDA) of the fungi were stored in a refrigerator at 4°C. A small piece of mycelium and agar was removed from the slant culture and was used to inoculate an agar plate (PDA), and the plate culture was allowed to grow for 1 week. A portion of the plate culture was used to inoculate a liquid culture (potato dextrose media, 250 mL), which was allowed to grow with constant shaking (160 rpm) for 1 week. Inocula (20 mL) from the small shake culture were used to inoculate still cultures grown in Fernbach flasks (1 L, media composition: *vide infra*), while inocula (25 mL) were used to inoculate large shake cultures (500 mL of media).

Trichoderma longibrachiatum strain UAMH 5068 was grown on still and shake culture using the following media: glucose 2%, yeast extract 0.5%, malt extract 0.5%, K_2HPO_4 0.25%, $MgSO_4$ 0.2%,

Can. J. Chem. Downloaded from www.nrcresearchpress.com by 109.225.110.28 on 09/08/12
For personal use only.

$(NH_4)_2SO_4$ 0.1%, bactopeptone 0.5%. The still culture was harvested after 26 days and the shake culture after 11 days of growth.

Trichoderma longibrachiatum strain UAMH 4159 was grown on still culture using the same media, but with lactose instead of glucose as the main carbon source. This growth was harvested after 27 days.

The mycelium was separated from the broth by gravity filtration through cheese cloth. The mycelial mass was dried for 24 h in a fume hood and then extracted for 24 h with $CHCl_3$:CH_2Cl_2 (1:1) in a percolator. The solvent was removed under reduced pressure to give the crude mycelial extract.

The broth was concentrated under reduced pressure to approximately one quarter of its original volume. Butanol was added to avoid excessive foaming during the evaporation. The concentrated broth was then extracted under stirring with chloroform (approx. 4 × 1/2 volume). The chloroform extract was concentrated under reduced pressure to give the crude broth extract as a gum.

Isolation of the metabolites of Trichoderma longibrachiatum

The crude mycelium extract (9.5 g) from a still culture of the *T. longibrachiatum* (UAMH 5068, 10 L) was separated in the following way. A Sephadex LH20 column (70 g, 36 × 2.8 cm i.d.) was packed in methanol, and increasing amounts of chloroform and petroleum ether were used to precondition the column and the column was rinsed with 250 mL of the least-polar solvent mixture to be used. Elution of the metabolites from the crude extract was accomplished using a stepwise increase in solvent polarity. The solvents used were petroleum ether:$CHCl_3$ 2:3 (500 mL), 1:2 (750 mL); petroleum ether:$CHCl_3$:acetone 1:2:1 (250 mL), 1:2:2 (250 mL); $CHCl_3$:acetone 1:1 (250 mL); and methanol. The first fraction (75 mL) was discarded, subsequent fractions (15–20 mL) collected, and like fractions (tlc) combined.

Trichodimerol (**1**) eluted in fractions 20–33 and 56–73 (0.86 g). Sorbicillin (**2**) eluted in fractions 33–44 as a 1:1 mixture with trichodimerol (0.26 g). Sorbiquinol coeluted with trichodimerol in fractions 45–55 (0.27 g). Crude bisvertinol (**3**) eluted in fractions 74–82 (3.5 g). Bisvertinol was purified further by column chromatography (Sephadex LH20, petroleum ether:$CHCl_3$:acetone 1:1:0.4) to give 470 mg of bisvertinol. An analytical sample, prepared by precipitation (twice) from petroleum ether:Et_2O gave bisvertinol, mp 151.5–152.5°C (82 mg). Column chromatography (silica gel; 1% EtOH:$CHCl_3$) of the fraction containing sorbicillin (60 mg) gave pure sorbicillin (20 mg). Column chromatography (silica gel; 2% EtOH:$CHCl_3$) of the fraction containing sorbiquinol (80 mg) afforded sorbiquinol, $C_{28}H_{32}O_7$ (19.4 mg), as a yellow solid, and, after increasing the polarity (6% EtOH:$CHCl_3$), trichodimerol (19.4 mg).

The broth extract (7.5 g) of the still culture of *T. longibrachiatum* (UAMH 5068) was separated as described above. Fractions 15–30 contained impure trichodimerol (0.76 g). Fractions 31–35 gave sorbicillin and trichodimerol (87 mg), 36–57 impure trichodimerol (0.6 g), and 58–69 impure bisvertinol (1.70 g). Sorbiquinol was not obtained. After repeating the Sephadex column with fractions 4–15 (3.25 g), 370 mg of bislongiquinolide, $C_{28}H_{32}O_8$, was obtained in fractions 79–85 as a yellow gum, and 100 mg of bisvertinolone (**4**) in fractions 87–90.

The crude broth extract (3.7 g) from the shake culture of *T. longibrachiatum* (UAMH 5068) was separated as before by Sephadex LH20 chromatography. Impure bisvertinolone (**4**) was obtained in fractions 56–65. This was precipitated from petroleum ether:Et_2O to give 350 mg of bisvertinolone as an amorphous powder, mp 153–155°C. The mycelial extract of the shake culture provided only trichodimerol.

The mycelium extract of *T. longibrachiatum* (UAMH 4159) (9.3 g) was separated by Sephadex LH20 chromatography as described above. Trichodermolide was found in fractions 1–3 and was purified by column chromatography (silica gel; Bz:Et_2O 10:1 to 5:1) to give 235 mg of pure trichodermolide, $C_{24}H_{28}O_4$, as a colorless wax. Fractions 11–18 contained almost pure trichodimerol (1.5 g), fractions 19–38 gave mainly a mixture (2.4 g) of trichodimerol, sorbicillin, and sorbiquinol, while fractions 58–66 contained impure bisvertinol (1.5 g).

The broth extract of *T. longibrachiatum* (UAMH 4159) (8 g) was separated by Sephadex chromatography as described above. Fractions 1–5 contained impure trichodermolide, which after column chromatography (silica gel; Bz:Et_2O 3:1) gave 71 mg of pure trichodermolide. Fractions 32–50 (1.2 g) were combined and subjected to further Sephadex LH20 chromatography using petroleum ether:$CHCl_3$:acetone (2:3:0.4) as eluant. The first 150 mL was discarded. 5-Hydroxyvertinolide, $C_{14}H_{18}O_5$, eluted in fractions 34–48, with fractions 39–40 containing pure 5-hydroxyvertinolide (40 mg).

Trichodimerol (1): $[\alpha]_D$ −376 (*c* 0.26, MeOH); ftir ν_{max} (cm^{-1}): 3420, 2970, 2920, 1613, 1546, 1414, 1288, 1251, 1150, 1125, 992, 935; uv (MeOH) λ_{max} nm (log ε): 362 (4.48), 307 (4.20), 295 (4.17), 240 (4.00); NaOH: 378 nm: HCl regenerated the original spectrum; cd (MeOH) $\lambda_{extremum}$ nm (Δε): 336 (+11), 382 (−14); amplitude (*A*) = −25; ord (MeOH) $\lambda_{extremum}$ nm ([ϕ]): 230 (+10 900), 296 (−22 800), 357 (+52 600), 408 (−20 000); ^{1}H nmr spectrum: see Table 1; ^{1}H nmr spectrum (C_6D_6, 360 MHz) δ: 1.42 (dd, 1.6, 7 Hz, 1H), 1.46 (s, 3H), 1.54 (s, 3H), 3.12 (s, 1H), 3.35 (br s, 1H), 5.55 (dq, 15, 7 Hz, 1H), 5.88 (ddq, 15, 11, 1.5 Hz, 1H), 6.25 (d, 15 Hz, 1H), 7.38 (dd, 11, 14.5 Hz, 1H), 17.14 (s, 1H); ^{13}C nmr spectrum ($CDCl_3$): see Table 2; hreims: 496.2090 (calcd. for $C_{28}H_{32}O_8$: 496.2098, 14%), 401 (3), 248 (22), 232 (7), 205 (30), 137 (33), 95 (C_6H_7O, 100); cims: 514 (M^+ +18, 0.4%), 497 (M^+ +1, 1.2%), 249 (1/2 M^+ +1, 30%); fabms: 497 (M^+ +1, 35%), 249 ($M/2^+$ +1, 30%); tlc: R_f 0.73 (CH_2Cl_2:acetone 3:1).

Sorbicillin (2): ftir ν_{max} (c^{-1}): 3360, 2920, 1640, 1620, 1559, 1480, 1383, 1281, 1154, and 990: uv (MeOH) ν_{max} nm (ε): 318 (27 000); NaOH: 405 (29 000); HCl regenerated the original spectrum; ^{1}H nmr spectrum δ: 1.92 (d, 6 Hz, 3H), 2.16 (s, 3H), 2.24 (s, 3H), 5.26 (br s, 1H), 6.32 (dq, 12, 6 Hz, 1H), 6.38 (dd, 10, 12 Hz, 1H), 6.98 (d, 15 Hz, 1H), 7.48 (dd, 10, 15 Hz, 1H), 7.48 (s, 1H), 13.58 (s, 1H); (C_6D_6, 200 MHz) δ: 1.44 (d, 6.5 Hz, 1H), 1.94 (s, 3H), 1.96 (s, 3H), 4.62 (br s, 1H, exhanges upon addition of D_2O), 5.70 (dq, 15, 6.5 Hz, 1H), 6.00 (ddq, 11, 15, 1.5 Hz, 1H), 6.73 (d, 14.5 Hz, 1H), 7.24 (s, 1H), 7.61 (dd, 10.5, 14.5 Hz, 1H), 14.42 (s, 1H); ^{13}C nmr spectrum δ: 7.0 (q), 15.1 (q), 18.4 (q), 109.9 (s), 113.0 (s), 113.9 (s), 121.3 (d), 128.2 (d), 130.0 (d), 140.6 (d), 144.0 (d), 158.2 (s), 162.0 (s), 192.0 (s); hreims: 232.1096 (calcd. for $C_{14}H_{16}O_3$: 232.1100, 97%), 217 (100), 191 (70), 189 (20), 175 (25), 165 (68), 136 (72), 95 (6); cims: 233 (M^+ +1, 100); tlc: R_f 0.41 (2% EtOH:$CHCl_3$), 0.63 (6%).

Bisvertinol (3): mp 151.5–152.5°C (power from petroleum ether:Et_2O, lit. (9) mp 139–141°C); $[\alpha]_D$ −1274 (*c* 0.99, MeOH) (lit. (9) $[\alpha]_D$ −1467 ($CHCl_3$)); ftir ν_{max} (cm^{-1}) 3400, 3010, 2975, 2925, 1616, 1556, 1445, 1411, 1379, 1022, 992, 974; uv (MeOH) λ_{max} nm (ε): 227 (9 900), 274 (15 400), 300 (15 000). 313sh, 400 (24 000); NaOH: 203 (74 000), 234 (14 200), 273 (17 300), 298 (14 700), 362 (18 000), 426 (17 000); HCl regenerated the original spectrum; cd (MeOH) $\lambda_{extremum}$ nm (Δε): 410 (−42), 353 (+33); *A* = −75; ord (MeOH) $\lambda_{extremum}$ nm ([ϕ]): 443 (−53 000), 379 (+227 000), 315 (+20 000), 276 (+31 000); ^{1}H nmr spectrum (MeOH-d_4, 360 MHz) δ: 1.19 (s, 3H), 1.26 (s, 3H), 1.40 (s, 3H), 1.42 (s, 3H), 1.85 (d, 7 Hz, 3H), 1.89 (d, 7 Hz, 3H), 2.44 (d, 14 Hz, 1H), 2.71 (d, 14 Hz, 1H), 3.63 (s, 1H), 6.09 (ddq, 10, 15, 1.5 Hz, 1H), 6.25–6.40 (m, 3H), 7.19 (dd, 10, 15, 1H), 7.20 (dd, 10, 15 Hz, 1H); ^{1}H nmr spectrum: 1.30 (s, 3H), 1.38 (s, 3H), 1.50 (s, 3H), 1.58 (s, 3H), 1.92 (d, 6 Hz, 6H), 2.62 (d, 14 Hz, 1H), 2.75 (d, 14 Hz, 1H), 3.68 (s, 1H), 3.98 (br s, 1H), 6.4 (m, 6H), 6.44 (d, 15 Hz, 1H), 7.34 (dd, 15, 11 Hz, 2H), 16.2 (s, 1H), 16.7 (s, 1H); ^{13}C nmr spectrum (MeOH-d_4, 75.5 MHz) δ: 7.1 (q), 18.8 (q), 18.9 (q), 20.0 (q), 22.7 (q), 25.8 (q), 36.5 (t), 54.9 (d), 60.3 (s), 74.2 (s), 80.4 (s), 102.5 (s), 106.0 (s), 107.2 (s), 110.6 (d), 121.7 (d) 2C, 132.2 (d), 137.2 (d), 139.3 (d), 140.5 (d), 143.3 (d),

Can. J. Chem. Downloaded from www.nrcresearchpress.com by 109.225.110.28 on 09/08/12
For personal use only.

168.4 (s), 170 (s), 179.7 (s), 193.3 (s), 194 (s) (all carbons within 0.4 ppm of reported (9) values).

*Bisvertinolone (**4**):* mp 153–155°C (diisopropyl ether), 124–125°C petroleum ether:Et_2O (lit. (9) mp 156–158°C); ftir ν_{max} (cm^{-1}) 3400, 3020, 2980, 2935, 1760w, 1663s, 1607, 1575, 1412, 1379, and 994; uv (MeOH) λ_{max} nm (ε): 272 (23 000), 294 (sh (23 000), 366 (24 000); NaOH: 276 (32 000), 394 (17 000); HCl regenerated the original spectrum; cd (MeOH) $\lambda_{extremum}$ nm (Δε): 402 (−22), 350 (+20); A = −42; ord (MeOH) $\lambda_{extremum}$ nm ([ϕ]): 437 (−23 500), 370 (+91 000), 325 (+12 000); ^{1}H nmr spectrum δ: 1.35 (s, 3H), 1.42 (s, 3H), 1.43 (s, 3H), 1.46 (s, 3H), 1.86 (d, 6 Hz, 1H), 1.89 (d, 5 Hz, 1H), 3.72 (s, 1H), 4.20 (br s, 1H, exchangeable), 4.54 (br s, 1H, exchangeable), 6.0–6.4 (m, 6H, 1H exchangeable), 7.31 (dd, 11, 15 Hz, 1H), 7.39 (d, 15 Hz, 1H), 7.56 (dd, 16, 10 Hz, 1H), 16.31 (s, 1H), 17.71 (s, 1H): ^{13}C nmr spectrum δ: 6.9 (1), 18.6 (q), 18.7 (q), 19.2 (q), 22.6 (q), 25.6 (q), 54.4 (d), 59.8 (s), 79.0 (s), 79.8 (s), 99.8 (s), 104.0 (s), 107.2 (s), 110.9 (s), 120.0 (d), 121.9 (d), 131.0 (d), 131.2 (d), 137.4 (d), 139.6 (d), 144.0 (d), 148.3 (d), 163.8 (s), 170.2 (s), 185.7 (s), 191.2 (s), 196.4 (s), 199.8 (s), (all carbons within 0.4 ppm of reported (9) values); nOe (C_6D_6): [1.19]: 1.56 (0.8%), OH approx. 6 (1.4%); [1.407]: 4.01 (0.4%), OH approx. 6 ppm (3.5%); [1.56]: 4.01 (0.5%), OH (4.4%), 6.12 (d, 15 Hz) (1%); [1.97]: OH (7.5%); [4.01]: 6.12 approx. (d, 15 Hz) (6.6%), 1.56 (2.6%), 1.407 (3.5%) ppm; nOe ($CDCl_3$): [3.72]: 6.38 (8%), 1.42–1.43 (7%); [1.46]: none; [1.42–1.43]: 3.72 (3.6%); [1.35]: none.

*Hydrogenation of trichodimerol (**1**)*

Trichodimerol (**1**) (170 mg) in ethyl acetate was hydrogenated over palladium on carbon at room temperature for 1 h. The reaction mixture was filtered, concentrated, and purified by column chromatography (silica gel; Bz:Et_2O 1:1) to give octahydrotrichodimerol (**6**) (105 mg): mp 147–149°C (EtOAc: petroleum ether), 124–125°C (Bz:Et_2O); $[\alpha]_D$ +184 (*c* 0.70, MeOH); ftir ν_{max} (cm^{-1}): 3420, 2960, 2940, 2910, 1580, 1265, 1129, and 1130; uv (MeOH) λ_{max} nm (ε): 340 (390), 294 (14 100); cd (MeOH) $\lambda_{extremum}$ nm (Δε): 311 (+28), 281 (−4.9); A = +32.9; ord (MeOH) $\lambda_{extremum}$ nm ([ϕ]): 323 (+64 000), 296 (−65 000); ^{1}H nmr spectrum: see Table 1; ^{13}C nmr spectrum: see Table 2; hreims: 504.2727 (calcd. for $C_{28}H_{40}O_8$: 504.2724, 26%), 253 (65), 252 (33), 237 (17), 236 (35), 235 (25), 193 (53), 181 (76), 165 (52), 154 (73), 99 (100), 83 (19), 71 (53); cims: 502 (12%), 501 (32%), 252 (100%), 251 (73%), 233 (19%); tlc: R_f 0.17 (2% EtOH/$CHCl_3$), 0.46 (6%).

*Acetylation of octahydrotrichodimerol (**6**)*

Octahydrotrichodimerol (129 mg), acetic anhydride (1.5 mL), pyridine (0.5 mL), and dimethylaminopyridine (one crystal) were refluxed in dichloromethane (15 mL) for 7 days. Methanol (5 mL) was added, and the reaction mixture was filtered and evaporated *in vacuo*. Traces of pyridine were removed by azeotropic evaporation with toluene. Purification by column chromatography (silica gel; 12 to 33% ethyl acetate:petroleum ether) afforded the monoacetyl derivative of the keto form (**7**) (3.1 mg), diacetyloctahydrotrichodimerol (**9**) (51.2 mg), triacetyloctahydrotrichodimerol (**10**) (32.3 mg), and impure monoacetyloctahydrotrichodimerol (**8**) (7.7 mg). Compound **8** was purified further by preparative tlc on silica gel (eluant: 4% EtOH:$CHCl_3$) to give pure monoacetyloctahydrotrichodimerol (**8**) (3 mg).

*Monoacetyloctahydrotrichodimerol (**7**):* ftir ν_{max} (cm^{-1}): 3400, 2960, 2935, 2895, 2860, 1728, 1605, 1588, 1380, 1262, 1138, 1110, 1041, 948; uv (MeOH) λ_{max} nm (log ε): 295 (4.08); NaOH: 203 (4.53), 307 (4.08); HCl regenerated the original spectrum; ^{1}H nmr spectrum: see Table 1; ^{13}C nmr spectrum: see Table 2; hreims: 546.2834 (calcd. for $C_{30}H_{42}O_9$: 546.2830, 90%), 528 (19), 486 (37), 468 (14), 261 (27), 253 (42), 252 (12), 237 (22), 236 (81), 235 (52), 223 (19), 218 (21), 207 (22), 180 (33), 165 (60), 154 (21), 149 (40), 99 (100), 71 (80); cims: 564 (M^++18, 29%), 547 (M^++1, 14%), 504 (66), 295 (100); tlc: R_f 0.56 (EtOH:$CHCl_3$ 1%), 0.78 (2%), 0.92 (6%).

*Monoacetyloctahydrotrichodimerol (**8**):* ftir ν_{max} (cm^{-1}): 3440, 2957, 2932, 2872, 2860, 1752, 1600, 1466, 1462, 1374, 1243, 1076; uv (MeOH) λ_{max} nm (log ε): 292 (4.20); NaOH: 204 (4.69), 308 (4.20); HCl regenerated the original spectrum; ^{1}H nmr spectrum: see Table 1; ^{13}C nmr spectrum: see Table 2; hreims: 546.2822 (calcd. for $C_{30}H_{42}O_9$: 546.2830, 7%), 486 (39), 443 (27), 415 (11), 291 (18), 263 (31), 251 (17), 236 (100), 218 (25), 209 (17), 192 (26), 180 (39), 167 (68), 165 (61), 99 (66), 71 (61); cims: 564 (M^++18, 100%), 547 (M^++1, 6%); tlc 0.65 (EtOH:$CHCl_3$ 4%).

*Diacetyloctahydrotrichodimerol (**9**):* ftir ν_{max} (cm^{-1}): 2957, 2885, 1753, 1599, 1580, 1466, 1252, 1231, 1197, 1078, 1064; uv (MeOH) λ_{max} nm (log ε): 290 (4.30); NaOH: 204 (4.74), 299 (4.34); HCl regenerated the original spectrum; ^{1}H nmr spectrum: see Table 1; ^{13}C nmr spectrum: see Table 2; hreims: 588.2931 (calcd for $C_{32}H_{44}O_{10}$: 588.2935, 93%), 447 (26), 370 (34), 317 (37), 279 (20), 278 (32), 272 (30), 263 (21), 251 (48), 237 (41), 236 (95), 235 (43), 233 (20), 223 (24), 218 (27), 192 (31), 180 (42), 167 (47), 165 (86), 99 (100); cims: 606 (M^++18, 100%), 589 (M^++1, 22%); tlc: R_f 0.63 (EtOH:$CHCl_3$ 2%), 0.87 (6%).

*Triacetyloctahydrotrichodimerol (**10**):* ftir ν_{max} (cm^{-1}): 2956, 2932, 2880, 2865, 1752, 1699, 1612, 1465, 1373, 1253, 1232, 1193, 1176, 1066; uv (MeOH) λ_{max} nm (log ε): 224 (3.90), 229 (3.90), 255 (4.08), 292 (4.00); NaOH: 205 (4.89), 248 (4.00), 304 (4.26); HCl regenerated the original spectrum; ^{1}H nmr spectrum: see Table 1; ^{13}C nmr spectrum: see Table 2; hreims: 630.3069 (calcd. for $C_{34}H_{46}O_{11}$: 630.3045, 5%), 604 (36), 588 (8), 468 (18), 401 (26), 370 (34), 359 (31), 317 (22), 252 (9), 251 (27), 236 (46), 235 (43), 233 (24), 218 (35), 180 (25), 165 (63), 99 (100), 83 (21), 71 (87); cims: 648 (M^++18, 45%), 631 (M^++1, 22%), 588 (M^+−42, 100%); tlc: R_f 0.32 (EtOH:$CHCl_3$ 2%), 0.73 (6%).

Natural abundance INADSYM

Octahydrotrichodimerol (600 mg) was dissolved in deuterated benzene (1.5 mL). Sixty-four FIDs of 2K points and 640 scans each were obtained with the program INADSYM of Bruker. The delays were optimized for a carbon–carbon coupling constant of 59 Hz. A relaxation delay of 2 s was used between scans. This required a total spectrometer time of 40 h. The spectral window used was of 4545 Hz, corresponding to 50 ppm at 90.56 MHz. A zero filling to 1024 W was done in F_1 and the spectra were Fourier-transformed with a Gaussian multiplication in F_1 (LB_1 = 100, GB_1 = 0.2), and a sinusoidal multiplication in F_2 followed by symmetrization.

Acknowledgements

We acknowledge with thanks the financial support provided by the Natural Sciences and Engineering Research Council of Canada, the International Development Research Centre, and the Alberta Heritage Foundation for Medical Research. We also thank Lynne Sigler, University of Alberta Microfungus Herbarium, for cultures and valuable discussion and Dr. Lois M. Browne for her interest and assistance.

1. M. A. Rifai. Mycol. Pap. Commonw. Mycol. Inst. **116**, 1 (1969).
2. W. B. Turner and D. C. Aldridge. Fungal Metabolites II. Academic Press, New York. 1983. p. 592.
3. R. W. Dunlop, A. Simon, K. Sivasithamparam, and E. L. Ghisalberti. J. Nat. Prod. **52**, 67 (1989), and references therein.
4. G. C. Papavizas. Annu. Rev. Phytopathol. **23**, 23 (1985).
5. W. A. Ayer and C. Dufresne. Bull. Soc. Chim. Belg. **95**, 699 (1986).
6. D. J. Cram. and M. Tishler. J. Am. Chem. Soc. **70**, 4238 (1948).
7. D. J. Cram. J. Am. Chem. Soc. **70**, 4240 (1948).
8. L. Trifonov, A. S. Dreiding, L. Hoesch, and D. M. Rast. Helv. Chim. Acta, **64**, 1843 (1981).
9. L. Trifonov, H. Hilpert, P. Floersheim, A. S. Dreiding, D.

M. Rast, R. Skrivanova, and L. Hoesch. Tetrahedron, **42**, 3157 (1986).
10. J. F. C. McOmie and M. S. Tute. J. Chem. Soc. 3226 (1958).
11. P. V. Demarco, E. Farkas, D. Doddrell, B. L. Mylari, and E. Wenkert. J. Am. Chem. Soc. **90**, 5480 (1968).
12. N. Harada and K. Nakanishi. Circular dichroic spectroscopy. Exciton coupling in organic stereochemistry. University Science Books, Mill Valley, Calif. 1983. pp. 3–8.
13. A. I. Scott. Interpretation of the ultraviolet spectra of natural products. Pergamon Press, New York. 1964. p. 69.
14. R. N. Henrie II, R. W. Creekmore, and W. Yeager. J. Org. Chem. **53**, 5977 (1988).
15. A. E. Derome. Modern NMR techniques for chemistry research. Pergamon Press, Oxford. 1987. pp. 234–239.
16. R. Freeman and D. L. Turner. J. Magn. Reson. **48**, 158 (1982).
17. R. M. Silverstein, C. G. Bassler, and T. C. Morrill. Spectrometric identification of organic compounds. 4th ed. 1981. p. 289.
18. L. Trifonov, J. H. Bieri, R. Prewo, A. S. Dreiding, D. M. Rast, and L. Hoesch. Tetrahedron, **38**, 397 (1982).
19. S. C. Jong and M. J. Gantt (*Editors*). American type culture collection of fungi/yeasts. 17th ed. American Type Culture Collection, Md. 1987. p. 386.

Can. J. Chem. Downloaded from www.nrcresearchpress.com by 109.225.110.28 on 09/08/12
For personal use only.

Solvent effects in the metal interchange of crown ether – alkali metal cation complexes. Transition from an associative exchange in nitromethane to a dissociative exchange in acetonitrile studied by ^{23}Na nuclear magnetic resonance

KATHLEEN M. BRIÈRE[1] AND CHRISTIAN DETELLIER[2]

Ottawa–Carleton Chemistry Institute, University of Ottawa Campus, Ottawa, Ont., Canada K1N 6N5

Received March 27, 1992

KATHLEEN M. BRIÈRE and CHRISTIAN DETELLIER. Can. J. Chem. **70**, 2536 (1992).

The role of the solvent in the dissociation kinetics and cation exchange mechanisms of the complex sodium–monobenzo-15-crown-5 $(Na:B15C5)^+$ was examined by ^{23}Na NMR. In nitromethane (NM), the cationic exchange between the complexes takes place via an associative metal interchange mechanism, I_M. In acetonitrile (AN), it takes place via a dissociative (dissociation/recombination) mechanism. In AN–NM binary mixtures, the rate constant of the dissociative exchange (k_{-1}) increases with the AN molar fraction, X_{AN}, from 1.1×10^{-2} s^{-1} for $X_{AN} = 0$ to 89×10^{-2} s^{-1} for $X_{AN} = 0.400$ (corresponding to a decrease of the free energy of activation, $\Delta G_{di}^{\neq}$ from 62.1 to 51.1 kJ mol^{-1} respectively, at 301.5 K). The activation parameters were $\Delta H_{di}^{\neq} = 48$ kJ mol^{-1} and $\Delta S_{di}^{\neq} = -20$ J K^{-1}, mol^{-1} for $X_{AN} = 0.200$. This rate increase was related to the concentration increase in solution of the AN monosolvated complex $(AN:Na:B15C5)^+$. In the whole range of AN mole fractions studied, the rate constant of the associative exchange, k_2, was not dependent upon X_{AN} in the error limits: $k_2 \approx 9 \times 10^4$ M^{-1} s^{-1} at 301.5 K ($\Delta G_{as}^{\neq} = 45$ kJ mol^{-1}). The activation parameters were determined to be $\Delta H_{as}^{\neq} = 23$ kJ mol^{-1} and $\Delta S_{as}^{\neq} = -75$ J K^{-1} mol^{-1}. These findings are in good agreement with an associative exchange controlled mainly by the conformational changes of the ligand during the concerted partial decomplexation of a sodium cation and partial complexation of a second one, while solvation of the complexed cation plays a major role in the dissociative mechanism.

KATHLEEN M. BRIÈRE et CHRISTIAN DETELLIER. Can. J. Chem. **70**, 2536 (1992).

Par RMN du ^{23}Na, on a étudié le rôle du solvant sur les cinétiques de dissociation et sur les mécanismes d'échange de cation dans le complexe sodium–monobenzo-15-couronne-5. Dans le nitrométhane (NM), l'échange cationique entre les complexes se fait par un mécanisme associatif d'interchange du métal, I_M. Dans l'acétonitrile (AN), il se fait par un mécanisme dissociatif (de dissociation/recombinaison). Dans les mélanges binaires AN–NM, la constante de vitesse de l'échange dissociatif (k_{-1}) s'accroît avec la fraction molaire d'AN, X_{AN}, de 1.1×10^{-2} s^{-1} pour $X_{AN} = 0$ à 89×10^{-2} s^{-1} pour $X_{AN} = 0.400$ (ce qui correspond à une diminution de l'énergie libre d'activation $\Delta G_{di}^{\neq}$ de 62.1 à 51.1 kJ mol^{-1} respectivement, à 301.5 K). Les paramètres d'activation sont $\Delta H_{di}^{\neq} = 48$ kJ mol^{-1} et $\Delta S_{di}^{\neq} = -20$ J K^{-1} mol^{-1} pour $X_{AN} = 0.200$. Cet accroissement de vitesse se corrèle avec un accroissement de la concentration en solution du complexe monosolvaté par AN (AN : Na : B15C5)$^+$. Dans tout le domaine étudié des fractions molaires en AN, la constante de vitesse de l'échange associatif, k_2, ne dépendait pas de X_{AN}, dans les limites des erreurs de mesure : $k_2 \approx 9 \times 10^4$ M^{-1} s^{-1} à 301.5 K ($\Delta G_{as}^{\neq} = 45$ kJ mol^{-1}). Les paramètres d'activation étaient $\Delta H_{as}^{\neq} = 23$ kJ mol^{-1} and $\Delta S_{as}^{\neq} = -75$ J K^{-1} mol^{-1}. Ces résultats sont en accord avec un mécanisme associatif contrôlé par des changements conformationnels du ligand durant la décomplexation partielle du cation complexé allant de concert avec la complexation partielle d'un second cation, alors que c'est la solvatation du cation complexé qui joue le rôle prépondérant dans le mécanisme dissociatif.

Introduction

Since the report on crown ethers by Pedersen in 1967 (1), a wealth of information has been published concerning alkali metal cation – macrocyclic ligand complexes (see, for example, ref. 2). The structural and behavioral similarities of these macrocyclic ligands to the larger natural antibiotic ionophores make the simpler crown ethers a choice model for the study of transport of important biological cations, such as sodium or potassium, across lipophilic membranes. To gain insight into the underlying selectivities of these ligands towards the alkali metal cations, it is necessary to define their mechanisms of association and dissociation. Although thermodynamic and structural studies are relatively abundant, the kinetic and mechanistic aspects have received little attention and therefore are still not well understood (3). They were investigated in recent years by a few research groups, using alkali metal NMR (3–10). So far, two limiting mechanistic hypotheses (11) have accounted for the kinetic results obtained for alkali metal cations (M^+) in the presence of crown ethers or cryptands (C) in nonaqueous solvents: a *dissociative* (eq. [1]; with the steps of dissociation (1*a*) and recombination (1*b*)) and an *associative* exchange (eq. [2]).

$$[1a] \quad (M:C)^+ \underset{k_1}{\overset{k_{-1}}{\rightleftharpoons}} M^+ + C$$

$$[1b] \quad M^{+}* + C \underset{k_{-1}}{\overset{k_1}{\rightleftharpoons}} (M^*:C)^+$$

$$[2] \quad (M:C)^+ + M^{+}* \overset{k_2}{\rightleftharpoons} (M^*:C)^+ + M^+$$

For a given cation – macrocyclic ligand system, the nature of the counteranion (12, 13) and that of the solvent (14, 15) were shown to affect the competition between the above mechanisms. We previously reported that whereas the metal interchange in $(Na:B15C5^+)$[3] proceeds via the associative pathway (eq. [2]) in the poorly donating solvent nitromethane (NM; donor number (DN) = 2.7 (16)), in acetonitrile (AN; DN = 14.1) the preferred route is dissociative (eq. [1])

[1]Present address: Institute for Biological Sciences, National Research Council, Ottawa, Ont., Canada K1A 0R6.

[2]Author to whom correspondence may be addressed.

[3]Monobenzo-15-crown-5 (B15C5): 2,3,5,6,8,9,11,12-octahydro-1,4,7,10,13-pentaoxabenzocyclopentadecin.

Can. J. Chem. Downloaded from www.nrcresearchpress.com by 109.225.110.28 on 09/08/12
For personal use only.

Can. J. Chem. Downloaded from www.nrcresearchpress.com by 109.225.110.28 on 09/08/12
For personal use only.

(4, 17). This was observed despite the many similarities between these two solvents: the dielectric constants are 35.9 for both solvents, the dipole moments are 3.53 and 3.56 D, and the solubility parameters (Hildebrand's δ) are 24.8 and 26.0 $MPa^{1/2}$ for AN and NM respectively (18). We therefore proceeded to investigate further this dramatic mechanistic difference by characterizing the exchange kinetics of sodium in $(Na:B15C5)^+$ in the binary solvent mixtures of AN and NM. The gradual change from the associative to the dissociative exchange in going from NM to AN is mainly controlled by the nature of the first coordination sphere of the complexed cation and by the organization of the solvation cage around the complex.

Experimental section

B15C5 (Aldrich 98%) was recrystallized from hexanes and vacuum-dried over P_2O_5 (303 K) for at least 24 h prior to use. $NaBPh_4$ (Aldrich 99%) was recrystallized from cyclohexane with a minimum amount of ethanol, and vacuum dried (353 K) over P_2O_5 for at least 24 h prior to use. NM (BDH, OmniSolv) and AN (BDH, certified ACS) were dried under reflux over calcium hydride for 3 h, distilled under nitrogen, and stored under argon. The NMR tubes containing the sample solutions were prepared under argon and sealed with Parafilm. All the spectra were recorded within 48 h after the preparation of the samples.

Binary mixtures of desired mole fraction composition were prepared by adding the appropriate mass of AN in preweighed amounts of NM. The mole fraction, X, of the minor component was calculated from the masses of each component. Since the volumes of the individual components were not actually measured, the concentration, in moles/litre, of the minor component was calculated using the density values for each solvent at ambient temperature (18) and assuming additive volumes in determining the total volume of the binary mixture.

^{23}Na NMR spectra and transverse and longitudinal relaxation times were obtained on a Varian XL-300 spectrometer, at 79.35 MHz. In the case of Lorentzian lineshapes, the transverse relaxation times (T_2) were determined directly from the linewidths. The longitudinal relaxation times (T_1) were determined using the inversion–recovery 180°–τ–90° pulse sequence and T_1 was obtained from a three-parameter nonlinear regression analysis on at least nine experimental data points. The 90° pulse width was systematically verified and depended upon the experimental conditions; it was in the range 20–30 μs. The temperature of the probe was measured with a thermocouple dipped in nitromethane in a nonspinning 10-mm NMR tube. For a temperature range between 240 and 310 K, the temperature of the sample was estimated to be reliable to ±0.5 K. Pseudo-first-order rate constants were obtained from a full line-shape analysis of the ^{23}Na NMR spectra for a two-site exchange (19, 21). This was carried out on an Amdahl mainframe system using a nonlinear regression procedure as described previously (20).

The errors reported on values that resulted from statistical regressions are the standard errors, σ, associated with the regressions: ±1σ reported for linear regressions and ±2σ for nonlinear regressions. The free energies of activation, $\Delta G^{\neq}$, and their respective errors (19) were calculated directly from the rate constants at 301.5 K.

The chemical shifts were referenced to sodium chloride (0.1 M NaCl) in 90:10 (v/v) $H_2O:D_2O$ and were corrected for differences in bulk magnetic susceptibilities between the sample solvent and aqueous reference (eq. [3]). The correction factors (c.f. = $(4\pi/3)(\chi_{ref} - \chi_{samp})$; χ_{ref} and χ_{samp} are the volume magnetic susceptibilities of the reference and sample solvents (22, 23)) were calculated to be respectively −1.374 ppm for NM and −0.775 ppm for AN.

$$[3] \qquad \delta = \delta_{obs} + \text{c.f.}$$

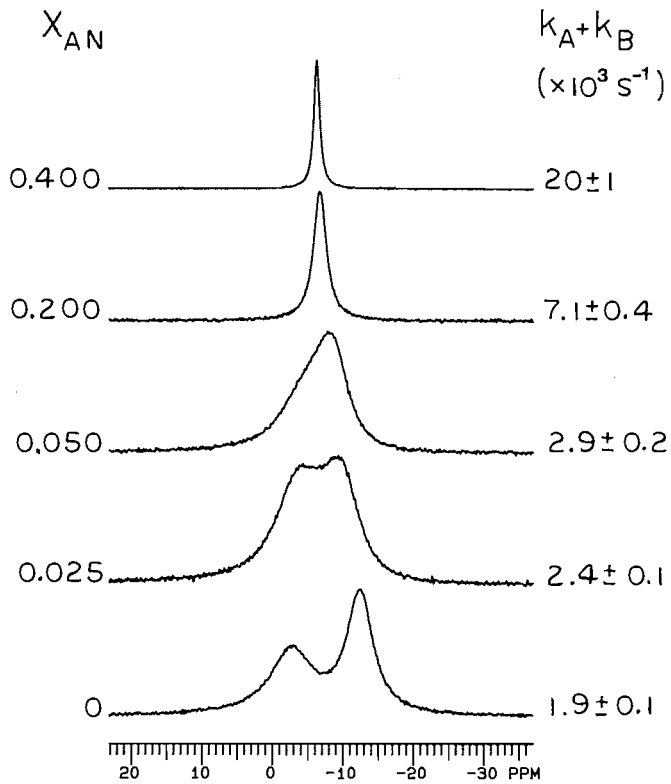

FIG. 1. ^{23}Na NMR spectra of samples containing equal populations of $(Na^+)_s$ and $(Na:B15C5)^+$ (ρ = 0.50) in AN–NM binary mixtures. $[NaBPh_4]_t$ = 20.0 mM and T = 301.5 ± 0.5 K. From top to bottom, the mole fraction of AN (X_{AN}) and ($k_A + k_B$) vary as shown.

For the binary solvent mixtures a weighted correction, determined from the values of the two neat solvents, was applied.

The viscosities of the binary mixtures were determined at 301 K using an Ostwald viscosimeter.

Results and discussion

In both AN and NM, the sodium cation forms quantitatively a 1:1 complex with B15C5 ($\log K_f > 4$) (4, 16, 24), so that it occupies two sites in solution (eq. [4]).

$$[4] \qquad A \underset{k_B}{\overset{k_A}{\rightleftharpoons}} B$$

Site A for the alkali metal cation is the solvated or "free" site, M^+, site B is the complexed alkali metal cation, $(M:C)^+$, and k_A and k_B are the pseudo-first order rate constants for the forward and reverse reactions respectively. In NM, at 300 K, this two-site exchange is slow on the ^{23}Na NMR chemical shift timescale, two separate peaks are observed, and a complete kinetic analysis from full lineshape analysis can be performed (4, 17). On the contrary, in AN, the exchange is very fast and a population weighted signal is observed, with no measurable exchange contribution to the linewidth (4). This can be observed in Fig. 1, which shows several ^{23}Na NMR spectra obtained at 301.5 K in a series of AN–NM binary solvent mixtures, for samples containing equal populations of solvated sodium (site A) and sodium complexed with B15C5 (site B). The bottom spectrum is that obtained in neat NM where a peak for each sodium site is observed (δ_A = −14.4 ppm; δ_B = −3.7 ppm). Upon in-

TABLE 1. Kinetic parameters for the dissociative (di) and associative (as) exchange of sodium with B15C5 in acetonitrile (AN)–nitromethane (NM) binary solvent mixtures[a]

X_{AN}[b]	$10^{-2}\,k_{-1}$ (s^{-1})	$\Delta G^{\neq}_{di}$ (kJ mol^{-1})	$\Delta H^{\neq}_{di}$ (kJ mol^{-1})	$\Delta S^{\neq}_{di}$ (J K^{-1} mol^{-1})	$10^{-4}\,k_2$ (M^{-1} s^{-1})	$\Delta G^{\neq}_{as}$ (kJ mol^{-1})	$\Delta H^{\neq}_{as}$ (kJ mol^{-1})	$\Delta S^{\neq}_{as}$ (J K^{-1} mol^{-1})
0[c]	1.1 ± 0.1	62.1 ± 0.3	n.d.[d]	n.d.	10.9 ± 0.4	44.8 ± 0.1	28 ± 3	−57 ± 3
0.025	3.5 ± 0.1	59.2 ± 0.1	n.d.	n.d.	8.4 ± 0.1	45.9 ± 0.1	25 ± 1	−66 ± 8
0.050	6.2 ± 0.9	57.8 ± 0.4	n.d.	n.d.	8.0 ± 0.8	45.6 ± 0.5	24 ± 2	−66 ± 8
0.100	10 ± 1	56.5 ± 0.2	n.d.	n.d.	9.7 ± 0.9	45.1 ± 0.5	n.d.	n.d.
0.200	27 ± 3	54.1 ± 0.3	48 ± 3	−20 ± 8	8 ± 4	45 ± 1	23 ± 2	−75 ± 8
0.300	46 ± 1	52.7 ± 0.1	52 ± 2	−2 ± 8	14 ± 4	44.1 ± 0.5	28 ± 2	−58 ± 8
0.400	89 ± 5	51.1 ± 0.2	n.d.	n.d.	2 ± 5	50 ± 8	n.d.	n.d.

[a]All values of k_{-1}, k_2, $\Delta G^{\neq}_{di}$, and $\Delta G^{\neq}_{as}$ are reported at 301.5 ± 0.5 K.
[b]X_{AN} is the mole fraction content of AN in the AN–NM binary solvent mixtures.
[c]In neat NM; ref. 17.
[d]Not determined.

Can. J. Chem. Downloaded from www.nrcresearchpress.com by 109.225.110.28 on 09/08/12
For personal use only.

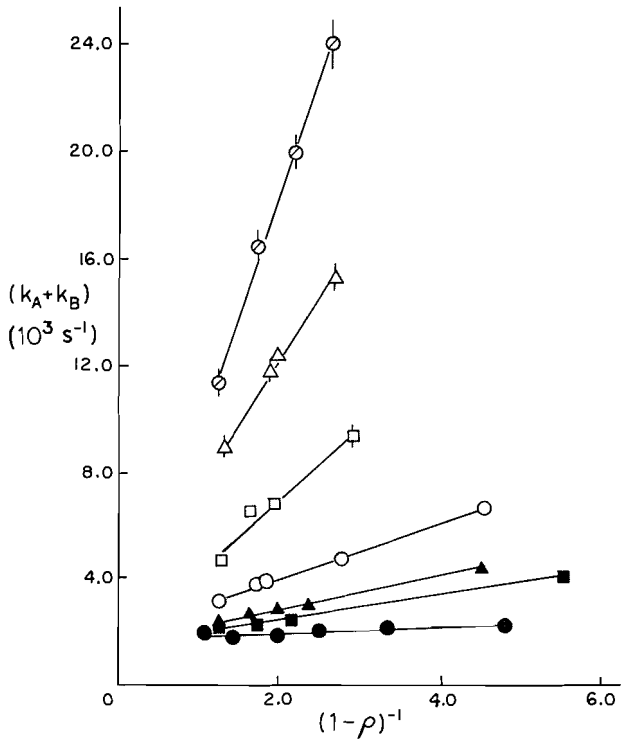

FIG. 2. $(k_A + k_B)$ as a function of $(1 - \rho)^{-1}$ for several AN–NM binary mixtures. $[NaBPh_4]_t$ = 20.0 mM and T = 301.5 ± 0.5 K. X_{AN}: (∅) 0.40; (△) 0.30; (□) 0.20; (○) 0.10; (▲) 0.050; (■) 0.025; (●) 0.

creasing the content of AN in the solvent, there is a coalescence of the two peaks around a mole fraction (X_{AN}) of 0.05, indicating an increase of the exchange rate.

For $X_{AN} < 0.2$, the pseudo-first-order rate constants were obtained from a complete lineshape analysis of the spectrum for an uncoupled two-site exchange case (19). The obtained lifetime (τ) is related to the pseudo-first-order rate constants as shown in eq. [5], since $P_A + P_B = 1$ (19, 21).

$$[5] \qquad \tau = P_A/k_B = P_B/k_A = (k_A + k_B)^{-1}$$

In eq. [5], P_A and P_B are the sodium populations in sites A and B respectively and τ is directly related to the lifetime of sodium in the two sites. For $0.2 \leq X_{AN} \leq 0.4$, the signal becomes Lorentzian, in the "moderately rapid" exchange limit, so that a comparison between the transverse relaxation rate (T_2^{-1}) and the longitudinal relaxation rate (T_1^{-1}) gives access to the pseudo-first-order rate constants (eq. [6]) (25–27).

$$[6] \qquad T_2^{-1} = 4\,P_A P_B\,\pi^2\,(\nu_A - \nu_B)^2\,(k_A + k_B)^{-1}$$

At $X_{AN} > 0.4$, a meaningful contribution to the exchange cannot be obtained.

The sum of the two pseudo-first-order rate constants, $(k_A + k_B)$, can be interpreted only if the corresponding mechanism of exchange is known. The two limiting mechanistic hypotheses (11), described in the introduction (eq. [1] and [2]), will be considered. They can be conveniently tested by the relationship between $(k_A + k_B)$ and the crown ether and salt concentrations, shown in eq. [7] (4, 21),

$$[7] \qquad k_A + k_B = k_{-1}(1 - \rho)^{-1} + k_2\,[Na^+]_t$$

where k_{-1} and k_2 are defined in eq. [1] and [2], $[Na^+]_t$ is the total concentration of sodium, and $\rho = [crown]_t/[Na^+]_t$.

Figure 2 shows plots of $(k_A + k_B)$ as a function of $(1 - \rho)^{-1}$ for several AN–NM binary mixtures varying in composition. In such linear plots, the slope is equivalent to k_{-1} whereas the intercept is related to k_2 (see eq. [7]) and one may thus separate the contributions of both mechanisms. In neat NM, this plot is near horizontal, indicating a mechanism predominantly associative. The slope increases as the content of AN in the solvent mixture increases, indicating a competition between both mechanisms. The linearity of all the plots is a good indication of the pertinence of this approach. It is noteworthy that all the plots extrapolate to the same value within experimental errors showing that k_2, the rate constant for the associative exchange, does not depend upon the nature of the solvent mixture, while k_{-1}, the rate constant for the dissociative exchange, displays a strong dependence upon X_{AN}. Table 1 contains the results obtained from linear regressions of the plots shown in Fig. 2, as well as the calculated free energies of activation, $\Delta G^{\neq}$, for the dissociative (di) and associative (as) exchange mechanisms: $\Delta G^{\neq}_{di}$ drops from 62 to 51 kJ mol^{-1} as X_{AN} increases to 0.40 while $\Delta G^{\neq}_{as}$ remains in the limits 44–46 kJ mol^{-1}. The extrapolation of the curve giving $\Delta G^{\neq}_{di}$ as a function of X_{AN} permits its estimation in neat AN: $\Delta G^{\neq}_{di} \sim$ 45–50 kJ mol^{-1}

Can. J. Chem. Downloaded from www.nrcresearchpress.com by 109.225.110.28 on 09/08/12
For personal use only.

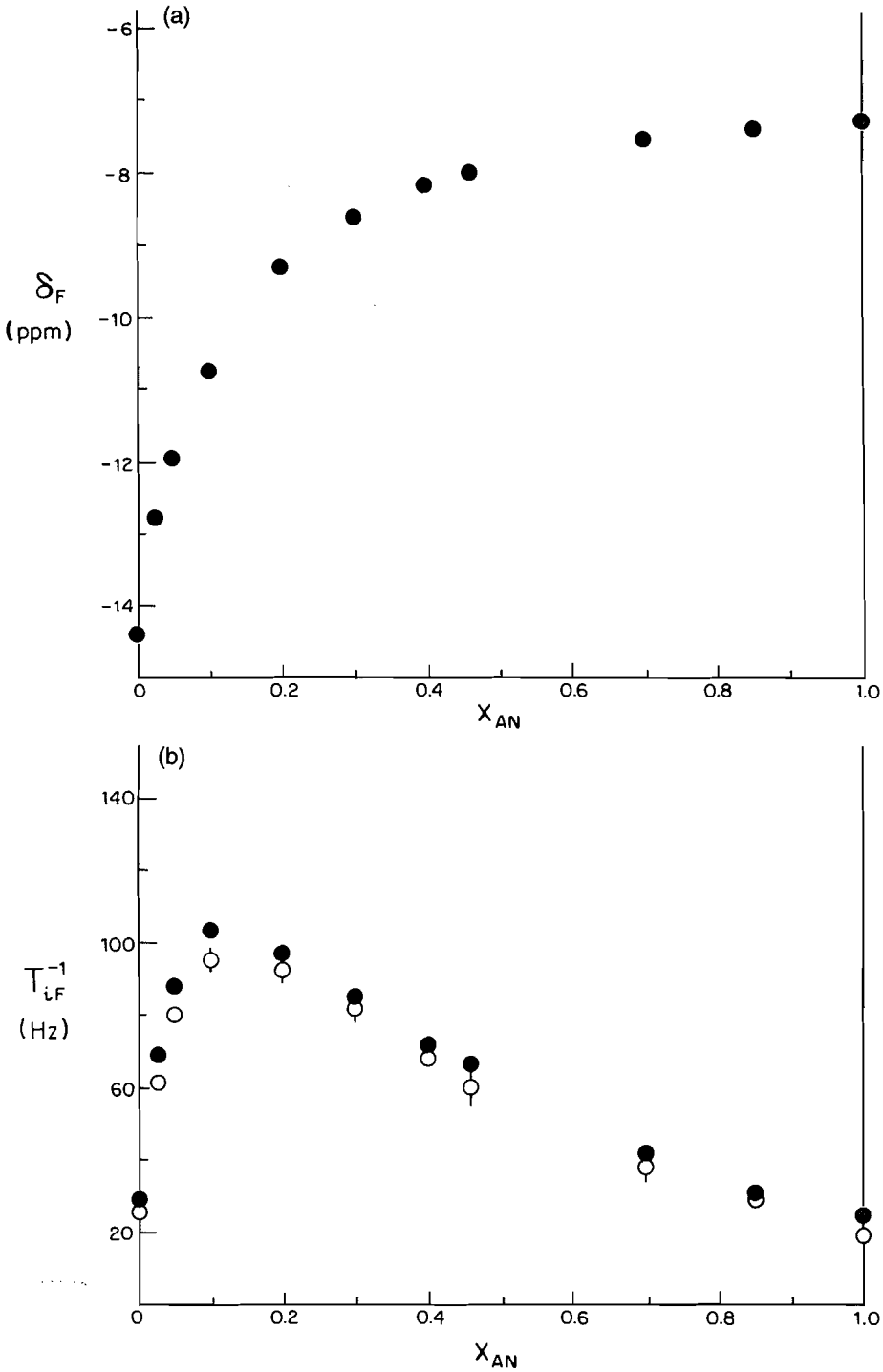

FIG. 3. (*a*) ^{23}Na NMR chemical shifts of $(Na^+)_s$, δ_F, as a function of the mole fraction of AN (X_{AN}). $[NaBPh_4]_t$ = 20.0 mM and T = 301.5 ± 0.5 K. (*b*) ^{23}Na NMR longitudinal (i = 1; ○) and transverse relaxation rate (i = 2; ●) of $(Na^+)_s$ as a function of the mole fraction of AN (X_{AN}). $[NaBPh_4]_t$ = 20.0 mM and T = 301.5 ± 0.5 K.

at 301.5 K. This can be compared with a value of 45.4 ± 0.4 kJ mol^{-1} previously reported at 258 K (4).

At this point, one should relate the exchange kinetics results with the nature of the various species in the binary mixtures. Figure 3 shows the variation of the solvated sodium cation, $(^{23}Na^+)_s$, chemical shift, δ_F, and of its transverse and longitudinal relaxation rates as a function of X_{AN}. The strong curvature of the chemical shift relationship towards low values of X_{AN} reflects a preferential solvation of the sodium cation by acetonitrile (28). The T_2^{-1} and T_1^{-1} values differ only by the instrumental inhomogeneities. While the relaxation rates are in the range 20–30 Hz in the neat solvents, a maximum value of 100 Hz is observed for X_{AN} ≅ 0.1. This value of X_{AN} (<0.5) indicates again a prefer-

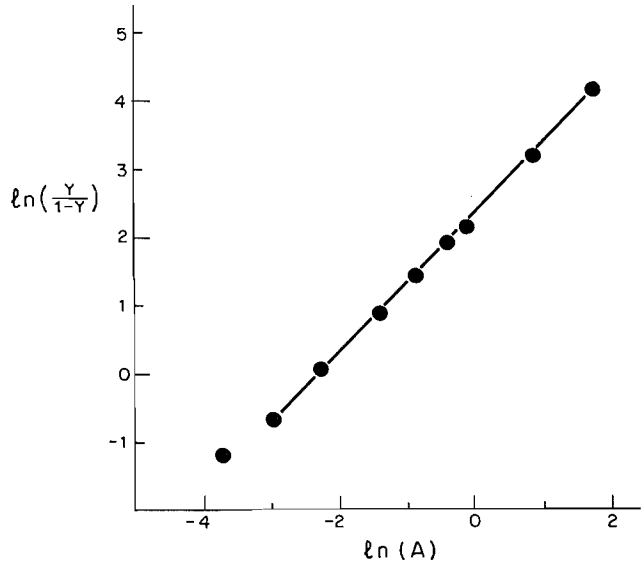

FIG. 4. Hill plot (see ref. 32) for AN–NM binary mixtures. $[NaBPh_4]_t$ = 20.0 mM and T = 301.5 ± 0.5 K.

ential solvation by AN (29). The maximum, as well as the general shape of the curve, reflects the dissymmetry of the sodium cation coordination sphere of the intermediate species $(Na^+(AN)_x(NM)_y)$ in the binary mixture (30). The application of the Hill formalism (31) has been extended to preferential solvation problems (32). Figure 4 gives the Hill plot for the ^{23}Na chemical shifts in the system AN–NM. The relationship is linear with a slope of 1.03 ± 0.03, indicating the absence of cooperativity (equality of the successive intrinsic constants) in the successive replacement of NM by AN molecules in the first sodium cation coordination sphere, as X_{AN} increases (32). This approach is based on the assumption that the ^{23}Na chemical shifts of the various solvates is additive (32–34). Since the process does not show any cooperativity, the Hill plot also yields the value of the intrinsic equilibrium constant of each step in the stepwise replacement of NM by AN molecules: K_s = 10.0 ± 0.3.

The ^{23}Na NMR parameters can also give information on the nature of the coordination sphere of sodium complexed with B15C5 (35). Figure 5 shows the relaxation rates corrected for the solvent viscosity, $R^* = T_2^{-1}/\eta$, as a function of X_{AN}. The simplicity of this curve is remarkable: no maximum, no inflection points are observed, and R^* decreases monotonically from 9.8×10^4 to 3.5×10^4 s^{-1} P^{-1}. For several binary solvent mixtures, the T_1^{-1} values were found to approximate the T_2^{-1} values within inhomogeneity, confirming the absence of any exchange contribution to the observed T_2^{-1}, which, except for inhomogeneity, has a purely quadrupolar origin ($T_2^{-1} = T_{2,inh}^{-1} + T_{2,q}^{-1}$; with $T_{2,inh}^{-1} << T_{2,q}^{-1}$) (30). In the case of a spin-3/2 nucleus, the quadrupolar relaxation rate in extreme narrowing conditions is given by eq. [8].

$$[8] \quad T_{2,q}^{-1} = T_{1,q}^{-1} = (2/5)\,\pi^2\chi^2\tau_c$$

where τ_c, which is related to the macroscopic viscosity through the Debye–Stokes–Einstein relationship (eq. [9]), is the correlation time characteristic of the quadrupolar relaxation and χ is the quadrupolar coupling constant (QCC) given by eq. [10].

$$[9] \quad \tau_c = 4/3\,\pi\,a^3\,(\eta/k_BT)f_r$$

$$[10] \quad \chi = (e^2qQ\,(1 + \gamma_\infty))/h$$

In eqs. [9] and [10], a is the molecular radius and f_r is a microviscosity coefficient, Q is the ^{23}Na nuclear quadrupole moment, q is the electric field gradient at the quadrupolar nucleus site, and $(1 + \gamma_\infty)$ is the Sternheimer antishielding factor. From eqs. [8]–[10], it appears that $T_{2,q}^{-1}$ is proportional to χ^2 and η. Since QCC is a very sensitive probe of the electronic distribution in the first coordination sphere

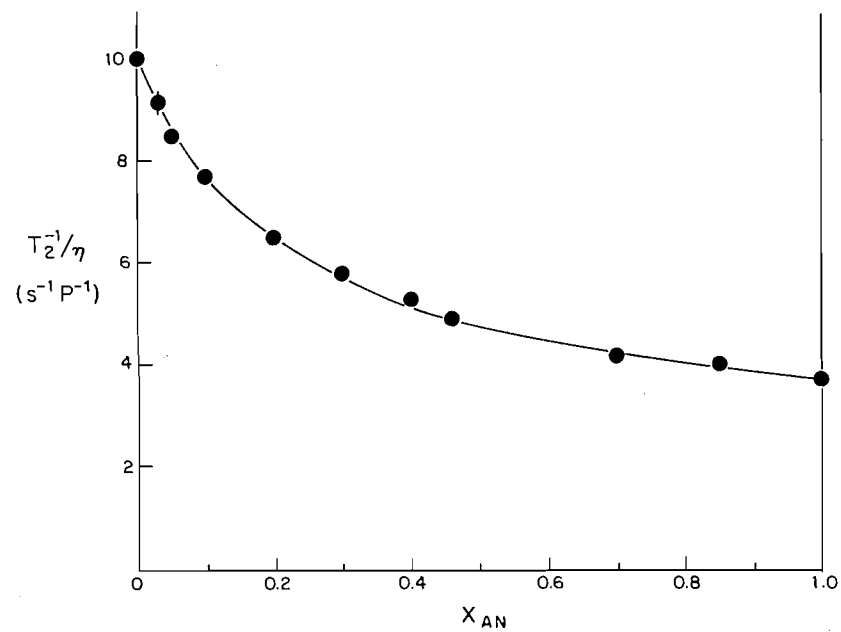

FIG. 5. ^{23}Na NMR transverse relaxation rates corrected for solvent viscosity, $R^* = T_2^{-1}/\eta$, of Na^+ complexed with B15C5 as a function of AN mole fraction in AN–NM binary mixtures. The data points are experimental and the curve is calculated (K_{CS} = 5.1; eq. [11]).

Can. J. Chem. Downloaded from www.nrcresearchpress.com by 109.225.110.28 on 09/08/12
For personal use only.

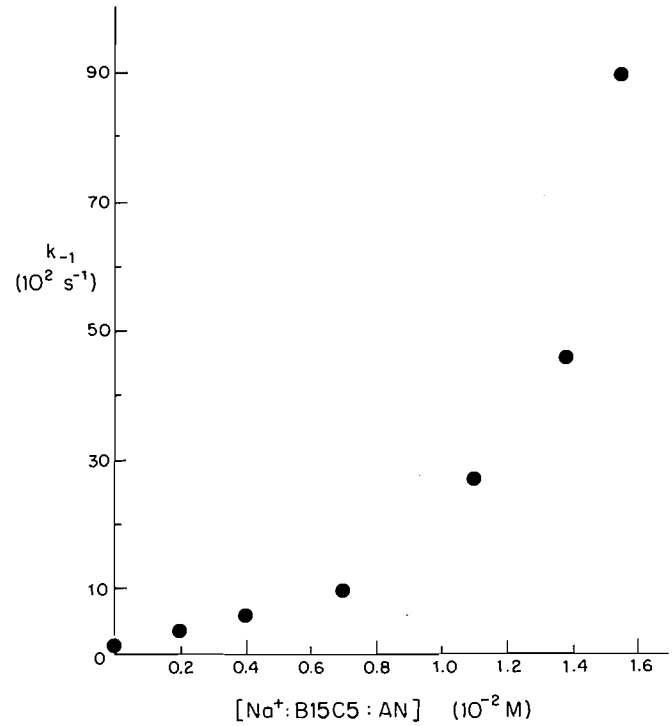

FIG. 6. The dissociative rate constant, k_{-1}, as a function of the concentration of the species $(AN:Na:B15C5)^+$.

of the sodium cation (30), R^* should be independent of X_{AN} if the environment of the sodium cation in the complex is invariant throughout the binary mixture range, as was shown previously for the systems $^{23}Na^+$–DB24C8 (36) and $^{39}K^+$–DB30C10 (37). So Fig. 5 shows the presence of more than one species in the binary mixtures. However, the smooth monotonic variation suggests no more than two species. Otherwise, one would expect the presence of a maximum such as that in Fig. 3*b*. The relationship between R^* and X_{AN} can be interpreted on the basis of a simple two-species model (eq. [11]):

$$[11] \quad (NM:Na:B15C5)^+ + AN \overset{K_{CS}}{\rightleftharpoons} (AN:Na:B15C5)^+ + NM$$

The observed T_2^{-1} is population averaged on the limiting values, obtained in neat solvents, for the two species shown in eq. [11]. Based on the above equilibrium, a nonlinear regression of the data shown in Fig. 5 gave the value 5.1 ± 0.5 for K_{CS}. This value is in the same order of magnitude as the intrinsic equilibrium constant for the replacement of one molecule of NM by one molecule of AN in the first coordination sphere of solvated sodium ($K_s = 10.0 \pm 0.3$). In Fig. 5, the data points are experimental and the curve is calculated. For any mole fraction, one can calculate the concentration of the species $(AN:Na:B15C5)^+$. Figure 6 shows a plot of the dissociative rate constant, k_{-1}, as a function of the concentration of $(AN:Na:B15C5)^+$. For values of $X_{AN} \leq 0.1$, corresponding to $[(AN:Na:B15C5)^+] \leq 7 \times 10^{-3}$ M (the total concentration of $Na^+ = 20.0 \times 10^{-3}$ M throughout this study), the relationship is linear. For higher values of X_{AN}, a strong increase of k_{-1} is observed. These results strongly suggest that the active species in the dissociative mechanism is the AN monosolvated complex (eq. [11]; $(AN:Na:B15C5)^+$) and that the first event in the dissociation process is the formation of this complex, governed by K_{CS}.

The global dissociation process is the result of a series of stepwise sodium–oxygen bond ruptures accompanied by sodium–solvent bond formations. This concept was recently discussed by Cox and Schneider (10). One can assume that the molecular composition of the solvation cage around the AN solvated complex (second solvation sphere of the sodium cation) roughly parallels the composition of the bulk solvent. Direct access to this information is not possible, since the ^{23}Na NMR parameters reflect the local solvent composition, at the $^{23}Na^+$ nucleus site. At low X_{AN} values, the solvation cage around the sodium complex is predominantly constituted of NM molecules. The general aspect of the plot shown in Fig. 6 is in good agreement with this model. Qualitatively, one should expect an increase of the rates in each of the discrete dissociative steps as the concentration of AN in the solvation cage of the complex increases, since AN is a stronger donor solvent than NM. Figure 6 is a reflection of this, since k_{-1} increases dramatically as X_{AN} increases. At low AN molar fractions, the nature of the solvation cage around the AN-solvated complex is mainly composed of NM molecules, and can be, at first approximation, considered as constant. The linear part of the plot, which one can visualize as the tangent to the plot at concentration 0, corresponds to a "clean" process in which the dissociating species can be identified to a supramolecular aggregate of a sodium cation complexed by a crown ether and coordinated by one acetonitrile molecule, encaged in a solvation shell of NM molecules. As the solvation cage is enriched in AN the global dissociation process is accelerated, in good agreement with Na^+—O bond ruptures concerted with Na^+–solvent bond formation.

To more completely characterize the competition between the dissociative and associative exchange mechanisms, variable temperature studies were performed in which values for the activation parameters of both competing mechanisms could be determined. Figure 7 shows four graphs of plots of $(k_A + k_B)$ as a function of $(1 - \rho)^{-1}$ (see eq. [7]) for four different values of X_{AN}. In each graph, the temperature is varied from 301.5 K (top) to 255.0 K (bottom). As in Fig. 2, the dissociative rate constant, k_{-1}, is obtained from the slope whereas the associative rate constant, k_2, is obtained from the *Y*-intercept. As expected, at each value of X_{AN}, both the k_{-1} and k_2 values increase with temperature. Reliable values of activation parameters for the dissociative process could be obtained only for $X_{AN} = 0.3$ and 0.2, since at the lower values of X_{AN}, the exchange is mainly controlled by the associative process. The results shown in Fig. 7 are also an illustration of an exchange process whose associative or dissociative nature is controlled by temperature. At the lower temperatures, the associative process, characterized by large negative entropies of activation, is favoured. As the temperature increases, the dissociative mechanism becomes competitive. A similar behaviour has been reported by Popoy and co-workers in the case of a diazacrown complex of sodium in tetrahydrofuran (38). Figure 8 shows the Eyring plots for the dissociative rate constant, k_{-1}. Table 1 gives the values of the activation parameters for both mechanisms at different values of X_{AN}. The activation

Can. J. Chem. Downloaded from www.nrcresearchpress.com by 109.225.110.28 on 09/08/12
For personal use only.

Can. J. Chem. Downloaded from www.nrcresearchpress.com by 109.225.110.28 on 09/08/12
For personal use only.

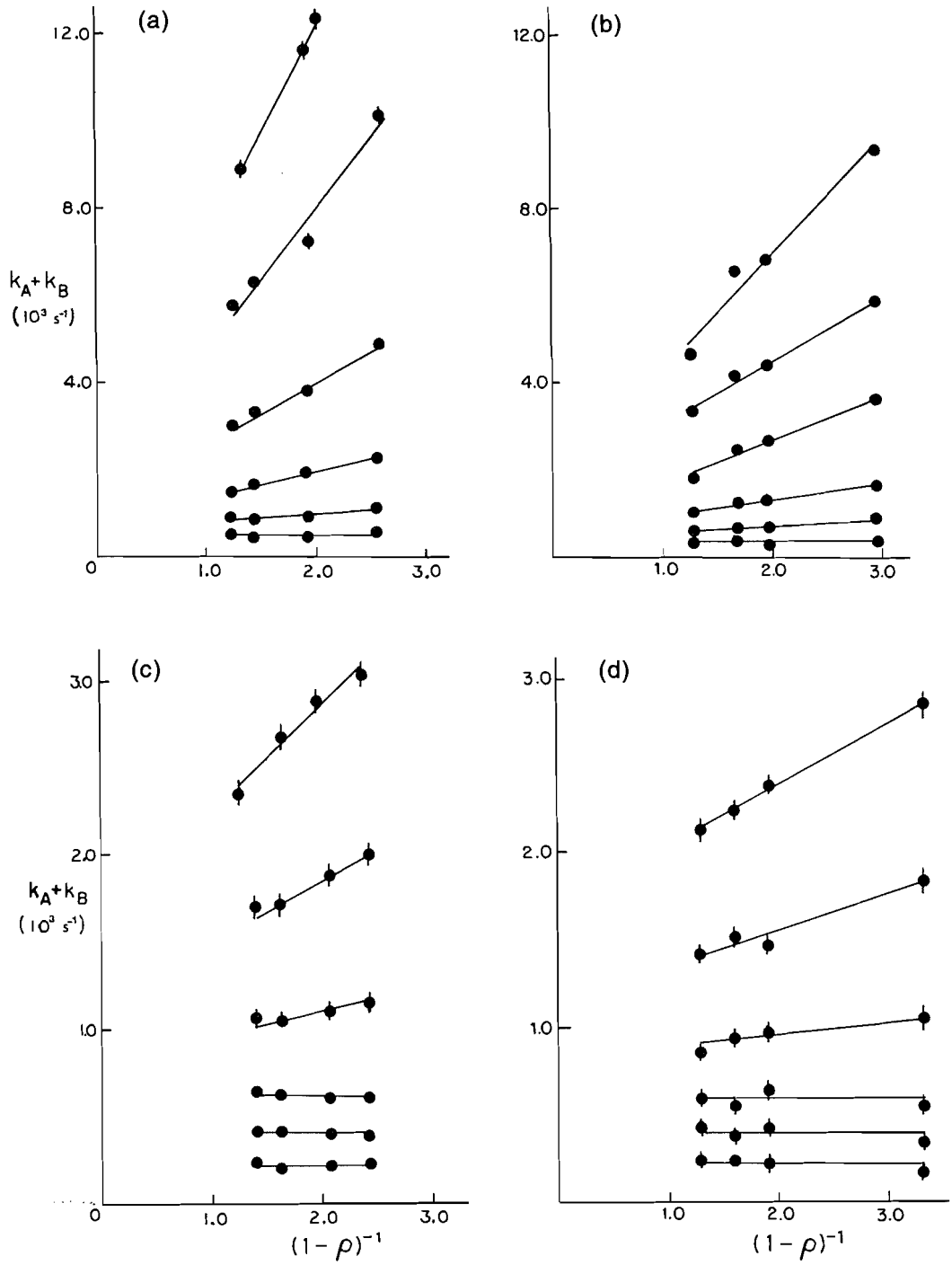

FIG. 7. (k_A + k_B) as a function of $(1 - \rho)^{-1}$ for a series of temperatures, at various mole fractions. (*a*) X_{AN} = 0.300; (*b*) X_{AN} = 0.200; (*c*) X_{AN} = 0.050; (*d*) X_{AN} = 0.025. In all four cases, from top to bottom, T = 301.5, 293.0, 284.0, 274.0, 264.5, 255.0 K.

parameters characterizing the associative process are essentially constant throughout the range of binary mixtures studied, in excellent agreement with our previous finding that this exchange process is mainly controlled by conformational factors (4, 5), which should be only slightly dependent upon the binary mixture composition. The large, negative value of $\Delta S^{\ddagger}_{as}$ is expected for an associative mechanism.

This study shows that the molecular role of the solvent in the kinetics and mechanisms of formation/dissociation of supramolecular entities in solution can be specified. The mechanistic difference that is observed between NM and AN could be related to the presence in solution of a species $(AN:Na:B15C5)^+$ strongly favoring the dissociation mechanism. A system in which a more strongly donating solvent molecule, such as dimethylformamide (DN = 26.6, compared to 14.1 for AN), would occupy the first coordination sphere of sodium in the solvent NM should permit us to specify further the nature and the role of the active species

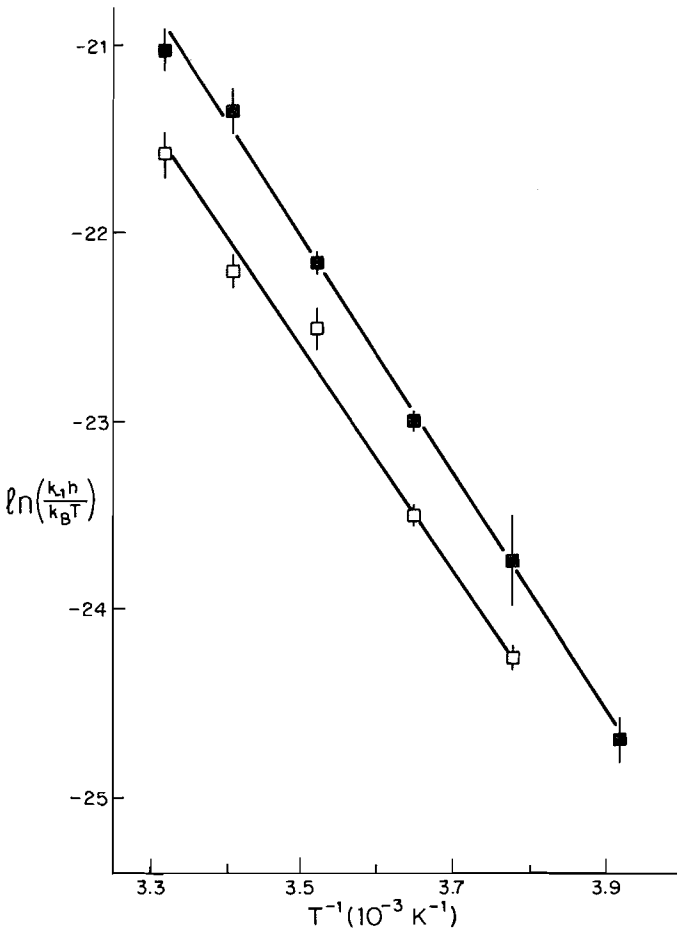

FIG. 8. Eyring plots for the dissociation rate constant of the complex $(Na:B15C5)^+$, k_{-1}, in AN–NM binary mixtures: X_{AN} = 0.300 (■); X_{AN} = 0.200 (□).

in the dissociation process. This work will be published in a forthcoming paper.

Acknowledgements

We gratefully acknowledge the financial support of the Natural Sciences and Engineering Research Council of Canada (NSERCC).

1. C. J. Pedersen. J. Am. Chem. Soc. **89**, 7017 (1967).
2. (*a*) G. A. Melson (*Editor*). Coordination chemistry of macrocyclic compounds. Plenum Press, New York. 1979; (*b*) S. Patai and Z. Rappoport (*Editors*). Crown ethers and analogs. John Wiley and Sons, Great Britain. 1989; (*c*) R. M. Izatt and J. J. Christensen (*Editors*). Synthetic multidentate macrocyclic compounds. Academic Press, New York. 1978.
3. C. Detellier, H. P. Graves, and K. M. Brière. Alkali metal NMR studies of synthetic an natural ionophore complexes. *In* Isotopes in the physical and biomedical science; isotopic applications in NMR studies. Vol. 2. *Edited by* E. Buncel and J. R. Jones. Elsevier, Amsterdam. 1991. Chap. 4; pp. 159–211.
4. K. M. Brière and C. Detellier. New. J. Chem. **13**, 145 (1989).
5. K. M. Brière and C. Detellier. J. Phys. Chem. **96**, 2185 (1992).
6. M. Shamsipur and A. I. Popov. J. Phys. Chem. **92**, 147 (1988).
7. A. Abou-Hamdan and S. F. Lincoln. Inorg. Chem. **30**, 462 (1991).
8. J. Bouquant, A. Delville, J. Granjean, and P. Laszlo. J. Am. Chem. Soc. **104**, 686 (1982).
9. R. C. Philips, S. Khazaeli, and J. L. Dye. J. Phys. Chem. **89**, 606 (1985).
10. B. G. Cox and H. Schneider. Pure Appl. Chem. **62**, 2259 (1990).
11. E. Shchori, J. Jagur-Grodzinski, Z. Luz, and M. Shporer. J. Am. Chem. Soc. **93**, 7133 (1971).
12. H. D. H. Stöver and C. Detellier. J. Phys. Chem. **93**, 3174 (1989).
13. B. O. Strasser, K. Hallenga, and A. I. Popov. J. Am. Chem. Soc. **107**, 789 (1985).
14. B. O. Strasser and A. I. Popov. J. Am. Chem. Soc. **107**, 7921 (1985).
15. H. P. Graves and C. Detellier. J. Am. Chem. Soc. **110**, 6019 (1988).
16. V. Gutmann. The donor–acceptor approach to molecular interactions. Plenum Press, New York. 1978.
17. K. M. Brière and C. Detellier. J. Phys. Chem. **91**, 6097 (1987).
18. J. A. Ridick, W. B. Bunger, and T. K. Sakano. *In* Organic solvents. 4th ed. Vol. 2. *In* Techniques of chemistry. *Edited by* A. Weissberger. Wiley Publishers, New York. 1986.
19. J. Sandström. Dynamic nmr spectroscopy. Academic Press, New York. 1982.
20. Z. Chen, H. D. Dettman, and C. Detellier. Polyhedron, **8**, 2029 (1989).
21. C. Detellier. Reaction kinetics and exchange. *In* Modern NMR techniques and their application in chemistry. Practical Spectroscopy Series. Vol. 11. *Edited by* A. I. Popov and K. Hallenga. Marcel Dekker, New York. 1990. Chap. 9.
22. J. Homer. J. Magn. Reson. **57**, 171 (1984).
23. R. C. Weast (*Editor*). Handbook of chemistry and physics. 63rd ed. CRC Press Inc., Boca Raton, Fla. 1982–1983.
24. J. D. Lin and A. I. Popov. J. Am. Chem. Soc. **103**, 3773 (1981).
25. (*a*) H. D. H. Stöver, A. Delville, and C. Detellier. J. Am. Chem. Soc. **107**, 4167 (1985); (*b*) A. Delville, H. D. H. Stöver, and C. Detellier. J. Am. Chem. Soc. **107**, 4172 (1985).
26. A. Delville, H. D. H. Stöver, and C. Detellier. J. Am. Chem. Soc. **109**, 7293 (1987).
27. D. E. Woessner. J. Chem. Phys. **35**, 41 (1961).
28. C. Detellier and P. Laszlo. Helv. Chim. Acta, **59**, 1333 (1976).
29. C. Detellier and P. Laszlo. Helv. Chim. Acta, **59**, 1346 (1976).
30. C. Detellier. Alkali metals. *In* NMR of newly accessible nuclei. Vol. 2. *Edited by* P. Laszlo. Academic Press, New York. 1983. Chap. 5; pp. 105–152.
31. A. V. Hill. J. Physiol. **40**, IV (1910).
32. A. Delville, C. Detellier, A. Gerstmans, and P. Laszlo. Helv. Chim. Acta, **64**, 547 (1981).
33. S. Chalais, A. Delville, C. Detellier, A. Gerstmans, and P. Laszlo. J. Solution Chem. **12**, 33 (1983).
34. C. Detellier and P. Laszlo. *In* Studies in physical and theoretical chemistry. Vol. 37. *Edited by* W. J. Orville-Thomas, H. Ratajczak, and C. N. R. Rao. Elsevier Science Publ., Amsterdam. 1985. pp. 291–336.
35. K. M. Brière, H. P. Graves, T. S. Rana, L. J. Maurice, and C. Detellier. J. Phys. Org. Chem. **3**, 435 (1990).
36. M. Bisnaire, C. Detellier, and D. Nadon. Can. J. Chem. **60**, 3071 (1982).
37. C. Detellier and M. Robillard. Can. J. Chem. **65**, 1684 (1987).
38. P. Szczygiel, M. Shamsipur, K. Hallenga, and A. I. Popov. J. Phys. Chem. **91**, 1252 (1987).

Can. J. Chem. Downloaded from www.nrcresearchpress.com by 109.225.110.28 on 09/08/12
For personal use only.

Synthesis, multinuclear NMR, and solution conformation of (η^5-indenyl)CoIR$_f$L complexes (L = CO, P-donor)

CHET R. JABLONSKI[1] AND ZHONGXIN ZHOU

Department of Chemistry, Memorial University of Newfoundland, St. John's, Nfld., Canada A1B 3X7

Received December 4, 1991

CHET R. JABLONSKI and ZHONGXIN ZHOU. Can. J. Chem. **70**, 2544 (1992).

The preparation, spectroscopic characterization, and conformational analysis of a series of Co(III) indenyl complexes, (C_9H_7)CoIR$_f$L (R$_f$ = C_3F_7, C_6F_{13}, L = CO, P-donor), **2–8**, are described. ^{13}C and ^{1}H NMR parameters are consistent with a slightly distorted η^5-C_9H_7 coordination. ^{1}H nuclear Overhauser effect difference (nOed) spectra indicate a preferred solution conformation in which the perfluoroalkyl group is *trans* to the C_{3a}—C_{7a} ring junction.

CHET R. JABLONSKI et ZHONGXIN ZHOU. Can. J. Chem. **70**, 2544 (1992).

On décrit la préparation, la caractérisation spectroscopique et l'analyse conformationnelle d'une série de complexes du Co(III) indényle, (C_9H_7)CoR$_f$L (R$_f$ = C_3F_7 et C_6F_{13}; L = CO et P-donneur), **2–8**. Les paramètres RMN du ^{1}H et du ^{13}C sont en accord avec une coordination η^5-C_9H_7 légèrement déformée. Les spectres de différence d'effet Overhauser nucléaire du ^{1}H (deOn) suggèrent une conformation privilégiée en solution dans laquelle le groupe perfluoroalkyle est *trans* par rapport à la jonction C_{3a}—C_{7a}.

[Traduit par la rédaction]

Introduction

Transition metal π-indenyl complexes have attracted a great deal of attention, compared to their isostructural cyclopentadienyl derivatives, because of their enhanced reactivity toward ligand substitutions and related reactions (1–10). The "indenyl effect" has been explained on the basis of the ability of the π-indenyl ligand to undergo facile $\eta^5 \leftrightarrow \eta^3$ "ring-slippage" (5–9, 11–22).

Compared to other transition metals, the π-indenyl chemistry of cobalt remains relatively underdeveloped. π-Indenyl complexes are known for cobalt in formal oxidation states III, II, and I with the very air-sensitive Co(I) derivatives formulated as (η^5-indenyl)CoL$_2$ (L = ethylene (23, 24), CO (25, 26), PPh_3 (27), PMe_3 (28), $P(OR)_3$ (29) or L$_2$ = cyclic and acyclic dienes (3, 4, 23) or vinylketenes (27)) being the most numerous. Fewer Co(III) complexes have been reported (21, 27, 28, 30) and only one crystal structure ((η^5-indenyl)Co($C_2B_9H_{11}$)) has been determined (21). The homoleptic examples [(indenyl)$_2$Co]PF_6 (30) and (indenyl)$_2$Co (31) serve to delineate bonding extrema observed for cobalt and to illustrate the dependence of indene distortion and hapticity on electronic configuration (32). Structural studies (32) establish that the 19e$^-$ Co(II) indenyl complex significantly distorts towards an η^3 bonding mode. ^{13}C NMR data (30, 32, 33) confirm that the 18e$^-$ Co(III) complex, [(indenyl)$_2$Co]PF_6, is a "true" η^5-indenyl species.

During studies of chiral induction from the asymmetric metal centre of pseudo octahedral cyclopentadienyl complexes in the Arbuzov-like dealkylation of Scheme 1, we found that reactivity and optical selectivity are subtly related to the stereoelectronic properties of the ligand sphere (34–36). Reasoning that the lowered symmetry of piano-stool π-indenyl compared to their isostructural cyclopentadienyl Co(III) complexes might restrict rotamer populations and result in more efficient Co→P chiral induction for the chemistry outlined in Scheme 1, we reported (37, 38) the preparation and resolution of $(-)_{436}$-(η^5-C_9H_7)CoI(C_3F_7)-($PPh_2NHCH(CH_3)Ph$), **9**. To more clearly define the influence of ligand properties on conformation preferences of indenyl complexes, we prepared the series **2–8** (η^5-C_9H_7)-CoIR$_f$L (R$_f$ = C_3F_7, C_6F_{13}; L = CO, P-donor). Herein we report the synthesis, spectroscopic properties, and solution conformation of these new complexes.

[1]Author to whom correspondence may be addressed.

Results and discussion

Synthesis and properties

Preparation of the title complexes was carried out according to Scheme 2. The known complex **1** was prepared (38) using a modification of the method originally described by Bönnemann (3) and Salzer and Taschler (26), which represents the most convenient route to **1**, the precursor for preparation of the new π-indenyl cobalt complexes. Oxidative additions of R$_f$I to **1** are slow but afford complexes **2** and **3** in good yield. Complexes **4–8** are then prepared by facile CO substitution in **2** and **3** by phosphorus donor ligands. Except for **7**, which decomposes at room temperature in the solid state within several days, all the π-indenyl cobalt(III) complexes prepared in this study are air stable in the solid state, but decompose gradually in solution at room temperature. They have been characterized by elemental analysis, infrared and multinuclear NMR spectroscopy, and, in the case of **3** and **6**, by X-ray diffraction.[2,3] Their physical properties are summarized in Table 1. The NMR spectra are discussed more fully below.

[2]Octahedral, slightly distorted η^5-structures for **3** and **6** were confirmed by X-ray crystallography. Problems encountered during data collection along with sample twinning resulted in relatively low-precision structures. The solid state and solution conformations were identical in the case of **3**. The solid state conformation of **6** places the $PPh(OCH_3)_2$ ligand *trans* to the indenyl 6-ring.

[3]Details of the structure refinements, crystal data, positional parameters, thermal factors, bond distances, intramolecular bond angles, Pluto diagrams, and intensity data have been deposited and may be purchased from: The Depository of Unpublished Data, Document Delivery, CISTI, National Research Council Canada, Ottawa, Canada K1A 0S2.

Tables of crystal data, positional parameters, bond distances and angles, and the Pluto diagrams have also been deposited with the Cambridge Crystallographic Data Centre, and can be obtained on request from The Director, Cambridge Crystallographic Data Centre, University Chemical Laboratory, 12 Union Road, Cambridge, CB2 IEZ, U.K.

Can. J. Chem. Downloaded from www.nrcresearchpress.com by 109.225.110.28 on 09/08/12
For personal use only.

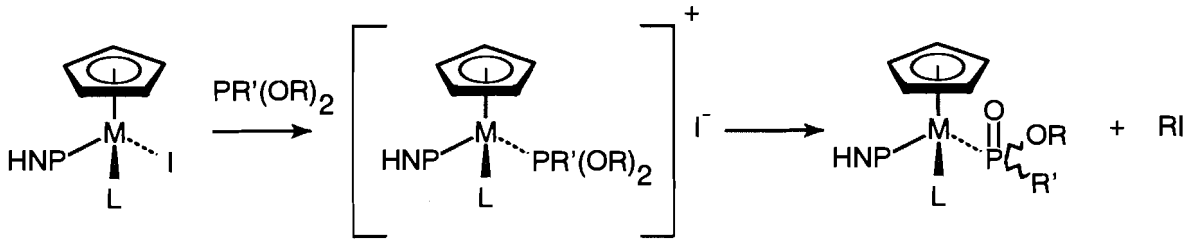

PNH=$PPh_2NHC^*H(CH_3)Ph$; M=Co, Rh

L=I, CF_3, C_3F_7, C_6F_{13}; R'=Ph; R=CH_3

SCHEME 1

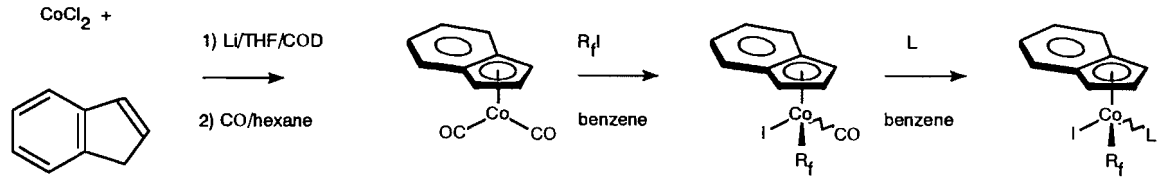

1 2,3 4-9

SCHEME 2

TABLE 1. Physical properties of (η^5-C_9H_7)Co(R_f)(I)(L)

No.	R_f	L	Formula	Yield[a] (%)	Appearance	Melting point[b] (°C)	Anal calcd. (found)	ν (CO)[c] (cm^{-1})
2	C_3F_7	CO	$C_{13}H_7CoF_7IO$	80	Black crystal (microcrystal)	dec. > 120	C:31.35(31.71) H: 1.42(1.83)	2081
3	C_6F_{13}	CO	$C_{16}H_7CoF_{13}IO$	75	Black rect. plate	dec. > 120	C:29.65(29.64) H: 1.09(0.88)	2081
4	C_3F_7	$P(OCH_3)_3$	$C_{15}H_{16}CoF_7IO_3P$	99	Black rect. plate (twinned)	142	C:30.32(30.01) H: 2.71(2.36)	
5	C_6F_{13}	$P(OCH_3)_3$	$C_{18}H_{16}CoF_{13}IO_3P$	82	Black rect. plate (twinned)	139	C:29.05(29.23) H: 2.17(2.04)	
6	C_3F_7	$PPh(OCH_3)_2$	$C_{20}H_{18}CoF_7IO_2P$	93	Black prism	145	C:37.52(37.14) H: 2.83(2.39)	
7	C_6F_{13}	$PPh(OCH_3)_2$	$C_{23}H_{18}CoF_{13}IO_2P$	84	Red-brown powder	112	[d]	
8[e]	C_6F_{13}	PNH[f]	$C_{35}H_{27}CoF_{13}INP$	25	Red-brown powder	103	C:45.42(45.14) H: 2.94(2.83) N: 1.51(1.53)	

[a]Yield obtained before crystallization calculated based on the cobalt reactant complexes (cf. experimental).
[b]Sealed (N_2) capillary.
[c]Methylene chloride, 0.1 mm cells.
[d]Samples decomposed at room temperature over a period of several days and were not analyzed.
[e]High R_f isomer.
[f]PNH = (S)-(−)-$PPh_2NHCH(CH_3)Ph$.

NMR spectroscopy

The NMR spectra of transition-metal indenyl complexes have been extensively studied (7, 19, 30, 33, 39–41). Both electronic (15, 42) and steric (39, 41, 43, 44) factors can influence the extent of η^5-indenyl ring distortion as well as the preferred conformation of the ligands relative to the indenyl ring in solution.

^1H and ^{13}C NMR data are given in Tables 2 and 3, respectively. The presence of a chiral Co centre requires that the indenyl ring atoms (1,3; 4,7; 5,6) be diastereotopic and, in general, well-separated resonances were observed in both the 7.05 tesla ^1H and ^{13}C NMR spectra. ^1H NMR assignments (cf. Table 2) are supported by nuclear Overhauser effect difference (nOed) spectra shown in Fig. 1 for the representative case

Can. J. Chem. Downloaded from www.nrcresearchpress.com by 109.225.110.28 on 09/08/12
For personal use only.

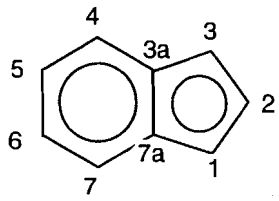

SCHEME 3

of complex **6**. Irradiation of the proton with δ = 4.88 ppm (Fig. 1*g*) results in enhancement of the peaks at δ = 5.68 and 7.16 ppm, but no enhancement of the peak at δ = 6.47 ppm. Irradiation of the proton with δ = 5.68 ppm (Fig. 1*f*) enhances the δ = 4.88 and 6.47 ppm signals. Irradiation of the proton at δ = 6.47 ppm (Fig. 1*e*) enhances the proton signals at δ = 5.68 and 7.53 ppm but no other enhancements were observed. Accordingly the three signals in the region of 4.5–7.0 ppm are assigned to H1 (4.88 ppm), H2 (5.68 ppm), H3 (6.47 ppm), respectively, and the higher-field doublet (δ = 7.16 ppm) is assigned to H7 while the lower-field doublet (δ = 7.53 ppm) corresponds to H4 (cf. Scheme 3 for numbering system). The ^{1}H NMR data for the remaining complexes were assigned on the basis of nOed data and by comparison with complex **6**. A similar method was employed by Coville and co-workers (39, 43, 44) to assign the ^{1}H NMR of a series of chiral indenyl ruthenium and iron complexes.

The ^{13}C spectra of complex **3** (cf. Table 3) were definitively assigned on the basis of 2-D ^{1}H/^{13}C ^1J heterocorrelation spectra, which correlate ^{13}C (95.37 ppm) with H2 (δ = 5.90 ppm), ^{13}C (87.95 ppm) with H3 (δ = 6.85 ppm), and ^{13}C (71.94 ppm) with H1 (δ = 5.80 ppm). Thus the indenyl carbon atoms are assigned as C1 (δ = 71.94 ppm), C2 (δ = 95.37 ppm), and C3 (δ = 87.95 ppm), respectively. Correlations of H4–H7 with C4–C7 were also clearly observed so that the assignments of the remaining indenyl carbons are unambiguous. Assignments for the remaining complexes in the series were made analogously.

The ^{19}F chemical shift assignments and coupling constants for the complexes investigated in this study are reported in Table 4. All compounds showed well-separated C_α–C_γ and C_α–C_ζ resonances for the perfluoropropyl and perfluorohexyl compounds, respectively. Due to the presence of the chiral Co centre and typically small vicinal couplings ($^3J_{FF}$ = 5–8 Hz), the ^{19}F spectra of the diastereotopic $(CF_2)_n$ groups are well approximated as a series of isolated AB spin systems. $^2J_{F_aF_b}$ values for F_a–C–F_b show a marked increase on passing from C_α to C_β but are relatively constant further along the perfluoroalkyl chain (cf. Fig. 2), pointing to a weakening of the C_α—F bond (45).

The ^{1}H and ^{13}C chemical shifts of η^5-indenyl are relatively insensitive to the perfluoroalkyl ligand in these complexes, suggesting that the electronic and steric requirements of C_3F_7 and C_6F_{13} are similar in determining the spectroscopic properties. However, the chemical shifts of the diastereotopic η^5-indenyl H1 and H3 protons correlate well with the electronic parameter (χ(cm^{-1})) (46, 47) of the phosphorus ligand (L) (cf. Fig. 3). The chemical shift of H1 decreases as the electronic donicity of L increases (the value of χ decreases) while the chemical shifts of H3 increase as the electronic donicity of L increases. The chemical shift of H2 is relatively insensitive to L. Thus, high donicity ligands result in a large difference of the chemical shifts for H1 and H3 (Δδ(H3–H1)) (cf. Fig. 3). Crabtree and coworkers (15, 42) argue that preferential weakening of the Co—C3a and Co—C7a bonds is expected to facilitate more significant stabilization via aromatization, hence strong *trans*-

TABLE 2. ^{1}H NMR data for indenyl complexes (η^5-C_9H_7)Co(R_f)(I)(L)[a,b,c,d]

Compound	H1	H2	H3	H4	H5	H6	H7	Others
2	5.80	5.90	6.84	7.74(d)	7.62(t)	7.43(t)	7.53(d)[e]	
3	5.80	5.90	6.85	7.74(d)	7.63(t)	7.42(t)	7.52(d)[f]	
4	5.27	5.79	6.38	7.51(d)[g]	7.28–7.40		7.42	CH_3 3.62(d, 10.3)[h]
5	5.28	5.78	6.37	7.50(d)[i]	7.27–7.41		7.42	CH_3 3.62(d, 10.4)[h]
6	4.88	5.68	6.47	7.53(d)[j]	7.24–7.50[k]		7.16(d)[j]	CH_3 3.56(d, 10.8)[h]
7	4.91	5.68	6.46	7.53(d)[j]	7.24–7.50[k]		7.17(d)[j]	CH_3 3.56(d, 10.9)[h]
8[l]	4.52	5.65	6.63		6.40–7.90[k]			CH 3.65(m) NH 3.00(m) CH_3 1.25(d, 6.8)[m]
9[n]	4.50	5.65	6.63		6.40–7.90[k]			CH 3.66(m) NH 2.98(m) CH_3 1.25(d, 6.5)[m]

[a]300 MHz, chemical shift in ppm relative to TMS.
[b]$CDCl_3$ solvent.
[c]Indenyl H1, H2, H3 peaks show small, unresolved coupling (0.3–1.5 Hz).
[d]Coupling constant (Hz) given in parentheses. d = doublet, t = triplet, m = multiplet.
[e] ^3J(HH) = 8.5 Hz.
[f] ^3J(HH) = 8.3 Hz.
[g] ^3J(HH) = 8.0 Hz.
[h] ^3J(PH).
[i] ^3J(HH) = 8.0 Hz.
[j] ^3J(HH) = 7.8 Hz.
[k]Overlapped with phenyl protons, and for **6** δ = 7.77 ppm (m, 2H) assigned to H_{ortho} of P-phenyl.
[l]High R_f isomer.
[m] ^3J(HH).
[n]Cf. refs. 37, 38.

Can. J. Chem. Downloaded from www.nrcresearchpress.com by 109.225.110.28 on 09/08/12
For personal use only.

TABLE 3. ^{13}C NMR data for indenyl complexes $(\eta^5\text{-}C_9H_7)Co(R_f)(I)(L)$[a,b,c]

Compound	C1	C2	C3	C3a, C7a	Phenyl	Other
2	71.79	95.34	87.88	111.63, 109.45	133.07(C_5) 132.25(C_6) 128.69(C_4) 124.04(C_7)	CO 197.86
3	71.94	95.37	87.95	111.65, 109.46	133.12(C_5) 132.31(C_6) 128.72(C_4) 124.12(C_7)	CO 197.78
4	68.94	94.67 (d, 5.9)	82.05 (d, 12.4)	112.34, 110.19	130.64(C_5) 130.53(C_6) 127.79(C_4) 126.33(C_7)	CH_3 55.64(d, 9.5)
5	69.07	94.63	81.92 (d, 11.9)	112.28, 110.22	130.63(C_5) 130.55(C_6) 127.81(C_4) 126.33(C_7)	CH_3 55.64(d, 7.8)
6[d]	70.72	94.82	79.82 (d, 11.3)	113.70, 109.92	130.08(C_5) 128.00(C_6) 127.46(C_4) 125.79(C_7)	CH_3 56.73(d, 9.0) 55.34(d, 9.0)
7	70.80	94.65	79.64 (d, 11.2)	113.65, 109.93	125.79–135.30	CH_3 56.68(d, 9.2) 55.41(d, 11.2)
8[e]	72.52	94.74 (d, 8.8)	78.16 (d, 8.2)	112.78, 111.27	124.32–145.37	CH 54.71(d, 12.4) CH_3 27.21(d, 4.0)
9[f]	72.56	94.82 (d, 8.1)	78.57 (d, 9.4)	112.53, 111.71	124.35–145.63	CH 54.69(d, 12.4) CH_3 27.24(d, 3.2)

[a]75.5 MHz, chemical shifts in ppm relative to $CDCl_3$.
[b]Coupling constants in Hz given in parentheses, ^2J(PC). d = doublet.
[c]Perfluoroalkyl carbons distributed in the chemical shift range; of 105–140 ppm with very weak intensity.
[d]For **6**, the resonances at 131.35, 131.06 assigned to C_{ortho}; 131.48, 131.17 to C_{meta}; 128.13 to C_{para}; and 134.94 (d, $^1J_{PC}$ = 54.0) to C_{ipso}
[e]High R_f isomer
[f]Cf. refs. 37, 38.

TABLE 4. ^{19}F NMR data for indenyl complexes $(\eta^5\text{-}C_9H_7)Co(R_f)(I)(L)$[a,b,c]

	$C_\alpha F_2$	$C_\beta F_2$	$C_\gamma F_2$	$C_\delta F_2$	$C_\epsilon F_2$	
Compound	F_a, F_b	F_a, F_b	F_a, F_b	F_a, F_b	F_a, F_b	CF_3
2	−47.59, −51.15 (d, 208.1)	−111.94, −115.70 (d, 278.0)				−79.73(s)
3	−47.16, −49.32 (d, 210.6)	−106.32, −112.39 (d, 286.6)	−120.63, −122.38 (d, 298.8)	−122.55, −123.62 (d, 301.0)	−126.06, −127.17 (d, 294.5)	−81.32(s)
4	−56.21, −63.29 (d, 228.3)	−112.95, −114.60 (d, 281.2)				−79.58(s)
5	−54.97, −63.25 (d, 230.6)	−107.78, −111.33 (d, 284.0)	−120.96, −122.18 (d, 295.3)	−122.48, −123.49 (d, 307.8)	−126.07, −127.07 (d, 294.6)	−81.31(s)
6	−57.02, −57.58 (d, 230.0)	−109.75, −112.70 (d, 279.1)				−79.73(s)
9[d]	−58.17, −58.57 (d, 247.6)	−107.86, −112.19 (d, 277.3)				−79.96(s)

[a]282.4 MHz, chemical shifts in ppm relative to $CFCl_3$.
[b]$CDCl_3$ solvent.
[c]$^2J(F_aF_b)$ given in parentheses (Hz). d = doublet, s = singlet. In some cases the CF_3 peak appears as triplet with $^3J_{FF}$ = 8.0–11.0 Hz.
[d]Cf. refs. 37, 38.

influence ligands will prefer a site *trans* to the indenyl 6-ring regardless of steric consequences. For complexes **2–8**, the strong *trans*-influence perfluoroalkyl ligands will then presumably select a conformation placing L between H1 and H7, *trans* to H3 of the indenyl ring as shown in Fig. 4.

The same conformational preference is deduced by examination of the ^{13}C NMR spectra. The C3 resonances (cf. Table 4) for complexes **4–9** are doublets with $^2J_{PC}$ equal to 10 ± 2 Hz while no coupling was observed for C1, which is *cis* to the phosphorus atom. In some cases coupling of C2 to phosphorus was also detected.

Support for these conformational preferences was ob-

Can. J. Chem. Downloaded from www.nrcresearchpress.com by 109.225.110.28 on 09/08/12
For personal use only.

Can. J. Chem. Downloaded from www.nrcresearchpress.com by 109.225.110.28 on 09/08/12
For personal use only.

FIG. 1. ^{1}H nOed spectra for **6**. (*i*) reference spectrum; (*a–h*) difference spectra (16x) for irradiation at the indicated (*) frequency; (*a*) H_{ortho}; (*b*) H4 and H_{meta}; (c) H5, H6, and H_{para}; (*d*) H7; (*e*) H3; (*f*) H2; (*g*) H1; (*h*) OCH_3.

tained from ^{1}H nOed (nuclear Overhauser effect difference spectra) experiments. The nOed spectra of complex **4** (cf. Fig. 5) unambiguously show that the $P(OCH_3)_3$ ligand bisects the H1 and H7 indenyl protons. Irradiation of the OCH_3 groups results in a strong enhancement to H1 and H7 and a very weak enhancement to H2, but *no* enhancement to H3 (cf. Fig. 5*f*). Successive irradiation of H1, H2, H3 reveal the proximal protons (Fig. 5*c*, *d*, *e*). Similar nOed results were observed for complex **5**.

The nOed spectra of complex **6** (cf. Fig. 1) are also in accord with the conformational arguments presented above.

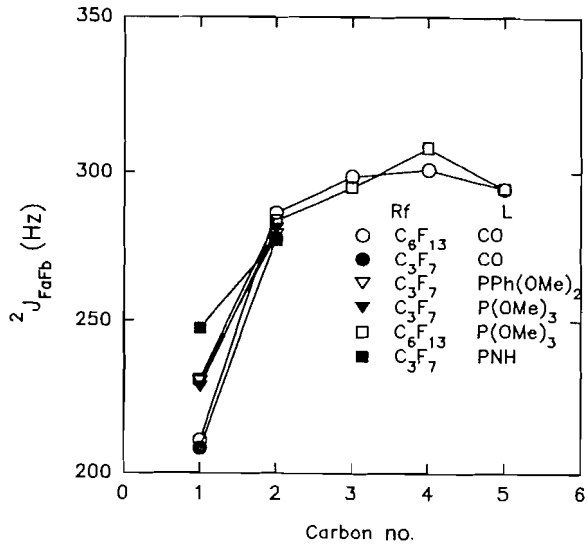

FIG. 2. Dependence of the ^{19}F coupling constants on position.

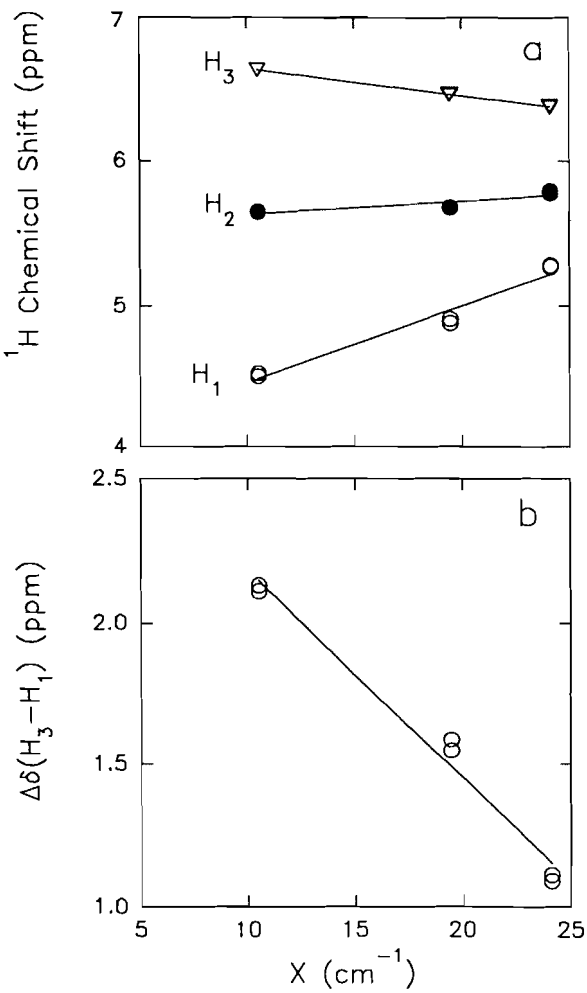

FIG. 3. Correlation of indenyl ^{1}H chemical shifts with χ.

Irradiation of the *ortho*-proton resonances of the $PPh(OCH_3)_2$ ligand results in strong enhancements for H7, H1, and OCH_3 (cf. Fig. 1*a*). Irradiation of H7 results in enhancement to the *ortho* protons and H1 (cf. Fig. 1*d*). Irradiation of OCH_3 (cf.

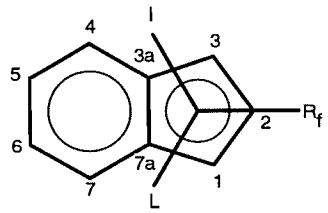

FIG. 4. Solution conformation of (η^5-indenyl)Co(R_f)(I)(L).

FIG. 5. ^{1}H nOed spectra for **4**. (*g*) reference spectrum; (*a–f*) difference spectra (32×) for irradiation at the indicated (*) frequency; (*a*) H4; (*b*) H7; (*c*) H3; (*d*) H2; (*e*) H1; (*f*) OCH_3.

Fig. 1*h*) affords a small but definitive enhancement to H1 and H7. The solution conformation of complex **9**, which was also determined by ^{1}H nOed, is the same as the complexes discussed above (37, 38).

Strong correlations between the indenyl ring junction (C3a, C7a) ^{13}C chemical shift and indenyl distortion have been reported (16, 18, 30, 32, 33). $\Delta\delta^{13}C_{3a,7a}$ ($\Delta\delta^{13}C_{3a,7a} = \delta^{13}C_{3a,7a}$(indenyl) $- \delta^{13}C_{3a,7a}$(Na^+indenyl$^-$)) has been demonstrated to be a reliable indicator of indene hapticity (16, 18, 32, 33) with values in the range -10 to -40 ppm and $+5$ to $+30$ considered diagnostic for η^5 and η^3 bonding, respectively (33). The calculated $\Delta\delta^{13}C_{3a,7a}$ parameters, determined from the chemical shifts of the diastereotopic ring junction carbons of the chiral complexes **2–9** (cf. Table 5), are in the range of -22 to -17 ppm, consistent with their description as slightly distorted η^5 complexes (32, 33), and are completely in accord with solid state results (see footnote 2).

TABLE 5. ^{13}C NMR indenyl distortion parameters

Compound	$\Delta\delta^{13}C_{3a,7a}$[a]
2	−19.07, −21.25
3	−19.05, −21.24
4	−18.36, −20.51
5	−18.42, −20.48
6	−17.00, −20.78
7	−17.05, −20.77
8	−17.92, −19.43
9[b]	−18.17, −18.99

[a] $\Delta\delta^{13}C_{3a,7a} = \delta^{13}C_{3a,7a}$(indenyl) $- \delta^{13}C_{3a,7a}$(Na^+indenyl$^-$).
[b] Cf. refs. 37, 38.

Summary

The preparation and spectroscopic characterization of a series of η^5-indenyl cobalt(III) complexes are described. Consistent with their 18e$^-$ configurations, the indenyl ring in these complexes is η^5-bonded but NMR parameters suggest a characteristic distortion towards η^3. ^{1}H nuclear Overhauser effect difference spectra show that all of these complexes prefer a solution conformation that places the perfluoroalkyl ligand *trans* to the indenyl 6-ring and the P-donor ligand *trans* to C3.

A good correlation is found for the ^{1}H chemical shift difference between H1 and H3 ($\Delta\delta$(H3–H1)) and the electron donicity (χ(cm^{-1})) of the *trans*-lying phosphorus ligand. The easily determined diastereotopic chemical shift difference ($\Delta\delta$(H3–H1)) reflects the extent of rotamer preference in the chiral-at-metal (η^5-indenyl)Co(III) complexes and, if ring-slip distortion is related to ligand electronic effects as has been suggested (15), may be a reactivity indicator.

Experimental section

Reagents and methods

All manipulations were performed under a dry, oxygen-free nitrogen or argon atmosphere using standard Schlenk techniques. Nitrogen gas was purified by passing through a series of columns containing DEOX (Alpha) catalyst heated to 120°C, granular P_4O_{10}, and, finally, activated 3A molecular sieves. THF, benzene, and hexane solvents were distilled under nitrogen from blue solutions of sodium benzophenone ketyl. Methylene chloride was distilled under nitrogen from P_4O_{10}. Anhydrous $CoCl_2$ was prepared by refluxing $CoCl_2 \cdot 6H_2O$ with thionyl chloride ($SOCl_2$, bp 77°C). Indene and 1,5-cyclooctadiene (COD) were vacuum distilled before use. C_3F_7I, $C_6F_{13}I$, and $PPh(OCH_3)_2$ were purchased from Aldrich and used as received. $P(OCH_3)_3$ (Strem) was distilled under vacuum before use. (*S*)-(−)-Diphenyl((1-phenylethyl)amino)phosphine (PNH) was prepared using the established procedure reported by Brunner and Doppelberger (48). Infrared spectra were measured on a Mattson Polaris Fourier transform spectrometer as solutions in KBr cells (0.1 mm) or as thin films deposited on a KBr

Can. J. Chem. Downloaded from www.nrcresearchpress.com by 109.225.110.28 on 09/08/12
For personal use only.

Can. J. Chem. Downloaded from www.nrcresearchpress.com by 109.225.110.28 on 09/08/12
For personal use only.

disk. Elemental analyses were performed by Guelph Chemical Laboratories Ltd. Melting points were determined in sealed capillaries and are uncorrected. NMR spectra were recorded on a GE 300-NB Fourier transform spectrometer operating at a proton frequency of 300.12 MHz. Complexes **1** and **9** were prepared as described previously (37, 38).

Proton nOed spectra were determined under steady state conditions on the GE 300-NB instrument. Data were collected using interleaved experiments of 16 or 32 transients cycled 12–16 times through the list of decoupling frequencies. In each experiment the decoupler was gated on in continuous wave (CW) mode for 6 s with sufficient attenuation to give an approximate 70–90% reduction in intensity of the irradiated peak. A 60 s delay preceded each frequency change. A set of four equilibrating scans was employed to equilibrate the spins prior to data acquisition. No relaxation delay was applied between successive scans of a given decoupling frequency. Difference spectra were obtained on 16 K or zero-filled 32 K data tables that had been digitally filtered with a 0.1 Hz exponential or Gaussian line broadening function. Quantitative data were obtained by integration.

Synthesis of (η^5-C_9H_7)$Co(CO)(I)(C_6F_{13})$, ***3***

Compound **1** (5.25 g, 22.8 mmol) was dissolved in 50 mL of benzene in an atmosphere of dry nitrogen. Perfluorohexyl iodide (10.8 g, 24.2 mmol) was injected into the solution via syringe and the solution stirred for 40 h at room temperature to afford a dark, red-brown solution containing some black precipitate. The reaction mixture was filtered through a Schlenk filter fitted with a 10 cm silica gel pad and washed with methylene chloride. TLC analysis (elution with benzene:hexane 2:1) showed the formation of a single product. Removal of solvent with the aid of a rotary evaporator left **3** as an air-stable, black powder (11.0 g, 75%). The crude product was dissolved in a small amount of methylene chloride and crystallized by slow diffusion of hexane at −20°C to give pure **3** as black, rectangular plates. Compound **2** was prepared from **1** and C_3F_7I using similar conditions.

Synthesis of (η^5-C_9H_7)$Co(R_f)(I)(L)$ ($R_f = C_3F_7$, C_6F_{13}; $L = P(OCH_3)$, $PPh(OCH_3)_2$, PNH) ***4–8***

All P-donor substituted complexes were synthesized using a procedure similar to that used for complex **6** described below. $PPh(OCH_3)_2$ (0.0912 g, 0.536 mmol) was added slowly via syringe with stirring to a solution of **2** (0.2547 g, 0.5102 mmol) in 10 mL benzene in a nitrogen atmosphere at room temperature. After stirring for 0.5 h, the solution was placed on an ice bath for 10 min. Removal of volatiles under oil-pump vacuum left the crude product as a dark powder (0.3043 g, 93%). The crude product was dissolved in a small amount of CH_2Cl_2 and crystallized by slow diffusion of hexane at −20°C to afford pure **6** as black prisms.

Acknowledgement

We thank the Natural Sciences and Engineering Research Council of Canada (NSERC) for financial support of this work. Z. Z. acknowledges the award of a graduate fellowship by Memorial University.

1. A. J. Hart-Davis and R. J. Mawby. J. Chem. Soc. A, 2403 (1969).
2. D. J. Jones and R. J. Mawby. Inorg. Chim. Acta, **6**, 157 (1972).
3. H. Bönnemann. Angew. Chem. Int. Ed. Engl. **24**, 248 (1985).
4. H. Bönnemann and W. Brijoux. Aspects Homogeneous Catal. **5**, 75 (1984).
5. T. C. Forschner and A. R. Cutler. J. Organomet. Chem. **361**, C41 (1989).
6. T. C. Forschner, A. R. Cutler, and R. K. Kullnig. Organometallics, **6**, 889 (1987).
7. A. Habib, R. S. Tanke, E. M. Holt, and R. H. Crabtree. Organometallics, **8**, 1225 (1989).
8. L.-N. Ji, M. E. Rerek, and F. Basolo. Organometallics, **3**, 740 (1984).
9. M. E. Rerek, L.-N. Ji, and F. Basolo. J. Chem. Soc. Chem. Commun. 1208 (1983).
10. T. B. Marder, D. C. Roe, and D. Milstein. Organometallics, **7**, 1451 (1988).
11. J. M. O'Connor and C. P. Casey. Chem. Rev. **87**, 307 (1987).
12. H. H. Hammud and G. M. Moran. J. Organomet. Chem. **307**, 255 (1986).
13. P. Caddy, M. Green, E. O'Brien, L. E. Smart, and P. Woodward. J. Chem. Soc. Dalton Trans. 962 (1980).
14. H. Eshtiagh-Hosseini and J. F. Nixon. J. Less-Common Met. **61**, 107 (1978).
15. J. W. Faller, R. H. Crabtree, and A. Habib. Organometallics, **4**, 929 (1985).
16. A. K. Kakker, S. F. Jones, N. J. Taylor, S. Collins, and T. B. Marder. J. Chem. Soc. Chem. Commun. 1454 (1989).
17. R. M. Kowaleski, A. L. Rheingold, W. Trogler C, and F. Basolo. J. Am. Chem. Soc. **108**, 2460 (1986).
18. T. B. Marder, J. C. Calabrese, D. C. Roe, and T. H. Tulip. Organometallics, **6**, 2012 (1987).
19. J. S. Merola, R. T. Kacmarcik, and D. V. Engen. J. Am. Chem. Soc. **108**, 329 (1986).
20. M. Mlekuz, P. Bougeard, B. G. Sayer, M. J. McGlinchey, C. A. Rodger, M. R. Churchill, J. W. Ziller, S. K. Kang, and T. A. Albright. Organometallics, **5**, 1656 (1986).
21. D. E. Smith and A. J. Welch. Organometallics, **5**, 760 (1986).
22. L. P. Szajek, R. J. Lawson, and J. R. Shapley, Organometallics, **10**, 357 (1991).
23. R. Benn, K. Cibura, P. Hofmann, K. Jonas, and A. Rufinska. Organometallics, **4**, 2214 (1985).
24. P. Binger, R. Milczarek, R. Mynott, C. Kruger, Y.-H. Tsay, E. Raabe, and M. Regitz. Chem. Ber. **121**, 637 (1988).
25. E. W. Abel and S. Moorhouse. J. Chem. Soc. Dalton Trans. 1706 (1973).
26. A. Salzer and C. Taschler. J. Organomet. Chem. **294**, 261 (1985).
27. M. A. Huffman and L. S. Liebeskind. J. Am. Chem. Soc. **112**, 8617 (1990).
28. H. Werner, J. Mahr, and G. Hoerlin. Z. Anorg. Allg. Chem. **577**, 283 (1989).
29. P. Diversi, A. Giusti, G. Ingrosso, and A. Lucherini. J. Organomet. Chem. **205**, 239 (1981).
30. F. H. Köhler. Chem. Ber. **107**, 570 (1974).
31. H. P. Fritz, F. H. Köhler, and K. E. Schwarzhans. J. Organomet. Chem. **16**, P14 (1969).
32. S. A. Westcott, A. K. Kakkar, G. Stringer, N. J. Taylor, and T. B. Marder. J. Organomet. Chem. **394**, 777 (1990).
33. R. T. Baker and T. H. Tulip. Organometallics, **5**, 839 (1986).
34. H. Brunner, C. R. Jablonski, and P. G. Jones. Organometallics, **7**, 1283 (1988).
35. C. R. Jablonski, T. Burrow, and P. G. Jones. J. Organomet. Chem. **370**, 173 (1989).
36. C. R. Jablonski and H. Ma. 74th Canadian Chemical Conference, June 2–6, Hamilton, Ontario. Abstr. no. 390 IN E1. (1991).
37. Z. Zhou and C. R. Jablonski. 74th Canadian Chemical Conference, June 2–6, Hamilton, Ontario. Abstr. no. 963 IN D1. (1991).
38. C. R. Jablonski, Z. Zhou, and J. Bridson. J. Organomet. Chem. **429**, 379 (1992).
39. L. Carlton, P. Johnston, and N. J. Coville. J. Organomet. Chem. **339**, 339 (1988).
40. H. P. Fritz and C. G. Kreiter. J. Organomet. Chem. **4**, 198 (1965).
41. M. S. Loonat, L. Carlton, and N. J. Coville. S. Afr. J. Chem. **41**, 72 (1988).

42. R. H. Crabtree and C. P. Parnell. Organometallics, **3**, 1727 (1984).
43. P. Johnston, M. S. Loonat, W. L. Ingham, L. Carlton, and N. J. Coville. Organometallics, **6**, 2121 (1987).
44. M. S. Loonat, L. Carlton, J. C. A. Boeyens, and N. J. Coville. J. Chem. Soc. Dalton Trans. 2407 (1989).
45. K. J. Karel, T. H. Tulip, and S. D. Ittel. Organometallics, **9**, 1276 (1990).
46. C. A. Tolman. Chem. Rev. **77**, 313 (1977).
47. T. Bartik, T. Himmler, H.-G. Schulte, and K. Seevogel. J. Organomet. Chem. **272**, 29 (1984).
48. H. Brunner and J. Doppelberger. Chem. Ber. **111**, 673 (1978).

Can. J. Chem. Downloaded from www.nrcresearchpress.com by 109.225.110.28 on 09/08/12
For personal use only.

2-Chloro-2,4-dioxo-3-methyl-1,3,2-thiazaphospholidine. Comments on its phosphorylating properties

AGNES M. MODRO AND TOMASZ A. MODRO[1]
Department of Chemistry, University of Pretoria, Pretoria 0002, South Africa

Received March 6, 1992

AGNES M. MODRO and TOMASZ A. MODRO. Can. J. Chem. **70**, 2552 (1992).

2-Alkoxy-2,4-dioxo-3-methyl-1,3,2-thiazaphospholidines undergo facile ring-opening reactions with chloride ion, and, in particular, with water. This reactivity may limit their value as first intermediates in the sequential synthesis of phosphoric diesters from the parent 2-chloro-2,4-dioxo-3-methyl-1,3,2-thiazaphospholidine.

AGNES M. MODRO et TOMASZ A. MODRO. Can. J. Chem. **70**, 2552 (1992).

Les 2-alkoxy-2,4-dioxo-3-méthyl-1,3,2-thiazaphospholidines subissent des réactions d'ouvertures de cycle faciles sous l'influence de l'ion chlorure et, en particulier, avec l'eau. Cette réactivité peut s'avérer une limite à leur utilité comme premiers intermédiaires dans la synthèse séquentielle de diesters phosphorique à partir de la 2-chloro-2,4-dioxo-3-méthyl-1,3,2-thiazaphospholidine parente.

[Traduit par la rédaction]

Can. J. Chem. Downloaded from www.nrcresearchpress.com by 109.225.110.28 on 09/08/12
For personal use only.

In a search for a versatile reagent for the synthesis of unsymmetrical dialkyl phosphates, Ugi and co-workers introduced 2-chloro-2,4-dioxo-3-methyl-1,3,2-thiazaphospholidine **1** as an ideal phosphorylating agent (1). Its value stemmed from a sequence of selective steps of the nucleophilic fission of the P—Cl, the P—N, and, finally, the P—S bond (Scheme 1).

The necessary conditions for the successful synthesis are that "the first phosphorylation step completely preserves the five-membered ring", and that "**2** does not react any further with alcohols, unless deliberately activated" (1); according to the reports, reagent **1** meets precisely these conditions. In our attempts to prepare dialkyl phosphates incorporating nitroimidazole drug moiety (2), we applied the above approach and found that it can present problems and requires very rigorous reaction conditions. We report here on some aspects of the reactivity of **1** that can complicate or limit its application as a multifunctional phosphorylating agent.

Results and discussion

Preparation of substrate **1** required some modification of the literature procedure, since under the reported conditions the reaction mixture solidifies due to freezing of the benzene solution. Compound **1** can, however, be prepared in benzene at 0°C (some frozen benzene serves as an internal cooling agent), or in CH_2Cl_2 at −30°C. We then reacted **1** with ethanol under conditions (1*a*) that should give pure 2-ethoxy-2,4-dioxo-3-methyl-1,3,2-thiazaphospholidine, **2***a* (**2**, R = Et) in 92% yield. The phosphorylation (the scale of the reactions was in the range of 1.5×10^{-4}–10^{-1} mol of **1**, and either pyridine or triethylamine was used as a base), however, repeatedly yielded a mixture consisting of three compounds (total yield 100%), that is, the required ester **2***a*, and the two ring-opened products, **4** and **5** (eq. [1]).

[1] $$\mathbf{1} \xrightarrow{\text{EtOH/amine}} \underset{78\text{–}80\%}{\mathbf{2}a} + \underset{\mathbf{4}}{\underset{2\text{–}4\%}{\text{MeNHC(O)CH}_2\text{SP(O)(OEt)Cl}}} + \underset{\mathbf{5}}{\underset{18\text{–}20\%}{\text{MeNHC(O)CH}_2\text{SP(O)(OEt)OH}}}$$

[1]Author to whom correspondence may be addressed.

Analogous results were obtained with *n*-butanol, where the corresponding products, **2***b* (**2**, R = *n*-Bu), and the *O*-*n*-butyl analogues of **4** and **5** (**4**′ and **5**′) were formed in 68, 11, and 21% yields, respectively.[2] Phosphorochloridates **4**, **4**′ are *not* the result of the nonselective reaction of an alcohol with **1** (P—N instead of the P—Cl bond cleavage), but of the subsequent ring opening in **2** by the tertiary ammonium chloride present in the system. When the reaction mixture (eq. [1]), instead of being filtered off and evaporated, was stirred at room temperature for periods of 16, 24, and 72 h, the proportion of **4** increased to 22, 48, and 71%, respectively. When the reaction of **1** with ethanol (or *n*-butanol) was carried out without any base, **4** (or **4**′) was virtually the exclusive product, formed via the fast cleavage of the P—N bond in **2** by free HCl (3). It is worth noting that **4** did not undergo any appreciable hydrolysis when it was kept in aqueous solution over a period of several days.[3]

Cyclic ester **2***a*, free of any phosphorochloridate **4**, could be prepared by carrying out the phosphorylation at −65°C and the work-up at a temperature not higher than −5°C. NMR spectroscopy (^{31}P, ^{1}H) showed complete absence of **4**, but even under these conditions, up to 7% of the acid **5** could be observed in the reaction product. It is possible, however, that at least some of **5** was formed during the preparation and handling of the sample for spectroscopic determinations (*vide infra*).

The most remarkable property of the cyclic intermediate **2** is its susceptibility to hydrolysis. Irrespective of the care taken to remove water from solvents, reagents, and reaction atmosphere, we were never able to avoid to formation of some of the ring-opened acid **5**. When **1** was reacted with two mol-equivalents of ethanol and amine in benzene, the expected *O*,*O*-diethylphosphorothiolate **3***a* (**3**, R = R′ = Et) was formed in 87% yield. It was, however, contaminated with 13% of **5**, formed via the competitive hydrolysis of **2**

[2]Products **2***b* and **5**′ were not isolated and fully characterized, but they were identified by their ^{31}P nmr signals (**2***b*: δ_P 36.3; 5′: δ 20.9), in analogy with the respective ^{31}P nmr spectra of **2***a* (δ 36.1) and **5** (δ 21.9).

[3]As one of the referees pointed out, it should be possible to arrive at products **3** from substrates **1** via intermediates **4**. We are currently investigating this approach to the preparation of unsymmetrical phosphates.

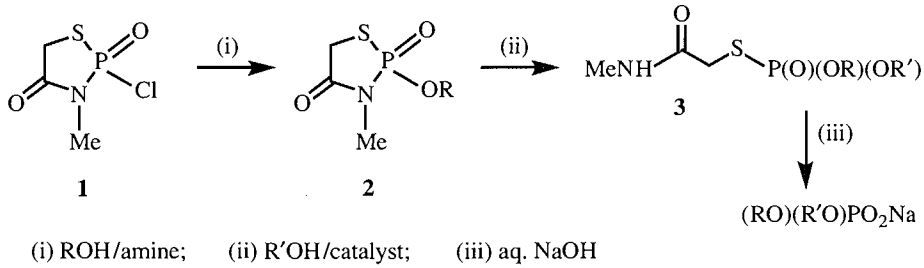

SCHEME 1

in a second phosphorylation step (Scheme 1, step (ii)). It seems that the reactivity of **2** in the ring opening decreases rapidly with an increase in the steric bulk of the nucleophile. In the reaction of **1** with ethanol/pyridine (one mol-equivalent), followed by 2-propanol/pyridine, the expected mixed ester **3***b* (**3**, R = Et; R′ = *i*-Pr) was formed in only 50% yield, the remaining components being the intermediate cyclic ester **2***a* (36%), and its hydrolysis product, **5** (14%). The non-catalyzed hydrolytic opening of the 2,4-dioxo-3-methyl-1,3,2-thiazaphospholidine ring is a very facile reaction, irrespective of the nature of the 2-substituent. When the equimolar mixture of **1** and **2***a* was subjected to the competitive hydrolysis with water (half mol-equivalent) in $CDCl_3$ yielding a mixture of the respective products, $MeNHC(O)CH_2SP(O)(OH)Cl$ and **5**, we found (by examining the composition of the mixture by ^{31}P nmr spectroscopy) **1** to be only approximately two times more reactive than **2***a*. Ester **2***a* is, on the other hand, much more hygroscopic than substrate **1**, which may explain its very facile hydrolysis. When pure samples of **2***a* and **1** were exposed to the atmosphere, the absorption of moisture by **2***a* was found to be 11 times faster than that of **1**.

Reaction of **1** with amines also did not lead to a single substitution product. When a benzene solution of **1** was treated at 0°C with two mol-equivalents of aniline, the product consisted of the expected 2-phenylamino-2,4-dioxo-3-methyl-1,3,2-thiazaphospholidine, **6** (77%), and the corresponding chloride-promoted ring-opened derivative, **7** (23%) (eq. [2]). Since the cyclic product **6** is not hygroscopic, the hydrolysis product was in this case absent, but when **6** was dissolved in water, it gave instantly and quantitatively the corresponding amino acid, $MeNHC(O)CH_2SP(NHPh)O_2H$.

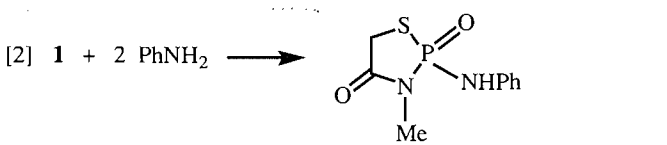

6

+ $MeNHC(O)CH_2S–P(O)(NHPh)Cl$

7

In conclusion, we demonstrated that cyclic ester **2**, the key intermediate in the phosphorylation sequence, is a less selective reagent than originally reported (1), and that it reacts smoothly without a catalyst with nucleophilic species, and with water in particular. The latter reaction can be highly detrimental from the synthetic point of view, as side-products of the type **5** can easily contaminate the final product of the phosphorylation. It is recommended, therefore, that step (ii) (Scheme 1) should be carried out immediately after the completion of the first step without isolation of **2**, at low temperature, and with the most rigorous exclusion of moisture.

Experimental section

Benzene (Merck, GR Grade) was stored and distilled over sodium wire and stored over molecular sieves (5A). Dichloromethane (Merck, GR Grade) was distilled from P_4O_{10} and stored over molecular sieves (4A). Pyridine (Merck, GR Grade) was stored over solid KOH for 2 weeks, fractionally distilled from KOH, and stored over molecular sieves (5A). Triethylamine (Aldrich, 99+%) was stored over solid KOH and distilled from P_4O_{10}. Ethanol, *n*-butanol, and 2-propanol (Merck, GR Grade) were purified with magnesium activated with iodine and fractionally distilled. Aniline (Aldrich, 99.5+%) was dried over KOH and distilled; sulfuryl chloride (Aldrich) was distilled immediately before use. *N*-Methylmercaptoacetamide was prepared in 83% yield from methyl mercaptoacetate following a literature procedure (4); bp 104–105°C (2 Torr; 1 Torr = 133.3 Pa). 2-Methoxy-3-methyl-4-oxo-1,3,2-thiazaphospholidine **8** was prepared as described by Richter and Ugi (1*a*) in 66% yield; bp 90–92°C (0.1 Torr); nmr (^1H and ^{31}P) spectra in full agreement with those reported (1*a*). The nmr spectra were recorded on a Bruker AC 300 MHz spectrometer and the chemical shift values are given relative to TMS (^1H) and 85% H_3PO_4 (^{31}P). Mass spectra were recorded on a Varian MAT-212 double-focusing direct-inlet spectrometer at an ionization potential of 70 eV. Only the molecular ion data are included.

2-Chloro-2,4-dioxo-3-methyl-1,3,2-thiazaphospholidine ***1***

Sulfuryl chloride (33.7 g, 0.25 mol) dissolved in CH_2Cl_2 (100 mL) was added slowly with stirring and cooling at −30°C to a solution of **8** (41 g, 0.25 mol) in CH_2Cl_2 (500 mL). Stirring was continued at room temperature for 10 h; the solution was concentrated under reduced pressure to approximately one-third volume and left overnight in a refrigerator. The product was collected by filtration, washed with dry CH_2Cl_2 and stored in a desiccator over P_4O_{10}. Yield 38.7 g (84%); δ_P 39.75 (lit. δ_P 39.06). ^1H nmr spectrum in full agreement with that reported (1*a*).

Reactions of ***1*** *with alcohols*

(*a*) Reactions were carried out under conditions reported in the literature. Pyridine or triethylamine was used as a base. After completion of the reaction and filtration, the solvent (benzene) was removed under reduced pressure and the crude product was examined by nmr (^1H, ^{31}P) spectroscopy. The proportions of individual components were determined from the relative intensities of the corresponding signals in the ^{31}P nmr spectra.

(*i*) Reaction with ethanol: 100%; **2***a* (78–80%), δ_P ($CDCl_3$) 36.1; ^1H nmr spectrum in full agreement with that given in ref. 1*a*; **4** (2–4%), δ_P 27.5; δ_H 2.72 (3H, br s, NMe), 3.35 (2H, d, J_{HP} 19.5 Hz, CH_2S), **5** (18–20%), δ_P 21.9; δ_H 2.83 (3H, br s, NMe), 3.50 (2H, d, J_{HP} 18.5 Hz, CH_2S).

(*ii*) Reaction with *n*-butanol: carried out as above, with pyridine

Can. J. Chem. Downloaded from www.nrcresearchpress.com by 109.225.110.28 on 09/08/12
For personal use only.

Can. J. Chem. Downloaded from www.nrcresearchpress.com by 109.225.110.28 on 09/08/12
For personal use only.

as a base. 100%; **2***b* (68%), δ_P ($CDCl_3$) 36.3; **4**′ (11%), δ_P 28.6; **5**′ (21%), δ_P 20.9.

(*iii*) Reaction with two mol-equivalents of ethanol in the presence of two mol-equivalents of triethylamine: 99%; **3***a* (87%), δ_P ($CDCl_3$) 24.2; δ_H 1.28 (6H, t, J_{HH} 7.1 Hz, 2 × Me of POEt), 2.75 (3H, br s, NMe), 3.37 (2H, d, J_{HP} 19.2 Hz, CH_2S), 4.09 (4H, quint, J_{HH}, J_{HP} 7.1 Hz, 2 × CH_2 of POEt), 7.04 (1H, br s, NH); spectral data in full agreement with those given in ref. 1*a*; **5** (13%), nmr (^1H, ^{31}P) spectra identical to those given above.

(*iv*) Reaction with ethanol, followed by 2-propanol: carried out as above using pyridine in both steps: 100%; **3***b* (50%), δ_P ($CDCl_3$) 20.7; ^1H nmr spectrum in full agreement with that given in ref. 1a; **2***a* (36%), δ_P 36.1; **5** (14%), δ_P 21.9.

(b) Modified synthesis of **2**a

A solution of equimolar quantities of ethanol and pyridine (or triethylamine) in CH_2Cl_2 (0.3 mL/mmol) was added slowly dropwise to a stirred solution of **1** in CH_2Cl_2 (7.5 mL/mmol) at −65°C. The mixture was then warmed to −10°C, evaporated at ca. 0°C and reduced pressure, benzene (5 mL/mmol) was added, and the mixture was filtered. After the evaporation of benzene under reduced pressure, **2***a* was obtained in 89% yield. The purity of the crude product (as determined by ^{31}P nmr spectroscopy) was 93–95%, the remaining 5–7% being product **5**.

Preparation of **4**

Ethanol (0.074 g, 1.62 mmol) in benzene (1 mL) was added slowly dropwise to a stirred solution of **1** (0.300 g, 1.62 mmol) in benzene (3 mL) at 0°C. The solution was left overnight in a refrigerator and evaporated under reduced pressure, yielding **4** as a viscous oil in quantitative yield. The nmr (^1H, ^{31}P) spectra were identical to those given above for the product of the experiment (*a*) (*i*); ms: *m/z* 231 (12%). The only other phosphorus containing product (≤5%) detected by ^{31}P nmr spectroscopy was **5** (δ_P 21.7).

When *n*-butanol was used instead of ethanol, **4**′ was obtained in almost quantitative yield. Oil; δ_P ($CDCl_3$) 28.5; δ_H 1.24 (3H, t, J_{HH} 7.1 Hz, Me of POBu), 1.36 (2H, m, γ-CH_2 of POBu), 1.68 (2H, m, β-CH_2 of POBu), 2.65 (3H, br s, NMe), 3.44 (2H, d, J_{HP} 19.0 Hz, CH_2S), 4.12 (2H, m, OCH_2 of POBu); ms: *m/z* 259 (1%).

Preparation of **5**

Compound **2***a* (0.70 g, 0.36 mmol) was dissolved in dioxane (7 mL), water (0.5 mL) was added to this solution, and the mixture was kept at room temperature for 43 h. The solution was evaporated to dryness under reduced pressure and the syrupy residue (98%) crystallized upon standing. It was purified by crystallization from chloroform/benzene (1:2); mp 81–83°C; nmr (^1H, ^{31}P) spectra identical to those given above; ms: *m/z* 213 (8%). Anal. calcd. for $C_5H_{12}NO_4PS$: C 28.2, H 5.6, N 6.6, S 15.0; found: C 29.1, H 5.8, N 6.6, S 14.8%.

Competitive hydrolysis of **1** *and* **2**a

Equimolar amounts (0.01 mmol) of **1** and **2***a* were dissolved in $CDCl_3$ (1.0 mL) and the ^{31}P nmr spectrum of this solution was recorded. A solution of water (0.11 mmol) in dioxane (0.1 mL) was added and the ^{31}P nmr spectra of this solution were recorded several times within a period of 1 h. The change in the **1**/**2***a* ratio (measured by the relative intensities of signals at δ_P 39.7 and 36.1) indicated that the disappearance of **1** was approximately two times faster than that of **2***a*.

Relative hygroscopic properties of **1** *and* **2**a

Samples of **1** and **2***a* (0.27 g each) were placed in identical containers and left exposed to the surrounding atmosphere. The increase of the mass of both samples was monitored periodically. The absorption of moisture by **2***a* was approximately 11 times faster than that by **1**; the ^{31}P nmr spectra of the samples, recorded after 72 h, corresponded mostly to the respective hydrolysis products.

Reaction of **1** *with aniline*

Aniline (0.10 g, 1.08 mmol) in benzene (5 mL) was added dropwise with stirring and cooling at 0°C to the solution of **1** (0.10 g, 0.54 mmol) in benzene (2 mL). The mixture was stirred at 0°C for 1.5 h, warmed up to room temperature, and filtered. After the evaporation of the solvent under reduced pressure, the crude product (0.087 g, 67%) was obtained as a yellow syrup. The ^{31}P nmr spectrum demonstrated the presence of two products: the major (77%, $CDCl_3$ δ_P 31.9) and the minor (23%, δ_P 25.7). Pure **6** was obtained by crystallization (ether/petroleum ether), mp 128–128.5°C; δ_P ($CDCl_3$) 31.9; δ_H 2.92 (3H, d, J_{HP} 7.7 Hz, NMe), 3.77 (1H, dd, J_{HH}, J_{HP} 16.3, 11.7 Hz, CH_AS), 3.92 (1H, dd, J_{HH}, J_{HP} 16.3, 6.5 Hz, CH_BS), 6.90–7.30 (5H, m, Ph), 7.73 (1H, br s, NH). Anal. calcd. for $C_9H_{11}N_2O_2PS$: C 44.6, H 4.6, N 11.6; found: C 44.4, H 4.5, N 11.3%.

When a sample of **6** was dissolved in D_2O, the nmr spectrum of this solution showed complete disappearance of **6** and the formation of the hydrolysis product, $MeNHC(O)CH_2SP(NHPh)O_2H$; δ_P (D_2O) 16.9; δ_H 2.67 (3H, s, NMe), 3.36 (2H, d, J_{HP} 14.4 Hz, CH_2S), 7.30–7.60 (5H, m, Ph).

The minor product obtained after crystallization of **6** (colorless oil) was identified as compound **7**: δ_P ($CDCl_3$) 25.7; δ_H 2.70 (3H, d, J_{HH} 6.9 Hz, NMe), 3.54 (2H, d, J_{HP} 9.2 Hz, CH_2S), 6.90–7.30 (5H, m, Ph); ms: *m/z* 278 (6%). Anal. calcd. for $C_9H_{12}ClN_2O_2PS$: C 38.7, H 4.3, N 10.0, Cl 12.7; found: C 38.1, H 4.4, N 9.6, Cl 11.9%.

Acknowledgement

Financial support from the University of Pretoria and the Foundation for Research Development is gratefully acknowledged.

1. (*a*) W. Richter and I. Ugi. Synthesis, 661 (1990); (*b*) I. Ugi, N. Bachmeier, R. Herrmann, P. Jacob, R. Karl, M. Klein, B. Landgraf, P. Lemmen, W. Richter, and U. Verfurth. Phosphorus, Sulfur, Silicon, **51/52**, 57 (1990); (*c*) W. Richter, R. Karl, and I. Ugi. Tetrahedron, **46**, 3167 (1990).
2. T. A. Modro and R. A. McClelland. Org. Prep. Proced. Int. **24**, 197 (1992).
3. J. Emsley and D. Hall. *In* The chemistry of phosphorus. Harper and Row, London. 1976. Chap. 10.1.
4. G. Barany and R. B. Merrifield. J. Am. Chem. Soc. **102**, 3084 (1980).

The negative ^7J(CHO, CH_3) in 4-methylbenzaldehyde. Ionicity of the carbonyl bond

TED SCHAEFER AND RUDY SEBASTIAN
Department of Chemistry, University of Mannitoba, Winnipeg, Man., Canada R3T 2N2

Received April 7, 1992

TED SCHAEFER and RUDY SEBASTIAN. Can. J. Chem. **70**, 2555 (1992).

The spin–spin coupling constant over seven bonds between the formyl and methyl protons in 4-methylbenzaldehyde is −0.030 Hz in CS_2/C_6D_{12}/TMS, and (−)0.035 Hz in acetone-d_6, solutions at 297 K. This unexpected result is rationalized in terms of a spin–spin coupling mechanism attributed to the importance of a valence bond structure with an ionic carbonyl bond. The result again emphasizes the sensitivity to substituent perturbations of the six-bond coupling constant in quasi-planar benzaldehyde derivatives. It can have either sign and presents a challenge to its computation from first principles.

TED SCHAEFER et RUDY SEBASTIAN. Can. J. Chem. **70**, 2555 (1992).

On a déterminé que, à 297 K, les constantes de couplage spin–spin à travers sept liaisons entre les protons du formyle et du méthyle du 4-méthylbenzaldéhyde sont de −0,030 Hz dans le CS_2/C_6D_{12}/TMS et de (−)0,035 Hz dans l'acétone-d_6. On rationalise ce résultat inattendu en fonction d'un mécanisme de couplage spin–spin attribué à l'importance d'une structure de liaison de valence avec une liaison carbonyle ionique. Ce résultat met à nouveau en relief la sensibilité des perturbations des substituants sur la constante de couplage à travers six liaisons dans des dérivés benzaldéhydes pratiquement plans. Elle peut prendre un signe ou l'autre et elle présente un défi pour ceux qui veulent la calculer à partir de principes fondamentaux.

[Traduit par la rédaction]

Introduction

The unprecedented properties of ^6J(H,CHO) ≡ ^6J, the coupling constant between the formyl and *para* ring protons, in benzaldehyde derivatives have been discussed recently (1, 2). While ^6J is negative in benzaldehyde itself, as expected for a σ–π mechanism dependent on $\sin^2\theta$, θ being the angle by which the formyl group twists out of the molecular plane, and while $^6J_0$ (θ = 0) most likely very nearly vanishes (2), it is as large as +0.086(3) Hz in the 3,5-difluoro derivative (1).

These positive ^6J values in some *meta*-substituted benzaldehydes are attributed (1) to a coupling mechanism associated with an ionic valence bond structure, here written[1] as **1**; crossed arrows denote proton spin states and the other

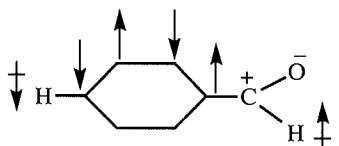

1

arrows refer to π electrons. In such derivatives, a linear relationship ^6J/Hz = 0.007 − 0.127 Σ $\sigma_{R,ST}$, exists (1) between ^6J and the standard residual resonance substituent constants (7) for *meta* substituents, $\sigma_{R,ST}$. It is therefore implied that substituents with residual π donor characteristics (7) at the *meta* position, such as F, Cl, OCH_3, CH_3, increase the importance of **1**. Although ^6J could not be determined for the 3,5-dimethyl derivative (1), a more recent determination of ^6J in 3-methylbenzaldehyde (8), possible because of the second-order and asymmetric properties of the spin system, gave +0.015(1) Hz via a very precise analysis of a highly resolved spectrum in acetone-d_6 solution. The linear regression yields +0.012(2) Hz. The considerable ionic character of the C=O bond in some molecules has been attested to recently by high-level molecular orbital computations (9).

The linear regression has ^6J as 0.007 Hz in the parent compound, yet ^6J is given as −0.018 (2) Hz in CS_2/C_6D_{12}/TMS and as −0.013 (1) Hz in acetone-d_6 solutions at 300 K (1). It is unlikely that, while unresolved, ^6J is positive in benzaldehyde (see below). Are the *meta* derivatives therefore unique in this respect? A measurement of ^7J(CHO,CH_3) in 4-methylbenzaldehyde (4MB) should provide a partial answer. For, if ^6J in benzaldehyde arises from the σ–π mechanism, proportional to $\sin^2\theta$, then, because $Q^H_{CH} = -Q^H_{CCH}$ in closed-shell aromatic molecules,[2] ^7J(CHO,CH_3) should be positive. If an unsuspected σ electron coupling mechanism accounts for ^6J in benzaldehyde, then ^7J should be severely attenuated relative to ^6J. Finally, if the methyl group enhances the importance of **1**, then ^7J may be negative.

Here we report that ^7J in 4MB is −0.030(0) Hz in CS_2/C_6D_{12} solution and is (−)0.035(0) Hz in acetone-d_6 solution at 297 K.

Experimental

Dilute solutions in CS_2/C_6D_{12}/TMS and (or) acetone-d_6/TMS solvent mixtures (see tables for details) were filtered into 5 mm o.d.

[1] Structure **1** is an alternative to that given previously (1); the present structure is a conflation that emphasizes the parallel spin states of the formyl proton and the π electron at the ipso carbon site. One way of picturing this arrangement is to note that the hyperfine parameter, $Q^H_{COH} < 0$, as based on the sign of isotropic shifts (3). Another way notes that $Q^C_{C'C} < 0$, where C′ is the ipso carbon atom (4), and that the hyperfine coupling constant is positive for the proton in the sigma radical, HCO (5, 6). In other words, positive spin density in the $2p_z$ orbital of the ipso carbon atom induces negative spin density in the sp^2 orbital near the formyl carbon atom, which, in turn, leads to negative spin density near the site of the formyl proton. In **1** the electron in the $2p_z$ orbital of the formyl carbon atom has moved to oxygen and is not involved in the spin polarization phenomena.

[2] ^6J(H,CH_3) is −0.602(2) Hz in toluene (10). In *p*-xylene, ^7J(CH_3,CH_3) is +0.60(3) Hz in a CS_2 solution (11, 12) and 0.596(9) Hz in acetone-d_6 solution (unpublished work in this laboratory). These coupling constants are proportional to $Q^H_{CH}Q^H_{CCH}$ and $(Q^H_{CCH})^2$, respectively (13–15).

Can. J. Chem. Downloaded from www.nrcresearchpress.com by 109.225.110.28 on 09/08/12
For personal use only.

Can. J. Chem. Downloaded from www.nrcresearchpress.com by 109.225.110.28 on 09/08/12
For personal use only.

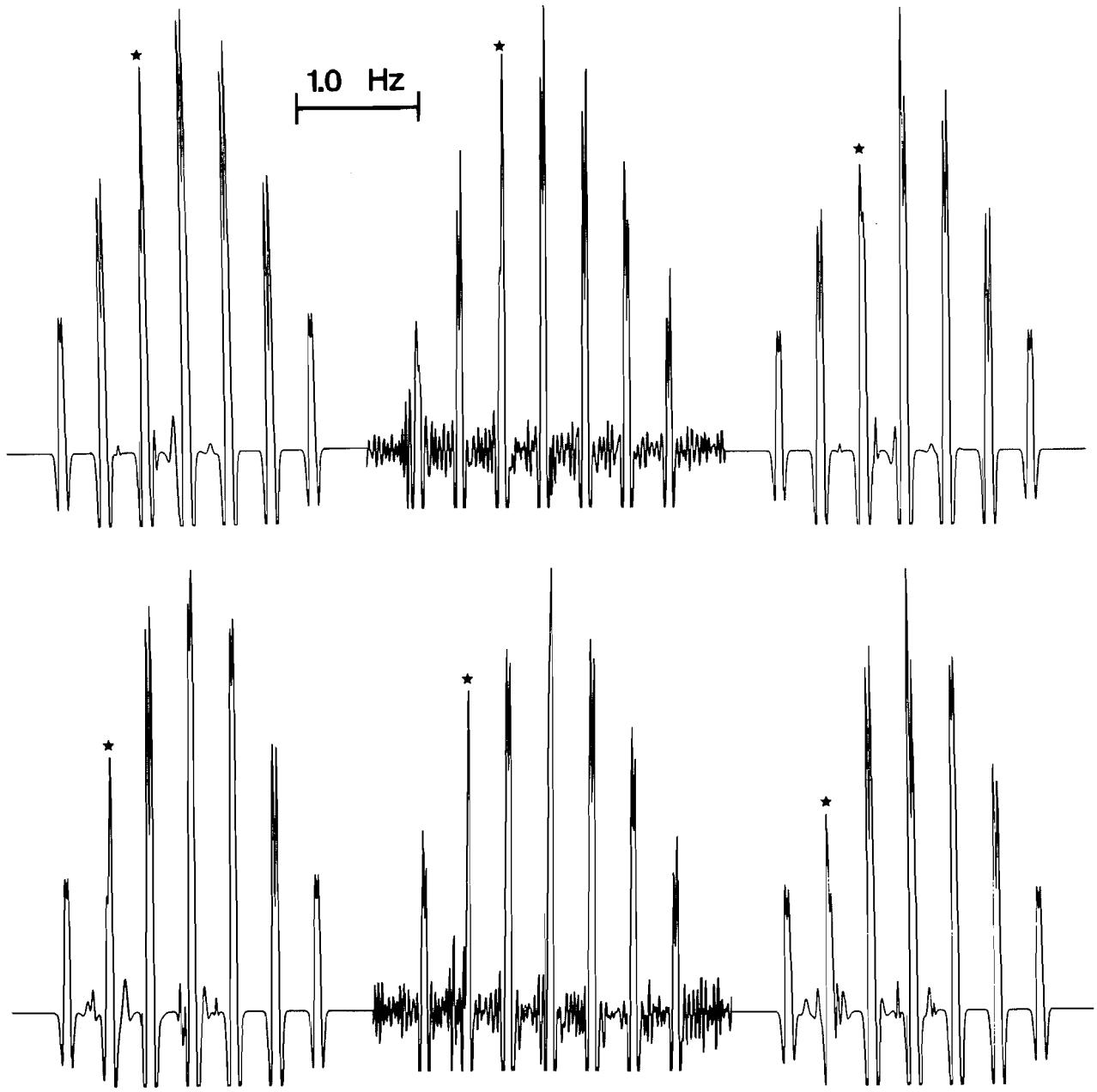

FIG. 1. Various $^1H\{^1H\}$ nmr spectra, experimental and theoretical, are displayed for the methyl protons of 4-methylbenzaldehyde as a 3.0 mol% solution in CS_2/C_6D_{12}/TMS at 300.135$_2$ MHz and 297 K. $^5J(H,CH_3)$ is 0.354(1) Hz and $^4J(H,CH_3)$ is −0.704(1) Hz, accounting for the gross pattern. The small splitting arises from $^7J(CHO,CH_3)$, which is 0.030(0) Hz in magnitude. The computed spectra on the left assume that $^7J < 0$ and those on the right, that $^7J > 0$, together with the spectral parameters in Table 1. In the top row, $\gamma B_2 \sim 0.2$ Hz at 2291.09 Hz relative to TMS, that is, a peak in the H-2 region is being weakly irradiated. In the experimental spectrum, shown to illustrate an artifact in addition to the expected perturbation of certain transitions, the doublet farthest to the left is distorted by interference between various frequencies (beats). The left-hand peak of the starred doublet has changed markedly in intensity (generalized Overhauser effect), as can be seen by comparison with the same doublet in the bottom row, for example. In the bottom row a weak irradiation field is applied in the H-3 region, at 2171.58 Hz; the theoretical spectra are consistent with $^7J < 0$. A series of 14 experiments confirmed this conclusion. The simulated and experimental spectra were processed with resolution enhancements of LB/GB = −0.190/0.625. Acquisition times were 45.5 s and digital resolution was 0.003–0.005 Hz/point. The resolution of the single-resonance spectra was somewhat better than that displayed here. The assumed linewidths above are 0.030 Hz.

nmr sample tubes. These were degassed by five cycles of the freeze–pump–thaw technique and were then sealed under vacuum to provide fairly symmetrical tops.

The ^1H nmr experiments utilized an AM300 Bruker spectrometer. Acquisition times for the free induction decays, acquired after final shimming on the decays of tetramethylsilane, were as long as 45.5 s. Data regions were set so as to provide, after zero-filling, a digital resolution of as high as 0.003 Hz/point when required or possible. Lower digital resolution, 0.005 Hz/point, was necessary in some $^1H\{^1H\}$ experiments.

The ^1H nmr spectra were analyzed with the computer program NUMARIT (16), extensively modified by R. Sebastian. Weak ir-

TABLE 1. The ^{1}H nmr spectral parameters for 4-methylbenzaldehyde in CS_2/C_6D_{12} and acetone-d_6 solutions at 297 K

Parameter	Solvent		Parameter	Solvent	
	CS_2/C_6D_{12}[a]	Acetone-d_6[b]		CS_2/C_6D_{12}[a]	Acetone-d_6[b]
υ(CHO)	2954.988[c]	2996.509	^4J(H,CH_3)	−0.704	−0.714
υ_2	2292.595	2343.636	^5J(H,CHO)	0.431	0.427
υ_3	2170.303	2222.583	^5J(H,CH_3)	0.354	0.357
$\upsilon(CH_3)$	723.178	728.115	^7J(CHO,CH_3)	−0.030	(−)0.035
$^3J_{23}$	7.825	7.858	Transitions calculated	512	512
$^4J_{26}$	1.824(1)[d]	1.853(1)	Assigned transitions	491	479
$^4J_{35}$	1.758(1)	1.762(1)	Peaks observed	227	225
$^5J_{25}$	0.560	0.568	Largest difference	0.017	0.016
^4J(H,CHO)	−0.163	−0.167	Root-mean-square deviation	0.004	0.004

[a]3.0 mol% in CS_2, containing also 10.0 mol% of C_6D_{12} and 0.5 mol% of tetramethylsilane (TMS)
[b]3.0 mol% in acetone-d_6, containing also 0.5 mol% of TMS.
[c]In Hz at 300.135$_2$ MHz to low frequency of internal TMS.
[d]The standard deviations in the spectral parameters were less than 0.001 Hz unless otherwise stated, as here. The solvent dependence of the intraring coupling constants is expected on the basis of experience with many molecules in this laboratory.

radiation experiments (17), ^{1}H{^{1}H}, were simulated with the program DOR (18), locally modified to deal with at least eight spin-$\frac{1}{2}$ nuclei.

Results and discussion

The ^{1}H nmr spectral parameters for 4MB are given in Table 1.

^7J(CHO,CH_3)

Figure 1 shows one example of a series of weak double irradiation or tickling experiments designed to determine the sign of ^7J(CHO,CH_3) ≡ ^7J. These experiments demonstrate that ^7J is −0.030(0) Hz in CS_2/C_6D_{12} solution at 297 K and, by inference from the data in Table 1, −0.035(0) Hz in acetone-d_6 solution at the same temperature.

A naive interpretation of these results combines $-Q^H_{CCH} = Q^H_{CH}$, the $\sigma_{R,ST}$ value of −0.19 for a *para* methyl substituent (7), and the linear relationship for *meta* substituents to give $^7J = -^6J = 0.007 - 0.127\sigma_{R,ST} = -0.031$ Hz, as measured. However, ^6J in benzaldehydye is certainly negative in these solutions (see below). As it happens, the sums of $-^6J$ in benzaldehyde and $-^7J$ in 4MB are +0.048(2) Hz in both solutions, perhaps implying that, in the 4-methyl derivative, the ionic mechanism has this magnitude. Whatever the true situation, it is clear that the methyl substituent enhances the importance of the coupling mechanism attributed to the ionic valence bond structure and that it dominates those mechanisms which contribute to a positive ^7J.

Remarks on ^{6}J *in benzaldehyde*

Further to discussions of the value of the unresolved ^6J in benzaldehyde (1, 2), a detailed reexamination of the spectral data (1) for an acetone-d_6 solution by iterative and simulative approaches has satisfied us that ^6J must indeed be negative. The present study emphasizes how sensitive ^6J in benzaldehydes is to substituent perturbations.

Acknowledgements

We thank the Natural Sciences and Engineering Research Council of Canada for financial assistance.

1. T. Schaefer and C. S. Takeuchi. Can. J. Chem. **67**, 827 (1989).
2. R. Laatikainen, K. Tuppurainen, Y. Hiltunen, and S. Lötjönen. Magn. Reson. Chem. **28**, 939 (1990).
3. D. R. Eaton, A. D. Josey, and R. E. Benson. J. Am. Chem. Soc. **89**, 4040 (1967).
4. M. Karplus and G. K. Fraenkel. J. Chem. Phys. **35**, 1312 (1961).
5. F. J. Adrian, E. L. Cochran, and V. A. Bowers. J. Chem. Phys. **43**, 462 (1965).
6. J. A. Pople and D. L. Beveridge. Approximate molecular orbital theory. McGraw–Hill, New York. 1970. p. 132.
7. G. F. Fadhil and M. Godfrey. J. Chem. Soc. Perkin Trans. 2, 133 (1988).
8. T. Schaefer, K. J. Cox, and R. Sebastian. Can. J. Chem. **69**, 908 (1991).
9. K. B. Wiberg and C. M. Breneman. J. Am. Chem. Soc. **114**, 831 (1992); see also footnote 20 of this reference.
10. T. Schaefer, R. Sebastian, and G. H. Penner. Can. J. Chem. **63**, 2597 (1985).
11. J. B. Rowbotham and T. Schaefer. Can. J. Chem. **52**, 496 (1974).
12. C. J. Macdonald and W. F. Reynolds. Can. J. Chem. **48**, 1002 (1970).
13. M. Barfield and B. Chakrabarti. J. Am. Chem. Soc. **91**, 4346 (1969).
14. H. M. McConnell. J. Chem. Phys. **30**, 126 (1959).
15. R. Wasylishen and T. Schaefer. Can. J. Chem. **50**, 1852 (1972).
16. J. S. Martin, A. R. Quirt, and K. E. Worvill. The NMR program library. Daresbury Laboratory, Daresbury, U.K.
17. R. Freeman and W. A. Anderson. J. Chem. Phys. **37**, 2053 (1962).
18. G. Govil and D. H. Whiffen. Mol. Phys. **12**, 449 (1967).

Can. J. Chem. Downloaded from www.nrcresearchpress.com by 109.225.110.28 on 09/08/12
For personal use only.

Analysis of minor constituents in fullerene soots by LC–MS using a heated pneumatic nebulizer interface with atmospheric pressure chemical ionization[1]

J. F. ANACLETO
Chemistry Department, Dalhousie University, Halifax, N.S., Canada B3H 4J3

R. K. BOYD, S. PLEASANCE,[2] AND M. A. QUILLIAM
Institute for Marine Biosciences, National Research Council, 1411 Oxford Street, Halifax, N.S., Canada B3H 3Z1

AND

J. B. HOWARD, A. L. LAFLEUR, AND Y. MAKAROVSKY
Center for Environmental Health Sciences, Department of Chemical Engineering and Energy Laboratory, Massachusetts Institute of Technology, 77 Massachusetts Avenue, Cambridge, MA 02139, U.S.A.

Received April 7, 1992

J. F. ANACLETO, R. K. BOYD, S. PLEASANCE, M. A. QUILLIAM, J. B. HOWARD, A. L. LAFLEUR, and Y. MAKAROVSKY. Can. J. Chem. **70**, 2558 (1992).

The minor constituents of toluene extracts of three fullerene-rich materials have been characterized by on-line LC–MS techniques, incorporating both positive and negative ion mass spectra obtained by atmospheric pressure chemical ionization. Two of the materials were soots, produced by resistive heating of graphite in an inert atmosphere, from different commercial suppliers. The third material was obtained as a condensate from a controlled laminar flame, and was shown previously (Anacleto *et al.*, Rapid Commun. Mass Spectrom. **6**, 214 (1992)) to contain significant quantities of compounds that behaved under the present LC–MS conditions as isomers of the C_{60} and C_{70} fullerenes, and which reverted to the latter upon heating. This finding was confirmed here, and extended to the higher clusters C_{76}, C_{84}, C_{90}, and C_{94}. One of the graphite-derived soots contained monoxides of the carbon clusters as the principal minor components, while the other soot contained hydrogenated species including $C_{60}H_2$, $C_{60}H_4$, $C_{70}H_2$, and $(C_{60} \cdot CH_4)$. The flame-generated material contained all of these minor constituents, together with complexes of C_{60} with larger aliphatic molecules as well as large quantities of polycyclic aromatic hydrocarbons and related species. Photo-oxidation of a purified C_{60} preparation, from the graphitic soot containing mostly monoxide impurities, was shown to lead to increased levels of the mono-, di-, and tri-oxides of C_{60}.

J. F. ANACLETO, R. K. BOYD, S. PLEASANCE, M. A. QUILLIAM, J. B. HOWARD, A. L. LAFLEUR et Y. MAKAROVSKY. Can. J. Chem. **70**, 2558 (1992).

Faisant appel à des techniques de LC–MS incorporant des spectres de masse des ions tant positifs que négatifs obtenus par des ionisations chimiques réalisées à la pression atmosphérique, on a caractérisé les constituants mineurs obtenus par extraction au toluène de trois matériaux riches en fullerène. Deux des matériaux étaient des suies fournies par différents fournisseurs commerciaux et obtenue par chauffage de graphite par résistance dans une atmosphère inerte. Le troisième matériel a été obtenu sous forme de produit de condensation d'une flamme laminaire contrôlée; il a été démontré antérieurement (Anacleto *et al.*, Rapid Commun. Mass Spectrom. **6**, 214 (1992)) que ce matériel contient des quantités importantes de produits qui se comportent, dans les conditions actuelles de LC–MS, comme des isomères des fullerènes en C_{60} et en C_{70} et qui se transforment en ces derniers par chauffage. On a confirmé cette conclusion dans le présent travail et on l'a étendue aux agrégats plus importants C_{76}, C_{84}, C_{90} et C_{94}. L'une des suies provenant du graphite contient des monoxydes des agrégats carbonés comme constituants mineurs principaux alors que l'autre contient des espèces hydrogénées incluant le $C_{60}H_2$, le $C_{60}H_4$, le $C_{70}H_2$ et $(C_{60} \cdot CH_4)$. Le matériel généré par une flamme contient tous ces constituants mineurs en plus de complexes du C_{60} avec des molécules aliphatiques plus grosses ainsi que des quantités importantes d'hydrocarbures aromatiques polycycliques et d'espèces apparentées. On a montré que la photo-oxydation d'une préparation purifiée de C_{60}, obtenue à partir de suie graphitique contenant principalement des monoxydes comme impuretés, conduit à la formation de quantités de plus en plus grandes de mono-, di- et tri-oxydes de C_{60}.

[Traduit par la rédaction]

Introduction

The remarkably stable carbon cluster C_{60}, first discovered (1) in vapour from laser irradiation of graphite and subsequently produced in macroscopic quantities by resistive heating of graphite under an inert atmosphere (2–5),[3] is now established (6) as possessing a truncated icosahedron ("soccer ball") structure, while the homologue C_{70} is assigned (6) an ellipsoidal cage structure ("rugby ball"). In this paper the terms "buckminsterfullerene" and "fullerene" are taken to refer to these highly symmetrical stable closed-cage carbon clusters (1–6). Recently (7) it was shown that C_{60} and C_{70} fullerenes, found in samples of condensible compounds and soot collected from controlled combustion of benzene in premixed laminar flames, were spectroscopically indistinguishable from fullerenes prepared from graphite. Analysis of the flame samples by high-performance liquid chromatography with ultraviolet spectroscopic detection also revealed the presence of several additional components with fullerene-like characteristics (7).

The most abundant of these additional fullerene-like components (7) were tentatively identified (8) as isomers of the stable C_{60} and C_{70} fullerenes, using high-performance liquid chromatography coupled on-line to mass spectrometry (LC–MS). It was necessary to use mild LC–MS condi-

[1]NRCC No. 34822.

[2]Present address: Wellcome Research Laboratories, Beckenham, Kent BR3 3BS, U.K.

[3]R. E. Smalley. The Almost Complete Buckminsterfullerene Bibliography. Private communication, June, 1991.

Can. J. Chem. Downloaded from www.nrcresearchpress.com by 109.225.110.28 on 09/08/12
For personal use only.

Can. J. Chem. Downloaded from www.nrcresearchpress.com by 109.225.110.28 on 09/08/12
For personal use only.

tions since it was also shown (8) that these compounds (putative fullerene isomers) were thermally converted to the corresponding stable fullerenes, with a half-life of about 1 h at 111°C (boiling toluene). The problem of converting relatively involatile and thermally labile analytes, in a condensed phase, into gaseous ions suitable for analysis by a mass spectrometer, is well known. Approaches include strategies whereby the analytes are pre-ionized in solution, and these analyte-derived ions are then transferred into the gas phase by mechanisms incorporating the effects of strong electric fields; the related techniques of electrospray and ionspray ionization (9–18) fall into this category. This approach will not be easily applicable to fullerenes and related compounds, although van Berkel *et al.* (19, 20) recently demonstrated ingenious methods whereby polycyclic aromatic hydrocarbons (PAHs) are ionized in solution via charge-transfer complex formation with appropriate electron acceptors or via electrochemical oxidation. A different approach was adopted in the LC–MS analysis of the flame-generated fullerenes (8). This approach exploits the fact that the equilibrium vapour pressure of a microscopic droplet, containing just a few molecules, can be many times greater than that of the same substance in the macroscopic bulk phase. This phenomenon reflects the much smaller binding forces exerted by its neighbours on a molecule in the surface layer of a microscopic droplet. While successful exploitation of this physical effect clearly requires that the analyte be somewhat volatile, it has proved effective for a wide variety of chemical compound types including polycyclic aromatic compounds (21) as well as the fullerenes of interest here (8). Briefly, the analyte solution (e.g., the effluent from an LC column) is nebulized at atmospheric pressure to form sub-micron sized droplets. When this is achieved in a pneumatic nebulizer surrounded by a heated tube, the solvent is rapidly evaporated from the droplets via interactions with the warm (100°C or so) gas, leaving behind extremely small particles of analyte. Remaining concerns (8), about identification of the thermally metastable compounds in the flame soot as C_{60} and C_{70} isomers, are centered on the question of whether the volatilization process was sufficiently mild and did not cause decomposition of unspecified labile adducts of the corresponding fullerenes. We believe that the subsequent ionization of the volatilized analytes (see below) was sufficiently soft that fragmentation of the gas-phase ions did not occur.

Soft-ionization of the volatilized analytes was achieved (8, 21) by atmospheric pressure chemical ionization (APCI) in a plasma sustained by a cold cathode discharge. In the absence of any other precautions, the dominant mechanism for formation of positive ions under these experimental conditions is proton transfer from protonated water clusters (21). However, it was found to be advantageous (8, 21), for the analytes of interest here, to separately introduce benzene at a controlled rate into the APCI source. In this way the dominant ionization mechanism for the fullerenes in positive-ion mode was found (8) to involve electron transfer to the $C_6H_6^{+\cdot}$ ions that dominated the APCI plasma. However, some degree of ionization via proton transfer from water clusters was also apparent (8). This competition between the two ionization mechanisms was even more apparent in the case of PAHs, for which the relative contributions of the two mechanisms were found (21) to reflect the trends in the ionization energies and proton affinities of the PAHs; protonation becomes relatively more important as PAH size increases. In negative-ion mode the benzene was omitted, and ionization mechanisms involved all of electron capture, proton abstraction (by OH^- and other anions present in the APCI plasma), and attachment of chloride ion derived from the dichloromethane used as one of the LC mobile phase components.

In the present work, additional details of the experimental arrangement are described. The power of the method is then illustrated by results obtained for minor constituents of the flame-generated material described previously (7, 8), and by comparable results obtained for extracts of two commercially available fullerene soots prepared by resistive heating of graphite in inert atmosphere (2–5 and footnote 3).

Experimental

Materials

The flame-generated soots and condensates were extracted with toluene at room temperature using low-power ultrasonic agitation (7). These solutions were the same as those characterized previously (7, 8). Samples of soot produced by resistive heating of graphite (2–5 and footnote 3), and of a purified extract of such a soot, containing C_{60} plus a few per cent of the C_{70} fullerene, were obtained from the Texas Fullerenes Corp. (TFC), Houston, Texas. A different soot was obtained separately from Materials and Electrochemical Research (MER) Corporation, Tucson, Arizona. Soot extracts were prepared by treatment with toluene, as described previously (7).

LC with UV–VIS spectroscopy

The column used was 25 cm long × 2.1 mm i.d., with Vydac 201TP C_{18} packing. The initial solvent was 100% acetonitrile for 5 min, then programmed linearly to 100% dichloromethane over 45 min, held for 5 min, then programmed back to initial composition over 5 min. The mobile phase flow rate was 0.2 mL/min, with an injection volume of 5 μL. A HP1090M liquid chromatograph (Hewlett Packard Co., Palo Alto, Calif.), equipped with a ternary DR5 solvent delivery system, a built-in HP1040A diode array detector, and a HP7994A data system, was used in all LC–UV–VIS analyses. As previously (8), the detector was configured for continuous full UV–VIS spectral acquisition (integrated over 220–600 nm) as well as for acquisition at 254 ± 2 nm.

LC with on-line mass spectrometry

The LC conditions were identical to those used in the LC–UV–VIS analyses. The LC–MS experiments employing APCI were conducted using an API III triple quadrupole instrument (SCIEX, Thornhill, Ontario), equipped with a heated pneumatic nebulizer interface (SCIEX). The pneumatic nebulizer is contained within a concentric quartz heating tube; itself located within the room temperature APCI source; the indicating thermocouple is located on the exterior surface of this heating tube, together with the heating element. Experiments conducted previously (8) on this nebulizer interface mounted on the bench but under conditions otherwise identical to those used in the LC–MS analyses, with a second thermocouple used to probe the gas temperatures within the interface, showed that the maximum temperatures experienced by the analytes under the conditions used fell in the range 80–100°C; estimates of analyte residence time in the warm gas indicate (8) a maximum of 5 s. A schematic illustration of the SCIEX heated nebulizer interface, as modified for the present work to permit post-column doping of the gas in the APCI source, is shown in Fig. 1. Medical quality air was normally used as the nebulizing gas, but was replaced by high-purity nitrogen for a few experiments; high-purity nitrogen was always used for the counter-current gas flow (the "gas curtain").

The APCI plasma was sustained by a cold corona discharge

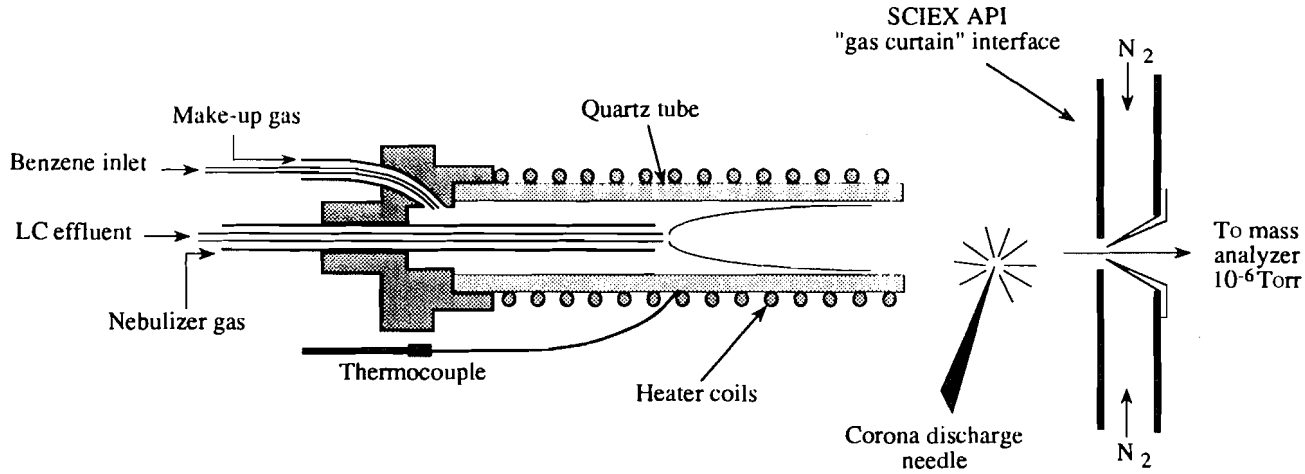

FIG. 1. Schematic illustration (not to scale) of modified heated pneumatic nebulizer interface used for LC–MS in conjunction with an APCI source. The microscopic droplets and particles of analyte are swept into the APCI plasma by the combined action of the nebulizer gas and make-up gas flows.

Can. J. Chem. Downloaded from www.nrcresearchpress.com by 109.225.110.28 on 09/08/12
For personal use only.

(stainless steel needle maintained at 3 kV). Introduction of 20 μL/min of benzene, as illustrated in Fig. 1, ensured that the dominant positive reactant ions in the plasma were $C_6H_6^{+\cdot}$, together with some water cluster ions from residual water in the system. Characterization of this APCI plasma in the absence of analytes also showed a significant population of benzene-derived ions at m/z 91, presumably $C_7H_7^+$ ions of tropylium structure. The benzene was not added when operating in negative-ion mode.

In preliminary survey experiments the mass spectrometer was usually scanned over a range m/z 600–1200, with a scan cycle time of 2 s. Having thus established the mass ranges of interest, improved signal/noise ratios could be achieved by scanning the quadrupole mass spectrometer in a piecemeal fashion, e.g., from m/z 1070 to 1090, then from m/z 1120 to 1140, in order to properly characterize the higher carbon clusters C_{90} and C_{94}. However, all of the other constituents described below could be characterized, with adequate ion statistics, in the full-scan mode (m/z 600–1200).

Mass spectrometric analyses of purified samples, without on-line HPLC, were obtained by flow-injection of a solution of the analyte into an acetonitrile–dichloromethane mobile phase with a composition and flow rate characteristic of conditions about halfway through an HPLC run, as specified above.

Results and discussion

A comparison of LC–UV–VIS chromatograms of extracts of three different fullerene materials is shown in Fig. 2. To exhibit the minor components, the intensity axes have been magnified so that LC peaks corresponding to the major components are well off-scale. The labelling of the major LC peaks in Fig. 2 is the same as that used previously (7, 8); peaks I and II were shown (8) to correspond to the stable C_{60} and C_{70} fullerenes, respectively, while peaks B and C are the compounds that have thus far behaved exactly as would be expected for thermally metastable C_{60} and C_{70} isomers (8). Peaks A and D were shown (8) to correspond to $C_{60}O$ and to C_{84}, respectively. The minor peaks labelled with Arabic numerals are those for which some information regarding the chemical nature of the eluting compounds could be obtained. The chemical identities of some of these compounds, e.g., those eluting after peak D in Fig. 2*c*, could not be satisfactorily determined due to a substantial degree of coelution of these high-mass compounds, and these peaks are therefore not numbered. To facilitate the discussion, Table 1 lists the annotated LC peaks together with their relative retention times and chemical identifications.

Major components: carbon clusters and their monoxides, and PAHs

As noted previously (7, 8) the flame-generated material is clearly very different from the two materials produced by resistive heating of graphite. The two extracts of graphite-derived soots (Fig. 2*a* and 2*b*) are very similar to one another with respect to their contents of C_{60} and C_{70} fullerenes (Peaks I and II), but show noticeable differences in the minor constituents.

Previously (8) it was shown that the flame-generated material contained significant proportions (0.5–1%) of the higher carbon clusters C_{76} and C_{84} (the former corresponding to peaks 10 and 11, and the latter to peak D). Figure 3 illustrates the dynamic range of the present LC–MS methodology in positive-ion mode, by comparing the reconstructed ion chromatograms (RICs) for m/z 720 and 840 (C_{60} and C_{70}, Figs. 3*a* and 3*c*) with those for even larger clusters C_{90} and C_{94} (m/z 1080 and 1128, Figs. 3*e* and 3*f*). Assuming equal LC–MS response factors for all of these carbon clusters, the data presented in Fig. 3 indicate that several chromatographically distinct forms of each of C_{90} and C_{94} are present in the extract of the flame-generated material (7), at levels 0.1% and 0.03% of those of the C_{60} clusters. The demonstrated dynamic range of 10^4, using piecemeal mass scanning (*not* selected ion monitoring, see experimental section), owes a great deal to the high molecular weights of the target analytes since there is almost no chemical noise in this mass range. It is worth noting that the same heat treatment (in boiling toluene under argon), which caused (8) conversion of peaks B and C (the putative metastable C_{60} and C_{70} isomers) to their stable fullerene counterparts (peaks I and II), also led to conversion of the early-eluting isomers of C_{76}, C_{90}, and C_{94} to later-eluting forms (data not shown). By way of contrast, the same heat treatment had almost no perceptible effect on the RIC for m/z 1008 ($C_{84}^{+\cdot}$) (8).

At m/z values above 700, the most important components in the flame-generated material, other than the carbon

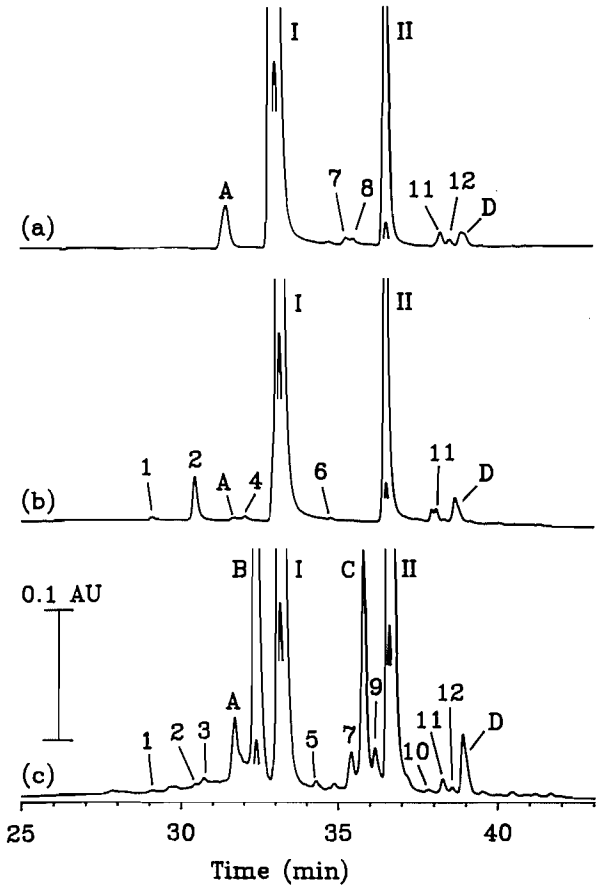

FIG. 2. LC–UV chromatograms (254 nm) of toluene extracts of fullerene-rich materials. The labelling of the LC peaks I and II (C_{60} and C_{70} fullerenes, respectively), and of peaks A–D, corresponds to that used previously (7, 8). Other annotations correspond to those in Table 1. In each case the complete chromatogram shown is a 10× expansion (vertical scale) of the chromatogram with all peaks on scale (shown as partial inserts for the major components). LC conditions are described in the text. (a) Graphite-derived soot, TFC, Houston. (b) Graphite-derived soot, MER, Tucson. (c) Flame-generated material (7, 8).

clusters themselves, were the monoxides (8). The complex RICs for *m/z* 736 and 856, corresponding to $C_{60}O^{+\cdot}$ and $C_{70}O^{+\cdot}$, respectively, are shown in Figs. 3*b* and 3*d*. The relevance of these complex chromatograms, as circumstantial evidence supporting the identification of peaks B and C as metastable isomers of the fullerenes, was discussed previously (8). Those peaks in the RICs for *m/z* 736 (Fig. 3*b*) and 856 (Fig. 3*d*), which apparently coelute with C_{60} and C_{70} compounds, were shown (8) to be APCI artifacts arising from oxidation of the carbon clusters in the APCI plasma. Replacement of air by high-purity nitrogen as the nebulizing gas resulted in a reduction of these oxide artifact peaks (annotated with asterisks in the appropriate figures) to negligible intensities, confirming previous observations (8) (see also discussion of Fig. 7, below).

At lower *m/z* values, and at elution times less than about 20 min, intense signals were observed in the chromatograms of the flame-generated material. Examples of these RICs are shown in Fig. 4, in the *m/z* range characteristic of PAHs. These RICs were computed to include the *m/z* values for both the molecular ions $M^{+\cdot}$ and the protonated molecules $(M + H)^+$, since it was shown previously (21) that both of these ionized forms are produced from PAHs under the present APCI conditions. The structures drawn in Fig. 4 are intended only to illustrate possible candidates for the compounds detected. At present no definite identifications of these PAHs have been made. Most of these constituents are present at apparently high levels relative to that of C_{60} (Fig. 4*g*), although it seems likely that the LC–MS response factors for these low-molecular weight components should be appreciably greater than for the large carbon clusters in view of their relative vapour pressures. At any rate, it is clear that formation of fullerenes and related compounds in the controlled flame (7) is accompanied by formation of large quantities of PAHs. It is worth noting here that the extracts of the two graphite-derived soots contained no detectable quantities of PAHs. The general increase in mass spectrometric background (chemical noise) at lower molecular weights can be seen in the RICs presented in Fig. 4. The increase in this background signal with increasing retention time reflects the gradient in mobile phase composition.

Each of the extracts of the two graphite-derived soots yielded evidence for fullerene monoxides. The appropriate evidence for the extract of the TFC soot is shown in Fig. 5. The RIC for *m/z* 736 (Fig. 5*b*, attributed to $C_{60}O^{+\cdot}$) shows an APCI artifact at the retention time for peak I (C_{60} fullerene). In addition to this artifact peak, only one other LC peak is observed in Fig. 5*b* (Peak A, Fig. 2) for *m/z* 736; this is in accord with expectations (8) based upon a unique monoxide structure for the fully symmetrical C_{60} fullerene (all carbon atoms equivalent). Recent work (22) has shown that an epoxide structure may be assigned to this unique monoxide of C_{60} fullerene. As emphasized previously (8), the flame-generated sample contains both the C_{60} fullerene plus the compound (peak B, Fig. 3*a*) postulated to be a necessarily less symmetrical isomer, and correspondingly also contains (Fig. 3*b*) several chromatographically distinguishable $C_{60}O$ isomers including peak A attributable to the fullerene monoxide (22). Similarly, the graphite-derived soot extract contains only the stable C_{70} fullerene (peak II, Fig. 5*c*) and correspondingly many fewer $C_{70}O$ isomers (Fig. 5*d*) than observed for the flame-generated material, which is known (8) to contain several forms of C_{70} including peak C (the putative metastable isomer) and the fullerene (peak II, Figs. 2 and 3*c*). The analytical results (not shown) for the other graphite-derived soot (obtained from MER) were similar to those shown in Fig. 5 except that the LC–MS peak A in the RIC for *m/z* 736, presumed to be due to the $C_{60}O$ monoxide, was only some 0.3% of the intensity of that of peak I (C_{60}) as compared with 6–7% in the case of the TFC soot extract (Fig. 5). The same trend was true of the RIC for $C_{70}O$ (*m/z* 856), i.e., the MER soot extract gave barely detectable signals for the monoxides, while that from the TFC soot (Fig. 5*d*) indicated the presence of at least two isomers. This suggests either that the soot obtained from MER was formed in a more reducing environment than that from TFC, or that the TFC soot had been exposed to light and air resulting in photo-oxidation (22, 23). This difference between the two graphite-derived soots will be referred to below. Small amounts of C_{76} and C_{84} were found in the extracts of both graphite-derived soots (Figs. 5*e* and 5*f*), as well as trace quantities of C_{90} (*m/z* 1080) and C_{94} (*m/z* 1128).

It was also of interest to analyse the solution of purified

Can. J. Chem. Downloaded from www.nrcresearchpress.com by 109.225.110.28 on 09/08/12
For personal use only.

TABLE 1. LC peak annotations, relative retention times (RRT), chemical identifications, relative molecular masses, and relative abundances estimated from positive-ion APCI LC-MS peak areas.

				Relative Levels		
Peak	**RRT**	**Compound(s)**	**Rel.mol.mass**	**Flame**	**TFC**	**MER**
I	1.000	C_{60} fullerene	720	100	100	100
II	1.105	C_{70} fullerene	840	20	8.0	9.5
A	0.956	$C_{60}O$ ($C_{60}.CH_4$)	736 (736)	10 (?)	6.4(ND)	(ND)(0.25)
B	0.978	C_{60} isomer	720	61	ND	ND
C	1.085	C_{70} isomer	840	7.0	ND	ND
D	1.174	C_{84} (2 isomers)	1008	0.65	0.26	0.46
1	0.878	$C_{60}H_4$	724	0.13	ND	0.32
2	0.921	$C_{60}H_2$	722	0.38	ND	5.0
3	0.931	$C_{60}(CH_4)_2$*	752	?	ND	ND
4	0.968	$C_{60}(C_7H_6)$*	810	?	ND	?
5	1.038	$C_{70}O$	856	0.88	ND	ND
6	1.052	$C_{70}H_2$	842	<0.1	<0.1	0.24
7	1.069	$C_{70}O$	856	1.8	0.66	ND
8	1.073	$C_{70}O$	856	1.0	0.58	ND
9	1.094	C_{70} isomer	840	2.8	ND	ND
10	1.128	C_{76}	912	0.51	ND	ND
11	1.154	C_{76}	912	0.99	0.78	0.72
12	1.163	C_{78}*	936	?	?	?
13	1.194	C_{90}	1080	0.02	ND	ND
14	1.225	C_{90}	1080	0.1	0.04	0.05
15	1.231	C_{90}	1080	0.05	<0.04	<0.05
16	1.234	C_{94}	1128	0.03	ND	ND
17	1.246	C_{94}	1128	0.03	ND	ND
18	1.257	C_{94}	1128	0.03	<0.02	<0.02

? Abundance could not be estimated from LC-MS data; usually detected only in negative ion mode.
* Tentative identification only.
ND, Not Detected.

C_{60} fullerene supplied by the Texas Fullerenes Corp. Figure 6*a* shows that the RIC for m/z 720 contains several small peaks with elution times shorter than that of C_{60} fullerene (peak I). One of these peaks has the same retention time (32 min) as peak B (Figs. 2*c* and 3*a*), and thus suggests the presence in this preparation of about 1% of the same putative metastable C_{60} isomer as was reported (8) in the flame-generated material. It is of interest that peak B was not observable in our own toluene extract of the TFC soot; this could reflect enrichment of the more soluble isomer (earlier retention time) during the TFC clean-up procedure used to prepare the fullerene solution, or possibly a different thermal history. Previous analyses of graphite-derived soots failed to observe peaks B and C due partly to the presumed low primary yields of these unstable compounds under the extreme conditions of the electrical discharge, and partly to the thermal conditions (boiling toluene for extended periods) used in most extraction procedures and which have been shown (8) to induce conversion of the putative isomers to the more stable fullerenes. The less intense peaks in the RIC for m/z 720 (Fig. 6*a* insert, peak annotated with #), at even earlier elution times, correspond to $C_{60}^{+\cdot}$ fragment ions of $C_{60}O^{+\cdot}$

Can. J. Chem. Downloaded from www.nrcresearchpress.com by 109.225.110.28 on 09/08/12
For personal use only.

Can. J. Chem. Downloaded from www.nrcresearchpress.com by 109.225.110.28 on 09/08/12
For personal use only.

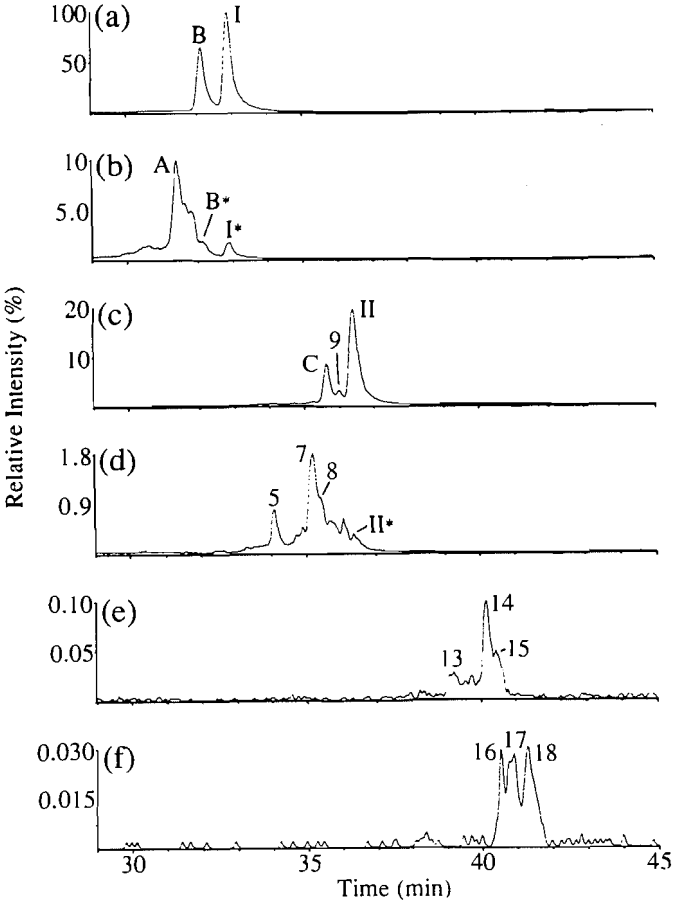

FIG. 3. Reconstructed ion chromatograms (RICs) from LC–MS analyses of a toluene extract of a fullerene-rich material generated by a controlled flame (7). Chromatographic conditions as described for Fig. 2. LC–MS coupling was by the heated pneumatic nebulizer interface (Fig. 1), and ionization was at atmospheric pressure and room temperature using electron transfer to $C_6H_6^{+\cdot}$ formed in a cold corona discharge (see text). Labelling of LC peaks is the same as in Fig. 2. Note the relative intensities of the various RICs. Peaks marked with asterisks in (*b*) and (*d*) are artifacts arising from oxidation of carbon clusters in the APCI:plasma. (*a*) *m/z* 720 ($C_{60}^{+\cdot}$); (*b*) *m/z* 736 ($C_{60}O^{+\cdot}$); (*c*) *m/z* 840 ($C_{70}^{+\cdot}$); (*d*) *m/z* 856 ($C_{70}O^{+\cdot}$); (*e*) *m/z* 1080 ($C_{90}^{+\cdot}$); (*f*) *m/z* 1128 ($C_{94}^{+\cdot}$).

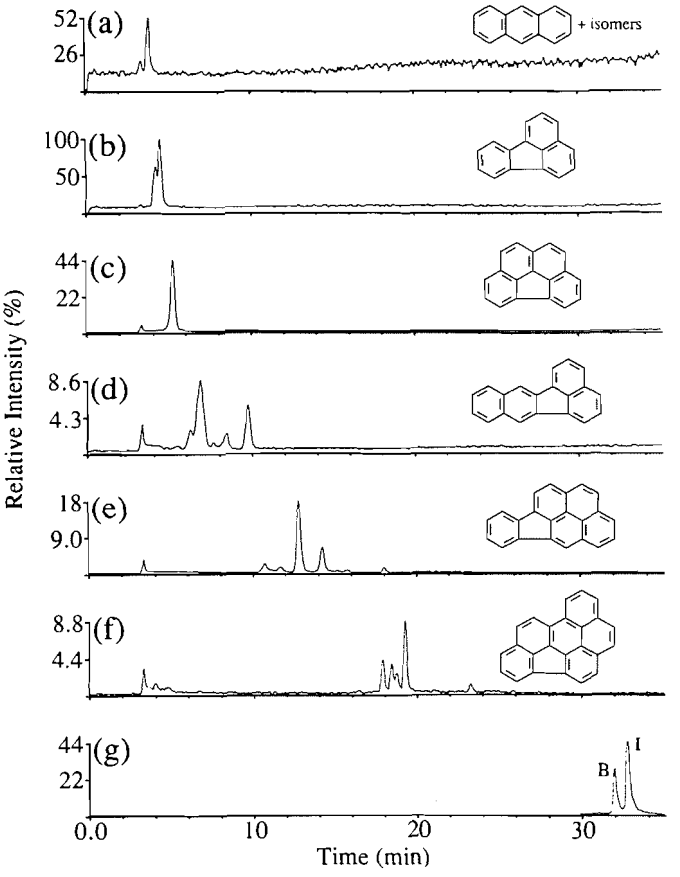

FIG. 4. RICs from LC–MS analyses of a toluene extract of a fullerene-rich material generated by a controlled flame (7). Chromatographic conditions as described for Fig. 2. LC–MS coupling was by the heated pneumatic nebulizer interface (Fig. 1), and ionization was at atmospheric pressure and room temperature using electron transfer to $C_6H_6^{+\cdot}$ formed in a cold corona discharge (see text). The structures shown are representative of the PAHs that possess the molecular masses detected in each case. Note the relative intensities of the various RICs: (*a*) *m/z* 178 plus 179; (*b*) *m/z* 202 plus 203; (*c*) *m/z* 226 plus 227; (*d*) *m/z* 252 plus 253; (*e*) *m/z* 276 plus 277; (*f*) *m/z* 300 plus 301; (*g*) *m/z* 720 plus 721 (C_{60} ions, for comparison of intensities). The t_0 is at 3.2 min, and can be observed in some of the RICs.

formed in the atmospheric pressure – vacuum interface region of the APCI mass spectrometer; this fragmentation reaction has been demonstrated previously (23) to occur at collision energies of a few tens of an electron volt. Comparison of Figs. 5*a*, 5*b*, and 5*c* with Fig. 6 shows that the purification procedure, used to obtain the commercial (TFC) purified solution, enriched $C_{60}O$ relative to C_{60}, but discriminated against C_{70}.

Minor components

The extract of the graphite-derived soot supplied by MER showed interesting differences from that of the TFC soot, other than the monoxide content discussed above. Mass spectra (Figs. 7*b* and 7*c*), acquired at retention times earlier than those of the corresponding fullerene, suggested the presence of $C_{60}H_2$ (peak 2) and of $C_{60}H_4$ (peak 1) at levels approximately 5% and 0.3%, respectively, of that of C_{60}. These constituents are well resolved chromatographically from peak I (C_{60}) and from each other. The patterns of mass peaks down to *m/z* 720 (Figs. 7*b* and 7*c*) are thus due to fragmentations induced in the APCI interface region, rather than to superimposed mass spectra of co-eluting $C_{60}H_2$ and $C_{60}H_4$ compounds. In the case where $C_{60}H_2$ was the dominant trace constituent (Fig. 7*b*), the $C_7H_7^+$ adduct ion was clearly observed at *m/z* 813 (compare the analogous adduct ion of C_{60} at *m/z* 811 in Fig. 7*a*).

Use of air as the nebulizing gas invariably resulted in greater sensitivity than use of high-purity nitrogen or argon, and for this reason air was used in most of the experiments reported here. This sensitivity effect was undoubtedly related to changes in the composition of the APCI plasma, which also resulted in marked changes in the APCI artifacts discussed above. These artifacts consisted of monoxides when air was present (see Fig. 3), but when air was excluded as far as possible the APCI artifacts changed from 16 Da adducts to 14 Da adducts; Fig. 7*a* exemplifies this general observation, in that *m/z* 734 now appears to replace *m/z* 736

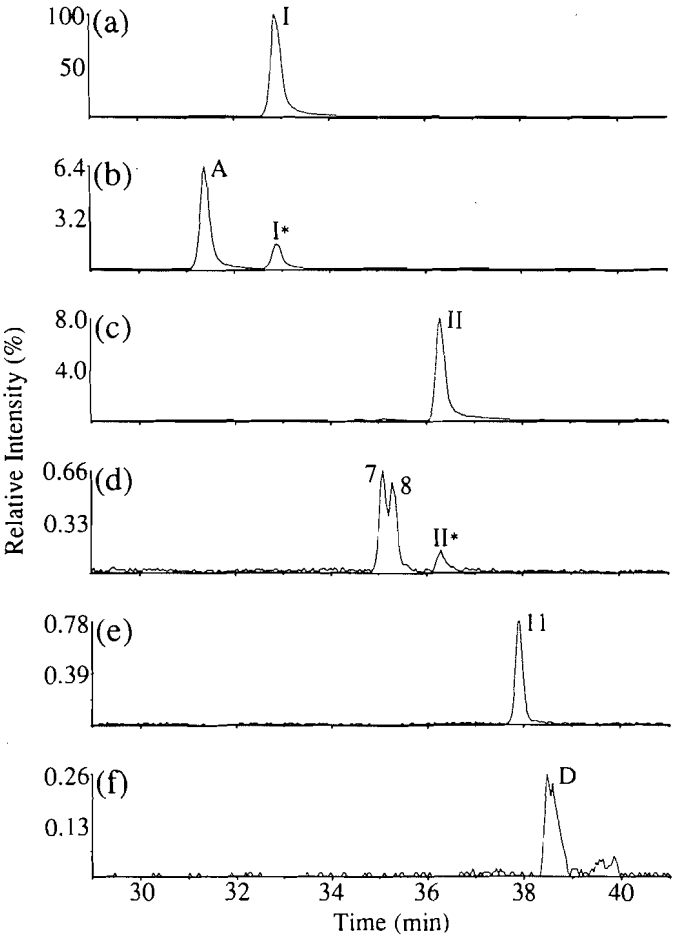

FIG. 5. RICs from LC–MS analyses of a toluene extract of a fullerene-rich material generated by resistive heating of graphite in an inert atmosphere (TFC). LC–MS conditions were identical to those used to obtain Fig. 4. Labelling of LC peaks is the same as in Fig. 2. Note the relative intensities of the various RICs. Peaks marked with asterisks in (*b*) and (*d*) are artifacts arising from oxidation of carbon clusters in the APCI plasma. (*a*) *m/z* 720 ($C_{60}^{+\cdot}$); (*b*) *m/z* 736 ($C_{60}O^{+\cdot}$); (*c*) *m/z* 840 ($C_{70}^{+\cdot}$); (*d*) *m/z* 856 ($C_{70}O^{+\cdot}$); (*e*) *m/z* 912 ($C_{76}^{+\cdot}$); (*f*) *m/z* 1008 ($C_{84}^{+\cdot}$).

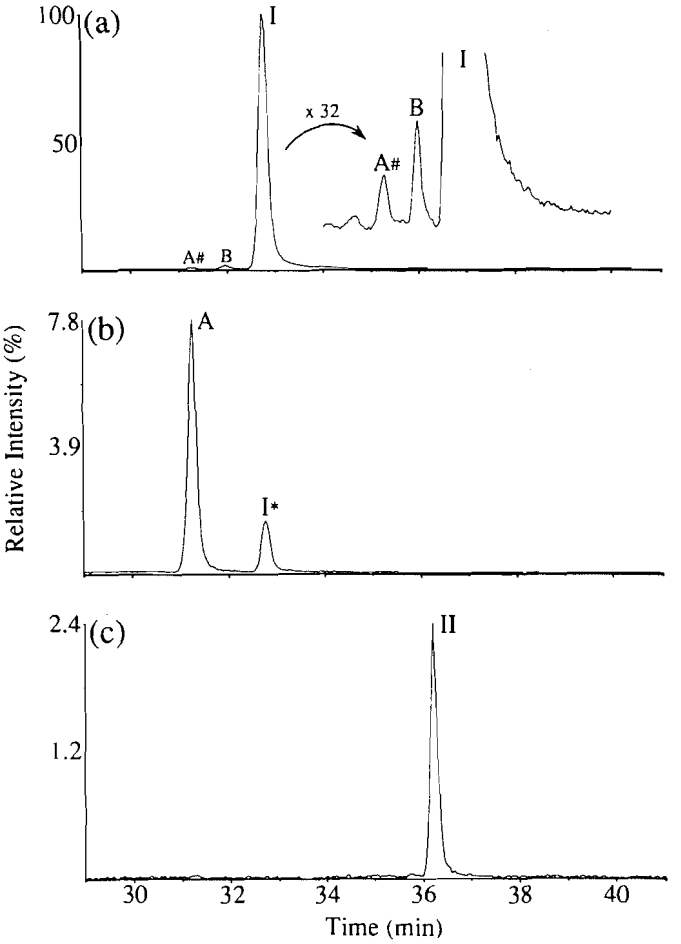

FIG. 6. RICs from LC–MS analyses of a commercial C_{60} solution (TFC) derived from a fullerene-rich material generated by resistive heating of graphite in an inert atmosphere. LC–MS conditions were identical to those used to obtain Fig. 4. Labelling of LC peaks is the same as in Fig. 2. Note the relative intensities of the various RICs. The peak marked with an asterisk in (*b*) is an artifact arising from oxidation of C_{60} in the APCI plasma, and that marked # in the insert in (*a*) is due to $C_{60}^{+\cdot}$ fragment ions formed by collision-induced dissociation of $C_{60}O^{+\cdot}$. (*a*) *m/z* 720 ($C_{60}^{+\cdot}$); (*b*) *m/z* 736 ($C_{60}O^{+\cdot}$); (*c*) *m/z* 840 ($C_{70}^{+\cdot}$).

in the spectrum of peak I. Attempts to establish that the APCI artifact at *m/z* 734 (Fig. 7*a*) had composition $C_{61}H_2^{+\cdot}$ (possibly the methylene adduct observed previously (23)), through flow-injection experiments on the purified fullerene extract obtained from TFC using perdeuterated versions of the mobile phase components (acetonitrile and dichloromethane) and of the benzene, yielded inconclusive results. The same was true of a corresponding experiment in which only the acetonitrile was replaced by its ^{15}N version, to investigate whether this minor component was $C_{60}N^{+\cdot}$, an ion for which some evidence has been presented previously (24). Interferences from other constituents in the sample were the cause of the ambiguity of the results obtained in both isotopic substitution experiments. Unfortunately use of the isotopically substituted mobile phases, in the corresponding experiments using LC–MS instead of flow-injection MS, was prohibitively expensive.

$C_{70}H_2$ was also observed (Fig. 7*d*) at extremely low levels, chromatographically well resolved (peak 6) from peak II (C_{70} fullerene). These hydrogenated carbon clusters were not detectable in the graphite-derived soot from TFC, supporting the above proposal that the MER material was produced in more reducing conditions than that from TFC. Possibly the graphite starting materials were significantly different. These hydrogenated forms were also observed, however, in the LC–MS analysis of the flame-generated material (Table 1).

The results described thus far are all derived from the positive-ion LC–MS data. The complementary negative-ion data did provide new insights. Figure 8 shows selected negative-ion mass spectra obtained by LC–MS analysis of the MER soot extract. The spectra in Fig. 8 should be compared to the corresponding positive-ion spectra for the same extract shown in Fig. 7. Figure 8*a* is similar to those shown previously (8) for LC peaks B and I in the LC–MS analysis of the flame-generated material; ionization of C_{60} by electron attachment (*m/z* 720) and by chloride attachment (*m/z* 755 and 757) are of comparable efficiencies. The fact that peaks B and I yield mass spectra indistinguishable from one

Can. J. Chem. Downloaded from www.nrcresearchpress.com by 109.225.110.28 on 09/08/12
For personal use only.

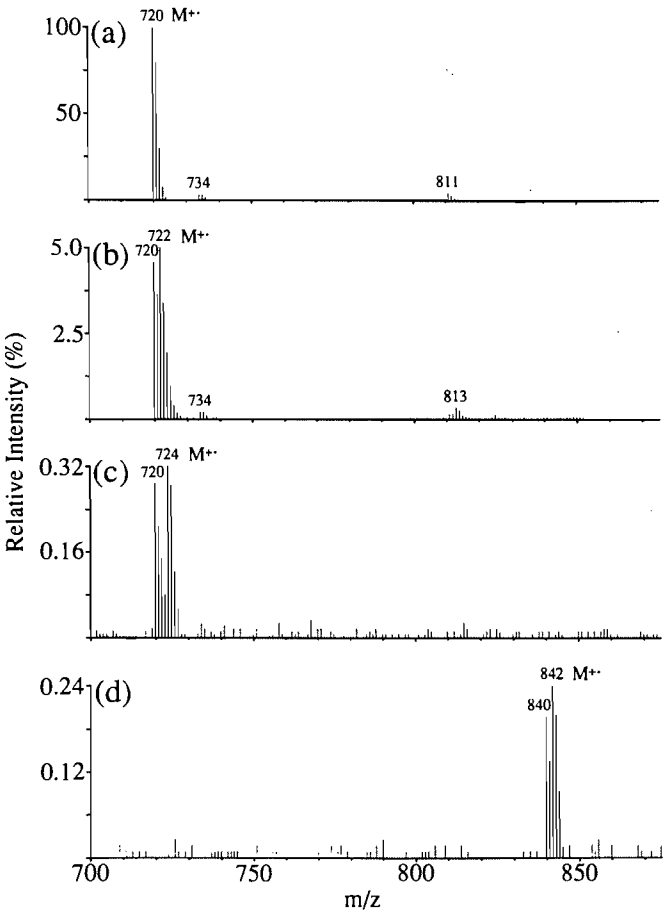

FIG. 7. Positive-ion mass spectra obtained during LC–MS analysis of the toluene extract of the graphite-derived soot from MER. LC–MS conditions were identical to those used to obtain Fig. 4, except that nitrogen replaced air as the nebulizing gas. (*a*) Spectrum acquired at the crest of peak I (C_{60} fullerene). (*b*) Spectrum acquired at the crest of peak 2 ($C_{60}H_2$). (*c*) Spectrum acquired at the crest of peak 1 ($C_{60}H_4$). (*d*) Spectrum acquired at the crest of peak 6 ($C_{70}H_2$).

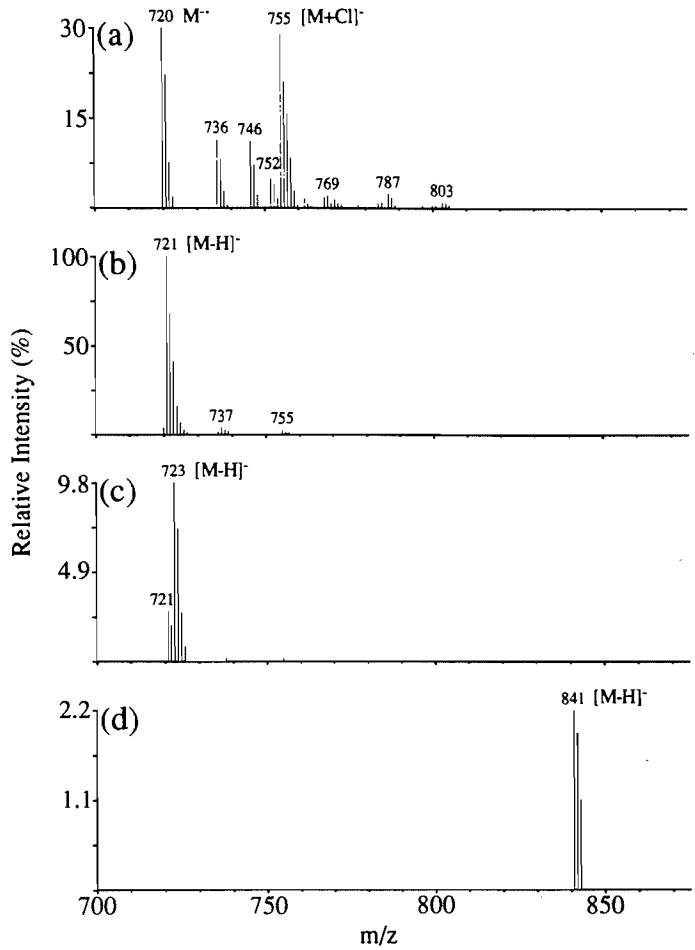

FIG. 8. Negative-ion mass spectra obtained during LC–MS analysis of the toluene extract of the graphite-derived soot from MER. LC–MS conditions were identical to those used to obtain Fig. 4, except that the post-column addition of benzene was omitted and negative ions were monitored. (*a*) Spectrum acquired at the crest of peak I (C_{60} fullerene). (*b*) Spectrum acquired at the crest of peak 2 ($C_{60}H_2$). (*c*) Spectrum acquired at the crest of peak 1 ($C_{60}H_4$). (*d*) Spectrum acquired at the crest of peak 6 ($C_{70}H_2$).

another in both positive- and negative-ion modes is strong evidence supporting the view (see Introduction) that, if peak B is *not* a C_{60} isomer, decomposition to C_{60} must have occurred prior to ionization in the APCI source. The corresponding negative-ion spectrum (not shown) for C_{70} (peak II) indicates that chloride attachment was about three times more efficient than electron attachment in this case. The ions at m/z 736 and 752 in Fig. 8*a* had greatly reduced relative intensities when high-purity nitrogen replaced air as the nebulizing gas (data not shown). This intensity dependence supports the interpretation of m/z 736 and 752 in Fig. 8*a* as being due to electron attachment ionization of $C_{60}O$ and $C_{60}O_2$ species formed as APCI artifacts. The electron capture efficiencies of these oxygenated species are expected to be higher than that of the parent C_{60} compound. The identity of the ion at m/z 746 could not be determined. Use of perdeuterated mobile phase components in flow-injection experiments again yielded disappointingly ambiguous results, and the corresponding LC–MS experiment, while desirable, was prohibitively expensive.

The hydrogenated species $C_{60}H_2$ (peak 2 and Fig. 8*b*) and $C_{60}H_4$ (peak 1 and Fig. 8*c*) appear to be efficiently ionized via proton abstraction to yield $C_{60}H^-$ and $C_{60}H_3^-$ ions at m/z 721 and 723. Note in Figs. 8*b* and 8*c* the reduced tendency of these anions to lose hydrogen atoms, compared with that of the corresponding cations (Figs. 7*b* and 7*c*). Identification of peak 5 as $C_{70}H_2$ (Table 1 and Fig. 7*d*) is based upon the negative-ion spectrum in Fig. 8*d*; the evidence for $C_{70}H^-$, derived from $C_{70}H_2$ by proton abstraction, is reasonably clearcut in Fig. 8*d* although this spectrum was obtained near the ion statistical limit.

The real surprise in the negative-ion data concerned the mass spectra acquired over LC peak A, thus far attributed solely to $C_{60}O$. While no direct evidence for this assignment was previously available (8), the only conceivable alternative ($C_{60} \cdot CH_4$) seemed much less appealing to chemical intuition. Nonetheless, the negative-ion spectra shown in Fig. 9 strongly suggest that both $C_{60}O$ and ($C_{60} \cdot CH_4$) can contribute to the signals at m/z 736 in the positive-ion spectra. The negative-ion spectrum in Fig. 9*a*, obtained for the graphite-derived soot from TFC, is consistent with ionization of $C_{60}O$ by competing electron-attachment and chloride-attachment mechanisms. In contrast, the corresponding

Can. J. Chem. Downloaded from www.nrcresearchpress.com by 109.225.110.28 on 09/08/12
For personal use only.

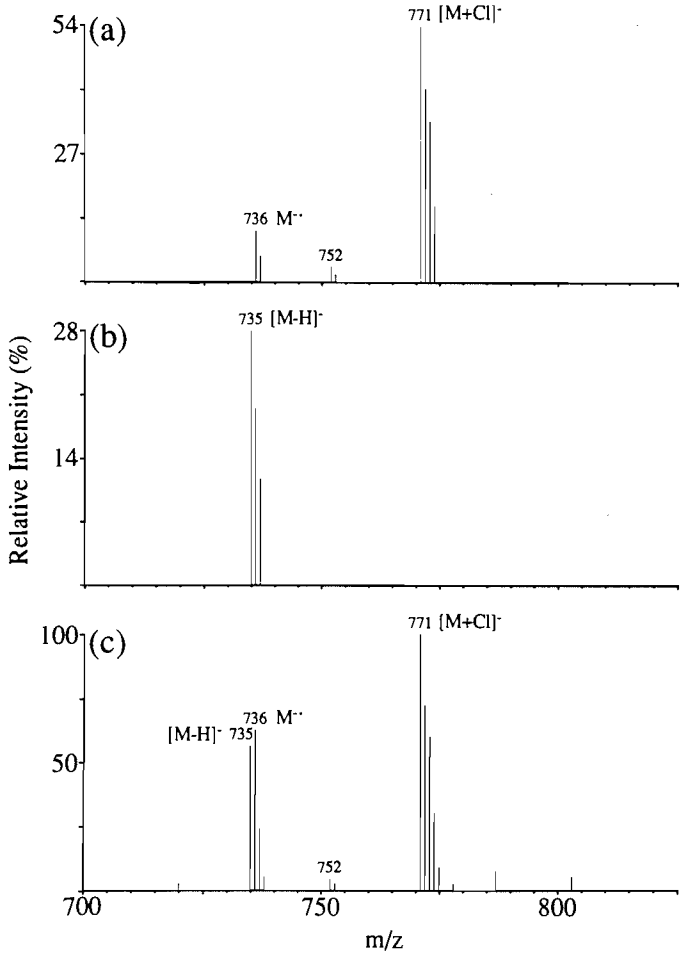

FIG. 9. Negative-ion mass spectra obtained during LC–MS analysis of the toluene extract of three fullerene-rich materials. LC–MS conditions were identical to those used to obtain Fig. 4, except that the post-column addition of benzene was omitted and negative ions were monitored. Spectra were acquired at the crests of LC peak A in each case. The relative intensities of the three spectra are not meaningful in this case. (*a*) Extract of graphite-derived soot from TFC. (*b*) Extract of graphite-derived soot from MER. (*c*) Extract of flame-generated material (8).

spectrum (Fig. 9*b*) for the graphite-derived soot from MER is precisely that which would be predicted for $(C_{60} \cdot CH_4)$ ionized via proton abstraction (e.g., by OH^-) to give a $C_{61}H_3^-$ anion with *no* observable $(M + Cl)^-$ ion. This difference between the two graphite-derived soots is again consistent with the suggestion that the material supplied by MER was produced in an atmosphere containing traces of hydrogen. It is interesting that the corresponding negative-ion mass spectrum for the flame-generated material (Fig. 9*c*) indicates significant quantities of both $C_{60}O$ (via m/z 736 and 771) and $(C_{60} \cdot CH_4)$ (m/z 735); the relative response factors are entirely unknown, and are quite possibly wildly different under these negative-ion conditions, so no definite conclusions concerning relative amounts can be drawn. However, comparison of the RIC for m/z 771 (negative-ion characteristic of Cl^- adduct of $C_{60}O$) with that shown in Fig. 3*b* (and previously (8)) for m/z 736 in the positive-ion analysis of the same flame-generated material, showed that the two traces were almost superimposable. On the other hand, the RIC for m/z 735 ($(M - H)^-$ ion characteristic of $C_{60} \cdot CH_4$) showed only a single peak co-eluting with peak A in the positive-ion RIC for m/z 736. These comparisons suggest that the CH_4 adduct was probably a minor constituent relative to the monoxides; ionization efficiencies of these compounds in positive-ion mode (electron transfer to $C_6H_6^{+\cdot}$) are not expected to differ wildly from one another, unlike those in negative ion mode (e.g., $C_{60}H_2^{+\cdot}$ at m/z 722 in Fig. 7*b* is only some 5% as intense as $C_{60}^{+\cdot}$ at m/z 720 in Fig. 7*a*, but the intensity of the corresponding $C_{60}H^{-\cdot}$ anion in Fig. 8*b* is three times as intense as $C_{60}^{-\cdot}$ at m/z 720 in Fig. 8*a*).

The nature of the $C_{60} \cdot CH_4$ complex is possibly analogous to that of the $C_{60}H_2$ species. It is possible to imagine the latter as being formed by a free-radical mechanism whereby two hydrogen atoms add successively across a C=C double bond. By analogy the $C_{60} \cdot CH_4$ complex could be formed by successive additions of a hydrogen atom and a methyl radical, and would thus be better described as $[C_{60}(H)(CH_3)]$. An alternative structure, described as $[C_{60}(CH_2)(H_2)]$, would correspond to a hydrogenated version of the methylene adduct of C_{60} (isoelectronic with $C_{60}O$) described previously (23); additions of monophenyl carbene (compare peak 4, Table 1), and of diphenylcarbene, to C_{60} have been characterized (25, 26). It is of interest that the flame-generated material also contained extremely low levels of a large number of constituents that appear to correspond to adducts of C_{60} and C_{70} with aliphatic molecules; these constituents were observed in the negative-ion LC–MS data as the corresponding anions formed by proton abstraction.

Finally, in view of the high ionization efficiency of the oxygenated fullerenes in negative-ion mode, a brief study of the photo-oxidation of the purified fullerene extract from TFC was conducted. Figure 10 shows selected mass spectra acquired, at well-resolved retention times, in the LC–MS analysis of an aliquot of this commercially purified solution, following exposure to daylight and air at room temperature for several weeks. The spectrum (not shown) acquired at the crest of peak I (C_{60}) was indistinguishable from that acquired prior to exposure (compare Fig. 8*a*). The same is true of the spectrum (Fig. 10*a*) acquired at the crest of peak A ($C_{60}O$, compare Fig. 9*a*). However, weak but well-resolved LC peaks corresponding to $C_{60}O_2$ and to $C_{60}O_3$ were observed in the exposed solution, but not in the original. Figures 10*b* and 10*c* show the mass spectra acquired at the crests of these LC peaks; that for $C_{60}O_3$ was obtained near the ion statistical limit, so the relative abundances of the isotopic variants are not in good agreement with predicted values. Comparison of these spectra suggests, interestingly, that electron attachment becomes progressively less competitive relative to chloride attachment as the degree of oxygenation increases. This trend cannot be accounted for by the different concentrations of dichloromethane in the mobile phase (and thus in the APCI reagent gas), since in fact the more highly oxygenated species eluted first. The RIC for m/z 736 ($C_{60}O^{-\cdot}$) showed only peak A in addition to the APCI artifact coincident with peak I, similar to Fig. 6*b* for this unexposed purified fullerene solution. However, the RIC for m/z 752 ($C_{60}O_2^{-\cdot}$, not shown) clearly indicated that two chromatographically distinguishable isomers were present, while that for m/z 768 ($C_{60}O_3^{-\cdot}$) demonstrated the presence of at least three isomers.

Estimate of absolute LC–MS sensitivity

The sensitivity of the LC–MS technique used here was estimated by calculating the concentration of the C_{60} fuller-

Can. J. Chem. Downloaded from www.nrcresearchpress.com by 109.225.110.28 on 09/08/12
For personal use only.

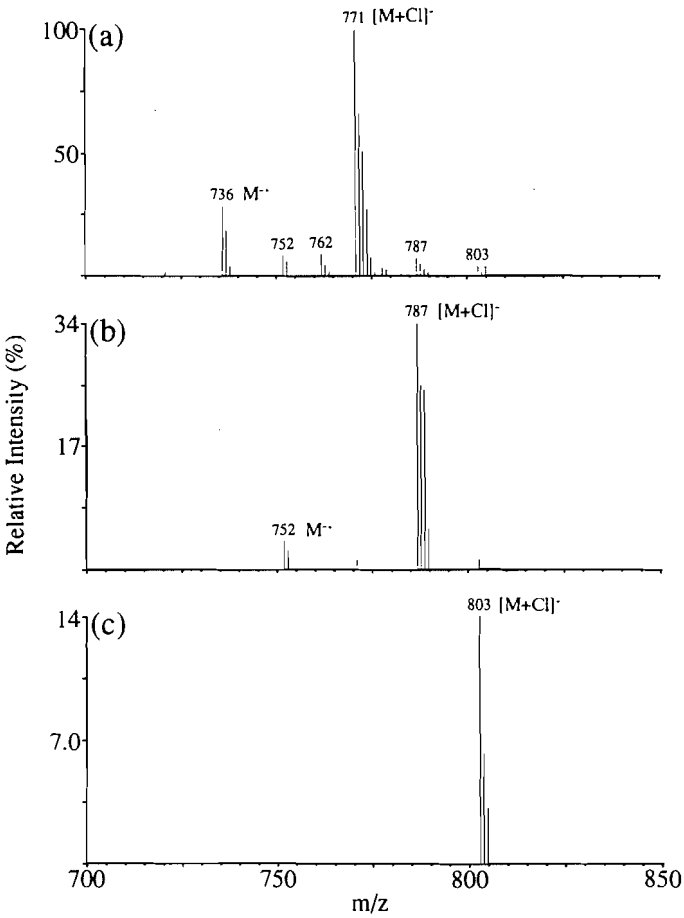

FIG. 10. Negative-ion mass spectra obtained during LC–MS analysis of the purified C_{60} solution prepared (TFC) from a graphite-derived soot, following prolonged exposure to light and air. LC–MS conditions were identical to those used to obtain Fig. 4, except that the post-column addition of benzene was omitted and negative ions were monitored. Spectra were acquired at the crests of the indicated LC peaks: (*a*) peak A ($C_{60}O$); (*b*) most intense peak in RICs for both m/z 752 (e^- attachment) and 787 (Cl^- attachment to $C_{60}O_2$); (*c*) most intense peak in RICs for both m/z 803 and 805 (Cl^- attachment to $C_{60}O_3$).

ene in the extracts analysed here by LC–UV. A value of the extinction coefficient at 257 nm is available (27), and this permitted an estimate of 500 ng as the amount of C_{60} fullerene injected on-column in the LC–MS experiment summarized in Figs. 3 and 4. This in turn implies that the quantity of C_{94} detected in Fig. 3*f* was less than 1 ng, assuming equal LC–MS response factors in positive-ion mode. In fact the volatilization efficiency within the heated nebulizer interface is likely to decrease with increasing size of the carbon clusters, so that the estimate of the amount of C_{94} is likely to be a lower limit.

Conclusions

It would be interesting to correlate the differences between the two commercially available graphite-derived soots, elucidated in the present work via analyses of the minor components, with details of their preparation. It is not surprising that the flame-generated material (7) is strikingly different from the other two, however. The presence in the flame-generated material of large quantities of polycyclic aromatic hydrocarbons, which were unobservable in the graphite-derived soots, reflects the different gaseous atmospheres under which compounds are formed in these two systems. This difference may lead to different mechanisms for control of formation of fullerenes, as might also be suggested by the discovery (7, 8) in the flame-generated material of large proportions of thermally labile compounds (peaks B and C), which revert to the C_{60} and C_{70} fullerenes on heating. The present work has added no further evidence for or against the proposal (8) that these thermally metastable compounds might be isomers of the C_{60} and C_{70} fullerenes, but has confirmed the conclusion that, if they are instead unstable adducts of some kind, dissociation to the fullerenes must have occurred *after* chromatographic separation but *before* ionization. Additional experiments designed to elucidate this problem are in progress.

The susceptibility of the fullerenes to form oxides upon photo-oxidation was confirmed here and shown to lead to mono-, di-, and tri-oxides of C_{60}. The presence of $C_{60} \cdot CH_4$ in some of these materials was masked by that of $C_{60}O$, and was revealed only through comparison of negative- and positive-ion mass spectra. It is probable that only a small amount of $C_{60} \cdot CH_4$, relative to that of $C_{60}O$, is present in the flame-generated material. This finding thus leaves unchanged the previous discussion (8) of the different multiplicities of the $C_{60}O$ isomers observed in the flame-generated material and in the TFC soot; this difference was presented (8) as circumstantial evidence supporting the tentative identification of peak B as a less symmetrical isomer of C_{60}.

The present work also illustrates the greatly superior power of the combined on-line LC–MS technique, relative to that of the two techniques applied separately. The LC–UV chromatograms of Fig. 2 clearly indicate that differences exist between the three solutions analysed, but the information content of the chromatograms and UV spectra (not shown) is very limited. Similarly, attempts to use mass spectrometry without pre-separation by HPLC failed to yield the desired information in the perdeuteration experiments conducted here, due to the obscuring effects of other more abundant constituents in the mixture.

Extension of the present technique, to other fractions of flame-derived materials, is in progress.

Acknowledgements

The authors thank Dr. J. Fetzer, Chevron Oil Co., for the gift of the graphite-derived soot supplied by Materials and Electrochemical Research Corporation. The combustion research was supported by the Division of Chemical Sciences, Office of Basic Energy Research, US Department of Energy under Grant No. DE-FG02-84ER13282. The M.I.T. Center for Environmental Health Sciences is supported by National Institute of Environmental Health Sciences Center Grant EHS-5P30-ES02109-10. The analytical work forms part of the Marine Analytical Chemistry Standards Program of the National Research Council of Canada. J.F.A. thanks the Natural Sciences and Engineering Research Council of Canada and Dalhousie University for graduate scholarships.

1. H. W. Kroto, J. R. Heath, S. C. O'Brien, R. F. Curl, and R. E. Smalley. Nature, **318**, 162 (1985).
2. W. Krätschmer, L. D. Lamb, K. Fostiropoulos, and D. R. Huffmann. Nature, **347**, 354 (1990).
3. R. Taylor, J. P. Hare, A. K. Abdul-Sada, and H. W. Kroto. J. Chem. Soc. Chem. Commun. 1423 (1990).

Can. J. Chem. Downloaded from www.nrcresearchpress.com by 109.225.110.28 on 09/08/12
For personal use only.

4. H. Ajie, M. M. Alvarez, S. J. Anj, R. D. Beck, F. Diederich, K. Fostiropoulos, D. R. Huffman, W. Krätschmer, Y. Rubin, K. E. Schriver, D. Sensharma, and R. L. Whetten. J. Phys. Chem. **94**, 8630 (1990).
5. R. E. Haufler, J. Conceicao, L. P. F. Chibante, Y. Chai, N. E. Byrne, S. Flanagan, M. M. Haley, S. C. O'Brien, C. Pan, Z. Xiao, W. E. Billups, M. A. Ciufolini, R. H. Hauge, J. L. Margrave, L. J. Wilson, R. F. Curl, and R. E. Smalley. J. Phys. Chem. **94**, 8634 (1990).
6. J. F. Stoddart. Angew. Chem. Int. Ed. Engl. **30**, 70 (1991); F. Diederich and R. L. Whetten. Angew. Chem. Int. Ed. Engl. **30**, 678 (1991).
7. J. B. Howard, J. T. McKinnon, Y. Makarovsky, A. L. Lafleur, and M. E. Johnson. Nature, **352**, 139 (1991).
8. J. F. Anacleto, H. Perreault, R. K. Boyd, S. Pleasance, M. A. Quilliam, P. G. Sim, J. B. Howard, Y. Makarovsky, and A. L. Lafleur. Rapid Commun. Mass Spectrom. **6**, 214 (1992).
9. J. V. Iribarne and B. A. Thomson. J. Chem. Phys. **64**, 2287 (1976).
10. B. A. Thomson, J. V. Iribarne, and P. Dziedzic. Anal. Chem. **54**, 2219 (1982).
11. M. L. Alexandrov, L. N. Gall, N. V. Krasnov, V. I. Nikolaev, V. A. Pavlenko, and V. A. Shkuzov. Dokl. Akad. Nauk SSR, **277**, 379 (1984).
12. C. M. Whitehouse, R. M. Dreyer, M. Yamashita, and J. B. Fenn. Anal. Chem. **57**, 675 (1985).
13. A. P. Bruins, T. R. Covey, and J. D. Henion. Anal. Chem. **59**, 2642 (1987).
14. G. Schmelzeisen-Redeker, L. Bütfering, and F. W. Röllgen. Int. J. Mass Spectrom. Ion Processes, **90**, 189 (1989).
15. J. A. Loo, H. R. Udseth, and R. D. Smith. Anal. Biochem. **179**, 404 (1989).
16. R. D. Smith, J. A. Loo, C. G. Edmonds, C. J. Barinaga, and H. R. Udseth. Anal. Chem. **62**, 882 (1990).
17. S. K. Chowdhury and B. T. Chait. Anal. Chem. **63**, 1660 (1991).
18. M. G. Ikonomou, A. T. Blades, and P. Kebarle. Anal. Chem. **63**, 1989 (1991).
19. G. J. Van Berkel, S. A. McLuckey, and G. L. Glish. Anal. Chem. **63**, 2064 (1991).
20. G. J. Van Berkel, S. A. McLuckey, and G. L. Glish. Anal. Chem. In press.
21. J. F. Anacleto, L. Ramaley, R. K. Boyd, S. Pleasance, M. A. Quilliam, P. G. Sim, and F. M. Benoit. Rapid Commun. Mass Spectrom. **5**, 149 (1991).
22. K. M. Creegan, J. L. Robbins, W. K. Robbins, J. M. Millar, R. D. Sherwood, P. J. Tindall, and D. M. Cox. J. Am. Chem. Soc. **114**, 1103 (1992).
23. J. M. Wood, B. Kahr, S. H. Hoke II, L. Dejarme, R. G. Cooks, and D. Ben-Amotz. J. Am. Chem. Soc. **113**, 5907 (1991).
24. T. Pradeep, V. Vijayakakrishnan, A. K. Santra, and C. N. R. Rao. J. Phys. Chem. **95**, 10564 (1991).
25. T. Suzuki, Q. Li, K. C. Khemani, F. Wudl, and O. Almarsson. Science, **254**, 1186 (1991).
26. F. Wudl. Acc. Chem. Res. **25**, 157 (1992).
27. J. P. Hare, H. W. Kroto, and R. Taylor. Chem. Phys. Lett. **177**, 394 (1991).

Can. J. Chem. Downloaded from www.nrcresearchpress.com by 109.225.110.28 on 09/08/12
For personal use only.

Second nearest-neighbor interactions in ternary regular solutions

MEGURU NAGAMORI
Centre de recherches minérales, Quebec Government, 2700 Einstein, Ste-Foy, Quebec, Canada G1P 3W8

Received January 21, 1992

MEGURU NAGAMORI. Can. J. Chem. **70**, 2569 (1992).

The concept of classical regular solutions has been expanded by considering both first and second nearest-neighbor interactions between randomly distributed molecules. While the present model requires an ideal entropy of mixing, as does the classic regularity model, its heat of mixing is expressed by a more flexible equation which attributes the second-order terms of the Margules formalism to first nearest-neighbor interactions, and the third-order terms to second nearest-neighbor interactions. The activity–composition relations have been expressed by a single equation of the grand partition function, which converges to that of the classical regularity with decreasing contributions from second nearest-neighbor molecules.

MEGURU NAGAMORI. Can J. Chem. **70**, 2569 (1992).

Le concept des solutions régulières classiques a été élargi en prenant en compte les interactions entre les paires moléculaires, non seulement les plus proches mais aussi les seconds plus proches, dans l'ensemble aléatoirement distribué. Bien que le présent modèle exige une entropie idéale de mélange, comme dans le modèle de régularité classique, l'enthalpie de mélange prend une expression qui attribue les termes de deuxième ordre de l'équation de Margules aux interactions moléculaires des plus proches voisins, et les termes de troisième ordre à celles des seconds plus proches voisins. La relation entre l'activité et la composition chimique a été exprimée par une grande fonction de partition, laquelle converge vers l'expression de la régularité classique à mesure que les contributions des seconds plus proches voisins diminuent.

Can. J. Chem. Downloaded from www.nrcresearchpress.com by 109.225.110.28 on 09/08/12
For personal use only.

1. Introduction

Despite the advent of many more sophisticated models, the classical regular solution model (regularity) is still in widest use for approximating organic, metallic, slag, and other solutions. In terms of statistical thermodynamics, the regularity is based on the configurational entropy of a random distribution of equal-sized spherical molecules (atoms) as well as on the internal energy of mixing of nearest-neighbor (nn) interactions (1, 2). Some attempts were made (3, 4) to improve the regularity model by including the contributions of second nn interaction energies as well. However, these models have not been put to practical use, because the obtained formulae were too complicated even for simple binary solutions.

The present note describes a novel method for counting first and second nn interactions, while remaining loyal to the classical regularity concept, yet dealing primarily with ternary and multicomponent solutions.

2. Configurational and vibrational complexions

Let us assume a ternary regular substitutional solution consisting of N_1 atoms (or molecules) of species 1, N_2 atoms of species 2, and N_3 atoms of species 3, which are randomly distributed over the lattice sites. The total number of complexions Ω for such a crystal may be expressed by the product of configurational and vibrational contributions (5): viz.

$$[1] \qquad \Omega = \frac{(N_1 + N_2 + N_3)!}{N_1!\, N_2!\, N_3!}\, q_1^{N_1}\, q_2^{N_2}\, q_3^{N_3}$$

where q_i refers to the vibrational partition function of an atom (or molecule) i, which remains unchanged in both pure solids and ternary mixtures in accordance with Neumann–Kopp's law.

3. Vectorial quartering of the second nn interactions

Let us consider, as an example, a face-centered cubic (fcc) solid solution whose lattice constants remain unchanged with varying composition. With respect to the central atom O, there are 12 first nn (or $z = 12$) and six second nn (or $s = 6$) atoms, as shown in Fig. 1. An atom in the second nn shell, say the atom X, has 4 nn atoms on the inner shell, or the atoms A, E, D, and J. Since the distance between the atoms O and X is 1.414 times the unit distance OA, the interaction energy between the second nn pair OX is 1/8 of that of the first nn pair OA, provided the interaction energy is inversely proportional to the sixth power of the distance of separation r (Lennard–Jones potential).

To take into account the interference of the second nn interaction (vector OX) by four window-forming atoms (A, E, D, and J) in the first nn shell, let us divide the vector OX into four equal portions and allocate a quarter each in the directions of OA, OE, OD, and OJ. Being of the same length in opposite direction, the vectors PQ and PR cancel out on the plane AOD, as shown in Fig. 1. A similar cancellation occurs on the plane EOJ as well.

4. Partial blockage of second nn interaction by first nn atoms

Let us single out the three atoms that are situated in the sites O, A, and X, and designate them by i, j, and k, respectively. By virtue of the vectorial quartering, the forces interacting between the atoms i, j, and k can be looked upon as being one-dimensional. The bond energy pertaining to an alignment ijk (called aligned energy E_{ijk}) may then be approximated as a sum of two interaction energy terms representing the atomic pairs i–j and i–k. It is convenient to first define both of the pairwise interaction energies, E_{ij} and E_{ik}, at a unit distance of $r = 1$, and then modify only the second nn pairwise energy E_{ik} by a multiplier compensating for a farther distance ($r > 1$) and the blockage effect of an intervening atom j. Under these conventions and the assumption of random distribution, the aligned atoms i, j, and k can now be either of species 1 or 2 or 3, independently.

The author tried and abandoned several different ideas for counting the second nn interaction energy before settling on the present method. The abandoned counting methods led to

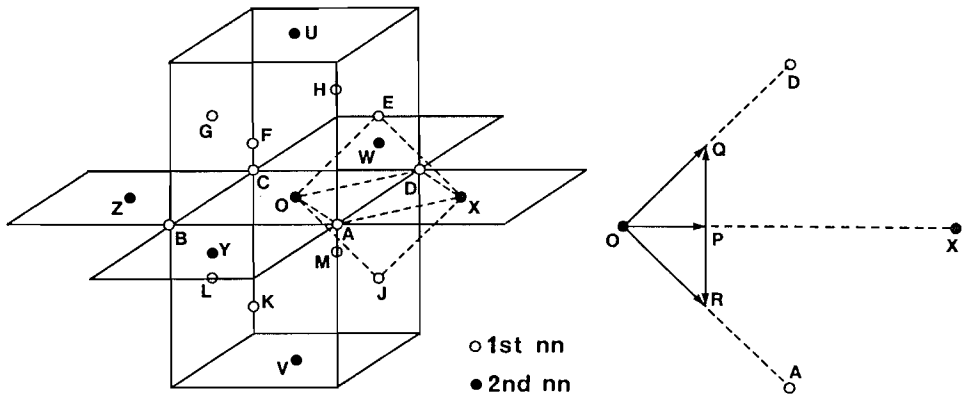

FIG. 1. The fcc structure and vectorial quartering.

complicated mathematical expressions of little practical merit. A simple expression for internal energy came about when the counting was made based on the following assumption: The force exerted upon the central atom i by a second nn atom k from the direction of OA is partially blocked by an intervening first nn atom j, and the extent of the blockage is a characteristic proper to the intervening atom j. The degree of such a partial blockage by an atom j, b_j, may be defined to range between 0 and 1; viz.

$$[2] \quad 0 < b_j < 1$$

It is to be noted that the classical regular solutions can be described as a limiting case where second nn interactions are totally blocked by the first nn shell, or $b_j = 1$.

The effects of the degree of blockage b_j and the distance r can be put together to define a new parameter f_j, which is named the permeation constant of atom j. If the potential energy beyond the first nn shell is proportional to r^{-6} in a fcc crystal, for example, its permeation constant f_j is expressed as

$$[3] \quad f_j = (1 - b_j)r^{-6} = (1 - b_j)/8$$

The interaction energy between the central atom i and the second nn atom k in an alignment ijk can then be given by $f_jE_{ik}/4$, where the coefficient 1/4 comes from the vectorial quartering.

As for the first nn interaction energy due to the atomic pair i–j, the same counting method as has been used in the traditional regularity theory is adopted here. Hence, only one half of the pairwise energy, or $E_{ij}/2$, is allocated to an alignment ijk, because the bond OA is counted twice as OAX and OAY, Fig. 1. Accordingly, the aligned energy E_{ijk} may be expressed by the following sum of first and second nn pairwise interaction energies:

$$[4] \quad E_{ijk} = 0.5(E_{ij}/2 + f_jE_{ik}/4) = E_{ij}/4 + f_jE_{ik}/8$$

where the coefficient 0.5 is to compensate for double counting of first nn (j) and second nn atoms (k) as central ones (i). The two pairwise components of an aligned energy E_{ijk} are shown schematically in Fig. 2.

5. Probability in random distribution

In a fcc regular crystal consisting of randomly distributed N_t ($=N_1 + N_2 + N_3$) atoms, the probability P_{ijk} of finding an atom i at the central site O, an atom j at the first nn site A, and an atom k at the second nn site X is given by

$$[5] \quad P_{ijk} = (N_i/N_t)\,(N_j/N_t)\,(N_k/N_t)$$

The number N_{ijk} of an alignment ijk over the sites OAX is given by the product of the total number of atoms N_t and the probability of occurrence P_{ijk}; viz.

$$[6] \quad N_{ijk} = N_t P_{ijk} = N_iN_jN_k/N_t^2$$

Each alignment ijk possesses an energy E_{ijk} as given by eq. [4]. Over the sites OAX, there are 27 possible different alignments ijk, as shown in Table 1. The bond energy of an alignment ijk is obtained by adding up the 27 aligned energies multiplied by each probabilistic weight, Table 1.

6. Internal energy of mixing

About the central site O, there is a total of $4s$ (=24) alignments equivalent to OAX, Fig. 1. Consequently, the internal energy η_{123} of the ternary fcc crystal is given by $4s$ times the weighted bond energy of the alignment OAX; viz.

$$[7] \quad \eta_{123} = 4s \Sigma (N_{ijk} E_{ijk})$$

For a fcc crystal of species 1 consisting of N_1 atoms, the internal energy, η_1, can be expressed by summing up the number of independent alignments 111, or $4sN_1$, times its aligned energy E_{111}; viz.

$$[8] \quad \eta_1 = 4s\,N_1(E_{11}/4 + f_1E_{11}/8)$$

Likewise, for pure fcc crystals of species 2 and 3 consisting of N_2 and N_3 atoms, respectively, we have

$$[9] \quad \eta_2 = 4s\,N_2(E_{22}/4 + f_2E_{22}/8)$$

$$[10] \quad \eta_3 = 4s\,N_3(E_{33}/4 + f_3E_{33}/8)$$

The internal energy of mixing ΔE can be given by the difference in internal energy before and after the mixing; viz.

$$[11] \quad \Delta E = \eta_{123} - \eta_1 - \eta_2 - \eta_3$$

The so-calculated expression of ΔE is shown in Table 2, where $z = 12$ and $s = 6$ for fcc crystals. The present solution, in which both first and second nn interactions are counted by using vectorial quartering, is called here the biregularity model, and the parameter e_{123} given by eq. [2.8] is named the biregular constant.

The internal energy of mixing for a biregular mixed crystal comprising 6×10^{23} ($=N_t$) atoms can be obtained by rewriting eq. [2.1], Table 2, as follows:

Can. J. Chem. Downloaded from www.nrcresearchpress.com by 109.225.110.28 on 09/08/12
For personal use only.

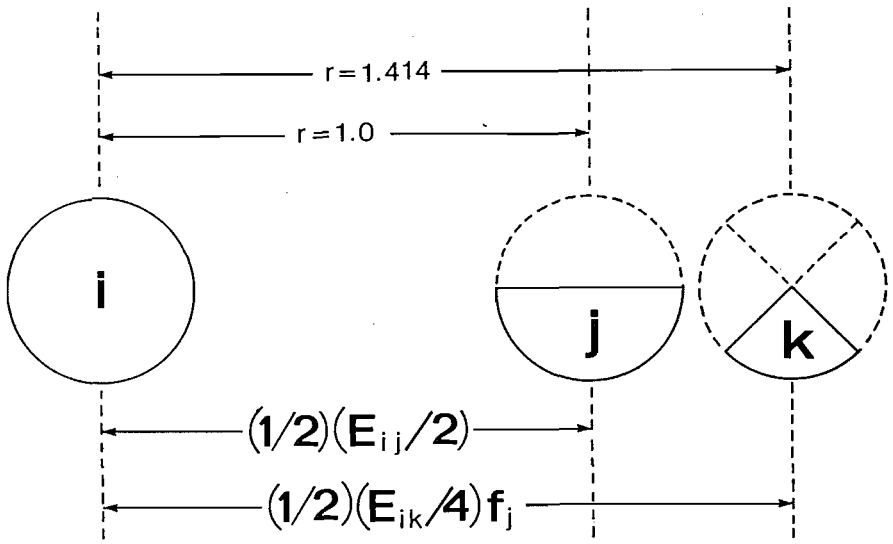

FIG 2. Aligned energy E_{ijk} in fcc structure. The symbols i, j, and k refer to the central, first nn, and second nn atoms.

TABLE 1. Number of possible alignments OAX and corresponding aligned energies in fcc ternary regular solutions

Aligned atoms			Total site number		Probability of site occupation				Aligned energy E_{ijk}
i	j	k			O	A	X		
1	1	1	N_t	×	(N_1/N_t)	(N_1/N_t)	(N_1/N_t)	×	$(E_{11}/4 + f_1 E_{11}/8)$
		2	N_t	×	(N_1/N_t)	(N_1/N_t)	(N_2/N_t)	×	$(E_{11}/4 + f_1 E_{12}/8)$
		3	N_t	×	(N_1/N_t)	(N_1/N_t)	(N_3/N_t)	×	$(E_{11}/4 + f_1 E_{31}/8)$
	2	1	N_t	×	(N_1/N_t)	(N_2/N_t)	(N_1/N_t)	×	$(E_{12}/4 + f_2 E_{11}/8)$
		2	N_t	×	(N_1/N_t)	(N_2/N_t)	(N_2/N_t)	×	$(E_{12}/4 + f_2 E_{12}/8)$
		3	N_t	×	(N_1/N_t)	(N_2/N_t)	(N_3/N_t)	×	$(E_{12}/4 + f_2 E_{31}/8)$
	3	1	N_t	×	(N_1/N_t)	(N_3/N_t)	(N_1/N_t)	×	$(E_{31}/4 + f_3 E_{11}/8)$
		2	N_t	×	(N_1/N_t)	(N_3/N_t)	(N_2/N_t)	×	$(E_{31}/4 + f_3 E_{12}/8)$
		3	N_t	×	(N_1/N_t)	(N_3/N_t)	(N_3/N_t)	×	$(E_{31}/4 + f_3 E_{31}/8)$
2	1	1	N_t	×	(N_2/N_t)	(N_1/N_t)	(N_1/N_t)	×	$(E_{12}/4 + f_1 E_{12}/8)$
		2	N_t	×	(N_2/N_t)	(N_1/N_t)	(N_2/N_t)	×	$(E_{12}/4 + f_1 E_{22}/8)$
		3	N_t	×	(N_2/N_t)	(N_1/N_t)	(N_3/N_t)	×	$(E_{12}/4 + f_1 E_{23}/8)$
	2	1	N_t	×	(N_2/N_t)	(N_2/N_t)	(N_1/N_t)	×	$(E_{22}/4 + f_2 E_{12}/8)$
		2	N_t	×	(N_2/N_t)	(N_2/N_t)	(N_2/N_t)	×	$(E_{22}/4 + f_2 E_{22}/8)$
		3	N_t	×	(N_2/N_t)	(N_2/N_t)	(N_3/N_t)	×	$(E_{22}/4 + f_2 E_{23}/8)$
	3	1	N_t	×	(N_2/N_t)	(N_3/N_t)	(N_1/N_t)	×	$(E_{23}/4 + f_3 E_{12}/8)$
		2	N_t	×	(N_2/N_t)	(N_3/N_t)	(N_2/N_t)	×	$(E_{23}/4 + f_3 E_{22}/8)$
		3	N_t	×	(N_2/N_t)	(N_3/N_t)	(N_3/N_t)	×	$(E_{23}/4 + f_3 E_{23}/8)$
3	1	1	N_t	×	(N_3/N_t)	(N_1/N_t)	(N_1/N_t)	×	$(E_{31}/4 + f_1 E_{31}/8)$
		2	N_t	×	(N_3/N_t)	(N_1/N_t)	(N_2/N_t)	×	$(E_{31}/4 + f_1 E_{23}/8)$
		3	N_t	×	(N_3/N_t)	(N_1/N_t)	(N_3/N_t)	×	$(E_{31}/4 + f_1 E_{33}/8)$
	2	1	N_t	×	(N_3/N_t)	(N_2/N_t)	(N_1/N_t)	×	$(E_{23}/4 + f_2 E_{31}/8)$
		2	N_t	×	(N_3/N_t)	(N_2/N_t)	(N_2/N_t)	×	$(E_{23}/4 + f_2 E_{23}/8)$
		3	N_t	×	(N_3/N_t)	(N_2/N_t)	(N_3/N_t)	×	$(E_{23}/4 + f_2 E_{33}/8)$
	3	1	N_t	×	(N_3/N_t)	(N_3/N_t)	(N_1/N_t)	×	$(E_{33}/4 + f_3 E_{31}/8)$
		2	N_t	×	(N_3/N_t)	(N_3/N_t)	(N_2/N_t)	×	$(E_{33}/4 + f_3 E_{23}/8)$
		3	N_t	×	(N_3/N_t)	(N_3/N_t)	(N_3/N_t)	×	$(E_{33}/4 + f_3 E_{33}/8)$

[12] $$\Delta E/N_t = x_1x_2(e_{12}x_1 + e_{21}x_2) + x_2x_3(e_{23}x_2 + e_{32}x_3) + x_3x_1(e_{31}x_3 + e_{13}x_1) + e_{123}x_1x_2x_3$$

where x_i refers to the atomic fraction of species i, or $x_i = N_i/N_t$. If volume change before and after the mixing is negligible, the internal energy ΔE becomes equal to the heat of mixing ΔH. Equation [12] can then be identified with the empirical Margules equation of the third order for the ternary heat of solution (6).

Equation [2.1] can also be derived for body-centered cubic (bcc) crystals with $z = 8$ and $s = 6$, as well as for ideal hexagonal close-packed (hcp) solids with $z = 12$ and $s = 6$. Liquids consisting of spherical molecules (atoms) of a similar size may be approximated by the coordination numbers

Can. J. Chem. Downloaded from www.nrcresearchpress.com by 109.225.110.28 on 09/08/12
For personal use only.

TABLE 2. Internal energy of mixing for ternary biregular solutions

$$\Delta E = (e_{12}N_1 + e_{21}N_2)N_1N_2/N_t^2 + (e_{23}N_2 + e_{32}N_3)N_2N_3/N_t^2 + (e_{31}N_3 + e_{13}N_1)N_3N_1/N_t^2 + e_{123}N_1N_2N_3/N_t^2 \quad [2.1]$$

where $$e_{12} = 2\left(\frac{z}{2} + f_1\frac{s}{2}\right)(E_{12} - E_{11}) + \left(\frac{z}{2} + f_2\frac{s}{2}\right)(E_{11} - E_{22}) \quad [2.2]$$

$$e_{21} = 2\left(\frac{z}{2} + f_2\frac{s}{2}\right)(E_{12} - E_{22}) + \left(\frac{z}{2} + f_1\frac{s}{2}\right)(E_{22} - E_{11}) \quad [2.3]$$

$$e_{23} = 2\left(\frac{z}{2} + f_2\frac{s}{2}\right)(E_{23} - E_{22}) + \left(\frac{z}{2} + f_3\frac{s}{2}\right)(E_{22} - E_{33}) \quad [2.4]$$

$$e_{32} = 2\left(\frac{z}{2} + f_3\frac{s}{2}\right)(E_{23} - E_{33}) + \left(\frac{z}{2} + f_2\frac{s}{2}\right)(E_{33} - E_{22}) \quad [2.5]$$

$$e_{31} = 2\left(\frac{z}{2} + f_3\frac{s}{2}\right)(E_{31} - E_{33}) + \left(\frac{z}{2} + f_1\frac{s}{2}\right)(E_{33} - E_{11}) \quad [2.6]$$

$$e_{13} = 2\left(\frac{z}{2} + f_1\frac{s}{2}\right)(E_{31} - E_{11}) + \left(\frac{z}{2} + f_3\frac{s}{2}\right)(E_{11} - E_{33}) \quad [2.7]$$

$$e_{123} = 2\left(\frac{z}{2} + f_1\frac{s}{2}\right)(E_{23} - E_{11}) + 2\left(\frac{z}{2} + f_2\frac{s}{2}\right)(E_{31} - E_{22}) + 2\left(\frac{z}{2} + f_3\frac{s}{2}\right)(E_{12} - E_{33}) \quad [2.8]$$

$z = 10$ and $s = 5$. Assuming a symmetrical distribution of molecules about the central site, the heat of mixing for such liquids can again be expressed by eq. [2.1].

7. Monoregular approximation for unknown biregular constant

As expressed by eq. [2.8], the biregular constant e_{123} contains terms involving all three species combined, such as the product $f_3(E_{12} - E_{33})$. Thus, e_{123} is a unique property of a given ternary system, and it cannot be calculated from the properties of the constituent binaries alone. Nonetheless, an approximate estimation of e_{123} may be attempted by assuming its regularity behavior; upon substituting $f_j = 0$ in eq. [2.8] only, we find

$$[13] \quad e_{123} = w_{12} + w_{23} + w_{31}$$

where

$$[14] \quad w_{mn} = z[E_{mn} - 0.5(E_{mm} + E_{nn})]$$

For a binary 1–2 solution, eq. [2.1] may be rewritten as

$$[15] \quad (\Delta E/N_t)/(x_1x_2) = e_{12}x_1 + e_{21}x_2 \equiv y$$

If the 1–2 binary is regarded as a regular solution, the value of w_{12} can be expressed by the average of y, eq. [15], over the entire 1–2 solution range; viz.

$$[16] \quad w_{12} = \int_0^1 y\, dx_2 = 0.5(e_{12} + e_{21})$$

Likewise, for the binary regular solutions of the systems 2–3 and 3–1, we have

$$[17] \quad w_{23} = 0.5(e_{23} + e_{32})$$

$$[18] \quad w_{31} = 0.5(e_{31} + e_{13})$$

Although eqs. [16], [17], and [18] are valid only for strictly regular solutions, they may be used to estimate approximately (called here monoregular approximation) an unknown value of e_{123}. Substituting them in eq. [13] yields

$$[19] \quad e_{123} = (e_{12} + e_{21} + e_{23} + e_{32} + e_{31} + e_{13})/2$$

The biregular constant e_{123} thus approximated assumes the same expression as that of Hillert (7), and it tends to provide better agreement with reality at middle concentrations than in terminal dilute solutions. The present biregular constant is slightly larger than the corresponding value given by the surrounded atom theory (7, 8), which has typically a coefficient of about $z/(3z - 1)$ as compared to $1/2$ in eq. [19].

8. Grand partition function for ternary biregular solutions

The grand partition function Ξ (GPF) can be constructed by combining the configurational and vibrational complexions Ω and the internal energy of mixing ΔE, as well as by introducing the absolute activity λ, as shown in Table 3. When a ternary biregular solution is in thermal equilibrium, the following conditions are satisfied (2, 5):

$$[20] \quad \partial \ln \Xi^0/\partial N_1 = 0; \qquad \partial \ln \Xi^0/\partial N_2 = 0; \qquad \partial \ln \Xi^0/\partial N_3 = 0$$

where Ξ^0 refers to the maximum term in the triple summation, Table 3. These partial differentiations may be carried out by using Stirling's formula $\ln N! = N \ln N - N$, and the results of such calculations are shown in Table 3.

When the Raoultian activity a_i is adopted (i.e., $a_i = 1$ for pure substance i), we find $a_i = q_i\lambda_i$. Each of the three conditions specified by eq. [20] then gives the expression for the Raoultian activity coefficient γ_i of constituent i, where $\gamma_i = a_i/x_i$ and $i = 1$, 2, or 3. When the internal energy of mixing is known for three constituent binaries, as each is expressed by a pair of e_{ij} values, together with an experimental (or monoregularly approximated) value of the biregular constant e_{123}, the Raoultian activities of all three components can be calculated from eqs. [3.3] through [3.5] for any ternary composition.

It is interesting to note that the GPF methodology entirely obliterates the Gibbs–Duhem integration, which is replaced by more straightforward partial differentiation, as given by eq. [20]. Thus, the problem of path dependence or

Can. J. Chem. Downloaded from www.nrcresearchpress.com by 109.225.110.28 on 09/08/12
For personal use only.

TABLE 3. Grand partition function of ternary biregular solutions and conditions for equilibrium

$$\Xi = \sum_{N_1}\sum_{N_2}\sum_{N_3}\frac{(N_1+N_2+N_3)!}{N_1!N_2!N_3!}\exp\left\{\frac{-1}{kT}\frac{1}{(N_1+N_2+N_3)^2}\{N_1N_2(e_{12}N_1+e_{21}N_2)+N_2N_3(e_{23}N_2+e_{32}N_3)+N_3N_1(e_{31}N_3+e_{13}N_1)\right.$$
$$\left.+e_{123}N_1N_2N_3\}\right\}(q_1\lambda_1)^{N_1}(q_2\lambda_2)^{N_2}(q_3\lambda_3)^{N_3} \quad [3.1]$$

$$\ln\Xi^0 = (N_1+N_2+N_3)\ln(N_1+N_2+N_3) - N_1\ln N_1 - N_2\ln N_2 - N_3\ln N_3 + N_1\ln(q_1\lambda_1) + N_2\ln(q_2\lambda_2) + N_3\ln(q_3\lambda_3)$$
$$-\frac{1}{kT}\frac{1}{(N_1+N_2+N_3)^2}\{N_1N_2(e_{12}N_1+e_{21}N_2)+N_2N_3(e_{23}N_2+e_{32}N_3)+N_3N_1(e_{31}N_3+e_{13}N_1)+e_{123}N_1N_2N_3\} \quad [3.2]$$

$$\frac{\partial\ln\Xi^0}{\partial N_1}=0 \quad ; \quad \ln\frac{q_1\lambda_1}{x_1}=\ln\gamma_1=-2A+x_2(D_{21}x_2+2D_{12}x_1)+x_3(D_{31}x_3+2D_{13}x_1)+D_{123}x_2x_3 \quad [3.3]$$

$$\frac{\partial\ln\Xi^0}{\partial N_2}=0 \quad ; \quad \ln\frac{q_2\lambda_2}{x_2}=\ln\gamma_2=-2A+x_3(D_{32}x_3+2D_{23}x_2)+x_1(D_{12}x_1+2D_{21}x_2)+D_{123}x_3x_1 \quad [3.4]$$

$$\frac{\partial\ln\Xi^0}{\partial N_3}=0 \quad ; \quad \ln\frac{q_3\lambda_3}{x_3}=\ln\gamma_3=-2A+x_1(D_{13}x_1+2D_{31}x_3)+x_2(D_{23}x_2+2D_{32}x_3)+D_{123}x_1x_2 \quad [3.5]$$

where $A \equiv x_1x_2(D_{12}x_1+D_{21}x_2)+x_2x_3(D_{23}x_2+D_{32}x_3)+x_3x_1(D_{31}x_3+D_{13}x_1)+D_{123}x_1x_2x_3$ [3.6]

NOTE: Ξ^0 = maximum term in Ξ; $x_i = N_i/(N_1+N_2+N_3)$; $D_{ij} = e_{ij}/kT$; $D_{123} = e_{123}/kT$; k = Boltzmann constant; T = temperature in Kelvin.

TABLE 4. Grand partition function of quaternary biregular solutions

$$\Xi = \sum_{N_1}\sum_{N_2}\sum_{N_3}\sum_{N_4}\frac{(N_1+N_2+N_3+N_4)!}{N_1!N_2!N_3!N_4!}(q_1\lambda_1)^{N_1}(q_2\lambda_2)^{N_2}(q_3\lambda_3)^{N_3}(q_4\lambda_4)^{N_4}\exp\left\{\frac{-1}{kT}\frac{1}{(N_1+N_2+N_3+N_4)^2}\right.$$
$$\times\{N_1N_2(e_{12}N_1+e_{21}N_2)+N_1N_3(e_{13}N_1+e_{31}N_3)+N_1N_4(e_{14}N_1+e_{41}N_4)+N_2N_3(e_{23}N_2+e_{32}N_3)$$
$$\left.+N_2N_4(e_{24}N_2+e_{42}N_4)+N_3N_4(e_{34}N_3+e_{43}N_4)+N_1N_2N_3e_{123}+N_1N_2N_4e_{124}+N_1N_3N_4e_{134}+N_2N_3N_4e_{234}\}\right\} \quad [4.1]$$

an arbitrary constant of integration is absent in the formulae derived based on the GPF method (2). All the thermodynamic functions of a ternary biregular solution can be derived from this sole equation of GPF, eq. [3.1].

Thermodynamically, eqs. [3.3]–[3.5] are valid for ternary solutions having an ideal entropy of mixing together with a weak intermolecular interaction. Mathematically, however, they are identical with the Margules formalism of the third order which has been used to approximate many real solutions having a non-ideal entropy of mixing. Equations [3.3]–[3.5] can be used, among others, in such applications as calculating the activity coefficients of the second and third constituents from the observed values of the first constituent, or estimating the activity coefficients at different temperatures. Biregularity can readily be applied to quaternary and multi-component solutions. As an example, the grand partition function of quaternary biregular solutions is shown in Table 4.

9. Conclusions

A solution model has been developed by taking into account the contributions of both first and second nearest-neighbor interactions, while observing faithfully the classical regularity concept. The present method of counting the second nearest-neighbor interactions did not lead to complicated mathematical relationships, differing from previous attempts, but it produced the same simple expression as the empirical Margules equation of the third order. The present biregularity model can be represented by a single equation, eq. [3.1], and it provides a slightly more flexible approximation for the heat of mixing than the classical regularity, although the entropy of mixing still has to be close to ideal.

Acknowledgements

The author wishes to thank Dr. J.-A. Boivin, Professor K. Ito, and Professor M. Tokuda for constructive discussions, and also the Centre de recherches minérales for permission to publish this work.

1. K. S. Pitzer and L. Brewer. *In* Thermodynamics (revised edition). G. N. Lewis and M. Randall. McGraw-Hill, New York, N.Y. 1961. p. 280.
2. M. Nagamori. Metall. Trans. B: **20B**, 434 (1989).
3. E. A. Guggenheim. Mixtures. Clarendon Press, Oxford. 1952.
4. J. Lumsden. Thermodynamics of alloys. Institute of Metals, London. 1952.
5. R. Fowler and E. A. Guggenheim. Statistical thermodynamics. University Press, Cambridge. 1965.
6. N. A. Gokcen. Statistical thermodynamics of alloys. Plenum Press, New York, N.Y. 1986.
7. I. Ansara. Int. Met. Rev. **24**, 20 (1979).
8. A. Vermandé, I. Ansara, and J. C. Mathieu. Ann. Chim. **5**, 535 (1980).

Can. J. Chem. Downloaded from www.nrcresearchpress.com by 109.225.110.28 on 09/08/12
For personal use only.

The *trans* effect: methodological musings[1]

OSVALD KNOP[2] AND S. C. CHOI
Department of Chemistry, Dalhousie University, Halifax, N.S., Canada B3H 4J3

AND

DAVID C. HAMILTON
Department of Mathematics, Statistics and Computer Science, Dalhousie University, Halifax, N.S., Canada B3H 4J3

Received April 15, 1992

OSVALD KNOP, S. C. CHOI, and DAVID C. HAMILTON. Can. J. Chem. **70**, 2574 (1992).

The *trans* effect (TE) in the present context refers to the electronic compensation which in collinear homoligand L—Z—L* *trans* bond pairs lengthens the Z—L* bond when the Z—L bond is shortened. The existence of a functional relation $d^* = f(d)$ between the conjugated bond lengths d(Z—L) and d^*(Z—L*) (d and d^* not equivalent by symmetry; population **A**) has been demonstrated for a variety of Z–L combinations, with Z mostly from Groups VI and V and L mostly a halogen. The two model functions investigated in detail are the empirical DPF (difference power fit), $d^* - d_0 = K(d - d_0)^{-c}$, and the semiempirical CSBO (constant sum of bond orders) based on a modified 3-centre 4-electron bond concept, $d^* - d_0 = -B \ln \{1 - \exp[-(d - d_0)/B]\}$, where $B = b_0 + b_1(d - d_0)$. Fitting DPF and CSBO to experimental d,d^* data sets involves 3-parameter nonlinear optimization; in this CSBO differs from the 2-parameter treatment of Sheldrick *et al.*, in which the limiting bond length d_0 was supplied externally. Modified versions of DPF and CSBO have been devised to accommodate, along with **A**, d,d^* pairs in which $d = d^*$ by symmetry (population **S**).

The relative merits of DPF and CSBO and the various aspects of TE quantification are discussed at length, among these the effect of the oxidation state of Z and of the presence of heteroligands on Z. The meaning of the parameters of optimization and the existence of "chemical" trends between them are examined as well as the importance of the symmetrically balanced bond length $d_e = d = d^*$ and of the total d range $\Delta = d_e - d_0$ resulting from the d,d^* regressions. Attempts to extend TE quantification to collinear heteroligand L_1—Z—L_2 *trans* bond pairs have provided insight into the nature of the bond-length variation in such systems. The very good DPF and CSBO fits to d,d^* sets obtained from 6-31G* optimizations of the equilibrium geometries of the OBOX, XOCN, and OCNY (X, Y = H, F, Cl, Li, Na, or no ligand) molecules and ions support the validity of the modified 3c4e model in accounting for the TE bond-length relationships.

OSVALD KNOP, S. C. CHOI et DAVID C. HAMILTON. Can. J. Chem. **70**, 2574 (1992).

Dans le présent contexte, l'effet *trans* (TE) se réfère à la compensation électronique qui, dans des paires de liaisons *trans* L—Z—L* d'homoligands colinéaires, provoque un allongement de la liaison Z—L* lorsque la liaison Z—L se raccourcit. On a démontré l'existence d'une relation fonctionnelle $d^* = f(d)$ entre les longueurs des liaisons conjuguées d(Z—L) et d^*(Z—L*) (d et d^* n'étant pas équivalents par symétrie; population **A**) d'une variété de combinaisons Z–L dans lesquelles Z représente principalement des éléments des groupes V et VI alors que L est généralement un halogène. Les deux fonctions modèles étudiées en détail sont la DPF empirique (ajustement de la différence des puissances), $d^* - d_0 = K(d - d_0)^{-c}$, et la CSBO constante (somme constante des ordres de liaison) semi-empirique basée sur un concept modifié de liaison à 4-électrons sur 3-centres, $d^* - d_0 = -B \ln \{1 - \exp[-d - d_0)/B]\}$ dans laquelle $B = b_0 + b_1(d - d_0)$. Un ajustement des DPF et CSBO avec les ensembles de données expérimentales pour d,d^* implique une optimisation non-linéaire de 3 paramètres; par cette procédure, la CSBO diffère du traitement à 2 paramètres de Sheldrick *et al.* dans lequel la valeur d_0 de la longueur de liaison limitante était fournit par une source extérieure. On a développé des versions modifiées de DPF et de CSBO pour accommoder, en plus de **A**, des paires d,d^* dans lesquelles $d = d^*$ par symétrie (population **S**).

On discute en détail des mérites relatifs des méthodes DPF et CSBO et de divers aspects de la quantification TE, en particulier de l'état d'oxydation de Z et de la présence d'hétéroligands sur Z. On a examiné la signification des paramètres d'optimisation et de l'existence de «tendances» chimiques entre ces paramètres ainsi que l'importance d'une longueur de liaison symétriquement balancée, $d_e = d = d^*$ et de l'ensemble de la plage $\Delta = d_e - d_0$ résultant des régressions d,d^*. Des essais dans le but d'étendre la quantification des TE à des paires de liaisons L_1—Z—L_2 d'hétéroligands colinéaires ont permis d'obtenir une compréhension de la nature de la variation de la longueur de liaison dans de tels systèmes. Les très bonnes corrélations des DPF et CSBO avec les ensembles d,d^* obtenues par optimisations 6-31G* des équilibres de géométrie des ions et molécules OBOX, XOCN et OCNY (X, Y = H, F, Cl, Li, Na ou aucun ligand) supporte la validité du modèle 3c4e modifié pour expliquer les relations entre le TE et les longueurs des liaisons.

[Traduit par la rédaction]

In this paper we investigate the presumed inherent connection (1) between the bond lengths d(Z—L) = d and d(Z—L*) = d^* ($d^* \geq d$) in collinear or nearly collinear L—Z—L* groups, where L and L* are atoms of the same element (here mostly a halogen). Unless the conjugated Z—L and Z—L* *trans* bonds are equivalent by symmetry at Z, $d \neq d^*$ except by accident. This inequality is commonly attributed to the existence of a compensating electronic mechanism (the *trans* effect, TE), which shortens Z—L and lengthens Z—L* relative to some real or supposed reference bond length $d = d^* = d_e$ (e, equal). The bond-length compensation is believed to be nonlinear.

Among the questions that can be asked are the following:

Q1. Are d and d^* connected through a functional relationship $d^* = f(d)$, i.e., to what extent can TE be quantified?

[1]Some of the results reported here were presented, in a much abbreviated form, at the 13th European Crystallographic Meeting, Trieste, 26–30 August, 1991.

[2]Author to whom correspondence may be addressed.

Can. J. Chem. Downloaded from www.nrcresearchpress.com by 109.225.110.28 on 09/08/12
For personal use only.

Can. J. Chem. Downloaded from www.nrcresearchpress.com by 109.225.110.28 on 09/08/12
For personal use only.

Q2. If such a relationship exists, what is this function, and does the relationship hold regardless of the cause of the disproportionation $d_e,d_e \rightarrow d,d^*$?

Q3. If d_e is the lower bound of d^*, what is the *upper* bound of d^* beyond which $d^* = f(d)$ ceases to correspond to an effective bonding interaction between Z and L*?

Q4. Other circumstances being equal, what distinguishes TE for one Z–L combination from TE for another such combination? In particular, what is the effect of the oxidation state of Z?

Q5. How do other ligands on Z affect TE in the L—Z—L* homoligand bond pair?

Q6. What is the effect of deviations from collinearity on the quantification of TE?

TE can be investigated from a preconceived theory or in a purely empirical manner. In either case the success and validity of the investigation will depend on the reliability of the experimental bond-length values. We shall be concerned mainly with examination of primary evidence for TE, with a minimum of recourse to particular and ad hoc schemes that may have been advanced to deal with TE in specific circumstances.

Limits of detection and quantification of TE

To quantify TE with confidence, the total bond-length range should be large and the d,d^* pairs should be distributed over it as uniformly as possible. These requirements are not easily met, since for a given Z–L the d,d^* sampling is limited by the Z–L chemistry and in practice is almost always the result of historical, haphazard accumulation of bond-length values. In particular, as is often the case, bond lengths from certain classes of closely related compounds or structures may be overrepresented, resulting in distorted weighting.

Quite apart from limitations of their range and distribution, the individual bond-length values suffer from uncertainties associated with the method and procedure with which the bond lengths were determined. The majority of bond-length values by far come from crystal-structure determinations. In addition to the esd's of the refined atom coordinates and to inaccuracies in the unit-cell dimensions there is the uncertainty involved in correcting a bond length for the effects of thermal motion. The correction is model-dependent and thus only partially reliable (cf. ref. 1); where it has been applied it increases the bond length, typically, by 0.01–0.03 Å.[3] In principle, the total uncertainty in the bond-length value can be minimized by lowering as much as advisable the temperature of the crystal and by increasing the volume and accuracy of the diffraction data. In practice, however, one finds that the bulk of the reported bond-length values comes from room-temperature determinations and a large proportion of these bond lengths have not been corrected for thermal motion. Faced with the choice between attempting to supply, with questionable results, thermal corrections for the several hundred uncorrected bond lengths in our d,d^* data sets and using the uncorrected values throughout, we have opted for the latter. This means that, realistically, our investigation of the existence and nature of a d,d^* correlation depends on a body of uncorrected bond lengths that are estimated to be no closer to the "true" values than 0.01 Å at best.[4]

This uncertainty in the bond-length values interferes with the detection of TE in the region where the difference $d^* - d$ is small and, more seriously for the present investigation, with the assessment of the suitability of a trial $d^* = f(d)$ model function at large d^* values. Further uncertainty is introduced into the d,d^* correlation by deviations from collinearity, the effect of which on TE does not appear to have been investigated to date. Clearly, the relative merits of different model functions can only be tested and compared within the accuracy of the d,d^* values in a set.

A. Model functions

Visual inspection of d^* vs. d plots (ref. 1 and **B**) leads to a strong presumption that d and d^* are correlated and that the correlation is not linear. The function $d^* = f(d)$ representing the correlation will therefore have $f'(d) < 0$ and because of $d^* \geq d$ will cease to have a physical meaning beyond the point of intersection with the $d = d^*$ line. A further requirement is that $f(d)_{d \rightarrow d_0} \rightarrow N$ $(0 < d_0 \leq d_{min})$, the upper bound of N being infinity and the lower bound a d^* value corresponding to the cut-off distance for effective Z—L bonding interaction.

Stipulation of the lower bound of N presents a vexing problem. This bound is probably smaller than the sum ΣvdWr of the van der Waals radii of Z and L, but this statement may amount to no more than tautology, as the tabulated van der Waals radii are average estimates for atoms in neutral molecules, not necessarily applicable to situations in which TE is observed. However, assigning a finite value to N in advance would preempt **Q3** and lead to a circular argument. Furthermore, with increasing $|f'(d)|$ the experimental uncertainties in d increasingly influence the estimation of the lower bound of N (see **C3**). In these circumstances the most reasonable compromise is to assume $N \rightarrow \infty$, i.e., the $d^* = f(d)$ curve converges to a vertical asymptote at $d = d_0$, and to investigate the cut-off problem in terms of σ of the goodness of fit to the model function.

The presumed $d^* = f(d)$ relationship can be represented, within the limitations imposed by experiment, by various empirical functions satisfying the above requirements. The functions eventually investigated in detail (cf. also ref. 1) were

PF1 (simple power fit):

$$[1] \quad d^* = Kd^{-c}$$

PF2:

$$[2] \quad d^* = K(d - d_0)^{-c}$$

DPF (difference power fit):

$$[3] \quad d^* - d_0 = K(d - d_0)^{-c}$$

CSBO (constant sum of bond orders):

$$[4] \quad d^* - d_0 = -[b_0 + b_1(d - d_0)] \ln \{1 - \exp\{-(d - d_0)/[b_0 + b_1(d - d_0)]\}\}$$

[3] In some cases the disparity of the corrections for different Z—L bonds at Z may effectively wipe out the differences between the uncorrected $d(Z—L_{ax})$ and $d(Z—L_{eq})$, e.g., in the IF_5 square pyramid in $XeF_2 \cdot IF_5$ (2).

[4] For the effect of thermal corrections on TE correlations see **D5**.

Can. J. Chem. Downloaded from www.nrcresearchpress.com by 109.225.110.28 on 09/08/12
For personal use only.

The first three are purely empirical representations of the d,d^* correlation. They were chosen over polynomial representations because of convenience of manipulation and because the parameters d_0, K, and c can be assigned simple physical meaning. The fourth, semiempirical model function CSBO is based on the 3-centre 4-electron (3c4e) bond concept. Its suitability has been demonstrated previously (see **A4**) and CSBO is therefore discussed in detail below. All four model functions satisfy the asymptotic requirements $d^* \rightarrow \infty$ and $f' = \mathrm{d}d^*/\mathrm{d}d \rightarrow \infty$ as $d \rightarrow d_0$ ($d_0 = 0$ in PF1 and $d_0 > 0$ in the other three functions). In the following we shall write $d_e - d_0 = \Delta$, the total d range.

1. Function PF1

Setting $d^* = d = d_e$ yields $K = {d_e}^{c+1}$, hence $d^*/d_e = (d/d_e)^{-c}$ or ${d^*}_{red} = {d_{red}}^{-c}$. Furthermore, $f' = -cd^*/d; f' = -c$ for $d^* = d = d_e, f' = -1$ for $d^*/d = 1/c$.

2. Function PF2

Setting $d^* = d = d_e$ yields $K = d_e\Delta^c$. Hence $d^*/d_e = [(d - d_0)/\Delta]^{-c}, f' = -cd^*/(d - d_0); f' = -1$ for $d^*/d = (d - d_0)/dc, f' = cd_e/\Delta$ for $d^*/d = 1$.

3. Function DPF

Setting $d^* = d = d_e$ yields $K = \Delta^{c+1}$, hence

$$[5] \qquad (d^* - d_0)/\Delta = [(d - d_0)/\Delta]^{-c}$$

or $(d^* - d_0)_{red} = (d - d_0)_{red}{}^{-c}$ when the differences are normalized to Δ.[5] Further, $f' = -c(d^* - d_0)/(d - d_0), f' = -c$ for $d^* = d = d_e$, and $f' = -1$ for $(d^* - d_0)/(d - d_0) = 1/c$, i.e., at $d^*/d = [d + d_0(c - 1)]cd$.

In the statistical treatment of actual d,d^* sets the parameters chosen for the unconstrained nonlinear optimizations were d_0, K, and c. However, the difference Δ, which defines the total range of d implicit in TE for a given Z–L combination, is a fundamental property of the combination and is therefore readily visualized as a natural parameter of the d,d^* correlation. In the fitting of actual d,d^* data sets PF2 and DPF were sometimes reparametrized to d_0, Δ, and c.

4. Function CSBO

When contemplating the d,d^* plot for conjugate Sb—Cl *trans* bonds in Sb(III) species with octahedral coordination Lipka (3, 4) suggested, in accordance with earlier (5–8) notions on 3c4e bonds traceable to Rundle (9), that Pauling's (10) relation $D(n) = D(1) - B \log n = D(1) - \log n^B$ can be modified (our notation) to

$$[6] \qquad d(s) = d_0 - B \ln s, \qquad d^*(s^*) = d_0 - B \ln s^*$$

with the assumption that $s + s^* = 1$, i.e., the sum of the bond orders in the conjugate *trans* bond pair is constant; d_0 was taken as the shortest Sb—Cl bond length in the $SbCl_3$ crystal. From this, $\exp[-(d^* - d_0)/B] + \exp[-(d - d_0)/B] = 1$ and

$$[7] \qquad d^* = d_0 - B \ln \{(1 - \exp[-(d - d_0)/B]\}$$

Setting $d^* = d = d_e$, $B = \Delta/\ln 2$. A similar treatment has been applied to P(III)—Br (11), As(III)—Cl (12), As(III)—Br (13), and Sb(III)—Cl (14) d,d^* data sets.

Testing the validity of eq. [7] on more complete d,d^* sets, first for As(III)—Br (15) and subsequently for Sb(III)—Hal (16), and equating d_0 with the experimental Z—Hal bond lengths in gaseous $ZHal_3$ (i.e., $d_0 = d_0$(expt)), Sheldrick *et al.* found that B was not constant but varied with $d - d_0$. This variation was assumed to be linear, $B = b_0 + b_1 (d - d_0)$. On optimizing b_0 and b_1 they obtained (subject to certain restrictions on the d,d^* data sets, see **C3**) very satisfactory agreement for As—Br, Sb—Br, and Sb—I bonds, while for the Sb—Cl set they found that B and $d - d_0$ were uncorrelated.

Equation [4] is a rearranged form of Sheldrick's model function. The parameters b_0 and b_1 are related by

$$[8] \qquad b_1 = (1/\ln 2) - (b_0/\Delta)$$

However, the optimization procedure used by Sheldrick *et al.* and that in the present work are not the same. In Sheldrick's procedure $d_0 = d_0$ (expt) is fixed at an *external* value and b_0 and b_1 are fitted. In our treatment d_0 is a parameter of refinement; d_0, b_0, and b_1 are optimized *simultaneously* by a nonlinear three-parameter procedure. The legitimacy of the assumptions implicit in the two procedures is examined in **C2**.

5. Symmetric conjugate bond pairs

Conjugate homoligand Z—L *trans* bonds that are equivalent by molecular or crystallographic symmetry generate a special category of d,d^* pairs, $d_s = d_s{}^*$. They constitute a statistical population **S** different from the population **A** formed by the asymmetric $d_a \neq d_a{}^*$ pairs, which of course are subject to TE. For a particular Z–L combination the distribution of experimental d_s values is due to factors that undoubtedly operate also on the **A** population, but the effect of which cannot be separated there from the consequences of TE (see **C1**).

The **S** distribution in some cases is surprisingly wide, e.g., for Te(IV)—Cl, Bi(III)—Br, or Te(II)—S bonds; its apparent narrowness for other Z—L bonds may simply be due to insufficient sampling. Among the factors which contribute to the d_s spread are experimental accuracy, ionic charge and coordination number,[6] Coulombic compression in ionic crystals, Jahn–Teller effect, hydrogen bonding to L, ligation of Z to other atoms, and (for C_2 and C_s symmetries at Z) deviations from collinearity. Depending on the coordination number and symmetry, the Z atom can be shared by two or three such symmetric conjugate L—Z—L bond pairs, which in turn can be distinct or equivalent among themselves (e.g., in octahedral ${ZHal_6}^{n-}$ anions), or the symmetric conjugate pair can be unique (e.g., in trigonal-bipyramidal ${ZHal_5}^{n-}$ species of D_{3h} or C_{3h} symmetry).

The d_s values in an **S** set may be assumed normally distributed and have a mean $\bar{d}_s$. This mean may or may not be identical with the d_e value computed from the correlation function fitted to the **A** + **S** set or to the **A** set alone. This raises question

Q7, is $\bar{d}_s$ numerically the same as d_e?

In CSBO no special provision is made for the existence of a distribution of d_s values, since $s = s^* = \frac{1}{2}$ when $d^* = d$. However, if the variation in d_s is assumed to reflect changes in the bond order in the **S** population, then the spread of the bond orders about $s = \frac{1}{2}$ can be expressed, from $s + s^* = 1 + 2\delta s$, as $2\delta s = \exp[-(d - \bar{d}_s)/\bar{B}] - 1$, where $\bar{B} = (\bar{d}_s - d_0)/\ln 2$. The variance of this distribution can then be

[5] In its logarithmic form eq. [5] is naturally suited for graphical presentation.

[6] For the relative magnitude of the effect of coordination number and ionic charge in M(III)—Cl species see ref. 17.

Can. J. Chem. Downloaded from www.nrcresearchpress.com by 109.225.110.28 on 09/08/12
For personal use only.

taken as a measure of the variability of the bond order in balanced (i.e., symmetric) conjugate *trans* bonds.

For each Z–L d,d^* set the sum $S[d^*(\text{obs})_i - d^*(\text{fit})_i]^2$ was minimized for the total **A** + **S** sample as well as for the **A** sample alone; for $n_S = 0$, of course, $S_{A+S} = S_A$. In addition to these **A** + **S** and **A** regressions, attempts were made to accommodate **S** as a separate population in the model functions. This was done (subject to the assumptions stated in **F**) by minimizing weighted combinations of $S_A[d_a^*(\text{obs})_i - d_a^*(\text{fit})_i]^2$ and $S_S[d_s(\text{obs})_i - d_c]^2$ in two ways, depending on the size of the **S** sample. For reasonably large n_S the combination to be minimized was

[9] $\quad n_A \log S_A + n_S \log S_S$

(regressions DPF(**A**,**S**) and CSBO(**A**,**S**)). For $n_S = 1$–4 the **S** sample is too small to estimate the **S** variance reliably. Assuming that the ratio of the **A** and **S** variances is λ, one can minimize the combination

[10] $\quad S_A + \lambda S_S$

(regressions DPF(**A**/**S**) and CSBO(**A**/**S**); initially λ was taken to be unity. Evaluation of r^2 and of error estimates is treated in **F**.

B. Individual Z–L combinations

Of the model functions investigated PF1 and PF2 (and even more so LIN, the linear function, cf. ref. 1) have generally been found inferior to or no better than DPF and CSBO, as judged by their respective r^2 and σ values. DPF and CSBO have therefore been adopted as the two standard model functions and evaluated (with the further elaboration allowing for **A** and **S** as separate populations) for the particular Z–L combinations considered in this work. The numerical results of the regressions are presented in Tables 1 and 2. Figures 1–4 contain plots of the experimental d,d^* pairs and the fitted DPF(**A** + **S**) curves. The corresponding CSBO(**A** + **S**) curves are not shown, as they are indistinguishable, on the scale of the drawings, from the DPF(**A** + **S**) curves. Sources of data are listed in **F**.

The Z–L data sets are for homoligand Z coordinations. The occasional d,d^* pairs in heterocoordinate Z species that are included in some of the sets are consistent with the body of the homoligand data (for the special case of Se(IV)—Cl(Ox) see below).

DPF(**A** + **S**) and CSBO(**A** + **S**) regressions have been obtained for all the Z–L data sets of Tables 1 and 2 except for Se(II)—Cl, As(III)—Cl, and As(III)—I (for the special case of P(III)—Br see below), which contain no d_s values and for which only the DPF(**A**) and CSBO(**A**) regressions are available. DPF(**A**,**S**) and CSBO(**A**,**S**) regressions were performed for data sets with $n_S \geq 2$. However, since the distribution of d_s values in very small **S** samples is likely to be unrepresentative, it would not be prudent to place too much confidence in the **A**,**S** regressions in such cases. For **S** samples with one to four d_s values, DPF(**A**/**S**) regressions (not listed in Table 1) were attempted as well, resulting in parameter values that did not differ from those obtained from the corresponding **A** or **A** + **S** regressions within the standard errors and that in most cases were numerically quite close to the latter.

Because of the incompleteness and deficiencies of some of the data sets it was thought most practical for comparison purposes to use the results of the **A** + **S** regressions throughout. While this is not the most logical choice when the different nature of the **A** and **S** populations is considered (see **A5**), it is justified by the fact that the parameter values from the **A** + **S** regressions are within at most 1.5σ of the corresponding values from the **A** or **A**,**S** regressions where the latter are available.

It should be noted that while each of the d,d^* data sets is adequately fitted by the regressions of Tables 1 and 2, the standard errors on the parameter estimates are large, at times comparable to or even exceeding the parameter value. In part, these large errors are the price to pay for universality, i.e., for the liberal inclusiveness of the data sets, both as concerns accuracy and chemical appropriateness of the bond lengths. This problem is illustrated by comparing the results of the present regressions for Se–Cl and Te–Hal with those for the much smaller but chemically homogeneous d,d^* sets for the μ_2–$Z_2Hal_{10}^{2-}$ dimers (Table III of ref. 1). The vintage of some of the literature d,d^* values is also a factor: older values, with larger than desirable esd's, tend to increase the scatter. However, the scatter is not the only factor responsible for the magnitude of the standard errors on the refined parameters (see **F**).

The comments below include (though not exhaustively) the bond lengths d_u for Z—L bonds with unopposed ligand (i.e., no *trans* ligand at an acceptable bonding distance, or a presumed lone pair, L—Z—LP). These bonds are often perpendicular or approximately perpendicular to the L—Z—L *trans* bond pair(s). Also cited are some "limiting" Z—L bond lengths, which may have bearing on the discussion of the d_0 values and which to some represent the "experimental" d_0 values, d_0(expt) (see **A4**).

Se(IV)–Cl(Ox). This set includes $Se_2O_2Cl_6^{2-}$, $SeOCl_3^-$, and $SeOCl_4^{2-}$. In all these species the Se—O bonds are perpendicular to the Se,Cl planes.

Se(II)–Cl, Se(II)–Br. The bond lengths in $SeCl_2$(g) and $SeBr_2$(g) are 2.157(3) and 2.32(2) Å, respectively (Table II of ref. 18).

Te(II)–S. This is the only experimental homoligand combination we have examined in which the ligand is not a halogen. The data set (Fig. 4) is interesting in several respects. Of the 107 d,d^* pairs 58 form the **S** sample (three of them corresponding to bond pairs of C_2 symmetry). Another 26 constitute an asymmetric **A1** sample, which corresponds to square-planar Te coordination with S—Te—S angles greater than 160° but which is skewed strongly toward 180° (mean S—Te—S angle, 172.2(56)°, $\gamma_1 = -0.77$, $\gamma_2 = 2.42$).[7] This is a true *trans* population, subject to TE. The remaining 23 pairs (population **A2**) correspond to quasi-*trans* S—Te—S* bonds associated with the trapezoidal-planar Te coordination.[8] In this sample the S—Te—S angle range is rather narrow, 145–152°, with a mean of 148.3(18)° and only a slightly skewed distribution ($\gamma_1 = 0.10$, $\gamma_2 = 1.88$). The existence of these two asymmetric populations with no angle overlap affords an opportunity to assess the effect of noncollinearity on TE. The regressions listed in Tables 1 and 2 are for **A1** and **S**. Regressions involving **A2** are discussed in **C5**.

P(III)–Br. There are only three d,d^* pairs in this set (points 2, 4, and 8 in Fig. 2 of ref. 11), so the parameter values in Tables 1 and 2 are for the exact fit. This set, although *statistically* not significant, has been included as a reference for tracing the effect of cyano heteroligands on the TE of P(III)—Br (see **C6**). Two of the three available d_u values, 2.217(1) Å (11), 2.221(3) Å (20), and 2.333(2) Å (11) (all three against LP), are marginally lower than the fitted d_0 values.

As(III)–Cl. This exclusively **A** data set does not contain d,d^* pairs sufficiently close to the expected d_c value and the point with the lowest d^* (and one that crucially affects the outcome of the d_c estimation)[9] appears to be spurious. Indeed, fitting this set to both DPF and CSBO ($r^2 = 0.917$, $\sigma = 0.045$ Å, $d_c = 2.443(25)$ Å) resulted in standard errors on the parameter values that were so large as to render the latter meaningless. A "synthetic" d_c value of

[7] γ_1, coefficient of skewness; $\gamma_1 < 0$, distribution skewed toward 180°, γ_2, coefficient of kurtosis; for a normal distribution $\gamma_2 = 3$.

[8] This coordination geometry is encountered with bidentate ligands of the $-CS_2$ type (cf. ref. 19).

[9] This point corresponds to a d,d^* pair in the heteroligand $As_2SCl_5^-$ anion (21).

TABLE 1. Optimized parameter values for the DPF model function[a]

n	r^2	σ, Å[b]	d_0, Å	K	c	d_c, Å	Δ, Å
				1. Se(IV)–Cl			
52	0.940	0.045	1.838(78)	0.271(56)	1.160(147)	2.384(8)	0.547(73)
48 + 4	0.920	45/9	1.845(61)	0.268(48)	1.143(98)	2.385(4)	0.541(59)
48	0.920	0.046	1.813(116)	0.286(84)	1.213(224)	2.381(12)	0.568(106)
				2. Se(IV)–Cl(Ox)			
16	0.954	0.049	1.842(302)	0.321(306)	1.413(412)	2.466(12)	0.624(295)
15	0.951	0.049	1.624(634)	0.612(1173)	1.697(586)	2.458(13)	0.834(624)
				3. Se(II)–Cl			
8	0.973	0.027	1.992(188)	0.212(115)	0.931(309)	2.440(13)	0.448(179)
				4. Se(IV)–Br			
52	0.945	0.035	2.008(99)	0.282(86)	1.120(122)	2.558(4)	0.550(96)
43 + 9	0.916	36/7	2.001(92)	0.288(86)	1.128(94)	2.558(2)	0.557(91)
43	0.916	0.038	2.001(142)	0.288(119)	1.129(198)	2.558(8)	0.557(136)
				5. Se(II)–Br[c]			
20	0.956	0.037	1.572(631)	1.052(1398)	1.159(239)	2.595(8)	1.024(628)
16 + 4	0.907	38/4	1.665(474)	0.865(914)	1.104(179)	2.598(2)	0.933(474)
				6. Te(IV)–Cl			
121	0.907	0.051	2.061(57)	0.207(37)	1.053(96)	2.525(3)	0.464(55)
81 + 40	0.877	61/11	2.087(53)	0.201(34)	0.974(84)	2.531(2)	0.443(52)
81	0.891	0.058	1.838(199)	0.382(239)	1.437(215)	2.511(5)	0.674(195)
				7. Te(IV)–Br			
41	0.943	0.029	2.180(138)	0.259(118)	1.047(140)	2.696(3)	0.516(138)
17 + 24	0.953	29/13	1.875(411)	0.638(700)	1.258(186)	2.695(2)	0.820(411)
17	0.954	0.031	1.695(762)	0.991(1785)	1.364(285)	2.692(6)	0.996(759)
				8. Te(IV)–I			
63	0.931	0.036	1.806(563)	1.336(1564)	1.324(154)	2.938(3)	1.133(562)
47 + 16	0.869	40/8	1.659(749)	1.788(2541)	1.366(149)	2.938(2)	1.278(749)
47	0.869	0.041	1.783(824)	1.401(2348)	1.316(258)	2.939(8)	1.157(819)
				9. Te(II)–S[d]			
84	0.953	0.044	2.297(17)	0.174(7)	0.845(53)	2.684(3)	0.387(16)
26 + 58	0.937	62/17	2.289(26)	0.178(11)	0.865(71)	2.685(2)	0.396(26)
26	0.940	0.065	2.259(53)	0.169(17)	1.008(195)	2.672(13)	0.412(44)
				10. As(III)–Cl[e]			
29[+1]	0.914	0.048	1.805(147)	0.512(155)	0.979(205)	2.517(19)	0.713(132)
				11. As(III)–Br			
42	0.950	0.041	2.128(65)	0.320(47)	0.842(106)	2.666(9)	0.539(60)
40 + 2	0.941	41/1	2.150(43)	0.312(35)	0.790(51)	2.672(1)	0.521(42)
40	0.942	0.042	2.118(76)	0.324(54)	0.863(127)	2.664(10)	0.546(69)
				12. As(III)–I			
17	0.921	0.048	2.380(126)	0.274(70)	0.874(262)	2.881(21)	0.502(110)
				13. Sb(III)–Cl			
84	0.830	0.087	1.829(287)	0.569(448)	1.447(311)	2.623(12)	0.794(278)
82 + 2	0.814	87/9	1.987(131)	0.384(143)	1.209(157)	2.635(6)	0.648(128)
82	0.817	0.088	1.725(409)	0.749(825)	1.568(383)	2.618(14)	0.893(398)

Can. J. Chem. Downloaded from www.nrcresearchpress.com by 109.225.110.28 on 09/08/12
For personal use only.

TABLE 1 (*concluded*)

n	r^2	σ, Å[b]	d_0, Å	*K*	*c*	d_e, Å	Δ, Å
			14. Sb(III)–Br				
16	0.982	0.032	2.452(19)	0.137(11)	0.823(103)	2.788(9)	0.337(14)
14 + 2	0.975	31/3	2.456(12)	0.140(4)	0.800(43)	2.791(2)	0.335(11)
14	0.975	0.034	2.446(31)	0.134(17)	0.860(175)	2.785(16)	0.339(18)
			15. Sb(III)–I				
88	0.894	0.056	2.532(72)	0.310(49)	0.775(114)	3.049(9)	0.517(66)
82 + 6	0.882	53/44	2.503(86)	0.331(64)	0.816(128)	3.047(10)	0.544(79)
82	0.882	0.054	2.511(93)	0.326(65)	0.800(147)	3.048(12)	0.537(84)
			16. Bi(III)–Cl				
60	0.864	0.041	2.308(87)	0.184(51)	0.840(135)	2.706(4)	0.398(85)
39 + 21	0.856	40/40	2.183(158)	0.271(139)	1.002(149)	2.704(3)	0.521(157)
39	0.878	0.039	2.342(81)	0.190(41)	0.706(148)	2.719(7)	0.377(77)
			17. Bi(III)–Br				
59	0.834	0.048	2.300(217)	0.310(206)	1.000(189)	2.856(5)	0.557(214)
46 + 13	0.795	47/20	1.966(598)	0.767(1115)	1.201(222)	2.853(5)	0.887(596)
46	0.800	0.048	2.302(282)	0.322(262)	0.950(263)	2.862(9)	0.559(275)
			18. Bi(III)–I				
35	0.895	0.035	2.585(197)	0.257(157)	0.932(210)	3.080(7)	0.495(192)
32 + 3	0.869	35/5	2.409(307)	0.422(382)	1.110(171)	3.074(3)	0.665(306)
32	0.875	0.036	2.659(157)	0.211(97)	0.820(227)	3.085(10)	0.426(150)
			19. Xe(II)–F				
9	0.888	0.055	1.700(128)	0.094(37)	0.928(418)	1.994(16)	0.293(120)
8	0.869	0.060	1.712(132)	0.097(37)	0.864(471)	1.998(21)	0.286(120)
			20. P(III)–Br[f]				
3	—	—	2.230	0.222	0.466	2.588	0.358

[a]First line refers always to DPF(**A** + **S**); second, DPF(**A**, **S**); third line, DPF(**A**). Otherwise the line with $n < n$[DPF(**A** + **S**)] refers to DPF(**A**) and the line with n(**A**) + n(**S**) refers to DPF(**A**,**S**).
[b]45/9 etc. stands for $10^3\sigma$(**A**)/$10^3\sigma$(**S**).
[c]Refinement for DPF(**A**) gave unreasonable parameter values.
[d]DPF(**A1** + **S**); DPF(**A1**,**S**); DPF(**A1**).
[e]See **B**.
[f]Fit to three d,d* pairs only (see **B** and **C6**).

2.535 Å estimated from the d_e(Z—Hal) vs. $r(Hal^-)$ correlation (see **C5** and Fig. 5) was therefore added and the set was reoptimized, yielding parameter values with acceptable standard errors. The reported d_u values are 2.179 Å (22), 2.189 Å (12), and 2.204 Å (21). The bond length in $AsCl_3$(g) is 2.161 Å (23).

As(III)–Br. This set is among the most consistent investigated here, with all the d,d* values coming from one laboratory. The reported d_u values are 2.335 Å (15), 2.347 Å (13), and 2.366 Å (15). In $AsBr_3$(g), d(As—Br) = 2.33 Å (23).

As(III)–I. The values in this set, too, come from one laboratory and, as for As(III)–Br, from recent investigations. No d_s value is available, but there are d,d* pairs reasonably close to d_e. The solitary d_u value is 2.585 Å (24). The bond length in AsI_3(g) is 2.55 Å (23).

Sb(III)–Cl. The scatter in this large set may be in part attributable to the lower accuracy of the older structure determinations. It is reflected in the smallest r^2 and the largest σ value in Tables 1 and 2, and in the very large standard errors on the parameter values. It is noteworthy that Sheldrick and Martin (16), who used a somewhat smaller d,d* set in their CSBO regression with a d_0 fixed at d_0 (expt) in $SbCl_3$(g) (cf. Table 2), failed to obtain a meaningful correlation between B and $d - d_0$. Accumulation of additional, accurate d,d* should make it possible to formulate objective rejection criteria for cleaning up the existing Sb(III)–Cl set and to determine to what extent the scatter is inherent, i.e., arising from differences in bonding specific to the Sb(III)–Cl combination (as held in ref. 16). Many d_u values have been reported (7, 14, 25–27), ranging from 2.338 to 2.385 Å. In a $SbCl_3$[crown] complex (28) the Sb—Cl bond lengths are 2.405, 2.412, and 2.423 Å; in $SbCl_3$(g), d(Sb—Cl) = 2.333 Å (23).

Sb(III)–Br. This set is poorly defined at low d and the uniformity of the d,d* sampling leaves something to be desired. The reported d_u values are 2.505 and 2.529 Å (29). The bond length in $SbBr_3$(g) is 2.49 Å (23).

Sb(III)–I. The d_s distribution has a considerable width. The d_u bond lengths are 2.767 and 2.773 Å (30). In SbI_3(g), d(Sb—I) = 2.719 Å (23).

Bi(III)–Cl. The d_u reported recently in $Bi_2Cl_8^{2-}$ is 2.500(6) Å (31). In $BiCl_3$(g) the bond length is 2.48 Å (23); the average bond length in a $BiCl_3$[12]crown-4 complex (31) is 2.52(1) Å.

Bi(III)–Br. The scatter in this sample is appreciable; the d,d* distribution gives the impression of being bimodal. The bond length in $BiBr_3$(g) is reported as 2.63 Å (23).

Cl–Bi(III)–S. The appreciable scatter in this set comes from

Can. J. Chem. Downloaded from www.nrcresearchpress.com by 109.225.110.28 on 09/08/12
For personal use only.

TABLE 2. Optimized parameter values for the CSBO model function[a]

n	r^2	σ, Å	d_0, Å	b_0, Å	b_1	d_c, Å	Δ, Å
				1. Se(IV)–Cl			
52	0.940	0.045	2.006(29)	0.601(71)	−0.147(98)	2.384(7)	0.378(25)
				2. Se(IV)–Cl(Ox)			
16	0.953	0.050	2.075(129)	0.695(321)	−0.335(280)	2.466(11)	0.391(122)
				3. Se(II)–Cl			
8	0.973	0.027	2.098(90)	0.482(186)	0.027(220)	2.439(13)	0.341(83)
				4. Se(IV)–Br			
52	0.944	0.035	2.177(46)	0.589(96)	−0.105(83)	2.558(4)	0.381(44)
				5. Se(II)–Br			
20	0.956	0.037	1.922(341)	1.052(636)	−0.119(169)	2.595(8)	0.673(338)
				6. Te(IV)–Cl			
121	0.906	0.052	2.185(26)	0.515(58)	−0.072(66)	2.525(3)	0.340(25)
				7. Te(IV)–Br			
41	0.943	0.029	2.329(72)	0.546(140)	−0.046(98)	2.696(3)	0.367(71)
				8. Te(IV)–I			
63	0.931	0.036	2.236(313)	1.181(597)	−0.239(109)	2.938(3)	0.702(312)
				9. Te(II)–S[b]			
84	0.948	0.046	2.357(7)	0.458(21)	0.043(41)	2.684(3)	0.327(7)
				10. As(III)–Cl[c]			
30	0.912	0.048	1.981(61)	0.781(141)	−0.017(146)	2.516(18)	0.535(50)
				11. As(III)–Br			
36	0.949	0.042	2.233(30)	0.586(64)	0.089(77)	2.666(8)	0.433(27)
40			[2.33]	0.395	0.303		
				12. As(III)–I			
17	0.920	0.048	2.483(51)	0.549(118)	0.059(190)	2.880(21)	0.397(40)
				13. Sb(III)–Cl[d]			
84	0.829	0.087	2.136(119)	0.873(295)	−0.353(210)	2.622(12)	0.486(111)
57			[2.325]				
				14. Sb(III)–Br			
16	0.980	0.033	2.503(6)	0.392(21)	0.060(86)	2.787(9)	0.284(8)
23			[2.49]	0.387(9)	0.13(4)		
				15. Sb(III)–I			
88	0.893	0.057	2.623(34)	0.550(70)	0.149(85)	3.049(9)	0.425(30)
65			[2.719]	0.360(5)	0.43(3)		
				16. Bi(III)–Cl			
60	0.863	0.041	2.393(45)	0.418(85)	0.108(97)	2.706(4)	0.313(43)
				17. Bi(III)–Br			
59	0.834	0.048	2.458(115)	0.578(211)	−0.007(132)	2.856(5)	0.399(112)

Can. J. Chem. Downloaded from www.nrcresearchpress.com by 109.225.110.28 on 09/08/12
For personal use only.

TABLE 2 (*concluded*)

n	r^2	σ, Å	d_0, Å	b_0, Å	b_1	d_e, Å	Δ, Å
				18. Bi(III)–I			
35	0.895	0.035	2.717(100)	0.507(183)	0.047(147)	3.080(7)	0.363(96)
				19. Xe(II)–F			
9	0.885	0.056	1.764(57)	0.326(133)	0.019(304)	1.994(16)	0.229(53)
				20. P(III)–Br[e]			
3			2.242	0.360	0.404	2.588	0.346

[a]First line, CSBO(**A** + **S**). Second line, Sheldrick *et al.* (15, 16); d_0 assumed equal to the Z—Hal bond length in $ZHal_3$(g).
[b]**A1** plus **S** data sets.
[c]d_e value supplied externally, see text.
[d]Reference 16 states that B and $d - d_0$ are uncorrelated.
[e]Fit to three d,d^* pairs only (see text).

limited experimental accuracy, from the involvement of the S ligands in other bonds, from the presence of other heteroligands on Bi, and from significant departures from collinearity. The shortest Bi—S distance in Bi_2S_3 is reported to be ~2.56 Å (32).

Xe(II)–F. The two *ab initio* $d = d^*$ values for XeF_2, 1.978 Å (33) and 1.985 Å (34), agree well with the d_e(**A** + **S**) = d_e[CSBO(**A** + **S**)] = 1.994(16) Å and d_e (**A**) = 1.998 (21) Å values calculated from the regressions. The *ab initio* (33) d,d^* pair for $Xe_2F_3^+$, 1.899 and 2.228 Å, is within 2σ of the regression. However, the *ab initio* d(Xe—F) estimates for XeF^+, 1.877 Å (33) and 1.886 Å (34), are higher than the asymptotic limit of the TE regressions, d_0(DPF) = 1.70 (13) Å and d_0(CSBO) = 1.76(6) Å, which seems to indicate that either the *ab initio* estimates are still too high or XeF^+ is not the correct asymptotic reference species for TE[Xe(II)–F], or both (see **C2** and Fig. 6).

B(III)–O. This combination was investigated only on 6–31G* *ab initio* values of d(B—O),d^*(B—O) in BO_2^-, OBO*X (X = H, F, Cl, Li), and B_2O_3 molecules. The data set for BO_2^- and OBO*X (n = 5) gave an almost exact fit to both DPF and CSBO; with *cis*-B_2O_3 and *trans*-B_2O_3 included (n = 7) the fit was considerably worse (see **D1**).

O–C–N. Like the preceeding, this combination was investigated only on 6–31G* *ab initio* values of the bond lengths, d(O—C),d(C—N), in OCN^-, XOCN, and OCNY (X, Y = H, F, Cl, Li, Na) species, and it too was found to give superior fits to the model functions (see **D3**).

Data sets with convergence problems

Fitting to DPF and CSBO was also attempted for the data sets assembled for Pb(II)–Br, Pb(II)–I, I(III)–Cl, and Ti(IV)–Cl. A significant fraction of the d,d^* pairs in these sets derives from entities that can only marginally be characterized as discrete. Although Figs. 1 and 3 show definite TE trends for these combinations, the data sets are small and ill-conditioned. Convergence could not be achieved for Pb(II)–Br (n = 5) and Ti(IV)–Cl (n = 17). For Pb(II)–I (n = 27) convergence was obtained for DPF (**A** + **S**) but the standard errors on the optimized parameter values were very large. The I(III)–Cl (n = 17) set contains a number of older d,d^* values of questionable accuracy. Regressions of the full set and of partial sets with some of the outliers omitted resulted in very large standard errors on the parameter values. However, the d_e values obtained in these regressions were reasonably consistent, with 2.508(13) Å as the best estimate.

Other Z–L combinations

The literature was searched also for d,d^* pairs of other Z–L combinations, especially in "planar" μ_2-bridged species. The results of our findings for TE in a number of transition-element μ_2-T_2Hal_{10} and μ_2-$T_2Hal_{10}^{2-}$ dimers are described in ref. 1. In planar Cu(II), Au(III), Pd(II), and Pt(II) μ_2-halogeno species the d,d^* inequality was found to be too small for a meaningful TE analysis; this is typical of T–Hal combinations in general. Scarcity of data was prohibitive for Ge(II) and Sn(II) combinations with the exception of Sn(II)–F where, however, other difficulties were encountered (see Sb(III)–F below). Such indications as there are point to the existence of TE ranges for Ge(II)–I and Sn(II)–I comparable to that for Pb(II)–I. For Pb(II)–Cl and Cd(II)–Cl the d,d^* pairs form ill-defined clusters with narrow d,d^* ranges, and the same seems true of Cd(II)–Br and Cd(II)–I.

Proper convergence could not be obtained for the Sb(III)–F set (n = 27). The scatter was large and difficult to trace to any one among the lower accuracy of the older structure determinations, large deviations from collinearity, and the lack of well-defined discrete character of the $Sb_pF_q^e$ entities. Indefiniteness of the Sb coordination and F–Sb–F "*trans*" angles as small as 130° are characteristic and inherent in crystal structures containing Sb(III)–F species. Similar problems are encountered with Sn(II)–F (cf. ref. 35 for an account of both Z–F combinations) and are endemic in oxide structures.[10]

C. Conclusions from data treatment

1. Examination of d_e *and* $\bar{d}_s$ *(Q7)*

The d_e (**A**) obtained from a DPF(**A**) regression represents the "best" estimate of the balanced Z—L bond length for the pertinent Z–L combination, provided the data set contains d,d^* pairs sufficiently close to the $d = d^*$ line. In that case the d_e(**A**) value has a remarkably small standard error and is very close to the d_e values calculated from the **A** + **S** and **A**,**S** regressions. When the d_e(**A**) values for the Z–Hal combinations are regressed linearly on Shannon's $r(Hal^-)$ radii, very good fits result. In the three series where all three halogens are represented, the regressions d_e(**A**) = a_0 + $a_1 r(Hal^-)$ give

[10]The d,d^* relationship for strongly angular *trans* bond pairs in oxides of Sb(III), Te(IV), and I(V) has been treated in terms of DPF with c = 1 in refs. 36 and 37 (cf. also ref. 38). Setting c = 1 implies $\Delta = d_e - d_0 = \sqrt{K}$. If $r(Cl^-) - r(O^{2-})$ is taken as 0.41 Å (Shannon's radii), d_e(Z—Cl) = $d_0 + \sqrt{K}$ + 0.41; using d_0 and K values from refs. 36 and 37 gives d_e estimates for Te(IV)—Cl and Sb(III)—Cl of 2.51 and 2.62 Å, respectively, in good agreement with the corresponding refined values in Table 1, 2.53 and 2.62 Å.

Can. J. Chem. Downloaded from www.nrcresearchpress.com by 109.225.110.28 on 09/08/12
For personal use only.

Can. J. Chem. Downloaded from www.nrcresearchpress.com by 109.225.110.28 on 09/08/12
For personal use only.

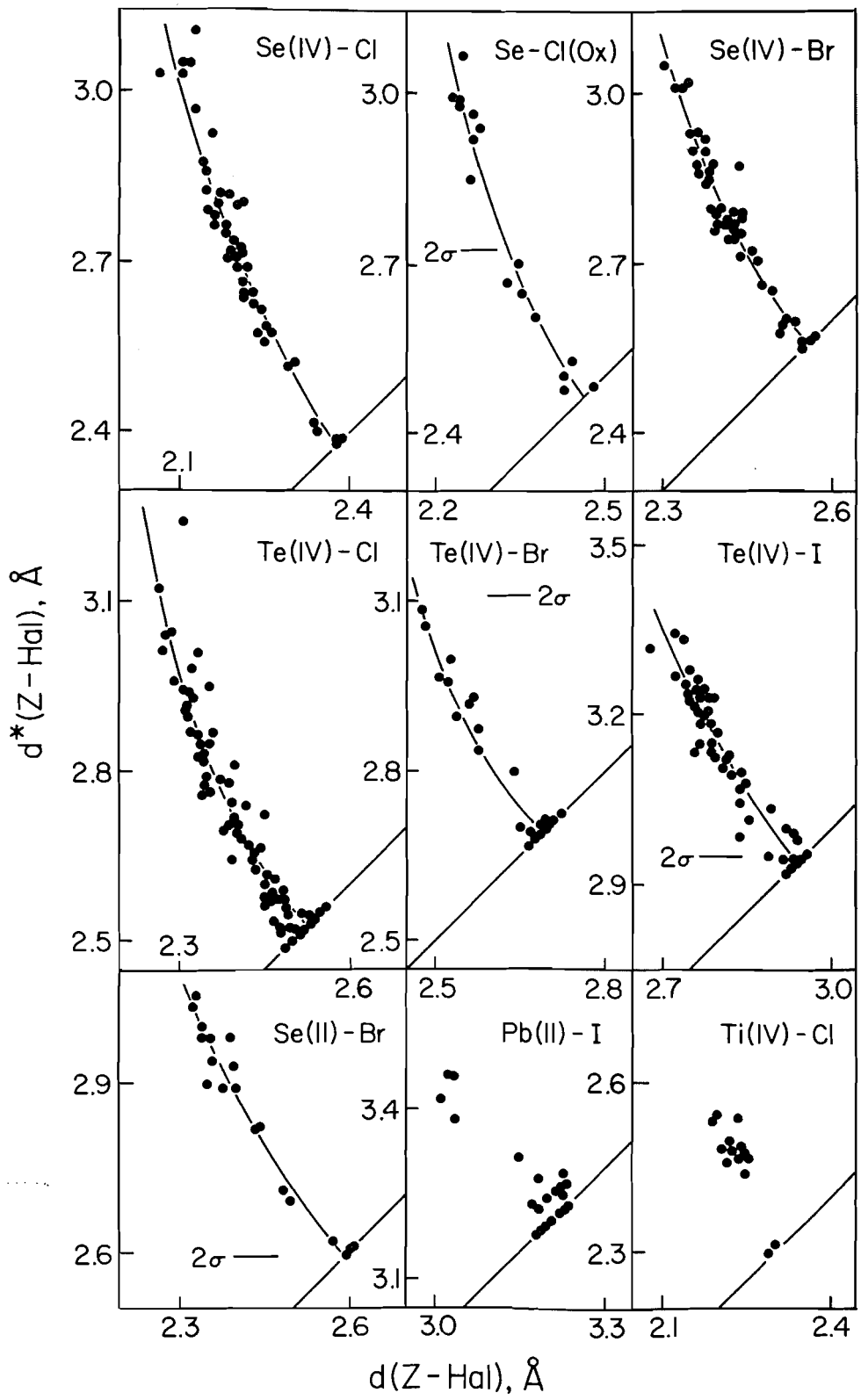

FIG. 1. d^* vs. d plots for conjugate Hal—Z—Hal* *trans* bonds in Se(IV), Te(IV), Se(II), Pb(II), and Ti(IV) halogeno compounds. Se–Cl(Ox) stands for Se(IV)–Cl(Ox). The correlation lines are for the DPF function. 1σ and 2σ indicate d^* values corresponding to $d = d_0(\text{CSBO}) + \sigma[d_0(\text{CSBO})]$ and $d = d_0(\text{CSBO}) + 2\sigma[d_0(\text{CSBO})]$, respectively; 0.05 indicates d^* corresponding to $d = d_0(\text{CSBO}) + 0.05$ Å; expt. indicates d^* corresponding to $d = d_0(\text{expt}) + 0.05$ Å; S&H indicates the d^* truncation limit of ref. 15 (see **C3**).

Can. J. Chem. Downloaded from www.nrcresearchpress.com by 109.225.110.28 on 09/08/12
For personal use only.

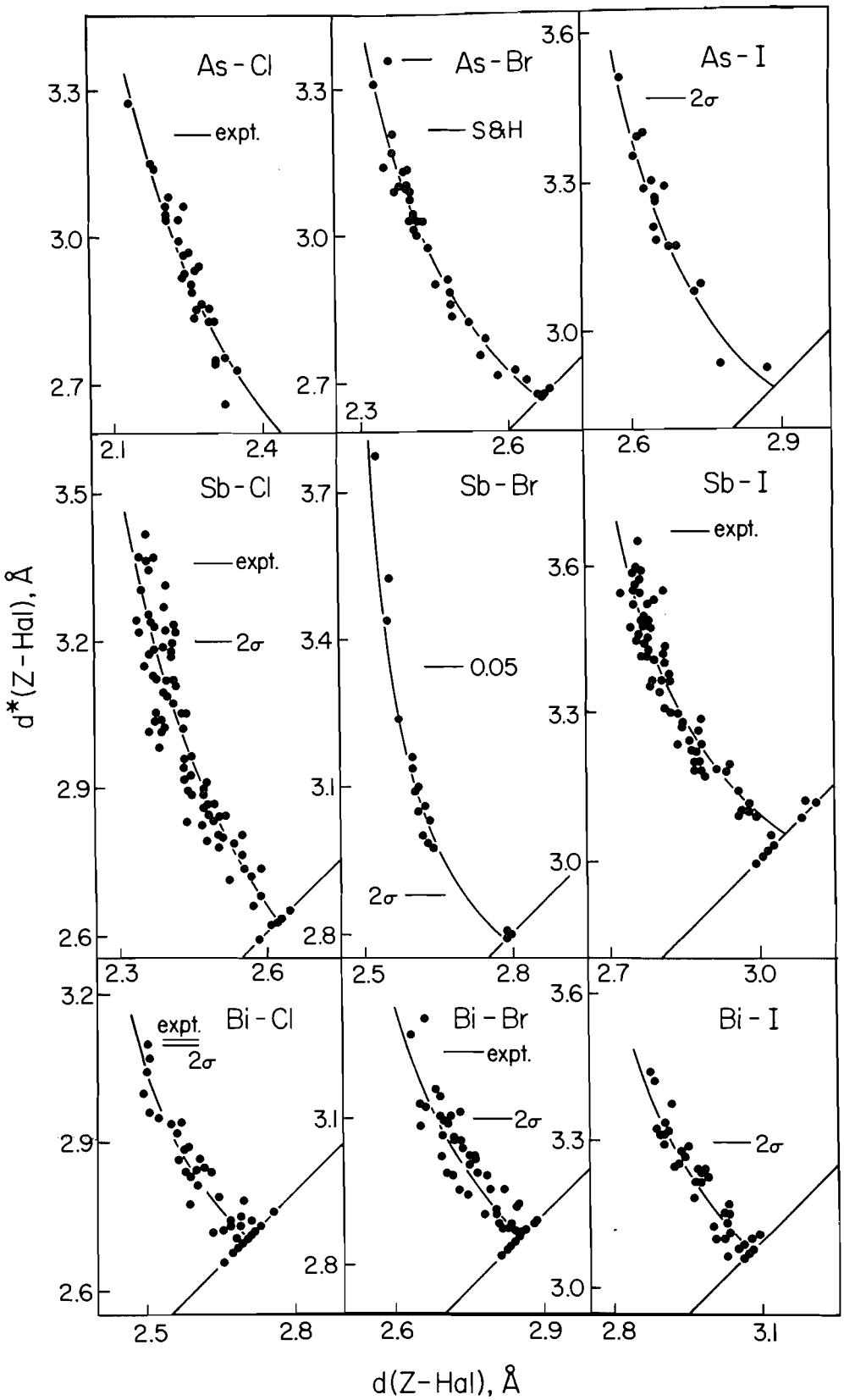

FIG. 2. d^* vs. d plots for conjugate Hal—Z—Hal* *trans* bonds in halogeno species of trivalent Group V elements (cf. caption of Fig. 1). The upper bar in the As–Br plot indicates d^* that corresponds to $d = d_0(\text{expt}) + 0.05$ Å.

Te(IV)–Hal:	$r^2 = 0.998$	$\sigma = 0.013$ Å,	$a_0 = 0.543(95)$ Å,	$a_1 = 1.091(48)$
Sb(III)–Hal:	1.000	0.001 Å	0.624(9) Å	1.102(5)
Bi(III)–Hal:	1.000	0.002 Å	1.023(13) Å	0.938(6)

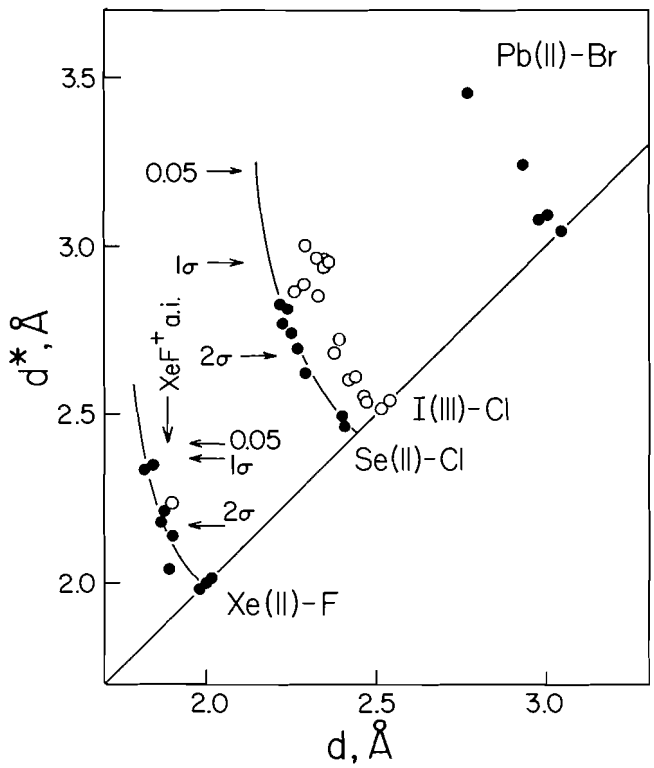

FIG. 3. d^* vs. d plots for conjugate Hal—Z—Hal* *trans* bonds in homoligand Se(II)–Cl, Xe(II)–F, I(III)–Cl, and Pb(II)–Br species (see caption of Fig. 1). Xe(II)–F: open circle, $Xe_2F_3^+$, *ab initio* value (33) not included in the regression.

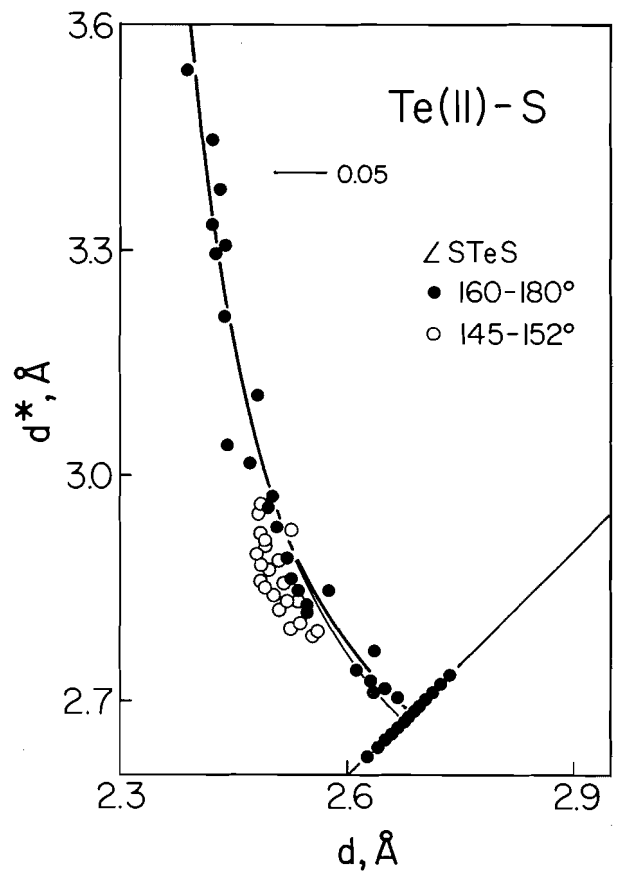

FIG. 4. d^* vs. d plot for conjugate S—Te—S *trans* bond pairs in Te(II)–S species. Full circles, **S** (on $d = d^*$ line) and **A1** data sets; open circles, **A2** data set. Thick line, DPF(**A1** + **S**) regression; thin line, DPF(**A1**) regression. For the 0.05 line see caption of Fig. 1.

Fits statistically indistinguishable from these are obtained when the d_e[CSBO(**A**)] or d_e(**A** + **S**) values are used; the latter give slightly lower error estimates. Since the regression lines for these three Z–Hal series are approximately parallel, one can roughly estimate the missing d_e values in those Z–Hal series where only two halogens are available (Fig. 5).

The estimated d_e(Z—F) obtained by extrapolation to $r(F^-)$ = 1.33 Å (Te(IV), 2.02–2.09 Å; Sb(III), 1.99–2.10 Å; Bi(III), 2.25–2.27 Å, depending on the TE regression used) all appear to be higher than the estimates from experiment (Fig. 5), but in view of the long extrapolation and of the various uncertainties involved these results should not be regarded as unreasonable.

The answer to **Q7** would be expected to be in the affirmative. By and large, the contributions to both **A** and **S** for the Z–Hal combinations examined originate in similarly-coordinate Z, although vagaries of uncontrolled sampling may be responsible for a disproportionate fraction of d_s values from discrete $ZHal_6^{n-}$ ions in some of the **S** sample populations. In the test of the d_e(**A**) and $\bar{d}_s$ values for equality (Table 3) a significance probability $P > 0.05$ indicates that the d_e(**A**) and $\bar{d}_s$ for that Z–L combination are statistically not distinct.[11] Inspection of the table reveals that with two exceptions P is always greater than the critical value, i.e., the test results confirm the above expectation of equality. The exceptions are Te(IV)–Cl and Bi(III)–Cl, for which P is very small. The reason for the low P values has not been investigated.

The statistical equivalence of d_e(**A**) and $\bar{d}_s$ thus legitimizes combining the **A** and **S** sample sets to one set, which can then be fitted to DPF(**A** + **S**) or DPF(**A**,**S**).

For the overall goodness of fit it is found that generally, for a given Z–L combination, $\sigma(\mathbf{S}) \sim \frac{1}{3}\sigma(\mathbf{A})$.

2. Problems involving d_0

In the empirical DPF model d_0 represents the asymptotic limit of d(Z—L) as defined by the Z–L sample used in the evaluation of TE(Z–L). Theoretically it should correspond to the limiting internuclear separation as determined by Z···L

[11]Hence d_e(**A** + **S**) and $\bar{d}_s$, too, must be statistically indistinguishable.

Can. J. Chem. Downloaded from www.nrcresearchpress.com by 109.225.110.28 on 09/08/12
For personal use only.

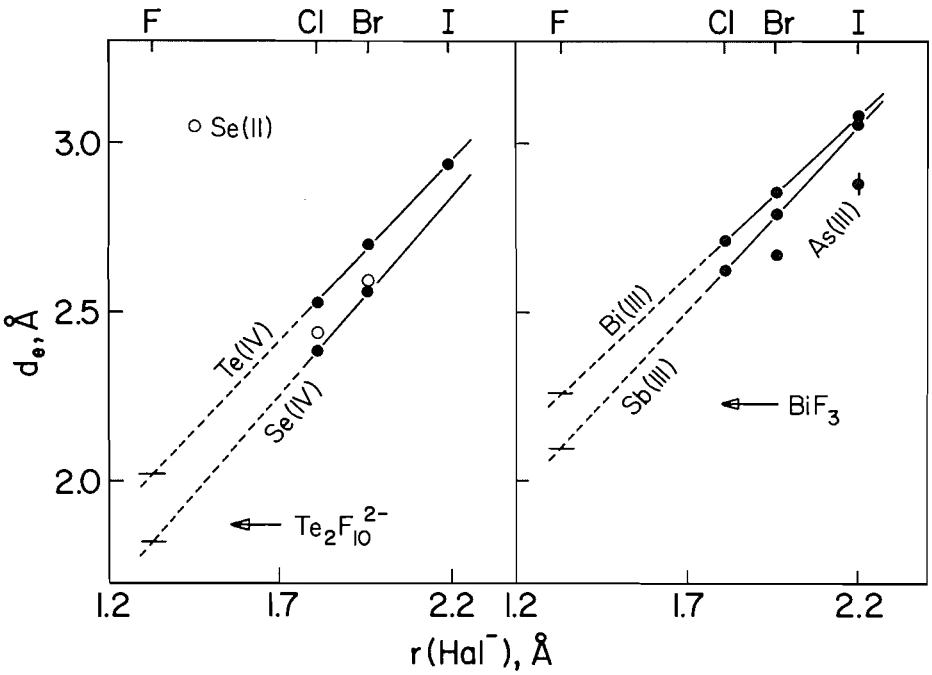

FIG. 5. Variation of d_e with the size of the halogeno ligand. BiF_3 indicates the smallest Bi—F bond length in BiF_3 (39) and $Te_2F_{10}^{2-}$ the smallest Te—F bond length in the pseudo μ_2-$[Te_2F_{10}]^{2-}$ dimer (18).

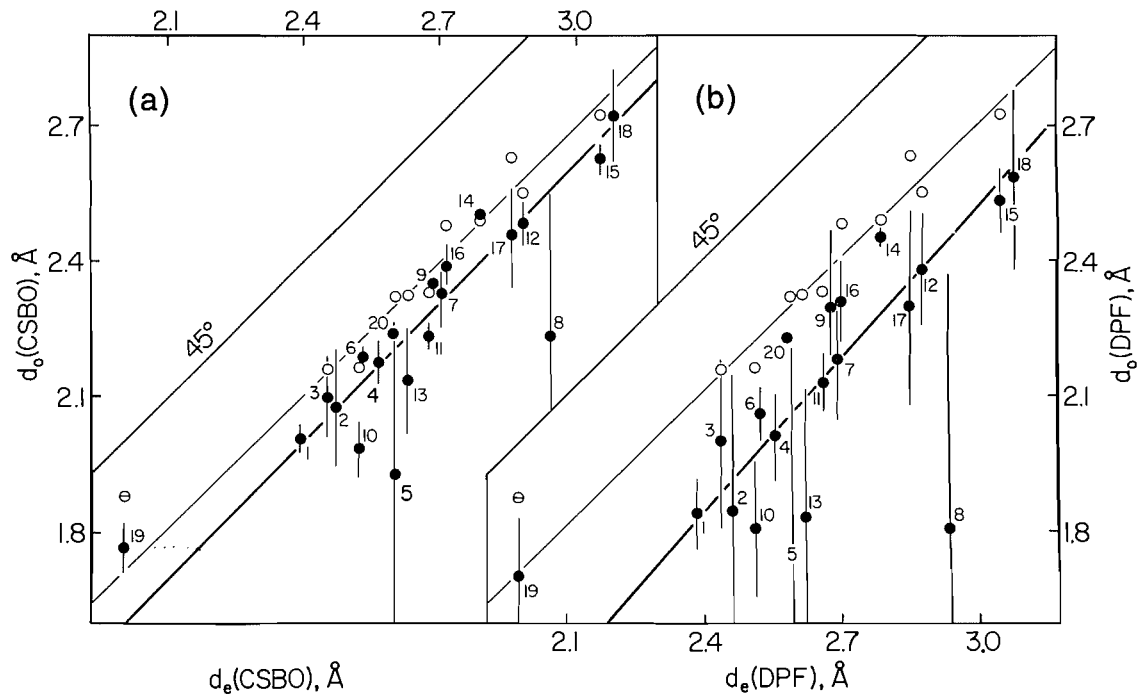

FIG. 6. Variation of d_0 with d_e for CSBO (*a*) and DPF (*b*). Full circles, optimized d_0; open circles, d_0(expt); circle with bar, *ab initio* d(Xe—F) in XeF^+ (not included in regressions). Thick line, regression of optimized d_0 on d_e with pairs 5, 8, and 19 excluded (see text). Thin line, regression of d_0(expt) on d_e. Numbering of Z–L combinations as in Tables 1 and 2.

repulsion at short range, but this is not possible to verify as we do not know how d(Z—L) in compounds of interest varies with external pressure. Clearly the confidence with which d_0 can be determined depends on the availability of d,d^* pairs at $d \rightarrow d_{0,\text{est}}$. The difficulty here is that in this region of the TE plot d^* increases steeply with d. Since all interatomic distances in a crystal are calculated from the same set of crystallographic parameters, the accuracy of d^* does not deteriorate as d^* increases. The problem is therefore one not of accuracy but of *eligibility* of large d^* for inclusion in the Z–L data set, especially in the presence of significant deviations from collinearity, i.e., when the coordination of Z at large Z · · · L distances is not sufficiently well defined. In doubtful cases one is therefore tempted to use extrapolation

Can. J. Chem. Downloaded from www.nrcresearchpress.com by 109.225.110.28 on 09/08/12
For personal use only.

TABLE 3. Likelihood-ratio test for equality of the d_e(**A**) and $\bar{d}_s$ values[a]

Z–L	n_A/n_S	d_e(**A**), Å	$\bar{d}_s$, Å	P
Se(IV)–Cl	48/4	2.381(12)	2.386(11)	0.717
Se(IV)–Br	43/9	2.558(8)	2.558(7)	0.995
Se(II)–Br	16/4	2.581(17)	2.598(4)	0.332
Te(IV)–Cl	81/40	2.511(5)	2.532(11)	0.001
Te(IV)–Br	17/24	2.692(6)	2.696(13)	0.524
Te(IV)–I	47/16	2.939(8)	2.937(8)	0.773
Te(II)–S	26/58	2.672(13)	2.685(17)	0.281
Sb(III)–Cl	82/2	2.618(14)	2.639(12)	0.186
Sb(III)–I	82/6	3.048(12)	3.043(47)	0.782
Bi(III)–Cl	39/21	2.719(7)	2.695(19)	0.001
Bi(III)–Br	46/13	2.862(9)	2.849(21)	0.203
Bi(III)–I	32/3	3.085(10)	3.072(6)	0.158

[a]n, number of d,d^* pairs in sample; P, significance probability (see **F**).

from the well-defined portion of the TE curve as a guide for the acceptance or rejection of large d^* values, thus ending up in a circular argument without improving the estimate of d_0. This matter is discussed in **C3**.

In CSBO d_0 by definition corresponds to the length of a Z—L bond of order one. This bond length should be accessible from experiment, but the precise meaning of this quantity is not clear. The d_0 (expt) values, for a particular Z–L combination, obtained by different experimental methods and under different conditions of temperature and aggregation will not be the same, and there is the problem of choice, availability, and experimental accuracy of the reference values. Thus for Z(III)–Hal of Group V previous authors (see **A4**) have used as d_0 the d_u bond lengths in $ZHal_3$, in the gas phase where available, otherwise in the crystal. Again, in $SeCl_4$ and $TeCl_4$ monomers the bond lengths are not known (the other $SeHal_4$ and $TeHal_4$, Hal ≠ F, monomers do not appear to exist in the vapour state), and the $SeHal_4$ and $TeHal_4$ tetramers that occur in the crystals do not contain Z—Hal bonds with unopposed ligands. The bond length in XeF^+, the presumed reference species for the Xe(II)–F set, has not yet been determined and *ab initio* estimates of unknown accuracy (see **B**) must serve instead as external d_0. In the circumstances the optimized, internally consistent d_0(CSBO) defined by the d,d^* sample itself seem a more satisfactory choice than d_0 values supplied externally. The d_0 (expt), d_0(CSBO), and d_0(DPF) sets are compared below.

The refined d_0(CSBO) as well as the d_0(DPF) are consistently smaller than the corresponding d_0(expt). When the d_u in $ZHal_3$ (23) and in $SeCl_2$(g) and $SeBr_2$(g) (18) are taken as d_0(expt) and regressed linearly on d_e one obtains d_0(expt) = −0.274(235) + 0.993(87)d_e, r^2 = 0.943, σ = 0.046 Å (Fig. 6),[12] from which, for the midpoint of the d_e = 2.4–3.1 Å range, Δ(expt) = 0.274 − 0.007d_e ~ 0.26 Å. A similar regression of d_0(CSBO) on d_e including all the Z–L sets of Table 2 except Xe(II)–F and P(III)–Br resulted in r^2 = 0.741. The d_0(CSBO) of Se(II)–Br and Te(IV)–I, because of their very large standard errors, tend to obscure the observed trend. Omission of these two points improved the correlation considerably while still accommodating the omitted d_0(CSBO) within their respective 1σ limits: d_0(CSBO) = −0.446(221) + 1.023(82)d_e, r^2 = 0.917, σ = 0.066 Å (Fig. 6*a*);[13] Δ(expt) ~ 0.38 Å at d_e = 2.75 Å. On the average, the refined d_0(CSBO) values are thus about 0.09 Å smaller than the d_u in the reference species, and the Δ(CSBO) about 0.12 Å larger than the Δ(expt). The mean difference d_0(CSBO) − d_0(expt) is just outside the joint 1σ of the two regressions and therefore statistically not significant.

The scatter in the d_0(DPF) vs. d_e plot (Fig. 6*b*) is more appreciable than for d_0(CSBO) but the trends are the same. Linear regression with the points for Xe(II)–F, Se(II)–Br, and Te(IV)–I omitted gave d_0(DPF) = −0.889 (931) + 1.136 (145) d_e, r^2 = 0.813, σ = 0.116 Å.[14] The d_0(DPF) values are thus consistently smaller than the corresponding d_0(CSBO) values, on the average by about 0.13 Å, and by about 0.22 Å smaller than the corresponding d_0(expt) values.

Comparison of the regression lines shows that while the d_0(expt) on d_e and the d_0(CSBO) on d_e regressions are statistically equivalent, the d_0(DPF) regression on d_e is equivalent to neither. This raises the question, is the difference in the fitted d_0 values due to the difference in the rate of the asymptotic convergence of DPF and CSBO and thus an artefact of the model, or is the difference real and the collective information content of the observed variation of d^* with d such that d_0(DPF) in fact represents an estimate of the asymptotic limit of the Z—L bond length as determined by nuclear repulsion at short range? The latter naturally would be smaller than the d_0(expt) obtained from the d_u of the reference species at ordinary pressures. At present no answer can be given (but see **C7**). However, the *practical* consequences of the differences in d_0 are not serious, for the d,d^* data sets are adequately fitted over the observed d ranges by both model functions, and either function can be used for predictive or verificative purposes up to the limit of chemical bonding between Z and L.

3. *Cut-off distance for effective bonding (Q3)*

The distance limit for effective chemical bonding is usually taken as ΣvdWr, the sum of the van der Waals radii of the two atoms involved in the putative bond. Although by its very nature this sum is not a precise quantity, it does provide an independent check on the reasonableness of the refined asymptotic bond-length limit d_0: the d(ΣvdWr) value conjugated to d^* = ΣvdWr and calculated from a TE regression should not exceed d_0. That this indeed is the case is demonstrated in Fig. 7, where the differences d(ΣvdWr) − d_0(CSBO) as well as d(ΣvdWr) are plotted against d_0(CSBO).[15] Since d^* = ΣvdWr falls on the steep portion of the TE curve, the d(ΣvdWr) value is not overly sensitive to variation in d^* = ΣvdWr. For As(III)–Br, for example, for which ΣvdWr ~ 3.95 Å, a decrease of 0.4 Å in d^* from 4.15 to 3.75 Å produces an increase in d of only 0.024 Å. Still, all the d(ΣvdWr) − d_0(CSBO) differences in Fig. 7 are greater than zero; the d(ΣvdWr) are, on the average, about 0.05 Å from the corresponding d_0(CSBO).

Sheldrick and Horn (15) consider that "the wide scatter of

[12]If the *ab initio* value for XeF^+ is included, the regression gives d_0(expt) = 0.124(171) + 0.848(64)d_e, r^2 = 0.951, σ = 0.057 Å.

[13]If Xe(II)–F is included, the regression gives d_0(CSBO) = −0.167(182) + 0.921(68)d_e, r^2 = 0.923, σ = 0.071 Å.

[14]With Xe(II)–F included, d_0(PDF) = −0.360(327) + 0.943 · (123)d_e, r^2 = 0.796, σ = 0.129 Å.

[15]Pauling's van der Waals radii; the value for Bi is taken as 2.25 Å.

Can. J. Chem. Downloaded from www.nrcresearchpress.com by 109.225.110.28 on 09/08/12
For personal use only.

Can. J. Chem. Downloaded from www.nrcresearchpress.com by 109.225.110.28 on 09/08/12
For personal use only.

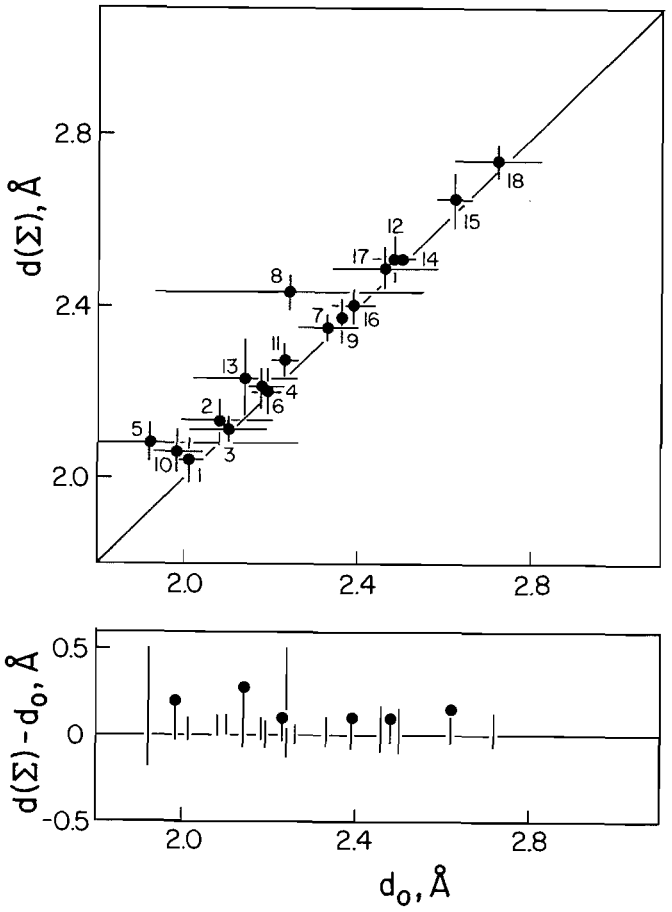

FIG. 7. Top: Comparison of d_0(CSBO) = d_0 with the bond length $d(\Sigma\text{vdWr}) = d(\Sigma)$ that results when d^* in the CSBO regression equation is equated with ΣvdWr, the sum of Pauling's van der Waals radii of Z and L. The uncertainty in $d(\Sigma\text{vdWr})$ does not include the uncertainty in the values of the radii themselves. Bottom: Variation of the difference $d(\Sigma\text{vdWr}) - d_0$(CSBO) with d_0(CSBO). Full circles, d_0(expt) values.

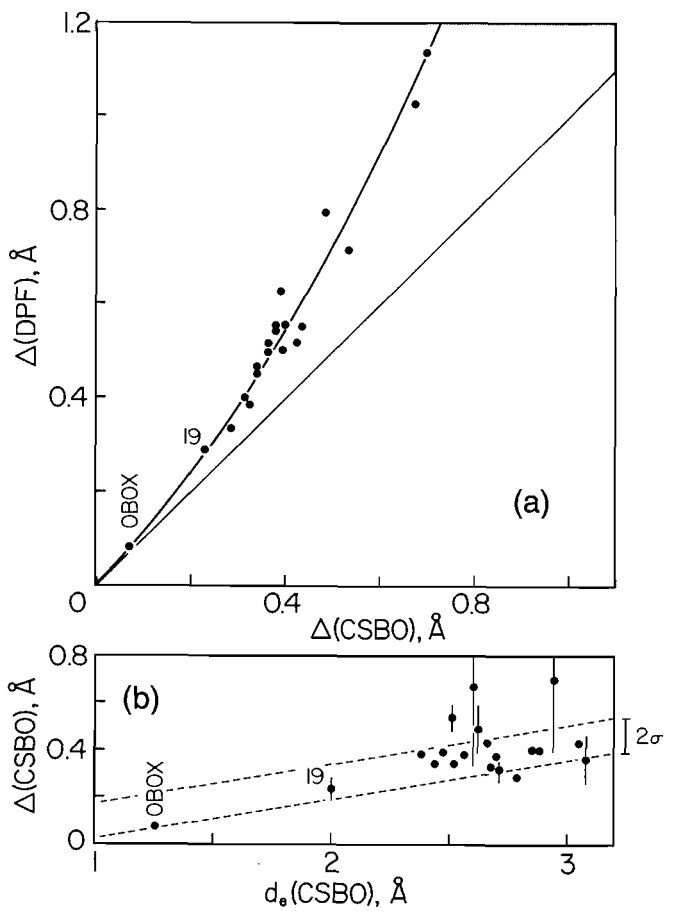

FIG. 8. (*a*) Comparison of Δ(DPF) and Δ(CSBO). (*b*) Variation of Δ(CSBO) with d_e(CSBO) over the extended d_e range.

d^* values observed for the extremely weak secondary bonds falsifies the observed [TE] trend."[16] In their treatment of the As(III)–Br set they therefore excluded d,d^* pairs for which $d - d_0(\text{expt}) \leq 0.05$ Å. Such truncation of course precludes in principle an answer to Q3, viz., can the cutoff for effective bonding be estimated from experimental data? Again, inclusion of d,d^* pairs that are only marginally governed by TE may vitiate this very endeavour.

To assess the effect of the above rejection criterion on a d,d^* sample set Figs. 1–4 indicate the d^* limits that correspond, respectively, to $d = d_0$(CSBO) + 0.05 Å, $d = d_0$(CSBO) + $\sigma[d_0(\text{CSBO})]$, $d = d_0$(CSBO) + $2\sigma[d_0(\text{CSBO})]$, and $d = d_0$(expt) + 0.05 Å, all as calculated from the CSBO regressions of Table 2; and, for As(III)–Br, also the d^* corresponding to $d = d_0$(expt) + 0.05 Å as calculated from the regression of ref. 15. The positions of these d^* limits vary from case to case and in several of the sets none of these limits is below the largest d^* value in the set (e.g., for Se(IV)–Cl, Se(IV)–Br, Sb(III)–I), but even where the limit is low, the scatter of the d,d^* points that are above the limit (i.e., candidates for rejection) is not appreciably worse than for the uncontested region of the TE curve. Rejection criteria based on such limits, if strictly applied, may therefore be unduly severe and may tend to eliminate much needed d,d^* pairs in the d region close to d_0.

4. Magnitude of TE and the involvement of lone pairs(s) on Z

As discussed in **C2**, the total variability Δ of d(Z—L) depends on d_0 and is therefore subject to the same uncertainty as the latter, with the result that Δ(DPF), Δ(CSBO), and Δ(expt) are not the same. The Δ(DPF) and Δ(CSBO) appear to be correlated: the difference between them increases with Δ and is satisfactorily represented by Δ(DPF) − Δ(CSBO) = $0.864[\Delta(\text{CSBO})]^2$ (Fig. 8*a*). Concomitant with this divergence of Δ(DPF) and Δ(CSBO), whether by accident or otherwise, is the general increase with Δ of the standard errors on the Δ values.

For Z–L combinations having d_e in the 2.4–3.1 Å range (i.e., all those in Fig. 4 except Xe(II)–F) Δ was found to vary only slightly with d_e (see **C2**). While this finding can be claimed to hold over that limited d_e range, given the large standard errors on d_0, its validity would not be expected to extend to low d_e values: the variability, for example, of d(Z—F) due to TE is significantly smaller than for other Z–Hal combinations (cf. ref. 1). In an attempt to elucidate this apparent discrepancy we have included, in the plot of

[16]As noted in **C2**, the accuracy of the large bond lengths is not significantly inferior to that of the short bond lengths, since all the interatomic distances in a crystal structure are calculated from the same set of atom coordinates and unit-cell dimensions. Hence by and large the scatter has other origins.

Can. J. Chem. Downloaded from www.nrcresearchpress.com by 109.225.110.28 on 09/08/12
For personal use only.

Δ(CSBO) against d_e(CSBO) (Fig. 8*b*), Xe(II)–F as well as the point for B(III)–O based on *ab initio* results for OBOX species (see **D1**). Although the trend that now emerges depends critically on the two additional points, it strongly suggests that, over a wider range of d_e, Δ increases with d_e. If a linear variation is assumed and the points for Se(II)–Br and Te(IV)–I are excluded from the regression because of their large errors (cf. **C2**), one obtains $\Delta(\text{CSBO}) = -0.067(113) + 0.166(44)d_e$, $r^2 = 0.474$, $\sigma = 0.075$ Å, from which it follows that $[\Delta(\text{CSBO})/d_e]_{\text{lim}} \sim 0.166$. This, qualitatively, is an important and plausible finding. For example, d_e for the N—N—N *trans* bond pair in azides and hydrazoic acid derivatives is 1.18 Å; the total variability of d(N—N) expected from Fig. 8*b* would be 0.13(8) Å. This is consistent with the experimental estimate of the upper bound of Δ(N—N), 0.08 Å (40); other examples can be adduced in support of this trend. The tentative conclusion thus is that the total spread Δ of d(Z—L) varies roughly linearly with d_e, the *strength* of TE then being determined by the magnitude of c (eq. [5]) or b_0 (eqs. [4] and [8]). The quasi-linear variation of Δ with d_e is also consistent with the variation of the bond-length difference $d_s - d_u$ with d_s observed in molecular species having certain geometries (see **D2**).

In mononuclear ZL_n^{ε} species an observable TE may arise from internal or from external causes. The bond length disproportionation in the discrete octahedral 14-valence-electron $ZHal_6^{n-}$ anions in asymmetric environments is largely (though not exclusively) the consequence of the stereochemical activity of the lone electron pair on Z (cf. ref. 41 and literature therein) and thus in the internal causes category. By contrast, in $XeF_2 \cdot MF_5$ and related adducts (Fig. 3) the Xe—F bond-length inequality is caused *externally*, by a weakening of one of the two Xe—F bonds through electron-abstracting interaction with MF_5, and with $[FXe]^+[FMF_5]^-$ as the extrapolation limit. The lone pairs on Xe are perpendicular to the F—Xe—F* *trans* bond pair and thus not involved in the bond-length compensation in any obvious way. Again, the TE in OBO*X (see **D1**), which results when $[OBO]^-$ forms a bond to X, cannot involve a lone pair as there are no lone pairs on the B atom. The conclusion would seem to be that TE depends on the stereochemical activity of a lone pair on Z only insofar as the lone pair is responsible for the formation of "secondary" bonds participating in conjugate *trans* bond pairs.

Let us now consider bridged halogeno species. Presence of a lone pair on Z seems to be essential in the discrete $[(\mu_2\text{-}Zi_2Hal_6)(Hal_\perp)_{0\text{-}4}]^{\varepsilon}$ dimers[17] in which large bridge asymmetry (and thus large TE) is observed. This is the case when Z is Se(IV), Se(II), Te(IV), I(III), or a Z(III) from Group V (15, 16; ref. 1 and literature therein). The bridge asymmetry decreases along the sequence Hal = (F), Cl, Br, I (1). When the lone pair is absent, the bridge asymmetry is generally small, sometimes negligible, and TE can vary considerably. Thus in the discrete $(Ti_2Cl_{10})^{2-}$ dimer (42, 43) the bridge asymmetry is small but the difference $\delta = d_{\text{bridge}} - d_{\text{terminal}}$ is ~0.23 Å (Fig. 1). In another $Z(d^0)$ species, $[Zr_2Cl_{10}]^{2-}$ (44), the bridge asymmetry is negligible and $\delta = 0.20$ Å (for other examples of and comments on μ_2-$[T_2Hal_{10}]^0$ and μ_2-$[T_2Hal_{10}]^{2-}$ dimers see ref. 1). In planar μ_2-$T_2Hal_6^{\varepsilon}$ (T = Au(III), Pd(II), Pt(II), Cu(II)) dimers the double bridge is practically symmetric and $\delta \leq 0.1$ Å, sometimes well below this value (45).[18]

*5. Effect of bond angle (**Q6**)*

Deviations from collinearity would be expected to play a rôle in TE, but this effect is difficult to establish with clarity. The bond angle in most of the Z–Hal data sets varies considerably, depending on the preponderance of the coordination geometries included in the sample. Typical distributions of the bond angles are illustrated by the following:[7]

			γ_1	γ_2
Se(IV)–Cl:	165.0–179.1°	⟨172.8(34)⟩°	−0.15	2.65
Se(IV)–Cl(Ox):	154.1–168.7°	⟨164.3(47)⟩°	−1.01	2.87
Se(II)–Cl:	169.7–178.8°	⟨174.4(26)⟩°	−0.10	2.41
As(III)–Br:	164.2–176.3°	⟨170.3(34)⟩°	−0.16	1.80
Bi(III)–Br:	161–179.9°	⟨173.5(47)⟩°	−0.79	2.87
Bi(III)–I:	163.9–176.7°	⟨171.8(33)⟩°	−0.63	2.45

(Centrosymmetric d_s, d_s pairs are not included in the range and means.)[19] These numbers indicate that unless the bond angle is constrained to 180° by symmetry at Z, it tends toward a mean value the difference of which from 180° reflects the stereochemical composition of the sample. This tendency is particularly noticeable in the Se(IV)–Cl(Ox) set, which is based on square-pyramidal $SeOCl_4$ units with O—Se—Cl angles greater than 90°.[20] All the above bond-angle distributions are skewed toward 180°, i.e., the tendency of the sample to noncollinearity is smaller than the mean would indicate.

Examination of several of the data sets for possible correlation between deviations from the fitted d^* values and the bond angles has so far proved inconclusive, although there appears to exist a very weak trend of the bond angle toward 180° as d tends toward d_e. On the whole, the less discrete the nature of the Z,Hal unit containing the *trans* bond pair(s), the larger the deviations of the bond angles from 180° and the greater their scatter, as evident in the Z–F sets, e.g., Sb(III)–F (35).

An unusual angle distribution is encountered for 4-coordinate Te in the Te(II)–S data set (see **B** and Fig. 4). The d,d^* pairs in the asymmetric **A1** subset are derived mostly from square-planar TeS_4 units with monodentate ligands, whereas those in the asymmetric **A2** subset come from trapezoidal-planar units in which the S atoms belong to two *cis*-S_2 pairs, each from a bidentate ligand molecule.[8] The latter arrangement is in fact an incomplete pentagonal-planar coordination, which accounts for the closeness of the S—Te—S angle in **A2** to $(360°/5) \times 2 = 144°$. The **A1** and **A2** angle distributions do not overlap.

Regressions for the **A1** + **S** subset show that this is a well-behaved d,d^* set, in fact one of the best examined here. The DPF(**A1**,**S**) and DPF(**A1**) regressions yield results that are statistically indistinguishable from DPF(**A1** + **S**). Keeping in mind that the goodness of fit σ for the reference regres-

[17]$Hal_\perp$ is perpendicular to the μ_2-Z_2Hal_6 bridge plane.

[18]Bonding in planar μ_2-$T_2Cl_6^{\varepsilon}$ d^8 dimers is considered in ref. 46, but its discussion there is unhelpful for understanding the magnitude of TE in these dimers.

[19]One of the noncentrosymmetric d_s pairs in the Bi(III)–Br set has an angle of 168.5° (C_2) and another, 178.0° (C_s); in the Bi(III)–I set, one d_s pair has an angle of 170.6° (C_2).

[20]The mean for 29 O—Se—Cl angles (ranging from 89.3 to 104.0°) in $SeOCl_4$ units (cf. ref. 1) is 98.0(40)°, $\gamma_1 = -0.47$, $\gamma_2 = 2.44$.

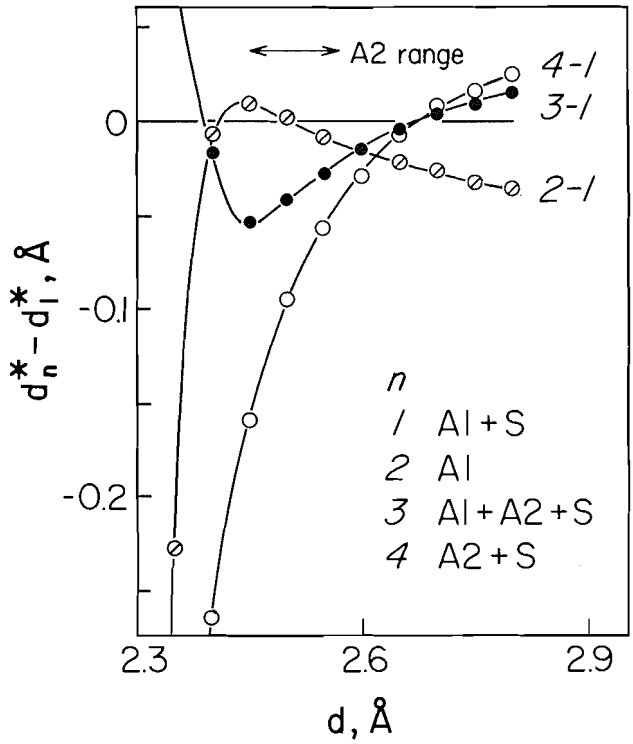

FIG. 9. Effect of bond angle on d,d^* correlations in Te(II)–S (see **B** and Fig. 4). **A1**, asymmetric *trans* population; **A2**, asymmetric quasi-*trans* population, S—Te—S = 145–152°; **S**, symmetric population. *2–1*, d^*[DPF(**A1**)] − d^*[DPF(**A1** + **S**]; *3–1*, d^*[DPF(**A1** + **A2**,**S**] − d^*[DPF(**A1** + **S**)]; *4–1*, d^*[DPF(**A2**,**S**)] − d^*[DPF(**A1** + **S**)]. Goodness of fit of the DPF(**A1** + **S**) regression, σ = 0.044 Å.

sion DPF(**A1** + **S**) is 0.044 Å, DPF(**A1**) and DPF(**A1**,**S**) are indistinguishable over the entire observed d,d^* range (Fig. 9). To test for the effect of the bond angle, regressions involving **A2** were attempted. Convergence was achieved for DPF and CSBO of **A2**,**S** (n_A = 23, n_S = 58) and **A1** + **A2**,**S** (n_A = 49, n_S = 58):

A2,**S**, σ_A = 0.033 Å, σ_S = 0.017 Å
DPF: r^2 = 0.957, d_0 = 2.329(110) Å, K = 0.198(71), c = 0.568(123), d_e = 2.685(2) Å, Δ = 0.356(110) Å
CSBO: r^2 = 0.957, d_0 = 2.358(77) Å, b_0 = 0.369(118) Å, b_1 = 0.314(98), d_e = 2.737(6) Å, Δ = 0.379(72) Å.

A1 + **A2**,**S**, σ_A = 0.072 Å, σ_S = 0.017 Å
DPF: r^2 = 0.931, d_0 = 2.337(11) Å, K = 0.168(5), c = 0.690(41), d_e = 2.684(2) Å, Δ = 0.347(11) Å
CSBO: r^2 = 0.922, d_0 = 2.370(5) Å, b_0 = 0.397(16) Å, b_1 = 0.181(36), d_e = 2.737(3) Å, Δ = 0.367(5) Å.

From Fig. 9 it is clear that the differences between the d^* calculated from DPF(**A1** + **S**) and the d^* calculated from DPF(**A1** + **A2**,**S**) are, over the observed d,d^* range, within 1σ of DPF(**A1** + **S**) and thus not significant. The d^* differences between DPF(**A2**,**S**) and DPF(**A1** + **S**) are large at small d values but quite small at large d; within the d(**A2**) range they are completely within 3σ of DPF(**A1** + **S**).

These comparisons and a statistical test (see **F**) lead to the conclusion that, statistically, the **A1** + **S** and **A2** populations are only marginally different, even though the two belong to different stereochemistries. This would be consistent with the visual impression of the *prima facie* evidence of Fig. 4 if one had no prior knowledge of the distinction between the **A1** and the **A2** points.

The lesson to be learnt here is that the *appearance* of a d,d^* plot may not, and probably will not, be sufficient to suggest the existence of two or more angle-differentiated populations in the d,d^* sample set if there is no *a priori* reason to suspect that the set is in fact composite. This would be so especially when the difference in the means of the stereochemically distinct angle distribution is relatively small or when the distributions significantly overlap. Inability to recognize and identify the d,d^* subsets may then lead to undifferentiated d,d^* regressions and to inferior TE correlations.

*6. Effect of heteroligands on TE (**Q3**)*

When the halogen coordination of Z in a Z–Hal species is not homoligand, the presence of non-halogen heteroligands (e.g., O, CH_3, CN) may affect TE in the conjugate Hal—Z—Hal *trans* bonds to a degree where the correlation equation for the pure homoligand species does not adequately accommodate the Z—Hal,Z—Hal* pairs in the heteroligand species. A case in point is TE for the homoligand Se(IV)–Cl species as compared to the square-planar $SeCl_4$ groupings with perpendicular Se—O bonds, specifically $Se_2Cl_{10}^{2-}$ (data set Se(IV)–Cl) vs. $Se_2O_2Cl_6^{2-}$ (data set Se(IV)–Cl(Ox)). In these centrosymmetric μ_2-dimers the bridge plane contains also four terminal Se—Cl bonds. The remaining four terminal Se—Cl bonds in $Se_2Cl_{10}^{2-}$ and the two Se—O bonds in $Se_2O_2Cl_6^{2-}$ are approximately perpendicular to the bridge plane (Fig. 1 of ref. 1). Statistical comparison of Se(IV)–Cl and Se(IV)–Cl(Ox) (see **F**) reveals that the Se—Cl,Se—Cl* bond-length pairs in these two sets *do not* come from the same population. This is not evident from the values of most of the regression parameters if their standard errors are taken into account, but for d_e (Se—Cl) the difference is immediately seen: the two d_e values differ by 0.085(19) Å, which is outside 3σ = 0.057 Å and thus clearly significant (but see **C7** for d_0).

A second example is TE in conjugate P(III)—Br *trans* bonds. Figure 2 of ref. 11 is a plot of $d^* - d_0$ vs. $d - d_0$ for PBr_4^-, PCl_4^-, and several heteroligand P(III)–Br anions. The $PBr_2(CN)_2^-$ anion in the solvated Na-[18]crown-6 salt (20) has C_2 symmetry (Br—P—Br, 171.4°), so that $d^* = d \sim d_e$ = 2.496(1) Å. The DPF and CSBO correlation curves defined by the three PBr_4^- pairs (see **B**) extrapolate to d_e = 2.588 Å, i.e., to a value ~0.09 Å higher. Because of the statistical inadequacy of this P(III)–Br set we have no error estimate for this value, but the difference of ~0.09 Å is believed to be significant.[21]

*7. Effect of oxidation state (**Q4**)*

A change in the oxidation state of Z entails the attendant changes in the coordination number and the effective size of Z. Since these changes are interdependent, differences in TE that may result on going from one oxidation state to another cannot be said to be specifically due to the change in the oxidation state. The overall effect on TE can at present be compared for the pairs Se(IV)–Cl/Se(II)–Cl and Se(IV)–Br/Se(II)–Br.

[21]This extrapolated d_e value is supported from a linear regression of d_e(CSBO) on d_0(expt) for Z(III)—Br (Z = P, As, Sb, Bi): r^2 = 0.922, σ = 0.013 Å, d_e(CSBO) = 1.117 + 0.665d_0(expt), from which d_e for P(III)—Br is 2.59 Å.

Can. J. Chem. Downloaded from www.nrcresearchpress.com by 109.225.110.28 on 09/08/12
For personal use only.

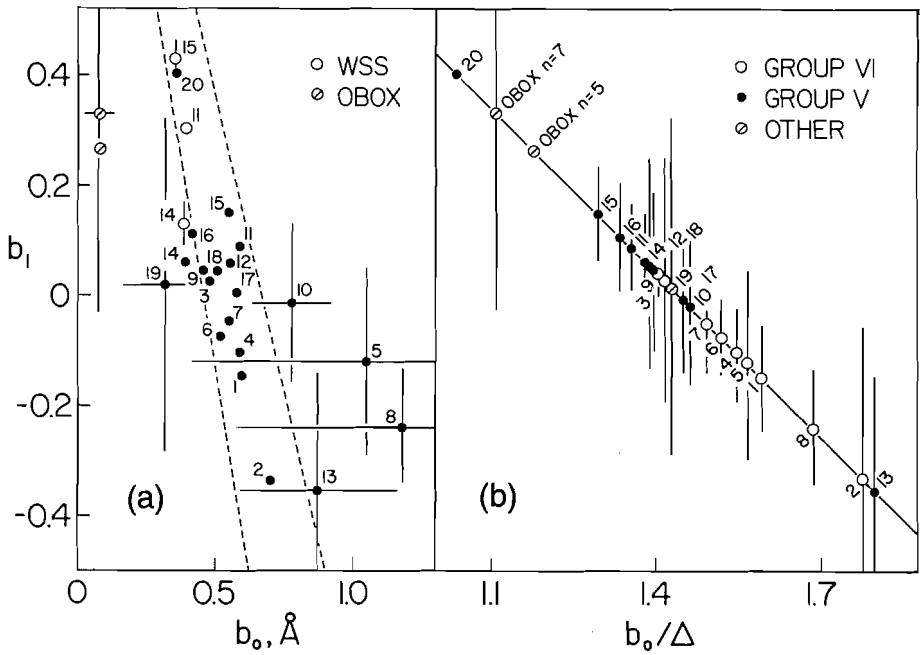

FIG. 10. Correlation of the optimized CSBO parameters b_0 and b_1. (*a*) WSS, Sheldrick *et al.* (15, 16); OBOX, *ab initio* values for OBO*X (see **D1**). For the broken lines see **C8**. Error bars shown only for points outside the region between the broken lines. (*b*) Plot of b_1 vs. b_0/Δ (eq. [8]). Standard error not available for P(III)–Br (no. 20, see text) and very small for OBOX, $n = 5$.

As would be expected, the d_e values are larger for Se(II) than for Se(IV). For the Cl pair the difference is 0.055(15) Å, i.e., ~0.06 Å > 3σ. For the Br pair the difference is smaller, 0.037(9) Å, i.e., ~0.04 Å > 3σ. However, the differences in the *refined parameters* are all smaller than the respective pooled esd's of the parameters and therefore statistically meaningless. This calls for testing the hypothesis that the Se(IV)–Cl and Se(II)–Cl samples come from the same population. Appropriate tests (see **F**) show that for the Cl pair this hypothesis can be rejected with considerable confidence and somewhat less strongly for the Br pair. The conclusion from the present data thus is that the change in the oxidation state affects TE in a significant way.

Closer scrutiny of the regression results for the three Se–Cl sets brings to light an additional interesting observation. The d_0(CSBO) values for Se(IV)–Cl, Se(IV)–Cl(Ox), and Se(II)–Cl are 2.006(29), 2.075(129), and 2.098(90) Å, respectively (Fig. 6*a*). All three are accommodated by the 1.5σ interval of the unweighted mean, 2.060(39) Å; a more comprehensive test (see **F**) shows that the three d_0 values are *not* significantly different even at the 0.10 level. This would suggest that, at least for the three cases considered, the *limiting* Se—Cl bond length as estimated by the CSBO treatment depends neither on the oxidation state nor on the presence of heteroligands on the Se atom. The same result is obtained with the Se(IV)–Br and Se(II)–Br sets, though less convincingly because of the very large standard errors on the d_0(CSBO) of Se(II)–Br. The implications of this finding are touched upon in **E**.

*8. Correlation of parameters (**Q4**)*

The values of the DPF and CSBO parameters would be expected to reflect the chemical regularities of the Z–L combinations. When b_1 is plotted against b_0 (Fig. 10*a*), the points for Z from Group VI appear to segregate roughly in the $b_1 < 0$ region of the plot and those for Z from Group V in the $b_1 > 0$ region, with most of the points falling within the area between the broken lines and defined, for $d_e = 2$ Å (right) and $d_e = 3$ Å (left), by the regression equations of **C2**. However, the expected consistency in the Cl, Br, I order in the Z–Hal triads is lacking. A similar situation is encountered in K vs. Δ(DPF) and log Δ(DPF) vs. log [K/Δ(DPF)] plots.

These observations are puzzling until it is realized that the three parameters each in the DPF and CSBO regressions are statistically very highly correlated. This correlation has its origin in the functional form of DPF and CSBO.[22] From eq. [8] we have $b_1 = (1/\ln 2) - (b_0/\Delta)$, which is the basis of the rectified plot, Fig. 10*b*. This plot displays the apparent segregation of the Group VI and Group V points, as well as the irregularities in the Z–Hal sequences, more dramatically than Fig. 10*a*. Because of the above algebraic constraint the triplet of b_0, b_1, and Δ values that results from a convergent CSBO optimization of any d,d^* sample set or subset will be accommodated on the straight line of Fig. 10*b*, regardless of how well the d,d^* sample represents the d,d^* population. For an *ideal* d,d^* population the regression would amount to a straightforward algebraic functional dependence: the positions of the Z–L points on the straight line would be exactly determined and presumably in the proper chemical order. The position of the point for a d,d^* *sample* set or subset, however, is determined by the requirement that the regression for that set converge to the model function, and the closeness of the point to the "true" position on the line thus depends on the magnitude of $\sigma(b_1)$. The order of the points in the sequence of Fig. 10*b* can then be changed by moving the points along the straight line within the projec-

[22]Very high correlations are to be expected for any model function in which the parameters of refinement are not separated.

Can. J. Chem. Downloaded from www.nrcresearchpress.com by 109.225.110.28 on 09/08/12
For personal use only.

tions of their respective $\sigma(b_1)$ intervals. The uncertainty in the ordering can be decreased only by reducing the errors on the parameters, i.e., by improving the selfconsistency of the individual d,d^* data sets. Considering the present uncertainty in the b_1 values it is difficult to know whether special significance should be ascribed to the sign of b_1, i.e., whether $b_1 = 0$ corresponds to a boundary between two chemically distinguished regions of the b_1 vs. b_0/Δ plot.[23] Much the same situation as for CSBO is encountered in the rectified c vs. (log K)/log Δ(DPF) plot.

9. Comparison of DPF and CSBO

For a given Z–L data set the figures of merit, r^2 and σ, of the DPF(**A** + **S**) and CSBO(**A** + **S**) regressions are the same, i.e., the d,d^* pairs in an individual Z–L set are fitted equally well by both, and the same is true of the **A**,**S** regressions. Furthermore, the difference between the d_e values from DPF(**A** + **S**) and CSBO(**A** + **S**) is smaller than 0.005 Å and thus statistically negligible. Because of this and because of the smallness of its standard error, d_e is the regression parameter in which we can place most confidence, and with respect to which we can assess differences between the DPE and CSBO treatments.[24]

In Fig. 11 c and b_1 are plotted against d_e. By themselves these two plots do not enhance any trends that may have been suggested by the previous figures. However, their quasi-mirror symmetry seems to indicate the existence of a direct relationship between c and b_1, i.e., between DPF and CSBO. Indeed, the plot of c vs. b_1 (Fig. 12) mutually corroborates the consistency of the results obtained by independent fitting of the data sets to the two model functions. It can be shown from eqs. [3] and [4] that a c,b_1 correlation line must pass through the point $c = 0,b_1 = 0$. We also have the c and b_1 values for the OBO*X ($n = 5$) set, for which each fit is extremely close (see **D1**). A straight line passing through these two points is seen to accommodate all the Z–L points within their respective 1σ intervals but in most cases much more closely. This quasi-linearity of the c,b_1 correlation would have been difficult to predict from the complicated implicit function of the parameters that is obtained by combining eqs. [3] and [4]. The order of the c,b_1 points along the correlation line follows that of Fig. 10*b*.

The relationship between DPF and CSBO suggested by Fig. 12 leads one to expect that the conclusions formulated for Z–L combinations on the basis of the CSBO regressions will not differ from those obtained from DPF. This is certainly true of both the values and the order of d_e and essentially true of d_0. However, the standard error on d_0(CSBO) is consistently about half that of the standard error on d_0(DPF). On balance, while for practical purposes a Z–L d,d^* set is equally well fitted by DPF and CSBO, the latter function is to be preferred to DPF if only because it is not purely empirical. This said, DPF is more convenient for manipulation, and if eq. [3] is recast to eq. [5] it can be interpreted in chemical terms, with d_0 the limiting bond-length value, Δ the total d bond-length range, and c the curvature-determining exponent. By contrast, the b_0 and b_1 parameters have a more implicit, less intuitive meaning.[25]

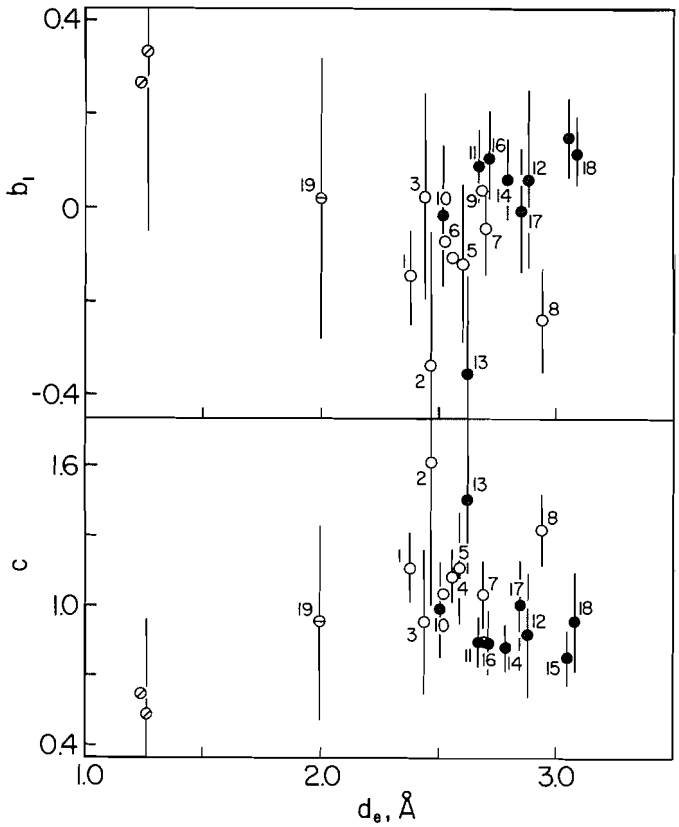

FIG. 11. Correlation of the parameters b_1 (top) and c (bottom) with d_e (**A** + **S** regressions). Open circles, Z from Group VI; full circles, Z from Group V; crossed circles, OBO*X.

D. General considerations

1. Support from ab initio *calculations (Q1, Q2)*

The existence and essential independence of the TE compensation and its regularity can be demonstrated on a centrosymmetric ZL_2 molecule in which the electron density in one of the bonds is decreased by formation of an L—X bond to a fourth atom, L—Z—L → L—Z—L*—X. An experimental LZL*X series suitable for the demonstration would be difficult to find, not to speak of interference from extraneous factors likely to confuse the expected trends. However, useful series can be generated by *ab initio* optimizations of the equilibrium ground-state geometries of LZL and LZL*X molecules, provided the calculations are self-con-

[23]For their As(III)–Br, Sb(III)–Br, and Sb(III)–I data sets Sheldrick *et al.* (15, 16) found $b_1 > 0$, in agreement with Table 2, but they failed to observe a $B,(d - d_0)$ correlation for their Sb(III)–Cl set (16). This presumably implies $b_1 \sim 0$. They explain this lack of correlation by an ad hoc argument involving the magnitude of the antibonding contribution of the Sb(5*s*) orbital. The result for our Sb(III)–Cl set is a negative, numerically large b_1, but the standard errors on b_1 and on the other refined parameters are large. A detailed reexamination of the Sb(III)–Cl d,d^* pairs seems desirable, especially if it is confirmed that in general b_1 can assume both negative and positive definite values, as found in our regressions.

[24]Sheldrick's (15, 16) d_e and Δ are not the same as ours. In the former, $d_e' - d_0(\text{expt}) = (b_0' \ln 2)/(1 - b_1' \ln 2)$, with b_0' and b_1' obtained from a linear optimization. In the latter, $d_e - d_0 = (b_0 \ln 2)/(1 - b_1 \ln 2)$, with d_0, b_0, and b_1 optimized simultaneously by a nonlinear regression (see **A4**).

[25]In this context even the meaning of B in Pauling's relation[4] ceases to be intuitive if the relation is written as $D(n) = D(1) - \ln n^B$, i.e., when B is formulated not as a scaling factor of ln n but as an empirical power of the bond order (cf. eq. [6]).

Can. J. Chem. Downloaded from www.nrcresearchpress.com by 109.225.110.28 on 09/08/12
For personal use only.

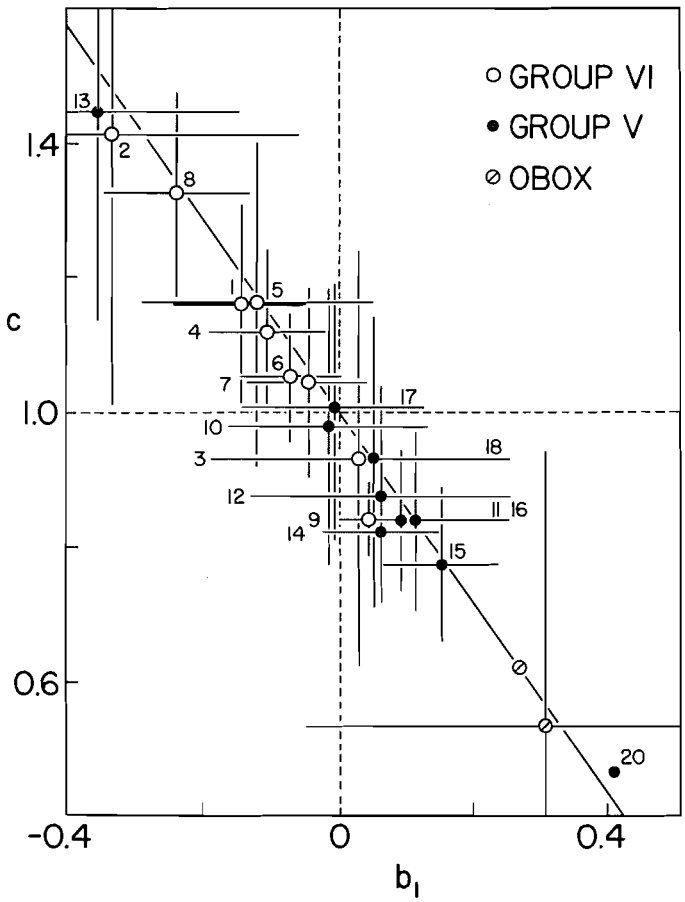

FIG. 12. Correlation of the parameters c and b_1 (**A** + **S** regressions). Standard errors not available for P(III)–Br (no. 20; see text).

sistent within the series and at a level that is known to yield reasonably realistic geometries. Halogens as ligands are a poor choice for this purpose because of chemical restrictions on the L–X combinations, but the series deriving from the 16-valence-electron BO_2^- metaborate ion monomer (isoelectronic with CO_2) is well suited to illustrate the operation of TE in isolated homoligand species.

The conjugate B—O bond lengths obtained from 6-31G* optimizations for BO_2^-, OBO*X (X = H, F, Cl, Li), and *cis*- and *trans*-B_2O_3 = OBO*BO (Table 4) are plotted against each other in Fig. 13*a*. The OBO angle in these molecules is either 180° by symmetry or within 3° of 180°. It is immediately obvious that the disposition of the d,d* points in this plot resembles Figs. 1–4. To demonstrate the concomitant variation of the electron density, the density ρ_c at the bond critical point is plotted in Fig. 13*b* against the corresponding bond length d(O—B) or d*(B—O*). This plot is expected to conform to the functional dependence $\rho_c = sd^{-v}$ for B—O bonds (cf. ref. 47); to support and strengthen this contention we have included 6-31G* points for seven BO^ϵ diatomics[26] as well as the neutral BO_2, the BO_3^{3-} ion, and $B(OH)_3$. The power fit to these 22 d,ρ_c pairs gave $r^2 = 0.989$, $\sigma = 0.0077$ au = 0.052 e/Å^3 ~ 4% of ρ_c range, leaving no doubt about the internal consistency of the compensation in the OBO*X molecules or molecule-ions.

[26]S. C. Choi and O. Knop. Unpublished results.

The d,d* pairs in Fig. 13*a* were fitted to DPF (*i*) without any assumption about d_0, and (*ii*) assuming that d_0 corresponds to $d(B—O)_{6\text{-}31G^*} = 1.160$ Å in the singlet BO^+ (Table 4), on the premise that progressive lengthening of the B—O* bond would end up in the eventual removal of an O*X$^-$ unit. Regression *ii* of d* on d resulted in $r^2 = 0.913$, $\sigma = 0.014$ Å ~ 13% of range; with *cis*- and *trans*-B_2O_3 omitted, $r^2 = 0.998$, $\sigma = 0.002$ Å ~ 2% of range. The unconstrained regression *i* gave $r^2 = 0.865$ and $d_0 = 1.169(33)$ Å for $n = 7$ and an almost exact fit for $n = 5$, with $d_0 = 1.1677(4)$ Å (Table 5). The CSBO regressions gave very similar results save for a slight difference in d_0. The closeness of $d_0 = d(BO^+)_{6\text{-}31G^*}$ and the d_0 obtained from the unconstrained regressions supports the above assumption about the dissociative process.

The analytic treatment of TE is thus validated also for free molecular species, at least to the extent their equilibrium geometries are described by the 6-31G* calculations. This provides further support for the view of the general nature of the bond-length compensatory mechanism and for the 3c4e bond concept, as well as an affirmative answer to the second part of **Q2**.

The OBO*X series also provides an opportunity for estimating the effect of the bond angle on the TE correlation. The geometry of OBO*H was reoptimized with the OBO* angle constrained successively to 170°, 165°, and 160°. As would be expected, the closing-up of the bond angle from its unconstrained equilibrium value produced a lengthening of both the O—B and the B—O* bonds (d*(B—O*) = −1.1486 + 2.0616d(O—B), $r^2 = 0.999$), but the lengthening was so slight that it amounted to only ~0.0009 Å per 5° decrease in OBO*, a variation that would at best be only marginally recognizable in an experimental d,d* data set as arising from a departure from collinearity.

2. *"Self-TE-calibrating" stereochemistries*

Homoligand molecules or ions with stereochemistries such as those in Fig. 14 are of particular interest for the treatment of TE. They contain one or two symmetric pairs of balanced Z—L *trans* bonds with bond lengths d_s, and one or more Z—L bonds with unopposed ligands and bond lengths d_u. If d_s is taken as an estimate of d_e and d_u as an estimate of d_0, we have $\Delta_{est} = d_s - d_u$. This means that the total d bond-length range for the particular Z–L combination can in principle be estimated from the dimensions of a single molecular species. Equation [5] can then be written as $(d^* - d_u)/\Delta_{est} = [(d - d_u)/\Delta_{est}]^{-c}$, leaving c as the only parameter to be determined.

Although the molecular dimensions of many such species are known (e.g., type A, ClF_3, BrF_3; type B, SF_4, SbF_4^-; type C, BrF_5, IF_5, XeF_5^+, TeF_5^-, $SbCl_5^{2-}$; type D, PF_5, AsF_5, PCl_5, $SbCl_5$, $InCl_5^{2-}$), of all these combinations only Sb(III)–Cl can be checked against our TE treatment. In $SbCl_5^{2-}$ (25), the difference of the uncorrected bond lengths $d_s' - d_u = 0.33$ Å, $\frac{1}{2}(d_s + d_s') - d_u = 0.28$ Å; Δ(DPF) = 0.80(30) Å, Δ(CSBO) = 0.45(13) Å, $d_e - d_0[SbCl_3(g)] = 0.30$ Å. In view of what has been said in **C2** about d_0 as a parameter of refinement, these estimates of Δ from the bond lengths in the anion are of the right order of magnitude. For TeF_5^- the mean differences (8 determinations) are $d_s' - d_u = 0.11(3)$ Å. $\frac{1}{2}(d_s + d_s') - d_u = 0.09(2)$

Can. J. Chem. Downloaded from www.nrcresearchpress.com by 109.225.110.28 on 09/08/12
For personal use only.

TABLE 4. 6-31G* optimized molecular parameters of OBO*X species in their ground states[a]

Species	P.G.	E	d(O—B)	d(B—O*)	OBO*	BO*X	ρ_c(O—B)	ρ_c(B—O*)
OBO*H	C_s	−175.07710	1.195	1.315	178.8	117.4	0.3187	0.2324
OBO*F	C_s	−273.77185	1.187	1.350	177.1	105.6	0.3248	0.2209
OBO*Cl	C_s	−633.89276	1.191	1.330	178.1	116.0	0.3215	0.2248
OBO*Li	C_s	−182.01867	1.213	1.275	180.0	178.5	0.3048	0.2559
BO_2^-	$D_{\infty h}$	−174.52937	1.245	1.245	180	—	0.2805	0.2805
trans-OBO*BO	C_{2h}	−274.13424	1.190	1.303	180.0	180	0.3234	0.2204
cis-OBO*BO[b]	C_{2v}	−274.13512	1.189	1.313	178.6	144.5	0.3237	0.2200
BO_2(d)	$D_{\infty h}$	−174.43104	1.254	1.254	180	—	0.2750	0.2750
BO^+(s)	$C_{\infty v}$	−99.03372	1.160	—	—	—	0.3294	—
$B(OH)_3$[c]	C_{3h}	−251.18172	1.358	—	120	112.6	0.2082	—
BO_3^{3-}	D_{3h}	−248.61832	1.419	—	120	—	0.1786	—

[a]Total electronic energy E and the electron densities ρ_c at the bond critical points are in au, the bond lengths are in Å, and the bond angles OBO* and BO*X are in degrees. Optimization constrained to point-group symmetry P.G. For experimental values of some of the parameters see ref. 23.
[b]V-shaped conformation. Optimization with the W-shaped C_{2v} initial conformation ended up in the V-shaped conformation.
[c]In $B(OD)_3$ crystal, d(B—O) = 1.367(15) Å, d(O—D) = 0.970(17) Å, BOD, ⟨113.3(8)⟩° (48).

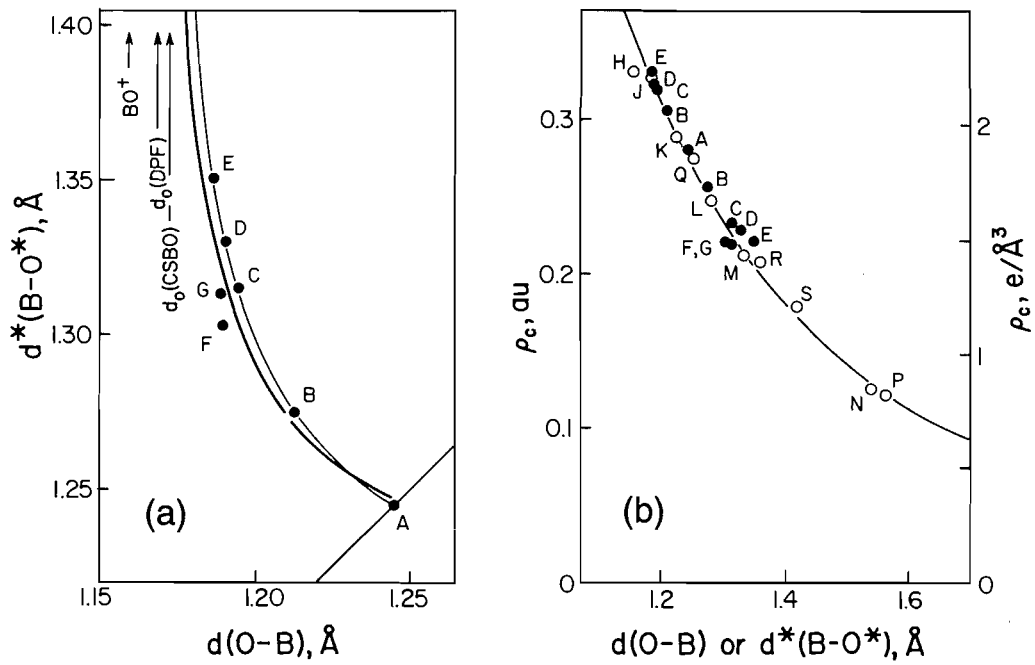

FIG. 13. (*a*) *Ab initio* conjugate bond lengths d(O—B) and d^*(B—O*) in OBO*X and related species. Thick line, DPF; thin line, DPF excluding points *F* and *G*. The corresponding CSBO curves are indistinguishable from the DPF curves on the scale of this drawing. (*b*) Electron density ρ_c at the bond critical point vs. d(O—B) and d^*(B—O*) in OBO*X and related species. *A*, BO_2^-; *B*, OBO*Li; *C*, OBO*H; *D*, OBO*Cl; *E*, OBO*F; *F*, *trans*-OBO*BO; *G*, *cis*-OBO*BO; *H*, BO^+(s); *J*, BO(d); *K*, BO^-(s); *L*, BO^-(t); *M*, BO^{2-}(d); *N*, BO^{3-}(s); *P*, BO^{3-}(t); *Q*, BO_2(d); *R*, $B(OH)_3$; *S*, BO_3^{3-}; s, singlet; d, doublet; t, triplet (see text and Table 4)

Å, i.e., much smaller than for $SbCl_5^{2-}$. This is generally true of F as against Cl as a ligand. The range of bond lengths in the pseudo dimer $Te_2Cl_{10}^{2-}$ (cf. Table II of ref. 1) is in agreement with these estimates. The success of estimating the total d bond-length range from single geometries may well be worth investigating further.

3. Extension to dissimilar ligands

Because of the different nuclear charges on the ligands, in a heteroligand L_a—Z—L_b *trans* bond pair the two bonds are chemically nonequivalent. While for a homoligand L—Z—L bond pair $d^* \geq d$, $d^* = d = d_e$, for the heteroligand pair $d^b = d$(Z—L_b) can be greater or smaller than $d^a = d$(Z—L_a), with a crossover at $d^b = d^a$. However, the $d^b = d^a$ equality now does not characterize a symmetrically balanced pair of conjugate bond lengths, i.e., $d^b = d^a = d_e$ is not a limiting bond length, and the total bond-length range $\Delta = d_e - d_0$ now becomes, for Z—L_a and Z—L_b separately, infinite, with d_0^a and d_0^b as the respective lower bounds.

If it is assumed that TE for the L_a—Z—L_b bond pair can be represented by a single smooth correlation function, the regression equations for DPF and CSBO will have to be rewritten as

$$[11] \quad d^b - d_0^b = K(d^a - d_0^a)^{-c}$$

and

Can. J. Chem. Downloaded from www.nrcresearchpress.com by 109.225.110.28 on 09/08/12
For personal use only.

TABLE 5. Regressions of d^* on d for OBO*X (cf. Table 4)[a]

	DPF		CSBO	
Parameter	$n = 5$	$n = 7$	$n = 5$	$n = 7$
r^2	1.000	0.865	1.000	0.866
σ, Å	0.0002	0.016	0.0004	0.016
d_0, Å	1.1677(4)	1.169(33)	1.1754(4)	1.173(20)
K	0.0158(2)	0.020(13)	—	—
c	0.6200(57)	0.529(416)	—	—
b_0, Å	—	—	0.0818(10)	0.081(41)
b_1	—	—	0.265(10)	0.330(382)
d_e, Å	1.2449(1)	1.246(10)	1.2449(3)	1.246(10)
Δ, Å	0.0773(3)	0.078(28)	0.0694(4)	0.073(18)

[a]$n = 5$ includes $[OBO]^-$ and OBO*X (X = H, F, Cl, Li); $n = 7$ includes in addition *cis*- and *trans*-OBO*BO.

[12] $$d^b - d_0^b = -B^b \ln\{1 - \exp[-(d^a - d_0^a)/B^a]\}$$

where B^a and B^b may be constants or $B^a = b_0^a + b_1^a(d^a - d_0^a)$, $B^b = b_0^b + b_1^b(d^b - d_0^b)$. The DPF thus becomes a 4-parameter regression and the CSBO a 4- or 6-parameter regression. The increase in the number of refinement parameters can be expected to place severe demands on the size and quality of the d^a, d^b data sets. However, simplification can be achieved by introducing certain assumptions.

If one accepts the tentative conclusion (see **C7**) that the refined limiting bond length d_0 for an L—Z—L d,d^* set is independent of the presence of other ligands on Z and of the oxidation state of Z, then d_0^a can be taken as the refined d_0 for the Z–L_a set and d_0^b as the refined d_0 for the Z–L_b set. When both d_0 values are available, the number of refinement parameters in eq. [11] will be reduced to two and that in eq. [12] to two and four, respectively.

As an indication of what may be expected from a generalization of the TE treatment we have examined the *trans* bond lengths in Cl—Bi(III)—S groupings (Fig. 15).[27] Attempts to obtain proper convergence for the 19 d^{Cl},d^S pairs in an unconstrained 4-parameter DPF regression (eq. [11]) were unsuccessful. However, a regression with d_0^{Cl} fixed at 2.35 Å gave $r^2 = 0.816$, $\sigma = 0.048$ Å, $K = 0.143(173)$, $c = 0.917(636)$, and $d_0^S = 2.457(200)$ Å.[28,29]

To test the above assumption that TE for L_a—Z—L_b obeys a single, smooth functional dependence a more selfconsistent d^a,d^b set is needed. To this end[27] we obtained a number of d(O—C),d(C—N) pairs in the isocyanate ion OCN^- and in XOCN and OCNY molecules from 6-31G* *ab initio* optimizations of the respective ground-state equilibrium geometries (Table 6). The optimized O—C—N angle in these species is either 180° or within 7° of 180°. A plot of d(C—N) against d(O—C) (Fig. 16) reveals that the bond-length variation in the *trans* bond pairs *cannot* be described by a single smooth DPF or CSBO function. Although the variation is monotonic, the OCNY and XOCN curves from a cusp at the OCN^- point. This unmistakable discontinuity owes its existence to the fact that the d,d^* correlation for the heteroligand bond pairs extends beyond $d^a = d^b$, and to the difference in the effect of bond formation on the OCN m.o. energy levels when X is added to $[OCN]^-$ on the O side in the one case and on the N side in the other, the nuclear charges on the O and N atoms not being the same. By contrast, the cusp that appears when a TE curve for a homoligand bond-pair set is folded symmetrically along the $d = d^*$ line on itself (e.g., OBOX, Figs. 13*a* and 16), arises from the termination of the TE curve at $d = d^* = d_e$ and is observed whenever the slope of the curve at d_e differs from -1 (for DPF this implies $c \neq 1$).

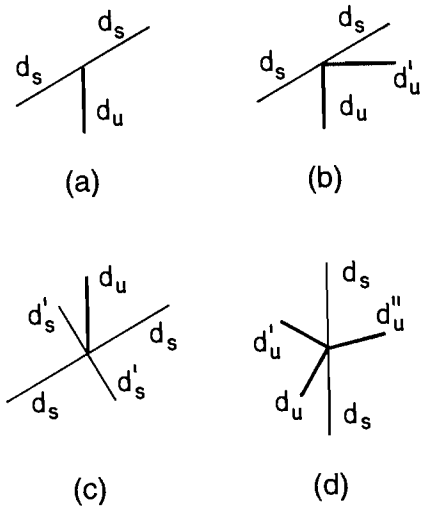

FIG. 14. Homoligand molecular geometries (schematic) containing balanced symmetric *trans* bond pairs as well as bonds with unopposed ligands. Symmetries: (*a*) and (*b*), C_{2v} or subgroups ($d_u \leq d_u'$); (*c*), C_{4v} or subgroups ($d_s \leq d_s'$); (*d*), D_{3h} or σ_h-retaining subgroups.

[27]Sufficiently extensive and selfconsistent Z–L_a,L_b sets are difficult to find. The appreciable scatter in the Bi(III)–Cl,S set comes from limited experimental accuracy, from the involvement of the S ligands in other bonds, from the presence of other heteroligands on Bi, and from significant deviations from collinearity. The data sets for Bi(III)–Br,S, Bi(III)–I,S, Sb(III)–I,S, and Te(II)–Cl,S are even worse in this respect. Paucity of data in any such series and the poor selfconsistency of the d^a,d^b pairs may in fact prove to be the greatest obstacle at present to a systematic investigation of TE in heteroligand *trans* bond pairs.

[28]The d^{Cl} bond length corresponding to point A in Fig. 15 (Cl—Bi—S, 165°; ref. 187, see **F**) is longer than any in the Bi(III)–Cl set. Points B and C correspond to bifurcated Cl—Bi—2S bonds, Cl—Bi—S ~ 144°. For point X see caption.

[29]A d,d^* regression for Bi(III)—S is not available. The mean of eight d_s[Bi(III)—S] values (refs. 188, 191, 192, and 258, see **F**) is 2.833(26) Å.

Can. J. Chem. Downloaded from www.nrcresearchpress.com by 109.225.110.28 on 09/08/12
For personal use only.

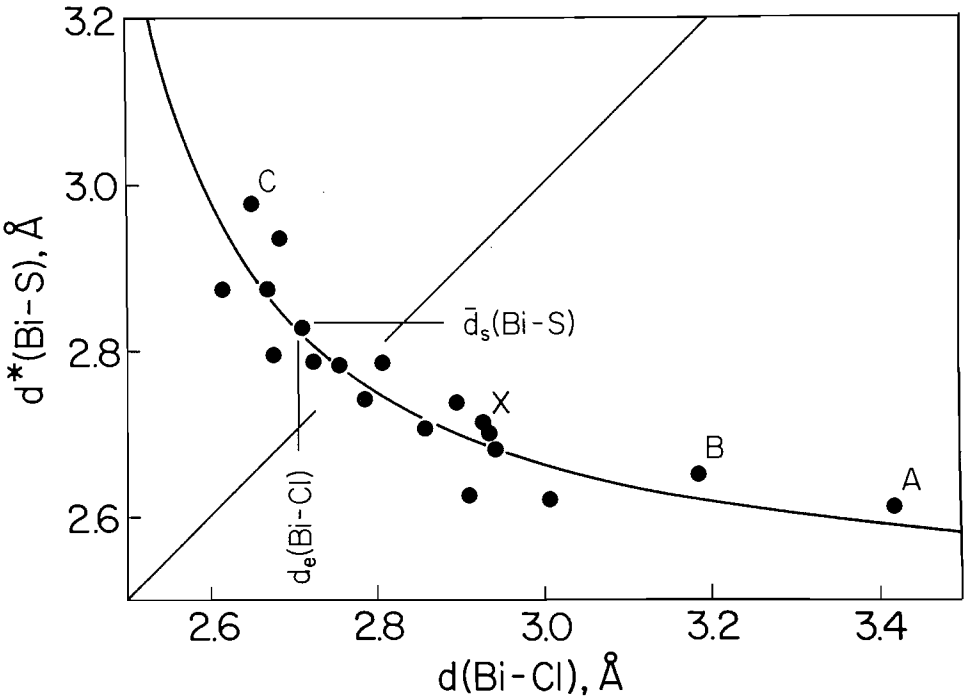

FIG. 15. Variation of d(Bi—S) with d(Bi—Cl) in heteroligand Cl—Bi(III)—S *trans* bond pairs. X, Cl—Bi—S in BiSCl (ref. 259, section **F**); A–C, see footnote 28; d_e(Bi—Cl), see no. 16 in Table 1; $\bar{d}_s$(Bi—S), see footnote 29.

TABLE 6. 6-31G* optimized bond lengths and bond angles in OCN^-, XOCN, OCNY, and related species in their ground states (47)[a]

	Bond length, Å				Bond angle, deg		
Species	O—C	C—N	X—O	N—Y	OCN	XOC	CNY
FOCN	1.299	1.134	1.375	—	176.8	106.9	—
ClOCN	1.291	1.135	1.686	—	177.6	114.0	—
HOCN	1.289	1.136	0.952	—	178.4	111.1	—
LiOCN	1.244	1.146	1.655	—	180.0	180.0	—
NaOCN	1.241	1.150	1.991	—	180.0	175.5	—
OCN^-	1.216	1.167	—	—	180	—	—
OCNNa	1.180	1.178	—	2.089	180.0	—	180.0
OCNLi	1.172	1.180	—	1.755	180.0	—	180.0
OCNH	1.148	1.200	—	0.944	174.2	—	125.3
OCNCl	1.141	1.217	—	1.694	173.8	—	120.2
OCNF	1.135	1.239	—	1.374	173.3	—	109.8
CO	1.114	—	—	—	—	—	—
CO_2	1.143	—	—	—	180[b]	—	—
NCN^{2-}	—	1.231	—	—	180[c]	—	—

[a]Molecular symmetry constrained to C_s (XOCN and OCNY), $C_{\infty v}$ (OCN⁻), and $D_{\infty h}$(CO_2, NCN^{2-}), respectively. For experimental values of some of the parameters see ref. 23.
[b]OCO angle.
[c]NCN angle.

The presence of the cusp necessitates fitting the two branches of the TE correlation curve of Fig. 16 separately. However, there is no a priori reason to think that the limiting d_0^{CO} bond length for the two branches will not be the same, and similarly for d_0^{CN}. Consequently eqs. [11] and [12] are still applicable, subject to the condition that both branches pass through the cusp point at $[OCN]^-$. This requirement reduces the number of optimization parameters by two; for DPF the convenient parameters to eliminate are K^{OCNY} and K^{XOCN}. Fitting the two XOCNY branches to eq. [11] simultaneously without additional constraints gave a very satisfactory result (fit A, Table 7). Repeating the regressions with d_0^{CO} fixed at the d(C—O)$_{6\text{-}31G^*}$ value in CO (Table 6; the matching *ab initio* d_0^{CN} value in CN was unobtainable), and again without *any* constraint for the OCNY plus $[OCN]^-$ branch only, gave essentially the same results. The d_0^{CO} value obtained from the unconstrained regressions was somewhat higher than the *ab initio* value for CO. Proper convergence could not be achieved for an unconstrained DPF fit to the XOCN plus $[OCN]^-$ only branch.

Can. J. Chem. Downloaded from www.nrcresearchpress.com by 109.225.110.28 on 09/08/12
For personal use only.

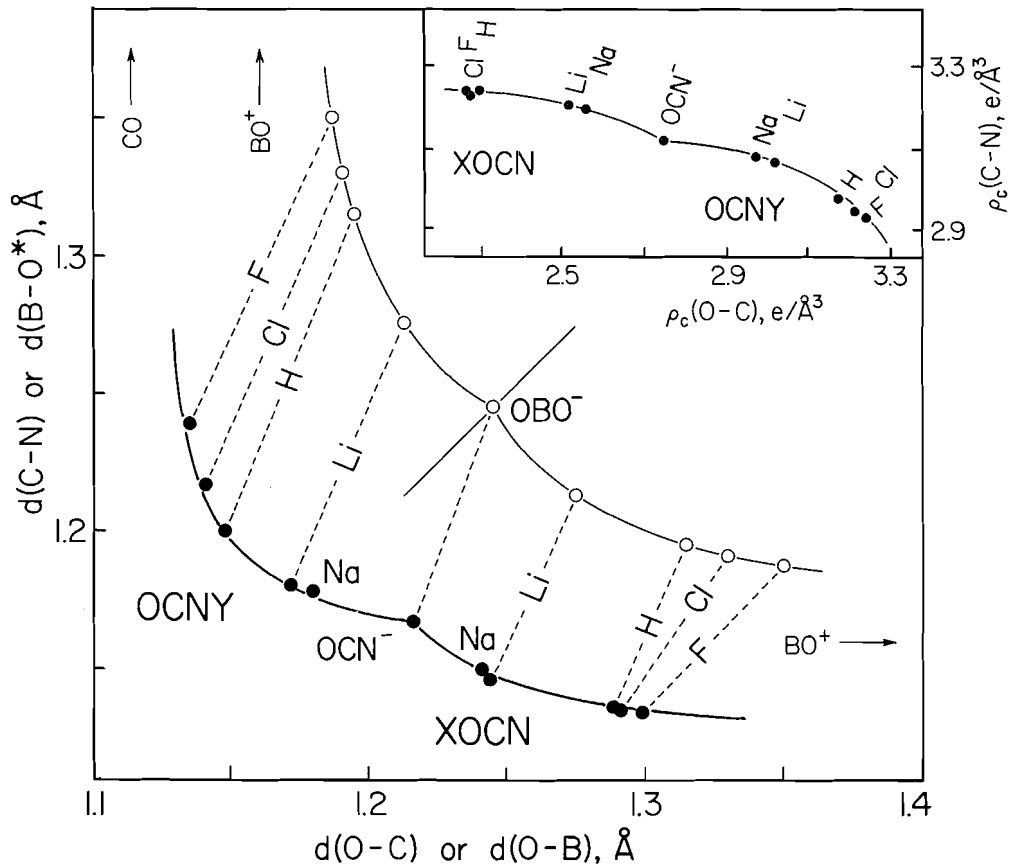

FIG. 16. Variation of d(C—N) with d(O—C) in $[OCN]^-$, XOCN, and OCNY (X, Y = H, F, Cl, Li, Na; 6-31G* *ab initio* bond lengths, see Table 7). The corresponding DPF curve for OBO*X (cf. Fig. 13*a*) is shown for comparison. Inset: correlation of the electron density ρ_c at the bond critical point in the O—C and the C—N bonds.

TABLE 7. DPF regressions of d(C—N) on d(O—C) for XOCN and OCNY (X, Y = H, F, Cl, Li, Na, or no substituent; cf. Table 6 and Fig. 16)[a]

Parameter	A[b]	B	C
r^2	0.9992	0.9745	0.9986
σ, Å	0.0013	0.0068	0.0016
d_0^{CO}, Å	1.125(4)	[1.114]	1.124(9)
d_0^{CN}, Å	1.127(1)	1.128(2)	1.144(26)
K^{OCNY}	[0.01474]	[9.220×10^{-3}]	$4.84(1117) \times 10^{-3}$
c^{OCNY}	0.416(39)	0.632(199)	0.668(565)
K^{XOCN}	[1.496×10^{-4}]	[5.357×10^{-5}]	—
c^{XOCN}	2.330(438)	2.887(308)	—

[a] $d^{CN} - d_0^{CN} = K(d^{CO} - d_0^{CO})^{-c}$; K^{OCNY}, c^{OCNY} refer to the OCNY branch, K^{XOCN}, c^{XOCN} to the XOCN branch of the correlation curve of Fig. 16. *A*, the OCNY and XOCN branches constrained to pass through the OCN^- point but otherwise unrestricted. *B*, d_0^{CO} fixed at 1.114 Å, otherwise as for the *A* regression. *C*, unrestricted fit to OCNY only (includes OCN^-).
[b] Smallest correlation matrix elements: d_0^{CO}–d_0^{CN}, −0.48; d_0^{CN}–c^{XOCN}, −0.51.

These results indicate that the d^{Cl},d^S data for Cl—Bi(III)—S should be refitted to take account of the presumed though not visible cusp. Point X in Fig. 15 represents the interatomic distances in the neutral BiSCl and may well correspond to the position of the cusp, but the overall quality of the existing Bi(III)–Cl,S data set is such that further treatment does not seem warranted at this time, in particular for the branch corresponding to large d(Bi—Cl) values.

4. Legitimacy of bond-length averaging

The problem with reporting a representative Z—L bond length when a significant TE is present is illustrated in the following two examples. In the centrosymmetric μ_2-$[Te_2Cl_{10}]^{2-}$ dimer there are three distinct d,d^* pairs at the 6-coordinate Te atom, the individual bond lengths ranging from ~2.34 to ~3.1 Å and clearly subject to TE (1). If these bond lengths are to be compared with other Te(IV)—Cl bond lengths, how is it to be done?

Can. J. Chem. Downloaded from www.nrcresearchpress.com by 109.225.110.28 on 09/08/12
For personal use only.

Can. J. Chem. Downloaded from www.nrcresearchpress.com by 109.225.110.28 on 09/08/12
For personal use only.

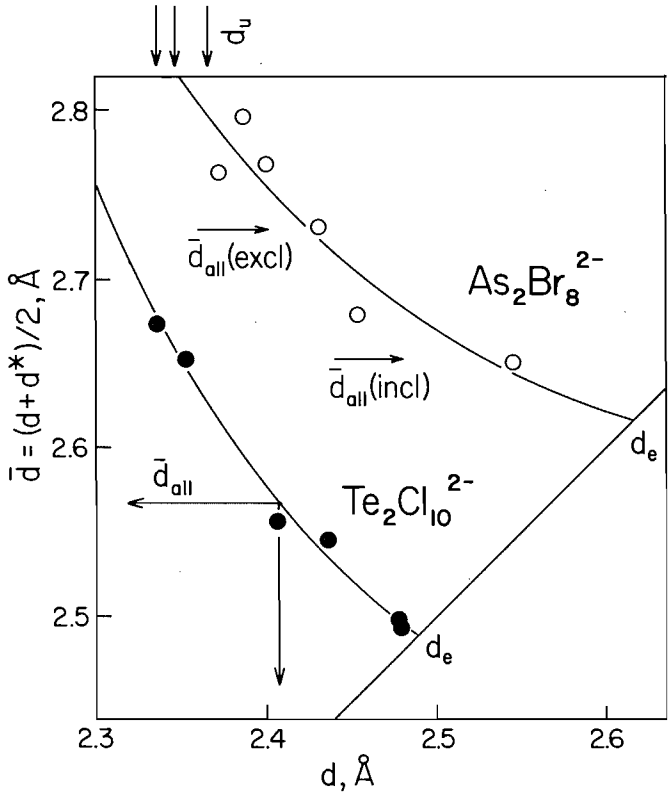

FIG. 17. Bond-length averaging in centrosymmetric μ_2-dimers $[Te_2Cl_{10}]^{2-}$ and $[As_2Br_8]^{2-}$ (see text). The curves represent the pairwise $\bar{d}_i = \frac{1}{2}(d_i + d^*_i)$ averages calculated from the DPF regressions. The d_u values are for $[As_2Br_8]^{2-}$.

A frequently encountered practice is to take the overall mean $\bar{d}_{all} = (\Sigma d_i)/n$, which is then assumed to be comparable to the bond length in a fully symmetric coordination, in the present case (as well as for strongly distorted $TeCl_6^{2-}$ anions) to the balanced d(Te—Cl) in $TeCl_6^{2-}$ of O_h symmetry.[30] This practice is justified when $d_i + d^*_i \sim 2d_e$, i.e., when the pairwise means $\bar{d}_i = \frac{1}{2}(d_i + d^*_i)$ are approximately the same, which would obtain when the d,d^* plot is approximately linear. However, this is generally not the case. In our example, the six available authentic d,d^* pairs for $Te_2Cl_{10}^{2-}$ can be fitted to DPF to $r^2 = 0.995$, $\sigma = 0.020$ Å (data set *a* of Table III, ref. 1).[31] As seen in Fig. 17, the d_i averages for these pairs are far from constant and at the far end considerably in excess of the $d_e = 2.489$ Å calculated from the regression. The $\bar{d}_{all}$ value is 0.08 Å above this d_e, i.e., significantly larger than the value that should be compared with d(Te—Cl) in $TeCl_6^{2-}(O_h)$. For other homoligand Te(IV)–Cl species the correlation line might be somewhat different as would $\bar{d}_{all}$, but the d_e calculated from the respective regressions would be essentially the same as for $Te_2Cl_{10}^{2-}$. All such d,d^* subsets would be contained in the global Te(IV)–Cl regressions, such as those of Table 1. In the overall context, there being only one d_e value for Te(IV)–Cl, viz. that from the global regression, the *trans* bond lengths in different Te(IV)–Cl species would differ from one another in the distribution of the $d_i,\bar{d}_i$ pairs but not in the d_e values. As long as the $d_i,\bar{d}_i$ pairs are consistent with the global regression line, no further comparisons are necessary, the bond-length differences between species being simply particular (but consistent) consequences of the operation of TE.

In the centrosymmetric μ_2-$[As_2Br_8]^{2-}$ dimer (13, 15) the situation is different in that the As atom is 5-coordinate. The As—Br bond approximately perpendicular to the bridge plane (actually the mean $Br_2As(Br)_2AsBr_2$ plane) is unopposed (Fig. 1 of ref. 1), of length d_u. It is thus shorter than either terminal As—Br bond (Fig. 17) and when included in $\bar{d}_{all}$ will result in a $\bar{d}_{all}$(incl.) value of ~2.654 Å, about 0.04 Å above the $d_e = 2.617$ Å calculated from the $As_2Br_8^{2-}$-only regression. However, when d_u is omitted, the $\bar{d}_{all}$ will increase to $\bar{d}_{all}$(excl.) = 2.730 Å. Neither $\bar{d}_{all}$ average is really satisfactory for comparisons. If the aim is to compare the d_u(As—Br) with other d_u(As—Br) bond lengths, there is no need for averaging, as these bond lengths can be compared directly. If the 5-coordination at As is regarded as an incomplete octahedral coordination, then $\bar{d}_{all}$(incl.) might be more appropriate for comparison with d_e.

5. Effect of thermal correction on TE parameters

So far the results and conclusions have been based on bond lengths uncorrected for the effect of thermal motion. The correction is typically in the 0.01–0.03 Å range and thus not negligible. We must now examine how it affects the quantification of TE.

For the purposes of this analysis let us assume that the corrected bond lengths can be written as

$$[13] \quad d^+ = pd + q, \quad d^{*+} = pd^* + q, \quad q > (1 - p)d$$

When the p,q pair is the same for every d,d^* pair in the Z–L set, the resulting DPF and CSBO fits for the d^+,d^{*+} set are entirely predictable, for the sums of squares functions for the corrected data $S_A{}^+(d_0{}^+, d_e{}^+, c)$ and $S_S{}^+(d_s{}^+)$ are made directly proportional to the sums of squares for the uncorrected data by simple transformations of the parameters. For DPF, choosing $d_0{}^+ = pd_0 + q$ and $d_e{}^+ = pd_e + q$ gives

$$S_A{}^+(d_0{}^+, d_e{}^+, c) = p^2 S_A(d_0, d_e, c)$$

and

$$S_S{}^+(d_s{}^+) = p^2 S_S(d_s)$$

Minimizing $S_A{}^+$ or $n_A \log S_A{}^+ + n_S \log S_S{}^+$ (see **A5**) therefore gives the same value for c, but for d_0 and d_e it gives values that are corrected in the same way as the data, viz. $d_0{}^+ = pd_0 + q$, $d_e{}^+ = pd_e + q$. The r^2 measure is the same for the corrected data, but the overall standard error σ now becomes $p\sigma$. For CSBO the same effect is achieved with the transformations $d_0{}^+ = pd_0 + q$, $b_0{}^+ = pb_0$.

In reality the thermal corrections are different for each d,d^* pair. However, the p and q can be considered to be mean values for the correction coefficients, and the resulting fit can be regarded as an approximate mean of the possible fits. Reliably corrected d,d^* values would be required to estimate $\langle p \rangle$ and $\langle q \rangle$ for each particular Z–L set.

Among the more important consequences of applying a correction for thermal motion is the reduction of the difference between d_0(expt) and d_0(CSBO) or d_0(DPF) (see **C2**). With the exception of BiI_3 the d_0(expt) in Fig. 6 are from the gas phase and therefore not subject to correction. The points

[30] The effect of ionic charge, though not negligible, is not dominant.

[31] The $Te_2Cl_{10}^{2-}$-only regression has a smaller dispersion than the global Te(IV)–Cl regression of Table 1, and similarly for the $As_2Br_8^{2-}$-only set.

Can. J. Chem. Downloaded from www.nrcresearchpress.com by 109.225.110.28 on 09/08/12
For personal use only.

that represent these values, when replotted against d_e^+, will undergo horizontal shifts toward higher d_e, whereas the d_0(CSBO),d_e(CBSO) and d_0(DPF),d_e(DPF) will be displaced both horizontally and vertically to $d_0^+ (> d_0)$,$d_e^+ (> d_e)$. As a result the difference D^+ between d_0(expt) and $d_0^+ = a_0^+ + a_1^+ d_e^+$ will be smaller than the difference D between d_0(expt) and $d_0 = a_0 + a_1 d_e$: $D^+ - D \sim -a_1[(p - 1)d_e + q]$. Although we have not attempted a quantitative evaluation of this difference, it is clear that the thermal correction will tend to reduce the discrepancy between the optimized and the experimental d_0.

E. Summary

In terms of answers to questions **Q1–Q7** posed initially, our findings can be summarized as follows.

Q1, Q2. The existence of TE as a functional relation between the conjugated bond lengths d and d^* in collinear homoligand L—Z—L* *trans* bond pairs has been demonstrated or confirmed for a variety of Z–L combinations, at the experimental level for *trans* bond pairs in discrete or quasi-discrete species with Z mainly from Groups VI and V, and at the 6-31G* *ab initio* level for a number of isolated molecules or molecule-ions (OBOX, XOCN, OCNY; X,Y = H, F, Cl, Li, Na, or no ligand). In all these cases the TE correlation has been found to hold regardless of the specific cause of the bond-length disproportionation $d_e, d_e \rightarrow d, d^*$.

For the Z–L combinations examined it can be claimed that d,d^* in experimental homoligand *trans* bond pairs ($d \leq d^*$, d and d^* not related by symmetry; population **A**) are highly correlated. The model functions that have been adopted for the correlation and investigated in detail are the purely empirical DPF. (eq. [3]) and the 3-centre 4-electron (3c4e) based CSBO (eq. [4]), both involving 3-parameter nonlinear optimizations. For DPF (**A**) the r^2 values are between 0.80 and 0.98 and the average goodness of fit measure σ is about 9% of the total d range. For CSBO (**A**) the corresponding figures are 0.80–0.97 and ~13%.

To take account of d,d^* bond lengths equivalent by symmetry ($d = d^*$; population **S**) the DPF and CSBO functions were modified to combine the suitably weighted **A** and **S** samples. This was done in two ways, DPF(**A**,**S**) and CSBO(**A**,**S**) (eq. [9]), and DPF(**A**/**S**) (eq. [10]). In addition, DPF and CSBO were optimized for the straightforward **A** + **S** sum of the two samples; these two fits are available for all the Z–L data sets examined.

The individual d,d^* sets are equally well fitted by DPF and CSBO. In particular, the d_e values resulting from the two fits for a Z–L combination are practically identical and statistically indistinguishable. However, the rates of convergence of the two model functions to the asymptotic limit $d \rightarrow d_0$, $d^* \rightarrow \infty$ are not the same, which results in somewhat different estimates of d_0. This discrepancy is discussed at some length. The difference $\Delta = d_e - d_0$ represents the total range of d subject to TE and is surmised to vary quasi-linearly with d_e (Fig. 8*b*).

The equal (and high) success of the purely empirical DPF and of CSBO in fitting the d,d^* data sets validates the use of the modified 3c4e bond concept in accounting for the quantitative aspects of TE, not only for experimental d,d^* data to which the concept has been applied previously (e.g., As(III)–Br) and in this investigation, but also for much simpler situations involving 6-31G* optimized equilibrium geometries of isolated molecules or molecule-ions with collinear homoligand *trans* bond pairs. While the *absolute* values of the 6-31G* bond lengths should be treated with reserve, the self-consistency of the OBOX, XOCN, and OCNY sets is such that the observed conformity to the model functions cannot be dismissed as fortuitous or as an artefact of the basis set and the H–F method. The goodness of fit of the 6-31G* regressions thus corroborates, on the one hand, the validity of the calculated bond lengths relative to one another and, on the other hand, vindicates the suitability of the modified 3c4e model function CSBO for quantifying TE.

The problems arising from the extension of TE correlations to heteroligand L_1—Z—L_2 *trans* bond pairs are in part practical (insufficient data, appreciable scatter of d(Z—L_1),d(Z—L_2) points), in part theoretical (the bond-length variation over the observed range is not representable by a single smooth function). These matters are discussed in **D3**, in relation to Cl—Bi(III)—S and to *ab initio* bond pairs.

Q3. The upper bound of d^* beyond which $d^* = \text{DPF}(d)$ or $d^* = \text{CSBO}(d)$ in homoligand *trans* bond pairs ceases to correspond to an effective bonding interaction between Z and L is difficult to evaluate, but generally it appears to be somewhat lower than the sum ΣvdWr of the tabulated van der Waals radii of Z and L (Fig. 7).

Q4, Q5. The optimized parameter values of DPF and CSBO are different for different Z–L combinations. There are indications (Figs. 10 and 12) that these values may reflect chemical trends and regularities of Z–L. Statistical comparison of the Se(IV)–Cl, Se(IV)–Cl(Ox), and Se(II)–Cl data sets shows that while the d,d^* in the three sets come from different populations and the d_e values for the three sets are different and statistically distinguishable, the three d_0 values are similar and statistically indistinguishable. The three sets thus appear to have a common limiting d_0 bond length that is independent of the oxidation state of Se and of the presence of heteroligands on the Se atom. Lack of suitable and sufficiently extensive experimental d,d^* sets has prevented us from determining whether this conclusion for Se–Cl is true of other Z–L combinations. If it is, then the d_0 from the regressions will of necessity be smaller than d_u(Z—L) in the reference species, as d(Se—Cl) in $SeCl_2$(g) is not expected to be the same as the (as yet unknown) d_u(Se—Cl) in $SeCl_4$(g).

Q6. Departures from collinearity would be expected to increase both d and d^*, though not by equal amounts. As a result the d,d^* point would move away from the TE regression line established for essentially collinear bond pairs. The bond angles for the d,d^* sets examined are generally 170–180°, yet no significant systematic deviations from the TE lines have been detected that could be attributed specifically to lack of collinearity. For the special case of Te(II)–S see **C5**.

Q7. Where an **S** sample exists, the mean $\bar{d}_s$ value in most (though not all) of the cases examined is very close to and statistically indistinguishable from the d_e value obtained from the corresponding **A** sample. The d_e constitutes a well-defined basic parameter of a d,d^* set and, for Z–Hal combinations, has been shown to correlate well with the empirical ionic radius of the ligand (Fig. 5).

Among the various other aspects of TE discussed in this

Can. J. Chem. Downloaded from www.nrcresearchpress.com by 109.225.110.28 on 09/08/12
For personal use only.

paper are the consequences of correcting d,d^* bond-length pairs for the effects of thermal motion.

F. Sources of data and statistical treatment

The data sets used in our treatment of the individual Z–L combinations are based on an extensive (though not exhaustive) search of the literature. All the d,d^* pairs from this search have been included in the regressions except for the very small number which gave *gross* visual misfits in the d^* vs. d plots and clearly did not belong to the respective sets. These were omitted from the final regressions and are not shown in Figs. 1–4.

To save space, papers cited previously in refs. 1 and 41 will be referred to only by the numbers under which the citations appear there; references marked *a* are from ref. 41 and those marked *b* from ref. 1. The very numerous additional papers not referred to in the text have been assigned running numbers between 100 and 300 and the citations have been deposited.[32]

Se(IV)–Cl: 18; *a*125; *b*13–*b*15; 100–104.
Se(IV)–Cl(Ox): 1; *b*9–11, *b*17; 105, 106.
Se(II)–Cl: *b*15; 107.
Se(IV)–Br: 18; *a*78; 104, 108–112.
Se(II)–Br: 110, 112–116.
Te(IV)–Cl: 1; *a*74, *a*77; *b*6, *b*9, *b*12, *b*19, *b*58; 104, 117–142.
Te(IV)–Br: 18; *a*71, *a*73, *a*75, *a*80; *b*8; 104, 143–152.
Te(IV)–I: 18; *a*50, *a*102; 104, 111, 153–161.
P(III)–Br: 11, 20:
As(III)–Cl: 12, 21, 22; 162–164.
As(III)–Br: 13, 15; 165.
As(III)–I: 24; 165.
Sb(III)–F: 35.
Sb(III)–Cl: 4, 5, 7, 8, 14, 25, 26, 28; *b*36; 166–173.
Sb(III)–Br: 6, 29; *a*88; 172, 174–177.
Sb(III)–I: 16, 29, 30; 178–183.
Bi(III)–Cl: 31; *a*90, *a*92; *b*42–44; 184–201.
Bi(III)–Br: *a*93; *b*45–47; 187, 200–212.
Bi(III)–I: *a*94; 178, 187, 189, 202, 213–221.
Te(II)–S: 222–257.
Bi(III)–Cl,S: 32; 185–188, 192, 195, 258–261.
Xe(II)–F: 33, 34; 262.
Pb(II)–Br: *a*119; 263, 264.
Pb(II)–I: *a*84, *a*115, *a*117, *a*118; 265–270.
I(III)–Cl: 271–276.
Ti(IV)–Cl: 41, 42; 277, 278.

Ab initio values (Tables 4 and 6): the total electronic energies, bond lengths and angles, net charges, critical radii, and electron densities at the bond critical points were obtained from in-house (see footnote 26) 6-31G* optimizations of the ground-state equilibrium molecular geometries. For methods see ref. 47.

Statistical treatment

The DPF and CSBO model functions are assumed to represent the conditional mean of d^* given d, and the variation of d^* about this mean is assumed to be Gaussian, with a standard deviation σ which is constant over the range of d values. With the additional assumption of statistical independence among the different d values, the method of nonlinear least squares (49, 50) is the appropriate technique for estimating the model parameters. An iterative algorithm minimizes the sum $S[d^*(\text{obs})_i - d^*(\text{fit})_i]^2$ and provides parameter estimates, standard errors for these estimates, and an estimate of the overall standard error σ. The latter and the proportion r^2 of the variation in d^* explained by the regression provide summaries that indicate the adequacy of the fit.

[32]The deposited material can be purchased from: The Depository of Unpublished Data, Document Delivery, CISTI, National Research Council Canada, Ottawa, Canada K1A 0S2.

The standard errors of the parameters derive from both σ and the model function and can be large even when the fit is adequate. For example, estimation of d_0 involves, for *any* suitable $d^* = f(d)$ model function, extrapolation to infinity and is inherently less accurate than estimation of d_e.

When **S** data are available, however, different methodology is required to accommodate possible differences between $\bar{d}_s$ and d_e and between σ_A and σ_S. Since in the **S** population $d^*_i = d_i$, it is only possible to consider the statistical fluctuations of d^* about its mean $\bar{d}_s$ rather than its variation about a conditional mean given d.

When $\bar{d}_s$ and d_e are assumed equal, a combined fit **A**,**S** is obtained by minimizing the weighted combination of eq. [9]. Estimates for σ_A^2 and σ_S^2 are then given by $\hat{S}_A/n_A$ and $\hat{S}_S/n_S$, respectively, $\hat{S}$ denoting evaluation at the optimal parameter values. Equation [9] is the negative of the maximized log likelihood function for the DPF and CSBO parameters, under the assumption that the **S** population is also Gaussian. For the **A**,**S** fit an r^2 measure was constructed using the **A** data only. The constrained or combined **A**,**S** fit is the appropriate one if estimates of $\bar{d}_s$ and d_e are deemed not to be significantly different. Standard errors on the parameter estimates will be smaller than for the fit to the **A** data only.

Test for equality of $\bar{d}_s$ *and* d_e

A statistical test for the equivalence of $\bar{d}_s$ and d_e was derived using the likelihood-ratio statistic, which is approximately distributed as a χ^2 with one degree of freedom. This statistic compares the fit to the data under the assumption that $\bar{d}_s = d_e$ to the unconstrained fit. The unconstrained fit involves fitting the model function to **A** data using nonlinear least squares and also estimating $\bar{d}_s$ and σ_S using the sample average and standard deviation from the **S** population. The test statistic is therefore

$$[14] \quad TI = n_A \log (S_{A,c}/S_{A,u}) + n_S \log (S_{S,c}/S_{S,u})$$

where c and u, respectively, indicate the constrained and unconstrained fit. Large values of TI, or small values of the significance probability P (cf. Table 3), suggest that the equality hypothesis may be untenable.

Testing for the effect of noncollinearity

The difference between the **A1**,**S** and **A2** Te(II)–S populations was assessed using the $n = n_{A2} = 23$ deviations $\mathbf{e} = (e_1, e_2 \ldots, e_{23})'$ of the d^*(**A2**) values from their corresponding predictions from DPF(**A1**,**S**). The quadratic form

$$[15] \quad Q = \mathbf{e}'\mathbf{M}\mathbf{e}/n = [\mathbf{e}'\mathbf{e} - \mathbf{e}'\mathbf{F}(\hat{\sigma}^2\mathbf{V}^{-1} + \mathbf{F}'\mathbf{F})^{-1}\mathbf{F}']/\hat{\sigma}^2$$

properly combines these deviations and is approximately distributed as a χ^2 with n degrees of freedom. Here $\mathbf{M} = [\hat{\sigma}^2\mathbf{I}_n + \mathbf{F}\mathbf{V}\mathbf{F}']^{-1}$ is the inverse of the estimated covariance matrix of the deviations, $\mathbf{V}$ is the estimated covariance matrix of the parameter estimates, $\hat{\sigma}^2$ is the estimated variance of the d^*(**A1**) values about the DPF curve, and $\mathbf{F}$ is the derivative matrix of DPF with respect to the parameters evaluated using the d(**A2**) values and the DPF(**A1**,**S**) parameter estimates of $\hat{K}$, $\hat{c}$, and $\hat{d}_0$.

The value of Q was calculated to be 32.34, which is exceeded with probability 0.09 in the χ^2_{23} distribution. We conclude that these results provide mild evidence of a difference between the **A1** and **A2** populations.

Testing for the effect of oxidation state and heteroligation

An overall test for comparing two populations can be constructed from the two sets of DPF parameter estimates $\hat{\Theta}_i = (\hat{d}_0, \hat{c}, \hat{d}_e)'$ and their covariance matrices $\hat{\Sigma}_i$ from each sample $i = 1,2$. The test statistic is given by

$$[16] \quad T2 = (\hat{\Sigma}_1^{-1} + \hat{\Sigma}_2^{-1})^{-1}(\hat{\Sigma}_1^{-1}\hat{\Theta}_1 + \hat{\Sigma}_2^{-1}\hat{\Theta}_2^{-1})$$

and has an approximate χ^2 distribution with three degrees of freedom under the hypothesis of equality of the population parameters.

Comparing Se(IV)–Cl and Se(IV)–Cl(Ox) in this way gives $T2 = 746.7$, while Se(IV)–Cl and Se(II)–Cl give 188.5. Both these values are much larger than $\chi^2_3(0.01) = 11.3$, so we conclude the population differences in both pairs are significant.

Similar tests for single parameter values indicate that d_e is significantly different at the 0.01 level in each pair: for the Se(IV)–Cl vs. Se(IV)–Cl(Ox) comparison, $T2 = 42.3$, and for Se(IV)–Cl vs. Se(II)–Cl $T2 = 15.5$. However, the values of d_0 in the three populations are *not* significantly different even at the 0.10 level, with $T2 = 0.5572$.

NOTE ADDED IN PROOF: In the recently reported $XeF_2 \cdot CrF_4$ (ref. 51; personal communication from Professor Leban), d(Xe—F) = 1.928 Å, d^*(Xe—F) = 2.123 Å. When this d,d^* pair is added to the Xe(II)–F set of Tables 1 and 2, the regressions ($n = 10$) give

DPF(**A**+**S**): $r^2 = 0.874$, $\sigma = 0.054$ Å, $d_0 = 1.690(142)$ Å, $K = 0.103(44)$, $c = 0.926(424)$, $d_e = 1.997(16)$ Å, $\Delta = 0.307(134)$ Å; for $d = 1.928$ Å, $d^*_{calc} = 2.079$ (54) Å.

CSBO(**A**+**S**): $r^2 = 0.872$, $\sigma = 0.055$ Å, $d_0 = 1.758(63)$ Å, $b_0 = 0.339(145)$ Å, $b_1 = 0.023(306)$, $d_e = 1.997(15)$ Å, $\Delta = 0.239(49)$ Å; for $d = 1.928$ Å, $d^*_{calc} = 2.080(550)$ Å.

With the d,d^* pair for $XeF_2 \cdot WOF_4$ (23) omitted ($n = 9$),

DPF(**A**+**S**): $r^2 = 0.957$, $\sigma = 0.033$ Å, $d_0 = 1.537(248)$ Å, $K = 0.182(165)$, $c = 1.200(357)$, $d_e = 1.998(9)$ Å, $\Delta = 0.461(244)$ Å; for $d = 1.928$ Å, $d^*_{calc} = 2.099(33)$ Å.

CSBO(**A**+**S**): $r^2 = 0.956$, $\sigma = 0.033$ Å, $d_0 = 1.690(117)$ Å, $b_0 = 0.494(252)$ Å, $b_1 = -0.163(247)$, $d_e = 1.998(9)$ Å, $\Delta = 0.309(113)$ Å; for $d = 1.928$ Å, $d^*_{calc} = 2.099(33)$ Å.

Acknowledgments

We are indebted to Professor H. Krebs and to the late Professor F. Lazarini for their generosity in providing us with details of a number of their crystal-structure determinations in advance of publication. This investigation was supported by grants from the Natural Sciences and Engineering Research Council of Canada.

1. M. A. James, O. Knop, and T. S. Cameron. Can. J. Chem. **70**, 1795 (1992).
2. G. R. Jones, R. D. Burbank, and N. Bartlett. Inorg. Chem. **9**, 2264 (1970).
3. A. Lipka. Z. Kristallogr. **159**, 88 (1982).
4. A. Lipka. Z. Anorg. Allg. Chem. **469**, 218 (1980).
5. S. K. Porter and R. A. Jacobson. J. Chem. Soc. A, 1359 (1970).
6. S. K. Porter and R. A. Jacobson. J. Chem. Soc. A, 1359 (1970).
7. R. K. Wismer and R. A. Jacobson. Inorg. Chem. **13**, 1678 (1974).
8. F. W. B. Einstein and A. C. MacGregor. J. Chem. Soc. Dalton Trans. 778 (1974).
9. R. E. Rundle. J. Am. Chem. Soc. **85**, 112 (1963).
10. L. Pauling. The nature of the chemical bond. 3rd ed. Cornell University Press, Ithaca, N.Y. 1960.
11. W. S. Sheldrick and J. Kiefer. Z. Naturforsch. **44**b, 609 (1989).
12. J. Kaub and W. S. Sheldrick. Z. Naturforsch. **39**b, 1252 (1984).
13. J. Kaub and W. S. Sheldrick. Z. Naturforsch. **39**b, 1257 (1984).
14. U. Ensinger, W. Schwarz, and A. Schmidt. Z. Naturforsch. **37**b, 1584 (1982).
15. W. S. Sheldrick and C. Horn. Z. Naturforsch. **44**b, 405 (1989).
16. W. S. Sheldrick and C. Martin. Z. Naturforsch. **46**b, 639 (1991).
17. O. Knop, T. S. Cameron, D. Adhikesavalu, B. R. Vincent, and J. A. Jenkins, Can. J. Chem. **65**, 1527 (1987).
18. B. Krebs and F.-P Ahlers. Adv. Inorg. Chem. **35**, 235 (1990).
19. B. F. Hoskins and C. D. Pannan. Aust. J. Chem. **29**, 2541 (1976).
20. W. S. Sheldrick, A. Schmidpeter, F. Zwaschka, K. B. Dillon, A. W. G. Platt, and T. C. Waddington. J. Chem. Soc. Dalton Trans. 413 (1981).
21. A. T. Mohammed and U. Müller. Z. Anorg. Allg. Chem. **523**, 45 (1985).
22. A. T. Mohammed and U. Müller. Acta Crystallogr. Sect. C: Cryst. Struct. Commun. **C41**, 329 (1985).
23. A. F. Wells. Structural inorganic chemistry. 5th ed. Clarendon Press, Oxford. 1984.
24. W. S. Sheldrick, H.-J. Häusler, and J. Kaub. Z. Naturforsch. **43**b, 789 (1988).
25. M. Webster and S. Keats. J. Chem. Soc. A, 298 (1971).
26. A. Lipka and D. Mootz. Z. Anorg. Allg. Chem. **440**, 231 (1978).
27. A. L. Rheingold, A. G. Landers, P. Dahlstrom, and J. Zubieta. J. Chem. Soc. Chem. Commun. 143 (1979).
28. E. Hough, D. G. Nicholson, and A. K. Vasudevan. J. Chem. Soc. Dalton Trans. 427 (1987).
29. S. Pohl, W. Saak, R. Lotz, and D. Haase. Z. Naturforsch. **45**b, 1355 (1990).
30. S. Pohl, W. Saak, and D. Haase. Angew. Chem. Int. Ed. Engl. **26**, 467 (1987).
31. N. W. Alcock, M. Ravindran, and G. R. Willey. J. Chem. Soc. Chem. Commun. 1063 (1989).
32. V. Kupčík and L. Veselá-Nováková. TMPM. Tschermaks Mineral. Petrogr. Mitt. **14**, 55 (1970).
33. D. A. Dixon, A. J. Arduengo III, and W. B. Farnham. Inorg. Chem. **28**, 4589 (1989).
34. P. J. MacDougall, G. J. Schrobilgen, and R. W. F. Bader. Inorg. Chem. **28**, 763 (1989).
35. J. F. Sawyer and R. J. Gillespie. Prog. Inorg. Chem. **34**, 65 (1986).
36. M. Trömel. Z. Kristallogr. **154**, 338 (1981).
37. M. Trömel. Acta Crystallogr. Sect. B: Struct. Sci. **B42**, 138 (1986).
38. I. D. Brown. J. Solid State Chem. **11**, 214 (1974).
39. O. Greis and M. Martinez-Ripoll. Z. Anorg. Allg. Chem. **436**, 105 (1977).
40. P. Klaeboe, C. J. Nielsen, H. Priebe, S. H. Schei, and C. E. Sjøgren. J. Mol. Struct. **141**, 161 (1986).
41. O. Knop, A. Linden, B. R. Vincent, S. C. Choi, T. S. Cameron, and R. J. Boyd. Can. J. Chem. **67**, 1984 (1989).
42. T. J. Kistenmacher and G. D. Stucky. Inorg. Chem. **10**, 122 (1971).
43. J. Eicher, P. Klingelhöfer, U. Müller, and K. Dehnicke. Z. Anorg. Allg. Chem. **514**, 79 (1984).
44. J. Eicher, U. Müller, and K. Dehnicke. Z. Anorg. Allg. Chem. **521**, 37 (1985).
45. R. D. Willett. Acta Crystallogr. Sect. B: Struct. Sci. **B44**, 503 (1988).

Can. J. Chem. Downloaded from www.nrcresearchpress.com by 109.225.110.28 on 09/08/12
For personal use only.

46. R. H. Summerville and R. Hoffmann. J. Am. Chem. Soc. **98**, 7240 (1976).
47. O. Knop, R. J. Boyd, and S. C. Choi. J. Am. Chem. Soc. **110**, 7299 (1988).
48. B. M. Craven and T. M. Sabine. Acta Crystallogr. **20**, 214 (1966).
49. D. M. Bates and D. G. Watts. Nonlinear regression analysis and its applications. Wiley, New York. 1988.
50. G. A. F. Seber and C. J. Wild. Nonlinear regression. Wiley, New York, 1989.
51. K. Lutar, I. Leban, T. Ogrin, and B. Žemva. Eur. J. Inorg. Solid State Chem. In press.

Can. J. Chem. Downloaded from www.nrcresearchpress.com by 109.225.110.28 on 09/08/12
For personal use only.

Preparation and ^{31}P NMR characterization of N-bonded complexes of platinum(II) with a phosphadithiatriazine: X-ray structure of *trans*-$PtCl_2(PEt_3)(\eta^1$-N-$Ph_2PS_2N_3)$

TRISTRAM CHIVERS,[1] ROBERT W. HILTS, AND IAN H. KROUSE
Department of Chemistry, The University of Calgary, Calgary, Alta., Canada T2N 1N4

AND

A. WALLACE CORDES, RANDAL HALLFORD, AND SYRONA R. SCOTT
Department of Chemistry and Biochemistry, University of Arkansas, Fayetteville, AR 72701, U.S.A.

Received April 1, 1992

TRISTRAM CHIVERS, ROBERT W. HILTS, IAN H. KROUSE, A. WALLACE CORDES, RANDAL HALLFORD, and SYRONA R. SCOTT. Can. J. Chem. **70**, 2602 (1992).

The reaction of $Ph_2PS_2N_3$ with $[Pt_2(\mu\text{-}Cl)_2(PEt_3)_4][BF_4]_2$ or $[PtCl_2(PEt_3)]_2$ in dichloromethane at 23°C produces the 1:1 adducts *cis*-$[PtCl(PEt_3)_2(Ph_2PS_2N_3)][BF_4]$, **3**, and *trans*-$[PtCl_2(PEt_3)(Ph_2PS_3N_2)]$, **4**, respectively, in good yields. The ^{31}P NMR data for **3** and **4** indicate that (*i*) the platinum is attached to a nitrogen atom adjacent to phosphorus in both these adducts, (*ii*) the PEt_3 ligands in **3** are in mutually *cis* positions, and (*iii*) the PEt_3 ligand in **4** is *trans* to the heterocyclic nitrogen. These structural features were confirmed by an X-ray analysis of **4**. Crystals of **4** are monoclinic, space group $P2_1/c$, with a = 14.920(3) Å, b = 8.966(5) Å, c = 19.103(5) Å, β = 109.32(2)°, V = 2411.6(16) Å^3, and Z = 4. The least-squares refinement with anisotropic thermal parameters for all non-hydrogen atoms converged at R = 0.050 and R_w = 0.053. The Pt—N bond length is 2.122(15) Å and the coordinated nitrogen atom is lifted ca. 0.63(2) Å out of the plane containing the other heterocyclic ring atoms. The attachment of a platinum(II) centre to the PN_3S_2 ring perturbs the S—N bond lengths significantly. The S—N distance involving the coordinated nitrogen is 1.672(16) Å, while the other S—N distances are 1.631(19), 1.555(19), and 1.562(19) Å, indicative of a localized sulfur diimide (-N=S=N-) structure. The UV–visible spectra of **3** and **4** in CH_2Cl_2 exhibit absorption bands at 514 and 528 nm, respectively, but dissociation of these adducts to give the free ligand $Ph_2PS_2N_3$ occurs readily in dilute solution.

TRISTRAM CHIVERS, ROBERT W. HILTS, IAN H. KROUSE, A. WALLACE CORDES, RANDAL HALLFORD et SYRONA R. SCOTT. Can. J. Chem. **70**, 2602 (1992).

Les réactions du $Ph_2PS_2N_3$ avec le $[Pt_2(\mu\text{-}Cl)_2(PEt_3)_4][BF_4]_2$ ou le $[PtCl_2(PEt_3)]_2$ effectuées dans la dichlorométhane, à 23°C, conduisent respectivement aux adduits 1 : 1 *cis*-$[PtCl(PEt_3)_2(Ph_2PS_2N_3)][BF_4]$, **3**, et *trans*-$[PtCl_2(PEt_3)(Ph_2PS_3N_2)]$, **4**, avec de bons rendements. Les données de la RMN du ^{31}P des composés **3** et **4** indiquent que (*i*) dans les deux cas, le platine est attaché à un atome d'azote adjacent de l'azote, (*ii*) les ligands PEt_3 du composé **3** sont dans des positions *cis* et (*iii*) le ligand PEt_3 du composé **4** se trouve en position *trans* par rapport à l'azote hétérocyclique. Ces caractéristiques structurales sont confirmées par une analyse du spectre de diffraction des rayons X du composé **4**. Les cristaux du composé **4** sont monocliniques, groupe d'espace $P2_1/c$, avec a = 14,920(3), b = 8,966(5) et c = 19,103(5) Å, β = 109,32(2)°, V = 2411,6(16) Å^3 et Z = 4. Un affinement, par la méthode des moindres carrés, des paramètres thermiques anisotropiques de tous les atomes qui ne sont pas des hydrogènes converge à R = 0,050 et R_w = 0,053. La longueur de la liaison Pt—N est égale à 2,122(15) Å et l'atome d'azote coordonné est déplacé de 0,63(2) Å au-dessus du plan contenant les autres atomes hétérocycliques du cycle. L'attachement d'un centre platine(II) au PN_3S_2 cycle perturbe fortement les longueurs des liaisons S—N. La distance S—N impliquant l'azote coordonné est égale à 1,672(16) Å alors que les autres distances S—N sont égales à 1,631(19), 1,555(19) et 1,562(19) Å et suggèrent l'existence d'une structure diimide de soufre (-N=S=N-) localisée. Les spectres UV–visible des composés **3** et **4**, déterminés dans le CH_2Cl_2, présentent des bandes d'absorption à 514 et 528 nm respectivement; toutefois, en solution diluée, la dissociation de ces adduits pour donner le ligand libre $Ph_2PS_2N_3$ se produit facilement.

[Traduit par la rédaction]

Introduction

The phosphadithiatriazine ring system **1** is an eight π-electron system, which readily undergoes cycloaddition with norbornadiene (1) or oxidative-addition with halogens (2). The interaction of **1** with Lewis or Brønsted acids gives adducts of the type **2** in which the electrophile (E) is attached to a nitrogen atom attached to a phosphorus atom (3). *Ab initio* Hartree–Fock–Slater SCF calculations indicate that the regiospecificity of these reactions is governed by electrostatic effects. An X-ray structural determination of the methylated derivative, **2***a*, reveals that coordination of **1** to an electrophile also imposes a marked perturbation on both the conformation of the ring and the S—N bond lengths (3). Specifically, the S—N bond involving the coordinated nitrogen is weakened substantially suggesting that electrophiles might be used to promote ring-opening reactions. It was of interest, therefore, to investigate the reactions of **1** with other electrophiles in order to compare the deformation of ring geometry induced by adduct formation with that observed upon N-methylation. In this study we describe the

1

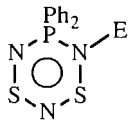

2*a* (E = Me^+)
2*b* (E = H^+)
2*c* (E = BCl_3)
2*d* (E = $SnCl_4$)[2]

[1]Author to whom correspondence may be addressed.

[2]In the $SnCl_4$ complex two molecules of **1** are coordinated to tin in a *trans* geometry.

Can. J. Chem. Downloaded from www.nrcresearchpress.com by 109.225.110.28 on 09/08/12
For personal use only.

Can. J. Chem. Downloaded from www.nrcresearchpress.com by 109.225.110.28 on 09/08/12
For personal use only.

synthesis and ^{31}P NMR characterization of two platinum(II) adducts, viz. *cis*-$[PtCl(PEt_3)_2(Ph_2PS_2N_3)][BF_4]$, **3**, and *trans*-$[PtCl_2(PEt_3)(Ph_2PS_2N_3)]$, **4**, and the X-ray structure of **4**.

Experimental

Manipulations of air-sensitive reagents and products were performed under an atmosphere of prepurified nitrogen or argon using standard Schlenk or dry box techniques. Solvents (THF, diethyl ether, hexane, and dichloromethane) were dried with the appropriate desiccant and purged with argon. The compounds $Ph_2PS_2N_3$ (4), $[PtCl_2(PEt_3)]_2$ (5), and $[Pt_2(\mu\text{-}Cl)_2(PEt_3)_4][BF_4]_2$ (6) were prepared by the literature procedures.

Infrared spectra were obtained as Nujol mulls (KBr plates) on a Mattson 4030 FTIR spectrometer. UV–visible spectra were determined by using a Cary 219 spectrophotometer. The ^{31}P $\{^1H\}$ and ^1H NMR spectra were recorded on a Bruker AM-400 spectrometer operating at 161.978 and 400.13 MHz, respectively. The elemental analyses were performed by the microanalytical service within the chemistry department of the University of Calgary.

Preparation of cis-*[PtCl(PEt$_3$)$_2$(Ph$_2$PS$_2$N$_3$)][BF$_4$], 3*

A purple solution of $Ph_2PS_2N_3$ (0.100 g, 0.343 mmol) in dichloromethane (10 mL) was added dropwise to a solution of $[Pt_2(\mu\text{-}Cl)_2(PEt_3)_4][BF_4]_2$ (0.190 g, 0.172 mmol) in dichloromethane (10 mL) at 23°C with the immediate formation of a transparent red solution. The solution was stirred for 1 h and then solvent was removed under vacuum to give a purple-pink solid. Recrystallization of this product from deoxygenated diethyl ether – dichloromethane (1:1) solution at 23°C afforded *cis*-$[PtCl(PEt_3)_2(Ph_2PS_2N_3)][BF_4]$, (0.188 g, 0.222 mmol) in 65% yield. Infrared: 1060 cm^{-1} (s, br, ν_{as} BF_4^-); ^1H nmr ($CDCl_3$, 23°C), δ (ppm): 7.39–8.15 (m, C_6H_5, 10H), ca. 1.9 (m, CH_2CH_3, 12H), and ca. 1.2 (m, CH_2CH_3, 18H). The ^{31}P nmr data are discussed in the Results and discussion section. Anal. calcd. for $C_{24}H_{40}BClF_4N_3P_3PtS_2$: C 34.11, H 4.77, N 4.97; found: C 33.38, H 5.07, N 4.18.

Preparation of trans-*[PtCl$_2$(PEt$_3$)(Ph$_2$PS$_3$N$_2$)], 4*

This adduct was obtained as red crystals in 75% yield, after two recrystallizations from hexane at 23°C, from the reaction of $Ph_2PS_2N_3$ with $[PtCl_2(PEt_3)]_2$ by using a procedure similar to that described above for **3**. ^1H nmr ($CDCl_3$, 23°C); δ (ppm) 7.54–8.11 (m, C_6H_5, 10H), 1.68 (m, CH_2CH_3, 6H), 0.96 (dt, CH_2CH_3, 9H), $^3J(PH)$ = 18 Hz, $^3J(HH)$ = 9 Hz. The ^{31}P nmr data are discussed in the Results and discussion section. Anal. calcd. for $C_{18}H_{25}Cl_2N_3P_2PtS_2$: C 32.00, H 3.73, N 6.22; found: C 31.56, H 3.42, N 6.04.

X-ray crystallographic analysis of 4

Crystals of **4** were obtained from hexane solution. The crystal was attached to a glass fibre with epoxy. The structure was determined by the application of standard procedures, and pertinent crystallographic data are listed in Table 1.

The unit cell was determined from the setting angles of 25 reflections with $17° < 2\theta < 19°$. All measurements were made on an Enraf–Nonius CAD4 diffractometer with the $\omega/2\theta$ scan technique and calculations were done using the NRCVAX system of programs (7). Psi scan absorption corrections were made. No general correction was made for extinction.

The structure was solved by Patterson techniques. All non-H atoms were refined anisotropically. H atoms were constrained to idealized positions (C—H = 0.95 Å) with isotropic B values of 1.2 times the B value of the attached C atom. In the full-matrix least-squares refinement, the function minimized was $\Sigma w(|F_o| - |F_c|)^2$ where $w^{-1} = [\sigma^2(I) + 0.02\,I^2]/4F^2$. Conventional atomic scattering factors, corrected for anomalous dispersion, were used (8). Positional parameters are given in Table 2 and selected bond distances and angles are summarized in Table 3.

Hydrogen atom parameters, anisotropic thermal parameters,

TABLE 1. Crystallographic parameters for *trans*-$PtCl_2(PEt_3)(\eta^1\text{-}NPh_2PS_2N_3)$, **4**

Formula	$C_{18}H_{25}Cl_2N_3P_2PtS_2$
fw	675.47
Crystal size (mm)	0.06 × 0.14 × 0.20
Space group	$P2_1/c$
a (Å)	14.920(3)
b (Å)	8.966(5)
c (Å)	19.103(5)
β (°)	109.32(2)
V (Å^3)	2411.6(16)
Z	4
D_{calcd} (g/cm^3)	1.86
Radiation, Å	MoKα (λ = 0.71073 Å) graphite monochromated
Temperature (K)	293
F(000)	1307.3
Scan range (°)	1.0 + 0.35 tan θ
Scan speed (° min^{-1})	4–16
Max θ (°)	25
Octants	$\pm h + k + l$
Unique reflections	4236
Observed reflections (>2.5σ)	2000
μ (MoKα) (cm^{-1})	64.1
Min/max absorption corr.	0.66–0.99
Parameters refined	253
GOF	1.21
R, R_w[a]	0.050, 0.053

[a] $R = \Sigma(||F_o| - |F_c||)/\Sigma|F_o|$; $R_w = [\Sigma w(|F_o| - |F_c|)^2/\Sigma w|F_o|^2]^{1/2}$.

TABLE 2. Positional parameters for **4**

	x	y	z	B_{iso}[a]
Pt	0.27532(5)	0.40689(9)	0.44311(4)	2.74(4)
Cl1	0.1864 (4)	0.6166 (6)	0.4448 (3)	5.1 (3)
Cl2	0.3744 (4)	0.2115 (6)	0.4434 (3)	4.4 (3)
S1	0.2936 (4)	0.8656 (6)	0.3525 (4)	4.9 (4)
S2	0.4270 (4)	0.6458 (6)	0.4264 (3)	4.2 (3)
P1	0.2061 (4)	0.2758 (7)	0.5091 (3)	3.4 (3)
P2	0.2839 (3)	0.5804 (7)	0.2948 (3)	3.15(25)
N1	0.3433 (10)	0.5257 (17)	0.3787 (8)	3.2 (8)
N2	0.2428 (11)	0.7504 (19)	0.2909 (9)	4.4 (10)
N3	0.3843 (12)	0.8149 (19)	0.4159 (9)	4.5 (10)
C1	0.3572 (13)	0.5690 (22)	0.2363 (10)	3.3 (10)
C2	0.4277 (16)	0.468 (3)	0.2503 (12)	4.9 (13)
C3	0.4825 (16)	0.4575 (25)	0.2032 (14)	5.2 (13)
C4	0.4610 (17)	0.548 (3)	0.1438 (14)	5.1 (15)
C5	0.3892 (19)	0.654 (3)	0.1289 (12)	5.3 (14)
C6	0.3378 (15)	0.6628 (23)	0.1752 (12)	4.4 (12)
C7	0.1864 (16)	0.459 (3)	0.2588 (12)	3.7 (12)
C8	0.2010 (15)	0.308 (3)	0.2621 (13)	4.7 (14)
C9	0.1251 (20)	0.210 (3)	0.2334 (14)	5.1 (14)
C10	0.0338 (21)	0.275 (4)	0.1964 (14)	7.0 (18)
C11	0.0229 (16)	0.423 (4)	0.1930 (14)	6.5 (16)
C12	0.0985 (17)	0.511 (3)	0.2245 (12)	5.0 (13)
C13	0.2770 (17)	0.273 (4)	0.6055 (14)	7.4 (17)
C14	0.2968 (22)	0.430 (4)	0.6403 (13)	8.9 (21)
C15	0.1976 (14)	0.078 (3)	0.4869 (11)	4.8 (12)
C16	0.1413 (17)	−0.0171 (25)	0.5226 (15)	6.3 (16)
C17	0.0859 (16)	0.333 (3)	0.4993 (14)	5.3 (14)
C18	0.0171 (15)	0.315 (3)	0.4207 (17)	8.0 (17)

[a] B_{iso} is the mean of the principal axes of the thermal ellipsoid.

Can. J. Chem. Downloaded from www.nrcresearchpress.com by 109.225.110.28 on 09/08/12
For personal use only.

TABLE 3. Selected bond lengths (Å) and bond angles (deg) for *trans*-$[PtCl_2(PEt_3)(Ph_2PS_2N_3)]$, **4**, $Ph_2PS_2N_3Me^+CF_3SO_3^-$, **2***a*, and *trans*-$(Ph_2PS_2N_3)_2SnCl_4$, **2***d*

Atoms	**4**	**2***a*	**2***d*[a]
S(1)—N(2)	1.562(19)	1.562(5)	1.564(4)
S(1)—N(3)	1.555(19)	1.549(7)	1.548(4)
S(2)—N(1)	1.672(16)	1.707(5)	1.712(3)
S(2)—N(3)	1.631(19)	1.644(6)	1.631(4)
P(2)—N(1)	1.629(15)	1.668(6)	1.648(3)
P(2)—N(2)	1.635(18)	1.649(5)	1.649(3)
P(2)—C(1)	1.807(20)	1.770(6)	1.780(4)
P(2)—C(7)	1.766(22)	1.771(5)	1.796(4)
Pt—Cl(1)	2.308(6)		
Pt—Cl(2)	2.291(5)		
Pt—P(1)	2.213(6)		
Pt—N(1)	2.122(15)		
N(2)—S(1)—N(3)	118.3(9)	117.2(3)	116.2(2)
N(1)—S(2)—N(3)	109.9(8)	106.8(3)	109.1(2)
N(1)—P(2)—N(2)	113.5(8)	108.7(3)	109.3(2)
S(2)—N(1)—P(2)	114.0(9)	110.3(3)	112.4(2)
S(1)—N(2)—P(2)	120.0(10)	121.1(1)	125.3(2)
S(1)—N(3)—S(2)	124.8(10)	125.5(4)	123.6(2)
Cl(1)—Pt—P(1)	92.62(21)		
Cl(1)—Pt—N(1)	89.2(4)		
Cl(2)—Pt—P—(1)	90.87(21)		
Cl(2)—Pt—N(1)	87.3(4)		
Pt—N(1)—S(2)	114.9(8)		
Pt—N(1)—P(2)	120.9(8)		

[a]See footnote 2.

torsion angles, least-squares planes, complete tables of bond lengths and bond angles, and structure factors have been deposited.[3]

Results and discussion

Synthesis and ^{31}P nmr characterization of 3 and 4

The reaction of $Ph_2PS_2N_3$, **1**, with either $[PtCl(PEt_3)_2]_2[BF_4]_2$ or $[PtCl_2(PEt_3)]_2$ in dichloromethane at room temperature results in the cleavage of the chloro bridges to give the 1:1 adducts **3** and **4**, respectively, as air-stable, red crystals. By contrast **1** does not react with the palladium dimer $[PdCl_2(PEt_3)]_2$ even at reflux in chloroform.

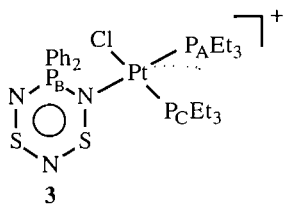

3

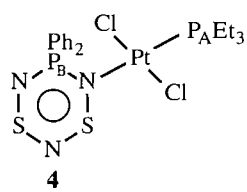

4

The $^{31}P\{^1H\}$ nmr spectrum of **3** indicates that platinum is coordinated to a nitrogen atom adjacent to the phosphorus atom of the heterocyclic ring (Fig. 1). The resonances at 6.8 and 10.7 ppm are readily assigned to the inequivalent PEt_3 ligands (P_A and P_C, respectively) on the basis of their large couplings to platinum, 3269 and 3607 Hz, respectively. In addition, these resonances exhibit a mutual coupling of 21 Hz, indicating that the PEt_3 ligands are attached to platinum in mutually *cis* positions.[4] The signal for P_A appears as a doublet of doublets due to a three-bond coupling of 11 Hz to the heterocyclic phosphorus atom, P_B. The resonance for P_B is observed at 2.3 ppm, ca. 23 ppm downfield from that of **1** (1). For comparison the ^{31}P nmr chemical shifts of **2***a–d* occur in the range 29–41 ppm downfield from that of **1**. The resonance for P_B exhibits ^{195}Pt satellites with $J(PtP_B)$ = 30 Hz. The observation of this coupling and the P_A–P_B coupling strongly suggests that the platinum is coordinated to one of the equivalent nitrogen atoms (i.e., adjacent to P_B) rather than to the unique nitrogen in **1**.

The ^{31}P nmr spectrum of **4** also indicates that the platinum is attached to a nitrogen atom adjacent to phosphorus. Two mutually coupled resonances, $^3J(P_AP_B)$ = 11 Hz, are observed at 2.7 and 2.4 ppm, each with flanking ^{195}Pt satellites. The low-field signal with $^1J(PtP)$ = 3728 Hz is assigned to the PEt_3 ligand while the high-field signal with $J(PtP)$ = 28 Hz is ascribed to the heterocyclic phosphorus P_B. The structure of **4** was determined by X-ray crystallography.

X-ray crystal structure of trans-*[$PtCl_2(PEt_3)(Ph_2PS_2N_3)$], 4*

The X-ray analysis of **4** confirms that platinum is attached to a nitrogen atom adjacent to phosphorus. An ORTEP drawing of the structure with the atomic numbering scheme is displayed in Fig. 2. The pertinent endocyclic and exocyclic bond lengths and bond angles of **4** are compared with the corresponding values for the related adducts **2***a* and **2***d* in Table 3. The structural determination confirms that the $PtCl_2(PEt_3)$ is η^1-N-bonded to the PS_2N_3 ring with PEt_3 *trans* to nitrogen.

The structural trends for all three adducts are similar, although the perturbation of the geometry of the PS_2N_3 ring caused by coordination to platinum(II) is somewhat less than that observed for **2***a* and **2***d*. Thus the S(2)—N(1) bond distance in **4** is elongated from 1.575(3) Å in **1** (1) to 1.672(16) Å in **4** (cf. 1.707(5) and 1.712(3) Å in **2***a* and **2***d*, respectively (3)). The P—N bond lengths of ca. 1.63 Å in **4** are not significantly changed from the value of 1.62 Å observed for **1** (1) and the endocyclic bond angle at phosphorus is also little affected in **4**. The S(2)—N(3)—S(1)—N(2)—P(2) segment of the ring is planar to within 0.05(2) Å in **4** while the coordinated nitrogen N(1) is displaced from this plane by 0.63(2) Å (cf. 0.78 and 0.71 Å for **2***a* and **2***d*, respectively (3)). The angles sums at N(1) in **4** are 349.8° compared to values of 339° for **2***a* and 358.3° for **2***d*. As for **2***a* and **2***d*, the S(1)—N bond lengths of 1.55–1.56 Å are indicative of a localized sulfur diimide structure -N=S=N- in **4**.[5]

The geometry about platinum in **4** is essentially square-planar with d(Pt—N) = 2.122(15) Å. For comparison, the Pt—N bond lengths in platinum(II) complexes of chelating

[3]Supplementary material mentioned in the text may be purchased from: The Depository of Unpublished Data, Document Delivery, CISTI, National Research Council Canada, Ottawa, Canada K1A 0S2.

Tables of hydrogen atom parameters and bond lengths and angles have also been deposited with the Cambridge Crystallographic Data Centre and can be obtained on request from The Director, Cambridge Crystallographic Data Centre, University Chemical Laboratory, 12 Union Road, Cambridge CB2 1EZ, U.K.

[4]*trans* ^2J(P–P) coupling constants are typically in the range 300–600 Hz (9).

[5]Typical S—N bond lengths in a *cis*, *cis*-sulfur diimide are ca. 1.52 Å (10).

Can. J. Chem. Downloaded from www.nrcresearchpress.com by 109.225.110.28 on 09/08/12
For personal use only.

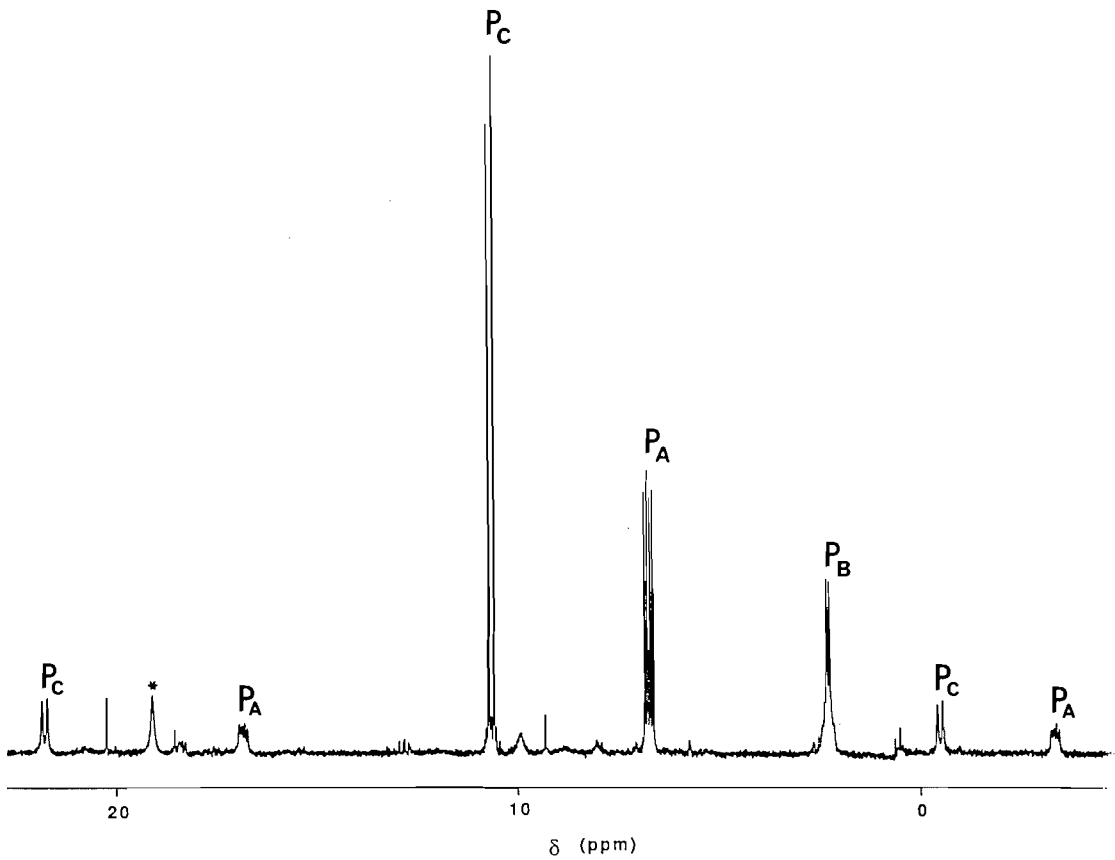

FIG. 1. ^{31}P NMR spectrum of *cis*-$[PtCl(PEt_3)_2(Ph_2PS_2N_3)][BF_4]$, **3**. Unreacted $[Pt_2(\mu\text{-}Cl)_2(PEt_3)_4][BF_4]_2$ is identified by an asterisk.

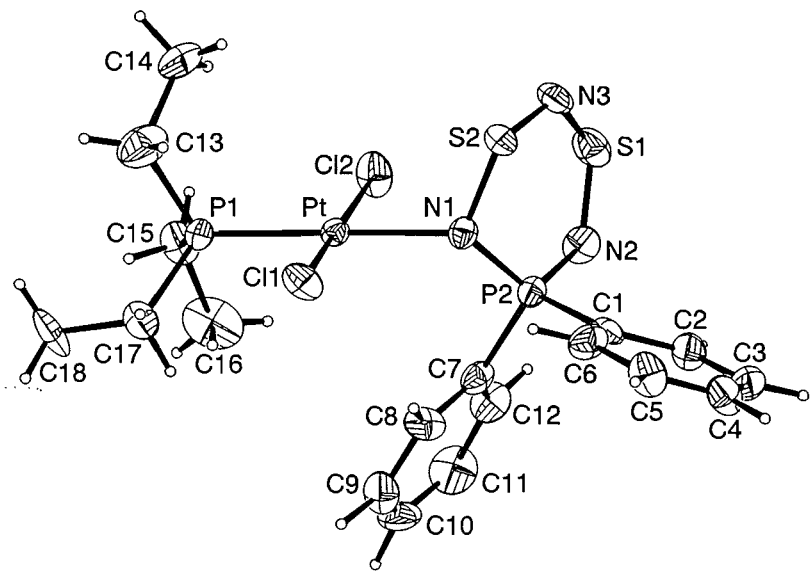

FIG. 2. ORTEP plot (30% probability ellipsoids) of *trans*-$[PtCl_2(PEt_3)(Ph_2PS_2N_3)]$, **4**.

S—N ligands are in the range 2.01–2.05 Å (11–13) and the Pt—N bond distance in the fluxional dimer $[Pt(PR_3)(1,5\text{-}Ph_4P_2N_4S_2)]_2$ is 2.089(7) Å (14). This centrosymmetric molecule undergoes a facile [1, 3] shift of platinum between vicinal nitrogen atoms of the $P_2N_4S_2$ ring. Thus the Pt—N bond length observed for **4** is indicative of a weak interaction as reflected in the ready dissociation of this adduct in solution (*vide infra*). The relatively large value (3728 Hz) for $^1J(Pt\text{–}PEt_3)$ in **4** is further evidence of the weakness of this interaction.[6]

[6] $^1J(Pt\text{–}P)$ values for closely related complexes with strong Pt—N bonds *trans* to PEt_3 are significantly smaller (3175–3355 Hz) (12, 13).

Electronic spectra of 3 and 4

The adducts **3** and **4** exhibit absorption bands at 514 and 528 nm, respectively, in methylene dichloride. The determination of an extinction coefficient for these absorptions was thwarted by the partial dissociation of the adducts to give **1** (λ_{max} 550 nm). The observed hypsochromic shift in the π^*(HOMO) $\rightarrow$ π^* (LUMO) transition of **1** upon coordination to platinum(II) is much less pronounced than that observed for the adducts **2***a–d*, for which absorption maxima are observed in the range 410–430 nm (3). Thus the visible spectroscopic data provide another manifestation of the relative weakness of the nitrogen–electrophile interaction in **4** compared to that in **2***a–d*.

Conclusions

The interaction of the phosphadithiatriazine **1** with platinum(II) electrophiles produces 1:1 adducts in which the metal is attached to a nitrogen atom adjacent to phosphorus in the PS_2N_3 ring. Coordination to platinum perturbs the conformation of the ring and the S—N bond lengths in a manner similar to that observed for other electrophiles. However, the interaction with platinum(II) is weaker than that observed for electrophiles such as $SnCl_4$ or upon methylation, as indicated by ^{31}P NMR and visible spectroscopic measurements and by the X-ray structural data.

Acknowledgements

We thank the Natural Sciences and Engineering Research Council of Canada, the National Science Foundation, and the State of Arkansas for financial support.

1. N. Burford, T. Chivers, A. W. Cordes, W. G. Laidlaw, M. Noble, R. T. Oakley, and P. N. Swepston. J. Am. Chem. Soc. **104**, 1282 (1982).
2. N. Burford, T. Chivers, R. T. Oakley, and T. Oswald. Can. J. Chem. **62**, 712 (1984).
3. T. Chivers, S. W. Liblong, J. F. Richardson, and T. Ziegler. Inorg. Chem. **27**, 860 (1988).
4. T. Chivers, K. S. Dhathathreyan, S. W. Liblong, and T. Parks. Inorg. Chem. **27**, 1305 (1988).
5. J. Chatt and L. M. Venanzi. J. Chem. Soc. 2787 (1955).
6. K. R. Dixon and D. J. Hawke. Can. J. Chem. **49**, 3253 (1971).
7. E. J. Gabe, Y. Lepage, J. P. Charland, F. L. Lee, and P. S. White. J. Appl. Crystallogr. **22**, 383 (1989).
8. D. T. Cromer and J. T. Waber. International tables for X-ray crystallography. Vol. IV. Kynoch Press, Birmingham, England. 1974.
9. A. Pidcock and J. F. Nixon. Annu. Rev. NMR Spectrosc. **2**, 345 (1969).
10. A. Gieren, H. Betz, T. Hübner, V. Lamm, M. Herberhold, and K. Guldner. Z. Anorg. Allg. Chem. **513**, 160 (1984).
11. R. Jones, C. P. Warrens, D. J. Williams, and J. D. Woollins. J. Chem. Soc. Dalton Trans. 907 (1987).
12. R. Jones, P. F. Kelly, D. J. Williams, and J. D. Woollins. J. Chem. Soc. Dalton Trans. 1569 (1988).
13. P. F. Kelly, A. M. Z. Slawin, D. J. Williams, and J. D. Woollins. Polyhedron, **9**, 2659 (1990).
14. T. Chivers, M. Edwards, P. N. Kapoor, A. Meetsma, J. C. van de Grampel, and A. Van Der Lee. Inorg. Chem. **29**, 3069 (1990).

Can. J. Chem. Downloaded from www.nrcresearchpress.com by 109.225.110.28 on 09/08/12
For personal use only.

Syntheses of model oligosaccharides of biological significance. XII.[1] Synthesis, NMR, and conformational analysis of trideuteriomethyl 4-*O*-(β-D-mannopyranosyl)-2-acetamido-2-deoxy-β-D-glucopyranoside: the use of DEPT ^{1}H to ^{13}C transfer for T_1 measurements and NOE assignments of tightly coupled ^{1}H nuclei

HO HUAT LEE[2] AND LIGAYA N. CONGSON[3]
Ludwig Institute for Cancer Research, Toronto Branch, Toronto, Ont., Canada

AND

DENNIS M. WHITFIELD, LAJOS R. RADICS,[4] AND JIRI J. KREPINSKY[5]
Department of Molecular and Medical Genetics, and Carbohydrate Research Centre, University of Toronto, Toronto, Ont., Canada M5S 1A8

Received October 28, 1991[6]

HO HUAT LEE, LIGAYA N. CONGSON, DENNIS M. WHITFIELD, LAJOS R. RADICS, and JIRI J. KREPINSKY. Can. J. Chem. **70**, 2607 (1992).

The title disaccharide Manp(β1–4)GlcpNAcβ1-OCD$_3$ has been prepared by a short synthetic sequence through the inversion of configuration from *gluco* to *manno* involving benzyl Glcp(β1–4)GlcpNAc. The disaccharide was subjected to detailed high-field ^{1}H and ^{13}C NMR study. First, conventional and 2D spectra were run to afford a complete set of assigned spectral parameters. Next, steady-state ^{1}H–{^{1}H} NOE and ^{1}H, ^{13}C spin lattice relaxation experiments were performed to infer dynamic spectral data related to molecular conformation. Owing to tight couplings and signal overlaps in the ^{1}H spectrum, proton relaxation and selected NOE data were obtained via ^{13}C NMR after transfer of the actual, non-equilibrium, proton magnetization to the ^{13}C frequency domain. Using this experimental approach it has been found that T_1's for Manp H-4 and GlcpNAc H-2 were substantially longer than those of the other sugar ring protons, and that the principal interresidue dipolar contact in Manp(β1–4)GlcpNAcβ1-OCD$_3$ takes place between Manp H-1 and GlcpNAc H-4. Subsequently, a conformational analysis of the disaccharide was executed by means of a semiempirical method comparing Boltzman-averaged computed observables with experimental T_1 and NOE values. The results suggest that the disaccharide has substantial conformational flexibility. Its *exo*-anomeric-stabilized conformational minimum at approximately $\phi = +50°$ ($\psi = 0 \pm 10°$) of the glycosidic rotational angle is significantly populated but this global minimum does not represent the only rotational form available to the molecule.

HO HUAT LEE, LIGAYA N. CONGSON, DENNIS M. WHITFIELD, LAJOS R. RADICS et JIRI J. KREPINSKY. Can. J. Chem. **70**, 2607 (1992).

On a préparé le disaccharide Manp(β1–4)GlcpNAcβ1-OCD$_3$ mentionné dans le titre en utilisant une courte voie de synthèse impliquant une inversion de configuration de *gluco* à *manno* sur le Glcp(β1–4)GlcpNAc de benzyle. On a soumis le disaccharide à une étude détaillée par RMN du ^{1}H et du ^{13}C à haut champ. Dans un premier temps, on a déterminé les spectres conventionnels et en 2D afin d'obtenir un ensemble complet des paramètres spectraux. Par la suite, dans le but de relier les données spectrales avec une conformation moléculaire, on a effectué des expériences d'EON ^{1}H-{^{1}H} à l'état stationnaire et de relaxation spin-réseau du ^{1}H et du ^{13}C. À cause des faibles couplages et des recouvrements de signaux dans le spectre du ^{1}H, on a déterminé la relaxation du proton et les données sélectives d'EON à l'aide de la RMN du ^{13}C après un transfert de la magnétisation réelle, non-équilibrée, du proton vers le domaine de fréquence du ^{13}C. Utilisant cette approche expérimentale, on a trouvé que les T_1 du H-4 du Manp et du H-2 du GlcpNAc sont beaucoup plus longs que ceux des autres protons du cycle du sucre et que le principal contact dipolaire inter-résidu dans le Manp(β1–4)GlcpNAcβ1-OCD$_3$ se produit entre le H-1 du Manp et le H-4 du GlcpNAc. Par la suite, on a effectué une analyse conformationnelle complète du disaccharide à l'aide d'une méthode semi-empirique permettant de comparer les valeurs moyennes de Boltzman calculées et les valeurs experimentales de T_1 et d'EON. Les résultats suggèrent que la disaccharide possède beaucoup de flexibilité conformationnelle. La population de sa conformation *exo*, stabilisée par anomérie et correspondant à un minimum d'énergie pour un angle de rotation glycosidique $\phi = +50°$ ($\psi = 0 \pm 10°$), est importante, mais ce minimum global ne représente pas nécessairement la seule forme rotationnelle disponible pour cette molécule.
[Traduit par la rédaction]

Introduction

The biological functions of the oligosaccharide moieties of glycoproteins depend on their 3-dimensional structures (1). Oligosaccharides bound to proteins by an amidic linkage to asparagine invariantly contain the core structure **I** as a base

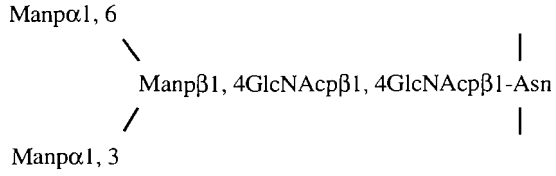

I

of enormous diversity of more complex structures. Such structures can in principle assume a variety of conformations, which can be further modified through interactions with

[1]For part 11, see ref. 39.
[2]Present address: Cancer Research Laboratory, School of Medicine, Auckland University, Auckland, New Zealand.
[3]Present Address: Department of Chemical Engineering, University of Toronto.
[4]Central Research Institute for Chemistry, Hungarian Academy of Sciences, Budapest, Hungary.
[5]Author to whom correspondence may be addressed.
[6]Revision received June 25, 1992.

Can. J. Chem. Downloaded from www.nrcresearchpress.com by 109.225.110.28 on 09/08/12
For personal use only.

Can. J. Chem. Downloaded from www.nrcresearchpress.com by 109.225.110.28 on 09/08/12
For personal use only.

suitable sites on the carrier peptidic chain. NMR spectroscopy is the method of choice for the determination of conformations of these substances in solution (2). However, NMR spectra become increasingly crowded as the molecules become more complex and resulting ambiguity in certain assignments makes it more difficult to draw conformational conclusions based on analysis of the spectra. This is further aggravated by tight coupling involving several ^1H nuclei as in the case of GlcpNAc substituted in β1–4 fashion (3). Since the understanding of smaller components assists in the studies of the larger molecule, we have examined the disaccharide Manp(β1–4)GlcpNAcβ1-OCD_3 (**II**) with the objective to determine its preferred conformation. One of our aims has been to solve the problem of signal assignments, including NOE measurement, in tight coupling situations. Furthermore, we were interested in agreement between the conformational conclusions derived from the NMR measurements and potential energy calculations.

Results and discussion

Synthesis

The synthetic design is summarized in Scheme 1. The only major problem in the synthesis of this saccharide is the formation of the *cis* glycosidic bond, i.e., the β-mannopyranoside (4). This is a difficult problem and a number of solutions has been proposed for its solution. All direct methods using a non-participating group for protection of O-2 of mannose result in formation of both α and β anomers and, depending on circumstances, different ratios of α:β anomers are obtained. The β anomers are formed predominantly (sometimes exclusively) with reactive hydroxyl groups, such as those in aliphatic alcohols: this has been observed in the case of the 2,3-;4,6-dicyclohexylidene derivative (5) and the 2,3-carbonate of mannose (6). The hydroxyl group on C-4 of 2-acetamido-2-deoxyglucopyranosides is relatively unreactive and in glycosylation reactions the above derivatives yield predominantly the *trans* product, i.e., α-mannopyranoside. When O-2 of mannose is protected by a benzyl group, and heterogenous promotion is used (silver silicate, silver zeolite, thallium zeolite), analogous observations have been made. An indirect method of formation of β-mannopyranoside is based on the preparation of β-glucopyranoside with the assistance of a participating protecting group on O-2 of glucopyranoside, and converting anomerically pure β-glucopyranoside into β-mannopyranoside by an inversion of the C-2 configuration (*gluco* to *manno*). This has been done by either S_N2 displacement (7) or oxidation–reduction sequences (8). Although the last mentioned procedure from the Jeanloz laboratory involving oxidation of HO-2 to a carbonyl and reduction of the latter with sodium borohydride afforded the *manno* configuration with a very good specificity, some *gluco* configuration has usually been obtained as well (8). We have found that L-Selectride (lithium tri-*sec*-butylborohydride) gave a reduction product in which the *gluco* configuration was consistently undetectable.

The accepting partner in the glycosylation reaction often reacts differently when it is presented to a glycosylating agent as an α- or β-glycoside. To determine which anomer would give higher yield and better purity in the coupling reaction, we have prepared pure both α- and β-benzyl 2-acetamido-2-deoxy-3,6-di-*O*-benzyl-D-glucopyranosides. Comparison of glycosylation reactions using both acceptors separately did not show any noticeable difference.

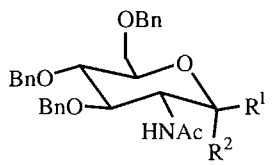

III*a*: R^1 = H, R^2 = OBn
III*b*: R^1 = OBn, R^2 = H

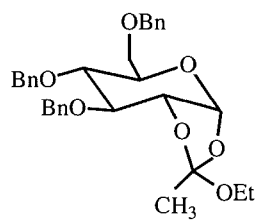

IV

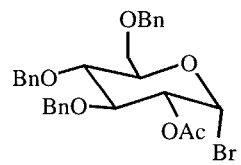

V

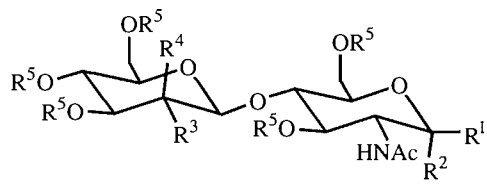

VI*a*: $R^1 = R^4$ = H; R^2 = OBn; R^3 = OAc; R^5 = Bn
VI*b*: R^1 = OBn; $R^2 = R^4$ = H; R^3 = OAc; R^5 = Bn
VI*c*: $R^1 = R^4$ = H; R^2 = OBn; R^3 = OH; R^5 = Bn
VI*d*: R^1 = H; R^2 = OBn; R^3, R^4 = O; R^5 = Bn
VI*e*: $R^1 = R^3$ = H; R^2 = OBn; R^4 = OH; R^5 = Bn
VI*f*: $R^1 = R^2$ = H, OAc; R^3 = H; R^4 = OAc; R^5 = Ac
VI*g*: $R^1 = OCD_3$; $R^2 = R^3$ = H; R^4 = OAc; R^5 = Ac
II : $R^1 = OCD_3$; $R^2 = R^3 = R^5$ = H; R^4 = OH

SCHEME 1

Can. J. Chem. Downloaded from www.nrcresearchpress.com by 109.225.110.28 on 09/08/12
For personal use only.

The starting materials **2** and **3** were prepared as reported previously: orthoester **IV** was made according to Kochetkov *et al.* (9) and transformed into the bromide **V** by a modification of the procedure of Hindsgaul *et al.* (10). Acceptors benzyl 2-acetamido-2-deoxy-3,6-di-*O*-benzyl-D-glucopyranosides α (8, 11) (**III***a*) and β (12) (**III***b*) were known as well, but their preparation was somewhat lengthy or involved a chromatographic separation of a differently substituted carbohydrate moiety, which would be tedious on a larger scale. Regioselective reductive opening of the 4,6-benzylidine derivative described by Garegg *et al.* (13) was promising as a simplification for the synthesis of these acceptors. Moreover, purification of individual intermediates on the pathway leading to **III***a* and **III***b* was substantially helped by no need for chromatography since they were all crystalline. Benzylidine derivatives were synthesized from benzyl anomers (α prepared by Fischer glycosidation (11); β by Koenigs–Knorr glycosylation (12*a*, 14), separately benzylated, and subjected to reductive opening of the 1,3-dioxane ring system. Although the yields may seem low, they could be substantially improved by purification of mother liquors after crystallization. However, this would make the synthesis more tedious and time consuming and, in light of the simplicity of the design and low costs of materials involved, not justified. The synthesis of the title compound **II** is portrayed in Scheme 1, and the synthesis of intermediates **III***a* and **III***b* is summarized in Scheme 2.

NMR spectrometry

Conformational studies by NMR methods usually require a prior complete assignment of the ^1H and ^{13}C spectra (2). Assignments were made by standard 1D and 2D procedures: first, homonuclear 2D chemical shift correlation (COSY) experiment indicated proton–proton connectivities within the individual sugar moieties. Next, 2D heteronuclear (H,C-COSY) experiment afforded the assignment of ^{13}C resonances. The assigned spectral parameters, i.e., ^1H and ^{13}C chemical shifts, and ^1H–^1H coupling constants, are collected in the experimental section.

Conformational analysis of oligosaccharides relies on conformation-related NMR parameters, such as interresidue ^1H–$\{^1H\}$ nuclear Overhauser enhancement (NOE) data and spin-lattice relaxation times of hydrogen nuclei, T_1^H, and carbons, T_1^C. The 400 MHz spectrum of the disaccharide Manp(β1–4)GlcpNAcβ1-OCD_3 (cf. Fig. 1) as obtained in a dilute D_2O solution is displayed in Fig. 2. It can be seen that under these conditions protons H-2, H-3, and H-4 of the GlcpNAc unit appear tightly coupled (3) (cf. the additional splitting of the resonance at 4.63 ppm assigned to H-1 of this unit) while other resonances of GlcpNAc overlap with signals of Manp protons. Although such spectral complexity, typical for certain oligosaccharides, causes no major difficulties in the assignment procedure, it makes it impossible to measure the individual relaxation times of more than a fraction of protons in the system. Moreover, it obviates determining which of the resonances due to the GlcpNAc unit become enhanced upon selective preirradiation of an isolated proton, e.g., the anomeric proton H-1 of the Manp unit. However, resonances in decoupled ^{13}C spectra of molecules of this size are generally well separated at frequencies employed in this study (100 MHz), and consequently it becomes convenient to monitor proton relaxation processes and steady-state NOE enhancements after transferring proton magnetizations to the ^{13}C domain prior to observation. This may be easily achieved using one of the known polarization transfer pulse sequences, a possibility recognized in the early 1980's by Avent and Freeman (15), who described a related proton relaxation experiment using 2D spectroscopy. Indirect measurement of proton relaxation rates by INEPT polarization transfer to ^{13}C has been reported by Morris (16) and more recently by Bigler (17), who used this technique to infer relaxation parameters of protons directly bound to ^{13}C nuclei.

The accuracy of indirectly measured proton relaxation rates, $1/T_1^{H(indir)}$, is limited by the fact that its value is obtained as a difference

$$1/T_1^{H(indirect)} = 1/T_1^{H(pt)} - 1/NT_1^C$$

where $T_1^{H(pt)}$ is the proton relaxation time measured via polarization transfer method, T_1^C represents the dipolar portion of the ^{13}C relaxation time, and N is the number of protons directly attached to a given carbon atom. This relationship reflects the fact that proton longitudinal relaxation rates of the ^{12}C and ^{13}C obtained, respectively, from direct and indirect T_1 experiments differ by an amount determined by the dipolar interaction between the ^{13}C and ^1H nuclei. This amount is given by the dipolar ^{13}C relaxation rate divided by the number of directly bound protons. In all reported cases, the two right-hand side terms were determined in two separate experiments. To improve accuracy of the indirect proton relaxation data, in this study we made two modifications to the known technique. First, we used the DEPT sequence as the polarization transfer method (known to provide distortionless and J_{CH}-independent transfer, and, second, we acquired the two data sets ($T_1H^{(DEPT)}$ and T_1^C in *one single experiment*). The effects of these modifications were tested on a sample of methyl α-D-glucopyranoside. Three subsequent measurements were performed in a queued serial run and the pertinent data are reported in Table 1. It can be seen that the accuracy of the indirectly measured T_1^H is about 10%, which compares well with the overall estimated error of 5% for the directly measured relaxation time values. The accuracy of indirect measurements performed on the disaccharide **II** is estimated to be of the same order.

The proton relaxation data obtained for the disaccharide using the direct and indirect methods are collected in Table 2. It can be seen that the indirect T_1 data agree well with the values obtained by direct measurements for all protons that exhibit no overlapping with other resonances. The data summarized in Table 2 also show that Manp H-4 and GlcNAc H-2 protons have significantly longer T_1 values than the other ring protons of the disaccharide **II**. This fact may reflect the *trans diaxial* relationship of these protons to their (vicinal) neighbours.

The NOE difference spectrum obtained for disaccharide **II** upon selective preirradiation of the resonance due to Manp H-1 is displayed in Fig. 3. Intra-residue enhancements of resonances due to Manp H-2′, H-3′, H-4′, and H-5′, as well as H-6′ and H6″ are readily recognized. However, as can be seen from Fig. 3, the spectrum gives no unambiguous answer as to which of the closely spaced H-2, H-3, and H-4 resonances of the GlcpNAc unit is responsible for the interglycosidic enhancement, a question of prime importance for the conformational analysis. Fourier transformation of the

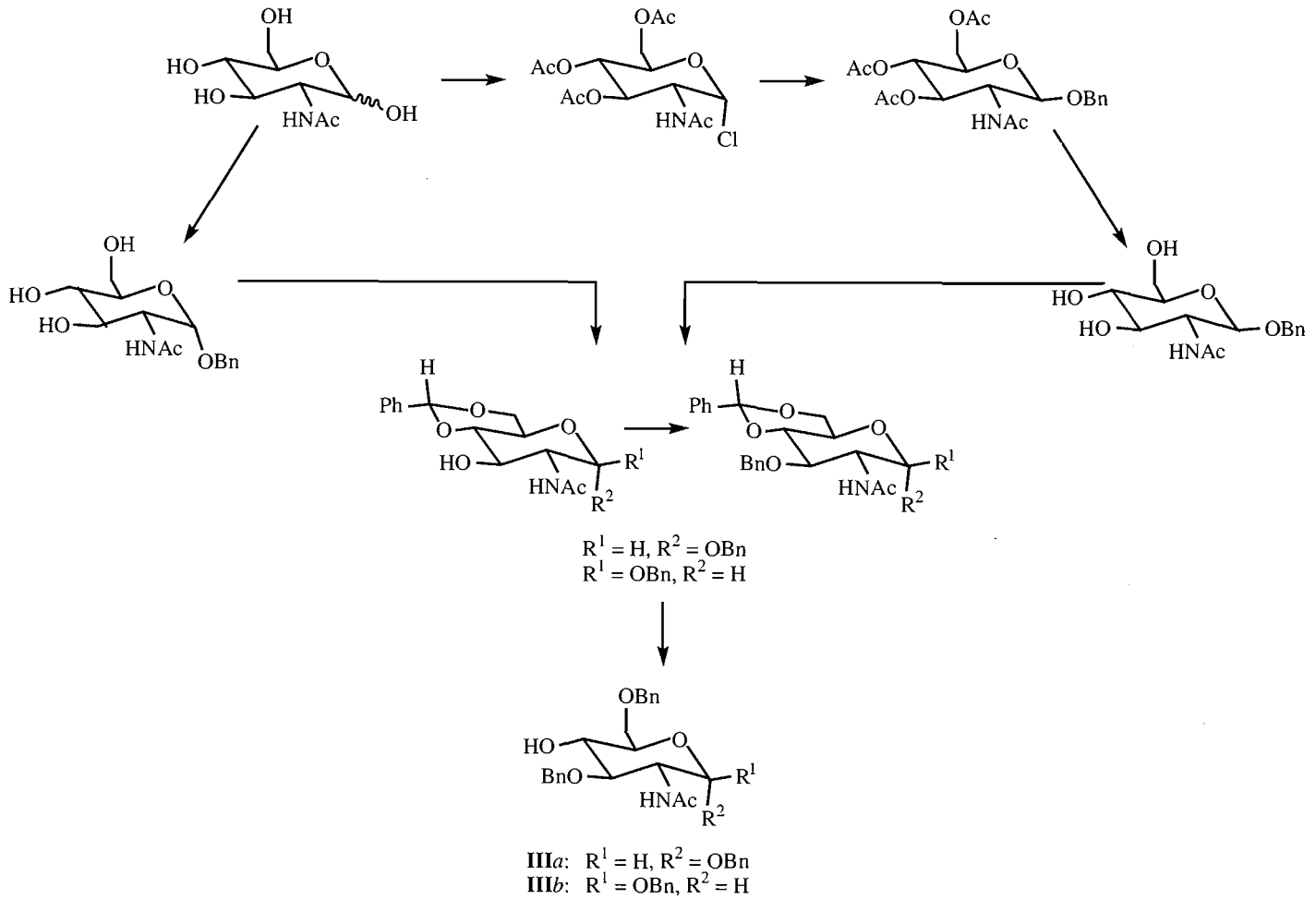

IIIa: $R^1 = H, R^2 = OBn$
IIIb: $R^1 = OBn, R^2 = H$

SCHEME 2

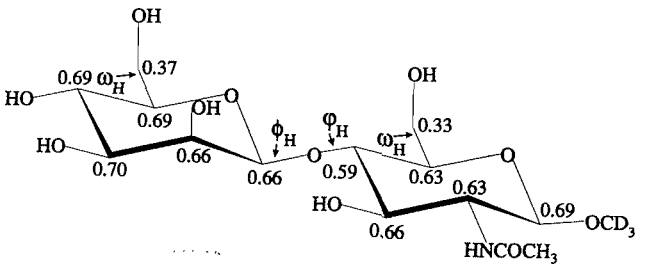

FIG. 1. Structure of the disaccharide **II** showing the glycosidic torsion angles ϕ_H and ψ_H, and the exocyclic ω_H hydroxymethylene torsion angles. Also shown are the direct ^{13}C T_1's measured with an accuracy of ±10%. The small variations between values is indicative of isotropic reorientation of the molecule as a whole.

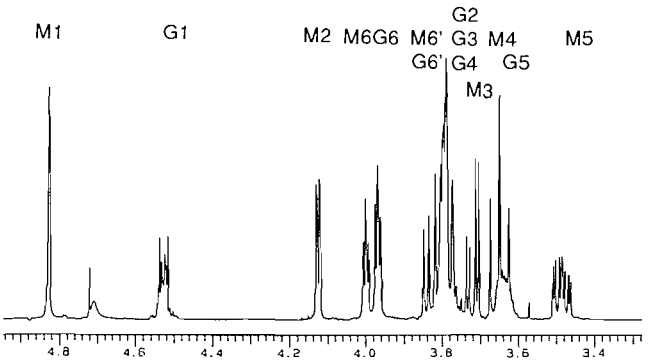

FIG. 2. Partial ^1H NMR spectrum of the disaccharide **II** in D_2O showing CH and CH_2 protons and their assignments. The virtual coupling in GlcpNAc H-1 and H-5 is readily apparent.

resolution-enhanced time-domain difference signal (cf. Fig. 4) suggested that most of the observed inter-glycosidic NOE is due to H-4 of the GlcpNAc unit.

To verify this conclusion, a method, analogous to the indirect T_1 experiment described above, was devised in which the non-equilibrium polarization of the proton spin system resulting from selective preirradiation of one of the proton resonances of interest was transferred to the ^{13}C domain via DEPT. The carbon spectrum measured with the unperturbed proton spin system was subtracted from the carbon spectrum thus obtained, and the difference spectrum obtained is displayed in Fig. 5 (for details, see the Experimental). It can be clearly seen that the NOE originating in the ^1H multiplet at 3.8 ppm (cf. Fig. 4) is mostly associated with GlcpNAc ^{13}C-4 at 80.2 ppm.

Conformational analysis

We used for conformational analysis the method, developed by Cumming and Carver, that compares Boltzman-averaged calculated observables, $\langle X \rangle$, with the experimental

Can. J. Chem. Downloaded from www.nrcresearchpress.com by 109.225.110.28 on 09/08/12
For personal use only.

Can. J. Chem. Downloaded from www.nrcresearchpress.com by 109.225.110.28 on 09/08/12
For personal use only.

TABLE 1. ^1H and ^{13}C relaxation times for methyl α-D-glucopyranoside[a]

Site	NT_1^C	$T_1^{H(DEPT)}$	$T_1^{H(ind)}$	$T_1^{H(dir)}$
1 (a)	1.20	0.80	2.42	
(b)	1.24	0.81	2.33	2.32 ± 0.12
(c)	1.26	0.79	2.16	
2 (a)	1.38	0.86	2.32	
(b)	1.34	0.84	2.25	2.25 ± 0.12
(c)	1.32	0.82	2.20	
3 (a)	1.34	0.94	3.20	
(b)	1.36	0.95	3.15	3.20 ± 0.14
(c)	1.30	0.92	3.24	
4 (a)	1.30	0.85	2.52	
(b)	1.36	0.88	2.49	2.43 ± 0.12
(c)	1.36	0.87	2.44	
5 (a)	1.34	0.78	1.92	
(b)	1.35	0.79	1.84	1.90 ± 0.11
(c)	1.29	0.77	1.94	
6 (a)	1.49	0.56	0.92	
(b)	1.53	0.56	0.88	0.83 ± 0.06
(c)	1.46	0.52	0.82	

[a]Direct proton relaxation times, $T_1^{H(dir)}$, were obtained with a relaxation delay of 10 s between subsequent scans, and 8 scans were accumulated for each of 15 variable delay values (varied between 0.025 and 8 s). In the polarization transfer experiment providing the $T_1^{H(DEPT)}$ and T_1^C data, 256 transients were accumulated for each pair of FID's using a relaxation delay of 8 s and 16 s values of variable delay ranging between 0.005 and 4 s. Prior to Fourier transformation, the time domain signals in both experiments were multiplied by an exponential window function with LB = 3 s. The three sets of data, (a), (b), and (c), were obtained in a queued serial experiment.

values (18). In this work we calculated P.E. surfaces considering the bonds of greatest flexibility, namely, the glycosidic torsion angles ϕ_H (H-1′, C-1′, O-1′, C-4) and ψ_H (C-1′, O-1′, C-4, H-4) and the exocyclic hydroxymethylene torsion angles ω_H (H-5, C-5, C-6, O-6) and (H-5′, C-5′, C-6′, O-6′). This simplification is usually invoked since the bonds of the pyranose rings are known to exhibit fluctuations of <10° (19). Thus the rings were fixed at their geometries determined by X-ray diffraction of model compounds (20, 21). This conformation is the $^4C_1$ chair conformation for both Manp and GlcpNAc and is supported by the observed coupling constants (see Experimental). Thus P.E. cubes were generated by calculating sixty 60 × 60 P.E. surfaces by varying ϕ_H, ψ_H, and ω_H in 6° intervals.

Three different P.E. equations were used. The first one, HS, has terms for van der Waals (Hard-Sphere) and the Exo-Anomeric (EA) effect only. The second uses these terms plus a Hydrogen bonding term and is denoted HH. The third uses Hard-Sphere but no EA term and it uses point charges to calculate an electrostatic term EL (dielectric = 1). The P.E. cubes HS, HH, or EL were then converted to probabilities using the Boltzman relation and subsequently to ⟨NOE⟩'s and $\langle T_1\rangle$'s by calculating the averaged $\langle 1/r^6\rangle$ distance matrix. The requisite isotropic correlation times were estimated to best fit the conformationally least-sensitive ^1H variables as 1.4×10^{-10} s, such as the ^1H T_1 of GlcpNAc H-1. In this way the isotropic relaxation matrix could be solved to yield ⟨NOE⟩'s and $\langle T_1\rangle$'s.

The results are tabulated in Tables 2 (T_1) and 3 (NOE) along with the experimental values. The reported values are for varying ϕ_H, ψ_H, and ω_H of the GlcpNAc residue. Similar values except for the NOE between Manp H-1′ and GlcpNAc H-6, H-6′ were calculated by varying the Manp ω_H instead of the GlcpNAc ω_H (not shown). Also shown in Tables 2 and 3 are values calculated using the correlation time 0.78×10^{-10} s calculated from the $^{13}CT_1$'s. The $^{13}CT_1$'s did not vary significantly among each other whereas the $^1HT_1$'s do so, suggesting that the $^{13}CT_1$'s are sensitive to the overall motion of the molecule while the $^1HT_1$'s are also sensitive to other motions. Figure 1 shows a drawing of disaccharide **II** with the direct $^{13}CT_1$'s marked on it, and the flexible torsion angles ϕ_H, ψ_H, and ω_H indicated.

The general agreement between calculated and experimental values is good considering the simplifications made in the calculations. The largest discrepancies are the T_1 of Manp H-4′ and the corresponding NOE to this proton from H-1′. This may reflect some bias caused by the crystal structure used to generate the coordinates. Small changes in

TABLE 2. 400 MHz ^1H NMR T_1's at 310 K for disaccharide **II** in s calculated with $\tau_c = 1.4 \times 10^{-10}$ or $\tau_c = 0.78 \times 10^{-10}$ (^{13}C in brackets)

Resonance	⟨HS⟩ (^{13}C)	⟨HH⟩ (^{13}C)	⟨EL⟩ (^{13}C)	Obsd.[a]	Obsd.[b]
Manp H-1′	0.46 (0.64)	0.47 (0.68)	0.44 (0.61)	0.53	0.47
Manp H-2′	1.06 (1.45)	1.06 (1.48)	0.91 (1.21)	1.16	1.09
Manp H-3′	0.80 (1.14)	0.80 (1.14)	0.80 (1.14)	0.98	0.99
Manp H-4′	1.61 (2.61)	1.61 (2.56)	1.61 (2.55)	1.20	3.70
Manp H-5′	0.61 (0.79)	0.61 (0.78)	0.62 (0.79)	0.84	1.04
Manp H-6′	0.33 (0.45)	0.33 (0.45)	0.33 (0.45)	0.44	0.44
GlcpNAc H-1	1.02 (1.46)	1.02 (1.46)	1.02 (1.46)	1.03	0.84
GlcpNAc H-2	2.02 (2.82)	2.02 (2.82)	2.00 (2.81)		2.52
GlcpNAc H-3	1.28 (1.82)	1.28 (1.81)	1.25 (1.79)		1.55
GlcpNAc H-4	0.73 (1.01)	0.72 (0.98)	0.60 (0.81)		0.92
GlcpNAc H-5	0.59 (0.92)	0.59 (0.92)	0.56 (0.92)		1.17
GlcpNAc H-6	0.29 (0.38)	0.29 (0.39)	0.30 (0.38)	0.44	0.44

[a]Measured directly at 310 K with accuracy ± 10%.

[b]Obtained via ^{13}C spectrum at 303 K and calculated as $1/T_1^{H(ind)} = 1/T_1^{H(DEPT)} - 1/NT_1^C$. NT_1^C (in s) values were as follows: Manp, C-1, 0.58; C-2, 0.58; C-3, 0.61; C-4, 0.59; C-5, 0.60; C-6, 0.63. GlcpNAc, C-1, 0.56; C-2, 0.54; C-3, 0.55; C-4, 0.53; C-5, 0.53; C-6, 0.56. The T_1^C and $T_1^{H(DEPT)}$ values were measured in a single experiment by alternately acquiring the two time-domain signals.

Can. J. Chem. Downloaded from www.nrcresearchpress.com by 109.225.110.28 on 09/08/12
For personal use only.

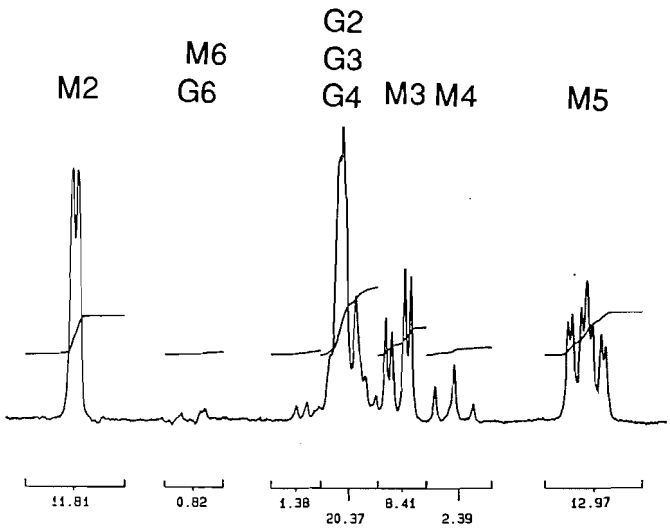

FIG. 3. The NOE of disaccharide **II** in D_2O showing the enhanced resonances after irradiation of Manp H-1′. The strongly coupled GlcNAc H-2, H-3, and H-4 at $\delta = 3.8$ ppm are readily apparent. The integral of irradiated Manp H-1′ was set to −100%.

either the ring dihedral angles or the C—H bond lengths will change the H—H separations. This factor was not further investigated since it should not markedly influence the glycosidic torsions.

To compare the various models, a statistical parameter Z (see eq. [1], where X_{obs} is the observed NMR observable, X_{calc} is the corresponding calculated NMR observable, and n is the number of observables) was determined for the variables sensitive to the glycosidic torsions, namely, the

$$[1] \quad Z = \left[\sum^{n} (X_{obs} - X_{calc}/X_{obs})^2 \right] \Big/ n$$

$^1HT_1$'s of Manp H-1′ and H-2′, and GlcpNAc H-4, and NOE's between Manp H-1′ and Manp H-2′ as well as across the linkage to GlcpNAc H-4 and H-6. The various values of Z are tabulated in Table 4, including those neglecting the NOE to GlcpNAc H-6. This last NOE depends on ω_H as well as ϕ_H and ψ_H, and ω_H is not well calculated by these P.E. surfaces. For example the coupling constants J_{56proR} and J_{56proS} of the GlcpNAc are calculated (22, 23) to be 5.3 ± 0.5 Hz and 5.9 ± 0.5 Hz by any of these P. E. surfaces compared to the experimental values of 5.2 Hz and 2.9 Hz respectively. The experimental values suggest averaging between the $\psi_H = -60°$ and 180° rotamers (24).

The HH surface with variation of GlcpNAc ω_H gives the best fit (lowest Z) to the experimental data although the distinction is small. If the NOE between Manp H-1′ and GlcNAc H-6 is neglected, then the HS model with variation of Manp ω_H gives the best fit. The EL model also fits the data well, suggesting that all three models give a satisfactory representation of the molecule. A contour plot of the EL surface, which shows the minimum and 10 1-kcal contours above the minimum, is shown in Fig. 6*a*. The corresponding probability plot, which shows contours for the minimum and the 10%, 25%, 50%, 90%, and 99.9% probability

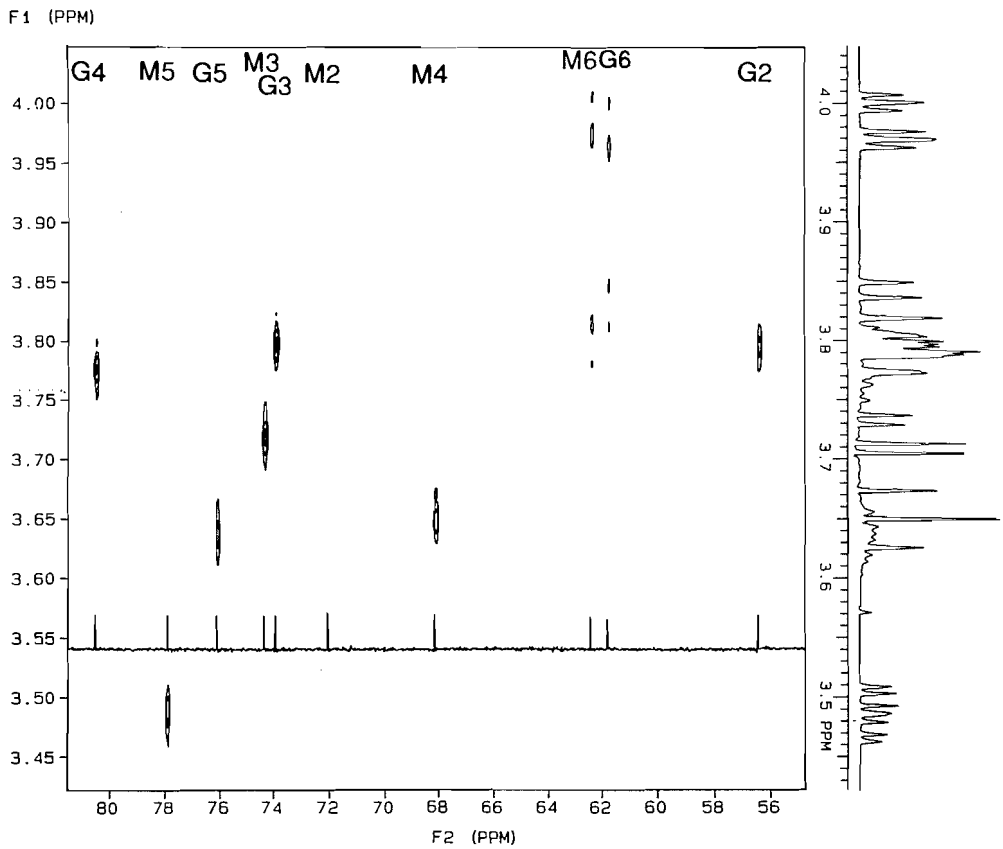

FIG. 4. Partial ^1H–^{13}H COSY spectrum of **II** in D_2O. The assignments are marked on the tracings of the 1-D spectra.

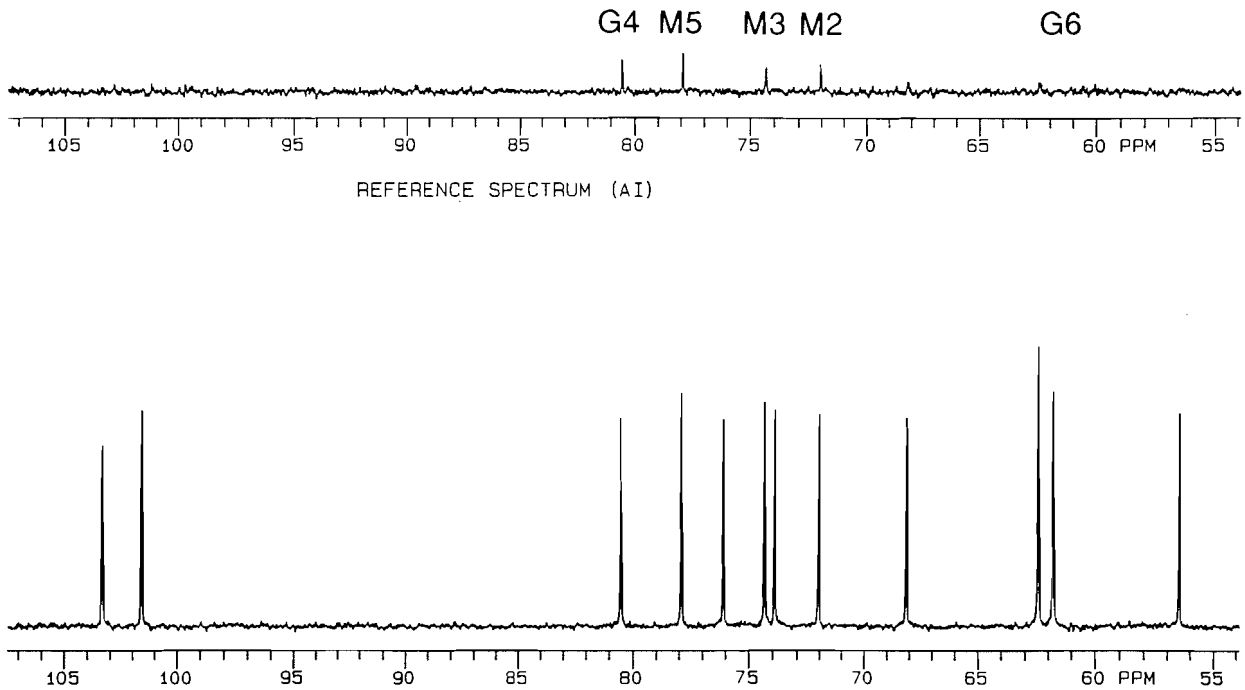

FIG. 5. The differential ^{1}H NOE spectrum of **II** after irradiation of Manp H-1′ monitored in the ^{13}C domain via DEPT transfer. The resonance at δ = 80.2 ppm shows that the main inter-residue NOE is to GlcpNAc H-4.

TABLE 3. 400 MHz ^{1}H NMR NOE's at 310 K for irradiation of Manp H-1′ calculated with $\tau_c = 1.4 \times 10^{-10}$ or $\tau_c = 0.78 \times 10^{-10}$ (^{13}C in parentheses)

Resonance	⟨HS⟩ (^{13}C)	⟨HH⟩ (^{13}C)	⟨EL⟩ (^{13}C)	Obsd. ± 10%
Manp H-2′	14.1 (15.5)	14.2 (15.9)	11.7 (12.3)	12.0
Manp H-3′	5.8 (6.4)	5.8 (6.4)	6.1 (6.3)	8.9
Manp H-4′	0.0 (−0.1)	0.0 (0.0)	0.1 (0.0)	2.7
Manp H-5′	11.7 (12.6)	11.7 (12.4)	11.9 (12.7)	13.5
Manp H-6′	−0.6 (−0.5)	−0.6 (−0.6)	−0.6 (−0.6)	−0.2
Manp H-6″	0.1 (−0.1)	0.1 (0.0)	0.1 (−0.1)	0.8
GlcpNAc H-4	14.5 (15.4)	14.9 (16.4)	19.4 (20.0)	12.0
GlcpNAc H-6	1.4 (0.4)	1.0 (1.6)	0.2 (1.3)	0.8

TABLE 4. Statistical evaluation using eq. [1] of the various P.E. models (the number of variables is given in parentheses)

Description	⟨HS⟩	⟨HH⟩	⟨EL⟩
Varying ω_H of GlcpNAc	0.11 (6) 0.02 (5)[a]	0.04 (6) 0.03 (5)[a]	0.18 (6) 0.11 (5)[a]
Varying ω_H of Manp	0.86 (6) 0.02 (5)[a]	0.11 (6) 0.02 (5)[a]	0.09 (6) 0.08 (5)[a]
Varying ω_H of Manp at ^{13}C τ_c	0.11 (6) 0.08 (5)[a]	0.26 (6) 0.11 (5)[a]	0.16 (6) 0.11 (5)[a]

[a]Calculated without considering the NOE between Manp H-1′ and GlcpNAc H-6.

contours is shown in Fig. 6*b*. This surface is entirely consistent with the results of Homans using the Amber force field (25). The more than 150° of ϕ_H and 80° of ψ_H occupied by the 99.9% probability contour suggests that this disaccharide is flexible. Figures 6*c* and 6*d* show the probability surfaces for the HS and HH surfaces respectively. These last two surfaces do not vary significantly from each other but do occupy a smaller volume of conformational space then the EL surface. The HH plot does suggest that a hydrogen bond can potentially stabilize the conformation. The plots in Fig. 6 are all taken at the minimum value of ω_H for the respective surface. The surfaces at different values of ω_H (not shown) do not differ qualitatively.

Taken together, these results suggest that the *exo*-anomeric (EA) stabilized minimum near $\phi_H = +50°$ ($\psi_H = 0 \pm 10°$) is significantly populated but is not the only conformation possible. These minima are also consistent with previous calculations for this linkage that did not implicitly consider flexibility (26–29). In two crystal structures of small molecules with this linkage this conformation is indeed found (20, 30). However, in a complex between an oligosaccharide containing the linkage in **II** and a lectin, the Manp(β1–4)GlcpNAc linkage is found in a second minimum (31). This result points to the importance of these other conformers. In fact, although not predicted to be populated in our "rigid" maps (22, 32) (which also neglect solvation), the EL PE surface in Fig. 6*a* shows that conformers with ψ_H near 180°

Can. J. Chem. Downloaded from www.nrcresearchpress.com by 109.225.110.28 on 09/08/12
For personal use only.

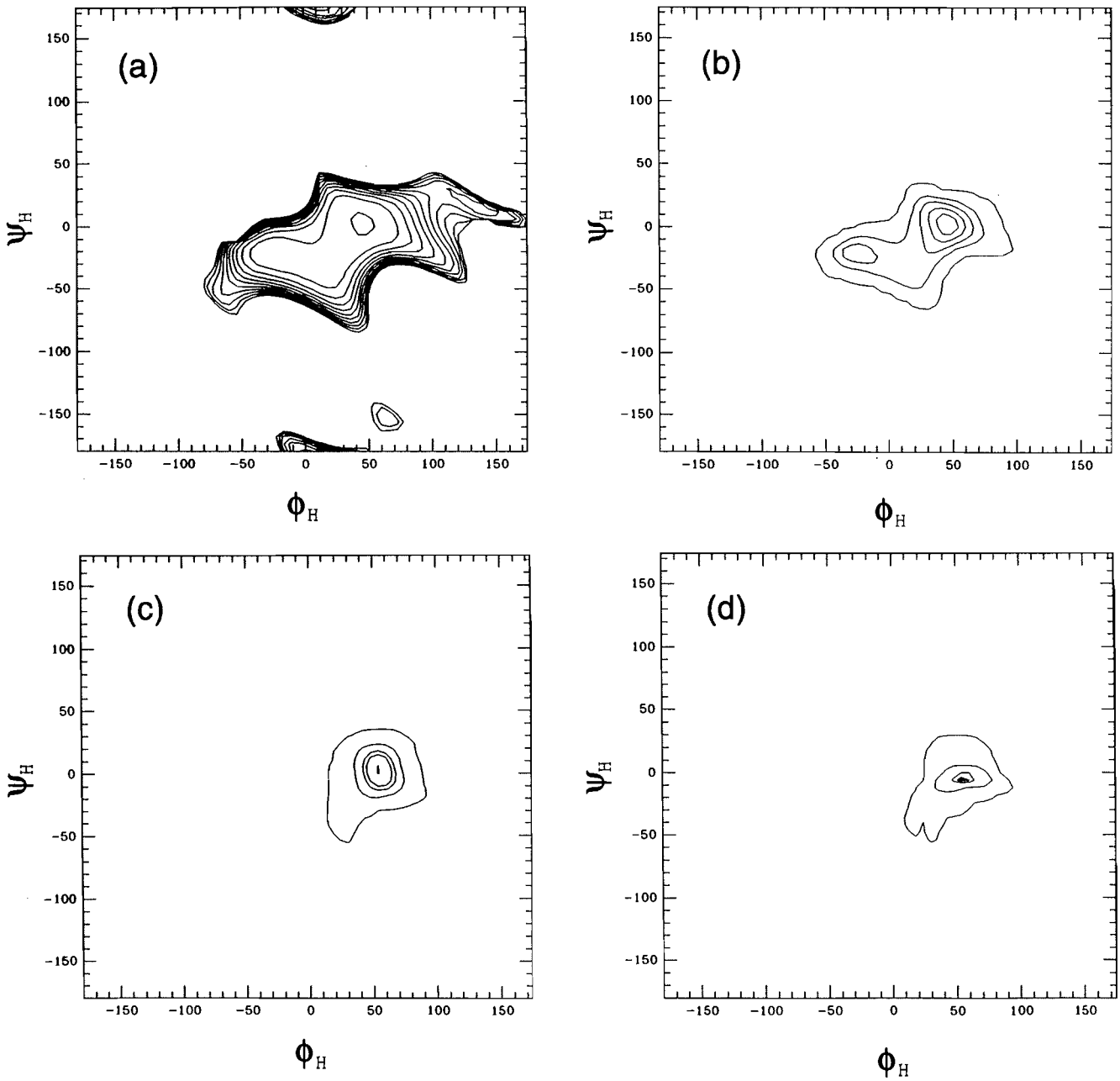

FIG. 6. Potential energy surfaces of the disaccharide **II**: (*a*) showing the EL surface as a function of the glycosidic torsion angles ϕ_H and ψ_H. The minimum and ten 1 kcal contours above the minimum are plotted. (*b*) The corresponding EL probability surface of **II**. The minimum and the 10%, 25%, 50%, 90%, and 99.9% probability contours are plotted. (*c*) The HS probability surface of **II**. The minimum and the 10%, 25%, 50%, 90%, and 99.9% probability contours are plotted. (*d*) The HH probability surface of **II**. The minimum and the 10%, 25%, 50%, 90%, and 99.9% probability contours are plotted.

are only a few kilocalories above the global minimum and probably easily accessible to the molecule.

Conclusions

In conclusion, we have designed an efficient synthesis of Manp(β1–4)GlcpNAc glycosides. Furthermore, we have developed an NMR method for unambiguously assigning ^{1}H–^{1}H NOE's in tight coupling situations by monitoring the effect in the ^{13}C domain using DEPT transfer, and applied it to this disaccharide. This confirmed that the NOE across the glycosidic linkage is mostly between Manp H-1′ and GlcpNAc H-4. This value and the T_1 values were then compared to calculated values, demonstrating that models in which the glycosidic torsion angles vary substantially are entirely consistent with the NMR data. This result strongly suggests that conformations other than the global minimum need to be considered when modelling larger oligosaccharides of the N-linked family that contain this linkage. It has also been shown that T_1's of certain ^{1}H nuclei are considerably longer than expected (this has significance for the choice of experimental conditions for NOE measurements).

Experimental

General methods

Melting points were determined on a Reichert Thermovar melting point apparatus and are uncorrected. Optical rotations were

Can. J. Chem. Downloaded from www.nrcresearchpress.com by 109.225.110.28 on 09/08/12
For personal use only.

Can. J. Chem. Downloaded from www.nrcresearchpress.com by 109.225.110.28 on 09/08/12
For personal use only.

measured with a Perkin–Elmer polarimeter (model 243B) at 26 ± °C. Microanalyses were performed by the Micro Analytical Laboratory Ltd., Markham, Ontario. IR spectra were recorded on a Perkin–Elmer (model 1430) spectrometer using thin film on NaCl plates.

Fast Atom Bombardment mass spectra (FAB-MS) were recorded with a VG Analytical ZAB-SE mass spectrometer at the Mass Spectrometry Laboratory of the Carbohydrate Research Centre, University of Toronto. The samples in thioglycerol were bombarded by neutral xenon atoms (8 keV and 1 mA anode current) generated by an Ion-Tech Saddle Field Ion Gun.

Thin-layer chromatography (TLC) was performed on silica gel $60F_{254}$ (Merck) plastic plates and visualized by spraying with 50% sulfuric acid and (or) 1% orcinol acidic ferric chloride and heating at 200°C. Silica gel (230–400 mesh; Toronto Research Chemicals) was used for flash chromatography. All starting materials were dried overnight under vacuum (10^{-3} Torr; 1 Torr = 133.3 Pa) prior to use and the solvents were distilled from appropriate drying agents. Solutions were concentrated at water aspirator pressure.

^{1}H NMR spectra of the synthetic intermediates were obtained with a Bruker AM 500-spectrometer at 19 ± 2°C either in $CDCl_3$ containing a trace of TMS (0 ppm, ^{1}H and ^{13}C) as the internal standard or in D_2O (99.98%, Aldrich) containing a trace of acetone (2.225 ppm relative to internal DSS, ^{1}H) as the internal standard using the δ(ppm) scale. ^{13}C spectra in D_2O were referenced to external dioxane (67.4 ppm relative to TMS). Samples for NMR analyses in D_2O were passed through a Chelex 100 (Bio-Rad) ion-exchange resin in doubly distilled H_2O to remove paramagnetic impurities, lyophilized, and then lyophilized three times with D_2O.

A Varian Associates model VXR-400 instrument was used to obtain the NMR spectra of the title disaccharide (**II**). All experiments were made with undegassed samples (10 mg in 0.7 mL D_2O). Absence of paramagnetic impurities was tested qualitatively by measuring the proton T_1 value of the residual HDO signal of the solvent. In all samples this was found to be longer than 18 s.

NMR spectrometry

Relaxation time measurements

The T_1^H data for protons involved in tight couplings, and (or) exhibiting their resonances in crowded spectral regions, were also measured by an indirect method. The pulse sequence employed in this study was similar to that published by Bigler (17) except that the polarization transfer step was achieved by means of DEPT (cf. Pegg *et al.* (35)). To decrease the overall errors of the indirect proton relaxation data, $T_1^{H(ind)}$, acquisition of the time domain signal pertinent to $T_1^{H(DEPT)}$, and T_1^C were acquired alternately in one experiment. To test the reliability, the modified sequence was applied to a sample of methyl α-D-glucopyranoside (20 mg in 0.7 mL of $CDCl_3$). First, $T_1^{H(dir)}$ values were obtained in a conventional proton inversion recovery experiment, then the contribution of the dipolar mechanism in ^{13}C relaxation was examined using a {^{1}H}–^{13}C heteronuclear NOE measurement. The values obtained were close the theoretically expected maximum (2.98) for each ring carbon signal, attesting to the predominance of a dipolar mechanism in the longitudinal relaxation of the monosaccharide. Values of $T_1^{H(DEPT)}$ and T_1^C were obtained next (cf. Table 1 for the summary of the relaxation data).

Homonuclear NOE experiments

Steady-state Overhauser enhancements of proton resonances exhibiting their signals in crowded spectral regions were conveniently monitored via ^{13}C NMR spectroscopy. A pulse sequence was employed, in which the DEPT polarization transfer step was preceded by a selective proton preirradiation period analogous to that employed in steady-state {^{1}H}–^{1}H NOE experiments. The non-equilibrium magnetization of the proton spin system, resulting from the selective preirradiation, is thus transferred to the ^{13}C frequency domain and detected as ^{13}C signal enhancement. As in the proton NOE difference spectroscopy, the ^{13}C signal enhancement is conveniently monitored in the difference mode. The reference intensity required is provided by ^{13}C resonance obtained through polarization transfer from the unperturbed proton spin system. In practical terms such a pulse sequence requires fast switching between low-power, multiple frequency, selective preirradiation (NOE) mode, and high-power pulsing mode (DEPT) while observing ^{13}C NMR, a condition readily met by modern dual broadband spectrometers fitted with computer-controlled attenuators. As the spectrometer at our disposal was of an earlier generation, in which multiple-frequency, low-power selective irradiation is available only with the ^{1}H observe set-up, the above experiment was conveniently performed in the "reversed" mode, i.e., by deriving both soft and hard proton pulses from the decoupler channel. In the actual pulse sequence the selective preirradiation was achieved by frequency-cycled, low-power DANTE pulse trains (36). This segment, terminated with optional, hard 90° decoupler read pulse, was used to set up the NOE part of the experiment (level, duration, frequencies of selective preirradiation). With the NOE setup completed, the NOE part of the pulse sequence was connected to the standard DEPT segment, preceded by a train of 90° ^{13}C pulses to destroy eventual proton–carbon correlation effects. With alternate acquisition, a reference ^{13}C DEPT spectrum with no proton preirradiation was also accumulated and the resulting two time-domain signals were used to obtain the NOE difference spectrum. Running these experiments in D_2O, particular attention had to be given to minor changes in the sample temperature when switching from the NOE setup to the NOE DEPT experiment. Since this experimental sequence uses broad-band decoupling, the sample temperature rises a few degrees over the temperature during the NOE setup, and a readjustment of the preirradiation frequency is required.

Computational methods

The computational methods used have been described in detail previously (18, 33, 37). (BIGST and NEWSIG400 are modifications of the original CCM program developed by Carver and co-workers, which uses a full relaxation matrix approach to calculate NOE's and T_1's (23). All programs, except MONGO and MODEV were written in Fortran at the University of Toronto (37). Calculations were performed on a Microvax.) Briefly, they entail using the coordinates (X-ray) for these monosaccharides (20, 21) as starting conformations. Then PE cubes were calculated using the program BIGTST using 60 6° increments for each of the torsion angles ϕ_H, ψ_H, and ω_H (i.e., sixty 60 × 60 PE surfaces). Electrostatic calculations used point charges. These PE cubes were next used to calculate Boltzman-averaged relaxation matrices using the programs QSET and NEWSIG400. Finally, the relaxation matrix was solved to calculate for NOE's and T_1's. Contour plots were made using the program MONGO (38). Coupling constants were calculated employing the calculated torsion angles using the equation 8E of Haasnoot *et al.* (22) and data analysis was done utilizing the BASIC program MODEV (computer code available on request) (33).

Chemical synthesis

2-O-Acetyl-3,4,6-tri-O-benzyl-D-glucopyranosyl bromide (V)

Bromide **V** (refs. 1, 2) was prepared from the ortho ester **IV** (refs. 9, 10) by a method of Lemieux and co-workers (10) modified as follows. A mixture of orthoester **IV** (2.69 g, 5.17 mmol) and acetyl bromide (30 mL) was stirred at room temperature for 0.5 h. Then it was diluted with toluene (100 mL) and evaporated to dryness to give **V** (2.9 g) as a pale brownish solid. TLC indicated that it contained mainly bromide **V**, R_F 0.45 (ethyl acetate – hexane = 1:4). The crude product **V** was dried over P_2O_5 *in vacuo* before using for the coupling reaction.

Benzyl 2-acetamido-2-deoxy-3,6-di-O-benzyl-α-D-glucopyranoside (IIIa)

To a solution of benzyl 2-acetamido-2-deoxy-α-D-glucopyranoside, mp 186–187°C (11), (4.39 g) in acetonitrile (200 mL), benzaldehyde dimethylacetal (10.00 mL) and *p*-toluenesulfonic (0.5 g) were added at room temperature, and the reaction mixture was stirred at 60°C under argon for 60 h. After pouring the reaction mixture into an ice-cold saturated aqueous $NaHCO_3$ solution,

Can. J. Chem. Downloaded from www.nrcresearchpress.com by 109.225.110.28 on 09/08/12
For personal use only.

the resulting benzyl 2-acetamido-4,6-*O*-benzylidene-2-deoxy-α-D-glucopyranoside was extracted into CH_2Cl_2, and after evaporation of the solvent and recrystallization from dioxane and isopropanol it was obtained pure (mp 263–264°C, 3.59 g, 62%). This benzylidene derivative (3.05 g) in dry. THF (8 mL) was added to a solution of NaH (0.58 g) in dry THF (5 mL), and stirred under argon to homogeneity. A solution of α-bromotoluene (1.43 mL) in dry THF (8 mL) was added slowly and this mixture was stirred until all the benzylidene derivative was consumed. Then CH_2Cl_2 was added, solids were filtered off, the solution was washed with aqueous NaCl, dried over $MgSO_4$, and the solution after concentration gave white crystalline benzyl 2-acetamido-3-*O*-benzyl-4,6-*O*-benzylidene-2-deoxy-α-D-glucopyranoside, mp 267–269°C (3.67 g, 63%). To a solution of this latter compound (4.17 g) and $NaCNBH_3$ (2.95 g) in dry THF (300 mL) containing molecular sieves 3A (10 g) was added dropwise Et_2O saturated with gaseous HCl (50 mL). After completion of the reaction in about 45 min, CH_2Cl_2 (300 mL) was added, the mixture was poured onto ice, and extracted four times with CH_2Cl_2, dried over $MgSO_4$, and concentrated to dryness. The benzyl 2-acetamido-2-deoxy-3,6-di-*O*-benzyl-α-D-glucopyranoside crystallized from hexane–ethanol at 5°C (mp 145–146°C, 1.4 g, 33.5%). An additional equal amount was obtained after chromatography of the mother liquors on a silica gel column using a gradient of MeOH in CH_2Cl_2.

*Benzyl 2-acetamido-2-deoxy-3,6-di-*O*-benzyl-β-D-glucopyranoside (**III**b)*

2-Acetamido-2-deoxy-D-glucopyranose (50 g) gave after overnight stirring with acetyl chloride (100 mL) 2-acetamido-2-deoxy-3,4,6-tri-*O*-acetyl-α-D-glycopyranosyl chloride (mp 118–120°C, 29.7 g, 36%), which was dissolved in dry benzyl alcohol (100 mL) together with $Hg(CN)_2$ (18.37 g) and $HgBr_2$ (3.5 g). This reaction mixture was stirred overnight, then it was diluted with $CHCl_3$ (400 mL), washed with saturated aqueous $NaHCO_3$, water, dried over $MgSO_4$, and evaporated to dryness. Chromatography on silica gel of the residue afforded benzyl 2-acetamido-2-deoxy-3,4,6-tri-*O*-acetyl-β-D-glycopyranoside, which after crystallization from ethanol gave 9.15 g (26%) of the compound, mp 165°C. The latter compound (12.83 g) was dissolved in dry methanol (50 mL, and to this was added dropwise a solution of NaOMe prepared by dissolving Na (0.7 g) in dry MeOH (50 mL) at room temperature. White crystals that formed during the reaction were collected and recrystallized from EtOH to give benzyl 2-acetamido-2-deoxy-β-D-glucopyranoside, mp 199–202°C (6.88 g). From this precursor were sequentially prepared benzyl 2-acetamido-4,6-*O*-benzylidene-2-deoxy-β-D-glucopyranoside, mp 267–270°C, benzyl 2-acetamido-3-*O*-benzyl-4,6-*O*-benzylidene-2-deoxy-β-D-glucopyranoside, mp 278–280°C, and benzyl 2-acetamido-2-deoxy-3,6-di-*O*-benzyl-β-D-glucopyranoside, mp 176–178°C, by the same procedures as described for the α anomer.

*Benzyl 2-acetamido-4-O-(2-O-acetyl-3,4,6-tri-O-benzyl-β-D-glucopyranosyl)-3,6-di-O-benzyl-2-deoxy-α-D-glucopyranoside (**VI**a) (ref. 8)*

To a mixture of acceptor **III***a* (500 mg, 1.02 mmol), $HgCl_2$ (500 mg), and molecular sieves (3A, 800 mg) in CH_3NO_2 (4 mL) stirred at room temperature under argon, a solution of crude bromide **V** (1.60 g, 2.88 mmol) in toluene (4 mL) was added (12*a*). The reaction mixture was stirred in the dark for an additional 46 h. Then another batch of $HgCl_2$ (300 mg) was added, and stirring continued for 71 h. The reaction mixture was diluted with CH_2Cl_2 (150 mL), filtered through Celite, the Celite cake was washed with additional CH_2Cl_2 (3 × 30 mL), and the combined filtrates after washing with H_2O (200 mL) were dried over $MgSO_4$ and evaporated to dryness. The residue was subjected to chromatography on silica gel (ethyl acetate – toluene = 1:2) and pure compound **VI***a* (719 mg, 73%) was obtained as a colorless solid, mp 128–129°C (from Et_2O–CH_2Cl_2); $[\alpha]_D$ + 79.9 (*c* 1.0, $CHCl_3$) (lit. (8) mp 128–129°C; $[\alpha]_D^{20}$ + 84 (*c* 3.0, $CHCl_3$)); R_f 0.32 (ethyl acetate – toluene, 1:2); IR (neat): 3300 and 1660 (NHCO), 1750 (RCOOR) cm^{-1}; ^1H NMR δ: 5.12 (d, 1H, *J* = 8.9 Hz, exchangeable with D_2O; N*H*); 4.98 (br t, 1H, *J* = 9.7 Hz, H-2′), 4.93 (d, 1H, *J* = 3.7 Hz, H-1), 4.46 (d, 1H, *J* = 10 Hz, H-1′), 4.17 = (t × d, 1H, *J* = 9.2 Hz and 3.7 Hz, H-2), 4.01 (t, 1H, *J* = 9.2 Hz, H-4) 3.48 (t, 1H, *J* = 9.3 Hz, H-3′), 3.30 (m, 1H, H-5′), 1.90 and 1.74 (2S, 6H, $COCH_3$).

*Benzyl 2-acetamido-4-O-(2-O-acetyl-3,4,6-tri-O-benzyl-β-D-glucopyranosyl)-3,6-di-O-benzyl-2-deoxy-α-D-glucopyranoside (**VI**a) and benzyl 2-acetamido-4-O-(2-O-acetyl-3,4,6-tri-O-benzyl-β-D-glucopyranosyl)-3,6-di-O-benzyl-2-deoxy-β-D-glucopyranoside (**VI**b): a comparison*

To assess the reactivity of acceptors **III***a* and **III***b* toward bromide **V**, control experiments were carried out under identical conditions (room temperature, 45 h). Two separate reactions were set up side by side, each using: acceptor (**III***a* or **III***b*, 60 mg), bromide **V** (205 mg of the same batch), $HgCl_2$ (60 mg), and molecular sieves (3A) (100 mg). Comparable yields of **VI***a* and **VI***b* (8, 12*a*) of similar purity were obtained.

*Benzyl 2-acetamido-3,6-di-O-benzyl-2-deoxy-4-O-(3,4,6-tri-O-benzyl-β-D-mannopyranosyl)-α-D-glucopyranoside (**VI**e) (ref. 8)*

A solution of crude ketone **VI***d* (70 mg. 0.076 mmol) (prepared from **VI***a* as described (8)) in THF (3 mL) (5) was added dropwise (34) to a 1 M solution of L-Selectride (lithium tri-sec-isobutylborohydride) in THF (Aldrich; 3 mL) under stirring at −78°C. After stirring the reaction mixture at this temperature for a further 5 h, the reaction was quenched by addition of MeOH (0.3 mL), followed by 30% aqueous H_2O_2 (0.5 mL). Then the solution was filtered through Celite, washed with CH_2Cl_2 (50 mL), and the solvent was evaporated to give a pale yellow syrup, which after chromatography on silica gel (ethyl acetate – toluene = 1:2) afforded pure **VI***e* (38 mg, 56%) as a colorless solid; mp 173.5–174.5°C (observable change into an amorphous wet solid started at 156°C); $[\alpha]_D$ +78.5 (*c* 1.0, $CHCl_3$); (lit. (8) mp 156–159°C; $[\alpha]_D^{20}$ + 80 (*c* 0.98, $CHCl_3$)); R_F 0.35 (fivefold development in the same solvent); ^1H NMR δ:7.27 (m, 30H, C_6H_5), 5.28 (d, 1H, *J* = 9.2 Hz, exchangeable with D_2O, N*H*), 4.93 (d, 1H, *J* = 4.0 Hz, H-1), 4.63 (br s, 1H, H-1′), 4.27 (br t × d, 1H, *J* = 9.6 Hz and 3.7 Hz, became a d × d after exchange with D_2O, H-2), 4.05(t, 1H, *J* = 9.2 Hz, H-4), 3.99 (br t, 1H, *J* = 2.8 Hz, became d after exchange with D_2O, H-2′), 3.35 (d × d, 1H, *J* = 9.2 Hz and 3.0 Hz, H-3′), 3.27 (m, 1H, H-5′), 2.50 (d, 1H, *J* = 2.9 Hz, exchangeable with D_2O, O*H*), and 1.79 (s, 3H, $COCH_3$). Anal. calcd. for $C_{56}H_{61}NO_{11}$ (924.090): C 72.79, H 6.65, N 1.52, found: C 72.68, H 6.53, N 1.46.

*Methyl-d_3 2-acetamido-2-deoxy-3,6-di-O-acetyl-4-O-(2,3,4,6-tetra-O-acetyl-β-D-mannopyranosyl)-β-D-glucopyranoside (**VI**g)*

Compound **VI***e* (327 mg, 0.354 mmol) in acetic acid – methanol (3:4, 70 mL) was stirred in an H_2 atmosphere with 10% Pd–C (250 mg) at room temperature for 23 h. After the usual work-up it gave a crude product that was subsequently treated with acetic anhydride (10 mL) in pyridine (10 mL) for 70 h. Ethyl acetate (100 mL) was added, the solution was washed with cold water (2 × 50 mL), dried over $MgSO_4$, and evaporated to give peracetylated compound **VI***f* (mixture of α and β, 263 mg) as an amorphous solid; R_F 0.52 (ethyl acetate – methanol = 20:1). Crude **VI***f* (263 mg) was dissolved in acetyl chloride – acetic acid (6:1, 35 mL) and the solution was saturated with HCl gas passing slowly through at 0°C for 6 h; stirring continued for another 85 h at room temperature. Then toluene (200 mL) was added, and the solvents were evaporated to give the chloride as a light-brown amorphous solid (R_F 0.58, ethyl acetate). The chloride, after drying over P_2O_5 *in vacuo*, was treated with $HgCl_2$ (300 mg), molecular sieves (3A; 600 mg), and methanol-d_3 (0.50 mL) in nitromethane–toluene (1:1, 5 mL) at room temperature for 6 h. It was diluted with ethyl acetate – dichloromethane (1:1, 100 mL); filtered through Celite, and washed with ethyl acetate (3 × 20 mL); the combined filtrates were evaporated to give a pale brown syrup. After chromatography on

a silica column (ethyl acetate), pure **VIg** (153 mg, 66% overall) was obtained as a colorless syrup; R_F 0.20 (same solvent); $[\alpha]_D$ −48.2 (*c* 0.57, $CHCl_3$); IR (neat): 3370 and 1670 (NHCO), 2210 and 2065 (CD), 1745 (RCOOR); ^{1}H NMR δ: 5.43 (d, 1H, *J* = 9.2 Hz, N*H*), 5.40 (d × d, 1H, *J* = 3.3 Hz and 0.6 Hz, H-2′), 5.21 (t, 1H, *J* = 9.9 Hz, H-4′), 5.12 (d × d, 1H, *J* = 10.4 Hz and 8.9 Hz, H-3), 5.03 (d × d, 1H, *J* = 10.4 Hz and 8.9 Hz, H-3), 5.03 (d × d, 1H, *J* = 9.9 Hz and 3.3 Hz, H-3′), 4.70 (d, 1H, *J* = 0.6 Hz, H-1′), 4.39 (d, 1H, *J* = 8.1 Hz, H-1), 3.97, (d × d × d, 1H, *J* = 10.3 Hz, 9.2 Hz, and 8.3 Hz, H-2), 3.85 (t, 1H, *J* = 9.1 Hz, H-4), 3.63 (m, 2H, H-5, H-5′), 2.14, 2.13, 2.10, 2.09, 2.04, 1.99, and 1.96 (7s, 21H, COC*H*$_3$). Anal. calcd. for $C_{27}H_{36}NO_{17}D_3$ (652.617): C 49.69, H 6.49, N 2.15; found: C 49.52, H 6.43, N 2.08.

*Methyl-*d$_3$ *2-acetamido-2-deoxy-4-*O*-β-*D*-mannopyranosyl-β-*D*-glucopyranoside (II)*

A solution of sodium methoxide in dry methanol (1%; 4 mL) was added to a solution of compound **VIg** (104 mg, 0.160 mmol) dissolved in dichloromethane–methanol (2:1, 6 mL). The reaction mixture was stirred for 25 min at room temperature, cooled to 0°C, and neutralized with acidic DOWEX 50 (H^+) resin (2.1 mL, 1.7 mg per mL). The resin was subsequently filtered off and washed with methanol (3 × 20 mL). The combined filtrates were evaporated to dryness, yielding a syrup that was taken up into distilled water (30 mL) and washed with hexane (30 mL). The aqueous solution was evaporated to give compound **II** (60 mg, 94%) as a colorless solid; mp 251–253°C (from methanol); R_F 0.25 ($CHCl_3$–MeOH = 1:1); $[\alpha]_D$ −48.5 (*c* 0.47, methanol–water, 2:1). ^{1}H NMR δ: 4.83 (d, 1H, *J* = 1.1 Hz, H-1′), 4.13 (d × d, 1H, *J* = 3.2 Hz and 1.1 Hz, H-2′), 3.72 (d × d, 1H, *J* = 9.6 Hz and 3.2 Hz, H-3′), 3.65 (d × d, 1H, *J* = 9.6 Hz and 9.6 Hz, H-4′), 3.49 (d × d × d, 1H, *J* = 2.4 Hz, 6.4 Hz, and 9.6 Hz, H-5′), 3.99 (d × d, 1H, *J* = 2.4 Hz and −12.3 Hz, H-6′), 3.80 (d, 1H, *J* = 6.4 Hz and −12.3 Hz, H-6″), 4.53 (d, 1H, *J* = 8.2 Hz, H-1), 3.8, (m, 3H, H-2, H-3, H-4), 3.64 (m, 1H, H-5), 3.95 (d × d, 1H, *J* = 2.9 Hz and −12.3 Hz, H-6), 3.83 (d × d, 1H, *J* = 5.2 Hz and −12.3 Hz, H-6′) 2.10 (s, 3H, NCOC*H*$_3$); ^{13}C NMR δ: 101.4 (C-1′), 71.8 (C-2′), 74.1 (C-3′), 67.9 (C-4′), 77.7 (C-5′), 62.2 (C-6′), 103.1 (C-1), 56.2 (C-2), 73.7 (C-3), 80.3 (C-4), 75.9 (C-5), 61.6 (C-6), 23.5 (CO*C*H$_3$), 170 (*C*OCH$_3$). *Anal.* calcd. for $C_{15}H_{24}NO_{11}D_3$ (400.395): C 45.00, H 7.55, N 3.50, found: C 44.83, H 7.45, N 3.46.

Acknowledgement

The part of this work done at the University of Toronto was been supported by Denison Mines Ltd. and the Protein Engineering Network of Centres of Excellence, Canada. Our particular thanks are due to Dr. J. P. Carver, whose continuous efforts created the environment at the Faculty of Medicine, University of Toronto, favourable for this and similar studies, for illuminating discussions over many years.

1. T. W. Rademacher, R. B. Parekh, and R. A. Dwek. Annu. Rev. Biochem. **57**, 785 (1988).
2. B. Meyer. Top. Curr. Chem. **154**, 141 (1990).
3. J.-R. Brisson and J. P. Carver. J. Biol. Chem. **257**, 11207 (1982); Can. J. Biochem. Cell Biol. **61**, 1067 (1983).
4. H. Paulsen and R. Lebuhn. Ann. Chem. 1047 (1983).
5. P. J. Garegg, T. Iversen, and R. Johansson. Acta Chem. Scand. B, **34**, 505 (1980).
6. D. S. Dime, E. Rachaman, C. E. Dime, A. A. Grey, J. P. Carver, and J. J. Krepinsky. J. Labelled Compd. Radiopharm. **24**, 725 (1987).
7. (*a*) S. David, A. Malleron, and C. Dini. Carbohydr. Res. **188**, 193 (1989); (*b*) M. H. S. Griffith and O. Hindsgaul. Abstracts, 15th Int. Carbohydr. Symp. Yokohama. 1990. p. 73.
8. C. D. Warren, C. Auge, M. L. Laver, S. Suzuki, D. Power, and R. W. Jeanloz. Carbohydr. Res. **82**, 71 (1980).
9. N. K. Kochetkov, B. A. Dmitriev, O. S. Chizhov, E. M. Klimov, N. N. Malysheva, A. Ya, Chernyak, N. E. Bayramova, and V. I. Torgov. Carbohydr. Res. **33**, C5–C7 (1974).
10. O. Hindsgaul, T. Norberg, J. Le Pendu, and R. U. Lemieux. Carbohydr. Res. **109**, 109 (1982).
11. C. D. Warren and R. W. Jeanloz. Carbohydr. Res. **53**, 67 (1977).
12. (*a*) M. A. E. Shaban and R. Jeanloz. Carbohydr. Res. **52**, 115 (1976); (*b*) R. Gigg and R. Connant. J. Chem. Soc. Perkin Trans. 1, 2006 (1977); (*c*) A. Hasegawa and H. G. Fletcher, Jr. Carbohydr. Res. **29**, 209 (1973); (*d*) P. Szabo. J. Chem. Soc. Perkin Trans. 1, 919, (1989); (*e*) F. Dasgupta and L. Anderson. Carbohydr. Res. **202**, 239 (1990).
13. (*a*) P. J. Garegg, H. Hultberg, and S. Wallin. Carbohydr. Res. **108**, 97 (1982); (*b*) J. Dahmen, T. Frejd, G. Magnusson, G. Noori, and A.-S. Carlström. Carbohydr. Res. **125**, 237 (1984).
14. P. Gross and R. W. Jeanloz. J. Org. Chem. **32**, 2759 (1967).
15. A. G. Avent and R. Freeman. J. Magn. Reson. **39**, 169 (1980).
16. G. A. Morris. J. Magn. Reson. **41**, 185 (1980).
17. P. Bigler. J. Magn. Reson. **75**, 162 (1987).
18. D. A. Cumming and J. P. Carver. Biochemistry, **26**, 6676 (1987).
19. G. A. Jeffrey. Acta Crystallogr. Sect. B: Struct. Sci. **B46**, 89 (1990).
20. V. Warin, F. Baert, R. Fouret, G. Strecker, G. Spik, B. Fournet, and J. Montreuil. Carbohydr. Res. **76**, 11 (1979).
21. F. Mo. Acta Chem. Scand. **A33**, 207 (1979).
22. C. A. G. Haasnoot, F. A. A. M. De Leeuw, and C. Altona. Tetrahedron, **36**, 2783 (1980).
23. J.-R. Brisson and J. P. Carver. Biochemistry, **22**, 3671 (1983).
24. Y. Nishida, H. Hori, H. Ohrui, and H. Meguro. Carbohydr. Res. **170**, 106 (1987).
25. S. W. Homans. Biochemistry, **29**, 9110 (1990).
26. H. Paulsen, T. Peters, V. Sinnwell, and B. Meyer. Carbohydr. Res. **165**, 251 (1987).
27. S. W. Homans, R. A. Dwek, and T. W. Rademacher. Biochemistry, **26**, 6553 (1987).
28. S. W. Homans, A. Pastore, R. A. Dwek, and T. W. Rademacher. Biochemistry, **26**, 6649 (1987).
29. K. Bock, J. Arnarp, and J. Lonngren. Eur. J. Biochem. **129**, 171 (1982).
30. Y. Bourne, P. Rouge, and C. Cambillau. J. Biol. Chem. **265**, 18161 (1990).
31. A. Imberty, V. Tran, and S. Perez. J. Comput. Chem. **11**, 205 1990.
32. V. Tran, A. Buleon, A. Imberty, and S. Perez. Biopolymers, **28**, 679 (1989).
33. D. M. Whitfield and B. Sarkar. Biopolymers, **32**, 597 (1992).
34. G. Ekborg and C. P. J. Glaudemans. Carbohydr. Res. **129**, 287 (1984).
35. D. T. Pegg, D. M. Doddrell, W. M. Brooks, and M. R. Randall. J. Magn. Reson. **44**, 32 (1981).
36. G. A. Morris and R. Freeman. J. Magn. Reson. **29**, 433 (1978).
37. J. P. Carver, D. Mandel, S. W. Michnik, A. Imberty, and J. W. Brady. *In* Computer modeling of carbohydrates (ACS Symp. Ser. **430**; A. D. French & J. W. Brady, Eds.), American Chemical Society, Washington, D. C. 1990. pp. 266–280.
38. T. J. Pearson. California Institute of Technology, Pasadena, CA.
39. H. H. Lee, J. A. B. Baptista, and J. J. Krepinsky. Can. J. Chem. **68**, 953 (1990).

Can. J. Chem. Downloaded from www.nrcresearchpress.com by 109.225.110.28 on 09/08/12
For personal use only.

Stereoselective deprotonation of tropinone and reactions of tropinone lithium enolate

MAREK MAJEWSKI[1] AND GUO-ZHU ZHENG
Department of Chemistry, University of Saskatchewan, Saskatoon, Sask., Canada S7N 0W0

Received April 30, 1992

MAREK MAJEWSKI AND GUO-ZHU ZHENG. Can. J. Chem. **70**, 2618 (1992).

Tropinone (**6**) was deprotonated with lithium diisopropylamide and with chiral lithium amides (**18–24**) and the resulting enolates (two enantiomers) were treated with electrophiles. The aldol reaction with benzaldehyde and deuteration were both diastereoselective. The former yielded only one isomer (*exo*, *anti*) of the aldol **8***a*; the latter proceeded from the *exo* face. This selectivity permitted us to probe the deprotonation of tropinone with lithium amides; it was concluded that the reaction involves predominantly the *exo* axial protons. The reaction of tropinone enolate with ethyl chloroformate led, via a ring opening, to the cycloheptenone derivative **9**. The reaction with methyl cyanoformate yielded, in the presence of silver acetate and acetic acid, the β-ketoester **8***b*; however, in the absence of these additives, and especially when 12-crown-4 was added to the enolate, a ring opening leading to the pyrrolidine derivative **10** occurred instead. Deprotonation of tropinone with chiral lithium amides proceeded with modest enantioselectivity. A synthesis of non-racemic anhydroecgonine via this strategy allowed establishing the absolute stereochemistry of deprotonation.

MAREK MAJEWSKI et GUO-ZHU ZHENG. Can. J. Chem. **70**, 2618 (1992).

On a déprotoné la tropinone (**6**) à l'aide du diisopropylamidure de sodium et des amidures de lithium chiraux (**18–24**) et l'on a traité les énolates qui se sont formés (deux énantiomères) avec des électrophiles. La réaction aldolique avec le benzaldéhyde ainsi que la deutération sont toutes les deux diastéréosélectives; la première ne fournit qu'un isomère (*exo*, *anti*) de l'aldol **8***a* alors que la dernière se produit par la face *exo*. Cette sélectivité a permis d'examiner la déprotonation de la tropinone avec des amidures de lithium; on en a conclu que la réaction implique principalement les protons axiaux *exo*. La réaction de l'énolate de tropinone avec le chloroformate d'éthyle conduit, par le biais d'une ouverture de cycle, au dérivé cyclohepténone **9**. La réaction avec le cyanoformate de méthyle, réalisée en présence d'acétate d'argent et d'acide acétique, conduit au β-cétoester **8***b*; toutefois, lorsque cette addition est réalisée en l'absence de ces additifs et particulièrement lorsqu'on ajoute de l'éther 12-couronne-4 à l'énolate, il se produit plutôt une ouverture de cycle conduisant au dérivé de la pyrrolidine **10**. La déprotonation de la tropinone sous l'influence d'amidures de lithium se produit avec une énantiosélectivité modeste. Une synthèse de l'anhydroecgonine non-racémique à l'aide de cette stratégie a permis d'établir la stéréochimie absolue de la déprotonation.

[Traduit par la rédaction]

Introduction

Reactions that differentiate efficiently between two enantiotopic groups are often encountered in bioorganic chemistry when enzymes are used as reagents (1). In more classical synthetic organic chemistry such reactions are rare (2). Indeed the scarcity of group-enantioselective reactions has led some researchers to caution against complications of synthetic problems arising from symmetry in starting materials (3). Development of methods for achieving enantiotopic group selectivity is thus important; one such method that emerged recently as a promising new synthetic tool involves enantioselective deprotonation of ketones (4). The method is shown in general terms in Scheme 1; an achiral (or *meso*) ketone **1**, which has an internal plane of symmetry and thus belongs to the C_s point group, reacts with a chiral lithium amide **2** to yield a non-racemic mixture of lithium enolates (**3s**, **r**) which further react with an electrophile to give a number of products (**4**, **5**; only one enantiomer of each of these compounds is shown in Scheme 1). The goal is to achieve control over reaction selectivity, i.e., one of the products should predominate.

In this paper we describe our studies on the deprotonation of tropinone (**6**) (5); apart from theoretical interest in studying the scope and limitations of enantioselective deprotonation, we hoped that deprotonation of this *meso* ketone, followed by reactions of the resulting enolates with electrophiles, might lead to the development of a synthetic strategy suitable for the construction of a number of tropane alkaloids (6) in a stereoselective manner.

Results and discussion

A metal enolate of tropinone has three electron-rich centers that could be attacked by an electrophile: the α-carbon, the oxygen, and the nitrogen; depending on the character of the electrophile either one of these centers can participate in the reaction (*vide infra*).

Deprotonation of tropinone with LDA

Relatively little is known about generation and reactions of tropinone lithium enolates (6); for that reason, and also to find a suitable method of determination of the enantiomeric excess of tropinone deprotonation, we first investigated reactions of this ketone with lithium diisopropylamide (LDA) followed by electrophilic attack (Scheme 2). The racemic mixture of tropinone lithium enolates, generated by mixing tropinone with LDA in THF at −78°C, was treated with a number of electrophiles. The results are summarized in Table 1 (the differences between yields presented in Table 1 and these in ref. 5*a* reflect the changes in experimental procedures made since preliminary results of this work were published).

Chlorotrimethylsilane (entry 1) and acetic anhydride (entry 2) yielded the racemic mixtures of the O-silylated and O-acetylated products **7***a* (E = $SiMe_3$) and **7***b* (E = COMe), respectively. In the first case the quality of chlorotrimethylsilane proved crucial. Use of a chlorotrimethylsilane–triethylamine mixture, from which the amine hydrochloride was removed by centrifugation, a common procedure in silyla-

[1]Author to whom correspondence may be addressed.

Can. J. Chem. Downloaded from www.nrcresearchpress.com by 109.225.110.28 on 09/08/12
For personal use only.

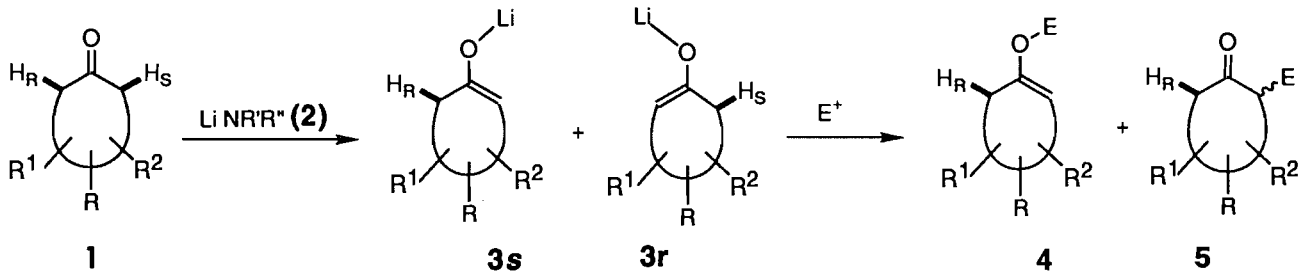

SCHEME 1

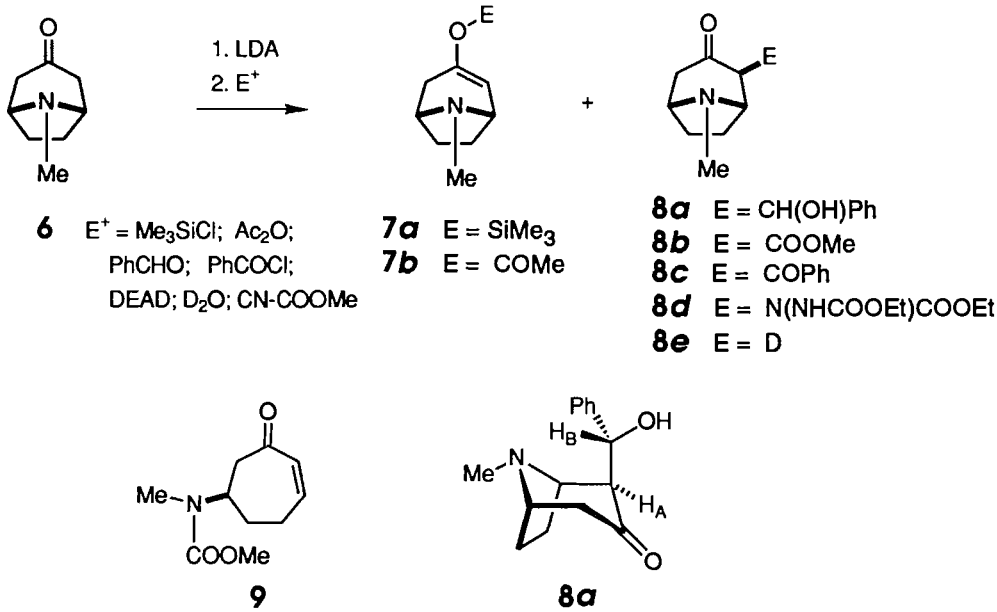

SCHEME 2

TABLE 1. Reactions of tropinone lithium enolate with electrophiles.

Entry	E^+	Product	Yield (%)[a]
1	Me_3SiCl	7*a*	88
2	Ac_2O	7*b*	54
3	PhCHO	8*a*	88
4	Cl-COOEt	9	87
5	CN-COOMe	8*b*	82
6	PhCOCl	8*c*	62
7	DEAD	8*d*	80
8	D_2O	8*e*	81

[a]Yields refer to isolated, pure products.

tion reactions, led to low yields both when Corey's internal quench (7) and the normal procedure of quenching the preformed enolate with one equivalent of chlorosilane were tried. This was, conceivably, due to triethylamine hydrochloride protonating the enolate. Good yield was achieved by purifying TMSCl by distillation from CaH_2 followed by storage over polyvinylpyridine (Reillex 402) (8), and using the internal quench procedure.

Benzaldehyde (entry 3), methyl cyanoformate (entry 5), benzoyl chloride (entry 6), and diethylazodicarboxylate (DEAD; entry 7) reacted at the carbon terminus. Interestingly, the reaction with benzaldehyde was highly stereoselective and gave only one diastereoisomer out of a possible four. Lithium enolates of cyclic ketones are known to give predominantly *anti* aldols (9); the vicinal coupling constant J_{AB} in the ^1H NMR of the aldol product **8***a* was, however, only 3 Hz, which suggested the *syn* configuration (9*a*). In agreement with both steric and stereoelectronic effects we expected this product to be the *exo* isomer; the *exo* face of tropinone should be less hindered sterically in analogy to norbornyl ring systems (10*a*). Alkylation of endocyclic six-membered enolates is known to proceed predominantly from the axial direction, which, in systems where steric constrains are absent, was rationalized by stereoelectronic effects (10, 11). We finally determined that the aldol **8***a* was indeed the *exo-anti* isomer by NMR studies on a cyclic derivative (5*a*) and by X-ray analysis of compound **8***a*, which fortunately was crystalline.[2] The low J_{AB} value is probably due to the fact that, in solution, the OH group of **8***a* is hydrogen-bonded to the nitrogen (similar hydrogen bonding is pseudotropine was reported before) (12).

To gain an entry into alkaloids related to cocaine we wanted to attach an ester synthon to the tropinone ring. Towards this end we treated the racemic mixture of tropinone lithium enolates with ethyl chloroformate, a reagent that was

[2]The X-ray data will be published elsewhere.

Can. J. Chem. Downloaded from www.nrcresearchpress.com by 109.225.110.28 on 09/08/12
For personal use only.

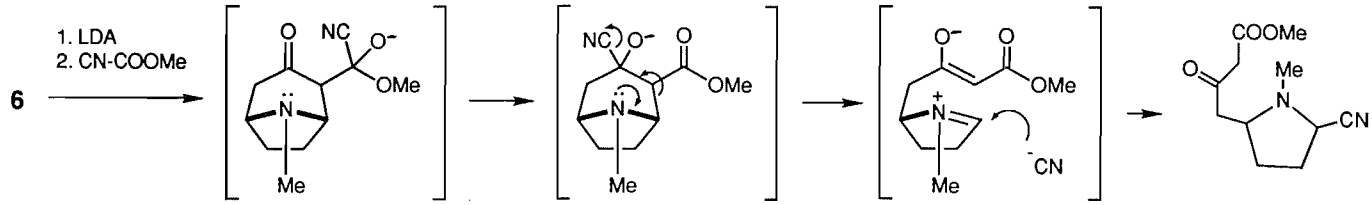

SCHEME 3

often used for carboethoxylation (13). Unexpectedly this led to formation of cycloheptenone **9** via ring opening.[3] Chloroformates are known to demethylate tropinone and other tertiary amines (14) but the reaction leading to **9** is clearly of a different type; it can be viewed as an electrophilic attack on nitrogen in tandem with E1cB elimination.

The reaction with chloroformate was thus unsuccessful as far as making of the β-ketoester was concerned. We next turned our attention to methyl cyanoformate, developed by Mander and co-workers as a reagent for α-carbomethoxylation of ketones (15*a*). Initially, reaction of tropinone lithium enolate with this reagent produced the desired β-ketoester **8***b*, which exists as a mixture of keto and enol forms, in low yield (45%). The major by-product isolated from this reaction was the substituted pyrrolidine **10** (Scheme 3, relative stereochemistry unknown). After a brief study of the reaction conditions we found that when, prior to addition of the cyanoformate reagent, one equivalent of 12-crown-4 was added to the enolate, the pyrrolidine derivative **10** became the major product (74% isolated yield) and only a small amount of the β-ketoester **8***b* was formed. When one equivalent of LiBr was added to the enolate, however, the amount of pyrrolidine **10** was much smaller and the yield of **8***b* increased to 70%. We rationalized these observations as follows:

Mander and Crabtree observed formation of ketone cyanohydrins of β-ketoesters in reactions of ketone enolates with cyanoformate (15). It seems, therefore, reasonable to envisage that intermediate **12** (Scheme 3) plays an important role in the reaction. This intermediate presumably undergoes Grob fragmentation (16), which leads to the undesired pyrrolidine **10**; to minimize this side reaction the formation of **12** has to be suppressed. The experiment with LiBr, addition of which increased the yield of the β-ketoester **8***b*, indicated that a Lewis acid retarded the Grob pathway; we attributed this to the LiBr complexation with the CN ion, which attenuated the nucleophilicity of this anion. In an effort to further decrease the ability of CN^- to attack the C=O, acetic acid was added to the reaction mixture instead of LiBr. The acid was expected to convert the cyanide to the less nucleophilic HCN: we subsequently added silver acetate to trap HCN as silver cyanide. This strategy worked; the desired β-ketoester **8***b* was now produced in 94% yield (82% after column chromatography).

Deuteration of tropinone lithium enolate with D_2O, using a second equivalent of *n*-BuLi to prevent "internal return" of the proton according to the procedure developed by Seebach and co-workers (17), showed the same face selectivity as the aldol reaction and yielded only one monodeuterated product **8***e*, the *exo* isomer. This allowed us to address the question: is the deprotonation of tropinone diastereoselective? Due to steric and stereoelectronic effects (*vide supra*) the axial *exo* protons should undergo abstraction faster than the equatorial ones.

Both ^1H and ^{13}C NMR spectra of tropinone were described before (18), however, there is some confusion in the literature concerning proton assignments (cf. difference in assignments in ref. 18*a* and ref. 18*b*). Since we intended to use NMR for the analysis of deuterated tropinones, we reinvestigated the proton NMR spectrum using nuclear Overhauser effects to help identify all the protons. The proton assignments and nOe's are shown in Fig. 1. It should be noted that the six-membered ring of tropinone is known to assume the chair conformation with the methyl group being equatorial (18).

Only one product (**8***e*) was isolated from lithiation of tropinone with LDA, followed by addition of one equivalent of *n*-BuLi and deuteration with D_2O (17). This product was the *exo* isomer, as evidenced by the 50% decrease in the intensity of the NMR signal at 2.69 ppm (the signal at 2.20 ppm remained unchanged). The *exo* **8***e* was then subjected to another deprotonation with LDA followed by treatment of the enolate with *n*-BuLi and then by quenching with D_2O. We envisaged that, if the base removed any of the equatorial protons, producing enolates **14** and (or) **15**, we should find the geminal bis-deuterotropinone **16** in the products (Scheme 4). The formation of the isomer **17**, with both deuterium atoms axial, could result from either axial or equatorial deprotonation. We did not detect compound **16** either by ^1H or by ^{13}C NMR which led us to the conclusion that the deprotonation of tropinone with LDA is highly diastereoselective: the axial (*exo*) protons are removed at least 12 times faster than the equatorial (*endo*) protons (assuming that deprotonation is not reversible and that NMR provides 5% detection level of **16**; if 5% of **16** was indeed produced this would indicate the relative rate of proton abstraction k_{Hax}/k_{Heq} of 12–17 depending on the magnitude of the primary deuterium isotope effect).

Deprotonation with chiral lithium amides

Abstraction of an α-proton from tropinone (**6**) with a chiral lithium amide (**18–24**), followed by quenching of the resulting non-racemic mixture of tropinone lithium enolates with benzaldehyde, yielded two enantiomers of the aldol product **8***a*. The enantiomeric excess (ee) was determined by NMR; when the ^1H and ^{13}C spectra of samples of **8***a* were taken in the presence of optically active shift reagent

[3]We later learned that this ring-opening reaction had also been observed by Simpkins, who reported it in a lecture, cf. ref. 4*b*.

Can. J. Chem. Downloaded from www.nrcresearchpress.com by 109.225.110.28 on 09/08/12
For personal use only.

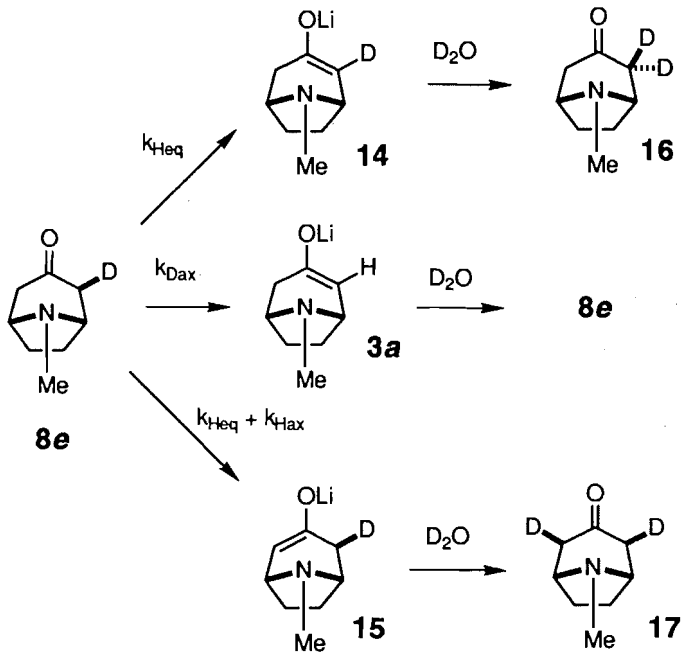

SCHEME 4

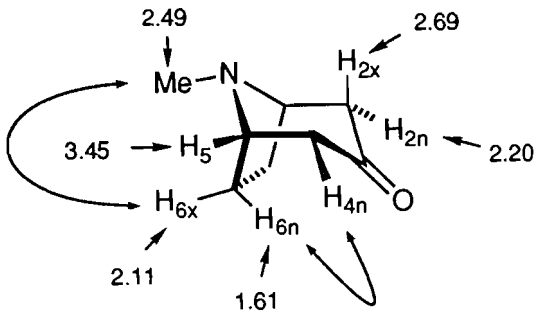

FIG. 1. Proton chemical shifts and nOe's (double-headed arrows) of tropinone (**6**).

(+)-Eu(tfc)$_3$, the splitting of the singlet corresponding to the N-Me group was observed. When the racemic **8***a*, obtained using LDA as the base, was analysed by this method the ratio of the peaks in the N-Me singlet split in the presence of Eu(tfc)$_3$ was 52:48, which provided some measure of the accuracy of this technique. The results of our enantioselective deprotonation experiments are shown in Table 2. The observed selectivities were modest with an optimum ee of 60%. We were able, however, to obtain an optically pure sample of compound **8***a* by fractional crystallization (19).

In an effort to improve enantioselectivity we investigated the effect of reaction conditions (bases **22** and **23** were used in this brief study). Lowering the reaction temperature to −100°C, as well as using two equivalents of base or an additional equivalent of *n*-BuLi, had no effect on enantioselectivity. Use of HMPA or sparteine as additives decreased the ee by up to three quarters (i.e., 10% ee instead 40% when base **23** was used in the presence of sparteine).

To establish the absolute stereochemistry of the proton abstraction with chiral lithium amides and also to highlight the potential practical utility of the method we synthesised non-racemic anhydroecgonine methyl ester (**27**), a natural product of known configuration (20*b*), via this enantioselective deprotonation strategy. The synthesis is shown in Scheme 5. A non-racemic sample of compound **8***b* was obtained in 95% yield according to the method described above (deprotonation of tropinone with base **22** followed by treatment with methyl cyanoformate, AcOH, and AcOAg). Due to tautomerism, compound **8***b* exists as a mixture of isomers with, presumably, the carboxymethyl group disposed equatorially in the major isomer. The keto group in **8***b* was reduced with sodium borohydride. It was found that under standard conditions ($NaBH_4$ in EtOH) only a small amount of **8***b* underwent reduction. However, upon lowering the reaction temperature to −60°C and addition of a small amount of aqueous NH_4Cl the reduction proceeded well (presumably due to the change in the keto–enol equilibrium of the starting material) and yielded a mixture of two products **25** and **26** in a ratio of 6:1 (80% yield). Compounds **25** and **26** were separated[4] and were then subjected to dehydration. It was found that compound **25** (but not **26**) underwent a facile dehydration with trifluoroacetic anhydride – triethylamine. Compound **26** (but not **25**) was easily dehydrated with triflic anhydride – triphenylphosphine oxide. Elimination of trifluoroacetate esters with Et_3N presumably proceeds via the E2 mechanism, hence compound **26**, in which the hydrogen atom and the OH group are *cis*, could not be easily dehydrated with the $(CF_3CO)_2O$–Et_3N mixture. The method utilizing triphenylphosphine and trifluoromethylsulfonic anhydride, developed by Hendrickson and Hussoin (21), presumably involves *syn* elimination. This would account for the easy dehydration of compound **26** under these conditions.

[4]The relative configurations of these compounds were assigned on the basis of the comparison of their NMR spectra with the spectra of cocaine and its isomers reported by Carroll *et al.*; cf. ref. 20*c*.

Can. J. Chem. Downloaded from www.nrcresearchpress.com by 109.225.110.28 on 09/08/12
For personal use only.

TABLE 2. Enantioselective deprotonation of tropinone with bases **18–24** followed by aldol addition

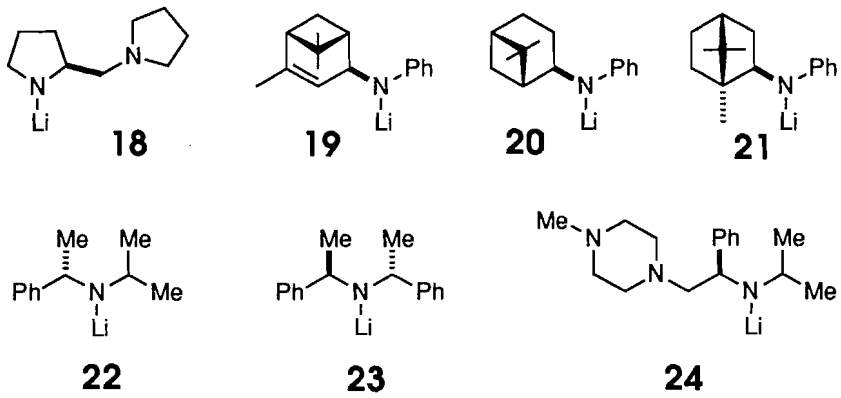

Entry	Base[a]	Yield (%)[b]	ee (%)[b]	Isomer[b,c]
1	**18**	85	8	(+)-2*R*
2	**19**	97	16	(−)-2*S*
3	**20**	70[d]	26	(−)-2*S*
4	**21**	75[d]	40	(−)-2*S*
5	**22**	88	34	(+)-2*R*
6	**23**	84	40	(−)-2*S*
7	**24**	64	60	(+)-2*R*

[a]Optically pure bases **18–24** were used (cf. Experimental).
[b]Yields and ee refer to compound **8***a*.
[c]The absolute stereochemistry was established by correlating the structure of **8***a* with that of ecgonine Me ester.
[d]A small amount (less than 5%) of the *endo-anti* isomer of **8***a* was observed.

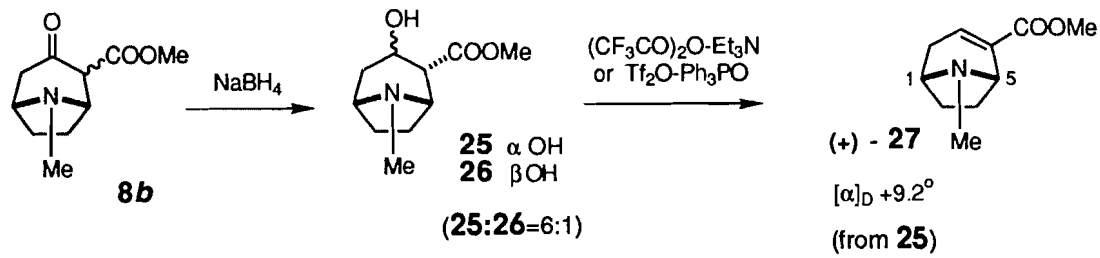

SCHEME 5

The optically active **27** was thus obtained, via the sequence described above, in 71% yield from an achiral starting material (tropinone) and had the optical rotation of +9.2. Since the optically pure levorotatory anhydroecgonine methyl ester, derived from cocaine, was reported (20*a*) to have $[\alpha]_D^{20}$ of −43, the optical purity of our sample was calculated to be 21% (the optical purity of compound **27** could not be measured by NMR as no separation of peaks due to enantiomers in the presence of optically active shift reagents was observed).

The absolute configuration of levorotatory anhydroecgonine methyl ester is known (6, 20); this isomer has the carbomethoxy group at C-2 (Scheme 5; tropane alkaloid numbering). This allowed us to determine the absolute stereochemistry of proton abstraction: bases **18**, **22**, and **24** remove preferentially the pro-*S* proton of tropinone (from C-4) and bases **19–21** and **23** deprotonate faster at C-2 (pro-*R* axial hydrogen); this was in agreement with the results of Simpkins (4*b*).

In conclusion, we have established that: (*i*) deprotonation of tropinone with LDA is diastereoselective and involves the axial (*exo*) protons. (*ii*) The aldol addition of tropinone Li enolate is also diastereoselective and produces the *exo-anti* aldol. (*iii*) Chloroformates react with the Li-enolate of tropinone to give a product of ring opening (**9**). (*iv*) Tropinone can be deprotonated enantioselectively with chiral lithium amides. Although the optical yields observed so far were modest, we are pursuing the potential use of this strategy in the stereoselective synthesis of tropane alkaloids. The strategy was highlighted by a short synthesis of non-racemic anhydroecgonine methyl ester (**27**).

Experimental

All moisture-sensitive reactions were carried out under argon. THF was distilled from a dark-blue solution containing sodium benzophenone ketyl under nitrogen atmosphere. Diisopropylamine, triethylamine, pyridine, DMF, TMEDA, and dichloromethane were distilled from calcium hydride under nitrogen atmosphere, and then stored in 100-mL Sure-seal™ bottles containing 4Å molecular sieves under argon. TMSCl was twice dis-

Can. J. Chem. Downloaded from www.nrcresearchpress.com by 109.225.110.28 on 09/08/12
For personal use only.

Can. J. Chem. Downloaded from www.nrcresearchpress.com by 109.225.110.28 on 09/08/12
For personal use only.

tilled from calcium hydride under argon atmosphere, and then stored in a 100-mL Sure-seal™ bottle with Reillex™ 402 (8). Acetic anhydride was distilled from calcium carbide (22), then redistilled before storing over 4Å molecular sieves under argon. Benzoyl chloride was stirred with oven-dried calcium carbonate powder for 2 days; the filtered liquid was then dried over sodium sulfate. After distillation, the purified benzoyl chloride was stored with 4Å molecular sieves under argon. Benzaldehyde was washed with 10% aqueous calcium carbonate solution and dried over calcium chloride prior to fractional distillation (22). Butyllithium was titrated periodically using 2,5-dimethoxybenzyl alcohol as indicator. Lithum bromide was flame-dried under vacuum and stored in a sealed flask under an argon atmosphere; it was used as a stock solution in THF (~3 M). Flash column chromatographic separations were performed with Merck Kieselgel 60 (230–400 mesh ASTM). All thin-layer chromatography (TLC) was carried out using precoated glass plates with Silica Gel 60 F254. The spots were detected by using UV light, or phosphomolybdic acid/$Ce(SO_4)_2$ solution followed by charring on a hot plate.

Melting points are uncorrected. Gas chromatography was performed using a Hewlett Packard 5890A with a HP-1 column (methyl silica gum, 5 m × 0.53 mm × 2.65 mm film thickness). The CHN elemental analyses were done using a Perkin Elmer 2400 CHN elemental analyzer. Low-resolution mass spectra were obtained using a VG Analytical retro-fitted MS-12. All NMR spectra were recorded on a Brucker AM 300 (^{1}H at 300 MHz; ^{13}C at 75 MHz) using $CDCl_3$ as solvent and TMS (tetramethylsilane) as internal standard (δ_{TMS} = 0.00 ppm).

3-Trimethylsiloxy-8-methyl-8-azabicyclo[3.2.1]oct-2-ene (7a)

TMSCl (5.5 mmol; 0.7 mL) was added to a solution of LDA (1.1 mmol) in THF (3.2 mL) followed by the dropwise addition of a solution of tropinone (1.0 mmol; 0.139 g) in THF (2 mL) over 15 min at −78°C. After 5 min the mixture was quenched with triethylamine (1.5 mL) and was then warmed to room temperature; the remaining TMSCl, triethylamine, and THF were removed on a rotary evaporator. The pure product (185 mg, 88%) was obtained after distillation from Kugelrohr apparatus: bp 218°C; IR (KBr) 3045, 2958, 2937, 2844, 2794, 1651, 1251, 893, 845 cm^{-1}; ^{1}H NMR δ: 4.92 (d, J = 5.6 Hz, 1H), 3.28 (d, J = 5.3 Hz, 1H), 3.26 (d, J = 5.7 Hz, 1H), 2.53 (dd, J_1 = 20.0 Hz, J_2 = 9.7 Hz, 1H), 2.37 (s, 3H), 2.13 (m, 1H), 2.00 (m, 1H), 1.83 (m, 1H), 1.58 (m, 2H), 0.20 (s, 9H); ^{13}C NMR δ: 147.1 (OC), 106.5 (CH), 57.9 (CH), 57.2 (CH), 35.7 (NCH_3), 35.3 (CH_2), 34.9 (CH_2), 29.8 (CH_2), 0.1 ($SiCH_3$); MS (CI–NH_3) m/z: 214 (8.3), 213 (25.3), 212 (100.0), 211 (9.1), 183 (18.8), 182 (37.8). Anal. calcd. for $C_{11}H_{21}NOSi$: C 62.50, H 10.01, N 6.63; found: C 62.40, H 10.22, N 6.81.

General procedure for generation of tropinone lithium enolate and its reaction with electrophiles

Diisopropylamine (0.155 mL; 1.1 mmol) was dissolved in THF (3.2 mL), and cooled to 0°C. *n*-Butyllithium (1.1 mmol; 0.48 mL of a 2.3 M solution in hexane) was added to the solution. The resulting, colourless, solution of LDA was stirred for 25 min at 0°C and was then cooled to −78°C. Tropinone **6** (0.139 g; 1.0 mmol), dissolved in THF (2 mL), was added dropwise over 15 min to the solution. The resulting mixture was stirred for 45 min at −78°C and was then treated with an appropriate electrophile. After the reaction mixture was stirred for a specified period of time the reaction was quenched with saturated aqueous NH_4Cl solution at −78°C. The reaction mixture was then allowed to warm to room temperature and was extracted with CH_3Cl (3 × 10 mL). The combined organic layers were washed with water, then dried over sodium sulfate, and the solvents were removed on a rotary evaporator to give the crude product.

3-Acetoxy-8-methyl-8-azabicyclo[3.2.1]oct-2-ene (7b)

Acetic anhydride (5.3 mmol; 0.5 mL) was added to a solution of tropinone lithium enolate (1.0 mmol) in THF (3.2 mL) and the mixture was stirred at −78°C for 1 h. After the standard work-up, the crude product **7***b* was obtained as a yellow oil (117 mg; 64%). Purification by chromatography (SiO_2; 5% MeOH in CH_3Cl) and bulb-to-bulb distillation (50°C/0.5 Torr; 1 Torr = 133.3 Pa) afforded **7***b* as a colourless oil (97 mg, 54%). IR (KBr) 2939, 2798, 1757, 1676, 1432, 1212, 1116 cm^{-1}; ^{1}H NMR δ: 5.46 (dd, J_1 = 1.3, J_2 = 4.2 Hz, 1H), 3.37 (m, 2H), 2.67 (dd, J_1 = 3.7 Hz, J_2 = 17.1 Hz, 1H), 2.44 (s, 3H), 2.18 (m, 1H), 2.11 (s, 3H), 2.05 (m, 1H), 1.91 (dt, J_1 = 8.9 Hz, J_2 = 2.5 Hz, 1H), 1.71 (d, J = 17.0 Hz, 1H), 1.66 (m, 1H); ^{13}C NMR δ: 169.1 (CO), 145.1 (OC), 116.4 (CH), 57.9 (CH), 57.2 (CH), 35.3 (NCH_3), 34.6 (CH_2), 29.9 (CH_2), 21.0 (CH_3); MS (El) m/z: 183 (0.3), 182 (3.4), 181 (19.4), 138 (19.3), 111 (27.5), 110 (100.0), 96 (27.3).

(1R, 2S*, 1'R*)-2-(1'-Hydroxybenzyl)-8-methyl-8-azabicyclo[3.2.1]octan-3-one (8a)*

The general procedure was followed with PhCHO as electrophile. The reaction mixture was stirred at −78°C for 15 min. After standard work-up, a yellowish solid was obtained (216 mg; 88%).

The crude product was dissolved in a minimum amount of chloroform in a warm water bath. Hexane was then added dropwise until the solution became cloudy. A small amount of $CHCl_3$ was added until the mixture became clear again. The clear solution was cooled down slowly to room temperature, and white needles of the racemate were collected (183 mg, 75%); m.p. 132.7°C; IR (KBr) 3399, 3086, 2954, 2880, 2807, 1711, 1491, 1452, 1077, 760, 701 cm^{-1}; ^{1}H NMR δ: 7.19–7.40 (m, 5H), 5.21 (d, J = 3.1 Hz, 1H), 3.57 (d, J = 6.6 Hz, 1H), 3.43–3.48 (m, 1H), 2.84 (ddd, J_1 = 15.6 Hz, J_2 = 4.6 Hz, J_3 = 1.5 Hz, 1H), 2.44 (s, 3H), 2.39–2.42 (m, 1H), 2.30 (ddd, J_1 = 15.7 Hz, J_2 = 2.0 Hz, J_3 = 2.0 Hz, 1H), 2.07–2.25 (m, 2H), 1.44–1.65 (m, 2H); ^{13}C NMR δ: 208.0 (CO), 141.7 (C), 128.0 (CH), 127.3 (CH), 125.2 (CH), 76.5 (CHOH), 67.1 (CHN), 63.8 (CHN), 61.5 (CH), 51.6 (CH_2), 40.5 (CH_3N), 26.3 (CH_2), 26.1 (CH_2); MS (CI, NH_3) m/z: 247 (17.7), 246 (100.0), 140 (51.9), 82 (20.1). Anal. calcd. for $C_{15}H_{19}NO_2$: C 73.44, H 7.81, N 5.71; found: C 73.50, H 8.06, N 5.70.

The ee was measured by ^{1}H NMR. Small amounts of (+)-$Eu(tfc)_3$ were added to the sample in $CDCl_3$ solution until a sufficient separation of the peak corresponding to the N-Me group (originally at 2.44 ppm) was achieved.

(+)-(1S, 2R, 1'S)-2-(1'-Hydroxybenzyl)-8-methyl-8-azabicyclo[3.2.1]octan-3-one (8a)

A solution of tropinone (1.0 mmol; 0.139 g) in THF (2 mL) was added dropwise over 15 min, to the preformed yellowish solution of lithium amide **22** (1.1 mmol) in THF (3.2 mL) and the mixture was stirred for 45 min at −78°C. Benzaldehyde (1.2 mmol; 0.127 mL) in THF (1 mL) was added to the reaction mixture at −78°C and, after 15 min, the reaction was quenched with saturated NH_4Cl solution (2 mL). After standard work-up, the crude mixture was placed under high vacuum for 2 days. A yellow solid was obtained (212 mg; 86% yield).

Optical purity of the crude **8***a* was 34% as measured by ^{1}H NMR using (+)-$Eu(tfc)_3$. The compound was recrystallized from $CHCl_3$–hexane as described above. White needles of the racemate were collected first and the solvent from the mother liquid was removed, and the remaining solid was again subjected to recrystallization. After repeating this procedure several times, an enantiometrically pure product was obtained as yellow rhombic crystals: mp 132–133°C; $[\alpha]_D^{20}$ + 23 (c 0.0173 g/mL, $CHCl_3$).

Methyl 8-methyl-3-oxo-8-azabicyclo[3.2.1]octane-2-carboxylate (8b) (ref. 20b)

Methyl cyanoformate (1.3 mmol; 0.1 mL) was added dropwise to a solution of tropinone lithium enolate (1.0 mmol) in THF (3.2 mL) at −78°C. The mixture was stirred at −78°C for 20 min. Glacial acetic acid (1 mL), and then silver acetate (1 mmol; 0.168 g) in glacial acetic acid (1 mL) were added to the mixture at −78°C. The mixture was warmed to room temperature, stirred for 30 min, and concentrated NH_4OH solution was added until the

Can. J. Chem. Downloaded from www.nrcresearchpress.com by 109.225.110.28 on 09/08/12
For personal use only.

mixture became clear. The resulting solution was extracted with $CHCl_3$ (5 × 30 mL), the combined organic extracts were washed with water, dried (Na_2SO_4), and the solvent was removed to give an off-white solid (187 mg; 95% yield).

Purification by flash chromatography (SiO_2, 5% MeOH in $CHCl_3$) yielded a white solid that was a mixture of keto and enol forms of **8***b* (161 mg, 82%): IR (KBr): 2951, 2851, 2799, 1741, 1718, 1652, 1615, 1443, 1227, 813 cm^{-1}; ^1H NMR δ: 3.78 (m, 1H), 3.76 (s, 64% 3H), 3.74 (s, 36% 3H), 3.37–3.66 (1H), 3.12–3.37 (1H), 2.67–2.93 (1H), 2.53 (s, 13% 3H), 2.38 (s, 22% 3H), 2.36 (s, 65% 3H), 2.03–2.32 (3H), 1.74–1.94 (1H), 1.48–1.66 (1H); MS (CI, isobutane) *m/z*: 198 (100), 166 (23). Anal. calcd. for $C_{10}H_{15}NO_3$: C 60.89, H 7.67, N 7.10; found: C 60.59, H 7.72, N 6.98.

2-Benzoyl-8-methyl-8-azabicyclo[3.2.1]oct-2-en-3-ol (8c)

The general procedure was followed with benzoyl chloride (2.6 mmol; 0.3 mL, 2.5 equivalents) as the electrophile. The mixture was stirred at −78°C for 30 min, before saturated NH_4Cl solution (2 mL) was added to the reaction mixture. Na_2CO_3 solution (40%) was added to the resulting yellow mixture until pH ~9. Extraction, followed by column chromatography (SiO_2, 5% MeOH in $CHCl_3$), yielded a yellow solid of **8***c* (150 mg; 62%); mp 75.2–77.2°C; IR (KBr) 3058, 2945, 2849, 2796, 1716, 1678, 1595, 1568, 1447, 1400, 1273, 1146, 697 cm^{-1}; ^1H NMR δ: 7.43–7.57 (m, 5H), 3.82 (d, J = 6.0 Hz, 1H), 3.41 (t, J = 6.1 Hz, 1H), 2.91 (ddd, J_1 = 19.3 Hz, J_2 = 5.5 Hz, J_3 = 1.9 Hz, 1H), 2.28–2.42 (m, 1H), 2.32 (s, 3H), 2.22 (t, J = 9.5 Hz, 2H), 2.02 (m, 1H), 1.70 (m, 1H); ^{13}C NMR δ: 195.6 (CO), 181.2 (OC=C), 135.6 (C), 130.6 (CH), 128.3 (CH), 128.1 (CH), 112.8 (C=C), 59.6 (CH), 58.0 (CH), 40.4 (CH_2), 37.1 (NCH_3), 33.9 (CH_2), 29.2 (CH_2); MS (EI) *m/z*: 245 (0.7), 244 (5.4), 243 (21.2), 215 (54.1), 214 (100.0), 136 (20.6), 110 (12.2), 105 (39.5), 82 (52.8). Anal. calcd. for $C_{15}H_{17}NO_2$: C 74.05, H 7.04, N 5.76; found: C 73.83, H 6.82, N 5.51.

2-(1, 2-Dicarbethoxyhydrazo)-8-methyl-8-azabicyclo[3.2.1]-octan-3-one (8d)

DEAD (1.9 mmol; 0.3 mL) was added to a solution of tropinone lithium enolate (1.0 mmol) in THF (3.2 mL) and the mixture was stirred at −78°C for 30 min. After standard work-up the yellowish, oily product **8***d* was obtained (295 mg, 94%). The product was purified by flash chromatography (SiO_2; 5% MeOH in $CHCl_3$). The purified product **8***d* was a yellow solid (250 mg, 80%): mp 81.2–82.2°C; IR (KBr) 3295, 3252, 2978, 2957, 2883, 2766, 1746, 1712, 1508, 1468, 1302, 1231, 1095 cm^{-1}; ^1H NMR δ: 6.81–7.09 (br, 1H), 4.99–5.21 (br, 1H), 4.13 (q, J = 7.0 Hz, 4H), 3.58–3.68 (br, 1H), 3.41 (br, 1H), 2.69 (d, J = 15.1 Hz, 1H), 2.52 (br, 3H), 2.23 (d, J = 15.3 Hz, 1H), 1.80–2.12 (br, 3H), 1.49 (m, 1H), 1.19 (two overlap. t, J = 7.0 Hz, 6H); ^{13}C NMR δ: 205.4 (CO), 204.9 (CO), 156.6 (COO), 156.0 (COO), 65.1 (CH), 64.8 (CH), 62.8 (OCH_2), 61.8 (OCH_2), 61.3 (CH), 61.0 (CH), 46.7 (CH_2), 46.4 (CH_2), 38.5 (CH), 37.4 (CH_3), 37.2 (CH_3), 27.9 (CH_2), 27.5 (CH_2), 24.5 (CH_2), 24.2 (CH_2), 14.4 (CH_3), 14.3 (CH_3); MS (CI (NH_3)) *m/z*: 316 (2.6), 315 (17.5), 314 (100.0), 313 (12.3), 225 (20.3), 85 (20.2), 83 (31.2), 82 (37.2). Anal. calcd. for $C_{14}H_{23}N_3O_5$: C 53.66, H 7.40, N 13.41; found: C 53.57, H 7.58, N 13.58.

(exo)-2-Deutero-8-methyl-8-azabicyclo[3.2.1]octan-3-one (8e)

n-Butyllithium (2.2 mmol; 1.05 mL of 2.1 molar solution in hexane), was added dropwise to a solution of tropinone lithium enolate (2.0 mmol) in THF (5.2 mL) at −78°C, and the mixture was then warmed to 0°C for 20 min. The reaction mixture was then cooled down to −78°C, D_2O (5 mL, 99% D) was added, and the mixture was warmed first to 0°C for 3 min, then to room temperature. Extraction and removal of the solvents using first a rotary evaporator and then high vacuum gave a greenish solid.

Pentane was added to the crude solid dropwise at 40°C until all the solid had dissolved. The solution was then cooled down to −30°C for several hours. The solvent was removed from the crystals at this low temperature via a syringe, and the crystals of the pure **8***e* were washed with cold pentane. Yield: 227 mg; 81%; mp 40.5–42.0°C; IR (KBr): 3387, 2934, 2882, 2855, 2802, 1714, 1592, 1476, 1348 cm^{-1}; ^1H NMR δ: 3.44 (br, 2H), 2.69 (dd, J_1 = 4.0 Hz, J_2 = 16.0 Hz, 1H), 2.49 (s, 3H), 2.20 (d, J = 15.3 Hz, 2H), 2.11 (m, 2H), 1.61 (m, 2H); ^{13}C NMR δ: 211.1 (CO), 60.7 (CH), 47.6 (CH_2), 47.3 (t, J = 18.2 Hz, CHD), 38.3 (CH_3), 27.6 (CH_2); MS (CI (NH_3)) *m/z*: 144 (18.0), 143 (20.3), 142 (69.8), 141 (100.0), 140 (84.2), 138 (17.0), 83 (91.9).

(exo, exo)-2,4-Dideutero-8-methyl-8-azabicyclo[3.2.1]octan-3-one (17)

2-Deuterotropinone (**8***e*) (1.0 mmol; 140 mg) in THF (1.2 mL) solution was added dropwise to a solution of LDA (1.1 mmol) in THF (3.2 mL) at −78°C. After 40 min, *n*-BuLi (1.1 mmol; 0.52 mL of 2.1 molar solution in hexane) was added slowly to the mixture at −78°C. The mixture was then warmed to 0°C for 20 min and cooled down to −78°C again. D_2O (5 mL, 99%D) was added to the reaction mixture at −78°C, and then warmed to 0°C for 3 min, then to room temperature. Extraction and removal of solvents by rotary evaporator, followed by high vacuum, gave a greenish solid (141 mg; 100%). The solid was purified by crystallization from pentane as described above. Yield: 110 mg (78%), mp 42–43°C; IR (KBr): 2932, 2882, 2856, 2802, 2216, 1702, 1475, 1344, 1146, 483, 453 cm^{-1}; ^1H NMR δ: 3.45 (br, 2H), 2.70 (dd, J_1 = 3.9 Hz, J_2 = 16.0 Hz, 33% of 2H), 2.50 (s, 3H), 2.20 (d, J = 15.4 Hz, 2H), 2.12 (m, 2H), 1.61 (m, 2H); ^{13}C NMR δ: 211.1 (CO), 60.7 (CH), 47.6 (CH_2), 47.3 (t, J = 18.2 Hz, CHD), 38.3 (CH_3), 27.6 (CH_2); MS (CI − NH_3) *m/z*: 145 (8.4), 144 (46.2), 143 (83.4), 142 (100.0), 141 (69.8), 140 (29.3).

6-(N-Carbethoxy-N-methyl)aminocyclohept-2-en-1-one (9)

Ethyl chloroformate (4.7 mmol; 0.45 mL) was added slowly to a solution of tropinone lithium enolate (1.0 mmol) in THF (3.2 mL) and stirred for 10 min at −78°C. Saturated NH_4Cl solution (2 mL) was added at −78°C, the mixture was warmed to room temperature, and 40% Na_2CO_3 solution (3 mL) was added to make the mixture basic. The organic layer was separated, and the aqueous layer was extracted with chloroform (4 × 5 mL). After drying (Na_2SO_4) and removal of the solvent from the combined organic layers the product was purified by chromatography (SiO_2, 4:1 hexane:AcOEt). Yellow oil (184 mg; 87%), bp 275°C; IR (KBr): 3022, 2978, 2936, 2872, 1693, 1667, 1483, 1405, 1314, 1155, 772 cm^{-1}; ^1H NMR δ: 6.64 (ddd, J_1 = 11.5 Hz, J_2 = 6.3 Hz, J_3 = 4.6 Hz, 1H), 6.04 (d, J = 12.1 Hz, 1H), 4.60 (br, 1H), 4.14 (q, J = 7.1 Hz, 2H), 2.84 (m, 2H), 2.80 (s, 3H), 2.42–2.68 (m, 2H), 1.87–2.14 (m, 2H), 1.26 (t, J = 7.1 Hz, 3H); ^{13}C NMR δ: 14.4 (OCH_2CH_3), 29.0 (CH), 30.4 (CH_2), 47.8 (CH_2), 50.9 (NCH_3), 61.0 (OCH_2CH_3), 132.2 (CH), 146.2 (CH), 155.6 (NCOO), 200.3 (CO); MS (EI, 20eV) *m/z*: 211 (60), 138 (66), 108 (95), 104 (100). Anal. calcd. for $C_{11}H_{17}NO_3$: C 62.54, H 8.11, N 6.63; found: C 62.70, H 8.38; N 6.76.

Methyl 4-[2'-(5'-cyano-1'-methylpyrrolidinyl)]-3-oxo-butyrate (10)

12-Crown-4 (1.1 mmol; 0.194 g) in THF (1 mL) was added to a solution of tropinone lithium enolate (1.0 mmol) in THF (3.2 mL) at −78°C. The mixture was warmed to 0°C for 10 min, and was then cooled to −78°C. Methyl cyanoformate (1.3 mmol; 0.1 mL) was added and the reaction mixture was stirred for 30 min at −78°C. After the standard work-up, and the removal of solvents, the crude product was purified by chromatography (SiO_2, 1:1 hexane:AcOEt), yielding a white solid (165 mg; 74%). Mp 78.8–79.8°C; IR (KBr): 2954, 2855, 2799, 2242, 1745, 1715, 1630, 1565, 1437, 1323, 1258, 1198, 1161, 1048 cm^{-1}; ^1H NMR δ: 3.93 (d, J = 6.7 Hz, 1H), 3.75 (s, 3H), 3.48 (s, 2H), 2.98 (m, 1H), 2.87 (dd, J_1 = 17.0 Hz, J_2 = 3.8 Hz, 1H), 2.58 (q, J = 8.5 Hz, 1H), 2.43 (s, 3H), 2.34 (m, 1H), 2.02–2.18 (m, 2H), 1.58 (m, 1H); ^{13}C NMR δ: 201.0 (CO), 167.4 (COO), 117.3 (CN), 58.3 (OCH3), 56.5 (CH), 52.4 (CH), 49.6 (CH_2), 47.0 (CH_2), 36.6 (NCH_3), 29.2 (CH_2), 28.0 (CH_2); MS (CI, NH_3) *m/z*: 227 (1.4), 226 (13.0), 225 (97.3), 224 (2.0), 198 (39.7), 109 (100.0), 82

Can. J. Chem. Downloaded from www.nrcresearchpress.com by 109.225.110.28 on 09/08/12
For personal use only.

(24.4), 225 (46.0), 198 (100.0), 109 (19.0), 82 (12.0). Anal. calcd. for $C_{11}H_{16}N_2O_3$: C 58.91, H 7.19, C 12.49; found: C 58.76, H 7.12, C 12.71.

*Methyl (*endo, endo*)-3-hydroxy-8-methyl-8-azabicyclo[3.2.1]-octane-2-carboxylate (**25**) and methyl (2-*endo, *3-*exo*)-3-hydroxy-8-methyl-8-azabicyclo[3.2.1]octane-2-carboxylate (**26**)*

Compound **8***b* (1.0 mmol; 0.197 g) was dissolved in absolute ethanol (2.5 mL) at room temperature, and the solution was then cooled down to −60°C. Sodium borohydride (5.3 mmol; 0.200 g) was added to the clear solution. A small amount of solid NH_4Cl was then added to the mixture followed by addition of saturated NH_4Cl solution (0.5 mL). The reaction mixture was stirred at −60°C for 3 h, was then allowed to warm to room temperature, and stirred overnight. The excess of $NaBH_4$ was destroyed by adding acetic acid (glacial) dropwise. The solvent and excess AcOH were removed on a rotary evaporator, and the residue was dissolved in $CHCl_3$ (10 mL). Na_2CO_3 (40% solution, 5 mL) was added and the mixture was then extracted with $CHCl_3$ (4 × 15 mL). After washing with water, the combined organic layers were dried (Na_2SO_4). The solvent was removed and the crude product was dried under high vacuum, yielding an oily solid (159 mg; 80%). ^{1}H NMR showed that the product contained 86% of **25** and 14% of **26**.

These two isomers were separated by flash chromatography (SiO_2, 5% MeOH in $CHCl_3$); **26** (20 mg; 10%) was eluted first followed by **25** (133 mg; 67%).

Compound **25**: IR (neat): 3700–3100, 1740 cm^{-1}; ^{1}H NMR δ: 4.28 (t, J = 4.5 Hz, 1H), 3.76 (s, 3H), 3.49 (br, 1H), 3.23 (br, 1H, OH), 3.17 (br, 1H), 3.00 (t, J = 3.5 Hz, 1H), 2.32 (s, 3H), 1.94–2.16 (m, 5H), 1.82 (m, 1H); ^{13}C NMR δ: 24.2 (CH_2), 25.8 (CH_2), 38.7 (CH_2), 40.0 (CH), 50.0 (CH), 52.0 (CH), 60.3 (NCH_3), 62.1 (CH), 64.9 (OCH_3), 173.9 (CO); MS (EI) *m/z*: 199 (15), 97 (58), 96 (78), 83 (58), 82 (100). Anal. calcd. for $C_{10}H_{17}NO_3$: C 60.28, H 8.60, N 7.03; found: C 60.05, H 8.67, N 6.78.

Compound **26**: IR (neat): 3700–3100, 1740 cm^{-1}; ^{1}H NMR δ: 4.12 (dt, J_1 = 10.3 Hz, J_2 = 6.6 Hz, 1H), 3.74 (s, 3H), 3.48 (dd, J_1 = 6.1 Hz, J_2 = 2.6 Hz, 1H), 3.24 (m, 1H), 2.72 (dd, J_1 = 9.9 Hz, J_2 = 2.9 Hz, 1H), 2.38 (s, 3H), 1.68–2.08 (m, 4H), 1.54 (q, J = 8.6 Hz, 2H); ^{13}C NMR δ: 25.0 (CH_2), 27.2 (CH_2), 36.1 (CH_2), 38.0 (CH), 52.1 (CH), 52.2 (CH), 60.1 (NCH_3), 62.0 (CH), 64.8 (OCH_3), 175.0 (CO); MS (Cl (NH_3)) *m/z*: 201 (12.3), 200 (100), 83 (24). Anal. calcd. for $C_{10}H_{17}NO_3$: C 60.28, H 8.60, N 7.03; found: C 60.17, H 8.90, N 6.78.

*Anhydroecgonine methyl ester (**27**) (ref. 20*a*)*

(*a*) (±)-(**27**): Triphenylphosphine oxide (0.4 mmol; 0.111 g) was dissolved in anhydrous dichloromethane (0.5 mL) and placed in a septum-sealed 10-mL round-bottom flask at 0°C, under argon. Trifluoromethanesulfonic anhydride (0.2 mmol; 34 mL) in anhydrous dichloromethane (0.5 mL) was added dropwise to the reaction mixture with constant stirring. The reddish colour of triphenylphosphine oxide solution disappeared immediately after the triflic anhydride had been added. Racemic compound **26** (0.1 mmol; 20 mg) in dry dichloromethane (0.5 mL) was added slowly at 0°C, and the reaction mixture was then warmed to room temperature and stirred for 15 min. Anhydrous triethylamine (0.5 mL) was added to the reaction mixture and the reddish color appeared again. After 15 min, the reaction was quenched with water (2 mL), and then extracted with diethyl ether (5 × 5 mL). The combined organic layers were dried over anhydrous sodium sulfate. After removal of the solvent, the residue was subjected to separation on a short column (SiO_2, 3% MeOH in $CHCl_3$), which yielded the purified product (15 mg; 83%).

(*b*) (+)-(**27**): Non-racemic **25** (5.5 mmol; 1.1 g), was prepared as previously described using chiral base **22**, and dissolved in anhydrous dichloromethane (4 mL) in a septum-sealed 10-mL round-bottom flask at 0°C, under argon. Anhydrous triethylamine (15.8 mmol; 2.2 mL) was added, followed by a catalytic amount of 4-(dimethylamino)pyridine in dichloromethane (1.2 mL) solution. The solution was stirred and trifluoroacetic anhydride (7.1 mmol, 1.0 mL) in dichloromethane (2.5 mL) was added dropwise during 20 min. After stirring for an additional 2 h at 0°C, the reaction mixture was warmed to room temperature and stirred for another 30 h. The reaction mixture was then cooled down to 0°C again, and treated with dilute Na_2CO_3 solution until the solution became basic. The mixture was extracted with chloroform (5 × 30 mL), and the combined organic layers were washed (H_2O), and then dried (Na_2SO_4). After removal of the solvent, the mixture was subjected to flash chromatography (SiO_2, 3% MeOH in $CHCl_3$). A colorless oil was obtained (925 mg; 93%): $[\alpha]_D^{20}$ + 9.2 (*c* 0.1084 g/mL, MeOH), IR (KBr): 2949, 2876, 2843, 2793, 1711, 1639, 1436, 1253, 1084, 753, 728 cm^{-1}; ^{1}H NMR δ: 1.52 (m, 1H), 1.85 (t, J = 9.8 Hz, 1H), 1.88 (dd, J_1 = 19.6 Hz, J_2 = 4.7 Hz, 1H), 2.18 (m, 2H), 2.37 (s, 3H), 2.65 (m, 1H), 3.28 (m, 1H), 3.75 (s, 3H), 3.83 (m, 1H), 6.83 (m, 1H); ^{13}C NMR δ: 30.1 (CH_2), 31.6 (CH_2), 34.5 (CH_2), 36.8 (CH), 51.8 (NCH_3), 57.0 (OCH_3), 134.0 (C), 136.2 (CH), 166.7 (CO); MS (CI (NH_3)) *m/z*: 182 (100), 181 (15.6), 152 (15.3).

Synthesis of chiral amines

(*S*)-(+)-1-(2-Pyrrolidinylmethyl)pyrrolidine **18***a*, which was the precursor to base **18**, was purchased from Aldrich and dried prior to use (CaH_2). Amines used for generating **21–24** were synthesized by methods reported in the literature (23). Amines that were the source of compounds **19** and **20** were synthesized by reductive amination (see below).

*(+)-(1S, 2S, 5S)-N-Phenyl-4,6,6-trimethylbicyclo[3.1.1]hept-3-enylamine (**19**a)*

Aniline (9.0 mmol; 0.83 g), and glacial acetic acid (15 mL) were placed under argon. (1*S*)-(−)-Verbenone (1.0 mmol; 0.154 mL) was then slowly added to this solution at room temperature and the reaction mixture was stirred for 4 h. Sodium borohydride (5.3 mmol; 200 mg) was then added in small portions and the turbid mixture was stirred at room temperature overnight under argon. Aqueous HCl solution (10%) was added to acidify the mixture, and acetic acid was then removed on a rotary evaporator. The residue was dissolved in chloroform (10 mL) and aqueous sodium carbonate solution (40%) was added until the mixture became basic. The mixture was then extracted with chloroform (4 × 20 mL). After washing with water, the combined organic layers were dried over anhydrous sodium sulfate. The solvent was removed and the crude product was purified by chromatography (SiO_2, 4:1 *n*-hexane:ethyl acetate). Yield: 191 mg, $[\alpha]_D^{20}$ + 25.0 (*c* 0.0162 g/mL, $CHCl_3$); IR (KBr): 3429, 3049, 2922, 2867, 1600, 1502, 1428, 746, 691 cm^{-1}; ^{1}H NMR δ: 7.17 (td, J_1 = 7.4 Hz, J_2 = 1.0 Hz, 2H), 6.68 (t, J = 6.4 Hz, 1H), 6.60 (d, J = 7.7 Hz, 2H), 5.38 (br, 1H), 4.30 (br, 1H), 3.90 (br, 1H (NH)), 2.50 (m, 1H), 2.43 (m, 1H), 2.01 (t, J = 6.2 Hz, 1H), 1.74 (t, J = 1.8 Hz, 3H), 1.41 (d, J = 8.8 Hz, 1H), 1.32 (s, 3H), 1.07 (s, 3H); ^{13}C NMR δ: 147.8 (C), 147.5 (C), 130.1 (CH), 118.4 (CH), 117.5 (CH), 113.5 (CH), 56.5 (CH), 47.8 (CH), 45.2 (CH), 39.0 (CH_2), 35.0 (CH_2), 27.0 (CH_3), 23.0 (CH_3), 22.8 (CH_3); MS (CI (NH_3)) *m/z*: 229 (14.6), 228 (77.5), 227 (13.2), 135 (50.1), 94 (100.0). Anal. calcd. for $C_{16}H_{21}N$: C 84.53, H 9.31, N 6.16; found: C 84.40, H 9.02, N 6.15.

*(−)-(1R), 2R, 5S)-N-Phenyl-6,6-dimethylbicyclo[3.1.1]-heptanylamine (**20**a)*

Analogous procedure using (1*R*)-(+)-nopinone (1.0 mmol) and aniline yielded a yellowish oil, **20***a* (204 mg, 95%). After purification by flash chromatography, a colorless liquid was obtained (189 mg; 88%): bp 302°C; $[\alpha]_D^{20}$ −75.3 (*c* 0.1142 g/mL, $CHCl_3$); IR (KBr): 3421, 3050, 2911, 2867, 1601, 1502, 1465, 1315, 746, 691 cm^{-1}; ^{1}H NMR δ: 7.15 (t, J = 7.5 Hz, 2H), 6.65 (t, 7.3 Hz, 1H), 6.34 (d, J = 8.5 Hz, 2H), 3.94 (m, 1H), 3.81 (br, 1H (NH)), 2.28–2.48 (m, 2H), 2.19 (br, 1H), 1.98 (m, 2H), 1.88 (m, 1H), 1.61 (m, 1H), 1.21 (s, 3H), 1.12 (s, 3H), 1.03 (d, J = 10.0 Hz, 1H); ^{13}C NMR δ: 23.2 (CH_3), 24.7 (CH_2), 25.2 (CH_2), 27.8 (CH_3),

30.0 (C), 38.0 (CH_2), 41.1 (CH), 45.6 (CH), 54.9 (CH), 113.1 (CH), 116.9 (CH), 129.4 (CH), 147.6 (C); MS (CI (NH_3)) *m/z*: 217 (17.2), 216 (100); Anal. calcd. for $C_{15}H_{21}N$: C 83.67, H 9.83, N 6.50; found: C 83.77, H 9.71, N 6.47.

Acknowledgement

The authors are grateful to the Natural Sciences and Engineering Research Council of Canada and the University of Saskatchewan for financial support.

1. Y.-F. Wang, C.-S. Chen, G. Girdaukas, and C. Sih. *In* Enzymes in organic synthesis. Ciba Foundation Symp. **111**, 128 (1985).
2. R. S. Ward. Chem. Soc. Rev. **19**, 1 (1990).
3. S. H. Bertz. J. Chem. Soc., Chem. Commun. 218 (1984).
4. (*a*) P. J. Cox and N. S. Simpkins. Tetrahedron: Asymmetry, **2**, 1 (1991); (*b*) N. S. Simpkins, J. Chem. Soc. Rev. **19**, 335 (1990).
5. (*a*) M. Majewski and G.-Z. Zheng. Synlett, 173 (1991); (*b*) T. Momose, N. Toyoka, S. Seki, and Y. Hirai. Chem. Pharm. Bull. **38**, 2072 (1990).
6. M. Lounasmaa. *In* The alkaloids. Vol. 33. *Edited by* A. Brossi. Academic Press, Toronto. 1988. Chap. 1.
7. E. J. Corey and A. W. Gross. Tetrahedron Lett. **25**, 495 (1984).
8. D. K. Hutchinson. Aldrichimica Acta **19**, 58 (1986).
9. (*a*) C. H. Heathcock. *In* Comprehensive organic synthesis. Vol. 2. Pergamon Press, Oxford. 1991. p. 181; (*b*) M. Majewski and D. M. Gleave. Tetrahedron Lett. **30**, 5681 (1989).
10. (*a*) D. A. Evans. *In* Asymmetric synthesis. Vol. 3. *Edited by* J. D. Morrison. Academic Press, New York. 1984. pp. 1 and 51; (*b*) D. Caine. *In* Comprehensive organic synthesis. Vol. 3. Pergamon Press, Oxford. 1991. p. 12; (*c*) J. Toullec. Adv. Phys. Org. Chem. **18**, 1 (1982).
11. P. Deslongchamps. Stereoelectronic effects in organic chemistry. Pergamon Press, Toronto. 1983. p. 274.
12. P. Hanisch, A. J. Jones, A. F. Casey, and J. E. Coates. J. Chem. Soc. Perkin Trans. 2, 1202 (1977).
13. D. Caine. *In* Carbon–carbon bond formation. *Edited by* R. L. Augustine. Marcel Dekker, New York. 1981. p. 250.
14. T. A. Montzka, J. D. Matiskella, and R. A. Partyka. Tetrahedron Lett. 1325 (1974).
15. (*a*) S. R. Crabtree, W. L. A. Chu, and L. A. Mander. Synlett, 169 (1990); (*b*) S. R. Crabtree. Ph.D. Thesis, Research School of Chemistry, Australian National University, Canberra. 1990.
16. C. A. Grob and W. Schwarz. Helv. Chim. Acta, **47**, 1870 (1964).
17. T. Laube, J. D. Dunitz, and D. Seebach. Helv. Chim. Acta, **68**, 1373 (1985).
18. (*a*) H. Ohashi, I. Morishima, K. Okada, and T. Yonezawa. J. Chem. Soc. Chem. Commun. 34 (1971); (*b*) Y. Kashman and S. Cherkez. Tetrahedron, **28**, 155 (1972); (*c*) R. J. Bishop, G. Fodor, A. R. Katritzky, F. Soti, L. E. Sutton, and F. J. Swinbourne. J. Chem. Soc.(C), 74 (1966); (*d*) E. Wenkert, J. S. Bindra, C.-J. Chang, D. W. Cochran, and F. M. Schell. Acc. Chem. Res. **7**, 46 (1974).
19. J. Jacques, A. Collet, and S. H. Wilen. Enantiomers, racemates and resolution. Wiley. New York. 1981. p. 423.
20. (*a*) H. F. Campbell, E. O. Edwards, and R. Kolt. Can. J. Chem. **55**, 1372 (1977); (*b*) S. P. Findlay. J. Org. Chem. **22**, 1385 (1957); (*c*) F. I. Carroll, M. L. Coleman, and A. H. Lewin. J. Org. Chem. **47**, 13 (1982).
21. J. B. Hendrickson and M. S. Hussoin. J. Org. Chem. **52**, 4137 (1987).
22. D. D. Perrin and S. P. Armarego. Purification of laboratory chemicals. 3rd ed. Pergamon Press, Toronto. 1988.
23. (*a*) A. Ando and T. Shioiri. Tetrahedron, **45**, 4969 (1989); (*b*) H.-F. Kim, H. Kawasaki, M. Makajima, and K. Koga. Tetrahedron Lett. **30**, 6537 (1989); (*c*) C. M. Cain, R. P. C. Cousins, G. Coumbarides, and N. S. Simpkins. Tetrahedron, **46**, 523 (1990).

Can. J. Chem. Downloaded from www.nrcresearchpress.com by 109.225.110.28 on 09/08/12
For personal use only.

Lewis acid mediated Diels–Alder reactions of 2*H*-thiopyrans

DALE E. WARD[1] AND YUANZHU GAI

Department of Chemistry, University of Saskatchewan, Saskatoon, Sask., Canada S7N 0W0

Received April 13, 1992

DALE E. WARD and YUANZHU GAI. Can. J. Chem. **70**, 2627 (1992).

Lewis acid mediated Diels–Alder reactions of 2*H*-thiopyrans with acrylate, crotonate, and methacrylate dienophiles have been investigated. Modest to good yields of predominantly *exo* adducts are obtained with 4-substituted 2*H*-thiopyrans. With 5-substituted 2*H*-thiopyrans, high *endo* selectivity is observed. No adducts were produced with methacrylate dienophiles. Relative to the thermal reactions, the *exo* selectivity is enhanced in the presence of Lewis acids. Unusually high *exo* selectivity is observed using "wet" Et_2AlCl as the promoter.

DALE E. WARD et YUANZHU GAI. Can. J. Chem. **70**, 2627 (1992).

On a étudié les réactions de Diels–Alder catalysées par des acides de Lewis entre des 2*H*-thiopyranes et des acrylate, crotonate et méthacrylate agissant comme diénophiles. Avec les 2*H*-thiopyranes substitués en position 4, on a obtenu des rendements allant de modestes à bons d'adduits principalement *exo*. Avec les 2*H*-thiopyranes substitués en position 5, on observe une sélectivité élevée de produits *endo*. Il ne se produit aucun adduit lorsque le méthacrylate agit comme diénophile. Comparées aux réactions thermiques, la sélectivité *exo* est améliorée en présence d'acide de Lewis. On observe une sélectivité anormalement élevée en faveur de l'*exo* lorsque du Et_2AlCl «humide» est utilisé comme promoteur.

[Traduit par la rédaction]

Can. J. Chem. Downloaded from www.nrcresearchpress.com by 109.225.110.28 on 09/08/12
For personal use only.

Introduction

The lack of reactivity associated with *cis*-substituted 1,3-dienes (1) is a significant limitation of the Diels–Alder reaction (2). In an effort to address this problem, we have recently investigated (3) a strategy involving the use of 2*H*-thiopyrans as functional equivalents to *cis*-dienes. Diels–Alder reactions of 2*H*-thiopyrans with dienophiles can provide adducts that, after desulfurization, are synthetically equivalent to an adduct derived from a *cis*-diene (3).

The reactions of various 2*H*-thiopyrans bearing electron-donating substituents with reactive dienophiles such as maleic anhydride or maleimide provide good to excellent yields of predominantly *endo* adducts. However, with less reactive dienophiles such as methyl acrylate or butenone the reactions are considerably slower and thermal decomposition of the dienes competes effectively with cycloaddition. Although the regioselectivity is high compared to reactions with related acyclic dienes (3*b*), the lower yields and poor stereoselectivity observed in the reactions of 2*H*-thiopyrans with less reactive dienophiles limits potential synthetic applications. In an attempt to improve yields and stereoselectivity by producing adducts at lower temperatures we have examined the effect of Lewis acids on these reactions (2, 4). The results are presented in Tables 1–3.

Results and discussion

Initially we investigated the reaction of **1***a* with methyl acrylate (**2***a*). The Diels–Alder reaction proceeds at 120°C in toluene (sealed tube) to give a 1.7:1 mixture of *endo* and *exo* adducts, **5***a* and **5***b* respectively, in 56% yield after 6 days (3) (Table 1, entry 1). The efficacy of various Lewis acids in promoting the reaction at lower temperatures was evaluated. The addition of various amounts of $TiCl_4$, $SnCl_4$, or Et_2AlCl to a solution of **1***a* and **2***a* in CH_2Cl_2 at −78°C or room temperature failed to produce the desired adducts; the only products resulted from hydrolysis of **1***a*. Eventually, we found that Diels–Alder adducts were produced at room temperature in the presence of $BF_3 \cdot Et_2O$ (Table 1, entry 5) or, better, $EtAlCl_2$ (Table 1, entries 6–9). The adducts obtained were a mixture of **5***a* and **5***b* together with their products of silyl enol ether hydrolysis, **7***a* and **7***b*. Analysis of the reaction products was simplified by employing an acidic work-up that effected the hydrolysis of **5***a* and **5***b* and resulted in the isolation of **7***a* and **7***b* as the only adducts.

The stereochemistry of **7** was readily determined, as previously (3*a*), by analysis of the coupling constants observed in the ^1H NMR spectra. The *endo* proton at C-5 was readily assigned based on its $^4J_{HH}$ with H-3_{anti} (2–2.5 Hz). The stereochemistry of the proton at C-6 was determined based on its $^3J_{HH}$ with H-5_{endo} (for **7***b*, J = 11 Hz; for **7***a*, J = 6 Hz) and its $^4J_{HH}$ with H-7_{exo} (for **7***b*, J = 0 Hz; for **7***a*, J = 2.5 Hz). Stereochemical assignments were independently confirmed by hydrolysis (CF_3CO_2H, CH_2Cl_2) of the individual isomers (3*a*) **5***a* and **5***b* to give **7***a* and **7***b*, respectively.[2]

The use of $EtAlCl_2$ was also effective in promoting the reaction of **1***a* with *N*-phenylmaleimide (**1***c*) to produce the *endo* adduct **11** in yields similar to that obtained in the thermal reaction (Table 1, cf. entries 10 and 12) (3*a*). Comparing with the reactions of **2***a*, the yield and stereoselectivity obtained in the reactions of *N*-phenylmaleimide were not as sensitive to the amount of Lewis acid employed. Other Lewis acids were not as effective in promoting the reaction. In contrast to the thermal reaction, the *exo* adduct could not be detected in the ^1H NMR spectrum of the crude product from the Lewis acid mediated reactions. Several attempts to effect reaction of **1***a* with methyl crotonate (**3***a*) or methyl methacrylate (**4***a*) were unsuccessful (Table 1, entries 15, 16).

In an effort to improve on both the scope and stereoselectivity of Diels–Alder reactions with acrylate derivatives we examined substrates incorporating an oxazolidone auxiliary (5). *N*-Alkenoyloxazolidones have been reported to be reactive acrylate equivalents (6) in Lewis acid mediated Diels–Alder reactions producing adducts with high stereoselectiv-

[1]Author to whom correspondence may be addressed.

[2]For a discussion of the determination of stereochemistry in these systems see ref. 3*a*. For related cases see ref. 18.

TABLE 1. Diels–Alder reactions of **1***a* with **2**, **3**, **4**, and *N*-phenylmaleimide (**1***c*)[a]

Entry	Dienophile[b]	Lewis acid[b]	Product	Yield (%)	*exo*:*endo*[c]
1.	**2***a* (2.5)	None[d]	**5**	56	0.6:1
2.	**2***a* (1.5)	$TiCl_4$ (0.7)	—	—	—
3.	**2***a* (1.5)	$SnCl_4$ (0.7)	—	—	—
4.	**2***a* (1.5)	Et_2AlCl (0.7)	—	—	—
5.	**2***a* (1.5)	$BF_3 \cdot Et_2O$ (0.7)	**7**	41	1.0:1
6.	**2***a* (1.5)	$EtAlCl_2$ (0.7)	**7**	77	1.1:1
7.	**2***a* (1.5)	$EtAlCl_2$(1.5)	**7**	44	1.5:1
8.	**2***a* (1.5)	$EtAlCl_2$(1.0)	**7**	54	1.6:1
9.	**2***a* (1.5)	$EtAlCl_2$(0.5)	**7**	79	1.2:1
10.	**1***c* (1.6)	None[e]	**11**[f]	77	0.1:1
11.	**1***c* (1.5)	$EtAlCl_2$ (1.0)	**11**	71	*endo*[g]
12.	**1***c* (1.5)	$EtAlCl_2$ (0.7)	**11**	78	*endo*[g]
13.	**1***c* (1.5)	$EtAlCl_2$ (0.5)	**11**	80	*endo*[g]
14.	**1***c* (1.0)	$TiCl_4$ (0.6)	**11**	19	*endo*[g]
15.	**3***a* (1.5)	$EtAlCl_2$(0.7)	—	—	—
16.	**4***a* (1.5)	$EtAlCl_2$(0.5)	—	—	—
17.	**2***b* (1.3)	None[h]	**8**[f]	66	1.0:1
18.	**2***b* (1.1)	Et_2AlCl(1.6)[i,j]	—	—	—
19.	**2***b* (1.1)	Me_2AlCl(1.6)[i,j]	**8**	26	1.7:1
20.	**2***b* (1.0)	$EtAlCl_2$(0.7)	—	—	—
21.	**2***b* (1.0)	$SnCl_4$ (0.7)	**8**	20	*exo*[k]
22.	**2***b* (1.0)	$TiCl_4$ (0.7)	**8**	46	1.0:1
23.	**2***b* (1.0)	$TiCl_4$ (0.7)[l]	**8**	44	1.8:1
24.	**2***b* (1.2)	$TiCl_4$ (0.8)[m]	**8**	33	2.3:1
25.	**2***b* (1.3)	$TiCl_4$ (1.0)	**8**	49	1.5:1
26.	**2***b* (1.3)	$TiCl_4$ (0.7)	**8**	67	1.2:1
27.	**2***b* (1.3)	$TiCl_4$ (0.5)	**8**	69	1.1:1
28.	**2***b* (1.3)	$TiCl_4$ (0.4)	**8**	54	1.1:1
29.	**2***b* (1.3)	$TiCl_4$ (0.7) $Ti(i\text{-}PrO)_4$(0.1)	**8**	62	1.6:1
30.	**2***b* (1.3)	$TiCl_4$ (0.7) $Ti(i\text{-}PrO)_4$(0.2)	**8**	70	2.4:1
31.	**2***b* (1.3)	$TiCl_4$ (0.7) $Ti(i\text{-}PrO)_4$(0.3)	**8**	55	3.1:1
32.	**3***b* (1.3)	$TiCl_4$(0.7)	**9**	61	2.5:1
33.	**3***b* (1.3)	$TiCl_4$ (0.5)	**9**	60	2.5:1
34.	**3***b* (1.3)	$TiCl_4$ (0.7) $Ti(i\text{-}PrO)_4$(0.2)	**9**	30	3.3:1
35.	**4***b* (1.3)	$TiCl_4$(0.7)	—	—	—
36.	**2***c* (1.3)	None[h]	**10**[f]	61	0.6:1
37.	**2***c* (1.1)	Me_2AlCl(1.6)[i]	**10**	59	2.7:1
38.	**2***c* (1.1)	Me_2AlCl (1.0)[i]	**10**	27	5:1
39.	**2***c* (1.1)	Me_2AlCl (0.7)[i]	**10**	19	*exo*[k]
40.	**2***c* (1.1)	Et_2AlCl (1.6)[i]	**10**	53	1.3:1
41.	**2***c* (1.3)	$EtAlCl_2$ (1.0)	**10**	30	*exo*[k]
42.	**2***c* (1.3)	$TiCl_4$ (1.0)	**10**	24	4:1
43.	**2***c* (1.1)	Et_2AlCl (1.0) H_2O(0.25)	**10**	84	16:1
44.	**3***c* (1.1)	Et_2AlCl(1.6)[i]	—	—	—
45.	**3***c* (1.1)	Me_2AlCl(1.6)[i]	—	—	—

[a]Reactions carried out with 0.1–0.15 mmol of **1***a* in CH_2Cl_2 (2 mL) at room temperature.
[b]The number of equivalents based on **1***a* indicated in parentheses.
[c]Measured by ^1H NMR or (for **7**) by weight of isolated adducts.
[d]Reaction carried out in toluene in a sealed tube (120°C, 144 h).
[e]Reaction carried out in xylene in a sealed tube (120°C, 48 h) (ref. 3*a*).
[f]The corresponding triisopropylsilyl enol ether was isolated.
[g]The *exo* isomer was not detected by ^1H NMR.
[h]Reaction carried out in $CDCl_3$ in a sealed tube (110°C, 120 h).
[i]Reaction at −78°C.
[j]At room temperature the diene was rapidly decomposed and no adducts were formed.
[k]The *endo* isomer was not detected by ^1H NMR.
[l]Reaction at 0°C.
[m]Reaction at −20°C.

Can. J. Chem. Downloaded from www.nrcresearchpress.com by 109.225.110.28 on 09/08/12
For personal use only.

ity (7–9). The results are presented in Table 1 (entries 17–45).

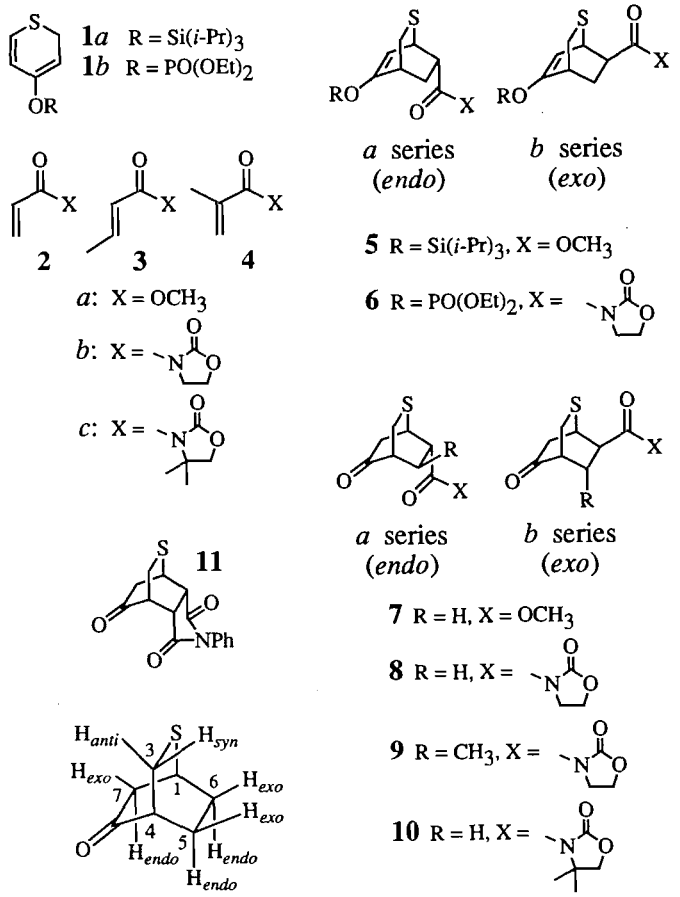

Surprisingly, the reaction of **1***a* with **2***b* in the presence of excess Et_2AlCl under the published conditions[3] did not produce an adduct after 1 h at −78°C or at room temperature (Table 1, entry 18). A similar reaction mediated by Me_2AlCl at −78°C gave a 1.7:1 mixture of the adducts **8***b* and **8***a* in low yield after work-up (Table 1, entry 19). The stereochemistry of the adducts was assigned on the basis of ^1H NMR as outlined above. The difference in the results obtained with Et_2AlCl and Me_2AlCl might be due to the higher propensity of the former to add to **2***b* in a 1,4 sense in competition with cycloaddition of **2***b* to an unreactive diene (7, 10).

A survey of various Lewis acids eventually revealed that the reaction of **1***a* with **2***b* could be effectively promoted by $TiCl_4$ (Table 1, entries 22–31). Best results were obtained by "buffering" the $TiCl_4$ with $Ti(i\text{-}PrO)_4$ (11). The yield of adducts was sensitive to the amount of $TiCl_4$ (Table 1, cf. entries 25–28) as well to the ratio of $TiCl_4$ to **2***b* (Table 1, cf. entries 22 and 26). The degree of *exo* stereoselectivity was enhanced in reactions conducted at lower temperatures (Table 1, cf. entries 22 and 23), with more $TiCl_4$ (Table 1, cf. entries 25 and 28), or with added $Ti(i\text{-}PrO)_4$ (Table 1, cf. entries 26 and 30).

Under similar conditions, a modest yield of Diels–Alder adducts was obtained from the reaction of **1***a* with **3***b* (Table 1, entries 32–34). By contrast, adducts were not detected in attempted reactions of **1***a* and **4***b*. The stereochemistry of the adducts **9***a* and **9***b* was evident based on analysis of the coupling constants between H-7_{exo} and H-6 (for **9***b*, ^4J = 0 Hz; for **9***a*, ^4J = 1 Hz) and between H-3_{anti} and H-5 (for **9***b*, ^3J = 0 Hz; for **9***a*, ^3J = 1 Hz). The coupling constants observed between H-6 and H-5 (for **9***b*, ^3J = 6.5 Hz; for **9***a*, ^3J = 7.5 Hz) were consistent with a *trans* relationship between the C-5 methyl group and the C-6 acyl group.

The low stereoselectivity observed in reactions with **2***b* prompted us to examine the dimethyl derivative **2***c* (8*c*). The results are presented in Table 1 (entries 36–45). The thermal reaction of **1***a* with **2***c* modest *endo* selectivity. Reactions mediated by various Lewis acids were consistently *exo* selective. After considerable experimentation we were able to produce the *exo* adduct **10***b* with high stereoselectivity and in good yield using "wet" Et_2AlCl as the mediator (5). Reactions of **1***a* with **3***c* failed to produce any cycloaddition products under a variety of conditions.

The major by-products in the above reactions resulted from the decomposition of the diene. The use of dienol phosphates as stable analogues of dienol silyl ethers has recently been reported (12). Diels–Alder adducts were not obtained in thermal reactions of **1***b* with acrylate derivatives (3*a*). We briefly examined the reaction of **1***b* with **2***b* in the presence of $TiCl_4$ and the results are presented in Table 2. At best, a modest yield of Diels–Alder adducts was obtained as a 1.5:1 mixture of *exo*:*endo* isomers. No adducts could be detected in similar reactions of **1***b* with **3***b* or with **4***b*.

The thermal Diels–Alder reactions of **1***a* with **2***a*, **2***b*, or **2***c* are unselective or show modest *endo* selectivity. Interestingly, in all of the Lewis acid mediated reactions examined the *exo* adducts are the major diastereomers produced.[4] By contrast, both thermal (13) and Lewis acid mediated (14) Diels–Alder reactions of 1,3-cyclohexadienes typically give predominantly *endo* adducts with varying levels of diastereoselectivity. Similarly, Diels–Alder reactions of both 1,2-dihyropyridines (15) and 2-pyranones (16) are typically *endo* selective. With the exception of reactions with methacrylate derivatives (17), very few examples of *exo*-selective Diels–Alder reactions of 1,3-cyclohexadienes have been reported (13*g*, 18, 19). Specifically, Diels–Alder reactions of 1,3-bis(trialkylsilyloxy)-1,3-cyclohexadienes are highly *exo* selective both under thermal (18, 19) and Lewis acid mediated (18) conditions; the reason(s) for this unusual behavior is unknown.

To test the generality of this *exo* selective process with 2*H*-thiopyrans we examined the Diels–Alder reactions of 5-triisopropylsilyloxy-2*H*-thiopyran (**12**) (3*a*). The propensity for **12** to rearrange into the unreactive 3-substituted isomer **13** precluded thermal reactions with acrylate dienophiles (3*a*). Lewis acid mediated reactions of **12** with *N*-phenylmaleimide, **2***a*, **2***b*, and **2***c* were repeated under conditions that

[3]Under these conditions cyclopentadiene reacts with **2***b* at −100°C "within seconds" to produce the *endo* adduct in quantitative yield (7).

[4]We assume that the observed *endo*:*exo* ratios result from kinetic control since: (*i*) the *endo*:*exo* ratios do not appear to change during the course of the reactions; (*ii*) samples of **5***a* and **7***a* treated with $EtAlCl_2$ were shown to be configurationally stable; (*iii*) a 1:1 mixture of the triisopropylsilyl enol ethers corresponding to **10***a*,*b* was unchanged after treatment with Me_2AlCl at room temperature; (*iv*) samples of **10***a* and **17***a* were unchanged after treatment with Me_2AlCl at room temperature.

Can. J. Chem. Downloaded from www.nrcresearchpress.com by 109.225.110.28 on 09/08/12
For personal use only.

TABLE 2. Diels–Alder reactions of **1***b* with **2***b*, **3***b*, and **4***b*[a]

Entry	Dienophile[b]	Lewis acid[b]	Product	Yield (%)	*exo*:*endo*[c]
1.	**2***b* (1.5)	$TiCl_4$(0.7)	**6**	Trace	—
2.	**2***b* (1.5)	$TiCl_4$(1.0)	**6**	38	1.5:1
3.	**2***b* (1.5)	$TiCl_4$(1.0)[d]	**6**	49	1.4:1
4.	**2***b* (1.5)	$TiCl_4$(1.0) $Ti(i\text{-}PrO)_4$(0.2)	**6**	41	1.6:1
5.	**2***b* (1.5)	$TiCl_4$(1.0) $Ti(i\text{-}PrO)_4$(0.2)[d]	**6**	51	1.5:1
6.	**2***b* (1.5)	$SnCl_4$(0.7)	**6**	Trace	—
7.	**3***b* (1.5)	$TiCl_4$(1.0)	—	—	—
8.	**4***b* (1.5)	$TiCl_4$(1.0)	—	—	—

[a]Unless otherwise noted, reactions carried out with 0.1–0.15 mmol of **1***b* in CH_2Cl_2 (2 mL) at room temperature.
[b]The number of equivalents based on **1***a* indicated in parentheses.
[c]Measured by weight of isolated adducts.
[d]Reaction carried out at 40°C.

proved successful for **1***a*. The results are presented in Table 3.

Reaction of **12** with *N*-phenylmaleimide (**1***c*) mediated by $EtAlCl_2$ gave the *endo* adduct **14** in low yield along with **13** (60%). The stereochemistry of the product was assigned based on the coupling observed in the ^1H NMR spectrum between H-8_{exo} and H-5 (^4J = 2 Hz) and was confirmed by hydrolysis (CF_3CO_2H, CH_2Cl_2) of the known (3*a*) *endo* triisopropylsilyl enol ether.

Reaction of **12** with **2***a* in the presence of $EtAlCl_2$ at room temperature gave a good yield of adducts as a 1.4:1 mixture of stereoisomers **15** (Table 3, entry 3). Severe congestion of resonances in the ^1H NMR spectrum of the adducts prevented definitive assignment of stereochemistry. Alternatively, reaction of **12** with **2***b* in the presence of $TiCl_4$ gave a single adduct that was identified as **16***a* together with rearranged diene **13** (30%) (Table 3, entries 4, 5). In the ^1H NMR spectrum of **16***a*, H-5 was coupled to H-8_{exo} (^4J = 1.5 Hz) but not to H-3_{anti} (*dd*, *J* = 3, 10.5 Hz). The stereochemistry of the major adduct from the reaction of **12** and **2***a* was assigned as *endo* (**15***a*) based on the close correspondence of its ^{13}C NMR spectrum with that of **16***a*. Reactions of **12** and **2***c* in the presence of Me_2AlCl or $TiCl_4$ were also highly *endo* selective (Table 3, entries 8, 9). Surprisingly, the same reaction mediated by "wet" Et_2AlCl (5) resulted in poor stereoselectivity (Table 3, entry 11). Adducts were not detected in similar reactions of **1***a* with **3***c*.

endo Addition is generally the preferred mode of the Diels–Alder reaction (1). Various factors have been proposed to rationalize the *endo*:*exo* ratios in Diels–Alder reactions including secondary orbital interactions, steric effects, and dipole–dipole interactions (1). The small difference in the activation energy of *endo* and *exo* transition states, however, means that relatively subtle changes in the transition

TABLE 3. Diels–Alder reactions of **12** with **2***a*, **2***b*, **2***c*, and *N*-phenylmaleimide (**1***c*)[a]

Entry	Dienophile[b]	Lewis acid[b]	Product	Yield (%)[c]	*endo*:*exo*[d]
1.	**1***c* (2.5)	None[e]	**14**[f]	57	*endo*[g]
2.	**1***c* (1.5)	$EtAlCl_2$(0.5)	**14**	20	*endo*[g]
3.	**2***a* (1.5)	$EtAlCl_2$(0.5)	**15**	71	1.4:1
4.	**2***b* (1.5)	$TiCl_4$(0.7)	**16**	40	*endo*[g]
5.	**2***b* (1.5)	$TiCl_4$(0.5)	**16**	41	*endo*[g]
6.	**2***b* (1.1)	Me_2AlCl(1.6)[h]	—	—	—
7.	**2***c* (1.1)	Et_2AlCl(1.6)[h]	—	—	—
8.	**2***c* (1.1)	Me_2AlCl(1.6)[h]	**17**	56	9:1
9.	**2***c* (1.1)	$TiCl_4$(0.5) $TiCl_4$(0.7)	**17**	30	10:1
10.	**2***c* (1.1)	$Ti(i\text{-}PrO)_4$(0.2) Et_2AlCl (1.0)	—	—	—
11.	**2***c* (1.1)	H_2O(0.25)	**17**	32	1.5:1

[a]Diene was a 4.5–5.1 mixture of **12** and **13**, respectively. Unless otherwise noted, reactions were carried out with 0.1–0.15 mmol of diene in CH_2Cl_2 (2 mL) at room temperature.
[b]The number of equivalents based on diene indicated in parentheses.
[c]Yield based on **12**.
[d]Measured by ^1H NMR.
[e]Reaction in a sealed tube in toluene-d_8 (110°C, 24 h).
[f]The corresponding triisopropylsilyl enol ether was isolated.
[g]The *exo* isomer was not detected by ^1H NMR.
[h]Reaction carried out at −78°C.

Can. J. Chem. Downloaded from www.nrcresearchpress.com by 109.225.110.28 on 09/08/12
For personal use only.

state structure can result in large changes in the *endo*:*exo* ratio (20). Lewis acid mediated Diels–Alder reactions typically display enhanced *endo* selectivity relative to their thermal counterparts (2, 4, 21). Compared to other cyclic dienes, **1***a* is unusual since the portion of *exo* adduct increases when reactions are conducted in the presence of Lewis acids.[4] This behavior is presumably due to structural and (or) mechanistic consequences resulting from the replacement of a methylene group in a 1,3-cyclohexadiene skeleton with a sulfur atom.

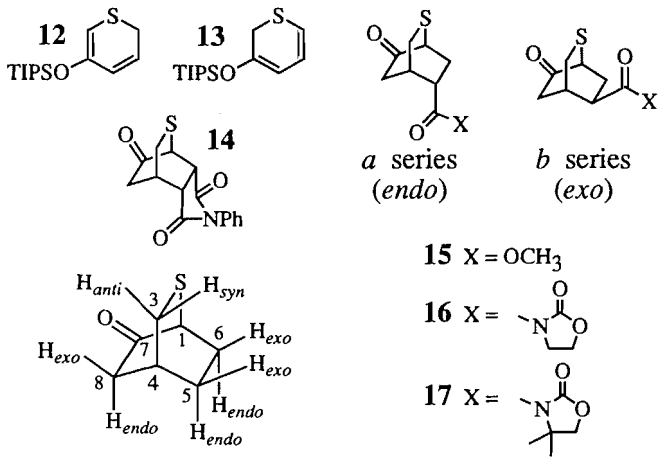

The 1,3-diene of 2*H*-thiopyran deviates significantly from planarity and shows little conjugation with the sulfur atom (22). Diels–Alder reaction with methyl acrylate (**2***a*), however, is completely regioselective and gives predominantly the *endo* adduct corresponding to **5***a* (i.e., **5***a* with OR = H) (23). The mechanism of Lewis acid mediated cycloaddition with silyloxy substituted 2*H*-thiopyrans **1***a* and **12** is uncertain. Several examples of cycloaddition reactions of both cyclic (14*c*–*e*) and acyclic (24; see also ref. 11*a*) silyloxy dienes with dienophiles in the presence of Lewis acids have been proposed to proceed through a stepwise double Michael reaction mechanism. The evidence presented in favor of the two-step mechanism typically involves the detection or isolation of an intermediate. We presume that a two-step mechanism for cycloaddition reactions with **1***b* is unlikely since, in contrast to silyl enol ethers (25), we are unaware of examples of Lewis acid promoted Michael reactions of enol phosphates. In no case have we detected or isolated any intermediate product in the Lewis acid mediated cycloaddition reactions of **1***a*, **1***b*, or **12**. The similar stereoselectivity observed in the $TiCl_4$ promoted reactions of **2***b* with **1***a* and **1***b* is consistent with similar reaction mechanisms. Interestingly, high *endo* stereoselectivity is typically observed in double Michael reactions both under acidic (14*c*–*e*, 24) and basic (26) conditions.

Several factors might be invoked to explain the increase in *exo* selectivity in the reactions of **1***a* with **2** under Lewis acid mediated conditions compared to the thermal reaction. The presence of the sulfur atom could result in reduced steric repulsions in the *exo* transition state.[5] Since coordination of the dienophile with a Lewis acid results in a larger effective size, the *exo* selectivity would increase under these conditions. Alternatively, secondary orbital interactions involving the sulfur atom might favor the *exo* transition state.[6] In the presence of Lewis acids these interactions become more important (21) and *exo* selectivity would be enhanced. Finally, the sulfur might act as a Lewis base. The *exo* mode of addition would be favored by the possibility of simultaneous coordination of the diene and the dienophile with a Lewis acid. With small revisions, all of these factors could be similarly applied to the second step in a double Michael reaction mechanism to rationalize *exo* selectivity.

Comparing the reactions of **1***a* with those of **12** is instructive. With both dienes reaction with *N*-phenylmaleimide is highly *endo* selective under thermal and Lewis acid mediated conditions. The reactions of **12** with acrylate derivatives are *endo* selective while the same reactions of **1***a* are *exo* selective. In general these results can be accommodated by a steric argument. Cases where the *exo* transition state develops a *gauche* interaction between a substituent on the dienophile and the CH_2 group on the diene (i.e., **1***a* with **1***c*, **12** with **1***c*, and **12** with **2**) favor the *endo* adduct. Cases where the only *gauche* interaction in the *exo* transition state is between a substituent on the dienophile and the sulfur atom on the diene (i.e., **1***a* and **1***b* with **2**) favor the *exo* adduct.

Rationalizing the differences in reactivity and stereoselectivity observed with different dienophile and Lewis acids combinations is difficult. The importance of the dienophile conformation (and the influence of the Lewis acid on dienophile conformation) on stereoselectivity has been discussed (6, 7, 8, 28). A major anomaly occurs in reactions mediated by aluminum Lewis acids, particularly "wet" Et_2AlCl. The reaction of water with Et_2AlCl is known (29) to produce $(ClEtAl)_2O$ (plus ethane). At present we feel that the unusual selectivity observed with this mediator is best rationalized by *exo* transition state with simultaneous coordination of the diene (via sulfur) and dienophile to a bidentate (or polydentate) Lewis acid related to $(ClEtAl)_2O$ (5).

Conclusion

Lewis acid mediated Diels–Alder reactions of 2*H*-thiopyrans are very sensitive to the nature of the dienophile and the Lewis acid. Under appropriate conditions, the reactions are highly stereoselective and can provide adducts that are unavailable in thermal reactions. Modest to good yields of predominantly *exo* adducts are obtained in Lewis acid mediated reactions of 4-triisopropylsilyloxy-2*H*-thiopyran (**1***a*) with acrylate and crotonate derivatives. Reactions of 5-triisopropylsilyloxy-2*H*-thiopyran (**12**) with acrylate derivatives give modest to good yields of predominantly *endo* adducts. In most cases the observed stereoselectivity can be rationalized by steric effects. Unusually high *exo* selectivity is observed in reactions of **2***c* in the presence of "wet" Et_2AlCl. We postulate that, in this case, the selectivity is due to simultaneous coordination of the diene (via sulfur) and dienophile to a bidentate (or polydentate) Lewis acid related to $(ClEtAl)_2O$.

Further experiments aimed at determining the nature of the *exo* selectivity and of the wet Et_2AlCl promoter are underway. Applications of the use of 2*H*-thiopyrans as surrogates

[5]In the *exo* transition state, a *gauche* interaction develops between the acyl group and the S while in the *endo* transition state the steric interaction is between the acyl group and an sp^2 CH. A sulfur atom is sterically much smaller than an sp^2 CH ($-SCH_3$, *A* value = 0.7; $-CH{=}CH_2$, *A* value = 1.35; ref. 27).

[6]For example, interaction of an occupied orbital on sulfur with the dienophile LUMO.

Can. J. Chem. Downloaded from www.nrcresearchpress.com by 109.225.110.28 on 09/08/12
For personal use only.

Can. J. Chem. Downloaded from www.nrcresearchpress.com by 109.225.110.28 on 09/08/12
For personal use only.

for *cis*-dienes are under active investigation and will be reported in due course.

Experimental[7]

The dienes **1***a*, **1***b*, and **12** were freshly prepared as described previously (*3a*). The ratio of **12**:**13** was 4.5–5:1. The dienophiles **2***b*, **2***c*, **3***b*, **3***c*, **4***b*, and **4***c* were prepared by acylation (*7*) of the corresponding oxazolidones (*30*). The dienophiles **2***a*, **3***a*, and **4***a* were distilled. CH_2Cl_2 was distilled from P_2O_5 and stored over 3Å molecular sieves under argon. The Lewis acids $EtAlCl_2$, Et_2AlCl, and Me_2AlCl were purchased as 1 M solutions in hexane and were of good quality as judged by calibration with a known example (*5*, *7*). $BF_3 \cdot Et_2O$ (neat) and $SnCl_4$ (1 M in CH_2Cl_2) were used as received. Solutions of $TiCl_4$ (0.2–0.25 M in CH_2Cl_2) were prepared from distilled (CaH_2) reagent. "Wet" Et_2AlCl (for reaction with 0.1 mmol of diene) was prepared as follows (*5*): a solution of H_2O in CH_2Cl_2 (0.11 M) was prepared by addition of H_2O (10 mg) to anhydrous CH_2Cl_2 (5 mL). Et_2AlCl (1 M in hexane, 0.1 mL) was added to an aliquot of this solution (0.23 mL, 0.25 mmol) in CH_2Cl_2 (1 mL). After stirring at ambient temperature for 15 min the dienophile was added, followed by the diene.

The IR spectra were obtained by diffuse reflectance infrared Fourier transform (DRIFT). Unless otherwise noted, the ^1H NMR and ^{13}C NMR spectra were obtained in $CDCl_3$ solution at 300 MHz and 75 MHz, respectively. Mass spectra were obtained at low resolution with ionization by electron impact at 70 eV (EI) or by chemical ionization (CI) using NH_3 as reagent gas.

General procedure for reactions

The Lewis acid was added via syringe to a stirred solution of the dienophile (0.11–0.25 mmol) in CH_2Cl_2 (1 mL) at the appropriate temperature. A solution of the diene (0.1–0.15 mmol) in CH_2Cl_2 (1 mL) was then added. The reactions were monitored by TLC and after 1 h the dienes typically were no longer detected. The reactions were quenched by addition of saturated $NaHCO_3$(aq) (ca. 1 mL). After extraction with CH_2Cl_2, the combined organic layers was dried over Na_2SO_4(s) and concentrated and the crude product analyzed by ^1H NMR for the presence of diene(s) and adducts. In successful reactions, various amounts of the silyl enol ether of the adduct(s) was detected. Addition of trifluoroacetic acid (ca. 2 drops) to a CH_2Cl_2 solution of the crude product gave complete hydrolysis of the enol ethers within 5–10 min. After concentration to dryness, the *endo*:*exo* ratio was determined by ^1H NMR. The crude products were fractionated by flash column chromatography and (or) by preparative thin-layer chromatography (ether/hexane mixtures as eluent) to give the individual adducts. Yields are based on isolated products.

*(1′*R*, 4′*R*, 6′*S*-3-(8′-Diethylphosphoryloxy-2′-thiabicyclo-[2.2.2]oct-7′-ene-6′-carbonyl)-2-oxazolidinone (**6***a*)*

IR: 3072, 1772, 1699, 1686, 1653, 1477, 1276 cm^{-1}; ^1H NMR δ: 6.00 (1H, dt, J = 2, 7.5 Hz, H-7′), 4.41 (2H, dt, J = 2.5, 8.5 Hz, H-5), 4.19 (1H, m, H-6′), 4.18 (4H, dq, J = 7, 7 Hz, OCH_2CH_3), 3.95 (2H, dt, J = 3, 8.5 Hz, H-4), 3.86 (1H, dd, J = 2, 7 Hz, H-1′), 3.24 (1H, m, H-4′), 3.05 (1H, dd, J = 3, 10 Hz, H-3′$_{syn}$), 2.85 (1H, ddd, J = 2, 2.5, 10 Hz, H-3′$_{anti}$), 2.16 (1H, ddd, J = 2, 10, 12 Hz, H-5′$_{exo}$), 1.98 (1H, m, H-5′$_{endo}$), 1.36 (6H, t, J = 7 Hz, OCH_2CH_3); ^{13}C NMR δ: 172.6 (S, C-6′ C=O), 153.0 (s, C-2), 151.1 (s, C-8′), 130.0 (d, C-7′), 64.5 (t, OCH_2CH_3), 62.2 (t, C-5), 47.7 (d, C-6′), 42.8 (t, C-4), 36.2 (d, C-4′), 34.6 (d, C-1′), 34.5 (t, C-3′), 29.5 (t, C-5′), 16.1 (q, OCH_2CH_3), (C-7′, 8′ show coupling to ^{31}P; J = 4–8 Hz); MS (EI), m/z (relative intensity): 391 ($[M]^+$, 19), 250 (52), 150 (100), 96 (76).

*(1′*R*, 4′*R*, 6′*R*)-3-(8′-Diethylphosphoryloxy-2′-thiabicyclo-[2.2.2]oct-7′-ene-6′-carbonyl)-2-oxazolidinone (**6***b*)*

IR: 3067, 1774, 1700, 1655, 1478, 1277, 1202 cm^{-1}; ^1H NMR δ: 6.16 (1H, dt, J = 2, 8 Hz, H-7′), 4.44 (2H, t, J = 8 Hz, H-5), 4.19 (4H, dq, J = 7, 7 Hz, OCH_2CH_3), 4.10 (2H, m, H-4), 3.95 (1H, dd, J = 3, 8 Hz, H-1′), 3.86 (1H, ddd, J = 3, 5, 11 Hz, H-6′), 3.17 (1H, m, H-4′), 3.07 (1H, dd, J = 3, 10 Hz, H-3′$_{syn}$), 2.82 (1H, ddd, J = 2.5, 3, 10 Hz, H-3′$_{anti}$), 2.39 (1H, ddd, J = 1.5, 5, 13 Hz, H-5′$_{exo}$), 1.78 (1H, dddd, J = 2.5, 3.5, 5, 13 Hz, H-5′$_{endo}$), 1.37 (6H, t, J = 7 Hz, OCH_2CH_3); ^{13}C NMR δ: 171.9 (s, C-6′ C=O), 153.2 (s, C-2), 151.2 (s, C-8′), 114.4 (d, C-7′), 64.6 (t, C-5), 62.3 (t, OCH_2), 46.2 (d, C-6′), 43.2 (t, C-4), 37.4 (d, C-1′), 34.1 (d, C-4′), 33.2 (t, C-3′), 26.1 (t, C-5′), 16.2 (q, OCH_2CH_3), (C-7′, 8′ show coupling to ^{31}P; J = 4–8 Hz); MS (EI), m/z (relative intensity): 391 ($[M]^+$, 23), 250 (87), 150 (63), 96 (100).

(1R, 4R*, 6S*)-2-Thiabicyclo[2.2.2]octan-8-one-6-carboxylic acid, methyl ester (**7**a)*

IR: 2996, 1729, 1218, 1175 cm^{-1}; ^1H NMR (C_6D_6) δ: 3.24 (3H, s, OCH_3), 2.99 (2H, m, H-6, H-1), 2.65 (1H, dd, J = 2.5, 19 Hz, H-7$_{endo}$), 2.59 (1H, ddd, J = 2.5, 3.5, 11 Hz, H-3$_{anti}$), 2.50 (1H, ddd, J = 2.5, 2.5, 19 Hz, H-7$_{exo}$), 2.32 (2H, m, H-3$_{syn}$, H-4), 2.09 (1H, dddd, J = 2.5, 2.5, 6, 14.5 Hz, H-5$_{endo}$), 1.56 (1H, ddd, J = 2.5, 11.5, 14.5 Hz, H-5$_{exo}$), ^{13}C NMR δ: 211.2 (s, C-8), 173.2 (s, C-6 C=O), 52.4 (q, OCH_3), 45.1 (t, C-7), 44.2 (d, C-6), 41.9 (d, C-4), 35.7 (d, C-1), 27.4 (t, C-3), 25.3 (t, C-5); MS (CI, NH_3), m/z (relative intensity): 218 ($[M + 18]^+$, 100).

(1R, 4S*, 6R*)-2-Thiabicyclo[2.2.2]octan-8-one-6-carboxylic acid, methyl ester (**7**b)*

IR: 1729, 1204, 1182 cm^{-1}; ^1H NMR δ: 3.78 (3H, s, OCH_3), 3.51 (1H, ddd, J = 3, 3, 6.5 Hz, H-1), 3.07 (2H, m, H-6, H-3$_{syn}$), 2.99 (1H, ddd, J = 2, 3, 11 Hz, H-3$_{anti}$), 2.88 (1H, dd, J = 3, 19 Hz, H-7), 2.73 (1H, dd, J = 3, 19 Hz, H-7), 2.67 (1H, m, H-4), 2.63 (1H, m, H-5$_{exo}$), 2.07 (1H, dddd, J = 2, 4, 11, 14.5 Hz, H-5$_{endo}$); ^{13}C NMR (75 MHz, CDCl3) δ: 211.8 (s, C-8), 172.8 (s, C-6 C=O), 52.5 (q, OCH_3), 48.0 (t, C-7), 43.9 (d, C-6), 41.3 (d, C-4), 37.0 (d, C-1), 27.4 (t, C-3), 24.1 (t, C-5); MS (CI, NH_3), m/z (relative intensity): 218 ($[M + 18]^+$, 100), 201 ($[M + 1]^+$, 24), 172 (16).

*(1′*R*, 4′*R*, 6′*S*)-3-(2′-Thiabicyclo[2.2.2]octan-8′-one-6′-carbonyl)-2-oxazolidinone (**8**a)*

Recrystallized from EtOAc to afford colorless needles (mp 147–149°C). IR: 1773, 1726, 1688 cm^{-1}; ^1H NMR δ: 4.48 (3H, m, H-6′, H-5), 4.03 (2H, t, J = 8.5 Hz, H-4), 3.34 (1H, m, H-1′), 3.09 (2H, m, H-3′), 2.98 (1H, dd, J = 3, 19 Hz, H-7′$_{exo}$), 2.77 (1H, m, H-4′), 2.73 (1H, ddd, J = 1.5, 3.5, 19 Hz, H-7′$_{endo}$), 2.39 (1H, ddd, J = 3, 10.5, 14 Hz, H-5′$_{exo}$), 2.27 (1H, dddd, J = 1.5, 3, 7, 14 Hz, H-5′$_{endo}$); ^{13}C NMR δ: 211.6 (s, C-8), 173.1 (s, C-6′ C=O), 153.0 (s, C-2), 62.2 (t, C-5), 44.9 (t, C-4), 43.0 (d, C-6′), 42.9 (t, C-7′), 42.0 (d, C-4′), 35.7 (d, C-1′), 27.3 (t, C-3′), 25.3 (t, C-5′); MS (EI), m/z (relative intensity): 255 ($[M]^+$, 60), 208 (46), 141 (60), 120 (100). Anal. calcd. for $C_{11}H_{13}NO_4S$: C 51.75, H 5.13; N 5.49; found: C 51.84, H 5.18, N 5.58.

*(1′*R*, 4′*R*, 6′*R*)-3-(2′-Thiabicyclo[2.2.2]octan-8′-one-6′-carbonyl)-2-oxazolidinone (**8**b)*

Recrystallized from EtOAc to afford colorless needles (mp 164–165°C). IR: 1769, 1725, 1698 cm^{-1}, ^1H NMR δ: 4.48 (2H, t, J = 7.5 Hz, H-5), 4.12 (3H, m, H-4, H-6′), 3.54 (1H, ddd, J = 3, 3, 6.5 Hz, H-1′), 3.13 (1H, dd, J = 3, 11 Hz, H-3′$_{syn}$), 2.99 (1H, ddd, J = 2.5, 3.5, 11 Hz, H-3′$_{anti}$), 2.87 (2H, m, H-7′), 2.79 (1H, ddd, J = 2.5, 5, 14 Hz, H-5′$_{exo}$), 2.73 (1H, m, H-4′), 1.96 (1H, dddd, J = 2.5, 4, 11, 14 Hz, H-5′$_{endo}$); ^{13}C NMR δ: 211.9 (S, C-8′), 172.2 (S, C-6′ C=O), 153.4 (S, C-2), 62.4 (t, C-5), 48.4 (t, C-4), 43.5 (d, C-6′), 43.1 (t, C-7′), 41.4 (d, C-4′), 37.1 (d, C-1′), 27.6 (t, C-3′), 23.1 (t, C-5′); MS (EI), m/z (relative intensity): 255 ($[M]^+$, 56), 208 (54), 149 (62), 121 (100). Anal. calcd. for $C_{11}H_{13}NO_4S$: C 51.75, H 5.13, N 5.49; found: C 51.82, H 5.26, N 5.28.

*(1′*R*, 4′*R*, 5′*S*, 6′*S*)-3-(5′-Methyl-2′-thiabicyclo[2.2.2]-octan-8′-one-6′carbonyl)-2-oxazalidinone (**9**a)*

IR: 1776, 1724, 1692 cm^{-1}; ^1H NMR δ: 4.45 (2H, t, J = 8 Hz, H-5), 4.16 (1H, dt, J = 7.5, 1 Hz, H-6′), 4.05 (2H, m, H-4), 3.25 (2H, m, H-3′$_{syn}$, H-1′), 2.94 (1H, ddd, J = 1, 4, 11.5 Hz, H-3′$_{anti}$),

[7]General experimental procedures have been recently described (*3a*).

2.86 (1H, m, H-5′), 2.73 (1H, dd, J = 3, 19 Hz, H-7′$_{endo}$), 2.60 (2H, m, H-7′$_{exo}$, H-4′), 1.18 (1H, d, J = 7 Hz, C-5′ CH_3); ^{13}C NMR δ: 211.3 (s, C-8′), 172.4 (s, C-6′ C=O), 153.0 (s, C-2), 62.1 (t, C-5), 51.3 (d, C-6′), 48.3 (d, C-4′), 43.4 (t, C-4), 43.1 (t, C-7′), 36.9 (d, C-1′), 28.0 (d, C-5′), 21.6 (t, C-3′), 18.1 (q, C-5′ CH_3); MS (CI, NH_3), m/z (relative intensity): 287 ([M + 18]$^+$, 100), 270 ([M + 1]$^+$, 19).

*(1′*R*, 4′*R*, 5′R*, 6′R*)-3-(5′-Methyl-2′-thiabicyclo[2,2,2]-octan-8′-one-6′-carbonyl)-2-oxazolidinone (**9**b)*

IR: 1767, 1725, 1693 cm^{-1}; ^1H NMR δ: 4.48 (2H, dt, J = 7, 7 Hz, H-5), 4.12 (2H, m, H-4), 3.16 (1H, dd, J = 2.5, 6.5 Hz, H-6′), 3.49 (1H, m, H-1′), 3.12 (1H, dd, J = 3.5, 11 Hz, H-3′$_{syn}$), 3.03 (2H, m, H-5′, H-3′$_{anti}$), 2.82 (2H, d, J = 3.5 Hz, H-7′), 2.55 (1H, m, H-4′), 0.97 (3H, d, J = 7 Hz, C-5′ CH_3); ^{13}C NMR δ: 211.5 (s, C-8′), 171.6 (s, C-6′ C=O), 153.4 (s, C-2), 62.4 (t, C-5), 53.0 (d, C-6′), 48.6 (d, C-4′), 48.3 (t, C-4), 43.1 (t, C-7′), 37.8 (d, C-1′), 30.9 (d, C-5′), 27.7 (t, C-3′), 21.9 (q, C-5′ CH_3); MS (EI), m/z (relative intensity): 269 ([M]$^+$, 36), 222 (21), 135 (100).

(1′R, 4′R*, 6′S*)-3-(2′-Thiabicyclo[2.2.2]octan-8′-one-6′-carbonyl)-4,4-dimethyl-2-oxazolidinone (**10**a)*

IR: 1773, 1727, 1697 cm^{-1}; ^1H NMR δ: 4.48 (1H, dddd, J = 1.5, 1.5, 7, 10.5 Hz, H-6′), 4.03 (2H, s, H-5), 3.25 (1H, m, H-1′), 3.08 (2H, m, H-3′), 2.98 (1H, dd, J = 3, 19 Hz, H-7′$_{endo}$), 2.76 (1H, m, H-4′), 2.73 (1H, ddd, J = 1.5, 3, 19 Hz, H-7′$_{exo}$), 2.36 (1H, ddd, J = 3, 10.5, 14 Hz, H-5′$_{exo}$), 2.21 (1H, dddd, J = 1.5, 2.5, 7, 14 Hz, H-5′$_{endo}$), 1.56 (6H, s, C4-CH_3); ^{13}C NMR δ: 211.7 (s, C-8′), 174.1 (s, C-6′ C=O), 153.4 (s, C-2) 75.3 (t, C-5), 60.8 (s, C-4), 45.0 (t, C-7′), 44.3 (d, C-6′), 42.2 (d, C-4′), 35.7 (d, C-1′), 27.3 (t, C-3′), 25.5 (t, C-5′), 24.8 (q, C4-CH_3), 24.7 (q, C4-CH_3); MS (CI), m/z (relative intensity): 301 ([M + 18]$^+$, 100), 284 ([M + 1])$^+$, 11), 133 (45).

(1′R, 4′R*, 6′R*)3-(2′-Thiabicyclo[2.2.2]octan-8′-one-6′-carbonyl)-4,4-dimethyl-2-oxazolidinone (**10**b)*

IR: 1768, 1727, 1703 cm^{-1}; ^1H NMR δ: 4.17 (1H, ddd, J = 3, 5, 11 Hz, H-6′), 4.03 (1H, d, J = 8.5 Hz, H-5), 4.00 (1H, d, J = 8.5 Hz, H-5), 3.39 (1H, ddd, J = 3, 3, 6.5 Hz, H-1′), 3.07 (1H, dd, J = 3, 11 Hz, H-3′$_{syn}$), 2.93 (1H, ddd, J = 2.5, 3, 11 Hz, H-3′$_{anti}$), 2.80 (2H, m, H-7′), 2.76 (1H, ddd, J = 2.5, 5, 14 Hz, H-5′$_{exo}$), 2.67 (1H, m, H-4′), 1.88 (1H, dddd, J = 2.5, 4, 11, 14 Hz, H-5′$_{endo}$), 1.59 (3H, s, C4-CH_3), 1.58 (3H, s, C4-CH_3); ^{13}C NMR δ: 212.2 (s, C-8′), 172.8 (s, C-6′ C=O), 154.0 (s, C-2), 75.4 (t, C-5), 61.1 (s, C-4), 48.4 (t, C-7′), 44.4 (d, C-6′), 41.5 (d, C-4′), 37.4 (d, C-1′), 27.5 (t, C-3′), 25.0 (q, C4-CH_3), 24.5 (q, C4-CH_3), 22.6 (t, C-5′); MS (CI, NH_3), m/z (relative intensity): 301 ([M + 18]$^+$, 90), 284 ([M + 1]$^+$, 100), 268 (14), 133 (34).

(1S, 4S*, 5R*,6R*)-N-Phenyl-2-thiabicyclo[2.2.2]octan-7-one-5,6-dicarboxylic acid imide (**14**)*

IR: 1711, 1494 cm^{-1}; ^1H NMR δ: 3.81 (1H, dd, J = 3.5, 10 Hz, H-6), 3.60 (1H, d, J = 3.5 Hz, H-1), 3.24 (2H, m, H-5, 4), 3.05 (2H, m, H-3), 2.68 (1H, ddd, J = 2, 2, 20 Hz, H-8$_{exo}$), 2.34 (1H, ddd, J = 1.5, 2, 20 Hz, H-8$_{endo}$); ^{13}C NMR δ: 199.7 (s, C-7), 176.1 (s, imide C=O), 174.1 (s, imide C=O), 129.4 (d × 2, N-C_6H_5), 129.2 (d, N-C_6H_5), 126.2 (d × 2, N-C_6H_5), 45.6 (d, C-6), 41.9 (d, C-5), 41.4 (d, C-1), 39.4 (t, C-8), 31.2 (d, C-4), 28.9 (t, C-3); MS (CI, NH_3), m/z (relative intensity): 305 ([M + 18]$^+$, 100).

(1S, 4S*, 5S*)-2-Thiabicyclo[2.2.2]octan-7-one-5-carboxylic acid, methyl ester (**15**a)*

IR: 1723 cm^{-1}; ^1H NMR δ: 3.72 (3H, s, OCH_3), 3.03 (1H, t, J = 3 Hz, H-1), 2.87 (4H, m, H-3, 4, 5), 2.55 (4H, m, H-8, 6); ^{13}C NMR δ: 204.2 (s, C-7), 174.3 (s, C-5 C=O), 52.3 (q, OCH_3), 40.6 (d, C-5), 39.5 (d, C-1), 39.4 (t, C-8), 32.0 (d, C-4), 30.4 (t, C-3), 28.9 (t, C-6); MS (CI, NH_3), m/z (relative intensity): 218 ([M + 18]$^+$, 85), 201 ([M + 1]$^+$, 100).

(1S, 4S*, 5R*)-2-Thiabicyclo[2.2.2]octan-7-one-5-carboxylic acid, methyl ester (**15**b)*

IR: 1719 cm^{-1}; ^1H NMR δ: 3.76 (3H, s, OCH_3), 2.99 (2H, m), 2.88 (2H, m), 2.75 (3H, m), 2.46 (2H, m); ^{13}C NMR δ: 204.5 (s, C-7), 173.5 (s, C-5 C=O), 52.4 (q, OCH_3), 42.7 (t, C-8), 40.3 (d, C-5), 39.9 (d, C-1), 31.7 (d, C-4), 28.3 (t, C-6), 24.9 (t, C-3); MS (CI, NH_3), m/z (relative intensity): 218 ([M + 18]$^+$, 36), 201 ([M + 1]$^+$, 100).

(1′S, 4′S*, 5′S*)-3-(2′-Thiabicyclo[2.2.2]octan-7′one-5′-carbonyl)-2-oxazolidinone (**16**a)*

IR: 1773, 1720, 1691 cm^{-1}; ^1H NMR δ: 4.45 (2H, t, J = 7 Hz, H-5), 4.04 (3H, m, H-4, 5′$_{exo}$), 3.09 (1H, ddd, J = 2, 3, 10.5 Hz, H-3′$_{syn}$), 3.06 (1H, m, H-1′), 2.88 (1H, dd, J = 3, 10.5 Hz, H-3′$_{anti}$), 2.76 (1H, m, H-4′), 2.70 (1H, ddd, J = 2.5, 6.5, 14 Hz, H-6′$_{endo}$), 2.65 (1H, ddd, J = 2, 3, 19 Hz, H-8′$_{endo}$), 2.53 (1H, m, H-6′$_{exo}$), 2.43 (1H, ddd, J = 1.5, 3, 19 Hz, H-8′$_{exo}$); in C_6D_6, δ: 3.82 (1H, m, H-5′$_{exo}$), 3.16 (2H, m, H-5), 2.92 (3H, m, H-4,1′), 2.77 (1H, ddd, J = 2, 3, 10.5 Hz, H-3′$_{syn}$), 2.56 (1H, ddd, J = 2.5, 6.5, 14 Hz, H-6′$_{endo}$), 2.46 (1H, ddd, J = 2, 3, 19 Hz, H-8′$_{endo}$), 2.39 (1H, dd, J = 3, 10.5 Hz, H-3′$_{anti}$), 2.17 (3H, m, H-8′$_{exo}$, 6′$_{exo}$, 4′); ^{13}C NMR δ: 204.3 (s, C-7′), 173.9 (s, C-5′ C=O), 153.2 (s, C-2), 62.2 (t, C-5), 42.9 (t, C-4), 40.7 (d, C-5′), 38.9 (t, C-8′), 38.2 (d, C-1′), 32.6 (d, C-4′), 30.3 (t, C-3′), 27.9 (t, C-6′); MS (EI), m/z (relative intensity): 255 ([M]$^+$, 100), 211 (26), 182 (44), 168 (98).

(1′S, 4′S*, 5′S*)-4,4-Dimethyl-3-(2′-thiabicyclo[2.2.2]octan-7′one-5′-carbonyl)-2-oxazolidinone (**17**a)*

Characterized as a 10:1 (^1H NMR) mixture of **17***a* and **17***b* IR: 1770, 1721, 1697 cm^{-1}; ^1H NMR δ: 4.03 (2H, s, H-5), 4.03 (1H, m, H-5′), 3.06 (1H, ddd, J = 1.5, 3, 10.5 Hz, H-3′$_{syn}$), 3.04 (1H, m, H-1′), 2.87 (1H, dd, J = 3, 10.5 Hz, H-3′$_{anti}$), 2.73 (1H, m, H-4′), 2.66 (1H, ddd, J = 3, 6.5, 14 Hz, H-6′$_{endo}$), 2.56 (1H, ddd, J = 1.5, 3, 19 Hz, H-8′$_{endo}$), 2.47 (1H, m, H-6′$_{exo}$), 2.43 (1H, ddd, J = 1, 3, 19 Hz, H-8′$_{exo}$), 1.56 (3H, s, CH_3), 1.54 (3H, s, CH_3); ^{13}C NMR δ: 204.3 (s, C-7′), 174.8 (s, C-5′ C=O), 153.7 (s, C-2), 75.2 (t, C-5), 60.8 (s, C-4), 40.9 (d, C-5′), 39.5 (d, C-1′), 38.8 (t, C-8′), 32.5 (d, C-4′), 30.4 (t, C-3′), 28.1 (t, C-6′), 24.9 (q, CH_3), 24.8 (q, CH_3); MS (EI), m/z (relative intensity): 283 ([M]$^+$, 100), 210 (88), 168 (95).

(1′S, 4′S*, 5′R*)-4,4-Dimethyl-3-(2′-thiabicyclo[2.2.2]octan-7′one-5′-carbonyl)-2-oxazolidinone (**17**b)*

A 1.5:1 mixture of **17***a* and **17***b* was fractionated by PTLC (ether, multiple elution) to give a sample that was a 0.2:1 mixture (^1H NMR) of **17***a* and **17***b*. IR: 1770, 1721, 1698 cm^{-1}; ^1H NMR (C_6D_6) δ: 3.73 (1H, m, H-5′; coupled to H-3′$_{anti}$, J = 1.5 Hz), 3.11 (2H, s, H-5), 2.79 (3H, m, H-1′, 3′$_{syn}$, 6′$_{exo}$), 2.42 (1H, dd, J = 3.5, 19 Hz, H-8′$_{exo}$), 2.31 (2H, m, H-4′, 8′$_{endo}$), 2.19 (1H, ddd, J = 1.5, 3.5, 11 Hz, H-3′$_{anti}$), 1.97 (1H, ddd, J = 4, 10.5, 15 Hz, H-6′$_{endo}$), 1.14 (3H, s, CH_3), 1.10 (3H, s, CH_3); ^{13}C NMR δ: 204.5 (s, C-7′), 173.9 (s, C-5′ C=O), 153.7 (s, C-2), 75.2 (t, C-5), 61.0 (s, C-4), 42.8 (d, C-8′), 40.5 (d, C-5′), 40.3 (d, C-1′), 31.9 (d, C-4′), 27.6 (t, C-6′), 24.8 (q, CH_3), 24.7 (q, CH_3), 24.2 (t, C-3′); MS (EI), m/z (relative intensity): 301 ([M + 18]$^+$, 100), 284 ([M + 1]$^+$, 88).

Acknowledgement

Financial support from the Natural Sciences and Engineering Research Council of Canada and the University of Saskatchewan is gratefully acknowledged.

1. (*a*) J. G. Martin and R. K. Hill. Chem. Rev. **61**, 537 (1961); (*b*) J. Sauer. Angew. Chem. Int. Ed. Engl. **6**, 17 (1967).
2. B. M. Trost and I. Flemming (*Editors*). Comprehensive organic synthesis. Vol. 5. Pergamon Press, Oxford. 1991. Chap. 4.
3. (*a*) D. E. Ward, Y. Gai, and W. M. Zoghaib. Can. J. Chem. **69**, 1487 (1991); (*b*) D. E. Ward, W. M. Zoghaib, C. K. Rhee, and Y. Gai. Tetrahedron Lett. **31**, 845 (1990).
4. (*a*) L. A. Paquette. *In* Asymmetric synthesis. Vol. 3. *Edited by* J. D. Morrison. Academic Press, New York. 1984. Chap. 7; (*b*) M. J. Tashner. *In* Organic synthesis—theory and applications. Vol. 1. *Edited by* T. Hudlicky. JAI Press, Greenwich, Conn. 1989. pp. 1–102; (*c*) V. D. Kiselev and A. I. Konovalov. Russ Chem. Rev. **58**, 230 (1989).

Can. J. Chem. Downloaded from www.nrcresearchpress.com by 109.225.110.28 on 09/08/12
For personal use only.

Can. J. Chem. Downloaded from www.nrcresearchpress.com by 109.225.110.28 on 09/08/12
For personal use only.

5. D. E. Ward and Y. Gai. Tetrahedron Lett. **33**, 1851 (1992).
6. G. Helmchen, R. Karge, and J. Weetman. *In* Modern synthetic methods. Vol. 4. *Edited by* R. Scheffold. Springer Verlag, Berlin. 1986. p. 261.
7. D. A. Evans, K. T. Chapman, and J. Bisaha. J. Am. Chem. Soc. **110**, 1238 (1988).
8. (*a*) E. J. Corey and Y. Matsumura. Tetrahedron Lett. **32**, 6289 (1991); (*b*) E. J. Corey, R. Imwinkelreid, S. Pikul, and Y. B. Xiang. J. Am. Chem. Soc. **100**, 5493 (1989); (*c*) K. Narasaka, N. Iwasawa, M. Inoue, T. Yamada, M. Nakashima, and J. Sugimori. J. Am. Chem. Soc. **111**, 5340 (1989); (*d*) C. Chapuis and J. Jurczak. Helv. Chim. Acta, **70**, 436 (1987).
9. (*a*) M. J. Martenelli. J. Org. Chem. **55**, 5065 (1990); (*b*) H. Matsunaga, K. Kimura, and T. Ishizuka. Tetrahedron Lett. **32**, 7715 (1991).
10. K. Rück and H. Kunz. Angew. Chem. Int. Ed. Engl. **30**, 694 (1991).
11. (*a*) T. Mukaiyama. Angew. Chem. Int. Ed. Engl. **16**, 817 (1977); (*b*) M. T. Reetz. *In* Organotitianium reagents in organic synthesis. Springer Verlag, Berlin. 1986.
12. (*a*) C. Koulklovsky, A. Pouilhés, and Y. Langois. J. Am. Chem. Soc. **112**, 6672 (1990); (*b*) T. Calogeropoulou and D. F. Weimer. J. Org. Chem. **53**, 2295 (1988); (*c*) H.-J. Liu and T. K. Ngooi. Can. J. Chem. **62**, 2676 (1984).
13. (*a*) C. M. Cimarusti and J. Wolinsky. J. Am. Chem. Soc. **90**, 113 (1968); (*b*) H. Nozaki, T. Yamuguti, S. Ueda, and K. Kondo. Tetrahedron, **24**, 1445 (1968); (*c*) A. J. Birch, P. L. Macdonald, and V. H. Powell. Tetrahedron Lett. 351 (1969); (*d*) I Alfaro, W. Ashton, L. D. McManus, R. C. Newstead, K. L. Rabone, N. A. J. Rodgers, and W. Kernick. Tetrahedron, **26**, 201 (1970); (*e*) T. W. Scott, W. Vetter, W. E. Oberhänsli, and A. Fürst. Tetrahedron Lett. 1719 (1972); (*f*) D. A. Evans, W. L. Scott, and L. K. Truesdale. Tetrahedron Lett. 121 (1972); (*g*) A. J. Birch and K. P. Dastur. Tetrahedron Lett. 4195 (1972); (*h*) J. Chem. Soc. Perkin Trans. 1, 1650 (1973); (*i*) G. M. Rubottom and D. S. Kruger. Tetrahedron Lett. 611 (1977); (*j*) M. E. Jung and C. A. McCombs. J. Am. Chem. Soc. **100**, 5207 (1978); (*k*) S. A. Monti, S.-C. Chen, Y.-L. Yang, S.-S. Yuan, and O. P. Bourgeois. J. Org. Chem. **43**, 4062 (1978); (*l*) M. E. Jung and Y.-G. Pan. Tetrahedron Lett. **21**, 3127 (1980); (*m*) W. C. Still and M.-Y. Tsai. J. Am. Chem. Soc. **102**, 3654 (1980).
14. (*a*) P. N. Devine and T. Oh. J. Org. Chem. **56**, 1966 (1991); (*b*) W. G. Early, E. J. Jacobsen, G. P. Meier, T. Oh, and L. E. Overman. Tetrahedron Lett. **29** 3781 (1988); (*c*) M. Asaoka, K. Ishibashi, W. Takahashi, and H. Takei. Bull. Chem. Soc. Jpn. **60**, 2259 (1987); (*d*) H. Hagiwara, A. Okano, and H. Uda. J. Chem. Soc. Chem. Commun. 1047 (1985); (*e*) M. Ihara, Y. Ishida, M. Abe, M. Toyota, K. Fukumota, and T. Kametani. J. Chem. Soc, Perkin Trans. 1, 1155 (1988).
15. (*a*) B. C. Ulf. *In* Comprehensive heterocyclic chemistry. Vol. 2. *Edited by* A. R. Katritzky and C. W. Rees. Pergamon, Oxford. 1984. Chap. 2.06; (*b*) G. R. Krow, Y. B. Lee, R. Raghavachari, and S. W. Szczepanski. Tetrahedron, **47**, 8499 (1991), and cited references.
16. G. H. Posner, T. D. Nelson, C. M. Kinter, and K. Afarinka. Tetrahedron Lett. **32**, 5295 (1991), and cited references.
17. K. Maruoka, K. Nonoshita, and H. Yamamoto. Synth. Commun. **18**, 1453 (1988).
18. (*a*) H. Lamy-Schelkens and L. Ghosez. Tetrahedron Lett. **30**, 5891 (1989); (*b*) H. Lamy-Schelkens, D. Giomi, and L. Ghosez. Tetrahedron Lett. **30**, 5887 (1989); (*c*) M. Rivera, H. Lamy-Schelkens, F. Sainte, K. Mbiya, and L. Ghosez. Tetrahedron Lett. **29**, 4573 (1988).
19. T. Ibuka, Y. Mori, T. Aoyama, and Y. Inubushi. Chem. Pharm. Bull. **26**, 456 (1978).
20. E. C. Angell, F. Fringuelli, L. Minuti, F. Pizzo, B. Porter, A. Taticchi, and E. Wenkert. J. Org. Chem. **51**, 2649 (1986).
21. (*a*) R. J. Loncharich, T. R. Schwartz, and K. N. Houk. J. Am. Chem. Soc. **109**, 14 (1987); (*b*) O. F. Guner, R. M. Ottenbrite, D. Shillady, and P. V. Alston. J. Org. Chem. **52**, 391 (1987), and cited references.
22. A. H. Ingall. *In* Comprehensive heterocyclic chemistry. Vol. 3. *Edited by* A. R. Katrinsky and C. W. Rees. Pergamon Press, Oxford. 1984. Chapter 2.25.
23. R. H. Flemming and B. H. Murray. J. Org. Chem. **44**, 2280 (1979).
24. T. Sato, Y. Wakahara, J. Otera, and H. Nozaki. Tetrahedron, **47**, 9773 (1991), and cited references.
25. (*a*) T. Mukaiyama, Y. Sagawa, and S. Kobayashi. Chem. Lett. 1821 (1986); (*b*) M. Ihara, M. Katogi, K. Fukumoto, and T. Kametani. J. Chem. Soc. Chem. Commun. 721 (1987); (*c*) H. Hagiwara, A. Okano, T. Akama, and H. Uda. J. Chem. Soc. Chem. Commun. 1333 (1987); (*d*) M. Ihara, T. Takahashi, N. Shimizu, Y. Ishida, I. Sudow, K. Fukumoto, and T. Kametani. J. Chem. Soc. Chem. Commun. 1467 (1987); (*e*) M. Ihara, K. Kirihara, A. Kawaguchi, M. Tsuruta, F. Keichiro, and T. Kametani. J. Chem. Soc. Perkin Trans. 1, 1719 (1987); (*f*) F. Richter and H.-H. Otto. Tetrahedron Lett. **28**, 2945 (1987); (*g*) S. Kobayashi, Y. Sagawa, H. Akamatsu, and T. Mukaiyama. Chem. Lett. 1777 (1988).
26. D. A. Oare and C. H. Heathcock. Top. Stereochem. **19**, 227 (1989).
27. J. A. Hirsch. Top. Stereochem. **1**, 199 (1967).
28. (*a*) R. K. Boeckman, Jr., S. G. Nelson, and M. D. Gaul. J. Am. Chem. Soc. **114**, 2258 (1992); (*b*) W. Oppolzer, G. Poli, C. Starkemann, and G. Bernardinelli. Tetrahedron Lett. **29** 3559 (1988); (*c*) G. Montaudo, V. Librando, S. Caccamese, and P. Maravigna. J. Am. Chem. Soc. **95**, 6365 (1973).
29. (*a*) M. Boleslawski, L. Siergiejczyk, and L. Synoradzki Przem. Chem. **65**, 141 (1986); Chem. Abstr. **106**, 18656k (1986); (*b*) V. D. Petrova, N. N. Rzhevskaya, N. V. Shcherbakova, Y. A. Sangalov, and K. S. Minsker. Izv. Akad. Nauk SSSR, Ser. Khim. 1373 (1978); Chem. Abstr. **89**, 109659k (1978); (*c*) B. B. Snider, M. K. Rodini, T. C. Kirk, E. A. Deutsch, R. Cordova, and R. T. Price. Tetrahedron, **37**, 3927 (1981); (*d*) M. P. Boleslawski. *In* Organometallic synthesis. Vol. 3. *Edited by* R. B. King and J. J. Eisch. Elsevier, Amsterdam. 1986. p. 472.
30. A. H. Homeyer. Chem. Abstr. **40**, P 4084^6 (1946).

The acidities of 4-arylsulfonylmethylpyridines and *N*-methyl and *N*-benzyl 4-arylsulfonylmethylpyridinium cations in aqueous solution

STEFAN WODZINSKI AND JOHN W. BUNTING[1]

Department of Chemistry, University of Toronto, Toronto, Ont., Canada M5S 1A1

Received March 23, 1992

STEFAN WODZINSKI and JOHN W. BUNTING. Can. J. Chem. **70**, 2635 (1992).

The pK_a values for the deprotonation of a series of 4-(X-phenylsulfonylmethyl)pyridines (**6**) (pK_a = 19.89 (X = H); ρ = 3.0) were determined in aqueous dimethyl sulfoxide solutions at 25°C using the H_0^q acidity function. The pK_a values were also measured for the corresponding series of *N*-methyl 4-(X-phenylsulfonylmethyl)pyridinium cations (**2**) (pK_a = 11.27 (X = H); ρ = 1.45) and also for a series of *N*-(X-benzyl) 4-phenylsulfonylmethylpyridinium cations (**7**) (pK_a = 10.70 (X = H); ρ = 0.65) in aqueous solution (ionic strength 0.1 at 25°C). Comparison of the substituent effects upon the pK_a values of the sulfonyl-activated carbon acids **2**, **6**, and **7** with the substituent effects upon the pK_a values of the corresponding three series of ketones gives insight into the electron-density distribution in the carbanionic conjugate bases of sulfone and ketone carbon acids. Extrapolation of a linear free energy relationship between the pK_a values of neutral sulfones and ketones allows the estimation of pK_a = 28.7 for the deprotonation of methyl phenyl sulfone in aqueous solution.

STEFAN WODZINSKI et JOHN W. BUNTING. Can. J. Chem. **70**, 2635 (1992).

Opérant à 25°C, dans des solutions de diméthylsulfoxyde aqueuses et faisant appel à la fonction d'acidité H_0^q, on a déterminé les valeurs de pK_a pour la déprotonation d'une série de 4-(X-phénylsulfonylméthyl)pyridines (**6**) (pK_a = 19,89 (X = H); ρ = 3,0). On a aussi mesuré les valeurs des pK_a pour la série correspondante des cations *N*-méthyl 4-(X-phénylsulfonylméthyl)pyridinium (**2**) (pK_a = 11,27 (X = H); ρ = 1,45) ainsi que pour une série de cations *N*-(X-benzyl) 4-(X-phénylsulfonylméthyl)pyridinium (**7**) (pK_a = 10,70 (X = H); ρ = 0,65) en solution aqueuse (force ionique de 0,1 à 25°C). Une comparaison des effets de substituants sur les valeurs de pK_a des acides carbonés **2**, **6** et **7**, activés par le sulfonyle, avec les effets de substituants sur les valeurs des pK_a des trois séries de cétones correspondantes éclaire notre compréhension de la distribution de la densité électronique dans les bases carbanioniques conjuguées des acides carbonés de sulfones et de cétones. Une extrapolation de la relation d'énergie libre linéaire entre les valeurs de pK_a des sulfones et des cétones neutres permet d'évaluer à 28,7 la valeur du pK_a pour la déprotonation de la méthyl phényl sulfone, en solution aqueuse.

[Traduit par la rédaction]

There have been relatively few quantitative measurements of the thermodynamic acidities of sulfonyl-activated carbon acids in aqueous solution. The acidities of bis(methylsulfonyl)methane ($(CH_3SO_2)_2CH_2$, pK_a = 12.5 (1–3)) and bis(phenylsulfonyl)methane ($(C_6H_5SO_2)_2CH_2$, pK_a = 11.21 (1)) have been measured in water, and related cyclic 1,3-disulfones have been found, depending upon ring size, to be up to 1.5 pK_a units more acidic (eight-membered ring) or less acidic (five-membered ring) than these acyclic sulfones (1). α-Methylation of disulfones leads to a significant decrease in acidity ($(C_2H_5SO_2)_2CHR$, pK_a = 12.20 for R = H, pK_a = 14.56 for R = CH_3 (3*a*); $(C_6H_5SO_2)_2CHR$, pK_a = 11.21 for R = H, pK_a = 13.76 for R = CH_3 (3*b*)); α-phenylation results in only a slight increase in acidity ($(C_2H_5SO_2)_2CHC_6H_5$, pK_a = 12.12 (3*a*)); α-bromination leads to a significant increase in acidity ($(C_2H_5SO_2)_2CHBr$, pK_a = 10.71 (3*a*)).

All of the above disulfones are significantly less acidic than the corresponding diketones (e.g., $(CH_3CO)_2CH_2$, pK_a = 8.87 (4); $(CH_3CO)_2CHCH_3$, pK_a = 10.9 (5); $(CH_3CO)_2CHBr$, pK_a ≈ 7.0 (6)). Greater thermodynamic acidity for a ketone than for the corresponding sulfone is also found for the picolinium cations **1** (pK_a = 7.66 for X = H (7)) and **2** (pK_a = 11.34 for X = H (8)), and for β-keto sulfones (e.g., $CH_3SO_2CH_2COCH_3$, pK_a = 9.90 (6, 9)) relative to disulfones (see above). Ketones are also known to be more acidic than the corresponding sulfones in dimethyl sulfoxide solution (10).

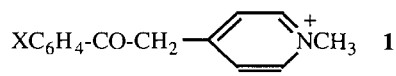

1

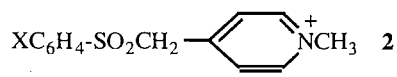

2

Apart from the examples quoted above, the only other sulfone-activated carbon acids for which we have been able to locate pK_a values in aqueous solution are six examples of cyclic β-keto sulfones (both exocyclic and endocyclic sulfones) (9), the α- and β-picolinium isomers of **2** (8), 3-phenyl-2*H*-thiopyran 1,1-dioxide (pK_a = 10.79 (11)) and its 6-methyl derivative (pK_a = 12.36 (11)), a variety of ring-substituted phenyl esters of methylsulfonylmethanesulfonic acid (e.g., $CH_3SO_2CH_2SO_3C_6H_5$, pK_a = 9.99 (12)), 3-methylsulfonyl-2,4-pentanedione ($(CH_3CO)_2CHSO_2CH_3$, pK_a ≈ 4.7 (6)), tris(methylsulfonyl)methane ($(CH_3SO_2)_3CH$, pK_a ≈ 0 (6, 13)), and a bicyclic trisulfone containing an acidic bridgehead hydrogen atom (pK_a = 3.30 (13)). In addition, data are available for several acyclic β-keto sulfones in 50% ethanol – 50% water (9), six ethoxycarbonyl-activated sulfones and disulfones in 60% acetonitrile – 40% water (14, 15), and also for a variety of ring-substituted phenacyl phenyl sulfones (**3**) in 95% ethanol – 5% water (16).

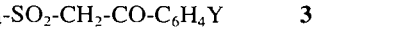

3

Substituent effects upon the acidities of 4-phenacylpyridines (**4**) and 4-phenacylpyridinium cations (**1** and **5**) have been shown (7) to be useful probes of the delocalization of

[1]Author to whom correspondence may be addressed.

Can. J. Chem. Downloaded from www.nrcresearchpress.com by 109.225.110.28 on 09/08/12
For personal use only.

Can. J. Chem. Downloaded from www.nrcresearchpress.com by 109.225.110.28 on 09/08/12
For personal use only.

electron density in the carbanionic conjugate bases of these species. We felt that similar insight into the electronic structure of the conjugate bases of the corresponding sulfonyl-activated carbon acids (**2**, **6**, and **7**) would also be of interest in view of the wide use of sulfonyl-stabilized carbanions as reagents in synthetic organic chemistry. Furthermore, in conjunction with our previous study of substituent effects upon the acidities of the ketones **1**, **4**, and **5** (7), such data would allow a detailed comparison of substituent effects upon the acidities of these two closely related series of carbonyl- and sulfonyl-activated carbon acids in aqueous solution. In particular, we felt that such a comparison might provide quantitative insight into the saturation of resonance effects that is commonly observed upon the acidities of carbon acids when successive activating substituents are introduced.

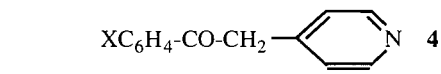

4

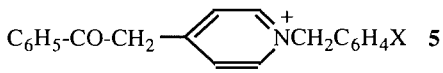

5

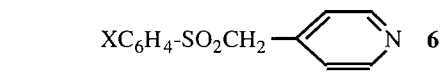

6

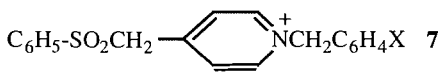

7

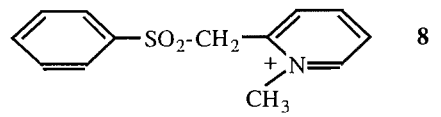

8

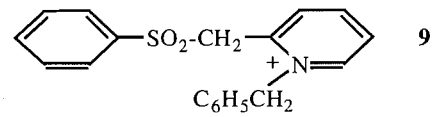

9

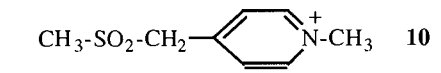

10

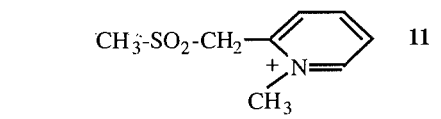

11

The current paper reports the synthesis and acidities of a wide range of ring-substituted 4-arylsulfonylmethylpyridines (**6**) and their *N*-methyl cations (**2**) and also *N*-(substituted benzyl) 4-phenylsulfonylmethylpyridinium cations (**7**). In addition, the pK_a values were measured for several other sulfonylmethylpyridinium cations (**8**–**11**) in aqueous solution. These data allow the estimation of the pK_a value of methyl phenyl sulfone in aqueous solution. To the best of our knowledge, this is the first estimate of the aqueous acidity of a simple sulfone, unactivated by other acidifying functional groups, on the basis of a linear free energy relationship that does not resort to assumptions (17) regarding the rates of the deprotonation reaction.

Experimental

*4-arylsulfonylmethylpyridines (**6**)*

All 4-arylsulfonylmethylpyridines (**6**), with the exception of the 4-bromo-3-nitrophenyl derivative (**6***j*) which is described below, were prepared from 4-picolyl chloride and the sodium salt of the appropriate arylsulfinic acid by a method based upon that described by Golding *et al.* (8). This method is outlined below for 4-phenylsulfonylmethylpyridine. In some cases the appropriate sodium arylsulfinate was commercially available; in other cases these salts were prepared from the appropriate arylsulfonyl chloride as described below for sodium 4-bromobenzenesulfinate.

Sodium 4-bromobenzenesulfinate

4-Bromobenzenesulfonyl chloride (10.0 g) was added to a solution of sodium sulfite (7.4 g) in water. The mixture was stirred at 70°C, with periodic addition of aqueous NaOH to maintain an alkaline solution. After complete dissolution of the sulfonyl chloride, the solution was heated at 100°C for 5 min, and then strongly acidified with concentrated hydrochloric acid. Upon cooling this solution in an ice bath, white crystalline 4-bromobenzenesulfinic acid was obtained. This product (5.4 g) was collected, washed with dilute hydrochloric acid, press-dried with filter paper, and immediately dissolved in aqueous NaOH (1 equivalent). All water was removed on the rotatory evaporator, whereupon sodium 4-bromobenzenesulfinate was obtained as a white powder.

Sodium salts of the following substituted benzenesulfinic acids were also prepared by this same general route: 4-methoxy; 4-nitro; 3-nitro; 3-chloro; 3,4-dichloro; 3,5-dichloro. The 4-nitrobenzenesulfinic acid did not precipitate from the acidified solution, and was extracted into diethyl ether, which was subsequently dried over magnesium sulfate and removed on the rotatory evaporator.

*4-Phenylsulfonylmethylpyridine (**6**a)*

4-Picolyl chloride hydrochloride (8.0 g), sodium benzenesulfinate (8.2 g), and sodium acetate trihydrate (13.3 g) were refluxed in 1-butanol (35 mL) for 6 h. The reaction mixture was poured into water (800 mL). The product (6.8 g), which precipitated as brown crystals was collected and recrystallized twice from ethanol to give white crystals; mp 202–203°C (lit (8) mp 203–204°C).

The other sulfones (**6***b*–**6***i*) were also prepared via this same general method in yields of 30–60%. The melting points and ^1H NMR spectra of all **6** are listed in Table 1. All **6** were also characterized by elemental analyses (C, H, N) (Huffman Laboratories, Golden, Colorado), which in all cases were within experimental error of the theoretical predictions.

*4-Bromo-3-nitrophenylsulfonylmethylpyridine (**6**j)*

Direct reduction of 4-chloro-3-nitrobenzenesulfonyl chloride to the sulfinic acid by the above method was unsuccessful. However, the 4-bromo-3-nitrophenylsulfonylmethylpyridine was readily prepared, based upon a method given by Nunn and Schofield (18), via direct nitration of the previously prepared 4-bromophenylsulfonylmethylpyridine (**6***d*).

4-Bromophenylsulfonylmethylpyridine (0.83 g) was shaken for 15 min with a solution containing 70% nitric acid (0.3 mL) in water (10 mL) that had been saturated with sodium nitrate. The reaction mixture was then kept at 0°C for 3 h. The white crystalline N-nitrate was collected by vacuum filtration, and then slowly added to ice-cooled concentrated sulfuric acid (20 mL). This mixture was heated to 50°C for 5 min, and then poured onto ice. Upon careful basification with aqueous ammonia, a yellow precipitate was obtained. The product (**6***j*; 0.64 g) was recrystallized from aqueous ethanol, and characterized as usual (Table 1).

*N-Methyl 4-arylsulfonylmethylpyridinium bromides (**2** · Br^-)*

The appropriate sulfone (**6**) was stirred with excess methyl bromide in acetone solution in a pressure bottle for 24 h. The precipitated products were collected and recrystallized from ethanol in 70–

TABLE 1. Characterization of 4-(X-phenylsulfonylmethyl)pyridines (**6**)

Sulfone	X	Melting point, °C	^{1}H NMR,[a] δ
6*a*	H	202–203[b]	4.31 (2H, s), 7.05 (2H, d), 7.44–7.70 (5H, m), 8.52–8.55 (2H, d)
6*b*	4-OCH_3	141–143	3.87 (3H, s), 4.27 (2H, s), 6.89–6.98 (2H, m), 7.03–7.07 (2H, m), 7.52–7.61 (2H, m), 8.53–8.56 (2H, m)
6*c*	4-CH_3	188–190	2.43 (3H, s), 4.29 (2H, s), 7.03–7.07 (2H, m), 7.26–7.30 (2H, m), 7.52–7.57 (2H, m), 8.52–8.55 (2H, m)
6*d*	4-Br	165–167	4.30 (2H, s), 7.05–7.08 (2H, m), 7.48–7.54 (2H, m), 7.61–7.66 (2H, m), 8.55–8.58 (2H, m)
6*e*	3-Cl	171–173	4.31 (2H, s), 7.07–7.10 (2H, m), 7.43–7.72 (4H, m), 8.57–8.58 (2H, m)
6*f*	3,4-Cl_2	166–168	4.31 (2H, s), 7.08–7.11 (2H, m), 7.41–7.46 (1H, m), 7.55–7.59 (1H, d), 7.79–7.80 (1H, d), 8.59–8.62 (2H, m)
6*g*	3,5-Cl_2	190–192	4.31 (2H, s), 7.10–7.13 (2H, m), 7.55–7.56 (2H, d), 7.62–7.64 (1H, t), 8.60–8.63 (2H, m)
6*h*	4-NO_2	211–212	4.37 (2H, d), 7.07–7.10 (2H, m), 7.86–7.90 (2H, m), 8.32–8.37 (2H, m), 8.58–8.61 (2H, m)
6*i*	3-NO_2	181–183	4.38 (2H, s), 7.09–7.12 (2H, m), 7.66–7.75 (1H, t), 7.90–7.91 (1H, m), 8.46–8.62 (4H, m)
6*j*	3-NO_2, 4-Br	169–171 (dec.)	4.36 (2H, s), 7.11–7.14 (2H, m), 7.57–7.63 (1H, q), 7.86–7.90 (1H, d), 8.15–8.16 (1H, d), 8.61–8.64 (2H, m)

[a]In $CDCl_3$; all chemical shifts are relative to tetramethylsilane.
[b]Literature (8) mp 203–204°C, (19) 199–200.5°C.

90% yields. The melting points and ^{1}H NMR spectra of all **2**.Br^- are collected in Table 2.

N-*(Substituted benzyl) 4-phenylsulfonylmethylpyridinium bromides (7 · Br^-)*

4-Phenylsulfonylmethylpyridine (1.0 g) was refluxed with the appropriate substituted benzyl bromide (1.1 equivalents) in acetone for 24 h. The products that precipitated were collected and recrystallized from ethanol in 65–85% yields. The melting points and ^{1}H NMR spectra of all **7** · Br^- are collected in Table 3.

Other sulfones

2-Phenylsulfonylmethylpyridine (mp 111–112°C (lit. (8) mp 111.5–112.5°C)) was prepared by a similar route to that described above for its 4-pyridyl isomer. This species was methylated and benzylated by the above general routes to give the bromide salts of **8** and **9**, respectively. 4-Methylsulfonylmethylpyridine (mp 137–138°C (lit. (19) mp 133.5–134.5°C)) and its 2-pyridyl isomer (mp 122–124°C (lit. (20) mp 121–122°C)) were prepared by the above route from the appropriate picolyl chloride and sodium methanesulfinate. The bromide salts of **10** and **11** were then prepared by methylation by the above procedure. The characterization of the bromide salts of **8**–**11** is reported in Table 4.

pK_a values

The pK_a values of all *N*-methyl and *N*-benzyl sulfonylmethylpyridinium cations (**2**, **7**–**11**) were measured spectrophotometrically in aqueous solution at ionic strength 0.1 and 25°C by the general method of Albert and Serjeant (21). Buffer solutions contained KOH + KCl for pH > 10.7 and Na_2CO_3 + $NaHCO_3$ for pH 9.4–10.7. pK_a values were evaluated from the pH-dependence of the absorbance of temperature-equilibrated solutions prepared by mixing equal volumes of a stock aqueous solution of the cationic sulfone (usually 0.06 mM) with double strength buffer solutions. Absorbances at λ_{max} in the spectrum of the conjugate base species were used for the evaluation of pK_a values.

As discussed below, the neutral sulfones (**6**) are quite weak acids and required the use of the acidity function (H_0^q) developed by Cox *et al.* (22) for mixtures of dimethyl sulfoxide and water containing a constant concentration of tetramethylammonium hydroxide (0.047 M). A stock solution of tetramethylammonium hydroxide (0.77 M) in water was prepared from a freshly opened bottle of the solid pentahydrate (99% purity as supplied by Aldrich Chemical Co., Milwaukee, Wisconsin). The exact hydroxide ion concentration of this stock solution was determined by titration with standard hydrochloric acid (0.1 M). Solutions of known H_0^q were prepared according to the compositions given in the table in ref. 22 using analytical grade dimethyl sulfoxide (BDH Chemicals, Toronto, Ontario), and were temperature-equilibrated for at least 10 min before the addition of a small aliquot (0.1 mL) of a stock solution of the sulfone (**6**) (3.0 mM). Absorbances of these basic solutions were then monitored for 5 min at λ_{max} of the conjugate base species, and extrapolated to the mixing time (t = 0) to correct for a slow decomposition of the carbanionic conjugate base species. The pK_a values of **6** were then calculated by fitting the initial absorbance (A) at H_0^q to eq. [1] by an iterative procedure based upon the Marquardt algorithm. The pK_a value, the absorbance (A_C) of the conjugate base, and the absorbance of the conjugate acid (A_{CH}) are treated as parameters to be evaluated in this iterative method. In all cases A_{CH} = 0 within experimental error, which is consistent with the observed transparency of the sulfone at wavelengths in the vicinity of the absorbance maximum in the spectrum of its conjugate base (e.g., Fig. 1).

$$[1] \quad H_0^q = pK_a + \log((A - A_{CH})/(A_C - A))$$

Results

4-Arylsulfonylmethylpyridines (6)

The electronic absorption spectra of the 4-arylsulfonylmethylpyridines (**6**) do not change between pH 7 and 14 in aqueous solution. To investigate the acidities of these weak carbon acids, we resorted to the acidity function (H_0^q) defined by Cox *et al.* (22) for aqueous solutions of 0.047 M tetramethylammonium hydroxide containing varying concentrations of dimethyl sulfoxide. The electronic absorption

Can. J. Chem. Downloaded from www.nrcresearchpress.com by 109.225.110.28 on 09/08/12
For personal use only.

TABLE 2. Characterization of the bromide salts of *N*-(methyl) 4-(X-phenylsulfonylmethyl) pyridinium cations (**2** · Br^-)

Bromide salt	X	Melting point, °C	^{1}H NMR,[a] δ
2*a*	H	255–256 (dec.)	4.38 (3H, s), 7.62–7.87 (7H, m), 8.72–8.76 (2H, m)
2*b*	4-OCH_3	248–250 (dec.)	3.92 (3H, s), 4.40 (3H, s), 4.99 (2H, m), 7.08–7.16 (2H, m), 7.62–7.70 (2H, m), 7.83–7.87 (2H, d), 8.74–8.78 (2H, d)
2*c*	4-CH_3	228–231 (dec.)	2.45 (3H, s), 4.37 (3H, s), 7.44–7.48 (2H, m), 7.61–7.66 (2H, m), 7.82–7.85 (2H, d), 8.71–8.75 (2H, d)
2*d*	4-Br	249–253 (dec.)	4.40 (3H, s), 7.64–7.68 (2H, m), 7.82–7.86 (2H, m), 7.87–7.90 (2H, d), 8.75–8.79 (2H, d)
2*e*	3-Cl	259 (dec.)	4.39 (3H, s), 7.57–7.73 (2H, m), 7.82–7.85 (1H, m), 7.88–7.91 (2H, d), 8.76–8.79 (2H, d)
2*f*	3,4-Cl_2	249 (dec.)	4.45 (3H, s), 7.68–7.73 (1H, m), 7.77–7.81 (1H, d), 7.98–8.01 (2H, d), 8.02 (1H, d), 8.84–8.87 (2H, d)
2*g*	3,5-Cl_2	250 (dec.)	4.39 (3H, s), 7.80–7.81 (2H, d), 7.91–7.94 (3H, m), 8.78–8.81 (2H, d)
2*h*	4-NO_2	239 (dec.)	4.39 (3H, s), 7.92–7.95 (2H, d), 8.05–8.09 (2H, m), 8.45–8.50 (2H, m), 8.77–8.80 (2H, d)
2*i*	3-NO_2	257 (dec.)	4.39 (3H, s), 7.87–7.96 (3H, m), 8.17–8.22 (1H, m), 8.62–8.68 (2H, m), 8.77–8.81 (2H, d)
2*j*	3-NO_2, 4-Br	244 (dec.)	4.41 (3H, s), 7.92–7.96 (3H, m), 8.14–8.18 (1H, d), 8.35–8.36 (1H, d), 8.79–8.82 (2H, d)

[a]In D_2O; all chemical shifts relative to sodium 2,2-dimethyl-2-silapentane-5-sulfonate; the methylene hydrogens are not seen due to deuterium exchange.

TABLE 3. Characterization of the bromide salts of *N*-(X-benzyl) 4-(phenylsulfonylmethyl) pyridinium cations (**7** · Br^-)

Bromide salt	X	Melting point, °C	^{1}H NMR,[a] δ
7*a*	H	178–179	5.84 (2H, s), 7.46–7.86 (10H, m), 7.86–7.92 (2H, d), 8.88–8.92 (2H, d)
7*b*	3-CH_3	196–197	2.36 (3H, s), 5.74 (2H, s), 7.22–7.82 (9H, m), 7.82–7.86 (2H, d), 8.82–8.85 (2H, d)
7*c*	4-CH_3	228–229 (dec.)	2.38 (3H, s), 5.75 (2H, s), 7.35 (4H, s), 7.55–7.77 (5H, m), 7.82–7.86 (2H, d), 8.82–8.86 (2H, d)
7*d*	4-Br	212–213 (dec.)	5.77 (2H, s), 7.32–7.82 (9H, m), 7.85–7.88 (2H, d), 8.83–8.86 (2H, d)
7*e*	3-F	225 (dec.)	5.81 (2H, s), 7.16–7.82 (9H, m), 7.86–7.89 (2H, d), 8.84–8.88 (2H, d)
7*f*	4-CN	242 (dec.)	5.91 (2H, s), 7.53–7.63 (4H, m), 7.72–7.87 (4H, m), 7.89–7.94 (3H, m), 8.87–8.91 (2H, d)
7*g*	3-NO_2	237 (dec.)	5.95 (2H, s), 7.54–7.63 (2H, m), 7.71–7.86 (5H, m), 7.89–7.93 (2H, m), 8.31–8.39 (2H, m), 8.89–8.93 (2H, d)
7*h*	4-NO_2	222 (dec.)	5.96 (2H, s), 7.55–7.63 (4H, m), 7.72–7.82 (3H, m), 7.90–7.94 (2H, d), 8.31–8.35 (2H, d), 8.89–8.92 (2H, d)

[a]In D_2O; all chemical shifts relative to sodium 2,2-dimethyl-2-silapentane-5-sulfonate; the hydrogens of the methylene group adjacent to the sulfonyl group are not seen due to deuterium exchange.

spectrum of **6***a*: X = H as a function of H_0^q is shown in Fig. 1. Although such solutions are unstable, the initial spectrum of each of these basic solution is readily measured. The initial intensity (*A*) of the band of λ_{max} = 350 nm is clearly dependent upon H_0^q; this band can be assigned to the carbanionic conjugate base **12***a*: X = H. The dependence of *A* upon H_0^q can be described by eq. [1], with the parameters A_{CH}, A_C, and pK_a being defined by fitting the data to this equation via an iterative regression analysis based upon the Marquardt algorithm. Similar observations were made for five other 4-arylsulfonylmethylpyridines. Spectral parameters and pK_a values that have been calculated for the deprotonation of each **6** are collected in Table 5. This table also includes individual pK_a values calculated from each absorbance measurement using the value of A_{CH} derived in the iterative fit to eq. [1].

Two of the 4-arylsulfonylmethylpyridines (**6***i* and **6***j*) underwent reactions in these highly basic solutions to give intensely colored species having absorption spectra that were quite different from the $\lambda_{max} \approx 350$ nm that are listed in Table

Can. J. Chem. Downloaded from www.nrcresearchpress.com by 109.225.110.28 on 09/08/12
For personal use only.

TABLE 4. Characterization of bromide salts of the pyridinium cations **8**–**11**

Compound	Melting point, °C	^{1}H NMR,[a] δ
8 · Br^-	255–257 (dec.)	4.41 (3H, s), 7.67–7.78 (3H, m), 7.86–7.93 (3H, m), 8.03–8.10 (1H, t), 8.41–8.49 (1H, t), 8.91–8.94 (1H, d)
9 · Br^-	159–160	5.96 (2H, s), 7.26–7.31 (2H, m), 7.50–7.53 (3H, m), 7.67–7.75 (2H, m), 7.85–7.94 (4H, m), 8.05–8.12 (1H, m), 8.48–8.56 (1H, m), 8.85–8.89 (1H, m)
10 · Br^-	116–118	3.22 (3H, s), 4.43 (3H, s), 8.14–8.18 (2H, d), 8.86–8.89 (2H, d)
11 · Br^-	183–184	3.38 (3h, s), 4.51 (3H, s), 8.06–8.23 (2H, m), 8.56–8.66 (1H, m), 8.94–8.98 (1H, m)

[a]In D_2O: all chemical shifts relative to sodium 2,2-dimethyl-2-silapentane-5-sulfonate.

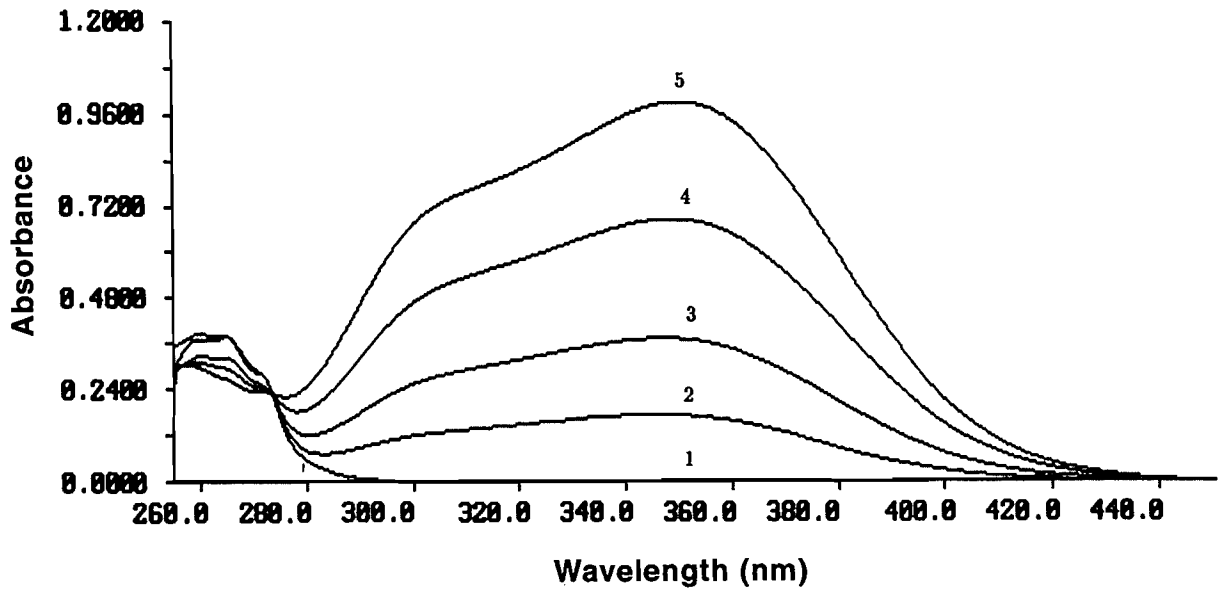

FIG. 1. Variation of the electronic absorption spectrum of **6***a* (0.1 mM) as a function of H_0^q in dimethyl sulfoxide – water solutions containing 0.047 M tetramethylammonium hydroxide. Curve 1, neutral dimethyl sulfoxide; 2, H_0^q = 18.81, 3, H_0^q = 19.41; 4, H_0^q = 20.10; 5, H_0^q = 20.97. Spectra were recorded immediately after mixing a neutral stock solution of **6***a* with each of the basic media.

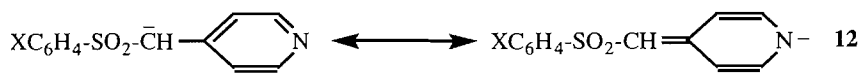

12

5. An example of this phenomenon is shown in Fig. 2 for **6***i* at H_0^q = 18.12, which displays an absorption maximum at 632 nm. We have not investigated these atypical reactions in detail. However, it seems significant that such species are only observed for phenyl rings having a 1,3-orientation of the nitro and sulfonyl substituents. This substitution pattern is well established as promoting nucleophilic addition reactions in these electron-deficient aromatic rings; i.e., Meisenheimer complex formation (23, 24). We suggest that a similar nucleophilic addition to the substituted phenyl ring probably occurs for **6***i* and **6***j* in these basic media. Our observations suggest that in these two cases the formation of Meisenheimer-type σ-adducts is thermodynamically more favourable than carbanion formation via the deprotonation of the α-methylene group of these two sulfones (**6***i* and **6***j*).

4-Arylsulfonylmethylpyridinium cations (2 and 7)

The pH-dependence of the electronic absorption spectrum of **2***a*: X = H is shown in Fig. 3. These spectra are cleanly reversible to the spectrum of **2***a* in neutral solution upon acidification of these basic solutions. The pH-dependent spectrum in Fig. 3 is quite typical of that observed for all **2** and **7**. The pH-dependence of the absorbance at constant wavelength describes a clean acid–base titration curve for all X-substituents. The pK_a value for each substituted derivative of **2** and **7**, and also the spectral characteristics of the absorption maximum of the corresponding conjugate base species, are collected in Table 6.

Other sulfones

Similar spectral observations to those described above for **2***a* were also made for the cationic sulfones **8**–**11**. The pK_a values for each of these species and spectral data for their conjugate bases are also included in Table 6. The *N*-benzyl cation is more acidic than the corresponding *N*-methyl cation in both the 2-pyridyl (ΔpK_a = 1.01) and 4-pyridyl (ΔpK_a = 0.57) cases, and the 4-phenylsulfonylmethyl de-

Can. J. Chem. Downloaded from www.nrcresearchpress.com by 109.225.110.28 on 09/08/12
For personal use only.

TABLE 5. pK_a values values for 4-(X-phenylsulfonylmethyl)pyridines (**6**)

Sulfone	λ_{max}[a]	log ϵ	H_o^q	A	pK_a calcd.[b]	pK_a[c]
			18.81	0.1817	19.89	
			19.12	0.2704	19.89	
6*a*	350	4.1	19.41	0.3908	19.91	19.89 ± 0.01
			19.75	0.6222	19.88	
			20.10	0.8626	19.90	
			20.97	1.2525	19.89	
			19.12	0.1020	20.34	
			19.41	0.1621	20.34	
6*c*	349	4.1	19.75	0.2994	20.30	20.34 ± 0.03
			20.10	0.4599	20.37	
			20.97	1.0247	20.34	
			18.25	0.1960	19.05	
			18.59	0.3134	19.02	
6*d*	360	4.0	18.81	0.4010	19.04	19.05 ± 0.02
			19.12	0.5386	19.08	
			19.75	0.8116	19.04	
			20.10	0.8830	19.05	
			17.89	0.1481	18.57	
	307	4.0	18.25	0.3328	18.51	
6*e*	360	4.0	18.59	0.4854	18.59	18.56 ± 0.06
			18.81	0.6173	18.58	
			19.41	0.8681	18.56	
			17.00	0.0474	18.34	
			17.89	0.2544	18.31	
	311	4.1	18.25	0.4275	18.30	
6*f*	370	3.9	18.59	0.5667	18.36	18.33 ± 0.03
			18.81	0.6573	18.38	
			19.12	0.7790	18.31	
			16.35	0.1593	17.55	
			16.70	0.2552	17.53	
6*h*	317	4.2	17.00	0.3774	17.55	17.55 ± 0.02
			17.36	0.5966	17.57	
			17.58	0.7963	17.53	
			18.12	1.1531	17.55	

[a]Absorption maximum (nm) in the spectrum of the conjugate base; log ϵ is calculated from A_C, which is evaluated as described in the text.

[b]pK_a values in this column were calculated for each individual solution from eq. [1] using A_C evaluated as described in the text.

[c]pK_a values in this column are from the iterative fit to eq. [1] that is described in the text.

rivative is more acidic than the corresponding 4-methylsulfonylmethyl derivative in both the *N*-methyl 2-pyridyl (ΔpK_a = 0.57) and 4-pyridyl (ΔpK_a = 0.63) cations. The 2-pyridyl cations are 0.96 to 1.40 pK_a units more acidic than their 4-pyridyl isomers.

Discussion

Each of the sulfones that were investigated in the present work displays a pH-dependent electronic absorption spectrum that is consistent with the equilibration of the sulfone with its conjugate base. Whereas the spectra of the sulfones contain only the ultraviolet absorption maxima that are expected for simply substituted benzene and pyridine chromophores, the conjugate bases display long-wavelength absorption maxima that are typical of more highly conjugated non-aromatic systems. Delocalization of carbanionic electron density into the pyridine (or pyridinium) ring as described in **12** is expected to be of considerable importance in these conjugate base species.

The weakly acidic neutral sulfones (**2**) only undergo deprotonation in highly basic media. We have found that the H_0^q acidity function that was developed (22) for the exocyclic deprotonation of ring-substituted pyridinium cations appears to be applicable to the deprotonation of these 4-arylsulfonylmethylpyridines. A major concern in the use of this acidity function is the question of whether the activity coefficient postulates that are inherent in the definition of H_0^q for pyridinium cations will also be applicable to neutral pyridines. The lack of any trend in individually calculated pK_a values as a function of H_0^q in Table 5 suggests that the inherent activity assumptions in H_0^q must be at least approximately applicable to the deprotonation of neutral pyridine carbon acids. The extensive electron delocalization into the pyridine ring in the conjugate base species is similar for both neutral and cationic pyridines, as exemplified by the similar λ_{max} in the absorption spectra of the conjugate bases of **2** and **7** (Tables 5 and 6). Such delocalization may be a major factor in determining the applicability of H_0^q to the neutral sulfones (**2**).

Can. J. Chem. Downloaded from www.nrcresearchpress.com by 109.225.110.28 on 09/08/12
For personal use only.

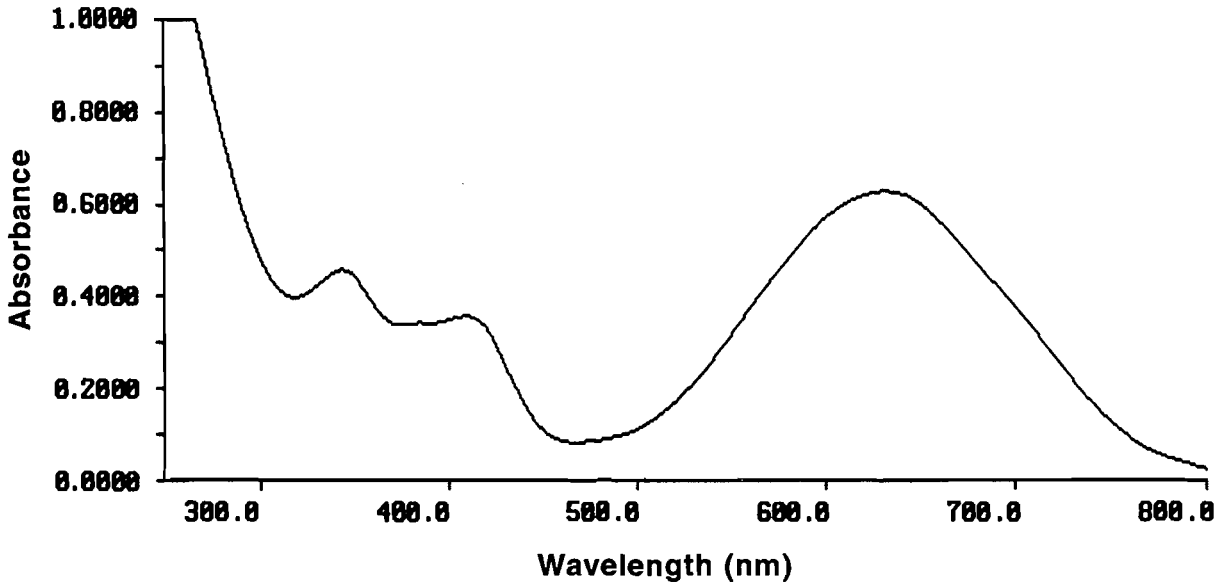

FIG. 2. The electronic absorption spectrum of **6*i*** (0.09 mM) in dimethyl sulfoxide – water containing 0.047 M tetramethylammonium hydroxide at $H_0^q = 18.12$.

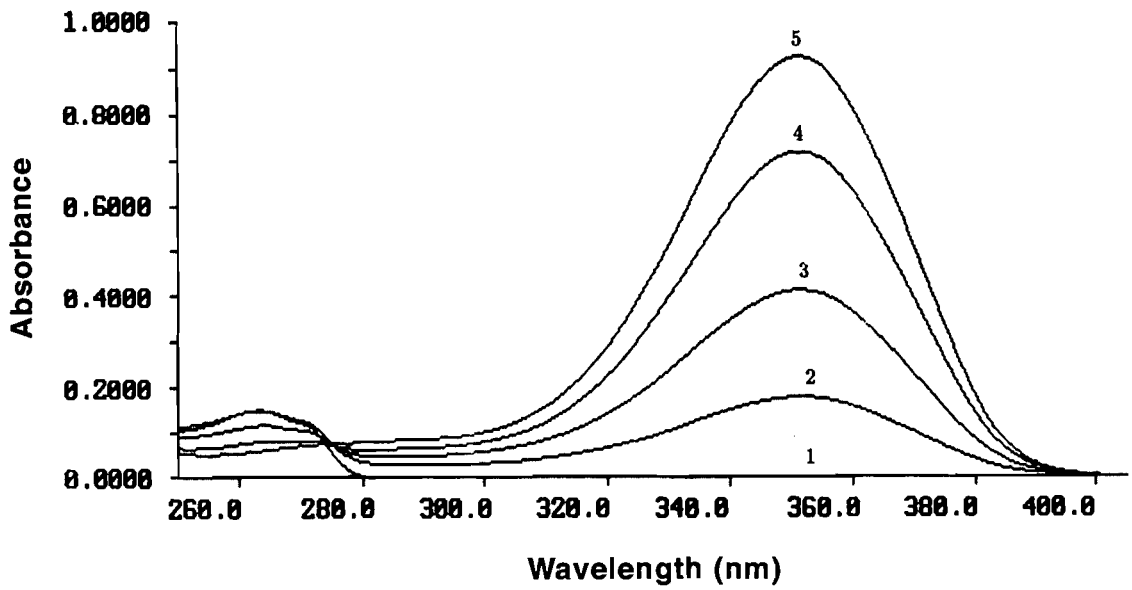

FIG. 3. Variation of the electronic absorption spectrum of **2*a*** (0.03 mM) as a function of pH in aqueous solution. Curve 1, pH = 10.0; 2, pH = 11.1; 3, pH = 11.55; 4, pH = 12.0; 5, pH = 13.0.

The reasons for the somewhat different λ_{max} that are observed for the 4-nitro derivatives than for all other X-substituents in the spectra of the conjugate bases of both **2** and **6** must reside in phenomena other than resonance effects (see below). The λ_{max} = 317 nm that is observed for **6*h***: X = 4-NO_2 appears to be a logical extension of the shoulder that is apparent in the vicinity of 310 nm in the spectrum of the conjugate base of **6*a*** (Fig. 1), and the maxima at 307 and 311 nm in the carbanions from **6*e*** and **6*f*** (Table 5). It seems likely that the spectra in Table 5 are influenced by the variation in solvent composition that is involved in the generation of the conjugate base species. One wonders whether preferential solvation of the pyridine nitrogen atom and (or) the sulfone group by dimethyl sulfoxide and water, similar to that established for the nitro group (25), may play a role in the observed λ_{max} of the spectra of the carbanions of **6** in Table 5. The conjugate base of **2*h*** in Table 6 is the only 4-arylsulfonylmethylpyridinium cation in this table to display a double maximum. The possibility of intramolecular charge-transfer complexation in the conjugate base of **2*h*** should be considered as a source of the unusual spectrum in this case.

Substituent effects upon the pK_a values of **2** (Fig. 4), **6** (Fig. 5), and **7** are closely correlated with Hammett σ constants for the X-substituents. Correlation equations are given in eqs. [2]–[4].

[2] $pK_a(\mathbf{2}) = -1.45(\pm 0.03)\,\sigma + 11.30(\pm 0.02)$,

$r = 0.998$

Can. J. Chem. Downloaded from www.nrcresearchpress.com by 109.225.110.28 on 09/08/12
For personal use only.

TABLE 6. pK_a values for 4-arylsulfonylmethylpyridinium cations[a]

Cation	X	pK_a	λ_{max}[b]	log ε
2*a*	H	11.27	352	4.47
2*b*	4-OCH_3	11.71	350	4.50
2*c*	4-CH_3	11.52	351	4.50
2*d*	4-Br	10.97	353	4.48
2*e*	3-Cl	10.82	354	4.41
2*f*	3,4-Cl_2	10.58	356	4.47
2*g*	3,5-Cl_2	10.27	355	4.46
2*h*	4-NO_2	10.14	333, 390	4.33, 3.92
2*i*	3-NO_2	10.28	354	4.45
2*j*	3-NO_2, 4-Br	10.05	355	4.41
7*a*	H	10.70	354	4.45
7*b*	3-CH_3	10.72	354	4.55
7*c*	4-CH_3	10.75	353	4.51
7*d*	4-Br	10.57	353	4.54
7*e*	3-F	10.47	353	4.56
7*f*	4-CN	10.24	354	4.53
7*g*	3-NO_2	10.21	355	4.60
7*h*	4-NO_2	10.18	355	4.49
8	—	10.31	362	3.96
9	—	9.30	366	3.96
10	—	11.93	338	4.43
11	—	10.88	286, 360	4.34, 3.84

[a]In aqueous solution, ionic strength 0.1, at 25°C.
[b]Absorption maximum (nm) in the spectrum of the conjugate base.

[3] $pK_a(\mathbf{6}) = -3.0(\pm 0.1)\,\sigma + 19.80(\pm 0.06)$, $r = 0.996$

[4] $pK_a(\mathbf{7}) = -0.65(\pm 0.02)\,\sigma + 10.68(\pm 0.01)$, $r = 0.995$

The clean correlation of substituent effects (eq. [3] and Fig. 5) that is obtained for **6** provides further support for the adequacy of H_0[9] for the evaluation of the acidities of these neutral sulfones. Equation [2] was evaluated using the σ constants recommended by Hansch *et al.* (26) for the 3,4-dichloro (**2***f*) and 4-bromo-3-nitro (**2***j*) derivatives. In each of these cases, the assumption of strict additivity of *meta* and *para* substituent constants for these 3,4-disubstituted rings leads to significant deviations from the correlation line established for the other X-substituents (Fig. 4).

It seems clear that the X-substituent effects upon the acidities of **2** and **6** do not contain contributions from resonance interactions between X and the carbanionic centre, since neither σ^+ parameters for the 4-methoxy or 4-methyl substituents nor the σ^- parameter for the 4-nitro substituent are appropriate. This result contrasts with the X-substituent effects upon the pK_a values for the corresponding ketones (**1**) in which both the 4-methoxy and 4-nitro substituents deviate significantly from the correlation line defined by other substituents (7).

Substituent effects upon the acidities of the neutral sulfones **6** (ρ = 3.0) are much larger than for the more strongly acidic *N*-methyl cation analogs **2** (ρ = 1.45). The reduced ρ value for **2** relative to **6** suggests much lower electron density on the formal carbanionic atom in the conjugate base of **2** than in the conjugate base of **6**. This observation is consistent with the ρ = 0.65 that is found for the *N*-(substituted benzyl) cations (**7**). This ρ = 0.65 indicates significant neutralization of the cationic charge upon the ring nitrogen atom as a result of electron delocalization from the carbanionic

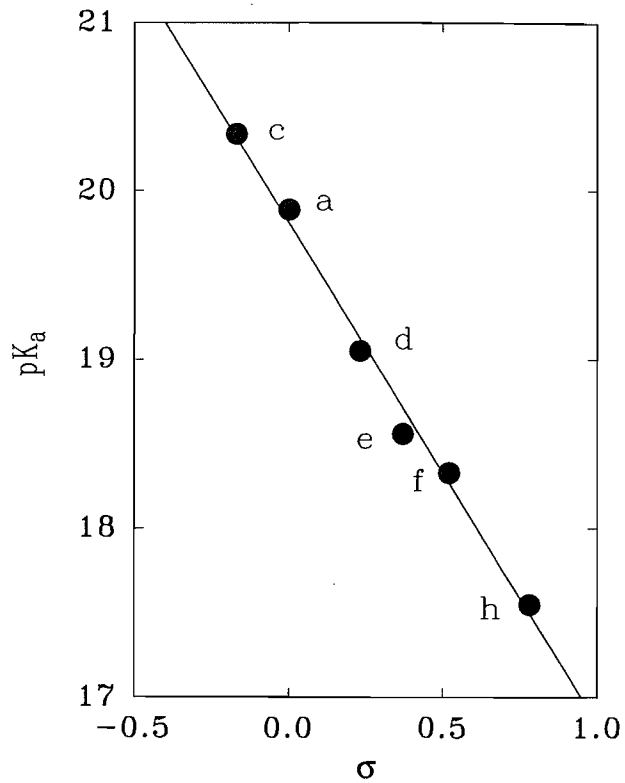

FIG. 4. Hammett correlation for the substituent dependence of the pK_a values of **6**.

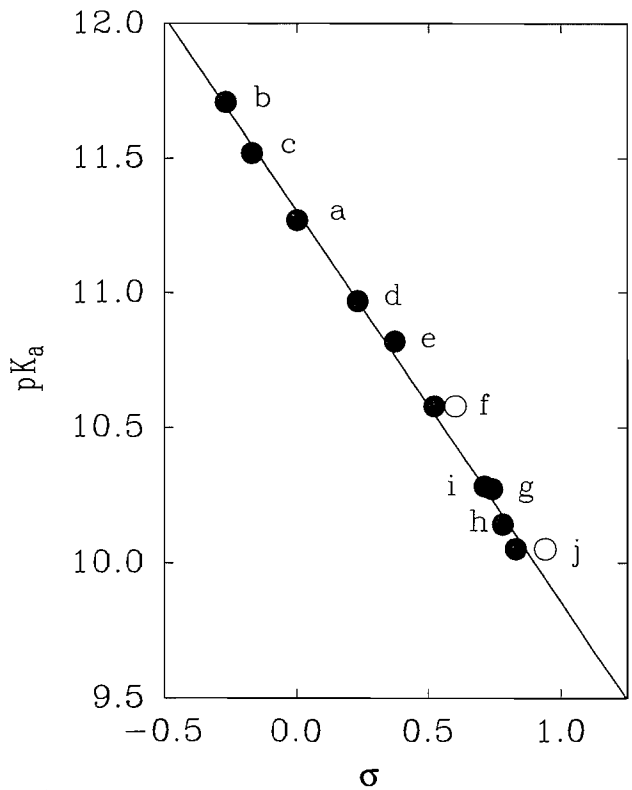

FIG. 5. Hammett correlation for the substituent dependence of the pK_a values of **2**. The empty circles for **2***f* and **2***j* refer to σ constants that assume strict additivity of substituent effects (see text).

Can. J. Chem. Downloaded from www.nrcresearchpress.com by 109.225.110.28 on 09/08/12
For personal use only.

TABLE 7. Thermodynamic acidities of sulfones and ketones in aqueous solution

Carbon acid	pK_a (X = H)	ΔpK_a	ρ
$C_6H_5SO_2CH_3$	28.7[a]		
$C_6H_5COCH_3$	18.31[b]	10.4	[c]
$XC_6H_4SO_2CH_2C_5H_4N$ (**6**)	19.89[d]		3.0
$XC_6H_4COCH_2C_5H_4N$ (**4**)	12.47[e]	7.42	2.03
$XC_6H_4SO_2CH_2C_5H_4\overset{+}{N}CH_3$ (**2**)	11.27[d]		1.45
$XC_6H_4COCH_2C_5H_4\overset{+}{N}CH_3$ (**1**)	7.66[e]	3.61	1.38
$C_6H_5SO_2CH_2C_5H_4\overset{+}{N}CH_2C_6H_4X$ (**7**)	10.70[d]		0.65
$C_6H_5COCH_2C_5H_4\overset{+}{N}CH_2C_6H_4X$ (**5**)	7.28[e]	3.42	0.47

[a]Estimated from eq. [6].
[b]From ref. 30.
[c]Guthrie *et al.* report (31) ρ = 1.95(±0.19) for $XC_6H_4COCH_3$ for which individual pK_a values are rather imprecise (± 0.5 logarithmic units).
[d]Current work.
[e]From ref. 7.

centre into the pyridinium ring (**13**). Relative to ρ = 1.14 for the deprotonation of *N*,*N*-dimethylbenzylammonium cations (27), the ρ = 0.65 for **7** suggests approximately 60% neutralization of the formal charge upon the pyridinium nitrogen atom of **7** upon deprotonation of the methylene group. Such extensive delocalization of negative charge into the pyridinium ring requires predominant sp^2-hybridization for the carbanionic carbon atom in **13**, and leaves little doubt that in the present case the carbanionic centre is planar rather than pyramidal (32).

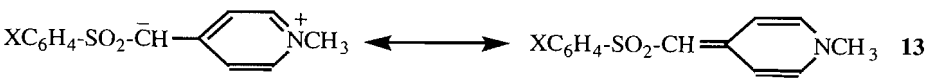

13

The cationic sulfones **2** with ρ = 1.45 are of similar acidity to phenacylsulfones (**3**) for which X-substituent effects have been reported (16) to have ρ = 2.01 in 95% ethanol – 5% water. This latter value may be corrected to ρ = 2.01/1.63 = 1.23 for aqueous solutions using ρ = 1.63 for the deprotonation of substituted benzoic acids in ethanolic solution (28). Substituent effects upon the pK_a values for ring-substituted benzenesulfonamides ($XC_6H_4SO_2NH_2$, pK_a 10.00 (X = H), ρ = 1.06) and benzenesulfonanilides ($XC_6H_4SO_2NHC_6H_5$, pK_a 8.31 (X = H), ρ = 1.15) are also of similar magnitude in aqueous solution (29) to those found for **2** in the current study.

Substituent effects upon the aqueous acidities of analogous series of pyridine and pyridinium activated sulfones and ketones are compared in Table 7. In all cases the ketones are more acidic than the corresponding sulfones, although the difference in acidity of these two series of carbon acids decreases with increasing acidity from ΔpK_a = 7.42 for the neutral species to only 3.42 for the N-benzyl cations. In all cases the ρ values are also smaller for the ketones than for the corresponding sulfones, although $\Delta\rho$ = 0.97 for the neutral species is reduced to only 0.07 for the N-methyl cations. The ΔpK_a = 4.81 observed upon N-methylation of the ketone is also considerably smaller than ΔpK_a = 8.62 that is found upon N-methylation of the sulfone. The ρ values of 0.65 and 0.47 for the sulfones (**7**) and ketones (**5**), respectively, suggest that delocalization of carbanionic charge into the pyridinium ring is more important for the conjugate bases of the sulfones than of the ketones. This latter result is presumably attributable to the much greater importance of enolate ion stabilization in the conjugate bases of the ketones, than the analogous delocalization of electron density into the sulfonyl group in the sulfone carbanions.

Combination of the Hammett correlation (eq. [3]) for substituent effects upon the acidity of the neutral 4-arylsulfonylmethylpyridines with the analogous Hammett correlation (eq. [5]) previously established (7) for the corresponding 4-phenacylpyridines (**4**) leads to eq. [6]. Extrapolation of this relationship to pK_a = 18.31 for acetophenone in aqueous solution (30) allows the estimation of pK_a = 28.7 for methyl phenyl sulfone in water. This appears to be the first estimate of the acidity of this sulfone in aqueous media, and is comparable with pK_a = 29.05 reported for this same sulfone (10) in dimethyl sulfoxide solution.

[5] $pK_a(\mathbf{4}) = 2.03\,\sigma + 12.50$

[6] $pK_a(\text{sulfone}) = 1.5\,pK_a(\text{ketone}) + 1.3$

The only previous estimate that we have been able to locate for the pK_a of a simple sulfone in aqueous solution is the value of 23 proposed by Pearson and Dillon (17) for dimethyl sulfone. This estimate was based on two separate assumptions regarding the kinetic acidity of this compound, including the assumption that the rate–equilibrium correlation for the deprotonation of ketones is also applicable to sulfones. This latter assumption almost certainly leads to a large overestimation of the acidity of dimethyl sulfone (i.e., too low pK_a) since the kinetic acidities of sulfones are known (2, 3, 17) to be considerably greater than those of ketones of similar thermodynamic acidity. Since we have shown above that methyl sulfones (**10** and **11**) are less acidic than their phenyl sulfone analogues (**2***a* and **8**) in aqueous solu-

Can. J. Chem. Downloaded from www.nrcresearchpress.com by 109.225.110.28 on 09/08/12
For personal use only.

tion, the above estimate for methyl phenyl sulfone requires $pK_a > 28.7$ (probably ≈ 30) for dimethyl sulfone in aqueous solution. The pK_a of dimethyl sulfone in dimethyl sulfoxide solution is reported to be 31.1 (10).

Acknowledgement

We appreciate the support of this work by the Natural Sciences and Engineering Research Council of Canada, and the award of a University of Toronto Open Fellowship to S. W.

1. E. J. Corey, H. Konig, and T. H. Lowry. Tetrahedron Lett. 515 (1962).
2. J. Hine, J. C. Philips, and J. I. Maxwell. J. Org. Chem. **35**, 3943 (1970).
3. (*a*) R. P. Bell and B. G. Cox. J. Chem. Soc. (B), 652 (1971); (*b*) F. Hibbert. J. Chem. Soc. Perkin Trans. 2, 1289 (1973).
4. R. P. Bell and D. J. Barnes. Proc. R. Soc. London, Ser. A, **318**, 421 (1970).
5. P. Alcais and R. Brouillard. J. Chem. Soc. Perkin Trans. 2, 1214 (1972).
6. G. Schwarzenbach and E. Felder. Helv. Chem. Acta, **27**, 1701 (1944).
7. D. Stefanidis and J. W. Bunting. J. Am. Chem. Soc. **112**, 3163 (1990).
8. S. Golding, A. R. Katritzky, and H. Z. Kucharska. J. Chem. Soc. 3090 (1965).
9. W. E. Truce, W. W. Bannister, and R. H. Knospe. J. Org. Chem. **27**, 2821 (1962).
10. F. G. Bordwell. Acc. Chem. Res. **21**, 456 (1988).
11. G. Gaviraghi and G. Pagani. J. Chem. Soc. Perkin Trans. 2, 50 (1973).
12. S. Thea, G. Guanti, A. R. Hopkins, and A. Williams. J. Org. Chem. **50**, 5592 (1985).
13. W. v. E. Doering and L. K. Levy. J. Am. Chem. Soc. **77**, 509 (1955).
14. R. Breslow and E. Mohacsi. J. Am. Chem. Soc. **83**, 4100 (1961).
15. R. Breslow and E. Mohacsi. J. Am. Chem. Soc. **84**, 684 (1962).
16. R. T. Amel and P. J. Marek. J. Org. Chem. **38**, 3513 (1970).
17. R. G. Pearson and R. L. Dillon. J. Am. Chem. Soc. **75**, 2439 (1953).
18. A. J. Nunn and K. J. Schofield. J. Chem. Soc. 583 (1952).
19. A. Fischer, M. J. King, and F. K. Robinson. Can. J. Chem. **56**, 3072 (1978).
20. A. Fischer, M. J. King, and F. K. Robinson. Can J. Chem. **56**, 3059 (1978).
21. A. Albert and E. P. Serjeant. The determination of ionization constants. 3rd ed. Chapman and Hall, London. 1984. Chap. 4.
22. R. A. Cox, R. Stewart, M. J. Cook, A. R. Katritzky, and R. D. Tack. Can. J. Chem. **54**, 900 (1976).
23. F. Terrier. Chem. Rev. **82**, 77 (1982).
24. M. R. Crampton, E. Buncel, M. J. Strauss, and F. Terrier. Electron-deficient aromatic- and heteroaromatic-base interactions. Elsevier Scientific Publishing, Amsterdam. 1984.
25. E. A. Walters. J. Phys. Chem. **81**, 1995 (1977).
26. C. Hansch, A. Leo, S. U. Unger, K. H. Kim, D. Nikaitani, and E. J. Lien. J. Med. Chem. **16**, 1207 (1973).
27. D. H. Rosenblatt, L. A. Hull, D. C. Deluca, G. T. Davis, R. C. Weglein, and H. K. R. Williams. J. Am. Chem. Soc. **89**, 1158 (1967).
28. M. Kilpatrick and W. H. Mears. J. Am. Chem. Soc. **71**, 3051 (1949).
29. A. V. Willi. Helv. Chim. Acta, **39**, 46 (1956).
30. J. R. Keeffe, A. J. Kresge, and J. Toullec. Can. J. Chem. **64**, 1224 (1986).
31. J. P. Guthrie, J. Cossar, and A. Klym. Can. J. Chem. **65**, 2154 (1987).
32. F. Hibbert. *In* Comprehensive chemical kinetics. Vol. 8. *Edited by* C. H. Bamford and C. F. H. Tipper. Elsevier, Amsterdam. 1977. pp. 145–153.

Can. J. Chem. Downloaded from www.nrcresearchpress.com by 109.225.110.28 on 09/08/12
For personal use only.

Viscosities and thermodynamics of viscous flow of binary liquid mixtures of 2-(2-butoxyethoxy)ethanol with aniline and *N*-alkyl anilines

PAUL WISEMAN,[1] MURRAY HEGGIE, AND RAMAMURTHY PALEPU[2]

Department of Mathematics and Natural Sciences, University College of Cape Breton, Sydney, N.S., Canada B1P 6L2

Received December 5, 1991

PAUL WISEMAN, MURRAY HEGGIE, and RAMAMURTHY PALEPU. Can. J. Chem. **70**, 2645 (1992).

Viscosities and densities of binary mixtures containing 2-(2-butoxyethoxy)ethanol with aniline and *N*-alkyl-substituted anilines have been determined at five different temperatures over the complete concentration range. Excess volumes, viscosities, and excess molar free energy of activation of flow were calculated and the departure from ideal behavior is explained on the basis of specific interactions between the components in these mixtures. McAllister's approach correlates the viscosity data with a significantly high degree of accuracy for all these systems.

PAUL WISEMAN, MURRAY HEGGIE et RAMAMURTHY PALEPU. Can. J. Chem. **70**, 2645 (1992).

Opérant à cinq températures différentes et sur l'ensemble des plages de concentration, on a déterminé les viscosités et les densités de mélanges binaires contenant du 2-(2-butoxyéthoxy)éthanol avec de l'aniline et des anilines *N*-alkylées. On a calculé les volumes et les viscosités en excès ainsi que l'énergie libre molaire d'activation en excès et on explique la déviation par rapport au comportement idéal en se basant sur des interactions spécifiques entre les composants de ces mélanges. Pour tous ces systèmes, l'approche de McAllister permet d'obtenir une très bonne corrélation entre toutes les données de viscosité.

[Traduit par la rédaction]

Can. J. Chem. Downloaded from www.nrcresearchpress.com by 109.225.110.28 on 09/08/12
For personal use only.

Introduction

In this work, viscosities of five nonelectrolyte binary mixtures at five different temperatures were measured. These mixtures were composed of 2-(2-butoxyethoxy)ethanol with aniline (ANL), *N*-methylaniline (MEA), *N*,*N*-dimethylaniline (DMA), *N*-ethylaniline (EAN), and *N*,*N*-diethylaniline (DEA).

Excess molar viscosities, volumes, and the free energies of activation for viscous flow were evaluated from the experimental data to examine the type and strength of interactions between the components in these mixtures.

Experimental

The methods used in our laboratory have been described previously (1–6). Densities were determined with a digital densimeter DMA 45 (Anton-Parr, Austria). A Sodev temperature controller bath (constant to 0.001°C) was used. Calibration was carried out with air and nanopure water with an error of $\pm 1 \times 10^{-4}$ g cm^{-3}. Viscosities at different temperatures were measured using modified Ostwald viscometers and a viscosity bath (Koehler instrumentation). The estimated error in the viscosity measurements was within ±0.005 cP.

Anilines used were the same as in earlier studies (1–6). 2-(2-Butoxyethoxy)ethanol, an Aldrich product, was purified by distillation under reduced pressure and stored over molecular sieves. The experimental density of 0.9521 g cm^{-3} at 298 K agrees well with the literature value of 0.9528 g cm^{-3} (7).

Results and discussion

The excess functions V^E, η^E and ΔG^{*E}, were calculated from the experimental values[3] using the following equations:

$$[1] \quad V^E = [(X_1M_1 + X_2M_2) \div \rho] - [X_1V_1 + X_2V_2]$$

$$[2] \quad \eta^E = \eta - \exp(X_1 \ln \eta_1 + X_2 \ln \eta_2]$$

$$[3] \quad \Delta G^{*E} = RT[\ln \eta V - (X_1 \ln \eta_1 V_1 + X_2 \ln \eta_2 V_2)]$$

where ρ, η, and V are the density, viscosity, and volume of the mixture, M_1, M_2, V_1, V_2, η_1, η_2, X_1, and X_2 are molar masses, volumes, viscosities, and mole fractions of the pure components 1 and 2, respectively.

The excess function (Y^E) for the binary systems could be represented by Redlich–Kister equation (8):

$$[4] \quad Y^E = X_1X_2 \sum_{j=1}^{n} a_j(1 - 2X_1)^{j-1}$$

where Y^E and a_j represent the excess functions V^E, η^E, ΔG^{*E} and the polynomial coefficients. The values of the coefficients were determined by the method of least squares. In each case, the optimum number of coefficients was ascertained from an examination of the variation of the standard error of estimate with n:

$$[5] \quad \sigma_y = [\Sigma(X^E_{ob} - X^E_{cal})^2 \div (n_{ob} - n)]^{1/2}$$

where n_{ob} is the number of measurements. The values of these coefficients along with standard error of estimate at 298 K are presented in Table 1. Figures 1–3 show the values of η^E, V^E, and ΔG^{*E} as a function of the mole fraction of the alcohol. The continuous curves were generated with the aid of the coefficients in Table 1.

Viscosity data for the liquid mixtures were used to test the empirical approach of McAllister (9). The McAllister correlation is based on a model proposed by Eyring and coworkers (10) which considers that interaction between layers of molecules as if the molecules were undergoing a chemical reaction and have to overcome a potential barrier of this

[1]Graduate student, Department of Chemistry, University of Western Ontario, London, Ontario.

[2]Author to whom correspondence may be addressed.

[3]Experimental data of viscosities and densities along with the values of a_j have been deposited as supplementary material and may be purchased from: The Depository of Unpublished Data, Document Delivery, CISTI, National Research Council Canada, Ottawa, Canada K1A 0S2.

TABLE 1. Coefficients for the least-squares fit of the results of eq. [4] at 298 K[a]

System	Y^E	A_1	A_2	A_3	A_4	A_5	A_6	σ
ANL + BEE	V^E	−2.314	−1.443	−1.252	−2.825			0.0090
	η^E	6.262	0.869	−0.279	−3.285			0.04
	ΔG^{*E}	3567.0	819.0	319.9	−1509.0			25
MEA + BEE	V^E	−0.431	−0.373	2.072	−4.106	1.013		0.0028
	η^E	3.099	−1.242	−0.929	0.248			0.01
	ΔG^{*E}	2458.0	126.0	−231.9	−258.5	−627.0		11
DMA + BEE	V^E	1.147	−0.382	3.319	−2.358			0.0083
	η^E	0.310	−0.758	0.018	0.077	−0.946		0.01
	ΔG^{*E}	405.5	−186.1	392.6	−1127.0	−2314.0		36
EA + BEE	V^E	−0.774	0.406	0.117	−1.964	0.870		0.0048
	η^E	3.276	−1.152	−0.654	−0.671			0.01
	ΔG^{*E}	2459.0	238.9	425.4	−792.8	−68.9		10
DEA + BEE	V^E	1.579	0.967	4.437	−2.705			0.033
	η^E	−0.076	−0.628	−0.493	−0.665			0.02
	ΔG^{*E}	−21.0	−492.5	−783.5	−981.9			18

[a]Units: V^E(cm^3/mol), η^E(cP), and ΔG^{*E}(J/mol).

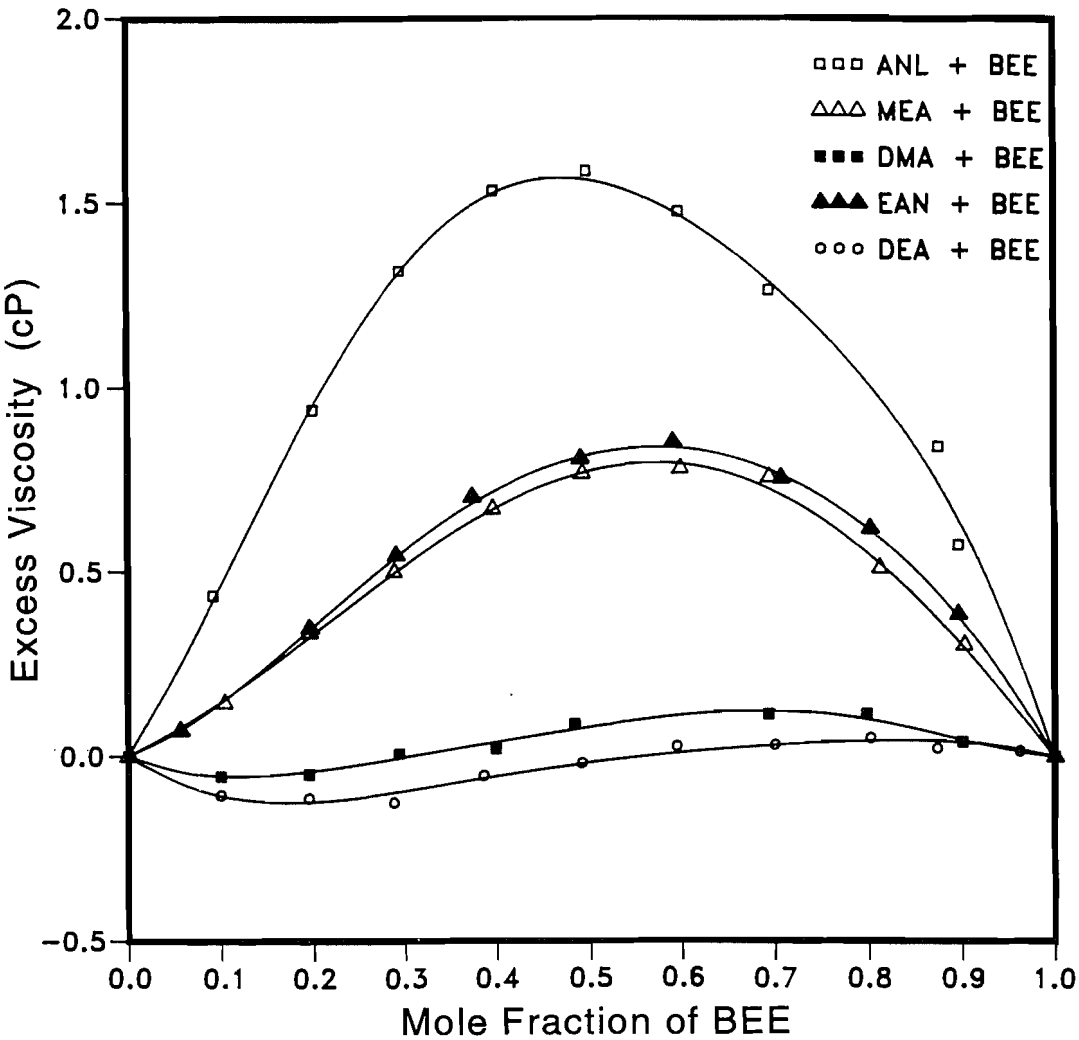

FIG. 1. Excess viscosities of the systems at 298.15 K.

process. For a binary mixture of A and B in which the molecular interactions of 1-1-1, 1-2-1, 1-1-2, 1-2-2, 2-1-2, and 2-2-2 types can be visualized, this approach yields the following equation for a three-body interaction.

$$[6] \quad \ln \nu = X_1^3 \ln \nu_1 + 3X_1^2X_2 \ln \nu_{12} + 3X_1X_2^2 \ln \nu_{21} + X_2^3 \ln \nu_2 + R_0$$

where

Can. J. Chem. Downloaded from www.nrcresearchpress.com by 109.225.110.28 on 09/08/12
For personal use only.

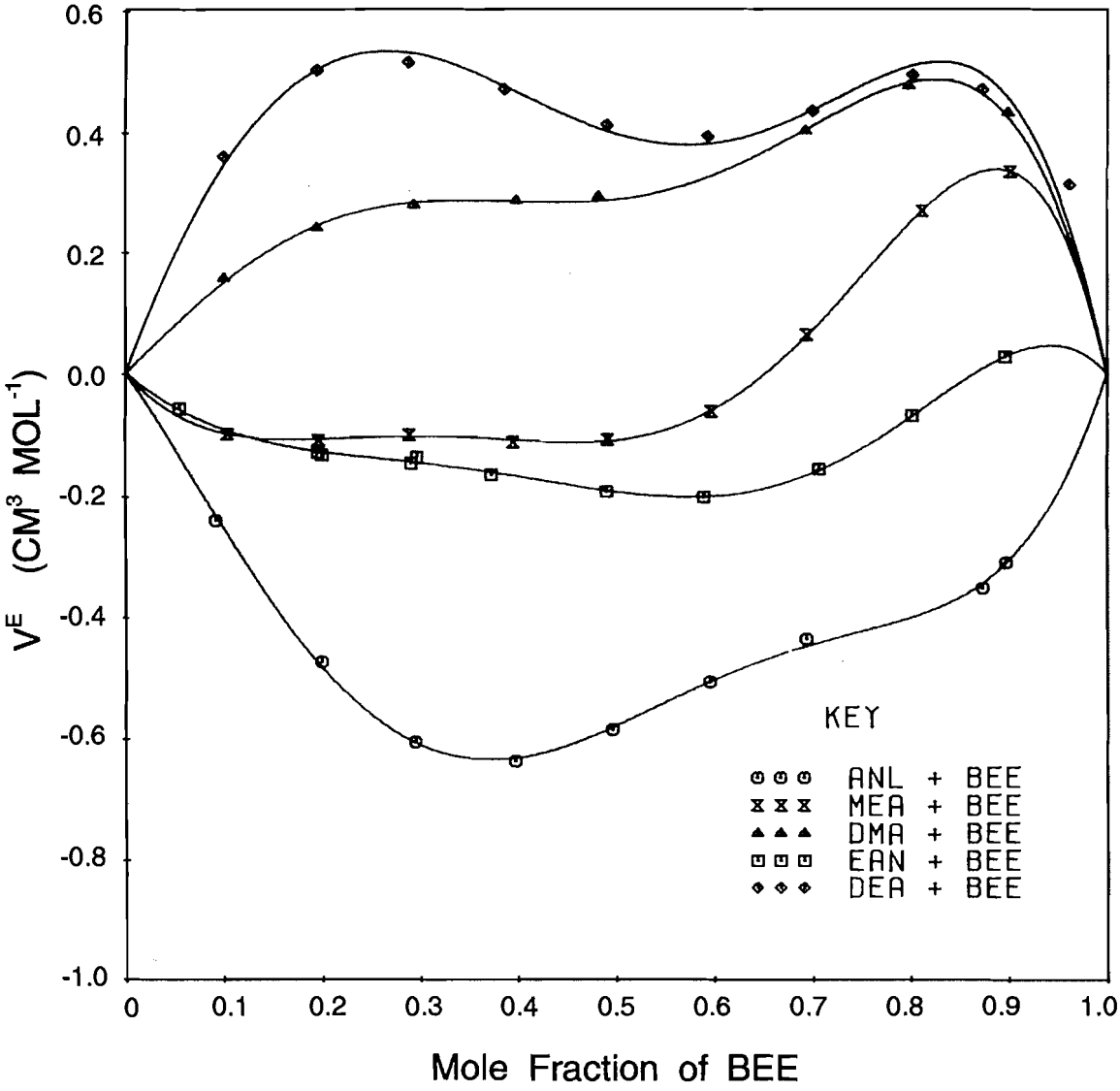

FIG. 2. Molar excess volumes of the systems at 298.15 K.

$$[7]\quad R_0 = -\ln\left[X_1 + \frac{X_2M_2}{M_1}\right] + 3X_1^2X_2\ln\left[\frac{2}{3} + \frac{M_2}{3M_1}\right] + 3X_1X_2^2\ln\left[\frac{1}{3} + \frac{2M_2}{3M_1}\right] + X_2^3\ln\left[\frac{M_1}{M_2}\right]$$

In eq. [6], ν_1, ν_2 and ν refer to the kinematic viscosities of the pure components 1, 2 and the mixture respectively. The interaction parameters ν_{12} and ν_{21} were determined by the methods of least squares from the experimental viscosity data. The values of ν_{12}, ν_{21}, absolute average error, and the ratio of radii r_2/r_1 at different temperatures are presented in Table 2. The use of a cubic equation is justified only if the ratio of the molecular radii of the two components in the mixture is less than 1.5. The interaction parameters ν_{12} and ν_{21} may be represented in terms of specific interactions between unlike molecules. It is possible in a simplified model to associate the parameter ν_{12} with the 1-1-2, 2-1-2 type and ν_{21} with the 1-2-1, 1-2-2 type of interaction. The relative intensities of these interactions between a central unit and the surrounding molecules or any other aggregates in any direction may be different for different neighboring arrangements. It is not unreasonable to expect the nature of these specific interactions to be about the same either for the 1 or 2 central species. Therefore the specific interaction terms ν_{12} and ν_{21} should have the same statistical weight at a given temperature. From the examination of the values of ν_{12} and ν_{21} in Table 2, it is obvious that the values are of the same order of magnitude but they do differ slightly from each other. However, McAllister's treatment proved to be reasonably accurate in predicting the viscosity data of the binary mixtures.

The excess viscosity values (Fig. 1) are positive for BEE with ANL, MEA, EAN and slightly negative for the DMA and DEA systems. The algebraic values of η^E may be represented in the following order: DMA < DEA < EAN < MEA < ANL. The sign and magnitude of η^E depend on the combined effect of factors such as molecular size, shape, and intermolecular forces (11). The positive values of η^E indicate the presence of a specific interaction such as the formation of weak hydrogen bonding of the type O—H---N or N—H---O. The negative values of η^E in the systems of BEE with DEA and DMA suggest that mutual loss of specific in-

Can. J. Chem. Downloaded from www.nrcresearchpress.com by 109.225.110.28 on 09/08/12
For personal use only.

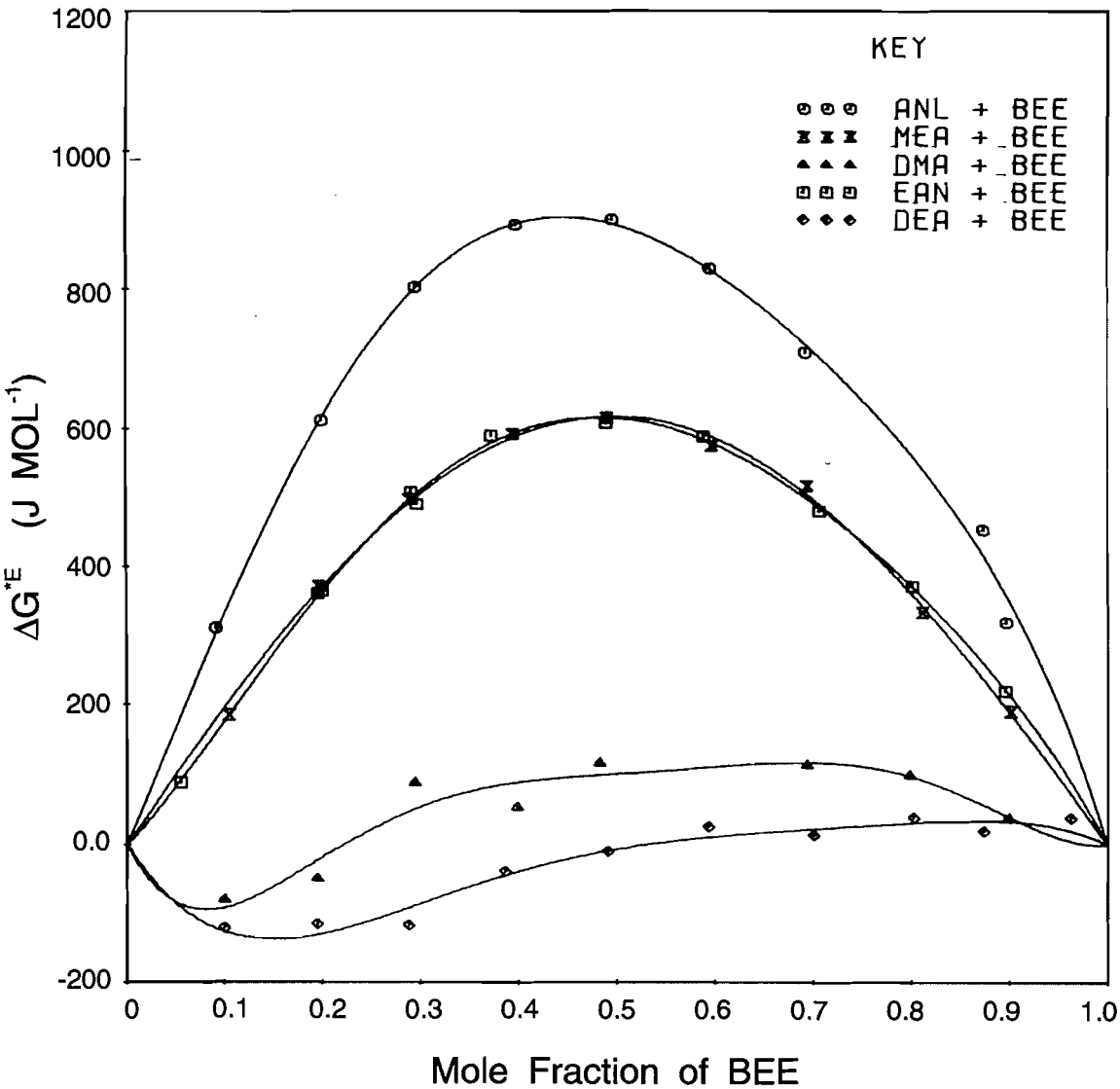

FIG. 3. Molar excess free energies of viscous flow for the systems at 298.15 K.

teractions in like molecules outweigh the specific interactions between unlike molecules (12, 13). The symmetric curve of η^E and ΔG^{*E} vs. mole fraction for ANL + BEE indicates that the energy necessary to break the hydrogen bonds in the mixing process for the pure liquids is similar for both components. For the systems BEE with MEA and EAN the excess viscosity becomes less positive and the maxima shifts toward the higher mole fraction of BEE. This indicates that the breaking energy of hydrogen bonding in BEE, when mixing with MEA and EAN, is not compensated by the weak N---H bonding of the base (14). In systems whose excess viscosity shows a well-marked maximum, the composition of the complex formed can be fixed at least to a first approximation from the mole ratio at the maximum (15). One can conclude from the analysis of Fig. 1 that, for the system ANL + BEE, there is evidence of a complex formation in the mole ratio of 1:1. For the other two systems, we can not find a molar relation because the maxima do not coincide.

The observed excess volume (V^E) values result from the balance of dipole–dipole interaction contributions leading to an expansion in volume and geometrical packing or free volume effects leading to contraction in volume (16). The curves in Fig. 2, indicate that the excess volumes are positive for BEE with DEA, DMA and negative for ANL, EAN systems in the entire concentration range and change sign for the MEA system. A negative value of V^E indicates strong interaction between the components of the mixture. The positive ΔG^{*E} values (Fig. 3) can be seen in binary systems as an indication of strength of interactions between molecules (17, 18). From the values of excess functions, one can conclude that the strength of specific interactions varies in the order ANL + BEE > MEA + BEE > EAN + BEE > DMA + BEE > DEA + BEE.

Acknowledgements

This work is supported by financial assistance from the Natural Sciences and Engineering Research Council (NSERC) of Canada and the Council of the Evaluation of Research Proposals of the University College of Cape Breton. One of the authors (P.W.) wishes to acknowledge the un-

Can. J. Chem. Downloaded from www.nrcresearchpress.com by 109.225.110.28 on 09/08/12
For personal use only.

TABLE 2. Values of McAllister's interaction parameters (ν_{12} and ν_{21}) and average absolute error (AAE) at different temperatures

System	T (K)	ν_{12}	ν_{21}	AAE[a]	r_2/r_1[b]
ANL + BEE	298	6.5989	6.8274	0.0076	0.812
	303	5.3778	5.5756	0.0056	0.812
	308	4.6064	4.5236	0.0052	0.812
	313	4.0164	3.5857	0.0089	0.812
	318	3.5482	2.9535	0.0154	0.812
MEA + BEE	298	3.7496	4.9233	0.0059	0.862
	303	3.1817	4.1965	0.0047	0.861
	308	2.9111	3.6779	0.0041	0.861
	313	2.7551	3.3253	0.0043	0.861
	318	2.6567	3.1000	0.0100	0.861
DMA + BEE	298	2.0647	3.5449	0.0112	0.907
	303	1.8367	3.0945	0.0109	0.907
	308	1.7449	2.7788	0.0098	0.907
	313	1.7189	2.5718	0.0059	0.907
	318	1.6761	2.4752	0.0064	0.907
EA + BEE	298	3.7891	5.0597	0.0053	0.906
	303	3.2397	4.3669	0.0053	0.905
	308	2.8410	3.7748	0.0041	0.905
	313	2.7396	3.3399	0.0071	0.905
	318	2.6539	3.1078	0.0134	0.905
DEA + BEE	298	2.4939	4.0306	0.0090	0.980
	303	2.1961	3.4376	0.0077	0.980
	308	2.0014	2.9148	0.0161	0.980
	313	1.8633	2.4591	0.0217	0.980
	318	1.7475	2.0322	0.0318	0.980

[a]Average absolute error $= \frac{1}{n}\sum^{n}\left[\frac{\nu_{exp} - \nu_{cal}}{\nu_{exp}}\right]$, where n is the number of measurements.

[b]$r_2/r_1 = \left[\frac{M_2\rho_1}{M_1\rho_2}\right]^{1/3}$.

dergraduate summer Research Fellowship (1987–1988) provided by NSERC of Canada.

1. R. Palepu, J. Oliver, and B. MacKinnon. Can. J. Chem. **63**, 1024 (1985).
2. R. Palepu and J. H. MacNeil. Aust. J. Chem. **41**, 791 (1988).
3. R. Palepu and J. H. MacNeil. Thermochim. Acta, **149**, 275 (1989).
4. R. Palepu, J. H. MacNeil, and P. Wiseman. Phys. Chem. Liq. **23**, 181 (1991).
5. R. Palepu, J. Oliver, and D. Campbell. J. Chem. Eng. Data, **30**, 355 (1985).
6. D. J. G. Irwin, R. Johnson, and R. Palepu. Thermochim. Acta, **82**, 277 (1984).
7. B. Sokolowski. Pol. J. Chem. **53**, 905 (1979).
8. O. Redlich and A. T. Kister. Ind. Eng. Chem. **40**, 345 (1948).
9. R. A. McAllister. Am. Inst. Chem. Eng. J. **6**, 427 (1960).
10. S. Glasstone, K. J. Laidler, and H. Eyring. The theory of rate processes. McGraw-Hill, New York. 1941.
11. J. Nath and A. K. Srinivastava. Fluid Phase Equilib. **28**, 97 (1986).
12. H. Illoekhani, K. D. Reddy, and M. V. P. Rao. Phys. Chem. Liq. **14**, 181 (1985).
13. R. J. Fort and W. R. Moore. Trans. Faraday Soc. **62**, 1112 (1966).
14. V. T. Deshpande and K. A. Pathki. Trans. Faraday Soc. **58**, 2134 (1962).
15. Y. Fialkov. Russ. J. Phys. Chem. **37**, 1051 (1963).
16. I. Prigogine. The molecular theory of solutions. North Holland Publishing Company, Amsterdam. 1957.
17. T. M. Reed and T. E. Taylor. J. Phys. Chem. **63**, 58 (1959).
18. R. Meyer, M. Meyer, J. Metzer, and A. Peneloux. J. Chim. Phys. **62**, 405 (1971).

Can. J. Chem. Downloaded from www.nrcresearchpress.com by 109.225.110.28 on 09/08/12
For personal use only.

The anomeric effect in thio derivatives of benzocycloheptene

S. DÉSILETS AND M. ST-JACQUES[1]

Département de chimie, Université de Montréal, C.P. 6128, Succ. A, Montréal (Québec), Canada H3C 3J7

Received January 30, 1992

S. DÉSILETS and M. ST-JACQUES. Can. J. Chem. **70**, 2650 (1992).

The conformational properties of six thio derivatives of benzocycloheptene were studied by ^1H and ^{13}C high-field NMR spectroscopy in solution at low temperature. Both parent compounds **2** and **6**, with sulfur at positions 3 and 1, respectively, were found to exist in the chair conformation. The 2-substituted derivatives of **2** (**3**: Y = OCH_3 and **4**: Y = Cl) revealed the presence of the Ca form only. In contrast, the 2-substituted derivatives of **6** (**7**: Y = OCH_3 and **8**: Y = Cl), with sulfur at position 1, showed mixtures of three conformers, namely Ca:Ce:TB (Ca = axial chair, Ce = equatorial chair, and TB = twist-boat), whose populations in CHF_2Cl were, respectively, 93:5:2 and 85:12:3. The predominance of the Ca form in both series argues in favour of a strong anomeric effect in spite of the large departure from coplanarity (~35°) in the :—S—C—Y fragment of both **7** and **8**. This noncoplanarity appears to weaken only slightly the n–σ^* overlap characteristic of the *endo*-anomeric effect, contrary to earlier observations for the :—O—C—Y fragment in **5**. The differences between the effects of O and S are discussed.

S. DÉSILETS et M. ST-JACQUES. Can. J. Chem. **70**, 2650 (1992).

Faisant appel à la RMN du ^1H et du ^{13}C à haut champ, on a étudié les propriétés conformationnelles à basse température de six dérivés sulfurés du benzocycloheptène en solution. On a trouvé que les deux composés parents **2** et **6** contenant du soufre respectivement dans les positions 3 et 1 existent dans la conformation chaise. Les spectres des dérivés du composés **2** substitués en position 2 (**3** : Y = OCE_3 et **4** : Y = Cl) ne révèlent la présence que de la forme Ca. Par ailleurs, les spectres des dérivés du composé **6** substitués en position 2 (**7** : Y = OCH_3 et **8** : Y = Cl) et portant un atome de soufre en position 1 montrent la présence des trois conformères suivants : Ca, Ce et TB (Ca = chaise axiale, Ce = chaise équatoriale et TB = bateau croisé) dont les populations dans le CHF_2Cl sont respectivement de 93 : 5 : 2 et 85 : 12 : 3. La prédominance de la forme Ca dans les deux séries suggère l'existence d'un effet anomère important malgré le fait que la molécule est loin d'être coplanaire (déviation de ≈35°) dans le fragment :—S—C—Y des deux composés **7** et **8**. Contrairement à ce qui a été observé antérieurement avec le segment :—O—C—Y du composé **5**, ce manque de coplanéité ne semble pas diminuer beaucoup le recouvrement n–σ^* caractéristique de l'effet anomère *endo*. On discute des différences dans les effets du O et du S.

[Traduit par la rédaction]

Stereoelectronic concepts are of fundamental importance in modern organic chemistry (1). Among these, the anomeric effect (2) is best known. It refers to the preference of an electronegative substituent for the axial rather than the sterically preferred equatorial position at the anomeric carbon in the tetrahydropyran ring (3). The major experimental results (4) used to characterize this effect were generated by studies of five- and six-membered heterocyclic compounds such as tetrahydrofuran and tetrahydropyran derivatives substituted on the α-carbon. Analogous studies were carried out (5) on the seven-membered cyclic molecules **1**, **5**, and **9** for which the electronegative α-substituent is OCH_3. These benzocycloheptene derivatives revealed the stabilization of the twist-boat (TB) conformer with large variations resulting from changes in the oxygen position of the seven-membered ring. Hence, this ring system is useful to probe conformational effects of stereoelectronic origin.

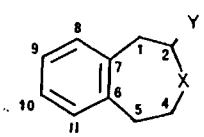

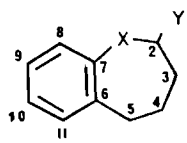

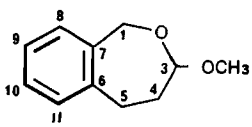

1 X=O , Y=OCH_3 **5** X=O , Y=OCH_3 **9**

2 X=S , Y=H **6** X=S , Y=H

3 X=S , Y=OCH_3 **7** X=S , Y=OCH_3

4 X=S , Y=Cl **8** X=S , Y=Cl

The anomeric effect for second-row atoms such as sulfur has received relatively little attention. Interesting work on six-membered molecules was reported by Pinto and co-workers (6) but none for seven-membered cyclic molecules. We therefore wish to report herein the conformational results of a low-temperature NMR investigation of six derivatives of thiobenzocycloheptene (**2**, **3**, and **4** constituting series 3 and **6**, **7**, and **8** referred to as series 1) whose substituents (Y) are all located at the anomeric carbon. The observed conformational differences will be discussed in light of interactions at the origin of the anomeric effect.

Spectral analysis and conformational results

High-field proton (^1H) and carbon (^{13}C) NMR spectra of

[1]Author to whom correspondence may be addressed.

Can. J. Chem. Downloaded from www.nrcresearchpress.com by 109.225.110.28 on 09/08/12
For personal use only.

TABLE 1. Carbon-13 chemical shifts of compounds **2**–**4** and **6**–**8** at high and low temperatures

Compound	T, °C	Solvent[a]	Conformer	C-1	C-2	C-3	C-4	C-5	C-6	C-7	C-8	C-9	C-10	C-11	OCH_3	α	β	γ	δ
2	−20	CHF_2Cl		41.8	30.6	—	30.6	41.8	143.4	143.4	131.0	127.7	127.7	131.0	—				
H	−143		C	41.4	29.9	—	29.9	41.4	143.5	143.5	131.1	127.7	127.7	131.1	—				
3	−20	CHF_2Cl		46.2	82.9	—	25.2	40.4	143.0	138.3	132.6	127.6	128.3	130.8	57.0				
OCH_3	−140		Ca	46.4	81.1	—	25.0	40.8	143.5	138.1	132.7	127.8	128.6	130.8	57.1	+51.2	+5.0	−4.9	−0.6
4	0	CHF_2Cl		49.4	63.7	—	26.8	40.0	142.5	137.5	133.4	127.2	127.7	130.9	—				
Cl	−120		Ca	49.0	63.7	—	26.1	40.3	143.2	137.4	133.7	127.6	128.8	131.0	—	+33.7	+7.6	−3.8	−1.1
6	0	CHF_2Cl		—	35.6	34.0	28.6	38.0	138.7	149.5	134.1	131.0	127.1	129.0	—				
H	−120			—	35.4	34.1	27.9	37.8	138.1	149.8	134.1	131.2	127.1	129.1	—				
7	0	CHF_2Cl		—	86.3	39.6	23.5	37.0	132.6	149.3	135.8	130.5	127.7	129.6	56.97				
OCH_3	−120		Ca(93%)[b]	—	84.1	40.3	21.5	37.4	131.0	140.8	136.3	130.3	127.8	130.0	56.95	+48.7	+6.2	−6.4	−0.4
			Ce(5%)	—	91.0	42.0	27.0	36.2	[c]	150.8	[d]	[d]	[d]	[d]	56.95	+55.6	+7.9	−0.9	−0.8
			TB(2%)	—	86.3	32.8	23.5	31.8	[c]	[c]	[c]	[c]	[c]	[c]	58.09				
8	0	CHF_2Cl		—	64.4	43.3	24.3	36.4	132.0	148.8	135.7	130.7	127.8	130.6	—				
Cl	−120		Ca(85%)[b]	—	64.3	43.6	21.6	37.1	131.0	149.5	136.0	131.0	127.7	130.7	—	+28.9	+9.5	−6.3	−0.7
			Ce(12%)	—	[d]	45.9	28.4	35.8	[d]	149.1	135.0	[d]	[d]	[d]	—	—	+11.8	+0.5	−2.0
			TB(3%)	—	[c]	33.7	26.0	30.1	[c]	[c]	[c]	[c]	[c]	[c]	—				

[a]Chemical shifts in CH_3OCH_3 are similar.
[b]Uncertainties on conformer populations were ±0.5.
[c]Low S/N or superposed with the major signals.
[d]Superposed with the majors signals.

compounds **2**–**4** (series 3) and **6**–**8** (series 1) were obtained at different temperatures between 0 and −143°C in two different solvent systems (CHF_2Cl and CH_3OCH_3).

The 100.6 MHz ^{13}C NMR decoupled spectrum of the parent compound **2** (Y = H) of series 3 shows five well-resolved signals at −20°C. No spectral change was observed when the temperature was lowered to −120°C.

This result clearly establishes that **2** exists as a single conformer. In support of this conclusion, the 400.1 MHz ^1H NMR spectrum at −143°C shows splittings characteristic of axial and equatorial protons of the single conformer. After assignment of the ^1H and ^{13}C signals at 25°C using normal (7) and long-range (8) HETCOR 2D spectra as summarized in Tables 1 and 2, the following proton–proton vicinal coupling constants were obtained for the C4—C5 bond at −20°C ($^3J_{aa}$ = 11.2 Hz; $^3J_{ee}$ = 7.0 Hz; $^3J_{ae}$ < 1.0 Hz). A comparison with similar benzocycloheptene derivatives (9) indicates that these parameters are characteristic of a chair conformation. The activation energy of the chair inversion determined (10) at the coalescence temperature of the H-2 signal (T_c = −127°C), is $\Delta G^{\neq}$ = 7.0 ± 0.3 kcal mol^{-1} in CHF_2Cl.

The 100.6 MHz ^{13}C and 400.1 MHz ^1H NMR spectra of derivatives **3** (Y = OCH_3) and **4** (Y = Cl) showed a slight broadening of the signals when lowering the temperature to −140°C. This observation is in accord with the presence of a single conformer. The assignment of the proton signals for these two compounds was readily made using the ^1H–^1H COSY 2D experiment (11) at −120°C, while the ^{13}C signal assignment was made by comparison with the chemical shifts of the parent compound **2**. The pertinent parameters are given in Tables 1 and 2.

The single conformer for each of **3** and **4** is found to have a chair geometry from consideration of the vicinal proton–proton coupling constants about the C4—C5 bond ($^3J_{aa}$ = 11.0 and 11.6 Hz; $^3J_{ee}$ = 6.6 and 6.8 Hz for both **3** and **4**; $^3J_{ae}$ < 1.0 Hz) obtained at −120°C. These values are similar to those determined for the chair form of compound **2**. The orientation of the polar substituents (OCH_3 for **3** and Cl for **4**) is then deduced as axial by the characteristic equatorial–equatorial vicinal coupling constants about the C1—C2 between H-2 and the two H-1 ($^3J_{ee}$ = 6.6 Hz for **3** and 6.2 Hz for **4**). The substituent chemical shift effects (12) α, β, γ were determined from the ^{13}C data at −120°C for the Ca forms of **3** and **4** as summarized in Table 1.

Decoupled 100.6 MHz ^{13}C NMR spectra of the parent compound **6** (Y = H) at variable temperature are also characteristic of a single conformer; indeed no spectral change is observed down to −120°C. Normal (7) and long-range (8) HETCOR 2D experiments at 25°C were used to assign the carbon peaks reported in Table 1.

As for compound **2**, the 400.1 MHz ^1H NMR spectrum of **6** at low temperature (−120°C) also shows splitting of the axial and equatorial proton signals that were assigned using COSY 2D data (11). The chair conformer is then deduced from the values of the vicinal coupling constants between H-4 and H-5, namely $^3J_{4a-5a}$ = 11.8 Hz; $^3J_{4e-5e}$ = 7.6 Hz; $^3J_{ae}$ < 1.0 Hz, which are found to be similar to those obtained for compounds **2**–**4**. $\Delta G^{\neq}$ is calculated for the inversion of the chair at the coalescence temperature (10) of H-2 (T_c = −45°C) and is equal 10.8 ± 0.3 kcal mol^{-1}.

On lowering the temperature, both the methoxy and chloro derivatives (**7** and **8**) showed changes in the 100.6 MHz ^{13}C NMR and also in the 400.1 MHz ^1H NMR spectra. For example, Fig. 1 shows that the aliphatic carbon signals (C-2 to C-5) of **7** split into three components of unequal intensities (93:5:2) at −120°C, while for compound **8** the intensities are 85:12:3 at −120°C, both in CHF_2Cl.

To show that for **7** the less abundant of the three peaks (2%) in CHF_2Cl is not an impurity but a real conformer signal, the saturation transfer technique (13) was used with selective excitation of the C-2 signals using the DANTE

Can. J. Chem. Downloaded from www.nrcresearchpress.com by 109.225.110.28 on 09/08/12
For personal use only.

Can. J. Chem. Downloaded from www.nrcresearchpress.com by 109.225.110.28 on 09/08/12
For personal use only.

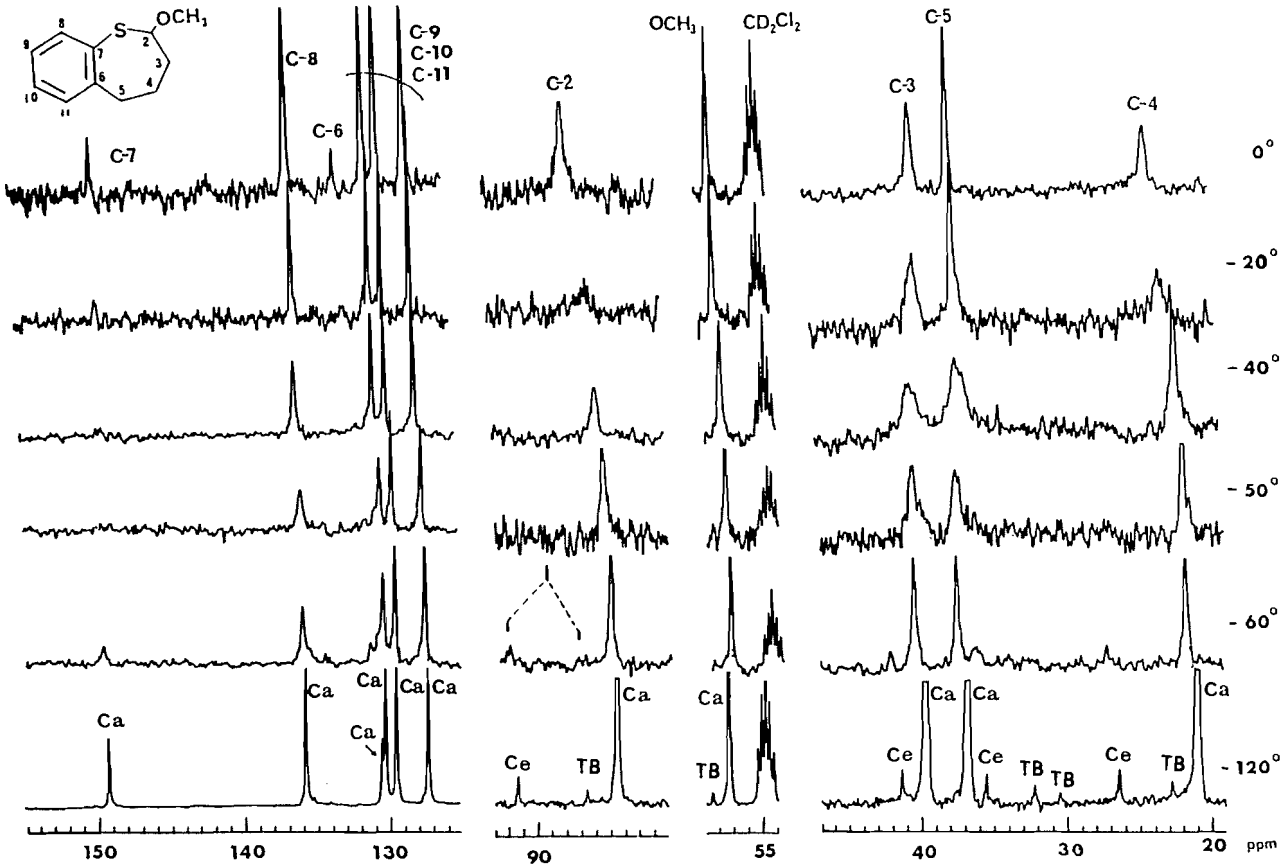

FIG. 1. Variable temperature 100.6 MHz ^{13}C NMR spectra of **7**, in CHF_2Cl (Ca = axial chair, Ce = equatorial chair, TB = twist-boat).

sequence (14) as illustrated in Fig. 2. At −85°C in CHF_2Cl, selective saturation of the minor peak at 86.3 ppm (Fig. 2*b*) effectively reduced the relative intensity of the other two peaks located at 84.1 and 91.0 ppm. Saturation of the major peak (84.1 ppm) was also accompanied by transfer of saturation that, as Fig. 2*c* shows, modified the other two signals. This transfer of saturation between the three signals confirms the presence of three equilibrating conformers.

The ^{13}C NMR spectrum of compound **8** at −120°C shows that the chemical shifts of the minor peaks (C-3 to C-5) are similar to those of **7** and therefore in accord with the presence of three conformers. The ^{13}C aliphatic signals for the two most abundant conformers of compounds **7** and **8** have been assigned by selective double irradiation of H-5 and H-4 respectively. A comparison with ^{13}C chemical shifts of the parent compound **6** was made to assign the aromatic carbons. From these results, the α, β, γ chemical shift parameters (12) were calculated and are summarized in Table 1. The γ parameter is the most reliable diagnostic (15) of the Ca or Ce forms. It is observed that this parameter for **7** is negative, larger for Ca (−6.4 ppm) than for Ce (−0.9 ppm), in accord with the value already observed (5) for the Ca (−6.8 ppm) and Ce (−2.2 ppm) forms of the reference methoxy derivative **5**. The chloro compound **8** also possesses a greater negative γ value for Ca (−6.3 ppm) than for Ce (+0.5 ppm) as commonly observed in many other analogs (16).

To support the conformational results obtained from the ^{13}C parameter analysis, the ^{1}H NMR spectra of **7** and **8** were also analyzed at −120°C. However, because the majority of the signals of the two less-populated conformers (namely the second and third conformer in order of decreasing population) overlap with those of the major conformer (namely the first conformer), complete spectral assignment for **7** was made using the ^{1}H–^{1}H COSY 2D experiment (11) at −120°C. Figure 3 shows the contour plot obtained at −120°C from the COSY 2D experiment together with the normal one-dimensional ^{1}H spectrum above it. The diagonal peaks correspond to the chemical shifts of the various signals in the normal spectrum while the off-diagonal peaks result from coherence transfer via *J* coupling.

The downfield signal H-2e at 4.6 ppm was taken as starting point for the assignment. This signal numbered 1 on the diagonal of the contour plot shows two correlations (2 and 3) that identify H-3e and H-3a. Next, the H-3e peak at 2.4 ppm gives rise to the two correlations 4 and 5 that identify H-4e and H4a. Finally, the two protons H-5a and H-5e were assigned using the two correlations 6 and 7. The assignment of axial and equatorial protons for **8** was similarly made and the data are presented in Table 2.

For the major conformer of **7** and **8**, the vicinal coupling constants between H-4 and H-5 agree with chair forms for which the substituent orientation is deduced as axial using the vicinal proton–proton coupling constant between H-2 and the two H-3 protons ($^{3}J_{2e-3e}$ = 3.7 Hz; $^{3}J_{2e-3a}$ = 2.6 Hz for **7** and $^{3}J_{2e-3e} = {}^{3}J_{2e-3a}$ = 3.0 Hz for **8**). The minor H-2 signals at 4.09 and 4.66 ppm for the second conformer of both compounds **7** and **8** showed only one large coupling con-

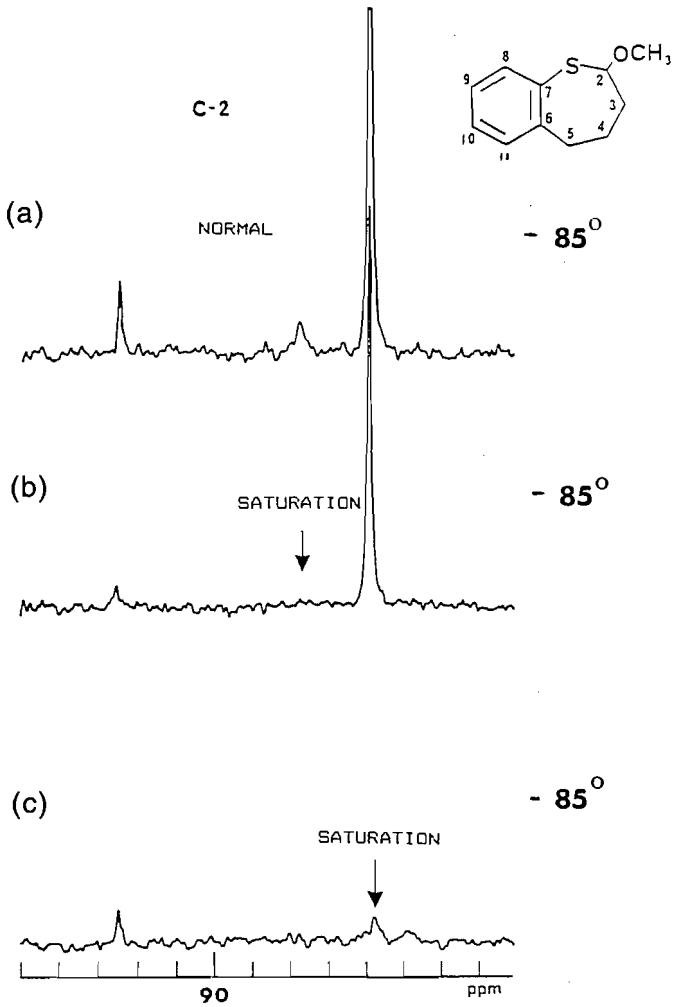

FIG. 2. Partial 100.6 MHz ^{13}C NMR spectra of **7** at −85°C with saturation transfer between the three conformers. (The intensities are normalized with the solvent signal.)

stant between H-2 and one of the two H-3 protons ($^3J_{2a-3a}$ = 11.3 Hz for **7** and 11.5 Hz for **8**) which is indicative of an equatorial orientation of the polar substituents (Y = OCH_3 for **7** and Y = Cl for **8**).

For the third and less populated conformer, no signal was detected in the ^1H spectra because of overlap with the major signals. However, based on the general behaviour for this family of compounds, the most likely conformer possible is the twist-boat form (TB).

In conclusion, the ^1H and ^{13}C NMR parameters for **7** and **8** are in accord with the presence of the three conformers, namely, Ca, Ce, TB, in the ratios summarized in Table 1.

The $\Delta G^{\neq}$ values were estimated (17) at the coalescence temperatures of signals in the ^{13}C NMR spectra. The results for **7** are $\Delta G^{\neq}$(Ca–TB) = 12 ± 1 kcal mol^{-1} (T_c = −20°C) and $\Delta G^{\neq}$(Ce–TB) = 9 ± 1 kcal mol^{-1} (T_c = −50°C), while for the chloro compound **8**, $\Delta G^{\neq}$(Ca–TB) = 10.7 ± 0.5 kcal mol^{-1} (T_c = 35°C) and $\Delta G^{\neq}$(Ce–TB) = 10.2 ± 0.5 kcal mol^{-1} (T_c = −40°C).

Discussion

Conformation of the parent compounds 2 and 6

The ^1H and ^{13}C NMR spectra of the parent compounds **2** and **6** revealed exclusively the presence of the chair (C) conformation. This large preference for C over TB is totally in accord with that observed for analogous benzoxepins (5) and is in accord with the relative conformational energies calculated for TB using the MM2 Molecular Mechanics computer program (18) (2.8 kcal mol^{-1} for **2** and 3.1 kcal mol^{-1} for **6**).

Conformational dynamics

The activation energies for the conformational exchange processes of the sulfur compounds are summarized in Table 3. While compound **2** (Y = H), with sulfur at the 3 position, shows a low barrier for the C ⇄ C* inversion (ΔG^* = 7.0 kcal mol^{-1}), the three derivatives with sulfur at the 1 position (**6**, Y = H; **7**, Y = OCH_3; **8**, Y = Cl) possess a higher free energy barrier for the C ⇄ C* process (10.7–12.0 kcal mol^{-1}). The observation that the 1,5-benzodithiepin series (19) showed a similar high free energy barrier (10.9–12.9 kcal mol^{-1}) suggests that rotation about the phenyl–S bond contributes to raise the barrier for conformational interconversion.

Anomeric effect in the methoxy derivatives 3 and 7

In a previous publication (20), Wolfe *et al.* using the theoretical PMO method for sulfur derivatives confirmed the large preference for the *gauche* form in the :—S—C—Y moiety (dihedral angle θ = 60°) over the *anti* form (θ = 180°). The stabilization energy resulting from an interaction between the occupied (n_s) and unoccupied (σ^*_{C-Y}) molecular orbitals is proportional to $S^2/\Delta E$ (where S is the overlap between the two orbitals and ΔE is the energy difference between these two orbitals). The analysis of the n_x–σ^*_{C-Y} orbital interaction within this framework (20) predicts better overlap for the n_O than the n_S free electron pair and it is suggested that this term should dominate over the energy gap term (ΔE). Consequently, the anomeric effect is expected to be greater for the :—O—C—Y than for :—S—C—Y moiety. *Ab initio* studies (21) made on the O—C—O and S—C—O fragments are in accord with the above *n*-σ* analysis. Furthermore, assuming that a longer C—Y bond is a reflection of a stronger anomeric effect (22), the observation that the C—Cl bond lengths in some six-membered rings (23) are longer for :—O—C—Cl (1.84 Å) than for :—S—C—Cl (1.80 Å), supports the above prediction on the relative strength of the anomeric effect.

In spite of these considerations, it is found that the axial conformer is more favored in cyclic six-membered sulfur compounds because the C—S (1.84 Å) bond is longer than C—O (1.45 Å) and this reduces steric repulsion in Ca. For example, the results for both the six-membered 2-methoxytetrahydropyran (3*a*) **10** and 2-methoxytetrahydrothiopyran (24) **11** showed an identical Ca:Ce population ratio at 25°C in the nonpolar solvent CCl_4 (83:17), while in the more polar acetonitrile the Ca:Ce ratio is 68:32 for **10** and 79:21 for the sulfur analog **11**.

Comparison of our results for the two methoxy benzothiepins (**3** and **7**) to the analogous methoxy benzoxepins (**1** and **5**, whose results are also reported in Table 3) show similar axial preference in the 3-hetero series (>98% for **3** and 94% for **1** at −120°C), while for the 1-hetero series the Ca amounts are strikingly different, 93% for **7** and 5% for **5**. This low Ca population for **5** was explained (5) by a weakening of the *endo*-anomeric effect produced by a large departure from coplanarity in the :—O—C—OMe fragment as revealed by calculated torsional angles. A stronger

Can. J. Chem. Downloaded from www.nrcresearchpress.com by 109.225.110.28 on 09/08/12
For personal use only.

Can. J. Chem. Downloaded from www.nrcresearchpress.com by 109.225.110.28 on 09/08/12
For personal use only.

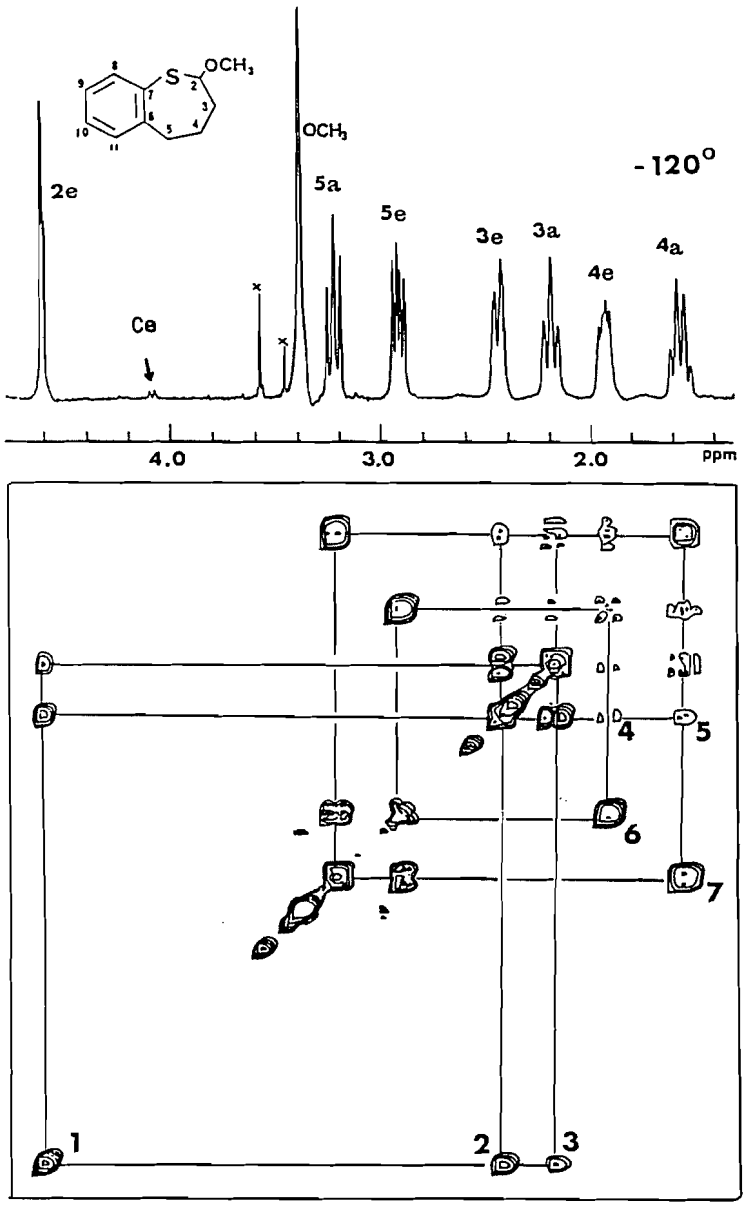

FIG. 3. Partial 400.1 MHz ^{1}H NMR 2D COSY spectrum of **7** at −120°C in CHF_2Cl. (X denotes impurity signals.)

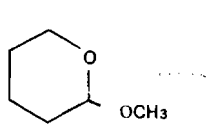

10

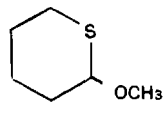

11

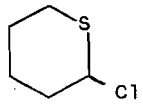

12

exo-anomeric effect was also expected to further stabilize the Ce form of **5**. In contrast, the departure from coplanarity in the :—S—C—OMe fragment of **7** does not appear to appreciably attenuate the n–σ* overlap from the *endo*-anomeric effect. In terms of free energy, the axial conformer of **7** is stabilized over the equatorial form by ΔG^0(a − e) = −1.0 kcal mol^{-1} while in **5** the situation is reversed with a destabilization ΔG^0(a − e) = 0.9 kcal mol^{-1}. Thus, the total energy difference between the Ca and Ce forms of **5** and **7** is estimated at about 1.9 kcal mol^{-1}. It would appear that the larger and more diffuse character of the n_S orbital relative to n_O orbital allows it to contribute more favorably to n–σ* overlap in spite of the appreciable departure from coplanarity as suggested by the torsion angle near 35° that is estimated for both **5** and **7** by the MM2 computer program (18).

Finally it appears that the stereoelectronic stabilization of the TB in compound **7**, mainly by the anomeric effect, is sufficient to lead to observable NMR signals (2%), while for compound **5** the attenuation of the anomeric effect (n–σ*$_{C—O}$) was not sufficient to lead to observable signals for the TB form (5*b*).

*Anomeric effect in the chloro derivatives **4** and **8***

The advantage of the chloro substituent over the methoxy group is that it has no particular rotamer favouring the *exo*-anomeric interaction (25). Now, without this contribution,

TABLE 2. Proton ^1H chemical shifts[a] of compounds **2–4** and **6–8** at high and low temperatures

Compound	T, °C	Conformer[a]	H-1	H-2	H-3	H-4	H-5	OCH_3
2	−20		2.68 (t, H1), J = 4.6 Hz	3.26 (t, H2), J = 4.6 Hz	—	See H2	See H1	—
	−143	C	2.60 (dd, H1a), $^2J_{1a-1e}$ = −14.6 Hz, $^3J_{1a-2a}$ = 11.2 Hz; 2.70 (dd, H1e), $^2J_{1e-1a}$ = −14.6 Hz; $^3J_{1e-2e}$ = 7.0 Hz	3.30 (dd, H2a), $^2J_{2a-2e}$ = −14.9 Hz, $^3J_{2a-1e}$ = 11.2 Hz; 3.14 (dd, H2e), $^2J_{2e-2a}$ = −14.9 Hz, $^3J_{2e-1e}$ = 7.0 Hz	—	See H2	See H1	—
3	0		[b]	[b]	—	[b]	[b]	[b]
	−120	Ca	3.73 (d, H1a), $^2J_{1a-1e}$ = −14.3 Hz; 3.49 (dd, H1e), $^2J_{1e-1a}$ = −14.3 Hz, $^3J_{1e-2e}$ = 6.6 Hz	4.67 (d, H2), $^3J_{2e-1e}$ = 6.6 Hz	—	2.73 (t, H5e), $^2J_{4a-4e}$ = −14.3 Hz, $^3J_{4a-5a}$ = 11.0 Hz; 2.60 (dd, H4e), $^3J_{4e-4a}$ = −14.3 Hz, $^3J_{4e-5e}$ = 6.6 Hz	3.21 (dd, H5e), $^2J_{5e-5a}$ = −14.3 Hz, $^3J_{5e-4e}$ = 6.6 Hz; [c] (H5a)	3.29
4	0		[b]	[b]		[b]	[b]	[b]
	−120	Ca	3.86 (d, H1a), $^2J_{1a-1e}$ = −14.3 Hz; 3.45 (dd, H1e), $^2J_{1e-1a}$ = −14.3 Hz, $^3J_{1e-2e}$ = 6.6 Hz	5.54 (d, H2), $^3J_{2e-1e}$ = 6.2 Hz	—	2.96 (t, H4a), $^2J_{4a-4e}$ = −14.1 Hz, $^3J_{4a-5a}$ = 11.6 Hz; 2.75 (dd, H4e), $^2J_{4e-4a}$ = −14.1 Hz, $^3J_{4e-5e}$ = 6.8 Hz	3.3–3.1 (H5e, H5a)	—
6	−20		—	2.73 (t, H2), J = 5.4 Hz	2.09 (m, H3)	1.79 (br, H4)	3.03 (t, H5), J = 5.3 Hz	—
	−120	C	—	2.53 (ddd, H2a), $^2J_{2a-2e}$ = −13.6 Hz, $^3J_{2a-3a}$ = 13.0 Hz, $^3J_{2a-3e}$ = 2.0 Hz; 2.89 (d, H2e), $^2J_{2a-2e}$ = −13.6 Hz	1.92 (qt, H3a), $^2J_{3a-3e}$ = −13.4 Hz, $^3J_{3a-2a}$ = 13.0 Hz, $^3J_{3a-4a}$ = 13.0 Hz, $^3J_{3a-4e}$ = 3.0 Hz; 2.28 (m, H3e)	1.28 (qd, H4a), $^2J_{4a-4e}$ = −13.2 Hz, $^3J_{4a-3a}$ = 13.0 Hz, $^3J_{4a-5a}$ = 11.8 Hz, $^3J_{4a-3e}$ = 3.4 Hz; 2.08 (m, H4e)	3.13 (t, H5a), $^2J_{5a-5e}$ = −13.7 Hz, $^3J_{5a-4a}$ = 11.8 Hz; 2.92 (dd, H5e), $^2J_{5e-5a}$ = −13.7 Hz, $^3J_{5e-4e}$ = 7.6 Hz	—
7	0		—	4.45 (br, H2)	2.23 (m, H3), 2.15 (m, H3′)	1.75 (m, H4, H4′)	3.15 (m, H5), 2.91 (m, H5′)	3.40
	−120	Ca	—	4.60 (dd, H2), $^3J_{2e-3a}$ = 2.6 Hz, $^3J_{2e-3e}$ = 3.7 Hz	2.19 (td, H3a), $^2J_{3a-3e}$ = −13.9 Hz, $^3J_{3a-4a}$ = 13.9 Hz, $^3J_{3a-2e}$ = 2.6 Hz; 2.45 (dd, H3e), $^2J_{3e-3a}$ = −13.9 Hz, $^3J_{3e-2e}$ = 3.7 Hz	1.56 (qd, H4a), $^2J_{4a-4e}$ = −13.9 Hz, $^3J_{4a-3a}$ = 13.9 Hz, $^3J_{4a-5a}$ = 11.8 Hz, $^3J_{4a-3e}$ = 1.7 Hz; 1.92 (m, H4e)	3.22 (dd, H5a), $^2J_{5a-5e}$ = −13.6 Hz, $^3J_{6a-4a}$ = 11.8 Hz; 2.91 (dd, H5e), $^2J_{5e-5a}$ = −13.6 Hz, $^3J_{5e-4e}$ = 7.6 Hz	3.39
		Ce	—	4.09 (d, H2), $^3J_{2a-3a}$ = 11.3 Hz	[c]	[c]	[c]	[c]
8	0		—	5.10 (br, H2)	2.36 (br, H3)	1.89 (br, H4), 1.73 (br, H4′)	3.09 (br, H5), 2.93 (br, H5′)	—
	−120	Ca	—	5.44 (t, H2), $^3J_{2e-3a}$ = 3.0 Hz, $^3J_{2e-3e}$ = 3.0 Hz	2.42 (t, H3a), $^2J_{3a-3e}$ = −13.2 Hz, $^3J_{3a-4a}$ = 13.2 Hz; 2.55 (dd, H3e), $^2J_{3e-3a}$ = −13.4 Hz, $^3J_{3e-4e}$ = 3.5 Hz	2.77 (q, H4a), $^2J_{4a-4e}$ = −13.2 Hz, $^3J_{4a-3a}$ = 13.2 Hz, s3J_{4a-5a} = 13.2 Hz; 1.98 (m, H4e)	3.15 (t, H5a), $^2J_{5a-5e}$ = −14.0 Hz, $^3J_{5a-4a}$ = 13.2 Hz; 2.96 (dd, H5e), $^2J_{5e-5a}$ = −14.0 Hz, $^3J_{5e-4e}$ = 8.0 Hz	—
		Ce	—	4.66 (d, H2), $^2J_{2a-3a}$ = 11.5 Hz	[c]	[c]	[c]	[c]

[a]C = chair, Ca = axial chair, Ce = equatorial chair.
[b]Parameters are similars to those at −120°C.
[c]Superposed with major conformer.

Can. J. Chem. Downloaded from www.nrcresearchpress.com by 109.225.110.28 on 09/08/12
For personal use only.

TABLE 3. Thermodynamic and kinetic data for compounds **1–8**

Compound	Solvent	Conformer	Population, %[a,b]	$-\Delta G^0$, kcal/mol (T, °C)	$\Delta G^{\neq}$, kcal/mol (T, °C)
1[c]	CHF_2Cl	Ca	94	0.84 (Ca/Ce, −120)	8.8 (Ca→Ce, −85)
		Ce	6		
2	CHF_2Cl	C	>98	>1.2 (C/TB, −143)	7.0 (C→C*, −127)
3	CHF_2Cl	Ca	>98	>1.2 (C/TB, −140)	—
4	CHF_2Cl	Ca	>98	>1.2 (C/TB, −120)	—
5[c]	CHF_2Cl	Ca	5	0.89 (Ce/Ca, −120)	8.4 (Ce→Ca, −90)
			95		
6	CHF_2Cl	C	>98	>1.2 (C/TB, −120)	10.8 (C→C*, −45)
7	CHF_2Cl	Ca	93	1.0 (Ca/Ce, −120)	12.0 (Ca→TB, −20)
		Ce	5	1.2 (Ca/TB, −120)	9.0 (Ce→TB, −50)
		TB	2	0.3 (Ce/TB, −120)	
8	CHF_2Cl	Ca	85	0.6 (Ca/Ce, −120)	10.7 (Ca→TB, −35)
		Ce	12	1.0 (Ca/TB, −120)	10.2 (Ce→TB, −40)
		TB	3	0.4 (Ce/TB, −120)	

[a]Populations in CH_3OCH_3 are similar for **2–6**, while for **7** and **8** populations are Ca:Ce:TB, 91:6:3 and Ca:Ce:TB, 80:17:3, respectively.
[b]Uncertainties on conformer populations were ±0.5.
[c]Data taken from ref. 5*b*.

the Ca/Ce ratio should be representative of the strength of *endo*-anomeric effect alone (25). Furthermore, the relative steric effect of both the methoxy and the chloro groups is expected to be similar as indicated by the similar conformational *A* values in the cyclohexane series (26).

Considering the relative energies of the σ^*_{C-Y} orbitals (lower for Y=Cl than for Y=OCH_3) (27), the energy gap ΔE for the n_S–σ^*_{C-Y} interaction suggests a better anomeric stabilization for the chloro substituent than for the methoxy group. Considering the similar electronegativity of Cl and OCH_3, it is expected (28) that both σ^*_{C-Cl} and σ^*_{C-OCH3} would provide the same overlap (S^2) with the n_S orbitals. Consequently for a six-membered ring, the 2-chlorotetrahydrothiopyran **12** shows a larger axial preference[2] with ΔG^0(a − e) = −1.75 kcal mol^{-1} than the methoxy analogue **11** for which ΔG^0(a − e) = −1.53 kcal mol^{-1}.

Our results for the thio derivatives **3** and **4** (>98% of Ca) are not sufficiently sensitive to show differences between the chloro and methoxy substituents. However, in compounds **7** and **8** a larger axial preference is observed for the methoxy derivative **7** relative to the chloro derivative **8**. This result is opposite to that reported earlier for six-membered rings.[2] An electrostatic interaction between the polar substituent (Cl or OCH_3) and the benzo group favouring the Ce form has been identified in the past (9) for the methoxy and chloro derivatives **13** and **14** of benzocycloheptene. Such an electrostatic interaction might also be responsible for the stronger axial preference for **7** (Y = OCH_3) than for **8** (Y = Cl).

Considering that in both compounds **4** and **8** the chloro group is located at the same ring position, then the difference in the Ca amounts should arise mainly from the change in the S-atom position in the seven-membered ring. With sulfur located at that 3 position (as in **4**), the large preference for the Ca (Ca/Ce > 49) is controlled by the *endo*-anomeric effect, while with sulfur at the 1 position (as in **8**) the preference for the axial form is reduced slightly (Ca/Ce = 7.7) and, possibly, as the result of a departure from coplanarity in the :—S—C—Cl moiety in **8**, which could lead to a slight reduction of the *endo*-anomeric effect and therefore shift the equilibrium towards the Ce conformer.

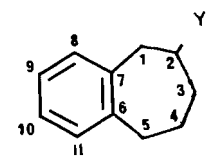

13 Y=OCH_3
14 Y=Cl

Finally, the *endo*-anomeric effect n_S–σ^*_{C-Cl} contributes to the stabilization of TB (3%) in **8** but not in **4**. This trend was also observed for the methoxy derivatives **3** and **7**.

Experimental

High-field variable temperature ^1H, ^{13}C, and COSY 2D NMR spectra were recorded with a Bruker WH-400 spectrometer equipped with a B-VT-100 variable temperature unit. Calibration using a copper–constantan thermocouple inside an NMR tube containing a solvent indicates that the temperatures reported are precise within ±3°C.

The samples used in the variable temperature ^1H experiment were prepared as a CHF_2Cl solution (15–20 mg in 0.55 mL of solution) containing 18% of CD_2Cl_2 (for locking purposes), 82% of CHF_2Cl, and a small quantity of Me_4Si in 5-mm tubes that were degassed and sealed. The degassed carbon-13 samples were prepared in CHF_2Cl or CH_3OCH_3 (120–180 mg in 2.2 mL of solution) containing 18% of CD_2Cl_2 (for locking purposes) and a small quantity of Me_4Si.

Reliable integrations from the ^{13}C spectra were obtained using a 0.1–0.2 s delay between pulses and by averaging at least three sets of carbon signals for each compound.

Normal and long-range HETCOR 2D NMR spectra were performed on a Varian VXR-300 spectrometer in $CDCl_3$, using the published pulse sequence (7, 8), for which 128 FID of 2K were recorded. A Gaussian function was applied and the final matrix was zero-filled to 256 × 2K. The digital resolution obtained was between 5–10 Hz/pt (F2, ^{13}C) and 2–4 Hz/pt (F1, ^1H).

Typical parameters for the COSY 2D spectra are as follows:

[2]Reference 2, p. 24.

Can. J. Chem. Downloaded from www.nrcresearchpress.com by 109.225.110.28 on 09/08/12
For personal use only.

Can. J. Chem. Downloaded from www.nrcresearchpress.com by 109.225.110.28 on 09/08/12
For personal use only.

128FID × 1K of 16 scans were acquired and the final matrix was treated with Gaussian multiplication and zero-filled to 1K × 1K matrix. The digital resolution was between 2 and 4 Hz/pt.

The high-resolution mass spectra were taken on a modified MS-50 spectrometer at 70 eV.

The molecular mechanics (MM2) calculations were obtained on an IBM/AT computer, using the PCMODEL program (18) purchased from Serena Software, Box 3076, Bloomington, IN 47402-3076.

Compounds **2–4** and **6–8** were prepared as follows:

1,2,4,5-Tetrahydro-3-benzothiepin (2)

This compound was prepared by the reaction of ditosylated 1,2-benzenediethanol (*5b*) (10 g, 24.4 mmol) in 150 mL of ethanol with sodium sulfide nonanhydrate (5.9 g, 24.5 mmol). The suspension was stirred vigourously for 6 h at room temperature and then filtered. The solvent was removed under vacuum and the remaining liquid was purified by flash chromatography on silica gel (230–400 mesh) using a mixture of CH_2Cl_2:hexanes/50:50 as eluant. The solid compound **2** (2.4 g), reported in the literature (29), was confirmed by the ^1H and ^{13}C NMR spectra listed in Tables 1 and 2. Mass spectrum EI, Exact Mass calcd. for $C_{10}H_{12}S$: 164.066; found: 164.066.

2-Chloro-1,2,4,5-tetrahydro-3-benzothiepin (4)

This compound was prepared by the reaction of 1,2,4,5-tetrahydro-3-benzothiepin (**2**) (0.78 g, 4.75 mmol) at −20°C for 2 h with *N*-chlorosuccinimide (0.65 g, 4.86 mmol) in 30 mL of carbon tetrachloride. The mixture was then filtered and the solvent evaporated under vacuum to give 0.93 g of liquid, identified by its proton NMR spectrum as a mixture (50:50) of compound **4** and 1,2-dihydro-3-benzothiepin. Many purification attempts by distillation, flash chromatography (silica, alumina, basic alumina), or gas chromatography were unsuccessful and led to 1,2-dihydro-3-benzothiepin. The ^1H and ^{13}C NMR parameters were obtained on the mixture and those of **4** are reported in Tables 1 and 2. Mass spectrum CI, *m/e*: 199 (M + 1); 163 (M − Cl).

2-Methoxy-1,2,4,5-tetrahydro-3-benzothiepin (3)

At −80°C, the chloro derivative (**4**) freshly prepared as above (0.54 g, 2.72 mmol) was dissolved in 100 mL of methanol and the solution was neutralized with $NaHCO_3$ (0.28 g of $NaHCO_3$ was added in excess). The solution was then stirred vigourously at −80°C and a solution of silver trifluoromethanesulfonate (0.7 g, 2.72 mmol) in 5 mL of methanol at −80°C was added dropwise. After 0.5 h, the mixture was filtered, poured into 100 mL of water, and extracted with 3 × 150 mL of ether. The organic layers were dried with magnesium sulfate, filtered, and evaporated under vacuum. Purification by flash chromatography on silica gel (230–400 mesh) eluting with (10% CH_2Cl_2/hexane) yielded 0.32 g of pure 2-methoxy-1,2,4,5-tetrahydro-3-benzothiepin (**3**). The ^1H and ^{13}C NMR parameters are reported in Tables 1 and 2. Mass spectrum EI, Exact Mass calcd. for $C_{11}H_{14}OS$: 194.076; found: 194.073; CI, *m/e*: 195 (M + 1), 163 (M − OCH_3).

2,3,4,5-Tetrahydro-1-benzothiepin (6)

This compound was prepared using thiophenol as starting material by a published method (30). The compound was purified by flash chromatography on silica gel (230–400 mesh) using a mixture of CH_2Cl_2 and hexane as eluant.

The ^1H and ^{13}C NMR parameters are reported in Tables 1 and 2. Mass spectrum EI, Exact Mass calcd. for $C_{10}H_{12}S$: 164.066; found: 164.063.

2-Chloro-2,3,4,5-tetrahydro-1-benzothiepin (8)

N-Chlorosuccinimide (0.68 g, 5.09 mmol) was added to a solution containing compound **6** (0.8 g, 4.87 mmol) in 15 mL of carbon tetrachloride. The mixture was stired overnight, filtered, and evaporated under vacuum to give 0.95 g of compound **8** as a liquid. The ^1H and ^{13}C data listed in Tables 1 and 2 showed the compound to be pure. Mass spectrum CI, *m/e*: 199 (M + 1), 163 (M − Cl).

2-Methoxy-2,3,4,5-tetrahydro-1-banzothiepin (7)

A solution of silver trifluoromethanesulfonate (0.65 g, 2.52 mmol) in 4 mL of methanol was added dropwise to a stirred solution of the chloro compound **8** (0.5 g, 2.52 mmol) in 30 mL of methanol. After 0.5 h the acid mixture was neutralized with $NaHCO_3$, filtered, and added to 10 mL of water. Extractions were made with 3 × 100 mL of ether and the organic fractions were dried with $MgSO_4$, filtered, and evaporated under vacuum. The mixture was purified on flash chromatography eluting with a mixture of 20% CH_2Cl_2:hexane to give 0.39 g of compound **7** as liquid. The ^1H and ^{13}C NMR data are listed in Tables 1 and 2. Mass spectrum EI, Exact Mass calcd. for $C_{11}H_{14}OS$: 194.076; found: 194.073; CI, *m/e*: 195 (M + 1), 163 (M − OCH_3).

Acknowledgments

We acknowledge the assistance of Dr. Phan Viet Minh Tan, Manager of the "Laboratoire de RMN à Haut Champ" at the Université de Montréal. We thank the Natural Sciences and Engineering Research Council of Canada for financial support.

1. P. Deslongchamps. Stereoelectronics effects in organic chemistry. Pergamon Press, Oxford. 1983.
2. A. J. Kirby. The anomeric effect and related stereoelectronic effect at oxygen. Springer-Verlag, New York. 1983.
3. (*a*) R. U. Lemieux, A. A. Pavia, J. C. Martin, and K. A. Watanabe. Can. J. Chem., **47**, 4427 (1969); (*b*) H. Booth and K. A. Khedhair. Tetrahedron, **43**, 4699 (1987); (*c*) J. Chem. Soc. Chem. Commun. 467 (1985); (*d*) J. Chem. Soc. Chem. Commun. 1047 (1982); (*e*) C. B. Anderson and D. T. Sepp. Tetrahedron, **24**, 1707 (1967).
4. (*a*) A. Cosse-Barbi and J. E. Dubois. J. Am. Chem. Soc. **109**, 1503 (1987); (*b*) B. Fuchs, L. Schleifer, and E. Tartakovsky. Nouv. J. Chim. **8**, 275 (1984).
5. (*a*) S. Désilets and M. St-Jacques. J. Am. Chem. Soc. **109**, 1641 (1987); (*b*) Tetrahedron, **44**, 7027 (1988).
6. (*a*) B. M. Pinto, J. Sandoval-Ramirez, R. Dev Sharma, A. C. Willis, and F. W. B. Einstein. Can. J. Chem. **64**, 732 (1986); (*b*) B. M. Pinto, B. D. Johnston, and R. Nagelkerke. J. Org. Chem. **53**, 5668 (1988); (*c*) B. M. Pinto, B. D. Johnston, R. Sandoval-Ramirez, and R. D. Sharma. J. Org. Chem. **53**, 3766 (1988); (*d*) B. M. Pinto, J. Sandoval Ramirez, and R. D. Sharma. Tetrahedron, **26**, 5235 (1985); (*e*) B. M. Pinto, H. B. Schlegel, and S. Wolfe. Can. J. Chem. **65**, 1658, (1987); (*f*) E. Juaristi, E. A. Gonzalez, B. M. Pinto, B. D. Johnston, and R. Nagelkerke. J. Am. Chem. Soc. **111**, 6745, (1989); (*g*) E. Juaristi, J. Tapia, and R. Mendez. Tetrahedron, **42**, 1253 (1986); (*h*) P. v. R. Schleyer, E. D. Jemmis, and G. W. Spitznagel. J. Am. Chem. Soc. **107**, 6393 (1985).
7. A. Bax and G. A. Morris. J. Magn. Reson. **42**, 501 (1981).
8. (*a*) W. F. Reynold, D. W. Hughes, M. Perpick-Dumont, and R. G. Enriques. J. Magn. Reson. **63**, 413 (1985); (*b*) G. E. Martin and A. S. Zektzer. Magn. Reson. Chem. **26**, 631 (1988).
9. D. Ménard and M. St-Jacques. Tetrahedron, **39**, 1041 (1983).
10. (*a*) D. Kost, E. H. Carlson, and M. Raban. J. Chem. Soc. Chem. Commun. 656 (1971); (*b*) J. R. Kurland, M. B. Rubin, and W. B. Wise. J. Chem. Phys. **40**, 2426 (1964).
11. (*a*) A. Kumar. Bull. Magn. Reson. **10**, 96 (1988); (*b*) A. Bax and R. Freeman. J. Magn. Reson. **44**, 542 (1981).
12. (*a*) T. Pehk and E. Lippmaa. Org. Magn. Reson. **3**, 679 (1971); (*b*) H. J. Schneider and V. Hoppen. Tetrahedron Lett. **7**, 579 (1974); (*c*) O. A. Subbotin and N. M. Sergeyev. J. Am. Chem. Soc. **97**, 1080 (1975).
13. J. Sandstrom. Dynamic NMR spectroscopy. Academic Press, New York. 1982. Chap. 4.

14. X. L. Wu, P. Xu, J. Friedrich, and R. Freeman. J. Magn. Reson. **81**, 206 (1989).
15. (*a*) J. B. Lambert and A. R. Vagenas. Org. Magn. Reson. **17**, 265 (1981); (*b*) H. Beierbeck and J. Saunders. Can. J. Chem. **55**, 2814 (1977).
16. H. O. Kalinowski, S. Berger, and S. Braun. Carbon-13 NMR spectroscopy. John Wiley and Sons, New York. 1988. Chap. 3. p. 259.
17. F. A. L. Anet and V. J. Basus. J. Magn. Reson. **32**, 339 (1978).
18. PCMODEL Software, Serena Software Box 3076, Bloomington, Ind.
19. D. Ménard and M. St-Jacques. Can. J. Chem. **64**, 2142 (1986).
20. S. Wolfe, M. H. Whangbo, and D. J. Mitchell. Carbohydr. Res. **69**, 1 (1979).
21. S. Vishveshwara and V. S. R. Rao. Carbohydr. Res. **104**, 21 (1982).
22. I. Tvaroska and T. Bleha. Adv. Carbohydr. Chem. Biochem. **47**, 45 (1989).
23. (*a*) N. De Wolf, C. Romers, and C. Altona. Acta Crystallogr. **22**, 715 (1967); (*b*) C. Altona, C. Knobler, and C. Robers. Acta Crystallogr. **16**, 1217 (1963); (*c*) H. T. Kalff and C. Romers. Acta Crystallogr. **18**, 164 (1965); (*d*) C. Altona and C. Romers. Recl. Trav. Chim. Pays-Bas, **82**, 1080 (1963).
24. N. S. Zefirov, S. Blagoveshchenskil, L. V. Kazimirchik, and O. P. Yakovleva. J. Org. Chem. USSR, **7**, 599 (1971).
25. (*a*) H. Booth and K. A. Khedhair. J. Chem. Soc. Chem. Commun. 467 (1985); (*b*) H. Booth, K. A. Khedhair, and S. A. Readshaw. Tetrahedron, **43**, 4699 (1987).
26. (*a*) F. R. Jensen, C. H. Bushweller, and B. H. Beck. J. Am. Chem. Soc. **91**, 344 (1969); (*b*) E. L. Eliel, N. L. Allinger, S. J. Angyal, and G. A. Morrison. Conformational analysis. John Wiley and Sons, New York. 1965 p. 44; (*c*) N. S. Zefirov, L. G. Gurvich, and A. S. Shashkov. Tetrahedron, **32**, 1211 (1976).
27. N. D. Epiotis, W. R. Cherry, S. Shaik, R. L. Yates, and F. Bernardi. Top. Curr. Chem. **70**, 1 (1977).
28. T. K. Brunck and F. Weinhold. J. Am. Chem. Soc. **101**, 1700 (1979).
29. W. E. Truce and F. J. Lotspeich. J. Am. Chem. Soc. **78**, 848 (1956).
30. V. J. Traynelis and R. F. Love. J. Org. Chem. **26**, 2728 (1961).

Can. J. Chem. Downloaded from www.nrcresearchpress.com by 109.225.110.28 on 09/08/12
For personal use only.

Thermal expansivities of aqueous solutions of 2-butoxyethanol in the water-rich region: transition of mixing scheme

JAMES V. DAVIES

Department of Chemistry, University College of the Cariboo, Kamloops, B.C., Canada V2C 5N3

AND

FRANKIE W. LAU, LOANNE T. N. LE, JOHN T. W. LAI, AND YOSHIKATA KOGA[1]

Department of Chemistry, University of British Columbia, Vancouver, B.C., Canada V6T 1Z1

Received September 19, 1991[2]

JAMES V. DAVIES, FRANKIE W. LAU, LOANNE T. N. LE, JOHN T. W. LAI, and YOSHIKATA KOGA. Can J. Chem. **70**, 2659 (1992).

Thermal expansivities of aqueous solutions of 2-butoxyethanol (BE) were measured at concentrations of $x_{BE} < 0.04$, where x_{BE} is the mole fraction of BE. Thermal expansivity is a second derivative of the Gibbs free energy. The composition derivatives of thermal expansivities, the third derivatives, show peak anomalies at the same loci as the other third derivatives of the Gibbs free energy reported earlier from this laboratory (Can. J. Chem. **67**, 671 (1989); J. Phys. Chem. **94**, 3879 (1990); J. Phys. Chem. **95**, 4119 (1991)). The loci of such anomalies form a boundary that separates two regions of totally different mixing schemes. The mixing scheme in the water-rich region seems to be consistent with the "iceberg formation," the "structure enhancement of H_2O by hydrophobic solute," and the "hydrophobic attraction." In the intermediate composition region, the hydrogen bond network of H_2O collapses due to the presence of too many molecules of BE, and H_2O and BE molecules interact with each other as normal liquid molecules.

JAMES V. DAVIES, FRANKIE W. LAU, LOANNE T. N. LE, JOHN T. W. LAI et YOSHIKATA KOGA. Can. J. Chem. **70**, 2659 (1992).

On a mesuré l'expansibilité thermique de solutions aqueuses du 2-butoxyéthanol (BE) à des concentrations de $x_{BE} < 0.04$ où x_{BE} est la fraction molaire du BE. L'expansibilité thermique est égale à la deuxième dérivé de l'énergie libre de Gibbs. Les dérivés de l'expansibilité thermique en fonction de la composition, les troisièmes dérivés, présentent des anomalies dans les pics aux mêmes endroits que les autres troisièmes dérivés de l'énergie libre de Gibbs rapportées antérieurement par ce laboratoire (Can. J. Chem. **67**, 671 (1989); J. Phys. Chem. **94**, 3879 (1990); J. Phys. Chem. **95**, 4119 (1991)). Les locations de ces anomalies forment une frontière qui sépare deux régions dans lesquelles les processus de mélange sont totalement différents. La processus dans la région riche en eau semble être en accord avec les concepts de «formation d'iceberg», de «rehaussement de la structure de l'eau par le soluté hydrophobe» et d'«attraction hydrophobe». Dans la région de composition intermédiaire, la présence d'une trop grande quantité de molécules de BE provoque une désagrégation du réseau de liaisons hydrogènes de l'eau et les molécules d'eau et de BE interagissent les unes avec les autres comme des molécules liquides normales.

[Traduit par la rédaction]

Introduction

In previous thermodynamic studies from this laboratory on aqueous solutions of 2-butoxyethanol (BE), the excess partial molar enthalpies, $H_m^E(i)$ (1, 2), entropies, $S_m^E(i)$ (3), and volumes, $V_m^E(i)$ (4, 7), were reported. Here i stands for BE or H_2O. These quantities were determined accurately and at small increments in mole fraction. Thus the derivatives of these quantities with respect to the amount of the ith species were evaluated with a reasonable accuracy, within several per cent. These derivatives signify the effect of an additional ith species on the respective partial molar quantity of the existing ith species. Thus, it was argued (1–4, 7) that they provide a measure of the ith species – ith species interaction in terms of enthalpy, entropy, or volume, respectively.

With the aid of these quantities, we pointed out that there are three composition regions in the single phase domain, in each of which the mixing scheme is qualitatively different from those in the other regions. Furthermore, we pointed out (1–4, 7) that the crossovers between the neighbouring regions are associated with anomalies in the third or the fourth derivatives of the Gibbs free energy. In particular, the transition from the water-rich to the intermediate composition regions was accompanied by peak anomalies in the third derivatives of the Gibbs free energy.

This work is a part of continuing efforts of learning how the other third derivatives behave across this boundary in mixing scheme. To this end we measured thermal expansivities of the BE–H_2O mixtures.

Experimental

2-Butoxyethanol (BE) used was supplied by Aldrich (99+%, spectroscopic grade). H_2O was freshly distilled. The mixtures were prepared by weighing. BE was weighed out, at least 3 g, to within 0.0001 g and H_2O, about 300 g, to 0.01 g for series I (see below), or to 0.1 g for series II. Thus the mole fraction was determined at worst within 0.05%, taking account of the effect of degassing noted below.

A home-made dilatometer is shown in Fig. 1. It is made of Pyrex glass with a volume of about 270 mL. A capillary of 1 mm diameter is fitted through a B19 ground joint. A standard wooden meter stick was fixed to the capillary by means of two plastic cord holders. The cross-sectional areas of the capillary at various positions of the meter stick were calibrated by using a small amount of mercury. It was found necessary to degas the sample immediately before filling the dilatometer. Otherwise, gas bubbles formed in the dilatometer. Degassing was accomplished by connecting the flask containing a sample solution to a 2 L flask evacuated to approxi-

[1]Author to whom correspondence may be addressed.

[2]Revision received June 3, 1992.

Can. J. Chem. Downloaded from www.nrcresearchpress.com by 109.225.110.28 on 09/08/12
For personal use only.

TABLE 1. Thermal expansivities of aqueous solutions of 2-butoxyethanol, series I

Temp. (°C):	α_p' (measured) (10^{-4} K^{-1})					α_p' (fitted) (10^{-4} K^{-1})		
x_{BE}	21.00	23.00	25.00	27.00	29.00	20.00	25.00	30.00
0	2.173	2.376	2.572	2.761	2.943	2.054	2.573	3.005
0.002000	2.247	2.466	2.667	2.834	3.032	2.157	2.664	3.166
0.004000	2.358	2.576	2.797	2.957	3.142	2.240	2.784	3.215
0.006000	2.475	2.701	2.900	3.059	3.234	2.362	2.894	3.300
0.008000	2.604	2.815	3.013	3.172	3.349	2.496	3.006	3.420
0.010000	2.746	2.954	3.152	3.309	3.484	2.639	3.144	3.554
0.012000	2.907	3.106	3.305	3.475	3.673	2.809	3.297	3.759
0.014000	3.086	3.296	3.496	3.676	3.837	2.972	3.495	3.912
0.016000	3.326	3.543	3.765	3.946	4.102	3.198	3.760	4.175
0.018000	3.631	3.842	4.042	4.193	4.345	3.515	4.035	4.404
0.019996	3.956	4.135	4.298	4.463	4.583	3.856	4.304	4.647
0.022000	4.169	4.321	4.466	4.578	4.704	4.090	4.460	4.753
0.024000	4.341	4.480	4.613	4.719	4.817	4.263	4.610	4.858
0.026000	4.483	4.607	4.737	4.834	4.937	4.413	4.730	4.981

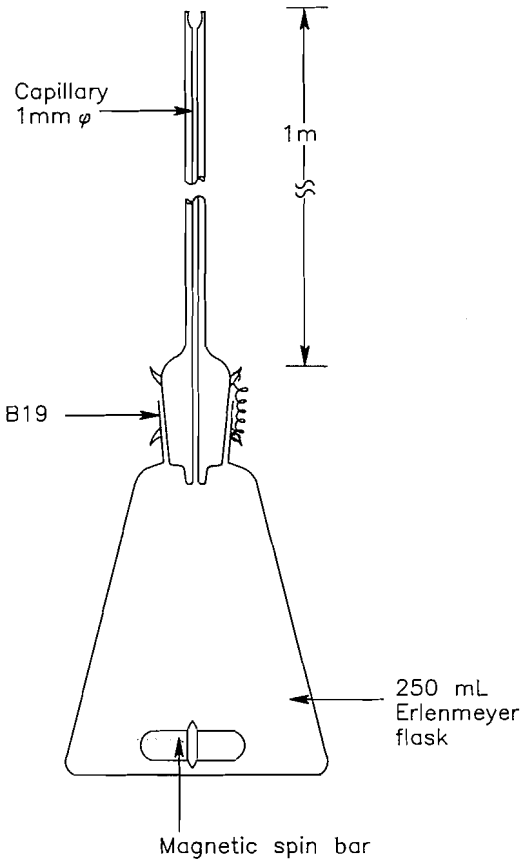

FIG. 1. Dilatometer.

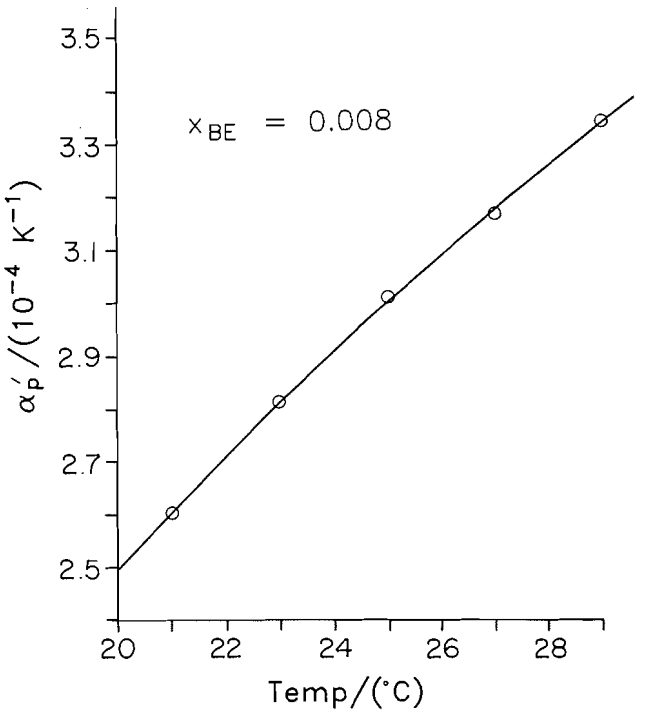

FIG. 2. Thermal expansibility, α_p', vs. temperature for x_{BE} = 0.008, series I.

mately 10 Torr (1 Torr = 133.3 Pa) and then immersing the flask in an ultrasonic bath for 3 min. The decrease in mass following this procedure was less than 0.03%, which was judged to cause a negligible change in solution composition. No problems associated with dissolved gases were subsequently detectable.

The dilatometer filled with a sample was immersed in a bath the temperature of which was controlled within ±0.001°C. The temperature of the bath was measured to 0.01°C by a mercury-in-glass thermometer, which had been calibrated at the ice point and the melting point of $Na_2SO_4 \cdot 10H_2O$, 32.383°C. After thermal equilibration, which was attained within an hour, the temperature of the bath was raised and the volume change was measured by the rise of the meniscus in the capillary.

Two series of measurements were performed. At lower mole fraction regions, the thermal expansivities turned out to be smaller than those at higher concentrations. Therefore, in the first series, after thermal equilibration at 20°C the temperature was raised successively by 2°C up to 30°C for the concentration region $x_{BE} < 0.026$. In the second series, $x_{BE} > 0.01$, the temperature was changed by 1°C from about 23.5 up to 26.5°C. In this way the meniscus rise for both series was typically from 10 to 20 cm, depending on the concentration of the sample. The meniscus rise was read to 0.01 cm by a magnifying glass. The temperature change was determined with a Beckmann thermometer to within 0.001°C. Thus with stem corrections for both the Beckmann thermometer and the

Can. J. Chem. Downloaded from www.nrcresearchpress.com by 109.225.110.28 on 09/08/12
For personal use only.

Can. J. Chem. Downloaded from www.nrcresearchpress.com by 109.225.110.28 on 09/08/12
For personal use only.

TABLE 2. Thermal expansivities, α_p', of aqueous solutions of 2-butoxyethanol, series II

x_{BE}	Temperature (°C)	α_p' (measured) (10^{-4} K^{-1})	α_p' at 25.00°C (10^{-4} K^{-1})
0.008899	24.01	2.943	
	25.01	3.054	3.047 ± 0.007
	26.01	3.153	
0.01101	24.00	3.150	
	25.00	3.269	3.29 ± 0.02
	26.01	3.442	
0.01300	24.01	3.245	
	25.00	3.379	3.36 ± 0.02
	26.01	3.463	
0.01482	24.00	3.449	
	25.00	3.592	3.57 ± 0.02
	26.00	3.663	
0.01600	24.00	3.678	
	25.00	3.794	3.784 ± 0.009
	26.00	3.881	
0.01742	24.00	3.832	
	25.00	3.940	3.929 ± 0.009
	26.00	4.016	
0.01810	24.00	3.836	
	25.01	3.991	3.95 ± 0.04
	26.00	4.027	
0.01894	24.01	4.045	
	25.01	4.131	4.137 ± 0.006
	26.01	4.236	
0.01955	24.01	4.105	
	25.01	4.231	4.21 ± 0.02
	26.01	4.292	
0.01955	24.00	4.166	
	25.05	4.262	4.25 ± 0.01
	26.05	4.318	
0.01966	24.05	4.177	
	25.00	4.308	4.27 ± 0.03
	26.00	4.335	
0.02101	24.00	4.307	
	24.99	4.368	4.38 ± 0.02
	26.01	4.460	
0.02200	24.00	4.343	
	25.00	4.461	4.44 ± 0.02
	26.00	4.505	
0.02308	24.00	4.471	
	25.00	4.576	4.56 ± 0.02
	25.99	4.626	
0.02400	24.00	4.537	
	25.00	4.624	4.61 ± 0.01
	26.00	4.663	
0.02500	24.00	4.606	
	24.99	4.704	4.69 ± 0.01
	26.00	4.760	
0.02570	24.10	4.734	
	25.00	4.753	4.76 ± 0.01
	26.00	4.820	
0.02616	24.01	4.645	
	25.01	4.778	4.75 ± 0.03
	26.00	4.790	
0.02765	24.00	4.779	
	25.00	4.857	4.84 ± 0.02
	26.00	4.890	
0.02900	24.00	4.860	
	25.00	4.913	4.919 ± 0.007
	26.00	4.985	
0.03200	24.00	4.998	
	25.00	5.084	5.06 ± 0.02
	26.00	5.099	
0.03500	24.00	5.140	
	25.00	5.215	5.205 ± 0.01
	26.00	5.245	
0.03800	24.00	5.275	
	25.00	5.340	5.31 ± 0.03
	26.00	5.328	

capillary of the dilatometer, the uncertainties were estimated to be less than 0.5%. Taking into account the thermal expansivity of Pyrex glass, we could indeed reproduce the thermal expansivity of pure H_2O within 0.25% of the literature values (6) in the temperature range from 20 to 30°C.

Results and discussion

The definition of thermal expansivity, α_p, is given by

$$[1] \quad \alpha_p = (1/V)(\partial V/\partial T)_p$$

As mentioned above, we used a dilatometer with its total volume, V_0, being kept constant. Thus, we actually measure the following quantity, α_p', given by

$$[2] \quad \alpha_p' = (1/V_0)(\partial V/\partial T) = (1/V_0)(\partial^2 G/\partial p \partial T)$$

which is therefore a second derivative of the Gibbs free energy. Thus, we wish to measure the values of α_p' in small increments in composition and to determine the following derivative, the third derivative of the Gibbs free energy:

$$[3] \quad (\partial \alpha_p'/\partial n_{BE})_{n_W} = (\partial x_{BE}/\partial n_{BE})_{n_W}(\partial \alpha_p'/\partial x_{BE})$$
$$= (1/N)(1 - x_{BE})(\partial \alpha_p'/\partial x_{BE})$$
$$= (1/V_0)(\partial^3 G/\partial p \partial T \partial n_{BE})$$

Here, $N = n_{BE} + n_W$, and n_{BE} and n_W are the amounts of BE and H_2O in the mixture.

Table 1 lists the results for series I. A typical plot of α_p' vs. temperature at a given mole fraction is shown in Fig. 2. The curve in the figure is a quadratic equation fit to the five values of α_p' determined at 21, 23, 25, 27, and 29°C. From such a curve fitting, the values of α_p' at 20.00, 25.00, and 30.00°C were obtained and are also listed in Table 1. For series II, since there are only three values, determined at 24, 25, and 26°C, a linear fit was used to estimate the value of α_p' at 25.00°C and the uncertainty for each mole fraction. Such values of α_p' at 25.00°C are listed in Table 2 together with all the measured values.

All of these data for α_p' are plotted against x_{BE} in Fig. 3. Inflection points are clearly apparent. The derivatives of eq.

Can. J. Chem. Downloaded from www.nrcresearchpress.com by 109.225.110.28 on 09/08/12
For personal use only.

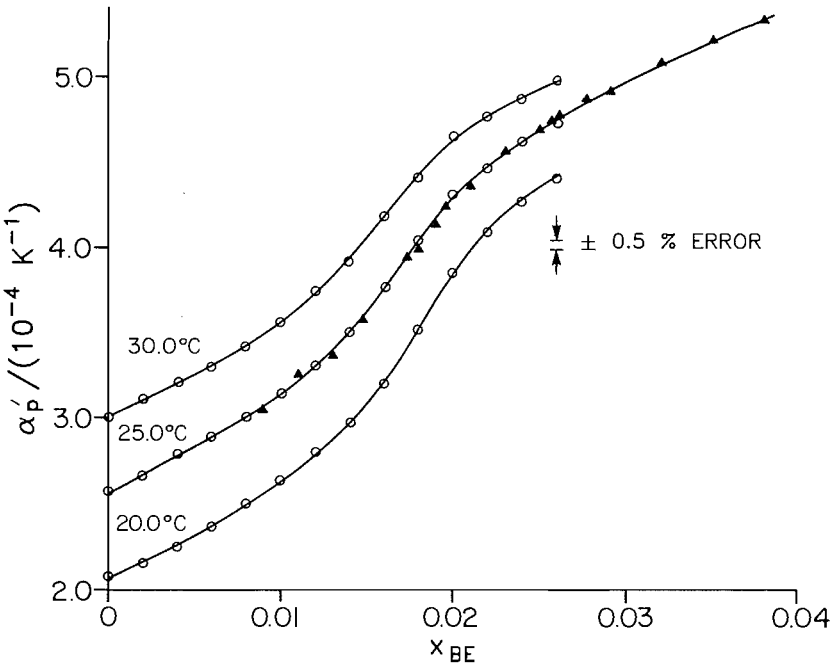

FIG. 3. Thermal expansibility, α_p', vs. mole fraction, x_{BE}. ○, series I; ▲, series II (see the text).

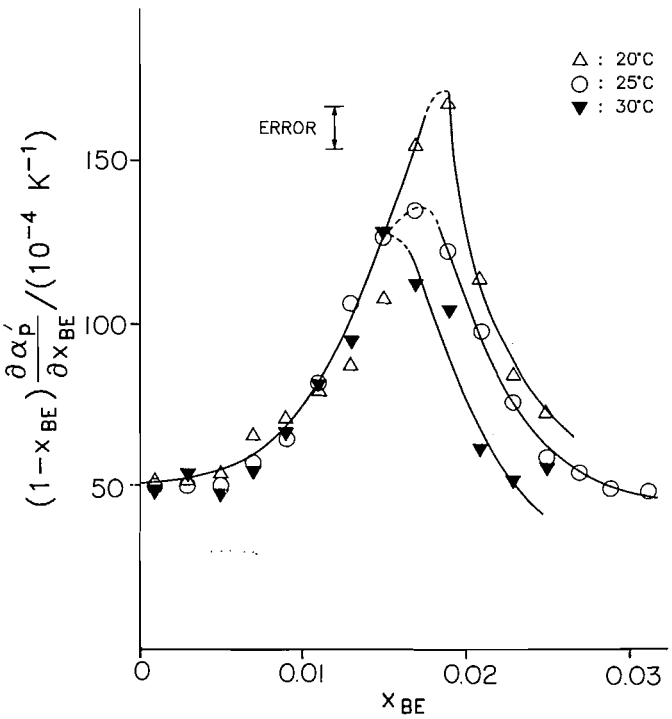

FIG. 4. The effect of additional BE on thermal expansibility, $(1 - x_{BE})(\partial\alpha_p'/\partial x_{BE})$, vs. mole fraction.

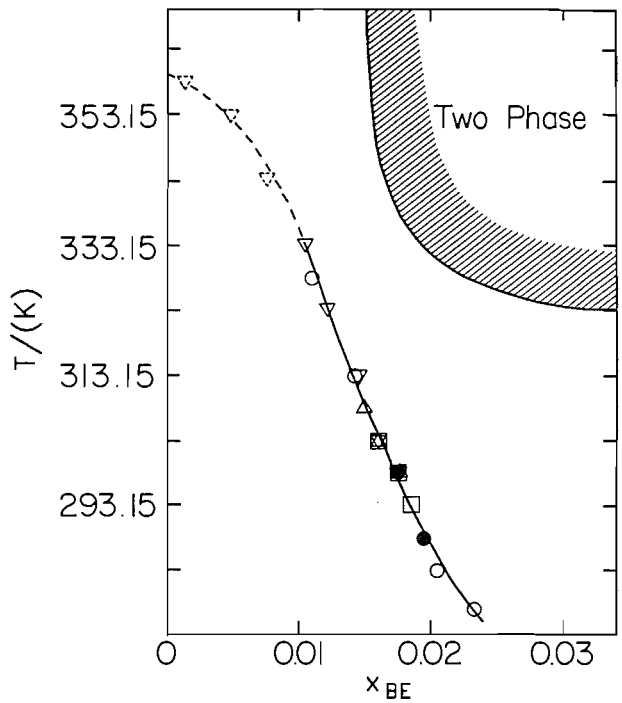

FIG. 5. The loci of peak or cusp anomalies in various third derivatives of Gibbs free energy: $\Delta\nabla$ ▽, $(\partial H_m^E(BE)/\partial n_{BE})$, refs. 1–3; ○, $C_p^E(BE)$, ref. 5; ●, $(\partial V_m^E(BE)/\partial n_{BE})$, ref. 7; □, $(\partial\alpha_p'/\partial n_{BE})$, this work.

[3] are graphically evaluated from Fig. 3. The results are plotted in Fig. 4 for N taken to be unity. An estimated uncertainty is shown in Fig. 4. The loci of the peak anomalies shown in Fig. 4 are plotted in Fig. 5 together with those of other third derivatives mentioned in the Introduction. They all seem to fall on the same boundary.

According to the discussion presented in the previous papers (1–4, 7), in the region to the left of the boundary shown in Fig. 5, the hydrogen bond network of H_2O is enhanced by BE molecules in the solution. In the intermediate concentration region, to the right of the boundary, H_2O loses its hydrogen bond network and behaves as a normal liquid. The fact that the values of α_p' are smaller in the water-rich region

than those in the intermediate region, as is apparent from Fig. 3, is perfectly consistent with the above interpretation. In the water-rich region, the volume increase due to thermal motion is compensated for by the volume decrease due to the breakage of hydrogen bonds on heating.

Acknowledgements

This work was supported by the Natural Sciences and Engineering Research Council of Canada. One of us (J.V.D.) thanks the University College of the Cariboo and the Faculty of Science, the University of British Columbia, for support for this research. Two of us (F.W.L. and L.T.N.L.) are grateful to the Governments of Canada and British Columbia for the Work Study Programme.

1. W. Siu and Y. Koga. Can. J. Chem. **67**, 671 (1989).
2. Y. Koga, W. W. Y. Siu, and T. Y. H. Wong. J. Phys. Chem. **94**, 3879 (1990).
3. Y. Koga. J. Phys. Chem. **95**, 4119 (1991).
4. Y. Koga, J. Kristiansen, and Aa. Hvidt. J. Chem. Thermodyn. In press.
5. G. Roux, G. Perron, and J. E. Desnoyers. J. Solution Chem. **7**, 639 (1978).
6. R. C. Weast (*Editor*). Handbook of chemistry and physics. 62nd ed. Chemical Rubber Co., Boca Raton, Fla. 1981/82, p. F-5.
7. Y. Koga. J. Phys. Chem. In press.

Can. J. Chem. Downloaded from www.nrcresearchpress.com by 109.225.110.28 on 09/08/12
For personal use only.

The acidic specific capsular polysaccharide of *Rhodococcus equi* serotype 3. Structural elucidation and stereochemical analysis of the lactate ether and pyruvate acetal substituents[1]

WAYNE B. SEVERN[2] AND JAMES C. RICHARDS

Institute for Biological Sciences, National Research Council of Canada, Ottawa, Ont., Canada K1A 0R6

Received May 1, 1992

WAYNE B. SEVERN and JAMES C. RICHARDS. Can. J. Chem. **70**, 2664 (1992).

The specific capsular polysaccharide produced by *Rhodococcus equi* serotype 3 was found to be a high-molecular-weight acidic polymer composed of D-glucose, D-galactose, D-glucuronic acid, 4-*O*-[(*S*)-1-carboxyethyl]-D-mannose, and pyruvic acid in equal molar proportions. Structural analysis, employing a combination of chemical and nuclear magnetic resonance techniques, established that the polysaccharide is composed of linear repeating tetrasaccharide units,

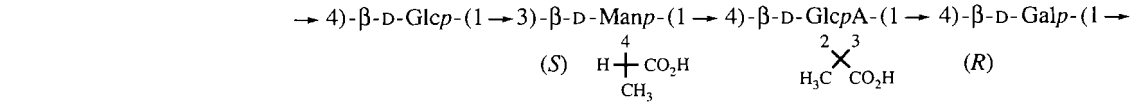

in which (*R*)-1-carboxyethylidene groups bridge the O-2 and O-3 positions of the β-D-glucuronic acid residues. The ^1H and ^{13}C NMR resonances of the native and depyruvulated serotype 3 polysaccharides were fully assigned by homo- and heteronuclear chemical shift correlation methods. The absolute configurations of the lactate-substituted mannopyranosyl residues and the pyruvate acetals were determined from ^1H–^1H NOE measurements on the intact polysaccharide. Unequivocal determination of the absolute chirality of the 4-*O*-[(*S*)-1-carboxyethyl]-β-D-mannopyranose residues was achieved by ^1H–^1H NOE measurements on an acetylated lactone derivative of the glycose.

WAYNE B. SEVERN et JAMES C. RICHARDS. Can. J. Chem. **70**, 2664 (1992).

On a trouvé que le polysaccharide capsulaire spécifique produit par le *Rhodococcus equi* du sérotype 3 est un polymère acide de poids moléculaire élevé, composé de D-glucose, de D-galactose, d'acide D-glucuronique, de 4-*O*-[(*S*)-1-carboxyéthyl]-D-mannose et d'acide pyruvique présents en proportions molaires égales. Une analyse structurale faisant appel à une combinaison de techniques chimiques et de la résonance magnétique nucléaire a permis d'établir que le polysaccharide est formé d'unités linéaires tétrasaccharides qui se répètent,

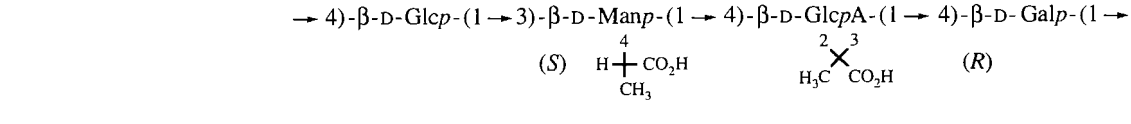

dans lesquelles des groupes (*R*)-1-carboxyéthylidènes forment un pont entre les positions O-2 et O-3 des résidus d'acide β-D-glucuronique. Les spectres RMN du ^1H et du ^{13}C des polysaccharides du sérotype 3, tant naturel que dépourvu d'acide pyruvique, ont été attribués par des méthodes de corrélation des déplacements chimiques homo- et hétéronucléaires. Les configurations absolues des résidus mannopyranosyles substitués par un lactate ainsi que les acétals pyruviques ont été déterminés par des mesures d'eOn ^1H–^1H sur le polysaccharide intact. On a réalisé une détermination univoque de la chiralité absolue des résidus 4-*O*-[(*S*)-1-carboxyéthyl]-β-D-mannopyranose grâce à des mesures d'eOn sur un dérivé lactone acétylé du glycose.

[Traduit par la rédaction]

Introduction

Rhodococcus equi (1) is a Gram-positive bacterial pathogen that causes serious, and often fatal, respiratory disease in 4 to 12 week old foals (2). The bacteria are encapsulated by negatively charged, carbohydrate polymers that are serotype specific (3, 4). By using a double immunodiffusion precipitation test (4) seven serotypes of the *R. equi* are currently recognised.

Capsular polysaccharide (CPS) is identified as a potential virulence factor of both Gram-positive and Gram-negative bacteria (5). In pathogenic bacteria, the capsular layer provides protection from the nonspecific host defense mechanisms, although the relationship between the presence of capsule and pathogenesis in *R. equi* has not been established.

In an attempt to understand the molecular basis for the antigenic diversity of the *R. equi* CPS, we have employed a combination of NMR and MS based strategies for their structural elucidation (6). The specific CPS's of serotypes 1 and 2 have been fully characterized (7, 8). Both were found to be high-molecular-weight heteroglycans composed of linear tetrasaccharide units containing D-glucuronic acid residues. In addition, the two polysaccharides contained acidic, non-carbohydrate components that could be related to their serological specificities. The serotype 1 polysaccharide was found to contain 1-carboxyethylidene (pyruvic acid) acetal groups while the serotype 2 polysaccharde carries biosynthetically related (9) 1-carboxyethyl (lactic acid) ether substituents.

Pyruvic acid acetals occur widely in bacterial polysaccharides (9) and are recognised (10) as immunodominant structural features. Although less frequently encountered, lactic acid ether substituted sugars have been reported as components of both lipo- and extracellular polysaccharides (9). The structural variability of the antigenic determinants

[1]Issued as NRCC No. 34279.

[2]NRCC Research Associate 1988–1990.

Can. J. Chem. Downloaded from www.nrcresearchpress.com by 109.225.110.28 on 09/08/12
For personal use only.

Can. J. Chem. Downloaded from www.nrcresearchpress.com by 109.225.110.28 on 09/08/12
For personal use only.

is influenced by: (1) the nature of the substituted monosaccharide residue, (2) the position(s) of substitution, and (3) the chirality of the substituent. These features were completely assigned for the components present in the *R. equi* serotype 1 and 2 polysaccharides. NMR spectroscopy led to the identification of (*S*)-1-carboxyethylidene acetal groups linked to the O-4 and O-6 positions of β-D-mannopyranosyl residues in the serotype 1 polysaccharide (7). For the serotype 2 CPS, a chemical approach was employed to establish the presence of 3-*O*-[(*S*)-1-carboxyethyl]-α-L-rhamnopyranosyl residues (8).

In the present investigation, the structural elucidation of the specific capsular polysaccharide produced by *R. equi* serotype 3 is reported. This polysaccharide is unusual in that it contains both the pyruvic acid and lactic acid moieties in a D-glucuronic-acid-containing tetrasaccharide repeating unit. The absolute stereochemistry of these chiral antigenic determinants was determined by proton nuclear Overhauser enhancement based methods.

Results and discussion

Isolation and purification

The specific capsular polysaccharide produced by *R. equi* serotype 3 was isolated from plate-grown cells by mechanical dissociation from the cellular material into 4 M sodium chloride solution. Following enzymatic digestion with ribonuclease, deoxyribonuclease, and proteinase K, the polysaccharide was purified via its insoluble cetyltrimethyl ammonium salt (8). Pure capsule was obtained by ion exchange chromatography on DEAE–Sephacel as a discrete band at the beginning of the sodium chloride gradient and was judged to be free from nucleic acids and proteins since neither ribose nor amino acids were detectable in its acid hydrolysis products. The polysaccharide had $[\alpha]_D$ −5.5 (*c* 1.2, water); Anal. found: C 40.76, H 5.45, N 0.00, ash 0.8%; and gave a single sharp precipitin line in immunodiffusion against rabbit antisera to *R. equi* serotype 3 cells (4). All subsequent analyses were made on the DEAE–Sephacel purified product.

Composition

The native serotype 3 CPS eluted as a sharp band at the void volume (K_{av} 0.09) of a Sephadex G-200 gel filtration system, indicating it to be a high-molecular-weight polymer. Qualitative analysis of the eluant revealed that the polysaccharide contained both neutral glycose (11) and hexuronic acid components (12).

Analysis of the polysaccharide hydrolysis products (2 M trifluoroacetic acid, 100°C, 16 h) by high-performance anion exchange (HPAE) chromatography (13) indicated the neutral glycoses to be galactose (R_G 0.95) and glucose (R_G 1.0) (eluant A), while pyruvic acid (R_G 2.6), glucuronic acid (R_G 3.9), and a fifth component (R_G 3.2) were identified (eluant B) as the acidic constituents in the hydrolyzate.

The pyruvic acid moiety could be easily released from the native *R. equi* serotype 3 CPS by treatment of the polymer with dilute acetic acid (2%, 100°C, 2 h), indicating that the substituent was linked as an acetal to a glycosyl residue (10). The depyruvulated polysaccharide had $[\alpha]_D$ −4.8 (*c* 1.25, water); Anal. found: C 40.20, H 5.39, N 0.00, ash 0.9%.

GLC analysis of the reduced and acetylated hydrolysis products (14), derived from the *R. equi* serotype 3 polysaccharide, indicated that the neutral glycosyl residues, which were identified as 1,2,3,4,5,6-hexa-*O*-acetyl derivatives of glucitol (T_{GA} 1.0) and galactitol (T_{GA} 1.1), were present in approximately equimolar proportions. Sequential treatment of the polysaccharide with methanolic HCl (1 M, 85°C, 14 h) and sodium borohydride was employed to effect carboxyl group reduction. Subsequent hydrolysis and formation of the alditol acetates indicated the presence of glucose and galactose in the ratio of 2:1. When carboxyl group reduction was carried out with sodium borodeuteride, MS analysis confirmed that the glucuronic acid component, identified as 1,2,3,4,5,6-hexa-*O*-acetyl glucitol-6,6-d_2, represented approximately one half of the derived glucitol hexaacetate. A molar equivalent of an additional component was identified by using the methanolysis procedure (T_{GA} 1.5). The EI-MS fragmentation pattern for the carboxyl-reduced ($NaBH_4$) alditol acetate derived from this component is depicted below (**1**).

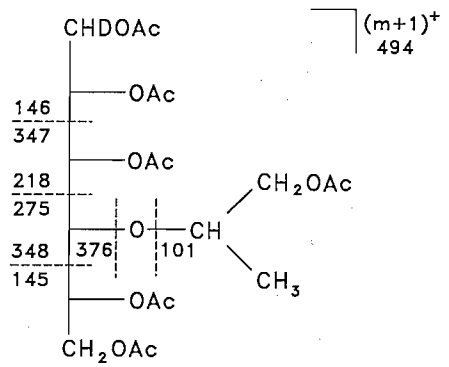

1

The primary fragment ion at *m/z* 101 is indicative of an acetoxypropyl moiety (15) and the shift of this fragment by two mass units to *m/z* 103 when carboxyl reduction was effected with $NaBD_4$ indicated it to be derived from a carboxyethyl moiety. Furthermore, peaks at *m/z* 145, 146, 218, 275, 347, 348, and 376 place this substituent at the 4-position of the alditol, establishing that the residue is a 4-*O*-(1-carboxyethyl)-hexose.

The absolute configurations of the unsubstituted glycoses were established from the characteristic GLC retention times of their trimethylsilylated *R*-2-butyl glycosides (16). In this way the glucosyl, galactosyl, and glucuronic acid residues were all assigned to the D-series.

Glycosyl linkage analysis

The methylated (17), reduced ($NaBH_4$) (18), and hydrolyzed, pyruvate-free, *R. equi* serotype 3 CPS afforded products that, after reduction ($NaBD_4$) and acetylation, furnished valuable mass spectral data on the positions of the linkages of the component glycosyl residues (Table 1). From this analysis it can be inferred that the capsular polysaccharide is composed of →4)-D-Glc*p*-(1→, →4)-D-Gal*p*-(1→, →4)-D-Glc*p*A-(1→ and a →3)-4-*O*-(1-carboxyethyl)-hex*p*-(1→, which form a linear tetrasaccharide unit. The hydrolysis products, analogously derived from the permethylated native polysaccharide, contained the same *O*-methylated derivatives for D-glucose, D-galactose, and the (1-carboxy-

TABLE 1. Methylation analysis data for the depyruvulated and native *R. equi* serotype 3 capsular polysaccharides

Methylated glycose derivatives[a]	T_{GM}[b]	Mole ratio
Depyruvulated polysaccharide		
2,3,6-Tri-*O*-methyl-D-glucose	1.00	1.00
2,3,6-Tri-*O*-methyl-D-galactose	1.05	0.95
2,3-Di-*O*-methyl-D-glucose	1.39	0.90
2,6-Di-*O*-methyl-4-*O*-[(*S*)-1-hydroxypropyl]-D-mannose	2.15	0.90
Native polysaccharide		
2,3,6-Tri-*O*-methyl-D-glucose	1.00	1.00
2,3,6-Tri-*O*-methyl-D-galactose	1.05	0.95
D-Glucose	1.90	0.72
2,6-Di-*O*-methyl-4-*O*-[(*S*)-1-hydroxypropyl]-D-mannose	2.15	0.90

[a]Determined as their carboxyl reduced [1-^{3}H] alditol acetates.
[b]Retention times relative to that of 1,4,5-tri-*O*-acetyl-2,3,6-tri-*O*-methyl-D-glucitol-1-*d*, using GLC program A.

ethyl)-hexose. However, D-glucose was obtained instead of 2,3-di-*O*-methyl-D-glucose, indicating that the pyruvate acetals were linked to the O-2 and O-3 positions of the O-4 substituted D-glucuronic acid units in the native polysaccharide.

Glycosyl sequence determination

High-resolution NMR techniques were employed to establish the sequence of the glycosyl residues. The general approach involved the initial complete assignment of the ^{1}H and ^{13}C NMR spectra of the intact polysaccharide from which the relative stereochemistry, ring size, and anomeric configuration of the component glycoses were identified and the location of the 1-carboxyethylidene substituent confirmed.

Solubilization of the native polysaccharide in D_2O produced viscous solutions (pD $\approx$ 2) that gave broad lines in the NMR spectra. Although better resolution was obtained at higher temperatures, autohydrolysis of the pyruvic acid acetals was observed. To reduce the extent of degradation, all NMR spectra of the native polysaccharide were recorded at 62°C in D_2O buffered at pD $\approx$ 6.2.

Examination of the ^{1}H and ^{13}C NMR spectra of the type 3 polysaccharide confirmed the polymer to be composed of a regular repeating tetrasaccharide unit. The ^{1}H NMR spectrum of the native polysaccharide exhibited anomeric ^{1}H resonances corresponding to the four glycosyl residues in the low-field region of the spectrum at 5.03 (d, ca. 1H, J = 7.5 Hz), 4.73 (s, ca. 1H, J = 1.2 Hz), 4.58 (d, ca. 1H, J = 7.5 Hz), and 4.49 ppm (d, 1H, J = 7.8 Hz). Four ^{13}C resonances were observed in the proton-decoupled ^{13}C NMR spectrum between 110 and 100 ppm (Fig. 1*a*). The lowest-field resonance in this grouping (109.88 ppm) could be attributed to the acetal carbon of the pyruvic acid moiety from the ^{1}H coupled or DEPT (19) ^{13}C NMR spectra, while the intensity of the peak at 100.73 ppm suggested it to be composed of two coincident resonances. The magnitude of the heteronuclear one-bond ^{13}C–^{1}H coupling constants ($^1J_{C,H}$) was found to be ca. 160 Hz for each of the anomeric resonances, which indicates that the anomeric configurations of all the linkages were β (20). In accord with compositional analysis, diagnostic ^{13}C resonances were observed at 19.08 and 23.87 ppm from the methyl carbons of the carboxyethyl and carboxyethylidene groups, respectively; and three signals at low field, 182.4, 177.2, and 175.6 ppm, indicated the presence of the three carboxyl groups within the repeating unit. Correspondingly, characteristic high-field resonances at 1.61 (s, 3H) and 1.40 ppm (d, 3H, J = 7.7 Hz) in the ^{1}H NMR spectrum could be assigned to the methyl protons of the respective carboxyethylidene and carboxyethyl groups. The methyl singlet from the carboxyethylidene moiety was absent in the ^{1}H NMR spectrum of the pyruvate-free polysaccharide.

Assignment of the proton resonances from the native and pyruvate-free polysaccharides was made from two-dimensional homonuclear chemical shift correlation (COSY (21) and Relayed COSY (22)) experiments. Subspectra corresponding to each of the four glycosyl residues were identified from the chemical shift (23) and the vicinal ^{1}H–^{1}H coupling constant values (24). The residues were labelled **a**, **b**, **c**, and **d** according to decreasing order of the chemical shifts from the H-1 resonances (25). The observed chemical shifts and coupling constants for the native and pyruvate-free polysaccharide are given in Tables 2 and 3. Unambiguous assignment of the corresponding ^{13}C resonances was effected by correlation with the ^{1}H resonances of the directly attached protons by heteronuclear ^{13}C–^{1}H chemical shift correlation experiments (26) and the data are recorded in Tables 4 and 5.

The contour plot of the ring proton region of the COSY spectrum obtained on the native polysaccharide is shown in Fig. 2. Five ^{1}H resonances were associated with the subspectrum from residue **a** and, from the large observed ring proton coupling constants ($^3J \approx 10$ Hz), it could be identified as the β-D-glucopyranosyluronic acid unit. Analogously, the subspectrum arising from residue **c** could be attributed to a pyranosyl residue having the β-gluco configuration. The spin system associated with this residue comprised seven ^{1}H resonances and was assigned to the β-D-glucopyranosyl unit.

The connectivity pathway relating H-1, H-2, H-3, and H-4 of residue **d** was readily discernible from the cross-peaks, and the ^3J-values (Table 2) were typical of a pyranoside unit possessing the β-D-*galacto* configuration.

Residue **b** could be identified as a *manno*-pyranosyl unit from the observed small magnitude of the vicinal cou-

Can. J. Chem. Downloaded from www.nrcresearchpress.com by 109.225.110.28 on 09/08/12
For personal use only.

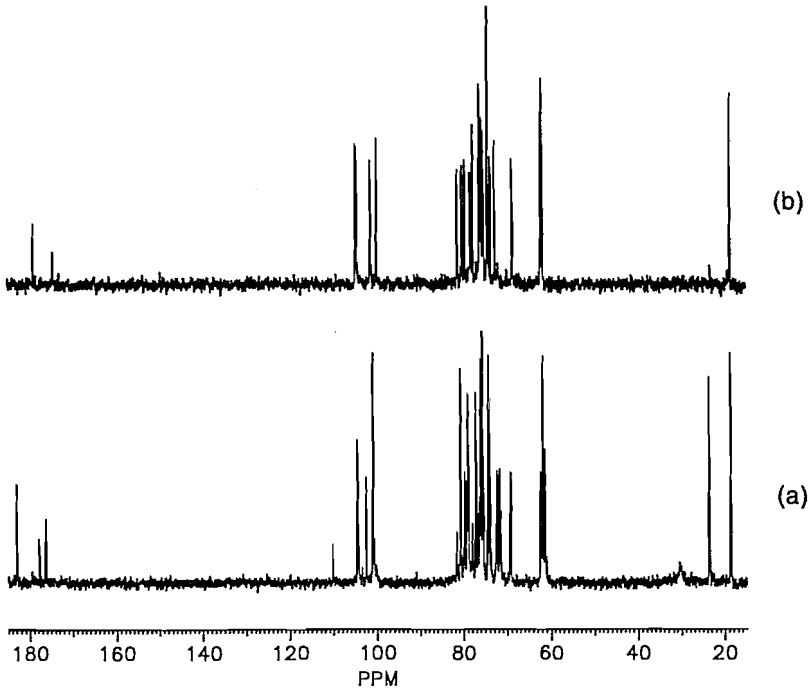

FIG. 1. ^{13}C NMR spectra of the (*a*), native and (*b*), depyruvulated *R. equi* Serotype 3 capsular polysaccharides recorded at 62°C.

TABLE 2. ^{1}H chemical shifts and coupling constants[a] (Hz) for the native *R. equi* serotype 3 capsular polysaccharide

Residue	Glycosyl residue	H-1 ($J_{1,2}$)	H-2 ($J_{2,3}$)	H-3 ($J_{3,4}$)	H-4 ($J_{4,5}$)	H-5	H-6 ($J_{5,6}$)	H-6′ ($J_{5,6'}$, $J_{6,6'}$)	Lactic acid residue: -CH_3 (J_{CH-CH_3})	Lactic acid residue: -CH	Pyruvic acid residue: CH_3
a	→4)-β-D-Glc*p*A-(1→ 2 3 (*R*) × H_3C CO_2H	5.03 (7.5)	3.48 (9.3)	3.75 (9.6)	4.17 (9.9)	3.79					1.61
b	→3)-β-D-Man*p*-(1→ 4 (*S*) H + CO_2H CH_3	4.73 (1.2)	4.16 (2.8)	4.03 (9.6)	3.66 (9.5)	3.48	3.79 (2.4)	3.97 (5.3, 12.5)	1.40 (7.7)	4.30	
c	→4)-β-D-Glc*p*-(1→	4.58 (7.5)	3.39 (9.0)	3.65 (9.6)	3.70 (9.6)	3.50	3.77 (2.3)	3.97 (5.3, 12.5)			
d	→4)-β-D-Gal*p*-(1→	4.49 (7.8)	3.67 (9.0)	3.76 (3.5)	4.21 (1.2)	3.76	3.76 (7.7)	3.76 (3.9, 10.7)			

[a]Observed first-order chemical shifts and coupling constants (Hz) measured at 62°C in D_2O/phosphate buffer (pD ≈ 6.2).

plings, $J_{1,2}$ (0.5 Hz) and $J_{2,3}$ (2.8 Hz). However, mannose was not detected in the polysaccharide acid hydrolysis products, which suggested this residue to be the *O*-(1-carboxyethyl)-substituted hexose. The AX_3 spin system associated with the carboxyethyl substituent of residue **b** was identified from cross-peaks in the full-scale COSY spectrum relating the methyl doublet at 1.40 ppm (J = 7.7 Hz) to the lactic acid H-2 quartet at 4.30 ppm. The low intensities of the cross peaks relating H-1 to H-2 of residue **b** and those relating H-4 to H-5 of residue **d** (Fig. 2) are attributed to the small values (ca. 1–3 Hz) for the scalar couplings, $J_{1,2}$ and $J_{4,5}$, typical of the *manno*- and *galacto*-pyranosyl configurations, respectively (18).

The ^{1}H NMR spectrum of the pyruvate-free polysaccharide lacked the characteristic signal due to the carboxyethylidene methyl protons that was observed for the native polysaccharide. In addition, H-1**a** and H-4**a** showed substantial upfield shifts (0.3–0.4 ppm) upon removal of the pyruvate group. With the exception of the protons associated with the glucopyranosyl uronic acid (residue **a**), the chemical shifts from residues **b**, **c**, and **d** (Table 3) were closely similar (within 0.1 ppm) to those observed for the native polysaccharide (Table 2).

In the ^{13}C NMR spectrum of the native polysaccharide, resonances at 182.40, 109.88, and 23.87 ppm were attributed to the respective carboxyl, acetal, and methyl carbons of the pyruvic acid moiety (Fig. 1*a*). These signals were absent in the spectrum of the depyruvulated polysaccharide (Fig.

Can. J. Chem. Downloaded from www.nrcresearchpress.com by 109.225.110.28 on 09/08/12
For personal use only.

TABLE 3. ^{1}H chemical shifts and coupling constants[a] (Hz) for the depyruvulated *R. equi* serotype 3 capsular polysaccharide

Residue	Glycosyl residue	H-1 ($J_{1,2}$)	H-2 ($J_{2,3}$)	H-3 ($J_{3,4}$)	H-4 ($J_{4,5}$)	H-5	H-6 ($J_{5,6}$)	H-6′ ($J_{5,6'}$,$J_{6,6'}$)	Lactic acid residue CH$_3$ (J_{CH-CH_3})	Lactic acid residue -CH
a	→4)-β-D-Glc*p*A-(1→	4.73 (7.6)	3.46 (9.1)	3.69 (9.4)	3.80 (9.7)	3.93				
b	→3)-β-D-Man*p*-(1→ 4 (*S*) H + CO_2H CH_3	4.67 (1.2)	4.18 (3.6)	4.07 (9.8)	3.74 (9.5)	3.48	3.78 (2.4)	3.94 (5.4, 12.1)	1.40 (7.7)	4.46
c	→4)-β-D-Glc*p*-(1→	4.59 (7.6)	3.37 (9.0)	3.66 (9.1)	3.62 (9.4)	3.54	3.78 (2.4)	3.96 (4.8, 12.1)		
d	→4)-β-D-Gal*p*-(1→	4.47 (7.8)	3.63 (9.1)	3.78 (3.6)	4.16 (1.1)	3.75	3.76 (7.6)	3.76) (4.5, 11.2)		

[a]Observed first-order chemical shifts and coupling constants (Hz) memasured at 62°C in D_2O (pD ≈ 2).

TABLE 4. ^{13}C chemical shifts and $^1J_{C,H}$ values (Hz)[a] for the native *R. equi* serotype 3 capsular polysaccharide

Residue	Glycosyl residue	C-1	C-2	C-3	C-4	C-5	C-6	Lactic acid residue -CH$_3$	Lactic acid residue -CH	Lactic acid residue -CO$_2$H	Pyruvic acid residue CH$_3$	Pyruvic acid residue C	Pyruvic acid residue CO$_2$H
a	→4)-β-D-Glc*p*A-(1→ 2 3 (*R*) × H_3C CO_2H	102.46 (162)	77.20	78.83	79.28	76.75	175.60[b]				23.87	109.88	182.40[b]
b	→3)-β-D-Man*p*-(1→ 4 (*S*) H + CO_2H CH_3	100.73 (160)	69.30	80.70	79.73	76.37	62.34[c]	19.08	77.92	177.20[b]			
c	→4)-β-D-Glc*p*-(1→	100.73 (160)	74.20	75.61	79.86	76.02	62.50[c]						
d	→4)-β-D-Gal*p*-(1→	104.29 (162)	72.36	75.75	79.01	74.08	61.91[c]						

[a]Measured at 62°C in D_2O/phosphate buffer (pD ≈ 6.2) and, unless indicated, assignments were determined by ^{13}C–^{1}H chemical shift correlation.
[b]Assignments may be reversed.
[c]Identified by DEPT experiment.

TABLE 5. ^{13}C chemical shifts[a] for the depyruvulated *R. equi* serotype 3 capsular polysaccharide

Residue	Glycosyl residue	C-1	C-2	C-3	C-4	C-5	C-6	Lactic acid residue -CH$_3$	Lactic acid residue -CH	Lactic acid residue -COOH
a	→4)-β-D-Glc*p*A-(1→	104.60	74.50	75.50	81.50	76.00	174.70[b]			
b	→3)-β-D-Man*p*-(1→ 4 (*S*) H + CO_2H CH_3	101.20	68.80	79.65	78.08	76.22	62.14[c]	19.12	77.86	178.60[b]
c	→4)-β-D-Glc*p*-(1→	99.83	74.40	75.73	80.28	76.14	62.14[c]			
d	→4)-β-D-Gal*p*-(1→	104.30	72.72	75.92	78.28	73.72	61.90[c]			

[a]Measured at 62°C in D_2O (pD ≈ 2) and, unless indicated, assignments were determined by ^{13}C–^{1}H chemical shift correlation.
[b]Assignments may be reversed.
[c]Identified by DEPT experiment.

1*b*). The low-field value of the acetal carbon (≈110 ppm) is indicative of the pyruvic acid acetal forming a five-membered ring system (27). A comparison of the ^{13}C NMR data from the native and the pyruvate-free polysaccharides (Tables 4 and 5) indicates that the β-D-glucopyranosyl uronic acid residue is substituted by the pyruvic acid moiety at the O-2 and O-3 positions, a result that is in accord with the methylation analysis data (Table 1). Following removal of the pyruvate, the corresponding carbon resonances, C-2 and C-3, showed significant upfield shifts of 2.7 and 3.3 ppm,

Can. J. Chem. Downloaded from www.nrcresearchpress.com by 109.225.110.28 on 09/08/12
For personal use only.

Can. J. Chem. Downloaded from www.nrcresearchpress.com by 109.225.110.28 on 09/08/12
For personal use only.

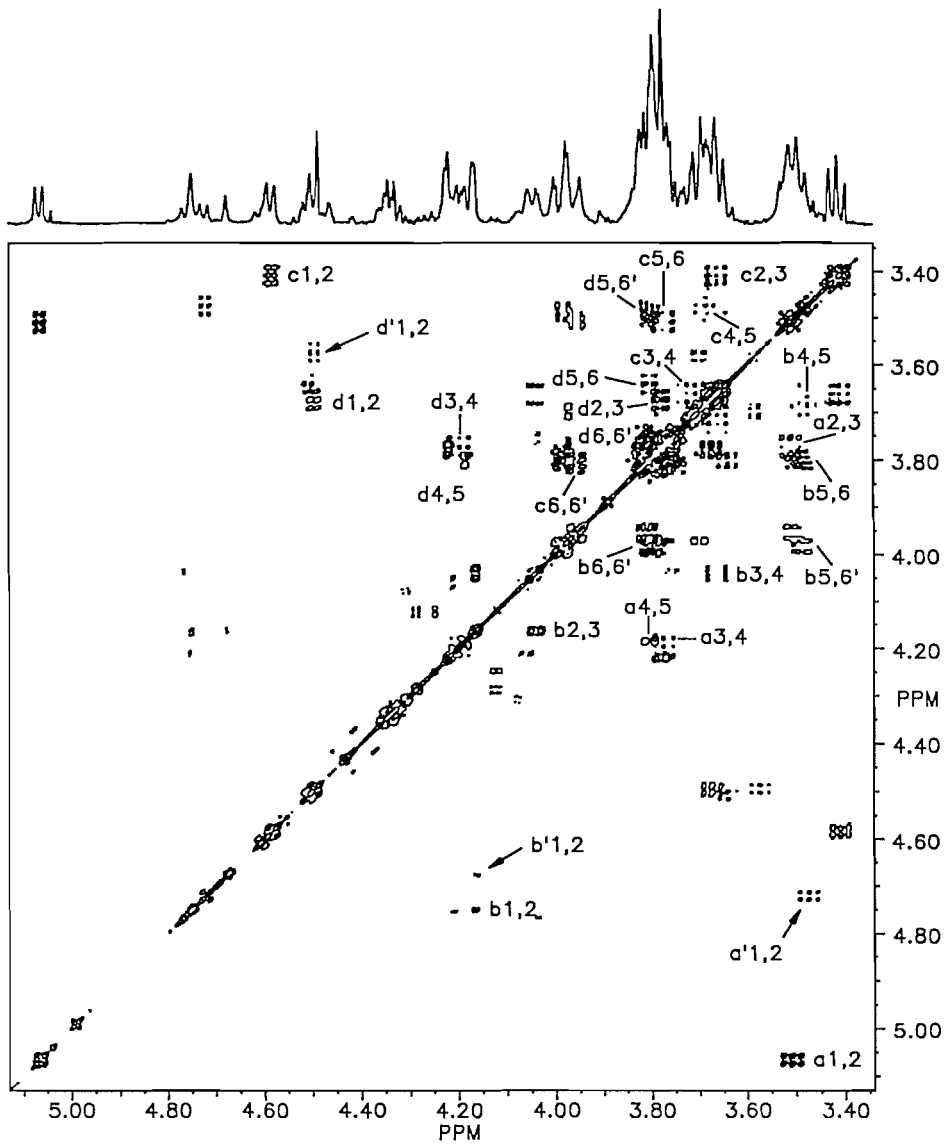

FIG. 2. Partial phase-sensitive COSY contour map of the native *R. equi* serotype 3 capsular polysaccharide recorded at 62°C, showing correlations of the ring protons from 3.3 to 5.1 ppm. Cross-peak assignments are indicated. **a**'1,2, **b**'1,2, **d**'1,2, and other minor peaks arise from partial depyruvulation of the polysaccharide.

respectively, while the adjacent carbons, C-1 and C-4, were shifted downfield by approximately 2.2 ppm. In addition, shielding effects experienced by C-3 and C-4 of residue **b**, i.e., upfield shifts of ≈1.0 and 1.6 ppm, respectively, may be attributed to conformational changes accompanying removal of the acetal substituent.

The arrangement of the four glycosyl residues within the repeating unit was determined from interresidue ^1H–^1H NOE measurements (28), which also served to confirm the positions of the glycosidic linkages (Table 6). NOE measurements were made using difference spectroscopy (29) (Fig. 3). The NOE were employed qualitatively to establish short (≥3 Å) through-space connectivities between the anomeric and aglyconic protons of the adjacent glycosidically linked residues. In addition, the occurrence of intraresidue NOE between H-1 andd H-3 and between H-1 and H-5 within the pyranose ring systems of each of the glycosyl residues was

TABLE 6. Proton NOE data for the *R. equi* serotype 3 capsular polysaccharide[a]

Anomeric proton	Observed proton: Intraresidue NOE	Observed proton: Interresidue NOE	Partial sequence	Linkage site
1**a**	3**a**/5**a**	4**d**	**a** → **d**	O-4 (**d**)
1**b**	2**b**,3**b**,5**b**	4**a**	**b** → **a**	O-4(**a**)
1**c**	3**c**,5**c**	2**b**,3**b**	**c** → **b**	O-3 (**b**)[b]
1**d**	3**d**,5**d**	4**c**	**d** → **c**	O-4 (**c**)

[a]Measured from the NOE difference spectra of the native polysaccharide at pD ≈ 6.2.

[b]Confirmed by methylation analysis and ^{13}C chemical shifts.

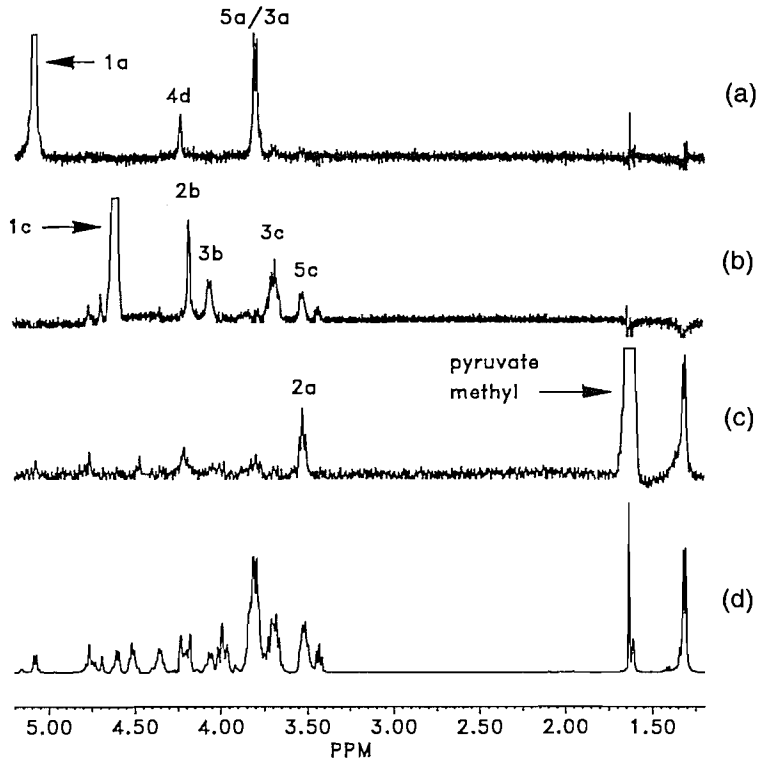

FIG. 3. NOE difference spectra measured on the native *R. equi* serotype 3 capsular polysaccharide. Spectrum arising from the irradiation of (*a*), H-1 of glucuronic acid unit (1**a**); (*b*), H-1 of glucosyl unit (1**c**); and (*c*), the methyl group of the pyruvate substituent. The off-resonance control spectrum is shown in (*d*).

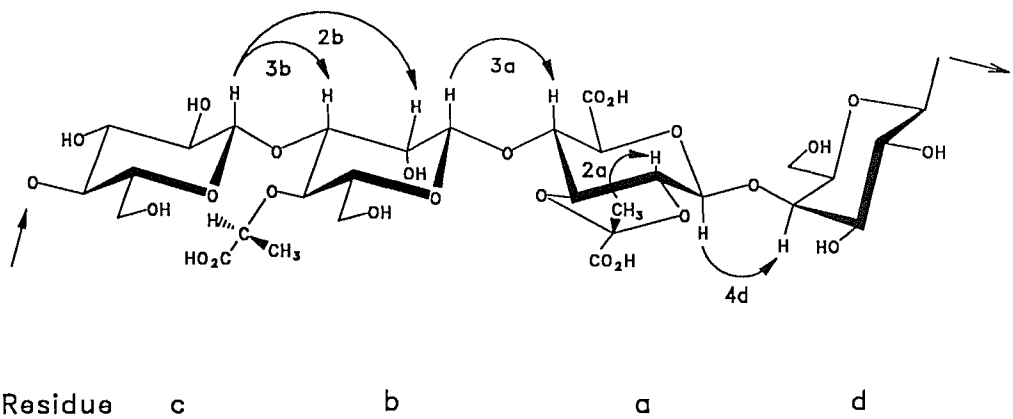

FIG. 4. The tetrasaccharide repeating unit of the *R. equi* serotype 3 capsular polysaccharide showing some of the observed NOE's.

indicative of their assigned β-configurations. Thus irradiation of the anomeric proton resonance (5.03 ppm) of the β-D-glucopyranosyluronic acid residue **a** showed strong NOE within the pyranose ring system to H-5**a** and (or) H-3**a** (≈3.79 ppm), and across the glycosidic bond to H-4**d** (4.21 ppm) of the D-galactopyranosyl residue (Fig. 3*a*). The connectivity established by the transglycosidic NOE (H1-**a**/H-4**d**), indicates the partial sequence **a**→**d** and further suggests that the β-D-glucopyranosyl uronic acid is linked to the O-4 position of the β-D-galactopyranosyl unit. The occurrence of interresidue NOE relating the H-1**d**/H-4**c**, H-1**c**/H-3**b**, and H-1**b**/H4**a** resonance pairs established the linear sequence of glycoses within the repeating tetrasaccharide unit as

[→**a**→**d**→**c**→**b**→]

The NOE connectivities are as shown in Fig. 4 and the indicated linkage positions (Table 6) are in agreement with the results from methylation analysis. Furthermore, the relatively deshielded values of the ^{13}C NMR resonances (≥79 ppm) from C-4**a**, C-3**b**, C-4**c**, and C-4**d** (Table 4) would indicate that the respective positions are glycosylated.

The conformation about the glycosidic linkage is to a large extent governed by the *exo*-anomeric effect (30). Thus, for a disaccharide in its minimum energy conformation, the internuclear distance between the anomeric and aglyconic protons of adjacent pyranose residues is of the

Can. J. Chem. Downloaded from www.nrcresearchpress.com by 109.225.110.28 on 09/08/12
For personal use only.

Can. J. Chem. Downloaded from www.nrcresearchpress.com by 109.225.110.28 on 09/08/12
For personal use only.

order of 3 Å, leading to a detectable NOE. In certain instances, interresidue NOE can be transferred to other protons on the aglycone. This can be realised when aglycone protons adjacent to the site of substitution occupy equatorial positions, viz., in 3-*O*-substituted mannopyranosyl or galactopyranosyl residues. Whether an NOE will be observed at an adjacent equatorial proton is dependent on the stereochemistry (D or L) of the two glycosyl residues (glycone and aglycone) and the configuration (α or β) of the adjoining glycosidic linkage. In the present context, significant NOE's were observed between H-1 of the β-D-glucopyranosyl residue **c** and both H-2 and H-3 of the lactate-substituted mannopyranosyl residue **b** (Fig. 3*b*). The absolute stereochemistry of the D-glucose residue was determined by chemical correlation with a standard of known chirality. The chirality of the 4-*O*-(1-carboxyethyl)-mannose residue was not evident by this method since appropriate standards were not available, but could be determined relative to that of the D-glucose residue from the observed $^1H-^1H$ NOE values.

The minimum energy conformations of the two disaccharide units, β-D-Glc*p*-(1→3)-β-D-Man*p* and β-D-Glc*p*-(1→3)-β-L-Man*p*, were calculated using the HSEA method (31) and the minimum energy molecules are shown in Fig. 5. A transglycosidic NOE would be expected between Glc H-1 and Man H-2 only in the disaccharide in which both glycosyl units possess the D-configuration (internuclear separation 2.8 Å) and not in the diastereoisomeric D-L disaccharide (separation 3.9 Å). The observation of an NOE between H-1**c** and H-2**b** of the β-D-1,3-linked **c**→**b** disaccharide unit of the native polysacchardie (Fig. 3*b*, Fig. 4) establishes that the 4-*O*-(1-carboxyethyl)-β-mannopyranose has the D-absolute configuration. A similar pattern of NOE was observed for the →4)-β-D-Glc*p*-(1→3)-β-D-Man*p*-(1→ unit in the *R. equi* serotype 1 polysaccharide in which the chirality of the mannose residue was established independently by chemical correlation (7).

Considerations of the conformation about the glycosidic bond of 1,3-linked disaccharides as a means of stereochemical assignment have previously been reported (32, 33).

Thus the tetrasaccharide unit of the *R. equi* S3 polysaccharide can be assigned the sequence shown in **2**.

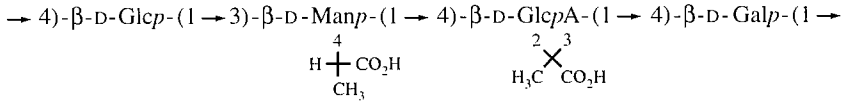

2

Partial acid hydrolysis

The foregoing structural conclusions were supported by analysis of the oligosaccharide fragments produced upon mild acid hydrolysis (2% TFA, 3 h, 100°C) of the CPS. Subsequent purification on Sephadex G-15 gave the disaccharides **3** (K_{av} 0.61) and **4** (K_{av} 0.53), and the trisaccharide **5** (K_{av} 0.23). Methanolysis followed by quantitative analysis of the carboxyl-reduced ($NaBD_4$) acid hydrolysis products gave the results recorded in Table 7. Structural information was obtained from the GLC–MS analysis of the methylated oligosaccharide alditol derivatives. The disaccharide **3** was composed of glucuronic acid and galactose. Methylation of the reduced **3** and subsequent GLC–EI-MS analysis showed diagnostic ions at *m/z* 233 (aA_1), 201 (aA_2), and 169 (aA_3), indicative of a hexopyranosyl uronate end group (34). Abundant fragment ions at 296 (J_1), 236 (bA_1), and 204 (bA_2) confirm the presence of a terminal hexitol, allowing **3** to be identified as

β-D-Glc*p*A-(1→4)-D-Gal

Glycose analysis indicated oligosaccharide **4** to contain 4-*O*-(1-carboxyethyl)-D-mannose and D-glucose. The EI-MS fragmentation pattern of the reduced, methylated disaccharide indicated nonreducing hexose (*m/z* 219, aA_1) and (1-carboxyethyl)-hexitol (*m/z* 308, bA_1) monomeric units consistent with **4** being assigned the structure

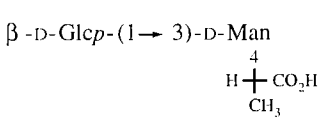

Identification of the two disaccharide fragments confirms the partial sequences, **a**→**d** and **c**→**b**, in the repeating unit **2** of the polysaccharide. The trisaccharide **5** was composed of GlcA, Gal, and Glc. The reduced methylated trisaccharide showed abundant ions in its EI-MS characteristic of terminal HexA (*m/z* 233, aA_1), HexA-Hex (*m/z* 437, abA_1), and hexitol end group (*m/z* 236, cA_1) fragments that permitted **5** to be identified as

β-D-Glc*p*A-(1→4)-β-D-Gal*p*-(1→4)-D-Glc

representative of the trisaccharide sequence **a**→**d**→**c** in the polysaccharide.

Absolute configuration of the carboxyethylidene and carboxyethyl substituents

Pyruvic acid acetals bridging the O-2 and O-3 positions of D-glucuronic acid residues are known as components of a number of *Klebsiella* polysaccharides, but the chiralities of these components has not been reported (35). The absolute configuration of the acetal carbon of cyclic pyruvate acetals involving 1,3-dioxane ring systems linked to the O-4 and O-6 positions of hexopyranosyl residues (Glc*p*, Man*p*, and Gal*p*) can be readily determined by comparison of ^{13}C NMR chemical shifts of the pyruvate methyl resonance with those of model compounds (27). However, assignment of the absolute configuration of cyclic pyruvate acetals involving 1,3-dioxolane ring systems is not as straightforward. When a 1-carboxyethylidene substituent is linked to the O-3 and O-4 positions of D-Gal*p*, no significant difference is observed for ^1H or ^{13}C chemical shifts of the methyl resonances in the *R* and *S* acetals (27). By analogy, the methyl resonances from the *R*- or *S*-2,3-(1-

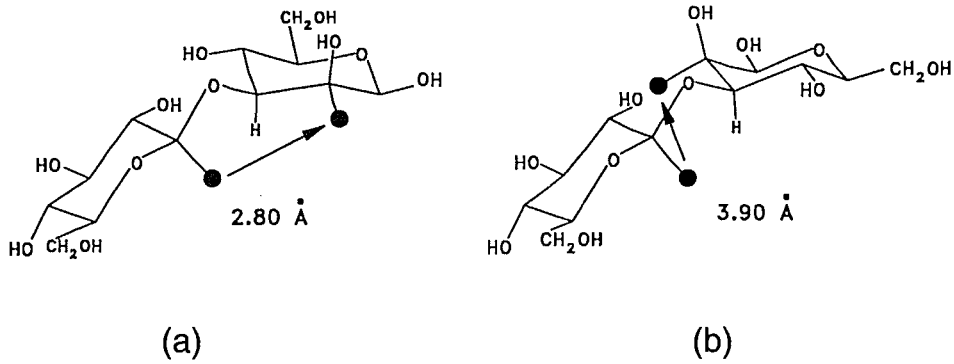

FIG. 5. The minimum energy conformation of the two disaccharide units, (*a*) β-D-Glc*p*-(1→3)-β-D-Man*p* ($\phi = 55°$, $\psi = 10°$) and (*b*) β-D-Glc*p*-(1→3)-β-L-Man*p* ($\phi = 55°$, $\psi = -5°$), calculated using the HSEA method. Internuclear distances between Glc H-1 and Man H-2 are indicated. A transglycosidic NOE would be expected only in the disaccharide in which both glycosyl units possess the D-configuration.

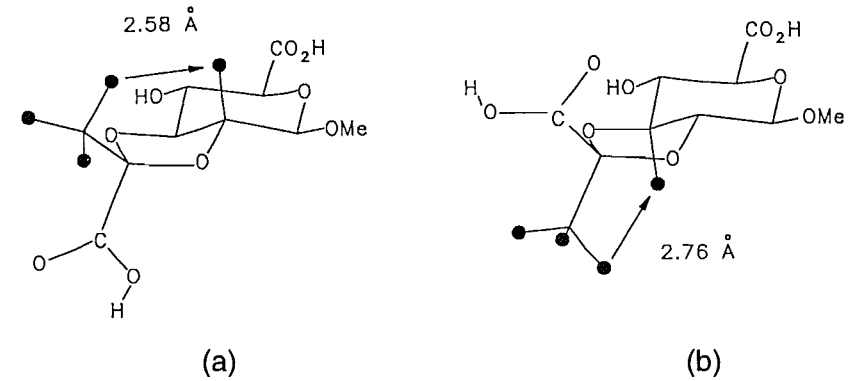

FIG. 6. Computer-generated models for the (*a*), *R*- and (*b*), *S*-2,3-pyruvate acetals of β-D-Glc*p*A. An NOE would be expected between the pyruvate methyl group and H-2 of the pyranose ring in the *R* isomer, whereas an NOE would be expected at the β-D-Glc*p*A H-3 in the *S* isomer.

TABLE 7. Sugar analysis data for the oligosaccharides obtained on partial hydrolysis of the *R. equi* serotype 3 polysaccharide

Compound	Derivatives[a]	T_{GA}	Mole ratio
3	Glucitol-6,6-d_2[b]	1.00	0.80
	Galactitol	1.01	1.00
4	Glucitol	1.00	1.00
	4-*O*-(1-Hydroxypropyl)-mannitol	1.48	0.95
5	Glucitol[b]	1.00	1.00
	Glucitol-6,6-d_2[b]	1.00	0.92
	Galactitol	1.01	0.95

[a]Determined as their carbonyl reducued alditol acetates.
[b]Determined by mass spectrometry.

carboxyethylidene) derivatives of D-Glc*p*A would not be expected to show significant stereochemical shift differences. Furthermore, suitable reference compounds are not readily available and chemical correlation is further complicated by the extreme acid lability of the *trans*-fused 1,3-dioxolane ring system (35).

It was envisaged that results from ^1H–^1H NOE experiments on the intact polysaccharide would provide a diagnostic indication of the orientation of the pyruvate methyl group and thereby lead to the desired stereochemical assignment (Fig. 6). This approach was recently applied to the stereochemical analysis of pyruvate acetals substituted at the O-2 and O-3 positions of α-D-Gal*p* residues (36).

Saturation of the pyruvate methyl resonance in the native polysaccharide resulted in an NOE at H-2 of the D-glucopyranosyl uronic acid residue **a** (Fig. 3*c*); no detectable NOE was observed at the H-1**a** or H-3**a** resonances. This result is consistent only with the pyruvate acid acetal

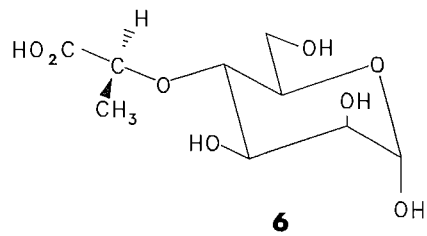

6

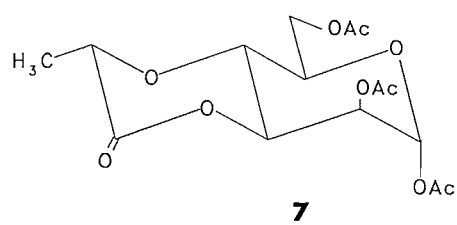

7

Can. J. Chem. Downloaded from www.nrcresearchpress.com by 109.225.110.28 on 09/08/12
For personal use only.

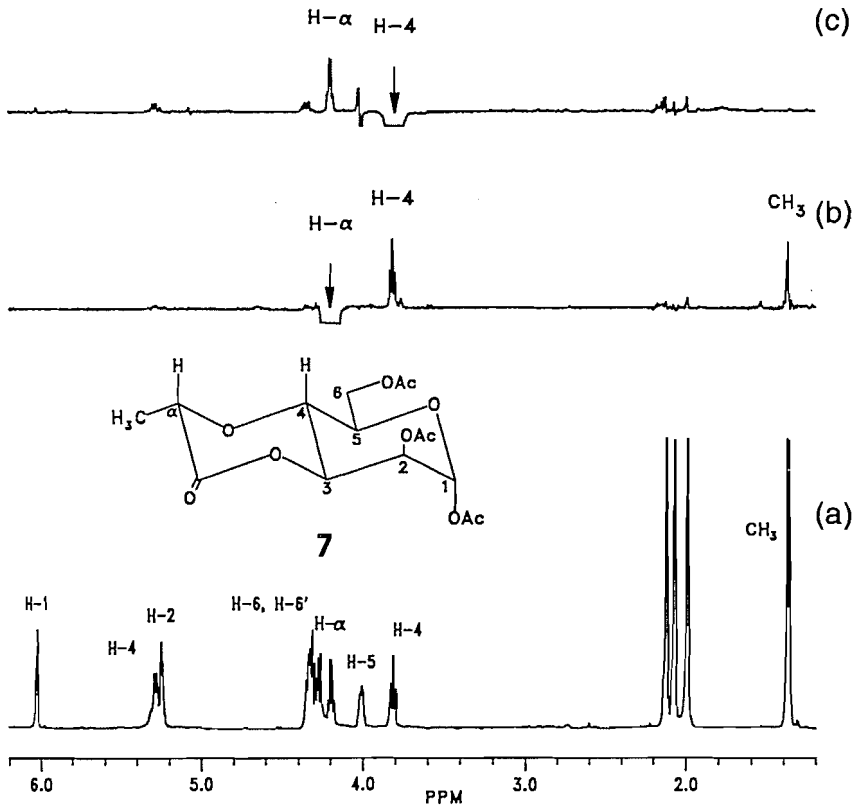

FIG. 7. NOE difference spectra measured on the lactone **7**. (*a*), off-resonance control spectrum showing assignments. Spectrum arising from the irradiation of (*b*), the lactate α-proton; and (*c*), H-4 of the mannopyranosyl ring.

having the *R* configuration in which the methyl group occupies a position on the same face of the D-glucopyranosyl ring system as the axial H-2 (Fig. 4, Fig. 6*a*).

The absolute configuration of the lactic acid moiety was determined from an NOE-based method that involved a conformationally rigid lactone derivative of the 4-*O*-(1-carboxyethyl)-α-D-mannopyranose.[3]

Periodate oxidation of the pyruvate-free polysaccharide followed by $NaBH_4$ reduction and acid hydrolysis (2 M TFA, 100°C, 12 h) afforded 4-*O*-(1-carboxyethyl)-D-mannose (**6**), which was obtained by Biogel P2 gel filtration. Treatment of the 4-*O*-(1-carboxyethyl) sugar ether (**6**) with acetic anhydride in the presence of pyridine afforded the 1,2,6-tri-*O*-acetyl lactone derivative (**7**), which was obtained pure by silica gel chromatography (see Experimental).

The chirality of the lactone α-carbon was correlated to that of the D-mannose residue from the observed $^1H-^1H$ NOE's in the acetylated lactone derivative (**7**) (Fig. 7). The ^1H NMR resonances were fully assigned (Fig. 7*a*) from a COSY experiment. Irradiation of the lactate α-proton resulted in an NOE at H-4 of the D-mannopyranosyl ring (Fig. 7*b*). Correspondingly, irradiation of the D-mannose H-4 resulted in an NOE at H-α (Fig. 7*c*), establishing the lactate moiety to have *S* chirality (as in **6**).

Conclusion

The accumulated evidence permits the repeating unit of the native *R. equi* S3 polysaccharide to be assigned the structure **8**.

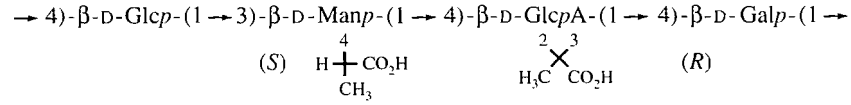

8

Immunodiffusion studies suggest that the 1-carboxyethylidene acetals are part of the immunodeterminant region of the serotype 3 polysaccharide. The native polysacchride (8) gave a strong positive precipitin reaction, whereas no precipitin line against serotype 3 specific rabbit antisera was obtained with the pyruvate-free polysaccharide. The stereochemistry of these substituents is undoubtedly important in determining the serological specificity (37). The stereochemistry of the 1-carboxyethylidene acetals was firmly established from $^1H-^1H$ NOE measurements in the intact polysaccharide.

An NOE-based strategy involving prior lactonization of

[3]W. B. Severn and J. C. Richards. Submitted for publication.

Can. J. Chem. Downloaded from www.nrcresearchpress.com by 109.225.110.28 on 09/08/12
For personal use only.

the lactone-substituted sugar enabled configurational analysis of this substituent. It is possible that the (*S*)-1-carboxyethyl substituents are also major epitopic features of the serotype 3 antigen.

Experimental

Bacterial culture

Rhodococcus equi serotype 3 (ATCC 33703), obtained from Dr. J. F. Prescott, University of Guelph, Guelph, Ontario, was grown on plates as previously described (8).

Capsular polysaccharide

The capsular polysaccharide was isolated from the cells (123 g, wet weight) by mechanical dissociation from the cellular material into 4 M sodium chloride solution. The cellular material was removed by centrifugation and the supernatant dialyzed until salt-free. Following enzymic digestion with ribonuclease, deoxyribonuclease, and proteinase K, the crude polysaccharide was precipitated with cetyltrimethyl ammonium bromide (38). The insoluble Cetavlon–polysaccharide complex was collected by centrifugation, redissolved in aqueous NaCl (4 M), and the polysaccharide component was recovered after precipitation with ethanol. Extensive dialysis afforded the sodium salt of the serotype 3 CPS (yield 490 mg, 0.4%).

Pure capsule was obtained by ion exchange chromatography. A sample (20 mg), dissolved in water, was applied to a column (1 × 40 cm) of DEAE–Sephacel (Pharmacia) equilibrated with 0.05 M Tris-HCl buffer (pH 7.2). The column was eluted with the same buffer (50 mL) followed by a 0–1 M NaCl gradient in the same buffer. Fractions (2 mL) were collected and assayed colourimetrically for neutral glycose (11) and hexuronic acid (12). Material purified in this way was deionized with Rexyn 101 (H^+ form) ion exchange resin followed by lyophilization of the eluant.

Polysaccharide samples (20 mg) were subjected to gel chromatography on columns (1 × 40 cm) of Sephadex G-200 (Pharmacia) eluted with pyridinium acetate (0.05 M, pH 4.5). Column eluants were continuously monitored for changes in refractive index by a Waters R403 differential refractometer and fractions were assayed colourimetrically (11, 12).

Polysaccharide samples were tested for serological activity by the gel diffusion test described by Prescott (4). Serotype 3 *R. equi* antisera was a gift from Dr. J. F. Prescott, University of Guelph.

Analytical methods

Quantitative colourimetric methods were used to analyse the column chromatography eluants for (*i*) neutral glycoses (11), (*ii*) hexuronic acids (12), and (*iii*) lactic-acid-containing glycoses (39).

Glycoses were determined directly by HPAE (13) or by GLC of their alditol acetate derivatives (14). Carbohydrate samples (0.2–0.5 mg) were hydrolyzed with trifluoroacetic acid (2 M, 0.5 mL) for 15 h at 100°C and evaporated to dryness *in vacuo* to obtain the free glycoses. For the GLC–MS estimation of acidic glycoses, polysaccharide samples (0.5 mg) were treated with methanolic HCl (1 M, 1 mL) for 15 h at 85°C. Excess methanolic HCl was removed *in vacuo* and the residues, in water (1 mL), were treated with $NaBD_4$ or $NaBH_4$ (15 mg) for 6 h at 25°C. Following neutralization with aqueous acetic acid (10% v/v), the mixtures were concentrated *in vacuo*, and borate was removed by repeated distillation of methanol (5 × 5 mL) from the residue. The products were deionized by passing the aqueous solution (2 mL) through a column containing Rexyn 101 (H^+ form) and then hydrolyzed (as stated). The free glycoses were reduced ($NaBH_4$) and borate was removed before the resultant alditols were acetylated by treatment with acetic anhydride (0.5 mL, 2 h, 115°C).

Absolute configurations of the glycoses were determined by GLC–MS of the corresponding trimethylsilyl *R*-2-butyl-glycoside derivatives (16). The identity of the glycose derivatives was established by comparison of their GLC retention times and mass spectra with those of authentic reference compounds.

Methylation analysis was performed on polysaccharide samples (2 mg) with methyl iodide in dimethyl sulfoxide containing an excess of sodium methylsulfinylmethanide (17). The methylated products were recovered by partitioning the reaction mixture between water and methylene chloride, followed by concentration of the organic phase. The methylated polysaccharide was treated with $NaBH_4$ in an ethanol:water mixture (1:4) at 25°C for 15 h and the carboxyl-reduced products were hydrolyzed, concentrated to dryness, reduced with $NaBD_4$, and acetylated (as stated).

GLC was performed with a Hewlett Packard model 5710A chromatograph fitted with a hydrogen flame detector and a model 3380A electronic integrator using a fused-silica capillary column (0.3 mm × 25 m) containing 3% OV17 with the following temperature programs: A, 2 min at 180°C, then 2°C/min to 240°C (methylated and acetylated alditols); B, isothermally at 175°C (trimethylsilyl 2-butyl-glycosides); and C, 2 min at 200°C, then 10°C/min to 320°C (methylated oligosaccharides). The carrier gas was dry nitrogen at 30 mL/min and retention times are quoted relative to D-glucitol hexaacetate (T_{GA}) or 1,4,5-tri-*O*-acetyl-2,3,6-tri-*O*-methyl-D-glucitol (T_{GM}).

GLC–MS was performed using a Hewlett Packard 5958B system employing the GLC program conditions A or C, by electron impact (EI) employing an ionization potential of 70 eV, or by chemical ionization (CI) with ammonia as the reagent gas.

HPAE was carried out using a Dionex BioLC carbohydrate system equipped with a column (4.6 × 250 mm) of Dionex Carbopac AS-6 pellicular anion exchange resin, and a AG-6 guard column with pulsed amperometric detection. Isocratic elution was performed using the following eluants: A, 15 mm sodium hydroxide, or B, 150 mM sodium hydroxide and 150 mM sodium acetate, at a flow rate of 1 mL/min at ambient temperature. Retention times are quoted relative to that of D-glucose (R_G).

Depyruvulation of the polysaccharide

The pyruvate acetal substituents were removed from the native capsular polysaccharide by heating a sample (120 mg) in aqueous acetic acid (2% v/v, 120 mL) at 100°C for 2 h. The modified polysaccharide was concentrated to dryness and purified by gel filtration on a G-200 column.

Partial acid hydrolysis

The serotype 3 CPS (50 mg), dissolved in 2% trifluoroacetic acid, was kept at 100°C for 3 h, then concentrated *in vacuo*. The hydrolyzate was fractionated by gel chromatography on a column (2.5 × 70 cm) of Sephadex G-15 with pyridinium acetate (0.05 M, pH 4.5) as eluant. The three oligosaccharides isolated, **3** (K_{av} 0.61), **4** (K_{av} 0.53), and **5** (K_{av} 0.23), were reduced ($NaBH_4$) and methylated before undergoing GLC–MS analysis (program C).

Isolation of the lactone derivative of 1,2,6-tri-O-acetyl-4-O-[(S)-1-carboxyethyl]-D-mannopyranose (7)

The depyruvulated *R. equi* serotype 3 polysaccharide (100 mg) was treated, in the dark, with aqueous sodium metaperiodate (0.12 M, 100 mL) at 4°C for 7 days. Following destruction of excess periodate with ethylene glycol (1 mL), the oxidized polysaccharide was reduced with $NaBH_4$ (200 mg) (6 h, 25°C); excess borohydride was then decomposed with aqueous acetic acid. The modified polysaccharide was purified by gel filtration on a column (1.6 × 100 cm) of Biogel P2 (-400 mesh) by using water as the eluant. The product was detected by assaying fractions (1 mL) colourimetrically for lactate-containing sugars (39).

A sample of the modified polysaccharide (40 mg) was hydrolyzed with trifluoroacetic acid (2 M, 100 mL) for 12 h at 100°C and concentrated to dryness, followed by repeated distillation from

Can. J. Chem. Downloaded from www.nrcresearchpress.com by 109.225.110.28 on 09/08/12
For personal use only.

water. Acetic anhydride (2 mL) was added to a suspension of the hydrolyzate in THF (10 mL). After the mixture had been stirred for 13 h, pyridine (2 mL) was added and the mixture stirred for an additional 8 h. The acetylated product (**7**) was purified on a column of silica gel (60 Å) eluted with ethyl acetate:hexane (4:1); yield, 10 mg (10%). ^{1}H NMR ($CDCl_3$): 6.05 (1H, d, J = 1.9 Hz, H-1), 5.31 (1H, dd, J = 9.7 Hz, H-3), 5.10 (1H, d, J = 2.3 Hz, H-2), 4.36 (1H, dd, J = 5.8 Hz, H-6′), 4.29 (1H, dd, J = 1.7, 12.5 Hz, H-6), 4.22 (1H, q, J = 6.8 Hz, H-α), 4.03 (1H, m, H-5), 3.83 (1H, t, J = 9.7 Hz, H-4), 2.13–2.00 (9H, s, Ac), 1.40 (3H, d, CH_3). ^{13}C NMR ($CDCl_3$): 90.8(C-1), 77.1 (C-α), 73.3 (C-2), 71.9 (C-4), 71.6 (C-3), 71.3 (C-5), 62.7 (C-6), 20.8 (Ac), 19.1 (CH_3).

NMR spectroscopy

Unless otherwise stated, nuclear magnetic resonance spectra were obtained on a Bruker AM-500 spectrometer equipped with an Aspect 3000 computer, using standard Bruker software. Solutions of polysaccharide samples in deuterium oxide (Merck, Sharp and Dohm, 99.8 at.%) or D_2O/phosphate buffer were prepared at a concentration of 10–40 mg/mL subsequent to lyophilization from D_2O. Proton and carbon-13 measurements were made on solutions (0.4 mL) of the polysaccharides (pD ≈ 2.0, or 6.5) in 5 mm tubes at 62°C.

^{1}H NMR spectra at 500 MHz were recorded using a spectral width of 2.5 kHz, an acquisition time of 3.2 s, and a 90° pulse. Resolution enhancement was achieved by using a Gaussian lineshape transformation (40). Chemical shifts are expressed relative to internal acetone (2.225 ppm).

NOE difference spectra were obtained using a selective low-power presaturation pulse applied to the proton resonance for 200 ms followed by a 90° observation pulse, where each line of a multiple resonance was irradiated sequentially for 25 ms during the presaturation delay (29).

Broad-band proton-decoupled ^{13}C NMR spectra were obtained at 125 MHz using a spectral width of 25 kHz and a 90° pulse, employing composite pulse proton decoupling (WALTZ) (41). Proton-coupled ^{13}C NMR spectra were determined by gated coupling (42). Chemical shifts are referenced to internal acetone (31.07 ppm).

Two-dimensional homonuclear proton correlation experiments, COSY (21), Relayed COSY (22), and NOESY (43), were measured with solvent suppression employing the conventional pulse sequences as previously described (8). A mixing time of 200 ms was employed for the NOESY experiment.

Heteronuclear ^{1}H–^{13}C chemical shift correlations were made using the CHORTLE pulse sequence (8, 26).

^{1}H and ^{13}C NMR spectra of the lactone **7** were obtained on a sample in $CDCl_3$ at 600 MHz and 150 MHz, respectively, using a Bruker AMX-600 spectrometer (see footnote 3). ^{1}H–^{1}H NOE measurements were made by selective irradiation of each line of the multiplet resonance for a total irradiation time of 1 s.

Molecular modeling

Molecular modeling was performed by using the PC-based program, Alchemy (Tripos Associates, Inc.). The minimum energy conformation about the glycosidic bond of the disaccharides was estimated by the HSEA method (30, 31). Structures were optimized by the MM2 algorithm (Allinger, QCPE, Indiana University) optimized for carbohydrates (44).

General methods

Commercial reagents and solvents were analytical grade. Concentrations were made under reduced pressure at bath temperatures below 40°C. Optical rotations were determined at 22°C in 10 cm microtubes using a Perkin–Elmer model 243 polarimeter.

Acknowledgements

We thank Dr. J. F. Prescott, University of Guelph, Guelph, Ontario, for providing *R. equi* serotype 3 bacterial culture and specific rabbit antisera. We also thank Mr. D. W. Griffith for the large-scale production of cells and Mr. F. P. Cooper for the GLC–MS analyses.

1. M. Goodfellow. Vet. Microbiol. **14**, 205 (1987).
2. M. D. Barton and K. L. Hughes. Vet. Bull. **50**, 65 (1980).
3. J. B. Woolcock and M. D. Mutimer. J. Gen. Microbiol. **109**, 127 (1978).
4. J. F. Prescott. Can. J. Comp. Med. **45**, 130 (1981).
5. H. J. Smith. Bacteriol. Rev. **41**, 475 (1977).
6. J. C. Richards and W. B. Severn. J. Cell Biochem. **16D**, 157 (1992).
7. R. A. Leitch and J. C. Richards. Biochem. Cell Biol. **68**, 778 (1990).
8. W. B. Severn and J. C. Richards. Carbohydr. Res. **206**, 311 (1990).
9. B. Lindberg. Adv. Carbohydr. Chem. Biochem. **48**, 279 (1990).
10. M. Heidleberger, W. F. Dudman, and W. Nimmich. J. Immunol. **104**, 1321 (1970).
11. M. Dubois, K. A. Gilles, J. K. Hamilton, P. A. Rebers, and F. Smith. Anal. Chem. **28**, 350 (1956).
12. N. Blumenkrantz and G. Asboe-Hansen. Anal. Biochem. **54**, 484 (1973).
13. M. R. Hardy, R. R. Townsend, and Y. C. Lee. Anal. Biochem. **170**, 54 (1988).
14. S. W. Gunner, J. K. N. Jones, and M. B. Perry. Can. J. Chem. **39**, 1892 (1961).
15. N. K. Kochetkov, B. A. Dmitriev, and V. L. Lvov. Carbohydr. Res. **54**, 253 (1977).
16. G. J. Gerwig, J. P. Kamerling, and J. F. G. Vliegenthart. Carbohydr. Res. **62**, 349 (1978).
17. S. Hakomori. J. Biochem. (Tokyo), **55**, 205 (1964).
18. J. C. Richards, M. B. Perry, and P. J. Kniskern. Biochem. Cell Biol. **67**, 1038 (1989).
19. D. M. Doddrell, D. T. Pegg, and M. R. Bendall. J. Magn. Reson. **48**, 323 (1982).
20. K. Bock and C. Pedersen. J. Chem. Soc. Perkin Trans. 2, 293 (1974).
21. A. Bax, R. Freeman, and G. Morris. J. Magn. Reson. **42**, 164 (1981).
22. A. Bax and G. Drobny. J. Magn. Reson. **61**, 306 (1985).
23. K. Bock and H. Thogersen. Annu. Rep. NMR Spectrosc. **13**, 1 (1982).
24. C. Altona and C. A. G. Haasnoot. Org. Magn. Reson. **13**, 417 (1980).
25. M. A. Bernstein, L. D. Hall, and S. Sukumar. Carbohydr. Res. **103**, C1 (1982).
26. G. A. Pearson. J. Magn. Reson. **64**, 487 (1985).
27. P. J. Garegg, P. E. Jansson, B. Lindberg, F. Lindh, J. Lönngren, I. Kvarnstrom, and W. Nimmich. Carbohydr. Res. **78**, 127 (1980).
28. J. M. Prestegard, T. A. W. Koerner, Jr., P. C. Demou, and R. K. Yu. J. Am. Chem. Soc. **104**, 4993 (1982); M. A. Bernstein and L. D. Hall. J. Am. Chem. Soc. **104**, 5553 (1982).
29. M. Kinnis and J. K. M. Sanders. J. Magn. Reson. **56**, 518 (1984).
30. H. Thogersen, R. U. Lemieux, K. Bock, and B. Meyer. Can. J. Chem. **60**, 44 (1982).
31. R. U. Lemieux, K. Bock, L. T. J. Delbaere, S. Koto, and V. S. Rao. Can. J. Chem. **58**, 631 (1981).
32. A. S. Shashkov, G. M. Lipkind, Y. A. Knirel, and N. K. Kochetkov. Magn. Reson. Chem. **26**, 735 (1988).
33. H. Baumann, P. E. Jansson, and L. Kenne. J. Chem. Soc. Perkin Trans 1, 209 (1988).

Can. J. Chem. Downloaded from www.nrcresearchpress.com by 109.225.110.28 on 09/08/12
For personal use only.

34. V. Kovacik, S. Bauer, and P. Kovac. Carbohydr. Res. **8**, 282 (1966).
35. C. Erbing, L. Kenne, B. Lindberg, J. Lönngren, and I. W. Sutherland. Carbohydr. Res. **50**, 115 (1976); G. G. S. Dutton and A. V. Savage. Carbohydr. Res. **84**, 297 (1980).
36. C. Jones. Carbohydr. Res. **198**, 353 (1990).
37. L. G. Bennett and C. T. Bishop. Immunochemistry, **14**, 693 (1977).
38. J. E. Scott. Methods Biochem. Anal. **8**, 145 (1960).
39. O. Hadzua. Anal. Biochem. **60**, 512 (1974).
40. A. G. Ferrige and J. C. Lindon. J. Magn. Reson. **31**, 337 (1978).
41. A. J. Shaka, J. Keeler, T. Frenkiel, and R. Freeman. J. Magn. Reson. **52**, 335 (1983).
42. O. A. Gansow and W. Schittenhelm. J. Am. Chem. Soc. **93**, 4292 (1971).
43. A. Kumar, R. R. Ernst, and K. Wuthrich. Biochem. Biophys. Res. Commun. **95**, 1 (1980).
44. G. A. Jeffrey and R. Taylor. J. Comput. Chem. **1**, 99 (1980).

Can. J. Chem. Downloaded from www.nrcresearchpress.com by 109.225.110.28 on 09/08/12
For personal use only.

Dielectric enrichment in binary solvent mixtures. The intramolecular hydrogen bond in *N*-alkyl-substituted *o*-nitroanilines. Substituent effects

ROSA CATTANA, JUANA J. SILBER, AND JORGE ANUNZIATA[1]

Departamento de Química y Física, Universidad Nacional de Río Cuarto, Estafeta Nro 9, Río Cuarto, Argentina

Received January 2, 1992

ROSA CATTANA, JUANA J. SILBER, and JORGE ANUNZIATA. Can. J. Chem. **70**, 2677 (1992).

In this work we report solvatochromism studies on *o*-nitroaniline and several *N*-alkyl-*o*-nitroaniline derivatives used as solutes in solvent mixtures of an "inert" nonpolar cosolvent, cyclohexane, and THF as a solvent with hydrogen bond acceptor ability. These studies allowed us to establish the competition between inter- and intramolecular hydrogen bond in solutes. This was done by comparing the magnitude of the local inhomogeneity induced by the solute-in-solvent mixture, that is, "preferential solvation," using Suppan's dielectric enrichment model as modified by us to be applied to electronic transitions. Since preferential solvation accounts for dielectric as well as specific interactions while dielectric enrichment only for the former, it was shown by comparison that it is possible to separate both effects and even quantify them. It was deduced that *N*-alkyl-*o*-nitroanilines form a strong intramolecular hydrogen bond, which remains unbroken even in polar solvents and hydrogen bond acceptors such as dimethyl sulfoxide. This was also confirmed by solvatochromic studies in pure solvents. On the other hand, a symmetrical dependence of the effects of alkyl substituents and solvents on the shifts of the absorption spectra was observed.

ROSA CATTANA, JUANA J. SILBER et JORGE ANUNZIATA. Can. J. Chem. **70**, 2677 (1992).

On a effectué des études de solvatochromisme sur des dérivés de l'*o*-nitroaniline et de plusieurs *N*-alkyl-*o*-nitroanilines utilisées comme solutés dans des mélanges d'un co-solvant non-polaire «inerte», le cyclohexane, et de THF agissant comme solvant capable d'accepter des liaisons hydrogènes. Ces études ont permis d'établir les quantités relatives de liaisons hydrogènes inter- et intramoléculaires dans les solutés. Ces conclusions ont été obtenues en comparant l'amplitude de l'inhomogénéité locale induite par le solvant dans le mélange, soit la «solvatation préférentielle», avec le modèle d'enrichissement diélectrique de Suppan tel que nous l'avons modifié pour l'appliquer aux transitions électroniques. Comme la solvatation préférentielle explique les interactions diélectriques et spécifiques alors que l'enrichissement diélectrique n'explique que les premières, on montre que, par comparaison, il est possible de différencier les deux effets et même de les quantifier. On a déduit que les *N*-alkyl-*o*-nitroanilines forment une forte liaison hydrogène intramoléculaire qui n'est pas brisée même dans des solvants polaires et accepteurs de liaisons hydrogènes comme le diméthylsulfoxyde. Cette conclusion a aussi été confirmée par des études solvatochromiques dans des solvants purs. Par ailleurs, on a observé une dépendance symétrique des effets de substituants alkyles et de solvants sur les déplacements du spectre d'absorption.

[Traduit par la rédaction]

Introduction

Solvent effects on the electronic spectrum of a molecule are due to the usually weak interactions between the solute and solvent molecules. These can be classified into nonspecific and specific interactions. Although it has been recognized that when specific interactions are present they tend to dominate the total effect (1), the greatest difficulty is usually to determine which is the predominating solvent effect.

To unravel this problem, empirical parameters are commonly used (1, 2). One of the most successful approaches is the solvatochromic comparison method of Kamlet, Taft, and co-workers (3). This allows us to quantify specific interactions and to separate them from polarity–polarizability effects.

Another useful approach to this problem might be the use of a binary mixture of solvents. As expected, the solute preferentially surrounds itself with the component in the mixture that leads to the most negative Gibbs energy of solvation (ΔG^0). The observation that the solvent shell has a composition other than the macroscopic ratio is termed selective or preferential solvation (4). These terms are generally used to describe molecular–microscopic local-solute-induced nonhomogeneity in a multicomponent solvent mixture. They include both (*i*) nonspecific solute–solvent association caused by dielectric enrichment in the solvent shell (5) and (*ii*) specific solute–solvent association such as hydrogen bonding or electron donor–acceptor (EDA) interactions.

The importance of such phenomena has been recognized not only for spectroscopic studies but also for the interpretation of equilibrium and kinetic data (6–9).

Perhaps the first thermodynamic treatment of the problem of preferential solvation was presented by Grunwald *et al.* (10), who were interested in the solvation of ions in mixtures of water and dioxane. This approach was further developed by Covington and Newman (11), who studied the immediate chemical environment of solute ions by measuring the NMR chemical shifts of alkali metal ions in binary solvent mixtures.

Although preferential solvation effects have been attributed mostly to specific interactions, Nitsche and Suppan (12) suggested that there is also a complete general mechanism, the "dielectric enrichment" model, to explain nonadditive polarity effects. Taking into consideration that the absorption band position depends on both the solute ground state dipole moment and the associated change by excitation (13), we have introduced a modification of this model. To distinguish pure dielectric effects from other specific solute–solvent interactions, we compared the preferential solvation approach with the theoretical results obtained by the dielectric enrichment model for *p*-nitroanilines (13).

On the other hand, there has been some controversy about solutes such as *o*-nitroanilines. There may be a competition between inter- and intramolecular hydrogen bond interactions in these solutes. Studies of the IR spectra of these

[1]Author to whom correspondence may be addressed.

Can. J. Chem. Downloaded from www.nrcresearchpress.com by 109.225.110.28 on 09/08/12
For personal use only.

Can. J. Chem. Downloaded from www.nrcresearchpress.com by 109.225.110.28 on 09/08/12
For personal use only.

compounds in different proton-accepting solvents (14) led to the conclusion that there is a moderately strong intramolecular hydrogen bond in *o*-nitroaniline that is completely broken in such solvents as dioxane, ethers, and amines. However, it was shown by UV–visible spectroscopy (15) that the intramolecular hydrogen bond in *o*-nitroaniline and *N*-methyl-*o*-nitroaniline does not break to form intermolecular hydrogen bonds in bases as strong as *N*-methylpyrrolidin-2-one. NMR and IR studies (16) have shown that *m*- and *p*-nitroanilines form dimers in carbon tetrachloride and chloroform by hydrogen bonding between the hydrogen of one molecule of amine and the nitro group of the other. This is not observed for *o*-nitroaniline, where the intramolecular hydrogen bond reduces the possibility of intermolecular interaction.

A set of hydrogen-bond rules from crystal chemistry and crystallographic data has recently been developed for organic compounds including nitroanilines. This is valid for solids and solutions (17). However, it is emphasized that the expected or typical hydrogen bonds may not occur for several reasons, including the presence of multiple competitive hydrogen-bond sites, steric overcrowding, or competing dipolar or ionic forces.

In this work we report solvatochromism studies in *o*-nitroaniline (**1**) and *N*-alkyl-*o*-nitroaniline derivatives (**2**–**10**) used as solutes in solvent mixtures of an "inert" nonpolar cosolvent, cyclohexane, and THF as a solvent with hydrogen-bond acceptor ability. These results are compared with those obtained for *p*-nitroaniline (13).

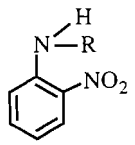

1 R = H
2 -$CH_2CH_2CH_3$
3 -$CH(CH_3)_2$
4 -$CH_2CH_2CH_2CH_3$
5 -$CH_2CH(CH_3)_2$
6 -$CH(CH_3)CH_2CH_3$
7 -$CH(CH_3)_3$
8

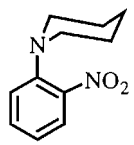

9

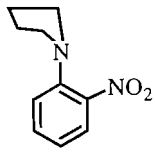

10

The studies were performed on a series of pure solvents and the data analyzed by the solvatochromic comparison method. We also considered the effect that the substituents may have upon the type or strength of the solute–solvent interactions. It is known (18) that solvent and substituent effects on the acidity of *p*-substituted anilines are mutually symmetrical. Thus, for a series of solvents, each solvent yields a regression coefficient for the acidity vs. the substituent, σ^*, and these coefficients subsequently correlate with solvent basicity. On the other hand, when the acidity of the amino group is correlated with solvent basicity the regression coefficient now correlates with the substituent constant.

These studies aim through the analysis of solute–solvent interactions, to yield further insight into the structure of those compounds which, having inherently large second-order polarizabilities, are good candidates for nonlinear optical materials (19).

Theoretical section

Model used in studies in binary solvent mixtures

(a) Preferential solvation

Following the model of Frankel *et al.* (20) for a solute in a binary mixture, the solvent is considered to be distributed between two phases, the bulk solvent and the solvation shell of the solute. It is assumed that the solvation shell is made up of independent sites that are always occupied. If the solvation number is considered to be the same for both solvents, there is a one to one replacement of solvent molecules. Considering that the solvation shell obeys the laws of regular solutions, eq. [1] can be derived (20).

$$[1] \quad Y_a/Y_b = K\,X_a/X_b$$

where Y_a and Y_b represent the mole fractions of solvents a and b in the solvation shell, respectively, and X_a and X_b refer to the bulk solvent.

The solvents a and b are considered to contribute in an additive manner to the total solvation energy. Then, if the frequency of the absorption maximum (ν_m) is a representative value for the mixture in the solvation phase, it can be assumed that (21):

$$[2] \quad \nu_m = \nu_a\,Y_a + \nu_b\,Y_b$$

and then:

$$[3] \quad \Delta\nu_m = \Delta\nu\,Y_a$$

where $\Delta\nu_m = \nu_m - \nu_b$; $\Delta\nu = \nu_a - \nu_b$; and $Y_b = 1 - Y_a$.

Since the experimentally known values are the molar fractions of the bulk solvents, a linear relation between $\Delta\nu_m$ and X_a is predicted only when $X_a = Y_a$. Any deviation from this relation ($K \neq 1$) may indicate preferential solvation effects.

(b) Dielectric enrichment

The initial model proposed by Suppan (5, 12), which we modified (13) for a better application to the study of solvent effects in electronic transitions, is described by the local thermodynamic equilibrium in a solvent under the influence of a polar, nonpolarizable solute.

Considering in the solvent mixture an element of volume dv, in which an electric dipole moment $d\boldsymbol{p}$ is induced by the permanent dipole moment $\boldsymbol{\mu}$ of the solute, the dielectric interaction energy dE is given by eq. [4] (22, 23).

$$[4] \quad dE = -\boldsymbol{F}(\boldsymbol{r}) \cdot d\boldsymbol{p} = \frac{3\mu^2 f(D)}{8\pi} \frac{(3\cos^2\theta + 1)}{r^6}\,dV$$

where $\boldsymbol{F}(\boldsymbol{r})$ is the dipolar electric field generated by the solute, $\boldsymbol{r}$ is the position vector of the element of volume with respect to the solute, and $f(D) = 2(D-1)/2D + 1$ is Onsager's function for the mixture (eq. [5])

$$[5] \quad f(D) = Y_p(\boldsymbol{r})\,f(D_p) + Y_N(\boldsymbol{r})\,f(D_N)$$

where D_p and D_N are the static bulk dielectric constants and $Y_p(\boldsymbol{r})$ and $Y_N(\boldsymbol{r})$ are the "*local*" molar fractions of the polar and nonpolar solvent, respectively.

Suppan derived an expression based on the ground state dipole moment of the solute from which it is possible to calculate the stabilization energy and, consequently, $Y_p(\boldsymbol{r})$ (5, 12).

However, since the absorption band position depends on

the ground state dipole moment (μ_g) and its associated change by excitation according the Franck–Condon principle (24), we have proposed that the dielectric enrichment energy (E_{en}) should be, for this purpose, better expressed by

$$[6] \quad E_{en} = (E_{ex} - E_g)_{local} - (E_{ex} - E_g)_{bulk}$$

where $E = -\int \boldsymbol{F}(\boldsymbol{r})\, d\boldsymbol{p}$ and the subscripts "ex" and "g" refer to excited and ground state, respectively.

To evaluate E_{ex} and E_g, eq. [4] is used. The value of $f(D)$ for the *local* is given in eq. [5] while $f(D)$ for *bulk* is calculated from the experimental values of X_p and X_N. Then, E_{en} is given explicitly by eq. [7].

$$[7] \quad E_{en} = -\frac{3}{4}\mu_g(\mu_{ex} - \mu_g)\int_a^{\infty} dr \int_{\phi}^{\pi} d\theta\, [(Y_p - X_p)f(D_p) + (Y_N - X_N)f(D_N)]\frac{(3\cos^2\theta + 1)\sin\theta}{r^4}$$

$$= \frac{-X_N X_P \Delta E_{lineal}}{8}\int_{-1}^{1} d\rho \int_{-1}^{1} du\, \frac{G(u)[1 - \exp(-G(u)\, z\rho^2)]}{X_p + X_N \exp(-G(u)\, z\rho^2)}$$

where

$$\frac{Y_N(r)}{Y_p(r)} = \frac{X_N}{X_p}\exp - [Z\, G(u)/r^6]$$

$$\Delta E_{lineal} = \frac{\mu_g(\mu_{ex} - \mu_g)\,\Delta f}{a^3}$$

a = cavity radius; the preferential solvatochromic index (5) is

$$Z = \frac{3\mu_g^2 \bar{M}\,\Delta f}{8\pi\, T\, \bar{\delta}\, R\, a^6}$$

where $\bar{M}$ is the average molecular weight and $\bar{\delta}$ the average density of the solvents in the mixture; $\Delta f = f(D_p) - f(D_N)$; $\rho = (a/r)^3$; $u = \cos\theta$; and $G(u) = 3u^2 + 1$.

Knowing a, μ_g and μ_{ex} for the solute and $f(D)$ for the corresponding solvents it is possible to evaluate, from eq. [7], the dielectric enrichment energy (E_{en}) for each pair of experimental values of X_N and X_p in every mixture studied. From these data a theoretical curve can be constructed. This curve gives an idea of the deviation from linearity of the solvatochromic shifts due only to dielectric enrichment.

Experimental section

o-Nitroaniline (**1**) from Carlo Erba was purified by sublimation under vacuum; mp 71.6°C (lit. (25) mp 71.5°C). Compounds **2–8** were synthesized and purified following the method already reported (26). Compounds **9** and **10** were synthesized and purified by a method reported elsewhere (27).

The solvents used: *n*-hexane (Hx), cyclohexane (CHx), benzene (Bz), dimethyl sulfoxide (DMSO), dimethylformamide (DMF), methanol (MeOH), ethanol (EtOH), isopropyl ether (iPE), acetonitrile (ACN), ethyl acetate (EtAc), and tetrahydrofuran (THF), were purified to spectroscopic quality by standard methods (28). The UV cutoff point in a UV cell of 10 mm against air was used as purity criterion.

The spectroscopic measurements were performed in a Cary 17 spectrophotometer at a temperature of 25 ± 0.2°C.

ν_{max} was measured by taking the midpoint between the two positions of the spectrum where the absorbance is equal to 0.90 A_{max} (29). Thus, the uncertainties in ν_{max} are ca. 100 cm^{-1}.

The least-squares correlation coefficients between π^* vs. α, π^* vs. β, and α vs. β for the solvent set used are 0.0327, 0.6439, and 0.3702 with high significance level. Thus, they may be considered mutually independent.

Data processing for the dielectric enrichment model as carried out using an IBM 3031 computer.

Results and discussion

(a) Studies in binary solvent mixtures

The behavior of *o*-nitroaniline (**1**) and *N*-alkyl-*o*-nitroanilines (**2–8**) was compared by measuring the position of the maximum of the longest wavelength absorption band in several solvent mixtures. This band, corresponding to a transition polarized in the *z* axis, has a strong charge transfer character and consequently, it is greatly influenced by polar solvents (30, 31).

Preferential solvation

The results for **1** and **2** in THF–CHx mixtures are shown in Figs. 1 and 2. As can be observed, the experimental points deviate from linearity, so preferential solvation for both solutes is detected in the solvent mixtures studied. The behavior for the other *N*-alkyl-*o*-nitroanilines is very similar.

It should be taken into account that the observed deviations are produced not only by the dielectric factors but also by the specific interactions that could be involved, mainly hydrogen bond formation. These global interactions may be quantified by calculating the preferential solvation constant, K, which according to eqs. [1]–[3] can be calculated by eq. [8].

$$[8] \quad K = X_{THF}(\nu_m - \nu_{CHx})/X_{CHx}(\nu_{THF} - \nu_m)$$

The results are shown in Table 1.

Dielectric enrichment

Solving eq. [7] by numerical integration with Gauss–Legendre quadrature (32), we calculated a theoretical curve for **1**, which represents the deviation from linearity due to dielectric enrichment (Fig. 1). The solute parameters used in these calculations are a = 3.36 Å and μ_g = 4.35 D (33). It is not necessary to know the value of μ_{ex} since it can be inferred from the experimental values of ΔE_{lineal}, a, Δf, and μ_g (eq. [7]).

There exists an extra energy of stabilization for **1**, as shown by a curvature of the experimental points greater than that predicted by dipolar effects (Fig. 1). To interpret these results we have considered that THF is a good hydrogen-bond acceptor solvent, as predicted by its β value (β = 0.55).

Moreover, **1** is capable of being a hydrogen bond donor (14, 18, 34) and, in fact, it has a value of α_2^H = 0.367 on the solute hydrogen-bond acidity scale of Abraham *et al.* (35). Thus it is expected that hydrogen bond formation with the solvent should be responsible for at least a part of the observed preferential solvation of THF toward **1**, as was observed for *p*-nitroaniline (13).

Can. J. Chem. Downloaded from www.nrcresearchpress.com by 109.225.110.28 on 09/08/12
For personal use only.

Can. J. Chem. Downloaded from www.nrcresearchpress.com by 109.225.110.28 on 09/08/12
For personal use only.

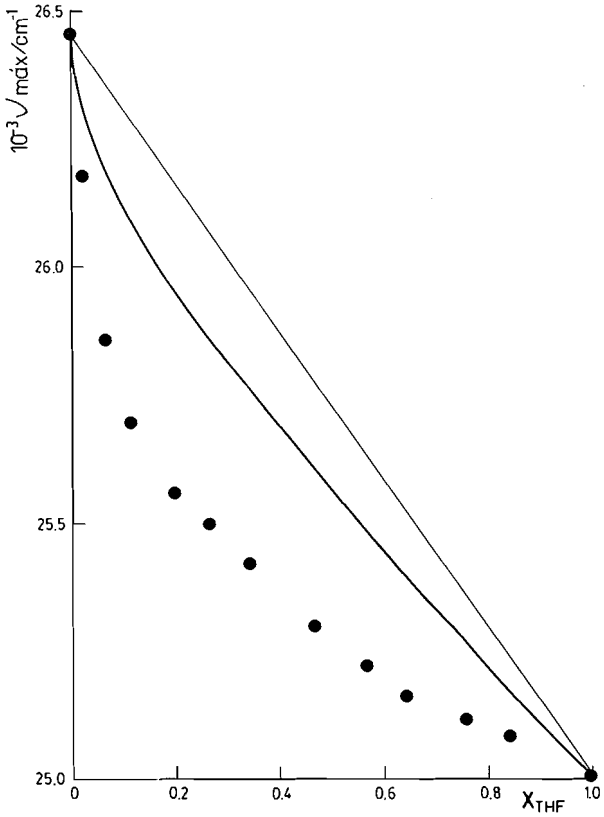

FIG. 1. ν_{max} vs. X_p for *o*-nitroaniline in THF–CHx solvent mixture. (——) Theoretical linear dependence for no preferential solvation; (——) curve predicted by dielectric enrichment model; (●) experimental data.

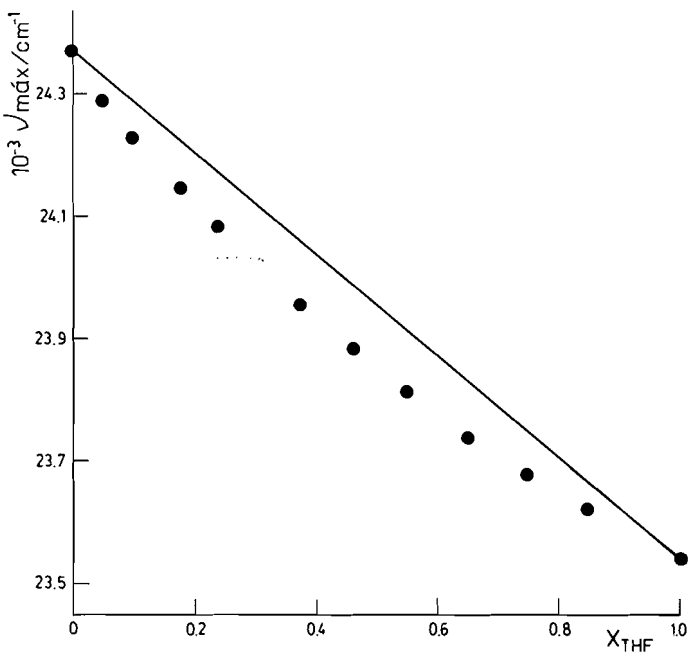

FIG. 2. ν_{max} vs. X_p for *N*-propyl-*o*-nitroaniline in THF–CHx solvent mixture. (——) Theoretical linear dependence for no preferential solvation; (●) experimental data.

TABLE 1. Preferential solvation constants (K) for compounds **2**–**8** in the CHx–THF solvent mixture

Compound	K
2	1.47 ± 0.03
3	1.49 ± 0.02
4	1.48 ± 0.04
5	1.48 ± 0.02
6	1.50 ± 0.03
7	1.52 ± 0.02
8	1.49 ± 0.04

To obtain a more quantitative picture of the dielectric effect of the solvent mixtures, we calculated the solvation constant, K_D, from the theoretical curve (Fig. 1), applying the same procedure used to calculate K in the preferential solvation model. This constant may be considered a measure of the dielectric enrichment in the polar solvent within the solvation shell.

The values of K_D for **1** and *p*-nitroaniline (13) are 1.44 ± 0.02 and 1.70 ± 0.02, respectively, while the corresponding values of K are 3.74 ± 0.03 and 4.09 ± 0.02.

As can be observed, the values of K_D for *p*-nitroaniline are higher than for **1**, as expected, since the former has a higher value of μ_g (33). The greater values of K for *p*-nitroaniline also reflect not only the higher dielectric effects but also a higher degree of intermolecular hydrogen bond formation than for **1** (α_2^H (*p*-nitroaniline) = 0.421).

The values of K for *N*-alkyl-*o*-nitroanilines are very similar to the value of K_D for **1**, which could indicate that the preferential solvation is mainly due to dipolar interaction of these solutes with THF and that there is no breaking of the intramolecular hydrogen bond in this medium.

On the other hand there is no significant variation of K with the *N*-alkyl substituents (R). This may be because of the relatively high polarity of THF that gives such strong dipole–dipole interactions with the solutes and that is insensitive to the small changes produced by the change of the substituent.

(b) Studies in pure solvents

The absorption maxima measured for the solutes **1**–**10** in different solvents are reported in Table 2. The correlations obtained by Taft and Kamlet's solvatochromic comparison method (3) are shown in eqs. [9]–[18]:

[9] $\nu(\mathbf{1}) = (26.57 \pm 0.03) - (1.75 \pm 0.06)\pi^* - (1.05 \pm 0.06)\beta, \quad r = 0.9987$

[10] $\nu(\mathbf{2}) = (24.50 \pm 0.05) - (1.65 \pm 0.08)\pi^* - (0.14 \pm 0.06)\alpha, \quad r = 0.9918$

[11] $\nu(\mathbf{3}) = (24.45 \pm 0.04) - (1.62 \pm 0.06)\pi^* - (0.14 \pm 0.05)\alpha, \quad r = 0.9945$

[12] $\nu(\mathbf{4}) = (24.41 \pm 0.05) - (1.58 \pm 0.07)\pi^* - (0.11 \pm 0.06)\alpha, \quad r = 0.9924$

[13] $\nu(\mathbf{5}) = (24.37 \pm 0.04) - (1.62 \pm 0.06)\pi^* - (0.13 \pm 0.04)\alpha, \quad r = 0.9899$

TABLE 2. Absorption spectra of compounds 1 through 10. Values given in $10^3\ \nu_{max}/cm^{-1}$

Solvent	Compound 1	2	3	4	5	6	7	8	9	10
Hx	26.46	24.57	24.51	24.45	24.39	24.33	24.21	24.21	25.25	26.20
Bz	25.44	23.47	23.47	23.47	23.42	23.36	23.31	23.25	24.04	24.50
DMSO	23.98	22.83	22.83	22.78	22.67	22.67	22.62	22.62	23.15	23.58
DMF	24.33	23.04	22.99	22.99	22.95	22.93	22.83	22.83	23.36	23.87
MeOH	24.84	23.35	23.36	23.31	23.27	23.20	23.15	23.25	23.87	24.69
EtOH	24.81	23.53	23.47	23.53	23.42	23.36	23.31	23.25	23.98	24.75
iPE	25.64	24.10	24.10	24.04	24.04	23.92	23.87	23.87	24.75	25.40
ACN	24.94	23.20	23.15	23.15	23.09	23.04	22.99	22.99	23.59	24.24
EtAc	25.19	23.75	23.64	23.58	23.53	23.53	23.42	23.42	24.10	24.81
THF	24.94	23.53	23.53	23.58	23.47	23.42	23.47	23.31	24.15	24.70

[14] $\nu(\mathbf{6}) = (24.28 \pm 0.04) - (1.55 \pm 0.07)\pi^* - (0.14 \pm 0.06)\alpha, \quad r = 0.9931$

[15] $\nu(\mathbf{7}) = (24.20 \pm 0.06) - (1.51 \pm 0.09)\pi^* - (0.13 \pm 0.07)\alpha, \quad r = 0.9866$

[16] $\nu(\mathbf{8}) = (24.17 \pm 0.05) - (1.52 \pm 0.07)\pi^* - (0.07 \pm 0.04)\alpha, \quad r = 0.9914$

[17] $\nu(\mathbf{9}) = (26.06 \pm 0.04) - (2.39 \pm 0.08)\pi^* - (0.10 \pm 0.04)\alpha, \quad r = 0.9954$

[18] $\nu(\mathbf{10}) = (25.20 \pm 0.06) - (2.00 \pm 0.07)\pi^* - (0.17 \pm 0.03)\alpha, \quad r = 0.9900$

There is a strong effect of the β parameter on **1** (eq. [9]), which coincides with literature data (14) and is interpreted as due to the hydrogen bond donor ability of the H amino group not involved in the intramolecular hydrogen bond.

On the contrary there is no effect on β in the solutes **2–8**. The values of *b* are smaller than its standard deviation and with a significance level higher than 40% according to the Student t-test. This means that the *b* values can be considered equal to zero.

This may indicate that there is no breaking of the intramolecular hydrogen bond in these *N*-alkyl-*o*-nitroanilines. Consequently, they have a similar behavior to solutes **9** and **10**, which do not have an H in the amino group.

The high and negative values of the π* sensitivity coefficients, *s*, are as expected, considering the important increase of dipole moment upon excitation for these solutes (36).

The value of *s* is higher for *N*,*N*-dialkyl-*o*-nitroanilines than for **1** and *N*-alkyl-*o*-nitroanilines. This has been explained by considering that polar solvents favor the coplanarity of the *ortho* group, producing a marked bathochromic effect (15). However, it is believed that this effect is due to the fact that, in the *N*-alkyl-*o*-nitroanilines, the intramolecular hydrogen bond aids in stabilizing, particularly, the excited state of these solutes and makes them less sensitive to the solvent polarity.

On the other hand, a negative value of the coefficient for α, *a*, in compounds **2–10** indicates the formation of an intermolecular hydrogen bond to the oxygen of the nitro group in protic solvents (37). However, the values of *a*, although statistically significant, are low. It is evident that for compounds **9** and **10** the non-coplanarity of the *ortho* groups weakens the intramolecular charge transfer from the amine to the nitro group. Thus the latter is a weak hydrogen bond acceptor. In the case of the *N*-alkyl-*o*-nitroanilines (compounds **2–8**), which are coplanar, *inter*molecular hydrogen bond formation competes unfavorably with the *intra*molecular bond formation. Moreover, it might be considered that the charge transfer from the amine to the nitro group (classical through-resonance) is only partial, as was calculated recently for *p*-nitroaniline (38).

(c) Substituent effects in the solvatochromism of N-*alkyl*-o-*nitroanilines*

Equations [9]–[16] show a variation of the sensitivity to solvent polarity, when the R group is changed.

To quantify the influence of inductive and steric effects, the values of the coefficient *s* were intended to be correlated with σ* and E_s (39) parameters, respectively.

Although the correlation of *s* with σ* is very poor ($r = 0.8368$), it shows the trend that the greater the inductive electron donor effect of the R substituent, the lesser the sensitivity to the solvent polarity. There is also no significant dependence on the steric parameters.

On the other hand, it was possible to determine for each solvent the dependence of the absorption band in *N*-alkyl-*o*-nitroanilines upon substituent parameters by a general equation such as:

[19] $\nu = \nu_0' + \rho \Sigma \overset{*}{\sigma} + a_1 E_s(R)$

This equation accounts for the effect exerted by the alkyl substituent on the stabilization of the positive charge on amine nitrogen in the excited state. The results are shown in Table 3.

As can be observed, only the inductive effect of the substituent is significant. The positive sign of ρ shows that, when the electron donor effect of the alkyl substituents increases, the excited state is more stable.

Also, by considering the correlations in Table 3, a dependence of ρ upon the solvent parameters was found, as shown in eq. [20]:

[20] $\rho = (3.24 \pm 0.07) - (0.25 \pm 0.13)\pi^* - (1.50 \pm 0.16)\beta, \quad r = 0.9818$

It is evident that when the polarity of the solvent increases, and consequently its interaction with the solutes, the dependence on the substituent is smaller. Moreover, the

Can. J. Chem. Downloaded from www.nrcresearchpress.com by 109.225.110.28 on 09/08/12
For personal use only.

TABLE 3. Correlation terms obtained by application of eq. [19] to compounds **1–8**[a]

Solvent	ν_0'	ρ	r
Hx	24.96 ± 0.07	3.31 ± 0.28	0.9788
Bz	23.92 ± 0.07	2.93 ± 0.27	0.9751
DMSO	23.04 ± 0.04	1.82 ± 0.18	0.9722
DMF	23.29 ± 0.04	2.01 ± 0.17	0.9800
MeOH	23.67 ± 0.04	2.27 ± 0.17	0.9836
EtOH	23.77 ± 0.05	2.03 ± 0.19	0.9750
iPE	24.41 ± 0.05	2.38 ± 0.20	0.9797
ACN	23.56 ± 0.05	2.66 ± 0.22	0.9795
EtAc	23.97 ± 0.05	2.37 ± 0.22	0.9760
THF	23.85 ± 0.06	2.08 ± 0.24	0.9622

[a]Confidence level of every correlation greater than 99.99%, according to Student *t*-test.

negative sign of the β coefficient can be explained by considering that the higher the β value for the solvent, the closer inductive effect of the H on **1** gets to the alkyl groups.

Summarizing, there seems to be a symmetrical dependence of the substituent and solvent effects on the shifts of the absorption band (18).

(d) Substituent effects on N,N-*dialkyl* o-*nitroanilines*

The results obtained by the solvatochromic comparison method for compounds **9** and **10** are compared with the correlations for the corresponding *p*-nitroaniline isomers from literature data (40). For *p*-nitropyrrolidino benzene (Pyr) eq. [21] is obtained:

$$[21]\quad \nu(\text{Pyr}) = (27.39 \pm 0.04) - (3.13 \pm 0.06)\pi^* - (0.56 \pm 0.08)\alpha, \qquad n = 9, \qquad r = 0.9873$$

and for *p*-nitropiperidino benzene (Pip) eq. [22]:

$$[22]\quad \nu(\text{Pip}) = (27.68 \pm 0.05) - (3.13 \pm 0.05)\pi^* - (0.49 \pm 0.06)\alpha, \qquad n = 9, \qquad r = 0.9901$$

When the values of the solvatochromic terms *s* and *a* are compared with those for the *ortho* isomers (eqs. [17] and [18]), it is clear that the *para* isomers are much more sensitive in both nonspecific and specific (hydrogen bond) solvent interactions. This could be attributed to the lack of planarity of the *ortho* compound, which implies lower charge delocalization and, thus, lower effect of solvent polarity and hydrogen bond formation capability.

1. C. Reichardt. Angew. Chem. Int. Ed. Engl. **4**, 29 (1965).
2. (*a*) M. J. Kamlet, J. L. Abboud, and R. W. Taft. J. Am. Chem. Soc. **99**, 6027 (1977); (*b*) R. W. Taft and M. J. Kamlet. J. Am. Chem. Soc. **98**, 2886 (1976); (*c*) J. Am. Chem. Soc. **98**, 337 (1976).
3. M. J. Kamlet, J. L. Abboud, M. H. Abraham, and R. W. Taft. J. Org. Chem. **48**, 2877 (1983).
4. C. Reichardt. *In* Solvents and solvent effects in organic chemistry. 2nd ed. V.C.H. Publishers, Weinheim. 1990.
5. P. Suppan. J. Chem. Soc. Faraday Trans. 1, **83**, 495 (1987).
6. K. Remerle and J. B. Engberts. J. Phys. Chem. **87**, 5449 (1983).
7. M. Muanda, J. B. Nagy, and O. B. Nagy. Tetrahedron Lett. **38**, 3421 (1974).
8. S. Kalsi, R. Laframboise, and R. M. Scott. Can. J. Chem. **65**, 563 (1978).
9. J.-L. M. Abboud, A. Douhal, M. J. Arin, M. T. Diez, H. Homan, and G. J. Guihéneuf. J. Phys. Chem. **93**, 214 (1989).
10. E. Grunwald, G. Baughman, and G. Kohnstam. J. Am. Chem. Soc. **82**, 5801 (1960).
11. A. K. Covington and K. E. Newman. Adv. Chem. Ser. **155**, 153 (1976).
12. M. J. Nitsche and P. Suppan. Chimia, **36**, 346 (1982).
13. R. Cattana, J. Perez, J. J. Silber, and J. D. Anunziata. Spectrochim. Acta, **47A**, 821 (1991).
14. G. Parimala Someswar. Indian J. Chem. **27A**, 947 (1988).
15. T. Yokoyama, R. W. Taft, and M. J. Kamlet. Aust. J. Chem. **36**, 701 (1983).
16. M. Nomura and S. Nakata. Nippon Kagaku Kaishi, **1**, 48 (1990).
17. M. C. Etter. J. Phys. Chem. **95**, 4601 (1991).
18. G. Launay, B. Wojtkowiak, and T. M. Krygowski. Can. J. Chem. **57**, 3065 (1979).
19. T. W. Panunto, Z. Urbánczyck-Lipkowska, R. Johnson, and M. C. Etter. J. Am. Chem. Soc. **109**, 7786 (1987).
20. L. S. Frankel, T. R. Stengle, and C. H. Lanford. J. Phys. Chem. **74**, 1376 (1970).
21. R. G. E. Morales. Spectrosc. Lett. **16**, 899 (1983).
22. H. B. Callen. Thermodinamica. Ed. AC, Libros Cientificos y Técnicos, Madrid. 1981.
23. J. D. Jackson. Electrodinámica Clásica. Ed. Alhambra S.A., Mexico. 1966.
24. W. Liptay. Angew. Chem. Int. Ed. Engl. **8**, 177 (1969).
25. R. C. Weast (*Editor*). CRC handbook of chemistry and physics. 65th ed. CRC Press Inc., Boca Raton, Fla. 1984.
26. S. M. Chiacchiera, J. O. Singh, J. D. Anunziata, and J. J. Silber. J. Chem. Soc. Perkin Trans 2, 987 (1987).
27. R. Cattana, J. O. Singh, J. D. Anunziata, and J. J. Silber. J. Chem. Soc. Perkin Trans. 2, 79 (1987).
28. J. A. Riddick and W. B. Bunger. Techniques of chemistry. Vol. II. Organic solvents. 3rd ed. Wiley–Interscience, New York. 1970.
29. M. J. Kamlet, J.-L. M. Abboud, and R. W. Taft. J. Am. Chem. Soc. **99**, 6027 (1977).
30. H. J. Freund and R. W. Bigelow. Chem. Phys. **55**, 407 (1981).
31. (*a*) H. E. Smith, W. I. Cozart, T. de Paulis, and F. M. Chen. J. Am. Chem. Soc. **101**, 5186 (1979); (*b*) W. von Niessen. J. Phys. Chem. **92**, 1035 (1988).
32. K. E. Atkinson. An introduction to numerical analysis. J. Wiley and Sons, New York. 1978.
33. B. Oscik-Mendyk. Chromatographia, **28**, 151 (1989).
34. M. J. Kamlet, M. E. Jones, R. W. Taft, and J.-L. M. Abboud. J. Chem. Soc. Perkin Trans. 2, 342 (1979).
35. M. H. Abraham, P. L. Grellier, D. V. Prior, P. P. Duce, J. J. Morris, and P. J. Taylor. J. Chem. Soc. Perkin Trans. 2, 699 (1989).
36. L. S. Prabhumirashi and S. S. Kunte. Spectrochim. Acta, **44A**, 213 (1988).
37. T. Yokoyama, R. W. Taft, and M. J. Kamlet. J. Am. Chem. Soc. **98**, 3233 (1976).
38. T. M. Krygowsky and J. Maurin. J. Chem. Soc. Perkin Trans. 2, 695 (1989).
39. C. Takayama, T. Fujita, and N. Nakajima. J. Org. Chem. **44**, 2871 (1979).
40. M. J. Kamlet, R. R. Minesinger, E. G. Kayser, M. H. Aldridge, and J. W. Eastes. J. Org. Chem. **36**, 3852 (1971).

Can. J. Chem. Downloaded from www.nrcresearchpress.com by 109.225.110.28 on 09/08/12
For personal use only.

The synthesis and structural characterization of a series of triphenyltin(IV) esters of *N*-arylidene-ω-amino acids

Y. C. TOONG, S. P. TAI, AND M. C. PUN
School of Chemical Sciences, Universiti Sains Malaysia, 11800 Penang, Malaysia

ROSEMARY C. HYNES
Chemistry Department, McGill University, Montreal, Que., Canada H3A 2T5

L. E. KHOO
NIE-Chemistry, Nanyang Technological University, 469 Bukit Timah Road, Singapore 1025

AND

F. E. SMITH[1]
Chemistry Department, Laurentian University, Sudbury, Ont., Canada P3E 2C6

Received March 13, 1992

Y. C. TOONG, S. P. TAI, M. C. PUN, ROSEMARY C. HYNES, L. E. KHOO, and F. E. SMITH. Can. J. Chem. **70**, 2683 (1992).

Methods of synthesis, elemental analyses, and IR and NMR spectroscopic data are reported for a series of triphenyltin esters of *N*-salicylidene-ω amino acids of the general formula: $Ph_3SnOCO(CH_2)_nN{=}CHAr$ (Ar = 2-HOC_6H_4- and 2-$HOC_{10}H_6$-; n = 1, 2, 3, and 5). The crystal structure of triphenyltin *N*-salicylidene-6-aminohexanoate was determined. The crystals are monoclinic, space group $P2_1/a$, with a = 16.3493(8) Å, b = 9.0675(7) Å, c = 18.8562(14) Å, β = 100.493(5)°, V = 2748.6(3) Å^3, Z = 4, and D_{calc} = 1.427 Mg m^{-3}. The final discrepancy factors are R_F = 0.033, and R_W = 0.036 for 2339 significant reflections. This compound, believed typical of the series described, adopts a polymeric *trans*-O_2SnC_3 trigonal bipyramidal geometry with the axial positions occupied by a carboxylate oxygen and the phenolic oxygen of an adjacent molecule. These compounds appear to be the first reported triphenyltin(IV) carboxylates with phenolic oxygen bridges.

Y. C. TOONG, S. P. TAI, M. C. PUN, ROSEMARY C. HYNES, L. E. KHOO et F. E. SMITH. Can. J. Chem. **70**, 2683 (1992).

On rapporte les méthodes de synthèse, les analyses élémentaires et les données spectroscopiques d'une série d'esters triphénylstanniques d'acides *N*-salicylidène-ω-aminés de formule générale : $Ph_3SnOCO(CH_2)_nN{=}CHAr$ (Ar = 2-HOC_6H_4- et 2-$HOC_{10}H_6$-; n = 1, 2, 3 et 5). On a déterminé la structure cristalline du *N*-salicylidène-6-aminohexanonate de triphénylétain. Les cristaux sont monocliniques, groupe d'espace $P2_1/a$, avec a = 16,3493(8), b = 9,0675(7) et c = 18,8562(14) Å, β = 100,493(5)°, V = 2748,6(3) Å^3, Z = 4 et D_{calc} = 1,427 Mg m^{-3}. On a affiné la structure jusqu'à des facteurs R_F = 0,033 et R_W = 0,036 pour 2339 réflexions significatives. Ce composé, considéré comme typique de la série décrite, adopte une géométrie bipyramidale trigonale polymérique du *trans*-O_2SnC_3 dans laquelle les positions axiales sont occupées par un oxygène du carboxylate et par l'oxygène phénolique d'une molécule adjacente. Ces composés semblent être les premiers carboxylates de triphénylétain(IV) comportant des ponts phénoliques oxygénés.
[Traduit par la rédaction]

Introduction

Structural studies on a range of triphenyltin carboxylates have yielded examples of monomeric and polymeric forms. For the monomers, depending on whether the chelating carboxylate group functions as a uni- or bi-dentate ligand, the tin atoms are found to be either four- or five-coordinate (1). However, in the polymeric forms the carboxylate ligands behave as bridging bidentate ligands and the pentacoordinate tin atoms have distorted trigonal bipyramidal geometries (1). Alternatives to carboxyl bridging have been sought in compounds containing either donor substituent groups or labile phenolic groups in the ester function. Among the earliest compounds successfully investigated was trimethyltin(IV) glycinate (2) whose crystal structure revealed a polymeric network built of Sn—N linkages. Polymeric triphenyltin(IV) carboxylates that contain unidentate carboxylate groups are rare. There are only three compounds reported, namely, triphenyltin(IV) pyridine-3-carboxylate (3), triphenyltin(IV) 3-ureidopropionate (4), and the triphenyltin(IV) ester of citraconic acid monopyrrolidide (5). The first compound involves an Sn—N linkage, while for the last two structures the Sn—O bridges occur through the uriedo and amido carbonyl oxygens, respectively, and not the carboxyl oxygen. X-ray structural analyses for $Ph_3SnOCOR$ where R contains a phenolic functional group as in $Ph_3SnOCOC_6H_4$-OH-*o* (6), $Ph_3SnOCOC_6H_4OCH_3$-*o* (6), $Ph_3SnOCOC_6H_4$-OPh-*o* (7), $Ph_3SnOCOC_6H_4(N_2C_6H_3MeOH)$ (the ligand in this complex is *o*-(2-hydroxy-5-methylphenylazo)-benzoate (8) failed to firmly establish the presence of an Sn—O(phenolic) linkage even though such a network was reported for the trimethyltin(IV) analogue, $Me_3SnOCOC_6H_4OH$-*o* (9). We describe here the synthesis and characterization by IR and NMR spectroscopic techniques of a series of triphenyltin derivatives of *N*-salicylidene-ω-amino acids, 2-HOC_6H_4-$CH{=}N(CH_2)_nCOOH$, and *N*-2-hydroxynaphthylidene-ω-amino acids, 2-$HOC_{10}H_6CH{=}N(CH_2)_nCOOH$ (n = 1, 2, 3, and 5). Each ligand contains a potential binding site in its phenolic fragment in addition to the carboxyl function that could engage the tin atom in either intra- or inter-molecular (polymeric) coordination. Since definitive establishment of the bonding behaviour in these situations must come from X-ray diffraction studies, we carried out an X-ray crystal structure determination on a representative compound in

[1]Author to whom correspondence may be addressed.

Can. J. Chem. Downloaded from www.nrcresearchpress.com by 109.225.110.28 on 09/08/12
For personal use only.

TABLE 1. Analytical data for $Ph_3SnOCO(CH_2)_nN{=}CHAr$

Compound		Yield	Melting point	Elemental analysis (%) found (calcd.)			
Ar	*n*	(%)	(°C)	C	H	N	Sn
$2\text{-}HOC_6H_4$	1	92	152–153	60.04 (61.39)	4.30 (4.40)	2.61 (2.65)	24.07 (22.47)
$2\text{-}HOC_6H_4$	2	73	130–132	60.56 (62.02)	4.64 (4.66)	2.73 (2.58)	21.45 (21.89)
$2\text{-}HOC_6H_4$	3	62	72–74	63.61 (62.61)	4.81 (4.90)	1.98 (2.52)	—
$2\text{-}HOC_6H_4$	5	85	118–119	62.19 (63.72)	5.26 (5.36)	2.95 (2.40)	—
$2\text{-}HOC_{10}H_6$	1	60	208–210	64.70 (64.38)	4.43 (4.37)	2.29 (2.42)	20.15 (20.53)
$2\text{-}HOC_{10}H_6$	2	65	170–171	66.80 (64.89)	4.71 (4.60)	1.92 (2.37)	20.83 (20.04)
$2\text{-}HOC_{10}H_6$	3	89	174–175	66.03 (65.37)	4.78 (4.83)	2.01 (2.31)	—
$2\text{-}HOC_{10}H_6$	5	70	128–130	65.80 (65.82)	5.00 (5.05)	2.02 (2.26)	—

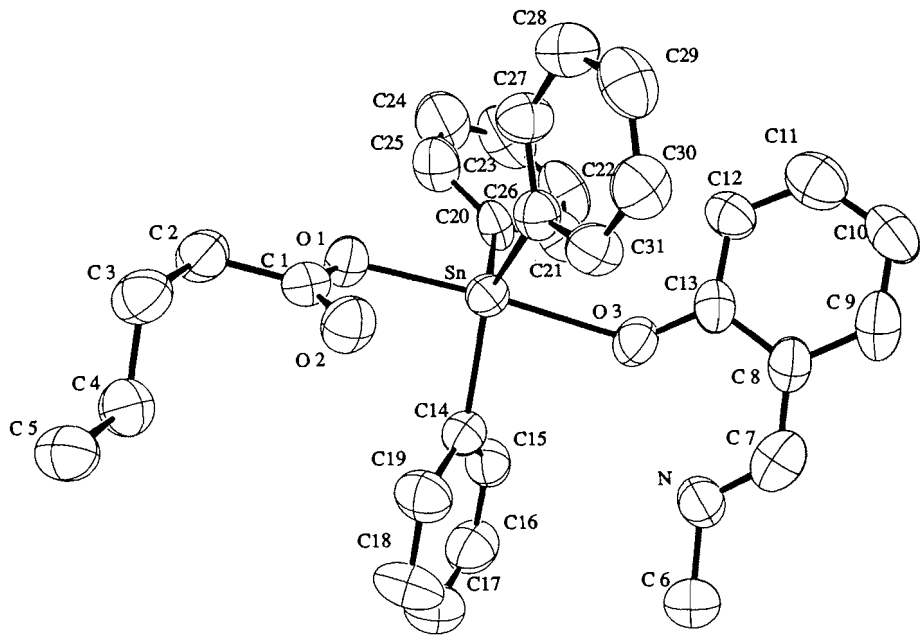

FIG. 1. An ORTEP plot showing the coordination at tin (ellipsoids are shown at 50% probability).

this series, namely, triphenyltin *N*-salicylidene-6-aminohexanoate. The results confirmed the presence of an Sn—O(phenolic) bridge with the carboxylate group functioning in the unidentate mode.

Experimental

Reagents

Bistriphenyltin oxide and other chemicals were purchased from the Aldrich Chemical Company, and used without further purification.

Preparation of ligands

Triphenyltin(IV) esters of *N*-arylidene-ω-amino acids were prepared by refluxing in absolute ethanol (ca. 90 mL) a mixture of bistriphenyltin oxide (10 mmol), ω-amino acid (20 mmol), and salicylaldehyde or 2-hydroxynaphthaldehyde (20 mmol). After refluxing for 6–8 h the reaction mixture was cooled and the product (if there was precipitation) was isolated via filtration, otherwise the reaction mixture was concentrated under reduced pressure before either toluene or petroleum ether (60–80°C) was added to induce precipitation. The isolated solid was recrystallized from benzene, petroleum ether, or ethanol to give the pure triphenyltin carboxylates whose yields and melting points are listed in Table 1.

A slowly evaporating solution (95% ethanol, 30 mL) of triphenyltin(IV) *N*-salicylidene-6-aminohexanoate (4 g) yielded crystals (1.2 g), mp 118–119°C, from which a thin yellow plate of dimensions 0.40 × 0.25 × 0.03 mm was selected for X-ray analysis.

TABLE 2. Carboxylate frequencies (cm^{-1}) of $Ph_3SnOCO(CH_2)_nN{=}CHAr$

Compound		IR(KBr)		
Ar′	*n*	ν_{ass}(OCO)	ν_{sym}(OCO)	$\Delta\nu$
$2\text{-}HOC_6H_4$	1	1640	1325	315
$2\text{-}HOC_6H_4$	2	1640	1350	290
$2\text{-}HOC_6H_4$	3	1630	1370	260
$2\text{-}HOC_6H_4$	5	1640	1390	250
$2\text{-}HOC_{10}H_6$	1	1640	1355	285
$2\text{-}HOC_{10}H_6$	2	1645	1295	350
$2\text{-}HOC_{10}H_6$	3	1635	1405	230
$2\text{-}HOC_{10}H_6$	5	1630	1370	260

Instrumentation

The IR spectra of the complexes were recorded in the region 4000–300 cm^{-1} with a Beckman IR 20A spectrophotometer with samples either as Nujol mulls or KBr discs.

Tin was determined gravimetrically as SnO_2. Carbon, hydro-

Can. J. Chem. Downloaded from www.nrcresearchpress.com by 109.225.110.28 on 09/08/12
For personal use only.

TABLE 3. Atomic parameters x, y, z and B_{iso}; esd's refer to the last digit printed

Atom	x	y	z	B_{iso}[a]
Sn	0.238424(24)	0.98873(5)	0.250144(23)	3.500(22)
O 1	0.1176 (3)	0.9007 (5)	0.20709 (25)	4.29 (22)
O 2	0.1776 (3)	0.8010 (5)	0.1221 (3)	4.90 (25)
O 3	0.3681 (3)	1.0952 (5)	0.2905 (3)	4.52 (23)
N	0.4579 (4)	1.2291 (7)	0.2109 (3)	4.6 (3)
C 1	0.1163 (4)	0.8212 (8)	0.1495 (4)	4.2 (3)
C 2	0.0328 (4)	0.7537 (9)	0.1202 (4)	5.1 (4)
C 3	0.0268 (5)	0.6818 (9)	0.0473 (4)	5.4 (4)
C 4	0.0287 (4)	0.7904 (8)	−0.0144 (4)	5.0 (4)
C 5	0.0299 (5)	0.7097 (8)	−0.0842 (4)	5.1 (4)
C 6	0.4681 (5)	1.3118 (9)	0.1463 (4)	5.2 (4)
C 7	0.5202 (5)	1.1728 (9)	0.2551 (5)	5.2 (4)
C 8	0.5143 (4)	1.0811 (8)	0.3145 (4)	4.5 (4)
C 9	0.5871 (4)	1.0228 (11)	0.3572 (5)	6.5 (5)
C10	0.5845 (5)	0.9315 (11)	0.4132 (5)	6.6 (5)
C11	0.5078 (6)	0.8986 (9)	0.4289 (4)	6.0 (5)
C12	0.4353 (4)	0.9531 (9)	0.3909 (4)	4.7 (4)
C13	0.4364 (4)	1.0451 (8)	0.3319 (4)	4.1 (3)
C14	0.2344 (4)	1.1538 (7)	0.1696 (4)	3.7 (4)
C15	0.2355 (4)	1.3004 (9)	0.1917 (4)	4.7 (4)
C16	0.2292 (5)	1.4155 (9)	0.1418 (5)	5.7 (5)
C17	0.2238 (5)	1.3875 (10)	0.0703 (5)	6.2 (5)
C18	0.2234 (6)	1.2437 (11)	0.0471 (4)	6.7 (5)
C19	0.2285 (5)	1.1279 (9)	0.0959 (4)	5.2 (4)
C20	0.1969 (4)	1.0613 (8)	0.3451 (3)	4.0 (3)
C21	0.2418 (5)	1.1636 (9)	0.3926 (4)	5.3 (4)
C22	0.2153 (6)	1.2072 (10)	0.4557 (4)	6.6 (5)
C23	0.1448 (7)	1.1482 (13)	0.4729 (5)	7.4 (6)
C24	0.0992 (5)	1.0468 (13)	0.4275 (5)	7.3 (6)
C25	0.1264 (4)	1.0035 (9)	0.3654 (4)	5.1 (4)
C26	0.2997 (4)	0.7829 (8)	0.2689 (3)	3.9 (3)
C27	0.2740 (4)	0.6880 (8)	0.3174 (4)	4.6 (4)
C28	0.3175 (5)	0.5581 (9)	0.3386 (4)	5.3 (4)
C29	0.3874 (5)	0.5241 (9)	0.3108 (4)	5.7 (4)
C30	0.4131 (5)	0.6157 (9)	0.2609 (4)	5.3 (4)
C31	0.3699 (4)	0.7434 (8)	0.2409 (4)	4.6 (4)

[a] B_{iso} is the mean of the principal axes of the thermal ellipsoid.

gen, and nitrogen microanalyses were performed at the Chemistry Department, National University of Singapore, Singapore.

X-ray analysis

Space group and cell dimensions

Empirical formula: $SnC_{31}H_{28}O_3N$ FW = 590.33

Monoclinic $P2_1/a$, a = 16.3493(8) Å, b = 9.0675(7) Å, c = 18.8562(14) Å, β = 100.493(5)°, V = 2748.6(3) Å^3. Cell dimensions were obtained from 25 reflections with 2θ in the range 90.00°–100.00°. Crystal dimensions: 0.40 × 0.25 × 0.03 mm. Z = 4, $F(000)$ = 1215.85, D_{calc} = 1.427 Mg m^{-3}, μ = 7.80 mm^{-1}, λ = 1.54056 Å (Cu Kα), $2\theta_{max}$ = 99.8°.

Data collection, structure solution and refinement

The intensity data were collected at 295 K on a Nonius diffractometer run by the NRCCAD diffractometer control program (10), using the θ/2θ scan mode and profile analysis (11). A total of 3027 reflections were measured, of which 2803 were unique. Of these, 2339 had $I > 2.5\sigma I_{net}$. Absorption corrections were made from 4 psi scans. The structure was solved by locating the tin from a Patterson synthesis. The inner coordination sphere was identified using the DIRDIF (12) programme. Hydrogen atoms were calculated. The remaining non-hydrogen atoms were located from a difference Fourier. The final least-squares cycle was calculated with 68 atoms, 326 parameters, and 2339 out of 2803 reflections. Unit weights were used. Final residuals are R_F = 0.033, R_W = 0.036 for data with $I_{net} > 2.5\sigma I_{net}$, R_F = 0.043, R_W = for all data. The goodness of fit was 1.35. Maximum shift/error was 0.006. In the last D-map, the top peak was 0.410 e/Å^3, and the deepest hole was −0.470 e/Å^3. Scattering factors were taken from the literature (13). All computation was performed using the NRCVAX system of crystal structure solving programmes (14).

Results and discussion

The triphenyltin carboxylates, $Ph_3SnOCO(CH_2)_nN{=}CHAr$ (n = 1, 2, 3, and 5), listed in Table 1, can be prepared by refluxing a mixture of bistriphenyltin oxide, an ω-amino acid, and the appropriate hydroxyaldehyde in absolute alcohol as shown by the equation below:

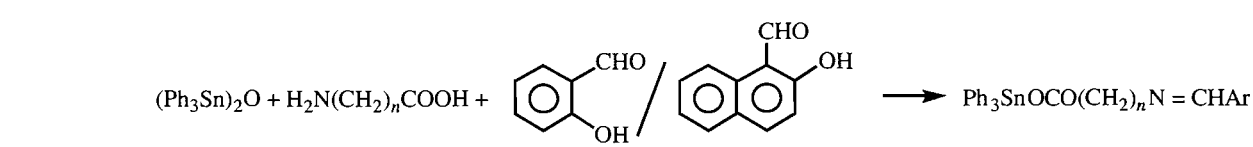

Can. J. Chem. Downloaded from www.nrcresearchpress.com by 109.225.110.28 on 09/08/12
For personal use only.

Can. J. Chem. Downloaded from www.nrcresearchpress.com by 109.225.110.28 on 09/08/12
For personal use only.

TABLE 4. Bond distances in angstroms

Sn—O(1)	2.148(4)	C(11)—C(12)	1.363(11)
Sn—O(3)	2.328(4)	C(12)—C(13)	1.393(10)
Sn—C(14)	2.124(7)	C(14)—C(15)	1.392(10)
Sn—C(20)	2.130(6)	C(14)—C(19)	1.396(10)
Sn—C(26)	2.118(7)	C(15)—C(16)	1.397(11)
O(1)—C(1)	1.300(9)	C(16)—C(17)	1.358(14)
O(2)—C(1)	1.222(9)	C(17)—C(18)	1.375(14)
O(3)—C(13)	1.321(8)	C(18)—C(19)	1.389(12)
N—C(6)	1.467(9)	C(20)—C(21)	1.401(11)
N—C(7)	1.297(11)	C(20)—C(25)	1.384(10)
C(1)—C(2)	1.507(10)	C(21)—C(22)	1.396(12)
C(2)—C(3)	1.509(10)	C(22)—C(23)	1.361(16)
C(3)—C(4)	1.528(11)	C(23)—C(24)	1.378(16)
C(4)—C(5)	1.508(10)	C(24)—C(25)	1.382(11)
C(5)—C(6)a	1.498(11)	C(26)—C(27)	1.376(10)
C(6)—C(5)b	1.498(11)	C(26)—C(31)	1.394(9)
C(7)—C(8)	1.413(12)	C(27)—C(28)	1.397(11)
C(8)—C(9)	1.413(11)	C(28)—C(29)	1.376(12)
C(8)—C(13)	1.411(10)	C(29)—C(30)	1.377(13)
C(9)—C(10)	1.348(14)	C(30)—C(31)	1.373(11)
C(10)—C(11)	1.373(13)		

Atoms labelled a and b are symmetry equivalent

C(6)a	0.03188	0.81179	−0.14625	0.500−x	−0.500+y	$-z$
C(5)b	0.47014	1.20973	0.08415	0.500−x	0.500+y	$-z$

The melting points and analytical data for the range of carboxylates synthesized are shown in Table 1. All the carboxylates listed in Table 1 were isolated as yellow solids that were stable in air.

The NMR signal from the azomethine proton in each of the free ligands (δ = 8.40–8.80 ppm) did not shift significantly on complex formation. For all the complexes, a broad signal observed at δ = 11–14 ppm was assigned to the phenolic proton. This assignment was substantiated by the broad infrared absorptions in the region 2600–3400 cm^{-1} which are reported to be due to intramolecular hydrogen bonding between the phenolic proton and the azomethine nitrogen (15).

The observed infrared absorption frequencies for the carboxylic antisymmetric, ν_{asym}(OCO), and symmetric, ν_{sym}(OCO), stretching vibrations are shown in Table 2. The assignment of the ν_{asym}(OCO) band is complicated by the presence of the ν(C=N) stretching vibration, which is observed in the region 1615–1625 cm^{-1}. Nevertheless, the magnitude of the ν_{asym}(OCO) − ν_{sym}(OCO) (i.e., Δν) separation is of interest. The observed values of Δν, which are in the range 230–350 cm^{-1}, indicate a unidentate bonding mode for the carboxylate moiety (16). For a bridging or chelating carboxylate group Δν would be expected to be ≤ 150 cm^{-1} (17), as widely observed in the infrared spectra of triorganotin carboxylates (18). This suggests that it is the phenolic group which occupies the fifth coordination site at the tin atom (19). Furthermore, the strong intramolecular hydrogen bonding between the imino nitrogen atom and the phenolic group would increase the likelihood of coordination by the phenolic oxygen to the tin atom. Thus the spectroscopic data suggest that the structures of these triphenyltin carboxylates may well involve bridging by phenolic oxygen atoms. This conclusion was confirmed by the the results of an X-ray structural analysis for triphenyltin(IV) *N*-salicylidene-6-aminohexanoate. Figure 1 is an ORTEP plot illustrating the coordination around the tin atom. The final fractional coordinates of non-hydrogen atoms with equivalent isotropic thermal parameters are listed in Table 3 while the bond lengths and bond angles for the complex are in Tables 4 and 5, respectively. Calculated and observed structure factors, calculated hydrogen atom parameters, and anisotropic thermal parameters have been deposited as Tables S-1, S-2, and S-3, respectively. The atom-numbering scheme and a stereo pair showing the packing arrangement in the unit cell have been deposited as Figs. S-1 and S-2.[2]

The tin is five-coordinate with the axial positions of the trigonal bipyramid being occupied by a carboxylate oxygen, O(1), and the phenolic oxygen, O(3), of an adjacent symmetry-related molecule. The sum of the carbon–tin–carbon angles in the trigonal plane of triphenyltin *N*-salicylidene-6-aminohexanoate is 358.2(3)° (114.2° + 133.8° + 110.2°). The apical angle subtended at tin is 176.20(17)°. The short tin–oxygen distances are Sn—O(1) = 2.148(4) Å and Sn—O(3) = 2.328(4) Å and are well within the range of Sn—O bond distances usually observed for triorganotin carboxylates (1). It is interesting to compare the phenolic oxygen–tin distance of 2.33 Å observed here with that of 3.04 Å reported for triphenyltin salicylate (6), which clearly corresponds to a much weaker interaction.

The Sn—O(2) distance is 2.973(5) Å, which explains the opening-up of the C(14)—Sn—C(26) angle to 133.8°. Such non-uniformity in CSnC angles has been observed before, and attributed to weak Sn...O contacts (20).

In contrast to the Sn—O(1)—C(1) angle of 113.3(4)° the Sn—O(3)—C(13) angle of the bridging oxygen atom is opened up to 132.2(4)° to accommodate the bulk of the salicylidene moiety. Even larger Sn—O′—C′ angles (where O′ refers to the bridging oxygen atom) have been observed for $Ph_3SnOCOCH_2CH_2NHCONH_2$, 144.1(2)° (4), $Ph_3SnOCOCH_3$, 142.7° (20), and $Ph_3SnOCOC_6H_4Cl$-2, 146.4 (21).

The short C=O distance of 1.222(9) Å indicates that the free carbonyl group on the ligand is not involved in coordination with another tin atom. Similar C=O bond lengths have also been reported for corresponding non-bridging carbonyl groups in the compounds $Ph_3SnOCOCH_2CH_2NHCONH_2$, 1.224(4) Å (4), and $Ph_3SnOCOCME{=}CHCON(CH_2)_4$, 1.222(5) Å (5). The *cis* configuration adopted by the salicylidene moiety is similar to that reported for 2-bromo-*N*-salicylidene aniline (22). Proton transfer from oxygen to nitrogen atoms via hydrogen bonding and the formation of zwitterion intermediates in similar molecules to those discussed here is quite commonly encountered (19, 23, 24). Thus the labile phenolic oxygen is rendered susceptible to coordination with the tin atom. This makes possible the formation of a series of Sn—O(phenolic) bridges leading to the zigzag polymeric structure of triphenyltin *N*-salicylidene-6-aminohexanoate, which has a repeat distance of 4.7140 Å (25, 26). Similarities in the spectroscopic data suggest that the other compounds in the series adopt similar structures.

This series appears to be the first reported example of such an arrangement in triphenyltin carboxylates.

[2]These tables and diagrams may be purchased from: The Depository of Unpublished Data, Document Delivery, CISTI, National Research Council Canada, Ottawa, Canada K1A 0S2.

The diagrams and table of hydrogen atom parameters have also been deposited with the Cambridge Crystallographic Data Centre, University Chemical Laboratory, 12 Union Road, Cambridge, CB2 1EZ, U.K.

TABLE 5. Bond angles in degrees

O(1)—Sn—O(3)	176.20(17)	C(11)—C(12)—C(13)	120.1(7)
O(1)—Sn—C(14)	94.88(21)	O(3)—C(13)—C(8)	119.0(6)
O(1)—Sn—C(20)	91.18(22)	O(3)—C(13)—C(12)	123.1(6)
O(1)—Sn—C(26)	96.33(21)	C(8)—C(13)—C(12)	117.9(6)
O(3)—Sn—C(14)	81.31(21)	Sn—C(14)—C(15)	117.5(5)
O(3)—Sn—C(20)	90.45(21)	Sn—C(14)—C(19)	125.5(5)
O(3)—Sn—C(26)	86.32(21)	C(15)—C(14)—C(19)	117.0(6)
C(14)—Sn—C(20)	114.2(3)	C(14)—C(15)—C(16)	121.1(7)
C(14)—Sn—C(26)	133.82(25)	C(15)—C(16)—C(17)	120.9(8)
C(20)—Sn—C(26)	110.2(3)	C(16)—C(17)—C(18)	119.3(8)
Sn—O(1)—C(1)	113.3(4)	C(17)—C(18)—C(19)	120.6(8)
Sn—O(3)—C(13)	132.2(4)	C(14)—C(19)—C(18)	121.2(7)
C(6)—N—C(7)	122.6(6)	Sn—C(20)—C(21)	122.2(5)
O(1)—C(1)—O(2)	123.1(6)	Sn—C(20)—C(25)	121.7(5)
O(1)—C(1)—C(2)	114.0(6)	C(21)—C(20)—C(25)	116.0(6)
O(2)—C(1)—C(2)	122.8(7)	C(20)—C(21)—C(22)	121.7(8)
C(1)—C(2)—C(3)	114.4(6)	C(21)—C(22)—C(23)	119.9(8)
C(2)—C(3)—C(4)	114.1(6)	C(22)—C(23)—C(24)	120.0(8)
C(3)—C(4)—C(5)	110.9(8)	C(23)—C(24)—C(25)	119.6(8)
C(4)—C(5)—C(6)a	112.8(6)	C(20)—C(25)—C(24)	122.7(8)
N—C(6)—C(5)b	110.9(6)	Sn—C(26)—C(27)	118.0(5)
N—C(7)—C(8)	125.6(7)	Sn—C(26)—C(31)	124.1(5)
C(7)—C(8)—C(9)	120.0(7)	C(27)—C(26)—C(31)	117.6(6)
C(7)—C(8)—C(13)	121.0(6)	C(26)—C827)—C(28)	121.1(6)
C(9)—C(8)—C(13)	119.0(7)	C(27)—C(28)—C(29)	119.6(7)
C(8)—C(9)—C(10)	122.1(7)	C(28)—C(29)—C(30)	120.2(7)
C(9)—C(10)—C(11)	117.6(7)	C(29)—C(30)—C(31)	119.4(7)
C(10)—C(11)—C(12)	123.3(8)	C(26)—C(31)—C(30)	122.0(7)

Atoms labelled a and b are symmetry equivalents

C(6)a	0.03188	0.81179	−0.14625	0.500−x	−0.500+y	−z
C(5)b	0.47014	1.20973	0.08415	0.500−x	0.500+y	−z

Can. J. Chem. Downloaded from www.nrcresearchpress.com by 109.225.110.28 on 09/08/12
For personal use only.

Acknowledgements

Financial support from Universiti Sains Malaysia (Grant No: 123/3203/2502) and the Laurentian University Research Fund (LURF) are gratefully acknowledged.

1. E. R. T. Tiekink. Appl. Organomet. Chem. **5**, 1 (1991).
2. B. Y. K. Ho, K. C. Molloy, J. J. Zuckerman, F. Reidinger, and J. A. Zubieta. J. Organomet. Chem. **187**, 213 (1980).
3. S. W. Ng, V. G. Kumar Das, F. Van Meurs, J. D. Schagen, and L. H. Straver. Acta. Crystallogr. Sect. C: Cryst. Struct. Commun. **C45**, 570 (1989).
4. K. M. Lo, V. G. Kumar Das, W. H. Yip, and T. C. W. Mak. J. Organomet. Chem. **412**, 21 (1991).
5. A. S. Lewis, P. J. Smith, J. H. Aupers, and D. C. Povey. J. Organomet. Chem. **402**, 319 (1991).
6. J. F. Voltano, R. O. Day, D. N. Rau, V. Chandrasekhar, and R. R. Holmes. Inorg. Chem. **23**, 3153 (1984).
7. S. W. Ng, V. G. Kumar Das, W. H. Yip, and T. C. W. Mak. Acta. Crystallogr. Sect. C: Cryst. Struct. Commun. **C47**, 1593 (1991).
8. P. G. Harrison, K. Lambert, T. J. King, and B. Majee. J. Chem. Soc. Dalton Trans. 363 (1983).
9. P. J. Smith, R. O. Day, V. Chandrasekhar, J. M. Holmes, and R. R. Holmes. Inorg. Chem. **25**, 2495 (1986).
10. Y. Le Page, P. S. White, and E. J. Gabe. Abstracts. Am. Crystallogr. Assoc. Annu. Meeting. 1986. p. 24.
11. D. F. Grant and E. J. Gabe. J. Appl. Crystallogr. **11**, 114 (1978).
12. P. T. Beurskeno, W. P. Basman, H. M. Daresburg, Th. E. M. van den Hark, P. A. J. Prick, J. H. Noordick, G. Beurskeno, R. O. Gould, and V. Parthasarati. Technical Report 1981/2, Crystallography Laboratory, Toernooiveld, 6525. Nijmegen, The Netherlands. 1981.
13. International tables for X-ray crystallography. 2nd ed. Vol. IV. Kynoch Press, Biringham, England. 1974. p. 99.
14. E. J. Gabe, Y. Le Page, J-P. Charland, F. L. Lee, and P. S. White. J. Appl. Crystallogr. **22**, 384 (1989).
15. E. C. Alyea and A. Malek. Can. J. Chem. **53**, 939 (1975).
16. G. B. Deacon, F. Huber, and R. J. Phillips. Coord. Chem. Rev. **33**, 227 (1980).
17. G. Micera, L. S. Erre, A. Pauzenelli, P. Piu, and F. Cariata. J. Coord. Chem. **13**, 231 (1984).
18. V. G. Kumar Das, C. K. Yap, S. W. Ng, C. Wei, and T. C. W. Mak. J. Organomet. Chem. **311**, 289 (1986).
19. J. P. Charland, F. L. Lee, E. J. Gabe, L. E. Khoo, and F. E. Smith. Inorg. Chim. Acta, **130**, 55 (1987).
20. K. C. Molloy, T. G. Purcell, K. Quill, and I. W. Nowell. J. Organomet. Chem. **267**, 237 (1984).
21. R. R. Holmes, R. O. Day, V. Chandrasekhar, J. F. Vollano, and J. M. Holmes. Inorg. Chem. **25**, 2490 (1986).
22. A. H. Burr and A. D. Hobson. Acta Crystallogr. Sect. B: Struct. Crystallogr. Cryst. Chem. **B25**, 2662 (1969).
23. J. J. Bullock, M. F. C. Ladd, D. C. Povey, and H. A. Tajmir-Raihi. Acta. Crystallogr. Sect. B: Struct. Crystallogr. Cryst. Chem. **B35**, 2013 (1979).
24. M. E. Kamwaya and L. E. Khoo. Acta. Crystallogr. Cryst. Sect. C: Cryst. Struct. Commun. **C41**, 1027 (1985).
25. S. W. Ng, C. Wei, and V. G. Kumar Das. J. Organomet. Chem. **345**, 59 (1988).
26. D. Tudela. Struct. Chem. **1**, 437 (1990).

Lambertellin, a metabolite of *Ciboria gordonii* Funk

GERALD ARTHUR POULTON,[1] GORDON WILLIAM BUSHNELL, AND YUN-LONG LI
Department of Chemistry, University of Victoria, Victoria, B.C., Canada V8W 3P6

Received January 7, 1992

GERALD ARTHUR POULTON, GORDON WILLIAM BUSHNELL, and YUN-LONG LI. Can. J. Chem. **70**, 2688 (1992).

Lambertellin, 9-hydroxy-3-methyl-2*H*-naphtho[2,3-*b*]pyran-2,5,10-trione, previously identified from species of *Lambertella* and *Pseudospiropes*, has been isolated from the discomycete *Ciboria gordonii* Funk, identified on needles of the western hemlock *Tsuga heterophylla*. Spectral data and a crystal structure are given for lambertellin, confirming the structure in the literature.

GERALD ARTHUR POULTON, GORDON WILLIAM BUSHNELL et YUN-LONG LI. Can. J. Chem. **70**, 2688 (1992).

On a isolé lambertelline, la 9-hydroxy-3-méthyl-2*H*-naphto[2,3-*b*]pyran-2,5,10-trione (antérieurement identifiée à partir d'espèces de *Lambertella* et de *Pseudospiropes*), à partir du discomycète *Ciboria gordonii* Funk, identifié sur les aiguilles de la ciguë *Tsuga heterophylla*. On rapporte les données spectrales de la lambertelline et on a déterminé sa structure cristalline, confirmant ainsi la structure proposée dans la littérature.

[Traduit par la rédaction]

Introduction

Funk (1) has identified the fungus *Ciboria gordonii* Funk from needles of the Western hemlock *Tsuga heterophylla* (Raf.) Sarg. Cultures of this fungus produce visible quantities of the metabolite lambertellin, 9-hydroxy-3-methyl-2*H*-naphtho-[2,3,*b*]-pyran-2,5,10-trione, **1**, production being best at 10°C. Lambertellin has been previously isolated from *Lambertellin hicoriae* Whetzel (2, 3), from *L. corni maris* (4), and later from *Pseudospiropes simplex* (5), and a synthesis reported (6). As our preliminary spectral data were not in agreement with literature data for lambertellin, a crystal structure determination was conducted to confirm identity.

Results and discussion

Lambertellin was first isolated and identified as a constituent of a number of different fungi more than 20 years ago (2–4). It is of low solubility in organic solvents and thus the ^{1}H NMR data reported in the literature (in CF_3COOH (6) or as the sodium salt in D_2O (4)) did not permit a simple comparison with spectra obtained on current FT machines in $CDCl_3$ or DMSO-d_6. Differences between our observed chemical shifts of the coupled grouping of methyl and olefinic proton (2.16 and 7.84 ppm in $CDCl_3$) and published data (2.71 and 6.77 ppm in D_2O (4); 2.41 and 7.85–8.4 ppm in CF_3COOH (6)), plus the unavailability of comparison ^{13}C data, prompted us to confirm the structure of our isolate through X-ray crystal structure determination.

Figure 1 is an ORTEP drawing of lambertellin, giving the atomic labelling scheme and a display of the thermal motion ellipsoids scaled to enclose 50% probability. Table 1 summarizes the crystal data for lambertellin. The fractional atomic coordinates are presented in Table 2 together with equivalent isotropic temperature parameters. The interatomic distances are given in Table 3. The A ring is aromatic, with a mean bond length of 1.39(2) Å. Ring B is distinctly quinonoid, with the four carbon–carbon bonds α to the carbonyl showing an average bond length of 1.476(10) Å and the two central partial double bonds being 1.348(3) Å and 1.418(3) Å, typical of naphthoquinone-type structures (7–10). Ring C exhibits C—O single bonds (1.397(3), 1.356(2) Å), C—C single bonds (1.426(3), 1.452(3) Å), and the isolated C=C double bond (1.344(3) Å) typical (11) of an α-pyrone ring.

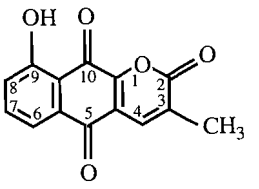

1

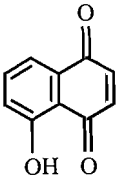

2

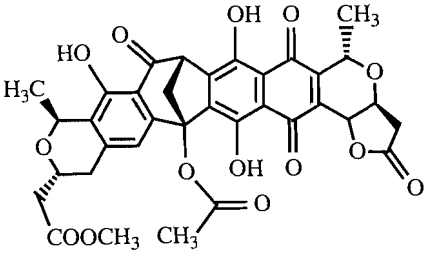

3

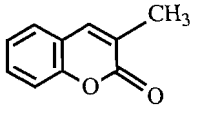

4

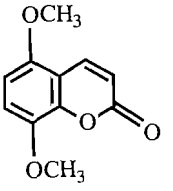

5

The carbonyl bond C(13)—O(4) is longer (1.228(2) Å) than the other two (1.216(2) Å, 1.202(2) Å), characteristic of a carbonyl group which is intramolecularly hydrogen bonded to a neighbouring hydroxyl group. Juglone (**2**) exhibits an analogous difference between the hydrogen-bonded carbonyl bond length (1.26(2) Å) and that of the non-hydrogen-bonded carbonyl (1.20(2) Å) (7).

Bond angles are listed in Table 4. As might be expected from a peri-naphthalene-type interaction, the C(11)—O(5) and C(13)—O(4) bonds are forced apart by steric interactions, the external angle of the C—O bond facing the carbonyl group being enlarged to 123.3(2)°, resulting in a

[1]Author to whom correspondence may be addressed.

Can. J. Chem. Downloaded from www.nrcresearchpress.com by 109.225.110.28 on 09/08/12
For personal use only.

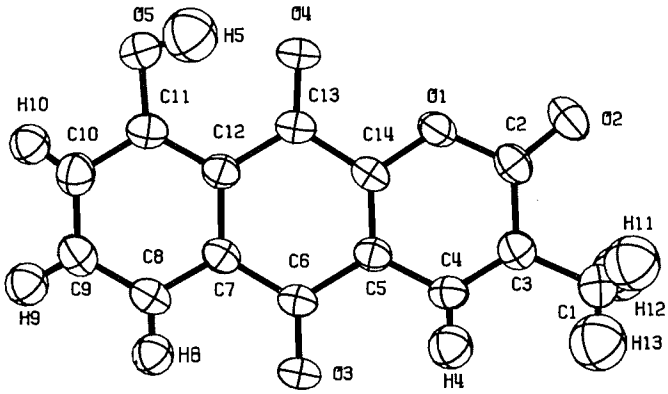

FIG. 1. An ORTEP drawing of the lambertellin molecule.

TABLE 1. Crystal data for lambertellin

Crystal system	Monoclinic
Space group	$P2_1/n$ (No. 14)
a	17.749(7) Å
b	6.437(5) Å
c	9.452(2) Å
β	90.15(5)°
V (cell)	1080(1) Å^3
T	28°C
Z	4 molecules/cell
D (meas.)	1.538 g cm^{-3}
D (calcd.)	1.576 g cm^{-3}
Formula	$C_{14}H_8O_5$
Mol. wt.	256.22
λ	0.71069 Å
μ	1.31 cm^{-1}

TABLE 2. Fractional atomic coordinates and temperature parameters[a]

Atom	x/a	y/b	z/c	U_{eq}
O(1)	4112(1)	−168(2)	3844(1)	447(5)
O(2)	3116(1)	−1902(3)	4581(2)	587(6)
O(3)	5714(1)	−2448(3)	209(2)	553(6)
O(4)	4985(1)	3129(2)	4184(2)	504(5)
O(5)	6116(1)	5530(3)	3430(2)	517(5)
C(1)	3292(2)	−5281(5)	2639(3)	600(9)
C(2)	3635(1)	−1891(4)	3768(2)	429(7)
C(3)	3813(1)	−3464(3)	2719(2)	429(7)
C(4)	4420(1)	−3223(4)	1888(2)	417(6)
C(5)	4904(1)	−1467(3)	2038(2)	374(6)
C(6)	5580(1)	−1203(3)	1142(2)	392(6)
C(7)	6060(1)	653(3)	1388(2)	391(6)
C(8)	6711(1)	911(4)	611(2)	468(7)
C(9)	7140(1)	2709(4)	775(2)	499(7)
C(10)	6924(1)	4238(4)	1690(3)	495(8)
C(11)	6282(1)	3990(3)	2527(2)	418(6)
C(12)	5842(1)	2188(3)	2383(2)	378(6)
C(13)	5176(1)	1891(3)	3263(2)	387(6)
C(14)	4729(1)	−9(9)	3007(2)	380(6)
H(4)	453(1)	−419(4)	122(3)	58(7)′
H(5)	573(2)	505(5)	389(3)	86(10)′
H(8)	684(1)	−18(4)	−7(2)	50(6)′
H(9)	761(1)	290(4)	22(2)	54(6)′
H(10)	718(1)	545(4)	182(2)	47(6)′
H(11)	279(2)	−474(5)	259(3)	87(10)′
H(12)	333(2)	−612(5)	347(3)	94(10)′
H(13)	342(2)	−624(5)	192(3)	94(10)′

[a]Estimated standard deviations are given in parentheses. Parameters ×10^n where n = 4 for O and C and n = 3 for H. U_{eq} = the equivalent isotropic temperature parameter. $U_{eq} = 1/3\ \Sigma_i\Sigma_j U_{ij} a_i^* a_j^* (a_i \cdot a_j)$. Primed values indicate that U_{iso} is given. $T = \exp -(8\pi^2 U_{iso} \sin^2\theta/\lambda^2)$.

TABLE 3. Interatomic distances (Å)[a]

Atoms	Distance	Atoms	Distance
C(2)—O(1)	1.397(3)	C(14)—O(1)	1.356(2)
C(2)—O(2)	1.202(2)	C(6)—O(3)	1.216(2)
C(11)—O(5)	1.342(2)	C(13)—O(4)	1.228(2)
C(3)—C(2)	1.452(3)	C(3)—C(1)	1.493(3)
C(4)—C(3)	1.344(3)	C(8)—C(7)	1.381(3)
C(14)—C(5)	1.348(3)	C(12)—C(7)	1.418(3)
C(5)—C(4)	1.426(3)	C(9)—C(8)	1.394(3)
C(6)—C(5)	1.480(3)	C(10)—C(9)	1.366(3)
C(7)—C(6)	1.486(3)	C(11)—C(10)	1.397(3)
C(13)—C(12)	1.460(3)	C(12)—C(11)	1.405(3)
C(14)—C(13)	1.477(3)		

[a]Estimated standard deviations are given in parentheses.

compression of the angle on the opposite side to 117.1(2)°. Analogous effects have been reported, e.g., for juglone (**2**) (7) and γ-naphthoquinone (**3**) (8). Least-squares plane calculations were done for the atoms in the three six-membered rings and for the atoms in each individual six-membered ring. These four calculations were repeated with the attached peripheral non-hydrogen atoms included in the set of atoms defining the plane. Not one of these calculations indicated planarity for the set of atoms considered, judged by the esd's of the fractional atomic coordinates. The plane defined by the 14 atoms of the three rings gives a concise description of the structure, and these results have been deposited (see footnote 3). The maximum deviation from this plane by an atom belonging to the defining set was 0.063 Å by C(8). The peripheral O atoms deviated from the plane slightly more, up to 0.130 Å for O(3). This plane of the molecule lies at a perpendicular distance of 0.034 Å from the centre of inversion (at 0.5, 0.5, 0.5 for the coordinates given).

Selected intermolecular distances have been deposited as supplementary Table 4 (see footnote 3). The shortest intermolecular distance is O(4)···O(4′) across an inversion centre. Figure 2 shows this intermolecular contact to be part of a bifurcated hydrogen bond which is repeated by the inversion centre to give a double bifurcation. Bifurcated hydrogen bonds are relatively rare (12).

The packing of the molecular structure can be explained in terms of the molecular pairs just described. Pairs of molecules are arranged across each origin and across points like (0.5, 0.5, 0.5), as shown in Fig. 2. This results in layers of parallel obliquely slanted molecules with differing orientations at the x = 0 and x = 0.5 levels. Since the unit cell angle β is close to 90°, the layers are approximately at right angles to the a axis. The short lengths of b and c are related to the packing efficiency of the almost planar structure of the molecular pairs. The three-dimensional methyl groups do not lie within the layers, but are located on their surfaces. C(1) lies at 0.003(3) Å from the principal mean plane described above and has no close intermolecular contacts.

Table 5 summarizes the ^{1}H NMR data obtained in this

Can. J. Chem. Downloaded from www.nrcresearchpress.com by 109.225.110.28 on 09/08/12
For personal use only.

TABLE 4. Bond angles (°)[a]

Atoms	Angle	Atoms	Angle
C(14)—O(1)—C(2)	121.4(2)	C(12)—C(7)—C(8)	119.9(2)
O(2)—C(2)—O(1)	115.9(2)	C(9)—C(8)—C(7)	119.9(2)
C(3)—C(2)—O(1)	117.1(2)	C(10)—C(9)—C(8)	120.9(2)
C(3)—C(2)—O(2)	126.9(2)	C(11)—C(10)—C(9)	120.4(2)
C(2)—C(3)—C(1)	116.5(2)	C(10)—C(11)—O(5)	117.1(2)
C(4)—C(3)—C(1)	123.9(2)	C(12)—C(11)—O(5)	123.3(2)
C(4)—C(3)—C(2)	119.6(2)	C(12)—C(11)—C(10)	119.6(2)
C(5)—C(4)—C(3)	121.1(2)	C(11)—C(12)—C(7)	119.1(2)
C(6)—C(5)—C(4)	121.5(2)	C(13)—C(12)—C(7)	120.6(2)
C(14)—C(5)—C(4)	118.7(2)	C(13)—C(12)—C(11)	120.3(2)
C(14)—C(5)—C(6)	119.8(2)	C(12)—C(13)—O(4)	123.0(2)
C(5)—C(6)—O(3)	120.0(2)	C(14)—C(13)—O(4)	120.2(2)
C(7)—C(6)—O(3)	122.0(2)	C(14)—C(13)—C(12)	116.8(2)
C(7)—C(6)—C(5)	117.9(2)	C(5)—C(14)—O(1)	122.0(2)
C(8)—C(7)—C(6)	119.6(2)	C(13)—C(14)—O(1)	113.7(2)
C(12)—C(7)—C(6)	120.5(2)	C(13)—C(14)—C(5)	124.3(2)

[a]Estimated standard deviations are given in parentheses.

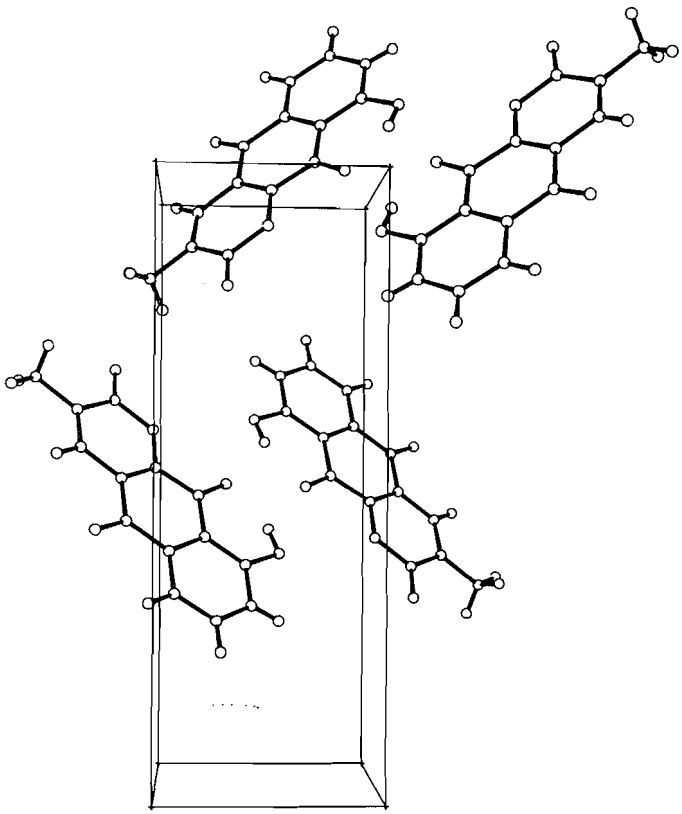

FIG. 2. Packing diagram for lambertellin. Unit cell outline is given with the origin at the lower, back, on the right-hand side. The *a* axis is vertically up, the *b* axis is across the page, right to left, and the *c* axis is toward the viewer. The molecules drawn are x, y, z; $1 - x, 1 - y, 1 - z$; $1.5 - x, -0.5 + y, 1.5 - z$; $0.5 + x, 0.5 - y, 0.5 + z$.

study and compares them with data reported in the literature for lambertellin and its methyl ether. In both $CDCl_3$ and DMSO, the methyl signal is observed upfield from all previously reported values, more in line with the values obtained for 3-methylcoumarins (e.g., 2.18 ppm for 3-methylcoumarin (**4**) itself (13)). Coupling constants and proton chemical shifts of the three coupled aromatic protons of ring A were confirmed by spectral simulation, and are in line with previously reported assignments (14).

Table 6 shows the ^{13}C data and assignments which are supported by 2D-COSY, DEPT, HETCOR, and HMBC data (15). Juglone (**2**) may be taken as an appropriate model for rings A and B, whereas 3-methylcoumarin (**4**) and 5,8-dimethoxycoumarin (**5**) are less accurate models for chemical shifts in an α-pyrone ring fused to a quinonoid ring.

Experimental

General

Melting points were determined on a Kofler hot stage and are uncorrected. Proton NMR spectra were obtained on a Perkin–Elmer R32 spectrometer at 90 MHz, a Bruker WM250 spectrometer at 250 MHz, or a Varian XL-300 spectrometer at 300 MHz. Carbon NMR spectra were determined on the Bruker WM250 spectrometer at 62.9 MHz, Varian XL-300 spectrometer at 75.4 MHz, or Varian VXR-500 spectrometer at 125.8 MHz. Infrared spectra were obtained on a Perkin–Elmer 283 spectrometer and ultraviolet spectra on the Beckman DU-8 spectrophotometer. Accurate mass measurements were kindly provided by the University of British Columbia Mass Spectrometry Centre using the Kratos MS-50 instrument.

Culture and extraction

Ciboria gordonii (1) was cultured on 2% malt extract (DIFCO) in Petri dishes at 10°C in the dark for 4 weeks. Mycelium and agar from 50 dishes were extracted by stirring with dichloromethane at room temperature (3 × 800 mL). The crude extract (120 mg) was washed with small amounts of acetone and the product recrystallized from acetone–hexane. Lambertellin was isolated as orange–red needles, mp 251–252°C (lit. (4) mp 253–254°C). Lambertellin showed ν_{max} (KBr): 3450, 3200–2500 br, 1750, 1650, 1610 cm^{-1}; λ_{max} (CH_3OH): 299 (log ϵ = 3.98), 270 nm (4.07); ^{1}HMR (250 MHz, $CDCl_3$): 11.8 (1H, s, OH, D_2O exchangeable), 7.84 (1H, q, J = 1.5 Hz, H4), 7.72 (1H, dd, J = 8.4, 7.5 Hz, H7), 7.65 (1H, dd, J = 7.5, 1.2 Hz, H6), 7.32 (1H, dd, J = 8.4, 1.2 Hz, H8), 2.29 (3H, d, J = 1.5 Hz, Me); ^{13}CMR: see Table 6; in a gated spectrum run in $CDCl_3$, the peaks at 137.4, 133.3, 125.3, and 119.9 ppm appeared as doublets; ms *m/z* (relative intensity, formula): 256.0370 (M+, 100, calculated for $C_{14}H_8O_5$ 256.0372), 228

Can. J. Chem. Downloaded from www.nrcresearchpress.com by 109.225.110.28 on 09/08/12
For personal use only.

TABLE 5. Proton NMR data

Compound	4	6	7	8	OH	CH_3	Solvent	Reference
Lambertellin	7.94[a]	7.6[b]	7.80[b]	7.40[b]	n.o.[c]	2.19[a]	DMSO-d_6	This work
	7.84[a]	7.65	7.72	7.32	11.77	2.16[a]	$CDCl_3$	This work
	---------- 8.4–7.85(m) ----------				n.o.	2.41[a]	CF_3COOH	6
Lambertellin Sodium salt	6.77[a]	---------- 8.26–7.42(m) ----------			n.o.	2.71[a]	D_2O	4
Lambertellin Methyl ether	8.06[a]	---------- 8.00–7.44(m) ----------			4.12 (OCH_3)	2.38[a]	CF_3COOH	6

[a] J = 1.5 Hz.
[b] $J_{6,7}$ = 7.5 Hz; $J_{6,8}$ = 1.2 Hz; $J_{7,8}$ = 8.4 Hz. Confirmed by spectral simulation.
[c] n.o. = not observed.

TABLE 6. Carbon NMR data

Compound	2	3	4	4a	5	5a	6	7	8	9	9a[b]	10	10a	CH_3	Solvent	Reference
1	159.8	131.3	133.9	148.6	180.0	131.7	119.2	137.4	124.7	160.8	114.9	180.3	152.7	17.0	DMSO-d_6	
1	n.o.[a]	131.0	133.3	n.o.	179.9	133.1	119.9	137.4	125.3	162.5	114.7	180.5	153.5	17.7	$CDCl_3$	
2				139.3	183.9	131.5	118.9	136.4	124.2	161.2	114.8	190.0	138.4		$CDCl_3$	16
4	162.1	125.7	139.2	119.6	127.0	124.3					130.4	116.3	153.2	17.1	$CDCl_3$	17
5	159.4	114.7*	138.2	110.2	149.5	103.7					114.9*	141.3†	144.7†		$CDCl_3$	18

[a] n.o. = not observed.
[b] The symbols *, † indicate the signals may be interchanged.

(35, $C_{13}H_8O_4$), 200 (98, $C_{12}H_8O_3$), 199 (96, $C_{12}H_7O_3$), 172 (12, $C_{11}H_8O_2$), 144 (12, $C_{10}H_8O$), 115 (30, C_9H_7), 92 (20, C_6H_4O).

X-ray measurements

The crystal was mounted on a glass fibre in the direction of its greatest length and photographed using Weissenberg and precession cameras with CuK_α radiation. The symmetry was found to be monoclinic and an approximate unit cell was established. The crystal was then transferred to a Picker 4-circle diffractometer using MoK_α radiation and automated with a PDP-11/10 computer on which all further work was done. The unit cell was refined by least squares from 14 pairs of reflections (at $\pm 2\theta$) in the range 2θ = 8–45°. The crystal data are presented in Table 1.

Intensity measurements were done for 1 quadrant ($k,l \geq 0$) in the range 2θ = 0–50°, using a stepped scan of 120 steps of 0.01° in 2θ counting for 0.50 s per step. Background counting was for 30 s at each end of the scan. A set of standards 043;406;216 were measured before each batch of 50 reflections; 2164 measurements consisting of 129 standards and 2035 reflections were obtained. Lorentz and polarisation corrections were applied and equivalent measurements were averaged to obtain a final file with 1901 unique reflections. Weak reflections were included. No absorption correction was applied.

Structure solution and refinement

The programs used were SHELX-76 (19) and ORTEP (20). The atomic scattering factors were those given in the SHELX-76 program (19, 21). The structure was solved using direct methods and refined by standard Fourier synthesis techniques and by least-squares minimizing $\Sigma w\Delta^2$ (where w is a weight derived from the counting statistics ($w = 1/(\sigma^2(F) + 0.001F^2)$ and $\Delta = ||F_o| - |F_c||$). Initially carbon atomic scattering factors were used for all the ring atoms. The O atoms were identified as such by abnormally low temperature parameters. The hydrogen atoms of the C(1) methyl group were first calculated and then the group as a whole was refined as a rigid body. The hydrogen atoms were treated as isotropic scatterers and the heavier atoms were allowed the freedom of anisotropic thermal motion. U_{iso} was refined for those hydrogen atoms whose positional coordinates were refined. The final residuals were R = 0.0599, R_w = 0.0715.[2] The convergence was good with the final maximum (shift/esd) = 0.009. The final difference map had no important features, maximum 0.22 e Å^{-3}, minimum −0.28 e Å^{-3}. The number of measurements, 1901, was sufficient to determine the 204 parameters well.

Supplementary tables containing hydrogen-atom fractional atomic coordinates and isotropic temperature parameters, interatomic distances for the hydrogen atoms, bond angles involving hydrogen atoms, selected intermolecular distances, anisotropic temperature parameters, least-squares plane results, and observed and calculated structure factor amplitudes have been deposited.[3]

Acknowledgements

The authors would like to thank Dr. A. Funk, of the Pacific Forestry Centre, Burnside Road, Victoria, B.C., for provision of the culture samples and the preparative scale cultures, and Professor R. H. Thompson for provision of an authentic sample. Continued financial support of the University of Victoria and of the Natural Sciences and Engineering Research Council of Canada is also acknowledged. Mr. Y.-L. Li was supported by the Government of the People's Republic of China during a leave from the Guanhzhou Institute of Chemistry, Academy of Science of China.

[2] $R = \Sigma||F_o| - |F_c||/\Sigma|F_o|$, $R_w = [\Sigma w\Delta^2/\Sigma wF_o^2]^{1/2}$.

[3] Copies of the supplementary tables may be purchased from: The Depository of Unpublished Data, Document Delivery, CISTI, National Research Council Canada, Ottawa, Canada K1A 0S2.

Tables of hydrogen atom coordinates, interatomic and intermolecular distances, and bond angles have also been deposited with the Cambridge Crystallographic Data Centre and can be obtained on request from the Director, Cambridge Crystallographic Data Centre, University Chemical Laboratory, 12 Union Road, Cambridge, CB2 1EZ, U.K.

Can. J. Chem. Downloaded from www.nrcresearchpress.com by 109.225.110.28 on 09/08/12
For personal use only.

1. A. Funk. Trans. Br. Mycol. Soc. **86**, 184 (1986).
2. T. Sproston, H. Tomlinson, G. E. Milo, and A. Jones. Phytopathology, **52**, 753 (1962).
3. T. B. Tijo, T. Sproston, and H. Tomlinson. Lloydia, **28**, 359 (1965).
4. J. J. Armstrong and W. B. Turner. J. Chem. Soc. 5927 (1965).
5. G. W. van Eijk and H. J. Roeymans. Phytochemistry, **17**, 1804 (1978).
6. P. M. Brown, V. Krishnamoorthy, J. W. Mathieson, and R. H. Thompson. J. Chem. Soc. C, 109 (1970).
7. P. D. Cradwick and D. Hall. Acta Crystallogr. Sect. B: Struct. Crystallogr. Cryst. Chem. **B27**, 1468 (1971).
8. E. Egert, M. Noltemeyer, G. M. Sheldrick, W. Saenger, H. Brand, and A. Zeeck. Liebigs Ann. Chem. 503 (1983).
9. M. Brufani and M. Dobler. Helv. Chim. Acta, **51**, 1269 (1968).
10. D. W. Cameron, S. R. Hall, C. L. Raston, and A. H. White. Aust. J. Chem. **30**, 2705 (1977).
11. G. Bravic and J. P. Bideau. Cryst. Struct. Commun. **7**, 633 (1978).
12. A. F. Wells. Structural inorganic chemistry. 4th ed. Oxford University Press, New York. 1975. p. 305.
13. P. Bouvier, J. Andrieux, H. Cunha, and D. Molho. Bull. Soc. Chim. Fr. 1187 (1977).
14. W. Steck and M. Mazurek. Lloydia, **35**, 418 (1972).
15. M. Kobayashi, Y. Terui, K. Tori, and N. Tsuji. Tetrahedron Lett. 619 (1976).
16. L. Ernst. J. Magn. Reson. **21**, 241 (1976).
17. H. Gunther, J. Prestien, and P. Joseph-Nathan. Org. Magn. Reson. **7**, 339 (1975).
18. M. A. Keniry and G. A. Poulton. Magn. Reson. Chem. **29**, 46 (1991).
19. G. M. Sheldrick. SHELX-76, a program for crystal structure determination. Anorganische-Chemische Institut der Universitat Göttingen. 1976.
20. C. K. Johnson. ORTEP: a Fortran thermal ellipsoid plot program for crystal structure illustrations. ORNL-3794, Revised. Oak Ridge National Laboratory, Oak Ridge, Tenn. 1965.
21. D. T. Cromer and J. T. Waber. International tables for X-ray crystallography. Vol. 4. Kynoch Press, Birmingham, England. 1974. pp. 99 and 149.

Can. J. Chem. Downloaded from www.nrcresearchpress.com by 109.225.110.28 on 09/08/12
For personal use only.

Spatial and temporal visualization of a pH-dependent complexation equilibrium by nuclear magnetic resonance imaging

B. J. BALCOM, T. A. CARPENTER, AND L. D. HALL[1]

Herchel Smith Laboratory for Medicinal Chemistry, Cambridge University School of Clinical Medicine, University Forvie Site, Robinson Way, Cambridge, CB2 2PZ, U.K.

Received June 8, 1992

B. J. BALCOM, T. A. CARPENTER, and L. D. HALL. Can. J. Chem. **70**, 2693 (1992).

Alteration of a chemical equilibrium, ethylenediaminetetraacetic acid chelation of aqueous copper, in response to a pH gradient that protonates the complexing agent, has been observed spatially and temporally by ^{1}H nuclear magnetic resonance. Protonation of the complexing agent shifted the complexation equilibrium towards free copper ion. Free and bound copper ions alter the spin lattice relaxation time (T_1) of water in the host polyacrylamide gel to different extents. Based on this difference, a T_1 weighted (fast repetition time, short echo time) two-dimensional spin-warp imaging sequence mapped out the distribution of the free and bound species. Addition of a pH 3 aqueous solution to the gel was insufficient to alter the equilibrium; a pH 1 aqueous solution liberated the complexed copper. Quantitative one-dimensional experiments gave a T_1 weighted profile that showed the reaction front is displaced a distance proportional to the square root of time.

B. J. BALCOM, T. A. CARPENTER et L. D. HALL. Can. J. Chem. **70**, 2693 (1992).

Utilisant la RMN du ^{1}H, on a pu observer la modification spatiale et temporale d'un équilibre chimique, la chélation du cuivre aqueux par de l'acide éthylènediaminetétraacétique sous l'influence d'un gradient de pH qui protone l'agent complexant. La protonation de l'agent complexant déplace l'équilibre de la complexation vers l'ion cuivre libre. Les ions de cuivre libres et liés altèrent de façons différentes les temps de relaxation spin-réseau (T_1) de l'eau du gel de polyacrylamide hôte. En se basant sur cette différence, une valeur moyenne de T_1 (temps de répétition rapide et temps d'écho court), il a été possible d'établir des séquences bidimensionnelles d'images déformées des spins qui définissent les contours de distribution des espèces libres et liées. L'addition d'une solution aqueuse de pH 3 n'est pas suffisante pour altérer l'équilibre; à un pH de 1, la solution aqueuse libère le cuivre complexé. Des expériences unidimensionnelles quantitatives ont permis de déterminer un profil moyen de T_1 qui montre que la front de la réaction se déplace d'une distance qui est proportionnelle à la racine carrée du temps.

[Traduit par la rédaction]

Can. J. Chem. Downloaded from www.nrcresearchpress.com by 109.225.110.28 on 09/08/12
For personal use only.

It is a fundamental tenet of the majority of chemical transformations that the reaction medium is spatially and temporally homogeneous. In practise this is generally ensured by dissolving the reagents in a suitable solvent, which is then stirred. However, fast reactions often cannot be stirred briskly enough to ensure that the reaction is homogeneous. This is commonly observed for many acid/base titrations. Recently we examined two irreversible chemical reactions (1) where the rate of reaction was limited in a controlled manner by diffusion of reagents in a gel medium. In this communication we examine by Nuclear Magnetic Resonance Imaging (2–6) (NMRI), the spatial and temporal behaviour of a chemical equilibrium in a gel matrix perturbed by a pH gradient. This experiment is effectively a spatial titration.

Ethylenediaminetetraacetic acid (EDTA) has a very high affinity for divalent cations; for example, the log stability constant of EDTA and aqueous Cu^{2+} is approximately 18 (7). The effective stability constant, however, is pH dependent (7, 8); decreasing the pH of the reaction medium protonates the binding sites of EDTA and shifts the equilibrium towards free Cu^{2+} ions. Relaxation of the Cu^{2+}–EDTA system to a new equilibrium is very rapid upon addition of acid[2] and therefore it can be anticipated that progress of the "titration" will be limited by the rate at which reagents diffuse together.

A time-varying pH gradient was induced in the reaction sample by adding an acidic solution (pH 1.2, sulfuric acid) to the axial void of a right cylinder formed from cross-linked polyacrylamide gel[3] doped with EDTA chelated Cu^{2+} (15 mM). The gel network acts to limit long-range convective mixing of the reagents (9) so that the concentration profile of migrating protons in this medium is predominantly controlled by aqueous diffusion (9, 10). Thus the polyacrylamide gel behaves in many respects like pure water but with a well-defined ultrastructure determined by the casting geometry.

[1]Author to whom correspondence may be addressed.

[2]Homogeneous test reaction at concentrations representative of this work. Colour of the Cu^{2+}–EDTA complex was the indicator.

[3]Polyacrylamide gels were formed, over 24 h, from a 90:9.5:0.5 mixture of water, acrylamide, and bis-acrylamide (9) employing ammonium persulphate as the initiator and *N*,*N*,*N*′,*N*′-tetramethyethylenediamine as the accelerator. Gels were cast as right cylinders (*i*) diameter 26 mm in a Perspex cylinder sealed at the bottom, with a 5-mm NMR tube placed concentric with the cylinder axis, (*ii*) diameter 16 mm in a Perspex cylinder sealed at the bottom. Water-soluble by-products of the reaction were removed by equilibration over several days in a large reservoir of distilled deionized water. Gels were doped with 15 mM Cu^{2+} (sulphate salt) and 15 mM EDTA (disodium salt) by a similar equilibration. The dopant solution was adjusted to pH 7 with aqueous NaOH prior to equilibration. Small diameter samples (1-D experiments) were cut to a square edge with a sharp wire and guide.

Can. J. Chem. Downloaded from www.nrcresearchpress.com by 109.225.110.28 on 09/08/12
For personal use only.

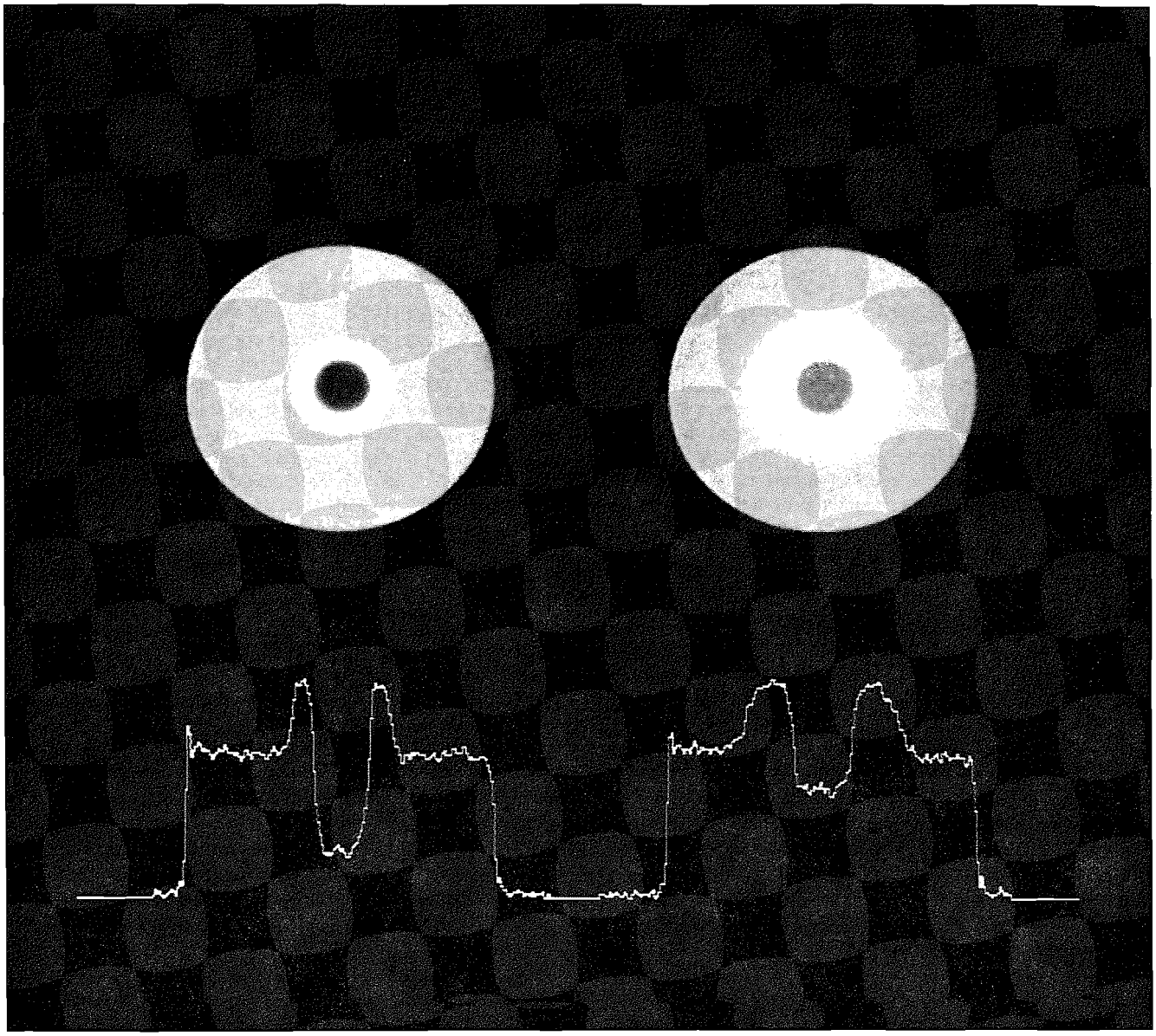

FIG. 1. Two-dimensional image illustrating the shift in complexation equilibrium Cu^{2+}–EDTA under the influence of a pH gradient. Areas of high image intensity map unbound Cu^{2+}. The left image corresponds to 4 min after addition of acid to the axial void, the right image 25 min. Profiles below both images reflect the intensity distribution along a line that bisects the center of each image horizontally.

As the local concentration of H^+ increases, the resultant, spatially dependent, shift in equilibrium can be imaged by utilizing the differential effect of complexed and free Cu^{2+} on the spin lattice relaxation time (T_1) of water in the gel media. Previously we examined contrast engendered through an alteration in the electronic structure of a contrast agent (1). In this work signal contrast is created through an alteration in the solvation of a contrast agent. Such effects with other paramagnetic metals are well known (11) and are presumed to reflect the reduced contact of the metal with its hydration sphere. Inversion recovery measurements of the proton spin lattice relaxation time at pH 7 (Cu^{2+} = 15 mM, EDTA = 15 mM) gave a T_1 of 0.38 s, whereas at pH 1.2 the T_1 was 0.19 s in the same system.

A conventional T_1 weighted spin-warp imaging sequence was employed (2) to visualize the molecular processes occurring in the gel. The analytical expression for the signal intensity at any point in the image is given by eq. [1], where TE is the time at which the spin echo is detected, TR is the repetition time, T_2 is the spin–spin relaxation time, and ρ is proton density. Since the gels under study are primarily water (90%), the proton density is very high and signal-to-noise in the resultant images is good.

$$[1] \quad S = \rho \exp(-TE/T_2)(1 - \exp(-TR/T_1))$$

The relaxation times for this system and the imaging parameters chosen (fast repetition rate, short TE) result in an image where contrast is strongly T_1 weighted and translates, to a first approximation, into a map of free and bound Cu^{2+}. Figure 1 shows two transverse slice images of the gel sys-

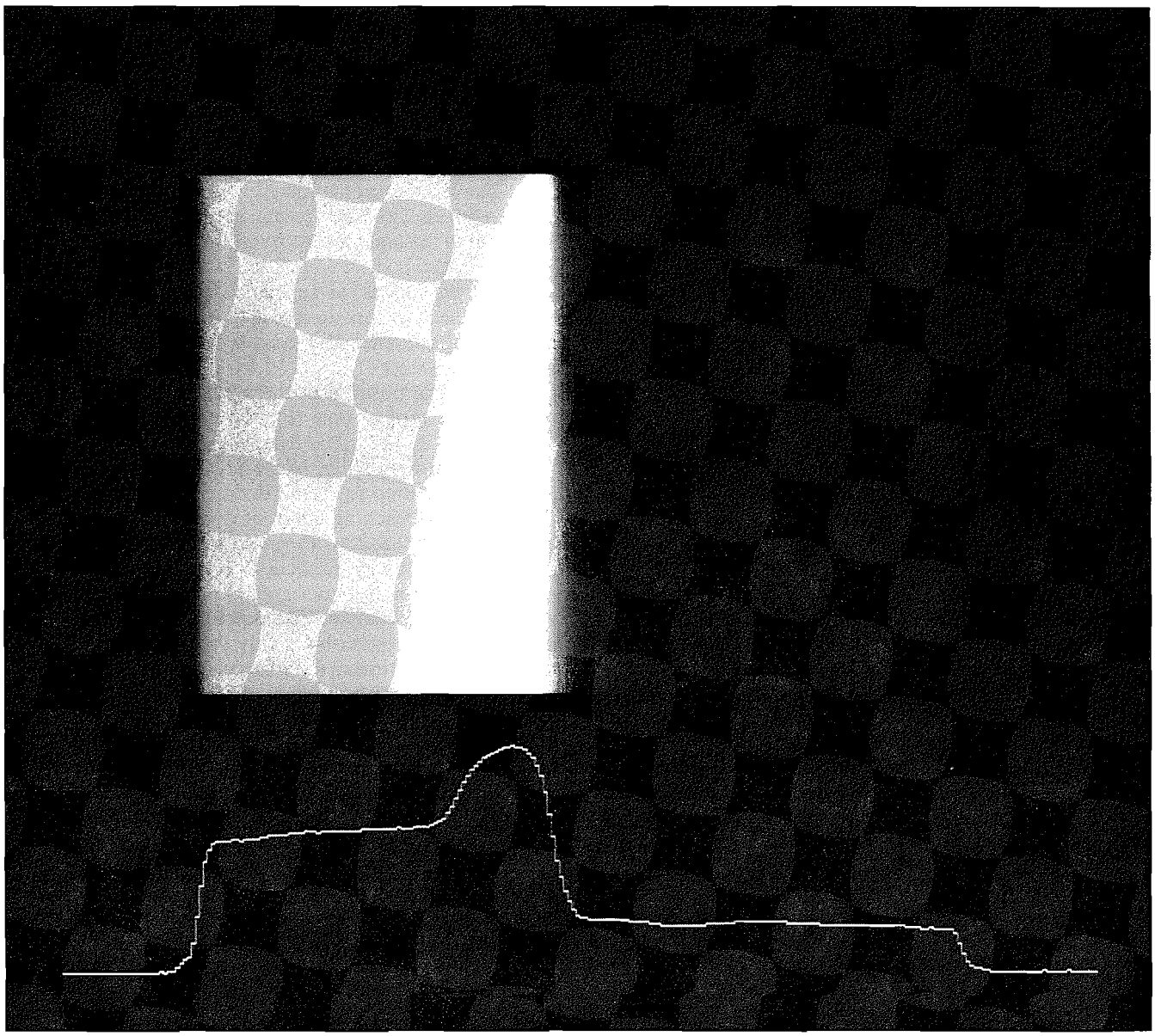

FIG. 2. One-dimensional magnetization profiles (x direction) acquired as a function of time (y direction) demonstrating the shift in complexation equilibrium Cu^{2+}–EDTA under the influence of a pH gradient. The reaction front moves right to left into the pre-doped aqueous gel as time increases. High signal intensities map unbound Cu^{2+}. The discrete profile shown is midway through the stack of 128. The uniform signal intensity in the aqueous reservoir shows it remains well mixed throughout the experiment.

Can. J. Chem. Downloaded from www.nrcresearchpress.com by 109.225.110.28 on 09/08/12
For personal use only.

tem,[4] acquired 4 and 25 min after addition of the acidic solution to the axial void. Regions of the sample without significant concentrations of free Cu^{2+} have weaker signal intensities due to partial saturation of their longitudinal magnetization under the influence of a fast repetition rate. Initially, bound copper and, therefore, low signal, predominates everywhere except in the immediate vicinity of the axial void.

With increasing time, the region of enhanced signal intensity spreads as the wave of aqueous protons migrates radially from the central void shifting the equilibrium between complexed and free Cu^{2+}. Back-diffusion of liberated Cu^{2+} into the axial void increases the signal from this part of the sample. Visual examination of the sample subsequent to imaging confirms that unbound copper predominates in the annular region of enhanced intensity. EDTA chelated copper in this sample displays a distinctive blue colour, which is diminished in the region of the sample corresponding approximately to the intense signal observed in Fig. 1. Cloudiness of the polyacrylamide gel (12), however, precludes more than a qualitative examination of the gel system based

[4]The NMR probe was a modified split-ring resonator (15) of 6.3 cm diameter. The imaging experiment was performed using an ORS Biospec 1 (83.7 MHz) instrument with a horizontal bore (31 cm) magnet and 20 cm home-built gradient set. The 2-D spin-warp sequence, with a hard 90° pulse and a slice-selective 180° pulse, had a repetition time of 0.3 s and an echo time of 15 ms. Slice thickness was 1 cm and the acquisition time 80 s for each 256 × 256 image. Field of view was 6 cm and pixel size 0.2 mm.

Can. J. Chem. Downloaded from www.nrcresearchpress.com by 109.225.110.28 on 09/08/12
For personal use only.

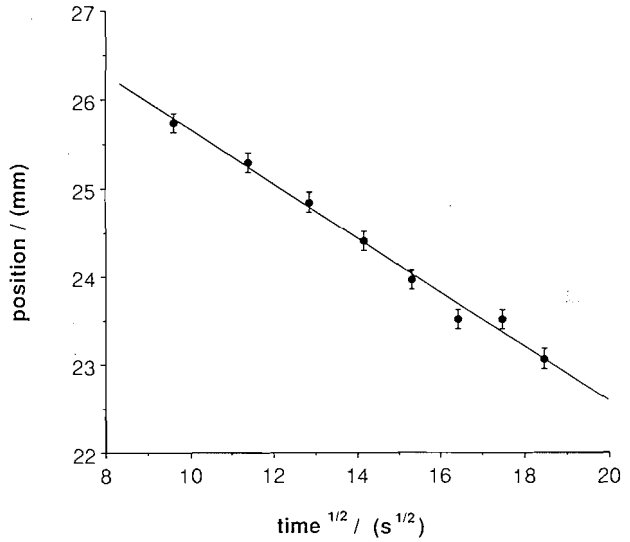

FIG. 3. Plot of the interface position as a function of the square root of time. The plot is linear in accord with theory. The uncertainty in each point is $\pm 1/2$ pixel (0.1 mm).

on colour changes. A less acidic solution (pH 3) added to the axial void gave no enhancement of NMR signal from the gel, which accords with the expectation that a pH 3 solution should be insufficient to manifest a substantial alteration in the Cu^{2+}–EDTA equilibrium. The Cu^{2+}–EDTA complex is known to be stable at approximately pH 3 (8).

The experiment shown in Fig. 1 illustrates that we are able to follow the moving boundary between free and bound Cu^{2+} that results from diffusion of H^+. The spread of the reaction front in this experiment, however, is difficult to quantify for two reasons: (1) The front moves a finite distance during data acquisition, which leads to a smearing of the front. The exact nature of this smearing in the image (frequency) domain is difficult to predict *a priori* because the image is reconstructed, via a Fourier transform, from data collected in the time domain (2). (2) H^+ in the axial void is of finite concentration. Most simple solutions to the reaction–diffusion equation presume a constant concentration reservoir. Both of these difficulties, along with the attendant mathematical complications of radial geometry (Bessel functions), are avoided if one works with a simple one-dimensional sample.

Roughton (13) has shown that fast reaction kinetics, in a one-dimensional sample, lead to the propagation of reaction fronts a distance proportional to the square root of time. To investigate the Cu^{2+}–EDTA system more thoroughly, we performed the one-dimensional analog to the experiment in Fig. 1. The sample was a cylinder of polyacrylamide, in a Perspex former, pre-doped with chelated copper; A roughly equivalent volume of pH 1.2 sulfuric acid was added to the top of the polyacrylamide gel. The reaction front moving into the gel was imaged by rapid repetition of a simple spin-echo imaging sequence[5] without a phase encode step (2). This sequence produced a one-dimensional magnetization profile of the sample along the cylinder axis. The signal intensity at a point is governed, as before, by eq. [1].

The experiment is shown in Fig. 2 where we have synthesized an image from a series of profiles acquired at 30-s intervals. In this composite image the discrete profiles (x direction) are displayed as a function of time (y direction). As before, regions of high intensity correspond to unbound Cu^{2+}. The left side of the image, with moderate intensity, is the gel with chelated Cu^{2+} while the dark right-hand side of the image is the aqueous reservoir. A representative profile from the image is displayed at the bottom of the figure. The reaction front moves, as expected, from the aqueous reservoir into the gel; the shorter acquisition time of the one-dimensional sequence (5 versus 80 s) freezes movement of the reaction zone.

A plot of the position of the reaction front as a function of the square root of time (Fig. 3) is a straight line as predicted by theory (13). The front position is chosen to be the point of maximum slope in the advancing wave; a difference approximation to the derivative (14) yields this point. This method of tracking the front is valid provided the front shape does not change with time. We have plotted only the first quarter of the experiment in Fig. 3 because the reservoir concentration does not greatly exceed the total amount of EDTA in the sample. The boundary condition outlined above (constant reservoir) is only valid early in the experiment. At longer times, the observed reaction front broadens, probably because the flux of H^+ has decreased.

Further studies with other reactions and imaging sequences are planned to investigate in more detail moving boundaries of chemical reactivity by NMRI. We conclude by noting this work provides a simple precedent for using paramagnetic chelates as a novel class of NMR-active indicators whereby the spatial variation of various chemical equilibria may be examined. It is conceivable that the approach can be used to study systems such as ion exchange beds where it may be impossible to sample aliquots or to insert any form of instrumental probe.

[5]The 1-D spin-echo sequence, with hard 90° and 180° pulses (16 per profile), had a repetition time of 0.3 s and an echo time of 10 ms. Profiles (128) of 256 pixels were collected every 30 s. The field of view and pixel size were approximately the same as the two-dimensional experiment.

Acknowledgements

We thank Dr. Herchel Smith for a generous endowment (T.A.C., L.D.H.) and the Natural Sciences and Engineering Research Council of Canada for a post-doctoral fellowship (B.J.B.). Andrew Derbyshire and Matthew Robson provided the profile differentiation routine.

1. B. J. Balcom, T. A. Carpenter, and L. D. Hall. J. Chem. Soc. Chem. Commun. 312, (1992).
2. P. Callaghan. Principles of nuclear magnetic resonance microscopy. Oxford Science, Oxford. 1991.
3. J. J. Attard, T. A. Carpenter, A. de Crespigny, S. L. Duce, L. D. Hall, R. C. Hawkes, R. J. Hodgson, and N. J. Herrod. Philos. Trans. R. Soc. London A, **333**, 477 (1990).
4. A. Tzalmona, R. L. Armstrong, M. Menzinger, A. Cross, and C. Lemaine. Chem. Phys. Lett. **174**, 199 (1990).
5. J. M. Listerud, S. W. Sinton, and G. P. Drobny. Anal. Chem. **61**, 23A (1989).
6. W. Kuhn. Angew. Chem. Int. Ed. Engl. **29**, 1 (1990).
7. G. Schwarzenbach and H. Flaschka (Translated by H. M. Irving). Complexometric titrations. Methuen, London. 1969. Chaps. 1, 2.
8. T. S. West. Complexometry. BDH, Poole. 1969. Chaps. 1, 2.
9. A. T. Andrews. Electrophoresis: theory, technique, and bio-

chemical and clinical applications. Oxford Science, Oxford. 1986. Chap. 2.
10. T. Yamaguchi, L. Kuhnert, Zs. Nagy-Ungvari, S. C. Muller, and B. Hess. J. Phys. Chem. **95**, 5831 (1991).
11. S. H. Koenig and R. D. Brown. *In* Magnetic resonance annual, 1987. *Edited by* H. Y. Kressel. Raven Press, New York. 1987. pp. 263–286.
12. J. Margolis and C. W. Wrigley. J. Chromatogr. **106**, 204 (1975).
13. F. J. W. Roughton. Prog. Biophys. Biochem. **9**, 55 (1959).
14. R. C. Gonzalez and P. Wintz. Digital image processing. Addison–Wesley, London. 1977. p. 155.
15. L. D. Hall, T. Marcus, C. Neale, B. Powell, J. Sallos, and S. L. Talagala. J. Magn. Reson. **62**, 525 (1985).

Can. J. Chem. Downloaded from www.nrcresearchpress.com by 109.225.110.28 on 09/08/12
For personal use only.

The thermodynamics of the vaporization of liquid indium(I) iodide by modified entrainment

PETER J. GARDNER AND STEVE R. PRESTON

Department of Chemistry, Royal Holloway and Bedford New College, University of London, Egham Hill, Egham, Surrey, TW20 0EX, U.K.

Received March 3, 1992

PETER J. GARDNER and STEVE R. PRESTON. Can. J. Chem. **70**, 2699 (1992).

The transport of gaseous In(I)I in an argon carrier gas was studied in the temperature range 723–887 K by the modified entrainment method. Combination of the entrainment results with a literature equation for the total vapour pressure above the liquid gave the following expressions for the temperature dependence of the vapour pressures of the monomer (InI) and dimer (In_2I_2) respectively: $\ln[p^0_1/p^0] = -(12\ 866 \pm 141)/T + (12.99 \pm 0.51)$ (720–810 K) and $\ln[p^0_2/p^0] = -(18\ 370 \pm 700)/T + (15.8 \pm 1.2)$ (720–790 K); $p^0 = 10^5$ Pa. The dimer concentration is ca. 2% and nearly constant from 720 to 810 K.

PETER J. GARDNER et STEVE R. PRESTON. Can. J. Chem. **70**, 2699 (1992).

Faisant appel à la méthode d'entrainement modifiée et opérant entre 728 et 887 K, on a étudié le transport du In(I)I gazeux dans de l'argon agissant comme gaz porteur. Une combinaison des résultats de l'entraînement avec une équation tirée de la littérature pour la pression de vapeur totale au-dessus du liquide a permis de tirer les expressions suivantes pour la relation entre la température et respectivement les pressions de vapeur du monomère (InI) et du dimère (In_2I_2) : $\ln[p^0{}_1/p^0] = -(12\ 866 \pm 141)/T + (12{,}99 \pm 0{,}51)$ (720–810 K) et $\ln[p^0{}_2/p^0] = -(18\ 370 \pm 700)/T + (15{,}8 \pm 1{,}2)$ (720–790 K); $p^0 = 10^5$ Pa. La concentration de dimère est approximativement égale à 2% et elle est pratiquement constante de 720 à 810 K.

[Traduit par la rédaction]

Introduction

There is considerable current interest in the thermodynamics of the complexation and polymerization of gaseous metal halides (1). Much of this interest is engendered by the lamp industry (2), which makes extensive use of these halides, e.g., of In, Na, Sc, Sn, etc., as dopants within the envelope of the current generation of "metal halide" mercury discharge lamps. Their presence improves significantly the spectral distribution and colour rendition of the discharge. Before the discharge is struck, the halide is present as a condensed phase and knowledge of its vaporization thermodynamics is crucial to proper lamp design. There has been a recent study (3) of the total vapour pressure over liquid indium(I) iodide from 646 to 958 K by quasi-static vapour pressure manometry. The results from this study have been used in combination with an examination of In(I)I(l) from 723 to 887 K by modified entrainment to yield separate vapour pressure equations for the monomer and dimer species. The techniques and data analysis are similar to those used in a recently reported study (4) of indium(I) bromide.

Experimental

Materials

Indium(I) iodide, an opaque purple crystalline material, was from the same batch (3) as that used for vapour pressure manometry; its synthesis and analysis have been reported (3). The material was handled in a dry-nitrogen-filled glove bag.

Argon was purified by passage through a commercial rare gas purifier (model RGP-4, B.O.C. Ltd.)

Apparatus

The modified entrainment apparatus has been described before (4). The principal difference between the modified entrainment method (MEM) and conventional entrainment is that in MEM the sample and the vapour in equilibrium with it are insulated from the irreproducible effects of the carrier gas (argon) by a narrow capillary (20 mm long × 1 mm diameter). This capillary acts as a diffusive resistance to the egress of sample vapour which is swept away by the carrier at the capillary orifice. The equilibrium vapour pressure obtains at the bottom of the capillary (5) above the sample surface and consequently the transport kinetics in the capillary may be formulated readily. The experimental parameter is the rate of mass loss ($\dot{w}$) at a preset temperature (T); the range studied was from 4.2×10^{-11} kg s^{-1} (at 723 K) to 1.6×10^{-9} kg s^{-1} (at 887 K). The diffusive resistance (length over cross-sectional area) of the channel was 24 120 ± 12 m^{-1}. Eighty-three data points were recorded using a modified protocol compared to that used in earlier work (4). The sample was allowed to cool from its maximum temperature of 887 K at 2 K min^{-1} and the rate of mass loss ($\dot{w}$) was logged digitally at 1 min intervals. Several points throughout the temperature range were repeated under isothermal conditions to confirm that thermal equilibrium is established during the dynamic recording protocol. The apparatus is operated at near atmospheric pressure.

Results and discussion

High-temperature mass spectroscopy, at 590 K, of the vapour above solid In(I)I (T_m = 632 K) indicates the presence of a low concentration (a few percent) of the dimer, In_2I_2 (3). The vapour composition was also examined by absorption spectroscopy (6, 7) but only the presence of the monomer was noted. Accordingly, our results were interpreted assuming the following equilibria

[1] $\quad InI(l) \rightleftharpoons InI(g) \qquad \Delta H_1, \Delta S_1$

[2] $\quad 2InI(g) \rightleftharpoons In_2I_2(g) \qquad \Delta H_2, \Delta S_2$

The solution to the flux equations for these equilibria is identical to that for the corresponding $InBr/In_2Br_2$ system, which has been described in detail (4) and will not be repeated here. Briefly, if the ratio of the dimer to monomer flux in the capillary (see Experimental) is β, then the partial pressures of the monomer (p^0_1) and dimer (p^0_2) are given by eqs. [3] and [4]

Can. J. Chem. Downloaded from www.nrcresearchpress.com by 109.225.110.28 on 09/08/12
For personal use only.

Can. J. Chem. Downloaded from www.nrcresearchpress.com by 109.225.110.28 on 09/08/12
For personal use only.

$$[3] \quad p_1^0 = \frac{P}{(1+\beta)}\left(1 - \exp\left(\frac{-\dot{w}RTl(1+\beta)}{D_1AM_1P(1+2\beta)}\right)\right)$$

$$[4] \quad p_2^0 = \frac{P\beta}{(1+\beta)}\left(1 - \exp\left(\frac{-\dot{w}RTl(1+\beta)}{D_2AM_1P(1+2\beta)}\right)\right)$$

In these equations, P is the argon carrier gas pressure (near atmosheric), $\dot{w}$ is the rate of mass loss at temperature T, l/A is the diffusive resistance, and M_1 is the monomer molecular mass. For the limiting cases of zero dimer ($\beta = 0$ in eqs. [3] and [4] and $i = 1$ in eq. [5]) or zero monomer ($\beta = \infty$ in eqs. [3] and [4] and $i = 2$ in eq. [5]), eqs. [3] and [4] reduce to eq. [5]

$$[5] \quad p_i^0 = P\left(1 - \exp\left(\frac{-\dot{w}RTl}{\mathcal{D}_iM_iAP}\right)\right)$$

In these equations D_i are ternary (InI, In_2I_2, Ar) diffusion coefficients and $\mathcal{D}_i$ are binary (InI or In_2I_2, Ar) diffusion coefficients. The total vapour pressure (p_T) is given by eq. [6].

$$[6] \quad p_T/\text{Pa} = p_1^0 + p_2^0 = \exp(-16\,683/T + 62.716 - 5.001 \ln T)$$

which was obtained by a weighted three-parameter regression of the experimental points (3) from quasi-static vapour pressure manometry; the weighting factor is p_T^2 (8). The temperature range for the study by Brumleve *et al.* (3) was 645–960 K, which encompasses our experimental range (723–887 K). The total vapour pressure above In(I)I has been reported many times in the past and the relative merits of these earlier determinations have been discussed (3). The presence of higher halides in the sample is a frequent cause of high results. We prefer to use the results of Brumleve *et al.* because they were obtained with a sample from the same batch as used in our work, and because of our first-hand knowledge of the experimental procedure of Brumleve *et al.*

If the diffusion coefficients (D_i) are known, then eqs. [3], [4], and [6] contain three unknowns, p_1^0, p_2^0, and β. The estimation of the diffusion coefficients is described in the Appendix. The equations were solved numerically at each experimental temperature using a bisections algorithm (9) to find the root of $F(\beta) = 0$ where

$$[7] \quad F(\beta) = p_T - p_1^0 - p_2^0$$

with an initial guess $0 < \beta < 10$. $F(\beta)$ is a monotonically increasing function from $\beta = -0.5$, approaches asymptotically a positive limit at large values of β and with one root in this range. During data processing it was noted that the proportion of dimer (and hence β) was small throughout the experimental range. Consequently, because of random error in $\dot{w}$, several negative roots for β (and hence p_2^0) were found; this problem has been noted before (4). This was circumvented by using analytic values of $\dot{w}$ from a weighted linear regression of the experimental data points, eq. [8]. This has the effect of smoothing the input data.

$$[8] \quad \ln[\dot{w}/\text{kg s}^{-1}] = -(4.74 \pm 0.19) - \frac{(13\,782 \pm 150)}{T}$$

Having found values for β at the experimental temperatures, values for p_1^0 and p_2^0 follow from eqs. [3] and [4]. These were used to generate vapour pressure equations, [9] and [10], for the monomer and dimer ($p^0 = 10^5$ Pa).

$$[9] \quad \ln[p_1^0/p^0] = (12.99 \pm 0.51) - (12\,866 \pm 141)/T \quad (720\text{–}810\ \text{K})$$

$$[10] \quad \ln[p_2^0/p^0] = (15.8 \pm 1.2) - (18\,366 \pm 698)/T \quad (720\text{–}790\ \text{K})$$

The uncertainty intervals in the coefficients of the vapour

TABLE 1. The first thirty experimental data points, derived[a] values of β, p_1^0, and p_2^0 (P = 763.8 Torr[b])

T/K	$10^{11}\ \dot{w}$ (kg s^{-1})	β[c]	p_1^0 (Pa)[d]	p_2^0 (Pa)[d]
723.1	4.27	0.0051	823.3	5.89
724.8	4.56	0.0052	858.5	6.32
727.1	5.01	0.0054	907.6	6.99
729.0	5.42	0.0057	952.2	7.63
730.8	5.09	0.0059	994.2	8.27
733.0	6.40	0.0062	1047.9	9.11
735.0	6.68	0.0064	1098.9	9.94
737.1	5.21	0.0067	1156.6	10.95
739.0	6.57	0.0070	1209.2	11.91
740.9	8.42	0.0072	1264.4	12.91
742.9	8.48	0.0073	1326.0	13.71
744.9	8.53	0.0076	1389.7	14.93
747.0	7.95	0.0079	1457.8	16.22
749.0	7.81	0.0082	1527.6	17.57
751.0	9.49	0.0084	1596.0	18.91
752.9	9.54	0.0087	1666.3	20.32
755.1	10.02	0.0089	1754.3	22.00
757.1	13.61	0.0092	1834.3	23.58
758.9	10.92	0.0094	1908.5	25.03
760.9	14.63	0.0096	1992.8	26.66
762.9	10.43	0.0097	2082.8	28.34
765.1	11.94	0.0099	2185.8	30.20
767.0	16.28	0.0100	2277.8	31.81
769.0	14.01	0.0101	2382.6	33.53
770.9	15.09	0.0102	2483.5	35.17
772.9	15.28	0.0102	2589.4	36.67
775.1	17.46	0.0102	2716.5	38.39
777.0	17.42	0.0101	2829.3	39.73
779.0	17.80	0.0100	2948.8	40.96
781.0	17.74	0.0098	3080.5	42.08

[a]These derived quantities were obtained from smoothed values of $\dot{w}$, eq. [8], see text.
[b]1 Torr = 133.3 Pa.
[c]β is the ratio of the fluxes of dimer to monomer in the capillary and is approximately equal to $p_2^0D_1/p_1^0D_2$; values of D_1 and D_2 may be estimated from eqs. [A2] and [A3].
[d]Redundant significant figures are included in these columns; the precision of these pressures is discussed in the text and shown in the figure.

TABLE 2. Enthalpy and entropy changes for reactions [1], [2], and [11] at 760 K obtained by a second law analysis

Reaction	ΔH (kJ mol^{-1})	ΔS (J K^{-1} mol^{-1})
[1] InI(l) $\rightleftharpoons$ InI(g)	107.0 ± 1.2	108.0 ± 4.2
[2] 2InI(g) $\rightleftharpoons$ In_2I_2(g)	−61 ± 6	−85 ± 11
[11] 2InI(l) $\rightleftharpoons$ In_2I_2(g)	153 ± 6	131 ± 10

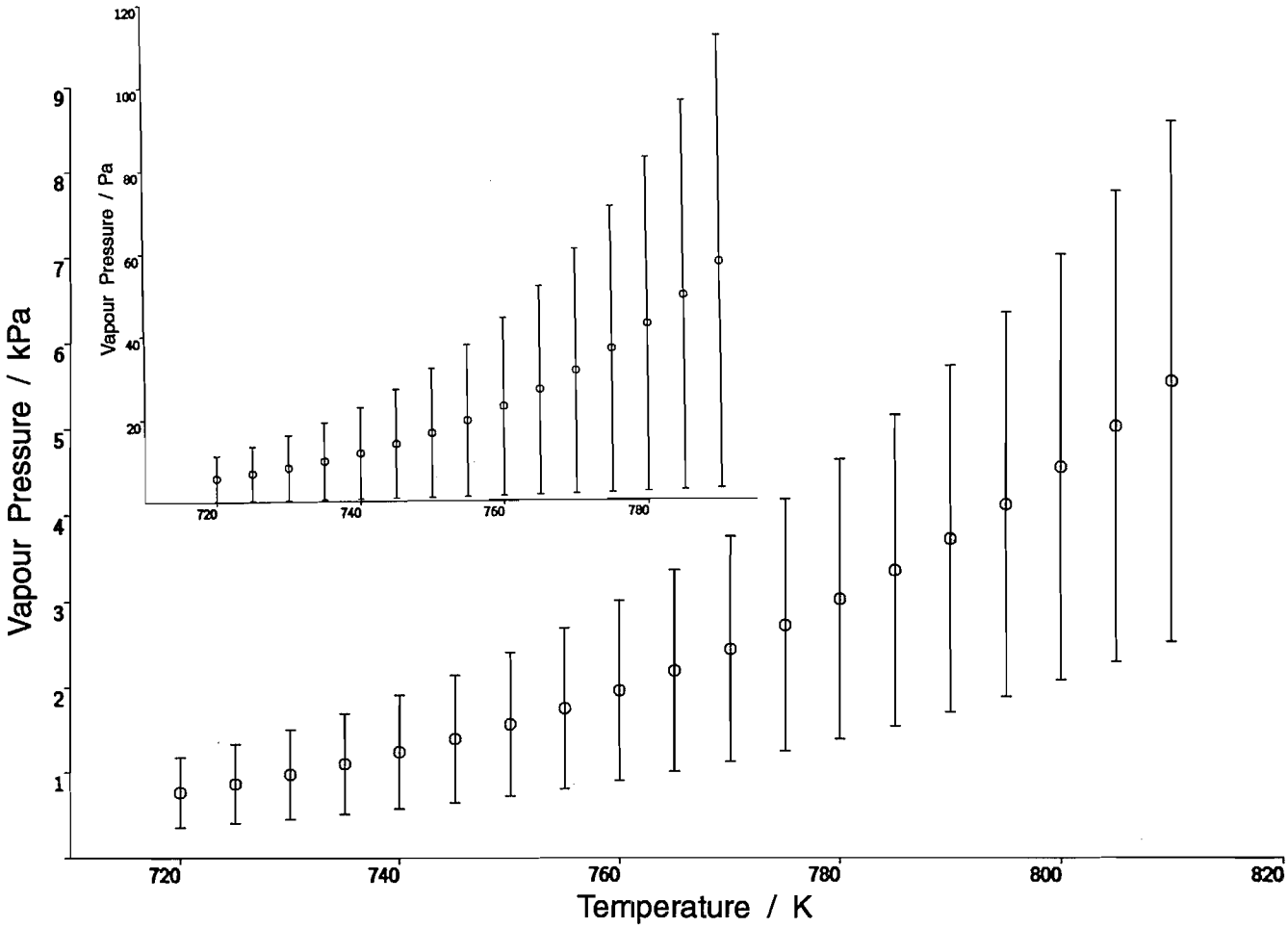

FIG. 1. Vapour pressures of InI(l) and In_2I_2(l)(inset) as a function of temperature. Error bars represent 50% confidence limits.

TABLE 3. Enthalpy changes for reactions [1], [2], and [11] for indium(I) chloride, bromide, and iodide at 298.15 K; comparison with literature results

Reaction	ΔH (kJ mol^{-1})		
	X = Cl	X = Br	X = I
[1] InX(l) $\rightleftharpoons$ InX(g)	104.9 ± 2.0[a]	107.9 ± 0.2(4)	120.2 ± 1.2
	104 ± 4(3)	110 ± 4[c](3)	118 ± 4[c](3)
[2] 2InX(g) $\rightleftharpoons$ In_2X_2(g)	−95.3 ± 0.4[b]	−144 ± 14[c](4)	−64 ± 6[c]
		−100 ± 13[d](14)	−71 ± 22[d](14)
[11] 2InX(l) $\rightleftharpoons$ In_2X_2(g)	110.5 ± 2.0[c]	72 ± 14(4)	177 ± 6
		128 ± 9[d](14)	157 ± 12[d](14)
Dimer pressure fraction, 800 K, %	Small(3)	4	2

[a]A third law result from ref. 15 combined with an enthalpy of fusion from ref. 3 where the wide range of reported values for this function is discussed.
[b]Observed directly by DeFoort *et al.* (15), reaction(4) in his Table 7.
[c]From eq. [12].
[d]These literature values are not mutually self-consistent via eq. [12] because, although they come from the same authors, they were reported independently (3, 14).

pressure equations are 68% confidence intervals and are composite terms that include the effect of the random fluctuations in $\dot{w}$, the uncertainty in the diffusive resistance, and an estimated (5%) uncertainty for the diffusion coefficients (see Appendix). Some experimental values of $\dot{w}(T)$ and the derived values of p_1^0, p_2^0, and β are collected in Table 1.

The vapour pressures are given in Fig. 1 with the error bars calculated using an estimated cross-correlation coefficient as in the earlier work (4). The pressure fraction of the dimer is small, changing from 0.9% (at 730 K) to 1.4% (at 780 K); the difference is not statistically significant and the conclusion is that the dimer concentration is approximately con-

Can. J. Chem. Downloaded from www.nrcresearchpress.com by 109.225.110.28 on 09/08/12
For personal use only.

Can. J. Chem. Downloaded from www.nrcresearchpress.com by 109.225.110.28 on 09/08/12
For personal use only.

stant and less than 2% in the range 720–810 K. Equation [10] refers to the equilibrium

[11] $2InI(l) \rightleftharpoons In_2I_2(g) \qquad \Delta H_{11}, \Delta S_{11}$

and the thermodynamic constants for this expression are related to those for eqs. [1] and [2] by eq. [12]; Table 2 summarizes our thermodynamic constants for these reactions.

[12] $\Delta H_2 = \Delta H_{11} - 2\Delta H_1$

Table 3 compares thermodynamic constants for the same three reactions for InX (X = Cl, Br, I) and includes some literature results. To permit comparison with literature results, the data in Table 2 and the corresponding earlier results (4) for InBr have been converted to apply to 298.15 K. The source of the C_p data for this conversion was as follows: for the liquid halides (10, 11), for InX(g) standard statistical thermodynamic routines with known (12) molecular parameters were used, and for $In_2X_2(g)$ scaling with $2.2C_p(InX)$ was used; this scaling factor is nearly temperature independent and is valid for the alkali metal halides and their dimers (13).

The enthalpy changes for reaction [1] given in Table 3 show a predictable trend and the agreement between various sources is satisfactory. For eqs. [2] and [11] there is agreement with literature sources only for InI; the disagreement for InBr is quite marked, especially for eq. [11].

The proportion of dimer in the vapour at 800 K is higher for InBr than for the other halides and InBr has a relatively high dimerization bond energy: In_2Cl_2 (47 kJ mol^{-1}), In_2Br_2 (72 kJ mol^{-1}), In_2I_2 (32 kJ mol^{-1}). As noted before (4), the dimerization bond energy for the bromide fits satisfactorily with the trend in this function vs. molecular mass for the alkali metal halide dimers but is clearly out of step with the other indium(I) halides; we can offer no explanation for this surprising fact.

Acknowledgement

The authors are grateful to Dr. S. A. Mucklejohn (Thorn Lighting Ltd.) for helpful discussion and the gift of materials and to Mr. J. Turner for skilful silica work.

1. K. Hilpert. Structure Bonding (Berlin), **73**, 97 (1990).
2. M. A. Cayless and A. M. Marsden. Lamps and lighting. 3rd ed. Edward Arnold, London. 1983.
3. T. R. Brumleve, S. A. Mucklejohn, and N. W. O'Brien. J. Chem. Thermodyn. **21**, 1193 (1989).
4. P. J. Gardner and S. R. Preston. Can. J. Chem. **69**, 1394 (1991).
5. P. J. Gardner and P. Pang. Can. J. Chem. **66**, 2137 (1988).
6. Y. K. Grinberg, V. A. Boryakova, V. F. Shevel'kov, and Z. S. Medvedeva. Izv. Akad. Nauk SSSR, Neorg. Mater. **8**, 67 (1972).
7. Y. K. Grinberg, V. A. Boryakova, and V. F. Shevel'kov. Izv. Akad. Nauk SSSR, Neorg. Mater. **12**, 402 (1976).
8. D. E. Sands. J. Chem. Educ. **51**, 473 (1974).
9. W. H. Press, B. P. Flannery, S. A. Tenkolosky, and W. T. Vetterling. Numerical recipes. C.U.P., London. 1986. p. 243.
10. P. J. Gardner and S. R. Preston. Thermochim. Acta, **180**, 281 (1991).
11. T. P. Chusova, G. G. Stenin, V. A. Titov, G. A. Kokovin, and T. D. Karpova. Izv. Sib. Otd. Akad. Nauk SSSR, Ser. Khim. Nauk, **6**, 62 (1983).
12. K. P. Huber and G. Herzberg. Molecular spectra and molecular structure; constants of diatomic molecules. Van Nostrand, New York. 1979.
13. M. W. Chase, C. A. Davies, J. R. Downey, D. J. Frurip, R. A. McDonald, and A. N. Syverud. JANAF thermochemical tables. 3rd ed. J. Phys. Chem. Ref. Data, **14**, Supp. No. 1 (1985).
14. T. M. Brumleve, S. A. Mucklejohn, and N. W. O'Brien. Proc. Symp. High Temp. Lamp Chem. 2, The Electrochemical Society, **96** (1988).
15. F. Defoort, C. Chatillon, and C. Bernard. J. Chem. Thermodyn. **20**, 1443 (1988).
16. D. Battat, M. M. Faktor, I. Garrett, and R. H. Moss. J. Chem. Soc. Faraday Trans. 1, **70**, 2293 (1974).
17. S. Chapman and T. G. Cowling. The mathematical theory of non-uniform gases. Cambridge Univ. Press, London. 1960.
18. P. J. Gardner and P. Pang. Can. J. Chem. **66**, 566 (1988).
19. P. Davidovitz and D. L. McFadden (*Editors*). Alkali halide vapours. Academic Press, New York. 1979.
20. J. G. Hartley and M. Fink. J. Chem. Phys. **87**, 5477 (1987).
21. J. E. Huheey. Inorganic chemistry. Harper and Row, New York. 1983. Table 6.1.
22. D. O. Welch, O. W. Lazareth, G. J. Dienes, and R. D. Hatcher. J. Chem. Phys. **64**, 835 (1976).
23. R. A. Svehla. NASA Tech. Rep. R-132. Lewis Research Centre, Cleveland, Ohio. 1962.
24. R. C. Reid, J. M. Prausnitz, and T. K. Sherwood. The properties of gases and liquids. McGraw-Hill, New York. 1977.
25. M. Rigby, E. B. Smith, W. A. Wakeham, and G. C. Maitland. The forces between molecules. Clarendon Press, Oxford. 1986.
26. P. D. Neufeld, A. R. Janzen, and P. A. Aziz. J. Chem. Phys. **51**, 1100 (1972).
27. V. G. Solomonik. Russ. J. Phys. Chem. **53**, 313 (1979).
28. P. J. Gardner and S. R. Preston. J. Chem. Soc. Faraday Trans. **88**, 1993 (1992).

Appendix

Diffusion coefficients

The simultaneous solution of eqs. [3], [4], and [6] at each experimental temperature to yield β and then p_1^0 and p_2^0 assumes that the ternary diffusion coefficients for the system $InI/In_2I_2/Ar$ are known. There are no experimental diffusion coefficients for this system but a second-order treatment (16) of ternary diffusion in the context of modified entrainment permits the effective ternary coefficients ($D_{i,mix}$) to be written in terms of the corresponding binary diffusion coefficients ($\mathcal{D}_{ij}$) with respect to the majority component, argon

[A1] $$D_{i,\text{mixture}} = \frac{\mathcal{D}_{i,Ar}}{\gamma_i}$$

In eq. [A1], γ_i is a function of β, molecular masses, and temperature; the analytical form has been given before (4) along with computational details. Numerical values commonly lie in the range $0.8 < \gamma_i < 1.1$. The binary diffusion coefficients were calculated from the Chapman–Enskog equation (17). Use of this equation requires collision diameters for the interdiffusing species, and for the indium iodides these were estimated from an empirical correlation between Lennard Jones (LJ) collision diameters and moments of inertia (18). To calculate moment of inertia, it is necessary to know the molecular structure and the problem of estimating $\mathcal{D}_{ij}$ reduces to the estimation of the molecular structure of In_2I_2. The corresponding structure for InI is known (r_e = 2.754 Å (12)) and there are well-established correlations between structural constants for the alkali metal halides and their dimers (19, 20). The structure of In_2I_2 was

assumed to be D_{2h} and the In—I bond length was interpolated (2.99 Å) from a plot of $r(\text{M—X})_{\text{mon}}$ vs. $r(\text{M—X})_{\text{dim}}$ for the alkali metal halides using $r(\text{In—I})_{\text{mon}}$ = 2.754 Å. The bond angle θ(I—In—I) was interpolated at 107.2° from a linear plot of θ(X—M—X) vs. $(R_M - R_X)$ for the alkali metal halides where R_i are covalent radii (21); a similar correlation has been noted by Welch *et al.* (22). The covalent radius for In was estimated from the bond lengths in InX (X = Cl, Br, I) as 1.38 Å. Using the moments of inertia calculated from the structures and the σ_{LJ} vs. $I^{1/2}$ correlation in ref. 18, $\sigma_{LJ}(\text{InI})$ = 4.92 Å and $\sigma_{LJ}(\text{In}_2\text{I}_2)$ = 5.99 Å. The Chapman–Enskog equation contains a collision integral, which is a weak function of k_BT/ϵ_{ij}, where ϵ_{ij} is the well-depth of the interdiffusing species and k_B is the Boltzmann's constant. Svehla's correlation (23) with normal boiling point was used to estimate ϵ/k_B, InI = 1173 K and ϵ/k_B, In_2I_2 = 1821 K. Values for the LJ constants for argon were taken from a tabulation by Reid *et al.* (24). With the Lorentz–Berthelot (25) combining rules for ϵ_{ij} and σ_{ij} and Neufeld's expression (26) for the collision integral, the diffusion coefficients were calculated and regressed to a power law in T (ϵ_{ij} and σ_{ij} are the Lennard–Jones intermolecular potential parameters). From 700 to 950 K, the expressions [A2] and [A3] apply.

$$[\text{A2}] \quad \mathcal{D}(\text{InI, Ar})/\text{m}^2\,\text{s}^{-1} = 5.70 \times 10^{-6}\left(\frac{T}{273}\right)^{1.805}$$

$$[\text{A3}] \quad \mathcal{D}(\text{In}_2\text{I}_2\text{, Ar})/\text{m}^2\,\text{s}^{-1} = 3.83 \times 10^{-6}\left(\frac{T}{273}\right)^{1.851}$$

The choice of molecular parameters for In_2I_2 will clearly influence the result, and a range of estimated parameters was explored to investigate the effect. Values for the In—I bond length in the dimer were varied by ±5% and the theoretically estimated parameters of Solomonik (27), r(In—I) = 3.078 Å and θ(I—In—I) = 95.9°, were also studied.[1] The effect of these changes is to alter $\sigma_{LJ}(\text{In}_2\text{I}_2)$ to within the range 5.86–6.12 Å and this in turn affects $\mathcal{D}(\text{In}_2\text{I}_2)$, β, and the proportion of dimer. For all these modifications, the percentage of dimer remained less than 2% throughout the experimental temperature range. The procedure described in this appendix, that of estimating diffusion coefficients from empirical LJ parameters, has been validated for the SnBr_2–Ar and SnI_2–Ar systems (28).

[1]We are indebted to a referee for drawing this reference to our attention.

Can. J. Chem. Downloaded from www.nrcresearchpress.com by 109.225.110.28 on 09/08/12
For personal use only.

Electrochemical studies on arylhydrazonomesoxalonitriles in nonaqueous media

G. M. ABOU-ELENIEN[1]
Chemistry Department, Faculty of Science, Cairo University, Giza, A.R. Egypt
N. A. ISMAIL AND M. M. HASSANIN
Chemistry Department, Faculty of Science, Zagazig University, Egypt
AND
A. A. FAHMY
National Research Centre, Dokki, Cario, Egypt

Received April 22, 1992

G. M. ABOU-ELENIEN, N. A. ISMAIL, M. M. HASSANIN, and A. A. FAHMY. Can J. Chem. **70**, 2704 (1992).

The substituted arylhydrazonomesoxalonitriles and *N*-methyl phenylhydrazonomesoxalonitrile are studied electrochemically in benzonitrile (BN) employing different voltammetric and coulometric techniques. They are oxidized in a single irreversible one-electron transfer leading to a dimerization reaction. The reduction process occurs in two irreversible one-electron uptakes followed by proton abstraction from the solvent to give the saturated azomethine linkage.

G. M. ABOU-ELENIEN, N. A. ISMAIL, M. M. HASSANIN et A. A. FAHMY. Can J. Chem. **70**, 2704 (1992).

Opérant en milieu benzonitrile et faisant appel à des techniques voltammétriques et coulométriques, on a étudié le comportement électrochimique d'arylhydrazonomesoxalonitriles substitués et du *N*-méthyl phénylhydrazonomesoxalonitrile. Ces produits sont oxydés par un transfert unique irréversible d'un électron conduisant à une réaction de dimérisation. Le processus de réduction se produit par le biais de deux acceptations irréversibles d'un électron, suivies de l'arrachement d'un proton du solvant pour conduire à la formation d'une liaison azométhine saturée.

[Traduit par la rédaction]

Introduction

The electrochemical behaviour of α-arylhydrazononitriles and their *N*-methylated derivatives has recently been reported in the literature (1–8). The increase of interest in the chemistry of this class of compounds arose from their reported biological activity (9–13). It was found that these compounds are more effective than cyanides in the uncoupling oxidative phosphorylation in mitochonderial systems (14, 15).

Despite the considerable interest in the polarographic reduction of these compounds at the DME in aqueous buffers (1, 2, 16, 17), little has been reported (5) about their electrochemical behaviour in nonaqueous media at solid electrodes. In the present work we report the reduction and oxidation properties of some *para*-substituted α-arylhydrazonomesoxalonitriles (**1***a–g*) and their unsubstituted *N*-methyl derivative (**2**) at a rotating platinum disc electrode and the effects of substituents on their redox characteristics.

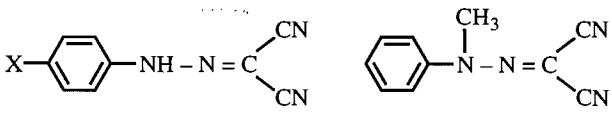

1*a - g*

2

1	*a*	*b*	*c*	*d*	*e*	*f*	*g*
X	H	Cl	Br	NO_2	CH_3	OCH_3	NH_2

Experimental

Reagents

Benzonitrile (BN) (Rotitainerm, West Germany) was purified by, first, distillation under vacuum from orthophosphoric acid, followed by repeated distillations from phosphorus pentoxide and final fractional distillation from potassium metal. The supporting electrolyte, tetra-*n*-butylammonium perchlorate (TBAP) (Fluka–Swiss), was crystallized several times from ethanol–water (9:1 v/v) mixture and dried *in vacuo* before use.

Organic syntheses

Compounds **1***a–g* were prepared following the procedure described by Lax (18). Compound **2** was prepared according to the procedure described by Cauquis *et al.* (5). The products obtained were purified by repeated crystallization from ethanol and the purity was checked by TLC. The structures of all the prepared compounds were confirmed by elemental analyses as well as by spectral data.

Apparatus and instruments

The voltammetric measurements were carried out using a potential scan generator VSG 72 as a potential source, potential control amplifier PCA 72C (Bank Electronic, Gottingen, West Germany) as a potentiostat, servogor XY (Metrawatt, Nurnberg, West Germany) as *X–Y* recorder, and a coulometer manufactured by Bank Electronic, Gottingen, West Germany. The rotating platinum disc electrode (RDE), was mounted to a rotating motor (750 rpm) (Metrohm, Swiss).

Measurements

The electrochemical measurements were carried out in dry benzonitrile (BN) containing 0.1 M tetra-*n*-butylammonium perchlorate (TBAP) as supporting electrolyte. The steady state voltammetry was carried out using a rotating platinum disc electrode (RDE), the cyclic voltammetry using a stationary platinum disc electrode. The number of electrons participating in each electrode process was obtained by controlled potential coulometry (CPC) in the same electrolyte using a platinum sheet electrode. Controlled potential electrolysis (CPE) experiments were carried out using a platinum net electrode either in dry benzonitrile or in acetonitrile with lithium perchlorate as supporting electrolyte.

The electrode potentials were measured against a saturated Ag/AgCl/Cl^- (BN) electrode, which was occasionally calibrated against the redox potential of the cobaltocenium/cobaltocene system (19). The standard potential of the Ag/AgCl/sat. Cl^- (BN)

[1]Author to whom correspondence may be addressed.

Can. J. Chem. Downloaded from www.nrcresearchpress.com by 109.225.110.28 on 09/08/12
For personal use only.

TABLE 1. DC voltammetric data of substituted phenylhydrazonomesoxalonitriles (**1***a–g*) and *N*-methyl phenylhydrazonomesoxalonitrile (**2**) in benzonitrile

Compound	Process[a]	$E_{1/2}$ (mV)	S^b	$E_{1/4} - E_{1/2}$	σ
1*a*	O_I	1963	107.97	150	0.00
	R_I	−447	84.17	90	
	R_{II}	−908	84.62	100	
1*b*	O_I	1637	128.7	155	0.227
	R_I	−518	121.13	170	
	R_{II}	−1095	50.67	50	
1*c*	O_I	2002	139.82	200	0.232
	R_I	−433	129.68	135	
	R_{II}	−993	139.34	120	
1*d*	O_I	1950	124.5	156	0.775
	R_I	−853	116.81	115	
	R_{II}	−1200	153.11	160	
1*e*	O_I	2022	153.6	300	−0.17
	R_I	−478	210.29	270	
	R_{II}	−1008	92.51	100	
1*f*	O_I	1890	215.04	270	−0.268
	R_I	−408	135.05	175	
	R_{II}	−1078	158.86	150	
1*g*	O_I	1892	112.1	140	−0.660
	O_{II}	2292	157.71	210	
	R_I	−493	196.3	170	
	R_{II}	−1058	129.16	105	
2	O_I	2072	73.53	120	
	R	−1193	194.34	160	

[a] O_I refers to the first electron oxidation, R_I and R_{II} to the first and second electron reductions, respectively.
[b] $S = dE/d \log ((i_d - i)/i)$.

Can. J. Chem. Downloaded from www.nrcresearchpress.com by 109.225.110.28 on 09/08/12
For personal use only.

electrode against the normal hydrogen electrode (NHE) is −176 mV (20, 21).

Controlled potential electrolysis (CPE)

Electrolysis of phenylhydrazonomesoxalonitrile (**1***b*) was carried out with 250 mg amounts of the starting material in both acetonitrile and benzonitrile. The potential was adjusted to a value corresponding to the limiting current plateau (+1.9 V for oxidation and −1.3 V for reduction). The electrolysis was stopped after the passage of a quantity of electricity corresponding to the uptake of 1 mole of electrons per mole of product for the oxidation and 2 moles for the reduction. In each case, after electrolysis, the resulting solution was evaporated at reduced pressure and the product was extracted with ethyl acetate, which was subsequently removed by evaporation. The mixture obtained was chromatographed on thin-layer silica gel plates using chloroform as solvent.

The oxidation product of CPE

Two main products with R_f = 0.71 and 0.84 were obtained. The zone with R_f value 0.71 was scraped off the plate, extracted with acetonitrile, filtered, and evaporated at reduced pressure. The resulting brownish solid compound (yield 60%; mp 250°C (dec.)) was identified as **3**; ir, cm^{-1} (KBr): 3200, 3300 (two NH); 2220 (CN); 1600 (C=N); 1220 (ClO_4); ^1H nmr ($CDCl_3$, TMS) δ, ppm: 7.2–7.4 (m, 8H, aromatic protons), 10.0 (s, br, 2H, two NH). Anal. calcd.: C 39.71, H 1.84, Cl 26.10, N 20.59%; found: C 39.68, H 1.75, Cl 25.66, N 20.37%.

The zone with R_f 0.84 was scraped and extracted as above. The faint orange-yellowish product obtained (yield 23%; mp 83°C) was identified as **4**; ir, cm^{-1} (KBr): 3200–3300 (two NH), 2220 (CN), 1600 (C=N); ^1H nmr ($CDCl_3$, TMS) δ, ppm: 7.25–7.44 (m, 6H, aromatic protons), 10.0 (s, br, 2H, two NH). Anal. calcd.: C 53.07, H 1.97, Cl 17.44, N 27.52%; found: C 53.15, H. 1.90, Cl 17.31, N 27.35%.

The reduction product of CPE

A quantitative yield of the original compound **1***b* was obtained (mp 102°C) when the reduction product was exposed to air; ir, cm^{-1} (KBr): 3240 (NH), 2220 (CN), 1600 (C=N); ^1H nmr ($CDCl_3$, TMS) δ, ppm: 7.2–7.5 (m, 4H, aromatic protons), 10.0 (s, br, 1H, NH). Anal. Calcd.: C 52.81, H 2.44, Cl 17.36, N 27.38%; found: C 52.63, H 2.38, Cl 17.28, N 27.25%.

Results and discussion

The electrochemical data for compounds **1***a–g* and **2** are summarized in Table 1. Figure 1 shows typical steady state voltammograms of these compounds, while Figs. 2*a* and *b* illustrate the corresponding cyclic voltammograms of the oxidation and reduction processes respectively, which are similar for compounds **1***a–f*. The oxidation occurs in a single irreversible one-electron process coupled with a consecutive chemical reaction (an EC mechanism). On the other hand, the reduction process occurs in two irreversible one-electron processes following an ECEC mechanism.

Compound **1***g* with an amino substituent is reduced similarly to the other members of the series, but the oxidation is accompanied by a second irreversible process corresponding to the oxidation of a primary aromatic amine. The reduction of the *N*-methylated derivative (**2**) occurs in a single two-electron wave instead in two irreversible one-elec-

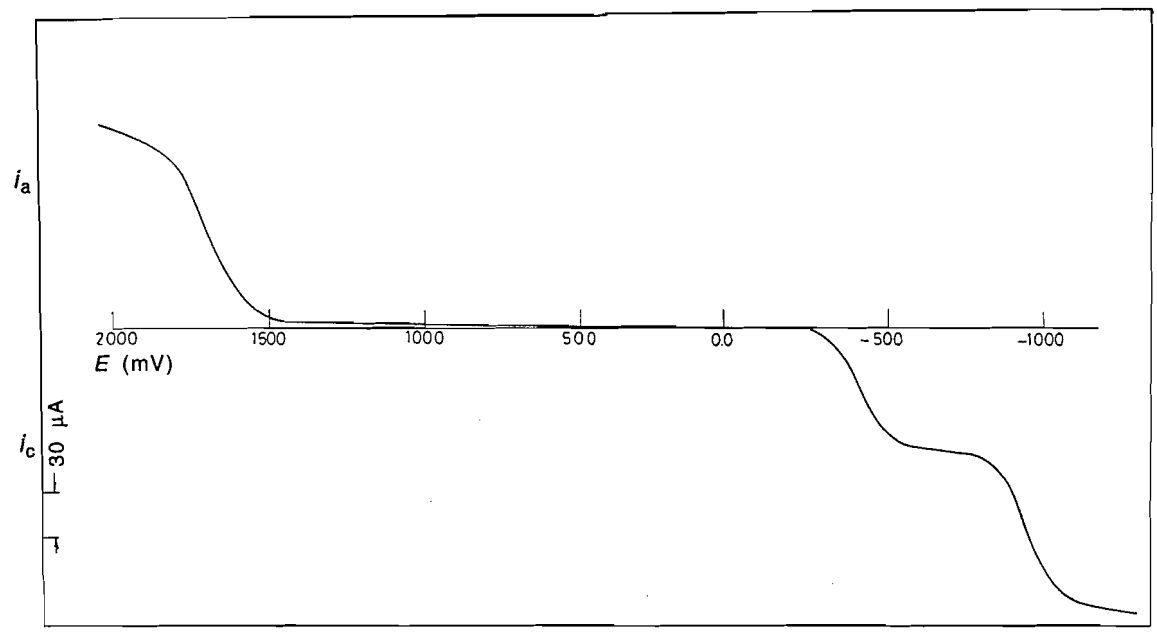

FIG. 1. DC voltamogram of compound **1***a* in BN.

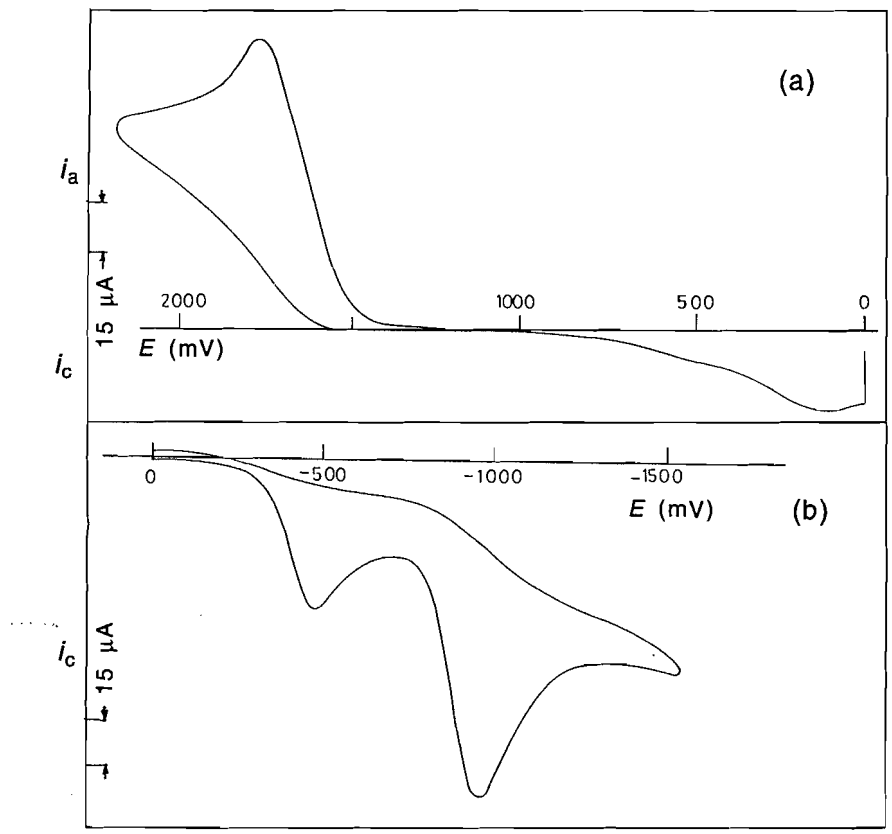

FIG. 2. Cyclic voltamogram of compound **1***a* in BN. (*a*) Oxidation. (*b*) Reduction. Scan rate = 100 mV/s.

tron waves. This two-electron process is accompanied by a chemical reaction (EC mechanism).

The substituted arylmesoxalonitriles **1***a–g* and (**2**) are thus oxidized in a single irreversible one-electron transfer process. This assumes that the coupled chemical reaction is dimerization. This is supported by isolation of 60% of the dimer **3** in the CPE (Scheme 1). The presence of 23% of the other dimeric species **4** indicates that under conditions of CPE, using a larger electrode over a prolonged period of time, the electrooxidation involves more than one electron per molecule of compound **1**.

The reduction of compounds **1***a–g* is assumed to occur on

Can. J. Chem. Downloaded from www.nrcresearchpress.com by 109.225.110.28 on 09/08/12
For personal use only.

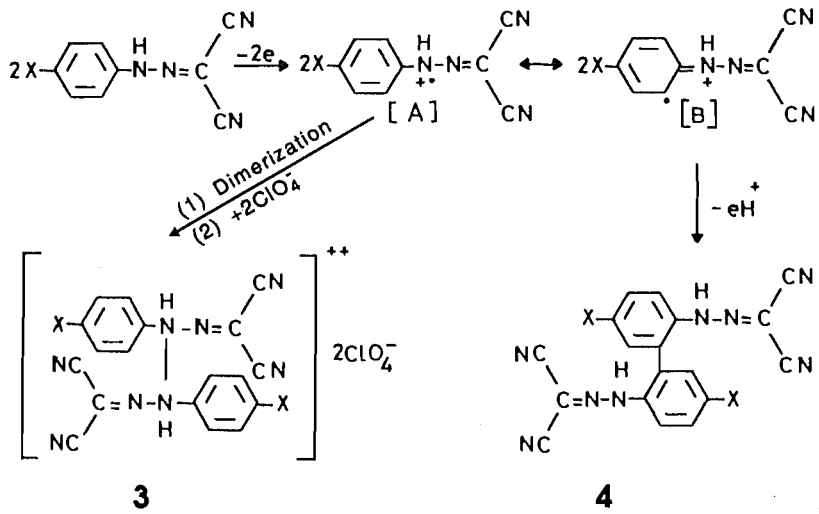

SCHEME 1

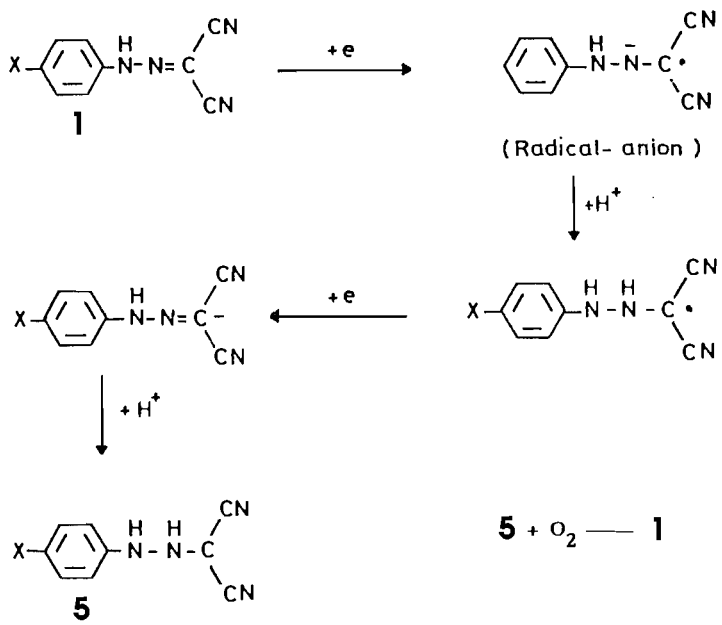

SCHEME 2

the -N=C double bond in two irreversible consecutive one-electron transfers, the potentials of which, for compound **2**, overlap. It is assumed that chemical reactions accompanying both electron transfers are proton abstractions — either from residual water in the solvent, from ions of the supporting electrolyte, or from the parent compound. Such a sequence is indicated in Scheme 2. The resulting hydrazine derivative **5** is unstable, especially in air, and is readily oxidized with air oxygen to the starting substance. This was the product obtained by CPE under aerobic conditions.

The introduction of the nitro group (Table 1, compound **1***d*) makes both reduction processes more difficult when compared with the unsubstituted parent compounds. This is contrary to the fact that usually the electron-attracting property of the nitro group lowers the electron density at the reduction centre. Also the presence of the electron-donating methoxy group has an effect opposite that usually observed (22) for electroreductions; it facilitates the first reduction process by 40 mV. Similar behaviour of the nitro and methoxy substituents was also found by Kass (23) in the reduction of different substituted arylaziridinium salts. The substitution by a methyl group on nitrogen (compound **2**) makes both oxidation and reduction processes more difficult than that of compound **1***a*. This may be explained by a steric effect of the methyl group at the reduction centre, which would hinder the approach of the reduction centre to the electrode surface.

1. M. H. Elnagdi and H. M. Fahmy. J. Electroanal. Chem. **84**, 149 (1977).
2. H. M. Fahmy and M. H. Elnagdi. Electrochim. Acta, **23**, 255 (1978).
3. H. M. Fahmy, M. A. Morsi, and M. H. Elnagdo. Gazz. Chim. Ital. **107**, 565 (1977).

Can. J. Chem. Downloaded from www.nrcresearchpress.com by 109.225.110.28 on 09/08/12
For personal use only.

4. G. Cauquis, H. M. Fahmy, G. Pierre, and M. H. Elnagdi. Electrochim. Acta, **24**, 391 (1979).
5. G. Cauquis, H. M. Fahmy, G. Pierre, and Z. E. Kandeel. J. Electroanal. Chem. **124**, 133 (1981).
6. M. A. Morsi, H. M. Fahmy, M. H. Elnagdi, and M. Abdel Azzem. J. Electroanal. Chem. **133**, 269 (1982).
7. M. A. Morsi, A. M. A. Helmy, and H. M. Fahmy. J. Electroanal. Chem. **148**, 123 (1983).
8. N. M. Abed, N. Nashed, H. M. Fahmy, and M. Abdel Azzem. Monatsh. Chem. **117**, 599 (1986).
9. T. Zsolnai. Biochem. Pharmacol. **13**, 285 (1964); Chem. Abstr. **60**, 13811 h (1964).
10. T. Zsolnai. Biochem. Pharmacol. **14**, 1325 (1965); Chem. Abstr. **63**, 15467d (1965).
11. T. Zsolnai. Biochem. Pharmacol. **14**, 1425 (1965); Chem. Abstr. **64**, 2686 h (1966).
12. M. W. Goldberg and A. I. Rachlin. U.S. Patent no. 265,889 (1953); Chem. Abstr. **49**, 1103 ġ (1955).
13. P. G. Heytler and W. W. Prichard. Biochem. Biophys. Res. Commun. **1**, 272 (1962).
14. B. Dienh and G. Tollin. Arch. Biochem. Biophys. **121**, 169 (1967).
15. E. S. Bamberger, C. C. Black, C. A. Fewson, and M. Gibbs. Plant Physiol. **38**, 483 (1963).
16. H. M. Sammour, H. M. Fahmy, and M. H. Elnagdi. J. Prakt. Chem. **317**, 257 (1975).
17. M. H. Elnagdi, H. M. Fahmy, and M. A. Morsi. J. Electroanal. Chem. **68**, 237 (1976).
18. W. Lax. J. Prakt. Chem. **63**, 1 (1901).
19. W. Summermann. Ph.D. Thesis, Freiburg, West Germany (1970). p. 10.
20. H. M. Koepp, H. Wendt, and H. Strehlow. Z. Elektrochem. **64**, 483 (1960).
21. G. Wilkinson. J. Am. Chem. Soc. **74**, 6142 (1952).
22. H. Lund. Acta Chem. Scand. **13**, 249 (1959).
23. M. B. Kass. J. Am. Chem. Soc. **95**, 959 (1973).

Can. J. Chem. Downloaded from www.nrcresearchpress.com by 109.225.110.28 on 09/08/12
For personal use only.

Coordination chemistry of thioether–pyridazine macrocycles II. Synthesis, structural and spectroscopic studies of dinuclear copper(II) and polynuclear copper(I) and silver(I) complexes of a tetrathiapyridazinophane macrocyclic ligand

LIQIN CHEN, LAURENCE K. THOMPSON,[1] AND JOHN N. BRIDSON
Department of Chemistry, Memorial University of Newfoundland, St. John's, Nfld., Canada A1B 3X7

Received May 19, 1992

LIQIN CHEN, LAURENCE K. THOMPSON, and JOHN N. BRIDSON. Can. J. Chem. **70**, 2709 (1992).

The preparation and properties of the thioether–pyridazine macrocycle (L3; $C_{11}H_{16}N_2S_4$) containing one pyridazine subunit, and its copper(II), copper(I), and silver(I) complexes are described. Magnetic susceptibility data (5–300 K) for the binuclear complexes $[CuL3Cl_2]_2$ (**I**) and $[CuL3Br_2]_2$ (**II**) have been fitted to the Friedberg magnetization expression with a molecular field correction. Intradimer antiferromagnetic exchange is weak ($-2J < 18$ cm^{-1}), with even weaker interdimer exchange ($-zJ' < 0.3$ cm^{-1}). The complexes $[CuL3Cl]_x$ (**III**) and $[AgL3ClO_4]_x$ (**V**) have been characterized by X-ray crystallography. **III** crystallizes in the triclinic system, space group $P\bar{1}$, with a = 9.410(2) Å, b = 10.291(2) Å, c = 9.208(2) Å, α = 108.56(1)°, β = 91.82(2)°, γ = 68.04(1)°, V = 780.1(2) Å^3, and $Z = 2$(R = 0.035, R_w = 0.031 for 1856 reflections). The ligand acts as a bidentate, S_2, bridge between dinuclear Cu_2Cl_2 units in a double stranded polymer. **III** crystallized in the monoclinic system, space group $P2_1/n$, with a = 9.382(4) Å, b = 19.274(4) Å, c = 10.190(3) Å, β = 106.35(3)°, V = 1768(1) Å^3, and $Z = 4$ (R = 0.036, R_w = 0.029 for 1776 reflections). The structure consists of a polymeric, two dimensional sheet structure, involving pseudo-tetrahedral silver ions linked by *exo*-bidentate, S_2, ligands and bidentate perchlorates.

LIQIN CHEN, LAURENCE K. THOMPSON et JOHN N. BRIDSON. Can. J. Chem. **70**, 2709 (1992).

On décrit la préparation et les propriétés du macrocycle thioéther-pyridazine (L3; $C_{11}H_{16}N_2S_4$) contenant une sous-unité pyridizane et de ses complexes avec le cuivre(II), le cuivre(I) et l'argent(I). On a ajusté les données de susceptibilité magnétique (5–300 K) des complexes binucléaires $[CuL3Cl_2]_2$ (**I**) et $[CuL3Br_2]_2$ (**II**) avec l'expression de magnétisation de Friedberg en faisant appel à une correction moléculaire du champs. L'échange antiferromagnétique intradimère est faible ($-2J < 18$ cm^{-1}) et l'échange interdimère est encore plus faible ($-zJ' < 0{,}3$ cm^{-1}). On a caractérisé les complexes $[CuL3Cl]_x$ (**III**) et $[AgL3ClO_4]_x$ (**V**) par cristallographie par rayons X. Le composé **III** cristallise dans le système triclinique, groupe d'espace $P\bar{1}$, avec a = 9,410(2), b 10,291(2) et c = 9,208(2)Å, α = 108,56(1), β = 91,82(2) et γ = 68,04(1)°, V 780,1(2)Å^3 et $Z = 2$ (R = 0,035 et R_w = 0,031 pour 1856 réflexions). Le ligand agit comme un pont bidentate, S_2, entre des unités dinucléaires Cu_2Cl_2 dans un polymère bicaténaire. Le composé **III** cristallise dans le système monoclinique, groupe d'espace $P2_1/n$, avec a = 9,382(4), b = 19,274(4) et c = 10,190(3) Å, β = 106,35(3)°, V = 1768(1) Å^3 et $Z = 4$ (R = 0,036 et R_w = 0,029 pour 1776 réflexions). La structure consiste en une feuille polymérique bidimensionnelle impliquant des ions argent pseuduo-tétraédriques liés entre eux par des ligands *exo*-bidentates, S_2, et des perchlorates bidentates.

[Traduit par la rédaction]

Introduction

Numerous studies have been carried out on homoleptic thioether complexes of copper (1–11). The coordination chemistry of chelating ligands with built in thioether and azole groups (12), and macrocyclic ligands with thioether and amino, amido, pyridine, furan and thiophene subunits have also been explored (13–23).

Our interest in mixed sulfur–nitrogen ligands involving thioether and diazine linkages stems from our earlier studies on open chain tetradentate (N_4) thioether–pyridazine ligands (24–29), which involved non-coordinating thioether linkages and formed binuclear copper(II) complexes with, in some cases, positive (0 → +0.5 V vs. SCE) reduction potentials. The combination of pyridazine and thioether groups, suitably disposed for simultaneous coordination, might be expected to produce binuclear copper(II) complexes with more positive reduction potentials, due to the softer nature of the sulfur donors and their affinity for copper(I). Our initial studies in this area have involved the synthesis and structural and spectroscopic studies of a series of copper(II) and copper(I) complexes of two oligomeric macrocyclic thioether–pyridazine ligands (L1, L2, Fig. 1) (30). For the copper(II) complexes the ligands act as nitrogen (pyridazine) donors only, while for the copper(I) derivatives coordination appears to involve just the sulfur atoms. The present paper describes the copper and silver coordination chemistry of the simple 1:1 macrocyclic ligand L3

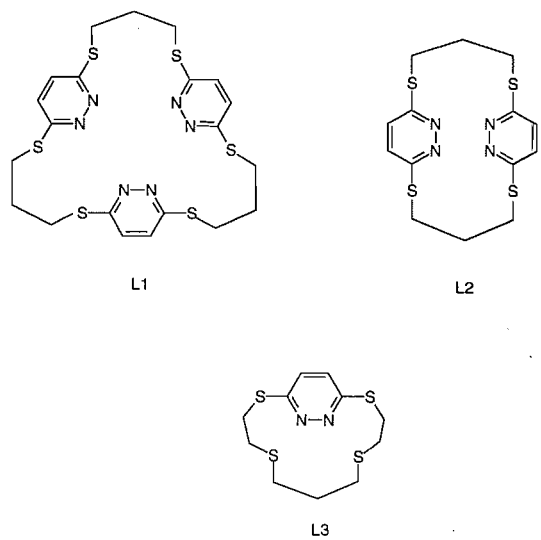

FIG. 1. Structural representation of the ligands.

[1]Author to whom correspondence may be addressed.

Can. J. Chem. Downloaded from www.nrcresearchpress.com by 109.225.110.28 on 09/08/12
For personal use only.

Can. J. Chem. Downloaded from www.nrcresearchpress.com by 109.225.110.28 on 09/08/12
For personal use only.

(Fig. 1), which produces unusual polymeric copper(I) and silver(I) derivatives.

Experimental section

Commercially available reagents (Aldrich) were used without further purification. Infrared spectra were recorded using a Mattson Polaris FT instrument and electronic spectra with a Cary 17 spectrometer. EPR spectra were recorded with a Bruker ESP 300 X-band spectrometer at room temperature and 77 K. Mass spectra were obtained using a VG Micromass 7070 HS spectrometer and nmr spectra using a GE 300 MHz instrument. X-ray diffraction data were collected using a Rigaku AFC6S instrument and room temperature magnetic susceptibility data were measured by the Faraday method using a Cahn 7600 magnetic susceptibility system. Variable temperature (5–300 K) magnetic data were obtained with an Oxford Instruments superconducting Faraday magnetometer with a Sartorius 4432 microbalance. A main solenoid field of 1.5 T and a gradient field of 10 T m^{-1} were employed. Elemental analyses were performed by Canadian Microanalytical Service, Delta, British Columbia, Canada.

Synthesis of ligand and complexes

Safety note

Perchlorate salts of metal complexes with organic ligands are potentially explosive. Only small amounts of material should be prepared and these should be handled with caution. The complexes described in this report have, so far, been found to be safe when used in small quantities.

L3

3,7-Dithianonane-1,9-diol (31) (5.70 g, 25.0 mmol) was added to anhydrous ethanol (100 mL) in which sodium metal (1.15 g, 50.0 mmol) had been dissolved, and the resulting solution was stirred for 30 min. 3,6-Dichloropyridazine (3.73 g, 25.0 mmol) was then dissolved in anhydrous ethanol (100 mL) and both solutions were added dropwise simultaneously to anhydrous ethanol (500 mL) by using pressure equalizing funnels, over a period of 6 h during which time a white precipitate formed. The mixture was stirred overnight and then filtered. The white solid was washed with ethanol and deionized water, dried *in vacuo*, and recrystallized from $CHCl_3$ to give white crystals. Yield 5.5 g (72%). MP 234–236°C. Mass spectrum, major mass peaks (*m/e* (relative intensity)) 304(20) P, 271(5), 202(8), 170(40), 133(100), 105(28), 41(42). ^1H nmr ($CDCl_3$) (δ (relative intensity)): 1.88(2) (multiplet, CH_2), 2.65(4) (multiplet, CH_2), 2.85(4) (multiplet, CH_2), 3.53(4) (multiplet, CH_2), 7.11(2) (singlet, pyridazine).

[CuL3Cl$_2$] (I) and [CuL3Br$_2$]$_2$ (II)

A solution of L3 (182 mg, 0.6 mmol) in $CHCl_3$ (20 mL) was added to a solution of $CuCl_2 \cdot 2H_2O$ (255.6 mg, 1.5 mmol) in MeOH (20 mL). The resulting solution was filtered and then refluxed for 20 min whereupon dark brown crystals formed. Yield 200 mg (76%). Anal. calcd. for $(C_{11}H_{16}N_2S_4CuCl_2)_2$: C 30.10, H 3.67, N 6.38; found: C 29.80, H 3.48, N 6.28. $[CuL3Br_2]_2$ (**II**) was prepared similarly by reaction of L3 with $CuBr_2$ and was obtained as dark brown crystals. Yield 210 mg (66%). Anal. calcd. for $(C_{11}H_{16}N_2S_4CuBr_2)_2$: C 25.02, H 3.05, N 5.31; found: C 24.98, H 3.00, N 5.29.

[CuL3Cl]$_x$ (III)

Cu powder (190.5 mg, 3.0 mmol) was added to a solution of $CuCl_2 \cdot 2H_2O$ (51.2 mg, 0.30 mmol) in CH_3CN (20 mL). The mixture was stirred for 6 h under N_2 and the resulting colourless solution filtered into a solution of L3 (91.2 mg, 0.3 mmol) in $CHCl_3$ (20 mL) under a nitrogen atmosphere. The pale yellow solution was left at room temperature overnight and colourless crystals formed. Yield 105 mg (87%). Anal. calcd. for $(C_{11}H_{16}N_2S_4CuCl)_x$: C 32.74, H 3.99, N 6.94; found: C 32.87, H 3.97, N 6.98.

[AgL3(ClO$_4$)]$_x$ (IV), [AgL3(ClO$_4$)]·CH$_3$CN (V) and [AgL3(NO$_3$)] (VI)

A solution of L3 (152 mg, 0.5 mmol) in $CHCl_3$ (20 mL) was added to a solution of $AgClO_4$ (250 mg, 1.2 mmol) in CH_3CN (20 mL). The combined solution was filtered and then allowed to stand at room temperature overnight. Colourless crystals formed which were filtered, washed with CH_3CN and $CHCl_3$, and dried in air. Yield 150 mg (63%). Anal. calcd. for $(C_{11}H_{16}N_2S_4AgClO_4)_x$: C 25.81, H 3.15, N 5.47; found: C 25.92, H 3.09, N 5.52. When the colourless crystals were kept in contact with the solution for several days they gradually become yellow crystals (**V**), which were found to contain one molecule of acetonitrile. Anal. calcd. for $(C_{11}H_{16}N_2S_4AgClO_4)\cdot CH_3CN$: C 28.24, H 3.46, N 7.60; found: C 28.06, H 3.35, N 7.53. $[AgL3(NO_3)]$ (**VI**) was prepared similarly by using $AgNO_3$ and obtained only as colourless crystals. Yield 127 mg (54%). Anal. calcd. for $C_{11}H_{16}N_2S_4AgNO_3$: C 27.85, H 3.40, N 8.86; found C 27.76, H 3.26, N 8.87.

X-ray crystallographic analysis of [CuL3Cl]$_x$ (III)

The diffraction intensities of a colourless parallelepiped crystal of $[CuL3Cl]_x$ of approximate dimensions 0.35 × 0.35 × 0.10 mm were collected using a Rigaku AFC6S diffractometer with graphite monochromatized MoKα radiation. Cell constants and the orientation matrix were obtained by the least squares refinement of the setting angles of 24 carefully centred reflections in the range $48.12° < 2\theta < 49.88°$. Based on a statistical analysis of the intensity distribution, and the successful solution and refinement of the structure, the space group was determined to be $P\bar{1}$. Machine and data collection parameters and crystal data are given in Table 1. The data were collected at 25 ± 1°C using the ω–2θ scan technique to a maximum 2θ value of 50.0°. Omega scans of several intense reflections, made prior to data collection, had an average width at half-height of 0.28° with a take-off angle of 6.0°. Scans of $(1.37 + 0.30 \tan\theta)°$ were made at a speed of 16.0°/min (in ω). The weak reflections ($I < 10.0\ \sigma(I)$) were rescanned (maximum of two rescans) and the counts were accumulated to assure good counting statistics. Stationary background counts were recorded on each side of the reflection. The ratio of peak counting time to background counting time was 2:1.

A total of 2932 reflections were collected. The intensities of three representative reflections, which were measured after every 150 reflections, remained constant during data collection (no decay correction applied). An empirical absorption correction was applied, using the program DIFABS (32), which resulted in transmission factors ranging from 0.75 to 1.36. The data were corrected for Lorentz and polarization effects.

The structure was solved by direct methods (33, 34). The non-hydrogen atoms were refined anisotropically. The final cycle of full-matrix least-squares refinement was based on 1856 observed reflections ($I > 3.00\ \sigma(I)$) and 173 variable parameters and converged with unweighted and weighted agreement factors of $R = \Sigma||F_o| - |F_c||/\Sigma|F_o| = 0.035$ and $R_w = [(\Sigma w(|F_o| - |F_c|)^2/\Sigma wF_o^2]^{1/2} = 0.031$. The standard deviation of an observation of unit weight was 1.63. The weighting scheme was based on counting statistics and included a factor ($p = 0.01$) to down weight the intense reflections. Plots of $\Sigma w(|F_o| - |F_c|)^2$ versus $|F_o|$, reflection order in data collection, $\sin\theta/\lambda$, and various classes of indices showed no unusual trends. The maximum and minimum peaks on the final difference Fourier map corresponded to 0.36 and −0.48 electrons/Å^3, respectively, and have no chemical significance. Neutral atom scattering factors (35) and anomalous dispersion terms (36, 37) were taken from the usual sources. All calculations were performed using the TEXSAN (38) crystallographic software package using a VAX 3100 workstation. Hydrogen atoms were located in a difference map but not refined. Thermal parameters were set at 1.2 times the isotropic thermal parameter of the bonded C atoms.

Atomic positional parameters are given in Table 2 and selected

TABLE 1. Summary of crystal data, intensity collection, and structure refinement for **III** and **IV**

Formula	**III** $C_{11}H_{16}CuClS_4N_2$	**IV** $C_{11}H_{16}AgClS_4N_2O_4$
Crystal colour (habit)	Colourless parallelepiped	Colourless, irregular
Formula weight	403.50	511.82
Crystal system	Triclinic	Monoclinic
Space group	$P\bar{1}$(No. 2)	$P2_1/n$(No. 14)
a (Å)	9.410(2)	9.382(4)
b (Å)	10.291(2)	19.274(4)
c (Å)	9.208(2)	10.190(3)
α (deg)	108.56(1)	—
β (deg)	91.82(2)	106.35(3)
γ (deg)	68.04(1)	—
Volume (Å^3)	780.1(2)	1768(1)
Density calcd. (g cm^{-3})	1.718	1.922
Z	2	4
Absorption coefficient, μ (cm^{-1})	20.78	17.52
Radiation, λ (Å)	0.71069	0.71069
Temperature (°C)	25	25
F_{000}	412	1024
Scan rate (deg min^{-1})	16.0	8.0
$2\theta_{max}$ (deg)	50.0	50.0
Data collected	2932	3419
Number of unique data ($I > 3.0\sigma(I)$)	1856	1776
Number of variables	173	208
Goodness of fit	1.63	1.34
R	0.035	0.036
R_w	0.031	0.029

bond distances and angles are given in Table 4. Thermal parameters (Table S-1), hydrogen atom parameters (Table S-2) a full listing of bond distances and angles (Table S-3) and observed and calculated structure factors ($10|F_o|$ and $10|F_c|$) (Table S-4) are deposited as supplementary material.[2]

*X-ray crystallographic analysis of [AgL3(ClO$_4$)]$_x$ (**IV**)*

The diffraction intensities of a colourless, irregular crystal of **V** of approximate dimensions 0.40 × 0.20 × 0.15 mm were collected in a similar manner to **III**. Crystal data, intensity collection and refinement details are summarized in Table 1. Atomic positional parameters are given in Table 3 and selected bond distances and angles are given in Table 5. Thermal parameters (Table S-5), hydrogen atom positional parameters (Table S-6), a full listing of bond distances and angles (Table S-7), and observed and calculated structure factors ($10|F_o|$ and $10|F_c|$) Table (S-8) are deposited as supplementary material.[2]

Results and discussion

The synthesis of L3 was achieved in high yield by a traditional high dilution cyclization reaction and no trace of any 30-membered macrocycle containing two pyridazine subunits was detected. The copper and silver complexes of L3 did not dissolve appreciably in any solvent and so were studied exclusively in the solid state.

[2]Supplementary Tables S-1 to S-8 may be purchased from: The Depository of Unpublished Data, Document Delivery, CISTI, National Research Council Canada, Ottawa, Canada K1A 0S2.

Tables S-2, S-3, S-6, and S-7 have also been deposited with the Cambridge Crystallographic Data Centre and can be obtained on request from The Director, Cambridge Crystallographic Data Centre, University Chemical Laboratory, 12 Union Road, Cambridge, CB2 1EZ, U.K.

TABLE 2. Positional parameters and B(eq) values (esd's) for [CuL3Cl]$_x$ (**III**)

Atom	x	Y	z	B(eq)
Cu(1)	0.49896(7)	0.46980(7)	0.83978(8)	3.17(4)
Cl(1)	0.3538(1)	0.4159(1)	0.9971(1)	2.97(7)
S(1)	0.6880(1)	0.2437(1)	0.6822(1)	2.60(7)
S(2)	1.3337(1)	0.0366(1)	0.9055(2)	2.82(7)
S(3)	1.3498(1)	−0.4200(1)	0.6789(1)	2.55(7)
S(4)	0.7373(1)	−0.2250(1)	0.5414(2)	3.19(8)
N(1)	0.9176(4)	0.0737(4)	0.7939(4)	2.4(2)
N(2)	1.0612(4)	0.0265(4)	0.8427(4)	2.4(2)
C(1)	0.8656(5)	0.1997(5)	0.7641(5)	2.1(3)
C(2)	0.9449(5)	0.2939(5)	0.7883(6)	2.7(3)
C(3)	1.0876(5)	0.2481(5)	0.8382(6)	2.6(3)
C(4)	1.1434(5)	0.1092(5)	0.8602(5)	2.1(3)
C(5)	1.3569(5)	−0.1527(5)	0.8800(5)	2.5(3)
C(6)	1.3667(5)	−0.2432(5)	0.7110(5)	2.6(3)
C(7)	1.1484(5)	−0.3598(5)	0.7441(6)	2.7(3)
C(8)	1.0415(5)	−0.3204(5)	0.6223(6)	2.7(3)
C(9)	0.8721(6)	−0.2636(5)	0.6818(6)	2.9(3)
C(10)	0.7397(5)	−0.0521(5)	0.5344(5)	2.6(3)
C(11)	0.6433(5)	0.0838(5)	0.6701(6)	2.8(3)

*Description of the structures of [CuL3Cl]$_x$ (**III**) and [AgL3(ClO$_4$)]$_x$ (**V**)*

The structure of [CuL3Cl]$_x$ (**III**) is illustrated in Figs. 2, 3. The overall structure is that on an infinite double stranded polymer with two *exo*-bidentate macrocyclic ligands bridging the dinuclear chloro-bridged copper groups. The ligands are bonded only by sulfur donor atoms and these include S1, which is attached to the pyridazine ring and S3.

Can. J. Chem. Downloaded from www.nrcresearchpress.com by 109.225.110.28 on 09/08/12
For personal use only.

Can. J. Chem. Downloaded from www.nrcresearchpress.com by 109.225.110.28 on 09/08/12
For personal use only.

TABLE 3. Positional parameters and B(eq) values (esd's) for $[AgL3(ClO_4)]_x$ (**IV**)

Atom	x	y	z	B(eq)
Ag(1)	0.91005(7)	0.20787(3)	0.40042(6)	3.66(3)
Cl(1)	0.0945(2)	0.1798(1)	0.7653(2)	3.09(8)
S(1)	0.7141(2)	0.11980(9)	0.3625(2)	2.27(7)
S(2)	0.6190(2)	0.24062(9)	0.8327(2)	2.78(7)
S(3)	0.6954(2)	0.0428(1)	1.0630(2)	3.8(1)
S(4)	0.7953(2)	−0.08963(9)	0.5422(2)	2.48(8)
O(1)	0.0490(7)	0.2315(3)	0.6624(5)	7.5(4)
O(2)	0.2501(6)	0.1783(3)	0.8193(8)	9.1(4)
O(3)	0.0452(6)	0.1132(3)	0.7133(5)	5.1(3)
O(4)	0.0312(7)	0.1958(3)	0.8721(6)	6.9(3)
N(1)	0.6515(6)	0.0272(3)	0.7952(5)	2.8(3)
N(2)	0.6731(6)	−0.0029(3)	0.6822(5)	2.5(2)
C(1)	0.5906(7)	0.1412(3)	0.4654(6)	2.3(3)
C(2)	0.6619(7)	0.1769(3)	0.6010(6)	2.6(3)
C(3)	0.5458(7)	0.1937(3)	0.6736(6)	2.5(3)
C(4)	0.7031(7)	0.1722(4)	0.9508(7)	3.1(3)
C(5)	0.5972(7)	0.1208(4)	0.9864(6)	3.0(3)
C(6)	0.7245(8)	0.0032(4)	0.9167(7)	2.9(3)
C(7)	0.823(1)	−0.0531(4)	0.9336(7)	4.4(4)
C(8)	0.8454(9)	−0.0820(4)	0.8211(7)	3.7(4)
C(9)	0.7676(7)	−0.0549(3)	0.6925(6)	2.3(3)
C(10)	0.7164(7)	−0.0211(3)	0.4210(6)	2.2(3)
C(11)	0.8114(6)	0.0434(3)	0.4487(6)	2.4(3)

TABLE 4. Selected bond distances (Å) and angles (deg) for $[CuL3Cl]_x$ (**III**)

Bond	Distance (Å)	Bonds	Angle (deg)
Cu(1)—Cl(1)	2.340(2)	Cl(1)—Cu(1)—Cl(1)	106.19(5)
Cu(1)—Cl(1)	2.350(1)	Cl(1)—Cu(1)—S(1)	108.41(5)
Cu(1)—S(1)	2.367(2)	Cl(1)—Cu(1)—S(3)	111.21(5)
Cu(1)—S(3)	2.280(1)	Cl(1)—Cu(1)—S(1)	102.90(5)
		Cl(1)—Cu(1)—S(3)	120.54(5)
		S(1)—Cu(1)—S(3)	106.84(5)

TABLE 5. Selected bond distances (Å) and angles (deg) for $[AgL3(ClO_4)]_x$ (**IV**)

Bond	Distance (Å)	Bonds	Angle (deg)
Ag(1)—S(1)	2.452(2)	S(1)—Ag(1)—S(2)	148.82(6)
Ag(1)—S(2)	2.463(2)	S(1)—Ag(1)—O(2)	101.0(1)
Ag(1)—O(1)	2.659(5)	S(1)—Ag(1)—O(1)	114.2(1)
Ag(1)—O(2)	2.655(6)	S(2)—Ag(1)—O(2)	90.2(1)
		S(2)—Ag(1)—O(1)	90.5(1)
		O(2)—Ag(1)—O(1)	104.2(2)

Each repeating unit of the polymer can be envisaged as a tetranuclear copper(I) entity, with the two ligands and the four coppers forming a most unusual metallocyclic arrangement. The copper atoms have a slightly distorted tetrahedral geometry with angles at copper in the range 102.90(5) to 120.54(5)°. The bond distances to sulfur (Cu1—S1 2.367(2) Å, Cu1—S3 2.280(1) Å) are within the range of other Cu(I) complexes of homoleptic thioether ligands (4, 5, 7, 9–11). The long Cu1—S1 bond may be associated with an inductive effect resulting from the proximity of S1 to the pyridazine ring. S1—C1 (1.772(4) Å) is significantly shorter than S3—C6 and S3—C7 (1.815(5) Å). The two copper chlorine distances are very similar (Cu1—Cl1 2.340(2), 2.350(1) Å) and can be compared with those in the polymeric complex $(C_3H_6S_3)_2$ $(CuCl)_3$ (2.30 to 2.413 Å) (39) which involves a canted $Cu_2S_4Cl_2$ dinuclear centre.

Homoleptic crown thioether complexes of silver(I) usually involve high coordination numbers. Examples include six-coordinate $[Ag([18]aneS_6)]^+$ (40) and $[Ag([9]aneS_3)_2]^+$ (41, 42), five-coordinate $[Ag_2L_2]^{2+}$ (L = 2,5,7,10-tetrathia[12](2,5)-thiophene) (43) and four-coordinate $[Ag_3([9]aneS_3)]^{3+}$ (44), $[Ag_2([15]aneS_5)_2]^{2+}$ (45), and $[Ag(16S6)]^+$ (16S6 = 1,3,6,9,11,14-hexathiacyclohexadecane) (46) species. Part of the structure of **IV** is illustrated in Fig. 4 and it involves a polymeric chain structure in which distorted tetrahedral silver(I) ions are bridged by *exo*-bidentate, macrocyclic ligands, that involve sulfur atoms S1 and S2 only as donors. The silver–sulfur distances (Ag1—S1 2.452(2) Å, Ag1—S2 2.463(2) Å) are about 0.1 Å shorter than those found in other Ag(I) thioether complexes with high coordination numbers (40–46), and about 0.1 Å longer than those in two-coordinate Ag(I) complexes (47, 48). Unlike the situation for **III**, where one thioether sulfur adjacent to the pyridazine ring was involved in coordination, only aliphatic thioether sulfurs act as donors in **IV**. The other two donor sites are provided by perchlorate oxygens (O1,O2) with relatively long silver oxygen bonds (Ag1—O1 2.659(5) Å, Ag1—O2 2.655(6) Å). However, the overall structure is most unusual and involves bidentate perchlorates, which cross link the polymeric S_2 chains with the formation of a 2-dimensional, polymeric sheet (Fig. 5). Bonded perchlorates involving silver thioether complexes are not common and in the case of the ligand cyclo(L-methionyl-L-methionyl) the distant silver–perchlorate contacts of 3.00 and 3.03 Å are questionable in terms of bonding interactions. Other silver–perchlorate bonds in, for example, isothiocyanate (49) and dimethyl sulfoxide (50) complexes of silver fall in the range 2.40–2.75 Å. The tetrahedral distortion at the silver ion is dominated by a large S1—Ag1—S2 angle of 148.82(6)°, with the smallest angle S2—Ag1—O1 of 90.5(1)°.

The coordination of L3 to both copper(I) and silver(I) by sulfur atoms only is clearly a reflection on the soft donor preferences of these ions. The exobidentate nature of the coordination of L3 to both copper(I) and silver(I) ions is consistent with the general trend for *exo*-dentate coordination observed for homoleptic, macrocyclic thioether complexes, which is related to the preferred "gauche" placement of the C—S linkages (51, 52). However, the incorporation of the rigid pyridazine subunit into the macrocycle sets ligands of this type apart from the symmetric, ethane bridged, homoleptic macrocyclic thioethers, and could lead to departures from the general trend of exodentate coordination. Molecular models indicate that L3 could encapsulate two metals acting as a tetradentate N_2S_2 ligand with endodentate aliphatic sulfur donors. Clearly more examples of structures of complexes of ligands of this sort are required to make reasonable comparisons with the aliphatic, macrocyclic thioethers.

Spectral and magnetic properties

The ligand L3 has an infrared absorption at 1568 cm^{-1}, associated with CN stretch in the pyridazine ring. A very

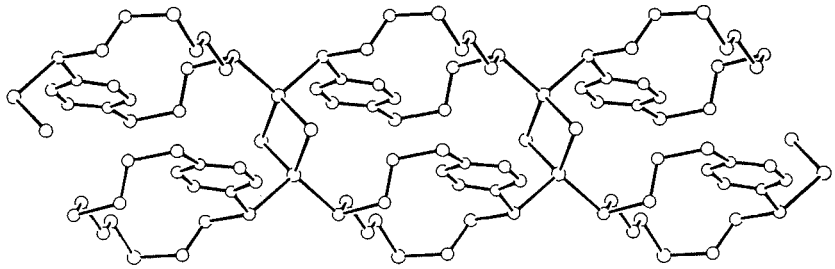

FIG. 2. Molecular structure of $[CuL3Cl]_x$ (**III**) illustrating the double stranded polymer.

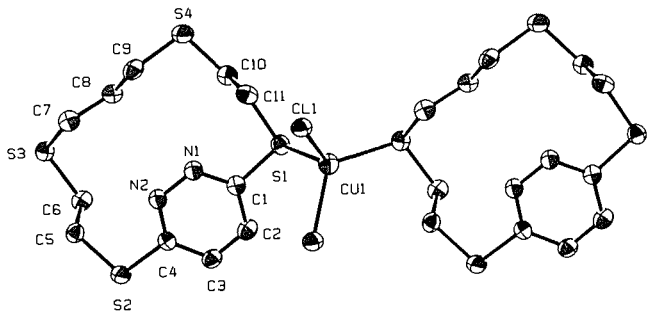

FIG. 3. Molecular structure of a fragment of $[CuL3Cl]_x$ (**III**).

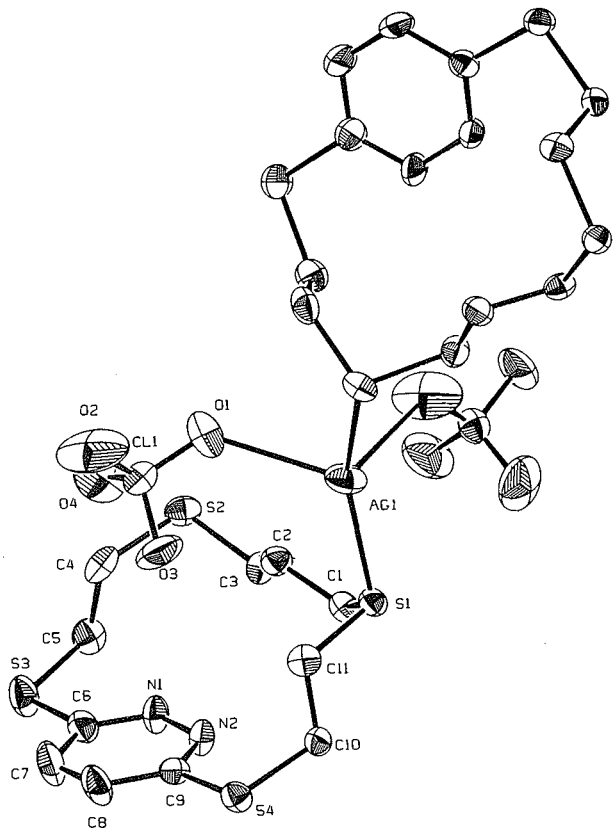

FIG. 4. Molecular structure of a fragment of $[AgL3(ClO_4)]_x$ (**IV**).

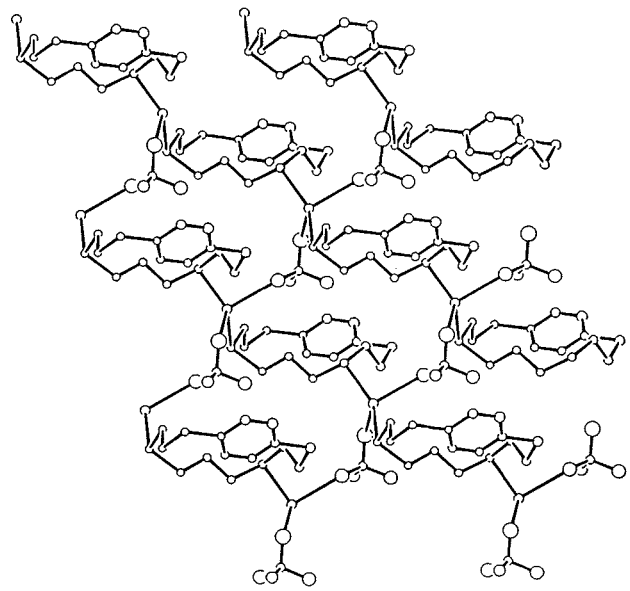

FIG. 5. Molecular structure of $[AgL3(ClO_4)]_x$ (**IV**) illustrating the 2-dimensional polymeric arrangement.

small shift is observed in this band by 7 cm^{-1} or less, in all the complexes (Table 6). The absence of pyridazine coordination in **III** and **IV** and the similarity in the position of this absorption in all the complexes suggests that pyridazine nitrogen atoms are not involved in coordination in the other complexes. Far infrared absorptions for **I** at 355 and 350 (sh) cm^{-1} are assigned to terminal copper–chlorine stretch, while bands at 280 and 260 cm^{-1} are assigned to bridging copper–chlorine bonds. Similar absorptions for **II** at 208 and 252 cm^{-1} are assigned to terminal copper–bromine stretch. In the range 4000–400 cm^{-1} the spectra of **I** and **II** are virtually identical, indicating structurally similar complexes.

The ν_3 perchlorate vibration for **IV** appeared as a strong, broad absorption centred at 1078 cm^{-1}, with little peak resolution. This might not have been anticipated based on the bidentate bridging nature of the perchlorate groups. A similar broad, strong absorption is observed for **V**. Overall the infrared spectra of **IV** and **V** are very similar, suggesting a similar structural arrangement. The presence of two CN stretching bands at 2293 and 2255 cm^{-1} suggests that the CH_3CN occupies a lattice position only and is not coordinated to silver. The nitrate complex **VI** has an overall infrared spectrum similar to the perchlorate complex, and in the nitrate combination band region an expanded spectrum reveals four bands at 1748, 1741, 1738, and 1731 cm^{-1}. The fairly narrow range of this group of bands (17 cm^{-1}) is probably indicative of two slightly different monodentate nitrate groups (53). Structurally **VI** maybe similar to **IV** with a polymeric exobidentate ligand bridging the Ag(I) ions,

Can. J. Chem. Downloaded from www.nrcresearchpress.com by 109.225.110.28 on 09/08/12
For personal use only.

TABLE 6. Spectral and magnetic data[a]

Compound	IR (cm^{-1})	μ_{eff} (RT) (BM)	UV/VIS[b] (cm^{-1})	Magnetic data[c]
$[CuL3Cl_2]_2$ (**I**)	1562 (νCN), 355, [350], 280, 260	1.74	[29400], 20400, [17900]	$g = 2.061(3)$, $-2J = 17.77(7)$ cm^{-1}, $zJ' = -0.51(5)$ cm^{-1}, $\rho = 0.045$, $10^2R = 1.1$
$[CuL3Br_2]_2$ (**II**)	1563 (νCN), 268, 252	1.83	28600, 19000, [15900]	$g = 2.010(2)$, $-2J = 8.56(6)$ cm^{-1}, $zJ' = -0.28(5)$ cm^{-1}, $\rho = 0.025$, $10^2R = 0.42$
$[CuL3Cl]_x$ (**III**)	1562 (νCN)	—	—	
$[AgL3(ClO_4)]_x$ (**IV**)	1564 (νCN), 1078 (νClO_4)	—	—	
$AgL3(ClO_4) \cdot CH_3CN$ (**V**)	2293, 2253 (νCH_3CN), 1562 (νCN), 1072 (νClO_4)	—	—	
$AgL3(NO_3)$ (**VI**)	1562 (νCN), 1748, 1742, 1738, 1731 (νNO_3)	—	—	

[a][ ]Shoulder.
[b]Mull transmittance.
[c]ρ fraction paramagnetic impurity; $R = \{\Sigma(\chi_{obs} - \chi_{calc})^2/\Sigma(\chi_{obs})^2\}^{1/2}$; $N\alpha = 60 \times 10^{-6}$ cgsu.

which are three coordinate with coordinated, monodentate nitrate.

Compounds **I**, **II** are dark brown in colour and are insoluble in common solvents. Solution can be effected in strong donor solvents like DMF, but decomposition occurs with the release of the ligand. Consequently the electronic spectra of **I** and **II** were only examined in the solid state as mulls. Intense high energy absorptions were observed in both cases (Table 6), which are clearly associated with charge transfer, rather than *d–d* transitions. Infrared data indicate that the ligand does not involve pyridazine–nitrogen coordination and that both complexes contain terminal and bridging halogen ligands. A reasonably structural suggestion for **I** and **II** would be a square-pyramidal dihalogen bridged dimer with L3 behaving as a bidentate S_2 donor in the square-pyramidal basal plane, with an axially bound halogen. The intense visible absorptions at 20 400 cm^{-1} (**I**) and 19 000 cm^{-1} (**II**) are associated with halogen to metal charge transfer because of their difference in energy, while the higher energy bands are likely to be associated with $\sigma S \rightarrow Cu$ charge transfer. A comparable ligand, 2,5,9,12-tetrathia[13]-(2,5)-thiophenophane (L), which involves the same S_4 thioether fragment bound to the 2- and 5-positions of a thiophene ring, formed a dinuclear, dichloro-bridged, square-pyramidal complex $[LCuCl_2]_2$ involving bidentate chelating S_2 ligands (54). Similar, intense visible and ultraviolet bands for this, and related complexes, were assigned to charge transfer transitions associated with the sulfur and chlorine donor atoms.

Magnetic moments for **I** and **II**, measured at room temperature (Table 6), exceed the spin only value for copper and do not give any clear indication of spin coupling and support for the proposed dimeric structures. Variable temperature magnetic measurements were therefore carried out on both **I** and **II** in the temperature range 4.5–300 K. Susceptibility/temperature profiles are both similar (see Fig. 6 for **I**) with a pronounced susceptibility maximum at low temperatures ($T_N \sim 18$ K for **I**; $T_N \sim 8$ K for **II**). Such behaviour is typical of weakly antiferromagnetically coupled copper(II) dimers, thus supporting the dimeric structures for **I** and **II**.

Magnetic interactions between copper(II) centres in isolated dinuclear species are described by the Bleaney–Bowers expression (eq. [1]) (55)

$$[1] \quad \chi_M = \frac{N\beta^2 g^2}{3k(T-\theta)}[1 + (1/3)\exp(-2J/kT)]^{-1} + N\alpha$$

using the isotropic (Heisenberg) exchange Hamiltonian ($H = -2J\mathbf{s}_1 \cdot \mathbf{s}_2$) ($\chi_M$ is expressed per mole of copper atoms and $N\alpha$ is the temperature-independent paramagnetism). Interdimer exchange can be accounted for by the inclusion of a Weiss-type correction (θ) (56). A non-linear regression analysis (57) of the magnetic data for **I** and **II** using eq. [1] indicated the presence of weak intradimer antiferromagnetic coupling ($-2J < 16$ cm^{-1} (**I**); $-2J < 5$ cm^{-1} (**II**)), but also significant interdimer exchange as well ($\theta \sim -5$ K). For weakly coupled copper(II) dimers where the singlet–triplet splitting is comparable with the Zeeman energy, $g\beta H$, the magnetization expression (eqs. [2], [3]) is considered to be more appropriate (58, 59).

Equation [2] can be corrected, in the molecular field approximation, for the presence of magnetic interactions between neighbouring dimers (eq. 4),

$$[2] \quad M = \frac{Ng\beta \sinh(g\beta H/kT}{\exp(-2J/kT) + 2\cosh(g\beta H/kT) + 1}$$

$$[3] \quad \chi_M = M/H + N\alpha$$

where z is the

$$\chi'_{Cu} = \frac{\chi_{Cu}}{1 - (2zJ'\chi_{Cu}/Ng^2\beta^2)}$$

number of nearest neighbor dimers and J' the interdimer exchange parameter. The variable temperature susceptibility data for **I** and **II** were fitted to an equation which combined eqs [2], [3], and [4] and was corrected for the presence of simple Curie law paramagnetic impurity components. The results are given in Table 6. Both compounds show weak intradimer antiferromagnetic coupling ($-2J = 17.77(7)$ cm^{-1} (**I**); $-2J = 8.08(4)$ cm^{-1} (**II**)). Very weak interdimer antiferromagnetic coupling is also apparent ($zJ' = -0.51(1)$ cm^{-1} (**I**); $zJ' = -0.29(1)$ cm^{-1} (**II**)), but because no structural details are available for these compounds little can be said concerning the mechanism of this exchange component, or how many dimers are involved. Comparable values of g and $-2J$ were obtained from both methods of data fit-

Can. J. Chem. Downloaded from www.nrcresearchpress.com by 109.225.110.28 on 09/08/12
For personal use only.

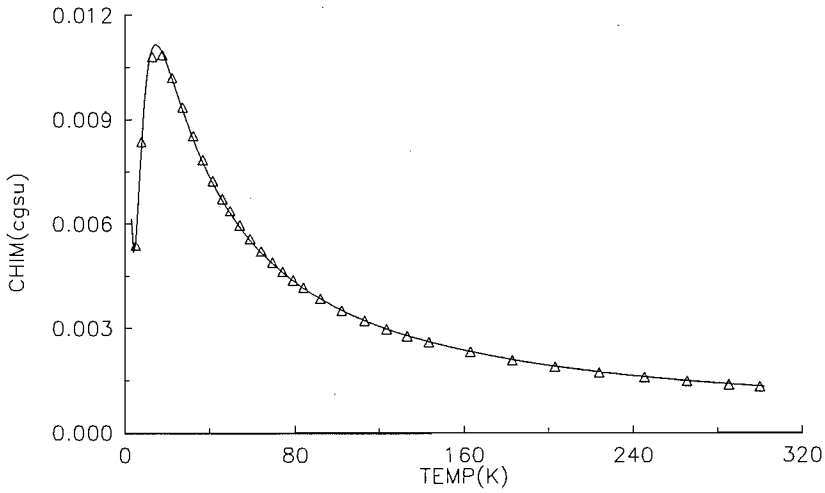

FIG. 6. Variable temperature magnetic data for $[CuL3Cl_2]_2$ (**I**). The solid line was calculated from eqs. [2], [3], [4] with $g = 2.061(3)$, $-2J = 17.77(7)$ cm^{-1}, $zJ' = -0.51(5)$ cm^{-1}, $\rho = 0.045$.

ting, but since lower residual factors were obtained with the magnetization equation, combined with the inherent problems of using the Bleaney–Bowers fit for weakly coupled copper(II) dimers, a more confident assessment of the exchange situation can be realised by the use of eqs. [2], [3], and [4]. Small amounts of Curie law paramagnetic impurities were necessary for reasonable data fits and these show up in the solid state EPR spectra of **I** and **II**. No half-field EPR transitions were observed that sometimes typify weakly coupled dinuclear copper(II) complexes. The experimental data and the theoretical line for **I**, calculated using eqs. [2], [3], and [4] for $g = 2.061(3)$, $-2J = 17.77(7)$ cm^{-1}, $zJ' = -0.51(5)$ cm^{-1}, $\rho = 0.045$ are shown in Fig. 6.

Weak antiferromagnetic coupling is typical for halogen bridged dimeric copper(II) complexes and in the case of dichloro-bridged square-pyramidal, $[LCuCl_2]_2$ (S_2) (54) and octahedral $[L'CuCl_2]_2$ (S_3) (54) complexes of some thiophenophane ligands $-2J$ values of 20.8 and 7.4 cm^{-1} are found for Cu—Cl—Cu bridge angles of 90.94° and 86.87°, respectively (22). The magnetic properties of **I** and **II** are therefore consistent with dimeric halogen bridged structures. The smaller exchange integral for the bromo-complex(II) would not be anticipated if **I** and **II** had similar structures, with comparable bridge angles, because of the demonstrated ability of bridging and terminal halogen ligands to modify exchange based on their electron polarizing effects (60, 61). On this basis a somewhat smaller bridge angle might be anticipated for **II**.

Acknowledgements

We thank the Natural Sciences and Engineering Research Council of Canada for financial support for this study, and for funds to purchase the Rigaku AFC6S X-ray diffractometer.

1. T. E. Jones, L. A. Ochrymowycz, and D. B. Rorabacher. J. Am. Chem. Soc. **98**, 4322 (1976).
2. M. D. Glick, D. P. Gravel, L. L. Diaddario Jr., and D. B. Rorabacher. Inorg. Chem. **15**, 1190 (1976).
3. E. R. Dockal, L. L. Diaddario Jr., M. D. Glick, and D. B. Rorabacher. J. Am. Chem. Soc. **99**, 4530 (1977).
4. P. W. R. Corfield, C. Ceccarelli, M. D. Glick, I. W-Y. Moy, L. A. Ochrymowycz, and D. B. Rorabacher. J. Am. Chem. Soc. **107**, 2399 (1985).
5. L. L. Diaddario Jr., E. R. Dockal, M. D. Glick, L. A. Ochrymowycz, and D. B. Rorabacher. Inorg. Chem. **24**, 356 (1985).
6. V. B. Pett, L. L. Diaddario Jr., P. W. Corfield, C. Ceccarelli, M. D. Glick, L. A. Ochrymowycz, and D. B. Rorabacher. Inorg. Chem. **22**, 3661 (1983).
7. J. R. Hartman and S. R. Cooper. J. Am. Chem. Soc. **108**, 1202 (1986).
8. S. C. Rowle, G. A. Admans, and S. R. Cooper. J. Chem. Soc. Dalton Trans. 93 (1988).
9. C. R. Lucas, S. Liu, M. J. Newlands, J-P. Charland, and E. J. Gabe. Can. J. Chem. **66**, 1506 (1988).
10. B. De Groot and S. J. Loeb. Inorg. Chem. **28**, 3573 (1989).
11. A. J. Blake, A. Taylor, and M. Schröder. Polyhedron, **9**, 2911 (1990).
12. E. Bouwman, W. L. Driessen, and J. Reedjik. Coord. Chem. Rev. **104**, 143 (1990).
13. N. Atkinson, A. J. Blake, M. G. B. Drew, G. Forsyth, A. J. Lavery, G. Reid, and M. Schröder. J. Chem. Soc. Chem. Commun. 984 (1989).
14. P. D. Beer, J. E. Nation, S. L. W. McWhinnie, M. E. Harman, M. B. Hursthouse, M. I. Ogden, and A. H. White. J. Chem. Soc. Dalton Trans. 2485 (1991).
15. A. J. Blake, G. Reid, and M. Schröder. J. Chem. Soc. Dalton Trans. 615 (1991).
16. E. Kimura, Y. Kurogi, T. Tojo, M. Shionoya, and M. Shiro. J. Am. Chem. Soc. **113**, 4857 (1991).
17. I. M. Helps, K. E. Matthes, D. Parker, and G. Ferguson. J. Chem. Soc. Dalton Trans. 915 (1989).
18. E. Weber and F. Vögtle. Liebigs Ann. Chem. 891 (1976).
19. J. S. Bradshaw and J. Y. K. Hui. J. Heterocycl. Chem. **11**, 649 (1974).
20. G. R. Newkome, J. D. Sauer, J. M. Roper, and D. C. Hager. Chem. Rev. **77**, 513 (1977).
21. C. R. Lucas, S. Liu, and M. J. Newlands. Can. J. Chem. **67**, 639 (1989).
22. C. R. Lucas, S. Liu, and L. K. Thompson. Inorg. Chem. **29**, 85 (1990).
23. M. M. Bernardo, M. J. Hegg, R. R. Schroeder, L. A. Ochrymowycz, and D. B. Rorabacher. Inorg. Chem. **31**, 191 (1992).
24. S. K. Mandal, L. K. Thompson, E. J. Gabe, J-P. Charland, and F. L. Lee. Inorg. Chem. **27**, 855 (1988).

Can. J. Chem. Downloaded from www.nrcresearchpress.com by 109.225.110.28 on 09/08/12
For personal use only.

25. L. K. Thompson, S. K. Mandal, J-P. Charland, and E. J. Gabe. Can. J. Chem. **66**, 348 (1988).
26. L. K. Thompson, S. K. Mandal, L. Rosenberg, F. L. Lee, and E. J. Gabe. Inorg. Chim. Acta, **133**, 81 (1987).
27. S. K. Mandal, L. K. Thompson, E. J. Gabe, F. L. Lee, and J-P. Charland. Inorg. Chem. **26**, 2384 (1987).
28. T. C. Woon, R. McDonald, S. K. Mandal, L. K. Thompson, S. P. Connors, and A. W. Addison. J. Chem. Soc. Dalton Trans. 2381 (1986).
29. S. K. Mandal, L. K. Thompson, M. J. Newlands, F. L. Lee, Y. LePage, J-P. Charland, and E. J. Gabe. Inorg. Chim. Acta, **122**, 199 (1986).
30. L. Chen, L. K. Thompson, and J. N. Bridson. Can. J. Chem. **70**, 1886 (1992).
31. E. Vedejs. Org. Synth. 150 (1987).
32. N. Walker and D. Stuart. Acta. Crystallogr. Sect. A: Found. Crystallogr. **A39**, 158 (1983).
33. C. J. Gilmore. J. Appl. Crystallogr. **17**, 42 (1984).
34. P. T. Beurskens. DIRDIF: Technical Report 1984/1, Crystallography Laboratory, Toernooiveld, 6525 Ed Nijmegen, Netherlands.
35. D. T. Cromer and J. T. Waber. International tables for X-ray crystallography. Vol. IV. The Kynoch Press, Birmingham, United Kingdom. 1974. Table 2.2A.
36. J. A. Ibers and W. C. Hamilton. Acta Crystallogr. **17**, 781 (1974).
37. D. T. Cromer. International tables for X-ray crystallography. Vol. IV. The Kynoch Press, Birmingham, United Kingdom. 1974. Table 2.3.1.
38. Texsan-Texray Structure Analysis Package, Molecular Structure Corporation, 1985.
39. A. Domenicano, R. Spagna, and A. Vaciago. J. Chem. Soc. Chem. Commun. 1291 (1968).
40. A. J. Blake, R. O. Gould, A. J. Holder, T. L. Hyde, and M. Schröder. Polyhedron, **8**, 513 (1989).
41. J. A. Clarkson, R. Yagabason, P. T. Blower, and S. R. Cooper. J. Chem. Soc. Chem. Commun. 950 (1987).
42. P. T. Blower, J. A. Clarkson, S. C. Rawle, J. R. Hartman, R. E. Wolf, R. Yagbason, S. G. Bott, and S. R. Cooper. Inorg. Chem. **28**, 4040 (1989).
43. C. R. Lucas, S. Liu, M. J. Newlands, J.-P. Charland, and E. J. Gabe. Can. J. Chem. **68**, 644 (1990).
44. H-J. Küppers, K. Wieghardt, Y. H. Tsay, C. Kruger, P. Nuber, and J. Weiss. Angew. Chem. Int. Ed. Engl. **26**, 575 (1987).
45. A. J. Blake, R. O. Gould, G. Reid, and M. J. Schröder. J. Chem. Soc. Chem. Commun. 974 (1990).
46. B. De Groot and S. J. Loeb. Inorg. Chem. **30**, 3103 (1991).
47. Y. Kojima, T. Yamashita, Y. Ishino, T. Hirashima, and K. Hirotsu. Chem. Lett. 453 (1983).
48. I. G. Dance, L. J. Fitzpatrick, A. D. Rae, and M. L. Scudder. Inorg. Chem. **22**, 3785 (1983).
49. A. Guitard, A. Mari, A. L. Beauchamp, Y. Dartiguenave, and M. Dartiguenave. Inorg. Chem. **22**, 1603 (1983).
50. N-O. Björk and A. Cassel. Acta Chem. Scand. **A30**, 235 (1976).
51. R. E. Wolf, Jr., J. R. Hartman, J. M. E. Storey, B. M. Foxman, and S. R. Cooper. J. Am. Chem. Soc. **109**, 4328 (1987).
52. S. R. Cooper. Acc. Chem. Res. **21**, 141 (1988).
53. A. B. P. Lever, E. Mantovani, and B. S. Ramaswamy. Can. J. Chem. **49**, 1957 (1971).
54. C. R. Lucas, S. Liu, M. J. Newlands, J-P. Charland, and E. J. Gabe. Can. J. Chem. **67**, 639 (1989).
55. B. Bleaney and K. D. Bowers. Proc. R. Soc. London, A, **214**, 451 (1952).
56. K. T. McGregor, J. A. Barnes, and W. E. Hatfield, J. Am. Chem. Soc. **95**, 7993 (1973).
57. R. G. Duggleby. Anal. Biochem. **110**, 9 (1981).
58. B. E. Myers, L. Berger, and S. A. Friedberg. J. Appl. Phys. **40**, 1149 (1969).
59. W. E. March, K. C. Patel, W. E. Hatfield, and D. J. Hodgson. Inorg. Chem. **22**, 511 (1983).
60. S. K. Mandal, L. K. Thompson, M. J. Newlands, E. J. Gabe, and K. Nag. Inorg. Chem. **29**, 1324 (1990).
61. L. K. Thompson, S. K. Mandal, J-P. Charland, and E. J. Gabe. Can. J. Chem. **66**, 348 (1988).

Can. J. Chem. Downloaded from www.nrcresearchpress.com by 109.225.110.28 on 09/08/12
For personal use only.

FT-infrared study of the interaction between all-*trans* retinylidene isopropylamine and model proton donors

P. MIGCHELS AND TH. ZEEGERS-HUYSKENS[1]

Department of Chemistry, University of Leuven, Celestijnenlaan 200F, B-3001 Heverlee, Belgium

Received March 10, 1992

P. MIGCHELS and TH. ZEEGERS-HUYSKENS. Can. J. Chem. **70**, 2717 (1992).

The interaction between all-*trans* retinylidene isopropylamine (*t*RiPA) and phenols covering a large pK_a domain is investigated by FT-infrared spectrometry. For phenols having pK_a between 10.2 and 8.18, only normal OH...N hydrogen bonds are formed. The thermodynamic parameters (K, $-\Delta H$, $-\Delta S^0$) determined in carbon tetrachloride solution show that *t*RiPA possesses a good proton acceptor ability. The spectral characteristics (frequency and integrated intensity) of the $\nu_{C=N}$ vibration are also investigated. From a pK_a of 6, proton transfer takes place. The proton transfer constants determined in 1,2-dichloroethane are linearly related to ΔpK_a (pK_a of the protonated base minus pK_a of the phenol). Comparison with previously studied imine systems shows that the proton transfer constant increases with the number of C=C double bonds in the base.

P. MIGCHELS et TH. ZEEGERS-HUYSKENS. Can. J. Chem. **70**, 2717 (1992).

L'interaction entre la toute-*trans* retinylidène isopropylamine (*t*RiPA) et des phénols couvrant un large domaine de pK_a est étudiée par spectrométrie infrarouge à transformée de Fourier Pour les phénols caractérisés par des pK_a variant de 10.20 à 8.18, seuls les complexes à liaison hydrogène normale OH...N sont formés. Les paramètres thermodynamiques (K, $-\Delta H$, $-\Delta S^0$), déterminés dans la tétrachlorure de carbone, montrent que la *t*RiPA possède un bon pouvoir accepteur de proton. Les caractéristiques spectrales de la vibration $\nu_{C=N}$ (fréquence, intensité intégrée) sont aussi étudiées. À partir d'un pK_a de 6, il y a formation de complexes par transfert de proton. Les constantes de transfert déterminées dans le 1,2-dichloroéthane sont linéairement correlées aux ΔpK_a (pK_a de la base protonée moins pK_a du phénol). La comparaison avec des systèmes d'imine étudiés antérieurement montre que la constante de transfert augmente avec le nombre de doubles liaisons présentes dans la base.

Can. J. Chem. Downloaded from www.nrcresearchpress.com by 109.225.110.28 on 09/08/12
For personal use only.

Introduction

In the light transduction mechanisms of both rhodopsin and bacteriorhodopsin, the bond between the retinal Schiff base nitrogen and a proton donor group in the opsin deserves particular attention and it is essential to know if the Schiff base is initially protonated or not (see, for example, ref. 1). Although resonance Raman spectra of rhodopsine indicate that the N atom is protonated (2–6), ^{13}C NMR (7) and differential kinetic IR measurements (8) oppose this view. Both extreme views can be reconciled by admitting a strong hydrogen bond with a double minimum potential function (9–15). This is in agreement with *ab initio* calculations (16, 17) on retinal chromophore modelling systems such as the alkylimine – formic acid system. It is thus essential to know the shape of the potential function governing the proton motion. In this work, the interaction between *trans* retinylidene isopropylamine (*t*RiPA) and phenol derivatives covering a large pK_a range (10.20–0.5) is investigated by FT-infrared spectroscopy.

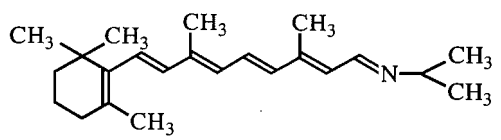

(*t*RiPA)

The phenols have been chosen as proton donors because they can serve as models for tyrosine (18) and, in this large pK_a domain, the following equilibria can be studied:

$$C{=}N + HO \overset{K_{HB}}{\rightleftharpoons} C{=}N...HO \overset{K_{PT}}{\rightleftharpoons} C{=}N\text{-}H^+...O^-$$

where K_{HB} refers to normal hydrogen bonds and K_{PT} to proton transfer complexes. There are some literature data on the interaction between *trans* retinylidene isobutylamine (*t*RiBu) and phenols. Kristoforov *et al.* have shown that *t*RiBu forms normal hydrogen bonds with *p*-cresol and that proton transfer complexes can be detected in excess of proton donor. The proton transfer equilibria have been studied in carbon tetrachloride for some phenol–*t*RiBu systems by Rastogi and Zundel (20). In methylcyclohexane, the ΔG^0_{PT} values at 295 K vary from +10.5 to 13.5 kJ mol^{-1} (K_{PT} from 0.013 to 0.004) and are not correlated with the pK_a of the proton donors (21). There seems, however, to exist a correlation between the enthalpies and entropies for the proton transfer processes and the proton donor ability of the phenols (20). In a recent work, the thermodynamic constants for hydrogen bonding and proton transfer were extensively discussed for the phenol–*t*RiBu system (22).

This literature overview shows that there is no systematic study on hydrogen bonding between retinal Schiff bases and phenols. Furthermore, the proton transfer constants are not always reliable. The present study was undertaken in order to investigate systematically the influence of the proton donor acidity on the K_{HB} and on the K_{PT} values, to discuss the characteristics of the $\nu_{C=N}$ vibration, and to establish the influence of the number of C=C bonds on the proton transfer constants.

Experimental

The infrared spectra were recorded on the Perkin Elmer 883 and on the Bruker FT-IR 88 spectrophotometers. The formation constants K were determined in carbon tetrachloride from the absorbance of the ν_{OH} stretching vibration at concentrations of proton donors ranging from 5 to 8 × 10^{-3} mol L^{-1}. The base was in excess. The proton transfer constants K_{PT} were determined in 1,2-dichloroethane from the intensity of the $\nu_{C=N}$ band. The intensity of the $\nu_{C=N\text{-}H^+}$ band of *t*RiPA picrate observed at 1651 cm^{-1}, where 100% proton transfer was supposed to occur, was taken as refer-

[1]Author to whom correspondence may be addressed.

TABLE 1. Equilibrium constants, enthalpies, and entropies of complex formation for the interaction between *t*RiPA and phenols. Solvent = carbon tetrachloride

Phenols[a]	K^{298K} (L mol^{-1})	K^{323K} (L mol^{-1})	$-\Delta H^b$ (kJ mol^{-1})	$-\Delta S^0$ (J mol^{-1} K^{-1})
4-CH_3O phenol (10.21)	78	32	27	55
Phenol (9.95)	98	42	28	55
4-Br phenol (9.34)	285	105	31	58
3-Br phenol (9.03)	360	115	33	62
3,4-Dichlorophenol (8.58)	725	230	35	63
3,5-Dichlorophenol (8.18)	1070	335	37	66

[a]The pK_a of the phenols are indicated in parentheses.
[b]Calculated from the K values computed from the least-squares correlations of log K vs. pK_a.

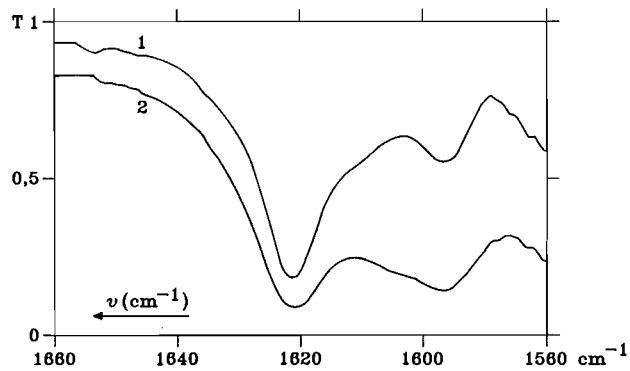

FIG. 1. FT–infrared spectra (1660–1580 cm^{-1}) of 1 *t*RiPA (c = 0.032 mol L^{-1}); 2 *t*RiPA (c = 0.032 mol L^{-1}) and 3,4-dichlorophenol (c = 0.034 mol L^{-1}). Solvent = carbon tetrachloride. Cell thickness = 0.1 cm.

ence. The total concentration of complexes was calculated from the intensity of the ν_{OH} stretching vibration in the same solvents.

*t*RiPA was synthesized by condensation of isopropylamine and all-*trans* retinal (19). The product was held at 5°C, in the dark and under nitrogen atmosphere. The solvents and the phenols were carefully dried and purified by the standard methods.

Results and discussion

1. Normal hydrogen bonds

For phenols having pK_a between 10.20 and 8.18, only one band at 1620–1621 cm^{-1} was observed. This suggests that only normal hydrogen bonds are formed. The thermodynamic parameters (K, $-\Delta H$, $-\Delta S^0$) determined in carbon tetrachloride solution are listed in Table 1.

The logarithms of the formation constants are linearly related to the pK_a of the proton donors:

$$\log K^{298K} = 7.80 - 0.58\ pK_a\ (r = 0.996)$$

$$\log K^{323K} = 6.72 - 0.51\ pK_a\ (r = 0.995)$$

It must be pointed out here that the thermodynamic data for the interaction between the *n*-butylamine retinal Schiff base and phenols having pK_a between 6 and 8 were measured in methylcyclohexane. The ΔG^0 values at 295 K vary from -8.7 to -13 kJ mol^{-1} (K_{HB} from 35 to 200 L mol^{-1}) but are not correlated to the acidity of the proton donors (21). The lowest value is obtained for the 2,4,6-trichlorophenol complex (K = 35 L mol^{-1}, pK_a = 6) and the highest one for the 2,4,5-trichlorophenol complex (K = 200 L mol^{-1}, pK_a = 6.72), the weakest proton donor 2,4-dichlorophenol (pK_a = 6.0) being characterized by a stability constant of 92 L mol^{-1}. These data were obtained in methylcyclohexane.

The thermodynamic data reported in Table 1 show that *t*RiPA possesses a good proton acceptor ability. The equilibrium constants have been recently reported for systems involving the same proton donors and other Schiff bases such as isobutylidene isopropylamine (iBiPA) (23), 2,4-hexadienylidene isopropylamine (HiPA) (24), and *trans*-butenylidene isopropylamine (*t*BiPA) (25). The K values are markedly higher for the *t*RiPA than for the iBiPA complexes where the Schiff base has no C=C double bond. There is, however, no systematic correlation between the thermodynamic data and the number of C=C double bonds.

The $\nu_{OH...N}$ band is broad and characterized by several submaxima. These spectroscopic features have also been

TABLE 2. Wavenumbers, integrated intensity (A), intensification factor (A^c/A^f), and dipole moment derivative ($\partial\mu/\partial Q$) of the $\nu_{C=N}$ vibration of *t*RiPA complexed with phenols. Solvent = carbon tetrachloride

Phenol	$\nu_{C=N}$ (cm^{-1})	A^a (L mol^{-1} cm^{-2})	A^c/A^f	$\pm\partial\mu/\partial Q$ (esu amu$^{-1/2}$)
None	1620	7250	—	101.6
4-CH_3O phenol	1621	8550	1.18	119.9
Phenol	1621	9710	1.34	136.1
4-Br phenol	1620	10150	1.40	142.2
3,4-Dichlorophenol	1620	10730	1.48	150.4
3,5-Dichlorophenol	1620	11140	1.52	156.2

[a]Integration limits: 1670–1575 cm^{-1}.

Can. J. Chem. Downloaded from www.nrcresearchpress.com by 109.225.110.28 on 09/08/12
For personal use only.

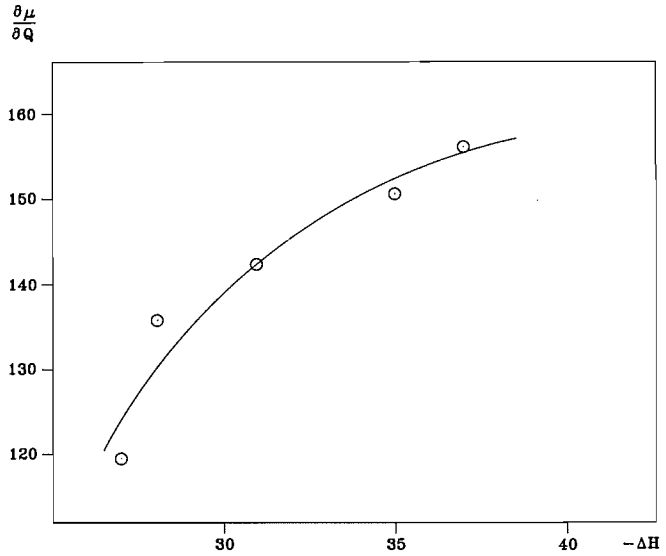

FIG. 2. $\partial\mu/\partial Q$ (esu amu$^{-1/2}$) as a function of $-\Delta H$ (kJ mol^{-1}).

observed for other complexed Schiff bases (22). Owing to the overlapping with the strong ν_{CH_3} and ν_{CH} bands, the maximum could not be estimated with precision. For the *t*RiPa–phenol complex, the maximum was localized at 3050 ± 50 cm^{-1}.

Characteristics of the $\nu_{C=N}$ vibration

The $\nu_{C=N}$ vibration is observed at 1620 cm^{-1} in carbon tetrachloride. As shown in Fig. 1, the frequency of this vibration is very insensitive to hydrogen bond formation. The $\nu_{C=N}$ band is indeed observed at 1621 cm^{-1} in the phenol complex and at 1620 cm^{-1} in the 3,4-dichlorophenol complex. A broadening of the band can be observed. This behaviour is in complete contrast with the $\nu_{C=O}$ vibration, which is shifted to lower frequencies by about 10–25 cm^{-1}. The insensitivity of the $\nu_{C=N}$ vibration to normal hydrogen bond formation has been explained by the fact that the perturbation induced by the formation of the bond is transmitted to the terminal group implanted on the double bond rather than on the double bond itself (23).

The integrated intensity (A) of the $\nu_{C=N}$ band in free *t*RiPA (A^f) and in some complexes (A^c) was obtained by deconvolution of the bands, because of the overlapping with the $\nu_{C=N}$ band of *t*RiPA and with $\nu_{8a,b}$ vibrations of the phenols. The values are indicated in Table 2, along with the intensity enhancement A^c/A^f.

The dipole moment derivatives with respect to the normal coordinate obtained by the relation

$$\frac{\partial\mu}{\partial Q} = \pm\left(\frac{3000\,C^2\,A}{\pi\,N}\right)^{1/2}$$

are also indicated in Table 2. As shown in Fig. 2, this derivative increases with the enthalpy of complex formation.

It is noteworthy that in the complexes involving the same proton donors and saturated Schiff bases, the intensity of the $\nu_{C=N}$ vibration does not increase upon hydrogen bond formation (23). The difference can be ascribed to the electronic delocalization in the retinylidene system, which increases upon complex formation.

3. Proton transfer complexes

From a pK_a value of 6, proton transfer takes place. This can be evidenced by the frequency increase of the $\nu_{C=N}$ vibration, which is observed at 1655 cm^{-1}. As shown in Fig. 3, the intensity of this band increases with the acidity of the proton donor. The proton transfer constant K_{PT}

$$K_{PT} = \frac{[O^-...H^+N]}{[OH...N]}$$

$[O^-...H^+N]$ and [OH...N] being the concentrations of the ionic pair and of the normal hydrogen bonds, is calculated from the intensity of the band at 1655 cm^{-1}. This method seems better than that based on the intensity decrease of the $\nu_{C=N}$ vibration, which strongly overlaps with the $\nu_{C=C}$ vibrations. The observation of both the $\nu_{C=N}$ and $\nu_{C=N\text{-}(H^+)}$ vibrations indicates a double minimum potential for the proton motion.

The proton transfer constants are usually discussed as a function of ΔpK_a, the difference between the pK_a of the acid conjugated to the base and that of the proton donor (24). The pK_a value of *t*RiPA is estimated from the shift of the ν_{OH} band

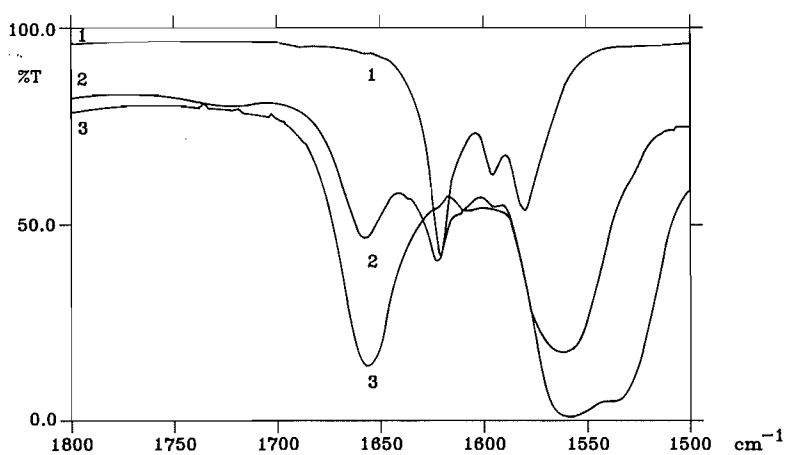

FIG. 3. FT–infrared spectra (1800–1500 cm^{-1}) of 1 *t*RiPA (c = 0.17 mol L^{-1}); 2 *t*RiPA (c = 0.17 mol L^{-1}) and 2,4,6-trichlorophenol (c = 0.19 mol L^{-1}); 3 *t*RiPA (c = 0.17 mol L^{-1}) and 2,4,5,6-tetrachlorophenol (c = 0.24 mol L^{-1}). Solvent = 1,2-dichloroethane. Cell thickness = 0.01 cm.

Can. J. Chem. Downloaded from www.nrcresearchpress.com by 109.225.110.28 on 09/08/12
For personal use only.

TABLE 3. ΔpK_a values, proton transfer constant (K_{PT}), and percentage proton transfer (%PT) for the complexes between *t*RiPA and some phenols. Solvent = 1,2-dichloroethane; T = 298 K

Phenol	ΔpK_a	K_{PT}	%PT
3-CF_3,4-NO_2 phenol	6.10	0.32	24
2,4,6-Trichlorophenol	5.99	0.39	28
2,3,4,5,6-Tetrachlorophenol	4.90	2.29	69
Pentachlorophenol	4.75	2.52	79
2,6-Dichloro-4-NO_2 phenol	3.55	10.19	91

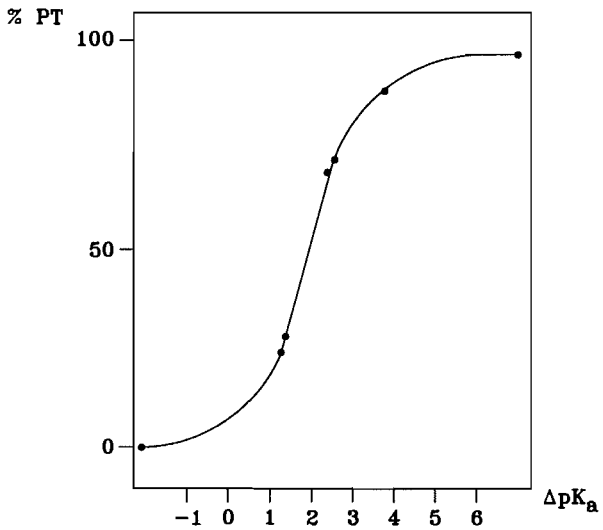

FIG. 4. %PT as a function of ΔpK_a

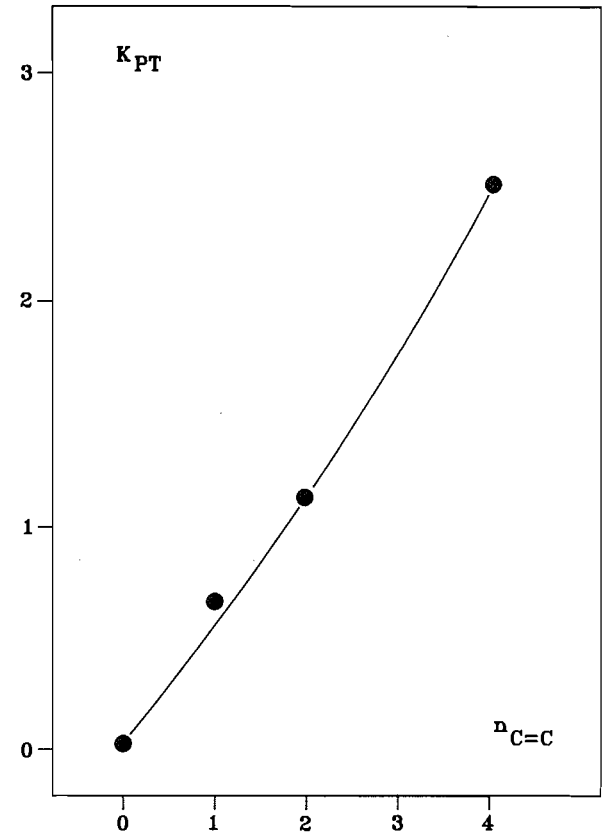

FIG. 5. K_{PT} as a function of the number of C=C bonds in the Schiff bases.

in the methanol complex (350 cm^{-1}) and the correlation between the $\Delta\nu_{OH}$ values and the pK_a for OH...N(sp^2) hydrogen bonds. The pK_a of *t*RiPA computed from this relation is 7.36.

Table 3 lists the ΔpK_a values, the proton transfer constants, and the percentage of proton transfer for the investigated systems. It must be pointed out here that for the interaction between *t*RiBu and phenols having pK_a between 6 and 8, Zundel and co-workers (21) obtained very low proton transfer constants (K_{PT}^{295K} between 0.004 and 0.013) in methylcyclohexane. These values are not correlated to the acidity of the phenol derivative but a linear correlation was obtained between the enthalpies and entropies for the proton transfer process. Although these experimental results are hardly explainable, the K_{PT} values are, as expected, much weaker in methylcyclohexane than in 1,2-dichloroethane (26).

The logarithms of the proton transfer constants are linearly related to ΔpK_a

$$\log K_{PT} = -1.20 + 0.60\ \Delta pK_a\ (r = 0.995)$$

Typical slopes between 0.4 and 1 have been obtained for the OH...N $\rightleftarrows$ O^-...H^+N equilibria. The slopes and intercepts of the above correlation depend on the nature of the interacting molecules, the solvents, and the temperature (26). Figure 4, where the percentage of proton transfer is plotted versus ΔpK_a, shows that 50% proton transfer is achieved for ΔpK_a = 2 or, in other words, when the pK_a of the proton donor is 5.35. For the interaction between the *n*-butylamine retinal Schiff base and carboxylic acids in carbontetrachloride, 50% proton transfer occurs at the same ΔpK_a value of 2 (27). For systems involving all-*trans* retinylidene *tert*-butylamine and substituted acetic acids, 65% proton transfer is achieved when the pK_a of the proton donor is about 4 (28).

In previous works (23–25) the proton transfer constants of various Schiff bases – phenol systems were determined in the same solvent and at the same temperature. It seemed to us interesting to investigate the influence of the number of C=C bonds on the proton transfer constants. The K_{PT} values for the pentachlorophenol and various Schiff bases are as follows:

	iBiPA	*t*BiPA	*t*HiPA	*t*RiPA
K_{PT}	0	0.69	1.13	2.52
$n_{C=C}$	0	1	2	4

Figure 5 shows that the K_{PT} values clearly increase with the number of C=C bonds in the Schiff base or, in other words, with the electronic delocalization in the polyene chain. It must be pointed out here that these results do not agree with those of Bissonnette *et al.* (13). These authors investigated the interaction of various carboxylic acids with *trans* heptadienylidene 2,4-*tert*-butylamine and all-*trans* retinylidene *tert*-butylamine by electronic and ^{1}H NMR spectroscopy. The percentage of protonation was very similar for the two imines. The results of the present work show that the K_{PT} values are higher for the *t*RiPA than for the *t*HiPA systems.

Can. J. Chem. Downloaded from www.nrcresearchpress.com by 109.225.110.28 on 09/08/12
For personal use only.

Acknowledgements

The authors thank the University of Leuven and the National Fund of Research of Belgium for financial support.

1. (*a*) A. Warshel. Photochem. Photobiol. **30**, 285 (1979); (*b*) B. Honig, T. Ebrey, R. J. Callender, U. Dinur, and H. Ottolenghi. Proc. R. Acad. Sci. **76**, 2503 (1979); (*c*) B. Honig. Annu. Rev. Phys. Chem. **29**, 31 (1978); (*d*) R. Uhl and E. W. Abrahamson. Chem. Rev. **81**, 291 (1981); (*e*) K. Nakanishi, V. Balogh-Nair, M. Arnaboldi, K. Tsujimota, and B. Honig. J. Am. Chem. Soc. **102**, 7945 (1983); (*f*) G. D. Mateesen and M. Igbal. Biochemistry, **23**, 3357 (1984), and references herein.
2. B. Aton, A. G. Doukas, R. H. Callender, B. Becker, and T. G. Ebrey. Biochemistry, **16**, 2995 (1977).
3. R. Mathies, A. R. Oseroff, and I. Streyer. Proc. Natl. Acad. Sci. USA, **73**, 1 (1976).
4. D. S. Oesterheldt and W. Stoeckenius. Proc. Natl. Acad. Sci. USA, **70**, 2853 (1973).
5. G. Massig, M. Stockburger, W. Gärtner, D. Oesterheldt, and P. Towner. J. Raman. Spectrosc. **12**, 287 (1982).
6. R. Lohrmann, I. Grieger, and M. Stockburger. J. Phys. Chem. **95**, 1993 (1991).
7. J. Shriver, G. Mateescu, R. Fager, D. Torchia, and E. W. Abrahamson. Nature, **270**, 271 (1977).
8. F. Siebert and W. Mäntele. Biophys. Struct. Mech. **6**, 147 (1980).
9. F. I. Harosi, J. Favrot, J. M. Leclercq, D. Vocelle, and C. Sandorfy. Rev. Can. Biol. **37**, 257 (1978).
10. J. M. Leclercq, D. Dupuis, and C. Sandorfy. Croat. Chem. Acta, **55**, 105 (1982).
11. J. M. Leclercq and C. Sandorfy. Photochem. Photobiol. **33**, 361 (1981).
12. P. Dupuis, F. I. Harosi, C. Sandorfy, J. M. Leclercq, and D. Vocelle. Rev. Can. Biol. **39**, 247 (1980).
13. M. Bissonnette, H. Le Thanh, and D. Vocelle. Can. J. Chem. **63**, 1480 (1985).
14. M. Bissonnette, J. Le Thanh, and D. Vocelle. Can. J. Chem. **63**, 1459 (1985).
15. M. Bissonnette, J. Le Thanh, and D. Vocelle. Can. J. Chem. **63**, 2298 (1985).
16. M. Hodoschek and D. Hadzi. Can. J. Chem. **63**, 1528 (1985).
17. F. Zuccarello, A. Raudino, and G. Buemi. J. Mol. Struct. (Theochem), **107**, 215 (1984).
18. P. Hillebrandt, R. A. Copeland, T. G. Spiro, J. Otlewski, M. Laskowski, and F. G. Prendergast. Biochemistry, **27**, 5426 (1988).
19. V. L. Kristoforov, E. N. Zvonkova, and R. P. Evstigneeva. J. Gen. Chem. USSR, **44**, 876 (1977).
20. F. P. Rastogi and G. Zundel. Biochem. Biophys. Rev. **99**, 804 (1981).
21. H. Schmideder, O. Kasende, H. Merz, P. R. Rastagi, and G. Zundel. J. Mol. Struct. **161**, 87 (1987).
22. P. E. Blatz and J. A. Tompkins. J. Am. Chem. Soc. **114**, 3951 (1992).
23. P. Migchels, Th. Zeegers-Huyskens, and D. Peeters. J. Phys. Chem. **95**, 7599 (1991).
24. P. Migchels, N. Leroux, and Th. Zeegers-Huyskens. Vib. Spectrosc. **2**, 81 (1991).
25. P. Migchels and Th. Zeegers-Huyskens. J. Mol. Struct. **247**, 173 (1991).
26. Th. Zeegers-Huyskens and P. Huyskens. *In* Molecular interactions. Vol. 2. *Edited by* H. Ratajczak and W. J. Orville-Thomas. John Wiley & Sons, New York. 1981. pp. 1–106.
27. H. Merz and G. Zundel. Biophys. Res. Commun. **138**, 819 (1986).
28. L. S. Lussier, C. Sandorfy, H. Le Thanh, and D. Vocelle. J. Phys. Chem. **91**, 2282 (1987).

Can. J. Chem. Downloaded from www.nrcresearchpress.com by 109.225.110.28 on 09/08/12
For personal use only.

Sedum alkaloids XII. Synthesis of the new piperidine alkaloids homosedinone and dihomosedinone

ALEX DURANT AND CLAUDE HOOTELÉ[1]

Service de chimie organique, Faculté des sciences, Université Libre de Bruxelles, B-1050 Bruxelles, Belgium

Received April 14, 1992

ALEX DURANT and CLAUDE HOOTELÉ. Can. J. Chem. **70**, 2722 (1992).

The new piperidine alkaloids homosedinone **2** and dihomosedinone **3**, isolated from *Sedum acre*, have been synthesized from (−)-norsedamine **7** by application of the sequence: anodic methoxylation – elimination – nucleophilic addition.

ALEX DURANT et CLAUDE HOOTELÉ. Can. J. Chem. **70**, 2722 (1992).

La synthèse de deux nouveaux alcaloïdes pipéridiniques, l'homosédinone **2** et la dihomosédinone **3**, isolés de *Sedum acre*, est décrite au départ de la (−)-norsédamine **7** par application de la séquence : méthoxylation anodique – élimination – addition nucléophile.

Introduction

Sedum acre constitutes a rich source of piperidine alkaloids (1). During a search for new bases from this species, we isolated two fractions, after repetitive counter-current and chromatography separations, whose spectral properties indicated two homologs of sedinone **1**. These fractions contained, respectively, homosedinone **2** and dihomosedinone **3** accompanied by their C-6 epimers **4** and **5**. The separation of the diastereoisomers was complicated owing to the facile epimerization (2, 3) of this type of base (β-amino ketones); **2** and **3** were eventually isolated in very minute amounts by TLC.[2] Definite evidence for structures **2** and **3**, which also represent the absolute configuration of the new alkaloids (2*S*,6*R*,8*S*), rests on the synthesis we describe in this paper.

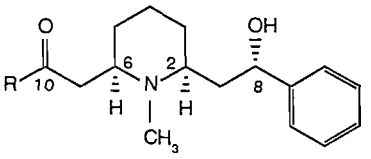

1 R = CH_3

2 R = CH_2-CH_3

3 R = CH_2-CH_2-CH_3

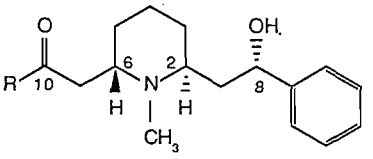

4 R = CH_2-CH_3

5 R = CH_2-CH_2-CH_3

6 4,5-dehydro, R = CH_3

Results and discussion

We have shown recently that the sequence of anodic methoxylation – elimination – nucleophilic addition (4) provides an efficient route for the synthesis of 2,6-disubstituted piperidine alkaloids (3) and we used this procedure for the synthesis of sedinone **1** and sedacrine **6**. The sedinone homologs **2** and **3** have now been obtained by application of the same methodology.

The α-methoxy carbamate **8** was prepared by anodic oxidation of the *N*-carbomethoxy derivative of (−)-norsedamine **7** as reported previously (3). Replacement of the 6-methoxy group in **8** by the desired side chain was carried out by treatment with an excess of 2-trimethylsilyloxybut-1-ene and 2-trimethylsilyloxypent-1-ene, respectively (synthesized according to the procedure of Corey and Gross (5)), at −78°C in dichloromethane in the presence of $TiCl_4$ as a Lewis acid. After chromatography two fractions containing at least 95% (by ^1H NMR) of the *cis*-2,6-disubstituted carbamates **9** and **10** were isolated in 78 and 85% yield, respectively; the principal by-product of these substitutions is the enecarbamate resulting from elimination of methanol from **8** (3).

The high stereoselectivity observed in the reactions of α-methoxy-*N*-acylpiperidines with nucleophiles is now well documented (3, 7, 8): the *cis* stereochemistry results from stereoelectronically preferred axial attack of the nucleophile on the iminium intermediate that contains the phenethyl chain in the axial orientation due to $A^{1,3}$ strain.

Without further purification **9** and **10** were transformed into the corresponding acetals **11** and **12**. Reduction of the acetals **11** and **12** with $LiAlH_4$ in THF gave the *N*-methyl derivatives **13** and **14**; acid hydrolysis of the acetal groups furnished two 85:15 mixtures of *cis*- and *trans*-piperidines **2**:**4** and **3**:**5** in 70% overall yield from the carbamates **9** and **10** respectively. The presence of 15% of the *trans* isomers **4** and **5** results from the epimerization at C-6 during the basic work-up after the deprotection step. Fractional crystallization of the above mixtures from hexane yielded pure homosedinone **2** and dihomosedinone **3**. The spectral properties and optical rotation of the synthetic compounds were identical to those of the alkaloids **2** and **3** from the natural source.

[1]Author to whom correspondence may be addressed.

[2]C. Hootelé, D. Vanderaa, and A. Durant. Unpublished results.

Can. J. Chem. Downloaded from www.nrcresearchpress.com by 109.225.110.28 on 09/08/12
For personal use only.

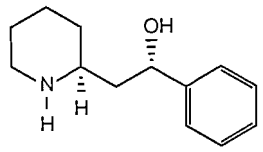

7

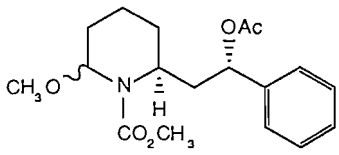

8

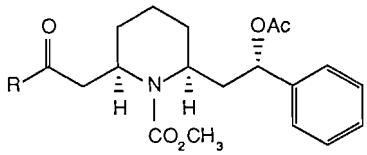

9 R = CH_2-CH_3

10 R = CH_2-CH_2-CH_3

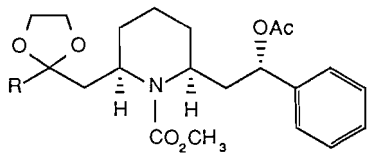

11 R = CH_2-CH_3

12 R = CH_2-CH_2-CH_3

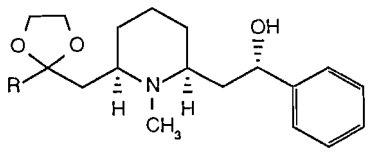

13 R = CH_2-CH_3

14 R = CH_2-CH_2-CH_3

Structure **2** (without stereochemical implications) was recently assigned to a base isolated from *Lobelia davidii*; comparison of the physical and spectral values reported (6) with those of **2** and **4** do not allow its stereochemistry to be established and we have not been able to obtain a specimen of the natural product for direct comparison with the synthetic material.

The facile epimerization of the β-amino ketones sedinone **1** and the homologs **2** and **3** deserves some comments. In methanol at room temperature these bases epimerize at C-6; the equilibrium (*cis*:*trans* ca. 1:1) is reached after a few hours, while the corresponding hydrochlorides (and the *N*-acyl derivatives **9** and **10**) are stereochemically stable under the same comditions. Epimerization is also fast in chloroform/ammonia and chloroform/MacIlvaine buffer pH 6 (precluding the use of these last conditions for the separation of the C-6 epimers by counter-current distribution) but much slower in pure chloroform. It is likely that the epimerization involves a reversible retro-Michael reaction by way of the six-membered ring chelate of an enol tautomer as depicted in Fig. 1 (3, 9).

Given the propensity for β-amino ketones to undergo epimerization in the conditions used during isolation of the bases, it is not established which epimers are present in *Sedum acre*.

Experimental

Melting points were determined on a Kofler microscope and are uncorrected. Mass spectral data were obtained on a Micromass 7070 spectrometer. Nuclear magnetic resonance spectra were recorded in $CDCl_3$ with TMS as internal standard on a Bruker WM 250 spectrometer. Optical rotations were measured on a Perkin Elmer 141 polarimeter.

Preparation of **9**

To a stirred solution of $TiCl_4$ (108 mg) in CH_2Cl_2 (2 mL) at −78°C, under a nitrogen atmosphere, was added dropwise a solution of **8** (172 mg) in the same solvent (2 mL). A solution of 2-trimethylsilyloxybut-1-ene (738 mg) was then added and the resulting reaction mixture was stirred for 1 h at −78°C and then allowed to reach room temperature (1 h). After addition of water and NH_4OH the mixture weas extracted twice with $CHCl_3$. The combined organic layers were evaporated and the residue was purified by chromatography on alumina ($CHCl_3$) to afford **9** (149 mg, 78% yield) and the enecarbamate resulting from elimination of methanol from **8** (26 mg, 17% yield), with spectral data as previously reported (3). **9** (oil): ^{1}H nmr δ: 7.3 (5H, m), 5.77 (1H, dd, J = 4 and 10 Hz, H8), 4.64 (1H, m, H6), 4.28 (1H, m, H2), 3.69 (3H, s), 2.61 (2H, m, H9), 2.45 (2H, m, H11), 2.09 (3H, s), 2.2–1.5 (8H, m), 1.03 (3H, t, J = 7 Hz); ^{13}C nmr δ: 209.3 (C10), 170.4, 156.3 (NCO), 140.7, 128.7, 128.2, 126.6, 73.8 (C8), 52.7 (CH_3), 47.6, 47.2 and 46.7 (C2, C6, C9), 41.4 (C7), 36.2 (C11), 28.1 and 27.4 (C3, C5), 21.3 (CH_3), 14.0 (C4), 7.8 (C12); ms, m/z: 375 (<0.5%), 315, 256, 212, 154, 140 (100).

Preparation of the acetal ***11*** *from* ***9***

A solution of **9** (126 mg), ethylene glycol (105 mg), and $TsOH \cdot H_2O$ (4 mg) in 20 mL of benzene was heated under reflux for 20 h in a Dean–Stark apparatus. After evaporation of the solvent, the residue was dissolved in water, basified with NH_4OH, and extracted with $CHCl_3$. The combined organic layers were evaporated and the residue was filtered through a short column of alumina ($CHCl_3$) to yield the acetal **11** (117 mg, 83%); **11** (oil): ^{1}H nmr δ: 7.3 (5H, m), 5.76 (1H, dd, J = 4 and 10 Hz, H8), 4.3 (2H, m, H2 and H6), 3.9 (4H, m), 3.69 (3H, s), 2.09 (3H, s), 2.2–1.3 (12H, m), 0.91 (3H, t, J = 7 Hz); ^{13}C nmr δ: 170.6, 156.1, 141.0,

Can. J. Chem. Downloaded from www.nrcresearchpress.com by 109.225.110.28 on 09/08/12
For personal use only.

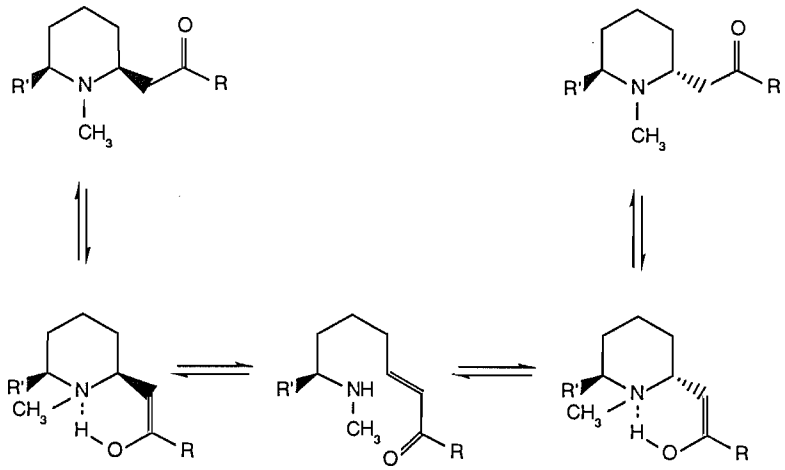

FIG. 1. Mechanism of epimerization of β-amino ketones.

128.7, 128.2, 126.7, 111.5, 74.0, 65.1, 64.7, 52.6, 47.8, 47.1, 41.5, 40.7, 30.0, 28.5, 27.7, 21.4, 14.2, 8.1; ms, *m/z*: 419 (0.5%), 390, 359, 304, 256, 244, 140 (100), 101.

$LiAlH_4$ reduction of ***11***

To a solution of the acetal **11** (108 mg) in THF (15 mL) was added $LiAlH_4$ (106 mg). The mixture was heated under reflux for 17 h. The excess of hydride was carefully destroyed by water and the mixture was filtered through Celite and evaporated to dryness. The residue was dissolved in 0.2 N aqueous HCl and washed twice with $CHCl_3$. The aqueous phase was then basified (NH_4OH) and extracted twice with $CHCl_3$. Evaporation of the organic phase afforded the *N*-methyl derivative **13** (75 mg, 88% yield). **13** (oil): ^1H nmr δ: 7.3 (5H, m), 4.94 (1H, dd, J = 3 and 9 Hz, H8), 3.9 (4H, m), 3.2–3 (2H, m, H2 and H6), 2.26 (3H, s), 2–1 (12H, m), 0.92 (3H, t, J = 7 Hz); ^{13}C nmr δ: 145.3, 128.1, 126.9, 125.6, 111.5, 76.1, 64.9, 64.8, 64.6, 58.8, 40.5, 40.4, 30.2, 26.3, 25.3, 24.1, 23.2, 7.5; ms, *m/z*: 333 (4%), 290, 218, 212 (100), 170, 101, 96.

Homosedinone ***2*** *from* ***13***

A solution of the acetal **11** (288 mg) in 0.12 N aqueous HCl (50 mL) was heated under reflux for 30 min. The mixture was then cooled, basified (NH_4OH), and extracted twice with $CHCl_3$. Evaporation of the combined organic layers afforded a 85:15 mixture (248 mg, 96% yield) of homosedinone **2** and 6-epihomosedinone **4**. Crystallization of the mixture from hexane afforded pure homosedinone **2** : mp 62–63°C; $[\alpha]_D^{20}$ −41 ($CHCl_3$, c = 1.5); ^1H nmr δ: 7.3 (5H, m), 4.93 (1H, dd, J = 3 and 11 Hz, H8), 3.6–3.1 (2H, m, H2 and H6), 2.7–2.3 (4H, m, H9 and H11), 2.26 (3H, s), 2–1 (8H, m), 1.06 (3H, t, J = 7 Hz); ^{13}C nmr δ: 209.5, 145.2, 128.3, 127.1, 125.7, 75.9 (C8), 64.6 (C6), 59.0 (C2), 47.7 (C9), 40.5 (C7), 36.3 (C11), 27.1 (NCH_3), 24.8, 23.5, and 23.4 (C3, C4, and C5), 7.9 (CH_3); ms, *m/z*: 289 (10%), 218, 168 (100), 96. These spectral values are virtually identical with those of **2** from *S. acre*: mp 62–63°C (mixture mp without depression), $[\alpha]_D^{20}$ −40 ($CHCl_3$, c = 0.2).

6-Epihomosedinone **4** : ^1H nmr δ: 7.3 (m), 4.89 (dd, J = 3 and 11 Hz), 2.48 (s); ^{13}C nmr δ: 209.3, 145.2, 128.3, 127.1, 125.7, 75.8 (C8), 60.7 (C6), 51.3 (C2), 46.6 (C9), 39.0 (C7), 36.3 (C11), 35.7 (NCH_3), 23.3 and 23.1 (C4 and C5), 20.5 (C4), 7.8 (CH_3); ms, *m/z*: 289; (these values were extracted from the spectra of a 1:1 mixture of **2** and **4**).

Preparation of ***10*** *and* ***8***

By use of a procedure similar to that described for the preparation of **9**, **8** (346 mg) was treated with $TiCl_4$ (241 mg) and 2-trimethylsilyloxypent-1-ene (1537 mg) to afford **10** (342 mg, 85% yield) and the enecarbamate resulting from the elimination of methanol (48 mg, 15% yield); **10** (oil): ^1H nmr δ: 7.3 (5H, m), 5.77 (1H, dd, J = 4 and 10 Hz, H8), 4.66 (1H, m, H6), 4.29 (1H, m, H2), 3.69 (3H, s), 2.62 (2H, m, H9), 2.41 (2H, m, H11), 2.09 (3H, s), 2.2–1.9 (2H, m, H7), 1.7–1.5 (8H, m), 0.90 (3H, t, J = 7 Hz); ^{13}C nmr δ: 209.4, 170.8, 156.7, 141.2, 129.2, 128.7, 127.3, 74.3, 53.2 (CH_3), 48.1 and 47.1 (C2 and C6), 48.0 and 45.4 (C9 and C11), 41.9 (C7), 28.6 and 27.9 (C3 and C5), 21.7 (CH_3), 17.7 (C12), 14.4 (C4), 14.2 (CH_3); ms, *m/z*: 389 (<0.5%), 329, 270, 142, 141; 140 (100), 85, 83.

Preparation of the acetal ***12*** *from* ***10***

The acetal **12** (386 mg, 81% yield) was prepared by a procedure similar to that described for **11** from **10** (428 mg), ethylene glycol (468 mg), and $TsOH \cdot H_2O$ (12 mg); **12** (oil): ^1H nmr δ: 7.3 (5H, m), 5.76 (1H, dd, J = 4 and 10 Hz, H8), 4.3 (2H, m, H2 and H6), 3.9 (4H, m), 3.69 (3H, s), 2.09 (3H, s), 2.2–1.3 (14H, m), 0.91 (3H, t, J = 7 Hz); ^{13}C nmr δ: 170.9, 156.7, 141.4, 129.1, 128.6, 127.1, 111.6, 74.4, 65.4, 65.0, 53.0, 48.2, 47.6, 42.0, 41.6, 39.9, 28.9, 28.1, 21.7, 17.5, 14.9, 14.6; ms, *m/z*: 433 (<0.5%), 390, 373, 304, 270, 244, 140 (100), 115.

$LiAlH_4$ reduction of ***12***

By use of a procedure similar to that described for the preparation of **13**, **12** (358 mg) was treated with $LiAlH_4$ (340 mg) in THF to afford the *N*-methyl derivative **14** (oil, 259 mg, 90% yield): ^1H nmr δ: 7.3 (5H, m), 4.94 (1H, dd, J = 2 and 9 Hz, H8), 3.9 (4H, m), 3.2–2.9 (2H, m, H2 and H6), 2.25 (3H, s), 2–1.1 (14H, m), 0.93 (3H, t, J = 7 Hz); ^{13}C nmr δ: 145.9, 128.8, 127.5, 126.2, 111.8, 76.7, 65.5, 65.4, 65.3, 59.4, 41.7, 41.1, 40.4, 26.9, 25.9, 24.7, 23.8, 17.8, 15.0; ms, *m/z*: 347 (8%), 304, 226, 218, 115, 98 (100), 96.

Dihomosedinone ***3*** *from* ***14***

By use of a procedure similar to that described for the preparation of **2**, a 85:15 mixture (204 mg, 94% yield) of **3** and **5** was obtained after hydrolysis of **14** (256 mg) in 0.12 N aqueous HCl. Crystallization from hexane afforded pure dihomosedinone **3**: mp: 67–68°C, $[\alpha]_D^{20}$ −43 ($CHCl_3$, c = 1.4); ^1H nmr δ: 7.3 (5H, m), 4.93 (1H, dd, J = 3 and 11 Hz, H8), 3.6–3.1 (2H, m, H2 and H6), 2.7–2.3 (4H, m, H9 and H11), 2.26 (3H, s), 2–1.1 (10H, m), 0.91 (3H, t, J = 7 Hz); ^{13}C nmr δ: 209.4, 145.7, 128.8, 127.6, 126.2, 76.4 (C8), 65.1 (C6), 59.3 (C2), 48.7 (C9), 45.8 (C11), 41.1 (C7), 27.8 (NCH_3), 25.4, 24.0, and 23.9 (C3, C4, and C5), 17.9 (C12), 14.3 (CH_3); ms, *m/z*: 303 (17%), 218, 182 (100), 98, 97, 96. These spectral values are virtually identical with those of dihomosedinone **3** from *S. acre* ($[\alpha]_D^{20}$ −42 ($CHCl_3$, c = 0.3)).

Can. J. Chem. Downloaded from www.nrcresearchpress.com by 109.225.110.28 on 09/08/12
For personal use only.

6-Epidihomosedinone **5** : ^{1}H nmr δ: 7.3 (m), 4.89 (dd, J = 3 and 11 Hz), 2.48 (s); ^{13}C nmr δ: 208.8, 145.7, 128.8, 127.6, 126.1, 75.8 (C8), 60.7 (C6), 51.2 (C2), 47.0 (C9), 45.2 (C11), 38.9 (C7), 35.7 (NCH_3), 23.3 and 23.1 (C3 and C5), 20.5 (C4), 17.3 (C12), 13.8 (CH_3); ms, m/z: 303 (these values were extracted from the spectra of a 1:1 mixture of **3** and **5**).

Acknowledgements

A.D. wishes to thank the Institut pour l'Encouragement de la Recherche Scientifique dans l'Industrie et l'Agriculture (IRSIA) for the award of a fellowship. C.H. is a Research Associate of the National Fund for Scientific Research (FNRS).

1. W. Ibebeke-Bomangwa and C. Hootelé. Tetrahedron, **43**, 935 (1987).
2. B. Colau and C. Hootelé. Can. J. Chem. **61**, 470 (1983).
3. F. Driessens and C. Hootelé. Can. J. Chem. **69**, 211 (1991).
4. T. Shono. Tetrahedron, **40**, 811 (1984), and references therein.
5. E. J. Corey and A. W. Gross. Tetrahedron Lett. **25**, 495 (1984).
6. M. Zhang, J. Wang, and S. Zhou. Phytochemistry, **29**, 1354 (1990).
7. K. Irie, A. Aoe, T. Tanaka, and S. Saito. J. Chem. Soc. Chem. Commun. 633 (1985).
8. T. Shono, Y. Matsumura, K. Tsubata, and K. Uchida. J. Org. Chem. **51**, 2590 (1986).
9. F. Galinovsky, G. Bianchetti, and O. Vogel. Monatsh. Chem. **84**, 1221 (1953).

Can. J. Chem. Downloaded from www.nrcresearchpress.com by 109.225.110.28 on 09/08/12
For personal use only.

A concise synthesis of (+)-muscarine

T. H. CHAN[1] AND C. J. LI
Department of Chemistry, McGill University, Montreal, Que., Canada H3A 2K6

Received March 31, 1992

T. H. CHAN and C. J. LI. Can. J. Chem. **70**, 2726 (1992).

(+)-Muscarine was synthesized from *S*-(−)-ethyl lactate in five steps with the application of a zinc-mediated allylation reaction in aqueous media. Reversal of chelation-control stereoselectivity was observed in the allylations of chiral α-alkoxy aldehydes in aqueous media.

T. H. CHAN et C. J. LI. Can. J. Chem. **70**, 2726 (1992).

Appliquant une réaction d'allylation réalisée en milieu aqueux et faisant intervenir du zinc, on a effectué la synthèse de la (+)-muscarine en cinq étapes à partir du *S*-(−)-lactate d'éthyle. Lors des allylations en milieu aqueux des α-alkoxy aldéhydes chiraux, on a observé un renversement du contrôle de stéréosélectivité de la chélation.

[Traduit par la rédaction]

Can. J. Chem. Downloaded from www.nrcresearchpress.com by 109.225.110.28 on 09/08/12
For personal use only.

Introduction

Muscarine (**1**, OH^- instead of I^-) is an alkaloid first isolated from the poisonous mushroom, *Amanita muscaria* (fly agaric) in 1954 (1). Its structure, chemistry and physiological activities have been extensively investigated (2). Muscarine acts as a selective agonist of the neurotransmitter acetylcholine on smooth muscles of the gastrointestinal tract, eye exocrine glands, and heart. As a consequence, the receptor responses in those tissues are termed muscarinic receptors. More recently, with the use of selective antagonists, distinct subtypes of muscarinic receptors were distinguished (3).

Synthesis of muscarine has been accomplished a number of times from different precursors (2–6). Recently, a chemoenzymatic synthesis of muscarine and its stereoisomers has been reported (7). The renewed interest in this molecule is due in part to the recent suggestion that various subtypes of muscarinic receptors may be implicated in Alzheimer disease (8). Because of our interest in this area, we report here an efficient synthesis of (+)-muscarine from the readily available *S*-(−)-ethyl lactate by taking advantage of a zinc-mediated allylation reaction in aqueous media (9, 10).

Results and discussion

S-(−)-Ethyl lactate (**2**) was converted into the 2,6-dichlorobenzyl ether **3** in 90% yield (Scheme 1). DIBAL reduction of **3** gave the aldehyde **4**. Treatment of the crude aldehyde **4** with allyl bromide and zinc powder in water with NH_4Cl as catalyst resulted in a *anti*:*syn* (71:29) mixture of diastereomers **5***a* and **5***b* in 85% combined yield. The two diastereomers were easily separated by flash chromatography (eluent: hexane:ethyl acetate, 20:1). Treatment of **5***a* with iodine in CH_3CN at 0°C gave the cyclized product **6***a* stereospecifically in 85% yield (for previous study of the iodocyclization reaction, see ref. 11). Finally, treatment of **6***a* with excess trimethylamine in ethanol gave (+)-muscarine (2*S*,4*R*,5*S*). A similar reaction sequence with **5***b* gave (+)-epimuscarine **7**. Compared to the previously reported syntheses in the literature, the present synthesis of muscarine offers the advantages of simplicity, good overall yield, and high optical purity of the product from a readily available chiral precursor.[2]

The stereoselectivity in the conversion of **4** and **5** deserves some comments. Normally, the stereoselectivity observed in the addition of *C*-nucleophiles such as organometallic reagents to chiral α-alkoxy aldehydes (and ketones) has been rationalized on the basis of chelation control (12, 13). The carbonyl compound **8** forms the chelate **9** as shown in Scheme 2. The *C*-nucleophile (R^-) attacks from the less-hindered side as indicated by the arrow, giving the chelation-controlled product **10** in preference to the non-chelation product **11** (Scheme 2). The chelation-control approach provides a useful and convenient synthesis of **10**. When this presumed chelation is diminished by the use of a bulky protecting R^2 or by the use of a non-chelating reagent, the non-chelation product **11** can predominate.[3]

Indeed, the reaction of **4** with allylmagnesium bromide in ether afforded the two diastereomers **5***a* and **5***b* in a ratio of 40:60 (*anti*:*syn*) as predicted by the chelation-control model. A similar reaction with diallylzinc in ether (15) resulted in a complicated mixture. The reversal in diastereoselectivity between organic and aqueous media appears to be a general result for several α-alkoxy aldehydes **8***a*, *b*, and *c*. The effects of solvent on diastereoselectivity are summarized in Table 1. We attribute this change to the disruption of chelation in the aqueous media. In support of this, it should be noted that in the case of α-methylphenylacetaldehyde (**12**), where there is no possibility of chelation, there was no significant difference in the diastereoselectivity between allylations in organic or aqueous media (16). However, it is possible that the observed stereoselectivity in the aqueous organometallic-type reactions may be due to factors associated with the metal surface in such heterogenous reactions (10).

The present synthesis of muscarine demonstrates that organometallic-type reactions in aqueous media can make a meaningful contribution to organic synthesis. Further applications of such reactions can be anticipated.

[1]Author to whom correspondence may be addressed.

[2]Synthesis of muscarine from lactate ester was not reported previously, presumably because of the difficulty in obtaining the intermediate **5***a* in the conventional organometallic allylation due to chelation control.

[3]Non-chelation-controlled additions can be achieved with alkyltitanium reagents of low Lewis acidity (see ref. 14*a*). For effects of protecting group on chelation control, see ref. 14*b*.

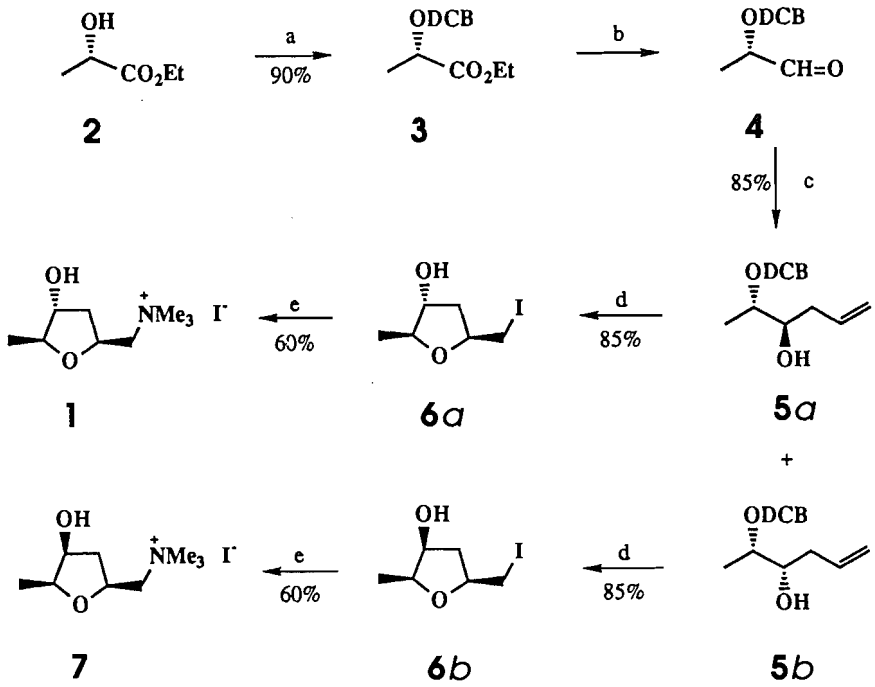

(a) DCBBr/Ag_2O/Et_2O/reflux/6 h; (b) DIBAL-H/Et_2O/-78°C/2 h; (c) CH_2=$CHCH_2Br$/Zn/H_2O/NH_4Cl/3 h; (d) I_2/CH_3CN/0°C/3 h; (e) NMe_3/EtOH/80°C/4 h

SCHEME 1

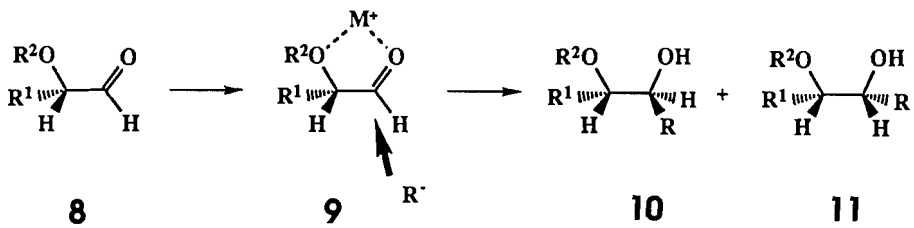

a: R^1=Ph, R^2=Bn
b: R^1=Bu, R^2=Bn
c: R^1=Me, R^2=Bn

SCHEME 2

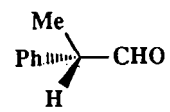

12

Experimental section

Melting points are uncorrected. Infrared spectra were obtained from films on NaCl plates for liquids and as a KBr pellet for solids on an Analect FTIR AQS-18 spectrophotometer. The ^1H NMR and ^{13}C NMR spectra were recorded on Varian XL-200, XL-300, and Gemini-200 instruments. Mass spectra were determined on a DuPont 21-492B spectrometer. High-resolution mass spectra were obtained on a VG ZAB-HS instrument. Optical rotations were measured on a JASCO DID-140 polarimeter. Column chromatography was performed on silica gel 60 (Merck and EM Science). Acetonitrile was dried by refluxing over CaH_2.

Ethyl (S)-2-(2',6'-dichlorobenzyloxy)-propionate (3)

Dry powdered silver oxide (1.3 g, 5.25 mmol) was added to a solution of ethyl *S*-(−)-lactate (559 mg, 5 mmol) and 2,6-dichlorobenzyl bromide (1.2 g, 5 mmol) in dry ether (50 mL) over a period of 40 min while stirring. The reaction was kept refluxing for 6 h until TLC showed complete disappearance of the starting lactate. Then the reaction mixture was filtered through Celite. Evaporation of the solvent resulted in a crude material, which was purified by flash chromatography (hexane:ethyl acetate, 20:1) to give 1.25 g (90%) of **3** as a colorless oil. IR(neat) *v*: 2986, 2901, 2886, 1746, 1581, 1564, 1436, 1373, 1268, 1197, 1139, 1116, 766 cm^{-1}; ^1H NMR ($CDCl_3$) δ: 1.30(t, *J* = 7.1, 3H), 1.41(d, *J* = 6.9, 3H), 4.1(q, *J* = 7.1, 1H), 4.2(q, *J* = 7.1, 2H), 4.7(d, *J* = 10.6, 1H), 5.02(d, *J* = 10.61, 1H), 7.25(m, 3H)ppm; HRMS, Exact Mass for $C_{12}H_{14}O_3Cl_2$ + H^+, calcd.: 277.0399; found: 277.0398.

(2S,3R)-2-(2',6'-Dichlorobenzyloxy)-5-hexen-3-ol (5a)

To a solution of the lactate **3** (556 mg, 2 mmol) in ethyl ether (20 mL) under argon, diisobutyl aluminium hydride (2.2 mL,

Can. J. Chem. Downloaded from www.nrcresearchpress.com by 109.225.110.28 on 09/08/12
For personal use only.

TABLE 1. Stereoselective allylation of chiral α-substituted aldehydes

Aldehyde	R^1	R^2O	Method[a]	*syn*:*anti*[b]	Combined yield(%)
8*a*	Ph	BnO	O(Mg)	67:33	75
8*a*	Ph	BnO	A(Zn)	43:57	50
8*b*	Bu	BnO	O(Mg)	60:40	60
8*b*	Bu	BnO	A(Zn)	24:76	80
8*c*	Me	BnO	O(Mg)	65:35	50
8*c*	Me	BnO	A(Zn)	35:65	85
4	Me	DCBO	O(Mg)	60:40	45
4	Me	DCBO	A(Zn)	29:71	85
12	Ph	Me	O(Mg)	60:40	90
12	Ph	Me	A(Zn)	68:32	85

[a]For Method, see experimental section.
[b]The ratio of *syn*:*anti* isomers was determined by ^{1}H nmr. See refs. 17 and 21.

1.0 M in hexane) was added dropwise by syringe over 40 min at −78°C. After stirring for 2 h, saturated aqueous ammonium chloride (10 mL) was added to quench the reaction, followed by the addition of 10% HCl (2 mL). The organic layer was separated and dried ($MgSO_4$). Evaporation of the solvent afforded the crude aldehyde **4**, which was used directly without purification. The crude aldehyde was transferred into a 100-mL flask and mixed with H_2O (50 mL). To the suspension was added allyl bromide (360 mg, 3 mmol) and zinc powder (192 mg, 3 mmol), followed by 1 mL of saturated aqueous ammonium chloride solution to catalyze the reaction. The reaction was continued until no aldehyde could be detected by TLC. The reaction mixture was extracted with ether. The ether extract was dried ($MgSO_4$). Evaporation of the solvent gave a mixture of diastereomers (2–3:1). Separation of the diastereomers was achieved by flash chromatography (hexane:ethyl acetate, 20:1). The major isomer proved to be **5***a*. ^{1}H NMR ($CDCl_3$) δ: 1.21(d, J = 6.3, 3H), 2.21(br, 3H), 3.50(m, 1H), 3.71(m, 1H), 4.75(AB, J = 10.2, 2H), 5.1(m, 2H), 5.8(m, 1H), 7.25(m, 3H) ppm; ^{13}C NMR ($CDCl_3$) δ: 13.9, 36.8, 65.3, 72.2, 77.7, 117.3, 128.3, 129.8, 133.3, 134.9, 136.6 ppm.

*(2S,3S)-2-(2′,6′-Dichlorobenzyloxy)-5-hexen-3-ol (**5**b)*

The minor product from the above reaction proved to be **5***b*. ^{1}H NMR ($CDCl_3$) δ: 1.23(d, J = 6.0, 3H), 2.21(br, 2H), 2.77(d, OH, J = 2.6, 1H), 3.41(m, 2H), 4.80(AB, J = 10.2, 2H), 5.1(m, 2H), 5.8(m, 1H), 7.25(m, 3H) ppm; ^{13}C NMR ($CDCl_3$) δ: 15.2, 37.1, 65.2, 74.2, 77.9, 116.9, 128.3, 129.9, 133.1, 134.6, 136.6 ppm.

*(2S,4R,5S)-2-Iodomethyl-5-methyl-tetrahydrofuran-4-ol (**6**a)*

A solution of **5***a* (266 mg, 0.97 mmol) in acetonitrile (15 mL) was treated with iodine (254 mg, 1.0 mmol) in small portions under an atmosphere of nitrogen at −5°C. After stirring for 3 h at 0°C, the mixture was diluted with ether, and washed with water and 10% sodium thiosulfate aqueous solution. After drying ($MgSO_4$), **6***a* was isolated by flash chromatography (hexane: EtOAc, 2:1) as a colorless oil (234 mg, 85%). IR(neat) ν: 3399(br, OH), 2970, 2930, 1733, 1445, 1358, 1249, 1096, 1063, 984, 992, 905 cm^{-1}; ^{1}H NMR ($CDCl_3$) δ: 1.21(d, J = 6.4, 3H), 1.88(m, 1H), 2.0(m, 1H), 2.6(s, br, 1H), 3.25(m, 2H), 3.9–4.2(m, 3H) ppm; ^{13}C NMR ($CDCl_3$) δ: 10.4, 19.7, 40.8, 77.0, 77.2, 83.2 ppm.

*(2S,4S,5S)-2-Iodomethyl-5-methyl-tetrahydrofuran-4-ol (**6**b)*

The compound was obtained from **5***b* by the same procedure as described above as a colorless needle crystal, mp 60–62°C (lit. (11) mp 62°C); IR(KBr) ν: 3435(br, OH), 2885, 1716, 1539, 1179, 1164, 1065, 1039, 1013 cm^{-1}; ^{1}H NMR ($CDCl_3$) δ: 1.28(d, J = 6.4, 3H), 1.75(br, 2H), 2.4(m, 1H), 3.35(m, 2H), 3.8–4.0(m, 2H), 4.16(m, 1H) ppm; ^{13}C NMR ($CDCl_3$) δ: 79.9, 76.7, 73.4, 41.4, 14.1, 11.8 ppm.

*(+)-Muscarine iodide (**1**)*

The iodoalcohol **6***a* (170 mg, 0.7 mmol) and excess of trimethylamine (~500 mg) were dissolved in 2 mL of ethanol, and heated to 80°C in an ampule for 4 h. On cooling, (+)-muscarine iodide (**1**) crystallized from solution as colorless needles. Recrystallization of the crude material twice from 2-propanol furnished colorless crystals (124 mg, 60%), mp 141–143°C; (lit. (7) mp 138–142°C); $[\alpha]_D^{20}$ +6.3 (*c* 1.0, EtOH) (lit. (7) $[\alpha]_D^{20}$ +6.36 (*c* 0.346, EtOH); IR(KBr) ν: 3374(br, OH), 3016, 2969, 2923, 2906, 2741, 1651, 1486, 1465, 1183, 1100, 1008, 970, 929 cm^{-1}; ^{1}H NMR (D_2O) δ: 1.23(d, J = 6.5, 3H), 2.1(m, 2H), 2.9(br, 1H), 3.25(s, 9H), 3.55(m, 2H), 4.15(m, 2H), 4.65(m, 1H) ppm; ^{13}C NMR (D_2O) δ: 86.9, 78.0, 74.8, 73.4, 56.9, 40.3, 22.0 ppm.

*(+)-Epimuscarine iodide (**7**)*

By the same procedure as described above, (+)-epimuscarine iodide (**7**) was obtained from **6***b* as colorless crystals, mp 169–170°C (lit. (11) mp 175°C); $[\alpha]_D^{20}$ +41.9 (*c* 0.34, EtOH) (lit. (11) $[\alpha]_D^{20}$ +43.23 (*c* 0.636, EtOH); IR(KBr) ν: 3428(br, OH), 2969, 2885, 1653, 1558, 1458, 1065, 1013 cm^{-1}; ^{1}H NMR (D_2O) δ: 1.25(d, J = 6.4, 3H), 1.65(m, 1H), 2.65(m, 1H), 3.20(s, 9H), 3.55(m, 2H), 3.96(m, 1H), 4.25(m, 1H), 4.45(m, 1H) ppm; ^{13}C NMR (D_2O) δ: 83.54, 74.23, 74.04, 73.03, 56.70, 47.55, 16.14 ppm.

Allylation studies

Method O(Mg): To a solution of the aldehyde (1 mmol) in ether (20 mL) at −78°C, allylmagnesium bromide (1 M, 3 mmol) was added dropwise. The mixture was worked up in the usual manner to give the product.

Method A(Zn): A mixture of the aldehyde (1 mmol), allyl bromide (1.5 mmol), and zinc powder (1.5 mmol) in water (20 mL) was stirred at room temperature for 3 h. A few drops of aqueous NH_4Cl was added at the beginning to initiate the reaction. The product was extracted with ether and purified in the usual manner.

*1-Benzyloxy-1-phenyl-5-penten-2-ol (**10**a, **11**a)*

The compound was obtained by Method A(Zn) or Method O(Mg). ^{1}H NMR ($CDCl_3$) δ: (*syn*) 2.05(m, 2H), 2.95(br, 1H), 3.8(m, 1H), 4.2(d, J = 7.7, 1H), 4.35(dd, J = 11.4, 39.3, 2H), 5.0(m, 2H), 5.8(m, 1H), 7.35(m, 10H) ppm; (*anti*) 2.5(m, 2H), 3.9(m, 1H), 4.3(d, J = 1.2, 1H) ppm. The stereochemistry was deduced from ^{1}H NMR spectra of the diols based on the empirical rule of J(CH-OH, *syn*) > J(CH-OH, *anti*) (17) on comparison with similar compounds (18).

*5-Benzyloxy-1-nonanen-4-ol (**10**b, **11**b)*

The compound was obtained by Method A(Zn) or Method O(Mg). ^{1}H NMR ($CDCl_3$) δ: (*syn*) 0.9(t, 3H), 1.35(br, 4H), 1.6(m, 2H), 2.1(br, 1H), 2.3(m, 2H), 3.3(q, J = 5.4, 1H), 3.65(m, 1H), 4.56(dd, J = 11.3, 21.2, 2H), 5.1(m, 2H), 5.85(m, 1H), 7.35(m, 5H) ppm; (*anti*) 3.4(m, 1H), 3.85(m, 1H), 4.6(br, 2H) ppm (19).

*2-Benzyloxy-5-hexen-3-ol (**10**c, **11**c)*

The compound was obtained by Method A(Zn) or Method O(Mg). ^{1}H NMR ($CDCl_3$) δ: (*syn*) 1.20(d, J = 6.0, 3H), 2.2–2.5(m, 2H), 3.5(m, 2H), 4.6(dd, 2H), 5.15(m, 2H), 5.85(m, 1H), 7.35(m, 5H) ppm; (*anti*) 1.19(d, J = 6.3, 3H), 2.25(m, 2H), 3.5(m, 1H), 3.8(m, 1H) ppm (20).

Acknowledgement

C.J.L. thanks the Faculty of Graduate Studies and Research for a Max Bell Fellowship and a Dalbir Bindra Fellowship. We thank the Natural Sciences and Engineering Research Council of Canada (NSERC), Fonds de la recherche en santé du Québec (FRSQ), and Fonds pour la formation de chercheurs et l'aide à la recherche (FCAR) for financial support.

Can. J. Chem. Downloaded from www.nrcresearchpress.com by 109.225.110.28 on 09/08/12
For personal use only.

1. C. H. Eugster and P. G. Waser. Experientia, **10**, 298 (1954).
2. P. C. Wang and M. M. Joullie. The alkaloids. Vol. XXIII. *Edited by* A. Brossi. Academic Press, New York. 1984. pp. 327–380.
3. R. R. Levine and N. J. M. Birdsdall. Trends Pharmacol. Sci. 10. Suppl. Subtypes Muscarinic Recept. IV. Elsevier, Cambridge. 1989.
4. M. C. Pirrung and C. V. DeAmicis. Tetrahedron Lett. **29**, 159 (1988).
5. J. Adams, M. A. Poupart, and L. Grenier. Tetrahedron Lett. **30**, 1753 (1989).
6. S. Tankano, Y. Iwabuchi, and J. Ogasawara. J. Chem. Soc. Chem. Commun. 1371 (1989).
7. M. D. Amici, C. D. Micheli, G. Molteni, D. Pitre, G. Carrea, S. Riva, S. Spezia, and L. Zetta. J. Org. Chem. **56**, 67 (1991).
8. R. Quirion, I. Aubert, P. A. Lapchak, R. P. Schaum, S. Teolis, S. Gauthier, and D. M. Araujo. *In* Trends Pharmacol. Sci. 10. Suppl. Subtypes Muscarinic Recept. IV. *Edited by* R. R. Levine and N. J. M. Birdsdall. Elsevier, Cambridge. 1989. pp. 80–88.
9. (*a*) K. Uneyama, N. Kamaki, A. Moriya, and S. Torii. J. Org. Chem. **50**, 5396 (1985); (*b*) C. Petrier, J. Einhorn, and J. L. Luche. Tetrahedron Lett. **26**, 1449 (1985); (*c*) C. Petrier and J. L. Luche. J. Org. Chem. **50**, 910 (1985); C. Einhorn and J. L. Luche. J. Organomet. Chem. **322**, 177 (1987); (*d*) S. R. Wilson and M. E. Guazzaroni. J. Org. Chem. **54**, 3087 (1989).
10. T. H. Chan and C. J. Li. Organometallics, **9**, 2649 (1990); C. J. Li and T. H. Chan. Organometallics, **10**, 2548 (1991).
11. S. Rychnovsky and P. A. Bartlett. J. Am. Chem. Soc. **103**, 3963 (1981); R. Amouroux, B. Gerin, and M. Chastrette. Tetrahedron Lett. **23**, 4341 (1982); Tetrahedron, **41**, 5321 (1985); J. Mulzer, A. Angermann, W. Munch, G. Schlichthorl, and A. Hentzschel. Ann. 7 (1987); S. Hatakeyama, K. Sakurai, and S. Takano. Heterocycles, **24**, 633 (1986).
12. D. J. Cram and F. A. Abd Elhafez. J. Am. Chem. Soc. **74**, 5828 (1952).
13. (*a*) M. T. Reetz. Angew. Chem. Int. Ed. Engl. **23**, 556 (1984); (*b*) C. H. Heathcock, S. I. Kiyooka, and T. A. Blumenkopf. J. Org. Chem. **49**, 4214 (1984); M. M. Midland and R. W. Koops. J. Org. Chem. **55**, 5058 (1990).
14. (*a*) B. Weidmann and D. Seebach. Angew. Chem. Int. Ed. Engl. **22**, 31 (1983); M. T. Reetz. Chem. Ind. (London), 541 (1981); (*b*) G. E. Keck, W. J. Hehre, and S. D. Kahn. Tetrahedron Lett. **28**, 279 (1987).
15. H. Nagaoka and Y. Kishi. Tetrahedron, **37**, 3873 (1981).
16. T. Kunz and H-U. Reizig. Liebigs Ann. Chem. 891 (1989).
17. M. Fujita and T. Hiyama. J. Am. Chem. Soc. **106**, 4629 (1984).
18. M. Asami and R. Kimura. Chem. Lett. 1221 (1985).
19. G. E. Keck and E. P. Boden. Tetrahedron Lett. **25**, 1879 (1982).
20. M. T. Reetz, K. Kesseler, S. Schmidtberger, B. Wenderoth, and R. Steinbach. Angew. Chem. Int. Ed. Engl. **22**, 989 (1983).
21. R. E. Ireland, S. Thaisrivongs, and P. H. Dussault. J. Am. Chem. Soc. **110**, 5768 (1980); W. C. Still and J. A. Schneider. Tetrahedron Lett. **21**, 1035 (1980); J. A. Marshall and G. P. Luke. J. Org. Chem. **56**, 483 (1981).

Can. J. Chem. Downloaded from www.nrcresearchpress.com by 109.225.110.28 on 09/08/12
For personal use only.

Competitive Diels–Alder and ene addition of *N*-arylmaleimides to 7-dehydrocholesteryl acetate

WILLIAM J. LEIGH,[1] DONALD W. HUGHES, AND D. SCOTT MITCHELL[2]
Department of Chemistry, McMaster University, Hamilton, Ont., Canada L8S 4M1

Received April 21, 1992

WILLIAM J. LEIGH, DONALD W. HUGHES, and D. SCOTT MITCHELL. Can. J. Chem. **70**, 2730 (1992).

Thermolysis of *N*-phenyl, *N-para*-biphenyl, and *N-para,para'*-terphenylmaleimide with 7-dehydrocholesteryl acetate in benzene solution at 200°C yields mixtures of four cycloadducts in relative yields that are essentially independent of the maleimide substituent. The three major products are those of ene addition to C_7 of the steroid with abstraction of the proton at C_9 or C_{14}. The α-*endo*-Diels–Alder adduct is formed as a minor product. The structures of the adducts have been elucidated on the basis of one- and two-dimensional ^1H and ^{13}C NMR spectroscopic techniques, including homonuclear ^1H decoupling, NOE, ^1H–^1H COSY, heteronuclear ^1H–^{13}C shift correlation, and TOCSY 2-D experiments, and the results of molecular mechanics (MMX) calculations. The combination of these techniques has made it possible to almost completely assign the ^1H and ^{13}C NMR spectra for two of the ene adducts and the Diels–Alder adduct from reaction of 7-dehydrocholesteryl acetate with *N*-phenyl maleimide.

WILLIAM J. LEIGH, DONALD W. HUGHES et D. SCOTT MITCHELL. Can. J. Chem. **70**, 2730 (1992).

La thermolyse des *N*-phényl, *N-para*-biphényl et *N-para,para'*-terphénylmaléimides en présence d'acétate du 7-déhydrocholestéryle, en solution dans le benzène, à 200°C, fournit des mélanges de quatre cycloadduits dont les rendements relatifs sont essentiellement indépendants du substituant de la maléimide. Les trois produits principaux correspondent à une addition ène sur la position C_7 du stéroïde, accompagnée d'un enlèvement de proton en C_9 ou en C_{14}. L'adduit de Diels–Alder α-*endo* se forme comme produit mineur. On a déterminé les structures à l'aide de techniques de RMN du ^1H et du ^{13}C, uni- et bidimensionnelles, comprenant des expériences de découplage homonucléaire du ^1H, d'eOn, de COSY ^1H–^1H, de corrélation hétéronucléaire de déplacements ^1H–^{13}C et des expériences TOCSY en 2-D, et de résultats de calculs de mécanique moléculaire (MMX). Grâce à l'ensemble de ces techniques, il a été possible d'attribuer pratiquement tous les spectres RMN du ^1H et du ^{13}C de deux des adduits ène et de l'adduit de Diels–Alder obtenus par la réaction de l'acétate du 7-déhydrocholestéryle avec la *N*-phénylmaléimide.

[Traduit par la rédaction]

Introduction

The reactions of steroidal dienes such as 7-dehydrocholesterol (**1**) and ergosterol (**2**) with common dienophiles have been studied in some detail (1–13). Acyclic dienophiles such as dialkyl azocarboxylates (1–3), dimethyl acetylenedicarboxylate (4), acrylonitrile (5), and carbonyl dicyanide (6) have been reported to undergo ene addition with **1** (1–5), **2** (6), and the corresponding acetate esters to the complete exclusion of Diels–Alder cycloaddition. Evidently, Diels–Alder addition is preferred only with particularly powerful dienophiles such as *N*-phenyltriazolinedione (7, 8), 1,4-phthalazinedione (9), or singlet oxygen (10), or with acyclic alkenes when the steroidal diene moiety is part of a higher conjugated system (11).

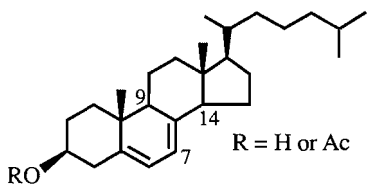

1

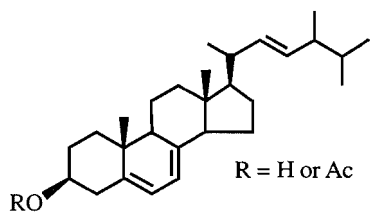

2

The reaction of maleic anhydride with ergosteryl acetate, which was first investigated almost 60 years ago (12), has been the subject of some confusion over the years (12–14). The reaction is now known to yield a mixture of the ene and Diels–Alder adducts shown in eq. [1] (14). The structures of the four products (**3–5**) have been assigned on the basis of derivativization studies and ^1H NMR spectroscopy (14), following the pioneering studies of Huisman and co-workers on the reactions of dienophiles with 7-dehydrocholesteryl acetate (**1**) (1, 3).

As part of our continuing studies of the effects of thermotropic liquid crystals on the reactivity of guest molecules (15), we have investigated the reaction of **1** with a series of *N*-aryl maleimides (**6–8**). A preliminary account of the reaction of **7** with **1** in isotropic and steroidal liquid crystalline solvents has been published (16). As is the case with maleic anhydride and **2**, a mixture of Diels–Alder and ene adducts are obtained as the major products from this reaction (eq. [2]). The three ene adducts were originally identified on the basis of diagnostic similarities between their ^1H NMR spectra and those of the ene adducts of **1** with acyclic dienophiles (1, 3).

[1]Natural Sciences and Engineering Research Council of Canada University Research Fellow, 1983–1993. Author to whom correspondence may be addressed.

[2]Present address: Uniroyal Chemical Limited, Guelph, Ont.

Can. J. Chem. Downloaded from www.nrcresearchpress.com by 109.225.110.28 on 09/08/12
For personal use only.

Can. J. Chem. Downloaded from www.nrcresearchpress.com by 109.225.110.28 on 09/08/12
For personal use only.

[1] 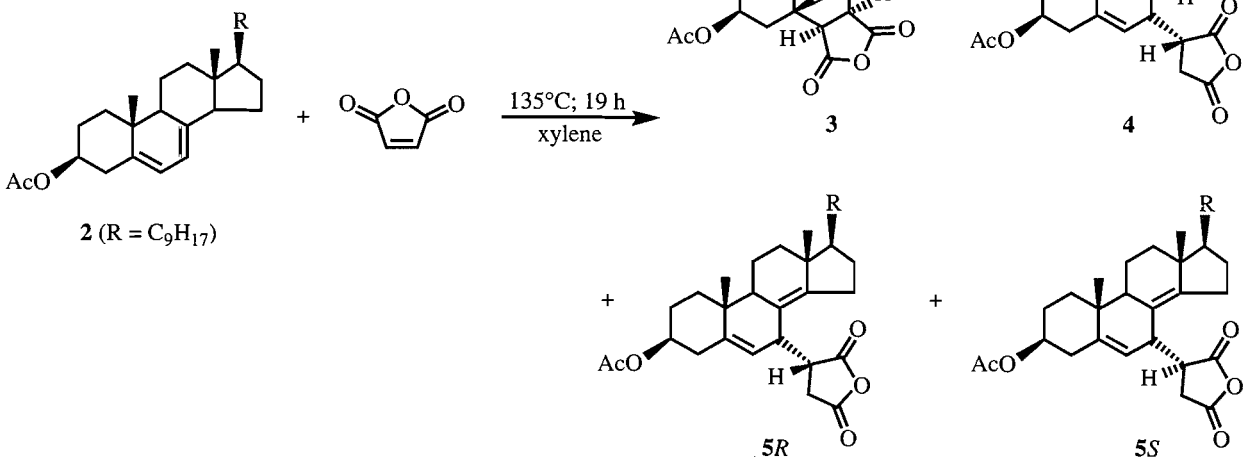

2 (R = C_9H_{17})

3 4 5R 5S

6 7 8

[2] 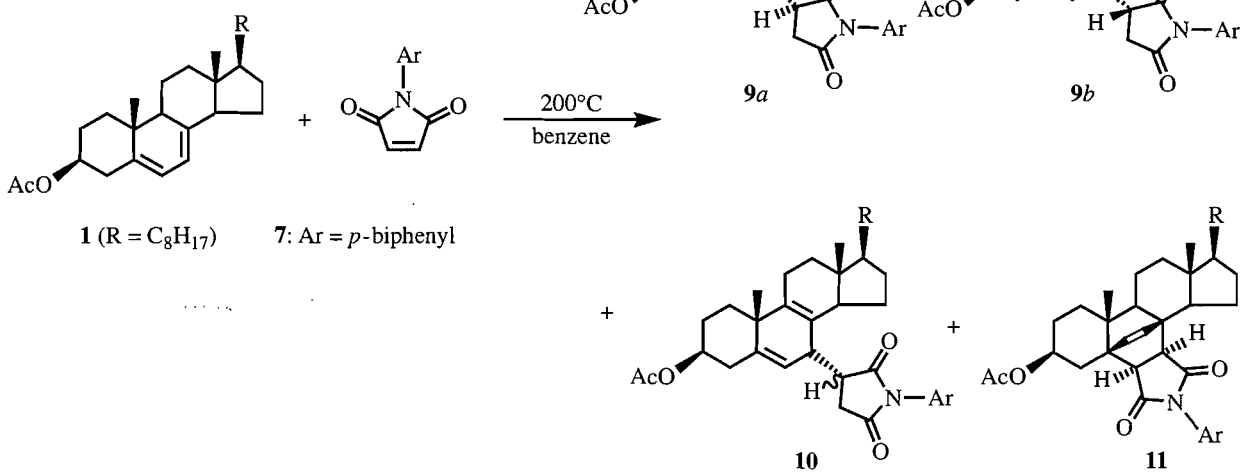

1 (R = C_8H_{17}) 7: Ar = *p*-biphenyl

9a 9b 10 11

In this paper, we report the results of a study of the reaction of **6–8** with **1** in benzene solution. We were particularly interested in rigorously verifying our structural assignments for **9** and **10**, which were made on the basis of ^{1}H chemical shift arguments following the rationale developed by Huisman and co-workers in identifying the ene adducts of **1** with dimethyl acetylenedicarboxylate (**12**) (eq. [3]) (4). The chemical shifts of the 18- and 19-methyl protons are very different in the ^{1}H NMR spectra of **13** and **14**. From examination of molecular models, Huisman and co-workers reasoned that the geometry of 18-CH_3 in relation to the C_8—C_9 double bond in **14** should result in its protons experiencing greater shielding than the corresponding ones in **13**. The methyl-proton regions of the ^{1}H NMR spectra of **9***a*,*b* and **10** (Ar = *para*-biphenyl) bear marked similarities to those of **13** and **14**, and our initial structural assignments were made on this basis. This same rationale has been used by numerous other workers in assigning the

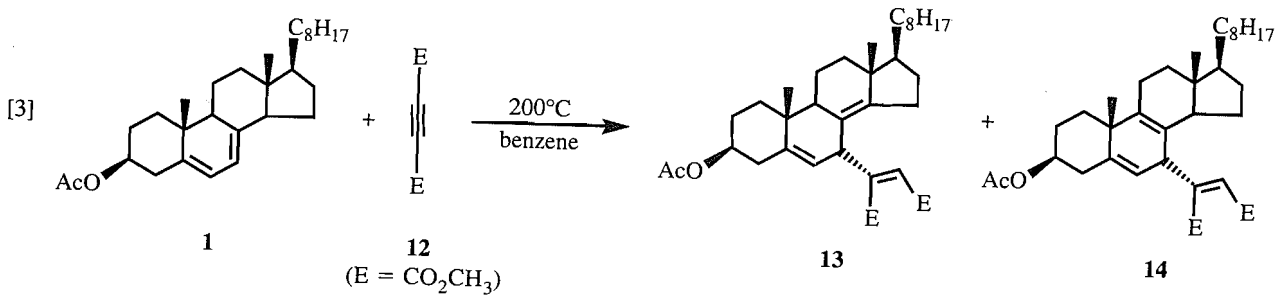

1 12 ($E = CO_2CH_3$) 13 14

structures of the products of ene additions to steroidal dienes (1–3, 5, 6, 14), but has evidently never been verified using modern NMR techniques.

In the present work, we attempted to verify our initial assignments using a more rigorous spectroscopic approach. We carried out various two-dimensional chemical shift correlation experiments, in order to assign the individual resonances in the rather complex ^1H and ^{13}C NMR spectra of these molecules. For three of the adducts, we also carried out homonuclear proton decoupling, NOE, and TOCSY 2-D experiments to help identify individual protons whose assignments on the basis of the other 2-D experiments are inconclusive. Molecular mechanics (MMX) calculations were also carried out in order to assist in our assignments in some cases. In particular, we wondered if it might be possible to conclusively identify the differences in the structures of the B and C rings in the two adduct types, through complete assignment of the B-, C-, and D-ring carbon and proton resonances. As shown in the partial structures below, differentiation of the two adduct structures is possible if the protons at C-11, C-12, C-15, and C-9/14 can be rigorously identified. We also employed these methods to establish the stereochemistry in the Diels–Alder adduct **11**, in order to verify the assignment made by Jones *et al.* for the Diels–Alder adduct (**3**) obtained from the reaction of ergosteryl acetate (**2**) with maleic anhydride (14).

The reaction of **1** and **6–8** in liquid crystalline solvents, which was the reason for our initial interest in this system, is described in a separate publication (17).

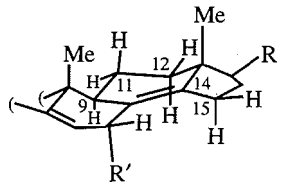

9

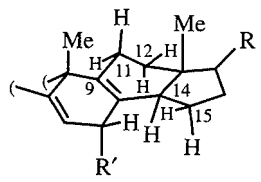

10

Results and discussion

N-Biphenyl- and *N*-terphenylmaleimide (**7** and **8**, respectively) were synthesized by condensation of the appropriate aromatic amine with maleic anhydride, following the method of Crivello (18).

Reaction of **6–8** with equimolar **1** was carried out at 200°C in benzene solution in sealed tubes. Monitoring the progress of small-scale runs in deuteriobenzene by ^1H NMR and high-performance liquid chromatography (HPLC) showed that the reaction proceeds to ca. 70% completion after 4 h under these conditions in each case. The products were isolated and purified by semi-preparative medium-pressure chromatography, using a combination of normal- and reverse-phase conditions. The reaction produced four main products in each case (eq. [2]), and one minor product in yields that were too low (6–7%) to enable isolation. The distribution of adducts is independent of the aryl substituent in **6–8**, within experimental error. Ene adducts **9***a* and **9***b* are formed in ca. 34 and 25% yield, respectively, ene adduct **10** is formed in ca. 13% yield, and the Diels–Alder adduct **11** is formed in ca. 20% yield. Product yields were determined by quantitative HPLC analyses. It is interesting to note that the distributions of adducts obtained from reaction of **1** with the series of *N*-aryl maleimides are very similar to that reported for the reaction of **2** with maleic anhydride (14).

Preliminary structure assignments for **9–11** (Ar = *para*-biphenyl) were made on the basis of their high-field ^1H and ^{13}C NMR spectra in deuteriochloroform solution, as well as their infrared and chemical ionization mass spectra. For each adduct, DEPT ^{13}C NMR spectra were recorded to distinguish between C/CH_2 and CH/CH_3 resonances. Heteronuclear ^1H-^{13}C shift correlated spectra, ^1H–^1H COSY, and TOCSY experiments were then recorded to establish ^1H–^{13}C and ^1H–^1H connectivities (19). The high-field ^1H and ^{13}C NMR spectra of the adducts were essentially independent of the *N*-aryl substituent, except of course in the aromatic regions.

The ^1H NMR spectra of ene adducts **9***a* and **10** and the Diels–Alder adduct **11** (Ar = phenyl) were investigated in greater detail, in an attempt to establish the differences in the structures of the B and C rings for the first two molecules, and to rigorously establish the stereochemistry of addition in the case of the third. Figure 1 shows the 500 MHz ^1H NMR spectra of **9***a* and **10**, illustrating the pronounced differences in the methyl proton resonances in the 0.8–1.3 ppm region for the two adduct types, and the slightly more subtle differences that occur elsewhere in the spectra. Figures 2 and 3 show contour plots obtained from the ^1H–^1H COSY and the ^1H–^{13}C shift-correlated spectra of adduct **9***a*, respectively. The pertinent details of our spectral assignments for compound **9***a* are presented below, along with a brief description of the assignments for **9***b*, **10**, and **11** where they differ from those of **9***a*. The ^1H and ^{13}C NMR spectra of **1** (which have been completely assigned (20)) and those of other, similar cholestane steroids (21–23) were especially helpful in deriving the spectral assignments for these compounds. It should be noted that while eq. [2] specifically identifies **9***a* as having *R* stereochemistry at C-1′ of the maleimide ring, we are actually not able to distinguish between the two diastereomers on the basis of our NMR data.

The TOCSY 2-D experiment provides a means of reveal-

Can. J. Chem. Downloaded from www.nrcresearchpress.com by 109.225.110.28 on 09/08/12
For personal use only.

Can. J. Chem. Downloaded from www.nrcresearchpress.com by 109.225.110.28 on 09/08/12
For personal use only.

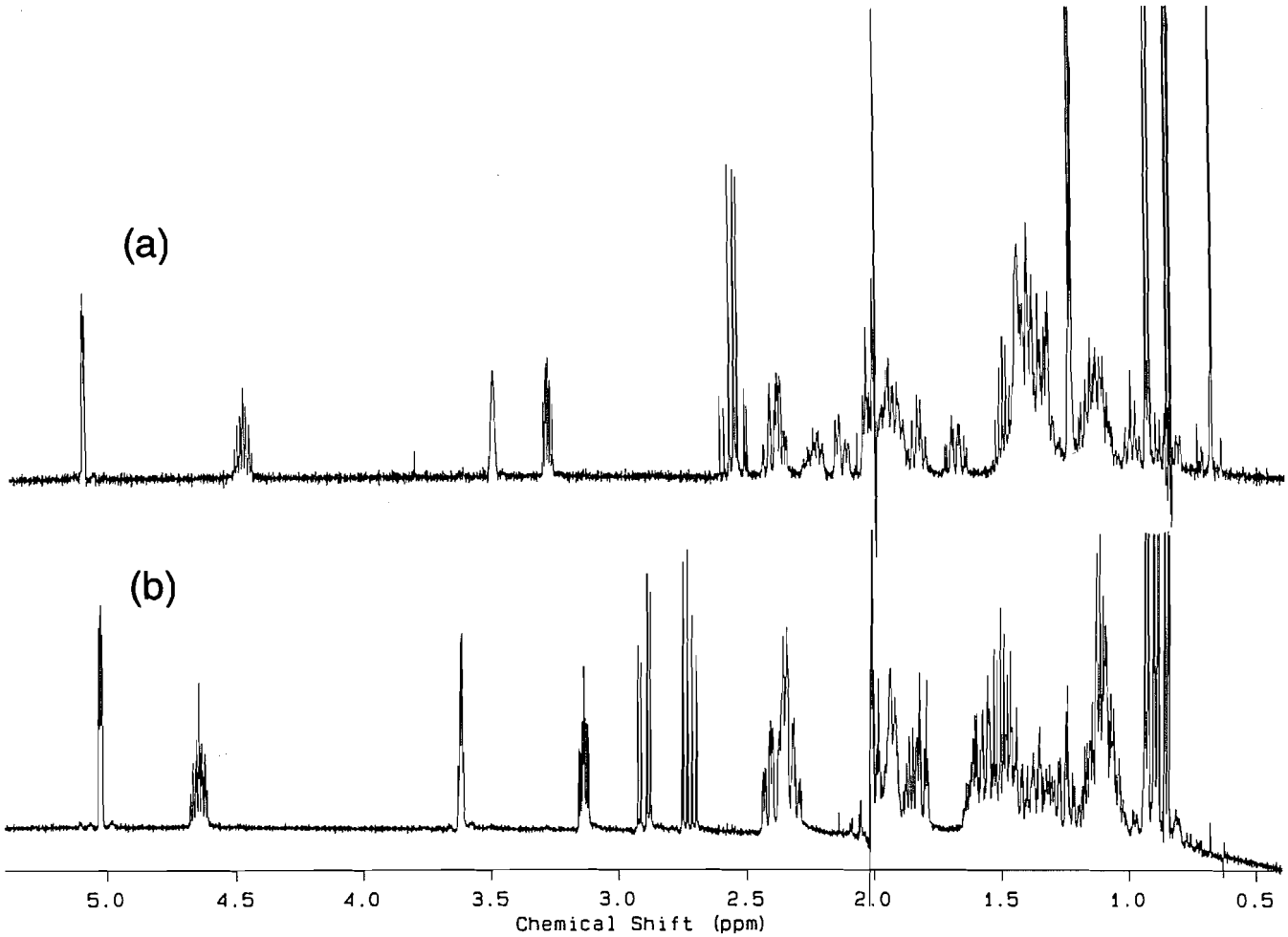

FIG. 1. High-field (500 MHz) ^{1}H NMR spectra (0–5.1 ppm region) of (*a*) **9***a* (Ar = phenyl) and (*b*) **10** (Ar = phenyl) in $CDCl_3$ solution.

ing coherence transfer throughout a spin system and will produce cross-peaks between protons that are not spin-coupled but belong to the same spin system. In principle, this technique should be able to resolve entire spin systems for specific steroid rings. To illustrate the application of the TOCSY method, Fig. 4 displays cross sections taken through the C-15 and C-3 protons of steroid **9***a*. For the former, correlations are observed not only to all the other ring-D protons but also to H-20 (overlapped by H-16α) and the 21-CH_3 protons. Similarly, all the A-ring protons were resolved by the observation of TOCSY correlations between H-3α and the C-1 protons. Figure 5 displays the TOCSY contour plot of Diels–Alder adduct **11**, obtained with an 80 ms spin-lock time.

The ^{1}H and ^{13}C NMR chemical shifts and ^{1}H–^{1}H spin coupling constants for **9***a*, **10**, and **11** (Ar = phenyl) are tabulated in Tables 1 and 2, respectively, while the results of the ^{1}H–^{1}H NOE experiments are listed in Table 3. The proton chemical shifts and coupling constants presented in Tables 1 and 2 were not refined by iterative spectral simulation. Interpretation of the information obtained from the NOE experiments was assisted by consideration of energy-minimized structures of the adducts determined from molecular mechanics (MMX) calculations. The results of these calculations are shown in Figure 6. Vicinal ^{1}H–^{1}H coupling constants, calculated from the energy-minimized structures of **9–11** using the equation included in the molecular mechanics software package (see experimental section), are included in Table 2 for comparison to the experimentally determined values. All of the adducts exhibited IR and mass spectral properties that were consistent with their proposed structures. ^{1}H and ^{13}C NMR assignments for **9***b* (Ar = *p*-biphenyl) are collected in the experimental section.

(i) Spectral assignments: ene adduct **9**a

The general strategy for assigning the ^{1}H spectrum was to begin with the olefinic proton H-6 at 5.03 ppm and H-3α at 4.65 ppm and establish both through-bond and through-space connectivities with neighbouring protons and then proceed into the adjacent ring spin systems. Through-space connectivity was provided by NOE difference experiments and this information was examined in relation to the energy-minimized structure of the molecule (Fig. 6*a*). In the COSY-45 contour plot of **9***a*, H-6 displayed cross-peaks with protons at 3.62 and 2.31 ppm. The 3.62 ppm multiplet correlates with a signal at 3.14 ppm that appears as the X part of an isolated ABX spin system arising from the C-1′ and C-2′ protons (3.14 and 2.90, 2.73 ppm, respectively) of the *N*-phenyl substituted imide ring. This dictates that the 3.62 ppm multiplet must be assigned to H-7.

Can. J. Chem. Downloaded from www.nrcresearchpress.com by 109.225.110.28 on 09/08/12
For personal use only.

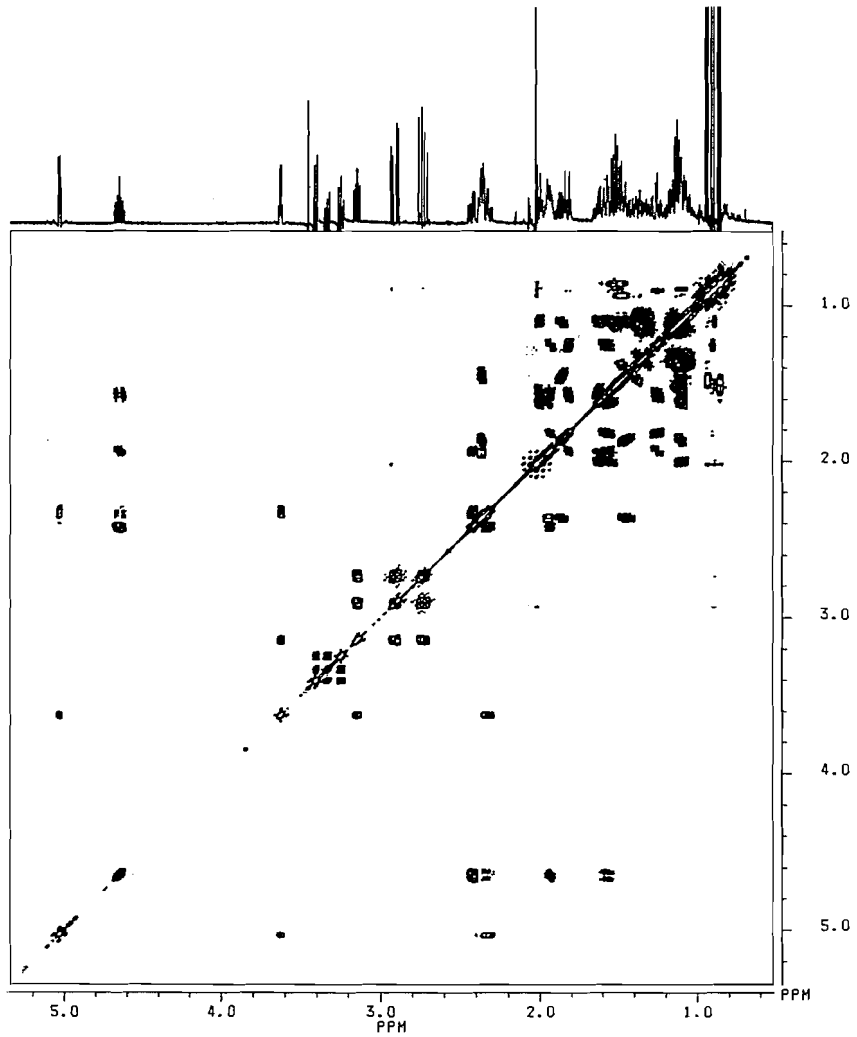

FIG. 2. COSY-45 spectrum of **9***a* in $CDCl_3$ solution.

Proton H-7 also shows a correlation with the complex multiplet at 2.31 ppm. Closer examination of the 2.31 ppm signal revealed that it overlaps with a two-proton multiplet and that it is coupled to the signal at 2.49 ppm as well as to H-3α at 4.65 ppm. Proton H-3α was also coupled to the signal at 2.49 ppm. These COSY connectivities suggest that the 2.31 and 2.49 ppm signals arise from the protons on C-4. Presumably, the cross-peaks between 2.31 ppm and H-6 and H-7 are due to long-range coupling over four and five bonds, respectively. Differentiation of the C-4 protons was achieved by NOE experiments. Saturation of the 19-CH_3 signal at 0.90 ppm resulted in an enhancement of the C-4 proton at 2.31 ppm, allowing it to be assigned to H-4β. Similarly, saturation of H-3α enhanced the H-4α signal at 2.49 ppm.

The identification of H-4β provided a means for determining if H-7 occupies an α or β position by using the stereochemical dependence of the five-bond homoallylic coupling between these protons. Maximum homoallylic coupling is observed when both coupled nuclei are 90° above or below the plane of the double bond (24). In this case with the geometry of H-4β being fixed, the 3.5 Hz five-bond coupling can only arise with H-7 being in a β position as shown in Fig. 6*a*. Furthermore, in an NOE experiment where H-7 was saturated there was an enhancement of a multiplet later identified as H-15α,β. This NOE result can be accounted for provided H-7 is in the β position. The structure in Fig. 6*a* indicates an average internuclear distance of 2.4 Å between H-7β and H-15α,β. During this NOE experiment H-6 and H-1′ were also enhanced.

The assignment of the A-rings protons was completed by following the cross-peaks in the COSY-45 spectrum from H-3α to the multiplets corresponding to the C-2 protons (1.93 and 1.57 ppm) and then from the C-2 protons to the C-1 methylene protons at 1.25 and 1.82 ppm. The α and β protons were identified in an NOE experiment where the 19-CH_3 was saturated (Tables 1 and 3). Additional confirmation of the H-2α assignment was provided by the observation of a four-bond W-type coupling (2.2 Hz) between H-4α and H-2α. A four-bond coupling was also detected between H-1α and the 19-CH_3 in the COSY spectrum.

Only a limited number of protons on the C and D rings and on the C-17 side chain could be identified from the ^1H spectrum because of the high degree of signal overlap in the 0.5–1.7 ppm region. A four-bond coupling resulted in a cross-peak being observed in the COSY-45 between the 18-CH_3 and H-12α (1.10 ppm) protons. Methyls 26 and 27 correlated with the H-25 multiplet centred at 1.51 ppm. Proton

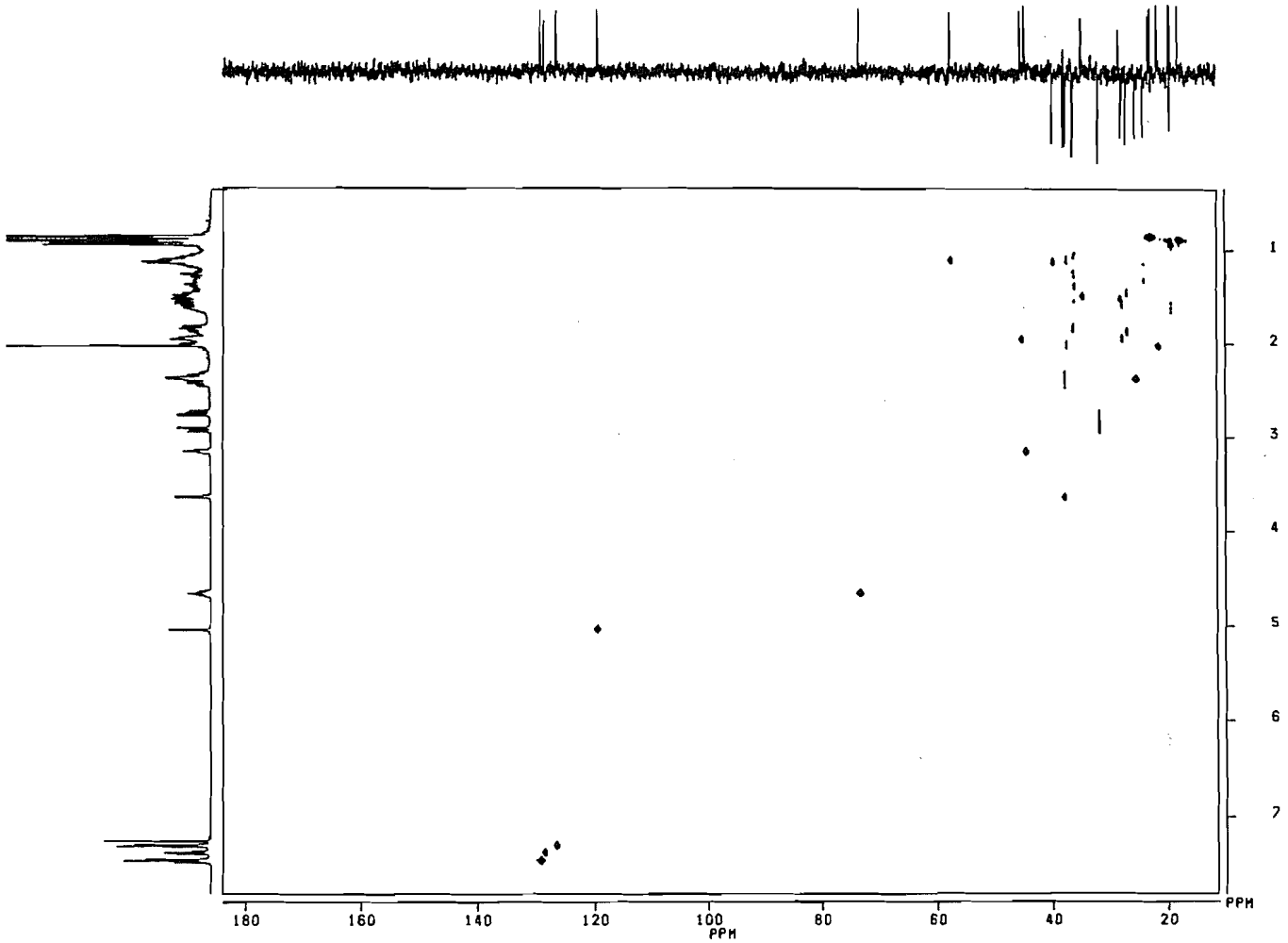

FIG. 3. $^{1}H-^{13}C$ shift correlation spectrum of **9***a* in $CDCl_3$ solution. The ^{13}C spectrum is shown as the DEPT spectrum.

H-20 was assigned to 1.48 ppm on the basis of its correlation with the 21-CH_3 doublet at 0.93 ppm.

The $^{1}H-^{13}C$ 2-D shift correlation experiment allows assignment of the remaining proton resonances and facilitates the analysis of the ^{13}C spectrum. A preliminary assignment of the ^{13}C NMR spectrum (Table 1) was achieved by the DEPT technique and by comparison with literature data (22, 23). Olefinic carbons 5 and 6 could be readily assigned by these methods to 145.9 and 119.3 ppm, respectively. However, the assignment of carbons 8 and 14 remains tentative.

Cross sections from the shift correlation spectra were particularly useful for assigning both the aliphatic carbons and their corresponding directly bonded protons. Since the A-ring protons were already identified, this simplified the assignment of carbons 1 through 4 (Table 1). There was an overlap of the C-4 and C-7 resonances. In the C ring, the previously assigned H-12α (1.10 ppm) was correlated with the carbon at 37.3 ppm. The cross section through this carbon resonance located H-12β (2.00 ppm), which was overlapped by the acetate methyl singlet. The C-11 methylene protons (1.63 and 1.53 ppm) were revealed in the COSY-45 spectrum by the cross-peaks with the C-12 protons. The C-11 carbon (19.1 ppm) was difficult to assign because of overlap with the 19-CH_3.

The resolution of the methine carbon signals between 40 and 75 ppm made it possible to assign the H-17α and H-9α protons (Table 1), which were obscured in the ^{1}H NMR spectrum. Identification of H-17α provided the means for assigning the other D-ring protons since a cross-peak was detected in the COSY spectrum to the multiplet eventually assigned to H-16β (1.83 ppm). The combination of the COSY and shift correlation data indicated that the C-16 methylene protons were at 1.83 and 1.46 ppm. Their designation as α (1.46 ppm) and β (1.83 ppm) is tentatively based on the coupling constants estimated from these multiplets (Table 3) (19, 22). However, it should be noted that this method of assignment is considered controversial (21). Both C-16 protons show correlations with an unresolved multiplet overlapping H-4β at 2.36 ppm; by elimination, this multiplet can be assigned to the H-15α,β protons. In the cross section through the shift correlation spectrum, H-15α,β appeared as a singlet connected to the carbon at 25.2 ppm, indicating that these methylene protons are in fact equivalent. The assignment of the C-17 side-chain protons and carbons relied on the COSY and shift correlation spectra and comparisons with literature data.

The TOCSY 2-D experiment, which produces cross-peaks between protons that are not coupled but belong to the same spin system, provided additional confirmation of some of the ^{1}H assignments. In particular, all the A-ring protons

Can. J. Chem. Downloaded from www.nrcresearchpress.com by 109.225.110.28 on 09/08/12
For personal use only.

Can. J. Chem. Downloaded from www.nrcresearchpress.com by 109.225.110.28 on 09/08/12
For personal use only.

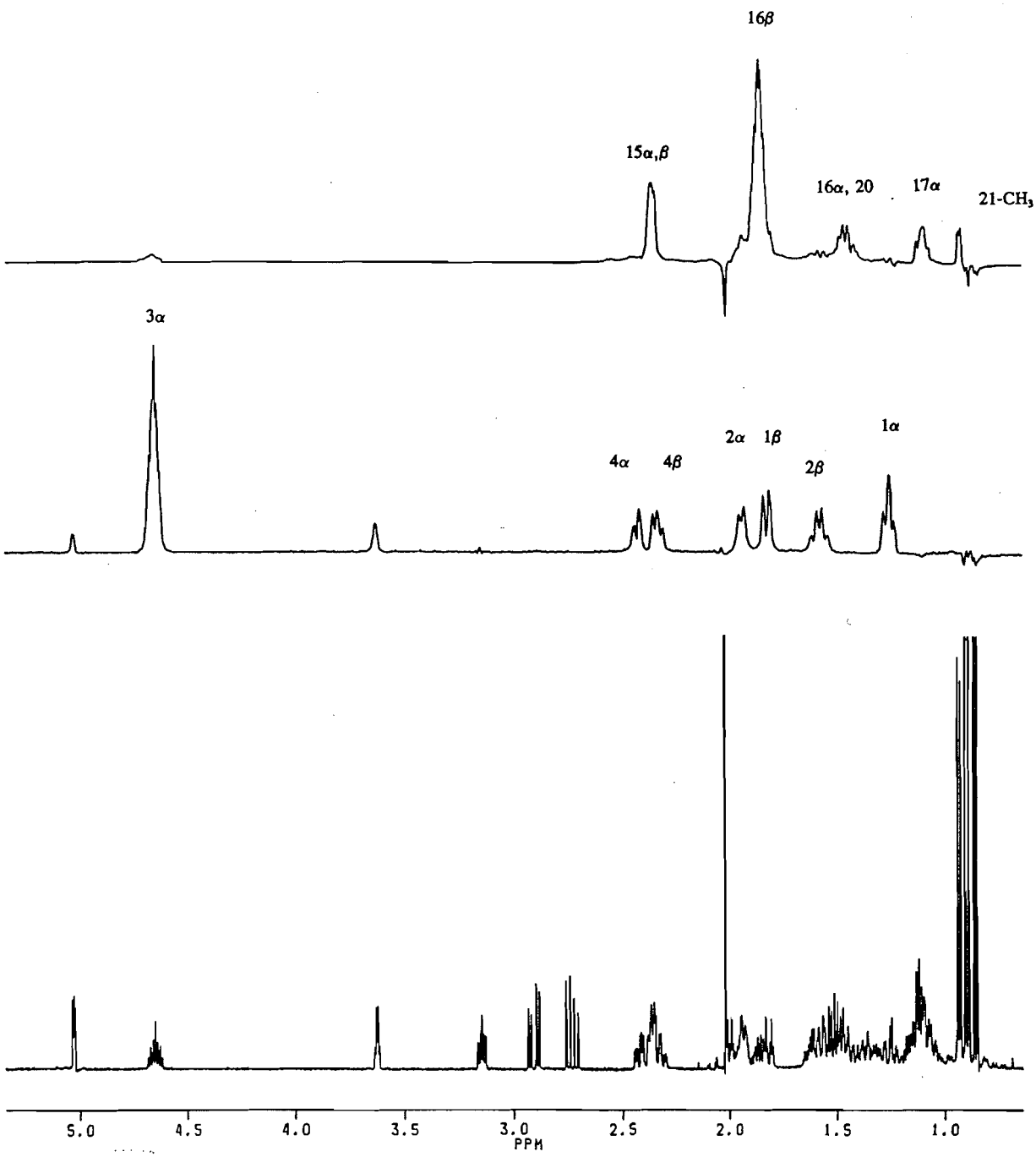

FIG. 4. Cross sections taken from the TOCSY spectrum of adduct **9***a* showing the resolution of the protons in rings A and D (middle and top spectra, respectively). The correlation between H-15α,β and the 21-CH_3 indicate coherence transfer occurring over six bonds.

could be identified by taking a cross section through the H-3α signal. In addition to the normal correlations with the C-2 and C-4 protons, H-3α also shows TOCSY cross-peaks to the C-1 protons at 1.25 and 1.82 ppm. An interesting result was the observation of TOCSY correlations through the entire D-ring spin system between 21-CH_3 and the C-15 protons (Fig. 4, top). In the cross section through 21-CH_3, the only proton not clearly observed was H-20, which was overlapped with the multiplet from H-16α. The H-15 to 21-CH_3 proton correlation indicates coherence transfer occurring between nuclei separated by six bonds. Unfortunately, the H-9/H-11/H-12 correlation could not be clearly observed due to overlap of the broad H-9 proton resonance with other signals.

(ii) Spectral assignments: ene adduct **9**b

The ^1H and ^{13}C spectra of **9***b* appear to be somewhat different from those of **9***a*, though they are essentially identical in the 0.8–1.0 ppm (methyl) regions. ^1H–^1H COSY and ^1H–^{13}C shift-correlated spectra of **9***b* (Ar = biphenyl), made in identical fashion to those for **9***a* (*vide supra*), allow sufficiently detailed assignment of the ^1H spectrum to conclude that the main differences between the spectra of **9***a*,*b* are associated with the B-ring carbons (C-6–C-9) and their corresponding protons. This is consistent with the identifi-

Can. J. Chem. Downloaded from www.nrcresearchpress.com by 109.225.110.28 on 09/08/12
For personal use only.

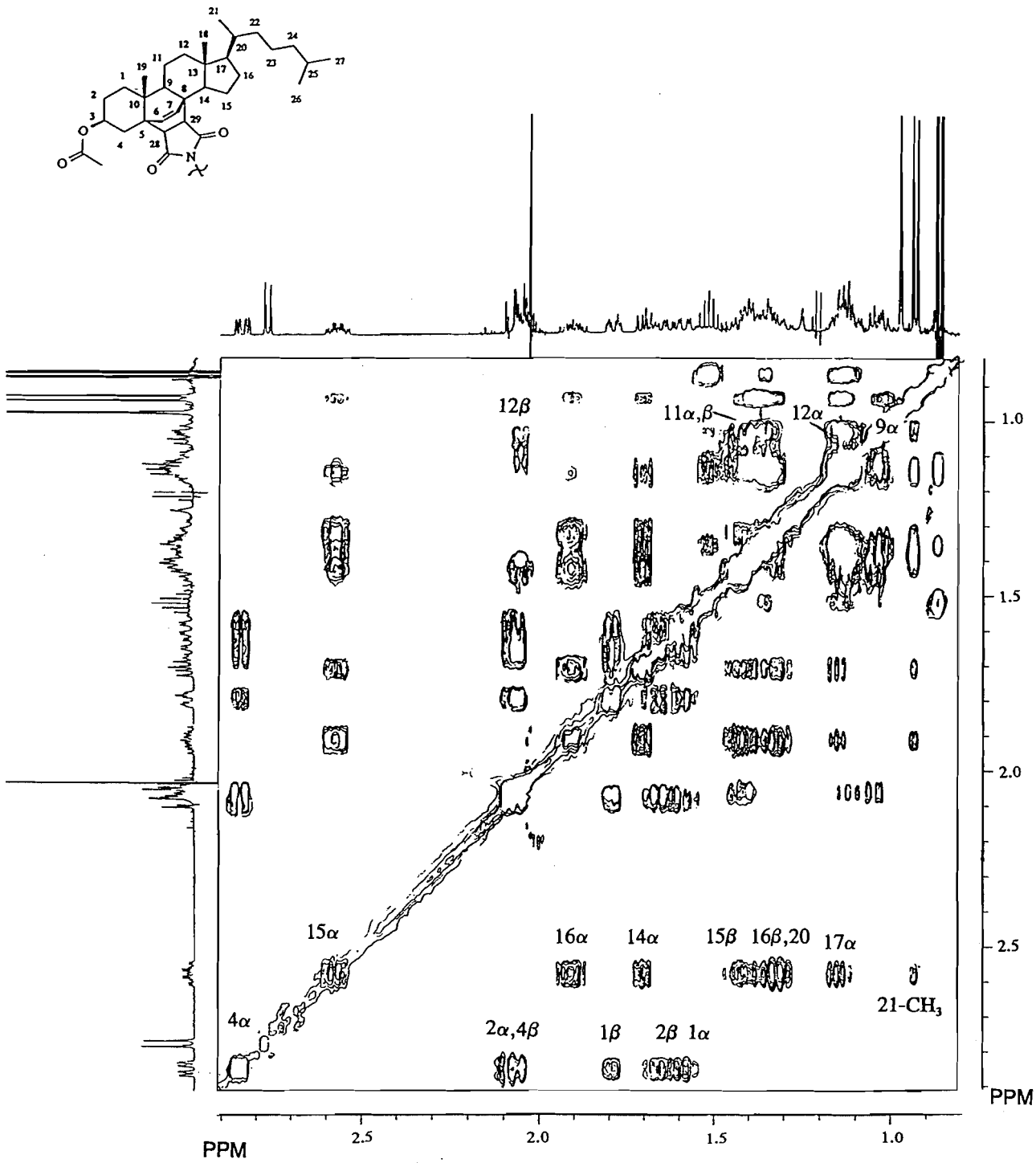

FIG. 5. TOCSY contour plot of the region from 0.8 to 2.9 ppm for adduct **11** (Ar = phenyl), recorded with an 80 ms spin-lock time.

cation of **9*a*** and **9*b*** as diastereomers differing only in the stereochemistry at the 1′-position of the maleimide ring. In the ^{1}H NMR spectrum of **9*b***, H-6 appears at 5.51 ppm (cf. 5.03 ppm in **9*a***), H-7β appears at 3.16 ppm (cf. 3.62 ppm in **9*a***), and H-9α appears at 2.25 ppm (cf. 1.94 ppm in **9*a***). Also, the H-15 protons are shifted to 2.17 and 2.27 ppm, from their position of 2.36 in **9*a***. The remaining protons in **9*b*** appear within 0.06 ppm of their positions in the spectrum of **9*a***.

The main differences in the ^{13}C spectrum are due to C-5 (143.6 ppm), C-6 (121.5 ppm), C-7 (39.9 ppm), C-8 (125.9 ppm), and C-9 (44.0 ppm), to be compared with the corresponding resonances in **9*a*** (145.9, 119.3, 37.6, 132.0, and 45.1 ppm, respectively). Also, the C-1′ and C-2′ resonances are shifted to 45.7 and 33.9 ppm, respectively, from their positions in the spectrum of **9*a***. The remaining resonances in the ^{13}C NMR spectrum of **9*b*** are within 0.4 ppm of their positions in the spectrum of **9*a***.

The assigned ^{1}H and ^{13}C resonances for this compound are listed in the experimental section.

TABLE 1. ^1H and ^{13}C chemical shifts for **9***a*, **10**, and **11** from NMR spectra in $CDCl_3$[a]

C/H	**9***a* Chemical shift (ppm)		**10** Chemical shift (ppm)		**11** Chemical shift (ppm)	
	^1H	^{13}C	^1H	^{13}C	^1H	^{13}C
1	1.25(α), 1.82(β)	36.0	1.40(α), 2.03(β)	36.2	1.56(α), 1.77(β)	34.5
2	1.93(α), 1.57(β)	27.7	1.96(α), 1.68(β)	27.7	2.04(α), 1.64(β)	26.7
3	4.65(α)	73.1	4.49(α)	74.1	5.30(α)	69.5
4	2.49(α), 2.31(β)	37.6	2.38(α), 2.42(β)	38.2	2.83(α), 2.05(β)	31.3
5	—	145.9	—	143.1	—	45.8[d]
6	5.03	119.3	5.11	117.5	5.81	135.7
7	3.62(β)	37.6	3.51(β)	38.9	6.22	130.5
8	—	132.0	—	126.2	—	44.9[d]
9	1.94(α)	45.1	—	136.5	1.03(α)	53.4
10	—	38.5	—	38.4	—	40.8[d]
11	1.63(α), 1.53(β)	19.1	2.13(α), 2.26(β)	22.8	1.39(α), 1.39(β)	22.8[d]
12	1.10(α), 2.00(β)	37.3	1.42(α), 1.96(β)	28.7	1.10(α), 2.05(β)	39.5
13	—	43.2	—	42.3	—	43.6[d]
14	—	125.3	1.92(α)	50.2	1.68	54.8
15	2.36(α), 2.36(β)	25.2	1.84(α), 1.42(β)	23.4	2.55(α), 1.40(β)	23.1
16	1.46(α), 1.83(β)	26.8	1.18(α), 1.92(β)	36.5	1.89(α), 1.30(β)	27.7
17	1.10(α)	57.4	1.19(α)	54.2	1.12	55.1
18-CH_3	0.89	17.8	0.69	11.6	0.73	12.4
19-CH_3	0.90	19.1	1.25	23.6	0.96	18.6
20	1.48	34.5	1.40	36.0	1.35	35.3[d]
21-CH_3	0.93	19.2	0.94	19.0	0.91	19.1
22	1.36, 1.03	36.0	1.36, 1.01	36.1	1.12, 1.35	36.0[d]
23	1.32, 1.14	23.8	1.34, 1.15	23.8	1.12, 1.35	23.8[d]
24	1.12	39.5	1.12	39.5	1.12, 1.35	38.9[d]
25	1.51	28.0	1.51	28.0	1.50	28.0
26, 27	0.86, 0.85	22.6, 22.8	0.86, 0.85	22.8, 22.5	0.85	22.8, 22.5
CH_3CO	2.02	21.3	2.01	21.3	2.01	21.9
CH_3CO	—	170.4	—	[c]	—	[c]
1′	3.14	44.4	3.29	42.9	3.38	42.3
2′	2.90, 2.73	31.5	2.59, 2.55	30.2	2.75	56.6
3′	—	175.7[b]	—	178.1	—	[c]
4′	—	177.8[b]	—	[c]	—	[c]

[a]Aromatic protons appeared in the 7.29–7.44 ppm range; aromatic carbons in the 126.4–147 ppm range.
[b]Assignments may be reversed.
[c]Signals not observed due to low sample concentration.
[d]Assignments tentative.

*(iii) Spectral assignments: ene adduct **10***

The chemical shifts and coupling constants for **10** were determined using procedures similar to those used for **9***a*. The ^1H and ^{13}C spectral assignments presented for this compound in Table 1 should be viewed with greater caution than those for **9***a*, since there was considerably greater overlap of signals in the ^1H spectrum of **10** and only a small number of coupling constants could be determined reliably. However, sufficient resolution was obtained to confirm the stereochemistry at C-7 and to give an indication of the change in position of the second double bond in ring B.

By analogy with the data for **9***a*, the homoallylic coupling (2.1 Hz) is consistent with H-7 occupying a β position. Therefore, the stereochemistry at C-7 in **10** appears to be the same as that in **9***a*.

The position of the C-8/C-9 double bond was determined by locating the C-11 protons and examining their geminal coupling. These protons (11α, 2.26 and 11β, 2.13 ppm) were identified in the COSY-45 spectrum and were differentiated in an NOE experiment where the 19-CH_3 was saturated. An evaluation of the geminal coupling from the H-11α multiplet showed it to be approximately −18.1 Hz. The substantial increase in the magnitude of the geminal coupling is consistent with the plane of the π-system bisecting the angle between the C-11 methylene protons (25–27). This result confirms that the double bond is in fact located between C-8 and C-9.

*(iv) Spectral assignments: Diels–Alder adduct **11***

The gross structure of the Diels–Alder adduct (**11**) is particularly easy to identify because of the AX patterns in the ^1H NMR spectrum due to the vinylic protons at C-6 and C-7 (5.81 and 6.22 ppm, respectively) and the maleimide protons at C-1′ and C-2′ (2.75 and 3.38 ppm, respectively). Assignment of the A- and C-ring protons (Table 1) was achieved by a combination of COSY-45 and TOCSY (Fig. 5) 2-D techniques as well as NOE difference spectra (Table 3). The C-ring assignments were complicated by the overlap of H-11α and H-11β.

The B-ring vinyl proton chemical shifts were assigned with the aid of NOE difference spectra in which the methyl signals at 0.73 and 0.96 ppm were saturated. In the experiment where the 0.93 ppm methyl resonance was irradiated, an enhancement of the 5.81 ppm doublet was observed.

Can. J. Chem. Downloaded from www.nrcresearchpress.com by 109.225.110.28 on 09/08/12
For personal use only.

TABLE 2. Observed and calculated[a] ^1H–^1H coupling constants (±0.5–1.0 Hz) for **9a**, **10**, and **11** in $CDCl_3$

	9a		**10**		**11**	
Protons	^2J	^3J	^2J	^3J	^2J	^3J
1α, 1β	−13.8		—		−13.2	
1α, 2α		3.8(3.6)		—		3.4(4.3)
1α, 2β		13.9(13.6)		13.3(13.4)		13.4(13.2)
1β, 2α		3.8(3.3)		—		3.2(2.7)
1β, 2β		3.8(3.2)		4.4(3.7)		3.2(4.1)
2α, 2β	−12.9		−13.3		−12.5	
2α, 3α		4.7(4.2)		—		5.2(5.5)
2β, 3α		11.6(11.4)		11.7(11.1)		11.6(10.6)
4α, 4β	−13.9		−12.4		−13.0	
4α, 3α		5.1(4.6)		5.6(4.9)		4.9(4.7)
4β, 3α		11.6(11.1)		12.0(10.7)		12.3(10.7)
6, 7		3.8(3.8)		3.3(3.6)		8.6
9α, 11α		7.2(7.3)		—		6.2(4.3)
9α, 11β		10.2(9.9)		—		11.9(12.0)[b]
11α, 11β	−14.1		−18.1			
11α, 12α		3.4(3.4)		—		4.8(3.4)[b]
11α, 12β		3.4(3.3)		—		
11β, 12α		14.0(13.2)		—		12.5(13.2)
11β, 12β		3.4(3.9)		—		3.7(4.0)
12α, 12β	−12.8		—		−12.5	
14α, 15α		—				7.2(6.0)
14α, 15β		—		—		12.3(11.5)
15α, 15β	—		—		−12.5	
15α, 16α		9.4[c](9.9)		—		10.6(11.7)
15α, 16β		5.9[c](8.6))		—		3.0(2.4)
15β, 16α		—		—		6.0(4.6)
15β, 16β		—		—		12.2(11.8)
16α, 16β	−13.3		—		−11.6	
16α, 17α		7.5(5.1)		—		9.5(6.8)
16β, 17α		12.9(12.0)		—		9.5(10.8)
17α, 20			—		—	9.5

[a]Calculated from the energy minimized structures (Fig. 6), using the equation supplied with PCModel Version 4.0. Calculated values are in parentheses following the observed values.
[b]Overlapping multiplets; coupling not resolved.
[c]Assignment uncertain.

Several other protons arising mainly from ring A were also enhanced (Table 3). Thus, the 0.93 ppm singlet must be assigned to the 19-CH_3 while the vinylic doublet at 5.81 ppm can be attributed to H-6. Saturation of the 18-CH_3 resonance (0.73 ppm) produced the corresponding enhancement of H-7 (6.22 ppm) (Table 3). These NOE results provide experimental verification of the agreement of our assignments of the C-18 and C-19 methyl resonances with those of Jones *et al.* for the Diels–Alder adduct from **2** and maleic anhydride (14). In addition, the NOE data also confirm the *endo*- stereochemistry of adduct **11** as shown in the MMX-derived structure in Fig. 6*c*. Methyl-19 is close to H-6 while the 18-CH_3 is in the proximity of H-7. Further support for this geometry was provided by NOE experiments that involved the saturation of H-1′ and H-2′ protons of the succinimidyl ring. Saturation of the 3.38 ppm signal produced an enhancement of H-3α at 5.30 ppm, thereby allowing the 3.38 ppm resonance to be assigned to H-1′. The neighbouring H-2′ proton (2.75 ppm) was enhanced along with the 1.56 ppm H-1α multiplet. Saturation of H-2′ resulted in NOE's to H-1′ and to the 1.03 ppm multiplet assigned to H-9α.

The D-ring protons were identified from the COSY-45 and TOCSY (Fig. 5) spectra. The isolated multiplet at 2.55 ppm correlates with the doublet of doublets at 1.68 ppm and with the multiplets at 1.89, 1.40, and 1.30 ppm. Measurement of the coupling constants for the 2.55 and 1.68 ppm multiplets indicated a 7.2 Hz coupling between these protons. The remaining 12.3 Hz coupling associated with the 1.68 ppm signal arises from an interaction with the proton at 1.40 ppm. These results were interpreted with H-14α being assigned to 1.68 ppm with an axial/pseudo-equatorial coupling (7.2 Hz) to H-15α (2.55 ppm), and an axial/pseudo-axial coupling (12.3 Hz) to H-15β (1.40 ppm). The 1.89 and 1.30 ppm signals were shown by NOE experiments involving saturation of H-15α (Table 3) to arise from H-16α and H-16β, respectively. The D-ring proton H-15β was also affected by saturation of the olefinic proton H-7 (6.22 ppm). This enhancement is consistent with the spatial geometry of these protons as shown in the MMX structure (Fig. 6*c*).

The TOCSY contour plot (Fig. 5) allowed the completion of the D-ring assignments by the observation of the correlation between H-15α and H-17α. The longer-range correlation was also detected between H-15α and the 21-CH_3 protons. The multiplet for H-20 was not observed because of overlap with the H-15β and H-16β signals.

Can. J. Chem. Downloaded from www.nrcresearchpress.com by 109.225.110.28 on 09/08/12
For personal use only.

TABLE 3. Summary of NOE experiments for **9***a*, **10**, and **11**

Compound	Saturated (ppm)	Enhanced (%[a])
9*a*	3α (4.65)	4α (5.8%), 2α (3.9%)
	6 (5.03)	4α (6.0%), 7β (8.4%)
	19-CH_3 (0.90)	1β (1.9%), 2β (9.9%), 4β (3.0%)
	7β (3.62)	6 (7.9%), 1′ (5.0%), 15 (3.6%)
10	19-CH_3 (1.25)	1β (1.8%), 4β (3.3%), 11β (2.7%)
	6 (5.11)	4α (3.4%), 7β (4.9%)
11	18-CH_3 (0.73)	7 (7.3%), 11β (18.0%)
	19-CH_3 (0.96)	6 (2.2%), 11β (12.0%), 4β (8.8%), 2β (2.0%), 1β (0.5 %)
	1′ (3.38)	2′ (4.5%), 3α (8.3%), 1α (3.2%)
	2′ (2.75)	1′ (4.6%), 9α (5.8%)
	6 (5.81)	7 (6.5%)
	7 (6.22)	6 (8.2%), 15β (4.7%)
	15α (2.55)	15β (17.9%), 16α[b]

[a]Intensities measured from the difference spectrum are reported relative to the saturated signal where the intensity was assigned to −100 for a single proton multiplet; the peaks of interest were then integrated. Since the samples were not degassed, these results cannot be considered quantitative and serve only as a general indication of the observed enhancement of the signals. For the applications in this study, the determination of a numerical value for the NOE was not critical since the detection of an enhancement in itself is sufficient to provide the required structural information (40).

[b]The percent change in peak intensity is not considered accurate due to overlap with other signals or baseline distortions resulting from incomplete subtraction of adjacent peaks.

Only a partial assignment of the alkyl side-chain protons was possible from the 2-D spectra. The 26,27-CH_3 protons displayed TOCSY cross-peaks to contours centered at 1.35 and 1.12 ppm. These cross-peaks are considered to arise from the protons on carbons 22, 23, and 24, but no further differentiation of these signals was possible.

Summary and conclusions

The reaction of 7-dehydrocholesteryl acetate (**1**) with *N*-aryl maleimides yields mixtures of ene and Diels–Alder adducts. There is very little variation in the relative yields of the adducts with *N*-aryl substituent throughout the series **6–8**, and the product distributions are similar to that reported previously for the reaction of ergosteryl acetate with maleic anhydride (14).

The structures of the ene-adducts **9** and **10** and Diels–Alder adduct **11** from the reaction of **1** and **6–8** have been elucidated by high-field ^1H and ^{13}C NMR spectroscopic techniques, employing 2-D chemical shift correlation experiments and molecular mechanics calculations to assist in the spectral assignments. The accuracy with which the latter is able to predict coupling constants in these systems is quite remarkable. In all cases, the present assignments verify the conclusions of previous workers, who employed differences in the chemical shifts of the C-18 and C-19 methyl protons to identify the structures of the various adduct types (1–4).

TOCSY spectra have been reported previously for a triterpenoid (39). However, to our knowledge, the present work represents one of the first demonstrations of the power of the TOCSY pulse sequence for resolving entire spin systems in steroids. This technique will undoubtedly find increasingly frequent use in the analysis of the ^1H NMR spectra of complex natural products.

Experimental

Melting points were determined using a Mettler FP82 hot stage (controlled by a Mettler FP80 central processor) mounted on an Olympus BH-2 microscope, and are corrected. Routine ^1H NMR spectra were recorded with Varian EM390 or Bruker AC200 NMR spectrometers, and referenced with internal tetramethylsilane. Infrared spectra were recorded as KBr pellets (except where noted otherwise) using a Perkin–Elmer model 283 infrared spectrometer, calibrated with the 1601.8 cm^{-1} polystyrene absorption. Mass spectra and exact masses were determined by electron impact (70 eV), using a VG analytical ZAB-E mass spectrometer with a source temperature of 200°C and direct probe injection. Combustion analyses were performed by Galbraith Laboratories, Inc.

Analytical high-performance liquid chromatographic analyses employed a Gilson Isocratic HPLC system consisting of a model 302 pump and 5-mL head, a model 802B manometric module, Holochrome variable wavelength detector, and a Rheodyne model 7125 loop injector. A detector wavelength of 235 nm was used for analysis of product mixtures from reaction of **1** and **6**. Analyses of those from reaction of **1** with **7** and **8** employed a detector wavelength of 280 nm. The detector was interfaced with a Unitron microcomputer (Apple II+ clone) through an Adalab® data acquisition/control card (Interactive Microware, Inc.). The 0–10 mV signal was amplified to 0–1 V using an Adaamp® analog amplifier (Interactive Microware, Inc.). Chromatogram acquisition and storage was performed using Chromatochart® (Interactive Microware, Inc.). Product yields were determined from the HPLC peak areas (calculated by triangulation), assuming identical detector responses for each set of adducts and are the averages of two runs each analysed in triplicate. Normal-phase separations employed a Merck Hibar (4.6 × 220 mm) Si60 (10 μm) column, while reverse-phase separations employed Alltech (4.6 × 250 mm) C18 (10 μm) or Brownlee (4.6 × 220 mm) RP-18 Spheri-10 columns.

Semi-preparative LC separations were performed with the above system equipped with a 50-mL recycling pump head and an Isco 254-nm single wavelength detector. Normal-phase separations were performed with an EM Lobar Si60 (2.5 × 25 cm) silica column,

Can. J. Chem. Downloaded from www.nrcresearchpress.com by 109.225.110.28 on 09/08/12
For personal use only.

Can. J. Chem. Downloaded from www.nrcresearchpress.com by 109.225.110.28 on 09/08/12
For personal use only.

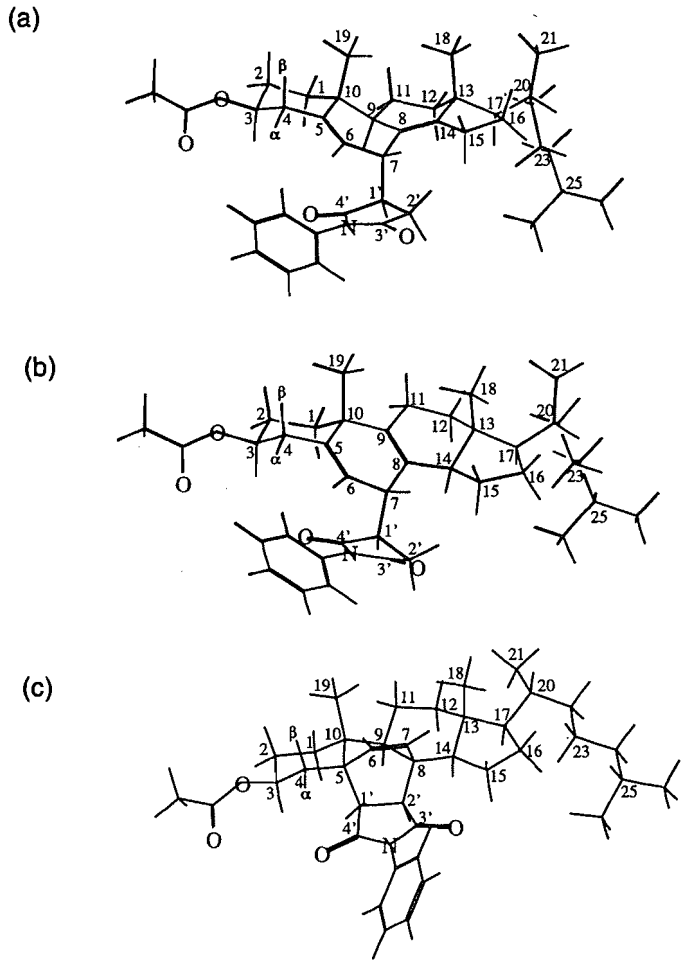

FIG. 6. Energy-minimized (MMX) structures of adducts **9***a* (*a*), **10** (*b*), and **11** (*c*).

while reverse-phase separations were performed using a Whatman Partisil M9 10/50 ODS-2 column.

High-resolution ^1H and ^{13}C NMR spectra were recorded on a Bruker AM500 spectrometer. Proton spectra were acquired at 500.135 MHz using a 5-mm dual frequency ^1H–^{13}C probe. Spectra were obtained in 64–88 scans in 32K data points over a 2.415–3.012 kHz spectral width (5.439–6.783 s acquisition times). The sample temperature was maintained at 30°C by a Bruker BVT-1000 variable temperature unit. The free induction decay (FID) was processed using Gaussian multiplication (line broadening: −2.0 Hz, Gaussian broadening factor: 0.15) for resolution enhancement and was zero-filled to 64K before Fourier transformation.

Absolute value proton COSY 2-D NMR spectra were recorded using the pulse sequence 90°–t_1–45°–ACQ. Spectra were acquired in 32 scans for each of the 512 FID's that contained 2K data points in F2 over the previously mentioned spectral widths. The ^1H 90° pulse width was 18.6 μs. A 2.0 s relaxation delay was employed between acquisitions. Zero-filling in F1 produced a 1K × 1K data matrix with a digital resolution of 2.359 or 2.941 Hz/point in both dimensions. During 2-D Fourier transformation a sine-bell squared window function was applied to both dimensions. The transformed data were then symmetrized.

TOCSY 2-D NMR spectra were acquired in the phase-sensitive mode using the MLEV-17 pulse sequence (28). Phase-sensitive data were obtained using time-proportional phase incrementation (TPPI) (29, 30). In the F2 dimension, 2K data points were used during the acquisition of the 256 FID's. Each FID was acquired in 16 scans for adduct **9***a* and 176 scans for **10**. A 2.415 kHz spectral width in the F2 dimension was used for both samples. The relaxation delays were 1.0 s for **9***a* and 0.7 s for **10**. The 90° ^1H pulse width used in the 5-mm broadband inverse probe was 26.0 μs. The length of the spin-lock mixing time was 80 ms plus two trim pulses of 2.5 ms. Zero-filling in the F1 dimension to 2K data points resulted in a digital resolution of 2.359 Hz/point in both dimensions. During the 2-D Fourier transformation, a sine-bell squared window function shifted by $\pi/2$ was applied to both dimensions. The transformed data were not symmetrized.

Proton–proton NOE difference spectra were acquired by subtraction of a control FID from an on-resonance FID. The decoupler in the control FID irradiated a position in the spectrum where there were no proton signals. The on-resonance FID was obtained with the proton of interest being selectively saturated. In both cases the same decoupler power and duration of saturation (5.0 s) were used. This saturation period also served as the relaxation delay for both the control and on-resonance FID's. The decoupler was gated off during acquisition. Eight scans were acquired for both the control and on-resonance FID's. The cycle of alternate acquisition of control and on-resonance FID's was repeated 8 times for a total of 64 scans for the complete difference FID. A 90° ^1H pulse width of 18.6 μs was used. The difference FID was processed using exponential multiplication (line broadening: 4.0 Hz) and was zero-filled to 32K before Fourier transformation. Samples were not degassed.

Carbon-13 NMR spectra were recorded at 125.759 MHz using the 5-mm dual frequency ^1H–^{13}C probe. The spectra were acquired over a 21.739 or 30.0 kHz spectral width in 16K or 32K data points (0.377–0.557 s acquisition time). Single pulse spectra used a ^{13}C pulse width of 2.5 μs (30° flip angle) and a 0.5 s relaxation delay. The DEPT pulse sequence was used for editing. The ^{13}C 90° pulse width was 6.4 μs while the ^1H 90° pulse width through the decoupler channel was 18.6 μs. The delays used in the DEPT pulse sequence were a 1.0 s relaxation delay and $1/2^1J_{CH}$ delay of 0.003571 s. The FID's were processed using exponential multiplication (line broadening: 4.0–5.0 Hz).

The ^{13}C–^1H 2-D chemical shift correlation spectra of **9** and **10** (Ar = phenyl) were acquired using the standard pulse sequence incorporating the BIRD pulse during the evolution period for ^1H–^1H decoupling in F1 (31–33). The spectra in the F2 (^1H) dimension were recorded over a spectral width of 3.106 kHz in 2–4K data points. The 256–512 FID's in the F1 (^{13}C) dimension were obtained over a 19.231 kHz spectral width. Each FID was acquired in 32 scans. The fixed delays in the pulse sequence were a 0.75–1.0 s relaxation delay, BIRD pulse and polarization transfer delays ($1/2^1J_{CH}$) of 0.003571 s, a refocussing delay ($1/4^1J_{CH}$) of 0.001786 s, and a 0.3 s delay between the BIRD pulse and the inverse pulse sequence. The 90° ^1H pulse was 9.2 μs while the 90° ^{13}C pulse was 10.1 μs. The data for **9** and **10** (Ar = phenyl) were processed using exponential multiplication (line broadening: 11.0 Hz) in F2 and unshifted sine bell in F1. Zero-filling in F1 resulted in a 2K × 1K data matrix.

The ^1H–^{13}C inverse detected shift correlation spectrum of **11** was acquired by using the HMQC pulse sequence with the BIRD pulse (34) in a 5-mm broadband inverse probe. The data were obtained in the phase sensitive mode using time-proportional phase incrementation (TPPI) (29, 30). The spectra in F2 were recorded over a spectral width of 2.415 KHz in 2K data points. In F1, each of the 186 FID's was acquired in 144 scans over the ^{13}C spectral width of 14.286 KHz. The fixed delays in the pulse sequence were a relaxation delay of 0.6 s, a BIRD pulse delay ($1/2^1J_{CH}$) of 0.003571 s, and the delay between the BIRD pulse and the HMQC pulse sequence was 0.35 s. The 90° ^1H pulse was 8.5 μs while the ^{13}C 90° pulse was 10.3 μs. Carbon-13 decoupling during acquisition was achieved by the GARP method (35). The data were processed using a sine-bell squared window function shifted by $\pi/2$ in both dimensions. In F1, the 2-D data were zero-filled to 2K.

Can. J. Chem. Downloaded from www.nrcresearchpress.com by 109.225.110.28 on 09/08/12
For personal use only.

The compounds used in the NMR experiments were dissolved in $CDCl_3$ (MSD Isotopes) to a concentration of about 0.05 M. Chemical shifts for the ^1H and ^{13}C spectra are reported in ppm relative to TMS using the residual solvent signals at 7.24 and 77.0 ppm as internal references for the ^1H and ^{13}C spectra, respectively.

Molecular mechanics calculations employed the MMX package supplied with PCModel Version 4.0 (Serena Software, Inc). Vicinal ^1H–^1H coupling constants were calculated using the equation supplied with the same software package, from the energy-minimized structures.

HPLC solvents acetonitrile (Caledon HPLC), dichloromethane (Caledon HPLC), ethyl acetate (BDH Reagent), and hexane (Caledon HPLC) were used as received from the suppliers, as were methanol (Mallinckrodt anhydrous), acetic anhydride (BDH Reagent), 1-nitropropane (Eastman), chlorobenzene (Fisher Reagent), toluene (Caledon Reagent), and carbon tetrachloride (Caledon Reagent or Fisher Spectroscopic). Absolute ethanol was prepared by refluxing 95% ethanol over magnesium turnings and iodine for 24 h followed by distillation. Benzene-d_6 and deuteriochloroform were used as received from MSD Isotopes. *N*-Phenylmaleimide (Sigma) was recrystallized twice from acetone and dried over phosphorus pentoxide (mp 89.5–90°C). 4-Aminobiphenyl, maleic anhydride, and *para*-terphenyl were used as received from Aldrich Chemical Co.

7-Dehydrocholesteryl acetate (**1**) was prepared from 7-dehydrocholesterol (Sigma) and acetic anhydride by the method of Prichard (36). The product was recrystallized thrice from acetone and washed with cold methanol (mp 125–127°C; lit. (37) mp 129–130°C).

N-Biphenylmaleimide (**7**) was prepared by the method of Crivello (18). The crude product was purified by column chromatography (silica; 2% acetonitrile – methylene chloride) followed by two recrystallizations from acetone, and obtained as bright yellow needles (mp 190.0–190.5°C; lit. (18) mp 189–190°C).

N-Terphenylmaleimide (**8**) was prepared by a modification of the procedure employed for the synthesis of **7** (18). Maleic anhydride (0.3 g, 3.1 mmol) was dissolved in acetone (4 mL) and 4-amino-*p*-terphenyl (38) (0.5 g, 2.04 mmol) was added, resulting in the immediate formation of a yellowish precipitate. The precipitate was collected by vacuum filtration, dried over phosphorus pentoxide in a vacuum desiccator for several hours, and then dissolved in a solution of acetic anhydride (5 mL) and anhydrous sodium acetate (0.1 g). The mixture was heated for 4 h at 90°C, during which time a yellow precipitate was formed. The mixture was cooled and the resulting solid collected and washed with acetone–water. Two recrystallizations from acetone yielded **8** as a pale yellow solid (0.55 g, 1.7 mmol, 83%); mp 293–303°C (dec.). IR (KBr) (cm^{-1}): 3095 (w), 1705 (s), 1503 (w), 1481 (m), 1394 (m), 1153 (w), 1139 (w), 1009 (w), 939 (w), 822 (m), 812 (m), 757 (w), 751 (w), 718 (w), 676 (m); ^1H NMR (200 MHz; $CDCl_3$) δ: 6.88 (s, 2H), 7.46 (m, 4H), 7.68 (s, 5H), 7.69 (m, 4H); ^{13}C NMR ($CDCl_3$) δ: 126.28, 127.02, 127.52, 127.74, 128.80, 130.29, 134.26, 139.00, 140.48, 169.50; MS *m/e*(*I*): 69(13), 169(9), 255(10), 271(11), 325(100), 326(6). Exact Mass calcd. for $C_{22}H_{15}NO_2$: 325.1103; found: 325.1105.

*Preparation and isolation of adducts from reaction of **1** and **6–8***

Preparative-scale thermolyses of **1** with **6** and **7** were carried out in the following fashion. 7-Dehydrocholesteryl acetate (**1**; 0.30 g, 0.7 mmol) and an equimolar amount of **6** or **7** were dissolved in benzene (35 mL). The resulting solution was divided among three 5/8-in. thick-walled Pyrex tubes which had been soaked in 10% aqueous sodium hydroxide for ca. 8 h, rinsed several times with distilled water, and oven-dried. The samples were degassed using three freeze–pump–thaw cycles, and the tubes were sealed under vacuum. They were then placed in a Parr model 4914 Pressure Reaction Apparatus and heated at 200°C for 4 h. The tubes were opened and the solvent was removed on the rotary evaporator.

Preparative-scale thermolysis of **1** and **8** was carried out using cholesteryl 4-chlorobenzoate (a cholesteric liquid crystal at 200°C) as solvent, in order to obtain a higher yield of adduct **10** than is afforded from the reaction in benzene solution (17). The diene **1** (0.15 g, 0.35 mmol), **8** (0.113 g, 0.35 mmol), and cholesteryl 4-chlorobenzoate (15 g) were dissolved in methylene chloride (15 mL). The volatile solvent was removed on the rotary evaporator, and the solid mixture which remained was placed in a 5/8-in. Pyrex tube, sealed under vacuum, and heated at 200°C for 4 h. The resulting mixture was flash-chromatographed on a silica gel column. The liquid crystal was eluted with 3:2 dichloromethane:hexanes, while the products were subsequently eluted as a mixture with starting materials with 2% acetonitrile in dichloromethane.

Isolation of the products from the thermolyses described above was carried out by cyclic semi-preparative liquid chromatography, using flow rates of 8–10 mL/min. The crude reaction mixtures were placed on the column. Three chromatographic cycles with methylene chloride as eluant separated the mixture into three fractions, which were collected and stripped of solvent. The first fraction, which consisted of the starting materials, was discarded. The second fraction consisted of a mixture of **9*a*** and **10**, while the third consisted of a mixture of **9*b***, **11**, and small quantities of a fifth (unidentified) adduct. Adducts **9*a*** and **10** were separated after three further cycles of the second fraction on the same column using methylene chloride as eluant. For the reaction with **6**, adducts **9*b*** and **11** were separated from the third fraction after two further cycles on the same column using 2% acetonitrile in dichloromethane as eluant. For the reaction with **7** and **8**, adducts **9*b*** and **11** were isolated by reverse-phase chromatography using 5% water in acetonitrile as eluant (7 mL/min) and a single pass through the column. The solvents were stripped from the purified adducts, and they were then recrystallized several times from methanol or chloroform–methanol mixtures. Analytical, physical, and spectroscopic data for each of the adducts are described below.

Product yields for the reaction of **1** with **6–8** in benzene solution were determined by HPLC analysis of small-scale (ca. 0.01 mmol) mixtures, which were thermolysed in base-washed, sealed 7-mm Pyrex tubes for 4 h in an oil bath at 200°C. After cooling to room temperature, the tubes were opened and aliquots were injected into the HPLC.

*Thermolysis of **1** and **6***

The adducts were separated on silica using 2% acetonitrile–dichloromethane as eluant and a flow rate of 1 mL/min. Under these conditions, the starting materials and products elute as follows: **1** (4 min); **6** (6 min); **9*a*** (13 min; 36%); **10** (14 min; 13%); **9*b*** (19 min; 25%); **11** (23.5 min; 19%); unidentified adduct (27 min; 6%).

The aryl regions in the ^1H and ^{13}C NMR spectra of the adducts were essentially identical (see **9*a*** (Ar = phenyl)).

9a *(Ar = phenyl):* mp 124–126°C; IR (cm^{-1}): 2959 (s,br), 2979 (m), 1715 (s), 1500 (m), 1467 (m), 1459 (m), 1385 (s), 1244 (s,br), 1215 (w), 1179 (s, br), 1034 (s), 949 (w), 931 (w), 799 (w), 755 (w), 742 (w), 693 (w); MS m/e(*I*): 599(0.5), 524(1), 424(3), 365(100), 349(15), 251(30), 197(18), 157(16). Exact Mass calcd. for $C_{39}H_{53}NO_4$: 599.3975; found: 599.3961. See Tables 1–3 for ^1H and ^{13}C NMR data for this compound.

9b *(Ar = phenyl):* mp 78.5–81.0°C; IR (cm^{-1}): 2960 (s, br), 2878 (m), 1719 (s,br), 1501 (m), 1468 (w), 1458 (w), 1378 (s), 1369 (s), 1260 (s), 1244 (s,br), 1174 (s, br), 1028 (s, br), 952 (w), 938 (w), 799 (m), 756 (w), 738 (w), 694 (w); ^1H NMR ($CDCl_3$): essentially identical to that of **9*b*** (Ar = biphenyl; *vide infra*), except in aryl region; ^{13}C NMR ($CDCl_3$): essentially identical to that of **9*b*** (Ar = biphenyl; *vide infra*), except in aryl region; MS *m/e*(*I*): 599(0.5), 524(2), 424(2), 365(100), 349(7), 251(10), 197(8), 157(7), 119(7). Exact Mass calcd. for $C_{39}H_{53}NO_4$: 599.3975; found: 599.3970.

Can. J. Chem. Downloaded from www.nrcresearchpress.com by 109.225.110.28 on 09/08/12
For personal use only.

10 *(Ar = phenyl):* mp 170.0–172.5°C; IR (cm^{-1}): 2957 (s, br), 2876 (m), 1714 (s,br), 1499 (m), 1467 (w), 1455 (w), 1395 (s), 1378 (m), 1359 (m), 1234 (s, br), 1209 (w), 1180 (s, br), 1158 (w), 1034 (s), 958 (w), 939 (w), 793 (m), 776 (w), 748 (w), 691 (m); MS *m/e(I)*: 599(0.8), 524(5), 424(2), 365(100), 349(5), 195(6), 157(33), 119(11), 95(10). Exact Mass calcd. for $C_{39}H_{53}NO_4$: 599.3975; found: 599.3967. See Tables 1–3 for ^1H and ^{13}C NMR data for this compound.

11 *(Ar = phenyl):* mp 96.5–98.0°C; IR (cm^{-1}): 2962 (s, br), 2879 (m), 1718 (s,br), 1500 (m), 1468 (w), 1458 (w), 1380 (s, br), 1368 (s), 1246 (s,br), 1186 (m), 1029 (m), 919 (w), 897 (w), 760 (w), 730 (w), 688 (w); MS *m/e(I)*: 599(1), 539(100), 524(20), 365(5), 351(4), 237(8), 174(50), 129(20). Exact Mass calcd. for $C_{39}H_{53}NO_4$: 599.3975; found: 599.3976. See Tables 1–3 for ^1H and ^{13}C NMR data for this compound.

*Thermolysis of **1** and **7***

The adducts were separated on silica gel using 2% acetonitrile–dichloromethane as eluant and a flow rate of 1 mL/min. Under these conditions, the starting materials and products elute as follows: **1** (4 min); **7** (5.5 min); **10** (7.5 min; 13%); ***9a*** (8.1 min; 32%); ***9b*** (11 min; 26%); and **11** (11 min; 22%); unidentified adduct (16 min; 7%).

The aryl regions in the ^1H and ^{13}C NMR spectra of the adducts were essentially identical (see ***9a*** (Ar = *para*-biphenyl)).

9a *(Ar = para-biphenyl):* mp 100.5–101.5°C; IR (cm^{-1}): 2956 (s,br), 2876 (m), 1714 (s, br), 1522 (m), 1485 (m), 1466 (w), 1434 (w), 1376 (s, br), 1241 (s,br), 1172 (m, br), 1027 (m,br), 833 (m), 757 (m), 692 (m), 662 (w); ^1H NMR: similar to ***9a*** (Ar = phenyl) (Fig. 1*a* and Table 1), except in aryl region; δ: 7.2–7.9 (m, 9H); ^{13}C NMR: similar to ***9a*** (Ar = phenyl) (Table 1), except in aryl region; δ: 127.2 (Bp-3′/5′), 127.8 (Bp-2′/6′), 128.2 (Bp-4′), 128.4 (Bp-3/5), 129.4 (Bp-2/6), 131.7 (Bp-1), 141.0 (Bp-1′), 142.1 (Bp-4); MS *m/e(I)*: 675(0.5), 615(2), 366(34), 365(100), 364(47), 251(25), 249(50), 237(17), 219(13), 195(32). Exact Mass calcd. for $C_{45}H_{57}NO_4$: 675.4287; found: 675.4281. Anal. calcd. for $C_{45}H_{57}NO_4$: C 79.96, H 8.50; found: C 79.44, H 8.52.

9b *(Ar = para-biphenyl):* mp 221.0–223.0°C; IR (cm^{-1}): 2959 (s,br), 2875 (m), 1716 (s, br), 1505 (w), 1486 (m), 1464 (w), 1444 (w), 1376 (s, br), 1243 (s,br), 1173 (m, br), 1025 (m), 817 (w), 759 (m), 690 (m), 664 (w); ^1H NMR ($CDCl_3$; assignments tentative in some cases); δ: 0.84 (d, 26), 0.85 (d, 27), 0.89 (s, 19), 0.90 (s, 18), 0.93 (d, 21), 1.03 and 1.36 (m, 22), 1.15 and 1.34 (m, 23), 1.11 (m(2H), 24), 1.15 (m, 17), 1.16 (dd, 12α), 1.24 (dd, 1α), 1.42 (m, 16α), 1.45 (m, 20), 1.51 (m, 25), 1.54 (m, 11β), 1.55 (m, 2β), 1.64 (m, 11α), 1.78 (ddd, 1β), 1.84 (m, 16α), 1.87 (m, 2α), 2.01 (dd, 12β), 2.17 (m, 15β), 2.25 (m, 9), 2.27 (m, 15α), 2.34 (m, 4β), 2.45 (ddd, 4α), 3.09 (m, 1′), 2.70 and 2.93 (dd(2H), 2′), 1.98 (s, CH_3CO), 3.16 (q, 7β), 4.61 (m, 3α), 5.51 (dd, 6), 7.2–7.9 (m, 9H); ^{13}C NMR ($CDCl_3$; assignments tentative in some cases); δ: 18.2 (18), 19.7 (11), 19.8 (19), 20.9 (21), 22.0 (CH_3CO), 23.1 (27), 23.4 (26), 24.6 (23), 26.7 (15), 27.3 (16), 28.3 (2), 28.6 (25), 34.4 (2′), 35.2 (20), 36.5 (22), 36.6 (1), 37.7 (12), 38.4 (4), 39.3 (10), 40.1 (24), 40.5 (7), 44.1 (13), 44.5 (9), 46.2 (1′), 58.3 (17), 73.8 (3), 122.0 (6), 125.9 (5), 127.4 (Bp-3′/5′), 127.9 (Bp-2′/6), 128.2 (Bp-4′), 128.7 (Bp-3/5), 129.4 (Bp-2/6), 131.7 (Bp-1), 141.0 (Bp-1′), 142.3 (Bp-4), 144.0 (14), 148.2 (8), 170.9 (CH_3CO), 176.2 (CO), 178.9 (CO); MS *m/e(I)*: 675(2), 616(14), 366(37), 365(100), 364(42), 251(22), 249(15), 237(4), 219(9) 195(19). Exact Mass calcd. for $C_{45}H_{57}NO_4$: 675.4287; found: 675.4284. Anal. calcd. for $C_{45}H_{57}NO_4$: C 79.96, H 8.50; found: C 79.57, H 8.40.

10 *(Ar = para-biphenyl):* mp 183.5–185.0°C; IR (cm^{-1}): 2957 (s,br), 2877 (m), 1716 (s, br), 1522 (m), 1486 (m), 1466 (w), 1451 (w), 1376 (s, br), 1245 (s,br), 1172 (m, br), 1026 (m), 836 (w), 758 (m), 692 (m), 660 (w); ^1H NMR: similar to **10** (Ar = phenyl) (Fig. 1*a* and Table 1), except in aryl region; ^{13}C NMR: similar to **10** (Ar = phenyl) (Table 1), except in aryl region; MS *m/e(I)*: 675(0.2), 616(1), 615(3), 600(4), 366(35), 365(100), 364(32), 251(22), 249(24), 195(15). Exact Mass calcd. for $C_{45}H_{57}NO_4$: 675.4287; found: 675.4314. Anal. calcd. for $C_{45}H_{57}NO_4$: C 79.96, H 8.50; found: C 79.96, H 8.56.

11 *(Ar = para-biphenyl):* mp 120.0–122.0°C; IR (cm^{-1}): 2956 (s,br), 2875 (m), 1715 (s, br), 1520 (m), 1486 (m), 1465 (w), 1445 (w), 1377 (s, br), 1244 (s,br), 1180 (m), 1027 (m), 832 (m), 760 (m), 739(m), 694 (m), 665 (w); ^1H NMR: similar to **11** (Ar = phenyl) (Table 1), except in aryl region; ^{13}C NMR: similar to **11** (Ar = phenyl) (Table 1), except in aryl region; MS *m/e(I)*: 675(48), 367(30), 366(100), 365(26), 364(15), 351(14), 253(18), 251(11), 250(19), 249(89), 195(16). Exact Mass calcd. for $C_{45}H_{57}NO_4$: 675.4287; found: 675.4289.

*Thermolysis of **1** and **8***

The adducts were separated on silica using 2% acetonitrile–dichloromethane as eluant and a flow rate of 1 mL/min. Under these conditions, the starting materials and products elute as follows: **1** (4 min); **8** (5.0 min); **10** (6 min; 15%); ***9a*** (7 min; 32%); ***9b*** (10 min; 26%); and **11** (10 min; 21%), unidentified adduct (13 min; 7%). Thermolysis of **1** and **8** in the cholesteric liquid-crystalline phase of cholesteryl-4-chlorobenzoate for 4 h at 200°C yields the same products, but in the following yields: **10** (40%), ***9a*** (21%), ***9b*** (13%), **11** (10%), unidentified adduct (16%).

The aryl regions in the ^1H and ^{13}C NMR spectra of the adducts were essentially identical (see ***9a*** (Ar = *para,para′*-phenyl)).

9a *(Ar = para,para′-terphenyl):* mp 147.5–1.49.5°C; IR (cm^{-1}): 2939 (s,br), 2861 (s), 1713 (s, br), 1508 (w), 1487 (m), 1465 (m), 1380 (s, br), 1240 (s,br), 1169 (m, br), 1029 (w), 820 (w), 760 (m), 730 (w), 691 (w); ^1H NMR: similar to ***9a*** (Ar = phenyl) (Fig. 1*a* and Table 1), except in aryl region; δ: 7.2–7.9 (m, 13H); ^{13}C NMR: similar to ***9a*** (Ar = phenyl) (Table 1), except in aryl region; MS *m/e(I)*: 751(1), 424(2), 367(6), 366(32), 365(100), 364(47), 325(21), 271(14), 157(10). Exact Mass calcd. for $C_{51}H_{64}NO_4$: 751.4601; found: 751.4579.

9b *(Ar = para,para′-terphenyl):* mp 182.0–185.0°C; IR (cm^{-1}): 2942 (s,br), 2862 (m), 1715 (s, br), 1478 (m), 1459 (w), 1370 (s, br), 1230 (m,br), 1167 (m, br), 1020 (m, br), 683 (w); ^1H NMR ($CDCl_3$): essentially identical to that of ***9b*** (Ar = biphenyl; *vide supra*), except in aryl region; ^{13}C NMR ($CDCl_3$): essentially identical to that of ***9b*** (Ar = biphenyl; *vide supra*), except in aryl region; MS *m/e(I)*: 751(1), 424(2), 367(8), 366(38), 365(100), 364(52), 325(34), 271(18). Exact Mass calcd. for $C_{51}H_{64}NO_4$: 751.4601; found: 751.4579.

10 *(Ar = para,para′-terphenyl):* mp 162–166°C; IR (cm^{-1}): 2937 (s,br), 2860 (m), 1715 (s, br), 1510 (m), 1485 (w), 1466 (m), 1384 (s), 1240 (s,br), 1166 (m, br), 1032 (m), 824 (m), 760 (m), 730 (w), 692 (w); ^1H NMR: similar to **10** (Ar = phenyl) (Fig. 1*a* and Table 1), except in aryl region; ^{13}C NMR: similar to **10** (Ar = phenyl) (Table 1), except in aryl region; MS *m/e(I)*: 751(0.5), 424(2), 367(7), 366(33), 365(100), 364(38), 325(21), 271(12), 213(17), 157(31). Exact Mass calcd. for $C_{51}H_{64}NO_4$: 751.4601; found: 751.4579.

11 *(Ar = para,para′-terphenyl):* mp 119.5–123.0°C; IR (cm^{-1}): 2959 (s,br), 2878 (s), 1715 (s, br), 1508 (w), 1485 (m), 1467 (m, br), 1379 (s, br), 1244 (s,br), 1179 (m, br), 1028 (w), 820 (m), 762 (m), 745 (w), 732 (w), 691 (m); ^1H NMR: similar to **11** (Ar = phenyl) (Table 1), except in aryl region; ^{13}C NMR: similar to **11** (Ar = phenyl) (Table 1), except in aryl region; MS *m/e(I)*: 751(77), 366(100), 325(82), 271(20), 195(12). Exact Mass calcd. for $C_{51}H_{64}NO_4$: 751.4601; found: 751.4606.

Acknowledgements

We wish to thank the McMaster University Regional Centre for Mass Spectrometry for the mass spectrometric analyses, and the Natural Sciences and Engineering Research Council of Canada for its generous financial support.

1. A. Van der Gen, J. Lakeman, M. A. M. P. Gras, and H. O. Huisman. Tetrahedron, **20**, 2521 (1964).
2. M. Anastasia, A. Fiecchi, and G. Galli. J. Org. Chem. **46**, 3421 (1981).
3. J. Lakeman, W. N. Speckamp, and H. O. Huisman. Tetrahedron, **24**, 5151 (1968).
4. A. Van der Gen, J. Lakeman, U. K. Pandit, and H. O. Huisman. Tetrahedron, **21**, 3641 (1965).
5. F. Snatzke and H. P. Wolff. Liebigs Ann. Chem. 468 (1985).
6. D. N. Jones, P. F. Greenhalgh, and I. Thomas. Tetrahedron, **24**, 5215 (1968).
7. D. H. R. Barton, T. Shioiri, and D. A. Widdowson. J. Chem. Soc. C, 1968 (1971).
8. M. Tada and A. Oikawa. J. Chem. Soc. Perkin Trans. 1, 1858 (1979).
9. M. K. Shakhova, V. A. Kostoglodova, and G. I. Samokhvalov. J. Gen. Chem. USSR, **46**, 1598 (1976).
10. D. H. R. Barton, G. LeClerc, P. D. Magnus, and I. D. Menzies. J. Chem. Soc. Chem. Commun. 447 (1972).
11. A. Van der Gen, W. A. Zunnebald, U. K. Pandit, and H. O. Huisman. Tetrahedron, **21**, 3651 (1965).
12. A. Windaus and A. Luttringhaus. Ber. Dtsch. Chem. Ges. **64**, 850 (1931).
13. (*a*) H. H. Inhoffen. Justus Liebigs Ann. Chem. **508**, 81 (1934); (*b*) E. M. Hicks, C. J. Berg, and E. S. Wallis. J. Biol. Chem. **162**, 654 (1946); (*c*) K. Schubert and K.-H. Bohme. Chem. Ber. **93**, 1878 (1960); (*d*) D. N. Jones and I. Thomas. J. Chem. Soc. 5206 (1964).
14. D. N. Jones, P. F. Greenhalgh, and I. Thomas. Tetrahedron, **24**, 297 (1968).
15. W. J. Leigh. *In* Liquid crystals. Applications and uses. Vol. II. *Edited by* B. Bahadur. World Scientific, Singapore. 1990; and references cited therein.
16. W. J. Leigh and D. S. Mitchell. J. Am. Chem. Soc. **110**, 1311 (1988).
17. W. J. Leigh and D. S. Mitchell. J. Am. Chem. Soc. **114**, 5005 (1992).
18. J. V. Crivello. J. Polymer Sci. Polymer Chem. Ed. **14**, 159 (1976).
19. (*a*) R. R. Ernst, G. Bodenhausen, and A. Wokaun. Principles of nuclear magnetic resonance in one and two dimensions. Oxford Science Publications, Oxford. 1987; (*b*) J. K. M. Sanders and B. K. Hunter. Modern NMR spectroscopy — A guide for chemists. Oxford University Press, Oxford. 1987.
20. (*a*) W. B. Smith. Org. Magn. Reson. **9**, 644 (1977); (*b*) R. E. Perrier and M. J. McGlinchey. Can. J. Chem. **66**, 3003 (1988).
21. D. N. Kirk, H. C. Toms, C. Douglas, K. A. White, K. E. Smith, S. Latif, and R. W. P. Hubbard. J. Chem. Soc. Perkin Trans. 2, 1567 (1990).
22. J. Drew, J.-R. Brisson, P. Morand, and A. G. Szabo. Can. J. Chem. **65**, 1784 (1987).
23. J. B. Stothers. Carbon-13 NMR spectroscopy. Academic Press, New York. 1972. pp. 439–443.
24. L. M. Jackman and S. Sternhell. Applications of nuclear magnetic resonance spectroscopy in organic chemistry. 2nd ed. Pergamon Press, Oxford. 1969. p. 325.
25. H. Booth. Prog. NMR Spectrosc. **5**, 149 (1969).
26. M. Barfield and D. M. Grant. J. Am. Chem. Soc. **85**, 1899 (1963).
27. A. A. Bothner-By. Advances in magnetic resonance. Vol. I. *Edited by* J. S. Waugh. Academic Press, New York. 1965. p. 195.
28. (*a*) L. Braunschweiler and R. R. Ernst. J. Magn. Reson. **53**, 521 (1983); (*b*) A. Bax and D. G. Davies. J. Magn. Reson. **65**, 355 (1985).
29. D. Marion and K. Wuthrich. Biochem. Biophys. Res. Commun. **113**, 967 (1983).
30. G. Bodenhausen, H. Kogler, and R. R. Ernst. J. Magn. Reson. **58**, 370 (1984).
31. A. Bax. J. Magn. Reson. **53**, 517 (1983).
32. V. Rutar. J. Magn. Reson. **58**, 306 (1984).
33. J. A. Wilde and P. H. Bolton. J. Magn. Reson. **59**, 343 (1985).
34. A. Bax and S. Subramanian. J. Magn. Reson. **67**, 565 (1986).
35. A. J. Shaka, P. B. Barker, and R. Freeman. J. Magn. Reson. **64**, 547 (1985).
36. W. W. Prichard. Org. Synth. **28**, 68 (1948).
37. H. Schaltegger. Helv. Chim. Acta, **33**, 2101 (1950).
38. R. G. Splies. J. Org. Chem. **26**, 2601 (1961).
39. R. W. Kriwacki and T. P. Pitner. Pharm. Res. **6**, 531 (1989).
40. D. Neuhaus and M. P. Williamson. *In* The nuclear Overhauser effect in structural and conformational analysis. VCH Publishers, New York. 1989.

Can. J. Chem. Downloaded from www.nrcresearchpress.com by 109.225.110.28 on 09/08/12
For personal use only.

The HLM method: a simple way to get the solid–liquid phase diagrams and enthalpies of transition of pure components and mixtures

FRANÇOIS QUIRION,[1] DANIEL LAMBERT, AND GÉRALD PERRON

Institut national de la recherche scientifique – Energie et matériaux, 1650 Montée Ste-Julie, Varennes (Qué.), Canada J3X 1S2

Received November 6, 1991[2]

FRANÇOIS QUIRION, DANIEL LAMBERT, and GÉRALD PERRON. Can. J. Chem. **70**, 2745 (1992).

A simple method of thermal analysis is described which gives the same information as differential scanning calorimetry. The method is based on the Heat-Leak-Modulus, HLM, of a sample cell placed in a constant temperature reservoir. In the present study, the HLM method is used for the investigation of pure components and mixtures from −190 to 50°C. The method allows the determination of glass-transition, crystallizations, solid–solid transition, eutectic, and melting temperatures with a reproducibility better than ±0.1°C. The enthalpy of a transition can be determined with a reproducibility of ±5%. The simplicity, the low cost, and the precision of the HLM method fills the gap between standard cooling curves and sophisticated differential scanning calorimetry experiments. The HLM method has numerous applications in physical chemistry, polymer science, metallurgy, and chemical engineering.

FRANÇOIS QUIRION, DANIEL LAMBERT et GÉRALD PERRON. Can. J. Chem. **70**, 2745 (1992).

Nous présentons une méthode d'analyse thermique donnant essentiellement la même information que la calorimétrie différentielle à balayage. La méthode est basée sur le «heat-leak-modulus» d'un échantillon placé dans un réservoir gardé à température constante et elle est utilisée pour l'étude des solvants et des mélanges de solvants entre −190 et 50°C. La méthode permet de déterminer les températures de transition vitreuse, de cristallisation, de transition solide–solide, d'eutectique et de fusion avec une reproductibilité meilleure que ±0.1°C. L'enthalpie associée à une transition peut être obtenue avec une reproductibilité de ±5%. La simplicité, la précision et le faible coût de la méthode en font une technique intermédiaire entre les courbes simples de refroidissement et la calorimétrie différentielle à balayage.

Can. J. Chem. Downloaded from www.nrcresearchpress.com by 109.225.110.28 on 09/08/12
For personal use only.

Introduction

In the past years, we have been involved in the optimization of aprotic solvent mixtures for low-temperature applications of lithium batteries. To identify systems that remain liquid at very low temperatures, solid–liquid phase diagrams were determined for numerous mixtures and many of them showed unusual heating curves that were difficult to interpret in terms of solid–liquid and solid–solid transitions. Consequently, we developed a simple method to analyse the time dependence of the temperature of the sample in term of the Heat-Leak-Modulus, HLM, of a sample cell placed in a reservoir kept at a constant temperature.

As will be shown, the HLM method provides essentially the same information as differential scanning calorimetry, DSC, the major difference being that DSC is more sensitive. However, the HLM setup is much less expensive and is as effective for the analysis of systems having heats of transition greater than 1 joule per gram of sample. This condition is almost always satisfied for the investigation of the solid–liquid phase diagrams of mixtures.

The present paper describes the HLM method and its application to the determination of phase diagrams and enthalpies of transition of pure components and mixtures.

Theoretical background

The heating rate of a cooled sample placed in a heat reservoir will depend on the thermal conductivity, k (J s^{-1} K^{-1} cm^{-1}), of the material between the reservoir and the sample. With air, the heating rate will be small and the temperature of the sample, T_S, will increase slowly. If the heat required to warm the sample is small compared to the amount of heat in the reservoir then the temperature of the reservoir, T_R, will remain constant. In these conditions, the time dependence of the temperature of the sample can be described by (1)

$$[1] \quad c_P \frac{dT_S}{dt} = k\,G(x)\,(T_R - T_S)$$

where $G(x)$ is a geometrical factor (cm) and c_P (J K^{-1}) is the heat capacity of the cell containing the sample. This equation can be rearranged in term of the Heat-Leak-Modulus, HLM, a parameter that varies less with the temperature of the sample.

$$[2] \quad \mathrm{HLM} = \frac{dT_S}{dt} \Big/ (T_R - T_S)$$

In the absence of transitions involving heat, the unperturbed Heat-Leak-Modulus, HLM_0 (s^{-1}), becomes (2)

$$[3] \quad \mathrm{HLM}_0 = \frac{k\,G(x)}{c_P}$$

Both the thermal conductivity of air and the heat capacity of the cell containing the sample increase with temperature, so that HLM_0 should not vary much with temperature. If the sample goes through an endothermic transition, $dH_S > 0$, the heat will be taken from the cell and the sample because of the poor thermal conductivity of the air layer surrounding the cell. In these conditions, the transition is assumed to proceed adiabatically and the contribution to the time dependence of the temperature of the sample becomes

$$[4] \quad \frac{dT_S}{dt} = -\frac{dH_S}{dt} \Big/ c_P$$

Adding this contribution to HLM gives

$$[5] \quad \mathrm{HLM} = \mathrm{HLM}_0 - \frac{1}{c_P\,(T_R - T_S)} \frac{dH_S}{dt}$$

[1]Author to whom correspondence may be addressed.

[2]Revision received May 11, 1992.

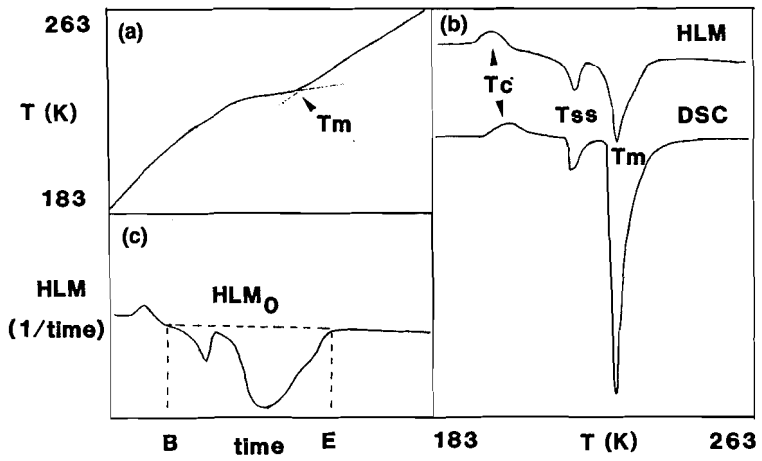

FIG. 1. Comparison of three representations of the time dependence of the temperature, for a sample of 0.25 cm^3 of acetonitrile. In (*a*), the usual temperature vs. time; in (*b*), the HLM vs. temperature curve is compared with a scan obtained by differential calorimetry using a DuPont calorimeter (model DSC 2910); in (*c*), the values of HLM shown in (*b*) are plotted against time and the beginning, B, and end, E, of the region of transition are shown.

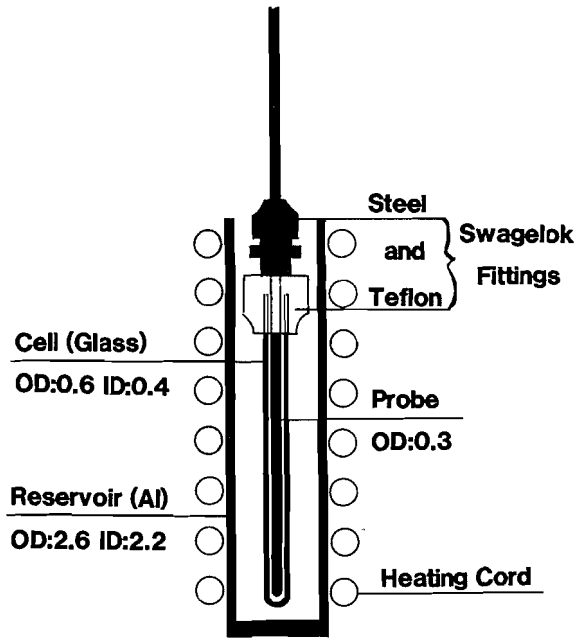

FIG. 2. Apparatus used in the present investigation. OB and ID stand for outer and inner diameter in cm, respectively. In the present work, the aluminum reservoir was 17 cm high and the length of the glass cell was about 8 cm.

Thus, an endothermic transition will produce a minimum in HLM while an exothermic transition will produce a maximum. The resulting dependence of HLM on temperature will essentially be identical to the one obtained with a more sophisticated differential scanning calorimeter. This is illustrated in Fig. 1 where three different approaches to the thermal analysis of acetonitrile are compared. First, the typical temperature vs. time curve shown in Fig. 1*a* allows a rough estimate of the melting temperature. In Fig. 1*b*, the same data are plotted as HLM vs. temperature and the resulting curve is compared to a DSC scan obtained with a Dupont calorimeter (DSC 2910). In both cases, the crystallization peak, the solid–solid transition, and the melting point of acetonitrile were detected.

In addition to the detection of a transition, one can also determine the heat associated with the transition through an appropriate analysis of the time dependence of the temperature of a sample as it is cooled or heated. Integration of eq. [5] leads to

$$[6] \quad g_S \Delta H_S = \int dH = -c_P \int (\mathrm{HLM} - \mathrm{HLM}_0)(T_R - T_S)\, dt$$

where ΔH_S (J g^{-1}) and g_S (g) are the enthalpy of transition and the mass of the sample. As with other calorimeters, the heat capacity of the system must be determined experimentally in the range of temperature of the investigation.

Experimental section

Chemicals

The origin and purity of the chemicals used are as follows: octane, nonane, dodecane, tetradecane, hexadecane, octadecane, and eicosane from Produits Chimiques Américain, >>99%; methanol and benzene from Produits Chimiques Américain, reagent anhydrous; heptane, decane, 1,4-dioxane, acetonitrile, and carbon tetrachloride from Caledon, distilled in glass; chloroform from Caledon, ACS spectro grade; toluene from Aldrich, ACS reagent; dichloromethane from Aldrich, HPLC grade.

Metholology

Figure 2 is a representation of the apparatus that was used in this investigation. The temperature probe (Omega, 100 ohm, platinum) is fixed to the glass cell with Swagelok fittings. In this configuration, the liquid sample is trapped as a film (~0.05 cm thick) between the temperature probe and the cell. The heat reservoir is an aluminum cylinder heated at a constant power with a powercord. The data acquisition unit consists of a multimeter (Keithley no. 196) driven by a compuer through an IEEE interface. This setup is flexible and other types of temperature probe, heating device, materials, or acquisition unit can be used.

The methodology consists of three very simple steps; loading, cooling, and analysis of the sample.

Loading

A volume of 0.25 cm^3 is weighed and placed into the glass cell. This fairly large volume reduces significantly the effect of humidity and evaporation encountered in differential scanning calorimetry when very small quantities of sample, ≈10 mg are weighed. The temperature probe is introduced into the glass cell, forcing the

Can. J. Chem. Downloaded from www.nrcresearchpress.com by 109.225.110.28 on 09/08/12
For personal use only.

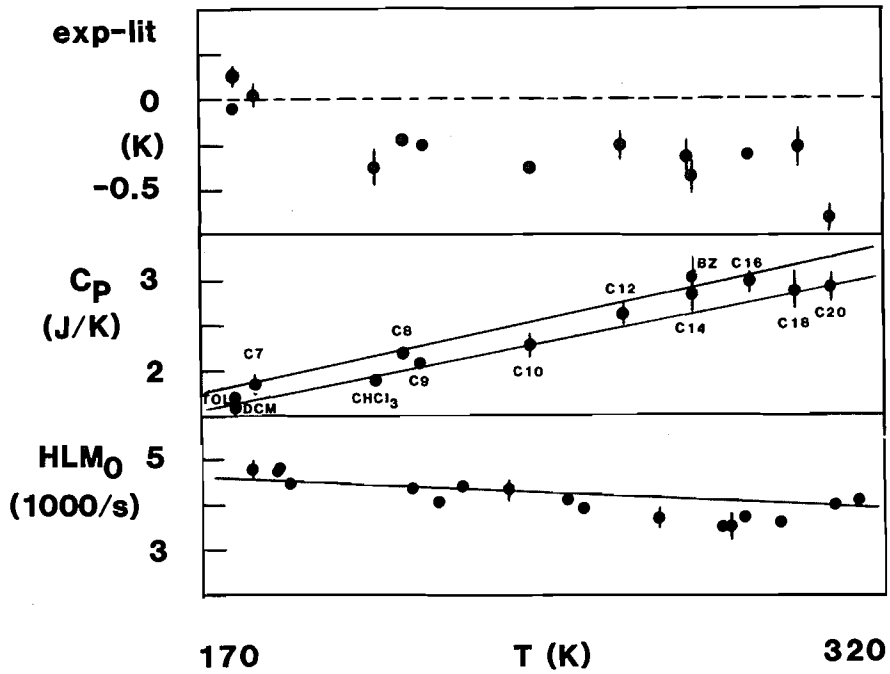

FIG. 3. Top; temperature dependence of the difference between the experimental and literature values of the temperature of transition. Middle; temperature dependence of the calibration constant, c_p, of the apparatus shown in Fig. 2. C*i* stands for aliphatic hydrocarbons with *i* carbon atoms and TOL, DCM, $CHCl_3$, and BZ stand for toluene, dichloromethane, chloroform, and benzene, respectively. Bottom; temperature dependence of the heat-leak-modulus in the absence of transition, HLM_0, as determined from the values of HLM_E. The solid line was calculated as described in the text.

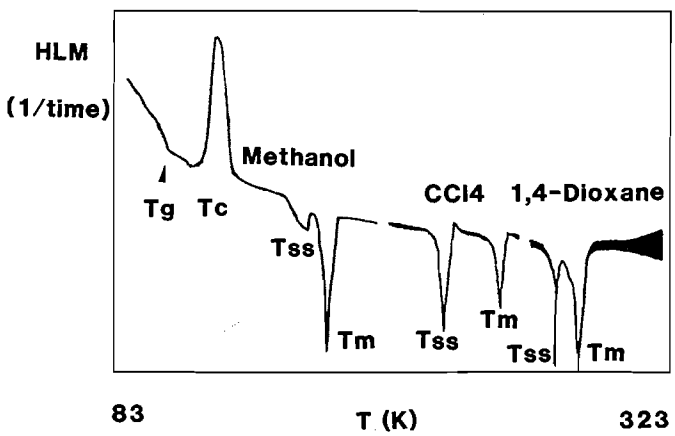

FIG. 4. HLM vs. temperature diagram showing portions of the curves obtained for methanol, carbon tetrachloride, and 1,4-dioxane. T_C, T_M, T_G, and T_{SS} stand for crystallization, melting, glass, and solid-solid transitions, respectively.

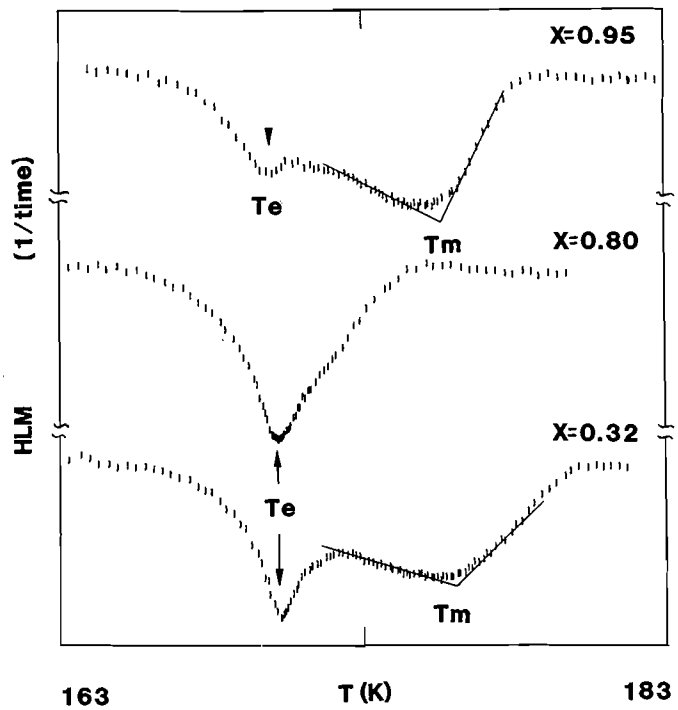

FIG. 5. Example of HLM vs. temperature curves obtained for three mixtures of heptane and toluene. The values of X is the mole fraction of toluene in the mixture. The eutectic temperature, T_E, is determined at the minimum of its corresponding peak while the melting temperature, T_M, is determined graphically.

volume of the liquid to rise as a film (thickness = 0.05 cm) between the probe and the glass cell.

Cooling

The cell is hermetically closed with Teflon and steel fittings to avoid evaporation and contamination of the sample. Then it is frozen by immersion in liquid nitrogen or another cryogenic mixture.

Analysis

The cell is transferred and fixed to the heat reservoir. The temperature of the sample is read at predetermined time intervals. Starting at the second value, the HLM is calculated and plotted on the screen. At the end, the scan can be analysed, printed, and saved for further analysis.

With the HLM method, it is not necessary to determine the absolute value of time because the array containing the temperature of the sample contains data that are equally spaced in time. That time interval, dt, is set to unity and HLM is calculated with eq. [2] where dT_S is the temperature difference between two successive

Can. J. Chem. Downloaded from www.nrcresearchpress.com by 109.225.110.28 on 09/08/12
For personal use only.

Can. J. Chem. Downloaded from www.nrcresearchpress.com by 109.225.110.28 on 09/08/12
For personal use only.

TABLE 1. Literature values of the temperature and enthalpy of fusion and solid–solid transition (in parentheses) and experimental values of the temperature of transition and calibration constant, c_p, of the apparatus. Unless otherwise specified, the reservoir was kept at 348 K

Systems[a]	T_F (K)	ΔH_F (J g^{-1})	$(T_F^{exp} - T_F^{lit})$ (K)	c_P (J K^{-1})
Heptane	182.54	141.3	+0.02 ± 0.06	1.86 ± 0.08
Octane	216.36	180.8	−0.23 ± 0.00	2.21 ± 0.05
Decane	243.4	202.2	−0.4 ± 0.0	2.27 ± 0.10
Dodecane	263.6	214.8	−0.2 ± 0.1	2.62 ± 0.12
Tetradecane[b]	267.29	229.9	−0.29 ± 0.04	2.84 ± 0.19
Hexadecane[b,c]	291.32	228.9	−0.29 ± 0.03	2.98 ± 0.10
Octadecane[c]	301.33	241.2	−0.25 ± 0.10	2.90 ± 0.18
Eicosane[c]	309.95	247.3	−0.64 ± 0.07	2.92 ± 0.13
Toluene	178.16	71.8	−0.05 ± 0.03	1.71 ± 0.04
Benzene	278.68	127.4	−0.42 ± 0.08	3.05 ± 0.18
Chloroforme	209.6	73.7	−0.4 ± 0.1	1.88 ± 0.04
Dichloromethane	178.0	70.7	+0.1 ± 0.1	1.60 ± 0.04
Nonane[b]	219.6	120.6	−0.3 ± 0.1	
	(217.18)	(48.9)	+0.69 ± 0.13	
		169.5[d]		2.08 ± 0.08
Methanol[b]	175.4	99.2	−0.3 ± 0.1	
	(157.4)	(19.8)	+6.4 ± 1.2	
Acetonitrile[b]	229.4	198.9	−0.1 ± 0.2	
	(217.2)	(21.9)	+1.2 ± 0.2	
Carbontetrachloride[b]	250.2	21.3	−0.1 ± 0.2	
	(225.2)	(29.8)	+0.4 ± 0.07	
1,4-Dioxane[b]	284.8	145.8	−0.3 ± 0.1	
	(272.8)	(26.7)	+2.4 ± 0.2	
Heptane + Toluene[e,f]	170.8 ± 0.1		−0.4 ± 0.3	
Toluene + Tetradecane[e]	178.1 ± 0.1		−0.5 ± 0.6	
Benzene + Tetradecane[e]	264.7 ± 0.1		−0.3 ± 0.2	

[a]From Handbook of Chemistry and Physics, 57th edition, CRC, 1976–77.
[b]From Lange's Handbook of Chemistry, 13th edition, McGraw–Hill, 1985.
[c]T_R = 373 K.
[d]Sum of both transitions.
[e]Eutectic temperatures from ref. 5.
[f]T_R = 303 K.

readings. The same arbitrary unit of time is used for the determination of the enthalpies of transition.

For integration purpose, HLM is plotted as a function of time (in arbitrary units) and the values are smoothed (3) over three equally spaced data with

$$[7] \quad HLM_I^{NEW} = HLM_{I-1}/4 + HLM_I/2 + HLM_{I+1}/4$$

Then the user selects the beginning and the end of a transition where HLM_B and HLM_E are determined, respectively. The baseline, HLM_0, is calculated by linear interpolation between HLM_B and HLM_E, as shown in Fig. 1*c*. The integral of eq. [6] is approximated (3) by a summation assuming linearity between equally spaced values of HLM. The integration becomes

$$[8] \quad \text{Area} = 1/2\,(A_B + A_E) + \sum_{I=B+1}^{E-1} A_I\,\Delta t$$

where $A(t) = (\text{HLM-HLM}_0)(T_R\text{-}T_S)$ and Δt is the arbitrary unit of time set to unity. With the resulting area (K), and knowing the calibration constant (J K^{-1}) and the mass of sample (g), the enthalpy of the transition (J g^{-1}) is calculated with the area resulting from the integration.

Results and discussion

Reproducibility of experiments

The temperatures and enthalpies of transition reported in this paper are values averaged over at least three runs with typical standard deviations of ±0.05 K and ±5%, respectively. From one sample to another, the reproducibilities of these results are ±0.1 K and ±3%, respectively.

Varying parameters such as the thickness of the reservoir, the cooling rate of the sample, and the period of acquisition does not affect the calibration constant, c_P, within the reproducibility limit of ±5%. The calibration is also independent of the temperature of the reservoir as long as it is at least 40 K higher than the temperature of the transition to be studied.

One very important parameter for the reproducibility of the data is the volume of sample in the cell since it determines the height of the liquid film and, consequently, the amount of cell material that contributes to the heat capacity. For instance, on going from 0.15 to 0.25 cm^3 of heptane, the calibration constant increases linearily with a slope of 8 J K^{-1} cm^{-3}. This value is much higher than the heat capacity of heptane because it also contains contributions from the glass cell and the probe. These contributions are very difficult to evaluate and, for that reason, it is important to always use the same volume of sample from one experiment to another to keep the calibration as constant as possible.

The melting temperatures of mixtures were determined graphically. The eutectic temperature and the temperature of

Can. J. Chem. Downloaded from www.nrcresearchpress.com by 109.225.110.28 on 09/08/12
For personal use only.

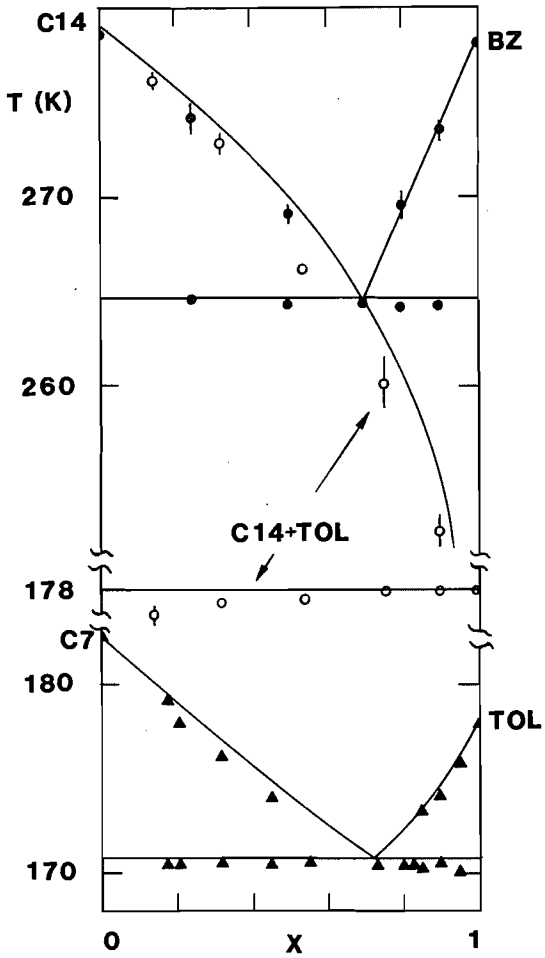

FIG. 6. Comparison of the solid–liquid phase diagram obtained with the HLM method with the results of Guieu et al. (5) (solid lines). Empty and filled circles are the melting and eutectic temperatures, respectively. C14, BZ, C7, and TOL stand for tetradecane, benzene, heptane, and toluene, respectively.

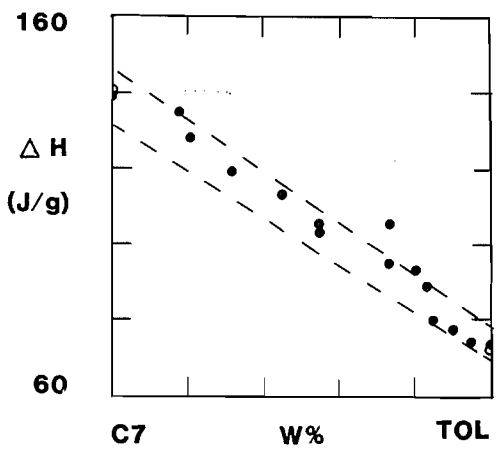

FIG. 7. Total enthalpy of melting, in joules per gram, of the mixtures of heptane and toluene as a function of the weight fraction of toluene. Dashed lines represent the +5% and −5% limits of the reproductibility. The calibration constant was taken as the average of the calibrations obtained with heptane and toluene.

melting of the pure components were defined as the temperatures at the minimum of the smoothed HLM vs. T curves. This procedure may lead to temperatures of transition that are different from the expected one because the minimum is not always symmetrical. This is shown in Fig. 3 where a difference of about −0.25°C is observed between the experimental and the literature values of the melting temperature. That small difference is rather systematic and it may also be the consequence of a miscalibration of the temperature probe. Nevertheless, the use of the minimum for the determination of the melting temperature is fast and convenient.

Temperature dependence of the calibration constant, c_P

The determination of the enthalpy of transition requires the calibration of the apparatus in term of its heat capacity (eq. [6]) in the temperature range to be investigated. We have determined the calibration constant of the present apparatus, c_P, with the literature value of the enthalpy of fusion, ΔH_F, and the experimental area (eq. [7]) of the peak at the melting point. The results are reported in Table 1 and plotted in Fig. 3 as a function of the melting temperature. The increase of the calibration constant with temperature is in accordance with the general temperature dependence of the heat capacity of materials. Moreover, most of the values fall within the ±5% limits of the linear trend. Thus, using the linear trend that describes the temperature dependence of the calibration constant, $c_P(T) = 1.54 + 0.0103(T\text{-}160)$, it is possible to measure the enthalpy of transition of an unknown within 5%.

Temperature dependence of HLM_0

Equation [3] shows that HLM_0 depends on a geometrical factor, $G(x)$, independent of the temperature, and on c_P and k, the heat capacity and the thermal conductivity of the system, which both depend on temperature. Thus, provided that the values of $G(x)$, c_P, and k are known, the temperature dependence of HLM_0 could be determined quantitatively. The geometrical factor was calculated with the value of HLM_0 just after the melting of heptane, and the values of c_P and k were also available at that temperature.

With the present geometry, the heat flux is normal to the surface of the components, so that the overall thermal conductivity of the system is limited by the component having the lowest thermal conductivity according to (1)

$$[9] \quad k^{-1} = \Sigma \Phi_i k_i^{-1}$$

where Φ_i is the volume fraction of component i. For the apparatus described in Fig. 2, the air layer accounts for about 93% of the volume while the remaining space is occupied by the sample cell. The thermal conductivity was calculated using the reported values of k for dry air, and the contribution of the sample cell was assumed to be negligible (less than 1%). Taking $G(x)$ as a constant, the temperature dependence of HLM_0 was calculated with eqs. [3] and [9] and the temperature dependence of c_P. The resulting curve is plotted as a solid line in Fig. 3 and it is in good agreement with the experimental values of HLM_E, which correspond to the values of HLM_0 after the melting of the samples. This shows that HLM_0 can be calculated quantitatively as a function of temperature provided that the geometry and the characteristics of the materials are well known.

Transitions in the solid state

The presence of transitions in the solid state is often difficult to observe with typical temperature vs. time curves. This was shown for acetonitrile in Fig. 1 and there exist many

Can. J. Chem. Downloaded from www.nrcresearchpress.com by 109.225.110.28 on 09/08/12
For personal use only.

other components that present solid–solid transitions. Figure 4 presents the experimental HLM vs. T curves of methanol, carbon tetrachloride, and 1,4-dioxane where such transitions are observed in the solid state.

The glass transition, T_G, corresponds to an increase of the heat capacity due to additional molecular motions in the solid state, and from eq. [3] it will appear as a sudden decrease of HLM_0. These molecular motions often lead to the exothermic crystallization, T_C, of the solid glass. For instance, see the curve for methanol in Fig. 4. Another type of transition in the solid state is the reorganization of the solid structure or the solid–solid transition, T_{SS}, that occurs at a temperature lower than the solid–liquid transition, T_M. As for acetonitrile, the HLM vs. temperature curves of Fig. 4 all show the presence of a solid–solid transition.

Solid–liquid phase diagram

In addition to the characterization of pure components, the HLM method is very effective for the investigation of the solid–liquid phase diagram of mixtures. This is shown in Fig. 5 where the scans obtained with the HLM method are presented for three mixtures of heptane and toluene. The shape of the curves obtained for the thermal analysis of that system is very similar to the scans obtained by DSC (4). For that single eutectic system, the eutectic mixture, as for the pure components, shows a single peak that has its minimum at the temperature of the transition. The HLM curves of the mixtures on both sides of the eutectic composition show a sharp peak at the eutectic temperature and a broad and asymmetric peak corresponding to the range of the solid–liquid equilibrium of the mixtures. Because of the asymmetry of the melting range, the melting temperature is determined by extrapolation.

The HLM method was used to determine the solid–liquid phase diagram of the systems heptane–toluene, tetradecane–benzene, and tetradecane–toluene. The resulting phase diagrams are shown in Fig. 6 and compared to those obtained by Guieu *et al.* (5). For the three systems, the difference between our value of the eutectic temperature and the literature value is within the experimental error. This is quite good, considering the fact that the thermal analyses reported in the literature were performed at a heating rate of 0.2 K min^{-1} while, in our case, the heating rate varied from 35 K min^{-1} at 170 K to about 20 K min^{-1} at room temperature.

The investigation of mixtures with the HLM method is not only a fast and accurate method for the determination of solid–liquid phase diagrams but it is also reliable for the determination of the total enthalpy of melting of a mixture. For instance, the method was applied to mixtures of heptane and toluene. The enthalpy of mixing should be small for these monpolar solvents so that the enthalpy of melting of that single eutectic system is expected to be linear from one component to the other. The calibration constant, c_P, was determined with the pure components, and the total enthalpy of melting of the mixture was determined with the integration procedure described using eqs. [6]–[8]. The results are shown in Fig. 7 and they are in accord with the expected behavior within the ±5% limits shown by the two straight lines.

Conclusions

The HLM method is a technique of thermal analysis based on the Heat-Leak-Modulus of the system. This parameter is not very dependent on the temperature and it provides a reproducible baseline from one experiment to another. The HLM method allows the identification of the glass-transition, crystallization, solid–solid transition, eutectic, and melting temperatures of a system with a precision better than 0.1 K. The apparatus is easy to calibrate in term of its heat capacity and the enthalpies of transition can be determined with a precision of ±5%.

The main difference between the HLM method and differential scanning calorimetry is the limit of detection, which is lower in the case of DSC. However, a wide variety of investigations do not require the high sensitivity of DSC. Moreover, the high sensitivity of DSC often forces the use of a very small amount of sample, which increases the relative error in the weight of sample and emphasizes the effect of evaporation and humidity.

The simplicity, low cost, and precision of the HLM method fill the gap between standard cooling curves and the sophisticated differential scanning calorimetry experiments. The HLM method has numerous applications in physical chemistry, polymer science, metallurgy, and chemical engineering.

Acknowledgements

The authors are grateful to the Natural Sciences and Engineering Research Council of Canada and to the Department of National Defence of Canada (contract no. 064SSW2207-9-AF01) for financial support.

1. W. D. Kingery, H. K. Bowen, and D. R. Uhlmann. *In* Introduction to ceramics. 2nd ed. John Wiley & Sons, New York. 1976. Chap. 12.
2. H. H. Bauer, G. D. Christian, and J. E. O'Reilly. *In* Instrumental analysis. Allyn & Bacon Inc., Boston. 1978. Chap. 17.
3. P. R. Bevington. *In* Data reduction and error analysis for the physical sciences. McGraw–Hill, New York. 1969. Chap. 13.
4. C. Grabrielle-Magdelmont and R. Perron. J. Colloid Interface Sci. **95**, 471 (1983).
5. R. Guieu, A. Faradjzadeh, L. Cabonnel, and P. Franzosini. Int. DATA Ser. Sel. Data Mixtures, Ser. A, **1**, 51 (1980).

Studies of the role of water on some imine–acid complexes by means of Raman spectroscopy

P. TURCOTTE, S. ALEX, AND D. VOCELLE[1]

Département de chimie, Université du Québec à Montréal, C.P. 8888, Succ. A, Montréal (Québec), Canada H3C 3P8

Received July 12, 1991[2]

P. TURCOTTE, S. ALEX, and D. VOCELLE. Can. J. Chem. **70**, 2751 (1992).

The percentages of protonation were determined for a conjugated Schiff base *trans,trans*-2,4-heptadienylidene *tert*-butylamine in the presence of 3-chloropropionic acid (CPR) and dichloroacetic acid (DCA) in three solvents of different polarities. In dioxane, a solvent of low polarity, protonation is only important for the strong acid DCA (50–60%). By using solvents of higher polarities, protonation is seen to increase and is almost complete for DCA in ethanol. When water molecules are added to these systems, hydrolysis of the Schiff base, measured inside the time span of the experiments (10 min), occurs readily in dioxane, is very slow in a chloroform–dioxane mixture (9:1), and is totally absent in a mixture of ethanol–dioxane (1:9). Results indicate that water does not mediate protonation in all three sets of solvent combinations. The results are also discussed in terms of the possible role that water molecules could have in the visual and bacterial pigments.

P. TURCOTTE, S. ALEX et D. VOCELLE. Can. J. Chem. **70**, 2751 (1992).

Les pourcentages de protonation ont été déterminés pour le cas d'une base de Schiff conjuguée, la *trans,trans*-2,4-heptadiénylidène *tert*-butylamine, en présence de l'acide 3-chloropropionique (CPR) et de l'acide dichloroacétique (DCA) dans trois solvants de différentes polarités. Dans le dioxane, un solvant de faible polarité, la protonation n'est importante que pour l'acide fort DCA (50–60%). En utilisant des solvants de polarité plus élevée, la protonation augmente et est à peu près complète pour le DCA dans l'éthanol. Quand de l'eau est ajoutée à ces systèmes, l'hydrolyse de la base de Schiff, mesurée à l'intérieur du temps d'enregistrement des spectres (10 min), est rapide dans le dioxane, est beaucoup plus lente dans un mélange de chloroforme–dioxane (9:1) et est totalement absente dans un mélange d'éthanol–dioxane (1:9). Les résultats indiquent que l'eau ne favorise aucunement la protonation et cela vaut pour les trois ensembles de solvants utilisés. Les résultats sont aussi discutés en terme du rôle que pourrait jouer l'eau dans les pigments visuels et bactériens.

Can. J. Chem. Downloaded from www.nrcresearchpress.com by 109.225.110.28 on 09/08/12
For personal use only.

Introduction

Protonation and deprotonation of a retinal Schiff base are essential events in the mechanism of proton translocation in visual and bacterial pigments. These two aspects have received wide interest on both theoretical and experimental grounds (1–10). It is now known that the protonating agent of the chromophore of rhodopsin (11-*cis* retinal linked to lysine 296 of the apoprotein) is glutamic acid 113 (11–13), whereas for the related bacterial pigment bacteriorhodopsin, it is a combination of three amino acids that are responsible for the protonation of the chromophore: Asp-85, Asp-212, and Arg-82 (14, 15). One of the most important features of these pigments that is still not fully understood is their capacity to absorb light in the 500–570 nm region. Model studies of Schiff base in organic solvents have shown that an unprotonated Schiff base has its maximum absorption (λ_{max}) at ca. 360 nm while protonated model Schiff bases (SB) are red-shifted to λ_{max} ca. 440–450 nm (16, 17). Considering that bovine rhodopsin (as an example) has its λ_{max} at 500 nm (18), it implies that the protonated chromophore is again red-shifted by about another 50 nm by interactions with the protein. This last bathochromic shift is called the opsin shift (19). Several hypotheses have been advanced to explain this shift (2, 16, 18), but lately, the emphasis has been placed on the relationship between the protonated Schiff base and its counterion; visualize $RetCH{=}N(R)H^{+}\cdots{}^{-}OOCR$, where Ret is the retinylidene portion of the Schiff base that could well explain totally or in part the opsin shift. Yet, model studies conducted in our laboratory (20–25) have indicated that a retinylidene Schiff base in nonpolar solvents or in methanol could not be fully protonated by acids having pK_a's in the 3–5 region as measured in water, which is the region where Glu or Asp have their pK_a's (4.25 and 3.89 respectively). Hence, some stabilizing factors must be present in the protein so that the system Schiff base/acid could be fully protonated ($SBH^{+}\cdots{}^{-}OOC^{-}$). We have suggested (26) and partly demonstrated (21, 25) that the concomitant presence of several molecules of acid acting like a proton relay transfer and (or) the presence of water molecules could possibly help the system to reach full protonation. In particular the role of water, apart from its obvious involvement in the hydrolysis of metarhodopsin II, remains intriguing, since pigments which have been made dry react quite differently than normal "wet" pigments (9, 10). However, these hypotheses are still controversial and more data must be gathered to confirm or invalidate these postulates.

At this moment, two schools of thought exist on this question. One favors the presence of water next to the Schiff base (2, 6–10), the other (27) rather promotes the excitonic model of Kriebel and Albrecht (1). Both models have advantages and drawbacks but neither one nor the other can rationalize all the physical and chemical properties of these pigments.

Furthermore, if water molecules are present near the protonated Schiff base, some additional factors must also be present to prevent these water molecules from reaching the protonated imine before the metarhodopsin II stage, since hydrolysis will occur readily. So far, the mechanism of hydrolysis of Schiff bases have received little attention. Cooper *et al.* (28) have reported a full kinetic analysis of the hydrolysis of a model of rhodopsin consisting of *N*-retinylidene

[1]Author to whom correspondence may be addressed.

[2]Revision received July 11, 1992.

Can. J. Chem. Downloaded from www.nrcresearchpress.com by 109.225.110.28 on 09/08/12
For personal use only.

n-butylamine in aqueous anionic, cationic, and neutral detergent micelle systems.

In the present study, the role of water, especially its ability to favor protonation and hydrolysis, will be explored. Since Papadopoulos *et al.* (29) have shown that four molecules of water are likely present near the chromophore, different ratios of water in the system, from 0 up to 4, will be added. To do this, a simpler model will be used. It consists of *trans,trans*-2,4-heptadienylidene *tert*-butylamine (SB hereafter) that will be protonated by two acids: dichloroacetic acid (DCA, pK_a 1.26) and 3-chloropropionic acid (CPR, pK_a 3.99). The SB and the acid will be dissolved in a solvent or mixtures of solvents (dioxane, chloroform, or ethanol) to which different amounts of water will be added. Protonation and the unwanted hydrolysis will be monitored by Raman spectroscopy. These experiments are expected to give a better knowledge of the behavior of such systems in various electrostatic media. In addition, these tests are meant to stress the importance of electrostatic interactions on the physical and chemical properties of protonated Schiff bases.

Experimental

The synthesis of *trans,trans*-2,4-heptadienylidene *tert*-butylamine ($CH_3CH_2CH{=}CHCH{=}CHCH{=}NC(CH_3)_3$, called SB) was carried out according to a well-established method (22). The aldehyde and amine were supplied by the Aldrich Chemical Co. (Milwaukee, Wis., U.S.A.). Since this SB is somewhat unstable, it must be used freshly prepared or redistilled. All experiments were done quickly, especially when water and acids were present so as to minimize hydrolysis. Solutions for Raman spectra were prepared by mixing 0.025 M of the SB with an equimolar quantity of the organic acid in a given solvent. The concentration of the imine was selected to reduce to a minimum the self-absorption on Raman intensities deriving from the tail of the $\pi-\pi^*$ electronic transition of the protonated imine seen at ca. 308 nm in chloroform (30). The $\pi-\pi^*$ electronic transition of the unprotonated form absorbs at 267 nm. Dioxane, chloroform, and ethanol were all of a spectrograde quality and were dried, as well as the acids, over molecular sieves for liquids and in a desiccator over anhydrous calcium chloride for solids. Chloroform was also eluted three times on a basic alumina column to remove traces of ethanol and hydrochloric acid.

In the experiments using water (HPLC grade), spectra were taken immediately after water addition in the solution. UV spectra were recorded on a Pye Unicam PU 8800 instrument while Raman spectra were obtained on a Spex Triplemate spectrograph coupled to an EG&G Princeton Applied Research detector, model 1422. Samples were excited with the 25–50 mW of the 488.8 nm laser line (Spectra Physics CW A^+, model 2016) to take full advantage of the preresonance effect. To improve the preresonance effect, attempts to use the 457.9 nm laser line were tried but were inconclusive because of the poor detector efficiency in this spectral region. The samples were put in a sealed capillary mounted on a thermally regulated sample holder maintained at 10°C. Resolution was 5 cm^{-1} at 1600 cm^{-1}. The spectra were recorded in 10 min and the fluorescence background was routinely substracted with an appropriate *n*th-order polynomial when necessary.

Results and discussion

In a first approximation, the SB/acid system obeys the simple equation written below, using symbolic notation:

[1] $C{=}C{-}C{=}C{-}C{=}N{-}R + HOOC{-}R_1 \rightleftharpoons C{=}C{-}C{=}C{-}C{=}N(R)H^+\cdots{}^-OOCR_1$

Depending on the acids and solvents used, the percentage of protonated SB (or PSB) varies and this particular point has already been investigated in pure chloroform and methanol solutions by means of FT-IR spectroscopy (23, 24). As a rule, the protonation is almost complete, providing that the proton source has a pK_a value less than to 2 units, especially when the solvents are polar and protic. Upon water addition, the PSB is known to hydrolyse to give irreversibly the parent aldehyde (2):

[2] $R{-}CH{=}N(R_1)H^+ + H_2O \rightleftharpoons R\text{-}CH{=}O + R_1\text{-}NH_3^+$

This is particularly true for the protonated SB since the unprotonated SB is expected to be more stable in the presence of water according to standard organic chemistry rules. Thus, hydrolysis is believed to be dependent on both the protonation state of the imine moiety and the electrostatic properties of the solvents. In the present work, the water effect will be tested to differently solvated PSB in order to characterize its action. Several solvents and combinations of solvents can be tested to carry out this study, but for this work we have chosen dioxane, chloroform, and ethanol for reasons that are explained later.

Generally speaking, in the actual pigments, the protonated chromophore may be located in a protein cavity falling into one of the following three categories.

(*1*) The protonated Schiff base lies in a nonpolar cavity and does not form H bonds within this pocket.

(*2*) The protonated Schiff base rests in a nonpolar but interactive cavity. For simplicity, the term interactive cavity will be used in the text when interactions are presumed to exist between the chromophore and the cavity.

(*3*) The protonated Schiff base is surrounded by a polar and interactive cavity.

To mimic the situations (*1*), (*2*), and (*3*), three solvents or mixtures of solvents could be used. For case (*1*), pure dioxane was selected even though some interactions are possible by the use of the lone pairs of electrons located at the two oxygen atoms. However, it is the only suitable nonpolar solvent (dielectric constant 2.21) that is able to dissolve the SB, the acid, and the water without inducing a phase separation. In case (*2*), a mixture of 90% of chloroform and 10% of dioxane was used, whereas for (*3*), a mixture of 10% ethanol and 90% dioxane was used. In the last case, ethanol was chosen instead of the customary methanol because fluorescence, always a nuisance in Raman, is less intense in that solvent. A few combinations of solvents were also tested and will be mentioned in the text when necessary.

First, Raman spectra of unprotonated and protonated model SB were collected in dioxane, chloroform, and ethanol in the absence of water in order to characterize their spectroscopic behaviour. Spectra of the SB and differently protonated SB in chloroform are displayed in Fig. 1. As can be seen, they are dominated by the C=C double bond stretching mode ($\nu_{C=C}$) of the conjugated system centered at ca. 1624 cm^{-1} and the C=N double bond stretching mode of the imine link ($\nu_{C=N}$) located at ca. 1641 cm^{-1} when unprotonated. Following addition of any organic acids, the $\nu_{C=N}$ vibration gradually disappears and is replaced by the weak $C{=}N^+$ stretching mode ($\nu_{C=N^+}$) detected at ca. 1679 cm^{-1}. Simultaneously, the Raman intensity of the $\nu_{C=C}$ band is enhanced, while its frequency position remains almost unchanged. It should be noted that when protonated, the intensity of the $\nu_{C=C}$ mode of the PSB gains intensity because the energy of its electronic transition becomes more coinci-

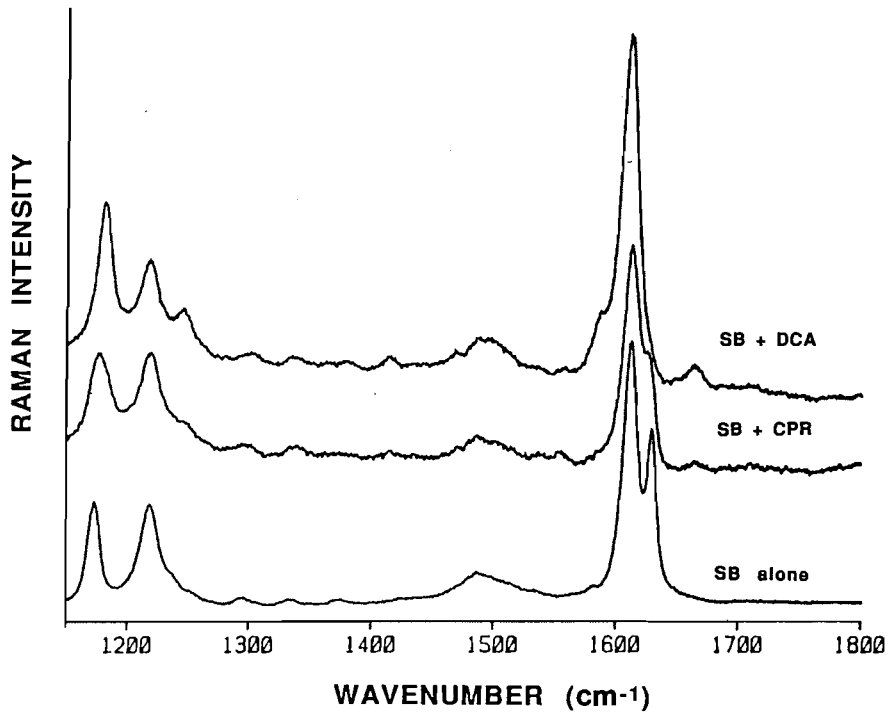

FIG. 1. Raman spectra of the SB (bottom trace) and of the SB complexed to organic acids (top traces) in chloroform excited with the 488 nm laser line at a concentration of 0.025 M.

TABLE 1. Percentages of protonation of several SB/acid systems in dioxane, chloroform, and ethanol

SB/acid	Dioxane (%)	Chloroform (%)	Ethanol (%)
SB/CPR	0–10	40–50	50–60
SB/MCA[a]	35–45	60–70	80–100
SB/DCA	50–60	80–90	100

[a]MCA stands for monochloroacetic acid.

dent with the energy of the 488 nm laser line, leading to a better preresonance Raman effect (viz. λ_{max} 308 nm for the PSB compared with λ_{max} 267 nm for the SB). This Raman regime also leaves the spectra of the complexes free of the contribution of the $\nu_{as\ COO^-}$-mode of the deprotonated organic acids, detected in the same spectral region. This makes the measurements of the percentage of protonation easily accessible and they are reported in Table 1 for chloroform, dioxane, and ethanol. The percentages of protonation have been calculated simply by measuring the peak heights of the $\nu_{C=N}$ of the SB that remains after protonation compared with the peak heights of the $\nu_{C=N}$ of the SB without the acid system, since all spectra have been obtained using the same concentration of the SB. This method is applicable as long as the $\nu_{C=N}$ band is visible, that is, for systems where the SB is moderately protonated. When protonation becomes large, the height of the $\nu_{C=N^+}$ band (at 1679 cm^{-1}) can be measured and compared with the height of this band for the fully protonated system. From Table 1, it can be seen that protonation increases with the strength of the acid used and the polarity of the solvent (dielectric constants of these three solvents are dioxane 2.21, chloroform 4.81, and ethanol 24.3). Maximum protonation occurs for DCA in ethanol, whereas the minimum is reached for CPR in dioxane. These results are comparable to those obtained by means of FT-IR for the same system in chloroform (23) and in methanol (24). Knowledge of the initial degree of protonation is important, as the reactions taking place following water addition are governed by its relative concentration compared with the one of either the PSB or the SB.

Addition of water

When water is added to the system, part of the protonated SB is destroyed and turned into its aldehyde form. The aldehyde (*trans,trans*-2,4-heptadienal) has two characteristic bands: the very intense $\nu_{C=C}$ at ca. 1637 cm^{-1} and the weaker $\nu_{C=O}$ at ca. 1681 cm^{-1}, which are unfortunately coincident with the $\nu_{C=N}$ band of SB (at 1641 cm^{-1}) and the $\nu_{C=N^+}$ band of PSB (at 1679 cm^{-1}), with the result that this study is less straightforward. The effect of the presence of the aldehyde in the SB spectrum can be seen in Fig. 2, corresponding to 30, 70, and 100% of hydrolysis. The spectra corresponding to 30 and 70% of hydrolysis are computerized versions using the pure SB and pure aldehyde spectra and correspond to the situations where respectively 30 and 70% of the SB would have been hydrolyzed. As can be seen, the intense $\nu_{C=C}$ of the dienal completely overlaps the $\nu_{C=N}$ of the SB. This deteriorates even more when the PSB is present, because then three products having almost the same Raman signature appear as shown experimentally in Fig. 3 for hydrated PSB and SB adducts in dioxane. As can be seen, the overlapping contribution from the aldehyde considerably alters the usual spectral response in the 1600–1700 cm^{-1} region. This makes it difficult to evaluate the percentage of protonation using the method quoted earlier, as well as the measurement of the extent of hydrolysis. It is not possible to solve this problem by substracting the alde-

Can. J. Chem. Downloaded from www.nrcresearchpress.com by 109.225.110.28 on 09/08/12
For personal use only.

Can. J. Chem. Downloaded from www.nrcresearchpress.com by 109.225.110.28 on 09/08/12
For personal use only.

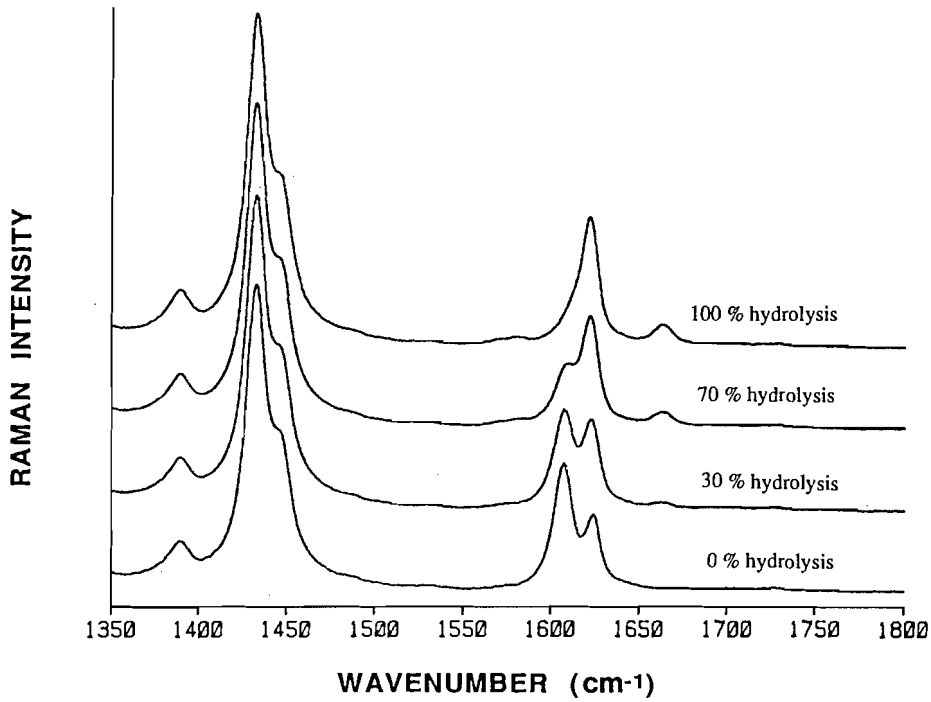

FIG. 2. Raman spectra of a 0.025 M dioxane solution of SB (bottom trace) and of a 0.025 M dioxane solution of its parent aldehyde (top trace) excited at 488 nm. Middle traces represent computer mixing of both spectra in various proportions as quoted (*vide infra*).

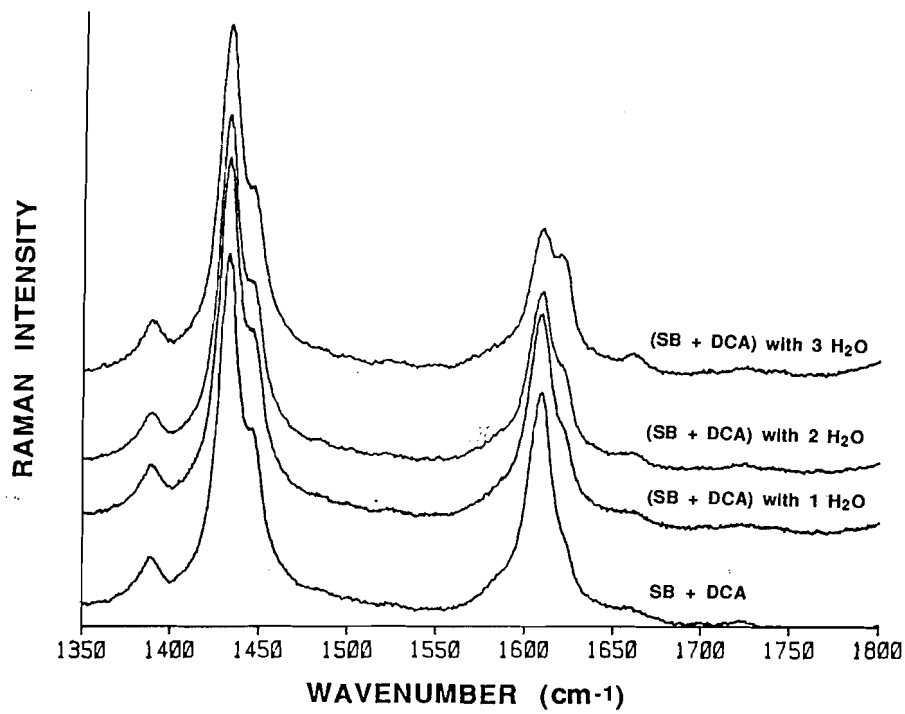

FIG. 3. Raman spectra of a 0.025 M solution of the SB complexed to dichloroacetic acid in the absence (bottom trace) and in the presence of water (top three traces) in dioxane (excitation wavelength 488 nm).

hyde contribution, firstly because all the aldehyde vibrations are coincident with either the SB or the PSB spectral response and secondly, because of a lack of an internal standard, an unmatched mass balance will result leading to a false estimation of the degree of protonation.

However, it is not necessary to monitor the exact changes in the degree of protonation of the SB in the presence of water; it is sufficient to have an indication of how the protonation state varies under the different conditions. Hence, the relative change in the percentage of protonation of the SB

TABLE 2. Calculation of the ratio R of an equimolar mixture of SB/acid in dioxane (0.025 M) in the presence of 0 to 4 times water compared with the initial concentration of SB

Water ratio added	SB alone	SB/CPR	SB/DCA
0	1.8	1.6	2.4
1	1.7	1.7	1.8
2	1.9	1.6	1.6
3	1.8	1.6	1.3
4	1.8	1.5	0.9

TABLE 3. Calculation of the ratio R of an equimolar mixture of SB/acid (0.025 M) in a chloroform/dioxane solution (90:10) in the presence of 0 to 4 times water compared with the initial concentration of SB

Water ratio added	SB alone	SB/CPR	SB/DCA
0	1.4	1.8	3.6
1	1.4	1.7	3.5
2	1.4	1.7	2.9
3	1.4	1.6	2.8
4	1.5	1.6	2.8

TABLE 4. Calculation of the ratio R of an equimolar mixture of SB/acid (0.025 M) in a solution of ethanol/dioxane (10:90) in the presence of 0 to 4 times water compared with the initial concentration of SB

Water ratio added	SB alone	SB/DCA
0	1.7	2.9
1	1.7	2.9
2	1.7	2.9
3	1.7	2.9
4	1.7	2.9

in the presence of water can be evaluated by considering the evolution of the different bands in the 1600–1700 cm^{-1} region. If protonation is favoured by water, the $\nu_{C=N}$ band at 1641 cm^{-1} will decrease, whereas the $\nu_{C=C}$ band at 1624 cm^{-1} will increase. Thus the intensity ratio of the $\nu_{C=C}$ band measured at 1624 cm^{-1} divided by the intensity of the $\nu_{C=N}$ at 1641 cm^{-1} will increase according to an increase of the degree of protonation. This ratio R can then be used as an indicator reflecting the protonation state of the SB. For 0% protonation, R ranges between 1.4 and 1.8, depending on the solvent, whereas for 100% protonation, R tends to infinity. However, when hydrolysis is present, R is directly affected since the dienal produced has its $\nu_{C=C}$ located at 1637 cm^{-1}, as previously described, and thus R is expected to decrease. This can be seen in Fig. 3 where four spectra of a SB/DCA in dioxane are shown. The first spectrum (bottom line) shows a band at ca. 1624 cm^{-1} and a shoulder at ca. 1641 cm^{-1}; the ratio R is 2.4, indicating that protonation is indeed present (R 2.4 compared with R 1.8 for 0% protonation). The other spectra relate to the addition of 1, 2, and 3 molecules of water. It shows that the 1620–1625 cm^{-1} band decreases whereas the ca. 1635 cm^{-1} band increases. R, measured always at 1624 and 1641 cm^{-1}, takes the value of 1.8, 1.6, and 1.3 respectively. This time, the denominator of R mostly represents the contribution (at 1641 cm^{-1}) of the $\nu_{C=C}$ of the dienal plus the contribution of the $\nu_{C=N}$ of the SB. The Raman signal deriving from the bending mode of water can also be detected in this same region, but its contribution is negligeable because, at the concentration range used, its signal is very weak. Thus R does not reflect the exact degree of protonation because of the presence of the aldehyde formed after hydrolysis. However, if an x% protonation of the SB is followed by the same x% hydrolysis, R can again be used by utilizing an experimentally derived equation (3):

$$[3] \quad \% \text{ of protonation} = \% \text{ of hydrolysis} = 114.0 - 70.4R$$

As an example, for R = 1.62, eq. (3) gives 0% hydrolysis; for R 0.2, a 100% hydrolysis. Therefore after water addition, if the value R corresponds to the initial percentage of protonation, then it means that water does not promote protonation. Table 2 reports the results obtained in dioxane using 0 to 4 molecules of water and Tables 3 and 4 refer respectively to chloroform–dioxane (9:1) and ethanol–dioxane (1:9) solvents.

In all three cases, as can be seen in Tables 2–4, results show that the heptadienylidene Schiff base without acids, but in the presence of water, is quite stable (R does not vary).

For 3-chloropropionic acid, a weak acid, Table 2 shows that R is very slightly different from the "standard" value (R 1.8), indicating that protonation, if any, is very small and that water molecules have, at the most, a very weak effect in promoting protonation in dioxane. With DCA, protonation is higher (R 2.4) and water molecules affect R directly (from 2.4 to 0.9). Using eq. [3], in the case of four molecules of water, the degree of protonation reaches around 50%, which corresponds to the initial degree of protonation, thus indicating that water has no effect in promoting protonation. In the time span of the experiments (some 10 min for each spectrum), these results indicate that it takes four molecules of water to cause the complete hydrolysis of one molecule of the protonated Schiff base.

In a chloroform–dioxane (9:1) mixture, CPR is more effective as a protonating agent (R 1.8 compared with 1.4). With water, R reaches only 1.6 (from 1.8), indicating that in the time span of the experiments water has almost no effect. For DCA, in the absence of water, R reaches 3.6, indicating some 80–90% protonation and showing that chloroform favors more protonation than dioxane (50–60%). Again, with water present, R drops only slightly from 3.5 to 2.8. For a protonation of 80% followed by complete hydrolysis, R should reach ca. 0.48 (as calculated using eq. [3]) instead of 2.8. From Table 3 then, it must be concluded that chloroform is rather effective in shielding the PSB from water and only a small fraction of the molecules of water can hydrolyze the PSB. Chloroform is known to cause the formation of tight ion-pairs (thus favoring protonation) and this has been described before (20, 24). Finally, the ratio of chloroform to dioxane was varied from 1:1 to 1:9 and the same results were obtained, that is, R was identical or greater than R obtained in pure dioxane.

In an ethanol–dioxane (1:9) mixture, only DCA was used. Table 4 shows that DCA gives only 60–70% protonation (R

Can. J. Chem. Downloaded from www.nrcresearchpress.com by 109.225.110.28 on 09/08/12
For personal use only.

Can. J. Chem. Downloaded from www.nrcresearchpress.com by 109.225.110.28 on 09/08/12
For personal use only.

2.9), that is, more than in dioxane (R 2.4) and less than in chloroform–dioxane (R 3.6). Other ratios of ethanol and dioxane were tested. Usually R increased with an increase in the ratio of ethanol to dioxane. Unfortunately, severe experimental limitations exist in this case because of the unavoidable fluorescence background present with alcoholic solutions. Upon water addition, R remains constant, meaning that the system is chemically stable: no hydrolysis is occurring as well as no additional protonation. This is quite different from the results obtained in pure dioxane where hydrolysis readily occurred. In fact, hydrolysis became important in this ethanol–dioxane mixture only when the concentration of water was at least 1% v/v water/solvent. The presence of ethanol promotes protonation when compared with dioxane alone and prevents hydrolysis. This means that some ethanol molecules lie close to the imine function and interact with the SB and the acid probably through hydrogen bonding, helping protonation to occur. Also, other ethanol molecules must interact with water, again through hydrogen bonding, and this time preventing water from diffusing near the protonated Schiff base.

This is not too surprising when one considers the action that water has when interacting either with dioxane or ethanol. Cennamo and Tartaglione (31) have studied by X-ray spectroscopy the behavior of water mixed with either dioxane or ethanol. In that work, they show that whatever the concentrations of water used, its structure is different from one solvent to the other. This can also be seen by examining the Raman spectra of mixtures of water–ethanol and water–dioxane. Figure 4 shows the spectrum obtained with a mixture of water–dioxane in a ratio of 1:9 (curve 1). This must be compared with the spectrum of pure water (also shown, curve 2). Dioxane is then seen to disturb greatly the structure of water with an enhancement of the 3420 cm^{-1} band relative to the 3260 cm^{-1} band. This is well documented and is assigned to a decrease of the in-phase intermolecular coupling of the OH oscillators (ref. 32 and references therein). It is believed that in such cases water is dispatched into micro domains. The spectrum of a 1:10 water–ethanol mixture is quite different from that obtained with a 1:10 water–dioxane mixture. The water vibrations in this region are again perturbed but the variation of the 3420 and 3260 cm^{-1} band system is less pronounced. However, in the case of the water–ethanol mixture, the analysis becomes more complex because of the presence of the stretching vibration mode of OH of the alcohol. Some information can be found in the region of the OH bending mode which appears in the 1600–1700 cm^{-1} region. For pure water, in the IR spectrum (this signal is too weak in the Raman spectrum), the band appears at ca. 1645 cm^{-1}. In a water–ethanol mixture (1:10), the band is at ca. 1656 cm^{-1} whereas for a 1:10 water–dioxane mixture, it is at ca. 1648 cm^{-1}. The 1648 cm^{-1} band being close to the 1645 cm^{-1} band implies that water molecules prefer to associate with themselves in dioxane in the same way they do in pure water, whereas in ethanol water molecules are seen to associate with molecules of ethanol, creating stronger H bonds; it must be noted that H bonding tends to increase the vibration frequency of a bending mode. This being so, the results obtained in dioxane and in an ethanol–dioxane mixture are perfectly understandable. Hydrolysis of the PSB is fast in dioxane since water does not associate with it and is very slow in ethanol–dioxane because water associates itself to ethanol and in doing so does not reach the PSB easily.

If we now look globally to the three systems, the addition of water does not seem to promote protonation. Of course, the water content is quite low compared with the solvents, but nevertheless it indicates that water is not attracted by the PSB/counterion system and hence plays no role.

These results also demonstrate that the protection of a

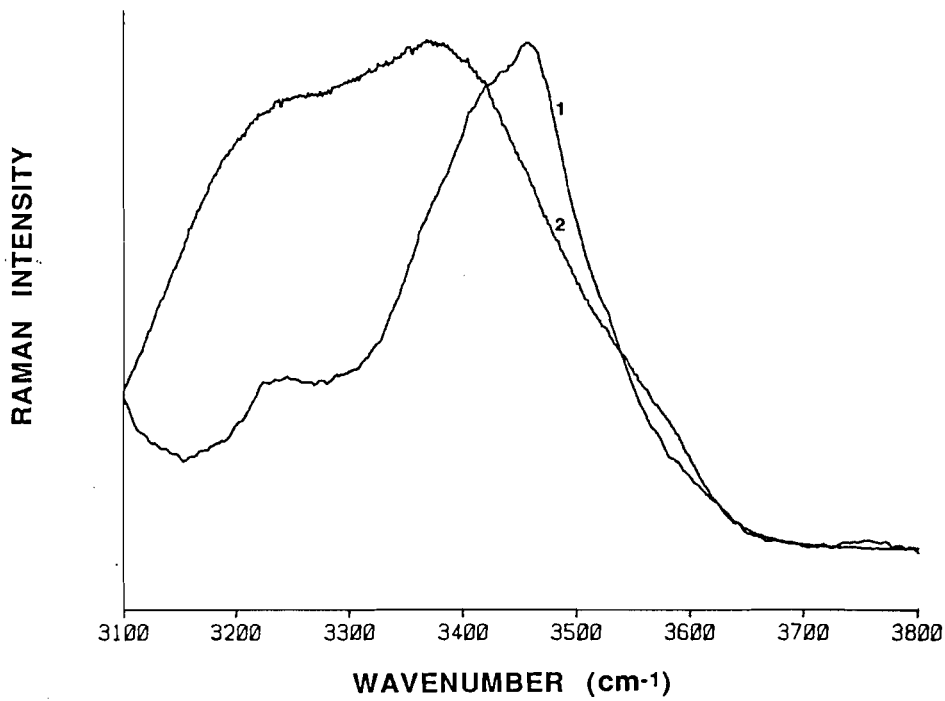

FIG. 4. Raman spectra of a 10:90 mixture of water in dioxane (1) and of neat water (2) in the region 3100–3800 cm^{-1} (excitation wavelength 488 nm).

protonated Schiff base from hydrolysis is assured by a protic medium and this protection is greater as the dielectric constant of the medium is large.

Our system has been devised to shed some light on how water molecules could react with the chromophore in the host cavity. It is evident that this model is quite different from the protein; dioxane, chloroform, and ethanol cannot mimic the protein moiety as such. However, the polarity of the cavity hosting the Schiff base portion of the chromophore is not known. Recently, the protonating agent has been found. It is Glu-113 (15), a rather weak acid which, as we have shown in the past (22–25), is unlikely to protonate fully the Schiff base chromophore unless some stabilizing factors are also present in the protein. Furthermore, water molecules are now known to be present near the chromophore (9, 10) and only very recently (33) their possible role in protonation has been advocated, much in the same way as we have predicted in the past. The present model, given all its shortcomings, can nevertheless show, we believe, some interesting inferences. In particular, our results indicate that the host cavity lodging the protonated Schiff base in the pigments could possibly be rich in groups that will be able to form an extensive hydrogen-bond network so as to offer a propitious environment for protonation. That is, the environment would stabilize the PSB, its counterion, and the water molecules. These groups could be Tyr, Ser, His, Glu, Asp, Arg and they could act in a fashion similar as the one found by Khorana *et al.* (14, 15) in bacteriodopsin where protonation of the SB seems to be due to the combined action of three amino acids. At different stages, especially for metarhodopsin II, it is possible to invoke the fact that the environment surrounding the chromophore could change from a protic medium to an aprotic one, thus liberating the water molecules that can now hydrolyze the Schiff base.

Can. J. Chem. Downloaded from www.nrcresearchpress.com by 109.225.110.28 on 09/08/12
For personal use only.

Acknowledgments

Our thanks are due to the Natural Sciences and Engineering Research Council of Canada and to the Université du Québec à Montréal for financial assistance. We also thank Mrs. Phuong Xue Trong for her contribution in the early stages of this work.

1. A. N. Kriebel and C. C. Albrecht. J. Chem. Phys. **65**, 4575 (1976).
2. C. Sandorfy and D. Vocelle. *In* Molecules in physics, chemistry and biology. Vol. IV. *Edited by* Jean Maruani. Kluwer Academic Publishers, Norwell, Mass. 1989. pp. 192–211.
3. D. Hadzi, J. Koller, and M. Hodoscek. J. Mol. Struct. (Theochem). **168**, 279 (1988).
4. J. Koller, M. Hodoscek, and D. Hadzi. J. Mol. Struct. (Theochem), **168**, 287 (1988).
5. G. Zundel. *In* Transport through membranes: Carriers, channels and pumps. *Edited by* A. Pullman *et al.* Kluwer Academic Publishers, Norwell, Mass. 1988. pp. 409–420.
6. G. Zundel. J. Mol. Struct. **177**, 43 (1988).
7. M. Eckert and G. Zundel. J. Phys. Chem. **92**, 7016 (1988).
8. U. M. Ganter, E. D. Schmid, and F. Siebert. J. Photochem. Photobiol. B, Biol. **2**, 417 (1988).
9. P. Hildebrandt and M. Stockburger. Biochemistry, **23**, 5539 (1984).
10. C. N. Rafferty and H. Shichi. Photochem. Photobiol. **33**, 229 (1981).
11. T. P. Sakmar, R. R. Franke, and H. G. Khorana. Proc. Natl. Acad. Sci. USA, **86**, 8309 (1989).
12. E. A. Zhukovsky and D. D. Oprian. Science, **246**, 928 (1989).
13. J. Nathans. Biochemistry, **29**, 9746 (1990).
14. S. Subramaniam, T. Marti, and H. G. Khorana. Proc. Natl. Acad. Sci. USA, **87**, 1013 (1990).
15. H. Otto, T. Marti, M. Holz, T. Mogi, L. J. Stern, F. Engel, H. G. Khorana, and M. P. Heyn. Proc. Natl. Acad. Sci. USA, **87**, 1018 (1990).
16. P. E. Blatz, J. Mohler, and H. Navangul. Biochemistry, **11**, 848 (1972).
17. C. Sandorfy and D. Vocelle. Can. J. Chem. **64**, 2251 (1986).
18. R. R. Birge. Biochim. Biophys. Acta, **1016**, 293 (1990).
19. B. Honig, U. Dinur, K. Nakanishi, V. Balogh-Nair, M. A. Gawinowicz, M. Arnaboldi, and M. G. Motto. J. Am. Chem. Soc. **101**, 7084 (1979).
20. S. Alex, P. Turcotte, R. Fournier, and D. Vocelle. Can. J. Chem. **69**, 239 (1991).
21. S. Alex, C. Sandorfy, and D. Vocelle. J. Phys. Chem. **95**, 3021 (1991).
22. L. S. Lussier, A. Dion, C. Sandorfy, H. Le-Thanh, and D. Vocelle. Photochem. Photobiol. **44**, 629 (1986).
23. L. S. Lussier, C. Sandorfy, H. Le-Thanh, and D. Vocelle. Photochem. Photobiol. **45**, 801 (1987).
24. C. Rhofir, D. Vocelle, and C. Sandorfy. Res. Chem. Intermed. **12**, 131 (1989).
25. H. Le-Thanh and D. Vocelle. Can. J. Chem. **68**, 1909 (1990).
26. P. Dupuis, F. I. Harosi, C. Sandorfy, J. M. Leclercq, and D. Vocelle. Rev. Ann. Biol. **39**, 247 (1980).
27. J. E. Draheim, N. J. Gibson, and J. Cassim. Biophys. J. **54**, 931 (1988).
28. A. Cooper, S. F. Dixon, M. A. Nutley, and J. L. Robb. J. Am. Chem. Soc. **109**, 7254 (1987).
29. G. Papadopoulos, N. A. Dencher, G. Zaccai, and G. Buldt. J. Mol. Biol. **214**, 15 (1990).
30. M. Bissonnette and D. Vocelle. Spectrosc. Int. J. **2**, 120 (1983).
31. F. Cennamo and F. Tartaglione. Nuovo Cimento, **11**, 401 (1959).
32. M. Lafleur, M. Pigeon, M. Pézolet, and J. P. Caillé. J. Phys. Chem. **93**, 1522 (1989).
33. R. Renthal and R. Regalado. Photochem. Photobiol. **54**, 931 (1991).

An efficient and general synthesis of alkyl alkynyl sulfoxides

SIDIMA T. KABANYANE AND DAVID I. MAGEE[1]
Department of Chemistry, University of New Brunswick, Bag Service No. 45222, Fredericton, N. B., Canada E3B 6E2

Received March 31, 1992

SIDIMA T. KABANYANE and DAVID I. MAGEE. Can. J. Chem. **70**, 2758 (1992).

A convenient one-step method for the preparation of alkynyl phenyl sulfides using diphenyl disulfide has been developed. The oxidation of the corresponding sulfides to the sulfoxides, and not sulfones, was achieved by using *trans*-(phenylsulfonyl)-3-phenyloxaziridine. A variety of other oxidizing reagents was also investigated.

SIDIMA T. KABANYANE et DAVID I. MAGEE. Can. J. Chem. **70**, 2758 (1992).

On a mis au point une méthode de préparation simple qui conduit en une étape du disulfure de diphényle aux sulfures d'alkynyle et de phényle. On a réalisé l'oxydation des sulfures en sulfoxydes correspondants — et non pas en sulfones — en utilisant de la *trans*-(phenylsulfonyl)-3-phényloxaziridine. On a aussi examiné une série d'autres agents d'oxydation.

[Traduit par la rédaction]

Introduction

In the course of our studies on the chemistry of acetylenic sulfoxides, the development of a general, high-yielding method for their preparation became necessary. A survey of the literature showed numerous methods for the preparation of acetylenic sulfides that, in turn, were oxidized to the required sulfoxides: dehydrohalogenation of olefinic compounds (1), elimination of mercaptans (2), isomerization with migration of multiple bonds (3), and the reaction of metal acetylides on alkyl or phenyl sulfenyl halides and thiosulfinates (4). The only direct method involved the reaction of an alkynyl anion with sulfinate esters (5). However, for our purposes these methods proved to be either low yielding, or incompatible with another functionality in our system. As a result of these difficulties, we investigated other means of synthesizing these compounds that would not only serve our purposes, but be of general utility.

Results and discussion

Our first attempt was the reaction of an acetylide anion with diphenyl disulfide; however, the sole product observed (85% yield) was a bis-sulfide (eq. [1]). The structural geometry of this compound was supported by a 5.5% nOe between the olefinic proton and the allylic methylene. This product, we believe, arose from nucleophilic attack of the lithium thiophenolate generated during the course of the reaction upon the acetylenic sulfide. This mechanism was further corroborated by the fact that treatment of pure acetylenic sulfide, synthesized via a different procedure, with lithium thiophenolate under identical reaction conditions gave the same bis-sulfide product. This result is not without precedent (4). Alkyl cuprates (6), sodium stannanes (7), trialkyl phosphites (8), tertiary amines (9), and a variety of other reagents (10) all undergo nucleophilic additions to this class of compounds as well. It then became quite evident that a successful approach required an efficient removal of the unwanted lithium thiophenolate.

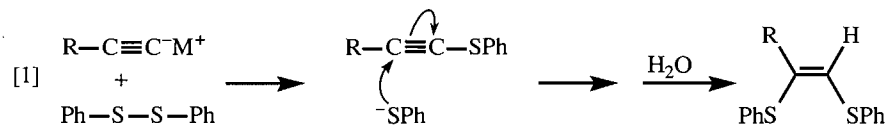

[1]

The conversion of sulfur compounds to stable sulfonium ions via S-alkylation is a well-known biological and chemical process used for the activation of certain centers towards nucleophilic addition. It occurred to us that we may utilize this property of sulfur for our purposes in the following way. Pretreatment of the disulfide with one equivalent of methyl iodide would generate the S-alkylated product that, in turn, should yield only the desired product and methyl phenyl sulfide on treatment with an alkynyl anion (path a, eq. [2]).

As a test of this hypothesis we treated diphenyl disulfide with methyl iodide in tetrahydrofuran (THF) at room temperature for 1 h, followed by cooling to −78°C and addition of the lithium alkynyl anion generated from MEM-protected propargyl alcohol. *As predicted, the crude ^{1}H NMR spectrum revealed only the alkynyl phenyl and methyl phenyl sulfides after a normal work-up procedure.* Silica gel chromatography provided the desired compound in 87% yield. Clearly methyl iodide was beneficial, but was its role as postulated (path a, eq. [2]), or simply as an efficient thiophenolate trap (path b, eq. [2])? We favor the latter explanation for the following reasons: (1) separate, simultaneous addition of methyl iodide and diphenyl disulfide to the alkynyl anion gave the same result as the premixed solution, and (2) ^{1}H NMR analysis of the premixed solution over various periods of time (i.e., 5 min – 1 h) showed no evidence of any intermediates.

Encouraged by this result, we investigated its generality and our results are presented in Table 1. As can be seen from the table, a variety of functional groups tolerate the reaction conditions. Notable examples are entries 2 and 4 where the phenyl sulfenyl group was only incorporated at the alkyne.

[1]Author to whom correspondence may be addressed.

Can. J. Chem. Downloaded from www.nrcresearchpress.com by 109.225.110.28 on 09/08/12
For personal use only.

TABLE 1. Sulfenation of alkynes with diphenyldisulfide and methyl iodide

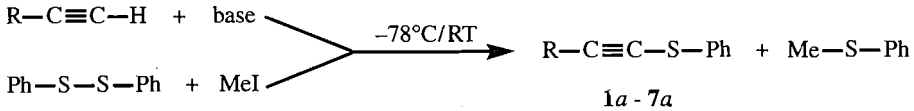

Entry	Alkyne	Base (temp, °C)	Yield (%)[a]	MeSPh (%)
1	$MEMOCH_2—C≡C—H$	*n*BuLi (−78)	87	90
2	$HOCH_2—C≡C—H$	*n*BuLi (−30)	90	89
3	$CH_3(CH_2)_5CH_2—C≡C—H$	*n*BuLi (−78)	68	71
4	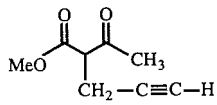	NaH, *n*BuLi (−30)	81	80
5	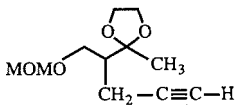	*n*BuLi (−78)	83	87
6	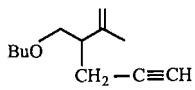	*n*BuLi (−78)	72	70
7	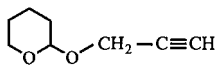	*n*BuLi (−78)	90	89

[a]All new compounds gave satisfactory ^1H NMR, IR, and high-resolution mass spectra.

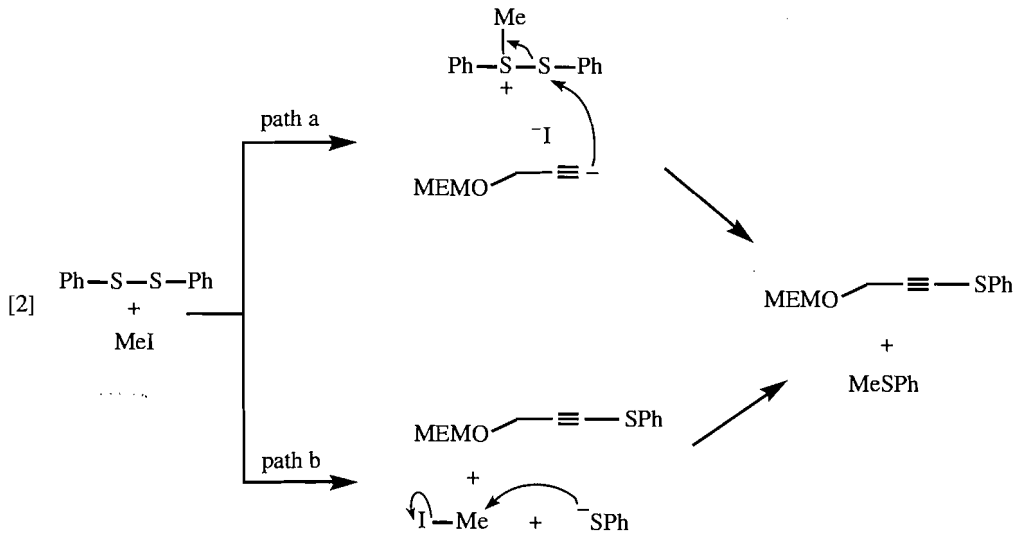

With the preparation of the sulfides in hand, the only task remaining was their oxidation to the corresponding sulfoxides. We anticipated no particular problems since there is ample literature precedent for performing this transformation (11). However, we decided to undertake a more rigorous investigation since the oxidation of sulfides to sulfoxides, and not sulfones, can be rather troublesome. The reagents chosen were the standard oxidants *m*CPBA, Oxone® (12), and sodium periodiate ($NaIO_4$) (13), as well as the recently introduced Davis reagent, *trans*-2-(phenylsulfonyl)-3-phenyloxaziridine (14). Our results are presented in Table 2.

Unexpectedly, neither phenylsulfonyloxaziridine nor $NaIO_4$ showed any reactivity towards the sulfides under normal oxidation conditions, even after extended periods of time (24 h at room temperature). Both of these reagents are known to oxidize alkyl and phenyl sulfides very readily and, in the case of oxaziridine, very cleanly and rapidly (14*a*). This result suggests that the alkyne plays a pivotal role in decreasing the nucleophilicity of the sulfur atom and thus its

Can. J. Chem. Downloaded from www.nrcresearchpress.com by 109.225.110.28 on 09/08/12
For personal use only.

TABLE 2. Oxidation of alkynyl phenyl sulfides

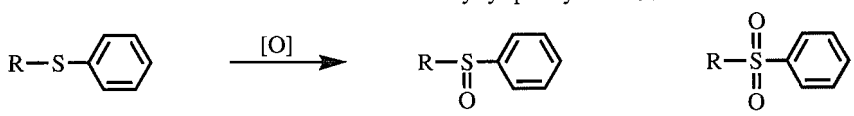

1a - 7a **1b - 7b** **1c - 7c**

Compound	Method[b]	Product *b*:*c* (yield%)[a]
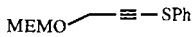 **1a**	*i*	100:0 (90)
	ii	100:0 (64)
	iii	100:0 (88)
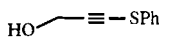 **2a**	*i*	100:0 (83)
	ii	90:10 (68)
	iii	100:0 (89)
$CH_3(CH_2)_5CH_2-C\equiv C-SPh$ **3a**	*i*	100:0 (80)
	ii	100:0 (96)
	iii	100:0 (73)
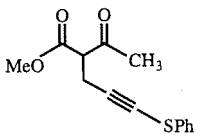 **4a**	*i*	* (70)
	ii	20:80 (62)
	iii	** (57)
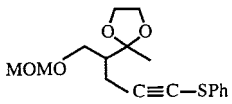 **5a**	*i*	88:12 (78)
	ii	60:40 (60)
	iii	100:0 (97)
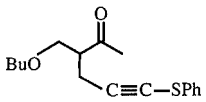 **6a**	*i*	10:90 (58)
	ii	20:80 (50)
	iii	100:0 (97)
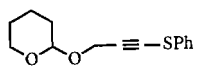 **7a**	*i*	80:20 (63)
	ii	95:5 (71)
	iii	100:0 (93)

[a]All new compounds gave satisfactory ^1H NMR, IR, and high-resolution mass spectra.
[b]Methods: *i*. *m*-CPBA/CH_2CL_2, 0°C; *ii*. oxone($KHSO_5$)/MeOH/H_2O, 0°C, RT; *iii*. phenylsulfonyloxaziridine/$CHCl_3$, reflux (60°C).
*See Text, compounds **8***a* and **8***b* were obtained.
See text, compound **8*a* was obtained.

Can. J. Chem. Downloaded from www.nrcresearchpress.com by 109.225.110.28 on 09/08/12
For personal use only.

susceptibility towards oxidation. The reason for this reduced reactivity is not readily apparent. While one can argue that a sulfur lone pair may be delocalized into the π orbitals of the alkyne, Davis *et al.* showed that diphenyl sulfide oxidizes instantaneously at 0°C with oxaziridine (14*a*). The neighbouring acetylene thus exerts a very specific deactivating effect.

We were, however, pleased to find that reactions with the Davis reagent at 60°C provided the desired products in high yields, Table 2. *In all cases attempted, no overoxidation was observed.* Surprisingly, olefin **6** showed no reaction of the double bond even though these are the conditions reported for epoxidation (14*b*). This method of oxidation solves the dilemma that we encountered with the use of *m*CPBA and (or) Oxone®. Although uniformly good yields of oxidized products were obtained, there was difficulty in achieving complete specificity (contrast the results for compound **1***a* with those for **4***a* and **5***a*, Table 2).

The oxidation of compound **4**, under any of the conditions, gave a more complicated result, which could prove of use for the synthesis of highly substituted furans. Treatment of **4** with oxaziridine gave, as expected, a sulfoxide, but spectroscopic investigations (i.e., $^1H-^1H$ decoupling, ^{13}C NMR, low-resolution MS, UV, IR) revealed the structure to be the vinyl ether **8***a*, Scheme 1. This product presumably arises by enolization of the β-keto ester, followed by Michael addition of the oxygen atom onto the acetylenic sulfoxide. Acid-catalyzed isomerization (*p*TSA, MeOH) of the exocyclic double bond cleanly furnished furan **4***b*, Scheme 1.

Since it was clear that an acid source was required to induce isomerization, we felt that treatment of acetoacetate **4***a* with either *m*CPBA or Oxone® should produce the furans directly. In the case of Oxone®, furan **4***b* could be obtained directly (see Table 2). However, the reaction could be intercepted to give compound **8***a*, the same vinyl ether as in the oxaziridine oxidation. *m*CPBA, as shown in Table 2, gave only compounds **8***a* and **8***b*, with the sulfone product predominating. Both of these products, when treated with *p*-

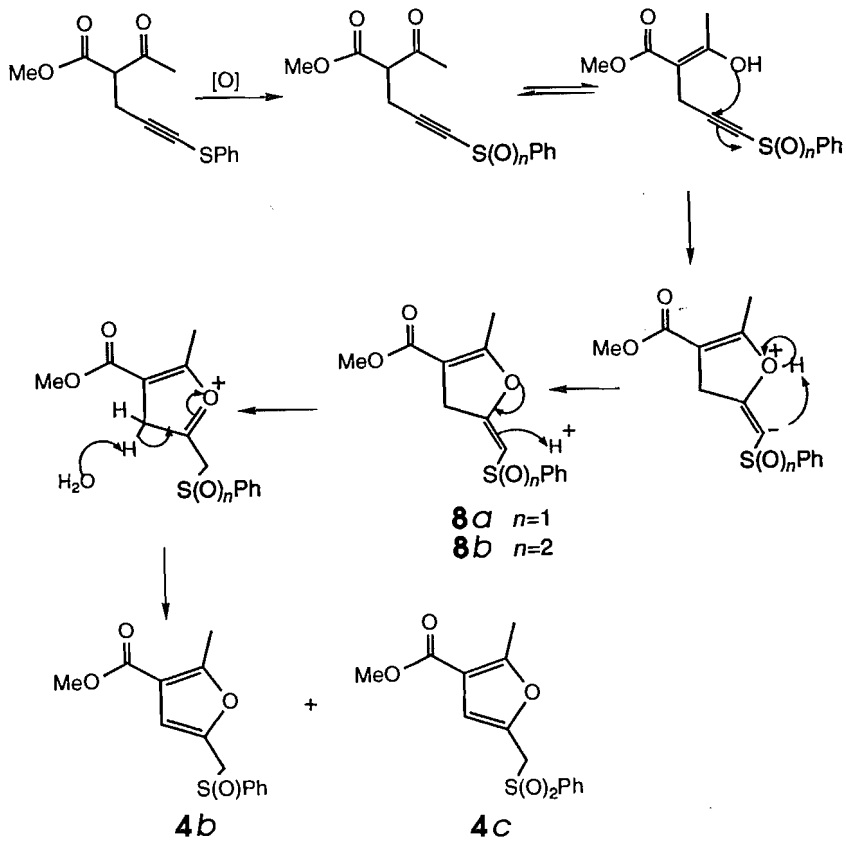

SCHEME 1

toluenesulfonic acid in methanol, isomerized to give furans **4***b* and **4***c*.

In conclusion, we have demonstrated that alkynyl sulfides can be prepared in generally high yields by treating a premixed solution of diphenyl disulfide and methyl iodide with various lithium alkynyl anions. The sulfides can then be oxidized exclusively to their sulfoxides by *trans*-2-(phenylsulfonyl)-3-phenyloxaziridine. Other oxidants such as *m*CPBA or Oxone® are also effective but, in some instances, mixtures or sulfones predominate. Further studies in this area, including the potential use of the resulting alkynyl sulfoxides (and sulfones) for intra- and intermolecular nucleophilic additions, are currently being pursued.

Experimental

All commercial reagents were purchased from Aldrich Chemicals (Milwaukee) and used without any further purification. Reaction solvents were dried according to established procedures (15). All reactions were performed in oven-dried glassware (120°C) under an atmosphere of nitrogen unless otherwise stated. Reaction temperatures refer to external baths.

Column chromatography was carried out according to the procedure of Still *et al.* (16), using Merck silica gel (230–400 mesh). Thin-layer chromatographic analyses were performed on Merck F_{254} 0.25 mm plates. Infrared (IR) spectra were recorded on a Bruker IFS25 FTIR and are reported in wave numbers (cm^{-1}). Low- and high-resolution mass spectra were measured on a Kratos MS50TC. All nuclear magnetic resonance (NMR) spectra were recorded on an XL200 (200 MHz) spectrometer with chemical shifts reported in ppm (δ) with tetramethylsilane as an internal standard. All coupling constants (J) are reported in Hz. Ultraviolet (UV) spectra were recorded on a Beckmann model 25 spectrometer with 4.5 mL capacity quartz cuvets and 95% ethanol as solvent.

General method for alkynyl sulfide preparation: 3-(methoxyethoxymethyl)-1-propynyl phenyl sulfide **1***a*

A solution of 3-(2-methoxyethoxymethyl)-1-propynyl ether (250 mg, 2.2 mmol) in 5 mL THF was cooled to −78°C. To this was added *n*-butyllithium (1.4 mL, 2.2 mmol) and the reaction was stirred for 30 min. A premixed solution (1 h at RT) of diphenyl disulfide (480 mg, 2.2 mmol) and methyl iodide (0.14 mL, 2.2 mmol) in THF (8 mL) was then added dropwise, and was stirred for 1 h at room temperature. It was then quenched with 20 mL of dilute aqueous NH_4Cl solution and extracted with diethyl ether (2 portions). The organic phase was dried with magnesium sulfate ($MgSO_4$) and concentrated *in vacuo*. The crude product was purified by SiO_2 chromatography (3:1 hexane:EtOAc) to give sulfide **1***a* (384 mg, 87%) as a colorless oil. IR (neat) cm^{-1}: 3075 (s), 2929 (s), 2183 (s), 1583 (s), 849 (s); ^1H NMR ($CDCl_3$) δ: 7.35 (m, 5H), 4.82 (s, 2H), 4.46 (s, 2H), 3.70 (t, 2H, J = 3.9), 3.55 (t, 2H, J = 3.9), 3.37 (s, 2H); HRMS: m^+/z_{obs} = 252.0814 (m^+/z_{calc} = 25.0821).

3-Hydroxy-1-propynyl phenyl sulfide **2**a

A solution of proparyl alcohol (200 mg, 3.5 mmol) and THF (10 mL) was cooled to −30°C. *n*-Butyllithium (4.7 mL, 7.5 mmol) was added dropwise and the reaction was stirred for 30 min. A premixed solution (1 h, RT) of diphenyl disulfide (785 mg, 3.6 mmol) and methyl iodide (0.3 mL, 3.8 mmol) in THF (5 mL) was then added dropwise. The reaction mixture was allowed to warm to room temperature and stir for 1 h. Aqueous work-up followed by SiO_2 chromatography (3:1 hexane:EtOAc) afforded sulfide **2***a* (530 mg, 90%) as a colorless oil. IR (neat) cm^{-1}: 3371 (b), 3020 (s), 2919 (s), 2186 (s), 1583 (s), 678 (s); ^1H NMR ($CDCl_3$) δ: 7.33 (m, 5H), 4.48 (s, 2H); HRMS: m^+/z_{obs} = 164.0296 (m^+/z_{calc} = 164.0296).

Can. J. Chem. Downloaded from www.nrcresearchpress.com by 109.225.110.28 on 09/08/12
For personal use only.

Can. J. Chem. Downloaded from www.nrcresearchpress.com by 109.225.110.28 on 09/08/12
For personal use only.

1-Nonynyl phenyl sulfide **3**a

1-Nonyne (200 mg, 1.6 mmol) was treated as described in the general procedure. SiO_2 chromatography (20:1 hexane:EtOAc) afforded sulfide **3***a* (252 mg, 68%) as a colorless oil. IR (neat) cm^{-1}: 3131 (w), 2927 (s), 2359 (w), 1583 (s); ^1H NMR ($CDCl_3$) δ: 7.26 (m, 5H), 2.48 (t, 2H, J = 6.7), 1.60 (m, 2H), 1.35 (m, 8H), 0.88 (t, 3H, J = 6.7); HRMS: m^+/z_{obs} = 232.1284 (m^+/z_{calc} = 232.1286).

Methyl-2-acyl-5-phenylthio-pentynoate **4**a

A suspension of sodium hydride (83.6 mg, 2.1 mmol) in THF (20 mL) was cooled to 0°C. To this was added β-keto acetylene **4** (300 mg, 1.9 mmol) in THF (5 mL). After complete addition and stirring for 10 min, the temperature was lowered to −30°C and *n*-butyllithium (1.3 mL, 2.1 mmol) was added dropwise. Stirring was continued for 30 min at this temperature. A premixed solution (1 h, RT) of diphenyl disulfide (414 mg, 1.9 mmol) and methyl iodide (0.14 mL, 2.3 mmol) in THF (5 mL) was added dropwise. The reaction mixture was stirred for 1 h at room temperature. Aqueous work-up followed by purification on SiO_2 chromatography (3:1 hexane:EtOAc) gave sulfide **4***a* (413 mg, 81%) as a colorless oil. IR (neat) cm^{-1}: 3063 (m), 2189 (w), 1744 (s), 1719 (s), 1583 (m); ^1H NMR ($CDCl_3$) δ: 7.32 (m, 5H), 3.75 (t, 1H, J = 7.5), 3.75 (s, 3H), 2.98 (d, 2H, J = 7.5), 2.29 (s, 3H); HRMS: m^+/z_{obs} = 262.0654 (m^+/z_{calc} = 262.0644).

4-(Methoxymethoxymethyl)-5-(1,3-dioxolane)-1-hexynyl phenyl sulfide **5**a

MOM-(1,3-dioxolane)-1-hexyne (300 mg, 1.4 mmol) was treated as described in the general procedure. Purification by SiO_2 chromatography (3:1 hexane:EtOAc) afforded sulfide **5***a* (374 mg, 83%) as a colorless oil. IR (neat) cm^{-1}: 3073 (m), 2984 (s), 2201 (w), 1583 (s), 1441 (m), 899 (s); ^1H NMR ($CDCl_3$) δ: 7.28 (m, 5H), 4.63 (s, 2H), 3.94 (m, 4H), 3.76 (dd, 2H, J = 6.0, J = 2.2), 3.35 (s, 3H), 2.73 (dd, 2H, J = 6.0, J = 2.2), 2.11 (m, 1H), 1.34 (s, 3H); HRMS: m^+/z_{obs} = 322.1245 (m^+/z_{calc} = 322.1239).

*4-*n*-Butoxymethyl-5-ethylene-1-hexynyl phenyl sulfide* **6**a

The corresponding alkyne (200 mg, 1.11 mmol) was treated as described in the general procedure. Chromatography on SiO_2 (3:1 hexane:EtOAc) afforded sulfide **6***a* (229 mg, 72%) as a colorless oil. IR (neat) cm^{-1}: 3087 (m), 2998 (s), 2929 (s), 2203 (w), 1648 (m), 1584 (m), 1449 (m); ^1H NMR ($CDCl_3$) δ: 7.30 (m, 5H), 4.91 (p, 1H, J = 1.5), 4.85 (p, J = 1.5), 3.48 (m, 4H), 2.65 (m, 3H), 1.77 (bs, 3H), 1.50 (m, 5H), 0.91 (t, 3H, J = 8.2); HRMS: m^+/z_{obs} = 288.1561 (m^+/z_{calc} = 288.1598).

3-Tetrahydropyranoxyl-1-propynyl phenyl sulfide **7**a

The corresponding alkyne (200 mg, 1.42 mmol) was treated as described in the general procedure. Chromatography on SiO_2 (20:1 hexane:EtOAc) gave sulfide **7***a* (318 mg, 90%) as a colorless oil. IR (neat) cm^{-1}: 3060 (m), 3005 (s), 2739 (s), 2136 (m), 1583 (s), 1441 (s); ^1H NMR ($CDCl_3$) δ: 7.29 (m, 5H), 4.87 (t, 1H, J = 3.1), 4.50 (s, 2H), 3.85 (m, 1H), 3.65 (m, 1H), 1.71 (m, 6H); HRMS: m^+/z_{obs} = 248.0864 (m^+/z_{calc} = 248.0871).

3-(Methoxyethoxymethyl)propynyl phenyl sulfoxide **1**b

General method 1

To a stirred solution of sulfide **1***a* (100 mg, 0.39 mmol) in methylene chloride (10 mL) at 0°C was added a solution of *m*-chloroperoxybenzoic acid (82 mg, 0.47 mmol) in methylene chloride (5 mL). The solution was stirred for 1 h at 0°C, added to 20 mL of $NaHCO_3$ solution, shaken, and separated into two layers. The aqueous layer was extracted with methylene chloride (2 portions) and the combined extracts washed with brine. The organic phase was dried with $MgSO_4$ and the solvent evaporated under reduced pressure. The crude product was purified by SiO_2 chromatography (3:1 hexane:EtOAc) to afford sulfoxide **1***b* (100 mg, 96%) as a colorless oil. IR (neat) cm^{-1}: 2926 (s), 2184 (m), 1445 (m), 1200 (b); UV λ_{max}: 226 (ϵ_{max} 6400); ^1H NMR ($CDCl_3$) δ: 7.75 (m, 2H), 7.53 (m, 3H), 4.72 (s, 2H), 4.39 (s, 2H), 3.34 (s, 3H); HRMS: $(m^+/z - CH_3OCH_2CH_2O)_{obs}$ = 209.0269 ($(m^+/z - CH_3OCH_2CH_2O)_{calc}$ = 209.0273).

3-Hydroxy-1-propynyl phenyl sulfoxide **2**b *and sulfone* **2**c

General method 2

Oxone® ($2KHSO_5 \cdot KHSO_4 \cdot K_2SO_4$, 132 mg, 0.44 mmol of $KHSO_5$) in water (4 mL) was added to a solution of sulfide **2***a* (60 mg, 0.36 mmol) in methanol (4 mL) at 0°C with vigorous stirring. A white precipitate formed immediately. The reaction mixture was allowed to warm to room temperature and was stirred until TLC showed complete disappearance of starting material. The solvent was removed *in vacuo* and the mixture was extracted with chloroform (3 portions). The organic phase was washed with water (10 mL) and brine (10 mL) and dried with $MgSO_4$. The solvent was removed and the crude product purified by SiO_2 chromatography (1:3 hexane:EtOAc) to give 45 mg (68%) of sulfoxide **2***b* and 5 mg of sulfone **2***c* as colorless oils.

2*b*: IR (neat) cm^{-1}: 3372 (b), 2182 (s), 1445 (s), 1048 (s); UV λ_{max}: 223 (ϵ_{max} 9300); ^1H NMR ($CDCl_3$) δ: 7.75 (m, 2H), 7.50 (m, 3H), 4.39 (s, 2H); HRMS: m^+/z_{obs} = 180.0234 (m^+/z_{calc} = 180.0245).

2*c*: IR (neat) cm^{-1}: 3296 (b), 3066 (s), 2957 (s), 2203 (s), 1312 (s); UV λ_{max}: 224 (ϵ_{max} 8100); ^1H NMR ($CDCl_3$) δ: 8.00 (m, 8H), 7.60 (m, 3H), 4.41 (s, 2H), 1.9 (bs, 1H); HRMS: m^+/z_{obs} = 196.0189 (m^+/z_{calc} = 196.0194).

1-Nonynyl phenyl sulfoxide **3**b

Oxidation of sulfide **3***a* according to general procedure 2 and purification on SiO_2 (3:1 hexane:EtOAc) gave sulfoxide **3***b* (96%) as a colorless oil. IR (neat) cm^{-1}: 3060 (s), 2953 (s), 2180 (s), 1457 (s); UV λ_{max}: 226 (ϵ_{max} 9200); ^1H NMR ($CDCl_3$) δ: 7.79 (m, 2H), 7.54 (m, 3H), 2.42 (t, 2H, J = 9.7), 1.53 (m, 2H), 1.25 (m, 8H), 0.87 (t, 3H, J = 5.9); HRMS: $(m^+/z + H)_{obs}$ = 249.1244 ($(m^+/z + H)_{calc}$ = 249.1250).

Methyl-(2-phenylthiomethyl sulfoxide)-5-methyl-furanoate **4**b *and methyl-(2-phenylthiomethyl sulfone)-5-methyl-furanoate* **4**c

General method 3

A solution of sulfide **4***a* (50 mg, 0.19 mmol) and *trans*-2-(phenylsulfonyl)-3-phenyloxaziridine (65 mg, 0.25 mmol) in 5 mL of chloroform was refluxed (60°C) for 3 h. The reaction mixture was then cooled and the solvent was removed *in vacuo*. The residue was purified by SiO_2 chromatography (1:1 hexane:EtOAc) to afford 30 mg of sulfoxide **8***a* (57%) as a colorless oil.

Sulfoxide **8***a* was then dissolved in 2 mL of MeOH and a catalytic amount of *p*-toluenesulfonic acid was added. The mixture was stirred at room temperature for 12 h and then diluted with 10 mL of water and extracted with ether (3 × 20 mL). The combined organic phases were dried ($MgSO_4$), filtered, and the solvent was evaporated under reduced pressure to furnish 30 mg of sulfoxide **4***b* (100%) as a colorless oil.

8*a*: IR (neat) cm^{-1}: 3057 (m), 2956 (s), 1717 (s), 1652 (s), 1049 (s); UV λ_{max}: 271 (ϵ_{max} 20 000); ^1H NMR ($CDCl_3$) δ: 7.66 (m, 2H), 7.51 (m, 3H), 5.63 (t, 1H, J = 2.3), 3.76 (s, 3H), 3.71 (dt, 2H, J = 2.2, J = 2.3), 2.41 (t, 3H, J = 2.2); MS (relative intensity): 246 (m^+ − 32, 2), 153 (100), 125 (7), 77 (8).

4*b*: IR (neat) cm^{-1}: 2986 (s), 1717 (s), 1615 (s), 1447 (s), 1052 (s), 636 (s); UV λ_{max}: 244 (ϵ_{max} 12 400); ^1H NMR ($CDCl_3$) δ: 7.49 (s, 5H), 6.43 (s, 1H), 4.00 (d, 2H, J = 6.4), 3.78 (s, 3H), 2.43 (s, 3H); HRMS: $(m^+/z - C_6H_5SO)_{obs}$ = 153.0560 ($(m^+/z - C_6H_5SO)_{calc}$ = 153.0552).

Oxidation of sulfide **4***a* according to general procedure 1 gave sulfone **8***b* (70%) as a colorless oil. Acid-catalyzed isomerization as above followed by SiO_2 chromatography (1:1 hexane:EtOAc) yielded furan sulfone **4***c* (100%) as a colorless oil.

8*b*: IR (neat) cm^{-1}: 3033 (s), 2950 (s), 1720 (s), 1651 (s), 1325

(s); ^{1}H NMR ($CDCl_3$) δ: 8.10 (m, 2H), 7.66 (m, 3H), 5.31 (s, 1H), 3.74 (s, 3H), 3.72 (s, 2H), 2.28 (s, 3H).

4*c*: IR (neat) cm^{-1}: 2988 (m), 1719 (s), 1647 (s), 1447 (s), 1324 (s), 1178 (m); UV λ_{max}: 226 (ϵ_{max} 12 900); ^{1}H NMR ($CDCl_3$) δ: 7.66 (m, 5H), 6.52 (s, 1H), 4.34 (s, 2H), 3.79 (s, 3H), 2.42 (s, 3H); HRMS: m^+/z_{obs} = 294.0571 (m^+/z_{calc} = 294.0562).

5-(1,3-Dioxolane)-4-methoxymethoxymethyl-1-hexynyl phenyl sulfoxide **5**b *and sulfone* **5**c

Oxidation of sulfide **5***a* according to general procedure 1, followed by SiO_2 chromatography (3:1 hexane:EtOAc), furnished sulfoxide **5***b* and sulfone **5***c* (78%, 7:1 ratio) as colorless oils.

5*b*: IR (neat) cm^{-1}: 3058 (s), 2984 (s), 2182 (s), 1048 (s), 896 (s); UV λ_{max}: 227 (ϵ_{max} 5200); ^{1}H NMR ($CDCl_3$) δ: 7.80 (m, 2H), 7.53 (m, 3H), 4.56 (d, 2H, J = 2.9), 3.90 (m, 4H), 3.64 (m, 2H), 3.28 and 3.27 (s, 3H, -OMe diastereoisomers), 2.70 (d, 2H, J = 6.5), 2.13 (m, 1H), 1.28 (s, 3H); HRMS: $(m^+/z - CH_3OCH_2O)_{obs}$ = 277.0896 ($(m^+/z - CH_3OCH_2O)_{calc}$ = 277.0899).

5*c*: IR (neat) cm^{-1}: 3016 (m), 2923 (s), 2202 (s), 1310 (s), 1111 (s); UV λ_{max}: 237 (ϵ_{max} 5300); ^{1}H NMR ($CDCl_3$) δ: 7.96 (m, 2H), 7.54 (m, 3H), 4.51 (s, 2H), 3.87 (m, 4H), 3.60 (m, 2H), 3.27 (s, 3H), 2.62 (d, 2H, J = 6.3), 2.10 (m, 1H), 1.22 (s, 3H); HRMS: $(m^+/z - CH_3)_{obs}$ = 339.0912 ($(m^+/z - CH_3)_{calc}$ = 339.0902).

*4-*n*-Butoxymethyl-5-ethylene-1-hexynyl phenyl sulfoxide* **6**b *and sulfone* **6**c

Oxidation of sulfide **6***a* according to general procedure 2, and SiO_2 chromatography (3:1 hexane:EtOAc) furnished sulfoxide **6***b* and sulfone **6***c* (50%, 1:4 ratio) as colorless oils.

6*b*: IR (neat) cm^{-1}: 2926 (s), 2202 (s), 1458 (s), 1032 (s); UV λ_{max}: 228 (ϵ_{max} 8500); ^{1}H NMR ($CDCl_3$) δ: 7.74 (m, 3H), 7.45 (m, 3H), 4.88 (bs, 1H), 4.75 (bs, 1H), 3.26 (m, 4H), 2.51 (m, 3H), 1.6 (s, 3H), 1.25 (m, 4H), 0.9 (t, 3H, J = 2.8); HRMS: $(m^+/z - C_4H_9OCH_2)_{obs}$ = 217.0688 ($(m^+/z - C_4H_9OCH_2)_{calc}$ = 217.0687).

6*c*: IR (neat) cm^{-1}: 3070 (m), 2926 (s), 2202 (s), 1309 (s), 1115 (s); UC λ_{max}: 227 (ϵ_{max} 8800); ^{1}H NMR ($CDCl_3$) δ: 7.92 (m, 2H), 7.50 (m, 3H), 4.74 (s, 1H), 4.73 (s, 1H), 3.31 (m, 4H), 2.45 (m, 3H), 1.58 (s, 3H), 1.42 (m, 4H), 0.84 (t, 3H, J = 4.1); HRMS: $(m^+/z - C_4H_9OCH_2)_{obs}$ = 233.0629 ($(m^+/z - C_4H_9OCH_2)_{calc}$ = 233.0636).

3-Tetrahydropyranyloxy-1-proprynyl phenyl sulfoxide **7**b *and sulfone* **7**c

Oxidation of sulfide **7***a* according to general procedure 2, followed by SiO_2 chromatography (1:2 hexane:EtOAc), afforded sulfoxide **7***b* and sulfone **7***c* (71%, 19:1 ratio) as colorless oils.

7*b*: IR (neat) cm^{-1}: 3384 (b), 2943 (s), 2189 (s), 1036 (s), 612 (m); UV λ_{max}: 227 (ϵ_{max} 6800); ^{1}H NMR ($CDCl_3$) δ: 7.82 (m, 2H), 7.56 (m, 3H), 4.76 (m, 1H), 4.48 (s, 2H), 3.79 (m, 1H), 3.52 (m, 1H), 1.70 (m, 6H); HRMS: $(m^+/z - OH)_{obs}$ = 247.0781 ($(m^+/z - OH)_{calc}$ = 247.0793).

7*c*: IR (neat) cm^{-1}: 3030 (m), 2945 (s), 2203 (s), 1311 (s), 1123 (s); UV λ_{max}: 226 (ϵ_{max} 7100); ^{1}H NMR ($CDCl_3$) δ: 8.00 (m, 2H), 7.63 (m, 3H), 4.70 (s, 1H), 4.39 (s, 2H), 3.74 (m, 1H), 3.50 (m, 1H), 1.62 (m, 6H); HRMS: $(m^+/z - H)_{obs}$ = 279.0687 ($(m^+/z - H)_{calc}$ = 279.0691).

Acknowledgements

Financial support by the Natural Sciences and Engineering Research Council of Canada and the University of New Brunswick is gratefully acknowledged. S.T.K. wishes to thank the South African Education Trust Fund (CIDA) for a scholarship. We thank Dr. Zdenek Valenta for helpful discussions. The contribution of Larry Calhoun and Dan Drummond through their helpful discussions and support on various spectroscopic matters is acknowledged.

1. A. Commercon, J. F. Normant, and J. Villiers. Tetrahedron, **36**, 1215 (1980).
2. (*a*) L. Brandsma, H. J. T. Bos, and J. F. Arens. Chemistry of acetylenes. Marcel Dekker, New York. 1969. p. 751; (*b*) R. H. Everhardus and L. Brandsma. Synthesis, 359 (1978).
3. S. Saito, S. Hamano, M. Ihaba, and T. Moriwake. Synth. Commun. **14**, 1105 (1984).
4. T. Hagama, S. Tomado, Y. Takeuchi, and Y. Nomure. Chem. Lett. 1249 (1982).
5. (*a*) S. Darvesh, A. S. Grant, D. I. Magee, and Z. Valenta. Can. J. Chem. **67**, 2237 (1989); (*b*) H. Kosugi, M. Kitoaka, K. Tagami, and H. Uda. Chem. Lett. 805 (1985).
6. P. Vermeer, C. De Graff, and J. Meijer. Recl. Trav. Chim. Pays-Bas, **93**, 24 (1974).
7. (*a*) V. S. Zavgorodnil, T. P. Zubova, and A. A. Petrov. Zh. Obshch. Khim. **43**, 115 (1973); (*b*) T. P. Zubova, V. S. Zavgorodnil, V. N. Strelets, and A. A. Petrov. Zh. Obshch. Khim. **41**, 1646 (1971).
8. (*a*) M. L. Petrov and A. A. Petrov. Zh. Obshch. Khim. **43**, 691 (1973); (*b*) Zh. Obshch. Khim. **42**, 2345 (1972).
9. A. Kh. Filippova, T. V. Kashik, and G. S. Lyashenko. Zh. Obshch. Khim. **53**, 1141 (1983).
10. S. I. Radchenko and A. A. Petrov. Russ. Chem. Rev. **58**, 948 (1989).
11. (*a*) M. Madesclaure. Tetrahedron, **42**, 5459 (1986); (*b*) E. Block. *In* The chemistry of ethers, crown ethers, hydroxyl groups and their sulphur analogues. Supplement E. *Edited by* S. Patai. Interscience, Chichester. 1980. pp. 539–608; (*c*) G. L. Russel and L. A. Ochrymowycz. J. Org. Chem. **35**, 2106 (1970); (*d*) V. I. Laba, A. V. Suiridova, and E. N. Prilezhaeva. Izv. Akad. Nauk SSSR Ser. Khim. **21**, 212 (1972); (*e*) J. Brimble. J. Chem. Soc. Perkin Trans. 1, 179 (1989).
12. B. M. Trost and D. P. Curran. Tetrahedron Lett. **22**, 1287 (1981).
13. R. G. Hisley and M. A. Harpold. J. Org. Chem. **32**, 3191 (1967).
14. (*a*) F. A. Davis, S. B. Awad, R. H. Jenkins, Jr., R. L. Billmers, and L. A. Jenkins. J. Org. Chem. **48**, 3071 (1983); (*b*) F. A. Davis, R. Jenkins, Jr., and S. G. Yocklovich. Tetrahedron Lett. 5171 (1978).
15. D. D. Perrin and W. L. F. Armarego. Purification of laboratory chemicals. 3rd ed. Pergamon Press, Toronto. 1988.
16. W. C. Still, M. Kahn, and A. Mitra. J. Org. Chem. **43**, 2923 (1978).

Can. J. Chem. Downloaded from www.nrcresearchpress.com by 109.225.110.28 on 09/08/12
For personal use only.

Fused heterocycles derived from pseudoephedrine and ephedrine

NORBERTO FARFÁN,[1] ROSA L. SANTILLAN, DOLORES CASTILLO, REYNA CRUZ, AND PEDRO JOSEPH-NATHAN
Departamento de Química, Centro de Investigación y de Estudios Avanzados del Instituto Politécnico Nacional, Apartado 14-740 México, 07000 D.F. México

AND

JEAN-CLAUDE DARAN
Laboratoire de chimie des metaux de transition, Université Pierre et Marie Curie, 4, Place Jussieu, Boite No. 42, 75252 Paris CEDEX 05, France

Received April 13, 1992

NORBERTO FARFÁN, ROSA L. SANTILLAN, DOLORES CASTILLO, REYNA CRUZ, PEDRO JOSEPH-NATHAN, and JEAN-CLAUDE DARAN. Can. J. Chem. **70**, 2764 (1992).

The formation of heterobicycles by condensation of (1*R*, 2*R*)-(−)-pseudoephedrine or (1*R*, 2*S*)-(−)-ephedrine with glyoxal is reported. In the case of pseudoephedrine, the nuclear magnetic resonance data of the crude reaction mixture indicate the presence of three isomeric compounds (**5**, **6**, and **7**), which were separated by fractional crystallization, while ephedrine afforded the oxazino-oxazine **8** and the known (5*S**,6*R**)-4,5-dimethyl-6-phenyl-1,4-oxazin-2-one (**9**). Conclusive spectroscopic evidence for the structures of the new compounds having the *cis*-[1,4]oxazino[3,2-*b*]-1,4-oxazine (**5** and **8**) and the 2,2′-bioxazolidine type structures (**6** and **7**) was obtained by measurement of the ^{13}C satellite coupling constants in the 300 MHz ^1H nmr spectra, combined with the evaluation of dihedral angles using a modified Karplus type relationship. Unequivocal ^1H and ^{13}C nmr spectral assignments for all new compounds were done using two-dimensional carbon–proton correlation experiments. Syntheses of the known 5a,6,11a,12-tetrahydro[1,4]benzoxazino[3,2-*b*]benzoxazine (**3***a*) whose crystal structure has been previously determined, as well as of its *N*,*N*′-diisopropyl derivative **3***b*, allowed us to corroborate the above observations for the six-membered ring heterocycles. Moreover, the structures of **3***b* and **7** were independently verified by single crystal X-ray diffraction studies, thus validating the structural conclusions deduced from nmr satellite multiplicity measurements.

NORBERTO FARFÁN, ROSA L. SANTILLAN, DOLORES CASTILLO, REYNA CRUZ, PEDRO JOSEPH-NATHAN et JEAN-CLAUDE DARAN. Can. J. Chem. **70**, 2764 (1992).

La formation d'hétérocycles par condensation de l'(1*R*,2*R*)-(−)-pseudoéphédrine et de l'(1*R*,2*S*)-(−)-éphédrine avec le glyoxal a été étudiée. Dans le cas de la pseudoéphédrine les données de la RMN sur le produit brut de la réaction sont en accord avec un mélange de trois isomères (**5**, **6** et **7**) qui ont été séparés par cristallisation fractionnée, alors que l'éphédrine conduit à l'oxazino-oxazine **8** et à la (5*S**,6*R**)-4,5-diméthyl-6-phényl-1,4-oxazin-2-one (**9**) déjà connue. La détermination des structures des *cis*-[1,4]oxazino[3,2-*b*]-1,4-oxazines (**5** et **8**) et des 2,2′-bioxazolidines (**6** et **7**) a été réalisée par la mesure des constantes de couplage observées sur les satellites ^{13}C des spectres RMN ^1H à 300 MHz, et par évaluation des angles dièdres au moyen d'une relation de type Karplus modifiée. L'attribution des signaux dans les spectres RMN ^1H et ^{13}C de tous les composés nouveaux a été déterminée sans ambiguïté par des expériences de corrélation à deux dimensions carbone–proton. La synthèse de la 5a,6,11a,12-tétrahydro[1,4]benzoxazino[3,2-*b*]-benzoxazine (**3***a*) dont la structure cristalline est connue, et son dérivé *N*,*N*′-diisopropyle **3***b* a permis de corroborer les observations précédentes relatives aux hétérocycles à six chainons. Les structures de **3***b* et **7** ont été verifiées par diffraction des rayons X sur monocristaux et vérifient les conclusions structurales déduites des mesures des constantes de couplage satellites.

Introduction

The condensation of *o*-aminophenol and glyoxal was initially thought (1) to provide glyoxal *bis*-(2-hydroxyanil) (**1**), but a structural reinvestigation (2) suggested that a 2,2′-bioxazolidine (such as **2**) is formed. Further studies (3) using various *o*-aminophenols, several α-dicarbonyl compounds and varying the molar ratio of the reactants revealed that the ease of condensation and the type of condensation products depend on the steric factors of the α-dicarbonyl compounds, as well as on the basicity of the amino group and the acidity of the hydroxyl group of the *o*-aminophenols; the 2 ,2′-bioxazolidines (**2**) being the condensation products of two moles of *o*-aminophenol with one mole of the α-dicarbonyl compounds.

Subsequent studies (4) showed that there were two additional conceivable structures (**3***a* and **4**) for the reaction of glyoxal with *o*-aminophenol. Structure **4** was excluded, based on the 270 MHz ^1H nmr spectrum, since for this isomer the two central C-H protons are not equivalent and should provide a complex signal pattern. However, since the proton spectrum does not allow a distinction between structures **2** or **3***a*, and photochemical experiments did not permit establishing the structure, the condensation product was definitively established as 5a,6,11a,12-tetrahydro-*cis*-[1,4]-benzoxazino[3,2-*b*][1,4]-benzoxazine (**3***a*) by a single crystal X-ray diffraction study (4).

Closely related studies report the reaction of 2-propyn-1-ols with 2-aminoalcohols and mercury(II) chloride (5), the reaction of 2-methylaminoethanol with glyoxal (6), and the reaction of 2-methylaminoethanol with *gem*-dibromoketones (7), which have been shown to proceed by highly stereoselective processes leading to *cis*-[1,4]oxazino[3,2-*b*]-[1,4]-oxazine derivatives. However, in all these cases the authors conclude that nmr techniques do not allow unequivocal distinction between the 2,2′-bioxazolidines (like **2**) or the actual *cis*-fused oxazino-oxazine structures (like **3**), and therefore the structures were established by single crystal X-ray analyses.

[1]Author to whom correspondence may be addressed.

Can. J. Chem. Downloaded from www.nrcresearchpress.com by 109.225.110.28 on 09/08/12
For personal use only.

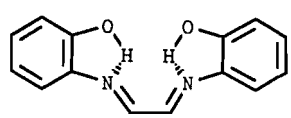

1

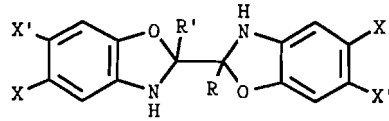

2

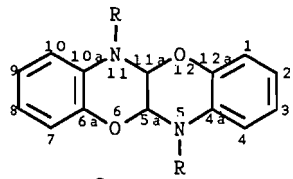

3a: R=H
3b: R=i-propyl

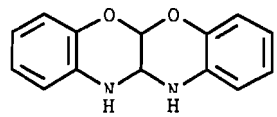

4

The aim of this study is to demonstrate that nmr techniques indeed allow unequivocal distinction between the *cis*-fused oxazino-oxazines (like **3**) and the bioxazolidine structures (like **2**) using the $^3J_{HH}$ values extracted from the ^{13}C satellites in the ^1H nmr spectra.

Experimental section

The ^1H and ^{13}C nmr spectra were recorded on Varian XL-300GS, Jeol GSX-270, and Jeol 90Q spectrometers in deuteriochloroform solutions containing internal TMS. The HETCOR standard pulse sequence, which incorporates quadrature detection in both domains, was used. The spectral windows of HETCOR experiments were adjusted in order to perform separate measurements for the aromatic and aliphatic regions. Mass spectra were obtained with a LKB 9000S/11E10 spectrometer and infrared spectra with a Nicolet MX-1 FT spectrophotometer. Melting points were determined in open capillaries and are uncorrected. Elemental analyses were performed by Oneida Research Services, Inc., New York.

(1*R*,2*R*)-(−)-Pseudoephedrine, (1*R*,2*S*)-(−)-ephedrine, and glyoxal (40%) were commercially available.

*5a,6,11a,12-Tetrahydro[1,4]benzoxazino[3,2-*b*]benzoxazine (**3**a)* was prepared as described in the literature (4); ^1H nmr ($CDCl_3$, 300 MHz): 6.84 (ddd, J = 7.5, 6.7, 2.0 Hz, 1H, H-3), 6.81 (dd, J = 8.2, 1.9 Hz, 1H, H-1), 6.79 (ddd, J = 8.1, 6.6, 1.5 Hz, 1H, H-2), 6.69 (ddd, J = 7.6, 1.7, 0.6 Hz, 1H, H-4), 5.33 (d, J = 3.7 Hz, 1H, H-5a), 4.88 (bd, J = 2.9, 1H, NH); ^{13}C nmr ($CDCl_3$, 75 MHz): 141.53 (C-12a), 128.52 (C-4a), 122.05 (C-3), 120.61 (C-2), 117.11 (C-1), 114.92 (C-4), 75.89 (C-5a).

*N,N'-Diisopropyl-5a,6,11a,12-tetrahydro[1,4]benzoxazino-[3,2-*b*]benzoxazine (**3**b)* was prepared from *N*-isopropyl-*o*-aminophenol (8) using the procedure described for the preparation of **3***a*, mp 195–198°C; ^1H nmr ($CDCl_3$, 90 MHz): 6.93–6.69 (m, 4H, H-1,2,3,4), 5.23 (s, 1H, H-5a), 4.17 (septet, J = 6.6, $CH(CH_3)_2$), 1.41 and 1.32 (d ea, J = 6.6, $CH(CH_3)_2$; ^{13}C nmr ($CDCl_3$, 22.5 MHz): 142.2 (C-12a), 130.5 (C-4a), 121.7 (C-3), 118.9 (C-2). 117.2 (C-1), 112.0 (C-4), 76.0 (C-5a).

Condensation of pseudoephedrine with glyoxal

To a solution of (1*R*,2*R*)-(−)pseudoephedrine (1 g, 6.05 mmol) in 50 mL benzene were added 0.5 g (3.0 mmol) of 40% aqueous glyoxal and a few iodine crystals and the solution was refluxed for 2 h using a Dean–Stark head. The solvent was evaporated and the solid residue (1.25 g, 2.6 mmol) consisting of a mixture of **5**, **7**, and **6** in a 6:3:1 ratio was recrystallized several times using methanol–hexane mixtures. The less soluble crystals afforded 454 mg (43%) of pure *(2R*,3R*,6R*,7R*)-2,6-diphenyl-3,4,7,8-tetramethyl-*cis*-perhydro[1,4]oxazino[3,2-*b*]-1,4-oxazine (**5**)*, mp 121–123°C; ir ν_{max} (KBr): 2955, 2876, 1641, 1451, 1378, 1332, 1232, 1090, 1052, 978, 891 cm^{-1}; ms, m/z (%): 352 (M^+, 7%), 353 (M^+, +1,1), 219(4), 190(11), 189(100), 176(12), 148(7), 118(39), 117(12), 91(4), 86(7), 84(11), and 49(17); Anal. calcd. for $C_{22}H_{28}N_2O_2$: C 74.97, H 8.01, N 7.95; found: C 75.07, H 7.75, N 7.90

Further crystallization yielded 191 mg (18%) of *(4R*,4'R*,5R*,5'R*)-5,5'-diphenyl-3,3',4,4'-tetramethyl-2,2'-bioxazolidine (**7**)*, mp 119–121°C; ir ν_{max} (KBr): 2965, 2927, 1453, 1378, 1222, 1177, 1051, 1013 cm^{-1}; ms, m/z (%) 352(M^+, 5%), 353(M^+ +1,1), 301(2), 219(7), 190(11), 189(100), 177(6), 176(42), 148(20), 133(3), 119(6), 118(42), 117(16), 91(10), 86(19), 84(28), and 49(18); Anal. calcd. for $C_{22}H_{28}N_2O_2$: C 74.97, H 8.01, N 7.95; found: C 75.21, H 7.85, N 7.97.

The final crystals yielded 21 mg (2%) of *(4R*,4'R*,5R*,5'R*)-5,5'-diphenyl-3,3',4,4'-tetramethyl-2,2'-bioxazolidine (**6**)*, mp 181–183°C; ir ν_{max} (KBr) 2969, 2844, 1452. 1357, 1221, 1776, 1092, 1073, 995 cm^{-1}; ms, m/z (%): 352 (M^+, 4%), 353(M^+ + 1,1), 219(9), 190(10), 189(100), 176(3), 148(5), 118(44), 117(13), and 91(4).

Condensation of ephedrine with glyoxal

Condensation of ephedrine with glyoxal was carried out using the procedure described in the case of pseudoephedrine. The reaction affords a mixture of **8** and **9** in a 7:3 ratio. The residue was evaporated to dryness and the solid dissolved in hexane–methanol mixtures to afford *(2R*,3S*,6R*,7S*)-2,6-diphenyl-3,4,7,8-tetramethyl-*cis*-perhydro[1,4]oxazino-[3,2-*b*]-1,4-oxazine (**8**)* (662 mg, 61%), which was recrystallized several times using methanol–hexane mixtures, mp 102–103°C; ir ν_{max} (KBr): 3292, 2887, 2865, 1439, 1378, 1156, 1128, 1068, 1006, 962 cm^{-1}. The remaining liquid was distilled under vacuum to give *(5S*,6R*)-4,5-dimethyl-6-phenyl-1,4-oxazin-2-one (**9**)* (284 mg, 26%), bp 135°C (0.5 Torr; 1 Torr = 133.3 Pa) (9). ^1H nmr ($CDCl_3$, 300 MHz): 7.27–7.40 (m, 5H, arom), 5.62 (d, J = 3.8 Hz, 1H, H-6), 3.43 and 3.49 (AB, J = 18.3 Hz, 2H, CH_2-3), 3.10 (dq, J = 6.8, 3.4 Hz, 1H, H-5), 2.36 (s, 3H, N-CH_3), 0.74 (d, J = 6.8 Hz, CH_3).

Results and discussion

In continuing our studies on the reaction of glyoxal with aminoalcohols (11) we decided to look more carefully into the reaction conditions for the condensation of pseudoephedrine or ephedrine with 40% aqueous glyoxal. The reaction of pseudoephedrine with glyoxal in a 2:1 ratio was carried out in benzene under reflux for 2 h. The crude reaction product is a mixture of (2R*,3R*,6R*,7R*)-2,6-diphenyl-3,4,7,8-tetramethyl-*cis*-perhydro[1,4]oxazino[3,2-*b*]-1,4-oxazine (**5**), mp 121–123°C, and two isomeric (4*R**,

Can. J. Chem. Downloaded from www.nrcresearchpress.com by 109.225.110.28 on 09/08/12
For personal use only.

4′*R**,5*R**,5′*R**)-5,5′-diphenyl-3,3′,4,4′-tetramethyl-2,2′-bioxazolidines, mp 181–183°C (**6**) and 119–121°C (**7**), which were separated by fractional crystallizations using hexane–methanol mixtures.

In contrast, reaction of ephedrine with glyoxal, under the same reaction conditions, affords a mixture of (2*R**,3*S**,6*R**,7*S**)-2,6-diphenyl-3,4,7,8-tetramethyl-*cis*-perhydro-[1,4]oxazino[3,2-*b*]-1,4-oxazine (**8**) and (5*S**,6*R**)-4,5-dimethyl-6-phenyl-1,4-oxazin-2-one (**9**) (9).

Contrary to all previous reports, differentiation between the two types of ring fusion can indeed be achieved by observation of the ^{13}C satellites of the ring fusion protons in the ^1H nmr spectra. This removes the equivalence of any pair of CH residues since one of the protons couples strongly to the ^{13}C atom and the probability that the other proton is also attached to a ^{13}C atom is very small. Thus the A_2 system, consequent to symmetry, gives rise to an ABX spin–spin system, with the ^{13}C atom as the X part. These experiments show that the H-2 signals at 4.06 (s) in **6** and at 4.31 (s) in **7** undergo additional splitting ($^3J_{HH}$ = 3.85 Hz), while in the case of the six-membered heterocycles the same protons, at 4.34 in **5** and 4.30 in **8**, respectively, show coupling constants of 0 and 1.28 Hz, respectively.

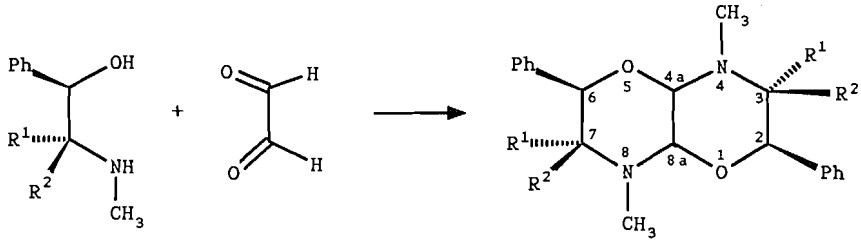

$R^1 = CH_3$ $R^2 = H$

$R^1 = H$ $R^2 = CH_3$

5 $R^1 = CH_3$ $R^2 = H$

8 $R^1 = H$ $R^2 = CH_3$

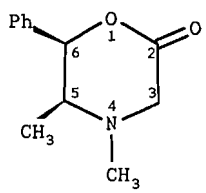

9

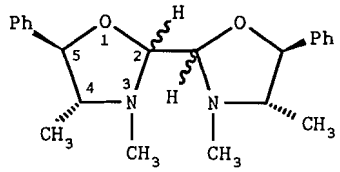

6 mp 181-183 °C

7 *(meso)* mp 119-121 °C

To establish a generalization of the above observations, compounds **3***a* and **3***b* were prepared and subjected to nmr studies. Comparison of the $^3J_{HH}$ values for 5a,6,11a,12-tetrahydro[1,4]benzoxazino[3,2-*b*][1,4]benzoxazine ($^3J_{HH}$ = 0.89) (**3***a*) and its *N*-isopropyl derivative ($^3J_{HH}$ = 0.95) (**3***b*) with those of compounds **5** and **8** shows reasonable agreement and allows definite attribution of the ring-type fusion based on the satellite spectrum (Fig. 1). Furthermore, the use of a generalized Karplus type relationship (12) in the latter compounds allows us to establish a *cis*-type fusion of these derivatives, since the corresponding *trans* derivatives should exhibit coupling constants in the order of 7 Hz, while for compounds of type **2** one would expect $^3J_{HH}$ around 3–4 Hz. The structure of **3***a* has already been established (4) by single crystal X-ray analysis and those of **3***b* and **7** were determined in this work. Perspective views of the molecular structures are depicted in Figs. 2 and 3, respectively, while the atom coordinates are given in Tables 1 and 2, respectively.

Unequivocal ^1H and ^{13}C nmr assignments for compounds **5–8** to the values shown in Tables 3 and 4, respectively, were achieved by 2D carbon–proton correlated experiments and comparison with model compounds (13). In general, the assignment of the ^1H spectra is trivial and the fact that the proton signal can be recognized readily allows attribution of the corresponding signals in the ^{13}C nmr spectra. Observation of Tables 3 and 4 shows that neither the ^1H nor the ^{13}C chemical shifts of the ring fusion atoms may be of diagnostic value to establish the ring size in these fused heterocycles. This is in contrast to previous reports on bidioxolane and tetraoxodecalin mixtures (14, 15) where it has been found that dioxalane acetal methine protons absorb at lower field relative to dioxane acetal methine protons.

Complete assignment of the ^{13}C and ^1H nmr spectra of **3***a* (see experimental) was achieved by 2D carbon–proton correlated experiments. The distinction between the C-1 and C-4 carbons was achieved by comparison of the coupled spectrum with that obtained after addition of D_2O, which shows increased intensity of the dd signal at 114.92 ppm, thus allowing attribution of this resonance to C-4; the corresponding H-4 proton appears as a double doublet of doublets at 6.69 ppm (J = 7.6, 1.7, 0.6 Hz) in the ^1H nmr spectrum. In turn C-1 resonates at 117.11 and is observed as dd in the ^1H nmr spectrum (J = 8.2, 1.9) at 6.81 ppm. The remaining

Can. J. Chem. Downloaded from www.nrcresearchpress.com by 109.225.110.28 on 09/08/12
For personal use only.

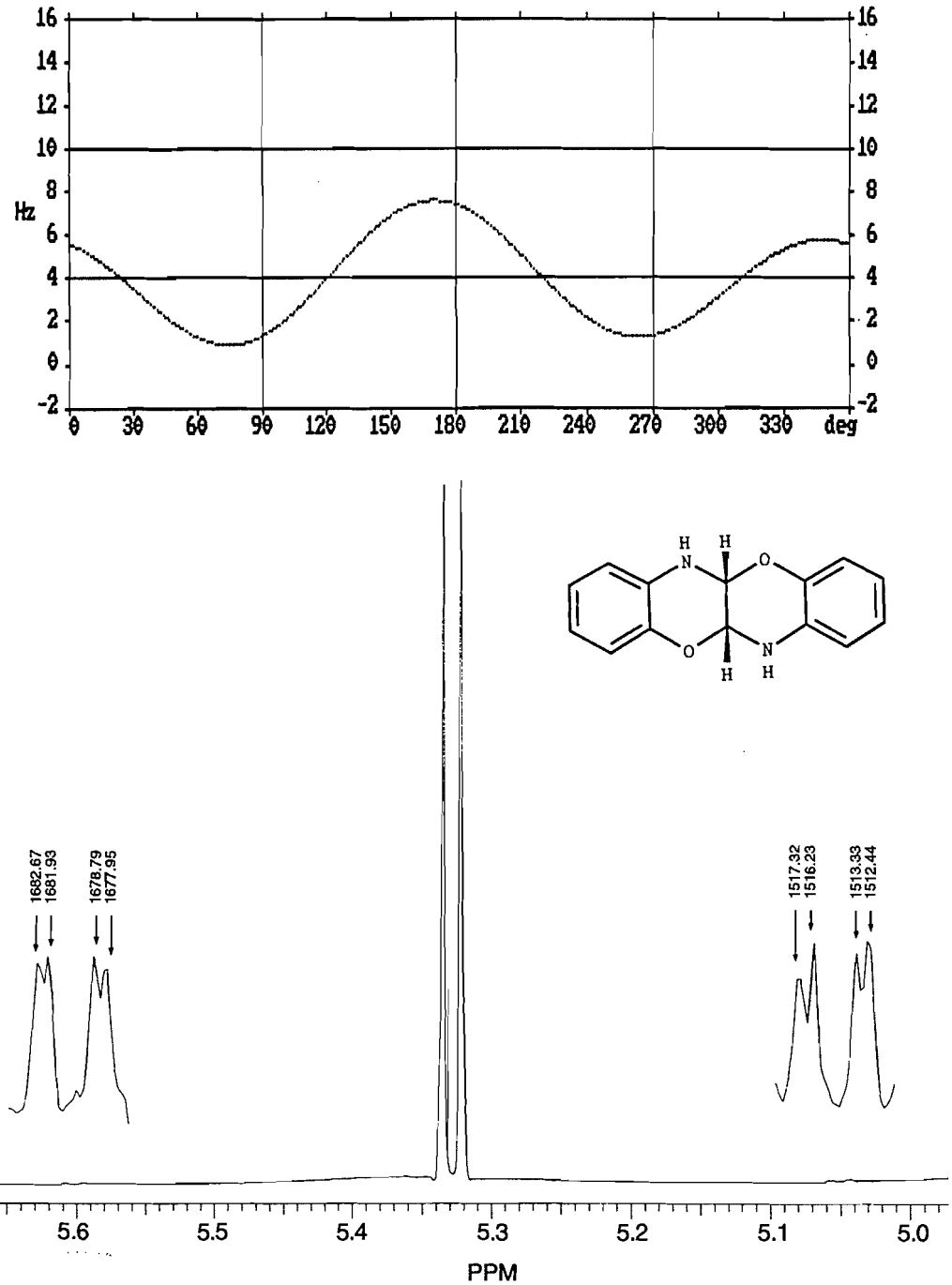

FIG. 1. ^{13}C satellite spectrum for the H—C(5a)—C(11a)—H fragment of **3***a* and plot generated by Altona. The program Altona (12) uses the relative stereochemistry of the fragment and electronegativity of atoms.

aromatic signals were assigned from the ^1H nmr spectrum, based on observation of the coupling pattern that allows us to distinguish the *meta* relationship. Thus the ddd (J = 7.5, 6.7, 2.0) at 6.84 ppm was attributed to H-3, which correlates to the carbon signal at 122.05, while the ddd (J = 8.1, 6.6, 1.5) at 6.79 corresponds to H-2, which is assigned to the carbon at 120.61 ppm.

The spectra of the *N*-isopropyl derivative **3***b* were assigned by comparison with those of **3***a*.

Assignment of the configuration of the 2,2′ protons in bioxazolidines **6** and **7** from nmr measurements was not possible due to the fact that the central -CH-CH- protons give rise to singlets at 4.06 and 4.31 ppm. These could not be resolved by addition of optically active shift reagents, by which one would expect two singlets for a *d,l* mixture or an AB system for a *meso* compound (16). However, the structure of **7** was established by X-ray analysis as the *meso* form.

Although it has been described that mass spectrometry provides a criterion for the differentiation of 1,4,5,8-tetraoxadecalin and bi(dioxolan-2-yl) derivatives (17) based on the observation of the molecular peak, which appears in the tetraoxadecalins but is virtually absent in the bi(dioxolanyl)

Can. J. Chem. Downloaded from www.nrcresearchpress.com by 109.225.110.28 on 09/08/12
For personal use only.

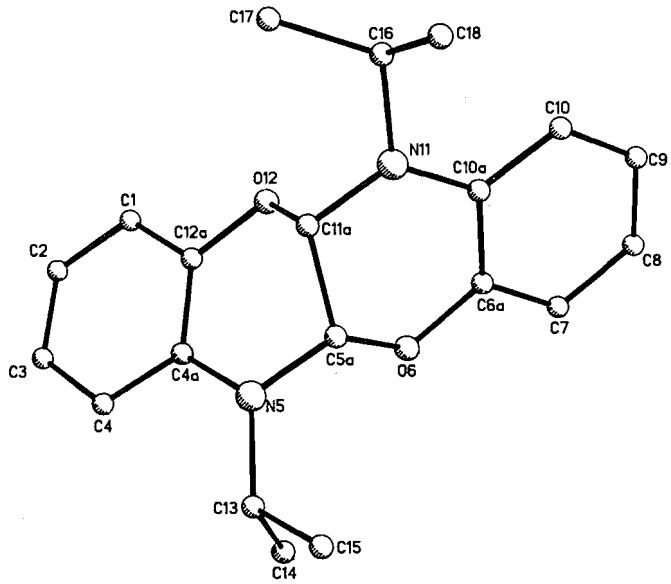

FIG. 2. Perspective view of the molecular structure of **3***b*.

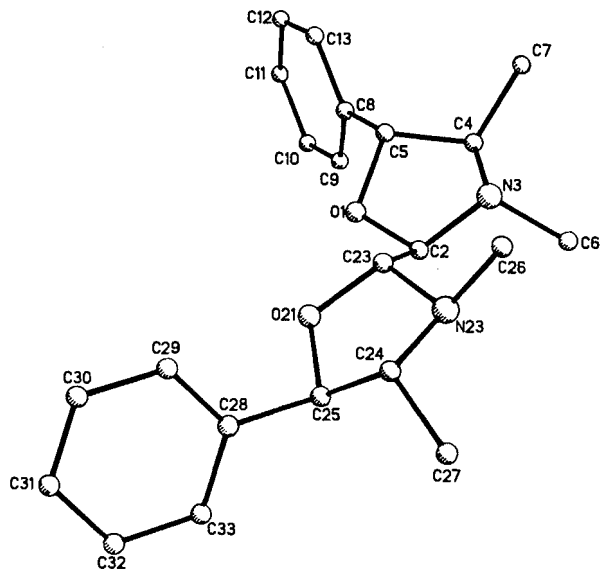

FIG. 3. Perspective view of the molecular structure of **7**.

derivatives, we are not aware of analogous mass spectral studies in the case of the bioxazolidines and oxazino-oxazine derivatives. However, we have found that this criterion has been used to establish the structure in the case of isomeric bibenzothiazole and [1,4]benzothiazino[3,2-*b*]-benzothiazine (18), based on the fact that the mass spectrum of the latter exhibits in addition to the M^+ and $M^+/2$ ions, two fragments that are 13 mass units above or below the $M^+/2$ peak, and such fragments have only been observed in ring systems like **3***a*.

In the case of the isomeric structures **5**, **6**, and **7** described in this study, the mass spectra show the M^+ and $M^+/2$ peaks in all cases. However, the most important fragment is at m/z 189, corresponding indeed to 13 mass units above the $M^+/2$ peak. The fact that this fragment was observed in all three isomers cast some doubts on the validity of such an approach to the general application of this methodology for

TABLE 1. Atomic positional parameters ($\times 10^4$) for *N*,*N*-diisopropyl-5a,6,11a,12-tetrahydro-[1,4]benzoxazino[3,2-*b*]-1,4-benzoxazine (**3***b*)[a]

Atom	*x*	*y*	*z*
C(1)	8200(4)	3205(5)	8024(4)
C(2)	9286(4)	2546(6)	9081(4)
C(3)	8855(4)	1473(6)	9768(4)
C(4)	7332(4)	1055(5)	9438(4)
C(4a)	6213(4)	1720(4)	8376(3)
N(5)	4676(3)	1315(4)	7975(3)
C(5a)	3642(4)	2108(4)	6920(3)
O(6)	3135(3)	3439(4)	7392(2)
C(6a)	2341(3)	4435(4)	6437(3)
C(7)	1483(4)	5486(5)	6765(4)
C(8)	690(4)	6558(5)	5866(4)
C(9)	752(4)	6517(5)	4628(4)
C(10)	1618(3)	5469(4)	4289(3)
C(10a)	2449(3)	4403(4)	5177(3)
N(11)	3361(3)	3328(4)	4887(3)
C(11a)	4378(3)	2550(4)	5934(3)
O(12)	5686(2)	3453(4)	6587(2)
C(12a)	6707(4)	2795(4)	7673(3)
C(13)	4113(4)	436(5)	8861(4)
C(14)	4152(6)	1323(6)	10062(4)
C(15)	2539(4)	−202(6)	8177(4)
C(16)	3580(4)	3368(4)	3598(3)
C(17)	5069(4)	2691(7)	3635(4)
C(18)	2275(5)	2646(7)	2570(4)

[a]Crystals: monoclinic, $P2_1$; a = 9.397(3), b = 9.017(3), c = 10.997(3) Å, β = 110.16(2)°; Z = 2.

TABLE 2. Atomic positional parameters ($\times 10^4$) for (4*R**,4′*R**,5*R**,5′*R**)-5,5′-diphenyl-3,3′,4,4′-tetramethyl-2,2′-bioxazolidine (**7**)[a]

Atom	*x*	*y*	*z*
O(1)	4933(8)	2689(3)	2435(2)
N(3)	4550(7)	4273(3)	2801(2)
C(2)	5871(9)	3436(3)	2773(2)
C(4)	3150(8)	4137(4)	2311(2)
C(5)	2932(9)	3045(4)	2311(2)
C(6)	5620(10)	5221(5)	2772(3)
C(7)	1228(10)	4711(5)	2402(2)
C(8)	2233(9)	2558(3)	1745(2)
C(9)	3472(10)	2498(4)	1261(3)
C(10)	2891(15)	2056(5)	739(3)
C(11)	976(16)	1677(5)	703(3)
C(12)	−301(11)	1722(5)	1174(3)
C(13)	299(10)	2162(4)	1702(3)
O(21)	7444(9)	2144(3)	3353(2)
N(23)	7218(7)	3657(3)	3811(2)
C(23)	6177(10)	2982(4)	3404(2)
C(24)	8534(9)	3026(4)	4169(2)
C(25)	9220(8)	2281(4)	3706(2)
C(26)	5794(10)	4216(5)	4191(3)
C(27)	10233(11)	3613(5)	4435(3)
C(28)	9842(8)	1272(4)	3925(2)
C(29)	8525(9)	636(5)	4186(2)
C(30)	9106(14)	−291(5)	4366(3)
C(31)	11037(15)	−593(4)	4297(3)
C(32)	12408(10)	47(5)	4041(3)
C(33)	11822(9)	974(4)	3860(3)

[a]Crystals: orthorombic, $P2_12_12_1$; a = 6.680(4), b = 13.474(13), c = 22.496(4) Å; Z = 4, using CRYSTALS (10).

Can. J. Chem. Downloaded from www.nrcresearchpress.com by 109.225.110.28 on 09/08/12
For personal use only.

TABLE 3. The ^{1}H nmr data for compounds **5**–**8** (in ppm)[a]

Compound (mp, °C)	H-2	H-3	H-4a	N-CH_3	CH_3	C_6H_5
5 (121–123)	4.17 (d, J = 9.3)	3.08 (dq, J = 9.3, 6.4)	4.34 (s)	2.45 (s)	0.80 (d, J = 6.4)	7.28–7.50
8 (102–103)	4.81 (d, J = 2.7)	2.96 (dq, J = 3.0, 6.7)	4.30 (s)	2.67 (s)	0.96 (d, J = 6.6)	7.20–7.33
	H-5	H-4	H-2	N-CH_3	CH_3	C_6H_5
6 (181–183)	4.82 (dd, J = 9.5)	2.52 (dq, J = 9.5, 6.2)	4.06 (s)	2.26 (s)	0.91 (d, J = 6.2)	7.27–7.41
	5.09[b] (d, J = 9.2)	2.45 (dq, J = 9.2, 6.1)	4.17 (s)	2.22 (s)	0.84 (d, J = 5.9)	7.37 (1H, J = 7.9, 1.3) 7.19–7.07 (m, 3H)
7(*meso*) (119–121)	4.59 (d, J = 8.8)	2.46 (dq, J = 8.9, 6.0)	4.31 (s)	2.52 (s)	1.09 (d, J = 6.1)	7.23–7.40 (m, 3H)
	4.67[b] (d, J = 8.6)	2.36 (dq, J = 8.6, 5.9)	4.44 (s)	2.39 (s)	0.95 (d, J = 5.9)	7.37 (J = 7.9, 1.3) 7.19–7.07 (m, 3H)

[a]Measured in $CDCl_3$ from TMS.
[b]Measured in C_6D_6.

TABLE 4. The ^{13}C nmr data for compounds **5**–**8** (in ppm)[a]

Compounds	C-2	C-3	C-4a	N-CH_3	CH_3	*ipso*	*ortho*	*meta*	*para*
5	83.42	55.15	87.44	39.07	14.89	140.45	127.95	128.18	[b]
8	79.37	56.69	86.95	38.98	10.06	140.39	125.60	128.02	126.77
	C-5	C-4	C-2	N-CH_3	CH_3	*ipso*	*ortho*	*meta*	*para*
6	76.00	62.16	87.12	36.27	15.22	139.91	128.11	128.37	[b]
7(*meso*)	86.05	69.32	97.98	38.78	14.40	139.26	127.02	128.16	127.91

[a]In $CDCl_3$ from TMS.
[b]Superimposed.

the differentiation of the type of isomers described in the present study.

The current interest in the study of the anomeric effect in ring systems containing the X-C-Y grouping, both experimentally and by computational studies (19–21), evidences the need to establish an unequivocal and simple approach for identifying and differentiating between isomeric systems.

Excepting an isolated report (22), the reaction of aminoalcohols with glyoxal (4, 6) as well as with various other compounds (5, 7, 23) have been shown to yield *cis*-oxazino-oxazine structures after X-ray analyses. These results, which imply a high degree of stereoselectivity, have been rationalized in terms of an anomeric effect (5) that favors those structures having the non-bonding lone pairs of the nitrogen atoms antiperiplanar to the C—O bonds.

Conclusions

It is apparent that neither the formation nor the ratio of the isomeric oxazino-oxazine (such as **3**) and bioxazolidine (such as **2**) products can be predicted. In the case of both ephedrine and pseudoephedrine, oxazino-oxazine type structures (as **3**) having the *cis* ring fusion are formed, while bioxazolidine (as **2**) formation occurred only in the latter aminoalcohol at higher temperatures. These results show that in addition to the reaction conditions, to the basicity of the amine and the acidity of the alcohol, the reaction outcome is also sensitive to stereochemical changes at the aminoalcohol portion.

The fact that the compounds having the bioxazolidine type structure (as **2**) isomerize in solution, or during chromatographic procedures, to the *cis*-oxazino-oxazine type structures (as **3**) gives evidence that the latter are thermodynamic products.

Detailed evaluation of the ^{1}H, ^{13}C, and mass spectral data for the isomeric five- and six-membered ring bis-heterocycles described in this study allows us to conclude that in the case of the bioxazolidine (as **2**) and oxazino-oxazine (as **3**) derivatives with hydyrogen atoms at the ring fusion, measurement of the ^{13}C satellites in the ^{1}H nmr spectra constitutes the simplest and most adequate criterion for their differentiation, as validated in the present study by the X-ray diffraction studies of **3***b* and **7**.

Acknowledgements

We are grateful to Rubén Ocampo Torres for the mass spectral analyses, to the Consejo Nacional de Ciencía y Tecnología (CoNaCyt), Consejo Superior Nacional de Educación Tecnológica (CoSNET), and Proyectos Estratégicos SEP for financial support.

1. E. Bayer. Chem. Ber. **90**, 2325 (1957).
2. I. Murase. Bull. Chem. Soc. Jpn. **32**, 827 (1959).
3. I. Murase. Bull. Chem. Soc. Jpn. **33**, 59 (1960).

Can. J. Chem. Downloaded from www.nrcresearchpress.com by 109.225.110.28 on 09/08/12
For personal use only.

4. E. Tauer, K. H. Grellmann, E. Kaufmann, and M. Noltemeyer. Chem. Ber. **119**, 3316 (1986).
5. J. Barluenga, F. Aznar, R. Liz, M. P. Cabal, F. H. Cano, and F. Foces-Foces. Chem. Ber. **119**, 887 (1986).
6. A. Le Rouzic, M. Maunaye, and P. L'Haridon. J. Chem. Res. (S), 35; (M), 0601 (1985).
7. P. L'Haridon and A. Le Rouzic. J. Chem. Res. (S), 244; (M), 2165 (1986).
8. H. R. Morales, M. Pérez-Juárez, L. Cuéllar, L. Mendoza, H. Fernández, and R. Contreras. Synth. Commun. **14**, 1213 (1984).
9. A. Flores-Parra, N. Farfán, A. I. Hernández-Bautista, L. Fernández-Sánchez, and R. Contreras. Tetrahedron, **47**, 6903 (1991).
10. D. J. Watkin, J. R. Carruthers, and P. W. Betteridge. CRYSTALS users guide. Chemical Crystallography Laboratory, University of Oxford, Oxford, England. 1986.
11. N. Farfán, J. M. Hernández, P. Joseph-Nathan, and R. Contreras. J. Heterocycl. Chem. **27**, 1745 (1990); N. Farfán, L. Cuéllar, J. M. Aceves, and R. Contreras. Synthesis, 927 (1987).
12. C. M. Cerda-García-Rojas, L. G. Zepeda, and P. Joseph-Nathan. Tetrahedron Comput. Methodol. **3**, 113 (1990).
13. M. A. Paz-Sandoval, F. Santiesteban, and R. Contreras. Magn. Reson. Chem. **23**, 428 (1985).
14. P. P. Castro, S. Tihomiro, and C. G. Gutiérrez. J. Org. Chem. **53**, 5181 (1988).
15. E. Caspi, T. A. Wittstruck, and N. Grover. Org. Chem. **8**, 763 (1963).
16. P. Joseph-Nathan and L. U. Román. Spectroscopy, **9**, 47 (1991).
17. B. Fuchs. Tetrahedron Lett. 1747 (1970).
18. E. Tauer and K. H. Grellmann. Chem. Ber. **123**, 1149 (1990).
19. R. Müller, W. von Philipsborn, L. Schleifer, P. Aped, and B. Fuchs. Tetrahedron, **47**, 1013 (1991).
20. B. Fernández, M. A. Ríos, and L. Carballeira. J. Mol. Struct. **246**, 301 (1991).
21. H. Senderowitz, P. Aped, and B. Fuchs. Helv. Chim. Acta, **73**, 2113 (1990).
22. B. Alcaide, R. Pérez-Ossorio, J. Plumet, M. Rico, and I. M. Rodríguez-Campos. Tetrahedron Lett. **27**, 1381 (1986); recently corrected in: B. Alcaide, J. Plumet, I. M. Rodríguez-Campos, S. García-Blanco, and S. Martínez-Carrera. J. Org. Chem. **57**, 2446 (1992).
23. P. L'Haridon, A. Le Rouzic, and M. Maunaye. J. Chem. Res. (S), 349 (1980).

Can. J. Chem. Downloaded from www.nrcresearchpress.com by 109.225.110.28 on 09/08/12
For personal use only.

Dinuclear cobalt(II) complexes of a polyhydroimidazole ligand. Dinuclear (2:1) non-metallocyclic derivatives and dinuclear (1:1) metallocyclic complexes with a large, unoccupied central cavity

SANTOKH S. TANDON, LAURENCE K. THOMPSON,[1] AND JOHN N. BRIDSON
Department of Chemistry, Memorial University of Newfoundland, St. John's, Nfld., Canada A1B 3X7

AND

JOHN C. DEWAN
Department of Chemistry, New York University, New York, NY 10003, U.S.A.

Received May 26, 1992

SANTOKH S. TANDON, LAURENCE K. THOMPSON, JOHN N. BRIDSON, and JOHN C. DEWAN. Can. J. Chem. **70**, 2771 (1992).

The ligand BTIM (1,2,4,5-tetrakis(4,5-dihydro-imidazol-2-yl)benzene) reacts with cobalt(II) salts to form two series of complexes. The 1:1, dinuclear, metallocyclic derivatives $[Co_2(BTIM)_2X_2]X_2$ (X = Cl (**I**), Br (**II**)) involve two bis-dentate ligands in a metallocyclic structure with a large unoccupied cavity. The 2:1, binuclear derivatives $[Co_2(BTIM)X_4]$ (X = Cl (**III**), Br (**IV**)) involve two metals bound to a single, bis-bidentate ligand. The crystal and molecular structures of **II** and **III** are reported. Compound **II** crystallized in the monoclinic system, space group $P2_1/c$, with a = 13.642(6) Å, b = 11.560(3) Å, c = 18.406(7) Å, β = 101.73(3)° and four formula units per unit cell. Refinement by full-matrix least squares gave final residuals of R = 0.060 and R_w = 0.062. Compound **III** crystallized in the triclinic system, space group $P\bar{1}$, with a = 8.367(2) Å, b = 14.254(3) Å, c = 7.649(2) Å, α = 100.99(2)°, β = 101.44(2)°, γ = 106.85(1)° and one formula per unit cell. Refinement by full-matrix least squares gave final residuals of R = 0.052 and R_w = 0.045. In the metallocyclic structure (**II**) the square-pyramidal cobalt(II) centres are separated by 7.599(4) Å, while in the 2:1 derivative the two tetrahedral cobalt(II) centres have a much larger separation (8.736(3) Å).

SANTOKH S. TANDON, LAURENCE K. THOMPSON, JOHN N. BRIDSON et JOHN C. DEWAN. Can. J. Chem. **70**, 2771 (1992).

Le ligand BTIM (1,2,4,5-tétrakis(4,5-dihydroimidazol-2-yl)benzène) réagit avec les sels de cobalt(II) pour former deux séries de complexes. Les dérivés métallocycliques dinucléaires 1 : 1 $[Co(BTIM)_2X_2]X_2$ (X = Cl (**I**) et Br (**II**)) impliquent deux ligands bis-dentates dans une structure métallocyclique et une cavité vide importante. Les dérivés binucléaires 2 : 1 $[Co_2(BTIM)X_4]$ (X = Cl(**III**) et Br (**IV**) impliquent des liaisons de deux métaux à un seul ligand bis-dentate. On a déterminé et on rapporte les structures moléculaires des composés **II** et **III**. Le composé **II** cristallise dans le système monoclinique, groupe d'espace $P2_1/c$, avec a = 13,642(6), b = 11,560(3) et c = 18,406(7) Å, β = 101,73(3)° et quatres molécules par unité. On a affiné la structure par la méthode des moindres carrés jusqu'à des valeurs finales de R = 0,060 et R_w = 0,062. Le composé **III** cristallise dans le système triclinique, groupe d'espace $P\bar{1}$, avec a = 8,367(2), b = 14,254(3) et c = 7,649(2) Å, α = 100,99(2), β = 101,44(2) et γ = 106,85(1)° et une molécule par unité. On a affiné la structure par la méthode des moindres carrés jusq'à une valeur de R = 0,052 et de R_w = 0,045. Dans la structure métallocyclique **II**, les centres en pyramide carrée du cobalt(II) sont séparés par 7,599(4) Å alors que dans le dérivé 2 : 1 les deux centres tétraédriques du cobalt(II) sont beaucoup plus séparés (8,736(3) Å).

[Traduit par la rédaction]

Introduction

The ligand BTIM (1,2,4,5-tetrakis(4,5-dihydroimidazol-2-yl)benzene) (Fig. 1) behaves in a tetradentate fashion in its copper coordination chemistry forming mainly 1:1 metallocyclic derivatives, e.g. $[Cu_2(BTIM)_2X_2]X_2$ (X = Cl, N_3), $[Cu_2(BTIM)_2(H_2O)_2](ClO_4)_4$, with two square pyramidal copper(II) centres bridged by two bis-dentate ligands, with large copper–copper separations (7.30, 7.42 Å) (1,2). The copper(II) centres were shown to be very weakly antiferromagnetically coupled with $-2J < 2$ cm^{-1}.

Reaction of BTIM with cobalt(II) salts led to the formation of two types of dinuclear complex, one similar to the copper derivatives with a 1:1 stoichiometry and the other with a 2:1 (metal:ligand) stoichiometry. The complexes have been characterized by infrared, electronic spectra and variable temperature magnetism and the structures of one example of each type of dinuclear complex have been confirmed by X-ray crystallography. The complex $[Co_2(BTIM)_2Br_2]$-$Br_2 \cdot 2CHCl_3 \cdot 4MeOH$ (II) has a dinuclear, metallocyclic (2:2) structure with dimensions comparable to the metallocyclic copper derivatives. The 2:1 complex $[Co_2(BTIM)Cl_4] \cdot$ 2DMF (**III**) involves a unique, open chain, dinuclear structure with the two tetrahedral cobalt(II) centres bridged by one ligand, with a much larger metal–metal separation (8.736(3) Å)). Variable temperature magnetic studies have been carried out on compounds **I**–**IV**, but are not really conclusive in terms of the presence of significant magnetic exchange between the cobalt centres.

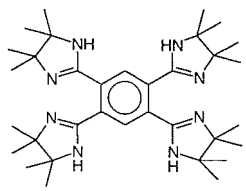

FIG. 1. Structural representation of the ligand BTIM.

Experimental section

Synthesis of the ligand and cobalt complexes

BTIM

A low yield synthesis of the ligand has already been reported (2). An improved synthesis is now described.

[1]Author to whom correspondence may be addressed.

Can. J. Chem. Downloaded from www.nrcresearchpress.com by 109.225.110.28 on 09/08/12
For personal use only.

Can. J. Chem. Downloaded from www.nrcresearchpress.com by 109.225.110.28 on 09/08/12
For personal use only.

Tetracyanobenzene (3) (6.0 g; 0.034 mol) was dissolved in hot (100°C) nitrobenzene (150 mL). A solution of ethane-1,2-diamine (25.0 mL) in nitrobenzene (50 mL) was added dropwise over a period of 2 h and the mixture stirred at 100°C for three days. A reddish brown solution formed, followed by the formation of a light brown solid, which was filtered off, after cooling and washed with nitrobenzene (2 × 20 mL) and acetone (3 × 50 mL). The solid was recrystallized from methanol/chloroform (3:1) mixture. Yield 50%, *m/e* 350, mp dec. 270–300°C.

$[Co_2(BTIM)_2Cl_2]Cl_2 \cdot 4H_2O$ (I)

BTIM (0.35 g, 0.001 mol) was dissolved in a boiling mixture of methanol (200 mL) and chloroform (200 mL) and the solution filtered into a solution of $CoCl_2 \cdot 6H_2O$ (0.48 g, 0.002 mol) in methanol (50 mL). The reaction mixture was boiled gently in a conical flask for 1–2 h so that some solvent evaporated. A brown solid separated from the hot solution, which was filtered, washed with methanol, and dried under vacuum. The blue filtrate was concentrated to a volume of about 100 mL and allowed to stand at room temperature overnight. More product appeared on standing as well formed red–brown crystals, which were filtered and washed with methanol and chloroform. The crystals crumble and lose solvent on exposure to air and are only stable in the presence of the mother liquor. The crystalline sample was dried under vacuum and analysed. Anal. calcd. for $[Co_2(C_{18}H_{22}N_8)_2Cl_2]Cl_2 \cdot 4H_2O$: C 41.87, H 5.04, N 21.71, Co 11.42; found: C 41.86, H 4.16, N 21.52, Co 11.23.

$[Co_2(BTIM)_2Br_2]Br_2 \cdot 2CHCl_3$ (**II**) was prepared in a similar manner. Anal. calcd. for $[Co_2(C_{18}H_{22}N_8)_2Br_2]Br_2 \cdot 2CHCl_3$: C 33.12, H 3.34, N 16.27, Co 8.56; found: C 32.78, H 3.24, N 16.11, Co 8.27. Crystals of **II** suitable for X-ray analysis were unstable and lost solvent on exposure to air, and so were kept in contact with the mother liquor. Both methanol and chloroform solvent molecules were found in the X-ray sample.

$[Co_2(BTIM)Cl_4]$ (III) and
$[Co_2(BTIM)_2Br_4] \cdot 0.5MeOH \cdot 0.5CHCl_3$ (IV)

The blue (**III**) and greenish blue (**IV**) filtrates obtained after separation of **I** and **II** were concentrated further to a small volume. Acetonitrile (50 mL) was added to the hot solutions and the mixtures boiled gently in an open conical flask for about 15 min. Dark blue (**III**) or greenish blue (**IV**) crystals separated on standing at room temperature and were filtered off, washed with acetonitrile (2 × 5 mL) and methanol (2 × 5 mL), and dried under vacuum. Anal. calcd. for $[Co_2(C_{18}H_{22}N_8)Cl_4]$: C 35.42, H 3.61, N 18.37, Co 19.32; found: C 35.21, H 3.65, N 17.93, Co 18.88. Crystals of **III** suitable for X-ray analysis were obtained by slow, vapour diffusion of ether into a DMF:MeOH (1:1) solution of the complex, and the sample was shown to have the composition $[Co_2(C_{18}H_{22}N_8)Cl_4] \cdot 2DMF$. Anal. calcd. for $[Co_2(C_{18}H_{22}N_8)Br_4] \cdot 0.5CHCl_3 \cdot 0.5MeOH$ (**IV**): C 26.40, H 2.84, N 12.97, Co 13.64; found: C 26.11, H 2.81, N 12.87, Co 13.20.

Physical measurements

Infrared spectra were recorded using a Mattson Polaris Fourier transform spectrometer and electronic spectra using a Cary 17 spectrometer. Room temperature magnetic moments were measured by the Faraday method using a Cahn 7600 magnetic susceptibility system. Variable temperature magnetic data were obtained in the temperature range 5–305 K with an Oxford Instruments superconducting Faraday magnetic susceptibility system with a Sartorius 4432 microbalance. A main solenoid field of 1.5 T and a gradient field of 10 T m^{-1} were employed. C, H, and N analyses were carried out by the Canadian Microanalytical Service, Delta, and cobalt was determined by EDTA titration.

Crystallographic data collection and refinement of the structures

$[Co_2(BTIM)_2Br_2]Br_2 \cdot 2CHCl_3 \cdot 4MeOH$ (II)

Crystals of **II** dried out, crumbled, and ceased to diffract X-rays if removed from their mother liquor. Accordingly, a red–brown crystal was mounted at the end of a glass fiber under a stream of cold nitrogen gas and coated with high vacuum grease. The crystal was then transferred to the nitrogen cold stream of a low temperature device mounted on the diffractometer, and maintained at −110 ± 1°C throughout the data collection. The crystal was quite stable under these conditions and the intensities of three standard reflections showed no decay during data collection.

The diffraction intensities of an approximately 0.48 × 0.40 × 0.25 mm crystal were collected with graphite monochromatized MoKα radiation and a 1.5 kW sealed tube X-ray source using a Rigaku AFC6S diffractometer. The data were collected at low temperature using the ω–2θ scan technique to a maximum 2θ value of 55.2° and a scan rate of 8.0°/min. Cell constants were obtained by the least-squares refinement of the setting angles of 25 carefully centred reflections with 2θ in the range 27.23–29.97°. A total of 7190 reflections were measured, of which 6910 were unique (R_{int} = 0.086), and 3277 were considered significant with $I_{net} > 2.0\sigma(I_{net})$. An empirical absorption correction was applied using the program DIFABS (4) and the data were corrected for Lorentz and polarization effects.

The structure was solved by direct methods and refined by full-matrix least squares using TEXSAN (5) to final residuals of R and R_w of 0.060 and 0.062 respectively ($R = \Sigma(|F_o| - |F_c|)/\Sigma(|F_o|)$; $R_w = [\Sigma(|F_o| - |F_c|)^2/\Sigma wF_o^2)]^{1/2}$), with weights based on counting statistics. Hydrogen atoms were placed in calculated positions (temperature factor 1.2 times B(eq) of atom to which they are bound) and the non-hydrogen atoms were refined anisotropically. Neutral atom scattering factors were taken from ref. 6. The final difference map had no peaks greater than 0.7 e/Å^3. One chloroform molecule (C(90), Cl(90), Cl(91), Cl(92)) and two methanol molecules (C(50), O(50); C(60), O(60)) have been identified in the asymmetric unit and included in the refinement. A summary of crystal data is given in Table 1 and atomic positional parameters are given in Table 2. Anisotropic thermal parameters (Table S1), hydrogen atom positional parameters (Table S2), a full listing of bond distances and angles (Table S3), a listing of structure factors (Table S4), and least-squares planes data (Table S9) are included as supplementary material.[2]

$[Co_2(BTIM)Cl_4] \cdot 2DMF$ (III)

The diffraction intensities of a blue needle of approximate dimensions 0.35 × 0.10 × 0.08 mm were collected on a Rigaku AFC6S diffractometer, with graphite monochromatized MoKα radiation. The data were collected at a temperature of 26 ± 1°C using the ω–2θ scan technique to a maximum 2θ value of 50.0° at a scan speed of 4.0°/min. Cell constants were obtained by the least-squares refinement of the setting angles of 25 carefully centred reflections with 2θ in the range 22.75–31.97°. A total of 3111 reflections were measured, of which 2893 were unique (R_{int} = 0.043), and 1558 were considered significant with $I_{net} > 3.0\sigma(I_{net})$. An empirical absorption correction was applied using the program DIFABS (4) and the data were corrected for Lorentz and polarization effects. The structure was solved by direct methods and refined by full matrix least squares using TEXSAN (5) to final residuals of R and R_w of 0.052 and 0.045, respectively, with the non-hydrogen atoms refined anisotropically. Neutral atom scattering factors were taken from ref. 6. The final difference map had no peaks greater than 0.44 e/Å^3. A summary of crystal data is given in Table 1 and atomic positional parameters are given in Table 3. Anisotropic thermal parameters (Table S5), hydrogen atom positional parameters (Table S6), a full listing of bond distances and

[2]Supplementary Tables S1–S9 may be purchased from: The Depository of Unpublished Data, Document Delivery, CISTI, National Research Council Canada, Ottawa, Canada K1A 0S2.

Tables S3, S7 (bond distances and bond angles) have also been deposited with the Cambridge Crystallographic Data Centre and can be obtained on request from the Director, Cambridge Crystallographic Data Centre, University Chemical Laboratory, 12 Union Road, Cambridge, CB2 1EZ, U.K.

TABLE 1. Crystallographic data for $[Co_2(BTIM)_2Br_2]Br_2 \cdot 2CHCl_3 \cdot 4MeOH$ (**II**) and $[Co_2(BTIM)Cl_4] \cdot 2DMF$ (**III**)

Parameter	II	III
Empirical formula	$C_{21}H_{29}Br_2Cl_3CoN_8O_2$	$C_{24}H_{28}Cl_4Co_2N_{10}O_2$
fw	750.61	748.23
Crystal system	Monoclinic	Triclinic
Space group	$P2_1/c$	$P\bar{1}$
a, Å	13.642(6)	8.367(2)
b, Å	11.560(3)	14.254(3)
c, Å	18.406(7)	7.649(2)
α, deg	—	100.99(2)
β, deg	101.73(3)	101.44(2)
γ, deg	—	106.85(1)
V, Å^3	2842(2)	825.2(3)
Z	4	1
ρ(calcd), g cm^{-3}	1.754	1.505
μ, cm^{-1}	37.07	13.68
Radiation; λ, Å	MoKα; 0.71069	MoKα; 0.71069
F_{000}	1500	380

TABLE 2. Positional parameters and B(eq) values for $[Co_2(BTIM)_2Br_2]Br_2 \cdot 2CHCl_3 \cdot 4MeOH$ (**II**)

Atom	x	y	z	B(eq)
Co	0.76249(8)	0.1138(1)	0.07438(7)	2.17(5)
Br(1)	0.94060(7)	0.1852(1)	0.12457(6)	3.21(4)
Br(2)	0.39385(7)	0.4393(1)	−0.18844(5)	2.76(4)
C(90)	0.699(1)	0.719(1)	−0.1527(7)	5.4(6)
Cl(90)	0.5792(2)	0.6598(3)	−0.1644(2)	5.9(2)
Cl(91)	0.7823(3)	0.6197(4)	−0.1817(2)	6.9(2)
Cl(92)	0.7411(3)	0.7579(3)	−0.0607(2)	6.0(2)
O(50)	0.968(1)	0.037(2)	0.2913(8)	15(1)
C(50)	1.047(2)	−0.039(2)	0.304(1)	15(2)
O(60)	0.910(1)	0.167(2)	0.407(1)	17(1)
C(60)	0.971(3)	0.124(3)	0.466(1)	24(3)
N(1)	0.6991(5)	0.2616(6)	0.0304(4)	1.9(3)
N(2)	0.5890(5)	0.3797(7)	−0.0365(4)	2.7(3)
N(3)	0.7779(5)	0.0742(6)	−0.0285(4)	2.0(3)
N(4)	0.7366(5)	0.0274(7)	−0.1478(4)	2.4(3)
N(5)	0.2957(5)	−0.1373(6)	−0.1650(4)	2.5(3)
N(6)	0.3942(5)	−0.1139(7)	−0.2466(4)	2.7(3)
N(7)	0.2150(5)	0.0519(7)	−0.1071(4)	2.4(3)
N(8)	0.2493(5)	0.2337(7)	−0.1307(5)	3.1(4)
C(1)	0.6188(6)	0.2700(8)	−0.0201(5)	2.0(4)
C(2)	0.6660(7)	0.4591(8)	−0.0006(5)	2.7(4)
C(3)	0.7275(7)	0.3798(9)	0.0541(5)	3.1(4)
C(4)	0.7060(6)	0.0626(8)	−0.0848(5)	2.0(4)
C(5)	0.8431(6)	0.023(1)	−0.1334(5)	3.4(5)
C(6)	0.8710(6)	0.046(1)	−0.0513(5)	3.4(5)
C(7)	0.3688(6)	−0.0827(8)	−0.1822(5)	2.1(4)
C(8)	0.2567(7)	−0.216(1)	−0.2264(5)	3.2(5)
C(9)	0.3325(7)	−0.209(1)	−0.2785(5)	3.6(5)
C(10)	0.2827(6)	0.1255(8)	−0.1154(5)	2.2(4)
C(11)	0.1412(7)	0.233(1)	−0.1452(6)	4.1(5)
C(12)	0.1209(7)	0.115(1)	−0.1175(7)	4.6(6)
C(13)	0.5589(5)	0.1725(7)	−0.0571(4)	1.5(3)
C(14)	0.5989(6)	0.0771(7)	−0.0866(4)	1.4(3)
C(15)	0.5342(6)	−0.0031(8)	−0.1244(4)	1.8(3)
C(16)	0.4304(6)	0.0066(8)	−0.1347(5)	1.8(4)
C(17)	0.3911(6)	0.1013(8)	−0.1049(4)	1.7(3)
C(18)	0.4560(6)	0.1825(8)	−0.0662(4)	1.8(4)

Can. J. Chem. Downloaded from www.nrcresearchpress.com by 109.225.110.28 on 09/08/12
For personal use only.

TABLE 3. Positional parameters and B(eq) values for $[Co_2(BTIM)Cl_4] \cdot 2DMF$ (**III**)

Atom	x	y	z	B(eq)
Co(1)	0.5093(1)	0.26407(9)	0.6768(2)	2.79(4)
Cl(1)	0.3046(3)	0.1309(2)	0.4602(4)	5.2(1)
Cl(2)	0.4125(3)	0.3207(2)	0.9132(3)	5.3(1)
O(1)	1.0905(9)	0.6907(5)	0.638(1)	6.2(3)
N(1)	0.7205(8)	0.2250(4)	0.7382(9)	2.7(2)
N(2)	0.9986(9)	0.2394(5)	0.801(1)	4.1(3)
N(3)	0.6121(7)	0.3739(5)	0.5647(8)	2.6(2)
N(4)	0.8024(8)	0.5084(5)	0.5269(9)	2.9(2)
N(5)	1.196(1)	0.8582(5)	0.782(1)	4.2(3)
C(1)	0.725(1)	0.1215(6)	0.673(1)	4.0(3)
C(2)	0.916(1)	0.1326(6)	0.724(1)	4.4(4)
C(3)	0.881(1)	0.2865(5)	0.806(1)	2.3(3)
C(4)	0.9360(9)	0.3970(5)	0.897(1)	2.1(3)
C(5)	0.8781(9)	0.4679(6)	0.822(1)	2.3(3)
C(6)	0.7623(9)	0.4472(5)	0.635(1)	2.3(3)
C(7)	0.675(1)	0.4689(6)	0.347(1)	3.7(3)
C(8)	0.539(1)	0.3846(6)	0.383(1)	3.2(3)
C(9)	0.944(1)	0.5692(6)	0.931(1)	2.5(3)
C(10)	1.071(1)	0.7727(8)	0.681(1)	5.1(4)
C(11)	1.371(1)	0.8573(7)	0.846(2)	6.3(5)
C(12)	1.171(1)	0.9560(8)	0.823(2)	6.8(5)

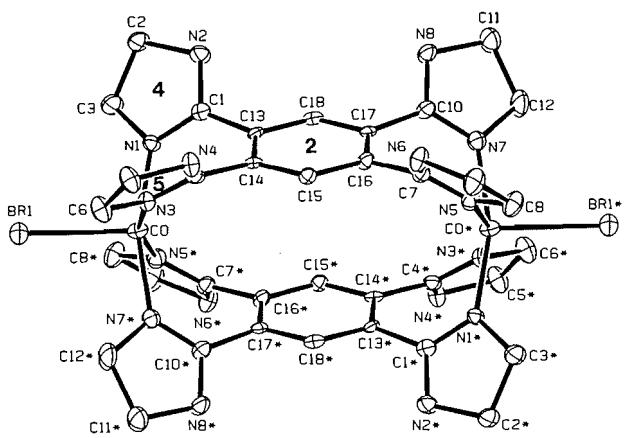

FIG. 2. Molecular structure of $[Co_2(BTIM)_2Br_2]Br_2 \cdot 2CHCl_3 \cdot 4MeOH$ (**II**).

angles (Table S7), a listing of structure factors (Table S8), and least-squares planes data (Table S9), are included as supplementary material.[2]

Results

Description of the structures of
$[Co_2(BTIM)_2Br_2]Br_2 \cdot 2CHCl_3 \cdot 4MeOH$ (II) and
$[Co_2(BTIM)Cl_4] \cdot 2DMF$ (III)

The structure of **II** is shown in Fig. 2 and bond lengths and angles relevant to the cobalt coordination spheres are listed in Table 4. Structurally **II** is analogous to several previously reported copper(II) complexes (2), where two BTIM molecules act as bridging, binucleating, tetradentate ligands and hold the two square-pyramidal metal centres in such a way as to create a large metallocyclic structure, with an unoccupied cavity bounded by the two parallel and eclipsed benzene rings and the MN_4 equatorial planes. **II** has a centre of symmetry at the centre of the cavity. The Co—N distances are essentially equal (ave. 2.006 Å) and compare

TABLE 4. Interatomic distances (Å) and angles (deg) relevant to the cobalt coordination spheres in $[Co_2(BTIM)_2Br_2]Br_2 \cdot 2CHCl_3 \cdot 4MeOH$ (**II**)

Atoms	Distance	Bonds	Angle
Co···Br(1)	2.555(2)	Br(1)—Co—N(1)	99.8(2)
Co···N(1)	2.010(7)	Br(1)—Co—N(3)	98.1(2)
Co···N(3)	2.001(7)	Br(1)—Co—N(5)	99.4(2)
Co···N(5)	2.007(7)	Br(1)—Co—N(7)	97.1(2)
Co···N(7)	2.014(8)	N(1)—Co—N(3)	86.1(3)
		N(1)—Co—N(5)	90.5(3)
		N(1)—Co—N(7)	163.1(3)
		N(3)—Co—N(5)	162.5(3)
		N(3)—Co—N(7)	91.5(3)
		N(5)—Co—N(7)	86.7(3)

closely with those reported for the copper derivatives (2). The equatorial donor atoms N(1), N(3), N(5), N(7) form an almost perfect plane (least-squares plane 1), with the cobalt displaced by 0.301 Å towards the apical bromine. The cobalt bromine distance of 2.555(2) Å compares closely with that found in the analogous copper chloride complex (2.504(3) Å) (2). The two cobalt atoms are separated by 7.599(4) Å and the benzene ring separation is 4.062 Å, thus creating a cavity of similar dimensions to that found in $[Cu_2(BTIM)_2Cl_2]Cl_2 \cdot 7H_2O$ (1, 2). The hydroimidazole rings (least-squares planes *4*, *5*) are twisted relative to the N_4 plane (plane *1*) and the benzene ring (least-squares plane *2*) (Fig. 2; dihedral angles between least-squares planes *1–2*, 90.2°; *1–4*, 69.7°; *2–4*, 133.6°; *1–5*, 68.6°; *2–5*, 135.0°; *4–5*, 77.0°). There are no close contacts between the solvent molecules in the lattice and the complex cation.

The structure of **III** is shown in Fig. 3 and bond lengths and angles relevant to the cobalt coordination spheres are listed in Table 5. The molecule is centrosymmetric, with the center of inversion at the center of the benzene ring of the BTIM ligand. The two cobalt atoms are four coordinate,

Can. J. Chem. Downloaded from www.nrcresearchpress.com by 109.225.110.28 on 09/08/12
For personal use only.

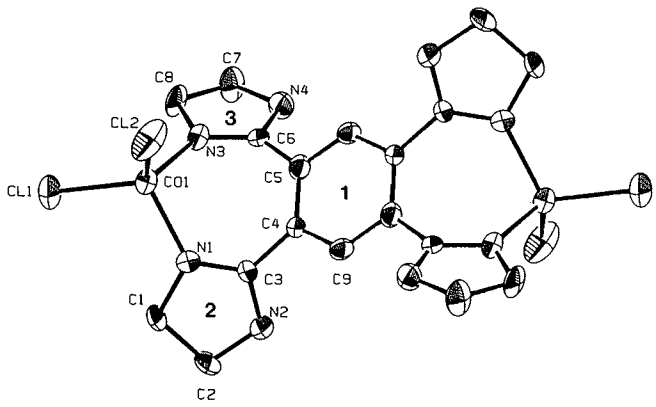

FIG. 3. Molecular structure of $[Co_2(BTIM)Cl_4] \cdot 2DMF$ (**III**).

TABLE 5. Interatomic distances (Å) and angles (deg) relevant to the cobalt coordination spheres in $[Co_2(BTIM)Cl_4] \cdot 2DMF$ (**III**)

Atoms	Distance	Bonds	Angle
Co(1)···Cl(1)	2.252(3)	Cl(1)—Co(1)—Cl(1)	112.6(1)
Co(1)···Cl(2)	2.232(3)	Cl(1)—Co(1)—N(1)	107.0(2)
Co(1)···N(1)	1.999(6)	Cl(1)—Co(1)—N(3)	110.9(2)
Co(1)···N(3)	1.988(6)	Cl(2)—Co(1)—N(1)	116.8(2)
		Cl(2)—Co(1)—N(3)	112.1(2)
		N(1)—Co(1)—N(3)	96.2(2)

bound to two nitrogen atoms and two chlorines on each side of the ligand. Each cobalt centre has a slightly distorted tetrahedral stereochemistry with angles at cobalt ranging from 96.2(2)° (N(3)—Co(1)—N(1)) to 116.8(2)° (Cl(2)—Co(1)—N(1)). The Co—N distances are almost equal (ave. 1.99 Å) and compare closely with those in **II**. The Co—Cl distances (Co(1)—Cl(1) 2.252(3) Å, Co(1)—Cl(2) 2.232(3) Å) are considered normal. The consequences of the 1,2-arrangement of the hydroimidazole rings is to create seven-membered chelate rings, with the result that the hydroimidazole rings themselves are mutually twisted and also twisted relative to the central benzene ring (Fig. 3; dihedral angles between least-squares planes *1–2*, 48.8°; *1–3*, 49.6°; *2–3*, 73.5°). Each half of the structure can be compared with that of the complex $Cu(OBT)Cl_2$, involving the related ligand 2,2′-*o*-phenylenebisbenzothiazole, which has a slightly distorted *cis*-square-planar structure involving very similar Cu—N and Cu—Cl distances (7). The DMF solvent molecule is hydrogen bonded via O(1) to hydrogen atom H(2), attached to the hydroimidazole nitrogen N(4), (N(4)—H(2) 1.067 Å; H(2)—O(1) 1.873 Å; N(4)—O(1) 2.829(9) Å).

Spectroscopy and magnetism

Characteristic infrared absorptions were observed for these complexes, associated with the ligand, in the range 3220–3320 cm^{-1}, due to the hydroimidazole N—H stretch, and in the range 1581–1606 cm^{-1} due to the hydroimidazole CN stretch. In the far infrared metal–nitrogen (hydroimidazole) stretching absorptions were identified in the range 290–310 cm^{-1}. For complexes **I** and **II** single absorptions associated with cobalt–halogen stretch were observed at 307 cm^{-1} (**I**) and 232 cm^{-1} (**II**), while for the 2:1 derivatives **III** and **IV** two clearly defined bands (308, 330 cm^{-1} (**III**); 215, 240 cm^{-1} (**IV**)) are assigned to cobalt–halogen stretch (Cl, Br, respectively) in a local C_{2v} environment. The solid state, mull transmittance, spectra (Table 6) of compounds **I**, **II** are characterized by the presence of two bands in the range 17 000 – 20 000 cm^{-1} and much weaker absorptions in the near infrared, which are assigned to *d–d* transitions in a square-pyramidal cobalt(II) centre. The higher overall absorption energies associated with **I** are consistent with an axially coordinated chlorine ligand. The general infrared and electronic spectral similarities between compounds **I** and **II** suggests a dinuclear metallocyclic structure for **I** similar to **II**. Compounds **III** and **IV** exhibit major solid state absorptions in the visible and near infrared regions, each clearly resolved into three components, and associated with the ν_3 and ν_2 transitions, respectively, in a C_{2v} distorted tetrahedral cobalt(II) centre. The lower energy absorptions in these regions associated with **IV** confirm the presence of coordinated bromine and suggest a structure similar to that in **III**. These spectral bands are typical of pseudo-tetrahedral cobalt(II) complexes with CoN_2X_2 chromophores and the absorption energies compare closely with bands observed for analogous, mononuclear complexes involving the ligands 1,2-bis(4,5-dihydroimidazol-2-yl)benzene(LP) and 1,2-bis(benzothiazol-2-yl)ethane(BBTE), which have very similar donor groups producing equivalent, seven membered chelate rings (8, 9). In DMF solution **III** and **IV** exhibit ν_3 and ν_2 transitions with almost identical absorption energies.

The 2:2 metallocyclic complexes **I**, **II** have high magnetic moments at room temperature (Table 6), typical of square-pyramidal or octahedral cobalt(II) compounds. The lower values observed for the 2:1 dinuclear complexes **III**, **IV** (4.47, 4.71 BM, respectively) are typical of pseudo-tetrahedral cobalt(II) species (10). Variable temperature magnetic studies were carried out on **I–IV** in the temperature range 5–305 K. Reciprocal susceptibility versus temperature plots showed that the Curie–Weiss law was obeyed in all cases over the full temperature range, with very small Weiss constants(θ = 0 to −7K). Such small values clearly do not signal the presence of very significant exchange interactions. For compounds **I** and **II** magnetic moments at 5 K exceeded 5.0 BM and so were not considered to have significant spin coupling between the cobalt(II) centres. The 1:1 metallocyclic, dinuclear copper(II) complexes of BTIM (2), which have the same structure as **II**, are very weakly antiferromagnetically coupled ($-2J < 2$ cm^{-1}), consistent with this observation. As a consequence the variable temperature magnetic data for these compounds were not analysed with respect to an exchange equation. A more pronounced decrease in magnetic moment (μ_{eff}) was observed for **III** and **IV** at low temperatures, and in the case of $[Co_2(BTIM)Br_4]$ (**IV**) the moment goes below the spin only value at about 7 K. The magnetic moment of cobalt(II) with a regular or slightly distorted tetrahedral geometry ($^4A_2$ ground state for T_d) is temperature independent, except at very low temperatures where zero field splitting may lead to some temperature dependence (11). Distinguishing such a situation from one involving very weak antiferromagnetic coupling is clearly difficult.

The magnetic data for **III** and **IV** were fitted to an exchange equation derived from the Van Vleck expression (12) for an isotropic, Heisenberg $S = 3/2,3/2$ pair. Very small negative J values ($-J$ = 0.432(8) cm^{-1} (**III**), $-J$ = 0.635(5) cm^{-1} (**IV**)) were obtained. However, since these J

Can. J. Chem. Downloaded from www.nrcresearchpress.com by 109.225.110.28 on 09/08/12
For personal use only.

TABLE 6. Spectral and magnetic data

Complex	Colour	μ_{eff} (RT) (BM)	Electronic spectra (cm^{-1}) (ε = $dm^3\ mol^{-1}\ cm^{-1}$)
$[Co_2(BTIM)_2Cl_2]Cl_2 \cdot 4H_2O$ (**I**)	Reddish brown	5.57	[7000], 8260, 17700, 18500, [24400][a]
$[Co_2(BTIM)_2Br_2]Br_2 \cdot 2CHCl_3$ (**II**)	Reddish brown	5.63	[6700], 7940, [15400], 17000, 18700, [25600], [28600][a]
$[Co_2(BTIM)Cl_4]$ (**III**)	Blue	4.47	5260, 7250, 10000, 15400, 16800, 18200[a] 15500(705), 16100(945), [17400](703)[b] 10300(53), 7400(194), 6020(75)
$[Co_2(BTIM)Br_4] \cdot 0.5MeOH \cdot 0.5CHCl_3$ (**IV**)	Greenish blue	4.71	5200, 6800, [9300], 14700, 15400, 16300, 24400, 28600[a] 15400(415), 16300(487), 17500(514)[b] 10100(60), 7200(220)

[a]Mull transmittance; [ ] shoulder (Dq = 420 cm^{-1} (**III**), 396 cm^{-1} (**IV**)).
[b]DMF solution.

values are very small and cannot readily be distinguished from zero field splitting effects, little can be said concerning intramolecular exchange in **III** and **IV** other than the fact that it is very weak.

Acknowledgement

We thank the Natural Sciences and Engineering Research Council of Canada for financial support for this study.

1. S. K. Mandal, L. K. Thompson, M. J. Newlands, E. J. Gabe, and F. L. Lee. J. Chem. Soc. Chem. Commun. 744 (1989).
2. S. K. Mandal, L. K. Thompson, M. J. Newlands, E. J. Gabe, and F. L. Lee. Inorg. Chem. **29**, 3556 (1990).
3. A. S. Bailey, B. R. Henn, and J. M. Langdon. Tetrahedron, **19**, 161 (1963).
4. N. Walker and D. Stuart. Acta Crystallogr. Sect. A: Found. Crystallogr. **A39**, 158 (1983).
5. Texsan-Texray Structure Analysis Package, Molecular Structure Corporation (1985), which includes versions of MITHRIL (C. J. Gillmore. J. Appl. Cryst. **17**, 42 (1984)) and DIRDIF (P. T. Beurkens. Crystallography Laboratory, Toernooiveld, 6525Ed Nijmegen, Netherlands).
6. D. T. Cromer and J. T. Weber. International tables for X-ray crystallography. Vol. IV. The Kynoch Press, Birmingham, England. 1974. Table 2.2A.
7. R. G. Ball and J. Trotter. Can. J. Chem. **57**, 1368 (1979).
8. A. B. P. Lever, B. S. Ramaswamy, S. H. Simonsen, and L. K. Thompson. Can. J. Chem. **48**, 3076 (1970).
9. G. C. Wellon, D. V. Bautista, L. K. Thompson, and F. W. Hartstock. Inorg. Chim. Acta, **75**, 271 (1983).
10. B. N. Figgis and R. S. Nyholm. J. Chem. Soc. 12 (1954).
11. C. J. O'Connor. *In* Progress in inorganic chemistry. Vol. 29. *Edited by* S. J. Lippard. John Wiley and Sons, New York. p. 203.
12. J. H. Van Vleck. The theory of electric and magnetic susceptibilities. Oxford University Press, London. 1932.

Can. J. Chem. Downloaded from www.nrcresearchpress.com by 109.225.110.28 on 09/08/12
For personal use only.

Nature and characterization of the singlet and triplet excited states of the dibenzylideneacetone and di-3-(*N*-ethylcarbazoylidene)acetone bridging ligands[1]

PIERRE D. HARVEY[2] AND BENOIT DAOUST

Département de chimie, Université de Sherbrooke, Sherbrooke (Québec), Canada J1K 2R1

Received March 13, 1992

PIERRE D. HARVEY and BENOIT DAOUST. Can. J. Chem. **70**, 2777 (1992).

The lowest energy singlet state in di-3-(*N*-ethylcarbazoylidene)acetone (dNECa), a luminescent model compound at room temperature for dibenzylideneacetone (dba), has been assigned to a charge transfer (CT) state using the medium polarity effect on $\lambda_{max}(F)$ and the fluorescence polarized spectra of dNECa at 77 K. The dNECa fluorescence quantum yields (ϕ_F) and lifetimes (τ_F) are solvent sensitive where both ϕ_F and τ_F tend to increase with polarity. The very weak and moderately structured phosphorences have been located for the first time for both dba and dNECa in the 550–800 nm range and are also assigned to a CT state. In this case the CT interactions are less pronounced than $\lambda_{(0\text{-}0)}P$ and τ_P are much less solvent sensitive. Finally, EHMO type calculations confirm that the CT transition is the lowest energy transition in dba and di-3-(*N*-methylindoylidene)acetone (a model compound for dNECa), but also suggest that the $n\pi^*$ state must lie near the CT state in dba.

PIERRE D. HARVEY et BENOIT DAOUST. Can. J. Chem. **70**, 2777 (1992).

En se basant sur l'effet de polarité du milieu sur le $\lambda_{max}(F)$ et sur les spectres de fluorescence polarisée de la dNECa à 77 K, on a attribué l'état singulet de base énergie de la di-3-(*N*-éthylcarbazoylidène)acétone (dNECa), un composé modèle de la dibenzylidèneacétone (dba) qui est luminescent à la température ambiante, à un état de transfert de charge (TC). Les rendements quantiques (Φ_F) et les temps de vie (τ_F) de la fluorescence de la dNECa dépendent tous les deux du solvant alors que Φ_F et τ_F ont tous les deux tendance à augmenter avec une augmentation de la polarité. Pour la première fois, on a pu localiser les phosphorescences très faibles et relativement bien structurées de la dba et de la dNECa dans la plage allant de 550 à 800 nm et on les a aussi attribuées à un état de TC. Dans ce cas, les interactions de TC sont moins prononcées et il en résulte $\lambda_{(0\text{-}0)}P$ et τ_P sont beaucoup moins sensibles aux effets de solvant. Enfin, des calculs du type orbitales moléculaires de HE confirment que la transition de TC est la transition de plus basse énergie dans la dba et la di-3-(*N*-méthylindoloylidène)acétone (un composé modèle de la dNECa) et suggèrent aussi que, pour la dba, l'état $n\pi^*$ doit se trouver près de l'état de TC.

[Traduit par la rédaction]

Introduction

The dibenzylideneacetone compound (dba) is a remarkable ligand that is particularly easy to synthesize and is capable of stabilizing Pd(0) and Pt(0) metals via coordination with the olefinic groups for preparing either mono- or binuclear species (1–6). In the free state the ligand adopts primarily the *s,cis–s,cis* conformation (7) and appears to be particularly photoreactive (8). Electron transfer and *cis,trans* isomerization reactions have been observed in the lowest-energy singlet (9) and triplet excited states, respectively (8). The luminescing singlet excited state has been assigned to a charge transfer (CT) state from the aryl groups to the ketone (9). There has been no spectroscopic evidence for an $n \rightarrow \pi^*$ transition associated with the presence of the carbonyl group although the molecule is closely related to benzophenone for which the lowest energy $n\pi^*$ singlet and triplet excited states are well known (10).

As mentioned, the dba ligand is photoreactive in solution. In the complexed state, our unreported results on the $M_2(dba)_3$ complexes (M = Pd, Pt) picosecond flash photolysis studies[3] have shown that the photoexcited binuclear complexes are efficiently deactivated, in part, via processes involving the bridging ligand. This investigation has an impact on the ongoing research on binuclear complexes substituted with electroactive pendant groups (11) in our laboratory. We recently showed that the excited state for $Pd_2(dba\text{-}Fc)_3$(dba-Fc = $(C_6H_5)CH{=}CH_2(CO)CH_2{=}CH(C_6H_4)(C_5H_4)Fe(C_5H_5)$) is due to metal-to-ligand charge transfer (MLCT) as in the $M_2(dba)_3$ complexes (M = Pd, Pt) (12), but appears to be ferrocenium localized in the oxidized form $[Pd_2(dba\text{-}Fc)_3]^{3+}$. Since the ferrocene molecule is an efficient deactivating agent for the triplet excited state (13), it became important to further investigate the nature of the dba excited states at this stage.

In this work we wish to report a number of experimental and theoretical results in order to address both singlet and triplet excited states, and the MO picture of the dba ligand. Since dba is not luminescent in solution at 298 K, the closely related model compound di-3-(*N*-ethylcarbazoylidene)acetone (dNECa) will be investigated (see Scheme 1 for structure). The CT fluorescence assignment will be spectroscopically demonstrated by polarity effects and polarization studies using dNECa. Furthermore, the very weak phosphorescences for dba and dNECa will be presented and assigned to a process arising from a CT state. The photophysical characterization of these two molecules is also made. Finally a qualitative MO analysis (via extended Hückel type calculations) will be examined for dba and di-3-(*N*-methylindoylidene)acetone (a model compound for dNECa) confirming the existence of the expected $n \rightarrow \pi^*$ and CT electronic transitions for both *s,cis–s,cis* and *s,cis–s,trans* conformations.

Experimental section

Materials

Dba (14) and dNECa (9) were prepared according to standard procedures. All the solvents: methanol (BDH), acetone (Fisher Scientific Company), acetonitrile (BDH), dimethyl sulfoxide (Fisher Scientific Company), dichloromethane (Fisher Scientific Com-

[1]For part one, see ref. 9.

[2]Author to whom correspondence may be addressed.

[3]S. M. Hubig, M. Drouin, A. Michel, and P. D. Harvey. Inorg. Chem. In press.

Can. J. Chem. Downloaded from www.nrcresearchpress.com by 109.225.110.28 on 09/08/12
For personal use only.

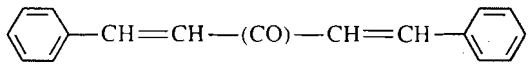

dba = dibenzylideneacetone

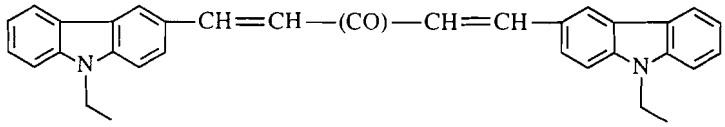

dNECa = di-3-(*N*-ethylcarbazoylidene)acetone

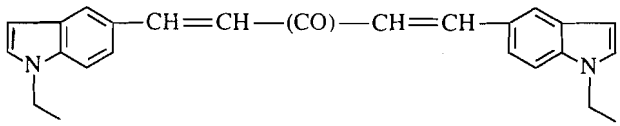

di-3-(*N*-methylindoylidene)acetone

SCHEME 1. Molecular structures of the investigated compounds.

TABLE 1. $\lambda_{max}(F)$ and Φ_F for dNECa at 298 K

Solvent	ε^a	$\lambda_{max}(F)^b$ (±1 nm)	Φ_F (±10%)
Carbon tetrachloride	2.2	476	0.0022
Chloroform	4.8	502	0.073[c]
Ethyl acetate	6.02	495	0.013
Dimethoxethane	7.1	498	0.013
Tetrahydrofuran	7.6	498	0.0046
Dichloromethane	9.0	509	0.090
Pyridine	12.3	505	0.066
Acetone	20.7	515	0.045
N-*N*-Dimethylformamide	38.0	517	0.037
Acetonitrile	38.0	528	0.13
Dimethyl sulfoxide	47.0	525	0.12

[a]The dielectric constants are from ref. 23.
[b]The emission spectra are corrected for the instrument response.
[c]Chloroform can be considered a protic solvent.

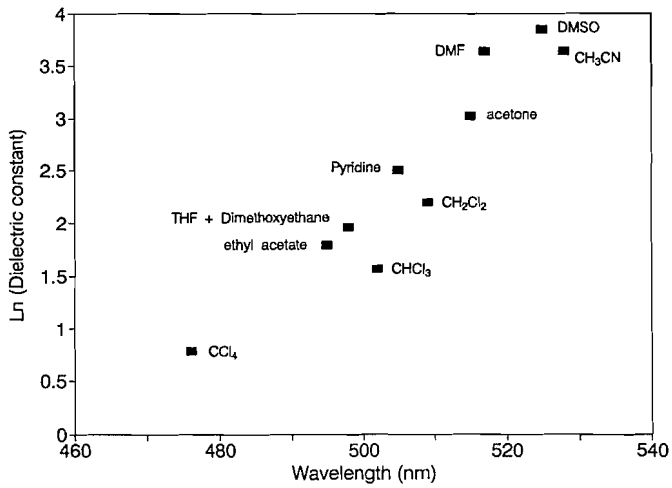

FIG. 1. $\lambda_{max}(F)$ vs. ε (ln scale) for dNECa in various solvents.

pany), dimethylformamide (BDH), chloroform (BDH), tetrahydrofuran (Aldrich Chemical Company), toluene (Mallinckrodt), benzene (Fisher Scientific Company), carbon tetrachloride (BDH), ehtyl acetate (BDH), dimethoxyethane (BDH), pyridine (BDH), butyronitrile (Aldrich Chemical Company), and 2-methyltetrahydrofuran (Aldrich Chemical Company), were purified according to standard procedures (15).

Apparatus

The absorption spectra were acquired on a Hewlett Packard 8452 A diode array spectrophotometer. The emission and excitation spectra were obtained using a Spex Fluorolog II spectrometer. The phosphorescence spectra and lifetime measurements were performed on a Spex 1934D phosphorimeter coupled with the Spex Fluorolog spectrometer. The fluorescence lifetimes were measured with a FL900 single photon counting fluorometer (Edinburgh Inst.) using a nF 900-ns flash-lamp source under the following conditions: electrode gap, 1.0 mm; gas, 0.5 bar of H_2(g) (1 bar = 100 kPa); applied EHT, 7.0 kV; repetition rate, 40 kHz.

Experimental procedures

The Φ_F values were measured using 9,10-diphenylantracene as standard (16). The polarization ratios (*N*) were measured according to literature procedures (see for examples ref. 17).

Computational details

All MO calculations were of the extended Hückel type (EHMO) using a modified version of the Wolfsberg–Helmholz formula (18). The atomic parameters used for C, O, and H are taken from ref. 19. The C—O, C—H, C=C, and C—C distances used for the computations are 1.23, 1.05, 1.31, and 1.46 Å as found crystallographically for the 2,2′-dimethyldibenzylideneacetone derivative in its *s,cis–s,cis* conformation. All angles were taken to be 120°, except for the torsional angle which was taken to be 0°. A detailed description of the graphic programs used in this work can

Can. J. Chem. Downloaded from www.nrcresearchpress.com by 109.225.110.28 on 09/08/12
For personal use only.

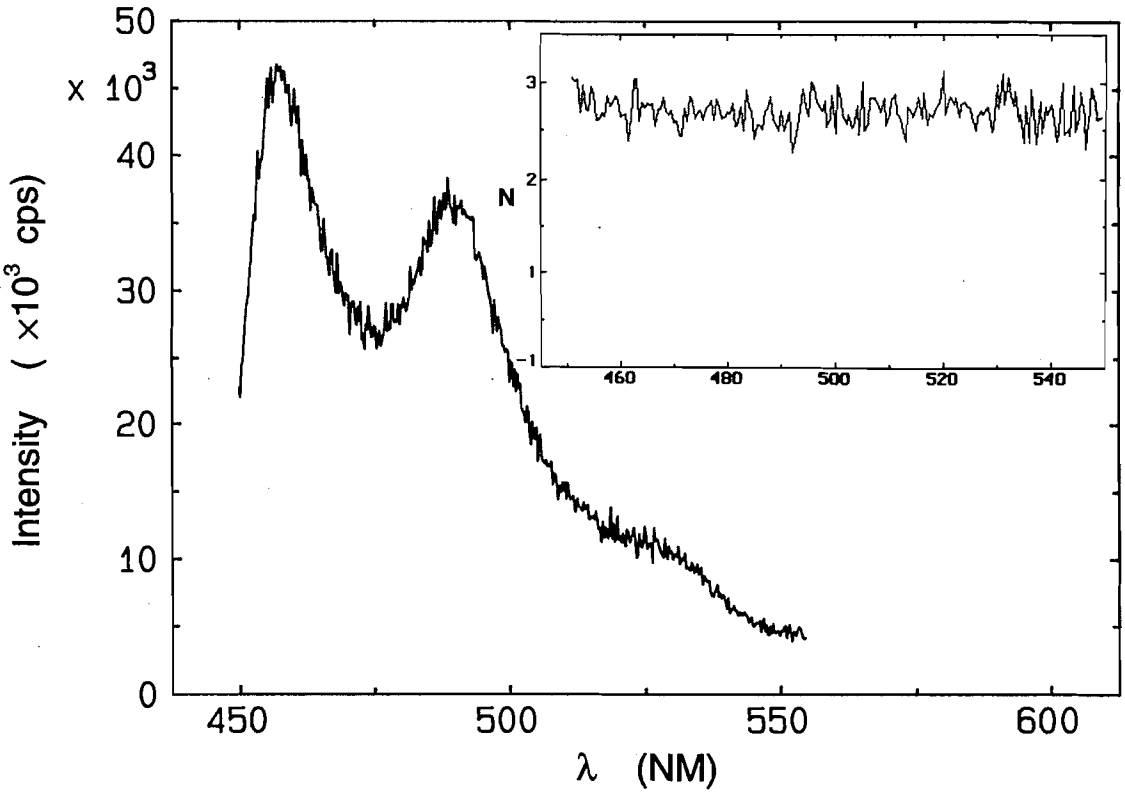

FIG. 2. Fluorescence spectrum of dNECa in 2-MeTHF at 77 K (concentration ~1 × 10^{-6} M). Insert: polarization ratio (N) as a function of λ using λ_{exc} = 447 nm (0-0 of the CT absorption band).

be found in ref. 20. Tables of atomic orbital contributions of the MO 41–45 for dba and 60–65 for di-3-(*N*-methylindoylidene)-acetone are provided as supplementary data.[4] Solution NMR studies proved that dba and dNECa have the *s,cis–s,cis* conformation (8, 9). The di-3-(*N*-methylindoylidene)acetone compound was used as a computational model for dNECa because the EHMO package (20) did not permit calculations for molecules exhibiting large numbers of MO's, and because the MO diagram would become more complicated than necessary for this work.

Results and discussion

1. CT Fluorescence assignment

The dNECa fluorescence appear as structureless symmetric bands that are sensitive to medium polarity. Table 1 lists the λ_{max}(F) values, the solvent dielectric constants (ε), and the Φ_F's for dNECa in various solvents at 298 K. The variation of λ_{max}(F) plotted against ε in the ln scale (Fig. 1) shows a clear increase in λ_{max}(F) (ranging from 476 to 525 nm = ~2070 cm^{-1}) with the medium polarity. For comparison purposes one should examine the spectroscopic data for some related monomeric compounds, particularly for 3-cyano-*N*-ethylcarbazole and 3-carboxyethyl-*N*-ethylcarbazole for which $\pi \rightarrow \pi$ fluorescences have been assigned (21). For the later, 60 and 170 cm^{-1} red shifts of the fluorescence bands for 3-cyano- and 3-carboxyethyl-*N*-ethylcarbazole, respectively, are reported for solvents going from 3-methylpentane to ethanol at 296 K (21). The particularly large polarity effect for dNECa is conclusively indicative of a CT fluorescence, and rules out the $n \rightarrow \pi^*$ emission. This CT assignment should be considered as a $\pi \rightarrow \pi^*$ transition in which a large charge separation is induced in the singlet excited state. The fluorescence quantum yield (Φ_F) also increases with the solvent polarity, but this increase is not as regular. The 77 K spectra are moderately vibrationally structured (Fig. 2) where the 0-0 band is easily recognized. Again the medium polarity induces large shifts in the fluorescence spectra as the 0-0 band shifts from 458 (toluene), to 462 (2-MeTHF), to 488 (butyronitrile), and to 492 nm (ethanol).

The second set of experiments involves the measurement of the polarization ratios (N). The CT assignment for the lowest energy absorption band has been established (9). The variation of the dipole moment should be polarized along the main (z) axis of dNECa in the C_{2v} point group (*s,cis–s,cis* conformation). According to the absorptivity data, ε ~21 000 M^{-1} cm^{-1} (9), this CT transition is allowed, and mixing of non-totally symmetric vibrational modes due to vibronic coupling is very unlikely. Theoretically, a value of N = 3 indicates that the emission is polarized parallel to the dipole moment change involved in the absorption process, while when N = 0.5, the luminescence is polarized perpendicular to the absorption. Figure 2 shows the fluorescence spectrum of dNECa at 77 K along with the polarization. The N values approach 3 all along the spectrum, clearly demonstrating that the emission does rise from the absorbing CT state and that no non-totally symmetric vibrational modes contribute to the intensity of the fluorescence, contrary to the substituted derivatives of carbazole

[4]Supplementary tables of atomic orbital contributions of the MO nos. 41–45 for dba and nos. 60–65 for di-3-(*N*-methyllindoylidene)acetone may be purchased from The Depository of Unpublished Data, Document Delivery, CISTI, National Research Council Canada, Ottawa, Canada K1A 0S2.

Can. J. Chem. Downloaded from www.nrcresearchpress.com by 109.225.110.28 on 09/08/12
For personal use only.

Can. J. Chem. Downloaded from www.nrcresearchpress.com by 109.225.110.28 on 09/08/12
For personal use only.

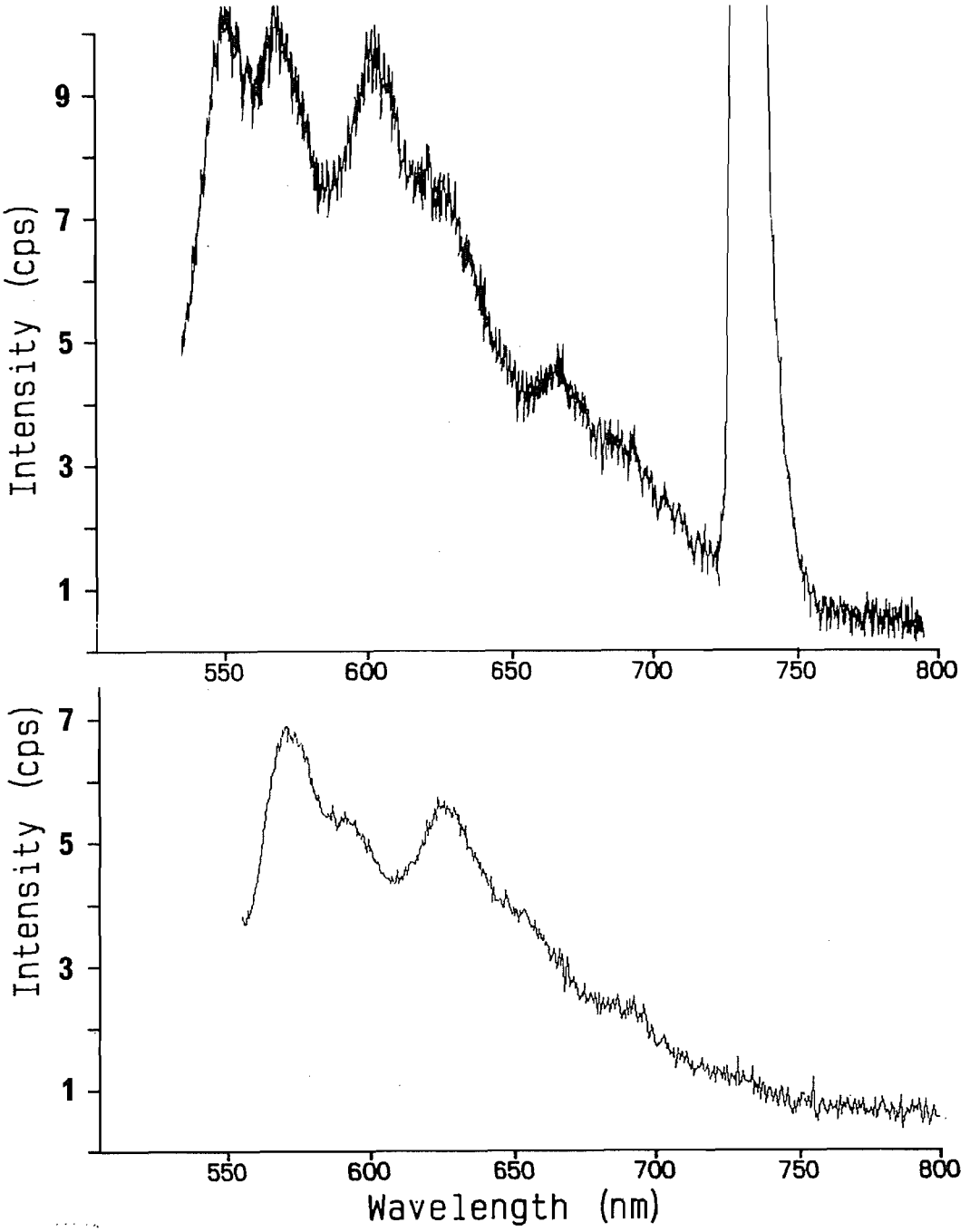

FIG. 3. Top: phosphorescence spectrum of dba in 2-MeTHF at 77 K (concentration $\sim 1 \times 10^{-4}$ M, λ_{exc} = 370 nm using a 450-W Xe lamp). Bottom: phosphorescence spectrum of dNECa in 2-MeTHF at 77 K (concentration $\sim 1 \times 10^{-5}$ M, λ_{exc} = 447 nm (0-0 of the CT absorption band) using a 450-W Xe lamp).

(17). The fact that N does not reach 3.0 (but rather ~2.7) for the 0-0 band is due to depolarization induced by glass imperfection and by solvent-induced depolarization.

The dba molecule could not be investigated as no emission was observed at 298 K and luminescence is very weak at 77 K ($\Phi_F < 0.01$). On the basis of the structural similarities (and the molecular orbital analysis; see the text below), the emissive singlet excited state is undoubtedly a CT state.

2. CT phosphorescence assignment

Very weak and moderately structured phosphorescence spectra were observed for dba and dNECa (Fig. 3) for which both band shapes and positions are very similar. The band positions are reported in Table 2. From the structured phosphorescence bands, two vibrational modes can be depicted, $\Delta\nu$ and $\Delta\nu'$ (Table 2) where the low- and high-frequency modes average ~540 ± 70 and ~670, and 1530 ± 70 and ~1540 cm^{-1} for dba and dNECa, respectively. The high-frequency modes are easily assigned to ν(C═C), not ν(C═O) (ν(C═O) = 1673 and 1694 cm^{-1} for dba and dNECa, respectively (9)). The IR and Raman spectra exhibit strong signals in this range where the closest frequencies are found at 1577 and 1576, and 1575 and 1550, for dba and dNECa,

TABLE 2. Phosphorescence spectra of dba and dNECa

dba				dNECa			
λ (±1 nm)	ν (cm^{-1})	Δν (cm^{-1})	Δν′(cm^{-1})	λ (±1 nm)	ν (cm^{-1})	Δν (cm^{-1})	Δν′ (cm^{-1})
554	18050 ± 35	540 ± 65	1520 ± 65	572	17480 ± 30	620 ± 60	1500 ± 60
571	17510 ± 30			593	16860 ± 30		
605	16530 ± 30	530 ± 60		626	15980 ± 30	690 ± 60	
625	16000 ± 30		1540 ± 60	654	15290 ± 30		~1580
667	14990 ± 30	560 ± 60		~695	~14400	~700	
693	14430 ± 30			~730	~13700		

TABLE 3. Fluorescence photophysical parameters for dNECa in various solvents at 298 K

Solvents	τ_F (ns)	χ^2	k_F (10^8 s^{-1})[a]	k_{nr} (10^8 s^{-1})[b]
Dichloromethane	0.27 ± 0.07	1.30	3.3 ± 1.2	33 ± 12
Acetone	0.33 ± 0.02	1.34	1.4 ± 0.2	29 ± 5
N,*N*-Dimethylformamide	0.31 ± 0.07	1.35	1.2 ± 0.4	31 ± 10
Acetonitrile	0.51 ± 0.04	0.93	2.5 ± 0.5	17 ± 3
Dimethyl sulfoxide	0.44 ± 0.04	1.38	2.7 ± 0.5	20 ± 4
Ethanol	1.34 ± 0.03	1.25	5.2 ± 0.6	2.2 ± 0.3
Methanol	0.215 ± 0.006 1.18 ± 0.03	1.20[c]	—	—

[a] $k_F = \Phi_F/\tau_F$; Φ_F ± 10%.
[b] $k_{nr} = (1 - \Phi_F)/\tau_F$; Φ_F ± 10%.
[c] Biexponential curve fitting with the short lifetime component intensity of 37.1% and the long one of 62.9%.

TABLE 4. Some spectroscopic and photophysical data for the 77 K dNECa fluorescence

Solvent	ε	λ_{0-0}(F)	λ_{0-1}(F)	Φ_F	τ (ns)	I[a′]	χ^2
Ethanol	24.3	492	530	0.19	0.17 1.35	90% 10%	1.31
Butyronitrile	22.23	488	525	0.065	—		
2-Methyltetrahydrofuran	7.6[b]	462	496	0.080	0.46 3.51	70% 30%	1.20
Toulene	2.4	458	485	—[c]	—		

[a] The relative intensity has been normalized.
[b] Dielectric constant for tetrahydrofuran.
[c] Φ_F not measured but qualitatively Φ_F (toulene) << Φ (butyronitrile).

respectively (9). The lower-frequency mode could be associated to ring deformation coupled with ν(C=C). No polarization measurement was attempted due to the weakness of the phosphorescence.

The 77 K phophorescence spectra do not appear to be especially sensitive to solvent polarity as a moderate 6-nm red shift is observed for dNECa going from toluene (570), to 2-methyltetrahydrofuran (574), to butyronitrile (576), and to ethanol (575 nm). The possibility of an $n \rightarrow \pi^*$ triplet excited state is also ruled out, and a CT assignment is preferred. The rather small red shift in the phosphorescence spectra in the polarity implies that this CT interaction is somewhat less extensive than that of the singlet excited state. The triplet state appears to possess significant $\pi\pi^*$ character, which is consistent with the *cis–trans* photoinduced isomerization in dba (8).

3. *Photophysical characterization*

As was the case for Φ_F (Table 1), the 298K τ_F values for dNECa in aprotic solvents vary with the medium polarity. The τ_F values are rather short as they range from 0.27 ± 0.07 to 0.51 ± 0.04 ns. Since the measurements are near the limit of the instrument, large uncertainties are induced. The radiative rate constants for fluorescence, $k_F(\Phi_F/\tau_F)$, and the non-radiative rate constants, k_{nr} ($(1 - \Phi_F)/\tau_F$), are listed in Table 3. Considering the experimental uncertainties, both k_F and k_{nr} are only weakly solvent dependent. The k_F values (ranging from (1.2 ± 0.4) × 10^8 to (3.3 ± 1.2) × 10^8 s^{-1}) compare reasonably with the theoretical value reported pre-

Can. J. Chem. Downloaded from www.nrcresearchpress.com by 109.225.110.28 on 09/08/12
For personal use only.

TABLE 5. Some spectroscopic and photophysical data for the 77 K dNECa phosphorescence

Solvent	ε	λ_{0-0}(P) (±1 nm)	τ_P (μs)
Ethanol	24.3	575	23.0 ± 0.3
Butyronitrile	22.23	576	24.1 ± 0.2
2-Methyltetrahydrofuran	7.6[a]	574	22.5 ± 0.3
Toluene	2.4	570	24.8 ± 0.3

[a]Dielectric constant for tetrahydrofuran.

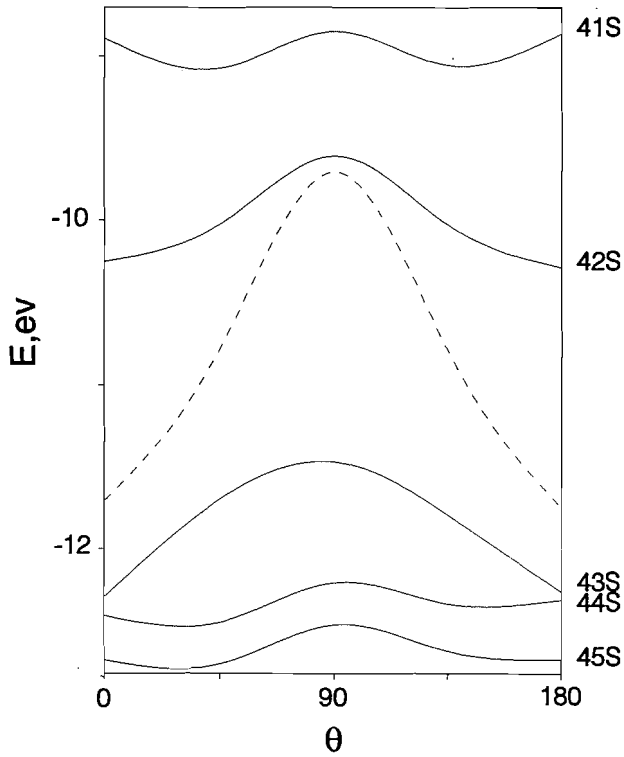

FIG. 4. Walsh diagram for the *s,cis–s,trans* (0°) → *s,cis–s,cis* (180°) conversion of dba around one of the (CO)—(C=C) bonds. MO no. 43 is the HOMO. The broken line is the total energy (1 div = 3 eV on this scale).

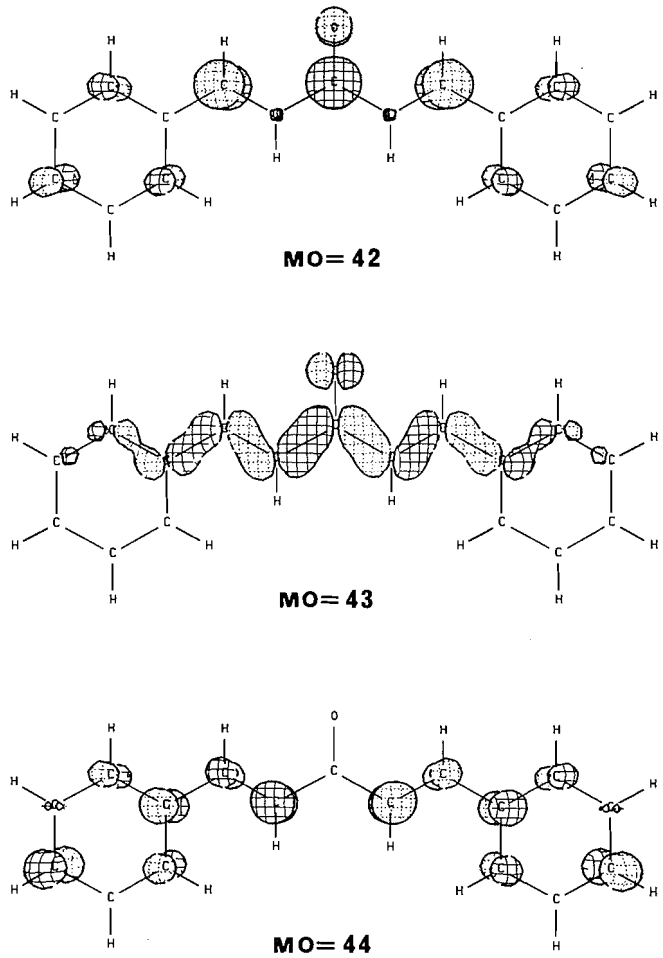

FIG. 5. MO diagram of the LUMO (no. 42), HOMO (no. 43), and HOMO-1 (no. 44) of *s,cis–s,cis* dba.

viously (3.9×10^8 s^{-1}) (9). At 77 K, both Φ_F and τ_F are also solvent dependent (Table 4) with the complication that the fluorescence decays exhibit biexponential kinetics. These biexponential kinetics were previously observed (9, 22) and tentatively interpreted in terms of *s,cis–s,cis* and *s,cis–s,trans* conformers (9). These conformers are in equilibrium, depending on both temperature and solvent (in the ground state) (6). The *s,cis–s,cis* form is the predominant form although a minor and non-negligible concentration of the second conformer exists (7). In this work no temperature dependence of the photophysical parameters is observed because one form is dominant over a very large temperature range. The dNECa phophorescence lifetimes (77 K; Table 5) are (like the $\lambda_{(0-0)}$P values) essentially solvent insensitive (and vary from 22.5 ± 0.3 to 24.8 ± 0.3 μs). The dba lifetime is similar but harder to measure; τ_p is 20 ± 2 μs in the same 77 K glasses. Interestingly, the low-energy triplet excited states in the diarylideneacetone compounds are not very sensitive to the meedium and do not appear to be strongly influenced by the nature of the aryl groups either.

4. MO Analysis

Assuming that the bond distances remain constant, a Walsh diagram is computed for dba undergoing the *s,cis–s,cis* (C_{2v}) ↔ *s,cis–s,trans* (C_s) conversion, via a rotation from 0° to 180° around one of the (CO)—(C=C) bonds (Fig. 4). In this graph the total energy (---) is plotted where a ~6.1 eV barrier to rotation is calculated with a maximum at θ = 90°. The *s,cis–s,cis* form is more stable (by only a few milli-electron volts), in agreement with previous observations (7). More importantly, the MO atomic contributions were also computed for both forms (Figs. 5 and 6). The LUMO's (no. 42; b_2 symmetry in the C_{2v} point group) have essentially the same atomic contributions and are delocalized π systems involving the C=O group. One other feature is that C_α and C_γ make little or no contribution to the MO. The MO contributions for the HOMO's and HOMO-1's (nos. 43 and 44, b_1 and a_2 symmetry in the C_{2v} point group, respectively) are inverted in the two conformers. This inversion does not appear as an MO crossing in the Walsh diagram, but rather appears as a gradual conversion from one set of atomic contributions to the other under the rotation. In the *s,cis–s,cis* form, the HOMO (no. 43) exhibits atomic contributions involving C—C σ-bonding and the nonbonding *p* orbital of the

Can. J. Chem. Downloaded from www.nrcresearchpress.com by 109.225.110.28 on 09/08/12
For personal use only.

Can. J. Chem. Downloaded from www.nrcresearchpress.com by 109.225.110.28 on 09/08/12
For personal use only.

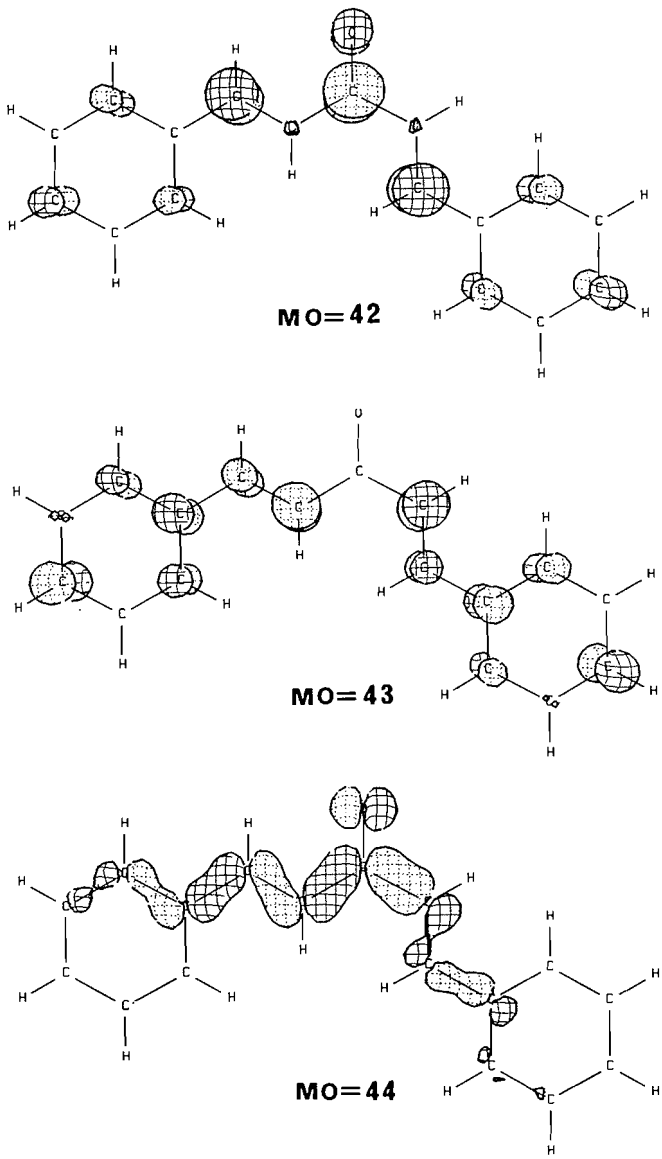

FIG. 6. MO diagram of the LUMO (no. 42), HOMO (no. 43), and HOMO-1 (no. 44) of *s,cis–s,trans* dba.

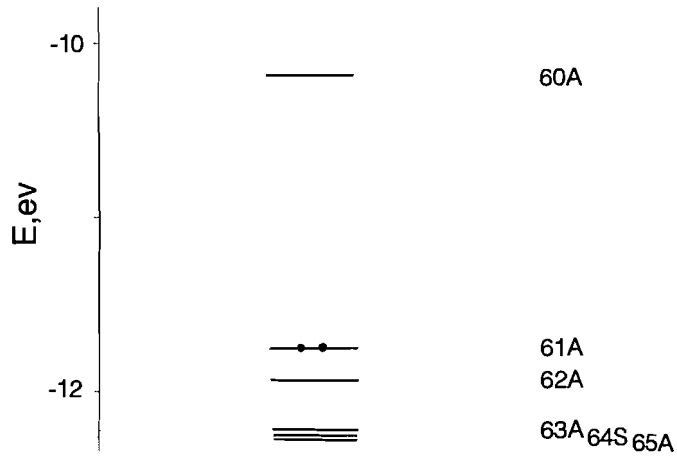

FIG. 7. Energy diagram for *s,cis–s,cis*-di-3-(*N*-methylindoylidene)acetone showing MO nos. 60 (LUMO) – 65. The atomic contributions for MO nos. 60–65 are provided as supplementary material (see footnote 3).

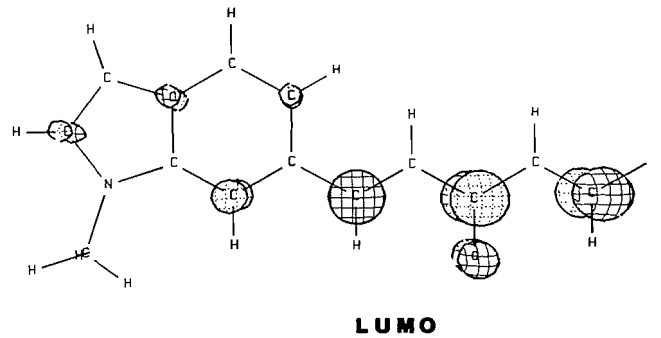

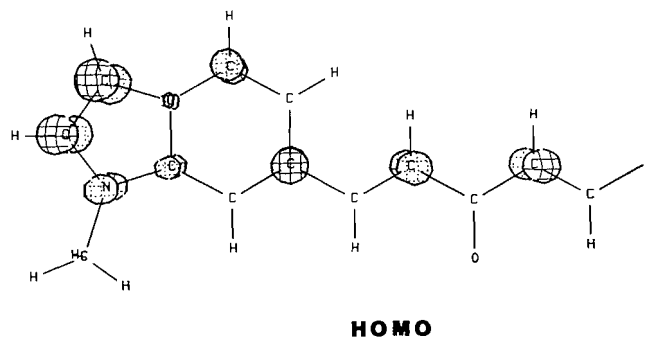

FIG. 8. MO diagram of the LUMO and HOMO for di-3-(*N*-methylindoylidene)acetone. The molecule is not shown completely since the LUMO exhibits a perpendicular miror plane at the C—O while the HOMO possess a C_2 axis along the C—O bond as is the case for dba.

O-atom, while the HOMO-1 is a π-delocalized system with no C=O contribution.

In the *s,cis–s,cis* form, the two lowest-energy transitions (HOMO → LUMO and HOMO-1 → LUMO; $^1A_1 \rightarrow {}^{1,3}A_2$ and $^1A_1 \rightarrow {}^{1,3}B_1$) are essentially the unobserved and orbitally forbidden $n \rightarrow \pi^*$ and a $\pi \rightarrow \pi^*$ type transition, respectively. In the latter case, the transition is polarized along the long axis of the molecule and induces a shift of the electronic density from the C_α-C_β-C_γ's to the C=O group and the C_β atoms that is indicative of a CT transition (from the ring to the C=O group), in agreement with our experimental observation. In the *s,cis–s,cis* form, the computed energy gap between the two MO's (nos. 43 and 44) is very small (0.047 eV) and is only indicative that they are close in energy.

To confirm that the luminescent dNECa is an appropriate model for dba, the *s,cis–s,cis* di-3-(*N*-methylindoylidene)-acetone compound (also C_{2v} point group; Fig. 7) is analyzed. The MO diagram (Fig. 7) exhibits a smaller LUMO (no. 60; b_1)–HOMO (no. 61; a_2) gap as expected, and the atomic contributions (Fig. 8) are very similar to the corresponding MO nos. 42 and 44 in *s,cis–s,cis* dba (Fig. 5). The two key features in this analysis are that the CT interaction during the lowest-energy electronic transition appears more

pronounced than in the dba case, and the energy gap between the HOMO and the MO corresponding to MO no. 43 in *s,cis–s,cis* dba (C—C σ-bonding + O nonbonding; no. 64 in this case) is now much greater (0.505 eV). The first result is perfectly consistent with the very large medium polarity effect on $\lambda_{max}(F)$ for dNECa, which appears not to be due to the presence of the heteroatom, but rather to extended π-delocalization. The second result implies that the $n\pi^*$-type excited states should definitely lie above the CT states in this case, as confirmed by the polarization experiments on dNECa.

Concluding remarks

While the lowest energy singlet excited state in dba is a CT state in nature, the triplet excited state possesses significant $\pi \rightarrow \pi^*$ character. These results are consistent with the photoinduced electron transfer and the typical *cis,trans*-isomerization reactivities of the dba singlet and triplet excited state, respectively. Since the τ_F and τ_P values are particularly short, excited state deactivation in their corresponding $M_2(dba)_3$ complexes (M = Pd, Pt) can be promoted if the process involve these (intraligand) states. Picosecond flash photolysis investigations on the $M_2(dba)_3$ (M = Pd, Pt) and $Pd_2(dba\text{-}Fc)_3$ complexes are in progress.

Acknowledgements

This research was supported by grants from the Natural Sciences and Engineering Research Council (NSERC) (Canada), Fonds pour la formation de chercheurs et l'aide à la recherche (FCAR) (Québec), and The Université de Sherbrooke (Bureau de la recherche).

1. Y. Takahashi, T. Ito, and Y. Ishii. J. Chem. Soc. Chem. Commun. 1065 (1970).
2. K. Moseley and P. M. Maitlis. J. Chem. Soc. Chem. Commun. 982 (1971).
3. M. C. Mazza and C. G. Pierpont. J. Chem. Soc. Chem. Commun. 207 (1973).
4. T. Ukai, H. Kawazura, Y. Ishii, J. J. Bonnet, and J. A. Ibers. J. Organomet. Chem. **65**, 253 (1974).
5. H. Tanaka and H. Kawazura. Bull. Chem. Soc. Jpn. **52**, 2815 (1979).
6. H. Tanaka and H. Kawazura. Bull. Chem. Soc. Jpn. **53**, 1743 (1980).
7. H. Tanaka, K.-I. Yamada, and H. Kawazura. J. Chem. Soc. Perkin Trans. 2, 231 (1978).
8. P. D. Harvey, C. Aubry, L. Gan, and M. Drouin. J. Photochem. Photobiol. A: Chem. **57**, 465 (1991).
9. P. D. Harvey, L. Gan, and C. Aubry. Can. J. Chem. **68**, 2278 (1990).
10. N. J. Turro. Modern molecular photochemistry. Benjamin/Cummings, London. 1978.
11. P. D. Harvey and J. G. Sharma. Can. J. Chem. **68**, 223 (1990).
12. P. D. Harvey and L. Gan. Inorg. Chem. **30**, 3239 (1991).
13. G. L. Geoffroy and M. S. Wrighton. Organometallic photochemistry. Academic Press, New York. 1979.
14. C. R. Conrad and M. A. Dolliver. Org. Synth. Collect. Vol. **2**, 167 (1943).
15. (*a*) D. D. Perrin, W. L. F. Armarego, and D. R. Perrin. Purifications of laboratory chemicals. Pergamon, Oxford. 1966; (*b*) A. J. Gordon and R. A. Ford. The chemist's companion, a handbook of practical data, techniques, and references. Wiley, New York. 1972. p. 436.
16. E. C. Lim, J. D. Laposa, and J. M. H. Yu. J. Mol. Spectrosc. **19**, 412 (1966), and references therein.
17. (*a*) B. Zelent, P. D. Harvey, and G. Durocher. Can. J. Spectrosc. **29**, 23 (1984); (*b*) Can. J. Spectrosc. **28**, 188 (1983); (*c*) P. D. Harvey, B. Zelent, and G. Durocher. Spectrosc. Int. J. **2**, 128 (1983).
18. J. H. Ammeter, H. B. Burgi, J. C. Thibeault, and R. Hoffmann, J. Am. Chem. Soc. **100**, 3686 (1978).
19. (*a*) R. Hoffmann and W. N. Lipscomb. J. Chem. Phys. **36**, 2179 (1962); (*b*) J. Chem. Phys. **37**, 2872 (1962); (*c*) R. Hoffmann. J. Chem. Phys. **39**, 1397 (1963).
20. C. Mealli and D. M. Prosperio. J. Chem. Educ. **67**, 399 (1990).
21. P. D. Harvey and G. Durocher. J. Lumin. **33**, 175 (1985).
22. J. Teply and J. Bursik. J. Radioanal. Nucl. Chem. **101**, 369 (1986).
23. R. C. Weast and J. Astle (*Editors*). CRC handbook of chemistry and physics. 60th ed. CRC Press, Boca Raton, Fla. 1973. pp. E56–58.

Can. J. Chem. Downloaded from www.nrcresearchpress.com by 109.225.110.28 on 09/08/12
For personal use only.

Kinetics and mechanism of oxidation of nickel(II) tetraazamacrocycles by the peroxydisulphate anion in aqueous and binary aqueous mixtures

ROBERT I. HAINES[1] AND SANDRA J. NORTHCOTT

Chemistry Department, Sir Wilfred Grenfell College, Memorial University of Newfoundland, Corner Brook, Nfld., Canada A2H 6P9

Received February 6, 1992

ROBERT I. HAINES and SANDRA J. NORTHCOTT. Can. J. Chem. **70**, 2785 (1992).

The kinetics of oxidation of several nickel(II) tetraazamacrocycles by the peroxydisulphate anion have been studied in water and in binary aqueous mixtures. The reactions proceed via an ion-pairing pre-equilibrium, followed by metal ion-assisted peroxy-bond fissure within the ion-pair solvent shell. The derived rate law is

$$\text{rate} = \frac{2k_4k_{ip}[S_2O_8^{2-}]\,[Ni(II)L]_{tot}}{1 + K_{ip}[S_2O_8^{2-}]}$$

Ion-pairing constants have been determined and have been found to be little influenced by steric factors, but do depend on solvent composition. Rate constants have been extracted using the rate expression and activation energies have been estimated from temperature dependences.

ROBERT I. HAINES et SANDRA J. NORTHCOTT. Can. J. Chem. **70**, 2785 (1992).

Opérant en milieux dans l'eau et dans des mélanges binaires aqueux, on a étudié la cinétique de l'oxydation, par l'anion peroxydisulfate, de plusieurs complexes de tétraazamacrocycles avec le nickel(II). Les réactions se produisent par le biais d'un pré-équilibre de paires d'ions, suivis d'un bris de la liaison peroxy assisté par l'ion métallique, à l'intérieur de la couche de solvant de la paire d'ions. La loi de vitesse qui en dérive est

$$\text{rate} = \frac{2k_4K_{ip}[S_2O_8^{2-}]\,[Ni(II)L]_{tot}}{1 + K_{ip}[S_2O_8^{2-}]}$$

On a déterminé les constantes de formation des paires d'ions et on a trouvé qu'elles ne sont pratiquement pas influencées par des facteurs stériques; elles dépendent toutefois de la composition du solvant. On a extrait les constantes de vitesse en utilisant une expression de vitesse et on a évalué les énergies d'activation à partir des dépendances sur la température.

[Traduit par la rédaction]

Introduction

There have been many kinetic studies of oxidations by the peroxydisulphate anion, $S_2O_8^{2-}$ (1). Although $S_2O_8^{2-}$ is a very strong two-electron oxidant (E^0 = 2.2 V vs SHE), its redox reactions are usually slow. This is because the rate-determining step is thermal dissociation of the peroxy anion into SO_4^- radicals. Examples include the oxidation of thallium(I) (2), manganese(II) (3), and cerium(III) (4). The SO_4^- radical is known to be a very electrophilic species that can undergo H-atom abstractions (5) and addition reactions (6) and acts as an efficient one-electron oxidant with many substrates (7). Peroxydisulphate oxidations are, however, catalyzed by the presence of silver(I) ions (1, 3, 8), where a silver(I)-peroxydisulphate complex is postulated. The reduction of $S_2O_8^{2-}$ by a disilver(I) porphyrin complex (9) was found to be first order in both reactants. The porphyrin complex was labile and catalytic decomposition of the oxidant by free Ag(I) was suggested. Reaction of $S_2O_8^{2-}$ with Ag^+ alone is thought to proceed by a chain mechanism involving Ag^{2+}, AgO^+, SO_4^-, and OH^- intermediates, with the production of molecular oxygen (10). Intramolecular electron-transfer-assisted decomposition of peroxydisulphate has been found for a binuclear iron/ruthenium system (11).

As an oxidant, the peroxydisulphate anion has been used to prepare aqueous solutions of nickel(III) polyazamacrocycles (12), but no mechanistic studies of these reactions have been published to date. Xu and McAuley have used $S_2O_8^{2-}$ preparatively to oxidize macrobicyclic nickel(II) complexes, but found the kinetics intractible due to side reactions of the SO_4^- radicals (A. McAuley, personal communication).

In this paper, the kinetics of oxidation of nickel(II) tetraazamacrocycles, $[Ni(II)L]^{2+}$, by $S_2O_8^{2-}$ in aqueous and binary aqueous mixtures are examined. The ligands L_1–L_3 used in this work are described structurally in the schematic.

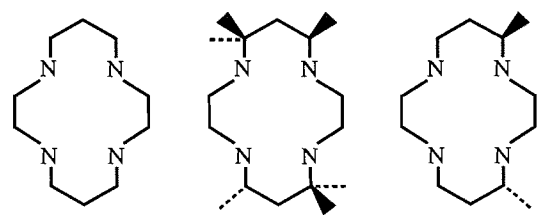

L_1 L_2 L_3

The mechanism of the reaction is described and the effects of added cosolvent are discussed in relation to solvent studies in other inorganic reaction mechanisms.

Experimental

Materials

The ligand L_1 (1,4,8,11-tetraazacyclotetradecane, 'cyclam') was used as received (Aldrich). L_2 (*meso*-5,7,7,12,14,14-hexamethyl 1,4,8,11-tetraazacyclotetradecane) and L_3 (2,3-dimethyl 1,4,8,11-tetraazacyclotetradecane) were synthesized according to the literature (13).

[1]Author to whom correspondence may be addressed.

Can. J. Chem. Downloaded from www.nrcresearchpress.com by 109.225.110.28 on 09/08/12
For personal use only.

TABLE 1. Observed first-order rate constants, k_{obs} (s^{-1}), for the oxidation of nickel(II)

$[S_2O_8^{2-}]$ (mol dm^{-3})	Complex = $[Ni(II)L_1]^{2+}$ 10^2 k_{obs} (s^{-1})			$[S_2O_8^{2-}]$ (mol dm^{-3})	Complex = 10^2 k_{obs}	
	T = 283.2 K	T = 293.2 K	T = 298.0 K		T = 285.3 K	T = 293.7 K
0.00250		1.23 ± 0.01	3.63 ± 0.02	0.00500	0.0281 ± 0.0004	0.0470 ± 0.0006
0.00500	1.33 ± 0.01	2.34 ± 0.01	6.67 ± 0.03	0.0100		
0.0100	2.50 ± 0.01	4.32 ± 0.02	11.4 ± 0.1	0.0150	0.0731 ± 0.0010	0.112 ± 0.0003
0.0150	3.60 ± 0.02	5.79 ± 0.02	14.5 ± 0.1	0.0200		
0.0200	4.54 ± 0.03	7.54 ± 0.03	15.4 ± 0.1	0.0250	0.0949 ± 0.0012	0.152 ± 0.0003
0.0250	5.01 ± 0.03		19.5 ± 0.2	0.0300	0.105 ± 0.0003	0.180 ± 0.0004
0.0300	5.37 ± 0.02	10.1 ± 0.1	23.0 ± 0.2	0.0350		
0.0350			25.4 ± 0.1	0.0400		
0.0400		11.8 ± 0.1	28.0 ± 0.2	0.0450		
0.0450			29.0 ± 0.1	0.0500		
0.0500		13.2 ± 0.1	30.6 ± 0.2			

The nickel(II) complexes were prepared as the perchlorate salts by standard literature methods (13) and recrystallized from water prior to use. AnalaR grade potassium peroxydisulphate (BDH) was first washed several times with distilled water, then recrystallized four times from cold water, rinsed with ice-water, and dried over P_4O_{10} *in vacuo*. This procedure was found necessary to obtain reproducible, clean kinetics. Lithium perchlorate was prepared by neutralization of perchloric acid with lithium carbonate and was thrice recrystallized from water. All other reagents and solvents were of AnalaR grade and were used without further purification. All solutions were prepared using double-distilled, deionized water.

Kinetics

Kinetics were performed under pseudo-first-order conditions, using an excess of peroxydisulphate. The concentration of the nickel(II) complexes used in all experiments was 5.00×10^{-6} mol dm^{-3}. Absorbance changes with time were measured using 1 cm path length quartz cells in the thermostatted cell compartment of a Beckman DU-65 recording spectrophotometer. Data were collected using Beckman Datacapture software on a Wise AT-compatible microcomputer. First-order rate constants, k_{obs}, were calculated from the slopes of linear regression plots of $\ln(A_\infty - A_t)$ versus time. Reported values of k_{obs} are the means of at least three measurements. For any given set of conditions, repetitive measurements gave observed rate-constant values invariant within 1%.

A constant perchloric acid concentration of 0.0100 mol dm^{-3} was maintained to help stabilize the nickel(III) products. The stabilization of nickel(III) complexes in acidic media, as well as in the presence of coordinating ligands, is well known from kinetic studies (12, 14). Decomposition of the tervalent species at low acidity has been attributed to intramolecular electron transfer involving nickel(II)-ligand radical species. Ionic strength was kept constant at 0.300 mol dm^{-3} for all kinetic runs, using lithium perchlorate. Absorbance measurements were made at wavelengths chosen between 370 and 400 nm, to avoid interference by some of the co-solvents.

Results

Stoichiometric titration of the nickel(II) L_2 complex with $S_2O_8^{2-}$ in aqueous solution gave a ratio of 2.02 ± 0.05 : 1. The same stoichiometry was found for the reaction in the binary aqueous solvent mixtures used. The UV/visible spectrum of the product corresponded to the monosulphatonickel(III) species, $[Ni(III)L_2(SO_4)]^+$ (15). In aqueous solution, a clean isosbestic point was observed at 256 nm, indicating no observable intermediates. Furthermore, the product precipitated on addition of an aqueous solution of $NaBPh_4$. No precipitate was formed on addition of Ph_4AsCl to the product solution. These observations indicate the Ni(III) species to be cationic and the overall reaction may be described as

$$[1] \quad 2[Ni(II)L]^{2+} + S_2O_8^{2-} \rightarrow 2[Ni(III)L(SO_4)]^+$$

Excellent first-order kinetics were observed over at least five half-lives for the appearance of the nickel(III) products, in all solvents studied. This is remarkable in light of the well-known deviations from first-order behaviour in oxidations by peroxydisulphate that arise from reactions of SO_4^- radicals generated during the reaction (16). Thus the rate law

$$[2] \quad \text{rate} = +\frac{1}{2}\frac{d[Ni(III)L]}{dt} = k_{obs}[Ni(II)L]$$

is obeyed.

Table 1 lists the observed first-order rate constants for oxidation of the three nickel(II) complexes studied, in water as a function of temperature and $S_2O_8^{2-}$ concentration. Oxidation of $[Ni(II)L_2]^{2+}$ was much slower than that of the L_1 and L_3 complexes, as expected from the difference in electrode potentials for the nickel(II/III) complex couples (+0.67, +0.87, and +0.68 V (versus $Ag/AgNO_3$ (0.1 M) in acetonitrile) for the L_1, L_2, and L_3 complexes respectively) (17). Rates were independent of acid between pH 4 and 2, indicating no protonation of the oxidant in this range. This observation is consistent with the known lack of hydrogen-ion dependence in the oxidation of iron(II) by $S_2O_8^{2-}$ up to an acid concentration of 0.010 mol dm^{-3} (18). The addition of a radical scavenger, allyl acetate (19), caused no change in rates, within experimental error. This suggests that the rate-determining step does not likely involve the SO_4^- species.

Figure 1 shows the dependence of k_{obs} on $S_2O_8^{2-}$ concentration for the L_2 complex at several temperatures. The marked curvature in the plots (found for all systems studied) suggests an equilibrium pre-association of the ionic reactants prior to a rate-determining electron transfer. The general pattern bears resemblance to the classic Eigen–Wilkins (I_D) mechanism (20). A simplified mechanism (ignoring, for the moment, interchange between possible inner-sphere solvent at the nickel(II) complex and peroxydisulphate) may be described schematically as

Can. J. Chem. Downloaded from www.nrcresearchpress.com by 109.225.110.28 on 09/08/12
For personal use only.

macrocycles as a function of $[S_2O_8^{2-}]$ and temperature (ionic strength 0.30 mol dm^{-3})

$[Ni(II)L_2]^{2+}$ (s^{-1})			$[S_2O_8^{2-}]$ (mol dm^{-3})	Complex = $[Ni(II)L_3]^{2+}$ $10^2 k_{obs}$ (s^{-1})			
T = 298.0 K	T = 304.0 K	T = 308.0 K		T = 283.2 K	T = 293.2 K	T = 298.2 K	T = 303.2 K
0.0714 ± 0.0011	0.110 ± 0.003	0.137 ± 0.003	0.00500	0.514 ± 0.007	0.944 ± 0.010	1.56 ± 0.02	1.92 ± 0.02
0.125 ± 0.002		0.266 ± 0.005	0.0100	0.887 ± 0.022			
0.195 ± 0.002	0.272 ± 0.004	0.352 ± 0.006	0.0150	1.42 ± 0.02	2.50 ± 0.04	3.62 ± 0.04	5.06 ± 0.06
0.235 ± 0.005	0.381 ± 0.005	0.454 ± 0.006	0.0250	1.85 ± 0.03	3.48 ± 0.05	5.52 ± 0.07	6.79 ± 0.05
0.276 ± 0.005		0.573 ± 0.012	0.0300		4.01 ± 0.09	6.38 ± 0.13	8.08 ± 0.10
0.280 ± 0.004	0.441 ± 0.006		0.0350		4.89 ± 0.09	6.90 ± 0.08	
0.326 ± 0.005	0.485 ± 0.011		0.0400				9.01 ± 0.07
0.345 ± 0.003							
0.352 ± 0.005							
0.375 ± 0.007							

Can. J. Chem. Downloaded from www.nrcresearchpress.com by 109.225.110.28 on 09/08/12
For personal use only.

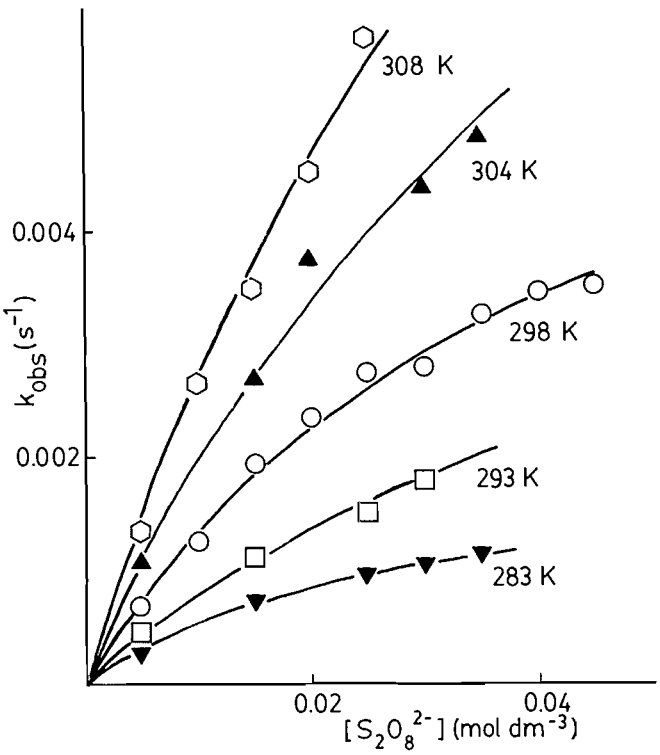

FIG. 1. Dependence of observed first-order rate constants on peroxydisulphate concentration for oxidation of the $[Ni(II)L_2]^{2+}$ cation at various temperatures.

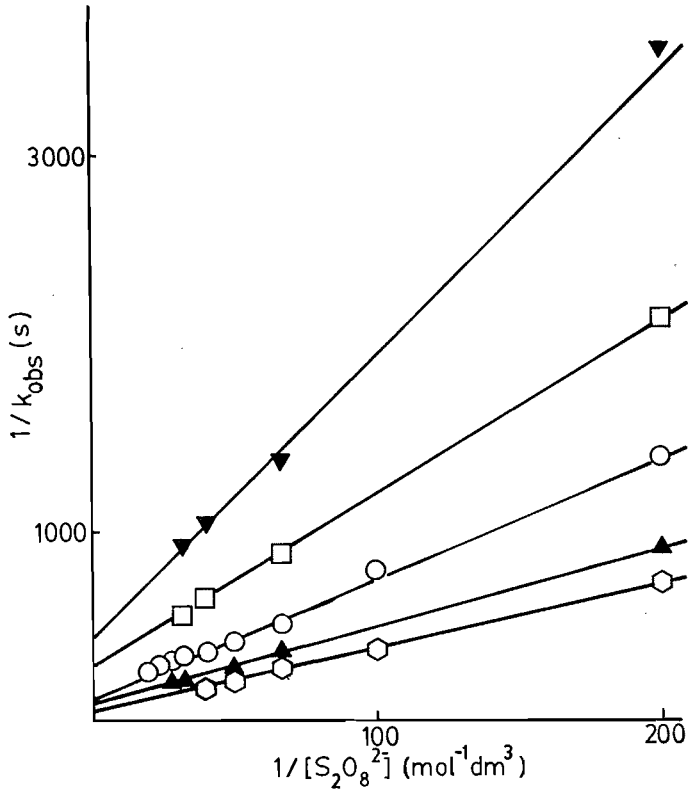

FIG. 2. Reciprocal plots for the data shown in Fig. 1.

$$[3] \quad [Ni(II)L]^{2+} + S_2O_8^{2-} \overset{K_3}{\rightleftharpoons} \{Ni(II)L^{2+}, S_2O_8^{2-}\} \quad \text{ion-pair}$$

$$[4] \quad \{Ni(II)L^{2+}, S_2O_8^{2-}\} \overset{k_4}{\rightarrow} [Ni(III)L(SO_4)]^+ + SO_4^-$$

$$[5] \quad [Ni(II)L]^{2+} + SO_4^- \overset{\text{fast}}{\rightarrow} [Ni(III)L(SO_4)]^+$$

The rate law derived from this scheme is

$$[6] \quad \text{rate} = \frac{2k_4K_{ip}[S_2O_8^{2-}]}{1 + K_{ip}[S_2O_8^{2-}]}[Ni(II)L]_{tot}$$

From eqs. [2] and [6], a plot of $1/k_{obs}$ versus $1/[S_2O_8^{2-}]$ should be linear, with a slope of $1/(2k_4K_{ip})$ and an intercept of $1/2k_4$. Figure 2 shows the inverse relationship for the L_2 complex at different temperatures. From such plots, the derived second-order rate constants, k_4, and ion-pairing constants, K_{ip}, for all reactions studied were computed using a linear least-squares fit. Table 2 lists these parameters for reaction of the three complexes in water as a function of temperature. From the temperature dependencies of the k_4 values, activation energies of 41.1 ± 1.3 and 34.9 ± 2.7 kJ mol^{-1} were calculated for the L_2 and L_3 complexes respectively.

Since the rates of reactions of the L_1 and L_3 complexes are near the measurable limit for the conventional kinetic equipment available to us, the L_2 complex was chosen for further study of solvation effects on the kinetics of the re-

TABLE 2. Oxidation rate constants (k_4) and ion-pairing constants (K_{ip}) as a function of temperature

	$[NiL_2]^{2+}$		$[NiL_2]^{2+}$		$[NiL_3]^{2+}$	
T (K)	k_4 (s^{-1})	K_{ip}	k_4 (s^{-1})	K_{ip}	k_4 (s^{-1})	K_{ip}
283.2	0.088 ± 0.004	26 ± 10			0.0294 ± 0.0014	19 ± 8
285.3			0.00127 ± 0.00005	25 ± 5		
288.2	0.089 ± 0.006	24 ± 10				
293.2			0.00187 ± 0.00004	29 ± 12	0.0580[a] ± 0.0032	18 ± 5[a]
298.0			0.00393 ± 0.00006	20 ± 8	0.0743[b] ± 0.0040	19 ± 6[b]
304.0			0.00615 ± 0.00010	20 ± 9	0.104[c] ± 0.006	20 ± 7[c]
308.0			0.0111 ± 0.0010	13 ± 10		

[a] T = 293.2 K.
[b] T = 298.2 K.
[c] T = 303.2 K.

TABLE 3. Observed first-order rate constants, k_{obs}, for the oxidation of $[Ni(II)L_2]^{2+}$ in binary aqueous mixtures

	$10^3 k_{obs}$ (s^{-1})				
	Methanol (%)			Acetone (%)	
$[S_2O_8^{2-}]$ (mol dm^{-3})	20	30	40	20	40
0.00500	2.13 ± 0.05	1.61 ± 0.04	1.39 ± 0.04	1.04 ± 0.02	0.851 ± 0.010
0.0100		2.64 ± 0.06	2.20 ± 0.05		1.07 ± 0.02
0.0150	3.81 ± 0.05	3.33 ± 0.03	2.60 ± 0.03	2.04 ± 0.02	1.63 ± 0.02
0.0200	4.48 ± 0.04	3.84 ± 0.04	3.33 ± 0.02		1.96 ± 0.03
0.0250	4.93 ± 0.06	4.37 ± 0.04	3.52 ± 0.04	2.96 ± 0.04	2.22 ± 0.04
0.0300	5.89 ± 0.08		3.73 ± 0.03		2.59 ± 0.04
0.0350			3.90 ± 0.06	3.09 ± 0.03	
0.0400			4.20 ± 0.06		

action. Table 3 lists k_{obs} for oxidation of the L_2 complex in a range of binary aqueous mixtures at 298 K. Figures 3 and 4 illustrate the effect of the added cosolvents methanol and acetone on the observed first-order rate constants. At first glance the data seem erratic, but reciprocal plots analogous to those in Fig. 2 yield the ion-pairing constants, K_{ip}, and second-order rate constants, k_4, listed in Table 4. The observed trend in these parameters with added cosolvent is consistent with that expected for increasingly hydrophobic media.

The magnitudes of the ion-pairing constants in all media studied are consistent with those expected for a 2+/2− pair (see Table 5), indicating the $S_2O_8^{2-}$ anion, not $HS_2O_8^-$, to be the reacting species.

Discussion

Mechanism

Reduction of peroxydisulphate characteristically proceeds via rate-determining fission of the peroxy bond (1), a step that may be assisted by the presence of a metal ion. In the present study, formation of an ion-pair provides a catalytic pathway for reduction of $S_2O_8^{2-}$ by the Ni(II) centre.

In the classic Eigen–Wilkins mechanism for complex formation, a rapid pre-equilibrium outer-sphere association (or ion-pairing) followed by rate-determining exchange of inner-sphere solvent with the incoming ligand obtains. This mechanism is summarized as

$$[7]\quad M(OH_2)_6^{n+} + L \overset{K_{os}}{\rightleftharpoons} \{M(OH_2)_6^{n+}, L\} \overset{k_{ex}}{\rightarrow} \{M(OH_2)_5L^{n+}\} + H_2O$$

The derived rate law for this scheme is

$$[8]\quad \frac{+d[ML^{n+}(aq)]}{dt} = \frac{K_{os}k_{ex}[M^{n+}][L]}{1 + K_{os}[L]}$$

Nickel(II) tetraazamacrocycles exist in aqueous solution as a mixture of low-spin square planar $[Ni(II)L]^{2+}$ and high-spin tetragonal $[Ni(II)L(OH_2)_2]^{2+}$ ions (21):

$$[9]\quad NiL^{2+}(aq) + 2H_2O(l) \overset{K_9}{\rightleftharpoons} NiL(OH_2)_2^{2+}$$

Electrostatic interaction of the peroxydisulphate anion with the square planar nickel(II) complex will occur according to eq. [3], and with the tetragonal bis-aquo species:

$$[10]\quad NiL(OH_2)_2^{2+} + S_2O_8^{2-} \overset{K_{10}}{\rightleftharpoons} \underset{\text{ion-pair}}{\{NiL(OH_2)_2^{2+}, S_2O_8^{2-}\}}$$

For intimate ion-pair formation, exchange between the inner-sphere solvent and $S_2O_8^{2-}$ must occur, analogous to that in eq. [7]:

$$[11]\quad \{NiL(OH_2)_2^{2+}, S_2O_8^{2-}\} \rightarrow \{NiL, S_2O_8^{2-}\} + 2H_2O$$

Estimated values of the rate of interchange of inner-sphere water with a variety of incoming ligands of varying charge have been tabulated by Burgess (22). The values fall in the range of 3–30 × 10^3 s^{-1}, which is close to the solvent exchange rate for water at $Ni^{2+}(aq)$ of 3 × 10^4 s^{-1} (23). It is reasonable to assume that like $Ni^{2+}(aq)$, interchange at the bis-aquo nickel(II) tetraazamacrocycle will be dissociative, with an exchange rate that is fast relative to the rate-

Can. J. Chem. Downloaded from www.nrcresearchpress.com by 109.225.110.28 on 09/08/12
For personal use only.

Can. J. Chem. Downloaded from www.nrcresearchpress.com by 109.225.110.28 on 09/08/12
For personal use only.

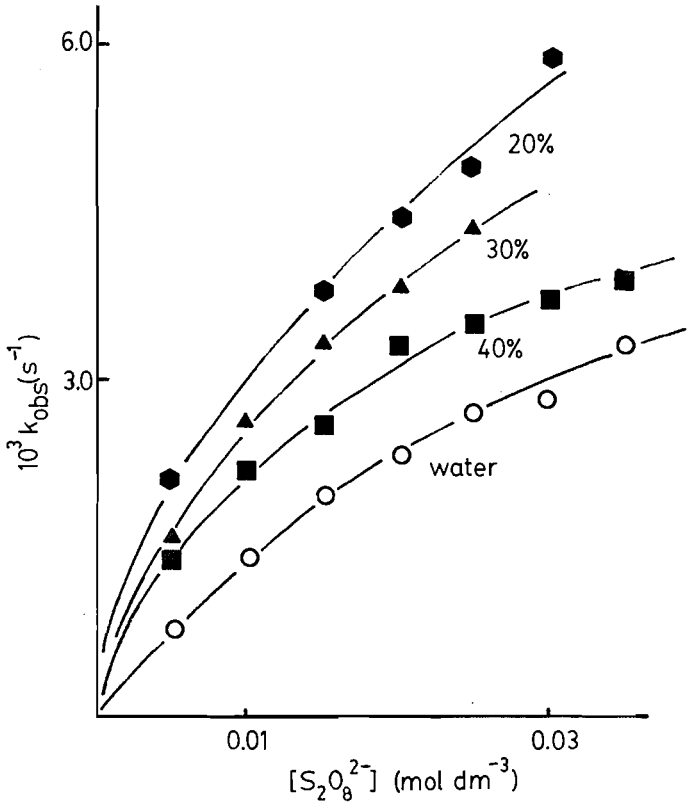

FIG. 3. Dependence of observed first-order rate constants on peroxydisulphate concentration for oxidation of the $[Ni(II)L_2]^{2+}$ cation in methanol–water mixtures (T = 298 K). Aqueous data are included for comparison.

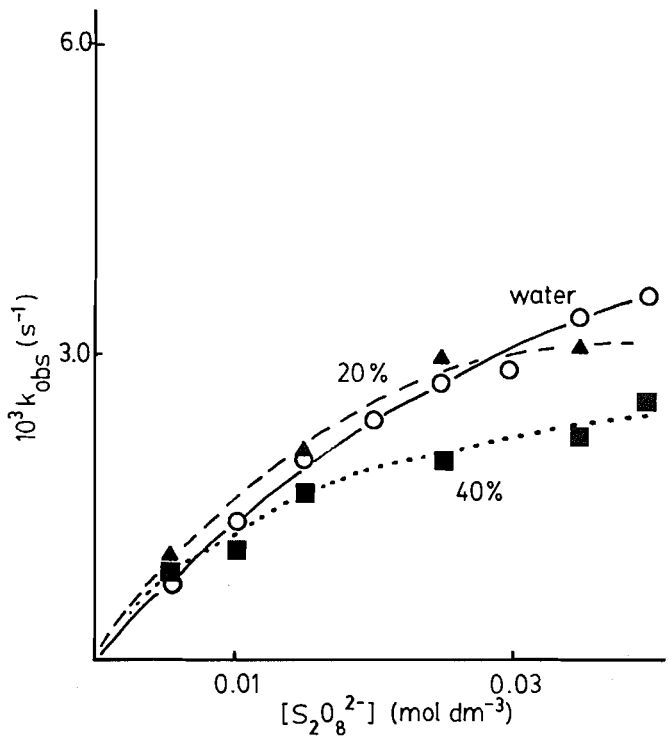

FIG. 4. Dependence of observed first-order rate constants on peroxydisulphate concentration for oxidation of the $[Ni(II)L_2]^{2+}$ cation in acetone–water mixtures (T = 298 K). Aqueous data are included for comparison.

determining peroxy-bond fissure in our system. The interchange rate at $Ni^{2+}(aq)$ for sulphate has been estimated as 1.0×10^4 s^{-1} at 20°C (24).

After formation of the intimate ion-pair, the redox step results in the formation of a sulphatonickel(III) complex. The lack of rate dependence on radical scavengers suggests that peroxy-bond fissure and Ni(III)–SO_4^{2-} bond formation occur concomitantly, according to eq. [4].

A rate law can be derived for the reaction, from eqs. [3]–[5] and [9]–[11]:

$$[12] \quad \text{rate} = \frac{2k_4K'[S_2O_8^{2-}]\,[Ni(II)L]_{tot}}{1 + K'[S_2O_8^{2-}]}$$

where $K' = (K_9K_{10} + K_3)$. The value of K_9 is small compared with K_3, whence $K' \approx K_3$ (which we have designated K_{ip}).

It is seen in Table 2 that the values of K_{ip} are little affected by the presence of substituents on the macrocyclic ligands. This indicates that the macrocycle does not impede the approach of the dianion to the metal centre, suggesting axial approach of the oxidant to the nickel in the ion-pair. The K_{ip}'s for the complexes agree well with that for pairing of aquonickel(II) with sulphate ion (Table 5), further supporting close approach of the $S_2O_8^{2-}$ to the nickel centre in the complexes without steric interference by the macrocyclic ligands. The precision of measuring K_{ip}'s is not good enough to detect subtle effects in the primary/secondary solvation shells of the complex (22). The activation energies (Table 2) are high for outer-sphere redox processes, but are approximately half the value expected for rate-determining peroxy-bond fissure (25). This is further evidence for assistance to peroxy-bond fissure by the macrocyclic complexes.

TABLE 4. Solvent effects on rate and equilibrium constants for the $[Ni(II)L_2]^{2+}/S_2O_8^{2-}$ system at 298 K

Solvent (% v/v)	k_4 (s^{-1})	K_{ip}
Water	0.00393 ± 0.00005	20 ± 6
Methanol		
20%	0.0038 ± 0.0002	78 ± 20
30%	0.0037 ± 0.0004	56 ± 15
40%	0.0028 ± 0.0003	65 ± 17
tert-Butyl alcohol		
20%	0.0051 ± 0.0004	22 ± 6
40%	0.0028 ± 0.0002	72 ± 12
50%	0.0030 ± 0.0002	83 ± 15
Acetone		
20%	0.0023 ± 0.0001	57 ± 8
40%	0.0017 ± 0.0002	61

Electrochemical and pulse radiolysis studies (26) have shown that in sulphate media nickel(III) tetraazamacrocycles are stabilized by axially coordinated sulphate(s). Axial proximity of the oxidant to the metal centre is expected to facilitate electron transfer from Ni(II) to the dianion, with concomitant peroxy-bond elongation in the transition state. Pennington and Haim (27) have shown that an inner-sphere mechanism obtains in the oxidation of chromium(II) by peroxodisulphate, with the formation of a mixture of $CrSO_4^+(aq)$ and $Cr^{3+}(aq)$.

TABLE 5. Ion-pairing constants for M^{n+}/X^{y-} systems in water at 298 K

M^{n+}	X^{y-}	K_{ip}	Reference
$Ni^{2+}(aq)$	$ImidH^+$	0.02	39
$Ni^{2+}(aq)$	$N\text{-Me-imid}^+$	0.02	39
$Ni^{2+}(aq)$	Histidine	0.15	39
$Ni^{2+}(aq)$	Imidazole	0.15	39
$Ni^{2+}(aq)$	HF	0.15	39
$Ni^{2+}(aq)$	$Hoxalate^-$	2	40
$Ni^{2+}(aq)$	$Oxalate^{2-}$	13	40
$[Ni(II)L_1]^{2+}$	$S_2O_8^{2-}$	24	This work
$[Ni(II)L_2]^{2+}$	$S_2O_8^{2-}$	20	This work
$[Ni(II)L_3]^{2+}$	$S_2O_8^{2-}$	19	This work

There appears to be little temperature dependence for the estimated values of K_{ip} (Table 2). However, the errors associated with their estimation precludes any confident interpretation of trends. The apparent lack of temperature dependence of K_{ip} on temperature indicates a near zero enthalpy for ion-pair formation. The entropy change for this process may be calculated as $+6.0\ J\ K^{-1}\ mol^{-1}$, using a value of 20 for K_{ip}. These values are not dissimilar to those obtained for ion-pair formation between the aquopentamminecobalt(III) cation and sulphate anion ($\Delta H = 0$ and $\Delta S = +68\ J\ K^{-1}\ mol^{-1}$ at zero ionic strength; $-1.3\ kJ\ mol^{-1}$ and $+14\ J\ K^{-1}\ mol^{-1}$ at ionic strength 1.0 mol L^{-1}) (28). The small entropy value is consistent with ion-pair formation rather than complexation, since fewer solvent molecules are released in the former case. Comparison of entropies of association for a series of ions forming inner- and outer-sphere associations has been made (29), showing significantly lower entropies for outer-sphere (ion-pairing) couples than inner-sphere (complexing) ones. Enthalpies of association for ion-pairing in these systems was also small, despite large charge neutralisations ($|z_+z_-| = 9$ or 10).

The most significant feature of our results is that within an order of magnitude the values of K_{ip} correspond to ion-pairing constants for $Ni^{2+}(aq)$–X^{2-}. Again, this supports the contention that the peroxydisulphate anion approaches the nickel(II) centre axially.

Solvent effects

Peroxydisulphate is known to oxidize organic solvents such as alcohols (30, 31), dimethyl sulphoxide (32), and acetone (33), particularly in the presence of metal-ion catalysts. These reactions have been shown to proceed by radical chain mechanisms, but are exceedingly slow compared with the rate of oxidation of the nickel complexes in this work and offer no interference.

Ion-pairing constants were found to increase with increasing organic content of the solvent mixture (Table 4). This behaviour is in accord with the electrostatic model of ion-pairing, where K_{ip} is dependent on the charge product of the component ions, the distance between the centres of the ions, and the dielectric constant of the medium (22).

The second-order rate constants, k_4, are relatively insensitive to bulk solvent composition, although there is a slight decrease in k_4 with increased organic component. For a second-order reaction between oppositely charged ions, it is expected that increasing the hydrophobic character of the medium would stabilize the free energy of the transition state relative to that of the initial state (34). Hence a reduction in the activation energy for the reaction in the more hydrophobic medium is expected relative to water. This would result in an increase in rate constants in the binary mixtures relative to those in water. Such effects have been observed, for example in the mixed-solvent study of the mercury(II)-catalysed aquation of hexachlororhenate (35).

In the present study, the slight changes in rate constants with increasing hydrophobicity of the medium suggests that the system has undergone any major electrostatic rearrangements that are likely, prior to the rate-determining step. Only slight solvation differences are apparent in the system before and after electron transfer. This agrees with the proposed mechanism, where concomitant nickel(II) oxidation peroxy-bond fissure occurs within the solvent cage of the ion-pair, oblivious to the solvation effects of the bulk medium. Retardation of rates on going from water to binary aqueous mixtures has been observed previously (36) for oxidation of tris-diimine iron(II) complexes. In those cases, trends in reaction rates with solvent composition were explained in terms of changes in initial-state versus transition-state energies.

Recently, there has been a series of reports on solvent effects on peroxydisulphate oxidations of transition-metal complexes (37, 38). In all of the systems studied, decreases in rates with increasing organic cosolvent were observed, in agreement with the present study. Holba *et al.* (36, 37) did not detect ion-pairing, which is not unexpected since their cationic complexes were singly charged.

Acknowledgements

We are grateful to the Natural Sciences and Engineering Research Council of Canada for financial support and to Sir Wilfred Grenfell College for the purchase of the spectrophotometer and the award of the Principal's Research grant.

1. D. A. House. Chem. Rev. **62**, 185 (1962).
2. H. Eiberberger, S. Steenken, P. O'Neill, and D. Schulte-Frohlinde. J. Phys. Chem. **82**, 749 (1978).
3. R. O. C. Norman, P. M. Storey, and P. R. West. J. Chem. Soc. B, 1087 (1978).
4. W. C. Vasudeva. J. Chem. Soc. Perkin Trans. 2, 697 (1975); M. E. Snook and G. A. Hamilton. J. Am. Chem. Soc. **97**, 1603 (1975).
5. M. Kimura, T. Akazome, K. Takenaka, and A. Kobayashi. Bull. Chem. Soc. Jpn. **53**, 1271 (1980).
6. K. A. Kumar, P. Sivawaroop, K. J. Rao, and P. V. K. Rao. Transition Met. Chem. **12**, 441 (1987).
7. S. Fronaeus and C. O. Ostman. Acta Chem. Scand. **9**, 902 (1955); **22**, 2827 (1968).
8. V. K. Gupta. Z. Phys. Chem. **270**, 297 (1989).
9. J. M. Okoh and M. Krishnamurthy. J. Chem. Soc. Dalton Trans. 449 (1986).
10. M. Kimura, T. Kawajiri, and M. Tanida. J. Chem. Soc. Dalton Trans. 726 (1980).
11. J. A. Olabe and A. Haim. Inorg. Chem. **28**, 3278 (1989).
12. R. I. Haines and A. McAuley. Coord. Chem. Rev. **39**, 77 (1981).
13. N. F. Curtiss, Y. M. Curtiss, and H. J. K. Powell. J. Chem. Soc. A, 1015 (1966).
14. R. I. Haines and A. McAuley. Inorg. Chem. **19**, 719 (1980).
15. E. Zeigerson, G. Ginzberg, N. Schwartz, Z. Luz, and D. Meyerstein. J. Chem. Soc. Chem. Commun. 241 (1979).
16. D. H. Irvine. J. Chem. Soc. 2977 (1959); D. Benson. *In* Mechanisms of inorganic reactions in solution, an introduction. McGraw–Hill, London. 1968. Chap. 5.
17. F. V. Lovecchio, E. S. Gore, and D. H. Busch. J. Am. Chem. Soc. **96**, 3109 (1974).

Can. J. Chem. Downloaded from www.nrcresearchpress.com by 109.225.110.28 on 09/08/12
For personal use only.

18. S. S. Gupta and Y. K. Gupta. Inorg. Chem. **20**, 454 (1981).
19. I. M. Kolthoff, E. J. Meehan, and E. M. Carr. J. Am. Chem. Soc. **75**, 1439 (1953); D. L. Ball, M. M. Crutchfield, and J. O. Edwards. J. Org. Chem. **25**, 1599 (1960).
20. H. Diebler and M. Eigen. Z. Phys. Chem. Frankfurt Ausg. **20**, 229 (1959); M. Eigen. Ber. Bunsen Ges. Phys. Chem. **67**, 753 (1963); M. Eigen and K. Tamm. Z. Elektrochem. **66**, 93, 107 (1962).
21. G. A. Melson and D. H. Busch. J. Am. Chem. Soc. **86**, 4830 (1964).
22. J. Burgess. Metal ions in solution. Ellis Horwood Ltd. London. 1978. Chap. 12, pp. 349–353.
23. J. Granot, A. M. Achlama, and D. Fiat. J. Chem. Phys. **61**, 3043 (1974); H. Strehlow and J. Frahm. J. Ber. Bunsen Ges. Phys. Chem. **79**, 57 (1975).
24. R. M. Fuoss. J. Am. Chem. Soc. **80**, 5059 (1958); M. Z. Eigen. Elektrochemie, **64**, 115 (1960).
25. M. T. Beck. *In* Chemistry of complex equilibria. Van Nostrand Reinhold, New York. 1970. Chap. 9. F. Basolo and R. G. Pearson. *In* Mechanisms of inorganic reactions. Wiley Interscience, New York. 1958. Chap. 9. R. M. Fuoss and C. A. Krauss. J. Am. Chem. Soc. **79**, 3304 (1957).
26. E. Zeigerson, I. Bar, J. Bernstein, L. J. Kirschenbaum, and D. Meyerstein. Inorg. Chem. **21**, 73 (1982), and references therein.
27. D. E. Pennington and A. Haim. J. Am. Chem. Soc. **90**, 3700 (1968).
28. F. A. Posey and H. Taube. J. Am. Chem. Soc. **78**, 15 (1956).
29. A. E. Martell (*Editor*). Coordination chemistry. Vol. 1. ACS Monograph 168. Van Nostrand Reinhold Co., New York. 1971. p. 469; A. R. Gallopo and J. O. Edwards. J. Org. Chem. **36**, 4089 (1971).
30. W. C. Vasudeva and S. Wasif. J. Chem. Soc. B, 960 (1970).
31. N. V. Fedorovich, M. D. Levi, B. B. Damaskin, and A. V. Shlepakov. Dokl. Akad. Nauk SSSR, **225**, 148 (1975).
32. S. C. Agarwal, SMT P. L. Agarwal, V. B. Agarwal, and V. Dwivedi. Rev. Roum. Chim. **27**, 265 (1982).
33. M. J. Blandamer and J. Burgess. Coord. Chem. Rev. **31**, 93 (1980).
34. M. J. Blandamer, J. Burgess, and R. I. Haines. J. Chem. Soc. Dalton Trans. 607 (1980).
35. M. J. Blandamer, J. Burgess, and R. I. Haines. J. Chem. Soc. Chem. Commun. 963 (1978); M. J. Blandamer, J. Burgess, P. P. Duce, and R. I. Haines. J. Chem. Soc. Dalton Trans. 2442 (1980).
36. V. Holba, J. Benko, O. Grancicova, and O. Vollarova. Transition Met. Chem. **10**, 84 (1985).
37. V. Holba, O. Grancicova, and A. Paulenova. Transition Met. Chem. **12**, 121 (1987).
38. J. Burgess, O. Vollarova, and J. Benko. Transition Met. Chem. **12**, 238 (1987).
39. J. E. Letter and R. B. Jordan. Inorg. Chem. **10**, 2692 (1971).
40. G. H. Nancollas and N. Sutin. Inorg. Chem. **3**, 360 (1964).

Can. J. Chem. Downloaded from www.nrcresearchpress.com by 109.225.110.28 on 09/08/12
For personal use only.

Azetinone formation is not competitive with intermolecular reactions of a β-lactam-4-ylidene

MICHEL ZOGHBI AND JOHN WARKENTIN[1]
Department of Chemistry, McMaster University Hamilton, Ont., Canada L8S 4M1

Received May 1, 1992

MICHEL ZOGHBI and JOHN WARKENTIN. Can. J. Chem. **70**, 2792 (1992).

3-Phenoxy-1-phenyl-2-azetidinon-4-ylidene (β-lactam-4-ylidene) **2***a*, was generated by thermolysis of a spiro-fused β-lactam oxadiazoline precursor (**1**). Fast 1,2-H migration, a characteristic reaction of singlet carbenes that would convert **2***a* to 3-phenoxy-1-phenyl-3-azetin-2-one (**4***a*) could not be demonstrated. Added 1, 3-diphenylisobenzofuran (**6**) did not afford the [4+2] cycloadduct (**7**) expected from **4***a* but, instead, the isomeric *E*- and *Z*-4-[1-(2-benzoylphenyl)-1-phenyl]-methylene-3-phenoxy-1-phenylazetidin-2-ones (**9**). Those compounds can be rationalized as the products of rearrangement of first-formed [2+1] adducts of **6** and the ylidene. The structure of the *Z* isomer of **9** was established by means of single crystal X-ray diffraction. Generation of **2***a* in methanol-d_4, either neat or 3.3 M in benzene, afforded the isomeric products of carbene insertion into the OD bond of methanol-d_4. Structural isomers expected from addition of methanol-d_4 to **4***a* could not be detected. The results suggest that 1,2-H migration in **2***a* is relatively slow, with $k_H \leq 1.4 \times 10^6$ s^{-1} at 100°C, which is slower than analogous rearrangement of benzylchlorocarbene by 200-fold or more.

MICHEL ZOGHBI et JOHN WARKENTIN. Can. J. Chem. **70**, 2792 (1992).

La thermolyse d'une oxadiazoline spiro-condensée à une β-lactame (**1**) conduit au 3-phénoxy-1-phényl-2-azétidon-4-ylidène (β-lactam-4-ylidène) (**2***a*). On n'a pas pu mettre en évidence de migration rapide 1,2-H, une réaction caractéristique des carbènes singulets qui permettrait de transformer le composé **2***a* en 3-phénoxy-1-phényl-3-azétin-2-one (**4***a*). L'addition de 1,3-diphénylisobenzofurane (**6**) n'a pas permis d'isoler le cycloadduit [4+2] (**7**) que l'on pourrait attendre à partir du produit **4***a*; on a plutôt obtenu les *E*- et *Z*-4-[1-(2-benzoylphényl)-1-phényl]-méthylène-3-phénoxy-1-phénylazétidin-2-ones isomères (**9**). On peut rationaliser la formation de ces produits par une transposition des adduits [2+1] du produit **6** et de l'ylidène qui se forment en premier. On a déterminé la structure de l'isomère *Z* du composé **9** grâce à la diffraction des rayons X par un cristal unique. La génération du composé **2***a* dans du méthanol-d_4, soit à l'état pur ou en solution 3,3 M dans le benzène, fournit des produits d'insertion du carbène dans la liaison OD du méthanol-d_4. On n'a pas pu détecter les isomères de structure que l'on pourrait attendre lors de l'addition du méthanol-d_4 sur le composé **4***a*. Les résultats suggèrent que la migration 1,2-H dans le composé **2***a* est relativement lente, alors que $k_H \leq 1{,}4 \times 10^6$ s^{-1}, à 100°C; cette valeur est 200 fois plus faible que celle observée lors de la transposition analogue du benzylchlorocarbène.

[Traduit par la rédaction]

Can. J. Chem. Downloaded from www.nrcresearchpress.com by 109.225.110.28 on 09/08/12
For personal use only.

Despite intense interest and activity in the area of β-lactam chemistry (for post-1980 reviews, see ref. 1), β-lactam-4-ylidenes, **2**, were described only recently (2). They can be generated efficiently and conveniently by heating spiro-β-lactam oxadiazolines (**1**) at ca. 100°C in solution, Scheme 1, and they have considerable potential for elaboration of the β-lactam system by both intramolecular and intermolecular reactions (2). Two potential intramolecular reactions of **2** include 1,2-H migrations leading to azetinones, **3** and **4**. With **1***a* (R^1 = Ph, R^2 = OPh, R^3 = H) in hand (2) we were in a position to generate **2***a* (R^1 = Ph, R^2 = OPh, R^3 = H) and to examine its fate. Azetinones are not stable species: An azetinone of type **4** has been observed at −5°C by spectroscopic methods (3) but none has ever been isolated despite attempts by several groups (4–6). Azetinones **3** have not been isolated either, but their existence as transients is a facet of postulated mechanisms of nucleophilic substitutions on β-lactams (7) bearing a leaving group (L) at C4, Scheme 2, and of the hetero-Diels–Alder reactions, to form **5**, reported by Meyers' group (8).

Methods, results, and discussion

In view of the limited stabilities of azetinones **4**, diphenyl isobenzofuran (**6**) was included to trap **4***a*, *in situ*, as the [4π+2π] cycloadduct **7**, Scheme 3.

Thermolysis of **1***a* in benzene containing **6** (0.5 M) did not take the course leading to **7**. Instead of **7**, two 1:1 adducts of **2***a* and **6** were isolated, each in 16% yield. Spectroscopic data (ir, ^{1}H nmr, ^{13}C nmr) indicated not only a higher β-lactam carbonyl frequency (1800 cm^{-1}) than in **1***a* (1792 cm^{-1}) and the presence of another carbonyl group (ca. 1665 cm^{-1}), but also a high probability of geometric isomerism. Single crystal X-ray diffraction showed that one of the products was *Z*-4-[1-(2-benzoylphenyl)-1-phenyl]-methylene-3-phenoxy-1-phenylazetidin-2-one, **9***a*.[2] The other product could then be identified, from its spectra, as the corresponding *E* isomer, **9***b*. In view of the fact that **2***a* and its analogues have been shown to add to CC double bonds, as in styrene (2) and 4-bromo-1-butene,[3] we propose an analogous cyclopropanation in the first step, to form **8**, presumably as a mixture of all possible isomers (Scheme 4). As a special divinylcyclopropane, with heteroatom substituents and phenyl groups as well, isomers **8** are not expected to be stable at 100°C. A reasonable mechanism for formation of **9** (Scheme 5) begins with an expected vinylcyclopropane bond cleavage in **8**, leading to diradical **10**, which undergoes β-scission to form **9***a* and **9***b*.

We were unable to find a precedent in the literature for formation of a 4-methylene-β-lactam by a carbene route. A few members of the family are known (9) but molecular structures of compounds containing that interesting ring

[1]Author to whom correspondence may be addressed.

[2]Full details of the crystal and molecular structures of **9***a* will be published elsewhere.

[3]M. Zoghbi and J. Warkentin. Unpublished observations.

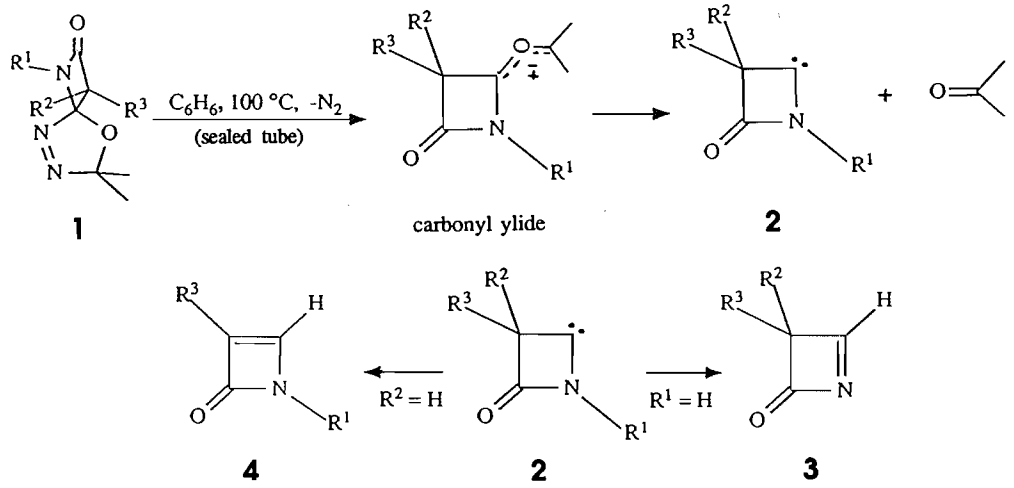

1 2 4 2 3

SCHEME 1

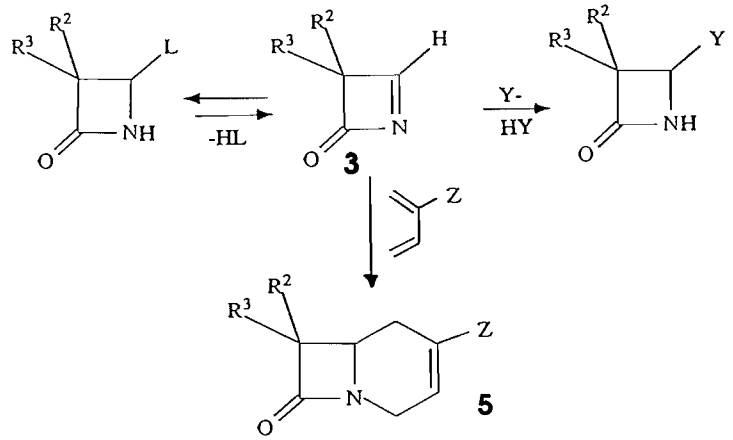

3 5

SCHEME 2

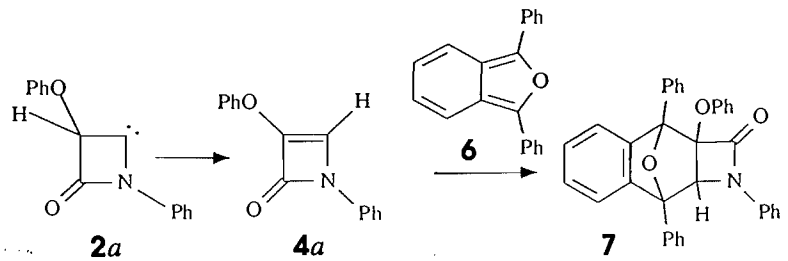

2a 4a 6 7

SCHEME 3

system have not been reported. Major structural features of the β-lactam portion of **9***a* (bond lengths and bond angles) are given in Fig. 1.[2]

Reactions of singlet carbenes with 1,3-diarylisobenzofurans, including 1,3-diphenylisobenzofuran (10, 11), are known. Thus dichloro, dibromo, and diiodocarbene react with **6** to afford the appropriate β,β-dihalo-[2-benzoyl]-styrenes (10). The authors (10) also proposed initial [2+1] cycloaddition and subsequent rearrangement of vinylcyclopropane systems analogous to **8**.

A second test for azetinone **4***a* involved generation of **2***a* in methanol-d_4. If carbene **2***a* were to rearrange to **4***a* in competition with its insertion into the OD bond of methanol-d_4, then geometric isomers **11***a* and **11***b* would be expected as well as their structural isomers, **12***a* and **12***b*, Scheme 6.

The system was calibrated by generating **2***a* in neat CH_3OH by thermolysis of **1***a* at 100°C. Insertion products **11***c* and **11***d* were formed quantitatively in the ratio **11***c* (*trans*): **11***d* (*cis*) = 2.6:1. Chemical shifts (δ) for the proton at C3 were: *trans*, 5.26 (s, br); *cis*, 5.30(J = 3.6 Hz). Three experiments with CD_3OD were then carried out with concentrations of CD_3OD (in benzene) at 0.06, 0.40, and 3.30 M as well as one experiment in neat CD_3OD. Products from the low-concentration runs (0.06 and 0.40) were very complex and inconclusive because products of insertion into CD_3OD (if any) could not be identified or isolated. However, the

Can. J. Chem. Downloaded from www.nrcresearchpress.com by 109.225.110.28 on 09/08/12
For personal use only.

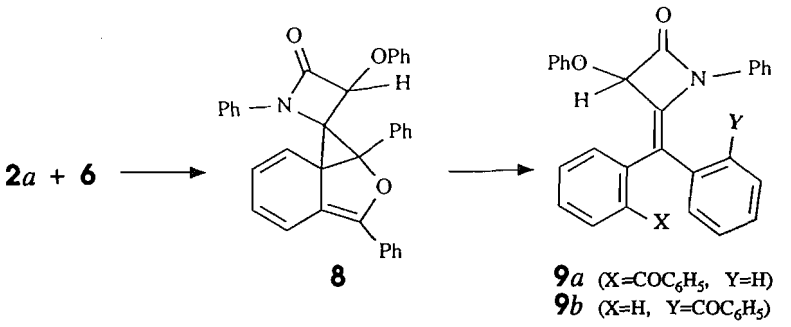

SCHEME 4

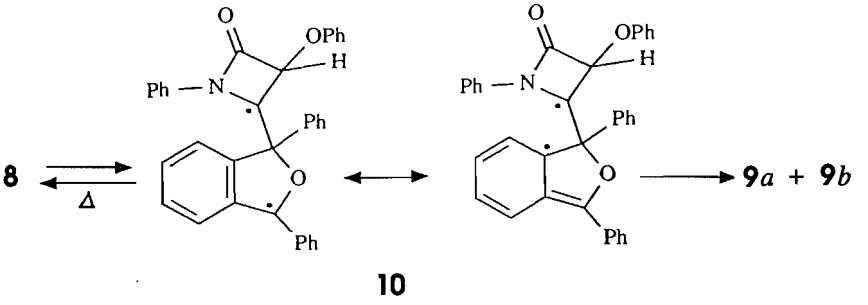

SCHEME 5

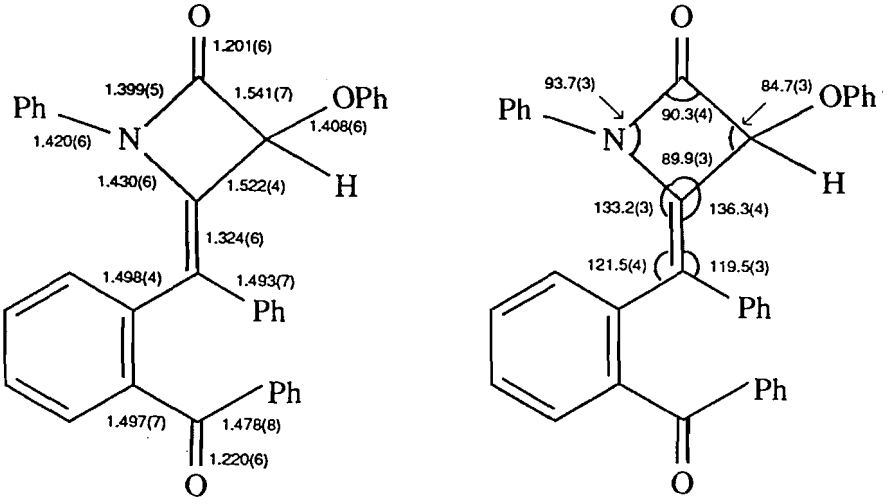

FIG. 1. Bond lengths (Å) and bond angles (degrees) of **9a**.

experiment with 3.30 M CD_3OD afforded **11***a* and **11***b* in ca. 70% yield and that with neat CD_3OD afforded the same products in quantitative yield. In both cases, the isomer ratio was 2.6:1 and the signals at δ 5.27 (*trans*) and 5.30 (*cis*) were singlets. Moreover, the signals from C4-H (*trans*, δ = 5.44, J = 0.63 Hz; *cis*, δ = 5.68, J = 3.6 Hz) in the ^{1}H nmr spectra of **11***c* and **11***d*, respectively, were absent from spectra of products formed in CD_3OD. Therefore, perdeuteromethanol afforded **11***a* and **11***b* from carbene **2***a* and not **12***a* and **12***b* from azetinone **4***a*.

Rearrangement of carbene **2***a* to azetinone **4***a* is probably slower than analogous 1,2-H migrations in other carbenes, because of strain in the azetinone. A rough estimate of the increase in strain (in units of displacement from ideal angles, in degrees) was obtained by assuming that actual internal bond angles in the carbene are 90° (N1), 93° (C2), 87° (C3), and 89° (C4) and that those in the azetinone are all 90°. The inherent carbene bond angle in an unconstrained singlet carbene was assumed to be that of singlet methylene, 102° (12), and inherent bond angles at the sp^2 and sp^3 carbons were taken to be 120° and 109°, respectively. Given these assumptions, the angle strain increase accompanying the rearrangement **2***a* → **4***a* is about 28°.[4] Some fraction of that increase in angle strain must be present at the transition state for migration, to reduce the rate constant for that step. Nevertheless, the absolute value of that rate constant could still be substantial, given that rearrangement of benzyl-

[4]Small changes in the assumed bond angles do not affect the sense of the change of angle strain.

Can. J. Chem. Downloaded from www.nrcresearchpress.com by 109.225.110.28 on 09/08/12
For personal use only.

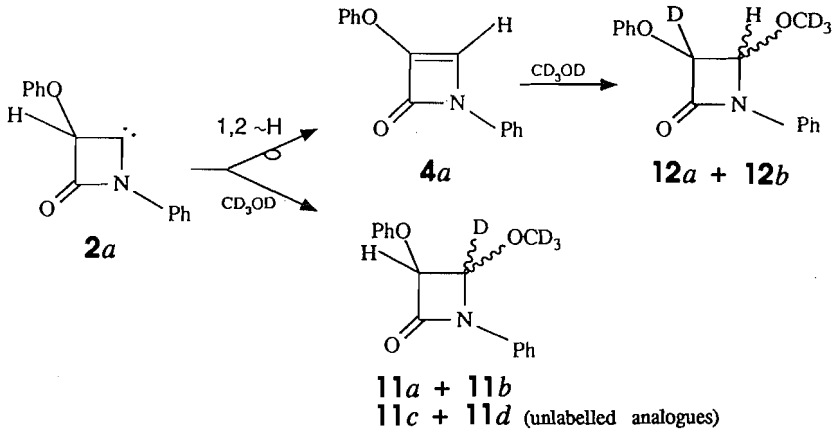

SCHEME 6

chlorocarbene occurs with k (100°C) $\simeq 2.9 \times 10^8$ s^{-1} (calculated from $A = 10^{11.1}$ s^{-1} and $E_a = 4.5$ kcal mol^{-1}) (13). If 1,2-H migration in **2***a* were slower by a factor of 100, bimolecular reaction of **2***a* with **6** would consume half of the carbene at [**6**] = 5×10^{-3} M, assuming that the rate constant for trapping of **2***a* with **6** is about the same as that for trapping of benzylchlorocarbene with tetramethylethylene (6×10^8 M^{-1} s^{-1} (13). Experiments with [**6**] = 5×10^{-3} M are out of the question, given that the yield was only 32% with 100-fold more concentrated **6**

The rate constant for trapping of singlet dimethoxycarbene with methanol has a value $\simeq 10^5$ M^{-1} s^{-1} at 20°C (14). Assuming that dimethoxycarbene is an adequate model for **2***a* and that the rate constant at 100°C would be about 10^6 M^{-1} s^{-1}, the experiment with 3.3 M methanol suggests that the rate constant for 1,2-H migration in **2***a* has a value $\leq 1.4 \times 10^6$ s^{-1} at 100°C. Those results also have a bearing on the lifetime of the carbonyl ylide precursor of carbene **2***a*, as discussed below.

A question that remains is the fate of the fraction of carbene **2***a* that is not trapped by **6** (0.5 M) or by methanol (≤3.3 M). In view of the fact that trapping by neat methanol was quantitative, bimolecular reactions of the carbonyl ylide (Scheme 7) are unlikely. Although **14** could be converted to the observed products in methanol, analogous compounds from genuine trapping of carbonyl ylides by methanol survive similar conditions (15). We assume, therefore, that the lifetime of the carbonyl ylide intermediate (Scheme 1) is very short. There are then two explanations for the fact that carbene trapping can be surprisingly inefficient without competition from azetinone formation. First, the carbene may undergo fast alternative unimolecular reactions, such as fragmentations or insertions (Scheme 8). Second, it is conceivable that some azetinone (**4***a*) is actually formed and that it undergoes unimolecular reactions (Scheme 9) fast enough to escape trapping by the reagents that were chosen. Azetinones **4** can rearrange rapidly to iminoketenes (6) and *N*-phenyliminoketenes undergo efficient electrocyclization (16) to 4-(1*H*)-quinolinones. Electrocyclic ring opening of cyclobutenones to ketenes is also well known (17) and serves as a second model for the potential ring opening of **4***a*. We were not able to isolate any 3-phenoxy-4-(1*H*)-quinolinone (Scheme 9) and fragmentation to phenylisocyanate can be ruled out, at least in the reactions where methanol was present, because methyl-*N*-phenylcarbamate was not obtained.

In summary, the potential 1,2-H migration that would rearrange β-lactam-4-ylidene **2***a* to azetinone **4***a* is slowed because of increased angle strain in the product and possibly because of reduced electrophilicity imparted by the nitrogen substituent. Moss *et al.* (18) recently reported that the methoxy group of cyclopropylmethoxy carbene retards ring expansion of that carbene. Although evidence for the intermediacy of **4***a* could not be obtained, it must be recognized that the high reactivity of the carbene precursor (**2***a*), not only in unimolecular reactions but also toward suitable traps for **4***a*, imposes severe restrictions on the choice of conditions.

The reaction of ylidene **2***a* with 1,3-diphenylisobenzofuran to form **9** constitutes the first example of the construction of the rare **4**-methylenazetidin-2-one unit by a carbene route. In view of the known reactions of rhodium carbenoids with simpler furans (19) there is some potential for the synthesis

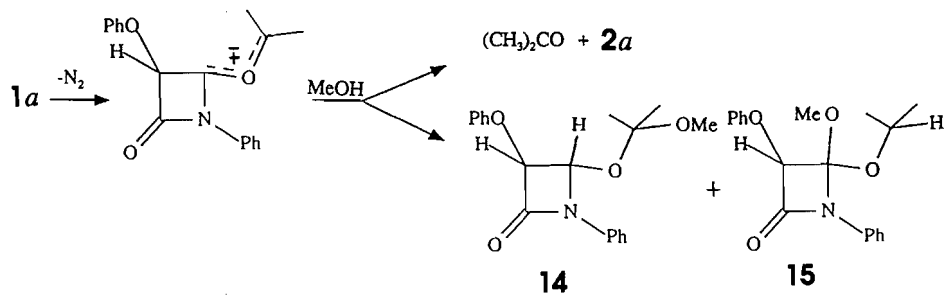

SCHEME 7

Can. J. Chem. Downloaded from www.nrcresearchpress.com by 109.225.110.28 on 09/08/12
For personal use only.

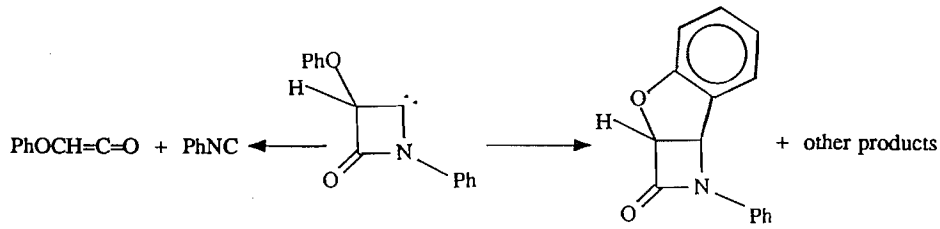

SCHEME 8

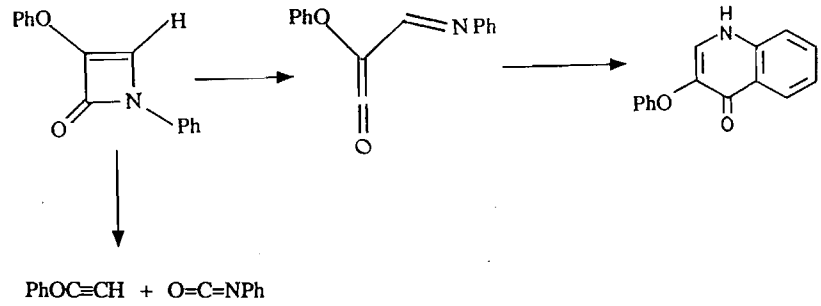

SCHEME 9

of additional 4-methylenazetidin-2-ones from **2***a* and its analogues.

Experimental

*1,7,8-Triaza-6,6-dimethyl-5-oxa-2-oxo-3-phenoxy-1-phenylspiro-[3·4] oct-7-ene (**1**)*

This compound, a spiro-fused β-lactam oxadiazoline (2), was synthesized by formal [2+2] cycloaddition of phenoxyketene to 5,5-dimethyl-2-phenylimino-Δ^3-1,3,4-oxadiazoline (**13**) (7*a*, 20).

Phenoxyacetyl chloride (0.51 g, 3.0 mmol) in dry CH_2Cl_2 (10 mL) was added, drop by drop and with stirring, to a solution of **13** (0.47 g, 2.5 mmol) and triethylamine (6.0 mmol) in dry CH_2Cl_2 (20 mL) under N_2 at −23°C. When addition was complete, the cold bath was removed but stirring was maintained overnight. The reaction solution was washed with saturated aqueous bicarbonate and with brine. Those aqueous layers were extracted twice with CH_2Cl_2 and the organic layers were combined. Removal of the solvent after drying over $MgSO_4$, and chromatography on silica (Chromatotron, 2-mm plate), afforded **1** as a white solid (98%), one diastereomer only, presumably *trans*, mp 95–96°C; ir (KBr) cm^{-1}: 1792 (CO), 1594 (N=N); ^1H nmr (200 MHz, $CDCl_3$) δ: 1.48 (s, 3H), 1.56 (s, 3H), 5.49 (s, 1H), 7.0–7.4 (m, 10H); ^{13}C nmr (126 MHz, $CDCl_3$) δ: 23.93 (CH_3), 24.35 (CH_3), 88.21 (C3), 122.85 (C6), 129.66 (C4), 116.14, 121.91, 123.13, 127.33, 129.30 (5 CH, aryl), 133.24 (N-C1, aryl), 156.99 (O-C1, aryl), 162.13 (CO); ms (ci) *m/z*: 267 ($M-N_2-CO$, 4%), 209 ($M-N_2-CO-C_3H_6O$, 87%), 180 (76%), 134 (20%), 105 (70%), 77 (100%); ms (ci, CH_4) *m/z*: 324 (M+1, 10%), 254 (9%), 230 (40%), 209 (100%), 180 (42%), 132 (46%), 104 (24%), 71 (75%). The *trans* geometry was confirmed by means of single crystal X-ray diffraction.

A minor fraction from the plate (ca. 1% yield) was a thick yellow oil to which the corresponding *cis* structure was assigned on the basis of its spectra; ir (film) cm^{-1}: 1785 (CO), 1595 (N=N); ^1H nmr (200 MHz, $CDCl_3$) δ: 1.38 (s, 3H), 1.56 (s, 3H), 5.79 (s, 1H), 6.96–7.40 (m, 10H); ^{13}C nmr (50.3 MHz, $CDCl_3$) δ: 24.08 (CH_3), 24.35 (CH_3), 84.20 (C3), 122.37 (C6), 122.57 (C4), 115.50, 121.14, 123.00, 127.14, 129.36, 129.75 (6 CH, aryl), 133.51 (N-C1, aryl), 156.75 (O-C1, aryl), 162.48 (CO); ms (ei) *m/z*: 209 ($M-N_2-CO-C_3H_6O$, 95%), 180 (100%), 132 (18%), 105 (33%), 77 (34%); ms (ci, NH_3) *m/z*: 341 ($M+NH_4$, 50%), 326 (7%), 308 (11%) 210 ($M+1-N_2-CO-C_3H_6O$, 100%), 180 (32%), 118 (11%).

Thermolysis in benzene

For attempted trapping with 1,3-diphenylisobenzofuran a solution of β-lactam oxadiazoline **1***a* (*trans* isomer, 27.6 mg, 0.085 mmol) and diphenylisobenzofuran **14** (70.0 mg, 0.256 mmol) in benzene (0.4 mL) was sealed into a glass tube after three cycles of freeze–pump–thaw degassing. The tube was then immersed in an oil bath (100 ± 0.2°C) for 1 h. Removal of the solvent afforded a yellow oily residue, which was chromatographed on silica (Chromatotron, 2-mm plate) with ether (5%) in hexane as eluent. Excess **14** was eluted first followed by **9***b* and **9***a*.

E-*4-[1-(2-Benzoylphenyl)-1-phenyl]-methylene-3-phenoxy-1-phenylazetidin-2-one,* **9**b

Yellow oil; ir (film) cm^{-1}: 1800 (CO, lactam), 1665 (CO, ketone); ^1H nmr (200 MHz, $CDCl_3$) δ: 5.61 (s, 1H), 6.72–7.58 (m, 24H); ^{13}C nmr (126 MHz, $CDCl_3$) δ: 84.68 (C3, −ve), 128.14 (C4), C5 not assigned, 117.24, 121.77, 123.01, 126.09, 127.09, 127.35, 127.79, 127.99, 128.31, 128.84, 129.44, 129.56, 129.84, 130.02, 132.32, 132.98 (16 CH, aryl, −ve), 130.02, 130.32, 139.85 (3 C, aryl, +ve), 162.10 (CO, lactam); ms (ei) *m/z*: 507 (M, 10%), 414 (6%), 388 (M-PhNCO, 34%), 370 (8%), 311 (10%), 270 (M−β-lactam, 100%), 241 (20%), 193 (9%), 165 (26%), 144 (27%), 116 (9%), 105 (56%), 77 (92%); ms (ci, NH_3) *m/z*: 508 (M+1, 100%), 388 (M−PhNCO, 12%), 270 (M−β-lactam, 10%).

Z-*4 [1-(2-Benzoylphenyl)-1-phenyl] methylene-3-phenoxy-1-phenylazetidin-2-one,* **9**a

Yellow oil; ir (film) cm^{-1}: 1800 (CO, lactam), 1740 (C=C, tentative), 1670 (CO, ketone); ^1H nmr (200 MHz, $CDCl_3$) δ: 6.07 (br s, 1H), 6.86–7.72 (m, 24H); ^{13}C nmr (126 MHz, $CDCl_3$) δ: 84.82 (C3), 118.10 (C5 or C4), 123.22 (C4 or C5), 122.39, 126.13, 126.57, 126.70, 127.79, 128.13, 128.33, 128.90, 129.29, 129.85, 130.02, 131.90, 132.67 (13 CH, aryl), 136.53 (C1, aryl), 137.14 (C1, aryl), 137.93 (2 C1, aryl), 157.34 (O-C1, aryl), 166.96 (CO, β-lactam), 189.28 (CO, ketone); ms (ei) *m/z*: 507 (M, 10%), 414 (12%), 388 (M−PhNCO, 69%), 311 (15%), 270 (M−lactam, 100%), 241 (10%), 209 (18%), 144 (30%); structure confirmed by single crystal X-ray diffraction on a crystal grown from hexane.

Thermolysis in methanol

Reactions were carried out in sealed nmr tubes of medium wall thickness. In a typical experiment, oxadiazoline **1***a* (32 mg,

Can. J. Chem. Downloaded from www.nrcresearchpress.com by 109.225.110.28 on 09/08/12
For personal use only.

0.1 mmol) in methanol (0.25 mL) was degassed by means of three freeze–pump–thaw cycles (10^{-2} Torr; 1 Torr = 133.3 Pa) before the tube was sealed. The tube was then immersed in oil (100 ± 0.2°C) for 55 min before it was opened and the excess solvent was removed by bulb-to-bulb distillation on the vacuum line. Reactions in which benzene was used to dilute the methanol were run in the same way.

The residue remaining after solvent removal was taken up in $CDCl_3$ for ^1H nmr and ^{13}C nmr spectroscopy. Those spectra were clean, indicating two isomeric products only, except for the cases where dilute methanol-in-benzene solutions were used. In those cases the nmr spectra were very complex and both assignments of the spectra and attempts to separate components of the product mixture failed.

4-Methoxy-3-phenoxy-1-phenylazetidin-2-one

The only product observed by ^1H nmr spectroscopy, following thermolysis of **1***a* in neat methanol were the *trans* and *cis* isomers **11***a* and **11***b* (*trans*: *cis* = 2.6:1) as a yellow oil. Spectra were obtained with the mixture; ir (film, cm^{-1}): 1770 (C=O); ^1H nmr (200 MHz, $CDCl_3$, *trans* isomer) δ: 3.55 (s, OCH_3), 5.28 (d, J = 0.8 Hz), 5.46 (d, J = 0.8 Hz), 7.06–7.57 (m); *cis* isomer, δ: 3.55 (s, OCH_3), 5.33 (d, J = 3.6 Hz), 5.71 (d, J = 3.6 Hz), 7.06–7.57 (m), total integrals (Σ doublets : Σ OMe : Σ ArH) in satisfactory ratios; ^{13}C nmr (50.3 MHz, $CDCl_3$, *trans* isomer) δ: 53.83 (OCH_3), 83.67 (C4, tent.), 84.61 (C3, tent.), 160.94 (CO); *cis* isomer, δ: 54.53 (OCH_3), 81.79 (C3, tent.), 88.23 (C4, tent.), 163.07 (CO), observed signals not assigned to a particular isomer, 115.56, 115.70, 117.47, 117.57, 122.55, 125.31, 125.34, 129.31, 129.65, 129.76 (10 CH, aryl, 136.70 (N-C1, aryl, both isomers), 157.07 and 157.40 (OC1, aryl); ms (ei), *m/z*: 269 (M, 13%), 150 (M−PhNCO, 100%), 135 (15%), 104 (15%), 84 (15%), 77 (60%); ms (ci, NH_3) *m/z*: 287 (M + NH_4, 100%), 270 (M + 1, 90%), 178 (18%), 150 (28%), 138 (5%), 136 (14%), 94 (11%); ms (high resolution) *m/z*: 269.1056; calcd. for $C_{16}H_{15}NO_3$: 269.1052.

Acknowledgement

This work was financed from a grant provided by the Natural Sciences and Engineering Research Council of Canada. We are grateful to Dr. C. S. Frampton for the X-ray crystallography.

1. (*a*) R. B. Sykes, C. M. Cimarusti, D. P. Bonner, K. Bush, D. M. Floyd, N. H. Geodopapadakou, W. H. Koster, W. C. Lin, W. L. Parker, P. A. Principle, M. L. Rathnum, W. A. Slusarchyk, W. H. Treo, and J. S. Wells. Nature, **291**, 489 (1981); (*b*) P. C. Cherry and C. W. Newall. *In* Chemistry and biology of β-lactam antibiotics. Vol. 2. *Edited by* R. B. Morin and M. Gorman. Academic Press, New York. 1982. pp. 361–408; (*c*) A. G. Brown and S. M. Roberts (*Editors*). Recent advances in the chemistry of β-lactam antibiotics. The Royal Society of Chemistry, Burlington House, London. 1984; (*d*) T. Kametani. Heterocycles, **25**, 729 (1987).
2. M. Zoghbi and J. Warkentin. J. Org. Chem. **56**, 3214 (1991).
3. R. A. Olofson, D. S. Morrison, and A. Banerji. J. Org. Chem. **49**, 2652 (1984).
4. T. Sheradsky and D. Zbaida. J. Heterocycl. Chem. **20**, 245 (1983).
5. (*a*) D. H. R. Barton, E. Buschmann, J. Haüsler, C. W. Holzapfel, T. Sheradsky, and D. A. Taylor. J. Chem. Soc. Perkin Trans. 1, 1107 (1977); (*b*) R. D. Allan, D. H. R. Barton, M. G. Girijavellabhan, P. G. Sammes, and M. V. Taylor. J. Chem. Soc. Perkin Trans. 1, 1182 (1973).
6. G. Kretschmer and R. N. Warrener. Tetrahedron Lett. 1335 (1975).
7. (*a*) D. E. Davis and R. C. Storr. *In* Comprehensive heterocyclic chemistry. Vol. 7. *Edited by* W. Lwowski. Pergamon Press, Oxford, England. 1984. p. 237; (*b*) K. Clauss, D. Grimm, and G. Prossel. Liebigs Ann. Chem. 539 (1974); (*c*) S. Mickel. Aldrichimica Acta, **18**, 95 (1985); (*d*) H. Fritz, P. Sutter, and C. D. Weis. J. Org. Chem. **51**, 558 (1986); (*e*) K. Prasad, K. Adlgasser, R. Sharma, and P. Stütz. Heterocycles, **19**, 2099 (1982); (*f*) D. J. Hart and D.-C. Ha. Tetrahedron Lett. **26**, 5493 (1985); (*g*) S. Uyeo and H. Itani. Tetrahedron Lett. **32**, 2143 (1991); (*h*) R. P. Attrill, A. G. M. Barett, P. Quayl, J. van der Westhuisen, and M. J. Betts. J. Org. Chem. **49**, 1679 (1984); (*i*) D. H. Hua and A. Verma. Tetrahedron Lett. **26**, 547 (1985); (*j*) Y. Kita, N. Shibata, N. Yoshida, and T. Tohjo. Tetrahedron Lett. **32**, 2375 (1991); (*k*) C. Nativi, E. Perrotta, A. Ricci, and M. Taddei. Tetrahedron Lett. **32**, 2265 (1991); (*l*) H. R. Pfaendler and H. Hoppe. Heteroycles, **23**, 265 (1985); (*m*) F. P. Cossio, B. Lecea, and C. Palomo. J. Chem. Soc. Chem. Commun. 1743 (1987); (*n*) A. Arrieta, B. Lecea, F. P. Cossio, and C. Palomo. J. Org. Chem. **53**, 2784 (1988); (*o*) L. R. Fedor. J. Org. Chem. **49**, 5094 (1984).
8. (*a*) A. I. Meyers, T. J. Sowin, S. Scholz, and Y. Ueda. Tetrahedron Lett. **28**, 5103 (1987); (*b*) T. J. Sowin and A. I. Meyers. J. Org. Chem. **53**, 4154 (1988).
9. (*a*) I. Yamamoto, I. Abe, M. Mozawa, M. Kotani, J. Motoyoshiya, H. Gotoh, and K. Matsuzaki. J. Chem. Soc. Perkin Trans. 1, 2297 (1983); (*b*) I. Yamamoto, I. Abe, M. Mozawa, J. Motoyoshiya, and H. Gotoh. Synthesis, 813 (1981).
10. E. V. Dehmlow, W. Broda, and N. H. Schladerbeck. Tetrahedron Lett. **25**, 5509 (1984).
11. K. Narasimhan and P. R. Kumar. Indian J. Chem. **23B**, 512 (1984).
12. (*a*) G. Herzberg and J. Shoosmith. Nature, **183**, 1801 (1959); (*b*) G. Herzberg. Proc. R. Soc. London, A: **262**, 291 (1961); (*c*) G. Herzberg and J. W. C. Johns. Proc. R. Soc. London, A: **295**, 107 (1966).
13. M. T. H. Lui and R. Bonneau. J. Am. Chem. Soc. **112**, 3915 (1990), and references therein.
14. X.-M. Du, H. Fan, J. L. Goodman, M. A. Kesselmayer, K. Krogh-Jesperson, J. A. LaVilla, R. A. Moss, S. Shen and R. S. Sheridan. J. Am. Chem. Soc. **112**, 1920 (1990).
15. M. Békhazi and J. Warkentin. J. Am. Chem. Soc. **103**, 2473 (1981).
16. H. J. Gordon, J. C. Martin, and H. McNab. J. Chem. Soc. Chem. Commun. 957 (1983).
17. S. T. Perri and H. W. Moore. J. Am. Chem. Soc. **112**, 1897 (1990), and references therein.
18. R. A. Moss, E. G. Jang, H. Fan, M. Wlostowski, and K. Krogh-Jespersen. J. Phys. Org. Chem. **5**, 104 (1992).
19. J. Adams and D. M. Spero. Tetrahedron, **47**, 1765 (1991).
20. (*a*) G. A. Koppel. *In* Heteroyclic compounds. *Edited by* A. Hassner. Wiley–Interscience, New York. 1983. p. 219; (*b*) K. S. Holden. *In* Chemistry and biology of β-lactam antibiotics. Vol. 2. *Edited by* R. B. Morin and M. Gorman. Academic Press, New York. 1982. p. 99; (*c*) A. K. Bose, B. Lai, and B. Dayal. Tetrahedron Lett. 2633 (1974); (*d*) D. A. Nelson. J. Org. Chem. **37**, 1447 (1972).

Can. J. Chem. Downloaded from www.nrcresearchpress.com by 109.225.110.28 on 09/08/12
For personal use only.

Computational and ultraviolet photoelectron spectroscopic studies of 5-substituted cyclopentadienes. Evidence that $n-\pi$ orbital mixing in the HOMO is not the source of the *syn* π-facial selectivity in Diels–Alder reactions

NICK H. WERSTIUK[1] AND JIANGONG MA
Department of Chemistry, McMaster University, Hamilton, Ont., Canada L8S 4M1

AND

JOHN B. MACAULAY AND ALEX G. FALLIS
The Ottawa–Carleton Chemistry Institute, Department of Chemistry, University of Ottawa, Ottawa, Ont., Canada K1N 6N5

Received April 14, 1992

NICK H. WERSTIUK, JIANGONG MA, JOHN B. MACAULAY, and ALEX G. FALLIS. Can. J. Chem. **70**, 2798 (1992).

A series of C5 monomethyl (**1***a*–**1***f*) and pentamethylcyclopentadienes (**2***a*–**2***f*) bearing stereogenic C5 heteroatom substituents (-NH_2, -OH, -OCH_3, and -SCH_3) have been studied computationally (*ab initio* and AM1) and with ultraviolet photoelectron (pe) spectroscopy. In the case of compounds **1***d*–**1***f* and **2***d*–**2***f*, the conformations **3** and **4** of C_s symmetry with the lone paris *anti* to the cyclopentadiene ring are computed to be the most stable geometries. On the other hand, the twisted-*anti* conformers **5***a* and **5***b* are the most stable geometries of **1***c* and **2***c*. Analysis of the computed MO eigenvalues (orbital energies), MO eigenvectors (orbital coefficients), and the pe spectra of cyclopentadienes **2***a*–**2***f* established that $n-\pi$ orbital mixing is not important in the HOMO's of **1***c*–**1***d* or **2***c*–**2***d*. That the ionization energy of the HOMO is found to be virtually independent of the substituent at C5 in the series **2***a*–**2***f*, provides support for the computational results. Because **2***c*–**2***d* undergo Diels–Alder reactions selectively, *syn* to the heteroatom substituent, $n-\pi$ orbital mixing in the HOMO cannot be the source of the π-facial selectivity observed for these compounds.

NICK H. WERSTIUK, JIANGONG MA, JOHN B. MACAULAY et ALEX G. FALLIS. Can. J. Chem. **70**, 2798 (1992).

Utilisant des calculs (*ab initio* et AM1) et la spectroscopie photoélectronique ultraviolette, on a étudié une série C5 de monométhyl (**1***a*–**1***f*) et de pentaméthylcyclopentadiènes (**2***a*–**2***f*) portant des substituants hétéroatomiques stéréogéniques en C5 (-NH_2, -OH, -OCH_3 et -SCH_3). Dans les cas des composés **1***d*–**1***f* et **2***d*–**2***f*, les calculs ont permis d'établir que les conformations **3** et **4** de symétrie C_s, dans lesquelles les paires libres sont *anti* par rapport au cycle cyclopentadiène, possèdent les géométries les plus stables. Par ailleurs, les conformères *anti* déformés, **5***a* et **5***b*, correspondent aux géométries les plus stables des composés **1***c* et **2***c*. Une analyse des valeurs propres calculées pour les OM (énergies des orbitales), des vecteurs propres des OM (coefficients des orbitales) et des spectres pe des cyclopentadiènes **2***a*–**2***f* a permis d'établir qu'un mélange d'orbitales $n-\pi$ n'est pas important dans les OM hautes occupées des produits **1***c*–**1***d* ou **2***c*–**2***d*. Le fait que l'énergie d'ionisation de l'OM haute occupée soit virtuellement indépendante de la nature du substituant en C5, dans la série **2***a*–**2***f*, confirme les résultats des calculs. Compte tenu du fait que les composés **2***c*–**2***d* subissent des réactions de Diels–Alder sélectivement *syn* par rapport au substituant hétéroatomique, on en conclut que le mélange d'orbitals $n-\pi$ dans l'OM haute occupée ne peut pas être la source de la sélectivité π-faciale observée pour ces composés.

[Traduit par la rédaction]

Introduction

The origin of the π-facial diastereoselectivity observed in Diels–Alder (DA) reactions of C5 heteroatom-substituted cyclopentadienes is still imperfectly understood. Consequently, to determine the key factors responsible, a wide range of substrates have been studied both experimentally (1–11) and computationally (11–18). These investigations revealed that a number of interrelated factors are important. Various suggestions have been advanced as possible sources for the pattern observed. These include steric effects, complexation between the diene and the dienophile, secondary orbital interactions, polarizability, electrostatic interactions, orbital mixing, and transition-state hyperconjugation. This latter interpretation, proposed originally by Cieplak (19) for reactions of cyclohexanones, is based on the concept of transition-state stabilization by σ-electron donation from the adjacent bond into the vacant σ orbital associated with the incipient bond. This explanation accounted for the *syn* approach of a butadiene to 5-fluoroadamantane-2-thione where the electrostatic model failed (20). Macaulay and Fallis and co-workers extended these ideas to Diels–Alder reactions of 2,5-dimethylthiophenes oxides (21) and C-5 substituted cyclopentadienes (22) to rationalize the preference observed for cycloaddition *anti* to the antiperiplanar σ bond that is the better donor.

The synthetic utility of the Diels–Alder reaction is well established (23). Nevertheless, the ability to control the facial selectivity without the use of a chiral auxiliary is often limited. Complete facial control renders the reaction enantioselective and with asymmetric, planar 1,3-dienes there exists a latent capacity to establish five or more chiral centres in one operation. Thus it is desirable to identify the factors that affect the π-facial diastereoselectivity so the stereochemistry of Diels–Alder reactions of C5 substituted cyclopentadienes can be predicted with certainty and the adducts utilized for the total synthesis of complex natural products.

We undertook a study of two groups of substituted cyclopentadienes. One group consisting of the C5 disubstituted cyclopentadienes **1***a*–**1***e* was studied computationally with *ab initio* and semiempirical methods. The other class, **2***a*–**2***f*, were synthesized earlier (9, 22) to establish experimentally the diastereoselective preferences in this series. The

[1]Author to whom correspondence may be addressed.

Can. J. Chem. Downloaded from www.nrcresearchpress.com by 109.225.110.28 on 09/08/12
For personal use only.

Can. J. Chem. Downloaded from www.nrcresearchpress.com by 109.225.110.28 on 09/08/12
For personal use only.

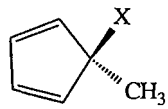

1

a, X = H
b, X = CH_3
c, X = NH_2
d, X = OH
e, X = OCH_3
f, X = SCH_3

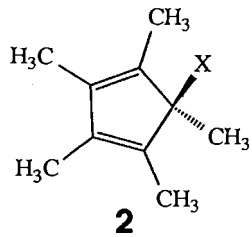

2

a, X = H
b, X = CH_3
c, X = NH_2
d, X = OH
e, X = OCH_3
f, X = SCH_3

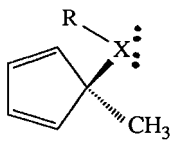

3

a, X = O; R = H or CH_3
b, X = S; R = CH_3

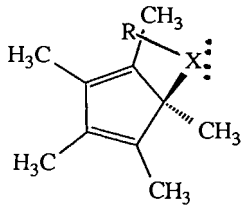

4

a, X = O; R = H or CH_3
b, X = S; R = CH_3

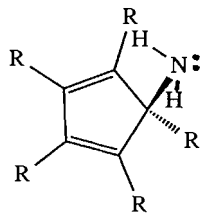

5

a, R = H
b, R = CH3

TABLE 1. Diastereoselectivities for Diels–Alder reactions of pentamethylcyclopentadienes with maleic anhydride

Compound[a]	Reaction time[b]	Addition ratio *syn*	Addition ratio *anti*
2*c*	<30 s	10	0
2*d*	<10 min	10	0
2*e*	3.5 h	10[c]	0
2*f*	27.5 h	1	9

[a]See ref. 9.
[b]Approximate time for diene disappearance (TLC); reactions were run at 22°C; ratios determined by integration of ^{1}H NMR spectra of the total reaction mixture.
[c]*N*-Phenylmaleimide adduct.

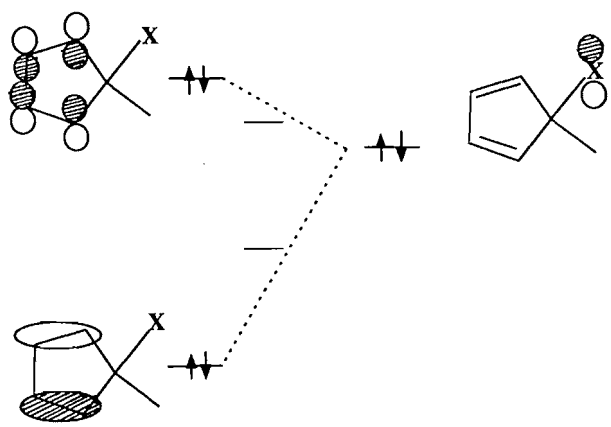

SCHEME 1

results are shown in Table 1. This group has been examined both computationally and experimentally with the aid of ultraviolet photoelectron spectroscopy (UPS) measurements. The objectives of the combined computational/UPS study were to determine the conformational preferences of the heteroatom substituents at C5 and gain information on the magnitude of the n–π orbital mixing in the HOMO in both series of compounds. This is important since it has been postulated that the latter effect is important in determining the *syn*-facial selectivity observed for reactions of cyclopentadienes bearing oxygen and chlorine substituents at C5 (13). According to the orbital mixing rule (13), for cyclopentadienes bearing heteroatom substituents at C5 the π-HOMO combines out of phase with the n- and σ-orbitals in such a way that the n-orbital mixes with the π-HOMO (Scheme 1). This produces a nonequivalent extension of the π-MO in the direction of the substituent and leads to preferential *syn* attack of the incoming dienophile. In view of the facial diastereoselectivities observed for **2***c*–**2***f* (9, 22), we anticipated that a computational study of compounds **1***a*–**1***f* and **2***a*–**2***f*, coupled with a UPS study of **2***a*–**2***f*, would establish whether n–π orbital mixing occurs in the HOMO of these compounds and thereby establish its importance in determining the π-facial selectivity of DA reactions of C5 heteroatom-substituted cyclopentadienes (cp's). Methyl substitution at C1, C2, C3, and C4 of the cp ring should differentially destablize the HOMO and lead to an increase in the ϵ_{HOMO}, ϵ_n gap ($\epsilon_{HOMO} > \epsilon_n$) in the series of compounds **2***c*–**2***f* relative to the 5,5-disubstituted cp's, **1***a*–**1***f*. In principle, this should reduce the magnitude of the n–π_{HOMO} interaction and, according to the orbital mixing model, result in a loss of facial diastereoselectivity.

In this paper we document and discuss the results of the *ab initio* and semiempirical calculations and analyze the

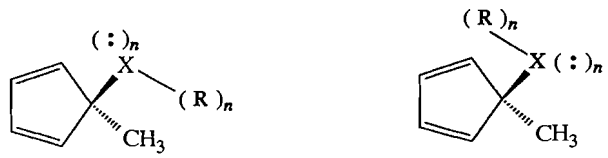

lp - *syn* (*n*=1 or 2) lp - *anti* (*n*=1 or 2)

SCHEME 2

TABLE 2. *Ab initio* relative energies of 5,5-disubstituted cyclopentadiene conformers

Diene	Relative energy (kcal mol^{-1})[a]		
	C_S *syn*	C_S *anti*	Twisted-*syn*
1*c*	2.99	3.93	0(−286.57908)[b]
1*d*	3.79	0(−306.39110)	2.61
1*e*	6.88	0(−345.37622)	3.33
1*f*	5.85	0(−667.70577)	1.74

[a]The total energy (hartrees) of the most stable conformation is given in parentheses. All calculations were done at the 4-31G**//4-31G level.
[b]This is the twisted-*anti* conformation of **1***c*.

photoelectron (pe) spectra of **2***a*–**2***f*. From the pe spectral data and the results of the *ab initio* and semiempirical computational studies, information was gained on the magnitude of the n–π interactions in dienes **2***c*–**2***f*. This has led to new insights and improved our predictive capability.

Results and discussion

Ab initio *calculations on 5,5-disubstituted cyclopentadienes*

Ab initio calculations (24, 25) were carried out on cyclopentadienes **1***a*–**1***e* (i) to determine the preferred orientation, *syn* or *anti* to the cp ring, of the lone pairs of X (Scheme 2), and (*ii*) to gain information on the degree of the interaction of the lone pairs with the π-system from computed eigenvectors (orbital coefficients) and eigenvalues (orbital energies) with no methyl substituents on the carbons of the π-system. Calculations were first carried out on conformations with the lone pair(s) *syn* and *anti* to the cp ring, with forced C_S symmetry in both cases. Optimizations were carried out with 3-21G and 4-31G basis sets, but the geometries obtained with the 4-31G calculations were used for single point calculations at the 4-31G** level. This was so because the differences in energy between the C_S *anti* and C_S *syn* conformers were computed to be smaller (in the order of 1 kcal mol^{-1}) with the 4-31G basis set than the 3-21G basis set. In fact, this led to a switch in the computed relative stabilities of the C_S *anti* and C_S *syn* conformers in the case of **1***c*. When the 3-21G basis set was used the C_S *anti* conformer was found to be slightly lower in energy (0.03 kcal mol^{-1}) than C_S *syn* conformer; with the 4-31G basis set the C_S *syn* conformer was 0.1 kcal mol^{-1} lower in energy than the *anti* conformer. Single point calculations at the 4-31G** level on the 4-31G geometries gave the results documented in Table 2. Polarization functions were added to hydrogens in addition to the heavy atoms simply to balance the basis set. When the 4-31G C_S geometries of the *anti* conformations of **1***d*, **1***e*, and **1***f* were used as starting points for full optimizations in the absence of the symmetry constraint, C_S symmetry was maintained. To establish with certainty that the C_S *anti* conformation is the global minimum for **1***d*–**1***f*, the CH_3—C(5)—O—CH_3 dihedral angle of **1***e* was set at 170° and the geometry was optimized with the 4-31G basis set without any symmetry constraints. That the dihedral angle was 179.9° in the optimized geometrical structure indicates that the C_S *anti* conformation is the global minimum of **1***e*. Furthermore a FORCE calculation on the 4-31G geometry gave no imaginary frequencies. Because the C_S *anti* conformations are computed to be the most stable geometrical structures of **1***d* and **1***f* as well, frequency calculations were not carried out on these compounds. When the *syn* conformations of these compounds were optimized without the C_S symmetry constraint, twisting occurred about the C5—X bond to relieve torsional strain. Table 2 lists the total and relative energies of three conformations of **1***c*, **1***d*, **1***e*, and **1***f*. Table 3 lists the torsional angles of the twist conformations and Table 4 documents the orbital energies of **1***a*–**1***f*. As is seen from the data in Table 2, except for the amino compound, the C_S *anti* conformers of **1***d*, **1***e*, and **1***f* are computed to be more stable than the C_S *syn* and twisted-*syn* conformers, which would be considered to be the most reactive in the orbital mixing model. For the amino compound **1***c*, the twisted-*syn* conformer **5***a* was computed to be

TABLE 3. Torsional angles of twisted cyclopentadiene conformers

Diene	H_3C—C5—X—R torsional angle (deg)	
	Ab initio (4-31G)	AM1
1*c*	175.4, −51.4	177.4, −58.6
1*d*	66.4	67.0
1*e*	69.9	64.3
1*f*	66.9	66.5
2*c*	[a]	175.0, −65.5
2*d*	53.1	70.0
2*e*	[a]	42.0
2*f*	37.5	51.4

[a]Not computed at the *ab initio* level.

TABLE 4. *Ab initio* orbital energies of 5,5-disubstituted cyclopentadienes

Diene	Orbital energy (eV)[a]			
	HOMO	HOMO-1	HOMO-2	HOMO-3
1*b*	8.19	11.02		
1*c syn*	8.20	9.90	11.34	
anti	8.31	9.86	11.35	
Twisted-*anti*	8.15	10.15	11.30	
1*d syn*	8.29	11.43	11.65	
anti	8.47	11.63	11.69	
Twisted-*syn*	8.39	11.44	11.84	
1*e syn*	8.21	10.96	11.31	
anti	8.45	11.09	11.53	
Twisted-*syn*	8.35	11.02	11.54	
1*f syn*	8.00	9.34	10.47	11.71
anti	8.23	9.22	10.51	11.69
Twisted-*syn*	8.37	9.05	10.58	11.82

[a]Computed with the 4-31G**//4-31G basis sets.

Can. J. Chem. Downloaded from www.nrcresearchpress.com by 109.225.110.28 on 09/08/12
For personal use only.

Can. J. Chem. Downloaded from www.nrcresearchpress.com by 109.225.110.28 on 09/08/12
For personal use only.

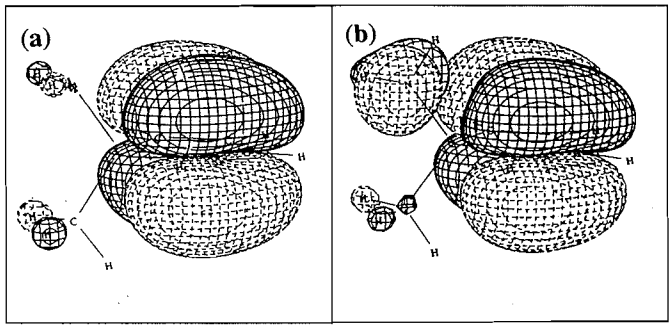

FIG. 1. Plots of the 0.025 au contours of the HOMO's of the C_S *syn* (*a*) and twisted-*anti* (*b*) conformers of **1***c*.

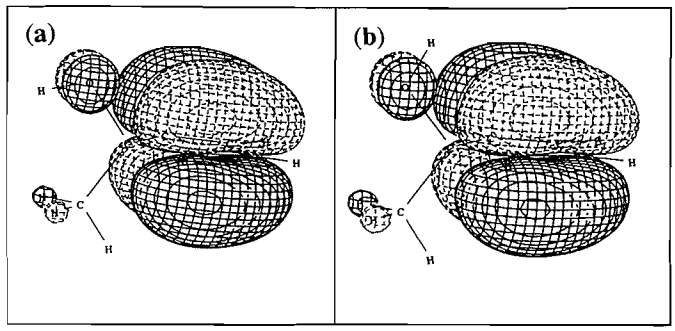

FIG. 2. Plots of the 0.025 au contours of the HOMO's of the C_S *syn* (*a*) and *anti* (*b*) conformers of **1***d*.

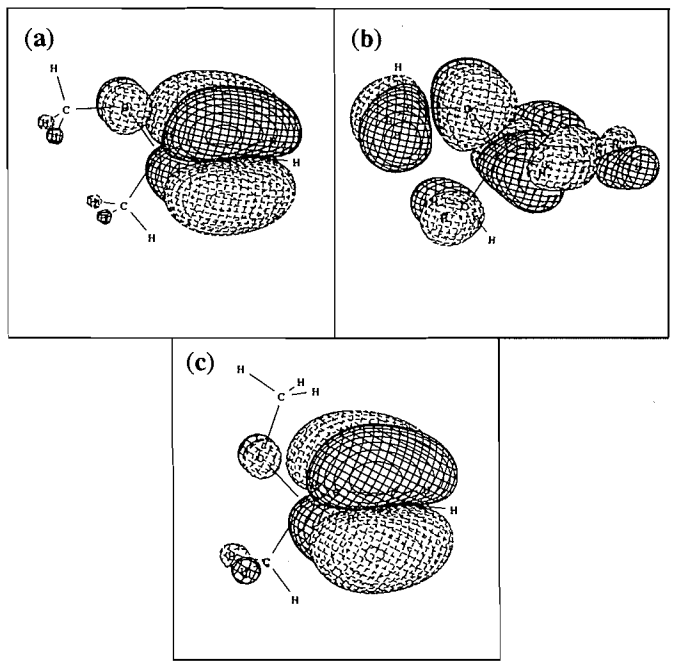

FIG. 3. Plots of the 0.025 au contours of the HOMO (*a*), and HOMO-1 (*b*) of the C_S *syn* conformer and the HOMO (*c*) of the C_S *anti* conformer of **1***e*.

lower in energy than the C_S *anti* conformer with the 4-31G**//4-31G basis sets.

Of importance is the nature of the three highest occupied MO's of **1***c*, **1***d*, **1***e*, and **1***f*. According to the *ab initio* (4-31G**) calculations, there is no significant interaction between the nitrogen and the π-system in the HOMO of the C_S *syn* conformer of **1***c*; the orbital coefficients at N are <0.03.[2] A plot of the HOMO that is diene π-type is given in Fig. 1(*a*). This plot, as well as the others obtained from *ab initio* calculations, was generated with PSI/88(26) and GAUSSIAN 90° checkpoint files; in this and all other examples, the 0.025 au contour is plotted. Because PSI/88 uses only STO-3G, 3-21G, and 6-31G basis sets, the MO's were obtained from single point calculations with the 3-21G(*) basis set on the 4-31G optimized geometry. It is important to note here that the orbital coefficients of the heavy atoms were virtually identical to the coefficients obtained with the 4-31G and 4-31G** basis sets. While the HOMO-1 is predominantly localized on N (coefficient 0.49) there are sizeable coefficients on the methyl carbon (0.20) and C5 (0.17) of the cp ring. There is little mixing with the cp π orbitals; the coefficients at C1, C2, C3, and C4 are less than 0.06. HOMO-2 predominantly cp π-type (orbital coefficients at C1(C4), 0.17; at C2(C5), 0.23), with a sizeable coefficient on N (0.11). For the twisted-*anti* conformer of **1***c* there is mixing of the N lp and the π orbitals in the HOMO as is seen in Fig. 1(*b*). The coefficients on N, C1(C4), and C2(C3) are 0.12, 0.28, and 0.23, respectively. For HOMO-1 the coefficients are 0.44 on N, 0.20 on the carbon (C1) *anti* to the lp, 0.14 on C4, and 0.1 on C5. As was the case for the C_S *syn* conformer, the HOMO-2 is predominantly cp ring π-type. The presence of an *n*–π interaction in the twisted conformation is supported by the fact that the HOMO is destabilized (0.16 eV) and the N lp is stabilized (0.29 eV) relative to the C_S *anti* conformer (Table 4). For the C_S *anti* conformer there is no significant mixing between the N l*p* and the π system in the HOMO. In accord with this result is the fact that the orbital energies (Table 4) do not change significantly relative to the *syn* conformer.

In the case of the C_S *anti* conformer of alcohol **1***d*, a weak interaction between the oxygen (orbital coefficient = 0.1) and the π-system in the HOMO is indicated by the *ab initio* calculations with the 4-31**//4-31G basis sets. This interaction is purely π-type. HOMO-1 is predominantly diene π_+ with some involvement of the oxygen (0.12) and CH_3 orbitals. The third MO involves mixing of oxygen (0.42) with the σ orbitals of the C1—C5 and C4—C5 bonds of the cp ring; at the 4-31G**//4-31G level $\epsilon_{\pi-} > \epsilon_{\pi+} > \epsilon_n$. A plot of the HOMO of **1***d* computed with the 3-21G(*) basis set (the orbital coefficients were virtually identical to the coefficients computed with the 4-31G**//4-31G basis sets) is given in Fig. 2(*a*). For the *anti* conformer the coefficients on oxygen and the carbons of the HOMO are virtually identical to the coefficients of the HOMO of the *syn* conformer, as is seen from a comparison of Fig. 2(*a*) and Fig. 2(*b*).

In going from the C_S *syn* conformer of **1***d* to the C_S *syn* conformer of the methoxy compound **1***e*, the computed energy of the HOMO increases only by 0.08 eV. Based on the magnitude of the coefficients on oxygen (0.12) and carbon, the interaction of the lp with the π-system of the diene (see Fig. 3(*a*)) is similar to the interaction in **1***d*. The HOMO-1 of **1***e* involves mixing of the oxygen orbitals within the framework of the cp ring (see Fig. 3(*b*). The shift of the HOMO-1 from 11.65 to 10.96 eV (Table 3) is as expected for methyl substitution on oxygen. For **1***e*, HOMO-2 is

[2]Since 4-31G** is a split-valence basis set, only the largest coefficient of the pairs of orbitals is given in each case.

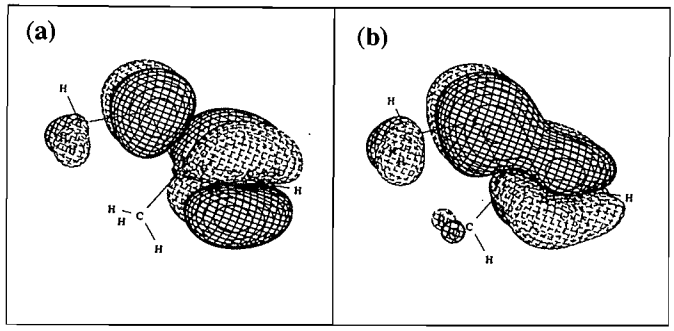

FIG. 4. Plots of the 0.025 au contours of the HOMO (*a*) and HOMO-1 (*b*) of the C_S *syn* conformer of **1***f*.

TABLE 5. AM1 relative energies of 5,5-disubstituted cyclopentadiene conformers

Diene	Relative heat of formation (kcal mol^{-1})		
	C_S *syn*	C_S *anti*	Twisted-*syn*
1*c*	1.61	1.15	0(40.52)[a]
1*d*	2.78	0(−6.68)	1.60
1*e*	3.08	0(0.02)	1.31
1*f*	1.77	0(39.24)	0.52
1	1.63	0(41.70)[b]	0.48

[a]This is the heat of formation of the twisted-*anti* conformation of **1***c*.
[b]These values were obtained using mixed parameters (C,H(AM1), S(MNDO)).

similar to the HOMO-2 of **1***d*: there is a minor degree of mixing of the oxygen and π carbon orbitals with the carbon coefficients predominating. For the C_S *anti* conformer, the oxygen orbital coefficient is reduced (0.06) relative to the C_S *syn* conformation. This is seen in a comparison of the HOMO's given in Fig. 3(*a*) and Fig. 3(*c*). The HOMO and HOMO-2 are stabilized by 0.24 and 0.22 eV, respectively and the HOMO-1 is stabilized by 0.13 eV.

For the C_S *syn* conformer of **1***f* the orbital coefficients define a significant interaction between the sulfur lone pair and the π-system of the cp ring in the HOMO (S, 0.37), and HOMO-1 (S, 0.5) (see Figs. 4(*a*) and 4(*b*). HOMO-2 and HOMO-3 also show considerable mixing of S and cp ring orbitals. An interaction between S and the cp ring is also computed for HOMO, HOMO-1, HOMO-2, and HOMO-3 of the *anti* conformer, as indicated by the coefficients on S and the ring carbons. In fact, based on the coefficients, the mixing is virtually identical to the mixing in the *syn* conformer.

AM1 calculations on 5,5-disubstituted cyclopentadienes

AM1 calculations (27) were also carried out on cyclopentadienes **1***c*–**1***f* as well as **1***a* and **1***b*. As seen from the data in Table 5, the conformational preferences of X-R computed by AM1 are the same as those computed for the series at the 4-31G** level. The *anti* conformations are the lowest-energy geometrical structures of **1***d*, **1***e*, and **1***f*, but the twisted-*anti* conformer of **1***c* is lower in energy than the *anti* or *syn* conformations. The orbital energies are given in Table 6.

TABLE 6. AM1 orbital energies of 5,5-disubstituted cyclopentadiene conformers

Diene	Orbital energy (eV)			
	HOMO	HOMO-1	HOMO-2	HOMO-3
1*a*	9.07	10.93		
1*b*	9.04	11.04		
1*c* *syn*	9.08	9.90	11.42	
anti	9.30	9.88	11.32	
Twisted-*anti*	9.21	9.95	11.32	
1*d* *syn*	9.16	11.43	11.65	
anti	9.39	11.00	11.55	
Twisted-*syn*	9.27	11.03	11.52	
1*e* *syn*	9.10	10.38	11.19	
anti	9.29	10.50	11.43	
Twisted-*syn*	9.22	10.50	11.32	
1*f* *syn*	8.31[a]	9.37	10.62	11.57
anti	8.47[a]	9.36	10.62	
Twisted-*syn*	8.48[a]	9.23	10.62	
1*f* *syn*	8.85[b]	9.43	10.62	
anti	9.05[b]	9.41	10.88	11.51

[a]These orbital energies were obtained using the AM1 parameters for C, H, and S.
[b]These orbital energies were obtained using mixed parameters (C,H(AM1); S(MNDO)).

TABLE 7. *Ab initio* relative energies of pentamethylcyclopentadiene conformers

Diene	Relative energy (kcal mol^{-1})[a]		
	syn	*anti*	Twisted-*syn*
2*d*	3.27	0(−462.40932)	2.63
2*f*	5.16	0(−823.72279)	4.12

[a]The total energies (hartrees) of the most stable conformations are given in parentheses.

TABLE 8. *Ab initio* orbital energies of pentamethylcyclopentadiene conformers

Diene	$-\epsilon_i$ (eV)[a]			
	HOMO	HOMO-1	HOMO-2	HOMO-3
2*b*	7.38	10.15		
2*d* *syn*	7.53	10.44	11.23	
anti	7.67	10.59	11.25	
Twisted-*syn*	7.59	10.48	11.36	
2*f* *syn*	7.53	9.00	10.00	11.30
anti	7.66	8.97	9.98	11.32
Twisted-*syn*	7.57	8.95	9.99	11.33

[a]Computed with the 4-31G**//4-31G basis sets.

Ab initio *calculations on pentamethylcyclopentadienes*

Ab initio calculations were also carried out on **2***b*, **2***d*, and **2***f* with the 4-31G**//4-31G basis sets. As is seen from the data in Table 7, the hydroxyl group of **2***d* has the same conformational preference as **1***d*; the *anti* conformer is more stable than the *syn* or twisted-*syn* conformers. The key point is that the HOMO is destabilized by 0.8 eV relative to **1***d* (Table 8), but HOMO-2 is affected only marginally (0.1 eV). The orbital energies are shown graphically in Fig. 5. For the

Can. J. Chem. Downloaded from www.nrcresearchpress.com by 109.225.110.28 on 09/08/12
For personal use only.

Can. J. Chem. Downloaded from www.nrcresearchpress.com by 109.225.110.28 on 09/08/12
For personal use only.

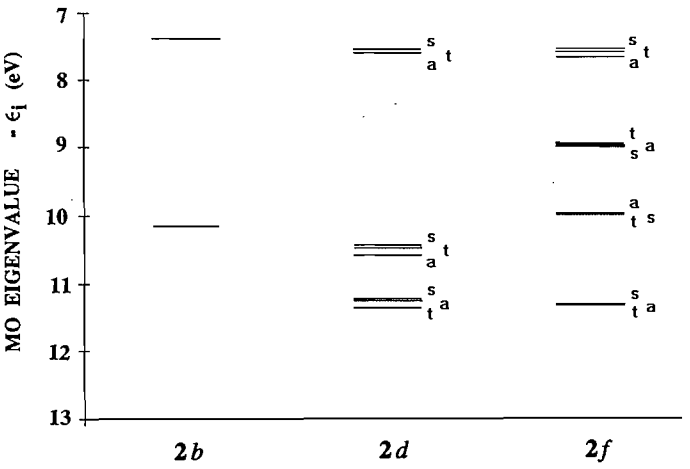

FIG. 5. Orbital energies of the *syn* (s), *anti* (a), and twist (t) conformers of **2***b* (HOMO and HOMO-1), **2***d* (HOMO, HOMO-1, and HOMO-2), and **2***f* (HOMO, HOMO-1, HOMO-2, and HOMO-3) computed with the 4-31G**//4-31G basis sets.

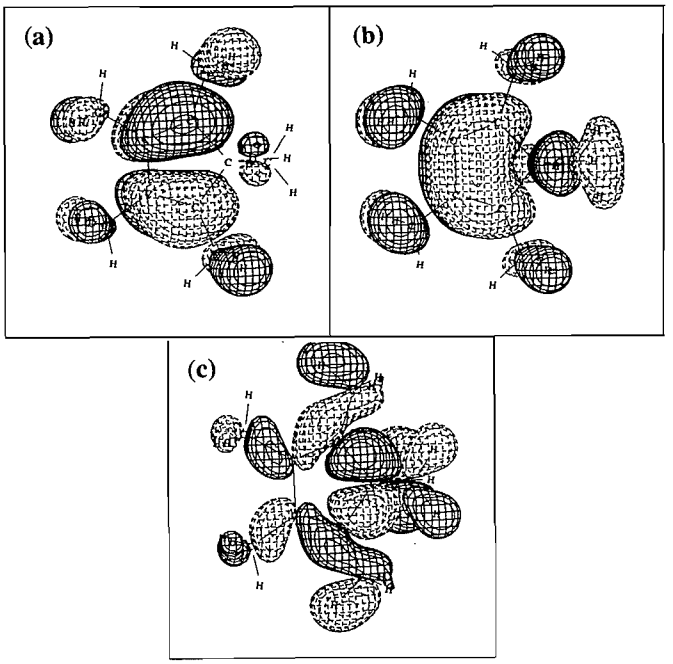

FIG. 6. Plots of the 0.025 au contours of the HOMO (*a*), HOMO-1 (*b*), and HOMO-2 (*c*) of the C_S *syn* conformer of **2***d*.

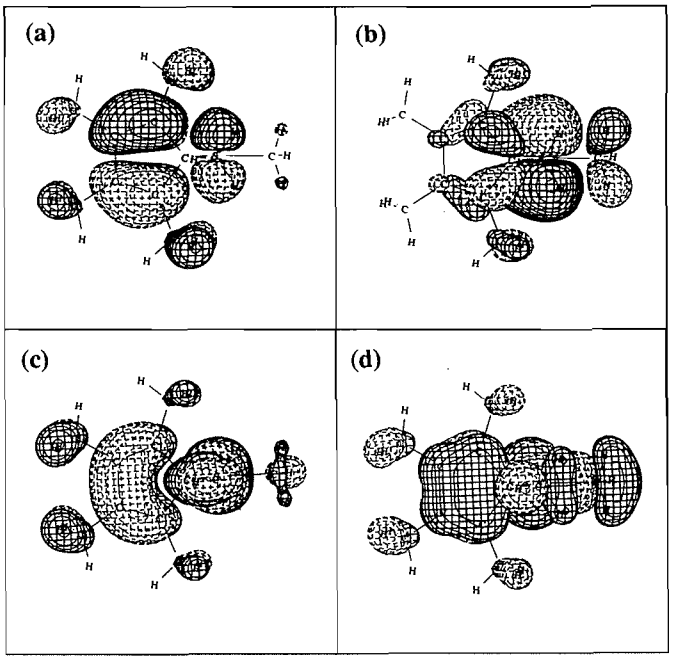

FIG. 7. Plots of the 0.025 au contours of the HOMO (*a*), HOMO-1 (*b*), and HOMO-2 (*c*), and HOMO-3 (*d*) of the C_S *syn* conformer of **2***f*.

TABLE 9. AM1 relative energies of pentamethylcyclopentadiene conformers

	Relative energies (kcal mol^{-1})[a]		
Diene	*syn*	*anti*	Twisted-*syn*
2*c*	1.98	1.15	0(8.15)[b]
2*d*	3.16	0(−38.95)	1.58
2*e*	3.29	0(−31.79)	2.05
2*f*	2.01	0(8.31)	0.82
2	1.86	0(10.92)	0.94[c]

[a]The heat of formation of the most stable conformer is given in parentheses.
[b]The heat of formation of the twisted-*anti* conformation.
[c]These values were obtained with mixed AM1 parameters (C, H(AM1); S(MNDO)).

anti conformation the coefficient on oxygen is smaller (0.06) than the coefficient for the *anti* conformation of **1***d* (0.10). Figures 6(*a*)–6(*c*) give the plots of HOMO, HOMO-1, and HOMO-2 of the C_S *syn* conformer of **2***d* and clearly show that there is no appreciable n–π orbital mixing in the HOMO and HOMO-1. On the other hand, the plot of HOMO-2 also shows that the mixing of the lp orbitals is n–σ, not n–π. Figures 7(*a*)–7(*d*) show the plots of the HOMO, HOMO-1, HOMO-2, and HOMO-3 of the *syn* conformer of **2***f*. In this case there is n–π mixing in the HOMO (S, 0.20; C1(C4), 0.26; C2(C3), 0.20). HOMO-1 is essentially n_S (S, 0.62; C1(C4), 0.098). HOMO-2 and HOMO-3 show a substantial amount of n–π mixing. The coefficients of the four highest occupied MO's of **2***f* are virtually identical to the coefficients of the HOMO, HOMO-1, HOMO-2, and HOMO-3 (plots not shown) of *syn*-**2***f*, as are the orbital energies (Table 8).

AM1 calculations on pentamethylcyclopentadienes

As is seen from the data in Table 9, the twisted-*anti* conformer of **2***c* was computed as the most stable geometry with AM1, in keeping with the results of the *ab initio* and AM1 calculations on **1***c*. The orbital energies given in Table 10 are shown graphically in Fig. 8. For **2***d*, **2***e*, and **2***f* the *anti* conformations are computed to be the most stable geometrical structures. These results are in accord with the *ab initio*/AM1 calculations on **1***d*, **1***e*, and **1***f* and the *ab initio* calculations on **2***d* and **2***f*. Plots of HOMO, HOMO-1, and HOMO-2 of twisted-*anti* - **2***c* (not shown), *syn*-**2***d* (Figs. 9(*a*)–9(*c*), and *syn*-**2***c* (not shown) were obtained with PSI/88 and the AMPAC gpt files. It is seen that the MO's (the 0.025 au contours are plotted) of *syn*-**2***d* are indistinguishable from

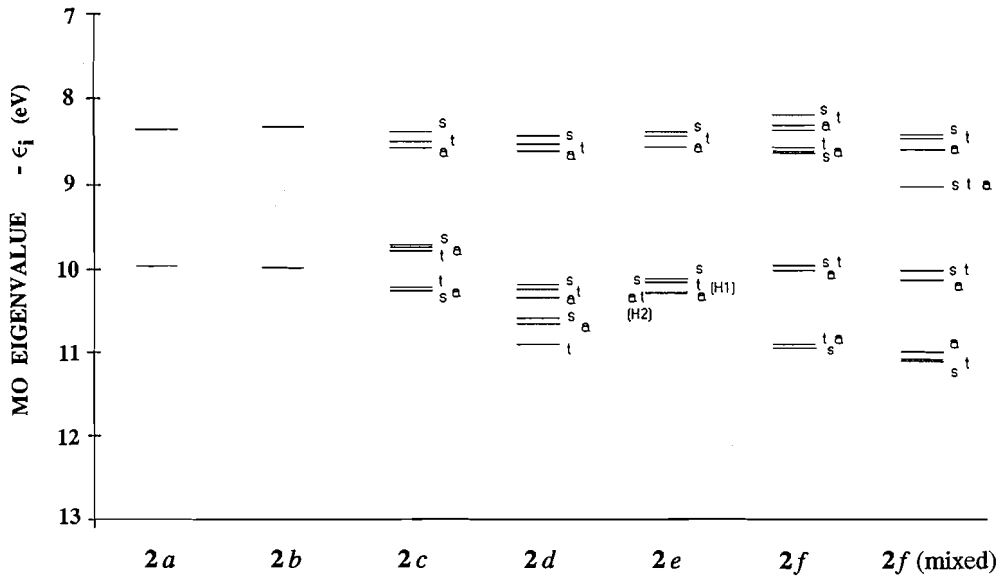

FIG. 8. Orbital energies of **2***a* (HOMO and HOMO-1), **2***b* (HOMO and HOMO-1), and the *syn* (s), *anti* (a), and twist (t) conformers of **2***c* (HOMO, HOMO-1, and HOMO-2), **2***d* (HOMO, HOMO-1, and HOMO-2), **2***e* (HOMO, HOMO-1, and HOMO-2), and **2***f* (HOMO, HOMO-1, HOMO-2, and HOMO-3) computed with AM1. H1 and H2 are the values for HOMO-1 and HOMO-2 of **2***e*. The values for **2***f* (mixed) were obtained with mixed parameters (C,H(AM1); S(MNDO)).

TABLE 10. AM1 orbital energies of pentamethylcyclopentadiene conformers

Diene	Orbital energies (eV) HOMO	HOMO-1	HOMO-2	HOMO-3
2*a*	8.35	9.95		
2*b*	8.33	9.99		
2*c syn*	8.38	9.71	10.26	
anti	8.57	9.74	10.24	
Twisted-*anti*	8.50	9.78	10.21	
2*d syn*	8.43	10.18	10.59	
anti	8.62	10.34	10.66	
Twisted-*syn*	8.53	10.24	10.91	
2*e syn*	8.39	10.12	10.16	
anti	8.55	10.27	10.27	
Twisted-*syn*	8.43	10.14	10.29	
2*f syn*	8.18	8.63	9.96	10.95
anti	8.36	8.60	10.02	10.91
Twisted-*syn*	8.30	8.55	9.96	10.91
2*f syn*	8.41[a]	9.02	10.02	11.91
anti	8.58	9.02	10.13	10.99
Twisted-*syn*	8.46	9.02	10.02	11.11

[a]These values were obtained using mixed AM1 parameters (C, H(AM1): S(MNDO)).

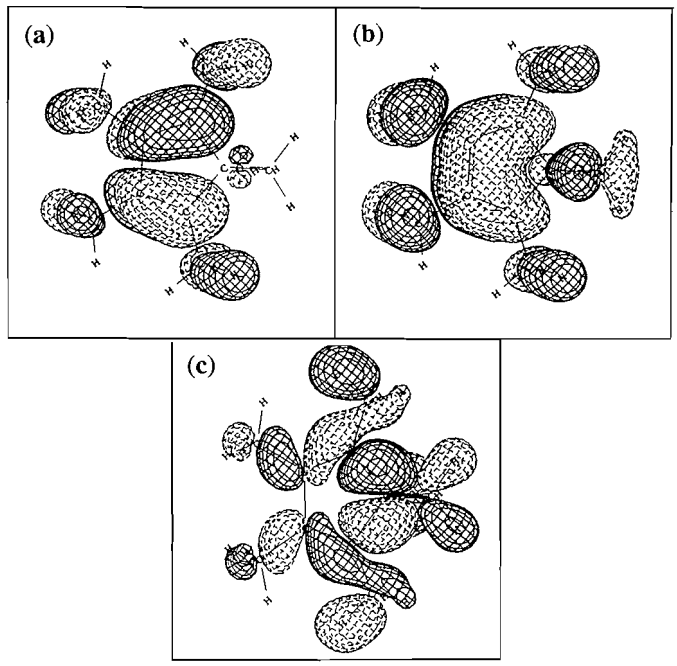

FIG. 9. Plots of the 0.025 au contours of the HOMO (*a*), HOMO-1 (*b*), and HOMO-2 (*c*) of the C_S *syn* conformer of **2***d* computed with AM1.

the 3-21G(*) MO's (Figs. 6(*a*)–6(*c*)). This is the case (not shown) for *syn*-**2***e* as well. The HOMO and HOMO-1 of **2***f* computed with AM1 parameters for C, H, and S are shown in Figs. 10(*a*) and 10(*b*). Based on the orbital energies (Fig. 5) and MO's computed with the 4-31G**//4-31G and 3-21G(*) basis sets, these AM1 calculations overestimate the n_S–π interaction, primarily because the n_S orbital energy is too high. This analysis is supported by the pe spectrum of **2***f* (*vide infra*). On the other hand, calculations with mixed AM1/MNDO parameters (C,H(AM1);S(MNDO) yielded results that compare closely to those obtained with *ab initio* calculations. The HOMO, HOMO-1, HOMO-2, and HOMO-3 or *syn*-**2***f* are shown in Figs. 11(*a*)–11(*d*). The π-type S lp is localized more when mixed parameters are used and the MO's closely resemble the 3-21G(*) MO's shown in Figs. 7(*a*)–7(*d*). This study was carried out to ascertain which set of parameters gives the best description of the orbital energies and MO's of **2***f* before a comprehensive AM1

Can. J. Chem. Downloaded from www.nrcresearchpress.com by 109.225.110.28 on 09/08/12
For personal use only.

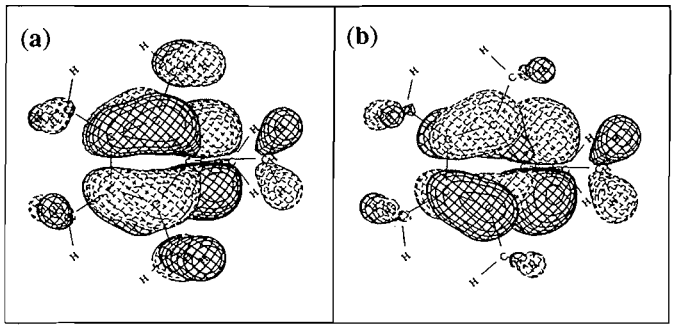

FIG. 10. Plots of the 0.025 au contours of the HOMO (*a*) and HOMO-1 (*b*) of the C_S *syn* conformer of **2***f* computed with AM1 parameters.

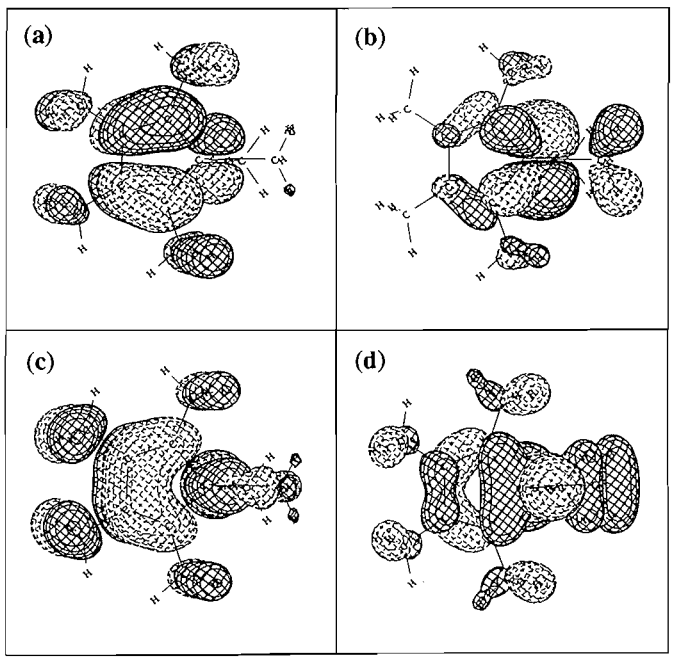

FIG. 11. Plots of the 0.025 au contours of the HOMO (*a*), HOMO-1 (*b*), HOMO-2 (*c*), and HOMO-3 (*d*) of the C_S *syn* conformer of **2***f* computed with AM1 using mixed parameters.

computational study[3] of the Diels–Alder addition of maleic anhydride to **2***a*, **2***c*, **2***d*, **2***e*, and **2***f* was initiated.

The *ab initio* and semiempirical computational studies clearly establish that n–π mixing is not important in the HOMO of **2***c*, **2***d*, and **2***e*. Furthermore, a comparison of the *ab initio* and semiempirical results shows that AM1 calculations give conformational preferences, eigenvalues (orbital energies), and eigenvectors (MO's) that compare favourably with the *ab initio* calculations at the 4-31G** level. This result suggests that AM1 calculations will be useful for studying conformational preferences, n–π orbital mixing in other heteroatom substituted cp's, and the DA reactions of **2***a*–**2***e* with maleic anhydride.

Photoelectron spectra of cyclopentadienes

The pe spectra of **2***a*–**2***f* are given in Figs. 12(*a*–12(*f*), respectively. The IE's are tabulated in Table 11 and shown graphically in Fig. 13. The π_+, π_- splittings of **2***a* and **2***b* are 2.07 ± 0.05 and 2.04 ± 0.05 eV, respectively. These values are similar to the splitting of 2.10 eV observed for 5,5-dimethylcyclopentadiene (28). In going from **2***a* to **2***b* there is a decrease of 0.08–0.10 eV in the π IE's. Relative to cyclopentadiene (28) the IE's of the HOMO and HOMO-1 decrease by 1.20 and 1.28 eV for **2***a* and 1.27 and 1.38 for **2***b*. Relative to 5,5-dimethylcyclopentadiene the shifts of the π_- and π_+ IE's of **2***b* are 1.17 and 1.23 eV, respectively. These results show that the addition of five or six methyls to the cyclopentadiene ring does not produce a significant differential destabilization of π_+ or π_-. According to the *ab initio*/AM1 calculations the HOMO's of **2***a* and **2***b* are basically diene π-type mixed with π-type orbitals of the methyl groups at C1, C2, C3, and C4. No On the other hand, the HOMO-1 does involve orbital mixing with the C—H and C—C bonds at C5.

For the amino compound **2***c*, the IE of the HOMO does not shift significantly relative to **2***a*, but HOMO-2 is stabilized by 0.23 eV (Fig. 12(*c*)). According to the *ab initio*/AM1 calculations, the band at 8.88 eV is due to the nitrogen lone pair. These experimental results are in accord with the AM1 calculations, which showed that there is no significant interaction between the lone pair and the π-system in the HOMO of **2***c* in either of the three conformations studied computationally.

For alcohol **2***d* the HOMO is stabilized relative to **2***a* and **2***b* by 0.17 and 0.24 eV (Fig. 12(*d*)). This is due to an inductive stabilization by oxygen. That the HOMO is stabilized is in accord with the calculations, which showed that there is no significant n–π interaction in the HOMO. The next two bands are closely spaced, as predicted by the *ab initio* calculations. According to the *ab initio*/AM1 calculations there is no significant n–π mixing in the HOMO-1, but HOMO-2 involves mixing of the lone pair orbitals and the σ (C1—C5 and C4—C5) orbitals of the cp ring. This explains why the bands due to HOMO-1 and HOMO-2 overlap rather than being split.

In going from **2***d* to **2***e*, the HOMO (Fig. 12(*e*)) is slightly destabilized (0.1 eV), in keeping with the results of the computational studies. HOMO-2 is stabilized by 0.28 eV relative to **2***a*, a consequence of an indictive effect and a weak n–π interaction with the oxygen lone pairs.

In the case of **2***f*, the lowest IE band (Fig. 12(*f*) is destabilized by 0.09 eV relative to the HOMO of **2***a*. This result is in keeping with the *ab initio*/AM1 calculations, which showed that there is an n–π interaction in the HOMO of **2***f*. Confirmation that this interaction is weak is provided by the fact that the second band, computed to be predominantely n_S, remains sharp (FWHM = 0.2 eV) like the n_S band of $(CH_3)_2S$ (FWHM = 12 eV) (29). The other sulfur lone-pair band is at 10.19 eV.

Because the computed orbital energies, both *ab initio* and AM1 (Tables 8 and 10) are insensitive to the dihedral angle as shown graphically in Figs. 5 and 8, the predicted confor-

[3]We (N.H.W. and J.M.) have found that *syn* approach of maleic anhydride to **2***f* is preferred when AM1 parameters are used for C, H, and S; on the other hand, when mixed parameters are used, *anti* addition is computed to be the low-energy pathway in keeping with the experimental results (Table 1). A manuscript documenting an AM1 computational study of the DA reaction of **2***b*–**2***f* with maleic anhydride is being written.

Can. J. Chem. Downloaded from www.nrcresearchpress.com by 109.225.110.28 on 09/08/12
For personal use only.

Can. J. Chem. Downloaded from www.nrcresearchpress.com by 109.225.110.28 on 09/08/12
For personal use only.

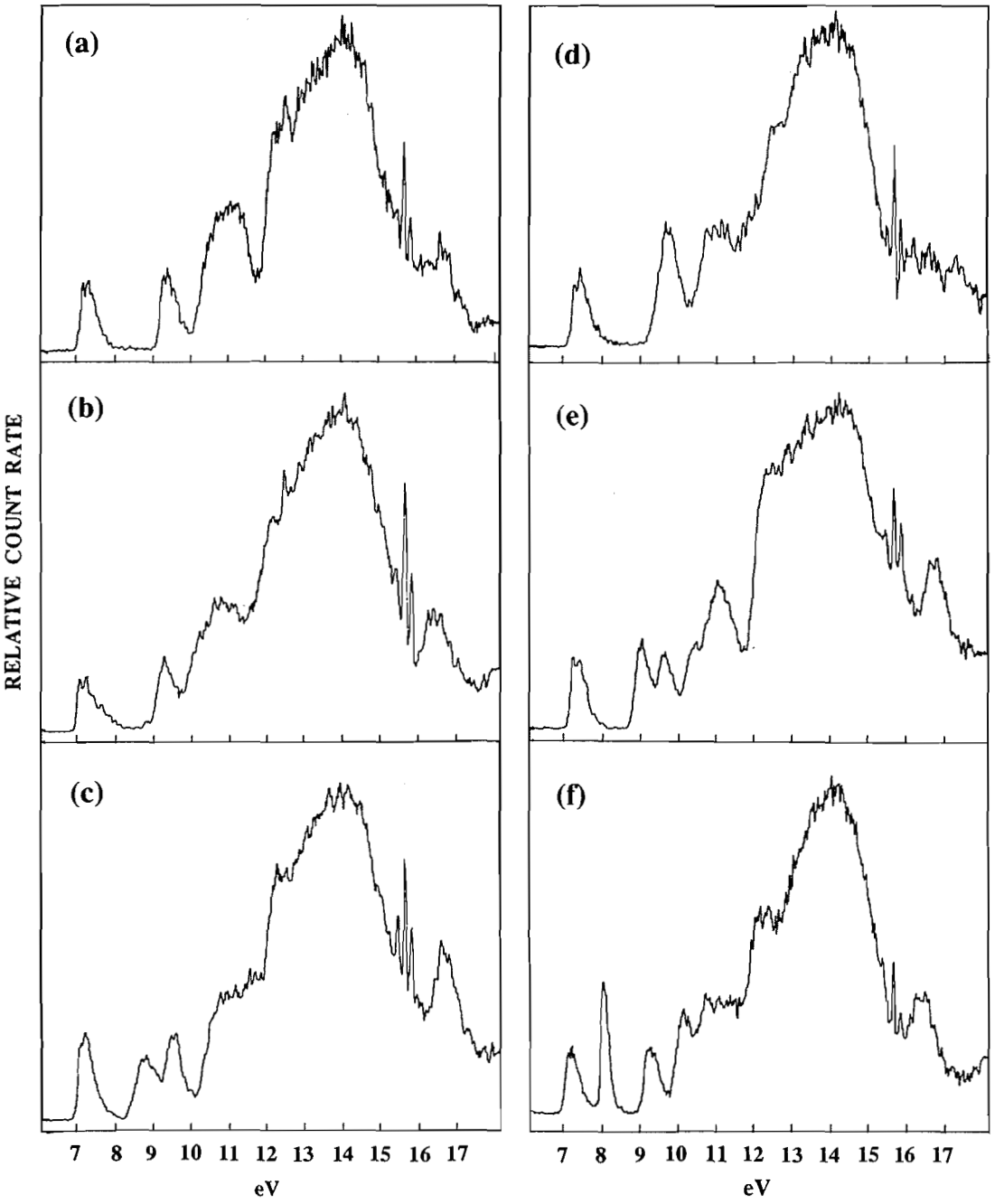

FIG. 12. Ultraviolet photoelectron spectra of **2***a* (*a*), **2***b* (*b*), **2***c* (*c*), **2***d* (*d*), **2***e* (*e*), and **2***f* (*f*).

mational preferences, twisted-*anti* for **2***c* and *anti* for **2***d*, **2***e*, and **2***f*, cannot be corroborated with the pes data.

As far as the correlation between the computed and experimental π_-,π_+ splittings of the dienes is concerned (Table 12), the *ab initio* calculations overestimated the splittings. Nevertheless, the IE's of the HOMO's are computed with good accuracy (Tables 8 and 11). AM1 overestimated the IE's of the HOMO's and underestimated the splittings by 0.4–0.5 eV. The key point is that both methods, assuming that Koopmans' theorem (30) holds, computed the insensitivity of energy of the HOMO to the nature of X at C5 of the cp ring, and this was corroborated by experiment.

Conclusions

The results of the computational studies on **1***a*–**1***f* and **2***a*–**2***f*, the pes studies on **2***a*–**2***f* and the study of the stereochemistry of the DA reactions with maleic anhydride/N-phenylmaleimide clearly show that $n-\pi$ orbital mixing in the HOMO proposed by Inagaki *et al.* (13) cannot be the source of the π-facial selectivity observed in the reactions of cyclopentadienes **2***c*–**2***f*. According to *ab initio*/AM1 calculations and pe spectroscopy there is no significant mixing of the lone-pair orbitals and the π-system in the HOMO's of **2***c*, **2***d*, and **2***e*, a requirement in the orbital mixing model, yet *syn* π-facial selectivity is observed in the DA reactions

TABLE 11. Vertical ionization energies of substituted cyclopentadienes

Diene	Ionization energy (eV)[a]			
	HOMO	HOMO-1	HOMO-2	HOMO-3
2*a*	7.35	9.42		
2*b*	7.28	9.32		
2*c*	7.32	8.88	9.65	
2*d*	7.52	~9.70	~9.90	
2*e*	7.42	9.11	9.70	
2*f*	7.26	8.10	9.32	10.19

[a]The estimated errors are ±0.025 eV.

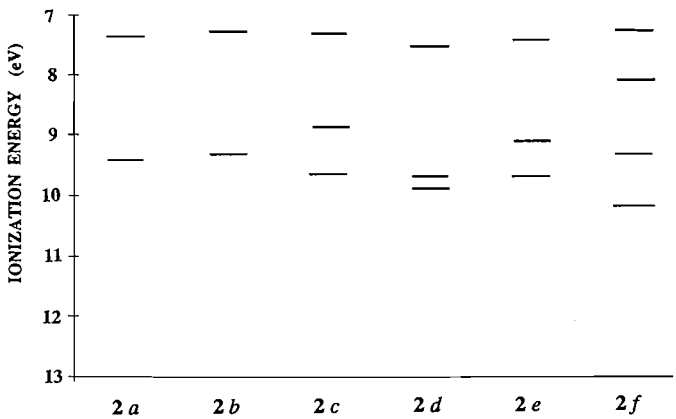

FIG. 13. Vertical ionization energies of **2***a*–**2***f*.

TABLE 12. Computed and experimental π_+, π_- splittings of substituted cyclopentadienes

Compound	*Ab initio*[a]	AM1[a]	UPS[a,b]
Cyclopentadiene	2.31[c]	1.79	2.15 (ref. 28)
5,5-Dimethylcyclopentadiene	2.41[c]	2.00	2.10 (ref. 28)
2*b*	2.77	1.60	2.04
2*c* twisted-*anti*	[d]	1.71	2.33
2*d*-*anti*	2.92	2.04	~2.4
2*e*-*anti*	[d]	1.72	2.28
2*f*-*anti*	2.32	1.66	2.16

[a]In electron volts (eV).
[b]The estimated errors are ±0.05 eV.
[c]Calculations done with the 4-31**//4-31G basis set; this work.
[d]Not computed at the *ab initio* level.

of these compounds (Table 1). Moreover, *anti* and not *syn* facial selectivity is observed for the sulfur compound **2***f* where the n_S orbital energy is close to π and $n-\pi$ mixing occurs in the HOMO.

Experimental

Computational studies

Calculations were carried out with the *ab initio* packages GAUSSIAN 90 (24) and GAMESS (25) running on Multiflow Trace 14/300 and IBM RS/6000 computers, respectively. AM1 calculations were carried out with AMPAC version 2.1 (27) ported to an IBM RS/6000 computer. The keyword PRECISE was used to tighten the convergence criteria. The MO plots were obtained with PSI/88 (26) ported to a SUN 3/60 computer.

Ultraviolet photoelectron spectroscopic studies

The pe spectra of the dienes synthesized previously (9, 22) were obtained on a non-commercial spectrometer described previously (31) by signal averaging 20–50 scans. The spectra were calibrated with argon.

Acknowledgements

We thank the Natural Sciences and Engineering Research Council of Canada for financial support. The PS/2, 70/486, 80/386, and RS/6000 computers used in this study were obtained under the auspices of an IBM Canada – McMaster University cooperative project. We also thank Professor W. L. Jorgensen for providing the PSI/88 computational package and Mr. S. Urqhart for porting the software to a Sun 3/60 computer.

1. S. Winstein, M. Shatavsky, C. Norton, and R. B. Woodward. J. Am. Chem. Soc. **77**, 4183 (1955).
2. D. W. Jones. J. Chem. Soc. Chem. Commun. 739 (1980).
3. (*a*) K. L. Williamson, Y. L. Hsu, R. Lacko, and C. H. Young. J. Am. Chem. Soc. **91**, 6129 (1969); (*b*) K. L. Williamson and Y. L. Hsu. J. Am. Chem. Soc. **92**, 7385 (1970); (*c*) G. Bianchi, C. De Micheli, A. Gamba, and R. Gandolfi. J. Chem. Soc. Perkin Trans. 1, 137 (1974).
4. (*a*) R. Breslow and J. M. Hoffman, Jr. J. Am. Chem. Soc. **94**, 2110 (1972); (*b*) R. Breslow, J. M. Hoffman, Jr., and C. Perchonock. Tetrahedron Lett. 3723 (1973).
5. M. Franck-Neumann and M. Sedrati. Tetrahedron Lett. 1391 (1983).
6. (*a*) D. J. Burnell and Z. Valenta. J. Chem. Soc. Chem. Commun. 1247 (1985); (*b*) F. K. Brown, K. N. Houk, D. J. Burnell, and A. Valenta. J. Org. Chem. **52**, 3050 (1987).
7. E. J. Corey, N. M. Weinshenker, T. K. Schaat, and W. Huber. J. Am. Chem. Soc. **91**, 5675 (1969).
8. L. A. Paquette, C. Vanucci, and R. D. Rogers. J. Am. Chem. Soc. **111**, 5792 (1989).
9. J. B. Macaulay and A. G. Fallis. J. Am. Chem. Soc. **110**, 4074 (1988).
10. M. Ishida, T. Aoyama, and S. Kato. Chem. Lett. 663 (1989).
11. A. G. Fallis and Y-F. Lu. Adv. Cycloaddit. In press.
12. N. T. Anh. Tetrahedron, **29**, 3227 (1973).
13. S. Inagaki, H. Fujimoto, and K. Fukui. J. Am. Chem. Soc. **98**, 4054 (1976).
14. R. Gleiter and L. A. Paquette. Acc. Chem. Res. **16**, 328 (1983).
15. (*a*) F. K. Brown and K. M. Houk. J. Am. Chem. Soc. **107**, 1971 (1985); (*b*) M. H. Padden-Row, N. G. Rondan, and K. N. Houk. J. Am. Chem. Soc. **104**, 7162 (1982).
16. (*a*) S. D. Kahn and W. J. Hehre. J. Am. Chem. Soc. **109**, 663 (1987); (*b*) J. Org. Chem. **53**, 301 (1988).
17. N. Kaila, R. W. Frank, and J. J. Dannenberg. J. Org. Chem. **54**, 4206 (1989).
18. M. Ishida, Y. Beniya, S. Inagaki, and S. Kato. J. Am. Chem. Soc. **112**, 8980 (1990).
19. (*a*) A. S. Cieplak. J. Am. Chem. Soc. **103**, 4540 (1981); (*b*) A. S. Cieplak, B. D. Tait, and C. R. Johnson. J. Am. Chem. Soc. **111**, 8447 (1989).
20. W.-S. Chung, N. J. Turro, S. Srivastava, H. Li, and W. J. le Noble. J. Am. Chem. Soc. **110**, 7882 (1988).
21. A. M. Naperstkow, J. B. Macaulay, M. J. Newlands, and A. G. Fallis. Tetrahedron Lett. 5077 (1989).
22. J. B. Macaulay and A. G. Fallis. J. Am. Chem. Soc. **112**, 1136 (1990).
23. (*a*) G. Desimoni, G. Tacconi, A. Bario, and G. P. Pollini. Natural product syntheses through pericyclic reactions. ACS Monograph 180. American Chemical Society, Washington, D.C. 1984. Chap. 5; (*b*) A. G. Fallis. Can. J. Chem. **62**, 183 (1984).

Can. J. Chem. Downloaded from www.nrcresearchpress.com by 109.225.110.28 on 09/08/12
For personal use only.

24. M. J. Frisch, M. Head-Gordon, G. W. Trucks, J. B. Foresman, H. B. Schlegel, K. Raghavachari, M. A. Robb, J. S. Binkley, C. Gonzalez, D. J. De Frees, D. J. Fox, K. A. Whiteside, R. Seeger, C. F. Melius, J. Baker, R. L. Martin, L. R. Kahn, J. J. P. Stewart, S. Topiol, and A. J. Pople. GAUSSIAN 90. Gaussian Inc., Pittsburgh, Pa. 1990.
25. M. W. Schmidt, K. K. Baldridge, I. A. Boatz, J. H. Jensen, S. Koseki, M. S. Gordon, K. A. Nguyen, T. L. Windus, and S. T. Elbert. GAMESS. Version April 4, 1991. QCPE Bull. **10**, 52 (1990).
26. W. L. Jorgensen and D. L. Severence. PSI/88 Version 1.0. Department of Chemistry, Yale University, New Haven, Conn.
27. Dewar Research Group and J. J. P. Stewart. Austin Method 1 Package 1.0. QCPE 506. QCPE Bull. **6**, 2 (1986).
28. C. Guimon, G. Pfister-Guillouzo, J. Dubac, A. Laporterie, G. Manuel, and H. Iloughmane. Organometallics, **4**, 636 (1985).
29. K. Kimura, S. Katsumata, Y. Achiba, T. Yamazaki, and S. Iwata. Handbook of HeI photoelectron spectra of fundamental organic molecules. Japan Scientific Societies Press, Tokyo; Halsted Press, New York. 1981. p. 126.
30. T. A. Koopmans. Physica, **1**, 104 (1933).
31. N. H. Werstiuk, D. N. Butler, and E. Shahid. Can. J. Chem. **65**, 760 (1986).

Can. J. Chem. Downloaded from www.nrcresearchpress.com by 109.225.110.28 on 09/08/12
For personal use only.

Structural studies of organoboron compounds. LVI.[1] 1-Benzyl-7-methyl-3,5-diphenyl-2,4,6-trioxa-1-azonia-3-bora-5-boratabicyclo[3.3.0]octane and 1,4,6,9-tetramethyl-2,7-diphenyl-3,8,11,12-tetraoxa-1,6-diazonia-2,7-diboratatricyclo[5.3.1.1^{2,6}]dodecane

WOLFGANG KLIEGEL AND GOTTFRIED LUBKOWITZ

Institut für Pharmazeutische Chemie der Technischen Universität Braunschweig, Beethovenstrasse 55, 3300 Braunschweig, Germany

AND

STEVEN J. RETTIG AND JAMES TROTTER

Department of Chemistry, University of British Columbia, 2036 Main Mall, Vancouver, B.C., Canada V6T 1Z1

Received December 9, 1991

WOLFGANG KLIEGEL, GOTTFRIED LUBKOWITZ, STEVEN J. RETTIG, and JAMES TROTTER. Can. J. Chem. **70**, 2809 (1992).

The preparation of the *N*-(2-hydroxypropyl)-*N*-alkylhydroxylamines, **6***a* (R = CH_3) and **6***b* (R = CH_2Ph), and their reactions with phenylboronic acid are described. Regardless of the molar ratios of reactants employed, the reaction with **6***b* leads to the 1:2 condensate 1-benzyl-7-methyl-3,5-diphenyl-2,4,6-trioxa-1-azonia-3-bora-5-boratabicyclo[3.3.0]-octane, **7**, while that with **6***a* gives rise to the 1:1 condensate 1,4,6,9-tetramethyl-2,7-diphenyl-3,8,11,12-tetraoxa-1,6-diazonia-2,7-diboratatricyclo[5.3.1.1^{2,6}]dodecane, **11** (the cyclic BONBON dimer of 4,6-dimethyl-2-phenyl-1,3-dioxa-4-aza-2-boracyclohexane, **9**). Compounds **7** and **11** both crystallize in the triclinic space group $P\bar{1}$: for **7**; a = 13.126(1), b = 15.337(1), c = 10.9469(5) Å, α = 91.727(5), β = 104.647(5), γ = 72.922(7)°, Z = 4; and for **11**; a = 9.0807(4), b = 9.1653(3), c = 6.4876(2) Å, α = 97.708(3), β = 108.830(3), γ = 89.188(4)°, Z = 1. The structures were solved by direct methods and were refined by full-matrix least-squares procedures to R = 0.038 and 0.032 for 5879 and 1827 reflections with $I \geq 3\sigma(F^2)$, respectively. Compound **7** has the expected bicyclic pyroboronate structure, but represents the first reported *N*-substituted example of this type of compound. Bond lengths involving boron in **7** are (C) O—B(sp^3) = 1.428(2) and 1.420(2), (B)O—B(sp^3) = 1.472(2) and 1.468(2), N—B(sp^3) = 1.737(2) and 1.762(2), C(phenyl)—B(sp^3) = 1.588(2) and 1.584(2), (N)O—B(sp^2) = 1.402(2) and 1.404(2), (B)O—B(sp^2) = 1.331(2) and 1.329(2), C(phenyl)—B(sp^2) = 1.555(3) and 1.553(2) Å. The X-ray analysis establishes a centrosymmetric, twofold N→B coordinated, dimeric structure in the solid state for **11** in which each B—O—N segment of a central six-membered BONBON ring is bridged by an O—C—C moiety. Compound **11** represents the first fully characterized example of a new type of "BONBON" compound. Bond distances involving the boron atom are (N)O—B = 1.465(1), (C)O—B = 1.428(1), N—B = 1.695(2), and C(phenyl)—B = 1.607(2) Å. Spectroscopic evidence indicates that in solution and in the gas phase this material exists predominantly as the monomer **9**.

WOLFGANG KLIEGEL, GOTTFRIED LUBKOWITZ, STEVEN J. RETTIG et JAMES TROTTER. Can. J. Chem. **70**, 2809 (1992).

On décrit la préparation des *N*-(2-hydroxypropyl)-*N*-alkylhydroxylamines (**6***a*, R = CH_3 et **6***b*, R = CH_2Ph) et leurs réactions avec l'acide phénylboronique. Quels que soient les rapports molaires de réactifs utilisés, la réaction du composé **6***b* conduit à une condensation 1:2 et à la formation du 1-benzyl-7-méthyl-3,5-diphényl-2,4,6-trioxa-1-azonia-3-bora-5-boratabicyclo[3.3.0]octane (**7**) alors que celle du composé **6***a* fournit une condensation 1:1 donnant naissance au 1,4,6,9-tétraméthyl-2,7-diphényl-3,8,11,12-tétroxa-1,6-diazonia-2,7-diboratatricyclo[5.3.1.1^{2,6}]dodécane (**11**) (le dimère cyclique BONBON du 4,6-diméthyl-2-phényl-1,3-dioxa-4-aza-2-boracyclohexane, **9**). Les composés **7** et **11** cristallisent tous les deux dans le groupe d'espace triclinique $P\bar{1}$; pour **7**, a = 13,126(1), b = 15,337(1) et c = 10,9469(5) Å, α = 91,727(5), β = 104,647(5) et γ = 72,922(7)° et Z = 4 alors que pour **11**, a = 9,0807(4), b = 9,1653(3) et c = 6,4876(2) Å, α = 97,708(3), β = 108,830(3) et γ = 89,188(4)° et Z = 1. On a résolu les structures par des méthodes directes et on les a affinées par la méthode des moindres carrés (matrice entière) jusqu'à des valeurs de R = 0,038 et 0,032 respectivement pour 5879 et 1827 réflexions avec $I \geq 3\sigma(F^2)$. Le composé **7** possède la structure pyroboronate bicyclique attendue, mais elle représente le premier exemple rapporté d'un composé de ce genre qui est *N*-substitué. Les longueurs de liaisons impliquant le bore du composé **7** sont (C)O—B(sp^3) = 1,428(2) et 1,420(2), (B)O—B(sp^3) = 1,472(2) et 1,468(2), N—B(sp^3) = 1,737(2) et 1,762(2), C(phényl)—B(sp^3) = 1,588(2) et 1,584(2), (N)O—B(sp^2) = 1,402(2) et 1,404(2), (B)O—B(sp^2) = 1,331(2) et 1,329(2) et C(phényl)—B(sp^2) = 1,555(3) et 1,553(2) Å. L'analyse par rayons X permet d'établir que dans le composé **11**, à l'état solide, il existe une structure dimère, centrosymétrique, comportant une coordination N→B binaire dans laquelle chaque segment B—O—N du cycle à six chaînons BONBON central est lié par un pont O—C—C. Le composé **11** représente le premier cas complètement caractérisé d'un nouveau type de composé "BONBON." Les distances impliquant l'atome de bore sont (N)O—B = 1,465(1), (C)O—B = 1,428(1), N—B = 1,695(2) et C(phényl)—B = 1,607(2) Å. Les données spectroscopiques indiquent que, en solution et en phase gazeuse, ce composé existe préférentiellement sous la forme du monomère **9**.

[Traduit par la rédaction]

Introduction

N-(2-Hydroxyalkyl)hydroxylamines, **1**, react with phenylboronic acid in a ratio of 1:2 resulting in a bicyclic condensation product **2** (1), the molecular structure of which has been confirmed by an X-ray crystallographic analysis of **2** (R^1 = R^2 = Me, R^3 = R^4 = H) (2). A similar bicyclic structure with a transannular N→B coordinative bond, **4**, has been established for the 1:2 condensates of *N*,*N*′-dialkyl-*N*,*N*′-dihydroxyaminals **3** with phenylboronic acid (3, 4).

[1]Previous paper in this series: ref. 27.

Can. J. Chem. Downloaded from www.nrcresearchpress.com by 109.225.110.28 on 09/08/12
For personal use only.

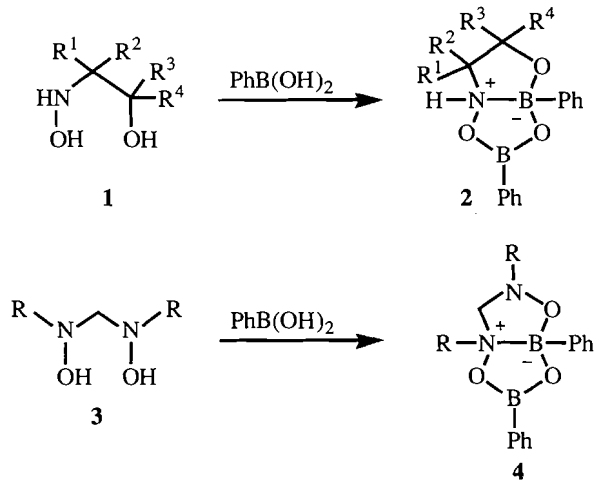

1 2 3 4

As an extension of our studies in this area we have synthesized the *N*-(2-hydroxypropyl)-*N*-alkylhydroxylamines **6** by reduction of the nitrones **5** (*a*: R = CH_3; *b*: R = CH_2Ph), obtained from 2-hydroxypropanal and *N*-methyl- or *N*-benzylhydroxylamine, respectively. Compounds **6** represent analogues of the bishydroxylamine **3** in which one of the nitrogen atoms has been replaced by a carbon atom. The condensation reaction of **6** with phenylboronic acid, however, gives (dependent on the nature of the *N*-alkyl substituent) differently composed crystalline products having elemental analyses and ^1H nmr spectra consistent with 1:1 and 1:2 condensates, respectively. The latter reaction product, obtained from **6***b* (R = CH_2Ph), could possess the bicyclic structure **7** analogous to the type **2** compounds that can be synthesized from various *N*-unsubstituted *N*-(2-hydroxyalkyl)hydroxylamines. The bicyclic ring system in **7**, like that in **2**, would be formed by intramolecular N→B coordination. This is confirmed by the ^{11}B nmr spectrum of **7** in $CDCl_3$ which displays two signals of nearly equal peak area at $\delta(Et_2OBF_3)$ = 13.3 and 28.0 ppm, indicating the presence of both tetracoordinate (sp^3) and trivalent (sp^2) boron species (5). The 1:1 reaction product,[2] obtained from **6***a* (R = CH_3), gives a ^1H nmr spectrum consistent with both of the cycloboronate structures **8** and **9**. The latter structure, having the potential for twofold O—B $pp(\pi)$ back donation, should be more stable than the five-membered cycloboronate **8** containing a borinic amide *N*-oxide function, presumably an unstable moiety expected to rearrange to the more stable six-membered boronate ring **9**. Cycloboronates of "1,3-diols" are well-documented in the literature (6).

The primary signal in the ^{11}B nmr spectrum of the product in $CDCl_3$ solution at $\delta(Et_2OBF_3)$ = 27.2 ppm indicates the presence of a trivalent boron species like **9** (or **8**). A second weak signal (3% of the total peak area) in the ^{11}B nmr spectrum at 13.6 ppm, however, suggests the presence of a small amount of a tetracoordinate boron compound. Two separate ^{11}B nmr signals indicating the presence of both tri- and tetracoordinate boron have also been observed in the spectra of the supposed BONBON dimers of borinic acid esters of oximes (7, 8). The tetracoordinate boron species in this case could originate from the dimerization of **8** to give the tricyclic compound **10** that resembles the dimerization product of salicylaldoxime phenylboronate, **12**, having a similar BONBON ring system (9). On the other hand, a stable six-membered cycloboronate **9** could dimerize to a tricyclic compound **11** containing tetracoordinate boron if there were stabilizing forces to overcompensate for the loss of O—B $pp(\pi)$ resonance energy. Another hint at a possible dimerization process comes from the infrared spectrum (KBr pellet) and provides further evidence in support of a tetrahedral boron atom, at least in the solid state. The characteristic ν_{16} phenyl ring stretching vibration at 1600 cm^{-1} which is normally found in the spectra of trigonal planar phenylboronates is very weak in this case, and the decrease in the intensity of the ν_{16} band corresponds to an increasing degree of "tetracoordination" at phenylboron centres (10).

In both the EI and FAB mass spectra the highest mass feature with highest abundance is the molecular ion of the monomer **8** or **9**. This could also be interpreted as a complete dissociation of the respective dimers **10** or **11**. Similar dissociations of BONBON dimers in the gas phase have been reported for various borinic acid esters of oximes (7, 8, 11). In view of the somewhat ambiguous spectroscopic data, an X-ray crystallographic analysis has been carried out to provide a definitive assignment to one of the monomer structures **8** or **9**, or to one of the dimeric structures **10** or **11**, at least in the solid state. In addition, an unambiguous proof of the bicyclic structure **7** was desirable and has been provided by an X-ray analysis.

Experimental

N-(2-Hydroxypropylidene)methanamine-N-oxide, **5**a *(R = CH_3)*

2-Hydroxypropanal (1.48 g, 20 mmol) and *N*-methylhydroxylammonium chloride (1.66 g, 20 mmol) are dissolved in 20 mL of ethanol (96%) and are mixed with a solution of K_2CO_3 (1.38 g, 10 mmol) in 5 mL of water. After 48 h the solvent is distilled off *in vacuo*. The remaining oil is not purified further. Yield: 1.85 g (90%). ^1H nmr (90 MHz, $CDCl_3$/TMS): δ (ppm) = 1.36 (d, *J* = 7 Hz, C—CH_3), 3.65 (s, N—CH_3), 4.70 (m_c, O—CH), 5.23 (s, broad, exchangeable, OH), 6.81 (d, *J* = 5 Hz, N=CH).

N-(2-Hydroxypropylidene)phenylmethanamine-N-oxide, **5**b *(R = CH_2Ph)*

2-Hydroxypropanal (1.11 g, 15 mmol) and *N*-benzylhydroxylammonium chloride (2.39 g, 15 mmol) are reacted as described above for **5***a*. The residue remaining after removal of the solvent is recrystallized from ethanol/ether. Yield: 2.55 g (95%); mp 97°C. Anal. calcd. for $C_{10}H_{13}NO_2$: C 67.02, H 7.31, N 7.82; found: C 67.14, H 7.34, N 7.69. Infrared (KBr): 3250 (O—H), 1600 cm^{-1} (—C=N). ^1H nmr (90 MHz, $CDCl_3$/TMS): δ (ppm) = 1.34 (d, *J* = 7 Hz, CH_3), 4.86 (m_C, O—CH and OH), 4.83 (s, N—CH_2), 6.76 (d, *J* = 5 Hz, N=CH), 7.39 (s, 5 aromatic H).

1-(N-Hydroxy-N-methylamino)-2-propanol, **6**a

N-(2-Hydroxypropylidene)methanamine-*N*-oxide, **5***a* (crude product, 1.03 g, 10 mmol), is dissolved in 30 mL of methanol. A solution of KBH_4 (1.08 g, 20 mmol) in 15 mL of water is added dropwise and the mixture is stirred for 24 h at room temperature. Excess KBH_4 is decomposed with tartaric acid, and the solution is brought to pH 9–10 by the addition of an aqueous solution of Na_2CO_3. After the removal of methanol *in vacuo*, the aqueous solution is extracted with dichloromethane (4 × 50 mL). The dichloromethane solution is dried over $MgSO_4$, and the solvent is then distilled off *in vacuo*. The residual oil is taken up in a small volume of absolute ethanol and cooled down until crystallization yields 0.60 g (57%) of colorless needles; mp 71°C (from absolute

[2]The equimolar ratio of the components in the condensation product still results even when a large excess of phenylboronic acid is employed in the reaction.

Can. J. Chem. Downloaded from www.nrcresearchpress.com by 109.225.110.28 on 09/08/12
For personal use only.

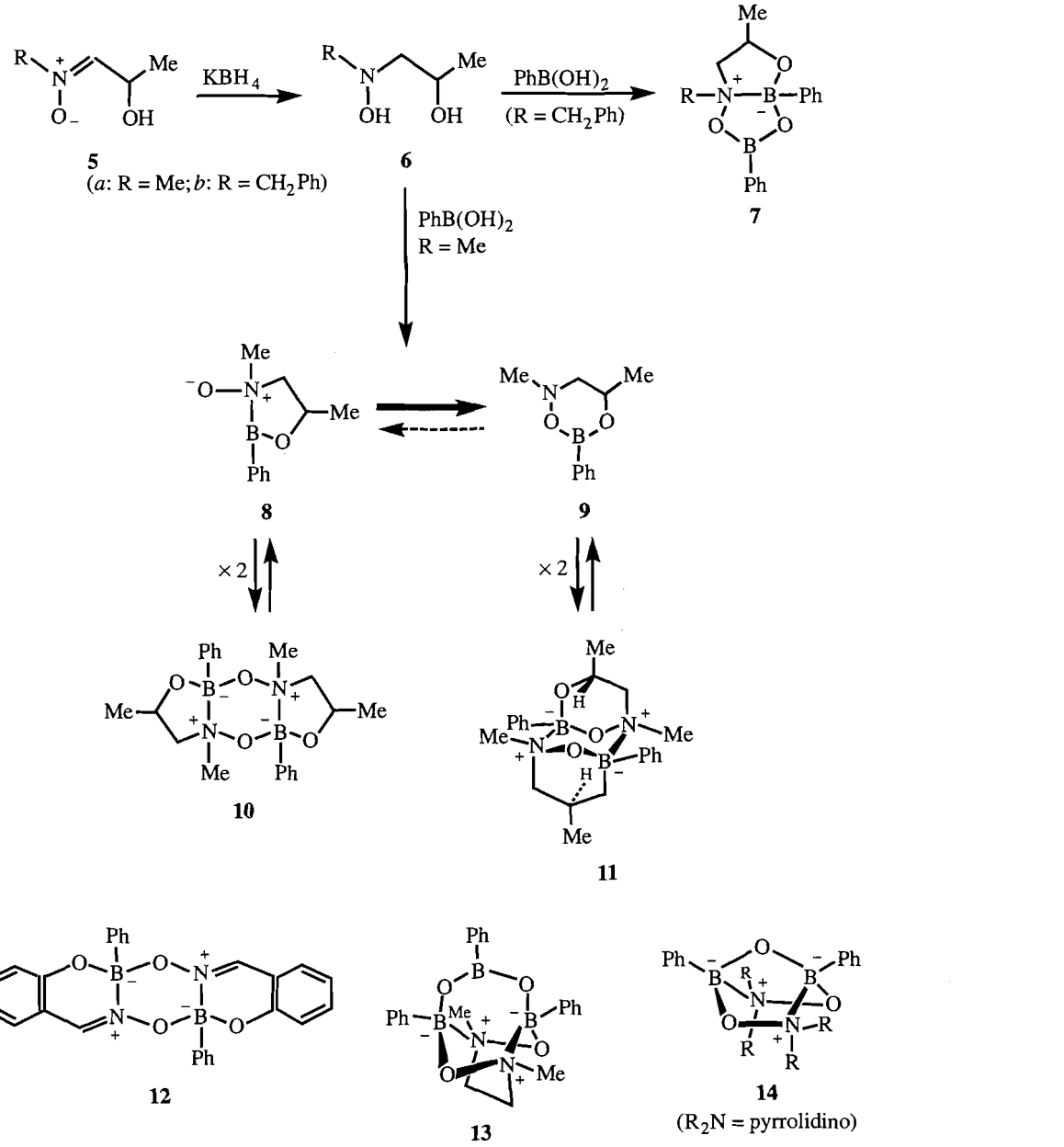

5
(*a*: R = Me; *b*: R = CH_2Ph)

6

7

8

9

10

11

12

13

14
(R_2N = pyrrolidino)

ethanol). Anal. calcd. for $C_4H_{11}NO_2$: C 45.70, H 10.55, N 13.32; found: C 45.65, H 10.66, N 12.96. Infrared (KBr): 3400 and 3160 cm^{-1} (O—H). ^1H nmr (90 MHz, $CDCl_3$/TMS): δ (ppm) = 1.20 (d, J = 7 Hz, C—CH_3), 2.72 (m_c, N—CH_3 and N—CH_2—C), 4.08 (m_c, O—CH), 6.25 (s, broad, exchangeable, 2 OH).

1-Benzyl-7-methyl-3,5-diphenyl-2,4,6-trioxa-1-azonia-3-bora-5-boratabicyclo[3.3.0]octane, 7

1-(*N*-Benzyl-*N*-hydroxyamino)-2-propanol, ***6b*** (0.36 g, 2 mmol), and phenylboronic acid (0.49 g, 4 mmol) are dissolved in 20 mL of benzene and refluxed for 1 h using a Dean–Stark trap for continuous removal of water. After evaporation of the solvent *in vacuo* the crystalline residue is recrystallized from CH_2Cl_2. Yield: 0.55 g (74%) of colorless crystals; mp 114–116°C. Anal. calcd. for $C_{22}H_{23}B_2NO_3$: C 71.21, H 6.25, B 5.83, N 3.78; found: C 71.22, H 6.31, B 5.98, N 3.79. Infrared (KBr): 1605 cm^{-1} (phenyl C=C). ^1H nmr (400 MHz, $CDCl_3$/TMS): δ (ppm) = 1.38 (d, J = 6 Hz, CH_3), 2.58 and 2.61 (d, J = 12 Hz and d, J = 11 Hz, 1/2 (O—C)—CH_2), 3.45 (d, J = 15 Hz, 1/2 Ph—CH_2), 3.92 (d, J = 15 Hz, 1/2 Ph—CH_2), 4.30 (m_c, O—CH), 7.30–7.50 (m, 11 aromatic H), 7.75–7.80 (m, 2 aromatic H), 7.92–7.98 (m, 2 aromatic H). ^{11}B nmr (64 MHz, $CDCl_3/Et_2OBF_3$): δ (ppm) = 28.0 ($w_{1/2}$ = 960 Hz) and 13.3 ($w_{1/2}$ = 770 Hz); ratio of peak areas: 1:1. Crystals suitable for X-ray analysis were obtained by slow crystallization form CH_2Cl_2.

*1,4,6,9-Tetramethyl-2,7-diphenyl-3,8,11,12-tetraoxa-1,6-diazonia-2,7-diboratatricyclo[5.3.1.$1^{2,6}$]dodecane, **11** (cyclic BONBON dimer of 4,6-dimethyl-2-phenyl-1,3-dioxa-4-aza-2-boracyclohexane, **9**)*

1-(*N*-Hydroxy-*N*-methylamino)-2-propanol, **6** (0.21 g, 2 mmol), and phenylboronic acid (0.25 g, 2 mmol) are dissolved in 20 mL of benzene and refluxed for 1 h using a Dean-Stark trap for continuous removal of water. The solvent is distilled off *in vacuo*, and the remaining oil is taken up in a small volume of absolute ethanol. Cooling down the ethanolic solution yields 0.26 g (68%) of colorless crystals; mp 107–108°C (from absolute ethanol). Anal. calcd.

Can. J. Chem. Downloaded from www.nrcresearchpress.com by 109.225.110.28 on 09/08/12
For personal use only.

Can. J. Chem. Downloaded from www.nrcresearchpress.com by 109.225.110.28 on 09/08/12
For personal use only.

TABLE 1. Crystallographic data[a]

	7	11
Formula	$C_{22}H_{23}B_2NO_3$	$C_{20}H_{28}B_2N_2O_4$
fw	371.05	382.08
Crystal system	Triclinic	Triclinic
Space group	$P\bar{1}$	$P\bar{1}$
a, Å	13.126(1)	9.0807(4)
b, Å	15.337(1)	9.1653(3)
c, Å	10.9469(5)	6.4876(2)
α (deg)	91.727(5)	97.708(3)
β (deg)	104.647(5)	108.830(3)
γ (deg)	72.922(7)	89.188(4)
V, Å^3	2035.7(3)	506.19(4)
Z	4	1
ρ_{calcd}, g/cm^3	1.211	1.253
F (000)	784	204
μ(Cu-K_α), cm^{-1}	5.87	6.48
Crystal size, mm	0.20 × 0.30 × 0.30	0.15 × 0.25 × 0.49
Transmission factors	0.86–1.00	0.90–1.00
Scan type	ω–2θ	ω–2θ
Scan range, deg in ω	1.20 + 0.20 tan θ	1.10 + 0.20 tan θ
Scan speed, deg/min	32	32
Data collected	$+h$, $\pm k$, $\pm l$	$+h$, $\pm k$, $\pm l$
$2\theta_{max}$, deg	155	155
Crystal decay	5.3%	7.3%
Total reflections	8690	2275
Total unique reflections	8314	2078
R_{merge}	0.016	0.012
No. of reflections with $I \geq 3\sigma(I)$	5879	1827
No. of variables	506	184
R	0.038	0.032
R_w	0.048	0.041
Goodness of fit (gof)	2.41	3.71
Max Δ/σ (final cycle)	0.001	0.09
Residual density e/Å^3	−0.13 to +0.15	−0.11 to +0.24

[a]Temperature 294 K, Rigaku AFC6S diffractometer, Cu-K_α radiation (λ = 1.54178 Å), graphite monochromator, takeoff angle 6.0°, aperture 6.0 × 6.0 mm at a distance of 285 mm from the crystal, stationary background counts at each end of the scan (scan/background time ratio 2:1, up to eight rescans), $\sigma^2(F^2) = [S^2(C + 4B) + (pF^2)^2]/Lp^2$($S$ = scan rate, C = scan count, B = normalized background count, p = 0.020 for **7** and 0.005 for **11**), function minimized $\Sigma w(|F_o| - |F_c|)^2$ where $w = 4F_o^2/\sigma^2(F_o^2)$, $R = \Sigma||F_o| - |F_c||/\Sigma|F_o|$, $R_w = (\Sigma w(|F_o| - |F_c|)^2/\Sigma w|F_o|^2)^{1/2}$, and gof = $[\Sigma w(|F_o| - |F_c|)^2/(m - n)]^{1/2}$. Values given for R, R_w, and gof are based on those reflections with $I \geq 3\sigma(I)$.

for $C_{20}H_{28}B_2N_2O_4$: C 62.87, H 7.39, N 7.33; found: C 62.88, H 7.58, N 7.29. ^{1}H nmr (90 MHz, $CDCl_3$/TMS): δ (ppm) = 1.34 (d, J = 6 Hz, C—CH_3), 2.64 (m_c, 1 H of N—CH_2—C), 2.82 (s, N—CH_3), 3.04/3.17 (dd, 1 H of N—CH_2—C), 4.43 (m_c, O—CH), 7.14–7.38 (m, 3 aromatic H), 7.60–7.78 (m, 2 aromatic H). ^{11}B nmr (64 MHz, $CDCl_3/Et_2OBF_3$): δ (ppm) = 27.2 ($w_{1/2}$ = 482 Hz) and 13.6 ($w_{1/2}$ = 290 Hz); ratio of peak areas: 32:1. EI-Mass spectrum (70 eV, 250°C): m/z = 191 (100%, 1/2 M$^+$), 176 (11%, 1/2 M$^+$ − CH_3), 104 (28%, C_6H_5BO). FAB-Mass spectrum (3-nitrobenzylalcohol [NBA], positive ion mode); m/z = 191 (100%, 1/2 M$^+$), 136 (47%, NBA − 17), 114 (34%, M$^+$ − 77), 105 (44%, PhBOH), 104 (24%, PhBO), 77 (34%, Ph), 72 (58%, M$^+$ − 77 − 42). Crystals suitable for X-ray analysis were obtained by slow crystallization from absolute ethanol.

X-ray crystallographic analyses of 7 and 11

Crystallographic data for **7** and **11** appear in Table 1. The final unit-cell parameters were obtained by least-squares on the setting angles for 25 reflections with 2θ = 93.8–101.9° for **7** and 106.2–112.6° for **11**. The intensities of three standard reflections, measured every 200 reflections throughout the data collections, showed a linear decays of 5.3% for **7** and 7.3% for **11**. The data were processed,[3] corrected for Lorentz and polarization effects, decay, and absorption (empirical, based on azimuthal scans for four reflections).

Both structure analyses were initiated in the centrosymmetric space group $P\bar{1}$ on the basis of E-statistics, the choices being confirmed by the subsequent successful solutions and refinements of the structures. The asymmetric unit of **7** contains two molecules. The structures were solved by direct methods, the coordinates of the non-hydrogen atoms being determined from E-maps or from subsequent difference Fourier syntheses. The non-hydrogen atoms were refined with anisotropic thermal parameters and the hydrogen atoms were fixed in idealized positions (C—H = 0.98 Å, $B_H = 1.2B_{bonded\ atom}$) for **7** and were refined with isotropic thermal parameters for **11**. Corrections for secondary extinction were applied for both structures, the final values of the extinction coefficients being 1.02×10^{-5} for **7** and 4.62×10^{-3} for **11**. Neutral atom

[3]TEXSAN/TEXRAY structure analysis package which includes versions of the following: DIRDIF, direct methods for difference structures, by P. T. Beurskens; ORFLS, full-matrix least-squares, and ORFFE, function and errors, by W. R. Busing, K. O. Martin, and H. A. Levy; ORTEP II, illustrations, by C. K. Johnson.

Can. J. Chem. Downloaded from www.nrcresearchpress.com by 109.225.110.28 on 09/08/12
For personal use only.

scattering factors for all atoms and anomalous dispersion corrections for the non-hydrogen atoms were taken from the International tables for X-ray crystallography (12). Final atomic coordinates and equivalent isotropic thermal parameters, bond lengths, and bond angles appear in Tables 2–4, respectively. Hydrogen atom parameters, anisotropic thermal parameters, torsion angles, intermolecular contacts, and least-squares planes, and measured and calculated structure factor amplitudes for the both structures are included as supplementary material.[4]

Results and discussion

The X-ray analyses establish structure **11** (Fig. 1) for the 1:1 reaction product of **6***a* and phenylboronic acid, and structure **7** (Fig. 2) for the 1:2 condensate of **6***b* and phenylboronic acid. It is not yet understood why the *N*-benzyl substituted educt **6***b* gives the expected bicyclic pyroboronate **7**, analogous to **2** and **4**, whereas the *N*-methyl derivative **6***a* leads to the six-membered cycloboronate **9** which associates to the dimer **11** in the solid state but appears to be present predominantly as the monomer in the $CDCl_3$ solution used for obtaining the ^{11}B nmr spectrum. Varying the molar ratios of the reactants does not change the results in either reaction. Several competitive factors such as O—B $pp(\pi)$ interactions, rehybridization energy ($sp^2 \rightarrow sp^3$) of N—B coordination, steric effects, hydrogen bonding, and crystal packing effects seem to control the formation of the particular crystalline product in each case.

Compound **7** is characterized by the bicyclo[3.3.0]octane ring skeleton, formed by a transannular N—B interaction in the eight-membered BOBONCCO ring which has a boat-boat ("saddle") conformation. Folding about the N—B bond divides the ring system into a pair of *cis*-fused five-membered rings. The angles between the normals to the mean planes of the nearly planar BOBON rings and the BOCN planes of the BOCCN rings (that have envelope conformations) are 113.7 and 114.0° in the two independent molecules of **7**, representing the "folding angle" of the bicyclic system. Similar "folding" of bicyclo[3.3.0]octane ring systems has been reported for the compounds **2** ($R^1 = R^2 =$ Me, $R^3 = R^4 =$ H) (2) and **4** (R = Me) (4). Until now, type **2** compounds had only been obtained from *N-un*substituted *N*-(2-hydroxyalkyl)hydroxylamines. Thus, the *N*-benzyl derivative **7** is the first example of an *N*-substituted type **2** compound.

There are two crystallographically independent molecules of **7**. Figure 2 depicts the 1*R*,5*S*,7*R*-enantiomer of the molecule containing B(1) and the 1*S*,5*R*,7*S*-enantiomer of the molecule containing B(3). Since this material crystallizes in a centrosymmetric space group, the respective enantiomers of each of the two independent molecules are also present in the crystal.

The N—B bonds in the two independent molecules of **7** are significantly different from one another, presumably as a result of packing effects. The N—B bonds of 1.737(2) and 1.762(2) Å observed for **7** are longer than the transannular N—B bond in the *N*-unsubstituted derivative **2** (1.688(2) Å) (2), probably a result of the steric requirements of the benzyl substituent, and are similar to those of 1.729(3) and 1.736(3) Å reported for the two independent molecules of **4**

[4]Supplementary material mentioned in the text may be purchased from the Depository of Unpublished Data, Document Delivery, CISTI, National Research Council Canada, Ottawa, Canada K1A 0S2.

TABLE 2. Final atomic coordinates (fractional) and B_{eq} (Å^2)[a]

Atom	*x*	*y*	*z*	B_{eq}
		7		
O(1)	0.76579(9)	0.43961(7)	0.2300(1)	4.21(5)
O(2)	0.75269(9)	0.45199(7)	0.4367(1)	4.55(6)
O(3)	0.82850(9)	0.58052(8)	0.4357(1)	4.84(6)
O(4)	0.29315(8)	0.16273(7)	1.1452(1)	4.38(6)
O(5)	0.20958(9)	0.21135(8)	0.9358(1)	4.62(6)
O(6)	0.08111(9)	0.33921(7)	1.0087(1)	4.74(6)
N(1)	0.7219(1)	0.53716(8)	0.2410(1)	3.63(6)
N(2)	0.1780(1)	0.20138(8)	1.1435(1)	3.96(6)
C(1)	0.8893(1)	0.5665(1)	0.3426(1)	4.35(8)
C(2)	0.8021(1)	0.5808(1)	0.2177(1)	4.08(8)
C(3)	0.9576(2)	0.6312(1)	0.3562(2)	5.9(1)
C(4)	0.6097(1)	0.5666(1)	0.1531(1)	4.13(8)
C(5)	0.6046(1)	0.5666(1)	0.0144(1)	4.13(8)
C(6)	0.6604(1)	0.4928(1)	−0.0430(2)	5.2(1)
C(7)	0.6525(2)	0.4982(2)	−0.1711(2)	6.1(1)
C(8)	0.5881(2)	0.5756(2)	−0.2430(2)	6.7(1)
C(9)	0.5290(2)	0.6475(2)	−0.1883(2)	7.1(1)
C(10)	0.5380(2)	0.6433(1)	−0.0598(2)	5.4(1)
C(11)	0.8133(1)	0.2902(1)	0.3502(2)	4.42(8)
C(12)	0.8226(2)	0.2430(1)	0.2406(2)	5.3(1)
C(13)	0.8528(2)	0.1489(1)	0.2417(2)	6.2(1)
C(14)	0.8740(2)	0.0998(1)	0.3523(3)	6.7(1)
C(15)	0.8661(2)	0.1434(1)	0.4617(2)	6.6(1)
C(16)	0.8366(1)	0.2385(1)	0.4616(2)	5.4(1)
C(17)	0.6266(1)	0.6179(1)	0.4297(1)	3.82(7)
C(18)	0.6250(1)	0.7069(1)	0.4611(2)	4.8(1)
C(19)	0.5322(2)	0.7692(1)	0.4837(2)	6.2(1)
C(20)	0.4379(2)	0.7448(1)	0.4735(2)	6.1(1)
C(21)	0.4361(1)	0.6580(1)	0.4417(2)	5.2(1)
C(22)	0.5302(1)	0.5952(1)	0.4213(1)	4.39(8)
C(23)	0.1518(1)	0.3605(1)	1.1199(2)	4.59(8)
C(24)	0.1677(1)	0.2852(1)	1.2155(2)	4.78(9)
C(25)	0.0996(2)	0.4536(1)	1.1617(2)	6.2(1)
C(26)	0.1438(1)	0.1298(1)	1.1964(2)	4.58(9)
C(27)	0.1966(1)	0.1039(1)	1.3345(2)	4.25(8)
C(28)	0.1411(1)	0.1404(1)	1.4247(2)	5.2(1)
C(29)	0.1880(2)	0.1168(1)	1.5516(2)	6.2(1)
C(30)	0.2916(2)	0.0568(1)	1.5897(2)	6.4(1)
C(31)	0.3476(2)	0.0194(1)	1.5016(2)	6.5(1)
C(32)	0.3006(2)	0.0425(1)	1.3747(2)	5.3(1)
C(33)	0.4203(1)	0.1417(1)	0.9997(2)	4.26(8)
C(34)	0.5131(1)	0.1033(1)	1.0959(2)	5.2(1)
C(35)	0.6169(2)	0.0797(2)	1.0755(2)	6.5(1)
C(36)	0.6301(2)	0.0951(2)	0.9591(2)	6.7(1)
C(37)	0.5398(2)	0.1331(1)	0.8613(2)	6.1(1)
C(38)	0.4360(1)	0.1554(1)	0.8810(2)	4.9(1)
C(39)	0.0131(1)	0.2062(1)	0.9221(1)	4.22(8)
C(40)	0.0287(1)	0.1212(1)	0.8688(2)	5.3(1)
C(41)	−0.0587(2)	0.0884(1)	0.8123(2)	6.2(1)
C(42)	−0.1647(2)	0.1405(2)	0.8052(2)	6.2(1)
C(43)	−0.1831(2)	0.2245(2)	0.8558(2)	6.4(1)
C(44)	−0.0951(1)	0.2564(1)	0.9141(2)	5.4(1)
B(1)	0.7766(1)	0.3963(1)	0.3456(2)	4.11(9)
B(2)	0.7338(1)	0.5485(1)	0.4019(2)	3.93(9)
B(3)	0.3030(2)	0.1731(1)	1.0221(2)	4.09(9)
B(4)	0.1126(2)	0.2444(1)	0.9869(2)	4.16(9)
		11		
O(1)	0.59129(8)	0.52907(8)	0.3648(1)	2.78(3)
O(2)	0.40051(8)	0.32714(8)	0.2075(1)	3.18(3)
N(1)	0.4690(1)	0.6288(1)	0.3831(1)	2.73(3)
C(1)	0.3311(1)	0.5833(1)	0.1843(2)	3.20(4)
C(2)	0.2743(1)	0.4257(1)	0.1680(2)	3.12(4)
C(3)	0.5286(2)	0.7750(1)	0.3659(2)	3.74(4)

TABLE 2 (*concluded*)

Atom	*x*	*y*	*z*	B_{eq}
C(4)	0.1617(1)	0.3775(2)	−0.0600(2)	4.09(5)
C(5)	0.6851(1)	0.2715(1)	0.3356(2)	2.85(3)
C(6)	0.8409(1)	0.3184(1)	0.4065(2)	3.54(4)
C(7)	0.9556(2)	0.2282(2)	0.3667(2)	4.36(5)
C(8)	0.9165(2)	0.0883(2)	0.2527(3)	4.84(5)
C(9)	0.7630(2)	0.0390(2)	0.1790(3)	4.90(5)
C(10)	0.6496(1)	0.1295(1)	0.2216(2)	3.87(4)
B(1)	0.5476(1)	0.3759(1)	0.3650(2)	2.69(4)

[a] $B_{eq} = (8/3)\pi^2\Sigma\Sigma U_{ij}a_i^*a_j^*(\mathbf{a}_i \cdot \mathbf{a}_j)$.

TABLE 3. Bond lengths (Å) with estimated standard deviations.

Atom	Atom	Distance	Atom	Atom	Distance
O(1)	N(1)	1.450(2)	O(4)	N(2)	1.448(2)
O(1)	B(1)	1.402(2)	O(4)	B(3)	1.404(2)
O(2)	B(1)	1.331(2)	O(5)	B(3)	1.329(2)
O(2)	B(2)	1.472(2)	O(5)	B(4)	1.468(2)
O(3)	C(1)	1.421(2)	O(6)	C(23)	1.426(2)
O(3)	B(2)	1.428(2)	O(6)	B(4)	1.420(2)
N(1)	C(2)	1.477(2)	N(2)	C(24)	1.477(2)
N(1)	C(4)	1.489(2)	N(2)	C(26)	1.484(2)
N(1)	B(2)	1.737(2)	N(2)	B(4)	1.762(2)
C(1)	C(2)	1.519(2)	C(23)	C(24)	1.514(2)
C(1)	C(3)	1.502(2)	C(23)	C(25)	1.504(3)
C(4)	C(5)	1.502(2)	C(26)	C(27)	1.506(2)
C(5)	C(6)	1.384(2)	C(27)	C(28)	1.383(2)
C(5)	C(10)	1.379(2)	C(27)	C(32)	1.382(2)
C(6)	C(7)	1.384(2)	C(28)	C(29)	1.381(3)
C(7)	C(8)	1.369(3)	C(29)	C(30)	1.367(3)
C(8)	C(9)	1.367(3)	C(30)	C(31)	1.371(3)
C(9)	C(10)	1.383(3)	C(31)	C(32)	1.380(3)
C(11)	C(12)	1.396(2)	C(33)	C(34)	1.381(2)
C(11)	C(16)	1.392(2)	C(33)	C(38)	1.397(2)
C(11)	B(1)	1.555(3)	C(33)	B(3)	1.553(2)
C(12)	C(13)	1.379(3)	C(34)	C(35)	1.378(2)
C(13)	C(14)	1.369(3)	C(35)	C(36)	1.365(3)
C(14)	C(15)	1.366(3)	C(36)	C(37)	1.371(3)
C(15)	C(16)	1.394(3)	C(37)	C(38)	1.374(2)
C(17)	C(18)	1.394(2)	C(39)	C(40)	1.393(2)
C(17)	C(22)	1.389(2)	C(39)	C(44)	1.384(2)
C(17)	B(2)	1.588(2)	C(39)	B(4)	1.584(2)
C(18)	C(19)	1.383(3)	C(40)	C(41)	1.384(3)
C(19)	C(20)	1.373(3)	C(41)	C(42)	1.370(3)
C(20)	C(21)	1.371(3)	C(42)	C(43)	1.365(3)
C(21)	C(22)	1.390(2)	C(43)	C(44)	1.386(3)
		11			
O(1)	N(1)	1.453(1)	C(2)	C(4)	1.513(2)
O(1)	B(1)	1.465(1)	C(5)	C(6)	1.393(2)
O(2)	C(2)	1.428(1)	C(5)	C(10)	1.395(2)
O(2)	B(1)	1.428(1)	C(5)	B(1)	1.607(2)
N(1)	C(1)	1.494(1)	C(6)	C(7)	1.388(2)
N(1)	C(3)	1.483(1)	C(7)	C(8)	1.381(2)
N(1)	B(1)[a]	1.695(2)	C(8)	C(9)	1.380(2)
C(1)	C(2)	1.519(2)	C(9)	C(10)	1.387(2)

[a] Symmetry operation: $1 - x, 1 - y, 1 - z$.

(4). As expected, the coordination about N(1)/N(2) and B(2)/B(4) is approximately tetrahedral, whereas the coordination at the trivalent boron atom B(1)/B(3) is planar within experimental error. The partial double bond character of both O—B bonds involving the trivalent boron atom in **7** is documented by the short bond lengths (O(2)—B(1) = 1.331(2), O(1)—B(1) = 1.402(2), O(5)—B(3) = 1.329(2), O(4)—B(3) = 1.404(2) Å) which further suggest O—B *pp*(π) interactions of differing strengths for the two bonds. The *B*-phenyl ring is nearly coplanar with the boronate group, an orientation which could facilitate a possible conjugation between the π-systems of the phenyl and boronate moieties. The (sp^2)B—C(phenyl) bonds are shorter by about 0.03 Å than the (sp^3)B—C(phenyl) bonds at B(2)/B(4), resulting from a combination of steric and hybridization effects and a weak π-interaction between the phenyl ring and the "vacant" p_z orbital of the adjacent sp^2-boron atom.

In the (sp^2)B—O—B(sp^3) anhydridic moiety, the characteristic difference between the very short (sp^2)B—O bond (1.331(2) and 1.329(2) Å) and the long (sp^3)B—O bond (1.472(2) and 1.468(2) Å) is consistent with that observed for other compounds of type **2** (2), **4** (4), and similar cyclic "pyroboronates" involving one trigonal boronate and one tetracoordinated borinic (13) or boronic acid group (14–17).

The 7-methyl substituent at C(1)/C(23) is positioned in a pseudo-equatorial orientation at the "flap" of the BOCCN ring "envelope." The hydrogen atom at C(1)/C(23) occupies the pseudo-axial position, but the distance between this hydrogen atom and the facing oxygen atom O(1)/O(4) is too long for an intramolecular C—H···O interaction that could play a role in the stabilization of the structure.

Structure **11**, a centrosymmetric twofold N→B coordinated dimer of the six-membered BONCCO ring **9**, represents the solid state structure of the simple cyclic phenylboronate **9**. A pair of enantiomers of **9** comprises the centrosymmetric dimer **11**, forming an "internal racemate." The chiral centres of the molecule depicted in Fig. 1 have the configurations B(1): *S*, C(2): *R*, N(1): *S*, B(1)*: *R*, C(2)*: *S*, N(1)*: *R*. The tricyclic ring system of **11** is composed of a central six-membered BONBON ring having O—C—C bridges spanning both of the B—O—N segments. This is a new type of "BONBON" compound. In addition to the simple BONBON dimers of open-chain B—O—N compounds (7, 8, 11, 15 and references therein, 18), the ring system **12** having two —O—C=C—C= anellations (one at each side of the central BONBON ring) (9) and two other types of bridged BONBON compounds **13** (15) and **14** (19) are known. The tricyclic ring system of **13** has an O—B—O bridge across the B—O—N—B fragment and a C—C bridge across the N—B—O—N fragment of the central BONBON ring. The bicyclic compound **14** contains a B—O—B bridge across the six-membered BONBON ring. Whereas the BONBON ring in **11** has a strain-free, nearly undistorted chair conformation, those in **12**, **13**, and **14** have more or less distorted boat conformations. To the best of our knowledge, compounds **11–14** are the only "BONBON" compounds which have as yet been structurally characterized by X-ray analysis with the exception of a preliminary communication of some crystallographic data (without details on the molecular structure) for the oxime derivative $Me_2C{=}N{-}O{-}BMe_2$ (11). These data, together with spectroscopic studies, led to the conclusion that the boron compound probably has a dimeric structure in the crystal, but is partially dissociated in solution and fully dissociated in the gas phase into the monomeric $Me_2C{=}N{-}O{-}BMe_2$.

The N—B bond length in **11** (1.695(2) Å) is similar to those observed for several cyclic N—B coordinated com-

Can. J. Chem. Downloaded from www.nrcresearchpress.com by 109.225.110.28 on 09/08/12
For personal use only.

TABLE 4. Bond angles (deg) with estimated standard deviations.

Atom	Atom	Atom	Angle	Atom	Atom	Atom	Angle
			7				
N(1)	O(1)	B(1)	107.9(1)	N(2)	O(4)	B(3)	107.6(1)
B(1)	O(2)	B(2)	112.8(1)	B(3)	O(5)	B(4)	114.3(1)
C(1)	O(3)	B(2)	113.5(1)	C(23)	O(6)	B(4)	111.9(1)
O(1)	N(1)	C(2)	107.8(1)	O(4)	N(2)	C(24)	107.5(1)
O(1)	N(1)	C(4)	107.0(1)	O(4)	N(2)	C(26)	107.2(1)
O(1)	N(1)	B(2)	103.6(1)	O(4)	N(2)	B(4)	104.8(1)
C(2)	N(1)	C(4)	116.1(1)	C(24)	N(2)	C(26)	114.4(1)
C(2)	N(1)	B(2)	103.0(1)	C(24)	N(2)	B(4)	102.7(1)
C(4)	N(1)	B(2)	118.3(1)	C(26)	N(2)	B(4)	119.3(1)
O(3)	C(1)	C(2)	104.3(1)	O(6)	C(23)	C(24)	103.9(1)
O(3)	C(1)	C(3)	110.8(1)	O(6)	C(23)	C(25)	110.6(1)
C(2)	C(1)	C(3)	113.1(1)	C(24)	C(23)	C(25)	112.4(1)
N(1)	C(2)	C(1)	104.1(1)	N(2)	C(24)	C(23)	105.1(1)
N(1)	C(4)	C(5)	116.3(1)	N(2)	C(26)	C(27)	115.3(1)
C(4)	C(5)	C(6)	123.4(1)	C(26)	C(27)	C(28)	120.4(2)
C(4)	C(5)	C(10)	118.1(2)	C(26)	C(27)	C(32)	121.4(2)
C(6)	C(5)	C(10)	118.5(1)	C(28)	C(27)	C(32)	118.2(2)
C(5)	C(6)	C(7)	120.1(2)	C(27)	C(28)	C(29)	121.2(2)
C(6)	C(7)	C(8)	120.6(2)	C(28)	C(29)	C(30)	119.9(2)
C(7)	C(8)	C(9)	119.8(2)	C(29)	C(30)	C(31)	119.8(2)
C(8)	C(9)	C(10)	120.0(2)	C(30)	C(31)	C(32)	120.4(2)
C(5)	C(10)	C(9)	120.9(2)	C(27)	C(32)	C(31)	120.6(2)
C(12)	C(11)	C(16)	117.3(2)	C(34)	C(33)	C(38)	117.4(2)
C(12)	C(11)	B(1)	120.6(2)	C(34)	C(33)	B(3)	122.0(1)
C(16)	C(11)	B(1)	122.1(2)	C(38)	C(33)	B(3)	120.5(1)
C(11)	C(12)	C(13)	121.7(2)	C(33)	C(34)	C(35)	121.2(2)
C(12)	C(13)	C(14)	119.8(2)	C(34)	C(35)	C(36)	120.3(2)
C(13)	C(14)	C(15)	120.4(2)	C(35)	C(36)	C(37)	120.1(2)
C(14)	C(15)	C(16)	120.2(2)	C(36)	C(37)	C(38)	119.7(2)
C(11)	C(16)	C(15)	120.7(2)	C(33)	C(38)	C(37)	121.3(2)
C(18)	C(17)	C(22)	116.6(1)	C(40)	C(39)	C(44)	116.1(2)
C(18)	C(17)	B(2)	120.3(1)	C(40)	C(39)	B(4)	122.3(1)
C(22)	C(17)	B(2)	123.0(1)	C(44)	C(39)	B(4)	121.5(1)
C(17)	C(18)	C(19)	121.6(2)	C(39)	C(40)	C(41)	121.9(2)
C(18)	C(19)	C(20)	120.3(2)	C(40)	C(41)	C(42)	120.2(2)
C(19)	C(20)	C(21)	119.8(2)	C(41)	C(42)	C(43)	119.4(2)
C(20)	C(21)	C(22)	119.6(2)	C(42)	C(43)	C(44)	120.2(2)
C(17)	C(22)	C(21)	122.0(2)	C(39)	C(44)	C(43)	122.1(2)
O(1)	B(1)	O(2)	115.4(1)	O(4)	B(3)	O(5)	115.9(1)
O(1)	B(1)	C(11)	116.1(1)	O(4)	B(3)	C(33)	118.0(1)
O(2)	B(1)	C(11)	128.6(1)	O(5)	B(3)	C(33)	126.1(2)
O(2)	B(2)	O(3)	115.8(1)	O(5)	B(4)	O(6)	115.5(1)
O(2)	B(2)	N(1)	97.8(1)	O(5)	B(4)	N(2)	97.1(1)
O(2)	B(2)	C(17)	115.4(1)	O(5)	B(4)	C(39)	114.7(1)
O(3)	B(2)	N(1)	99.8(1)	O(6)	B(4)	N(2)	99.2(1)
O(3)	B(2)	C(17)	113.6(1)	O(6)	B(4)	C(39)	114.4(1)
N(1)	B(2)	C(17)	112.1(1)	N(2)	B(4)	C(39)	113.4(1)
			11				
N(1)	O(1)	B(1)	111.75(7)	C(6)	C(5)	B(1)	123.3(1)
C(2)	O(2)	B(1)	119.33(8)	C(10)	C(5)	B(1)	119.8(1)
O(1)	N(1)	C(1)	105.96(8)	C(5)	C(6)	C(7)	121.8(1)
O(1)	N(1)	C(3)	104.20(8)	C(6)	C(7)	C(8)	120.0(1)
O(1)	N(1)	B(1)[a]	106.80(7)	C(7)	C(8)	C(9)	119.6(1)
C(1)	N(1)	C(3)	108.80(9)	C(8)	C(9)	C(10)	119.9(1)
C(1)	N(1)	B(1)[a]	118.74(8)	C(5)	C(10)	C(9)	121.9(1)
C(3)	N(1)	B(1)[a]	111.20(9)	O(1)	B(1)	O(2)	114.34(9)
N(1)	C(1)	C(2)	113.37(9)	O(1)	B(1)	N(1)[a]	104.98(8)
O(2)	C(2)	C(1)	111.33(9)	O(1)	B(1)	C(5)	109.02(8)
O(2)	C(2)	C(4)	108.3(1)	O(2)	B(1)	N(1)[a]	106.81(8)
C(1)	C(2)	C(4)	109.7(1)	O(2)	B(1)	C(5)	111.72(9)
C(6)	C(5)	C(10)	116.8(1)	N(1)	B(1)	C(5)	109.67(8)

[a]Symmetry operation: $1 - x$, $1 - y$, $1 - z$.

Can. J. Chem. Downloaded from www.nrcresearchpress.com by 109.225.110.28 on 09/08/12
For personal use only.

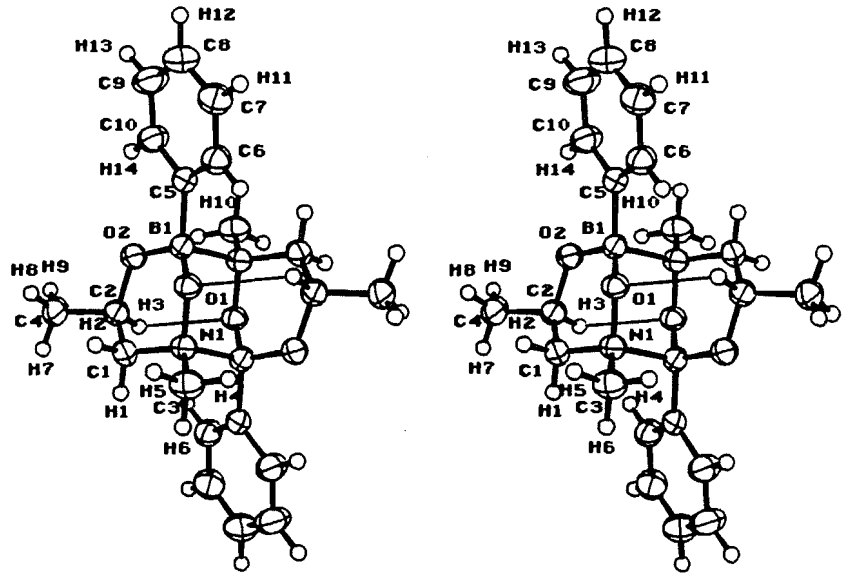

FIG. 1. Stereoview of **11**; 33% probability thermal ellipsoids are shown for the non-hydrogen atoms.

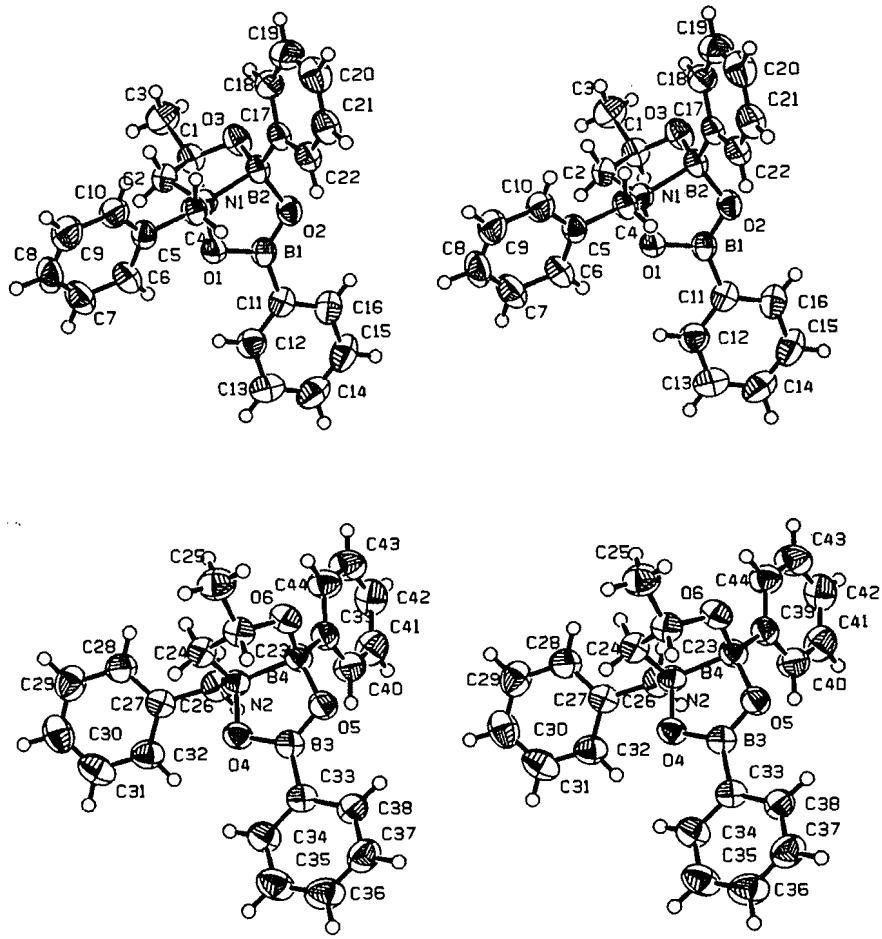

FIG. 2. Stereoviews of the two crystallographically independent molecules of **7**; 33% probability thermal ellipsoids are shown for the non-hydrogen atoms.

Can. J. Chem. Downloaded from www.nrcresearchpress.com by 109.225.110.28 on 09/08/12
For personal use only.

pounds like **2** ($R^1 = R^2 = Me$, $R^3 = R^4 = H$) (1.688(2) Å) (2) and the "BONBON" derivative **14** (1.703(3) Å) (19), but is somewhat shorter than the N—B bonds in other tetrahedral "$PhBO_2N$" compounds having sterically hindered N—B bonds like **4** (R = Me) (1.729(3) and 1.736(3) Å) (4) and **7** (1.737(2) and 1.762(2) Å) (this work) and similar bicyclic systems with N—B bond lengths ranging from 1.706(2) to 1.759(3) Å (14, 16, 17). Shorter N—B bonds than those in the BONBON dimer **11** are found in the polycyclic BONBON compounds **12** (mean 1.586(3) Å) (9) and **13** (mean 1.654(8) Å) (15). The sum of the bond lengths about the boron atom in **11**, 6.170 Å, is at the lower end of the range 6.191–6.297 Å observed previously for compounds of the type "$PhBO_2N(sp^3)$" (15, 20). This is consistent with a relatively low overall strain about the boron atom (15).

The dimeric structure of **11** in the solid state is additionally stabilized by weak transannular C—H···O hydrogen bonds between C(2)—H(3) of one of the BONCCO rings and O(1) of the second such ring. The intramolecular C···O distance of 2.853(1) Å is significantly shorter than the sum of van der Waals radii (about 3.3 Å). The existence of short C—H···O interactions in crystals is well-documented, these interactions being considered attractive (21–23). Spectroscopic (24) and crystallographic evidence (25) document the influence of intramolecular C—H···O interactions on the conformational preferences and on the general geometry of both open-chain and cyclic compounds. The distance between the transannular hydrogen H(3) and the BON oxygen atom O(1) in the eight-membered BONBOCCN ring portion of **11** is 2.37(1) Å. A similar distance (2.34 Å) has been observed for the transannular C—H···O interaction in the ten-membered ring system of nonanolactone (25). The C—H···O angle of 108.0(8)° in **11** is similar to the corresponding value of 109.5° in nonanolactone (25). Including these C—H···O hydrogen bonds, the complete three-dimensional array of the crystalline form of **11** has an approximate diamond-lattice conformation resembling the skeleton of "diamantane" ("congressane") (26). There is also a second pair of weaker intramolecular C—H···O interactions present in **11**: C(3)—H(4)···O(2)*, H···O = 2.47(2) Å, C···O = 2.911(2) Å, and C—H···O = 106(1)°. All intermolecular distances correspond to normal van der Waals interactions.

Acknowledgements

We thank the Natural Sciences and Engineering Research Council of Canada and the Fonds der Chemischen Industrie, Frankfurt am Main, for financial support. We are grateful to the nmr laboratory of the Chemische Institut der Technischen Universität, Braunschweig, for running the ^{11}B nmr spectra.

1. W. Kliegel and H. Becker. Chem. Ber. **110**, 2090 (1977); W. Kliegel, B. Enders, and H. Becker. Ann. Chem. 1712 (1982).
2. S. J. Rettig, J. Trotter, W. Kliegel, and H. Becker. Can. J. Chem. **54**, 3142 (1976).
3. W. Kliegel. J. Organomet. Chem. **253**, 9 (1983).
4. W. Kliegel, S. J. Rettig, and J. Trotter. Can. J. Chem. **62**, 515 (1984).
5. H. Noth and B. Wrackmeyer. Nuclear magnetic resonance spectroscopy of boron compounds. Springer-Verlag, Berlin. 1978.
6. W. Kliegel, G. Lubkowitz, S. J. Rettig, and J. Trotter. Can. J. Chem. **69**, 234 (1991), and references therein.
7. W. Maringgele and A. Meller. Monatsh. Chem. **106**, 1369 (1975).
8. D. W. Palmer and K. Niedenzu. Synth. React. Inorg. Met.-Org. Chem. **9**, 13 (1979).
9. W. Kliegel and D. Nanninga. Monatsh. Chem. **114**, 465 (1983); S. J. Rettig and J. Trotter. Can. J. Chem. **61**, 206 (1983).
10. W. Kliegel. Liebigs Ann. Chem. **763**, 61 (1972); W. Kliegel and E. Ahlenstiel. J. Organomet. Chem. **277**, 173 (1984).
11. J. R. Jennings and K. Wade. J. Chem. Soc. Sect. A, 1333 (1967).
12. International tables for X-ray crystallography Vol. IV. Kynoch Press, Birmingham, U.K. Present distributor: Kluwer Academic Publishers, Dordrecht, The Netherlands. 1974 pp. 99–102 and 149.
13. W. Kliegel, D. Nanninga, S. J. Rettig, and J. Trotter. Can. J. Chem. **61**, 2329 (1983).
14. W. Kliegel, D. Nanninga, S. J. Rettig, and J. Trotter. Can. J. Chem. **62**, 845 (1984).
15. H. Amt, W. Kliegel, S. J. Rettig, and J. Trotter. Can. J. Chem. **66**, 1117 (1988).
16. H. Amt, W. Kliegel, S. J. Rettig, and J. Trotter. Can. J. Chem. **68**, 1791 (1990).
17. W. Kliegel, G. Lubkowitz, S. J. Rettig, and J. Trotter. Can. J. Chem. **70**, 2027 (1992).
18. R. Köster. *In* Houben-Weyl, Methoden der organischen chemie. Band 13, Teil 3b Organobor-Verbindungen II. Thieme Verlag, Stuttgart. 1983. p. 586.
19. W. Kliegel, U. Riebe, S. J. Rettig, and J. Trotter. Can. J. Chem. **69**, 1222 (1991).
20. E. Ebeling, W. Kliegel, S. J. Rettig, and J. Trotter. Can. J. Chem. **67**, 933 (1989); S. J. Rettig and J. Trotter. Can. J. Chem. **53**, 1393 (1975).
21. D. J. Sutor. J. Chem. Soc. 1105 (1963).
22. R. Taylor and O. Kennard. J. Am. Chem. Soc. **104**, 5063 (1982).
23. G. R. Desiraju. Acc. Chem. Res. **24**, 290 (1991).
24. S. Zushi, Y. Kodama, K. Nishihata, K. Umemura, M. Nishio, J. Uzawa, and M. Hirota. Bull. Chem. Soc. Jpn. **53**, 3631 (1980).
25. K. B. Wiberg, R. F. Waldron, G. Schulte, and M. Saunders. J. Am. Chem. Soc. **113**, 971 (1991).
26. T. M. Gund, E. Osawa, Van Zandt Williams, and P. v. R. Schleyer. J. Org. Chem. **39**, 2979 (1974).
27. W. Kliegel, G. Lubkowitz, S. J. Rettig, and J. Trotter. Can. J. Chem. **70**, 2033 (1992).

Can. J. Chem. Downloaded from www.nrcresearchpress.com by 109.225.110.28 on 09/08/12
For personal use only.

Mechanistic studies on the formation of aminoxyl radicals from 5,5-dimethyl-1-pyrroline-*N*-oxide in Fenton systems. Characterization of key precursors giving rise to background ESR signals

KEISUKE MAKINO,[1] AKIFUMI HAGI, HIROSHI IDE, AND AKIRA MURAKAMI

Department of Polymer Science and Engineering, Kyoto Institute of Technology, Matsugasaki, Sakyo-ku, Kyoto 606, Japan

AND

MASATOSHI NISHI

Faculty of Pharmaceutical Sciences, Setsunan University, Nagaotouge-cho, Hirakata, Osaka 573-01, Japan

Received April 30, 1992

KEISUKE MAKINO, AKIFUMI HAGI, HIROSHI IDE, AKIRA MURAKAMI, and MASATOSHI NISHI. Can. J. Chem. **70**, 2818 (1992).

To assign unidentified ESR signals obtained in a Fenton system with a spin trap, 5,5-dimethyl-1-pyrroline-*N*-oxide (DMPO), fundamental reactions of DMPO have been thoroughly investigated. When the concentration of Fe^{2+} in Fenton systems exceeded 1% of that of DMPO, background ESR signals totally distinguishable from 2-hydroxy-5,5-dimethyl-1-pyrrolidinyloxy (DMPO-OH) appeared, and simultaneously absorbance at 520 nm increased, which was characteristic of hydroxamic acids complexed with Fe^{3+}. To prove the postulated formation of hydroxamic acid as a key intermediate, DMPO was subjected to Fenton reaction or was treated with Fe^{3+} in aqueous solution to produce DMPO-OH (Makino *et al.* Biochem. Biophys. Res. Commun. **172**, 1073 (1990)), and a major product was isolated by RPLC. Based on ^1H, ^{13}C NMR and MS measurements, the structure of the major product was assigned to 1-hydroxy-5,5-dimethyl-1-pyrrolid-2-one (HDMPN) having a hydroxamic acid structure. Temperature dependence of NMR spectra and careful analysis of the fragmentation patterns in MS further revealed that HDMPN was present in equilibrium with 2-hydroxy-5,5-dimethyl-1-pyrroline-*N*-oxide (HDMPO), a tautomer of HDMPN. It has also been shown that the oxidation of DMPO yielding HDMPN and HDMPO occurs via DMPO-OH and is driven by Fe^{3+}. These oxidation products (HDMPN and HDMPO) were readily converted to the corresponding ESR visible aminoxyl radicals by oxidation and $^{\cdot}OH$ addition in aqueous solution, respectively, and superimposition of the ESR signals arising from these radicals accounts for the background signals observed in Fenton systems with DMPO as a spin trap.

KEISUKE MAKINO, AKIFUMI HAGI, HIROSHI IDE, AKIRA MURAKAMI et MASATOSHI NISHI. Can. J. Chem. **70**, 2818 (1992).

Dans le but d'attribuer les signaux RPE non-identifiés obtenus dans un système de Fenton avec un piège à spin, le *N*-oxyde de 5,5-diméthyl-1-pyrroline (DMPO), on a étudié à fond les réactions fondamentales du DMPO. Lorsque la concentration de Fe^{2+} dans les systèmes de Fenton dépasse 1% de celle du DMPO, des signaux RPE totalement différents de ceux du 2-hydroxy-5,5-diméthyl-1-pyrrolidinyloxy (DMPO-OH) apparaissent avec une augmentation simultanée de l'absorption à 520 nm, caractéristique des acides hydroxamiques complexés par le Fe^{3+}. Afin de prouver la formation postulée d'acide hydroxamique comme intermédiaire clé, on a soumis le DMPO à une réaction de Fenton ou on l'a traité par du Fe^{3+} en solution aqueuse pour obtenir du DMPO-OH (Makino *et al.* Biochem. Biophys. Res. Commun. **172**, 1073 (1990)) et on a isolé le produit principal par RPLC. En se basant sur la RMN du ^1H et du ^{13}C et des mesures de spectrométrie de masse, on conclut que le produit majeur est la 1-hydroxy-5,5-diméthyl-1-pyrrolidin-2-one (HDMPN) possédant une acide hydroxamique dans sa structure. La relation entre la température et les spectres RMN ainsi qu'une analyse soigneuse des patrons de fragmentation de SM ont aussi permis de démontré que le HDMPN est présent à l'équilibre avec l'oxyde de 2-hydroxy-5,5-diméthyl-1-pyrroline (HDMPO), un tautomère du HDMPN. On a aussi montré que l'oxydation du DMPO, conduisant à la HDMPN et au HDMPO, se produit par l'intermédiaire du DMPO-OH et que cette réaction est provoquée par le Fe^{3+}. L'oxydation du HDMPN et l'addition de $^{\cdot}OH$ à une solution aqueuse de HDMPO permettent de transformer ces deux produits d'oxydation en radicaux aminoxyl correspondants, visibles par RPE; la superposition des signaux RPE qui résultent de ces réactions explique les signaux de fond qui sont observés dans les systèmes de Fenton avec du DMPO comme piège à spin.

[Traduit par la rédaction]

Introduction

The method of spin trapping is a powerful tool to detect short-lived free radicals that are not detectable by conventional ESR.[2] In this method, through reaction with spin traps, short-lived free radicals are converted to relatively stable aminoxyl radicals (spin adducts) that are ESR detectable (1). Recently this method has been widely applied to the detection of free radicals in biological systems in attempts to correlate the free-radical formation to the initiation of various diseases (2) since a large body of accumulated evidence indicates that free-radical-induced damage of cellular constit-

[1]Author to whom correspondence may be addressed.

[2]Abbreviations: ESR, electron spin resonance spectroscopy; DMPO, 5,5-dimethyl-1-pyrroline-*N*-oxide; $^{\cdot}OH$, hydroxyl radical; DMPO-OH, 2-hydroxy-5,5-dimethyl-1-pyrrolidinyloxy; HDMPN, 1-hydroxy-5,5-dimethyl-1-pyrrolid-2-one; NMR, nuclear magnetic resonance spectroscopy; M_3PO, 2,5,5-trimethyl-1-pyrroline-*N*-oxide; EIMS, electron ionization mass spectrometry; TMS, tetramethylsilane; TSP-d_4, 3-(trimethylsilyl)propionic-2,2,3,3-d_4 acid, sodium salt; DMPO-OOH, 2-hydroperoxy-5,5-dimethyl-1-pyrrolidinyloxy; MS, mass spectrometry; RPLC, high performance reversed phase liquid chromatography; amu, atomic mass unit; HDMPO, 2-hydroxy-5,5-dimethyl-1-pyrroline-*N*-oxide; DMPOX, 5,5-dimethyl-1-pyrrolidin-2-one-1-oxy; HDMPO-OH, 2,2-dihydroxy-5,5-dimethyl-1-pyrrolidinyloxy; M_3PO-OH, 2-hydroxy-2,5,5-trimethyl-1-pyrrolidinyloxy.

Can. J. Chem. Downloaded from www.nrcresearchpress.com by 109.225.110.28 on 09/08/12
For personal use only.

Can. J. Chem. Downloaded from www.nrcresearchpress.com by 109.225.110.28 on 09/08/12
For personal use only.

uents such as DNA and membrane is critical to such initiation steps. In these studies, 5,5-dimethyl-1-pyrroline-*N*-oxide (DMPO, **1** in Fig. 1) has been used almost exclusively as a spin trap since its solubility in water is sufficiently high that the high concentration of the spin trap can be used to detect short-lived free radicals present in very low concentrations. Another advantage is that this spin trap is sufficiently potent to trap oxygen-centered free radicals, especially hydroxyl radicals ($^{\cdot}OH$) and superoxide anion radicals (O_2^{-}) (3). Furthermore, compared to other spin traps (4), it exerts relatively low toxicity to cells.

It is known, however, that ESR spectra obtained with DMPO are often difficult to assign due to coexistence of unidentified signals (1*c*, 5). This is particularly the case when systems containing metal ions (for example, the Fenton reaction) are utilized to initiate free-radical reaction. These undesirable background ESR signals have hampered accurate analysis of ESR spectra and the origin of the spectra remains unidentified. Thus, to make the spin trapping method more accurate and reliable, it is extremely important to characterize all of the species giving rise to the background signals and to clarify the mechanism of their production.

To address these questions, we have conducted basic studies regarding the type of impurities contained in commercial preparations of DMPO that lead to undesirable artifactual ESR signals, and the reactions DMPO undergoes in the presence of metal ions to yield ESR detectable species. For the first question, we have shown that a DMPO derivative, a hydroxyl amine having an epoxy ring (**2** in Fig. 1), is contained in commercial DMPO preparations and this compound is readily oxidized to give an aminoxyl radical whose characteristic ESR spectrum is composed of six lines with equal intensities (6). For the second question, we have reported a preliminary study demonstrating that DMPO is converted to 2-hydroxy-5,5-dimethyl-1-pyrrolidinyloxy (DMPO-OH, **3** in Fig. 1), which is the same compound as a hydroxyl radical adduct of DMPO via the nucleophilic addition of a water molecule to the double bond of DMPO complexed with Fe^{3+} (7).

In the present study, we have carried out further detailed studies to elucidate the entire mechanism for the reaction of DMPO in the presence of iron ions. The present results will be useful not only for accurate assignment of complicated ESR spectra obtained with DMPO in biological studies, but also for designing improved spin traps that do not undergo the undesirable side reactions.

Materials and methods

Materials

High purity DMPO was obtained from Mitsui-Toatsu Co. (Tokyo, Japan) and used without further purification (6). Other reagents of reagent grade were purchased from Wako Pure Chemicals (Osaka, Japan). Water was purified sequentially by Milli R/Q and Milli QII (Millipore, Mass. U.S.A.).

1-Hydroxy-5,5-dimethyl-1-pyrrolid-2-one (HDMPN) was synthesized by modification of the procedure reported previously (8): a mixture of methyl acrylate (1.12 mol) and 2-nitropropane (3.35 mol) was stirred at 30°C for 14 days in the presence of triethylamine (0.56 mol). The methyl 4-methyl-4-nitropentanate obtained was distilled under reduced pressure (69–71°C at 0.7 Torr; 1 Torr = 133.3 Pa) (yield, 80%). To the 50% aqueous ethanol solution (300 mL) containing distilled 4-methyl-4-nitropentanate (0.25 mol) and NH_4Cl (0.25 mol), Zn powder (1.0 mol) was added at 10°C for 3 h with stirring. This mixture was filtered and the solvent was removed by evaporation. The remaining oil was dissolved in 2 N HCl (100 mL) and extracted with chloroform (100 mL, 5 times). After drying the chloroform layer over $MgSO_4$, the solvent was removed by evaporation. Crude HDMPN was purified by column chromatography on silica (Wakogel C-300) with $CHCl_3$:methanol (10:1) as eluent, and subsequently recrystallized from ether:petroleum ether (yield, 50%). This product was identified and examined for its purity by ^1H NMR and RPLC and no additional lines or peaks due to impurities were detected.

2,5,5-Trimethyl-1-pyrroline-*N*-oxide (M_3PO, **4** in Fig. 1) was synthesized by the modification of reported procedures (8*a*, 9). An ether solution (300 mL) of 3-butene-2-one (0.3 mol), 2-nitropropane (0.6 mol), and Triton B (24 mL) was refluxed for 5 h and subsequently shaken sequentially with 0.5 N HCl (100 mL), 10% Na_2CO_3 (100 mL), water (100 mL), and water saturated with NaCl (100 mL). The ether layer containing 5-methyl-5-nitro-2-hexanone was dried over Na_2SO_4 and the ether was then removed by evaporation. The residue was distilled under reduced pressure (59–60°C at 1 Torr). To an aqueous NH_4Cl solution (0.8 M, 300 mL) was added prepared 5-methyl-5-nitro-2-hexanone (0.225 mol). Zn powder (0.9 mol) was added to this suspension under vigorous stirring for 1 h at 0°C and then this solution kept at 20°C for 2 h with vigorous stirring. The reaction mixture was condensed *in vacuo* and was extracted with chloroform. After drying the chloroform layer over Na_2SO_4, chloroform was removed. The crude product was purified by column chromatography similar to that used above for the synthesis of HDMPN (yield, 50%). This product was identified and examined for its purity by ^1H NMR and RPLC and no additional lines or peaks due to impurities were observed.

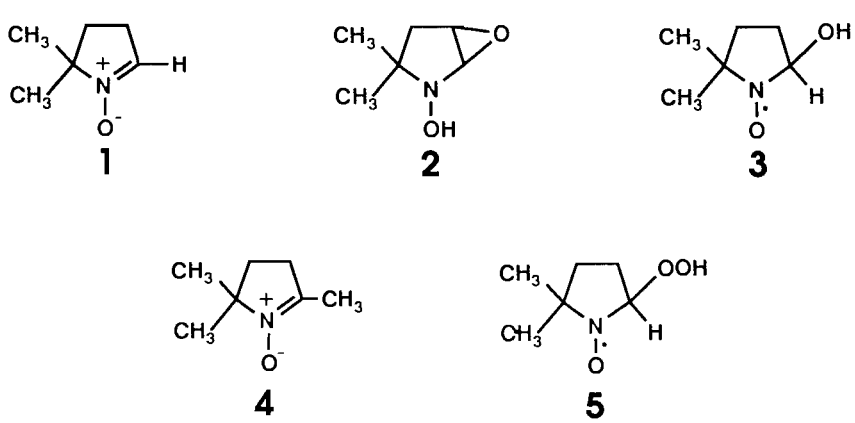

FIG. 1. DMPO and its derivatives appearing in this paper. For HDMPN and HDMPO, see Scheme 1.

Can. J. Chem. Downloaded from www.nrcresearchpress.com by 109.225.110.28 on 09/08/12
For personal use only.

Methods

Free radicals were generated by sonolysis or photolysis, except for Fe^{3+}-catalyzed DMPO-OH formation in the dark. For sonication, a Bransonic model B-2200 cleaning bath was used. A sample tube was set in the center of the bath and argon gas was bubbled (500 mL/min) during the sonication to enhance ESR signals (10). Photolysis was carried out on an XC-500 tunable irradiator (Koken Kogyo, Saitama, Japan) equipped with a 500-W xenon lump. These experiments were performed at room temperature.

ESR spectra were measured at room temperature on a Jeol model PE-3X spectrometer (X-band, 100-kHz field modulation, Jeol, Tokyo). Mn^{2+} was used as a marker for the measurements of hyperfine splitting constants (hfsc) and *g*-values. An aqueous flat quartz cell (1.6 mm in thickness, 10.0 mm in width, and 180.0 mm in length) was used. ESR settings used are represented in the figure legends. Spin concentrations were calculated with 2,2,6,6-tetramethylpiperidine-*N*-oxyl as a standard.

^1H and ^{13}C NMR spectra were obtained on a JNM GSX-400 NMR spectrometer (400 MHz, Jeol) coupled with a variable temperature unit. Standards used for the measurements of chemical shifts were tetramethylsilane (TMS) in $CDCl_3$ (internal reference) and 3-(trimethylsilyl)propionic-2,2,3,3-d_4 acid, sodium salt (TSP-d_4) in D_2O (external reference).

A JMS DX-300 MS spectrometer (Jeol) was used to measure *m/z* values. The electron ionization mass spectrometry (EIMS) was coupled with a temperature rise in the sample probe. The conditions for MS measurements were as follows: ionization energy, 30 eV; temperature rise, 16°C/min from 25°C; pressure, 10^{-6} Torr.

For RPLC analyses, a combination of Hitachi L-6000 and L-6200 pumps equipped with a photodiodearray L-3000 detector (Hitachi, Tokyo) was utilized. An Inertsil ODS column (GL Science, Tokyo) was used. The chromatographic conditions are shown in the figure legend.

Absorption spectra were obtained on a Shimadzu UV 260 spectrophotometer (Shimadzu, Kyoto, Japan). Concentrations of Fe^{2+} and Fe^{3+} were measured with 1,10-phenanthroline (ε_{510} = 9720 cm^{-1} M^{-1}) and potassium thiocyanate (ε_{480} = 9100 cm^{-1} M^{-1}) as coloring reagents, respectively.

All experiments were carried out in the dark to avoid photochemically induced reactions of DMPO (11).

Results and discussion

Background ESR signals in Fenton systems

The reaction of DMPO (0.01, 0.1, or 1 M) in Fenton systems (eqs. [1]–[3]) consisting of H_2O_2 and $FeSO_4$ was investigated by ESR at room temperature under atmospheric conditions.

$$[1]\quad Fe^{2+} + H_2O_2 \rightarrow Fe^{3+} + {}^{\cdot}OH + OH^-$$

$$[2]\quad {}^{\cdot}OH + H_2O_2 \rightarrow {}^{\cdot}OOH + H_2O$$

$$[3]\quad Fe^{3+} + {}^{\cdot}OOH \rightarrow Fe^{2+} + O_2 + H^+$$

The concentrations of H_2O_2 and $FeSO_4$ were varied from 1 mM to 1 M and 10 μM to 10 mM, respectively. When the concentration of Fe^{2+} was less than 1% of that of DMPO, an ESR spectrum composed of a 1:2:2:1 quartet attributable to a spin adduct of hydroxyl radicals (DMPO-OH, a_N = $a_{\beta H}$ = 1.50 mT) was obtained (Fig. 2*A*) (12). On the other hand, additional lines appeared when the concentration of Fe^{2+} exceeded 1% of that of DMPO. Figure 2*B* shows an ESR spectrum taken immediately after the sample preparation. The additional lines consisted of a 1:1:1 triplet of 1:1 doublets further split into a 1:1 doublet, and was assigned as a spin adduct of the hydroperoxyl radical of DMPO (DMPO-OOH, a_N = 1.43 mT, $a_{\beta H}$ = 1.15 mT, and $a_{\gamma H}$ = 0.13 mT, **5** in Fig. 1) (12). With increasing storage time, the ESR spectrum obtained immediately after the sample preparation (storage time ca. 1 min) changed further, and two sets of ESR lines appeared consisting of a 1:1:1 triplet (a_N = 1.53 mT, signal (*i*)) and a 1:1:1 triplet of 1:2:1 triplet

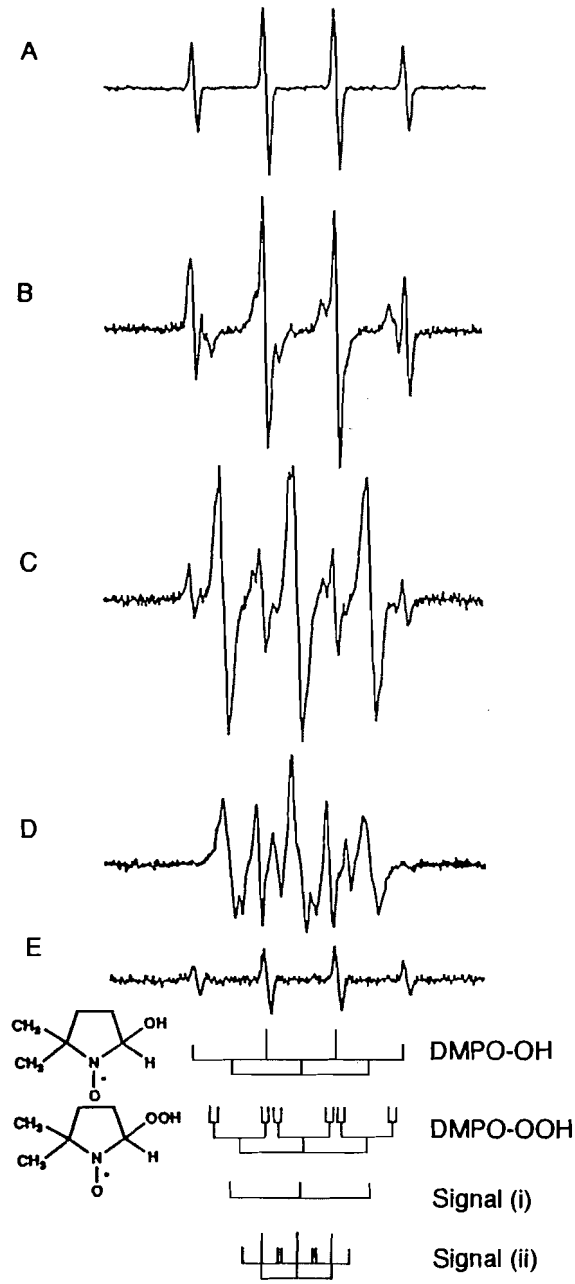

FIG. 2. ESR spectra obtained from aqueous DMPO solutions (100 mM) containing (*A*, *B*, *C*, and *D*) $FeSO_4$ (10 μM for *A* and 3 mM for *B*, *C*, and *D*) and H_2O_2 (900 mM), and (*E*) $FeNH_4(SO_4)_2$ (1 mM). Storage time was (*A*) 2 h, (*B*) 3 min, (*C*) 2 h, (*D*) 3 h, and (*E*) 1 min. Each component is explained by the stick diagrams in this figure. Hyperfine splitting constant values obtained for each of the ESR components are as follows: a_N = $a_{\beta H}$ = 1.50 mT for DMPO-OH, a_N = 1.43 mT, $a_{\beta H}$ = 1.15 mT, and $a_{\gamma H}$ = 0.13 mT for DMPO-OOH, a_N = 1.53 mT for signal (*i*), and a_N = 0.72 mT and $a_{\gamma H}$ = 0.41 mT (2H) for signal (*ii*). ESR settings are as follows: modulation amplitude, 0.05 mT; receiver gain, ×500 for *A*, *B*, *C*, and *D* and ×1000 for *E*; time constant, 0.3 s; sweep time, 16 min for *B*, *C*, and *D* and 8 min for *A* and *E*.

(a_N = 0.72 mT and a_H = 0.41 mT, signal (*ii*)) after 1 h (Fig. 2*C*) and 3 h (Fig. 2*D*), respectively. All the ESR components appearing in Figs. 2*A–D* are explained by the stick diagrams illustrated in Fig. 2. In the present study, the unidentified signals (*i*) and (*ii*) have been studied in detail to clarify their origin and formation mechanisms.

First we explored the possibility that the background signals (*i*) and (*ii*) might arise through reactions between DMPO and Fe^{2+} or Fe^{3+} oxidized from Fe^{2+} in Fenton systems. No reaction was observed for an aqueous DMPO solution containing Fe^{2+} (as $FeSO_4$). In an aqueous DMPO solution (100 mM) containing Fe^{3+} (as $FeNH_4(SO_4)_2$, 1 mM), an ESR spectrum consisting of a 1:2:2:1 quartet appeared (Fig. 2*E*) and diminished over several 10-min intervals. This species has been assigned to the same compound as a DMPO spin adduct of $^{\cdot}OH$ (DMPO-OH), and is formed by the nucleophilic addition of a water molecule to DMPO (7). These results suggest that other reactions, probably involving conversion of initially formed DMPO-OH, are responsible for the production of the background ESR signals.

Absorption spectra were also measured for Fenton systems that gave rise to the background ESR signals (*i*) and (*ii*). As shown in Fig. 3*A*, a Fenton system ($FeSO_4$ (3 mM) and H_2O_2 (900 mM)) containing DMPO (100 mM) showed an absorption at 520 nm, which increased with increasing storage time. A similar spectrum was obtained from an aqueous solution containing $FeNH_4(SO_4)_2$ (10 mM) and DMPO (10 mM) (Fig. 3*B*). These results imply that the same species absorbing at 520 nm is formed in both systems, and that the appearance of the background ESR signals may be related to the increment of the absorbance.

A possibility that the species absorbing at 520 nm is a complex between DMPO and Fe^{3+} has been ruled out since we already demonstrated that the formation of a DMPO–Fe^{3+} complex occurs instantly at room temperature (7, 13), while the complex absorbing at 520 nm formed slowly at a rate in the order of 1 h. Elsworth and Lamchen (14) have reported that cyclic nitrones including DMPO undergo two-electron reduction in the presence of $FeCl_3$ to yield directly the corresponding hydroxamic acids, and that a hydroxamic acid derivative of DMPO (1-hydroxy-5,5-dimethyl-1-pyrrolid-2-one, HDMPN) complexed with Fe^{3+} has absorption at 544 nm (ε = 1075 cm^{-1} M^{-1}). Although the absorption maximum observed in this study was slightly blue-shifted (520 nm) relative to that reported (544 nm), HDMPN was likely to be produced in the present systems. Accordingly, we decided to reexamine in more detail the formation of the hydroxamic acid (HDMPN) from DMPO or DMPO-OH to clarify the relation with the generation of background ESR signals.

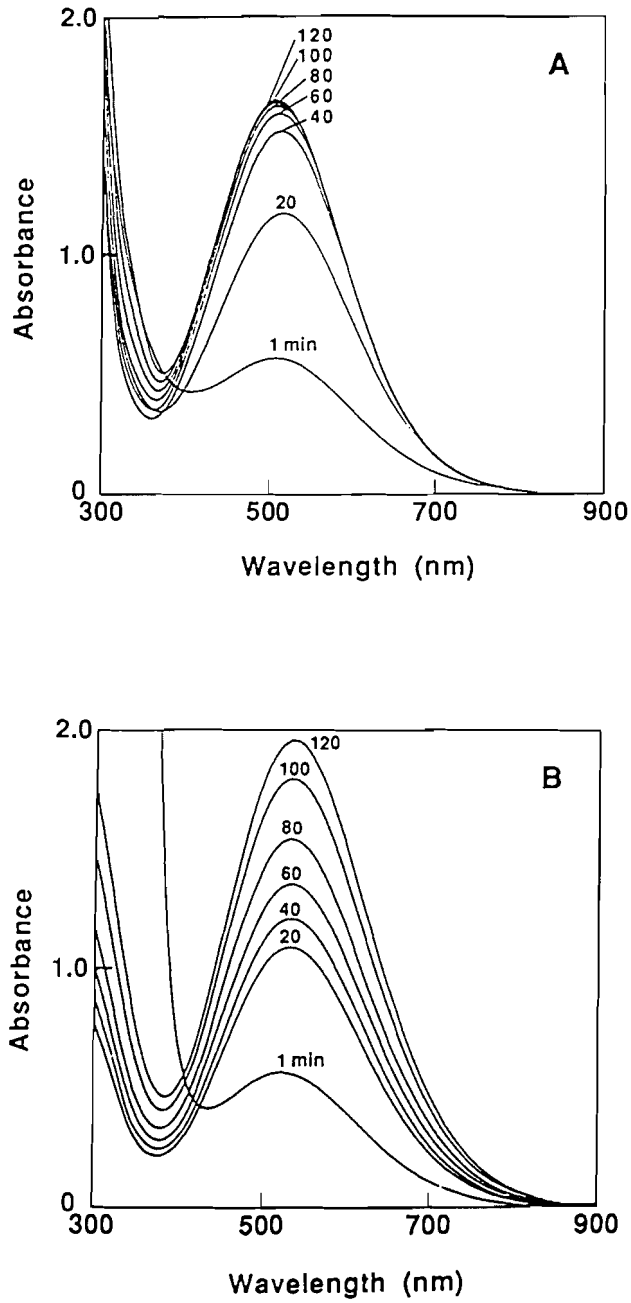

FIG. 3. Progressive change in the absorbance at 520 nm occurring in aqueous solutions containing (*A*) DMPO (100 mM), $FeSO_4$ (3 mM), and H_2O_2 (900 mM) and (*B*) DMPO (10 mM) and $FeNH_4(SO_4)_2$ (10 mM). The path length of the cell used was 0.5 cm for *A* and 1.0 cm for *B*.

Characterization of intermediates giving rise to background ESR signals

To examine the formation of HDMPN from DMPO or DMPO-OH, ^1H NMR measurements were first performed in a D_2O solution containing $FeNH_4(SO_4)_2$ (10 mM) and DMPO (10 mM), and the time course of the reaction was followed. A typical spectrum obtained is depicted in Fig. 4. Similar spectra were obtained from Fenton systems that gave the absorbance maximum at 520 nm. A set of lines with chemical shifts of 8.43 (CH at C2), 4.06 (CH_2 at C3), 3.37 (CH_2 at C4), and 2.57 (CH_3 at C5) ppm was assigned to DMPO: the chemical shifts were low-field shifted and line shapes broadened due to the presence of paramagnetic Fe^{3+}, in comparison with those for DMPO in D_2O free of ferric ions (7.23 (CH at C2), 2.76 (CH_2 at C3), 2.24 (CH_2 at C4), and 1.42 (CH_3 at C5) ppm). The rest of the signals with chemical shifts of 3.58, 3.13, and 2.43 ppm were probably due to the postulated complex between HDMPN and Fe^{3+}. The signal intensities of DMPO (asterisked) decreased as that of the complex increased. This conversion proceeded in the order of 1 h, corresponding to the slow change of the ESR lines appearing in Fig. 2.

Product analysis was also carried out for a system com-

Can. J. Chem. Downloaded from www.nrcresearchpress.com by 109.225.110.28 on 09/08/12
For personal use only.

Can. J. Chem. Downloaded from www.nrcresearchpress.com by 109.225.110.28 on 09/08/12
For personal use only.

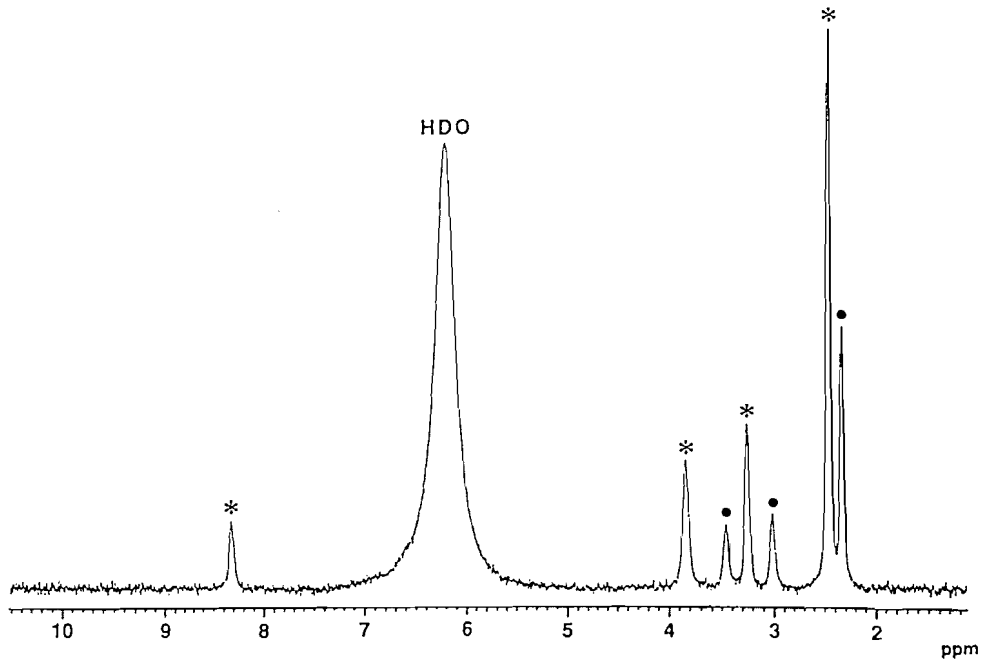

FIG. 4. A typical ^1H NMR spectrum obtained from a D_2O solution containing DMPO (10 mM) and $FeNH_4(SO_4)_2$ (10 mM). The peaks indicated by asterisks and closed circles are due to DMPO and a product from DMPO, respectively.

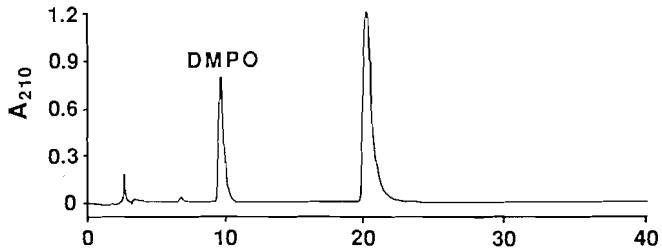

FIG. 5. An RPLC chromatogram obtained from an aqueous DMPO solution (10 mM) containing $FeNH_4(SO_4)_2$ (10 mM). Reaction time was 3 h. The first peak, eluted at 9.5 min, is due to DMPO. Chromatographic conditions are as follows: column, Inertsil ODS (4.6 mm i.d. × 250 mm long); eluent, (*a*) $CH_3CN:H_2O$ (5%) and (*b*) $CH_3CN:H_2O$ (25%); gradient, held in (*a*) for 10 min, linear from (*a*) to (*b*) for 20 min, and held in (*b*); flow rate, 1.0 mL/min; detection, 210 nm.

prising DMPO and ferric ions. DMPO (10 mM) was allowed to react in an aqueous solution containing $FeNH_4(SO_4)_2$ (10 mM) for 1 day at room temperature, and product analysis was performed periodically by RPLC. A typical chromatogram is shown in Fig. 5. Analogous chromatograms were obtained for the Fenton system containing DMPO. The intensity of the peak due to the major reaction product eluted at 20.5 min increased with the decrease in the peak of DMPO eluted at 9.5 min. The stoichiometry between DMPO and the major product was consistent with that obtained by the ^1H NMR measurement. The major product eluted at 20.5 min was collected and measured by ^1H NMR and MS. Fe^{3+} that disturbed the measurements was separated during the elution from the RPLC column. By the EIMS coupled with temperature rise, two peaks appeared at 170 and 194°C in the MS chromatogram and the major MS peaks were obtained from these peaks as follows: (*m/z*) 36, 98, 114, and 129 (M^+) at 170°C and 86, 114, and 129 (M^+) at 194°C. The second set of *m/z* values indicates the formation of HDMPN, which has a mass number of 129 and has methyl (15 amu) and carbonyl (28 amu) groups. The first set indicates that this molecule has a mass number of 129 and has methyl (15 amu) and hydroxyl (16 amu) groups. This compound is tentatively assigned to 2-hydroxy-5,5-dimethyl-1-pyrroline-*N*-oxide (HDMPO), a tautomer of HDMPN (see Scheme 1 for the structures of HDMPN and HDMPO). To confirm these assignments, ^1H and ^{13}C NMR spectra of the isolated product were measured in $CDCl_3$ and D_2O, respectively. The ^1H NMR spectrum of the major product consisted of signals with chemical shifts of 10.02 (N-OH), 2.40 (CH_2 at C3), 1.90 (CH_2 at C4), and 1.31 (CH_3 at C5) ppm (Fig. 6*A*). These values coincide exactly with those of authentic HDMPN. Consistent assignment was also obtained from the ^{13}C NMR spectrum (Fig. 6*B*): 174.73 (C=O at C2), 64.75 (C5), 32.79 (CH_2 at C4), 28.80 (CH_2 at C3), and 26.91 (CH_3 at C5) ppm. From these results, the major product is assigned to HDMPN. Since HDMPO is a tautomer of HDMPN, an equilibrium between HDMPN and HDMPO may exist. To elucidate the possibility, ^1H NMR measurements were performed in $CDCl_3$ by lowering the temperature to suppress structural exchange between HDMPN and HDMPO. As shown in Fig. 6*C*, at −20°C and below a broad singlet emerged around 5.5 ppm, which is characteristic of an enolic OH group, and the signal is attributed to an OH proton of HDMPO. The ratio of HDMPN:HDMPO calculated from the spectrum obtained at −60°C was roughly 8:1.

Since HDMPN is a hydroxylamine as well as a hydroxamic acid that can be converted to an aminoxyl radical under oxidative conditions, and HDMPO is a nitrone spin trap, ESR signals should arise when these compounds are oxidized by $^{\cdot}OH$. Thus an aqueous solution of authentic HDMPN (100 mM) was photo-irradiated at 260 nm in the presence of

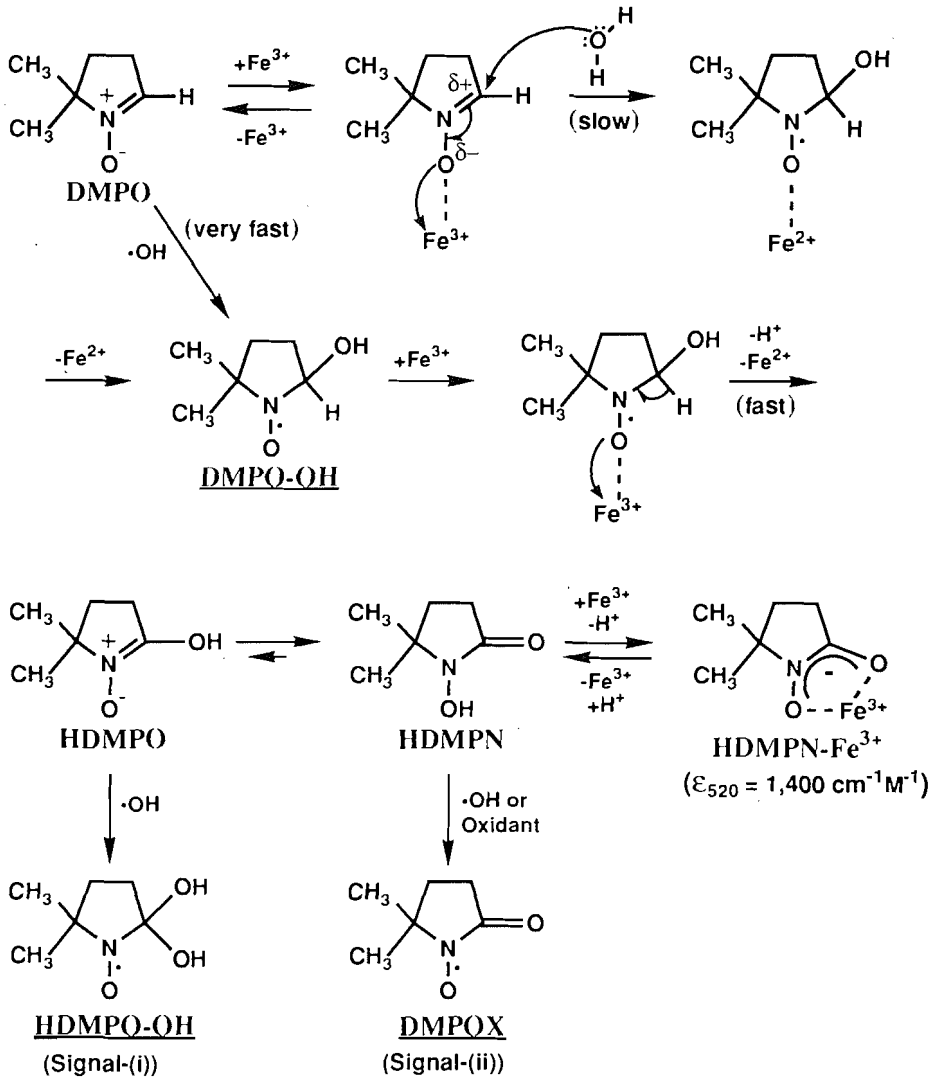

SCHEME 1. Overall reaction mechanism of DMPO spin trapping in Fenton systems. ESR detectable species are underlined.

H_2O_2 (100 mM). An ESR spectrum obtained from the sample is represented in Fig. 7*A*: the stick diagrams indicate that this spectrum is composed of two sets of lines (Fig. 7*B*). One is a 1:1:1 triplet (a_N = 0.72 mT) of a 1:2:1 triplet ($a_{\gamma H}$ = 0.41 mT, 2H). It should be noted that this spectrum was previously assigned to an aminoxyl radical referred to DMPOX (5*d*, 15). The other spectrum consists of a 1:1:1 triplet (a_N = 1.53 mT) of a 1:3:3:1 quartet ($a_{\gamma H}$ = 0.12 mT, 3H). The quartet that is not clear in Fig. 2 is obvious in this spectrum because of line sharpening in the absence of paramagnetic iron ions, and this spectrum is tentatively assigned to an HDMPO spin adduct of •OH. We suspect that the three hydrogen atoms of the two methyl groups at C5 fit the structural coordination of the W plan (16), with which hfsc values are relatively large via long-range interaction. A computer simulation (Fig. 7*B*) using the above hfsc values nicely reproduced the observed spectrum (Fig. 7*A*). Accordingly the two sets of ESR lines arising from HDMPO-OH and DMPOX are consistent with the background signals (*i*) and (*ii*) in Fig. 2. It was also confirmed that addition of Fe^{3+} to an aqueous HDMPN solution led to an absorption spectrum identical with that represented in Fig. 3. Assuming that both HDMPN and HDMPO form the complex (for convenience, referred to here as HDMPN–Fe^{3+}) with Fe^{3+} in the presence of excess Fe^{3+}, the molar absorption coefficient (ε) of the complex was revised here to be 1400 cm^{-1} M^{-1}, which was slightly higher than that reported previously (1075 cm^{-1} M^{-1}) (14*b*).

In summary, when DMPO is used in a solution containing Fe^{3+}, HDMPN and HDMPO are produced, which are ESR silent (the reactions to yield HDMPN and HDMPO are discussed below). However, when •OH is generated in solutions such as Fenton systems, HDMPN is converted to the corresponding aminoxyl radical (DMPOX), and HDMPO traps •OH to form an HDMPO spin adduct (HDMPO-OH), both of which are ESR detectable (Scheme 1). The absorption at 520 nm observed in the presence of Fe^{3+} is due to the complex between Fe^{3+} and HDMPN (and (or) HDMPO).

Precursor of HDMPN and HDMPO

As mentioned earlier in this text, the formation of DMPO-OH was detected by ESR in a solution containing DMPO and Fe^{3+}. Therefore, it is very likely that DMPO-OH is a pre-

Can. J. Chem. Downloaded from www.nrcresearchpress.com by 109.225.110.28 on 09/08/12
For personal use only.

Can. J. Chem. Downloaded from www.nrcresearchpress.com by 109.225.110.28 on 09/08/12
For personal use only.

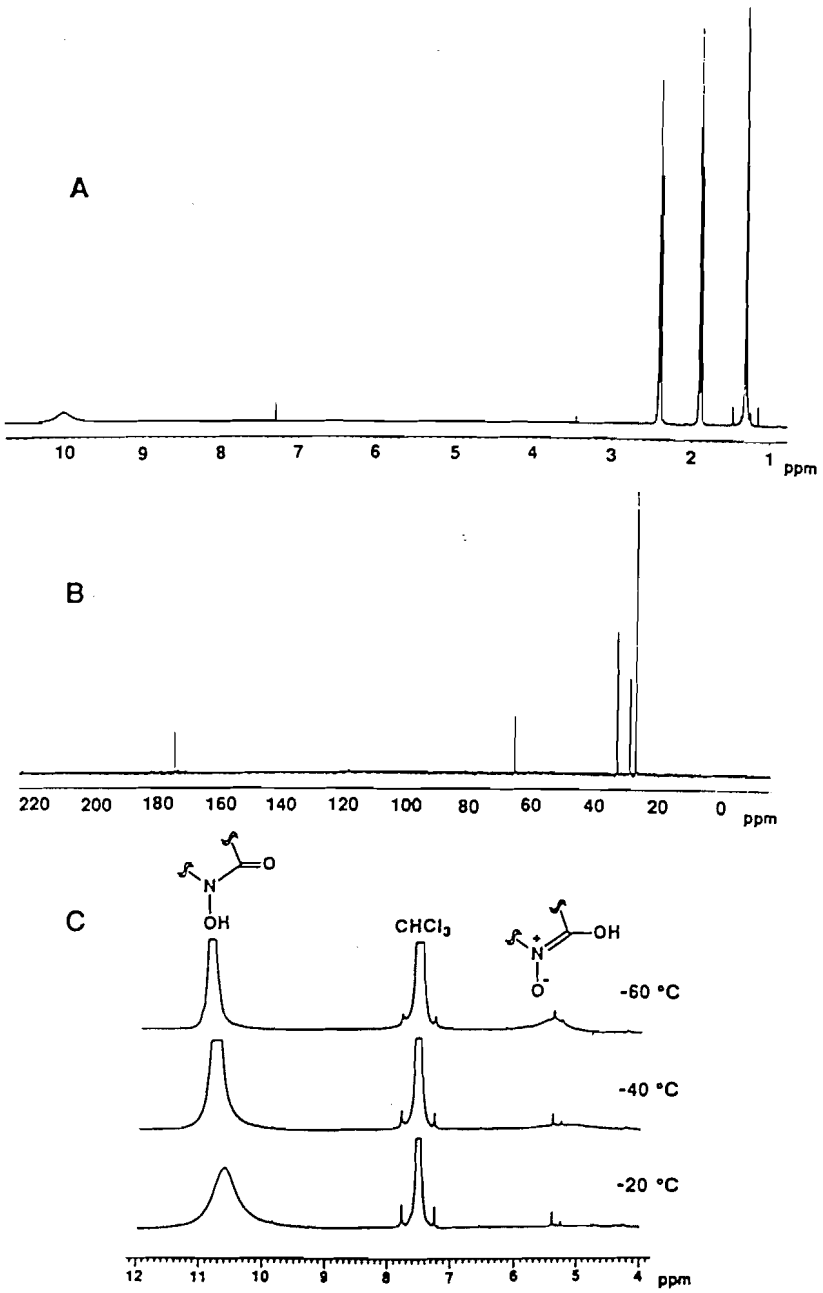

FIG. 6. ^1H and ^{13}C NMR spectra obtained from the second peak in the chromatogram shown in Fig. 5. (*A*) ^1H NMR spectrum obtained in $CDCl_3$ (reference, TMS (internal)). (*B*) ^{13}C NMR spectrum in D_2O (reference, TSP-d_4 (external)). (*C*) ^1H NMR spectrum obtained in $CDCl_3$ at lowered temperature (reference, TMS (internal)).

cursor of HDMPN and HDMPO. To prove this, DMPO-OH (ca. 50 μM based on ESR measurement) was generated by sonolysis in an aqueous DMPO solution (10 mM). Sonolysis of water gives rise to $^{\bullet}OH$ and $^{\bullet}H$ by homolytic cleavage of water molecules and thus DMPO-OH and DMPO-H are formed (10). It is noted that possible involvement of DMPO-H in the reactions discussed below was ruled out since essentially the same results were obtained in photolysis of an aqueous DMPO solution containing H_2O_2 and Fe^{3+}. After addition of Fe^{3+} (1 mM as $FeNH_4(SO_4)_2$) to the sonicated solution, the absorption at 520 nm increased for the first 30 min and reached a plateau, then decreased slightly (Fig. 8). The absorbance (520 nm) of the sonicated sample was always larger than that of non-sonicated one by 0.07 (in absorbance units). Using the ε value of the HDMPN–Fe^{3+} complex determined here (1400 cm^{-1} M^{-1}), the absorbance difference can be translated into 50 μM of the complex, which is in good agreement with the concentration of the ligand (HDMPN) expected from the initial yield of DMPO-OH (ca. 50 μM). The amount of Fe^{2+} reduced from Fe^{3+} was also monitored by colorimetric analysis and an analogous difference (ca. 50 μM) in the amount of Fe^{2+} was found between the samples with and without sonication. This result strongly supports that the precursor for HDMPN (and HDMPO) is DMPO-OH. The plateau and slight decrease in the concentration of the HDMPN–Fe^{3+} complex observed for both solutions after 30 min (Fig. 8) is probably due to the consumption of Fe^{3+} in these systems.

Can. J. Chem. Downloaded from www.nrcresearchpress.com by 109.225.110.28 on 09/08/12
For personal use only.

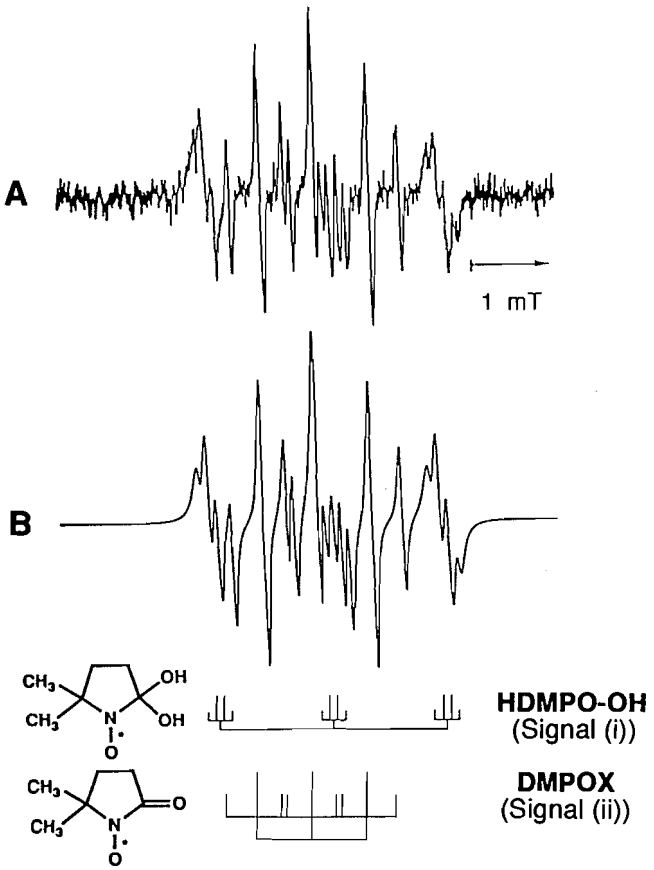

FIG. 7. (*A*) An ESR spectrum obtained from a UV-irradiated (at 260 nm for 3 s) HDMPN solution (100 mM) in the presence of H_2O_2 (100 mM) and (*B*) a computer simulation spectrum for *A*. ESR parameters used for the simulation are as follows: a_N = 1.53 mT, $a_{\gamma H}$ = 0.12 mT (3H), and g = 2.0063 for HDMPO-OH (denoted as signal (*i*) in Fig. 2), and a_N = 0.72 mT, $a_{\gamma H}$ = 0.41 mT (2H), and g = 2.0072 for DMPOX (denoted as signal (*ii*) in Fig. 2). The line width (ΔH_{pp}) taken was 0.05 mT for DMPOX and 0.08 mT for HDMPO-OH and the intensity ratio of DMPOX:HDMPO-OH was 1:1. ESR settings are follows: modulation amplitude, 0.025 mT; receiver gain, ×2000; time constant, 1.0 s; sweep time, 32 min.

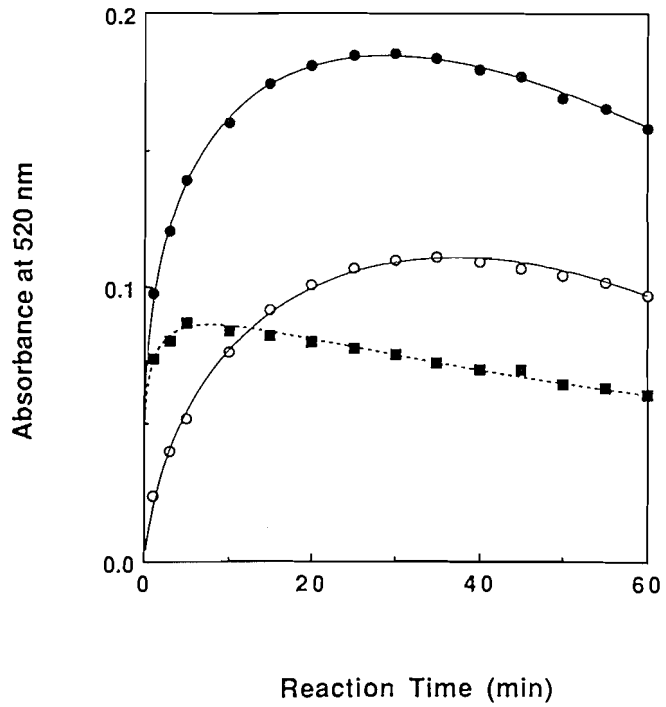

FIG. 8. Time courses for the formation of the HDMPN–Fe^{3+} complex in aqueous DMPO solutions (10 mM) containing (●) DMPO-OH (ca. 50 μM) and $FeNH_4(SO_4)_2$ (1 mM) and (○) $FeNH_4(SO_4)_2$ (1 mM). A broken line (□) representing a concentration of HDMPN–Fe^{3+} originating from the sonication was obtained by subtracting the concentration of the complex in the non-sonicated solution (○) from that in the sonicated one (●). DMPO-OH was generated immediately prior to the sample preparation by sonicating (for 5 min) an aqueous DMPO solution (10 mM) with Ar bubbling (500 mL/min). The concentration of the complex is calculated using the molar extinction coefficient (ε) of 1400 cm^{-1} M^{-1} (at 520 nm).

In the sonicated solution, DMPO-OH produced both by the sonication and the dark reaction is involved in the formation of the HDMPN–Fe^{3+} complex, while only the latter is responsible in the non-sonicated solution. Accordingly, the apparent rate of formation of the complex from DMPO-OH initially formed by the sonication can be roughly estimated by the initial slope of a curve (broken line) obtained by subtracting the concentration of the complex in the non-sonicated solution from that in the sonicated one (Fig. 8). The calculated rate is 53 μM/min. It should be noted that the calculated value is obviously a minimum estimate of a real rate: the first data point of the curve obtained is already in a late stage of the conversion reaction of DMPO-OH produced by the sonication and, additionally, the lifetime of DMPO-OH at pH 3 has been estimated to be several minutes in a γ-irradiated aqueous DMPO solution (17). The rate of complex formation by the dark reaction in the non-sonicated solution is also estimated as 17 μM/min. It follows that the formation of the HDMPN–Fe^{3+} complex from DMPO-OH initially formed by the sonication occurred at least 3-fold faster than that in the dark reaction. Assuming that the formation of DMPO-OH is a rate-determining reaction for the formation of the HDMPN–Fe^{3+} complex, the rates of formation of the complex in the conversion of DMPO-OH and in the dark reaction should be approximately proportional to k_1[DMPO-OH][Fe^{3+}] and k_2[DMPO][Fe^{3+}], respectively, where k_1 and k_2 are apparent rate constants. Using [DMPO-OH] = 50 μM, [DMPO] = 10 mM, [Fe^{3+}] = 1 mM, and k_1[DMPO-OH][Fe^{3+}]/k_2[DMPO][Fe^{3+}] ≃ 3, k_1/k_2 is roughly estimated as 660. This result implies that the reaction between DMPO-OH and Fe^{3+} to produce HDMPN proceeds at least two or three orders of magnitude more efficiently than that between DMPO and Fe^{3+} to produce DMPO-OH.

The reactions for the formation of HDMPN and HDMPO from DMPO in the presence of Fe^{3+} are summarized in Scheme 1. According to the scheme, the amount of the reduced Fe^{3+} should be twice as large as that of converted DMPO. To see if this is the case, the changes in the concentrations of Fe^{3+} and DMPO were measured for a sample consisting of equimolar $FeNH_4(SO_4)_2$ (10 mM) and DMPO (10 mM). The time profile for the conversion of Fe^{3+} and DMPO is shown in Fig. 9. It is evident from Fig. 9 that the amount of reduced Fe^{3+} is twice as large as that of the converted DMPO throughout the course of the reaction. This result is consistent with the proposed scheme.

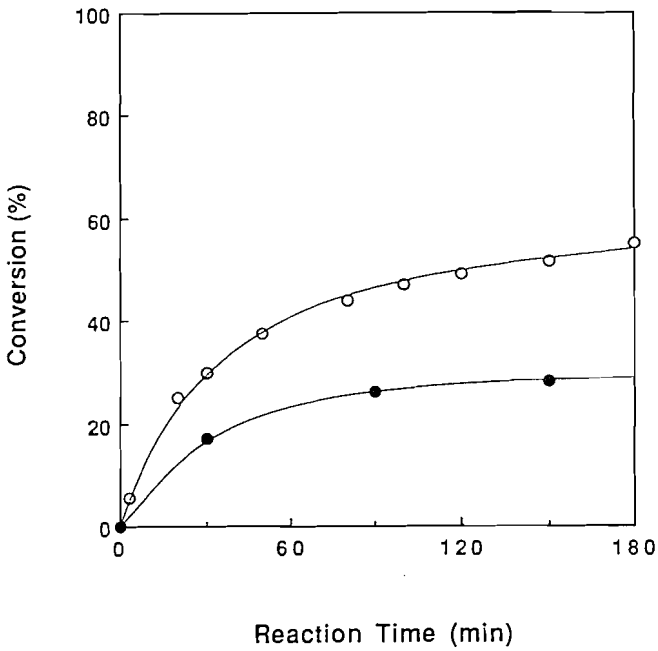

FIG. 9. Time courses for the decreases of (●) DMPO and (○) ferric ions in an aqueous DMPO solution (10 mM) containing $FeNH_4(SO_4)_2$ (10 mM). The contents of DMPO and ferric ions were measured by RPLC analysis and colorimetric determination with potassium thiocyanate, respectively.

Effect of methyl substitution at C2 on the formation of HDMPN and HDMPO

In the proposed scheme, elimination of a hydrogen atom from C2 in DMPO-OH is involved. This suggests that if the hydrogen atom is replaced by an alkyl group at C2, no reaction should take place after the hydroxylation of the double bond. To confirm this, reaction of M_3PO (18) having a methyl group at C2 was investigated in the presence of Fe^{3+}. M_3PO (10 mM) was allowed to stand in an aqueous solution in the presence of $FeNH_4(SO_4)_2$ (10 mM) at room temperature. However, no absorption appeared around 520 nm in up to 50 h, implying that compounds analogous to HDMPN and HDMPO for DMPO were not formed. From the same sample, an ESR spectrum composed of a 1:1:1 triplet (a_N = 1.52 mT) was obtained, indicating the formation of M_3PO-OH. Probably, as for DMPO-OH, M_3PO-OH is produced by the nucleophilic addition of a water molecule to the double bond. Also, RPLC analysis showed an extremely slight decrease in the concentration of M_3PO: this decrease may correspond to the amount of the produced spin adduct (in the order of 1 μM). These results indicate that M_3PO-OH does not undergo further proton elimination.

In summary, in the presence of Fe^{3+}, DMPO is initially converted to ESR detectable DMPO-OH by the addition of a water molecule and subsequently, through hydrogen elimination from DMPO-OH, HDMPN and HDMPO are formed. When $^{\bullet}OH$ is present, HDMPN is converted to the corresponding aminoxyl radical (DMPOX) and HDMPO traps $^{\bullet}OH$ to yield HDMPO-OH. These two species give rise to the background ESR signals (*i*) and (*ii*) in Fig. 2. This makes it difficult to analyze the ESR signals obtained. Since a series of reactions shown in Scheme 1 are accelerated when H_2O_2 coexists in the systems to produce DMPO-OH by $^{\bullet}OH$ addition, assignment of ESR signals obtained in biological systems should be carried out with great care. Such undesirable side reactions can be avoided by using spin traps having CH_3 groups at C2 in a pyrroline ring.

Acknowledgments

We thank Dr. Hiroaki Ohya-Nishiguchi for valuable discussion and Dr. Yashige Kotake for useful suggestions for the synthesis of M_3PO. This work was supported in part by the Grant-in-Aid for Scientific Research on Priority Areas No. 01540476 from the Ministry of Education, Science, and Culture, Japan.

1. (*a*) E. G. Janzen. Acc. Chem. Res. **4**, 31 (1971); (*b*) E. G. Janzen and B. J. Blackburn. J. Am. Chem. Soc. **91**, 4481 (1969); (*c*) E. G. Janzen. Methods Enzymol. **105**, 188 (1984); (*d*) C. A. Evans. Aldrichimica Acta, **12**, 182 (1979).
2. (*a*) B. Halliwell and J. M. C. Gutteridge. Free radicals in biology and medicine. 2nd ed. Oxford University Press, New York. 1989. pp. 416–508; (*b*) Y. Kuchino, F. Mori, H. Kasai, H. Inoue, S. Iwai, K. Miura, E. Ohtsuka, and S. Nishimura. Nature, **327**, 77 (1987); (*c*) J. M. McCord. Science, **185**, 529 (1974); (*d*) C. M. Arroyo, J. H. Kramer, B. F. Dickens, and W. B. Weglicki. FEBS Lett. **221**, 101 (1987); (*e*) S. Inoue and S. Kawanishi. Cancer Res. **47**, 6522 (1987); (*f*) M. Yamada, T. Okigaki, and M. Awai. Cell Struct. Funct. **12**, 407 (1987); (*g*) Y. Ebina, S. Okada, S. Hamazaki, F. Ogino, J.-I. Li, and O. Midorikawa. J. Natl. Cancer Inst. **76**, 107 (1986); (*h*) D. N. Granger, G. Rutili, and J. M. McCord. Gastroenterology, **81**, 22 (1981); (*i*) M. B. Grisham, L. A. Hernandez, and D. N. Granger. Am. J. Physiol. **251**, G567 (1986); (*j*) J. M. McCord. Fed. Proc. **46**, 2402 (1987).
3. (*a*) S. Pou, D. J. Hassett, B. E. Britigan, M. S. Cohen, and G. M. Rosen. Anal. Biochem. **177**, 1 (1989); (*b*) G. M. Rosen and E. J. Rauckman. Methods Enzymol. **105**, 198 (1984).
4. M. J. Hampton, R. A. Floyd, E. G. Janzen, and R. V. Shetty. Mutat. Res. **91**, 279 (1981).
5. (*a*) J. C. Evans, S. K. Jackson, C. C. Rowlands, and M. D. Barratt. Tetrahedron, **41**, 5191 (1985); (*b*) E. Finkelstein, G. M. Rosen, and E. J. Rauckman. Arch. Biochem. Biophys. **200**, 1 (1980); (*c*) R. A. Floyd and L. M. Soong. Biochem. Biophys. Res. Commun. **74**, 79 (1977); (*d*) G. M. Rosen and E. J. Rauckman. Mol. Pharmacol. **17**, 233 (1980); (*e*) S. Tero-Kubota, Y. Ikegami, T. Kurokawa, R. Sasaki, K. Sugioka, and M. Nakano. Biochem. Biophys. Res. Commun. **108**, 1025 (1982).
6. K. Makino, H. Imaishi, S. Morinishi, T. Hagiwara, T. Takeuchi, and A. Murakami. Free Radical Res. Commun. **6**, 19 (1989).
7. K. Makino, T. Hagiwara, A. Hagi, M. Nishi, and A. Murakami. Biochem. Biophys. Res. Commun. **172**, 1073 (1990).
8. (*a*) R. Bonnett, R. F. C. Brown, V. M. Clark, I. O. Sutherland, and A. Todd. J. Chem. Soc. 2094 (1959); (*b*) M. C. Kloetzel. J. Am. Chem. Soc. **70**, 3571 (1948).
9. K. Hideg and L. Lex. J. Chem. Soc. Perkin Trans. 1, 1431 (1986).
10. (*a*) K. Makino, M. M. Mossoba, and P. Riesz. J. Am. Chem. Soc. **104**, 3537 (1982); (*b*) J. Phys. Chem. **87**, 1369 (1983).
11. R. Bonnett, V. M. Clark, and A. Todd. J. Chem. Soc. 2102 (1959).
12. G. R. Buettner. Free Radical Biol. Med. **3**, 259 (1987).
13. K. Makino, T. Hagiwara, H. Imaishi, M. Nishi, S. Fujii, H. Ohya, and A. Murakami. Free Radical Res. Commun. **9**, 233 (1990).
14. (*a*) J. F. Elsworth and M. J. S. Lamchen. J. Chem. Soc. (C), 1477 (1966); (*b*) Afr. Chem. Inst. **XXIV**, 196 (1971).

Can. J. Chem. Downloaded from www.nrcresearchpress.com by 109.225.110.28 on 09/08/12
For personal use only.

15. H. G. Aurich and J. Trosken. Liebigs Ann. Chem., **745**, 159 (1971).
16. (*a*) F. W. King. Chem. Rev. **76**, 157 (1976); (*b*) G. A. Russell, J. J. McDonnell, P. R. Whittle, R. S. Givens, and R. G. Keske. J. Am. Chem. Soc. **93**, 1452 (1971); (*c*) F. Moriya, K. Makino, N. Iguchi, N. Suzuki, S. Rokushika, and H. Hatano. J. Phys. Chem. **88**, 2373 (1984).
17. A. J. Carmichael, K. Makino, and P. Riesz. Radiat. Res. **100**, 222 (1984).
18. (*a*) E. Finkelstein, G. M. Rosen, and E. J. Rauckman. J. Am. Chem. Soc. **102**, 4994 (1980); (*b*) E. G. Janzen, R. V. Shetty, and S. W. Kunanec. Can. J. Chem. **59**, 756 (1981); (*c*) E. G. Janzen, C. A. Evans, and J. I.-P. Liu. J. Magn. Reson. **9**, 513 (1973).

Can. J. Chem. Downloaded from www.nrcresearchpress.com by 109.225.110.28 on 09/08/12
For personal use only.

Additions covalentes de nucléophiles sur les pyrido-as-triazines

NELLY PLÉ, ALAIN TURCK ET GUY QUEGUINER[1]

Laboratoire de chimie organique fine et hétérocyclique, Institut de recherches en chimie organique fine, Institut national des sciences appliquées, Unité de recherche associée au Centre national de la recherche scientifique, n° 1429, BP 08, 76131 Mont Saint Aignan CEDEX France

Reçu le 26 février 1991[2]

NELLY PLÉ, ALAIN TURCK et GUY QUEGUINER. Can. J. Chem. **70**, 2828 (1992).

L'addition covalente de divers nucléophiles sur les pyrido-as-triazines a été étudiée; la structure des σ-adduits a été determinée par RMN. Nous avons decelé une exceptionnelle réactivité des pyrido-as-triazines comportant un atome d'azote pyridinique en β vis-à-vis des nucléophiles carbonés. Cette aptitude à former des σ-adduits avec ces réactifs est comparable à celle des ptéridines. Nous avons observé une régiosélectivité de l'attaque nucléophile sur le cycle pyridinique en péri du cycle triazinique.

NELLY PLÉ, ALAIN TURCK, and GUY QUEGUINER. Can. J. Chem. **70**, 2828 (1992).

Covalent addition of various nucleophiles to pyrido-as-triazines was studied and the σ-adduct structures were determined by NMR. A remarkable reactivity toward carbon nucleophiles has been highlighted for pyrido-as-triazines bearing a pyridinic nitrogen in the β position: only in the pteridine series has a similar reactivity been encountered. Complete regioselectivity of the nucleophilic attack on the pyridine nucleus peri to the triazine was observed.

Can. J. Chem. Downloaded from www.nrcresearchpress.com by 109.225.110.28 on 09/08/12
For personal use only.

Introduction

L'addition covalente de réactifs nucléophiles est une réaction caractéristique des systèmes polyazaaromatiques (1–4). Divers exemples d'hydratations covalentes observés avec des composés naturels comportant un hétérocycle polyazoté comme la xanthoptérine (5) ont suscité un vif intérêt pour l'étude de cette réaction. Parmi les polyazanaphtalénes, les pyrazino[2,3-*d*]pyrimidines ou ptéridines présentes dans un grand nombre de composés naturels ont été plus largement étudiées (15).

Les pyrido-as-triazines que nous avons synthétisées (13*c*) ont des structures proches de celle des ptérines et il apparait intéressant d'essayer de cerner leur réactivité vis-à-vis des nucléophiles. Dans la série des pyrido-as-triazines il existe quatre hétérocycles différents comportant un cycle as-triazine condensé à la pyridine par une liaison carbone–carbone. Notre étude porte sur trois d'entre eux, les hétérocycles **1**, **2** et **3**.

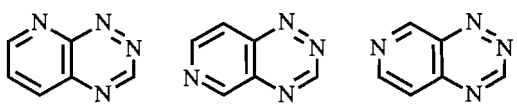

1 **2** **3**

Hydratation

Milieu neutre et acide

Les spectres RMN ^1H de ces hétérocycles restent inchangés dans D_2O et CD_3OD pendant un laps de temps supérieur à 1 semaine à température ambiante. En milieu neutre les pyrido-as-triazines étudiées, **1**, **2** et **3**, sont donc stables dans l'eau et dans le méthanol. Cependant l'addition de DCl provoque une perte très rapide de résolution du spectre RMN ^1H vraisemblablement due à des équilibres rapides entre formes protonées et neutres.

En milieu acide et anhydre (CF_3COOD) aucune modification du spectre RMN ^1H des pyrido-as-triazines n'a été observée à température ambiante pendant un temps relativement long (96 h). Ce résultat traduit une stabilité des cations anhydres $\mathbf{1}^+$, $\mathbf{2}^+$ et $\mathbf{3}^+$ dont la structure a pu être établie par ailleurs à l'aide de spectres RMN ^{13}C (14).

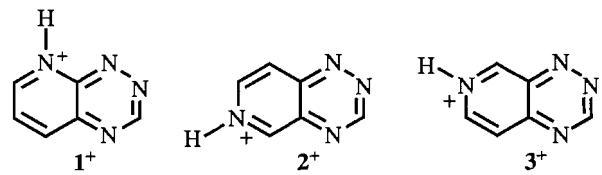

$\mathbf{1}^+$ $\mathbf{2}^+$ $\mathbf{3}^+$

L'addition d'eau ou de méthanol à une solution de pyrido-as-triazine dans l'acide trifluoroacétique entraîne la formation de nouvelles espéces comme le démontre en RMN la diminution des signaux des pyrido-as-triazines et l'apparition de nouveaux signaux dans une région de champs plus forts. La complexité des spectres ne nous a cependant pas permis d'établir la structure des composés obtenus.

En présence d'eau l'évolution des spectres se fait plus rapidement pour $\mathbf{3}^+$ ($t_{1/2}$ = 10 min) et $\mathbf{2}^+$ ($t_{1/2}$ = 30 min) que pour $\mathbf{1}^+$ ($t_{1/2}$ = 2 h 30),

Milieu basique

L'addition d'une base forte comme $NaOCD_3$ ou NaOD à température ambiante à des solutions de pyrido-as-triazines dans D_2O provoque la disparition progressive en 1 h à 1 h 30 des signaux des spectres RMN ^1H et ^{13}C. En RMN ^1H la disparition totale des signaux se fait avec une quantité de base équivalente à 1/10 de la quantité stoéchiométrique.

L'extraction par $CDCl_3$ de la solution basique (D_2O/NaOD) pour laquelle nous n'obtenons plus de signal RMN permet d'obtenir une phase organique dont le spectre RMN ^1H est identique à celui de l'hétérocycle initial. Nous avons pu vérifier ainsi que la disparition des signaux en RMN ^1H ou ^{13}C n'était pas due à la destruction de l'hétérocycle mais vraisemblablement à l'existence d'équilibres relativement rapides entre l'hétérocycle et des formes hydratées.

Nous avons tenté de déterminer la nature des produits d'addition formés en déplaçant ces équilibres par oxydation des σ-adduits par un excès de ferricyanure de potassium à température ambiante. Cette méthode a été précisément utilisée pour déterminer le site d'hydratation de triazanaphtalènes (6).

Dans ces conditions nous avons pu isoler les composés **6**

[1]Auteur correspondant.

[2]Révision reçue le 1er juin 1992.

TABLEAU 1. Données spectrales RMN ^{1}H des composés **1–3** et **5–7**

Composé	H3	H5	H6	H7	H8	H_{mob}	$J_{5,6}$	$J_{6,7}$	$J_{7,8}$
1[a]	10,2	8,6	8,1	9,4	—	—	9	4	—
2[a]	10,2	9,8	—	9,1	8,4	—	—	—	6
3[a]	10,1	7,9	9,0	—	10,0	—	6	—	—
5[b]	9,9	—	6,9	8,6	—	7,6	—	6	—
6[b]	10	—	—	8,1	7,25	7,7	—	—	6
7[b]	9,8	6,85	8,2	—	—	8,15	6	—	—

[a]Solvant $CDCl_3$.
[b]Solvant DMSO-d_6.

et **7** après un temps de réaction de 24 h tandis que le composé **5** est obtenu en 5 jours.

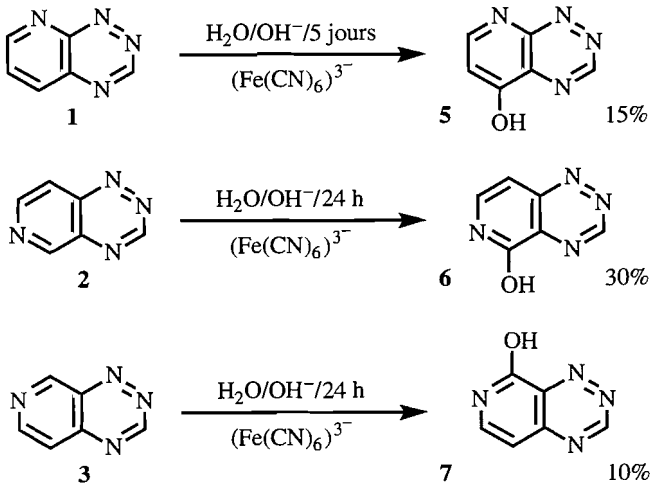

L'analyse des spectres RMN ^{1}H des composés **5–7** (tableau 1) révèle pour chacun de ces composés l'existence d'un proton mobile attribuable à un OH ou un NH. On observe également la présence d'un singulet dans la région des champs forts (δ 10–9, 8 ppm) que nous pouvons attribuer au proton H3.

Nous observons pour chacun des composés l'existence d'un spectre AB avec un déplacement chimique plus faible ($\Delta\delta \sim 1$ ppm vers les champs forts) que celui des protons équivalents dans l'hétérocycle de départ.

Ces remarques nous permettent d'envisager une attaque nucléophile sur le cycle pyridinique exclusivement. Pour les hétérocycles **2** et **3** l'attaque nucléophile se fait sans ambiguïté en α de l'azote pyridinique pour donner les composés **6** et **7** (en équilibre tautomère entre formes lactame–lactime).

Dans le cas du composé **5** deux structures ***5a*** et ***5b*** sont compatibles avec un spectre RMN ^{1}H comportant un AB et correspondent à une attaque nucléophile en C5 ou C7.

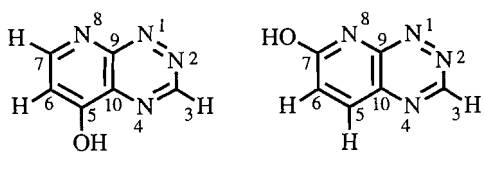

5a ***5b***

L'étude du spectre RMN ^{13}C du composé **5** (tableau 2) effectué à 400 MHz nous permet de lever l'indétermination.

Parmi les valeurs des constantes de couplage $^1J_{CH}$ et $^3J_{CH}$ du cycle pyridinique données dans la littérature (7) on observe les valeurs $^3J_{C2-H4} = 7$ Hz et $^3J_{C4-H2} = 4$ Hz ainsi qu'une valeur particulièrement élevée $^3J_{C2-H6} = 12$ Hz caractéristique de la présence d'un hydrogène sur un carbone en α de l'atome d'azote. L'étude comparative des constantes $^3J_{C-H}$ des composés **5** et **6** (tableau 2) nous permet d'observer 12 Hz pour la constante $^3J_{C5-H7}$ du composé **6** et 14 Hz pour la constante $^3J_{C9-H7}$ pour le carbone quaternaire C9 à 153,0 ppm du composé **5**. Cette forte valeur de la constante de couplage de ce carbone (situé en α de l'atome d'azote pyridinique en raison de son déplacement chimique) ne peut être expliquée que par une structure de type ***5a***. On note par ailleurs que les autres constantes de couplage observées sont en accord avec les valeurs données dans la littérature (7).

Cette étude nous permet de conclure que l'hydratation covalente des pyrido-as-triazines en milieu basique se fait exclusivement sur le cycle pyridinique. On observe que la position de l'atome d'azote pyridinique influe sur la vitesse de la réaction et la régiosélectivité : les composés **2** et **3** pour lesquels l'azote pyridinique est en β s'hydratent plus vite que **1**, l'attaque nucléophile se fait alors en α de l'azote pyridinique et en péri du cycle triazine. Pour le composé **1** dont l'azote pyridinique est en position α l'addition est plus lente et l'hydratation a lieu également sur le sommet péri libre (addition 1–4). Il est remarquable que le cycle monoazoté soit plus réactif que la triazine dans ces trois hétérocycles.

Action de différents nucléophiles

Action du bisulfite de sodium

Des nucléophiles soufrés comme le bisulfite de sodium, l'acide thiobarbiturique et les thiophénols forment des σ-adduits avec certains dérivés des ptéridines qui sont inactifs avec l'eau ou les alcools (3*a*, 8).

L'action du bisulfite de sodium dans l'eau à température ambiante a été étudiée sur les hétérocycles **1** et **2**. Seul le composé **2** fournit après un long temps de réaction (5 jours) un dérivé d'addition. Nous observons la précipitation d'un solide rouge **8**; la microanalyse nous permet d'établir pour ce composé la formation d'un adduit 1 : 1.

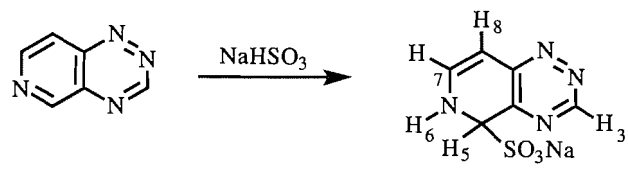

2 **8** 20%

Can. J. Chem. Downloaded from www.nrcresearchpress.com by 109.225.110.28 on 09/08/12
For personal use only.

TABLEAU 2. Données spectrales RMN ^{13}C des composés **5** et **6** dans le DMSO-d_6.

Composé		C3	C5	C6	C7	C8	C9	C10
	δ	151,6	156,4	106,6	155,9	—	153,0	129,2
5	^1J	207,2	—	164,5	177	—	—	—
	^3J	—	7,5	8	—	—	14	6
	δ	153,6	159,1	—	147,7	106,1	127,1	150,1
6	^1J	210,2	—	—	177	170,6	—	—
	^3J	—	12	—	—	—	<2	3

TABLEAU 3. Données spectrales ^1H des composés **8–15**. Les protons échangeables par D_2O sont indiqués par un astérisque

Composé	H3	H5	H6	H7	H8	CH_3	CH_2	CH	NH	$J_{7,8}$	$J_{5,6}$	$J_{6,8}$
8	9,4	6,16	7,5*	7,1	5,46	—	—	—	—	6	3	—
9	8,5	6,16	7,3*	7.6	5.4	1.83	—	—	—	6	3	—
10	8,6	6,3	7,15*	7,4	5,66	—	—	—	9,7	6	3	—
11	9,45	—	7,2*	7,0	6,45	1,3	4,2	6,2	—	7	—	—
12	9,85	—	8,1*	7,85	7,1	1,25	4,2	—	—	7	—	—
13*a*	10,1	—	—	8,9	8,3	3,8	—	6*	—	6	—	—
13*b*	9,6	—	7,3*	7,4	6,75	3,8	—	—	—	—	—	1–2
14*a*	10,1	—	—	8,9	8,3	1,3	4,2	6*	—	6	—	—
14*b*	9,52	—	7,3*	7,35	6,7	1,3	4,2	—	—	7	—	1–2
15*a*	10,1	7,9	9,0	—	—	3,7	—	6,2*	—	—	5	
15*b*	9,5	6,33	7,56	7,33*	—	3,7	—	—	—	—	7	

Le spectre RMN ^1H du composé **8** révèle la présence d'un spectre AB à 5,46 et 7,1 ppm avec une constante de couplage de 6 Hz attribuée aux protons H7 et H8.

Le glissement des déplacements chimiques de ces protons vers les champs forts ainsi que la constante de couplage voisine de celle observée dans les dihydro-1,2 pyridines (9) indique la formation d'un σ-adduit sur la liaison C5—N6. Ici encore, l'hétérocycle **2** qui présente un atome d'azote en β est plus réctif que l'isomére **1** qui lui a l'azote pyridinique en α.

Action de nucléophiles carbonés

L'addition de nucléophiles carbonés sur la ptéridine **16** (3*b*) et sur divers dérivés de cet hétérocycle (3*a*, 3*c*, 8*a*) conduit à deux types d'adduits différents, sans que toutefois une rationalisation de la régiosélectivité ait été proposée.

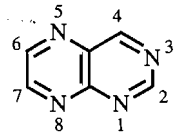

16

*Adduits 1 : 1 en N_3–C_4 du cycle pyridinique avec dans certains cas un réarrangement conduisant à des dérivés de la pyrido[2,3-*b*]pyrazine (10)

*Adduits 2 : 1 en N_5–C_6 et C_7–N_8 du cycle pyrazinique (11)

Nous avons fait agir sur les pyrido-as-triazines **1**, **2** et **3** les différents nucléophiles carbonés actifs avec la ptéridine et ses dérivés. Dans les conditions opératoires indiquées seuls les composés **2** et **3** ont conduit à la formation de σ-adduits.

Action de l'acide barbiturique et de l'acétylacétone

L'action de l'acide barbiturique et de l'acétylacétone sur la pyrido[3,4-*e*]as-triazine **2** dans l'eau à température ambiante nous a permis d'isoler deux adduits 1 : 1 possédant des caractéristiques voisines en RMN ^1H (tableau 3).

Les microanalyses établies pour les composés **9** et **10** permettent de conclure à la formation d'adduits 1 : 1.

Les spectres RMN ^1H de **9** et **10** présentent des analogies avec celui du composé **8** et nous permettent de conclure à une addition sur la liaison C5—N6.

Dans le cas des composés **9** et **10** nous n'avons pas pu observer le proton aliphatique H_α et nous notons par ailleurs l'absence de couplage du proton H5. Ces données RMN peuvent s'expliquer par l'existence d'un équilibre cétone–énol; nous n'avons toutefois pas pu confirmer l'existence de cet équilibre par RMN ^{13}C.

Action de l'acétylacétate d'éthyle et du cyanacétate d'éthyle

L'action de l'acétylacétate d'éthyle sur l'hétérocycle **2** conduit au composé **11**. Sa composition centésimale permet de lui attribuer la formule brute $C_{10}H_{10}N_4O_2$.

Le spectre IR présente un pic intense à 1660 cm^{-1} attribuable à un ν(C=O) associé, correspondant à une configuration *Z*.

Le spectre RMN ^1H dans le chloroforme deutérié (tableau 3) révèle l'absence de groupement méthyle non couplé, qui peut s'expliquer par une réaction de désacylation.

Les déplacement chimiques de H7 et H8 et leur constante de couplage $J_{8,7}$ sont comparables à ceux du système AB observé dans les pyridones-2 (12). Une étude comparative des spectres RMN ^1H de **11** avec ceux des σ-adduits **8–10** précédemment décrits révèle pour **11** l'absence de signal du proton H5 et un déblindage des protons H3 et H8. Ces éléments plaident en faveur d'une structure de type pyrilidène. Cette hypothèse est confirmée par le spectre RMN ^{13}C

Can. J. Chem. Downloaded from www.nrcresearchpress.com by 109.225.110.28 on 09/08/12
For personal use only.

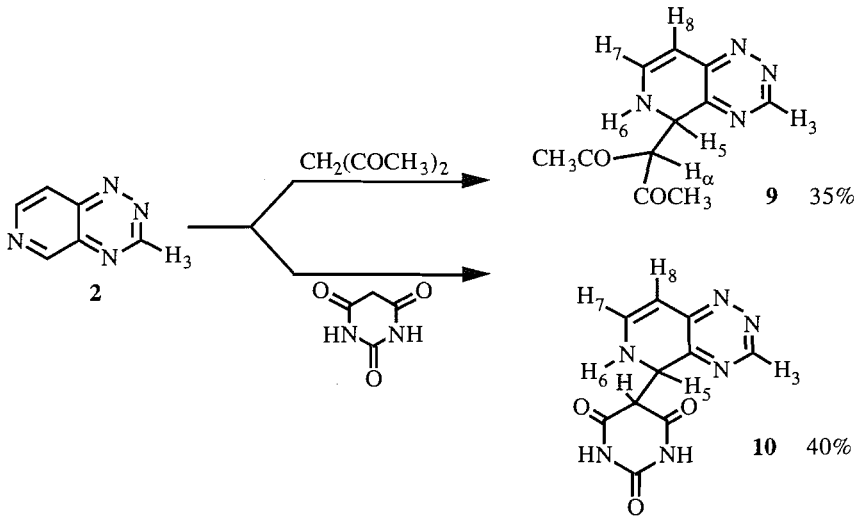

qui présente un carbone vinylique à 86,9 ppm ($^1J_{CH}$ = 167 Hz).

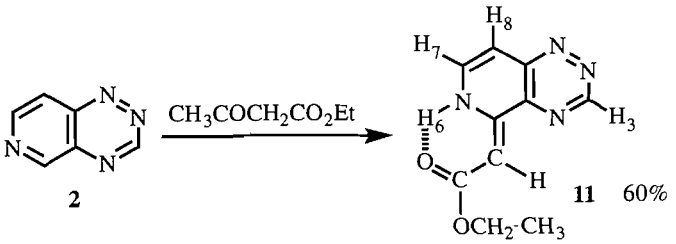

Les données spectrales RMN ^1H du composé **12** obtenu par action du cyanacétate d'éthyle sur l'hétérocycle **2** sont très voisines de celles décrites pour le composé **11** et permettent de lui attribuer également une structure pyrilidène. Le spectre IR révèle la présence d'un pic à 1635 cm^{-1} attribuable à un ν(C=O) associé, indiquant l'existence d'une configuration *Z*.

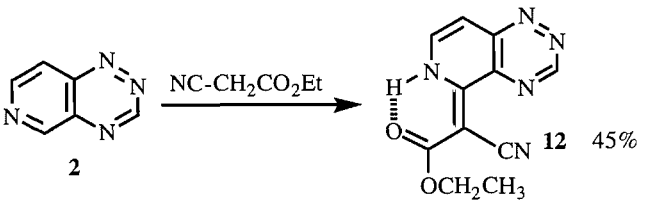

Action du malonate de diéthyle et de diméthyle

L'action des esters maloniques sur la pyrido[3,4-*e*]-as-triazine **2** conduit à la formation de dérivés dont la composition centésimale indique qu'il s'agit d'adduit 1 : 1.

Les spectres IR présentent deux bandes ν(C=O), l'une à 1730–1720 cm^{-1} et une autre moins intense à 1685–1670 cm^{-1}

Les spectres RMN ^1H relativement complexes révèlent l'existence de deux formes tautomères pour l'adduit formé.

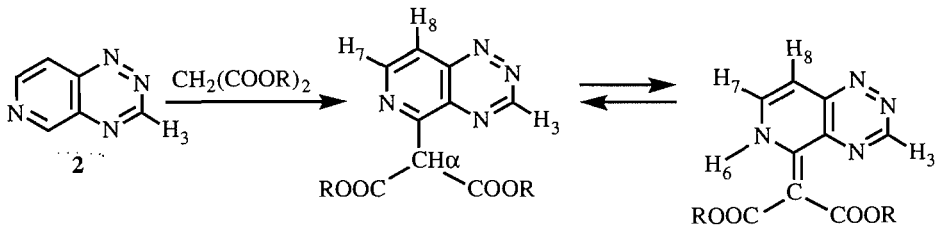

R = C_2H_5 **13***a* **13***b* 60%

R = CH_3 **14***a* **14***b* 65%

Dans la forme **13***a*, le spectre RMN ^1H indique que le cycle pyridinique est aromatique; en effet nous observons pour les protons H3, H8 et H7 de la pyrido-as-triazine des déplacements chimiques voisins de ceux de l'hétérocycle **2** (tableau 3). Dans la forme **13***b*, le cycle pyridinique est sous forme pyrilidène : nous observons un glissement des déplacements chimiques des protons H3, H8 et H7 vers les champs forts comparables à ceux observés dans les composés **11** et **12** précédemment décrits. L'addition de D_2O entraîne la disparition assez rapide du signal à 7,3 ppm et de la petite constante de couplage (*J* = 1–2 Hz) du signal à 6,75 ppm, ce qui permet d'attribuer le signal à 7,3 ppm au proton H6 de la forme **13***b*.

Par action de D_2O le singulet situé à 6 ppm disparaît également lentement au cours du temps (55 h pour une disparition totale) et peut être attribué au proton CH_α de la forme **13***a*.

Afin de vérifier l'existence d'une tautomérie entre les

Can. J. Chem. Downloaded from www.nrcresearchpress.com by 109.225.110.28 on 09/08/12
For personal use only.

formes **13***a* et **13***b* nous avons réalisé les spectres RMN ^{1}H dans le DMSO-d_6 et $CDCl_3$ et évalué le pourcentage de l'une et l'autre forme par intégration des différents signaux.

Solvant	**13***a*	**13***b*
$CDCl_3$	40%	60%
DMSO-d_6	24%	76%

La forme non aromatique **13***b* majoritaire est vraisemblablement stabilisée par une liaison hydrogène entre l'hydrogène H6 et les doublets libres des oxygènes de la fonction ester proche.

L'action du malonate de diméthyle à température ambiante sur la pyrido[4,3-*e*]-as-triazine **3** permet d'obtenir avec l'hétérocycle **2** la formation d'un adduit 1 : 1 **15** dont le spectre RMN ^{1}H révèle également l'existence de deux formes tautomères.

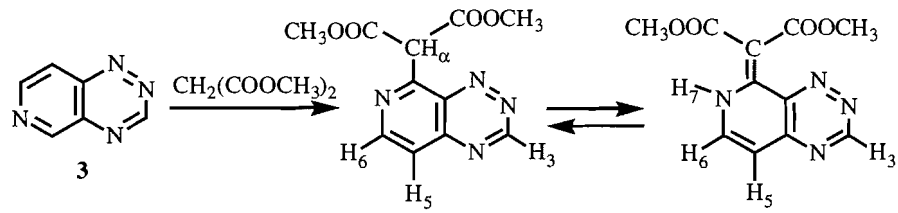

3 **15***a* 30% **15***b* 70%

L'analyse du spectre de RMN ^{1}H du composé **15** à température ambiante dans le chloroforme deutérié permet d'établir un pourcentage de 30% pour la forme aromatique **15***a* et 70% pour **15***b*.

Conclusion

L'action des nucléophiles carbonés sur la pyrido[3,4-*e*]-as-triazine **2** conduit essentiellement à deux types de composés.

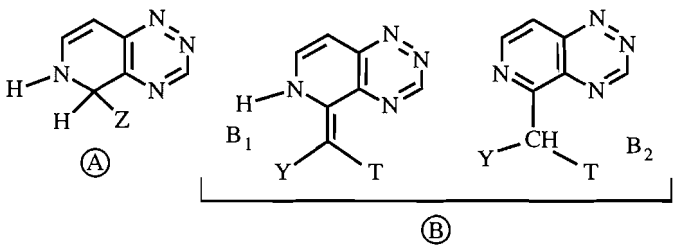

Les composés de type A résultent de l'addition primaire sur la liaison 5–6 et sont des dérivés de la dihydro-5,6 pyrido[3,4-*e*]-as-triazine. Les composés de type B résultent également d'une addition suivie d'une oxydation. Nous avons pu mettre en évidence des équilibres tautomères pour certains composés de type B.

Si la littérature relate l'existence de plusieurs polyazanaphtalènes capables de donner des σ-adduits avec des nucléophiles comme l'eau, les thiophénols ou les ions amidures, on peut noter l'exceptionnelle réactivité des ptéridines seules capables d'établir des σ-adduits avec des nucléophiles carbonés désignés dans la littérature en terme de réactifs de Michaël.

Cette étude de réactivité des pyrido-as-triazines vis-à-vis de divers nucléophiles permet de mettre en évidence pour les composés **2** et **3** une exceptionnelle aptitude à former des σ-adduits qui est comparable à celle des ptéridines.

Dans les pyrido-as-triazines la présence du cycle triazinique orthocondensé semble activer le cycle pyridinique vis-à-vis des nucléophiles et lui conférer cette remarquable réactivité.

On observe pour les pyrido-as-triazines étudiées une régiosélectivité totale des attaques nucléophiles sur le cycle pyridinique en péri du cycle triazinique. On peut également noter une réactivité accrue pour les composés possédant l'azote pyridinique en position β.

Partie expérimentale

Les points de fusion ont été déterminés sur un banc de Kofler et ne sont pas corrigés. Les spectres infrarouges ont été enregistrés sur un spectrographe Beckman IR 4250 à réseau. Les spectres de RMN de ^{1}H ont été enregistrés à l'aide de spectromètre Varian A60 et EM360, Varian XL 100-12 WG et Bruker AM 400 (Aspect 3000). Les déplacements chimiques (ppm) sont mesurés par rapport au tétraméthylsilane (TMS) dans $CDCl_3$ et par rapport à l'hexaméthyldisiloxane (HMDS) dans DMSO-d_6. Les spectres de RMN de ^{13}C ont été enregistrés sur un spectromètre Bruker WH 90 à 22,69 MHz et AM 400. Les déplacements chimiques sont reportés en ppm vers les champs faibles par rapport au TMS ou au HMDS. Les spectres de masse ont été enregistrés sur un spectromètre Jeol JMS-D 100. Les microanalyses ont été effectuées sur un appareil Technicon CHN par Monsieur Ecolivet au laboratoire d'analyse de l'Institut National des Sciences Appliquées.

Préparation des pyrido-as-triazines

Les composés **1**–**3** ont été préparés selon le mode opératoire donné dans la littérature (13).

Hydroxypyrido-as-triazines

À une solution de 0.5 g (3,78 mmol) de pyrido-as-triazine **1**, **2** ou **3** dans 10 mL d'ammoniaque (d = 0,9), on ajoute une solution de 1,62 g (5 mmol) de ferricyanure de potassium dans 15 mL d'eau. On laisse sous agitation à température ambiante pendant 48–60 h. Il apparait un précipité rouge orangé d'hydroxypyrido-as-triazine qui est isolé par filtration.

4-Hydroxypyrido[3,2-e]-as-triazine **5** : Rdt = 15%; F = 265°C; IR (KBr) : 3300, 3180, 2960, 1650 cm^{-1}; RMN ^{1}H (DMSO-d_6) δ ppm : 6,9 (d, 1H, $J_{6,7}$ = 6 Hz, H6), 7,6 (s, 1H, mob. NH), 8,6 (d, 1H, H7), 9,9 (s, 1H, H3); RMN ^{13}C (DMSO-d_6) δ ppm : 156.4 (d, C5, $^3J_{CH}$ = 7.5), 155,9 (d, C7, $^1J_{CH}$ = 177 Hz), 153.0 (d, C9, $^3J_{CH}$ = 14), 151,6 (d, C3, $^1J_{CH}$ = 207.2), 129.2 (d, C10, $^3J_{CH}$ = 6), 106,6 (dd, C6, $^1J_{CH}$ = 162 Hz, $^3J_{CH}$ = 9 Hz). Anal. calc. pour $C_6H_4N_4O$: C 48,64; H 2,70; N 37,83; trouvé : C 48,21; H 2,9; N 38,1%.

5-Hydroxypyrido[3,4-e]-as-triazine **6** : Rdt = 30%; F = 215°C; IR (KBr) : 3320, 3100, 1650, 1580 cm^{-1}; RMN ^{1}H (DMSO-d_6) δ ppm : 7,25 (d, 1H, $J_{7,8}$ = 6 Hz, H8), 7,7 (s, 1H, mob.), 8,1 (d, 1H, H7), 10 (s, 1H, H3); RMN ^{13}C (DMSO-d_6) δ ppm : 159.1 (d, C5, $^3J_{CH}$ = 12), 153,6 (d, C3, $^1J_{CH}$ = 210.2), 150.1 (d, C10,

Can. J. Chem. Downloaded from www.nrcresearchpress.com by 109.225.110.28 on 09/08/12
For personal use only.

$^3J_{CH}$ = 3), 147.7 (d, C7, $^1J_{CH}$ = 177), 127.1 (d, C9, ^3J = 2), 106,1 (d, C8, $^1J_{CH}$ = 170.6 Hz). Masse : 148 (M^+), 147 (100%, $M^+ - H$), 120 ($M^+ - N_2$), 93 (95%, $M^+ - N_2 - HCN$). Anal. calc. pour $C_6H_4N_4O$: C 48,64; H 2,70; N 37,83; trouvé : C 48,4; H 2,8; N 38,0%.

8-Hydroxypyrido[4,3-e]-as-triazine **7** : Rdt = 10%; *F* = 240°C; IR (KBr) : 3310, 3100, 2900, 1710, 1680, 1540; RMN ^{1}H (DMSO-d_6) δ ppm : 6,85 (d, 1H, $J_{5,6}$ = 6 Hz, H5), 8,15 (s, 1H mob.), 8,2 (d, 1H, H6), 9,8 (s, 1H, H3); RMN ^{13}C (DMSO-d_6) δ ppm : 157,1 (C3), 157,1 (C6), 106,6 (C5). Anal. calc. pour $C_6H_4N_4O$: C 48,64; H 2,70; N 37,83; trouvé : C 48,4; H 3,0; N 38,2%.

Action des nucléophiles

Combinaison bisulfitique **8**

À une solution de 0,90 g de bisulfite de sodium dans 10 mL d'eau, on ajoute 0,35 g de pyrido[3,4-*e*]-as-triazine **2**. Le mélange est agité pendant 30 min à température ambiante, filtré, puis à nouveau laissé sous agitation à température ambiante pendant 5 jours. Il apparait un précipité qui est séparé par filtration; Rdt = 20%; *F* > 260°C; IR (KBr) : 3340, 3240–3150, 1640, 1580, 1565, 1500 cm^{-1}; RMN ^{1}H (DMSO-d_6) δ ppm : 5,46 (d, 1H, $J_{7,8}$ = 6 Hz, H8), 6,16 (d, 1H, $J_{5,6}$ = 3 Hz, H5), 7,1 (d, 1H, H7), 7,5 (m, 1H, H6), 9,4 (s, 1H, H3); RMN ^{13}C (DMSO-d_6) δ ppm : 141,6 (s, C3), 141,2 (d, C7, J_{CH} = 178 Hz), 100,6 (dd, C8, $^1J_{CH}$ = 168 Hz, $^3J_{CH}$ = 7 Hz). Anal. calc. pour $C_6H_5N_4SO_3Na$: C 30,50; H 2,11; N 23,72; trouvé : C 30.1; H 2,4; N 23,2%.

Condensation avec l'acétylacétone **9**

À une solution de 0,35 g (2,6 mmol) de pyrido-as-triazine **2** dans 10 mL d'eau, on ajoute 0,4 g (3 mmol) d'acétylacétone. Le mélange est agité à température ambiante pendant 3 jours. Il apparait un précipité qui est filtré, puis lavé au chloroforme et à l'éthanol; Rdt = 35%; *F* = 245°C (dec); IR (KBr) : 3100, 2900, 1650, 1580, 1500 cm^{-1}; RMN ^{1}H (DMSO-d_6) δ ppm : 1,85 (s, 6H, CH_3), 5,85 (d, 1H, $J_{7,8}$ = 6 Hz, H8), 6,16 (d, 1H, $J_{5,6}$ = 3 Hz, H5), 7,3 (s large, 1H, H6), 7.7 (d, 1H, H7), 8.05 (s, 1H, H3). Anal. calc. pour $C_{11}H_{12}N_4O_2$: C 56,89; H 5,21; N 24,12; trouvé : C 56,8; H 5,2; N 24,2%.

Condensation avec l'acide barbiturique **10**

Une suspension de 0,35 g de pyrido[3,4-*e*]-as-triazine **2** et 0,5 g de dimédone dans 20 mL d'eau est portée 1 h à 50°C, puis agitée à température ambiante pendant 2 jours. On obtient un précipité brun clair isolé par filtration puis lavé à l'eau; Rdt = 40%; *F* = 260°C (dec.); IR (KBr) : 3200–3000 (large), 1730, 1580 cm^{-1}; RMN ^{1}H (DMSO-d_6) δ ppm : 5,66 (d, 1H, $J_{7,8}$ = 6 Hz, H8), 6,3 (d, 1H, $J_{5,6}$ = 3 Hz; H5), 7,15 (d, 1H, *J* = 3 Hz, H6), 7,4 (m, 1H, H7), 8,6 (s large, 1H, H3); 9,7 (s large, 2H, NH); RMN ^{13}C (DMSO-d_6) δ ppm : 163,6; 151,0; 149,8 (C=O); 142,0 (C3); 138,7 (C7); 98,9 (C8); 129,7; 123,5; 80,5 (C_{4aires}). Anal. calc. pour $C_{10}H_8N_6O_3 \cdot H_2O$: C 43,13; H 3,59; N 30,21; trouvé : C 43,5; H 3,4; N 30,0%.

Condensation avec l'acétylacétate d'éthyle **11**

Une solution de 0,35 g de pyrido[3,4-*e*]-as-triazine **2**, 0,40 g d'acétylacétate d'éthyle dans 20 mL d'eau est agitée à température ambiante pendant 2 jours. On obtient un précipité rouge vif, recristallisé dans l'éther éthylique; Rdt = 60%; *F* = 210°C; IR (KBr) : 3200, 1660, 1640 cm^{-1}; RMN ^{1}H($CDCl_3$) δ ppm : 1,3 (t, 3H, *J* = 7 Hz, CH_3), 4,2 (q, 2H, CH_2), 6,2 (s, 1H, =CH), 6,45 (d, 1H, $J_{7,8}$ = 7 Hz, H8), 7,1 (d, 1H, H7), 7,2 (s, 1H, H6), 9,45 (s, 1H, H3); RMN ^{13}C ($CDCl_3$) δ ppm : 14,1 (CH_3), 59,9 (CH_2O), 86,9 (d, =CH, J_{CH} = 157 Hz), 100,9 (d, C8, J_{CH} = 167 Hz), 134,4 (d, C7, J_{CH} = 184 Hz), 154,7 (d, C3, J_{CH} = 202 Hz), 154,2 (s, C5), 146,9 (s, C10), 119,4 (s, C9), 170 (s, C=O). Masse : 218 (90%, M^+), 190 ($M^+ - C_2H_5$), 172 ($M^+ - C_2H_5$), 144 ($M^+ - COOC_2H_5$), 116 (100%, $M^+ - COOC_2H_5$-N_2). Anal. calc. pour $C_{10}H_{10}N_4O_2$: C 55,04; H 4,62; N 25,67; trouvé : C 54,5; H 4,5; N 24,8%.

Condensation avec le cyanacétate d'éthyle **12**

Une suspension de 0,35 g de pyrido[3,4-*e*]-as-triazine **2**, 0,40 g de cyanacétate d'éthyle dans 20 mL d'eau est agitée à température ambiante pendant 24 h. On obtient un solide rouge vif qui est séparé par filtration, puis lavé au chloroforme et à l'éthanol; Rdt = 45%; *F* = 240°C; IR (KBr) : 3100, 3000, 2200, 1635, 1530 cm^{-1}; RMN ^{1}H (DMSO-d_6) δ ppm : 1,25 (t, 3H, *J* = 7 Hz, CH_3), 4,2 (q, 2H, CH_2), 7,1 (d, 1H, $J_{7,8}$ = 7 Hz, H8), 7,85 (d, 1H, H7), 8,1 (s, 1H, H6), 9,85 (s, 1H, H3). Masse : 243 (85%, M^+), 215 ($M^+ - CN$), 198 ($M^+ - OC_2H_5$), 188 ($M^+ - CN - N_2$), 160 (100%). Anal. calc. pour $C_{11}H_9N_5O_2$: C 54,32; H 3,73; N 28,79; trouvé : C 54,7; H 3,6; N 28,3%.

Condensation avec les esters maloniques

Une suspension de 0,35 g de pyrido-as-triazine, 0,5 g d'ester malonique et 20 mL d'eau est agitée à température ambiante pendant 24 h. Le précipité obtenu est filtré, lavé au chloroforme puis à l'éther froid. Recristallisation dans l'éther éthylique.

Condensation avec le malonate de diéthyle **13** : Rdt = 60%; *F* = 240°C; IR (KBr) : 3140, 3040, 2920, 1720, 1685, 1615 cm^{-1}. Anal. calc. pour $C_{13}H_{13}N_4O_4$: C 53,97; H 4,49; N 19,37; trouvé : C 54,5; H 4,6; N 19,8%.

Condensation avec le malonate de diméthyle **14** : Rdt = 65%; *F* = 230°C; IR (KBr) : 3100, 2980, 1730, 1680, 1615, cm^{-1}. Anal. calc. pour $C_{11}H_{10}N_4O_4$: C 50,38; H 3,84; N 21,37; trouvé : C 49,9; H 3,6; N 21,0%.

Condensation de la pyrido[4,3-e]-as-triazine avec le malonate de diméthyle **15** : Rdt = 30%; *F* = 234°C; IR (KBr) : 3140, 2960, 1730, 1670, 1605, 1540 cm^{-1}: Masse : 262 (40%, M^+); 231 ($M^+ - OCH_3$); 207 (100%). Anal. calc. pour $C_{11}H_{10}N_4O_4$: C 50,38; H 3,84; N 21,37; trouvé : C 50,7; H 3,7; N 21,0%.

1. (*a*) A. Albert et K. Ohta. J. Chem. Soc. C: 2357 (1971); (*b*) A. Albert et H. Mizuno. J. Chem. Soc. B: 2423 (1971).
2. (*a*) D. D. Perrin. J. Chem. Soc. 645 (1962); (*b*) A. Albert et W. L. Armarego. Adv. Heterocycl. Chem. **4**, pp. 1 (1965); (*c*) D. D. Perrin. Adv. Heterocycl. Chem. **4**, 43 (1965); (*d*) A. Albert. Adv. Heterocycl. Chem. **20**, 117 (1976).
3. (*a*) A. Albert et J. J. Mc Cormack. J. Chem. Soc. 6930 (1965); (*b*) A. Albert et H. Mizuno. J. Chem. Soc. Perkin Trans. 1, 1615 (1973); (*c*) 1974 (1973).
4. (*a*) U. Ewers, H. Günther et L. Jaenicke. Angew. Chem. Int. Ed. Engl. **14**, 354 (1975); (*b*) K. R. Davis et R. Wolfenden, J. Org. Chem. **48**, 2280 (1983); (*c*) W. W. Paudler et T. K. Chen. J. Heterocycl. Chem. **7**, 767 (1970); (*d*) W. W. Paudler et J. Lee. J. Org. Chem. **36**, 3921 (1971).
5. (*a*) A. Albert et F. Reich. J. Chem. Soc. 127 (1961); (*b*) Y. Inoue et D. D. Perrin. J. Chem. Soc. 2600 (1962).
6. (*a*) A. Albert et G. B. Barlin. J. Chem. Soc. 5156 (1963); (*b*) 5737 (1963).
7. E. Breitmaier et W. Voelter. Carbon-13 NMR spectroscopy. 3^e éd. Weinheim, New York. 1987. p. 145.
8. (*a*) A. Albert et J. J. McCormack. J. Chem. Soc. Perkin Trans. **1**, 2630 (1973); (*b*) T. Rowan, H. C. S. Wood et P. Hemmerich. Proc. Chem. Soc. London, 261 (1961).
9. M. Saunders et E. H. Gold. J. Org. Chem. **27**, 1439 (1962).
10. J. Hamer et R. E. Holliday. J. Org. Chem. **28**, 2488 (1963).
11. (*a*) R. C. de Selms et H. S. Mosher. J. Am. Chem. Soc. **82**, 3762 (1960); (*b*) A. Albert, J. J. Batterham et J. J. McCormack. J. Chem. Soc. B: 1105 (1966); (*c*) J. P. Geerts, A. Nagel et H. C. van der Plas. Org. Magn. Reson. **8**, 607 (1976).
12. (*a*) C. J. Turner et G. W. H. Cheeseman. Org. Magn. Reson. **6**, 633 (1974). (*b*) U. Vögeli et W. von Philipsborn. Org. Magn. Reson. **5**, 551 (1973).
13. (*a*) A. Lewis et R. G. Shepherd. J. Heterocycl. Chem. **8**, 41 (1971); (*b*) **8**, 47 (1971); (*c*) N. Plé, G. Queguiner et P. Pastour. J. Heterocycl. Chem. **10**, 1073 (1973).
14. N. Plé. Thèse de Doctorat d'État, Université de Rouen. (1987).
15. A. R. Katritzky et C. W. Rees (*Éditeurs*). Comprehensive heterocyclic chemistry. Vol. 3. Pteridines. Pergamon Press, New York. 1984. p. 263.

Can. J. Chem. Downloaded from www.nrcresearchpress.com by 109.225.110.28 on 09/08/12
For personal use only.

Isomerism in the diphosphirane series

JEAN-PIERRE FAYET AND DANIÈLE MERMILLOD-BLARDET
Laboratoire de chimie des matériaux inorganiques (Unité de recherche associée n° 1311), Université Paul Sabatier, 118 - Route de Narbonne, 31062 Toulouse CEDEX, France

AND

CHRISTINE TACHON, GUITA ETEMAD-MOGHADAM, AND MAX KOENIG[1]
Laboratoire de synthèse, structure et réactivité de molécules phosphorées (Unité de recherche associée n° 454), Université Paul Sabatier, 118 - Route de Narbonne, 31062 Toulouse CEDEX, France

Received March 2, 1992

JEAN-PIERRE FAYET, DANIÈLE MERMILLOD-BLARDET, CHRISTINE TACHON, GUITA ETEMAD-MOGHADAM, and MAX KOENIG. Can. J. Chem. **70**, 2834 (1992).

The *cis/trans* stereochemistry of diphosphiranes **1***a–g*, **2***a*, and **2***h* is investigated by MNDO calculations in terms of substituent effects on intracyclic phosphorus and carbon atoms. This approach is completed by calculations of dipole moments. These results are compared to experimental dipole moment measurements of the synthesized diphosphiranes **3***a–f*.

JEAN-PIERRE FAYET, DANIÈLE MERMILLOD-BLARDET, CHRISTINE TACHON, GUITA ETEMAD-MOGHADAM et MAX KOENIG. Can. J. Chem. **70**, 2834 (1992).

La stéréochimie *cis/trans* des diphosphiranes **1***a–g*, **2***a* et **2***h* est étudiée en terme d'effets de substituants sur les atomes de carbone et de phosphore intracycliques. Cette approche, complétée par des calculs de moments dipolaires, est effectuée par la méthode MNDO. Ces résultats sont comparés aux mesures expérimentales de moments dipolaires de diphosphiranes **3***a–f*, synthétisées par ailleurs.

Can. J. Chem. Downloaded from www.nrcresearchpress.com by 109.225.110.28 on 09/08/12
For personal use only.

Introduction

During the past few years, our project has focused on the replacement of one or several carbon atoms of cyclopropane by heteroatoms such as phosphorus, following the work of Baudler and co-workers (1). It is now well established that the stability of small strained rings such as diphosphiranes depends mainly on the influence of the substituent (2). We report here a comparative study of the stereochemistry of diphosphiranes, carried out by MNDO calculations (energies, dipole moments, charges) and experimental investigations.

Experimental

Diphosphiranes **3***a–f*, bearing bulky substituents on the phosphorus atoms, were prepared according to the procedure already described (3). For the theoretical approach, we used more simplified models, i.e., diphosphiranes **1***a–g* with methyl substituents, and **2***a* and **2***h* with a phenyl group on the phosphorus atom instead of the bulky tris-2,4,6-*tert*-butylphenyl substituents, which are too large for computational approaches (Scheme 1).

Calculations were carried out on diphosphiranes **1***a–g*, **2***a*, and **2***h*. The basic approximations of the MNDO (modified neglect of diatomic overlap) method included a semi-empirical model for the two-center integrals (4). We used a Control Data Cyber 860-180 NOS/VE system of the CICT (Centre Inter-Universitaire de Calcul de Toulouse). For the purpose of this paper, we collected energy values (eV), dipole moments (D), net atomic charges, and optimized parameters (Table 1).

The dipole moments of **3***a–f* were measured in benzene at 25°C by a WTW dipole meter (Table 2). The Debye formula was used, as in the Halverstadt and Kumler extrapolation method, for calculation of total polarization (5), with $\alpha = (d\varepsilon/d\omega_2)_{\omega_2 \to 0}$, $\beta = (dv/d\omega_2)_{\omega_2 \to 0}$, and $0.001 < \omega_2 < 0.050$. ε is the dielectric constant, ω_2 the mass fraction of the sample, and v the density. Electronic polarizations can be replaced by the molecular refractions R_{MD}.

[1]Author to whom correspondence may be addressed.

Results

To accomplish stabilization of unstable and unusual organophosphorus compounds in a low coordination state (6), the use of sterically bulky moieties as protective groups is extremely effective. Diphosphiranes **3***a–f* in refluxing toluene solution undergo a ring-opening reaction by preferential P—P bond rupture, leading to 1,3-diphosphapropenes (7). The determination of the kinetic parameters of the ring-opening reactions at 100°C in C_7D_8 was carried out by ^{31}P NMR. The free enthalpy of activation for the ring-opening reactions is in the range of 30 kcal mol^{-1} (Table 3) (8), so that the stabilities of diphosphiranes **3***a–f* can be established according to the following order: **3***e* > **3***c* > **3***d* > **3***a* > **3***f*.

This order of stability concerns solely the thermal ring-opening reactions of diphosphiranes **3***a–f* in the *trans* configuration. Calculations show that the *trans* configuration is thermodynamically the most stable isomer (about 4 kcal mol^{-1}) for **1***a–c* and **2***a*, while the preferential *cis* configuration is obtained for **1***d*, **1***f*, and **1***g*. Notable effects are observed in the case of **1***e*, in which the change of the intracyclic carbon configuration involves a change of the *cis/trans* stability.

Experimentally, the reaction of carbenoids with *trans* diphosphene was used as a stereoselective synthesis of diphosphiranes **3** (3). In each case, only the *trans* isomer was obtained. The $^{31}P\{^1H\}$ NMR spectra, reported as a singlet for **3***a*, **3***c*, and **3***f* and as an AB system for **3***d*, **3***e*, are consistent with a *trans* configuration. The X-ray analysis confirms this configuration (9).

Dipole moment calculations of **1** and **2** show a large difference between the *cis* and *trans* configurations. As expected, generally higher values (≅ 2D) are observed for the *cis* configuration. Substitution of a methyl by a phenyl group (**1***a* and **2***a*, respectively) does not induce a substantial modification of the dipole moment values.

Experimental values for **3** are in the range 0.46–1.81 D (Table 2). Higher values (1.81 and 1.75 D) correspond to

TABLE 1. Theoretical determination of dipole moments and total energies of diphosphiranane models **1***a–g*, **2***a*, and **2***h*

Compound		*cis*		*trans*		$\Delta E_{(trans\text{-}cis)}$ (kcal mol^{-1})
		μ (D)[a]	E_T (eV)[b]	μ (D)[a]	E_T (eV)[b]	
1*a*		3.07	−810.02580	1.32	−810.21031	4.26
1*b*		3.32	−1739.94999	1.30	−1740.14548	4.52
1*c*		2.96	−1490.24803	0.96	−1490.44821	4.62
1*d*	*A*[c]	1.17	−1972.77143	1.88	−1972.46907	−6.98
1*e*	*A*[c]	1.48	−1306.41939	1.40	−1305.78174	−14.73
	B[c]	4.12	−1305.07525			16.32
1*f*		2.88	−1088.46841	1.28	−1087.30812	−26.80
1*g*		3.04	−1121.13057	1.56	−1120.89017	−5.55
2*a*		3.19	−1476.46018	1.24	−1476.63381	4.01
2*h*	*A*[c]	1.98	−1816.40985	–	[d]	–
	B[c]	4.24	−1816.96142	–	[d]	–

[a]μ = dipole moment.
[b]Total energy.
[c]See Scheme 2.
[d]Sterically hindered.

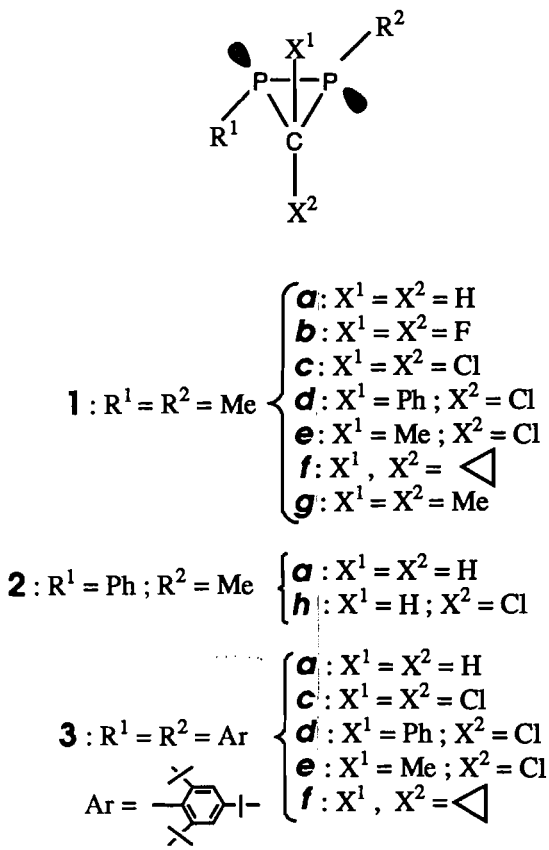

SCHEME 1. Structure of diphosphiranes **1***a–g*, **2***a*, **2***h*, and **3***a–f*.

monohalogenated diphosphiranes **3***d*, **3***e*, whereas the value observed in the case of *gem*-dichlorodiphosphirane **3***c* (0.46 D) is close to that for spirodiphosphirane **3***f* (0.60 D).

Discussion

Since the results of Lutsenko and co-workers (10) and Baudler and Saykowski (11), it is well established that diphosphiranes substituted by isopropyl or *tert*-butyl on the phosphorus atoms are somewhat unstable and susceptible to dimerization reactions. This dimerization, arising from biradical intermediates, is never observed for **3***a–f*, whatever the substituents on the intracyclic carbon atoms (3, 12). In the case of **3***f*, we have demonstrated that the diphosphanyl biradical intermediate leads to the ring extension product (diphosphacyclobutane) and the rearrangement product (diphosphanorbornadiene), without any dimerization (13).

We commonly notice a small difference in energy between *cis* and *trans* structures (≅ 4 kcal mol^{-1}); however, the *trans* forms are usually the more stable. Comparison between measurements performed on **3** and calculations carried out on **1***a–c* and **2***a* provides further support for the presence of *trans* isomers as the main products.

For the diphosphiranes **1***d* and **1***e*, the *cis* forms, in which

TABLE 2. Experimental dipole moment values of diphosphiranes **3** in benzene at 25°C

Compound	α	β	R_{MD}	$P_{2\infty}$[a]	μ (D)
3*a*	0.87	−0.40	171.55	218.50	1.51
3*c*	0.15	−0.26	181.18	185.47	0.46
3*d*	0.41	−0.10	196.02	263.03	1.81
3*e*	0.77	−0.30	181.01	243.94	1.75
3*f*	0.19	−0.21	178.79	186.26	0.60

[a]$P_{2\infty}$ = total molar polarization at infinite dilution.

TABLE 3. Free enthalpy of activation for the ring-opening reactions of diphosphiranes **3***a–f* in deuterated toluene at 100°C

Compound	$\Delta G^{\ddagger}$ (kcal mol^{-1})
3*e*	31.5
3*c*	29.8
3*d*	29.3
3*a*	29.0
3*f*	28.3

Can. J. Chem. Downloaded from www.nrcresearchpress.com by 109.225.110.28 on 09/08/12
For personal use only.

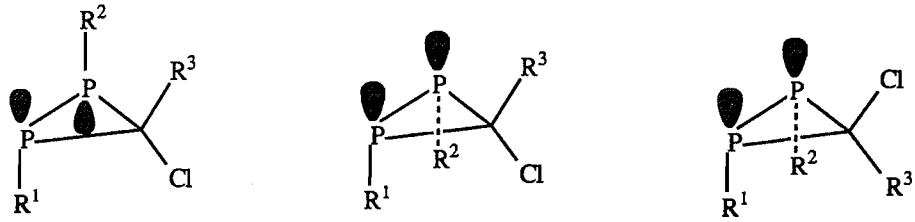

SCHEME 2. Configurations of mono-halogenated diphosphiranes.

TABLE 4. Influence of the rotation of the phenyl substituent on the dipole moment values

θ(°):	160	40	−77 (optimized value)
μ (D):	1.15	1.30	1.24

the chloride atom is *syn* with respect to the methyl substituents of the phosphorus atoms, are the more stable isomers. Such stabilization resulting from an attractive interaction between the methyl group and the negative dipole C–Cl has been reported for rotational isomerism of 1,2-dichloroethane (14). On the other hand, for **3***d* and **3***e*, the presence of bulky substituents (2,4,6-tri-*tert*-butylphenyl) induces a large steric hindrance, which involves a *trans* configuration.

For the spiro derivative, the large difference between *cis* and *trans* calculated energy values is probably the consequence of the particular strain energy of the spiro derivative **1***f* (15). Our method does not allow any accurate evaluation of the different ring-strain energies. Recently, Liu and Bachrach have estimated, by *ab initio* studies, the ring-strain energy of the parent diphosphirane (15 kcal mol^{-1}) using homodesmic reactions (16). For the same model, we obtain an energy value of 50 ± 20 kcal mol^{-1}, by MNDO calculations. Consequently, taking into account the inherent uncertainty in the calculated values, the energy levels for **1***f* cannot be adequately interpreted. Nevertheless, comparisons can be realized for the calculated and experimental dipole moments.

Thus the experimental dipole moment of **3***a* (1.51 D) is close to the calculated value for *trans* **1***a* (1.32 D) whereas the *cis* isomer has a much higher calculated dipole moment (3.07 D). The calculated dipole moment for *trans* **1***c* (0.96 D) is also in good agreement with the experimental value for **3***c* (0.46 D). For **1***d*, calculation of the dipole moment of the *cis* isomer in the *A* and *B* configurations excludes the *B* configuration (Scheme 2). In the case of **3***d*, the experimental dipole moment is nearly the same as the value calculated for *trans* **1***d*. In contrast to **3***d*, the two calculated values for *cis* and *trans* **1***e* are close to the experimental dipole moment determined for **3***e*. In this case, to determine the exact configuration of **3***e*, the dipole moment measurements must be completed by other appropriate methods.

Replacement of a methyl by a phenyl group on either a phosphorus atom or an intracyclic carbon atom affects the dipole moment slightly: 1.32 D for **1***a* (*trans*) and 1.24 D for **2***a* (*trans*) or 1.75 D for **3***e* (*trans*) and 1.81 D for **3***d*, respectively. The variation of μ induced by the possible boat conformation of the aryl substituents was estimated by MNDO calculations as 0.4 D. The θ angle value (dihedral angle CCPC), corresponding to the rotation of a phenyl group around the P—C bond, has almost no influence on the dipole moment values ($1.15 < \mu < 1.30$ D) (Table 4).

The optimized value of the angle (θ = −77°) corresponds quite well to the value given by X-ray structural analysis of **3***c* (θ = −72°) (9). This preferential conformation in the solid state disappears when compounds **3***a–f* are in solution. Thus variable temperature ^{1}H NMR studies clearly demonstrate a free rotation of the aryl groups. The rotation-barrier energy depends on the intracyclic carbon atom substituents. The lower rotation barriers measured for **3***a* and **3***f* are 10.9 and 10.0 kcal mol^{-1}, respectively, whereas the barrier for **3***c* is 17 kcal mol^{-1}. In diphosphirane **3***d*, only the aryl substituent in a *cis* position vs. the chlorine atom is able to rotate with a barrier equal to 19.6 kcal mol^{-1}. This rotation, occurring in solution at room temperature, has no noticeable effect on the experimental dipole moment measurements (Table 4).

In conclusion, the calculated dipole moments correspond to the *trans* geometry. Similarly, the experimental dipole moment values show the presence of preferential *trans* isomers, probably due to the stereoselective cyclopropanation reaction (17), but also to the presence of bulky substituents attached to each phosphorus atom. However, the calculations allow us to predict the formation of *cis* isomers for the sterically less-hindered diphosphiranes. Recently we have shown that, under ultrasonic irradiation, **3***d* undergoes a substitution of the aryl group by a chlorine atom on the phosphorus atom without ring opening (18). For **3***c*, under the same conditions, we observe the formation of two cyclic isomers (^{31}P NMR data: δ −12; −76; $^1J_{P-P}$ = 80 Hz, and δ −16; −59; $^1J_{P-P}$ = 143 Hz) in what are, most probably, the *trans* and *cis* configurations. This hypothesis will be experimentally investigated in the future.

1. (*a*) R. Gleiter, W. Schäfer, and M. Baudler. J. Am. Chem. Soc. **107**, 8043 (1985); (*b*) M. Baudler and J. Simon. Chem. Ber. **121**, 281 (1988); (*c*) M. Baudler. Angew. Chem. Int. Ed. Engl. **27**, 1059 (1988).
2. F. Mathey. Chem. Rev. **90**, 997 (1990).
3. G. Etemad-Moghadam, J. Bellan, C. Tachon, and M. Koenig. Tetrahedron, **43**, 1793 (1987).
4. M. J. S. Dewar and W. Thiel. J. Am. Chem. Soc. **99**, 4899 (1977).
5. I. F. Halverstadt and W. D. Kumler. J. Am. Chem. Soc. **64**, 2988 (1942).
6. (*a*) M. Yoshifuji, I. Shima, N. Inamoto, K. Hirotsu, and T. Higuchi. J. Am. Chem. Soc. **103**, 4587 (1981); (*b*) A. H. Cowley. Polyhedron, **3**, 389 (1984).

Can. J. Chem. Downloaded from www.nrcresearchpress.com by 109.225.110.28 on 09/08/12
For personal use only.

7. M. J. Hervé, G. Etemad-Moghadam, M. Gouygou, D. Gonbeau, M. Koenig, and G. Pfister-Guillouzo. In press.
8. M. Gouygou. Thèse d' Université, Toulouse. 1989.
9. M. Gouygou, C. Tachon, M. Koenig, A. Dubourg, J. P. Declercq, J. Jaud, and G. Etemad-Moghadam. J. Org. Chem. **55**, 5750 (1990).
10. (*a*) Z. S. Novikova, A. A. Prishchenko, and I. F. Lutsenko. Zh. Obshch. Khim. **49**, 471 (1979); (*b*) I. F. Lutsenko. Z. Chem. 345 (1984).
11. (*a*) M. Baudler and F. Saykowski. Z. Naturforsch. **33B**, 1208 (1978); (*b*) M. Baudler. Z. Chem. 352 (1984).
12. J. Bellan, G. Etemad-Moghadam, M. Payard, and M. Koenig. Tetrahedron Lett. **27**, 1145 (1986).
13. C. Garot, G. Etemad-Moghadam, J. P. Declercq, A. Dubourg, and M. Koenig. Angew. Chem. Int. Ed. Engl. **31**, 625 (1992).
14. S. Mizushima, Y. Morino, and M. Takeda. J. Chem. Phys. **9**, 826 (1941).
15. K. B. Wiberg. Angew. Chem., Int. Ed. Engl. **25**, 312 (1986).
16. M. Liu and S. M. Bachrach. Phosphorus, Sulfur, Silicon, **53**, 7 (1990).
17. C. Tachon, M. Gouygou, M. Koenig, M. J. Hervé, D. Gonbeau, and G. Pfister-Guillouzo. Inorg. Chem. **31**, 2414 (1992).
18. G. Etemad-Moghadam, M. Rifqui, P. Layrolle, J. Berlan, and M. Koenig. Tetrahedron Lett. **32**, 5965 (1991).

Can. J. Chem. Downloaded from www.nrcresearchpress.com by 109.225.110.28 on 09/08/12
For personal use only.

The 1992 Alcan Award Lecture
Excursions around the periodic table: ligand design in inorganic chemistry[1]

MICHAEL D. FRYZUK[2]

Department of Chemistry, University of British Columbia, 2036 Main Mall, Vancouver, B. C., Canada V6T 1Z1

Received June 23, 1992

MICHAEL D. FRYZUK. Can. J. Chem. **70**, 2839 (1992).

An overview is given on the strategy used to come up with the design of a new type of ligand that is appropriate for coordination to both the late metals and the early metals. The coordination chemistry of the potentially tridentate ligand $^{-}N(SiMe_2CH_2PR_2)_2$ is developed starting with the Ni triad and then the heavier members of group 9, namely rhodium and iridium. It is with iridium that reactive fragments such as methylene and vinylidene have been stabilized and their chemistry examined. Extension to groups 3, 4, and the lanthanides is also discussed. With these elements, phosphine coordination imparts new reactivity patterns such as alkane elimination with group 3 and dinitrogen activation with group 4. In addition, the side-on binding mode for N_2 attached to a dinuclear zirconium system is also presented.

MICHAEL D. FRYZUK. Can. J. Chem. **70**, 2839 (1992).

On présente une vue d'ensemble de la stratégie utilisée pour mettre au point un nouveau ligand pouvant donner une coordination avec les derniers et les premiers métaux. On a développé la chimie de coordination du ligand potentiellement tridentate $^{-}N(SiMe_2CH_2PR_2)_2$ en utilisant au départ la triade du nickel et ensuite les membres de masse plus élevée du groupe 9, soit le rhodium et l'iridium. Avec l'iridium, les fragments réactifs, tels le méthylène et le vinylène, sont stabilisés et on a examiné leur chimie. On discute aussi de l'extension aux groupes 3 et 4 et aux lanthanides. Avec ces éléments, la coordination avec la phosphine provoque de nouveaux types de réactivité, tels l'élimination d'alcane avec le groupe 3 et l'activation du diazote avec le groupe 4. De plus, on a passé en revue le mode de fixation par lé côté du N_2 attaché à un système dinucléaire du zirconium.

[Traduit par la rédaction]

Introduction

An invitation by the editors of the Canadian Journal of Chemistry to submit a personal account of some of our research presented in the ALCAN Award Lecture is a welcome one since it will give me an opportunity to thank many of the people who have enthusiastically carried this work to its present state. This particular project involves some very straightforward ideas but does need some background to set them in perspective.

When I arrived at UBC in 1979 there were so many projects that I wanted to tackle that I had to make some decisions on which avenues to concentrate given the limited manpower available for a new assistant professor. Although there was an apparently unfettered choice of research projects available to me, there were a few unwritten rules to abide by. The most important one was to avoid at all costs what you did for your Ph.D. work. For me that meant staying away from chiral chelating phosphine ligands and their associated rhodium complexes and catalytic asymmetric hydrogenation (1–3). Another related rule was to avoid what you did while you were a postdoctoral fellow. For me that meant staying away from zirconium and hafnium hydrides stabilized by pentamethylcyclopentadienyl ligands (4). As it turns out I probably ended up disobeying both of these rules, but I'm getting ahead of myself.

In 1979 a paper appeared which I found astounding (5). It reported the preparation of the three-coordinate rhodium complex $Rh(PPh_3)_2[N(SiMe_3)_2]$. What made this short communication so interesting was the claim that this was the first ever preparation of an amide ligand bound to rhodium. Even more important was the claim that amide ligands were still not known for complexes of Pd, Os, and Ir (and a few other metals). The amide ligand, defined as a deprotonated amine of the general formula $^{-}NR_2$ (R = alkyl, aryl, silyl, or H), is well known to bind to the early metals (groups 3–5) and the lanthanides (6) but the fact that its coordination chemistry with the later transition elements (groups 8–10) was so lacking was intriguing.

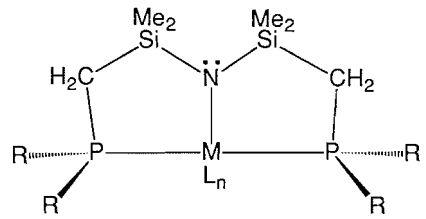

I

SCHEME 1

About this same time I had also noticed that phosphine ligands (PR_3) were not generally associated with complexes of the early transition metals and the lanthanides. In contrast, phosphine complexes of the later transition elements are ubiquitous. This observation was probably my way of disobeying the two unwritten rules for a new assistant professor, namely that I wanted to apply some of the expertise in phosphine chemistry obtained from my Ph.D. work to the experience with early metal chemistry picked up in my postdoctoral stint.

It was the dichotomy in the coordination behavior of these two ligand types, the amide group and the phosphine donor, that provided the incentive to develop a hybrid ligand system that incorporated both ligand types into one chelating array. The ligand system aimed for is shown in Scheme 1. It seemed possible that such a ligand would allow us to

[1]This is an invited personal review article based on Professor Fryzuk's Alcan Award lecture, presented at the 1992 Annual Conference of the Canadian Society for Chemistry, Edmonton, Alberta.

[2]E. W. R. Steacie Fellow (1990–1992).

Can. J. Chem. Downloaded from www.nrcresearchpress.com by 88.255.202.194 on 09/08/12
For personal use only.

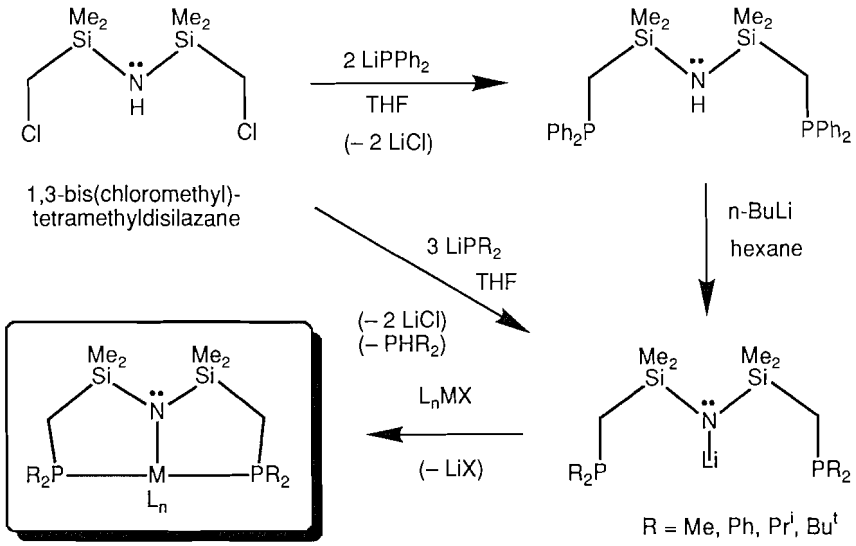

SCHEME 2

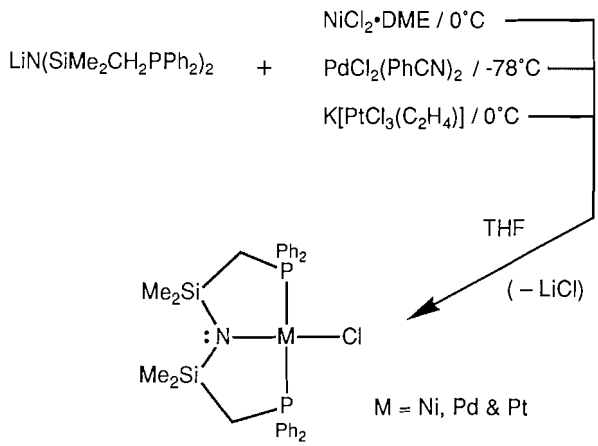

SCHEME 3

overcome the apparent coordination chemistry mismatches in the following way: phosphine complexes of the early metals and the lanthanides would be accessible since the amide portion of the tridentate ligand would anchor the ligand to the metal and force coordination of the phosphine donor by virtue of the chelate effect; in addition, amides of the later transition elements would also be accessible with this ligand system since now the phosphine interaction would help stabilize the amide ligation. More importantly, if the reactivity patterns of a metal complex are a function of its coordination environment then it was hoped that this ligand system would result in the observation of new and unusual chemistry because this was a brand new type of ligand.

A few final words of introduction are in order. The preparation of the actual target ligand was facilitated by the discovery that the proposed starting material was commercially readily available at reasonable prices. If at some point luck had to rear its head, why not at the beginning of a new project? In our excursion around the periodic table the vehicle will be the coordination complex **I** shown in Scheme 1. The rest of the account will summarize aspects of the coordination chemistry of this ligand with various metals across the periodic table, hopefully giving due credit to my co-workers.

Ligand synthesis

The preparation of various forms of the ligand is shown in Scheme 2; the range of substituents at phosphorus from phenyl to *tert*-butyl has provided some limited variability in steric and electronic effects. In general we use the lithium form of the deprotonated amide as the starting material in concert with some halide precursor complex containing the metal of choice; in a few cases the corresponding potassium salt has also been used.

Coordination chemistry: late metals

My first graduate student at UBC, Patricia MacNeil, was the person who initiated work on this ligand system. She began this trip around the periodic table at the nickel(II) complex $NiCl[N(SiMe_2CH_2PPh_2)_2]$ prepared by the reaction of the lithium salt with $NiCl_2 \cdot DME$ (DME = 1,2-dimethoxyethane); she then prepared the analogous Pd(II) and Pt(II) derivatives as outlined in Scheme 3 (7, 8). The palladium complex was the first mononuclear palladium amide to be structurally characterized, based on what was claimed earlier (5, 6). Interestingly, a review undertaken by ourselves did uncover some prior palladium amide complexes (9), but there are, to our knowledge, no other crystal structural analyses. Aside from some peculiar CO migratory insertion behavior for the Ni derivatives (10), the chemistry of the group 10 derivatives was rather predictable; however, this work did provide the groundwork for our later studies.

Patricia MacNeil then went on to synthesize rhodium and iridium derivatives using this ligand system (11–17). The preparation mirrors that for the group 10 triad; as shown in Scheme 4 the key starting material for the heavier members of group 9, namely rhodium and iridium, is the cyclooctene complex $M(\eta^2\text{-}C_8H_{14})[N(SiMe_2CH_2PPh_2)_2]$ since this allows access to a variety of derivatives in both the +1 and +3 oxidation states. Without a doubt it has been the iridium derivatives stabilized by this tridentate ligand system that have provided the enduring chemistry for the late metals. As outlined in Scheme 4, access to iridium(I) species incorporating

Can. J. Chem. Downloaded from www.nrcresearchpress.com by 88.255.202.194 on 09/08/12
For personal use only.

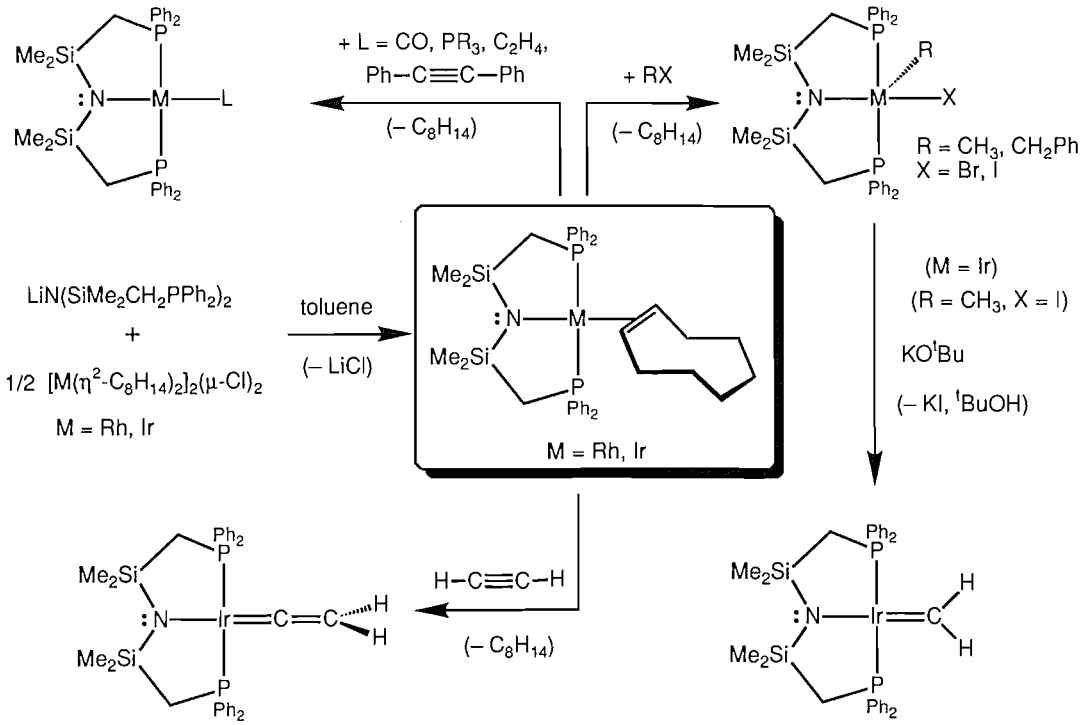

SCHEME 4

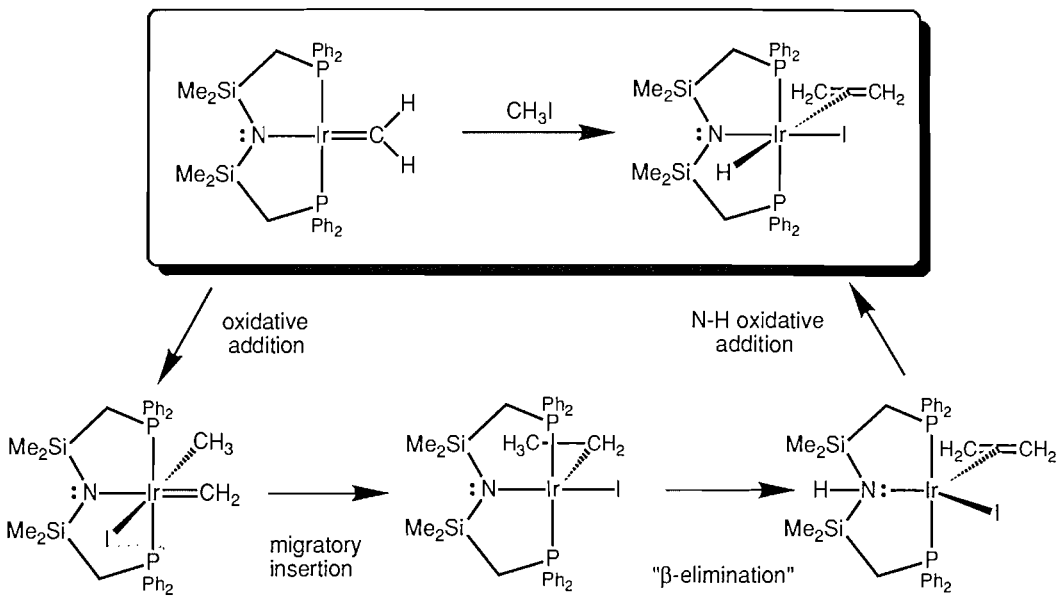

SCHEME 5

the very reactive methylene (=CH_2) (14) and vinylidene (=C=CH_2) (18) fragments has allowed the chemistry of these very unstable moieties to be examined. For example, Kiran Joshi showed that addition of CH_3I to the methylene complex resulted in the generation of the ethene-hydride derivative as a result of a carbon–carbon bond formation via migratory insertion; similarly, Dr. Neil McManus and Dr. Graham White showed that the vinylidene derivative also underwent migratory insertion with CH_3I to generate the corresponding allyl derivative (19). These reactions are shown in Schemes 5 and 6 respectively. What is significant in this work is that we have identical metals and ligand environments with which to compare the relative reactivity of the methylene and the vinylidene moieties. As shown by their reactivity with CH_3I there are intriguing similarities as well as differences and these are still being evaluated in my group. For example, in both of Schemes 5 and 6, the amide donor is shown to be involved in the mechanism by formation of amine derivative via intramolecular proton abstraction from a coordinated hydrocarbyl group; this "β-elimination" to the amide donor has precedent in some of our earlier work in the heterolytic activation of H_2 by related group 9 complexes (16).

Can. J. Chem. Downloaded from www.nrcresearchpress.com by 88.255.202.194 on 09/08/12
For personal use only.

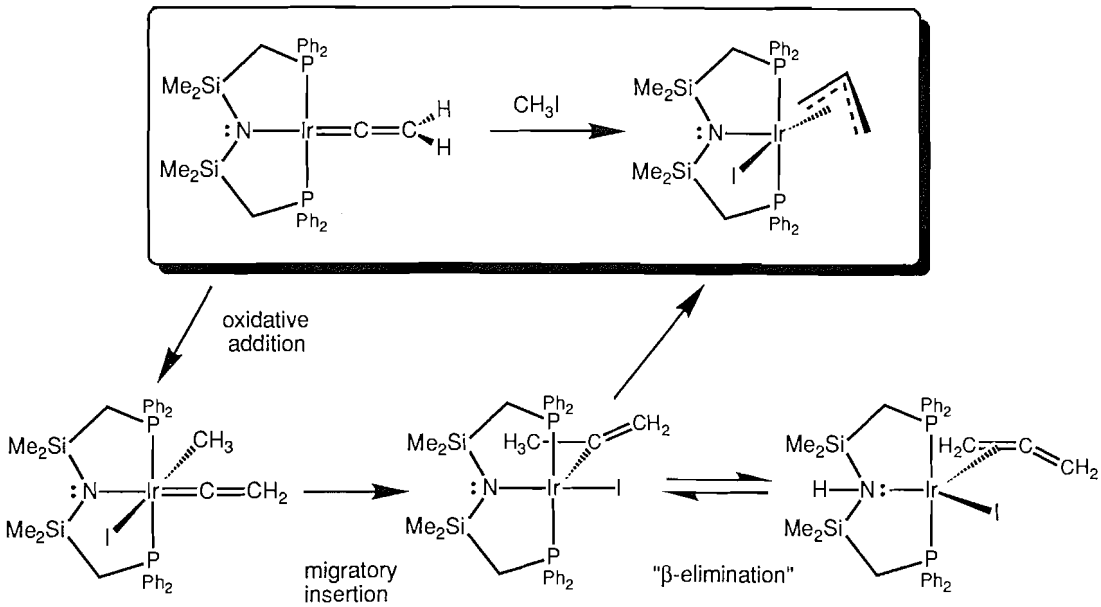

SCHEME 6

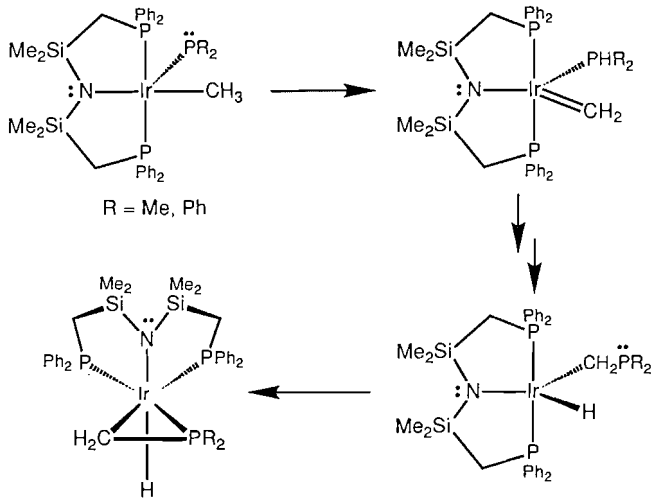

SCHEME 7

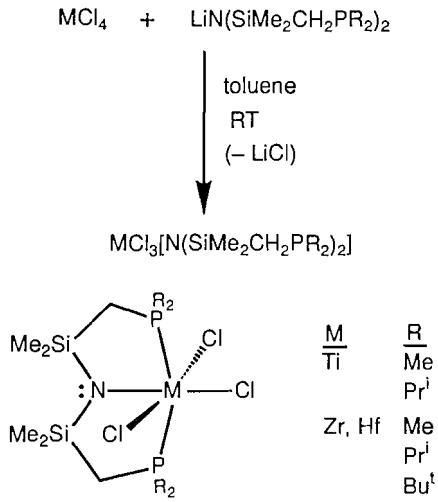

SCHEME 8

We have found that iridium–carbon double-bonded species occur in other chemistry involving the iridium fragment $Ir[N(SiMe_2CH_2PPh_2)_2]$ as well. Both the thermal transformation of, and the reaction of hydrogen with, phosphido-alkyl iridium species would appear to involve iridium–methylene type intermediates at crucial points in the sequence (20, 21). For example, Kiran Joshi showed (20) that in the thermal decomposition of iridium phosphido–methyl complexes, the formation of cyclometalated hydride derivatives can be rationalized by proton abstraction from the methyl ligand by the coordinated phosphide to generate an intermediate phosphine methylene; as shown in Scheme 7, subsequent rearrangement (by a number of hypothetical steps) produces the cyclometalated phosphine hydride.

It would appear that the combination of iridium and this ligand system is special since we have been able to access a variety of reactive organic fragments such as methylene and vinylidene and study their chemistry. In future, our efforts will be the focused on other reactive fragments such as silylene (=SiR_2), and silene (η^2-SiR_2SiR_2).

Coordination chemistry: early metals and the lanthanides

The other aspect of our ligand design was the use of this system to generate phosphine complexes of the early metals (22). In 1981, my second graduate student, Hugh Williams, was the first person to try bonding this ligand type to the early metals. His first success was in the preparation of bis(ligand) derivatives of zirconium(IV) and hafnium(IV), $MCl_2[N(SiMe_2CH_2PR_2)_2]_2$ (M = Zr, Hf; R = Me, Ph) (23); although these complexes were of stereochemical interest, they showed little reactivity. Hugh did find that hydride complexes of hafnium(IV) could be prepared (24) via the formation of a monoligand starting material having the approximate formula $HfCl_3[N(SiMe_2CH_2PMe_2)_2] \cdot HfCl_4$. A German post-

Can. J. Chem. Downloaded from www.nrcresearchpress.com by 88.255.202.194 on 09/08/12
For personal use only.

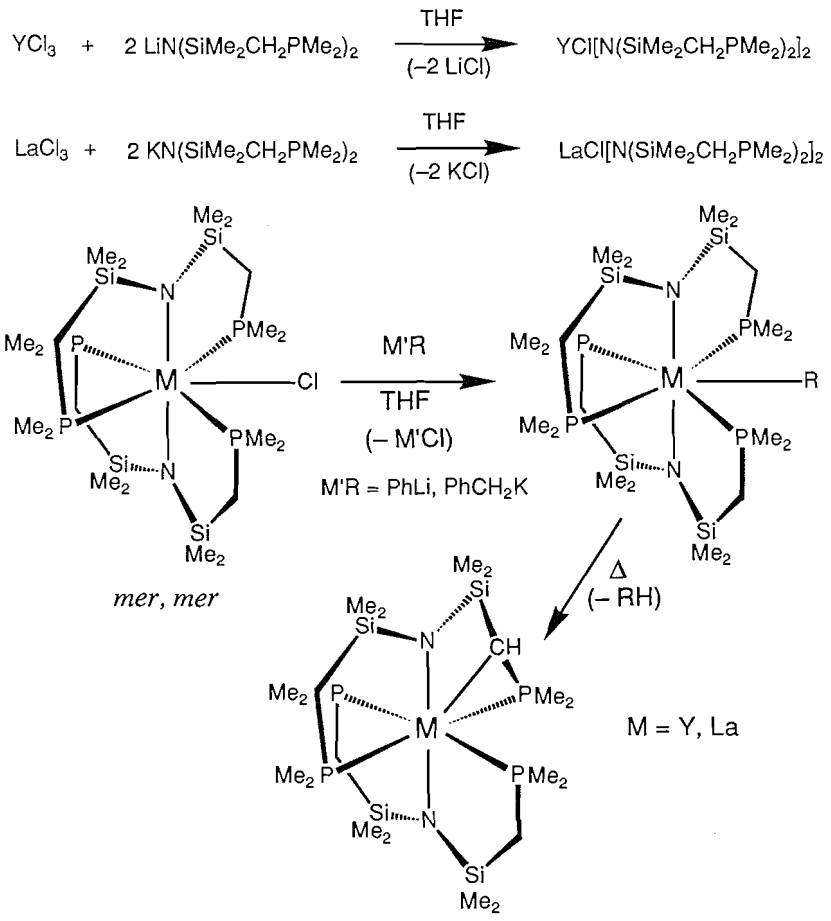

SCHEME 9

doctoral fellow, Dr. Axel Westerhaus, solved a lot of our problems in this area by coming up with straightforward syntheses of monoligand staring materials for Zr(IV) and Hf(IV) with a variety of substituents at phosphorus (25); this is outlined in Scheme 8. These monoligand derivatives turned out to be exceedingly versatile as we were able to prepare dinuclear hydride complexes (26), derivatives containing the η^4-butadiene moiety (27, 28), and trimethyl complexes of Zr and Hf (29). Tim Haddad prepared the η^4-butadiene complexes as part of his M.Sc. thesis and showed that the butadiene-allyl derivatives, $M(\eta^4\text{-}C_4H_6)(\eta^3\text{-}C_3H_5)[N(SiMe_2CH_2PR_2)_2]$ (M = Zr, Hf, R = PR^i, Me), underwent carbon–carbon coupling to generate a new hydrocarbon fragment bound $\eta^4{:}\eta^1$ to the group 4 metal centre (27). For his Ph.D., Tim moved the coordination chemistry of this ligand even further to the left in the transition series by preparing group 3 complexes (30, 31). Here again, we started off by preparing the bis(ligand) derivatives $MCl[N(SiMe_2CH_2PMe_2)_2]_2$ for M = Y and La; $^{31}P\{^1H\}$ NMR spectroscopy has turned out to be quite crucial in these systems since it can provide information on stereochemistry. We anticipated that these seven-coordinate derivatives would be rather unreactive in analogy to the group 4 complexes; however, we were pleasantly surprised to find that the remaining chloride could be metathesized by PhLi and $PhCH_2K$ to generate the corresponding hydrocarbyl derivatives, $YR[N(SiMe_2CH_2PMe_2)_2]_2$ (32). These hydrocarbyl complexes were found to thermally eliminate hydrocarbon to generate cyclometalated

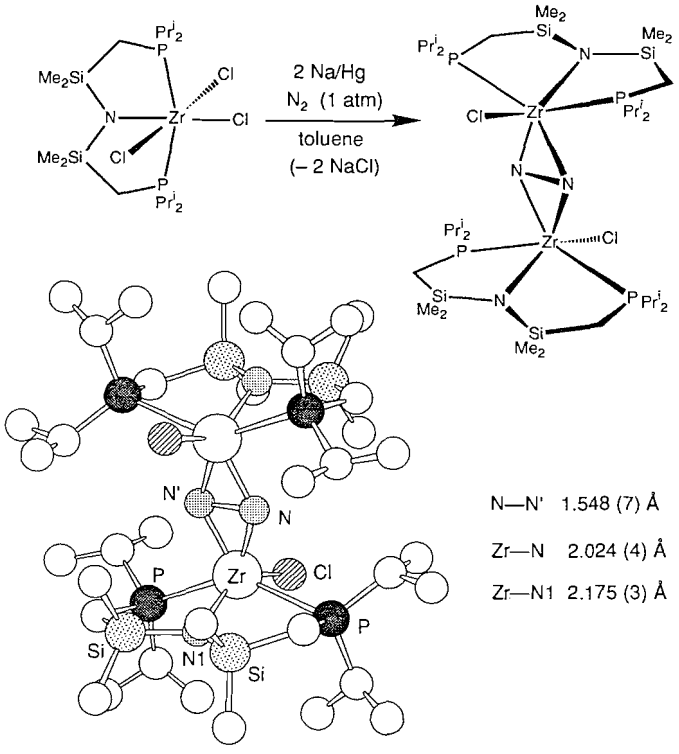

SCHEME 10

Can. J. Chem. Downloaded from www.nrcresearchpress.com by 88.255.202.194 on 09/08/12
For personal use only.

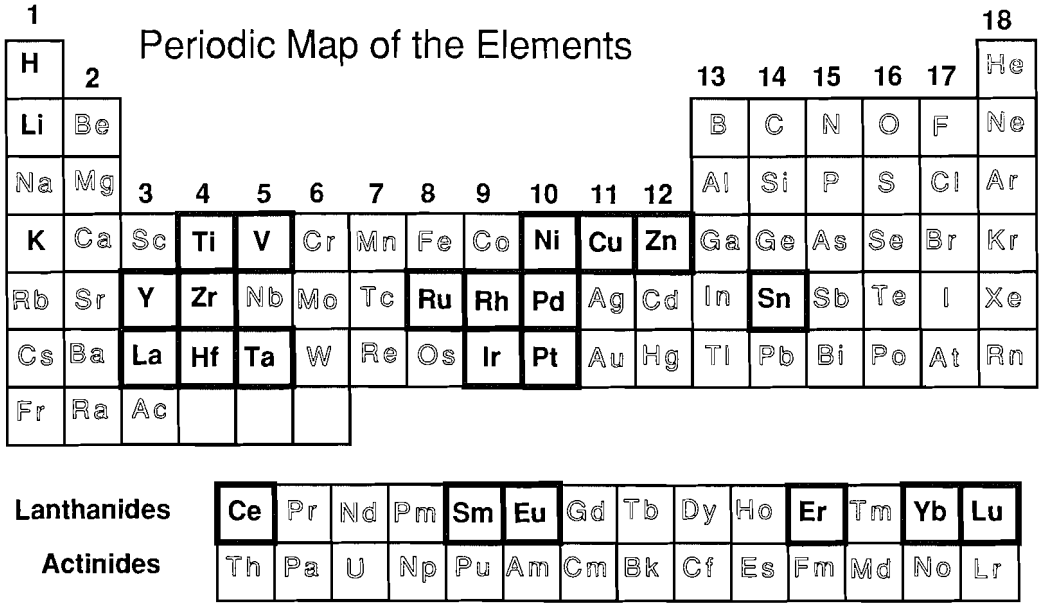

SCHEME 11

complexes; in fact, the lanthanum hydrocarbyl derivative could not be isolated, as it spontaneously formed the cyclometalated complex. The group 3 chemistry is summarized in Scheme 9.

Because of the similarity between the chemistry of the group 3 elements and the lanthanide metals, Dr. David Berg was able to open up the corresponding chemistry of the rare earth elements using this ligand system. He was able to prepare the bis(ligand) derivatives $MCl[N(SiMe_2CH_2PR_2)_2]_2$ for M = Ce, Sm, Er and Yb with R = Me and Ph; he also prepared bis(ligand) derivatives $M[N(SiMe_2CH_2PMe_2)_2]_2$ for the divalent metals M = Sm(II), Eu(II), and Yb(II). Noteworthy is the $^{31}P\{^1H\}$, NMR spectrum of the diamagnetic, divalent ytterbium derivative $Yb[N(SiMe_2CH_2PMe_2)_2]_2$, which shows a singlet with ^{171}Yb satellites (^{171}Yb has $s = 1/2$ and 14.3% natural abundance); the $^1J_{Yb-P}$ of 665 Hz is the first ever one-bond coupling recorded for these spin-active nuclei (22).

Phosphine complexes of group 4 are still being pursued in our group. One of the final accomplishments of Tim Haddad for his Ph.D. degree was to make a dinitrogen complex of zirconium. The reduction of $ZrCl_3[N(SiMe_2CH_2PPr^i_2)_2]$ with two or more equivalents of Na/Hg under an atmosphere of dinitrogen generates a deep blue material, which we have characterized as $\{[(Pr^i_2PCH_2SiMe_2)_2N]ZrCl\}_2(\mu\text{-}\eta^2\text{:}\eta^2\text{-}N_2)$ (33). This complex is remarkable since it contains the dinitrogen in the very rare side-on mode bridging between the two zirconium centres (Scheme 10). Even more remarkable is the extremely long N—N bond distance of 1.548(7) Å for the bridging N_2 unit; this is by far the longest N—N bond length ever recorded for dinitrogen complexes (34–36).

In an attempt to try and gain a deeper understanding of this side-on mode of bonding for a dinitrogen ligand, David McConville and M. Mylvaganam carried out semi-empirical molecular orbital calculations, backed up by synthetic studies (37). What they discovered was that the side-on mode is a direct result of the tridentate ligand's bonding requirements since the amide donor binds to one of the *d*-orbitals that would normally be used to form a π-bond with the end-on form of the N_2 ligand. This was verified by the preparation of a variety of derivatives; for example, the cyclopentadienyl derivative $\{[(Pr^i_2PCH_2SiMe_2)_2N]Zr(\eta^5\text{-}C_5H_5)\}_2(\mu\text{-}N_2)$ shows a linear end-on mode of coordination that is consistent with the molecular orbital analysis. Pauline Chow has recently extended the dinitrogen chemistry to titanium and vanadium (38); in these dinuclear systems, $\{[(Pr^i_2PCH_2SiMe_2)_2N]MCl\}_2(\mu\text{-}N_2)$ (M = Ti, V), the dinitrogen bridges in a linear end-on fashion due to steric constraints as a result of the smaller metal centres and the rather bulky ancillary ligand.

Future prospects

In Scheme 11, a periodic table is shown with those elements highlighted that have been studied with this ligand system. I have not discussed all of our efforts; rather I have tried to detail how this excursion got started and then travel across the periodic table with minimal stopovers at particular elements. However, it should be obvious that there are destinations in the periodic map of the elements that must be visited; for example, it is rumored that adventures will abound in the main group elements. And what about the actinides? This excursion is certainly not over.

Acknowledgments

The support of the Natural Sciences and Engineering Research Council of Canada (NSERC) since 1980 is gratefully acknowledged. Acknowledgment is also made to the donors of the Petroleum Research Fund, administered by the American Chemical Society, for partial support of this work. Johnson Matthey is thanked for their generous loans of precious metals (Pd, Pt, Ru, Rh, and Ir). I would also like to thank ALCAN International for their continued support of chemistry in Canada. Dr. Steven J. Rettig is also thanked for his enthusiastic expertise in solving crystal structures.

Can. J. Chem. Downloaded from www.nrcresearchpress.com by 88.255.202.194 on 09/08/12
For personal use only.

1. M. D. Fryzuk and B. Bosnich. J. Am. Chem. Soc. **99**, 6262 (1977).
2. M. D. Fryzuk and B. Bosnich. J. Am. Chem. Soc. **100**, 5491 (1978).
3. M. D. Fryzuk and B. Bosnich. J. Am. Chem. Soc. **101**, 3043 (1979).
4. D. M. Roddick, M. D. Fryzuk, P. F. Seidler, G. L. Hillhouse, and J. E. Bercaw. Organometallics, **4**, 97 (1985).
5. B. Cetinkaya, M. F. Lappert, and S. Torroni. J. Chem. Soc. Chem. Commun. 843 (1979).
6. M. F. Lappert, P. P. Power, A. R. Sanger, and R. C. Srivastava. Metal and metalloid amides. Ellis–Horwood, Chichester. 1980.
7. M. D. Fryzuk and P. A. MacNeil. J. Am. Chem. Soc. **103**, 3592 (1981).
8. M. D. Fryzuk, P. A. MacNeil, S. J. Rettig, A. S. Secco, and J. Trotter. Organometallics, **1**, 918 (1982).
9. M. D. Fryzuk and C. D. Montgomery. Coord. Chem. Rev. **95**, 1 (1989).
10. M. D. Fryzuk and P. A. MacNeil. J. Am. Chem. Soc. **106**, 6993 (1984).
11. M. D. Fryzuk and P. A. MacNeil. Organometallics, **2**, 355 (1983).
12. M. D. Fryzuk and P. A. MacNeil. Organometallics, **3**, 185 (1983).
13. M. D. Fryzuk, P. A. MacNeil, and S. J. Rettig. Organometallics, **4**, 1145 (1985).
14. M. D. Fryzuk, P. A. MacNeil, and S. J. Rettig. J. Am. Chem. Soc. **107**, 6708 (1985).
15. M. D. Fryzuk, P. A. MacNeil, and S. J. Rettig. Organometallics, **5**, 2469 (1986).
16. M. D. Fryzuk, P. A. MacNeil, and S. J. Rettig. J. Am. Chem. Soc. **109**, 2803 (1987).
17. M. D. Fryzuk, P. A. MacNeil, and N. T. McManus. Organometallics, **6**, 822 (1987).
18. M. D. Fryzuk, N. T. McManus, S. J. Rettig, and G. S. White. Angew. Chem. Int. Ed. Engl. **29**, 73 (1990).
19. M. D. Fryzuk, L. Huang, N. T. McManus, P. Paglia, S. J. Rettig, and G. S. White. Organometallics. **11**, 2979 (1992).
20. M. D. Fryzuk, K. Joshi, R. J. Chadha, and S. J. Rettig. J. Am. Chem. Soc. **113**, 8724 (1991).
21. M. D. Fryzuk and K. Bhangu. J. Am. Chem. Soc. **110**, 961 (1988).
22. M. D. Fryzuk, T. S. Haddad, D. J. Berg, and S. J. Rettig. Pure Appl. Chem. **63**, 845 (1991).
23. M. D. Fryzuk, S. J. Rettig, and H. D. Williams. Inorg. Chem. **22**, 863 (1983).
24. M. D. Fryzuk and H. D. Williams. Organometallics, **2**, 162 (1983).
25. M. D. Fryzuk, A. Carter, and A. Westerhaus. Inorg. Chem. **24**, 642 (1985).
26. M. D. Fryzuk, S. J. Rettig, A. Westerhaus, and H. D. Williams. Inorg. Chem. **24**, 4316 (1985).
27. M. D. Fryzuk, T. S. Haddad, and S. J. Rettig. Organometallics, **7**, 1224 (1988).
28. M. D. Fryzuk, T. S. Haddad, and S. J. Rettig. Organometallics, **8**, 1723 (1989).
29. M. D. Fryzuk, A. Carter, and S. J. Rettig. Organometallics, **11**, 469 (1992).
30. M. D. Fryzuk and T. S. Haddad. J. Am. Chem. Soc. **110**, 8263 (1988).
31. M. D. Fryzuk and T. S. Haddad. J. Chem. Soc. Chem. Commun. 1088 (1990).
32. M. D. Fryzuk, T. S. Haddad, and S. J. Rettig. Organometallics, **10**, 2026 (1991).
33. M. D. Fryzuk, T. S. Haddad, and S. J. Rettig. J. Am. Chem. Soc. **112**, 8185 (1990).
34. R. L. Richards. *In* The biology and biochemistry of nitrogen reduction. *Edited by* M. J. Dilworth and A. R. Glenn. Elsevier, Amsterdam. 1991. p. 58.
35. J. R. Dilworth and R. L. Richards. *In* Comprehensive organometallic chemistry. Vol. 8. *Edited by* G. Wilkinson, F. G. A. Stone, and E. W. Abel. Pergamon, Oxford. 1982. p. 1073.
36. R. A. Henderson. Transition Met. Chem. **15**, 330 (1990).
37. M. D. Fryzuk, T. S. Haddad, M. Mylvaganam, D. H. McConville, and S. J. Rettig. J. Am. Chem. Soc. In press.
38. M. D. Fryzuk, P. Chow, and S. J. Rettig. Unpublished work (1992).

Can. J. Chem. Downloaded from www.nrcresearchpress.com by 88.255.202.194 on 09/08/12
For personal use only.

Preparation and structure of chloro-copper(II) complexes of 7-azaindole

JACQUES POITRAS AND ANDRÉ L. BEAUCHAMP[1]

Département de chimie, Université de Montréal, C.P. 6128, Succ. A, Montréal, Qué., Canada H3C 3J7

Received April 6, 1992

JACQUES POITRAS and ANDRÉ L. BEAUCHAMP. Can. J. Chem. **70**, 2846 (1992).

The light green *trans*-$CuCl_2(Haza)_2$ adduct precipitates immediately from mixtures of $CuCl_2 \cdot 2H_2O$ with excess 7-azaindole (Haza) in methanol. Upon standing in azaindole-rich solution, this solid is replaced by a deep green $Cu_2Cl_4(Haza)_6$ compound, whose crystal structure (orthorbombic, *Fdd*2, a = 26.558, b = 23.750, c = 12.727 Å, Z = 8, R = 0.068, R_w = 0.066) shows the presence of square-planar $[Cu(Haza)_4]^{2+}$ and *trans*-$[CuCl_2(Haza)_2]$ units connected by bridging Cl^- ions, making each Cu atom (4 + 2)-coordinated. Azaindole is bonded to the metal via the pyridine N7 site, whereas the five-membered ring retains its N1—H proton. The azaindole ligands are disordered over two orientations in the $[CuCl_2(Haza)_2]$ unit. The square-planar Cu species and apical Cl^- ions lie on a twofold axis and define along c an infinite chain based on the $\cdots Cl\cdots[Cu(Haza)_4]\cdots Cl\cdots[CuCl_2(Haza)_2]\cdots$ pattern. Equimolar mixtures of azaindole and $CuCl_2 \cdot 2H_2O$ yield a brown $Cu_4OCl_6(Haza)_4$ compound. The crystal structure of its ethyl acetate solvate (monoclinic, $P2_1/c$, a = 11.661, b = 22.415, c = 15.077 Å, β = 109.85°, Z = 4, R = 0.048, R_w = 0.054) shows the presence of a tetranuclear cluster consisting of a μ_4-oxide ion surrounded by a tetrahedron of Cu(II) atoms bridged in pairs by chlorine atoms. The trigonal-bipyramidal coordination of each copper atom is completed by a monodentate N7-bonded azaindole molecule hydrogen bonded to bridging chlorines via N1—H. The influence of complexation on the infrared spectrum of azaindole is discussed.

JACQUES POITRAS et ANDRÉ L. BEAUCHAMP. Can. J. Chem. **70**, 2846 (1992).

Le composé d'addition vert clair *trans*-$CuCl_2(Haza)_2$ précipite immédiatement lors du mélange de $CuCl_2 \cdot 2H_2O$ avec le 7-azaindole (Haza) en excès dans le méthanol. En le laissant reposer dans une solution riche en azaindole, ce solide est remplacé par un composé vert foncé $Cu_2Cl_4(Haza)_6$, pour lequel la structure cristalline (orthorhombique, *Fdd*2, a = 26,558, b = 23,750, c = 12,727 Å, Z = 8, R = 0,068, R_w = 0,066) indique la présence d'espèces planes carrées $[Cu(Haza)_4]^{2+}$ et *trans*-$[CuCl_2(Haza)_2]$ reliées par des ions Cl^- pontants, qui confèrent à chaque atome de Cu une coordination (4 + 2). L'azaindole est lié au métal par l'intermédiaire de l'azote pyridinique N7, alors que le cycle à cinq chaînons conserve son proton N1—H. Les ligands azaindole sont désordonnés selon deux orientations dans le motif $[CuCl_2(Haza)_2]$. Les espèces planes carrées du cuivre et les ions Cl^- axiaux se trouvent sur un axe de rotation d'ordre deux et définissent selon c une chaîne infinie basée sur la séquence $\cdots Cl\cdots[Cu(Haza)_4]\cdots Cl\cdots[CuCl_2(Haza)_2]\cdots$. Le mélange équimolaire d'azaindole et de $CuCl_2 \cdot 2H_2O$ conduit au composé brun $Cu_4OCl_6(Haza)_4$. La structure cristalline du solvate d'acétate d'éthyle (monoclinique, $P2_1/c$, a = 11,661, b = 22,415, c = 15,077 Å, β = 109,85°, Z = 4, R = 0,048, R_w = 0,054) indique la présence d'un agrégat tétranucléaire comprenant un ion μ_4-oxyde entouré d'un tétraèdre d'atomes Cu(II) pontés deux à deux par des atomes de chlore. La coordination bipyramidale trigonale de chaque atome de cuivre est complétée par une molécule d'azaindole monodentate liée par N7, dont le proton N1—H participe à des liaisons hydrogène avec des chlores avoisinants. L'influence de la coordination sur le spectre infrarouge de l'azaindole a également été étudiée.

Introduction

The ligating properties in 7-azaindole (Haza, scheme 1)[2] have attracted relatively little attention. Previous reports from this laboratory described the preparation and structural characterization of three types of complexes with the CH_3Hg^+ cation (1, 2). In most of the remaining compounds structurally characterized so far, the azaindole anion acts as a bi-

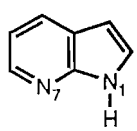

SCHEME 1

nucleating agent by bridging a pair of metal atoms as carboxylate ligands do. However, in contrast with carboxylates and other common assembling ligands, the two donor sites of azaindole are not equivalent, being part of five- and six-membered rings, respectively. For this reason, we often get mixtures of many stereoisomers which are difficult to separate and crystallize. Furthermore, when crystalline materials are obtained, structural studies are complicated by the fact that the ligands generally show disorder due to ring orientation. Peng and co-workers (3, 4) have shown that Cu and Ni compounds originally prepared by Brookes and Martin (5) are indeed "windmill" tetra(azaindolate)dimetal units. A similar binding mode has recently been reported for a dichromium system (6). Azaindole anions can be used to stabilize metal–metal bonds, as observed in quadruply-bonded dimolybdenum compounds (7, 8). Bridging is also observed in the $Cu_4O(aza)_4(OCH_3)_4(dmf)_2$ and $Co_4(aza)_6$ clusters (3).

In the neutral form, the lone pair of N7 in the six-membered ring is the only one available. The presence of the N1—H bond in the other ring, roughly parallel to the N7 lone pair, results in very unusual hydrogen-bonding features for the free ligand, which has recently been shown to exist in the solid state as a unique hydrogen-bonded tetramer (1). Complexes of formally neutral azaindole have been described for CH_3Hg^+ (1, 2) and Zn^{2+} (9). An adduct of dirhodium tetrapropionate has also been reported (10). When the ligand is

[1]Author to whom correspondence may be addressed.

[2]Unparenthesized symbols are used to identify the ligand atoms in general. When referring to specific atomic positions in crystal structures, the parenthesized symbols given in Tables 2 and 3 are used.

Can. J. Chem. Downloaded from www.nrcresearchpress.com by 88.255.202.194 on 09/08/12
For personal use only.

Can. J. Chem. Downloaded from www.nrcresearchpress.com by 88.255.202.194 on 09/08/12
For personal use only.

bonded via N7, the adjacent N1—H bond points inside the metal coordination sphere, where it can interact with other ligands. While exploring the coordinating ability of azaindole, the reactions with copper(II) chloride in methanol were examined under conditions that did not lead to ligand deprotonation. Three compounds were isolated and characterized. The crystallographic work carried out on two of these compounds shows that hydrogen bonding has a particular influence on the structure of these materials.

Experimental section

Reactants and methods

$CuCl_2 \cdot 2H_2O$ (BDH) and 7-azaindole (Aldrich) were used as received. The solvents were of reagent grade. Chlorine was analyzed by potentiometric titration with $AgNO_3$.

Infrared spectra (4000–220 cm^{-1}) were recorded as KBr or CsI pellets with a Perkin-Elmer 783 spectrophotometer. Magnetic susceptibilities were measured at room temperature with a Johnson-Matthey balance, calibrated with $HgCo(SCN)_4$ ($\chi = 16.44 \times 10^{-6}$ c.g.s.e.m.u.). The data were corrected for diamagnetism of the ligands using Pascal's constants (11).

Reactions

$CuCl_2(Haza)_2$

To a solution of $CuCl_2 \cdot 2H_2O$ (0.49 g, 2.9 mmol) in methanol (30 mL) was added a solution of 7-azaindole (1.01 g, 8.5 mmol) in methanol (30 mL) at room temperature. A light green precipitate formed immediately. The resulting mixture was stirred for several minutes and the product was collected by filtration, washed with methanol, and dried *in vacuo* at room temperature Yield: 0.78 g (73%). Anal. calcd. for $C_{14}H_{12}CuCl_2N_4$: Cl 19.14; found: 19.21. $\mu = 2.02$ BM. The same compound also formed in lower yields when the reaction was run at room temperature with a 2:1 or 1:1 ligand:Cu ratio.

$Cu_2Cl_4(Haza)_6$

A solution of 7-azaindole (1.00 g, 8.5 mmol) in methanol (30 mL) was added to a solution of $CuCl_2 \cdot 2H_2O$ (0.36 g, 2.1 mmol) dissolved in methanol (20 mL). The above light green precipitate of $CuCl_2(Haza)_2$ appeared immediately. The mixture was heated near the boiling point until the precipitate redissolved to give a clear dark green solution. Dark green prismatic crystals were obtained upon cooling. Yield: 0.94 g (91%); $\mu = 1.95$ BM (per copper atom).

$Cu_4OCl_6(Haza)_4$

A solution of 7-azaindole (2.00 g, 16.9 mmol) in methanol (30 mL) was added dropwise to a hot solution of $CuCl_2 \cdot 2H_2O$ (2.88 g, 16.9 mmol) in methanol (50 mL). The green solution gradually darkened and a brown solid formed. Heating was continued for several minutes. After cooling to room temperature, the product was collected by filtration, washed with methanol, and dried *in vacuo* at room temperature. Yield: 2.90 g (73%). Anal. calcd. for $C_{28}H_{24}Cu_4Cl_6N_8O$: Cl 22.26; found: 21.65. $\mu = 1.81$ BM (per cooper atoms). Single crystals were obtained as the ethyl acetate solvate $Cu_4OCl_6(Haza)_4 \cdot 0.5C_4H_8O_2$ by recrystallization from a chloroform – ethyl acetate mixture.

Crystallographic measurements and structure determination

The crystallographic work was done with an Enraf-Nonius CAD-4 diffractometer. A set of 25 centered reflections was used to determine the reduced cell, which was checked with axial photographs. A primitive monoclinic cell was obtained for $Cu_4OCl_6(Haza)_4 \cdot 0.5C_4H_8O_2$. The systematic absences ($h0l$, $l \neq 2n$; $0k0$, $k \neq 2n$), agreed with the intensity data set, uniquely defining $P2_1/c$ as the space group. For $Cu_2Cl_4(Haza)_6$, the Niggli matrix indicated an F-centred orthorhombic cell, which agreed with the axial photographs. The systematic absences (hkl, $h + k$, $h + l$, $k + l \neq 2n$; $0kl$, $k + l \neq 4n$; $h0l$, $h + l \neq 4n$) uniquely defined its space group as $Fdd2$.

Crystal data are given in Table 1. The intensities were measured as described earlier (12). Six standard reflections were monitored for crystal decay every hour and for misorientation every 200 reflections. For $Cu_4OCl_6(Haza)_4 \cdot 0.5C_4H_8O_2$, four octans ($hkl$, $hk\bar{l}$, $h\bar{k}l$, $h\bar{k}\bar{l}$ were collected (15883 reflections). Averaging ($R_{av} = 0.041$) yielded a set of 7020 independent hkl and $hk\bar{l}$ data. For $Cu_2Cl_4(Haza)_6$, 3941 hkl and $h\bar{k}l$ reflections were measured. Averaging yielded a set of 1997 unique hkl data ($R_{av} = 0.040$). The raw data were corrected for the effects of Lorentz, polarization and absorption (Gaussian integration, grid $10 \times 10 \times 10$).

Similar strategies were applied to solve and refine both structures. Details specific to each compound are provided in the supplementary material.[3] The Cu atoms were first located from a Patterson map or direct methods. The non-hydrogen atoms were then found from ΔF maps. Full-matrix least squares were used to refine all non-hydrogen atoms isotropically. The function minimized was $\Sigma w(|F_o| - |F_c|)^2$, with individual weights w based on counting statistics. The Cl and Cu atoms were first allowed to refine anisotropically, while the remaining non-hydrogen atoms were kept isotropic. Disorder was found to occur for an azaindole ligand in $Cu_2Cl_4(Haza)_6$ (Fig. 1) and the lattice ethyl acetate molecule in $Cu_4OCl_6(Haza)_4 \cdot 0.5C_4H_8O_2$. Occupancy factors were determined at this stage and fixed for the rest of the refinement. Hydrogens were introduced at idealized positions (C—H = 0.95 Å, N—H = 0.87 Å). Their parameters were not refined, but their coordinates were recalculated after each least-squares cycle. In the last stage, anisotropic temperature factors were refined for the non-hydrogen atoms.

The scattering curves were taken from standard sources (13, 14). The anomalous dispersion terms of Cu and Cl were taken from Cromer (15). The calculations were done with NRCVAX (16), SHELX-76 (17), and local utility programs (18). The refined coordinates for the two structures are listed in Tables 2 and 3, respectively.

Result and discussion

In the absence of a good proton acceptor, the very poorly acidic N1—H proton of 7-azaindole is not expected to dissociate or to be displaced by the metal in methanol. The ligand is indeed found to behave as a typical monodentate aromatic *N*-heterocycle like pyridine. Mixing methanol solutions of $CuCl_2 \cdot 2H_2O$ and a threefold excess of azaindole at room temperature produces a dark green solution from which a good yield of light green needles of composition $CuCl_2(Haza)_2$ precipitates immediately. The compound ex-

[3]The supplementary material includes details on structure determinations, tables of refined temperature factors, hydrogen coordinates, distances and angles in the disordered azaindole rings, distances and angles for hydrogen bonds, least-squares plane calculations and structure factor amplitudes for both structures, diagrams (disordered ethyl acetate and unit cell) for $Cu_4OCl_6(Haza)_4 \cdot 0.5C_4H_8O_2$, together with a list of infrared frequencies (62 pages). Complete set of data may be purchased from: The Depository of Unpublished Data, Document Delivery, CISTI, National Research Council Canada, Ottawa, Canada K1A 0S2.

Structure resolution and refinement, Figure S-1 (disordered ethyl acetate molecule), Figure S-2 (stereoview of the unit cell), Table S-2 (idealized coordinates of the hydrogen atoms), Table S-3 (distances and angles in the azaindole ligands), Table S-4 (distances and angles for the hydrogen bonds) for $Cu_4OCl_6(Haza)_4 \cdot 0.5C_4H_8O_2$, and structure resolution and refinement, Table S-9 (idealized coordinates of the hydrogen atoms), Table S-10 (distances and angles in the azaindole ligands), Table S-11 (distances and angles for the hydrogen bonds) for $Cu_2Cl_4(Haza)_6$ have also been deposited with the Cambridge Crystallographic Data Centre and can be obtained on request from The Director, University Chemical Laboratory, 12 Union Road, Cambridge, CB2 1EZ, U.K.

Can. J. Chem. Downloaded from www.nrcresearchpress.com by 88.255.202.194 on 09/08/12
For personal use only.

TABLE 1. Crystal data and conditions for data collection

Parameter	$Cu_2Cl_4(Haza)_6$	$Cu_4OCl_6(Haza)_4 \cdot 0.5C_4H_8O_2$
Formula	$C_{42}H_{36}Cu_2Cl_4N_{12}$	$C_{30}H_{28}Cu_4Cl_6N_8O_2$
Formula weight	977.73	999.51
Crystal system	Orthorhombic	Monoclinic
Space group	*Fdd*2	$P2_1/c$
a, Å	26.5580(6)	11.661(2)
b, Å	23.750(2)	22.415(7)
c, Å	12.7271(8)	15.077(4)
α, deg	90	90
β, deg	90	109.85(2)
γ, deg	90	90
V, Å^3	8027.7	3706.7
D_{calc}, g cm^{-3}	1.618	1.791
Z	8	4
Radiation, λ (Å)	CuKᾱ, 1.54178	CuKᾱ, 1.54178
Scan technique	ω/2θ	ω/2θ
Scan range, Δω (deg)	0.80° + 0.14 tan θ	0.80° + 0.14 tan θ
Scan speed, deg (ω) min^{-1}	3.3	3.3
F(000)	3984	1992
μ, cm^{-1}	42.0	69.9
Crystal size, mm (faces)	0.25 (010–0$\bar{1}$0)	0.09 (010–0$\bar{1}$0)
	0.11 (100–$\bar{1}$00)	0.15 (100–$\bar{1}$00)
	0.32 (001–00$\bar{1}$)	0.23 (001–00$\bar{1}$)
Transmission range	0.37–0.63	0.37–0.56
2θ max, deg	140.0	140.0
No. unique reflections measured	1997	7020
No. observed reflections	1741	4573
Rejection criterion, $I/\sigma(I) <$	3.00	3.00
T, K	293	293
Residual electron density, e Å^{-3}		
General background	±0.2	±0.35
Maximum		1.3 (ethyl acetate)
R^a	0.068	0.048
$R_w{}^a$	0.066	0.054
Goodness-of-fit ratio	2.23	2.17

$^aR = \Sigma||F_o| - |F_c||/\Sigma|F_o|$, $R_w = [\Sigma w(|F_o| - |F_c|)^2/\Sigma w|F_o|^2]^{1/2}$.

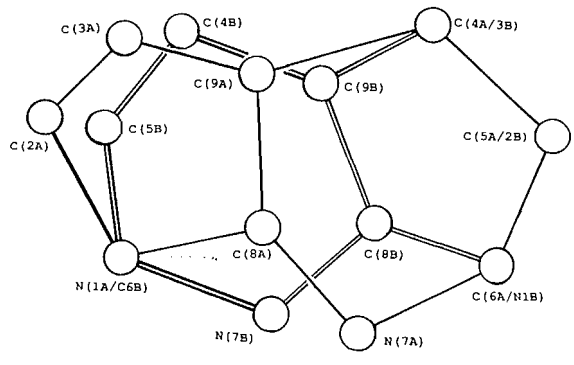

FIG. 1. Disorder of the coordinated azaindole ligand in the *trans*-$[CuCl_2(Haza)_2]$ unit of $Cu_2Cl_4(Haza)_6$ (occupancies 0.50/0.50).

hibits a normal magnetic moment of 2.02 BM. A similar green solid was isolated with imidazole (19) and found to consist of square-planar *trans*-$CuCl_2L_2$ units with one of the Cl ligands bridging the units into an infinite chain of (4 + 1)-coordinated Cu centres. The structure of $CuCl_2(Haza)_2$ was not determined, but it very likely corresponds to the same *trans*-square-planar structure, which is also found for pyridines (20–23), dimethylnaphthyridine (24) and related ligands (25).

The light green compound could also be isolated as a pure material from azaindole–$CuCl_2 \cdot 2H_2O$ mixtures with ratios between 6:1 and 1:1, provided the precipitate initially formed was filtered immediately. When attempts were made to grow single crystals by leaving the dark green filtrate of the above preparations to stand overnight in closed container at room temperature, deep green prismatic crystals were obtained instead of the needles. A quicker way to obtain the dark green prismatic solid is by boiling a 6:1 mixture. The composition of this material was shown by X-ray diffraction (see below) to be $CuCl_2(Haza)_3$, which should be formulated as $[CuCl_2(Haza)_2][Cu(Haza)_4]Cl_2$. The magnetic moment of 1.95 BM (per Cu atom) is consistent with this structure. This same compound was eventually prepared from a 3:1 ligand:metal mixture from which the fluffy precipitate initially formed was not filtered. After several hours, the precipitate had redissolved, to be replaced by the prismatic deep green solid. Interestingly, even when the reaction was carried out with four- to six-fold excess of ligand, the same $CuCl_2(Haza)_3$ compound was the only complex isolated. We were unable to obtain $[Cu(Haza)_4]Cl_2$, even though such $[CuL_4]X_2$ compounds are known with imidazoles (26–30) and pyridines (31).

Neither of the above green compounds formed when the reaction was carried out with excess copper. Under stoi-

Can. J. Chem. Downloaded from www.nrcresearchpress.com by 88.255.202.194 on 09/08/12
For personal use only.

TABLE 2. Refined coordinates ($\times 10^4$) and equivalent isotropic temperature factors ($Å^2 \times 10^3$) for $Cu_2Cl_4(Haza)_6$

Atom	x	y	z	U_{eq}
Cu(1)	2500	2500	2500	50
Cu(2)	2500	2500	7409(5)	73
Cl(1)	1647(1)	2508(2)	2387(4)	73
Cl(2)	2500	2500	4715(4)	57
Cl(3)	2500	2500	9720(3)	52
N(1A/C6B)	2960(4)	1371(4)	3474(11)	45
N(7A)[a]	2397(6)	1676(7)	2159(15)	29
C(2A)[a]	3141(13)	800(13)	3873(27)	38
C(3A)[a]	2968(11)	482(13)	3418(27)	51
C(4A/3B)	2210(6)	430(5)	1737(15)	81
C(5A/2B)	1909(5)	883(5)	1108(15)	63
C(6A/N1B)	2065(5)	1407(6)	1385(11)	70
C(8A)[a]	2614(7)	1251(9)	2701(18)	35
C(9A)[a]	2642(10)	625(10)	2698(24)	28
N(7B)[a]	2632(8)	1600(8)	2593(21)	47
C(4B)[a]	2829(14)	454(14)	3092(18)	52
C(5B)[a]	2977(14)	841(22)	3601(38)	75
C(8B)[a]	2358(8)	1234(9)	2060(18)	38
C(9B)[a]	2486(11)	664(11)	2348(25)	28
N(11)	2188(4)	1333(4)	5935(10)	51
N(17)	1976(3)	1927(3)	7457(8)	42
C(12)	2092(5)	819(5)	5531(11)	54
C(13)	1753(5)	536(4)	6249(12)	50
C(14)	1351(4)	953(4)	7918(11)	46
C(15)	1348(5)	1400(6)	8568(14)	63
C(16)	1652(5)	1891(6)	8317(10)	62
C(18)	1920(4)	1419(4)	6852(9)	34
C(19)	1653(4)	988(4)	7086(10)	40
N(21)	2794(4)	1370(4)	8837(9)	42
N(27)	3058(3)	1866(3)	7370(9)	45
C(22)	2924(4)	807(5)	9189(11)	51
C(23)	3225(4)	584(5)	8587(14)	56
C(24)	3631(5)	942(6)	6811(12)	67
C(25)	3651(4)	1449(5)	6258(11)	52
C(26)	3342(4)	1868(4)	6526(10)	46
C(28)	3033(4)	1450(4)	7946(9)	38
C(29)	3342(4)	898(3)	7733(11)	38

[a]Occupancy factor: 0.50.

TABLE 3. Refined coordinates (10^4, Cu, Cl $\times 10^5$) and equivalent isotropic temperature factors ($Å^2 \times 10^3$) for $Cu_4OCl_6(Haza)_4 \cdot 0.5C_4H_8O_2$

Atom	x	y	z	U_{eq}
Cu(1)	37970(9)	22611(4)	23637(7)	38
Cu(2)	52984(8)	32432(4)	17527(7)	33
Cu(3)	36198(9)	35823(4)	29313(7)	35
Cu(4)	25325(9)	31857(5)	7690(7)	43
Cl(1)	55585(18)	21703(7)	19236(14)	53
Cl(2)	40267(15)	36453(7)	2812(12)	42
Cl(3)	35728(19)	26690(7)	37241(13)	52
Cl(4)	19867(15)	40365(8)	17481(13)	47
Cl(5)	56814(16)	39143(8)	30441(13)	46
Cl(6)	18511(18)	22484(9)	10347(15)	63
O(1)	3802(4)	3070(2)	1963(3)	29
N(11)	5960(6)	1271(3)	3589(5)	55
C(12)	6679(9)	799(4)	4053(7)	75
C(13)	5956(11)	320(4)	4064(7)	81
C(14)	3633(10)	231(3)	3392(7)	71
C(15)	2614(9)	563(4)	2934(7)	69
C(16)	2709(7)	1146(3)	2655(6)	55
N(17)	3789(6)	1425(2)	2813(4)	44
C(18)	4781(7)	1091(3)	3299(5)	44
C(19)	4753(9)	495(3)	3599(6)	55
N(21)	6313(6)	2658(3)	185(5)	52
C(22)	6914(9)	2417(4)	−373(6)	68
C(23)	8068(9)	2626(4)	−105(7)	75
C(24)	9116(8)	3374(4)	1216(7)	74
C(25)	8894(7)	3706(4)	1897(7)	69
C(26)	7778(7)	3675(3)	2037(6)	53
N(27)	6854(5)	3335(2)	1505(4)	38
C(28)	7083(7)	3027(3)	823(5)	45
C(29)	8209(7)	3020(4)	647(7)	58
N(31)	3789(6)	5026(2)	3253(4)	48
C(32)	3788(8)	5618(3)	3496(7)	62
C(33)	3578(7)	5684(3)	4307(6)	53
C(34)	3181(8)	4851(4)	5368(6)	62
C(35)	3083(9)	4242(4)	5395(6)	73
C(36)	3226(8)	3891(3)	4698(6)	54
N(37)	3455(5)	4107(2)	3945(4)	40
C(38)	3541(6)	4697(3)	3918(5)	38
C(39)	3405(6)	5102(3)	4607(5)	42
N(41)	1023(6)	4353(3)	−408(5)	58
C(42)	289(9)	4770(4)	−1014(7)	68
C(43)	−453(9)	4516(5)	−1799(7)	79
C(44)	−632(9)	3402(5)	−2268(7)	89
C(45)	−143(11)	2865(5)	−1951(7)	97
C(46)	762(8)	2813(4)	−1069(6)	63
N(47)	1190(5)	3292(3)	−483(5)	55
C(48)	738(7)	3815(3)	−819(6)	52
C(49)	−229(8)	3908(5)	−1729(6)	65
O(1)[a]	108(10)	−276(5)	1008(9)	70
C(1)[a]	882(18)	−1170(8)	281(14)	86
C(2)[a]	267(32)	−496(12)	338(22)	246
O(2/C3)	179(14)	223(7)	837(11)	74
C(4)[a]	−303(30)	794(10)	582(24)	197

[a]Occupancy factor: 0.50.

chiometric conditions, a brown solid shown to be the tetranuclear cluster $Cu_4OCl_6(Haza)_4$ (see X-ray work below) was isolated when a hot solution of the ligand was slowly added to a hot solution of $CuCl_2 \cdot 2H_2O$. Fast addition of mixing in the opposite order resulted in immediate formation of some light green $CuCl_2(Haza)_2$ material. The magnetic moment (1.81 BM per Cu atom) similar to those found for this type of cluster (32) indicates that the copper atoms are not appreciably coupled. The central μ_4-oxide ligand undoubtedly originates from the relatively large amount of water introduced via the $CuCl_2 \cdot 2H_2O$ reactant, the two expelled protons being quenched by azaindole molecules (pK_a of $H_2aza^+ = 4.6$) (33). Infrared bands characteristic of the azaindolium ion are found in the spectrum of the residue obtained from filtrate evaporation.

Crystal structure of $Cu_2Cl_4(Haza)_6$

Two features commonly encountered in Cu(II) complexes (34) are observed in this crystal structure: (*1*) the primary coordination of the metal consists of four strong bonds in an roughly square-planar arrangement; and (*2*) one or two weaker axial bonds with halogen atoms belonging to adjacent units provide bridging interactions between the square planes, resulting in square-pyramidal (4 + 1) or elongated octahedral (4 + 2) overall coordinations.

The asymmetric unit includes two symmetry-independent copper atoms, both lying on a crystallographic twofold axis and belonging to square-planar *trans*-$[CuCl_2(Haza)_2]$ and $[Cu(Haza)_4]^{2+}$ species, respectively (Fig. 2). The azaindole

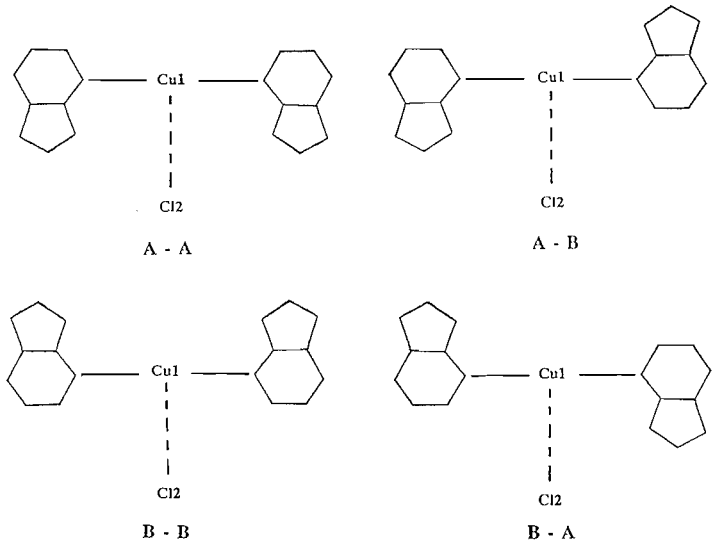

SCHEME 2

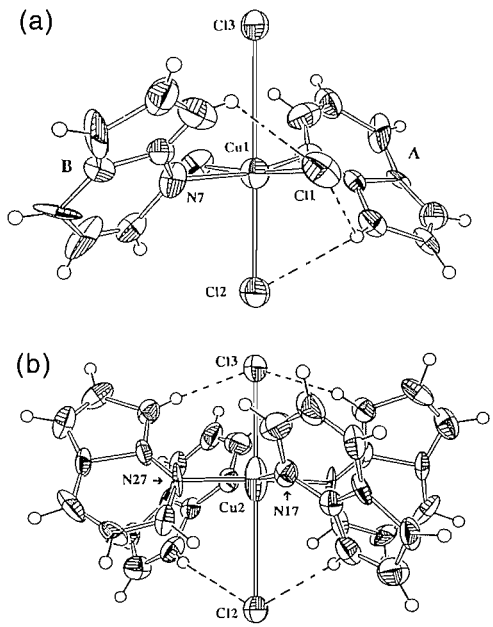

FIG. 2. Coordination of the metal atoms in $Cu_2Cl_4(Haza)_6$. (*a*) $CuCl_2(Haza)_2$ unit formed by Cu(1) and (*b*) $[Cu(Haza)_4]^{2+}$ ion formed by Cu(2). In $CuCl_2(Haza)_2$, the azaindole ligands are disordered over two orientations A and B (see text). About both Cu atoms, longer apical Cu···Cl bonds are formed with bridging Cl(2) and Cl(3) ions. Thermal ellipsoids correspond to 50% probability. Hydrogens are shown as spheres of arbitrary size. Dashed lines represent hydrogen bonds.

ligands are all formally neutral and coordinated to copper via N7. The square planes, roughly perpendicular to the twofold axis, are bridged by chloride ions lying on the same axis, which complete an overall (4 + 2)-coordination about the metal. Selected interatomic distances and bond angles are listed in Table 4.

(a) Environment of Cu(1): trans-*[$CuCl_2(Haza)_2$]*

The azaindole ligand is involved in a twofold disorder (Fig. 1) leading to two equally populated orientations of the five-membered ring with respect to the coordination plane: labels A and B (Fig. 2*a*) correspond to five-membered rings pointing toward Cl(2) and away from Cl(2), respectively. The crystallographic results are consistent with the presence of four possible combinations of these two orientations, namely A–A, B–B, A–B, and B–A (Scheme 2), which all possess a roughly square-planar *trans*-$CuCl_2N_2$ coordination. The B–A/A–B pair actually corresponds to the same molecule rotated by 180° about the Cu(1)–Cl(2) direction (crystallographic twofold axis). As chlorine is not disordered, the Cl(1)—Cu(1)—Cl(1) is 172.7(1)° in all cases. The N7 donor atoms are not coincident in A and B, so that different patterns of distances and angles are obtained around Cu(1) (Table 5). Departure from planarity is large and the bond angles deviate very significant from ideality. We tend to prefer the A–B/B–A structure, because all molecules would then show a small square-pyramidal distortion displacing Cu(1) by 0.121 Å toward the relatively close Cl(2) bridging atom. Also, the A–B/B–A molecule is statistically twice as probable as either A–A or B–B.

The ORTEP drawing (Fig. 2*a*) shows an A–B molecule. The Cu(1)—Cl(1) distance (2.270(2) Å) (Table 4) compares well with those reported for *trans*-$CuCl_2N_2$ molecules with 2,3- and 2,6-dimethylpyridine (2.254(2) and 2.264(2) Å, respectively), where the chlorines do not participate in bridging (20, 21). Because of the disorder, the Cu(1)—N7 bond lengths are less reliable. The Cu(1)—N(7A) distance (2.02(2) Å) is similar to those found in analogous complexes with related ligands (19–22, 24). The long Cu(1)—N(7B) distance is undoubtedly an artifact due to disorder. Individual distances and angles for the disordered Haza ligand are listed in the supplementary material.

(b) Environment of Cu(2): $[Cu(Haza)_4]^{2+}$ (Fig. 2b)

The Cu—N bonds in the square plane (mean 2.030 Å) are comparable with those stated above and they lie in the range (1.98–2.05 Å) found for imidazole complexes (26, 35, 36) containing CuN_4 units. The N—Cu—N *cis* bond angles are essentially equal to the ideal 90° value for a square-planar geometry. The *trans* angles (176.4(4), 177.3(4)°) show significant, but small, departure from 180°, indicating a

Can. J. Chem. Downloaded from www.nrcresearchpress.com by 88.255.202.194 on 09/08/12
For personal use only.

TABLE 4. Selected interatomic distances and bond angles in $Cu_2Cl_4(Haza)_6$

Atoms	Distance (Å)	Atoms	Distance (Å)
Cu(1)—Cl(1)	2.270(2)	Cu(2)—Cl(2)	3.429(8)
Cu(1)—Cl(2)	2.819(5)	Cu(2)—Cl(3)	2.941(8)
Cu(1)—Cl(3)	3.538(4)	Cu(2)—N(17)	1.947(8)
Cu(1)—N(7A)	2.023(18)	Cu(2)—N(27)	2.113(8)
Cu(1)—N(7B)	2.169(20)		
Bonds	**Angle (deg)**	**Bonds**	**Angle (deg)**
Cl(1)—Cu(1)—Cl(2)	93.63(12)	Cl(3)—Cu(1)—N(7B)	93.1(6)
Cl(1)—Cu(1)—Cl(3)	86.37(11)	N(7A)—Cu(1)—N(7A)[a]	155.2(7)
Cl(1)—Cu(1)—N(7A)	81.9(5)	N(7A)—Cu(1)—N(7B)[a]	160.6(8)
Cl(1)—Cu(1)—N(7B)	100.0(6)	N(7B)—Cu(1)—N(7B)[a]	173.7(9)
Cl(1)—Cu(1)—Cl(1)[a]	172.74(14)	Cl(2)—Cu(2)—Cl(3)	180.0
Cl(1)—Cu(1)—N(7A)[a]	96.5(5)	Cl(2)—Cu(2)—N(17)	91.8(3)
Cl(1)—Cu(1)—N(7B)[a]	80.4(6)	Cl(2)—Cu(2)—N(27)	88.7(3)
Cl(2)—Cu(1)—Cl(3)	180.0	Cl(3)—Cu(2)—N(17)	88.2(3)
Cl(2)—Cu(1)—N(7A)	102.4(5)	Cl(3)—Cu(2)—N(27)	91.4(3)
Cl(2)—Cu(1)—N(7B)	86.9(6)	N(17)—Cu(2)—N(27)	90.2(4)
Cl(3)—Cu(1)—N(7A)	77.6(5)	N(17)—Cu(2)—N(17)[a]	176.4(4)
N(17)—Cu(2)—N(27)[a]	89.9(4)	N(27)—Cu(2)—N(27)[a]	177.3(4)
Cu(2)—N(17)—C(16)	120.6(8)	Cu(2)—N(27)—C(26)	114.8(8)
Cu(2)—N(17)—C(18)	130.0(7)	Cu(2)—N(27)—C(28)	121.3(8)

[a] $1/2 - x, 1/2 - y, z$.

TABLE 5. Geometry of the three possible *trans*-$CuCl_2N_2$ molecules consistent with the disorder

Bonds	Angle (deg) A–A	Angle (deg) B–B	Angle (deg) A–B/B–A
Cl(1)—Cu(1)—Cl(1)[a]	172.74(14)	172.74(14)	172.74(14)
N(7)—Cu(1)—N(7)	155.2(7)	173.7(9)	160.6(8)
Cl(1)—Cu(1)—N(7)	81.9(5)	100.0(6)	81.9(6)
N(7)—Cu(1)—Cl(1)[a]	96.5(5)	80.4(6)	100.0(6)
Cl(1)[a]—Cu(1)—N(7)[a]	81.9(5)	100.0(6)	80.4(6)
N(7)[a]—Cu(1)—Cl(1)	96.5(5)	80.4(6)	96.5(5)

Atom	Distance (Å) to the $CuCl_2N_2$ plane A–A	B–B	A–B/B–A
Cu(1)	−0.231	−0.010	−0.121
Cl(1)	−0.087(5)	0.134(5)	0.009(5)
Cl(1)[a]	−0.087(5)	0.134(5)	0.009(5)
N(7)	0.203(19)	−0.129(27)	0.047(19)
N(7)[a]	0.203(19)	−0.129(27)	0.044(27)
Cl(2)	−3.050(5)	−2.829(5)	−2.915(5)
Cl(3)[a]	3.307(4)	3.528(4)	3.386(4)

[a] $1/2 - x, 1/2 - y, z$.

small tetrahedral distortion. The atom-to-plane distances are as follows: Cu(2), 0.003(7); N(17), −0.058(10); N(27), 0.053(11) Å.

The bond lengths for the two independent azaindole ligands in the $[Cu(Haza)_4]^{2+}$ moieties (supplementary material) show differences greater than the experimental error. Appreciable differences are also noted with respect to the free ligand (1) or other N7-bonded complexes (9, 10). This suggests that some disorder, milder than above, might be present in this case as well, in spite of the fact that it has not been possible to identify resolved atomic positions.

(c) Molecular packing

A view of an *ac* layer of the unit cell is given in Fig. 3. The ···Cl(3)···Cu(1)···Cl(2)···Cu(2)···Cl(3)··· chain is perfectly linear, all atoms lying on the crystallographic twofold axis. The CuN_4 and $CuCl_2N_2$ planes are roughly perpendicular to this chain and occur in alternance. They are bridged by Cl^- ions, but bridging is highly dissymmetric. Cl(2) forms a normal "semi-bond" of 2.819(5) Å with Cu(1), but its contact with Cu(2) is very long (3.429(8) Å). Similarly, Cl(3) is more strongly bonded to Cu(2) (2.941(8) Å) than to Cu(1) (3.538(4) Å). Similar features have been encountered in various alkylammonium salts of chlorocopper(II) anions containing linear Cu···Cl···Cu bridging units (37). Thus, although each Cu atom is surrounded by six neighbours in an octahedral arrangement, a square-pyramidal (4 + 1)-coordination including only one axial chlorine would be a more appropriate description from the electronic point of view.

All azaindole N1—H protons are hydrogen bonded to Cl atoms.[3] If the ligands were in the $CuCl_2N_2$ plane, extremely short H1···Cl(1) distances would result. This strain is relieved by rotating the ligand ~45° around the Cu—N7 bond, leading to a reasonably strong N1—H···Cl(1) hydrogen bond (N···Cl = 3.177(12) Å for A, 3.114(15) Å for B) (38). In this orientation, weaker hydrogen bonding can simultaneously take place with an apical chloride ion: N1···Cl(2) = 3.343(12) Å for ligands A, N1···Cl(3) = 3.545(14) Å for ligands B. In the $[Cu(Haza)_4]^{2+}$ unit, the ligands make angles of ~58° with the coordination plane. Two of these ligands form hydrogen bonds of 3.283(11) Å with Cl(2) on one side of the square plane, whereas the other two interact with Cl(3) at 3.013(10) Å on the other side.

This compound presents two unusual features: the chain is built up from two types of Cu(II) species and the ···Cl···Cu(1)···Cl···Cu(2)···Cl··· backbone is perfectly linear. These peculiarities can be regarded as a conse-

Can. J. Chem. Downloaded from www.nrcresearchpress.com by 88.255.202.194 on 09/08/12
For personal use only.

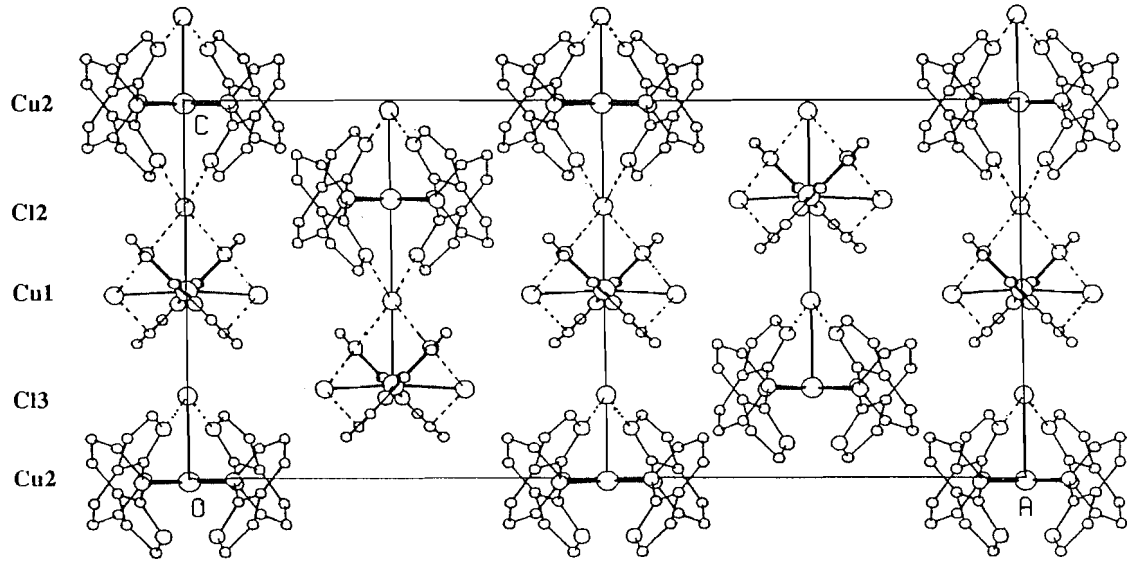

FIG. 3. View of a layer of the unit cell of $Cu_2Cl_4(Haza)_6$ down the *b* axis (thickness *b*/2). The Cu atoms and bridging Cl ions lie on crystallographic twofold axes. The labels on the left hand side refer to the Cl and Cu atoms on the *c* axis. The square planes around copper are perpendicular to these axes and seen edgewise in the figure. Hydrogen bonds are shown as dashed lines.

quence of the roughly parallel orientation of the N7 lone pair with the N1—H bond, which restricts the hydrogen bonding capability of coordinated azaindole to the regions just above and below the coordination plane. Figure 3 indeed shows that hydrogen bonding occurs only inside the chains, all inter-chain interactions consisting of normal van der Waals contacts. The ligands in the $[Cu(Haza)_4]^{2+}$ unit can rotate about the Cu—N7 bond so as to make efficient hydrogen bonds with chloride ions forming the apical Cu···Cl semi-bonds with the metal. This takes place without appreciably disturbing the Cu—N7 bond, the difference between the C6—N7—Cu(2) and C8—N7—Cu(2) angles remaining below 10° (Table 4). Other heterocyclic ligands like pyridine or imidazoles would be unable to give a similar stabilizing effect. Steric crowding would even destabilize the system with α-alkylated imidazoles and pyridines, or with a two-ring system like benzimidazole, which are devoid of properly oriented hydrogen-bond donors. In contrast, in the $[Cu(Haza)_4]^{2+}$ unit, two of the rings are rotated above the square plane and two are rotated below, thereby stabilizing a chloride ion on each side of the plane. The chain can then be propagated by approaching extra square planar species at each end of this ···Cl···$[Cu(Haza)_4]$···Cl··· nucleus, since the terminal Cl^- ions are not sterically crowded. However, if the stoichiometry were $[Cu(Haza)_4]Cl_2$, only half of the Cl^- ions could be part of such a chain, so that the remaining ions would have to sit elsewhere in the unit cell, where they would have to interact via van der Waals contacts with hydrophobic regions of azaindole in the outer part of the chain. In the present compound, a neutral $[CuCl_2(Haza)_2]$ unit is inserted between ···Cl···$Cu(Haza)_4$···Cl··· segments, allowing the system to use the residual basicity of the sterically accessible Cl^- ions to fill the apical positions of the $[CuCl_2(Haza)_2]$ unit and favour chain propagation. This could explain the unusual stoichiometry found for this deep green complex and the fact that the $[Cu(Haza)_4]Cl_2$ salt known with other ligands could not be obtained.

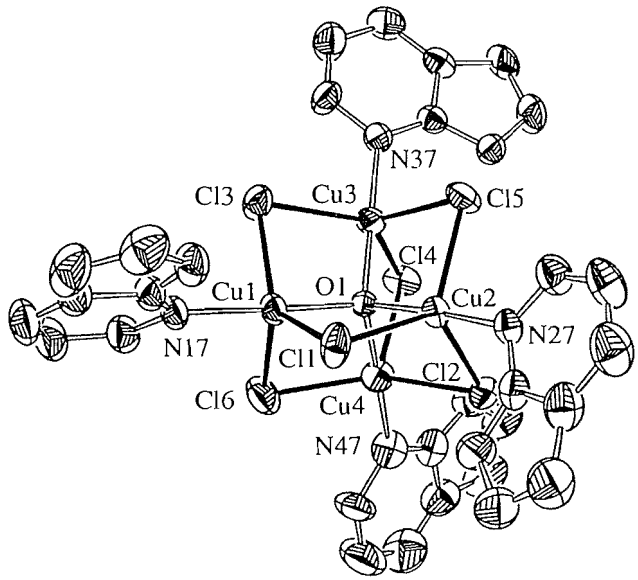

FIG. 4. ORTEP drawing of the $Cu_4OCl_6(Haza)_4$ molecule. Thermal ellipsoids correspond to 50% probability. Hydrogens are omitted for clarity.

Crystal structure of $Cu_4OCl_6(Haza)_4 \cdot 0.5C_4H_8O_2$

The molecule contains the Cu_4OCl_6 core consisting of a μ_4-oxygen atom coordinated tetrahedrally to four Cu atoms, which are bridged in pairs by six chlorine atoms (Fig. 4). A trigonal-bipyramidal coordination about each of these four Cu atoms is completed by 7-azaindole ligands bonded via the N7 lone pair. Disordered ethyl acetate molecules not bonded to the cluster are also present (Fig. S-1).[3] Selected distances and angles are listed in Table 6.

Structural results are available for similar clusters containing pyridines (32, 39), imidazoles (40–42) and other ligands (40, 43–45). Norman and co-workers (40) have

Can. J. Chem. Downloaded from www.nrcresearchpress.com by 88.255.202.194 on 09/08/12
For personal use only.

TABLE 6. Interatomic distances and bond angles in $Cu_4OCl_6(Haza)_4 \cdot 0.5C_4H_8O_2$

Atoms	Distance (Å)	Atoms	Distance (Å)
Cu(1)—Cl(1)	2.372(3)	Cu(3)—Cl(3)	2.381(2)
Cu(1)—Cl(3)	2.340(2)	Cu(3)—Cl(4)	2.353(2)
Cu(1)—Cl(6)	2.465(2)	Cu(3)—Cl(5)	2.467(2)
Cu(1)—O(1)	1.912(4)	Cu(3)—O(1)	1.925(4)
Cu(1)—N(17)	1.994(6)	Cu(3)—N(37)	1.989(6)
Cu(2)—Cl(1)	2.427(2)	Cu(4)—Cl(2)	2.347(2)
Cu(2)—Cl(2)	2.387(2)	Cu(4)—Cl(4)	2.619(2)
Cu(2)—Cl(5)	2.380(2)	Cu(4)—Cl(6)	2.329(2)
Cu(2)—O(1)	1.916(5)	Cu(4)—O(1)	1.921(4)
Cu(2)—N(27)	1.983(6)	Cu(4)—N(47)	2.016(7)
Bonds	**Angle (deg)**	**Bonds**	**Angle (deg)**
Cl(1)—Cu(1)—Cl(3)	130.08(8)	Cl(3)—Cu(3)—Cl(4)	127.01(8)
Cl(1)—Cu(1)—Cl(6)	114.66(8)	Cl(3)—Cu(3)—Cl(5)	114.39(8)
Cl(1)—Cu(1)—O(1)	84.1(1)	Cl(3)—Cu(3)—O(1)	84.0(1)
Cl(1)—Cu(1)—N(17)	96.8(2)	Cl(3)—Cu(3)—N(37)	95.6(2)
Cl(3)—Cu(1)—Cl(6)	111.78(8)	Cl(4)—Cu(3)—Cl(5)	116.14(7)
Cl(3)—Cu(1)—O(1)	85.4(1)	Cl(4)—Cu(3)—O(1)	87.3(1)
Cl(3)—Cu(1)—N(17)	93.1(2)	Cl(4)—Cu(3)—N(37)	93.6(2)
Cl(6)—Cu(1)—O(1)	81.7(1)	Cl(5)—Cu(3)—O(1)	82.9(1)
Cl(6)—Cu(1)—N(17)	99.0(2)	Cl(5)—Cu(3)—N(37)	96.6(2)
O(1)—Cu(1)—N(17)	178.5(2)	O(1)—Cu(3)—N(37)	179.1(2)
Cu(1)—N(17)—C(16)	119.1(5)	Cu(3)—N(37)—C(36)	122.4(5)
Cu(1)—N(17)—C(18)	126.7(5)	Cu(3)—N(37)—C(38)	122.5(5)
Cl(1)—Cu(2)—Cl(2)	119.25(7)	Cl(2)—Cu(4)—Cl(4)	101.85(7)
Cl(1)—Cu(2)—Cl(5)	123.89(8)	Cl(2)—Cu(4)—Cl(6)	141.53(8)
Cl(1)—Cu(2)—O(1)	82.5(1)	Cl(2)—Cu(4)—O(1)	86.3(1)
Cl(1)—Cu(2)—N(27)	91.9(2)	Cl(2)—Cu(4)—N(47)	94.5(2)
Cl(2)—Cu(2)—Cl(5)	113.99(7)	Cl(4)—Cu(4)—Cl(6)	113.43(8)
Cl(2)—Cu(2)—O(1)	85.2(1)	Cl(4)—Cu(4)—O(1)	80.1(1)
Cl(2)—Cu(2)—N(27)	96.0(2)	Cl(4)—Cu(4)—N(47)	100.5(2)
Cl(5)—Cu(2)—O(1)	85.5(1)	Cl(6)—Cu(4)—O(1)	85.2(1)
Cl(5)—Cu(2)—N(27)	99.2(2)	Cl(6)—Cu(4)—N(47)	93.8(2)
O(1)—Cu(2)—N(27)	174.2(2)	O(1)—Cu(4)—N(47)	179.0(2)
Cu(2)—N(27)—C(26)	123.2(5)	Cu(4)—N(47)—C(46)	120.5(5)
Cu(2)—N(27)—C(28)	121.7(5)	Cu(4)—N(47)—C(48)	123.3(6)
Cu(1)—Cl(1)—Cu(2)	81.71(7)	Cu(1)—O(1)—Cu(2)	110.2(2)
Cu(2)—Cl(2)—Cu(4)	80.56(6)	Cu(1)—O(1)—Cu(3)	108.3(2)
Cu(1)—Cl(3)—Cu(3)	82.38(7)	Cu(1)—O(1)—Cu(4)	109.9(2)
Cu(3)—Cl(4)—Cu(4)	79.82(6)	Cu(2)—O(1)—Cu(3)	110.2(2)
Cu(2)—Cl(5)—Cu(3)	81.09(7)	Cu(2)—O(1)—Cu(4)	105.8(2)
Cu(1)—Cl(6)—Cu(4)	81.70(8)	Cu(3)—O(1)—Cu(4)	112.5(2)

collected these data and noted that the geometry of the Cu_4O tetrahedron is relatively constant. The departure from tetrahedral geometry about oxygen is usually small: the O—Cu—O angles have been found to lie in the range 106.3–115.8°, with a mean value of 109.4°. Our Cu—O—Cu angles (105.8(2)–112.5(2)°, mean 109.5°) fit well with these earlier results. The Cu—O bond lengths are not very sensitive to the external ligand present: our results (1.912(4)–1.925(4) Å, mean 1.918 Å) are in good agreement with the literature (1.869–1.939 Å, mean 1.908 Å) (40). The Cu—N bond lengths show greater variation. Our distances (1.983(6)–2.016(7) Å, mean 1.998(6) Å) suggest that azaindole has steric requirements similar to pyridines (mean 1.98 Å) (32, 39) and greater than imidazoles (mean 1.94 Å) (40, 41).

The coordination of copper is best described as a distorted trigonal bipyramid. The O—Cu—N angles (174.2(2)–179.1(2)°) are close to the ideal 180° value. As found for similar molecules (40), the O—Cu—Cl angles (mean 84.2°) are ~10° less than the N—Cu—Cl angles (mean 95.9°). Thus, the Cu atom is displaced ~0.24 Å from the plane of the three Cl atoms, toward N7. Angular distortions in the equatorial plane are large. The Cu—Cl distances and Cl—Cu—Cl angles can vary over a broad range in such systems (40). Around Cu(1), Cu(2), and Cu(3), the Cl—Cu—Cl angles range from 111.8(1) to 130.1(1)° (mean 119.0°), whereas the Cu—Cl distances are found between 2.340(2) and 2.467(2) Å (mean 2.397 Å). Such variations can be regarded as normal for this type of framework. In contrast, the more severe distortions around Cu(4) are somewhat unusual. The Cl(2)—Cu(4)—Cl(6) angle (141.5(1)°) is much larger, although not quite as large as some of those found in Cu_4OCl_6(2-methylpyridine)$_4$ (32), where the metal coordination has been described as intermediate between a trigonal bipyramid and a square pyramid. The less regular environment of Cu(4) also includes an unusually long Cu(4)—Cl(4) bond of 2.619(2) Å, almost as long as the

Can. J. Chem. Downloaded from www.nrcresearchpress.com by 88.255.202.194 on 09/08/12
For personal use only.

Can. J. Chem. Downloaded from www.nrcresearchpress.com by 88.255.202.194 on 09/08/12
For personal use only.

2.679(8) Å bond found in the 2-methylpyridine complex. In spite of this long bond, the mean Cu—Cl distance (2.432 Å) about Cu(4) is not much greater than about the three other Cu atoms, since one of the bonds to Cu(4) (2.329(2) Å) is the shortest in the structure. Large distortions in similar clusters have been ascribed to packing effects (39, 40) and they probably have the same origin here (see below).

The geometry of the four non-equivalent azaindole ligands (see supplementary material) is normal (1, 9, 10). If coordination took place exactly along the lone pair direction, the metal would lie in the plane of the ligand and the two Cu—N7—C angles would be equal. The copper-to-plane distances are relatively small (Cu(1), 0.042(1) Å; Cu(2), 0.175(1) Å; Cu(3), 0.046(1) Å; Cu(4), 0.024(1) Å), whereas the maximum in-plane distortion corresponds to 3.8° (ligand 1).

Coordination of azaindole to the axial site of the trigonal bipyramid places the N1—H bond in a suitable orientation to form hydrogen bonds with the equatorial Cl atoms. Five of the six Cl atoms participate in such intramolecular interactions.[3] Ligands 1 and 4 each form one moderately strong (38) hydrogen bond (N···Cl < 3.13 Å) with a single chlorine. This corresponds to relatively small N(11)—N(17)—Cu(1)—Cl(1) and N(41)—N(47)—Cu(4)—Cl(4) torsion angles of 39.1(3) and 33.7(3)°, respectively. For ligands 2 and 3, the torsion angles are close to 60°, so that the N—H bonds are roughly equidistant from two chlorines, with which they form bifurcated hydrogen bonds.

A packing pattern is given in Figure S-2.[3] The molecules are held in the crystal mainly by normal van der Waals contacts. Contribution from hydrogen bonding is restricted to the N(21)—H···Cl(3) bond of 3.289(7) Å. The cavity occupied by the ethyl acetate molecule is delimited by azaindole rings and Cl(6) atoms of various cluster molecules. It is probably to make room for the solvent that Cl(6) is the only chlorine not participating in hydrogen bonding and this part of the cluster is distorted. Also, since the ethyl acetate molecule is disordered, it possibly induces minor disorder in the Cu(4)—Cl(6) region, leading to greater temperature factors for these atoms.

Infrared spectra of the azaindole complexes

The infrared spectrum of 7-azaindole has been discussed elsewhere (2, 7). A list of frequencies and tentative assignments is provided in the supplementary material. Since the state of protonation is not changed, the spectra of the complexes are not drastically different. Various shifts are noted in the 1600–1400 cm^{-1} region of the ring stretching modes. The best diagnostic for coordination to netural azaindole via N7 is provided by the well-defined ring out-of-plane vibrations at 428/419 cm^{-1}, which are replaced in the complexes by a weak component at 449 cm^{-1} and a stronger band at ~434 cm^{-1}.

The complexes can be differentiated from the 700–800 cm^{-1} region: 789/762/715 cm^{-1} for Haza, 781/746/699 cm^{-1} for $CuCl_2(Haza)_2$, 794/781/735/711/701 cm^{-1} for $Cu_2Cl_4(Haza)_6$, and 799/786/723 cm^{-1} for $Cu_4OCl_6(Haza)_4$. Differences in hydrogen bonding also introduce noticeable spectral variations for N1—H bands. The strong multi-component ν(N—H) region (2300–3200 cm^{-1}) of free Haza is replaced in $CuCl_2(Haza)_2$ by a better defined strong band at 3330 cm^{-1}. The weak N1—H out-of-plane bending band, observed near 850 cm^{-1} in the free ligand, shifts to 530 cm^{-1} and becomes much stronger in the complex. These displacements are indicative of weaker hydrogen bonding than in the free ligand. The same effect has been noted for azaindole adducts of $TaCl_5$ and $NbCl_5$ (46). For the N1—D derivatives, obtained by dissolution in CD_3OD, these N—H vibrations are shifted down to 2490 and 400 cm^{-1}, respectively, as expected. The greater number of independent ligands in $Cu_2Cl_4(Haza)_6$ leads to extra components at 3200 and 3145 cm^{-1}. For $Cu_4OCl_6(Haza)_4$, the ν(N—H) band occurs at 3110 cm^{-1}, but the γ(N—H) band expected at 530 cm^{-1} is masked by a metal-centered band (see below).

The ligand shows no vibrations in the 240–400 cm^{-1} range. The single broad band of medium intensity observed at 289 cm^{-1} for $CuCl_2(Haza)_2$ and $Cu_2Cl_4(Haza)_6$ originates from Cu–ligand motion, but it cannot be safely assigned. A strong ν(Cu—N) band has been found at this frequency for $[CuL_4]^{2+}$ species with pyridines (47) and imidazoles (27–30, 47, 48). For various $CuCl_2L_2$ compounds with the same ligands, the ν(Cu—N) and ν(Cu—Cl) bands are believed to occur in the same region (28–30, 49, 50). Our band at 289 cm^{-1} probably includes both vibrations. The low-frequency region also exhibits a band at ~230 cm^{-1}, mentioned for many similar systems. There is no consensus concerning its assignment, but it undoubtedly originates from a metal-centered mode. $Cu_4OCl_6(Haza)_4$ produces a new strong band at 558 cm^{-1}, observed for other clusters containing the Cu_4O core (32, 45, 51) and assigned to Cu—O stretching. The 289 cm^{-1} band mentioned above seems to have shifted down to ~250 cm^{-1}, where three components are observed at 263, 249, and 239 cm^{-1}. A similar pattern has been noticed for the 2-methylpyridine cluster (32) and assigned to general M-ligand stretching. It probably correspond mainly to Cu—N motion, since the comparison of a pair of analogous chloro and bromo compounds (45) identified the 225 cm^{-1} band as due to cluster ν(Cu—Cl) vibration.

Acknowledgments

We wish to thank M. Leduc for preparing the compounds, and M. Simard and F. Bélanger-Gariépy for their assistance in solving the X-ray structures. The support of the Natural Sciences and Engineering Research Council of Canada is gratefully acknowledged.

1. P. Dufour, Y. Dartiguenave, M. Dartiguenave, N. Dufour, A. M. Lebuis, F. Bélanger-Gariépy, and A. L. Beauchamp. Can. J. Chem. **68**, 193 (1990).
2. N. Dufour, A. M. Lebuis, M. C. Corbeil, A. L. Beauchamp, P. Dufour, Y. Dartiguenave, and M. Dartiguenave. Can. J. Chem. In press.
3. S. M. Peng and Y. N. Lin. Acta Crystallogr. Sect. C: Cryst. Struct. Commun. C**42**, 1725 (1986).
4. S. M. Peng and C. H. Lai. J. Chin. Chem. Soc. Taipei, **35**, 325 (1988).
5. R. W. Brookes and R. L. Martin. Aust. J. Chem. **27**, 1569 (1974).
6. J. J. H. Edema, S. Gambarotta, A. Meetsma, F. van Bolhuis, A. L. Spek, and W. J. J. Smeets. Inorg. Chem., **29**, 2147 (1990).
7. F. Allaire and A. L. Beauchamp. Inorg. Chim. Acta, **156**, 241 (1989).
8. F. A. Cotton, D. G. Lay, and M. Millar. Inorg. Chem. **17**, 186 (1978).
9. W. S. Sheldrick. Z. Naturforsch. **37B**, 653 (1982).

10. F. A. Cotton and T. R. Felthouse. Inorg. Chem. **20**, 600 (1981).
11. R. S. Drago. Physical methods in chemistry. Saunders, Philadelphia. 1977. p. 413.
12. F. Bélanger-Gariépy and A. L. Beauchamp. J. Am. Chem. Soc. **102**, 3461 (1980).
13. International tables for X-ray crystallography Vol. III. Kynoch Press, Birmingham, England. 1968.
14. D. T. Cromer and J. T. Waber. Acta Crystallogr. **18**, 104 (1965); R. F. Stewart, E. R. Davidson, and W. T. Simpson. J. Chem. Phys. **42**, 3175 (1965).
15. D. T. Cromer. Acta Crystallogr. **18**, 17 (1965).
16. E. J. Gabe, Y. Le Page, J. P. Charland, and F. L. Lee. J. Appl. Crystallogr. **22**, 384 (1989).
17. G. Sheldrick. SHELX-76, Crystallographic Program System. Cambridge University, U.K. 1976.
18. M. Authier-Martin and A. L. Beauchamp. Can. J. Chem. **55**, 1213 (1977).
19. B. K. S. Lundberg. Acta Chem. Scand. **26**, 3977 (1972).
20. W. Stählin and H. R. Oswald. Acta Crystallogr. Sect. B: Struct. Crystallogr. Cryst. Chem. B**27**, 1368 (1971).
21. J. A. Campbell, C. L. Raston, J. N. Varghese, and A. H. White. Aust. J. Chem. **30**, 1947 (1977).
22. W. E. Marsh, E. J. Valente, and D. J. Hodgson. Inorg. Chim. Acta, **51**, 49 (1981).
23. B. Morosin. Acta Crystallogr. Sect. B: Struct. Crystallogr. Cryst. Chem. B**31**, 632 (1975); W. E. Marsh, W. E. Hatfield, and D. J. Hodgson. Inorg. Chem. **21**, 2679 (1982); M. Laing and E. Horsfield. Chem. Commun. 735 (1968).
24. C. Mealli and L. Sacconi. Acta Crystallogr. Sect. B; Struct. Crystallogr. Cryst. Chem. B**33**, 710 (1977).
25. W. E. Marsh, D. S. Eggleston, W. E. Hatfield, and D. J. Hodgson. Inorg. Chim, Acta, **70**, 137 (1983); W. E. Estes, D. P. Gavel, W. E. Hatfield, and D. J. Hodgson. Inorg. Chem. **17**, 1415 (1978); D. P. Gavel and D. J. Hodgson. Acta Crystallogr. Sect. B: Struct. Crystallogr. Cryst. Chem. B**35**, 2704 (1979); W. E. Marsh, W. E. Hatfield, and D. J. Hodgson. Inorg. Chem. **27**, 1819 (1988).
26. F. Akhtar, D. M. L. Goodgame, M. Goodgame, G. W. Rayner-Canham, and A. C. Skapski. Chem. Commun. 1389 (1968).
27. D. M. L. Goodgame, M. Goodgame, P. J. Hayward, and G. W. Rayner-Canham. Inorg. Chem. **7**, 2447 (1968).
28. D. M. L. Goodgame, M. Goodgame, and G. W. Rayner-Canham. Inorg. Chim. Acta, **3**, 399 (1969); **3**, 406 (1969).
29. W. J. Eilbeck, F. Holmes, C. E. Taylor, and A. E. Underhill. J. Chem. Soc. A, 128 (1968).
30. B. C. Cornilsen and K. Nakamoto. J. Inorg. Nucl. Chem. **36**, 2467 (1974).
31. W. Ludwig and F. Gasser. Helv. Chim. Acta, **52**, 107 (1969).
32. N. S. Gill and M. Sterns. Inorg. Chem. **9**, 1619 (1970).
33. E. P. Serjeant and B. Dempsey. Ionisation constants of organic acids in aqueous solution. Pergamon Press. 1979. p. 367.
34. B. J. Hathaway. Comprehensive coordination chemistry. *Edited by* G. Wilkinson, R. D. Gillard, and J. A. McCleverty. Pergamon Press. 1987. Chap. 53.
35. D. L. McFadden, A. T. McPhail, C. D. Garner, and F. E. Mabbs. J. Chem. Soc. Dalton Trans. 263 (1975).
36. W. Vreugdenhil, P. J. M. W. L. Birker, R. M. ten Hoedt, G. Verschoor, and J. Reedijk. J. Chem. Soc. Dalton Trans. 429 (1984).
37. L. Antolini, G. Marcotrigiano, L. Menabue, and G. C. Pellacani. J. Am. Chem. Soc. **102**, 5506 (1980); D. N. Anderson and R. D. Willett. Inorg. Chim. Acta, **8**, 167 (1974); J. P. Steadman and R. D. Willett. Inorg. Chim. Acta, **4**, 367 (1970).
38. G. H. Stout and L. H. Jensen. X-ray structure determination, a practical guide. Macmillan, London. 1968. p. 303.
39. B. T. Kilbourn and J. D. Dunitz. Inorg. Chim. Acta, **1**, 209 (1967).
40. R. E. Norman, N. J. Rose, and R. E. Stenkamp. Acta Crystallogr. Sect. C: Cryst. Struct. Commun. C**45**, 1707 (1989).
41. A. Erdonmez, J. H. van Diemen, R. A. G. de Graaff, and J. Reedijk. Acta Crystallogr. Sect. C: Cryst. Struct. Commun. C**46**, 402 (1990).
42. W. Clegg, J. R. Nicholson, D. Collison, and C. D. Garner. Acta Crystallogr. Sect. C: Cryst. Struct. Commun. C**44**, 453 (1988).
43. S. Brownstein, N. F. Han, E. Gabe, and F. Lee. Can. J. Chem. **67**, 551 (1989).
44. M. R. Churchill, B. G. DeBoer, and S. J. Mendak. Inorg. Chem. **14**, 2496 (1975).
45. R. C. Dickinson, F. T. Helm, W. A. Baker Jr., T. D. Black, and W. H. Watson, Jr. Inorg. Chem. **16**, 1530 (1977).
46. J. Poitras and A. L. Beauchamp. Can. J. Chem. Submitted.
47. J. Reedijk, Recl. Trav. Chim. Pays-Bas, **88**, 1451, (1969).
48. J. B. Hodgson, G. C. Percy, and D. A. Thornton. J. Mol. Struct. **66**, 81 (1980).
49. J. A. C. van Ooijen and J. Reedijk. Inorg. Chim. Acta, **25**, 131 (1977).
50. P. T. T. Wong and D. G. Brewer. Can. J. Chem. **46**, 139 (1968).
51. R. Belford, D. E. Fenton, and M. R. Truter. J. Chem. Soc. Dalton Trans. 2345 (1972).

Can. J. Chem. Downloaded from www.nrcresearchpress.com by 88.255.202.194 on 09/08/12
For personal use only.

Basicity of substituted 2-pyridyl-1,1,3,3-tetramethylguanidines and aminopyridines in acetonitrile and water solvents

NASER FOROUGHIFAR,[1] KENNETH T. LEFFEK, AND YONG GU LEE[2]
Department of Chemistry, Dalhousie University, Halifax, N. S., Canada B3H 4J3

Received June 17, 1992

NASER FOROUGHIFAR, KENNETH T. LEFFEK, and YONG GU LEE. Can. J. Chem. **70**, 2856 (1992).

A series of substituted 2-pyridyl-1,1,3,3-tetramethylguanidines has been synthesized and the pK_a of each has been measured in acetonitrile and water solvents, together with the pK_a of the corresponding aminopyridine. A relationship between the pK_a's in these two solvents has been derived that allows the estimation of a pK_a in acetonitrile from that in water. The results were fitted to the Hammett equation, giving $\rho = 2.31 \pm 0.14$ and 1.64 ± 0.11 for the pyridylguanidines in acetonitrile and water, respectively, and 6.16 ± 0.4 and 5.24 ± 0.2 for the aminopyridines in the same solvents.

NASER FOROUGHIFAR, KENNETH T. LEFFEK et YONG GU LEE. Can. J. Chem. **70**, 2856 (1992).

On a synthétisé une série de 2-pyridyl-1,1,3,3-tétraméthylguanidines substituées et on a mesuré les pK_a de chacune dans l'acétonitrile et dans l'eau ainsi que les pK_a des aminopyridines correspondantes. On a établi une corrélation entre les pK_a dans ces deux solvants; elle permet d'évaluer un pK_a dans l'acétonitrile à partir de celui dans l'eau. On a ajusté les résultats avec l'équation de Hammett, obtenant des valeurs de $\rho = 2{,}31 \pm 0{,}14$ et $1{,}64 \pm 0{,}11$ pour les pyridylguanidines dans l'acétonitrile et l'eau, respectivement, et de $6{,}16 \pm 0{,}4$ et $5{,}24 \pm 0{,}2$ pour les aminopyridines dans les mêmes solvants.

[Traduit par la rédaction]

Can. J. Chem. Downloaded from www.nrcresearchpress.com by 88.255.202.194 on 09/08/12
For personal use only.

Introduction

The basicity of a series of phenyl-substituted 2-phenyl-1,1,3,3-tetramethylguanidines was measured (1) in order to provide a series of strong organic bases to complement the weaker aniline and pyridine bases for use in physical-organic research. Acetonitrile was chosen as the solvent since it is an aprotic solvent that is easy to purify and has a wide range of applicability in physical-organic measurements. The present work extends the range of strong bases to 1,1,3,3-tetramethylguanidines (TMG) substituted with various pyridyl groups at the N-2 position and also provides pK_a values of the conjugate acids of a series of aminopyridine bases in both acetonitrile and water solvents. The first objective is to provide a quantitative relationship between the pK_a in the solvents to allow a more reliable estimate of the pK_a of the conjugate acid of a particular base in acetonitrile from that in water. Coetzee and Padmanabhan (2) found no such quantitative relationship for a series of amines consisting mainly of aliphatic bases, but they did find that the pK_a's of the conjugate acids correlated with the Taft substituent constants, $\Sigma\sigma^*$, with the same slopes in acetonitrile solvent as those determined by Hall (3) in water.

It has been known for a long time (4) that Hammett σ constants, determined using phenyl-substituted substrates, could be used to correlate substituted pyridines. The second objective of the pK_a determinations for the aminopyridines is to demonstrate the validity of Hammett correlations in multiply-substituted pyridines and provide a body of data that will allow the standard methods of predicting pK_a's in water (5) to be used directly in acetonitrile.

Results and discussion

Table 1 presents the pK_a values of the conjugate acids of the bases in acetonitrile and water solvents, together with the pK_a differences between the two solvents. All the bases are stronger in acetonitrile than in water, as previously observed (1, 2), probably due to the weaker proton acceptor power of acetonitrile relative to water (2). It was shown (1) that the procedure of simply averaging the ΔpK_a values was not a satisfactory method of estimating the pK_a in one solvent from a measurement in the other, since the error may be more than half a pK_a unit. Uncertainties of this magnitude are usually too large for meaningful discussion of kinetic or other data.

The relationship between the pK_a values in acetonitrile and water for the bases in the present study is represented by eq. [1], with a correlation coefficient (c.c.) of 0.994.

$$[1] \quad pK_a^{AN} = (1.23 \pm 0.03)pK_a^{W} + 6.2 \pm 0.2$$

This relationship is complementary to the phenylTMG series previously published (1) and gives a range of bases in acetonitrile from a pK_a of 3.0 up to 23.9 (for DBU (1)). Schesinger (8) reported a value for DBU (1,8-diazabicyclo[5.4.0]undec-7-ene) of 24.32 in acetonitrile and also two 2,4-diaminovinamidines with pK_a values of 26.22 and 26.92 in the same solvent. Thus there is a wide range of nitrogen bases of known pK_a in acetonitrile over a scale of about 24 pK_a units.

If the 22 bases reported for the phenylTMG series (1) are combined with the 16 bases in Table 1, the relationship (c.c. 0.982) between pK_a^{AN} and pK_a^{W} is given by eq. [2].

$$[2] \quad pK_a^{AN} = (1.11 \pm 0.03)pK_a^{W} + 7.0 \pm 0.3$$

It is interesting to note that all the bases fall on the same correlation line despite the fact that the aminopyridine bases are protonated on the ring nitrogen atom, while the pyridylTMG bases are protonated on the N-2 atom of the TMG group, although no doubt considerably delocalized onto the N-1 and the N-2 atoms (9). Thus the solvent effect does not depend on the environment of the proton in the conjugate acid of the base, nor does it depend upon specific solvation of the picrate anion, since Coetzee and Padmanabhan (2) found

[1]Visiting Scientist (1991–1992) from Arak University, Arak, Iran.

[2]Postdoctoral Fellow (1991–1992).

TABLE 1. pK_a values for derivatives of TMG and pyridine bases in acetonitrile and water solvents

No.	Compound	pK_a^{AN}	pK_a^{W}	ΔpK_a^{AN-W}	$\Sigma\sigma$
1.	2-(2′-Pyridyl)TMG	19.61±0.13	10.49±0.05	9.12	0.56
2.	2-(3′-Pyridyl)TMG	18.99±0.12	10.59±0.05	8.40	0.73
3.	2-(4′-Pyridyl)TMG	18.48±0.11	10.17±0.08	8.31	0.83
4.	2-(5′-Methyl-2′-pyridyl)TMG	19.74±0.13	10.80±0.03	8.94	0.42
5.	2-(5′-Chloro-2′-pyridyl)TMG	18.79±0.12	10.19±0.11	8.60	0.80
6.	2-(5′-Bromo-2′-pyridyl)TMG	18.86±0.12	10.18±0.09	8.68	0.78
7.	2-(5′-Nitro-2′-pyridyl)TMG	16.60±0.09	8.56±0.67	8.04	1.82
8.	2-(4′,6′-Dimethyl-2′-pyridyl)TMG	19.82±0.11	10.92±0.01	8.90	0.44
9.	2-Aminopyridine	14.51±0.05	6.82[a]	7.69	−0.27
10.	3-Aminopyridine	14.12±0.05	6.04[a]	8.08	−0.16
11.	4-Aminopyridine	17.44±0.10	9.11[a]	8.33	−0.66
12.	2-Amino-5-methylpyridine	14.88±0.06	7.05±0.1	7.83	−0.33
13.	2-Amino-5-chloropyridine	12.00±0.02	4.7[b]	7.30	0.10
14.	2-Amino-5-bromopyridine	12.07±0.02	4.80±0.02	7.27	0.12
15.	2-Amino-5-nitropyridine	10.04±0.06	2.96±0.01	7.62	0.47
16.	2-Amino-4,6-dimethylpyridine	15.44±0.07	7.87±0.05	7.57	−0.54

[a]From ref. 6.
[b]From ref. 7.

Can. J. Chem. Downloaded from www.nrcresearchpress.com by 88.255.202.194 on 09/08/12
For personal use only.

virtually the same pK_a values for picrates and perchlorates. This confirms that the solvent effect must be due to the poorer proton-accepting ability of acetonitrile relative to water.

Equation [2] may be used to estimate pK_a values in water for strong bases that are affected by the levelling effect in water. We previously estimated the pK_a of DBU in water as 14.3 from a pK_a^{AN} of 23.9, but the application of eq. [2] gives a value of 15.2±0.5. If the Schesinger value of 24.3 in acetonitrile is used, DBU would have a pK_a in water of 15.7. Since DBU has a similar structure to the bases correlated by eq. [2], these values should be better estimates than our previous one. The large uncertainty in such an estimate demonstrates the need to measure pK_a values directly whenever this is possible.

Hammett plots may be constructed for all of the pyridylTMG compounds in Table 1 using the σ values for the =N— group of the pyridine ring given by Perrin *et al.* (ref. 5, p. 139) and the normal σ values (1, 5) for the substituents on the pyridine ring, both relative to the position of the TMG group, to give Σσ in Table 1. These are described by eqs. [3] (c.c. 0.989) and [4] (c.c. 0.987) for acetonitrile and water solvents, respectively.

$$[3] \quad pK_a^{AN} = -(2.31\pm0.14)\sigma + 20.7\pm0.1$$

$$[4] \quad pK_a^{W} = -(1.64\pm0.11)\sigma + 11.5\pm0.1$$

The intercepts of eq. [3] and eq. [4] should be equal to the pK_a of phenylTMG in acetonitrile and water, respectively. The agreement in acetonitrile, between 20.7±0.1 from eq. [3] and the literature value of 20.6±0.1(1) is very good, but in water eq. [4] gives 11.5±0.1, whereas Pruszynski found 12.18±0.02 (10). In acetonitrile, at least, the pK_a of a substituted pyridylTMG could, therefore, be predicted with good accuracy from that of phenylTMG. The ρ values are very similar to those found for the substituted phenylTMG compounds, i.e., ρ = 2.18±0.16 in CH_3CN (1) and 1.84±0.05 in water (10). Within ±σ they are the same in CH_3CN and differ by only a little more than this in water. The ρ values are clearly different in the two solvents, unlike the observation for aliphatic bases (2, 3).

It is concluded that the electronic effects governing the base strengths of pyridyl-substituted tetramethylguanidines generally parallel those of the phenyltetramethylguanidines.

Hammett plots for the aminopyridines in Table 1 are described by eqs. [5] and [6], with correlation coefficients of 0.983 and 0.999 respectively.

$$[5] \quad pK_a^{AN} = -(6.16\pm0.40)\sigma + 12.8\pm0.2$$

$$[6] \quad pK_a^{W} = -(5.24\pm0.20)\sigma + 5.34\pm0.08$$

The correlation found in water confirms earlier work of Charton (11), who obtained ρ = 5.70 and an intercept of 5.39, and also that of Clark and Perrin (12), who found ρ = 5.90 and an intercept of 5.25 for pyridinium ions in water. The pK_a of pyridine in water is 5.23 (6). The ρ value of 6.16 in acetonitrile shows that the sensitivity of this reaction constant to solvent change is less for pyridinium ions than it is for the tetramethylguanidinium ions. The intercept of 12.8 is somewhat higher than the pK_a of pyridine in acetonitrile, which was reported by Coetzee and Padmanabhan (2) as 12.33. Thus the pyridine bases are not as well correlated in acetonitrile as they are in water and also not as well correlated as the TMG bases in acetonitrile. Therefore, the prediction of the pK_a of a pyridine base in acetonitrile can be done only with moderate accuracy.

Experimental

Substituted 2-pyridyl-1,1,3,3-tetramethylguanidines were synthesized using a modification of the procedure of Bredereck (13). A solution of 1,1,3,3-tetramethylurea (0.1 mol) (Aldrich, dried over 4A molecular sieve) in dry benzene (100 mL) was treated dropwise with a solution of $POCl_3$ (0.2 mol) in dry benzene (30 mL). The reaction was stirred at room temperature overnight and a solution of the appropriate aminopyridine (0.15 mol) in dry benzene (80 mL) was added in several portions. The reaction mixture was stirred for 20 h at 75–80°C, after which the solid was separated and washed several times with benzene. The solid was then dissolved in water and 2 N NaOH solution was added to bring the pH to about 14, followed by extraction with benzene, drying over anhydrous sodium sulphate, evaporation, and vacuum distillation under reduced pressure. In some cases further purification was carried out

by tlc. The amount of $POCl_3$ used was larger than that reported by Bredereck (13) and this increased the yield calculated on the amount of tetramethylurea used.

2-Amino, 3-amino, and 4-aminopyridine were commercially availale (Aldrich) and were dried and further purified as necessary.

Picrates of the bases under study were obtained by mixing equimolar amounts of the bases and picric acid in 95% ethanol. This mixture was refluxed for 30 min, cooled to room temperature, and poured into an excess of water. The fine yellow crystals that precipitated were crystallized from ethanol and were dried in a vacuum desiccator. These preparations were carried out on a small scale and the picrates were handled carefully with due regard to the fact that ammonium picrate has been used in the explosive warhead of some naval shells.

The melting points were measured using a Fisher–Johns melting point apparatus and are uncorrected. The ^1H and ^{13}C nmr spectra were run in chloroform-*d*, unless otherwise stated, with TMS as the internal reference, using a Nicolet 360 NMR spectrometer with Fourier transform, at the Atlantic Resonance Centre, Dalhousie University. The mass spectra were recorded on a modified Du Pont CEC model 21-104 mass spectrometer at 70 eV. The ^{13}C nmr signals are reported in the sequence presented on structure I, followed by the signals for substituents on the heterocyclic part of the molecule.

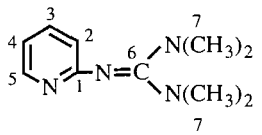

I

2-(2'-Pyridyl)-1,1,3,3-tetramethylguanidine

Yield 38%; bp 110–115°C/0.3 Torr (1 Torr = 133.3 Pa); ^1H nmr δ: 8.2(1H, d, 5.0 Hz), 7.4(1H, t, 6.0 Hz), 6.68(2H, m), 2.7(12H, s); ^{13}C nmr δ: 162.0, 114.7, 137.1, 116.7, 148.4, 163.7, 39.7; ms. (rel. int., %): 193(8), 177(4), 148(61), 78(100). Picrate: mp 148–150°C; ^1H nmr N^+H δ: 10.05(1H, bs).

2-(3'-Pyridyl)-1,1,3,3-tetramethylguanidine

Yield 36%; bp 112–115°C/0.3 Torr; ^1H nmr δ: 8.07(1H, d, 5.0 Hz), 7.99 (1H, s), 7.12 (1H, t, 5.0 Hz), 7.03 (1H, d, 6.0 Hz), 2.8(12H, s); ^{13}C nmr δ: 140.9, 148.1, 128.1, 123.5, 143.7, 160.7, 39.7; ms (rel. int., %): 193(6), 192(46), 177(10), 148(100), 78(25). Picrate: mp 141–144°C; ^1H nmr N^+H δ: 10.00(1H, bs).

2-(4'-Pyridyl)-1,1,3,3-tetramethylguanidine

Yield 30%; bp 118–120°C/0.3 Torr; ^1H nmr δ: 8.15(2H, d, 5.0 Hz), 6.41(2H, d, 5.0 Hz), 2.57(12H, s); ^{13}C nmr δ: 149.9, 116.8, 158.8, 116.8, 149.9, 161.2, 39.7; ms. (rel. int., %): 193(7), 192(37), 177(7), 148(100), 78(26). Picrate: mp 153–155°C; ^1H nmr N^+H δ: 10.41 (1H, s).

2-(5'-Methyl-2'-pyridyl)-1,1,3,3-tetramethylguanidine

Yield 40%; bp 115–120°C/0.3 Torr; ^1H nmr δ: 7.9(1H, d, 2.0 Hz), 7.2(1H, dd, 2 and 8 Hz), 6.6(1H, d, 8 hz), 2.8(12H, s); ^{13}C nmr δ: 161.3, 116.1, 138.0, 123.5, 148.1, 161.6, 39.6, 17.6; ms. (rel. int., %): 206(88), 162(71), 148(100), 119(12), 92(79). Picrate: mp 146–147°C; ^1H nmr N^+H δ: 8.4(1H, bs).

2-(5'-Chloro-2'-pyridyl)-1,1,3,3-tetramethylguanidine

Yield 42%; bp 120–125°C/0.3 Torr; ^1H nmr δ: 8, 9(1H, d, 2 Hz), 7.3(1H, dd, 2 and 8 Hz), 6.6(1H, d, 8 Hz), 2.8(12H, s); ^{13}C nmr δ: 162.0, 117.5, 136.9, 121.8, 146.6, 162.4, 39.7; ms (rel. int., %): 226(65), 182(80), 139(10), 127(43), 112(100), 77(38). Picrate: mp 138–139°C; ^1H nmr N^+H δ: 11.4(1H, bs).

2-(5'-Bromo-2'-pyridyl)-1,1,3,3-tetramethylguanidine

Yield 45%; bp 120–125°C/0.3 Torr; ^1H nmr δ: 8.2(1H, d, 2 Hz), 7.6(1H, dd, 2 and 8 Hz), 6.6 (1H, 8 Hz), 2.8(12H, s); ^{13}C nmr δ: 162.3, 118.2, 139.6, 109.7, 148.9, 162.4, 39.7; ms (rel. int., %): 271(92), 227(97), 211(100), 190(80), 157(95), Picrate: mp 135–136°C; ^1H nmr N^+H δ: 10.7(1H, bs).

2-(5'-Nitro-2'-pyridyl)-1,1,3,3-tetramethylguanidine

Yield 38%; bp 130–138°C/0.3 Torr; ^1H nmr δ: 9.1(1H, d, 2 Hz), 8.2(1H, dd, 2 and 8 Hz), 6.6(1H, d, 8 Hz), 2.8(12H, s); ^{13}C nmr δ: 164.9, 115.5, 132.3, 136.1, 146.6, 167.4, 40.0; ms. (rel. int., %) 237(100), 193(88), 179(99), 147(66), 124(7). Picrate: mp 123–125°C; ^1H nmr N^+H δ: 9.6(1H, bs).

2-(4',6'-Dimethyl-2'-pyridyl)-1,1,3,3-tetramethylguanidine

Yield 45%; bp 118–125°C/0.3 Torr; ^1H nmr δ: 6.3(1H, s), 6.2(1H, s), 2.6(12H, s), 2.3(3H, s), 2.1(3H, s); ^{13}C nmr δ: 161.2, 113.6, 147.8, 115.7, 156.3, 162.6, 39.7, 24.5, 20.8; ms (rel. int., %) 220(82), 176(42), 162(100), 121(36), 106(55). Picrate: mp 141–142°C; ^1H nmr N^+H δ: 8.9(1H, bs).

Tetraethylammonium perchlorate was recrystallized from benzene and dried in a vacuum oven at 60°C.

Acetonitrile was prepared by the method of O'Donnell *et al.* (14), followed by fractional distillation from P_2O_5 and calcium hydride.

The pK_a measurements in acetonitrile solvent were carried out using the potentiometric method of Coetzee and Padmanabhan (2, 15). The H-type cell and the detailed method have been described previously (1).

The pK_a measurements in water were carried out spectrophotometrically using a Cary 219 uv–vis instrument equipped with a thermostated cell, as previously described by Pruszynski (10).

1. K. T. Leffek, P. Pruszynski, and K. Thanapaalasingham. Can. J. Chem. **67**, 590 (1989).
2. J. F. Coetzee and G. R. Padmanabhan. J. Am. Chem. Soc. **87**, 5005 (1965).
3. H. H. Hall, Jr. J. Am. Chem. Soc. **79**, 5441 (1957).
4. H. H. Jaffe and G. D. Doak. J. Am. Chem. Soc. **77**, 4441 (1955).
5. D. D. Perrin, B. Dempsey, and E. P. Sergeant. pK_a prediction for organic acids and bases. Chapman and Hall, London. 1981.
6. A. Albert and E. P. Serjeant. The determination of ionization constants. 3rd ed. Chapman and Hall, London. 1984.
7. E. C. Taylor and R. O. Kan. J. Am. Chem. Soc. **85**, 776 (1963).
8. R. Schesinger. Angew. Chem. Int. Ed. Engl. **26**, 1164 (1987).
9. P. Pruszynski, K. T. Leffek, B. Borecka, and T. S. Cameron. Acta Crystallogr. Sect. C: Cryst. Struct. Commun. **C48**, 1638 (1992).
10. P. Pruszynski. Can. J. Chem. **65**, 626 (1987).
11. M. Charton. J. Am. Chem. Soc. **86**, 2033 (1964).
12. J. Clark and D. D. Perrin. Q. Rev. Chem. Soc. **18**, 295 (1964).
13. H. Bredereck and K. Bredereck. Chem. Ber. **94**, 2278 (1961).
14. J. F. O'Donnell, J. T. Ayres, and C. K. Mann. Anal. Chem. **37**, 1161 (1965).
15. J. F. Coetzee and G. R. Padmanabhan. J. Phys. Chem. **66**, 1708 (1962).

Can. J. Chem. Downloaded from www.nrcresearchpress.com by 88.255.202.194 on 09/08/12
For personal use only.

Excess properties for acetylacetone + pentanols systems at 298.15 K

ROQUE RIGGIO,[1] HECTOR E. MARTINEZ, AND NORMA Z. DE SALAS
Facultad de Ciencias Naturales, Universidad Nacional de Salta, Buenos Aires 177, 4400 Salta, Repūblica Argentina

Received October 17, 1991[2]

ROQUE RIGGIO, HECTOR E. MARTINEZ, and NORMA Z. DE SALAS. Can. J. Chem. **70**, 2859 (1992).

From experimental densities, viscosities, and refractive indexes for the acetylacetone + 1-pentanol, + 2-Pentanol, + isoamyl alcohol, and + *tert*-amyl alcohol systems at 298.15 K, the excess molar volumes, excess viscosities, excess molar free energies of activation of flow, and excess internal pressures were calculated over the whole concentration range. Conclusions about the molecular interactions in these mixtures were drawn from the variations of the excess functions with the composition.

ROQUE RIGGIO, HECTOR E. MARTINEZ et NORMA Z. DE SALAS. Can. J. Chem. **70**, 2859 (1992).

Utilisant les densités, les viscosités et les indices de réfractions expérimentaux des systèmes acétylacétone + pentan-1-ol, + pentan-2-ol, + alcool isoamylique et + alcool *tert*-amylique, à 298,15 K, on a calculé les volumes molaires en excès, les viscosités en excès, les énergies libres d'activation molaires en excès de l'écoulement et les pressions internes en excès, pour l'ensemble des concentrations. En se basant sur les variations des fonctions en excès en fonction de la composition, on a pu tirer des conclusions relativement aux interactions moléculaires présentes dans ces mélanges.

[Traduit par la rédaction]

Can. J. Chem. Downloaded from www.nrcresearchpress.com by 88.255.202.194 on 09/08/12
For personal use only.

Introduction

The excess properties of binary liquid solutions are fundamental for the design of industrial equipment and for the interpretation of the liquid state, particularly when polar–polar liquids are the components of the mixtures. Continuing our study on these types of systems (alcohols + ketones) (1–3) we report here the excess properties: molar volumes (V^E), viscosities (η^E), molar free energies of activation of flow (G^{*E}), and internal pressures (Pi^E), for the following mixtures: (*i*) acetylacetone (AA) + *n*-pentanol (P_1), (*ii*) acetylacetone (AA) + 2-pentanol (P_2), (*iii*) acetylacetone (AA) + isoamyl alcohol (IA), and (*iv*) acetylacetone (AA) + *tert*-amyl alcohol (TAA).

Experimental

Materials

Acetylacetone, *n*-pentanol, 2-pentanol, isoamyl alcohol, and *tert*-amyl alcohol (all Merck Darmstadt p.a.) were dried over anhydrous K_2CO_3 and fractionally distilled under a nitrogen atmosphere. In each case the middle fraction was collected and stored over 0.3 nm molecular sieve for alcohols and 0.4 nm molecular sieve for acetylacetone to prevent water absorption. The mixtures were prepared by mixing accurately weighed quantities of the pure liquids. Caution was taken to prevent evaporation.

Density (ρ)

Densities were determined with an Anton Paar DMA46 calculating density meter with a built-in thermostat. We estimated that the reported densities were accurate to within ± 0.1 kg m^{-3}.

Viscosity (η)

The measurements were carried out with a Cannon–Fenske viscosimeter calibrated with doubly distilled water and benzene (accuracy $\pm 0.5\%$).

Refractive index (n_D)

The refractive indexes of the pure components (sodium D line) were measured with a Jena dipping refractometer with an accuracy of ± 0.00002. For viscosity and refractive index, a thermostatically controlled bath, constant to ± 0.01°C, was used.

[1]Author to whom correspondence may be addressed.
[2]Revision received June 26, 1992.

Results

The experimental physical properties of the pure liquids are reported in Table 1, along with the literature values for comparison. Densities, viscosities, and refractive indexes of the binary mixtures can be calculated from the experimental data, knowing the mole fraction, by the following equation:

$$[1] \quad A = x_iA_i + x_jA_j + x_ix_j \sum_{\substack{k=0 \\ i<j}}^{n} a_k(x_i - x_j)^k$$

where A_i and A_j are the properties of the pure components. Table 2 shows the values of the coefficients a_k as well as their standard deviation, calculated by the method of least squares.

The excess functions of the binary systems can be represented by a Redlich–Kister form of the type:

$$[2] \quad X^E = x_ix_j \sum_{k=0}^{n} a_k(2x_i - 1)^k$$

where X^E represents V^E, η^E, G^{*E}, and Pi^E, x_i and x_j the mole fractions of the components *i* and *j*, respectively, and a_k the polynomial coefficients. The least-squares method was used to determine the values of the coefficients. In each case, the optimum number of coefficients was ascertained from an examination of the variation of the standard error of estimate with *n*:

$$[3] \quad \sigma_y = [\Sigma(X^E_{obs} - X^E_{cal})^2/(n_{obs} - n)]^{1/2}$$

where n_{obs} is the number of measurements.

The excess functions were calculated with the following equations:

$$[4] \quad V^E = V - (x_1V_1 + x_2V_2) = [(x_1M_1 + x_2M_2)/\rho] - (x_1V_1 + x_2V_2)$$

$$[5] \quad \eta^E = \eta - \eta^{id} = \eta - \exp(x_1 \ln \eta_1 + x_2 \ln \eta_2)$$

$$[6] \quad G^{*E} = RT[\ln \eta V - (x_1 \ln \eta_1V_1 + x_2 \ln \eta_2V_2)]$$

$$[7] \quad Pi^E = \frac{2^{1/6}RT}{2^{1/6}V - dN^{1/3}V^{2/3}} - \left[x_1 \frac{2^{1/6}RT}{2^{1/6}V_1 - d_1N^{1/3}V_1^{2/3}} + x_2 \frac{2^{1/6}RT}{2^{1/6}V_2 - d_2N^{1/3}V_2^{2/3}}\right]$$

TABLE 1. Experimental physical properties of the pure liquids at 298.15 K[a]

Component	ρ		η		n_D	
	Expt.	Lit. (ref.)	Expt.	Lit. (ref.)	Expt.	Lit. (ref.)
AA	968.3	—	0.700	—	1.44893	—
P_1	811.1	811.5 (18)	3.35	3.347 (18)	1.40791	1.4079 (18)
P_2	805.3	805.4 (18)	3.45	3.445 (19)	1.40431	1.4044 (18)
IA	806.6	807.1 (18)	3.48	—	1.40521	1.4052 (18)
TAA	805.0	805.0 (18)	3.52	3.548 (19)	1.40242	1.4024 (18)

[a]Units: ρ, kg m^{-3}; η, mPa s.

TABLE 2. Coefficients a_k for eq. [1] and standard deviations for the binary systems at 298.15 K[a]

Systems		a_0	a_1	a_2	a_3	a_4	σ_y
AA + $P1$	ρ	−0.015	−0.001	—	—	—	0.0
	η	−3.84	1.90	−0.63	1.24	−0.94	7×10^{-3}
	n_D	−0.0031	−0.0032	0.0008	0.0053	−0.0033	7×10^{-5}
AA + $P2$	ρ	−0.027	—	—	—	—	8×10^{-5}
	η	−4.37	4.00	−2.73	0.27	—	7×10^{-3}
	n_D	−0.0050	−0.0035	−0.0022	0.0051	0.0018	6×10^{-5}
AA + IA	ρ	−0.018	−0.002	−0.001	—	—	4×10^{-5}
	η	−4.11	2.39	−0.78	−0.14	—	7×10^{-3}
	n_D	−0.0038	−0.0018	0.0002	0.0014	−0.0007	1×10^{-5}
AA + TAA	ρ	−0.023	−0.004	−0.004	—	—	1×10^{-4}
	η	−4.53	3.16	−1.97	0.17	0.62	5×10^{-3}
	n_D	−0.0037	−0.0017	−0.0003	0.0016	0.0002	2×10^{-5}

[a]Units: ρ, kg m^{-3}; η, mPa s.

where V and η are the molar volumes and the viscosities of the mixtures; V_1, V_2, η_1, and η_2 are the molar volumes and viscosities of the pure components, respectively; η^{id} is the viscosity of ideal mixture. The excess internal pressures (Pi^E) of the liquid mixture have been obtained (4) by the equation:

$$[8] \quad Pi^E = P_i - (x_1 Pi_1 + x_2 Pi_2)$$

where Pi, Pi_1 and Pi_2 are the internal pressures of the mixture and the pure components, respectively, and can be obtained from the Buchler–Hirschfelder–Curtis equation of state (5):

$$[9] \quad Pi = \frac{2^{1/6}RT}{2^{1/6}V - dN^{1/3}V^{2/3}}$$

N is Avogadro's number and d the molecular diameter of the mixture or the pure components, calculated by following relation (6):

$$[10] \quad d = 2\left[\frac{n_D^2 - 1}{n_D^2 + 2} V \frac{3}{4\pi N}\right]^{1/3}$$

n_D are the refractive indexes of the mixtures or the pure components.

Table 3 shows the values of the coefficients a_k for the excess functions of the binary systems and their standard deviation, calculated by the method of least squares.

Discussion

All the alcohols are considered to be associated substances (7, 8), but when the alcohols are mixed with polar solvents (in our case a ketone), a breakdown of the alcohol's associated structure occurs and specific interactions could be present (9). In this paper, we report the values of the following excess properties: molar volumes (V^E), viscosities (η^E), free energies of viscous flow (G^{*E}), and internal pressures (Pi^E).

For the excess molar volumes, there are two factors that explain the behavior of this property as related to the composition in these mixtures. (*a*) The disruption of the hydrogen-bonded alcohol structure gives rise to a positive contribution to V^E. The positive contribution depends on the dielectric constant of the ketone (10), and on the chain length (11) and the degree of branching in the alcohol (12). (*b*) The fact that the interactions between unlike molecules in all the systems are weaker than the interactions between like molecules also produces a positive contribution to V^E.

Factors that make a negative contribution to V^E are (*a*) the geometrical fitting of the ketone into the remaining alcohol structure (13, 14) and (*b*) unlike specific interactions due to formation of new chemical species in the mixtures.

The excess volumes V^E measured at 298.15 K are plotted vs. composition in Fig. 1. V^E are positive for all systems and we can conclude that in all cases the positive contributions to V^E arise from the breaking of the self-associated alcohol structure with the ketone acting as a diluent. From the analysis of Fig. 1, we observe that V^E's are greater when the said

Can. J. Chem. Downloaded from www.nrcresearchpress.com by 88.255.202.194 on 09/08/12
For personal use only.

TABLE 3. Coefficients a_k from eq. [2] and standard deviations for the binary systems at 298.15 K[a]

Systems	Coefficients	$V^E \times 10^6$	η^E	G^{*E}	Pi^E
AA + P_1	a_0	0.8524	−1.819	−844.17	−0.0158
	a_1	−0.0051	1.401	15.10	−0.0052
	a_2	0.0438	−1.142	87.12	−0.0021
	a_3	—	1.214	295.84	0.0072
	σ_y	3×10^{-3}	1×10^{-2}	3.88	6×10^{-5}
AA + P_2	a_0	2.0969	−2.283	−1072.97	−0.0289
	a_1	−0.2584	3.578	941.22	−0.0042
	a_2	0.2745	−2.620	−149.39	−0.0033
	a_3	—	—	−752.97	0.0056
	σ_y	1×10^{-2}	1×10^{-2}	5.77	7×10^{-5}
AA + IA	a_0	1.0908	−1.992	−892.31	−0.0196
	a_1	0.0384	1.770	46.03	−0.0030
	a_2	0.1195	−0.674	172.43	−0.0013
	σ_y	4×10^{-3}	9×10^{-3}	5.58	6×10^{-5}
AA + TA	a_0	1.6879	−2.397	−1119.76	−0.0245
	a_1	0.1840	2.665	363.52	−0.0044
	a_2	0.4844	−1.444	149.62	−0.0041
	a_3	—	—	−286.27	—
	σ_y	1×10^{-2}	1×10^{-2}	5.01	1×10^{-4}

[a]Units: V^E, $m^3\ mol^{-1}$; η^E, mPa s; Pi^E, kbar.

Can. J. Chem. Downloaded from www.nrcresearchpress.com by 88.255.202.194 on 09/08/12
For personal use only.

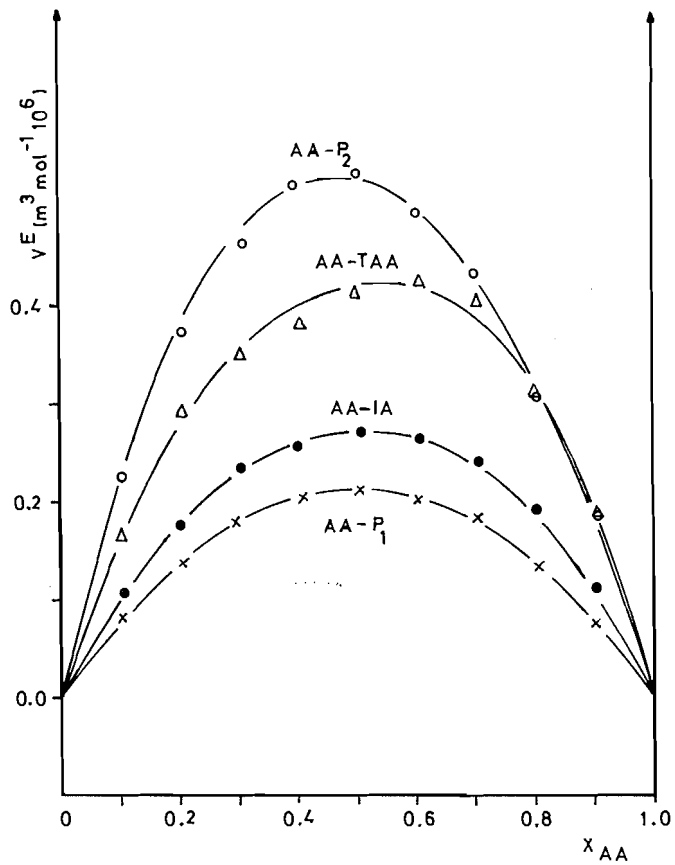

FIG. 1. Molar excess volumes of the systems at 298.15 K.

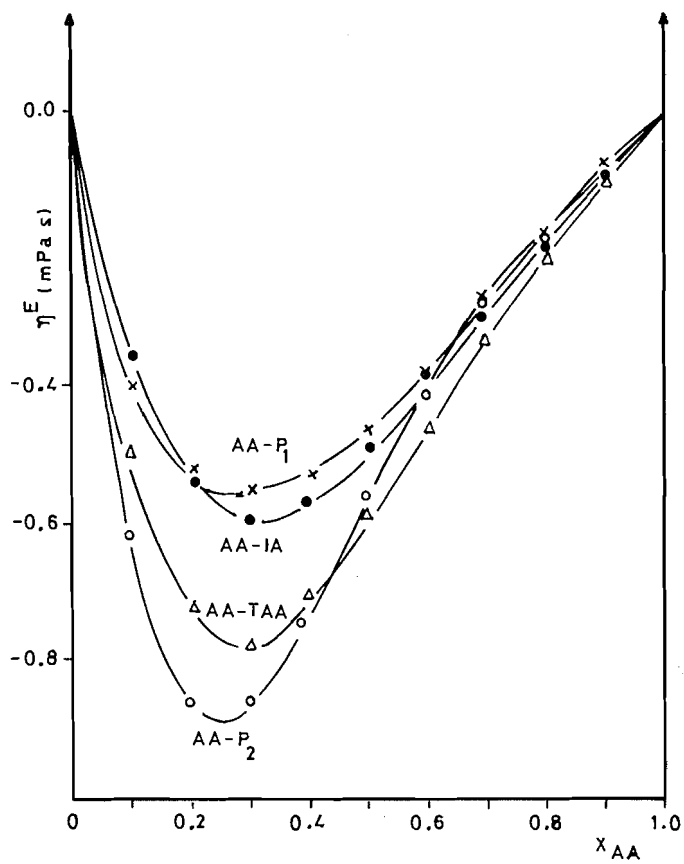

FIG.2. Excess viscosities of the systems at 298.15 K.

compounds are mixed with secondary and tertiary alcohols than when mixed with primary alcohols, it being evident from our results that the (OH) alcohol function at the secondary or tertiary carbon and the branched alcohols produces a less negative contribution to V^E on mixing. The typical contributions appearing in these types of systems are due to those

Can. J. Chem. Downloaded from www.nrcresearchpress.com by 88.255.202.194 on 09/08/12
For personal use only.

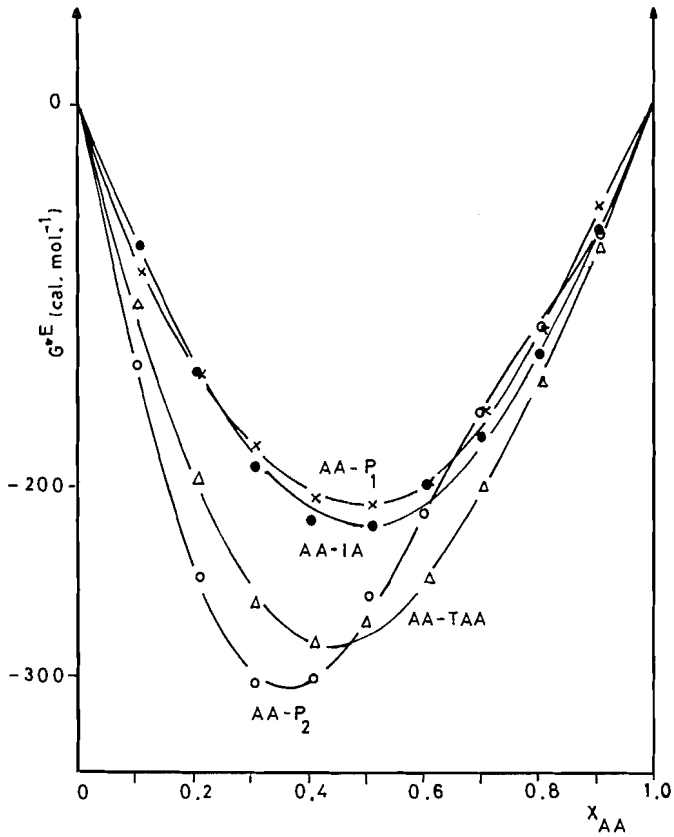

FIG. 3. Molar excess free energies of viscous flow activation by the systems at 298.15 K.

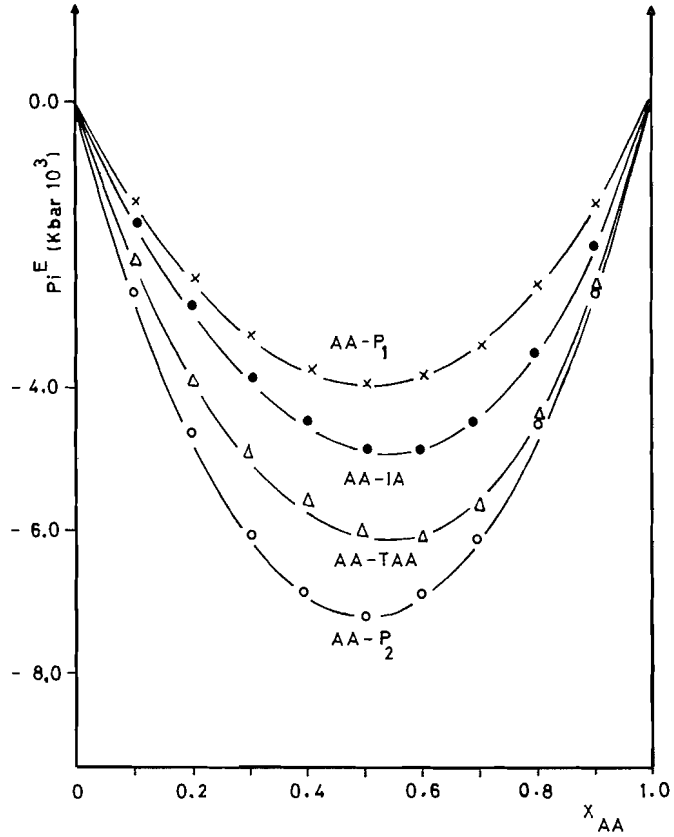

FIG. 4. Excess internal pressures of the systems at 298.15 K.

caused by the dipole–dipole interaction and, on the other hand, that caused by the effect of the self-association of the alcohol. This self-association effect seems to predominate over the former when the alcohol is not primary. The increments for the V^E's, with respect to the negative contribution, are in the following order:

$$AA + P_1 > AA + IA > AA + TAA > AA + P_2$$

which are according to ref. 15.

The smooth representation of the η^E values is presented in Fig. 2 and shows negative values for the excess viscosities for all the systems, which are interpreted in terms of dominant dispersion forces (16). The values obtained for η^E show the following decreasing order:

$$AA + P_1 < AA + IA < AA + TAA < AA + P_2$$

Such an excess function lets us draw conclusions about interactions present in the mixtures. Negative deviations occur when dispersion forces are responsible, according to the order given above, which is in complete agreement with the conclusions reached for the V^E's.

From the analysis of the dependence of G^{*E} upon composition (Fig. 3), we observed an increment of negative deviations in the following order:

$$AA + P_2 < AA + TAA < AA + IA < AA + P_1$$

It is known that the strength of interactions increases as G^{*E} diminishes, and the data obtained indicate that interactions decrease in the given order, in total accord with the conclusions pointed out previously.

Figure 4 shows negative deviations for the Pi^E's over the whole concentration range, for all the systems, in this sequence:

$$AA + P_2 < AA + TAA < AA + IA < AA + P_1$$

The negative values of the Pi^E's indicate in a qualitative way that the repulsion forces are greater than the forces of attraction, on the other hand, positive Pi^E values imply the forces of attraction are greater than those of repulsion. The values obtained for excess internal pressures present good agreement with the Dunlap and Scott (17) prediction that the systems with a positive maximum in the V^E will exhibit a minimum in the Pi^E.

If we compare the V^E and η^E values in this study with those of methylisobutylketone (MIK), already published for the same alcohols (1–3), we conclude: (*a*) V^E for the mixtures with MIK are less positive than V^E for the mixtures with AA; (*b*) η^E for the mixtures with MIK are less negative than the η^E for the mixtures with AA. This shows that more interaction exists between the alcohols and MIK than with AA. In principle, three types of interactions appear when mixing an alcohol + AA. These are (*a*) keto–enol, (*b*) keto–alcohol, and (*c*) enol–alcohol effects. The more predominant effects in our systems are the keto–enol interactions.

Acknowledgements

We wish to thank INENCO-CONICET-UNSa, Repūblica Argentina, for financial support.

1. H. N. Sólimo, R. Riggio, and H. E. Martinez. J. Solution Chem. **15**, 283 (1986).
2. R. Riggio, H. E. Martinez, and H. N. Sólimo. Can. J. Chem. **64**, 1595 (1986).

3. R. Riggio, H. E. Martinez, and N. Sólimo. An. Asoc. Quím. Argent. **4**, 409 (1987).
4. J. D. Pandey, N. Pant, and B. R. Chaturvedi. Chem. Scr. **18**, 224 (1981).
5. J. O. Hirschfelder, C. F. Curtis, and R. B. Bird. Molecular theory of gases and liquids. John Wiley & Sons, New York. 1954. p. 286.
6. S. Glasstone. Text-book of physical chemistry. MacMillan & Co. Ltd., London. 1962.
7. H. C. Van Ness, J. Van Winkle, H. H. Richtol, and H. E. Hollinger. J. Phys. Chem. **71**, 1483 (1967).
8. G. C. Pimentel and A. L. McClellan. The hydrogen bond. W. H. Freeman and Co., San Francisco. 1960.
9. J. E. House. J. Trans. Ill. State Acad. Sci. **59**, 123 (1966).
10. M. V. P. Rao and P. R. Naidu. Indian J. Chem. **11**, 242 (1973).
11. A. J. Treszczanowicz and G. C. Benson. J. Chem. Thermodyn. **10**, 967 (1978).
12. K. Nakanishi and H. Shirai. Bull. Chem. Soc. Jpn. **43**, 1634 (1970).
13. D. E. G. Jones, I. A. Weeks, S. C. Anand, R. W. Wetmore, and G. C. Benson. J. Chem. Eng. Data, **17**, 501 (1972).
14. G. C. Benson and O. Kiyohara. J. Chem. Eng. Data, **21**, 362 (1976).
15. M. Kato and N. Suzuki. J. Chem. Thermodyn. **10**, 435 (1978).
16. R. J. Fort and W. R. Moore. Trans. Faraday Soc. **62**, 1112 (1966).
17. R. D. Dunlap and R. L. Scott. J. Phys. Chem. **66**, 631 (1962).
18. J. A. Riddic and W. B. Bunger. Organic solvents. Vol. II. 3rd ed. Wiley–Interscience, New York. 1970.
19. A. D'Aprano, D. I. Donato, and V. Agrigento. J. Solution Chem. **10**, 673 (1981).

Can. J. Chem. Downloaded from www.nrcresearchpress.com by 88.255.202.194 on 09/08/12
For personal use only.

Solubility measurements and determination of Setschenow constants for the pesticide carbaryl in seawater and other electrolyte solutions

MIGUEL ANGEL HUERTA-DIAZ[1] AND SILVIO RODRIGUEZ
Department of Chemistry, University of the Pacific, Stockton, CA 95211, U.S.A.

Received February 21, 1992

MIGUEL ANGEL HUERTA-DIAZ and SILVIO RODRIGUEZ. Can. J. Chem. **70**, 2864 (1992).

Accurate solubility measurements covering the range 278–318 K were obtained for the carbamate pesticide carbaryl (1-naphthyl-*N*-methylcarbamate) in water, natural and artificial seawater, and NaCl, Na_2SO_4, $CaCl_2$, and $(CH_3)_4NBr$ electrolyte solutions. Carbaryl solubilities were determined using a combination of a generator column method and spectrophotometric techniques. In all cases the solubility of carbaryl in water and in the electrolyte solutions increased with an increase in temperature. The salt effect on the pesticide solubility as a function of temperature was obtained by calculating the Setschenow constants for each one of the electrolyte solutions. Salting-out was observed in solutions prepared with NaCl, Na_2SO_4, and $CaCl_2$ as well as in natural and artificial seawater, whereas salting-in was observed with $(CH_3)_4NBr$ solutions.

MIGUEL ANGEL HUERTA-DIAZ et SILVIO RODRIGUEZ. Can. J. Chem. **70**, 2864 (1992).

Opérant à des températures allant de 278 à 318 K, on a déterminé avec précision la solubilité du carbaryl (1-naphtyl-*N*-méthylcarbamate), un pesticide de la famille des carbamates, dans l'eau, dans des eaux de mer naturelle et artificielle et dans des solutions de NaCl, de Na_2SO_4, de $CaCl_2$ et de $(CH_3)_4NBr$ agissant comme électrolytes. On a déterminé les solubilités du carbaryl en utilisant une combinaison d'une méthode de colonne génératrice et de techniques spectrophotométriques. Dans tous les cas, la solubilité du carbaryl dans l'eau et dans les solutions d'électrolytes augmente avec une augmentation de la température. On a déterminé l'effet de sel sur la solubilité du pesticide en fonction de la température en calculant les constantes de Setschenow pour chacune des solutions d'électrolytes. On a observé un relargage dans les solutions préparées avec du NaCl, du Na_2SO_4 et du $CaCl_2$ ainsi qu'avec les eaux de mers naturelle et artificielle; l'inverse a été observé avec les solutions de $(CH_3)_4NBr$.

[Traduit par la rédaction]

Introduction

The extent to which aquatic biota are exposed to a toxicant such as a pesticide is largely controlled by its aqueous solubility (1). Solubility measurements can also be used to predict or extrapolate such parameters as transfer coefficients from residence in soils into runoff and ground water, systemic penetration into aqueous tissues, and distributions from formulations into aqueous spray carriers (2). In addition, solubilities are of thermodynamic interest since they can provide information fundamental in understanding hydrophobic interactions and in calculating the transfer properties of solutes between various solvents.

Since most pesticides are organic compounds of low molecular weight they show a hydrophobic character, having water solubilities in the ppm or even ppb range (3). Solubility measurements can be affected either by the temperature or by the ionic strength of the dissolving medium. Hence, the presence of a third component such as an electrolyte may substantially change the solubility of nonpolar molecules. This is the case of the salting-out effect of sodium chloride and other salts present in seawater (1). The magnitude of this effect can be calculated by using the empirical relationship developed by Setschenow (4)

$$[1] \quad \log(S_0) - \log(S) = k_S C_e$$

where k_S is the Setschenow constant, and S_0 and S represent the solubilities in mol kg^{-1} of the nonelectrolyte in water and in the electrolyte solution of concentration C_e, respectively. A positive value for k_S indicates salting-out and a negative one indicates salting-in.

Salt effect studies provide considerable information of theoretical importance concerning the complex interactions of ions and neutral molecules and the unique nature of water as a solvent. Additionally, knowledge of salting-out effects can have practical applications on the separation of nonelectrolytes from water solutions (5).

Carbaryl, the common name for the carbamate pesticide 1-naphthyl-*N*-methylcarbamate, is a white crystalline solid soluble in most polar solvents (6). It was introduced in 1956 under the trade name "Sevin" and since then its toxicity (refs. 7–11) as well as its physicochemistry (refs. 12–20) has been documented by several researchers. Carbaryl is currently used as a preharvest pesticide for the protection of fruits, vegetables, and field crops and is one of the most widely used carbamate insecticides (21). Carbaryl has also been employed in the aquatic environment to control the pests and predators of oysters (e.g., starfish, oyster drills (6)). However, some deleterious secondary effects have been observed. For example, Brown (22) noted that concentrations as low as 1 ppb of carbaryl could inhibit the development of clam eggs. Other studies (23) have indicated that carbaryl may be teratogenic. It is thus important to have reliable information on the solubility of this pesticide in natural water systems in order to make a proper assessment of its toxic implications for the aquatic fauna and the environment.

This paper reports solubility data of the pesticide carbaryl in water, natural and artificial seawater, and in solutions prepared with the major seawater salt components NaCl, Na_2SO_4, and $CaCl_2$. In addition, the quaternary salt $(CH_3)_4NBr$ (tetramethylammonium bromide) was utilized to investigate the salting-in effects of this compound on the solubility of carbaryl. All solubilities were measured as a function of temperature and electrolyte concentration and

[1]Current address: INRS–Eau, Université du Québec, C. P. 7500, Sainte-Foy (Québec), Canada G1V 4C7.

Can. J. Chem. Downloaded from www.nrcresearchpress.com by 88.255.202.194 on 09/08/12
For personal use only.

Can. J. Chem. Downloaded from www.nrcresearchpress.com by 88.255.202.194 on 09/08/12
For personal use only.

were subsequently used to evaluate salt-induced effects through the calculation of Setschenow constants.

Experimental

All reagents used were analytical grade or better and were used as received without further purification. Carbaryl was obtained from Chem Service as an analytical standard. All solutions were prepared with deionized water distilled in an all-glass still with a dissolved organic carbon content of <0.2 ppm (<0.02 μmol mL^{-1}). Natural seawater was IAPSO standard seawater (Institute of Oceanographic Sciences, Surrey, England) with a stated chlorinity of 19.3770‰. Artificial seawater was prepared according to the recipe given by Kester *et al.* (24). The maximum electrolyte concentrations utilized were selected based on their abundance in natural seawater.

The concentration of carbaryl in the different solutions was determined spectrophotometrically using a Varian model Cary 219 UV–VIS spectrophotometer equipped with a double beam, with a nominal slit of 0.5 nm and a special attachment to the cell holder that allowed the use of a thermoregulated bath. All measurements were made using 1-m matched quartz cells. Temperature measurements were done with a digital telethermometer (Bailey, model BAT-12) with a resolution of 0.1°C.

The solubilities of carbaryl at different temperatures in water and in electrolyte solutions of varying concentrations were measured using the method developed by May *et al.* (25, 26). This method has successfully been used by other researchers (1, 27–31) and, briefly, it consists in the generation of saturated solutions of nonelectrolytes produced by passing the solution acting as solvent through a column packed with glass beads previously covered with the nonelectrolyte. In this way the surface area is greatly increased and the time necessary for reaching saturation is decreased substantially.

For our analyses 4.0 g of carbaryl were dissolved with approximately 200 mL of methylene chloride. The resulting solution was then mixed with 100 g of glass beads 60–80 mesh and rotoevaporated to dryness. The beads were then packed into a 100-cm^3 Allihn condenser with a water jacket 300 mm in length. The condenser was connected to a thermoregulated circulating bath (Lauda, model B-1) with an operating range of 30–100°C and an accuracy of 0.03°C. An immersion cooler (Neslab, Cryocool model CC-60II) was used to lower the temperature of the circulating water below 30°C. Water or electrolyte solutions were pumped through the column at an estimated flow rate of 2 mL min^{-1}.

Each new column was initially conditioned by passing 500 mL of distilled water at 50°C. After this initial step the column could be reset to any desired temperature and solutions could be passed through and collected in the quartz cell for measurement. It was found by experience that after this initial equilibration step 100 mL of each new solution had to be pumped through before collecting the first sample. Each time a new temperature was set, 30–35 mL of the solution had to be passed through the column before taking a sample for analysis.

Results

Carbaryl shows two distinct peaks in the absorbance spectrum, one at 269 nm and the maximum at 279 nm. Values for the solubility concentrations were obtained by constructing a standard calibration curve (linear up to 0.5 μmol kg^{-1}) and reading at 279 nm. These values were corrected for temperature-induced volume changes by using the equation developed by Lo Surdo *et al.* (32). The estimated standard error ($\sigma \times 10^{-6}$) of this equation over the molality range zero to saturation and temperature range 273–323 K are 20.3 and 14.8 for NaCl and Na_2SO_4, respectively. In the special case of $CaCl_2$ and $(CH_3)_4NBr$, for which no high-accuracy density data as a function of temperature are available, the correction factors used were the same as those used for Na_2SO_4. This assumption seems supported by the findings of Ikono (33), who showed that the difference in density between two 0.5 molal solutions, one of $MgCl_2$ and the other of $CaCl_2$, was less than 0.6% in the temperature range 15–45°C, and this difference was even smaller for more dilute solutions. Furthermore, the magnitude of the correction in all our data in no case exceeded 0.8% of the value. Similar corrections were made for seawater (SW) and artificial seawater (ASW) following the equations developed by Leyendekkers (34).

Table 1. Solubility of carbaryl in water between 278 and 318 K

T (K)	$S \times 10^4$ (mol kg^{-1})
278	2.71 ± 0.08
283	3.15 ± 0.09
288	3.74 ± 0.11
293	4.45 ± 0.13
298	5.21 ± 0.18
303	6.52 ± 0.19
308	7.86 ± 0.24
313	8.99 ± 0.27
318	10.06 ± 0.31

Salinity of standard seawater was calculated using the equation recommended by UNESCO (35). The "molality" m_s of seawater, defined as the sum of the molalities of each one of the electrolyte components, was calculated using the equation (34):

$$[2] \quad m_s = \frac{S'}{M' - 10^{-3} M'S}$$

where S' stands for salinity and M' can be considered as the "corrected" molecular mass of sea salt. For convenience, seawater can be considered as a solution constituted of different electrolytes according to a specific "recipe." In this work, the recipe chosen for ASW was the one developed by Kester *et al.* (24) in which $M' = 68.08$ g "mol^{-1}."

All solubilities represent the mean of at least three measurements for each temperature, with the estimated experimental error expressed as one standard deviation. Error propagation methods (36) were used throughout this work along with the usual standard statistical techniques.

Table 1 shows that, as expected, the solubility values obtained for carbaryl in water increased with temperature from $(2.71 \pm 0.08) \times 10^{-4}$ mol kg^{-1} at 278 K to $(10.06 \pm 0.31) \times 10^{-4}$ mol kg^{-1} at 318 K. Solubility values at different temperatures taken from the literature (37–41) show a wide range of values, probably reflecting the lack of reliable solubility data for this pesticide. Swann *et al.* (41), who used the same generator column method, obtained a value of 82.6 ppm at 298 K. The difference between their value and the corresponding solubility determined in this work ($5.21 \times 10^{-4} \approx$ 105 ppm) might be attributed to the different amounts of glass beads and pesticide used in each experiment. During the course of this work it was observed that the carbaryl concentration values increased each time larger amounts of glass beads and pesticide were used. This trend continued up to a

Can. J. Chem. Downloaded from www.nrcresearchpress.com by 88.255.202.194 on 09/08/12
For personal use only.

TABLE 2. Solubility of carbaryl in sodium chloride and in tetramethylammonium bromide between 278 and 318 K

T (K)	$S \times 10^4$ (mol kg^{-1})	$S \times 10^4$ (mol kg^{-1})
	NaCl, m = 0.2559	$(CH_3)_4NBr$, m = 0.01007
278	2.25 ± 0.06	3.30 ± 0.10
283	2.67 ± 0.08	3.74 ± 0.11
288	3.14 ± 0.09	4.26 ± 0.13
293	3.76 ± 0.11	4.85 ± 0.14
298	4.50 ± 0.13	5.66 ± 0.19
303	5.59 ± 0.17	6.57 ± 0.19
308	6.51 ± 0.19	7.72 ± 0.24
313	7.53 ± 0.22	8.91 ± 0.26
318	8.59 ± 0.25	10.41 ± 0.30
	NaCl, m = 0.5031	$(CH_3)_4NBr$, m = 0.05211
278	1.97 ± 0.06	3.34 ± 0.10
283	2.28 ± 0.07	3.75 ± 0.11
288	2.72 ± 0.08	4.33 ± 0.13
293	3.29 ± 0.11	4.98 ± 0.16
298	3.97 ± 0.12	5.72 ± 0.18
303	5.06 ± 0.15	6.81 ± 0.20
308	5.84 ± 0.17	8.01 ± 0.23
313	6.74 ± 0.20	9.49 ± 0.28
318	7.64 ± 0.23	11.00 ± 0.33
	NaCl, m = 0.7525	$(CH_3)_4NBr$, m = 0.1014
278	1.68 ± 0.05	3.62 ± 0.11
283	2.01 ± 0.06	4.07 ± 0.14
288	2.36 ± 0.07	4.46 ± 0.14
293	2.85 ± 0.09	5.20 ± 0.15
298	3.43 ± 0.10	6.00 ± 0.18
303	4.30 ± 0.13	7.16 ± 0.21
308	5.08 ± 0.16	8.26 ± 0.24
313	5.81 ± 0.17	9.94 ± 0.29
318	6.76 ± 0.20	11.63 ± 0.35

TABLE 3. Solubility of carbaryl in sodium sulfate and in calcium chloride between 278 and 298 K

T (K)	$S \times 10^4$ (mol kg^{-1})	$S \times 10^4$ (mol kg^{-1})
	Na_2SO_4, m = 0.04987	$CaCl_2$, m = 0.06122
278	2.67 ± 0.08	2.72 ± 0.09
283	3.07 ± 0.09	3.12 ± 0.09
288	3.55 ± 0.11	3.62 ± 0.11
293	4.18 ± 0.14	4.17 ± 0.12
298	4.90 ± 0.15	4.93 ± 0.15
	Na_2SO_4, m = 0.1016	$CaCl_2$, m = 0.07887
278	2.50 ± 0.08	2.72 ± 0.08
283	2.79 ± 0.09	3.10 ± 0.11
288	3.21 ± 0.10	3.50 ± 0.11
293	3.80 ± 0.12	4.08 ± 0.12
298	4.44 ± 0.13	4.80 ± 0.14
	Na_2SO_4, m = 0.1514	$CaCl_2$, m = 0.09997
278	2.16 ± 0.07	2.67 ± 0.10
283	2.47 ± 0.07	2.99 ± 0.09
288	2.87 ± 0.09	3.45 ± 0.10
293	3.37 ± 0.10	4.04 ± 0.13
298	4.00 ± 0.12	4.80 ± 0.14

TABLE 4. Solubility of carbaryl in natural and artificial seawater between 278 and 298 K

T (K)	$S \times 10^4$ (mol kg^{-1})	$S \times 10^4$ (mol kg^{-1})
	Seawater, m = 0.05199	Artificial seawater, m = 0.05298
278	2.48 ± 0.07	2.64 ± 0.08
283	2.94 ± 0.09	3.03 ± 0.09
288	3.42 ± 0.10	3.64 ± 0.11
293	4.15 ± 0.12	4.28 ± 0.13
298	4.93 ± 0.14	5.18 ± 0.15
	Seawater, m = 0.1029	Artificial seawater, m = 0.1069
278	2.22 ± 0.07	2.45 ± 0.07
283	2.77 ± 0.08	2.91 ± 0.09
288	3.30 ± 0.10	3.47 ± 0.10
293	3.96 ± 0.12	4.11 ± 0.12
298	4.88 ± 0.14	4.94 ± 0.14
	Seawater, m = 0.5329	Artificial seawater, m = 0.5365
278	1.78 ± 0.05	1.91 ± 0.06
283	2.10 ± 0.06	2.26 ± 0.07
288	2.52 ± 0.07	2.69 ± 0.08
293	3.01 ± 0.09	3.22 ± 0.09
298	3.62 ± 0.11	3.87 ± 0.11

certain point at which further increases in their respective amounts did not change the solubility values obtained. Furthermore, concentrations similar to those reported by Swann *et al.* (41), within experimental error, were obtained each time their glass beads/pesticide ratio was used.

Tables 2–4 show the solubilities of carbaryl as a function of temperature and electrolyte concentration for the solutions made of NaCl, $(CH_3)_4NBr$, Na_2SO_4, $CaCl_2$ and for natural and artificial seawater. As a rule, carbaryl solubilities increased with increasing temperature and decreased with increasing electrolyte concentration. Only the tetramethylammonium bromide solutions showed an increase in carbaryl solublity with increasing electrolyte concentration (Table 2). These results were as expected since the solubility of nonelectrolytes in water is generally reduced by common inorganic salts, whereas the tetramethylammonium salts often have the opposite effect.

To measure the magnitude of the salting-in or the salting-out effect of the different electrolytes, the Setschenow constants (k_S) were calculated by fitting the different solubilities to eq. [1] using least squares. The results as a function of temperature are given in Figs. 1*a*–1*e*. As expected, the values of the Setschenow constant for carbaryl were positive in all the electrolyte solutions except in tetramethylammonium bromide where salting-in was observed.

The Setschenow constants for NaCl (Fig. 1*a*) generally decreased with increasing temperature. Similar results but opposite in trend were obtained for the salting-in of carbaryl in tetramethylammonium bromide as shown in Fig. 1*d*. The k_S values for sodium sulfate and tetramethylammonium bromide (Figs. 1*b* and 1*d*) remained essentially constant throughout the temperature range considered. Calcium chloride values for k_S (Fig. 1*c*) showed a maximum at 288

Can. J. Chem. Downloaded from www.nrcresearchpress.com by 88.255.202.194 on 09/08/12
For personal use only.

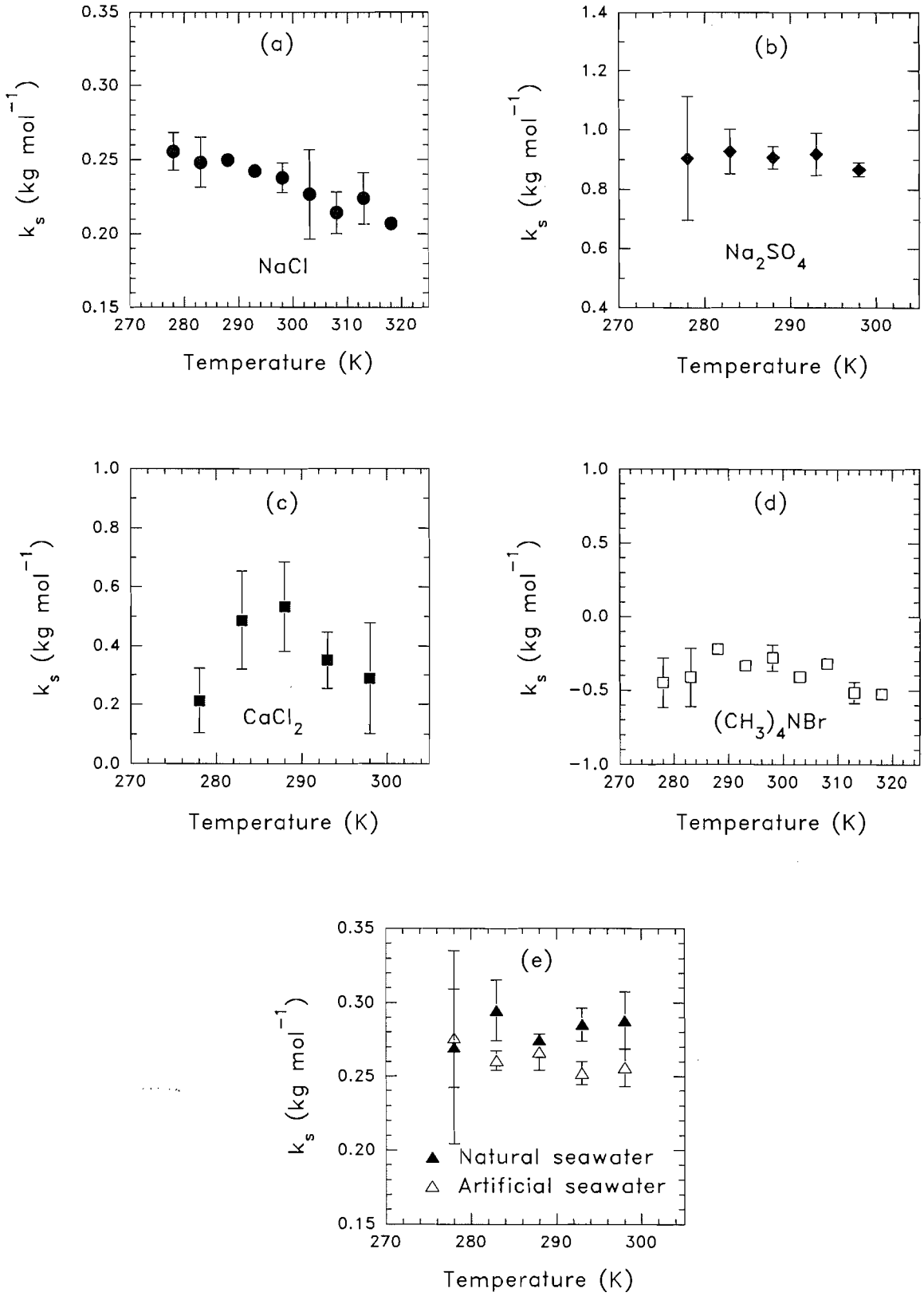

FIG. 1. Setschenow constants (k_S) as a function of temperature for (*a*) sodium chloride, (*b*) sodium sulfate, (*c*) calcium chloride, (*d*) tetramethylammonium bromide, and (*e*) natural and artificial seawater. Error bars correspond to ± (one standard deviation).

K but no conclusion can be reached due to the high uncertainty associated with each value.

As shown in Fig. 1*e*, the Setschenow constants for natural and artificial seawater were approximately constant for the measured temperature range (average of 0.282 ± 0.010 and 0.262 ± 0.009 kg mol^{-1}, respectively). They were also

Can. J. Chem. Downloaded from www.nrcresearchpress.com by 88.255.202.194 on 09/08/12
For personal use only.

similar to those obtained for sodium chloride (average of 0.247 ± 0.007 kg mol^{-1}), the dominant ionic species in seawater, although the trend of the values is somewhat different, reflecting perhaps the combined contributions of the other major constituents of seawater. Setschenow constants in natural and artificial seawater were determined in order to find if there was any effect due to organic matter that might be present in natural seawater. Considering the experimental uncertainty of the individual k_S values, the observed difference between the temperature variation of the Setschenow constant in natural and artificial seawater (Fig. 1*e*) was not clearly established.

Conclusions

Accurate solubility measurements for carbaryl in water, seawater, and different electrolyte solutions were obtained using a generator column system. This method was demonstrated to be a simple, reliable, and reproducible method for determining solubilities of nonpolar molecules like the pesticide carbaryl.

Setschenow parameters of carbaryl were measured as a function of temperature for several salts. We found that generally an increase in temperature decreased the k_S values for sodium chloride solutions and remained essentially constant for sodium sulfate, tetramethylammonium bromide, and natural and artificial seawater. General trends in the Setschenow constants for calcium chloride solutions were not clear due to the high uncertainty associated with each value.

Because sodium chloride is the dominant ionic species in seawater, we would expect a decrease in the solubility of the pesticide carbaryl (and other similar toxic compounds) once it reaches more saline, carbonate-enriched waters like coastal areas. However, this effect could be neutralized in organic-enriched natural waters or waters in which highly polarizable compounds, similar to $(CH_3)_4NBr$ (e.g., borates) are present. To have a better understanding of the behavior of pesticides in our environment more research must be done on this subject.

Acknowledgements

We thank Jean-Christian Auclair and two anonymous reviewers for their comments which helped to improve the original manuscript.

1. W. E. May. *In* Advances in chemistry series. Vol. 185. *Edited by* L. Petrakis and F. T. Weiss. American Chemical Society, Washington, D.C. 1980. pp. 143–192.
2. F. A. Gunther, W. E. Westlake, and P. S. Jaglan. Res. Rev. **20**, 1 (1968).
3. R. Haque and V. H. Freed. Res. Rev. **52**, 89 (1974).
4. R. Battino, T. R. Rettich, and T. Tominaga. J. Phys. Chem. Ref. Data, **12**, 163 (1983).
5. F. A. Long and W. F. McDevit. Chem. Rev. **51**, 119 (1952).
6. H. Martin and C. R. Worthing. Pesticide manual. British Crop Protection Council, England. 1977.
7. N. E. Stewart, R. E. Millerman, and W. P. Breese. Trans. Am. Fish. Soc. **96**, 25 (1967).
8. T. B. Shea and E. S. Berry. Bull. Environ. Contam. Toxicol. **30**, 99 (1983).
9. T. B. Shea and E. S. Berry. Bull. Environ. Contam. Toxicol. **31**, 526 (1983).
10. T. W. Lohner and S. W. Fisher. Aquat. Toxicol. **16**, 335 (1990).
11. W. H. Benson and S. F. Long. Ecotoxicol. Environ. Safety, **21**, 301 (1991).
12. O. M. Aly and M. A. El-Dib. *In* Advances in chemistry series. Vol. 111. *Edited by* R. F. Gould. American Chemical Society, Washington, D.C. 1972. pp. 211–243.
13. J. B. Addison, P. J. Silk, and I. Unger. Int. J. Environ. Anal. Chem. **4**, 135 (1975).
14. J. B. Addison, G. P. Semeluk, and I. Unger. J. Luminesc. **15**, 323 (1977).
15. G. P. Semeluk and I. Unger. J. Luminesc. **17**, 211 (1978).
16. J. B. Addison. Anal. Lett. **12**, 1103 (1979).
17. J. S. Devgun and G. P. Semeluk. Spectrosc. Lett. **12**, 109 (1979).
18. H. W. Dorough and S. K. Ballard. *In* Biodegradation of pesticides. *Edited by* F. Matsumura and C. R. K. Murti. Plenum Press, New York. 1982. pp. 3–20.
19. C. Cruces-Blanco and F. Garcia-Sanchez. J. Photochem. Photobiol. A: **42**, 357 (1988).
20. J. Sancenón, J. L. Carrión, and M. de la Guardia. Fresenius J. Anal. Chem. **336**, 389 (1990).
21. P. Yañez-Sedeño, C. N. Nova, and L. M. P. Díez. Microchem. J. **38**, 370 (1988).
22. A. W. A. Brown. Ecology of pesticides. John Wiley, New York. 1978.
23. R. J. Bushway. J. Chromatogr. **211**, 135 (1981).
24. D. R. Kester, I. W. Duedall, D. N. Connors, and R. M. Pytkowicz. Limnol. Oceanogr. **12**, 176 (1967).
25. W. E. May, S. P. Wasik, and D. H. Freeman. Anal. Chem. **50**, 175 (1978).
26. W. E. May, S. P. Wasik, and D. H. Freeman. Anal. Chem. **50**, 997 (1978).
27. H. DeVoe, M. M. Miller, and S. P. Wasik. J. Res. Nat. Bur. Stand. (U.S.), **86**, 361 (1981).
28. Y. B. Tewari, M. M. Miller, and S. P. Wasik. J. Res. Nat. Bur. Stand. (U.S.), **87**, 155 (1982).
29. Y. B. Tewari, M. M. Miller, S. P. Wasik, and D. E. Martre. J. Chem. Eng. Data, **27**, 451 (1982).
30. W. E. May, S. P. Wasik, M. M. Miller, W. B. Tewari, J. M. Brown-Thomas, and R. N. Goldberg. J. Chem. Eng. Data, **28**, 197 (1983).
31. R. A. Velapoldi, P. A. White, W. E. May, and K. R. Eberhardt. Anal. Chem. **55**, 1896 (1983).
32. A. Lo Surdo, E. M. Alzola, and F. J. Millero. J. Chem. Thermodyn. **14**, 649 (1982).
33. T. Ikono. J. Chem. Eng. Data, **29**, 45 (1983).
34. J. V. Leyendekkers. Thermodynamics of seawater. Marcel Dekker, New York. 1976.
35. UNESCO. Second report of the Joint Panel on Oceanographic Tables and Standards. UNESCO Tech. Pap. Mar. Sci. **4**, 1 (1966).
36. P. R. Bevington. Data reduction and error analysis for the physical sciences. McGraw–Hill, New York. 1969.
37. W. A. L. David, R. L. Metcalf, and M. Winston. J. Econ. Entomol. **53**, 1021 (1960).
38. J. B. Weber. *In* Advances in Chemistry Series. Vol. 111. *Edited by* R. F. Gould. American Chemical Society, Washington, D.C. 1972, pp. 55–120.
39. G. S. Hartley and I. J. Graham-Bryce. Physical principles of pesticide behavior. Vol. 2. Academic Press, London. 1980.
40. G. C. Briggs. J. Agric. Food Chem. **29**, 1050 (1981).
41. R. L. Swann, D. A. Laskowski, P. J. McCall, K. van der Kuy, and H. J. Dishburger. Res. Rev. **85**, 17 (1983).

A physicochemical study on organic eutectics and addition compound; benzidine–pyrogallol system

U. S. Rai and Santhi George

Chemistry Department, Banaras Hindu University, Varanasi - 221 005, U.P. India

Received July 8, 1991[1]

U. S. Rai and Santhi George. Can J. Chem. **70**, 2869 (1992).

The phase diagrams of the binary organic system of benzidine–pyrogallol was determined by the thaw–melt method. The solidification behaviour of the pure components, their eutectics, and the addition compound were studied by measuring the movement of growth front in a capillary. From the data on X-ray diffraction, thermal and microscopic investigations it can be inferred that the eutectics are not simple mechanical mixtures of the components involved. The IR and NMR spectral investigations were carried out to throw light on the nature of bonding between the two components forming the addition compound.

U. S. Rai et Santhi George. Can. J. Chem. **70**, 2869 (1992).

Faisant appel à la méthode de fusion, on a déterminé les diagrammes de phase du système organique binaire benzidine/pyrogallol. En mesurant le mouvement de croissance du front dans la capillaire, on a étudié le comportement lors de leur solidification des composants purs, de leurs eutectiques et de leur composé d'addition. En se basant sur des études thermiques, microscopiques et de diffraction des rayons X, on peut déduire que les eutectiques ne sont pas de simples mélanges des composants impliqués. Des études par spectroscopies IR et RMN ont été entreprises afin de faire la lumière sur la nature des liaisons entre les deux composants formant le composé d'addition.

[Traduit par la rédaction]

1. Introduction

The past decade has witnessed (1–6) an immense activity both in the fundamental understanding of the solidification and properties of polyphase alloys and in the technological developments of *in situ* composites for particular applications. Owing to the low transformation temperature, ease in purification, transparency, minimised convection effects and wider choice of materials, the organic systems (7–12) are being used as model systems for a detailed investigation of the parameters which control solidification, which in turn, govern the properties of materials. As the organic eutectics and the molecular complexes are analogues of metal eutectics and intermetallic compounds, respectively, a systematic physicochemical study of a model system involving organic compounds may be of potential importance in unravelling the mysteries of solidification, bonding, and microstructure, among others. In view of this, a binary organic system involving benzidine (BZ) and pyrogallol (PG) has been chosen to study its phase diagram, linear velocity of crystallization, thermochemistry, microstructure, X-ray diffraction, and spectral behaviour.

2. Experimental

2.1 Materials and purification

AR grade benzidine (CDH, India) was directly used in the present investigation. Pyrogallol (S.d. Fine-Chem Pvt Ltd., India) was purified by repeated distillation under reduced pressure and was stored in a coloured bottle to avoid exposure to light. The melting point of each compound (benzidine, 127°C and pyrogallol, 134°C) was compared with its literature value (benzidine, 128°C and pyrogallol, 134°C) to assess its purity.

2.2 Phase diagram

The phase diagram of the benzidine–pyrogallol system was determined by the thaw–melt method (13, 14). In this method, mixtures of two components covering the entire range of composition were prepared in different long-necked test tubes. These mixtures were homogenized by melting in silicone oil followed by chilling in ice. Their thaw and melting temperatures were determined using a Toshniwal melting point apparatus equipped with a precision thermometer which could read correctly up to ±0.5°C.

2.3 Linear velocity of crystallization

The linear velocity of crystallization data for the pure components, the eutectics, and the addition compound were determined (15, 16) at different undercooling temperatures by measuring the movement of the solid-liquid interface in the capillary tube of 15 cm length and 0.5 cm inner diameter.

2.4 Heat of fusion

Heats of fusion of the pure components, the eutectics, and the addition compound were determined (17) by using a Dupont-9900 thermal analysis DSC apparatus.

2.5 Microstructure

Microstructures of the eutectics and the addition compound were recorded (18, 19) by placing the slide containing unidirectionally solidified sample on the platform of a Leitz Labourlux D optical microscope attached with a camera.

2.6 X-ray diffraction

X-ray diffraction patterns of the pure components, the eutectics, and the addition compound were recorded (20, 21) on a computerized X-ray diffraction unit, PW 1710 model, using CuK_α radiation.

2.7 Spectral studies

Infrared spectra of the pure components, the eutectics, and the addition compound were recorded (22) in the region 4000–625 cm^{-1} in Nujol mull using a Perkin-Elmer 783 infrared spectrometer. $CDCl_3$ was used as a solvent for recording the PMR spectra on Jeol FX 90 Q Fourier Transform NMR spectrometer.

3. Results and discussion

3.1 Phase diagram

The solid–liquid equilibrium data on the BZ–PG system are given in Fig. 1 in the form of a temperature–composition curve. The plot shows the formation of a 1:1 addition compound with congruent melting point surrounded by two eutectics E_1 and E_2, containing 0.902 and 0.139 mole fractions of benzidine, respectively. The melting point of pure benzidine is 127.0°C and it decreases continuously with the

[1]Revision received July 28, 1992.

Can. J. Chem. Downloaded from www.nrcresearchpress.com by 88.255.202.194 on 09/08/12
For personal use only.

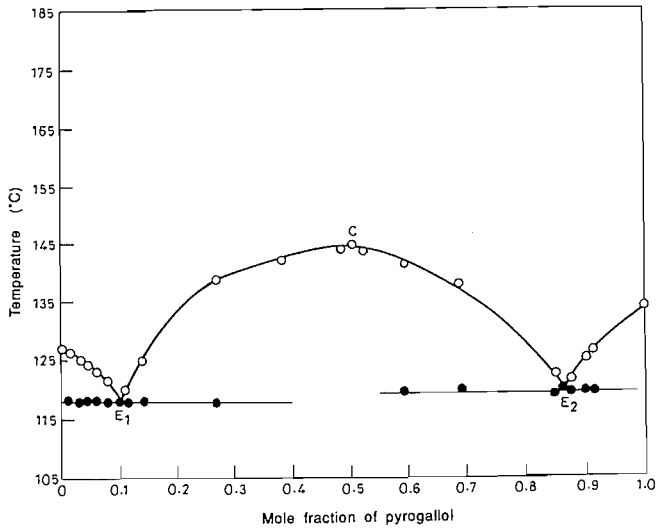

FIG. 1. Phase diagram of the benzidine–pyrogallol system. ○, Melting temperature; ●, thaw temperature.

addition of pyrogallol and attains a minimum at E_1 (118.0°C). With continued addition of pyrogallol the melting point rises to a maximum of 145.0°C at C after which it decreases to a minimum of 120.5°C at E_2. At point C the solid and the corresponding liquid have identical composition. This phase diagram may be viewed as consisting of two simple eutectic type phase diagrams placed side-by-side. The flatness in the maximum at C suggests that the addition compound is dissociated (23, 24) in the molten state.

3.2 Linear velocity of crystallization

According to Hillig and Turnbull (25), the linear velocity of crystallization (v) of each of the pure components, the eutectics, and the addition compound is related to the undercooling (T) by the equation

$$[1] \quad v = u(\Delta T)^n$$

where u and n are constants. The constants u and n are calculated from the linear plots (Fig. 2) of log v versus log ΔT and the values are reported in Table 1. It is evident from the table that most of the n values are close to 2, thereby suggesting a square relationship between v and ΔT. However, the deviations in the values of n from 2, observed in some cases, may be due to the difference in the bath temperature and the temperature of the growing interface. In the present investigation, both components have a high enthalpy of fusion, consequently each crystallization step results in a release of heat causing the interface to attain a higher temperature than the bath.

From the values of u (Table 1) for the pure components and the addition compound, it can be inferred that the crystallization rate of the addition compound of the BZ–PG system is less than that of the parent components. Studies on the crystal morphology of the addition compounds indicate that they crystallize as a definite chemical entity. However, during crystallization, the two components of the melt have to enter the crystal lattice simultaneously in such a way that the composition of the melt conforms to the respective molar ratios of the components. Thus the linear velocity of crystallization of the addition compound may be expected to be of the order of the growth velocity of the species crystallizing with the lower rate. The value of u for E_1 (formed between benzidine and the addition compound) is higher than that of either component while for E_2 (formed between the addition compound and pyrogallol) it lies between the corresponding components. These results may be explained on the basis of the mechanism proposed by Winegard *et al.* (26) and substantiated by others. Accordingly, the solidification of both the eutectics of BZ–PG system takes place by the side-by-side growth of the two components. In the eutectics under investigation the addition compound behaves as one of the components, and its melting point is higher than those of the components it nucleates first.

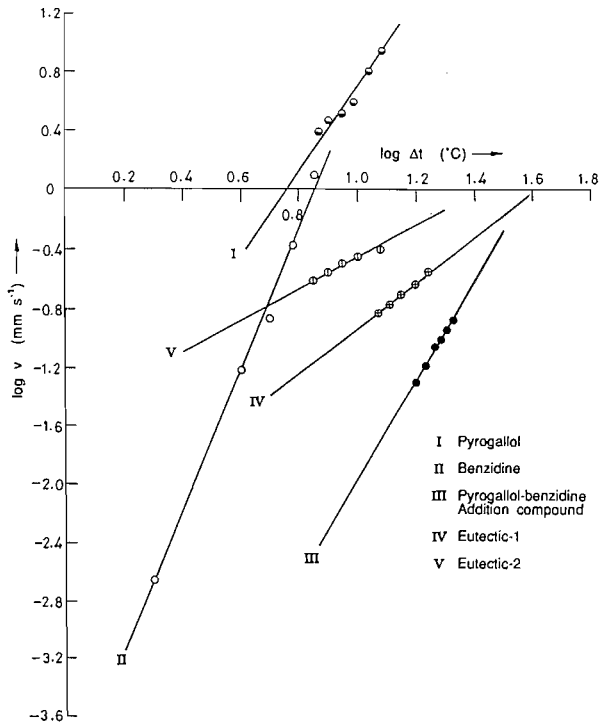

FIG. 2. Linear velocity of crystallization of the benzidine–pyrogallol system.

TABLE 1. Values of u and n of benzidine–pyrogallol system

Material	u (mm s^{-1} deg^{-1})	n
Benzidine	0.000105	4.00
Pyrogallol	0.007244	2.50
Eutectic-1	0.000724	1.86
Eutectic-2	0.006918	1.50
1:1 Addition compound	0.000005	3.33

3.3 Thermochemical studies

One may get an idea on the mode of crystallization, structure of eutectic melt, and the nature of interaction between two components forming the eutectics and the addition compound from their heats of fusion. For the purpose of comparison, the experimental and calculated values of heat of fusion for the eutectics are reported in Table 2. It is evident from the data in the table that the calculated (27) values of the heat of fusion are higher than the experimental

Can. J. Chem. Downloaded from www.nrcresearchpress.com by 88.255.202.194 on 09/08/12
For personal use only.

TABLE 2. Heat of fusion and heat of mixing of benzidine–pyrogallol system

Material	Heat of fusion (kJ mol^{-1})	Entropy of fusion (kJ mol^{-1} K^{-1})	Roughness parameter $\Delta S_f/R$	Heat of mixing (kJ mol^{-1})
Benzidine	19.10	0.0478	5.77	—
Pyrogallol	18.55	0.0456	5.51	—
Eutectic-1				
(exptl.)	16.67	0.0426	5.15	−4.72
(calcd.)	21.39			
Eutectic-2				
(exptl.)	21.68	0.0551	6.66	−0.17
(calcd.)	21.85			
1:1 Addition compound				
(exptl.)	21.19	0.0507	6.13	−16.43
(calcd.)	37.62			

values. If an eutectic is a simple mechanical mixture of two components involving no heat of mixing or any type of association in the melt, the heat of fusion will be simply given by the mixture law (19). However, when a solid eutectic melts there is considerable likelihood of association and mixing, both causing violation of the mixture law. The difference between the experimental and calculated values can be attributed to the formation of clusters in the eutectic melt. In the present eutectic system where one component has an $—NH_2$ group and the other contains an —OH group, both the end members have a tendency for hydrogen bond formation, resulting in a favourable condition for cluster (28) formation in the melt. The values of heat of mixing (29) (ΔH_m), which is the difference between the experimental and calculated values of the heat of fusion, were calculated for both eutectics and the data are reported in Table 2. It is clear that the values are highly negative. According to thermochemical studies (13) the structure of the eutectic melt depends on the sign and magnitude of the enthalpy of mixing. Three types of structures are suggested; quasieutectic $\Delta H_m > 0$, clustering of molecules for $\Delta H_m < 0$, and molecular solution for $\Delta H_m = 0$. The negative values of ΔH_m for the eutectics of the BZ–PG system suggest clustering of molecules in the eutectic melt. To see a small value of heat of mixing in the case of E_2 of the system, one might be tempted to consider the formation (30) of a molecular solution instead of a weak interaction. It may be noted that this system is quite different from simple eutectic systems where merely ordering of the parent phases has been suggested in the melts. It seems that there is considerable enhancement in the interactions due to the presence of molecular complex in the melt.

The experimental values of the heat of fusion of the addition compound determined by the DSC method are reported in Table 2. Its theoretical value was calculated by a method reported earlier (28). It is evident from Table 2 that the heat of mixing is highly negative. This suggests (30) that the presence of an addition compound enhances the attraction among the components. The association is also favoured by the presence of hydroxyl and amino groups in the components.

The deviation from ideal behaviour can best be expressed in terms of excess thermodynamic functions which give more quantitative ideas about the nature of the molecular interactions. It is defined as the difference between the thermodynamic function of mixing for a real system and the corresponding value for an ideal system at the same temperature and pressure. To understand the nature of interaction between two components forming the eutectics, some thermodynamic functions such as excess free energy (g^E), excess enthalpy (h^E) and excess entropy (S^E) were calculated by a method reported earlier (27). The positive g^E values (Table 3) suggest (31) that the interaction between like molecules is stronger than that between unlike molecules. The values of h^E and s^E correspond to the excess free energy and are a measure of the excess enthalpy of mixing and excess entropy of mixing, respectively.

TABLE 3. Excess thermodynamic functions for benzidine–pyrogallol system

Material	g^E (J mol^{-1})	h^E (J mol^{-1})	S^E (J mol^{-1} K^{-1})
Eutectic-1	580.02	1201.28	1.62
Eutectic-2	712.32	4383.36	9.34

3.4 Microstructure

It is well known that in a polyphase material the microstructure provides data on the size, shape and orientation of the grains in addition to the distribution of the phases involved. The arrangement of grains and phases in a material controls its mechanical properties and decides its various applications. The shape (32) that a crystal adopts in the melt subsequent to nucleation is controlled by the way in which atoms molecules are added onto the solid, which in turn is determined by the atomic/molecular structure of the solid–liquid interface. However, the interface structure depends upon the chemical character of the material in question and also upon the thermal environments in which the crystal is growing. For a material with entropy of fusion less than $2R$ (where R is the gas constant), the interface which is about 50% populated is atomically rough and results in non-faceted growth. On the other hand, for a material with entropy of fusion greater than $2R$, the interface is perfect with a few atoms missing from it, and results in faceted growth. In the present investigation, the pure components have their entropy of fusion greater than $2R$, thereby resulting in faceted growth. The morphology of eutectics developed in each case is influenced by the entropy of fusion of the phases involved. The microstructures of the eutectics under investi-

Can. J. Chem. Downloaded from www.nrcresearchpress.com by 88.255.202.194 on 09/08/12
For personal use only.

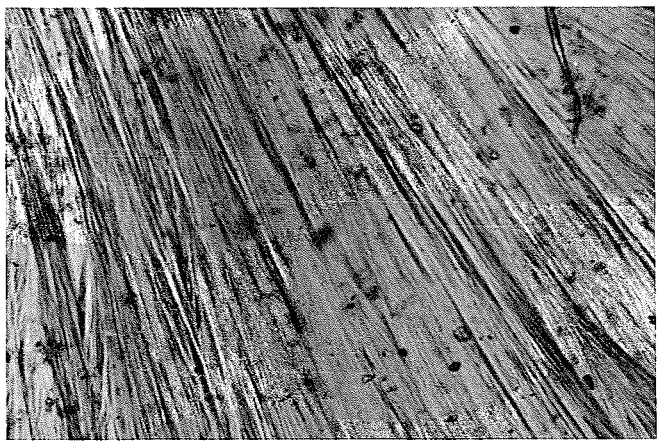

FIG. 3. Microstructure of the benzidine–pyrogallol eutectic (E_1) × 100.

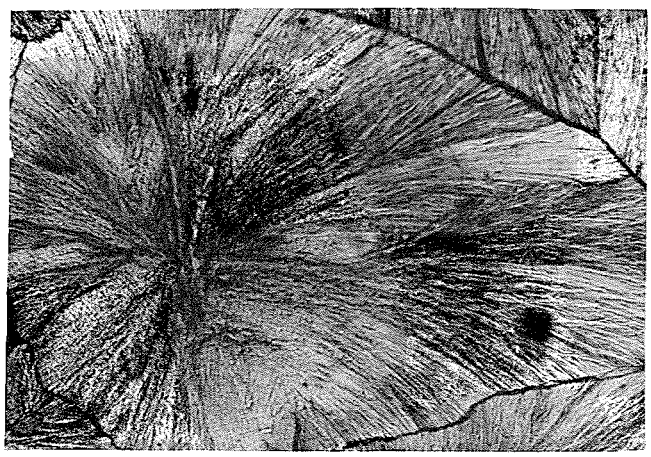

FIG. 4. Microstructure of the benzidine–pyrogallol eutectic (E_2) × 100.

gation are given in Figs. 3 and 4. While the eutectics E_1 of the BZ–PG system given in Fig. 3 shows lamellar growth, the second eutectic E_2 (Fig. 4) of this system indicates that one of the phases nucleates first and the other phase radiates outward perpendicularly. The microstructure of the addition compound (Fig. 5) shows faceted growth like pure components.

3.5 X-ray diffraction

A critical scanning of the current literature (19) reveals that there are two conflicting ideas about the nature and bonding in eutectics. While one group of workers believes that a binary eutectic is a mixture of two kinds of crystals, favourably oriented with respect to each other, the other group is of the opinion that the eutectic grains do not exhibit a fixed orientational relationship. To clarify this, the X-ray diffraction patterns of the pure components, the eutectics, and the addition compounds were recorded and the results are reported in Tables 4 and 5. It is evident from the reported data that the number of reflections of pure components and the addition compounds is comparable with the number of reflections of their corresponding eutectics. It can be inferred from this observation that they belong to the same crystal system and have similar lattices. It is evident from the results reported in Table 4 that for the BZ–PG system strong reflections of benzidine and the addition compound are either absent in the eutectic E_1 or show a variation of intensity. Accordingly, reflections of benzidine and *d* values 4.82, 4.45, 3.12 Å show an increase in intensity and those at 4.23, 3.83, and 3.35 Å show a decrease in intensity in the eutectic E_1. Similarly, reflections of the addition compound at *d* values 5.25, 4.47, 4.35, 3.94, 3.84, 3.30, and 3.14 Å show a decrease in intensity and those at *d* values 4.58, 3.53, and 3.10 Å show an increase in intensity in the eutectic E_1.

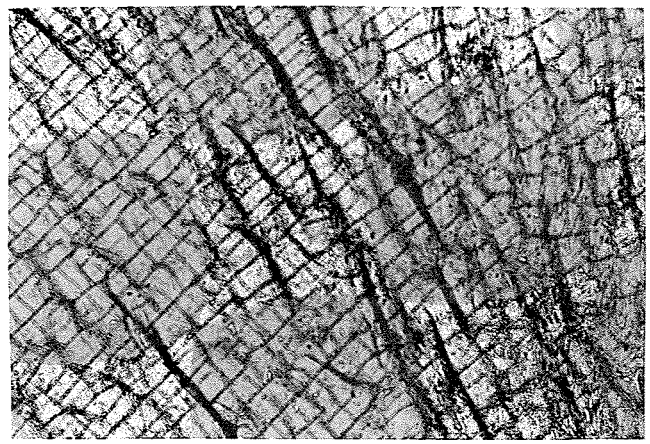

FIG. 5. Microstructure of the benzidine–pyrogallol addition compound (A) × 100.

The X-ray patterns of the two components should be exactly superimposed on the eutectic composite if a eutectic is a simple mechanical mixture of two components. From the diffraction data on the pure components, the eutectics, and the addition compound, it can be inferred that there is a marked difference in the interplanar distance and the relative intensity. The variation in relative intensity of the reflections of pure components in the eutectics and the absence of reflections of pure components in eutectics and those of eutectics in pure components suggest that the eutectics are not simply a mechanical mixture of two components. There is orientation of some atomic planes during the formation of the eutectics.

3.6 Spectral studies

The IR spectrum of benzidine in Nujol shows three bands at (*i*) 3190, (*ii*) 3320, and (*iii*) 3400 cm^{-1} due to NH stretching vibrations. The IR spectrum of the pyrogallol in Nujol exhibits four bands at (*i*) 3280, (*ii*) 3250, (*iii*) 3380, and (*iv*) 3480 cm^{-1} due to OH stretching vibration in the compound. The addition compound gives four peaks: (*i*) 3300, (*ii*) 3355, (*iii*) 3380, and (*iv*) 3485 cm^{-1}. This may be attributed to the merging of a peak of benzidine at 3190 cm^{-1} and that of pyrogallol at 3280 cm^{-1} resulting a new peak at 3300 cm^{-1} in the addition compound because of intermolecular interaction between the two components. However, no definite conclusion can be drawn from the IR data. The proton NMR spectrum of benzidine shows a peak at δ 3.52 due to NH proton, and the ring protons are obtained as multiplets in the range δ 6.48 – δ 7.37. Pyrogallol gives a proton signal at δ 1.6. The molecular complex of the BZ–PG system gives a broad band in the range δ 1.58 – δ 1.14 and shows the disappearance of the OH proton signal which may

Can. J. Chem. Downloaded from www.nrcresearchpress.com by 88.255.202.194 on 09/08/12
For personal use only.

TABLE 4. *d* values and relative intensity (RI) of benzidine, eutectic-1 and the addition compound of the benzidine–parogallol system

Benzidine		Eutectic-1		1:1 Addition compound	
d (Å)	RI	*d* (Å)	RI	*d* (Å)	RI
14.35	3	—	—	—	—
10.20	4	—	—	—	—
9.49	4	—	—	—	—
9.03	3	—	—	—	—
—	—	8.97	11	8.99	8
—	—	8.56	5	—	—
—	—	7.96	10	8.00	8
7.01	4	—	—	—	—
—	—	6.86	9	6.85	10
—	—	6.58	11	6.57	12
6.28	12	—	—	—	—
—	—	5.86	15	5.85	15
5.74	20	—	—	5.70	9
5.42	29	—	—	—	—
5.40	30	—	—	—	—
—	—	5.34	19	5.34	18
—	—	5.25	21	5.25	24
—	—	—	—	5.01	23
5.07	20	—	—	—	—
4.94	22	4.91	43	4.90	43
4.82	60	4.84	100	4.84	100
4.79	34	—	—	—	—
—	—	4.58	47	4.58	45
—	—	4.53	52	4.53	51
4.45	39	4.48	51	4.47	54
4.40	100	—	—	—	—
—	—	4.34	55	4.35	57
4.23	70	4.19	34	—	—
4.12	73	4.11	72	4.11	73
4.04	28	—	—	—	—
—	—	—	—	3.98	24
—	—	3.94	34	3.94	37
3.86	19	—	—	—	—
3.83	40	3.84	29	3.84	31
—	—	3.82	32	—	—
3.72	21	3.76	22	3.76	22
—	—	3.65	11	3.60	14
3.58	15	3.54	19	3.53	17
3.47	13	—	—	—	—
3.42	19	3.39	37	3.39	37
3.35	40	3.35	38	3.35	39
3.25	8	3.30	13	3.30	20
3.18	11	3.23	19	3.20	21
3.12	20	3.14	29	3.14	32
—	—	3.10	27	3.10	24
3.04	10	3.06	30	3.06	31
—	—	3.03	24	3.03	25

TABLE 5. *d* values and relative intensity (RI) of benzidine, eutectic-2, and the addition compound of the benzidine–pyrogallol system

Pyrogallol		Eutectic-2		1:1 Addition compound	
d (Å)	RI	*d* (Å)	RI	*d* (Å)	RI
—	—	17.20	5	—	—
12.30	100	—	—	—	—
—	—	10.70	100	—	—
—	—	—	—	8.99	8
8.70	30	—	—	—	—
—	—	8.42	9	—	—
—	—	—	—	8.00	8
6.80	10	—	—	6.85	10
—	—	—	—	6.57	12
6.10	60	—	—	—	—
—	—	5.99	19	—	—
—	—	—	—	5.85	15
—	—	—	—	5.70	9
—	—	5.57	11	—	—
—	—	5.57	11	—	—
5.50	50	5.50	29	—	—
—	—	5.34	44	5.34	18
—	—	—	—	5.25	24
—	—	—	—	5.01	23
—	—	—	—	4.90	43
—	—	—	—	4.84	100
—	—	4.60	7	4.58	45
—	—	4.51	9	4.53	51
—	—	—	—	4.47	54
—	—	4.40	14	4.35	57
4.08	20	4.10	7	4.11	73
—	—	—	—	3.98	24
3.91	20	—	—	3.94	37
—	—	—	—	3.84	31
—	—	—	—	3.76	22
3.67	30	3.65	26	—	—
—	—	—	—	3.60	14
3.52	100	3.56	7	3.53	17
—	—	—	—	3.39	37
3.35	20	3.36	14	3.35	39
3.23	75	3.27	27	3.30	20
—	—	3.21	9	3.20	21
—	—	3.17	12	3.14	32
—	—	—	—	3.10	24
—	—	—	—	3.06	31
3.01	50	—	—	3.03	25
—	—	—	—	2.98	17
—	—	—	—	2.92	10
2.85	40	—	—	2.84	9

be due to a slow exchange (33) between the OH and NH protons. This upfield shift of NH proton signal may be due to intermolecular hydrogen bonding between N of NH_2 and H of OH of pyrogallol.

Acknowledgement

We thank Professor K. N. Mehrotra, Head, Chemistry Department, Banaras Hindu University, for providing research facilities.

1. R. Elliott. Eutectic solidification processing. Butterworths, London. 1983.
2. M. M. Schwartz. Composite materials hand book. McGraw Hill Book Company, New York. 1984.
3. K. A. Jackson. Mater. Sci. Eng. **65**, 7 (1984).
4. C. Schafer, M. H. Johnson, and R. A. Parr. Acta Metall. **31**, 1221 (1983).
5. R. Elliott. Cast iron. Butterworths, London. 1988.
6. W. Kurz and R. Trivedi. Proc. Third Int. Conf. on Solidification Processing, Sheffield. 1987. p. 1.
7. N. B. Singh and K. D. Dwivedi. J. Sci. Ind. Res. **41**, 98 (1982).
8. R. P. Rastogi, D. P. Singh, N. Singh, and N. B. Singh. Mol. Cryst. Liq. Cryst. **73**, 7 (1981).

Can. J. Chem. Downloaded from www.nrcresearchpress.com by 88.255.202.194 on 09/08/12
For personal use only.

9. K. Pigon and A. Krajewska. Thermochim. Acta, **58**, 299 (1982).
10. M. E. Glicksman, N. B. Singh, and M. Chopra. Manuf. Space, **11**, 207 (1983).
11. N. B. Singh, N. N. Singh, and R. K. Laidlaw. J. Solid State Chem. **71**, 530 (1987).
12. H. Song and A. Hellawell. Metall. Trans. **20A**, 171 (1989).
13. U. S. Rai, K. D. Mandal, and N. P. Singh. J. Thermal Anal. **35**, 1687 (1989).
14. B. M. Shukla, N. P. Singh, and N. B. Singh. Mol. Cryst. Liq. Cryst. **104**, 265 (1984).
15. N. B. Singh and N. B. Singh. Krist. Tech. **13**, 1175 (1978).
16. U. S. Rai and K. D. Mandal. Bull. Chem. Soc. Jpn. **63**, 1496 (1990).
17. U. S. Rai, O. P. Singh, and N. B. Singh. Can. J. Chem. **65**, 2639 (1987).
18. R. P. Rastogi and V. K. Rastogi. J. Cryst. Growth, **5**, 345 (1969).
19. U. S. Rai and K. D. Mandal. Mol. Cryst. Liq. Cryst. Liq. Cryst. **182**, 387 (1990).
20. U. S. Rai and K. D. Mandal. Thermochim. Acta, **138**, 219 (1989).
21. N. P. Singh and B. M. Shukla. Cryst. Res. Technol. **20**, 345 (1985).
22. U. S. Rai and K. D. Mandal. Curr. Sci. **58**, 784 (1989).
23. R. P. Rastogi. J. Chem. Educ. **41**, 443 (1964).
24. M. Radomska and R. Radomski. Thermochim. Acta, **40**, 415 (1980).
25. W. B. Hillig and D. Turnbull. J. Chem. Phys. **24**, 914 (1954).
26. W. C. Winegard, S. Mojka, B. M. Thall, and B. Chalmers. Can. J. Chem. **29**, 320 (1957).
27. U. S. Rai, O. P. Singh, N. P. Singh, and N. B. Singh. Thermochim. Acta, **71**, 373 (1983).
28. R. P. Rastogi, N. B. Singh, and K. D. Dwivedi. Ber. Bunsenges. Phys. Chem. **85**, 85 (1981).
29. U. S. Rai and K. D. Mandal. Mat. Sci. Forum, **50**, 117 (1989).
30. N. P. Singh, B. M. Shukla, N. Singh, and N. B. Singh. J. Chem. Eng. Data, **30**, 49 (1985).
31. J. Wisniak and A. Tamir. Mixing and excess thermodynamic properties. Elsevier, New York. 1978.
32. G. A. Chadwick. Metallography of phase transformations. Butterworths and Co. Publishers Ltd., London. 1972.
33. R. M. Silverstein, G. C. Basslev, and T. C. Morill. Spectrometric identification of organic compounds. 4th ed. John Wiley & Sons, Inc., New York. 1981. pp. 95–105.

Can. J. Chem. Downloaded from www.nrcresearchpress.com by 88.255.202.194 on 09/08/12
For personal use only.

Vibrational spectroscopic study of the interaction of metal ions with diethyl phosphate, a model for biological systems

JANUSZ STANGRET[1] AND RODRIGUE SAVOIE[2]
Department of Chemistry, Laval University, Québec (Qué.), Canada G1K 7P4

Received June 3, 1991

JANUSZ STANGRET and RODRIGUE SAVOIE. Can. J. Chem. **70**, 2875 (1992).

We have studied, using Raman and infrared spectroscopy, the interaction of various monovalent, divalent, and trivalent metal cations with the PO_2^- group of diethyl phosphate in aqueous solution, at metal:phosphate ratios ranging from 1:40 to 6:1. The results show that the metal cations interact with the phosphate groups in various ways and to different extents. Spectral characteristics for some specific types of interactions are presented, namely, for direct metal binding by one of the oxygen atoms in the PO_2^- group, the formation of water-separated ion pairs, and non-specific electrostatic interactions.

JANUSZ STANGRET et RODRIGUE SAVOIE. Can. J. Chem. **70**, 2875 (1992).

Nous avons étudié par spectroscopie Raman et infrarouge l'interaction de divers cations métalliques monovalents, divalents et trivalents avec le groupe chargé PO_2^- du phosphate de diéthyle en solution aqueuse, à des rapports métal : phosphate variant de 1 : 40 à 6 : 1. Les résultats démontrent que les ions se distinguent tant par leur affinité pour le groupement phosphate que par leur façon d'interagir avec celui-ci. On présente diverses caractéristiques spectrales permettant d'identifier certains types d'interaction, notamment la fixation directe par l'un des atomes d'oxygène du groupement phosphate, la formation de paires d'ions séparées par molécules d'eau et les interactions non spécifiques de nature électrostatique.

Can. J. Chem. Downloaded from www.nrcresearchpress.com by 109.225.110.28 on 09/08/12
For personal use only.

Introduction

Phosphate groups are of prime importance in biological systems, as they are present in major classes of compounds, such as nucleic acids, phospholipids, etc. In DNA, they play a structural role in the linking of subunits through a phosphodiester bridge of the type $R_1O—PO_2^-—OR_2$. They can also interact with positively charged species, such as basic proteins and metal ions, through the negative charge on the PO_2^- groups. Although many metal cations can interact with the bases as well as with the phosphate groups in nucleic acids, the latter type of interaction is particularly important as it stabilizes the DNA double helix (1, 2). From theoretical considerations (3), phosphate groups also appear to be the most likely association sites for water in nucleic acids. Furthermore, the manner in which water molecules are organized around DNA through PO_2^-–metal–water interactions seems to be an important factor in the stabilization of specific DNA conformations (4).

Vibrational spectroscopy, particularly Raman spectroscopy, has been used extensively for the study of nucleic acids (5–8). The symmetric stretching vibration of the PO_2^- groups gives a moderately strong and sharp band near 1090 cm^{-1} in the Raman spectrum of DNA. This peak is relatively insensitive to the conformation of the polynucleotide and many investigators have followed the suggestion of Tsuboi *et al.* (9) that it be used as an internal standard in conformational studies. On the other hand, Raman studies of aqueous DNA solutions have shown that this band can be affected in intensity as well as in frequency when metal ions are present in the solution (10–12). Just how these changes are related to the extent and type of metal binding by the phosphate groups is not completely understood. It is the purpose of the present study to investigate this behavior with a very simple model compound, the diethyl phosphate anion ($(C_2H_5O)_2PO_2^-$), in the presence of different types of metal cations. The vibrational spectra of various salts of DEP have been reported previously (13–16) and they have been the subject of force constant calculations (14, 15, 17). This molecule has also been used as a model for the calculation of the vibrational frequencies of the DNA backbone (14, 18) and of the phosphate group in phospholipids (2).

Experimental

Diethyl phosphate (DEP, acid form) was purchased from Eastman Kodak and used without further purification. Metal salts were reagent grade and used as supplied. Stock solutions were prepared by mixing weighted amounts of diethyl phosphate in demineralized water and neutralizing with aqueous NaOH (or LiOH or KOH). The pH was measured with a micro-electrode and an Orion Research Model 721 pH-meter. These DEP solutions, at 0.1 or 0.3 M concentration, were used to obtain the reference spectra. Weighted amounts of the solid metal chlorides were dissolved in the reference solutions to prepare mixed samples at various metal:DEP ratios. The series of $NiCl_2$ solutions at appropriate Ni^{2+} concentrations were prepared by mixing equal volumes of a DEP reference solution and solutions of $NiCl_2$ (from the same original stock solution) at the appropriate molar concentration. The pH was not adjusted following the mixing; it varied from 7.5 for the pure DEP solution to 5.5 for a solution at 6:1 Ni:DEP molal ratio.

The Raman spectra were obtained from the aqueous samples contained in sealed capillary cells placed in a temperature-regulated holder (19). These spectra were recorded on a microcomputer-controlled Spex Model 1400 spectrometer, with either a conventional photomultiplier detection system or a multichannel detector (CCD9000 system from Photometrics Ltd., with 1152 × 298 pixels Thompson TH7895 detector). The spectra were excited by the 514.5 nm line from a Spectra Physics Model 2020 argon ion laser at an average power of 300 mW at the sample. The dispersive spectra were obtained at a spectral resolution of 5 cm^{-1}, the data being collected at 2 cm^{-1} intervals. The total integration time was 25s per point, resulting from the summation of 5 spectra obtained at 5s per point. The spectra obtained with the multichannel detector (1152 data points) covered a spectral region of ca. 500 cm^{-1} with 1200 grooves/mm gratings or ca. 2000 cm^{-1} with

[1]Permanent address: Department of Physical Chemistry, Institute of Inorganic Chemistry and Technology, Technical University of Gdańsk, 80-952 Gdańsk, Poland.

[2]Author to whom correspondence should be addressed.

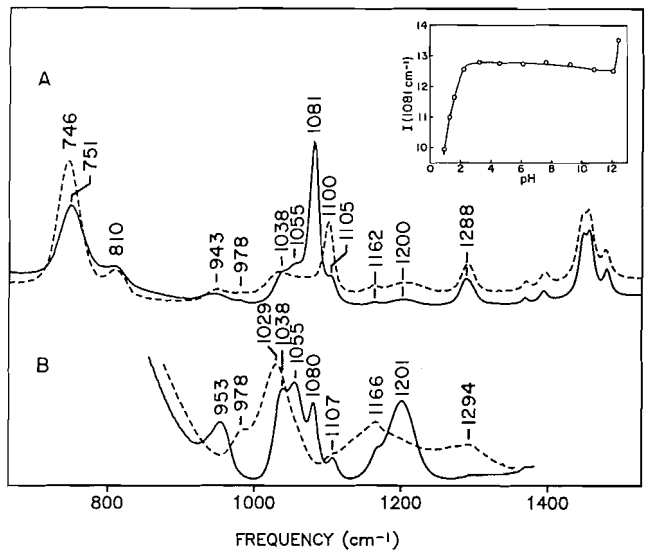

FIG. 1. (*A*) Raman and (*B*) infrared spectra of an aqueous solution of diethyl phosphate at 20°C; (—) 0.3M solution at pH 7 and (- - -) 1M solution in 4M HCl (pH < 0). Insert: variation in intensity of the 1081 cm^{-1} Raman band of the anion as a function of pH.

300 grooves/mm gratings. Intensity corrections were made for the transmission of the spectrometer and of the filter (holographic edge filter from Physical Optics Corporation, Torrance, CA, U.S.A.). The frequency calibration was achieved using emission lines from a neon spectral lamp (20), with an estimated accuracy of 1 cm^{-1} or better. The entrance slit of the spectrometer was adjusted to yield the maximum resolution consistent with channel separation in the detector (ca. 0.5 and 2 cm^{-1}, respectively, with the two types of gratings). The acquisition time was 10 min on the average.

The infrared spectra were obtained from samples contained between two BaF_2 windows separated by a 10 μm-thick Mylar spacer. They were recorded on a commercial BOMEM Model DA3.02 interferometer with MCT detector. These spectra were typically taken at a spectral resolution of 2 cm^{-1} by summation of 1000 interferograms and using a Bartlett apodisation function.

Spectral manipulations were performed with the *SpectraCalc* program (Galactic Industries Corporation, Salem, New Hampshire, U.S.A.).

Results

The Raman and infrared spectra of neutral (sodium salt) and strongly acidic aqueous solutions of diethyl phosphate are reproduced in Fig. 1. At neutral pH, the phosphate group of this molecule is ionized, giving the $(C_2H_5O)_2PO_2^-$ anion. Previous studies (13, 17) have shown that the stretching vibrations of the phosphate group in this species occur in two different regions: the charged PO_2^- group gives a symmetric mode (ν_s) responsible for the strong Raman band and medium intensity infrared peak near 1080 cm^{-1}, whereas the antisymmetric mode (ν_a) gives a strong infrared band, with little corresponding Raman activity, at ca. 1200 cm^{-1}. The phosphodiester —O—P—O— group is also characterized by symmetric and antisymmetric components, which give, respectively, a strong maximum near 750 cm^{-1} and a weaker band at 810 cm^{-1} in the Raman spectrum. The two strong bands at 1038 and 1055 cm^{-1} in the infrared, with relatively weak Raman counterparts, are usually assigned to C—O vibrations, and that at 953 cm^{-1} to a C—C stretching mode (2, 13, 14, 16). The weak band at 1105 cm^{-1}, present in both types of spectra, has generally been identified as a component of the $\nu_s(PO_2^-)$ vibration in the solid phase spectra. Its presence in the solution spectra, its absence in the spectra of dimethyl phosphate, and the fact that it is only weakly active in the spectra of methyl ethyl phosphate (15, 16) suggest that the band corresponds to a fundamental vibration of the ethyl group. Most of the weaker bands at frequencies higher than 1100 cm^{-1} arise from vibrations of alkyl groups.

Normal coordinate calculations have indicated that vibrational frequencies of the phosphate group in DEP vary with the molecular conformation (14, 15, 17). However, these effects are small and we have assumed that the spectral changes resulting from the addition of metal cations to DEP were not caused by changes in the distribution of these structures in the solutions.

Protonation of DEP causes important changes in the vibrations of the PO_2^- group. The infrared and Raman bands at 1080 cm^{-1}, caused by the ν_s vibration of this group, are practically absent from the spectra of a strongly acidic solution (Fig. 1). Similarly, the strong infrared band at 1201 cm^{-1}, assigned to ν_a, and that at 1055 cm^{-1} show an appreciable loss in intensity, whereas the band at 1105 cm^{-1} in the Raman spectrum displays the opposite behaviour. It seems that the addition of another single P—O bond to the system affects the mixing of P—O, C—O, and C—C stretching vibrations, displacing the 1080 and 1055 cm^{-1} bands of the anion to 1030 cm^{-1}, while the C—C vibrational band at 953 cm^{-1} loses most of its intensity. The composite band at 1029 cm^{-1} in the infrared spectrum of the acid solution has appreciable intensity, but the corresponding band in the Raman spectrum is quite weak. In a previous study on the interaction of Ag^+ ions with dialkylphosphates (13), it was proposed that the ν_a vibrational band of the anion at 1200 cm^{-1} in neutral solution is displaced to ca. 1150 cm^{-1} upon covalent neutralisation of the phosphate group. We rather believe that the 1200 cm^{-1} band is displaced, with reduced intensity, to ca. 1270 cm^{-1} in the infrared spectrum of the acid solution, the increased intensity in the 1150 cm^{-1} region being due, at least in part, to the ν_2 vibration of H_3O^+ ions (21). One also notes that the Raman band due to the symmetric stretching mode of the phosphodiester —O—P—O— group is shifted to 746 cm^{-1} at low pH, its intensity being enhanced in the process. The relative height of the 1081 cm^{-1} Raman band of the DEP anion shows that this species remains ionized in the pH range 2.5–12 (see insert, Fig. 1).

The changes occurring in the infrared and Raman spectra of DEP as a result of interaction with metal ions are usually small, especially at low metal concentration. Minor spectral modifications are more easily seen in the difference spectra, which are obtained by subtracting the spectrum of DEP from that of the corresponding solutions in the presence of metal ions. This can be done in a straightforward manner with infrared spectra if the sample thickness and concentration are very accurately known, which is seldom the case. In Raman spectroscopy, to determine the proper value of the constant to be used in the subtraction operation ([DEP + metal] − $K\times$[DEP]), a band present in both spectra and insensitive to the effect of the metal ions is needed as a reference intensity standard. We have used the Raman bands of the alkyl groups in the 1280–1500 cm^{-1} range for this purpose, since they should not be affected by perturbations of the PO_2^- group. In what follows, we will use a *normalized multiplication constant, K*, which is chosen in each case to yield the value

Can. J. Chem. Downloaded from www.nrcresearchpress.com by 109.225.110.28 on 09/08/12
For personal use only.

Can. J. Chem. Downloaded from www.nrcresearchpress.com by 109.225.110.28 on 09/08/12
For personal use only.

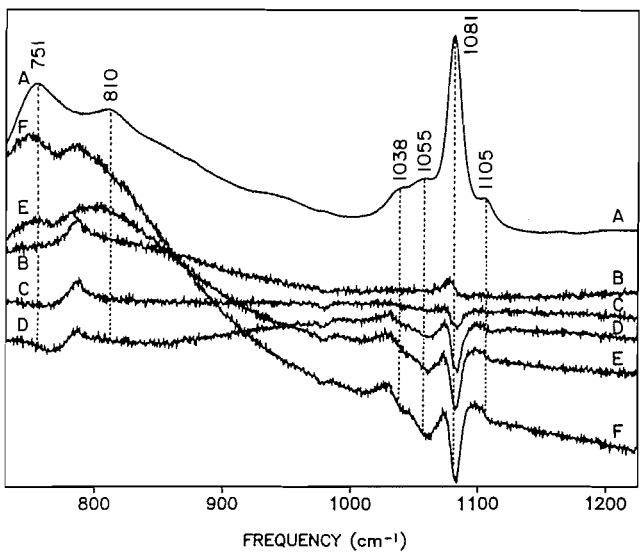

FIG. 2. (*A*) Raman spectrum of an aqueous solution of diethyl phosphate (0.1M, pH 7.5) at 20°C. (B–F) Difference spectra (intensity multiplied by 6) obtained in the presence of $NiCl_2$ at a Ni:DEP molar ratio of (*B*) 0.025, (*C*) 0.25, (*D*) 1.5, (*E*) 3.0, and (*F*) 5.0.

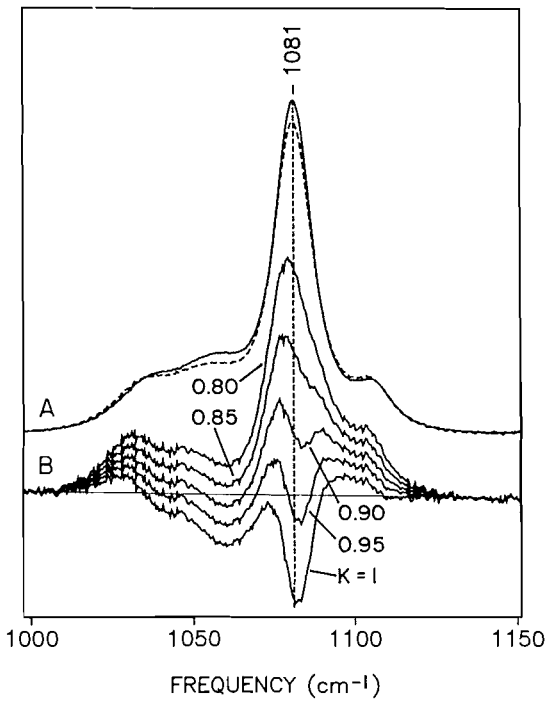

FIG. 3. (*A*) Raman spectrum of an aqueous solution of (—) diethyl phosphate (DEP) (0.1M, pH 7.5) and (- - -) the same solution with added $NiCl_2$ (DEP + metal) at a Ni:DEP molar ratio of 6:1. (*B*) Subtracted spectra (intensity multiplied by 5) ([DEP + metal] − K × [DEP]) for different values of the normalized multiplication constant K (see text).

1 (100%) when the reference bands used as intensity standards are completely annulled in the difference spectrum.

As an example of the use of difference spectra, the curves obtained from aqueous solutions of DEP in the presence of Ni(II) at metal:DEP ratios varying from 0.025:1 to 5:1 are given in Fig. 2. These difference spectra show that the spectral changes depend on the relative metal concentration. At very low metal:DEP ratio, one observes a slight shift to lower frequency of the $\nu_s(PO_2^-)$ band at 1081 cm^{-1} and a weak perturbation in the phosphodiester vibrational region near 800 cm^{-1}. At higher metal concentration, on the other hand, the $\nu_s(PO_2^-)$ band is shifted to higher frequency, with some loss in intensity. Band shifts and intensity changes are also apparent in the 1020–1060 cm^{-1} region (C-O stretching vibrations).

Another way in which spectral changes can be more easily visualized is through the "affected spectrum" (22–24), obtained by incompletely subtracting the reference spectrum to yield a positive difference curve in the region of interest. This is illustrated in Fig. 3, which shows the difference spectra obtained by subtracting the spectrum of an aqueous solution of DEP (0.1M) from that of the same solution in the presence of Ni(II) at a Ni:DEP molar ratio of 6:1, for various values of the normalized multiplication constant K. In the present study, the retained affected spectrum for the mixed solution with Ni(II) was the positive difference spectrum, obtained with the maximum value of K, which could be fitted with calculated band components. The program used for curve fitting was the FIT program from Spectrum Square Associates, Inc. (Ithaca, NY, U.S.A.), run under SpectraCalc (Galactic Industries Corporation, Salem, NH, U.S.A.). The difference between calculated and experimental spectra was taken to be:

$$\chi^2 = \frac{\sum_{i=1}^{N} [(\text{data}\ (\nu_i) - \text{calc}\ (\nu_i))/\text{Rms}]^2}{N - F}$$

in which N is the number of data points, F is the number of degrees of freedom, ν is the frequency, and Rms is a measure of the noise in the spectrum.

Taking Fig. 3 as an example, it was observed that negative peaks occurred in the difference curves for values of K approximately higher than 0.88. To fit the difference spectra for this value of K and lower, five components (of mixed Gaussian and Lorenztian shape) were needed. The fit between calculated and experimental spectra, as determined from the value of χ^2, decreased by an order of magnitude as K was lowered from 0.88 to 0.85. At this point the value of χ^2 as a function of K passed through a minimum, and the difference spectrum obtained with $K = 0.85$ was therefore taken as the affected spectrum. This procedure worked well in general, although in some cases the function $\chi^2 = f(K)$ gave a very broad minimum or merely levelled off with decreasing K. The calculated spectrum for the example given above is compared with the affected spectrum in Fig. 4-*D*. It is obvious that the manipulations of the spectral data needed for the complete analysis of the effect of a particular type of metal ion on the spectrum of DEP were very time-consuming, so that the whole procedure was used only in the case of Ni(II) in the present study. In the other cases, qualitatively affected spectra chosen by visual inspection were retained.

The affected spectrum can be very meaningful for a system limited number of discrete components. In this case, the above example is interpreted as follows. Since the final value of K was 0.85, we surmise that 85% of the spectrum of DEP remained unaffected by the metal ions under our experimental conditions. We also conclude that the affected spec-

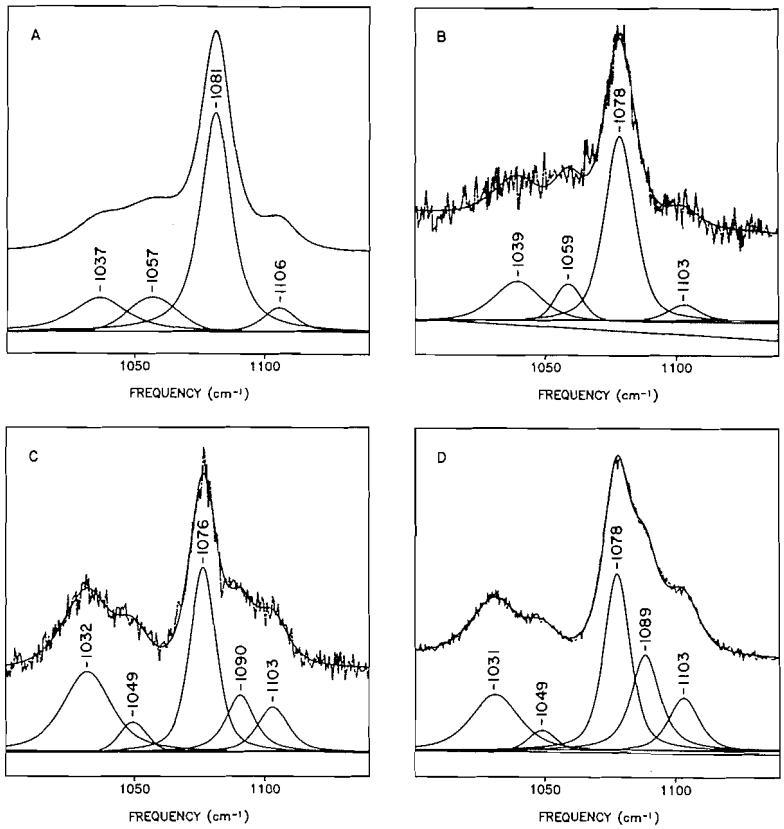

FIG. 4. Band fitting of (*A*) the Raman spectrum of aqueous diethyl phosphate (DEP) (0.1M, pH 7.5) and of (B–D) the affected spectra obtained from solutions of DEP containing $NiCl_2$ at a Ni:DEP molar ratio of (*B*) 0.1:1, (*C*) 2:1, and (*D*) 6:1. (—) Calculated spectra.

trum obtained by the subtraction procedure (at $K = 0.85$) represents 15% of DEP molecules. This interpretation can be questionable, particularly in the case of weak band shifts caused by bulk effects in the solution and affecting all solute molecules. It remains, however, that the affected spectrum in these conditions constitutes a very sensitive indicator of the band shift.

The affected Raman spectra in the 1000–1150 cm^{-1} of solutions of DEP in the presence of Ni(II) at various metal:DEP ratios (Fig. 4) are particularly revealing. Theoretical band fitting of the spectrum in aqueous DEP alone necessitates four components, the major one being associated to the $\nu_s(PO_2^-)$ vibration at 1081 cm^{-1} (Fig. 4-*A*). For the affected spectrum from the solution at Ni:DEP ratio of 1:40 (Fig. 4-*B*), the same number of components is needed, but the main band is shifted to a lower frequency by 3 cm^{-1}, which is consistent with the effect observed in the difference spectrum (Fig. 2-*B*). At higher metal:DEP ratio (Fig. 4-*C*, *D*), an extra component is needed at 1089 cm^{-1} to fit the affected spectra. This extra band becomes progressively more important as the metal concentration is increased. A shift to lower frequency of the 1037 and 1056 cm^{-1} bands of DEP, with enhancement of the lower frequency peak, is also observed in the affected spectra, in accordance with the derivative features present in the different spectra for these solutions (Fig. 2). This behavior, which will be discussed more fully below, indicates that DEP interacts with Ni(II) in different ways, depending on the concentration of the metal cation in the solution. In an attempt to determine the number of components required to explain the spectral data, we have performed a factor analysis using the 1000–1140 cm^{-1} region of the Raman spectra of 16 solutions of DEP (0.1 M) in the presence of Ni^{2+}, at metal:DEP ratios ranging from 6:1 to 0 (pure DEP). (The analysis was done using the PLSPLUS option of SpectraCalc; see ref. 25 for details on factor analysis.) The results of this analysis suggested that four major components are necessary to adequately describe the chosen ensemble.

Difference and affected Raman spectra for solutions of DEP (0.3M) in the presence of the cations K^+, Ca^{2+}, and Cu^{2+}, at a metal:DEP ratio of 1:1, are illustrated in Fig. 5. The corresponding curves for a solution at pH = 1 (effect of the H_3O^+ ion) are also reproduced. (The affected spectra for these mixtures are qualitative only, as they were not subjected to the band fitting procedure used with the Ni(II) solutions.) The subtracted spectra generally consist of a differential feature in the 1080 cm^{-1} region, indicative of a shift to higher frequency of the $\nu_s(PO_2^-)$ vibrational mode, and a slight positive peak at 750 cm^{-1}, resulting from an increased intensity of the band due to the symmetric phosphodiester stretch. The difference spectra of the divalent metal cations also show a decreased intensity in the 1081 cm^{-1} region and extra components on the low-frequency side of the main peak. The difference spectrum obtained with a solution at pH 1 versus that at pH 7, which shows the effect of protonation, is very similar to that obtained from a $CaCl_2$ solution, although the intensity loss at 1080 cm^{-1} is much larger for the acid solution. The affected spectrum, on the other hand, closely resembles the raw spectrum of a DEP solution at very low pH (Fig. 1), as expected.

Can. J. Chem. Downloaded from www.nrcresearchpress.com by 109.225.110.28 on 09/08/12
For personal use only.

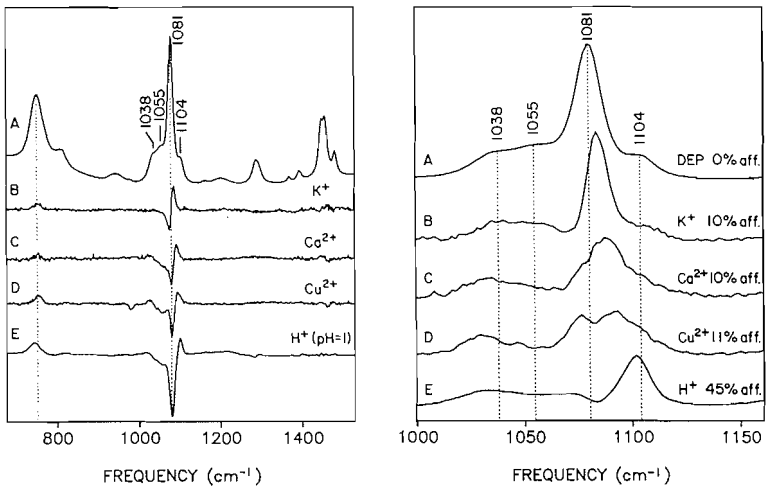

FIG. 5. (*A*) Raman spectrum of an aqueous solution of diethyl phosphate (DEP) (0.3M, pH adjusted to 7 with NaOH). Difference (left) and affected (right) spectra (intensity multiplied by 3) obtained from solutions of DEP in the presence of (*B*) KCl, (*C*) $CaCl_2$, and (*D*) $CuCl_2$ at a cation:DEP ratio of 1:1. (*E*) Corresponding curves (intensity multiplied by 1) for a solution of DEP at pH 1. The % values indicate the amount of affected spectrum (see text).

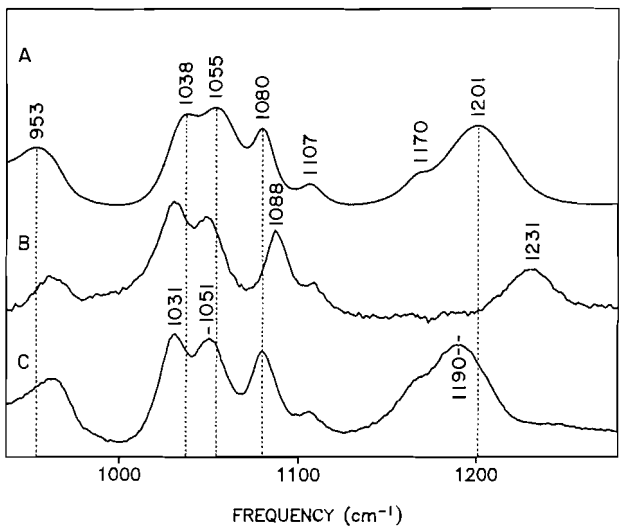

FIG. 6. (*A*) Infrared spectrum of an aqueous solution of diethyl phosphate (DEP) (0.1M, pH 7). Affected spectra obtained from solutions of DEP in the presence of (*B*) $CaCl_2$ and (*C*) $NiCl_2$ at a metal:DEP ratio of 1:1.

The information provided by the affected spectra in infrared are complementary to those provided by the Raman technique. An example of application is shown in Fig. 6, which shows the PO_2^- stretching vibrational region of the affected spectra obtained from DEP (0.1M) in the presence of Ca^{2+} and Ni^{2+} at a metal:DEP ratio of 1:1. The Ca^{2+}-affected spectrum is typical in that it shows a shift to lower frequency of the bands at 1038 and 1055 cm^{-1}, whereas the peaks at 1080 and 1201 cm^{-1}, arising from the stretching vibrations of the PO_2^- group, are shifted in the opposite direction. The effect of Ni^{2+} is clearly different, the $\nu_s(PO_2^-)$ mode at 1080 cm^{-1} remaining essentially invariant, while the $\nu_a(PO_2^-)$ mode at 1201 cm^{-1} is shifted to a lower frequency.

The pH of the solution has some effect on the frequency and intensity of the bands of DEP within the range in which the phosphate group is ionized. The effect of metal ions also differ from that at neutral pH. This is illustrated in Fig. 7, where the spectra of solutions brought to pH near 12 by addition of LiOH, NaOH, and KOH are compared with a solution adjusted to pH 7 with the same base. Increasing the pH to 12 results in a shift to lower frequency of the $\nu_s(PO_2^-)$ band.

Discussion

As shown in Fig. 5, the difference and affected spectra obtained from a series of solutions of DEP in the presence of different metal ions indicate that the complexation of this type of cations by ionized phosphate groups depends on the nature of the metals. As our measurements have been particularly extensive on the DEP–Ni^{2+} system, this particular case will be discussed first, so that the conclusions can be extended to other systems.

DEP – Ni^{2+} system

The vibrational spectroscopic results gathered in this study indicate that the interaction of Ni^{2+} cations with the phosphate group of DEP is a function of metal concentration. This is particularly evident when one compares the difference and affected spectra (Figs. 2 and 4) obtained from solutions at metal:DEP ratios of 0.025:1 and 6:1. We believe that the four spectral components indicated by the factor analysis for this ensemble reflect the existence of phosphate groups of DEP in four different types of environment, which we tentatively identify as follows:

Species A:

These are ionized PO_2^- groups as they are found in neutral aqueous DEP (Na^+ salt). They are for the most part hydrogen-bonded to water molecules and they interact electrostatically with their neighboring Na^+ counterion. These interactions are, on average, symmetrical with respect to the two oxygen atoms of the charged phosphate groups. Such a system is characterized by an intense $\nu_s(PO_2^-)$ Raman band at 1081 cm^{-1} (Fig. 4-*A*).

Species B:

These species consist of ionized PO_2^- groups interacting with Ni^{2+} ions through water molecules (outer-sphere inter-

Can. J. Chem. Downloaded from www.nrcresearchpress.com by 109.225.110.28 on 09/08/12
For personal use only.

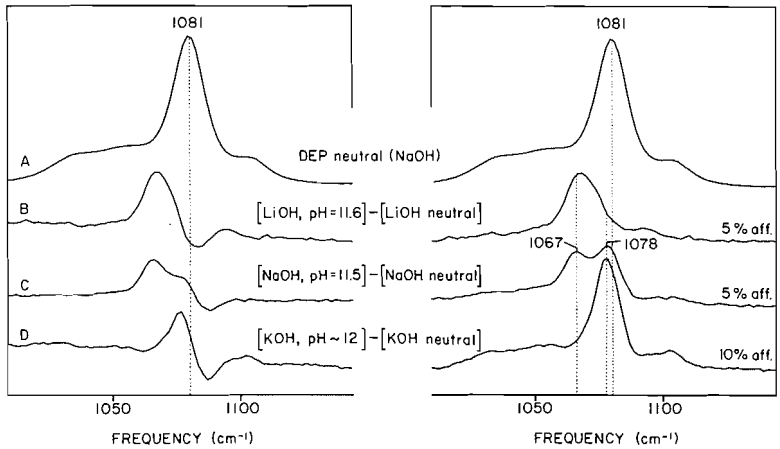

FIG. 7. (*A*) Raman spectrum of an aqueous solution of diethyl phosphate (DEP) (0.3M, pH 7). B–D (left) difference and (right) affected spectra (intensity multiplied by 6) obtained from solutions of DEP at high pH (conditions indicated). The % values indicate the amount of affected spectrum (see text).

Can. J. Chem. Downloaded from www.nrcresearchpress.com by 109.225.110.28 on 09/08/12
For personal use only.

actions or, more generally, formation of water-separated ions pairs). The effect of the metal cation in this $Ni^{2+}\cdots O(H)—H\cdots {}^{-}O_2P(OEt)_2$ type of aggregate is to increase the acidity of the water molecule and to strengthen the hydrogen bond affecting the phosphate group, causing a decrease in frequency of the $\nu_s(PO_2^-)$ vibration. Typically, the spectrum of such species corresponds to the affected spectrum obtained at very low metal:DEP ratio, such as in Fig. 4-*B*. Note that this spectrum is very similar to that of aqueous DEP alone, except for the displacement of the $\nu_s(PO_2^-)$ vibrational band to 1078 cm^{-1}. Another noteworthy difference is the absolute intensity of this peak, which is increased considerably in the presence of the metal cation. This causes a positive peak to appear in the difference spectrum, as in Fig. 2-*B*. The effect is also apparent when the intensity of the $\nu_s(PO_2^-)$ band of DEP near 1080 cm^{-1} is plotted as a function of the relative metal concentration, which shows a maximum at a Ni:DEP ratio of 0.25:1 (Fig. 8-*B*).

The increased intensity of the 1078 cm^{-1} band for the B-type species, compared to that of the corresponding band at 1081 cm^{-1} for the A-type variety, has to be taken into account when attempts are made to relate the intensity of the 1078 cm^{-1} component (see Fig. 8-*C*) to the actual concentration of the B-type species in solutions of various metal:DEP ratios. Even so, this curve displays a very peculiar shape in low metal concentrations, an effect which is reflected in the graph giving the total proportion of DEP affected by Ni^{2+} ions (Fig. 8-*A*), as determined by the band-fitting procedure described in the "results" section above. These findings, which are even more striking when one takes into account the total amount of affected DEP (Fig. 8-*D*), clearly show that the number of DEP molecules linked to Ni^{2+} ions by outer-sphere coordination is proportionally much larger at low metal concentrations. This can be explained by the fact that this type of bonding is favored on an entropy basis: when the metal concentration is small, it is relatively easy for the Ni^{2+} ions to find, within a few layers of water molecules, one or several phosphate groups with which it can interact through these solvent molecules. As the metal concentration is increased, more and more metal ions find their way close to the phosphate groups, and more direct interactions take place, at the expense of outer-sphere coordination.

Species C:

These are $Ni^+—O—P(=O)(O—Et)_2$ species, analogous to protonated DEP, with the acid proton replaced by the metal cation. The Raman spectrum of these unsymmetrically bound ion pairs are likely similar to that of protonated DEP (see Fig. 1), which is characterized by a 90% reduction in intensity at 1081 cm^{-1} and a 40% reduction at 1055 cm^{-1}, a shift to 1031 cm^{-1} of the band at 1038 cm^{-1} in DEP solution at pH 7, and an increase by a factor of 2.3 of the intensity of the peak at 1105 cm^{-1}, which is shifted to 1100 cm^{-1}. The frequency shift of the low-frequency band from 1039 to 1031 cm^{-1}, and the increased intensity of this band and of that near 1100 cm^{-1} when the Ni:DEP ratio is raised from 0.025 to 1 (Fig. 4-*B*, *C*), are likely due to the formation of these metallated species. Even more characteristic is the negative component at ca. 1081 cm^{-1} in the difference spectra (Fig. 2), which shows the decrease in intensity of the $\nu_s(PO_2^-)$ band as the metal:DEP ratio is raised. Also apparent in these spectra are the reduced intensity at 1055 cm^{-1} and the shift to lower frequency of the 1038 cm^{-1} band.

Species D:

The existence of these species has to be inferred to account for the component growing at 1090 cm^{-1} in the affected spectra at high metal concentrations (Fig. 8-*C*, *D*). The intensity of this band grows more slowly than that of the other components of the affected spectra at low metal:DEP ratios, but it does not level off at Ni:DEP ratios >3 as the others do. This suggests that the concentration of the species responsible for the 1090 cm^{-1} band become proportionally more important at high metal concentrations. We believe that species of this type are ionized phosphate groups which interact in a non-specific electrostatic way with metal cations. A partial disruption of the hydrogen bond network with water molecules in the neighborhood of the phosphate groups probably results from these interactions at increased metal concentrations. The effect is then equivalent to a partial dehydration of the PO_2^- groups, which is known to displace the $\nu_s(PO_2^-)$ vibrational frequency to higher values (17, 26). It is also possible that the PO_2 angle of the charged

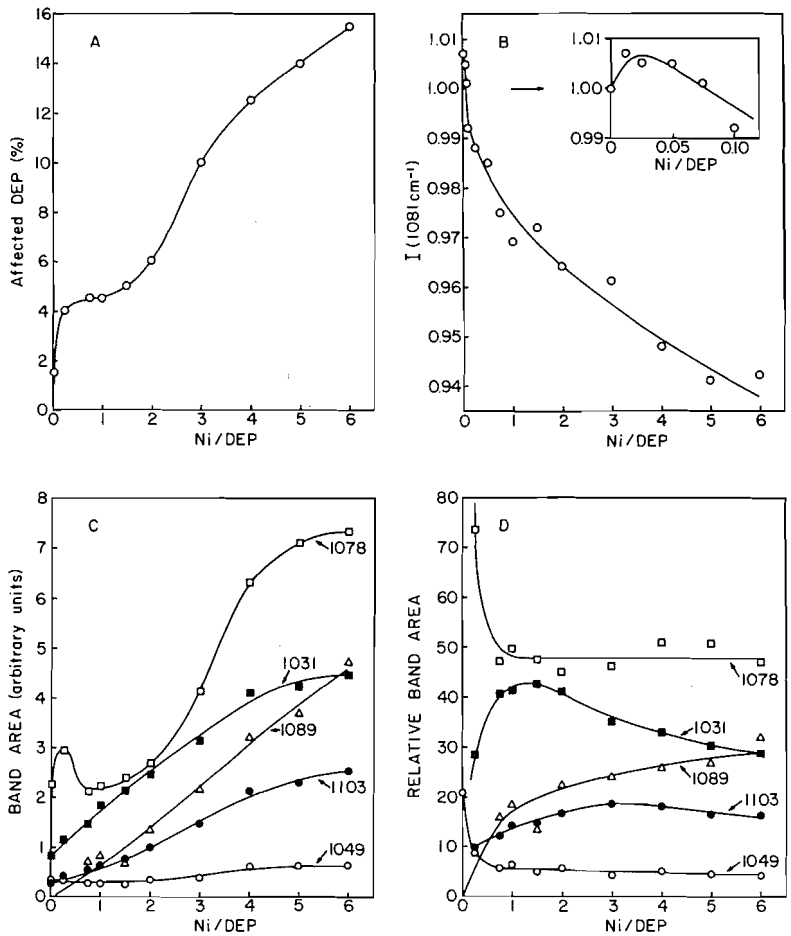

FIG. 8. Variation of spectral parameters obtained from a 0.1M aqueous solution of DEP with added $NiCl_2$ as a function of the Ni:DEP ratio. (*A*) Fraction of the spectrum affected, (*B*) relative peak-height intensity of the 1081 cm^{-1} Raman band, (*C*) intensity of calculated spectral components, and (*D*) intensity of calculated spectral components (given in *C*) divided by the fraction of affected spectrum (given in *A*).

phosphate group in DEP is modified by the presence of the metal cations, causing a modification of the vibrational frequencies of this group (17). Note that type-A species are equivalent to those of type D, except that the statistically symmetrical interactions involved in the latter case are more important or consequential than with the Na^+ counterions used in the reference solution (DEP-Na solution at pH 7).

DEP – other metal-ion systems

The conclusions from our analysis of the Ni^{2+}–DEP spectra can now be extended to the other metal–DEP systems. Unless otherwise specified, the spectra discussed below are for a 1:1 metal chloride:DEP ratio; indicated pH values refer to the cation/DEP solutions. The simplest metal ions to be considered are those of the alkaline metals: Li^+ (pH = 6.4), Na^+ (pH = 7.4) and K^+ (pH = 7.2). As shown in Fig. 5, the difference and affected Raman spectra for K^+ are indicative of a mere shift, with no loss in intensity, of the $\nu_s(PO_2^-)$ vibrational band. This is corroborated by the shape of the affected spectrum, which is very similar to that of the original DEP spectrum. The frequency shift is rather small (ca. 2 cm^{-1}) for K^+ and Na^+ (as determined from a Na^+ solution at 2:1 Na:DEP ratio), and slightly larger (ca. 4 cm^{-1}) for Li^+. These results show that the alkaline-metal ions interact electrostastically in a general manner with charged phosphate groups, these interactions being essentially symmetrical with respect to the two oxygen atoms. It is interesting to note that in a solution at a much larger Na^+:DEP ratio of 18, the frequency of the $\nu_s(PO_2^-)$ band (spectrum not shown) is essentially identical to that at a metal:DEP ratio of 2:1 (ca. 1083 cm^{-1}). The affected spectrum at high metal ion content, however, shows an increased scattering at 1031 cm^{-1}, with corresponding intensity decrease at 1055 cm^{-1}. This observation, together with the decrease in intensity (by approximately 5%) at 1081 cm^{-1}, suggests that unsymmetrical interactions (analogous to those yielding type-C species) take place to some extent at high salt concentrations.

Alkaline-earth metal ions appear to have an intermediate behavior towards DEP, by comparison with alkaline and transition metal ions. As shown in Fig. 5-*C* for Ca^{2+} (pH = 6.7), the frequency shift of the $\nu_s(PO_2^-)$ band is positive, but larger than with K^+ (1088 versus 1083 cm^{-1}), indicating generally stronger interactions with the PO_2^- groups. A slight overall decrease in intensity is also revealed in the $\nu_s(PO_2^-)$ region of the difference spectrum, suggesting some degree of asymmetrical interaction with the oxygen atoms of the phosphate groups. The decrease intensity at 1055 cm^{-1} in the affected spectrum supports this conclusion. Note that the difference spectrum in this case bears some resemblance to that for a solution of DEP at pH 1 (Fig. 5-*E*), for which a

Can. J. Chem. Downloaded from www.nrcresearchpress.com by 109.225.110.28 on 09/08/12
For personal use only.

Can. J. Chem. Downloaded from www.nrcresearchpress.com by 109.225.110.28 on 09/08/12
For personal use only.

good proportion of the phosphate groups are protonated. The affected spectrum (not shown) for a Mg^{2+}–DEP solution (pH = 6.8) shows an extra component at 1077 cm^{-1}, indicating that this metal cation is more involved than Ca^{2+} ions in the formation of water-separated ion pairs with the phosphate groups.

Transition metal ions, such as Ni^{2+} (pH = 6.2) (Figs. 3 and 4), Cu^{2+} (pH = 3.4) (Fig. 5-*D*), Zn^{2+} (pH = 5.1), and Cd^{2+} (pH = 6.3) (spectra not shown) behave in the same manner. Their affected spectrum contains a high-frequency component at ca. 1092 cm^{-1}, characteristic of symmetric electrostatic interactions with the PO_2^- groups, as well as a low-frequency band resulting from outer-sphere coordination. Their difference spectrum further shows a decrease in intensity in the $\nu_s(PO_2^-)$ region, indicating asymmetric interactions with the oxygen atoms of the phosphate groups. This contrasting behavior compared to alkaline-earth metal ions is especially obvious in the $\nu_a(PO_2^-)$ region of the affected infrared spectrum (Fig. 6), where the band at 1201 cm^{-1} in aqueous DEP is shifted to 1231 cm^{-1} in the presence of Ca^{2+} and 1190 cm^{-1} in a Ni^{2+} solution.

The affected spectra (not shown) of DEP solutions in the presence of Ag^+ (from $AgClO_4$; pH = 6) and Pb^{2+} (pH = 4.2) unexpectedly display a low-frequency component only, at ca. 1078 cm^{-1}. This is particularly surprising in the case of Ag^+, as the infrared spectrum for the solid silver salt of DEP is suggestive of the formation of a partly covalent (therefore asymmetrical) bond with PO_2^- groups (13). The present results suggest that both Ag^+ and Pb^{2+} in solution have a relatively high affinity for water molecules, and that they interact with the phosphate groups through the solvent molecules, forming water-separated ions pairs (type-B species).

The trivalent cations La^{3+} (pH = 3.5) and Al^{3+} (pH = 6,1) also behave in a peculiar way, their affected spectrum (not shown) containing mainly a high-frequency component at 1090 cm^{-1} with very weak accompanying peak at 1078 cm^{-1}. However, the fraction of affected spectrum with these cations (25–30%) is much higher than with monovalent and divalent metal ions. Furthermore, a considerable intensity loss occurs at 1081 cm^{-1}, suggesting that these ions can also interact directly, in an asymmetric way with the oxygen atoms of the PO_2^- groups. Otherwise, the interactions of the phosphate groups with these highly charged species, which are no doubt extensively solvated, appear to be non specific. It is also worth mentioning that the mixture with $AlCl_3$ at pH = 3.3 yields an affected spectrum which is quite similar to that obtained with DEP at pH 1 (Fig. 5-*E*). This probably results from a partial protonation of DEP under these circumstances.

Effect of high pH

The neutralization of aqueous solutions of DEP with either LiOH, NaOH, or KOH has the same effect on the vibrational spectra of this compound. In particular, the frequency of the $\nu_s(PO_2^-)$ in the resulting solutions is the same (within 1 cm^{-1}). However, raising the pH of such solutions to ca. 12 has a marked influence on this frequency, even though the concentration of OH^- ions is much lower than that of DEP. As shown in Fig. 7, the effect depends on the nature of the cation.

The frequency shift of the $\nu_s(PO_2^-)$ vibrational mode in the affected spectrum from the LiOH solution is quite large (14 cm^{-1}), suggesting a strong perturbation of the phosphate groups in the ca. 5% affected DEP molecules. We tentatively explain this behavior by the formation of $OH^- \cdot Li^+ \cdot {}^-O{-}P(=O)(O{-}Et)_2$ species, in which a LiOH molecule comes in close contact with one of the two oxygen atoms of the charged phosphate group. The effect is different in the KOH solution, which causes only a small frequency shift (3 cm^{-1}) of the $\nu_s(PO_2^-)$ mode. This minor effect probably results from small changes in the distribution of charged species in the vicinity of phosphate groups, as the affinity of K^+ cations for OH^- ions is not expected to be exactly the same as that for the negatively charged phosphate groups. The affected spectrum from the NaOH solution shows peaks at both 1067 and 1078 cm^{-1}, indicating that both types of structures are present in the mixture.

Conclusion

The present results indicate that metal cations have different affinities for charged phosphate groups and also that they interact in different ways with these groups. The vibrational spectra show that such interactions can have different and even opposite effects on the intensity and frequency of the vibrational bands of the PO_2^- unit. These changes can be interpreted in terms of direct metal binding by one of the oxygen atoms of the PO_2^- groups, non-specific electrostatic interactions, and formation of water-separated ion pairs with the phosphate groups. It can be concluded from these observations that the decrease in intensity of the band due to the symmetrical stretching mode of charged phosphate groups, which is prominent near 1080 cm^{-1} in the spectra of several types of biomolecules (phospholipids, nucleic acids. . .), is only partially characteristic of the extent of metal binding by these groups, as it arises mainly from interactions of the first kind.

Acknowledgements

We are indebted to the Natural Sciences and Engineering Research Council of Canada and to the Ministère de l'Éducation du Québec for financial support.

1. J. K. Barton and S. J. Lippard. *In* Nucleic acid – metal ion interactions. *Edited by* T. G. Spiro. Wiley, New York. 1980. pp. 31–113.
2. L. G. Marzilli, T. J. Kistenmacher, and G. L. Eichhorn. *In* Nucleic acid – metal ion interactions. *Edited by* T. G. Spiro. Wiley, New York. 1980. pp. 179–250.
3. M. de Oliveira Neto. J. Comput. Chem. **7**, 629 (1986).
4. S. Adam, J. Liquier, J. A. Taboury, and E. Taillandier. Biochemistry, **25**, 3220 (1986).
5. T. G. Spiro (*Editor*). Biological applications of Raman spectroscopy. John Wiley & Sons, Inc., New York. 1987.
6. R. J. H. Clark and R. E. Hester (*Editors*). Advances in spectroscopy. Vol. 13. Spectroscopy of biological systems. John Wiley & Sons, Inc., New York. 1986.
7. A. T. Tu. Raman spectroscopy in biology: principles and applications. John Wiley & Sons Inc., New York. 1982.
8. P. C. Carey. Biochemical applications of Raman and resonance Raman spectroscopies. Academic Press, Inc. New York. 1982.
9. M. Tsuboi, S. Takahashi, S. Muraishi, T. Kaijiura, and S. Nishimura. Science **174**, 1142 (1971).
10. H. A. Tajmir-Riahi, M. Langlais, and R. Savoie. Nucleic Acids Res. **16**, 751 (1988).
11. S. Alex and P. Dupuis. Inorg. Chim. Acta, **157**, 271 (1989).

12. M. Langlais, H. A. Tajmir-Riahi, and R. Savoie. Biopolymers, **30**, 743 (1990).
13. C. Garrigou-Lagrange, O. Bouloussa, and C. Clement. Can. J. Spectrosc. **21**, 75 (1976).
14. E. B. Brown and W. L. Peticolas. Biopolymers, **14**, 1259 (1975).
15. K. Taga, K. Miyagai, N. Hirabayashi, T. Yoshida, and H. Okaboyashi. J. Mol. Struct. **245**, 1 (1991).
16. T. Shimanouchi, M. Tsuboi, and Y. Kyogoku. Adv. Chem. Phys. **7**, 435 (1964).
17. W. Pohle, M. Bohl, and H. Böhlig. J. Mol. Struct. **242**, 333 (1990).
18. K. C. Lu, E. W. Prohofsky, and L. VanZandt. Biopolymers, **16**, 2491 (1977).
19. M. Pézolet, B. Boulé, and D. Bourque. Rev. Sci. Instrum. **54**, 1364 (1983).
20. R. Savoie and M. Pigeon-Gosselin. Can. J. Spectrosc. **28**, 133 (1983).
21. P. A. Giguère and J. G. Guillot. J. Phys. Chem. **86**, 3231 (1982).
22. O. Kristiansson and J. Lindgren. J. Phys. Chem. **95**, 1488 (1991).
23. H. Kleeberg. J. Mol Struct. **237**, 187 (1990).
24. J. Stangret and M. Męcik. J. Mol. Liquids, **46**, 83 (1990).
25. H. H. Harman. Modern factor analysis. 3rd ed. The University of Chicago Press, Chicago. 1976.
26. D. Hadži, M. Hodošček, J. Grdadolnik, and F. Avbelj. J. Mol. Struct. **266**, 9 (1992).

Can. J. Chem. Downloaded from www.nrcresearchpress.com by 109.225.110.28 on 09/08/12
For personal use only.

Tetrakis(trimethylgermyl)silane and tris(trimethylgermyl)silyllithium

KIM M. BAINES,[1] KEVIN A. MUELLER, AND TSUN K. SHAM
Department of Chemistry, University of Western Ontario, London, Ont., Canada N6A 5B7

Received July 20, 1992

KIM M. BAINES, KEVIN A. MUELLER, and TSUN K. SHAM. Can. J. Chem. **70**, 2884 (1992).

Tetrakis(trimethylgermyl)silane can be synthesized by the addition of four equivalents of trimethylgermyllithium to tetrachlorosilane. Treatment of tetrakis(trimethylgermyl)silane with methyllithium gives tris(trimethylgermyl)silyllithium, which was trapped with aqueous hydrochloric acid, chlorotrimethylsilane or methyl iodide to yield tris(trimethylgermyl)silane, tris(trimethylgermyl)(trimethylsilyl)silane, or methyltris(trimethylgermyl)silane, respectively. Chlorination of tris(trimethylgermyl)silane affords dichlorobis(trimethylgermyl)silane.

KIM M. BAINES, KEVIN A. MUELLER et TSUN K. SHAM. Can. J. Chem. **70**, 2884 (1992).

On peut synthétiser le tétrakis(triméthylgermyl)silane par addition de quatre équivalents de triméthylgermyllithium au tétrachlorosilane. Le traitement du tétrakis(triméthylgermyl)silane avec du méthyllithium fournit du tris(triméthylgermyl)silyllithium que l'on a piégé avec de l'acide chlorhydrique aqueux, du chlorotriméthylsilane ou de l'iodure de méthyle pour obtenir respectivement du tris(triméthylgermyl)silane, du tris(triméthylgermyl)(triméthylsilyl)silane ou du méthyltris(triméthylgermyl)silane. La chloration du tris(triméthylgermyl)silane fournit du dichlorobis(triméthylgermyl)silane.

[Traduit par la rédaction]

Can. J. Chem. Downloaded from www.nrcresearchpress.com by 88.255.202.194 on 09/08/12
For personal use only.

Introduction

Over the last decade, tris(trimethylsilyl)silyllithium has been used extensively for the synthesis of a variety of main group (for example, see ref. 1) and transition metal (for example, see ref. 2) silyl compounds. The tris(trimethylsilyl)silyl group is often the substituent of choice when a sterically encumbered ligand is required. The silyllithium reagent is readily prepared by the treatment of tetrakis(trimethylsilyl)silane (3) with MeLi in tetrahydrofuran (THF) and can be used either in situ (4) or isolated as its THF adduct (5) before use.

In addition to being a convenient precursor to $(Me_3Si)_3SiLi$, $(Me_3Si)_4Si$ has been used as a molecular model compound of a silicon surface (6) and proposed as a chemical shift standard for solid-state NMR spectroscopy (7).

Recently, the synthesis of tris(trimethyl*stannyl*)silyllithium, by the treatment of tetrakis(trimethyl*stannyl*)silane with MeLi, and its use in the synthesis of transition metal silyl complexes was reported (8). Given the interest shown in the $(Me_3M)_3Si$— (M = Si or Sn) group as a ligand in organometallic chemistry, we decided to investigate the synthesis of tetrakis(trimethyl*germyl*)silane and its conversion to tris(trimethyl*germyl*)silyllithium. In addition, $(Me_3Ge)_4Si$ was of interest because of possible applications in metal-organic chemical vapour deposition (MO–CVD) where, recently, compounds containing a silicon–$(carbon)_n$–germanium chain have been synthesized as potential CVD precursors (9). $(Me_3Ge)_4Si$ may also aid in the structural analysis of Si–Ge atomic layer superlattices (10).

Results and discussion

To investigate the synthesis of $(Me_3Ge)_4Si$, a high yield route to chlorotrimethylgermane was required. Although the synthesis of Me_3GeCl has been reported to occur in good yield by the demethylation of tetramethylgermane using concentrated sulfuric acid, followed by treatment with ammonium chloride (11); in our hands, yields significantly lower than that reported in the literature were consistently obtained. Thus, an alternative route to Me_3GeCl utilizing the redistribution reaction between tetraalkylgermanes and tetrachlorostannane was developed. Tetramethylgermane and tetrachlorostannane, when heated at 150°C for several hours in a Carius tube, yield Me_3GeCl quantitatively. This procedure is similar to that employed by Grobe and Hendriock (12) except that a catalyst is not required.

Analogous to the one-pot synthesis of $(Me_3Si)_4Si$ (3) from $SiCl_4$, Me_3SiCl, and lithium, the one-pot coupling reaction between $SiCl_4$ and Me_3GeCl using lithium metal seemed to be a viable route to $(Me_3Ge)_4Si$. However, attempts at the one-pot procedure gave hexamethyldigermane as the major product and only a trace amount of the desired compound (0.4% yield). Apparently, the formation of Me_3GeLi followed by coupling to Me_3GeCl occurs much more readily than the formation of Cl_3SiLi, leading to the formation of significant amounts of Me_6Ge_2.

$$[1]\quad SiCl_4 + 4Me_3GeCl + 8Li \xrightarrow{THF} \underset{\text{major}}{(Me_3Ge)_2} + \underset{\text{trace}}{(Me_3Ge)_4Si}$$

We therefore attempted the synthesis of $(Me_3Ge)_4Si$ by the addition of a solution of Me_3GeLi to $SiCl_4$. Two commonly used methods for the preparation of Me_3GeLi are the treatment of either Me_3GeCl or Me_6Ge_2 with two equivalents of lithium metal in hexamethylphosphoramide (HMPA) (13). More recently, HMPA/THF (14) or HMPA/Et_2O (15) has been used as the solvent. It was found that the preparation of Me_3GeLi in 1/1.2 HMPA/Et_2O from Me_3GeCl, followed by coupling to $SiCl_4$ in pentane, gave the best yield of $(Me_3Ge)_4Si$ (19%). Hexamethyldigermane, however, was still the major product formed (30%).

$$[2]\quad Me_3GeCl + 2Li \xrightarrow{HMPA/Et_2O} Me_3GeLi + LiCl$$

$$[3]\quad 4Me_3GeLi + SiCl_4 \xrightarrow{pentane} (Me_3Ge)_4Si + (Me_3Ge)_2$$

Tetrakis(trimethylgermyl)silane is a colourless, waxy solid. The ^{29}Si NMR chemical shift of the central silicon atom of $(Me_3Ge)_4Si$ (−104.62 ppm) falls between that of $(Me_3Si)_4Si$ (−135.5 ppm) (16) and $(Me_3Sn)_4Si$ (−69.2 ppm) (8).

The reaction between $(Me_3Ge)_4Si$ and MeLi gives $(Me_3Ge)_3SiLi$, analogous to the synthesis of $(Me_3Si)_3SiLi$ (4) and

[1]Author to whom correspondence may be addressed.

$(Me_3Sn)_3SiLi$ (8). Although this compound was not isolated, its presence was confirmed by trapping reactions with the following electrophiles: aqueous acid, Me_3SiCl, and MeI to give tris(trimethylgermyl)silane, tris(trimethylgermyl)(trimethylsilyl)silane, and methyltris(trimethylgermyl)-silane, respectively. In this way, $(Me_3Ge)_3SiLi$ proved to be a convenient reagent for the preparation of new compounds containing the $(Me_3Ge)_3Si$— group.

[4] $(Me_3Ge)_4Si + MeLi \xrightarrow{THF} (Me_3Ge)_3SiLi + GeMe_4$

[5] $(Me_3Ge)_3SiLi \xrightarrow{H_3O^+} (Me_3Ge)_3SiH$

$(Me_3Ge)_3SiLi \xrightarrow[pentane]{Me_3SiCl} (Me_3Ge)_3Si\text{-}SiMe_3$

$(Me_3Ge)_3SiLi \xrightarrow[pentane]{MeI} (Me_3Ge)_3Si\text{-}Me$

$(Me_3Ge)_3SiH$, the product resulting from the acidic hydrolysis of $(Me_3Ge)_3SiLi$, can be readily chlorinated to give $(Me_3Ge)_2SiCl_2$, in much the same manner as $(Me_3Si)_3SiH$ (17).

[6] $(Me_3Ge)_3SiH \xrightarrow[-78°C]{Cl_2/pentane} (Me_3Ge)_2SiCl_2$

The dichlorosilane will allow for further functionalization at the silicon centre using nucleophilic reagents.

Conclusions

The one-pot coupling reaction involving $SiCl_4$, Me_3GeCl, and Li metal in THF was not a satisfactory method for the preparation of $(Me_3Ge)_4Si$. However, a moderate yield of $(Me_3Ge)_4Si$ is obtained when four equivalents of Me_3GeLi are added to $SiCl_4$. As expected, the treatment of $(Me_3Ge)_4$-Si with MeLi gave $(Me_3Ge)_3SiLi$ which, when trapped with electrophiles, gave new compounds containing the $(Me_3Ge)_3Si$— group. The chlorination of $(Me_3Ge)_3SiH$ afforded $(Me_3Ge)_2SiCl_2$, which is a precursor to other new compounds containing silicon–germanium bonds.

Experimental

All glassware was thoroughly flame-dried and the apparatus kept under a dry argon atmosphere over the course of each reaction. THF and Et_2O were distilled from sodium and benzophenone immediately before use. Pentane and HMPA were distilled from $LiAlH_4$ and CaH_2, respectively, and stored under an atmosphere of dry argon prior to use. $SiCl_4$, Me_3SiCl, and MeI were distilled from $CaCl_2$ immediately before use. Me_4Ge was used as received from Toronto Research Chemicals Inc. Chromatography was performed on silica gel plates using a Chromatotron (Harrison Research Co.; model 8924) or by dry column flash chromatography (18). Acidic work-up refers to the slow addition of 1 M HCl to the reaction mixture, followed by separation of the two layers and extraction of the aqueous layer with Et_2O. The organic layers were subsequently combined, washed successively with water and brine, and dried over $MgSO_4$. When HMPA was used in the reaction, the organic layer was initially extracted several times with 1 M HCl.

Infrared spectra were recorded on a Bruker IFS 32 FTIR spectrometer, controlled by an IBM System 9000 computer. Nuclear magnetic resonance spectra were recorded on either a Gemini 200, Varian XL-200 or XL-300 NMR spectrometer, using C_6D_6 as the solvent. Electron impact mass spectra were recorded on a Finnegan MAT model 8230 spectrometer, using an ionizing voltage of 70 eV. Elemental analyses were performed by Galbraith Laboratories Inc., Knoxville, TN. A Hewlett-Packard 5830 GC, equipped with a DB 5 capillary column, was used to obtain the gas chromatographs. The yield of hexamethyldigermane given is based on the amount of chlorotrimethylgermane used.

Chlorotrimethylgermane

Me_4Ge (6.96 g, 52.5 mmol) and $SnCl_4$ (13.65 g, 52.4 mmol) were introduced into a Carius tube. The Carius tube was then sealed under vacuum and heated for 46 h at 150°C. Simple distillation (under a dry argon atmosphere) of the reaction mixture gave a quantitative yield of Me_3GeCl (8.02 g, 52.4 mmol) as a clear, colourless liquid (bp 102°C, atmospheric pressure; lit. (11) 102–103°C, 760 Torr; 1 Torr = 133.3 Pa). ^1H NMR (ppm) 0.35 (s) (lit. (11) (C_6D_6) 0.39 (s)).

Tetrakis(trimethylgermyl)silane

(a) One-pot Synthesis

Me_3GeCl (3.00 g, 19.6 mmol), THF (25 mL), and pounded lithium (0.39 g, 56 mmol) were mechanically stirred at −78°C. To this stirred suspension, was added a solution of $SiCl_4$ (0.75 g, 4.4 mmol) in THF (10 mL) from a pressure-equalizing funnel. After stirring at −78°C for 3 h, the cold bath was removed and the reaction mixture was left to stir overnight. As the reaction proceeded, the reaction mixture went from light-green to dark-brown and opaque in appearance. After filtration through Celite and acidic work-up; dry column flash chromatography (silica gel; hexanes), followed by Kugelrohr distillation (pot temperature: 100°C, 0.4 Torr), a crude, white solid was obtained. This was then sublimed (90°C, 0.5 Torr) to give $(Me_3Ge)_4Si$ (0.008 g, 0.4%) as a white, waxy solid.

(b) Using trimethylgermyllithium prepared from chlorotrimethylgermane

Lithium metal (0.21 g, 30 mmol), pounded into small, flat pieces (ca. 1 cm in diameter), was placed into a 100 mL three-neck round-bottom flask. HMPA (5 mL) was then added and the resulting HMPA/Li mixture was stirred vigorously until the solution turned from clear to blue-grey in colour. At this point, a solution of Me_3GeCl (1.65 g, 10.8 mmol) in Et_2O (6 mL) was added, dropwise. The resulting solution gradually acquired a dark-brown colour, with a yellow tinge. After 3.5 h of stirring at room temperature, the germyllithium solution was added dropwise (ca. 1 drop every 3 s) to a solution of $SiCl_4$ (0.44 g, 2.59 mmol) in pentane (50 mL) at −78°C. After the addition was complete, the reaction mixture was allowed to warm to room temperature and stirred overnight. Acidic work-up of the chocolate-brown solution, followed by removal of the solvents by simple distillation, resulted in a crude reaction mixture containing HMPA, $(Me_3Ge)_2$, and $(Me_3Ge)_4Si$. The residual HMPA was removed by dry column flash chromatography (silica gel, pentane). The $(Me_3Ge)_2$ and $(Me_3Ge)_4Si$ were then separated by trap-to-trap distillation (room temperature, 0.7 Torr) to yield $(Me_3Ge)_2$ (0.38 g, 30%) as a clear, colourless liquid. The pot residue, $(Me_3Ge)_4Si$, was purified by sublimation (62°C, 0.7 Torr) to yield 0.24 g (19%) of a white, waxy solid; mp 245°C (dec., sealed tube); IR (KBr pellet, cm^{-1}) 2969 (s), 2905 (s), 2797 (m), 1404 (s), 1229 (s); ^1H NMR (ppm) 0.38 (s); ^{13}C NMR (ppm) 1.98 (q, J = 126 Hz); ^{29}Si NMR (ppm) −104.62; MS m/e (%) 500 (15, M^+), 485 (36, $M^+ - Me$), 381 (41, $M^+ - GeMe_3$), 279 (26), 177 (36), 119 (30, $GeMe_3$), 73 (100, $SiMe_3$); Anal. calcd. for $C_{12}H_{36}Ge_4Si$: C 28.89, H 7.29, found: C 29.07, H 7.08.

Tris(trimethylgermyl)silyllithium and tris(trimethylgermyl)silane

Methyllithium (2.3 mL of a 1.3 M solution in Et_2O) was added, via pipet,[2] to a stirred solution of $(Me_3Ge)_4Si$ (0.21 g, 0.43 mmol)

[2]A glass pipet fitted with a 3-valve pipet filler (Aldrich Cat. no. Z13,647-6) is repeatedly flushed with argon in the following manner: the gas in the bulb is expelled by pressing simultaneously on the bulb and valve "A" on top of the bulb, followed by drawing argon up into the pipet and bulb by pressing the "S" valve on the stem. After expelling argon from the bulb, the liquid is then drawn up into the pipet by pressing valve "S" and, after transfer to the appropriate flask, the liquid is expelled from the pipet by squeezing the argon-filled bulb and then pressing valve "S."

Can. J. Chem. Downloaded from www.nrcresearchpress.com by 88.255.202.194 on 09/08/12
For personal use only.

Can. J. Chem. Downloaded from www.nrcresearchpress.com by 88.255.202.194 on 09/08/12
For personal use only.

in THF (12 mL). After stirring overnight at room temperature, the light-yellow $(Me_3Ge)_3SiLi$ solution was added dropwise to 15 mL of a rapidly stirring 1 M HCl solution. After the addition was complete, the aqueous layer was extracted with Et_2O. The combined organic layers were then washed with water, followed by brine, dried over $MgSO_4$, and the solvent removed by rotary evaporation. Purification by chromatography (Chromatotron; hexanes) yielded 0.12 g (72%) of $(Me_3Ge)_3SiH$ as a clear, colourless liquid. IR (neat, cm^{-1}) 2068 (s, Si—H); ^1H NMR (ppm) 0.37 (s, 27 H, Ge—CH_3), 3.10 (s, 1 H, Si—H); ^{13}C NMR (ppm) 1.05 (q, J = 126 Hz); ^{29}Si NMR (ppm) −96.95; MS *m/e* (%) 382 (6, M^+), 367 (8, M^+ − Me), 293 (22), 177 (20), 119 (24, $GeMe_3$), 73 (100, $SiMe_3$); high resolution MS: calcd. for *m/e* $C_9H_{28}{}^{28}Si^{72}Ge_2{}^{74}Ge$ 381.9614; found: 381.9662.

Tris(trimethylgermyl)(trimethylsilyl)silane

MeLi (0.4 mL of a 1.3 M solution in Et_2O) was added to a stirred solution of $(Me_3Ge)_4Si$ (0.09 g, 0.18 mmol) in THF (12 mL). After stirring overnight at room temperature, the light-yellow silyllithium reagent was transferred to a pressure-equalizing funnel and added, dropwise, to a solution of Me_3SiCl (0.13 g, 1.2 mmol) in pentane (35 mL) at −78°C. The cold bath was then removed and the reaction mixture stirred overnight. Acidic work-up and removal of the solvent by rotary evaporation gave a crude, white solid. Sublimation (55°C, 1.15 Torr) resulted in the isolation of 0.043 g (53%) of $(Me_3Ge)_3Si(SiMe_3)$ as a white, waxy solid. IR (KBr, cm^{-1}) 2967 (s), 2905 (s), 2797 (m), 1404 (m), 1260 (m), 1244 (s), 1229 (s), 814 (s), 687 (m), 625 (m), 586 (s), 558 (s); ^1H NMR (ppm) 0.24 (s, 9 H, Si—CH_3), 0.39 (s, 27 H, Ge—CH_3); ^{13}C NMR (ppm) 2.02 (q, Ge—CH_3, J = 126 Hz), 2.46 (q, Si—CH_3, J = 119 Hz); ^{29}Si NMR (ppm) −8.44 (sextet, $SiMe_3$, J = 7 Hz), −112.45 (m, $(Me_3Ge)_3Si$); MS *m/e* (%) 454 (4, M^+), 439 (10, M^+ − Me), 335 (12, M^+ − $GeMe_3$), 235 (12), 177 (8), 119 (11, $GeMe_3$), 73 (100, $SiMe_3$); high resolution MS: calcd. for *m/e* $C_{12}H_{36}{}^{28}Si_2{}^{72}Ge_2{}^{74}Ge$: 454.0009; found: 453.9991.

Methyltris(trimethylgermyl)silane

$(Me_3Ge)_3SiLi$ was prepared, as described previously, by the addition of MeLi (0.7 mL of a 1.3 M solution in Et_2O) to a stirred solution of $(Me_3Ge)_4Si$ (0.09 g, 0.19 mmol) in THF (12 mL) and stirring the resulting mixture overnight at room temperature. The light-yellow silyllithium reagent was then added dropwise to a solution of MeI (0.23 g, 1.6 mmol) in pentane (40 mL) at −78°C. The reaction mixture was then allowed to warm to ambient temperature and stirred overnight. After acidic work-up, purification by chromatography (Chromatotron; hexanes) gave 0.05 g of a white, waxy solid which contained a mixture of $(Me_3Ge)_3Si$—Me and $(Me_3Ge)_4Si$ in a 4:1 ratio (by GC). These two compounds could not be separated; however, preparative GC allowed for the isolation of a mixture containing 91% $(Me_3Ge)_3Si$—Me (by GC). Characterization for $(Me_3Ge)_3Si$—Me, containing approximately 20% $(Me_3Ge)_4Si$: ^1H NMR (ppm) 0.22 (s, 3 H, Si—CH_3), 0.31 (s, 27 H, $GeCH_3$); ^{13}C NMR (ppm) −0.53 (q, Ge—CH_3, J = 126 Hz), −11.26 (q, Si—CH_3, J = 124 Hz); ^{29}Si NMR (ppm) −63.18; MS *m/e* (%) 396 (31, M^+), 381 (56, M^+ − Me), 279 (83, M^+ − $GeMe_3$), 177 (75), 119 (30, $GeMe_3$), 73 (100, $SiMe_3$); high resolution MS: calcd. for *m/e* $C_{10}H_{30}{}^{28}Si^{72}Ge_2{}^{74}Ge$: 395.9770; found: 395.9796.

Dichlorobis(trimethylgermyl)silane

Chlorine gas was bubbled (ca. 1 bubble every 5 s) through a stirred solution of $(Me_3Ge)_3SiH$ (0.053 g, 0.14 mmol) in pentane (15 mL) at −78°C. The reaction was monitored by gas chromatography and was found to be complete after 16 min of chlorination. The solvent was then removed by rotary evaporation and the product purified by trap-to-trap distillation (room temperature, 0.5 Torr). This afforded 0.043 g (92%) of $(Me_3Ge)_2SiCl_2$ as a clear, colourless liquid. IR (neat, cm^{-1}) 2965 (s), 2936 (s), 2876 (m), 1458 (m), 1381 (m), 1237 (w), 822 (s), 652 (m), 600 (s); ^1H NMR (ppm) 0.28 (s); ^{13}C NMR (ppm) −3.27 (q, J = 128 Hz); ^{29}Si NMR (ppm) 40.83; MS *m/e* (%) 334 (5, M^+), 319 (4, M^+ − Me), 197 (15), 119 (100, $GeMe_3$), 73 (69, $SiMe_3$); high resolution MS: calcd. for *m/e* $C_6H_{18}{}^{28}Si^{72}Ge^{74}Ge^{35}Cl_2$: 333.8987; found: 333.8965.

Acknowledgements

The financial support of the Natural Sciences and Engineering Research Council of Canada, the University of Western Ontario, the J. P. Bickell Foundation, and the Ontario Centre for Materials Research is gratefully acknowledged.

1. Y. Derouiche and P. D. Lickiss. J. Organomet. Chem. **407**, 41 (1991); S. P. Mallela and R. A. Geanangel. Inorg. Chem. **30**, 1480 (1991); B. O. Dabbousi, P. J. Bonasia, and J. Arnold. J. Am. Chem. Soc. **113**, 3186 (1991); S. P. Mallela and R. A. Geanangel. Inorg. Chem. **29**, 3525 (1990); M. L. Sierra, V. S. J. De Mel, and J. P. Oliver. Organometallics, **8**, 2312 (1989); A. G. Brook, S. C. Nyburg, F. Abdesaken, B. Gutekunst, G. Gutekunst, R. K. M. R. Kallury, Y. C. Poon, Y.-M. Chang, and W. Wong-Ng. J. Am. Chem. Soc. **104**, 5667 (1982).
2. B. K. Campion, R. H. Heyn, and T. D. Tilley. J. Am. Chem. Soc. **112**, 2011 (1990); L. S. Chang, M. P. Johnson, and M. J. Fink. Organometallics, **8**, 1369 (1989); B. K. Campion, J. Falk, and T. D. Tilley. J. Am. Chem. Soc. **109**, 2049 (1987); D. M. Roddick, T. D. Tilley, A. L. Rheingold, and S. J. Geib. J. Am. Chem. Soc. **109**, 945 (1987); M. H. Chisolm, H. T. Chiu, K. Folting, and J. C. Huffman. Inorg. Chem. **23**, 4097 (1984).
3. H. Gilman and C. L. Smith. J. Organomet. Chem. **8**, 245 (1967).
4. H. Gilman and C. L. Smith. J. Organomet. Chem. **14**, 91 (1968).
5. A. G. Brook, G. Gutekunst, and K. M. Baines. Organomet. Synth. **4**, 385 (1988).
6. D. G. J. Sutherland, G. M. Bancroft, and K. H. Tan. Surf. Sci. Lett. **262**, L96 (1992).
7. J. V. Muntean, L. M. Stock, and R. E. Botto. J. Magn. Reson. **76**, 540 (1988).
8. R. H. Heyn and T. D. Tilley. Inorg. Chem. **29**, 4051 (1990).
9. P. Mazerolles, A. Reynes, S. Sefiani, and R. Morancho. J. Anal. Appl. Pyrolysis, **22**, 95 (1991); H. Schmidbaur and J. Rott. Z. Naturforsch. **45***b*, 961 (1990).
10. P. Aebi, T. Tyliszczak, A. P. Hitchcock, T. K. Sham, K. M. Baines, J. Xiong, K. A. Mueller, J. M. Chen, B. X. Yang, T. E. Jackman, J. M. Baribeau, and Z. H. Lu. To be published.
11. J. Barrau, G. Rima, and J. Satgé. Organomet. Synth. **4**, 534 (1988).
12. J. Grobe and J. Hendriock. Synth. React. Inorg. Met. Org. Chem. **5**, 393 (1975).
13. E. J. Bulten and J. G. Noltes. J. Organomet. Chem. **29**, 397 (1971).
14. K. Mochida, T. Kugita, and Y. Nakadaira. Polyhedron, **9**, 2263 (1990).
15. K. Mochida and N. Matsushige. J. Organomet. Chem. **229**, 11 (1982).
16. H. Marsmann. *In* NMR basic principles and progress. Vol. 17. *Edited by* P. Diehl, E. Fluck, and R. Kosfeld. Springer-Verlag, New York. 1982. p. 65.
17. B. H. Boo and P. P. Gaspar. Organometallics, **5**, 698 (1986).
18. L. M. Harwood. Aldrichimica Acta, **18**, 25 (1985).

Nonlinearity of the maximum entropy method in resolution enhancement[1]

J. K. KAUPPINEN
Department of Applied Physics, University of Turku, Vesilinnantie 5, SF-20500 Turku, Finland

AND

D. J. MOFFATT AND H. H. MANTSCH[2]
Institute for Biodiagnostics, National Research Council, Winnipeg, Man., Canada R3B 1Y6

Received April 16, 1992

J. K. KAUPPINEN, D. J. MOFFATT, and H. H. MANTSCH. Can. J. Chem. **70**, 2887 (1992).

The nonlinear behavior of the filter-type Maximum Entropy Method (MEM) was investigated from a theoretical and a practical point of view. The integrated intensity of the output spectral lines of MEM was probed as a function of the input intensity pattern, the filter length, and the S/N ratio of the input spectrum. The nonlinear behavior of MEM has been explained and the results compared with those derived by another method, LOMEP (Lineshape Optimized Maximum Entropy linear Prediction). The study was carried out with the aim of resolution enhancement of spectra that have high signal-to-noise ratio.

J. K. KAUPPINEN, D. J. MOFFATT et H. H. MANTSCH. Can. J. Chem. **70**, 2887 (1992).

On a étudié le comportement non-linéaire de la Méthode d'Entropie Maximale d'un point de vue tant théorique que pratique. On a examiné l'intensité intégrée des raies spectrales de sortie MEM en fonction du patron de l'intensité à l'entrée, de la longueur du filtre et du rapport signal/bruit du spectre d'entrée. On a expliqué le comportement non-linéaire du MEM et on a comparé les résultats avec ceux obtenus à l'aide d'une autre méthode, LOMEP (prédiction linéaire à partir de l'information sur l'entropie maximale et la forme de la courbe). On a réalisé l'étude afin d'augmenter la résolution de spectres ayant des rapports signal/bruit élevés.

[Traduit par la rédaction]

Introduction

The basic principle of the Maximum Entropy Method (MEM) (1–3) is to perform a least-squares fit with an extra constraint, maximization of the information entropy. Simpler techniques, which use as the only constraint the standard deviation of a least-squares fit, will not yield a unique solution. The most probable solution will be the one that has a maximum information entropy. Thus, by maximizing the entropy of the spectrum for a given standard deviation one obtains the best solution for a given set of data. This operation, known as iterative MEM, has been shown to be suitable for *fitting* a spectrum (1–8); however, it is not well suited for resolution enhancement.

There exists another type of MEM, based on filter theory, in which the output spectrum is computed simply from a maximum entropy power spectral estimator, which is proportional to the power spectrum of the transfer function of the filter. There are many variations of this MEM that differ only in the model of the filter and in the method used to solve the resulting equations. Most common (1–3, 9) are the autoregression (AR), moving-average (MA), and autoregression/moving-average (ARMA) models. As this type of MEM has been used for resolution enhancement, we will make it the focus of our discussion. In a previous report (10) we tested the use of the AR method of Burg's MEM (11, 12) as a resolution enhancement technique; we now explain why it should never be used for this purpose. We show that in AR, MA, and ARMA information regarding the intensity of the input lines is highly degraded. Moreover, other methods in which the power spectral estimator is proportional to the power of a transfer function, such as MUSIC (13, 14) or MINIMUM NORM (14), will also suffer from this disadvantage.

[1]NRCC No. 32853.

[2]Author to whom correspondence may be addressed.

Theory

Part A. Filter-type maximum entropy method

In the ARMA method (1–3, 9) the time domain model is given by

$$[1] \qquad I_j = -\sum_{k=1}^{M} a_k I_{j-k} + \sum_{k=0}^{P} b_k e_{j-k}, \qquad b_0 = 1$$

where, using an interferometric notation, $I_j = I(j\Delta x)$ is the time domain data point at $j\Delta x = j/(2\nu_{max})$, and e_j is the corresponding error at this point. The ARMA model in eq. [1] can be considered as a filter with a transfer function given by

$$[2] \qquad H(z) = \frac{1 + \sum_{k=1}^{P} b_k z^{-k}}{1 + \sum_{k=1}^{M} a_k z^{-k}}$$

where

$$[3] \qquad z = \exp\left(-i\frac{\pi\nu}{\nu_{max}}\right)$$

The power spectral estimation (2, 9) has been defined as

$$[4] \qquad P(\nu) = \sigma_M^2 H^*(\nu) H(\nu)$$

where σ_M is the standard deviation of the errors e_j and H^* stands for a complex conjugate of H.

In a spectrum with a high signal-to-noise ratio the $b_k e_{j-k}$ terms can be approximated to zero (for $k > 0$) and the method

Can. J. Chem. Downloaded from www.nrcresearchpress.com by 109.225.110.28 on 09/08/12
For personal use only.

Can. J. Chem. Downloaded from www.nrcresearchpress.com by 109.225.110.28 on 09/08/12
For personal use only.

becomes the autoregression AR model. Thus eq. [1] reduces to

$$[5] \quad I_j = -\sum_{k=1}^{M} a_k I_{j-k} + e_j$$

or

$$[6] \quad I_j - e_j = I'_j = -\sum_{k=1}^{M} a_k I_{j-k} = \sum_{k=1}^{M} h_k I_{j-k}$$

where $a_k = -h_k$ $(k > 0)$. Thus eqs. [2]–[4] yield

$$[7] \quad H(z) = \frac{1}{1 + \sum_{k=1}^{M} a_k z^{-k}}$$

and

$$[8] \quad P(\nu) = \frac{\sigma_M^2}{\left| \sum_{k=0}^{M} a_k \exp\left(\frac{i\pi\nu k}{\nu_{max}}\right) \right|^2}, \qquad a_0 = 1$$

$P(\nu)$ is referred to as the maximum entropy power spectral estimator. It has been demonstrated (15) that the information entropy has a maximum for $P(\nu)$ if the prediction-error coefficients $\{a_k\}$ are derived from eq. [5], i.e., by fitting the data I_j according to eq. [5].

The procedure known as Burg's MEM is based on eqs. [5] and [8]. Because under certain conditions the power spectrum $P(\nu)$ defined by eq. [8] produces narrow spectral lines this method is sometimes referred to as "super-resolution MEM." However, the method is highly nonlinear and therefore often misleading. If line narrowing were to take place correctly in eq. [8] then this would be equivalent to linear prediction in the time domain. We will show that this is never the case.

Part B. True linear prediction and LOMEP

Let us now consider a new approach to the problem of linear prediction. Instead of using Burg's method we derive a theoretical impulse response $\{h_k\}$ of the linear prediction based on eq. 5.[3] Equation [6] can be rewritten as a convolution:

$$[9] \quad I_p(x) = [D(x)h(x)] * I(x) = \int_{-\infty}^{\infty} D(x')h(x')I(x - x')\,dx'$$

where $I_p(x)$ is a predicted signal and $D(x)h(x)$ is the desired impulse response, if

$$[10] \quad D(x) = \begin{cases} 1 & 0 < x \leq M\Delta x \\ 0 & \text{elsewhere} \end{cases}$$

Let us assume that we know the true signal $I(x)$ in the interval $(0, M\Delta x)$ and that it consists of *noise-free* undamped cosine waves, i.e.,

$$[11] \quad I(x) = \sum_i A_i \cos(2\pi\nu_i x)$$

where A_i is the integrated intensity of a line at ν_i. A true linear prediction is possible if and only if we have a stationary case where the theoretical coefficients $\{a_k\}$ do not depend on the shift of the input data (see below). It can be shown[3] that if $e_j = 0$, then the simplest solution of eq. [5] is given by

$$[12] \quad h(x) = \sum_i \alpha_i \cos(2\pi\nu_i x + \phi_i)$$

where the scaling constants α_i and the phase adjustments ϕ_i can be derived from the constraint:

$$[13] \quad \mathcal{H}(\nu) = \mathcal{F}\{D(x)h(x)\} = 1 \qquad \text{at} \qquad \nu = \nu_i$$

where $\mathcal{F}\{\ \}$ is the Fourier transform operator. This is a necessary and sufficient condition for $h(x)$ to be a solution of eq. [5]. Furthermore, it can be shown[3] that the constants α_i and ϕ_i depend only on the frequencies ν_i of the spectral lines and on M; thus the filter coefficients $a_k = -h_k = -h(k\Delta x)$ *do not contain information concerning the line intensities* A_i. Hence, under these ideal conditions (a noise-free input spectrum) eq. [8] will not contain any intensity information and therefore the *filter-type MEM cannot give correct intensities of the spectral lines and eqs. [4] and [8] cannot be accurate estimates of the power spectrum* $P(\nu)$.

The only way to realize significant resolution enhancement with correct line intensities A_i is to perform a true linear prediction. This is accomplished by applying eq. [5] inductively (with the assumption $e_j = 0$) to extrapolate the time domain starting with the $M + 1$ known (measured) data I_j $(j = 0, 1, 2, \ldots M)$. We have given this resolution enhancement method the name "LOMEP" (10, 16) (Lineshape Optimized Maximum Entropy linear Prediction). LOMEP consists of three procedures: Fourier Self-Deconvolution FSD (17), Burg's MEM, and this true linear prediction, LP. Now, maximum resolution enhancement can only be achieved by extrapolation of undamped cosine waves as assumed in eq. [11]. In practice, the intrinsic lineshape of spectroscopic lines (e.g., Lorentzian or Gaussian) corresponds to damped cosine waves in the time domain. Therefore the first step in LOMEP is the use of FSD to change the damped cosine waves to undamped ones according to the following equation:

$$[14] \quad E(\nu) = \mathcal{F}\left\{\frac{\mathcal{F}^{-1}\{W_0(\nu)\}\,\mathcal{F}^{-1}\{E_{in}(\nu)\}}{\mathcal{F}^{-1}\{W(\nu)\}}\right\}$$

where $E_{in}(\nu)$ is the input spectrum with lineshape function $W(\nu)$, $\mathcal{F}\{\ \}$ and $\mathcal{F}^{-1}\{\ \}$ are the Fourier transform and inverse Fourier transform, respectively. Line narrowing will be achieved if the imposed output lineshape $W_0(\nu)$ is narrower than $W(\nu)$. The line-narrowing factor K, loosely referred to as the "resolution enhancement factor," is given by

$$[15] \quad K = \frac{\text{FWHH}(W)}{\text{FWHH}(W_0)}$$

where FWHH(W) and FWHH(W_0) are the full width at half-height of $W(\nu)$ and $W_0(\nu)$, respectively. In practice K is limited by the signal-to-noise ratio (S/N) of $E_{in}(\nu)$, i.e., $K < \log_{10}(\text{S/N})$. In LOMEP the output lineshape $W_0(\nu)$ is a sinc function meaning that FSD changes the damped time-domain signals to undamped ones. This lineshape optimization is the key step in LOMEP, enabling it to achieve resolution enhancement (10).

[3] J. K. Kauppinen, P. E. Saarinen, and D. J. Moffatt. To be published.

Can. J. Chem. Downloaded from www.nrcresearchpress.com by 109.225.110.28 on 09/08/12
For personal use only.

The next step in LOMEP is to compute the prediction-error coefficients $\{a_k\}$ ($k = 1, 2, 3, \ldots M$) of a prediction-error filter. This is done by using Burg's method (11, 12) and $M + 1$ known data I_j ($j = 0, 1, 2, \ldots M$). After this we are able to predict new data I_j($j > M$) by using eq. [5] and $M + 1$ known data I_j ($j = 0, 1, 2 \ldots M$) assuming that $e_j = 0$. In principle, Burg's MEM gives $\{a_k\}$ so that the error power $\Sigma^M |e_j|^2$ has a minimum. Unfortunately, this minimum error power depends very strongly and chaotically on the filter length M. The innovation in LOMEP is to optimize the filter length M using a simple test of the prediction coefficients a_k. This can be done by predicting backward the data I'_{-j} ($j = 1, 2, 3 \ldots M$) using the input data I_j ($j = 0, 1, 2, \ldots M$). From those predicted data I'_{-j} we are able to compute the quality factor of prediction given by:

$$[16] \quad q(M) = 1 - \sqrt{\frac{\sum_{j=1}^{M} (I'_{-j} - I_{-j})^2}{\sum_{j=1}^{M} (I_{-j})^2}}$$

This is possible, because $I_{-j} = I_j$ and the forward and backward prediction coefficients are the same, if the input signal consists of undamped cosine waves. Unfortunately, in all but the most trivial cases, the theoretical minimum M for which $q(M) = 1$ is larger than the number of usable data points in the time-domain signal. The practical solution is to search for an optimum filter length M_0 for which $q(M_0)$ has a maximum. The choice of M_0 can greatly affect the quality of the LOMEP output in terms of lineshape.

The next step of LOMEP is a linear prediction applying eq. [5] inductively to the initial input signal I_j ($j = 0, 1, 2, \ldots M_0$). The final signal is the input signal plus the predicted one I_j ($j = M_0 + 1, M_0 + 2, \ldots, N$) where the practical limit, N, to extrapolation is determined mainly by $q(M_0)$ and the degree of distortion allowable in the output spectrum. To obtain a more desirable lineshape than sinc we apodize the final signal. Thus the lineshape ($W_L(\nu)$) of the LOMEP output spectrum is simply the Fourier transform of the apodization function. The line-narrowing factor K of LOMEP is FWHH(W)/FWHH(W_L) and it is proportional to N.

Comparison of Burg's MEM with LOMEP as methods for resolution enhancement

The only step common to both MEM and LOMEP is the use of Burg's MEM to compute the coefficients $\{a_k\}$ using the same model eq. [5]. Thereafter LOMEP and MEM differ substantially, the former once again using eq. [5] to accomplish a true linear prediction, with the latter using the maximum entropy power spectral estimator given by eq. [8]. Therefore LOMEP output spectra are amplitude (true) spectra whereas MEM spectra are power spectra. In LOMEP, lineshape optimization is always performed with the help of FSD, while MEM is applied to spectra without use of any lineshape information. In this work we apply FSD before MEM, because in this case MEM works better (10). Further, in LOMEP we optimize the filter length and use the quality factor $q(M_0)$ to guarantee the reliability of the final prediction. The closer $q(M_0)$ is to 1, the less distorted are the output lines. In LOMEP the output lineshape and the line narrowing factor K are easily adjusted by apodization and the length (N) of the final signal, whereas in MEM lineshape and linewidth are not under our control.

Let us now compare the properties of Burg's MEM with the true linear prediction of LOMEP, by applying eq. [5] to synthesized data. This comparison was carried out by varying (*i*) the integrated intensity of the individual input spectral lines (see Fig. 1), (*ii*) the filter length M (see Fig. 2), and (*iii*) the S/N ratio of the input spectrum (see Fig. 3). The test spectra are comprised of Lorentzian lines (FWHH = 40) at positions $\nu_1 = 600$, $\nu_2 = 900$, $\nu_3 = 1600$, and $\nu_4 = 1650$ with a sampling interval of 1. The integrated intensities of the input spectra and those of the various output spectra are listed in Table 1; measured intensities were integrated 25 points to either side of the input line positions. In all three figures, the MEM spectra are magnitude spectra and the LOMEP spectra have a Bessel lineshape.

Figure 1 shows the FSD, LOMEP, and MEM output spectra with $M = 152$, $N = 153$. Because the theoretical impulse response $D(x)h(x)$, defined in eqs. [10] and [12], depends only on M and the frequencies ν_i, we may compute the $\{a_k\}$ coefficients for the input spectrum of Fig. 1A only, and then use these coefficients to compute LOMEP outputs for all four input spectra. The LOMEP spectra, even with a high K (resolution enhancement factor) value of 10, are quite reasonable, both in terms of lineshape (lack of distortion) and integrated intensity. As evident from Table 1-I, the intensities are accurate to within 0.1%. The output lineshape is controlled by apodization of the extrapolated signal. The fact that the impulse response calculated from spectrum 1A can be successfully employed for the linear prediction of all four spectra proves that the impulse response does not contain intensity information. It is to be noted that LOMEP also gives correct intensities in the case of negative lines.

On the other hand, the relative integrated intensities of the MEM spectra in Fig. 1 deviate from the input values by as much as two orders of magnitude. Furthermore, some lines have undergone splitting and even those that did not, do not possess uniform lineshapes. This clearly demonstrates that neither the impulse response nor the magnitude spectrum $(P(\nu))^{1/2}$ in eq. [8] contains significant intensity information. In this simulation the ratio M/N is approximately one. As it has been shown (2, 3), this is not an optimal situation for MEM. Figure 2 illustrates the behavior of LOMEP and MEM as a function of the filter length (M), using spectrum 1B as input. Again, the intensities of the spectral lines are retained in the LOMEP output while MEM produces a variation of between +3 and −51% around the input values (see Table 1-II). Spurious lines are also evident in the MEM output, and the lines at 1600 and 1650 often appear split. In this example the number of points, N, used in MEM was 153, while for LOMEP this number was $M + 1$. The discrete M values used in the calculations are given in Fig. 2. Now the M to N ratio is closer to the optimal value (2, 3) for MEM but not for LOMEP. For small values of M ($M << M_0$), the LOMEP procedure appears to suffer from lack of information, which results in lineshape distortions, but no degradation of the integrated intensity information.

Figure 3 compares the output of LOMEP with that of MEM as a function of S/N using again the intensities and frequencies in spectrum 1B as a model. The measured integrated intensities of the output spectra are given in Table

Can. J. Chem. Downloaded from www.nrcresearchpress.com by 109.225.110.28 on 09/08/12
For personal use only.

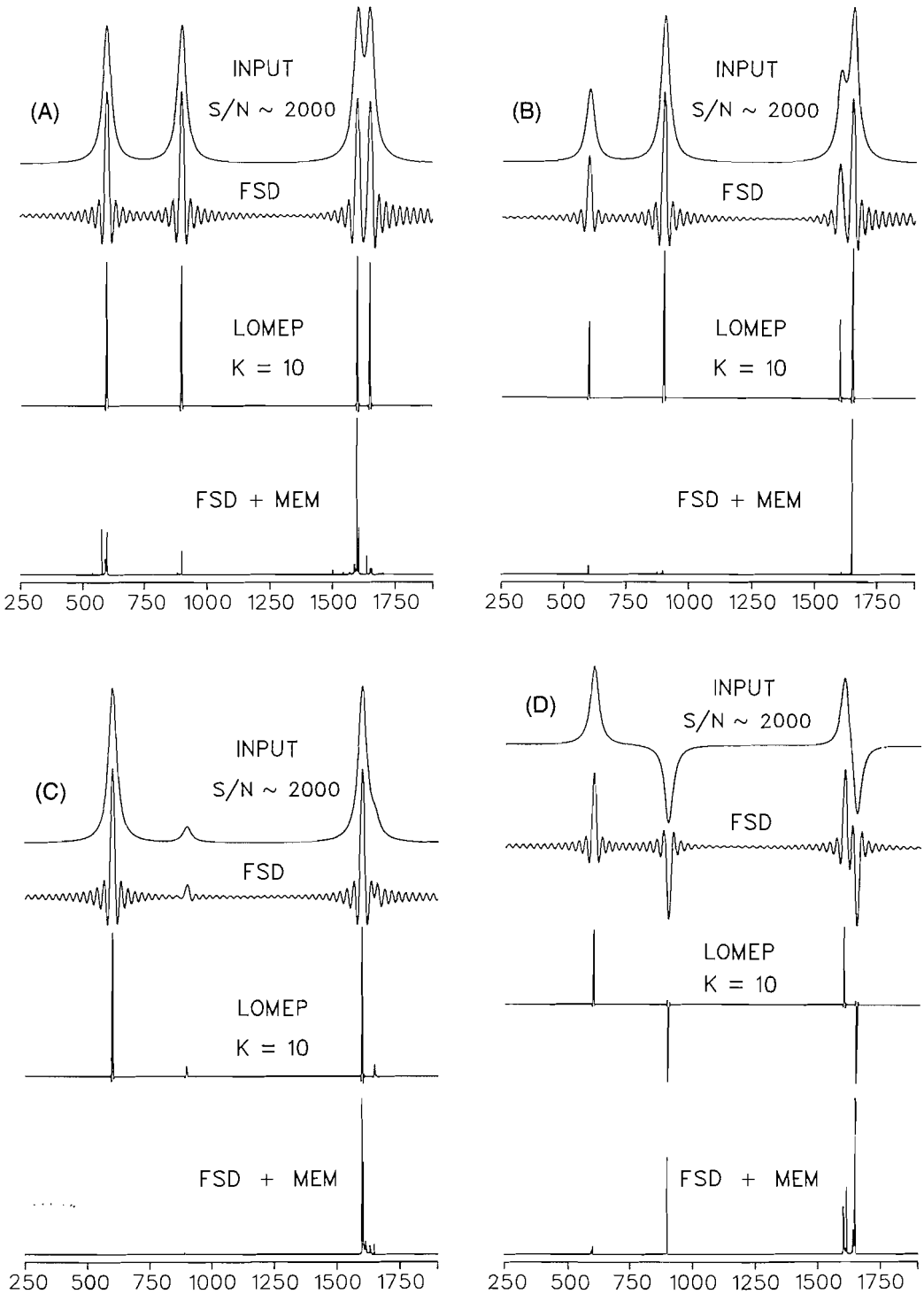

FIG. 1. Burg's MEM and LOMEP output spectra at various input line intensity patterns. The input lines at 800, 900, 1600, and 1650 have the following relative integrated intensities (A) 1, 1, 1, 1; (B) 1/2, 1, 1/2, 1; (C) 1, 1/10, 1, 1/10; (D) 1, −1, 1, −1. The peak-to-peak S/N was 2000.

1-III. Once more it is evident that LOMEP performs well, giving accurate intensities and output lineshapes even in the examples with low input S/N, though some output noise is evident in these cases. The MEM output spectra on the other hand have quite inaccurate intensities. In addition, this figure demonstrates a peculiar characteristic of filter MEM: its output appears to improve as the input S/N decreases. For example, with S/N = 2 or 20 the intensity errors are ~25%, while at S/N = ∞ the intensity errors are almost two orders of magnitude. This is further evidence that the maximum entropy power spectral estimator given in eqs. [4] and [8] is incorrect. Another odd characteristic of MEM is the apparent absence of noise in the output, regardless of the input S/N. This is because the link between the input spectrum and the output is very tenuous, depending only upon a smooth Fourier transform of the filter coefficients, $\{a_k\}$. Comparing

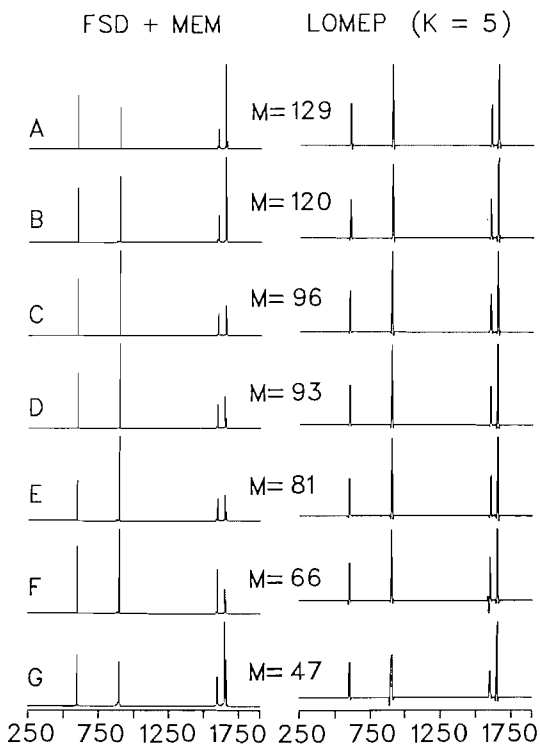

FIG. 2. Illustration of the effect of filter length, $M\Delta x$, on MEM and LOMEP output spectra. The input spectrum is that from Fig. 1B with $N = 153$ for MEM and $N = M + 1$ for LOMEP.

the LOMEP and MEM output at low S/N (Fig. 3E), MEM gives a better looking spectrum while LOMEP gives a more accurate representation of the input along with some output noise.

Discussion

Part A. Why can LOMEP perform a true linear prediction?

In LOMEP one uses a linear filter, as in eqs. [5] and [9], applied to the measured time domain signal, $I(x)$, after FSD. Upon Fourier transformation eq. [9] becomes:

$$[17] \quad E_p(\nu) = \mathcal{H}(\nu)E(\nu)$$

where the transfer function of the filter is given by

$$[18] \quad \mathcal{H}(\nu) = \mathcal{F}\{D(x)h(x)\}$$

According to eq. [11], $I(x)$ consists of infinitely long cosine waves even though only a short segment of this signal is known (between 0 and $M\Delta x$). Now if the condition in eq. [13], i.e., $\mathcal{F}\{D(x)h(x)\} = \mathcal{H}(\nu) = 1$, is exactly valid, at least at all the frequencies (ν_i) where lines occur in the spectrum $E(\nu)$, one can continue $I_p(x)$ ad infinitum, $I_p(x) = I(x)$, and eq. [17] can be rewritten:

$$\begin{aligned}[19] \quad E_p(\nu) &= \mathcal{H}(\nu)E(\nu) \\ &= \mathcal{H}(\nu) \sum_i A_i \{(1/2)\,\delta(\nu + \nu_i) \\ &\quad + (1/2)\,\delta(\nu - \nu_i)\} \\ &= \sum_i A_i \{(1/2)\,\delta(\nu + \nu_i) \\ &\quad + (1/2)\,\delta(\nu - \nu_i)\} = E(\nu)\end{aligned}$$

because $\mathcal{H}(\nu) = 1$ at $\pm \nu_i$ and $E(\nu) = \mathcal{F}\{I(x)\}$. This means that LOMEP gives an exactly correct spectrum including the intensities A_i and the frequencies ν_i. Though $h(x)$ may include frequencies that are not in $I(x)$, the LOMEP result will not contain lines at these frequencies. LOMEP is inherently a more reliable method because it will produce an output line at a given frequency, ν_ω, if and only if $\mathcal{H}(\nu_\omega) = 1$, and the spectrum, $E(\nu_\omega)$, has significant intensity at ν_ω according to eq. [19]. This practically eliminates the possibility of spurious lines, which are quite common in MEM. Moreover, LOMEP will in general yield more accurate frequencies than MEM because in linear prediction both the input signal and the impulse response contain frequency information.

Part B. What's wrong with MEM?

Burg's MEM is based on the maximum entropy power spectral estimator given by eq. [8]. Its predecessor, eq. [5], can be expressed in a continuous form as

$$[20] \quad I(x) = [D(x)h(x)]*I(x) + e(x)$$

or as

$$[21] \quad E(\nu) = \mathcal{H}(\nu)\,E(\nu) + \varepsilon(\nu)$$

where $\varepsilon(\nu)$ is an error spectrum that includes noise. Hence,

$$[22] \quad E(\nu) = \frac{\varepsilon(\nu)}{1 - \mathcal{F}\{D(x)h(x)\}} = \frac{\varepsilon(\nu)}{1 - \mathcal{H}(\nu)}$$

In Burg's MEM one first derives the impulse response $\{a_k\}$ of the so-called prediction-error filter by minimizing errors. If $\varepsilon(\nu)$ were known, the output spectrum could then be computed by direct application of the transfer function $1/(1 - \mathcal{H}(\nu))$. Because the absolute value of the error spectrum, $|\varepsilon(\nu)|$, is not known, the constant value, σ_M, has been used instead, i.e.,

$$[23] \quad |\varepsilon(\nu)| \approx \sigma_M = \sqrt{\frac{1}{2\nu_{\max}} \int_{-\nu_{\max}}^{\nu_{\max}} |\varepsilon(\nu)|^2 d\nu}$$

Using this approximation the power spectrum becomes:

$$[24] \quad P(\nu) = |E(\nu)|^2 \approx \frac{\sigma_M^2}{|1 - \mathcal{H}(\nu)|^2} = \frac{\sigma_M^2}{\left|\sum_{k=0}^{M} a_k e^{i2\pi\nu k\Delta x}\right|^2}$$

which is the well-known maximum entropy power spectral estimator. However, it turns out that this approximation in eq. [23] is very poor, especially at the line positions, ν_i, where the difference between σ_M and $|\varepsilon(\nu_i)|$ can be several orders of magnitude. Also, the error spectrum, $|\varepsilon(\nu)|$, is not merely noise, but contains intensity information not contained in the prediction-error constants. Rearranging eq. [22],

$$[25] \quad \varepsilon(\nu) = E(\nu)[1 - \mathcal{H}(\nu)]$$

we see that $\varepsilon(\nu)$ depends not only on $E(\nu)$, but also on how close $\mathcal{H}(\nu)$ is to unity, i.e., the validity of the linear prediction condition.

We will now explore how this erroneous approximation explains much of the anomalous behavior of MEM. Let us take a few numerical examples. For convenience, we rewrite eq. [24] as follows:

Can. J. Chem. Downloaded from www.nrcresearchpress.com by 109.225.110.28 on 09/08/12
For personal use only.

Can. J. Chem. Downloaded from www.nrcresearchpress.com by 109.225.110.28 on 09/08/12
For personal use only.

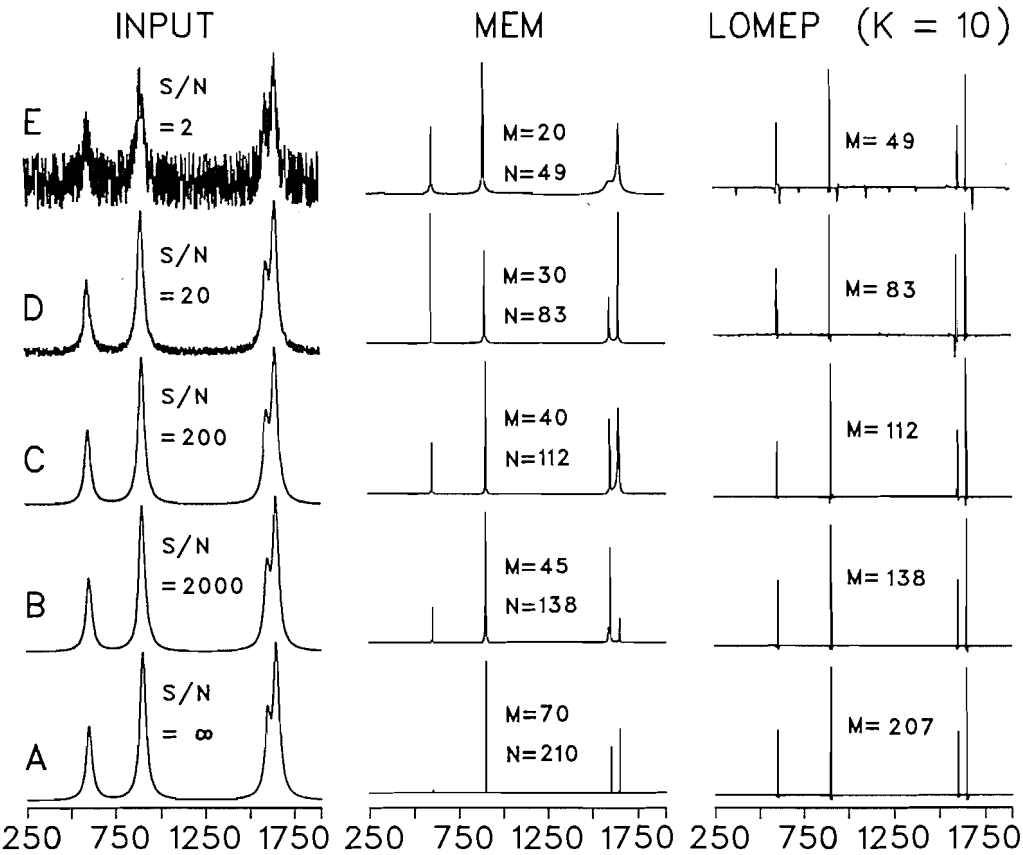

FIG. 3. Burg's MEM and LOMEP output spectra at various input signal-to-noise ratios. The intensity pattern is that used in Fig. 1B.

TABLE 1. Relative integrated intensities of the lines A_i in Figs. 1–3

		Input value				LOMEP output				MEM output					
		A_1	A_2	A_3	A_4	A_1	A_2	A_3	A_4	A_1	A_2	A_3	A_4	M	S/N
	Fig. 1A	1	1	1	1	0.9996	1.0000	1.0000	0.9996	0.67	0.14	1.00	0.20		
I	Fig. 1B	1/2	1	1/2	1	0.4996	1.0000	0.5000	0.9997	0.07	0.07	0.05	1.00		
	Fig. 1C	1	1/10	1	1/10	0.9996	0.0999	1.0000	0.0995	0.006	0.01	1.00	0.12		
	Fig. 1D	1	−1	1	−1	0.9991	−0.9997	0.9995	−1.0000	0.06	0.34	0.64	1.00		
	Fig. 2A	1/2	1	1/2	1	0.5012	1.0000	0.5052	0.9989	0.25	0.50	0.35	1.00	129	
	Fig. 2B	1/2	1	1/2	1	0.4976	0.9970	0.4994	1.0000	0.50	1.00	0.47	0.49	120	
	Fig. 2C	1/2	1	1/2	1	0.4983	1.0000	0.4997	0.9989	0.38	1.00	0.40	0.54	96	
II	Fig. 2D	1/2	1	1/2	1	0.4996	1.0000	0.5000	0.9997	0.48	1.00	0.42	0.60	93	
	Fig. 2E	1/2	1	1/2	1	0.4999	1.0000	0.4997	0.9997	0.48	1.00	0.40	0.55	81	
	Fig. 2F	1/2	1	1/2	1	0.5005	1.0000	0.4998	0.9998	0.41	0.83	0.53	1.00	66	
	Fig. 2G	1/2	1	1/2	1	0.5005	1.0000	0.4995	0.9999	0.44	0.61	0.46	1.00	47	
	Fig. 3A	1/2	1	1/2	1	0.5000	1.0000	0.5000	1.0000	0.03	1.00	0.55	0.46		∞
	Fig. 3B	1/2	1	1/2	1	0.4999	1.0000	0.5006	0.9994	0.16	1.00	0.59	0.11		2000
III	Fig. 3C	1/2	1	1/2	1	0.4982	0.9963	0.4989	1.0000	0.20	0.36	0.38	1.00		200
	Fig. 3D	1/2	1	1/2	1	0.4951	0.9836	0.4732	1.0000	0.42	1.00	0.74	0.89		20
	Fig. 3E	1/2	1	1/2	1	0.4920	1.0000	0.5790	0.9828	0.37	0.76	0.46	1.00		2

[26] $$P(\nu) = |E(\nu)|^2 \approx \frac{\sigma_M^2}{|1 - \mathcal{H}(\nu)|^2}$$

$$= \frac{\sigma_M^2}{[1 - \mathrm{Re}(\nu)]^2 + [\mathrm{Im}(\nu)]^2} = \frac{\sigma_M^2}{|\Delta(\nu)|^2}$$

where $\mathrm{Re}(\nu)$ and $\mathrm{Im}(\nu)$ are the real and imaginary parts, respectively, of $\mathcal{H}(\nu)$. Assuming the linear prediction condition (eq. [13]) is exactly valid, i.e., $\mathrm{Re}(\nu) = 1$ and $\mathrm{Im}(\nu) = 0$ at all the line positions, then, according to eq. [26], all the corresponding peak heights in MEM will be infinite. It is now easy to understand why on average the closer $[\Delta(\nu)]^2$ is to

Can. J. Chem. Downloaded from www.nrcresearchpress.com by 109.225.110.28 on 09/08/12
For personal use only.

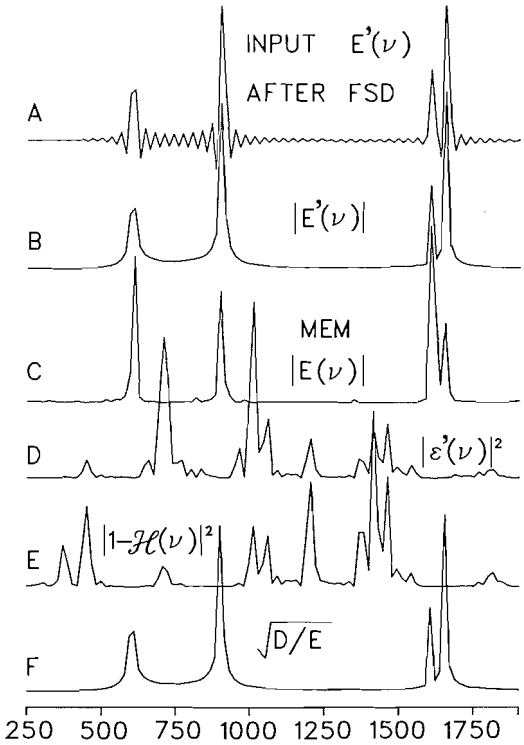

FIG. 4. Demonstration of the inaccurate approximation $|\epsilon(\nu)| \approx \sigma_M$ using eq. [22].

zero, the narrower will be the output line (compare Figs. 3A and 3E).

Figure 4 illustrates the behavior of the function $\Delta(\nu)$ and demonstrates eq. [22]. Figure 4A shows the FSD spectrum of the input spectrum from Fig. 3C with a S/N of 200, Fig. 4B is the corresponding magnitude spectrum $|E'(\nu)|$, and Fig. 4C is Burg's MEM spectrum with $M = 127$, $N = 128$. Again, the MEM output spectrum exhibits degradation of intensity information. Figures 4D and 4E show the power spectra of $\varepsilon'(\nu)$ and $1 - \mathcal{H}(\nu)$, respectively. An estimate, $\varepsilon'(\nu)$, is computed as the discrete Fourier transform of

$$e_j = \sum_{k=0}^{M} a_k I'_{j-k}$$

which means that $\varepsilon'(\nu) = E'(\nu)[1 - \mathcal{H}(\nu)] \approx E(\nu)[1 - \mathcal{H}(\nu)] = \varepsilon(\nu)$ with $E'(\nu) = \mathcal{F}^{-1}\{I'(x)\}$. This approximation, necessary because neither the fitted $I(x)$ nor $E(\nu)$ is known, is quite valid, because, at this S/N, $E'(\nu)$ and $E(\nu)$ differ by less than 1%. According to eq. [22], taking the square root of the ratio of spectrum D to E should yield $|E'(\nu)|$; this is shown to be the case in Fig. 4F. Hence we can conclude that the reason for the erroneous intensities in MEM spectra is the fact that $|\varepsilon(\nu)|^2$ is not a constant (σ_M). In this example, the measured values of $|\varepsilon'(\nu)|^2$ at 600, 900, 1600, and 1650 are 1.01×10^{-11}, 1.30×10^{-10}, 1.33×10^{-11}, and 2.90×10^{-10}, respectively. This represents a change of more than one order of magnitude from line to line.

A study of the value $|\Delta(\nu)|^2$ at the known line positions will further clarify the behavior of the filter-type MEM. For example, if one follows the MEM output spectra as a function of S/N in Fig. 3, it is clear that, at high S/N, $|\Delta(\nu)|^2$ is so small that slight changes in $\mathrm{Re}(\nu)$ and $\mathrm{Im}(\nu)$ can modulate the quantity $1/|\Delta(\nu)|^2$ by a few orders of magnitude. In extreme cases, e.g., Fig. 3A where $\log(|\Delta(\nu)|^2)$ ranges from -10 to -13, the peak height may even be markedly affected by small computational errors. As the S/N decreases, the value $|\Delta(\nu)|^2$ increases, resulting in smaller changes in the output; the range for $\log(|\Delta(\nu)|^2)$ in Fig. 3C is -5.7 to -6.6 and at S/N = 2 it is -2.2 to -4.2. From Table 1–III one can see that at very low S/N (2 and 20) there exists a slight correlation between the integrated intensities of MEM lines and the true intensities. The reason is that the transfer function $\mathcal{H}(\nu)$ is distorted by the noise. Statistically, the stronger the line is at ν_i, the closer $\mathcal{H}(\nu_i)$ is to unity. In other words, $|\Delta(\nu_i)|^2$ is statistically proportional to $(\mathrm{S/N})^{-2}$ at ν_i, resulting in a smaller intensity distortion at low S/N.

Part C. The importance of lineshape

Throughout this discussion the input signal has been assumed to be composed of undamped cosine waves corresponding to a sinc lineshape in the frequency domain. The filter-type MEM has been used for fitting the observed data in cases where the lineshape is not a sinc function, with the goal of increased S/N with any resolution enhancement as a serendipitous bonus. In such cases, where the time domain signal will consist of damped cosine waves, the AR model in eq. [5] is not generally applicable. According to the AR model, eq. [5] should hold for any M contiguous data points, $I_j, I_{j+1}, I_{j+2}, \ldots, I_{j+M-1}$, regardless of the starting point, j. The only function that can satisfy this criterion is the exponential: $A_i(x) = A_i \exp(-2\pi\tau x)$. This means that the AR model, eq. [5], may be applied only to spectra composed of Lorentzian lines. Now eq. [8] can be seen as being applicable only to the special case (implied by eq. [3]) where the Lorentzian lines have zero width with the sinc lineshape resulting from the time domain truncation inherent in all discrete sample data. Attempts to apply eq. [8] directly to Lorentzian lines (or any other lineshape) that correspond to damped cosine waves in the time domain, while not exhibiting as much degradation of intensity information as discussed herein, will often result in inaccurate output frequencies and the splitting of component lines that is a well-known characteristic of Burg's MEM.

Concluding remarks

Herein we have made a comparison between Burg's MEM and LOMEP as resolution enhancement techniques by examining their effect on line intensities. We compare the two techniques in three different ways, by varying the pattern of line intensities, the filter length (M), and the S/N ratio of the input. These trial tests demonstrate that MEM completely degrades intensity information, except at low-input S/N where there is a loose correlation between input and output intensities. At low S/N the coefficients $\{a_k\}$ will be degraded, resulting in the possibility of at least a statistical relationship between $\Delta(\nu_i)$ and the input intensity A_i.

By calculating an approximate error spectrum $|\varepsilon(\nu)|^2$, we have demonstrated the large inaccuracy in the approximation $|\varepsilon(\nu)|^2 \approx (\sigma_M)^2$ in eq. [8]. Furthermore, we point out that this approximation accounts for all the anomalous behavior of MEM. We conclude that for data having a high S/N ratio (>100) treatments such as Burg's MEM, and similar techniques that approximate the power spectral estimator as being proportional to the power spectrum of the transfer function, will retain little, if any, information of line intensities. The

prediction-error coefficients $\{a_k\}$, which are quite efficiently calculated by the Burg's algorithm, can be much better utilized for a true linear prediction as is accomplished in the LOMEP technique, which is shown to retain intensity information.

1. D. S. Stephenson. *In* Progress in nuclear magnetic resonance spectroscopy. *Edited by* J. W. Emsley, J. Feeney, and L. H. Sutcliffe. Pergamon Press, Oxford. 1988. pp. 515–626.
2. A. G. Marshall and F. R. Verdun. Fourier transforms in NMR, optical, and mass spectrometry: a user's handbook. Elsevier Science Publ., Amsterdam. 1990.
3. S. Haykin (*Editor*). Top. Appl. Phys. **34** (1979).
4. S. Sibisi. Nature, **301**, 134 (1983).
5. J. Skilling and R. K. Bryan. Mon. Not. R. Astron. Soc. **211**, 111 (1984).
6. S. F. Gull and J. Skilling. IEE Proc. **131**, 646 (1984).
7. E. D. Lane, J. Skilling, and J. Staunton. J. Magn. Reson. **63**, 418 (1985).
8. J. F. Martin. J. Magn. Reson. **65**, 291 (1985).
9. R. Jordan and S. A. Dyer. Appl. Spectrosc. **43**, 750 (1989).
10. J. K. Kauppinen, D. J. Moffatt, M. R. Hollberg, and H. H. Mantsch. Appl. Spectrosc. **45**, 411 (1991).
11. J. P. Burg. A new analysis technique for time series data. NATO ASI Ser. Signal Processing. Enschede, The Netherlands, 1968.
12. J. P. Burg. Ph.D. Dissertation, Stanford University, Stanford, Calif. (1975).
13. S. A. Meyer, D. L. Orth, M. A. Morgenstern, and D. W. Noid. J. Magn. Reson. **86**, 406 (1990).
14. G. P. Abousleman, R. Jordan, and R. H. Griffey. Appl. Spectrosc. **45**, 202 (1991).
15. K. Minami, S. Kawata, and S. Minami. Appl. Opt. **24**, 162 (1985).
16. J. K. Kauppinen, D. J. Moffatt, M. R. Hollberg, and H. H. Mantsch. Appl. Spectrosc. **45**, 1516 (1991).
17. J. K. Kauppinen, D. J. Moffatt, H. H. Mantsch, and D. G. Cameron. Appl. Spectrosc. **35**, 271 (1981).

Can. J. Chem. Downloaded from www.nrcresearchpress.com by 109.225.110.28 on 09/08/12
For personal use only.

Static dielectric constants of the *N,N*-dimethylformamide/2-methoxyethanol solvent system at various temperatures

FULVIO CORRADINI, LUIGI MARCHESELLI, LORENZO TASSI,[1] AND GIUSEPPE TOSI
Department of Chemistry, University of Modena, via G.Campi, 183 41100 Modena, Italy

Received April 2, 1992

FULVIO CORRADINI, LUIGI MARCHESELLI, LORENZO TASSI, and GIUSEPPE TOSI. Can. J. Chem. **70**, 2895 (1992).

Measurements of static dielectric constants (ε) have been made for binary liquid mixtures of *N,N*-dimethylformamide (DMF)/2-methoxyethanol (ME) at 19 temperatures ranging from −10 to +80°C. Some empirical equations of the type $\varepsilon = \varepsilon(T)$, $\varepsilon = \varepsilon(X_1)$, and $\varepsilon = \varepsilon(T,X_1)$ have been applied to check their validity. The ε^E values, which refer to the deviation of the dielectric constants of the binaries from the values arising from mole fraction mixture law, have been calculated. Deviations from ideal behaviour have been found to be positive at all temperatures. The positive ε^E values are attributed to a specific interaction between unlike molecules, which leads to the formation of complexes between DMF and ME in the liquid state. These *n*DMF·*m*ME complex moieties were found to have the stoichiometric ratios 2:1, 1:1, and 1:2 in the temperature range of −10 to +80°C.

FULVIO CORRADINI, LUIGI MARCHESELLI, LORENZO TASSI et GIUSEPPE TOSI. Can. J. Chem. **70**, 2895 (1992).

On a déterminé les constantes diélectriques statiques (ε) de mélanges liquides binaires *N,N*-diméthylformamide(DMF)/2-méthoxyéthanol(ME), à 19 températures allant de −10 à +80°C. Dans le but d'évaluer leur validité dans le cas présent, on a appliqué quelques équations empiriques du type $\varepsilon = \varepsilon(T)$, $\varepsilon = \varepsilon(X_1)$ et $\varepsilon = \varepsilon(T,X_1)$. On a calculé les valeurs de la quantité ε^E qui se réfère à la déviation des constantes diélectriques des binaires par rapport aux valeurs découlant de la loi de mélange des fractions molaires. On a trouvé que, à toutes les températures étudiées, le déplacement par rapport au comportement idéal est positif. On a attribué les valeurs positives de ε^E à l'existence d'une interaction spécifique, entre les molécules dissemblables, conduisant à la formation de complexes entre le DMF et le ME, à l'état liquide. On a détecté que les rapports stoechiométriques de ces entités complexes *n*DMF·*m*ME passent de 2:1 à 1:1, puis à 1:2 lorsqu'on fait varier la température de −10 à +80°C.

[Traduit par la rédaction]

Introduction

The static dielectric constant of materials in the liquid state represents a measure of polarization character. When working with polar liquids, this property can provide much useful information about the local structure due to the orientation of the molecules and to reciprocal interactions between neighbouring units. Furthermore, the dielectric data over a wide temperature range for pure liquids, and binary or more complex mixtures employed as solvents, are required to estimate the electrostatic ion–solvent interactions on the basis of the electrostriction theory for ionic solutions, the Debye–Hückel law coefficients for volumes, and other thermodynamic properties (1).

Although dielectric constants as a function of temperature and composition of binary mixtures have been measured for a lot of solvent systems, there are very few available experimental data in the literature on amido-alcholic solvent systems. Thus this study was designed to extend our knowledge on the dielectric behaviour of *n,n*-dimethylformamide (DMF)/2-methoxyethanol (ME) binaries in the temperature range −10 to +80°C, and covering the whole miscibility field expressed in mole fraction of DMF ($0 \leq X_1 \leq 1$).

This solvent system could also be used in electroanalytical chemistry, e.g., for measuring acid–base dissociation constants. In a recent paper, we reported the dissociation constant of picric acid, obtained experimentally using the conductometric method under the same experimental conditions as above (2).

N,N-Dimethylformamide is a nonaqueous solvent of particular interest because it has no hydrogen bonding in the pure state. It therefore acts as an aprotic protophilic medium with a large dipole moment (μ = 3.86 D at 25°C) (3) and a high dielectric constant (ε = 37.51 at 25°C). Consequently, according to Charlot (4) DMF may be classified as a dissociating solvent. Thus DMF and its binary mixtures with hydroxy compounds may be useful to study the effect of the solvent structure on the solvation properties of solutes.

2-Methoxyethanol is amphiprotic, a potentially acidic medium with a low autoprotolysis constant ($pK_{autoprot}$ = 20.5 at 20°C) (5) and a low dielectric constant (ε = 16.94 at 25°C). It is therefore hardly a dissociating solvent (6–10) either for ionogen or ionophore solutes. Because of its dipolar character (μ = 2.36 D) (11), ME shows a tendency to polymerize and form a hydrogen-bonded network.

Based on the arguments above, we are able to study the properties of this binary solvent system systematically, using a range of mixtures ranging from the very structured solvent (pure ME) to a solvent with no structural effects (pure DMF) (12).

Chemists often study the variation of thermomechanical parameters versus solvent composition to characterize liquid mixtures. In a strongly interacting system, this is not a linear relationship. Thus if one merely interpolates the ε values, one may incur serious errors, particularly if there were not a lot of experimental data used in the interpolation.

This paper reports on our findings of the relationship between dielectric constant, temperature, and mole fraction of one component in the system (X_1).

Experimental section

Materials

N,N-Dimethylformamide and 2-methoxyethanol (containing both <0.10% and 0.05% water by weight, respectively, found by Karl-Fischer titrations) were of Carlo Erba (Milan) high purity grade. The solvents were purified by passage through neutral almuina

[1]Author to whom correspondence may be addressed.

Can. J. Chem. Downloaded from www.nrcresearchpress.com by 88.255.202.194 on 09/08/12
For personal use only.

Can. J. Chem. Downloaded from www.nrcresearchpress.com by 88.255.202.194 on 09/08/12
For personal use only.

TABLE 1. Binary compositions of the *N*,*N*-dimethylformamide/2-methoxyethanol solvent system

System	X_1	V_{DMF}/V_{ME} (%)
A	1.0000	100/0
B	0.9021	90/10
C	0.8038	80/20
D	0.7053	70/30
E	0.6060	60/40
F	0.5063	50/50
G	0.4062	40/60
H	0.3053	30/70
I	0.2044	20/80
L	0.1025	10/90
M	0.0000	0/100

column before use, and the final purity was checked by gaschromatography (99.8% DMF, 99.7% ME), confirming that no other significant organic components were present.

Apparatus and procedures

The solvent mixtures were prepared by weight using a Mettler PM 4800 Δ-range balance in dry nitrogen to avoid contact with atmospheric moisture, and then preserved on 3A molecular sieves. The probable error in the DMF mole fraction (X_1) is estimated to be less than 1.5×10^{-4}.

Dielectric constant measurements were carried out at 2 MHz by the heterodyne beat method using a Wissenschaftlich, Technischen Werkstätten GMBH dipolmeter Model DM01 (WTW, Weilheim Oberbayern, Germany). The thermostated stainless steel measuring cells were of MFL 2 ($7 < \varepsilon < 21$) and MFL 3 ($21 < \varepsilon < 90$) type. The sample cells are of the covered coaxial capacitor type with vacuum capacitances of 2 pF (MFL 2) and 0.5 pF (MFL 3). These are adequate to cover the dielectric constant range of DMF/ME mixtures over the whole temperature range studied ($-10 \leq t/°C \leq 80$).

It was checked that good overlap was obtained when passing from the MFL 2 to MFL 3 measuring cell, the difference always lies within the experimental accuracy of the equipment. The cells were calibrated with standard pure liquids, such as dichloromethane, pyridine, butan-1-ol, and acetone (MFL 2); methanol, ethanol, glycerol, and deionized water (MFL 3). With the exception of the Millipore deionized water, all these solvents were of spectrograde quality or more higher. The dielectric constants for the standards were taken from literature (13).

All experiments were performed at least for 10 replicate runs for each composition and at each temperature the confidence level was 95%; the results were averaged.

The measurements were reproducible to within ±0.02 dielectric constant unit. The thermostated measuring cells were embodied in a polyurethane protective jacket, and a Lauda K2R controlled the temperature of the thermostatic bath to ±0.02°C. A thermoresistance Pt 100 (Tersid, Milan) immersed in the sample inside the measuring cells ensured that the temperature was constant and a Wayne Kerr 6425 Precision Component Analyzer measured the resistance. An automatic titration system (Crison model KF 431) equipped with a digital buret (Crison model 738) was used for Karl-Fischer titrations.

Results and discussion

We measured the dielectric constants of the two pure solvents and nine binary mixtures at 19 temperatures in the $-10 \leq t/°C \leq +80$ at 5°C intervals. The compositions are identified by the letters A,B,C,...M, and their ε values are presented in Table 1.

Table 2 reports the experimentally determined dielectric constants and ln ε was fitted to a linear equation in T (13)

$$[1] \quad \ln \varepsilon = \alpha_0 + \alpha_1 T \qquad T/K$$

The above procedure yields the results summarized in Table I, which includes the standard deviation σ(ln ε) at each temperature, has been supplied as supplementary material.[2] The average uncertainty $\overline{\Delta\varepsilon}$, as calculated by

$$[2] \quad \overline{\Delta\varepsilon} = \frac{\sum_N |\varepsilon_{calcd} - \varepsilon_{exptl}|}{N}$$

where N is the number of data points, equals $\pm 0.02\varepsilon$ units, this shows eq. [1] to be an adequate representation of the experimental data.

Figure 1 shows the nonlinear nature of ε as a function of X_2.

An early attempt to express ε as a function of X_1 was in the form of a polynomial:

$$[3] \quad \ln \varepsilon = \beta_0 + \beta_1 X_1 + \beta_2 X_1^2 + \ldots + \beta_n X_1^n$$

Here our best results were obtained for $n = 2$. The relative coefficients β_j are listed in Table II (supplementary material),[2] along with the corresponding standard deviations σ(ln ε) at each experimental temperature. The average uncertainty $\overline{\Delta\varepsilon}$ of the ε values estimated by eq. [3] was approximately ±0.03 ε unit.

The rational equation suggested by King and Queen (14) ε takes the form:

$$[4] \quad \ln \varepsilon = \frac{a_0 + a_1 X_1 + a_2 X_1^2 + \ldots + a_m X_1^m}{b_0 + b_1 X_1 + b_2 X_1^2 + \ldots + b_n X_1^n}$$

with some limiting conditions. Firstly, mole fraction X_1 is defined in the range [0,1] that corresponds to a likely optimum condition on the number of terms provided by $m = n$, and also the sum of the quantities in the denominator can never be zero. Reduced forms of the rational equation [4] are used by imposing the condition $b_0 = 1$ (known as the Padè approximant (14)), and improved by making $a_0 = 1$ (15) (the reciprocal Padè approximant). Thus rational equation becomes

$$[5] \quad \ln \varepsilon = \frac{a_0 + a_1 X_1}{b_0 + b_1 X_1}$$

It is noteworthy that eq. [5] reproduces the dielectric constant values of the two pure components, at the respective limits $X_1 = 0$ and $X_1 = 1$, being assumed $a_0 = 1$, and b_0 necessarily equal to $(\ln \varepsilon_2)^{-1}$ at each investigated temperature. Thus we only needed to determine two coefficients a_1 and b_1, which are the true adjustment parameters (Table III of supplementary material).[2] The experimental ε values in Table 2 are reproduced with an average uncertainty $\overline{\Delta\varepsilon}$ of $\pm 0.02\varepsilon$ unit.

Finally we suggest that rational functions like [5] fit experimental ε values for the DMF/ME binary solvent system better than the polynominal [3], even both are within experimental uncertainly and both have two adjustable coefficients. Equation [3] has two true adjustment coefficients because $\beta_0 = \ln \varepsilon_2$.

The dielectric constant and all thermomechanical properties of a binary system are functions of two variables:

[2]A complete set of tables may be purchased from: The Depository of Unpublished Data, Document Delivery, CISTI National Research Council Canada, Ottawa, Canada K1A 0S2.

TABLE 2. Experimental dielectric constants (ε) for the *N*,*N*-dimethylformamide/2-methoxyethanol binary mixtures at various temperatures

	System										
t (°C)	A	B	C	D	E	F	G	H	I	L	M
−10	44.19	42.99	40.95	39.01	37.20	34.92	32.86	30.20	26.50	23.65	20.03
−5	42.99	41.98	39.99	38.00	36.33	34.05	32.05	29.35	25.85	23.03	19.55
0	42.06	40.95	39.07	37.11	35.47	33.25	31.21	28.60	25.20	22.51	19.08
5	41.16	40.04	38.14	36.25	34.63	32.35	30.40	27.90	24.60	21.98	18.63
10	40.24	39.05	37.30	35.43	33.77	31.62	29.62	27.16	24.03	21.42	18.19
15	39.29	38.20	36.40	34.62	33.01	30.83	28.88	26.46	23.43	20.91	17.75
20	38.45	37.25	35.56	33.77	32.19	30.08	28.16	25.75	22.88	20.37	17.35
25	37.59	36.40	34.75	33.03	31.43	29.37	27.42	25.04	22.30	19.88	16.94
30	36.74	35.55	33.97	32.18	30.67	28.74	26.75	24.41	21.78	19.39	16.54
35	35.78	34.79	33.23	31.46	30.01	27.98	26.10	23.76	21.26	18.97	16.17
40	34.94	34.01	32.38	30.73	29.27	27.39	25.48	23.20	20.77	18.47	15.76
45	34.16	33.21	31.72	30.03	28.61	26.66	24.81	22.53	20.26	18.06	15.38
50	33.36	32.45	30.91	29.31	27.88	26.06	24.24	22.00	19.81	17.58	15.02
55	32.64	31.68	30.28	28.65	27.29	25.38	23.58	21.37	19.31	17.19	14.68
60	31.94	30.96	29.55	28.00	26.60	24.81	22.99	20.84	18.89	16.75	14.32
65	31.19	30.22	28.90	27.33	26.02	24.18	22.42	20.26	18.40	16.33	14.05
70	30.50	29.57	28.25	26.73	25.41	23.61	21.91	19.73	17.98	15.97	13.71
75	29.88	28.82	27.60	26.04	24.81	23.07	21.36	19.24	17.56	15.58	13.34
80	29.09	28.16	26.96	25.46	24.22	22.53	20.78	18.71	17.15	15.16	13.01

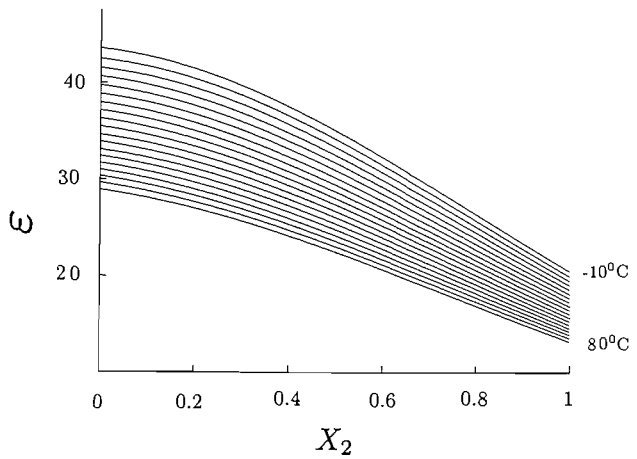

FIG. 1. Isothermal best-fit curves of the static dielectric constant for the *N*,*N*-dimethylformamide/2-methoxyethanol binary system calculated by eq. [5] at various composition.

temperature and composition. A general expression of this dependence is

$$[6] \quad \varepsilon = \varepsilon(T,X_1)$$

By algebraic manipulation of eqs. [1] and [5], eq. [6] may be expressed as

$$[7] \quad \ln \varepsilon(T,X_1) = \left[\frac{\sum_{i=0}^{1}\sum_{j=0}^{1} \gamma_{ij} T^i X_1^j}{(\ln \varepsilon_2)^{-1} + \gamma_{0\bar{1}} X_1} \right]^{1/2}$$

This three-dimensional correlation model, whose coefficients (Table 3) were evaluated by the least-squares method on a TSP computer package (16), fits the experimental data to within $\overline{\Delta\varepsilon} = \pm 0.08$ ε unit over the entire experimental temperature ($-10 \leq t/°C \leq +80$) and composition ($0 \leq X_1 \leq 1$) ranges.

TABLE 3. Coefficients γ_{ij} of the model equation $\varepsilon = \varepsilon(T,X_1)$ for the *N*,*N*-dimethylformamide/2-methoxyethanol solvent system

ij	Variable quantity	γ
00		16.42615
01	X_1	27.87694
10	T	-2.81728×10^{-2}
11	TX_1	-3.63106×10^{-2}
0$\bar{1}$	X_1	0.90008

The excess function

The dielectric behaviour of the DMF/ME system is far from ideal. This deviation from ideal behaviour may be measured by assuming a linear dependence of ε on composition for an ideal mixture. Payne and Theodorou (17) used the following equation for this measurement:

$$[8] \quad \varepsilon = \varepsilon^E + \varepsilon_1 X_1 + \varepsilon_2 X_2$$

where ε^E is the excess function; $\varepsilon_1,\varepsilon_2$ represent the values for the pure components at each experimental temperature; and X_1,X_2 are the mole fractions, respectively.

Table 4 lists the ε^E values that have been extensively used (18, 19).

Figure 2 shows plots of ε^E versus X_2, in which the data were obtained by fitting ε^E values in the following equation (20):

$$[9] \quad \varepsilon^E = X_1 X_2 \sum_{k=0}^{6} c_k (X_2 - X_1)^k$$

Table IV in the Depository of Unpublished Data[2] lists the c_k values in eq. [9] and the standard deviations $\sigma(\varepsilon^E)$ at each experimental temperature. Values of ε^E calculated from Eq. [9] are in good agreement with the experimental values listed

Can. J. Chem. Downloaded from www.nrcresearchpress.com by 88.255.202.194 on 09/08/12
For personal use only.

TABLE 4. Excess dielectric constants (ε^E) for the *N*,*N*-dimethylformamide/2-methoxyethanol binary mixtures at various temperatures

	System								
t (°C)	B	C	D	E	F	G	H	I	L
−10	1.19	1.53	1.93	2.57	2.65	3.01	2.82	1.52	1.15
−5	1.15	1.49	1.87	2.48	2.56	2.88	2.66	1.46	1.10
0	1.11	1.46	1.81	2.41	2.46	2.75	2.51	1.42	1.06
5	1.08	1.42	1.75	2.33	2.38	2.63	2.37	1.37	1.01
10	1.04	1.39	1.70	2.26	2.29	2.51	2.23	1.32	0.97
15	1.01	1.36	1.65	2.19	2.20	2.39	2.10	1.28	0.93
20	0.97	1.33	1.59	2.12	2.12	2.28	1.97	1.23	0.89
25	0.94	1.29	1.54	2.05	2.04	2.17	1.85	1.19	0.85
30	0.91	1.26	1.50	1.99	1.97	2.07	1.73	1.15	0.81
35	0.88	1.23	1.45	1.92	1.89	1.97	1.62	1.11	0.78
40	0.85	1.21	1.40	1.86	1.82	1.88	1.51	1.07	0.74
45	0.82	1.18	1.36	1.80	1.75	1.78	1.40	1.04	0.71
50	0.79	1.15	1.32	1.74	1.69	1.69	1.30	1.00	0.67
55	0.77	1.12	1.27	1.69	1.62	1.61	1.21	0.97	0.64
60	0.74	1.10	1.23	1.63	1.56	1.53	1.12	0.93	0.61
65	0.71	1.07	1.19	1.58	1.50	1.45	1.03	0.90	0.58
70	0.69	1.05	1.16	1.53	1.44	1.37	0.94	0.87	0.56
75	0.67	1.02	1.12	1.48	1.38	1.30	0.86	0.84	0.53
80	0.64	1.00	1.08	1.43	1.33	1.22	0.78	0.81	0.50

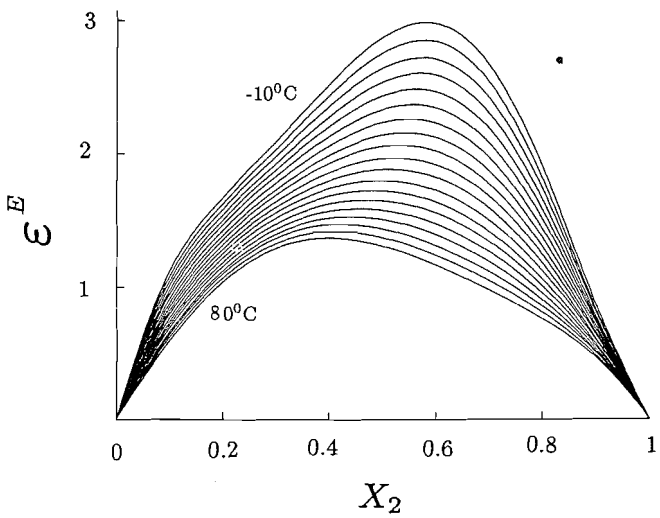

FIG. 2. Isothermal best-fit curves of the excess dielectric constant for the *N*,*N*-dimethylformamide/2-methoxyethanol binary system calculated by eq. [6] at various temperatures.

in Table 4, with $\overline{\Delta\varepsilon^E} = \pm 0.04\varepsilon$ units.

Figure 2 shows that the ε^E values are always positive. At the lower temperatures, ε^E reaches a maximum at $X_2 \simeq 0.65$. As the temperature increases, the maximum becomes more flattened and shifts to $X_2 \simeq 0.5$ at about 50°C. Above this temperature, the maximum becomes pronounced and shifts to $X_2 \simeq 0.35$ at 80°C.

It has been pointed out in literature that small shifts of dielectric behaviour of mixed solvents from ideality ($\varepsilon^E \leq 5$) may be attributed to two causes: (*i*) weak depolar associations between unlike molecules and (or) (*ii*) homoconjugations of the highest dipole moment component induced by the presence of the apolar or quasi-apolar cosolvent (17). Since we have two very polar components, it is less likely that there are homoconjugations between similar molecules but more likely that there are weak dipolar associations between unlike molecules.

Petersen (21) agreed with our opinion. He pointed out that the hydrogen bonds between the water molecules and the carbonyl oxygen atoms are stronger than those formed between the water molecules themselves. In the case of DMF, this effect may be enhanced by the presence of a nitrogen atom in the α-position of the carbonyl group, and by the negative charge on the oxygen in a resonance form:

The maxima values in Fig. 2 may also serve as an index of thermostability of the adducts formed in solution.

We therefore conclude that the probable compositions of the adducts are in DMF:ME = 1:2, 1:1, and 2:1 mole ratios over the temperature range of −10 to +80°C.

Acknowledgments

The authors gratefully thank Professor C. Preti for helpful suggestions, the Hospal s.p.a. (Bologna, Italy) for a grant to one of us (L.M.), and the Ministero dell'Università e della Ricerca Scientifica e Tecnologica (M.U.R.S.T.) of Italy for financial support.

1. D. J. Bradley and K. S. Pitzer. J. Phys. Chem. **83**, 1599 (1979).
2. A. Marchetti, C. Preti, M. Tagliazucchi, L. Tassi, and G. Tosi. Can. J. Chem. **69**, 509 (1991).
3. M. H. Hutchinson and L. H. Sutton. J. Chem. Soc. 4382 (1958).
4. G. Charlot and B. Tremillon. *In* Les reactions chimiques dans les solvants et les sels fondus. *Edited by* Gauthier-Villars. Masson et Cie, Paris. 1963.
5. A. P. Kreshkov, M. T. Smolova, A. Veveris, and B. Spince. Zh. Fiz. Khim. **51**, 1827 (1977).

Can. J. Chem. Downloaded from www.nrcresearchpress.com by 88.255.202.194 on 09/08/12
For personal use only.

6. G. C. Franchini, E. Ori, C. Preti, L. Tassi, and G. Tosi. Can. J. Chem. **65**, 722 (1987).
7. G. C. Franchini, L. Tassi, and G. Tosi. J. Chem. Soc. Faraday Trans. 1, **83**, 3129 (1987).
8. G. C. Franchini, A. Marchetti, C. Preti, L. Tassi, and G. Tosi. J. Chem. Soc. Faraday Trans. 1, **85**, 1697 (1989).
9. A. Marchetti, E. Picchioni, L. Tassi, and G. Tosi. Anal. Chem. **61**, 1971 (1989).
10. G. C. Franchini, A. Marchetti, L. Tassi, and G. Tosi. Anal. Chem. **62**, 1004 (1990).
11. P. Buckley and M. Brochu. Can. J. Chem. **50**, 1149 (1972).
12. S. J. Bass, W. I. Nathan, R. M. Meighan, and R. H. Cole. J. Phys. Chem. **68**, 509 (1964).
13. A. A. Maryott and E. R. Smith. Table of dielectric constant of pure liquids. Natl. Bur. Stand. Circ. No. 514. 1951.
14. M. King and N. Queen. J. Chem. Eng. Data, **24**, 178 (1979).
15. O. W. Kolling. Anal. Chem. **59**, 674 (1987).
16. B. H. Hall (*Editor*). TSP - Time Series Processor. User's Guide. TSP International. Stanford, Calif. 1987.
17. R. Payne and I. Theodorou. J. Phys. Chem. **76**, 2892 (1972).
18. J. Rowlinson and F. L. Swinton. *In* Liquids and liquid mixtures. Academic Press, New York. 1981.
19. G. Moumouzias, D. K. Panopoulos, and G. Ritzoulis. J. Chem. Eng. Data, **36**, 20 (1991).
20. O. Redlich and A. T. Kister. Ind. Eng. Chem. **40**, 341 (1948).
21. R. C. Petersen. J. Phys. Chem. **64**, 184 (1960).

Can. J. Chem. Downloaded from www.nrcresearchpress.com by 88.255.202.194 on 09/08/12
For personal use only.

CP-MAS ^{13}C NMR investigation of phase structure in mixtures of poly(ethyl acrylate) ionomers with sodium palmitate

A. NATANSOHN[1]

Department of Chemistry, Queen's University, Kingston, Ont., Canada K7L 3N6

AND

C. G. BAZUIN[1] AND X. TONG

Département de chimie, Centre de recherche en science et ingénierie des macromolecules, Université Laval, Cité Universitaire (Qué.), Canada G1K 7P4

Received April 9, 1992

A. NATANSOHN, C. G. BAZUIN, and X. TONG. Can. J. Chem. **70**, 2900 (1992).

A solid-state NMR study of mixtures of poly(ethyl acrylate) (PEA) or poly(ethyl acrylate-co-sodium acrylate) (PEA-i) with sodium palmitate (SP) shows that (1) there is a change in the electron density of the carboxylate carbons of SP in the mixtures compared to pure SP; (2) the $T_{1\rho H}$ value for SP in the mixtures with PEA or PEA-i is depressed in comparison with pure SP for mixtures containing over 4 mol% SP. This can be interpreted as a result of interfacial magnetization transfer from the protons of PEA or PEA-i to the protons of SP; (3) deuterated SP (D-SP) shows a similar growth in magnetization as a function of contact time when pure or when mixed with PEA. The growth is significantly slower in its mixtures with PEA-i. All these findings can be explained by a PEA-i:SP mixture morphology involving bilayers of carboxylate ions at the interface; the same tendency exists in the PEA:SP mixtures, only in this case the ester groups of PEA are preferentially located at the interface.

A. NATANSOHN, C. G. BAZUIN et X. TONG. Can. J. Chem. **70**, 2900 (1992).

Une étude, par spectroscopie RMN à l'état solide, de mélanges de poly(acrylate d'éthyle) (PEA) ou de poly(acrylate d'éthyle-co-acrylate de sodium) (PEA-i) avec du palmitate de sodium (SP) montre que : (1) dans le SP en mélange comparé au SP à l'état pur, il y a un changement dans la densité électronique des atomes de carbones des groupements carboxylate; (2) pour des mélanges avec le PEA et le PEA-i contenant plus de 4% molaire de SP, les valeurs de $T_{1\rho H}$ du SP sont plus faibles que celles du SP à l'état pur. On peut interpréter ce fait comme resultant d'un transfert interfacial de magnétisation des protons de PEA ou de PEA-i vers les protons du SP; (3) le SP deutérié (D-SP), tant à l'état pur qu'en mélange avec du PEA, présente une augmentation semblable de la magnétisation en fonction du temps de contact; par contre, l'augmentation est nettement plus lente dans les mélanges avec le PEA-i. On peut expliquer tous ces résultats par une morphologie du mélange PEA-i/SP impliquant des bicouches d'ions carboxylate à l'interface. La même tendance existe dans les mélanges de PEA/SP; toutefois, dans ce cas, les groupes esters du PEA se retrouvent préférentiellement à l'interface avec les ions carboxylate du SP.

[Traduit par la rédaction]

One of the more recent methods used to analyze the phase structure in polymer blends, mixtures, and composites is high-resolution solid-state NMR obtained with cross-polarization and magic angle spinning. A recent review of its applications to heterogeneous materials (1) emphasizes that spin diffusion can be used to obtain information on a scale between 1 and 200 nm. A variety of experimental techniques are available in solid-state NMR for obtaining information about spin diffusion (2), and the literature making use of them is constantly growing. Two of those techniques are employed in this paper to investigate mixtures of sodium palmitate with poly(ethyl acrylate) and poly(ethyl acrylate-co-sodium acrylate). This is part of a more general effort taking place in our laboratory to investigate the phase structure of polymer blends, mixtures, and composites by solid-state NMR.

The first technique is measurement of $T_{1\rho H}$, the rotating frame proton spin-lattice relaxation time constant. It is now well established that $T_{1\rho H}$ is a reliable probe for the phase structure of various materials based on polymers (3). A recent review of the literature on polymer blends is included in one of our previous publications (4). $T_{1\rho H}$ can be directly related to the distance the spin travels during the spin-lattice relaxation process, hence it may be used as an indirect measure of proton density in the analyzed phase (5). Our investigations on charge transfer interacting polymer blends confirmed that the physical distance between protons is more important for $T_{1\rho H}$ than are mobility factors (6).

The second technique is polarization transfer between nonbonded regions in a sample. This is usually employed in mixtures in which one of the components lacks protons, and hence its magnetization has to come from the other component, the protonated one, by physical proximity and nonbonding interactions. Another condition that must be satisfied for the magnetization to be transmitted is a relatively low mobility of both components. Except for very low T_g rubber materials, this condition is usually satisfied in the solid state. There are many examples of such studies, some of them reviewed in ref. 1. We have employed this technique in a study of compatibilization of a polymer pair through ionic interactions (7).

In a previous paper (8), mixtures of sodium palmitate (SP) with poly(ethyl acrylate) (PEA), and with an ionomer of PEA, namely poly(ethyl acrylate-co-sodium acrylate) (PEA-i), obtained by partial saponification of PEA, were investigated by differential scanning calorimetry (DSC) and dynamic mechanical thermal analysis. The fact that the DSC transitions of the pure soap phase are not perturbed in the mixtures shows that the soap remains phase-separated in the mixtures, and that the soap phase is virtually identical to that

[1]Authors to whom correspondence may be addressed.

Can. J. Chem. Downloaded from www.nrcresearchpress.com by 88.255.202.194 on 09/08/12
For personal use only.

Can. J. Chem. Downloaded from www.nrcresearchpress.com by 88.255.202.194 on 09/08/12
For personal use only.

of pure soap. Furthermore, neither the glass transition of either polymer nor the biphasic morphology of the ionomer was affected by the presence of the soap. On the other hand, there were certain indications that there may be physical interfacial interactions between the soap phase and either polymer. In particular, the rubbery region was significantly reinforced in modulus by addition of SP, roughly to the same extent for both polymers, leading to the supposition that there are interactions between SP carboxylate groups at the surface of the crystalline domains of the soap and the ester groups of either polymer. In the case of the ionomer, although the total effect of the interfacial interactions is similar to that obtained for PEA, it was supposed that interactions between carboxylate groups of the ionomer and those of the soap may also take place, but without significantly affecting the ionomer microdomain structure. However, no indication of interactions between the two components was observed through infrared spectroscopy. We will show in this paper that the two NMR techniques mentioned above provide new evidence for interfacial interactions.

Experimental

Synthesis of the polymer and ionomer and preparation of the mixtures are described in previous publications (6, 8). Briefly, the mixtures were prepared by dissolving the two components in a 1% benzene/methanol (50:50 v/v) solution, stirring for about 15 h, freeze-drying, and further drying at about 70°C under reduced pressure for several days. The PEA-i used in the present study is a poly(ethyl acrylate) ionomer containing 10 mol% sodium acrylate co-units. Deuterated palmitic acid (MSD Isotopes, 97.7 at.% D) was converted to deuterated sodium palmitate.

Sodium palmitate was prepared for NMR measurements by being subjected to the same processing procedures as were its mixtures with PEA or PEA-i. Thermal history, especially in a crystalline substance, can produce changes in the relaxation behaviour; hence all samples analyzed have a similar thermal history. Deuterated sodium palmitate (D-SP) was mixed with PEA and PEA-i, respectively, following the same general procedures.

The NMR spectra were recorded on a Bruker CXP-200 spectrometer operating at 50.307 MHz. A typical cross-polarization pulse sequence had a preparation delay of 10 s, a proton 90° pulse of 3.7 μs, a contact time of 1 ms, a decoupling time of 0.09 s, and an acquisition time of 0.1024 s. Two hundred scans were recorded for each spectrum and spinning was performed at ca. 4 kHz, leading to the complete absence of spinning side-bands. Proton spin-lattice relaxation in the rotating frame time constants and intermolecular cross-polarization rates were monitored by increasing contact times. Depending on the sample, contact times were varied between 0.2 and 200 ms. No external reference for the chemical shift was employed; all signals were measured in comparison to the sharp CH_3 peak (15 ppm).

Results and discussion

The spectrum of sodium palmitate is presented in Fig. 1, along with the assignments. There are three groups of signals. The carboxylate carbon resonates in a sharp peak at 187 ppm. The methyl carbon resonates at 15 ppm, while the various CH_2 carbons give a signal centered around 32 ppm, which is the resonance of all-*trans* methylene carbons, similar to polyethylene (9). The spectrum of PEA-i is presented in Fig. 2 together with its assignments. The backbone resonates at about 40 ppm in a broad peak, and the CH_3 peak (at 15 ppm) is again sharp, due to significant motional averaging. The glass transition temperature of this ionomer is 5°C according to DSC heating scans of 20°C/min (8), which

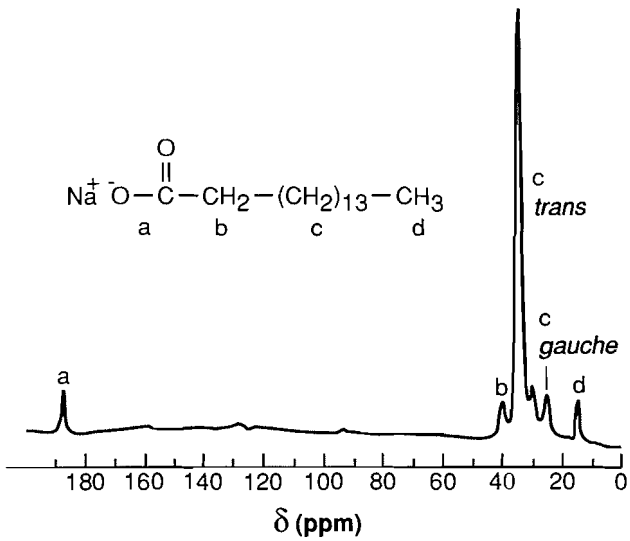

FIG. 1. CP-MAS ^{13}C NMR spectrum of sodium palmitate.

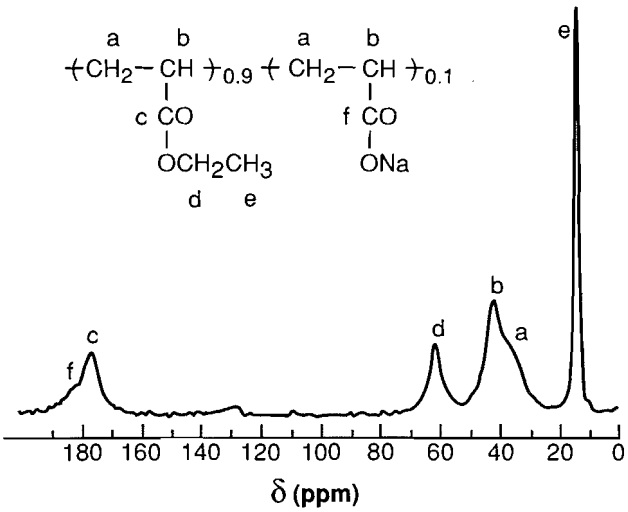

FIG. 2. CP-MAS ^{13}C NMR spectrum of a copolymer of ethyl acrylate with 10 mol% sodium acrylate (PEA-i).

means that even the segmental motion is significant at room temperature. The ester CH_2 resonates at about 60 ppm and the ester carbonyl at about 177 ppm. The carboxylate carbon appears as a shoulder on the low-field side of the carbonyl. Its chemical shift in the ionomer is 182 ppm, much higher than that in the sodium palmitate. A spectrum of PEA, not presented here, is very similar to the spectrum in Fig. 2. The main difference is the absence of the carboxylate carbon signal.

Figure 3 presents the ^{13}C NMR spectrum of a mixture of PEA-i and sodium palmitate (SP) containing 35 wt.% SP. As expected, the spectrum is essentially a weighted average sum of the spectra presented in Figs. 1 and 2. The CH_3 groups of the two components resonate together at 15 ppm, while the CH_2 signal of SP overlaps with the backbone resonances of PEA-i. The carboxylate carbons of the two components also seem to resonate together at 183 ppm. Two of the PEA-i signals resonate separately: the ester carbonyl at 177 ppm and the ester CH_2 at 60 ppm.

Although the carboxylate carbon signal, which belongs

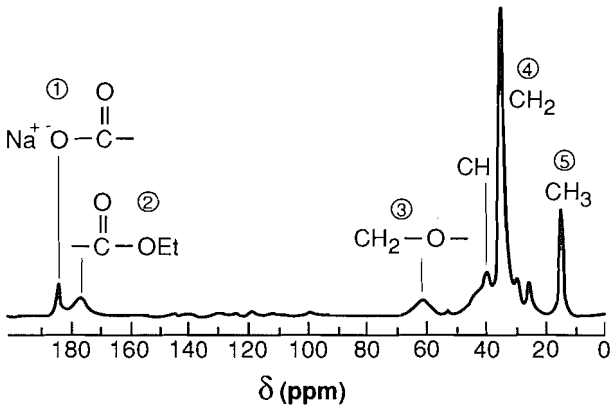

FIG. 3. CP-MAS ^{13}C NMR spectrum of a mixture of PEA-i containing 35 wt.% sodium palmitate.

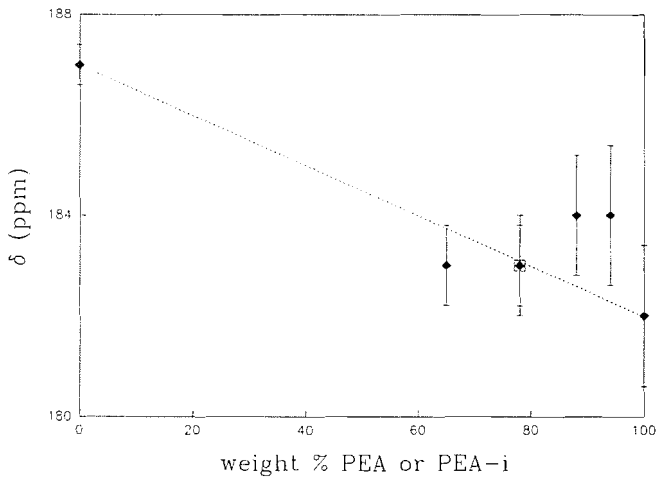

FIG. 4. Chemical shift of the carboxylate carbons as a function of composition for various mixtures of PEA-i with SP (◆) and for one mixture of PEA containing 22 wt.%. SP (□).

mainly to SP, overlaps the carbonyl signal of PEA-i, the resonance of the former can be readily identified and measured because of its rather sharp signal. A plot of its chemical shift as a function of the mixture composition is presented in Fig. 4. The principal result is that the carboxylate carbon soap signal in all of the mixtures resonates upfield from the signal of the pure soap. The dashed line suggests that this signal moves linearly upfield toward the pure ionomer signal as a function of composition. However, it is obvious that this cannot be confirmed by our data, since the error in measuring the chemical shift is relatively large and increases as the soap content decreases.

A PEA:SP mixture containing 22 wt.% SP is included in the five mixtures reported in Fig. 4. The chemical shift of its carboxylate carbons is seen to be identical to that in the PEA-i:SP mixture of the same composition. In both cases, this apparent chemical shift can be interpreted as a change in the electronic environment of the carboxylate carbon in going from the pure soap to the mixture with the polymer or ionomer. This is assuming, of course, that the chemical shift is dictated primarily by the electron density around the resonating nucleus, and does not take into account other factors that can affect carbon chemical shifts. If this assumption is accepted, one could explain the shift in the ionomer mixtures by considering the composition and resulting morphology of the ionomer. PEA-i, like many ionomers, shows two-phase behaviour (8). It is generally accepted that the ionic groups of the ionomer tend to aggregate to form ion-rich domains that lead to the appearance of the second phase (10). When SP is mixed with the ionomer, it is possible that at least some of its carboxylate groups tend to be in close proximity to the ion-rich domains, perhaps even mixed preferentially with carboxylate groups of the ionomer. The SP carboxylate groups would thus be surrounded by more electron density and therefore resonate at higher field when mixed with the ionomer than in pure SP. On the other hand, the chemical shift data in Fig. 4 also suggest that the SP carboxylate groups are as shielded in the polymer without carboxylate groups (PEA) as they are in the ionomer. The shielding of the SP carboxylate groups in the PEA mixture may indicate a preference for neighbouring ester carbonyl groups. If neighbouring ester groups have similar effects on the SP carboxylate groups as do neighbouring carboxylate groups, then, based on the chemical shift data, one cannot rule out that the SP groups may be mixed preferentially with ester groups in the ionomer mixtures as well.

One factor to be considered in the above is that the chemical shift of the carboxylate carbons in all soap mixtures contains a distribution of many possible shifts at the interfaces, in various environments, and in a bulk phase. Hence it is reasonable to suppose that the actual chemical shift of the soap carboxylate carbons present at the interface with PEA or PEA-i is much lower than the average read in the spectrum. Possibly this indicates the presence of carboxylate–carboxylate or carboxylate–ester bilayers.

To measure the proton spin-lattice relaxation time constant in the rotating frame ($T_{1\rho H}$), the contact time can be increased systematically and the spectrum monitored for magnetization decay. Figure 5 shows an example of a plot of ln(magnetization) as a function of contact time for a mixture of PEA-i and SP containing 22 wt.% SP. The numbers on each curve correspond to the signals in Fig. 3 and represent the magnetization decays for each of those signals. The only "pure" signals in Fig. 3, numbers 2 and 3, belong to PEA-i. They decay very fast, as fast as in the pure ionomer, and from the slope one can determine a $T_{1\rho H}$ of 2.8 ms. The remaining three signals contain both components and, consequently, their decay is nonexponential. Nevertheless, one can clearly distinguish a long relaxation time component (48 ms for this sample) and subtract this component from the overall decay to obtain the fast component, which is similar to that of the "pure" PEA-i signals. The contribution of PEA-i to signals 1 and 4 is minor, as one would expect from the intensity ratios in Fig. 2. For CH_3 (signal 5), however, PEA-i has the most important contribution, and this explains why the nonexponential decay is the most obvious here.

The most important conclusion to be drawn from Fig. 5 is that, as expected (8), the two components do not mix at the molecular level. They form separate phases, which relax independently, and there is a hindrance to magnetization transfer across phase boundaries. The actual $T_{1\rho H}$ values as a function of the composition of the mixtures were also determined. Figure 6 presents the results. However, some caution must be exercised when interpreting them. Two points in particular must be dealt with.

First, it is to be noted from the figure that, for a given composition, more than one $T_{1\rho H}$ values are obtained from

Can. J. Chem. Downloaded from www.nrcresearchpress.com by 88.255.202.194 on 09/08/12
For personal use only.

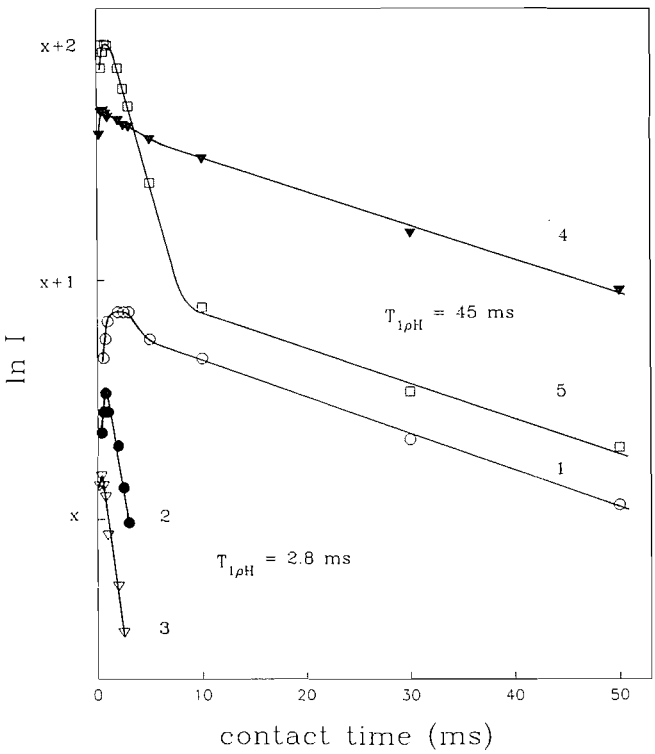

FIG. 5. Magnetization decay as a function of contact time for a mixture of PEA-i containing 22 wt.% SP. The numbers correspond to the signal numbers in Fig. 3.

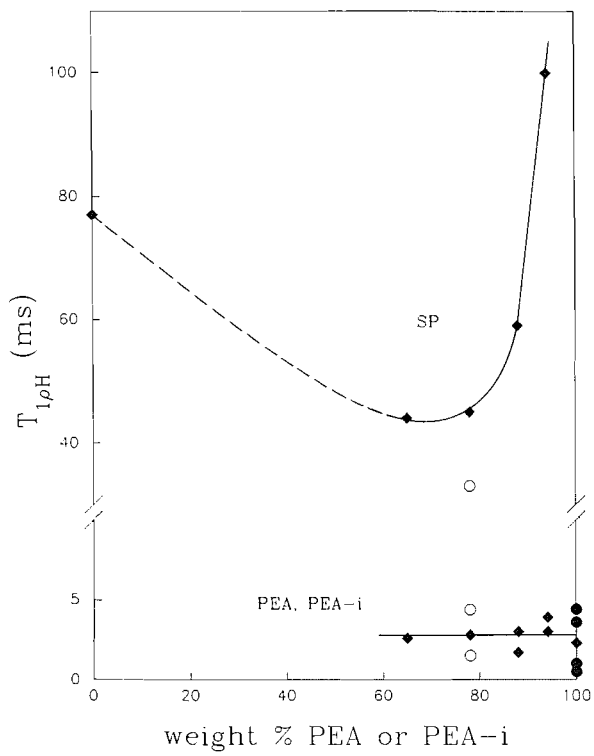

FIG. 6. $T_{1\rho H}$ values as a function of concentration for several PEA-i/SP mixtures (◆) and one PEA/SP mixture (○). The upper symbols are for the values obtained from SP signals, the lower symbols from PEA-i or PEA signals. The $T_{1\rho H}$ values for the signals of pure PEA are also shown (●). See text for more detailed explanation.

the polymer or ionomer signals in some cases. Mixtures containing PEA-i with 35 wt.% and 22 wt.% soap show the same slope for all signals, as does the pure ionomer. However, the two PEA-i mixtures of lower soap content, the only PEA mixture, and PEA itself show different slopes for different signals. This is, in fact, a well-known phenomenon for polymers above their T_g (11); and PEA, PEA-i, and all of the mixtures have glass transitions below room temperature (8). In this situation, the presence of different slopes does not mean that there are various phases within the polymer domains.

Second, care must be taken when measuring $T_{1\rho H}$ values for crystalline substances, which SP is. The presence of spin–spin relaxation mechanisms can prevent measurement of the actual $T_{1\rho H}$ value. To avoid errors in the measurements, especially to eliminate the local dipolar field, a spin-lock experiment can be used only with relatively high spin-locking fields. Analyzing other soaps at higher temperatures, Bonekamp *et al.* (12) demonstrated that there is a minimum acceptable field for this experiment. A variable field experiment confirmed that for our sample at room temperature the minimum admissible field is 4.5 G, clearly well below the 16 G field (corresponding to the 90° pulse of 3.7 μs) used by us. As supportive evidence, the $T_{1\rho H}$ values plotted in Fig. 6 are of the same order of magnitude as those measured on sodium *n*-butyrate (12).

Now, the data in Fig. 6 show that PEA and PEA-i are not influenced very much by the presence of the soap. Their $T_{1\rho H}$ values stay more or less constant. SP, on the other hand, undergoes significant changes when mixed with the polymer or ionomer. Except for the sample containing 6 wt.% SP, which shows an increase in the $T_{1\rho H}$ value, all mixtures have lower $T_{1\rho H}$ values than SP itself. It is generally accepted that in miscible systems $T_{1\rho H}$ takes a value that is intermediate between the values of the two components. Phase-separated systems can show some kind of "communication" at the interface, which affects the $T_{1\rho H}$ value of the slower relaxing component (4). This means that, if the two components of a system present some kind of physical interaction at the interface that separates the two phases, and that if this interaction can translate into a limited diffusion of spins across the interface, then, at the interface, the slowest-relaxing component will be partly relaxed by the fastest-relaxing component. This will translate into an overall decrease of $T_{1\rho H}$ for the slow-relaxing component. Such occurrences have been observed for charge-transfer interacting polymer blends (4), as well as for interpenetrating epoxy composites containing lignin (13).

If this is true in the case studied here, Fig. 6 indicates that there is some communication at the interface if the amount of soap in the mixture with PEA-i exceeds ca. 10 wt.% (ca. 4 mol%). Furthermore, there seems to be more communication in the mixture with PEA than in the mixture with the ionomers.

One explanation for the data in both Figs. 4 and 6 may be related to how the soap molecules arrange themselves at the interface with the polymer or ionomer. Soaps such as SP generally form a solid phase bilayer structure with interdigitated ionic groups; i.e., the ion pairs form an ionic double layer, where each half contains anions and cations that are arranged alternately both within the half-layer and between

Can. J. Chem. Downloaded from www.nrcresearchpress.com by 88.255.202.194 on 09/08/12
For personal use only.

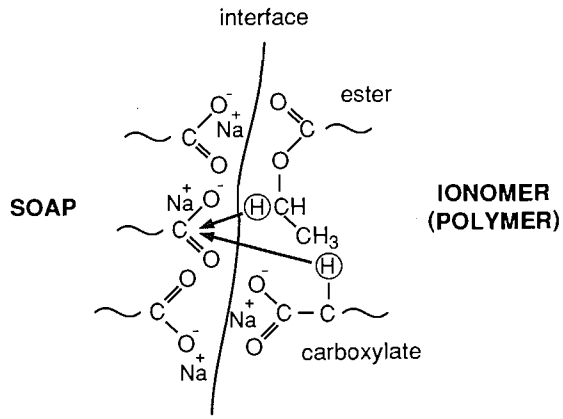

FIG. 7. Schematic view of the interface between the polymer (ionomer) and the soap domains. Arrows indicate the distance the spin is required to travel to allow for magnetization transfer.

the two half-layers (14). The DSC studies of the mixtures of SP with PEA and PEA-i indicated that the bulk structure of the SP phase is essentially unperturbed in the mixtures (8). However, given the tendency of the ionic groups to form bilayers, it is reasonable to assume that in the mixtures with PEA and PEA-i, which are polar media, the SP molecules at the surface of the soap domains are arranged such that the sodium carboxylate ion pairs face the surrounding polymer or ionomer. In the case of the ionomer, this allows for direct contact between its carboxylate groups and those at the SP surface; in fact, the SP and PEA-i carboxylate groups may even tend to form an interfacial ionic double layer. If the proportion of soap in the mixture is very low, the SP domains would be very small in size and number; under these conditions the interfacial separation between the soap and ionomer domains may consist solely of soap and ionomer carboxylate groups. This could explain why, in Fig. 6, a composition with the lowest amount of SP shows an increase in $T_{1\rho H}$ compared with the pure soap, unlike all other compositions, which present a depression of $T_{1\rho H}$. With the addition of more soap, ester carbonyl groups are likely to replace ionomer carboxylate groups at the interface with the soap phase. This would allow more contacts between the protonated part of the ionomer and the soap, and probably also some communication of the carbons in the soap with the protons in the ionomer.

In the mixtures with PEA, the carboxylate surface of the soap domains would be primarily in contact with the ester carbonyl groups of PEA, which are less polar than the carboxylate groups and may allow for more contact with the soap than in the case of PEA-i. This would explain why the $T_{1\rho H}$ of the soap is more depressed in the presence of 78 wt.% PEA than in the presence of 78 wt.% PEA-i. This hypothesis is also consistent with the chemical shifts in Fig. 4, as noted above. A schematic illustration to clarify the possible contacts at the interface is presented in Fig. 7.

To test this hypothesis, experiments were carried out using deuterated SP. In the same experimental conditions as were employed for the $T_{1\rho H}$ measurements, the magnetization of the carbon nuclei increases with increasing contact time, because now the protons are a diluted species and the physical distance between two protons is greater than the distance previously measured for spin diffusion. Figure 8*a*

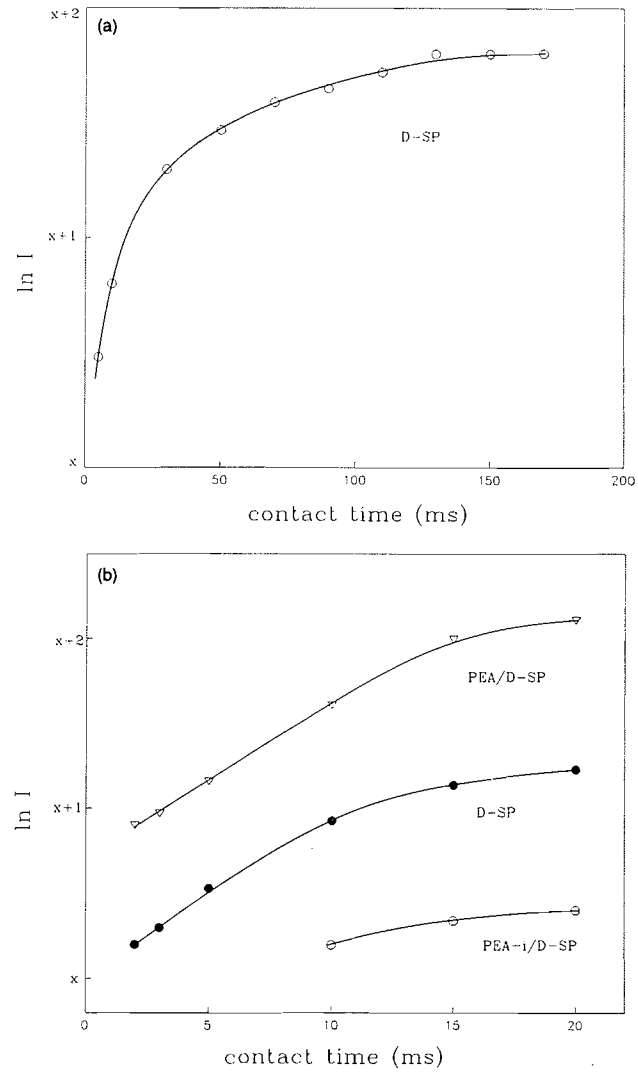

FIG. 8. Buildup of magnetization (*a*) in deuterated soap and (*b*) in D-SP, PEA:D-SP, and PEA-i:D-SP as a function of contact time. The vertical axis is shifted arbitrarily.

shows the magnetization buildup for one of the D-SP signals. There are small differences in this buildup for various carbons, due to different distances from protons. Figure 8*b* shows the initial part of this magnetization buildup curve for D-SP in comparison with two mixtures containing 22 wt.% D-SP: one with PEA and the other with PEA-i. The first obvious conclusion is that there are no significant changes in the buildup pattern for the mixtures as compared to the pure D-SP, which confirms phase separation and lack of spin diffusion across interfaces. Intimate molecular mixing would have allowed magnetization transfer from the protons of PEA or PEA-i to the carbons of D-SP, and the signals of D-SP carbons would have grown much faster.

Because the vertical scale in Fig. 8*b* is arbitrarily drawn, a better comparison between the samples can be made using Table 1, which presents the signal/noise ratios for the methylene carbons of D-SP at various contact times. The signal/noise ratio depends on several factors, the most important in our case being sample quantity. The same spinner is filled with pure D-SP or with a mixture containing only 22 wt.% D-SP (lines 2 and 3). One would expect a decrease

Can. J. Chem. Downloaded from www.nrcresearchpress.com by 88.255.202.194 on 09/08/12
For personal use only.

TABLE 1. Signal/noise ratios for the deuterated soap and its mixtures at various contact times

Sample	Signal/noise ratio			
	10 ms	15 ms	20 ms	10 ms/20 ms
D-SP	6.7	9.8	10.6	1.6
PEA-D-SP	7.5	8.4	15.8	2.1
PEA-i-D-SP	2.5	3.3	3.9	1.6

of the signal/noise ratio for the mixed samples, but this happens only for the mixture with the ionomer. This last mixture has such a weak signal that it cannot be measured out of the noise at contact times lower than 10 ms. The fact that the mixture with PEA has a higher signal/noise ratio than the pure D-SP suggests that there is some cross-polarization transferred through the soap–polymer interface. From Fig. 7, the closest contacts can be achieved with the ester methylene protons. They are not nearly as efficient in transmitting magnetization in the ionomer samples, which suggests that, in the ionomer mixtures, the carboxylate groups rather than the ester groups dominate at the interface with the soap domains. A carboxylate–carboxylate interface would have very few protons present, thus being an effective barrier for magnetization transmission.

The last column in Table 1 compares the signal/noise ratios at 10 and 20 ms contact times, and is an indication of growth during this interval. All samples are behaving similarly, as shown in Fig. 8*b*, with the mixture containing PEA showing a higher growth.

In conclusion, all three findings presented above can be explained by the presence of separated soap domains dispersed within a continuous polymer or ionomer phase. The soap molecules at the surface of the soap domains are arranged such that the carboxylate groups preferentially face the polymer phase. The carboxylate groups of the ionomer and the ester groups of the polymer are closer than the less polar groups to the soap domains, thus causing a chemical shift of the carboxylate carbon signal to a higher field in the mixtures than in pure soap. In the ionomer mixtures, a carboxylate–carboxylate bilayer tends to form at the interface separating the two domains, probably supplemented by a carboxylate–ester layer; this decreases or prevents magnetic communication between the protons of the ionomer and the carbons of the soap. If the amount of soap is very small, no communication is noted between even the protons of the two phases. In the polymer mixtures, the carboxylate–ester bilayer allows for more communication between the magnetic nuclei of the two phases than in the ionomer mixtures. Thus, although the bulk phase of neither component is significantly perturbed in the mixtures, as was shown in ref. 8, the above results strongly indicate the presence and type of interfacial interactions between the two components for both the polymer and ionomer mixtures.

Acknowledgments

We thank the Natural Sciences and Engineering Research Council of Canada (NSERC) for funding of this project. A. N. thanks the Government of Ontario and C. G. B. the Government of Québec for funding an exchange project. We also thank Michel Couturier (U. Laval) for neutralizing the deuterated palmitic acid.

1. B. Blumich. Adv. Mater. (Weinheim), **3**, 237 (1991).
2. H. W. Spiess. Chem. Rev. **91**, 1321 (1991).
3. A. Natansohn. Polym. Eng. Sci. **32**, 1711 (1992).
4. A. Simmons and A. Natansohn. Macromolecules, **24**, 3651 (1991).
5. V. J. McBrierty. *In* Comprehensive polymer science. Vol. 1. *Edited by* G. Allen. Pergamon Press, Oxford. 1989. p. 397.
6. A. Simmons and A. Natansohn. Macromolecules, **25**, 3881 (1992).
7. X. Zhang, A. Natansohn, and A. Eisenberg. Macromolecules, **23**, 412 (1990).
8. X. Tong and C. G. Bazuin. Chem. Mater. **4**, 370 (1992).
9. A. Natansohn. Chem. Mater. **4**, 182 (1992).
10. A. Eisenberg, B. Hird, and R. B. Moore. Macromolecules, **23**, 4098 (1990).
11. R. Voelkel. Angew. Chem. Int. Ed. Engl. **27**, 1468 (1988).
12. J. E. Bonekamp, T. Eguchi, S. Plesko, and J. Jonas. J. Chem. Phys. **79**, 1203 (1983).
13. D. Feldman, D. Banu, A. Natansohn, and J. Wang. J. Appl. Polym. Sci. **42**, 1537 (1991).
14. S. Plesko, M. L. Phillips, R. Cassell, and J. Jonas. J. Chem. Phys. **80**, 5806 (1984).

Can. J. Chem. Downloaded from www.nrcresearchpress.com by 88.255.202.194 on 09/08/12
For personal use only.

Influence of metal–metal interaction on magnetic and redox properties in different series of heterodinuclear copper(II), nickel(II), and zinc(II) complexes

BHAMIDI SRINIVAS AND PANTHAPPALLY S. ZACHARIAS[1]
School of Chemistry, University of Hyderabad, Hyderabad - 500 134, India

Received January 13, 1992

BHAMIDI SRINIVAS and PANTHAPPALLY S. ZACHARIAS. Can. J. Chem. **70**, 2906 (1992).

Different series of heterodinuclear complexes, viz., $[CuNiL](ClO_4)_2 \cdot nH_2O$, $[CuZnL](ClO_4)_2 \cdot nH_2O$, $[NiCuL](ClO_4)_2 \cdot nH_2O$, and $[NiZnL](ClO_4)_2 \cdot nH_2O$ complexes where L is a dinucleating Schiff base ligand derived from the condensation of 1 mole of 2-hydroxy-5-methylbenzene-1,3-dicarbaldehyde, 1 mole of 1,3-diaminopropane, and 2 moles of *ortho*- or *para*-substituted aniline, have been synthesized and investigated. The μ_{eff} values of the CuNiL and NiCuL series of complexes suggest presence of weak antiferromagnetic coupling in them. In MeCN and DMF the CuNiL and NiCuL series of complexes exhibit two reversible one-electron redox couples at two different potentials. The large separation between the two redox couples is attributed to the antiferromagnetic interaction between the metal centres in the complexes. In the NiCuL series of complexes, the observed shift of 100–150 mV in E_1 to more negative values in complexes with potential donor groups such as OMe, OEt, SMe, etc. in the *ortho* position of the phenyl group of L is explained on the basis of weak bonding interactions of these groups with the copper centre. The CuNiL series of complexes do not exhibit such shift in E_1 values since there is no significant change in the square planar geometry of the copper centre. The CuZnL and NiZnL series of complexes exhibit only single one-electron redox couple as could be anticipated.

BHAMIDI SRINIVAS et PANTHAPPALLY S. ZACHARIAS. Can. J. Chem. **70**, 2906 (1992).

On a synthétisé et étudié différentes séries de complexes hétérodinucléaires, comme $[CuNiL](ClO_4)_2 \cdot nH_2O$, $[CuZnL](ClO_4)_2 \cdot nH_2O$, $[NiCuL](ClO_4)_2 \cdot nH_2O$ et $[NiZnL](ClO_4)_2 \cdot nH_2O$, dans lesquels L est un ligand bidentate formé d'une base de Schiff provenant de la condensation d'une mole de 2-hydroxy-5-méthylbenzène-1,3-dicarbaldéhyde, une mole de 1,3-diaminopropane et deux moles d'anilines *ortho* ou *para* substituées. Les valeurs de μ_{eff} des complexes des séries CuNiL et NiCuL suggèrent la présence d'un faible couplage antiferromagnétique. Dans le MeCN et le DMF, les complexes des séries CuNiL et NiCuL présentent deux couples rédox réversibles à un électron, à deux potentiels différents. La grande séparation entre les deux couples rédox est attribuée à l'interaction antiferromagnétique entre les centres métalliques des complexes. Le déplacement de 100–150 mV observé vers des valeurs plus négatives de E_1 pour les complexes de la série NiCuL portant des groupes donneurs, comme OMe, OEt, SMe, etc., dans la position *ortho* du groupe phényle L est expliqué par les faibles interactions de liaison de ces groupes avec les centres cuivriques. Les complexes des séries CuNiL ne présentent pas de déplacement dans les valeurs de E_1 puisqu'il n'y a pas de changements significatifs dans la géométrie plan carré du centre cuivrique. Comme on pouvait s'y attendre, les complexes des séries CuZnL et NiZnL ne présentent qu'un seul couple rédox à un électron.

[Traduit par la rédaction]

Introduction

Dinuclear metal complexes are important in the investigation of interactions between metal ions in dinuclear metal centres of proteins (1–4) and that of multimetallic species at active bio sites (5–9). Various types of dinucleating ligands have been used in the preparation of dimetallic complexes, of which Schiff base ligands derived from 2-hydroxy-5-methylbenzene-1,3-dicarbaldehyde are of considerable interest since they provide two metal ions in close proximity (<3.0 Å) for direct metal–metal interaction. Dinuclear copper(II) complexes of these ligands show interesting magnetic and redox behaviour (10–19). The dicopper complex of macrocyclic Schiff base ligand obtained from the condensation of 2-hydroxy-5-methylbenzene-1,3-dicarbaldehyde and 1,3-diamino-propane exhibits reversible one-electron transfers at two different potentials, although both copper centres are identical with respect to ligand environment and geometry (20). This has been ascribed to the magnetic exchange coupling between the copper(II) centres and its resultant stabilizing influence on $Cu^{I}Cu^{II}$ intermediate complex species (20). Compared to the bulk of literature available on dicopper(II) complexes, very little has been reported on heterodimetallic complexes of these ligands, probably due to the difficulties involved in the syntheses of such complexes (21, 22). The heterodimetallic complexes, having copper(II) as one metal centre and the other metal centre varying among Mn(II), Fe(II), Co(II), and Ni(II), have been shown to exhibit considerable antiferromagnetic coupling between the metal centres. In this article we wish to report the syntheses, characterization of a series of heterodinuclear Cu(II), Ni(II), and Zn(II) complexes (general structure is shown in **2** of Scheme 1), and their spectral, magnetic, and redox properties.

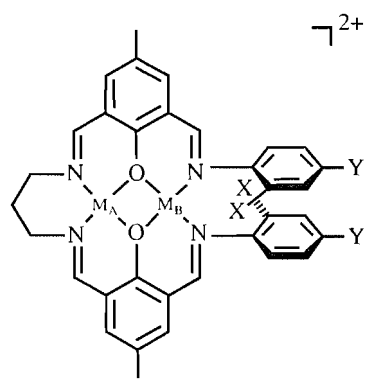

$M_AM_BL(ClO_4)_2 \cdot nH_2O$

[1]Author to whom correspondence may be addressed.

Can. J. Chem. Downloaded from www.nrcresearchpress.com by 88.255.202.194 on 09/08/12
For personal use only.

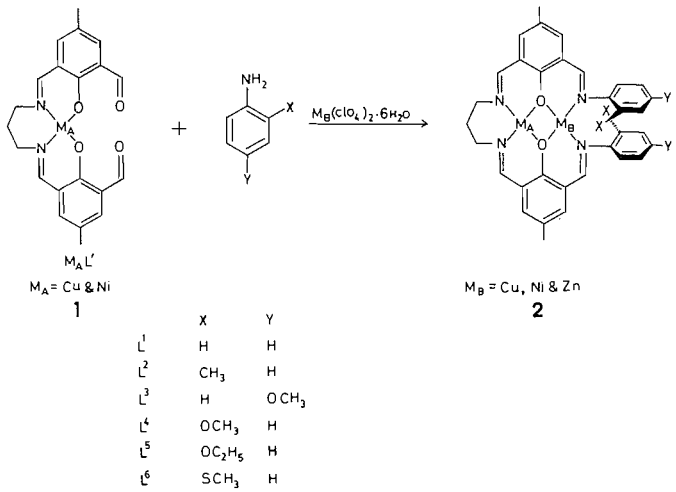

	X	Y
L^1	H	H
L^2	CH_3	H
L^3	H	OCH_3
L^4	OCH_3	H
L^5	OC_2H_5	H
L^6	SCH_3	H

SCHEME 1

It can be seen from the structure that the ligands provide two nonequivalent O_2N_2 coordination sites, which share two phenolato groups. While the substitution on the phenylazomethine group can be expected to influence the redox behaviour of the metal at the M_B site, it is not likely to do so at the M_A sites.

Experimental

Syntheses of complexes

All reagents and solvents were purchased from commercial sources and utilized after distillation or recrystallization. 2-Hydroxy-5-methylbenzene-1,3-dicarbaldehyde was prepared according to a reported procedure (13). For electrochemistry, MeCN was treated successively with $CaCl_2$ and P_2O_5 and DMF was dried over CaH_2 and distilled. They were stored on type 4A molecular sieves. The heterodinuclear Cu(II), Ni(II), and Zn(II) complexes, $CuNiL(ClO_4)_2\cdot 3H_2O$, $CuZnL(ClO_4)_2\cdot H_2O$, $NiCuL(ClO_4)_2\cdot 3H_2O$, and $NiZnL(ClO_4)_2\cdot 2H_2O$ were prepared from the precursor complexes CuL′ and NiL′ as shown in the Scheme 1.

The precursors CuL′ and NiL′ complexes were prepared according to reported procedure (21). In a typical preparation, a suspension of CuL′ (0.420 g, 1 mmol) in MeOH (20 cm^3) was added to the respective aniline (3 mmol) and solid $Ni(ClO_4)_2\cdot 6H_2O$ (0.365 g; 1 mmol) and stirred. The stirring was continued for 2 h, and the yellowish green product of $CuNiL(ClO_4)_2\cdot H_2O$ was collected by filtration, washed with diethyl ether, and dried *in vacuo* for 12 h. $NiCuL(ClO_4)_2\cdot 3H_2O$ complexes were prepared from NiL′ complex, the respective anilines and $Cu(ClO_4)_2\cdot 6H_2O$ by following a similar procedure adopted for the preparation of $CuNiL(ClO_4)\cdot 3H_2O$. The $CuZnL(ClO_4)_2\cdot H_2O$, $NiZnL(ClO_4)_2\cdot 2H_2O$ type complexes were also prepared by the same procedure.

Caution: The perchlorate salts are potential explosives and should be handled with care.

Physical measurements

The CHN analyses were carried out on a Perkin–Elmer 240 C Elemental Analyser. Metal estimations were carried out on an inductively coupled plasma spectrometer (Labtem-Australia). Infrared spectra were recorded on a Perkin–Elmer IR 283 spectrophotometer in the range 4000–200 cm^{-1} in KBr pellets. Electronic absorption spectra were recorded on a Perkin–Elmer Lambda 3B UV-Vis spectrophotometer in the 900–200 nm wavelength region and on a Cary 17D spectrophotometer in the near ir region in MeCN and DMF. Magnetic susceptibility measurements were made by the Faraday method, at ambient temperature using a CAHN magnetic balance setup. Diamagnetic corrections were made using Pascal's constants (23).

Cyclic voltammetric experiments were carried out on a PAR electrochemistry system consisting of a 174 A polarographic analyzer and a single compartment cell. Solutions of the strengths (1×10^{-3} mol dm^{-3}) in MeCN (acetonitrile) or DMF (*N*,*N*-dimethylformamide) were used. The supporting electrolyte was 0.1 mol dm^{-3} tetraethylammonium perchlorate (TEAP), which was prepared as described (24), recrystallised twice from H_2O, and dried under vacuum at 40°C. All experiments were performed under a blanket of dry nitrogen at 27°C, using a three-electrode assembly, a hanging mercury drop electrode (hmde) as working electrode, Pt wire as auxiliary electrode, and standard calomel electrode (sce) as reference electrode. All potentials are referred to the sce and are uncorrected for liquid junction potential.

Results and discussion

Synthesis and characterisation

Synthetic details of the heterodinuclear copper(II), nickel(II), and zinc(II) complexes are given in the experimental section and are outlined in Scheme 1. Syntheses of pure heterodinuclear complexes of these series are often difficult because of the presence of homodinuclear species. However, by maintaining proper experimental conditions such as reaction time, stoichiometry, etc., analytically pure complexes could be synthesised. All the complexes are soluble in common organic solvents and most of the complexes are obtained as hydrates.

The complexes discussed here will be abbreviated as CuNiL, NiCuL, CuZnL, and NiZnL. The first and the second metal centres are represented as M_A and M_B sites in the general structure of the complexes shown in Scheme 1. L represents the generalised ligand structure. Depending upon the substituents on the anilines these ligands are represented as L^1, L^2, and L^3, etc., and are shown in Scheme 1. A special feature of the present set of complexes is that the metal centres are in different ligand environments while in the case of heterodinuclear complexes derived from 2-hydroxy-5-methylbenzene-1,3-dicarbaldehyde and diamines reported in the literature, the metal centres have equivalent ligand environment.

Infrared spectra of the present complexes are similar since the ligand systems do not differ much from one another. For most of the complexes, the presence of water molecules is evident from the broad bands observed in the region 3550–3400 cm^{-1}. All the complexes exhibit two strong absorptions at 1620 and 1550 cm^{-1} characteristic of metal coordinated C=N and C---O (phenolato) groups. Presence of ionic perchlorate is evident from the observation of ir bands at 1100 and 625 cm^{-1}. Analytical data for the complexes are presented in Table 1 and they agree with the structure shown in **2** of Scheme 1.

Electronic spectra and magnetic moments

Electronic spectra were recorded in MeCN and DMF. Better spectral profiles are obtained for most of the complexes in MeCN. For all the complexes, a strong band in the wavelength region 430–400 nm is observed and is attributed to a combination of ligand to metal or interligand charge transfers. From the general structure of the dinuclear complexes shown in Scheme 1 it is apparent that the M_A site is close to planar geometry while the M_B site is more nonplanar. However, they can assume square pyramidal or octahedral geometry depending upon the number of co-ordinated water molecules.

The CuNiL complexes exhibit spectral bands at 590 nm, a shoulder at 750 nm, and another band at 960 nm. For

Can. J. Chem. Downloaded from www.nrcresearchpress.com by 88.255.202.194 on 09/08/12
For personal use only.

TABLE 1. Analytical data for the complexes

Complex	Found (calcd.)					
				Metal		
	C	H	N	Cu	Ni	Zn
$CuNiL^1(ClO_4)_2 \cdot 3H_2O$	44.42	3.88	6.30	7.02	6.52	—
	(44.54)	(4.08)	(6.29)	(7.14)	(6.60)	—
$CuNiL^2(ClO_4)_2 \cdot 3H_2O$	45.67	4.36	6.02	6.81	6.32	—
	(45.80)	(4.39)	(6.10)	(6.92)	(6.40)	—
$CuNiL^3(ClO_4)_2 \cdot 3H_2O$	44.08	4.17	5.82	6.55	6.07	—
	(44.26)	(4.24)	(5.89)	(6.69)	(6.18)	—
$CuNiL^4(ClO_4)_2 \cdot 3H_2O$	44.22	4.07	5.82	6.58	6.09	—
	(44.26)	(4.24)	(5.89)	(6.69)	(6.18)	—
$CuNiL^5(ClO_4)_2 \cdot 3H_2O$	44.94	4.26	5.80	6.44	5.94	—
	(45.45)	(4.53)	(5.73)	(6.50)	(6.00)	—
$CuNiL^6(ClO_4)_2 \cdot 3H_2O$	42.72	4.00	5.66	6.33	5.82	—
	(42.81)	(4.10)	(5.70)	(6.47)	(5.98)	—
$CuZnL^1(ClO_4)_2 \cdot H_2O$	46.02	3.70	6.50	7.22	—	7.46
	(46.06)	(3.75)	(6.51)	(7.38)	—	(7.60)
$CuZnL^2(ClO_4)_2 \cdot H_2O$	47.30	3.98	6.25	7.00	—	7.27
	(47.31)	(4.08)	(6.30)	(7.15)	—	(7.36)
$CuZnL^3(ClO_4)_2 \cdot H_2O$	45.44	3.92	6.01	6.75	—	7.03
	(45.67)	(3.94)	(6.08)	(6.90)	—	(7.10)
$CuZnL^4(ClO_4)_2 \cdot H_2O$	45.42	3.79	5.98	6.78	—	6.98
	(45.67)	(3.94)	(6.08)	(6.90)	—	(7.10)
$CuZnL^5(ClO_4)_2 \cdot H_2O$	46.52	4.11	5.83	6.64	—	6.86
	(46.95)	(4.25)	(5.90)	(6.70)	—	(6.98)
$CuZnL^6(ClO_4)_2 \cdot H_2O$	45.14	3.81	6.04	6.60	—	6.82
	(44.98)	(3.67)	(5.99)	(6.67)	—	(6.88)
$NiCuL^1(ClO_4)_2 \cdot H_2O$	46.25	3.72	6.44	7.40	6.81	—
	(46.42)	(3.77)	(6.56)	(7.44)	(6.88)	—
$NiCuL^2(ClO_4)_2 \cdot 3H_2O$	45.72	4.35	5.98	6.88	6.34	—
	(45.80)	(4.39)	(6.10)	(6.92)	(6.40)	—
$NiCuL^3(ClO_4)_2 \cdot 3H_2O$	44.12	4.20	6.02	6.83	6.09	—
	(44.26)	(4.24)	(5.89)	(6.90)	(6.18)	—
$NiCuL^4(ClO_4)_2 \cdot 3H_2O$	44.30	4.22	5.82	6.81	6.10	—
	(44.26)	(4.24)	(5.89)	(6.90)	(6.18)	—
$NiCuL^5(ClO_4)_2 \cdot 3H_2O$	45.22	4.43	5.66	6.44	5.97	—
	(45.45)	(4.53)	(5.73)	(6.50)	(6.00)	—
$NiCuL^6(ClO_4)_2 \cdot 3H_2O$	42.82	4.04	5.56	6.39	5.92	—
	(42.81)	(4.10)	(5.70)	(6.47)	(5.98)	—
$NiZnL^1(ClO_4)_2 \cdot 2H_2O$	45.22	4.07	6.33	—	6.70	7.22
	(45.37)	(3.92)	(6.41)	—	(6.72)	(7.50)
$NiZnL^2(ClO_4)_2 \cdot 2H_2O$	46.22	4.15	6.10	—	6.44	7.21
	(46.42)	(4.25)	(6.21)	—	(6.51)	(7.25)
$NiZnL^3(ClO_4)_2 \cdot 2H_2O$	45.00	4.12	5.91	—	6.23	7.03
	(45.02)	(3.10)	(6.07)	—	(6.29)	(7.00)
$NiZnL^4(ClO_4)_2 \cdot 2H_2O$	44.91	4.12	6.18	—	6.51	7.05
	(45.02)	(4.10)	(6.07)	—	(6.29)	(7.00)
$NiZnL^5(ClO_4)_2 \cdot 2H_2O$	46.00	4.33	5.77	—	6.11	6.77
	(46.21)	(4.41)	(5.82)	—	(6.10)	(6.80)
$NiZnL^6(ClO_4)_2 \cdot 2H_2O$	44.82	3.91	5.90	—	6.00	6.72
	(45.02)	(4.10)	(6.00)	—	(6.08)	(6.77)

CuZnL complexes there is only one band at 625 nm with a shoulder at 750 nm. The mononuclear copper complex CuL′ of the same ligand system where copper is in planar geometry has an absorption band at 598 nm. Therefore, the origin of the 590 nm band and 750 nm shoulder in CuNiL complex is due to the inner copper centre. The 990 band originates from the *d–d* transition of the nickel centre. The spectral pattern of CuNiL complexes suggests square-pyramidal geometry for the metal centre (25, 26) arising from the possible coordination of water molecules. It may be pointed out that all the dinuclear complexes discussed here have at least two water molecules (Table 1). The NiCuL complexes exhibit a band at 748 nm with a broad shoulder at ca. 1000 nm. The 748 nm band corresponds to the *d–d* transition of the copper(II) centre in square pyramidal geometry and the 1000 nm band to the nickel centre. These bands may be compared with the spectral bands of $[CuNiL_2Cl_2] \cdot 2H_2O$ type complexes which have bands at 1000

Can. J. Chem. Downloaded from www.nrcresearchpress.com by 88.255.202.194 on 09/08/12
For personal use only.

TABLE 2. Electronic spectral and magnetic data for heterodinuclear complexes

Complex	Electronic spectral data χ/nm (ε/dm^3 mol^{-1} cm^{-1}) In MeCN	In DMF	Magnetic moment[a] (μ_B)
$CuNiL^1(ClO_4)_2 \cdot 3H_2O$	970 (16) 593 (80)	965 (15), 750 (sh) 621 (77)	3.03
$CuNiL^2(ClO_4)_2 \cdot 3H_2O$	952 (18) 590 (67)	950 (12), 747 (sh) 619 (87)	2.91
$CuNiL^3(ClO_4)_2 \cdot 3H_2O$	962 (21) 590 (95)	970 (18), 748 (sh) 621 (105)	2.89
$CuNiL^4(ClO_4)_2 \cdot 3H_2O$	968 (28) 590 (68)	967 (22), 750 (sh) 605 (140)	2.90
$CuNiL^5(ClO_4)_2 \cdot 3H_2O$	944 (14) 586 (91)	948 (17), 752 (sh) 605 (136)	3.09
$CuNiL^6(ClO_4)_2 \cdot 3H_2O$	[b]	747 (sh), 620 (85)	2.86
$CuZnL^1(ClO_4)_2 \cdot H_2O$	618 (66)	620 (76)	1.91
$CuZnL^2(ClO_4)_2 \cdot H_2O$	614 (69)	606 (102)	1.93
$CuZnL^3(ClO_4)_2 \cdot H_2O$	605 (67)	620 (82)	1.95
$CuZnL^4(ClO_4)_2 \cdot H_2O$	617 (76)	629 (79)	1.84
$CuZnL^5(ClO_4)_2 \cdot H_2O$	629 (67)	626 (90)	1.96
$CuZnL^6(ClO_4)_2 \cdot H_2O$	655 (52)	626 (68)	1.92
$NiCuL^1(ClO_4)_2 \cdot H_2O$	748 (125) 1000 (sh)	744 (169) 1000 (sh)	3.08
$NiCuL^2(ClO_4)_2 \cdot 3H_2O$	748 (101) 1000 (sh)	748 (116) 1000 (sh)	2.98
$NiCuL^3(ClO_4)_2 \cdot 3H_2O$	748 (95) 1000 (sh)	745 (109) 1000 (sh)	2.97
$NiCuL^4(ClO_4)_2 \cdot 3H_2O$	1000 (sh)	745 (115) 1000 (sh)	3.06
$NiCuL^5(ClO_4)_2 \cdot 3H_2O$	745 (106) 1000 (sh)	745 (104) 1000 (sh)	3.12
$NiCuL^6(ClO_4)_2 \cdot 3H_2O$	748 (147) 1000 (sh)	747 (172) 1000 (sh)	3.08
$NiZnL^1(ClO_4)_2 \cdot 2H_2O$	988 (19)	1000 (17)	3.50
$NiZnL^2(ClO_4)_2 \cdot 2H_2O$	1012 (18)	1006 (14)	3.81
$NiZnL^3(ClO_4)_2 \cdot 2H_2O$	975 (24)	998 (22)	3.76
$NiZnL^4(ClO_4)_2 \cdot 2H_2O$	1020 (17)	1012 (29)	3.92
$NiZnL^5(ClO_4)_2 \cdot 2H_2O$	987 (21)	982 (16)	3.67
$NiZnL^6(ClO_4)_2 \cdot 2H_2O$	997 (23)	989 (20)	3.46

[a]Magnetic moment per molecule for heterodinuclear complexes; values are uncorrected for TIP; error limits ±0.02 μ_B; field strength 7 K Gauss.
[b]Peaks absent.

and 725 nm. The 725 nm band is reported to originate from square pyramidal geometry for the copper(II) center (27) arising from the possible coordination of water molecules. The NiZnL complexes show an absorption band at 980 nm which can be attributed to a square pyramidal nickel centre (25).

Room temperature magnetic moments obtained for CuNiL and NiCuL complexes are in the range 2.86–3.09 μ_B per complex molecule against the spin-only value of 3.31 μ_B per complex molecule for noninteracting CuNiL and NiCuL complexes. The lower μ_{eff} values indicate the presence of antiferromagnetic coupling between Cu(II) and Ni(II) centres in these series of complexes. Antiferromagnetic interactions exists in heterodinuclear CuNi complexes derived from 3-formylsalicylic acid and diamines and are reflected in their μ_{eff} values (3.05 μ_B). The CuZnL and NiZnL complexes exhibit magnetic moments in the ranges 1.84–1.93 μ_B and 3.5–3.8 μ_B, corresponding to square-planar copper(II) and high-spin nickel(II) centres, respectively. Magnetic interactions are not expected in these complexes because of the presence of a zinc atom with a d^{10} configuration. The magnetic moment values for the complexes are collected in Table 2.

Electrochemical data

Cyclic voltammetric data for the complexes were collected in MeCN and DMF in the potential range +0.4 to −1.6 V vs. sce using the hmde working electrode at various scan rates (20–200 mV/s) (Table 3). In general, better cyclic voltammetric profiles were obtained in MeCN. In MeCN, CuNiL complexes exhibit two redox couples, one at ca. −0.48 V, which is close to reversible ($\Delta E_1 \approx 70$ mV) at higher scan rates, with the second redox couple in the potential range −1.29 to −1.33 V. The i_c/i_a ratio is close to unity for both redox couples. The CuZnL complexes exhibit only one redox couple in the potential range −0.35 to 0.39 V in MeCN with ΔE values of 160–220 mV. The first

Can. J. Chem. Downloaded from www.nrcresearchpress.com by 88.255.202.194 on 09/08/12
For personal use only.

Can. J. Chem. Downloaded from www.nrcresearchpress.com by 88.255.202.194 on 09/08/12
For personal use only.

TABLE 3. Cyclic voltammetric data for the heterodinuclear complexes at scan rate of 100 mV/s

Complex	Solvent	First electron transfer			Second electron transfer		
		E_1	ΔE_p	$-i_c/i_a$	E_2	ΔE_p	$-i_c/i_a$
$CuNiL^1(ClO_4)_2\cdot 3H_2O$[a]	MeCN	−0.456	70	1.0	−1.30	100	1.0
	DMF	−0.49	80	1.0	−1.30	80	1.0
$CuNiL^2(ClO_4)_2\cdot 3H_2O$[a]	MeCN	−0.495	70	1.0	−1.34	80	1.0
	DMF	−0.51	80	1.2	−1.30	80	1.0
$CuNiL^3(ClO_4)_2\cdot 3H_2O$[a]	MeCN	−0.49	80	1.2	−1.30	80	1.0
	DMF	−9.515	70	1.0	−1.33	80	1.0
$CuNiL^4(ClO_4)_2\cdot 3H_2O$[a]	MeCN	−0.46	80	1.2	−1.29	80	1.0
	DMF	−0.445	70	1.0	—	—	—
$CuNiL^5(ClO_4)_2\cdot 3H_2O$[a]	MeCN	−0.43	60	1.2	−1.29	80	1.0
	DMF	−0.445	70	1.0	−1.26	80	1.0
$CuNiL^6(ClO_4)_2\cdot 3H_2O$[a]	MeCN	−0.47	70	1.1	−1.32	100	1.2
	DMF	−0.49	100	1.1	−1.31	80	1.1
$CuZnL^1(ClO_4)_2\cdot H_2O$	MeCN	−0.39	180	0.86	—	—	—
	DMF	—	—	—	—	—	—
$CuZnL^2(ClO_4)_2\cdot H_2O$	MeCN	−0.39	200	0.85	—	—	—
	DMF	−0.39	irrev	—	—	—	—
$CuZnL^3(ClO_4)_2\cdot H_2O$	MeCN	−0.41	220	0.90	—	—	—
	DMF	−0.56	irrev	—	—	—	—
$CuZnL^4(ClO_4)_2\cdot H_2O$	MeCN	−0.39	140	0.90	—	—	—
	DMF	−0.53	irrev	—	—	—	—
$CuZnL^5(ClO_4)_2\cdot H_2O$	MeCN	−0.37	160	0.90	—	—	—
	DMF	−0.55	irrev	—	—	—	—
$CuZnL^6(ClO_4)_2\cdot H_2O$	MeCN	−0.38	190	1.0	—	—	—
	DMF	−0.56	irrev	—	—	—	—
$NiCuL^1(ClO_4)_2\cdot H_2O$	MeCN	−0.25	60	1.0	−1.38	70	1.0
	DMF	−0.175	70	0.94	−1.32	60	1.0
$NiCuL^2(ClO_4)_2\cdot 3H_2O$	MeCN	−0.20	80	1.0	−1.42	60	1.0
	DMF	−0.13	60	0.98	−1.31	80	1.0
$NiCuL^3(ClO_4)_2\cdot 3H_2O$	MeCN	−0.25	60	1.0	−1.40	80	1.0
	DMF	−0.19	60	0.94	−1.34	80	1.0
$NiCuL^4(ClO_4)_2\cdot 3H_2O$	MeCN	−0.385	80	1.0	−1.38	70	1.0
	DMF	−0.36	80	1.0	−1.32	60	1.0
$NiCuL^5(ClO_4)_2\cdot 3H_2O$	MeCN	−0.385	70	1.0	−1.39	60	1.0
	DMF	−0.33	60	1.0	−1.32	80	1.0
$NiCuL^6(ClO_4)_2\cdot 3H_2O$	MeCN	−0.355	70	1.0	−1.36	70	1.1
	DMF	−0.30	100	1.0	−1.31	70	1.0
$NiZnL^1(ClO_4)_2\cdot 2H_2O$	MeCN	−0.88	100	1.0	—	—	—
	DMF	−0.96	80	1.0	—	—	—
$NiZnL^2(ClO_4)_2\cdot 2H_2O$	MeCN	−0.90	120	1.0	—	—	—
	DMF	−0.98	80	1.0	—	—	—
$NiZnL^3(ClO_4)_2\cdot 2H_2O$	MeCN	−0.95	120	1.0	—	—	—
	DMF	−0.96	90	1.0	—	—	—
$NiZnL^4(ClO_4)_2\cdot 2H_2O$	MeCN	−0.92	80	1.0	—	—	—
	DMF	−0.97	80	1.0	—	—	—
$NiZnL^5(ClO_4)_2\cdot 2H_2O$	MeCN	−0.93	80	1.0	—	—	—
	DMF	−0.945	70	1.0	—	—	—
$NiZnL^6(ClO_4)_2\cdot 2H_2O$	MeCN	−0.925	70	1.0	—	—	—
	DMF	−1.0	80	1.0	—	—	—

[a] E_1 values obtained after immediately reversing the scan after the first reduction peak.
[b] Peak absent.

redox couple of CuNiL complexes (E_1) therefore corresponds to a copper-centred redox process, $Cu^{II}Ni^{II}$–$Cu^{I}Ni^{II}$. The observation that this couple is reversible only at higher scan rates indicates that $Cu^{I}Ni^{II}L$ species is not very stable. At low scan rates (<50 mV/s) large current in the range −0.90 to −1.10 V implies decomposition of the $Cu^{I}Ni^{II}L$ species. The instability of the electrogenerated $Cu^{I}Ni^{II}L$ complex species should be related to square-planar based geometry of the copper environment which destabilises the intermediate species. It is observed that if the forward scan is reversed immediately after the first reduction peak (at −0.60 V), the E_1 redox couple becomes more reversible in behaviour. These features are shown in Fig. 1. The second redox couple (E_2) corresponds to a nickel-centred redox

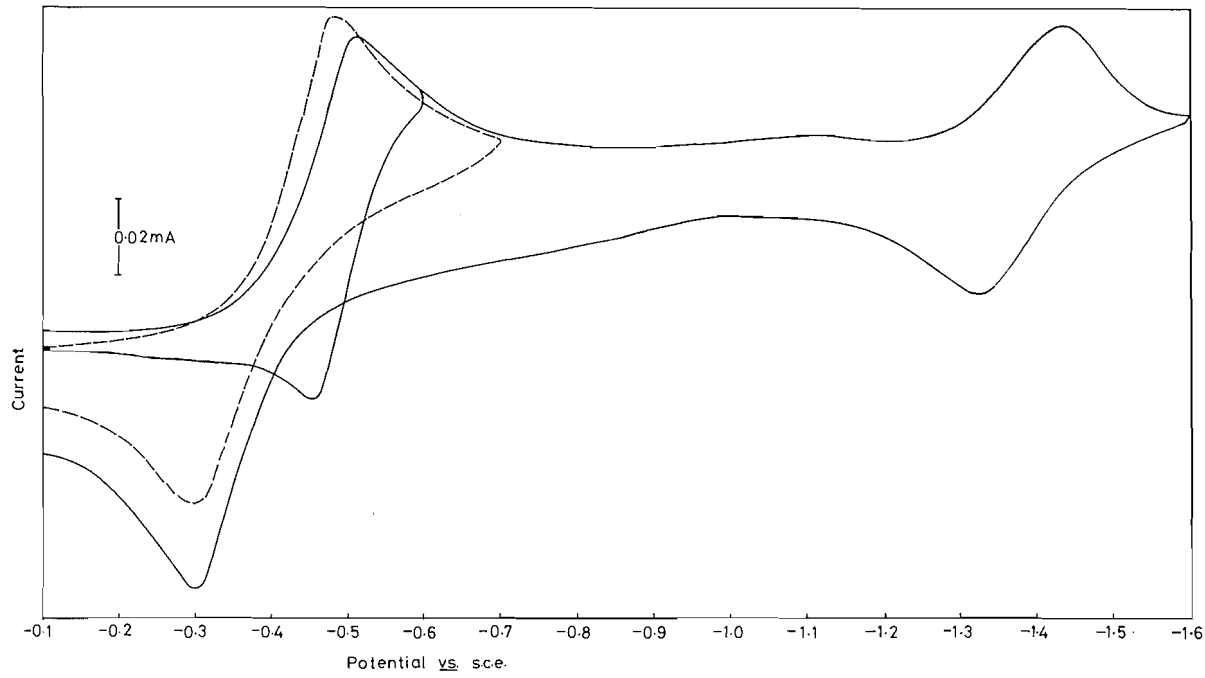

FIG. 1. Cyclic voltammograms of the complexes $CuNiL^2(ClO_4)_2 \cdot 3H_2O$ (—) and $CuZnL^2(ClO_4)_2 \cdot H_2O$ (----) in MeCN using a hmde working electrode at the scan rate 100 mV s^{-1}. Concentration of complex: 1×10^{-3}; supporting electrolyte: NEt_4ClO_4 (0.1 M).

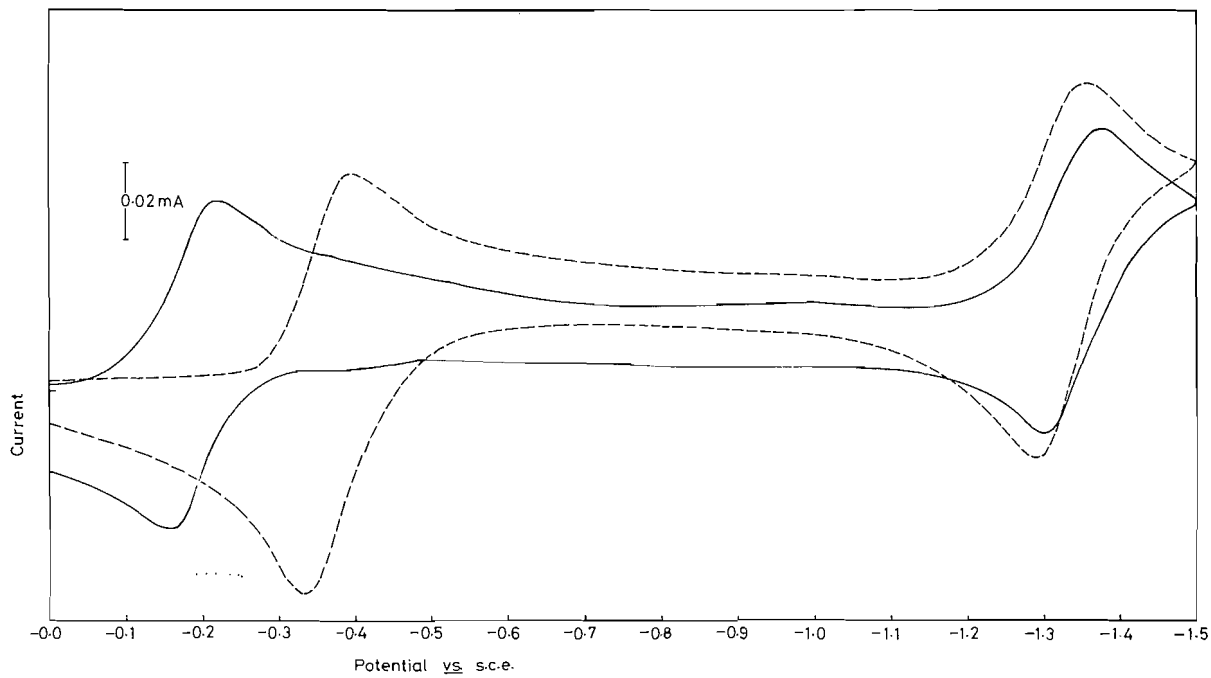

FIG. 2. Cyclic voltammograms of $NiCuL^1(ClO_4)_2 \cdot 3H_2O$ (—) $NiCuL^4(ClO_4)_2 \cdot 3H_2O$ (----) in MeCN, using a hmde working electrode at the scan rate 100 mV s^{-1}. Concentration of complex: 1×10^{-3} M; supporting electrolyte: NEt_4ClO_4 (0.1 M).

process, $Cu^{I}Ni^{II}$–$Cu^{I}Ni^{I}$, and is also close-to-reversible only at high scan rates. In DMF both redox couples are observed at high scan rates (>100 mV/s) at −0.48 and −1.30 V with ΔE_p at ca. 70 mV. The quasireversibility of the redox couple at ca. 0.35 V in CuZnL complexes can be explained to arise from the instability of the intermediate species because of the square-planar based geometry around the copper(II) ion. These complexes also exhibit a strong current in the potential range −0.90 to −1.10 V similar to CuNiL complexes, indicating decomposition/demetallation of the electrochemically generated $Cu^{I}Zn^{II}$ species. In DMF the redox couple is observed at a more negative potential (ca. −0.50 V). A cyclic voltammetric profile for a representative CuZnL complex is also shown in Fig. 1.

The NiCuL complexes in MeCN exhibit two reversible one-electron redox couples in the potential range −0.20 to −0.39 V (E_1) and −1.37 to −1.42 V (E_2). The redox couple E_1 corresponds to the copper-centred reduction $Ni^{II}Cu^{II}$–

Can. J. Chem. Downloaded from www.nrcresearchpress.com by 88.255.202.194 on 09/08/12
For personal use only.

Can. J. Chem. Downloaded from www.nrcresearchpress.com by 88.255.202.194 on 09/08/12
For personal use only.

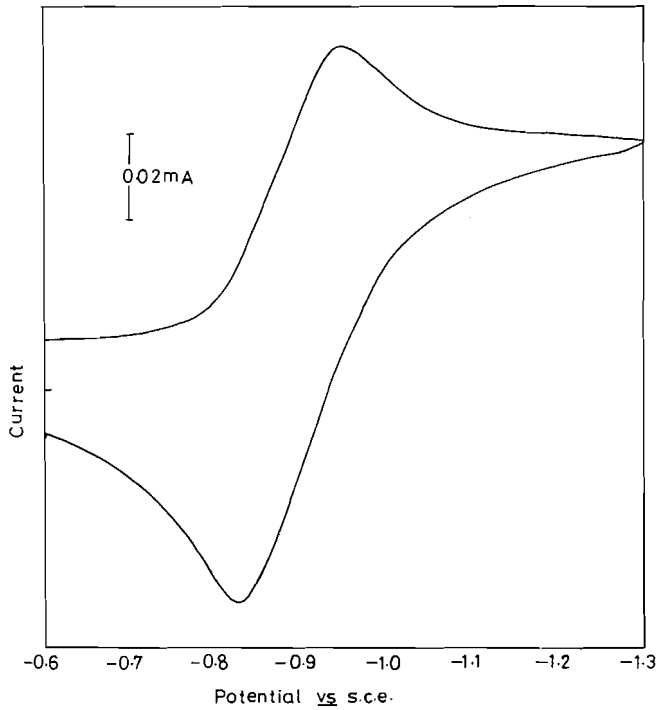

FIG. 3. Cyclic voltammogram of $NiZnL^1(ClO_4)_2 \cdot 2H_2O$ in MeCN using a hmde working electrode at the scan rate 100 mV s^{-1}. Concentration of complex: 1×10^{-3} M; supporting electrolyte: $NEt_4 \cdot ClO_4$ (0.1 M).

$Ni^{II}Cu^{I}$ and the other couple E_2 corresponds to the nickel-centred reduction $Ni^{II}Cu^{I}L$–$Ni^{I}Cu^{I}L$. The NiZnL complexes exhibit only a nickel-centred redox couple at ca. −0.90 V. These features are shown in Fig. 3. For both series, good cyclic voltammetric profiles are obtained at both low and high scan rates which suggests that the electrogenerated species are more stable on a cyclic voltammetric time scale against decomposition/demetallation. In DMF the first redox couple for NiCuL complexes is observed in the −0.13 to −0.36 V potential range and the second at ca. −1.32 V. It has been reported for the dicopper complexes of ligands L^1 and L^3 with strong antiferromagnetic interaction ($\mu_{eff} \sim 0.90\mu_B$) (28) the first reduction of $Cu^{II}Cu^{II}$–$Cu^{I}Cu^{II}$ is close to reversible and occurs at −0.05 and −0.07 V in DMF. The observed shift of ca. 120 mV towards more negative potentials for $NiCuL^1(ClO_4)_2 \cdot 3H_2O$ and $NiCuL^3(ClO_4)_2 \cdot 3H_2O$ complexes in comparison to their dicopper analogues can be explained by the weak antiferromagnetic coupling in the NiCuL complexes. The copper-centred reduction in complexes where there is no magnetic interaction occurs at more negative potential, ca. −0.50 V.

The NiCuL complexes of ligands L^2, L^4, L^5, and L^6 which have *ortho* substituents on the phenylazomethine group, viz., Me, OMe, OEt, and SMe, respectively, can be influenced by inductive, steric, and other effects due to substitutions. If steric is the only factor influencing the redox behaviour, all these complexes should show a shift of similar magnitude for the copper-centred electron transfer potential (E_1) to less negative values, since Cu(I) species become more stable in tetrahedral geometry, resulting from the presence of *ortho* substituents. The E_1 value for $NiCuL^2$ (2-Me) is −0.13 V while the other complexes have the following E_1 values: $NiCuL^4$ (2-OMe), −0.36; $NiCuL^5$ (2-OEt), −0.33 V; $NiCuL^6$ (2-SMe), −0.30 V. While the $NiCuL^2$ complex may attain pseudotetrahedral geometry for the copper centre because of steric interaction, the copper centre in $NiCuL^4$, $NiCuL^5$, and $NiCuL^6$ will be of different geometry because of the coordinating ability of the *ortho* substituents. The negative shift in E_1 potentials in $NiCuL^4$, $NiCuL^5$, and $NiCuL^6$ complexes can be attributed to this change in geometry. Cyclic voltammetric profiles for representative *ortho*- and *para*-substituted complexes in dmf are shown in Fig. 2. A similar behaviour has also been observed for the corresponding dicopper(II) complexes (29). Another significant observation is that for all the complexes, the second electron transfer, $Ni^{II}Cu^{I}$–$Ni^{I}Cu^{I}$, occurs in the narrow potential range −1.31 to −1.34 V, unlike the E_1 values. This is due to the similarity of the nickel–ligand environment in all the complexes. Although the general features are unchanged, the E_1 and E_2 values in MeCN are shifted by ca. 70–80 mV towards more negative values, compared to the corresponding values in DMF, possibly due to variation in solvent interaction with the central metal ions.

Comparison of the nickel-centred redox potentials in NiZnL complexes with those of CuNiL and NiCuL complexes reveals a shift of the potential to less negative values for NiZnL complexes. This arises from the difference in the charge of the reduced species, since for CuNiL and NiCuL complexes, the reduction at the nickel centre occurs after the first electron-transfer at the copper centre, i.e., reduction occurs from $Cu^{+}NiL$ and $NiCu^{+}L$ species, respectively.

Conclusion

In conclusion, it can be pointed out that the magnetic moments of the CuNiL and NiCuL series of complexes indicate weak antiferromagnetic coupling between the metal centres. The copper-centred reduction (E_1) occurs at −0.45 V for CuNiL and −0.38 V for NiCuL complexes. These E_1 values are in between the E_1 values observed for the strongly coupled dicopper system ($E_1 \sim 0.05$ V) and the noninteracting copper centres ($E_1 \sim -0.54$ V). In NiCuL complexes, ligands with donor groups such as OMe, OEt, and SMe influence the E_1 values. Magnetic and cyclic voltammetric results of our complexes show that weak magnetic interaction can exist even in heterodinuclear complexes analogous to the homodinuclear systems.

Acknowledgement

Financial assistance from University Grants Commission, New Delhi, is gratefully acknowledged by one of us (B.S.).

1. Y. Journaux, O. Kahn, J, Zarembowitch, J. Galy, and J. Jaudi. J. Am. Chem. Soc. **105**, 7585 (1983).
2. S. L. Lambert, C. L. Spiro, R. R. Gagne, and D. N. Hendrickson. Inorg. Chem. **21**, 68 (1982).
3. T. N. Sorrel, C. J. O'Connor, O. P. Anderson, and J. H. Reibenspies. J. Am. Chem. Soc. **107**, 4199 (1985).
4. K. D. Karlin and Y. Gultneh. J. Chem. Educ. **62**, 983 (1985).
5. L. Calabrese, D. Cocco, and A. Desideri. FEBS Lett. **106**, 142 (1979).
6. E. I. Solomon. *In* Binuclear copper active site. Copper proteins. *Edited by* T. G. Spiro. Wiley Interscience, New York. 1981. Chap. 2.
7. D. J. Spira, M. E. Winkler, and E. I. Solomon. Biochem. Biophys. Res. Commun. **107**, 721 (1982).

8. C. D. Lubien, M. E. Winkler, T. J. Thamann, R. A. Scott, M. S. Co, K. O. Hodgson, and E. I. Solomon. J. Am. Chem. Soc. **103**, 7014 (1981).
9. M. E. Winkler, D. J. K. Spira, C. D. Lubien, T. J. Thamann, and E. I. Solomon. Biochem. Biophys. Res. Commun. **107**, 727 (1982).
10. S. L. Lambert and D. N. Hendrickson. Inorg. Chem. **18**, 2683 (1979).
11. A. W. Addison. Inorg. Nucl. Chem. Lett. **12**, 899 (1976).
12. R. R. Gagne, R. P. Kreh, and J. A. Dodge. J. Am. Chem. Soc. **101**, 6917 (1979).
13. R. R. Gagne, C. L. Spiro, T. J. Smith, C. A. Hamann, W. R. Thies, and A. K. Shiemke. J. Am. Chem. Soc. **103**, 4073 (1981).
14. R. C. Long and D. N. Hendrickson. J. Am. Chem. Soc. **105**, 1513 (1983).
15. S. K. Mandal and K. Nag. Inorg. Chem. **22**, 2567 (1983).
16. R. S. Drago, M. J. Desmond, B. B. Corden, and K. A. Miller. J. Am. Chem. Soc. **105**, 2287 (1983).
17. W. Mazurek, A. M. Bond, K. S. Murray, M. J. O'Connor, and A. G. Wedd. Inorg. Chem. **24**, 2484 (1985).
18. S. K. Mandal, B. Adhikary, and K. Nag. J. Chem. Soc. Dalton Trans. 1175 (1986).
19. S. K. Mandal, L. K. Thompson, K. Nag, J. P. Charland, and E. J. Gabe. Inorg. Chem. **26**, 1391 (1987).
20. R. R. Gagne, C. A. Koval, and T. J. Smith. J. Am. Chem. Soc. **99**, 8367 (1977).
21. R. R. Gagne, C. L. Spiro, T. J. Smith, C. A. Hamann, W. R. Thies, and A. K. Shiemke. J. Am. Chem. Soc. **103**, 4073 (1981).
22. S. L. Lambert, C. L. Spiro, R. R. Gagne, and D. N. Hendrickson. Inorg. Chem. **21**, 68 (1982).
23. A. Earnshaw. Introduction to magnetochemistry. Academic Press, London. 1968. pp. 9–12.
24. H. O. House, E. Feng, and N. Peet. J. Org. Chem. **36**, 2371 (1971).
25. N. H. Pilkington and R. Robson. Aust. J. Chem. **23**, 2225 (1970).
26. R. Murassi, I. Bertini, and L. Sacconi. Coord. Chem. Rev. **11**, 343 (1973).
27. B. Adhikary, A. K. Biswas, K. Nag, P. Zanello, and A. Cinquantini. Polyhedron, **6**, 897 (1987).
28. B. Adhikary, S. K. Mandal, and K. Nag. J. Chem. Soc. Dalton Trans. 935 (1988).
29. B. Srinivas and P. S. Zacharias. Polyhedron. In press.

Can. J. Chem. Downloaded from www.nrcresearchpress.com by 88.255.202.194 on 09/08/12
For personal use only.

Complexation of 7-azaindole by the methylmercury(II) cation

NATHALIE DUFOUR, ANNE-MARIE LEBUIS, MARIE-CLAUDE CORBEIL, AND ANDRÉ L. BEAUCHAMP[1]
Département de chimie, Université de Montréal, C.P. 6128 Succ. A, Montréal (Qué.), Canada H3C 3J7

AND

PASCAL DUFOUR, YVES DARTIGUENAVE, AND MICHÈLE DARTIGUENAVE
Laboratoire de chimie inorganique, Université P. Sabatier, 118 route de Narbonne, 31062 Toulouse, France

Received May 28, 1992

NATHALIE DUFOUR, ANNE-MARIE LEBUIS, MARIE-CLAUDE CORBEIL, ANDRÉ L. BEAUCHAMP, PASCAL DUFOUR, YVES DARTIGUENAVE, and MICHÈLE DARTIGUENAVE. Can. J. Chem. **70**, 2914 (1992).

Complexes of the types $[CH_3Hg(aza)]$, $[CH_3Hg(Haza)]X$, and $[(CH_3Hg)_2(aza)]X$ are obtained by reacting CH_3HgOH and/or CH_3HgX (X = NO_3, ClO_4) with 7-azaindole (Haza). The weakly acidic N1-H proton on the pyrrole ring is displaced by the hydroxide, whereas the perchlorate and nitrate salts lead to CH_3Hg^+ coordination to the N7 lone pair on the pyridine ring. Detailed analysis of the infrared spectra of the complexes and their *N*-deuterated derivatives provides diagnostic regions for eventual prediction of the coordination mode in other systems. All compounds are characterized by means of ^1H, ^{13}C, and ^{199}Hg NMR spectra in DMSO solution and solid-state CP-MAS ^{13}C spectra. Comparison of the solution and solid-state ^{13}C spectra show that the species present in the solids remain undissociated in DMSO. Each type of complex can be identified from a characteristic pattern of large displacements of the ligand ^{13}C signals. The ^1H spectra are less informative because substitution of the N1-H proton by CH_3Hg^+ induces only minor shifts. Metal solvation appears to have a major influence on the ^{13}C and ^{199}Hg chemical shifts of the CH_3Hg^+ groups.

NATHALIE DUFOUR, ANNE-MARIE LEBUIS, MARIE-CLAUDE CORBEIL, ANDRÉ L. BEAUCHAMP, PASCAL DUFOUR, YVES DARTIGUENAVE et MICHÈLE DARTIGUENAVE. Can. J. Chem. **70**, 2914 (1992).

Les complexes $[CH_3Hg(aza)]$, $[CH_3Hg(Haza)]X$ et $[(CH_3Hg)_2(aza)]X$ sont obtenus par réaction de CH_3HgOH et/ou CH_3HgX (X = NO_3, ClO_4) avec le 7-azaindole (Haza). L'hydroxyde déplace le proton peu acide N1-H du cycle pyrrolique, alors que le perchlorate et le nitrate conduisent à une coordination de CH_3Hg^+ au doublet libre de l'atome N7 du cycle pyridinique. L'analyse détaillée des spectres infrarouges des complexes et de leurs dérivés N-deutérés permet d'identifier les régions caractéristiques du mode de coordination, résultat qui pourra être étendu à d'autres systèmes. Tous les composés sont caractérisés au moyen des spectres RMN ^1H, ^{13}C et ^{199}Hg en solution dans le DMSO et RMN ^{13}C CP-MAS à l'état solide. La comparaison des spectres ^{13}C des solutions et des solides montre que les espèces présentes dans les solides demeurent intactes dans le DMSO. Chaque type de complexe peut être identifié d'après un ensemble caractéristique de déplacements importants des signaux ^{13}C du ligand. Les spectres ^1H sont moins révélateurs, parce que la substitution du proton N1-H par CH_3Hg^+ ne produit que de faibles déplacements. La solvatation autour du métal semble exercer une grande influence sur les déplacements chimiques ^{13}C et ^{199}Hg des groupes CH_3Hg^+.

Introduction

Our interest has been attracted by the ability of multidentate nitrogen donors in rigid ligands like purines (**I**) to stabilize dinuclear metal–metal bonded systems. Since 7-azaindole[2] (**II**) consists of fused six- and five-membered rings with a pair of nitrogen atoms having the same arrangement as N3 and N9 in purines, the reactions with this simple model ligand were examined in the first place.

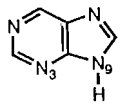

I

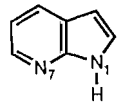

II

We previously reported (1) the crystal structures of a substitution product of dimolybdenum tetraacetate in which two carboxylates have been replaced by deprotonated azaindole units bridging the molybdenum atoms. The related $Mo_2Cl_2(aza)_2(PEt_3)_2$ complex has also been studied by Cotton and coworkers (2). Compounds of the type $M_2(aza)_4$ have been prepared for M = Ni(II) and Cu(II) by Brookes and Martin (3, 4), who proposed in both cases the presence of discrete dimeric units of the "copper acetate" or "paddle-wheel" type. This structure was confirmed for copper and nickel by Peng and co-workers (5), who also examined azaindole-containing clusters of copper and cobalt. The structure of a similar dinuclear chromium(II) compound has been recently reported (6). On the other hand, azaindole can act in a unidentate manner, for instance as axial ligand in dirhodium tetracarboxylates (7, 8). The crystal structure of a monodentate zinc complex has also been described by Sheldrick (9).

In the crystal structures containing bridging deprotonated azaindole, ligand disorder is almost always found to occur, because the two rings, although not identical, are sufficiently similar to lead to a random distribution of ligand direction in the crystal. Probably for this reason, getting crystals of dinuclear compounds suitable for X-ray work is difficult. Thus, reliable spectroscopic diagnostics are needed to establish the binding mode of this ligand.

Our previous work on nucleobases (10, 11) has revealed that the CH_3Hg^+ cation is a useful probe to evaluate the relative coordinating ability of the various sites in multidentate ligands. The three anticipated types of methylmercury complexes of azaindole were prepared and used to "calibrate" the NMR and vibrational spectroscopic results. The crystal structures of two of these complexes have been reported in a previous paper (12).

Experimental

Preparations

CH_3HgOH was obtained from Alfa as 1 M aqueous solution. 7-Azaindole was used as received from Aldrich. All other

[1]Author to whom correspondence may be addressed.
[2]1*H*-Pyrrolo[2,3-*b*]pyridine.

Can. J. Chem. Downloaded from www.nrcresearchpress.com by 88.255.202.194 on 09/08/12
For personal use only.

Can. J. Chem. Downloaded from www.nrcresearchpress.com by 88.255.202.194 on 09/08/12
For personal use only.

chemicals were reagent grade. C, H, N analyses were done by Schwazkopf Laboratories, New York.

[$CH_3Hg(aza)$], 1

CH_3HgOH (1.0 mL, 1.0 mmol) was added at room temperature to a solution of 118 mg (1.0 mmol) of azaindole in 13 mL methanol. After slow evaporation at room temperature to 2–3 mL in a well ventilated hood, a colourless precipitate appeared, which was filtered, quickly washed with methanol, and dried *in vacuo* at room temperature. Yield: 237 mg (71%). Anal. calcd. for $C_8H_8HgN_2$: C 28.88, H 2.42, N 8.42; found: C 29.07, H 2.57, N 8.28.

*[$CH_3Hg(Haza)$]NO_3, 2*a

CH_3HgOH (1.0 mL, 1.0 mmol) was added to a solution containing 118 mg (1.0 mmol) of azaindole in 13 mL methanol and 1.0 mL 1 M (1 mmol) aqueous HNO_3. Volume was reduced to 2–3 mL by slow evaporation at room temperature and the white solid was treated as above. Yield: 363 mg (92%). Anal. calcd. for $C_8H_9HgN_3O_3$: C 24.28, H 2.29, N 3.00; found: C 24.42, H 2.11, N 2.88.

*[$CH_3Hg(Haza)$]ClO_4, 2*b

Same procedure as for **2***a*, $HClO_4$ was used instead of HNO_3. Yield: 386 mg (89%). Anal. calcd. for $C_8H_9ClHgN_2O_4$: C 22.18, H 2.09, N 6.46; found: C 22.29, H 2.01, N 6.42.

*[$(CH_3Hg)_2(aza)$]NO_3, 3*a

CH_3HgOH (2.0 mL, 2.0 mmol) was added to a solution of 118 mg (1.0 mmol) of azaindole in 13 mL methanol and 1 mL 1 M (1.0 mmol) aqueous HNO_3. Volume was reduced to 2–3 mL by slow evaporation at room temperature. The white solid was isolated as above. Yield: 485 mg (79%). Anal. calcd. for $C_9H_{11}Hg_2N_3O_3$: C 17.71, H 1.82, N 6.88; found: C 17.98, H 1.77, N 6.81.

*[$(CH_3Hg)_2(aza)$]ClO_4, 3*b

Same procedure as for **3***a*, except that $HClO_4$ was used instead of HNO_3. Yield: 568 mg (87%). Anal. calcd. for $C_9H_{11}ClHg_2N_2O_4$: C 16.69, H 1.71, N 4.32, Cl 5.47; found: C 16.65, H 1.77, N 4.26, Cl 5.40. The unit cell parameters of this compound were determined with a CAD-4 diffractometer, following the standard procedure used for single crystals (12): monoclinic, space group *Cc* or *C2/c*, a = 19.292(7), b = 10.840(5), c = 14.002(7) Å, β = 114.78(4)°, Z = 8, D_{calcd} = 3.25 g cm^{-3}.

Instruments

The solution NMR spectra were recorded at ambient probe temperature using DMSO-d_6 (Silanor, from Merck, Sharp & Dohme Canada) as solvent. The ^1H spectra were recorded at 90 MHz with a Bruker WH-90 spectrometer, and the ^{13}C spectra at 20.17 MHz with a Bruker WP-80 instrument. Me_4Si (δ = 0) was used as internal standard in both cases. The ^1H–^{13}C heteronuclear shift-correlation experiment was done on a Varian VXR spectrometer (^1H frequency = 300 MHz, ^{13}C frequency = 75.43 MHz, spectral width = 4825 Hz, Mixing time = 1 s). The ^{199}Hg spectra were obtained at 72.57 MHz with the Bruker WH-400 instrument of the Laboratoire Régional de Résonance Magnétique Nucléaire, located at the Université de Montréal. The chemical shifts were referenced to an external 1.0 M CH_3HgCl solution in DMSO (δ = −848 ppm) (13).

The solid-state CP-MAS ^{13}C NMR spectra were recorded at ambient probe temperature on a Varian VXR instrument (^{13}C frequency = 75.43 MHz), using external hexamethylbenzene as reference (δ = 132.1 ppm). Relaxation delays were 80 s for Haza, 20 s for [CH_3Hg(aza)], 12 s for [CH_3Hg(Haza)]NO_3, and 40 s for [$(CH_3Hg)_2$(aza)]ClO_4. Spectra were recorded using a sideband suppression routine. Spinning rates were typically ~4 kHz.

The infrared spectra (4000–400 cm^{-1}) were recorded as KBr pellets with a Perkin–Elmer 783 spectrophotometer.

Results and discussion

The reactions are carried out in methanol, in which CH_3HgOH and the acid (HNO_3 or $HClO_4$) are introduced as 1 M aqueous solutions. Under the mild conditions used, no substitution occurs on azaindole carbon atoms and three types of *N*-bonded complexes are isolated.

The neutral [CH_3Hg(aza)] complex (**1**) is prepared by using CH_3HgOH as the metal reactant, whereby the weakly

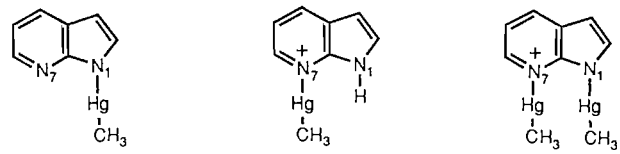

acidic proton of azaindole is neutralized and replaced by the metal on the five-membered ring, as indicated by X-ray work (12). This same compound has been reported by Kline and co-workers (14). On the other hand, if CH_3HgNO_3 or CH_3HgClO_4 (from the hydroxide + HNO_3 or $HClO_4$) is used in the reaction, the proton is not removed and a [CH_3Hg(Haza)]$^+$ salt (**2**) is obtained. In this case, the crystallographic results (12) show that the proton remains on the five-membered ring, whereas the CH_3Hg^+ group is bound to the lone pair of the pyridine nitrogen. Finally, if the reaction is conducted with one mole of each CH_3HgOH and CH_3HgNO_3 (or CH_3HgClO_4) per mole of azaindole, salts of the [$(CH_3Hg)_2$(aza)]$^+$ complex (**3**) are isolated, in which both nitrogens bear a metal atom.

Infrared spectroscopy

To obtain fingerprints for these three complexation patterns in the solid state, infrared spectra (4000–400 cm^{-1}) were recorded. The wavenumbers are listed in Table S-1 (supplementary material)[3] and compared with those of azaindole. The N1—D deuterated compounds are also included for the free ligand and the [CH_3Hg(Haza)]X complexes. The tentative assignments used are those proposed previously (1) by comparison with earlier work on indole by Lautié and co-workers (15) and Takeuchi and Harada (16).

Since complexation is accompanied by deprotonation or changes in hydrogen bonding, the vibrations involving the N—H bond were first identified by means of *N*-deuteration. Azaindole gives rise to a broad ν(N—H) absorption at ~2900 cm^{-1}, displaced to ~2300 cm^{-1} in the N1—D derivative. The δ(N1—H) vibration is expected at ~1150 cm^{-1}. The 1230–1100 cm^{-1} region includes four bands (1205, 1193, 1121, and 1103 cm^{-1}), one of which, probably at 1193 cm^{-1}, should correspond mainly to δ(N—H) motion. Only three bands (1220, 1174, and 1115 cm^{-1}) are left in the deuterated derivative, and the relatively large effect of deuteration suggests that appreciable coupling with N—H motion is present for all these modes in non-deuterated azaindole. Also, the new band at 1392 cm^{-1} in the deuterated compound is probably one of the ring modes at 1400–1450 cm^{-1} shifted to lower wavenumber by loss of N—H coupling. The δ(N—D) band is found at 850 cm^{-1}. The out-of-plane γ(N—H) vibration gives rise to the broad feature around 850 cm^{-1} for azaindole. The γ(N—D) vibration could correspond to the very broad absorption underlying other li-

[3]Table of infrared data for azaindole, the CH_3Hg^+ complexes, and N—D deuterated derivatives (four pages) may be purchased from: The Depository of Unpublished Data, Document Delivery, CISTI, National Research Council Canada, Ottawa, Canada K1A 0S2.

Can. J. Chem. Downloaded from www.nrcresearchpress.com by 88.255.202.194 on 09/08/12
For personal use only.

gand bands between 550 and 600 cm^{-1}, or to the very weak feature at 535 cm^{-1}.

In the spectra of the complexes, the CH_3Hg^+ groups produce the usual distinctive features: sharp ν(C—H) bands at 2930 cm^{-1}, strong $\delta(CH_3)$ bands at ~1195 cm^{-1}, and broader $\rho(CH_3)$ absorptions near 790 cm^{-1}. The weak ν(Hg—C) vibrations normally occur at 555 cm^{-1}, but ligand bands interfere in this region.

For the charged complexes, nitrate and perchlorate salts were studied to reveal all the ligand and CH_3Hg^+ bands, some of which are masked by the anion. The nitrate bands occur where they are expected (17): strong and broad ν_3 absorption at 1370 cm^{-1} and weaker doublet for ν_2 at ~820 cm^{-1}. Low site symmetry probably imparts some intensity to the normally IR-inactive ν_1 mode that seems to appear weakly at ~1050 cm^{-1}. For the perchlorate, the very strong ν_3 band is found at ~1080 cm^{-1}, as well as the weaker ν_4 vibration at 625 cm^{-1}. Weak features are also observed at 920 cm^{-1} for ν_1 and probably at 455 cm^{-1} for ν_2 in $[(CH_3Hg)_2(aza)]ClO_4$.

For the N1-protonated/N7-mercurated $[CH_3Hg(Haza)]X$ complexes, the most important perturbations in the ligand bands are probably due to changes in hydrogen bonding. The high-wavenumber region clearly shows that hydrogen bonding is much weaker in the perchlorate than in the nitrate: the ν(N1—H) mode produces a massif centred at ~3100 cm^{-1} (2300 cm^{-1} after deuteration) for the nitrate, but the absorption is sharper and at higher energy (3320 cm^{-1} N—H, 2480 cm^{-1} N—D) for the perchlorate. The γ(N—H) band is shifted to 880 cm^{-1}.

A few spectral changes can be used to distinguish between the free ligand and the complexes. The strong ligand band at 1422 cm^{-1} loses most of its intensity, whereas the barely visible 1450 cm^{-1} absorption is replaced by a sharp and strong band at 1441 cm^{-1}. In addition, the following significant shifts occur on ligand bands: 1498 (+12), 428 (+12), and 419 (+11) cm^{-1}.

Substitution of the N1—H proton leads to more spectacular changes for $[CH_3Hg(aza)]$ and the $[(CH_3Hg)_2(aza)]X$ salts. The high-frequency region is simplified by the disappearance of the broad ν(N—H) band. The weak γ(N—H) band at 850 cm^{-1} is also removed. No clear indication can be extracted from the δ(N—H) region, because the strong δ band of CH_3Hg^+ interferes. In the low-frequency region, where the spectra are particularly clear, the ring out-of-plane vibrations of azaindole at 428 and 419 cm^{-1} are shifted to 474 and 442 cm^{-1}, respectively. The 952/917/897 cm^{-1} set is displaced to 964/940/911 cm^{-1}. The strong 878 cm^{-1} band loses most of its intensity, whereas the equally strong 789 cm^{-1} band is displaced to 810 cm^{-1}. These characteristics common to $[CH_3Hg(aza)]$ and $[(CH_3Hg)_2(aza)]X$ can be regarded as good diagnostics for N1—H substitution.

The two kinds of *N*1-substituted compounds show a number of spectral differences (Table S-1). The in-plane azaindole ring mode at 1583 cm^{-1} is displaced to 1585 cm^{-1} in the 1:1 and to 1563 cm^{-1} in the 2:1 complexes. Also, the band at 1468 cm^{-1} for $[(CH_3Hg)_2(aza)]^+$ occurs 12 cm^{-1} higher for $[CH_3Hg(aza)]$. Between 1250 and 1350 cm^{-1}, the three bands occur at 1304 (vs), 1285 (s) and 1242 (vw) for the 1:1 compound, but at 1342 (s), 1272 (sh), and 1263 (s) cm^{-1} for the 2:1 complexes. Various other differences are found at lower wavenumbers, namely at 630 cm^{-1}, where the 2:1 nitrate compound is displaced −20 cm^{-1} with respect to the 1:1 complex.

These diagnostic regions in the infrared spectra can be used to identify the type of coordination taking place on 7-azaindole.

Solution NMR spectroscopy

^1H, ^{13}C, and ^{199}Hg NMR spectra were obtained with DMSO solution. The data are collected in Tables 1–3.

The ^1H and ^{13}C spectra of 7-azaindole were assigned by Cox and Sankar from data in $CDCl_3$ (18). Their assignments can be applied directly to our results, since the chemical shifts and coupling constants are not greatly affected by the change of solvent. An extra broad signal is observed at 11.6 ppm for the N1—H proton. The mutually coupled (^3J = 3.3 Hz) resonances of H2 (7.49 ppm) and H3 (6.45 ppm) show further coupling with this proton (^3J(H1—H2) = 1.5, ^4J(H1—H3) = 2.6 Hz). These features due to the N1—H proton, also observed in DMF (1), have not been mentioned for $CDCl_3$ solution (18).

For the complexes, the ^1H signals can be safely identified by comparison with the ligand chemical shifts and coupling constants. The three protons of the six-membered ring are mutually coupled and H5 is readily recognized as a doublet of doublets with ^3J couplings of ~7.7 Hz with H4 and ~5 Hz with H6. The difference in coupling constants makes it possible to identify H4 and H6. This is particularly useful for the N7-mercurated complexes, where the H4 and H6 signals are close together. In the five-membered ring, the H3 resonance always occurs ~1 ppm upfield from H2. For the $[CH_3Hg(Haza)]X$ salts, they both consist of doublets of doublets similar to those of the free ligand. For $[CH_3Hg(aza)]$ and the $[(CH_3Hg)_2(aza)]X$ compounds, substitution of the N1—H proton removes the broad low-field signal at 11.6 ppm, whereas H2 and H3 appear as simple doublets, due to loss of coupling with H1. In the ^{13}C spectra, the quaternary carbons C8 and C9 give low-intensity signals sufficiently separated as not to be confused. The remaining resonances can usually be identified by comparison with the free ligand. The ^1H and ^{13}C spectra also include high-field signals for the CH_3Hg^+ groups.

Coordination of CH_3Hg^+ to the N7 lone pair is expected to render the N1—H proton more acidic. This is reflected by the shift of the corresponding signal to 12.6 ppm for the $[CH_3Hg(Haza)]^+$ ions (Table 1). The positive charge on this complex displaces all azaindole resonances downfield. The largest shifts are found for H4 (+0.47 ppm) and H5 (+0.40 ppm), whereas the resonance of H6, adjacent to the coordination site, is displaced by only +0.28 ppm. Thus, the H2 and H3 protons on the other ring, both shifted by +0.25 ppm, are almost as sensitive as H6 to N7-coordination. A similar pattern of shifts is noted when azaindole is

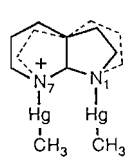

IV

7-methylated (**III**),[4] but the $\Delta\delta$ values are ~40% greater (18). Another similarity with the 7-methyl derivative is the ~1 Hz

[4]7-Methyl-1*H*-pyrrolo[2,3-*b*]pyridinium.

TABLE 1. ^{1}H NMR data for 7-azaindole and the methylmercury complexes[a]

Compound	^{1}H NMR					
	H1	H2	H3	H4	H5	H6
Haza	11.65	7.49 (3.3; 1.5)	6.45 (3.3; 2.6)	7.95 (7.7; 1.5)	7.05 (4.4; 7.7)	8.22 (4.4; 1.5)
$[CH_3(Haza)]^{+b}$		7.83 (3.5) [0.34]	6.87 (3.5) [0.42]	8.56 (7.7) [0.61]	7.52 (6.5; 7.7) [0.47]	8.61 (6.5) [0.39]
$[CH_3Hg(aza)]$		7.49 (2.9) [+0.00]	6.37 (2.9) [−0.08]	7.91 (7.7; ~1) [−0.04]	6.91 (4.7; 7.7) [−0.14]	8.10 (4.6; ~1) [−0.12]
$[CH_3Hg(Haza)]^{+c}$	12.65	7.74 (3.3; ~2) [+0.25]	6.70 (3.3; 1.8) [+0.25]	8.42 (7.7; ~1.5) [+0.47]	7.45 (5.5; 7.7) [+0.40]	8.50 (5.5; ~1.5) [+0.28]
$[(CH_3Hg)_2(aza)]^{+c}$		7.75 (2.9) [+0.26]	6.65 (2.9) [+0.20]	8.41 (7.7; ~1.5) [+0.46]	7.33 (5.5; 7.3) [+0.28]	8.44 (5.5; ~1.5) [+0.22]

[a]In ppm vs. $(CH_3)_4Si$, in DMSO-d_6. Coupling constants, in Hz, in parentheses. Displacement with respect to free azaindole within square brackets.
[b]7-Methylazaindolium cation, iodide salt; H1–H2, H1–H3, and H4–H6 couplings not found (18).
[c]Values averaged from the spectra of nitrate and perchlorate salts. Individual chemical shifts are within 0.02 ppm.

TABLE 2. ^{13}C NMR chemical shifts for 7-azaindole and the methylmercury(II) complexes[a]

Compound	^{13}C NMR						
	C2	C3	C4	C5	C6	C8[d]	C9[d]
HAza	126.1	99.9	128.2	115.5	142.6	148.6	119.7
$[CH_3(Haza)]^{+b}$	129.6 (+3.5)	103.4 (+3.5)	136.8 (+8.6)	115.9 (+0.4)	137.3 (−5.3)	139.4 (−9.2)	125.8 (+6.1)
$[CH_3Hg(aza)]$	135.7 (+9.6)	99.4 (−0.5)	127.2 (−1.0)	114.3 (−1.2)	140.8 (−1.8)	154.7 (+6.1)	121.0 (+1.3)
$[CH_3Hg(Haza)]^{+c}$	128.1 (+2.0)	101.8 (+1.9)	133.5 (+5.3)	116.0 (+0.5)	141.6 (−1.0)	145.0 (−3.6)	123.8 (+4.1)
$[(CH_3Hg)_2(aza)]^{+c}$	138.2 (+12.1)	101.3 (+1.4)	132.6 (+4.4)	114.3 (−1.2)	140.4 (−2.2)	149.9 (+1.3)	126.5 (+6.8)

[a]In ppm vs. $(CH_3)_4Si$, in DMSO-d_6. Displacement with respect to free azaindole within parentheses.
[b]7-Methylazaindolium cation, iodide salt (18).
[c]Mean values obtained with the nitrate and perchlorate salts. Individual chemical shifts are within 0.2 ppm.
[d]C8 and C9 interchanged in labelling scheme used by Cox and Sankar (18).

TABLE 3. NMR data for the CH_3Hg^+ groups[a]

Compound	NMR data					
	^{1}H[b]		^{13}C		^{199}Hg	
	N1	N7	N1	N7	N1	N7
$[CH_3Hg(aza)]$	0.79 (192)		1.5		−732	
$[CH_3Hg(Haza)]^{+c}$		0.97 (234)		1.9		−902
$[(CH_3Hg)_2(aza)]^{+c}$	0.85 (199)	0.94 (222)	2.3[d]	2.9[d]	−639	−761

[a]In ppm vs. $(CH_3)_4Si$ (^{1}H and ^{13}C), vs. $(CH_3)_2Hg$ (^{199}Hg); DMSO-d_6 solutions.
[b]Within parentheses, $^2J(^{199}Hg{-}{-}^1H)$ coupling constants in Hz.
[c]Mean value for NO_3^- and ClO_4^- salts.
[d]These assignments could be interchanged.

Can. J. Chem. Downloaded from www.nrcresearchpress.com by 88.255.202.194 on 09/08/12
For personal use only.

Can. J. Chem. Downloaded from www.nrcresearchpress.com by 88.255.202.194 on 09/08/12
For personal use only.

increase of the ^3J(H5—H6) coupling constant. In the ^{13}C spectra, CH_3Hg^+ coordination induces a pattern of shifts similar to methylation, but much smaller (Table 2). For instance, the adjacent carbons undergo shifts of −1.0 ppm (C6) and −3.6 ppm (C8) upon N7-mercuration, whereas the shifts are −5.3 and −9.2 ppm, respectively, for 7-methylation. The greatest displacements for this type of complex are found for C4 (+5.3 ppm) and C9 (+4.1 ppm).

Substitution of the N1—H proton in [CH_3Hg(aza)] removes the low-field ^1H resonance for this atom, but introduces only small shifts on the other signals. Surprisingly, the H2 proton, next to the substitution site, has not moved (7.49 ppm), even though an appreciable shift of −0.21 ppm has been noted for this complex in $CDCl_3$ (14). The largest shifts in DMSO are found for the protons most remote from the substitution site, that is, H5 (−0.14 ppm) and H6 (−0.12 ppm). The ^{13}C assignments given in Table 2 are based on a 2D ^1H–^{13}C experiment. Large downfield shifts are noted for the adjacent atoms C8 (+6.1 ppm) and C2 (+9.6 ppm).

Combined N1—H substitution and N7-coordination in the [$(CH_3Hg)_2$(aza)]X salts lead to roughly additive effects for both the ^1H and ^{13}C spectra. Large ^{13}C upfield shifts with respect to azaindole are observed for C2 (+12.1 ppm), C9 (+6.8 ppm), and C4 (+4.4 ppm). In the ^1H spectra, the chemical shifts are relatively close to those of [CH_3Hg-(Haza)]$^+$. This is normal, since N7-complexation introduces much larger shifts than N1—H substitution. As expected for [$(CH_3Hg)_2$(aza)]$^+$, the low-field N1—H signal is absent and simple doublets are found for H2 and H3.

The resonances of the CH_3Hg^+ groups are collected in Table 3. The two non-equivalent groups in [$(CH_3Hg)_2$(aza)]$^+$ produce two well-resolved signals in the ^1H, ^{13}C, and ^{199}Hg spectra, indicating slow exchange of the two types of groups.

The ^1H signal of [CH_3Hg(aza)] (0.79 ppm) occurs in the 0.7–0.8 ppm range found for complexes with monoanionic imidazoles (19) and purines (10, 11, 20, 21) in DMSO. Solvent effect is appreciable, since the signal is displaced to 0.93 ppm in $CDCl_3$ (14). Coordination to the less basic pyridine-type nitrogen results in a downfield shift to 0.97 ppm for the [CH_3Hg(Haza)]$^+$ compounds. For [$(CH_3Hg)_2$(aza)]$^+$, the two resonances get closer together than those of the above 1:1 compounds. The same behaviour is shown by the $^2J(^{199}Hg—^1H)$ coupling constants, which are generally regarded as good probes for the nucleophilic character of the mercuration site. Various workers (10, 19, 22–24) proposed linear equations relating this ^2J constant with either the log of the complex formation constant or the pK_a of the corresponding protonated ligand. The relationship $^2J = 248.5 - 3.88$ pK_a, based on complexes with heterocyclic nitrogen ligands in DMSO solutions (19), seems to be the most appropriate for the present system. When applied to the [CH_3Hg(Haza)]$^+$ species (^2J = 234 Hz), the predicted pK_a values for the N7-protonated $(H_2aza)^+$ ion is ~4, which is reasonably close to the value of 4.6 reported earlier (25), considering the anticipated reliability of such a crude relationship. Using this same equation with the 192 Hz constant for [CH_3Hg(aza)], a pK_a of ~15 is predicted for the N1—H proton of neutral azaindole, an acceptable value since the electro-attracting N7 atom should make the N1—H proton more acidic than in indole (pK_a ~17) (26). In the [$(CH_3Hg)_2$(aza)]$^+$ ion, the coupling constants, like the chemical shifts, have moved together. With a ^2J constant of 199 Hz, N1 behaves as though its pK_a had decreased by ~2 units, whereas that of N7 (222 Hz) had increased by ~3 units. Thus, electron density transferred from the five- to the six-membered ring has diminished the basicity difference between the two sites. However, this effect alone cannot account for the ^{13}C and ^{199}Hg results.

From data on a series of purine complexes, it was concluded (27) that the ^{13}C chemical shift of CH_3Hg^+ decreases as the $^2J(^{199}Hg—^1H)$ constant increases. Combining this with the above ^2J vs. pK_a relationship, it is predicted that $\delta(^{13}C)$ should *increase* with pK_a. Therefore, the ^{13}C data in Table 3 for [CH_3Hg(aza)] (1.5 ppm, pK_a ~15) and [CH_3Hg(Haza)]$^+$ (1.9 ppm, pK_a 4.6) are not in the expected order. In addition, the two signals of [$(CH_3Hg)_2$(aza)]$^+$ are displaced downfield by ~1 ppm compared with the corresponding 1:1 compounds, instead of moving together as observed for the ^1H resonances. Similarly, the ^{199}Hg chemical shifts cannot be rationalized solely from considerations on donor basicity. In this case, the 1:1 complexes occur in the order expected from earlier studies on purines and imidazoles (28): [CH_3Hg(Haza)]$^+$ (−902 ppm) is observed at higher field than [CH_3Hg(aza)] (−732 ppm). For [$(CH_3Hg)_2$(aza)]$^+$, the two signals are closer together than those of the 1:1 compounds, but the predominant effect is the very large downfield shift of both resonances.

The [$(CH_3Hg)_2$(aza)]$^+$ cation undoubtedly adopts structure **3**, similar to those of various adenine complexes (29, 30), with two roughly parallel CH_3Hg^+ groups lying in the molecular plane. The obvious peculiarity of this structure is the presence of two Hg atoms lying close together. The $^4J(^{199}Hg—^{199}Hg)$ coupling, detected for a dinuclear compound with bridging bis(diphenylphosphino)methane (31), could give an idea of the extent of interaction between the metals, but our compound was not soluble enough to produce observable features for the small population (<3%) of $^{199}Hg/^{199}Hg$ isotopomer. Metal–metal bonding is ruled out, because the Hg–Hg separation, probably similar to those observed in the adenine complexes (~3.2 Å), should be greater than the sum of the van der Waals radii. Even at this distance, the electric field of one Hg atom could be felt by the other nucleus, but the magnitude of this effect on the ^{199}Hg chemical shifts is hard to predict. On the other hand, direct interaction is not required to explain the large downfield shifts observed, since solvent effect was invoked to rationalize anomalies in ^{199}Hg data for other systems, namely for [CH_3Hg(py)]$^+$ complexes examined by Canty and co-workers (32). The −1159 ppm[5] signal of the pyridine complex was found to be drastically shifted in the compounds with 2-methylpyridine (−1014 ppm) and 2,6-dimethylpyridine (−975 ppm), even though ligand basicity had not changed appreciably. This was ascribed to reduced solvation of Hg due to the steric effect of the *ortho* methyl groups, restricting access of the good donor solvent molecules to the "equatorial" region around mercury. Similarly, data on a series of $(CH_3)_2Hg$ solutions in various solvents showed that replacing coordinating solvents like DMSO or DMF by hydrocarbons produced ~100 ppm downfield shifts, also ascribed to desolvation (33). In the case of [$(CH_3Hg)_2$(aza)]$^+$, the presence of two adjacent CH_3Hg^+ groups in near van der Waals contact is anticipated to severely perturb solvation

[5]These results, referenced to CH_3HgNO_3, were converted to the convention used here (δ = 0 for $(CH_3)_2Hg$) by subtracting 1146 ppm (39).

TABLE 4. Solid-state CP/MAS ^{13}C NMR chemical shifts for azaindole and the methylmercury complexes[a]

Compound	^{13}C NMR Shifts							
	C2	C3	C4	C5	C6	C8	C9	CH_3Hg[b]
HAza	128.0	99.3 101.0	129.6	113.9 ~115.0	141.5	148.4	121.1	
	(+1.9)	(+0.2)	(+1.4)	(−1.5)	(−1.1)	(−0.2)	(+1.4)	
$[CH_3Hg(aza)]$	134.9 133.6	102.8 100.6 98.5	129.1 126.9 126.2	114.2	143.7 140.2	155.1 152.6	121.1	4.4 (1530) −1.4 (1350)
	(−1.5)	(−1.2)	(−0.2)	(+0.1)	(+1.1)	(−0.9)	(+0.1)	
$[CH_3Hg(HAza)]NO_3$	130.1 (+2.0)	105.3 (+3.5)	138.6 (+5.3)	116.8 (+0.8)	141.2 (−0.4)	145.3 (+0.3)	124.7 (+0.9)	4.3 (1650)
$[(CH_3Hg)_2(aza)]ClO_4$	136.8[c]	104.1	136.8[c]	116.3 115.3	141.4	150.1	128.9	7.1 4.9
	(−1.4)	(+2.8)	(+3.8)	(+1.5)	(+1.0)	(+0.2)	(+2.4)	

[a]In ppm, vs. $(CH_3)_4Si$; within parentheses, displacement with respect to DMSO solution.
[b]$^1J(^{199}Hg—^{13}C)$ coupling constant in Hz within parentheses, estimated error = 100 Hz.
[c]Not resolved.

around the metal, since each Hg atom blocks access of solvent molecules to one side of the other Hg atoms. This effect likely makes a significant contribution to the observed downfield shifts in $[(CH_3Hg)_2(aza)]^+$, compared with the 1:1 compounds where no similar steric hindrance to solvation is present. Although centred on the metal, this effect is probably transmitted to some extent to the carbon atom and could explain the small downfield shift of the ^{13}C resonances.

Solid-state NMR

The ^{13}C signals for the solid compounds (Table 4) have been interpreted by comparison with the solution spectra.

For free azaindole, the resonances are relatively broad, often dissymmetric, and splitting in two resolved components is visible for C3 and C5. These effects are not due to poor spectrum quality or artefacts of data acquisition. They result from the presence of eight symmetry-independent azaindole molecules in the crystal. X-ray work (12) has shown that the solid contains two crystallographically non-equivalent types of hydrogen-bonded tetramers, in which the azaindole molecules are in similar, but not identical, environments. Thus, each peak can be regarded as resulting from eight close, but not exactly coincident, components. The mild disorder observed in the crystal can also contribute to signal broadening. The mean chemical shifts for the solid differ by <2 ppm from those observed for DMSO solution.

Similarly, for $[CH_3Hg(aza)]$, the mean chemical shifts of the ring carbons deviate by <1.5 ppm from those found in DMSO, confirming that the same species is present in both phases. The signals are much sharper than those of the free ligand, but most of them are split in two or three resolved components (Table 4). This is consistent with the crystal structure reported earlier (12), since the unit cell contains three non-equivalent monomeric molecules with appreciable differences in intermolecular interactions.

The high-field region of $[CH_3Hg(aza)]$ includes two CH_3Hg^+ peaks at 4.4 and −1.4 ppm (Table 4) in a roughly 2:1 ratio. The strongest component is shifted downfield by 2.9 ppm with respect to the DMSO solution. $[CH_3Hg(Haza)]NO_3$ and $[(CH_3Hg)_2(aza)]ClO_4$ also exhibit downfield shifts of 2–4 ppm in the solid state. It is tempting to relate this trend to the desolvation effect mentioned above, since the metal in the solid is presumably not as efficiently surrounded by good donors as in DMSO. Weak equatorial Hg—O(nitrate) contacts of ~2.95 Å in $[CH_3Hg(Haza)]NO_3$ should play a role similar to solvation and shift the resonance back to high field, but this does not seem to balance efficiently the effect of desolvation, since the signals remain downfield in the solid. Similarly, in the case of $[CH_3Hg(aza)]$, where moderately strong Hg···N7 "semi-bonds" of ~2.85 Å with adjacent molecules are found for *two* of the three independent molecules, the stronger signal remains downfield. Therefore, such dipolar interactions cannot explain the presence of the high-field signal at −1.4 ppm. The unit cell was carefully examined for other differences that would single out one of the groups. Molecule A (Fig. 1) was found to differ from the other two not only by the lack of intermolecular Hg···N contacts within 3.3 Å, but also by the position of its CH_3Hg^+ carbon at ~3.4 Å, just above the six-membered ring of a molecule B, where the anisotropic effect of the aromatic system is expected to be maximized. This could displace the corresponding signal for A upfield from those of the other two molecules, which do not overlook an aromatic ring. A recent study on CH_3Hg^+ complexes with amino acids supports this assumption. The ^{13}C signal (in water) of the amino-coordinated CH_3Hg^+ group appears at −1.9 ppm for serine (34), but it is shifted upfield to −4.3 ppm in presence of the aromatic substituent in tryptophan (35). This was ascribed to the anisotropic effect of the aromatic system, since the conformation observed in the solid, with the CH_3Hg^+ group above the indole ring, was shown to be predominant in solution (36).

In cationic complexes, the solid-state and the DMSO solution spectra show greater differences for some of the ring signals. For instance, with $[CH_3Hg(Haza)]NO_3$, differences of +5.3, +3.5, and +2.0 ppm are found for C3, C4, and C2, respectively. At the moment, these various shifts cannot be individually interpreted in terms of detailed structural effects. However, the presence of the charged NO_3^- ion can

Can. J. Chem. Downloaded from www.nrcresearchpress.com by 88.255.202.194 on 09/08/12
For personal use only.

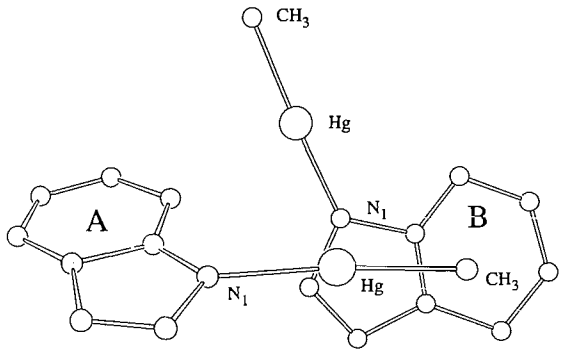

FIG. 1. Position of the CH_3Hg^+ group of molecule A above the azaindole ring of molecule B (in the plane of the figure) in the unit cell of [CH_3Hg(aza)]. The drawing is based on the X-ray work of ref. 12. Hydrogens are omitted for simplicity.

conceivably give rise, in the solid, to strong, localized, dipolar interactions that would not survive in solution.

The crystal structure of the $[(CH_3Hg)_2(aza)]ClO_4$ salt has not been determined, but the cation certainly adopts structure **3** similar to those found for adenine complexes (29, 30). This compound belongs to space group *C2/c* (assuming that it is centric, which is very likely). Thus the eight molecules in the unit cell should all be symmetry equivalent. Despite this fact, shoulders are found for almost all resonances, particularly for C5. This is probably due to crystal disorder, which is expected for this type of compound. Indeed, even though the two halves of the $[(CH_3Hg)_2(aza)]^+$ ion are different, the van der Waals envelope of this planar species is not greatly modified if it is rotated by 180° about the common C8—C9 bond (**IV**). As a result, the cation is probably randomly distributed over the two orientations in the crys-

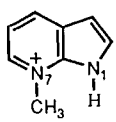

III

tal, as found whenever the two N atoms have similar environments, such as in neutral 7-azaindole (12), salts containing the azaindolium cation (37), and various complexes in which azaindole is bridging two metal atoms (1, 5, 38). Disorder in $[(CH_3Hg)_2(aza)]ClO_4$ would create non-uniform environments at the molecular level and introduce local non-equivalencies, which would explain the splitting shown by the solid-state spectrum.

Concluding remarks

The structures proposed for [CH_3Hg(aza)] and the [CH_3Hg(Haza)]X salts in the solid-state are based on X-ray diffraction work published earlier (12). As to the $[(CH_3Hg)_2$-(aza)]X salts, full X-ray diffraction was not deemed worthwhile, but structure **3** is very likely in view of the presence of the similar structure observed for related ligands. In our detailed analysis of the infrared spectra, the vibrations due to the anions and the CH_3Hg^+ groups were first identified. Patterns of spectral changes in the ligand bands were then proposed to provide characteristic diagnostics for each of the three types of coordination. While interpreting the ^1H spectra in DMSO, it was found that a large shift is not a reliable indication that coordination takes place at a nearby site, since the H5 and/or H4 signals are the most affected for all coordination patterns. Thus, the largest displacements observed upon N1—H substitution in the five-membered ring of [CH_3Hg(aza)] are found for protons of the other ring. Moreover, it is difficult to differentiate between $[(CH_3Hg)_2(aza)]^+$ and $[CH_3Hg(Haza)]^+$ from the ^1H spectra. The ^{13}C ligand signals are better suited to identify the binding mode, large displacement being noted on a specific set of carbons for each type of complex. On the other hand, the CH_3Hg^+ resonances seem to be very sensitive to metal solvation, so that relationships between donor basicity and ^{13}C or ^{199}Hg chemical shifts should be used with great care. The infrared and NMR diagnostics developed here are hoped to be useful to identify the coordination mode in non-crystalline materials for which X-ray diffraction information could not be obtained.

Acknowledgments

We wish to thank R. Mayer for assistance in recording solid-state NMR spectra, and the Natural Sciences and Engineering Research Council of Canada for financial support. A travel grant for P. Dufour provided by the Programme d'Échange Interuniversitaire Franco-québecois is also acknowledged.

1. F. Allaire and A. L. Beauchamp. Inorg. Chim. Acta, **156**, 241 (1989).
2. F. A. Cotton, D. G. Lay, and M. Millar. Inorg. Chem. **17**, 186 (1978).
3. R. W. Brookes and R. L. Martin. Aust. J. Chem. **27**, 1569 (1974).
4. R. W. Brookes and R. L. Martin. Inorg. Chem. **14**, 528 (1975).
5. S. M. Peng and Y. N. Lin. Acta Crystallogr. Sect. C: Cryst. Struct. Commun. **C42**, 1725 (1986); S. M. Peng and C. H. Lai. J. Chin. Chem. Soc. Taipei, **35**, 325 (1988).
6. J. J. H. Edema, S. Gambarotta, A. Meetsma, F. Van Bolhuis, A. L. Spek, and W. J. J. Smeets. Inorg. Chem. **29**, 2147 (1990).
7. F. A. Cotton and T. R. Felthouse. Inorg. Chem. **20**, 600 (1981).
8. F. Allaire and A. L. Beauchamp. To be published.
9. W. S. Sheldrick. Z. Naturforsch. **37B**, 653 (1982).
10. J. P. Charland, M. T. Phan Viet, M. St-Jacques, and A. L. Beauchamp. J. Am. Chem. Soc. **107**, 8202 (1985).
11. J. P. Charland and A. L. Beauchamp. Inorg. Chem. **25**, 4870 (1986).
12. P. Dufour, Y. Dartiguenave, M. Dartiguenave, N. Dufour, A.-M. Lebuis, F. Bélanger-Gariépy, and A. L. Beauchamp. Can. J. Chem. **68**, 193 (1990).
13. M. A. Sens, N. K. Wilson, P. D. Ellis, and J. D. Odom. J. Magn. Reson. **19**, 323 (1975).
14. R. J. Kline, L. F. Sytsma, and D. R. Shackle. Inorg. Nucl. Chem. Lett. **7**, 311 (1971).
15. A. Lautié, M. F. Lautié, A. Grucher, and S. A. Fakhri. Spectrochim. Acta, **36A**, 85 (1980).
16. H. Takeuchi and I. Harada. Spectrochim. Acta, **42A**, 1069 (1986).
17. K. Nakamoto. Infrared and Raman spectra of inorganic and coordination compounds. 4th ed. Wiley-Interscience, New York. 1986. pp. 124, 138.
18. R. H. Cox and S. Sankar. Org. Magn. Reson. **14**, 150 (1980).
19. A. R. Norris, E. Buncel, and S. E. Taylor. J. Inorg. Biochem. **16**, 279 (1982).
20. A. R. Norris, R. Kumar, E. Buncel, and A. L. Beauchamp. J. Inorg. Biochem. **21**, 277 (1984).

Can. J. Chem. Downloaded from www.nrcresearchpress.com by 88.255.202.194 on 09/08/12
For personal use only.

21. E. Buncel, B. K. Hunter, R. Kumar, and A. R. Norris. J. Inorg. Biochem. **20**, 171 (1984).
22. D. L. Rabenstein. Acc. Chem. Res. **11**, 100 (1978).
23. R. Sheffold. Helv. Chim. Acta, **52**, 56 (1969).
24. A. J. Canty and C. V. Lee. Inorg. Chim. Acta, **54**, L205 (1981). Organometallics, **1**, 1063 (1982).
25. J. V. Greenhill. Comprehensive heterocyclic chemistry. *Edited by* C. W. Bird and G. W. H. Cheeseman. Pergamon Press, Oxford. 1984. Chap. 3.09, p. 501; T. K. Adler and A. Albert. J. Chem. Soc. 1794 (1960).
26. E. P. Serjeant and B. Dempsey. Ionisation constants of organic acids in aqueous solution. Pergamon Press, Oxford. 1979. p. 367.
27. E. Buncel, A. R. Norris, W. J. Racz, and S. E. Taylor. Inorg. Chem. **20**, 98 (1981).
28. A. R. Norris and R. Kumar. Inorg. Chim. Acta, **93**, L63 (1984).
29. L. Grenier, J. P. Charland, and A. L. Beauchamp. Can. J. Chem. **66**, 1663 (1988).
30. J. P. Charland and A. L. Beauchamp. Inorg. Chem. **25**, 4870 (1986); J. Hubert and A. L. Beauchamp. Can. J. Chem. **58**, 1439 (1980); J. Hubert and A. L. Beauchamp. Acta Crystallogr. Sect. B: Struct. Crystallogr. Cryst. Chem. **B36**, 2613 (1980).
31. P. A. W. Dean and R. S. Srivastava. Can. J. Chem. **63**, 2829 (1985).
32. A. J. Canty, P. Barron, and P. C. Healy. J. Organomet. Chem. **179**, 447 (1979).
33. M. A. Sens, N. K. Wilson, P. D. Ellis, and J. D. Odom. J. Magn. Reson. **19**, 323 (1975).
34. M. C. Corbeil and A. L. Beauchamp. Can. J. Chem. **66**, 1379 (1988).
35. M. C. Corbeil and A. L. Beauchamp. Can. J. Chem. **66**, 2458 (1988).
36. M. C. Corbeil. Thèse de Ph.D., Université de Montréal. 1987.
37. J. Poitras, J. Young, and A. L. Beauchamp. Can. J. Chem. Submitted.
38. L. A. Oro, M. A. Ciriano, B. E. Villaroya, A. Tiripicchio, and F. J. Lahoz. J. Chem. Soc. Dalton Trans. 1891 (1985).
39. J. J. Dechter. Prog. Inorg. Chem. **33**, 393 (1985).

Can. J. Chem. Downloaded from www.nrcresearchpress.com by 88.255.202.194 on 09/08/12
For personal use only.

Total synthesis and establishment of the absolute stereochemistry of (+)-mostueine. Addition of chiral nucleophiles to 3,4-dihydro-2-methyl-9-(*p*-toluenesulfonyl)-β-carbolinium iodide[1]

ALLAN W. REY AND WALTER A. SZAREK[2]
Department of Chemistry, Queen's University, Kingston, Ont., Canada K7L 3N6

AND

DAVID B. MACLEAN[2]
Department of Chemistry, McMaster University, Hamilton, Ont., Canada L8S 4M1

Received May 14, 1992

ALLAN W. REY, WALTER A. SZAREK, and DAVID B. MACLEAN. Can. J. Chem. **70**, 2922 (1992).

A highly convergent synthesis of the pentacyclic indole alkaloid (+)-mostueine (**1**) is described. The key step involved the coupling of the dianion derived from (1′*S*)-3-(1′-hydroxyethyl)-4-methylpyridine (**4**) with the iminium salt 3,4-dihydro-2-methyl-9-(*p*-toluenesulfonyl)-β-carbolinium iodide (**3**). Low asymmetric induction (15% de) at the C-1 position of the β-carboline ring system (C-3 of mostueine) was obtained. The nonfermenting baker's yeast-mediated reduction of 3-acetyl-4-methylpyridine provided the hydroxyethylpyridine component in acceptable yield (67%) and high optical purity (99.0% ee). This synthesis of **1** has established that the absolute stereochemistry of mostueine is (3*S*,19*R*).

ALLAN W. REY, WALTER A. SZAREK et DAVID B. MACLEAN. Can. J. Chem. **70**, 2922 (1992).

On décrit une synthèse hautement convergente de l'alcaloïde indolique pentacyclique (+)-mostuéine (**1**). L'étape clé implique le couplage du dianion dérivé de la (1′*S*)-3-(1′-hydroxyéthyl)-4-méthylpyridine (**4**) avec le sel iminium (**3**), l'iodure de 3,4-dihydro-2-méthyl-9-(*p*-toluènesulfonyl)-β-carbolinium. On a obtenu une faible induction asymétrique (15% de) à la position C-1 du système cyclique β-carboline (C-3 de la mostuéine). La réduction de la 3-acétyl-4-méthylpyridine, sous l'influence de la levure pâtissière qui ne fermente pas, fournit la portion hydroxyéthylpyridine avec un rendement acceptable (67%) et une grande pureté optique (99,0% ee). Cette synthèse du composé **1** a établi que la stéréochimie absolue de la mostuéine est (3*S*,19*R*).

[Traduit par la rédaction]

Introduction

The structurally interesting pentacyclic indole alkaloid mostueine (**1**) (also referred to as 3,14-dihydrodecussine) is composed of a β-carboline skeleton possessing an azepino ring attached to a pyridine ring. Mostueine, a weak muscle relaxant, was originally isolated from the leaves of *Mostuea brunonis* (2). It has also been found to be a constituent in the root and stem bark of *Strychnos decussata, S. dale, S. elaecarpa* (3) and, most recently, *S. johnsonii* (4). The pharmacologically more active compound decussine (**2**) is identical with mostueine except for a site of unsaturation at C-3—C-14. It is noteworthy that mostueine has been reported to be converted into decussine (3, 5) on storage (3).

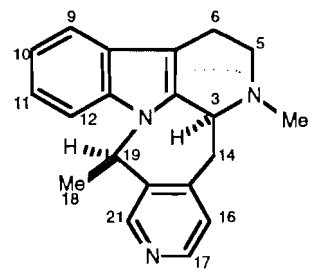

1

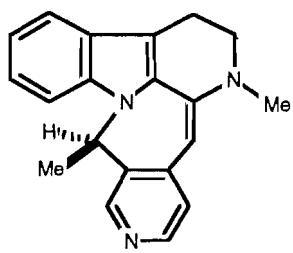

2

The total synthesis of (±)-mostueine was accomplished by McGee *et al.* (6) and by Onanga and Khuong-Huu (7), and their combined studies have established the relative configuration at C-3 and C-19 to be 3*SR*,19*RS*. These syntheses are strategically similar in that they both rely upon the alkylation of the indole nitrogen to close the azepino ring as the last step. Herein we report another more convergent and enantioselective synthesis of mostueine.

The addition of nucleophiles to iminium salt electrophiles has been effectively exploited by us and others for the synthesis of a variety of alkaloids (8). It became apparent that this reaction may permit an efficient synthesis of mostueine as shown retrosynthetically in Scheme 1. Furthermore, this strategy would establish the absolute stereochemistry at C-3. Another more general and synthetically interesting question was the extent of asymmetric induction at the C-1 position of the β-carboline ring system (C-3 of mostueine) upon addition of the chiral nucleophile **4**. In any event, the diastereomeric-adduct mixture should be readily resolvable by chromatography, thereby providing an enantioselective route to mostueine.

Results and discussion

Synthesis of **4**

The synthesis of (1′*S*)-3-(1′-hydroxyethyl)-4-methylpyridine (**4**) is outlined in Scheme 2. The starting material, 3-cyano-4-methylpyridine (**6**), was prepared in gram quantities using the 3-step procedure developed by Bobbitt and Scola (9). The conversion of **6** into 3-acetyl-4-methylpyridine (**8**) was originally accomplished by Webb and Corwin (10). However, this transformation necessitated 3 steps and the overall yield was 30%. Another higher-yielding but longer sequence involved conversion of **6** into 4-methylnicotinaldehyde (3 steps, 71% yield) (10, 11). This aldehyde was then converted into the desired methyl ketone **8** by way of its trimethysilylcyanohydrin derivative in 63% yield (12). In

[1]A preliminary account of a part of this work has appeared (1).
[2]Authors to whom correspondence may be addressed.

Can. J. Chem. Downloaded from www.nrcresearchpress.com by 88.255.202.194 on 09/08/12
For personal use only.

Can. J. Chem. Downloaded from www.nrcresearchpress.com by 88.255.202.194 on 09/08/12
For personal use only.

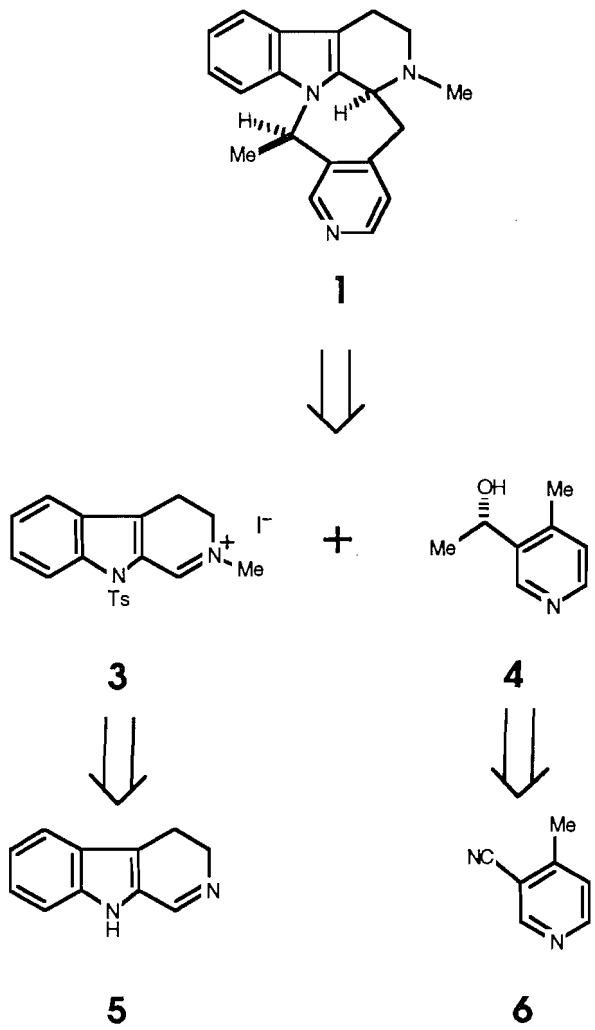

SCHEME 1

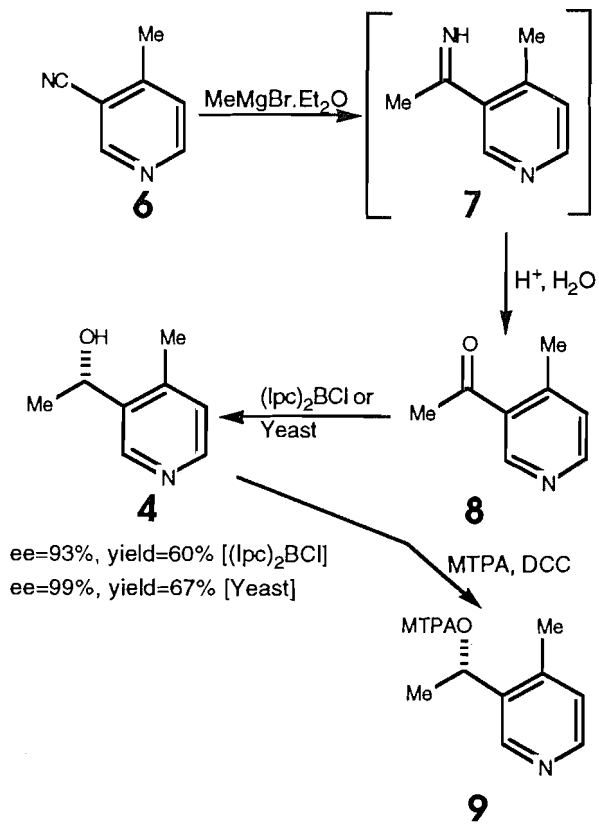

SCHEME 2

contrast to these methods, we have found that a more direct route was the Grignard addition of methylmagnesium bromide (3.0 M solution in diethyl ether) to the nitrile **6** followed by *in situ* acid-catalyzed hydrolysis of the presumed imine intermediate **7**. This protocol, based upon work done by Canonne *et al.* (13), conveniently furnished 3-acetyl-4-methylpyridine in 83% yield.

With acetylpyridine **8** in hand, the next challenge was the stereoselective reduction to form the (*S*)-alcohol **4**. Our initial notion was to employ methodology developed by Brown and co-workers (14) for the asymmetric reduction of aralkyl ketones. Thus, treatment of 3-acetyl-4-methylpyridine with (−)-*B*-chlorodiisopinocampheylborane [(−)-$(Ipc)_2BCl$], and subsequent removal of the boron moiety with diethanolamine, gave (1′*S*)-3-(1′-hydroxyethyl)-4-methylpyridine (**4**). The overall yield was 60% and the enantiomeric excess was 93%. This result is consistent with Brown and co-workers' (14) reduction of 3-acetylpyridine (65% yield and 92% ee). It is pertinent to note that, in each case, 2.3 equivalents of the (−)-$(Ipc)_2BCl$ reagent were required, presumably because of complex formation.

Owing to the expense of the (−)-$(Ipc)_2BCl$ reagent, we examined the possibility of a yeast-mediated reduction. Thus, treatment of the substrate **8** with Fleischmann's Baker's yeast (170:1 yeast to **8** ratio (w/w)) for 4 days at 32°C provided **4** in 67% yield and 99.0% ee ($[\alpha]_D$ −53.5; *c* 1.0, $CHCl_3$). The product was isolated by extractive processing, and the reaction was performed on a 5-gram scale. Another salient feature was that this reduction was accomplished using nonfermenting yeast (i.e., glucose or sucrose was *not* added), thereby facilitating processing. This modification was based upon work done by Bucciarelli *et al.* (15) and by Rasor and Rüchardt (16). An interesting point is that, under almost identical conditions, Takeshita *et al.* (17) found that the yeast-mediated reduction of 3-acetylpyridine gave (1′*S*)-3-(1′-hydroxyethyl)pyridine in 40% yield and 67% ee. Clearly, the 4-methyl group in substrate **8** has a profound effect on the stereochemical outcome of this reduction.

The enantiomeric excesses were determined by conversion of the crude alcohol products into their corresponding diastereomeric (*S*)-α-methoxy-α-(trifluoromethyl)phenylacetate derivatives (**9**) using *S*-MTPA (Aldrich) and *N*,*N*′-dicyclohexylcarbodiimide as the coupling agent. The ee was then assessed by high-resolution ^1H nmr (400 MHz) integration of the well-resolved signals ($\Delta\delta$ = 20 Hz) of the diastereomeric 4-methyl protons.

The absolute stereochemistry of **4** was ascertained to be *S* by ^1H nmr analysis of its *S*-MTPA and *R*-MTPA esters (18). This conclusion is consistent with Brown and co-workers' observation (14) that reduction of similar compounds with (−)-$(Ipc)_2BCl$ leads to the *S* enantiomer. Furthermore, yeast reductions of aralkyl ketones give predominantly the *S*-alcohol (19).

It has not escaped our attention that the enantiopure compound, (1′*S*)-3-(1′-hydroxyethyl)-4-methylpyridine, may be of value as a synthetic intermediate in the synthesis of various pyrido-alkaloids and other natural products. Further-

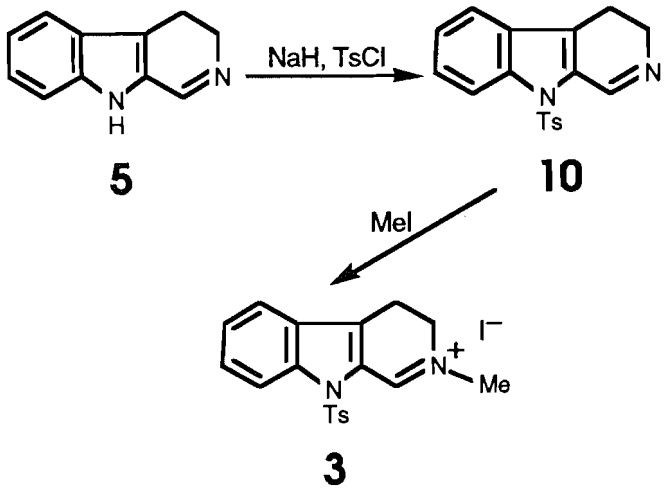

SCHEME 3

more, its *N*-benzyl salt may be of therapeutic value (20) as a possible antineoplastic agent.

Synthesis of ***3***

The synthesis of the intermediate of which the β-carboline portion of mostueine is comprised, specifically the iminium salt, 3,4-dihydro-2-methyl-9-(*p*-toluenesulfonyl)-β-carbolinium iodide (**3**), is depicted in Scheme 3. The starting material was the known 3,4-dihydro-β-carboline (or norharmalan) (**5**), which is readily accessible by way of the Bischler–Napieralski reaction of N^b-formyltryptamine (21). Protection of the indole nitrogen as its tosylamide presented some difficulty. Initially, phase-transfer catalytic methods (22) were examined; however, the yields were low (<30%) owing to formation of side products. Finally, reproducible yields (65%) of the desired 3,4-dihydro-9-(*p*-toluenesulfonyl)-β-carboline (**10**) were obtained by formation of the sodium salt of the indole (sodium hydride, DMF, −10°C, 30 min) followed by addition of *p*-toluenesulfonyl chloride (−60°C, 1.5 h). The major by-product resulted from sulfonylation at the C-3 position of the indole nucleus (C-7 of mostueine). This procedure is an adaptation of a method developed by Langlois *et al.* (23) for the *N*-benzylation of **5**. Methylation of the imine nitrogen of **10** by treatment with iodomethane (THF, room temperature, 12 h) and subsequent filtration provided the iminium salt **3** in 91% yield.

Coupling of ***3*** *and* ***4*** *and completion of the synthesis of* ***1***

The remaining steps in this convergent synthesis of mostueine are shown in Scheme 4. The critical coupling of **3** and **4** went as predicted and afforded adducts **11***a* (3*S*, 19*S*) and **11***b* (3*R*, 19*S*) as a 1.35:1.00 mixture, respectively, and in 62% yield. Considerable effort was spent optimizing this reaction and it was found that the use of a combination of potassium *tert*-butoxide and lithium diisopropylamide afforded the highest yield. A 30-min reaction time at −78°C was found to be sufficient; longer reaction periods led to a reduced yield. The diastereomeric compounds **11***a* and **11***b* were readily separable by silica gel flash chromatography.

We were somewhat disappointed by the low degree of asymmetric induction (de = 15%) obtained for the addition of enantiopure **4** to the iminium salt **3**. Preliminary efforts were made to improve the diastereoselection of this process by varying the hydroxyl protecting group (*tert*-butyldimethylsilyl ether and methoxymethyl ether) on **4** and the indole protecting group (benzyl and free indole). No improvement in the asymmetric induction was obtained for the coupling of these modified compounds (all combinations were tried). These results suggest that the stereocenter on **4** is too remote to offer significant stereoinduction upon addition of this nucleophile.

Compounds **11***a* and **11***b* in racemic form were also isolated by McGee *et al.* (6) in their synthesis of (±)-mostueine. Of significance is that our high-resolution ^{1}H nmr data obtained for (+)-**11***a* and (−)-**11***b* correspond exactly with the literature (6). Their work demonstrated that the racemic modifications of the (3*S*,19*S*) diastereomer **11***a* can be cyclized under forcing conditions (potassium *tert*-butoxide in THF) to provide (±)-mostueine. Mechanistically, this reaction is consistent with the transfer of the *p*-toluenesulfonyl group from the indole nitrogen to the C-19 alkoxide followed by S_N2 displacement of the *p*-toluenesulfonyloxy group by the indole nitrogen (for a related example of this type of cyclization, see ref. 24). Thus, treatment of **11***a* with potassium *tert*-butoxide in anhydrous THF provided (+)-mostueine in 13.5% yield. The major product of the reaction was the imine **12** (40% yield) presumably formed by *C*-alkylation of the intermediary C-19 tosylate. Our results are consistent with those obtained by others (6, 7). The relative (and in this case the absolute) configuration of **12** was established by ^{1}H nmr nOe experiments. For instance, a significant enhancement (6.8%) of the H-14ax signal was observed upon presaturation at the signal for H-19. Additionally, presaturation at the signal for the H-18 methyl protons gave a 7.5% intensity enhancement of the H-21 signal.

Attempts to improve the yield of mostueine were unsuccessful. For instance, the adduct corresponding to **11***a* deprotected at N-9 was oxidized (MnO_2, CH_2Cl_2, reflux, 36 h, 42%) at C-19 to provide the ketone. Unfortunately, conditions to reductively aminate the indole nitrogen with the ketone were not found.

The spectral data for the synthetically prepared (+)-mostueine were identical with the data for a sample of the natural product that was kindly provided by Prof. F. Khuong-Huu. Also, the optical rotation for mostueine synthesized by this method was +186 (*c* 1.0, $CHCl_3$), a value that closely corresponds to the optical rotation of natural mostueine (+196 (2)). This result unambiguously demonstrates that the absolute stereochemistry of **1** is (3*S*,19*R*), an assignment that is consistent with the proposed biosynthesis (4) of mostueine from strictoside.

In summary, the enantioselective synthesis of the indole alkaloid mostueine has been accomplished in a convergent and efficient manner. This work shows that the absolute configuration of mostueine is (3*S*,19*R*) as depicted.

Experimental

Apparatus, materials, and methods

The ^{1}H nmr spectra were recorded at 200 MHz and 400 MHz (as indicated) on Bruker AC-F200 and AM-400 spectrometers, respectively. The samples were dissolved in either $CDCl_3$ or DMSO-d_6 (as indicated). The proton chemical shifts are quoted in parts per million (ppm) downfield relative to the internal standard, tetramethylsilane (δ scale). The ^{13}C nmr spectra were recorded at 50.3 MHz on a Bruker AC-F200 spectrometer. The carbon chemical shifts are quoted in ppm with reference to $CDCl_3$ (77.00 ppm). The multiplicities of signals were determined by JMOD experiments. The analyses were done as a first-order ap-

Can. J. Chem. Downloaded from www.nrcresearchpress.com by 88.255.202.194 on 09/08/12
For personal use only.

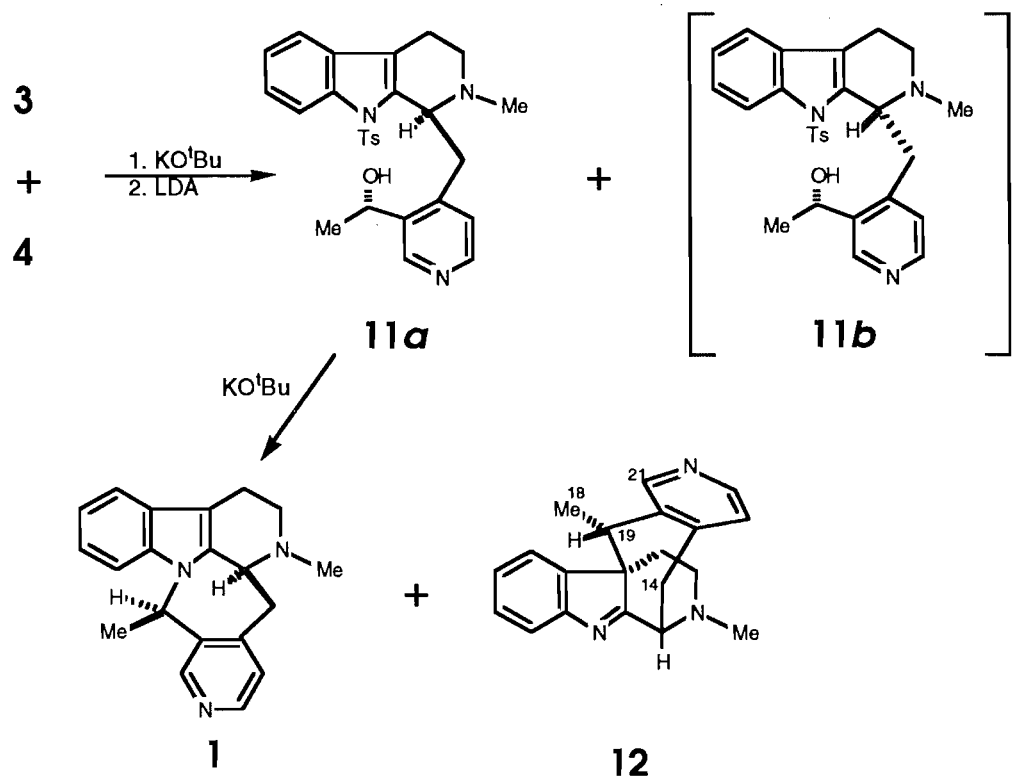

SCHEME 4

proximation. The ir spectra were determined using KBr disks or taken from films on sodium chloride plates (as indicated) on a BOMEM MB-120 ft-ir spectrophotometer at room temperature.

EI (electron ionization) mass spectra were recorded at 70 eV on a VG Analytical ZAB-E mass spectrometer equipped with a VG 11-250 data system. CI (chemical ionization) spectra were recorded on the same instrument using NH_3 at ~1 Torr (1 Torr = 133.3 Pa) as reagent gas. The peak intensities are given as a percent of the base peak (100%) intensity. High-resolution mass spectra (hrms) measurements were performed on the above instrument under EI conditions.

Melting points were determined using a Fisher–Johns apparatus and are uncorrected. Optical rotations were measured on a Perkin–Elmer 241 polarimeter and were run at room temperature (~23°C). Thin-layer chromatography was performed using silica gel 60-F_{254} plates (E. Merck No. 5714) of 0.25 mm thickness. Preparative-layer chromatographic (ptlc) separations were accomplished on silica gel 60-F_{254} plates (E. Merck No. 5717) of 2 mm thickness. For flash chromatography, silica gel 60 (230–400 mesh, E. Merck No. 9385-5) was employed.

All reactions involving lithiation were performed in apparatus dried in the oven at 140°C for at least 12 h and assembled hot under a stream of argon. Septa and syringes were used for transfer of reagents. Solvents and reagents were reagent grade and, when required, further purifications were accomplished following published procedures (25). Titrations of the organolithium reagents were done using diphenylacetic acid (26).

3-Acetyl-4-methylpyridine (8)

To a stirred solution of 3-cyano-4-methylpyridine (**6**) (5.01 g, 42.5 mmol) (prepared according to ref. 9) in benzene (30 mL) at 0°C and under an argon atmosphere was added a 3.0 M solution of MeMgBr in diethyl ether (42.0 mL, 126 mmol). The solution was stirred at 0°C for 2 h, the temperature was then raised to room temperature, and the stirring was continued a further 16 h. The mixture was cooled to 0°C, the excess of MeMgBr was carefully quenched, and the solution acidified to pH ~2 by addition of 4 M HCl. This solution was stirred for 2 h, at which point it was basified to pH ~10 using concentrated NH_4OH solution (aq.). The aqueous layer was extracted with ethyl acetate (6 × 60 mL), the combined organic extracts were dried over $MgSO_4$ (anhydrous), and the solvent was removed *in vacuo*. The crude red oil (5.14 g) was purified by silica gel flash chromatography (ethyl acetate – hexane (2:3, v/v)) to furnish the acetylpyridine **8** (4.75 g, 83% overall yield from **6**) as a colorless oil (this material is slightly volatile and, thus, should not be exposed to reduced pressure for prolonged periods); bp 57–58°C (1–2 Torr); ν_{max} (film): 3052, 2979, 2928, 1687, 1592, 1358, 1270 cm^{-1}; ^1H nmr (200 MHz, $CDCl_3$) δ: 2.53 (3H, s, CH_3CO), 2.62 (3H, s, CH_3 at C-4), 7.17 (1H, d, J = 5.0 Hz, H-5), 8.51 (1H, d, J = 5.0 Hz, H-6), 8.92 (1H, s, H-2); ^{13}C nmr (50.3 MHz, $CDCl_3$) δ: 20.8 (CH_3 at C-4), 29.1 (CH_3CO), 126.6 (C-5), 132.8 (C-4), 147.8 (C-3), 150.2 (C-6), 151.5 (C-2), 199.2 (CH_3CO); ms (EI), m/z (%): 135 (52) $[M]^+$, 120 (100), 92 (82), 65 (37). Exact Mass calcd. for C_8H_9NO $[M]^+$: 135.0684; found (hrms): 135.0692.

(1′S)-3-(1′-Hydroxyethyl)-4-methylpyridine (4)

Method 1. (−)-(Ipc)$_2$BCl reduction

To a solution of (−)-*B*-chlorodiisopinocampheylborane ((−)-(Ipc)$_2$BCl, Aldrich, 5.95 g, 18.5 mmol) in THF (20 mL) at −20°C and under an argon atmosphere was added 3-acetyl-4-methylpyridine (**8**) (1.00 g, 7.41 mmol). The reaction mixture was stirred for 17 h and the volatiles were removed under vacuum. The residue was dissolved in diethyl ether (30 mL) and diethanolamine (4.29 g, 40.8 mmol) was added. This mixture was stirred for 3 h and the solid that precipitated was removed by filtration through a sintered-glass funnel (medium porosity). The filter cake was washed twice with pentane and the combined filtrate and washings were concentrated *in vacuo*. To remove the remaining α-pinene, the oil was taken up in 0.2 M HCl (40 mL) and washed with ethyl acetate (60 mL). The aqueous layer was basified with $NaHCO_3$ (s) and extracted with ethyl acetate (5 × 50 mL). The combined extracts

Can. J. Chem. Downloaded from www.nrcresearchpress.com by 88.255.202.194 on 09/08/12
For personal use only.

Can. J. Chem. Downloaded from www.nrcresearchpress.com by 88.255.202.194 on 09/08/12
For personal use only.

were dried over $MgSO_4$ and the solvent removed *in vacuo*. The remaining oil was purified by silica gel flash chromatography (ethyl acetate – methanol (95:5, v/v)) to yield 0.61 g (60% yield) of the chiral alcohol **4** (ee = 93.0%) as a colorless oil; $[\alpha]_D$ −50.2 (*c* 1.0, $CHCl_3$).

Method 2. Yeast reduction

Six 500-mL side-arm Erlenmeyer flasks, each containing a mixture of the ketone **8** (0.85 g, 6.3 mmol) and dry baker's yeast (Fleischmann's Yeast Limited, "Traditional Active Dry Yeast") (145 g) in tap water (250 mL), were shaken on a wrist-action shaker for 4 days at 32°C. The solutions were combined and centrifuged (13,000 rpm, 10 min, 4°C). The supernatant aqueous layers were decanted, more water was added to the centrifuge tubes, and the yeast re-suspended. This mixture was centrifuged as above and the supernatant aqueous layers were collected. All aqueous extracts were combined and passed through a 2-cm bed of Celite. Extraction of the aqueous phase with ethyl acetate (6 × 400 mL), followed by drying of the combined organic layers over Na_2SO_4 and removal of the solvent *in vacuo*, gave a slightly-yellow oil. This material was further purified by silica gel flash chromatography (ethyl acetate – methanol (95:5, v/v)) to provide 3.45 g (67% yield) of the (*S*)-alcohol **4** (ee = 99.0%) as a colorless oil; $[\alpha]_D$ −53.5 (*c* 1.0, $CHCl_3$); ν_{max} (film): 3296, 2975, 2926, 1603, 1449, 1416, 1373, 1096, 1071 cm^{-1}; ^1H nmr (200 MHz, $CDCl_3$) δ: 1.46 (3H, d, *J* = 6.5 Hz, C-2′ H's), 2.30 (3H, s, CH_3 at C-4), 4.80 (1H, br s, D_2O-exchangeable, OH), 5.06 (1H, q, *J* = 6.5 Hz, H-1′), 6.98 (1H, d, *J* = 4.8 Hz, H-5), 8.18 (1H, d, *J* = 4.8 Hz, H-6), 8.51 (1H, s, H-2); ^{13}C nmr (50.3 MHz, $CDCl_3$) δ: 18.1 (C-2′), 23.4 (CH_3 at C-4), 64.5 (C-1′), 125.0 (C-5), 140.0 (C-4), 144.3 (C-3), 145.7 (C-6), 146.3 (C-2); ms (EI), *m/z* (%): 137 (28) $[M]^+$, 122 (100), 94 (50), 93 (13), 92 (12), 65 (14). Exact Mass calcd. for $C_8H_{11}NO$ $[M]^+$: 137.0841; found (hrms): 137.0851.

(1′S)-3-[1′-O-(S-MTPA)ethyl]-4-methylpyridine (9)

To *S*-(+)-α-methoxy-α-(trifluoromethyl)phenylacetic acid (101 mg, 0.430 mmol) in dichloromethane (15 mL) were added *N*,*N*′-dicyclohexylcarbodiimide (114 mg, 0.553 mmol), 4-dimethylaminopyridine (10 mg, 0.082 mmol), and the chiral alcohol **4** (42.0 mg, 0.306 mmol), and the solution was stirred for 16 h. The white precipitate was removed by filtration through a sintered-glass funnel (fine porosity) and washed with pentane (2 × 15 mL). The filtrate was diluted with dichloromethane (20 mL) and sequentially washed with saturated aqueous solutions of $NaHCO_3$ and NaCl (15 mL of each). The organic layer was dried over $MgSO_4$ and the solvent removed *in vacuo* to afford 76.8 mg (71% yield) of the acetate **9** as a colorless oil (the spectral data for the (1′*S*,*R*) diastereomer are given in parentheses if they are different from those of the (1′*S*,*S*) diastereomer); ^1H nmr (400 MHz, $CDCl_3$) δ: 1.56 (1.63) (3H, d, *J* = 6.7 Hz, C-2′ H's), 2.38 (2.33) (3H, s, CH_3 at C-4), 3.45 (3.55) (3H, q, *J* = 1.2 Hz, OCH_3), 6.27 (6.23) (1H, q, *J* = 6.7 Hz, H-1′), 7.06 (7.03) (1H, d, *J* = 5.0 Hz, H-5), 7.30–7.45 (5H, m, Ph), 8.39 (8.37) (1H, d, *J* = 5.0 Hz, H-6), 8.53 (8.35) (1H, s, H-2); ^{13}C nmr (50.3 MHz, $CDCl_3$) δ: 18.4 (18.3) (C-2′), 21.1 (21.0) (CH_3 at C-4), 55.3 (55.5) (OCH_3), 70.5 (70.4) (C-1′), 120.4 (*C*CF_3), 125.4 (125.2) (C-5), 126.2 (CF_3), 127.2, 128.3, 129.6, 131.8 (127.0, 128.4) (Ph), 134.4 (134.3) (C-3), 144.2 (C-4), 147.6 (147.4) (C-6), 149.1 (149.0) (C-2), 165.6 (165.8) (R*C*O_2R′); ms (EI), *m/z* (%): 354 (5) $[M + H]^+$, 224 (12), 189 (65), 143 (14), 120 (100); ms (CI), *m/z* (%): 354 (100) $[M + H]^+$, 120 (15). Exact Mass calcd. for $C_{18}H_{19}NO_3F_3$ $[M + H]^+$: 354.1316; found (hrms): 354.1322.

4,9-Dihydro-9-(p-toluenesulfonyl)-3H-pyrido-[3,4-b]indole (10)

At −10°C, the 3,4-dihydro-β-carboline **5** (see ref. 21 for preparation, 1.40 g, 8.23 mmol) was added slowly to a suspension of NaH (0.58 g, 60% in mineral oil, 14.6 mmol) in DMF (20 mL) and under an argon atmosphere. (**Caution**: various 3,4-dihydro-β-carbolines and 3,4-dihydro-2-methyl-β-carbolinium salts have recently been implicated in provoking the neuronal degeneration underlying idiopathic Parkinson's disease (27).) The mixture was stirred for 30 min and then cooled to −60°C at which time *p*-toluenesulfonyl chloride (3.15 g, 16.5 mmol) was added. The reaction mixture was acidified after 1.5 h using 0.2 M HCl (40 mL) and extracted with diethyl ether (2 × 30 mL). The combined organic layers were extracted with 0.2 M HCl (25 mL) and the combined aqueous extracts made basic with concentrated NH_4OH solution (aq.). Extraction with dichloromethane (2 × 60 mL) and subsequent drying over $MgSO_4$ and removal of the solvent *in vacuo* provided a solid amorphous material. This solid was purified by silica gel flash chromatography (ethyl acetate – hexane (7:3 v/v)) to yield 1.74 g (65%) of the tosylamide **10**, which was recrystallized from ethyl acetate – hexane; mp 143–145°C; ν_{max} (KBr): 3048, 2936, 2849, 1596, 1554, 1444, 1365, 1230, 1167 cm^{-1}; ^1H nmr (200 MHz, $CDCl_3$) δ: 2.31 (3H, s, Ts-CH_3), 2.75 (2H, app t, *J* = 8.7 Hz, H-4), 3.84 (2H, td, *J* = 2.2, 8.8 Hz, H-3), 7.16 (2H, d, *J* = 8.2 Hz, Ts), 7.28 (1H, t, *J* = 7.5 Hz, H-6), 7.43 (1H, t, *J* = 7.8 Hz, H-7), 7.47 (1H, d, *J* = 7.9 Hz, H-5), 7.65 (2H, d, *J* = 8.2 Hz, Ts), 8.18 (1H, d, *J* = 8.3 Hz, H-8), 8.99 (1H, app s, H-1); ^{13}C nmr (50.3 MHz, $CDCl_3$) δ: 18.7 (C-4), 21.4 (Ts-CH_3), 47.1 (C-3), 115.1 (C-8), 120.1 (C-5), 124.1 (C-6), 125.6 (C-4a), 126.5 (Ts), 127.3 (C-7), 127.8 (C-4b), 128.6, 129.8 (Ts), 134.7 (C-9a), 136.8 (C-8a), 145.1 (Ts), 150.9 (C-1); ms (EI), *m/z* (%): 324 (24) $[M]^+$, 169 (100), 142 (22), 115 (21), 91 (19). Exact Mass calcd. for $C_{18}H_{16}N_2O_2S$ $[M]^+$: 324.0932; found (hrms): 324.0926.

4,9-Dihydro-2-methyl-9-(p-toluenesulfonyl)-3H-pyrido-[3,4-b]indolinium iodide (3)

To a solution of the tosylamide **10** (501 mg, 1.54 mmol) in tetrahydrofuran (25 mL) was added iodomethane (0.49 mL, 7.7 mmol) with stirring and at room temperature, and the mixture was allowed to stand overnight. The solid precipitate **3** was isolated by filtration through Whatman filter paper (hardened) and the filter cake washed with hexane (2 × 20 mL) to provide 0.653 g (91% yield) of the bright-yellow crystalline 3,4-dihydro-2-methyl-β-carbolinium salt **3**; mp 195–197°C; ν_{max} (KBr): 3077, 3035, 2994, 2970, 1640, 1540, 1434, 1370, 1171, 1096 cm^{-1}; ^1H nmr (200 MHz, DMSO-d_6) δ: 2.31 (3H, s, Ts-CH_3), 3.37 (2H, app t, *J* = 9.0 Hz, H-4), 3.89 (3H, s, *N*-CH_3), 4.16 (2H, t, *J* = 9.1 Hz, H-3), 7.16 (2H, d, *J* = 8.4 Hz, Ts), 7.45 (1H, app t, *J* = 7.9 Hz, H-6 or H-7), 7.70 (1H, app t, *J* = 7.9 Hz, H-6 or H-7), 7.87 (1H, d, *J* = 7.9 Hz, H-5), 7.99 (2H, d, *J* = 8.4 Hz, Ts), 8.07 (1H, d, *J* = 8.6 Hz, H-8), 9.47 (1H, s, H-1); ^{13}C nmr (50.3 MHz, DMSO-d_6) δ: 19.0 (C-4), 21.0 (Ts-CH_3), 47.7 (*N*-CH_3), 49.8 (C-3), 114.6 (C-8), 123.2 (C-5), 125.4 (C-6), 125.8, 125.9 (C-4a, C-4b), 127.4, 130.4 (Ts), 131.6 (C-7), 132.5 (C-9a), 134.1 (Ts), 138.7 (C-8a), 146.5 (Ts), 155.1 (C-1); ms (EI), *m/z* (%): 340 (17) $[M - I + H]^+$, 185 (100), 184 (73), 183 (36), 157 (18), 156 (18), 142 (61), 139 (24), 92 (51), 91 (64). Exact Mass calcd. for $C_{19}H_{20}N_2O_2S$ $[M - I + H]^+$: 340.1245; found (hrms): 340.1234.

Tosylamide adducts 11a[(1S,1″S)-2,3,4,9-tetrahydro-1-{[3′-(1″-hydroxyethyl)-4′-pyridinyl]methyl}-2-methyl-9-(p-toluenesulfonyl)-1H-pyrido[3,4-b]indole] and 11b[(1R,1″S)-2,3,4,9-tetrahydro-1-{[3′-(1″-hydroxyethyl)-4′-pyridinyl]methyl}-2-methyl-9-(p-toluenesulfonyl)-1H-pyrido[3,4-b]indole]

Under an argon atmosphere and at −10°C, the hydroxypyridine **4** (228 mg, 1.66 mmol) in tetrahydrofuran (20 mL) was treated with potassium *tert*-butoxide (1.5 M in tetrahydrofuran, 1.44 mL, 2.16 mmol). The solution was stirred at this temperature for 10 min at which time it was cooled to −78°C and lithium diisopropylamide (1.5 M in tetrahydrofuran, 1.44 mL, 2.16 mmol) was added; the solution became yellow. After 25 min, the solution was added dropwise using a cannula to a vigorously stirred suspension of the 2-methyl-β-carbolinium salt **3** (519 mg, 1.11 mmol) in tetrahydrofuran (20 mL) at −78°C. The reaction was quenched after 0.5 h by addition of saturated NaCl (aq.) (2 mL) and then diluted with dichloromethane (40 mL). This mixture was washed sequentially with saturated $NaHCO_3$ (aq.) (15 mL) and saturated NaCl (aq.) (15 mL), dried over $MgSO_4$, and the solvent removed *in vacuo*. The

Can. J. Chem. Downloaded from www.nrcresearchpress.com by 88.255.202.194 on 09/08/12
For personal use only.

residual oil was purified by silica gel chromatography (ethyl acetate – methanol (95:5, v/v)) Silica gel flash chromatography (dichloromethane – 95% ethanol (20:1, v/v)) afforded the diastereomers **11***a* (188 mg) and **11***b* (139 mg) (62% overall yield) as slightly yellowish crystals. (The numbering system used for both ^{1}H nmr and ^{13}C nmr assignments for **11***a* and **11***b*, and for the following two compounds (**12** and **1**), refers to mostueine numbering, as shown in the structural formula for **1**.)

11*a*: mp 85–90°C; $[\alpha]_D$ +68 (*c* 1.0, $CHCl_3$); ν_{max} (KBr): 3363, 2967, 2933, 2847, 1597, 1450, 1366, 1170, 754 cm^{-1}; ^{1}H nmr (400 MHz, $CDCl_3$) δ: 1.60 (3H, d, *J* = 6.6 Hz, C-18 H's), 2.29 (3H, s, Ts-C*H*$_3$), 2.35 (3H, s, *N*-C*H*$_3$), 2.31–2.40 (1H, m, H-5 or H-6), 2.48–2.83 (3H, m, C-5 H's, C-6 H's), 3.34 (1H, dd, A of ABX, *J* = 7.4, 14.2 Hz, H-14), 3.53 (1H, dd, B of ABX, *J* = 3.5, 14.2 Hz, H-14′), 4.46 (1H, dd, *J* = 3.2, 7.3 Hz, H-3), 5.15 (1H, q, *J* = 6.6 Hz, H-19), 7.11 (2H, d, *J* = 8.4 Hz, Ts), 7.22 (1H, d, *J* = 5.1 Hz, H-16), 7.29–7.41 (3H, m, H-9, H-10, H-11), 7.50 (2H, d, *J* = 8.1 Hz, Ts), 8.22 (1H, d, *J* = 7.8 Hz, H-12), 8.32 (1H, d, *J* = 5.1 Hz, H-17), 8.61 (1H, s, H-21); ^{13}C nmr (50.3 MHz, $CDCl_3$) δ: 15.9 (C-6), 19.9 (Ts-*C*H$_3$), 21.4 (C-18), 36.5 (C-14), 41.3 (*N*-*C*H$_3$), 43.1 (C-5), 62.5, 62.9 (C-3, C-19), 115.7 (C-12), 118.6 (C-9), 118.9 (C-7), 124.2 (C-10), 125.2 (C-11), 125.7 (C-16), 126.1, 129.5, 130.0 (Ts), 134.5 (C-8), 137.1 (C-2), 137.2 (C-13), 138.8 (C-20), 144.9 (C-15), 146.9 (C-17), 147.0 (Ts), 148.7 (C-21); ms (EI), *m/z* (%): 476 (<1) $[M + H]^+$, 339 (100), 184 (47), 183 (36), 122 (23), 91 (35). Exact Mass calcd. for $C_{27}H_{30}N_3O_3S$ $[M + H]^+$: 476.1993; found (hrms): 476.2008.

11*b*: $[\alpha]_D$ −149 (*c* 1.0, $CHCl_3$); ν_{max} (KBr): 3378, 2969, 2935, 2849, 2801, 1596, 1450, 1368, 1170, 753 cm^{-1}; ^{1}H nmr (400 MHz, $CDCl_3$) δ: 1.68 (3H, d, *J* = 6.5 Hz, C-18 H's), 2.25 (3H, s, *N*-C*H*$_3$), 2.29 (3H, s, Ts-C*H*$_3$), 2.51–3.40 (4H, m, C-5 H's, C-6 H's), 3.16 (1H, dd, A of ABX, *J* = 10.0, 14.2 Hz, H-14), 3.37 (1H, d, *J* = 14.2 Hz, H-14′), 4.23 (1H, br d, *J* = 9.8 Hz, H-3), 5.02 (1H, q, *J* = 6.5 Hz, H-19), 7.10 (2H, d, *J* = 8.0 Hz, Ts), 7.26–7.41 (3H, m, H-9, H-10, H-11), 7.49 (2H, d, *J* = 8.4 Hz, Ts), 7.88 (1H, d, *J* = 5.2 Hz, H-16), 8.24 (1H, d, *J* = 8.1 Hz, H-12), 8.55 (1H, d, *J* = 5.1 Hz, H-17), 8.76 (1H, s, H-21); ^{13}C nmr (50.3 MHz, $CDCl_3$) δ: 16.4 (C-6), 21.4 (Ts-*C*H$_3$), 23.1 (C-18), 36.6 (C-14), 42.3 (*N*-*C*H$_3$), 44.1 (C-5), 61.4 (C-3), 65.4 (C-19), 115.7 (C-12), 118.6 (C-9), 119.9 (C-7), 124.2 (C-10), 125.0 (C-11), 126.0 (C-16), 126.2, 129.5, 130.2 (Ts), 134.4 (C-8), 134.8 (C-2), 137.2 (C-13), 139.5 (C-20), 144.8 (C-15), 146.3 (Ts), 148.0 (C-17), 148.1 (C-21).

Imine ***12*** *[(6*S*, 12*R*)-5,12-dihydro-12,15-dimethyl-6*H*-6,11b-(iminoethano)pyrido[3′,4′:4,5]cyclohept[1,2-*b*]indole] and (+)-mostueine (**1**) [(8*R*, 13a*S*)-1,2,3,8,13,13a-hexahydro-1,8-dimethyl-1,7b,10-triazabenzo[5,6]cyclohepta[1,2,3-jk]fluorene]*

To a stirred solution of the tosylamide **11***a* (163 mg, 0.343 mmol) in tetrahydrofuran (15 mL) at 0°C was added potassium *tert*-butoxide (231 mg, 2.06 mmol). The medium was allowed to warm slowly to room temperature and, after 5 h, was diluted with dichloromethane (40 mL) and washed with saturated NaCl (aq.) (20 mL). The organic layer was dried over $MgSO_4$ and the solvent removed *in vacuo*. The residual solid was purified by ptlc (diethyl ether – 95% ethanol – diethylamine (90:3:7, v/v)). The major product isolated was the imine **12** (40.3 mg, 40%) along with mostueine **1** (14.0 mg, 13.5%).

12: $[\alpha]_D$ −42.8 (*c* 1.0, $CHCl_3$); ν_{max} (KBr): 2930, 2859, 2794, 1593, 1451, 1325, 1143, 920 cm^{-1}; ^{1}H nmr (200 MHz, $CDCl_3$) δ: 1.72 (3H, d, *J* = 7.2 Hz, C-18 H's), 1.96–2.37 (4H, m, C-5 H's, C-6 H's), 2.38 (3H, s, *N*-C*H*$_3$), 2.78 (1H, q, *J* = 7.2 Hz, H-19), 3.11 (1H, dd, A of ABX, *J* = 6.3, 14.9 Hz, H-14), 3.47 (1H, dd, B of ABX, *J* = 1.9, 14.9 Hz, H-14′), 4.12 (1H, dd, *J* = 2.0, 6.4 Hz, H-3), 7.23 (1H, td, *J* = 1.2, 7.3 Hz, H-10 or H-11), 7.24 (1H, d, *J* = 4.8 Hz, H-16), 7.37 (1H, td, *J* = 1.3, 7.5 Hz, H-10 or H-11), 7.46 (1H, d, *J* = 7.5 Hz, H-9), 7.64 (1H, d, *J* = 7.3 Hz, H-12), 8.47 (1H, d, *J* = 4.8 Hz, H-17), 8.58 (1H, s, H-21); ^{13}C nmr (50.3 MHz, $CDCl_3$) δ: 18.5 (C-18), 30.6 (C-6), 36.0 (C-14), 38.2 (*N*-C*H*$_3$), 42.1 (C-7), 42.3 (C-19), 47.1 (C-5), 60.7 (C-3), 121.0 (C-12), 124.9 (C-11), 125.1 (C-10), 125.8 (C-9), 128.1 (C-16), 137.1 (C-20), 144.9 (C-8), 148.2 (C-17), 148.3 (C-15), 148.7 (C-21), 154.2 (C-13), 187.3 (C-2); ms (EI), *m/z* (%): 303 (82) $[M]^+$, 288 (8), 260 (23), 184 (100); ms (CI), *m/z* (%): 304 (100) $[M + H]^+$, 184 (18), 183 (18). Exact Mass calcd. for $C_{20}H_{21}N_3$ $[M]^+$: 303.1735; found (hrms): 303.1741.

1:[3] $[\alpha]_D$ +186 (c 1.0, $CHCl_3$); ν_{max} (KBr): 2920, 2850, 2790, 1596, 1457, 1320, 1192, 1051, 747 cm^{-1}; ^{1}H nmr (200 MHz, $CDCl_3$) δ: 1.67 (3H, d, *J* = 7.0 Hz, C-18 H's), 2.54 (3H, s, *N*-C*H*$_3$), 2.62–2.79 (1H, m, H-6), 2.90–3.00 (1H, m, H-5 or H-6), 3.10–3.38 (2H, m, C-5 H's or C-6 H's), 3.15 (1H, dd, *J* = 2.1, 13 Hz, H-14), 3.52 (1H, t, *J* = 12.7 Hz, H-14′), 3.85 (1H, dd, *J* = 2.1, 12.7 Hz, H-3), 5.79 (1H, q, *J* = 7 Hz, H-19), 7.19 (1H, t, *J* = 7.0 Hz, H-10), 7.28 (1H, d, *J* = 4.9 Hz, H-16), 7.29 (1H, t, *J* = 7.0 Hz, H-11), 7.47 (1H, d, *J* = 8.3 Hz, H-9), 7.52 (1H, d, *J* = 7.5 Hz, H-12), 8.55 (1H, d, *J* = 4.9 Hz, H-17), 8.62 (1H, s, H-21); ^{13}C nmr (50.3 MHz, $CDCl_3$) δ: 18.7 (C-6), 22.8 (C-18), 36.8 (C-14), 37.3 (*N*-C*H*$_3$), 53.1 (C-5), 55.3 (C-19), 60.8 (C-3), 108.2 (C-7), 109.5 (C-12), 118.4 (C-11), 119.6 (C-10), 121.8 (C-9), 125.1 (C-16), 126.8 (C-8), 133.7, 134.8 (C-2, C-20), 136.3 (C-13), 147.1 (C-15), 149.4, 150.2 (C-17, C-21); ms (EI), *m/z* (%): 303 (100) $[M]^+$, 288 (33), 260 (56), 184 (74); ms (CI), *m/z* (%): 304 (100) $[M + H]^+$, 183 (37). Exact Mass calcd. for $C_{20}H_{21}N_3$ $[M]^+$: 303.1735; found (hrms): 303.1738.

Acknowledgements

We thank Prof. F. Khuong-Huu for a sample of natural mostueine and the Natural Sciences and Engineering Research Council of Canada for financial support of this work through grants to W. A. S. and D. B. M. We are also indebted to Ms. S. L. Blake (Queen's University) for performing some nmr experiments and to Dr. R. W. Smith (McMaster University) for mass spectra.

1. A. W. Rey, W. A. Szarek, and D. B. MacLean. 13th International Congress of Heterocyclic Chemistry, Corvallis, Oreg. 1991.
2. M. Onanga and F. Khuong-Huu. C. R. Seances Acad. Sci. Sér. C: **291**, 191 (1980).
3. W. N. A. Rolfsen, A. A. Olaniyi, R. Verpoorte, and L. Bohlin. Nat. Prod. **44**, 415 (1981).
4. G. Massiot, P. Thépenier, M.-J. Jacquier, L. Le Men-Olivier, R. Verpoorte, and C. Delaude. Phytochemistry, **26**, 2839 (1987).
5. W. N. A. Rolfsen, A. A. Olaniyi, F. Sandberg, and A. H. Kvick. Acta Pharm. Suec. **17**, 105 (1980).
6. L. R. McGee, G. S. Reddy, and P. N. Confalone. Tetrahedron Lett. **25**, 2115 (1984).
7. M. Onanga and F. Khuong-Huu. Tetrahedron Lett. **24**, 3627 (1983).
8. A. W. Rey, W. A. Szarek, and D. B. MacLean. Heterocycles, **32**, 1143 (1991); M. Nakagawa, T. Kawate, H. Yamazaki, and T. Hino. J. Chem. Soc. Chem. Commun. 991 (1990); D. B. Repke, Jahangir, R. D. Clark, J. T. Nelson, and D. B. MacLean. Tetrahedron, **45**, 2541 (1989); D. B. Repke, Jahangir, R. D. Clark, and J. T. Nelson. Heterocycles, **27**, 2289 (1988); D. B. Repke, Jahangir, R. D. Clark, and D. B. MacLean. J. Chem. Soc. Chem. Commun. 439 (1988); Jahangir, M. A. Brook, D. B. MacLean, and H. L. Holland.

[3]In the present work **1** was isolated as a low-melting solid. Of the five publications (2–4, 6, 7) in which the isolation of mostueine has been reported, only in the case of ref. 3 has a melting point been cited (mp 78–82°C).

Tetrahedron, **43**, 5761 (1987); Jahangir, M. A. Brook, D. B. MacLean, and H. L. Holland. J. Chem. Soc. Chem. Comm. 1608 (1986).
9. J. M. Bobbit and D. A. Scola. J. Org. Chem. **25**, 560 (1960).
10. J. L. Webb and A. H. Corwin. J. Am. Chem. Soc. **66**, 1456 (1944).
11. A. Shariff and S. McLean. Can J. Chem. **61**, 2813 (1983).
12. K. Deuchert, U. Hertenstein, and S. Hünig. Synthesis, 777 (1973).
13. P. Canonne, G. B. Foscolos, and G. Lemay. Tetrahedron Lett. **21**, 155 (1980).
14. J. Chanrasekharan, P. V. Ramachandran, and H. C. Brown. J. Org. Chem. **50**, 5446 (1985).
15. M. Bucciarelli, A. Forni, I. Moretti, and G. Torre. Synthesis, 897 (1983).
16. J. P. Rasor and C. Rüchardt. Chem. Ber. **122**, 1375 (1989).
17. M. Takeshita, K. Terada, N. Akutsu, S. Yoshida, and T. Sato. Heterocycles, **26**, 3051 (1987).
18. I. Ohtani, T. Kusumi, Y. Kashman, and H. Kakisawa. J. Am. Chem. Soc. **113**, 4092 (1991), and references cited therein.
19. R. Csuk and B. I. Glänzer. Chem. Rev. **91**, 49 (1991).
20. A. C. Lovesey. J. Med. Chem. **13**, 693 (1970).
21. N. Whittaker. J. Chem. Soc. (C), 85 (1969).
22. Y. Kikugawa. Synthesis, 460 (1981); V. O. Illi. Synthesis, 136 (1979); V. Bocchi, G. Casnati, A. Dossena, and F. Villani. Synthesis, 414 (1976).
23. Y. Langlois, A. Pouilhès, D. Génin, R. Z. Andriamialisoa, and N. Langlois. Tetrahedron, **39**, 3755 (1983).
24. M. Rubiralta, A. Diez, J. Bosch, and X. Solans. J. Org. Chem. **54**, 5591 (1989).
25. D. D. Perrin, W. L. F. Armarego, and D. R. Perrin. *In* Purification of laboratory compounds. 2nd ed. Pergamon Press, London. 1980.
26. W. G. Kofron and L. M. Baclawski. J. Org. Chem. **41**, 1879 (1976).
27. G. Druker, K. Raikoff, E. J. Neafsey, and M. A. Collins. Brain Res. **509**, 125 (1990).

Can. J. Chem. Downloaded from www.nrcresearchpress.com by 88.255.202.194 on 09/08/12
For personal use only.

The effect of Lewis acids on the intramolecular Diels–Alder reaction of the furan diene

CHRISTINE ROGERS AND BRIAN A. KEAY[1]

Department of Chemistry, University of Calgary, Calgary, Alta., Canada T2N 1N4

Received May 15, 1992

CHRISTINE ROGERS and BRIAN A. KEAY. Can. J. Chem. **70**, 2929 (1992).

A general method is described for effecting the intramolecular Diels–Alder reaction of the furan diene in which the side arm connecting the diene to the dienophile contains four carbon atoms. The use of 1.1 equivalents of methylaluminum dichloride at −78°C for 2–8 h shifts the Diels–Alder equilibrium towards the products and provides the oxatricyclo adducts in good to excellent yield. Catalytic quantities of methylaluminum dichloride (10 mol%) provided a higher quantity of adduct than excess Lewis acid when the enone was substituted with alkyl groups. The scope was extended to include a precursor containing a five carbon atom side arm, and two examples containing acetylenic dienophiles that were activated by a carbonyl moiety on the side arm. Precursors having a four carbon atom side arm provided only oxatricyclo adducts having the side arm *syn* to the oxygen bridge. The assignment of the stereochemistry of the oxatricyclo adducts is discussed in detail.

CHRISTINE ROGERS et BRIAN A. KEAY. Can. J. Chem. **70**, 2929 (1992).

On décrit une méthode générale d'effectuer une réaction intramoléculaire de Diels–Alder avec des dièmes furaniques portant une chaîne latérale de quatre atomes de carbone qui relie le diène au diénophile. L'utilisation de 1,1 équivalent de dichlorure de méthylaluminium, à −78°C, pendant 2–8 h, déplace l'equilibre de Diels–Alder vers les produits et les adduits oxatricyclo avec des rendements allant de bons à excellents. Lorsqu'on substitue l'énone avec des groupes alkyles, les quantités d'adduit formées lorsqu'on utilise des quantités catalytiques de dichlorure de méthylaluminium (10 mol%) sont plus grandes que celles obtenues avec un excès d'acide de Lewis. On a étendu le champ d'application à un précurseur contenant une chaîne latérale de cinq atomes de carbone et à deux exemples contenant des diénophiles acétyléniques activés par une portion carbonyle sur la chaîne latérale. Les précurseurs portant une chaîne latérale contenant quatre atomes de carbone ne fournissent que les adduits oxatricyclo dans lesquels la chaîne latérale est *syn* par rapport au pont oxygène. On discute en détail de l'attribution de la stéréochimie des adduits oxatricyclo.

[Traduit par la rédaction]

Can. J. Chem. Downloaded from www.nrcresearchpress.com by 88.255.202.194 on 09/08/12
For personal use only.

The intramolecular Diels–Alder (IMDA) reaction is a widely utilized synthetic strategy for the simultaneous formation of two rings with high stereo- and regio-control (1). The use of a furan moiety as the diene component in the IMDA reaction leads to the creation of an oxygenated cyclohexane ring in a rigid cycloadduct that has potential application for the synthesis of natural products. The intramolecular Diels–Alder reaction of the furan diene (IMDAF) has been studied extensively both when the tether connecting the diene and dienophile consists of three carbon atoms (1, 2), and when the tether contains a heteroatom and is either three (n = 1) or four (n = 2) atoms in length (eq. 1) (1, 3). The IMDAF reaction of precursors that have a side arm containing four (n = 2) (1, 4) or five (n = 3) (1, 5) carbon atoms have been studied to a lesser extent, and are generally reported to have equilibria that lie toward starting material. Methods employed to overcome the unfavourable equilibrium have included heat (4*a*), β-cyclodextrin (6), aqueous solutions (4*h*, 7), substituted side arms (3*g*, 3*h*, 4*k*, 4*m*, 4*n*, 5*b*, 8) and high pressure (4*b*, 4*c*, 4*j*). The success of these methods has been variable. The first four methods have produced increased starting material:adduct (SM:A) ratios for precursors with unsubstituted dienophiles but usually required long reaction times (2–14 days). High pressure (1.0–1.2 GPa) has been successful in overcoming the unfavourable equilibrium with both unsubstituted and substituted dienophiles; however, the isolated yields of the adducts have been poor, the reaction scale is limited, and access to specialized equipment is necessary. We therefore sought a generally applicable method for performing the IMDAF reaction that would overcome these limitations.

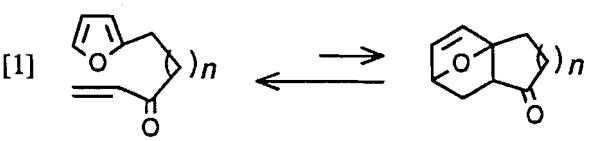

***n*=1 (a CH_2 may be substituted by an S, O, or N atom)**
***n*=2 (a CH_2 may be substituted by an O or N atom)**

Lewis acids have been used extensively in the *intermolecular* Diels–Alder reaction of the furan diene (9) to increase both the regioselectivity and the rate of reaction. Lewis acids have also been used to accelerate the rate of the *intramolecular* Diels–Alder reaction (10); however, their successful use in the IMDAF reaction (4*i*, 5*a*, 11) has been limited to only two reports: one employing an internally coordinated magnesium salt (12), and the second an application of zinc iodide (13). The paucity of examples of Lewis acid-mediated IMDAF reactions may be due to competing side reactions such as: (*a*) the polymerization of the furan ring or the dienophile (14), (*b*) the susceptibility of the furan ring to Friedel–Crafts-type reactions (14), and (*c*) the aromatization of the oxatricyclo adducts (15). We recently reported that the IMDAF reaction, in which the side arm contained four or five carbon atoms, is accelerated by the Lewis acid methylaluminum dichloride at low temperatures to provide the oxatricyclo adducts in good to excellent yield (16). We herein provide a full account of this work.

Preparation of IMDAF precursors ***1–17***

Precursors **1–8** were prepared as outlined in Scheme 1. Lithiation of either furan **18** or 2-methylfuran **19** under

[1]Author to whom correspondence may be addressed.

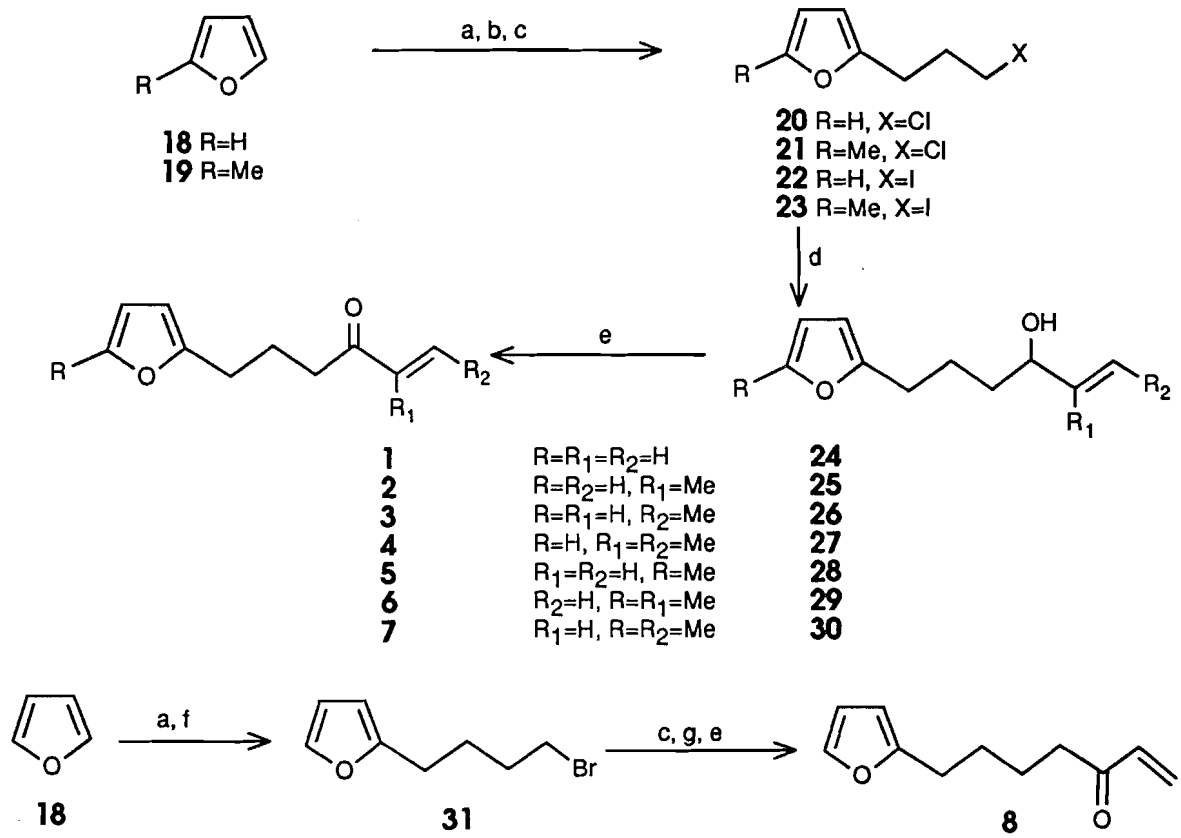

Reagents: (a) 1.2 equiv. n-BuLi, THF, 0°C, 1.5h; (b) 1-bromo-3-chloropropane; (c) NaI, acetone, reflux; (d) 2.2 equiv. t-BuLi, Et_2O, -78°C; then, acrolein, methacrolein, crotonaldehyde or tiglic aldehyde; (e) Swern [O]; (f) 1,4-dibromobutane; (g) 2.2 equiv. t-BuLi, Et_2O, -78°C; then acrolein

SCHEME 1

standard conditions (17) followed by trapping of the resultant anion with 1-bromo-3-chloropropane, afforded alkylated furans **20** (63%) and **21** (95%), respectively. Conversion of the chlorides **20** and **21** into the iodides **22** and **23** was accomplished in excellent yield under Finkelstein conditions (18). Halogen–metal exchange of the iodides **22** and **23** with *tert*-butyllithium (19) followed by quenching of the resulting carbanion with acrolein, methacrolein, crotonaldehyde, or tiglic aldehyde provided allylic alcohols **24–30**. Swern oxidation (20) of the allylic alcohols **24–30** yielded the IMDAF precursors **1–7** respectively. Furan **8** was prepared by reaction of the anion of furan **18** with 1,4-dibromobutane to provide bromide **31**, which was converted to furan **8** by the identical sequence described above (Scheme 1).

The synthesis of IMDAF precursors **9–15** is summarized in Scheme 2. Ismail and Hoffman (21) have reported that Friedel–Crafts alkylation of either furan **18** or 2-methylfuran **19** with 4-methyl-2-oxo-3-pentenenitrile **32** (22) in the presence of aluminum trichloride in benzene provided esters **33** and **34**, respectively, in reasonable yield after the reaction mixture was quenched with methanol. Our attempts to repeat this reaction provided esters **33** and **34** in poor yield (<20%) due to the competing Friedel–Crafts alkylation of the solvent benzene. Changing the solvent to carbon disulfide provided esters **33** and **34** in 30 and 66% yield, respectively. The yield of ester **33** was diminished due the formation of the 2,5-dialkylated product **35**. Attempts to prevent formation of **35** by blocking one α-site of furan with a *tert*-butyldimethylsilyl moiety were unsuccessful; the silylated furan did not undergo Friedel–Crafts reactions when subjected to a variety of Friedel–Crafts conditions.

Although Lipshutz and co-workers (23*a*) reported successful 1,4 additions of the higher-order cyanocuprate of 2-lithiofuran to α,β-unsaturated ketones, we were unsuccessful in effecting the same reaction on 3-methyl-2-butenal, methyl 3-methyl-2-butenoate, or dimethyl isopropylidenemalonate. The failure of these reactions may be due to both the low reactivity of the cuprate reagent (23*b*), and to the hindered nature of the position to be attacked.

Reduction of esters **33** and **34** with lithium aluminum hydride provided alcohols **36** and **37**, respectively, which were converted to the corresponding iodides **38** and **39** via the tosylates (18). The iodides **38** and **39** were then converted to precursors **9–12** and **13–15** via: (*a*) halogen–metal exchange, (*b*) quenching the anion with an α,β-unsaturated aldehyde to give allylic alcohols **40–46**, and (*c*) Swern oxidation.

The acetylenic precursors were prepared by treating the anion formed by halogen–metal exchange of iodide **38** with either 3-(trimethylsilyl)propynal **47** (24) or 2-butynal **48** (Scheme 2) (25). Swern oxidation provided compounds **16** and **17** in good yield.

Results and discussion

Compound **2** was treated with a number of Lewis acids (26) that had been reported to accelerate both inter- (9*c*, 27)

Can. J. Chem. Downloaded from www.nrcresearchpress.com by 88.255.202.194 on 09/08/12
For personal use only.

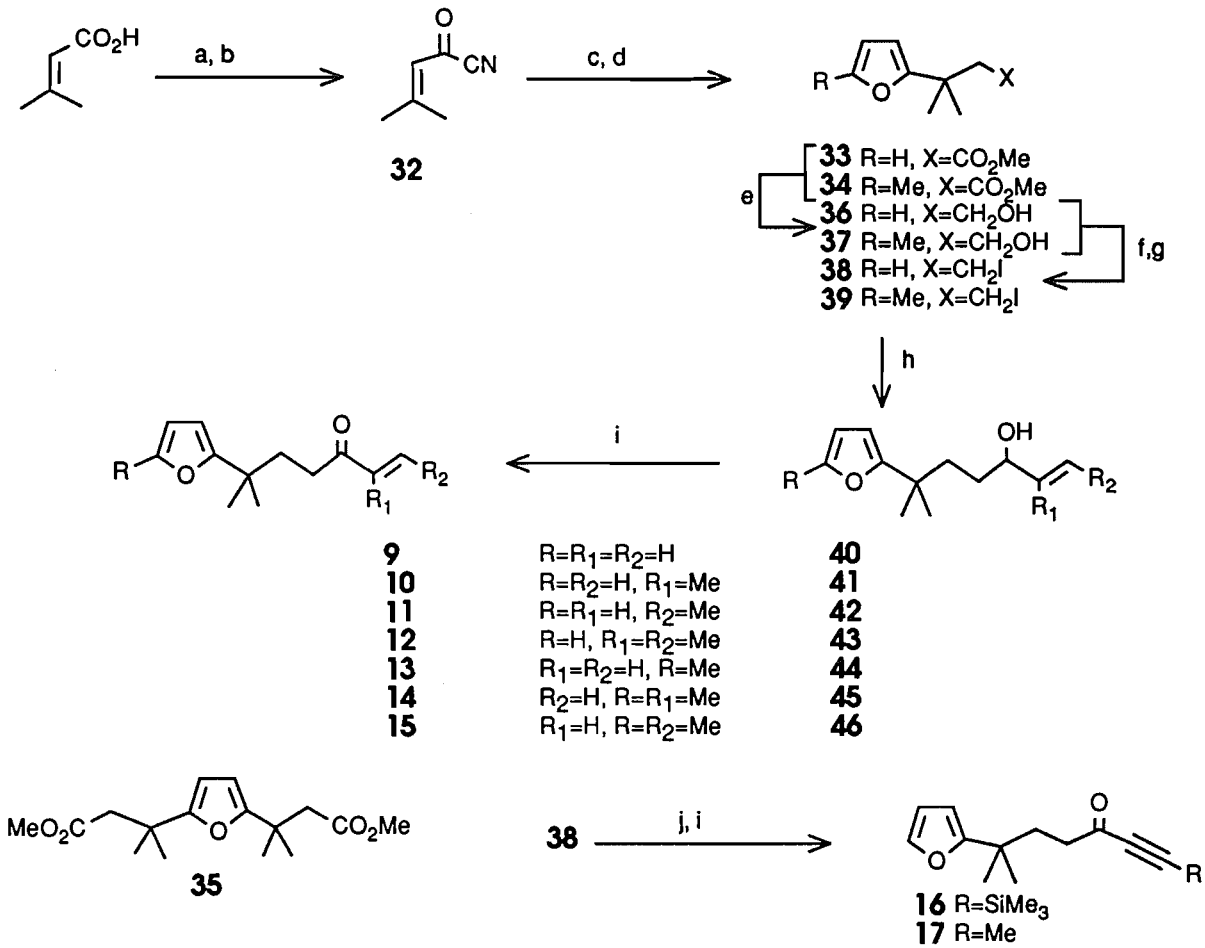

Reagents: (a) oxalyl choride, hexane; (b) CuCN, MeCN; (c) 0.25 equiv. $AlCl_3$, CS_2, furan **18** or 2-methylfuran **19**; (d) MeOH; (e) $LiAlH_4$, Et_2O; (f) TsCl, DMAP, CH_2Cl_2; (g) NaI, acetone, reflux; (h) 2.2 equiv. t-BuLi, Et_2O, -78°C; then acrolein, methacrolein, crotonaldehyde, or tiglic aldehyde; (i) Swern [O]; (j) 2.2 equiv.t-BuLi, Et_2O, -78°C; then TMSC≡CCHO (**47**) or MeC≡CCHO (**48**).

SCHEME 2

and intra-molecular (10*m*, 13, 28) Diels–Alder reactions (Table 1). Compound **2** was chosen for this model study since it had previously shown reluctance to undergo the IMDAF reaction when treated with Florisil either in methylene chloride or aqueous 2.0 M $CaCl_2$ solutions (entries 9 and 10) (4*h*). In each example, 1.1 equivalents of Lewis acid was added to a dilute solution (0.02–0.03 M) of compound **2** in methylene chloride at −78°C. Aliquots were removed from the reaction mixture and their ^{1}H NMR spectra were measured. The reaction was stirred at a particular temperature until there was no further change in the starting material to adduct (SM:A) ratio by ^{1}H NMR. The reaction was then warmed another 10 or 15°C, and the process repeated until a temperature was reached at which decomposition was detected. The aliquots removed from the reaction mixture were quenched with cold 10% sodium bicarbonate to prevent re-equilibration and to neutralize acidic by-products. The SM:A ratios were measured by integration of the ^{1}H NMR spectrum of the crude reaction mixture, in particular by comparison of the integral of the vinyl protons of the adduct **50** (δ 6.48 and 6.14) and that due to the β-furan protons of the starting material **2** (δ 6.28 and 6.00).

The results are summarized in Table 1. Zinc iodide (entry 1) was the least effective Lewis acid examined, which was surprising in light of its proven synthetic utility for accelerating both the intermolecular Diels–Alder reaction of the furan diene (9*c*) and an IMDAF reaction in which the side arm contained three carbon atoms (13). Although some adduct was produced within 3 h at room temperature, the equilibrium still favoured starting material. The ratio of SM:A did not change significantly after 39 h and decomposition products were detected by ^{1}H NMR. These findings are attributed to the unfavourable heterogeneous nature of the reaction mixture when zinc iodide is used. Tin(IV) chloride (entry 2) provided a favourable SM:A ratio of 24:76 within 1 h at −78°C; however, extensive decomposition was also observed (by ^{1}H NMR). The remaining Lewis acids (entries 3–8) provided SM:A ratios favouring adduct after only 2 h at either −78 or −50°C; decomposition was evident at temperatures above −50°C for all Lewis acids examined. The yields of the adduct were in excess of 95% (based on recovered starting material) after flash chromatography (29), indicating that decomposition below −50°C was insignificant. For ease of handling and reaction work-up, methylaluminum dichloride was chosen as the Lewis acid to continue the study.

Can. J. Chem. Downloaded from www.nrcresearchpress.com by 88.255.202.194 on 09/08/12
For personal use only.

TABLE 1. Effect of various Lewis acids on the IMDAF reaction of compound **2**

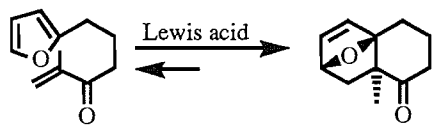

2 **50**

	Lewis acid	Conditions	2:50 Ratio
1	ZnI_2	1 h, −78°C	100:0
		3 h, r.t.	69:31
		39 h, r.t.	65:35[a]
2	$SnCl_4$	1 h, −78°C	24:76[b]
3	$BF_3 \cdot Et_2O$	2.5 h, −78°C	28:72
		3.5 h, −50°C	28:72[c]
4	$TiCl_4$:$Ti(O^iPr)_4$	4.5 h, −78°C	32.68
		2.5 h, −50°C	32.68[d]
5	$EtAlCl_2$	2.5 h, −78°C	35:65
		2.5 h, −50°C	35:65[d]
6	$MeAlCl_2$	2.5 h, −78°C	35:65
		2.5 h, −50°C	35:65[d]
7	Et_2AlCl	2.5 h, −50°C	35:65
8	Me_2AlCl	2.5 h, −50°C	32:68
9	Florisil/CH_2Cl_2	14 days, r.t. or 40°C	100:0
10	2.0 M $CaCl_2$	4 days, r.t.	50:50

[a]Some decomposition after 64 h (by ^{1}H NMR).
[b]Extensive decomposition (by ^{1}H NMR).
[c]Some decomposition after 3.5 h (by ^{1}H NMR).
[d]Decomposition occurred above −50°C.

The effect of solvent on the Lewis acid-mediated IMDAF reaction was also examined. Treatment of compound **2** in hexane with methylaluminum dichloride resulted in the formation of a gummy precipitate. Both ^{1}H NMR and TLC indicated that no IMDAF reaction had occurred. Toluene was also unsuitable as a solvent because many unidentified products formed even at −78°C. All subsequent reactions were therefore performed in methylene chloride.

The results from treating precursors **1–7** and **9–15** with methylaluminum dichloride at −78°C are summarized in Tables 2 and 3 respectively. Previous results from our lab (4*h*) using Florisil are also included for comparison purposes. Several observations are noteworthy. The use of 1.1 equivalents of methylaluminum dichloride with precursors **1**, **2**, **5**, and **6** provided their corresponding oxatricyclo adducts in excellent yields. Both compounds **1** and **5**, which have unsubstituted dienophiles, provided adducts **49** and **53** in 99% yield after only 1 h at −78°C. Compounds **2** and **6**, which were unreactive with Florisil, gave adducts **50** and **54** in 63 and 80% yields, respectively. In contrast, precursors **3**, **4**, and **7**, which have substitution at the terminus of the dienophile, had SM:A ratios in favour of starting material. The unreactive nature of these dienophiles in the IMDAF reaction is well precedented in the literature (4*i*), and may be a result of both increased steric interactions in the transition state as well as increased electron density of the carbon–carbon double bond.

The geminally substituted precursors **9** and **13** (Table 3) provided adducts **56** and **60** in 88% yield, respectively, upon treatment with Florisil alone after only 1 day at room temperature, and therefore were not treated with methylaluminum dichloride. Compounds **10**, **11**, **14**, and **15** provided varying SM:A ratios when Florisil was employed; however, in all cases adduct was detected and isolated. This finding is in contrast to the results from the corresponding unsubstituted precursors **2**, **3**, **6**, and **7** (Table 1) in which no adduct was detected after 6 days. The increased reactivity of the substituted precursors may be due to the *gem*-dialkyl effect (3*g*, 3*h*, 4*m*, 8, 30).

Treatment of compounds **10**, **11**, **14**, and **15** with 1.1 equivalents of methylaluminum dichloride provided SM:A ratios in favour of starting material; increased quantities of adduct were formed relative to the results from using Florisil, except for compound **14**. The lower SM:A ratios for compounds **10** and **14** (Table 3) when compared to the SM:A ratios for compounds **2** and **6** (Table 2) can be explained by unfavourable 1,3-diaxial methyl interactions present in adducts **57** and **61**, which are absent in adducts **50** and **54**. Thus the 1,3-diaxial interactions may be promoting the retro Diels–Alder reaction. Compound **12** provided no adduct with 1.1 equivalents of methylaluminum dichloride.

We then sought a means of overcoming the unfavourable equilibrium for precursors containing more hindered dienophiles. A survey of the literature revealed very few examples in which catalytic quantities of Lewis acids had been employed to accelerate IMDA reactions (10*h*, 10*j*, 10*k*, 28*c*, 31) and no examples involving the IMDAF reaction. Dramatic improvements in the SM:A ratios were observed when compounds **3**, **6**, **7** (Table 2), **10**, **11**, and **14** (Table 3) were exposed to 0.1 equivalents of methylaluminum dichloride at −78°C. In all cases the SM:A ratios favoured the adducts (SM:A ratios ranged from 40:60 to 0:100) and provided the oxatricyclo adducts in good to excellent yield. The SM:A ratios of compound **4** and **15** improved only slightly when compared to the results from the use of 1.1 equivalents of Lewis acid, and the tiglic precursor **12** did not react at all. These findings therefore represent the first examples of Lewis acid-catalyzed IMDAF reactions. In addition, these are also the first examples of Lewis acid-catalyzed IMDA reactions involving systems containing an internally activated dienophile.

The greatly improved SM:A ratios obtained when 0.1 equivalents of methylaluminum dichloride was employed, when compared with 1.1 equivalents, were rationalized by considering the effect that the amount of Lewis acid present has on the reaction equilibria. Our IMDAF reactions were shown to be under thermodynamic control: the reaction of pure adduct **50** with 1.1 equivalents of methylaluminum dichloride at −78°C for 2.5 h provided the same ratio of compounds **2**:**50** (35:65) that was obtained when pure precursor **2** was treated under the identical conditions (Scheme 3). The proposed equilibria are illustrated in Scheme 4. In the presence of 1.1 equivalents of Lewis acid the starting material and adduct are essentially complexed with Lewis acid and therefore both the forward and reverse Diels–Alder reactions are accelerated, leading to a thermodynamic ratio of Lewis acid complexed starting material **A*** and adduct **B***. Treatment of the reaction mixture with a bicarbonate quench at −78°C destroys the Lewis acid and provides, in the case of compound **3**, a SM:A ratio of 78:22 (Table 2). This ratio

Can. J. Chem. Downloaded from www.nrcresearchpress.com by 88.255.202.194 on 09/08/12
For personal use only.

TABLE 2. Effect of methylaluminum dichloride on IMDAF reactions

Starting Material	Conditions	Time (h)	SM:Adduct Ratio	Yield[a] (%)	Adduct
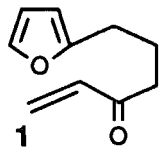 **1**	Florisil	144	10:90	71 (79)	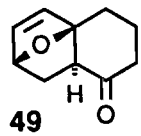 **49**
	1.1 eq. $MeAlCl_2$	1	0:100	99	
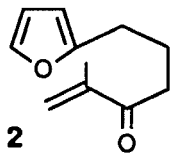 **2**	Florisil	144	100:0	0	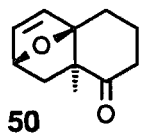 **50**
	1.1 eq. $MeAlCl_2$	2.5	35:65	63 (96)	
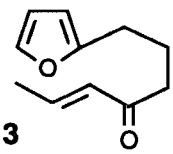 **3**	Florisil	144	100:0	0	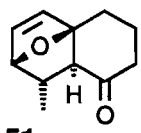 **51**
	1.1 eq. $MeAlCl_2$	8	78:22	11 (65)	
	0.1 eq. $MeAlCl_2$	2	31:69	69	
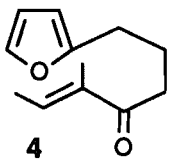 **4**	1.1 eq. $MeAlCl_2$	2	100:0	0	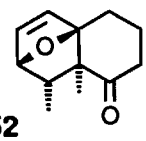 **52**
	0.1 eq. $MeAlCl_2$	2	95:5	4	
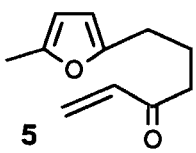 **5**	Florisil	336	12:88	65 (72)	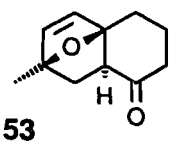 **53**
	1.1 eq. $MeAlCl_2$	1	0:100	99	
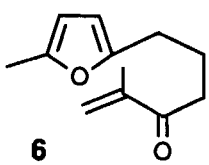 **6**	Florisil	144	100:0	0	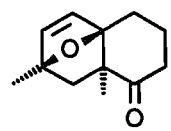 **54**
	1.1 eq. $MeAlCl_2$	8	19:81	80 (97)	
	0.1 eq. $MeAlCl_2$	2	0:100	99	
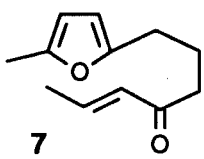 **7**	Florisil	144	100:0	0	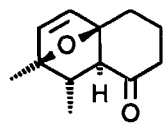 **55**
	1.1 eq. $MeAlCl_2$	8	82:18	18 (97)	
	0.1 eq. $MeAlCl_2$	2	24:76	74	

[a]Yield in parentheses is based on recovered starting material.

is therefore indicative of the **A***:**B*** ratio in solution, since it has been shown that compound **3** and adduct **51** do not interconvert in the absence of Lewis acid or upon work-up at room temperature. When catalytic quantities of methylaluminum dichloride are employed, the Lewis acid should preferentially complex with the more basic enone in the starting material **A** (Scheme 4) rather than with the saturated ketone in the adduct **B** (32). The dissociation of the Lewis acid from the adduct **B*** and complexation with **A** thus not only slows the rate of the reverse Diels–Alder reaction but accelerates the forward reaction, leading to a shift in the equilibrium towards adduct. The SM:A ratio for compound **3**:**51** increased to 31:69 (Table 2) with 0.1 equivalents of Lewis acid. Attempts to probe the nature of the species in solution by ^1H NMR studies have been inconclusive to date. Further work is in progress to establish support for the above hypothesis.

The utility of mild Lewis acids in the IMDAF reaction was not limited to either a four carbon atom side arm or dienophiles comprising enones. Compound **8**, containing a five carbon atom side arm, provided two oxatricyclo adducts **63** and **64** in a ratio of 84:8 in favour of the *endo* isomer in addition to unreacted starting material when treated with 0.1 equivalents of methylaluminum dichloride at −78°C for 2 h (Table 4). The stereochemistry of the major isomer (**63**) was determined by comparison of the ^1H NMR spectrum of **63**

Can. J. Chem. Downloaded from www.nrcresearchpress.com by 88.255.202.194 on 09/08/12
For personal use only.

TABLE 3. Effect of $MeAlCl_2$ on the IMDAF reaction of geminally substituted precursors

Starting Material	Conditions	Time (h)	SM:Adduct Ratio	Yield[a] (%)	Adduct
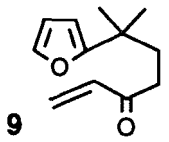 **9**	Florisil	12	0:100	88	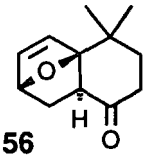 **56**
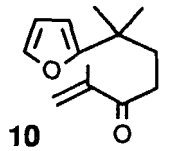 **10**	Florisil	24	83:17	16 (68)	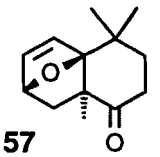 **57**
	1.1 eq. $MeAlCl_2$	8	68:32	31 (96)	
	0.1 eq. $MeAlCl_2$	2	40:60	60	
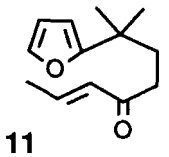 **11**	Florisil	192	87:13	12 (67)	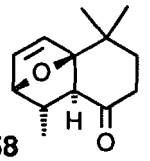 **58**
	1.1 eq. $MeAlCl_2$	8	73:27	22 (94)	
	0.1 eq. $MeAlCl_2$	2	27:73	70	
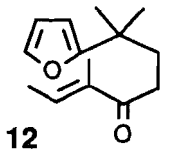 **12**	1.1 eq. $MeAlCl_2$	2	100:0	-	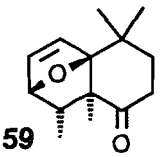 **59**
	0.1 eq. $MeAlCl_2$	2	100:0	-	
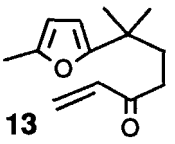 **13**	Florisil	12	0:100	96	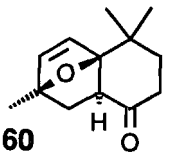 **60**
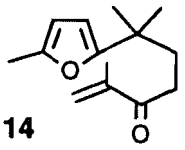 **14**	Florisil	240	77:23	19 (68)	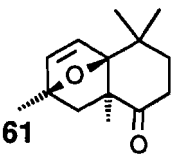 **61**
	1.1 eq. $MeAlCl_2$	8	78:22	22 (97)	
	0.1 eq. $MeAlCl_2$	2	23:77	75	
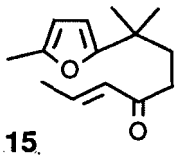 **15**	Florisil	336	85:15	13 (62)	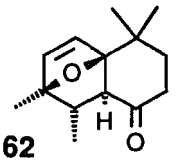 **62**
	1.1 eq. $MeAlCl_2$	8	78:22	18 (93)	
	0.1 eq. $MeAlCl_2$	2	69:31	30	

[a]Yield in parentheses is based on recovered starting material.

with that reported by Harwood and co-workers (5*a*). Interestingly, compound **8** has been previously reported to provide adducts **63** and **64** only at 1.2 GPa and in a ratio of 1:1 (5*a*).

Acetylenic precursors **16** and **17** provided the strained adducts **65** (88%) and **66** (97%), respectively, when treated with 1.1 equivalents of dimethylaluminum chloride at −50°C for 2.5 h (Scheme 5). The weaker Lewis acid dimethylaluminum chloride (26) was employed to minimize possible side reactions such as aromatization of the adducts. The use of internally activated acetylenic dienophiles in either the IMDA or IMDAF reaction is rare (1, 33), and no successful examples have been reported with the IMDAF reaction (4*l*). Usually the acetylene has been activated from the terminus by an ester moiety (1, 10). Thus, the reactions of compounds **16** and **17** are the first successful IMDA reactions involving internally activated acetylenic dienophiles. Adduct **65** was easily purified by flash chromatography, while adduct **66** was not as stable and partially isomerized to compound **67**, which contains an exocyclic double bond, upon standing.

Stereochemistry of the adducts

The stereochemistry of all the adducts formed in the Lewis acid accelerated IMDAF reactions containing a four-carbon

Can. J. Chem. Downloaded from www.nrcresearchpress.com by 88.255.202.194 on 09/08/12
For personal use only.

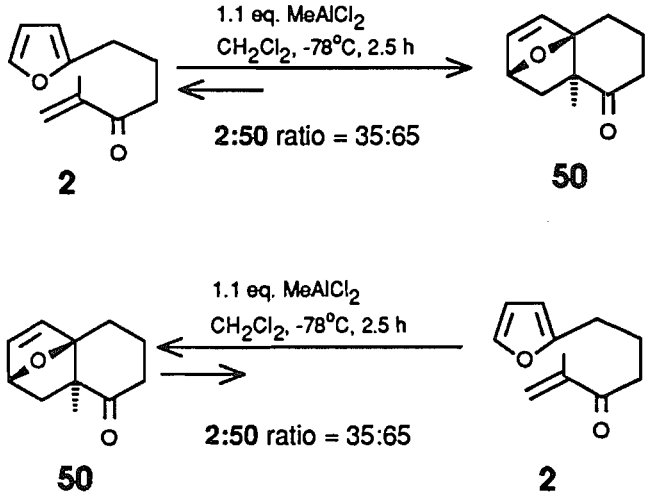

SCHEME 3

side arm had the side arm orientated *syn* with respect to the oxygen bridge resulting from an *exo* mode of attack. This is not surprising since (1) the calculated $\Delta G^0 = +12.9$ kJ/mol (PCModel 4), for the equilibration between the *exo* adduct **49** and the corresponding *endo* adduct, favours the *exo* adduct and (2) the reactions are under thermodynamic control (*vide supra*). This stereochemistry is consistent with that reported by others in the literature for tethers consisting of four carbon atoms with an internally activated dienophile (4*a*,*f*). The delineation of the stereochemistry in adducts **49–51** and **53–55** (Scheme 6) will be described in detail as representative examples. The stereochemistry of the remaining adducts arising from either acrolein-, methacrolein-, or crotonaldehyde-type dienophiles were determined in a similar manner.

The stereochemistry of adducts **49** and **53** was determined by ^{1}H NMR based on the coupling constants of protons H-6α, H-7α, and H-7β (Scheme 6). The bridge proton in adduct **49** H-8 (δ 4.91) was coupled to both H-7β (3.8 Hz) and H-9 (0.9 Hz). Coupling of H-8 to H-7α was not observed since the dihedral angle of H-8—C-8—C-7—H-7α was 90°. Proton H-7β (δ 2.49) was a multiplet with couplings of 3.0 Hz, 3.8 Hz, and 11.8 Hz to protons H-6α (δ 2.28), H-8, and H-7α (δ 1.49), respectively. The 3.0 Hz coupling constant observed between H-7β and H-6α was indicative of a 60° dihedral angle, thereby placing the side arm *syn* to the oxygen bridge. If the side arm was orientated *anti* to the oxygen bridge then the C-6 proton would have a dihedral angle of 0°C to the C-7α proton and a coupling constant of approximately 8 Hz would be expected (34). The 8.3 Hz coupling observed between H-7α and H-6α therefore confirmed our assignment of the relative stereochemistry. Since compound **53** has a methyl group at C-8, proton H-7α was identified by its upfield shift as the doublet of doublets at δ 1.61. This upfield shift was observed in compound **49** for H-7α, and was probably due to the diamagnetic anisotropy of the carbon–carbon double bond. The coupling constants of 11.8 Hz to H-7β and 8.2 Hz to H-6α again confirmed the *syn* orientation of the side arm to the oxygen bridge in compound **53**.

The determination of the stereochemistry of the side arm with respect to the oxygen bridge in adducts **50** and **54** could not be directly related to coupling constants since a methyl group is attached at C-6 (Scheme 6). If the adducts were formed from the mode of cyclization in which the side arm was orientated *exo*, the C-6 methyl substituent would be *anti* (i.e., *endo*) to the oxygen bridge and be shielded by the C-9—C-10 double bond. The methyl group at C-6 had an upfield chemical shift of δ 1.11 and δ 1.08 for adducts **50** and **54**, respectively, which is indicative of *endo* orientated methyl groups in oxatricyclo adducts (35). The proton H-7β was a doublet of doublets at δ 2.86 in compound **50**, due to vicinal coupling with the bridge proton H-8 (5.1 Hz) and geminal coupling to H-7α (11.8 Hz). Proton H-7α coupled only geminally to H-7β (11.8 Hz), and was highly shielded at δ 1.00 due to the anisotropy of the carbon–carbon double bond. Similarly, protons H-7α and H-7β appeared as an AB quartet (11.8 Hz) at δ 1.12 and δ 2.55, respectively, in compound **54**.

The crotonaldehyde-derived adducts **51** and **55** contain an additional stereocenter at C-7. Since IMDAF reactions catalyzed by Lewis acids have a concerted mechanism (36), the

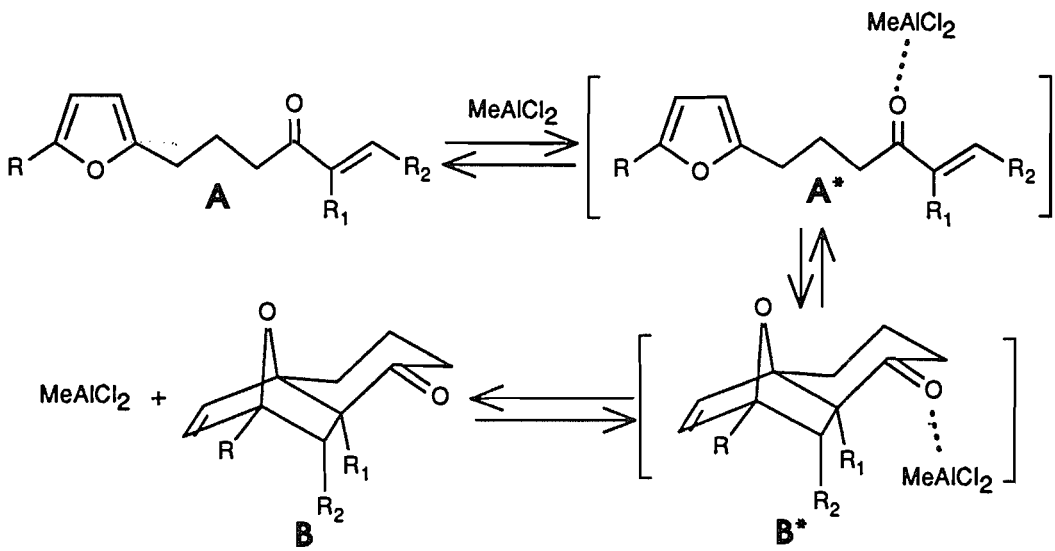

SCHEME 4

Can. J. Chem. Downloaded from www.nrcresearchpress.com by 88.255.202.194 on 09/08/12
For personal use only.

TABLE 4. IMDAF reaction of compound **8**

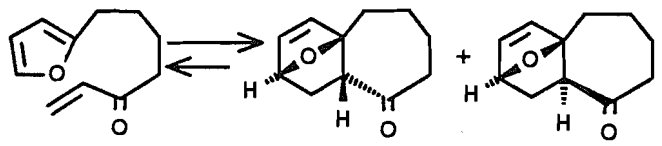

8 **63** *endo* **64** *exo*

	Temperature (°C)	SM : *endo* : *exo*
0.1 eq. $MeAlCl_2$	-78	8 : 84 : 8
	-65	8 : 81 : 11

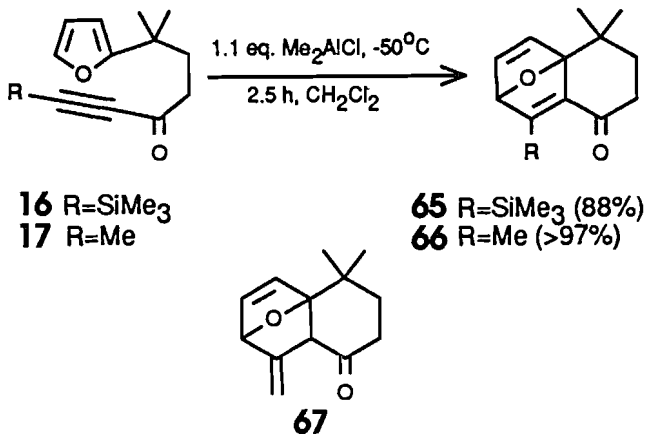

16 R=$SiMe_3$
17 R=Me

65 R=$SiMe_3$ (88%)
66 R=Me (>97%)

67

SCHEME 5

methyl group at C-7 should be *anti* to the oxygen bridge (Scheme 6) if an *exo* mode of cyclization had occurred. Proton H-8 (δ 4.69) in adduct **51** was a doublet of doublets coupled to H-9 (1.6 Hz) and H-7β (4.7 Hz), indicating that the methyl group at C-7 was indeed *anti* to the oxygen bridge. If the C-7 methyl group was *syn* to the oxygen bridge, the protons H-8 and H-7 would form a 90° dihedral angle, and would therefore show no coupling (34). This stereochemical assignment was also supported by the highly shielded chemical shift of the C-7 methyl doublet (δ 0.93) due to the anisotropy of the C-9—C-10 carbon–carbon double bond. Proton H-6 was a doublet (4.0 Hz, δ 1.73) and coupled to H-7β (δ 2.79). The 4.0 Hz coupling constant was indicative of a 60° dihedral angle, thereby placing H-6 *anti*, and the side arm *syn*, with respect to the oxygen bridge. The stereochemistry of compound **55** was assigned in a similar manner. The C-7 methyl group appeared as an upfield doublet at δ 0.95, consistent with the moiety being *anti* to the oxygen bridge. Proton H-6 (δ 1.89) was a doublet with 4.2 Hz coupling to H-7, indicating the side arm was *syn* with respect to the oxygen bridge.

Conclusions

We have shown that Lewis acids are effective reagents for promoting the IMDAF reaction in which the diene and dienophile are connected by four or five carbon atoms. The reaction conditions are also applicable to acetylenic dienophiles internally activated by a carbonyl moiety. The use of methylaluminum dichloride makes the IMDAF reaction a viable synthetic transformation since: (1) the time for the reaction to reach equilibrium is reduced to a few hours from 4 to 14 days; (2) the isolated yields of adducts are very high, and (3) only one adduct is formed with up to four asymmetric centres of known relative stereochemistry. Synthetic applications of this methodology are currently in progress.

Experimental

General methods

Melting points were determined using an Electrothermal melting point apparatus and are uncorrected. Boiling points refer to the air-bath temperature using Kugelrohr distillation apparatus, and are also uncorrected. Infrared spectra were obtained as either thin films (oils) on either NaCl or KBr plates, or as KBr pellets (solids). The infrared spectra were recorded on either a Nicolet 5-DX FT-IR spectrophotometer or a Mattson model 4030 FT-IR.

Nuclear magnetic resonance spectra were obtained on one of three instruments: Bruker AC-300 (^1H 300 MHz, ^{13}C 75 MHz), Bruker ACE-200 (^1H 200 MHz, ^{13}C 50 MHz), or a Bruker AM-400 spectrometer (^1H 400 MHz). Deuterochloroform was used both as the solvent, and the internal standard (^1H, δ 7.27; ^{13}C, δ 77.0) un-

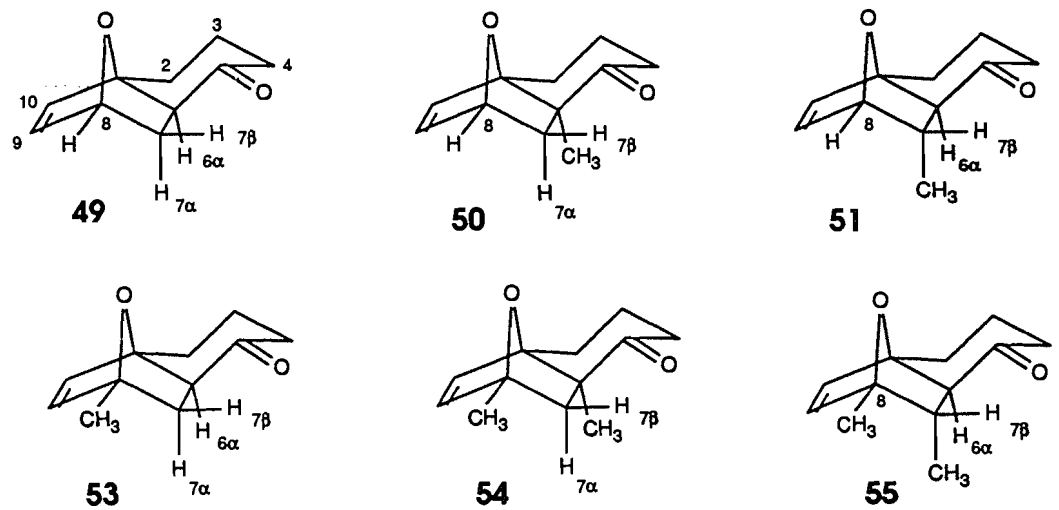

SCHEME 6

Can. J. Chem. Downloaded from www.nrcresearchpress.com by 88.255.202.194 on 09/08/12
For personal use only.

Can. J. Chem. Downloaded from www.nrcresearchpress.com by 88.255.202.194 on 09/08/12
For personal use only.

less otherwise stated. All ^{1}H NMR spectra listed will have the following format: chemical shift (in ppm), (multiplicity, number of protons, coupling constants (Hz), assignment). The abbreviations used to describe the multiplicities are as follows: br = broadened, s = singlet, d = doublet, t = triplet, q = quartet, qu = quintet, and ABq refers to a quartet due to an AB spin system. The ^{13}C NMR spectra listed will have the following format: chemical shift (in ppm), (number of attached protons as determined by DEPT experiments).

Low-resolution mass spectra were recorded using either a Varian CH5 spectrometer, or a VG 7070 instrument. The data are listed as mass (*m/e*), (relative intensity, assignment). The spectra were obtained either by the electron-impact (EI) method or field ionization (FI), and the method will only be listed if FI was used. High-resolution mass spectra were recorded on a Kratos MS80 spectrometer. Microanalyses were performed either by Guelph Chemical Laboratories Limited, Guelph, Ontario, or by Mrs. D. Fox, Department of Chemistry, University of Calgary.

Solvents were either dried by standard methods (37), then distilled prior to use, or were purchased as anhydrous solvents in Sure-Seal® bottles from the Aldrich Chemical Company. THF was dried over sodium and benzophenone, as was diethyl ether. Methylene chloride, diisopropyl amine, and triethylamine were dried over CaH_2. Methanol was refluxed with Mg^0 metal for 12 h, then distilled. DMSO was dried over NaOH. Acetonitrile, DMF, and diethyl ether were purchased as anhydrous solvents, and HPLC-grade acetone was used.

The Lewis acids employed in this study were used as purchased, with no further purification. Boron trifluoride etherate and titanium(IV) chloride were used as neat liquids. The aluminum-containing reagents were purchased as molar solutions in hexane from Aldrich.

All glassware and syringes were dried in a 120°C oven for at least 4 h, then cooled under a stream of Ar, or in a desiccator containing Drierite. Reactions that were sensitive to moisture or atmospheric conditions were performed under an Ar atmosphere.

General procedure 1: conversion of tosylate or chloride to iodide

The tosylate or chloride (10 mmol) and NaI (25 mmol) were dissolved in HPLC-grade acetone (75 mL) and heated to reflux for 24 h under Ar. The reaction was cooled, and the solvent removed *in vacuo*. Diethyl ether (100 mL) and water (75 mL) were then added to dissolve the crude material. The aqueous layer extracted with Et_2O (3 × 100 mL) and the combined organic layers were dried over Na_2SO_4 (anhydrous), filtered, and the solvent removed *in vacuo* to provide the crude iodide. The iodide was purified either by flash chromatography, or distillation.

General procedure 2: coupling of iodide with unsaturated aldehydes

The iodide was purified by filtration through basic alumina, then distillation just prior to use. The iodide (1.0 mmol) was dissolved in anhydrous Et_2O (10 mL), and the solution was cooled to −78°C in a Dry Ice – acetone bath. *tert*-Butyllithium (2.2 mmol) was added dropwise to the cooled solution by syringe, and the reaction was stirred for 1 h at −78°C. The α,β-unsaturated aldehyde was distilled from Na_2SO_4 under Ar, and was added neat (1.5 mmol) by syringe to the reaction. The reaction was continued for a further 30 min (or until monitoring by TLC showed no starting material was present), then was quenched at low temperature with saturated NH_4Cl (10 mL). After warming to room temperature, the aqueous layer was extracted with Et_2O (3 × 25 mL) and CH_2Cl_2 (2 × 25 mL). The combined organic layers were dried over Na_2SO_4, filtered, and the solvent removed *in vacuo* to provide the crude coupled product, which was purified by flash chromatography, then distillation.

General procedure 3: Swern oxidation

The method of Swern (20) was used to oxidize the allylic alcohols to the enones. Oxalyl chloride (11 mmol) was dissolved in dry CH_2Cl_2 (25 mL) and cooled to −60°C (Dry Ice – chloroform) in an Ar-purged 3-neck round-bottom flask equipped with a dropping funnel. Freshly distilled alcohol (10 mmol) was dissolved in dry CH_2Cl_2 (10 mL) and placed in the dropping funnel. DMSO (22 mmol) was added neat (by syringe) to the oxalyl chloride solution, the reaction was stirred for 2 min, and then the alcohol solution was added within 5 min. The mixture was stirred an additional 15 min, then Et_3N (50 mmol) was added and stirring was continued for another 5 min before warming the reaction to room temperature. Water (50 mL) was added, and the aqueous layer was extracted with CH_2Cl_2 (5 × 25 mL). The combined organic layers were washed with 5% HCl (15 mL), 5% Na_2CO_3 (15 mL), and water (15 mL), dried over Na_2SO_4, filtered, and the solvent removed *in vacuo* to provide the crude bad-smelling product, which was purified by flash chromatography, then distilled.

General procedure 4: IMDAF reactions in Florisil

The freshly distilled enone (1 mmol) was dissolved in dry CH_2Cl_2 (15 mL) and placed in an Ar-purged round-bottom flask. To this was added Florisil (100–200 mesh, 10 weight equivalents to the enone). The reaction was wrapped in foil and stirred at the appropriate temperature for the required length of time. The reaction was then filtered, the Florisil washed well with EtOAc (20 mL), and the solvent removed *in vacuo* without external heating to provide the crude product, which could be purified by flash chromatography.

General procedure 5: IMDAF reactions using Lewis acid

The freshly distilled enone (0.2 mmol) was dissolved in dry CH_2Cl_2 (10 mL), placed in an Ar-purged 3-necked flask, and cooled to the appropriate temperature. Methylaluminum dichloride (1.0 M in hexane) was added to the cooled enone solution, and the reaction was stirred for the appropriate length of time. The reaction was quenched with 10% $NaHCO_3$ (10 mL), and warmed until no frozen material remained. The aqueous layer was extracted with CH_2Cl_2 (4 × 10 mL), then the organic layer was washed with H_2O (15 mL), dried over Na_2SO_4, filtered, and the solvent removed *in vacuo* without external heating to provide the crude product, which was purified by flash chromatography.

*3-(2-Furyl)-1-chloropropane (**20**)*

Furan **18** (6.0 mL, 82.5 mmol) was dissolved in dry THF (140 mL) under Ar and cooled to −78°C. Butyllithium (2.5 M in hexanes, 39.6 mmol) was added, then the solution was warmed to 0°C and stirred for 2 h. The 1-bromo-3-chloropropane (15.5 g, 98.7 mmol) was passed through basic alumina, then distilled before being added dropwise to the yellow anion solution. The reaction was stirred at room temperature overnight. The solvent was removed *in vacuo*, then ether (100 mL) and saturated NH_4Cl (100 mL) were added to the oily residue. The aqueous layer was extracted with ether (3 × 100 mL), dried over Na_2SO_4, and the solvent removed *in vacuo*. Distillation under aspirator provided compound **20** as a clear, colourless oil (9.1 g, 63.1 mmol), 76% yield; bp 60–70°C/20 Torr (1 Torr = 133.3 Pa); IR (neat) cm^{-1}: 2959–2850(C-H), 735(C-Cl); ^{1}H NMR (200 MHz): 2.12(qu, 2H, J = 7.0 Hz), 2.82(t, 2H, J = 7.0 Hz), 3.57(t, 2H, J = 7.0 Hz), 6.05(dd, 1H, J = 0.8 Hz, J = 3.0 Hz), 6.30(dd, 1H, J = 1.8 Hz, J = 3.0 Hz), 7.33(dd, 1H, J = 0.8 Hz, J = 1.8 Hz); ^{13}C NMR (50 MHz): 25.07(t), 30.86(t), 44.01(t), 105.55(d), 110.09(d), 141.13(d), 154.29(s); mass spectrum: 144(15, $M^{+\cdot}$), 81(100, M − $(CH_2)_2Cl$). Exact Mass calcd. for C_7H_9ClO: 144.0342; found: 144.0352.

*3-(2-(5-Methylfuryl))-1-chloropropane (**21**)*

2-Methylfuran **19** (7.9 mL, 80.0 mmol) was dissolved in dry THF (140 mL) under Ar and cooled to −78°C. Butyllithium (2.5 M in hexanes, 38.4 mmol) was added, then the solution was warmed to 0°C and stirred for 2 h. The 1-bromo-3-chloropropane (17.0 g, 108.2 mmol) was passed through basic alumina, then distilled before being added dropwise to the yellow anion solution. The reaction was stirred at room temperature overnight. The solvent was removed *in vacuo*, then ether (100 mL) and saturated NH_4Cl (100 mL) were added to the oily residue. The aqueous layer was

Can. J. Chem. Downloaded from www.nrcresearchpress.com by 88.255.202.194 on 09/08/12
For personal use only.

extracted with ether (3 × 100 mL), dried over Na_2SO_4, and the solvent removed *in vacuo*. Distillation under aspirator provided chloride **21** as a clear, colourless oil (12.3 g, 77.5 mmol), 97% yield, bp 75–85°C/20 Torr; IR (neat) cm^{-1}: 2956–2867(C-H), 653(C-Cl); ^1H NMR (200 MHz): 2.10(qu, 2H, J = 6.9 Hz), 2.27(s, 3H), 2.76(t, 2H, J = 7.2 Hz), 3.58(t, 2H, J = 6.5 Hz), 5.87(d, 1H, J = 3.0 Hz), 5.92(d, 1H, J = 3.0 Hz); ^{13}C NMR (50 MHz): 13.27(q), 25.02(t), 30.87(t), 43.96(t), 105.66(d), 106.02(d), 150.43(s), 152.25(s); mass spectrum: 158(11, $M^{\cdot+}$), 95(100, M − $(CH_2)_2Cl$). Exact Mass calcd. for $C_8H_{11}OCl$: 158.0498; found: 158.0501.

3-(2-Furyl)-1-iodopropane (22)

Using general procedure 1, chloride **20** (9.1 g, 63.1 mmol) was converted to iodide **22** (14.1 g, 59.7 mmol) in 95% yield after distillation; bp 20–30°C/0.04 Torr; IR (neat) cm^{-1}: 3144–3001(C-H), 2953–2843(C-H); ^1H NMR (200 MHz): 2.15(qu, 2H, J = 7.0 Hz), 2.77(t, 2H, J = 7.0 Hz), 3.20(t, 2H, J = 7.0 Hz), 6.06(dd, 1H, J = 0.8 Hz, J = 3.1 Hz), 6.29(dd, 1H, J = 1.8 Hz, J = 3.1 Hz), 7.32(dd, 1H, J = 0.8 Hz, J = 1.8 Hz); ^{13}C NMR (50 MHz): 5.79(t), 28.57(t), 31.61(t), 105.70(d), 110.09(d), 141.16(d), 153.92(s); mass spectrum: 236(51, $M^{\cdot+}$), 81(100, M − $(CH_2)_2I$). Exact Mass calcd. for C_7H_9IO: 235.9697; found: 235.9704.

3-(2-(5-Methylfuryl))-1-iodopropane (23)

Using general procedure 1, chloride **21** (3.75 g, 23.6 mmol) was converted to the iodide **23** (5.60 g, 22.4 mmol) in 95% yield after distillation; bp 100°C/20 Torr; IR (neat) cm^{-1}: 3102(C-H), 2942–2845(C-H); ^1H NMR (300 MHz): 2.13(qu, 2H, J = 6.8 Hz), 2.26(s, 3H), 2.71(t, 2H, J = 6.8 Hz), 3.21(t, 2H, J = 6.8 Hz), 5.85 and 5.89(ABq, 2H, J = 3.0 Hz); ^{13}C NMR (50 MHz): 5.88(t), 13.42(q), 28.63(t), 31.72(t), 105.78(d), 106.28(d), 150.50(s), 151.94(s): mass spectrum: 250(51, $M^{\cdot+}$), 95(100, M − $(CH_2)_2I$). Exact Mass calcd. for $C_8H_{11}IO$: 249.9855; found: 249.9857.

6-(2-Furyl)-1-hexen-3-ol (24)

Using general procedure 2, iodide **22** (0.59 g, 2.50 mmol) was treated with *tert*-butyllithium (3.23 mL, 5.5 mmol) and acrolein (0.25 mL, 3.74 mmol) to produce compound **24** (0.22 g, 1.32 mmol) as a clear, colourless oil in 53% yield after purification by flash chromatography (5:1) and distillation; bp 60–68°C/0.04 Torr; IR (neat) cm^{-1}: 3385 (O-H); ^1H NMR (200 MHz): 1.52–1.84(overlapping m, 6H), 2.67(t, 2H, J = 7.1 Hz), 4.13(m, 1H, J = 6.2 Hz), 5.12(ddd, 1H, J = 1.3 Hz, J = 1.3 Hz, J = 10.3 Hz), 5.23(ddd, 1H, J = 1.3 Hz, J = 1.3 Hz, J = 17.2 Hz), 5.90(ddd, 1H, J = 6.2 Hz, J = 10.3 Hz, J = 17.2 Hz), 6.00(dd, 1H, J = 0.8 Hz, J = 3.1 Hz), 6.28(dd, 1H, J = 1.8 Hz, J = 3.1 Hz), 7.30(dd, 1H, J = 0.8 Hz, J = 1.8 Hz); ^{13}C NMR (50 MHz): 23.87(t), 27.80(t), 36.39(t), 72.93(d), 104.85(d), 110.05(d), 114.72(t), 140.77(d), 141.09(d), 155.98(s); mass spectrum: 166(9, $M^{\cdot+}$), 148(10, M − H_2O), 94(100, M − CH_2=C(OH)CH=CH_2). Exact Mass calcd. for $C_{10}H_{14}O_2$: 166.0994; found: 166.0994.

6-(2-Furyl)-2-methyl-1-hexen-3-ol (25)

Using general procedure 2, iodide **22** (0.51 g, 2.18 mmol) was treated with *tert*-butyllithium (2.82 mL, 4.79 mmol) and methacrolein (0.27 mL, 3.26 mmol) to produce compound **25** (0.22 g, 1.20 mmol) as a clear, colourless oil in 55% yield after purification by flash chromatography (5:1) and distillation; bp 130°C/0.1 Torr; IR (neat) cm^{-1}: 3397(OH); ^1H NMR (200 MHz): 1.55–1.80(m, 5H), 1.72(t, 3H, J = 1.1 Hz, J = 1.1 Hz), 2.67(t, 2H, J = 7.2 Hz, H-4), 4.08(br q, 1H), 4.85(qu, 1H, J = 1.6 Hz), 4.95(m, 1H, J = 1.0 Hz, J = 1.6 Hz), 5.99(dd, 1H, J = 0.8 Hz, J = 3.1 Hz), 6.28(dd, 1H, J = 1.8 Hz, J = 3.1 Hz), 7.30(dd, 1H, J = 0.8 Hz, J = 1.8 Hz); ^{13}C NMR (50 MHz): 17.45(q), 24.06(t), 27.76(t), 34.22(t), 75.85(d), 104.82(d), 110.03(d), 111.10(t), 140.75(d), 147.40(s), 156.00(s); mass spectrum: 180(10, $M^{\cdot+}$), 94(100, M − $CH_2CH(OH)C(Me)$=CH_2, McLafferty rearr.). Exact Mass calcd. for $C_{11}H_{16}O_2$: 180.1151; found: 180.1150.

(E-7-(2-Furyl)-2-hepten-4-ol (26)

Using general procedure 2, iodide **22** (0.60 g, 2.56 mmol) was treated with *tert*-butyllithium (3.32 mL, 5.64 mmol) and crotonaldehyde (0.32 mL, 3.84 mmol) to produce compound **26** (0.31 g, 1.72 mmol) as a clear, colourless oil in 67% yield after purification by flash chromatography (9:1) and distillation; bp 52–68°C/0.035 Torr; IR (neat) cm^{-1}: 3443(O-H); ^1H NMR (200 MHz): 1.47–1.84(m, 5H), 1.70(dd, 3H, J = 0.9 Hz, J = 6.0 Hz), 2.65(t, 2H, J = 7.1 Hz), 4.06(br q, 1H, J = 6.3 Hz), 5.48(ddq, 1H, J = 0.9 Hz, J = 6.0 Hz, J = 15.3 Hz), 5.67(ddq, 1H, J = 1.5 Hz, J = 6.8 Hz, J = 15.3 Hz), 5.99(dd, 1H, J = 0.8 Hz, J = 3.1 Hz), 6.28(dd, 1H, 1.9 Hz, J = 3.1 Hz), 7.30(dd, 1H, J = 0.8 Hz, J = 1.9 Hz); ^{13}C NMR (50 MHz): 17.62(q), 24.00(t), 27.81(t), 36.63(t), 72.84(d), 104.78(d), 110.02(d), 126.97(d), 134.11(d), 140.72(d), 156.05(s); mass spectrum: 180(8, $M^{\cdot+}$), 162(39, M − H_2O), 94(100, M − $CH_2CH(OH_2)$-CH=CHMe). Anal. calcd. for $C_{11}H_{16}O_2$: C 73.30, H 8.95; found: C 73.10, H 9.02.

(E)-7-(2-Furyl)-3-methyl-2-hepten-4-ol (27)

Using general procedure 2, iodide **22** (1.56 g, 6.63 mmol) was treated with *tert*-butyllithium (8.58 mL, 14.58 mmol) and tiglic aldehyde (0.96 mL, 9.94 mmol) to produce compound **27** (0.58 g, 3.00 mmol) as a clear, colourless oil in 45% yield after purification by flash chromatography (7:1) and distillation; bp 72–78°C/0.1 Torr; IR (neat) cm^{-1}: 3365(O-H); ^1H NMR (200 MHz): 1.49(br, s, 1H), 1.50–1.80(m, 10H), 2.65(t, 2H, J = 5.0 Hz), 4.01(br m, 1H), 5.47(br q, 1H), 5.99(dd, 1H, J = 0.7 Hz, J = 3.1 Hz), 6.28(dd, 1H, J = 1.9 Hz, J = 3.1 Hz), 7.30(dd, 1H, J = 0.7 Hz, J = 1.9 Hz); mass spectrum: 194(23, $M^{\cdot+}$), 176(42, M − H_2O), 94(100, M − $CH_2CH(OH)C(Me)$=CHMe). Anal. calcd. for $C_{12}H_{18}O_2$: C 74.19, H 9.34; found: C 73.91, H 9.32.

6-(2-(5-Methylfuryl))-1-hexen-3-ol (28)

Using general procedure 2, iodide **23** (0.59 g, 2.34 mmol) was treated with *tert*-butyllithium (3.03 mL, 5.15 mmol) and acrolein (0.24 mL, 3.51 mmol) to produce compound **28** (0.25 g, 1.40 mmol) as a clear, colourless oil in 60% yield after purification by flash chromatography (5:1) and distillation; bp 130–135°C/12 Torr; IR (neat) cm^{-1}: 3400(C-O), 1021(C-O); ^1H NMR (200 MHz): 1.53–1.81(overlapping m, 6H), 2.26(s, 1H), 2.61(t, 2H, J = 7.2 Hz), 4.13(br, m, 1H, J = 6.2 Hz), 5.12(dt, 1H, J = 1.3 Hz, J = 1.3 Hz, J = 10.3 Hz), 5.23(dt, 1H, J = 1.3 Hz, J = 1.3 Hz, J = 17.2 Hz), 5.85(ABq, 2H), 5.87(ddd, 1H, J = 6.2 Hz, J = 10.3 Hz, J = 17.2 Hz); ^{13}C NMR (50 MHz): 13.41(q), 23.96(t), 27.85(t), 36.42(t), 72.93(d), 105.40(d), 105.73(d), 114.73(t), 141.10(d), 150.16(s), 154.08(s); mass spectrum: 180(31, $M^{\cdot+}$), 162(7, M − H_2O), 108 (100, M − CH_2=C(OH)CH=CH_2). Anal. calcd. for $C_{11}H_{16}O_2$: C 73.30, H 8.95; found: C 73.08, H 9.21.

6-(2-(5-Methylfuryl))-2-methyl-1-hexen-3-ol (29)

Using general procedure 2, iodide **23** (0.52 g, 2.07 mmol) was treated with *tert*-butyllithium (2.67 mL, 4.55 mmol) and methacrolein (0.26 mL, 3.10 mmol) to produce compound **29** (0.28 g, 1.45 mmol) as a clear, colourless oil in 70% yield after purification by flash chromatography (5:1) and distillation; bp 69–77°C/0.04 Torr; IR (neat) cm^{-1}: 3405 (O-H); ^1H NMR (200 MHz): 1.55–1.70(m, 5H), 1.72(dd, 3H, J = 0.9 Hz, J = 1.2 Hz), 2.25(s, 3H), 2.61(t, 2H, 7.0 Hz), 4.08(br t, 1H, J = 7.5 Hz), 4.84(m, 1H, J = 1.7 Hz), 4.95(m, 1H, J = 0.8 Hz, J = 1.7 Hz), 5.85(ABq, 2H); ^{13}C NMR (50 MHz): 13.42(q), 17.44(q), 24.19(t), 27.84(t), 34.35(t), 75.66(d), 105.40(d), 105.79(d), 110.99(t), 147.48(s), 150.13(s), 154.16(s); mass spectrum: 194(14, $M^{\cdot+}$), 108(100, M − $CH_2CH(OH)C(Me)$=CH_2). Anal. calcd. for $C_{12}H_{18}O_2$: C 74.19, H 9.34; found: C 73.82, H 9.38.

(E)-7-(2-(5-Methylfuryl))-2-hepten-4-ol (30)

Using general procedure 2, iodide **23** (0.79 g, 3.18 mmol) was treated with *tert*-butyllithium (4.10 mL, 6.99 mmol) and crotonaldehyde (0.53 mL, 6.35 mmol) to produce compound **30**

Can. J. Chem. Downloaded from www.nrcresearchpress.com by 88.255.202.194 on 09/08/12
For personal use only.

(0.52 g, 2.66 mmol) as a clear, colourless oil in 84% yield after purification by flash chromatography (9:1) and distillation; bp 72–78°C/0.1 Torr; IR (neat) cm^{-1}: 3417(O-H); ^1H NMR (200 MHz): 1.50–1.70(m, 5H), 1.70(dd, 3H, J = 0.9 Hz, J = 6.3 Hz), 2.25(s, 3H), 2.58(t, 2H, J = 7.5 Hz), 4.06(br m, 1H), 5.46(ddq, 1H, J = 1.2 Hz, J = 6.8 Hz, J = 15.3 Hz), 5.68(ddq, 1H, J = 0.9 Hz, J = 5.9 Hz, J = 15.3 Hz), 5.85(ABq, 2H); ^{13}C NMR (50 MHz): 13.46(q), 17.82(q), 24.12(t), 27.88(t), 36.68(t), 72.88(d), 105.35(d), 105.72(d), 126.91(d), 134.14(d), 150.12(s), 154.20(s); mass spectrum: 194(16, $M^{+\cdot}$), 178(36, M − H_2O), 108(100, M − $CH_2CH(OH)CH{=}CHMe$). Anal. calcd. for $C_{12}H_{18}O_2$: C 74.19, H 9.34; found: C 73.86, H 9.29.

6-(2-Furyl)-1-hexen-3-one (1)

Compound **24** (0.19 g, 1.18 mmol) was oxidized according to general procedure 3 to provide compound **1** (0.18 g, 1.10 mmol) as a clear, colourless oil in 93% yield after purification by flash chromatography (20:1) and distillation; bp 50–55°C/0.08 Torr. The ^1H NMR spectrum always contained >10% bridged adduct **49**, therefore compound **1** was not analyzed but treated with either Florisil or methylaluminum dichloride to provide adduct **49**.

6-(2-Furyl)-2-methyl-1-hexen-3-one (2)

Compound **25** (0.65 g, 3.58 mmol) was oxidized according to general procedure 3 to provide compound **2** (0.60 g, 3.36 mmol) as a clear, colourless oil in 94% yield after purification by flash chromatography (20:1) and distillation; bp 58–60°C/0.045 Torr; IR(neat) cm^{-1}: 1677(C=O); ^1H NMR (200 MHz): 1.87(dd, 3H, J = 0.8 Hz, J = 1.4 Hz), 1.97(qu, 2H, J = 7.3 Hz), 2.67(t, 2H, J = 7.3 Hz), 2.72(t, 2H, J = 7.3 Hz), 5.75(dq, 1H, J = 0.8 Hz, J = 1.4 Hz), 5.92(m, 1H, J = 1.4 Hz), 6.00(dd, 1H, J = 0.8 Hz, J = 3.0 Hz), 6.28(dd, 1H, J = 2.0 Hz, J = 3.0 Hz), 7.30(dd, 1H, J = 0.8 Hz, J = 2.0 Hz); ^{13}C NMR(50 MHz): 17.55(q), 22.80(t), 27.27(t), 36.44(t), 105.18(d), 110.06(d), 124.27(t), 140.91(d), 144.53(s), 155.46(s), 199.52(s); mass spectrum: 178(21, $M^{+\cdot}$), 94(100, M − $CH_2{=}C(OH)C(Me){=}CH_2$, McLafferty rearr.). Exact Mass calcd. for $C_{11}H_{14}O_2$: 178.0994; found: 178.0998.

(E)-7-(2-Furyl)-2-hepten-4-one (3)

Compound **26** (0.27 g, 1.48 mmol) was oxidized according to general procedure 3 to provide compound **3** (0.23 g, 1.29 mmol) as a clear, colourless oil in 88% yield after purification by flash chromatography (20:1) and distillation; bp 60–70°C/0.05 Torr; IR (neat) cm^{-1}: 1672 and 1696(C=O); ^1H NMR (200 MHz): 1.89(dd, 3H, J = 1.6 Hz, J = 6.8 Hz), 1.96(qu, 2H, J = 7.2 Hz), 2.57(t, 2H, J = 7.2 Hz), 2.66(t, 2H, J = 7.2 Hz), 6.00(dd, 1H, J = 0.6 Hz, J = 3.1 Hz), 6.11(dq, 1H, J = 1.6 Hz, J = 15.7 Hz), 6.28(dd, 1H, J = 1.9 Hz, J = 3.0 Hz), 6.83(dq, 1H, J = 6.8 Hz, J = 15.7 Hz), 7.30(dd, 1H, J = 0.6 Hz, J = 1.9 Hz); ^{13}C NMR (50 MHz): 18.09(q), 22.50(t), 27.26(t), 38.92(t), 105.18(d), 110.04(d), 131.91(d), 140.89(d), 142.31(d), 155.44(s), 199.74(s); mass spectrum (FI): 178(100, $M^{+\cdot}$). Anal. calcd. for $C_{11}H_{14}O_2$: C 74.13, H 7.92; found: C 74.18, H 7.98.

(E)-7-(2-Furyl)-3-methyl-2-hepten-4-one (4)

Compound **27** (0.69 g, 3.55 mmol) was oxidized according to general procedure 3 to provide compound **4** (0.62 g, 3.24 mmol) as a clear, colourless oil in 91% yield after purification by flash chromatography (20:1) and distillation; bp 60–70°C/0.045 Torr; IR (neat) cm^{-1}: 1666 (C=O); ^1H NMR (200 MHz): 1.77(d, 3H, J = 1.1 Hz), 1.84(d, 3H, J = 6.9 Hz), 1.96(qu, 2H, J = 7.2 Hz), 2.66 and 2.68(overlapping t, 4H, J = 7.2 Hz), 5.99(dd, 1H, J = 0.7 Hz, J = 3.1 Hz), 6.27(dd, 1H, J = 1.8 Hz, J = 3.1 Hz), 6.69(qq, 1H, J = 1.1 Hz, J = 6.9 Hz), 7.29(dd, 1H, J = 0.7 Hz, J = 1.8 Hz); ^{13}C NMR (50 MHz): 10.78(q), 14.51(q), 22.92(t), 27.19(t), 35.90(t), 104.94(d), 109.90(d), 136.88(d), 138.02(s), 140.68(d), 155.40(s), 200.94(s); mass spectrum (FI): 192(51, $M^{+\cdot}$), 94(100 − CH=C(OH)C(Me)=CHMe, McLafferty rearrangement). Anal. calcd. for $C_{12}H_{16}O_2$: C 74.97, H 8.39; found: C 74.85, H 8.43.

6-(2-(5-Methylfuryl)-1-hexen-3-one (5)

Compound **28** (0.24 g, 1.34 mmol) was oxidized according to general procedure 3 to provide compound **5** (0.15 g, 0.84 mmol) as a clear, colourless oil in 63% yield after purification by flash chromatography (20:1) and distillation; bp 60–70°C/0.04 Torr; IR (neat) cm^{-1}: 1684(C=O); ^1H NMR (200 MHz): 1.96(qu, 2H, J = 7.5 Hz), 2.25(s, 3H), 2.59–2.70(t, 2H each, J = 7.5 Hz), 5.85(m, 2H), 6.19(dd, 1H, J = 1.5 Hz, J = 16.5 Hz), 6.38(dd, 1H, J = 10.1 Hz, J = 16.5 Hz); ^{13}C NMR (50 MHz): 13.42(q), 22.33(t), 27.24(t), 38.57(t), 105.74(d), 105.86(d), 127.87(t), 136.50(d), 150.36(s), 153.36(s), 200.34(s); mass spectrum: 178(13, $M^{+\cdot}$), 108(100, M − $CH_2{=}C(OH)CH{=}CH_2$, McLafferty rearrangement).

6-(2-(5-Methylfuryl))-2-methyl-1-hexen-3-one (6)

Compound **29** (0.28 g, 1.45 mmol) was oxidized according to general procedure 3 to provide compound **6** (0.27 g, 1.42 mmol) as a clear, colourless oil in 98% yield after purification by flash chromatography (20:1) and distillation; bp 60–68°C/0.045 Torr; IR (neat) cm^{-1}: 1680(C=O); ^1H NMR (200 MHz): 1.87(dd, 3H, J = 0.7 Hz, J = 1.3 Hz), 1.94(qu, 2H, J = 7.3 Hz), 2.24(s, 3H), 2.61(t, 2H, J = 7.3 Hz), 2.73(t, 2H, J = 7.3 Hz), 5.75(m, 1H, J = 0.7 Hz, J = 1.4 Hz), 5.84(ABq, 2H), 5.93(m, 1H, J = 1.3 Hz, J = 1.4 Hz); ^{13}C NMR (50 MHz): 13.41(q), 17.54(q), 22.95(t), 27.37(t), 36.52(t), 105.78(d), 124.19(t), 144.57(s), 150.33(s), 153.56(s), 201.61(s); mass spectrum: 192(62, $M^{+\cdot}$), 108(100, M − $CH_2{=}C(OH)C(Me){=}CH_2$, McLafferty rearrangement). Exact Mass calcd. for $C_{12}H_{16}O_2$: 192.1150; found: 192.1158.

(E)-7-(2-(5-Methylfuryl))-2-hepten-4-one (7)

Compound 30 (0.30 g, 1.54 mmol) was oxidized according to general procedure 3 to provide compound **7** (0.24 g, 1.23 mmol) as a clear, colourless oil in 80% yield after purification by flash chromatography (20:1) and distillation; bp 70–82°C/0.045 Torr; IR (neat) cm^{-1}: 1695–1670(C=O); ^1H NMR (200 MHz): 1.89(dd, 3H, J = 2.5 Hz, J = 7.5 Hz), 1.95(qu, 2H, J = 7.0 Hz), 2.25(s, 3H), 2.55(t, 2H, J = 7.0 Hz), 2.60(t, 2H, J = 7.0 Hz), 5.84(ABq, 2H), 6.11(dq, 1H, J = 1.6 Hz, J = 15.8 Hz), 6.83(dq, 1H, J = 6.8 Hz, J = 15.8 Hz); ^{13}C NMR (50 MHz): 13.39(q), 18.08(q), 22.59(t), 27.38(t), 38.96(t), 105.74(d), 105.78(d), 131.90(d), 142.24(d), 150.28(s), 153.49(s), 199.88(s); mass spectrum: 192(10, $M^{+\cdot}$), 108(100, M − $CH_2{=}C(OH)CH{=}CHMe$, McLafferty rearrangement). Exact Mass calcd. for $C_{12}H_{16}O_2$: 192.1151; found: 192.1138.

1-Bromo-4-(2-furyl)butane (31)

Furan **18** (5.0 mL, 68.7 mmol) was dissolved in dry THF (80 mL) in an Ar-purged flask and cooled to −78°C in a Dry Ice – acetone bath. To this solution was added *n*-butyllithium (20.0 mL, 50.0 mmol), then the reaction was stirred at room temperature for 1 h. Freshly distilled 1,4-dibromobutane (10.0 g, 46.3 mmol) was added to the orange anion, and the reaction was stirred overnight. Saturated NH_4Cl (50 mL) was used to quench the reaction. The aqueous layer was extracted with ether (3 × 100 mL), then the combined organic layers were dried over Na_2SO_4, filtered, and the solvent removed *in vacuo*. The crude product was distilled using a fractionating column under aspirator pressure, collecting the fraction boiling from 95 to 100°C to give compound **31** (2.54 g, 12.5 mmol) in 25% yield; IR (neat) cm^{-1}: 2943–2864(C-H); ^1H NMR (200 MHz): 1.67–2.08(m, 4H), 2.68(t, 2H, J = 7.1 Hz), 3.43(t, 2H, J = 7.1 Hz), 6.02(dd, 1H, J = 0.8 Hz, J = 3.0 Hz), 6.30(dd, 1H, J = 1.7 Hz, J = 3.0 Hz), 7.33(dd, 1H, J = 0.8 Hz, J = 1.7 Hz); ^{13}C NMR (50 MHz): 26.56(t), 27.00(t), 32.04(t), 33.34(t), 105.03(d), 110.06(d), 140.88(d), 155.38(s); mass spectrum: 202 (6, $M^{+\cdot}$), 81(100, M − $(CH_2)_3Br$). Exact Mass calcd. for $C_8H_{11}BrO$: 201.9993; found: 201.9982.

7-(2-Furyl)-1-hepten-3-one (8)

General procedure 1 was used to convert bromide **31** (3.55 g, 17.5 mmol) to the corresponding iodide (4.16 g, 16.6 mmol) in 95% yield after distillation; bp 60–68°C/0.08 Torr; IR (neat) cm^{-1}:

Can. J. Chem. Downloaded from www.nrcresearchpress.com by 88.255.202.194 on 09/08/12
For personal use only.

2936–2860(C-H); ^{1}H NMR (200 MHz): 1.64–2.01(m, 4H), 2.68(t, 2H, J = 7.5 Hz), 3.21(t, 2H, J = 7.5 Hz), 6.02(dd, 1H, J = 0.7 Hz, J = 3.1 Hz), 6.29(dd, 1H, J = 1.7 Hz, J = 3.1 Hz), 7.31(dd, 1H, J = 0.7 Hz, J = 1.7 Hz); ^{13}C NMR (200 MHz): 6.50(t), 26.80(t), 28.87(t), 32.78(t), 105.03(d), 110.06(d), 140.88(d), 155.35(s); mass spectrum: 250(22, $M^{\cdot+}$), 123(30, M-I), 81(100, M − $(CH_2)_3$I). Exact Mass calcd. for $C_8H_{11}IO$: 249.9851; found: 249.9851.

Using general procedure 2, the above iodide (0.58 g, 2.32 mmol) was treated with *tert*-butyllithium (3.0 mL, 5.09 mmol) and acrolein (185 μL, 2.78 mmol) to produce the corresponding allylic alcohol (0.29 g, 1.61 mmol) as a clear, colourless oil in 69% yield after purification by flash chromatography (7:1) and distillation; bp 50–60°C/0.05 Torr; ^{1}H NMR (200 MHz): 1.39–1.75(m, 7H), 2.64(t, 2H, J = 7.2 Hz), 4.11(br, m, 1H), 5.11(dt, 1H, J = 1.2 Hz, J = 1.2 Hz, J = 10.3 Hz), 5.22(dt, 1H, J = 1.2 Hz, J = 1.2 Hz, J = 17.2 Hz), 5.91(ddd, 1H, J = 6.2 Hz, J = 10.3 Hz, J = 17.2 Hz), 5.99(dd, 1H, J = 0.7 Hz, J = 3.0 Hz), 6.28(dd, 1H, J = 1.9 Hz, J = 3.0 Hz), 7.30(dd, 1H, J = 0.7 Hz, J = 1.9 Hz).

The above allylic alcohol (133.9 mg, 0.74 mmol) was oxidized according to general procedure 3 to provide compound **8** (113.3 g, 0.64 mmol) as a clear, colourless oil in 86% yield after purification by flash chromatography (20:1) and distillation; bp 80°C/0.06 Torr; ^{1}H NMR (200 MHz): 1.56–1.83(overlapping m), 2.50–2.76(overlapping m), 5.83(dd, 1H, J = 2.5 Hz, J = 10.1 Hz), 5.98(dd, 1H, J = 0.7 Hz, J = 3.0 Hz), 6.20(d of ABq, 1H, J = 2.5 Hz, J = 17.5 Hz), 6.25(dd, 1H, J = 1.8 Hz, J = 3.0 Hz), 6.37(d of ABq, 1H, J = 10.1 Hz, J = 17.5 Hz), 7.30(dd, 1H, J = 0.7 Hz, J = 1.8 Hz).

4-Methyl-2-oxo-3-pentenenitrile (32)

Freshly distilled acid chloride of 3-methyl-2-butenoic acid (2.19 g, 18.5 mmol) was dissolved in dry acetonitrile (15 mL) under Ar. To this solution was added anhydrous CuCN (2 equiv.), and the suspension was heated to reflux (oil bath, 90°C) for 30 min, during which time a clear, brown solution was formed. The solution was cooled to room temperature, and the solvent was removed using a rotary evaporator (no heat), followed by an Ar back-purge. The desired compound was then distilled from the remaining brown solid, along with some acetonitrile. Conversion was confirmed by ^{1}H NMR, then the acyl cyanide **32** was used directly for the next step, bp 70–80°C/20 Torr; ^{1}H NMR (200 MHz): 2.07 and 2.30(s, 3H each), 6.25(s, 1H).

Methyl 3-(2-furyl)-3-methylbutanoate (33)

A modification of the method of Ismail and Hoffmann (21) was used for the preparation of furan **33**. The acyl cyanide **32** (3.52 g, 32.3 mmol) was dissolved in CS_2 (120 mL) under Ar and cooled in an ice bath. To this solution was added $AlCl_3$ (1.08 g, 8.10 mmol), resulting in a gummy precipitate. After stirring for 1 h at room temperature, furan **18** (12.0 mL, 165.0 mmol) was added neat, and the reaction was stirred for 24 h, after which time anhydrous methanol (100 mL) was added to the solution. The reaction was then stirred for an additional 24 h. Evaporation of the CS_2, followed by removal of methanol *in vacuo*, resulted in a viscous brown material. The crude product was taken up in ether (200 mL) and water (100 mL) followed by washing with 10% Na_2CO_3 (2 × 100 mL), then water (2 × 100 mL), dried (Na_2SO_4), and the ether removed *in vacuo*. Distillation of the crude brown oil provided **33** (27% from 3-methyl-2-butenoic acid), bp 40–44°C/0.03 Torr (lit. (21) bp 40°C/0.03 Torr); IR (neat) cm^{-1}: 1738 (C═O), 1077 (C—O); ^{1}H NMR (200 MHz): 1.40(s, 6H), 2.61(s, 2H), 3.58(s, 3H), 6.01(dd, 1H, J = 0.8 Hz, J = 3.2 Hz), 6.26(dd, 1H, J = 1.9 Hz, J = 3.2 Hz), 7.32 (dd, 1H, J = 0.8 Hz, J = 1.9 Hz); ^{13}C NMR (50 MHz): 2 × 28.70(q), 34.96(s), 45.73(t), 51.11(q), 103.12(d), 108.80(d), 140.66(d), 161.27(s), 171.58(s); mass spectrum: 182(58, $M^{\cdot+}$), 109(100, M − CH_2CO_2Me). Exact Mass calcd. for $C_{10}H_{14}O_3$: 182.0942; found: 182.0935.

Methyl 3-(2-(5-methylfuryl))-3-methylbutanoate (34)

The acyl cyanide **32** (1.82 g, 16.7 mmol) was dissolved in CS_2 (60 mL) under Ar and cooled in an ice bath. To this solution was added $AlCl_3$ (0.56 g, 4.2 mmol), resulting in a gummy precipitate. After stirring for 1 h at room temperature, 2-methylfuran **19** (7.0 mL, 70.5 mmol) was added neat, and the reaction was stirred for 24 h, after which time anhydrous methanol (70 mL) was added to the crimson solution. The reaction was then stirred for an additional 24 h. Evaporation of the CS_2, followed by removal of methanol *in vacuo*, resulted in a viscous brown material. The crude product was taken up in ether (200 mL) and water (100 mL), followed by washing with 10% Na_2CO_3 (2 × 100 mL), then water (2 × 100 mL), dried (Na_2SO_4), and the ether removed *in vacuo*. Distillation of the crude brown oil provided **34** (66%), bp 100–120°C/15 Torr; IR (neat) cm^{-1}: 1738(C═O), 1385,1365(CMe_2) 1198(C—O); ^{1}H NMR (200 MHz): 1.37(s, 6H), 2.25(d, 3H, J = 0.75 Hz), 2.58(s, 2H), 3.60(s, 3H), 5.87(d of ABq, 2H, J = 0.8 Hz, J = 3.1 Hz); ^{13}C NMR (50 MHz): 13.43(q), 2 × 26.69(q), 34.89(s), 45.82(6), 71.08(q), 103.64(d), 105.57(d), 150.33(s), 159.568s), 171.77(s); mass spectrum: 196(53, $M^{\cdot+}$), 123(100, M − CH_2CO_2Me). Anal. calcd. for $C_{11}H_{16}O_3$: C 67.32, H 8.22; found: C 66.84, H 8.18.

3-(2-Furyl)-3-methyl-1-butanol (36)

To $LiAlH_4$ (0.51 g, 9.3 mmol), suspended in ether (25 mL) at 0°C under Ar, was added dropwise a solution of freshly distilled **33** (1.42 g, 7.8 mmol) in ether (8 mL). The reaction was warmed to room temperature and stirred for 12 h. After cooling to 0°C, the reaction was quenched using water (0.5 mL), 15% NaOH (0.5 mL), then water (1.5 mL). The white mixture was then filtered through Celite, and the solvent removed *in vacuo* to provide a clear, colourless oil. The oil was purified by flash chromatography (1:1), then distilled to yield compound **36** (92%), bp 48°C/0.07 Torr; IR (neat) cm^{-1}: 3333(OH), 1385,1363(CMe_2), 1077, 1059(C—O); ^{1}H NMR (200 MHz): 1.30(s, 6H), 1.51(s, 1H), 1.89(t, 2H, J = 7.2 Hz), 3.54(t, 2H, J = 7.2 Hz), 5.99 (dd, 1H, J = 0.9 Hz, J = 3.2 Hz), 6.28(dd, 1H, J = 1.5 Hz, J = 3.2 Hz) 7.32(dd, 1H, J = 0.9 Hz, J = 1.5 Hz); ^{13}C NMR (50 MHz): 2 × 27.20(q), 34.57(s), 44.61(t), 59.92(t), 103.24(d), 108.61(d), 140.64(d), 163.32(s); mass spectrum: 154(35, $M^{\cdot+}$), 109(100, M − $(CH_2)_2OH$). Anal. calcd. for $C_9H_{11}O_2$: C 70.09, H 9.15; found: C 69.66, H 9.00.

3-(2-(5-Methylfuryl))-3-methyl-1-butanol (37)

Compound **34** (2.03 g, 10.4 mmol) was reduced to alcohol **37** (1.76 g, 10.1 mmol) by the method described for compound **36** in 97.5% yield after distillation, bp 60–70°C/0.1 Torr; IR (neat) cm^{-1}: 3334(OH), 1384,1365(CMe_2), 1059,1021(C—O); ^{1}H NMR (200 MHz): 1.28(s, 6H), 1.38(br s, 1H), 1.87(t, 2H, J = 7.1 Hz), 2.26(d, 3H, J = 0.8 Hz), 3.58(t, 2H, J = 7.1 Hz), 5.85(ABq, 2H); ^{13}C NMR(50 MHz): 13.45(q), 2 × 27.22(q), 34.36(s), 44.55(t), 59.97(t), 103.62(d), 105.51(d), 150.31(s), 160.46(s); mass spectrum: 168(60, $M^{\cdot+}$), 123(100, M − $(CH_2)_2OH$). Anal. calcd. for $C_{10}H_{16}O_2$: C 71.39, H 9.59; found: C 71.37, H 9.43.

3-(2-Furyl)-1-iodo-3-methylbutane (38)

Distilled compound **36** (1.05 g, 6.80 mmol) was dissolved in dry CH_2Cl_2 (20 mL), and cooled in an ice bath. To this solution was added *p*-toluenesulfonyl chloride (2.59 g, 13.6 mmol) and DMAP (1.66 g, 13.6 mmol), and the reaction was stirred for 12 h. The mixture was poured into water (50 mL), then the organic layer was washed with 5% HCl (2 × 50 mL), and water (3 × 50 mL), then dried over Na_2SO_4. The solvent was removed *in vacuo* to yield a viscous clear oil, which was then purified by flash chromatography (7:1) to provide the tosylate of compound **36** (2.03 g, 6.58 mmol) in 98% yield. This decomposed when stored at room temperature; IR (neat) cm^{-1}: 3093–3035(C—H), 1364, 1187(SO_2st.); ^{1}H NMR (200 MHz): 1.25(s, 6H), 1.97(t, 2H, J = 7.3 Hz), 2.45(s, 3H), 3.93(t, 2H, J = 7.3 Hz), 5.91(dd, 1H, J = 0.7 Hz, J = 3.3 Hz), 6.22(dd, 1H, J = 1.8 Hz, J = 3.3 Hz), 7.25(d, 1H, J = 0.7 Hz, J = 1.8 Hz), 7.33 and 7.74(AA′XX′, 4H);

Can. J. Chem. Downloaded from www.nrcresearchpress.com by 88.255.202.194 on 09/08/12
For personal use only.

^{13}C NMR (50 MHz): 21.56(q), 2 × 27.02(q), 34.61(s), 40.34(t), 87.95(t), 103.78(d), 109.76(d), 127.64(d), 129.71(d), 133.40(s), 144.52(s), 141.05(d), 160.92(s); mass spectrum: 308(6, $M^{\cdot+}$), 109(100, M − $(CH_2)_2OTs$).

General procedure 1 was used to convert the above tosylate (2.00 g, 6.5 mmol) to iodide **38** (1.56 g, 5.91 mmol) in 91% yield after distillation, as a clear, colourless oil; bp 54–56°C/0.06 Torr; IR (neat) cm^{-1}: 1386, 1364(CMe_2); ^{1}H NMR (200 MHz): 1.28(s, 6H), 2.26(m, 2H), 2.96(m, 2H), 6.00(dd, 1H, J = 0.7 Hz, J = 3.2 Hz), 6.27(dd, 1H, J = 1.8 Hz, J = 3.2), 7.33(dd, 1H, J = 0.7 Hz, J = 1.8 Hz); ^{13}C NMR (50 MHz): 0.35(t), 2 × 26.41(q), 38.14(s), 47.22(t), 103.92(d), 109.78(d), 141.13(d), 160.82(s); mass spectrum: 264(36, $M^{\cdot+}$), 109(100, M − $(CH_2)_2I$). Anal. calcd. for $C_9H_{13}IO$: C 40.93, H 4.96; found: C 40.93, H 4.98.

*3-(2-(5-Methylfuryl))-1-iodo-3-methylbutane (**39**)*

The tosylate of alcohol **37** (2.70 g, 8.37 mmol) was prepared by the same method as above, in 87% yield after purification by flash chromatography (9:1) as a white, crystalline solid; mp 45–46°C; IR (KBr) cm^{-1}: 3087–3035(C—H), 1358 and 1191(SO_2); ^{1}H NMR (200 MHz): 1.22(s, 6H), 1.94(t, 2H, J = 7.3 Hz), 2.20(s, 3H), 2.46(s, 3H), 3.95(t, 3H, J = 7.3 Hz), 5.77(ABq, 2H), 7.33 and 7.75(AA′XX′, 4H); ^{13}C NMR (50 MHz): 13.41(q), 21.55(q), 2 × 27.05(q), 34.45(s), 40.29(t), 66.14(t), 104.37(d), 105.54(d), 127.64(d), 129.70(d), 133.24(s), 144.49(s), 150.52(s), 159.07(s); mass spectrum: 322(6, $M^{\cdot+}$), 123(100, M − $(CH_2)_2OTs$).

General procedure 1 was used to convert the above tosylate (2.70 g, 8.37 mmol) to iodide **39** (2.09 g, 7.51 mmol) in 90% yield after distillation, as a clear, colourless oil; bp 40–44°C/0.04 Torr; IR (neat) cm^{-1}: 1385,1366(CMe_2); ^{1}H NMR (200 MHz): 1.25(s, 6H), 2.23(m, 2H), 2.26(d, 3H, J = 0.8 Hz), 2.99(m, 2H), 5.84(m, 2H); ^{13}C NMR (50 MHz): 0.71(t), 13.52(q), 26.42(q), 37.98(s), 47.19(t), 104.50(d), 105.56(d), 150.53(s), 158.95(s); mass spectrum: 278(30, $M^{\cdot+}$), 123(100, M − $(CH_2)_2I$). Exact Mass calcd. for $C_{10}H_{15}IO$: 278.0168; found: 278.0153.

*6-(2-Furyl)-6-methyl-1-hepten-3-ol (**40**)*

Using general procedure 2, iodide **38** (250.1 mg, 0.947 mmol) was treated with *tert*-butyllithium (1.16 mL, 1.96 mmol) and acrolein (72 μL, 1.08 mmol) to produce compound **40** (89.1 mg, 0.458 mmol) as a clear, colourless oil in 48% yield after purification by flash chromatography (5:1); IR (neat) cm^{-1}: 3356(OH), 1644(C═C), 1385,1363(*gem*-CH_3), 1012(C—O); ^{1}H NMR (200 MHz): 1.26(s, 6H), 1.28–1.80(m, 5H), 3.99(q, 1H, J = 6.5 Hz), 5.10(dt, 1H, J = 1.2 Hz, J = 10.6 Hz), 5.18(dt, 1H, J = 1.2 Hz, J = 17.1 Hz), 5.80(ddd, 1H, J = 7.0 Hz, J = 10.6 Hz, J = 17.1 Hz), 5.98(dd, 1H, J = 0.8 Hz, J = 3.1 Hz), 6.25(dd, 1H, J = 1.7 Hz, J = 3.1 Hz), 7.30(dd, 1H, J = 0.8 Hz, J = 1.7 Hz); ^{13}C NMR (50 MHz): 26.75(q), 26.87(q), 32.25(t), 35.42(s), 37.46(t), 73.41(d), 103.31(d), 109.63(d), 114.58(t), 140.62(d), 141.13(d), 162.59(s); mass spectrum: 194(9, $M^{\cdot+}$), 176(10, M − H_2O), 161(37, M − H_2O and CH_3), 109(100, M − $(CH_2)_2CH(OH)CH{=}CH_2$). Exact Mass calcd. for $C_{12}H_{18}O_2$: 194.1307; found: 194.1296.

*6-(2-Furyl)-2,6-dimethyl-1-hepten-3-ol (**41**)*

Using general procedure 2, iodide **38** (201.1 mg, 0.761 mmol) was treated with *tert*-butyllithium (0.93 mL, 1.58 mmol) and methacrolein (72 μL, 1.08 mmol) to produce compound **41** (108.7 mg, 0.522 mmol) as a clear, colourless oil in 68.6% yield after purification by flash chromatography (5:1) and distillation; bp 56°C/0.035 Torr; IR (neat) cm^{-1}: 3373(OH), 1650(C═C), 1384,1364(CMe_2), 1013(C—O); ^{1}H NMR (200 MHz): 1.26(s, 6H), 1.29–1.75(m, 5H), 1.64(s, 3H), 3.96(br t, 1H, J = 6.3 Hz), 4.83(overlapping dd, 1H, J = 1.5 Hz), 4.91(dd, 1H, J = 1.6 Hz), 5.97(d, 1H, J = 3.2 Hz), 6.26(dd, 1H, J = 1.8 Hz, J = 3.2 Hz), 7.31(d, 1H, J = 1.8 Hz); ^{13}C NMR (50 MHz): 17.29(q), 26.71(q), 26.98(q), 30.02(t), 35.45(s), 37.61(t), 76.27(d), 103.35(d), 109.67(d), 111.18(t), 140.64(d), 147.33(s), 162.66(s); mass spectrum: 208(13, $M^{\cdot+}$), 190(4, M − H_2O), 175(10, M − H_2O and Me), 109(100, M − $(CH_2)_2CH(OH)C(Me){=}CH_2$). Anal. calcd. for $C_{13}H_{20}O_2$: C 74.96, H 9.68; found: C 74.93, H 10.08.

*(E)-7-(2-Furyl)-7-methyl-2-octen-4ol (**42**)*

Using general procedure 2, iodide **38** (247.3 mg, 0.936 mmol) was treated with *tert*-butyllithium (1.21 mL, 2.06 mmol) and crotonaldehyde (116 μL, 1.40 mmol) to produce compound **42** (166.4 mg, 0.800 mmol) as a clear, colourless oil in 84% yield after purification by flash chromatography (5:1) and distillation; IR (neat) cm^{-1}: 3350(OH), 1673(C═C), 1077(C—O); ^{1}H NMR (200 MHz): 1.26(s, 6H), 1.27–1.76(m, 5H), 1.69(dd, 3H, J = 1.3 Hz, J = 6.2 Hz), 3.93(br. q, 1H, J = 4.4 Hz), 5.44(dq, 1H, J = 1.8 Hz, J = 6.9 Hz, J = 15.3 Hz), 5.64(dq, 1H, J = 0.7 Hz, J = 6.2 Hz, J = 15.3 Hz), 5.96(dd, 1H, J = 0.9 Hz, J = 3.2 Hz), 6.26(dd, 1H, J = 1.8 Hz, J = 3.2 Hz), 7.31(dd, 1H, J = 0.9 Hz, J = 1.8 Hz); ^{13}C NMR (50 MHz): 17.59(q), 26.79(q), 26.91(q), 32.56(t), 35.50(s), 37.70(t), 73.41(d), 103.31(d), 109.65(d), 126.78(d), 134.28(d), 140.64(d), 162.74(s); mass spectrum: 208(15, $M^{\cdot+}$), 190(17, M − H_2O), 175(43, M − H_2O and Me), 109(100, M − $(CH_2)_2CH(OH)CH{=}CHMe$). Anal. calcd. for $C_{13}H_{20}O_2$: C 74.96, H 9.68; found: C 74.85, H 9.79.

*(E)-7-(2-Furyl)-3,7-dimethyl-2-octen-4-ol (**43**)*

Using general procedure 2, iodide **38** (346.1 mg, 1.466 mmol) was treated with *tert*-butyllithium (1.90 mL, 3.23 mmol) and tiglic aldehyde (212 μL, 2.20 mmol) to produce compound **43** (193.3 mg, 0.869 mmol) as a clear, colourless oil in 59.3% yield after purification by flash chromatography (9:1) and distillation; bp 68–72°C/0.045 Torr; IR (neat) cm^{-1}: 3353(OH), 1671(C═C), 1382,1363(CMe_2), 1076(C—O); ^{1}H NMR (200 MHz): 1.25(s), 1.28–1.70(m, 5H), 1.52(dq, 3H, J = 1.0 Hz, J = 2.2 Hz), 1.61(dq, 3H, J = 0.9 Hz, J = 6.7 Hz), 3.88(br t, 1H, J = 6.0 Hz), 5.43(qq, 1H, J = 0.9 Hz, J = 6.7 Hz), 5.96(dd, 1H, J = 0.9 Hz, J = 3.2 Hz), 6.26(dd, 1H, J = 1.9 Hz, J = 3.2 Hz), 7.30(dd, 1H, J = 0.9 Hz, J = 1.9 Hz); ^{13}C NMR (50 MHz): 10.65(q), 12.97(q), 26.67(q), 27.00(q), 29.96(t), 35.47(s), 37.97(t), 78.37(d), 103.29(d), 109.64(d), 120.94(d), 137.79(s), 140.60(d), 162.74(s); mass spectrum: 222(38, $M^{\cdot+}$), 204(17, M − H_2O), 189(30, M − H_2O and Me), 109(100, M − $(CH_2)_2CH(OH)CMe{=}CHMe$). Exact mass calcd. for $C_{14}H_{22}O_2$: 222.1621; found: 222.1609.

*6-(2-(5-Methylfuryl))-6-methyl-1-hepten-3-ol (**44**)*

Using general procedure 2, iodide **39** (297.9 mg, 1.07 mmol) was treated with *tert*-butyllithium (1.40 mL, 2.36 mmol) and acrolein (143 μL, 2.14 mmol) to produce compound **44** (154.5 mg, 0.742 mmol) as a clear, colourless oil in 69% yield after purification by flash chromatography (7:1); IR(neat) cm^{-1}: 3408(OH), 1388,1365(CMe_2), 1019(C—O); ^{1}H NMR (300 MHz): 1.20(s, 6H), 1.29–1.66(m, 5H), 2.22(s, 3H), 3.98(br q, 1H, J = 6.3 Hz), 5.07(dt, 1H, J = 1.4 Hz, J = 10.4 Hz), 5.17(dt, 1H, J = 1.2 Hz, J = 17.2 Hz), 5.79(ABq, 2H), 5.7(ddd, 1H, J = 6.2 Hz, J = 10.4 Hz, J = 17.2 Hz); ^{13}C NMR (75 MHz): 13.54(q), 26.78(q), 26.89(q), 32.21(t), 37.37(t), 35.24(s), 73.53(d), 103.66(d), 105.38(d), 114.63(t), 141.08(d), 150.02(s), 160.76(s); mass spectrum: 208(11, $M^{\cdot+}$), 190(6, M − H_2O), 175(19, M − H_2O and CH_3), 123(100, M − $(CH_2)_2CH(OH)CH{=}CH_2$). Exact Mass calcd. for $C_{13}H_{20}O_2$: 208.1464; found: 208.1467.

*6-(2-(5-Methylfuryl))-2,6-dimethyl-1-hepten-3-ol (**45**)*

Using general procedure 2, iodide **39** (253.7 mg, 0.912 mmol) was treated with *tert*-butyllithium (1.20 mL, 2.01 mmol) and methacrolein (151 μL, 2.01 mmol) to produce compound **45** (113.4 mg, 0.510 mmol) as a clear, colourless oil in 56% yield after purification by flash chromatography (7:1) and distillation; bp 60°C/0.065 Torr; IR (neat) cm^{-1}: 3369(OH), 1652(C═C), 1384,1366(CMe_2), 1021(C—O); ^{1}H NMR (300 MHz): 1.20(s, 6H), 1.29–1.59(m, 5H), 1.62(t, 3H, J = 1.1 Hz), 2.22(d, 3H, J = 0.8 Hz), 3.94(br t, 1H), 4.81(m, 1H, J = 1.6 Hz), 4.88(m, 1H), 5.80(ABq, 2H); ^{13}C NMR (75 MHz): 13.53(q), 17.16(q), 26.67(q), 27.02(q), 29.84(t), 37.38(t), 35.27(s), 76.29(d), 103.89(d), 105.37(d), 111.33(t), 147.20(s), 149.98(s), 160.78(s); mass

Can. J. Chem. Downloaded from www.nrcresearchpress.com by 88.255.202.194 on 09/08/12
For personal use only.

spectrum (FI): 222.28. Exact Mass calcd. for $C_{14}H_{22}O_2$: 222.1620; found: 222.1620.

(E)-7-(2-(5-Methylfuryl))-7-methyl-2-octen-4-ol (46)

Using general procedure 2, iodide **39** (270.4 mg, 0.972 mmol) was treated with *tert*-butyllithium (1.26 mL, 2.14 mmol) and crotonaldehyde (161 μL, 1.94 mmol) to produce compound **46** (194.3 mg, 0.874 mmol) as a clear, colourless oil in 90% yield after purification by flash chromatography (9:1) and distillation; IR (neat) cm^{-1}: 3457–3427(OH), 1675(C═C), 1384, 1367(CMe_2), 1077(C—O); ^1H NMR (300 MHz): 1.20(s, 6H), 1.24–1.68(m, 5H), 1.66(dd, 3H, J = 0.9 Hz, J = 6.2 Hz), 2.22(s, 3H), 3.90(m, 1H, J = 6.6 Hz), 5.43(dd, 1H, J = 0.9 Hz, J = 6.6 Hz, J = 15.0 Hz), 5.57(dq, 1H, J = 6.2 Hz, J = 15.0 Hz), 5.79(s, 2H); ^{13}C NMR (75 MHz): 13.53(q), 17.62(q), 26.77(q), 26.89(q), 32.46(t), 37.53(t), 35.27(s), 73.44(d), 103.81(d), 105.37(d), 126.76(d), 134.19(d), 149.97(s), 160.88(s); mass spectrum: 222(13, $M^{\cdot+}$), 123(100, M − $(CH_2)_2CH(OH)CH$═CMe). Anal. calcd. for $C_{14}H_{22}O_2$: C 75.63, H 9.97; found: C 75.25, H 9.99.

6-(2-Furyl)-6-methyl-1-hepten-3-one (9)

Compound **40** (169.4 mg, 0.872 mmol) was oxidized according to general procedure 3 to provide compound **9** (118.8 mg, 0.618 mmol) in 71% yield as a clear, colourless oil after purification by flash chromatography (9:1) and distillation; bp 50–56°C/0.05 Torr; IR (neat) cm^{-1}: 1703 and 1680(C═O), 1615(C═C); ^1H NMR (200 MHz): 1.28(s, 6H), 1.88–1.96(m, 2H), 2.37–2.45(m, 2H), 5.77(ddd, 1H, J = 1.5 Hz, J = 10.6 Hz), 6.00(dd, 1H, J = 3.2 Hz), 6.11(dd, 1H, J = 1.5 Hz, J = 17.3 Hz), 6.28(dd, 1H, J = 10.6 Hz, J = 17.3 Hz), 6.30(m, 1H), 7.32(dd, 1H, J = 0.9 Hz); ^{13}C NMR (50 MHz): 2 × 26.46(q), 35.09(s), 35.26(t), 35.56(t), 103.47(d), 109.44(d), 127.38(t), 136.12(d), 140.81(d), 161.56(s), 200.34(s); mass spectrum: 192(18, $M^{\cdot+}$), 109(100, M − $(CH_2)_2C(O)CH$═CH_2). Anal. calcd. for $C_{13}H_{18}O_2$: C 75.69, H 8.80; found: C 75.45, H 9.26.

6-(2-Furyl)-2,6-dimethyl-1-hepten-3-one (10)

Compound **41** (83.1 mg, 0.399 mmol) was oxidized according to general procedure 3 to provide compound **10** (63.1 mg, 0.306 mmol) in 77% yield as a clear, colourless oil after purification by flash chromatography (9:1) and distillation; bp 50–56°C/0.04 Torr; IR (neat) cm^{-1} 1679,1672(C═O), 1630(C═C), 1385,1367(CMe_2); ^1H NMR (200 MHz): 1.28(s, 6H), 1.83(dd, 3H, J = 0.8 Hz, J = 1.4 Hz), 1.86–1.95(m, 2H), 2.46–2.54(m, 2H), 5.70(m, 1H), 5.81(m, 1H), 5.99(dd, 1H, J = 0.8 Hz, J = 3.2 Hz), 6.26(dd, 1H, J = 1.8 Hz, J = 3.2 Hz), 7.31(dd, 1H, J = 0.8 Hz, J = 1.8 Hz); ^{13}C NMR (50 MHz): 17.60(q), 2 × 26.79(q), 33.35(t), 35.44(s), 36.60(t), 103.67(d), 109.72(d), 124.09(t), 140.84(d), 144.40(s), 162.00(s), 202.03(s); mass spectrum: 206(7, $M^{\cdot+}$), 109(100, M − $(CH_2)_2C(O)C(Me)$═CH_2). Exact Mass calcd. for $C_{13}H_{18}O_2$: 206.1307; found: 206.1283.

(E)-7-(2-Furyl)-7-methyl-2-octen-4-one (11)

Compound **42** (166.4 mg, 0.807 mmol) was oxidized according to general procedure 3 to provide compound **11** (124.7 mg, 0.604 mmol) in 76% yield as a clear, colourless oil after purification by flash chromatography (20:1) and distillation; IR(neat): 3143–3013(C—H), 2969–2871(C—H), 1697, 1673(C═O), 1634(C═C), 1379,1365(CMe_2); ^1H NMR(200 MHz): 1.26(s, 6H), 1.84(dd, 3H, J = 1.6 Hz, J = 6.8 Hz), 1.84–1.92(m, 2H), 2.29–2.37(m, 2H), 5.97(dd, 1H, J = 0.7 Hz, J = 3.2 Hz), 6.04(dq, 1H, J = 1.6 Hz, J = 15.8 Hz), 6.25(dd, 1H, J = 1.9 Hz, J = 3.2 Hz), 6.72(dq, 1H, J = 6.8 Hz, J = 15.8 Hz), 7.29(dd, 1H, J = 0.7 Hz, J = 1.8 Hz); ^{13}C NMR (50 MHz): 17.96(q), 2 × 26.68(q), 35.31(s), 35.76(t), 35.96(t), 103.59(d), 109.62(d), 131.72(d), 140.75(d), 142.00(d), 161.89(s), 200.22(s); mass spectrum: 206(36, $M^{\cdot+}$), 109(100, M − $(CH_2)_2C(O)CH$═$CHMe$). Exact Mass calcd. for $C_{13}H_{18}O_2$: 206.1307; found: 206.1307.

(E)-7-(2-Furyl)-3,7-dimethyl-2-octen-4-one (12)

Compound **43** (153.2 mg, 0.689 mmol) was oxidized according to general procedure 3 to provide compound **12** (144.2 mg, 0.654 mmol) in 95% yield as a clear, colourless oil after purification by flash chromatography (20:1) and distillation; bp 80–90°C/0.06 Torr; IR(neat) cm^{-1}: 1667(C═O), 1644(C═C), 1379,1363(CMe_2); ^1H NMR (200 MHz): 1.28(s, 6H), 1.74(d, 3H, J = 1.0 Hz), 1.82(d, 3H, J = 6.9 Hz), 1.85–1.94(m, 2H), 2.42–2.5(m, 2H), 5.99(dd, 1H, J = 0.7 Hz, J = 3.2 Hz), 6.20(dd, 1H, J = 1.8 Hz, J = 3.2 Hz), 6.58(m, 1H, J = 1.0 Hz, J = 6.9 Hz), 7.32(dd, 1H, J = 0.8 Hz, J = 1.8 Hz); ^{13}C NMR (50 MHz): 10.98(q), 14.59(q), 2 × 26.77(q), 32.95(t), 36.87(t), 35.44(s), 103.60(d), 109.89(d), 136.66(d), 138.05(s), 140.77(d), 162.10(s), 201.76(s); mass spectrum: 220(45, $M^{\cdot+}$), 109(100, M − $(CH_2)_2C(O)CMe$═$CHMe$). Exact Mass calcd. for $C_{14}H_{20}O_2$: 220.1464; found: 220.1461.

6-(2-(5-Methylfuryl))-6-methyl-1-hepten-3-one (13)

Compound **44** (122.0 mg, 0.586 mmol) was oxidized according to general procedure 3 to provide compound **13** (80.9 mg, 0.392 mmol) in 67% yield as a clear, colourless oil after purification by flash chromatography (9:1) and distillation; bp 52–58°C/0.03 Torr; IR (neat) cm^{-1}: 1682(C═O), 1614(C═C); ^1H NMR (300 MHz): 1.22(s, 6H), 1.84–1.89(m, 2H), 2.22(d, 3H, J = 0.9 Hz), 2.37–2.42(m, 2H), 5.75(dd, 1H, J = 1.3 Hz, J = 10.4 Hz), 5.80(dq, 1H, J = 1.0 Hz, J = 3.0 Hz), 5.83(d, 1H, J = 3.0 Hz), 6.10(dd, 1H, J = 1.3 Hz, J = 17.6 Hz), 6.26(dd, 1H, J = 10.4 Hz, J = 17.6 Hz); ^{13}C NMR (75 MHz): 13.55(q), 2 × 26.62(q), 35.23(s), 35.62(t), 35.79(t), 104.34(d), 105.47(d), 127.76(t), 136.44(d), 150.37(s), 159.98(s), 201.01(s); mass spectrum: 206(24, $M^{\cdot+}$), 123(100, M − $(CH_2)_2C(O)CH$═CH_2). Exact Mass calcd. for $C_{13}H_{18}O_2$: 206.1307; found: 206.1294.

6-(2-(5-Methylfuryl))-2,6-dimethyl-1-hepten-3-one (14)

Compound **45** (90.2 mg, 0.406 mmol) was oxidized according to general procedure 3 to provide compound **14** (88.3 mg, 0.401 mmol) in 99% yield as a clear, colourless oil after purification by flash chromatography (9:1) and distillation; bp 60°C/0.055 Torr; mp 27.5–30°C; IR (neat) cm^{-1}: 1677(C═O), 1625(C═C); ^1H NMR (300 MHz): 1.22(s, 6H), 1.81(d, 3H, J = 1.1 Hz), 1.82–1.87(m, 2H), 2.21(d, 3H, J = 0.8 Hz), 2.45–2.51(m, 2H), 5.68(m, 1H), 5.80(m, 3H); ^{13}C NMR (75 MHz): 13.53(q), 17.67(q), 2 × 26.63(q), 33.43(t), 36.56(t), 35.30(s), 104.28(d), 105.47(d), 124.29(t), 144.31(s), 150.29(s), 160.1(s), 202.39(s); mass spectrum: 220(18, $M^{\cdot+}$), 123(100, M − $(CH_2)_2C(O)C(Me)$═CH_2). Exact Mass calcd. for $C_{14}H_{20}O_2$: 220.1463; found: 220.1473.

(E)-7-(2-(5-Methylfuryl))-7-methyl-2-octen-4-one (15)

Compound **46** (199.8 mg, 0.899 mmol) was oxidized according to general procedure 3 to provide compound **15** (169.3 mg, 0.768 mmol) in 86% yield as a clear, colourless oil after purification by flash chromatography (20:1) and distillation, bp 62–64°C/0.055 Torr; IR (neat) cm^{-1}: 3034(CH), 2988–2869(CH), 1697, 1674(C═O), 1634(C═C), 1385, 1366(*gem*-Me); ^1H NMR (300 MHz): 1.25(s, 6H), 1.82–1.91(overlapping m, 5H), 2.25(s, 3H), 2.32–2.40(m, 2H), 5.84(m, 2H), 6.06(dq, 1H, J = 1.6 Hz, J = 15.7 Hz), 6.74(dq, 1H, J = 6.8 Hz, J = 15.7 Hz); ^{13}C NMR (75 MHz): 13.56(q), 18.16(q), 2 × 26.82(q), 35.27(s), 35.95(t), 36.01(t), 104.30(d), 105.45(d), 131.84(d), 142.22(d), 150.29(s), 160.12(s), 200.66(s); mass spectrum: 220(16, $M^{\cdot+}$), 123(100, M − $(CH_2)_2C(O)CH$═$CHMe$). Exact Mass calcd. for $C_{14}H_{20}O_2$: 220.1463; found: 220.1462.

6-(2-Furyl)-6-methyl-1-(trimethylsilyl)-1-heptyn-3-one (16)

Using general procedure 2, iodide **38** (285.1 mg, 1.08 mmol) was treated with *tert*-butyllithium (1.40 mL, 2.37 mmol) and aldehyde **47** (202.6 mg, 1.61 mmol) to produce the corresponding allylic alcohol (187.6 g, 0.71 mmol) as a clear, colourless oil in 66% yield after purification by flash chromatography (7:1) and distillation; bp 80–88°C/0.065 Torr; IR (neat) cm^{-1}: 3380(O—H), 1055(C—O); ^1H NMR (200 MHz): 0.18(s, 9H), 1.28(s, 6H), 1.47–1.81(overlapping m, 5H), 4.27(br q, 1H, J = 5.9 Hz), 5.99(dd, 1H, J = 0.8, J = 3.2 Hz), 6.27(dd, 1H, J = 1.9, J = 3.2 Hz),

Can. J. Chem. Downloaded from www.nrcresearchpress.com by 88.255.202.194 on 09/08/12
For personal use only.

7.31(dd, 1H, J = 0.8, J = 1.9 Hz); ^{13}C NMR (50 MHz): −0.14(q), 2 × 26.88(q), 33.24(t), 37.22(t), 63.12(d), 89.40(s), 106.80(s), 103.37(d), 109.66(d), 140.73(d), 162.43(s); mass spectrum: 264(4, $M^{\cdot+}$), 249(15, M − Me), 109(100, M − $(CH_2)_2CH(OH)$-C≡CSiMe$_3$). Exact Mass calcd. for $C_{15}H_{24}O_2Si$: 264.1546; found: 264.1535.

The above alcohol (123.3 mg, 0.47 mmol) was oxidized according to general procedure 3 to provide compound **16** (116.6 mg, 0.44 mmol) as a clear, colourless oil in 95% yield after purification by flash chromatography (20:1) and distillation; bp 68–74°C/0.04 Torr: IR (neat) cm^{-1}: 2151(C≡C), 1679(C=O); ^{1}H NMR (200 MHz): 0.25(s, 9H), 1.28(s, 6H), 1.90–2.04(m, 2H), 2.33–2.50(m, 2H), 6.00(dd, 1H, J = 0.8 and 3.0 Hz), 6.29(dd, 1H, J = 1.7 and 3.0 Hz), 7.33(dd, 1H, J = 0.8 and 1.7 Hz); ^{13}C NMR (50 MHz): 0.80(q), 2 × 26.73(q), 35.20(s), 35.38(t), 41.34(t), 97.50(s), 101.93(s), 103.82(d), 109.70(d), 140.99(d), 161.47(s), 187.51(s); mass spectrum: 262(5, $M^{\cdot+}$), 247(15, M − Me), 109(100, M − $(CH_2)_2C(O)C{\equiv}CSiMe_3$). Exact Mass calcd. for $C_{15}H_{22}O_2Si$: 262.1389; found: 262.1385.

*7-(2-Furyl)-7-methyl-2-octyn-4-one (**17**)*

Using general procedure 2, iodide **38** (601.5 mg, 2.28 mmol) was treated with *tert*-butyllithium (2.95 mL, 5.01 mmol) and aldehyde **48** (620.1 mg, 9.12 mmol) to produce the corresponding alcohol (378.8 g, 1.84 mmol) as a clear, colourless oil in 81% yield after purification by flash chromatography (7:1) and distillation; bp 70–80°C/0.045 Torr; IR (neat) cm^{-1}: 3520(O*H*), 1054(C—O); ^{1}H NMR (200 MHz): 1.28(s, 6H), 1.44–1.83(overlapping m, 5H), 1.84(d, 3H, J = 2.2 Hz), 4.22–4.25(br m, 1H), 5.98(dd, 1H, J = 0.7 Hz, J = 3.2 Hz), 6.26(dd, 1H, J = 1.8 Hz, J = 3.2 Hz), 7.31(dd, 1H, J = 0.7 Hz, J = 1.8 Hz); ^{13}C NMR (50 MHz): 3.37(q), 2 × 26.74(q), 33.46(t), 35.26(t), 37.19(t), 62.76(d), 80.37(s), 80.73(s), 103.24(d), 109.56(d), 140.59(d), 162.42(s); mass spectrum: 206(10, $M^{\cdot+}$), 109(100, M − $(CH_2)_2CH(OH)$-C≡CCH$_3$). Exact Mass calcd. for $C_{13}H_{18}O_2$: 206.1307; found: 206.1307.

The above alcohol (213.1 mg, 1.03 mmol) was oxidized according to general procedure 3 to provide compound **17** (200.9 mg, 0.98 mmol) as a clear, colourless oil in 95% yield after purification by flash chromatography (20:1) and distillation; bp 76–80°C/0.08 Torr. IR (neat) cm^{-1}: 2218(C≡C), 1673(C=O); ^{1}H NMR (200 MHz): 1.27(s, 6H), 1.90–1.98(m, 2H), 2.00(s, 3H), 2.34(m, 2H), 5.99(dd, 1H, J = 0.8 Hz, J = 3.2 Hz), 6.27(dd, 1H, J = 1.9 Hz, J = 3.2 Hz), 7.32(dd, 1H, J = 0.8 Hz, J = 1.9 Hz); ^{13}C NMR (50 MHz): 3.96(q), 2 × 26.70(q), 35.22(s), 35.54(d), 41.44(d), 80.18(s), 89.78(s), 103.75(d), 109.70(d), 140.96(d), 161.61(s), 187.86(s); mass spectrum: 204(11, $M^{\cdot+}$), 109(100, M − $(CH_2)_2C(O)C{\equiv}CCH_3$) Exact Mass calcd. for $C_{13}H_{16}O_2$: 204.1150; found: 204.1151.

*(6α,8α-H)-11-Oxatricyclo[6.2.1.0^{1,6}]undec-9-en-5-one (**49**)*

General procedure 5 was used for the Lewis acid-mediated IMDAF reaction of compound **1**. Thus, enone **1** (54.1 mg, 0.329 mmol) was treated with MeAlCl$_2$ (362 μL, 0.362 mmol) at −78°C for 1 h to provide adduct **49** (54.0 mg, 0.329 mmol) in 99% yield as white, crystalline solid; mp 25–27°C; IR (KBr) cm^{-1}: 1708(C=O), 1153(C—O); ^{1}H NMR (400 MHz): 1.47(dd, 1H, $J_{7\alpha,6\alpha}$ = 8.2 Hz, J_{gem} = 11.8 Hz, H-7α), 1.79–2.08(m, 2H), 2.28(dd, 1H, $J_{6\alpha,7\beta}$ = 3.0 Hz, $J_{6\alpha,7\alpha}$ = 8.2 Hz, H-6α), 2.49(ddd, $J_{7\beta,6\alpha}$ = 3.0 Hz, $J_{7\beta,8}$ = 4.8 Hz, J_{gem} = 11.8 Hz, H-7β), 2.20–2.58(m, 4H), 4.89(dd, 1H, $J_{8,9}$ = 1.6 Hz, $J_{8,7\beta}$ = 4.8 Hz, H-8), 6.27 (d, 1H, $J_{10,9}$ = 5.7 Hz, H-10), 6.42(dd, 1H, $J_{8,9}$ = 1.7 Hz, $J_{9,10}$ = 5.7 Hz, H-9); ^{13}C NMR(50 MHz): 21.73, 28.17, 29.10 and 41.66(t, C-2, C-3, C-4 and C-7), 50.30(d, C-6), 78.08(d, C-8), 90.40(s, C-1), 136.92 and 138.20(d, C-9 and C-10), 209.30(s, C-5); mass spectrum (FI): 164(100, $M^{\cdot+}$). Exact Mass calcd. for $C_{10}H_{12}O_2$: 164.0838; found: 164.0819.

*(8α-H)-6α-Methyl-11-oxatricyclo[6.2.1.0^{1,6}]undec-9-en-5-one (**50**)*

General procedure 5 was used to perform the Lewis acid-mediated reaction of compound **2**. Thus, enone **2** (66.6 mg, 0.374 mmol) was treated with MeAlCl$_2$ (411 μL, 0.411 mmol) at −78°C for 2.5 h to provide a SM:A ratio of 22.78 with 98% recovery of material. Adduct **50** was characterized as a pale yellow, crystalline solid, mp <22°C; IR (neat) cm^{-1}: 1707(C=O); ^{1}H NMR (400 MHz): 1.01(d, 1H, J_{gem} = 11.8 Hz, H-7α), 1.12(s, 3H, -CH$_3$), 1.91–2.03(m, 2H), 2.25–2.28(m, 2H), 2.42(dt, 1H, $J_{2\beta,3\alpha}$ = 2.9 Hz, $J_{2\beta,3\alpha}$ = 2.9 Hz, J_{gem} = 14.4 Hz, H-2β), 2.62(dd, 1H, $J_{3\alpha,4\alpha}$ = 14.4 Hz, J_{gem} = 19.4 Hz, H-4β), 2.86(dd, 1H, $J_{7\beta,8}$ = 5.1 Hz, J_{gem} = 11.8 Hz, H-7β), 4.82(dd, 1H, $J_{8,9}$ = 1.6 Hz, $J_{8,7\beta}$ = 5.1 Hz, H-8), 6.14(d, 1H, $J_{10,9}$ = 5.7 Hz, H-10), 6.49(dd, 1H, $J_{9,8}$ = 1.6 Hz, $J_{9,10}$ = 5.7 Hz, H-9); ^{13}C NMR (50 MHz): 20.94, 25.67, 37.34 and 38.28(t, C-2, C-3, C-4 and C-7), 22.44(q, -CH$_3$), 54.18(s, C-6), 78.03(d, C-8), 91.70(s, C-1), 135.13 and 138.81(d, C-9 and C-10), 213.00(s, C-5); mass spectrum: 178(14, $M^{\cdot+}$), 94(100, M − $CH_2{=}C(OH)C(Me){=}CH_2$, retro IMDAF–McLafferty rearr.). Exact Mass calcd. for $C_{11}H_{14}O_2$: 178.0994; found: 178.0990.

*(6α,8α-H)-7α-Methyl-11-oxatricyclo[6.2.1.0^{1,6}]undec-9-en-5-one (**51**)*

General procedure 5 was used to perform the Lewis acid-mediated reactions of compound **3**. Quantitative reaction: precursor **3** (107.6 mg, 0.604 mmol) was treated with MeAlCl$_2$ (664 μL, 0.664 mmol) at −78°C for 8 h to provide a SM:A ratio of 78:22 with quantitative recovery of material. Flash chromatography (7:1) provided starting material (40.8 mg) and adduct **51** (11.2 mg). Catalytic reaction: enone **3** (121.6 mg, 0.682 mmol) was treated with MeAlCl$_2$ (68 μL, 0.068 mmol) at −65°C for 2 h to provide a SM:A ratio of 31:69 with 99% recovery of material. Flash chromatography (9:1) provided precursor **3** (39.4 mg) and **51** (77.8 mg) as a clear, colourless oil; IR (neat) cm^{-1}: 1706(C=O); ^{1}H NMR (400 MHz): 0.93(d, 3H, J = 7.0 Hz, C-7-CH$_3$), 1.73(d, 1H, $J_{6\alpha,7\beta}$ = 4.0 Hz, H-6α), 1.82–2.01(m, 2H), 2.21(dt, 1H, $J_{2\alpha,3\alpha}$ = 4.7 Hz, $J_{2\alpha,3\beta}$ = 12.3 Hz, J_{gem} = 12.7 Hz, H-2α), 2.27–2.38(m, 2H), 2.47(ddt, 1H, $J_{4\beta,2\beta}$ = 1.6 Hz, $J_{4\beta,3\alpha}$ = 3.7 Hz, $J_{4\beta,3\beta}$ = 3.7 Hz, J_{gem} = 14.4 Hz, H-4β), 2.79(ddq, 1H, $J_{7\beta,6\alpha}$ = 4.0 Hz, $J_{7\beta,8}$ = 4.7 Hz, J = 7.0 Hz, H-7β), 4.69(dd, 1H, $J_{8,9}$ = 1.6 Hz, $J_{8,7\beta}$ = 4.7 Hz, H-8), 6.24(d, 1H, $J_{10,9}$ = 5.7 Hz, H-10), 6.37(dd, 1H, $J_{9,8}$ = 1.6 Hz, $J_{9,10}$ = 5.7 Hz, H-9); ^{13}C NMR (50 MHz): 17.23(q), 21.45, 28.50 and 41.54(t, C-2, C-3, and C-4), 37.40(d, C-7), 58.59(d, C-6), 81.80(d, C-8), 91.12(s, C-1), 135.80 and 138.32(d, C-9 and C-10), 209.76(s, C-5); mass spectrum: 178(16, $M^{\cdot+}$), 94(100, M − $CH_2{=}C(OH)CMe{=}CHMe$, retro IMDAF–McLafferty rearr.). Exact Mass calcd. for $C_{11}H_{14}O_2$: 178.0994; found: 178.1002.

*(8α-H)-6α,7α-Dimethyl-11-oxatricyclo[6.2.1.0^{1,6}]undec-9-en-5-one (**52**)*

General procedure 5 was used to perform the Lewis acid-mediated reaction of compound **4**. Quantitative reaction: enone **4** (38.1 mg, 0.198 mmol) was treated with MeAlCl$_2$ (218 μL, 0.218 mmol) at −65°C for 2 h to provide a SM:A ratio of 100:0. Catalytic reaction: compound **4** (143.8 mg, 0.747 mmol) was treated with MeAlCl$_2$ (75 μL, 0.075 mmol) at −65°C for 2 h to provide a SM:A ratio of 95:5 (99% recovery, 142.2 mg). Starting material **4** (130.0 mg) could be separated from the product **52** (6.0 mg), a yellow oil, using flash chromatography (9:1) (no bp due to decomposition); ^{1}H NMR (400 MHz): 0.78(d, 3H, J = 7.4 Hz, C-7-CH$_3$), 0.93(s, 3H, C-6-CH$_3$), 1.88–2.00(m, 2H), 2.20–2.26(m, 1H), 2.40(dt, 1H, $J_{4\beta,3\alpha}$ = 3.0 Hz, $J_{4\beta,3\beta}$ = 3.0 Hz, J_{gem} = 14.7 Hz, H-4β), 2.55–2.62(m, 1H), 2.64(dt, 1H, $J_{4\alpha,3\alpha}$ = 7.2 Hz, $J_{4\alpha,3\beta}$ = 14.7 Hz, J_{gem} = 14.7 Hz, H-4α), 2.99(dq, 1H, $J_{7\beta,8}$ = 4.8 Hz, $J_{7\beta,12}$ = 7.4 Hz, H-7β), 4.71(dd, $J_{8,9}$ = 1.7 Hz, $J_{8,7\beta}$ = 4.8 Hz, H-8), 6.22(d, 1H, $J_{10,9}$ = 5.8 Hz, H-10), 6.45(dd, 1H, $J_{9,8}$ = 1.7 Hz, $J_{9,10}$ = 5.8 Hz, H-9); ^{13}C NMR (50 MHz): 13.29(q), 17.86(q), 20.72, 26.18 and 38.20(t, C-2 to C-4), 39.27(d,

Can. J. Chem. Downloaded from www.nrcresearchpress.com by 88.255.202.194 on 09/08/12
For personal use only.

C-7), 60.35(s, C-6), 81.92(d, C-8), 92.68(s, C-1), 137.11(d, C-9 and C-10), 214.25(s, C-5).

(6α-H)-8α-Methyl-11-oxatricyclo[6.2.1.0^{1,6}]undec-9-en-5-one (53)

General procedure 5 was used to perform the Lewis acid-mediated reaction of compound **5**. Thus, enone **5** (58.9 mg, 0.33 mmol) was treated with $MeAlCl_2$ (0.36 mL, 0.36 mmol) at −78°C for 1 h to provide adduct **53** (58.9 mg, 0.33 mmol) in >99% yield as yellow oil (no bp due to decomposition on heating); IR (neat) cm^{-1}: 1710(C=O); ^{1}H NMR (400 MHz): 1.58(s, 3H, -CH_3), 1.61(dd, 1H, $J_{6\alpha,7\alpha}$ = 8.2 Hz, $J_{7\alpha,7\beta}$ = 11.8 Hz, H-7α), 1.88–2.04(m, 2H), 2.20(dd, 1H, $J_{7\beta,6\alpha}$ = 3.5 Hz, J_{gem} = 11.8 Hz, H-7β), 2.23(dt, 1H, $J_{2\alpha,3\alpha}$ = 5.2 Hz, $J_{2\alpha,3\beta}$ = 12.4 Hz, J_{gem} = 12.4 Hz, H-2α), 2.39(dd, 1H, $J_{6\alpha,7\beta}$ = 3.5 Hz, $J_{6\alpha,7\alpha}$ = 8.2 Hz, H-6α), 2.35–2.44(m, 2H), 2.52(dddt, 1H, $J_{4\beta,2\beta}$ = 1.6 Hz, $J_{4\beta,3\alpha}$ = 3.6 Hz, $J_{4\beta,3\beta}$ = 3.6 Hz, J_{gem} = 14.1 Hz, H-4β), 6.15 and 6.25(ABq, 1H, J = 5.6- Hz, H-9 and H-10); ^{13}C NMR (50 MHz): 18.71(q, -CH_3), 21.68, 28.54, 35.42, and 41.86(t, C-2, C-3, C-4, and C-7), 53.77(d, C-6), 85.96 and 90.83(s, C-1 and C-8), 137.69 and 141.18(d, C-9 and C-10), 209.70(s, C-5); mass spectrum (FI): 178. Exact mass calcd. for $C_{11}H_{14}O_2$: 178.0994; found: 178.0986.

6α,8α-Dimethyl-11-oxatricyclo[6.2.1.0^{1,6}]undec-9-en-5-one (54)

General procedure 5 was used to perform the Lewis acid-mediated reactions of compound **6**. 1.1 Equivalents of $MeAlCl_2$ reaction: precursor **6** (80.5 mg, 0.419 mmol) was treated with $MeAlCl_2$ (461 μL, 0.461 mmol) at −78°C for 8 h to provide a SM:A ratio of 19:81 with quantitative recovery of material. Flash chromatography (9:1) provided starting material (12.6 mg) and adduct **54** (59.0 mg). Catalytic reaction: enone **6** (37.4 mg, 0.192 mmol) was treated with $MeAlCl_2$ (19 μL, 0.019 mmol) at −65°C for 2 h to provide a SM:A ratio of <1:>99 with 99% recovery of material. Flash chromatography (9:1) provided precursor **6** (2.6 mg) and **54** (34.6 mg) as a clear, colourless oil; IR (neat) cm^{-1}: 1708(C=O); ^{1}H NMR (400 MHz): 1.08(s, 3H, C-6-CH_3), 1.10(d, 1H, $J_{7\alpha,7\beta}$ = 5.5 Hz, H-7α), 1.50(s, 3H, C-8-CH_3), 1.82–2.04(m, 2H), 2.16–2.23(m, 2H), 2.38(dt, 1H, $J_{3\beta,4\beta}$ = 3.2 Hz, $J_{3\alpha,4\beta}$ = 3.2 Hz, $J_{4\alpha,4\beta}$ = 14.4 Hz, H-4β), 2.51–2.67(m, 1H), 2.55(d, 1H, $J_{7\alpha,7\beta}$ = 11.8 Hz, H-7β), 6.13(d, 1H, $J_{10,9}$ = 5.6 Hz, H-10), 6.27(d, 1H, $J_{9,10}$ = 5.6 Hz, H-9); ^{13}C NMR (50 MHz): 18.87 and 22.24(q, -CH_3's), 20.84, 25.86, 38.22, and 43.66(t, C-2, C-3, C-4, and C-7), 57.41(s, C-6), 85.69 and 92.09(s, C-1 and C-8), 135.87 and 141.65(d, C-9 and C-10), 213.33(s, C-5); mass spectrum: 192(5, M$^{\cdot+}$), 108(100, M − CH_2=C(OH)C(Me)=CH_2, retro IMDAF–McLafferty rearr.). Exact Mass calcd. for $C_{12}H_{16}O_2$: 192.1150; found: 192.1141.

(6α-H)-7α,8α-Dimethyl-11-oxatricyclo[6.2.1.0^{1,6}]undec-9-en-5-one (55)

General procedure 5 was used to perform the Lewis acid-mediated reaction of compound **7**. Quantitative reaction: enone **7** (63.7 mg, 0.331 mmol) was treated with $MeAlCl_2$ (364 μL, 0.364 mmol) at −78°C for 8 h to provide a SM:A ratio of 82:18 with 98% recovery of material. Flash chromatography (7:1) provided enone **7** (46.9 mg) and adduct **55** (15.2 mg). Catalytic reaction: compound **7** (51.4 mg, 0.267 mmol) was treated with $MeAlCl_2$ (27 μL, 0.027 mmol) at −65°C for 2 h to provide a SM:A ratio of 24:76 (92% recovery, 47.5 mg). Starting material **7** (10.7 mg) could be separated from the product **55** (32.1 mg), a yellow solid, using flash chromatography (9:1), mp 28–30°C; IR (KBr) cm^{-1}: 1709(C=O), 1136(C—O); ^{1}H NMR (400 MHz): 0.95(d, 3H, J = 7.1 Hz, C-7-CH_3), 1.52(s, 3H, C-8-CH_3), 1.89(d, 1H, $J_{6\alpha,7\beta}$ = 4.3 Hz, H-6α), 1.90–1.99(m, 2H), 2.17(ddd, 1H, $J_{2\alpha,3\alpha}$ = 5.3 Hz, $J_{2\alpha,3\beta}$ = 12.1 Hz, J_{gem} = 14.7 Hz, H-2α), 2.29–2.38(m, 2H), 2.46(dq, 1H, $J_{7\beta,6\alpha}$ = 4.1 Hz, J = 7.0 Hz, H-7β), 2.5(dddt, 1H, $J_{4\beta,2\beta}$ = 1.6 Hz, $J_{4\beta,3\alpha}$ = 3.7 Hz, $J_{4\beta,3\beta}$ = 3.7 Hz, J_{gem} = 14.3 Hz, H-4β), 6.20(d, 1H, $J_{9,10}$ = 5.6 Hz, H-10), 6.26(d, 1H, $J_{9,10}$ = 5.6 Hz, H-9); ^{13}C NMR (50 MHz): 17.07(q), 17.12(q), 21.38, 28.62, and 41.53(t, C-2, C-3, and C-4), 43.10(d, C-7), 61.51(d, C-6), 88.63 and 90.09(s, C-1 and C-8), 138.80 and 138.87(d, C-9 and C-10), 210.14(s, C-5); mass spectrum: 192(13, M$^{\cdot+}$), 108(100, M − CH_2=C(OH)CH=CHMe, retro IMDAF–McLafferty rearr.). Exact Mass calcd. for $C_{12}H_{16}O_2$: 192.1151; found: 192.1132.

(6α,8α-H)-2,2-Dimethyl-11-oxatricyclo[6.2.1.0^{1,6}]undec-9-en-5-one (56)

The IMDAF reaction of compound **9** (52.9 mg, 0.275 mmol) was performed according to general procedure 4 to provide adduct **56** (46.5 mg, 0.242 mmol) after 12 h in 88% yield as a white solid, mp 57–60°C; IR (KBr) cm^{-1}: 1705(C=O), 1663(C=C), 1390, 1369(*gem*-Me); ^{1}H NMR (400 MHz): 1.08 and 1.36(s, 6H, 2 × CH_3), 1.55(dd, 1H, $J_{7\alpha,6\alpha}$ = 8.5 Hz, J_{gem} = 11.8 Hz, H-7α), 1.61(ddd, 1H, $J_{3\alpha,4\beta}$ = 2.7 Hz, $J_{3\alpha,4\alpha}$ = 5.8 Hz, J_{gem} = 13.9 Hz, H-3α), 1.99(dt, 1H, $J_{3\beta,4\beta}$ = 4.3 Hz, $J_{3\beta,4\alpha}$ = 13.9 Hz, J_{gem} = 13.9 Hz, H-3β), 2.27(dd, 1H, $J_{6\alpha,7\beta}$ = 3.2 Hz, $J_{6\alpha,7\alpha}$ = 8.5 Hz, H-6α), 2.37–2.42(overlapping m, 2H, H-4β and H-7β), 2.58(dt, 1H, $J_{4\alpha,3\alpha}$ = 5.8 Hz, $J_{4\alpha,3\beta}$ = 15.1 Hz, $J_{4\alpha,4\beta}$ = 15.1 Hz, H-4α), 4.88(dd, 1H, $J_{8,9}$ = 1.5 Hz, $J_{8,7\beta}$ = 4.9 Hz, H-8), 6.24(d, 1H, $J_{10,9}$ = 5.8 Hz, H-10), 6.43(dd, 1H, $J_{9,8}$ = 1.5 Hz, $J_{9,10}$ = 5.8 Hz, H-9); ^{13}C NMR (50 MHz): 24.24 and 25.96(q, -CH_3), 30.98, 34.88, and 37.84(t, C-3, C-4, and C-7), 31.98(s, C-2), 47.90(d, C-6), 77.90(d, C-8), 95.90(s, C-1), 133.47, 138.83(d, C-9 and C-10), 210.20(s, C-5); mass spectrum: 192(48, M$^{\cdot+}$), 109(100, M − $(CH_2)_2$C(O)CH=CH_2). Exact Mass calcd. for $C_{12}H_{16}O_2$: 192.1150; found: 192.1148.

(8α-H)-2,2,6α-Trimethyl-11-oxatricyclo[6.2.1.0^{1,6}]undec-9-en-5-one (57)

The IMDAF reaction of compound **10** (221.2 mg, 1.07 mmol) was performed according to general procedure 4 to provide after 96 h precursor **10** (186.4 mg, 0.903 mmol) and adduct **57** (19.8 mg, 0.096 mmol) after purification by flash chromatography (9:1) in 93% total recovery.

General Procedure 5 was used to perform the Lewis acid-mediated reactions of compound **10**. Thus, enone **10** (55.3 mg, 0.268 mmol) was treated with quantitative $MeAlCl_2$ (295 μL, 0.295 mmol) at −78°C for 8 h to provide a SM:A ratio of 68:32 with a quantitative recovery of material. Enone **10** (161.9 mg, 0.785 mmol) was treated with catalytic $MeAlCl_2$ (79 μL, 0.079 mmol) (according to general procedure 5) at −65°C for 2 h to provide a SM:A ratio of 40:60 with quantitative recovery. Flash chromatography (9:1) provided enone **10** (64.5 mg) and adduct **57** (92.3 mg) in 97% recovered yield. Adduct **57** was characterized as a white solid, mp 44–55°C; IR (KBr) cm^{-1}: 3078, 3021(C-H), 2982–2858(C-H), 1699(C=O), 1389, 1369(*gem*-Me); ^{1}H NMR (200 MHz): 0.99(d, 1H, J = 11.7 Hz, H-7α), 1.03(s, C-6-CH_3), 1.16 and 1.39(s, 3H each, 2 × CH_3), 1.61(ddd, 1H, $J_{3\alpha,4\beta}$ = 2.8 Hz, $J_{3\alpha,4\alpha}$ = 5.8 Hz, $J_{3\alpha,3\beta}$ = 13.4 Hz, H-3α), 2.01(dt, 1H, $J_{3\beta,4\beta}$ = 4.1 Hz, $J_{3\beta,4\alpha}$ = 14.3 Hz, $J_{3\beta,3\alpha}$ = 13.6 Hz, H-3β), 2.35(ddd, 1H, $J_{4\beta,3\alpha}$ = 2.8 Hz, $J_{4\beta,3\beta}$ = 4.0 Hz, $J_{4\beta,4\alpha}$ = 15.3 Hz, H-4β), 2.82(dt, 1H, $J_{4\beta,3\beta}$ = 5.8 Hz, J_{gem} = 14.5 Hz, H-4α), 2.85(dd, 1H, $J_{7\beta,8}$ = 3.8 Hz, $J_{7\beta,7\alpha}$ = 11.8 Hz, H-7β), 4.77(dd, 1H, $J_{8,9}$ = 1.6 Hz, $J_{8,7\beta}$ = 5.2 Hz, H-8), 6.33(d, 1H, $J_{10,9}$ = 5.9 Hz, H-10), 6.48(dd, 1H, $J_{9,8}$ = 1.7 Hz, $J_{9,10}$ = 5.9 Hz, H-9); ^{13}C NMR (50 MHz): 23.85(q), 24.44(q), 27.48(q), 32.70(s, C-2), 35.10, 35.29, and 39.78(t, C-3, C-4, and C-7), 54.18(s, C-6), 77.39(d, C-8), 97.10(s, C-1), 132.15 and 138.70(d, C-9 and C-10), 213.94(s, C-5); mass spectrum: 206(10, M$^{\cdot+}$), 109(100, M − $(CH_2)_2$C(O)CMe=CH_2). Exact Mass calcd. for $C_{13}H_{18}O_2$: 206.1307; found: 206.1290.

(6α,8α-H)-2,2,7α-Trimethyl-11-oxatricyclo[6.2.1.0^{1,6}]undec-9-en-5-one (58)

The IMDAF reaction of compound **11** (54.9 mg, 0.266 mmol) was performed according to general procedure 4 to provide a SM:A ratio of 87:13 with quantitative recovery of material after 192 h. General procedure 5 was used to perform the Lewis acid–mediated reactions of compound **11**. Thus, enone **11** (104.1 mg, 0.504 mmol) was treated with quantitative $MeAlCl_2$ (555 μL, 0.555 mmol) at −78°C for 8 h to provide a SM:A ratio of 73:27

Can. J. Chem. Downloaded from www.nrcresearchpress.com by 88.255.202.194 on 09/08/12
For personal use only.

and enone **11** (60.5 mg) and adduct **58** (24.7 mg) with 82% recovery after separation by flash chromatography (9:1). Enone **11** (124.7 mg, 0.604 mmol) was treated with catalytic $MeAlCl_2$ (60 μL, 0.060 mmol) at −65°C for 2 h according to general procedure 5 to provide a SM:A ratio of 27:73 with a quantitative recovery of material. Adduct **58** was characterized as a solid, mp 35–37°C; IR (KBr) cm^{-1}: 3012(CH), 2968–2871(CH), 1698(C=O), 1389, 1368(*gem*-Me); ^1H NMR (200 MHz): 0.98(d, $J_{7\beta,14}$ = 7.0 Hz, C-7-CH_3), 1.07 and 1.31(s, 3H each), 1.59(ddd, 1H, $J_{3\alpha,4\beta}$ = 3.1 Hz, $J_{3\alpha,4\alpha}$ = 5.7 Hz, $J_{3\alpha,3\beta}$ = 13.4 Hz, H-3α), 1.77(d, 1H, $J_{6\alpha,7\beta}$ = 4.0 Hz, H-6α), 2.01(dt, 1H, $J_{3\beta,4\beta}$ = 5.2 Hz, $J_{3\beta,4\alpha}$ = 13.4 Hz, $J_{3\alpha,3\beta}$ = 13.4 Hz, H-3β), 2.40(ddd, 1H, $J_{3\alpha,4\beta}$ = 3.1 Hz, $J_{3\beta,4\beta}$ = 5.2 Hz, $J_{4\alpha,4\beta}$ = 16.3 Hz, H-4β), 2.54(ddd, 1H, $J_{3\alpha,4\alpha}$ = 6.6 Hz, $J_{3\beta,4\alpha}$ = 13.4 Hz, $J_{4\beta,4\alpha}$ = 16.2 Hz, H-4α), 2.74(ddq, 1H, $J_{7\beta,6\alpha}$ = 4.2 Hz, $J_{7\beta,8}$ = 4.8 Hz, $J_{7\beta,14}$ = 7.0 Hz, H-7β), 4.73(d, 1H, $J_{7\beta,8}$ = 4.6 Hz, H-8), 6.40(ABq, 2H, H-9 and H-10); ^{13}C NMR (50 MHz): 17.51(q), 24.23(q), 25.78(q), 31.91(s, C-2), 34.47 and 37.55(t, C-3 and C-4), 39.72(d, C-7), 56.28(d, C-6), 81.57(d, C-8), 96.47(s, C-1), 134.95, 136.32(d, C-9 and C-10), 211.29(s, C-5); mass spectrum: 206(20, $M^{\cdot+}$), 109(100, M − $(CH_2)_2C(O)CMe{=}CH_2$). Exact Mass calcd. for $C_{13}H_{18}O_2$: 206.1307; found: 206.1305.

*(6α-H)-2,2,8α-Trimethyl-11-oxatricyclo[6.2.1.0^{1,6}]undec-9-en-5-one (**60**)*

The IMDAF reaction of compound **13** (62.1 mg, 0.301 mmol) occurred at 0°C as a neat oil to provide adduct **60** (62.1 mg, 0.301 mmol) as a white, crystalline solid, mp 52–54°C; IR (KBr) cm^{-1}: 1707(C=O); ^1H NMR (300 MHz): 1.08 and 1.33(s, 3H each), 1.55(s, 3H C-8-CH_3), 1.60(ddd, 1H, $J_{3\alpha,4\beta}$ = 2.7 Hz, $J_{3\alpha,4\alpha}$ to 5.8 Hz, $J_{3\alpha,3\beta}$ = 13.9 Hz, H-3α), 1.68(dd, 1H, $J_{7\alpha,6\alpha}$ = 8.4 Hz, $J_{7\alpha,7\beta}$ = 11.8 Hz, H-7α), 2.01(dt, 1H, $J_{3\beta,4\beta}$ = 4.3 Hz, $J_{3\beta,4\alpha}$ = 13.9 Hz, $J_{3\beta,3\alpha}$ = 13.9 Hz, H-3β), 2.12(dd, 1H, $J_{7\beta,6\alpha}$ = 3.3 Hz, $J_{7\beta,7\alpha}$ = 11.8 Hz, H-7β), 2.38(dd, 1H, $J_{6\alpha,7\beta}$ = 3.3 Hz, $J_{6\alpha,7\alpha}$ = 8.4 Hz, H-6α), 2.40(ddd, 1H, $J_{4\beta,3\alpha}$ = 2.8 Hz, $J_{4\beta,3\beta}$ = 4.3 Hz, $J_{4\beta,4\alpha}$ = 13.2 Hz, H-4β), 2.56(dt, 1H, $J_{4\alpha,3\alpha}$ = 5.8 Hz, $J_{4\alpha,4\beta}$ = 13.2 Hz, $J_{4\alpha,3\beta}$ = 13.9 Hz, H-4α), 6.25(ABq, 2H, H-9 and H-10); ^{13}C NMR (75 MHz): 18.77(q), 24.08(q), 26.05(q), 32.10(s, C-2), 34.88, 37.40, and 37.89(t, C-3, C-4, and C-7), 51.24(d, C-6), 85.63 and 96.09(s, C-1 and C-8), 134.16 and 141.77(d, C-9 and C-10), 210.83(s, C-5); mass spectrum: 206(43, $M^{\cdot+}$), 191(13, M − Me), 123(100, M − $(CH_2)_2C(O)CH{=}CH_2$). Exact Mass calcd. for $C_{13}H_{18}O_2$: 206.1307; found: 206.1297.

*2,2,6α,8α-Tetramethyl-11-oxatricyclo[6.2.1.0^{1,6}]undec-9-en-5-one (**61**)*

The IMDAF reaction of compound **14** (58.4 mg, 0.265 mmol) was performed according to general procedure 4 to provide a SM:A ratio of 88:12 in 82% recovery of material after 336 h. Starting material (40.9 mg) and adduct (6.8 mg) were isolated by flash chromatography (9:1). General procedure 5 was used to perform the Lewis acid-mediated reactions of compound **14**. Thus, enone **14** (48.8 mg, 0.222 mmol) was treated with quantitative $MeAlCl_2$ (244 μL, 0.244 mmol) at −78°C for 8 h to provide a SM:A ratio of 78:22 with quantitative recovery of material. Enone **14** (30.1 mg) and adduct (9.0 mg) were isolated by flash chromatography (9:1). Enone **14** (32.7 mg, 0.148 mmol) was treated with catalytic $MeAlCl_2$ (15 μL, 0.015 mmol) (according to general procedure 5) at −65°C for 2 h to provide a SM:A ratio of 23:77 with quantitative recovery. Adduct **61** was characterized as a solid; IR (KBr) cm^{-1}: 2986–2873(C—H), 1708(C=O), 1384,1371(*gem*-Me); ^1H NMR (300 MHz): 1.01(s, 3H, C-6-CH_3), 1.09(d, 1H, $J_{7\alpha,7\beta}$ = 11.7 Hz, H-7α), 1.12 and 1.33(s, 3H each), 1.46(s, 3H, C-8-CH_3), 1.56(ddd, 1H, $J_{3\alpha,4\beta}$ = 2.7 Hz, $J_{3\alpha,4\alpha}$ = 5.8 Hz, $J_{3\alpha,3\beta}$ = 13.6 Hz, H-3α), 1.99(dt, 1H, $J_{3\beta,4\beta}$ = 4.1 Hz, $J_{3\beta,3\alpha}$ = 13.6 Hz, $J_{3\beta,4\alpha}$ = 14.4 Hz, H-3β), 2.32(ddd, 1H, $J_{4\beta,3\alpha}$ = 2.7 Hz, $J_{4\beta,3\beta}$ = 4.1 Hz, $J_{4\beta,4\alpha}$ = 15.3 Hz, H-4β), 2.53(d, 1H, J = 11.7 Hz, H-7β), 2.77(ddd, 1H, $J_{4\alpha,3\alpha}$ = 5.8 Hz, $J_{4\alpha,3\beta}$ = 14.4 Hz, $J_{4\alpha,4\beta}$ = 15.3 Hz, H-4α), 6.25(d, 1H, $J_{10,9}$ = 5.7 Hz, H-10), 6.30(d, 1H, $J_{9,10}$ = 5.7 Hz, H-9); ^{13}C NMR (75 MHz): 18.93(q), 23.75(q), 24.27(q), 27.51(q), 32.78(s, C-2), 35.00 and 35.31(t, C-3 and C-7), 46.21(t, C-4), 57.37(s, C-6), 84.76 and 97.29(s, C-1 and C-8), 132.76 and 141.69(d, C-9 and C-10), 214.39(s, C-5); mass spectrum: 220(18, $M^{\cdot+}$), 123(100, M − $(CH_2)_2C(O)CMe{=}CH_2$). Exact Mass calcd. for $C_{14}H_{20}O_2$: 220.1464; found: 220.1462.

*(6α-H)-2,2,7α,8α-Tetramethyl-11-oxatricyclo[6.2.1.0^{1,6}]undec-9-en-5-one (**62**)*

General procedure 5 was used to perform the Lewis acid-mediated reactions of compound **15**. Thus, enone **15** (14.6 mg, 0.066 mmol) was treated with catalytic $MeAlCl_2$ (6.6 μL, 0.066 mmol) at −65°C for 2 h to provide a **15**:**62** ratio of 69:31 with 72% recovery; IR (KBr) cm^{-1}: 2960–2868(C-H), 1706(C=O), 1384,1368(*gem*-Me); ^1H NMR (400 MHz): 0.97(d, 3H, $J_{14,7\beta}$ = 7.0 Hz, H-14), 1.08 and 1.28(s, 3H each), 1.50(s, 3H, C-8-CH_3), 1.56(ddd, 1H, $J_{3\alpha,4\beta}$ = 2.8 Hz, $J_{3\alpha,4\alpha}$ = 6.0 Hz, $J_{3\alpha,3\beta}$ = 13.5 Hz, H-3α), 1.88(d, 1H, $J_{6\alpha,7\beta}$ = 4.1 Hz, H-6α), 2.01(dt, 1H, $J_{3\beta,4\beta}$ = 4.8 Hz, $J_{3\beta,4\alpha}$ = 13.6 Hz, $J_{3\beta,3\alpha}$ = 13.6 Hz, H-3β), 2.35(dq, 1H, $J_{7\beta,6\alpha}$ = 4.1 Hz, $J_{7\beta,14}$ = 7.0 Hz, H-7β), 2.40(ddd, 1H, $J_{4\beta,3\alpha}$ = 2.8 Hz, $J_{4\beta,3\beta}$ = 4.8 Hz, $J_{4\beta,4\alpha}$ = 16.2 Hz, H-4β), 2.51(ddd, 1H, $J_{4\alpha,3\alpha}$ = 6.0 Hz, $J_{4\alpha,3\beta}$ = 13.6 Hz, $J_{4\alpha,4\beta}$ = 16.2 Hz, H-4α), 6.20(d, 1H, $J_{10,9}$ = 5.7 Hz, H-10), 6.37(d, 1H, $J_{9,10}$ = 5.7 Hz, H-9); ^{13}C NMR (50 MHz): 17.20(q), 17.40(q), 24.06(q), 25.86(q), 31.94(s, C-2), 34.40 and 37.55(t, C-3 and C4), 45.65(d, C-7), 59.21(d, C-6), 88.25 and 95.38(s, C-1 and C-8), 135.41 and 139.34(d, C-9 and C-10), 211.59(s, C-5); mass spectrum: 220(8, $M^{\cdot+}$), 123(100, M − $(CH_2)_2C(O)CH{=}CHMe$). Exact Mass calcd. for $C_{14}H_{20}O_2$: 220.1464; found: 220.1465.

*(7β,9α-H)-12-Oxatricyclo[7.2.1.0^{1,7}]dodec-10-en-6-one (**63**)*

General procedure 5 was used to perform the Lewis acid-mediated reaction of compound **8**. Thus, enone **8** (63.5 mg, 0.356 mmol) was treated with $MeAlCl_2$ (36 μL, 0.036 mmol) at −78°C for 2 h to provide a SM:A ratio of 8:92 with 98% recovery of material. Some retro-IMDAF reaction occurred upon attempted purification by flash chromatography (9:1). Adduct **63** was characterized as a white crystalline solid; ^1H NMR (200 MHz): 1.38–1.67(m, 2H), 1.75–2.30(overlapping m, 6H), 2.38–2.70(overlapping m, 2H), 3.20(dd, 1H), 4.90(dd, 1H, H-9), 6.02(d, 1H, $J_{11,10}$ = 6.2 Hz, H-11), 6.41(dd, 1H, $J_{10,9}$ = 1.2 Hz, $J_{10,11}$ = 6.2 Hz, H-10).

*2,2-Dimethyl-7-(trimethysilyl)-11-oxatricyclo[6.2.1.0^{1,6}] undec-6,9-dien-5-one (**65**)*

General procedure 5 was used for the Lewis acid-mediated IMDAF reaction of compound **16**. Thus, enone **16** (100.9 mg, 0.384 mmol) was treated with $MeAlCl_2$ (423 μL, 0.423 mmol) at −50°C for 2.5 h to provide a SM:A ratio of 12.88. Adduct **65** (76.4 mg, 0.482 mmol) was obtained in 89% yield (based on recovered starting material) as a golden crystalline solid, after purification by flash chromatography; mp 85–94°C; IR (Kbr) cm^{-1}: 1660(C=O); ^1H NMR (200 MHz): 0.19(s, 9H), 1.09 and 1.22(s, 3H each, C-2-CH_3's), 1.79(ddd, 1H, $J_{3\alpha,4\beta}$ = 2.6 Hz, $J_{3\alpha,4\alpha}$ = 6.6 Hz, J_{gem} = 14.2 Hz, H-3α), 1.95(ddd, 1H, $J_{3\beta,4\beta}$ = 5.6 Hz, $J_{3\beta,4\alpha}$ = 12.5 Hz, J_{gem} = 14.2 Hz, H-3β), 2.43(ddd, 1H, $J_{4\beta,3\alpha}$ = 2.6 Hz, $J_{4\beta,3\beta}$ = 5.6 Hz, J_{gem} = 19.1 Hz, H-4β), 2.63(ddd, 1H, $J_{4\alpha,3\alpha}$ = 6.6 Hz, $J_{4\alpha,3\beta}$ = 12.5 Hz, J_{gem} = 19.1 Hz, H-4α), 5.60(d, 1H, $J_{8,9}$ = 1.9 Hz, H-8), 6.98(dd, 1H, $J_{9,8}$ = 1.9 Hz, $J_{9,10}$ = 5.4 Hz, H-9), 7.05(d, 1H, $J_{10,9}$ = 5.4 Hz, H-10); ^{13}C NMR (50 MHz): −2.15(q), 25.76(q), 22.29(q), 31.63(s, C-2), 34.20 and 36.16(t, C-3 and C-4), 86.48(d, C-8), 99.87(s, C-1), 144.16 and 144.44(d, C-9 and C-10), 160.77 and 174.23(s, C-6 and C-7), 195.64(s, C-5); mass spectrum: 262(15, $M^{\cdot+}$), 247(50, M − Me), 109(100, M − $C_8H_{16}OSi$). Exact Mass calcd. for $C_{15}H_{22}O_2Si$: 262.1389; found: 262.1376.

*2,2,7-Trimethyl-11-oxatricyclo[6.2.1.0^{1,6}]undec-6,9-dien-5-one (**66**)*

General procedure 5 was used for the Lewis acid-mediated IMDAF reaction of compound **17**. Thus, enone **17** (99.1 mg, 0.485 mmol) was treated with $MeAlCl_2$ (553 μL, 0.553 mmol) at −60°C for 0.5 h to provide adduct **66** (98.5 mg, 0.482 mmol) in

99% recovery as a white, crystalline solid, which could not be purified by flash chromatography without isomerization of the C-6, C-7 double bond; IR (neat) cm^{-1}: 1666(C=O); ^1H NMR (200 MHz): 1.10 and 1.21(s, 3H each), 1.75(ddd, 1H, $J_{3\alpha,4\beta}$ = 3.0 Hz, $J_{3\alpha,4\alpha}$ = 6.7 Hz, J_{gem} = 12.9 Hz, H-3α), 1.89(dt, 1H, $J_{3\beta,4\beta}$ = 3.0 Hz, $J_{3\beta,4\alpha}$ = J_{gem} = 12.9 Hz, H-3β), 2.31(s, 3H, C-8-CH_3), 2.43(ddd, 1H, $J_{4\beta,3\alpha}$ = 3.0 Hz, $J_{4\beta,3\beta}$ = 3.0 Hz, J_{gem} = 16.3 Hz, H-4β), 2.50–2.75(m, 1H, H-4α), 5.10(d, 1H, $J_{8,9}$ = 1.8 Hz, H-8), 7.04(dd, 1H, $J_{9,8}$ = 1.8 Hz, $J_{9,10}$ = 5.4 Hz, H-9), 7.09(d, 1H, $J_{10,9}$ = 5.4 Hz, H-10); ^{13}C NMR (50 MHz): 15.63(q), 22.02(q), 25.44(q), 31.64(s, C-2), 34.20(t), 36.16(t), 86.12(d, C-8), 99.28(s, C-1), 142.04 and 145.57(d, C-9 and C-10), 171.98(s, C-6 and C-7), 196.32(s, C-5); mass spectrum: 204(14, $M^{\cdot+}$), 163(24, M − HC≡CH), 109(100, M − $(CH_2)_2C(O)C{\equiv}CCH_3$). Exact Mass calcd. for $C_{13}H_{16}O_2$: 204.1150; found: 204.1146.

Acknowledgements

We thank the Natural Sciences and Engineering Research Council of Canada (NSERC), the University of Calgary, and the University of Windsor for financial support, and NSERC for a post-graduate scholarship (to C.R.).

1. (*a*) G. Brieger and J. N. Bennett. Chem. Rev. **80**, 63 (1980); (*b*) R. Sustman and J. Sauer. Angew. Chem. Int. Ed. Engl. **19**, 779 (1980); (*c*) A. G. Fallis. Can. J. Chem. **62**, 183 (1984); (*d*) E. Ciganek. Org. React. **32**, 1 (1984); (*e*) D. F. Taber. Intramolecular Diels–Alder reactions and Alder ene reactions. Springer-Verlag, New York. 1984; (*f*) K. Hayakawa and K. Kanematsu. J. Synth. Org. Chem. Jpn. **44**, 109 (1986); (*g*) D. Craig. Chem. Soc. Rev. **16**, 187 (1987).
2. S. Cauwberghs, P. J. De Clercq, B. Tinant, and J. P. Declercq. Tetrahedron Lett. **29**, 2493 (1988); T. Ghosh and H. Hart. J. Org. Chem. **54**, 5073 (1989); A. Padwa, Y. S. Kulkarni, and L. W. Terry. J. Org. Chem. **55**, 2478 (1990); A. P. Kozikowski and W. Tuckmantel. J. Org. Chem. **56**, 2826 (1991); K. Fischer and S. Hunig. J. Org. Chem. **52**, 564 (1987); B. L. Feringa, O. J. Gelling, and L. Meesters. Tetrahedron Lett. **31**, 7201 (1990); W. M. Grootaert and P. J. De Clercq. Tetrahedron Lett. **27**, 1731 (1986); F. Nuyttens, G. Appendino, and P. J. De Clercq. Synlett, 526 (1991).
3. (*a*) J. Moursounidis and D. Wede. Tetrahedron Lett. **27**, 3045 (1986); (*b*) W. M. Best and D. Wege. Aust. J. Chem. **39**, 635 (1986); (*c*) Aust. J. Chem. **39**, 647 (1986); (*d*) Y. Yamaguchi, J. Yamada, K. Hayakawa, and K. Kanematsu. J. Org. Chem. **52**, 2040 (1987); (*e*) H. Finch, L. M. Harwood, G. M. Robertson, and R. C. Sewell. Tetrahedron Lett. **30**, 2585 (1989); (*f*) K. H. Dotz, R. Noack, K. Harms, and G. Muller. Tetrahedron, **46**, 1235 (1990); (*g*) M. E. Jung. Synlett, **1**, 186 (1990); (*h*) M. E. Jung and J. Gervay. J. Am. Chem. Soc. **113**, 224 (1991); (*i*) W. Blokzijl, M. J. Blandamer, and J. B. F. N. Engberts. J. Am. Chem. Soc. **113**, 4241 (1991).
4. (*a*) P. J. De Clercq and L. A. Van Royen. Synth. Commun. **9**, 771 (1979); (*b*) L. M. Harwood, S. A. Leeming, N. S. Isaacs, G. Jones, J. Pickard, R. M. Thomas, and D. A. Watkin. Tetrahedron Lett. **29**, 5017 (1988); (*c*) L. M. Harwood, G. Jones, J. Pickard, R. M. Thomas, and D. Watkin. Tetrahedron Lett. **29**, 5825 (1988); (*d*) L. A. Van Royen, R. Mijngheer, and P. J. De Clercq. Tetrahedron Lett. **23**, 3283 (1982); (*e*) Tetrahedron Lett. **24**, 3145 (1983); (*f*) Bull. Soc. Chim. Belg. **93**, 1019 (1984); (*g*) Tetrahedron, **41**, 4667 (1985); (*h*) B. A. Keay. J. Chem. Soc. Chem. Commun. 419 (1987); (*i*) P. Missiaen and P. J. De Clercq. Bull. Soc. Chim. Belg. **96**, 105 (1987); (*j*) P. W. Dibble and B. A. Keay. Tetrahedron Lett. **30**, 1045 (1989); (*k*) C. Rogers and B. A. Keay. Tetrahedron Lett. **30**, 1349 (1989); (*l*) P. Missiaen and P. J. De Clercq. Bull. Soc. Chim. Belg. **99**, 271 (1990); (*m*) G. Appendino, J. Hoflack, P. J. De Clercq, G. Chiari, and M. Calleri. Tetrahedron, **44**, 4605 (1988); (*n*) S. G. Cawberghs and P. J. De Clercq. Tetrahedron Lett. **29**, 6501 (1988).
5. (*a*) S. J. Burrell, A. E. Derome, M. S. Edenborough, L. M. Harwood, S. A. Leeming, and N. S. Isaacs. Tetrahedron Lett. **26**, 2229 (1985); (*b*) L. M. Harwood, G. Jones, J. Pickard, R. M. Thomas, and D. Watkin. J. Chem. Soc. Chem. Commun. 605 and 608 (1990); (*c*) L. M. Harwood, T. Ishikawa, H. Phillips, and D. Watkin. J. Chem. Soc. Chem. Commun. 527 (1991).
6. D. D. Sternbach and D. M. Rossana. J. Am. Chem. Soc. **104**, 5853 (1982).
7. D. D. Sternbach and D. M. Rossana. Tetrahedron Lett. **23**, 303 (1982).
8. M. E. Jung and J. Gervay. J. Am. Chem. Soc. **111**, 5469 (1989); Tetrahedron Lett. **29**, 2429 (1988); D. D. Sternbach and D. M. Rossana. Tetrahedron Lett. **26**, 591 (1985); J. Org. Chem. **49**, 3428 (1984).
9. (*a*) B. H. Lipshutz. Chem. Rev. **86**, 795 (1986); (*b*) W. A. Nugent, R. J. McKinney, and R. L. Harlow. Organometallics, **3**, 1315 (1984); (*c*) F. Brion. Tetrahedron Lett. **23**, 5299 (1982); (*d*) H. Kotsuki, K. Asao, and H. Ohnishi. Bull. Soc. Chem. Jpn. 3339 (1984); (*e*) E. Vieira and P. Vogel. Helv. Chim. Acta, **65**, 1700 (1982); (*f*) J. A. Moore and E. M. Partain. J. Org. Chem. **48**, 1105 (1983).
10. (*a*) D. A. Smith and K. N. Houk. Tetrahedron Lett. **32**, 1549 (1991); (*b*) K. Takeda, T. Kobayashi, K. Saito, and E. Yoshii. J. Org. Chem. **53**, 1092 (1988); (*c*) W. R. Roush and R. Riva. J. Org. Chem. **53**, 710 (1988); (*d*) W. R. Roush, A. P. Essenfeld, and J. S. Warmus. Tetrahedron Lett. **28**, 2447 (1987); (*e*) J. A. Marshall. B. G. Shearer, and S. L. Crooks. J. Org. Chem. **52**, 1236 (1987); (*f*) J. A. Marshall, J. Grote, and J. E. Audia. J. Am. Chem. Soc. **109**, 1186 (1987); (*g*) D. A. Smith, K. Sukan, and K. N. Houk. Tetrahedron Lett. **27**, 4877 (1986); (*h*) J. A. Marshall, J. E. Audia, J. Grote, and B. G. Shearer. Tetrahedron, **42**, 2893 (1986); (*i*) J. A. Marshall, J. E. Audia, and J. Grote. J. Org. Chem. **49**, 5279 (1984); (*j*) K. Sakan and D. A. Smith. Tetrahedron Lett. **25**, 2081 (1984); (*k*) K. J. Shea and J. W. Gilman. Tetrahedron Lett. **24**, 657 (1983); (*l*) W. R. Roush and H. R. Gillis. J. Org. Chem. **47**, 4825 (1982); (*m*) W. R. Roush, H. R. Gillis, and A. I. Ko. J. Am. Chem. Soc. **104**, 2269 (1982); (*n*) W. R. Roush and S. E. Hall. J. Am. Chem. Soc. **103**, 5200 (1981).
11. K. A. Parker and M. R. Adamchuk. Tetrahedron Lett. 1689 (1978).
12. T. Takebayashi, N. Iwasawa, and T. Mukaiyama. Bull. Chem. Soc. Jpn. **56**, 1107 (1983); T. Mukaiyama and T. Takebayashi. Chem. Lett. 1013 (1980); T. Mukaiyama, T. Tsuji, and N. Iwasawa. Chem. Lett. 697 (1979).
13. B. L. Feringa, O. J. Gelling, and L. Meesters. Tetrahedron Lett. **31**, 7201 (1990).
14. P. Bosshard and C. H. Eugster. Adv. Heterocycl. Chem. **7**, 378 (1966); F. M. Dean. Adv. Heterocycl. Chem. **30**, 168 (1982); **31**, 238 (1982).
15. B. A. Keay, D. Rajapaksa, and R. Rodrigo. Can. J. Chem. **62**, 1093 (1984).
16. C. Rogers and B. A. Keay. Tetrahedron Lett. **32**, 6477 (1991); Synlett, 353 (1991).
17. B. J. Wakefield. Organolithium methods. Academic Press, Toronto. 1988.
18. E.-I. Negishi, L. D. Boardman, H. Sawada, V. Bagheri, A. T. Stoll, J. M. Tour, and C. L. Rand. J. Am. Chem. Soc. **110**, 5383 (1988).
19. W. F. Bailey, T. T. Nurmi, J. J. Patricia, and W. Wang. J. Am. Chem. Soc. **109**, 2442 (1987).
20. A. J. Mancuso and D. Swern. Synthesis, 165 (1981).
21. Z. M. Ismail and H. M. R. Hoffmann. Angew. Chem. Suppl. 985 (1983).

Can. J. Chem. Downloaded from www.nrcresearchpress.com by 88.255.202.194 on 09/08/12
For personal use only.

22. J. F. Normant and C. Piechuk. Bull. Soc. Chim. Fr. 2402 (1972).
23. (*a*) J. S. Ng, J. R. Behling, A. L. Campbell, D. Nguyen, and B. Lipshutz. Tetrahedron Lett. **29**, 3045 (1988); (*b*) K. Mori and M. Matsui. Tetrahedron, **22**, 2883 (1966).
24. T. K. Jones and S. E. Denmark. Org. Synth. **64**, 182 (1985); G. Piancatteli, A. Sattri, and M. D'Auria. Synthesis, 245 (1982).
25. L. Brandsma. Preparative acetylene chemistry. Elsevier, Amsterdam. 1971.
26. B. B. Snider, D. J. Rodini, M. K. Karras, T. C. Kirk, E. A. Deutsch, R. Cordova, and R. T. Price. Tetrahedron, **37**, 3927 (1981).
27. H. Kotsuki. Bull. Chem. Soc. Jpn. **57**, 3339 (1984).
28. (*a*) M. Kakushima, J. Espinosa, and Z. Valenta. Can. J. Chem. **54**, 3304 (1976); (*b*) W. Oppolzer, C. Chapuis, G. M. Dao, D. Reichlin, and T. Godel. Tetrahedron Lett. **23**, 4781 (1982); (*c*) K. Sakan and B. A. Craven. J. Am. Chem. Soc. **105**, 3732 (1983).
29. W. C. Still, M. Kahn, and A. Mitra. J. Org. Chem. **43**, 2923 (1978).
30. R. M. Beesley, C. K. Ingold, and J. F. Thorpe. J. Chem. Soc. **107**, 1080 (1915); C. K. Ingold. J. Chem. Soc. **119**, 305 (1921); N. L. Allinger and V. Zalkow. J. Org. Chem. **25**, 701 (1960); T. C. Bruice and U. K. Pandit. J. Am. Chem. Soc. **82**, 5858 (1960).
31. W. R. Roush and H. R. Gillis. J. Org. Chem. **45**, 4267 (1980).
32. B. P. Susz. Bull. Soc. Chem. Fr. 2671 (1965); T.-L. Ho. Chem. Rev. **75**, 1 (1975); J. March. Advanced organic chemistry. 3rd ed. Wiley and Sons, New York. 1985. pp. 218–223.
33. S. J. Hecker and C. H. Heathcock, J. Org. Chem. **50**, 5159 (1985); S. E. Hall and W. R. Roush. J. Org. Chem. **47**, 4611 (1982); W. R. Roush and S. M. Peseckis. J. Am. Chem. Soc. **103**, 6696 (1981); P. A. Jacobi and D. G. Walker. J. Am. Chem. Soc. **103**, 4611 (1981); P. A. Jacobi, D. G. Walker, and I. M. A. Odeh. J. Org. Chem. **46**, 2065 (1981); G. A. Kraus. J. Am. Chem. Soc. **102**, 1974 (1980); L. H. Klemm, T. M. McGuire, and K. W. Gopinath. J. Org. Chem. **41**, 2571 (1976).
34. B. A. Keay, H. P. Plaumann, D. Rajapaksa, and R. Rodrigo. Can. J. Chem. **61**, 1987 (1983); R. M. Silverstein, G. C. Bassler, and T. C. Morrill. Spectrometric identification of organic compounds. 5th ed. Wiley and Sons, Toronto. 1991.
35. T. Mukayama and T. Takebayashi. Chem. Lett. 1013 (1980).
36. I. Fleming. Frontier orbitals and organic chemical reactions. Wiley and Sons, New York. 1976. pp. 86–181.
37. D. D. Perrin and W. L. F. Armarego. Purification of laboratory chemicals. 3rd ed. Pergamon Press, Toronto. 1988.

Can. J. Chem. Downloaded from www.nrcresearchpress.com by 88.255.202.194 on 09/08/12
For personal use only.

The effect of tensioactive agents on the kinetics of hydrogen evolution at a nickel electrode

RICHARD MENINI,[1] PIOTR K. WRONA,[2] HUGUES MÉNARD, AND OLIVIER VITTORI[1]
Département de chimie, Université de Sherbrooke, Sherbrooke (Qué.), Canada J1K 2R1

Received November 29, 1991

RICHARD MENINI, PIOTR K. WRONA, HUGUES MÉNARD, and OLIVIER VITTORI. Can. J. Chem. **70**, 2948 (1992).

The effect of tensioactive agents (TSA = SDS, BRIJ35, BRIJ78, BRIJ99, and CTAB) on the kinetics of hydrogen evolution at a rotating nickel electrode in 0.2 M solutions of Na_2SO_4 was investigated. It was found that at higher concentrations of TSA, their presence inhibited the reaction although their adsorption behaviour at the nickel electrode is different. We concluded that BRIJ35 and CTAB should show better performance in the hydrogenation of organic compounds than SDS.

RICHARD MENINI, PIOTR K. WRONA, HUGUES MÉNARD et OLIVIER VITTORI. Can. J. Chem. **70**, 2948 (1992).

On a étudié l'influence de divers agents tensioactifs (STA = SDS, BRIJ35, BRIJ78, BRIJ99 et CTAB) sur la cinétique de la réaction d'évolution d'hydrogène à une électrode tournante, dans des solutions 0,2 M de Na_2SO_4. On a trouvé que, à des concentrations élevées de TSA, leur présence inhibe cette réaction de façons semblables, même si leur comportement d'adsorption à l'électrode de nickel est différent. On en conclut que, lors de l'hydrogénation de composés organiques, le BRIJ35 et le CTAB devraient donner de meilleures performances que le SDS.

[Traduit par la rédaction]

Introduction

Tensioactive agents (TSA) are frequently used in electrochemistry. Since these compounds usually show strong adsorption at the mercury electrode, they have been widely used in polarography as maxima suppressors (1). It has also been found (2) that TSA (gelatin and methyl red) show significant influence on the kinetics of reactions occurring at the electrodes. Many TSA show self-organization and at higher concentrations they spontaneously form micelles (3). Micellized TSA (4) were used by Proske to solubilize nonpolar organic compounds in water for electrochemical measurements. This idea was similar to that described (5) by Behr and Dojlido. These authors have found that the adsorption of benzene at mercury electrodes increased many times in the presence of small (5%) amounts of ethyl alcohol, although in the bulk of solution, ethyl alcohol had very small effect (an increase of less than 3%) on the solubility of benzene.

At present the TSA micelles are used widely to modify organic chemical and electrochemical reactions (6, 7). For example, it has been found (8) that after the addition of a nonionic surfactant (BRIJ35), a single four-electron polarographic wave of the reduction of substituted nitrobenzene at pH $\geq$ 9 splits into two waves. The product of the first one-electron wave has been identified as a nitrobenzene free radical. Similar results were obtained (9) in 1952 by Holleck and Exner, who used camphor and triphenylphosphine. They also obtained a single, one-electron reduction wave of nitrobenzene to nitrobenzene radical (see also ref. 10).

The use of cationic micelles of cetyltrimethylammonium bromide to reduce 4-bromobiphenyl to biphenyl by 9-phenylanthracene radical has been recently described (11).

TSA may also enhance the hydrogenation of organic compounds. Many organic, and mostly aromatic compounds, after reduction, could be used as a source of hydrogen. Various applications of this idea have been described by Lessard and co-workers (12). For hydrogenation reactions these authors used mostly nickel, copper, and other composite electrodes. Recently, Ménard *et al.* have described (13, 14) the use of composite nickel powder electrodes bonded with $AlPO_4$ and $LaPO_4$ polymers. These electrodes have very large active surfaces and have been used successfully in many electrochemical organic syntheses. The long-range purpose of our work was to determine the effect of TSA micelles on the hydrogenation of organic compounds at composite nickel electrodes. Since in the presence of TSA the organic substances are often reduced at higher overvoltages, our first problem is to find a TSA with as little effect as possible on the electrode kinetics, and that is strongly adsorbed at the electrode surface. This paper describes the first part of our work, i.e., to measure the effect of TSA micelles on the kinetics of hydrogen evolution reaction (HER) at nickel electrodes. We found that all TSA used anionic, cationic, and non-ionic, inhibit the HER in a similar way, but their adsorption at the nickel electrode is markedly different.

Experimental

The rotating disk electrode was made from high purity nickel rod, mounted in KEL-F. The surface of the electrode was 0.126 cm^2. The electrode was polished by alumina before every experiment, later rinsed in 1 M H_2SO_4 for 15 s or introduced into the cell without washing. When the electrode was not washed, its potential was 100 mV more negative than the formal potential of the Ni/Ni^{2+} redox couple. The pH of the solution was measured before every experiment.

The cell was made of Pyrex glass and the anodic compartment was separated by a Nafion membrane M-901 CATH/MD (DuPont). A Luggin capillary was used to minimize the ohmic drop. Since the current was of the order of 0.2 mA, and the resistivity did not exceed 40 Ω, the *IR* was smaller than 10 mV.

The reference electrode was a calomel electrode with saturated KCl. The electrode was separated from the experimental cell by a salt bridge containing the solution under study. The counter electrode was a graphite rod with a high surface area.

Most experiments were conducted in 0.2 M solution of Na_2SO_4

[1]On leave from Université Lyon I, Laboratoire d'électrochimie analytique, 43 Bd. du 11 Novembre 1918, 69622 Villeurbanne, France.

[2]On leave from Department of Chemistry, University of Warsaw, Pasteura 1, 02-093 Warsaw, Poland.

[3]Revision received June 26, 1992.

Can. J. Chem. Downloaded from www.nrcresearchpress.com by 88.255.202.194 on 09/08/12
For personal use only.

TABLE 1. Characteristics of the tensioactive agents used in this work

Type	Chemical formula and abbreviation	Critical micelles concentration (M)	Kraft temperature (°C)
Anionic	Sodium dodecylsulfate (SDS) $CH_3—(CH_2)_{11}—SO_3^-Na^+$	8.1×10^{-3}	23
	0.05 M Na_2SO_4[a]	1.5×10^{-3}	
	0.2 M Na_2SO_4[a]	4.2×10^{-4}	
Cationic	Cetyltrimethylammonium bromide $CH_3—(CH_2)_{15}—N(CH_3)_3^+Br^-$ (CTAB)	9.2×10^{-3}	26
	0.2 M Na_2SO_4[a]	1×10^{-5} (est)	
Non-ionic	Polyethylene oxide dodecanol $CH_3—(CH_2)_n—(OCH_2CH_2)_k—OH$		
	BRIJ-35 ($n = 11$, $k = 23$)	$(6–9) \times 10^{-5}$	
	0.05 M Na_2SO_4[a]	9.5×10^{-4}	
	BRIJ-78 ($n = 17$, $k = 20$) $CH_3(CH_2)_n—CH=CH—(OCH_2CH_2)_kOH$		
	BRIJ-99 ($n = 15$, $k = 20$)		
	0.05 M Na_2SO_4[a]	5.6×10^{-4}	

[a]Values determined in this work using the surface tension method (15).

at pH 3.4. The sodium sulfate used was of high purity (Na_2SO_4, anhydrous, BDH). In the case of Na_2SO_4 manufactured by Anachemia (Na_2SO_4, anhydrous) and $Na_2SO_4 \cdot 10H_2O$ (BDH) the current–potential wave appeared at potentials ~100 mV more negative. This shift can be explained by the presence of Cl^- ions in solutions prepared from $Na_2SO_4 \cdot 10H_2O$. The concentration of chlorine ions was 10 times higher in $Na_2SO_4 \cdot 10H_2O$ than in Na_2SO_4. Similar shift in potential occurred when a 10 mg/L solution of sodium chloride was added to the 0.2 M Na_2SO_4 solution. However, this phenomenon needs additional studies. Solutions were prepared using deionized water (Barnstead Nanopure). Oxygen was removed by passing nitrogen through the cell. All experiments were carried out at 25°C.

Results

Description of the surface active agents

The TSA used in this work are listed in Table 1. Physicochemical properties of these compounds in water and in organic solvents have been described by Lardet and Thomalla (15) and Berthod (16). Berthod has found that for ionic TSA, the critical micelles concentration (CMC) depends on the type of the salt, and decreases linearly with the salt concentration. The lowest CMC was found for Na_2SO_4. In the case of BRIJ, almost no dependence of CMC on salt concentration was found. Values of CMC corresponding to $\mu = 0$ M are presented in Table 1. We therefore measured the CMC at higher concentrations of Na_2SO_4 using the surface tension method (15). In all cases one observed the CMC at much lower concentrations of TSA.

Measurements of the formal potentials of the H^+/H_2 redox couple

The formal potentials of the electrode reaction

$$[1] \quad H_3O^+ + e \rightarrow 1/2\, H_2 + H_2O$$

were measured in Na_2SO_4 solutions at $\mu = 0.2$ M in the range of pH from 2.6 to 3.4 at a large Pt electrode kept in a stream of H_2. The dependence of E_f^0 on pH was described by a linear relation:

$$[2] \quad E_f^0 = -0.246\ (\mp 0.002) + 0.058(\mp 0.004)\ \text{pH}$$

with correlation coefficient $R = 0.989$. Both the slope and the E_f^0 value for pH = 0 were in accord with theoretical predictions.

Stability of the nickel electrode

Typical cyclic current–potential curves recorded with the use of the nickel-rotating electrode in 0.2 M solution of Na_2SO_4 at pH 3.4 are presented in Fig. 1. In the region of potentials more negative than −0.4 V (SCE), one observes a very well developed wave of H^+ ion reduction, and at more negative potentials, the reduction of water.

At potentials more positive, one observes a small oxidation peak. Since at these pH's the formal potential of the Ni^{2+}/Ni redox couple is close to 0 V/SCE (−0.25 V vs. SHE) (17), it follows from the Pourbaix diagrams (17) that the nickel electrode should be oxidized to Ni^{2+} ions. Interpretation of these small peaks is difficult. Formation of these peaks was also observed by Reshetnikov (18) and Kesten and Feller (19). Probably the peaks correspond to the formation of a monolayer of nickel hydroxide.

Though the electrode potential was always more negative than −0.4 V (when it was dipped into the solution), we have experienced some problems with the reproducibility of the *I–E* curves. For example, the second curve, recorded immediately after the first one, was usually located at potentials more negative. This can not be attributed to the formation of NiO which facilitates the reduction of hydrogen (20). Therefore some poisoning of the electrode surface has occurred. To achieve reproducibility, we have analyzed the effect of several electrochemical pre-treatments on the *I–E* curves under the following conditions: (*i*) no additional electrochemical pre-treatment; (*ii*) by passing a cathodic current 2 mA for 30 min; (*iii*) by imposing a potential in the region of limiting current of H^+ for 15 min; (*iv*) by keeping the electrode in solution at the open circuit for 30 min; and (*v*) by cycling the potential from zero current to reduction of water.

Before every experiment the electrode was polished on alumina and washed in 1 M solution of H_2SO_4 for 15 s.

Reproducible results were obtained only in case (*ii*). Here when the cathodic current was flowing through the nickel

Can. J. Chem. Downloaded from www.nrcresearchpress.com by 88.255.202.194 on 09/08/12
For personal use only.

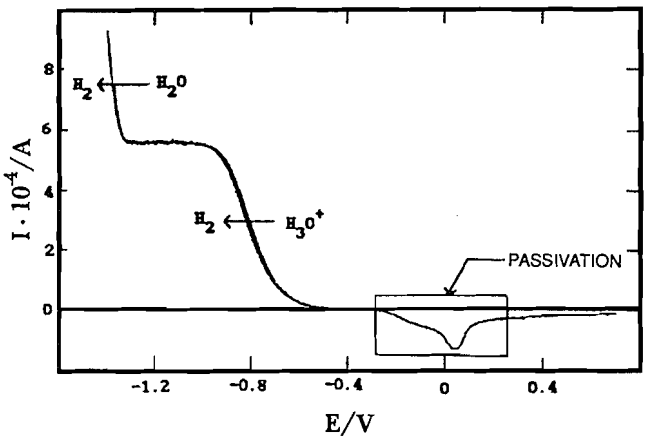

FIG. 1. The current-potential curves recorded in 0.2 M solution of Na_2SO_4 at pH 3.52 at the rotating nickel disk electrode: f = 3000 rev min^{-1}, v = 10 mV s^{-1}.

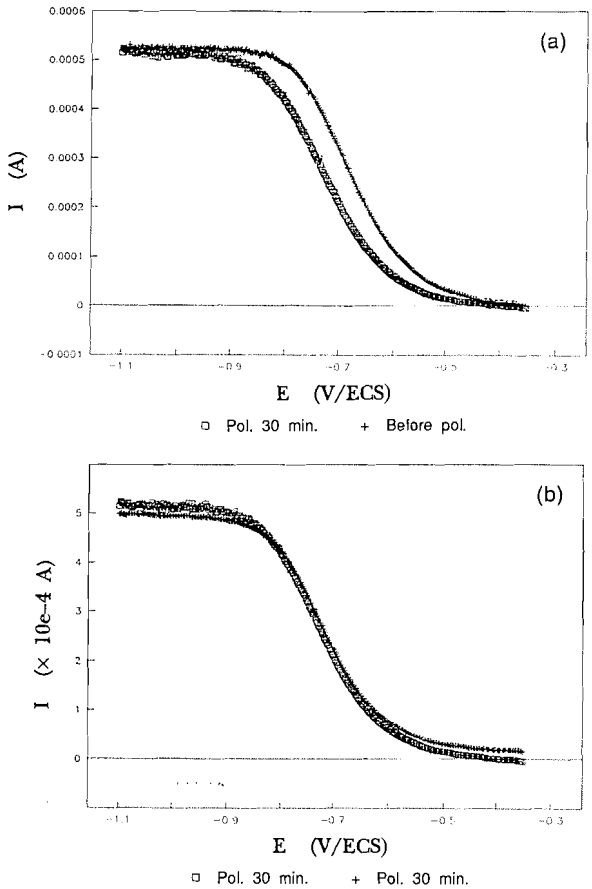

FIG. 2. (*a*) Comparison of *I–E* curves before and after pre-treatment (*ii*); (*b*) two *I–E* curves recorded at Ni RDE after treatment (*ii*) (see text): pH 3.4, 0.2 M Na_2SO_4, temperature 25°C.

electrode, its potential slowly changed towards more negative values, and later stabilized. This behaviour was similar to that observed by Bockris and Conway (21) and Amosé and Barbieri (22). These authors have also reported a loss in the activity of the nickel electrode during cathodic polarization, and ascribed this effect to the adsorption of traces of impurities (Bockris and Conway) or the dissolution of hydrogen

TABLE 2. The kinetic parameters of the hydrogen evolution reaction at the nickel electrode and parameters of the double layer

C_{TSA} (mM)	$E_{1/2}$ (V)	$-\log k_f^0$	α	C_{dl} (μF cm^{-2})	$(1-\varphi)$ (deg)
SDS pH 3.4, μ = 0.2 M					
0	0.696	3.40	0.50	39±6	10
8.5×10^{-2}	0.689	3.25	0.41	40	9
6.2×10^{-1}	0.689	3.44	0.52	33	11
7.3×10^{-1}	0.703	3.26	0.45	34	8
1.6	0.737	3.61	0.50	29	8
1.8	0.722	3.45	0.46	33	10
4.1	0.713	4.15	0.44	29	8
4.5	0.708	4.01	0.61	33	9
6.2	0.701	4.02	0.63	28	8
8	0.695	4.01	0.66	29	8
SDS pH = 3.1					
8.4×10^{-2}	0.729	3.51	0.44	40	14
3.1×10^{-1}	0.718	3.59	0.48	39	14
8.0×10^{-1}	0.722	3.68	0.49	35	14
1.4	0.703	3.75	0.54	35	14
2.7	0.722	3.61	0.47	40	14
BRIJ-35					
1.8×10^{-2}	0.712	3.61	0.50	29	11
6.2×10^{-2}	0.728	3.61	0.47	20	8
1.5×10^{-1}	0.741	3.53	0.44	20	9
3.0×10^{-1}	0.747	3.56	0.44	17	10
7.6×10^{-1}	0.734	3.60	0.47	13	9
1.4	0.791	4.00	0.47	12	8
BRIJ-78					
1.8×10^{-2}	0.721	3.43	0.45	40	16
8.1×10^{-2}	0.720	3.48	0.46	38	16
1.9×10^{-1}	0.736	3.28	0.40	39	16
3.4×10^{-1}	0.732	3.34	0.42	39	15
BRIJ-99					
1.9×10^{-2}	0.734	3.28	0.40	29	11
7.3×10^{-2}	0.721	3.36	0.43	31	12
1.8×10^{-1}	0.740	3.33	0.40	29	12
3.8×10^{-1}	0.797	3.63	0.39	22	11
CTAB					
8.2×10^{-2}	0.716	3.35	0.52	27	19
2.8×10^{-1}	0.720	3.64	0.40	24	19
6.6×10^{-1}	0.722	3.88	0.51	25	19
1.8	0.756	3.70	0.43	23	19
2.5	0.757	3.83	0.60	24	19
3.6	0.752	3.88	0.51	22	19

in the electrode (Amosé and Barbieri). We are unable to distinguish between these two possibilities. Our earlier results seem to confirm the first version (23). Undoubtedly freshly prepared electrodes have slightly higher activity than those that have undergone pre-treatment, since the reduction wave of the H^+ ions appeared at fresh electrodes at potentials more positive by ~50 mV (Fig. 2*a*). However, we decided to sacrifice a higher activity of the electrode to achieve reproducible results. An example of the *I–E* curves obtained is shown in Fig. 2*b*.

The dependence of limiting current on the concentration of H^+ ions for f = 3000 rev min^{-1} is described by the fol-

Can. J. Chem. Downloaded from www.nrcresearchpress.com by 88.255.202.194 on 09/08/12
For personal use only.

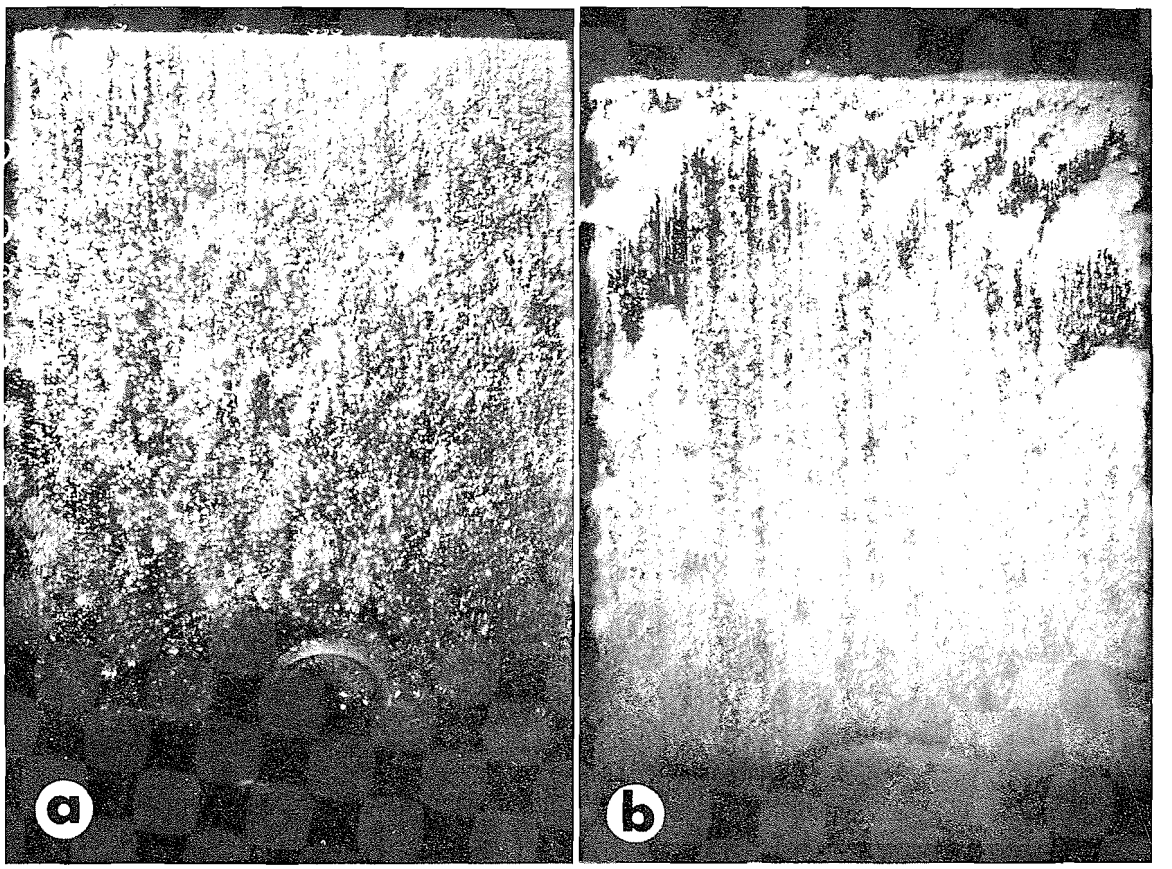

FIG. 3. Evolution of hydrogen at Ni electrode in 0.2 M solution of Na_2SO_4 (*a*) without and (*b*) in the presence of SDS (10^{-2} mol L^{-1}).

lowing equation: I_{lim} (mA) = (6.0 ± 2.7) × 10^{-2} + (4.96 ± 0.25) × 10^{-1} $C(H^+)$ (mM). From the Levich equation (24):

$$[3] \quad I_{lim} = 0.62nFAD_{H^+}^{2/3}\,\omega^{0.5}\,\delta^{-1/6}\,C_{H^+}$$

one may calculate the diffusion coefficient of the H^+ ions. The value obtained (D_{H^+} = (7.2 ± 0.5) × 10^{-5} cm^2 s^{-1}) was in good agreement with that reported (25) by Vielstich and Jahn (7.5 × 10^{-5} cm^2 s^{-1}).

Influence of various TSA on the kinetics of H^+ ion reduction at the nickel electrode

The experiments were conducted in 0.2 M solution of Na_2SO_4. The TSA was introduced to deoxygenated solution and its concentration was increased up to the moment when visible turbidity appeared. Up to 10 mM concentration of SDS could be obtained. Other TSA had much lower solubilities: 3.6 mM (CTAB), 1.4 mM (BRIJ35), and ~0.35 mM (BRIJ78 and BRIJ99).

The half-wave potentials, determined from the semi-logarithmic analysis (log $(i/(i_l - i)) - E$) are presented in Table 2. Table 2 also lists the kinetic parameters (logarithm of the formal rate constants and the cathodic transfer coefficients α) of reaction [1]. Since hydrogen evolution was in all cases irreversible, we could calculate the formal rate constants using the following equation (24):

$$[4] \quad k_{fh} = \frac{I_{lim}}{nFAC_{H^+}} \times \frac{I}{I_{lim} - I}$$

From the dependence of log k_{fh} on E, the α values were calculated. The log k_{fh}^0 values correspond to log k_{fh} at E_f^0.

Most of the TSA caused a shift of $E_{1/2}$ towards more negative potentials. In the presence of SDS, at lower concentrations almost no change in $E_{1/2}$ was observed, and at higher concentrations they shifted slightly towards more positive values. At the same time, in the region of intermediate concentrations, one observed an increase in α from 0.5 to 0.66.

All TSA (including SDS) significantly affect the sizes of the evolving hydrogen bubbles. In the absence of TSA, hydrogen evolved as large bubbles, causing erratic variations in the limiting currents. Occasionally, large bubbles of hydrogen formed and sticked to the nickel electrode, causing the current to drop to almost zero. In the presence of TSA, hydrogen evolved uniformly in the form of very small bubbles, which could be easily removed from the electrode. In these cases the limiting current did not show any irregularities. Changes of the form of bubbles in the presence of the TSA are presented in Fig. 3.

Changes in capacities of the nickel electrode caused by TSA at potentials more positive than the reduction of the H^+ ions

To measure the effect of TSA on capacities of the nickel electrode we attempted to measure the ac impedance in the region of hydrogen evolution. Since the ac measurements lasted for 10 min, we did our measurements while recording the current–time curves at various potentials. The results showed that the current slowly dropped with time for more than 5% of its original value, indicating a slow decrease in the activity of this electrode. We were therefore unable to measure the ac impedance in these potentials re-

Can. J. Chem. Downloaded from www.nrcresearchpress.com by 88.255.202.194 on 09/08/12
For personal use only.

Can. J. Chem. Downloaded from www.nrcresearchpress.com by 88.255.202.194 on 09/08/12
For personal use only.

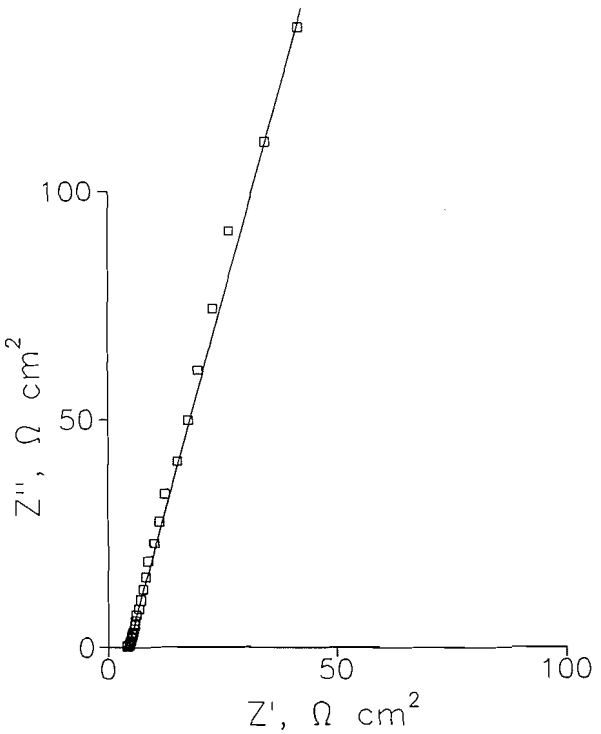

FIG. 4. The Nyquist plot for the Ni RDE in 0.4 M solution of Na_2SO_4 at pH 3.4.

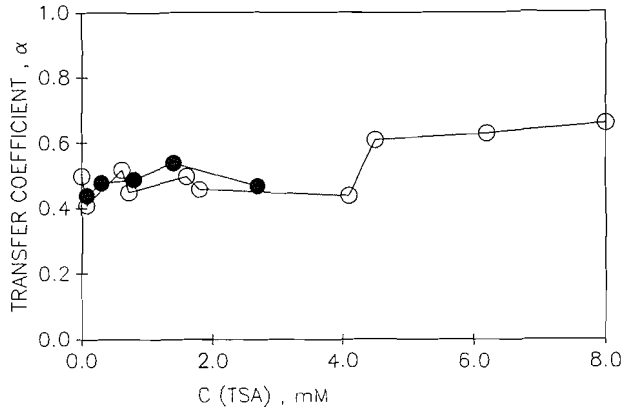

FIG. 5. Dependence of the transfer coefficient α on C_{TSA} for SDS at two pH values; ●, 3.1; ○, 3.4.

gion, since a change in activity affected the ac impedance. The ac impedance was therefore measured in a region of potentials more positive than the wave of the H^+ reduction, at zero current and $E = -450$ mV.

The impedance of the nickel electrode showed frequency dispersion (Fig. 4) which is typical for a solid electrode (26). Appearance of the frequency dispersion is most probably the result of electrode inhomogenity (27). In such a case one may use (28) the equivalent circuit consisting of the solution resistivity (R_s) and the constant phase element (CPE) in series. The total impedance ($\hat{Z}$) could be described by the following equation:

$$[5] \quad \hat{Z} = R_s \frac{1}{(j\omega)^{\alpha} T}$$

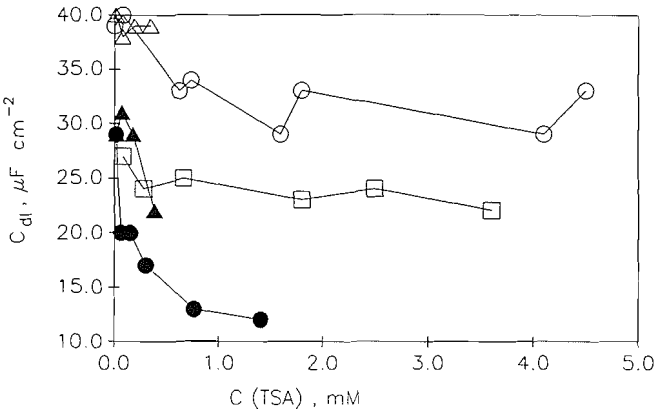

FIG. 6. Changes in the double layer capacity of the Ni RDE in the presence of various concentrations of TSA (pH = 3.4 and 0.2 M Na_2SO_4): ●, BRIJ 35; △, BRIJ 78; ▲, BRIJ 99; □, CTAB; ○, SDS.

The capacity of the double layer was calculated from the equation given by (29) Brug *et al.*:

$$[6] \quad T = C_{dl}^{\phi} \left(\frac{1}{R_s}\right)^{(1-\phi)}$$

The calculated capacities are given in Table 2.

Discussion

Changes in the formal rate constant of the hydrogen evolution reaction at nickel electrode, observed during the additions of increasing amounts of TSA, are presented in Table 2. All these changes have similar character. In regions of small concentrations of TSA, the formal rate constants increase by a factor of 2 and later decrease almost by a factor of 3. Changes in pH has small effect on the kinetic parameters and the adsorption of SDS on the nickel electrode.

Changes in the transfer coefficient α are presented in Fig. 5 for SDS and Table 2 for the other TSA. Results presented in Fig. 5 indicate that in the presence of SDS, in the region of intermediate concentrations, one observes an increase in α from 0.5 to 0.66, whereas the effect of all other TSA on this parameter is rather small (Table 2). Thus we may conclude that the presence of SDS facilitates the evolution of hydrogen to a greater degree than other substances.

Usually, the changes in the kinetics of electrode reactions in the presence of various organic compounds have been explained by different adsorption behaviours of these compounds. The changes in capacity of the nickel electrode caused by increasing amounts of TSA are presented in Fig. 6. All capacity measurements have been conducted in a region slightly more positive than the potential of zero charge for the nickel electrode (17) (E_{pzc}(Ni) = −0.55 V). Results presented in Fig. 6 indicate that SDS has small effect on capacity. Higher concentrations of CTAB lower the capacity of the nickel electrode by about 25%, whereas the maximum lowering in C_{dl}, equal to about 60%, was observed in the case of BRIJ35.

Thus we expect that these two compounds to have maximum effect on hydrogenation of organic substances, since they do not change much the kinetic of the hydrogen evolution, but they should facilitate adsorption of organic substances at the vicinity of the electrode and improve their hydrogenation.

SDS should not show similar properties. However, since in its presence one observes some increase in the transfer coefficient, it is possible that it could be used for the evolution of hydrogen.

Acknowledgments

We thank the Natural Sciences and Engineering Research Council of Canada and the Quebec government (Ministère de l'enseignement supérieur et de la science and Ministère des affaires internationales) for financial support.

1. H. H. Bauer, *In* Electroanalytical chemistry. Vol. 8. *Edited by* A. J. Bard. Dekker, New York. 1975. p. 169.
2. J. E. B. Randles. *In* Electrode processes, general discussions Faraday Society. p. 11.
3. K. Shinoda. *In* Colloidal surfactants. *Edited by* K. Shinoda, T. Nakagawa, B-I. Tamamushi, and T. Isemura. Academic Press, New York and London. 1963. p. 1.
4. G. E. O. Proske. Anal. Chem. **24**, 1834 (1952).
5. J. Dojlido and B. Behr. Rocz. Chem. **37**, 1044 (1963).
6. (*a*) K. L. Mittal and E. J. Fendler (*Editors*). Solution behavior of surfactants. Plenum Press, New York and London. 1982; (*b*) D. R. Karsa. (*Editor*). Industrial applications of surfactants. Royal Society of Chemistry Special Publications. 1987. p. 59.
7. K. L. Mittal (*Editor*). Solution chemistry of surfactants. Plenum Press. New York and London. 1979. p. 59.
8. S. Bencheikh-Sayarh, A.-M. Martre, G. Mousset, and P. Pouillen. Bull. Soc. Chim. Fr. No. 11–12. I-329 (1984).
9. L. Holleck and H. J. Exner. Z. Elektrochem. **56**, 46 (1952); 56, 677 (1952).
10. W. Kemula and T. M. Krygowski. *In* Encyclopedia of electrochemistry of the elements. Vol. XIII. *Edited by* A. J. Bard and H. Lund. Marcel Dekker, New York and Basel. 1979. p. 77.
11. G. N. Kamau and J. F. Rusling. J. Electroanal. Chem. **240**, 217 (1988).
12. P. Chambrion, J. Lessard, J. Mailhot, and M. Thomalla. J. Electrochem. Soc. Submitted.
13. E. Potvin, H. Ménard, J.-M. Lalancette, and L. Brossard. J. Appl. Electrochem. **20**, 252 (1990).
14. H. Dumont, P. K. Wrona, L. Brossard, J. M. Lalancette, and H. Ménard. J. Appl. Electrochem. In press.
15. D. Lardet and M. Thomalla. Bull. Soc. Chim. Fr. **3**, 524 (1988).
16. A. Berthod. J. Chim. Phys. **80**, 407 (1983).
17. A. J. Arvia and D. Posadas. *In* Encyclopedia of electrochemistry of the elements. Vol. III. *Edited by* A. J. Bard. Dekker, New York. 1975. p. 212.
18. S. M. Reshetnikov. Zh, Prikl. Khim. **54**, 1530 (1981).
19. M. Kesten and H. G. Feller. Electrochim. Acta, **16**, 763 (1971).
20. A. Lasia and A. Rami. J. Electroanal. Chem. **294**, 123 (1990).
21. J.'O. M. Bockris and B. E. Conway. Trans. Faraday Soc. **46**, 989 (1950).
22. J. Amosé and M. J. Barbieri. Electrochim. Acta, **11**, 1045 (1966).
23. P. K. Wrona, A. Lasia, M. Lessard, and H. Ménard. Electrochim. Acta, **37**, 1283 (1992).
24. Z. Galus. Fundamentals of electrochemical analysis. Ellis Harwood, Ltd., Chichester. 1976. Chap. 6.
25. W. Vielstich and D. Jahn. Z. Elektrochem. **64**, 43 (1960).
26. P. Delahay. Double layer and electrode kinetics. Interscience Publishers, New York-Sidney. 1965.
27. (*a*) T. I. Borisova, B. V. Ershler, and A. N. Frumkin. Zh. Fiz. Khim. **22**, 925 (1948); (*b*) E. O. Ayazyan. DAN SSSR, **100**, 473 (1955); (*c*) T. I. Borisova and B. V. Ershler. Zh. Fiz. Khim. **24**, 337 (1950).
28. J. R. Macdonald (*Editor*). Impedance spectroscopy. Wiley, New York. 1987.
29. G. J. Brug, A. L. G. van der Eeden, M. Sluyters, and J. Sluyters. J. Electroanal. Chem. **176**, 275 (1984).

Can. J. Chem. Downloaded from www.nrcresearchpress.com by 88.255.202.194 on 09/08/12
For personal use only.

The chemistry of copper(I) β-diketonate compounds. Part V. Syntheses and characterization of (β-diketonate)CuL_n species where L = PBu_3, PPh_3, and PCy_3; n = 1 and 2; crystal and molecular structures of (acac)Cu(PCy_3), (tfac)Cu(PCy_3), (hfac)Cu(PCy_3), and (hfac)Cu(PCy_3)$_2$

H.-K. SHIN, M. J. HAMPDEN-SMITH,[1] AND E. N. DUESLER

Department of Chemistry and Center for Micro-Engineered Ceramics, University of New Mexico, Albuquerque, NM 87131, U.S.A.

AND

T. T. KODAS[1]

Department of Chemical Engineering and Center for Micro-Engineered Ceramics, University of New Mexico, Albuquerque, NM 87131, U.S.A.

Received June 4, 1992

H.-K. SHIN, M. J. HAMPDEN-SMITH, E. N. DUESLER, and T. T. KODAS. Can. J. Chem. **70**, 2954 (1992).

The compounds (β-diketonate)Cu(PR_3)$_n$, where β-diketonate = 1,1,1,5,5,5-hexafluoroacetylacetonate, hfac; 1,1,1-trifluoroacetylacetonate, tfac; and acetylacetonate, acac; R = *n*-butyl (*n*-Bu), phenyl (Ph), and cyclohexyl (Cy); n = 1 and 2, have been prepared. The monotriorganophosphine adducts were prepared in high yield by the reaction of the sodium salt of the corresponding β-diketonate with [ClCu(PR_3)] with elimination of sodium chloride. The bis(triorganophosphine) adducts were prepared by the reaction of (β-diketonate)Cu(PR_3) with one equivalent of triorganophosphine. These species were characterized by ^{1}H, ^{13}C, and ^{31}P NMR spectroscopy, FTIR spectroscopy, mass spectroscopy, and by combustion elemental analysis. Four examples were structurally characterized by single crystal X-ray diffraction in the solid state. (acac)CuPCy_3 crystallizes in the triclinic crystal system, space group $P\bar{1}$, where a = 13.502(6) Å, b = 13.691(6) Å, c = 5.781(6) Å, α = 71.05(3)°, β = 67.50(3)°, γ = 64.81(3)°, Z = 4, and R = 5.42%. (tfac)CuPCy_3 crystallizes in the monoclinic crystal system, space group $P2_1/n$, where a = 9.639(3) Å, b = 22.717(7) Å, c = 12.045(5) Å, β = 111.67(3)°, Z = 4, and R = 7.22%. (hfac)CuPCy_3 crystallizes in the monoclinic crystal system, space group $P2_1/c$, where a = 9.870(2) Å, b = 17.314(4) Å, c = 15.586(3) Å, β = 99.74(2)°, Z = 4, and R = 5.29%. (hfac)Cu(PCy_3)$_2$ crystallizes in the monoclinic crystal system, space group $P2_1/n$, where a = 13.645(6) Å, b = 19.252(13) Å, c = 16.875(9) Å, β = 102.02(4)°, Z = 4, and R = 7.20%. The compounds (β-diketonate)Cu(PCy_3) are all monomeric in the solid state and possess approximately trigonal-planar copper coordination environments, although (tfac)Cu(PCy_3) is significantly distorted from trigonal geometry. The Cu—O bond distances are significantly different in this species. The compound (hfac)Cu(PCy_3)$_2$ is monomeric in the solid state and possesses a distorted tetrahedral copper coordination environment. The distortion is believed to be due to the large steric demands of the PCy_3 ligands that result in long Cu—P bond distances of 2.251(3) and 2.277(3) Å, a large P—Cu—P angle of 141.3(1)°, long Cu—O distances of 2.213(5) and 2.251(5) Å, and a small O—Cu—O angle of 80.8(2)° compared to the corresponding values for (hfac)Cu(PCy_3). No trends in Cu—O bond distances between the compounds can be discerned, within the limits of error on the data, that would clearly enable a comparison of thermodynamic parameters such as bond length – bond strength relationships as a function of the β-diketonate substituents. However, the spectroscopic data revealed a number of trends as a function of the β-diketonate substituents, including an increase of ν(C=O and ν(C=C) in the order acac < tfac < hfac, analogous to the increase in their Lewis acidity. An increase in shielding of the ^{31}P resonance of the triorganophosphine ligands was observed in the order hfac < tfac < acac, consistent with expected inductive effects based on the electronegativity of the β-diketonate substituents.

H.-K. SHIN, M. J. HAMPDEN-SMITH, E. N. DUESLER et T. T. KODAS. Can. J. Chem. **70**, 2954 (1992).

On a préparé les composés (β-dicétonate)Cu(PR_3)$_n$ dans lesquels β-dicétonate = 1,1,1,5,5,5-hexafluoroacétylacétonate (hfac), 1,1,1-trifluoroacétylacétonate (tfac) et acétylacétonate (acac); R = *n*-butyle (*n*-Bu), phényle (Ph) et cyclohexyle (Cy); n = 1 et 2. On a préparé les adduits monotriorganophosphines avec d'excellents rendements par la réaction du sel de sodium du β-dicétonate correspondant avec le [ClCu(PR_3)], avec élimination de chlorure de sodium. On a préparé les adduits bis(triorganophosphine) par la réaction des (β-dicétonate)Cu(PR_3) avec un équivalent de triorganophosphine. On a caractérisé ces espèces par RMN du ^{1}H, du ^{13}C et du ^{31}P, par spectroscopie infrarouge par transformée de Fourier, par spectroscopie de masse et par analyse élémentaire par combustion. On a caractérisé les structures de quatre exemples par le biais de la diffraction des rayons X par un cristal unique à l'état solide. Les cristaux du (acac)CuPCy_3 sont tricliniques, groupe d'espace $P\bar{1}$, avec a = 13,502(6), b = 13,691(6) et c = 5,781(6) Å, α = 71,05(3), β = 67,50(3) et γ = 64,81(3)°, Z = 4 et R = 5,42%. Ceux du (tfac)CuPCy_3 sont monocliniques, groupe d'espace $P2_1/n$, avec a = 9,639(3), b = 22,717(7) et c = 12,045(5) Å, β = 111,67(3)°, Z = 4 et R = 7,22%. Ceux du (hfac)CuPCy_3 sont monocliniques, groupe d'espace $P2_1/c$, avec a = 9,870(2), b = 17,314(4) et c = 15,586(3) Å, β = 99,74(2)°, Z = 4 et R = 5,29%. Les cristaux du (hfac)Cu(PCy_3)$_2$ sont monocliniques, groupe d'espace $P2_1/n$, avec a = 13,645(6), b = 19,252(13) et c = 16,875(9) Å, β = 102,02(4)°, Z = 4 et R = 7,20%. À l'état solide, tous les composés (β-dicétonate)Cu(PCy_3) sont monomériques et leurs environnements de coordination du cuivre sont approximativement plan trigonal même si la géométrie trigonale du (tfac)Cu(PCy_3) est très déformée. Dans ces espèces, les distances Cu—O sont très différentes. Le composé (hfac)Cu(PCy_3) est monomérique et l'environnement de coordination du cuivre est tétraédrique déformé. On croit que la distorsion est causée par les grandes demandes stériques des ligands PCy_3 qui

[1]Authors to whom correspondence may be addressed.

Can. J. Chem. Downloaded from www.nrcresearchpress.com by 88.255.202.194 on 09/08/12
For personal use only.

allongent les distance Cu—P (2,251(3) et 2,277(3) Å), élargissent l'angle P—Cu—P (141,3(1)°), allongent les distances Cu—O (2,213(5) et 2,251(5) Å) et amenuisent l'angle O—Cu—O (80.8(2)°) par rapport aux valeurs correspondantes du (hfac)Cu(PCy_3). Aux limites expérimentales près, on n'a pas observé de tendances dans les distance Cu—O entre les divers composés qui auraient pu permettre d'établir une comparaison avec des paramètres thermodynamiques comme les relations longueur de liaison/force de liaison en fonction des substituants des β-dicétonates. Toutefois, les données spectroscopiques ont révélé un certain nombre de tendances en fonction des substituants des β-dicétonates, y compris une augmentation de ν(C=O) et ν(C=C) dans l'ordre acac < tfac < hfac, analogue à celui de la variation de leur acidité de Lewis. On a observé une augmentation dans le blindage de la résonance ^{31}P des ligands triorganophosphines dans l'ordre hfac < tfac < acac qui est en accord avec les effets inductifs attendus sur la base de l'électronégativité des substituants des β-dicétonates.

[Traduit par la rédaction]

Introduction

It has been demonstrated that β-diketonate complexes of copper(I) and copper(II) exhibit suitable physical properties to be precursors for the Chemical Vapor Deposition (CVD) of copper metal. Copper(II) β-diketonate complexes have been studied extensively (1–5). However, while their volatility is high (Cu(hfac)$_2$ exhibits an equilibrium vapor pressure of ~250 mTorr (1 Torr = 133.3 Pa) at 60°C) (6), they do not thermally decompose below 340°C and, above 390°C, significant incorporation of carbon impurities into copper films is observed. The presence of hydrogen gas during deposition increases the purity of the deposit, but drastically alters the selectivity (4, 5).

On the other hand, it has recently been shown that copper(I) β-diketonate complexes, (β-diketonate)CuL_n, where L = a Lewis base such as a triorganophosphine, an olefin, or an alkyne, undergo thermally induced disproportionation reaction (Eq. [1]) (7–9) over a temperature range 80–400°C and, in some cases, deposit copper selectively (7–15). Selective copper deposition from (β-diketonate)CuL compounds onto the metals Pt, W, and Cu in the presence of SiO_2 and the minimum deposition temperature are strongly influenced by the nature of the β-diketonate substituents and Lewis base ligands, L. For example, (hfac)CuPMe_3 selectively deposits copper onto W and not SiO_2 in the temperature range 150–300°C. Above 300°C, selectivity is lost and deposition is observed on SiO_2 as well. However, (tfac)Cu(PMe_3) and (acac)Cu(PMe_3) selectively deposit copper at 100–150°C and <80°C, respectively, on W in the presence of SiO_2 (7, 16). Above these temperatures selectivity is lost. In contrast, (hfac)Cu(1,5-COD) and (hfac)Cu(2-butyne) deposit copper on both W and SiO_2 over the temperature range 120–200°C. Below 120°C, no deposition is observed (16, 17). Furthermore, the compounds (hfac)Cu(PR_3)$_2$, R = Me, Et, show substantially higher thermal stability than their monophosphine counterparts and do not deposit copper below 350°C (16). To gain a better understanding of those factors that affect the bonding of β-diketonate ligands to the copper(I) center and that play a crucial role in CVD, we have undertaken studies of the structural chemistry and reactivity of (β-diketonate)CuL_n complexes.

[1] $2(\beta\text{-diketonate})Cu^{(I)}L \rightarrow Cu^{(0)} + Cu^{(II)}(\beta\text{-diketonate})_2 + 2L$

Despite the enormous amount of work devoted to synthesis and characterization of copper(II) β-diketonate complexes, there are relatively few reports devoted to the corresponding Cu(I) complexes. Reports of monotriorganophosphine adducts, (β-diketonate)Cu(PR_3), are particularly rare. Copper(I) acetylacetonate was reported previously (18–20) and shown to undergo disproportionation to copper metal and copper(II) bisacetylacetonate compounds in the absence of stabilizing ligands (19). A number of stable complexes of general formula (β-diketonate)CuL_n (L = isonitriles, ammonia, and phosphines; n = 2 or 2.5) were synthesized and characterized by Nast and Lepel (21). In early 1970, Carty and co-workers (22, 23) also prepared a number of copper(I) β-diketonate complexes containing two triorganophosphine ligands bonded to each copper. Doyle et al. (24) reported preparation of (β-diketonate)Cu(CO) from Cu_2O and β-diketones, and observed that only one CO is absorbed per copper atom. The yellow-green solution of (hfac)Cu(CO) is only stable if stored under a CO atmosphere; otherwise, it disporportionates to form copper metal and copper(II) β-diketonate according to Scheme 1. These β-diketonate copper(I) carbonyl complexes react with triorganophosphines, amines, and isonitriles to produce the corresponding bis(Lewis base) species, (β-diketonate)CuL_2.

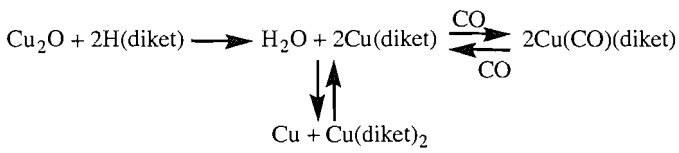

SCHEME 1

It was also shown previously that the addition of triorganophosphine ligands to the copper(I) coordination sphere can displace a uninegative oxygen donor ion. For example, the copper(I) nitrate complexes (NO_3)CuL_2, (NO_3)CuL_3, and (NO_3)CuL_4 exhibit bidentate, monodentate, and ionic nitrate ligand binding modes, respectively (22, 25). Furthermore, we recently demonstrated that addition of an excess of PMe_3 to the mononuclear, distorted trigonal-planar complex (β-diketonate)Cu(PMe_3) results in displacement of the β-diketonate ligand from the copper coordination sphere to form [β-diketonate]$^-$[Cu(PMe_3)$_4$]$^+$ (26). In this work we report the syntheses and characterization of a number of (β-diketonate)Cu(PR_3)$_n$ species, where R = Bu, Ph, and Cy; n = 1 and 2. Included is a solid state structural study of (β-diketonate)Cu(PCy_3), where β-diketonate = 1,1,1,5,5,5-hexafluoroacetylacetonate (hfac), 1,1,1-trifluoroacetylacetonate (tfac), and acetylacetonate (acac); Cy = cyclohexyl and (hfac)Cu(PCy_3)$_2$, to probe the changes in β-diketonate coordination as a function of the β-diketonate ligand and the degree of substitution with a sterically demanding phosphine ligand.

Experimental section

General procedures

All manipulations were carried out under an atmosphere of dry (molecular sieves) dinitrogen using standard Schlenk techniques. All hydrocarbon and ethereal solvents were dried and distilled from

Can. J. Chem. Downloaded from www.nrcresearchpress.com by 88.255.202.194 on 09/08/12
For personal use only.

Can. J. Chem. Downloaded from www.nrcresearchpress.com by 88.255.202.194 on 09/08/12
For personal use only.

sodium benzophenone ketyl and stored over 4 Å molecular sieves. Copper(I) chloride, sodium hydride, and tertiary phosphines were purchased from Aldrich Chemical Co. and used without further purification. Copper(I) chloride was obtained from Fischer Scientific Company and recrystallized by the literature method (27) prior to use. The β-diketone starting materials were purchased from Aldrich Chemical Co. and were distilled under nitrogen and stored over 4 Å molecular sieves before use. Sodium salts of β-diketones were prepared by the reaction of the free acid with sodium hydride, as previously described (28). The compounds [ClCu(PR_3)] were prepared by methods previously described in the literature (28). Elemental analyses were performed by Ms. R. Ju at the Department of Chemistry, University of New Mexico. NMR data were recorded on a Bruker AC-250P NMR spectrometer by using the protio impurities of the deuterated solvents as references for the ^{1}H NMR, and the ^{13}C resonance of the solvents as the reference for ^{13}C NMR spectroscopy. Temperatures were calibrated with either ethylene glycol or methanol. ^{31}P NMR data were recorded on the same instrument using phosphoric acid as reference. ^{31}P NMR chemical shifts are quoted using the high frequency = positive sign convention. Infrared data were recorded on a Perkin–Elmer model 1620 FTIR spectrophotometer. Mass spectra were recorded on a Finnegan GC mass spectrometer. The melting points were determined using a digital melting point apparatus purchased from Electrothermal England Ltd.

Syntheses

Similar synthetic procedures were employed to prepare the two classes of compounds described here, (β-diketonate)Cu(PR_3)$_n$, n = 1 and 2. A typical example of an experimental procedure is given for each, followed by the spectroscopic data.

(acac)CuPBu$_3$

The liquid ClCuPBu_3 (4.26 g, 14.14 mmol) and 2.30 g (18.84 mmol) of Na^+(acac$^-$) were placed in a 250 mL Schlenk flask, and 100 mL of dry pentane was added under dry nitrogen. The white solution immediately turned pale yellow. After stirring at room temperature for 2 h, the solution was filtered, the white precipitant was washed with two 10-mL portions of pentane, and the filtrates were combined. The volatile components were removed *in vacuo* to give 4.83 g (94% yield) of very pale yellow liquid, which was characterized as Cu(acac)(PBu_3).

(hfac)Cu(PCy_3)$_2$

PCy_3 (0087 g, 0.31 mmol) and 0.155 g (0.31 mmol) of (tfac)Cu(PCy_3) were placed in a 100 mL Schlenk flask, and 10 mL of dry pentane was added under dry nitrogen. The light yellow solution was stirred at room temperature for 2 h. The volatile components were removed *in vacuo* to give 0.221 g (91.7% yield) of greenish yellow powder, which was characterized as Cu(hfac)(PCy_3)$_2$. Chartreuse crystalline (hfac)Cu(PCy_3)$_2$ was prepared by cooling a pentane solution in the freezer (−30°C), overnight.

Spectroscopic and analytical data

Representative spectroscopic data are provided here for (hfac) compounds. ^{1}H, ^{13}C{^{1}H}, and ^{31}P{^{1}H} NMR data, IR and mass spectral data for the other compounds are available as supplementary materials (see footnote 2).

(hfac)CuP^{n}Bu$_3$

Orange liquid. Yield: 90%. IR data (KBr disc, cm^{-1}): 2962(s), 2934(s), 2875(m), 1642(s), 1590(w), 1549(m), 1522(m), 1483(s), 1467(m), 1415(w), 1381(w), 1342(w), 1256(s), 1198(s), 1147(s), 1096(m), 1051(w), 1007(w), 969(w), 946(w), 910(w), 794(m), 765(w), 741(w), 727(w), 668(s), 583(m), 527(w). ^{1}H NMR δ: 6.30 (s, 1H, CH), 1.10 (m, 18H, P($C_3H_6CH_3$)$_3$), 0.78 (t, 7 Hz, 9H, P($C_3H_6CH_3$)$_3$); ^{13}C{^{1}H} NMR δ: 177.4 (q, 34 Hz, CO), 118.6 (q, J(C–F) = 286 Hz, CF_3), 89.5 (s, CH), 27.5 (d, J(C–P) = 3 Hz, PBu_3), 24.8 (d, J(C–P) = 26 Hz, PBu_3), 24.4 (d, J(C–P) = 14 Hz, PBu_3), 13.7 (s, PBu_3); ^{31}P{^{1}H} NMR δ: −8.57 (s, br). Mass spectral data (70 eV, m/e): 472, 7%, [(hfac)CuPBu_3]$^{+\cdot}$; 467, 5%, [Cu(PBu_3)$_2$]$^{+\cdot}$; 403, <1%, [($O_2C_2CHCF_3$)CuPBu_3]$^{+\cdot}$; 265, 100%, [CuPBu_3]$^{+\cdot}$; 209, 7%, [CuP(H)Bu_2]$^{+\cdot}$; 202, 44%, [PBu_3]$^{+\cdot}$; 201, 2%, [Cu($O_2C_2CHCF_3$)]$^{+\cdot}$ or [(O_2C_2CH)$_2$Cu]$^{+\cdot}$; 187, 3%, [PBu_2(C_3H_6)]$^{+\cdot}$; 173, 14%, [PBu_2(C_2H_4)]$^{+\cdot}$; 160, 28%, [PBu_2(CH_3)]$^{+\cdot}$; 151. 5%, [CuPBu]$^{+\cdot}$; 146, 53%, [P(H)Bu_2]$^{+\cdot}$; 131, 5%, [P(H)Bu(C_3H_6)]$^{+\cdot}$; 118, 19%, [P(H)Bu(C_2H_5)]$^{+\cdot}$; 109, 12%, [CF_3COCH]$^{+\cdot}$; 104, 12%, [P(H)Bu(CH_3)]$^{+\cdot}$; 103, 7%, [(OCCH)Cu]$^{+\cdot}$; 89.7%, [P(H)Bu]$^{+\cdot}$; 69, 1%, [CF_3]$^{+\cdot}$; 63.3%, [Cu]$^{+\cdot}$; 57, 1%, [C_4H_9]$^{+\cdot}$. Anal. calcd. for $C_{17}H_{28}O_2F_6PCu$ (mol. wt. 472.93): C 43.18, H 5.97; found: C 43.55, H 6.19.

(tfac)CuP^{n}Bu$_3$

Chartreuse liquid. Yield: 98%. Anal. calcd. for $C_{17}H_{31}F_3O_2PCu$ (mol. wt. 418.96): C 48.74, H 7.46; found: C 49.14, H 7.55.

(acac)CuP^{n}Bu$_3$

Light-yellow liquid. Yield: 94%. Anal. calcd. for $C_{17}H_{34}O_2PCu$ (mol. wt. 364.99): C 55.94, H 9.39; found: C 56.24, H 9.31.

(hfac)CuPPh$_3$

Color: orange. Yield: 93%; mp 145°C. IR data (KBr disc, cm^{-1}): 3057(w), 3020(w), 2987(w), 1646(s), 1585(w), 1576(w), 1548(s), 1519(s), 1488(s), 1457(w), 1436(s), 1419(w), 1387(w), 1337(m), 1310(m), 1257(s), 1211(s), 1150(s), 1102(s), 1097(s), 1090(s), 1073(w), 1028(m), 998(m), 980(w), 973(w), 944(w), 927(w), 852(w), 846(w), 807(w), 792(s), 753(s), 738(s), 708(s), 696(s), 670(s), 618(w), 586(m), 537(s), 509(s), 493(s), 443(w), 436(w), 420(w). ^{1}H NMR δ: 7.32 (m, 6H, PPh_3(o)), 6.90 (m, 9H, PPh_3(m/p)), 6.31 (s, 1H, CH); ^{13}C{^{1}H} NMR δ: 177.6 (q, 33 Hz, CO), 134.0 (d, 13 Hz, PPh_3(b)), 131.5 (d, 43 Hz, PPh_3(a)), 130.7 (s, PPh_3(d)), 129.1 (s, br, PPh_3(c)$^+$), 118.6 (q, J(C–F) = 288 Hz, CF_3), 89.8 (s, CH); ^{31}P{^{1}H} NMR δ: 9.22 (s, br). Mass spectral data (70 eV, m/e): 595, <1%, [(hfac)Cu_2PPh_3]$^{+\cdot}$; 587, <1%, [Cu(PPh_3)$_2$]$^{+\cdot}$; 532, 1%, [(hfac)CuPPh_3]$^{+\cdot}$; 445, <1%, [(OC-$CHCF_3$)CuPPh_3]$^{+\cdot}$; 325, 4%, [CuPPh_3]$^{+\cdot}$; 262, 100%, [PPh_3]$^{+\cdot}$; 201, 4%, [Cu($O_2C_2CHCF_3$)]$^{+\cdot}$ or [(O_2C_2CH)$_2$Cu]$^{+\cdot}$; 183, 48% [PPh_2]$^{+\cdot}$; 108, 19%, [PPh]$^{+\cdot}$; 69, <1%, [CF_3]$^{+\cdot}$; 63, 3%, [Cu]$^{+\cdot}$. Anal. calcd. for $C_{23}H_{16}O_2F_6PCu$ (mol. wt. 533.59): C 51.77, H 3.02; found: C 52.13, H 2.97.

(tfac)CuPPh$_3$

Color: chartreuse. Yield: 92%; mp 131°C. Anal. calcd. for $C_{23}H_{19}F_3O_2PCu$ (mol. wt. 479.62): C 57.60, H 3.99; found: C 57.62, H 4.11.

(acac)CuPPh$_3$

Color: white. Yield: 94%; mp 109 (dec.). Anal. calcd. for $C_{23}H_{22}O_2PCu$ (mol. wt. 425.65): C 64.90, H 5.21; found: C 64.80, H 5.12.

(hfac)CuPCy$_3$

Color: orange. Yield: 75%; mp 111°C. IR data (KBr disc cm^{-1}): 2925(s), 2853(S), 1675(m), 1640(s), 1580(w), 1545(s), 1535(w), 1517(s), 1492(s), 1461(w), 1457(w), 1446(s), 1343(w), 1325(w), 1302(w), 1294(w), 1256(s), 1204(s), 1177(w), 1142(s), 1101(m), 1050(w), 1044(w), 1003(w), 946(w), 917(w), 890(w), 853(m), 845(w), 820(w), 806(w), 790(s), 760(m), 756(w), 741(w), 736(w), 707(w), 668(s), 583(m), 525(m), 517(w), 473(w), 460(w), 432(w), 419(w), 410(w), 404(w). ^{1}H NMR δ: 6.32 (s, 1H, CH), 1.8–0.9 (m, 33H, PCy_3); ^{13}C{^{1}H} NMR δ: 177.3 (q, 33 Hz, CO), 119 (q, J(C–F) = 286 Hz, CF_3), 89.6 (s, CH), 31.8 (d, J(C–P) = 21 Hz, PCy_3), 30.9 (d, J(C–P) = 3.0 Hz, PCy_3), 27.0 (d, J(C–P) = 10.4 Hz, PCy_3), 26.1 (s, PCy_3); ^{31}P{^{1}H} NMR δ: 30.34 (s, br). Mass spectral data (70 eV, m/e): 624, <1%, [Cu(PCy_3)$_2$]$^{+\cdot}$; 550, 7%, [(hfac)CuPCy_3]$^{+\cdot}$; 481, <1%, [($O_2C_2CHCF_3$)CuPCy_3]$^{+\cdot}$; 343, 9%, [CuPCy_3]$^{+\cdot}$; 280, 23%, [PCy_3]$^{+\cdot}$; 261, 8%, [Cu(PCy_2H)]$^{+\cdot}$; 198, 100%, [PCy_2H]$^{+\cdot}$; 177, 7%, [CuPCy]$^{+\cdot}$; 117, 37%, [$PCyH_2$]$^{+\cdot}$; 97, 2%, [CF_3CO]$^{+\cdot}$; 83, 9%, [Cy]$^{+\cdot}$; 81, 10%, [C_6H_9]$^{+\cdot}$; 55, 16%, [C_4H_7]$^{+\cdot}$. Anal. calcd. for $C_{23}H_{34}O_2F_6PCu$ (mol. wt. 551.04): C 50.14, H 6.22; found: C 50.38, H 6.28.

Can. J. Chem. Downloaded from www.nrcresearchpress.com by 88.255.202.194 on 09/08/12
For personal use only.

(tfac)CuPCy$_3$

Color: chartreuse. Yield: 75%; mp 104°C. Anal. calcd. for $C_{23}H_{37}O_2F_3PCu$ (mol. wt. 497.07): C 55.58, H 7.50; found: C 55.91, H 7.94.

(acac)CuPCy$_3$

Color: white. Yield: 82%; mp 92°C. Anal. calcd. for $C_{23}H_{40}O_2PCu$ (mol. wt. 443.10): C 62.35, H 9.10; found: C 62.49, H 9.34.

(hfac)Cu(P^{n}Bu$_3$)$_2$

Orange liquid. Yield: 89%. ^{1}H NMR δ: 6.02 (s, 1H, CH), 1.31 (m, 36H, $P(C_3H_6CH_3)_3$), 0.89 (t, 7.0 Hz, 18H, $P(C_3H_6CH_3)_3$); $^{13}C\{^1H\}$ NMR δ: 175.9 (q, J(C–F) = 31 Hz, CO), 119 (q, J(C–F) = 289 Hz, CF_3), 86.3 (s, CH), 27.5 (d, J(C–P) = 3.0 Hz, PBu_3), 25.5 (d, J(C–P) = 14.5 Hz, PBu_3), 25.0 (d, J(C–P) = 12.2 Hz, PBu_3), 13.9 (s, CH_3, PBu_3); $^{31}P\{^1H\}$ NMR δ: −19.5 (s, br). Anal. calcd. for $C_{29}H_{55}F_6O_2P_2Cu$ (mol. wt. 674.78): C 51.61, H 8.15; found: C 51.47, H 8.40.

(tfac)Cu(P^{n}Bu$_3$)$_2$

Chartreuse liquid. Yield: 93%. Anal. calcd. for $C_{29}H_{58}F_3O_2P_2Cu$ (mol. wt. 620.78): C 56.11, H 9.34; found: C 56.05, H 9.27.

(acac)Cu(P^{n}Bu$_3$)$_2$

Light-yellow liquid. Yield: 96%. Anal. calcd. for $C_{29}H_{61}O_2P_2Cu$ (mol. wt. 566.78): C 61.45, H 10.76; found: C 61.64, H 11.26.

(hfac)Cu(PPh$_3$)$_2$

Orange solid. Yield: 93%. ^{1}H NMR δ: 7.47 (m, 12H, PPh_3), 6.95 (m, 18H, PPh_3), 6.04 (s, 1H, CH); $^{13}C\{^1H\}$ NMR δ: 176.8 (q, J(C–F) = 32.5 Hz, CO), 134.0 (s, br, PPh_3), 133.1 (s, br, PPh_3), 129.9 (s, PPh_3), 128.8 (s, br, PPh_3), 118.7 (q, J(C–F) = 288.3 Hz, CF_3), 87.4 (s, CH); $^{31}P\{^1H\}$ NMR δ: −2.22 (s, br). Anal. calcd. for $C_{41}H_{31}F_6O_2P_2Cu$ (mol. wt. 794.90): C 61.95, H 3.90; found: C 62.13, H 4.06.

(tfac)Cu(PPh$_3$)$_2$

Chartreuse solid. Yield: 96%. Anal. calcd. for $C_{41}H_{34}F_3O_2P_2Cu$ (mol. wt. 740.90): C 66.46, H 4.59; found: C 66.42, H 4.36.

(acac)Cu(PPh$_3$)$_2$

Light-yellow solid. Yield: 86%. Anal. calcd. for $C_{41}H_{37}O_2P_2Cu$ (mol. wt. 686.90): C 71.68, H 5.39; found: C 71.62, H 5.46.

(hfac)Cu(PCy$_3$)$_2$

Color: orange. Yield: 97%; mp 148°C. IR data: 2931(s), 2851(s), 1653(s), 1646(m), 1517(s), 1515(m), 1507(w), 1448(m), 1251(s), 1188(s), 1138(s), 1084(w), 1005(w), 942(w), 915(w), 889(w), 852(w), 818(w), 799(w), 784(w), 753(w), 668(m), 662(s), 577(w), 525(w), 517(w), 418(w), 403(w). ^{1}H NMR δ: 6.25 (s, 1H, CH), 2.0–1.1 (m, 66H, PCy_3); $^{13}C\{^1H\}$ NMR δ: 175.5 (q, J(C–F) = 32 Hz, CO), 119 (q, J(C–P) = 289 Hz, CF_3), 86.9 (s, CH), 32.8 (s, br, PCy_3), 30.4 (s, br, PCy_3), 28.0 (s, br, PCy_3), 26.6 (s, PCy_3); $^{31}P\{^1H\}$ NMR δ: 9.45 (s, br). Mass spectral data (70 eV, *m/e*): 624, <1%, $[Cu(PCy_3)_2]^{+\cdot}$; 550, 2%, $[(hfac)CuPCy_3]^{+\cdot}$; 481, <1%, $[(O_2C_2CHCF_3)CuPCy_3]^{+\cdot}$; 343, 6%, $[CuPCy_3]^{+\cdot}$; 280, 31%, $[PCy_3]^{+\cdot}$; 261, 4%, $[Cu(PCy_2H)]^{+\cdot}$; 198, 100%, $[PCy_2H]^{+\cdot}$; 177, 4%, $[CuPCy]^{+\cdot}$; 117, 70%, $[PCyH_2]^{+\cdot}$; 97, 1%, $[CF_3CO]^{+\cdot}$; 83, 14%, $[Cy]^{+\cdot}$; 81, 6%, $[C_6H_9]^{+\cdot}$; 55, 23%, $[C_4H_7]^{+\cdot}$. Anal. calcd. for $C_{41}H_{67}O_2F_6P_2Cu$ (mol. wt. 831.48): C 59.23, H 8.12; found: C 58.98, H 8.42.

(tfac)Cu(PCy$_3$)$_2$

Color: chartreuse. Yield: 92%; mp 137°C. Anal. calcd. for $C_{41}H_{70}O_2F_3P_2Cu$ (mol. wt. 777.51): C 63.34, H 9.08; found: C 63.40, H 9.38.

(acac)Cu(PCy$_3$)$_2$

Color: white. Yield: 88%; mp 129°C. Anal. calcd. for $C_{41}H_{73}O_2P_2Cu$ (mol. wt. 723.54): C 68.06, H 10.17; found: C 67.98, H 10.76.

X-ray crystallographic studies

Single crystal X-ray difffraction studies of (acac)Cu(PCy$_3$), (tfac)Cu(PCy$_3$), (hfac)Cu(PCy$_3$), and (hfac)Cu(PCy$_3$)$_2$ were carried out for comparative purposes. A summary of the crystal data and experimental details for the X-ray diffraction studies of these compounds is presented in Table 1. A general description of the experimental procedure is presented here, with more details available as supplementary material.[2]

Crystals of each compound were grown from *n*-pentane solution at −30°C. Suitable crystals were selected and sealed in glass capillaries at room temperature in a glove box under nitrogen atmosphere. X-ray data were collected on a Nicolet R3m/V diffractometer and the structures solved by direct methods using Shelxtl Plus and refined by the full-matrix least-squares method.

(acac)Cu(PCy$_3$)

Refinement of the non-hydrogen atoms showed that the cyclohexane ring corresponding to C(18)–C(23) had large anisotropic U's. This is indicative of some positional disorder. Attempts to refine the ring as two disordered cyclohexanes with isotropic U's on the disordered ring positions yielded higher R-factors than by simply refining all these ring positions anisotropically. In the final model, all non-hydrogen atoms were treated anisotropically, and all hydrogen atoms were included in idealized positions (riding model) with their isotropic U's set to 1.25 times the U(equiv) of their parent atoms.

(tfac)Cu(PCy$_3$)

Refinement of the non-hydrogen atoms showed that the F's had very large anisotropic U's. Close inspection of a difference Fourier map showed two sets of F's corresponding to two CF_3 positions rotated slightly from one another. All the F's share one isotropic U, which was not varied at first to determine the relative occupancies of the two sets of F's. The occupancies refined to 0.6767 and 0.3233 for the sets F(1)–F(3) and F(1′)–F(3′), respectively. Fixing the occupancies on the disordered F's, the final refinement model used anisotropic U's on all non-hydrogen atoms except the disordered F's, which were refined isotropically with a common U. All hydrogens were included in idealized positions (riding model) with isotropic U's set to 1.25 times U(equiv) of their parent atoms.

(hfac)Cu(PCy$_3$)

Refinement of the model went smoothly without any problems. The final model: anisotropic refinement on all non-hydrogen atoms, all hydrogen atoms included in idealized positions (riding model) with isotropic U's set to 1.25 times U(equiv) of their parent atoms.

(hfac)Cu(PCy$_3$)$_2$

Refinement of the non-hydrogen atoms showed large anisotropic U's for F(2), F(3), F(4), F(5), F(6), and particularly C(17). Study of difference Fourier maps showed that C(17) could be disordered over two sites, while no other sites for the F's could be picked out except for their original positions. Fixing a common isotropic U for C(17) and its other site C(17′), varying the relative occupancies, gave the resulting site occupancies for C(17) and C(17′) as 0.675 and 0.325. The final model refined all non-hydrogen atoms anisotropically except for C(17) and C(17′), which had fixed occupancies and a common, but variable isotropic U, and included all hydrogen atoms (allowing for disorder on C(17) and C(17′)) in idealized positions (riding model) with isotropic U's set to 1.25 times U(equiv) of parent atom, except for those on C(17) and C(17′), which were set to 1.25 times the common isotropic U of C(17) and C(17′).

[2]The supplementary material referred to in the text may be purchased from: The Depository of Unpublished Data, Document Delivery, CISTI, National Research Council Canada, Ottawa, Canada K1A 0S2.

Tables of crystal data, bond lengths and angles, hydrogen-atom coordinates, and crystal packing diagrams for each of the four compounds have also been deposited with the Cambridge Crystallographic Data Centre and can be obtained on request from The Director, Cambridge Crystallographic Data Centre, University Chemical Laboratory, 12 Union Road, Cambridge, CB2 1EZ, U.K.

TABLE 1. Summary of crystal data and experimental details for X-ray diffraction studies[a]

	(acac)Cu(PCy_3)	(tfac)Cu(PCy_3)	(hfac)Cu(PCy_3)	(hfac)Cu(PCy_3)$_2$
M	443.1	497.0	551.0	831.4
Crystal size/mm	0.23 × 0.460 × 0.736	0.230 × 0.575 × 0.713	0.230 × 0.345 × 0.552	0.250 × 0.360 × 0.650
T/°C	20	20	20	20
Unit cell dimensions				
a (Å)	13.502(6)	9.639(3)	9.870(2)	13.645(6)
b (Å)	13.691(6)	22.717(7)	17.314(4)	19.252(13)
c (Å)	15.781(6)	12.045(5)	15.586(3)	16.875(9)
α (deg)	71.05(3)			
β (deg)	67.50(3)	111.67(3)	99.74(2)	102.02(4)
χ (deg)	64.81(3)			
V (Å^3)	2392.7(15)	2451.03(14)	2629.18(93)	4335.9(41)
D_c (g cm^{-3})	1.230	1.347	1.392	1.274
F(000)	952	1048	1144	1768
Z	4	4	4	4
Space group	$P\bar{1}$	$P2_1/n$	$P2_1/c$	$P2_1/n$
Crystal system	Triclinic	Monoclinic	Monoclinic	Monoclinic
Reflections collected	7876	4736	4630	6970
Reflections used ($F > 3.0(F)$)	4928	2944	2513	4222
2θ Range (deg)	2.0–48.0	2.0–50.0	2.0–50.0	2.0–47.0
μ (mm^{-1})	0.993	0.994	0.949	0.632
R	0.0542	0.0722	0.0529	0.0720
R'	0.0580	0.0882	0.0651	0.0832

[a]Details in common: radiation, Mo-K_α (λ = 0.71069Å); weighting scheme, $w^{-1} = \sigma^2(F) + g F^2$ (see supplementary materials for value of g).

Final difference Fourier maps were essentially featureless at the end of final refinements for all structures. Atomic coordinates are presented in Tables 2–5, and bond lengths and angles are presented in Tables 6–9. Full details of the structural data are available as supplementary materials (footnote 2).

Results and discussion

Synthesis

The complexes (β-diketonate)Cu(PR_3), where β-diketonate = hfac, tfac, and acac, R = Bu, Ph, and Cy, were prepared by the reactions of [Cu(Cl)(PR_3)] with the corresponding sodium β-diketonate salt according to eq. [2]. This method avoided the problems of formation of the bis(triorganophosphine) complexes described in the Introduction. The complexes (β-diketonate)Cu(PR_3)$_2$ were prepared from *n*-pentane or diethyl ether solutions of (β-diketonate)CuPR_3 by reaction with PR_3, in 1:1 molar ratio as shown in eq. [3]. These reactions resulted in the formation of the desired product in high yield.

[2] $[ClCuPR_3] + Na^+\beta\text{-diketonate}^- \rightarrow (\beta\text{-diketonate})CuPR_3 + NaCl$

[3] $(\beta\text{-diketonate})CuPR_3 + PR_3 \rightarrow (\beta\text{-diketonate})Cu(PR_3)_2$

In addition to the methods described in the Introduction, several other methods of preparing triorganophosphine adducts copper(I) compounds have been described in the literature. However, these methods do not result in formation of mono(triorganophosphine) species. The reduction of β-diketonate copper(II) complexes with the tertiary phosphine (22, 23, 29) results in formation of bis(triorganophosphine) adducts, and the reduction of copper(II) acetate with Grignard reagents in the presence of a triorganophosphine results in the formation of either tris(triorganophosphine) complexes or ionic salts when small phosphines such as PMe_3 and PMe_2Ph are used, as described by eq. [4] (30).

[4] $Cu_2(O_2CMe)_4 + 2MgR_2 + \text{excess L} \rightarrow$ [Cu(L)$_4$][CuR_2], L = PMe_3, PMe_2Ph; or CuRL_3, L = $PMePh_2$

The reaction of $ClCuPPh_3$ with the thallium(I) β-diketonate (1:1 molar ratio) led surprisingly to the formation of bisphosphine complexes (31) as shown in Eq. [5], and not to the expected monophosphine adduct.

[5] $Tl^+\beta\text{-diketonate}^- + ClCuPPh_3 \rightarrow 0.5(\beta\text{-diketonate})Cu(PPh_3)_2 + TlCl + ?$

Recently, Doyle *et al.* (24) prepared a number of β-diketonate copper(I) olefin and carbonyl complexes, but reported that displacement of the carbonyl ligand, with L = triorganophosphines, amines, or isonitriles, gave derivatives of the type (β-diketonate)CuL_2. The reaction of eq. [2] seems to be a convenient, high-yield, general route to a variety of (β-diketonate)Cu(PR_3) complexes.

The reaction of eq. [3] resulted in formation of the bis(triorganophosphine) products, generally in high yields. However, where PR_3 = PMe_3, the addition of an excess of phosphine ligand resulted in displacement of the β-diketonate ligand from the copper(I) coordination sphere to form the salt [(β-diketonate)]$^-$[Cu(PMe_3)$_4$]$^+$ (26), analogous to the observations of Dempsey and Girolami (30). Unexpectedly, the very sterically hindered species (β-diketonate)Cu(PCy_3)$_2$ (PCy_3, cone angle = 170°C) was prepared and isolated by reaction of eq. [3], and one example, (hfac)Cu(PCy_3)$_2$, was structurally characterized by single crystal X-ray diffrac-

Can. J. Chem. Downloaded from www.nrcresearchpress.com by 88.255.202.194 on 09/08/12
For personal use only.

TABLE 2. Atomic coordinates ($\times 10^4$) and equivalent isotropic displacement coefficients ($Å^2 \times 10^3$) for (hfac)Cu(PCy_3)

Atom	x	y	z	U(eq)[a]
Cu	4078(1)	2512(1)	1649(1)	55(1)
O(1)	3066(4)	3117(2)	660(3)	60(2)
O(2)	2575(4)	1704(2)	1497(3)	60(2)
C(1)	1926(7)	2942(4)	216(4)	54(3)
C(2)	1166(7)	2287(4)	287(5)	60(3)
C(3)	1550(6)	1717(4)	914(5)	55(3)
C(4)	1371(9)	3521(6)	−473(6)	82(4)
F(1)	1695(9)	4200(3)	−265(5)	227(5)
F(2)	52(5)	3528(3)	−690(3)	132(3)
F(3)	1775(7)	3389(5)	−1188(4)	192(4)
C(5)	646(10)	1009(6)	908(9)	109(5)
F(4)	1295(7)	387(3)	1005(5)	178(4)
F(5)	−277(8)	935(4)	236(6)	220(5)
F(6)	−13(9)	1025(5)	1541(7)	243(6)
P	5892(1)	2599(1)	2628(1)	39(1)
C(6)	6371(6)	1679(3)	3193(4)	44(2)
C(7)	5098(7)	1331(3)	3516(4)	56(3)
C(8)	5427(8)	552(4)	3938(5)	74(3)
C(9)	5981(8)	−9(4)	3335(5)	78(3)
C(10)	7239(7)	315(4)	3033(5)	73(3)
C(11)	6933(7)	1101(3)	2591(4)	57(3)
C(12)	5622(6)	3306(3)	3466(4)	44(2)
C(13)	6435(6)	3176(3)	4384(4)	53(3)
C(14)	6175(7)	3816(4)	5004(4)	70(3)
C(15)	4656(8)	3900(4)	5028(5)	73(3)
C(16)	3840(6)	4040(4)	4140(5)	64(3)
C(17)	4086(6)	3413(4)	3495(4)	57(3)
C(18)	7427(6)	2925(3)	2198(4)	47(2)
C(19)	8709(6)	3071(4)	2868(4)	64(3)
C(20)	9933(7)	3271(5)	2424(6)	94(4)
C(21)	9607(9)	3952(5)	1808(6)	104(5)
C(22)	8326(8)	3793(5)	1143(5)	93(4)
C(23)	7112(7)	3602(4)	1587(5)	72(3)

[a]Equivalent isotropic U defined as one third of the trace of the orthogonalized U_{ij} tensor.

Can. J. Chem. Downloaded from www.nrcresearchpress.com by 88.255.202.194 on 09/08/12
For personal use only.

tion. This molecule is of interest because the bulky tricyclohexylphosphine groups are likely to exert a large steric effect on the copper(I) coordination environment.

The addition of other Lewis base ligands such as pyridine, NEt_3, THF, and H_2O to electronically unsaturated complexes (β-diketonate)$CuPR_3$ in greater than tenfold excess did not lead to any reaction. This observation is not surprising, since these ligands, although less sterically demanding than PCy_3, are weaker (hard) lewis bases with respect to the "soft" copper(I) cation. However, the result of a proton NMR study in which pyridine-d_5 was reacted with (hfac)$CuPMe_3$ revealed that addition of one drop of pyridine-d_5 to a benzene-d_6 solution of (hfac)$CuPMe_3$ caused the ^1H resonance of the coordinated PMe_3 to be deshielded by 0.41 ppm, and dissolution of (hfac)$CuPMe_3$ in pyridine-d_5 resulted in further deshielding of 0.72 ppm. We previously observed that the coordination of the Lewis bases to the copper(I) center is dominated by the σ-donor ability, not the π-acceptor ability, as evidenced by the small change in carbon–carbon bond lengths of olefin and alkyne ligands on coordination to the (β-diketonate)Cu(I) moiety (8, 32).

Depending on the particular phosphine and β-diketonate groups, the complexes have varying stability with respect to air oxidation, but all are moisture insensitive. In general the complexes derived from hfacH are more stable with respect to aerial oxidation and thermolysis than those prepared from tfacH and acacH. For example (acac)$CuP(n\text{-}Bu)_3$ thermally decomposed during attempted sublimation. The compounds (hfac)$Cu(PR_3)_n$, (tfac)$Cu(PR_3)_n$, and (acac)$Cu(PR_3)_n$, in general, are orange-yellow, chartreuse, and light-yellow solids or liquids, respectively. The complexes (β-diketonate)$Cu(PBu_3)_n$, where $n = 1$ and 2, are viscous liquids at room temperature, whereas the other derivatives are solids with melting points that vary from 92°C to 148°C as described in the experimental section. In general (β-diketonate)$Cu(PR_3)_2$ compounds are more thermally stable than their (β-diketonate)$Cu(PR_3)$ analogues.

Characterization and trends

The compounds (β-diketonate)CuL that were characterized previously were shown to be monomeric in the solid state and in solution (8, 28, 32, 33), and thus the (β-diketonate)$Cu(PR_3)$ complexes described here were expected to exhibit a similar trigonal-planar arrangement of ligands about the central copper(I) atom. The species (β-diketonate)$Cu(PR_3)_2$ were expected to be monomeric, four-coordinate, and tetrahedral by comparison to the literature data for analogous complexes, assuming that the β-diketonate ligand remains chelating (22, 25). β-Diketonate ligands can exhibit a great variety of coordination modes in metal-organic complexes. The solution phase ^1H, ^{13}C, and

TABLE 3. Atomic coordinates ($\times 10^4$) and equivalent isotropic displacement coefficients ($Å^2 \times 10^3$) for (tfac)Cu(PCy_3)

Atom	x	y	z	U(eq)[a]
Cu	1547(1)	8799(1)	5456(1)	45(1)
P	938(2)	8958(1)	6989(1)	32(1)
O(1)	1718(5)	8974(2)	3934(4)	54(2)
O(2)	2663(6)	8010(2)	5572(5)	63(2)
C(1)	2354(7)	8650(3)	3427(6)	48(3)
C(2)	3048(8)	8115(3)	3769(7)	59(3)
C(3)	3177(9)	7819(3)	4849(7)	59(3)
C(4)	2379(10)	8904(4)	2268(7)	68(4)
C(5)	4055(13)	7252(4)	5164(9)	100(6)
F(1)	1076(11)	8845(4)	1407(8)	104
F(2)	3308(11)	8625(4)	1827(8)	104
F(3)	2842(12)	9436(4)	2382(8)	104
F(1′)	3709(21)	9098(9)	2327(17)	104
F(2′)	1624(23)	9452(8)	1915(17)	104
F(3′)	2049(24)	8543(9)	1361(17)	104
C(6)	1821(7)	8389(3)	8146(6)	39(2)
C(7)	1183(7)	7780(3)	7692(6)	46(3)
C(8)	1997(9)	7294(3)	8580(8)	65(4)
C(9)	3637(9)	7307(3)	8848(8)	68(4)
C(10)	4296(9)	7911(3)	9365(7)	69(3)
C(11)	3509(7)	8293(3)	8460(6)	49(3)
C(12)	−1091(6)	8890(3)	6635(5)	39(2)
C(13)	−1613(8)	8949(3)	7687(6)	57(3)
C(14)	−3266(9)	8817(4)	7293(8)	78(4)
C(15)	−4180(8)	9211(4)	6266(8)	77(4)
C(16)	−3650(8)	9181(4)	5230(7)	66(3)
C(17)	−1990(7)	9292(3)	5623(7)	58(3)
C(18)	1480(8)	9686(3)	7722(6)	43(3)
C(19)	1841(9)	9723(3)	9047(6)	56(3)
C(20)	2180(11)	10341(4)	9516(8)	85(4)
C(21)	3268(11)	10650(4)	9131(9)	87(5)
C(22)	2888(11)	10619(3)	7799(9)	82(5)
C(23)	2621(10)	9989(3)	7351(8)	65(4)

[a]Equivalent isotropic U defined as one third of the trace of the orthogonalized U_{ij} tensor.

Can. J. Chem. Downloaded from www.nrcresearchpress.com by 88.255.202.194 on 09/08/12
For personal use only.

^{31}P NMR and solid state IR spectral data were consistent with chelation through both oxygen atoms in these phases. Table 10 lists the IR spectroscopic data of some (β-diketonate)Cu(PR_3)$_n$ species in the double bond stretching region (1500–1700 cm^{-1}).[3] The β-diketones themselves exist in keto–enol tautomerism where electron-withdrawing substituents, such as CF_3 and C_6H_5, displace the equilibrium in favor of the enol tautomer, while electron-donating substituents (CH_3) favor the keto form (35). The observed increase in ν(C=C) frequency in the order acac < tfac < hfac is consistent with the increasing Lewis acidity of β-diketones (36, 37). It is also noteworthy that when CH_3 groups in β-dikeotnate complexes are replaced by CF_3 groups, the carbonyl stretching frequency increases (i.e., acac < tfac < hfac). These observations have previously been interpreted in terms of weakening of the Cu—O bond on complexation as the frequency of the perturbed carbonyl band was raised in the case of Cu(II) β-diketonate complexes (38–40). Comparison of the ν(C—O and ν(C—C) bands in (β-diketonate)Cu(PR_3)$_n$, n = 1 and 2, compounds show that ν(C—O) is higher and ν(C—C) is lower for n = 2 than for n = 1. These changes are consistent with a greater contribution of the keto form to (β-diketonate)Cu(PR_3)$_2$ compounds.

In the ^{1}H and ^{13}C NMR data of (β-diketonate)Cu(PR_3)$_n$, the downfield chemical shifts of the central methine protons and carbons of the β-diketonate ring, the upfield shifts of the phosphine protons, and the increasing $^2J_{P-H}$ in the order hfac > tfac > acac may be ascribed to the rehybridization of phosphorus (more electron-withdrawing substituents on the β-diketonate may cause the Cu(β-diketonate) moiety to be more electron withdrawing), as expected on the basis of Bent's rules (41). The ^{31}P NMR chemical shifts of phosphine ligands in the title species are generally quite broad and follow the order of shielding hfac < tfac < acac-. This trend could reasonably be interpreted in terms of inductive effects (more electron-withdrawing substituents on the β-diketonate ligand result in more deshielding of the ^{31}P resonance) due to the highly electronegative CF_3 group. The observation of broadened singlet ^{31}P NMR resonances may be the result of quadrupolar broadening (42, 43) due to the presence of ^{63}Cu or ^{65}Cu (44) or the possibility of an exchange process (45) involving either the triorganophosphine or β-diketonate ligands. Solutions containing excess triorganophosphines also exhibit a broad single resonance at the weighted-average resonance of the complexed and free phosphine at room temperature. These results are indicative of reversible

[3]There has been some discussion about these band assignments in the literature. For a normal coordinate analysis, see ref. 34.

TABLE 4. Atomic coordinates ($\times 10^4$) and equivalent isotropic displacement coefficients ($Å^2 \times 10^3$) for (acac)Cu(PCy_3)

Atom	x	y	z	U(eq)
Cu(1)	753(1)	3138(1)	4073(1)	59(1)
O(1)	1748(3)	3627(3)	2881(3)	57(2)
O(2)	2051(3)	2139(4)	4612(3)	74(3)
C(1)	2825(5)	3297(5)	2681(4)	51(3)
C(2)	3476(5)	2529(5)	3259(5)	62(4)
C(3)	3087(5)	1983(5)	4161(5)	62(4)
C(4)	3434(5)	3740(6)	1708(4)	74(4)
C(5)	3933(6)	1142(6)	4666(5)	87(4)
P(1)	−1014(1)	3361(1)	4789(1)	49(1)
C(6)	−1289(4)	3036(4)	6071(3)	47(3)
C(7)	−599(5)	1838(5)	6393(4)	59(3)
C(8)	−752(6)	1565(5)	7436(4)	70(4)
C(9)	−466(6)	2344(5)	7729(4)	73(4)
C(10)	−1133(6)	3524(5)	7426(4)	68(4)
C(11)	−980(5)	3800(5)	6374(4)	63(4)
C(12)	−1987(5)	4787(5)	4537(4)	63(3)
C(13)	−3252(5)	5021(5)	5003(4)	67(3)
C(14)	−3943(5)	6226(6)	4816(5)	92(4)
C(15)	−3659(6)	6784(6)	3823(5)	88(4)
C(16)	−2401(6)	6531(5)	3365(4)	78(4)
C(17)	−1718(6)	5343(5)	3554(5)	84(4)
C(18)	−1509(6)	2429(7)	4526(4)	92(5)
C(19)	−2552(5)	2186(5)	5185(4)	65(4)
C(20)	−2822(8)	1410(9)	4889(6)	145(8)
C(21)	−2236(9)	994(9)	4129(7)	163(9)
C(22)	−1241(7)	1304(6)	3472(5)	95(5)
C(23)	−995(10)	2086(10)	3756(8)	225(12)
Cu(2)	−3232(1)	7123(1)	773(1)	52(1)
O(4)	−3411(3)	5852(3)	1775(3)	60(2)
O(3)	−4542(3)	7309(3)	366(3)	56(2)
C(24)	−4197(5)	5469(5)	1969(4)	52(3)
C(25)	−5033(5)	5859(5)	1521(4)	61(4)
C(26)	−5151(5)	6715(5)	758(4)	53(3)
C(27)	−4167(6)	4479(5)	2765(4)	85(4)
C(28)	−6122(6)	6983(6)	375(5)	83(4)
P(2)	−2078(1)	8027(1)	183(1)	40(1)
C(29)	−2265(4)	8986(4)	−925(3)	43(3)
C(30)	−3505(4)	9789(5)	−771(4)	53(3)
C(31)	−3718(5)	10566(5)	−1676(4)	62(4)
C(32)	−3420(5)	9931(5)	−2412(4)	70(4)
C(33)	−2200(5)	9146(5)	−2584(4)	66(4)
C(34)	−1959(5)	8360(5)	−1686(4)	57(3)
C(35)	−575(4)	7095(4)	−96(3)	41(3)
C(36)	−301(5)	6237(4)	766(4)	51(3)
C(37)	902(5)	5389(5)	515(4)	57(3)
C(38)	1799(5)	5929(5)	−1(4)	62(4)
C(39)	1519(5)	6769(5)	−846(4)	59(3)
C(40)	333(4)	7638(4)	−584(4)	50(3)
C(41)	−2180(4)	8855(4)	964(3)	42(3)
C(42)	−1835(5)	9879(5)	487(4)	56(3)
C(43)	−1900(6)	10435(5)	1210(5)	73(4)
C(44)	−3061(6)	10712(5)	1921(5)	73(4)
C(45)	−3402(6)	9701(5)	2389(4)	66(4)
C(46)	−3365(5)	9166(5)	1668(3)	51(3)

triorganophosphine dissociation that is rapid on the NMR time scale at room temperature.

The mass spectral data of the title compounds were studied to investigate the oligomerization in the vapor phase since these species have potential to exist as oligomers bridged through the β-diketonate oxygen as a result of steric crowding (46). As we observed previously, ions corresponding to [(β-diketonate)$Cu_2(PR_3)_2]^+$ were observed with low intensities. Molecular ions were observed for (β-diketonate)-Cu(PR_3) compounds in every case, and the highest intensity ion was attributed to either $[Cu(PR_3)]^+$ or $[PR_3]^+$. The mass spectra were generally dominated by fragmentation of the PR_3 ligands. However, molecular ions were not observed for (β-diketonate)Cu$(PR_3)_2$ compounds, and their fragmentation was

Can. J. Chem. Downloaded from www.nrcresearchpress.com by 88.255.202.194 on 09/08/12
For personal use only.

Can. J. Chem. Downloaded from www.nrcresearchpress.com by 88.255.202.194 on 09/08/12
For personal use only.

TABLE 5. Atomic coordinates ($\times 10^4$) and equivalent isotropic displacement coefficients ($Å^2 \times 10^3$) for (hfac)Cu(PCy_3)$_2$

Atom	x	y	z	U(eq)[a]
Cu	−64(1)	2415(1)	7070(1)	43(1)
O(1)	−887(4)	1421(3)	6838(3)	54(2)
O(2)	501(4)	1893(3)	8272(3)	53(2)
C(1)	−772(6)	886(4)	7245(5)	50(3)
C(2)	−254(6)	778(4)	8024(5)	56(3)
C(3)	338(6)	1293(4)	8482(4)	52(3)
C(4)	887(8)	1098(6)	9322(6)	73(4)
C(5)	−1323(10)	262(6)	6801(7)	87(5)
F(1)	918(8)	1586(4)	9841(4)	176(5)
F(2)	545(6)	583(4)	9651(3)	147(4)
F(3)	1802(6)	951(5)	9344(4)	182(5)
F(4)	−1232(6)	−317(3)	7202(4)	148(4)
F(5)	−875(7)	96(4)	6192(5)	162(5)
F(6)	−2216(6)	357(4)	6489(6)	193(5)
P(1)	−962(1)	3242(1)	7540(1)	35(1)
C(6)	−2276(5)	2989(3)	7530(4)	38(3)
C(7)	−2797(5)	2731(4)	6688(4)	51(3)
C(8)	−3895(6)	2558(5)	6676(5)	72(4)
C(9)	−3969(7)	2008(5)	7292(5)	78(4)
C(10)	−3424(6)	2222(5)	8129(5)	68(4)
C(11)	−2342(5)	2415(4)	8147(4)	49(3)
C(12)	−1056(6)	4120(4)	7059(5)	60(3)
C(13)	−107(6)	4330(4)	6806(5)	61(3)
C(14)	−144(9)	5027(6)	6405(8)	151(7)
C(15)	−988(9)	5277(6)	5976(8)	131(7)
C(16)	−1934(8)	5090(5)	6221(7)	98(5)
C(17)[b]	−1980(9)	4302(6)	6430(7)	54(3)
C(17′)	−1767(17)	4595(12)	7073(14)	54(3)
C(18)	−423(5)	3390(3)	8620(4)	37(3)
C(19)	692(5)	3586(4)	8760(4)	45(3)
C(20)	1169(6)	3567(4)	9685(4)	54(3)
C(21)	612(6)	4030(4)	10159(4)	54(3)
C(22)	−501(6)	3868(4)	9994(4)	52(3)
C(23)	−971(5)	3884(4)	9096(4)	48(3)
P(2)	903(1)	2247(1)	6138(1)	38(1)
C(24)	1394(5)	1355(3)	6244(4)	40(3)
C(25)	2086(6)	1248(4)	7074(4)	54(3)
C(26)	2303(6)	486(4)	7245(5)	66(4)
C(27)	2751(7)	156(4)	6576(6)	75(4)
C(28)	2097(7)	275(4)	5752(5)	68(4)
C(29)	1880(6)	1040(4)	5585(4)	55(3)
C(30)	152(5)	2296(3)	5091(4)	40(3)
C(31)	−354(6)	3009(4)	4935(5)	62(3)
C(32)	−988(7)	3078(5)	4082(5)	78(4)
C(33)	−1754(7)	2495(5)	3919(5)	81(4)
C(34)	−1267(6)	1791(5)	4057(5)	72(4)
C(35)	−641(6)	1724(4)	4920(4)	53(3)
C(36)	1996(7)	2821(5)	6115(5)	73(4)
C(37)	2459(6)	2831(5)	5402(5)	69(4)
C(38)	3339(8)	3270(6)	5436(6)	109(5)
C(39)	3583(8)	3791(5)	6040(8)	108(6)
C(40)	3154(8)	3750(5)	6751(6)	88(5)
C(41)	2255(7)	3328(6)	6709(6)	105(5)

[a]Equivalent isotropic U defined as one third of the trace of the orthogonalized U_{ij} tensor.
[b]C(17) and C(17′) represent disordered positions of C(17) with occupancies of 0.675 and 0.325, respectively. The positions of H(12a), H(16a), H(16b) are the idealized hydrogen atom positions for C(17) and its corresponding hydrogens H(17a) and H(17b). The positions of H(12b), H(16c), and H(16d) are the idealized hydrogen atom positions for C(17′) and its corresponding hydrogens H(17c) and H(17d).

similar to that of their monophosphine analogues. Variation in the mass spectral parameters, such as reducing the ionization potential (70 to 30 eV), increasing the sample size, and decreasing the sample heating rate, did not result in the observation of the expected monomeric parent ion, (β-diketonate)Cu(PCy_3)$_2^+$. These observations probably result

Can. J. Chem. Downloaded from www.nrcresearchpress.com by 88.255.202.194 on 09/08/12
For personal use only.

TABLE 6*a*. Selected bond lengths (Å) for (hfac)Cu(PCy_3)

Cu—O(1)	1.987(4)	Cu—O(2)	2.026(4)
Cu—P	2.152(2)	O(1)—C(1)	1.255(7)
O(2)—C(3)	1.239(7)	C(1)—C(2)	1.376(10)
C(1)—C(4)	1.504(11)	C(2)—C(3)	1.397(10)
C(3)—C(5)	1.517(12)	P—C(6)	1.845(6)
P—C(12)	1.844(6)	P—C(18)	1.846(6)

TABLE 6*b*. Selected bond angles (deg) for (hfac)Cu(PCy_3)

O(1)—Cu—O(2)	90.7(2)	O(1)—Cu—P	139.6(1)
O(2)—Cu—P	129.5(1)	Cu—O(1)—C(1)	125.9(4)
Cu—O(2)—C(3)	124.3(4)	O(1)—C(1)—C(2)	127.2(6)
O(1)—C(1)—C(4)	114.7(6)	C(2)—C(1)—C(4)	118.1(6)
C(1)—C(2)—C(3)	123.6(6)	O(2)—C(3)—C(2)	128.1(6)
O(2)—C(3)—C(5)	113.3(7)	C(2)—C(3)—C(5)	118.6(7)
Cu—P—C(6)	113.2(2)	Cu—P—C(12)	110.2(2)
C(6)—P—C(12)	107.0(3)	Cu—P—C(18)	113.6(2)
C(6)—P—C(18)	106.2(3)	C(12)—P—C(18)	106.2(3)

TABLE 7*a*. Selected bond lengths (Å) for (tfac)Cu(PCy_3

Cu—P	2.164(2)	Cu—O(1)	1.942(6)
Cu—O(2)	2.068(5)	P—C(6)	1.860(6)
P—C(12)	1.848(6)	P—C(18)	1.858(6)
O(1)—C(1)	1.252(10)	O(2)—C(3)	1.229(12)
C(1)—C(2)	1.374(10)	C(1)—C(4)	1.520(12)
C(2)—C(3)	1.428(12)	C(3)—C(5)	1.511(12)

TABLE 7*b*. Selected bond angles (deg) for (tfac)Cu(PCy_3)

P—Cu—O(1)	156.3(2)	P—Cu—O(2)	112.7(2)
O(1)—Cu—O(2)	91.0(2)	Cu—P—C(6)	109.3(2)
Cu—P—C(12)	112.7(2)	C(6)—P—C(12)	105.5(3)
Cu—P—C(18)	115.9(3)	C(6)—P—C(18)	107.0(3)
C(12)—P—C(18)	105.8(3)	Cu—O(1)—C(1)	124.6(4)
Cu—O(2)—C(3)	126.4(5)	O(1)—C(1)—C(2)	130.2(7)
O(1)—C(1)—C(4)	113.7(6)	C(2)—C(1)—C(4)	116.1(8)
C(1)—C(2)—C(3)	123.9(8)	C(2)—C(3)—C(5)	118.9(9)
H(2)—C(2)—C(3)	118.0(5)	O(2)—C(3)—C(2)	123.8(7)
O(2)—C(3)—C(5)	117.3(8)		

from weak coordination of the second phosphine ligand, consistent with the observed lengthening (weakening) of the Cu—P bonds in the solid state structure of (hfac)Cu(PCy_3)$_2$ compared to that observed for (β-diketonate)CuPCy_3 compounds.

Solid state structural data

The solid state structures of (hfac)Cu(PCy_3), (tfac)Cu(PCy_3), and (acac)Cu(PCy_3) were determined by single crystal X-ray diffraction and the ORTEP plots are shown in Figs. 1–3 respectively. All three compounds are monomeric with three-coordinate copper in the solid state. The copper coordination environment is distorted trigonal planar and none of molecules possesses any symmetry elements in the solid state. The compound (tfac)Cu(PCy_3) is most distorted from trigonal-planar geometry with O—Cu—P angles of 156.3(2)° and 112.7(2)°. The two Cu—O bond distances are significantly different, within the limits of error

TABLE 8*a*. Selected bond lengths (Å) for (acac)Cu(PCy_3)

Cu(1)—O(1)	1.950(4)	Cu(1)—O(2)	2.002(4)
Cu(1)—P(1)	2.146(2)	O(1)—C(1)	1.265(7)
O(2)—C(3)	1.261(7)	C(1)—C(2)	1.383(8)
C(1)—C(4)	1.502(8)	C(2)—C(3)	1.390(8)
C(3)—C(5)	1.499(9)	P(1)—C(6)	1.847(5)
P(1)—C(12)	1.846(5)	P(1)—C(18)	1.879(11)
Cu(2)—O(4)	1.966(4)	Cu(2)—O(3)	1.995(5)
Cu(2)—P(2)	2.147(2)	O(4)—C(24)	1.271(9)
O83)—C(26)	1.255(8)	C(24)—C(25)	1.383(10)
C(24)—C(27)	1.518(8)	C(25)—C(26)	1.385(8)
C(26)—C(28)	1.507(11)	P(2)—C(29)	1.847(5)
P(2)—C(35)	1.848(4)	P(2)—C(41)	1.862(7)

TABLE 8*b*. Selected bond angles (deg) for (acac)Cu(PCy_3)

O(1)—Cu(1)—O(2)	93.7(2)	O(1)—Cu(1)—P(1)	141.5(1)
O(2)—Cu(1)—P(1)	124.9(1)	Cu(1)—O(1)—C(1)	124.5(3)
Cu(1)—O(2)—C(3)	123.6(4)	O(1)—C(1)—C(2)	125.7(5)
O(1)—C(1)—C(4)	116.1(5)	C(2)—C(1)—C(4)	118.2(5)
C(1)—C(2)—C(3)	127.3(5)	O(2)—C(3)—C(2)	125.0(6)
O(2)—C(3)—C(5)	115.5(5)	C(2)—C(3)—C(5)	119.5(5)
Cu(1)—P(1)—C(6)	111.7(2)	Cu(1)—P(1)—C(12)	113.8(2)
Cu(1)—P(1)—C(18)	112.2(2)	O(4)—Cu(2)—O(3)	93.9(2)
O(4)—Cu(2)—P(2)	137.1(2)	O(3)—Cu(2)—P(2)	128.9(1)
Cu(2)—O(4)—C(24)	123.5(4)	Cu(2)—O(3)—C(26)	123.4(4)
O(4)—C(24)—C(25)	126.3(5)	O(4)—C(24)—C(27)	114.6(6)
C(25)—C(24)—C(27)	119.1(7)	C(24)—C(25)—C(26)	126.6(7)
O(3)—C(26)—C(25)	126.3(7)	O(3)—C(26)—C(28)	116.5(5)
C(25)—C(26)—C(28)	117.2(6)	Cu(2)—P(2)—C(29)	112.9(2)
Cu(2)—P(2)—C(35)	111.3(2)	Cu(2)—P(2)—C(41)	114.5(2)

TABLE 9*a*. Selected bond lengths (Å) for (hfac)Cu(PCy_3)$_2$

Cu—O(1)	2.213(5)	Cu—O(2)	2.251(5)
Cu—P(1)	2.251(3)	Cu—P(2)	2.277(3)
O(1)—C(1)	1.230(9)	C(1)—C(2)	1.373(10)
C(3)—O(2)	1.244(10)	C(2)—C(3)	1.403(11)
C(1)—C(5)	1.528(13)	C(3)—C(4)	1.507(11)
P(1)—C(6)	1.855(7)	P(1)—C(12)	1.869(8)
P(2)—C(30)	1.852(6)	P(1)—C(18)	1.839(6)
P(2)—C(24)	1.839(7)	P(2)—C(36)	1.862(10)

TABLE 9*b*. Selected bond angles (deg) for (hfac)Cu(PCy_3)$_2$

O(1)—Cu—O(2)	80.8(2)	C(1)—O(1)—Cu	128.6(4)
C(2)—C(1)—O(1)	130.0(7)	C(3)—C(2)—C(1)	122.8(7)
O82)—C(3)—C(2)	128.1(7)	Cu—O(2)—C(3)	128.6(4)
P(1)—Cu—O(2)	96.2(2)	P(2)—Cu—O(1)	95.7(2)
P(1)—Cu—P(2)	141.3(1)	O(2)—Cu—P(2)	114.8(2)
C(2)—C(1)—C(5)	116.9(7)	C(2)—C(3)—C(4)	117.3(8)
O(1)—Cu—P(1)	112.4(2)	O(1)—C(1)—C(5)	113.1(7)
C(1)—C(2)—H(2)	118.6(5)	O(2)—C(3)—C(4)	114.6(7)
Cu—P(1)—C(6)	114.0(2)	C(6)—P(1)—C(12)	104.8(3)
Cu—P(2)—C(30)	111.6(2)	Cu—P(2)—C(36)	120.8(3)
Cu—P(2)—C(24)	108.5(2)	C(24)—P(2)—C(30)	104.9(3)
Cu—P(1)—C(12)	118.6(3)	Cu—P(1)—C(18)	108.9(2)

Can. J. Chem. Downloaded from www.nrcresearchpress.com by 88.255.202.194 on 09/08/12
For personal use only.

TABLE 10. IR spectral data for (β-diketonate)Cu(PR_3)$_n$ complexes. Assignments based on literature data (34)

Compounds	ν(C=O)	ν(C=C)
(hfac)Cu(PMe_3)	1672(s)	1548(s)
(tfac)Cu(PMe_3)	1623(s)	1526(s)
(acac)Cu(PMe_3)	1587(s)	1513(s)
(hfac)Cu(PMe_3)$_2$	1675(s)	1539(s)
(tfac)Cu(PMe_3)$_2$	1642(s)	1521(s)
(acac)Cu(PMe_3)$_2$	1613(s)	1512(s)
(hfac)Cu(PCy_3)	1640(s)	1545(s)
(tfac)Cu(PCy_3)	1625(s)	1524(s)
(acac)Cu(PCy_3)	1591(s)	1513(s)
(hfac)Cu(PCy_3)$_2$	1653(s)	1517(s)
(tfac)Cu(PCy_3)$_2$	1632(s)	1514(s)
(acac)Cu(PCy_3)$_2$	1605(s)	1510(m)

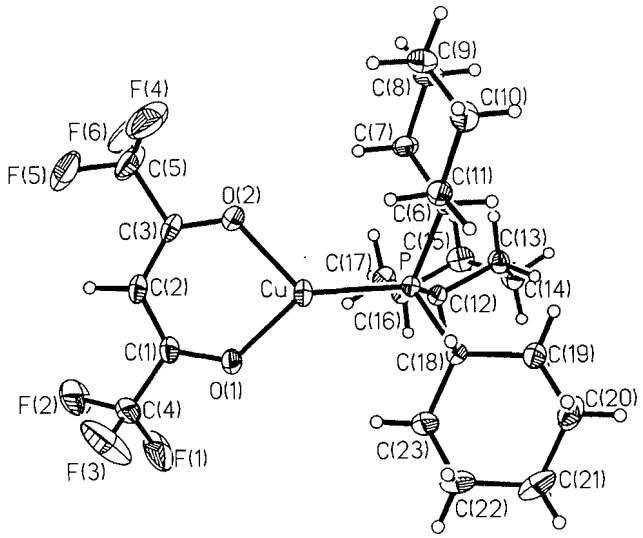

FIG. 1. ORTEP plot for (hfac)Cu(PCy_3).

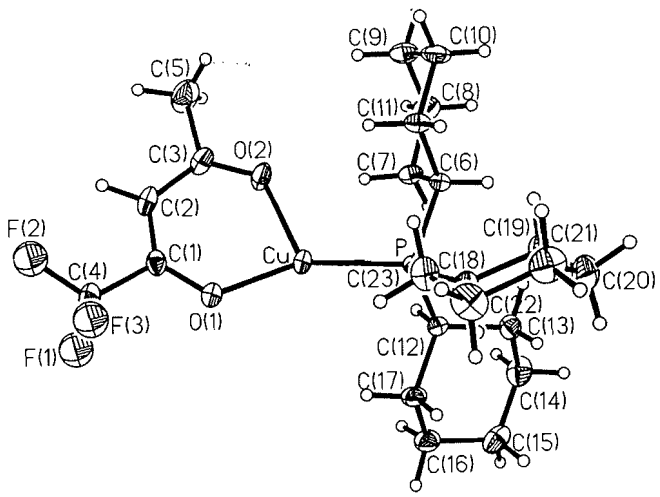

FIG. 2. ORTEP plot for (tfac)Cu(PCy_3).

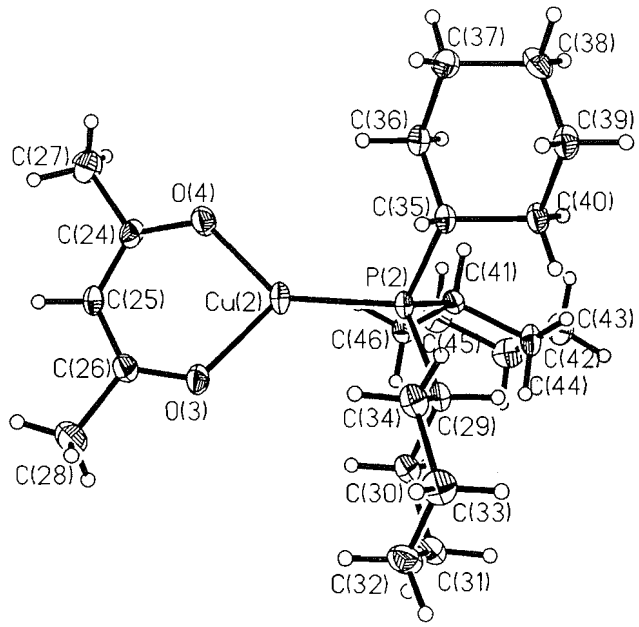

FIG. 3. ORTEP plot for (acac)Cu(PCy_3).

on the data, with Cu—O(1), close to the CF_3 substituent, 1.942(6) Å, shorter than Cu—O(2), close to the CH_3 substituent, 2.068(5) Å. However, no trends in Cu—O bond distances between the compounds can be discerned, within the limits of error on the data, that would clearly enable a comparison of thermodynamic parameters such as bond length – bond strength relationships as a function of the β-diketonate substituents. The bite angles of the β-diketonate ligands of ~91°–~94° and the Cu—O bond lengths of ~2.00 Å are similar to other copper(I) β-diketonate complexes bearing one Lewis base adduct (8, 28, 32, 33). Similarly, no unambiguous trends in Cu—P bond lengths or C—O and C—C bond lengths and angles, within the limits of error of the data, were observed that would enable comparison to the spectroscopic trends observed.

The crystal structure of (hfac)Cu(PCy_3)$_2$ was determined by single crystal X-ray diffraction. The ORTEP drawing is shown in Fig. 4 and the structural data confirm that this compound is monomeric and adopts a distorted tetrahedral geometry, although the bulky tricyclohexylphosphine ligands exert a large steric effect. The steric effects are evident from the long Cu—P bond distances of 2.251(3) and 2.277(3) Å (hfacCu(PCy_3) derivative = 2.15 Å), the large P—Cu—P angle of 141.3(1)°, the long Cu—O distances of 2.213(5) and 2.251(5) Å (~2.01 Å for (hfacCu(PCy_3)), and the small O—Cu—O angle of 80.8(2)° (90.7(2)° for (hfacCu(PCy_3)) compared to the monotricyclohexylphosphine-substituted derivative (Tables 6 and 9). The Cu—P bond lengths are analogous to those observed in other tetrahedrally coordinated copper(I) compounds with two-phosphine ligands (47). The P—Cu—P bond angle, 141.3(1)°, is close to that of the four-coordinate nitrate complex (NO$_3$)Cu(PCy_3)$_2$, 140(1)°, but it is significantly larger than those typically reported for systems with the less bulky PPh_3 groups: 127(1)° in (tfac)Cu(PPh_3)$_2$ (25), 131.2(1)° in (NO$_3$)Cu(PPh_3)$_2$ (22), and 123.26(6)° in (BH_4)Cu(PPh_3)$_2$ (23). Furthermore, the O—Cu—O angle, 80.8(2)°, of the hexafluoroacetylacetonate ligand is significantly smaller than

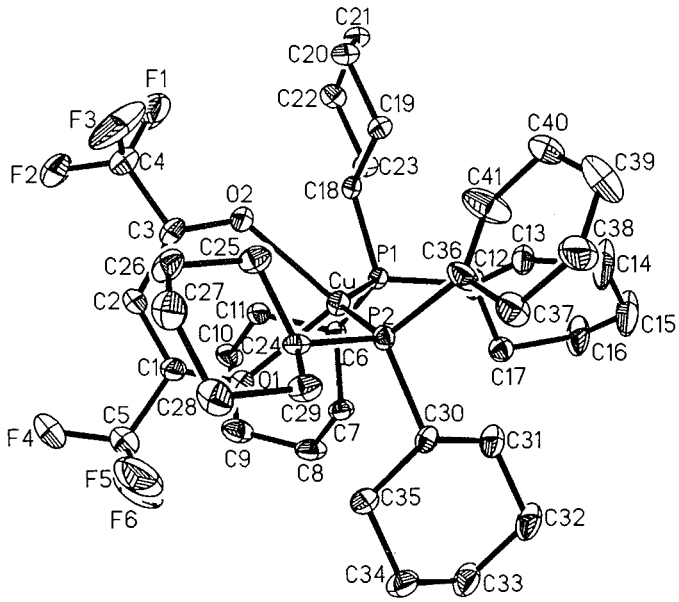

FIG. 4. ORTEP plot for (hfac)Cu(PCy_3)$_2$.

that of (hfac)CuPCy_3 (90.7(2)°). Since the tricyclohexylphosphine is very bulky, steric factors exert a strong influence on the coordination environment of copper in the compound (hfac)Cu(PCy_3)$_2$. These results are consistent with the cone angle data derived for PPh_3 (145°) and PCy_3 (170°) (46). Within the limits of error on the X-ray diffraction data, the changes in tautomerism predicted for the β-diketonate ligands in (hfac)Cu(PCy_3) compared to (hfacCu(PCy_3)$_2$, based on the spectroscopic data, could not be unambiguously established.

Conclusions

A general synthesis of a variety of new monotriorganophosphine adducts of copper(I) β-diketonates of general formula (β-diketonate)Cu(PR_3), prepared by the salt elimination reaction between [ClCu(PR_3)] and Na (β-diketonate), results in high purity and high yields. These species can then be reacted with one equivalent of the corresponding triorganophosphine to yield the adducts (β-diketonate)Cu(PR_3)$_2$ in virtually quantitative yield. Trends in the NMR and FTIR data suggested that the strength of binding of the β-diketonate and phosphine ligands to the copper(I) center increases in the order acac < tfac < hfac. This trend is also consistent with the observed qualitative trends in thermal and oxidative stability of these species. The ν(C—O) band is weakened markedly along the series hfac > tfac > acac. On addition of PR_3 to (β-diketonate)Cu(PR_3) compounds, the FTIR data are consistent with a stronger contribution of the keto form of the β-diketonate ligand compared to the starting material.

Attempts were made to confirm these trends by comparison of the metrical parameters of the species (hfac)Cu(PCy_3), (tfac)Cu(PCy_3), and (acac)Cu(PCy_3). However, while the Cu—O bond lengths in (tfac)Cu(PCy_3) were significantly different within the limits of error of the X-ray diffraction data, with Cu—O adjacent to the CF_3 substituent being shorter, the compounds (hfac)Cu(PCy_3) and (acac)Cu(PCy_3) exhibited values that covered a larger range of bond distances and did not exhibit any trends. As a result, care should be taken when interpreting these data as dependent on crystal packing forces (although no short intermolecular distances were observed).

The species (hfac)Cu(PCy_3)$_2$ was also characterized by single crystal X-ray diffraction in the solid state and revealed a distorted, tetrahedral copper(I) coordination environment. The distortion was believed to be the result of the two sterically demanding PCy_3 groups, which resulted in significant lengthening of the Cu—O bonds. These results are valuable for comparison to the thermally induced disproportionation of (β-diketonate)CuL compounds that is being examined as a method for the CVD of copper. The trends in FTIR data can be compared to the changes observed in coordination of these species on silica surfaces to provide insight into the mode of adsorption. Steric overcrowding of the copper(I) center resulting in lengthening of the Cu—O bonds of the β-diketonate ligand until it is finally completely displaced from the copper(I) coordination sphere, as in the case of [(β-diketonate)]$^-$ [CuL_4]$^+$ compounds, may provide insight into the β-diketonate ligand transfer during thermally induced disproportionation. Further studies are in progress.

Acknowledgements

We thank the National Science Foundation (NSF) (No. CHE-9107035) and Motorola Inc. for financial support of this research. M. J. Hampden-Smith thanks the NSF Chemical Instrumentation program for the purchase of a low-field NMR spectrometer. T. T. Kodas acknowledges support from a NSF Presidential Young Investigator Award No. CTS90558538.

1. D. Temple and A. Reisman. J. Electrochem. Soc. **136**, 3525 (1989).
2. R. L. Van Herment, L. B. Spendlove, and R. E. Sievers. J. Electrochem. Soc. **112**, 1123 (1965).
3. Y. Arita. Mater. Res. Soc. Symp. Proc. VLSI V, 335 (1990).
4. A. E. Kaloyeros, A. Feng, J. Garhart, K. C. Brooks, S. K. Gosh, A. N. Saxena, and F. Luethers. J. Electron. Mater. **19**, 271 (1990).
5. W. G. Lai, Y. Xie, and G. L. Griffin. J. Electrochem. Soc. **138**, 3449 (1991).
6. W. R. Wolf, R. E. Sievers, and G. H. Brown. Inorg. Chem. **11**, 1195 (1972).
7. H. K. Shin, K.-M. Chi, M. J. Hampden-Smith, T. T. Kodas, M. F. Paffett, and J. D. Farr. Angew. Chem. Adv. Mater. **3**, 246 (1991).
8. K.-M. Chi, H. K. Shin, M. J. Hampden-Smith, T. T. Kodas, and E. N. Duesler. Polyhedron, **10**, 2293 (1991).
9. A. Jain, M. J. Hampden-Smith, T. T. Kodas, M. F. Paffett, and J. D. Farr. Chem. Mater. **3**, 995 (1991).
10. S. K. Reynolds, C. J. Smart, E. F. Baran, T. H. Baum, C. E. Larson, and P. J. Brock. Appl. Phys. Lett. **59**, 2332 (1991).
11. R. Kumar, A. W. Maverick, F. R. Fronczek, W. G. Lai, and G. L. Griffin. Precursors for chemical vapor deposition of copper. 200th Am. Chem. Soc. Meet. Atlanta, April 1991. Abstract INOR 256.
12. J.A.T. Norman, B. A. Muratore, P. N. Dyer, D. A. Roberts, and A. K. Hochberg. J. Phys. Colloq. IV, 1, C2–271 (1991).
13. A. Jain, M. J. Hampden-Smith, T. T. Kodas, M. F. Paffett, and J. D. Farr. J. Mater. Res. **7**, 261 (1992).
14. T. H. Baum and C. E. Larson. C. E. Chem. Mater. **4**, 365 (1992).
15. M. E. Gross and V. M. Donnelly. *In* Advanced metallization for ULSI applications. *Edited by* V. S. Rana and R. V. Joshi. Materials Research Society, Pittsburgh, Pa. 1991. p. 355.

Can. J. Chem. Downloaded from www.nrcresearchpress.com by 88.255.202.194 on 09/08/12
For personal use only.

16. H. K. Shin, K.-M. Chi, M. J. Hampden-Smith, T. T. Kodas, M. F. Paffett, and J. D. Farr. Chem. Mater. **4**, 788 (1992).
17. H. K. Shin, K.-M. Chi, M. J. Hampden-Smith, T. T. Kodas, M. F. Paffett, and J. D. Farr. Proc. SPIE Conf. Metallization: Performance and Reliability Issues for VLSI and ULSI. San Jose, Calif. 1991. vol. 1596. p. 23.
18. B. Emmert, H. Gsottochneider, and H. Stanger. Chem. Ber. **69**, 1319 (1936).
19. R. Nast, R. Mohr, and C. Schultze. Chem. Ber. **96**, 2127 (1963).
20. Y. L. Chow and G. E. Buono-Core. Can. J. Chem. **61**, 795 (1983).
21. R. Nast and W.-H. Lepel. Chem. Ber. **102**, 3224 (1969).
22. W. A. Anderson, A. J. Carty, G. J. Palenik, and G. Schreiber. Can. J. Chem. **49**, 761 (1971).
23. R. J. Restivo, A. Costin, G. Ferguson, and A. J. Carty. Can. J. Chem. **53**, 1949 (1975).
24. G. Doyle, K. A. Eriksen, and D. Van Engen. Organometallics, **4**, 830 (1985).
25. M. Bartlett and J. Palenik. Acta Crystallogr. Sect. A: Cryst. Phys. Diffr. Theor. Gen. Crystallogr. **25**, s173 (1969).
26. H. K. Shin, J. Farkas, M. J. Hampden-Smith, T. T. Kodas, and E. N. Duesler. J. Chem. Soc. Dalton Trans. In press.
27. D. D. Perrin, W. L. F. Armargo, and D. R. Perrin. Purification of laboratory chemicals. Pergamon Press, New York. 1980; A. Osterlof. Acta Chem. Scand. **4**, 375 (1950).
28. H. K. Shin, J. Farkas, K. M. Chi, M. J. Hampden-Smith, T. T. Kodas, and E. N. Duesler. Inorg. Chem. **31**, 424 (1992).
29. D. Gibson, B. F. G. Johnson, and J. Lewis. J. Chem. Soc. (A), 367 (1970); F. Cariati and L. Naldini. Gazz. Chim. Ital. **3**, 95 (1965).
30. D. F. Dempsey and G. S. Girolami. Organometallics, **7**, 1208 (1988).
31. F. Cariati and L. Naldini. Gazz. Chim. Ital., **3**, 95 (1965).
32. K. M. Chi, H. K. Shin, M. J. Hampden-Smith, T. T. Kodas, and E. N. Duesler. Inorg. Chem. **30**, 4293 (1991).
33. H. K. Shin, M. J. Hampden-Smith, T. T. Kodas, and E. N. Duesler. Polyhedron, **6**, 645 (1991).
34. K. Nakamoto, Y. Morimoto, and A. E. Martell. J. Phys. Chem. **66**, 346 (1962); K. Nakamoto. *In* Infrared and Raman spectra of inorganic and coordination compounds. John Wiley and Sons, New York. 1986. p. 259.
35. S. Kawaguchi. Variety in coordination modes of ligands in metal complexes. Springer-Verlag, New York. 1987. p. 75.
36. D. P. Graddon. Coord. Chem. Rev. 4, **1**, (1969).
37. L. L. Funck and T. R. Ortolano. Inorg. Chem. **7**, 567 (1968).
38. N. A. Bailey, D. E. Fenton, M. V. Franklin, and M. Hall. J. Chem. Soc. Dalton Trans. 984 (1980).
39. M. A. V. Ribero da Silva and M. L. C. C. H. Ferrao. Pure Appl. Chem. **60**, 1225 (1988).
40. L. L. Funck and T. R. Ortolano. Inorg. Chem. **7**, 567 (1968).
41. H. A. Bent. J. Chem. Educ. **37**, 616 (1960); Chem. Rev. **61**, 275 (1961); J. E. Huheey. Inorganic chemistry. 3rd ed. Harper & Row Publishers, New York. 1983. p. 230.
42. R. K. Harris. Nuclear magnetic resonance spectroscopy. Pitman, London. 1983.
43. G. A. Bowmaker, B. W. Skelton, A. H. White, and P. C. Healy. J. Chem. Soc. Dalton Trans. 2825 (1988).
44. J. A. Dean. Lange's handbook of chemistry. 13th ed. McGraw–Hill, London. 1985.
45. M. Kubota, A. Miyashita, S. Komita, and A. Yamamoto. J. Organomet. Chem. **139**, 111 (1977).
46. C. A. Tolman. Chem. Rev. **77**, 313 (1977).
47. J. T. Gill, J. J. Mayerle, P. S. Welcker, D. F. Lewis, D. A. Ucko, D. J. Barton, D. Stowens, and S. L. Lippard. Inorg. Chem. **15**, 1155 (1976).

Can. J. Chem. Downloaded from www.nrcresearchpress.com by 88.255.202.194 on 09/08/12
For personal use only.

Spiro fused β-lactam cyclopropenes

MICHEL ZOGHBI AND JOHN WARKENTIN[1]
Department of Chemistry, McMaster University, Hamilton, Ont., Canada L8S 4M1

Received May 6, 1992

MICHEL ZOGHBI and JOHN WARKENTIN. Can. J. Chem. **70**, 2967 (1992).

Δ^3-1,3,4-Oxadiazolines (**1**) that share their C2 with C4 of a β-lactam ring in a spiro fusion were prepared. The structures were established through single crystal X-ray diffraction of **1***a* and by infrared, ^{1}H, and ^{13}C nuclear magnetic resonance spectroscopies. Thermolysis of **1** at 100°C, in benzene containing dimethyl acetylenedicarboxylate, afforded spiro-fused β-lactam cyclopropene **12** in 33% yield. Similar thermolysis of **1***b* in the presence of ethyl phenylpropiolate gave spiro-fused β-lactam cyclopropene **13** (32%). The molecular structure of **12**, determined by single crystal X-ray diffraction, has the two ester carbonyl carbons out of the plane of the cyclopropene ring by about 0.17 Å, indicating substantial nonbonded steric interactions and suggesting unusually high strain energy. At 154.5°C, **12** underwent isomerization to **19**, presumably through a vinyl carbene intermediate.

MICHEL ZOGHBI et JOHN WARKENTIN. Can. J. Chem. **70**, 2967 (1992).

On a préparé les Δ^3-1,3,4-oxadiazolines (**1**) qui partagent leur carbone-2 avec le carbone-4 d'un cycle β-lactame pour donner une fusion spiro. On a déterminé leurs structures par diffraction des rayons X par un cristal unique de **1** et par spectroscopies infrarouge et résonance magnétique nucléaire du ^{1}H et du ^{13}C. La thermolyse de **1**, à 100°C, dans du benzène contenant de l'acétylènedicarboxylate de diméthyle, fournit le cyclopropène spiro-condensé à un β-lactame, **12**, avec un rendement de 33%. Une thermolyse semblable de **1***b* en présence de phénylpropiolate d'éthyle conduit au cyclopropène spiro-condensé à un β-lactame, **13**, avec un rendement de 32%. La structure moléculaire de **12**, déterminée par diffraction des rayons X par un cristal unique, montre que les carbones des deux groupes carbonyles des esters sont à 0,17 Å du plan du cyclopropène, indiquant qu'il existe des interactions stériques non-liées importantes et suggérant la présence d'une énergie de tension anormalement élevée. À 154,5°C, le composé **12** s'isomérise en **19**, probablement par l'intermédiaire d'un carbène vinylique.

[Traduit par la rédaction]

Introduction

Recently we reported the preparation and thermolysis of some spiro β-lactam oxadiazolines, **1** (1). Such compounds undergo thermal decomposition to afford β-lactam-4-ylidene intermediates (**2**) that can be trapped by intermolecular cycloaddition to alkenes and alkynes (1). The product from reaction with an alkyne (Scheme 1) is a novel species (**3**) embodying not only the ring strains of a β-lactam and a cyclopropene but also the additional strain engendered by virtue of the spiro ring fusion. The latter feature prevents the bond angle between substituents at the tetracoordinate carbon of the cyclopropene from adopting the large value characteristic of small ring compounds.

We now report details of the synthesis and characterization of two compounds of the families **1** and **3** and the thermolysis chemistry of one of the spiro β-lactam cyclopropenes (**3**).

Methods, results, and discussion

Spiro β-lactam oxadiazolines **1***a* and **1***b* were prepared by the route outlines in Scheme 2. The preparation of 4-substituted ketone semicarbazones, including **4**, has been described (2) and their cyclization by oxidizing agents, including Pb^{IV}, to 2-imino-Δ^3-1,3,4-oxadiazolines (e.g., **5**) is well known (2, 3). Only the *Z* isomers of **5** were obtained, as shown in Scheme 2 (3*a*, 4). On treatment with diphenylacetyl chloride and triethylamine at −20°C, **5***a* was converted to **1***a* in 90% yield. Similarly, **5***b* afforded **1***b* in 80% yield.

While the structures of **1***a* and **1***b* could be inferred from their infrared and nmr spectra, an unequivocal proof of the connectivity was needed to rule out isomeric structures as well as compounds derived from **1** through loss of N_2. To that end, the structure of **1***a* was confirmed by X-ray diffraction. The main features of the molecular structures are illustrated in Fig. 1.[2] Bond lengths and bond angles for the β-lactam ring of **1***a* are not significantly different from those reported (4) for 1-(2-bromophenyl)-azetidinone.

Oxadiazoline **1***a* is stable at room temperature but it decomposes in benzene solution at 100°C (sealed tube) with a half-life of 41 min. Its decomposition was followed conveniently by ^{1}H nmr spectroscopy, which showed the decay of the methyl singlets of **1***a* (δ = 1.42 and 1.44) and the growth of the singlet from acetone at δ = 1.95, relative to the internal toluene reference signal at δ 2.50. By analogy to the mechanism of thermolysis of other Δ^3-1,3,4-oxadiazolines (5, 6) we propose that the first step is a concerted, suprafacial, 1,3-dipolar cycloreversion to N_2 and a carbonyl ylide (**6**), Scheme 3. Again, on the basis of analogy, **6** might be expected to undergo 1,4-sigmatropic rearrangement to **7** (7, 8), electrocyclization to oxirane **8** (9–11), and fragmentation to carbonyl compounds and carbenes (8, 9, 12), Scheme 3. Compound **7**, which should be stable under the reaction conditions, was not detectable by ^{1}H nmr spectroscopy. Oxirane **8**, which might survive at 100°C, was also not observed. Oxiranes spiro-fused to C4 of a β-lactam ring have not been reported, to the best of our knowledge, but a thiirane analogue is known (13). Imide **10** was not obtained either, nor was there any evidence for the formation of propene, the expected product from fast rearrangement of 2-propylidene (**11**) (12*b*). On the other hand, the high yield of acetone (>95%) implies that **6** fragments rapidly, and essentially unidirectionally, to **9** and acetone. That fragmen-

[1]Author to whom correspondence may be addressed.

[2]Full details of the crystal and molecular structure will be published elsewhere.

Can. J. Chem. Downloaded from www.nrcresearchpress.com by 88.255.202.194 on 09/08/12
For personal use only.

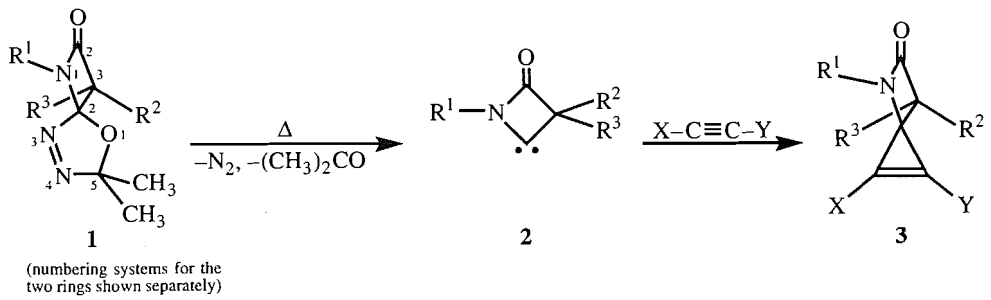

SCHEME 1

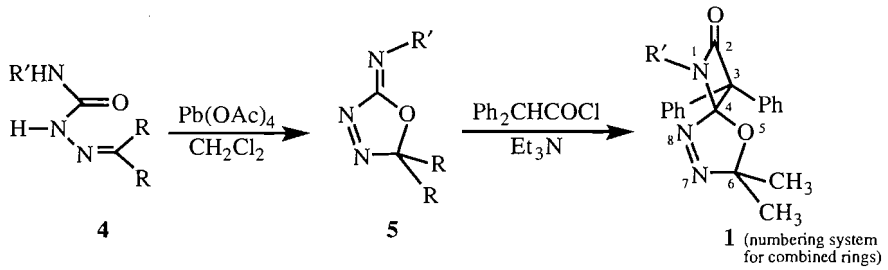

(*a*: R = CH_3, R′ = Ph; *b*: R = CH_3, R′ = CH_2Ph; *c*: R = p-C_6H_4Br; *d*: R = R′ = Ph; *c* and *d* apply to **4** and **5** only)

SCHEME 2

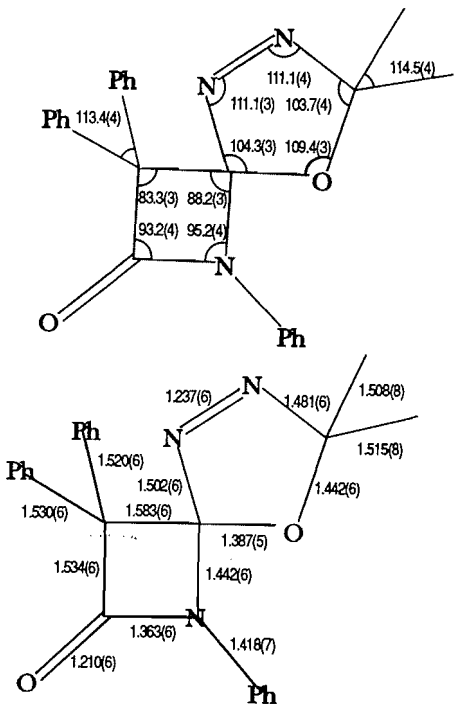

FIG. 1. Selected bond angles (deg) and bond lengths (Å) for spiro-β-lactam oxadiazoline **1***a*, with estimated standard deviations in parentheses.

tation, potentially reversible (12*b*), is presumably driven by two factors. First, **6** is heavily substituted in the β-lactam ring and must be twisted out of the planar conformation (14) to accommodate nonbonded interactions. Such twisting must reduce the bond order of at least one of the ylide O—C bonds. Second, the higher ground state energy of **6** is complemented by enhanced transition state stabilization from partial formation of the strong carbonyl double bond and a singlet aminocarbene (**9**).

Ylidene **9** probably undergoes a number of unimolecular reactions as well as reactions with **1***a* and with itself in the absence of good carbenophiles. The numerous products from thermolysis of **1***a* in benzene were not characterized[3] because of our greater interest in trapping **9** by cycloaddition.

Thermolysis of **1***a* at 100°C in benzene containing dimethyl acetylenedicarboxylate (3.1 M) and of **1***b* in the presence of ethyl phenylpropiolate (3.0 M) afforded **12** and **13** in 33 and 32% yields, respectively (Scheme 4). Both were characterized by means of ir spectroscopy, ^{13}C nmr spectroscopy, and mass spectrometry. A single crystal of **12** was used to confirm its structure, by X-ray diffraction.

Major aspects of the molecular structure of **12** are shown in Fig. 2.[2] The most striking feature is the distortion of the bonds holding the ester groups to the cyclopropene ring. The carbonyl carbons of these ester groups are out of the cyclopropene ring plane (0.180 Å for one, 0.155 Å for the other) in the direction toward the lactam nitrogen, as emphasized in the drawing (Fig. 2). Presumably nonbonded repulsions between those ester groups and the phenyl groups at C6 are responsible.

Thermolysis of **12** at 154.5°C in benzene afforded a product to which structure **19** could be assigned. Formation of **19** can be rationalized as depicted in Scheme 5. The well-known ring opening of cyclopropenes to vinyl carbenes (15) is the first step, forming **17** and its geometric isomer, not shown. Both carbenes presumably revert to **12** (15*a*) but **17**

[3]Except to exclude **7**, **8**, and **10** as reaction products and to confirm that a major product was acetone.

Can. J. Chem. Downloaded from www.nrcresearchpress.com by 88.255.202.194 on 09/08/12
For personal use only.

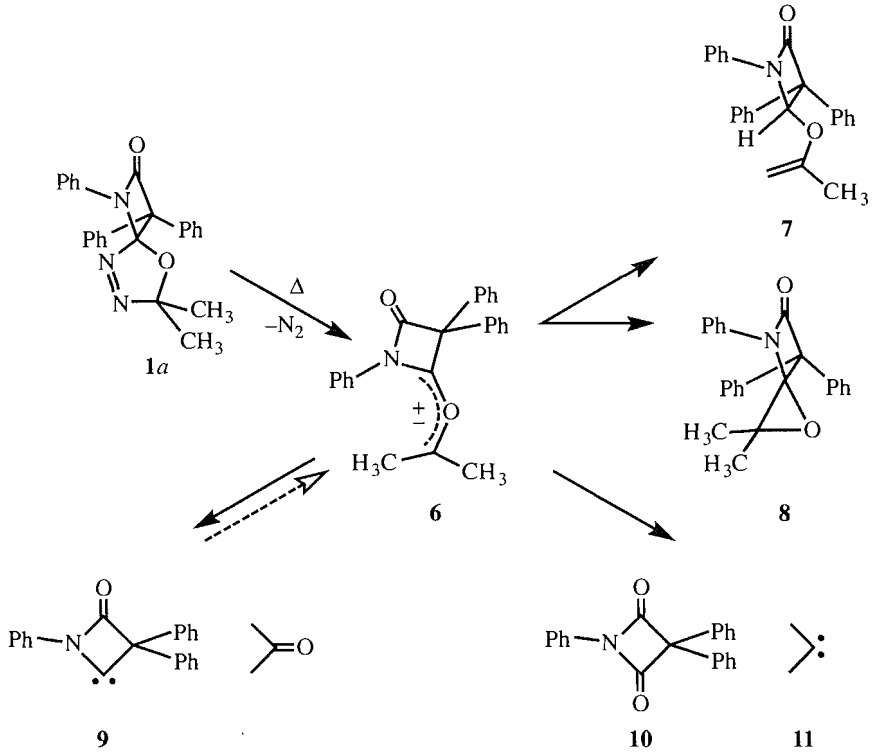

SCHEME 3

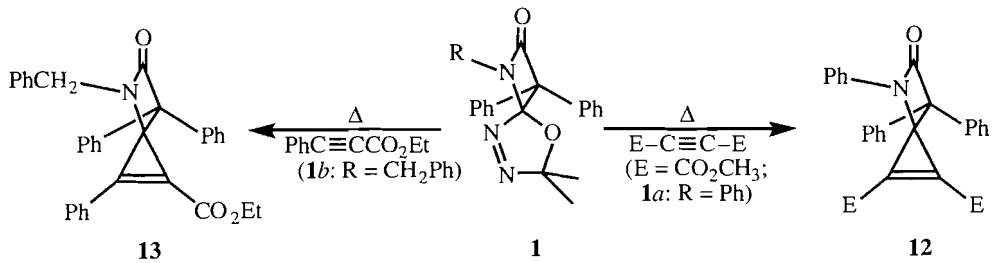

SCHEME 4

also inserts into a phenyl CH bond to form **18**, which undergoes allylic rearrangement to the more stable **19**. That carbene attack had occurred on a *C*-phenyl and not on the *N*-phenyl group was clear from the mass spectrum, which did not contain the signal for diphenylketene radical cation characteristic of **1**, **12**, and **13**. The infrared spectrum showed that the β-lactam ring had remained intact (1810 cm^{-1}) and both the uv spectrum as well as the ^1H and ^{13}C nmr spectra indicated that the product cannot have structure **18**. Although **18** would appear to be a necessary intermediate, isomerization to the more stable **19** is not surprising given that the H moiety that migrates is allylic, benzylic, and ester-activated in **18**.

Experimental

2-Phenylimino-5,5-dimethyl-Δ^3-1,3,4-oxadiazoline, **5**a, *and 2-benzylimino-5,5-dimethyl-Δ^3-1,3,4-oxadiazoline,* **5**b

These compounds were prepared from the appropriate 4-substituted semicarbazones of acetone as described in the literature (2).

*1,7,8-Triaza-6,6-dimethyl-5-oxa-2-oxo-1,3,3-triphenyl-spiro[3.4]oct-7-ene (**1**a)*

To a solution of **5***a* (0.96 g, 2.5 mmol) and triethylamine (6.0 mmol) in dry methylene chloride (20 mL) under nitrogen at ca. −23°C was added, drop by drop, a solution of diphenylacetyl chloride (0.69 g, 3.0 mmol) in dry methylene chloride (10 mL). The cold solution was stirred during the addition and, thereafter, overnight after the cold bath had been removed. The solution was washed with saturated sodium bicarbonate solution and with brine and the aqueous layers were extracted twice with methylene chloride. The combined organic layers were dried over $MgSO_4$. Filtration and evaporation of the solvent afforded β-lactam **1***a* in nearly pure form. Centrifugal chromatography (Chromatotron, 2-mm silica-coated plate, elution with ether (1 part) in hexanes (4 parts)) afforded pure **1***a* (90%), mp 154°C; ir (KBr) cm^{-1}: 1770 (C=O), 1595 (N=N); ^1H nmr (500 MHz, $CDCl_3$) δ: 1.38 (s, 3H), 1.39 (s, 3H), 7.10–7.50 (m, 15H); ^{13}C nmr (126 MHz, $CDCl_3$) δ: 24.30 (CH_3), 24.40 (CH_3), 76.13 (C3), 122.61 (C6), 125.17 (C4), 123.27, 127.57, 128.02, 128.33, 128.42, 128.69, 128.75, 129.39 (8 aryl CH), 133.38 (C1 of Ar), 134.61 (C1 of Ar), 136.39 (N-C1 of Ar), 166.80 (C=O); ms (ei, low resolution) *m/z*: 355 (M − N_2, 1%), 269 (M − N_2 − C_3H_6O, 68%), 236 (M − N_2 − PhNCO, 7%),

Can. J. Chem. Downloaded from www.nrcresearchpress.com by 88.255.202.194 on 09/08/12
For personal use only.

Can. J. Chem. Downloaded from www.nrcresearchpress.com by 88.255.202.194 on 09/08/12
For personal use only.

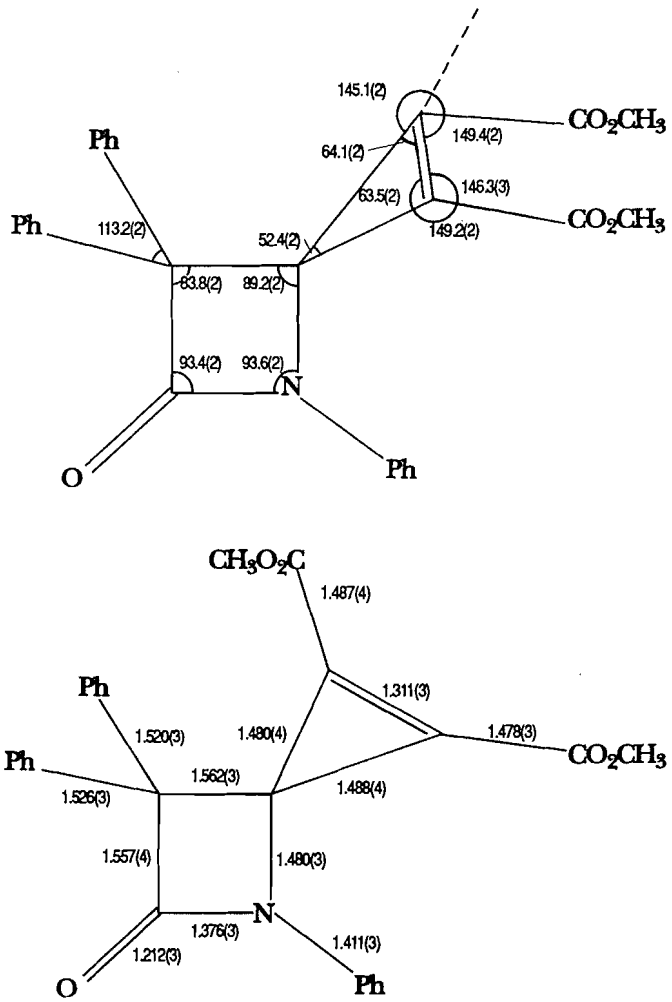

FIG. 2. Selected bond angles (deg) and bond lengths (Å) for spiro-β-lactam cyclopropene **12**, with estimated standard deviations in parentheses.

194 (Ph_2CCO, 60%), 119 (PhNCO, 35%), 165 ($C_{13}H_9$ = 9-fluorenyl, 100%); ms(ci, NH_3) *m/z*: 384 (M + 1, 100%); structure confirmed by single crystal X-ray diffraction.

*1,7,8-Triaza-1-benzyl-6,6-dimethyl-5-oxa-2-oxo-3,3-diphenylspiro[3.4]oct-7-ene (**1**b)*

The procedure described above gave, from **5***b* and diphenylacetyl chloride, spiro-β-lactam oxadiazoline **1***b* in 80% yield as a white solid, mp 101–102°C; ir (KBr) cm^{-1}: 1770 (C=O), 1600 (N=N); ^1H nmr (500 MHz, $CDCl_3$) δ: 1.35 (s, 3H), 1.45 (s, 3H), 4.53 (d, *J* = 15 Hz, 1H), 4.66 (d, *J* = 15 Hz, 1H), 7.20–7.55 (m, 15H); ^{13}C nmr (126 MHz, $CDCl_3$) δ: 24.32 (CH_3), 24.67 (CH_3), 76.03 (C3), 122.31 (C6), 124.82 (C4), 127.65, 127.80, 128.00, 128.36, 128.41, 128.60, 128.73 (7 aryl CH), 135.13 (C1 of Ar), 135.36 (C1 of Ar), 136.80 (C1 of Ar), 168.53 (CO); ms (ei) *m/z*: 397 (M, 3%), 341 (M − N_2 − CO, 11%), 265 (9%), 236 (18%), 194 (Ph_2CCO, 100%), 165 ($C_{13}H_9$, 9-fluorenyl, 83%), 132 (30%), 91 ($PhCH_2$, 87%); ms (ci, NH_3) *m/z*: 415 (M + NH_4, 28%), 398 (M + 1, 100%), 360 (11%), 345 (27%), 302 (71%), 267 (20%), 206 (32%), 194 (Ph_2CCO, 17%), 167 (43%), 108 (15%), 99 (40%).

*Thermolysis of β-lactam oxadiazolines in presence of alkynes. Preparation of **12** and **13***

For the preparation of **12**, a solution of spiro-β-lactam oxadiazoline **1***a* (0.038 g, 0.10 mmol) and dimethyl acetylenedicarboxylate (0.14 g, 1.0 mmol) in benzene (0.25 mL), in a medium-walled nmr tube sealed to a ground glass joint, was degassed by means of three freeze–pump–thaw cycles at 10^{-2} Torr (1 Torr = 133.3 Pa). The tube was sealed and immersed in an oil bath, maintained at 100 ± 0.2°C, for 10 h. Bulb-to-bulb transfer of the excess alkyne and benzene (vacuum line) left a residue that was chromatographed on silica (Chromatotron, 2-mm plate) using ether (25%) in hexane for elution.

Compound **13** was prepared by the same procedure, from **1***b* and ethyl phenylpropiolate.

*4-Aza-1,2-bis(methoxycarbonyl)-5-oxo-4,6,6-triphenylspiro[2.3]hex-1-ene (**12**)*

Yellow solid, 33% yield; mp 128–129°C; ir (KBr) cm^{-1}: 1720, 1730 (2 × CO, ester), 1750 (CO, lactam); uv (CH_2Cl_2), λ_{max}: 248 nm (log ε = 4.32); ^1H nmr (500 MHz, $CDCl_3$), δ: 3.75 (s, 6H), 7.11–7.46 (m, 15H); ^{13}C nmr (126 MHz, $CDCl_3$) δ: 53.43 (OCH_3), 64.13 (C3 or C6), 66.03 (C6 or C3), 119.81 (C1, C2); 125.55, 127.24, 127.79, 128.02, 128.53, 129.46 (6 aryl C), 135.82 (N − C1, Ar), 137.00 (2C1, Ar), 158.33 (2CO, ester), 167.63 (CO, lactam); ms (EI) *m/z*: 439 (M, trace), 411 (M − CO, 11%), 379 (13%), 348 (18%), 320 (M − PhNCO, 100%), 293 (24%), 249 (13%), 178 (31%), 165 ($C_{13}H_9$ = 9-fluorenyl, 73%), 119 (PhNCO, 15%), 77 (47%), ms (CI, NH_3), *m/z*: 457 (M + NH_4, 16%), 440 (M + 1, 100%), 410 (23%), 382 (5%), 352 (6%), 323 (7%), 294 (6%), 246 (5%), 167 (28%), 119 (10%), 94 (12%); confirmation of structure by single crystal X-ray diffraction.

*4-Aza-4-benzyl-1-ethoxycarbonyl-5-oxo-2,6,6-triphenylspiro[2.3]hex-1-ene (**13**)*

Yellow oil, 35% yield; ir (film) cm^{-1}: 1710 (CO, ester), 1745 (CO, lactam); ^1H nmr (200.1 MHz, $CDCl_3$) δ: 1.26 (t, *J* = 7.2 Hz, 3H), 4.04–4.41 (m, 4H, CH_2Ph and CH_2CH_3), 701–7.46 (m, 20H); ^{13}C nmr (50.32 MHz, $CDCl_3$) δ: 14.08 (CH_3), 43.02 ($PhCH_2$), 60.92 (C6), 61.45 (OCH_2), 70.97 (C3), 112.51 (C1), 125.00 (C2); 127.16, 127.29, 127.32, 127.50, 127.67, 128.29, 128.35, 128.56, 128.69, 131.50, 131.70, (11 aryl C); 135.97, 137.24, 138.20, 138.69 (4 × C1 of Ar), 159.46 (CO, ester), 169.55 (CO, lactam); ms (EI), *m/z*: 485 (M, 6%), 457 (M − CO, 9%), 384 (M − CO − CO_2Et, 7%), 352 (M − $PhCH_2NCO$, 19%), 322 (12%), 194 (Ph_2CCO, 11%), 165 ($C_{13}H_9$ = 9 − fluorenyl, 27%), 133 (Ph-CH_2NCO, 29%), 105 (22%), 91 ($PhCH_2$, 100%); ms (CI, NH_3), *m/z*: 503 (M + NH_4, 3%), 486 (M + 1, 100%), 353 (M − Ph-CH_2NCO − H, 5%), 167 (17%), 108 (18%), 91 (20%); ms (HR), *m/z*: calcd. for $C_{33}H_{27}NO_3$: 485.1991; found: 485.2000.

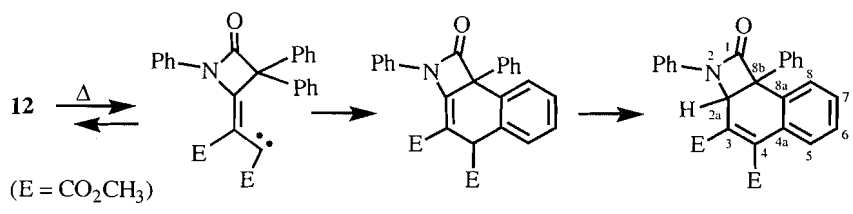

SCHEME 5

*3,4-bis(Methoxycarbonyl)-2,8b-diphenyl-2a,8b-dihydro-[2,1-b]azet-1(2H)one (**19**)*

Thermolysis of **12** (0.86 g, 1.95 mmol) was carried out in dry degassed benzene (5 mL) in a sealed tube. The tube was heated with refluxing anisole (154°C). After about 3 min the solution turned from pale yellow to dark green but the yellow colour returned on cooling the contents of the tube to room temperature. After 4 h of heating, the green colour, presumably from a reactive intermediate, faded, and the solution was again yellow. After heating for 4 additional hours the tube was opened, the solvent was evaporated, and the residue was examined by tlc to reveal two fluorescent spots and some highly polar material. Centrifugal chromatography (Chromatotron, 2-mm silica plate) using ether (25%) in hexane gave the least polar fluorescent material as a white solid, mp 165–166°C, in 25% yield; ir (KBr) cm^{-1}: 1685 (C=C), 1712 (CO, ester), 1732 (CO, ester), 1810 (CO, lactam); uv (λ_{max}, CH_2Cl_2) nm: 232 (log ε = 4.16), 258 (log ε = 4.05); ^1H nmr (200.1 MHz, $CDCl_3$) δ: 3.50 (s, 3H, OMe), 3.73 (s, 3H, OMe), 4.96 (s, 1H, CH), 7.22–7.56 (m, 14H); ^{13}C nmr (126 MHz, $CDCl_3$) δ: 44.11 (C2a), 51.11 (OMe), 52.74 (OMe), 78.12 (+ve, C8b), 98.87 (+ve, C3), 121.16 (+ve, Ar), 117.18 to 130.94 (series of 10 −ve Ar peaks), 130.26 (+ve, C4), 135.18 (+ve, Ar), 135.69 (+ve, Ar), 150.64 (+ve, C4a), 164.70 (+ve, CO), 165.41 (+ve, CO), 171.89 (+ve, CO lactam; ms (EI), *m/z*: 439 (M, 3%), 411 (M − CO, 5%), 380 (M − CH_3CO_2, 26%), 352 (M − CO − CH_3CO_2, 100%), 320 (M − PhNCO, 38%), 291 (15%), 160 (8%), 84 (35%); ms (CI, NH_3), *m/z*: 457 (M + NH_4, 100%), 440 (M + 1, 40%), 412 (M + 1 − CO, 40%), 380 (22%), 352 (40%), 320 (9%),; ms (HR), *m/z*: calcd. for $C_{27}H_{21}NO_5$: 439.1420; found: 439.1418.

Acknowledgements

This work was supported by the Natural Sciences and Engineering Research Council of Canada. We thank Dr. C. S. Frampton for the X-ray crystallography.

1. M. Zoghbi and J. Warkentin. J. Org. Chem. **56**, 3214 (1991).
2. A. M. Cameron, P. R. West, and J. Warkentin. J. Org. Chem. **34**, 3230 (1969).
3. (*a*) S. L. Lee, G. B. Gubelt, A. M. Cameron, and J. Warkentin. Chem. Commun. 1074 (1970); (*b*) S. L. Lee, A. M. Cameron, and J. Warkentin. Can. J. Chem. **50**, 2326 (1972); (*c*) J. K. Landquist. J. Chem. Soc. C, 63 (1970); (*d*) J. Chem. Soc. C, 323 (1970); (*e*) A. R. Katritzky, H. M. Faid-Allah, H. Aghabozorg, and G. R. Palenik. Chem. Scr. **23**, 134 (1984).
4. A. Prakash, C. Calvo, A. M. Cameron, and J. Warkentin. J. Cryst. Mol. Struct. **3**, 71 (1973).
5. H. Fujiwara, R. L. Varley, and J. M. van der Veen. J. Chem. Soc. Perkin Trans. 2, 547 (1977).
6. M. Békhazi, P. J. Smith, and J. Warkentin. Can. J. Chem. **62**, 1646 (1982).
7. M. W. Majchrzak and J. Warkentin. Can. J. Chem. **67**, 1753 (1989).
8. A. P. Hitchcock, S. Zweep, T. Steel, M. Békhazi, and J. Warkentin. Can. J. Chem. **60**, 2914 (1982).
9. (*a*) M. Békhazi and J. Warkentin. Can. J. Chem. **61**, 619 (1983); (*b*) H. Tomioka, T. Miwa, S. Suzuki, and T. Izawa. Bull. Chem. Soc. Jpn. **53**, 753 (1980); (*c*) N. Shimizu and P. D. Bartlett. J. Am. Chem. Soc. **100**, 4260 (1978).
10. P. C. Wong, D. Griller, and J. C. Scaiano. J. Am. Chem. Soc. **104**, 6631 (1982).
11. R. Huisgen. Angew. Chem. Int. Ed. Engl. **16**, 572 (1977).
12. (*a*) M. Békhazi and J. Warkentin. J. Am. Chem. Soc. **103**, 2473 (1981); (*b*) J. Am. Chem. Soc. **105**, 1289 (1983); (*c*) M. Békhazi, P. A. Risbood, and J. Warkentin. J. Am. Chem. Soc. **105**, 5675 (1983); (*d*) D. Keus, M. Kaminski, and J. Warkentin. J. Org. Chem. **49**, 343 (1984).
13. (*a*) I. Yamamoto, I. Abe, M. Mozawa, J. Motoyoshiya, and H. Gotoh. Synthesis, 813 (1981); (*b*) I. Yamamoto, I. Abe, M. Mozawa, M. Kotani, J. Motoyoshiya, H. Gotoh, and K. Matsuzaki. J. Chem. Soc. Perkin Trans. 1, 2297 (1983).
14. K. N. Houk, N. S. Rondan, C. Santiago, C. J. Gallo, R. Gandour, and G. W. Griffin. J. Am. Chem. Soc. **102**, 1504 (1980).
15. (*a*) E. J. York, W. Dittmar, J. R. Stevenson, and R. G. Bergman. J. Am. Chem. Soc. **95**, 5680 (1973); (*b*) J. A. Pincock, R. Morchat, and D. R. Arnold. J. Am. Chem. Soc. **95**, 7536 (1973); (*c*) J. A. Pincock and R. J. Boyd. Can. J. Chem. **55**, 2482 (1977); (*d*) M. G. Steinmetz, R. Srinivasan, and W. J. Leigh. Rev. Chem. Intermed. **5**, 57 (1984); (*e*) I. D. Domnin, J. Kopf, S. Keyaniyan, and A. De Meijere. Tetrahedron, **41**, 5377 (1985); (*f*) J. Al-Dulayymi, M. S. Baird, and H. H. Hussein. Tetrahedron Lett. **30**, 2009 (1989); (*g*) A. Padwa, U. Chiacchio, Y. Garreau, J. M. Kassir, K. E. Krumpe, and A. M. Shoffstall. J. Org. Chem. **55**, 414 (1990).

Can. J. Chem. Downloaded from www.nrcresearchpress.com by 88.255.202.194 on 09/08/12
For personal use only.

Cycloaddition reactions of $SNSAsF_6$ with aryl nitriles and diphenylacetylene; the preparation and characterization of aryl 1,3,2,4- and 1,2,3,5-dithiadiazole radicals

JACK PASSMORE,[1] XIAOPING SUN, AND SIMON PARSONS
Department of Chemistry, University of New Brunswick, Bag Service no. 45222, Fredericton, N. B., Canada E3B 6E2

Received June 2, 1992

JACK PASSMORE, XIAOPING SUN, and SIMON PARSONS. Can. J. Chem. **70**, 2972 (1992).

The SNS^+ cation (in $SNSAsF_6$) underwent symmetry-allowed concerted cycloadditions with the aryl nitriles RCN (R = 2,5-$Me_2C_6H_3$, Ph, *p*-$O_2NC_6H_4$, and 3,5-$(O_2N)_2C_6H_3$) and diphenylacetylene. The cycloadducts $RCNSNSAsF_6$ (R = 2,5-$Me_2C_6H_3$, Ph, *p*-$O_2NC_6H_4$, and 3,5-$(O_2N)_2C_6H_3$) and $PhCSNSCPhAsF_6$ were characterized by elemental analyses and IR and NMR (^1H, ^{13}C, ^{14}N) spectroscopies. The reduction of $RCNSNS^+$ gave the corresponding 1,3,2,4-dithiadiazoles RCNSNS·, which in turn rearranged to the corresponding 1,2,3,5-dithiadiazoles RCNSSN·. The rate of this rearrangement was correlated with the ionization potentials of the corresponding nitriles. The radicals RCNSNS· (R = Ph, *p*-$O_2NC_6H_4$) were isolated as pure compounds, and characterized by mass spectrometry, IR, FT-Raman, and ESR spectroscopies. The reduction of $PhCSNSCPh^+$ led to neutral radical PhCSNSCPh·, which is stable in solution up to ca. 0.5 M, but decomposes at higher concentrations.

JACK PASSMORE, XIAOPING SUN et SIMON PARSONS. Can. J. Chem. **70**, 2972 (1992).

Le cation SNS^+ (du $SNSAsF_6$) donne des cycloadditions concertées, permises par la symétrie, avec les nitriles aromatiques RCN (R = 2,5-$Me_2C_6H_3$, Ph, *p*-$O_2NC_6H_4$ et 3,5-$(O_2N)_2C_6H_3$) et le diphénylacétylène. On a caractérisé les cycloadduits $RCNSNSAsF_6$ (R = 2,5-$Me_2C_6H_3$, Ph, *p*-$O_2NC_6H_4$ et 3,5-$(O_2N)_2C_6H_3$) et $PhCSNSCPhAsF_6$ grâce aux analyses élémentaires et par spectroscopies IR et RMN du ^1H, du ^{13}C et du ^{14}N. La réduction des cations $RCNSNS^+$ fournit les 1,3,2,4-dithiadiazoles RCNSNS· correspondants qui, à leur tour, se réarrangent en 1,2,3,5-dithiadiazoles RCNSSN· correspondants. Il existe une corrélation entre la vitesse de cette transformation et les potentiels d'ionisation des nitriles correspondants. On a isolé les radicaux RCNSNS· (R = Ph, *p*-$O_2NC_6H_4$) à l'état pur et on les a caractérisé par spectrométrie de masse et par spectroscopie IR, Raman-TF et RPE. La réduction du cation $PhCSNSCPh^+$ conduit au radical neutre PhCSNSCPh· qui est stable en solution jusqu'à une concentration d'environ 0,5 M; toutefois, à des concentrations plus élevées, il se décompose.

[Traduit par la rédaction]

Introduction

We previously showed (1–5) that SNS^+ (as the AsF_6^- salt) undergoes extensive, quantitative, symmetry-allowed cycloaddition reactions with aliphatic alkynes, nitriles, alkenes, and SN^+. In this paper we report the cycloaddition reactions of SNS^+ with aryl nitriles and diphenylacetylene, which give $RCNSNSAsF_6$ (R = 2,5-$Me_2C_6H_3$, Ph, *p*-$O_2NC_6H_4$, and 3,5-$(O_2N)_2C_6H_3$) and $PhCSNSCPhAsF_6$. The quantitative kinetic aspects of these reactions have been reported elsewhere (5).

Reduction of the alkyl derivatives of $RCNSNS^+$ led to the corresponding neutral 7π radicals RCNSNS·, but at higher concentrations RCNSNS· rearranged to the thermodynamically more stable 7π radicals RCNSSN· (2, 6, 7). However, we were able to isolate small amounts of CH_3CNSNS· at low temperature (6) and the paramagnetic liquid Bu^{t}CNSNS· in the dark (7). Since then, some related diradicals have been prepared (8). We were interested in understanding RCNSNS· and its novel rearrangement to RCNSSN·. Therefore we attempted the preparation and isolation of the aryl derivatives of RCNSNS· and investigated the dependence of the rearrangement rate on the nature of the substituent. The results are reported below.

Reduction of alkyl derivatives of $R'CSNSCR''^+$ in dilute solution gave the corresponding 7π radicals R′CSNSCR″· (1, 9). At higher concentrations a large number of diamagnetic products were detected (1, 9), except in the case of $CF_3CSNSCCF_3$, which was isolated as a thermally stable green liquid under a blue gas (10). Since then NCCSNSCCN· has been prepared (11) by a different route. The related radical benzo-1,3,2-dithiazole is stable (12), as well as other more complex derivatives (e.g., benzobisdithiazole) (13). The preparation of PhCSNSCPh· in solution at high concentration and a study of its stability is reported below.

Experimental

Unless otherwise specified, reagents and techniques used are as described in ref. 5. The purity of the reagents RCN (R = 2,5-$Me_2C_6H_3$, Ph, *p*-$O_2NC_6H_4$, and 3,5-$(O_2N)_2C_6H_3$) and PhCCPh (Aldrich Chemical Company) was established by their infrared and NMR (^1H, ^{13}C and ^{14}N) spectra. $SNSAsF_6$ and $H_2CSNSCH_2AsF_6$ were prepared as described (3, 14). The multinuclear NMR (^1H, ^{13}C, ^{14}N) spectra were obtained as described (15). IR spectra were obtained as Nujol mulls with KBr plates in the 4000–200 cm^{-1} region using a Perkin–Elmer 683 IR spectrometer. ESR spectra were recorded at room temperature with a locally modified version of the Varian E-4 spectrometer using DPPH as a field marker. The FT-Raman spectra were acquired on solid samples in a 5-mm NMR

[1]Author to whom correspondence may be addressed.

Can. J. Chem. Downloaded from www.nrcresearchpress.com by 88.255.202.194 on 09/08/12
For personal use only.

TABLE 1. Data for the reactions of $SNSAsF_6$ with aryl nitriles or PhCCPh in liquid SO_2 at room temperature

Nitrile or PhCCPh (g, mmol)	$SNSAsF_6$ (g, mmol)	SO_2 (g)	Colour change	Apparent reaction time	Purified product: Appearance	Purified product: Weight (g, mmol)	Purified product: Isolated yield (%)	Impure fraction: Colour	Impure fraction: Weight (g)	Elemental anal. calcd. (top) obsd. (bottom): C (%)	H (%)	N (%)	S (%)
2,5-$Me_2C_6H_3CN$ (0.674,5.13)	1.39, 5.21	4.32	Clear yellow →orange	15 min	Orange crystals	1.55, 3.89	76	Yellow	0.38	27.2 27.3	2.3 2.4	7.0 7.0	16.1 16.3
PhCN (2.815,7.91)	2.13, 7.99	5.32	Clear yellow →dark green → brown	2 hrs	Bright yellow crystalline plates	2.51, 6.78	86	Green	0.324	22.7 22.9	1.4 1.4	7.6 7.8	17.3 18.1
P-$O_2NC_6H_4CN$ (1.07,7.24)	1.96, 7.32	5.58	Clear yellow →brown	20 hrs	Yellow crystals	2.66, 6.41	88	Brown	0.310	20.3 20.6	1.0 1.0	10.1 10.1	15.4 15.9
3,5-$(O_2N)_2C_6H_3CN$ (0.439,2.27)	0.687, 2.57	3.05	Clear yellow →brown	3 days	Yellow crystals	0.74, 1.61	71	Brown	0.27	18.3 18.4	0.66 0.73	12.2 12.2	13.9 14.0
PhC≡CPh (0.780,4.38)	1.20, 4.48	7.68	Clear yellow →black	3 min	Black powder	1.88, 4.22		Black		37.7 37.5	2.3 2.3	3.2 3.2	14.4 14.5

Can. J. Chem. Downloaded from www.nrcresearchpress.com by 88.255.202.194 on 09/08/12
For personal use only.

tube using the FT-IR spectrometer IFS 66 (Bruker) equipped with the FT-Raman accessory FRA 101 using the 1.064 μm exciting line of a Nd: YAG laser (70 mW; resolution: 2 cm^{-1}; 300 scans). The mass spectra were obtained at room temperature in the electron-impact mode using 70 eV ionizing voltage on a Kratos MS-50TC instrument.

All the reactions were performed in liquid SO_2 in a two-bulbed reaction vessel, incorporating a sintered glass frit and J. Young Teflon valve. ESR spectra were obtained using a rigorously dried 4-mm quartz tube connected via a J. Young valve. Reactions carried out *in situ* were quickly warmed up to room temperature to prevent tube breakage.

Preparation of aryl $\overline{RCNSNS}AsF_6$ *(R = 2,5-*$Me_2C_6H_3$*, Ph, p-*$O_2NC_6H_4$*, and 3,5-*$(O_2N)_2C_6H_3$*) and* $\overline{PhCSNSCPh}AsF_6$ *by the reactions of* $SNSAsF_6$ *with RCN or PhCCPh*

Liquid nitriles RCN (R = 2,5-$Me_2C_6H_3$ and Ph) were dissolved in SO_2, and the solutions poured onto $SNSAsF_6$; in the case of solid nitriles RCN (R = *p*-$O_2NC_6H_4$ and 3,5-$(O_2N)_2C_6H_3$) and PhCCPh, SO_2 was condensed onto the solid mixtures of $SNSAsF_6$ and the corresponding nitriles or PhCCPh at −196°C, and the mixtures warmed up to room temperature. These five reactions led to intensely coloured solutions as shown in Table 1. The colour change for 2,5-$Me_2C_6H_3CN$ and PhCCPh took place within the specified apparent reaction times (Table 1). In the case of PhCN, the first colour change from clear yellow to dark green took place quickly after the two reactants were mixed at room temperature, the second colour change from dark green to brown occurred in 2 h. For *p*-$O_2NC_6H_4CN$ and 3,5-$(O_2N)_2C_6H_3CN$, the colour change took place immediately with rapid dissolution of the nitriles after the reactants were mixed at room temperature. However, the $SNSAsF_6$ did not completely dissolve until the indicated reaction times (Table 1). All the products (except $\overline{PhCSNSCPh}AsF_6$) were recrystallized *in situ* as previously described (1, 5), giving purified crystals of $\overline{RCNSNS}AsF_6$ with different colours in the different yields (Table 1), which were characterized by chemical analyses (Table 1), IR (Table 2), and multinuclear NMR (Table 3). In the case of $\overline{PhCNSNS}AsF_6$, the trace amounts of dark green and brown impurities were removed by more than 10 recrystallizations, leading to a pure bright yellow product.[2] In other cases, fewer recrystallizations were needed to remove the intensely coloured impurities. The decomposition points of the first four products are all ca. 213 ± 3°C. The IR and ^1H NMR spectra of the impure fractions were identical to those of the corresponding pure fractions except that NH_4 peaks (only ca. 0.1 wt.%) were also observed in the ^1H NMR spectra (6.07 ppm, 1:1:1 triplet, $^1J(H-^{14}N)$ = 109.1 Hz) of the impure fractions. Traces of other impurities were not observed (^1H NMR) in reactions carried out *in situ*. The gross yields (pure + impure) for all the five preparations were higher than 95%.

The preparation of $\overline{PhCSNSCPh}AsF_6$ *by the reaction of PhCCPh with* $\overline{H_2CSNSCH_2}AsF_6$

SO_2 (5.35 g) was condensed onto a mixture of PhCCPh (0.089 g, 0.5 mmol) and $\overline{H_2CSNSCH_2}AsF_6$ (0.296 g, 1.0 mmol), giving a brown solution, which was stirred for 24 h. The volatiles were removed, leaving a brown solid (0.391 g) (^1H NMR in SO_2 with CH_2Cl_2 internal concentration standard: 7.8 ($\overline{PhCSNSCPh}^+$, multiplet, 10H), 3.7 and 3.1 ($S_2N(C_2H_4)_2^+$, d, *J* = 6.6 Hz, 8H). The brown solid was extracted four times with CH_2Cl_2 (4.66 g). After removal of the solvent it gave a brown soluble amorphous solid and a white insoluble solid (identified as $S_2N(C_2H_4)_2^+$ by IR). The brown solid was identified as $\overline{PhCSNSCPh}AsF_6$ by its IR spectrum: 1596(mw), 1578(w), 1496(mw), 1437(sh), 1421(m), 1311(vw), 1291(mw), 1181(w), 1151(w), 1095(w), 1088(sh), 1078(m), 1046(vw), 1032(vw), 1024(w), 1002(w), 969(w), 836(w), 794(m), 769(m), 757(ms), 690(s,$\nu_3AsF_6^-$), 679(sh), 669(sh), 626(w), 579(w), 541(w), 524(w), 464(w), 390(s,

[2] $\overline{PhCNSNS}AsF_6$ was simultaneously prepared elsewhere, but reported (16) to be green.

Can. J. Chem. Downloaded from www.nrcresearchpress.com by 88.255.202.194 on 09/08/12
For personal use only.

TABLE 2. The infrared spectral data for $R\overline{CNSNS}AsF_6$ (R = 2,5-$Me_2C_6H_3$ (*a*), Ph (*b*), *p*-$O_2NC_6H_4$ (*c*), and 3,5-$(O_2N)_2C_6H_3$ (*d*))[a]

a (cm^{-1})	*b* (cm^{-1})	*c* (cm^{-1})	*d* (cm^{-1})	Assignment
1612(w)	1620(w)	1609(m)	1632(s)	
1562(m)	1596(s)	1601(m)	1597(m)	
	1560(w)	1529(vs)	1493(w)	C=C stretch
1502(ms)	1494(w)	1499(m)		in aryl rings
		1425(s)	1406(m)	
1403(w)	1405(vs)	1402(s)	1365(w)	
	1345(w)	1355(vs)	1343(vs)	
		1324(s)	1321(m)	
	1327(w)	1307(w)		
1292(m)	1296(w)	1295(w)		
1235(w)	1212(w)	1250(vw)	1251(w)	C—H in-plane bend
1212(m)	1189(m)	1210(m)	1230(w)	in aryl rings
1166(w)	1169(w)	1188(m)	1131(m)*	*S—N asym. stretch[b]
1147(w)*	1101(w)	1123(m)*	1092(m)	
1033(w)	1074(w)*	1110(w)	1039(m)	
	1000(m)	1013(m)	1001(vw)	
977(ms)	986(s)	991(s)		
		980(vw)	945(w)	
934(w)	915(m)	922(m)	919(s)	
904(ms)	889(m)	888(m)	886(m)	-$\overline{CNSNS}^+$ ring
834(w)	840(w)	860(s)		vibrations
824(s)	798(s)	853(s)	836(m)	
815(w)		829(w)		
788(s)	773(vs)	804(s)	799(vs)	S—N sym stretch[b]
		752(m)	729(vs)	
		709(vs)	719(vs)	
694(vs,br)	700(vs,br)	693(vs,br)	689(vs,br)	$\nu_3AsF_6^-$
		683(w)		
675(w)	676(vs)	674(vs)	670(s)	$\nu_1AsF_6^-$
655(ms)	649(m)	623(s)	628(vs)	
640(w)	634(s)	596(ms)	585(w)	
587(m)	611(w)	575(m)		-$\overline{CNSNS}^+$ ring
521(m)	591(m)	535(w)		vibrations
465(w)	575(w)	474(w)	453(m)	
431(w)	440(m)	444(m)	425(w)	
397(vs)	339(vs)	400(vs)	395(vs)	$\nu_4AsF_6^-$

[a]Actual spectra deposited. See footnote 3.

[b]Based on the assignments of the symmetric stretches, the asymmetric stretches are then assigned according to Banister's equation (17) $\nu_{asym} = 1.51\ \nu_{sym} - 73.1$.

$\nu_4AsF_6^-$). The ^{13}C NMR spectrum of a similar reaction carried out in 1:1 stoichiometry in a 10-mm NMR tube showed resonances at 183.9, 134.4, 131.2, 130.3, 123.3 (Ph$\overline{CSNSC}Ph^+$, see Table 3); 132.5, 129.8, 129.7, 123.5, 91.5 (PhCCPh), and 46.8 ppm ($S_2N(C_2H_4)_2^+$ (3)).

The generation and ESR study of 4-aryl-1,3,2,4-dithiadiazoles $R\overline{CNSNS}\cdot$ *(R = 2,5-$Me_2C_6H_3$, Ph, p-$O_2NC_6H_4$, 3,5-$(O_2N)_2C_6H_3$)*

SO_2 (0.100 g) and $CFCl_3$ (0.500 g) were successively condensed onto a mixture of $R\overline{CNSNS}AsF_6$ (7 mg), $SbPh_3$ (7 mg), and NMe_4Cl (7 mg) in an ESR tube, giving a blue solution of $R\overline{CNSNS}\cdot$ ($(3.0 \pm 0.5) \times 10^{-2}$ M) at room temperature. A duplicate set of samples was also prepared. One set of the samples was continuously exposed to room light, while the other set was kept in the dark. ESR spectra of both sets of samples were recorded at room temperature once every 1 or 2 days until the rearrangement was completed as indicated by the yellow colour of all the solutions. The results are given in Table 4, and the data for the rearranged disulfides are given in Table 5.

ESR study of the rearrangement of $R\overline{CNSNS}\cdot$ *(R = 2,5-$Me_2C_6H_3$, Ph, p-$O_2NC_6H_4$, 3,5-$(O_2N)_2C_6H_3$) to* $R\overline{CNSSN}\cdot$ *in the solid state*

SO_2 (0.5 g) was condensed onto a solid mixture of $R\overline{CNSNS}AsF_6$ (7 mg), $SbPh_3$ (7 mg), and NMe_4Cl (7 mg) at −196°C. The samples were rapidly warmed up to room temperature and after 3 min the solvent was quickly removed under dynamic vacuum with solutions kept in the dark at all times. The solid mixtures (containing $R\overline{CNSNS}\cdot$) were exposed to room light for 1 or 2 days and then dissolved in a mixture of SO_2 (0.100 g) and $CFCl_3$ (0.500 g) (in the dark). Their ESR spectra were recorded immediately. The solvent was quickly removed (in the dark) and the above procedure was repeated on each of the samples until the rearrangement was completed. The spectral data are shown in Table 4.

Preparation of $R\overline{CNSNS}\cdot$ *(R = Ph, p-$O_2NC_6H_4$) by reduction of* $R\overline{CNSNS}^+$

$Ph\overline{CNSNS}\cdot$: SO_2 (6.30 g) was condensed onto the solid mixture of $Ph\overline{CNSNS}AsF_6$ (0.881 g, 2.38 mmol) and $Na_2S_2O_4$ (0.873

TABLE 3. The multinuclear NMR spectral[a] data for aryl $R\overline{CNSNS}^+$ and $Ph\overline{CSNSCPh}^+$

Compound	^{1}H NMR[a,b] δ (ppm) (relative intensity %)	^{13}C NMR δ (ppm) (No. of assigned C atom)[b]	^{14}N NMR[a] δ (ppm) ($\nu_{1/2}$ (Hz))
2,5-$Me_2C_6H_3\overline{CNSNS}^+$	8.15(23); H6 7.64(7), 7.60(16) } H3 7.55(20), 7.51(9) } H4 2.78(100); *o*-CH_3 2.45(90); *m*-CH_3	205.2(7),139.3(2),139.0(6) 138.8(5),134.(3),133.9(4) 125.8(1), 22.0(*o*-CH_3),20.2(*m*-CH_3)	−34(1750), N′, N″ a shoulder superimposed on the lower field side of the peak
$Ph\overline{CNSNS}^+$	8.38(m,90); H2, H6 7.97(m,55); H4 7.80(m,100); H3, H5	205.4(7),137.8(2,6),130.5(3,5) 129.8(4),125.0(1)	−46.4(750), N′ 20(560), N″
p-$O_2NC_6H_4\overline{CNSNS}^+$	AA′BB′ type 8.60(21), 8.55(100) } H2, H6 8.53(100), 8.48(21) } H3, H5	204.3(7),153.0(4),133.0(3,5) 130.9(1),126.2(2,6)	−13.9(280), N′, N″, NO_2 asymmetric peak
3,5-$(O_2N)_2C_6H_3\overline{CNSNS}^+$	AX_2 type 9.48(d, J_{42} = 1.9Hz,100); H2; H6 9.42(t, J_{24} = 1.9Hz,38); H4	202.1(7), 150.1(1),131.3(2,6) 128.6(3,5),126.2(4)	−19.5(190), N′, N″, NO_2 asymmetric peak
$Ph\overline{CSNSCPh}^+$	7.87(m), 10 H	184.1(7),134.7(4),131.6(3,5) 130.8(2,6),123.6(1)	No signal detected

[a]Actual spectra deposited (see footnote 3). The ^{1}H NMR spectra of the aryl derivatives of $R\overline{CNSNS}^+$ and $Ph\overline{CSNSCPh}^+$ exhibit complex second-order multiplets due to aryl ring protons with the exception of 3,5-$(O_2N)_2C_6H_3\overline{CNSNS}^+$, which has a simple AX_2 type of coupling between *ortho* and *para* protons. These spectra indicate that both H2, H6 and H3, H5 are equivalent, respectively. Correspondingly, the ^{13}C spectra show the equivalence between C2 and C6 and between C3 and C5 (except 2,5-$Me_2C_6H_3\overline{CNSNS}^+$). The results suggest that the aryl rings of all the cycloadducts can freely rotate about C—C single bonds in solution at room temperature.

[b]C7 stands for the carbon atoms in the -$\overline{CNSNS}^+$ or -$\overline{CSNSC}^+$- rings. The carbon and hydrogen atoms in the aryl rings are numbered in accordance with IUPAC rules as shown, e.g., for $Ph\overline{CNSNS}^+$ and $Ph\overline{CSNSCPh}^+$:

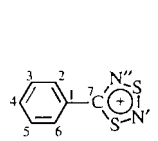

$Ph\overline{CNSNS}^+$

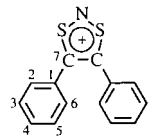

$Ph\overline{CSNSCPh}^+$

g, 5.01 mmol) at −196°C and then the reactants warmed up to room temperature and stirred overnight in the dark. The colour of the solution became near-black. The soluble material was poured through a frit into the other bulb and the SO_2 was removed by evacuation at −15°C. Black crystalline $Ph\overline{CNSNS}\cdot$ (0.375 g, 2.07 mmol) was recovered with a yield of 87%. IR:[3] 1597w, 1502vw, 1406vw, 1334w, 1227w, 1178w, 1152vw, 1099w, 1074w, 1056vw, 1027m, 1000w, 984w, 970w, 929m, 914m, 825w, 800w, 776s, 765s(sh), 757s, 705s, 680vs, 650m, 634m, 605w, 595m, 542w, 508m, 395s cm^{-1}. EI mass spectrum (*m/e* (int%)>7%): 181 (M^+, 70), 135 ($PhCNS^+$, 27), 103 ($PhCN^+$, 100), 78 (SNS^+, 47). ESR: identical to that of $Ph\overline{CNSNS}\cdot$ generated in 4-mm ESR tube *in situ* (see Table 4).

p-*$O_2NC_6H_4\overline{CNSNS}\cdot$*: SO_2 (12.9 g) was condensed onto the solid mixture of *p*-$O_2NC_6H_4\overline{CNSNS}AsF_6$ (1.288 g, 3.10 mmol), $SbPh_3$ (1.011 g, 2.86 mmol), and Me_4NCl (0.989 g, 9.02 mmol) at −196°C. The contents were warmed up to room temperature. The colour of the solution, which contained $SbPh_3Cl_2$ and Me_4NCl, became brown very quickly, and a black solid (insoluble in SO_2, $CFCl_3$, and C_6H_6) was formed. The reactants were stirred for 10 min at room temperature in the dark to allow the reduction to be completed, but to avoid any rearrangement taking place. The black powder was washed five times with SO_2 to remove the coloured solubles and then the colour of the solution became very light. The SO_2 was removed by evacuation and the black powdered *p*-$O_2NC_6H_4\overline{CNSNS}\cdot$ (0.589 g, 2.60 mmol) was recovered in the yield of 84%. IR:[3] 3100w, 3070w, 3053vw, 2722w, 2351vw, 1912vw, 1682vw, 1605ms, 1595ms, 1574w, 1524vs, 1503w, 1487w, 1408m, 1342vs, 1322m, 1310m, 1298w, 1227w, 1113m, 1105m, 1008w, 961w, 933ms, 855s, 850s, 824w, 792m, 751s, 705s, 683s, 651m, 613w, 592m, 542vw, 461m, 393vw cm^{-1}. FT-Raman:[3] 654.0vw, 721.9vw, 796.3s, 1105.3vw, 1181.6m, 1341.7w, 1405.7s, 1478.9m, 1506.5vs, 1515.4vs, 1595.5vs, 2392.6vw, 2819.0vw, cm^{-1}. EI mass spectrum (*m/e* (int%)>4%): 226 (M^+, 24.4), 180 ($M^+ - NO_2$, 5.4), 148 (*p*-$O_2NC_6H_4CN^+$, 4.2), 134 (*p*-$O_2NC_6H_4C^+$, 4.8), 102 ($C_6H_4CN^+$, 12.3), 78 (SNS^+, 100). Elemental anal. (%) calcd.: C 37.2, H 1.8, N 18.6, S 28.3; found: C 37.1, H 1.9, N 18.6, S 28.5. ESR: The spectrum was obtained in

[3]Actual spectrum deposited as supplementary data. Supplementary material mentioned in the text may be purchased from: The Depository of Unpublished Data, Document Delivery, CISTI, National Research Council Canada, Ottawa, Canada K1A 0S2.

Can. J. Chem. Downloaded from www.nrcresearchpress.com by 88.255.202.194 on 09/08/12
For personal use only.

TABLE 4. ESR spectral data of aryl RCNSNS· and their rearrangements in dilute solution and in the solid state

RCNSNS·	R			
	2,5-$Me_2C_6H_3$	Ph	p-$O_2NC_6H_4$	3,5-$(O_2N)_2C_6H_3$
Type of ESR spectrum	1:1:1 triplet	1:1:1 triplet	1:1:1 triplet	1:1:1 triplet
g	2.0048(2)	2.0068(3)	2.0066(2)	2.0060(4)
$a^{N'}$ (mT)	1.11(1)	1.10(3)	1.11(2)	1.11(1)
Rearrangement time[a] in solid state in light	5 days	>3 days	>3 days	>1 days
Rearrangement time[a] in $CFCl_3/SO_2$ in light	5–6 days	4 days	3 days	<1 days
Rearrangement time[a] in $CFCl_3/SO_2$ in the dark	No rearrangement	No rearrangement	>35 days	5 days
I.P. value (eV) of the corresponding RCN (5)	11.62	12.09	12.63	13.4

[a]Here rearrangement time indicates the period over which the above rearrangement of RCNSNS· to RCNSSN· was completed, i.e., RCNSNS· were not detectable by ESR even under high receiver gain.

TABLE 5. ESR spectral data of aryl RCNSSN·

RCNSSN·	R			
	2,5-$Me_2C_6H_3$	Ph[a]	p-$O_2NC_6H_4$	3,5-$(O_2N)_2C_6H_3$
Type of ESR spectrum	1:2:3:2:1 pentet	1:2:3:2:1 pentet	1:2:3:2:1 pentet	1:2:3:2:1 pentet
g	2.0113(3)	2.0110(4)	2.0111(3)	2.0102(3)
a^N(mT)	0.53(3)	0.51(2)	0.51(2)	0.50(2)

[a]Identical parameters to those in ref. 18.

Can. J. Chem. Downloaded from www.nrcresearchpress.com by 88.255.202.194 on 09/08/12
For personal use only.

saturated $CFCl_3$ solution at room temperature, and was identical to that of p-$O_2NC_6H_4$CNSNS· generated in a 4-mm ESR tube *in situ* (see Table 4).

Preparation of RCNSSN· (R = Ph, 3,5-$(O_2N)_2C_6H_3$) by the rearrangement of RCNSNS·

PhCNSSN·: SO_2 (5.24 g) was condensed onto $Na_2S_2O_4$ (0.325 g, 1.87 mmol) and PhCNSNSAsF_6 (R = Ph) (0.343 g, 0.927 mmol). The colour of the solution changed from yellow to dark brown after 10 min at room temperature, but the solution was stirred for 20 h to allow complete reduction and rearrangement. The SO_2 was then removed by evacuation and the soluble material extracted with dry benzene into the second bulb, giving a black crystalline product PhCNSSN· (0.13 g) in 81% recovered yield (IR and mass spectrum (19), ESR (18)). FT-Raman:[3] 3064.1s, 3010.7vw, 2136.2vw, 1915.4vw, 1673.8vw, 1599.4vs, 1553.6w, 1498.6m, 1375.2s, 1363.0m, 1325.0m, 1268.3w, 1159.1w, 1140.4vw, 1026.9w, 1003.3s, 805.6m, 777.2m, 662.9m, 618.5w, 508.7w, 473.0w, 430.5m (S–S stretch),[4] 310.8m, 263.5w, 219.6m, 152.9m, 116.9s cm^{-1}.

3,5-$(O_2N)_2C_6H_3$CNSSN·: SO_2 (4.33 g) was condensed onto the solid mixture of 3,5-$(O_2N)_2C_6H_3$CNSNS AsF_6 (0.518 g, 1.12 mmol), $SbPh_3$ (0.285 g, 1.86 mmol), and Me_4NCl (0.265 g, 2.43 mmol) at −196°C. The contents were warmed up to room temperature, the colour of the solution (which contained $SbPh_3Cl_2$ and Me_4NCl) became brown very quickly, and black solid was precipitated. The reactants were stirred for 10 min at room temperature to allow the reduction to be completed. The black powder was washed five times with SO_2 to remove the coloured solubles and then the colour of the solution became very light. The SO_2 was pumped off and the black powder of rearranged 3,5-$(O_2N)_2C_6H_3$CNSSN· was recovered. Mass spectrum (*m/e* (int%)): 271 (M^+, 100), 225 (M^+ − SN or NO_2, 70), 193 (3,5-$(O_2N)_2C_6H_3CN^+$, 44), 179 ($M^+ - N_2S_2$, 75), 147 ($O_2NC_6H_3CN^+$, 16), 101 ($C_6H_3CN^+$, 33), 78 (SNS^+, 66). ESR: the spectrum was acquired in $CFCl_3$ solution at room temperature and was identical to that of 3,5-$(O_2N)_2C_6H_3$CNSSN· generated *in situ* (see Table 5).

Preparation and stability of PhCSNSCPh·

In an initial experiment, SO_2 was condensed onto a mixture of PhCSNSCPhAsF_6 (ca. 1 mg), $SbPh_3$, and NMe_4Cl in an ESR tube. After allowing the reduction to proceed for 4 min the SO_2 was removed by dynamic vacuum, and replaced with degassed $CFCl_3$. The ESR spectrum at room temperature was the same as reported previously for PhCSNSCPh· (hyperfine coupling constants: ^{14}N, 10.71 G: ^{15}N, 15.02 G; ^{33}S, 3.92 G: g = 2.0065).

PhCSNSCPh· is transparent royal blue in dilute $CFCl_3$ solution, but opaque deep green when concentrated. In an attempt to prepare 1 M solution of PhCSNSCPh·, SO_2 was condensed onto a

[4]ν_{S-S} = 432.3 cm^{-1} based on Steudel's equation (20): d_{S-S} = 2.53 − (1.041 × 10^{-3}) ν_{S-S} ($300 < \nu_{S-S} < 530$); d_{S-S} = 2.08 Å for PhCNSSN· (23).

Can. J. Chem. Downloaded from www.nrcresearchpress.com by 88.255.202.194 on 09/08/12
For personal use only.

mixture of $PhCSNSCPhAsF_6/S_2N(C_2H_4)_2AsF_6$ (1.549 g, containing 2.0 mmol of $PhCSNSCPhAsF_6$), $SbPh_3$ (0.708 g, 2.01 mmol), and NMe_4Cl (0.538 g, 4.91 mmol), giving a brown solution, which was stirred in the dark for 30 min. The SO_2 was removed, leaving a brown solid lump, which was stirred in the dark with $CFCl_3$ (20 mL) overnight to extract the $PhCSNSCPh\cdot$. The deep green solution was filtered into a second bulb (where several flakes of a black precipitate began to form), and then into an NMR tube (containing 0.015 g of CH_2Cl_2 as an internal concentration standard), and an ESR tube. The samples were kept frozen at −196°C until the first spectra were acquired (at room temperature). Then on storing at −20°C, a thin grey film slowly formed on the walls of the tubes. The ESR spectrum of the solution was monitored over 600 h. The intensities (arbitrary units) of the ESR signal (determined by double integration of the spectra) varied with time (after the addition of SO_2): 15.5 h, 7.1; 88.9 h, 6.0; 155.9 h, 4.5; 256.4 h, 4.1; 417.4 h, 4.1; 615.8 h, 4.1. The ^1H NMR spectrum of the solution exhibited resonances due to $SbPh_3Cl_2$ (8.4 ppm, multiplet), $SbPh_3$ (7.9 ppm, multiplet), NMe_4^+ (1.8 ppm, singlet), and some radical decomposition products (7.6 ppm, multiplet). The intensities of these resonances did not change relative to that of the CH_2Cl_2 internal standard over 49 days.

Results and discussion

The cycloaddition reactions between SNS^+ and aryl nitriles and PhCCPh

The reactions of $SNSAsF_6$ with the aryl nitriles RCN (R = 2,5-$Me_2C_6H_3$, Ph, *p*-$O_2NC_6H_4$, and 3,5-$(O_2N)_2C_6H_3$) and PhCCPh gave analytically and spectroscopically pure cycloaddition products $RCNSNSAsF_6$ and $PhCSNSCPhAsF_6$, which were established by good elemental analyses (Table 1) and IR (CN, SN, CS, and AsF_6^- vibrations, Table 2) and multinuclear NMR (^1H, ^{13}C and ^{14}N, Table 3) spectroscopies. Although the initial unpurified products were highly coloured, the experimental results show that only traces of impurity were formed.[5] Therefore the aryl rings in $RCNSNS^+$ (R = 2,5-$Me_2C_6H_3$, Ph, *p*-$O_2NC_6H_4$ and 3,5-$(O_2N)_2C_6H_3$) and $PhCSNSCPh^+$ essentially remain intact during the cycloaddition reactions, and the cycloadditions between SNS^+ and aryl nitriles and PhCCPh are essentially quantitative symmetry-allowed cycloaddition reactions (5).

The NMR spectra of the cycloadducts showed aryl substituent resonances at higher frequency than in the corresponding unreacted nitrile due to the formation of the cationic rings. However, the identity of the ring systems is best established by the ^{13}C chemical shifts of C7 (202–205 ppm for the aryl derivatives of $RCNSNS^+$ and 184 ppm for $PhCSNSCPh^+$), which are characteristic for $-CNSNS^+$ and $-CSNSC-^+$ by comparison with the ^{13}C chemical shift values of related cations (5). The ^{14}N NMR spectrum of $PhCNSNS^+$ shows two broad peaks at −46 and 20 ppm, assignable to the two inequivalent nitrogen atoms in the five-membered ring. The peaks in the ^{14}N spectrum of 2,5-$Me_2C_6H_3CNSNS^+$ are broad and they appear to be superimposed. In the cases of $RCNSNS^+$ (R = *p*-$O_2NC_6H_4$ and 3,5-$(O_2N)_2C_6H_3$), the ^{14}N spectrum shows only one narrow asymmetric peak, presumably due to the superimposition of the resonances due to NO_2, N′, and N″. The ^1H and ^{13}C NMR spectra also show that there is free rotation of the aryl groups in solution at room temperature (see footnote (*a*) in Table 3).

We were unable to remove the traces of black impurity present in $PhCSNSCPhAsF_6$ given by the reaction of PhCCPh and $SNSAsF_6$. However, the material was analytically pure with IR and NMR (^1H, ^{13}C) identical to the pale brown material produced according to eq. [1]:

$$[1]\quad 2\,S_2N(C_2H_4)AsF_6 + PhCCPh \rightarrow PhCSNSCPhAsF_6 + S_2N(C_2H_4)_2AsF_6$$

Reaction [1] was shown to proceed quantitatively by an *in situ* ^{13}C NMR experiment. However, the isolated yield of $PhCSNSCPhAsF_6$ was lower than that in the direct cycloaddition reaction (100%) because of separation problems using CH_2Cl_2 as a solvent.

Aryl 1,3,2,4-dithiadiazole radicals and their rearrangements to 1,2,3,5-dithiadiazoles

Dilute solutions (ca. 10^{-2} M) of $RCNSNS\cdot$ (R = 2,5-$Me_2C_6H_3$, Ph, *p*-$O_2NC_6H_4$, 3,5-$(O_2N)_2C_6H_3$) were prepared according to reaction [2]:

$$[2]\quad RCNSNSAsF_6 + 1/2\,SbPh_3 + Me_4NCl \xrightarrow{SO_2/CFCl_3} RCNSNS\cdot + 1/2\,Ph_3SbCl_2 + Me_4NAsF_6$$

The radicals were identified by their ESR spectra, which showed *g* and a^N values very similar to those reported for the alkyl derivatives (6, 7); the spectral data are given in Table 4. Like the alkyl derivatives, they also undergo rearrangements to the corresponding disulfide isomers, the ESR parameters of which are given in Table 5. $RCNSNS\cdot$ (R = 2,5-$Me_2C_6H_3$ and Ph) (like the Bu′ derivative) only rearrange in the light. However, $RCNSNS\cdot$ (R = *p*-$O_2NC_6H_4$, 3,5-$(O_2N)_2C_6H_3$) (like the CF_3 derivative) rearrange in the dark, although at a much slower rate than in the light. The rates of rearrangement given in Table 4 can be correlated with the ionization potential of the RCN nitrile, and the electronegativity of R. This kind of correlation is also obtained for the aliphatic derivatives of $RCNSNS\cdot$ (R = CH_3, Bu′, CF_3, and I), i.e., the rearrangement rates of $RCNSNS\cdot$ follow the order Bu′ < CH_3 < CF_3 < I (6, 9). It is likely that the higher the electronegativity of R (which corresponds to a higher ionization potential of RCN and also of $RCNSNS\cdot$), the faster the rate of rearrangement of $RCNSNS\cdot$ to $RCNSSN\cdot$ (although on this basis the CF_3 derivative would have been expected to rearrange faster than the iodo derivative). This rearrangement has been quantitatively determined to be a bimolecular process for $RCNSNS\cdot$ (R = Ph,

[5]The highly coloured impurities may be produced from the slow side reaction of SNS^+ with the aryl rings of $RCNSNS^+$ (R = 2,5-$Me_2C_6H_3$, Ph, *p*-$O_2NC_6H_4$, and 3,5-$(O_2N)_2C_6H_3$) and $PhCSNSCPh^+$. A slow reaction is observed between SNS^+ and benzene to give highly coloured products (J. Passmore, M. J. Schriver, and X. Sun, unpublished results) (cf. reaction of ONO^+ with C_6H_6 (21)). The related cycloaddition reactions of SNS^+ with aliphatic nitriles and alkynes led to either colourless or yellow cycloadducts (1, 2, 5).

Can. J. Chem. Downloaded from www.nrcresearchpress.com by 88.255.202.194 on 09/08/12
For personal use only.

p-$O_2NC_6H_4$), which will be reported elsewhere).[6] Further studies of the rearrangement of RCNSNS· to RCNSSN· are in progress. We have prepared spectroscopically (IR, Raman, and ESR) pure PhCNSSN· by the quantitative rearrangement of PhCNSNS·. PhCNSSN· was first synthesized by Banister and co-workers (16, 19, 23) by the reduction of the corresponding cation. Since then various other RCNSSN· (e.g., CF_3 (24) and Me_2N (25)) have been synthesized by the same route. We have also synthesized RCNSSN· (R = Bu^t and CF_3) on a preparative scale by the quantitative rearrangement of the corresponding RCNSNS· (6). The rearrangement of 3,5-$(O_2N)_2C_6H_3$CNSNS·, like CF_3CNSNS·, was rapid, and we were unable to isolate it. The reduction of 3,5-$(O_2N)_2C_6H_3$CNSNS$^+$ on a preparative scale led directly to the precipitation of rearranged radical 3,5-$(O_2N)_2C_6H_3$CNSSN·, which was identified by ESR and mass spectrometry.

Isolation and properties of solid RCNSNS· (R = Ph, p-$O_2NC_6H_4$)

Although RCNSNS· undergoes facile rearrangement to RCNSSN·, we were able to isolate unrearranged radicals RCNSNS· (R = Ph, p-$O_2NC_6H_4$) as pure solid materials on a preparative scale by allowing them to quickly form in the solid state. Their identity was established by the combination of several experimental techniques, including mass spectrometry, ESR, IR and FT-Raman spectroscopies, and X-ray crystallographic analysis. The mass spectra of RCNSNS· (R = Ph, p-$O_2NC_6H_4$) showed intense SNS^+ (47% for Ph and 100% for p-$O_2NC_6H_4$ derivatives) and (or) RCN^+ (100% for Ph and 4% for p-$O_2NC_6H_4$[7] derivatives) peaks from the fragments for both of the radicals. This characteristic fragmentation pattern for RCNSNS· is supported by the observation of their photolysis into RCN and SNS· (22). Although the mass spectra of RCNSSN· gave peaks due to the fragments SSN (same m/e as SNS) and RCN, they were less intense than those of the corresponding molecular ions. The X-ray crystallographic analysis for PhCNSNS·[8] showed that its unit cell parameters and crystal system are completely different from those of the disulfide PhCNSSN· (23). In addition, PhCNSNS· also has different IR data from those of PhCNSSN· (19). The FT-Raman spectrum of p-$O_2NC_6H_4$CNSNS· did not give an S–S stretch, which was strong in PhCNSSN· at 430.5 cm^{-1}. This is, as far as we are aware, the first report of Raman spectra of these or related highly coloured radicals, now obtainable by using FT-Raman spectroscopy, which is likely to prove very useful in this and related areas. RCNSNS· (R = Ph, p-$O_2NC_6H_4$) are unambiguously characterized by their ESR spectral data (1:1:1 triplet for both derivatives) in solution, showing that the isolated solid compounds were unrearranged radicals RCNSNS· (R = Ph, p-$O_2NC_6H_4$). The crystallographic studies also showed that PhCNSNS· and PhCNSSN· possess essentially the same volumes of the molecular unit (389.9(1) Å^3 for PhCNSNS· and 382.4(1) Å^3 for PhCNSSN· (23)). This suggests that PhCNSNS· forms similar sulfur-based π^*–π^* dimers in the solid state as observed for PhCNSSN· (23). The attempted reduction of 2,5-$Me_2C_6H_3$CNSNS$^+$ resulted in an intractable tar.

RCNSNS· (R = 2,5-$Me_2C_6H_3$, Ph, p-$O_2NC_6H_4$, and 3,5-$(O_2N)_2C_6H_3$) not only undergo photochemical rearrangement in dilute solution, but also rearrange to RCNSSN· in the solid state in the light at room temperature. PhCNSNS· even completely rearranges to its disulfide isomer PhCNSSN·· in the solid state in the dark at −20°C after a week. We have also found that Bu^{t}CNSNS· completely rearranges to Bu^{t}CNSSN· in the liquid state in the dark at room temperature after ca. 20 h (7). Banister and co-workers (26) recently reported that p-C_6H_4(CNSNS)$_2$·· undergoes thermal rearrangement to its disulfide isomer p-C_6H_4(CNSSN)$_2$·· in the solid state at 150°C. All of these results suggest that this rearrangement is a general process for 1,3,2,4-dithiadiazoles in the solid state. Energetic difference obviously exists between the rearrangement of RCNSNS· to RCNSSN· in the light and in the dark. This suggests that the thermal rearrangement (low-energy process) may be related to a different reaction pathway from that of the photochemical rearrangement (high-energy process). p-$O_2NC_6H_4$CNSNS· is infinitely stable in the solid state in the dark at room temperature. However, the attempted crystal growth by sublimation at 90°C resulted in thermolysis to p-$O_2NC_6H_4$CN (detected by IR), presumably due to the loss of SNS· (22).

Generation and stability of PhCSNSCPh·

The PhCSNSCPh· was previously prepared in dilute solution by Sutcliffe and co-workers by the reaction of PhCCPh with S_4N_2, and characterized in dilute CCl_4 solution by ESR (27–31). We prepared it by the reduction of PhCSNSCPhAsF$_6$ with $SbPh_3$/NMe_4Cl according to eq. [3]:

$$[3]\quad \text{PhCSNSCPhAsF}_6 + 1/2\ \text{SbPh}_3 + \text{NMe}_4\text{Cl} \rightarrow \text{PhCSNSCPh·} + \text{NMe}_4\text{AsF}_6 + 1/2\ \text{SbPh}_3\text{Cl}_2$$

The ESR parameters obtained in this study were in good agreement with those obtained by Sutcliffe and co-workers (29–31).

PhCSNSCPh· decomposed to an insoluble diamagnetic solid when an attempt was made to isolate it. It is also unstable as a 1 M solution, decomposing to some soluble (^{1}H NMR) and insoluble products. The decomposition appeared

[6]N. Burford, J. Passmore, and X. Sun. Manuscript in preparation. See also ref. 22.

[7]The very low intensity of the p-$O_2NC_6H_4CN^+$ peak is conceivably attributed to the lower intensity of the M^+ peak than that of the Ph derivative and the more branched fragmentations of M^+ and p-$O_2NC_6H_4CN^+$ due to the existence of the nitro group.

[8]Crystallographic unit cell parameters for PhCNSNS·: monoclinic, a = 6.156(5) Å, b = 15.581(5) Å, c = 8.659(5) Å, $\alpha = \gamma = 90°$, β = 110.13(6)°, V = 779.8(1) Å^3, Z = 2, volume of molecular unit 389.9(1) Å^3. Determination of the full crystal structure was unsuccessful because of its crystallinity loss during attempted data collection, possibly due to the rearrangement on an irradiation by the X-ray beam.

to cease (in this case after 70 h) when the radical concentration reached a certain critical level, which we estimated to be about 0.5 M, by monitoring the intensity of the ESR signal of a 1 M solution of PhCSNSCPh· as a function of time in the dark. The stability of R′CSNSCR″· is comparable with that of its nitroxide analogue R′R″NO·. R_2NO· (R = Bu^t, CF_3) is a stable species (32, 33). Ph_2NO· is unstable and not isolable (33, 34), but it decomposes to diphenylamine and *N*-phenyl-*p*-benzoquinonime *N*-oxide in solution under normal preparative concentrations (34). This suggests that the stability of R′CSNSCR″· parallels that of the nitroxides R′R″NO·.

Conclusions

We previously showed the generality of quantitative symmetry-allowed cycloaddition reactions of SNS^+ with aliphatic alkynes and nitriles (1–5). This generality has now been extended to simple aryl derivatives to give the corresponding pure cycloadducts RCNSNS$^+$ (R = 2,5-$Me_2C_6H_3$, Ph, *p*-$O_2NC_6H_4$, and 3,5-$(O_2N)_2C_6H_3$) and PhCSNSCPh$^+$.

Reduction of RCNSNS$^+$ in dilute solution gives the neutral 7π radical RCNSNS·. We were able to isolate solid RCNSNS· (R = Ph, *p*-$O_2NC_6H_4$). The novel rearrangement of RCNSNS· to RCNSSN· was previously studied for some alkyl derivatives (6, 7). In this work, we determined the relative rates of this rearrangement for some related aryl derivatives and found that the lower the electronegativity of R, the slower the rearrangement. This discovery may lead to a better understanding of the mechanism of this rearrangement. It also aids us in the planned syntheses of more stable RCNSNS· mono- and multi-radical containing species that are of interest in their own right and as potentially useful materials.

The study of the stability of PhCSNSCPh· showed that PhCSNSCPh· is stable in solution up to ca. 0.5 M. It seems to be intermediate in stability between $CH_3CSNSCCH_3$·, which is only detectable by ESR spectroscopy in very dilute solution (1), and RCSNSCR· (R = CF_3 (10), CN (11)), which are isolable as stable materials.

Acknowledgements

We thank Dr. P. Boyle for crystallographic data of PhCNSNS·, Dr. G. Schatte for obtaining the FT-Raman spectra, and Mr. D. Drummond for the mass spectra. We also thank the Natural Sciences and Engineering Research Council of Canada (NSERC) and the University of New Brunswick (X.S.) for financial support, and the Canadian Commonwealth Scholarship and Fellowship Committee for a graduate scholarship (S.P.).

1. G. K. MacLean, J. Passmore, M. N. S. Rao, M. J. Schriver, P. S. White, D. Bethell, R. S. Pilkington, and L. H. Sutcliffe. J. Chem. Soc. Dalton Trans. 1405 (1985).
2. G. K. MacLean, J. Passmore, M. J. Schriver, P. S. White, D. Bethell, R. S. Pilkington, and L. H. Sutliffe. J. Chem. Soc. Chem. Commun. 807 (1983).
3. N. Burford, J. P. Johnson, J. Passmore, M. J. Schriver, and P. S. White. J. Chem. Soc. Chem. Commun. 966 (1986).
4. J. Passmore and M. J. Schriver. Inorg. Chem. **27**, 2749 (1988).
5. S. Parsons, J. Passmore, M. J. Schriver, and P. S. White. J. Chem. Soc. Chem. Commun. 369 (1991); S. Parsons, J. Passmore, M. J. Schriver, and X. Sun. Inorg. Chem. **30**, 3342 (1991).
6. N. Burford, J. Passmore, and M. J. Schriver. J. Chem. Soc. Chem. Commun. 140 (1986).
7. W. V. F. Brooks, N. Burford, J. Passmore, M. J. Schriver, and L. H. Sutcliffe. J. Chem. Soc. Chem. Commun. 69 (1987).
8. A. J. Banister, J. M. Rawson, W. Clegg, and S. L. Birkby. J. Chem. Soc. Dalton Trans. 1099 (1991).
9. M. J. Schriver. Ph. D. Thesis, University of New Brunswick, Fredericton, Canada (1988).
10. E. G. Awere, N. Burford, C. Mailer, J. Passmore, M. J. Schriver, P. S. White, A. J. Banister, H. Oberhammer, and L. H. Sucliffe. J. Chem. Soc. Chem. Commun. 66 (1987).
11. G. Wolmershauser and G. Kraft. Chem. Ber. **123**, 881 (1990).
12. E. G. Awere, N. Burford, R. C. Haddon, S. Parsons, J. Passmore, J. V. Waszczak, and P. S. White. Inorg. Chem. **29**, 4821 (1990).
13. (*a*) K. A. Williams, M. J. Nowak, E. Dormann, and F. Wudl. Synth. Met. **14**, 233 (1986); (*b*) G. Wolmershauser, M. Schnauber, and T. Wilhelm. Synth. Met. **14**, 239 (1986); (*c*) E. Dormann, M. J. Norak, K. A. Williams, R. O. Angus, Jr., and F. Wudl. J. Am. Chem. Soc. **109**, 2594 (1987).
14. E. G. Awere and J. Passmore. J. Chem. Soc. Dalton Trans. 1343 (1992).
15. S. Parsons, J. Passmore, M. J. Schriver, and P. S. White. Can. J. Chem. **68**, 852 (1990).
16. M. I. Hansford. Ph. D Thesis, University of Durham, Durham, U.K. (1989).
17. A. J. Banister. Phosphorus Sulfur, **5**, 147 (1978).
18. F. L. Lee, K. F. Preston, A. J. Williams, L. H. Sutcliffe, A. J. Banister, and S. T. Wait. Magn. Reson. Chem. **27**, 1161 (1989).
19. A. J. Banister, N. R. M. Smith, and R. G. Hey. J. Chem. Soc. Perkin Trans. 1, 1181 (1983).
20. R. Steudel. Angew. Chem. Int. Ed. Engl. **14**, 655 (1975).
21. G. A. Olah, R. Malhotra, and S. C. Narang. Nitration: methods and mechanisms. VCH Publishers, New York. 1989.
22. S. Mattar, J. Passmore, and X. Sun. Abstr. 75th Chem. Inst. Can. Conf. May 31 – June 4, 1992, Edmonton, Alta.
23. A. Vegas, A. Perez-Salazar, A. J. Banister, and R. G. Hey. J. Chem. Soc. 1812 (1980).
24. H.-U. Hofs, J. W. Bats, R. Gleiter, G. Hartmann, R. Mews, M. Eckert-Maksic, H. Oberhammer, and G. M. Sheldrick. Chem. Ber. **118**, 3781 (1985).
25. A. W. Cordes, J. D. Goddard, R. T. Oakley, and N. P. C. Westwood. J. Am. Chem. Soc. **111**, 6147 (1989).
26. C. Aherne, A. J. Banister, A. W. Luke, J. Rawson, and R. J. Whitehead. J. Chem. Soc. Dalton Trans. 1227 (1992).
27. S. A. Fairhurst, R. S. Pilkington, and L. H. Sutcliffe. J. Chem. Soc. Faraday Trans. 1, **79**, 925 (1983).
28. S. A. Fairhurst, R. S. Pilkington, and L. H. Sutcliffe. J. Chem. Soc. Faraday Trans. 1, **79**, 439 (1983).
29. S. R. Harrison, R. S. Pilkington, and L. H. Sutcliffe. J. Chem. Soc. Faraday Trans. 1, **80**, 669 (1984).
30. S. A. Fairhurst and L. H. Sutcliffe. J. Chem. Soc. Faraday Trans. 1, **76**, 1490 (1980).
31. K. F. Preston, J. P. B. Sandall, and L. H. Sutcliffe. Magn. Reson. Chem. **26**, 755 (1988).
32. A. K. Hoffmann and A. T. Henderson. J. Am. Chem. Soc. **83**, 4671 (1961).
33. A. Calder and A. R. Forrester. J. Chem. Soc. Chem. Commun. 682 (1967).
34. A. R. Forrester and R. H. Thomson. Nature, **203**, 74 (1964).

Can. J. Chem. Downloaded from www.nrcresearchpress.com by 88.255.202.194 on 09/08/12
For personal use only.

Organometallic intermediates in the group 4 metallocene-catalyzed dehydrocoupling of organosilanes. 2. Variations in the intermediates of dimethyltitanocene reactions with several silanes

J. F. HARROD[1] AND YING MU

Chemistry Department, McGill University, 801 Sherbrooke Street West, Montréal, Que., Canada H3A 2K6

AND

E. SAMUEL

Laboratoire de chimie organométallique de l'École nationale supérieure de chimie de Paris (Unité de recherche associée n° 403 du Centre national de la recherche scientifique), 11, rue P. et M. Curie, 75005 Paris, France

Received June 12, 1992

J. F. HARROD, YING MU, and E. SAMUEL. Can. J. Chem. **70**, 2980 (1992).

As previously described, organosilanes react with dimethyltitanocene (DMT) to give three reduced titanium intermediates, $Cp_2Ti(\mu\text{-}SiRR'H)(\mu\text{-}H)TiCp_2$, **1**, $[Cp_2Ti(\mu\text{-}SiRR'H)]_2$, **2**, and $[Cp_2Ti(H)]_2(\mu\text{-}H)$, **3**. When R = Me and R′ = *n*-Bu, the DMT is quantitatively converted to **1**, which is persistent at room temperature. When R′ = H, DMT is initially converted quantitatively to **1**, which then rapidly declines to give an equilibrium mixture of **1**, **2**, and **3**, with **2** as the dominant species. When R = Ph and R′ = Ph or Me, **1** is again produced quantitatively, but it rapidly declines to produce an unidentified paramagnetic product, rather than **2** or **3**. It is believed that **2** is unstable with respect to dissociation in these cases due to the steric bulk of the substituents.

J. F. HARROD, YING MU et E. SAMUEL. Can. J. Chem. **70**, 2980 (1992).

Comme on l'a démontré antérieurement, les organosilanes réagissent avec le diméthyltitanocène (DMT) pour donner trois intermédiaires réduits du titane, $Cp_2Ti(\mu\text{-}SiRR'H)(\mu\text{-}H)TiCp_2$, **1**, $[Cp_2Ti(\mu\text{-}SiRR'H)]_2$, **2**, et $[Cp_2Ti(\mu\text{-}SiRR'H)]_2(\mu\text{-}H)$, **3**. Lorsque R = Me et R′ = *n*-Bu, le DMT est transformé quantitativement en **1** qui est persistant à la température ambiante. Lorsque R′ = H, le DMT est initialement converti quantitativement en **1** qui disparaît alors rapidement pour donner un mélange à l'équilibre des composés **1**, **2** et **3** dans lequel le composé **2** prédomine. Lorsque R = Ph et R′ = Ph ou Me, **1** est encore une fois produit d'une façon quantitative, mais sa concentration diminue rapidement pour donner un produit paramagnétique inconnu plutôt que les produits **2** ou **3**. Dans ce cas, on croit que le composé **2** est instable et qu'il se dissocie à cause de l'encombrement stérique des substituants.

[Traduit par la rédaction]

Introduction

The intermediates in the group 4 metallocene-catalyzed dehydrocoupling reactions of organosilanes are quite different for titanium (1, 2) and for zirconium (3, 4). In a number of studies, we have used the dimethylmetallocenes of group 4 as the catalyst precursor (1, 3, 5). In these cases, the chemistry of the transformation of the precursor into the active catalytic species constitutes an important part of the chemistry. Tilley and Woo have carried out extensive studies with pre-synthesized silylzirconocene(IV) and hafnocene(IV) complexes that provide convincing evidence for the role of silylhydridozirconocenes(IV) as the key catalytic species (4). They also showed that the induction periods typical of dimethylmetallocene catalysts are not observed with silylhydridozirconocene catalysts. Finally, all studies have concluded that the zirconium remains mainly in the oxidation state IV throughout the reaction and only small amounts of Zr(III) species are detected.

The titanocene-catalyzed reaction differs in two important ways from the zirconocene and hafnocene systems. In the first place, one cannot use either dihydrotitanocene(IV) or hydridosilyltitanocene(IV) complexes as catalysts, since such compounds are too unstable to isolate and manipulate (6, 7). Secondly, once the induction period for transformation of DMT into the active catalyst is complete, all of the detectable titanium is in the form of Ti(III) (1, 2). Despite this fact, it was concluded from a study of the kinetics of a number of DMT-catalyzed reactions that the most probable species for the true catalyst was the hydridosilyltitanocene(IV), **4** (8). In no case has **4** ever been directly observed. However, Buchwald and his collaborators have recently succeeded in isolating and structurally characterizing trimethylphosphine coordinated **4** (R = R′ = Ph).[2] From these results, it appears likely that the true catalyst is generated by an equilibrium splitting of the dimer **1** by silane as shown in eq. [1].

[1] $$\underset{\mathbf{1}}{Cp_2Ti(\mu\text{-}H)(\mu\text{-}SiHRR')TiCp_2} + RR'SiH_2 \rightarrow 2\,\underset{\mathbf{4}}{Cp_2Ti(SiHRR')H}$$

In earlier reports, we described the manner in which DMT reacts rapidly with organosilanes, following an induction period, to give **1** initially, then $[Cp_2Ti(SiRR'H)]_2$, **2**, and finally the mixed valence hydride $Cp_2Ti_2H_3$, **3** (1, 2). We have now systematically followed these species in the course of the reactions of several organosilanes, by monitoring their ^1H NMR spectra.

Results and discussion

The reactions of primary silanes

The profile of a reaction of a catalytic amount of DMT with phenylsilane is shown in Fig. 1. The amounts of **1***a* and **2***a*

[1]Author to whom correspondence may be addressed.

[2]S. Buchwald, personal communication.

Can. J. Chem. Downloaded from www.nrcresearchpress.com by 88.255.202.194 on 09/08/12
For personal use only.

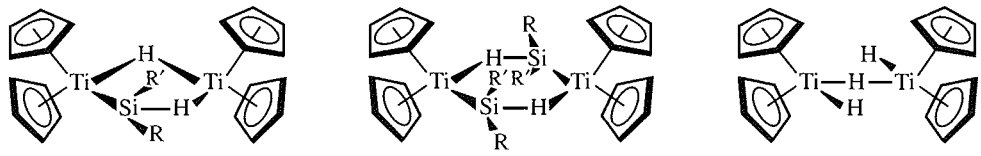

1 2 3

a: R = Ph; R′ = H
b: R = Me; R′ = H
c: R = Me; R′ = n-Bu
d: R = Ph; R′ = Ph
e: R = Ph; R′ = Me

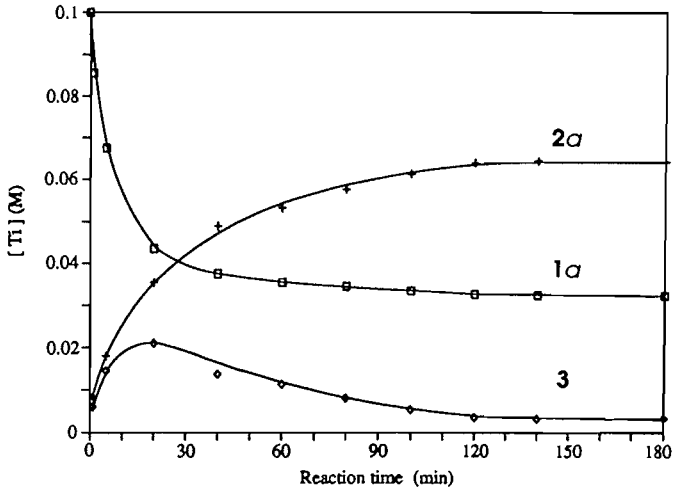

FIG. 1. Evolution of the concentrations of compounds **1***a*, **2***a*, and **3** with time. $[DMT]_i = 0.1$ M; $[PhSiH_3]_i = 1.0$ M in benzene-d_6 at 20°C.

were calculated directly from integration of NMR spectra. The third curve, believed to be mainly due to the presence of **3**, was obtained by subtraction of the amount of **1***a* + **2***a* from the total amount of titanium. The zero of time in this figure corresponds to the time at which the blue colour, signalling the end of the induction period, was first observed. It is evident from these results that DMT is transformed rapidly and completely to **1***a* in the first few seconds of the reaction. The concomitant formation of one equivalent of $PhMeSiH_2$, some oligophenylsilane, and some CH_4 was also evident from the ^1H NMR spectra. The initial reaction in the presence of excess silane is then:

$$[2] \quad 2\,Cp_2TiMe_2 + 4\,PhSiH_3 \rightarrow Cp_2Ti(H)(HPhSiH)TiCp_2 + 3\,MeH + PhMeSiH_2 + 2/n\,H(PhSiH)_nH$$

Immediately following its rapid formation, **1***a* begins to decay to the other two products. The decay continues until a steady state of all species is reached after about 2 h. At the steady state, under ambient conditions, the dominant species is **2***a* (ca. 65%) and **1***a* is about 30% of the total titanium present.

When isolated, **1***a* is used as a catalyst for phenylsilane polymerization, there is no induction period, and the rate of dehydrocoupling is initially high. The rate then declines as the **1***a* is converted into **2***a*. When isolated, **2***a* is used a catalyst, the reaction is initially very slow, but accelerates as the **2***a* is converted to **1***a*. This conversion is evident from the change in colour from the dark greenish-grey of **2***a* to the royal blue of **1***a*. The ^1H NMR spectrum of the reaction mixture shows that about 30% of **2***a* is converted to **1***a* over a period of several hours. Thus, the same steady state composition is achieved irrespective of the starting complex.

The course of a reaction of methylsilane with DMT is very similar to that of phenylsilane. At the steady state, which was achieved after ca. 3 h with 0.1 M DMT and 1.0 M $MeSiH_3$ in C_6D_6, the concentrations of **1***b* and **2***b* were again ca. 35% and 60% of the total titanium.

The reaction of n-*butylmethylsilane*

The reaction of *n*-butylmethylsilane is somewhat different from those of the primary silanes. Following the induction period, the reaction mixture does turn royal blue and the ^1H NMR spectrum shows the formation of CH_4, $BuMe_2SiH$, and the complex **1***c*. There is, however, no evidence for transformation of **1***c* into any other species and its concentration remains constant for at least several hours.

The ^1H NMR spectrum of **1***c* is similar to that of **1***a* (1). At room temperature, the four resonances of the inequivalent Cp groups are already sharp in **1***c*, while the bridging hydride resonances only sharpen up at lower temperature, as illustrated in Fig. 2. The presence of a paramagnetic species in solutions of **1***c* is signalled by a marked paramagnetic broadening of the resonances of the metal complex, excess $BuMeSiH_2$, and the solvent. The effect of concentration on the Cp resonances of **1***c* is shown in Fig. 3.

Studies by EPR of a solution of **1***c* in toluene showed a broad featureless singlet at room temperature with $g_{iso} = 1.984$, and did not provide further clarification as to the structure of the paramagnetic species responsible for the line broadening of the NMR signal.

The reactions of diphenylsilane and methylphenylsilane

The initial reactions of diphenylsilane and phenylmethylsilane with DMT gave CH_4, the methylated silanes, and quantitative conversion of DMT to **1***d* and **1***e*, respectively. In both cases, **1** begins to decay immediately, but there is no evidence in the NMR spectrum for the formation of **2**. The EPR spectra of reacting solutions reveal the presence of **3**, together with an intense broad singlet of unassigned origin. When the reactions are carried out in hexane as solvent, a black microcrystalline precipitate is recovered after several hours, which from its EPR spectrum and chemical analysis appears to be mainly **3**. Curves showing the disappearance of **1***d* and **1***e* with time are shown in Fig. 4.

The mechanism of formation of **1** *and* **2** *and their implication in DMT-catalyzed dehydrocoupling*

In earlier reports we described some aspects of the reactions of DMT with organosilanes and organogermanes (1,

Can. J. Chem. Downloaded from www.nrcresearchpress.com by 88.255.202.194 on 09/08/12
For personal use only.

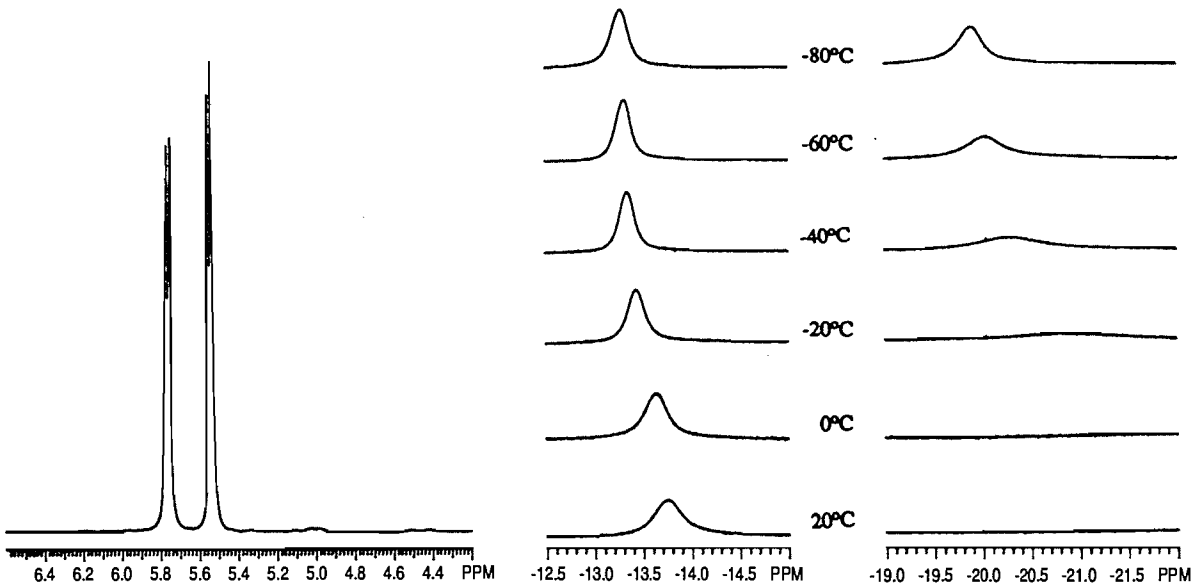

FIG. 2. ^{1}H spectrum of **1***c* at different temperatures. [**1***c*] = 0.1 M in toluene-d_8.

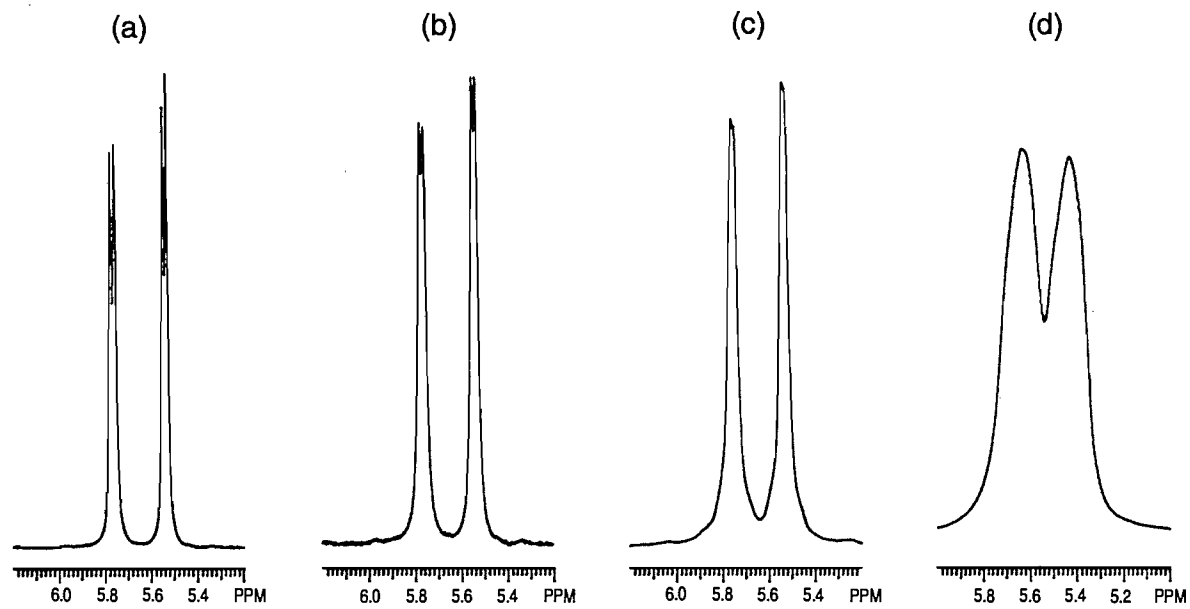

FIG. 3. ^{1}H NMR spectrum of **1***c* in the Cp region at different concentrations of the complex. (*a*) 0.1 M; (*b*) 0.2 M; (*c*) 0.3 M; (*d*) 0.6 M.

9). The critical feature of the DMT reactions, and one which distinguishes DMT from its zirconium and hafnium analogues, is the explosive nature of the reaction that leads to reduced titanium species. In its strongly autocatalytic nature and its spatially inhomogeneous propagation, this reaction is very similar to the reaction of H_2 with DMT (6, 10). It is likely in both cases that titanocene is the chain carrier that is responsible for the branched chain character of these reactions. Bercaw *et al.* were able to show unequivocally that this was the case for the reaction of H_2 with $Cp^*_2TiMe_2$ (11). We have shown that the explosive reduction, in the case of silanes, is suppressed by CO (1). When CO is present, instead of the catastrophic reduction to Ti(III) dimers, there is a slow, non-autocatalytic formation of $Cp_2Ti(CO)_2$. If there is only a small amount of CO available, the slow accumulation of the dicarbonyl continues until the CO is exhausted and then the catastrophic reduction to Ti(III) dimers occurs.

When a sterically undemanding, basic phosphine, such as Me_3P, is added to the DMT/silane reaction mixture, the product is not (as might be anticipated from the CO result) the titanocene(II)bis(phosphine) (12), but a titanocene(III)-silyl(phosphine) complex (2). The same products are observed on reaction of **1** or **2** with Me_3P or CO. Since **1** and **2** interconvert, it is not easy to distinguish whether these reactions involve specifically **1** or **2**.

The new results described above confirm that complexes **1** are the initial products of the reduction reactions of silanes with DMT. They also indicate that the origin of the low activities of secondary silanes with respect to catalyzed dehydrocoupling is different in the case of butylmethylsilane from

Can. J. Chem. Downloaded from www.nrcresearchpress.com by 88.255.202.194 on 09/08/12
For personal use only.

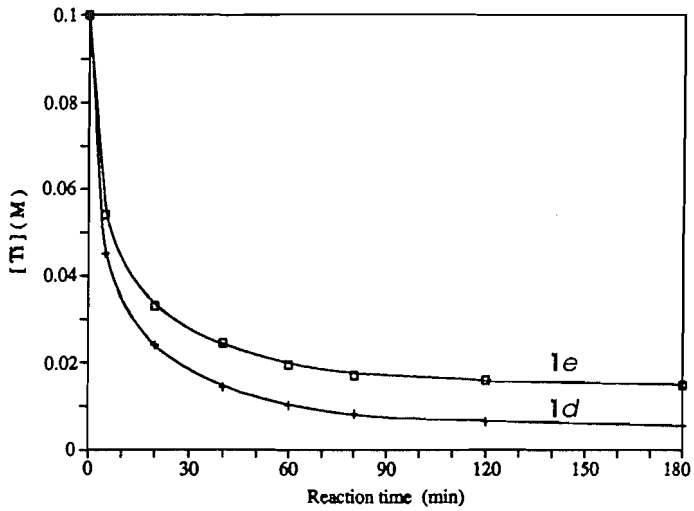

FIG. 4. Evolution of the concentrations of **1***d* and **1***e* with time. $[DMT]_i = 0.1$ M; $[Ph_2SiH_2] = 0.7$ M; $PhMeSiH_2 = 0.9$ M. At 20°C in benzene-d_6.

the cases of diphenyl- and phenylmethyl-silanes. The inactivity of the former is due to the inordinate stability of **1***c*, while that of the secondary arylalkylsilanes seems related to the inordinate labilities, or instabilities, of **1***d* and **1***e*. The abnormal stability of **1***c* may arise from the greater electron-releasing character of the alkyl substituents, giving rise to stronger bridging bonds. It may also be partly due to steric inhibition of reaction [1]. By the same reasoning, it may be concluded that the arylalkyl- and diaryl-silanes dissociate more readily into mononuclear species, due to the greater electron deficiency of the bridges, but that the formation of **4** (eq. [1]) is slowed down, perhaps by steric effects, to the point that the mononuclear intermediate decomposes via an unproductive channel. The more rapid disappearance of **1***d* and **1***e*, relative to **1***a*, may also be linked to a more facile dissociation of these bimetallic into monometallic complexes. In this case, however, the dissociation may be a disproportionation into titanocene(II) and a hydridosilyltitanocene(IV) complex (1, 8).

The failure to observe **2***d* and **2***e* by NMR does not prove that they are absent, since they may dissociate into paramagnetic monomers, according to eq. [3]. Even a small

[3] $[Cp_2Ti(SiRR'H)]_2 \rightleftharpoons 2\ Cp_2Ti(SiRR'H)$

amount of dissociation could cause extreme broadening of NMR resonances, provided the equilibrium was rapid. There is also ample evidence that dissociation of **2** can occur in the presence of donor ligands (2). This explanation is still not very convincing, however, when it is recognised that **2***a* and **2***b* have unbroadened resonances at room temperature, while neither **2***d* nor **2***e* can be detected in reaction mixtures down to −80°C.

The activity of primary silanes can then be rationalized in terms of an optimum ease of dissociation of **1** and a rate of conversion of the resulting mononuclear complex into **4** that precludes its decomposition by a nonproductive reaction. Although **2** is not an efficient source of the primary catalyst, its formation correlates with high catalytic activity. This is presumably because the processes that are prerequisite to the formation of **4** are also prerequisite to the formation of **2**. All of this leads to the conclusion that only a small fraction of the titanium is in the form of primary catalytic species and that the true activity of the primary catalyst is very much higher than the apparent activity. We are therefore concentrating our continuing efforts on the development of Cp-related ligands that inhibit dimerization of the hydride and silyl intermediates, and slow down their spontaneous decomposition, without unduly slowing down the dehydrocoupling process.

Experimental

The general procedures for the purification of solvents, synthesis of reactants and catalysts, and carrying out reactions, are the same as described previously (1).

Reactions of primary and secondary silanes with DMT

All of the reactions were followed by ^{1}H NMR. The standard conditions, except for methylsilane, were as follows. To a solution of DMT (10 mg; 0.048 mmol) in degassed benzene-d_6, containing one drop of cycylohexane as calibrant, was added the reactant silane (0.06 mL). The mixture was sealed in an NMR tube and placed in the temperature-controlled cavity of a 300 MHz NMR spectrometer. The concentrations of **1** and **2** were monitored periodically by comparison of the integrals of their Cp resonances with the cyclohexane standard. In the case of methylsilane, the same amount of DMT was dissolved in benzene-d_6 (0.48 mL) containing a drop of cyclohexane. The methylsilane gas was bubbled into the solution until it turned deep blue. The NMR tube was then sealed and the reaction was followed by the same method as for the other silanes.

Synthesis of $[Cp_2Ti(\mu\text{-}SiH_2Me)]_2$, **2**b

Methylsilane was bubbled into a solution of DMT (100 mg; 0.48 mmol) in toluene (2 mL). Within a few minutes a rapid colour change from orange to deep blue occurred, accompanied by a vigorous gas evolution. The solution was left under an atmosphere of methylsilane for 24 h to complete the conversion of **1***b* to **2***b*. The supernatant liquid was then decanted and the crystalline product was washed three times with 2-mL portions of cold toluene and dried under vacuum (yield: 34 mg; 35% based on **2***b*). The ^{1}H NMR spectrum of the product, in toluene-d_8, revealed only peaks due to the two isomers of **2***b*, in a ratio of 1.2:1. Major isomer (ppm): Cp: 4.594 (s) and 4.492 (2); Si-H terminal: 4.777 (m), $^2J_{H,H}$: 4.48 Hz; $^3J_{H,H}$: 4.50 Hz; CH_3: 0.765 (dd), $^3J_{H,\mu\text{-}H}$: 1.85 Hz; Si-H-Ti: −10.16 (br s). Minor isomer (ppm): Cp 4.586 (s) and 4.518 (s); Si-H (terminal): 4.866 (m), $^2J_{H,H}$: 4.48 Hz; $^3J_{H,H}$: 4.50 Hz; CH_3: 0.739 (dd), $^3J_{H,\mu\text{-}H}$: 1.85 Hz.; Si-H-Ti: −10.16 (br s). The spectral parameters for Si-H (terminal) and CH_3 resonances are cited for the spectra observed while decoupling at 0.765, 0.739, and −10.16 ppm respectively. The major isomer is tentatively assigned the *cis* structure on the basis of the larger difference in chemical shift between the two Cp resonances for this isomer. Although the NMR spectrum indicated only the presence of **2***b* in solution, satisfactory analyses for this compound were not obtained (Anal. calcd. for $C_{22}H_{30}Si_2Ti_2$: C 59.19, H 6.77, Si 12.58, Ti 21.46; found: C 55.57, H 6.25, Si 9.94, Ti 21.87). The poor analysis can be attributed in part to the presence of **3**, which is NMR silent, but it is also common for compounds containing Ti and Si to give poor analyses due to the formation of refractory titanium silicide. Although the mass spectra of the products contained many expected fragments, parent peaks were not observed and it was concluded that the compounds are not in general stable enough to carry out structure confirmation by high-resolution MS.

Several attempts to isolate **1***b* in a relatively pure state were frustrated by the facile decomposition of **1***b* into **2***b*. However, **1***b* was readily observed in solution by its ^{1}H NMR spectrum. At room temperature, all resonances were very broad, including the Cp resonances. Contrary to the spectra of all other complexes of **1** so far observed, **1***b* only exhibits three separate Cp resonances in the

Can. J. Chem. Downloaded from www.nrcresearchpress.com by 88.255.202.194 on 09/08/12
For personal use only.

TABLE 1. ^{1}H NMR data for $Cp_2Ti(\mu\text{-}H)(\mu\text{-}HSiMeH)TiCp_2$, **1***b*[a]

Temperature (°C)	Chemical shifts, ppm				
	C_5H_5	Si-H	CH_3	Si-H-Ti	Ti-H-Ti
20	5.62,[b] 5.45[b]	3.93[b]	0.16	−13.30 (42)	[c]
−40	5.62, 5.53, 5.33	4.05 (16)[d]	0.24	−13.12 (14)	−19.62 (50)
−80	5.61, 5.52, 5.30	4.10 (20)	0.28	−13.09 (16)	−19.50 (16)

[a]In toluene-d_8 with TMS standard.
[b]Very broad.
[c]Not observed.
[d]Figures in parentheses are peak widths at half height (Hz).

ratio of 1:1:2, due to the accidental degeneracy of the two higher field resonances. ^{1}H NMR data for **1***b* at different temperatures are summarized in Table 1.

*Synthesis of $Cp_2Ti(\mu\text{-}SiBuMeH)(\mu\text{-}H)TiCp_2$, 1*c

DMT (150 mg) was dissolved in pure degassed *n*-$BuMeSiH_2$ (1.0 mL). The solution changed colour rapidly from orange to dark blue with a vigorous gas evolution. After about 30 min, the supernatant liquid was decanted and the residual precipitate was washed three times with 2-mL portions of cold hexane and dried under vacuum to give a black powder (102 mg, 63% based on **1***c*). Satisfactory analyses were not obtained (calcd. for $C_{25}H_{34}SiT_2$: C 65.50, H 7.48, Si 6.13, Ti 20.9; found: C 62.7, H 7.01, Si 5.31, Ti 20.64). The ^{1}H NMR spectrum of the product gave only resonances in the Cp and hydride regions that were attributable to **1***c*. The *n*-C_4H_9 and CH_3 resonances of the complex were slightly obscured by small amounts of free $BuMeSiH_2$, also apparent from its Si-H resonance. The ^{1}H NMR spectrum of **1***c* is described in detail in the discussion. No parent peak for **1***c* was observed in the mass spectrum.

Acknowledgements

We thank the Natural Sciences and Engineering Research Council of Canada and the Fonds pour la formation de chercheurs et l'aide à la recherche (FCAR) du Québec for funding of this work. J.F.H. and E.S. thank N.A.T.O. for an International Collaborative Research Grant.

1. C. A. Aitken, J. F. Harrod, and E. Samuel. J. Am. Chem. Soc. **108**, 4059 (1986).
2. E. Samuel, Y. Mu, J. F. Harrod, Y. Dromzee, and Y. Jeannin. J. Am. Chem. Soc. **112**, 3435 (1990).
3. Y. Mu, B. Cote, C. A. Aitken, J. F. Harrod, and E. Samuel. Can. J. Chem. **69**, 264 (1990).
4. H-G. Woo and T. D. Tilley. J. Am. Chem. Soc. **111**, 8043 (1989); J. Am. Chem. Soc. **111**, 3757 (1989); T. D. Tilley. Comments Inorg. Chem. **10**, 37 (1990).
5. C. A. Aitken, J.-P. Barry, F. Gauvin, J. F. Harrod, A. Malek, and D. Rousseau. Organometallics, **8**, 1732 (1989).
6. G. E. Toogood and M. G. H. Wallbridge. Adv. Inorg. Chem. Radiochem. **25**, 267 (1982).
7. J. E. Bercaw and H. H. Brinzinger. J. Am. Chem. Soc. **91**, 7301 (1969).
8. J. F. Harrod and S. S. Yun. Organometallics, **6**, 1381 (1987).
9. C. A. Aitken, J. F. Harrod, A. Malek, and E. Samuel. J. Organomet. Chem. **349**, 285 (1988); J. F. Harrod, A. Malek, F. Rochon, and R. Melanson. Organometallics, **6**, 2117 (1987).
10. K. Klaus and H. Bestian. Liebigs Ann. Chem. **654**, 8 (1962).
11. J. E. Bercaw, R. H. Marvich, L. G. Bell, and H. H. Brintzinger. J. Am. Chem. Soc. **94**, 1219 (1972).
12. L. B. Kool, M. D. Rausch, H. G. Alt, M. Heberhold, U. Thewalt, and B. Wolf. Angew. Chem. Int. Ed. Engl. **24**, 394 (1985).

Can. J. Chem. Downloaded from www.nrcresearchpress.com by 88.255.202.194 on 09/08/12
For personal use only.